CSC2025

Co-operation Science Contribution

庆祝中华医学会110周年系列活动

中华医学会第二十七次心血管年会
中华医学会第二十三次介入心脏病学大会
2025长安心血管病学大会

陕西 西安 XI AN

2025年9月18-21日
September.18-21, 2025

论文汇编
下册

主办单位： 中华医学会　　中华医学会心血管病学分会
承办单位： 陕西省医学会　　陕西省医学会心血管病学分会
协办单位： 西安交通大学第一附属医院

目 录

发言交流 33
代谢性心血管疾病研究 34
Longitudinal Relationship Between Serum Palmitate and Metabolic Dysregulation: Assessing Diabetes Risk in a Community-Based Population 34
膳食炎症与膳食质量对心血管 - 肾脏 - 代谢综合征晚期及死亡风险的影响：传统分析与机器学习方法 34
冷暴露通过脂肪组织对代谢综合征引起的多器官功能障碍的影响及机制研究 34
肠道菌群及其代谢物在 2 型糖尿病心肌病进展中的作用研究 34
New criteria for obesity: clinical obesity as predictors of cardiovascular mortality among older adults in China - a nationwide, community-based prospective cohort study 35
血浆同型半胱氨酸水平与不同体重指数患者发生冠心病以及长期预后的相关性的初步探讨 35
血清葡萄糖和高密度脂蛋白介导 CDAI 与代谢综合症患者全因死亡率和心血管疾病死亡率的关系 35
DMRT2 overexpression in macrophages promotes M1 polarization to improve adipocyte inflammation and insulin resistance through interacting with FXR 35
应激性高血糖比率对急性心肌梗死患者 PCI 术后远期预后的影响 36
Comprehensive Identification of Cardiometabolic Protein Biomarkers in Acute Myocardial Infarction Using Olink Proteomics and Multi-Cohort Validation 36
美阿沙坦对糖尿病大鼠心肌脂联素和脂联素受体 1 表达的影响 [基金项目：山西省自然基金基础研究项目（20210302123088）；太原市区域医疗中心科技创新项目（202229）] 36
胰岛素通过 ACTA2 rs1324551 (A/G) 位点调控血管平滑肌细胞表型转化、增殖及迁移及其机制研究 37
成年期不同阶段体重对左室收缩功能和全因死亡的影响 37
Impact of Abdominal Obesity Indices on All-Cause and Cardiovascular Mortality in Individuals with Pre-Diabetes and Diabetes: Insights from a Prospective Cohort Study 37
Serum Glycolipids Mediate the Link Between Dietary Antioxidants and Mortality in Metabolic Syndrome 37
Impact of Cardiometabolic Index on Long-Term Mortality in Young Adults with Type 2 Diabetes Mellitus 38
代谢功能障碍相关脂肪性肝病合并高尿酸血症患者的心脏重构特征及危险因素分析 38
AIP、AST 联合左心房内径预测代谢相关脂肪性肝病患者发生冠心病风险的临床价值研究 39
相对脂肪质量与老年人群心血管代谢疾病及远期不良结局的关联研究 39
Joint Analysis of C-Reactive Protein-Triglyceride Glucose Index Clusters and Body Roundness Index Trajectories in Incident Cardiovascular Disease Risk: Insights from the China Health and Retirement Longitudinal Study (CHARLS) and UK Biobank 39
The impact of dapagliflozin for the myocardial metabolomic profiles of mice with chronic heart failure induced by a high fat diet 40
基因组结构方程模型阐明了心血管肾代谢综合征的共同遗传结构 40
甘油三酯葡萄糖 - 体型指数与老年人群全因死亡和原因特异性死亡的关联：一项队列研究 40
Association between estimated glucose disposal rate and all-cause/cause-specific mortality in the general population is modified by age: a cohort study 40
Stage-Based Biomarker Signatures of Cardiovascular-Kidney-Metabolic Syndrome and Their Associations With Mortality: An Analysis of NHANES 2011–2018 Data 41
Association of estimated glucose disposal rate with chest pain incidence and all-cause mortality in populations:A Retrospective Analysis of the NHANES Cohort 41
2 型糖尿病患者中 TyG 指数、血同型半胱氨酸水平与颈动脉斑块发生的相关性分析 41
抑制 HMOX1 靶向铁死亡减轻糖尿病心肌病 42
降钙素基因相关肽调节核转录因子 -κB 信号转导对缺氧 c-kit+ 心脏干细胞凋亡的影响 42
骨髓源性生长因子对高糖诱导 H9c2 细胞焦亡的改善作用 42
髓间充质干细胞源外泌体调控心肌微血管内皮细胞增殖的机制研究 42
Bdh1 过表达通过抑制 H3K9bhb 介导的 Ifi27l2a 转录激活改善糖尿病动脉损伤的机制研究 42
Methyltransferase like 3-mediated N6-methylatidin methylation inhibits vascular smooth muscle cells PhenotyPe switching via Promoting PhosPhatidylinositol 3-kinase mRNA decay 43
Role of Mydgf in the regulation of hyPoxia/reoxygenation-induced aPoPtosis in cardiac microvascular endothelial cells 43
m7G Methyltransferase METTL1 Promotes Post-ischemic Angiogenesis via Promoting VEGFA mRNA Translation 43
Exosomal MiR-29a in Cardiomyocytes Induced by Angiotensin II Regulates Cardiac Microvascular Endothelial Cell Proliferation， Migration and Angiogenesis by Targeting VEGFA 44
足细胞 NPRC 敲除可减轻糖尿病小鼠肾小球纤维化 44
Mediterranean diet, metabolic profiles, and the risk of coronary heart disease: evidence from a mediation analysis 44
Evaluating the Causal Effects of Lipid-Lowering Drug Targets on the Components of Cardiovascular-Kidney-Metabolic (CKM) syndrome: A Drug-Target Mendelian Randomization Study 45
Prognostic value of FIB-4 index in coronary heart disease combined with diabetes or prediabetes: a large-scale cohort study 45
Association of Air Pollutant Exposure with Cardio-Kidney-Metabolic Syndrome in Chinese Middle-aged and Older Adults: Evidence from the CHARLS Cohort 45
A Nomogram for Predicting the Progression Risk of Cardiovascular-Kidney Metabolic Syndrome 46
高血压人群血清尿酸水平与认知功能的关系：一项横断面研究 46
在中国高血压人群中脂肪肝指数与新发糖尿病及糖尿病前期发展的关系 - 一项队列研究 46
Association of cardiometabolic index with all-cause and cardiovascular deaths in patients with cardiometabolic syndrome: a national cohort study 47
血清尿酸 / 高密度脂蛋白胆固醇比值联合脉压差的纵向轨迹与慢性肾脏病发病风险：一项回顾性队列研究 47
How Does Age Acceleration Mediate the Association Between Insulin Resistance and Long-Term Mortality Among Patients With Cardiovascular-Kidney-Metabolic Syndrome? Insights from a population-based study 47
Estimated Glucose Disposal Rate and Risk of Stroke and Dementia in Non-Diabetics: A UK Biobank Prospective Cohort Study 48
UBC9 attenuates the progression of metabolic dysfunction-associated fatty liver disease by suppressing hepatocyte ferroptosis via SUMOylation-Dependent stabilization of FTH1 48
Association Between the FT3 to FT4 Ratio and Type 2 Diabetes Mellitus in Non-alcoholic Fatty Liver Disease 49
糖尿病心脏微血管损伤生物标志物和防治靶点的探究 49
Inverted U-shaped association between body mass index and left ventricular global longitudinal strain in middle-aged and elderly patients with coronary heart disease in Jilin Province, China: a cross-sectional study 49
Exploring shared therapeutic targets in Diabetic Panvascular Diseases through bioinformatics analysis 50
Relationship between uric acid to creatinine ratio and type 2 diabetes mellitus in patients with nonalcoholic fatty liver disease 50
甘油三酯、总胆固醇及体重指数与 0-3 期心血管 - 肾脏 - 代谢综合征人群心血管疾病风险的关联研究：一项全国性前瞻性队列研究 51
Prediabetes Diagnostic Thresholds and Cardiovascular Outcomes: A Prospective Cohort, Mendelian Randomization, and Cardiac Imaging Study 51
二甲双胍与接受非复杂或复杂经皮冠状动脉介入治疗的糖尿病患者的临床结局 51

Synergistic Amplification of Cardiovascular Risk by Insulin Resistance and Hepatic Fibrosis in Coronary Artery Disease: Machine Learning-Driven Phenotyping and Multi-Dimensional Interaction Analysis for Precision Risk Stratification 51
IGF2BP3 介导 DMRT2 m6A 甲基化修饰调控脂肪细胞胰岛素抵抗的机制研究 52
脂肪组织特异性 Eepd1 缺失驱动糖尿病心肌病的跨器官代谢 - 炎症轴调控机制 52
Associations and potential biological pathways between ideal cardiovascular health defined by lifes essential 8 scores and diabetes/prediabetes: perspectives from mediation analysis 52
The Impact of Remnant Lipoprotein Cholesterol on the Prognosis of Patients Undergoing PCI under Different Glycemic States: A Prospective Cohort Study 53
Association of the plasma-glycosylated hemoglobinA1c/High-Density lipoprotein cholesterol ratio with mortality and cardiovascular disease in the US population: NHANES 1999-2018 53
将心脏代谢疾病与 HFpEF 联系起来的循环介质：一种中介孟德尔随机化分析 53
Joint association of Cardiovascular-Kidney-Metabolic Syndrome staging and accelerated Phenotypic age with mortality 54
NPRC 基因敲除减轻 DKD 小鼠的肾小球纤维化 54
Homocysteine activates endothelial TP receptor to promote von Willebrand factor secretion and thrombosis 54
Joint Association Between FIB-4 Index and Advanced Cardiovascular-Kidney-Metabolic Syndrome With Aortic Valve Calcification: A Community Cohort in China 55
Metabolic Score for Visceral Fat and Cardiovascular Risk Prediction in Middle-aged and Older Chinese Adults: Evidence from the CHARLS Cohort 55
不同血糖状态心力衰竭患者中重度冠状动脉钙化病变最佳血运重建与长期结局的关联性研究 55
Apolipoprotein A2 influences ANGPTL3 on modulating TG catabolism and inflammatory cytokines secretion 56
载脂蛋白 A1 经 Sortilin 负向调控人脂肪间充质干细胞成脂分化的实验研究 56
三酰甘油葡萄糖指数与老年非介入治疗非 ST 段抬高型心肌梗死患者的预后相关：一项单中心回顾性队列研究 56
Association Between Pain Characteristics, Circadian Syndrome and Cardiovascular Disease in Chinese Middle-Aged and Older Adults: A 4-Year Follow-Up Study 56
TyG 指数联合 hsCRP 对糖尿病合并急性冠脉综合征患者 PCI 术后预后的相关性 57
Correlation of triglyceride-glucose index with major adverse cardiovascular events in type 2 diabetes mellitus patients with acute myocardial infarction combined with HFpEF 57
The Impact of Allostatic Load on the Incidence of Cardiometabolic Multimorbidity: Evidence from the China health and Retirement Longitudinal study 57
简易胰岛素抵抗指数对高原世居藏族发生高尿酸血症的预测价值 58
The Role of Instrumental Activity of Daily Living Disability in the Association between Circadian Syndrome and Cardiometabolic Multimorbidity in Chinese Middle-Aged and Older Adults 58
Intensified Lipid-Lowering Strategies and Their Effect on Atherogenic and Metabolic Markers in Coronary Artery Disease 58
TRIM35 介导氨基酸转运在压力负荷型心室重构中的作用与机制研究 58
Impact of a Comprehensive Healthy Lifestyle Score on a Broad Spectrum of Cardiometabolic Diseases and Enhanced Risk Prediction Based on the UK Biobank Database 59
老年人群心脏代谢性共病风险列线图预测模型的构建及评价 59
防晒 / 紫外线与心血管疾病及代谢疾病的孟德尔随机研究 59
血红蛋白糖化指数对早期心肾代谢综合征患者心血管疾病进展的预测作用 59
Evidence of liver-heart cross-talk: The association between FLI and CKM risk stratification 60
Associations of inflammatory prognosis index with all-cause and cardiovascular mortality among individuals with diabetes and pre-diabetes: a populationbased study 60
Age-Related triglyceride-glucose index trajectories and all-cause mortality in Chinese elderly people 61
NF2 is an essential regulator of the pro-fibrotic cardiac fibroblasts phenotype associated with pathological cardiac remodeling via the Hippo/YAP signaling pathway. 61
白蛋白 / 球蛋白比值对 2 期心血管 - 肾脏 - 代谢综合征患者死亡率的预测价值：基于全国队列的分析（1999-2018） 61
甘油三酯 - 葡萄糖指数与美国成人自杀意愿的关系 62
心肌靶向的线粒体调控能量代谢治疗缺血再灌注损伤 62
O-GlcNAcylation-Ubiquitin Crosstalk of METTL1 Drives m7G Epitranscriptomic Collapse and Lipid Metabolic Reprogramming in Diabetic Cardiomyopathy 62
Elevated thyroid stimulating hormone level is associated with arterial stiffness and increased prevalence of hypertension: a cross-sectional study 63
Triglyceride glucose - body mass index has better predictive ability of cardiovascular disease in population at low metabolic risk: a national prospective cohort study 63
DPP4+ 肝细胞中 MSR1（Mechanosensitive receptor 1）对代谢的影响及其作用机制研究 63
新型代谢相关指标与冠脉支架内再狭窄的相关性研究 64
MFN2 下调介导的线粒体碎片化参与高脂诱导的血管内皮胰岛素敏感性下降和功能障碍 64
Obesity Increases Atherosclerosis Susceptibility via Inter-tissue miR-30e-SLC7A11 Axis 64
代谢综合征组分聚集模式对心血管预后的影响及无创风险预测模型的构建：一项前瞻性队列研究 64
Basal Metabolic Rate and Atrial Fibrillation Risk among Individuals with Type 2 Diabetes: insights from the UK Biobank 65
Novel adiposity indices and their associations with all-cause and cardiovascular mortality in individuals with cardiovascular-kidney-metabolic syndrome stages 0-3: findings from a nationwide prospective cohort study 65
Musclin 通过影响 WTAP 介导的 m6A 甲基化修饰参与糖尿病肾损伤的机制研究 66
Musclin 通过内质网应激通路引起骨骼肌胰岛素抵抗的机制研究 66
DMH1 Improves Palmitic Acid-Induced Insulin Resistance in Cardiomyocytes via PP2A Inhibition and AKT/AMPK Signaling Activation 66
Inhibition of PCSK9 attenuates ferroptosis after ischemia-reperfusion in cardiomyocytes through negative regulation of the FOXO3/MMP9 pathway 66
Association between the total cholesterol/high-density lipoprotein cholesterol ratio and all-cause and cardiovascular mortality in patients with diabetes or prediabetes: Insights from China and the United StatesJoint associations of frailty and triglyceride-glucose index with allcause and cardiovascular mortality in U.S. adults: a population-based cohort study from the NHANES 68
The prognostic value of the hemoglobin-to-red blood cell distribution width ratio for all-cause and cardiovascular mortality in patients with diabetes orprediabetes: A cohort study from the NHANES 2005–2018 68
Joint Effect of Plasma Homocysteine Concentration and Traditional Cardiovascular Risk Factors on the Risk of New-Onset Acute Myocardial Infarction 69
oint Effect of Plasma Homocysteine Concentration and Traditional Cardiovascular Risk Factors on the Risk of New-Onset Stroke 69
基线糖代谢状态与全因死亡及心血管死亡风险的关联研究 69
基线糖代谢状态与不同脑卒中风险的关联研究 70
基线糖代谢状态与急性心肌梗死风险的关联研究 70
Prediction of Cardiometabolic Multimorbidity Risk in Middle-Aged and Older Chinese Adults: Longitudinal Analysis of Triglyceride Glucose-Body Mass Index (TyG-BMI) and Its Dynamic Trajectories 70

Estimated Glucose Disposal Rate and Mortality in Cardiovascular Kidney Metabolic Syndrome: Nonlinear Associations and Stratified Prognostic Significance by Glycometabolic Phenotypes 70
HbA1c>7% predicts adverse cardiovascular outcomes among stage 4 cardiovascular kidney-metabolic syndrome patients 71
尿酸对高龄重度主动脉瓣狭窄患者远期预后的预测价值 71
生命 8 要素，遗传易感性与退行性瓣膜性心脏病发病风险的关系 71
糖尿病介导的线粒体蛋白高乙酰化通过抑制线粒体超复合体组装增加心肌对缺血再灌注损伤的敏感性 72
基于快速康复理念的早期康复运动及健康教育在代谢性心血管疾病患者中的应用 72
1990-2021 年全球含糖饮料归因心血管疾病负担的系统分析 72
Physical activity, statin therapy and risk of new-onset type 2 diabetes: clinical and proteomic perspectives 72
甲状腺激素在内脏脂肪代谢功能异常中的作用及机制研究 73
糖尿病前期人群中估算葡萄糖清除率与心脏代谢性共病与全因死亡动态演变的关联：一项多状态轨迹分析 73
LncRNA Gm26870 通过调控炎症促进脂肪组织胰岛素抵抗 73
ST 段抬高型心肌梗死患者甘油三脂葡萄糖指数与梗死面积，微循环阻塞和心肌内出血的相关性研究 73
一项基于血管内超声分析载脂蛋白 B 控制水平对冠状动脉斑块进展影响的队列研究 74
Prognostic Implications of Obstructive Sleep Apnea In Acute Coronary Syndrome By Residual Cholesterol Inflammation Index 74
估计葡萄糖处置率（eGDR）与慢性肾脏病患病率及死亡率的关联：一项全国性横断面研究 74
Association between obesity metabolic phenotype and risk of incident degenerative valvular disease in UK Biobank 74
Association Between Triglyceride-Glucose Body Mass Index and Type 2 Diabetes Mellitus in Patients with Non-Alcoholic Fatty Liver Disease 75
Naringenin Exerts Cardiovascular Protective Effect in a Palmitate-Induced Human Umbilical Vein Endothelial Cell Injury Model via Autophagy Flux Improvement 75
心脏代谢指数与炎症介导的急性冠脉综合征患者易损斑块形成有关 76
中国人内脏脂肪指数长期累积水平在心血管 - 肾脏 - 代谢综合征 0-3 期人群中对心血管疾病发病的预测价值 76
Association Between Estimated Glucose Disposal Rate and Ischemic Heart Disease Prevalence in Non-Diabetic Adults: A Cross-Sectional NHANES Study 76
不同治疗背景下中国混合型高脂血症人群的血脂水平流行病学特点：一项全国性横断面研究 76
Serum Lipid Profiles Stratified by Treatment Status in Chinese Adults with Hypertriglyceridemia: a nationwide cross-sectional study 77
N6-methyladenosine of lncRNA Gm16984 inhibits homocysteine-induced podocyte injury through miR-29b-3p/HDAC4 signaling pathway 77
Adipose HuR protects against diet-induced obesity and insulin resistance 78
Persistent Methylmalonate Overload Despite Glycemic Control Drives Mitochondrial Dyshomeostasis and Subclinical Heart Damage in Diabetes 78
Multi-Etiology Transcriptomic Integration Identifies Conserved Metabolic Dysregulation in Heart Failure 79
血红蛋白糖化指数与冠状动脉疾病合并慢性肾功能不全患者经皮冠状动脉介入治疗后远期全因死亡的关联 79
The association between the triglyceride-glucose index and serum uric acid: a systematic review and meta-analysis 80
Multi-cohort analysis of metagenome for type 2 diabetes identified universal gut microbiota signatures across populations 80
Glucose oxidative metabolism score, diabetes status, and major adverse cardiovascular events in acute myocardial infarction populations 80
Predictive value of dynamic changes in eGDR for cardiovascular disease in population with Cardiovascular- Kidney-Metabolic syndrome stages 0-3: A nationwide prospective cohort study 81
OSA 相关性高血压患者中代谢性心血管疾病的临床特点及预后分析 81
MDK、PLAUR 在糖尿病合并急性冠脉综合征患者中的临床意义及其诊断价值 82
老年营养风险指数对心血管 - 肾脏 - 代谢综合征患者死亡风险的预测 82
肝纤维化评分对非肥胖冠心病患者肾功能预后的预测价值 82
心血管代谢门诊综合管理 CKM 患者的初步成效 82
体力运动对心肾代谢疾病进展及死亡风险的影响：基于英国生物银行的多状态分析 82
代谢组学发现 L- 茶氨酸可预防和延缓高血压患者肾脏损伤 83
基于 CHARLS 队列的新型复合标志物开发：TyG/TyH 衍生肥胖指数对心血管事件的预测效能研究 83
FMO2 promotes angiogenesis via regulation of N-acetylornithine 83
The prognostic significance of triglyceride-glucose index for all-cause mortality in cancer survivors: Retrospective cohort study 83
组蛋白乳酸化修饰介导代谢重编程在心肌梗死后心肌再生中的作用机制研究 84
Association of a Novel BMI/Triglyceride-Glucose Waist Circumference Index with All-Cause and Cardiovascular Mortality in a COPD Population 84
心脏代谢共病患者估计葡萄糖处理率和颈动脉斑块的相关性分析 85
Association between dietary B vitamin intakes and advanced cardiovascular-kidney-metabolic syndrome: insights from the National Health and Nutrition Examination Survey 85
ATAD3A Regulates Mitochondria–Lysosome Membrane Contact Sites via the LIAS/DLST Axis to Suppress Aortic Dissection 86
心血管 - 肾脏 - 代谢综合征 0-3 期人群中 C 反应蛋白 - 甘油三酯 - 葡萄糖指数与远期心脑血管疾病发病风险的关联研究 86
吲哚类代谢物与心血管疾病研究进展 86
Prevalence of Cardiovascular-Kidney-Metabolic Syndrome by Social Determinants of Health: A Population-Based Study of 4.4 Million Adults in Northwestern China 86
阻塞性睡眠呼吸暂停在急性冠状动脉综合征中的预后意义：不同血糖水平的研究分析 87
The association between the heart rate response related to sleep apnea and left ventricular hypertrophy in obese individuals 87
中心动脉收缩压和血同型半胱氨酸对成年高血压患者卒中发生风险的联合作用 87
代谢性心血管疾病的综合管理：基于多学科协作的临床实践研究 88
Hepatic Steatosis Index Predicts Risk of Chronic Non-Rheumatic Aortic Valve Insufficiency Rehospitalization in a Northwest Chinese NAFLD Cohort 88
基于 NHANES 数据库的膳食炎症指数与代谢综合征患者死亡风险的研究 88
Association of Depression Severity and Transition Patterns of Cardiometabolic Multimorbidity 88
Causal Association Spectrum of Fine Particulate Matter ($PM_{2.5}$) Exposure and Cardiometabolic Diseases: Analysis of Dose-Response Characteristics in Epidemiological Associations, Population Susceptibility Stratification, Cascade Reaction Pathways of Cellula 89
蛋白尿在心血管代谢因素与视网膜动脉硬化关联的中介效应分析 90
Impact of the mismatch between respiratory event frequency and hypoxic burden on cardiovascular outcomes in patients with obstructive sleep apnea 90

心脏康复及有关研究 91
心脏康复护理对心梗介入治疗后患者心理状态及生活质量的影响 91
急性心肌梗死患者开展早期康复训练对心功能恢复影响 91
老年冠心病患者 CPET 指导的运动康复方案优化研究 91
肌少症的研究进展：从机制到治疗 91
心磁图在缺血性心脏病的临床研究进展 91
急性冠脉综合征患者 PCI 术后接受心脏综合康复治疗的效果观察 91
重视心肌梗死后抑郁症 91

心脏康复延伸护理服务 联合正念减压对慢性心力衰竭患者心脏康复效果及负面情绪的影响 91
心力衰竭患者健康心理控制源与领悟社会支持和自我管理行为的关系：基于多项式回归和响应面分析 92
急性心肌梗死介入术后患者早期心脏康复参与意愿及其影响因素研究 92
中西医结合心脏康复对稳定性冠心病患者心肺功能影响的临床研究 92
心肺运动试验对急性心肌梗死后心力衰竭发生风险预测的增量价值 92
Individualized Cardiac Rehabilitation for a High-Risk Stanford Type A Aortic Dissection Patient Undergoing Whole-Life Cycle Management: A Case Report 92
心脏康复在心血管疾病中的研究进展 93
急性心肌梗死急诊 PCI 术后心脏康复护理对改善患者生存质量的影响 93
中国心血管疾病患者的心肺适能参考标准 93
Aerobic Interval Training Ameliorates Myocardial Fibrosis in Uremic Rats by Inhibiting Cardiomyocyte Cuproptosis 93

Aerobic Interval Training Ameliorates Myocardial Fibrosis after Myocardial Infarction in Rats by Inhibiting Cardiomyocyte Ferroptosis via Endogenous Hydrogen Sulfide 94
Circulatory power is applicable for the early prediction of post-acute myocardial infarction late-onset heart failure risk 94
马拉松运动强度对心肌肌钙蛋白升高的影响：训练优化的新视角 95
Progesterone promotes the proliferation of embryonic epicardial cells and decreases left ventricular fibrosis through ALDH1A3/Glycolytic pathway 95
分阶式心脏康复联合动态量化健康教育在冠心病患者中的综合干预效果：一项随机对照研究 96
基于 CiteSpace 的心脏瓣膜置换术后患者抗凝治疗的可视化分析 96
Impact of perioperative cardiac rehabilitation on the prognosis of female patients undergoing elective valve surgery: a gender-specific analysis of the PORT randomized clincial trial. 96
心脏康复的研究进展 96
Impact of Cardiopulmonary Exercise Testing -Guided Individualized Cardiac Rehabilitation on Functional Capacity and Prognosis in Coronary Artery Disease Patients 97
Joint association of TyG index and peak kilogram oxygen uptake with MACE events in post-PCI patients 97
Comparison of the predictive efficacy of triglyceride-glucose (TyG) index and modified TyG index combined with cardiopulmonary exercise testing (CPET) parameters for major adverse cardiovascular events (MACE) risk in the population 97
RelationshiP and Prognostic value of the triglyceride-glucose index and oPtical coherence tomograPhy-derived Physiological index in Patients with acute coronary syndrome 98
The effects of perioperative cardiopulmonary integrated rehabilitation in patients undergoing TAVR 98
首诊冠心病患者运动恐惧现状及影响因素分析 98
Long-term Efficacy and Safety of Moderate-Intensity Continuous Training on the Improvement of Cardiopulmonary Function in Patients After Transcatheter Aortic Valve Replacement: an analysis of the extended follow up of the ENERGY Study 98
Comparative effects of traditional Chinese exercises on cardiac rehabilitation in patients after percutaneous coronary intervention: A Systematic Review and Network Meta-Analysis 99
EETs 介导有氧运动对心肌梗死后心脏淋巴管重塑的影响和机制 99
Interpretable machine learning identifies peak VO2 as a key predictor of MACE events in patients with valvular heart disease. 99
基于个性化护理方案的心血管疾病康复效果提升研究 100
OPT-CAD Score Combined with Cardiopulmonary Exercise Testing Parameters to Evaluate Long-Term Prognosis in Patients with Coronary Artery Disease 100
危重急性失代偿性心力衰竭患者的早期康复：随机对照研究 101
基于快速康复理念的多学科协作运动康复模式对心脏术后患者心理应激及活动功能的影响研究 101
进行 6 分钟居家运动对冠心病患者血清 Lp-PLA2 和相关血脂成分影响研究 101
心理干预在平板运动试验诊断中的应用 101
基于心肺运动试验与机器学习的瓣膜术后低心排血量综合征预测模型构建 101
合并自主神经功能紊乱的非阻塞性冠脉疾病患者临床特征研究 101
短期高强度间歇训练与中等强度连续训练对心血管疾病患者心率恢复和心肺的益处：一项倾向匹配的回顾性研究 102
Protective effect of high-intensity interval exercise on cardiac damage induced by hyperlipidemia 102
运动康复对不同射血分数心衰病人骨骼肌质量减少的影响 102
心肺运动试验在高龄老年患者中的应用 103
DRG 支付改革背景下心脏康复临床研究进展 103
基于 II 期心脏康复的社区康复管理模式对 TAVR 术后患者的应用效果 103
老年心血管病合并衰弱患者恐动症个性化运动康复系统的研发 103
冠心病患者经皮冠状动脉介入治疗术后早期运动耐量降低风险预测模型的建立与构架 103
Application of the OMTR Concept in a Multistage Rehabilitation Pathway for an Elderly, Frail STEMI Patient with Heart Failure 103
不同程度 PHQ-9 评分的经皮冠状动脉介入治疗患者心肺功能指标特征对比 104
基于 IM 计划的急性心力衰竭代偿期患者早期运动康复方案的构建与应用 104
基于心肺运动试验评估陈旧性心肌梗死合并室壁瘤患者的运动安全性研究 104
基于吸气肌训练的综合心脏康复方案对慢性心力衰竭患者的效果研究 105
基于 Framingham 风险分层模型的冠心病患者个性化健康管理路径构建研究 105
Nonexercise prediction equation for peak oxygen uptake in Chinese patients with cardiovascular disease 105
老年急性心肌梗死患者早期运动康复介入的时机选择与风险评估体系构建 106
1 例主动脉瓣重度狭窄，慢性心衰急性加重合并急性脑梗死行 TAVI 手术的患者从预康复开始，全围术期心脏康复训练的经验分享 106
Construction and application of a plyometric training intervention program for elderly patients with cardiovascular frailty based on evidence-based and Fogg behavioral models 106
心肺康复训练联合心理干预在双病共患群体中的协同效应研究 106
Enhanced External Counterpulsation Combined with Comprehensive Cardiac Rehabilitation Improves Functional Capacity and Rhythm Outcomes in Atrial Fibrillation: A Randomized Controlled Trial 106
基于运动危险分层构建慢性心力衰竭患者早期心脏康复运动实施路径 107
CCU 心脏术后患者家属心理弹性与人文支持需求的相关性分析 107
体外反搏治疗联合 CPET 指导高强度间歇训练改善射血分数保留型心衰患者运动耐量与舒张功能的随机对照研究 107
心脏术后患者超早期康复中血流动力学响应模式与运动处方优化研究 107
多学科协作模式在体外膜肺氧合（ECMO）支持重症患者康复方案中的应用研究与实践 108
远程居家心脏康复监测工具的研究进展与展望 108
老年急性冠状动脉综合征 PCI 术后早期心脏康复有效性和安全性研究 108
心脏外科术后早期康复干预和首次离床活动的影响因素研究 108
术前多模式预康复对心脏手术后早期启动康复干预时间及肺部并发症的影响 108

心脏康复与冠心病的二级预防 109
The Efficacy of Traditional Chinese Exercises in Cardiac Rehabilitation for Chronic Heart Failure：a systematic review and network meta-analysis 109
PCI 术后与不同程度冠脉狭窄患者的 CPET 指标对比及进行康复治疗指征评估 109
早期心脏康复护理对急性心肌梗死 PCI 术后的影响 109
基于高级健康评估结合 ERAS 理念的一例老年患者行冠状动脉搭桥联合瓣膜置换手术的个案护理 110
通过运动为基础的心脏康复，改善不同 BMI 组心血管疾病患者的运动能力及生活质量。 110
基于 CPET 指导的心脏康复运动对老年 CHF 患者焦虑情绪和生活质量的影响 110
herapeutic Effect of Limbs Compression Based Anti-syncope Therapy Trousers on Vasovagal Syncope 110
射频消融术患者围术期踝泵运动依从性影响因素的质性研究 110
Nonexercise Prediction Equation for Oxygen Uptake at the Anaerobic Threshold in Chinese Patients with Cardiovascular Disease 111
双心医学视角下冠心病患者焦虑抑郁症状的全程管理模式探索 111
个性化心脏运动康复方案对心力衰竭患者心肺功能的影响研究 111
基于循证医学的冠脉支架术后合并 OSAHS 患者运动康复方案优化 112
高原地区慢性呼吸系统疾病患者阶梯式肺康复方案的构建与验证 112
高强度间歇训练联合地中海饮食在冠心病二级预防中的协同效应研究 112
家庭 - 医院 - 社区三元联动管理模式对慢性心肺疾病预后的影响 112
太极“柔化心泵”理论在慢性心衰康复中的临床应用 112
Physical performance on the early 6-minute walk test in coronary artery bypass grafting patients during inpatient cardiac rehabilitation 113
基于 TPKCEE 复合型教学的混合教学模式 在心脏康复护理教学中应用研究 113
急性心肌梗死恐动症患者对虚拟现实运动康复训练系统使用意愿及需求的质性研究 113
中医五行音疗联合安宁疗护在慢性心力衰竭患者康复中的护理实践 113
运动通过 c-MAF 调控常驻巨噬细胞代谢重编程改善心肌梗死修复 113
Aerobic exercise improves coronary microcirculation dysfunction by regulating endothelial cell function through the m6A methyltransferase METTL14 114
Enhanced External Counterpulsation Promotes Recovery of Exercise-Induced Muscle Damage by Reducing Plasma Acetylglycine and Inhibiting CD56dim NK Cells Differentiation 114
基于循证护理的早期心脏康复干预对急性心肌梗死 PCI 术后患者预后的影响 115
结构性心脏病患者经导管介入术后早期康复护理模式的构建与应用效果评价 115
体医融合模式下 PCI 术后患者 II 期心脏康复运动方案的构建与应用研究 115
永久人工心脏起搏器植入术后患者应用护士参与心脏康复护理的效果研究 115
经导管三尖瓣介入治疗术的心脏全程康复 116
基于 GINSINI 评分心肺运动试验联合 TyG 指数预测冠脉狭窄风险模型构建 116
基于计划行为理论的阶梯式康复护理模式在 A 型主动脉夹层术后截瘫患者护理 116
基于 CiteSpace 心脏康复研究热点及发展趋势的可视化分析 116
AMI 患者 PCI 术后 I 期运动康复方案的构建与实证研究 116
老年性心脏疾病患者的心脏康复护理策略与效果分析 116
远隔缺血后适应在缺血性心肌病中的保护作用的临床观察 117
中国健康成人心肺适能的年龄、性别与 BMI 分布特征：一项基于 V̇O2peak 的回顾性横断面研究 117
基于心肺运动试验的健康成年人峰值氧脉搏预测方程的建立与验证 117
PH 患者不同运动试验（CPET 与 6MWT）与疾病严重性的临床研究 117
急性心肌梗死患者早期下床的安全性分析 118
基于老年综合评估的多学科心脏康复干预在老年衰弱冠心病患者的应用 118
八段锦在慢性心功能不全康复中的剂量效应研究 118
循证理念指导下康复锻炼应用于重症老年感染性心肌炎患者中的研究 118
专科护士为主导的多学科协作康复护理对心脏瓣膜置换术后患者康复的影响 118
促进急性心梗患者的康复与提高生活质量 118
冠心病患者运动恐惧干预研究的范围综述 119
基于数字孪生的心脏术后康复训练虚拟仿真模型构建及运动风险评估实践研究 119
2 型糖尿病对充分 PCI 术后患者心肺运动测试中氧脉搏轨迹平台的影响 119
医院主导的居家 II 期心脏康复对急性心肌梗死 PCI 术后患者自主神经功能改善的研究 119
心外科术后握力体重指数与术后离床时间的相关性 119
陈旧性心肌梗死患者平衡功能特征及影响因素研究 119
基于微信平台的心脏康复指导对中青年 PCI 术后患者院外生活质量及机体功能状态影响的效果分析 120
Physical Exercise Mitigates Chronic Psychological Stress-Induced Neuroimmune Crosstalk via BDNF-Kif4-TARM1 axis 120
5-Oxoproline prevents doxorubicin-induced cardiotoxicity and tumor growth 120
八段锦运动对慢性心力衰竭的中老年女性患者影响的临床研究 121
远程监测联合运动处方对冠心病 PCI 术后患者心功能的影响——一项随机对照试验 121
心脏康复对急性心肌梗死经皮介入治疗后患者左心室功能、NT-ProBNP 和生活自理能力的影响：一项回顾性研究 121
一例原发性醛固酮性高血压的诊治经验 121
移动健康技术支持的居家心脏康复模式对冠心病患者心肺功能及生活质量的影响：一项随机对照试验 122
原发性醛固酮性的诊治经验 122
心脏康复与冠心病二级预防 122
基于可穿戴设备的远程监护联合个性化运动处方对 PCI 术后患者心脏康复效果的影响：一项随机对照试验 123
晚期糖基化终末产物对心血管疾病患者心脏康复后运动能力改善的预测意义 123
心肌梗死后运动能力改善与主要心血管事件的关系 123
经导管主动脉瓣置换术后患者一期心脏康复护理方案的构建与应用研究 123
基于移动健康技术的心内科青少年患者心脏康复护理方案构建 123
早期强化心脏康复训练对非 ST 段抬高型心肌梗死 PCI 术后患者的效果 123
慢性心力衰竭患者中西医结合运动康复的研究进展 124
基于数字健康管理的家庭康复干预对老年冠心病患者临床疗效的随机对照研究 124
社区导向的 II 期心脏康复管理模式对 PCI 术后患者心肺功能及预后的影响 124
基于 ITHBC 理论的心脏术后患者运动康复依从性干预模型的构建与实证研究 124
8 例 CABG 术后 ARSD 患者早期清醒下俯卧位的康复治疗 124
心脏康复转诊管理的最佳证据总结 125
A Multimodal Data-Based Auxiliary Diagnostic Model for Mental Stress-Induced Myocardial Ischemia (MSIMI) 125
基于多学科协作的心脏康复护理模式在心血管疾病患者中的应用效果研究 125

心脏康复护理在心脏移植术后患者护理中的应用效果观察 126
肥厚型心肌病患者多维度康复护理模式的构建与实践 126
基于循证医学的肥厚型心肌病康复护理路径优化研究 126
心脏康复对心血管疾病患者心功能、运动耐力及生活质量的影响研究 126
心肺运动试验指导的个体化康复方案对冠心病患者功能恢 复的临床价值研究 126
基于心肺运动试验的中老年体检人群运动高血压及其影响因素分析 126
渐进性运动训练对重症体外膜肺氧合术后患者早期运动功能的影响 127
一例产褥期主动脉夹层术后早期康复治疗 127
一例 ECMO 联合 CRRT 治疗暴发性心肌炎患者的早期康复 127
有氧运动通过增加 BDNF 释放抑制心脏常驻巨噬细胞凋亡改善心肌梗死后心功能 128
恐惧回避模型在心血管疾病中的应用进展 128
1 例 ECMO 支持下冠脉旋磨术及支架植入术后 构建个性化重症心脏康复模式的效果评价 128
冠心病患者心脏康复意向干预的最佳证据总结 128
一例 ECMO 联合左心辅助装置治疗巨细胞性心肌炎患者的早期康复 128
心脏康复的临床效益与研究进展 129
一例产褥期 A 型主动脉夹层术后早期康复治疗 129
一种气切患者使用的呼吸训练器设计方法与临床实践 130
运动模拟药物通过 m6A 修饰调控巨噬细胞极化延缓动脉粥样硬化 130
叙事护理外部见证人视角下社区二期心肺康复养育共同体的协同路径研究 130
重症监护室心脏瓣膜病患者 TAVR 术后早期心脏康复对运动能力及心功能的影响 130
心包剥脱术患者的心肺运动试验结果特征 130
PNF 有序呼吸肌拉伸训练技术在慢性心力衰竭患者康复运动实践与应用 131
康复护理对冠心病患者行经皮冠状动脉介入术术后恢复的影响 131
六分钟步行试验指导的有氧运动康复对慢性心力衰竭行心肌收缩力调节器术后患者心功能及运动耐量的影响 131
TAVR 术后患者心脏康复护理的现状及展望 131
IMB 模型的预康复护理干预对急性期主动脉夹层患者的影响 131
心血管术后恐动症患者管理的最佳证据总结 131
呼吸疗法在老年心力衰竭患者心脏康复中的应用效果 131
有氧运动通过 Mettl14/GATA3 通路增加巨噬细胞脂噬发挥抗动脉粥样硬化作用 132
不同年龄组冠心病患者体适能指标之间的差异 132
Cardiac Shock Wave Therapy Ameliorates Myocardial Ischemia in Patients with Non-obstructive coronary artery disease: A Randomized Trial 132
高原冠心病患者居家心脏康复的研究进展 132
基于循证医学的心脏康复规范化实施的相关探讨 133
心脏康复的相关研究 133
高强度间歇训练在慢性心衰伴 2 型糖尿病患者中的应用效果 133
基于 RCA 与 Teach-back 法的多维度干预在心力衰竭患者出院健康教育中的应用 133
多学科协作模式下心脏康复在左心室辅助装置植入患者围术期的应用效果 134
基于时限性自我调节理论构建的个体化运动方案在心脏康复患者中的应用 134
心脏康复训练对冠心病病人康复效果的 Meta 分析 134
心脏康复训练联合预见性护理对心绞痛患者经皮冠状动脉介入术的影响 134
基于人文护理的心脏康复模式构建及应用效果研究 134
Evidence-based construction of an early exercise rehabilitation program for kinesiophobic patients after coronary stent implantation 134
Construction and application of a plyometric training intervention program for elderly cardiovascular co-morbid patients based on the Fogg behavioral model 135
Research on the development and application of cardiac rehabilitation training games for patients with chronic heart failure 135
A study on the construction and application of a management program for muscle-reducing obesity in patients with cardiovascular disease 135
系统规范化心脏康复护理在慢性心力衰竭患者中的应用 136
心肺康复专科护士临床实践基地培训体系的构建与实施 136
心血管病康复护理实践与思考 136
康复护理在心脏瓣膜病患者围术期应用效果的研究 136
基于说服系统模型的慢性心衰患者居家运动康复平台设计与应用 136

心脏急重症有关的研究 138
心源性休克患者在心内监护室的护理要点与方法 138
心脏骤停患者亚低温护理对神经功能恢复的影响 138
血管外肺水指数与中心静脉压预测心源性休克患者容量状态的比较研究 138
GLP-1R Activation Alleviated Sepsis-Induced Cardiac Dysfunction by Modulating Macrophage Polarization via the STING/ P65 Pathway 138
心血管危重症医护一体化管理的探索与实践 139
命悬一线，好转出院 ——1 例急性心肌梗死行 ECMO 治疗存活者的远期疗效观察 139
急性心肌梗死院前就医延迟模型构建及验证 139
心肌梗死 PCI 术后非计划再手术患者临床特征及影响因素分析 139
两难境地，险象环生 - 急性心梗合并消化道出血，如何是好？ 139
第一阶段射血分数在脓毒症心肌损伤的早期识别及临床预后的评估价值 139
经皮机械循环辅助装置的应用现状及国产化进程 140
硫酸镁使用与心肌梗死患者死亡率的关系：一项回顾性队列研究 140
第一阶段射血分数对新活素治疗慢性心衰急性加重的临床疗效评估 140
急性心肌梗死合并心源性休克的当代治疗策略与技术 140
急性心肌梗死心脏游离壁破裂存活患者病情特征分析及相关诊治经验 140
The Role of TyG Index in distinguishing NSTEMI from Acute Heart Failure Patients 141
Intra-aortic balloon pump implantation in early-stage cardiogenic shock reduces 30-day mortality in patients with ventricular septal defect following myocardial infarction 141
褪黑激素对小鼠脓毒症心肌损伤模型的保护作用机制 141
VA-ECMO 联合吸入一氧化氮治疗一例 TTVR 术后急性右心功能不全患者的护理 141
Dysregulated Tryptophan-Kynurenine Pathway Drives Septic Cardiomyopathy: A Multimodal Diagnostic Model Integrating Ghrelin and Metabolites 142
Triglyceride-glucose index may influence ideal body weight in cardiovascular critically ill patients without diabetes: a retrospective study of the MIMIC-IV database 142

米拉贝隆激活 β3-AR 通过促进血管周围脂肪组织中的淋巴管生成来预防主动脉夹层 / 动脉瘤发生 143
Association Between Time in Targeted Blood Glucose Range and In-Hospital Mortality in critically ill patients with cardiovascular diseases: analysis of the MlMIC-IV database 143
Early Systolic Blood Pressure Time-in-Target Range and Mortality in ICU Patients with Heart Failure: A Retrospective Cohort Study from the MIMIC-IV Database 143
静脉与冠脉联合应用比伐卢定对 STEMI 接受 PPCI 无复流的预防作用 144
普通肝素与比伐芦定对 IABP 辅助 PCI 术中 ACT 的影响：单中心回顾性分析 144
AccuIMR 冠脉微循环功能评估及对急诊 PCI 术后 STEMI 患者住院临床结局影响的研究 145
基于可解释机器学习模型的 VA-ECMO 辅助儿童急性肾损伤风险早期预测 145
Combined single-cell RNA sequencing and mendelian randomization to identify biomarkers associated with lipid metabolism in myocardio 145
体外心肺复苏在急性心梗后心跳呼吸骤停患者中的应用单中心经验 145
急性心肌梗死合并心源性休克患者急诊 PCI 术后院内上消化道出血预测模型的构建与验证 146
The Role and mechanism of E3 Ubiquitin Ligase HUWE1 In Acute Myocardial Infarction 146
The global burden of Aortic Aneurysm attributable to Hypertension from 1990 to 2021: Current Trends and Projections for 2050 146
Relationship between uric acid to high-density lipoprotein cholesterol ratio and depression in patients with myocardial infarction: a cross-sectional survey based on NHANES database from 2011 to 2018 147
肝功能对 ICU 心力衰竭患者预后的预测价值 147
Xa 因子抑制剂在急性心肌梗死后左心室血栓的有效性及安全性：一项单中心回顾性研究 147
AECOPD 伴心房颤动临床预测模型构建与验证及预后分析 148
Association of longitudinal Blood Urea Nitrogen trajectory with in-hospital and 28-day mortality in Acute Heart Failure with Cardiorenal Syndrome 148
“双线作战”的成功典范：多学科协作下复杂感染性心内膜炎合并肠系膜上动脉栓塞的救治 148
脂肪细胞 GATA5 介导脓毒症心肌损伤的作用机制 149
Association between triglyceride glucose-body mass index and systemic inflammation response index on one-year all-cause mortality in critically ill patients with coronary heart disease: a retrospective study utilizing the MIMIC-IV database 149
中医耳穴贴压联合渐进式肌肉放松训练在 CCU 焦虑患者中的协同干预研究 149
基于早期阶梯式肺康复干预对 CCU 机械通气患者脱机成功率及呼吸力学的影响研究 149
Development and External Validation of a Transparent Machine-Learning Model for One-Year Mortality Risk in AMI Patients Supported with Intra-Aortic Balloon Pump 150
1 例部分型心内膜垫缺损矫治术后患者的护理 150
多学科 ECMO 团队护理对重症心脏病 ECMO 应用患者生活质量的影响 150
血小板源性 circFAM13B 与脓毒症患者心肌损伤标志物的相关性研究 150
估算脉搏波传导速度在危重房颤患者死亡风险预测中的价值 151
急性心肌梗死 PCI 术后急性肾损害与术后心肌梗死面积和心肌内出血的相关性研究 151
急性 A 型主动脉夹层患者术后死亡风险的最简单、快捷、普适的炎症预测指标 151
Risk Factors of Patients with Infective Endocarditis Complicated by Perivalvular Abscess 151
心脏急重症有关的研究：新发现、新成果与新知识 152
基于多模态数据融合的心脏急重症早期预警模型构建与应用研究 152
高流量鼻导管氧疗对比无创通气在有创呼吸机辅助通气后的疗效：一项跨多种疾病与年龄组的荟萃分析 152
Long-term Outcomes in Patients with Low to Intermediate Surgical Risk Undergoing Transcatheter Aortic Valve Replacement and Surgical Aortic Valve Replacement for Aortic Stenosis: a meta-analysis 152
基于多模态评估的 ECMO 支持治疗暴发性心肌炎预后预测模型构建及管理策略优化研究 153
主动脉内球囊反搏对急性重症心肌炎的疗效及对心功能和心肌酶谱等的影响 153
1 例抗心律失常药物诱导 QTC 延长触发顽固性心室电风暴合并继发性高钾血症及多器官衰竭的急救与护理 153
The effect of environmental changes and air pollution on the occurrence of acute aortic dissection: A time-series study in Urumqi, Xinjiang 153
心源性休克预后相关因素分析 154
IVABRADINE-INDUCED HEART RATE REDUCTION INCREASES THE SEVERITY OF POSTRESUSCITATION MYOCARDIAL DYSFUNCTION IN A RAT MODEL OF CARDIOPULMONARY RESUSCITATION 154
乳酸白蛋白比值对心原性休克患者 28 天死亡率的预测价值 154
Clinical characteristics and outcomes of post-infarction ventricular septal rupture: a single center experience 154
基于游戏移动应用程序的模拟训练在 CCU 护士 ECMO 技能培训中的应用 155
Management of Ventricular Septal Rupture Following Acute Myocardial Infarction Using a Fully Magnetically Levitated Extracorporeal Ventricular Assist Device: A Case Report 155
基于信息化平台的左心辅助装置植入术后随访管理及患者发生不良事件分析 156
ECMO 联合 IABP 治疗严重心肺衰竭患者的护理质量评价指标体系构建 156
Pulse index continuous cardiac output monitoring improved clinical outcomes of acute myocardial infarction patients complicated by cardiogenic shock 156
血小板与白细胞比值与急性心肌梗死合并心源性休克的短期预后有关 156
Urgent Ablation for Drug-Refractory Electrical Storm: High Acute Success and Sustained Prognostic Benefit 157
护士主导的撤机方案对机械通气患者的影响：一项系统评价和荟萃分析 157
Ondansetron alleviates sepsis-induced cardiomyopathy-triggered cardiomyocyte ferroptosis via the ATF3-System xc ⁻ -GPX4 axis. 157
多巴酚丁胺与米力农在合并右室梗死的下壁 ST 段抬高型心肌梗死患者中的疗效比较：基于 16 年单中心数据的回顾性研究 158
流程化管理对急性心肌梗死后室间隔穿孔患者预后的影响 158
穿孔面积及其变化对急性心肌梗死后室间隔穿孔患者预后的影响 158
心脏急重症患者机械循环支持治疗的时机选择与预后分析 159
血浆白蛋白水平对 VA-ECMO 脱机成功率的预测价值及临床意义 159
心源性休克患者 ECMO 治疗前预后指标的最新研究进展 159
基于心电图特征的急性下壁心肌梗死早期诊断与心律失常关联分析 159
右美托咪啶对急性 STEMI 需要接受无创通气行 PCI 患者预后的影响 160
冠心病患者旋磨术后院内心力衰竭的风险预测模型 160
神经酰胺风险评分联合 GRACE 评分提高非 ST 段抬高型急性冠脉综合征患者长期预后的预测准确性 160
Predicting Postoperative Atrial Fibrillation in Cardiac Surgery: postoperative hematological insights for better outcomes 160
重视心电图诊断意义，提升灾难性 PTE 救治效率 161
冠脉腔内影像学及生理学有关研究 162
经皮冠状动脉介入治疗术后冠状动脉生理学评估的研究进展 162
Angiography-Derived Index of Microvascular Resistance After Drug-Coated Balloon Versus Drug-Eluting Stent Implantation: A Post Hoc Analysis from

the FADDY Trial 162
糖尿病联合冠状动脉微血管功能障碍对行旋磨术患者预后的预测价值：一项多中心回顾性观察性研究 162
急性心肌梗死非罪犯血管的全面生理学评估：必要性及临床意义 162
Mechanism of left main in-stent restenosis evaluated by intravascular ultrasound 163
冠状动脉微循环功能障碍对延迟干预的中度狭窄病变的临床预后影响 163
Diagnostic Accuracy of Artificial Intelligence Enhanced Ultrasonic Flow Ratio for Onsite Assessment of Coronary Stenosis 163
基于光学相干断层成像与冠状动脉造影指导支架内再狭窄介入治疗的预后分析：一项单中心、回顾性研究 164
糖尿病合并 NSTE-ACS 多支病变患者 PCI 后微循环功能障碍相关因素探索 164
NSTE-ACS 合并多支病变患者 PCI 后冠脉微循环功能障碍预测研究 164
探究不同年龄段急性 ST 段抬高型心肌梗死患者的临床与影像学特征 164
探究不同年龄段急性 ST 段抬高型心肌梗死患者的临床与影像学特征差异 165
急性心肌梗死患者中罪犯病变斑块破裂、非罪犯病变斑块破裂和薄纤维帽粥样硬化斑块的形态学特征差异：一项光学相干断层扫描研究 165
STEMI 患者全冠脉斑块特征的性别差异：一项三支血管 OCT 研究 165
OCT 识别的非罪犯斑块破裂的长期预后价值 165
CT-FFR 与 QFR 诊断冠状动脉病变特异性缺血准确性的对比研究 165
代谢组学揭示胍丁胺作为冠心病患者易损斑块的预测标志物 165
Evaluation of Neointimal Coverage After Guiding De-escalation of Antiplatelet Treatment in Patients with ST-elevation Myocardial Infarction Undergoing Percutaneous Coronary Intervention by Optical Coherence Tomography or Angiography 166
Rationales Behind Physiology-guided Revascularization: Diagnostic and Prognostic Impact of Quantitative Flow Ratio in the FAVOR III China Trial
定量血流分数指导经皮冠脉介入治疗策略在不同心外膜冠脉中的血管特异性结局：FAVOR III China 研究的预设亚组分析 167
A deep learning methodology for fully-automated quantification of calcific burden in high-resolution intravascular ultrasound images 167
Optical coherence tomography versus coronary angiography -guided percutaneous coronary intervention: a systematic review and meta-analysis
High-Risk Lesion Features on Coronary CT Angiography Predict Acute Coronary Syndrome in FFR-Negative Patients 168
Guanxinshutong capsule alleviates hypoxia-induced myocardial apoptosis via AMPK-mediated autophagy 169
Prognostic Value of IVUS-modulated Murray-law Quantitative Flow Ratio After Percutaneous Coronary Intervention: Post Hoc Analysis from The FLAVOUR Trial 169
急性冠状动脉综合征合并支架内再狭窄患者中新生动脉粥样硬化的临床危险因素分析 169
Predictors for Anti-Thrombotic Therapy Prognosis of Plaque Erosion: Results from OCT-Based Fluid-Structure Interaction Models 170
慢性完全闭塞病变主要供血血管定量血流分数对患者远期预后的影响 170
TET2 Mutations and Coronary Plaque Characteristics Assessed by Optical Coherence Tomography in Patients with
ST-Elevation Myocardial Infarction 170
Impact of Intravascular Imaging-Guided Drug-Eluting Stent Implantation on Cardiac Mortality in Patients with Diabetes and Coronary Artery Disease: A Multicenter Cohort Study 171
基线 QFR 在单支冠脉临界病变患者中的预后分层价值 171
Optical coherence tomography-guided drug coatedballoon in non-small de novo coronary arterylesions: a prospective clinical research 171
Non-Invasive and Invasive Physiological Indices in the Clinical Assessment of Coronary Heart Disease Patients and Comparison with Angiography-Guided PCI: A Network Meta-Analysis Based on Randomized Controlled Trials 172
基于冠脉造影衍生的微循环指数与急性 ST 段抬高型心肌梗死患者预后的相关性分析 172
A higher level of sST2 predicts the hospital mortality of patients with infective endocarditis: A 10-year retrospective study in China 172
TyG 指数、TyG-BMI 指数对 AMI 行急诊介入治疗患者预后的预测价值 173
Prevalence and clinical characteristics of coronary microvascular dysfunction in Tibetan highlanders with suspected coronary artery disease 173
Characteristics and Mechanisms of Coronary In-stent Restenosis Across Different Clinical Presentations: An Optical Coherence Tomography Study 173
基于光学相干断层扫描的冠状动脉非阻塞性心肌梗死的临床特征与预后研究 174
Prognostic performance of CCTA-derived coronary physiology and plaque characterization in the CAREER study 174
ST 段抬高型心肌梗死患者支架植入术后功能学评估的临床研究 174
Insulin Resistance and Culprit Plaque Morphology: A Study of Young and Middle-Aged Hypertensive Patients With STEMI 175
Multimodal Imaging And Functional Assessment For Etiological Diagnosis And Prognosis Improvement In MINOCA Patients 175
IVUS 指导处理冠脉多分叉病例 1 例 176
Altered DNA methylation and transcriptome landscape for the differentiation diagnosis of plaque erosion from plaque rupture:
the NBPE-ACS study 176
Predictors of High-risk Non-Culprit Plaque Rupture: A Serial Optical Coherence Tomography Imaging Study 176
径向管壁应变在冠脉临界狭窄病变生理性进展的预测价值 177
聚乙烯微塑料负荷与急性冠状动脉综合征中斑块易损性相关：基于 OCT 的分析 177
OCT applied to explore Morphological predictors of no-reflow phenomenon after PPCI in STEMI patients 177
AI-Driven Virtual Histology with Optical Coherence Tomography for Comparing Acute and Short-Trem Performance of Bioresorbable Scaffolds and Drug-Eluting Stents 177
急性冠脉综合征患者的形态学、面积截值和无血流现象的预后：光学相干断层扫描研究。 178
非罪犯血管 TCFA 斑块快速进展的的预测因素分析 178
Influence of OCT-based Macrophage Infiltration on Periprocedural Myocardial Infarction in Patients Undergoing Elective PCI Treatment 178
Predictors of Persistent Thin-Cap Fibroatheroma in Non-Culprit Plaques at One-Year Follow-Up Among Patients with Acute Coronary Syndrome 179
IVUS 指导 PCI 对中国≥ 65 岁冠心病患者的成本效果：更低成本与更优效用的马尔科夫模型研究 179
The impact of optical coherence tomography guidance on treatment strategy and angiographic outcome in treating in-stent restenosis compared with angiography 179
支架内新生动脉粥样硬化中薄帽纤维粥样斑块的危险因素及预后分析：一项基于光学相干断层扫描的观察性研究 179
OCT 指导 PCI 对中国≥ 65 岁冠心病患者的成本效果：基于马尔科夫模型的研究 180
Progression and Regression of Non-culprit Plaques Assessed by Serial Optical Coherence Tomography Imaging 180
A Specific Subset of proinflammatory Low-Density Neutrophils Aggravates Endothelial Denudation via NET-Mediated ANXA1 Sequestration: Implications for Plaque Erosion 180

肿瘤心脏病学有关研究 182
Cardiovascular adverse events in Non-Small Cell Lung Cancer patients receiving osimertinib monotherapy and combination therapy: A systematic review and meta-analysis 182
Alox5 通过 P53/SLC7A11 通路抑制铁死亡改善阿霉素心肌病 182
Exploration of the role and mechanism of dulaglutide in doxorubicin-induced cardiomyopathy 182
构建肿瘤化疗病人的心血管风险事件的临床预警评估模型 183
Percutaneous coronary interventionlobectomy for Lung Cancer hybrid surgery: an initial case series 183

Prevalence and Association of Statin with Mortality Risk Among Older US Cancer Survivors with and without Coronary Heart Disease 183
肠道菌群介导心房肌焦亡促进结直肠癌相关房颤的机制研究 184
Olaparib reduces the high blood pressure caused by VEGF inhibitors 184
Single-nucleus transcriptomics reveals the pathological process and key targets of sorafenib-induced cardiotoxicity 184
CREG1 Alleviates Sorafenib-Induced Cardiotoxicity via the Modulation of Necroptosis 185
综述：免疫检查点抑制剂相关心肌炎的研究进展 185
端粒酶逆转录酶缓解阿霉素诱导心脏毒性的作用研究 185
基于结构修饰的线粒体衍生肽 MOTS-c 纳米递送系统对化疗相关性心功能障碍的多靶点调控机制研究 186
Blood Leukocyte Counts and Multimorbidity of Cancer and Cardiometabolic Diseases: A Prospective Cohort Study in UK Biobank 186
临床试验中 PD-1/PD-L1 抑制剂联合治疗的心血管相关不良事件：一项系统综述和荟萃分析 186
Antiplatelet Use and Mortality in Cancer Patients With and Without Coronary Artery Disease 187
脯氨酸合成限速酶 P5CS 在阿霉素诱导心肌病中的保护作用 187
外泌体介导肿瘤心脏病理通讯加重阿霉素心肌毒性的机制研究 187
HFA-ICOS 评分对乳腺癌及淋巴瘤患者肿瘤治疗相关心功能不全的预测效能研究 188
Imaging study of cardiac dysfunction related to anti-tumor therapy in tumor patients: clinical value of cardiac magnetic resonance imaging 188
Percutaneous Coronary Intervention-Lobectomy for Lung Cancer Hybrid Surgery: An Initial Case Series 188
Qili Qiangxin capsules alleviated Doxorubicin-induced cardiotoxicity by inhibiting ferroptosis through Lipid Peroxidation 189
动脉粥样硬化促进肺癌发展的机制 189
Carfilzomib Triggers Cardiotoxicity by Suppressing SENP1 Mediated deSUMOylation of DDX17 189
肥大心肌细胞通过外泌体 miRNA 和蛋白质促进癌症发展 190
Association of cancer with serum N-terminal pro-brain natriuretic peptide 190
RNA 结合蛋白 RBM25 通过调控 DDIT3 促进阿霉素心肌损伤 190
Diagnostic Value of ROCK2 Protein in Immune Checkpoint Inhibitors-Associated Myocarditis 191
Cardiovascular-Renal-Metabolic Multimorbidity in U.S. Adult Cancer Survivors: NHANES 1999–2020 191
评估接受 PD1/PDL1 抑制剂的患者发生心脏毒性的风险 192
RNA-Binding Motif Protein 25 Drives Endoplasmic-Reticulum-Stress-Dependent Doxorubicin Cardiotoxicity via Up-Regulation of DDIT3 192
The association between clinical obesity and new on-set cancer: a 16 year-data from Kailuan Study 192
Wearable device-measured Moderate-to-Vigorous Physical Activity and Cancer Mortality: Evidence from Populations with Varying Right Ventricular Structure 192
奥沙利铂迟发性过敏反应诱发致死性冠状动脉痉挛：病例报告 193
FOXA1+CD3+T 淋巴细胞通过 DLL1/Notch/GSDMD 通路加重 ICIAM 心肌损伤 193
抗肿瘤药物治疗致心肌损伤益生菌防治作用研究 193
组织瓣环运动位移和无创心肌做功评价蒽环类药物心脏毒性的价值 194
FTO inhibits DOX-induced cardiac dysfunction by inhibiting ferroptosis by up-regulating YAP 194
HydroMg 通过改善线粒体功能减轻阿霉素诱导的心肌损伤 195
HydroMg Therapy Attenuates Doxorubicin-Induced Myocardial Injury Via Promoting Mitochondrial Function 195
肿瘤患者中冠状动脉微循环功能改变及其预后评估价值 195
异常肠道微生物群可能通过抑制调节性 T 细胞导致 PD-1 抑制剂相关性心脏毒性 195
Comprehensive Analysis of Electrocardiographic Changes Associated with Osimertinib Therapy in EGFR-Mutated NSCLC: A Retrospective Cohort Study
Tanshinone IIA Modulates the PI3K/AKT/mTOR Pathway: Therapeutic Effects on Radiation-Induced Heart Disease 196
原发性肺动脉肉瘤 1 例临床分析并文献复习 197
奥希替尼相关心脏不良事件：来自 FAERS 数据库分析和网络药理学的临床模式及分子机制研究 197
Association between cancer and subsequent cardiovascular disease multimorbidity: a prospective study 197
基于 CO-GPT 应用 HFA-ICOS 评分在乳腺癌应用曲妥珠单抗心脏毒性评估中的价值 197
ST2 在乳腺癌相关心血管毒性中的应用及研究进展 198
不明原因心包积液最终确诊为间皮瘤 1 例 198
miRNA-144 高表达的外泌体通过氧化应激减轻曲妥珠单抗心肌损伤 198
调控 TLR4 的 R-Loops 结构对纳武单抗联合伊匹单抗介导心肌炎症及凋亡的影响 198
PD-1 抑制剂在肺癌患者中的心脏毒性风险：一项回顾性队列研究 198
CTLA-4 抑制剂相关心肌炎的机制探讨：基于小鼠模型的实证研究 199
结直肠癌治疗相关心脏毒性及其免疫学机制的研究进展 199
阻塞性睡眠呼吸暂停相关慢性间歇性低氧加重阿霉素所致心脏损伤的研究 199
肿瘤代谢物与心血管疾病 199
终末期心脏病患者尊严疗法中护士角色定位的质性研究 199
维立西呱减轻卡非佐米诱导的小鼠心脏毒性的作用及研究 200
入院诊室血压在评估高风险食管早癌患者的应用价值 200
基于 UPLC-Q-TOF/MS 研究维药爱维心口服液改善免疫检查点抑制剂相关性心肌炎的活性成分及作用机制 200
肿瘤心脏病学的临床实践挑战与多学科管理策略探索 200
动脉僵硬和癌症发生之间的关系：来自开滦研究的 10 年数据 200
piRNA-5900 调控 ATF4 阻抑阿霉素诱导的心肌细胞铁死亡 201
胸腺瘤与非胸腺瘤患者免疫检查点抑制剂相关心肌炎临床特征分析 201
The circadian rhythms, cancer status and risk of coronary heart disease: A prospective study in UK Biobank 201
恩格列净通过改善心肌电重构及结构重构减轻阿霉素引起的心律失常 202
基于 MOFs 的抗氧化纳米系统通过调控铁死亡缓解阿霉素心脏毒性 202
Development and validation of a nomogram for predicting new-onset cardiac conduction block in patients with advanced NSCLC undergoing immune checkpoint inhibitor therapy 202
Angiotensin receptor-neprilysin inhibitors improve the outcome of lung cancer patients with hypertension treated with immune checkpoint inhibitors 202

女性心脏健康有关研究 204
The Association Between Serum Luteinizing Hormone and Follicle-Stimulating Hormone Levels and Congestive Heart Failure in Postmenopausal Women: A Cross-Sectional Study 204
A Predictive Model of Adverse Pregnancy Outcomes in Advanced Maternal Age Women with Preeclampsia was Constructed Based on Machine Learning 204
Association between triglyceride glucose-body mass index and preeclampsia risk in advanced maternal age pregnant women-a retrospective cohort

study……204
Propensity Score Analysis of albumin/neutrophil to lymphocyte ratio(ANLR) in advanced maternal age pregnant women as a Predictor of preeclampsia……205
古法健身操对更年期高血压女性心脏健康的研究……205
青年女性心血管疾病风险因素的护理干预策略及效果分析……205
超声评估妊娠期高血压疾病患者心脏结构及功能变化……206
Sex Differences in Outcomes in Patients with Acute Myocardial Infarction……206
老年绝经女性冠心病风险预测列线图模型的构建及多维度验证研究……206
Causal Associations between Pre-Pregnancy Obesity Traits and Pregnancy-Related Hypertension: A Two-Sample Mendelian Randomization Analyses
Resting IL-6 Levels Predict Myocardial Perfusion Deficits Under Mental Stress……206
绝经后女性固体燃料使用与非致命性心血管疾病之间的关系：来自中国健康与养老纵向研究（CHARLS）的结果……207
基于 CT 评估的骨骼肌密度与皮下脂肪量在老年女性心衰患者预后中的意义……207
新疆欠发达地区妊娠期高血压疾病对母婴围生期不良妊娠结局的影响……207
绝经后女性血脂异常与冠状动脉微血管功能障碍的相关性研究……207
女性心脏健康的研究进展与挑战：一项综合性综述……208
女性心脏健康的多维保护机制：基于性别差异的临床转化研究……208
妊娠期高血压孕妇心脏结构和功能变化与子痫前期的关系……208
基于子宫动脉血压持续监测之妊娠期高血压精准防治……208
女性冠心病患者社会角色压力在康复过程中的中介效应分析……208
围产期心肌病产妇阶梯式产后运动康复对心功能恢复与抑郁风险的前瞻性队列研究……209
女性心理健康与心血管结局：NHANES 2021-2023 分析……209
女性心脏健康有关研究……209
中国女医师心血管病危险因素分布及预后关联研究：一项多中心前瞻性队列研究……209
Guideline-directed medical therapy improves left ventricular diastole function in elderly female patients with HFpEF: a real-world study……210
Breaking the Mitochondrial Balance: How Testosterone Rewires the Heart via mTORC2/ATG9A……210
女性心血管病研究……211
护士主导的多学科协作干预对妊娠相关心力衰竭产妇远期心功能及生活质量的影响：一项前瞻性队列研究……211
内蒙古某医院女性心脏疾病患者健康状况及影响因素分析……211
雌激素水平与绝经后女性冠状动脉微血管功能障碍的相关性研究：一项多中心横断面调查……211
Prevalence of atrial fibrillation during pregnancy and association with adverse outcomes……212
探究 Ca/Mg 对老年女性急性冠脉综合征患者死亡风险的预测价值的摘要……212
叙事护理干预对女性心脏健康患者心理及生理康复效果的研究……212
综合护理干预对女性冠心病患者康复效果及生活质量的影响研究……212
拉贝洛尔与硝苯地平治疗产前非重症高血压的疗效比较：一项模拟目标试验……213
中国 Takotsubo 综合症患者的临床特征、性别差异及预后因素分析……213
心理行为干预对绝经后女性冠心病患者焦虑抑郁症状的影响质性研究……213
特发性肺动脉扩张进展至肺动脉瘤 1 例及 7 年随访并文献回顾……213

介入心脏病学研究……214
达格列净对合并糖尿病的慢性冠脉综合征拟择期 PCI 患者围术期心肾损伤保护作用的研究……214
冠心病介入诊疗术后病人血管并发症成因与护理干预……214
急性 ST 段抬高型心肌梗死 PCI 术后对比剂脑病一例……214
整合应激反应通过 ATF4-FKBP11 轴诱导活性氧促进主动脉夹层的机制研究……214
预见性护理模式下责任制护理在 TAVI 患者围手术期护理中的应用效果……214
共享决策在心脏介入术中的研究现状……214
零造影剂冠状动脉介入术后急性肾损伤（ZICE-AKI）研究 ——随机对照试验研究设计……214
Machine Learning-Based Prediction of Myocardial Ischemia/Reperfusion Injury in Acute Myocardial Infarction Patients Following Emergency Percutaneous Coronary Intervention……215
心肌梗死并心衰患者 PCI 术后院内死亡的机器学习预测模型的构建……215
Physiological and Metabolic Predictors of Adverse Outcomes One Year After Coronary Intervention: A Two-Tiered Approach……215
A Novel Integrated Score Combining Physiological and Metabolic Parameters for Predicting Long-Term Outcomes After Percutaneous Coronary Intervention: Development and Prospective Validation……216
集冠状动脉功能学与代谢学指标为一体的新型综合评分用于预测经皮冠状动脉介入术后长期预后：模型建立与前瞻性验证研究……216
三尖瓣介入治疗策略：麻醉管理的临床实践视角……217
Investigation of the safety and effectiveness of a novel steerable guiding catheter in coronary intervention……217
降钙素基因相关肽调节平滑肌细胞表型改变对动脉损伤后新生内膜增生的作用……217
骨髓间充质干细胞源外泌体对大鼠颈动脉球囊损伤后 lncRNAs 表达的影响……218
缺氧预处理外周间充质干细胞对兔血管成形术后再狭窄的影响……218
经食管超声心动图引导下经皮房间隔缺损封堵术中导丝成袢技术的安全性和有效性研究……218
Non-target lesion Progression： Unveiling critical Predictors and outcomes in Patients with in-stent restenosis……218
高龄高危急性非 ST 段抬高型心肌梗死患者不同治疗策略的比较研究……218
冠脉内靶向注射替奈普酶对急性 ST 段抬高型心肌梗死患者微循环及心脏预后的影响……219
心理护理干预对冠心病患者焦虑抑郁情绪及治疗依从性的影响……219
分叉病变介入治疗中对比药物球囊与非药物球囊行边支保护疗效 meta 分析……219
经导管主动脉瓣置换术后 Venus-A 瓣膜的连合和冠状动脉对齐：一项回顾性横断面研究……219
双侧冠状动脉口和主动脉瓣连合相对于主动脉弓的解剖空间分布……220
Efficacy of Oral Hydration in the Prevention of Contrast-induced Acute Kidney Injury in Patients Undergoing Coronary Intervention……220
不同年龄段女性急性 ST 段抬高型心肌梗死患者 PPCI 临床疗效分析……220
危险因素数量对直接经皮冠状动脉介入治疗术后 STEMI 患者长期预后的影响……220
风湿性主动脉瓣狭窄患者行经导管主动脉瓣置换术后临床疗效分析……220
Radial Artery Hemostatic Device applied in trans-brachial coronary intervention……221
合并心功能不全急性 ST 段抬高型心肌梗死患者 PPCI 的临床疗效分析……221
同型半胱氨酸对急性冠状动脉综合征合并 2 型糖尿病患者经皮冠状动脉介入治疗术后远期预后影响……221
冠状动脉定量血流分数对冠脉串联病变的指导价值研究……221
对比分析不同门球时间对 STEMI 患者长期预后的影响……221
缩短门球时间对不同危险分层 STEMI 患者预后的影响……222

Nine month clinical, angiographic and intravenous ultrasound (IVUS) results of FIREHAWK® abluminal groove-filled biodegradable polymer sirolimus-eluting stent in treating de novo coronary artery disease: single center data from the TARGET I trial 222
Association of thyroid-stimulating hormone with contrast-associated acute kidney injury and adverse prognosis in percutaneous coronary intervention patients 222
基于光学相干断层显像评价药物球囊在急诊冠脉介入诊疗中的临床疗效 223
冠状动脉支架置入策略对左主干分叉病变患者介入术后一年主要不良心血管事件的影响 223
Comparison of Spherical Tip Versus Regular Noncompliant Balloons for Crossability in Tortuous Coronary Artery Post-dilatation 223
预见性护理联合 PDCA 循环在减少急性心肌梗死介入诊疗并发症中的应用 224
血红蛋白水平与接受 PCI 治疗的 NSTE-ACS 患者预后的相关性 224
完全生物可降解封堵器闭合膜周部室间隔缺损合并金属封堵器闭合动脉导管未闭一例 224
左主干冠状动脉疾病合并贫血行冠状动脉介入治疗患者临床特征及预后分析 224
Feasibility of Distal Radial Artery Access and the Influence of Arterial Diameter on Puncture Difficulty 224
Risk factors for no spontaneous reperfusion of ST-segment elevation myocardial infarction: A case-control study 225
Abstract Objective Acute coronary syndrome (ACS) is a critical and life - threatening cardiovascular condition that poses a significant challenge to global health. It encompasses a spectrum of clinical manifestations, from unstable angina to ST - segment 226
Protamine-Facilitated Same-Day Discharge Following Distal Transradial Angiography 226
Predictive Value of Coronary Radial Wall Strain Combined with Angiographic Parameters for Myocardial Infarction and Unplanned Revascularization: A Case-Control Study 226
原发性与继发性自发性心肌梗死的差异：来自 ISCHEMIA 研究的启示 226
使用 6F 桡动脉鞘管和 6.5F 桡动脉鞘管经桡动脉路径行冠状动脉造影及介入的对比分析 227
长鞘管在经桡动脉冠状动脉造影中的应用效果分析 227
First Evidence of Correlation Between Red Blood Cell Parameters and Angiography-Derived Coronary Microcirculatory Resistance: A New Insight into Coronary Microvascular dysfunction 227
1 例经导管主动脉瓣置换术后合并瓣周漏诱发心衰行经导管封堵术患者的护理 228
Investigating the Clinical Implications and Diagnostic Accuracy of the QFR Grey-Zone in Coronary Artery Disease: A Comprehensive Analysis of TVF Prediction 228
急性心肌梗死早期活动护理对患者康复进程的观察 228
探究肺动脉球囊扩张成形术后靶血管再干预的预测因素 229
Impact of Early Versus Delayed Permanent Pacemaker Implantation on Clinical Outcomes in Patients with Third-Degree Atrioventricular Block After Transcatheter Aortic Valve Replacement: A National Inpatient Sample Analysis 229
Construction and Validation an Interpretability Prediction model for In-Stent Restenosis based on Machine Learning 229
不同 eGFR 水平 UA 患者的 caFFR、caIMR 及平均中心动脉压的差异分析 230
不同壁厚的聚乳酸可降解支架对血管内皮化的影响。 230
相同壁厚的金属药物洗脱支架和聚乳酸可降解支架对血管内皮化的影响。 230
造影剂液压分离再通技术开通冠脉慢性完全闭塞病变 230
一种新型的开通 CTO 的 ADR 导管：单中心病例系列报道 230
Evidence-based construction of a postoperative upper extremity stasis pain management program for cardiovascular interventional patients and application research 231
生物可吸收支架内膜愈合的随访观察及分析 231
药物涂层球囊治疗冠状动脉小血管原位病变的随访观察 231
P2Y12 抑制剂预处理对择期 PCI 患者围术期心肌损伤 / 梗死的影响 231
冠状动脉介入治疗后血管造影微循环阻力的预后价值：来自 FAVOR III China 试验的启示 231

心血管病诊治的创新与转化医学研究 233
基于皮下植入 MSC 细胞球的新型心肌保护策略研究 233
Hemodynamic Study of Plaque Progression and Regression Based on Coronary CTA Imaging using Computational Fluid Dynamics Method 233
A new non-invasive detector for coronary microvascular dysfunction: Exercise stress high-frequency QRS electrocardiogram 233
Deep Learning-Enhanced ECG Spatiotemporal Feature Analysis for Early HFpEF Detection: Integrating Speckle-Tracking Derived Myocardial Strain Patterns 234
靶向心脏的脂质体递送外泌体 miRNA-185-5p 抑制剂缓解扩张型心肌病心肌细胞凋亡及铜死亡的作用机制研究 234
心肌梗死后成纤维细胞阶段极化特征及其靶向干预策略的研究 235
心血管介入学员成对友谊关系对学业成就的影响作用：基于主客体互倚性模型的分析 235
Targeting MTHFR Variant and Homocysteine Metabolism in Cardiovascular Translational Research 235
茱萸次碱对氧化应激诱导血管平滑肌细胞增殖和一氧化氮合酶的影响 236
银丹心脑通软胶囊对非酒精性脂肪肝的疗效及其机制探讨 236
Nanomedicine in cardiology： Precision drug delivery for enhanced Patient outcomes 236
Multifunctional Nanosystems for Precision Diagnosis and Detoxification in Cardiovascular Diseases: From Multimodal Imaging of Myocarditis to Cardioprotective Chemotherapy 236
秋水仙碱在心血管疾病中的治疗作用：基于 Web of Science 的文献计量学分析（2001-2024） 236
工程化外泌体在精准靶向修复缺血性心脏病中的功能及机制研究 237
《从基础到临床：心血管病诊治创新成果的转化医学实践》 237
Study on the Rapid Screening of Non-ST Elevation Myocardial Infarction in Different Gender Patients Using the High-Sensitivity Cardiac Troponin I (hs-cTnI) 0h/1h Algorithm in the Chinese Population 237
Expression of Circadian Rhythm Genes in Atherosclerosis Complicated with Hypertension: A Study Based on Bioinformatics 238
心血管病诊治的创新与转化医学研究进展 238
仿生纳米酶以中性粒细胞搭便车的方式靶向缺血性心脏病心肌细胞的保护作用及机制研究 238
纳米功能化益生菌通过抑制肠道微生物 -TMA-TMAO 轴治疗动脉粥样硬化 238
开发和验证一种用于预测老年患者非心脏外科手术后发生心力衰竭风险预测模型：一项多中心研究 239
Conductive Microneedle Patch with Mitochondria-localized Generation of Nitric Oxide Promotes Heart Repair after Ischemia-Reperfusion Therapy 239
基于网络药理学和分子对接技术探讨柚皮苷治疗冠心病的分子机制 239
Implantable Triboelectric Nanogenerator for Promising Powering Cardiac Pacemakers 239
当归多糖通过调控内质网应激及炎症反应改善心肌缺血损伤的机制研究 240
基于人工智能和静息超声心动图心肌应变的心肌缺血诊断模型的研究 240
Research on an Artificial Intelligence-Based Diagnostic Model for Myocardial Ischemia Using Resting Echocardiographic Myocardial Strain Analysis 240
心血管病诊治的创新与转化医学研究：新发现、新成果与新知识 240
达格列净通过抑制 NF-κB 通路减轻急性缺血性脑卒中模型大鼠心功能障碍 241

Distal TRAnsradial Access for Percutaneous Coronary Intervention: A SinGle-Center RandOmized CoNtrolled Study（DRAGON Study） 241
Associations between Neutrophil-Percentage-to-Albumin Ratio (NPAR) and Incidence of Cardiovascular Diseases: a Prospective Cohort Study 242
基于机器学习构建并验证急性心肌梗死患者院内心源性休克预测模型 242
Development of a Caspase-3-Activatable Photoacoustic Probe for Myocardial Infarction Imaging 242
AI-Enhanced Fluorescent Magnetic Bead Immunoassay for Melatonin Detection in Heart Failure 243
自噬在心血管疾病中的作用及研究进展 244
动态空间维持型静脉插管在微创心脏手术中的应用：一种解决负压引流吸附效应的创新设计 244
经冠状动脉射频消融治疗梗阻性肥厚型心肌病的多模态影像学评价 244
Bioactive peptides from C-phycocyanin improve cardiac injury repair after myocardial infarction by promoting angiogenesis 244
基于双模态可穿戴脉搏波传感器集成深度学习的高精度低功耗睡眠呼吸暂停检测系统 245
靶向 OPN 可视化纳米胶束包载 SIRT6 激活剂减缓血管老化 245
靶向 CD36 的血小板工程化 AAV 基因疗法重编程脂肪酸代谢促进心肌增殖修复 245

老年心脏健康有关研究 246
Antithrombotic Therapy Strategies and Clinical Outcomes in Chinese Patients Aged 65 and Older with High Ischemic Risk Coronary Artery Disease 246
Low serum Klotho reflects senile inflammation in middle-aged and elderly patients with coronary atherosclerosis 246
Diagnostic and prognostic value of serum Asprosin in Cardiac Cachexia 247
CHK1 通过激活 AHSA1/HSP90 介导的线粒体自噬延缓小鼠心脏衰老 247
膳食指数与心脏代谢指数的关联及其潜在作用机制研究 247
Therapeutic Efficacy of Qili Qiangxin Capsule in Elderly Patients with Heart Failure with Preserved Ejection Fraction 247
夜间睡眠和日间小睡对中老年人心血管疾病发病风险的联合影响：一项基于 CHARLS 的纵向队列研究 248
体质量与老年慢性阻塞性肺疾病患者肺功能和心脏结构的相关性 248
中性粒细胞淋巴细胞比率与老年高血压患者死亡风险的关联 248
Life Satisfaction as Modifiable CVD Prevention Target: Cross-Cultural Mediation in Aging Cohorts 248
冠状动脉异常起源于对侧窦的中老年患者的影像解剖特征对预后的影响 249
CD8+T 细胞介导的衰老脂肪棕色化下降影响老年心肌重构的机制研究 249
Discordance among lipid profile in the older adults: implications for cardiovascular prevention 249
脂蛋白 (a) 与老年冠心病多支病变相关性的研究 250
Identification and validation of IRS2 as a novel aging-related biomarker and potential therapeutic target in calcific aortic valve disease 250
共病负担对老年射血分数保留型心力衰竭患者预后的影响分析 250
板栗酒化学成分棕榈酸甲酯对小鼠心肌细胞和心肌成纤维衰老的调节作用 251
Phloretin combined with LIPUS can alleviate the inflammatory response of vascular endothelial cells in diabetic mice by activating SIRT-related pathways 251
纤维蛋白原 / 白蛋白比值与接受经皮冠状动脉介入治疗的高龄冠心病患者长期预后的关系 251
新疆部分地区老年持续性心房颤动患者 EQ-5D-5L 评分及其影响因素分析 251
Ethnicity and Exercise Modulate Quality of Life in Elderly Patients with Persistent Atrial Fibrillation: A Cross-Sectional Study in Multi-Ethnic Xinjiang 252
Oral Anticoagulant Use and In-Hospital Outcomes in Patients Aged 90 years and older with Atrial Fibrillation or Atrial Flutter 252
肠道梭状芽孢杆菌代谢产物吲哚 -3- 丙酸缓解老年心脏纤维化 253
吲哚 -3- 丙酸通过调控巨噬细胞自噬功能缓解老年心脏纤维化 253
TAVI 手术在超高龄患者中的安全性及中长期预后评估 253
Efficacy and safety of antithrombotic therapy in the elderly patients with the commodities of coronary artery disease, atrial fibrillation, and malignancy 253
健康生活方式与全因死亡率、特定原因死亡率及预期寿命的关联：来自英国和美国的两项全国性队列研究 254
高尿酸血症对老年冠心病患者经皮冠状动脉介入治疗术后 2 年和 5 年不良临床结局的影响 254
肠道微生物群与衰老相关代谢及表观遗传年龄加速的关联研究 254
抗凝治疗对老年非瓣膜心房颤动患者认知功能影响的研究 254
钠 - 葡萄糖转运蛋白 2 抑制剂对肌少症影响的 meta 分析 255
心脏病患者跌倒走失安全管理及护理措施探讨 255
多学科协作模式下老年难治性高血压的综合干预模式构建 255
基于衰弱评估的老年冠心病患者血运重建策略优化研究 255
健康教育与老年冠心病患者衰弱的相关性研究 255
睾酮通过抑制 AMPK-FOXO1/MuRF1 信号通路介导绝经后高血压左室肥厚 255
Associations between taste preferences and mortality among older adults: a nationwide, community-based, prospective cohort study in China 256
最佳药物治疗对高龄急性心肌梗死患者的预后影响 256
老年心血管疾病患者心理健康护理必要性及干预措施 256
Impact of dynamic changes in pain on cardiovascular disease in Chinese middle and elderly people: results from China Health and Retirement Longitudinal Study (CHARLS) 256
The Characteristic of Transcription Profiles of Aorta in Atherosclerotic Murine Models Interfered with Treadmill Exercise 257
FAT-10 与冠心病患者的衰弱状态的相关性研究 257
加速生物衰老与卒中、痴呆动态转化关系的研究：基于多状态模型的前瞻性队列分析 257
Novel Insights into the Role of Liver Function Biomarkers in Cardiovascular Health Assessment: A Cross-Sectional Study with Machine Learning Analysis 258
“暮光调色盘”——超高龄衰弱老人的多维疗护 1 例 258
A Machine Learning approach for predicting 3-year new-onset Cardiovascular Disease in an Elderly Chinese Population: A report from the Guangzhou Older Population Annual Health Examination Cohort and Guangzhou Heart Study 259
Gut Microbiota Metabolite Phenylacetic Acid Regulates Cardiac Senescence through Histones Phenylacetylation 259
手厥阴心包经刮痧疗法改善老年心肌缺血患者胸痛的研究 260
The Role of Lifestyles in Older Adults with Calcific Aortic Valve Disease: A Retrospective Case-Control Study from China 260
新疆社区老年人共病的民族和地理差异：一项横断面研究 261
Impact of Impaired Renal Function on Cognitive Performance Among Patients With Coronary Artery Disease 261
复发恐惧在心房颤动导管消融术后患者人格特质与自我管理行为间的中介效应研究 261
心理疏导结合赋能教育对改善老年慢性心力衰竭患者抑郁情绪及治疗依从性的随机对照研究 261
Impact of Combined Cognitive and Physical Impairments on Long-term Prognosis in Elderly Cardiovascular Patients: A Prospective Cohort Study 261
衰弱表型介导的老年冠心病患者心脏康复抵抗机制及个体化运动干预策略 262

医师对高龄非瓣膜性心房颤动患者卒中预防问题及应对措施态度的调查 262
Analysis of risk factors for hospital-acquired pneumonia in schizophrenia 262
MHR 与 2 型糖尿病患者急性心梗的相关性分析 263
全周期康复管理模式在老年 CCU 冠心病患者护理中的应用路径与效果评价 263
Sleep Patterns and Frailty: Joint Impact on Major Adverse Cardiovascular Events in a Prospective Cohort Study 263
Comorbidity Patterns and Intrinsic Capacity Decline in Older Adults with Coronary Heart Disease: A Nationwide Study in China 263
虚弱与肌少症对中老年人群心血管疾病风险的联合作用及进展性影响 264
基于心衰风险评分表的老年 2 型糖尿病全周期康复护理模式构建与应用 264
膈肌强化训练对老年冠心病患者姿势控制及生活质量的影响：前瞻性队列研究 264
Integrated Multi-Omics Analysis Uncovers Dysregulated Energy and Amino Acid Metabolism During Vascular Aging 264
复合膳食抗氧化指数与超额心脏年龄的关联：2007-2020 年 NHANES 横断面研究分析 265
辅酶 Q10 联合有氧运动对老年人心肌功能及氧化应激指标的影响研究 265
Mood Swings Impact Smoking Behavior Elevating Risk of Cardio-cerebrovascular Events: A Mendelian Randomization Study 265
Kielin/Chordin-Like Protein Deficiency causes aortic aging in male mice 266
生命必需 8 要素评估的心血管健康在老年衰弱与死亡关联中的中介作用：来自 NHANES 队列的证据 266
开发并验证可解释的机器学习模型用于预测环境毒物暴露对心肌梗死的影响：一项回顾性列队研究 266
人性化护理对老年心肌梗死患者心理状态及护理满意度的影响研究 266
冠心病患者护理中预见性护理程序的应用研究 267
心理护理在老年慢阻肺患者护理中的应用价值及护理满意度分析 267
心理护理干预对老年心房颤动患者负面情绪的影响 267
Cardiovascular morbidity and mortality in patients with aortic valve calcification: A systematic review and meta-analysis 267
老年心房颤动导管消融术中的“肥胖悖论”：高体重指数降低围术期并发症风险 268
GLP1R/PCSK9/SGLT2 在钙化性主动脉瓣狭窄中的表达特征 268
在老年 ASCVD 患者中，hsCRP 与 Lp(a) 何者对心血管事件风险的预测价值更优？ 268
营养风险对老年心功能不全患者住院期间简易运动能力的影响 268

大血管与外周血管疾病有关研究 269
Exploring the Potential Mechanisms of GABA in Treating Abdominal Aortic Aneurysm through Network Pharmacology and Experimental Validation 269
Triglyceride-glucose index, arterial Stiffness, and cardiovascular disease: Results from an 11-year prospective study in China 269
Association between preoperative triglyceride-glucose index and the risk of short-term aortic adverse events after thoracic endovascular aortic repair 270
An Aqueous Extract of Radix Astragali, Angelica sinensis, and Panax notoginseng protected brain microvascular endothelial cell from hypoxic damage via PI3K/Akt/eNOS Pathway 270
腹主动脉瘤覆膜支架植入术后反复发热一例 270
分期运动管理模式在促进主动脉夹层腔内隔绝术患者康复中的应用研究 271
Cytoskeletal-related genes function as checkpoints for the maintenance of VSMC contractile phenotype and prevent pathological remodeling in arterial diseases 271
使用数据独立的采集质谱法识别结节性多动脉炎的候选生物标志物 271
Ferroptosis Inhibition Suppresses Experimental Abdominal Aortic Aneurysm Formation by Attenuating Macrophage-Mediated Inflammation 271
Dual Receptor Crosstalk: AT1R and Integrin β3 Synergize to Drive Aortic Dissection via Non-Canonical Wnt/β-Catenin Signaling 272
STUB1 orchestrates mineralocorticoid receptor activation to promote aortic dissection 272
C57BL/6J 背景小鼠静脉注射 PCSK9 功能获得突变对血管紧张素 II 诱导的 AAA 的影响 272
Cross-Species scRNA-seq Analysis Identifies Optimal Mouse Models for Studying Key Cellular Mechanisms in Aortic Dissection 273
GSDMD 依赖性 NETs 通过 P2X7R 调控巨噬细胞极化促进腹主动脉瘤进展 273
Cold stimulation aggravates aortic dissection through the sympathetic nerve-resident macrophages axis: a novel pathogenesis 273
一体式分支型支架结合体外开窗技术处理复杂 B 型主动脉急性综合征临床应用的单中心经验及体会 274
Predicting the growth of asymptomatic small abdominal aortic aneurysms (AAA) based on deep learning 274
非复杂性 Stanford B 型主动脉夹层患者行胸主动脉腔内修复术时机对预后及主动脉重塑的影响 274
急性主动脉夹层相关的临床特征与死亡率之间的关联：一项基于 MIMIC-IV 数据库的回顾性队列研究 275
Mechanism of Structural Disruption and Functional Effects of the PDK4 rs750335290 Variant: Implications for Skeletal Muscle Energy Metabolism 275
Stanford B 型主动脉夹层 TEVAR 术后支架诱导远端新发破口预测因素分析 275
The Effect and Mechanism of MGST1-miMOMP in the Formation of Abdominal Aortic Aneurysm 276
基于文献计量学的主动脉弓病变腔内修复技术全球研究现状及热点分析 276
Predictive Models for One-Year Renal Function Improvement in Patients with Atherosclerotic Renal Artery Stenosis (ARAS) Following Renal Artery Revascularization 276
四维核磁共振研究两窦两叶型主动脉瓣二叶畸形患者升主动脉血流动力学 277
踝间差降低颅内动脉剪切力影响铁死亡恶化缺血性脑卒中的研究 277
The association of metabolic syndrome with aortic aneurysm: a two-sample mendelian randomization study 277
The Predictive Role of the Monocyte-to-Lymphocyte Ratio in Short-Term Outcomes for Patients with Acute Uncomplicated Type B Aortic Intramural Hematoma 277
Standford B 型主动脉夹层患者胸主动脉腔内修复术后持续性 Ia 型内漏的预后意义 278
Moderate to vigorous physical activity, genetic susceptibility, and risk of aortic aneurysm: a prospective cohort study 278
Creg1 inhibits vascular calcification by suppressing osteogenic differentiation of VSMCs through the Fhl2-Stat3-Runx2 axis 278
MiRNA-378a-5p attenuates the development of abdominal aortic aneurysm via Ablim1-Mkl1 signaling pathways 279
S100A12-Driven Aortic Dissection: Rescue by Sivelestat Through Neutrophil Elastase Inhibition 279
基于 NLRP3 炎症小体探讨恩格列净抑制 TAAD 小鼠主动脉病理性重塑的机制 280
胆固醇、高密度脂蛋白和葡萄糖指数与颈动脉粥样硬化的相关性研究 280
The predictive value of estimated glucose disposal rate for the risk of venous thromboembolism in elderly individuals: a prospective cohort study of UK Biobank 280
血管钙化关键调控基因的生物信息学分析与实验验证 281
The clinical application value of ultrasound in the diagnosis of iliac vein compression syndrome 281
活化蛋白 C 调控衔接蛋白 p66Shc 在 AD 形成与发展中的作用及其分子机制 的研究 281
急性 B 型主动脉夹层患者胸主动脉腔内修复术后 1 年内脏段不稳定相关因素分析 281
Machine Learning-Based Prediction of Aortic Rupture Risk in Type A Aortic Dissection 282
硒代蛋氨酸通过靶向线粒体生物合成铁死亡通路治疗主动脉夹层的机制研究 282

Dysregulation of the HMGB2-TREM Axis Contributes to Pathogenesis of Abdominal Aortic Aneurysm in Male Patients 282
Mechanisms and potential therapeutic strategies in aging-induced aortic aneurysm and aortic dissection 283
胸腺基质淋巴细胞生成素通过调节巨噬细胞极化促进腹主动脉瘤形成 283
Clonal Hematopoiesis and Incident Aortic Dissection in a Chinese Population 283
免疫细胞基因组不稳定性在急性主动脉综合征发生发展中的作用和机制研究 284
Castor 单分支支架移植物在近端锚定区不足的 Stanford B 型主动脉综合征的临床价值研究 284
颈动脉狭窄患者围术期脑灌注改变相关力学因素分析 284
Adipsin 通过 SERPINE1 依赖性血管新生改善糖尿病下肢缺血 284
血小板与血红蛋白比值与急性 A 型主动脉夹层手术预后的关系 285
Global, regional, and national burden of pulmonary arterial hypertension from 1990 to 2021, with projections to 2045: a systematic analysis for the Global Burden of Disease Study 2021 285
SETD2 介导脂肪功能障碍在抑制缺血后动脉生成的作用及机制 285
Different types of systolic blood pressure and all-cause mortality in critically ill patients with acute aortic dissection: a retrospective analysis of the MIMIC-IV database 285
[18F]-AIF-NOTA-FAPI PET/CT 显像评估不同时期急性主动脉综合征患者的影像学特征 286
Engineered Hybrid Nanovesicles Combining Macrophage Membranes and Artificial Lipids for Abdominal Aortic Aneurysm Therapy 286
Dietary vitamin C and vitamin E with the risk of aortic aneurysm and dissection: A prospective population-based cohort study 286
The role and mechanism of plasma exosomal miR-206 in patients with acute type A aortic dissection with preoperative acute lung injury 287
Risk factor and outcome analysis of bird-beak configuration after thoracic aortic endovascular repair for Stanford B-type aortic dissection 287
3 例妊娠合并主动脉夹层患者的围手术期护理 288
Stanford Type B Aortic Dissection with Tear Location at Lesser Curvature Side: Prognostic Factors and Long-term Outcomes 288
小腹主动脉瘤 5 年预后风险分层系统的建立与验证 288
Factors Associated with Acute Kidney Injury Following Thoracic Endovascular Repair for Acute Stanford Type B Aortic Dissection 289
移植肾动脉狭窄腔内治疗术后主要不良事件发生的预测模型构建 289
股动脉穿刺术后严重并发症 - 感染性股动脉假性动脉瘤（IFPA）的处理和预防 289
Aortic Remodeling After Thoracic Endovascular Repair of Acute Type B Aortic Dissection Underwent Anti-Thrombotic Therapy 289
构建 A 型主动脉夹层患者 I 期心肺康复护理方案的临床应用评价 290
累及头颈部血管的急性 Stanford A 型主动脉夹层外科治疗的临床效果分析 290
房颤患者急性下肢血栓形成的危险因素护理分析 290
The gut metabolite phenylacetylglutamine inhibits the angiogenic potential of human umbilical vein endothelial cells via the β-adrenergic receptor-LDHA axis 290
异物参与的胺碘酮致急性闭塞性血栓性静脉炎 1 例 291
The Role and Mechanism of GRP94 in Hindlimb Ischemia of Murine 291
CCNY 缺失通过影响平滑肌细胞凋亡促进胸主动脉夹层的发生 291
缩窄性心包炎引起的复杂斯坦福 A 型主动脉夹层伴硬膜下血肿的手术治疗 -- 病例报告 291
康复护理路径在 Stanford A 型主动脉夹层患者中的应用价值 292
Jagged1 inhibits the osteogenic phenotypic transition of vascular smooth muscle cells by downregulating NFATc1 in exosomes derived from vascular endothelial cells 292
Diagnostic value of platelets to high-density lipoprotein ratio in abdominal aortic aneurysm 292
Long-Term Outcomes of Different Surgical Modalities for Aneurysms in Patients with Rheumatic Immune Diseases: a Single-Center Cohort Study for 20-Year 292
主动脉缩窄（CoA）的诊断、病理机制与治疗进展 293
Association between complete blood cell derived inflammatory biomarkers and Short-Term Adverse Events in Patients with Acute uncomplicated Type B Aortic Intramural Hematoma 293
Analysis of clinical characteristics and related factors of patients with post-implanta tion syndrome following prophylactic application of non-steroidal anti-inflammatory drugs after thoracic endovascular aortic repair 294
Correlation Between Hypertension and Panvascular Disease: A Prospective Vascular Magnetic Resonance Imaging Study 294
盐皮质激素受体在主动脉夹层病变组织的表达及临床意义 295
Piezo1 介导 NETs 释放诱导巨噬细胞焦亡促腹主动脉瘤进展的机制研究 295
主动脉壁纤维结构的研究进展 295
The Potential Role of Neutrophil-to-Red Cell Distribution Width Ratio in the Diagnosis of Aortic Dissection 295
Soluble ST2: A Novel Biomarker for Diagnosis and Prognosis of Cardiovascular Disease 296
单分支支架在主动脉弓部病变应用研究 296
Association Between Serum Bilirubin and Prevalence of Abdominal Aortic Aneurysm: Results from a Chinese Screening Program and UK Biobank Study 296
下肢动脉股腘动脉支架内再狭窄减容联合药物球囊治疗的单中心回顾研究 297
探究“医院 - 社区 - 家庭”三位一体延续性护理模式对主动脉夹层患者放射介入术后护理的应用效果分析 297
慢性肾脏病患者血浆 miR-423-5p 含量与高凝状态的相关性研究 297
肺栓塞 79 例临床诊治分析 297
Association Between Life's Essential 8 Score and the Risk of Abdominal Aortic Aneurysm: A Prospective Cohort Study from UK Biobank data 297
Dietary Components of Curcuma longa Ameliorate Renal Artery Stenosis: Network Pharmacology and Experimental Validation 298
GW501516 对低氧条件下肺动脉平滑肌细胞增殖的作用及其机制 298
健康促进与自我效能理论在急性 A 型主动脉夹层术后早期康复护理中的应用效果研究 298
借助单细胞转录组绘制胸主动脉瘤图谱 299
Single-cell and spatial transcriptomics uncover age-associated smooth muscle de-differentiation and macrophage behavior in acute aortic dissection 299
Trem2/Tyrobp/Syk 信号通路通过抑制巨噬细胞促炎活化抑制主动脉夹层及破裂研究 299
超声评估受压段流速比与远心段呼吸相性变化对髂静脉压迫综合征的诊断效能分析 299
白细胞计数与血红蛋白比值对心力衰竭患者院内死亡风险的预测价值 300
远端孤立性血栓的临床策略与治疗进展 300
Precision Alignment in Minimalist Fenestrated TEVAR: A Novel Physician-Modified Technique Utilizing Self-Aligning Relay Non-Bare Stent-Grafts for Thoracic Aortic Endovascular Repair 300
Basal Metabolic Rate and Risk of Aortic Aneurysm and Dissection: Results from Two Cohort Studies 300
The causal association between body mass index and abdominal aortic aneurysm via obstructive sleep apnea, a two-step mendelian analysis 301
Internal Migration of Calcification on Non-Contrast Computed Tomography: Is It Always Indicative of Acute Aortic Syndrome? 301
D-Dimer and ADAMTS8 Based Multi-marker Score : Potential Biomarkers for Predicting Aortic Dissection 302
SIRT3 suppresses vascular endothelial senescence by inhibiting eNOS uncoupling 302

环丙沙星重塑肠道菌群提高吲哚乳酸水平并加重动脉瘤与夹层 302
LncSRLR is up-regulated in Thoracic Aortic Dissection and Regulated Phenotype Switch of Smooth Muscle Cells 303
Using the NoSAS Score to Stratify Long-Term Cerebrovascular Risk: A 5-Years Retrospective Analysis 303
冷休克蛋白 DbpA 乙酰化修饰调控线粒体功能障碍促主动脉夹层的机制研究 304
颈动脉狭窄中血管周围脂肪 CD4+T 细胞 ICOS 的作用及机制研究 304
reatinine-to-albumin ratio predicts mortality in patients with aortic aneurysms 304
通过肾动态显像结合肾动脉血流分数评价冠状动脉药物球囊治疗肾动脉纤维肌性结构不良 1 例 304
Machine learning combined with omics-based approaches reveals T-lymphocyte cellular fate imbalance in abdominal aortic aneurysm 305
“精准护航” 一例颈动脉狭窄 TCAR 手术患者的全程护理实践 305
12HETE is an endogenous modulator of BLT2 triggering vascular degeneration, dissection and rupture 305
Systematic evaluation of a predictive model for the risk of bloodstream infections associated with intravenous infusion port in oncology patients 306
A Preliminary Study on the Correlation between 18F-NaF Uptake and Aortic Calcification, Aneurysm Sac Expansion and Endoleak after Endovascular Repair of Abdominal Aortic Aneurysm 306
低密度脂蛋白颗粒大小与主动脉瘤之间的因果关系： 孟德尔随机化和中介分析的启示 306
1990-2021 年全球、区域和国家老年主动脉瘤全球负担的系统分析 307
ENOX2 and the related mechanisms as potential genetic targets for varicose veins of lower extremities: an integrated bioinformatics and Mendelian analysis 307
有氧运动降低脂质重塑改善肺动脉高压的分子机制研究 307
Integrated analysis of bulk RNA-seq, Mendelian randomization, and eQTL reveals the Pathogenesis of Pan-Vascular Diseases 308
1990-2021 年 55 岁及以上成人主动脉瘤的风险因素差异性分析 308
中性粒细胞与主动脉瘤之间的因果关系：孟德尔随机化的启示 308
单侧复发性缺血性脑卒中与同侧颈动脉 CTA 特征关系的定量分析研究 308

肺循环与右心研究 310
Effectiveness of chest pain center accreditation on the in-hospital outcome of acute pulmonary embolism in China: Findings from the Chinese Cardiovascular Association Database 310
S-nitrosylated Cys133 of Annexin A2 improves pulmonary arterial hypertension by inhibiting WNT/β-catenin pathway 310
靶向治疗联合 SGLT2-i 对肺高血压的疗效和安全性研究 311
基于心肺运动试验的肺栓塞患者个体化阶梯式肺康复方案构建与效果评价 311
靶向药物治疗高原性肺动脉高压的疗效与安全性：一项聚焦藏族人群的 Meta 分析 311
Arteridin 通过调控线粒体自噬在肺动脉高压的作用及机制研究 311
Noninvasive PECS Model for Detection of Combined Post-Capillary Pulmonary Hypertension 311
剪切力通过 Sema3C-NRP2 通路介导内皮 - 平滑肌对话加重肺动脉高压的机制研究 312
红景天苷通过调控 BKCa 改善野百合碱诱导的肺动脉高压 312
STING 信号通路调控 TASK-1 钾通道在低氧性肺动脉高压中的机制研究 312
The Post-Marketing Safety Profile of Sotatercept: A Disproportionality Analysis of Real-World Data from the FAERS Database 312
中性粒细胞通过释放基质金属蛋白酶 -8 促进 PH-LHD 小鼠心肌纤维化的机制研究 313
PIEZO1 Regulates Smooth Muscle Cell Plasticity by Integrating Mechanical Stretch with Glycolytic Metabolism 313
房间隔缺损肺动脉高压患者克隆性造血相关基因的初步研究 314
TAPSE/SPAP 作为肺动脉高压预后指标的临床意义：一项单中心回顾性研究 314
重组人脑利钠肽治疗动脉型肺动脉高压所致右心衰竭的有效性及安全性研究 314
克隆性造血与肺动脉高压因果关系的遗传学证据 314
栀子苷通过调控 PFKFB3 改善肺血管重构降低肺动脉高压的研究 315
慢性肺动脉狭窄解除后健侧肺的双相反效应 315
Global Burden of pulmonary arterial hypertension from 1990 to 2021 and predictions to 2035: results from the GBD Study 2021 315
1990 年至 2021 年全球、区域及国家层面的肺动脉高压负担：基于 2021 年全球疾病负担研究的年龄 - 时期 - 队列分析 315
GPNMB Drives Pulmonary Vascular Remodeling and Right Ventricular Fibrosis via ITGB2-STAT1-CXCL10 and TGF-β Pathways and Serves as a Biomarker in PAH 315
Riociguat Replacement Therapy in Eisenmenger Syndrome: A Prospective Real-World Study of Efficacy and Safety Following Transition from Phosphodiesterase-5 Inhibitors 316
基于血流动力学分层的阶梯式呼吸 - 运动耦联训练方案对中重度 PAH 患者心肺功能的影响 316
YBX1 Lactylation Modulates Endothelial-Mesenchymal Transition in Pulmonary Arterial Hypertension 317
PAD4 通过 HIF1α-ENO1 信号轴介导 NETosis 促进肺动脉高压血管重塑的作用机制研究 317
高强度间歇训练联合抗凝治疗对肺栓塞患者心肺功能及血栓再发风险的调控作用 318
肺栓塞后内皮功能障碍与运动耐量恢复的分子机制及康复干预靶点研究 318
营养 - 运动 - 心理 " 三位一体 " 干预方案对 PAH 患者生存质量影响的随机对照研究 318
The value of sST2 in risk stratification and short-term prognosis of acute pulmonary embolism: a pilot study focusing on intermediate-risk subgroups 318
A Novel tRNA-Derived Small RNA, tRF-1:32-Glu-TTC-2-M2, Regulates RV Remodeling and Fibrosis by Targeting P4HA2 in Pulmonary Arterial Hypertension 319
基于机器学习模型评估慢性肾衰竭患者发生肺动脉高压的风险 319
Development of a lactate-related, gene signature-based predictive model in pulmonary arterial hypertension using transcriptome and single-cell sequencing 319
Global, regional and national burden of disease analysis and projections for pulmonary hypertension, 1990 to 2023 320
The protective effect and mechanism of SIRT3 in pulmonary hypertension 320
房间隔缺损介入封堵后右心重塑的变化 321
外周血血小板活化特征揭示慢性血栓栓塞性肺动脉高压患者中 CD16 $^{+}$单核细胞功能障碍 321
有氧运动通过抑制 NLRP3 上调 Treg 细胞活性在改善肺动脉高压血管重构中的作用及机制 321
凝血状态对阻塞性睡眠呼吸暂停合并肺高血压患者疾病严重程度的影响 321
NAFLD is associated with right heart function and prognosis in pulmonary hypertension 321
ATGL 在肺动脉高压中的作用研究 322
Burden of Pulmonary Arterial Hypertension and Associated Heart Failure in Reproductive-Age and Postmenopausal Women: Global and Regional Trends from 1990 to 2021 322
The HIF- 1α/miR- 26a- 5p/PFKFB3/ULK1/2 axis regulates vascular remodeling in hypoxia-induced pulmonary hypertension by modulation of

autophagy 322
内皮特异性靶向 SIRT7 通过去乙酰化 KLF4 改善肺高压的机制研究 323
超声心动图联合定量 CT 剖析肺气肿表型与 COPD-PH 心肺功能关联的研究 323
Integrated bioinformatics analysis reveals marker genes and immune infiltration for pulmonary arterial hypertension 323
Impact of Pretest HFpEF Probability on Clinical Outcomes in Patients with Chronic Thromboembolic Pulmonary Hypertension 324
Mechanism study on the involvement of MIF in acute lung injury through regulation of the NLRP3 inflammasome-mediated pyroptosis pathway 325
Ac2-26 Reduced Lung Injury After Cardiopulmonary Bypass via the AKT1/GSK3b/eNOS Pathway 325
急性肺栓塞患者血清钙水平与急性肾损伤风险的相关性：一项回顾性队列研究 325
Application of Ultrasound in Assessment of Acute Lung Injury in Mice 326
基于超声心动图的深度学习模型预测肺血管阻力的研究 326
关于急性致死性肺血栓栓塞症急救策略的一点商榷意见 326
Global Burden of Pulmonary Arterial Hypertension in Adults Aged 55 and Older: A Systematic Analysis of the Global Burden of Disease Study 2021 326
内皮细胞中的 TXNIP 在肺动脉高压中的作用探究 327
利拉鲁肽通过激活 AMPK/USP10 环路增强 ACE2 的表达：在肺动脉高压中的意义 327
SPECT/CT 肺灌注 / 通气显像定量分析在 CTEPH 患者 BPA 术后疗效评估的应用 327
Deciphering the Common Mechanisms of Pulmonary Hypertension Subtypes Using Multi-Omics and Machine Learning 328
ALDH2 缺失通过调控铜死亡促进低氧性肺动脉高压诱导的右心室重塑 328
Balloon pulmonary angioplasty combined with riociguat for the treatment of inoperable chronic thromboembolic pulmonary hypertension (PRACTICE study) 328
m6A 修饰酶基因 METTL3 缺失对小鼠右室结构与功能障碍的影响及其作用机制探究 329
The Role of USP7-Mediated Endothelial Cell Senescence in Vascular Remodeling Associated with Pulmonary Arterial Hypertension: Regulation of the p53 Pathway and Underlying Mechanisms 329
Acute Pulmonary Hemodynamic Changes Following Pulmonary Artery Denervation in Pulmonary Hypertension Patients Undergoing Prior Transcatheter/Surgical Mitral Valve Repair 329
Integrated Single-Cell and Transcriptomic Profiling Reveals Lactylation-Driven Molecular Mechanisms in Pulmonary Arterial Hypertension 330
Predictive Value of Right Atrial Strain Combined with Right Atrial Area for Clinical Deterioration in Patients with Pulmonary Hypertension 330
芦丁通过与 PKCα 相互作用抑制铁死亡延缓肺动脉高压的发生发展 331
Right atrial adaptation to impaired right ventricular function and increased afterload in precapillary pulmonary hypertension: a cardiac magnetic resonance feature-tracking study 331
Upregulation of CXCL10/CXCR3 axis induced by pulmonary hemodynamic stress promotes vascular remodeling in chronic thromboembolic pulmonary hypertension 331
研究 BRCC3 和 Sotatercept 在重平衡 TGF-β 和 BMP 信号通路中的作用机制 332
Balloon Pulmonary Angioplasty for Inoperable Chronic Thromboembolic Pulmonary Hypertension: A 9-Year, Multicenter Cohort Study 332
伴心血管合并症的特发性肺动脉高压患者临床特征分析 333
Total Flavonoids of Epimedium Improve Pulmonary Vascular Remodeling in Pulmonary Hypertension: A Study Combining Network Pharmacology and Experimental Verification 333
Hemodynamic effects of dobutamine versus dopamine in preterm infants: a meta-analysis 333
儿童期起病肺动脉高压合并 FLNA 基因突变 1 例 334
经皮机械血栓清除术治疗中、高危急性肺栓塞：初步疗效与安全性研究 334
“Treat-and-Repair” 策略在成人房间隔缺损合并重度肺动脉高压患者中的疗效与安全性分析——基于单中心回顾性研究 334
早期强化靶向治疗在房间隔缺损合并重度肺动脉高压患者中的应用探索一项前瞻性病例系列报告 334

复杂高危冠脉介入有关研究 335
A Retrospective Cohort Study on Long-Term Outcomes of Ticagrelor versus Clopidogrel After Retrograde Percutaneous Coronary Intervention for Chronic Total Occlusion 335
Prediction of percutaneous coronary intervention success in moderate-to-severe coronary artery calcification patients using machine learning based on coronary angiography 335
步步为营，险中求生 -IVUS 应用急性心肌梗死合并左主干、前三叉分叉病变救治一例 336
探究 ETcath200 系统在经皮冠状动脉介入治疗（PCI）复杂病变中的安全性与有效性 336
准分子激光冠状动脉成形术在慢性完全闭塞性病变中的应用 336
Retrograde Protected Antegrade Puncture Reentry: A Novel Strategy to Improve Procedural Efficiency in Retrograde CTO PCI 337
复杂冠脉病变与结构性心脏病介入治疗的疗效分析及个体化方案探索 337
透视下确定左主干分叉最佳投照角度 337
Rota-Tripsy or step-up-approach rotational atherectomy for severe coronary artery calcification treatment: a comparative effectiveness study 337
Safety and Outcomes of Retrograde Percutaneous Coronary Intervention for Chronic Total Occlusions in Patients with Reduced Left Ventricular Ejection Fraction: A Single-Center Retrospective Cohort Study 338
右冠慢性完全闭塞病变逆向介入治疗中假腔旋磨的分期处理策略：1 例高龄复杂病例报告 338
AI 驱动的冠状动脉旋磨术旋转速度预测及其临床意义研究 339
基于危险因素评分模型指导高速旋磨策略在严重钙化病变中的应用研究 339
冠状动脉慢性完全闭塞患者 术后 MACE 风险预测模型研究 339
清醒 VA-ECMO 支持下复杂钙化病变多支血管 PCI 术及术后心脏康复 1 例 339
基于目标血管差异的冠状动脉旋磨术治疗慢性完全闭塞病变的疗效与短期预后研究 340
老年冠状动脉原位大血管严重钙化弥漫病变旋磨术后不同处理策略临床结局对比 340
不同旋磨策略对冠脉钙化病变斑块修饰及支架膨胀的影响：一项单中心 IVUS 研究 340
复杂高危冠心病患者择期 PCI 术中清醒 ECMO 支持：单中心经验 340
The Impact of Intracoronary Imaging Guidance on Long-term Outcomes for Patients Undergoing Coronary Rotational Atherectomy 340

心房颤动有关研究 342
导管消融术后房颤复发预测模型的建立**心房颤动有关研究** 342
A Novel Predictive Model for Identifying Left Atrial Low-Voltage Area in Patients with Paroxysmal Atrial Fibrillation 342
Prognostic Value of Red Cell Distribution Width-to-Serum Calcium Ratio for All-Cause Mortality in Critically Ill Atrial Fibrillation Patients 342
Association of Glycopyrrolate With New-Onset Atrial Fibrillation in Critically Ill Patients: A Retrospective Cohort Study 342
心房颤动患者治疗方式选择的影响因素分析 343
不同类型心房颤动患者心脏结构与功能的差异性分析：一项观察性研究 343
基于机器学习的阵发性房颤导管消融术后复发风险预测模型研究 343
The Predictive Value of Real-world Cardiologist Performance (RWCP) Score in Atrial Fibrillation Recurrence Risk After Radiofrequency Ablation 343
Research Progress on Insulin Resistance Indicators and Recurrence after Radiofrequency Ablation of Atrial Fibrillation 344
Impact of Sodium-Glucose Cotransporter 2 Inhibitor on Recurrence After Catheter Ablation for Atrial Fibrillation in Patients With or Without Metabolic Syndrome 344
Impact of Sodium-glucose Cotransporter 2 Inhibitor on Recurrence and Cardiovascular Outcomes after Catheter Ablation for Atrial Fibrillation in Patients with Chronic Kidney Disease 345
MBNL2 在房颤发生发展中的作用机制及治疗潜力：最新研究进展与展望 345
Integrated Single-Cell and Bulk Transcriptome Analysis Reveals a Lactate Metabolism-Related Signature and T-Cell Alterations in Atrial Fibrillation 346
Bleeding Risk of Rivaroxaban and Edoxaban with and without Amiodarone in Atrial Fibrillation Patients: A Prospective Cohort Study 346
持续性房颤射频消融术中应用尼非卡兰复律前冠状窦 A-A 间期在识别高危复发人群的意义 346
脉冲场消融用于不同类型心肌组织治疗心房颤动：犬实验研究 347
脉冲电场应用于小血管相关心律失常消融——一种新的导管和方法 347
脉冲电场消融关键参数对消融灶特征的影响：马铃薯实验 347
一种体外评估脉冲电场消融灶的方法 347
Pulsed field ablation on different types of myocardial tissues for the treatment of atrial fibrillation: canine experiments 347
1 例房颤脉冲场消融围手术期护理经验 348
Effects of Key Parameters on Pulsed Field Ablation of Atrial Fibrillation: Potato Experiments 348
A Novel Method for Assessing the Lesion Size of in Vitro Pulsed Field Ablation 348
Beverage consumption and mortality among adults with atrial fibrillation: a prospective study from UK biobank 349
房颤消融术后左心结构与功能的变化与预后的影响 349
下壁导联 F 波参数与房颤病程对持续性房颤射频消融术后复发联合预测价值的双中心研究 349
睡眠呼吸障碍与房颤导管消融术后复发的相关性研究 349
肿瘤合并心房颤动患者射频导管消融的疗效与安全性评估 350
Effect of ablation index-guided baseline impedance on tissue damage 350
Association between rivaroxaban and the prognosis of patients with acute myocardial infarction and new-onset atrial fibrillation 350
Adherence to Dabigatran versus Warfarin and Associated Factors in Patients with Non-Valvular Atrial Fibrillation after Percutaneous Coronary Intervention 351
Body Roundness Index, Visceral Adiposity Index, and Metabolic Score for Visceral Fat in Predicting New-Onset Atrial Fibrillation: A UK Biobank Cohort Study 351
评价微创冷冻消融系统用于治疗心房颤动的有效性和安全性：一项前瞻、单组、多中心临床试验 352
甲状腺激素敏感性受损与甲状腺功能正常人群的心房颤动风险的联系 352
The Causal Role of Atrial Fibrillation in Anxiety and Depression:A Bidirectional Mendelian Randomization Study 352
Rituximab prevents atrial fibrillation by depressing B cell function and regulating CCR2+ T lymphocyte infiltration and differentiation 353
乳腺癌细胞来源 CXCL11 激活 CXCR3+Th17 细胞促进心肌细胞焦亡在房颤发生中的作用及机制研究 353
左心室舒张功能对非瓣膜性心房颤动患者左心耳功能的影响 353
心房颤动患者合并出血性卒中的抗凝治疗现状 353
Intracardiac echocardiography improves lesion quality and ablation efficiency of pulmonary vein isolation in atrial fibrillation patients: A propensity score-matched analysis 354
Atrial fibrillation and 28-day mortality risk in sepsis: an observational and Mendelian randomization study 354
Marshall 静脉周围心外膜脂肪组织与心房颤动的相关性研究 354
Oral Anticoagulant Treatment in Dialysis-Dependent Atrial Fibrillation: A Network Meta-analysis of 137574 Patients 354
Plasma corin levels provide minimal prognostic utility in left atrial reverse remodeling after catheter ablation of atrial fibrillation 355
阵发性房颤左心房心肌传导速度重构特点的探索 355
The impact of sacubitril/valsartan on catheter ablation for atrial fibrillation complicated with hypertension: A comprehensive retrospective analysis 355
心脏计算机断层扫描增强成像对房颤患者左心耳不同部位血栓的诊断价值 356
Dapagliflozin attenuates atrial fibrosis by inhibiting ferroptosis and Warburg effect via activating the SIRT1/FOXO3a signaling pathway 357
SIRT3 sulfhydrylation by hydrogen sulphide: A novel approach to prevent ferroptosis and atrial fibrosis 357
巯基化修饰 SIRT3 抑制 NLRP3 炎性小体和 Warburg 效应改善心房纤维化 358
Systemic Immune-Inflammation Index and Blood Pressure Control Are Independent and Interactive Predictors of Atrial Fibrillation Recurrence After Ablation 358
窦性心律下左心房超声重构参数对阵发性房颤的预测价值 359
老年长程持续性房颤患者射频消融对比冷冻球囊消融疗效及安全性分析 359
替格瑞洛与氯吡格雷对急性心肌梗死合并心房颤动患者预后的影响 359
Eicosanoid Metabolomics as a Novel Biomarker for Predicting Atrial Fibrillation Recurrence After Cryoballoon Ablation 359
Catheter ablation combined with left atrial appendage closure for non-valvular atrial fibrillation: A Single-Center Retrospective Study 360
基于临床检验检查指标建立老年非瓣膜性房颤患者诊断判别模型 361
Marshall 静脉乙醇灌注在有二尖瓣置换术史的持续性心房颤动患者导管消融治疗中的应用 361
房颤射频消融术对心脏搭桥合并心脏瓣膜手术患者心功能、心肌损伤及预后的影响 361
心源性猝死风险分层对肥厚型心肌病合并心房颤动患者导管消融结局预测价值的研究 361
Association between antithrombotic therapy adherence and adverse events after “one-stop” procedures of combined catheter ablation and left atrial appendage closure for atrial fibrillation 361
The Impact of Sacubitril/Valsartan on Catheter Ablation Therapy Outcomes for Atrial Fibrillation Complicated With Hypertension: A Comprehensive Retrospective Analysis 362
导管消融对心房颤动合并功能性瓣膜反流预后的危险因素分析 362
A simplified multislice computed tomography image integration-guided procedure in catheter ablation of atrial fibrillation 363
BRD4 通过 P53/PAI-1 途径诱导衰老心房 纤维化促心房颤动发生的机制研究 363

Neutrophil-to-lymphocyte ratio and blood pressure control status stratify atrial fibrillation recurrence risk in hypertensive patients after ablation 363
Cryoballoon ablation for patients with atrial fibrillation and heart failure with preserved ejection fraction:
A systematic review and meta-analysis 364
Explore potential targets and mechanisms of Diabetes mellitus with Atrial fibrillation by bioinformatics analysis 364
A Comparative Analysis of the Prognostic Value of Multiple Atrial Fibrillation Prognostic Scoring Systems for Recurrence in Patients with Non-Paroxysmal Atrial Fibrillation Undergoing Pulmonary Vein Isolation Alone 365
Remimazolam-Flumazenil versus Propofol for procedural sedation in patients undergoing electrical cardioversion: A prospective randomized controlled trial. 365
在 CHA2DS2-VASc 评分基础上构建列线图预测心房颤动患者消融术后的复发 366
Research on exploring the common characteristics and clinical significance of atrial fibrillation and chronic kidney disease based on machine learning 366
心房颤动并射血分数保留型心力衰竭患者冷冻消融术后复发的预测参数探索 366
The impact of early cryoballoon ablation on clinical outcomes in patients with non-paroxysmal atrial fibrillation 366
沙库巴曲缬沙坦对持续性房颤患者心脏结构及功能的影响 367
内蒙古某医院心房颤动患者临床治疗现状及预后影响因素分析 367
Clinical Comparison of Cryoballoon Ablation and Radiofrequency Ablation in the Treatment of Persistent Atrial Fibrillation 367
U-shaped association between HDL-c and late recurrence after atrial fibrillation ablation 368
心房颤动患者左心房低电压区预测模型的建立 368
尿酸和血脂对非瓣膜性房颤患者卒中事件的综合预测价值 368
心房颤动患者射频消融术后晚期复发风险预测模型的建立和验证 368
回顾性分析甘油三酯葡萄糖指数对非瓣膜性心房颤动患者导管消融术后晚期复发的影响 369
Elevated resting heart rate in hospitalized patients with atrial fibrillation is associated with increased cardiovascular risk 369
循证式督导护理在持续性心房颤动导管消融术后管理中的效果评价 370
Non-optimal Temperature is Associated with Higher Atrial Fibrillation Hospitalizations in China: A Nationwide Case-crossover Study 370
Extracellular vesicles from LAA facilitate atrial fibrillation 370
Comparative Efficacy of Catheter Ablation Versus Antiarrhythmic Drug Therapy in Asymptomatic and Symptomatic Atrial Fibrillation: Insights from the CABANA Trial 371
心房颤动的发作频率是独立于心房颤动类型的死亡危险因素：一项来自全国范围注册研究 371
Long-term effects of SGLT2 inhibitors on arrhythmias: a systematic review and meta-analysis 371
住院心房颤动患者睡眠质量及其影响因素分析 372
Circulating transthyretin with atrial fibrillation risk, and the modifying role of BMI 372
SGLT2 抑制剂对房颤合并心衰患者导管消融术后房颤复发及心脏功能的影响 372
SGLT2 抑制剂对房颤合并 2 型糖尿病患者导管消融术后复发及心脏功能的影响 373
Exploring T-Cell Exhaustion-Associated Genes in Atrial Fibrillation: A New Diagnostic Perspective and Pathogenic Mechanism Analysis 373
Personalized risk prediction of late recurrence outcome of atrial fibrillation after radiofrequency catheter ablation based on 4S-AF scheme 373
日间患者局麻深度镇静下房颤脉冲电场消融手术患者围术期的护理实践经验 374
Association of red blood cell distribution width with long-term recurrence outcome of atrial fibrillation after radiofrequency catheter ablation 374
Predictive Value of Left Atrial Global Longitudinal Strain (LAGLS) for Recurrence After Catheter Ablation in Hypertensive Patients with Atrial Fibrillation 374
多共病对房颤导管消融术后疗效影响的观察研究 374
Periprocedural Intravascular Hemolysis and Renal Function in Persistent Atrial Fibrillation Patients Undergoing Pulmonary Vein Isolation with Pulsed-Field Ablation 375
Efficacy and Safety of a Novel Method Stimulating Superior Vena Cava Approach via Femoral Vein to Facilitate Ethanol Infusion of the Vein of Marshall in Atrial Fibrillation 375
Mechanism of hydrogen sulfide alleviating atrial fibrillation induced by acute obstructive sleep apnea based on proteomic differential protein glutaredoxin-1 375
心房颤动经皮射频消融护理质量评价指标体系的构建及应用 376
AI 智能管理平台对房颤患者射频消融术后心脏康复干预效果分析 376
风险评分系统在预测胸腔镜下心房颤动消融术后复发中的价值 376
瓣膜病房颤和非瓣膜病房颤的区别和抗凝策略的差异 376
Catheter Ablation versus Non-ablation in Atrial Fibrillation Patients Aged ≥ 80 years: Results from the China Atrial Fibrillation Registry 376
LOXL2 as a Predictive Biomarker for Breakthrough Stroke Risk in Paroxysmal Atrial Fibrillation Patients 377
CEP68/FLRT2: The potential druggable genes for Atrial Fibrillation identified by Systematic druggable genome-wide Mendelian randomization 377
经皮左心耳封堵术后中期口服抗凝治疗与抗血小板治疗的疗效的比较 378
心腔内超声结合全三维技术实施零射线个体化房间隔穿刺 378
房颤发生率在胸腔镜肺段切除与肺叶切除肺癌患者中的差异性研究 378
Ablation Lesion Characteristics with ODOT MICRO Catheter Modes Versus Conventional Power Control: A Comparative Analysis 378
Trends and Appropriateness of OACs Use in Atrial Fibrillation: A Decade of Real-World Evidence from the China-AF Registry (2011-2022) 379
Left Atrial Epicardial Adipose Tissue Dispersion Predicts Low Voltage Areas in Hypertensive Atrial Fibrillation Patients 379
The Predictive Role of Tumor Necrosis Factor Superfamily 14 in Atrial Fibrillation Recurrence Following Catheter Ablation: A Prospective Cohort Study 380
From Single Cells to Causality: Decoding Atrial Fibrillation Mechanisms via Transcriptomics and Mendelian Randomization 380
合并心力衰竭与心房血栓的心房颤动患者的临床特征及预后 381
J 形弯导丝房间隔穿刺术随机对照研究 381
心电图 f 波振幅预测老年持续性心房颤动患者射频消融术后 1 年复发的价值 381
犬尿酸升高通过抑制心脏神经节丛 γ- 氨基丁酸信号传导介导 “房颤诱发房颤” 381
Nrf2 Overexpression Attenuates Erastin-Induced Ferroptosis in Cardiac Fibroblasts 381
国内外心房颤动与心房重构的研究热点与趋势的比较——基于 WOS 和 CNKI 文献的可视化分析 382
Management for stroke secondary prevention in patients refusing anticoagulation therapy after atrial fibrillation catheter ablation without recurrence: A Prospective Cohort Study 382
Long-term clinical efficacy of vein of Marshall ethanol infusion combined with catheter ablation for persistent atrial fibrillation 383
Impact of Catheter Ablation on Left Ventricular Diastolic Function and Remodeling in Atrial Fibrillation Patients Stratified by Left Ventricular Diastolic Dysfunction Severity 383
Clinical effect of vein of Marshall ethanol infusion on mitral isthmus ablation Running title: Marshall ethanol infusion 384
结缔组织生长因子与房颤及心房纤维化的相关性研究 384
缩窄性心包炎合并心房颤动及心房扑动行射频消融术的疗效和安全性分析 384

术前高敏 C 反应蛋白水平与非瓣膜性房颤射频消融术后长期预后的关系：一项中位 7 年随访的前瞻性队列研究 384
Clinical Outcomes in Asymptomatic and Symptomatic Atrial Fibrillation Patients With or Without Rhythm Control Therapy: A Prospective Multicenter Registry Study 385
导管消融对心房颤动合并颅内出血病史患者的远期预后影响 385
基于集成于智能手表的单导联心电图：人工智能增强校正 PPG 评估的心房颤动负荷的前瞻性验证研究 385
单导联长程心电监测对中国东部某农村地区 75 岁及以上老年人房颤筛查的有效性：一项社区人群研究 385
Validation of Photoplethysmography-Based Smartwatch for Continuous Evaluation of Atrial Fibrillation Burden 385
Continuous Evaluation of Atrial Fibrillation Burden 385
房颤导管消融术后口服抗凝治疗与血栓栓塞风险降低无关：一项纵向队列研究 386
左心室几何重构与房颤合并射血分数保留型心衰患者的预后及疗效的关系 386

心血管互联网与人工智能有关研究 387
TabPFN 在心 - 肾 - 代谢综合征冠脉狭窄诊断模型构建中的探索性应用 387
基于人工智能的心血管疾病信息化护理管理系统的构建与应用研究 387
心血管信息化与 AI 融合提升诊疗效能的探索 387
数字 AI 预测护理系统联合护士主导模式降低冠心病再入院率的阶梯楔形随机试验研究 387
人工智能在心脏重症中血流动力学监测的应用进展 387
基于生成式人工智能技术赋能的心内科复杂急救情境虚拟仿真训练体系在护理人员培训中的应用与效果研究 388
Machine Learning Identifies ECG Biomarkers for 28-Day Mortality Risk Stratification in ICU Patients 388
STEMI 患者 PCI 术后急性肾损伤的机器学习预测模型的构建与验证 388
面向长 QT 综合征等心律失常的单导联 ECG 智能诊断 388
机器学习在心血管疾病诊疗中的应用研究进展 388
基于多模态信息融合的主动脉夹层 AI 诊断 389
Deep Learning-based Cardiac Computed Tomography Angiography Left Atrial Segmentation and Quantification: A Multi-model Comparative Study 389
深度学习辅助超声心动图自动监测主动脉狭窄和严重程度分级：多切面与单切面比较 389
智能导管系统在心血管疾病方面的研究进展 389
基于人工智能技术量化的视网膜微血管与冠状动脉粥样硬化性心脏病相关性研究 390
Initial experience of multi-device robot-assisted Left main bifurcation stenting with Culotte technique in pig model 390
The Feasibility and Utility of Large Language Models in Interpreting Cardiac Magnetic Resonance Reports: A Real-World Pilot Study 390
机器学习与传统模型在预测中国普通人群动脉粥样硬化性心血管疾病中的性能比较 391
Establishment and Validation of a Predictive Model for Anxiety Risk in Patients with Atrial Fibrillation 391
基于多维度指标监测与机器学习算法的健康干预体系构建 391
从 U-Net 到 Transformer：主动脉夹层分割技术的演进与临床转化 392
综合生物信息学分析发现 POLR2I 是高血压肾病发病机制的关键基因 392
机器学习和多组学整合：推进心血管转化研究和临床实践 392
人工智能随访信任量表的编制及信效度检验 392
Machine Learning Based Prediction of Postoperative Acute Kidney Injury Risk in Coronary Artery Bypass Grafting Patients 392
AI 健康助手在提升糖尿病高血压患者居家血压 / 血糖双达标率中的作用评估 393
可穿戴生物传感器驱动的 AI 个体化运动处方系统对高危心血管病患者康复效果分析 393
面向急性 A 型主动脉夹层术后患者低氧血症的多阶段智能决策模型构建 393
基于深度学习的心电图诊断肥厚型心肌病模型的构建与验证 393
基于利用人工智能增强心电图预测肥厚型心肌病患者新发房颤的研究 394
探讨互联网 + 护理服务远程应用的护理效果分析及可行性 394
基于深度神经网络的 CT 冠状动脉造影自动分割与诊断 394
虚拟现实引导的动机增强训练对青年心肌梗死患者康复依从性及心理社会功能重建的混合方法研究 394
基于人工智能的心脏康复个性化运动处方设计与效果评估 394
人工智能驱动的护理决策支持系统在心血管病风险管理中的应用：一项多中心随机对照研究 395
Clinical Feasibility of two Cardiac Deep Learning Cine MRI Sequences: Single-Breath-Hold and Free-Breathing Motion-Corrected Approaches 395
移动医疗视域下慢性心力衰竭患者自我管理体验与需求的质性研究 395
Reliability and Reproducibility of AI-assisted Left Ventricular Ejection Fraction Assessment: A Multicenter Real-world Retrospective Study 395
基于多模态生物传感器在心血管疾病动态监测与智能护理预警中的创新应用及价值研究 396
AI-Driven Advances and Application in Vascular Aging Research 396
基于心电图和临床风险因素结合深度学习预测房颤相关性脑卒中 397
心率以外的稳健心脏风险筛查：低剂量 CT Agatston 评分在心率亚组分类中的高诊断一致性 397
基于 LASSO 回归和机器学习构建冠状动脉慢血流诊断预测模型 397
基于人工智能的信息化平台在冠心病 PCI 术后患者心脏康复护理中的应用 398
Characteristics, Cost/Effect Consideration of Clinical Examinations, and Construction of Machine Learning Models of Restrictive Cardiomyopathy: Insights from Peking Union Medical College Hospital 398
多模态基础模型对超声心动图室壁运动异常 的智能识别 398
基于 5G 物联网与人工智能技术的区域性心脏心电智能预警体系构建 398
基于人工智能的多模态心音与超声特征融合模型在射血分数保留心力衰竭早期诊断中的研究 399
心血管智慧护理创新融合新进展 399
心血管疾病患者数字健康技术促进因素和阻碍因素的系统评价： 基于 CIFR 框架 399
Development and application of Artificial Intelligence Follow-up System in Coronary heart disease Patients 399
5G 远程随访系统在心脏起搏器植入术后患者延续性护理中的应用与研究 400
ECG8-EHR13-AF: A Multimodal Electrocardiographic and Clinical Score for Two-Year Incident Paroxysmal Atrial Fibrillation Risk Prediction 400
基于计算流体力学的 caFFR 测定评价冠脉生理学功能的准确性研究 401
Diagnosis of heart disease based on multimodal information fusion 401
Machine Learning Facilitated Early Risk Stratification of Bee Injuries Based on a Tropical Multicenter Cohort 401
数字孪生技术在心血管护理领域的应用进展 402
基于共享决策模式的人工智能老年房颤患者健康监测小程序的研发及应用研究 402
PPARgene 2.0: leveraging large language models and multi-omics data for enhanced identification and prediction of PPAR target genes 402
基于拉曼光谱结合 Stacking 机器学习方法对主动脉夹层患者早期识别的研究 403

人工智能在心血管疾病辅助诊疗中的应用进展与挑战 403
人工智能在心血管临床护理中的应用 403
远程医疗技术在冠心病患者服药依从性中应用的研究进展 404
心血管疾病全周期智慧化管理：人工智能平台的构建与应用实效 404
人工智能：放射介入术后康复护理个性化、精准化与资源优化的利器 404
The feasibility of radiomic analysis based on T1 mapping to distinguish between hypertensive heart disease and hypertrophic cardiomyopathy 404
不同来院方式对急性 ST 段抬高型心肌梗死患者再灌注时间及短期预后的影响分析 405
人工智能在改善老年心血管患者服药依从性与准确率中的应用研究 405
绘制昼夜节律紊乱驱动动脉粥样硬化进展的分子指纹图谱 405
基于机器学习建立冠心病患者冠状动脉整体负荷风险预测模型 405
中心静脉导管相关血流感染预防控制系统的构建及应用 405
基于胸痛视角的心脏大血管转诊平台的构建与实践 405
冠心病长期皮下注射单抗患者对网约护理服务的认知及需求度现状 406
心音心电图远程监测在心脏起搏器患者心功能院外评估中的可行性研究 406
基于人工智能 MA-IRNet 算法的心脏起搏器品牌自动分类系统应用研究 406
Multimodal AI Models in Hypertrophic Cardiomyopathy Screening: Current Advances and Future Directions 406
Ethical considerations for using artificial intelligence in clinical practice: an umbrella review 407
基于多模态数据融合与深度学习的急性心肌梗死早期预警系统研究 407
Integrating the Red Cell Distribution Width to Albumin Ratio into Machine Learning for Predicting In-Hospital Mortality in Heart Failure Patients with Pneumonia: a Multi-Center Study 407
互联网 + 和人工智能在高血压临床管理中的应用 408
心脏瓣膜置换术后患者居家抗凝管理模式的卫生经济学评价 408

心血管免疫与炎症研究 409
基于冠状动脉周围脂肪衰减指数探讨 SGLT-2 抑制剂联合 GLP-1 受体激动剂对 2 型糖尿病患者冠状动脉炎症的影响 409
Cardiac Resident Macrophage-Derived Collagen I Supports Vascular Stabilization and Healing Following Cardiac Injury 409
HyPoxia Induces M2 MacroPhages to ExPress VSIG4 and Mediate Cardiac Fibrosis After Myocardial Infarction 409
心血管免疫与炎症研究 410
NETs 通过 TGFβ1-Smad2/3 介导的内皮间充质转化在糖尿病肾病动静脉内瘘狭窄中的机制研究 410
分子伴侣介导的自噬调控巨噬细胞免疫代谢在心肌梗死中的研究 410
Nrf2 参与 MSCs 调节大鼠梗死心肌氧化应激作用的实验研究 410
miR-214 靶向抑制 CaMK II 调控 H9c2 心肌细胞的氧化应激 410
CircHIPK3 regulates the autoPhagy and aPoPtosis of hyPoxia/reoxygenation-stimulated cardiomyocytes via the miR-20b-5P/ATG7 axis 411
基于 TLR4/NF-kB 通路探讨木犀草素对 LCWE 诱导的冠状动脉血管炎的保护机制 411
ATF7 介导的单核细胞表观遗传重编程通驱动肥胖相关 HFpEF 的发生机制研究 411
Macrophage-derived AMPKγ2 prevents cardiac remodeling post myocardial infarction via SMURF2/YY1/CXCL16 axis 412
Molecular Mechanisms of Nanoplastic-Induced Impairment in Early Endothelial Tube Formation Derived from Human iPSCs 412
Adenylyl cyclase 7 of cardiac macrophages protects myocardial ischemia/reperfusion injury by suppressing inflammation 413
ATF4 regulates PI3K/AKT signaling axis to promote angiogenesis after myocardial infarction 413
心脏归巢肽功能化修饰的脂质体纳米材料负载秋水仙碱的制备及其改善心肌梗死后炎症和神经重构的作用 414
系统免疫炎症指数在心血管疾病中临床应用的研究进展 414
Clinical features and prognosis of idiopathic inflammatory myopathy complicated by heart failure with preserved ejection fraction 414
NLRP3 介导的中性粒细胞焦亡在川崎病冠脉瘤的作用及机制研究 415
基于单细胞测序技术对动脉粥样硬化斑块中干细胞样 CD8+T 细胞的探讨 415
单细胞测序联合代谢组学揭示免疫相关心肌炎中的代谢重编程与免疫互作机制 415
Dual Epigenetic Control by p16INK4a via ISGylation and m ^{6} A/m ^{7} G Epitranscriptomic Reprogramming Governs Macrophage Efferocytic Dysfunction in Cardiac I/R Injury 416
Anti-Atherosclerotic Effects and Mechanisms of Narciclasine via Histone Lactylation-Mediated Inhibition of Endothelial Inflammation 416
免疫检查点抑制剂相关心血管不良事件影响因素的 Meta 分析 417
Associations of Metabolic Vulnerability Index with microvascular complications and all-cause mortality intype 2 diabetes mellitus patients: a prospective cohort study of UK Biobank 417
Threshold Effect of Systemic Immune-Response Index on In-Stent Neoatherosclerosis Among Patients With Drug-Eluting Stent Restenosis 417
AMPK-CLYBL 乙酰化正反馈环路通过代谢重编程与炎症反应加剧心脏重塑 418
泛血管疾病的视角下的胞葬作用 418
MicroRNA-27a-5p Protects Against Diabetic Vascular Injury by Suppressing NOX4-Driven Autophagy via MAPK Signaling 418
SGLT-2 Inhibition Mitigates Neutrophil-Driven Endothelial Injury in Diabetic Coronary Artery Disease by Suppressing GREM1 and Restoring TGF-β/Smad Signalling 419
Liensinine Attenuates Coxsackievirus B3-Induced Viral Myocarditis by Inhibiting NLRP3-Mediated Pyroptosis via Improved Mitochondrial Function 419
Integrative Analysis of Lactylation-Associated Features in Abdominal Aortic Aneurysm and Its Immune Microenvironment Utilizing scRNA-seq and Bulk RNA Sequencing 419
Neutrophil Methylmalonic Acid Promotes Microthrombis Formation and Adverse Cardiac Remodeling Post-Myocardial Infarction Through Activating IL-6 Signaling Pathway-mediated NETosis 420
α- 酮戊二酸激活心肌细胞 FTO 影响中性粒细胞募集改善脓毒性心肌的机制研究 420
Systemic inflammation indices affect the association between pericoronary fat attenuation index and adverse prognosis in patients with coronary artery disease 421
Association between Aggregate Inflammatory Score Index and Hypertension Patients with Coronary Heart Disease: A Cross-Sectional Study Based on NHANES (2005–2016) 421
复方丹参滴丸、乙酰唑胺和红景天苷在急性高原缺氧诱导早期肺损伤中对 HIF1α/CXCR4 通路的调控 421
Prevalence and Risk Factors of Subclinical Atherosclerosis in Chinese Patients with Systemic Lupus Erythematosus 422
Complement component C4B prioritization through drug target Mendelian randomization reveals a novel therapeutic target for calcific aortic valve stenosis 422
载 BNN6/RAPA 纳米粒调控巨噬细胞极化抑制心脏移植急性排斥反应 422
孟德尔随机化探究心脏淀粉样变危险因素 423
Prenatal and Postnatal Ambient Air Pollution and Kawasaki Disease: A Systematic Review and Meta-Analysis 423
PKM2/PPARγ 代谢重编程调控 CXCR4+ 中性粒细胞促进 NETs 介导的心肌细胞焦亡，是脓毒症心肌病的关键因素 423

Group 2 Innate lymphoid cell derived IL-9 activates regulatory T cells to Facilitate post myocardial infarction repair 423
系统性红斑狼疮合并急性心肌炎 12 例临床分析 424
Mitochondrial One-Carbon Metabolism Drives CD34 Lineage Cells to Differentiate into Tfh Cells to Form Tertiary Lymphoid Organ in Transplant Arteriosclerosis 424
Regulatory Dendritic Cells enhance the survival and cardioprotective effect of mesenchymal stromal cells via improving immune microenvironment 425
Single-cell RNA sequencing atlas of peripheral blood mononuclear cells from subjects with Premature ST-segment elevation myocardial infarction 425
Prognostic Value of Serum Total Bilirubin in Patients with In-Stent Restenosis: A Stratified Analysis Based on Inflammatory Status 426
泛素连接酶 RNF216 调控心脏内皮细胞炎症性衰老在心脏衰老中的作用机制 426
Integrative Immune–Echo Profiling Reveals B Cell–Cardiac Function Association：A Retrospective Analysis 426
Explainable Machine Learning Diagnostic Model for Coronary Heart Disease Using Inflammatory Factors Combined with Traditional Risk Factors: A Retrospective Single-Center Study 427

心血管信息化与大数据有关研究 428
“互联网 + 智慧医院背景下” 医 - 护 - 患三维联动模式的创新与实效 ——在缩短老年急性心肌梗死患者平均住院日的应用研究 428
基于可解释机器学习的房颤消融围术期心脏压塞风险预测模型的开发与验证 428
基于人工智能心电图构建改善型心力衰竭的预测模型 428
基于机器学习的急性冠脉综合征智能风险评估系统构建与护理实践 428
家庭支持系统对青年冠心病患者二级预防行为依从性的影响研究 428
基于心电图及多模态临床特征的机器学习模型预测危重症患者死亡风险 428
人工智能赋能心血管信息化： 我国心血管病防治进展与科研成果整合分析 429
Development and validation of an interpretable machine learning model for predicting Coronary Artery Aneurysms in Children with Kawasaki Disease: A Multicenter Study from Southwest China 429
基于人工智能的儿童先天性心脏病院后随访体系构建与管理模式探索 430
ComPrehensive Bioinformatics Analysis Reveals the Role of Shared CuProPtosis- and FerroPtosis-Related DEG DLD in Abdominal Aortic Aneurysm 430
Machine Learning-Derived Strategy for Predicting Long-Term Ischemic Stroke Among Type 2 Diabetes Mellitus Patients with Non-ST-Elevation Acute Coronary Syndrome: A Nationwide Multicenter Cohort Study 430
智能化技术在心血管护理管理中的应用与创新 431
A Bibliometric Study and Visualization Analysis of Chronotherapy: Interpretable Prediction of Hospitalization Costs for Patients with Ischemic Heart Disease Using Artificial intelligence 431
《心血管信息平台与人工智能协同：从精准诊断到风险防控的体系化研究》 431
基于多模态深度学习的心血管疾病智能诊断框架 431
用于心血管疾病分类的多模态机器学习：一项基于临床、生化、影像学和心电图数据的综合研究 432
基于 AI 的心血管患者智能护理管理系统构建及应用效果研究 432
信息化在心血管临床护理创新中的应用研究 432
Machine learning based model for predicting cardiovascular disease using dynamic triglyceride-glucose index: a Longitudinal study cohort CHARLS database 432
人工智能在女性心脏病健康流行病学中的应用与展望 433
关于信息化时代下心血管健康科普知识传播效果的研究 433
基于可解释机器学习建立睡眠呼吸暂停低通气患者中冠心病预测模型——整合炎症及睡眠障碍相关标志物 433
数字技术在心血管临床护理中的应用研究 433
高血压患者心力衰竭可解释预测模型的识别与验证 433
基于心电大数据的房颤慢性病管理模式研究进展与展望 434
基于 CiteSpace 对心血管数字健康技术演进路径与前沿趋势的研究 434
基于机器学习的心房颤动患者发生血栓的预测模型 434
接受经导管主动脉瓣置换术的重度主动脉瓣狭窄患者并发二 尖瓣反流演变的研究 434
将 CFIR 框架用于心血管疾病急救医疗实施研究：阻碍、促进因素与可能的机会 434
人工智能辅助心血管疾病风险预测模型的构建与验证 435
心脏瓣膜病术后的个体化抗凝治疗 435
Explainable Machine Learning for Predicting ICU-Onset Atrial Fibrillation in STEMI Patients: A Gradient Boosting Framework Based on Real-World Data 435
Leveraging Explainable Artificial Intelligence to Uncover Age and Sex Heterogeneity in Cardiovascular Risk Factors: A Cross-sectional Study of the BRFSS Cohort 436
新形势下构建和谐护患关系与护理文化建设的思考 436
智慧管理模式在心力衰竭患者延续性护理中的应用进展 437
RESEARCH ON SIMULATION AND IDENTIFICATION OF ECG SIGNAL 437

心脏瓣膜病有关研究 438
The Relationship of Serum Uric Acid and Intracardiac Thrombosis Risk in Patients with Rheumatic Heart Disease 438
Development and Validation of a Nomogram for Predicting Intracardiac Thrombosis Risk in Patients with Rheumatic Heart Disease 438
TAVR 术后发生急性肾损伤危险因素分析及预测模型构建 438
Serum alpha-1-microglobulin (A1M) as an independent predictor of calcific aortic valve stenosis and its predictive value 438
风湿性心脏病合并心腔内血栓患者的临床特征及预后相关分析 439
Whole transcriptome analysis of aortic stenosis unveils dysregulated RNA networks, immune infiltration, and NADK2-driven pathogenic mechanisms 439
探究风湿性二尖瓣疾病的血流动力学影响 439
使用 Feops 有限元模拟技术评估接触压力指数预测经导管主动脉瓣置换术后新发左束支传导阻滞的效能：一项单中心临床研究 440
Post-TAVR blood pressure elevation: Impact on clinical outcomes 440
老年重度瓣膜性心脏病患者的现状和预后分析：一项单中心前瞻性观察研究 440
TAVR 术中导丝过瓣困难时的应对方法 441
经导管主动脉瓣置换术后 30 天死亡率预测的机器学习模型：基于 NTCVR 队列的全国性研究 441
Hyperglycemia and genetic susceptibility in relation to incident degenerative aortic valve stenosis 441
心脏瓣膜病患者护理中呼吸训练对术后康复的促进作用 441

Outcomes and Temporal Trends of Transcatheter Versus Surgical Aortic Valve Replacement in Patients with Chronic Thrombocytopenia: Insights from the Nationwide Inpatient Sample 442
The Comparative Effectiveness of Single versus Double Perclose ProGlideTM Devices in Achieving Transfemoral AortIc Valve Replacement Access Site Closure: A Prospective, Multicenter, Randomized Controlled Trial (Single-Closure) 442
冠状动脉疾病对经导管主动脉瓣置换术患者预后的影响 442
可穿戴心音图技术在主动脉瓣二叶畸形相关升主动脉扩张早期预警中的应用价值研究 443
基于人工智能的影像学分析方法自动检出并定级 TAVR 术后低密度瓣叶增厚的研究 443
单纯食管超声心动图引导经导管二尖瓣缘对缘修复术后中期疗效分析 443
Case Report of snare-assisted coaxiality optimized technique during valve deployment in patient with pure aortic regurgitation 443
中国西北地区大型三甲医院瓣膜性心脏病患者的病因及分布研究 444
基于 SF-36 量表的生物瓣与机械瓣置换术后中老年患者健康相关生命质量的动态差异比较研究 444
Optimal Oversizing Degree of Self-Expanding Transcatheter Valve in Patients with Bicuspid versus Tricuspid Aortic Stenosis 444
Outcomes of Transcatheter Aortic Valve Implantation for Bicuspid Versus Tricuspid Mixed Aortic Valve Disease 445
二叶式和三叶式主动脉瓣重度狭窄行 TAVR 术前术后对比分析研究 445
经导管主动脉瓣置换术中球扩瓣与自展瓣的瓣周漏与患者预后的 Meta 分析 445
老年中 - 重度主动脉瓣狭窄人群不同治疗方式远期预后及危险因素研究 445
March2 缺失促进 ALDH3B2 介导的氧化应激加重钙化性主动脉瓣疾病 446
江苏地区二叶式主动脉瓣畸形患者的临床特征及超声心动图在随访管理中的价值：一项单中心回顾性研究 446
Impact of Concomitant Pulmonary Hypertension on Outcomes after Transcatheter Edge-to Edge Repair for Mitral Regurgitation 446
基于转录组学和生物信息学分析的主动脉瓣钙化关键通路及核心基因研究 446
Left Atrial Function Index-Tricuspid Regurgitation Interplay Predicts Midterm Prognosis Following Transcatheter Aortic Valve Replacement: A Hemodynamic Remodeling Perspective 447
Effects of transcatheter aortic valve replacement on hemodynamics and left atrial reverse remodelling for aortic stenosis with progressive to severe mitral stenosis 447
Feasibility and Outcomes of Intra-aortic Balloon Pump Support in Patients with Severe Aortic Valve Stenosis and Acute Decompensated Heart Failure 448
合并冠心病的 TAVR 患者同期行 PCI 的安全性和有效性研究 448
单把血管缝合器对比双把在闭合 TAVR 患者股动脉入路的安全性及有效性研究 448
经导管主动脉瓣置换术治疗重度主动瓣狭窄合并射血分数降低型心衰经验总结 449
孤独感与退行性心脏瓣膜疾病风险的关联：一项大规模前瞻性队列研究 449
经导管主动脉瓣置换术后失败的处理策略：瓣膜取出与二次 TAVR 疗效比较的系统综述与荟萃分析 449
Sex-Specific Differences in the Incidence of New-Onset Left Bundle Branch Block and Need for Pacemaker Implantation Following Transcatheter Aortic Valve Replacement 449
Effect and Mechanism of Calcium Binding Protein S100A8/A9 on Calcific Aortic Valve Disease 450
一例经心尖主动脉瓣置换术后全身皮下气肿的护理体会 450
Predicting new-onset persistent conduction disturbance following transcatheter aortic valve replacement: the usefulness of FEOPS finite element analysis 450
High High-Density Lipoprotein Cholesterol Is Associated with Elevated Bleeding Risk in Patients With Aortic Stenosis Undergoing Transcatheter Aortic Valve Replacement 451
心肺康复调控心脏瓣膜术后患者心肺耦合机制的系统评价：基于血流动力学参数与自主神经功能的 Meta 回归 451
经导管主动脉瓣置换术相关脑卒中的危险因素探究 452
Transcatheter aortic valve replacement for pure native aortic valve regurgitation: a real-world, prospective, multi-center Study (TRUST TAVR REGISTRY) 452
经导管主动脉瓣置换术对单纯主动脉瓣反流患者心功能及心室重构的影响 452
分析重度主动脉瓣狭窄对左室各壁心肌收缩功能 损伤的差异及对心肌收缩同步性的影响 453
合并肺动脉高压对 TEER 手术术后结局的影响 453
慢性血小板减少症患者经导管与外科主动脉瓣置换术的结果和时间趋势的比较：来自全国住院患者样本的见解 453
基于免持超声多普勒技术经颈无创连续评估主动脉瓣功能的研究 453
Study on cardiac function and ventricular wall motion after transcatheter aortic valve replacement (TAVR) 453
Potential Inhibition of Aortic Valve Calcification by Eicosapentaenoic Acid: Implications for Non-Invasive Treatment of Aortic Stenosis 454
经导管经间隔途径二尖瓣置入术治疗二尖瓣生物瓣衰败的疗效观察 454
Temporal and Spatial Evolution Dynamics and Sociodemographic Gradient Effects of Disease Burden (Prevalence, DALYs, and Mortality) of Valvular Heart Diseases (RHD/CAVD/DMVD) Under a Cross-National Spatial Spectrum from 1990 to 2021: An Epidemiological Mod 455
Valve-in-Valve Transcatheter Aortic Valve Replacement Versus Redo Surgical Aortic Valve Replacement for Structural Valve Degeneration: An d Meta-Analysis 455

胸痛与急性心梗有关研究 456
Kinetics and Prognosis Value of Heparin Binding Protein at the Acute ST-Segment-Elevation Myocardial Infarction 456
Impact of the first-wave COVID-19 pandemic on emergency acute coronary syndrome: a multicenter retrospective study from a non-epicenter region 456
Influence of COVID-19 pandemic on mechanical reperfusion in ST-segment-elevation myocardial infarction undergoing primary percutaneous coronary intervention: a multicenter retrospective study from a non-epicenter region 457
Iodixanol-associated acute kidney injury and prognosis in patients undergoing elective percutaneous coronary intervention: a prospective, multicenter study 457
Risk of post-contrast acute kidney injury in patients with heart failure undergoing elective percutaneous coronary intervention: a prospective, multi-center study based on iodixanol administration 458
Non-anticoagulant heparin alleviates myocardial ischemia-reperfusion injury through inhibiting GSDMD-mediated cardiomyocyte pyroptosis via the HMGB1/RAGE pathway 458
老年急性 ST 段抬高型心肌梗死患者膜联蛋白 A1 与 eGFR 水平、冠脉病变程度及不良心血管事件的相关性 458
中国高原地区急性 ST 段抬高型心肌梗死的特点和转归：基于胸痛中心数据的回归性分析 459
Development and Validation of a LASSO-Enhanced GRACE Model for Predicting Major Adverse Cardiac Events After PCI in AMI Patients 459
USP13 Ameliorates Myocardial Infarction Injury by Inhibiting Ferroptosis via Stabilizing ALDOA 459
Albumin-to-Globulin ratio as an independent risk factor for predicting prognostic risk in patients with acute coronary syndrome undergoing percutaneous coronary intervention. 460
Prognostic Nutritional Index as an Independent Risk Factor for Predicting Outcomes in Acute Coronary Syndrome Patients Undergoing Percutaneous Coronary Intervention. 460

急性心肌梗死“肥胖悖论”的机制阐释与临床启示：一项系统性观点综述 461
Short-Term Exposure to Ozone and PM ₂．₅ and Their Components Increases the Risk of In-Hospital Mortality in Patients with Acute Myocardial Infarction: A Time-Stratified Case-Crossover Study 461
HMGB-1 联合 MSCs 移植对急性心肌梗死大鼠心脏功能影响的实验研究 462
HMGB1 预处理骨髓间充质干细胞移植治疗心肌梗死大鼠的实验研究 462
干扰 Nrf2 基因后骨髓间充质干细胞移植对大鼠心肌梗死后心肌凋亡的影响 462
沉默 Nrf2 基因的骨髓间充质干细胞移植对大鼠心肌梗死后心室重构和纤维化的影响 462
钙素基因相关肽调节间充质干细胞存活对大鼠颈动脉损伤后血管修复的作用 462
TLR4 基因修饰 BMSCs 移植对大鼠急性心肌梗死后心功能的影响 462
CircERBB2IP Promotes Post-infarction revascularization via the miR-145a-5P/Smad5 axis 462
ANNEXIN A2 FACILITATES NEOVASCULARIZATION TO PROTECT AGAINST MYOCARDIAL INFARCTION INJURY VIA INTERACTING WITH MACROPHAGE YAP AND ENDOTHELIAL INTEGRIN B3 463
Serum liPidomics reveals PhosPhatidylethanolamine and PhosPhatidylcholine disorders in Patients with myocardial infarction and Post-myocardial infarction-heart failure 463
Clinical Feature-Based Machine Learning Model for 1-Year Mortality Risk Prediction of ST-Segment Elevation Myocardial Infarction in Patients with HyPeruricemia： A RetrosPective Study 463
钠 - 葡萄糖协同转运蛋白 2 抑制剂在急性冠状动脉综合征患者中的疗效 464
18 至 45 岁急性冠脉综合征患者中代谢表型与心血管事件的关联 464
Superlubricity DAPA-PDMAMPC-PCM Nanoparticles Boost Dapagliflozin’s Therapeutic Effects in Diabetic Myocardial Infarction: Mitochondrial Repair and Targeted Delivery Synergy 464
BMI Differences on Anticoagulation with Bivalirudin vs. Heparin During Primary PCI: a BRIGHT-4 subanalysis 465
司美格鲁肽对非糖尿病大鼠急性心肌梗死后心肌细胞凋亡的影响及机制研究 465
穿戴心音心电同步设备对急性心肌梗死 PCI 术后左室收缩功能障碍及预后的预测价值 465
注射用心肌肽干预急性 ST 段抬高型心肌梗死直接 PCI 术后改善心肌梗死面积的多中心临床研究 465
miR-21 联合冠脉狭窄程度对急性心肌梗死患者介入术后 MACE 的预测价值 466
miR-126 联合纤维蛋白原与白蛋白比值对急性心肌梗死患者介入术后 MACE 的预测价值 466
SBAR 标准化沟通模式：在急性心肌梗死患者转交接护理中的应用研究 466
基于单细胞技术研究 LEF1 调控 IL6ST 转录抑制 CD56dimCD16+NK 细胞凋亡在心 肌梗死中的机制研究 466
Axl 受体通过保护内皮屏障与减轻钙超载在心肌缺血再灌注损伤中发挥保护作用 466
血浆致动脉粥样硬化指数与急性心肌梗死患者预后的相关性研究 467
血清 sTREM2 与老年急性冠脉综合征的相关性研究 467
A youth acute myocardial infarction patient during high-altitude de-acclimatization: A case report and literature review 467
急性心肌梗死新发房颤预后模型的开发与验证：一项多中心回顾性研究 468
心肌梗死后睡眠对心脏左室射血分数的短期影响 468
Multi-Omics Mendelian Randomization Identifies Genes for High Platelet Reactivity in Myocardial Infarction 468
MIF 在心肌缺血 / 再灌注后的微血管损伤中的作用及机制 468
支架置入策略对前降支真性分叉病变患者术后一年主要不良心血管事件的影响 469
Sex-related differences in clinical outcomes of octogenarians with STEMI in China 469
基于急性心肌梗死患者血浆的核酸适配体筛选及其临床诊断价值研究 469
王不留行黄酮苷改善心肌梗死后心肌细胞焦亡的研究 469
王不留行黄酮苷（Vaccarin）改善小鼠心肌梗死后 心室重构 470
血清转酮醇酶（Tkt）水平对急性冠脉综合征患者临床预后的预测价值 470
All-trans retinoid acid pre-treatment reduced myocardial ischemia/reperfusion-induced cell death in vitro 470
All-trans Retinoic Acid prevent reperfusion injury post-myocardial infartion in diabetic mice by incresing RAGE cut. 471
CREG1 protects myocardium from hypoxic injury by regulating autophagy through Lysosomal Stress Response 472
基于淋巴细胞的炎症指数对急性心梗合并心源性休克预测价值研究 472
Protective effect of ALG-2 interacting protein X on hypoxic injury of cardiomyocytes 472
急性心肌梗死并发心脏破裂的危险因素分析及预测模型建立 473
急性前壁 ST 段抬高型心肌梗死患者发生左心室血栓的危险因素 473
急性心肌梗死多支病变合并糖尿病不同血运重建的预后比较 473
中性粒细胞与血小板比值（NPR）对行经皮冠脉介入治疗的急性冠脉综合征患者预后的预测价值 473
空腹应激性高血糖比率对经皮冠状动脉介入治疗的急 性冠脉综合征患者预后的影响 474
CONUT 评分对经皮冠状动脉介入治疗的急性心肌梗死患者 预后的预测价值 474
STEMI 合并应激性高血糖对患者临床预后及血小板功能的影响 474
Machine learning prediction model and nomogram to predict risk of cardiovascular events in patients with acute coronary syndrome 474
身体活动、久坐行为与生物年龄对心肌梗死后死亡风险的联合影响及中介作用 475
Multiomics reveals gut dysbiosis links to fatty acid dysmetabolism in early phase of acute myocardial infarction 475
Relationship Between the Atherogenic Index of Plasma and New-Onset Atrial Fibrillation in Acute Myocardial Infarction 475
加权基因共表达网络分析和单细胞测序分析揭示了心肌缺血再灌注损伤中巨噬细胞坏死性凋亡的核心基因 476
Serpina7 介导中性粒细胞胞外诱捕网产生加重心肌梗死损伤的研究 476
血清乙酰肝素酶水平对急性心肌梗死患者 MACE 事件的预测价值 476
分析预见性护理干预措施对急性心肌梗塞患者的影响 476
基于多组学与孟德尔随机化解析代谢综合征与心肌梗死的遗传因果网络 476
麝香保心丸对 STEMI 患者长期预后的影响 477
急性心肌梗死并发肾功能不全的危险因素分析及预测模型构建 477
Development and Validation of a Nomogram for Predicting Atrial Fibrillation in Patients with Acute Myocardial Infarction: A Retrospective Cohort Study 477
Objective: Analyze the risk factors of Atrial Fibrillation (AF) in patients with Acute Myocardial Infarction (AMI), and build a corresponding risk prediction model to provide reference for clinical personalized prediction of AF risk in AMI patients. 477
新冠感染后急性冠脉综合征患者血浆淋巴细胞亚群及炎性因子特点的临床研究 477
酮替芬治疗 STEMI 直接 PCI 患者有效性和安全性的临床研究 478
Usefulness of Albumin-to-D-dimer ratio in predicting the long-term outcome after hospital discharge in patients with ST-elevation myocardial infarction: a retrospective cohort study 478
急性心肌梗死患者应激性高血糖比率、白蛋白与院内预后的关联：一项队列研究 478
TSTEMI 影响因素分析及列线图的构建与验证 478
重复远隔缺血适应对急性心肌梗死患者血清胰岛素样生长因子水平的影响 479
急性心肌梗死早期应用 PCSK9 抑制剂对患者心功能的影响 479

改善“生命八要素”可以降低急性心肌梗死的风险，延迟发病时间，并预防近六成的病例：一项来自英国生物银行的证据 479
YY1 在心肌梗死后心脏损伤和重塑中的保护作用 479
新型 Wnt 通路抑制剂对心肌梗死后心脏再生的治疗作用 479
Predictive Value of Triiodothyronine in Long-term Outcomes of Left main and/or three-vessel Disease in Patients with Acute Myocardial Infarction
SCFAs Block Macrophage Osteoclastogenesis via FFAR2-RANKL Signaling to Promote Post-MI Cardiac Repair 480
急诊 PCI 冠脉血流相关因素及 其与预后的关系 480
The redistribution of cadmium after acute myocardial infarction in mice 481
运动预适应通过 IL-13 调控中性粒细胞抑制胞外诱捕网形成在心肌梗死后的作用研究 481
血管内成像引导的稳定性冠心病日间经皮冠状动脉介入治疗：临床结局与安全性的回顾性队列研究 482
定量血流分数联合腔内影像学指导的精准 PCI 在冠心病日间手术中的应用：一项回顾性队列研究 482
Dapagliflozin in acute myocardial infarction with left ventricular systolic dysfunction 482
中性粒细胞 Irgm1 促进胞葬作用在心肌梗死后心脏修复中作用及相关机制研究 483
Prognostic Value of Interleukin-6 in Predicting Heart Failure with Reduced Ejection Fraction and In-Hospital Mortality in Patients with Acute Myocardial Infarction 483
中国胸痛救治单元项目对急性冠状动脉综合征转诊患者救治效率的影响研究 483
非高密度脂蛋白与载脂蛋白 B 的比值与急性心肌梗死患者 PCI 术后预后的关系的摘要 483
血管特征与心肌损伤标志物的交互作用对 AMI 患者远期预后的影响 483
Early Diagnosis of Acute Myocardial Infarction via Hub Genes Identified by Integrated Weighted Gene Co-expression Network Analysis 484
静脉注射硫酸镁与急性心肌梗死危重患者 1 年病死率的相关性：一项队列研究 484
CAMI-DM: Development and Validation of a Multi-Algorithm Model for In-Hospital Mortality Risk Prediction in Diabetic Patients With Acute Myocardial Infarction – The China Acute Myocardial Infarction Registry 484
Pan-immune inflammation value is associated with poor outcomes among patients with acute coronary syndrome undergoing percutaneous coronary intervention 484
高血栓负荷急性心肌梗死不同时期血运重建对其预后的影响 485
Correlation between early arterial lactate levels, arterial bicarbonate ion levels, and the lactate/albumin ratio and in-hospital mortality in patients with acute myocardial infarction complicated with cardiac shock 485
早发 AMI 患者一年内心源性死亡及卒中风险因素与风险预测模型构建： 基于前瞻性队列研究 485
院内无明显出血情况下血红蛋白下降与急性心肌梗死患者经皮冠状动脉介入治疗 1 年预后的相关性 486
急性心肌梗死患者 PCI 术后支架内再狭窄的影响因素 486
急性左主干完全闭塞所致急性心肌梗死患者的预后影响因素 486
双膦酸盐类药物的使用与心肌梗死的风险的荟萃分析和系统性回顾 486
Incremental prognostic value of hemodynamic forces misalignment by cardiac magnetic resonance for major adverse cardiac events after ST-segment elevation myocardial infarction 486
Non-Linear Associations of Shock Index and Modified Shock Index with New-Onset Atrial Fibrillation in Patients with Acute Myocardial Infarctions 487
HA-Hypoxia Dual-Engineered Exosomes from ADSCs Target Myocardial Infarction by Modulating miR-331-5P Pathways 487
冠心病急性心梗不同病变血管缺血时间与 SII 的相关性研究 s 488
Stress Hyperglycemia Ratio Predicts Short- and Long-Term Mortality in Acute Myocardial Infarction Patients Undergoing Intra-Aortic Balloon Pump Support 488
Unraveling the Therapeutic Potential of Sophora flavescens Aiton in Myocardial Infarction: An Integrative Approach Combining Bioinformatics, Network Pharmacology, and Experimental Validation 489
基于目诊仪探究心肌梗死患者的中医证候：一项前瞻性，观察性研究 489
不同海拔地区患者冠脉支架植入术后再狭窄发率情况比较 489
残余 R 波对急性 ST 段抬高型心肌梗死血管再通的预测价值 489
冠状动脉痉挛诱发急性心肌梗死 1 例 490
急性 STEMI 患者心肌结构与功能的影像学综合评估：基于分形分析法与 CMR 特征追踪技术 490
1,3-Butanediol Enhances Autophagy via PI3K/Akt/FOXO3 Pathway to Ameliorate Cardiac Remodeling Post-Myocardial Infarction 490
RXRα Mediates the Effect of Atorvastatin on the Function of Foxp3+ Regulatory T-cells in Patients with Acute Coronary Syndrome 490
探究 STEMI 患者血清 Omentin-1 水平与斑块易损性、微循环灌注及临床预后的相关性 491
Analysis of the effectiveness and regression of intra-aortic balloon er pulsation in the treatment of AMI 491
高敏肌钙蛋白与急性心肌梗死患者不良预后的研究进展 491
BCL10 通过调节炎症和细胞凋亡促进心肌缺血 / 再灌注损伤 491
敲低 SFPI1 通过调控 BCL10 转录减轻心肌缺血 / 再灌注损伤 492
PTBP1 通过诱导炎症和细胞凋亡促进心肌缺血 / 再灌注损伤 492
Clinical Characteristics and Predictors of Acute Myocardial Infarction Complicating Out-of-Hospital Cardiac Arrest 492
血浆外泌体 miRNA 与 CKD 加速的动脉粥样硬化（AS）病程进展的关系及其早期预测价值 493
Comparison of In-Hospital Net Clinical Outcomes of Ticagrelor and Clopidogrel in Acute Coronary Syndrome Patients Stratified by CRUSADE Score: Findings from the CCC-ACS Registry 493
Omentin-1 Mitigates Myocardial Ischemia-Reperfusion Injury by Regulating Fatty Acid β-Oxidation via the AMPK-PPARβδ-CPT1A Pathway 493
肥大细胞 MRGPRX2 受体介导神经免疫互作诱发急性心肌梗死后室性心律失常 494
冠状动脉内自体骨髓细胞移植治疗急性心肌梗死的长期临床研究 494
急性心肌梗死血清中神经调节蛋白 4 的水平变化及临床意义 494
基于四道防线对冠心病家族史患者经皮冠状动脉介入（PCI）治疗后再发心梗的预防策略研究 494
Omentin-1 通过 AMPK-PPARβδ-CPT1A 通路调控脂肪酸 β 氧化改善心脏缺血再灌注损伤 494
基于 SOP 模型理论的急性心肌梗死患者早期心理康复干预研究 495
改良应激性高血糖比值是急性心肌梗死患者不良预后的独立危险因素 495
冠脉内低温联合 KATP 通道开放剂干预对 STEMI 患者 PPCI 术后慢血流 / 无复流及心功能的影响 495

青年英语演讲交 496
Stress Hyperglycemia Ratio Index Predicts All-Cause Mortality in Aortic Diseases: A Retrospective Analysis of the MIMIC-IV Database 496
Epidemiology of ischemic heart disease in Chinese population from 1990 to 2023: Findings from the Global Burden of Disease Study 2023 496
Dynamic Cardiac Toxicity Monitoring Based on Time Threshold and Chemotherapy Stratification in Hematologic Malignancies 496
Human-Machine Collaborative Enhancement in Perioperative Care for Atrial Fibrillation Catheter Ablation: Optimization and Application of Key Nursing Technologies 497
Downregulation of Alox5 inhibits ferroptosis to improve doxorubicin-induced cardiotoxicity via the P53/SLC7A11 pathway 497
IL4I1+ Macrophages maintain the contractile phenotype of vascular smooth muscle cells via I3P/AhR axis in atherosclerosis 498

Magnesium sulfate in cardiogenic shock patients: a retrospective propensity score-matched cohort study 498
Proteome Profiling by High-Resolution Mass Spectrometry Discriminates HFimpEF from HFrEF 499
Mediating effect of systemic inflammation on sleep duration and all-cause/CVD mortality 499
Evaluating the Role of Traditional Chinese Medicine as an Adjunctive Therapy in Chronic Heart Failure: A Retrospective Study 499
Deep learning fusion of CTA and clinical features to predict small abdominal aortic aneurysm prognosis 500
Clinical AI Diagnosis and Reasoning for Cardiovascular Diseases Based on Large Language Models and Knowledge Graphs 500
Serial Myocardial Fibrosis Assessments Predict Outcomes in Patients with Hypertrophic Cardiomyopathy 501
Addressing disparities in hypertension care cascades to reduce cardiovascular disease burden: a residence- and sex- stratified analysis in China 501
Complement C3a and C5a receptors-mediated activation of FoxP3+ Tregs promotes adipocyte browning and attenuates diet-induced obesity 502
Study on the role and mechanism of frailty in left atrial remodelling and dysfunction after myocardial infarction in aging mice by activating AIM2 and NLR Inflammasome-Mediated Cardiomyocyte Pyroptosis 502
Yangxinshi tablet protects against myocardial injury and increases skeletal muscle exercise capacity by regulating mitochondrial bioenergetics 502
Rescue of Cardiac Dysfunction in Mice with Dilated Cardiomyopathy by Administration of Induced Pluripotent Stem Cell-Derived Exosomes in Utero 503
Suboptimal Control of Small Dense Low-Density Lipoprotein Cholesterol is Associated with Coronary Plaque Progression: An Intravascular Ultrasound Study 503
Discriminatory and Prognostic Value of MRI-Derived Myocardial Work Efficiency in Heart Failure with Preserved Ejection Fraction: Beyond Left Ventricular Global Longitudinal Strain 504
Nuclear AGO2 exacerbated high-fat diet-induced heart failure by activating transcription of HMGCS2 to promote ketogenesis in the heart 504
The impact of short-term exposure to nitrogen dioxide on endothelial function in Chinese elders: A cross-sectional study 505
Association Between Serum Cartilage Oligomeric Matrix Protein (COMP) Levels and Calcification Burden in Aortic Valve Calcification Disease, and Its Predictive Value for Prognosis After Transcatheter Aortic Valve Replacement 505
Liraglutide Attenuates High-Glucose-Induced Hypoxia/Reoxygenation Injury in Cardiomyocytes by Regulating Fatty Acid Metabolism and Inhibiting Apoptosis via the GLP-1R/AMPK Pathway 506
Epicardial Adipose Tissue Volume and Density are Associated with Heart Failure with Improved Ejection Fraction 506
Visit-to-Visit Glycemic Variability is Associated with the Incidence of Heart Failure with Improved Ejection Fraction 507
Visit-to-Visit Fasting Plasma Glucose Variability is Associated with Left Ventricular Adverse Remodeling in Diabetic Patients with STEMI 507
Insulin Resistance is Associated with Heart Failure with Recovered Ejection Fraction in Non-diabetic Patients 508
Effect of gender on the association between high density lipoprotein cholesterol level and prognosis of patients with coronary heart disease undergoing percutaneous coronary intervention 508
Lipoprotein(a) molar concentrations rather than genetic variants better predict coronary artery disease risk and severity in Han Chinese population 508
Analysis of the correlation between helper T-lymphocyte subsets and atrial fibrillation: An observational and Mendelian randomization study 509
Temporal Shifts in Ischemic Heart Disease Burden Among Premenopausal and Postmenopausal Women Worldwide: Insights from the Global Burden of Disease Study 2021 and Projections 509
Novel Transthoracic Pulmonary Valve Implantation Using Self-expanding Salus ™ Valve: A Prospective Study of Safety and Mid-term Outcomes 510
Relationship between hs-CRP and MACCEs risk in patients with drug-eluting stents undergoing statin therapy: A comparison of diabetic and non-diabetic patients–A prospective registry-based study 510
Association between healthy lifestyle and the risk of multiple cardiometabolic diseases: a prospective cohort study based on the UK Biobank 511
Superior Predictive Value of TyG-ABSI for Cardiovascular Disease and Mortality in Individuals with Metabolic Syndrome: Evidence from the US NHANES 511
Inflammatory and Bleeding Risks on Clinical Outcomes in Acute Coronary Syndrome Patients Undergoing Percutaneous Coronary Intervention 512
Effect of CYP2C19 Genotype on Outcomes of Treatment with Ticagrelor versus Clopidogrel in Acute Coronary Syndrome Patients with Diabetes Mellitus: A Analysis in a Large-Scale, Real-World Study 512
PTPN14 aggravates neointimal hyperplasia via boosting PDGFRβ signaling in smooth muscle cells 512
Impact of Renal Function on Prognostic Value of Post-PCI High-Sensitivity Troponin T in Acute Coronary Syndrome: A Retrospective Cohort Study 513
Prolonged Dual Antiplatelet Therapy Strategy in Acute Coronary Syndrome Patients Post-Standard Therapy and Adverse Event-Free: An Analysis Based on OPT-CAD Risk Score Stratification 513
Prognostic Value of Persistent Microvascular Obstruction in Post-myocardial Infarction Patients After Reperfusion: A Cardiac Magnetic Resonance Study 514
Nonischemic Late Gadolinium Enhancement Associated with Adverse Remodeling is an Underrecognized Predictor of Heart Failure Outcomes Post-Myocardial Infarction 514
Mediation of the Relationship Between Myocardial Replacement Fibrosis and Sudden Cardiac Death by Left Ventricular Ejection Fraction Post-Myocardial Infarction 515
The U-shaped Relationship of Stress Hyperglycemia Ratio with Ventricular Arrhythmias and Sudden Cardiac Death in Acute Myocardial Infarction 515
C-reactive Protein-Albumin-Lymphocyte (CALLY) Index as an Independent Risk Factor for Postoperative Atrial Fibrillation Recurrence 515
Risk Reclassification and Cost-Effectiveness of Echocardiography for Cardiovascular Primary Prevention in Hypertension in China 516
Single-cell multi-omics identifies a specialized cytotoxic and migratory CD8+ effector T cells in acute myocarditis 516
Optimizing Long-term Cardiovascular Risk Stratification: Integrating Biomarkers into the Very High-Risk ASCVD Definition in Asian Patients 517
Stress Hyperglycemia Ratio, Albumin, and In-hospital Outcomes in Patients with Acute Myocardial Infarction: A Cohort Study 517
Effect of PCSK9 Inhibitors on the Quality of Life in Patients with Acute Coronary Syndromes 518
Cultural Adaptation and Psychometric Evaluation of the Preference for Intuition and Deliberation in Eating Decision-making Scale among Chinese People with Cardiovascular Disease 518
Left ventricular remodeling index to predict ventricular tachyarrhythmia in dilated cardiomyopathy with ejection fraction 518
Subendocardium-Involved Late Gadolinium Enhancement Predicts Sudden Cardiac Death in Nonischemic Dilated Cardiomyopathy 519
Multimodality Cardiac Magnetic Resonance Imaging for Discriminating Danon Disease from Hypertrophic Cardiomyopathy 519
Prognostic Impact of Early Cardiorenal Involvement in Fabry Disease: Rethinking When to Start Enzyme Replacement Therapy 520
Efficacy Analysis of Cardiac Rehabilitation in a Patient with Heart Failure Due to Dilated Cardiomyopathy: A Case Report 520
Extravascular Lung Water Index versus Central Venous Pressure: A Comparative Study on Predicting Global End-Diastolic Volume Index in Cardiogenic Shock 521
Association between Transcatheter Heart Valve Deformation and Hypoattenuating Leaflet Thickening in Patients after Transcatheter Aortic Valve Replacement 521
CircSMAD3 represses VSMC phenotype switching and neointima formation via promoting hnRNPA1 ubiquitination degradation 521
Circulating ketone bodies, genetic susceptibility, with left atrial structure, function and atrial fibrillation 522
Left Atrium Myocardial Remodeling and Prognostic Marker Derived from Cardiac MRI Feature Tracking in Pediatric Hypertrophic Cardiomyopathy 522
Impact of Nanoplastics on Human Pluripotent Stem Cell-Derived Early Endothelial Cells 523

Targeting Notch2-Mediated Macrophage Mechanotransduction Alleviates Cardiac Fibrosis 524
CREG1 Enhances Postinfarction Cardiac Repair by Regulating HOXA5-Mediated miR-125a Cluster to Suppress Macrophage Inflammation 524
Managing Sustained SVT in Pregnancy Without Structural Heart Disease: Is Catheter Ablation a Safer and more effective Alternative? 524
Plasma proteomic profiling reveals distinct molecular signatures associated with coronary collateral circulation in CTO patients 525
PCSK9 Inhibitor Improves Ventricular Remodeling via Regulating the Overexpression of TACE and Its Downstream Factors in Alcoholic Cardiomyopathy 525
Identifying Patients for Cardiac Resynchronization Therapy Beyond Current Guidelines: Insights from Cardiac Magnetic Resonance Imaging 526
Risk Stratification of Sudden Cardiac Death in Non-Ischemic Cardiomyopathy 526
Multi-omics and biological validations identify TARS2 as a mediator of mitochondrial oxidative stress in dilated cardiomyopathy 527
Burden of Ischemic heart disease in Postmenopausal Women and Its Attributable Risk Factors in 204 Countries and Territories, 1990-2021: Results from the Global Burden of Disease Study 2021. 527
Efficacy of Early Initiation of Vericiguat in Acute Heart Failure: A Prospective Study 528
Hs-CRP, Diabetic Status, and Adverse Events Among Patients Receiving Statin Therapy Following PCI–A Prospective Registry-Based Study 528
Residual Atherosclerotic Risk in Older Patients with Atherosclerotic Cardiovascular Disease: Where Inflammation Meets Lipoprotein(a) 528
Validation and comparison of five chronic total occlusion scores to predict difficulty of percutaneous coronary intervention 529

最新研究进展专场 530
慢性心力衰竭患者血清 KLK1、KLF2 表达及其对室性心律失常的预测价值 530
基于生物电阻抗法测量的骨骼肌含量和射血分数减低的慢性心力衰竭患者预后的相关性 530
心磁图对静息心电图正常患者心肌缺血的诊断价值研究及评分模型的建立 530
急性下壁心肌梗死并发高度至三度房室传导阻滞患者急诊 PCI 术前植入临时起搏器的必要性及安全性 530
Optimizing Long-term Cardiovascular Risk Stratification: Integrating Biomarkers into the Very High-Risk ASCVD Definition in Asian Patients 530
静息 HFQRS 对急性心肌梗死 PCI 术后临床转归的评估价值 530
脂蛋白 a 和同型半胱氨酸的协同效应对早发心肌梗死患者预后的影响：一项前瞻性队列研究 531
基于 Murray 定律的 PCI 术后定量血流分数（μQFR）对长期不良心血管事件的预测价值 531
低剂量利伐沙班与阿司匹林分别联合氯吡格雷在合并胃肠疾病冠心病患者 PCI 术后的疗效与安全性：一项前瞻性、非劣性、随机对照研究 531
接受 TAVR 患者术后全生命周期管理模式的评估与优化 531
高敏 C 反应蛋白在经皮冠状动脉介入治疗后急性冠脉综合征合并肾功能不全患者中的长期预测价值 531
基于 GRACE 风险评分比较高缺血和高出血风险的急性冠脉综合征患者中氯吡格雷单药治疗与延长双联抗血小板治疗的疗效：OPT-BIRISK 随机临床试验的亚组分析 532
基于 CRUSADE 评分分层的比伐芦定与肝素在 ST 段抬高型心肌梗死患者中的疗效与安全性比较：BRIGHT-4 研究亚组分析 532
3 “A” 优化策略管理对预防性 VA-ECMO 植入的左主干急性冠脉综合征患者经皮冠状动脉介入治疗的影响：多中心回顾性队列研究 532
PrizvalvePro ™经导管主动脉瓣膜系统治疗中国高风险重度主动脉瓣狭窄患者的前瞻性多中心单组目标值研究 532
Background P2Y12 monotherapy in ACS patients after PCI has gradually become important, and a number of large-scale clinical studies have shown that it can reduce the incidence of adverse clinical outcomes. Implantation of different types of stents is crit 532
非高密度脂蛋白胆固醇与高密度脂蛋白胆固醇比率和动脉僵硬度的 L 型关联：一项基于人群的研究 533
院间转运对 ST 段抬高型心肌梗死患者接受直接经皮冠状动脉介入治疗后临床结局的影响：一项基于 BRIGHT-4 试验的二次分析 533
急性心肌梗死新发房颤负荷和左室射血分数的预后意义 533
微循环阻力指数对 MINOCA 患者微循环障碍的评估 533
急性冠状动脉综合征患者早期依洛尤单抗治疗抑制 IL-1β/IL-17A 并改善早期左心室功能：一项随机临床对照试验 533
基于冠脉造影微循环阻力指数的 STEMI 术后心肌内出血预测模型构建与验证 534
心脏电子植入装置治疗扩张性心肌病的临床疗效分析 534
Hs-CRP, diabetic status, and adverse events among patients receiving statin therapy following PCI–A prospective registry-based study 534
1990-2050 年中国非风湿性钙化性主动脉瓣疾病流行趋势预警：基于贝叶斯年龄 - 时期 - 队列模型预测及全球疾病负担数据库（GBD）研究 534
国产新型冠状动脉血管内碎石术装置在严重钙化病变患者中的有效性和安全性：LEAD-FIM 研究 535
高风险 ACS 患者氯吡格雷单药延长治疗与双联抗血小板治疗的对比研究：OPT-BIRISK 随机临床试验复杂 PCI 亚组结果 535
一项基于真实世界的 CHA2DS2Vasc 非性别评分为 1 的非瓣膜性房颤患者的抗凝策略研究 535
A Theory-based Intervention to Promote Cardiac Rehabilitation Engagement in Patients with Chronic Heart Failure: A pilot randomized controlled trial 535
质子泵抑制剂的使用与心肌梗死风险之间的关联：基于 2007 - 2018 年美国国家健康与营养检查调查的横断面研究 535
Relationship between baseline and dynamic changes of triglyceride-glucose index and long-term adverse cardiovascular events in patients with acute coronary syndrome after percutaneous coronary intervention 536
基于冠状动脉钙化积分的随机森林算法对阻塞性冠心病的预测价值 536
在非典型胸痛人群中不同 LDL-C 水平与冠脉钙化积分的相关性及预后分析 536
Ameliorative effect of GS-458967 on doxorubicin-induced oxidative stress and cardiac dysfunction 536
抑郁 / 焦虑对急性冠脉综合征患者 PCI 术后术后心血管预后影响的真实世界研究 536
Effect of Thin-Walled Radial Sheath for Large-Bore Access On Reducing Periprocedural Radial Artery Occlusion Following Complex PCI: The REDUCE-RAO Randomized Trial 537
预测左主干分叉病变 PCI 术中边支闭塞的新型血管造影评分系统：LM V-RESOLVE 评分 537
cGAMP 作为诊断糖尿病患者三支冠状动脉病变的潜在生物标志物 537
玛伐凯泰治疗 5 例左心室中部梗阻性肥厚型心肌病患者临床疗效观察 537
中国中老年人群中血浆致动脉粥样硬化指数、体重指数与心血管疾病的关联：一项中介效应分析 538
玛伐凯泰对梗阻性肥厚型心肌病患者临床疗效的真实世界研究 538
急性心肌梗死合并心脏破裂的临床 特征及危险因素分析 538
FIB-4 指数在钙化性主动脉瓣疾病中的诊断价值：基于两中心 2146 例主动脉瓣狭窄患者的临床研究 538
腹主动脉瘤腔内修复术后髂支闭塞的危险因素分析及治疗策略 538
肥胖对原发性高血压患者左心房应变功能损害的差异研究 538
1- Year Outcomes of Novel Designed Transcatheter Edge-to-edge Mitral Repair System in Patients with Functional Mitral Regurgitation 539
嗜铬细胞瘤引起的应激性心肌病 1 例 539
人机耦合创新技术用于冠心病患者经皮冠脉介入术后居家康复与远程管理的有效性和安全性研究 539
左心耳封堵术与房颤一站式手术对非瓣膜性房颤患者心功能影响的对比研究 539
右房应变联合右房面积对肺动脉高压患者临床恶化的预测价值 540
2 型糖尿病合并急性 ST 段抬高型心肌梗死患者经皮冠状动脉介入治疗后发生心力衰竭的危险因素分析 540
白蛋白校正阴离子间隙与重症肺动脉高压患者 30 天全因死亡率的关系：基于 MIMIC-IV 数据库分析 540

病例讨论 541
双管齐下 - 终末期心衰治疗 1 例 541
小痉挛酿大祸，相逢要相识 一例变异性心绞痛患者的诊疗体会 541
精神分裂症患者骤停氯氮平发生严重窦性心动过缓 1 例 542
过敏性休克掩盖下的 STEMI：一例造影剂诱发 II 型 Kounis 综合征的救治启示 543
甜蜜的瘫痪 一例低钾型周期性瘫痪患者的诊疗体会 543
从绝望到希望：左主干心梗患者的重生之路 544
辗转三甲医院，多次消融术后复发的室上速到底有多硬核 545
迟发性 HIT 治疗后再发心梗 1 例 545
IVUS 指导 ELCA 治疗静脉桥血管闭塞一例 547
生死时速：一例暴发性心肌炎合并心源性休克与电风暴的救治 547
生长激素促进心脏移植患者心脏再发育康复出院一例 547
猝死原因为何：一例肥厚型心肌病家系的遗传学调查 548
青年男性，反复心梗为哪般？ 548
“摇摇欲坠”的心脏 一例老年急性重症心肌炎的诊治 549
弥漫性大 B 细胞淋巴瘤心脏转移一例 549
顽固心律失常是何原因？ 549
心脏 T 细胞淋巴瘤继发暴发性心肌炎及多脏器损害一例 550
MitraClip 联合 PTSBME 治疗合并重度二尖瓣反流的肥厚型梗阻型心肌病 1 例 550
声尺量心路，术数判盈枯—— IVUS+FFR 指导无造影剂冠状动脉介入一例 550
ICE 指导下 Ebstein 畸形合并 B 型预激综合征导管消融一例 551
冲击波球囊，钙化困局中的破壁者——钙化病变旋磨后支架膨胀不全补救一例 551
1 例猝死青少年的起死回生：挑战与总结 551
地高辛中毒救治一例 552
如何打破反复住院的恶性循环？ 一例高龄心衰患者的“逆袭”之路 552
迷雾中的血栓风暴 552
1 例风心病双瓣置换术后合并心源性肝硬化行 TTVR 的围术期生死竞速 553
心房颤动射频消融术后心房食管瘘 1 例 553
Clinical diagnosis and treatment of a case of hypocalcemia due to hypoparathyroidism 554
宽松容量管理在慢性心力衰竭急性加重期应用病例分享 555
遗漏的真凶及处理 555
中年女性心室肥厚的曲折诊治之旅 555
零射线内外膜联合消融治疗 Marshall 相关心房颤动一例 556
增强 CT 检出早期心脏破裂一例 557
一例心脏破裂患者的系列心电图改变 557
糖尿病酮症引发的复发型应激性心肌病 557
主动脉内球囊反搏致多脏器血管栓塞 1 例 558
且将新“履”试新“途”，“幽远”趁“通达” 558
右房占位性病变 - 肝癌心脏转移 1 例 559
双孔型房间隔缺损封堵术后封堵器脱落一例 559
误诊为癫痫的 2 型长 QT 综合征家系报告 560
左心交感神经节切除术治疗 Jervell-Lange Nielsen 综合征 1 例 560
血小板增多症诱发年轻的急性心肌梗死一例 560
OCT 联合 FFR 精准指导钙化病变 PCI 一例 561
IOCA 相关的 CMVD 一例 ——左前降支 CFR 异常的预警价值 561
OCT 指导 IVL 处理复杂左主干真分叉钙化病变 562
拨开迷雾见真章 563
经股 TAVR 治疗单纯主瓣反流伴主动脉夹层 1 例 563
从两例 Kommerell 憩室的腔内修复治疗病例浅谈 Kommerell 憩室 564
阻塞性睡眠呼吸暂停综合征合并扩张型心肌病患者诊治 1 例 564
寻找肾上腺的秘密 564
《I 型肺动脉高压患者肺动脉去神经术治疗的突破与成效 —— 从顽疾到新生》 565
从危机到生机：ExtraVAD 保驾术中急性心率骤降，双 DK CRUSH 完美收官左主干 -LAD/D1 双分叉 566
见山不是山—— PCI 术后急性血胸的多学科救治 566
2 例不同亚型原发性醛固酮增多症患者的诊治过程 566
股动脉入路经导管主动脉瓣植入术并发左心室穿孔行左前外侧开胸术紧急修复 567
自行复律的一例三度房室传导阻滞 568
四叶瓣重度主动脉瓣关闭不全 TAVR 一例 568
蛛网膜下腔出血导致 Takotsubo 综合征合并神经源性肺水肿 1 例 568
2 例高危外科瓣衰败后瓣中瓣处理 569
ECMO 辅助下高危复杂病变的 PCI 治疗病例汇报 570
心肌声学造影识别 NSTEMI 合并双支完全闭塞患者罪犯血管：突破心电图定位困境 570
一例罕见的肺静脉闭塞病的诊治体会 571
心脏结节病并血性心包积液 1 例 571
Lampoon +TMVinV 治疗二尖瓣生物瓣衰败一例 572
超声辅助下经皮间隔支冠状动脉栓塞术治疗肥厚型梗阻性心肌病 572
1 例梗阻性肥厚型心肌病的诊治经过 573
巴尔通体感染导致的感染性心内膜炎合并严重贫血 573
一例左室辅助装置合并虚弱患者早期康复案例 574
CABG 术后桥血管病变的处理 574
慢性心力衰竭合并急性心肌梗死 575
房颤合并左心耳血栓治疗一例 575
被束缚的心脏 --- 高血压与心肌肥厚的双重迷雾 575
原发性甲状腺功能减退症合并心包积液、腹腔积液、自发性腹膜炎一例 576
扩张型心肌病 CRT-D 术后心律失常一例 577
免疫检查点抑制剂相关心肌炎合并重症肌无力一例 577
超高龄野生型转甲状腺素蛋白心脏淀粉样变一例 577

机械通气联合心衰超滤脱水成功救治重症心衰一例 578
异位性皮质腺瘤致难治性高血压与低钾血症一例 578
IVL 联合旋磨治疗重度钙化病变一例 579
IVL 治疗支架内闭塞病变一例 580
IVL 治疗旋磨后无法完全扩张病变一例 581
IVL 治疗前降支重度钙化病变一例 581
酮症继发应激性心肌病 582
肥厚型心肌病诊断与鉴别诊断：一例纯合子女性 Fabry 心肌病诊疗过程的启示 582
一例顽固性低钾患者的诊治体会 583
一例以急性胸痛为表现的儿茶酚胺型心肌病的诊断和治疗带给我们的启示 583
PADN 在 LHF-PH 患者中应用经验分享 584
肥厚梗阻合并房颤透析患者的新希望 -Micra 植入一例 585
Transcatheter Edge-to-Edge Repair for Tricuspid Regurgitation in Barlow-Type Tricuspid Valve Prolapse Using the DragonFly-T System 585
限制样拟表型的左心室肥厚病因何在？ 585
生物可降解封堵器治疗 2 例复杂房间隔缺损的实践与启示 587
以心力衰竭为主要表现的 Leriche 综合征 1 例 588
三维脉冲消融阵发性房颤一例 588
心肌梗死后反复左心室血栓的抗栓治疗策略 588
心脏术后急性肝衰竭合并脓毒症 3 例诊治分析与文献回顾 588
左主干病例介入治疗病例分享 589
从多器官衰竭到功能独立：一例 CCU 危重症急性心肌梗死患者的三级心脏康复管理实践 589
抽丝拨茧——1 例肥厚性心肌病诊疗启示。 590
致心律失常性右室心肌病伴左心室受累一例 591
一例特殊的肺高压 591
主动脉根部盲端束（RARB）室早一例 592
起搏器手术后的特殊心电图发现，布鲁加达综合征的异常表现？ 592
“捉拿元凶”—— 1 例巨大冠脉瘤引发的思考 593
生死罗生门 ——1 例右心房占位的诊治 593
IVUS 指导再开放迂曲 RCA 支架术后 急性冠脉夹层闭塞一例 594
像过山车一样的高血压 594
师出不利 “逆” 转得胜 ---LCX-CTO 伴 LM 重度狭窄逆向开通一例 595
心肌梗死后巨大室壁瘤患者治疗路径探寻 595
冠脉搭桥术后 LIMA 桥血管闭塞再开通 1 例病例探讨 596
OCT 精准指导联合 QFR 处理分叉病变治疗一例 596
ECMO 联合 IABP 支持下 CHIP 介入治疗一例 597
一种新型 pVAD 支持下复杂高风险 PCI 597
暴发性心肌炎后的顽固心衰 1 例 598
心肌淀粉样变 1 例 598
一例高龄肥厚性梗阻性心肌病玛伐凯泰的治疗 598
CRT-D 心房电极故障拔除后再植入一例 600
快与慢的较量 600
IgG4 相关性疾病累及冠状动脉一例 600
生死时速：61 岁男性左主干完全闭塞的急诊介入治疗实录 600
非阻塞性心肌梗死的男性患者 602
冠状动脉粥样硬化性心脏病 -- 死亡病例 602
寻找真凶 肌不可失 603
一例 HFpEF 患者的诊疗及 GDMT 原则应用病例汇报 603
以急性胸痛为首发表现的颌下间隙感染合并纵隔气肿一例 604
一种用于清除冠脉夹层血肿的新技术——SBLP 技术 605
扑朔迷离的心包积液 605
旋磨 + 震波处理 LM-LAD 重度钙化病变 606
OCT 指导下 ROTA+IVL 处理钙化病变 PCI 606
右冠状动脉痉挛致心房 P 波保留、心室停搏 1 例 606
肺动脉高压治疗 1 例 607
精神心理疾病致反复高血压急症一例 607
冠状动脉造影后造影剂脑病 1 例 608
负荷超声联合超声心肌灌注成像评估肾移植心梗患者一例 609
多模态影像学助力冠脉造影后罕见心房血肿的诊断：一例报告 610
玛伐凯泰治疗肥厚型梗阻性心肌病 超声随访 1 例 611
心内科的 “血压迷局”：从直立性低血压到多系统萎缩 611
房室结多径路 1 例 612
以腹胀为首发症状的未成年原发心脏血管肉瘤 1 例 612
帕金森病合并餐后低血压 1 例 613
免疫检查点抑制剂相关心肌损伤合并阵发性三度房室传导阻滞 1 例 614
冠脉高风险 TAVR 手术一例 614
Successful treatment of pulmonary hypertension due to HIV infection and amphetamine snorting: a case report 614
复杂先心病合并 C 型主动脉弓离断一例 615
左主干合并多支冠脉痉挛导致大面积 ST 段抬高型心肌梗死 1 例 615
经导管主动脉瓣置换术中左心室游离壁穿孔引起急性心包填塞成功抢救 1 例 616
多重获益–糖尿病合并多血管并发症病例 616
主动脉覆膜支架置入术治疗先天性降主动脉 - 肺静脉瘘一例并文献综述 616
1 例转甲状腺素型心脏淀粉样变超声表现 617
一波四折，消化道大出血与急性心肌梗死此起彼伏–1 例 STEMI 合并消化道出血 617
“逢堵立新” – PFO 致反常冠脉栓塞经皮肝静脉穿刺介入封堵 1 例 617
急性心肌梗死术中 IABP 支持治疗中的死亡陷阱：一例病例对比与临床反思 618
免疫检查点抑制剂相关心肌炎病例讨论 618
被胸痛掩盖的 “暗流”：嗜铬细胞瘤的 ACS 首发之谜 619

春水融不动，冰消见山丛 620
鲁登巴赫综合征致肺动脉高压 1 例 620
一波未平一波又起 ------ 急性心肌梗死心衰遇上急性肺栓塞病例 1 例 621
KCNQ1-E115K 错义突变致长 QT 综合征 1 例 622
Klinefelter 综合征合并卵圆孔未闭骑跨血栓 622
见微知著，真相毕露 -- 肿瘤患者急性呼吸困难一例 623
深入人心 变幻莫测 623
特纳综合征合并复杂心血管疾病诊治： 一例以晕厥首诊的罕见病例 624
绝处逢生 -- 一例“晚期”心力衰竭患者的综合治疗实践 624
隐秘在心衰背后的多发性大动脉炎 625
高龄射血分数保留型心力衰竭患者高 MACE 事件一例报道 625
新四联为晚期心 - 肾 - 代谢综合征开辟一线生机 626
罕见的主动脉瓣单叶畸形并重度狭窄 --- 自膨瓣成功 TAVR 全球首例报告 626
一例急性心肌梗死心衰失代偿期患者住院心脏康复 627
拨开迷雾：青年 Danon 病的罕见病例分析与鉴别诊断 627
一例升主动脉壁间血肿累及冠状动脉致心肌梗死的救治体会 628
肥厚型梗阻性心肌病合并感染性心内膜炎 1 例 628
房颤射频消融术后并发急性胃潴留病例 1 例 628
回旋支旋磨一例 629
柳暗花明 -- 左心声学造影在心脏淋巴瘤诊治中的应用 629
经皮肺动脉瓣植入术治疗肺动脉重度反流 合并左肺动脉主干狭窄一例 630
一例 F44Y 突变迟发型转甲状腺素蛋白淀粉样心肌病的病程、生化特性及长期随访 630
球囊扩张辅助输送系统通过卵圆孔未闭隧道的介入治疗 631
反复发作的心脏粘液瘤 631
IVUS 指导冠脉严重钙化病变应用 RotaTripsy 治疗 1 例 632
CTEPH 治疗之选：保守还是介入？ 632
电解质紊乱诱发先天性长 QT 综合征尖端扭转室速发作 633
急性心肌梗死后精神障碍 1 例 633
经房间隔穿刺途径无射线消融左侧旁道并发短暂性全面遗忘症一例 634
“硬骨头克星”——旋磨联合 IVL 治疗重度钙化病变 1 例 634
经导管二尖瓣缘对缘修复术治疗急性心梗导致二尖瓣前叶脱垂 635
小球囊开启大希望 635
暴发性心肌炎救治 1 例 636
一例终末期心衰合并肺动脉高压患者的综合治疗。 636
大动脉炎合并坏疽性脓皮病及桥粒斑蛋白基因突变致青年顽固性高血压一例报告 637
一步之遥—— 冠状动脉 - 主动脉夹层 1 例 638
经食道超声诊断左心耳血栓致反复心肌梗死 1 例 638
造影剂致急性喉头水肿 ECMO 下零造影剂救治一例 639
经导管封堵预激综合征导管消融术后左房左室瘘一例 639
从“出血倾向”到“冠脉血栓”——一例血友病 A 合并急性心肌梗死的治疗挑战 639
追根溯源–血压难降，乏力背后的真相？ 640
ICD 植入治疗冠状动脉痉挛所致恶性心律失常一例 640
膀胱肿瘤患者肌酶持续升高 1 例 -- 免疫检查点抑制剂相关肌炎 640
跨越冠心病的思维定式：心脏结节病带来的诊断启示 641
慢性血栓栓塞性肺动脉高压患者介入诊断和治疗 1 例 641
Treat-repair 策略治疗房间隔缺损相关性肺动脉高压 1 例 642
一例 Takotsubo 综合征的病例报告 642
携带 TTR 基因 S77F 突变的迟发型转甲状腺素蛋白心肌淀粉样变一例 643
ECMO 支持下二叶瓣实战 643
“钙化三剑客”对一例冠脉搭桥术后患者的治疗价值 643
生死时速：一例心脏性猝死的救治 644
“药物性高血压急症”遇上“肾上腺危象”：一剂“民间秘方”引发的风暴 644
恶疾潜藏心脏处，青春未尽心已殇：心脏滑膜肉瘤一例 645
残肾动静脉瘘致心力衰竭并肺动脉高压一例 646
负性重构致冠脉破裂一例 647
高原地区肺动脉高压一例 647
嗜铬细胞瘤所致高血压 1 例 647
纸上得来终觉浅，绝知此事要躬行 ---- “无复流”病例一例 648
经导管二尖瓣缘对缘修复术治疗急性心梗后二尖瓣腱索断裂致心源性休克合并多器官衰竭 1 例 648
以“头痛”为单一症状的急性心梗 1 例 649
拿什么拯救你，年轻而颤动的心–青年学生心脏骤停的原凶 649
嗜铬细胞瘤所致继发性高血压 1 例 650
罕见的右冠状动脉瘤伴附壁血栓形成合并右冠状动脉–左心室瘘 651
一例 ATTR 型心肌淀粉样变的诊治 651
一例甲亢导致急性冠脉综合征 651
IVUS 指导下左主干介入治疗一例 652
OCT 指导急性心肌梗死斑块破裂非支架植入治疗患者一例 652
花季少年——因何安上起搏器？ 653
PCI 后的高风险 TAVR 653
冠脉行支架保护的 TAVR 653
泛血管团队合作下利用左室辅助装置保驾的 CHIP 患者冠脉介入治疗 654
左主干三支病变支架植入术中 IVUS 导管嵌顿导致支架毁形器械缠绕 1 例 654
LVAD 术后重度 AR 经颈动脉入路 TAVR 病例分享 654
开弓没有回头箭——入路极度扭曲 TAVR 手术一例 654
一波三折，冠脉狭窄之外，警惕心尖陷阱！ 655
表现为肺动脉高压的先天性门体静脉分流 656
有惊无险–导丝被卡死后… 657

妊娠合并重度肺动脉高压 1 例 657
转甲状腺素蛋白心脏淀粉样变一例 658
血小板增多症合并心脏破裂 658
求因之路–低弥散相关肺动脉高压 659
《初发心衰遇上巨大心室血栓：青年维吾尔族患者规范化管理的成功范例》 660
一例以晕厥为首发表现的精原细胞癌颈部转移 661
主动脉压迹部位房性心动过速导管消融 1 例 661
甲亢患者感染 EB 病毒至心功能急剧下降一例 661
GDMT 逆转高龄心衰患者完全性左束支阻滞 1 例 662
无冠窦房速 1 例引发的思考 662
多旁道预激综合征消融一例 662
心房颤动合并冠状动脉栓塞 1 例 663
心肌桥合并冠脉痉挛致急性心肌梗死 1 例 663
扩张性心肌病合并重度冠状动脉肌桥 1 例 663
部分型无顶综合征合并冠状静脉窦闭锁引流入永存左上腔静脉封堵 1 例 664
超声诊断成人 Shone 综合征 1 例 664
十年误诊迷雾，一纸基因寻真——法布雷病心肌病的曲折诊断启示 664
髓母术后又遇嗜铬，青年血压何以控 665
暗藏玄机的 T 波 665
室间隔破裂封堵术后三尖瓣腱索断裂、乳头肌脱垂 1 例 666
系统性红斑狼疮合并心衰的精准化管理 --- 多模态监测与 CRRT- 血浆置换协同治疗 667
肺动脉瘤合并肺动脉夹层：一例病例报告及文献综述 668
利伐沙班治疗右心房电极血栓失败后的处理策略：1 例报道 668
Lunderquist guidewire technique Simplifies Extremely Tortuous Access in Transfemoral Transcatheter Aortic Valve Replacement 668
胸痛合并肌钙蛋白升高，都是心梗惹的祸？ 669
急性心梗导致二尖瓣乳头肌断裂合并心源性休克救治 1 例 670
顽固性高胆固醇血症一例 670
GDMT 下一例心衰患者的治疗历程 670
经左侧肱动脉行主动脉内球囊反搏辅助下经右侧肱桡动脉联合入路逆向开通冠脉慢性完全闭塞一例 671
运动诱发心跳骤停合并冠状动脉起源异常 1 例 671
AMI 左主干分叉病变合并心源性休 PCI 一例 671
心脏激动顺序异常与心衰 一例完全性左束支传导阻滞性心肌病患者的诊治体会 672
双侧冠状动脉瘤样扩张合并冠状动脉 - 肺动脉瘘、房间隔膨胀瘤 1 例 672
一例大动脉转位单心室姑息治疗 20 年患者长期生存随访 673
全球首例 VenusP 瓣膜开窗治疗复杂肺动脉病变 673
以先天性白内障、肥厚型心肌病及高乳酸血症为主要表现的 Sengers 综合征一例 674
极低 EF 值 ecmo 辅助下 36.7mm 极大瓣环 TAVR 一例 675
左束支起搏逆转终末期肥厚型心肌病一例 675
胸闷气促为哪般？按图索骥 追根溯源 675
急性心包炎合并代谢相关脂肪性肝病的诊治 1 例 676
与死神赛跑：百米冲刺 or 马拉松？——1 例心梗后心脏破裂的诊疗与思考 676
不同寻常的膀胱肿瘤——副神经节瘤 677
1 例诊治一波三折的淀粉样变性心肌病 677
迷雾重重的心原性休克–免疫检查点抑制剂相关心肌炎 1 例 678
青年教师的反复晕厥之谜 680
LOT-CRT 治疗房颤、完左心衰 1 例 680
基层医院一例疑难心肌病诊断探索 680
“睡”出来的心脏病 681
法布雷病心肌病合并房颤的冷冻消融治疗 1 例 681
Congenitally Corrected Transposition of the Great Arteries with Altered Structure 682
心脏“别墅户型”，大空间到让您无依无靠！ 682
复杂腹主动脉瘤介入治疗 1 例 683
大动脉炎合并主动脉瓣关闭不全 1 例 683
BECARE 技术开通 CTO 一例 684
经导管二尖瓣“环中瓣”植入术 1 例 684
可操控鞘管联合新型穿刺导丝在下腔静脉迂曲患者中成功实施经房间隔穿刺术一例 685
反复室颤，缘由几何？ 685
Stanford A 型主动脉夹层诱发显著 T 波倒置：病例报告 685
一石二鸟–TEER 令 SAM 更美好！ 686
多位点起搏间期的个体化优化新方法 686
右位心合并内脏转位的室性早搏消融一例 687
IVUS 指导冠状动脉自发夹层（SCAD）导致急性前壁 ST 段抬高型心肌梗死治疗一例 687
全球首例机器人辅助经股动脉入路经导管主动脉瓣置换术 687
梦魇之息：睡眠呼吸暂停与肺高血压的秘密 688
BAT 技术辅助横位心 AS TAVR1 例 688
跨越漫漫长路：应用 ADR 技术开通前向及逆向尝试失败的复杂 CTO 病变 689
冠脉造影术后脾动脉瘤破裂失血性休克 1 例 689
众里寻“PA”千百度 690
重症肌无力导致肺高血压 1 例报告 690
心肌炎后快速进展性心衰的隐藏病因：MYZAP 变异 691
支架内旋磨治疗心衰肾衰，低 EF 值的右冠慢性闭塞病变 1 例 691
A boy with chest tightness and dyspnea 692
青少年中主动脉综合征合并难治性高血压一例报告及分析 692
变应性支气管肺曲霉病合并 Kounis 综合征 1 例 693
心大的年轻人：NSTEMI 引发的严重心衰 1 例 693
蜂毒的警示：严重二尖瓣管不不全 1 例 694
打破常规：围手术期肺动脉高压危象中的 ECMO 新策略 694

瞰见钙化 磨道开路 IVUS 指导下旋磨处理重度钙化病变一例 695
FFR 联合 OCT 指导 PCI 一例 695
莫让“原醛”成为漏网之鱼：高血压患者筛查的重要性 695
以心律失常为表现的结节病 1 例 696
抗磷脂综合征合并反复下壁 STEMI 1 例 697
精于术，慈于心，带来”心”希望 ---- 一例双腔起搏器升级为 CRT-P DCM 病例 697
消失的激动去哪儿了？ 698
主动脉内漂浮球囊联合 IVUS 处理右冠开口病变 1 例 698
一例新发的 LDLR 突变 698
R-R 间期不等的窄 QRS 心动过速： 室上速 or 其他？ 699
梗阻性肥厚型心肌病合并妇科肿瘤诊治一例 699
免疫检查点抑制剂引起的以心肌炎为首发症状的多系统衰竭 699
孤独”右心衰 - 最熟悉的陌生人 700
继发性高血压：隐匿性颈动脉体瘤一例 700

发言交流

代谢性心血管疾病研究

Longitudinal Relationship Between Serum Palmitate and Metabolic Dysregulation: Assessing Diabetes Risk in a Community-Based Population

Yu-Xin Nong, Ya-Feng Zhou

The Fourth Affiliated Hospital of Soochow University

Objective:

This study aimed to comprehensively investigate the association between plasma palmitic acid (PA) levels and insulin resistance (IR) as well as diabetes mellitus (DM) in a general adult population. As the most abundant saturated fatty acid in human plasma, PA has been implicated in metabolic dysregulation, but its precise role in diabetes pathogenesis remains controversial. Our study sought to clarify this relationship using a large, nationally representative cohort while controlling for key confounding factors. Additionally, we examined the long-term prognostic value of PA levels for mortality outcomes, and explored potential effect modifications by demographic and metabolic characteristics. These findings could provide important insights for diabetes prevention strategies and risk stratification in clinical practice.

Methods:

We conducted a rigorous population-based cohort study utilizing data from 6,578 adults aged ≥ 20 years participating in the National Health and Nutrition Examination Survey (NHANES) during 2003-2004, 2011-2012, and 2013-2014 cycles. Plasma PA levels were quantitatively measured using gas chromatography-mass spectrometry (GC-MS), the gold standard method for fatty acid analysis, and categorized into quartiles (Q1-Q4) for comparative analysis. IR was defined using the homeostasis model assessment (HOMA-IR) with established cut-off values, while diabetes status was determined through a combination of fasting glucose levels, HbA1c measurements, and self-reported physician diagnosis.

Multivariable logistic regression models were constructed to assess the independent associations between PA levels and metabolic outcomes, adjusting for potential confounders including age, sex, race/ethnicity, BMI, physical activity, smoking status, alcohol consumption, and dietary patterns. To account for potential nonlinear relationships, we employed restricted cubic splines with three knots. For survival analysis, we linked participants to mortality data from the National Death Index and performed Kaplan-Meier survival analysis to evaluate differences in all-cause mortality across PA quartiles over a maximum follow-up period of 200 months. All statistical analyses incorporated appropriate sampling weights to ensure nationally representative estimates and were conducted using specialized survey procedures in statistical software.

Results:

Our comprehensive analysis yielded several important findings. First, we observed a strong positive dose-response relationship between plasma PA levels and HbA1c (β=0.21, P<0.001), indicating that higher PA concentrations were associated with poorer long-term glycemic control. Participants in the highest PA quartile (Q4) exhibited substantially increased risks of both IR (OR=2.76, 95% CI: 2.19-3.49, P<0.001) and diabetes (OR=1.75, 95% CI: 1.29-2.37, P<0.001) compared to those in the lowest quartile (Q1), even after full adjustment for potential confounders. The restricted cubic spline analysis revealed a nonlinear relationship, with steeper increases in diabetes risk observed at higher PA concentrations.

Long-term follow-up data demonstrated significantly higher overall mortality in the Q4 group (24.0%) versus Q1 (11.0%, log-rank P<0.001), with the survival curves diverging markedly after approximately 120 months of follow-up. Interestingly, no significant difference in mortality was observed during the first 100 months of follow-up (7.8% vs 5.8%, P=0.264), suggesting that the adverse effects of elevated PA may require longer durations to manifest clinically. Subgroup analyses revealed important variations in the PA-diabetes association, with particularly strong effects observed among overweight/obese individuals (BMI ≥ 25; P for interaction=0.02), younger adults (<50 years; P for interaction=0.03), and women (P for interaction=0.04). These findings suggest that certain populations may be more vulnerable to the metabolic effects of elevated PA levels.

Conclusion:

This large, population-based cohort study provides compelling evidence that elevated plasma PA levels are independently associated with increased risks of IR and diabetes, particularly in overweight, younger, and female populations. The observed dose-response relationships and long-term mortality associations strengthen the biological plausibility of PA as an important contributor to metabolic dysfunction. Our findings suggest that PA may serve as a valuable biomarker for diabetes risk assessment and could potentially inform targeted prevention strategies in high-risk groups. The delayed emergence of mortality differences implies that early interventions to modify PA levels might yield long-term health benefits. Future research should focus on elucidating the underlying mechanisms, including potential effects on β-cell function and systemic inflammation, as well as evaluating whether dietary modifications or pharmacological interventions targeting PA metabolism could improve metabolic outcomes. These findings contribute significantly to our understanding of fatty acid metabolism in diabetes pathogenesis and may help refine current approaches to diabetes prevention and management.

膳食炎症与膳食质量对心血管 - 肾脏 - 代谢综合征晚期及死亡风险的影响：传统分析与机器学习方法

鲍伟 刘学波

上海市同济医院（同济大学附属同济医院）

目的

美国心脏协会最新定义的心血管 - 肾脏 - 代谢（CKM）综合征，是由共同炎症通路介导的心血管、肾脏与代谢紊乱的复杂症候群。本研究探讨膳食炎症指数（DII）与健康饮食指数（HEI）对 CKM 进展及死亡风险的影响，解析炎症标志物的中介作用，并识别关键膳食预测因子。

方法

我们分析了 1999-2020 年美国国家健康与营养调查（NHANES）中 19,742 名具有完整膳食与临床数据的参与者。DII 与 HEI 基于 24 小时膳食回顾计算：DII 选取 28 种膳食成分，HEI 采用 2015 版健康饮食指数的 13 项成分评估膳食指南依从性。主要结局为晚期 CKM 综合征（3-4 期）和全因死亡率。采用：1）多变量 logistic/Cox 回归评估 DII/HEI 与结局的关联；2）中介分析检验炎症标志物作用；3）机器学习结合 SHAP 分析识别关键膳食成分。

结果

高 DII 增加晚期 CKM 综合征风险（OR=1.081，95%CI：1.039-1.124）和死亡风险（HR=1.092，95%CI：1.040-1.148），而 HEI 显示保护作用（OR=0.990，95%CI：0.985-0.994；HR=0.993，95%CI：0.987-0.998）。聚类分析显示，与抗炎高质量膳食相比，促炎低质量膳食组的 CKM 风险增加 49%（OR=1.492），死亡风险升高 39%(HR=1.392)。中性粒细胞介导了 26.50%(DII)和 24.48%(HEI)的晚期 CKM 风险，以及 11.16%（DII）和 14.72%（HEI）的死亡风险。机器学习识别出维生素 B6、维生素 D、烟酸、单不饱和脂肪酸（MUFA）和多不饱和脂肪酸（PUFA）是 CKM 分期和死亡风险的关键预测因子。

结论

促炎膳食增加而高质量膳食降低 CKM 进展与死亡风险，中性粒细胞是重要中介因子。维生素 B6、维生素 D、烟酸、MUFA 和 PUFA 作为关键膳食因素，为 CKM 精准营养管理提供了策略依据。

冷暴露通过脂肪组织对代谢综合征引起的多器官功能障碍的影响及机制研究

陈思喆 张澄

山东大学齐鲁医院

研究目的 1. 研究冷暴露对 MetS 小鼠 BAT、皮下白色脂肪（subWAT）、内脏白色脂肪(eWAT)及 机体代谢的影响; 2. 研究冷暴露是否改善 MetS 引发的心血管、肝肾等器官功能障碍； 3. 探讨冷暴露是否通过脂肪组织产热代谢对 MetS 产生影响及其分子机制。

研究方法 1. 动物实验分组 。 2. 小鼠葡萄糖耐量检测、胰岛素耐量检测 3. 小鼠代谢率检测 4. 小鼠超声心动图检测 5. 组织病理学检测： 对脂肪组织进行 HE 染色、UCP1 免疫组化染色、CD31 免疫荧光染色、Endomucin 免疫荧光染色；对心肌、肾脏、肝脏组织进行 HE 染色、天狼猩红染色、Col I 免疫组化染色、Col III 免疫组化染色。

虽然已有一些分子靶点被发现可用于针对 MetS 的治疗，但其临床应用仍非常有限，并 有显著的副作用。适度寒冷暴露通过神经反射，激活脂肪组织的 β3 肾上腺素能受体，进而 激活脂肪组织产热过程，是自然存在的机体消耗能量保持体温的机制，本研究旨在明确冷 暴露是否可以作为一种改善代谢综合征及其多器官并发症的有效手段及其临床应用潜力。

研究结论 1. 冷暴露改善 MetS 小鼠的胰岛素敏感性和葡萄糖代谢。 2. 冷暴露降低 MetS 小鼠血糖及血脂水平并增强代谢。 3. 冷暴露改善 MetS 小鼠多器官功能学和组织学损伤。 4. 脂肪组织棕色化及线粒体解偶联蛋白 UCP1 的生热作用是冷暴露改善代谢综合征及其 并发症的重要作用机制。

肠道菌群及其代谢物在 2 型糖尿病心肌病进展中的作用研究

王金鑫 刘宏斌

中国人民解放军总医院 / 解放军医学院

目的：明确肠道菌群与糖尿病心肌病进展的相关性，筛选与糖尿病心肌病变相关的标志性菌属。探索粪便代谢物与糖尿病心肌病进展的相关性，筛选与糖尿病心肌病变相关的代谢物及代谢通路。明确糖尿病心肌病变肠道菌群与代谢物的相关性。

方法：从 22 例 2 型糖尿病合并心力衰竭患者、25 例 2 型糖尿病合并左室舒张功能障碍患者、37 例 2 型糖尿病无心功能障碍患者和 32 例例健康对照者中采集粪便样本，同时收集血糖、NT-proBNP 等临床指标。粪便样品采用 16S rDNA 基因测序、高通量靶标代谢组学测定，并将差异肠道菌群、代谢物和临床指标进行相关性分析。

结果：（1）四组人群的肠道微生物组成不同。Monoglobus、Roseburia 等菌属的丰度在健康对照组、糖尿病无心功能障碍组、糖尿病合并左室舒张功能障碍

组、糖尿病合并心力衰竭组逐渐下降。（2）相关性分析发现，Monoglobus、Roseburia 等菌属与血糖、NT-proBNP 呈负相关。（3）四组人群的粪便代谢物水平存在明显改变。（4）与健康对照组相比，其余三组在嘧啶代谢通路中，有 2 个下调的差异代谢物，7 个上调的差异代谢物；在半胱氨酸和蛋氨酸代谢通路中，有 2 下个调的差异代谢物，3 个上调的差异代谢物。（5）相关性分析发现，差异代谢物与 Monoglobus、Roseburia 等菌属具有较强相关性。（6）差异代谢物与血糖、NT-proBNP 等具有较强相关性。

结论：糖尿病无心功能障碍患者、糖尿病合并左室舒张功能障碍患者、糖尿病合并心力衰竭患者与健康对照者之间肠道微生物组成不同，且粪便代谢物水平存在差异，改变的代谢物可能通过影响嘧啶代谢通路和半胱氨酸和蛋氨酸代谢等通路参与糖尿病心肌病的进展。特征性改变的肠道菌群可能通过菌群功能通路影响粪便代谢物水平，从而影响血糖、NT-proBNP 等临床表型，进而参与糖尿病心肌病的发生发展。

New criteria for obesity: clinical obesity as predictors of cardiovascular mortality among older adults in China - a nationwide, community-based prospective cohort study

HaiYan Ruan[1,3], Liu Yang[2], Halmira Alimjan[2], Ke-Xin Wang[1], Yi Zheng[1], Sen He[1,2]

1. West China Hospital of Sichuan University, Chengdu, China.

2. Karamay Hospital of Integrated Chinese and Western Medicine, Karamay, China.

3. Hospital of Traditional Chinese Medicine, Shuangliu District, Chengdu, China.

Background: Recently (Jan 2025), the Lancet Diabetes & Endocrinology Commission redefined clinical obesity as a disease condition and introduced novel diagnostic standards. This redefinition is intended to assist healthcare professionals in making informed decisions and prioritizing treatment plans and public health initiatives. Despite these advancements, the correlation between clinical obesity and cardiovascular mortality in the elderly population of China has not been explored. To bridge this knowledge gap, we undertook a comprehensive nationwide, community-centered, longitudinal study in China.

Methods: A total of 747 participants, with a median age of 85. years (interquartile range: 76.–93.) and 46.% males, were included in the study from the Chinese Longitudinal Healthy Longevity Survey conducted between 2011 and 2014, with follow-up until 2018. The exposure variable under investigation was clinical obesity, defined according to the criteria set by the Lancet Diabetes & Endocrinology Commission. The primary outcome of interest was cardiovascular mortality. The cause of death for each participant was determined using the International Classification of Diseases, 10th revision. Detailed information on the cause of death was available for 131 participants, among whom 336 deaths were attributed to cardiovascular causes (coded as I00-I99), while 974 were due to non-cardiovascular reasons. Additionally, 2247 participants had an unknown cause of death. To analyze the association between obesity and cardiovascular mortality, participants were categorized as "deceased" if they died from cardiovascular disease, and as "censored" if they survived, died from non-cardiovascular causes, or had an unknown cause of death. The study assessed the relationship between clinical obesity and mortality using Cox regression models. Furthermore, the impact of clinical obesity on life expectancy for individuals aged 65 to 100 years was estimated through a two-step analysis involving flexible parametric survival models.

Results: During a median follow-up period of 3.5 years (interquartile range: 2.6–6.5 years), the study recorded 336 cardiovascular deaths, accounting for 4.5% of the total. Participants with preclinical obesity did not exhibit a significant association with mortality risk compared to those without obesity, as indicated by adjusted hazard ratios (HR) of 1.00 (95% CI: .71–1.42). In contrast, individuals with clinical obesity showed a notably higher mortality risk, with an adjusted HR of 1.95 (95% CI: 1.15–3.29). Moreover, at the age of 65 years, participants without obesity were found to have the longest remaining cardiovascular life expectancy, estimated at 32.1 years (95% CI: 31.2–32.8). In comparison, individuals with preclinical obesity at the same age had a reduced remaining life expectancy by 1.6 years (95% CI: .1–3.), while those with clinical obesity faced a further reduction of 2.6 years (95% CI: -.1 to 5.5).The study also investigated the relationship between cardiovascular mortality risk and body mass index (BMI), revealing a significant increase in risk at lower BMI levels. However, this association did not reach statistical significance, likely due to limited statistical power. Additionally, the combined assessment of BMI and waist circumference as indicators of obesity did not show any significant association with mortality in the study population.

Conclusion: In the older adult population of China, the presence of clinical obesity has been found to be closely linked to an increased risk of cardiovascular mortality and a decrease in overall life expectancy. It is crucial to emphasize the importance of implementing targeted therapeutic approaches and public health initiatives to effectively tackle clinical obesity in order to mitigate the disparities in mortality rates within this demographic.

血浆同型半胱氨酸水平与不同体重指数患者发生冠心病以及长期预后的相关性的初步探讨

陈家元

广州医科大学第二附属医院

目的：探讨血浆同型半胱氨酸（Hcy）水平与不同 BMI 患者发生冠心病以及长期预后的相关性。

方法：第一部分为回顾性横断面研究，选取 2015-2023 年于广州医科大学附属第二医院住院并接受冠脉造影的 40-65 岁患者，根据 BMI 分为正常体重组（18-25 kg/m^2）、超重组（25-28 kg/m^2）及肥胖组（大于 28 kg/m^2）。logistic 回归分析筛选不同 BMI 患者发生冠心病（CAD）的危险因素。第二部分为前瞻性验证试验，招募 80 名受试者，将其分为非 CAD 肥胖、CAD 肥胖和非 CAD 正常体重组，靶向氨基酸代谢组学进一步鉴定差异表达物。第三部分采取美国国家健康和营养检查调查（NHANES）2007-2018 年数据，分析 Hcy 对不同 BMI 受试者全因死亡的影响。

结果：第一部分：纳入 936 例患者，结果显示：以正常体重和低 Hcy 血症（小于 10.7mmol/L）组合为对照，肥胖合并高 Hcy 血症患者的 CAD 发生率是最高（HR:5.99, P < 0.001）。而在肥胖受试者亚组，合并高 Hcy 血症的 CAD 发生率是低 Hcy 血症的 7 倍。第二部分：靶向代谢组学进一步证实了蛋氨酸及其代谢产物（Hcy）在非 CAD 肥胖和 CAD 肥胖之间存在显著性差异（P < 0.001）。第三部分：从 NHANE 数据库入选 6410 个病例，生存曲线及 COX 回归分析显示，在肥胖受试者中，与低 Hcy 血症相比，高 Hcy 血症与全因死亡率的风险有更高相关性（HR:2.28, P < 0.001）。令人意外的是，与正常体重高 Hcy 血症组相比，肥胖的高 Hcy 血症组全因死亡率显著性降低（HR：0.66，P=0.006），而超重的高 Hcy 血症的全因死亡率进一步降低（HR: 0.57, P < 0.001）。

结论：高 Hcy 血症是肥胖并发冠心病以及全因死亡的独立危险因素，而超重的高 Hcy 患者的长期预后可能优于正常体重及肥胖人群，需要进一步研究证实。

血清葡萄糖和高密度脂蛋白介导 CDAI 与代谢综合症患者全因死亡率和心血管疾病死亡率的关系

李爱华

中南大学湘雅医院

目的：尽管饮食调整日益被视为干预代谢综合征（MetS）的策略，但复合饮食抗氧化指数（CDAI）与代谢综合征人群长期健康结局的关系仍不明确。为了明确 CDAI 和代谢综合症患者全因死亡率和心血管死亡率的关联，我们进行研究探索它们之间的关系。

方法：我们分析了美国国家健康与营养检查调查（NHANES，1999-2020）中 4756 名代谢综合征成人的数据。采用加权 Cox 比例风险回归模型评估风险比（HR）及 95% 置信区间（CI），通过限制立方样条（RCS）曲线分析非线性关系，并进行分层分析和中介效应分析。

结果：在中位随访 103.4 个月期间，发生 838 例死亡，其中 262 例为心血管原因死亡。校正混杂因素后，与 CDAI 最低四分位数组相比，最高四分位数组参与者的全因死亡率 HR 为 0.74（95% CI：0.57-0.97，p=0.030），心血管死亡率 HR 为 0.65（95% CI：0.45-0.96，p=0.030）。RCS 分析显示 CDAI 与死亡率呈线性负相关。分层分析支持上述结果，且无显著交互作用。中介分析表明，血清葡萄糖和高密度脂蛋白胆固醇（HDL-C）介导了 CDAI 与死亡率的关系。

结论：较高的 CDAI 与代谢综合征患者较低的全因死亡率和心血管死亡率相关，其机制可能通过调节糖脂代谢介导。

DMRT2 overexpression in macrophages promotes M1 polarization to improve adipocyte inflammation and insulin resistance through interacting with FXR

xian Wei, Jing Tao, Ming Liu, Yi-Tong Ma

The First Affiliated Hospital of Xinjiang Medical University

The well-established pathophysiological link between obesity and the development of insulin resistance (IR) is fundamentally intertwined with chronic, low-grade inflammation originating within adipose tissue (AT). Central to this inflammatory milieu is the dysregulated polarization state of infiltrating macrophages, where a shift from the anti-inflammatory M2 phenotype towards a dominant pro-inflammatory M1 state exacerbates adipocyte dysfunction and systemic metabolic impairment. While the double-sex and mab-3 related transcription factor 2 (DMRT2) has been previously implicated in ameliorating adipocyte insulin resistance, its specific regulatory function concerning macrophage polarization dynamics within the adipose niche, and the underlying molecular mechanisms, remained largely undefined. This investigation comprehensively elucidates the mechanistic role of macrophage-specific DMRT2 overexpression and its consequential impact on mitigating adipocyte inflammation and systemic insulin sensitivity, revealing a critical interaction with the farnesoid X receptor (FXR).

Utilizing a well-characterized high-fat diet (HFD)-induced murine model of obesity and insulin resistance in male C57BL/6 mice, we achieved targeted DMRT2 overexpression specifically within macrophages via advanced transduction techniques. This macrophage-specific intervention demonstrably improved critical whole-body metabolic parameters compared to HFD controls. These significant improvements encompassed enhanced glucose tolerance (as assessed by intraperitoneal glucose tolerance tests, IPGTT), markedly increased insulin sensitivity (confirmed by insulin tolerance tests, ITT, and homeostasis model assessment of

insulin resistance, HOMA-IR), favorable alterations in body composition (reduced fat mass percentage), and profound amelioration of adipose tissue histopathology. Histological analyses revealed reduced adipocyte hypertrophy, diminished crown-like structures indicative of macrophage infiltration, and decreased overall inflammatory infiltrates within epididymal white adipose tissue (eWAT).

Mechanistically, DMRT2 overexpression within AT macrophages significantly skewed their polarization balance away from the pro-inflammatory M1 phenotype. This crucial reprogramming was evidenced by a marked downregulation of canonical M1 surface markers (CD86) and associated pro-inflammatory cytokines (e.g., TNF-α, IL-6), concomitant with a significant upregulation of markers associated with the alternative, anti-inflammatory, and tissue-reparative M2 activation state (CD163, CD206, Arg1). To dissect the direct paracrine crosstalk, a sophisticated co-culture system was employed, comprising primary macrophages overexpressing DMRT2 and insulin-resistant 3T3-L1 adipocytes. Strikingly, DMRT2 overexpression in macrophages substantially enhanced insulin sensitivity in adjacent adipocytes. This improvement was quantified by elevated basal and insulin-stimulated 2-deoxyglucose uptake, increased plasma membrane translocation of the insulin-responsive glucose transporter GLUT4 (confirmed by immunofluorescence and cell fractionation), and heightened phosphorylation of AKT at Ser473 - a central node and critical activation step in the canonical insulin signaling cascade.

Crucially, the study uncovered a pivotal molecular interaction underpinning DMRT2's effects. RNA interference-mediated knockdown of the nuclear bile acid receptor, farnesoid X receptor (FXR), specifically within macrophages, significantly attenuated or partially abrogated the beneficial metabolic effects conferred by DMRT2 overexpression. This attenuation included a blunted shift away from M1 polarization and a reduced improvement in co-cultured adipocyte insulin sensitivity. This key finding establishes a critical, previously unrecognized functional interaction and likely co-regulatory relationship between DMRT2 and FXR within macrophages, essential for mediating the observed improvements in polarization balance and insulin sensitivity.

Collectively, these multifaceted results robustly identify macrophage-expressed DMRT2 as a pivotal transcriptional regulator governing adipose tissue inflammation and systemic metabolic homeostasis. Its action, operating at least partially through a cooperative interaction with FXR, modulates the intricate crosstalk between macrophage phenotypic commitment, adipose inflammatory tone, and insulin signaling fidelity. Consequently, targeting the DMRT2 pathway, particularly its interplay with FXR in macrophages, emerges as a promising and mechanistically grounded therapeutic strategy for ameliorating obesity-associated metabolic disorders, including type 2 diabetes.

应激性高血糖比率对急性心肌梗死患者 PCI 术后远期预后的影响

王彤 丛洪良

天津市胸科医院

目的

探讨应激性高血糖比率对于接受 PCI 治疗的 ST 段抬高型心肌梗死和非 ST 段抬高型心肌梗死患者远期预后的影响。

方法

纳入了 2019 年 1 月 1 日至 2019 年 12 月 31 日在天津市胸科医院成功行 PCI 手术的急性心肌梗死患者 734 例。主要研究终点为 MACCE。在 399 名 STEMI 患者中，依据入院 SHR 三分位数分为 T1、T2、T3 三组，其中低 SHR 组（T1、T2 组，SHR < 0.917，n = 266），高 SHR 组（T3 组，SHR ≥ 0.917，n = 133）。在 335 名 NSTEMI 患者中，同样分为 T1、T2、T3 三组，低 SHR 组（T1、T2 组，SHR < 0.926，n = 222），高 SHR 组（T3 组，SHR ≥ 0.926，n = 113）。分别比较 STEMI 及 NSTEMI 人群高 SHR 与低 SHR 患者基线资料及预后，使用单因素和多因素 Cox 比例风险模型分析 SHR 对成功行 PCI 术的急性心肌梗死患者远期预后的影响，并根据患者是否合并糖尿病进行亚组分析，探讨 SHR 对不同糖代谢状态下急性心肌梗死患者预后的影响。

结果

经过 4.8 年的中位随访，共发生 57 例（7.8%）全因死亡，41 例（5.6）心源性死亡，以及 173 例（23.6%）MACCE。多因素 COX 回归分析，在成功接受 PCI 术的 STEMI 患者中，高 SHR 组比低 SHR 组发生 MACCE 的风险更高 (HR: 1.886, 95%CI: 1.253-2.713, P=0.042)。在 STEMI 合并糖尿病的患者中也发现较高的 SHR 是 MACCE 事件的独立预测因素 (HR: 4.153, 95%CI: 1.519-11.350, P=0.006)。在 STEMI 合并非糖尿病，以及 NSTEMI 无论是否合并糖尿病的患者中，SHR 对不良预后没有显著影响（P 值均 >0.05)。

结论

接受 PCI 的 STEMI 及 STEMI 合并糖尿病患者，SHR 是远期 MACCE 事件的独立预测因素，SHR 的测量有利于风险分层及预后评估。

Comprehensive Identification of Cardiometabolic Protein Biomarkers in Acute Myocardial Infarction Using Olink Proteomics and Multi-Cohort Validation

Xin Tan, Shuai Xu, An-Chen Xu, Ya-Feng Zhou

Department of Cardiology, The Fourth Affiliated Hospital of Soochow University, Suzhou Dushu Lake Hospital, Medical Center of Soochow University

Background:

Acute myocardial infarction (AMI) is a leading cause of death and disability worldwide. Despite advances in reperfusion therapy, metabolic injury remains a major contributor to poor outcomes. Cardiometabolic dysfunction—characterized by impaired energy metabolism, inflammation, and oxidative stress—plays a key role in AMI pathogenesis. However, reliable biomarkers reflecting this metabolic damage are lacking. This study aimed to identify and validate cardiometabolic protein biomarkers for AMI using Olink proteomics and genetic causal analysis.

Methods:

We conducted a proteomic analysis of coronary plasma samples obtained from 20 patients diagnosed with AMI and 10 age- and sex-matched healthy controls using the Olink Cardiometabolic panel, which quantifies 92 targeted proteins implicated in cardiovascular metabolism. Differentially expressed proteins (DEPs) were identified using t-tests with false discovery rate (FDR) correction. Bioinformatics analyses, including Gene Ontology (GO), Kyoto Encyclopedia of Genes and Genomes (KEGG) pathway enrichment, and protein-protein interaction (PPI) network construction, were performed to investigate biological functions. Validation was conducted using enzyme-linked immunosorbent assay (ELISA) in an independent cohort of 125 AMI patients and 120 controls. Diagnostic performance was evaluated using receiver operating characteristic (ROC) curves derived from multiple public datasets, including GSE66360, GSE48060, GSE5406, GSE57388, and GSE57345. Additionally, we employed two-sample Mendelian randomization (MR) using genetic variants associated with protein levels from large-scale genome-wide association studies (GWAS) in the FinnGen consortium to infer potential causal associations between candidate biomarkers and AMI risk.

Results:

Among the 92 proteins profiled, 32 were found to be significantly differentially expressed between AMI patients and healthy controls ($p < 0.05$), including 12 upregulated and 20 downregulated proteins. GO and KEGG enrichment analyses revealed that these proteins were enriched in biological pathways related to collagen fibril organization, vascular smooth muscle cell development, PI3K-AKT signaling, and immune regulation. The five selected upregulated proteins—PCOLCE, FCN2, REG1A, DEFA1, and CRTAC1—were functionally linked to extracellular matrix remodeling, complement activation, inflammatory response, and cellular stress regulation. ELISA results confirmed significantly increased levels of these proteins in AMI patients compared with controls (all $p < 0.01$). ROC curve analyses based on GEO datasets demonstrated that these proteins had good diagnostic value, with area under the curve (AUC) values ranging from 0.678 to 0.825 across different cohorts, including both acute and chronic ischemic cardiomyopathy populations. Correlation analyses showed that levels of the core proteins were significantly associated with key clinical indicators such as left ventricular ejection fraction (LVEF), left ventricular fractional shortening (LVFS), NT-proBNP, CK-MB, cTnT, and body mass index (BMI), suggesting their clinical relevance in assessing myocardial injury severity and metabolic stress. Notably, MR analysis identified a statistically significant causal association between genetically predicted FCN2 levels and AMI risk (OR = 1.514, 95% CI: 1.095–2.095, p = 0.012), as well as between DEFA1 and AMI (OR = 1.179, 95% CI: 1.024–1.358, p = 0.022). The other three proteins exhibited suggestive but non-significant causal relationships. Sensitivity analyses, including MR-Egger and leave-one-out tests, supported the robustness of the findings and excluded pleiotropic effects.

Conclusions:

This study successfully identified and validated five cardiometabolic protein biomarkers—PCOLCE, FCN2, REG1A, DEFA1, and CRTAC1—that are significantly elevated in patients with acute myocardial infarction. These proteins are functionally involved in key pathological processes such as extracellular matrix remodeling, immune activation, and metabolic stress responses. The diagnostic performance of these markers was confirmed in multiple independent datasets, and FCN2 and DEFA1 were further demonstrated to have a causal relationship with AMI risk through Mendelian randomization. These findings provide important insights into the mechanisms of metabolic damage in AMI and suggest that these proteins may serve as promising candidates for early diagnosis, risk stratification, and therapeutic targeting. Further prospective multicenter studies are warranted to validate these findings and explore their utility in clinical decision-making and precision medicine.

美阿沙坦对糖尿病大鼠心肌脂联素和脂联素受体 1 表达的影响 [基金项目：山西省自然基金基础研究项目（20210302123088）；太原市区域医疗中心科技创新项目（202229）]

付德明

山西医科大学附属太原中心医院 / 太原市中心医院

目的 研究美阿沙坦酯（Azil）对糖尿病（DM）大鼠心肌脂联素（ ADPN）和脂联素受体 1（AdipoR1）表达影响，探讨心肌保护的可能机制。

方法 SD 大鼠分为 Sham+Vehicle、DM+Vehicle、DM+Azil、Sham+Azil 组。Azil 干预 12 周测量大鼠体重，测定血清 FBG、FINS、TG、TC，计算 LVMI、RVMI，光镜观察心肌病理变化，ELISA 测定心肌 ADPN、AdipoR1、MCP-1、NF-κB、GLUT-1、TGF-β_1；RT-PCR 和 Western blot 测定心肌 AdipoR1 mRNA 和蛋白表达水平。

结果 DM+Vehicle 组大鼠 FBG、FINS、TG、TC 水平高于 Sham+Vehicle 组，ADPN 水平低于 Sham+Vehicle 组；DM+Azil 组 FBG、FINS、TG、TC 水平低于 DM+Vehicle 组，ADPN 水平高于 DM+Vehicle 组。DM+Vehicle 组大鼠心肌 LVMI 较 Sham+Vehicle 组升高，DM+Azil 组 LVMI 较 DM+Vehicle 组降低。DM+Vehicle 组大鼠心肌 AdipoR1 表达低于 Sham+Vehicle 组，DM+Azil 组 AdipoR-1 表达则升高。DM+Vehicle 组大鼠心肌 AdipoR1 表达较 Sham+Vehicle 组降低，而 MCP-1、NF-κB、GLUT-1、TGF-β_1 较 Sham+Vehicle 组升高；DM+Azil 组大鼠心肌 AdipoR1 表达较 DM+Vehicle 组升高，而 MCP-1、NF-κB、GLUT-1、TGF-β_1 表达降低。

结论 Azil 可改善 DM 大鼠糖脂代谢紊乱，通过上调心肌 ADPN 和 AdipoR1 表达，下调 MCP-1、NF-κB、GLUT-1、TGF-β_1 表达，发挥心肌保护作用。

胰岛素通过 ACTA2 rs1324551 (A/G) 位点调控血管平滑肌细胞表型转化、增殖及迁移及其机制研究

陈芯尧 谢凤 闫庆凯 于长青

重庆市璧山区人民医院

目的 探讨胰岛素刺激血管平滑肌细胞（VSMCs）ACTA2 rs1324551 (A/G) 位点突变对细胞表型转化、增殖及迁移的影响。**方法** 分离 SD 大鼠原代 VSMCs，构建 ACTA2 rs1324551 (A/G) 位点慢病毒转染 VSMCs；将 VSMCs 细胞分组为常规培养组与胰岛素（10^{-7}mol/L）培养组，采用 CCK-8 试剂盒检测胰岛素刺激后细胞增殖水平，采用细胞划痕实验、Transwell 实验检测胰岛素刺激后细胞迁移水平；利用生物信息学对 rs1324551 区域进行分析，荧光素酶报告基因实验检测激活蛋白 -1（activating protein-1，AP-1）调控 ACTA2 rs1324551 (A/G) 位点表达；进一步检测胰岛素刺激后 VSMCs 的 MAPK/ERK/AP-1 信号通路及 SM-α 的蛋白表达。**结果** 胰岛素刺激后突变型 VSMCs 细胞的增殖水平较野生型 VSMCs 细胞显著增高（P<0.05）；细胞划痕实验、Transwell 实验发现胰岛素刺激后突变型 VSMCs 细胞的迁移水平较野生型 VSMCs 细胞显著增加（P<0.05）；荧光素酶报告基因显示 AP-1 可与 ACTA2 rs1324551 (GG) 位点结合并抑制 ACTA2 基因表达，同时胰岛素刺激后 MAPK/ERK/AP-1 通路激活，SM-α 蛋白表达下调。**结论** 胰岛素通过激活 VSMCs AP-1，抑制 ACTA2 基因 rs1324551 (GG) 位点的表达，因此 rs1324551 (GG) 可能是 SM-α 蛋白表达一个新的顺式调控位点，在 II 型糖尿病合并动脉粥样硬化患者的疾病发生发展中起重要调控作用。

成年期不同阶段体重对左室收缩功能和全因死亡的影响

杜家琦 [1] 公威 [2] 聂绍平 [1]

1. 首都医科大学附属北京安贞医院

2. 北京医院

目的：探究成年期不同阶段体重对左室结构、收缩功能和全因死亡风险是否存在不同影响。

方法：本研究纳入了动脉粥样硬化多种族研究中接受心脏磁共振检查的 3004 名参与者。所有参与者在入组时回忆了其 20 岁和 40 岁的体重，同时在每次 Exam 中均测量了身高和体重，以此计算各阶段的身体质量指数（BMI）。在本研究中，成年早期定义为 20-40 岁，成年中期定义为 40 岁至 Exam 1（中位年龄 59 岁），成年晚期定义为 Exam 1 及以后。使用多变量线性回归和限制性立方样条探究成年期 BMI 对左室结构和收缩功能的影响；采用 Cox 回归评估 BMI 与全因死亡率之间的关系，并通过中介分析探究左室射血分数（LVEF）在肥胖和全因死亡之间的中介作用。

结果：线性回归分析表明，左室质量和容积随成年期 BMI 增加而增大，且这一结果独立于晚年 BMI 存在。收缩功能方面，成年早期 BMI 较高与晚年 LVEF 降低独立相关，而成年中晚期 BMI 与 LVEF 则无此关联。Cox 回归分析表明，成年早期 BMI 较高是全因死亡的独立危险因素，而成年晚期 BMI 较高则是保护因素。中介分析表明，成年早期 BMI 对全因死亡的影响部分由 LVEF 介导。

结论：成年期不同阶段的 BMI 对左室收缩功能和全因死亡风险有着不同影响。成年早期较高的 BMI 与晚年 LVEF 降低密切相关，进而部分介导了全因死亡的发生。因此，应积极倡导成年早期体重控制，以降低肥胖对晚年心脏功能和死亡风险的不良影响。

Impact of Abdominal Obesity Indices on All-Cause and Cardiovascular Mortality in Individuals with Pre-Diabetes and Diabetes: Insights from a Prospective Cohort Study

Aihua Li, Qilin Ma

central south university

Abstract

Aims:

This study aimed to comprehensively evaluate the associations between key indices of abdominal obesity—specifically the Visceral Adiposity Index (VAI), Lipid Accumulation Product (LAP), and Waist Circumference (WC)—and the risks of all-cause and cardiovascular disease (CVD) mortality. Crucially, it sought to determine whether these relationships varied significantly across populations with distinct glucose metabolism statuses: normal glucose regulation (NGR), prediabetes (Pre-DM), and established diabetes mellitus (DM).

Methods:

Utilizing data from the National Health and Nutrition Examination Survey (NHANES) cycles spanning 1999 to 2018, this prospective cohort analysis included 17,727 adult participants. Mortality outcomes, including specific causes of death (all-cause and CVD mortality), were ascertained by linking participants to the National Death Index records up to December 31, 2019. Participants were stratified into three groups based on their baseline glucose metabolism status: DM, Pre-DM, or NGR. Separately, participants were categorized into sex-specific quartiles (Q1-Q4, with Q1 being the lowest and Q4 the highest) for each abdominal obesity index (VAI, LAP, WC). Cox proportional hazards regression models were employed to quantify the hazard ratios (HRs) and 95% confidence intervals (CIs) for the associations between glucose metabolism status, abdominal obesity indices (both individually and in combination), and mortality outcomes. Models were adjusted for relevant demographic, lifestyle, and clinical covariates. Restricted cubic splines (RCS) with three knots were applied to explore potential non-linear dose-response relationships between the continuous obesity indices and mortality risk. To evaluate the incremental predictive utility of LAP and WC beyond standard risk factors within each glucose metabolism group, C-statistics (area under the receiver operating characteristic curve, AUC) were calculated and compared between baseline prediction models and models incorporating each abdominal obesity index.

Results:

Over a median follow-up duration of 9.4 years, 2,687 deaths were recorded, of which 847 were attributed to CVD. Cox regression analyses demonstrated that both Pre-DM and DM status were significant independent predictors of increased all-cause and CVD mortality compared to NGR. Regarding abdominal obesity indices, higher WC was significantly associated with elevated risks of both all-cause and CVD mortality. Higher LAP was significantly associated with increased all-cause mortality, but not independently with CVD mortality after adjustments. VAI did not show consistent independent associations. Joint effect analyses revealed a pronounced risk elevation: individuals with Pre-DM or DM in the highest quartile (Q4) of WC or LAP exhibited significantly greater risks of all-cause mortality compared to the reference group (NGR individuals in the lowest quartile, Q1, of the respective obesity index). Assessment of model discrimination showed that incorporating WC into baseline predictive models significantly improved the C-statistic for all-cause mortality specifically within the Pre-DM subgroup, indicating enhanced predictive accuracy for this population.

Conclusions:

Waist Circumference (WC) and Lipid Accumulation Product (LAP) emerge as significant predictors of mortality risk in this nationally representative cohort. WC demonstrates associations with both all-cause and CVD mortality, while LAP is specifically linked to all-cause mortality. The detrimental impact of high levels of these abdominal obesity indices is particularly pronounced among individuals with impaired glucose metabolism (Pre-DM and DM). Critically, the inclusion of WC significantly improves the ability to predict all-cause mortality risk within the Pre-DM population. These findings underscore the critical importance of integrating assessments of abdominal obesity, particularly WC and LAP, alongside evaluations of glucose metabolic health (including Pre-DM status) for comprehensive risk stratification and the development of targeted preventive strategies aimed at reducing mortality.

Keywords: Abdominal obesity indices, Pre-diabetes, Diabetes, All-cause and cardiovascular mortality, NHANES

Serum Glycolipids Mediate the Link Between Dietary Antioxidants and Mortality in Metabolic Syndrome

Aihua Li, Qilin Ma

中南大学湘雅医院

Abstract

Background: Metabolic syndrome (MetS), characterized by interrelated cardiometabolic risk factors including abdominal obesity, dyslipidemia, hypertension, and hyperglycemia, represents a significant global public health burden associated with increased morbidity and mortality. Dietary modification is recognized as a cornerstone strategy for MetS intervention. Oxidative stress is a key pathophysiological mechanism underlying MetS complications, prompting interest in dietary antioxidants. While the Composite Dietary Antioxidant Index (CDAI), a holistic measure reflecting the combined intake of key dietary antioxidants (vitamins A, C, E, zinc, selenium, manganese, and copper), offers a comprehensive assessment of antioxidant capacity, its specific association with long-term survival outcomes—particularly all-cause and cardiovascular mortality—in indi-

viduals already diagnosed with MetS remains inadequately elucidated. This study aimed to investigate these critical relationships within a nationally representative cohort of U.S. adults with MetS.

Methods: We conducted a prospective cohort analysis utilizing data from 4,756 adults with confirmed MetS, drawn from the National Health and Nutrition Examination Survey (NHANES) cycles spanning 1999 to 2020. Mortality status and underlying causes of death (all-cause and cardiovascular disease [CVD] mortality) were ascertained by linkage to the National Death Index records through December 31, 2019. The CDAI was calculated from 24-hour dietary recall data. Participants were categorized into quartiles (Q1-Q4) based on their CDAI score, with Q1 representing the lowest intake. Weighted Cox proportional hazards regression models were employed to calculate hazard ratios (HRs) and 95% confidence intervals (CIs) for the associations between CDAI quartiles and mortality outcomes, using Q1 as the reference group. Multivariable models were sequentially adjusted for key confounders including age, sex, race/ethnicity, education, income, smoking status, physical activity, BMI, individual MetS components, and pre-existing CVD or cancer. Restricted cubic spline (RCS) curves with three knots were fitted to explore potential non-linear dose-response relationships between continuous CDAI scores and mortality risk. Stratified analyses were performed across key subgroups (e.g., age, sex, smoking status, diabetes status) to assess consistency, with interaction terms tested for significance. Formal mediation analysis quantified the proportion of the observed association between CDAI and mortality potentially mediated by serum glucose and high-density lipoprotein (HDL) cholesterol levels.

Results: Over a median follow-up period of 103.4 months (approximately 8.6 years), 838 deaths occurred, including 262 specifically attributed to cardiovascular causes. After comprehensive adjustment for all potential confounders, participants in the highest CDAI quartile (Q4) exhibited a statistically significant 26% reduced risk of all-cause mortality (adjusted HR = 0.74, 95% CI: 0.57–0.97, p = 0.030) and a 35% reduced risk of cardiovascular mortality (adjusted HR = 0.65, 95% CI: 0.45–0.96, p = 0.030) compared to those in the lowest quartile (Q1). RCS analysis confirmed a consistent, approximately linear, inverse relationship between increasing continuous CDAI scores and decreasing risks of both all-cause and cardiovascular mortality, with no evidence of a threshold effect or non-linearity. Stratified analyses across diverse demographic and clinical subgroups consistently demonstrated protective associations for higher CDAI, with no significant interactions detected (all p-interaction > 0.05), reinforcing the robustness of the findings. Mediation analysis revealed that serum glucose levels mediated approximately 14.3% of the association between CDAI and all-cause mortality, while HDL cholesterol mediated approximately 11.7% of the association between CDAI and cardiovascular mortality, suggesting these metabolic pathways partially explain the protective effect.

Conclusions: This large, nationally representative study demonstrates that a higher Composite Dietary Antioxidant Index (CDAI), indicative of greater combined dietary intake of key antioxidants, is independently associated with significantly lower risks of both all-cause mortality and cardiovascular mortality among adults with metabolic syndrome. The inverse association exhibits a linear dose-response pattern. The protective effects appear consistent across diverse population subgroups and are partially mediated through beneficial effects on serum glucose homeostasis and HDL cholesterol levels. These findings underscore the potential clinical and public health importance of promoting diets rich in diverse antioxidants as part of a comprehensive strategy to improve long-term survival outcomes in individuals managing MetS. Further research is warranted to confirm causality and elucidate specific mechanisms.

Keywords: Composite dietary antioxidant index; Metabolic syndrome; Glycolipid; NHANES

Impact of Cardiometabolic Index on Long-Term Mortality in Young Adults with Type 2 Diabetes Mellitus

Aihua Li, Qilin Ma

central south university

Abstract

Background: Metabolic syndrome (MetS), characterized by interrelated cardiometabolic risk factors including abdominal obesity, dyslipidemia, hypertension, and hyperglycemia, represents a significant global public health burden associated with increased morbidity and mortality. Dietary modification is recognized as a cornerstone strategy for MetS intervention. Oxidative stress is a key pathophysiological mechanism underlying MetS complications, prompting interest in dietary antioxidants. While the Composite Dietary Antioxidant Index (CDAI), a holistic measure reflecting the combined intake of key dietary antioxidants (vitamins A, C, E, zinc, selenium, manganese, and copper), offers a comprehensive assessment of antioxidant capacity, its specific association with long-term survival outcomes—particularly all-cause and cardiovascular mortality—in individuals already diagnosed with MetS remains inadequately elucidated. This study aimed to investigate these critical relationships within a nationally representative cohort of U.S. adults with MetS.

Methods: We conducted a prospective cohort analysis utilizing data from 4,756 adults with confirmed MetS, drawn from the National Health and Nutrition Examination Survey (NHANES) cycles spanning 1999 to 2020. Mortality status and underlying causes of death (all-cause and cardiovascular disease [CVD] mortality) were ascertained by linkage to the National Death Index records through December 31, 2019. The CDAI was calculated from 24-hour dietary recall data. Participants were categorized into quartiles (Q1-Q4) based on their CDAI score, with Q1 representing the lowest intake. Weighted Cox proportional hazards regression models were employed to calculate hazard ratios (HRs) and 95% confidence intervals (CIs) for the associations between CDAI quartiles and mortality outcomes, using Q1 as the reference group. Multivariable models were sequentially adjusted for key confounders including age, sex, race/ethnicity, education, income, smoking status, physical activity, BMI, individual MetS components, and pre-existing CVD or cancer. Restricted cubic spline (RCS) curves with three knots were fitted to explore potential non-linear dose-response relationships between continuous CDAI scores and mortality risk. Stratified analyses were performed across key subgroups (e.g., age, sex, smoking status, diabetes status) to assess consistency, with interaction terms tested for significance. Formal mediation analysis quantified the proportion of the observed association between CDAI and mortality potentially mediated by serum glucose and high-density lipoprotein (HDL) cholesterol levels.

Results: Over a median follow-up period of 103.4 months (approximately 8.6 years), 838 deaths occurred, including 262 specifically attributed to cardiovascular causes. After comprehensive adjustment for all potential confounders, participants in the highest CDAI quartile (Q4) exhibited a statistically significant 26% reduced risk of all-cause mortality (adjusted HR = 0.74, 95% CI: 0.57–0.97, p = 0.030) and a 35% reduced risk of cardiovascular mortality (adjusted HR = 0.65, 95% CI: 0.45–0.96, p = 0.030) compared to those in the lowest quartile (Q1). RCS analysis confirmed a consistent, approximately linear, inverse relationship between increasing continuous CDAI scores and decreasing risks of both all-cause and cardiovascular mortality, with no evidence of a threshold effect or non-linearity. Stratified analyses across diverse demographic and clinical subgroups consistently demonstrated protective associations for higher CDAI, with no significant interactions detected (all p-interaction > 0.05), reinforcing the robustness of the findings. Mediation analysis revealed that serum glucose levels mediated approximately 14.3% of the association between CDAI and all-cause mortality, while HDL cholesterol mediated approximately 11.7% of the association between CDAI and cardiovascular mortality, suggesting these metabolic pathways partially explain the protective effect.

Conclusions: This large, nationally representative study demonstrates that a higher Composite Dietary Antioxidant Index (CDAI), indicative of greater combined dietary intake of key antioxidants, is independently associated with significantly lower risks of both all-cause mortality and cardiovascular mortality among adults with metabolic syndrome. The inverse association exhibits a linear dose-response pattern. The protective effects appear consistent across diverse population subgroups and are partially mediated through beneficial effects on serum glucose homeostasis and HDL cholesterol levels. These findings underscore the potential clinical and public health importance of promoting diets rich in diverse antioxidants as part of a comprehensive strategy to improve long-term survival outcomes in individuals managing MetS. Further research is warranted to confirm causality and elucidate specific mechanisms.

Keywords: Cardiometabolic index; Diabetes Mellitus; NHANES

代谢功能障碍相关脂肪性肝病合并高尿酸血症患者的心脏重构特征及危险因素分析

周可然

盘锦市中心医院

一、目的

探讨代谢功能障碍相关脂肪性肝病（Metabolic Dysfunction-Associated Fatty Liver Disease, MAFLD）合并高尿酸血症（Hyperuricemia,HUA）患者的心脏结构改变及其独立危险因素。

二、方法

采用回顾性病例对照研究，纳入盘锦市中心医院 2024 年 4 月 -2025 年 4 月就诊的 MAFLD 患者 206 例，分为对照组（单纯 MASLD，n=103）和观察组（MAFLD 合并 HUA，n=103，高尿酸以男性血尿酸 >420 μmol/L，女性 >360 μmol/L，绝经女性 > 420 μmol/L 为诊断依据）。收集两组一般资料（年龄、性别、体重指数（BMI）、有无高血压、有无糖尿病病史），血生化指标：空腹血糖（FBG）、糖化血红蛋白（HbA1c）、甘油三酯（TG）、总胆固醇（TC）、低密度脂蛋白胆固醇（LDL-C）、高密度脂蛋白胆固醇（HDL-C）、尿白蛋白 / 肌酐比值（UACR）、血小板（PLT）、血肌酐（SCr）及心脏超声参数：室间隔厚度（IVSd）、舒张末期左心室内径（LVEDD）、收缩期末期左心房前后径（LAD）、左心室后壁厚度（LVPWd）、左心室射血分数（LVEF）、E/A（舒张早期与晚期二尖瓣血流速度比值）。采用多因素 Logistic 回归分析 HUA 危险因素，Spearman 相关分析评估尿酸（连续变量）与心脏指标的关系。

三、结果

1、心脏结构差异：

观察组 LAD[35(32,37)mm vs 33(30,35)mm, P=0.002] 和 IVSd[11(10,12) mm vs 10(10,11) mm, P<0.001] 显著高于对照组，但在性别、年龄、左室射血分数（LVEF）和 E/A 比值差异无统计学意义（均 P>0.05）。

尿酸连续变量分析显示：UA 与 LAD（Rho=0.238, P=0.001）、IVSd（Rho=0.247, P<0.001）呈显著正相关。

2、代谢与肾功能：

观察组空腹血糖 [9.33(7.31,12.15)mmol/L vs 8.52(7.26,10.0)mmol/L, P=0.046]、甘油三酯 [2.64(1.88,4.13) mmol/L vs 2.01 (1.22,3.34)mmol/L, P<0.001]、血肌酐 [72(59,89) μmol/L vs 11.18(6.32，28.36) μmol/L, P<0.001] 均显著升高。

3、MAFLD 患者发生 HUA 独立危险因素：

多因素 Logistic 回归显示，空腹血糖（OR=1.284, 95%CI 1.117-1.476, P<0.001）、血肌酐（OR=1.038, 95%CI 1.018-1.059, P<0.001）和尿白蛋白 / 肌酐比（OR=1.014, 95%CI 1.004-1.024, P=0.004）为独立危险因素。

4、心脏重构方面：

观察组中 LAD 与 IVSd（Rho=0.342, P<0.001）、左室内径（Rho=0.361, P<0.001）显著相关。UA 作为连续变量与 LAD、IVSd 的关联提示尿酸可能直接参与左房扩大和室间隔肥厚进程。

四、结论

1.MAFLD 合并 HUA 患者存在显著代谢 - 肾功能异常（血糖↑、TG↑、Scr↑）。

2. 高血糖（FPG）和肾功能损害（Scr、UACR）是 HUA 的独立危险因素（均 P<0.05，OR>1）。

3.MAFLD 合并 HUA 患者以左房扩大和室间隔肥厚为特征，且尿酸水平与这两种重构独立相关（均 P<0.01），提示尿酸可能通过容量负荷和心肌纤维化直接影响心脏重构。

AIP、AST 联合左心房内径预测代谢相关脂肪性肝病患者发生冠心病风险的临床价值研究

苗苗

盘锦市中心医院

一、目的：代谢相关脂肪性肝病（MAFLD）是一种由于代谢异常导致的慢性肝脏疾病，MAFLD 能显著增加心血管疾病风险，患有 MAFLD 的患者全因死亡率更高。目前单一的生物标志物对 MAFLD 患者发生冠心病风险的预测价值有限，因此本研究旨在探讨血浆只动脉粥样硬化指数（AIP）、天门冬氨酸氨基转移酶（AST）、左心房内径（LAD）三项指标联合预测 MAFLD 患者发生 CHD 的预测价值，为早期识别高危人群、优化心血管风险分层提供新的诊断工具。

二、方法：选取 2023 年 9 月份到 2024 年 9 月份于盘锦市中心医院心内科及内分泌科患者为研究对象，共收取 201 例患者，根据是否患有冠心病分为 MAFLD 合并 CHD 组 98 例和单纯 MAFLD 组 101 例，收集患者的一般资料及临床资料，包括性别、年龄、吸烟史、饮酒史、高血压病史、冠心病病史、白细胞、中性粒细胞百分比、白蛋白、ALT、AST、HDL-C、TG、尿酸、LAD、射血分数、E/A 比值，比较三者指标在不同组间的差异性及三者指标单独及联合指标对代谢相关性脂肪性肝病与冠心病的预测价值。

三、结果

3.1 一般资料对比：

一般资料显示：2 组患者在性别差异上无统计学意义（p>0.05）；MAFLD 合并 CHD 组与单纯 MAFLD 组的年龄、吸烟史、饮酒史、高血压病史方面差异有统计学意义（p<0.05）。

3.2 实验室指标对比：

实验室指标对比结果显示：2 组患者 ALT、GGT 水平比较差异无统计学意义（p=0.208>0.05），其余在白细胞水平、中性粒细胞百分比、尿酸、AST、TG、HDL-C、AIP、LAD、E/A、UHR 水平上有统计学意义，差异较显著（p<0.05）。

3.3 AIP、AST、LAD 对 NAFLD 患者发生 CHD 的预测效能

ROC 曲线图分析结果显示：（1）AIP 预测 MAFLD 患者发生 CHD 的最佳截断值为 0.4557，曲线下面积（AUC）为 0.651（95%CI：0.525~0.682），敏感度为 54.1%，特异度为 72.8%；（2）AST 预测 MAFLD 患者发生 CHD 的最佳截断值为 33.500，曲线下面积（AUC）为 0.604（95%CI：0.525~0.682）敏感度为 32.7%，特异度为 87.4%；（3）LAD 预测 MAFLD 患者发生 CHD 的最佳截断值为 38.500，曲线下面积（AUC）为 0.604（95%CI：0.52~0.685），敏感度为 53.1%，特异度为 72.8%。

3.4 三者联合指标多 MAFLD 患者发生 CHD 的预测效能

三者指标联合预测 MAFLD 患者发生 CHD 的最佳截断值为 0.519，曲线下面积（AUC）为 0.752（95%CI：0.685~0.819），敏感度为 60.2%，特异度为 82.5%。

四、结论

1. 单纯 MAFLD 组与 MAFLD 合并 CHD 组患者在性别方面差异上无统计学意义（p>0.05）；MAFLD 合并 CHD 组与单纯 MAFLD 组的年龄、吸烟史、饮酒史、高血压病史方面差异有统计学意义；单纯 MAFLD 组与 MAFLD 合并 CHD 组患者 ALT、GGT 水平比较差异无统计学意义（p=0.208>0.05），在白细胞计数、中性粒细胞百分比、尿酸、AST、TG、HDL-C、AIP、LAD、E/A、UHR 水平上有统计学意义，差异较显著（p<0.05）。

2.AIP、AST 联合左心房内径三者指标在对 MAFLD 患者发生 CHD 的预测性能比单一指标的预测性能好。

相对脂肪质量与老年人群心血管代谢疾病及远期不良结局的关联研究

王静 [1,2] 李心晴 [2]

1. 南京市第一医院

2. 北京协和医学院 中国医学科学院阜外医院

目的：老年人群肥胖患病率呈持续增长趋势。体重指数常用于评估肥胖，但其无法区分脂肪组织和去脂组织，并忽略了机体构成和脂肪分布的性别差异。相对脂肪质量（relative fat mass，RFM）是一种基于身高和腰围的新型性别特异性肥胖评估指标。迄今为止，尚无研究探索 RFM 对老年人群全因死亡和心血管死亡的预测价值。本研究基于具有全国代表性的美国老年人群，旨在探索：1）RFM 与老年人群机体构成及脂肪分布的相关性；2）RFM 与老年人群心血管代谢疾病患病率的关联；3）RFM 与老年人群远期全因死亡和心血管死亡风险的关联，并进一步探讨潜在的性别差异。

方法：本研究基于美国国家健康与营养调查（National Health and Nutrition Examination Survey，NHANES）数据库，纳入参加 NHANES 1999-2010 的老年受访者（≥ 60 岁）。双能 X 射线吸收测定法检测机体构成及脂肪分布。采用复杂抽样数据的 Pearson 相关性分析评估 RFM 与老年男性和女性机体构成及脂肪分布的相关性。分别在老年男性和女性中根据 RFM 分布进行分组，采用加权多因素 logistic 回归模型评估 RFM 与心血管危险因素及心血管疾病（cardiovascular disease，CVD）患病率的相关性；采用加权多因素 Cox 比例风险模型评估 RFM 与全因死亡和心血管死亡风险的关联。

结果：本研究共纳入 9261 名老年参与者，中位年龄 69.0 岁，女性加权占比 55.6%。老年女性 RFM 显著高于老年男性（43.0[39.4-46.1] vs 30.7[28.0-33.2]，P<0.001）。在老年男性和女性中，RFM 与全身脂肪百分比和躯干脂肪百分比均呈显著强正相关，RFM 与心血管危险因素（2 型糖尿病、高血压及血脂异常）以及 CVD（心力衰竭、缺血性心脏病和脑卒中）患病率均独立相关。中位随访时间 11.4 年，多因素校正后，与 RFM 在 25-30 范围的老年男性相比，RFM<25 和 RFM ≥ 35 的老年男性全因死亡风险分别增加 53%（风险比 [hazard ratio，HR]=1.53，95% 置信区间 [confidence interval，CI]：1.29-1.83）和 48%（HR=1.48，95%CI：1.25-1.75）；RFM 在 30-35 范围及 RFM ≥ 35 的老年男性心血管死亡风险分别增加 31%（HR=1.31，95%CI：1.02-1.67）和 52%（HR=1.52，95%CI：1.06-2.18）。然而，在老年女性中，RFM 与全因死亡和心血管死亡风险无显著关联。

结论：在老年男性和女性中，RFM 与全身脂肪百分比和躯干脂肪百分比均呈显著正相关，高 RFM 与心血管代谢疾病患病率增加均独立相关。RFM 与全因死亡和心血管死亡风险的关联存在性别差异。

Joint Analysis of C-Reactive Protein-Triglyceride Glucose Index Clusters and Body Roundness Index Trajectories in Incident Cardiovascular Disease Risk: Insights from the China Health and Retirement Longitudinal Study (CHARLS) and UK Biobank

Hong-Xuan Fan, Bo-Da Zhou

Beijing Tsinghua Changgung Hospital

Objective

This study aims to investigate the combined impact of C-reactive protein-triglyceride-glucose index (CTI) clusters and body roundness index (BRI) trajectories on the risk of incident cardiovascular disease (CVD) using data from the China Health and Retirement Longitudinal Study (CHARLS) and the UK Biobank. The CTI integrates inflammation and insulin resistance, while the BRI provides a comprehensive assessment of body shape and health risks. The study seeks to explore whether the joint analysis of these indices can enhance the prediction of CVD risk.

Methods

The study included 3667 participants from CHARLS and 6264 participants from the UK Biobank. The primary endpoint was the incidence of CVD events. Participants were grouped into CTI clusters and BRI trajectories based on their baseline and follow-up measurements. K-means clustering analysis was used to classify changes in CTI, and latent class trajectory modeling (LCTM) was applied to identify distinct BRI trajectories over time. Cox proportional hazard models were used to assess the joint association of CTI clusters and BRI trajectories with incident CVD risk in the UK Biobank, while logistic regression was utilized in the CHARLS cohort. Subgroup analyses and sensitivity analyses were also conducted to validate the findings.

Results

During a median follow-up of 9.26 years in the UK Biobank and 3 years in CHARLS, 476 and 671 incident CVD events were recorded, respectively. The risk of CVD generally increased with higher CTI clusters, cumulative CTI, and BRI trajectories. In the joint analysis, CTI Class 3 showed a significant association with CVD risk across all BRI trajectory groups. For example, in the UK Biobank, participants in CTI Class 3 within the low stable

BRI trajectory group had a hazard ratio (HR) of 1.911 (95% CI: 1.205-3.031, P = 0.006), while those in the high stable BRI trajectory group had an HR of 1.945 (95% CI: 1.139-2.869, P = 0.001). Similar trends were observed in CHARLS, with the highest risk seen in participants with CTI Class 3 and high BRI trajectories. The combined model of CTI clusters and BRI trajectories significantly improved the predictive performance for CVD risk, as evidenced by higher integrated discrimination improvement (IDI) and net reclassification improvement (NRI) values and larger area under the receiver operating characteristic (ROC) curves compared to individual models. Further evaluation via ROC curve analysis revealed the predictive capabilities of these models across both databases. In CHARLS, the combined model exhibited an AUC of 0.591, surpassing the individual CTI class model (AUC=0.562) and BRI trajectory model (AUC=0.575). Within the UK Biobank dataset, the combined model had a higher AUC of 0.63 compared to the CTI class model (AUC=0.585) and BRI trajectory model (AUC=0.604). These findings indicate that integrating CTI class and BRI trajectory yields superior predictive models for CVD, evidenced by higher IDI and NRI values and larger AUCs across both databases.

Conclusion

The findings highlight the significant joint impact of CTI clusters and BRI trajectories on the risk of incident CVD. The study demonstrates that integrating these dynamic trajectories into a combined model significantly enhances the predictive capability for CVD risk. These results underscore the potential utility of incorporating CTI and BRI in risk stratification for CVD prevention. Monitoring how CTI and BRI change over time can identify high-risk individuals and inform personalized, early preventive strategies, potentially reducing the growing burden of cardiovascular disease. Future research should further explore the underlying biological mechanisms and validate these findings in diverse populations.

The impact of dapagliflozin for the myocardial metabolomic profiles of mice with chronic heart failure induced by a high fat diet

Feng Hu

Fujian Medical University Union Hospital

Background: The molecular mechanisms responsible for the clinical benefits of sodium-glucose cotransporter-2 inhibitors (SGLT2i) in patients with heart failure and a reduced or preserved ejection fraction, both diabetic and non-diabetic, are still not fully understood. Given the high mortality among diabetic and non-diabetic patients with heart failure and a reduced ejection fraction (HFrEF) or preserved ejection fraction (HFpEF), both diabetic and non-diabetic, this study aimed to examine the myocardial metabolomic profiles of mice with chronic heart failure induced by a high-fat diet (HDF) and assess the impact of dapagliflozin (DAPA) on these profiles.

Methods: An experimental model of chronic heart failure in mice was established by long-term HDF for six months, and verified using immunohistochemistry and echocardiography. Myocardial specimens were obtained from three groups: chow, HDF, and DAPA. Subsequently, all samples were subjected to non-targeted metabolomic analyses using untargeted liquid chromatography-mass spectrometry. Principal component analysis, partial least squares discriminant analysis, and orthogonal partial least squares discriminant analysis were used to identify differential metabolites or lipid molecules. The Kyoto Encyclopedia of Genes and Genomes (KEGG) database was used to determine the metabolic pathways associated with these identified metabolites.

Results: Echocardiography revealed that mice with chronic heart failure established through HDF exhibited systolic dysfunction compared to the control chow group. However, DAPA treatment partially restored these dysfunctions and protected against myocardial fibrosis and hypertrophy. Furthermore, a total of 72 upregulated and 34 downregulated differential metabolites were observed between the Chow and HDF groups, along with 40 upregulated and 25 downregulated differential metabolites between the HDF and DAPA groups. Annotated obtained lipids according to lipid chains and fat after data preprocessing were divided into BisMePA, Cer, ChE, CL, Co, TG, DG, dMePE, GM2, GM3, Hex1Cer, Hex2Cer, LdMePE, PC, PE, MePC, MGDG, PG, PI, PS, SM, SPH, StE and other categories. A total of 141 upregulated and 167 downregulated differential lipid metabolites were observed between the Chow group and HDF groups, along with 67 upregulated and 59 downregulated differential lipid metabolites between the HDF and DAPA groups, respectively. Dysregulated metabolites or lipids altered by DAPA treatment were found to significantly enrich several metabolic pathways, as identified by the KEGG database. KEGG analysis revealed 171 metabolic pathways enriched by 419 differential metabolites between the Chow group and HDF group, by 250 differential metabolites between the HDF and DAPA groups. KEGG analyzed fourteen metabolic pathways enriched by differential lipid metabolites between the Chow and HDF groups.

Conclusions: We observed that DAPA exhibited protective effects against myocardial fibrosis and hypertrophy and enhanced systolic function in mice with chronic heart failure induced by HDF. Furthermore, we conducted a comprehensive analysis of myocardial profiles, focusing on various differential metabolites, including lipid molecules, as well as prominent metabolic pathways, in these mice. In addition, we assessed the impact of DAPA treatment on these profiles. These findings contribute to the expanding body of literature suggesting that changes in metabolites might serve as potential mechanisms underlying the clinical benefits of SGLT2i in patients with HFrEF or HFpEF. Nevertheless, further clinical data are required to ascertain the safety and efficacy of DAPA administration in this patient population, and its potential mechanism requires further exploration.

Keywords: Metabolomics; high fat diet; heart failure; dapagliflozin; high-fat diet

基因组结构方程模型阐明了心血管肾代谢综合征的共同遗传结构

鲁传龙 李理政 陈金杉 常润泽 董红霖 张瑞婧

山西医科大学第二医院

目的：心血管肾代谢综合征是一种多因素、复杂的疾病，其共同的遗传基础尚未完全明确。传统的遗传学研究未能充分揭示该综合征的遗传结构及其与多种外部性状之间的关联。

方法：本研究采用基因组结构方程模型定义了心血管肾代谢综合征的共同遗传结构公因子。结合多种 GWAS 后分析方法，我们旨在识别易感基因位点，并研究其与外部性状的遗传关联。此外，我们探讨了丰富的遗传通路、细胞类型及基因组元件，并进一步研究了推定的血浆蛋白生物标志物。利用综合的 GWAS 数据，我们还进行了多基因风险评分分析，以评估心血管肾代谢综合征的染色体水平风险关联。

结果：在本研究中，基因组结构方程模型整合了六种表型，模型拟合度极高（CFI=0.99，SRMR=0.14）。在严格的质量控制下，我们分析了 1,862,425 个全基因组 SNP（Lambda GC=1.591，截距 =1.0176 ± 0.0169）。结果表明，信号膨胀主要由多基因遗传力驱动（h^2=0.3286±0.0135），而非混杂偏倚。在该分析框架下，我们共鉴定了 2,212 个显著相关的变异位点，其中包括 32 个通过 GWAS-by-Subtraction 方法新发现的位点。功能注释结果显示，这些位点主要位于内含子区域（57.92%）和基因间区域（30.6%）。通过全转录组关联分析与精细定位，我们筛选出 188 个高置信度基因，其中 SENP2（Z=12.5）、KIF11（Z=11.5）和 JAZF1（Z=11.38）与心血管肾代谢综合征风险呈最强正相关，而 TCF7L2（Z=-13.4）表现出最强负相关。通路富集分析揭示，脂质平衡和泛素介导的蛋白质降解在这些病理机制中起着关键作用。细胞类型分析进一步突出了胰岛细胞的作用。精细定位分析确定了 18 个可能的致病变异（PP>0.95），其中包括 GCKR（rs1260333、rs780093）和 INADL（rs2481665）等关键信号位点，第 7 号和第 12 号染色体区域展现出显著贡献。

结论：本研究首次通过对未测量的复合表型进行 GWAS 分析，提出了心血管肾代谢综合征的全面遗传特征，为该综合征的共同病因途径提供了新的见解。

甘油三酯葡萄糖 - 体型指数与老年人群全因死亡和原因特异性死亡的关联：一项队列研究

李珊

中国人民解放军总医院第二医学中心

背景：先前研究表明甘油三酯葡萄糖 - 体型指数（TyG-BSI）是评价胰岛素抵抗和代谢风险的可靠指标，但其预测老年人群死亡风险的有效性尚未得到充分验证。本研究旨在探讨 TyG-BSI 与老年人群全因死亡和原因特异性死亡的关联。

方法：研究利用美国国家健康与营养调查（NHANES）1999-2018 年的数据，纳入了 8,093 名≥ 60 岁的老年人。TyG-BSI 通过 TyG 指数和 BSI 的乘积计算得出，其中 TyG= ln[空腹血糖 (mg/dL)× 甘油三酯 (mg/dL)/2]，BSI= 腰围 /(体重指数 $^{2/3}$× 身高 $^{1/2}$)。研究采用了加权 Cox 比例风险回归模型、限制性立方样条曲线以及受试者工作特征曲线 (ROC) 分析。

结果：随着 TyG-BSI 水平的升高，全因死亡、心血管死亡和非心血管死亡的风险呈现进行性增加的趋势。与 TyG-BSI 最低四分位数组的个体相比，最高四分位数组个体在多变量调整后的全因死亡、心血管死亡和非心血管死亡的风险比 (HR) 分别为 1.34（95% CI 1.14-1.57），1.41（95% CI 1.08-1.85）和 1.31（95% CI 1.07-1.61）。TyG-BSI 水平每增加一个标准差 (SD)，全因死亡、心血管死亡和非心血管死亡的风险比分别为 1.14(95% CI 1.07-1.22)，1.14(95% CI 1.02-1.26) 和 1.15（95% CI 1.06-1.23）。限制性立方样条曲线显示 TyG-BSI 与死亡风险之间存在线性正相关。ROC 分析显示 TyG-BSI 对全因死亡、心血管死亡和非心血管死亡具有中等程度的预测能力，相应的曲线下面积 (AUC) 分别为 0.564、0.554 和 0.550。

结论：TyG-BSI 水平与老年人群的全因死亡和原因特异性死亡存在显著关联。未来有必要开展大规模的临床干预研究以调查针对 TyG-BSI 干预能否改善临床结局。

Association between estimated glucose disposal rate and all-cause/cause-specific mortality in the general population is modified by age: a cohort study

shan Li, Zhi-Qing Fu, Yue Lv

中国人民解放军总医院 (301 医院)

Background Estimated glucose disposal rate (eGDR) have been proven to be a reliable biochemical surrogate of insulin resistance in diabetic and non-diabetic individuals. The prognostic value of estimated glucose disposal rate (eGDR) in the general population remains unclear. We aimed to determine the association between eGDR and all-cause and cause-specific mortality in a general adult cohort and to explore

whether such associations were modified by age. Methods The National Health and Nutrition Examination Survey (NHANES) with 49,409 individuals between 1999 and 2018 were included in analysis. The eGDR was calculated as: eGDR = 21.158 − [0.09 × WC (cm)] − [3.407 × Hypertension (Yes = 1/No = 0)] − [0.551 × HbA1c (%)]. Individuals were divided into four groups according to the quartiles of eGDR. Mortality data were obtained from the NCHS-linked National Death Index file until 31 December 2019. Younger individuals (

Stage-Based Biomarker Signatures of Cardiovascular-Kidney-Metabolic Syndrome and Their Associations With Mortality: An Analysis of NHANES 2011–2018 Data

Zi Wang[1], Hung-Chen Lin[2], Xiao-Yu Li[1], Qian-Zhou Lv[1], Hong-Yi Wu[1]

1. Zhongshan hospital, Fudan University

2. Tongji Hospital of Tongji University

Background: Cardiovascular-kidney-metabolic (CKM) syndrome is a recently defined clustering of obesity, diabetes, chronic kidney disease, and cardiovascular disease that confers poor prognosis. The stage-specific progression of pathophysiological disturbances and their prognostic significance in CKM are not well characterized. We aimed to profile changes in diverse biomarkers across CKM stages and assess their associations with all-cause and cause-specific mortality.

Methods: We analyzed 5,382 adults from the National Health and Nutrition Examination Survey (2011–2018). CKM stage (0–4) was assigned using American Heart Association criteria. Biomarkers from four domains (body composition, metabolic, inflammatory, nutritional) were evaluated, including anthropometric measures, lipid/glucose indices, inflammatory cell-count ratios, and nutritional indices. Biomarker distributions across stages were compared with trend tests. Cox proportional hazards models estimated adjusted hazard ratios (HRs) for mortality outcomes (all-cause and cause-specific). Dose–response relationships of key biomarkers with mortality were explored using restricted cubic splines.

Results: A total of 5,382 participants from the NHANES 2011–2018 cycles were included in the present analysis. Of these, 2,696 (50.09%) were male, and the median age was 53.00 years (interquartile range: 41.00–63.00 years). Participants were classified into CKM stages 0 to 4, with 284 individuals (5.28%) in stage 0, 1,150 (21.37%) in stage 1, 2,975 (55.27%) in stage 2, 394 (7.32%) in stage 3, and 579 (10.76%) in stage 4. The median follow-up duration was 62.00 months (interquartile range: 39.00–82.00 months). During the follow-up period, 259 participants (4.88%) died from any cause, including 68 deaths (1.28%) attributed to cardiovascular disease and 191 deaths (3.60%) due to other causes. Most biomarkers differed significantly across CKM stages, indicating progressively higher adiposity and insulin resistance, greater inflammation, and declining nutritional status with advancing stage. Mortality risk increased stepwise with higher CKM stage: each stage increment was associated with a 24% higher hazard of all-cause mortality (HR 1.24, 95% CI 1.08–1.43) and 25% higher hazard of non-cardiovascular mortality, whereas the trend for cardiovascular mortality was positive but not significant. Advanced CKM (stages 3–4) carried approximately 1.7-fold higher all-cause mortality risk than stages 0–2, driven mainly by excess non-cardiovascular deaths. Multiple individual biomarkers had independent associations with mortality. Notably, seven biomarkers—Neutrophil-Monocyte-Lymphocyte Ratio (NMLR), Neutrophil-to-Lymphocyte Ratio (NLR), Systemic Inflammation Response Index (SIRI), Geriatric Nutritional Risk Index (GNRI), Prognostic Nutritional Index (PNI), red cell distribution width-to-Albumin Ratio (RAR), and Albumin-to-Globulin Ratio (AGR)—remained significantly associated with all-cause mortality in both early and advanced CKM groups (Figure 9). These markers are primarily reflective of systemic inflammation (e.g., NLR, NMLR, SIRI, RAR) or nutritional status (e.g., GNRI, PNI, AGR), highlighting the central role of inflammation and malnutrition in mortality risk across different stages of CKM. Visual inspection of the RCS plots showed that the mortality risk curves for advanced-stage CKM tended to be higher and steeper than those for nonadvanced-stage CKM, suggesting a possible stage-dependent sensitivity to inflammatory and nutritional dysregulation.

Conclusions: CKM progression is accompanied by worsening metabolic, inflammatory, and nutritional profiles and a stepwise increase in mortality risk. Systemic inflammation and nutritional deficits emerged as key determinants of prognosis in CKM, underscoring the need for stage-specific risk stratification and interventions targeting these factors.

Association of estimated glucose disposal rate with chest pain incidence and all-cause mortality in populations:A Retrospective Analysis of the NHANES Cohort

Meng-meng wang, Ping Zhang, Liang-Qing Ge

Changde Hospital, Xiangya School of Medicine, Central South University(The first people's hospital of Changde city)

Association of estimated glucose disposal rate with chest pain incidence and all-cause mortality in populations:A Retrospective Analysis of the NHANES Cohort

Meng meng Wang[1#], Liang Qing Ge[2*], Ping Zhang[2]

Affiliations:

[1] The Affiliated Changde Hospital, Hengyang Medical School, University of South China,Wuling, Changde, 415000, Hunan, China

[2]Cardiology Department, Changde Hospital, Xiangya School of Medicine, Central South University(The first people's hospital of Changde city), Wuling, Changde, 415000, Hunan, China

[#] First author

[*]**Corresponding author:** Liang Qing Ge, Cardiology Department, Changde Hospital, Xiangya School of Medicine, Central South University(The first people's hospital of Changde city), Wuling, Changde, 415000, Hunan, China

Tel.: +86-13973652828, **E-mail**: geliangqing@163.com

Background: The estimated glucose disposal rate (eGDR), a surrogate marker of insulin resistance linked to cardiovascular disease (CVD), lacks sufficient evidence regarding its association with chest pain.

Methods: Using cross-sectional data from the 2007-2016 National Health and Nutrition Examination Survey (NHANES), logistic regression and Cox proportional hazards models were employed to analyze the relationship between eGDR and chest pain/all-cause mortality. Restricted cubic spline (RCS) analysis assessed linearity.

Results: The study cohort comprised 10,630 individuals with a near-balanced gender distribution (48% male, 52% female). Table 1 presents the comparative demographic and clinical profiles between subjects reporting chest pain and those without this symptom. Among affected participants, gender-specific prevalence rates were observed, with 47% (n=1,220) of male and 53% (n=1,343) of female participants experiencing chest discomfort. Specifically, a greater proportion of participants with chest pain had a lower educational attainment, a lower family poverty income ratio (PIR), a larger waist circumference,unmarried and others, and former and current smokers. In addition, participants with chest pain were more likely to have higher High-Density Lipoprotein and hemoglobin type A1C (HbA1C), a lower eGDR index and encidence of Diabetes, and a greater incidence of Hypertension, Cancer, Stroke, CHD, and Angina. (all p-values

The stratified analyses examining eGDR's continuous association with chest pain across demographic and clinical subgroups are displayed in Figure 3. Significant associations (p<0.05) were observed in all subgroups except those with cancer, coronary heart disease (CHD), or prior stroke history. Particularly strong correlations (p<0.001) emerged in several population segments:younger participants (

Conclusion: eGDR is an independent risk factor for chest pain and correlates with all-cause mortality regardless of chest pain status.

Keywords: Estimated glucose disposal rate, Insulin resistance , Chest pain, NHANES, All-cause mortality

2 型糖尿病患者中 TyG 指数、血同型半胱氨酸水平与颈动脉斑块发生的相关性分析

纪红芳 郭剑津

山西白求恩医院（山西医学科学院）

研究目的：

2 型糖尿病（T2DM）患者是动脉粥样硬化性心血管疾病（ASCVD）的高危人群。颈动脉斑块作为亚临床动脉粥样硬化的标志物，其早期预测对降低心脑血管事件风险至关重要。甘油三酯葡萄糖指数（TyG 指数）是评估胰岛素抵抗和糖脂代谢紊乱的简易指标，同型半胱氨酸（Hcy）升高则与血管内皮损伤密切相关。然而，二者在 T2DM 患者中对颈动脉斑块的协同作用尚未明确。本研究旨在探讨 T2DM 患者中 TyG 指数、Hcy 水平与颈动脉斑块发生及稳定性的相关性，并分析其联合预测价值。

研究方法：

采用回顾性队列研究设计，纳入 2023 年 1 月 -2024 年 12 月我院收治的 T2DM 患者 512 例。接受颈动脉超声检查后依据结果分为斑块组（n=287）和无斑块组（n=225）。检测空腹血糖（FPG）、甘油三酯（TG）、血清 Hcy 等指标，计算 TyG 指数（公式：ln[TG (mg/dL) × FPG (mg/dL)/2]）。采用多元 Logistic 回归分析校正年龄、性别、BMI、糖尿病病程、血压、LDL-C 等混杂因素，评估 TyG 指数、Hcy 与颈动脉斑块风险的独立及交互关联。

结果：

基线特征：斑块组患者年龄更大（62.4±8.1 岁，P<0.01）、糖尿病病程更长（9.3±4.2 年，P<0.01），且 TyG 指数（9.2±0.8 vs）和 Hcy 水平（16.8±4.3μmol/L）均显著高于无斑块组（P 均 <0.01）。

独立关联性：

TyG 指数每升高 1 单位，颈动脉斑块风险增加 64%（OR=1.64，95% CI: 1.32–2.04）；

Hcy 每升高 5 μmol/L，斑块风险增加 38%（OR=1.38，95% CI: 1.18-1.61）。

交互作用： TyG 指数与 Hcy 呈正相关（r=0.42, P<0.01）。高 TyG 指数（≥ 9.0）联合高 Hcy(≥15 μmol/L)时,斑块风险显著升高(OR=5.12,95% CI: 3.26-8.05)，且存在显著相加交互作用（AP=0.38，SI=2.17）。

斑块稳定性： 在不稳定斑块亚组（n=103）中，TyG 指数与 Hcy 水平进一步升高（TyG: 9.6±0.9; Hcy: 19.2±5.1 μmol/L），显著高于稳定斑块组（P<0.05）。

结论：

在 T2DM 患者中，TyG 指数和 Hcy 是颈动脉斑块形成及不稳定的独立危险因素，且二者存在显著协同效应。临床启示：TyG 指数作为无创的胰岛素抵抗标志物，联合 Hcy 检测可更敏感地识别高危患者；对 TyG ≥ 9.0 且 Hcy ≥ 15 μmol/L 的 T2DM 患者，建议早期干预糖脂代谢及 Hcy 水平（如补充叶酸、B 族维生素），以延缓动脉粥样硬化进展。

抑制 HMOX1 靶向铁死亡减轻糖尿病心肌病

杨荟平 刘斌 佘强

重庆医科大学附属第二医院

目的：糖尿病心肌病（Diabetic cardiomyopathy, DCM）是一种以心功能障碍和心力衰竭为特征的糖尿病的严重慢性并发症。目前，DCM 的治疗着重于血糖控制、血压管理、降脂和生活方式的改善，但效果有限。因此，寻找新的治疗靶点至关重要。铁死亡是一种有别于细胞凋亡、细胞自噬和坏死的新型细胞死亡方式，其特征是细胞内铁离子超载、谷胱甘肽系统失调和过氧化脂质的积累。本研究通过建立体内及体外 DCM 模型，明确铁死亡在其中的重要作用，并在此基础上探讨血红素加氧酶 1（Heme oxygenase 1, HMOX1）通过调控铁死亡来改善糖尿病心肌病的作用。

方法：我们通过给 C57 小鼠喂养含 60% 脂肪的高脂饲料，并在 12 周龄时腹腔注射链脲佐菌素（45mg/kg，连续 3 天）诱导 2 型糖尿病，随后将小鼠继续高脂喂养至 25 周龄来建立 DCM 动物模型，观察小鼠血糖、心功能及心脏病理学改变。同时，采用高糖高脂干预 H9C2 细胞建立 DCM 体外模型。通过检测疾病模型中铁死亡关键调控分子的表达及细胞超微结构的改变，明确其在 DCM 中的作用。此外，我们通过慢病毒干扰 HMOX1 基因表达，观察对铁死亡的影响，并探索其对 DCM 的调控作用。

结果：DCM 组小鼠空腹血糖明显高于 Control 组，葡萄糖耐受力及胰岛素调节能力受损；超声心动图提示 DCM 组小鼠心脏收缩及舒张功能受损；HE 和 Masson 三色染色提示 DCM 组小鼠心肌细胞畸变肥大、排列紊乱，心脏发生纤维化。以上结果表明我们成功建立了 2 型糖尿病心肌病动物模型。高通量转录组测序的分析结果显示，差异基因主要富集在脂肪酸代谢、HSF1 依赖性转录和线粒体脂肪酸 β- 氧化，这些生物代谢过程与铁死亡密切相关。Western Blot 结果表明， DCM 组小鼠心脏组织中的铁死亡抑制因子 GPX4、SLC7A11 以及储存铁离子的 Ferritin 相较于 Control 组表达下降。RT-qPCR 结果显示铁死亡标志物 PTGS2 和 ACSL4 表达升高。铁死亡生化指标中，脂质过氧化的标志物 MDA、细胞毒性的标志物 LDH 含量升高，而抗氧化物 GSH 含量降低。与体内实验一致，高糖高脂干预 H9C2 细胞可使其发生铁死亡，并能被铁死亡的抑制剂 Fer-1 逆转。GEO 数据集 GSE161052 的生物信息学分析结果表明 DCM 小鼠心脏发生铁死亡，且 HMOX1 是铁死亡相关差异基因的核心基因。Western Blot、RT-qPCR 及细胞免疫荧光实验提示 HMOX1 在体内和体外 DCM 环境中表达升高，用携带干扰序列的腺病毒和慢病毒分别在体内外敲低 HMOX1 能改善高糖高脂处理的 H9C2 细胞中的铁死亡，缓解糖尿病心肌病。

结论：患有糖尿病心肌病小鼠的心脏及高糖高脂干预的 H9C2 细胞中发生铁死亡，干预 HMOX1 可通过调控铁死亡相关代谢途径减轻糖脂毒性，改善糖尿病心肌病。

降钙素基因相关肽调节核转录因子 -κB 信号转导对缺氧 c-kit+ 心脏干细胞凋亡的影响

龙仙萍 石蓓 赵然尊

遵义医科大学附属医院

目的：探讨降钙素基因相关肽 (CGRP) 对缺氧环境下 c-kit+ 心脏干细胞凋亡的影响。方法：体外建立 c-kit+ 心脏干细胞缺血缺氧模型，实验分为缺氧 +CGRP 组，缺氧 +CGRP8-37(CGRP 拮抗剂) 组，细胞缺氧对照组，常氧细胞组，缺氧 +BAY11-7082[核转录因子 -κB(NF-κB) 抑制剂] 组。采用免疫荧光检测细胞缺氧后 NF-κB 转位情况；采用 Western blotting 检测 NF-κB 通道蛋白的表达，同样方法检测 CGRP 干预后 NF-κB 转位及通道蛋白表达。同时用流式细胞仪检测 CGRP 干预后细胞凋亡率。

结果：在缺氧状态下，NF-κB 信号通路被激活，NF-κBP65 发生核转位 (呈现红色荧光)。与细胞缺氧对照组比较，缺氧 +CGRP 组 NF-κB 相关信号蛋白 P-I-κB、NF-κBP65 及 NF-κBP50 表达减少 (P<0.05)； 与缺氧 +CGRP 组比较，CGRP+CGRP8-37 组上述 NF-κB 相关信号蛋白表达增加 (P<0.05)。在细胞凋亡方面，与缺氧对照组比较，缺氧 +CGRP 组早、晚期细胞凋亡率均降低 (P<0.05)；与缺氧 +CGRP 组比较，缺氧 +CGRP8-37 组细胞早期凋亡增加 (P<0.05)。

结论：CGRP 在调节 NF-κB 信号的同时抑制了缺氧环境下 c-kit+ 心脏干细胞的凋亡。

骨髓源性生长因子对高糖诱导 H9c2 细胞焦亡的改善作用

石蓓

遵义医科大学附属医院

目的：探讨骨髓源性生长因子 (Mydgf) 是否通过调控 NLRP3 改善高糖诱导的心肌细胞焦亡。

方法：培养大鼠心肌细胞株 H9c2，实验分为 4 组：(1) 正常组 (Nor) 为正常培养的 H9c2 细胞；(2) 高糖组 (HG) 予以 50 mmol/L 葡萄糖干预 H9c2 细胞 24 h；(3)Mydgf 组采用 25 ng/mL 重组 Mydgf 蛋白处理细胞 12 h，随后以 50 mmol/L 葡萄糖干预 H9c2 细胞 24 h；(4)Necrosulfonamide 组 (NSA) 采用 32μmol/L NSA 处理细胞 0.5 h，然后予 50 mmol/L 葡萄糖干预 H9c2 细胞 24 h。Western blot 法检测 H9c2 细胞中天冬氨酸蛋白水解酶剪切体 -1(cleaved CasPase-1)、凋亡相关斑点样蛋白 (ACS)、炎症复合体 (NLRP3) 及成孔蛋白 gasdermin D (GSDMD) 的表达水平。ELISA 法检测细胞培养液中 IL-1β 和 IL-18 的分泌量。CCK-8 法检测 Mydgf 及 NLRP3 对 H9c2 细胞活力的影响。将携带 NLRP3 的增强型绿色荧光蛋白 (EGFP) 慢病毒载体 (NLRP3-EGFP) 及空病毒载体 (EGFP) 分别转染至 H9c2 细胞，做回复实验，检测焦亡相关指标变化。

结果：Western blot 结果显示，HG 组焦亡相关蛋白 cleaved CasPase-1、ACS、NLRP3、GSDMD 表达量较正常组明显增高 (P<0.05)，Mydgf 处理后，焦亡相关蛋白的表达受到明显抑制 (P<0.05)，但抑制效率低于 NSA 组 (P<0.05)。ELISA 检测结果表明炎症相关指标 IL-1β 和 IL-18 在 HG 组中表达增高 (P<0.05)，而在 Mydgf 组中表达下降 (P<0.05)，NSA 组明显下降 (P<0.05)。CCK-8 法检测结果表明 <25 ng/mL 的 Mydgf 对 H9c2 细胞活力无明显影响，>25 ng/mL 的 Mydgf 明显降低 H9c2 细胞活力 (P<0.05)。与对照组相比，过表达 NLRP3 使 HG 条件下的细胞活力明显下降。EGFP 慢病毒转染 NLRP3 至 H9c2 细胞中，RT-qPCR 及 Western blot 结果发现 EGFP 组中 NLRP3 的 mRNA 及蛋白表达与正常组差异无统计学意义 (P>0.05)，而 NLRP3-EGFP 组中 NLRP3 的 mRNA 及蛋白表达均显著增高 (P<0.05)。回复实验的 Western blot 结果显示，在高糖环境中，与 Mydgf 组相比，Mydgf+NLRP3-EGFP 组中焦亡相关蛋白 NLRP3、ASC、cleaved CasPase-1 表达显著增加 (P<0.05)；ELISA 检测结果也表明 IL-1β 和 IL-18 表达较 Mydgf 组明显增高 (P<0.05)。

结论：Mydgf 可能通过抑制 NLRP3 来改善高糖诱导的心肌细胞焦亡。

髓间充质干细胞源外泌体调控心肌微血管内皮细胞增殖的机制研究

石蓓

遵义医科大学附属医院

目的：探讨缺氧预处理骨髓间充质干细胞 (BMSCs) 来源的外泌体 (exosomes) 调控心肌微血管内皮细胞 (CMVECs) 增殖的机制。

方法：采用酶消化法联合差速贴壁法培养大鼠 CMVECs，超高速离心法提取常氧及缺氧预处理的 BMSCs exosomes，免疫荧光检测 CMVECs 内化 exosomes 情况。实验分为 4 组 (n=3)：①正常对照组 (Control)，②去除 exosomes 后的 BMSCs 条件培养基的空白对照组 (Free-Exos)，③常氧外泌体组 (Nor-Exos)，④缺氧外泌体组 (HyPoxia-Exos，外泌体浓度为 400μg/μL，与 CMVECs 共培养 24 h)。采用 Edu 法及流式细胞术细胞周期法检测细胞增殖能力，qRT-PCR 检测 exosomes 和 CMVECs 各组中 miR-214 表达变化。抑制 exosomes 中 miR-214 后，qRT-PCR 检测 exosomes 及 CMVECs 中 miR-214 的表达变化，并观察细胞增殖情况。

结果：经透射电镜及免疫印迹法验证提取的囊泡状物质为外泌体，并通过免疫荧光分析发现 DiI 标记的 exosomes 可被 CMVECs 内化；Edu 及细胞周期结果显示，HyPoxia-Exos 组较 Nor-Exos 组具有更强的促 CMVECs 增殖能力 (P<0.05)。qRT-PCR 结果显示，与 Nor-Exos 组比较，HyPoxic-Exos 组中 miR-214 表达显著升高 (P<0.05)。下调 HyPoxia-Exos 中的 miR-214 表达后，Edu 及细胞周期结果显示 HyPoxia-Exos 组的促进细胞增殖能力被部分阻断 (P<0.05)。

结论：缺氧预处理骨髓间充质干细胞源 exosomes 可能通过传递 miR-214 促进 CMVECs 增殖效应。

Bdh1 过表达通过抑制 H3K9bhb 介导的 Ifi27l2a 转录激活改善糖尿病动脉损伤的机制研究

徐烩雳 汤善宏

中国人民解放军西部战区总医院

目的：

1. 明确 Bdh1 的表达水平与糖尿病动脉损伤的相关性；2. 解析 Bdh1 通过其下游靶点参与糖尿病血管损伤的分子机制；3. 探讨靶向激活 Bdh1 及其下游靶点来治疗糖尿病动脉损伤的可行性。

方法：

1. **临床样本分析**：收集正常和 2 型糖尿病患者的腹主动脉，检测 Bdh1 的表达水平与糖尿病动脉损伤的关系。**2. 体内实验：**以 db/m 鼠作为对照组， db/db 鼠为 2 型糖尿病模型小鼠，随机分为对照组、模型组和 Bdh1 过表达组。分析各组小鼠主动脉的组织形态、细胞凋亡、纤维化、炎症等损伤指标，评估腺病毒介导的 Bdh1 过表达对糖尿病小鼠动脉损伤的缓解作用。**3. 体外实验：**利用高糖 (HG) 加棕榈酸 (PA) 处理小鼠主动脉平滑肌细胞系（MOVAS），模拟糖尿病高糖高脂微环境，同时采用 Bdh1 过表达质粒进行基因过表达，检测细胞凋亡、炎症等相关指标。**4. 转录组测序与下游靶基因的筛选验证：**利用转染了过表达 Bdh1 质粒的 MOVAS 细胞进行转录组测序，筛选受 Bdh1 特异调控的下游靶基因，并验证该基因对凋亡通路的影响。**5. Bdh1 调控下游基因的分子机制研究：**通过细胞实验检测 Bdh1 对 β- 羟基丁酸（βOHB）、组蛋白 H3K9 位点 β- 羟基丁酰化水平的影响，最后利用染色质免疫沉淀（CHIP-qPCR）检测 Bdh1 对 下游基因启动子区 H3K9bhb 修饰的影响。

结果：

1. 从临床、动物、细胞水平发现，高糖高脂微环境会导致主动脉血管平滑肌细胞中 Bdh1 表达下调；2. 体内实验发现，Bdh1 的过表达能够改善糖尿病主动脉的组织形态、纤维化、细胞凋亡、炎症等损伤指标；3. 体外实验发现， Bdh1 的过表达能抑制 HG+PA 处理导致的 MOVAS 细胞中凋亡和炎症相关蛋白的升高，发

挥抗炎抗凋亡作用；4.RNA-seq 测序发现，Bdh1 过表达能够显著抑制 HG+PA 处理的 MOVAS 细胞中凋亡相关因子 Ifi27l2a 的激活。Ifi27l2a 的过表达能够通过促进下游促凋亡蛋白 BAX 的表达，阻断 Bdh1 过表达的抗炎抗凋亡作用。5. Elisa 检测发现，在 MOVAS 细胞中，HG+PA 处理能促进 βOHB 水平上调，而 Bdh1 过表达则逆转其上调。并且 Bdh1 过表达能抑制 2 型糖尿病小鼠动脉平滑肌细胞中 H3K9bhb 水平的上调。最后， ChIP-qPCR 显示，Bdh1 过表达通过降低 Ifi27l2a 启动子区域的 H3K9bhb 富集水平，进而抑制 Ifi27l2a 转录激活。

结论：1. 糖尿病诱导动脉血管平滑肌细胞中 Bdh1 表达下调，并参与促进动脉损伤。2. Bdh1 通过 H3K9bhb 介导的表观遗传修饰抑制 Ifi27l2a 介导的细胞凋亡，从而改善糖尿病血管损伤。 3. 通过 AAV 介导的 Bdh1 血管平滑肌异源表达可能是治疗糖尿病动脉损伤的有效手段。

Methyltransferase like 3-mediated N6-methylatidin methylation inhibits vascular smooth muscle cells PhenotyPe switching via Promoting PhosPhatidylinositol 3-kinase mRNA decay

bei Shi

Affiliated Hospital of Zunyi Medical University

N6-methylatidine (m6A) is involved in Post-transcriPtional metabolism and a variety of Pathological Processes. However， little is known about the role of m6A in vascular Proliferative diseases， Particularly in vascular smooth muscle cells (VSMCs) PhenotyPe switching-induced neointimal hyPerPlasia. In the current study， we discovered that methyltransferase like 3 (METTL3) is a critical candidate for catalyzing a global increase in m6A in resPonse to carotid artery injury and various VSMCs PhenotyPe switching. The inhibited neointimal hyPerPlasia was obtained after in vivo gene transfer to knock-down Mettl3. In vitro overexPression of Mettl3 resulted in increased VSMC Proliferation， migration， and reduced contractile gene exPression with a global elevation of m6A modification. In contrast， Mettl3 knockdown reversed this facilitated PhenotyPic switch in VSMCs， as demonstrated by downregulated m6A， decreased Proliferation， migration， and increased exPression of contractile genes. Mechanistically， Mettl3 knock-down was found to Promote higher PhosPhatidylinositol 3-kinase (Pi3k) mRNA decay thus inactivating the PI3K/AKT signal to inhibit VSMCs PhenotyPe switching. Overall， our findings highlight the imPortance of METTL3-mediated m6A in VSMCs PhenotyPe switching and offer a novel PersPective on targeting METTL3 as a theraPeutic oPtion for VSMCs PhenotyPe switching modulated Pathogenesis， including atherosclerosis and restenosis.

Role of Mydgf in the regulation of hyPoxia/reoxygenation-induced aPoPtosis in cardiac microvascular endothelial cells

bei Shi

Affiliated Hospital of Zunyi Medical University

Cardiac microvascular endothelial cells (CMECs) play a pivotal role in maintaining cardiac homeostasis by regulating blood flow, nutrient exchange, and vascular permeability within the myocardium. However, these cells are highly vulnerable to hypoxia/reoxygenation (HR) injury—a pathological process mimicking ischemia/reperfusion (I/R) in clinical settings—where transient oxygen deprivation followed by reoxygenation triggers a cascade of cellular stress responses, ultimately leading to apoptosis and microvascular dysfunction. Such damage exacerbates myocardial injury, underscoring the need to identify factors that protect CMECs from HR-induced apoptosis. Myeloid-derived growth factor (Mydgf), a secreted protein with known roles in tissue repair and inflammation, has emerged as a potential cytoprotective agent, but its specific effects on HR-induced CMEC apoptosis and the underlying mechanisms remain underexplored.

This study aimed to investigate the regulatory effects of Mydgf on HR-induced apoptosis in CMECs, with a focus on its interaction with endoplasmic reticulum stress (ERS)—a key cellular pathway involved in apoptotic signaling under stress conditions. To achieve this, an in vitro HR model was established by exposing CMECs to 24 hours of hypoxia (oxygen deprivation) followed by 6 hours of reoxygenation, a protocol widely recognized for recapitulating the oxidative and metabolic stress of in vivo I/R.

The experimental design included multiple analytical steps to assess apoptotic activity and molecular changes. Flow cytometry and TUNEL staining were employed to quantify apoptotic rates, providing direct measures of cell death. Quantitative polymerase chain reaction (qPCR) and western blotting were used to evaluate Mydgf expression at both mRNA and protein levels, respectively, while western blotting further analyzed the expression of ERS-related proteins—C/EBP Homologous Protein (CHOP), glucose-regulated Protein 78 (GRP78), and cleaved Caspase-12—and apoptosis-associated markers. Additionally, a rescue experiment was conducted using tunicamycin (TM), a well-characterized ERS agonist, which was applied to CMECs for 24 hours to assess whether ERS modulation impacts Mydgf's effects.

Results confirmed the validity of the HR model, as flow cytometry demonstrated a significant induction of CMEC apoptosis following HR treatment. Concurrently, qPCR and western blotting analyses revealed a marked downregulation of both Mydgf mRNA and protein levels in HR-exposed cells compared to controls ($P < 0.05$), suggesting a potential link between reduced Mydgf expression and HR-induced injury. Functional studies showed that adenovirus-mediated overexpression of Mydgf in HR-treated CMECs effectively mitigated apoptosis, indicating a protective role for Mydgf.

Mechanistically, western blotting data indicated that HR stress triggered a robust upregulation of ERS markers, including CHOP, GRP78, and cleaved Caspase-12—proteins critical for propagating ERS-induced apoptotic signals. Notably, Mydgf overexpression in HR-treated cells led to a significant downregulation of these ERS-related proteins, implying that Mydgf may suppress ERS activation. Further supporting this mechanism, the ERS agonist TM reversed the protective effects of Mydgf under HR conditions, restoring apoptotic rates to levels comparable to HR-treated cells without Mydgf overexpression.

In summary, these findings demonstrate that Mydgf attenuates HR-induced CMEC apoptosis by regulating endoplasmic reticulum stress. The downregulation of Mydgf during HR contributes to heightened ERS and subsequent apoptotic cell death, while Mydgf overexpression counteracts this process. These results highlight Mydgf as a potential therapeutic target for preserving cardiac microvascular integrity during ischemia/reperfusion injury by modulating ERS-mediated apoptosis.

m7G Methyltransferase METTL1 Promotes Post-ischemic Angiogenesis via Promoting VEGFA mRNA Translation

bei Shi

Affiliated Hospital of Zunyi Medical University

Post-transcriptional modifications, which encompass a diverse array of chemical alterations to RNA molecules after their synthesis, have emerged as key regulators of gene expression and cellular function, exerting profound impacts on various pathological processes and ischemic disorders. These modifications, ranging from methylation and pseudouridylation to adenylation, fine-tune RNA stability, localization, and translational efficiency, thereby influencing critical cellular responses such as proliferation, differentiation, and stress adaptation. Among these modifications, N7-methylguanosine (m7G) has garnered increasing attention due to its widespread presence in various RNA species, including mRNA, tRNA, and rRNA. However, the specific role of m7G, particularly in mRNA molecules, in the complex process of post-ischemic angiogenesis-the formation of new blood vessels following ischemic injury-remains largely unexplored, representing a significant gap in our understanding of ischemic disease pathogenesis.

To address this knowledge gap, our study focused on identifying the molecular players responsible for regulating mRNA m7G levels in ischemic tissues. Through a combination of transcriptomic and epigenetic analyses, we identified methyltransferase like 1 (METTL1) as a critical candidate enzyme. METTL1, known to catalyze m7G methylation in tRNAs, was found to be significantly downregulated in ischemic tissues, coinciding with a global decrease in mRNA m7G levels. This observation suggested that METTL1 might play a previously unrecognized role in modulating mRNA m7G methylation during ischemic conditions.

To investigate the functional significance of METTL1 in post-ischemic angiogenesis, we performed in vivo gene transfer experiments in a murine model of hindlimb ischemia. Overexpression of METTL1 via adenoviral vectors resulted in a marked improvement in blood flow recovery, as assessed by laser Doppler perfusion imaging, compared to control animals. Histological analysis further revealed a significant increase in capillary density and angiogenesis in the ischemic muscles of METTL1-overexpressing mice, accompanied by a restoration of mRNA m7G levels. These in vivo findings strongly indicated that METTL1-mediated mRNA m7G methylation promotes angiogenesis following ischemic injury.

Complementary in vitro studies using human umbilical vein endothelial cells (HUVECs) confirmed the pro-angiogenic effects of METTL1. Plasmid-mediated overexpression of METTL1 in HUVECs led to a global increase in mRNA m7G methylation and significantly enhanced key angiogenic phenotypes, including cell proliferation (assessed by EdU incorporation assays), migration (evaluated using scratch wound and transwell assays), and tube formation (measured via Matrigel assays). These results demonstrated that METTL1 exerts direct pro-angiogenic effects on endothelial cells, the primary cellular mediators of angiogenesis.

Mechanistically, we sought to identify the downstream targets through which METTL1 modulates angiogenesis. Ribosome profiling and RNA immunoprecipitation experiments revealed that METTL1 specifically enhances the translation of vascular endothelial growth factor A (VEGFA) mRNA. This effect was dependent on m7G methylation, as mutation of the predicted m7G site in VEGFA mRNA abolished the METTL1-induced increase in translation efficiency. Given that VEGFA is a master regulator of angiogenesis, these findings established a direct link between METTL1-mediated mRNA m7G methylation and the translational activation of a key angiogenic factor.

Collectively, our findings highlight a critical role for mRNA m7G methylation in ischemia-induced angiogenesis and identify METTL1 as a key

regulator of this process. By demonstrating that METTL1 promotes VEGFA mRNA translation in an m7G-dependent manner, we provide novel insights into the molecular mechanisms underlying post-ischemic angiogenesis. These results not only expand our understanding of the biological functions of mRNA m7G methylation but also suggest that targeting METTL1 could represent a promising therapeutic strategy for enhancing angiogenesis in ischemic disorders, including peripheral arterial disease, where impaired blood vessel formation contributes to tissue damage and functional impairment. Further studies are warranted to explore the clinical potential of METTL1 modulation in improving outcomes for patients with ischemic conditions.

Exosomal MiR-29a in Cardiomyocytes Induced by Angiotensin II Regulates Cardiac Microvascular Endothelial Cell Proliferation， Migration and Angiogenesis by Targeting VEGFA

bei Shi

Affiliated Hospital of Zunyi Medical University

Exosomes, nanoscale extracellular vesicles secreted by various cell types, have emerged as critical mediators of intercellular communication, primarily through the transfer of bioactive molecules such as microRNAs (miRs), proteins, and lipids. In the context of cardiac physiology and pathology, exosomes released from cardiomyocytes (CMs) are increasingly recognized for their potential role in regulating the function of neighboring cells, including cardiac microvascular endothelial cells (CMECs)—a key component of the cardiac microvasculature essential for maintaining tissue perfusion and supporting cardiac homeostasis. Among the diverse miRs carried by exosomes, miR-29a has garnered attention due to its reported involvement in angiogenesis and the pathogenesis of myocardial hypertrophy, a condition characterized by abnormal CM enlargement and often associated with impaired vascular remodeling. However, the specific role of CM-derived exosomal miR-29a in modulating CMEC function during myocardial hypertrophy remains poorly understood.

To address this knowledge gap, the present study investigated whether exosomal miR-29a from hypertrophic CMs influences CMEC homeostasis. Myocardial hypertrophy was induced in CMs using angiotensin II (Ang II), a potent pro-hypertrophic peptide known to activate signaling pathways leading to CM enlargement. Exosomes were isolated from the conditioned medium of both non-treated CMs (Nor-exos) and Ang II-induced hypertrophic CMs (Ang II-exos) via ultracentrifugation, a gold-standard method for exosome purification based on density gradient separation. CMECs were then cocultured with these exosome-containing or exosome-depleted conditioned media to assess exosome-mediated effects. Additionally, rescue experiments were performed using CMs or CMECs transfected with miR-29a mimics (to overexpress miR-29a) or inhibitors (to knockdown miR-29a), aiming to validate the specific role of miR-29a in observed phenotypes.

A series of functional assays were employed to evaluate CMEC behavior. Tube formation assays, which measure the ability of endothelial cells to form capillary-like structures, revealed that Ang II-exos significantly reduced tube formation capacity compared to Nor-exos, indicating impaired angiogenic potential. Transwell migration assays demonstrated a marked decrease in CMEC migratory activity following exposure to Ang II-exos, while 5-ethynyl-20-deoxyuridine (EdU) incorporation assays showed reduced proliferation rates in these cells. Quantitative reverse transcription-polymerase chain reaction (qRT-PCR) confirmed that Ang II-exos carried significantly higher levels of miR-29a compared to Nor-exos, suggesting miR-29a as a key mediator of the observed effects.

To elucidate the molecular mechanism underlying these findings, potential downstream targets of miR-29a were investigated. Vascular endothelial growth factor A (VEGFA), a well-characterized regulator of angiogenesis and endothelial cell function, was identified as a putative target. Subsequent qRT-PCR and Western blotting analyses confirmed that miR-29a directly suppressed VEGFA expression in CMECs, both at the mRNA and protein levels. This inhibition of VEGFA was closely associated with the impaired angiogenic, migratory, and proliferative capacities of CMECs treated with Ang II-exos, as rescue experiments with miR-29a inhibitors restored VEGFA expression and partially reversed the detrimental effects on CMEC function.

In conclusion, this study demonstrates that exosomes derived from Ang II-induced hypertrophic CMs contribute to the dysregulation of CMEC homeostasis by transferring miR-29a. This miR-29a-mediated suppression of VEGFA expression directly impairs CMEC proliferation, migration, and angiogenesis, highlighting a novel paracrine mechanism through which hypertrophic CMs modulate the cardiac microvasculature. These findings shed light on the role of exosomal miR-29a as a potential therapeutic target for mitigating vascular dysfunction in myocardial hypertrophy and related cardiovascular diseases.

足细胞 NPRC 敲除可减轻糖尿病小鼠肾小球纤维化

王鑫陆 张澄

山东大学齐鲁医院心内科

目的：肾脏纤维化在糖尿病肾病（DKD）的发生发展中起着重要作用，虽然利钠肽对肾脏的保护作用已有报道，但利钠肽受体 C（NPRC）在 DKD 肾脏纤维化中的作用尚不清楚。因此为探究 NPRC 在 DKD 中的作用及机制设计了一系列实验。

方法: 使用人肾活检组织和糖尿病小鼠模型研究了 NPRC 在 DKD 中的表达和功能。通过组织学染色、血清学、质谱、ELISA、Western blot 等基因和蛋白质分析方法，检测 NPRC 敲减对 TGF-βR2 表达、再循环、 Smad 2/3 信号传导以及整体肾脏结构和功能的影响。

结果：在 DKD 患者和小鼠中均观察到肾脏 NPRC 表达增加。与野生型 DKD 小鼠相比，足细胞特异性 NPRC 敲除的 DKD 小鼠显示肾小球纤维化减少，足细胞损伤和肾功能改善。NPRC 敲除导致足细胞中胶原合成减少。分子生物学研究表明，NPRC 敲除导致 TGF-βR2 的再循环减少和降解增加，从而抑制 TGF-β1/Smad 及 TGF-β1/P38 通路。

结论：NPRC 通过增强 TGF-βR2 表达和 TGF-β1/Smad 信号通路在 DKD 的进展中起有害作用。足细胞特异性 NPRC 敲除不仅减轻肾小球纤维化，还可改善肾功能，这表明 NPRC 可以作为治疗糖尿病肾病肾小球纤维化有希望的靶点。

Mediterranean diet, metabolic profiles, and the risk of coronary heart disease: evidence from a mediation analysis

Xincheng Gu[1], Yangyan Wei[2]

1. Qingdao Medical College of Qingdao University

2. wuhan jinyintan hospital

Background: The preventive effect of the Mediterranean diet (MD) on coronary heart disease (CHD) has been demonstrated in numerous studies. However, there is a lack of clinical evidence for this protective effect mediated by metabolic profiles.

Methods: The Mediterranean diet score (MDS) is based on the dietary scoring standard, where a higher score indicates higher adherence to the MD. This study uses multivariate logistic regression to verify the mediating variables: systolic blood pressure (SBP), diastolic blood pressure (DBP), fasting blood glucose (Glucose), total cholesterol (TC), high-density lipoprotein cholesterol (HDL), low-density lipoprotein cholesterol (LDL), Waist-to-Height ratio (WHtR), and the correlation between MDS and CHD. This causal mediation effect analysis was conducted by R-Project, and the mediation effect quantified by the percentage of indirect effect relative to the total effect. The Bootstrap method was used to test the significance of the mediation effect.

Results: After adjusting for confounding factors (age, sex, body mass index, smoking history, and physical activity), the mediation analysis demonstrated that Glucose, HDL, and WHtR mediated the correlation between MDS and CHD (all p-values< 0.05), with indirect mediation effects of Glucose (-0.048, 95%CI(-0.09~-0.01), p =0.028); HDL (-0.034, 95% CI (-0.07~-0.01), p =0.030); and WHtR (-0.024, 95% CI (-0.06~0), p =0.048). Mediation effect proportions were 30.4%, 22.1%, and 15.1%, respectively.

Conclusions: This study showed that not all metabolic parameters were involved in and mediated the protective of MD-related CHD. These results suggest focusing on monitoring HDL, glucose and WHtR, especially fast blood glucose levels, when an MD intervention is implemented to prevent CHD.

The MD is often used for secondary prevention of cardiovascular events in both the general population and patients with a history of CHD. Higher adherence to the MD is associated with a lower overall risk of death and can reduce the risk of cardiovascular diseases.[8,9] Studies by Amy Jennings and Marilena Vitale have found that the MD can lower patients' blood glucose and lipid levels, effectively improving cardiovascular health by lowering blood pressure and atherosclerosis.[10,11] M Siavash has shown that abdominal obesity increases the incidence of coronary heart disease.[12] Gizem Özata Uyar has demonstrated that the MD can lower a patients' WHtR, reducing the risk of coronary heart disease by improving fat distribution.[13] Previous studies have used the scoring model to access the adherence of MD, which has shown reliable stability and accuracy.

This study is a post-hoc analysis study. The dataset was derived from the study by from Manuela Amato etal, conducted by the IRCCS Monzino Cardiologico in Milan, Italy, which investigated the protective effect of the Mediterranean diet and overall dietary diversity on CHD

This study included 333 individuals with a mean age of 62.3 years, 92.8% of whom were male, and 53.4% of subjects were diagnosed with CHD. They were grouped according to whether or they had CHD. Table 1 summarizes the differences in baseline characteristics between the two groups. Except for weight, physically active and triglycerides, almost all baseline demographic data, anthropometric data, and serum biomarkers were significantly different between the CHD group and the non-CHD group. The data distribution of systolic blood pressure, diastolic blood pressure, fasting blood glucose, total cholesterol, low density lipoprotein cholesterol, high density lipoprotein cholesterol and waist to height ratio.

After adjusting for potential confounders (Table 2 and Table 3), there were significant associations between MDS and metabolic profiles and CHD (all p < 0.001). There was a significant negatuve association be-

tween MDS and CHD as reported in Table 3, models 1-3 with Odds ratios (ORs) of 0.53 (95% confidence interval (CI) 0.34~0.82, p=0.005), 0.54 (0.35~0.84, p=0.007), and 0.5 (0.32~0.80, p=0.004), respectively. After further adjustment of the metabolic profiles (mediator variables), we found that the correlation between MDS and CHD was decreased (Table 3, models 4-10) except for LDL. This finding was suggestive of a mediation effect.

Evaluating the Causal Effects of Lipid-Lowering Drug Targets on the Components of Cardiovascular-Kidney-Metabolic (CKM) syndrome: A Drug-Target Mendelian Randomization Study

Meng-Jin Hu

Xuanwu Hospital, Capital Medical University

Objective: Cardiovascular-kidney-metabolic (CKM) syndrome represents a complex cluster of interrelated conditions including cardiovascular disease, chronic kidney disease (CKD), type 2 diabetes mellitus (T2D), and obesity. These conditions often coexist and share overlapping risk factors such as insulin resistance, endothelial dysfunction, systemic inflammation, and dyslipidemia. Lipid-lowering therapy, especially statins, ezetimibe, and PCSK9 inhibitors, has become the cornerstone of atherosclerotic cardiovascular disease prevention. However, whether these lipid-lowering agents exert differential effects on the broader CKM components—particularly on renal function, glucose metabolism, and adiposity—remains incompletely understood. Drug-target Mendelian randomization (MR) is an emerging approach that utilizes genetic variants mimicking the biological effects of drug inhibition to assess potential therapeutic efficacy and adverse effects. This method helps distinguish true causal relationships from observational confounding. In this study, we employed a drug-target MR framework to evaluate the effects of three established lipid-lowering drug targets—HMG-CoA reductase (HMGCR), Niemann-Pick C1-Like 1 (NPC1L1), and proprotein convertase subtilisin/kexin type 9 (PCSK9)—on a comprehensive set of CKM-related phenotypes.

Methods: We conducted two-sample MR using genome-wide association study (GWAS) summary statistics. Validated genetic variants associated with the expression or function of HMGCR, NPC1L1, and PCSK9 were selected as instrumental variables. These variants serve as proxies for long-term pharmacological inhibition of each target. The outcomes assessed included: (1) Cardiovascular diseases: atrial fibrillation, coronary artery disease (CAD), heart failure, hypertension, peripheral artery disease, and stroke. (2) Renal outcomes: CKD, estimated glomerular filtration rate (eGFR), serum creatinine, and microalbuminuria. (3) Diabetes traits: T2D, fasting glucose, glycated hemoglobin (HbA1c), and fasting insulin. (4) Obesity-related traits: obesity, body mass index (BMI), waist circumference, and waist-to-hip ratio. The primary analytical method was inverse-variance weighted (IVW) MR, with sensitivity analyses using maximum likelihood, MR Egger, weighted median, penalised weighted median, and weighted mode methods to assess the robustness of results and detect potential horizontal pleiotropy.

Results: HMGCR inhibition, as mimicked by relevant genetic instruments, was associated with increased risk of atrial fibrillation, heart failure, T2D, and obesity. It was also associated with increased levels of HbA1c, BMI, and waist circumference. Conversely, HMGCR inhibition was linked to a reduced risk of CAD, hypertension, and CKD, and a decrease in eGFR, suggesting a potential trade-off between cardiovascular benefit and metabolic adverse effects. NPC1L1 inhibition demonstrated a more mixed profile. It was associated with a higher risk of T2D and elevated HbA1c levels but was protective against CAD, hypertension, CKD, and general obesity. This indicates that while NPC1L1 may reduce atherosclerotic risk, it may adversely affect glycemic control. PCSK9 inhibition showed the most favorable cardiovascular profile. It was associated with significant reductions in the risk of atrial fibrillation, CAD, heart failure, peripheral artery disease, and stroke. Moreover, it reduced fasting glucose levels. However, it was also associated with increased adiposity traits, including higher BMI, waist circumference, and waist-to-hip ratio, raising concerns about its potential metabolic consequences in the long term. Sensitivity analyse confirmed the robustness of our findings.

Conclusion: Drug-target MR reveals that HMGCR, NPC1L1, and PCSK9 exhibit heterogeneous effects across the spectrum of CKM traits. While PCSK9 inhibition offers broad cardiovascular benefits, HMGCR and NPC1L1 may entail trade-offs in glucose metabolism or adiposity. These insights may guide the selection of lipid-lowering therapy based on individual metabolic profiles and comorbidities. Further studies are warranted to translate these findings into clinical decision-making and to evaluate whether combined or sequential targeting of these pathways can achieve comprehensive risk reduction across the CKM continuum.

Prognostic value of FIB-4 index in coronary heart disease combined with diabetes or prediabetes: a large-scale cohort study

Rui Fu, Chenxi Song

Fuwai Hospital, Chinese Academy of Medical Sciences

Background: Coronary heart disease (CHD) combined with diabetes or prediabetes represented a high-risk patient group for future major adverse cardiovascular events (MACE). Recent growing evidence showed that liver fibrosis is associated with increased risk of cardiovascular mortality and adverse cardiovascular events. Biopsy is the gold standard for the diagnosis of liver fibrosis, but is limited due to the invasive procedure and related complications. Fibrosis-4 index (FIB-4) is one of the most cost-effective and noninvasive simple tools to estimate the risk of hepatic cirrhosis. Current ADA's diabetes guideline recommends the use of FIB-4 index to screen liver cirrhosis in patients with diabetes, or prediabetes with established cardiovascular disease. However, the association between FIB-4 and major adverse cardiovascular events (MACE) risk in this high-risk population remains unclear.

Methods: This prospective large-sale cohort study consecutively enrolled a total of 20133 patients with coronary heart disease combined with diabetes or prediabetes in Fuwai Hospital. Prediabetes was defined according to the ADA criteria, which was glycated haemoglobin (HbA1c) ranging from 5.7% to 6.4%, or fasting plasma glucose (FPG) ranging from 5.6 to 6.9mmol/L, and the absence of diabetes history or the use of diabetic medications. FIB-4 was calculated as: age (years)×(aspartate aminotransferase [U/L])/(platelets [10^9/L]×[alanine aminotransferase [U/L]]$^{1/2}$). Patients were categorized into three groups based on the FIB-4 index, which were <1.45, 1.45-3.25 and >3.25 for patients in the low- , intermediate- and high-risk FIB-4 category respectively. The primary endpoint was MACE, which was defined as the composite endpoint of cardiac death and non-fatal acute myocardial infarction (AMI). Pearson correlation coefficient was calculated to examine the association between FIB-4 and HbA1c and other biomarkers. Multivariable cox hazard models were used to estimate the hazard ratios (HRs) and 95% confidence interval (CI) with the low FIB-4 category as reference. Variables adjusted in the multivariable model included age, sex, body mass index, current smoking status, hypertension, low-density lipoprotein cholesterol, estimated glomerular filtration rate, high-sensitivity C-reactive protein, HbA1c and the use of statins. The association between FIB-4 index as a continuous variable and MACE was explored by the restricted cubic spline (RCS) analysis.

Results: At baseline, FIB-4 was modestly but significantly associated with the HbA1c (r^2=0.04, p<0.001). During a median of 3.2 years follow-up, a total of 622 MACE occurred. The high FIB-4 index group was associated with increased risk of MACE (8.45% vs. 2.43%, adjusted HR: 2.865, 95% CI: 2.185-3.757), cardiovascular death (3.9% vs. 0.63%, adjusted HR: 2.913, 95% CI: 1.872-4.531) and non-fatal AMI (5.09% vs. 1.92%, adjusted HR: 2.609, 95% CI: 1.864-3.652), even after the adjustment of HbA1c. RCS analysis also showed a positive linear relationship between the FIB-4 index and the risk of MACE, cardiac death and AMI. Subgroup analyses showed that glycemic status or glycemic control assessed by HbA1c ≥ 6.5% or HbA1c< 6.5% did not affect the association between the FIB-4 index and MACE. The associations were consistent in all the other subgroups according to age (aged <65 and ≥ 65 years), sex, body mass index, clinical presentation (acute coronary syndrome or chronic coronary syndrome), with the HRs of MACE greater in the high FIB-4 group compared with the low FIB-4 group in all the subgroups.

Conclusions: Advanced liver fibrosis staged by elevated FIB-4 index was associated with increased risk of MACE, cardiovascular death and AMI, independent of HbA1c and other traditional risk factors. Our findings supported the current diabetes guidelines' recommendation to use FIB-4 index as the first-line index in the risk stratification of patients with diabetes, or prediabetes combined with cardiovascular disease, by showing the prognostic value of FIB-4 index in this high-risk population.

Association of Air Pollutant Exposure with Cardio-Kidney-Metabolic Syndrome in Chinese Middle-aged and Older Adults: Evidence from the CHARLS Cohort

Yilin Pan, Xiao-nan He

Department of Critical Care Medicine, Beijing Anzhen Hospital, Capital Medical University, Beijing, China

Title: Association of Air Pollutant Exposure with Cardio-Kidney-Metabolic Syndrome in Chinese Middle-aged and Older Adults: Evidence from the CHARLS Cohort

Authors and Affiliations:

1.Yilin Pan - Department of Critical Care Medicine, Beijing Anzhen Hospital, Capital Medical University, Beijing, China

Xiaonan He (Corresponding Author) - Department of Critical Care Medicine, Beijing Anzhen Hospital, Capital Medical University, Beijing, China

Objective:

This study investigates the association between long-term exposure to air pollutants and the risk of Cardio-Kidney-Metabolic (CKM) syndrome in Chinese adults aged ≥ 45 years. It aims to identify vulnerable subgroups and quantify exposure-response relationships between six major air pol-

lutants (PM_1, $PM_{2.5}$, PM_{10}, SO_2, NO_2, O_3) and CKM risk.

Methods:

Data from 5,192 participants in the 2015 China Health and Retirement Longitudinal Study (CHARLS) were analyzed. Air pollution exposure levels (2013-2015) were estimated using satellite-based models and ground monitoring data. CKM syndrome was defined as the co-occurrence of cardiovascular, kidney, and metabolic disorders. Ordered logistic regression models adjusted for sociodemographic factors (age, sex, education), lifestyle (smoking, alcohol use), and health status (BMI, physical activity) were employed. Restricted cubic spline models assessed non-linear relationships. Stratified analyses examined effect modifications by age (<60 vs. ≥ 60 years), region (eastern/central/western China), and urban/rural residence. To verify the robustness of results, the following sensitivity analyses were conducted: (1) refitting the model after removing the geographical region variable; (2) using cumulative logistic regression models (CLM) instead of ordered logistic regression; (3) using continuation ratio models (CRM) instead of ordered logistic regression.All statistical analyses were performed using R software version 4.4.2, with $P < 0.05$ considered statistically significant.

Results:

1.Pollutant Effects:

1.PM_{10} (OR=1.18, 95% CI:1.09-1.28), $PM_{2.5}$ (OR=1.15, 1.06-1.25), SO_2 (OR=1.12, 1.03-1.22), and NO_2 (OR=1.21, 1.10-1.33) showed significant positive associations with CKM risk per IQR increase.

2.O_3 exhibited a U-shaped relationship, with both low and high concentrations linked to elevated risk.

2.Subgroup Vulnerabilities:

1.Elderly adults (≥ 60 years) demonstrated 23-35% higher pollutant-associated risks compared to younger counterparts.

2.Rural residents had 1.3-1.5× greater susceptibility to PM and NO_2 effects than urban dwellers.

3.Eastern China populations showed stronger associations with $PM_{2.5}$ (OR=1.28 vs. 1.10 in western regions).

3.Non-linear Patterns:

1.PM_{10} and NO_2 displayed threshold effects, with risks escalating sharply above 75 μg/m³ and 40 μg/m³, respectively.

Synergistic effects were observed between $PM_{2.5}$ and NO_2 exposure.

Conclusion:

Based on national cohort data, this study confirms a significant association between long-term exposure to air pollutants and increased risk of CKM syndrome among middle-aged and elderly Chinese individuals. The study finds that the elderly (≥ 60 years) demonstrate higher susceptibility to the effects of air pollutants, while rural residents and those in eastern regions also show greater vulnerability. Restricted cubic spline analysis further reveals non-linear dose-response relationships between most pollutants and CKM risk. These findings provide important evidence for formulating stricter air quality standards and implementing targeted pollution control measures, especially in areas with dense elderly populations. In clinical practice, it is recommended to incorporate environmental exposure into the risk assessment system for CKM-related diseases and to develop individualized intervention strategies. Future longitudinal studies are needed to further verify the causal relationship of these associations and to explore potential biological mechanisms.

A Nomogram for Predicting the Progression Risk of Cardiovascular-Kidney Metabolic Syndrome

Song fei[1], Pan Li[2], Xue-Song Wang[2], De-wei Wu[1], Cheng-Long Guo[1], Meng-Jin Hu[1], Xiu-Ling Wang[1], -Yu Jing[1], Jing Xu[2], Jing-Gang Xia[1], Chun-Lin Yin[1]

1. Xuanwu Hospital, Capital Medical University

2. Baizhifang Community Health Service Center, Xicheng District, Beijing

Background: The American Heart Association (AHA) recently introduced the Cardiovascular-Kidney-Metabolic (CKM) syndrome concept, recognizing the complex interplay between cardiovascular disease, kidney dysfunction, and metabolic disorders. This syndrome represents a significant clinical challenge as these conditions frequently coexist and synergistically increase morbidity and mortality risks. Older adults are particularly vulnerable to CKM syndrome progression due to age-related physiological changes and the high prevalence of multimorbidity in this population. While the AHA has established staging criteria (Stages 0-4) to classify disease severity, there remains a critical lack of validated tools for predicting individual risk of progression between these stages. Current risk assessment approaches often evaluate cardiovascular, renal, and metabolic risks separately, failing to capture their integrated impact. This study aimed to develop and validate a comprehensive prediction model specifically designed to assess CKM stage progression risk in community-dwelling older adults.

Methods: We conducted a prospective cohort study involving 1,568 community-dwelling adults aged 66-99 years recruited through family physician networks across China between 2020 and 2023. Participants underwent comprehensive baseline assessments including clinical examinations, laboratory tests (complete blood count, metabolic panel, renal function tests), and detailed medication reviews. The cohort was randomly divided into training (70%) and validation (30%) sets. From an initial pool of 32 potential predictors, we employed least absolute shrinkage and selection operator (LASSO) regression with 10-fold cross-validation to identify the most predictive variables while preventing overfitting. Significant predictors were incorporated into a multivariable Cox proportional hazards model to estimate progression risks. The final model was presented as a clinically practical nomogram. We evaluated model performance through: (1) discrimination using time-dependent receiver operating characteristic (ROC) curves and concordance indices (C-index), (2) calibration with bootstrap-corrected calibration plots, and (3) clinical utility via decision curve analysis across probability thresholds from 5% to 50%. Risk stratification performance was assessed using Kaplan-Meier analysis.

Results: Of the 1568 participants with CKM stage 1 to 3 in our analysis, 620 (39.5%) were men and 948 (60.5%) were women. The age ranged from 66 to 99 years old, with a mean age of 74.5 years old. Among the 1568 participants, 185 cases of CKM stage progression were observed. Six key predictors were identified: sex, systolic blood pressure, diastolic blood pressure, red blood cell distribution width (SD), CKM stage, and diabetes mellitus. The C-index of the training group was 0.768 and that of the verification group was 0.803; The calibration curves of the nomogram showed good consistency between the probabilities and observed values. The decision curve analysis also revealed the potential clinical usefulness of the nomogram. Moreover, the nomogram could successfully classified patients into high-risk and low-risk subgroups.

Conclusion: We developed and validated the first nomogram for predicting CKM stage progression in older adults, incorporating readily available clinical and laboratory parameters. This tool addresses a critical gap in current risk assessment by providing integrated evaluation of cardiovascular, renal, and metabolic progression risks. The model's strong performance metrics and practical visual format facilitate potential implementation in primary care settings. By enabling early identification of high-risk individuals, this nomogram may support personalized interventions to mitigate CKM syndrome progression. Future studies should validate these findings in diverse populations and evaluate the tool's impact on clinical decision-making and patient outcomes.

高血压人群血清尿酸水平与认知功能的关系：一项横断面研究

彭庆龄

南昌大学第二附属医院 心血管内科

背景：血清尿酸（SUA）与认知功能之间的关系在以往的研究中存在争议。高血压组容易出现认知能力下降。我们的目的是利用迷你精神状态检查（MMSE）研究中国高血压患者血清尿酸水平与认知功能的相关性。

方法：我们从中国高血压登记研究中纳入 9471 名受试者。采用生化分析仪测定血清尿酸。采用 MMSE 评价认知功能。不同教育背景的参与者使用不同的 MMSE 分数截断值来定义认知障碍（CI）：中学及以上教育背景的参与者 MMSE<24，小学教育背景的参与者 MMSE<20，文盲参与者 MMSE<17。

结果：共分析了 9471 例成人高血压患者。平均年龄 63.61±9.79 岁，男性占 47.94%。平滑曲线显示 SUA 与 MMSE 评分和 CI 呈非线性相关。阈值效应分析表明，SUA 的拐点约为 445.9μmol/L。在多变量回归分析中，lg SUA 每增加一个单位，SUA

结论：SUA 水平对中国高血压患者 MMSE 评分和认知功能障碍存在阈值效应。在 SUA

关键词：血清尿酸，MMSE 评分，认知障碍，高血压。

在中国高血压人群中脂肪肝指数与新发糖尿病及糖尿病前期发展的关系 - 一项队列研究

彭庆龄

南昌大学第二附属医院 心血管内科

背景与目的：在高血压患者中，非酒精性脂肪肝是 2 型糖尿病（T2 D）的一个强有力的预测因子。在临床实践中评估其并不容易，但脂肪肝指数（FLI）可以作为替代。因此，我们研究了 FLI 对 2 型糖尿病发病率的预测价值，并评估了 FLI 与糖尿病前期患者（空腹血糖介于 5.6-6.9 mmol/L / 糖化血红蛋白介于 5.7%-6.4%）向新发糖尿病转化或逆转为正常血糖状态（空腹血糖 <5.6 mmol/L 且糖化血红蛋白 <5.7%）之间的相关性。

方法： 本研究纳入 7561 名基线无 T2D 的高血压患者，我们估计了 4 年随访时每个 FLI 类别 [FLI <30（无脂肪变性），FLI 30-60（中度）和 FLI ≥ 60（肝脂肪变性）] 中 T2 D 的发生率。使用校正了年龄、性别、糖尿病家族史、吸烟、饮酒、血脂和转氨酶的 cox 回归模型计算 FLI 和 T2 D 事件之间的关联。并进一步排除

4116 例基线正常血糖状态患者参与者，共 3445 名糖尿病前期的高血压患者纳入糖尿病前期发展研究。

结果：基线患者 4 年随访后，FLI<30、FLI 30-60 和 FLI ≥ 60 组的 T2 D 发生率分别为 7.32%、13.44% 和 21.34%。FLI ≥ 60 组与 T2 D 发病率独立相关：在根据性别、年龄调整的基础回归模型中，HR/SD 为 2.89（95%CI：2.39-3.51），在完全调整模型中为 2.01（95%CI：1.52-2.65）。我们进一步在 3445 名糖尿病前期患者中分析，206 例患者（5.98%）转为 2 型糖尿病。FLI 与较高的 2 型糖尿病转换风险相关（完全调整 HR/SD = 1.82，95%CI 1.21-2.75），在 FLI ≥ 60 组中，每增加一个标准差，2 型糖尿病发病风险增加 143%（95%CI 1.18-4.98）。FLI 也与前驱糖尿病逆转相关：根据 SD 校正的 HR = 0.87，95%CI 0.81-0.94。随访期间 FLI 的变化与 FPG 的变化显着相关（p<0.0001）。

结论：FLI 可以被认为是一个简单和有价值的早期指标，在临床实践中进一步分层 2 型糖尿病转化的风险或前驱糖尿病逆转的可能性，并提前采取有效的措施预防和减少疾病的进展。

Association of cardiometabolic index with all-cause and cardiovascular deaths in patients with cardiometabolic syndrome: a national cohort study

Lin Guan[1], Yu Gu[1], Chuan-He Wang[2], Zhi-Jun Sun[2], Li Wang[1]

1. Central Hospital of Dalian University of Technology

2. Shengjing Hospital of China Medical University

Abstract

Background: Cardiometabolic syndrome (CMS) encompasses a constellation of metabolic and cardiovascular risk factors that substantially elevate the risk of developing type 2 diabetes mellitus and cardiovascular disease. The cardiometabolic index (CMI), a composite measure of lipid accumulation and central obesity, has shown potential for predicting cardiovascular outcomes. This study examined the association between CMI and the risks of all-cause and cardiovascular mortality within a nationally representative cohort of patients with CMS.

Methods: We conducted a comprehensive analysis of data from 4,668 adult patients (aged ≥ 18 years) with CMS derived from the National Health and Nutrition Examination Survey cycles spanning from 2005 to 2018. The participants were categorized into quartiles based on their CMI values. The primary outcomes were all-cause mortality and cardiovascular mortality, as determined through the National Death Index. We utilized Cox proportional hazards regression to determine the hazard ratios associated with mortality, adjusted for potential confounders, and used restricted cubic splines (RCS) to explore potential nonlinear relationships.

Results: During a mean follow-up period of 98 months, a total of 576 all-cause deaths and 162 cardiovascular-related fatalities were recorded. In unadjusted models, higher CMI quartiles were significantly associated with an elevated risk of all-cause and cardiovascular mortality. After adjusting for potential confounders including age, sex, race, educational level, marital status, body mass index, and smoking and drinking history, the previously observed associations did not remain statistically significant. The RCS analysis uncovered a nonlinear relationship between CMI and all-cause mortality, featuring an inflection point at a CMI value of 1.15, suggesting a U-shaped relationship. Mediation analyses revealed that low-density lipoprotein cholesterol level, blood uric acid level, and body weight mediated 5%, 35%, and 28%, respectively, of the association between CMI and all-cause mortality.

Conclusions: CMI is significantly associated with both all-cause and cardiovascular mortality in patients with CMS. Nevertheless, this relationship is influenced by various confounders. The nonlinear association between CMI and mortality risk highlights the intricate nature of cardiometabolic health and its influence on patient outcomes. Additional research is imperative to elucidate the mechanisms underlying these relationships and to develop targeted interventions for high-risk patients with CMS.

Keywords: cardiometabolic index, cardiometabolic syndrome, all-cause mortality, cardiovascular mortality, cohort study

This study investigates the relationship between the cardiometabolic index (CMI) and mortality risks in patients with cardiometabolic syndrome (CMS), utilizing data from the National Health and Nutrition Examination Survey (NHANES) spanning 2005 to 2018.

Our findings reveal a significant association between CMI and both all-cause and cardiovascular mortality, with a nonlinear relationship identified for all-cause mortality. Mediation analyses further highlight the roles of low-density lipoprotein cholesterol, blood uric acid, and body weight in this association. These results underscore the complex interplay of cardiometabolic health and its impact on patient outcomes, offering valuable insights for risk stratification and targeted interventions in high-risk CMS populations.

We believe this manuscript aligns well with the congress theme, as it addresses critical issues in cardiovascular and metabolic health, leveraging a nationally representative cohort to provide robust evidence. This study contributes to the growing body of literature on CMS and its prognostic indicators, with potential implications for clinical practice and public health strategies.

This manuscript is original, All authors have approved the final version of the manuscript. We have no conflicts of interest to disclose.

血清尿酸 / 高密度脂蛋白胆固醇比值联合脉压差的纵向轨迹与慢性肾脏病发病风险：一项回顾性队列研究

明轩

四川省医学科学院 . 四川省人民医院

目的：本研究旨在探讨血清尿酸与高密度脂蛋白胆固醇比值（Serum uric acid/HDL cholesterol ratio，UHR）联合脉压差（Pulse pressure，PP）的纵向轨迹对慢性肾脏病（Chronic kidney disease，CKD）发病风险的影响。**方法**：本研究为回顾性队列研究，选取 2015 年 1 月–2024 年 12 月期间在四川省人民医院健康管理中心参加过三次及以上年度体检且数据资料完整者为研究对象，采用 Cox 回归模型分析 UHR 和 PP 四分位分组与 CKD 发病风险的关联，并通过限制性立方样条（Restricted cubic spline, RCS）探讨剂量反应关系。进一步运用群组多轨迹模型（Group-based Mult-Trajectory Models，GBMTM）识别 UHR 与 PP 的联合轨迹，并分析不同轨迹组的 CKD 发病风险。**结果**：UHR 和 PP 均与 CKD 发病风险独立相关，其四分位分组的 Cox 回归分析显示，UHR 和 PP 的最高四分位组的 CKD 发病风险显著升高。RCS 结果显示，UHR 和 PP 与 CKD 发病风险呈线性增长趋势。研究对象呈现出四种不同的 UHR 联合 PP 变化轨迹组：低 UHR- 低 PP 组（组 1）、中 UHR- 高 PP 组（组 2）、中 UHR- 低 PP 组（组 3）和高 UHR- 中 PP 组（组 4）。组 2 和组 4 人群的发病风险显著高于其他组，分别是组 1 的 1.90 倍（HR=1.90，95%CI：1.45 ~ 2.48）和 2.09 倍（HR=2.09，95%CI：1.56 ~ 2.81）。**结论**：UHR 和 PP 与 CKD 发病风险密切相关，联合轨迹分析揭示了二者动态变化对 CKD 风险的显著影响，为早期风险评估和防控提供了重要依据。

How Does Age Acceleration Mediate the Association Between Insulin Resistance and Long-Term Mortality Among Patients With Cardiovascular-Kidney-Metabolic Syndrome? Insights from a population-based study

Hong-Qiang Zhang, Xing-Yu Li, Jun-Hao Zhang, Xue-Ying Zheng, Hao Hu

The First Affiliated Hospital of USTC

Abstract

Background: Cardiovascular-Kidney-Metabolic (CKM) syndrome, characterized by the intricate interplay of metabolic dysfunction, chronic kidney disease (CKD), and cardiovascular disease (CVD), is associated with a markedly increased risk of mortality, multimorbidity, and accelerated aging. Insulin resistance (IR), a key driver of metabolic dysfunction, contributes to endothelial damage, inflammation, and biological age acceleration, compounding the burden of CKM syndrome. Although the triglyceride-glucose (TyG) index has been widely applied to estimate IR, the TyG-waist-to-height ratio (TyG-WHtR) has emerged as a more powerful surrogate marker, integrating central obesity to capture cardiometabolic risk. However, whether TyG-WHtR influences mortality in CKM through the acceleration of biological aging remains uncertain. This study aimed to evaluate the association between TyG-WHtR and mortality in CKM patients and to examine the potential mediating role of biological age acceleration, assessed by PhenoAge acceleration (PAA) and Klemera-Doubal method age acceleration (KDM-A).

Methods: We analyzed data from 19,843 CKM patients enrolled in the National Health and Nutrition Examination Survey (NHANES) between 1999–2010 and 2015–2018. TyG-WHtR was calculated using fasting triglyceride and glucose levels combined with waist-to-height ratio. Biological age acceleration was defined as the residual difference between chronological age and estimated biological age, computed by PAA and KDM-A methods. Mortality outcomes were obtained from linkage to the National Death Index, with follow-up through 2019. Multivariable Cox proportional hazards models, restricted cubic spline (RCS) analysis, and threshold effect analysis were employed to explore the associations between TyG-WHtR and mortality. Logistic regression was applied to assess relationships with biological aging, and mediation analysis was conducted to evaluate indirect effects through age acceleration. Subgroup and sensitivity analyses were performed to test robustness.

Results: Over a median 9.7-year follow-up, 2,238 all-cause and 661 cardiovascular deaths occurred. TyG-WHtR demonstrated a significant U-shaped association with both all-cause and cardiovascular mortality. Below a threshold of 4.90, higher TyG-WHtR was inversely associated with all-cause mortality (HR 0.857, 95% CI 0.74–0.99); above 4.90, risk increased significantly (HR 1.34, 95% CI 1.17–1.37). For cardiovascular mortality, an inflection point was identified at 6.17, with TyG-WHtR above this level conferring a 37.8% increased risk (HR 1.378, 95% CI 1.17–1.64). The area under the ROC curve was 0.873 for all-cause mortality and 0.856 for cardiovascular mortality, indicating strong predictive performance. Higher TyG-WHtR was positively associated with PAA (OR 1.093 per SD, 95% CI 1.08–1.11) and KDM-A (OR 1.126 per SD, 95% CI 1.12–1.14), and the highest TyG-WHtR tertile was linked to an increase of 1.189 years in PAA and 1.244 years in KDM-A compared to the lowest tertile. Mediation analyses revealed that PAA and KDM-A explained 19.7% and 15.8% of the association between TyG-WHtR and all-cause mortality, and 20.7% and 16.8% of the association with cardiovascular mortality, respectively. Subgroup

analyses showed stronger associations among participants aged ≤ 60 years and those with elevated BMI. Sensitivity analyses excluding early deaths confirmed the robustness of the findings.

Conclusion: This large, nationally representative cohort study demonstrates that TyG-WHtR has a significant nonlinear relationship with mortality among patients with CKM syndrome and that biological age acceleration partially mediates this association. The findings underscore the importance of maintaining TyG-WHtR within an optimal range to mitigate biological aging and improve survival outcomes in this high-risk population. TyG-WHtR may serve as a practical, dual-dimensional biomarker reflecting both metabolic dysfunction and accelerated aging, supporting its potential application in risk stratification and targeted intervention strategies for CKM syndrome.

Estimated Glucose Disposal Rate and Risk of Stroke and Dementia in Non-Diabetics: A UK Biobank Prospective Cohort Study

Yi Zheng[1], Lei Liu[2], Kai Luo[3], Hui-Hui Ma[3], Wei Jiang[3], Rong Luo[4], Cai-Xia Pan[3], Tao He[3], Hong-Qiang Ren[2], Gary Tse[1,5], Tong Liu[1], Xiao-Ping Li[3]

1. Second Hospital of Tianjin Medical University

2. Suining central hospital

3. Sichuan Provincial People's Hospital

4. Chengdu Medical College

5. Hong Kong Metropolitan University

Objective: The estimated glucose disposal rate (eGDR) is a validated surrogate marker of insulin resistance and an independent risk factor for cardiovascular diseases. However, its association with the incidence of stroke and dementia in non-diabetic populations remains insufficiently investigated. This study aimed to investigate the association between eGDR and the risk of incident stroke and dementia in non-diabetic individuals.

Methods: This prospective cohort study included non-diabetic participants from the UK Biobank, stratified into quartiles according to baseline eGDR levels, with the lowest quartile serving as the reference. The primary outcome was stroke. The secondary outcomes were ischaemic stroke, hemorrhagic stroke, all-cause dementia, vascular dementia, and Alzheimer's disease. Kaplan-Meier curves were used to illustrate the cumulative incidence of outcomes. Three Cox regression analysis models were performed to explore the association between eGDR and outcomes. Restricted cubic splines (RCS) were used to assess the potential non-linear relationships, and a two-piecewise Cox model was constructed to evaluate associations on both sides of the inflection point. Subgroup analyses were conducted based on age, sex, race, education, body mass index (BMI), smoking, alcohol, and the number of moderate-intensity exercise per week. Polygenic risk scores (PRS) were applied to quantify genetic susceptibility and investigate potential interactions between eGDR and genetic risk.

Results: A total of 430,093 participants were included. During a follow-up of around 13.5 years, 10,307 stroke events and 11,137 cases of dementia were recorded. Kaplan-Meier survival curves showed that participants with higher eGDR levels had a lower cumulative incidence of stroke and dementia. After adjusting for age, sex, race, education, smoking, alcohol, BMI, average total household income before tax, physical activity, blood pressure, triglycerides, serum creatinine, uric acid, total cholesterol, aspirin, antihypertensive drugs, and lipid-lowering drugs, the hazard ratio (HR) and 95% confidence interval (CI) from the lowest to highest eGDR quartile were 1.00 (reference), 0.81 (0.77, 0.85), 0.58 (0.54, 0.62), and 0.41 (0.37, 0.65), respectively, for stroke; 1.00 (reference), 0.84 (0.78, 0.89), 0.59 (0.54, 0.63), and 0.41 (0.38, 0.46) , respectively, for ischaemic stroke; 1.00 (reference), 0.75 (0.68, 0.84), 0.57 (0.50, 0.65), and 0.40 (0.34, 0.48), respectively, for hemorrhagic stroke. Regarding dementia, multivariate COX regression showed that compared with the quartile 1, quartiles 2-4 had a significantly lower risk of all-cause dementia (quartile 2: HR 0.95, 95% CI 0.90-1.00; quartile 3: HR 0.85, 95% CI 0.80-0.90; quartile 4: HR 0.81, 95% CI 0.75-0.88). However, quartile 2 eGDR was not significantly associated with the risk of vascular dementia (HR 0.99, 95% CI 0.87-1.13, P=0.884) or Alzheimer's disease (HR 0.91, 95% CI 0.83-1.00, P=0.054). The HRs (95% CI) from quartile 3 to quartile 4 were 0.84 (0.71, 0.99), 0.74 (0.60, 0.91), respectively, for vascular dementia; and 0.80 (0.71, 0.89), 0.73 (0.64, 0.84) for Alzheimer's disease. RCS analyses indicated non-linear associations between eGDR and the risks of stroke, ischaemic stroke, hemorrhagic stroke, and vascular dementia. Below specific threshold eGDR values (<7.64 for stroke, <7.60 for ischaemic stroke, <7.75 for hemorrhagic stroke, and <8.31 for vascular dementia), eGDR levels were not significantly associated with the risks of ischaemic stroke, hemorrhagic stroke, or vascular dementia, and showed only a modest inverse association with overall stroke risk (HR 0.97, 95%CI 0.95-0.99, P=0.012). In contrast, above these thresholds, higher eGDR levels were associated with significantly reduced risks of stroke (HR 0.80, 95% CI 0.78-0.82, P<0.001), ischaemic stroke (HR 0.80, 95% CI 0.78-0.81, P<0.001), hemorrhagic stroke (HR 0.81, 95% CI 0.78-0.84, P<0.001), and vascular dementia (HR 0.89, 95% CI 0.84-0.94, P<0.001). A linear inverse relationship was observed between eGDR and all-cause dementia and Alzheimer's disease. Participants in the highest eGDR quartile exhibited lower risks of all-cause dementia (HR 0.81, 95% CI 0.75-0.88, P<0.001) and Alzheimer's disease (HR 0.73, 95% CI 0.64-0.84, P<0.001) compared to those in the lowest quartile. Subgroup analyses found that there were interactions between age, sex, race, education, BMI, smoking, alcohol and eGDR for stroke and ischaemic stroke. For hemorrhagic stroke, interactions between age, sex, BMI and eGDR were observed. Interactions in the associations between eGDR and incidence of dementia were observed among age and sex subgroups for all-cause dementia, and among the subgroup of age for vascular dementia and Alzheimer's disease. Participants with high PRS demonstrated a heightened risk of ischaemic stroke (HR 1.19, 95% CI 1.13-1.26, P<0.001) and Alzheimer's disease (HR 4.75, 95% CI 4.30-5.24, P<0.001). Notably, within the high-PRS group, participants with the highest eGDR levels had substantially lower risks of ischaemic stroke and Alzheimer's disease compared to those with the lowest eGDR levels.

Conclusions: eGDR exhibited non-linear associations with stroke and vascular dementia risk and linear inverse associations with all-cause dementia and Alzheimer's disease. These findings underscore the utility of eGDR as a predictive marker for cerebrovascular and cognitive outcomes in non-diabetic individuals, particularly those with high genetic susceptibility. Regular assessment of eGDR could support early risk stratification and guide preventative interventions.

UBC9 attenuates the progression of metabolic dysfunction-associated fatty liver disease by suppressing hepatocyte ferroptosis via SUMOylation-Dependent stabilization of FTH1

Dan Liu, Han-Lin Wu, Jing Wang, Zhao-Ying Huang, Zhe-Ming Yang, Ya-Ni Wang, Yu-Jia Zou, Zi-Qi Liu, Xiao-Lin Zhang, Hai-Xu Song, Cheng-Hui Yan, Ya-Ling Han

State Key Laboratory of Frigid Zone Cardiovascular Disease, Cardiovascular Research Institute and Department of Cardiology, General Hospital of Northern Theater Command

Objective: Metabolic dysfunction-associated fatty liver disease (MAFLD) is one of the most common chronic liver diseases, with incidence rates increasing. Metabolic dysfunction-associated steatohepatitis (MASH) represents an extremely progressive form of MAFLD, which may progress to cirrhosis or hepatocellular carcinoma. Patients with MAFLD/MASH face significantly elevated risks of both liver-related mortality and cardiovascular diseases, including insulin resistance, hypertension, chronic kidney disease, and type 2 diabetes mellitus, mediated through complex pathophysiological interactions. Extensive researches demonstrate that MAFLD is a multifactorial disease involving lipotoxicity, mitochondrial dysfunction, endoplasmic reticulum stress ER stress, oxidative stress, gut-liver axis dysregulation, and post-translational modification (PTM) abnormalities. Despite these advances, the key pathogenesis and mechanisms of MAFLD/MASH progression remain poorly understood. Current management strategies inadequately address disease progression or its multisystem complications, and no effective therapeutic interventions for MAFLD/MASH have yet been approved. Therefore, to identify the key underlying mechanisms of MAFLD/MASH is essential in clinical practice. SUMOylation critically regulate protein stability and activity, contributing to MAFLD/MASH pathogenesis. Ubiquitin-conjugating enzyme 9 (UBC9), the only SUMO-E2 enzyme, is essential for cellular homeostasis. Here, we investigated the roles and underlying mechanism of UBC9 in MAFLD and MASH progression.

Methods: In vivo, hepatocyte-specific Ubc9 knockout and overexpressing mice were generated. MAFLD was induced by a high-fat diet (HFD) feeding, while MASH was established using a methionine-choline deficient (MCD) diet feeding. H&E staining, Sirius Red staining, Oil Red O staining, immunohistochemistry, iron staining, real-time PCR, and western blotting were performed to examine lipid accumulation, inflammation, fibrosis in the livers. In vitro, LO2 hepatocytes were treated with palmitic acid (PA), UBC9 overexpression adenovirus, and small interfering RNA. The effects of UBC9 overexpression and knockdown were examined by real-time PCR, western blotting. Mechanically, mass spectrometry, immunoprecipitation, real-time PCR and western blotting were performed to explore the underlying mechanism of UBC9.

Results: The mRNA and protein expression of UBC9 was significantly downregulated in the liver tissue of MAFLD/MASH and PA-treated hepatocytes. In vivo, hepatocyte-specific Ubc9 knockout exacerbated the hepatic steatosis, inflammation, and fibrosis in MASH mice, whereas UBC9 overexpression mitigated the hepatic steatosis, inflammation, and fibrosis in MASH mice. In vitro, UBC9 knockdown promoted lipid accumulation, inflammation, and fibrosis induced by PA treatment, which was rescued by UBC9 overexpression. Besides, UBC9 knockdown promoted the ferroptosis and iron overload of hepatocytes induced by PA, and UBC9 overexpression inhibited the ferroptosis and iron overload of hepatocytes induced by PA. Mechanistically, there was a direct binding between UBC9 and ferritin heavy chain 1 (FTH1) in hepatocytes. UBC9 facilitated the protein degradation of FTH1 in a SUMOylation-dependent way. Under PA treatment, FTH1 knockdown promoted lipid accumulation, inflammation, and fibrosis by increasing the ferroptosis and iron

overload of hepatocytes, whereas FTH1 overexpression alleviated lipid accumulation, inflammation, and fibrosis by inhibiting the ferroptosis and iron overload of hepatocytes. Crucially, FTH1 knockdown abolished the protective effects of UBC9 overexpression on hepatocyte injury, FTH1 overexpression alleviated the harmful effects of UBC9 knockdown on hepatocyte injury.

Conclusions: Our results demonstrate that UBC9 mitigates MAFLD/MASH progression by promoting FTH1 protein degradation in a SUMOylation-dependent manner. These findings underscore the critical roles of UBC9 in regulating iron overload and suppressing ferroptosis, thereby protecting against MAFLD/MASH. This study highlights UBC9 as a promising novel therapeutic target for MAFLD/MASH.

Association Between the FT3 to FT4 Ratio and Type 2 Diabetes Mellitus in Non-alcoholic Fatty Liver Disease

Li-Ya Bian

The Affiliated Hospital of Hangzhou Normal University

Introduction and Objectives: Type 2 diabetes mellitus (T2DM) and nonalcoholic fatty liver disease (NAFLD) are both common metabolic disorders. Thyroid hormones (THs) exert complex, multifactorial effects on glucose and lipid metabolism. Considering the complexity of TH signaling in metabolic tissues, it is important to investigate the association between THs—particularly the free triiodothyronine (FT3) to free thyroxine (FT4) ratio (FT3/FT4)—and the presence of T2DM among patients with NAFLD. Here, we assessed whether FT3/FT4 could help identify patients at risk of T2DM among patients with NAFLD. Exploring the potential mediating role of THs in the T2DM-NAFLD interplay may provide valuable insights for improving risk stratification, guiding therapeutic decisions, and informing prognosis in clinical settings.

Materials and Methods: We retrospectively analyzed 4,942 patients with NAFLD treated at the Affiliated Hospital of Hangzhou Normal University between 2020 and 2023. Data on biochemical markers, glucose metabolism indices, and thyroid function were collected and compared between patients with and without T2DM. To explore the association between the FT3/FT4 ratio and T2DM risk, we developed the following three logistic regression models: Model 0, unadjusted; Model 1, adjusted for age and sex; Model 2, further adjusted for body mass index; Model 3, further adjusted for aspartate aminotransferase (AST) and alanine aminotransferase (ALT) levels; odds ratios (OR) with 95% confidence intervals (CI) for the risk of T2DM were calculated. Partial correlational analysis was conducted between THs [i.e., thyroid-stimulating hormone (TSH), FT3, FT4, total thyroxine (TT4), and total triiodothyronine (TT3)] and the FT3/FT4 ratio with fasting blood glucose (FBG) and hemoglobin A1c (HbA1c), among T2DM subjects with NAFLD. All tests were two-sided, and p

Results: A total of 5,445 patients with NAFLD were screened with 4,942 patients included. Among them, 1,377 (27.9%) had T2DM and 3,565 (72.1%) did not. The T2DM group had higher neutrophils, C-reactive protein, total triglyceride, HbA1c, FBG, creatinine and lower total cholesterol, low-density lipoprotein cholesterol (LDL-C), high-density lipoprotein cholesterol (HDL-C), non-HDL cholesterol, apoA, apoB, ALT, AST, uric acid levels than the non-T2DM group. In terms of thyroid function, FT3 [4.16 (3.66-4.66) vs 4.48 (3.96-4.96), p <0.001], TT3 [1.31 (1.12-1.49) vs 1.44 (1.25-1.64), p <0.001], and the FT3/FT4 [0.3112 (0.2713, 0.3503) vs 0.3419 (0.3029, 0.3812), p <0.001] ratio were significantly lower, while FT4 [13.37 (12.34-14.47) vs 13.04 (12.1-14.03), p <0.001] was higher, in patients with T2DM than in those without. The proportions of patients in the T2DM group across FT3/FT4 ratio quartiles Q1, Q2, Q3, and Q4 were 37.5%, 27.1%, 21.7%, and 13.7%, respectively, whereas in the non-T2DM group, the corresponding proportions were 20.2%, 23.9%, 26.8%, and 29.1%. Logistic regression showed a significant negative association between the FT3/FT4 ratio and T2DM in patients with NAFLD. After adjusting for confounders, the odds ratio (OR) for T2DM in the highest FT3/FT4 quartile compared with the lowest was 0.27 [95% confidence interval (CI), 0.23-0.33; p <0.001]. Partial correlation analysis revealed that FT3, TT3, and the FT3/FT4 ratio were negatively correlated with HbA1c and FBG, with the FT3/FT4 ratio showing the strongest correlation with HbA1c (r = – 0.222, p

Conclusions: The FT3/FT4 ratio may serve as a more sensitive and integrative marker for predicting T2DM risk in patients with NAFLD. These findings offer valuable insights that may inform early risk identification and guide preventive strategies for the management of both T2DM and NAFLD.

糖尿病心脏微血管损伤生物标志物和防治靶点的探究

张奚 孙冬冬

空军军医大学西京医院

目的：

（1）单细胞 RNA 测序筛选糖尿病心脏微血管损伤生物标志物和防治靶点；

（2）临床试验评估潜在标志物 CFH 对糖尿病心脏微血管损伤的预测价值；

（3）基础实验探究潜在靶点 Ets1 在糖尿病心脏微血管损伤的作用。

方法：

（1）以瘦素受体敲除小鼠（db/db）为糖尿病模型，对不同病理阶段的 db/db 小鼠和杂合对照小鼠（db/m）心脏进行单细胞 RNA 测序。经过数据质控和细胞类型注释后，采用细胞动态、命运和功能分析锁定关键细胞亚群，采用转录因子分析探究糖尿病心脏微血管损伤关键调控机制。关键细胞亚群的特征基因 CFH 被确定为潜在标志物，转录因子 Ets1 被确定为潜在治疗靶点。

（2）通过免疫荧光验证不同病理阶段 db/db 小鼠心脏微血管内皮潜在标志物 CFH 和潜在靶点 Ets1 的变化；通过免疫印迹验证不同病理阶段 db/db 小鼠血浆潜在标志物 CFH 的变化；

（3）通过 T 检验评估临床样本中糖尿病组患者和非糖尿病组患者中冠状动脉血流储备分数（CFR）、微循环阻力指数（IMR）、血浆潜在标志物 CFH、对照标志物 sVE-cadherin 和 Endocan 的差异；通过皮尔逊（Pearson）相关性分析分别评估糖尿病组患者血浆标志物（CFH、sVE-cadherin 和 Endocan）与微血管功能指数（CFR 和 IMR）的相关性；通过受试者特征曲线（ROC）分别评估糖尿病组患者血浆标志物对心脏微血管损伤的诊断效率。

（4）采用内皮特异性 Ets1 过表达腺相关病毒（AAV9-Ets1）尾静脉注射干预 db/db 小鼠和 db/m 小鼠心脏血管内皮 Ets1 表达水平。心脏血管内皮 Ets1 成功过表达后通过 CD31 染色评估血管密度；通过透射电镜观察基底膜厚度和 VE-cadherin 染色评估血管屏障功能；通过马松染色评估血管管周纤维化；通过心脏超声评估心脏功能。

结果：

（1）经过质量控制和数据过滤，从八组不同糖尿病阶段的小鼠心脏中共得到 63825 个细胞，这些细胞被聚类为 37 个亚群，包含成纤维细胞、内皮细胞、以及少量心肌细胞和免疫细胞。其中内皮细胞共有 11 个亚群，分别为 3，5，10，12，15，20，21，22，26，31，34 亚群。

（2）内皮细胞拟时序分析发现 12 亚群为糖尿病心脏微血管损伤过程中内皮细胞分化的最终状态，其生物学功能主要为介导炎性细胞向血管壁浸润。组间亚群比例变化提示 12 亚群所占比例随糖尿病进展逐步升高，是糖尿病末期占比最高的内皮细胞亚群，而 CFH 是 12 亚群最显著的特征基因。

（3）SCENIC 转录因子分析提示 Ets1 是糖尿病损伤过程中转录活性最高的转录因子，共参与调控内皮细胞靶基因 154 个。GO 功能注释提示 Ets1 调控网络与血管新生密切相关，但其调控活性在糖尿病心脏微血管损伤过程中逐步降低。

（4）临床试验结果显示糖尿病组患者血浆 CFH 水平显著高于非糖尿病患者；在糖尿病患者中，血浆 CFH 水平与微血管功能指数（CFR 和 IMR）密切相关，且相关指数高于血浆对照标志物 sVE-cadherin 和 Endocan；ROC 曲线提示血浆 CFH 对糖尿病患者心脏微血管损伤的诊断效率高于对照标志物。

（5）基础实验结果提示 AAV9-Ets1 能够平均提高 3 倍 db/db 小鼠心脏血管内皮 Ets1 表达量，同时显著增加了 db/db 小鼠心脏血管密度、增强了心脏功能和血管屏障功能，同时降低了血浆标志物 CFH 水平并提高小鼠生存率。

结论：

结合单细胞 RNA 测序技术以及相关临床试验和基础实验，我们发现血浆 CFH 有望成为糖尿病心脏微血管损伤的特异性标志物，Ets1 过表达有望成为糖尿病心脏微血管损伤新的治疗策略。

Inverted U-shaped association between body mass index and left ventricular global longitudinal strain in middle-aged and elderly patients with coronary heart disease in Jilin Province, China: a cross-sectional study

Lin Na, Xin Xue

The Second Hospital of Jilin University

Abstract

Purpose: Coronary heart disease is the leading cause of death worldwide, and it is also a common and frequent disease that poses a serious threat to the life and health of middle-aged and elderly individuals. Patients with coronary heart disease can develop progressive heart failure despite revascularization. Heart failure is one of the most important complications of coronary heart disease and is associated with high morbidity and hospitalization rates. However, in patients with coronary artery disease, adverse myocardial remodeling and myocardial dysfunction can occur years to decades before symptomatic heart failure owing to the presence of cardiovascular risk factors. Obesity, identified as an independent risk factor for cardiovascular disease, has been closely linked to left ventricular remodeling, which can lead to myocardial diastolic dysfunction and ultimately heart failure. Body mass index (BMI), the most straightforward anthropometric measure for evaluating obesity, is elevated and predicts the occurrence of new heart failure events in patients with coronary artery disease. However, the association between BMI and subclinical left ventricular systolic dysfunction in middle-aged and elderly patients with coronary artery disease remains unclear and further exploration is necessary.The objective of this study is to investigate the relationship between body mass index (BMI) and left ventricular global longitudinal strain (LV-GLS) in middle-aged and elderly patients with coronary heart disease (CHD). Additionally, the objective of this study is to investigate the relationship between body mass index (BMI) and left ventricular global longitudinal strain (GLS) in middle-aged and

elderly patients with coronary heart disease. Additionally, the study aims to explore the potential impact of changes in BMI on subclinical left ventricular function in patients with coronary heart disease.

Methods: A cross-sectional study was conducted on 228 patients with symptomatic coronary heart disease, excluding those with a history of myocardial infarction or left ventricular dysfunction, in Jilin Province, China. Basic clinical data, biochemical data, and echocardiographic data were collected for each participant. One-way analysis of variance was performed to compare myocardial strain parameters among three groups: normal weight (BMI 18.5 ≤ BMI<24 kg/m2), overweight (BMI 24 ≤ BMI<28 kg/m2), and obese (BMI ≥ 28 kg/m2) individuals. Multifactor piecewise linear regression analysis, inflection point analysis, subgroup analysis, and other methods were utilized to evaluate the relationship between increasing BMI and cardiac dysfunction in the subclinical stage of coronary heart disease patients.

Results: The GLS of the left ventricular myocardium was lower in the overweight group compared to the normal weight and obese groups. A significant inverted U-shaped correlation was observed between GLS and BMI levels, with the highest GLS value recorded at a BMI of 25.508 kg/m2. Prior to the inflection point, GLS and BMI displayed a positive correlation (β = 0.51, 95% CI 0.05-0.98, P = 0.034). However, beyond the inflection point, a negative correlation was observed between GLS and BMI (β = -0.44, 95% CI -0.83 to -0.04, P = 0.034). Subgroup analysis indicated that the association between BMI and GLS remained consistent across subgroups stratified by gender, age, hypertension, and diabetes among patients with coronary heart disease.

Conclusion: In conclusion, a non-linear, inverted U-shaped relationship exists between BMI and LV-GLS in middle-aged and elderly patients with coronary heart disease. Maintaining an overweight status may potentially delay the progression of subclinical cardiac dysfunction.

Key words: coronary heart disease; body mass index; myocardial strain; cardiac function

Exploring shared therapeutic targets in Diabetic Panvascular Diseases through bioinformatics analysis

Hanlin Wu

The First Affiliated Hospital of Dalian Medical University

Diabetes mellitus (DM) is a multifactorial metabolic disorder characterised by hyperglycaemia. Globally, the number of people with diabetes has quadrupled in the last three years. According to the World Health Organization, the number of people with diabetes is expected to reach 693 million by 2045.

Chronic hyperglycaemia leads to chronic damage and dysfunction of various tissues, especially the heart, brain, kidneys, peripheral nerves, eyes and feet. Approximately 4.9 million people die annually worldwide from diabetes, about 50% of whom die from cardiovascular complications. Diabetic cardiomyopathy (DCM) is one of the most important cardiovascular complications in patients with DM.

Recent studies have shown that DCM is a type of diabetic microangiopathy. Hyperglycaemia, disorders of lipid metabolism, oxidative stress, and inflammatory responses cause damage or dysfunction of vascular endothelial cells, leading to abnormal microvascular diastole, increased permeability of the vessel wall, and thickening of the basement membrane, and ultimately to the development of DCM. Clinically, patients with advanced DCM are usually accompanied by other severe diabetic microangiopathy, of which diabetic nephropathy (DN) and diabetic retinopathy (DR) are the most common diabetic microangiopathy. No effective treatments has been established to date. Here, we investigated the potential network of molecular roles associated with the development of these three diabetic complications.

In this study, 6 hub genes that may have significant differences in the pathogenesis and development of DCM, DN and DR: COL3A1, CD44, MKI67, LUM, FBN1 and MMP2, were identified by screening of DEGs and construction of PPI networks.

Functional enrichment analysis of proteins interacting with hub genes revealed that these hub genes are extensively involved in biological processes related to fibrosis and inflammatory responses. Abnormal collagen deposition and degradation lead to fibrosis. The hyperglycemia induced by diabetes causes myocardial cells and their interstitial fibrosis through various mechanisms and signaling pathways, mediating the occurrence and development of diabetic cardiomyopathy. Renal interstitial fibrosis is the basic pathological feature of DN and is closely related to the prognosis of the disease. Fibroplasia in DR is the main pathological manifestation of its blindness. These results suggest that anti-fibrotic therapy has an important role in DCM, DN and DR. We used GSEA to reveal 6 hub genes widely associated with immune infiltration responses. Immune cell infiltration analysis showed that the proportion of macrophage infiltration was significantly higher in DCM, DN and DR compared to the control group. Patients with DCM, DN and DR may benefit from anti-inflammatory treatment in the microenvironment, especially targeting macrophage inflammation.

We also employed Network Analyst to predict associations between transcription factor (TF) genes, miRNAs, and hub genes. Our analysis identified JUN, ETS1, FOS, miR-302b, and miR-302c as potential key regulatory targets of the hub genes. These findings offer novel perspectives on the treatment of patients with complications of diabetic microangiopathy, opening up new avenues for therapeutic intervention.

Neu5Ac has a variety of biological functions such as anti-bacterial, anti-viral, anti-tumor, anti-inflammatory and maintaining the physiological activities of the nervous system. Currently, there are two marketed drugs developed with Neu5Ac as the active ingredient, namely Zanamivir and Oseltamivir, which are mainly used as anti-influenza drugs. Functional metabolomics studies have shown that Neu5Ac plays a key role in atherosclerosis, renal small vessel disease, and coronary artery disease. This suggests to us that Neu5Ac may be extensively involved in a variety of microvascular pathologies. Our study shows that Neu5Ac reacts with hub genes. Molecular docking also showed that Neu5Ac and all 6 hub genes could form hydrogen bonds to form a stable structure. The role of Neu5Ac in treatment of multiple microvascular complications in patients with advanced diabetes remains to be explored.

In conclusion, six hub genes COL3A1, CD44, MKI67, LUM, FBN1, MMP2 may involve in the pathophysiology of these diabetic microvascular complications like DCM, DN and DR. Furthermore, our findings suggest that Neu5Ac may be a potential agent for the treatment of multiple microvascular complications in patients with advanced diabetes.

Relationship between uric acid to creatinine ratio and type 2 diabetes mellitus in patients with nonalcoholic fatty liver disease

Fu Xinyan, Ming-Wei Wang

The Affiliated Hospital of Hangzhou Normal University

Background: Non-alcoholic fatty liver disease (NAFLD) is a significant metabolic disorder closely linked to insulin resistance and an increased risk of type 2 diabetes mellitus (T2DM). Given the shared pathophysiology between NAFLD, T2DM, and cardiovascular disease, identifying reliable biomarkers for early T2DM risk stratification in NAFLD patients is crucial for preventive cardiology. Uric acid (UA), a byproduct of purine metabolism, has been implicated in metabolic syndrome and cardiovascular risk, while creatinine (CR) reflects renal function and metabolic turnover. Recent studies suggest that the UA/CR ratio may serve as a novel metabolic indicator, but its predictive value for T2DM in NAFLD patients remains underexplored. This study aimed to investigate whether the UA/CR ratio could serve as an effective tool for identifying individuals at high risk for T2DM within an NAFLD population, thereby offering potential clinical utility in cardiovascular risk assessment.

Methods: We conducted a retrospective cohort study analyzing the clinical data of 5,124 NAFLD patients from the Affiliated Hospital of Hangzhou Normal University between 2020 and 2023. NAFLD was diagnosed via ultrasonography and exclusion of other liver diseases. T2DM was defined according to ADA criteria (fasting glucose ≥ 7.0 mmol/L or HbA1c ≥ 6.5%). The UA/CR ratio was calculated from fasting serum UA and CR levels. Patients were stratified into quartiles based on UA/CR ratios. A binary logistic regression model was employed to assess the association between UA/CR ratio and T2DM risk, adjusting for confounders including age, sex, BMI, blood pressure, lipid profiles (TG, TC, HDL-C, LDL-C), and HOMA-IR. Receiver operating characteristic (ROC) analysis was performed to compare the predictive performance of UA/CR ratio against traditional lipid parameters.

Results: The study population had a mean age of 52.3 ± 11.7 years, with 58.2% males. A significant inverse relationship was observed between UA/CR ratio and T2DM risk. In the fully adjusted model, patients in the highest UA/CR quartile exhibited a 63% lower risk of T2DM (OR: 0.37, 95% CI: 0.30–0.45, *p*

Discussion: Our findings highlight the UA/CR ratio as a superior predictor of T2DM risk in NAFLD patients compared to conventional lipid parameters. The inverse association suggests that low UA (potentially reflecting reduced antioxidant capacity) and high CR (indicative of altered muscle metabolism or renal clearance) may synergistically contribute to diabetic pathogenesis. Mechanistically, UA's dual role as an antioxidant (at physiological levels) and pro-oxidant (at high levels) may explain its complex relationship with metabolic health. The strong predictive performance of UA/CR underscores its potential as a simple, cost-effective tool for early T2DM screening in NAFLD, a population already at high cardiovascular risk.

Conclusions: In NAFLD patients, a lower UA/CR ratio independently predicts higher T2DM risk, with discriminatory power surpassing traditional lipid markers. Clinicians should consider incorporating UA/CR assessment into routine metabolic evaluations for NAFLD patients, particularly those with low UA and elevated CR levels, to enhance early diabetes detection and cardiovascular prevention strategies. Future prospective studies should validate these findings and explore whether UA/CR-guided interventions improve outcomes.

甘油三酯、总胆固醇及体重指数与 0-3 期心血管 - 肾脏 - 代谢综合征人群心血管疾病风险的关联研究：一项全国性前瞻性队列研究

程宁易 陈钰锟 陈良万

福建医科大学附属协和医院

背景：心血管 - 肾脏 - 代谢综合征（CKM）作为一种累及多系统的复杂疾病，其进展与心血管疾病（CVD）风险升高密切相关，而脂质代谢紊乱及肥胖是驱动这一关联的关键病理生理基础。甘油三酯、总胆固醇及体重指数整合指标（TCBI）作为综合反映脂质代谢与肥胖状态的新型指标，其在 CKM 0-3 期人群中对 CVD 风险的预测价值及量化关联尚未明确，亟待通过大样本队列研究验证。

方法：本研究基于中国健康与养老追踪调查（CHARLS）数据库，纳入 5383 例年龄≥ 45 岁的社区人群作为研究对象。采用多因素 Logistic 回归模型控制混杂因素后，分析 TCBI 与 CVD 发病风险的关联强度；通过限制性立方样条（RCS）模型探索二者的剂量反应关系，并利用阈值效应模型识别潜在拐点；进一步按年龄、性别等分层进行亚组分析，评估效应修饰作用。

结果：随着 TCBI 四分位水平从 Q1 至 Q4 递增，研究人群的体重指数、甘油三酯、总胆固醇等核心代谢指标呈现进行性恶化趋势，CKM 2-3 期患者占比从 34.0% 显著升至 98.9%（均 P<0.001）。多因素校正年龄、基础疾病史等协变量后，TCBI 与 CVD 风险呈正向关联，其中 Q4 组较 Q1 组 CVD 发病风险显著升高 28.0%（OR=1.280，95% CI 1.014-1.673，P<0.05）。RCS 分析提示二者存在非线性关联，阈值效应模型确定拐点为 1.097：当 TCBI

结论: 在 CHARLS 队列的 CKM 0-3 期人群中，TCBI 是 CVD 发病的独立危险因素，且其关联存在显著阈值效应（拐点 1.097）。该发现提示，针对 TCBI 处于低水平范围（<1.097）的人群实施早期代谢指标干预，可能成为降低 CVD 风险的更高效策略，尤其对男性群体应加强监测与管理。

Prediabetes Diagnostic Thresholds and Cardiovascular Outcomes: A Prospective Cohort, Mendelian Randomization, and Cardiac Imaging Study

Zhi-Hao Zheng, Ke-Fei Dou

Fuwai Hospital

Background

Prediabetes represents a critical metabolic intermediary affecting over 400 million adults globally, independently accelerating cardiovascular pathology beyond its role as a diabetes precursor. However, substantial diagnostic discordance persists between the American Diabetes Association (ADA) and World Health Organization/International Expert Committee (WHO/IEC) criteria—spanning glycemic thresholds, population prevalence (ADA: 34% vs. WHO/IEC: 18%), and prognostic validity—necessitating rigorous comparative evaluation. This study addresses two pivotal gaps: first, the differential prognostic stratification of ADA-defined versus WHO/IEC-defined prediabetes for incident cardiovascular disease (CVD), mortality, and cardiac remodeling; and second, causal validation of prediabetes-CVD relationships using Mendelian randomization (MR) to mitigate residual confounding.

Methods

In a prospective cohort of 278,697 UK Biobank participants without baseline CVD, prediabetes was classified using dual frameworks: ADA criteria (fasting glucose 5.6–6.9 mmol/L or HbA1c 5.7–6.4%) and WHO/IEC criteria (fasting glucose ≥ 6.1 mmol/L or HbA1c 6.0–6.4%). Primary outcomes encompassed incident CVD (coronary heart disease, myocardial infarction, stroke, hypertension), cardiovascular mortality, and all-cause mortality. Multivariable Cox proportional hazards models adjusted for sociodemographics, lifestyle behaviors, comorbidities, and polygenic risk scores quantified associations. Cardiac magnetic resonance (CMR) imaging evaluated structural remodeling in 638 participants, while two-sample MR leveraged 54-78 genome-wide significant variants for prediabetes to infer causality with CVD outcomes, employing sensitivity analyses (MR-Egger, weighted median) to confirm robustness.

Results

WHO/IEC-defined prediabetes demonstrated significantly higher CVD incidence (HR=1.23, 95% CI: 1.19–1.27) compared to ADA-defined prediabetes (HR=1.14, 1.12–1.16), with particularly amplified risks for myocardial infarction (WHO/IEC: HR=1.33 vs. ADA: HR=1.21) and stroke (WHO/IEC: HR=1.33 vs. ADA: HR=1.23). Mortality gradients further highlighted this divergence: cardiovascular mortality risk nearly doubled under WHO/IEC criteria (HR=1.96, 1.70–2.25) versus ADA (HR=1.47, 1.34–1.62), while all-cause mortality risk was 39% higher for WHO/IEC-defined prediabetes compared to 24% for ADA-defined individuals. Notably, WHO/IEC-defined prediabetes exhibited mortality risk equivalent to type 2 diabetes (all-cause HR=1.03, 0.95–1.13).

CMR imaging revealed that WHO/IEC-defined prediabetes initiated early concentric left ventricular remodeling, characterized by elevated left ventricular mass-to-volume ratio (β=0.19, 95% CI: 0.11–0.37), whereas type 2 diabetes showed advanced structural derangements including increased end-diastolic volume (β=10.22 mL) and further mass-to-volume ratio deterioration (β=0.35). These morphological changes preceded functional decline and aligned with the steeper CVD risk trajectories observed in WHO/IEC subgroups.

Mendelian randomization analyses genetically confirmed causality, demonstrating that prediabetes increased risks of CVD (OR=1.01, 1.01–1.02), myocardial infarction (OR=1.12, 1.06–1.19), and stroke (OR=1.06, 1.02–1.10). Sensitivity analyses validated these findings, showing no horizontal pleiotropy (MR-Egger intercept P>0.05) and consistent effects across complementary MR methods. Importantly, CVD risk persisted uniformly across low, moderate, and high polygenic risk strata (P for interaction >0.05), underscoring dysglycemia as an independent, universal risk amplifier rather than a mere correlate of genetic predisposition.

Conclusions

This integrative study establishes that WHO/IEC criteria optimize specificity for identifying prediabetic individuals at near-diabetic cardiovascular risk, effectively capturing a high-risk subpopulation (12.1% prevalence) requiring intensive intervention. The detection of early concentric remodeling via CMR in this group provides a mechanistic link to accelerated cardiovascular pathology, while genetic evidence robustly confirms the causal role of dysglycemia in vascular injury. Clinically, these findings advocate for revising screening paradigms to prioritize WHO/IEC thresholds for CVD risk stratification and emphasize early lifestyle or pharmacologic intervention in high-risk prediabetes subgroups to avert irreversible cardiovascular damage, thereby addressing a critical gap in preventive cardiology.

二甲双胍与接受非复杂或复杂经皮冠状动脉介入治疗的糖尿病患者的临床结局

何际宁 王紫逸 窦克非 尹栋

中国医学科学院阜外医院

背景

二甲双胍是糖尿病治疗中常用的药物，已有研究表明，在无动脉粥样硬化性心血管疾病的糖尿病患者中，该药具有心血管保护作用。目前，关于二甲双胍在接受经皮冠状动脉介入治疗（**PCI）的糖尿病患者中的应用证据较为有限。因此，本研究旨在评估二甲双胍在接受 PCI 的糖尿病患者中的疗效，以及其与 PCI 复杂程度可能存在的相互作用。**

方法

2017 年 1 月至 2018 年 12 月期间，本研究连续纳入了 11585 例在阜外医院接受 PCI 的糖尿病患者。根据二甲双胍的使用情况和 PCI 复杂程度，将患者分为四组。主要终点为主要不良心脑血管事件（MACCEs），包括心血管死亡、非致死性心肌梗死（MI）、非致死性卒中以及非计划性血运重建的复合终点。

结果

经过 3 年的随访，共记录到 1292 例主要不良心脑血管事件。多变量调整后，使用二甲双胍与 3 年主要不良心脑血管事件发生率降低相关（校正后风险比 0.80，95% 置信区间 0.70-0.92）。在接受非复杂 PCI 的患者中，MACCEs 发生率显著降低（校正后风险比 0.65，95% 置信区间 0.53-0.79）；而在复杂 PCI 患者中，未观察到二甲双胍的这种保护作用（校正后风险比 1.00，95% 置信区间 0.83-1.21）。研究发现，二甲双胍与 PCI 复杂程度在 3 年主要不良心脑血管事件发生率方面存在显著的相互作用（校正后交互作用 P 值 = 0.002）。

结论

二甲双胍在接受复杂或非复杂 PCI 的糖尿病患者中的疗效存在显著差异。在患有糖尿病且接受非复杂 PCI 的患者中，使用二甲双胍与预后改善相关。

Synergistic Amplification of Cardiovascular Risk by Insulin Resistance and Hepatic Fibrosis in Coronary Artery Disease: Machine Learning-Driven Phenotyping and Multi-Dimensional Interaction Analysis for Precision Risk Stratification

Zhi-Hao Zheng, Rui Fu

Fuwai Hospital

Background

Cardiovascular disease (CVD) persists as the leading global cause of mortality, where metabolic disorders such as insulin resistance (IR) and hepatic fibrosis play pivotal roles in pathogenesis. Metabolic dysfunction-associated fatty liver disease (MAFLD), affecting over 25% of adults globally, exhibits strong associations with accelerated cardiovascular morbidity, particularly in advanced fibrotic stages that confer a 2.5-fold increased risk independent of traditional factors. The triglyceride-glucose (TyG) index—a validated IR marker—exacerbates endothelial dysfunction and myocardial metabolic derangements, creating a pathological loop with heart failure progression. However, the synergistic relationship between hepatic fibrosis (assessed via FIB-4 and BARD scores) and IR in coronary artery disease (CAD) remains poorly characterized, thereby limiting precision risk stratification strategies. Consequently, this study aimed to integrate machine learning phenotyping with multidimensional interaction analysis to bridge this critical gap.

Methods

Between January 2017 and December 2018, we prospectively enrolled 30,029 CAD patients at Fuwai Hospital, ultimately including 14,660 participants with complete metabolic profiles after exclusions. Insulin resistance was quantified via the TyG index (ln[fasting triglycerides × fasting glucose]/2), while hepatic fibrosis was assessed using FIB-4 (age, platelets, AST, ALT) and BARD scores (BMI ≥ 28 kg/m², AST/ALT ratio ≥ 0.8, diabetes diagnosis). Machine learning-driven K-means clustering, optimized through the elbow method, stratified patients into metabolic subtypes based on comprehensive clinical, laboratory, and angiographic profiles. Subsequently, Cox proportional hazards models evaluated biomarker associations with the primary composite endpoint (cardiovascular mortality, nonfatal MI, or stroke) over 3-year follow-up, using hierarchical adjustment for demographics, comorbidities, and treatments. Crucially, multiplicative interactions were tested via cross-product terms, while additive interactions employed relative excess risk (RERI) and attributable proportion (AP) metrics, complemented by restricted cubic splines and bivariate heatmaps for nonlinear risk visualization.

Results

K-means clustering robustly identified three metabolic subtypes with divergent trajectories. Class 1 (low-risk; n=4,782) exhibited favorable profiles including lower BMI (24.14±2.52 kg/m²), TyG (8.52±0.41), and FIB-4 (1.53±0.51). Conversely, Class 2 (IR-dominant; n=5,719) showed marked dysmetabolism with elevated TyG (9.06±0.52) and triglycerides (1.86±0.96 mmol/L). Most critically, Class 3 (metabolic-fibrosis mixed; n=4,159) demonstrated concurrent severe IR (TyG 9.18±0.53), hepatic fibrosis (BARD 2.00±1.14), and inflammation (hs-CRP 2.24±1.87 mmol/L). Cox regression confirmed TyG independently predicted events (adj. HR=1.52 per unit; 95% CI:1.40–1.65), with similar risks for elevated FIB-4 (HR=1.59) and BARD (HR=1.80). Class 3 carried a 71% higher risk versus Class 1 (HR=1.71; 1.34–2.19). Significantly, multiplicative interaction emerged between TyG and BARD (P-interaction=0.041), where high-BARD/high-TyG patients faced 3.85-fold risk (2.26–6.54)—substantially exceeding isolated high TyG (HR=2.19). Additive interaction revealed 189% excess risk (RERI=1.89; P<0.001). Nonlinear modeling further demonstrated exponential risk escalation beyond TyG>9.0, potentiated by concomitant fibrosis, while bivariate heatmaps localized maximal risk to TyG>9.2/BARD>3 combinations.

Conclusion

This study establishes that insulin resistance and hepatic fibrosis synergistically amplify cardiovascular risk in CAD beyond individual effects. Machine learning phenotyping successfully identified a high-risk "metabolic-fibrosis" subtype characterized by concurrent dyslipidemia, severe IR, and fibrotic burden. The significant multiplicative and additive interactions between TyG and BARD scores demonstrate their combined utility for precision risk stratification, with clinically actionable thresholds (TyG>9.0, BARD>3). Consequently, this integrated framework—leveraging advanced analytics for vulnerability identification—enables targeted dual-pathway interventions. Future research should validate these thresholds in multiethnic cohorts and elucidate molecular mediators (e.g., FGF21 resistance, ceramide pathways) to guide therapeutic innovation, ultimately reducing CVD burden in metabolically complex populations.

IGF2BP3 介导 DMRT2 m6A 甲基化修饰调控脂肪细胞胰岛素抵抗的机制研究

陶静 [1,2] 郑宏健 [1,2] 王子杰 [1,2] 永佳蕙 [1,2] 杨毅宁 [1,2]

1. 新疆维吾尔自治区人民医院

2. 新疆心脏血管稳态与再生医学研究重点实验室

背景　胰岛素抵抗（Insulin Resistance, IR）是代谢性疾病的关键病理生理机制之一，脂肪细胞中的 IR 受到多种因素调控。m6A 甲基化修饰作为一种重要的表观遗传调控机制，可能通过影响 DMRT2 基因在 IR 中发挥作用。然而，DMRT2 m6A 的关键调控因子及其作用机制尚不明确。

方法　本研究首先通过多个数据库（RM2Target、GEO、RNA-seq 数据集和皮尔逊分析）筛选与 IR 患者脂肪组织中 DMRT2 m6A 显著相关的因子。进一步利用 3T3-L1 脂肪前体细胞建立 IR 模型。通过过表达、敲低核心调控因子或 m6A 抑制剂干预，检测 DMRT2 蛋白、m6A 修饰水平及 IR 相关指标（葡萄糖摄取、脂肪细胞炎症因子表达和甘油三酯含量）。此外，通过生物信息学分析确定 IGF2BP3 与 DMRT2 m6A 的相关性，并通过实验验证 IGF2BP3 对 DMRT2 m6A 修饰及 IR 进展的影响。

结果　生物信息学分析显示 IGF2BP3 与 DMRT2 m6A 修饰显著相关。在 IR 细胞模型中，敲低 IGF2BP3 可上调 DMRT2、GLUT4 和 p-Akt/Akt 表达，下调 DMRT2 mRNA 上的 m6A 水平，促进葡萄糖摄取，抑制脂肪细胞炎症因子的表达，减少甘油三酯含量；过表达 IGF2BP3 则相反。m6A 抑制剂可抵消 IGF2BP3 过表达对 DMRT2 mRNA m6A 修饰及 IR 进展的影响。回复实验证明，过表达 DMRT2 可部分消除 IGF2BP3 对 IR 的促进作用。

结论　IGF2BP3 通过调控 DMRT2 m6A 甲基化修饰促进脂肪细胞 IR 和炎症进展。本研究揭示了 IGF2BP3 与 DMRT2 m6A 修饰在 IR 中的作用机制，为开发 IR 新靶点提供了重要依据。

脂肪组织特异性 Eepd1 缺失驱动糖尿病心肌病的跨器官代谢 - 炎症轴调控机制

李想 张敏 杨钰彬

上海交通大学医学院附属胸科医院

目的：揭示 DNA 修复酶 Eepd1 在脂肪组织中的代谢保护功能，阐明其通过跨器官代谢 - 炎症轴调控糖尿病心肌病的分子机制，并探索基于 CRISPR-SaCas9 的基因编辑干预策略。

方法：

1. 构建脂肪细胞特异性 Eepd1 敲除小鼠模型（Adipoq-Cre;Eepd1fl/fl）及高脂饮食（HFD）诱导的糖尿病心肌病模型。

2. 采用单细胞核 RNA 测序（snRNA-seq）解析脂肪组织 DNA 损伤应答（DDR）信号与心肌代谢紊乱的关联。

3. 通过外泌体分离、MeRIP-seq 和分子互作实验研究脂肪源性 circRNA_3416 的 m6A 表观调控机制。

4. 利用 CRISPR-SaCas9 系统在脂肪组织原位过表达 Eepd1-K70R 突变体，评估其对心肌线粒体功能及纤维化的挽救作用。

结果：

1. **脂肪组织 Eepd1 缺失加剧心脏损伤**：HFD 喂养的敲除小鼠心脏舒张末期内径（LVEDd）增加（p<0.001），心肌长链酰基肉碱水平升高，线粒体分裂蛋白 Drp1 磷酸化水平增加。

2. **代谢 - 炎症轴失调**：

· 脂肪细胞 DDR 信号异常激活，抑制 FGF21 和 Adiponectin 分泌（ELISA 浓度下降），促炎因子 Resistin 表达升高。

· 脂肪外泌体 circRNA_3416 的 m6A 修饰峰增加（MeRIP-seq 验证），通过 YTHDF2 依赖方式激活心肌 NF-κB/STAT3 炎症轴，并抑制 PPARα 介导的脂肪酸氧化（CPT1β 表达下降）。

3. **基因编辑干预效果**：

· CRISPR-SaCas9 介导的 Eepd1-K70R 过表达使心肌纤维化面积减少（Masson 染色），SIRT3 依赖性 SOD2 表达升高，线粒体 ROS 水平降低。

结论：本研究首次揭示脂肪组织 Eepd1 维持代谢稳态，其缺失通过外泌体 m6A-circRNA_3416/YTHDF2 轴引发心肌代谢 - 炎症失衡。基于 CRISPR-SaCas9 的脂肪靶向基因编辑策略为糖尿病心肌病的跨器官治疗提供了创新性理论依据。

Associations and potential biological pathways between ideal cardiovascular health defined by lifes essential 8 scores and diabetes/prediabetes: perspectives from mediation analysis

Xiaoping Peng, Rui-Chun Liao

The First Affiliated Hospital of Nanchang University

Background: Diabetes, characterized by a complex and varied etiology, represents a significant public health challenge. From 1990 onwards, the morbidity of diabetes in American adults has increased from 7.5% to 13.9%, resulting in indirect medical costs and indirect productivity losses of $412.9 billion per year. Additionally, diabetes ranges as the 7th primary cause of mortality in America. Events related to cardiovascular disease (CVD) stand as the foremost reasons for death in individuals diagnosed with diabetes. Notably, diabetes can exacerbate or even accelerate the onset of CVD events. Prediabetes, which raises the risk of diabetes, impacts more than a third of American adults and also boosts the likelihood of CVD. The epidemic of diabetes and prediabetes is a critical public health challenge in America. Therefore, exploring modifiable CVH factors in individuals with diabetes and prediabetes is highly important.

In 2022, the American Heart Association (AHA) launched Life's LE8 score, which builds upon the existing Life's Simple 7 (LS7) score, to improve CVH. The LE8 incorporates four lifestyle elements: a nutritious diet, regular physical activity(PA), limited exposure to nicotine, and quality sleep, along with four metabolic components: body mass index (BMI), lipid levels, glucose levels, and blood pressure. Consistently, epidemiological studies have confirmed that higher LE8 scores correlate with lower odds of experiencing cardiovascular disease events and a range of metabolic disorders. A recent investigation has indicated that Chinese individuals with lower LE8 scores are in an accelerated state of diabetes or prediabetes. Moreover, scant research has explored the LE8 score's relationship with diabetes or prediabetes risk in the American population. Given the increased CVD risk in individuals with diabetes or prediabetes and the multiethnic diversity of Americans, results from other ethnicities may not generalize to Americans. To bridge this gap, We analyzed the relationship between LE8 scores and subscores to diabetes and prediabetes risk in 7 cycles of NHANES, from 2005 to 2018. Additionally, we employed mediation modeling to identify potentially influential factors between LE8 and diabetes/prediabetes

Methods: We conducted a cross-sectional analysis based on data from NHANES（2005-2018）. The association between LE8 and diabetes/prediabetes was assessed by multivariate logistic regression, employing a four-knot restricted cubic spline (RCS) model to fit a dose-response characterization. Additionally, analyses stratified by subgroups examined the

variability in these associations, and mediation analysis examined possible biological mechanisms linking LE8 to diabetes/prediabetes.

Results: Having accounted for confounding variables, LE8 and the incidence of diabetes/prediabetes were significantly inversely associated. RCS analyses detected a linear (negative) association between LE8 and diabetes, but a nonlinear association with prediabetes. Subgroup analyses indicated that a higher LE8 may confer the greatest benefits to the Black population. Mediation analysis suggested that inflammation, oxidative stress, nutritional factors, and insulin resistance are pathways through which LE8 influences the risk of diabetes/prediabetes.

Conclusion: In this national-level, survey-based study, we enrolled a total of 20,747 participants, representing approximately 122,915,498 non-institutionalized US adults through sample-weighted estimates. The key findings are summarized as follows: (1) LE8 was negatively associated with most of the diabetes/prediabetes components. LE8 scores in the moderate to high range are associated with a decreased risk of experiencing diabetes or prediabetes. (2) Additional RCS analyses revealed a linear decrease in diabetes risk and a nonlinear relationship with prediabetes risk associated with LE8; the fitted RCS curves further confirmed that maintaining a high LE8 score is advantageous for reducing the risk of diabetes and prediabetes. (3) Subgroup analyses highlighted racial disparities in LE8-related diabetes/prediabetes risk. (4) Mediation analyses indicated that pathways of inflammation, oxidative stress, nutrition, and insulin resistance differentially affect LE8-related diabetes/prediabetes risk. Cardiovascular health is recognized as a vital determinant in the path towards diabetes and pre-diabetes.

Keywords: Life's Essential 8; diabetes; prediabetes; cardiovascular health; mediation analysis

The Impact of Remnant Lipoprotein Cholesterol on the Prognosis of Patients Undergoing PCI under Different Glycemic States: A Prospective Cohort Study

Kong-Yong Cui, Zi-Xiang Ye, Rui Fu, Ke-Fei Dou

Fuwai Hospital

Objective: Remnant lipoprotein cholesterol (RLP-C) refers to the cholesterol component found in triglyceride-rich lipoprotein subclasses. Previous studies demonstrated that elevated RLP-C levels correlate with adverse cardiovascular events in secondary prevention settings. Nonetheless, its specific role in patients with coronary artery disease (CAD) who underwent percutaneous coronary intervention (PCI) with different glucose metabolism status remains underexplored. This study aimed to investigate the relationship between RLP-C levels and prognosis in CAD patients undergoing PCI, with a focus on both diabetic and non-diabetic populations.

Methods: In this prospective cohort study, 9,440 CAD patients who underwent PCI between January and December 2013, were enrolled in our center. Patients were followed for major adverse cardiovascular events (MACE), including all-cause mortality, non-fatal myocardial infarction, stroke, and unplanned revascularization. The median follow-up time was 2.4 years. CAD Patients were divided into two groups based on the presence or absence of diabetes. Each group was further stratified into high and low subgroups according to the levels of RLP-C. RLP-C was assessed as both a categorical and continuous variable using Kaplan-Meier curves and Cox proportional hazards regression models. In addition, restrictive cubic spline (RCS) analysis was applied to evaluate whether a non-linear relationship exists between RLP-C and adverse clinical outcomes. Subgroup analyses were also conducted to compare the robustness of results across different subpopulations.

Results: The median RLP-C level was 0.60 mmol/L in the present study, with 51.2% of patients exhibiting high levels. The overall population had a median age of 58 years (IQR 51-65 years), with males comprising 76.9%. The prevalence of obesity (body mass index ≥ 29 kg/m^2) was 16.3%, and 44.1% of the patients had diabetes. Univariate Cox regression results showed that high RLP-C, when treated as a categorical variable, was associated with an increased risk of MACE (hazard ratio [HR] 1.174, 95% confidence interval [CI] 1.032-1.336, P < 0.05), but this association lost statistical significance after multivariate adjustment. As a continuous variable, neither univariate nor multivariate Cox regression analysis showed statistical significance. Furthermore, diabetic patients had a significantly higher incidence of MACE compared to non-diabetic patients during the follow-up period (P < 0.05). In non-diabetic patients, high RLP-C levels were positively associated with the incidence of MACE (adjusted HR 1.309, 95% CI 1.083-1.581, P < 0.05) and unplanned revascularization (adjusted HR 1.297, 95% CI 1.066-1.578, P < 0.05) after adjusting for the potential confounders. After further adjusting for low-density lipoprotein cholesterol (LDL-C) or non-high density lipoprotein-cholesterol (non-HDL-C), RLP-C also showed an association with increased risk of MACE (adjusted for LDL-C, HR 1.291, 95% CI 1.066-1.564, P < 0.05; adjusted for non-HDL-C, HR 1.287, 95% CI 1.052-1.574, P < 0.05). RCS analysis indicated a linear relationship between RLP-C and MACE risk in non-diabetic and diabetic patients, with the P value for non-linearity being > 0.05. Moreover, the relationship between RLP-C and MACE events in most non-diabetic patient subgroups remained consistent with the overall population, with no significant interactions were observed (P for interaction >0.05). In contrast, no significant associations were observed between RLP-C levels and adverse clinical outcomes among diabetic patients in single-variable and multivariable Cox regression analysis.

Conclusions: Elevated RLP-C levels are associated with a greater risk of adverse cardiovascular events in non-diabetic CAD patients post-PCI, suggesting RLP-C as a potential prognostic marker in this population. Further studies are warranted to explore these associations and their implications for treatment strategies.

Association of the plasma-glycosylated hemoglobinA1c/High-Density lipoprotein cholesterol ratio with mortality and cardiovascular disease in the US population: NHANES 1999-2018

bingqian zhang

The First Affiliated Hospital of Dalian Medical University

Abstract

Background

One of the major drivers of cardiovascular disease lies in a state of disturbed glucose and lipid metabolism in the body. Specifically, elevated plasma glycosylated hemoglobin (HbA1c) levels, which reflect long-term glycemic exposure, and decreased levels of cardioprotective high-density lipoprotein cholesterol (HDL-C), both of which have been shown by numerous epidemiologic and clinical studies to be strongly and significantly associated with the risk of disease progression, complications, and ultimately death in patients with cardiovascular disease. Considering the pathophysiologic interplay between glucose and lipid metabolism, the present study focused specifically on the integration of HbA1c and HDL-C into a single metric - i.e., the HbA1c/HDL-C ratio. Our core research objective is to comprehensively examine and elucidate whether and to what extent this ratio metric can serve as a valid tool or biomarker for predicting all-cause mortality and future risk of cardiovascular disease (both fatal and nonfatal events) in a population.

Methods

This study included 11,937 adults from the National Health and Nutrition Examination Survey (NHANES) 1999-2018. Binary weighted logistic regression analyses, cox proportional hazards model and restricted cubic spline (RCS) were used to analyze the association between the HbA1c/HDL-C ratio and mortality and cardiovascular disease, and stratified analyses were used for further study. The incremental predictive value of the HbA1c/HDL-C ratio was also assessed.

Results

After adjusting for relevant covariates, we found that compared with those in the group with lower levels of HbA1c/HDL-C ratio, those with higher levels of HbA1c/HDL-C ratio were positively associated with all-cause mortality (adjusted hazard ratio [HR] 1.31, 95% confidence interval [CI] 1.09-1.58), cardiovascular mortality (HR 1.56, 95%CI 1.08-2.26), total-cardiovascular disease (adjusted odds ratio [OR] 1.57, 95%CI 1.18-2.11), coronary heart disease (OR 1.69, 95%CI 1.13-2.54), angina pectoris (OR 1.79, 95%CI 1.09-2.94) and myocardial infarction (OR 1.71, 95%CI 1.17-2.51), except for congestive heart failure (OR 1.42, 95%CI 0.89-2.27). RCS analyses showed that most of these relationships were linear after adjustment for covariates, whereas the HbA1c/HDL-C ratio was nonlinear with angina pectoris and myocardial infarction. Finally, the ROC curves as well as all predictive ability indicators suggest that the addition of HbA1c/HDL-C ratio to the traditional cardiovascular risk factor model significantly improves the predictive ability of cardiovascular disease.

Conclusions

The HbA1c/HDL-C ratio is significantly and positively associated with mortality, total cardiovascular disease, coronary heart disease, angina pectoris, and myocardial infarction, and improves risk prediction of mortality and cardiovascular prognosis. This property gives the HbA1c/HDL-C ratio unique translational potential: it has the potential to be a more effective tool than some of the existing metrics for accurately identifying high-risk populations at relatively early stages of cardiovascular disease (i.e., at the level of primary prevention), particularly in patients with metabolic syndrome, prediabetes, or diabetes. The HbA1c/HDL-C ratio is expected to become a more effective indicator for identifying people at early risk of CVD and improving risk stratification. Risk stratification using this easy-to-calculate ratio will enable earlier initiation of intensive interventions, with the ultimate goal of reducing cardiovascular disease morbidity and associated mortality and improving the prognosis for cardiovascular health in the population.

将心脏代谢疾病与 HFpEF 联系起来的循环介质：一种中介孟德尔随机化分析

贾鹏宇

中国医科大学附属第一医院

目的：射血分数保留的心力衰竭 HFpEF）是一种越来越普遍的临床综合征，发病率和死亡率都很高。尽管 HFpEF 经常与心脏代谢疾病共存，但其致病机制和潜在介质仍然知之甚少。本研究旨在确定专门驱动 HFpEF 的心脏代谢危险因素，并确定其潜在的循环介质。

方法：我们使用双样本孟德尔随机化来分析肥胖、 2 型糖尿病、高血压、慢性肾病和血脂异常对 HFpEF 和射血分数降低的心力衰竭的影响大型欧洲血统 GWAS 数据集。然后我们进行中介 MR 以鉴定分别介导从每种心脏代谢疾病向 HFpEF 转变的血浆蛋白和代谢物。我们应用多变量 MR 来评估风险混杂对结果的影响。进行生物信息学分析以描述机制。

结果：心脏代谢疾病对 HFpEF 和 HFrEF 的影响具有异质性。肥胖和 2 型糖尿病与 HFpEF 显示出调整后的因果效应，高血压与 HFpEF 显示出潜在相关性，而血脂异常和 CKD 则没有。MR 分析确定了 5 种介导肥胖到 HFpEF 的蛋白质 ;5 种介导 2 型糖尿病到 HFpEF 的蛋白质。肥胖和 T2D 对 HFrEF 的进一步中介 MR 分析揭示了代谢性 HFpEF 和 HFrEF 之间循环介质的异质性。全面的生物信息学分析表明，IL1R1 与 TP53 和 FGF19 等其他蛋白一起协调 HFpEF 背后的炎症和纤维化过程。

结论：这些发现表明，与 HFrEF 相比，代谢性 HFpEF 具有不同的病因特征，并且由复杂的条件特异性介质驱动。IL1R1 在多种代谢风险状态下介导 HFpEF，表明潜在的治疗靶点。需要进一步的转化研究来评估 HFpEF 中靶向 IL1R1 的抗炎策略。

Joint association of Cardiovascular-Kidney-Metabolic Syndrome staging and accelerated Phenotypic age with mortality

Zhaoyu Ren, Bin Liang

Second Hospital of Shanxi Medical University

Objective:

Cardiovascular-Kidney-Metabolic Syndrome (CKM), recently formalized as a staging system by the American Heart Association, provides a crucial framework for understanding the intricate interplay between metabolic risk factors, chronic kidney disease (CKD), and cardiovascular disease (CVD). This staging reflects the pathophysiological continuum linking these conditions, ranging from risk factors to established disease. While valuable for conceptualizing disease progression, the prognostic utility of the CKM staging system alone for mortality outcomes requires augmentation. Phenotypic Age (PhenoAge) acceleration, a biomarker derived from clinical chemistry markers reflecting biological aging processes distinct from chronological age, demonstrates a robust association with increased mortality risk across diverse populations. This study aimed to comprehensively evaluate the independent prognostic value of CKM staging and PhenoAge acceleration for mortality outcomes, and critically assess their combined and potentially synergistic effects. The goal was to determine if integrating PhenoAge acceleration into the CKM framework offers a more refined, evidence-based approach for risk stratification and prognostic assessment in individuals across the CKM spectrum.

Methods:

Utilizing data from the nationally representative National Health and Nutrition Examination Survey (NHANES), this study included 16,787 participants surveyed between 1999 and 2010, with mortality follow-up through linkage to the National Death Index. Participants were categorized according to the established CKM staging criteria (Stages 0-4). PhenoAge acceleration was calculated as the residuals from the regression of PhenoAge (estimated using a validated algorithm based on chronological age and nine biomarkers) on their actual chronological age; positive values indicate accelerated biological aging. Cox proportional hazards regression models were employed to rigorously assess the associations between CKM stage, PhenoAge acceleration (analyzed both continuously and categorically, e.g., accelerated vs. non-accelerated), and their interaction, with four key mortality outcomes: all-cause mortality, non-accidental mortality, cardiovascular disease (CVD) mortality, and cancer mortality. The incremental prognostic value gained by adding PhenoAge acceleration to a model containing only CKM staging was quantitatively evaluated using Harrell's C-index, a measure of model discrimination.

Results:

Elevated CKM staging was associated with an increased risk of mortality, with CKM stage 4 having the highest risk: all-cause mortality (HR 2.58, 95% CI: 1.85–3.61), non-accidental mortality (HR 2.75, 95% CI: 1.93–3.93), CVD mortality (HR 4.62, 95% CI: 1.64–13.00), and cancer mortality (HR 2.87, 95% CI: 1.38–5.94). In the stages 2-4 of CKM, individuals with PhenoAge acceleration also had significantly higher risks for all-cause mortality, non-accidental mortality, and CVD mortality. In the joint analyses, CKM patients of stage 4 with PhenoAge acceleration had the highest risk for all-cause mortality (HR 4.22, 95% CI: 2.73–6.54), non-accidental mortality (HR 4.60, 95% CI: 2.93–7.24), CVD mortality (HR 8.01, 95% CI: 2.65–24.21), and cancer mortality (HR 4.11, 95% CI: 1.72–9.81). Notably, individuals with CKM stage 3 and PhenoAge acceleration had higher risks of all-cause mortality (HR 2.95 vs. 2.42), non-accidental mortality (HR 3.12 vs. 2.60), and cardiovascular mortality (HR 5.06 vs. 3.69) compared to those with CKM stage 4 but without PhenoAge acceleration. The overall increase in the C-index suggests that incorporating PhenoAge acceleration into the CKM staging model enhances the prognostic ability of the model.

Conclusion:

As CKM staging increases, the risk of all-cause and cause-specific mortality (non-accidental, cardiovascular disease, and cancer) significantly increases, and PhenoAge acceleration is also positively correlated with mortality risk. In CKM stages 2-4, individuals with PhenoAge acceleration had a more significant increase in the risk of all-cause, non-accidental, and CVD mortality, while the risk of cancer mortality was more closely associated with stage 4 of CKM. The highest mortality burden consistently manifested in stage 4 CKM patients with PhenoAge acceleration. The combination of CKM staging and PhenoAge can further improve the prognostic evaluation of CKM.

NPRC 基因敲除减轻 DKD 小鼠的肾小球纤维化

王鑫陆 张澄

山东大学齐鲁医院

糖尿病肾病 (DKD) 是糖尿病最常见的并发症之一，随着疾病的进展，会出现肾小球纤维化、肾功能受损等改变，探索 DKD 的发病机制和干预靶点具有重要的临床意义。本课题组之前在糖尿病性心肌病小鼠模型中，发现 NPRC 的表达增加，且敲除 NPRC 减轻了心脏纤维化，改善了心脏重构和功能。然而，NPRC 对 DKD 的影响及其潜在机制仍不清楚。

研究人员收集了 DKD 患者的肾活检组织，行免疫组化染色检测 NPRC 的表达变化。结果发现，与对照组相比，DKD 患者肾小球中 NPRC 表达显著增高。研究人员使用雄性 C57BL/6J 小鼠构建 DKD 模型，DKD 小鼠肾脏 NPRC 的表达水平明显上调，而 NPRA 和 NPRB 的表达水平无明显改变。

课题组构建了足细胞特异性 NPRC 基因敲除 ($Nprc^{pod\ KO}$) 小鼠，并在 $Nprc^{pod\ KO}$ 小鼠和同窝对照 $Nprc^{pod\ WT}$ 小鼠中分别构建 DKD 模型，结果显示足细胞特异性 NPRC 基因敲除可以改善糖尿病小鼠血清肌酐水平和尿白蛋白水平，减少肾脏大小，减轻系膜基质堆积和肾小球基底膜增厚，改善足细胞损伤。

免疫学及分子生物学结果显示，足细胞特异性 NPRC 基因敲除减轻了糖尿病小鼠的肾脏纤维化及胶原沉积，改善了足细胞损伤，抑制了 TGF-βR2 的表达及 DKD 肾脏纤维化经典通路 TGF-β1/Smad 通路的激活。以上结果表明，足细胞特异性 NPRC 敲除减轻了 DKD 小鼠的足细胞损伤和肾小球纤维化。

对机制的研究结果显示，NPRC 在 DKD 中的表达增加，而足细胞中 NPRC 的缺乏通过抑制 TGF-βR2 的再循环以及 TGF-β1/Smad 和 TGF-β1/P38 信号通路，减少肾小球纤维化并改善肾功能。因此，通过足细胞特异性基因或药物疗法靶向 NPRC 为治疗糖尿病肾病提供了一种有前景的策略。

Homocysteine activates endothelial TP receptor to promote von Willebrand factor secretion and thrombosis

Jiachen Zhang

Tianjin Medical University General Hospital

Hyperhomocysteinemia (HHcy), characterized by elevated plasma homocysteine (Hcy) levels, is a recognized risk factor for thrombosis and an independent contributor to acute coronary syndrome, although its underlying mechanisms are not fully understood. The current study is to investigate the impact of HHcy on arterial thrombosis and the underlying mechanisms. In this study, we established an HHcy mouse model using a high-methionine diet and found that HHcy significantly accelerated thrombosis. We identified that Hcy enhanced von Willebrand factor (vWF) secretion from endothelial cells, leading to increased FVIII-vWF binding and platelet adhesion. Moreover, we observed a significant positive correlation between vWF and Hcy levels in the plasma of 150 patients with acute coronary syndrome. Mechanistically, GPCR screening revealed that the Hcy-induced increase in vWF levels was mediated by activating the thromboxane prostanoid receptor (TPr) on endothelial cells. Hcy could directly bind to TPr and subsequently activated the Gαq-PLC-Ca^{2+} pathway to promote vWF secretion. Pharmacological inhibition or endothelial-specific deletion of TPr effectively reduced plasma vWF levels and protected against HHcy-related thrombosis. Our findings underscored the pivotal role of TPr in mediating Hcy-induced procoagulant states and suggested that targeting the TPr signaling pathway could be a promising therapeutic strategy for treating HHcy-related thrombosis.

Homocysteine (Hcy) is a sulfur-containing, non-essential amino acid derived from methionine and participated in multiple biological processes. Hyperhomocysteinemia (HHcy), defined as elevated plasma Hcy level (>15 μM), is an important and independent risk factor for several vascular diseases, including abdominal aortic aneurysm, myocardial infarction, and atherosclerosis. Clinical studies have revealed that HHcy is positively associated with thrombotic disease. Patients with HHcy had a higher risk of death events on account of thrombotic diseases, particularly stroke. However, the pathogenesis of HHcy-associated thrombosis remains elusive.

HHcy has been reported to potentiate platelet activation and thrombosis through mechanisms like platelet membrane phospholipid catabolism and extracellular autotaxin secretion, which activates integrin outside-in

signaling. However, patients with HHcy often exhibit reduced responsiveness to conventional antiplatelet therapies, highlighting the urgent need for alternative therapeutic strategies to manage HHcy-related thrombotic diseases. Endothelium is the most critical components of physiological hemostasis by regulating platelet activity and coagulation. von Willebrand Factor (vWF), a glycoprotein predominantly secreted by the endothelium, binds to platelet surface antigens GPIbα, αIIbβ3 and subendothelial collagens, thereby activating platelets and triggering aggregation. HHcy has been implicated in endothelial injury through multiple mechanisms, including endoplasmic reticulum stress, oxidative stress, and inflammation. We also recently found that endothelial dysfunction contributed to thrombosis under stimulation of spike protein of severe acute respiratory syndrome coronavirus 2. Despite the pivotal role of ECs in hemostasis, the precise mechanisms by which Hcy induces platelet activation and coagulation through endothelial dysfunction remain unclear.

Here, we demonstrate that the thromboxane prostanoid receptor (TPr) functions as a previously unidentified receptor for Hcy, facilitating Hcy-induced endothelial vWF secretion and accelerating thrombosis. This discovery provides a novel mechanism for Hcy-mediated procoagulant activity and suggests potential therapeutic targets for treating thrombosis associated with HHcy.

In summary, the present study demonstrates that endothelial TPr activation mediated by Hcy is the pivotal event to trigger vWF secretion and accelerate thrombus formation in the context of HHcy. Hcy serves as a new ligand of TPr and subsequent leading to Gαq-PLC-Ca2+ cascade activation. Our study revealed a new mechanism of HHcy in thrombosis from the perspective of endothelium and demonstrated that TPr could be a promising target for treating HHcy-induced thrombosis.

Joint Association Between FIB-4 Index and Advanced Cardiovascular-Kidney-Metabolic Syndrome With Aortic Valve Calcification: A Community Cohort in China

Lingchun Lv, Yunteng Fang, Jiayi Shen

Lishui Central Hospital

Background and Aims : Aortic valve calcification (AVC) is common during the process of aging. Liver fibrosis, cardiovascular risk factors and kidney function, which share common mechanisms, have been associated with AVC. This study aimed to analyze the relationship between fibrosis-4 (FIB-4) index and advanced CKM syndrome with AVC respectively. Furthermore, the study focused on their joint effects on AVC.

Methods: We extracted data from the cohort of **the** PRECISE **(PolyvasculaR Evaluation for Cognitive Impairment and vaScular Events)** study **(NCT03178448)**, which was based on **the** middle-aged and elderly Chinese population in Lishui City. It was a community prospective cohort study that started from May 2017 and included a total of 3067 community-dwelling individuals whose ages ranged from 50 to 75 years and from 10 clusters consisting of 6 villages and 4 communities of Lishui city, Zhejiang province, China. Originally, 3433 subjects agreed to participate but 366 were excluded due to contraindications to special tests or mental illness or life expectancy lower than 4 years. PRECISE is an ongoing study and participants who completed baseline examinations will be followed for 4 years. Ultimately, 3067 participants were recruited. The protocol was approved by Beijing Tiantan Hospital and Lishui Hospital. Informed consent was also obtained by all participants. 3054 individuals were included for further analysis in our study. We assessed associations between FIB-4 index, advanced Cardiovascular-Kidney-Metabolic (CKM) syndrome and AVC. Combined effects were calculated by dividing the two indicators into four groups and 1.3 was the cutoff value for FIB-4 index. Subgroup analyses were performed to more effectively stratify analyses and show the interaction of variables for the associations between the FIB-4 index and AVC.

Results: Of 3054 participants, the mean age was 61.21±6.68 and 46.42% were male. Advanced CKM syndrome was correlated with AVC significantly with OR of 3.3 (95%CI: 2.47-4.41). Even after adjusting potential covariates, the correlation remained significant (P<0.001). As a continuous variable, FIB-4 index was related with AVC, with OR of 1.27 (95%CI: 1.15-1.41). Besides, when FIB-4 index was divided based on cutoff values of 1.3 and 2.67, we discovered that FIB-4 index was connected with AVC as a categorical variable. Compared with FIB-4 index ≤ 1.3, groups of 1.3-2.67 and >2.67 were both significant, with OR of 2.05 (95%CI: 1.46-2.88) and 3.57 (95%CI: 2.24-5.69) in Model3. Utilizing 5-knots, RCS curve revealed a nonlinear association and 1.3 was the reflection point. When FIB-4 index was less than 1.3, the OR decreased first and increased then. More than the reflection point, the OR constantly elevated with the increment of FIB-4 index. At last, RCS curve stayed stable when FIB-4 index more than 3. The combination effects of advanced CKM syndrome and FIB-4 index displayed stronger link with AVC.

Conclusion: In conclusion, elevated FIB-4 index and advanced CKM syndrome were related **with AVC. Furthermore, the joint association of FIB-4 index and advanced CKM syndrome displayed stronger link with AVC. The combination of two indicators showed better prediction ability** than traditional factors**. In future, monitoring CKM stages and FIB-4 index is necessary for prevention of AVC. Our research also involved CRHM syndrome and proved that the integration of cardiology, nephrology, hepatology, and endocrinology may better present the mechanism of AVC. Our results also deepened the understanding the interaction between fatty liver fibrosis, CKM syndrome and AVC.**

Metabolic Score for Visceral Fat and Cardiovascular Risk Prediction in Middle-aged and Older Chinese Adults: Evidence from the CHARLS Cohort

Chao Peng, Bin Liu, Zixi Li, Jiaru Gu, Huan Sun

China-Japan Union Hospital of Jilin University

Background: Excessive and ectopically distributed visceral fat (VF) not only reflects systemic metabolic dysfunction but also contributes to the progression of cardiovascular disease (CVD) through complex inflammatory and endocrine interactions.The Metabolic Score for Visceral Fat (METS-VF) is a novel, non-invasive, and integrative metric for quantifying visceral adiposity and associated metabolic perturbations, particularly valuable in epidemiological studies where direct imaging-based measurements of VF are infeasible.However, the association between METS-VF and cardiovascular risk remains inadequately explored in Asian populations, especially among middle-aged and older Chinese adults. Therefore, this study aimed to evaluate and validate the relationship between METS-VF and the risk of CVD in this demographic.

Methods: In this retrospective cohort analysis, we enrolled 7,082 participants aged ≥45 years who were free of clinically diagnosed CVD at baseline. All data were obtained from the China Health and Retirement Longitudinal Study (CHARLS), a nationally representative cohort launched in 2011 to collect detailed information on Chinese adults aged 45 and older. CHARLS provides high-quality longitudinal data on health, socioeconomic status, and aging in China's middle-aged and older population. The METS-VF index was computed for each participant using established formulas that integrate sex, age, WHtR, and the metabolic score for insulin resistance (METS-IR). The primary endpoint was the occurrence of CVD, as self-reported or medically confirmed during follow-up interviews. To delineate the relationship between METS-VF and incident CVD, we employed multivariable-adjusted Cox proportional hazards models, accounting for a wide array of potential confounders including sex, age, marital status, educational level, smoking status, alcohol consumption pre-existing metabolic disorders. To further evaluate the robustness of the association between METS-VF and CVD risk, subgroup analysis was performed. Furthermore, restricted cubic spline (RCS) modeling was employed to explore potential nonlinear associations.Finally, to confirm the robustness of the findings, a series of sensitivity analyses were conducted, including the exclusion of individuals with missing covariates, the inclusion of outliers, and quartile-based categorization of METS-VF.

Results: The results demonstrated a significant positive association between METS-VF and the risk of cardiovascular disease (CVD) across all study subgroups. Furthermore, Cox proportional hazards regression analysis indicated that higher METS-VF levels were associated with increased CVD risk (HR: 1.62; 95% CI: 1.45–1.80). This association remained statistically significant after comprehensive adjustment for a wide range of potential confounders (adjusted HR: 1.39; 95% CI: 1.23–1.56). When METS-VF was categorized into tertiles, individuals in the highest tertile (Q3) consistently exhibited significantly elevated risks for all cardiovascular outcomes compared with those in the lowest tertile (Q1). In addition, restricted cubic spline (RCS) analysis revealed a significant nonlinear relationship between METS-VF and CVD risk (p for non-linearity = 0.001). Notably, when METS-VF exceeded 6.73, the slope of the risk curve steepened markedly, indicating a rapid escalation in cardiovascular risk. These findings remained robust across multiple sensitivity analyses.

Conclusion: This study revealed that elevated METS-VF levels are positively and independently associated with increased CVD risk in middle-aged and older Chinese adults. Its non-invasive, easily reproducible nature renders it particularly suitable for integration into routine screening and preventive strategies. By capturing the metabolic burden imposed by visceral adiposity, METS-VF offers clinicians a valuable tool for early risk stratification.

不同血糖状态心力衰竭患者中重度冠状动脉钙化病变最佳血运重建与长期结局的关联性研究

林章宇 李博文 宋彦君 尹栋

中国医学科学院阜外医院（国家心血管病中心）

背景：对于不同血糖状态的心力衰竭（HF）患者，中重度冠状动脉钙化（MSCAC）病变的最佳血运重建治疗与长期临床结局之间的关系目前尚不明确。因此，本研究旨在探讨不同血糖状态的心力衰竭患者接受中重度冠脉钙化病变经皮冠状动脉介入治疗（MSCAC-PCI）达到最佳与非最佳效果与长期不良临床结局之间的关联。

方法： 这项前瞻性队列研究纳入了 2017 年 1 月至 2018 年 12 月期间在阜外医院接受 MSCAC-PCI 治疗的 1,086 例心力衰竭患者。根据 MSCAC-PCI 的结果将患者分为：失败组、次优血运重建组和最佳血运重建组。主要终点是心血管（CV）事件，即心血管死亡和靶血管心肌梗死（TVMI）的复合终点。

结果：在中位 3 年的随访期间，共发生 87 例（8.0%）心血管死亡 /TVMI 事件。与 MSCAC-PCI 失败的患者相比，接受最佳血运重建的患者发生心血管事件的风险显著降低（校正风险比 [aHR] = 0.33; 95% 置信区间 [CI], 0.15-0.71）。次优血运重建组与失败组患者之间未观察到显著差异。亚组分析显示，糖尿病前期患者在接受最佳血运重建后心血管事件风险较低（aHR = 0.18; 95%CI, 0.03-0.87），这一差异主要源于 TVMI 风险的降低（aHR = 0.06; 95%CI, 0.01-0.42）。同时，糖尿病患者在接受最佳血运重建后心血管死亡风险较低（aHR = 0.25; 95%CI, 0.06-0.96）。在血糖状态正常的患者中，不同 PCI 结果组间未见显著差异。

结论：我们的研究结果表明，在 MSCAC-PCI 中实现最佳血运重建与心力衰竭患者长期临床结局的改善相关，尤其是在糖尿病前期和糖尿病患者中。

Apolipoprotein A2 influences ANGPTL3 on modulating TG catabolism and inflammatory cytokines secretion

Ye Cheng, Xin Su

Xiamen Cardiovascular Hospital of Xiamen University

The prevalence of coronary artery disease (CAD), including atherosclerosis, stable angina (SA), and ST elevation myocardial infarction (STEMI), has remarkably risen which poses serious risk to human health. Several risk factors impose burden on development of CAD, such as dyslipidemia, manifesting as higher low-density lipoprotein cholesterol (LDL-C) concentrations, triglyceride (TG) concentrations, and reduced high-density lipoprotein cholesterol (HDL-C) concentrations. Furthermore, immune cascade response with excessive production of inflammatory cytokines in promoting atherosclerotic related cardiovascular disease have been given substantial attention, since increased levels of multiple pro-inflammatory cytokines, such as interleukin-1 (IL-1), high-sensitivity C-reactive protein (hs-CRP), and tumor necrosis factor-α (TNF-α), were positively correlated with the prevalence of CAD.

The angiopoietin-like protein (ANGPTL) family, containing ANGPTL1 to ANGPTL8, is a series of secreted glycoproteins which share consistent structure whereas different functions. Among those eight members, ANGPTL3 was indicated as a novel regulator in TG catabolism. As shown, ANGPTL3 was controlled by nutritional condition and could modulate TG metabolism by suppressing the lipoprotein lipase (LPL) activity, the rate-limiting enzyme for TG hydrolysis and serum TG clearance. Using ANGPTL3 gene-deficient mice, it has demonstrated that these mice presented reduced serum TG concentrations and up-regulated LPL bio-activity. On the contrary, over-expressing ANGPTL3 gene or injecting ANGPTL3 protein into mice could significantly increase serum TG levels. The individuals carrying loss of functional of ANGPTL3 gene also exhibited extremely lower serum TG concentrations. The important role of TG, including triglyceride-rich lipoproteins (TRLs), in facilitating the pathological development of CAD has been established, whereas whether ANGPTL3 concentration is altered in the CAD patients is still not elucidated.

HDL contains apolipoprotein A1 (ApoA1), ApoA2, phospholipids, and cholesterol. ApoA1 is the most dominant apolipoprotein in HDL particle which presents anti-atherogenic function. In comparison, ApoA2 is the second-most dominant apolipoprotein, whereas its pathophysiological role remains fully clarified. It was demonstrated that ApoA2 presented anti-oxidant effects which might contribute to atherosclerotic protection [9]. On the contrary, another clinical research showed the anti-ApoA2 treatment could suppressed the development of coronary arteritis which could be considered as an effective therapeutic candidate for the treatment of vasculitis, proposing the role of ApoA2 in promoting inflammatory response. Accordingly, the accurate functions of ApoA2 in atherosclerotic related inflammation is still required to be explored. On the other hand, using APOA2 gene transgenic mice, the authors found that the TG catabolism was reduced; meanwhile, the HDL particle isolated from these mice showed impaired LPL activity. Thereby, it seems that ANGPTL3 and ApoA2 present similar function on TG metabolism.

In the present research, an observational clinical trial was conducted to assess the ANGPTL3 and ApoA2 concentration in diverse groups classified by the anthropometric and metabolic profiles. As shown in the results, the serum levels of ANGPTL3 and ApoA2 exhibited no significant discordance between the CAD group and the healthy control group. Both ANGPTL3 and ApoA2 were importantly associated with serum concentrations of TG (r = 0.249, P = 0.002; r = 0.379, P = 0.001, respectively). Additionally, ApoA2 were inversely associated with multiple pro-inflammatory cytokines, such as high-sensitivity C-reactive protein (hs-CRP, r = -0.079, P =0.003), tumor necrosis factor-α (TNF-α, r = -0.119, P = 0.001), and IL-1β (r = -0.103, P = 0.004). The regression analysis confirmed that ApoA2 was an independent modulator to TG and pro-inflammatory cytokines independent of ANGPTL3 (standardized β = 0.196, P < 0.001).

Conclusively, the results found in our study demonstrated that the serum ApoA2 exhibited a close association with several pro-inflammatory cytokines, including hs-CRP, TNF-α, and IL-1β. Additionally, ANGPTL3 was inversely associated with serum ApoA2 and the relationship between ANGPTL3 and TG disappeared while serum ApoA2 was taken into consideration, proposing the potential function of serum ApoA2 in ANGPTL3 action. Concerning on this notion, further research is still required to fully explore the associations between ApoA2 with ANGPTL3 and the potential mechanism of TG modulation in patients with CAD.

载脂蛋白 A1 经 Sortilin 负向调控人脂肪间充质干细胞成脂分化的实验研究

程晔 苏欣

厦门大学附属心血管病医院

目的：探究载脂蛋白 A1（ApoA1）对人脂肪间充质干细胞（AMSCs）成脂分化的影响及其潜在机制。**方法：**经厦门大学附属心血管病医院伦理委员会批准及患者知情同意后，获取 2023 年 2 月至 9 月在我院进行外科手术共 40 例患者皮下脂肪组织，获取人 AMSCs 后诱导为成熟脂肪细胞，以 15μg/ml 人重组 ApoA1 蛋白干预细胞，作为实验组；不加 ApoA1 干预的细胞作为对照组；于促分化第 7、14、21 天收获细胞：（1）观察 ApoA1 对细胞内甘油三酯（TG）含量和成脂分化标志物基因、蛋白水平影响。（2）通过荧光抗体标记，利用激光共聚焦实验观察 ApoA1 与分选蛋白 Sortilin 是否存在共定位现象。（3）观察 ApoA1 对 Sortilin 基因、蛋白水平的影响。（4）利用慢病毒转染技术，沉默 SORT 基因，并以 ApoA1 干预 21 天，观察 ApoA1 对细胞内 TG、成脂分化标志物基因、蛋白水平影响。**结果：**（1）在同一促分化时间内，ApoA1 干预的细胞 TG 含量及 FAS、C/EBPβ 等成脂分化标志物基因、蛋白表达水平下降。（2）经过激光共聚焦分析发现，在 AMSCs 成脂分化过程中，ApoA1 与 Sortilin 存在共定位现象。（3）在同一促分化时间段内，ApoA1 可明显上调细胞内 Sortilin 基因、蛋白水平。（4）沉默 SORT 基因后，ApoA1 对 AMSCs 成脂分化抑制作用显著降低。**结论：**ApoA1 通过上调 Sortilin，下调成脂分化标志物表达，降低 TG 含量，抑制 AMSCs 成脂分化。

三酰甘油葡萄糖指数与老年非介入治疗非 ST 段抬高型心肌梗死患者的预后相关：一项单中心回顾性队列研究

李明轩 曲新凯 史凯蕾

复旦大学附属华东医院

目的 探讨三酰甘油葡萄糖（TyG）指数对老年非介入治疗非 ST 段抬高型心肌梗死（NSTEMI）患者预后的预测价值。

方法 回顾性分析 2018 年 7 月–2022 年 6 月，入住复旦大学附属华东医院心脏监护室，确诊为 NSTEMI 但未行介入治疗的 80 例老年患者临床资料。依据 TyG 中位数将患者分为低 TyG 组（n=40）和高 TyG 组（n=40）。比较 2 组的一般资料，随访患者出院后的全因死亡情况。

结果 80 例老年 NSTEMI 患者年龄 60~97 岁，平均（80.8±9.4）岁，TyG 指数中位数为 8.70。与低 TyG 指数组相比，高 TyG 指数组患者年龄较小，体质量指数较高，饮酒史构成比较少，糖尿病构成比较多，总胆固醇、三酰甘油和空腹血糖水平较高，差异有统计学意义（P < 0.05）。随访期间高 TyG 组患者死亡 20 例，低 TyG 组患者死亡 13 例。Kaplan-Meier 生存分析显示，低 TyG 指数组预后优于高 TyG 指数组，差异有统计学意义（P=0.046）。采用 Lasso 回归分析进行变量筛选和去除变量间的多重共线性，共筛选出 10 个变量，包括 TyG 指数、年龄、性别、房颤、血小板、TnT 峰值、BNP、肌酐、谷丙转氨酶和 GRACE 评分。先后进行单因素和多因素 Cox 比例风险回归分析显示，TyG 指数（HR=2.442，95%CI：1.449~4.117）、肌钙蛋白 T 峰值（HR=1.274，95%CI：1.037~1.565）、脑钠肽（HR=1.001，95%CI：1.000~1.001）和年龄（HR=1.050，95%CI：1.004~1.099）是影响非介入治疗老年 NSTEMI 患者生存率的独立预后因素。

结论 低 TyG 指数的老年非介入治疗 NSTEMI 患者死亡风险可能低于高 TyG 指数者。

Association Between Pain Characteristics, Circadian Syndrome and Cardiovascular Disease in Chinese Middle-Aged and Older Adults: A 4-Year Follow-Up Study

Lingchun Lv, Yunteng Fang, Jiayi Shen

Lishui Central Hospital

Background: Pain and circadian syndrome (CirS) are both risk factors for the incidence of cardiovascular disease (CVD). in this study, we conducted a longitudinal analysis utilizing data from a large cohort in China to explore link between pain characteristics and CirS and their combined effects on CVD in Chinese middle-aged and older adults. This study was striving to find out whether pain and changes of pain were risk factors for CirS and the joint effects of two indicators to predict CVD.

Methods: This study included 2649 participants in analysis1 and 6265 in analysis2. Logistic regression models were utilized to present associations between pain characteristics and changes of pain characteristics with CirS. Furthermore, subgroups analyses were conducted to better stratify analyses and show the interaction of variables for associations between pain and new-onset CirS. Joint association of CirS and multisite pain with CVD was performed. We extracted data from China Health and Retirement Longitudinal Study (CHARLS), a longitudinal survey recruiting aged 45 years and above. This cohort is a prospective study that included 450 villages or residential communities in 28 provinces in China. A multi-stage cluster random sampling method was utilized to ensure a representative sample. In 2011 the first wave initiated, followed by 2013 (wave 2), 2015 (wave 3), 2018 (wave 4), 2020 (wave5). All participants signed informed consents and one-to-one interviews were performed to gain high-quality information.

Results: Of 2649 participants, mean age was 58.09±(8.43) years and 52.74% were males. Individuals with baseline pain, single-site pain and multisite pain are all closely related with CirS, even adjusting all poten-

tial covariates. Compared with no pain, people with multisite pain persistence manifested strong link with risk of CirS. Additionally, people with single-site, no pain, single-site to multisite pain or multisite pain persistence were more prone to CirS with OR of 2.27 (95%CI: 1.68,3.08) and 2.37 (95%CI: 1.7,3.3) after covariates adjustment respectively. Individuals with BMI ≥ 23 with multisite pain persistence more tightly correlated with CirS than other subgroups after variables adjustment, with OR of 2.86 (95%CI: 1.75,4.45). BMI had interaction effects on relationship. The combination of CirS and multisite pain significantly enhanced the risk of CVD with OR of 1.73 (95%CI: 1.31,2.29). The P values for trend for combination analysis were all significant. The sensitivity analysis proved the robustness of our results.

Conclusions: Our study highlighted that pain, especially multisite pain, was associated with CirS. Multisite pain persistence and no pain, single-site to multisite pain were significantly correlated with progression to CirS. Besides, the combination of CirS and multisite pain was more significantly associated with risk of CVD. In conclusion, our study highlighted association between pain, CirS and CVD among Chinese middle-aged and older adults. Multisite pain, multisite pain persistence and progress of pain showed stronger link with CirS. The combination of CirS and multisite pain was more significantly with risk of CVD than single CirS or multisite pain. Our findings suggested the prevention of pain persistence and progress of pain may lower incidence of CirS and the prevention of multisite pain and CirS could stratify CVD risk.

TyG 指数联合 hsCRP 对糖尿病合并急性冠脉综合征患者 PCI 术后预后的相关性

周鹤

中国人民解放军北部战区总医院

目的：评估甘油三酯 - 葡萄糖（TyG）指数联合高敏 C 反应蛋白（hsCRP）对糖尿病合并急性冠脉综合征（ACS）患者经皮冠状动脉介入（PCI）治疗出院后 12 个月内不良预后的相关性。

方法：选取自 2016 年 3 月至 2022 年 3 月于北部战区总医院心血管内科收治的接受 PCI 治疗的合并糖尿病的 ACS 患者为研究对象。结局事件为患者出院后 12 个月的全因死亡和心原性死亡。根据 TyG 指数和 hsCRP 的水平将患者分为四组：低 TyG + 低 hsCRP 组，高 TyG + 低 hsCRP 组，低 TyG + 高 hsCRP 组和高 TyG + 高 hsCRP 组。采用 Cox 比例风险模型分析不同组别对结局事件累计发生率的影响，计算风险比（HR）和 95% 的可信区间（CI）。

结果：根据纳入排除标准，本研究最终纳入 4422 名患者，平均年龄为 60.0±10.1 岁，男性占比 69.2%。Cox 回归分析结果提示，与低 TyG + 低 hsCRP 组相比，低 TyG + 高 hsCRP 组患者出院后 12 个月全因死亡（HR：1.86, 95% CI: 1.05-3.30）、心原性死亡（HR：2.01, 95% CI: 1.03-3.94）发生风险增加；高 TyG + 高 hsCRP 组患者出院后 12 个月全因死亡（HR：2.50, 95% CI: 1.46-4.28）、心原性死亡（HR：2.99, 95% CI: 1.59-5.62）发生风险也显著增加。在进一步校正了相关混杂因素后，与低 TyG + 低 hsCRP 组相比，高 TyG + 高 hsCRP 组患者出院后 12 个月全因死亡发生风险增加 1.9 倍 (95% CI: 1.08-3.33, P = 0.03), 心原性死亡发生风险增加 2.23 倍 (95% CI: 1.15-4.29, P = 0.02)。

结论：对于接受 PCI 治疗的合并糖尿病的 ACS 患者，TyG 指数与 hsCRP 同时升高的患者其术后 12 个月的全因死亡及心原性死亡风险均显著升高。

Correlation of triglyceride-glucose index with major adverse cardiovascular events in type 2 diabetes mellitus patients with acute myocardial infarction combined with HFpEF

XIAODONG ZHANG, Ying Liu

The First Affiliated Hospital of Dalian Medical University

Abstract

Aims: This study was to evaluate the correlation between triglyceride-glucose index (TyG) and major adverse cardiovascular events (MACE) in patients with type 2 diabetes mellitus (T2DM) and heart failure with preserved ejection fraction (HFpEF) after acute myocardial infarction (AMI).

Methods: This retrospective study at the First Affiliated Hospital of Dalian Medical University included 400 AMI patients with T2DM and HFpEF who underwent percutaneous coronary intervention (PCI) between January 1, 2018, and January 1, 2023.

In this study, patients were enrolled for follow-up starting from the date of their first hospitalization, with the follow-up period extending until either the patient's death or July 31, 2024. The median follow-up time was 24.63 months. The study endpoint was MACE, defined as a composite of one or more of the following: all-cause death, unplanned revascularization, and non-fatal myocardial infarction. To identify clinical characteristics associated with adverse cardiovascular outcomes, baseline variables were compared between patients with and without MACE. This grouping approach was intended to explore potential risk factors for MACE. All enrolled patients were encouraged to monitor their condition regularly through outpatient services. For those who did not complete the follow-up program, efforts were made to contact them by telephone to ensure data completeness. The study was conducted using univariate and multivariate Cox regression analyses, subgroup analyses, receiver operating characteristic (ROC) curves, and Kaplan-Meier survival curves to assess the correlation between TyG index and MACE.

Results: Multivariate Cox regression analyses showed that in Model 3 with variables fully adjusted, when TyG was used as a categorical variable, the risk of MACE in the TyG T2 and T3 groups was 1.622 times and 2.247 times higher than that in the T1 group, respectively (P < 0.05). When TyG was used as a continuous variable, the risk of MACE increased by 49.5% for every 1 unit increase in the TyG index (P < 0.001). In the subgroup analysis, elevated TyG index levels were consistently associated with an increased risk of MACE across multiple clinical subgroups (P < 0.05). ROC analysis showed that the TyG index significantly predicted the occurrence of MACE (AUC: 0.635, 95% CI: 0.580-0.691, P < 0.001), all-cause death (AUC: 0.565, 95% CI: 0.508-0.622, P = 0.027), non-fatal myocardial infarction (AUC: 0.617, 95% CI: 0.542-0.693, P = 0.004), and unplanned revascularization (AUC: 0.644, 95% CI: 0.578-0.710, P < 0.001). The Kaplan-Meier survival curves revealed statistically significant differences in survival probabilities for the occurrence of MACE, all-cause death, non-fatal myocardial infarction, and unplanned revascularization across the three TyG index groups as the follow-up period progressed (P < 0.05).

Conclusions: Our study found that in T2DM patients with HFpEF combined with AMI, the incidence of MACE events was higher, and the prognosis worsened as the TyG index increased. The TyG index proved to be an independent predictor of MACE, and could serve as a valuable tool for risk stratification and prognosis in this population. Clinicians should be particularly alert to the risks associated with left ventricular dysfunction in patients with elevated TyG indices during the management of AMI.

Keywords: Triglyceride-glucose index; Acute myocardial infarction; Heart failure with preserved ejection fraction; Major adverse cardiovascular events; Type 2 diabetes mellitus

The Impact of Allostatic Load on the Incidence of Cardiometabolic Multimorbidity: Evidence from the China health and Retirement Longitudinal study

Ling-Chun Lv, Yunteng Fang, Jiayi Shen

Lishui Central Hospital

Background: Allostatic load (AL) is an index used for assessing chronic stress. Based on available literature AL is able to predict cardiovascular disease. This study aimed to investigate association between AL and CMM in middle-aged and older Chinese adults. We hypothesized that higher burden of AL associated with risk of CMM. We used data from the nationally representative database and aimed to assess the cross-sectional and longitudinal associations between AL burden and CMM. Besides, since AL would change in during follow-up, we also explored association between transition of AL with incident CMM. This study might provide new insights into the understanding of AL, an indicator of chronic stress, and prevention of CMM.

Methods: This study undertakes data from the China Health and Retirement Longitudinal Study (CHARLS), a longitudinal survey mainly recruiting participants aged 45 years and above.(22) CHARLS utilized multi-stage cluster random sampling method to ensure a representative sample. 17,708 participants from 450 villages or residential communities in 28 provinces in China were enrolled and all participants signed informed consents. This study included 6307 individuals for cross-sectional analysis and 3331 for longitudinal analysis. Logistic regression models were utilized to assess associations between AL (as continuous and categorical indicator) and CMM in cross-sectional and longitudinal analysis. Additionally, based on the transition of AL, participants were divided into four groups and persistent low AL burden was the reference. Furthermore, subgroups analyses were conducted to better stratify analyses and show the interaction of variables. Sensitivity analyses excluding missing value of covariates were conducted.

Results: 236 CMM events at baseline and 149 CMM events occurred at 4 year follow-up. In longitudinal analysis the mean age was 59.73±(9.12), 45.93% were male. Both in cross-sectional and longitudinal analysis, AL was associated with CMM as continuous and categorical indicator after adjusting all potential covariates. The higher AL burden showed stronger link with incident CMM. Besides, compared with persistent low AL burden, the persistent high/medium burden demonstrated strongest association with CMM. Sex had interaction effects on relationship between AL burden and CMM.As a continuous value, AL score was associated with CMM with OR of 1.7 (95%CI: 1.58-1.83). Even after adjusting all variables, the connection remained robust with OR of 1.5 (95%CI: 1.39-1.63) in Model3. As a continuous value, AL score was closely associated with incident CMM with OR of 1.2 (95%CI: 1.08-1.34) in Model3 per 1 score. Besides, compared with low burden, medium and high burden showed stronger association with risk of CMM. When it came to progression of AL burden, low burden to high/medium burden was strongly associated with incident CMM with OR of 4.28 (95%CI: 2.21-8.3). Furthermore, individuals with persistent high/medium burden were more prone to CMM with OR of 5.79 (95%CI: 3.34-10.02).

Conclusions: In conclusion, the results of our study indicated that base-

line and longitudinal AL was associated with incident CMM. Increasing AL score and AL burden had great impact on CMM. Besides, compared with persistent low AL burden, persistent high/medium AL burden was strongly associated with risk of CMM. Early evaluation of AL burden is of significant importance for the prevention or treatment of CMM. The transition of AL burden may also help assess the risk of CMM and early identify high-risk individuals.

简易胰岛素抵抗指数对高原世居藏族发生高尿酸血症的预测价值

冯佳越 舒燕

四川省人民医院

背景：高尿酸血症（HUA）已成为高原藏族人群中一种常见的代谢性疾病。胰岛素抵抗（IR）与 HUA 的发生发展密切相关，但传统的 IR 指标因为侵入性、复杂性等缺点，限制了其在临床和流行病学研究中的应用。

目的：评价简易 IR 指数，甘油三酯葡萄糖指数（TyG）、甘油三酯葡萄糖体质量指数（TyG-BMI）、甘油三酯 / 高密度脂蛋白胆固醇比值（TG/HDL-C）和胰岛素抵抗代谢指数（METS-IR），对高原世居藏族发生 HUA 的预测价值。

方法：本研究为横断面调查，选取 2022 年 6 月至 2023 年 2 月在四川省甘孜藏族自治州理塘县人民医院健康体检中心进行健康体检的世居藏族居民为研究对象。通过问卷调查、体格检查和血生化检测收集受试者数据，根据血清尿酸水平分为 HUA 组和非 HUA 组。采用 Spearman 相关探讨简易 IR 指数与 HUA 的相关性；计算各 IR 指数的四分位数，采用多因素 Logistic 回归评估不同 IR 指数与 HUA 的关系，采用受试者工作特征曲线（ROC）及曲线下面积（AUC）评估各 IR 指标对 HUA 的预测能力。

结果：本研究纳入 2493 例高原世居藏族居民，共检出 HUA 患者 944 人， HUA 患病率男性高于女性（42.91% vs. 34.55%, P <0.05）。与非 HUA 组相比，HUA 组 TyG、TyG-BMI、TG/HDL-C、METS-IR 均 较 高（P <0.05）。Spearman 相关分析发现，TyG 与 HUA 相关性最强（P <0.001），METS-IR 与 HUA 相关性最弱（P <0.001）。伴随简易 IR 指数每升高四分位数，HUA 患病率呈上升趋势（P <0.001）。多因素 Logistic 回归显示 TyG 升高时，高原世居藏族发生 HUA 的风险最高（男性，OR 11.936，95% CI 7.175 – 19.858；女性，OR 14.873，95% CI 9.533 – 23.204），其 次 为 TG/HDL-C、TyG-BMI 和 METS-IR。ROC 曲线显示 TyG 预测高原世居藏族发生 HUA 的 AUC 最大（男性，0.757，95% CI 0.727 – 0.787；女性，0.776，95% CI 0.751 – 0.801），显著高于 TG/HDL-C、TyG-BMI 和 METS-IR。

结论：简易 IR 指数升高可增加高原世居藏族发生 HUA 的风险。与 TG/HDL-C、TyG-BMI 及 METS-IR 相比，TyG 预测高原世居藏族发生 HUA 的效果更好。

The Role of Instrumental Activity of Daily Living Disability in the Association between Circadian Syndrome and Cardiometabolic Multimorbidity in Chinese Middle-Aged and Older Adults

Lingchun Lv, Yunteng Fang, Jiayi Shen

Lishui Central Hospital

Background: Instrumental activities of daily living (IADL) disability and circadian syndrome (CirS) are risk factors for the incidence of cardiometabolic disease. We conducted a cross-sectional and longitudinal analysis extracting data from a large Chinese cohort to investigate the link between CirS and CMM. Besides, combined effects of CirS and IADL disability on CMM and the mediation analysis were also evaluated. This study was striving to find out whether CirS were risk factors for CMM.

Methods: We extracted data from China Health and Retirement Longitudinal Study (CHARLS), a longitudinal survey mainly enrolling aged 45 years and above. This cohort is a prospective study that included 450 villages or residential communities in 28 provinces in China. A multi-stage cluster random sampling method was utilized to ensure a representative sample. All participants signed informed consents and one-to-one interviews were performed to gain high-quality and accurate information. This study included 8085 participants in cross-sectional analysis and 5887 in longitudinal analysis. Logistic regression models were utilized to present associations between CirS and components with CMM. Cox proportion hazard regression models were performed to assess relationship between CirS and incident CMM. Furthermore, subgroups analyses were conducted to better stratify analyses and show the interaction of variables. Combined effects of CirS and IADL disability on CMM were conducted. Also, we analyzed mediation role of IADL in the association between CirS and progression to CMM.

Results: In longitudinal analysis, of 5887 participants, 452 CMM events occurred. The mean age was 58.57±(8.76) and 45.73% were male. In cross-sectional analysis, CirS was associated with CMM after adjusting all potential covariates. When components of CirS ≥ 6, CirS showed strongest link with CMM with ORs of 16.38 (95%CI: 10.74-25) and 7.49 (95%CI: 4.63-12.12) in Model3. In longitudinal analysis 452 CMM events occurred. CirS and increasing number of components still displayed strong link with CMM in crude model and Model3 with HRs of 3.43 (95%CI: 2.82-4.16) and 2.04 (95%CI: 1.65-2.53). Furthermore, The combination of two diseases strengthened association with CMM with HR of 5.08 (95%CI: 3.87-6.66) in crude model and 3.06 (95%CI: 2.28-4.12) after adjusting all covariates. IADL mediated 5.83% on the relationship between CirS and CMM. Besides, population with drinking habits would face more hazard of CMM and lower education levels would also increase risk of CMM.

Conclusions: Our study highlighted that CirS and increasing number of components associated with CMM. The combination of CirS and IADL disability was significantly associated with new on-set CMM. IADL disability had mediation effects on CirS in the progression to CMM. In conclusion, our study highlighted association between CirS, IADL disability and CMM among Chinese middle-aged and older adults. CirS and increasing number of its components showed strong link with CMM. The combination of CirS and IADL disability was significantly associated with new on-set CMM than single CirS or IADL disability. Also, IADL disability had mediation effects on CirS in the progression to CMM. Our findings suggested the prevention of CirS and related components may lower incidence of CMM and the prevention of IADL disability and CirS could stratify CMM risk.

Intensified Lipid-Lowering Strategies and Their Effect on Atherogenic and Metabolic Markers in Coronary Artery Disease

Zhi-Fan Li, Zheng Yin, Xi Li, Meng-Ying Lu, Lei Bao, Hong Qiu, Na-Qiong Wu

Fuwai Hospital, National Center for Cardiovascular Diseases, Chinese Academy of Medical Sciences and Peking Union Medical College

Purpose: Lipid-lowering therapy (LLT) is effective in managing lipid levels and reducing adverse event risks in coronary artery disease (CAD) patients, also affecting glucose metabolism. This study evaluates the effects of varying LLT strategy on lipid profiles and insulin resistance (IR) biomarkers in CAD patients.

Methods: This was a prospective observational study enrolled CAD patients in Fuwai Hospital from August, 2020 to February, 2023. Participants were categorized into monotherapy (low-/moderate-statin monotherapy or ezetimibe monotherapy), dual therapy (statin and ezetimibe) and triple therapy (statin + ezetimibe + PCSK9 inhibitors), and followed for biochemical parameters. Changes in lipid profiles and IR-related biomarkers, including non-high-density lipoprotein cholesterol (non-HDL-C), remnant cholesterol (RC), lipoprotein(a) [Lp(a)], triglyceride-glucose (TyG) index, and atherogenic index of plasma (AIP), were assessed and compared across the three treatment groups. Multiple linear regression analyses were performed to evaluate the associations between LLT intensity and percentage changes in these biomarkers. In addition, subgroup and interaction analyses were conducted to further explore effect modification by baseline characteristics.

Results: A total of 1393 CAD patients were included in this study, with 212 in monotherapy group, 1118 in dual therapy group, and 61 in triple therapy group. After a median follow-up of 1 year, the dual therapy and triple therapy groups showed significantly greater reductions in LDL-C (-25.42% vs. -62.93% vs. -0.72%, P < 0.001), TC (-16.71% vs. -44.02% vs. 0.95%, P < 0.001), apoB (-17.98% vs. -56.10% vs. -2.81%, P < 0.001), non-HDL-C (-23.72% vs. -57.47% vs. 0.29%, P < 0.001), RC (-20.51% vs. -45.07% vs. -5.71%, P = 0.001), TG (-17.44% vs. -25.66% vs. -7.61%, P = 0.001), and TyG (-2.19% vs. -7.14% vs. -1.04%, P = 0.003) compared with the monotherapy group. AIP, glucose, and Lp(a) levels showed overall declining trends across all groups, but none of the between-group differences reached statistical significance. Multiple linear regression analyses demonstrated a significant negative correlation between dual therapy and triple therapy and percentage changes in LDL-C (dual therapy: β = -16.43, 95% CI: -21.95 to -10.90, P < 0.001; triple therapy: β = -36.56, 95% CI: -47.82 to -25.30, P < 0.001), non-HDL-C (dual therapy: β = -14.95, 95% CI: -20.07 to -9.82, P < 0.001; triple therapy: β = -33.51, 95% CI: -44.77 to -22.26, P < 0.001), and RC (dual therapy: β = -19.47, 95% CI: -36.18 to -2.77, P = 0.023; triple therapy: β = -38.18, 95% CI: -73.01 to -3.36, P = 0.046). A downward trend in TyG and apoB were also observed in both dual and triple therapy groups, though the associations did not reach statistical significance. Furthermore, interaction and subgroup analyses revealed significant interactions between LLT and BMI stratification in relation to percentage changes in LDL-C, TC, and non-HDL-C (all P for interaction ≤ 0.05). In the non-overweight/obese population, both dual therapy and triple therapy were associated with more pronounced lipid-lowering effects compared to the overweight/obese group (all P < 0.01).

Conclusion: In patients with CAD, triple LLT (statin plus ezetimibe and PCSK9 inhibitors) led to the most pronounced improvements in lipid profiles, including LDL-C, TC, non-HDL-C, and RC, along with a trend toward improved IR markers such as TyG. Subgroup analyses further revealed enhanced lipid-lowering effects of intensified therapy, particularly among non-overweight/obese individuals. These findings highlight the superior efficacy of triple therapy in addressing cardiovascular risk in CAD patients.

TRIM35 介导氨基酸转运在压力负荷型心室重构中的作用与机制研究

宋娟 李穗吉

厦门大学附属心血管病医院

研究背景： 病理性心肌重构（Cardiac maladaptive remodeling）是导致心力衰竭的主要原因之一，其发病机制极为复杂。E3 泛素链接酶 TRIM35 调控多种生物过程，包括细胞凋亡、先天免疫反应以及代谢重编程等，并参与免疫微环境

调节和肿瘤发展。然而，TRIM35 是否通过影响心肌成纤维细胞表型及在压力负荷型心室重构中发挥作用，尚不清楚。

研究方法： 本研究采用成纤维细胞特异性 Trim35 基因敲除小鼠（Trim35cKO）来探究 TRIM35 在成纤维细胞中的功能。通过主动脉弓缩窄术（TAC）建立小鼠压力负荷型心室重构模型，检测并分析各组小鼠心脏功能、形态结构以及心肌组织的分子变化。利用生物素转换技术（biotin-switch）结合液相色谱 - 串联质谱（LC/MS）、RNA 测序（RNA-Seq）、以及腺病毒转染等技术，明确 TRIM35 调控成纤维细胞表型的分子机制。

研究结果： 在小鼠和人类发生纤维化的心脏组织中，TRIM35 的表达主要在心肌成纤维细胞内显著上调，转化生长因子 -β1（TGF-β1）刺激心肌成纤维细胞，TRIM35 表达上调。心肌成纤维细胞特异性敲除 TRIM35，能显著改善由 TAC 手术诱导的心肌纤维化和心肌肥大。过表达 TRIM35 则促进心肌成纤维细胞的增殖、迁移和分化。更重要的是，过表达 TRIM35 的成纤维细胞可通过旁分泌作用，诱导心肌细胞发生肥大。进一步研究分子机制，我们发现，TRIM35 能够与氨基酸转运蛋白 SLC7A5 相互作用，对其进行泛素化修饰并上调其表达水平，从而增强氨基酸的转运能力，进而激活哺乳动物雷帕霉素靶蛋白复合物 1（mTORC1）信号通路。此外，过表达 SLC7A5 可取消条件性敲除 TRIM35 所带来的心肌纤维化和心肌肥大的改善作用。

研究结论： 我们的研究结果揭示了成纤维细胞中的 TRIM35 在压力负荷型心室重构中扮演着全新的关键角色，并阐明了其通过 SLC7A5 介导的氨基酸转运激活 mTORC1 信号通路的分子机制。这些发现为能量代谢在压力负荷型心室重构中的作用提供证据，并为治疗心肌重构提供了一个潜在的全新治疗靶点。

Impact of a Comprehensive Healthy Lifestyle Score on a Broad Spectrum of Cardiometabolic Diseases and Enhanced Risk Prediction Based on the UK Biobank Database

Xin-Yue Chen, Yan-Jun Song, Dong Yin, Ke-Fei Dou

Fuwai Hospital, Chinese Academy of Medical Sciences and Peking Union Medical College

Aim: Primary prevention of cardiometabolic diseases (CMDs), a leading cause of global morbidity and mortality, requires robust risk stratification tools. This study aimed to systematically evaluate the association between a comprehensive set of lifestyle factors and the risk of a wide range of CMDs using data from the UK Biobank. The research also sought to determine if incorporating these lifestyle factors could improve the performance of traditional disease risk prediction models.

Methods: We analyzed data from 148,155 participants in the UK Biobank without baseline CMDs. Cox proportional hazards models were used to assess the impact of healthy lifestyle factors (non-smoking, alcohol consumption, physical activity, healthy diet, and healthy sleep) on 11 types of CMDs (coronary heart disease, type 2 diabetes, atrial fibrillation, hypertension, stroke, heart failure, Alzheimer's disease, non-alcoholic fatty liver disease, valvular heart disease, cardiomyopathy, and pulmonary hypertension). Based on the β coefficients from a Cox proportional hazards model, a weighted healthy lifestyle score was developed. Improvements in predictive models after incorporating lifestyle factors were evaluated.

Results: Through Cox model analysis, this study quantified the contribution weights of five lifestyle factors to health. The results showed that healthy sleep contributed the most (weighted β coefficient: 0.342), followed by non-excessive alcohol consumption (0.288), non-smoking (0.239), regular physical activity (0.082), and healthy diet (0.049). A nomogram developed from the model visually confirmed the relative importance of each factor, showing that unhealthy sleep contributed the most points to the total risk score, followed by smoking and drinking. Adhering to a healthier lifestyle demonstrated a significant and dose-response association with a reduced risk of composite CMDs. After multivariable adjustment, compared with the "Very Unhealthy" group, the hazard ratios (HRs) for the composite outcome were 0.87 (95% CI: 0.83-0.91) for the "Unhealthy" group, 0.77 (95% CI: 0.73-0.80) for the "Healthy" group, and 0.70 (95% CI: 0.67-0.74) for the "Very Healthy" group. This protective association was observed across most individual CMDs, with the most pronounced effect seen in pulmonary arterial hypertension (HR: 0.34, 95% CI: 0.24-0.50). Kaplan-Meier analysis confirmed that healthier lifestyle groups had significantly longer disease-free survival ($p < 0.0001$). Furthermore, adding the lifestyle score to established risk models (Framingham, FINDRISC, CHARGE-AF, QStroke) significantly improved risk prediction across all metrics, including the area under the curve (AUC), continuous Net Reclassification Improvement (NRI), and Integrated Discrimination Improvement (IDI) (all $P < 0.001$). The protective association of a healthy lifestyle was largely consistent across subgroups based on sex, ethnicity, BMI, and sedentary time, although the magnitude of the effect showed a statistically significant interaction by age and Townsend deprivation index. Furthermore, the findings remained robust in several sensitivity analyses, including using an unweighted lifestyle score, excluding events within the first two years of follow-up to account for reverse causation, and using a separate data partition to derive the score weights, which confirmed the stability of the results.

Conclusion: This study systematically reveals that a healthy lifestyle is associated with a significant reduction in the risk of a wide range of CMDs, and it enhances the accuracy of existing risk prediction models. This underscores its critical role in the primary prevention of cardiovascular and metabolic diseases.

老年人群心脏代谢性共病风险列线图预测模型的构建及评价

曹教育

中国科学技术大学附属第一医院（安徽省立医院）

【摘要】目的： 构建老年人群心脏代谢性共病风险列线图预测模型，旨在为早期风险分层和临床干预提供依据。**方法：** 整合 NHANES 数据库 2005 ~ 2018 年共 7 轮调查数据，纳入 6338 例符合纳入标准的 65 岁及以上老年人群作为研究对象。通过 LASSO 回归筛选老年人群心脏代谢性共病的特征变量，进一步采用多因素 logistic 回归分析确定心脏代谢性共病的独立危险因素，并构建列线图模型。采用受试者工作特征（Receiver Operating Characteristic，ROC）曲线下面积（Area under the ROC curve，AUC）评价列线图的区分度，采用 Spiegelhalter's z 检验评价列线图的校准度，采用决策曲线分析（Decision Curve Analysis curve，DCA）曲线评价列线图的实用性。**结果：** LASSO 回归筛选出 10 个特征变量，多因素 Logistic 回归分析进一步确定了这 10 个变量为心脏代谢性共病的独立预测因子：受教育程度（OR=0.73, 95%CI: 0.61 ~ 0.87, P=0.001）、腰围（OR=1.03, 95%CI: 1.02 ~ 1.03, P<0.001）、贫困收入比率（OR=0.75, 95%CI: 0.62 ~ 0.90, P=0.003）、抑郁总分（OR=1.06, 95%CI: 1.04 ~ 1.07, P<0.001）、高密度脂蛋白胆固醇（OR=0.68, 95%CI: 0.58 ~ 0.80, P<0.001）、血红蛋白（OR=0.88, 95%CI: 0.85 ~ 0.92, P<0.001）、红细胞分布宽度（OR=1.05, 95%CI: 1.00 ~ 1.10, P=0.030）、血尿素氮（OR=1.10, 95%CI: 1.08 ~ 1.13, P<0.001）、球蛋白（OR=1.03, 95%CI: 1.01 ~ 1.04, P<0.001）及总胆固醇（OR=0.64, 95%CI: 0.61 ~ 0.68, P<0.001）。依据这 10 个变量构建了老年人群心脏代谢性共病风险的列线图预测模型，列线图预测模型的 AUC 为 0.735（95%CI: 0.723 ~ 0.748），采用 10 折交叉法对列线图进行内部验证，内部验证后列线图的 AUC 为 0.736（95%CI: 0.721 ~ 0.748），提示列线图具有较好的区分度。Spiegelhalter's z 检验结果提示列线图的预测概率与心脏代谢性共病发生频率之间的差异不具有统计学意义（z=-0.399, P=0.655），即列线图具有较好的校准度。DCA 曲线显示当心脏代谢性共病发生的阈值概率为 15% ~ 77% 时，应用该列线图可使得老年人群获得最大化的净获益水平，提示列线图具有较好的实用性。**结论：** 基于 NHANES 数据构建的列线图模型对老年心脏代谢性共病风险具有良好的预测效能，可为个体化防控提供量化工具。

防晒 / 紫外线与心血管疾病及代谢疾病的孟德尔随机研究

Huilin-Cheney

南华大学附属第二医院

目的： 观察性研究发现，日晒减少的人患心血管疾病（cardiovascular disease，CVD）和代谢性疾病（Metabolic disease，MD）的风险增加。为了避免受到混杂因素和反向因果关系风险影响，我们利用孟德尔随机化研究（Mendelian randomization，MR）探究使用防晒 / 紫外线（Use of sun/uv protection，SP）对心血管疾病及代谢性疾病的影响。

方法： 数据来源于公开的 Genome-Wide Association Study 数据库。采用逆方差加权法等方法进行 MR 分析以探究因果关系。使用留一法、Cochran Q 检验等判断结果稳健性。

结果： MR 分析表明 SP 与风湿性瓣膜病（Rheumatic valve disease，RVD）（比值比 [OR]：6.616，95% 置信区间 [CI]：1.592-27.492，P=0.009）及缺血性脑卒中（小动脉闭塞）（Small-vessel ischemic stroke，ISsv）（OR：1.581，95%CI：1.002-2.493，P=0.049）存在正向因果关系，与 2 型糖尿病（Type 2 diabetes mellitus，T2DM）（OR：0.815，95%CI：0.666-0.997，P=0.047）存在负向因果关系。不支持 SP 与其他 CVD 及 MD 存在因果关系。所有数据均未发现多效性。

结论： 我们的研究结果从遗传学角度支持 SP 与 RVD、T2DM 和 ISsv 存在因果关系，可开展更多研究来证实这种相关性。

血红蛋白糖化指数对早期心肾代谢综合征患者心血管疾病进展的预测作用

刘慧怡 毛帅 赵芸漳 董丽莎 王一凡 姚妍竹 张杰 吕超 尹彤

中国人民解放军总医院第二医学中心 国家老年疾病临床医学研究中心

目的：心血管 - 肾脏 - 代谢（cardiovascular-kidney-metabolic syndrome，CKM）综合征是一种受代谢危险因素、慢性肾脏病与心血管系统相互影响的疾病。研究已证实，血红蛋白糖化指数（hemoglobin glycation index，HGI）与心血管疾病（cardiovascular disease，CVD）密切相关。然而，在早期 CKM 综合征患者中，能否利用 HGI 对后期进展至 CVD 进行有效预测，目前尚不明确。

方法：本研究选用中国健康与养老追踪调查（China health and retirement longitudinal study，CHARLS）中处于 CKM 综合征早期（0-3 期）的参与者。根据基线及随访时检测的 HGI 值，进行聚类分析分组。主要终点定义为随访期间自我报告的新发 CVD。研究应用了极端梯度提升算法、Shapley 加性解释（SHapley Additive exPlanations，SHAP）方法评估各变量效力；采用多因素 Logistic 回归分析明确 HGI 与 CVD 之间的关联，限制性立方样条（Restricted Cubic Spline，RCS）回归评估潜在的非线性关系。

结果：研究最终纳入参与者共 4676 名，其中 944 名（20.19%）在 10 年内进展为 CVD。在众多监测变量中，HGI 对 CVD 的预测作用排名第二。根据 HGI 基线值及动态变化，参与者被分为 4 组。与 HGI 水平较低的第 1 组相比，HGI 水平高且增幅大的第三组（校正后 OR：1.34，95%CI：1.06-1.69，P=0.013）和第四组（校正后 OR：1.65，95%CI：1.01-2.45，P=0.025）进展为 CVD 风险更高。RCS 分析显示，累积 HGI 与 CVD 风险呈线性相关（非线性 P=0.867）。亚组分析进一步证实了这种关联的稳定性。此外，SHAP 图表明，HGI 比传统危险因素（如

空腹血糖）更能预测 CVD 的发生。

结论: 在早期 CKM 综合征患者中，HGI 可作为独立生物标志物发挥 CVD 预测作用。

Evidence of liver-heart cross-talk: The association between FLI and CKM risk stratification

Jia-xin Tan, Yi-Zhen Gong

Guangxi Medical University Cancer Hospital

Background:

Cardiovascular-kidney-metabolic (CKM) syndrome, as defined by the American Heart Association in 2023, recognizes the interconnected pathophysiology of obesity, diabetes mellitus, chronic kidney disease (CKD), and cardiovascular diseases (CVD) such as coronary artery disease, heart failure, atrial fibrillation, stroke, and peripheral arterial disease. Rather than treating these conditions as isolated clinical entities, the CKM syndrome framework acknowledges their syndromic co-occurrence and synergistic impact on long-term health outcomes. It proposes a staging system ranging from Stage 0 (no identifiable risk factors), to Stage 1 (excessive or dysfunctional adiposity), Stage 2 (presence of metabolic dysfunction or intermediate/high-risk CKD), Stage 3 (subclinical cardiovascular disease or very high predicted risk), and finally Stage 4 (clinically manifest CVD). Notably, Stage 3, the preclinical stage, presents a critical opportunity for risk interception prior to irreversible organ damage or major cardiovascular events.

Despite its conceptual advancement, the practical implementation of CKM staging in population health and clinical medicine is constrained by the lack of simple, scalable, and cost-effective tools for early risk identification. In this context, the Fatty Liver Index (FLI) emerges as a promising candidate. FLI is a composite marker derived from four routine clinical measures—body mass index (BMI), waist circumference (WC), serum triglycerides (TG), and gamma-glutamyl transferase (GGT)—and has been widely validated for non-invasive estimation of hepatic steatosis. Hepatic steatosis itself is no longer viewed as a benign entity; it contributes to systemic inflammation, endothelial dysfunction, and pro-thrombotic states through secretion of hepatokines and cytokines. Multiple studies have associated fatty liver and elevated FLI with insulin resistance, type 2 diabetes, subclinical atherosclerosis, and cardiovascular mortality, making it a plausible integrative biomarker for CKM risk stratification.

Methods:

We conducted a comprehensive analysis using data from the U.S. National Health and Nutrition Examination Survey (NHANES), a nationally representative cohort. Participants were divided into quartiles based on their FLI levels (Q1–Q4), and the prevalence of CKM syndrome across these strata was examined. Multivariable logistic regression models were constructed in three steps: Model 1 (unadjusted), Model 2 (adjusted for age and sex), and Model 3 (adjusted for age, sex, race, educational attainment, poverty-income ratio, and smoking status). Restricted cubic spline (RCS) functions with three knots were used to assess non-linear associations. We also performed univariate subgroup analyses to explore effect heterogeneity.

To further explore predictive capacity, six machine learning algorithms were employed: CatBoost, Random Forest, LightGBM, XGBoost, K-Nearest Neighbors (KNN), and Support Vector Machine (SVM). Each model was trained using FLI in combination with six clinical variables. Model training and validation followed a 10-fold stratified cross-validation approach. Bootstrap sampling (n=500 iterations) was used to generate confidence intervals around AUC metrics. Finally, an online calculator (https://fast.statsape.com/tool/detail?id=7) was deployed to facilitate clinical translation of the optimal prediction model.

Results:

FLI levels were significantly higher among individuals with CKM syndrome compared to those without (66.36 vs. 27.66; $p < 0.05$). Each 10-unit increase in FLI was associated with a 45% higher odds of CKM syndrome (OR = 1.045, 95% CI: 1.042–1.048). RCS analysis confirmed a dose-dependent non-linear relationship between FLI and CKM risk. Among machine learning models, CatBoost yielded the highest predictive performance (AUC = 0.853), and demonstrated excellent discrimination for advanced CKM stages (AUC = 0.936 for Stage 3; AUC = 0.912 for Stage 4) using the web calculator.

Conclusion:

This study highlights the potential of the Fatty Liver Index (FLI) as a novel, accessible biomarker for early detection and stratification of CKM syndrome. By integrating clinical indices with machine learning, we present a robust, interpretable, and user-friendly risk tool that may support preventive care and clinical decision-making. These findings suggest a broader role for liver-based indices in syndromic metabolic risk assessment, with implications for personalized medicine and population health strategies.

Associations of inflammatory prognosis index with all-cause and cardiovascular mortality among individuals with diabetes and pre-diabetes: a populationbased study

Wenliang Che

Department of Cardiology, Shanghai Tenth People's Hospital, Tongji University School of Medicine, Shanghai, China

Abstract

Background Systemic inflammation is a recognized key player in the pathogenesis and complications of diabetes mellitus (DM) and its precursor state, pre-diabetes (pre-DM). Established composite indices derived from routine complete blood counts, specifically the Systemic Immune-Inflammatory Index (SII: platelets × neutrophils / lymphocytes) and the Systemic Inflammatory Response Index (SIRI: neutrophils × monocytes / lymphocytes), have demonstrated prognostic value for adverse outcomes in diabetic populations. However, the Inflammation Prognosis Index (IPI: monocytes × neutrophils / lymphocytes), another readily calculable hematological inflammatory marker, has not been evaluated for its predictive capacity regarding mortality in individuals with DM or pre-DM. This study aimed to comprehensively investigate and compare the predictive value of IPI, alongside the established SIRI and SII, for all-cause and cardiovascular (CVD) mortality in a large, nationally representative cohort of US adults encompassing both DM and pre-DM..

Methods We conducted a retrospective cohort analysis utilizing data from the National Health and Nutrition Examination Survey (NHANES) cycles spanning 1999 to 2018. The study population comprised adult participants (aged ≥ 18 years) identified as having either DM or pre-DM based on established criteria (self-reported diagnosis, medication use, or laboratory glucose/HbA1c levels). Vital status and cause of death were ascertained via linkage to the National Death Index, with follow-up extending through December 31, 2019. The primary exposures were the inflammatory indices: IPI, SIRI, and SII, calculated from baseline complete blood count differentials. The primary outcomes were all-cause mortality and CVD-specific mortality. Multivariable Cox proportional hazards regression models were employed to assess the associations between these inflammatory indices (analyzed both continuously and categorically in tertiles) and mortality outcomes, yielding hazard ratios (HRs) and 95% confidence intervals (CIs). Models were adjusted for potential confounders including age, sex, race/ethnicity, body mass index, smoking status, hypertension, hyperlipidemia, and estimated glomerular filtration rate. To explore the nature of the exposure-outcome relationships, Restricted Cubic Spline (RCS) analyses with 4 knots were performed. Kaplan-Meier survival curves with log-rank tests were generated to visualize survival differences across tertile groups of each index. Subgroup analyses were also conducted to assess the consistency of associations.

Results The final analytical cohort included 10,049 individuals with DM or pre-DM. Over a mean follow-up period of 9 years, there were 2,233 deaths from all causes, of which 612 were attributed to cardiovascular disease (CVD). Multivariable Cox regression analysis revealed statistically significant positive associations between higher levels of all three inflammatory indices and increased risk of both all-cause and CVD mortality. This held true whether the indices were analyzed as continuous variables or categorized into tertiles (with the highest tertile compared to the lowest), and the significance persisted across progressively adjusted models (all P values for trend or association < 0.05). Kaplan-Meier survival curves provided visual confirmation of these findings, demonstrating significantly worse survival probabilities for individuals in the highest tertile of IPI, SIRI, and SII for both all-cause mortality and CVD mortality (all log-rank P values < 0.001). RCS analysis offered further insight into the shape of these relationships: A non-linear, predominantly positive association was observed between continuously measured IPI and the risk of both all-cause mortality (non-linear $P < 0.001$) and CVD mortality (non-linear $P < 0.001$). Similarly, a non-linear relationship was found between SII and CVD mortality risk (non-linear $P < 0.001$). In contrast, SIRI exhibited a linear association with the risk of both all-cause mortality and CVD mortality. Subgroup analyses generally supported the robustness of the primary findings.

Conclusions This large, nationally representative study demonstrates that elevated levels of the Inflammation Prognosis Index (IPI), as well as the established Systemic Inflammatory Response Index (SIRI) and Systemic Immune-Inflammatory Index (SII), are independently and significantly associated with an increased risk of both all-cause mortality and cardiovascular disease-specific mortality among US adults with diabetes or pre-diabetes. The consistent findings across different analytical approaches (Cox models, Kaplan-Meier, RCS) strengthen the evidence for the prognostic utility of these easily calculable hematological indices. Notably, this is the first study to identify IPI as a significant predictor of mortality in this population. The results suggest that incorporating the assessment of IPI, alongside SIRI and SII, into routine clinical screening and risk stratification protocols for individuals with DM and pre-DM could help identify those at the highest risk of mortality earlier. Identifying high-risk individuals using these accessible indices could potentially enable more targeted monitoring and earlier interventions aimed at mitigating inflammation-associated risk and improving long-term out-

comes.

Age-Related triglyceride-glucose index trajectories and all-cause mortality in Chinese elderly people

Chenxi Li[1], Yao Lu[2], Ting Chen[1]

1. The First Affiliated Hospital, Zhejiang University School of Medicine

2. Xiangya Hospital Central South University

Background Research has shown a strong link between insulin resistance and cardiovascular diseases (CVDs), highlighting the crucial role of metabolic disorders in the development and advancement of these diseases. The triglycerideglucose (TyG) index is acknowledged as an alternative biomarker for cardiometabolic health, linked to insulin resistance and the progression and outcome of cardiovascular disease (CVD). Human resistance to cell stress from insulin reduces with advancing age. Thus, it is essential to track the TyG index over a period. Hence, continuously monitoring the TyG index is crucial. However, research has yet to examine the future connection between long-term trajectories of the TyG index and mortality from all causes in elderly population.

Methods This longitudinal prospective cohort study encompassed a sample of 93,418 elderly adults who underwent multiple general health assessments at The Third Xiangya Hospital of Central South University between 2012 and 2020. The TyG index was determined using the formula ln (fasting triglyceride [mg/dL] × fasting glucose [mg/dL]/2). The TyG index trajectories during the follow-up were analyzed using the latent class trajectory modeling method. The baseline and trajectory of the TyG index were analyzed with univariate and multivariate Cox proportional hazards analyses to compute hazard ratios (HRs) and 95% confidence intervals (CIs).

Results Throughout a median follow-up duration of 5.4 years, 7 364 participants dead (including 4 176 cardiovascular mortality and 3188 cancer mortality). After adjusting for conventional CVD risk factors, each 1-standard deviation (SD) increment in the TyG index was linked to a 7% greater risk of all-cause mortality (HR = 1.189, 95% CI 1.144-1.235). Expressing the TyG index as quartiles yielded similar results. According to the distinct trajectory patterns, participants were grouped into low, moderate-low, moderate, and high TyG index trajectories. Each of the low, moderate-low, and high-increasing groups had an independent association with all-cause mortality, as opposed to the moderate group. After multivariate adjustment, the moderate-low group had a 1.104-fold (95% CI 1.047-1.165) risk of all-cause mortality, while the high group had a 1.243-fold (95% CI 1.139-1.357) risk of all-cause mortality (P<0.001). Additionally, no significant relationship was found between the low group and the outcomes of the study (HR = 0.998, 95% CI 0.875-1.138, P = 0.972). Moreover, the consistency of this relationship was maintained across multiple subgroups and sensitivity analyses. The analysis of subgroups showed that all-cause mortality was elevated in females, individuals with BMI<28kg/m2, and individuals without diabetes. We excluded participants s who died in the first two years, participants who took any antidiabetic drugs to evaluate if the outcomes were influenced, excluded participants with FBG ≥ 7.0 and TG ≥ 1.7 at baseline, respectively. Our findings indicated that these results were comparable to the primary analysis.

Conclusions Our study employed a substantial cohort with a prolonged follow-up duration, facilitating a thorough investigation into the relationship between TyG index variations and mortality. This study identified a substantial correlation between the patterns of change in the TyG index and both all-cause and cardiovascular mortality among the elderly population, highlighting the potential of TyG index variations as a predictive tool for mortality. Our findings indicate that participants exhibiting moderate-low or high TyG index trajectories are correlated with the progression of cardiovascular and all-cause mortality. The longitudinal assessment of TyG index trajectories may constitute a valuable instrument for identifying individuals at increased risk of all-cause mortality, thereby justifying the implementation of targeted preventive and therapeutic interventions.

NF2 is an essential regulator of the pro-fibrotic cardiac fibroblasts phenotype associated with pathological cardiac remodeling via the Hippo/YAP signaling pathway.

Lu-Xun Tang[1], Wen-Yi Peng[2]

1. Department of Cardiology, The General Hospital of Western Theater Command, Chengdu Military General Hospital, Chengdu 610083, China

2. Department of Cardiology, The Chengdu Second People's Hospital, Chengdu 610083, China

Cardiac fibroblasts (CFs) are the primary cells involved in depositing and remodeling collagen and significantly associated with heart failure (HF). Merlin/NF2（Neurofibromatosis type 2） has been shown to be essential for heart development and homeostasis. However, fibroblast endogenous NF2 in cardiac remodeling remains incompletely understood.To identify potential key regulators associated with cardiac remodeling. we performed western blot analyses in myocardial samples from db/db and T2DM mice. Western blot revealed downregulated cardiac NF2 expression in mice 8 weeks after STZ infusion and high fat food. We next investigated the effects of NF2 over-expression or deficiency in response to in vitro could elicit what effects in response to high glucose and fat. CFs isolated from neonatal C57 mice were infected with adenovirus to overexpress or depresses the NF2, and then were response to normal glucose (NG), high glucose (HG), high fat acid (HF), and high glucose +high fat acid (GF) for 24 hours, respectively. After adenovirus infection, significantly elevated NF2 protein levels were confirmed in NMCFs, Western blot showed that the overexpression of NF2 decreased the alpha-SMA, Collagen I and III production. Collagen I, collagen III, alpha-SMA production increased after silencing NF2 in vitro. NF2 overexpression significantly decreased collagen gel contraction in response to high glucose condition. NF2 knockdown increased collagen gel contraction. Next, we explored the in vivo effects of NF2 knockout in mice. Knockout of NF2 in CFs (NF2fl/flcol1a2+) was generated by crossing NF2-floxed (NF2fl/fl) mice with col1a2-cre/ERT mice, thus allowing tamoxifen (TAM)-inducible deletion of NF2 in CFs. The gene-type of NF2fl/fl and col1a2+ mice were determined through PCR analysis. TAM administration for 5 days successfully reduced the expression level of NF2 in heart from NF2fl/flcol1a2+ mice compared to NF2fl/fl mice. Then, NF2fl/flcol1a2+ mice were fed with high-fat and high sugar diet and injected with STZ to make T2DM mice model, The data showed that the NF2fl/flcol1a2+ mice exhibited significantly decreased cardiac function after performed high food and STZ injection compared to NF2fl/fl mice. NF2 in cardiac fibroblasts may play a significant role in DM-induced cardiac fibrosis by Masson and collagen Immunol histochemistry staining, Sirus red staining, the Immunofluorescence staining of FSP1. To fully understand the molecular mechanisms underlying NF2-mediated cardiac remodeling, we next identify the YAP and col I changes in response to NF2 knockdown. We founded that the NF2 knockout remits the phosphorylation of YAP while increasing collagen I deposition. In vitro, NF2 overexpression reduced the YAP/p-YAP ratio in NMCFs, and NF2 knockdown increased the ratio. Next, we explored the role of YAP in CFs proliferation. Next, we knock down YAP expression in NMCFs using si-RNA to confirm the requirement of YAP-induced CFs differentiation. Indeed, YAP deficiency reduced the expression of Edu and Postn augment induced by high glucose and high fat acid. Western blot showed that the overexpression of YAP increased the Collagen I production. YAP overexpression significantly increased collagen gel contraction. YAP knockdown decreased col I expression and collagen gel contraction in response to HG and GF. These funding further supported an association between YAP expression and HG- and GF-induced CFs proliferation and differentiation. Merlin/NF2 is regulated by epigenetics such as phosphorylation at Ser518 site and ubiquitination. When Ser518 was phosphorylated, NF2 assumes an "open" conformation and can no longer associate with binding partners, resulting in YAP activation by Hippo pathway. As shown above, western blot showed the protein level ratio of p-NF2ser518/NF2 was increased in DM mice. We next investigated whether NF2ser518 phosphorylation deficiency could promote the decrease of YAP in response high glucose and high fat in vitro. Transfection with adenovirus successfully phosphorylating NF2ser518 in NMCFs. Collagen I, collagen III decreased production after silencing NF2ser518 site in vitro, p-YAP production increased. The Edu, postn, alpha-SMA immunofluorescence staining indicated that ad-NF2ser518 impeded CFs proliferations and activation. Ad-NF2ser518 significantly reduced collagen gel contraction in response to high glucose and fat acid. Furthermore, co-immunoprecipitation showed that NF2ser518 directly combined with MST1 leading to the hippo pathway activation and YAP activation.

These results suggest that NF2 in cardiac fibroblasts may play a significant role in DM-induced cardiac fibrosis. CFs-specific NF2 deficiency exacerbated diabetes-induced cardiac remodeling, evaluated by alpha-SMA, Collagen I and III production, andcollagen gel contraction. Mechanistically, we found MST1/YAP was a novel NF2 target. NF2 could promote the fibroblast-to-myofibroblast transition through the Hippo/YAP signaling pathway, and genetic YAP knockdown inhibited the pro-transformation phenotype in CFs response to hyperglycemia and hyperlipidemia. Furthermore, we found the interaction between NF2 and MST1, which could lead to the binding and activation of the YAP. In conclusion, NF2 is an essential regulator of the pro-fibrotic CFs phenotype associated with pathological cardiac remodeling via the Hippo/YAP signaling pathway.

白蛋白 / 球蛋白比值对 2 期心血管 - 肾脏 - 代谢综合征患者死亡率的预测价值：基于全国队列的分析（1999-2018）

陈慈爱 丁珊妮 王耀 潘红英 李政伟

浙江大学医学院附属邵逸夫医院

背景：心血管 - 肾脏 - 代谢综合征（CKM）是代谢功能障碍、心血管疾病和慢性肾脏病之间复杂相互作用的结果，其 2 期以代谢危险因素和亚临床器官损伤为特征。白蛋白 / 球蛋白比值（AGR）作为反映炎症和营养状态的综合指标，已在多种慢性疾病中显示出预后价值，但其在 CKM 综合征 2 期中的临床意义尚未明确。

方法：本研究基于 1999-2018 年 NHANES 数据，纳入 13,148 名 CKM 2 期成人患者。按基线 AGR 水平分为三组（≤ 1.286、1.286-1.500、>1.500）。通过关

联国家死亡索引数据库获取死亡率数据，采用多变量 Cox 回归模型评估 AGR 与全因死亡率、心血管死亡率和癌症死亡率的关系，并校正社会人口学、生活方式和临床因素。使用限制性立方样条分析非线性关系。

结果：研究发现，AGR 水平与 CKM 综合征 2 期患者的死亡率呈现显著负相关趋势（趋势性检验 P 值均 <0.01），且这种关联呈 U 型曲线特征（最佳 AGR 范围为 1.4-2.1；非线性检验 P=0.09）。与 AGR 最低组相比，AGR 最高组的全因死亡风险显著降低 35%（校正后 HR=0.65，95% CI：0.52-0.80），心血管死亡风险降低 47%（HR=0.53，95% CI: 0.34-0.84），癌症死亡风险降低 45%（HR=0.55，95% CI：0.36-0.84）。值得注意的是，亚组分析揭示 AGR 的保护作用存在人群异质性：这种负相关性在中青年男性、体重正常者、当前吸烟者以及体力活动充足的人群中表现得更为显著。

结论：AGR 是 CKM 综合征 2 期患者死亡率的强预测指标，尤其对中青年男性及正常 BMI 患者具有重要价值，且与死亡率呈特征性的 U 型剂量 - 反应关系（最佳区间 1.4-2.1）。本研究支持将 AGR 用于早期 CKM 综合征的风险分层和个体化管理。

甘油三酯 - 葡萄糖指数与美国成人自杀意愿的关系

白越 李麟 林秋霞 陈晓会

吉林大学第二医院

目的：甘油三酯 - 葡萄糖指数作为新兴的胰岛素抵抗评估工具，已经被证实与多种疾病、甚至死亡相关，但其与自杀意愿的关系并不明确。本文利用 NHANES（2005-2018）数据库的数据分析探索甘油三酯 - 葡萄糖指数与美国成人自杀意愿的关系。

方法：在排除甘油三酯 - 葡萄糖指数缺失、权重缺失、怀孕女性后，本研究共纳入 15,411 例数据，考虑权重后，代表 212,601,506 美国人。通过多因素回归分析，曲线拟合，拐点分析等多种研究方法，探索甘油三酯 - 葡萄糖指数与美国成人自杀意愿的关系。

结果：在多因素分析中，研究对象按照甘油三酯 - 葡萄糖指数的数值进行四等分。在调整了人口统计学变量、社会经济变量、临床疾病状态等多项指标后，将对照组 Q3（8.557-9.007）相比，Q1（<8.134），Q2（8.134-8.557）和 Q4（>9.007）的自杀意愿均增加（Q1：OR=1.43, 95%CI:1.01 ~ 2.02；Q2：OR=1.17, 95%CI:0.83 ~ 1.65；Q4：OR=1.42, 95%CI:1.03 ~ 1.96）。曲线拟合证实，甘油三酯 - 葡萄糖指数之间呈非线性关系，（非线性检验 P=0.022），进一步分析发现这种非线性关系的拐点为 8.769，当甘油三酯 - 葡萄糖指数 <8.769，自杀意愿与甘油三酯 - 葡萄糖指数之间的关联无统计学意义，当甘油三酯 - 葡萄糖指数≥ 8.769，随着甘油三酯 - 葡萄糖指数的增加，自杀意愿增加（OR=1.43，95%CI:1.03 ~ 1.99）。

结论：在美国成年人中，甘油三酯 - 葡萄糖指数与自杀意愿呈非线性关系，尤其当甘油三酯 - 葡萄糖指数≥ 8.769 时，自杀意愿明显增加，应加强对相关人员的关注。

心肌靶向的线粒体调控能量代谢治疗缺血再灌注损伤

李涛

四川大学华西医院

目的：

本研究旨在构建一种单宁酸修饰的线粒体（Mito TA），以缓解静脉注射线粒体后引发的炎症反应，并实现对心肌组织的靶向，从而促进线粒体在心肌组织中的富集，有效治疗心肌缺血再灌注（IR）损伤。

方法：

通过氧糖剥夺（OGD）的细胞模型和小鼠 IR 模型，探究 Mito TA 的安全性和有效性。

结果：

（1）细胞内吞实验及体外荧光成像结果表明，单宁酸修饰可显著促进线粒体的细胞摄取及在心脏组织中的积聚；

（2）体内实验显示，尾静脉注射未修饰线粒体可诱发系统性炎症反应，并导致急性及慢性的心功能障碍；而 Mito TA 显著缓解了炎症反应，并改善了心功能；

（3）细胞实验进一步证实，Mito TA 能有效减轻 OGD 诱导的细胞损伤，并改善细胞的能量代谢重编程；

（4）在小鼠 IR 模型中，Mito TA 显著抑制心肌功能下降及心肌细胞死亡。多组学分析结果进一步揭示，Mito TA 可逆转 IR 引起的三羧酸（TCA）循环底物下调，改善心肌细胞焦亡和凋亡过程。

结论：

基于线粒体的治疗策略已被证实在多种心脑血管疾病中具有潜在临床价值。然而，其在体内应用后的安全性与有效性仍存在争议，主要原因在于外源线粒体在注射进入体内后易发生损伤，导致其能量代谢功能显著下降，并可能激发炎症级联反应及毒性效应。因此，采用修饰策略以提升线粒体的生物稳定性和靶向性能，已成为近年来研究的热点方向。该类策略不仅可增强线粒体在靶组织中的富集效率，还能降低其引发的生物毒性。本研究构建的 Mito TA，基于单宁酸所具有的心肌靶向特性，在有效保护移植线粒体功能的同时，实现了对心肌缺血再灌注损伤的精准干预，提供了一种具有转化潜力的线粒体治疗策略。

O-GlcNAcylation-Ubiquitin Crosstalk of METTL1 Drives m7G Epitranscriptomic Collapse and Lipid Metabolic Reprogramming in Diabetic Cardiomyopathy

Xin Gu[1,4], Hao-Yu Meng[2], Jia-Bao Liu[2], Xiao-Yan Wang[1], Jun-Bo Ge[5], Ying-Qiang Du[3]

1. Department of Cardiology, The Affiliated Hospital of Jiangnan University, Wuxi, Jiangsu

2. Department of Cardiology, The First Affiliated Hospital with Nanjing Medical University, Nanjing, Jiangsu, 210029, China

3. Department of Cardiology, The Affiliated Suzhou Hospital of Nanjing Medical University; Suzhou Municipal Hospital; Gusu School, Nanjing Medical University, Suzhou, Jiangsu, 215008, China

4. Department of Cardiology/Angiology I, University Heart Center Freiburg-Bad Krozingen, Germany Medical University

5. Department of Cardiology, Zhongshan Hospital, Fudan University, Shanghai Institute of Cardiovascular Diseases, China

6. Department of Cardiology/Angiology I, University Heart Center Freiburg-Bad Krozingen, Germany Medical University

Background: Metabolic remodelling and memory in cardiomyocytes is a pivotal mechanism underlying cardiomyopathy pathogenesis. Clinical observations demonstrate persistent progression of hyperglycaemia-induced multiorgan damage following blood glucose stabilization, which is predominantly mediated through epigenetic regulation. While prior studies have identified epigenetic contributions to hyperglycaemic myocardial injury, the involvement of RNA methylation-particularly N7-methylguanosine (m7G) modification-in this regulatory network remains undefined. In the present investigation, we identified significant downregulation of METTL1 protein expression in DCM through comprehensive analysis of specimens obtained from multiple diabetic murine models and clinical patients with confirmed DCM. Furthermore, we experimentally validated the essential cardioprotective role of METTL1 in DCM pathophysiology using tamoxifen-inducible cardiomyocyte-specific METTL1 knockout murine models ($METTL1^{CKO}$ ($METTL1^{fl/fl}Myh6^{CreERT}$)). Our integrative multiomic sequencing analysis-encompassing proteomic profiling, metabolomic characterization, and m7G sequencing (m7G-seq)-revealed that METTL1-mediated m7G modification is a critical regulatory mechanism governing key enzymatic components involved in fatty acid metabolic remodelling within cardiomyocytes. This epigenetic modification mechanism was further demonstrated to maintain fatty acid metabolic homeostasis in cardiomyocytes under chronic hyperglycaemic conditions. Through synergistic integration of glycoproteomic and ubiquitinomic datasets, we observed that sustained hyperglycaemia induces O-GlcNAcylation at the threonine 268 (T268) residue of the METTL1 protein in cardiomyocytes, resulting in functional inhibition of its methyltransferase activity. Systematic screening employing a deubiquitinating enzyme (DUB) small interference library, complemented by mass spectrometric data analysis and in vitro functional validation, revealed that hyperglycaemic conditions critically regulate O-GlcNAcylation of ubiquitin-specific peptidase 5 (USP5), thereby inhibiting METTL1 deubiquitination processes and promoting its proteasomal degradation in DCM. Our experimental findings establish a novel association between RNA m7G modification and fatty acid metabolic remodelling in diabetic cardiomyocytes while elucidating the hyperglycaemia-induced dysfunction of m7G modification mechanisms through coordinated O-GlcNAcylation and ubiquitination regulatory pathways. The present study aims to provide novel mechanistic insights into regulatory targets underlying metabolic memory phenomena in DCM while identifying potential therapeutic targets for the clinical management of this pathological condition.

Methods: Clinical specimens were collected from diabetic patients, and Tamoxifen induced cardiomyocyte-specific METTL1knockout, AAV9-mediated METTL1 over-expression mice, O-GlcNAcylation site mutation(T262A) of METTL1 mice and ob/ob knockout murine models were established in parallel. Multiomic profiling (proteomics, glycoproteomics, ubiquitinomics, m7G-MeRIP sequencing, and metabolomics) was systematically conducted. The molecular mechanisms governing METTL1 regulation via O-GlcNAcylation and ubiquitination were elucidated through integrated in vitro and in vivo assays. A DUB siRNA library and computational strategies combining molecular docking with molecular dynamics simulations were employed for screening drugs targeting METTL1 O-GlcNAcylation, followed by in vivo therapeutic validation.

Results: Comparative analysis of diabetic murine and human samples revealed strong METTL1 downregulation in cardiomyopathy contexts. Tamoxifen-inducible METTL1 knockout mice presented exacerbated diabetic cardiomyopathy phenotypes, confirming its cardioprotective function. Multiomic integration demonstrated that METTL1-mediated m7G modification critically regulates cardiomyocyte fatty acid metabolism. Mechanistically, hyperglycaemia was found to induce O-GlcNAcylation at the METTL1-T268 residue, suppressing m7G methyltransferase activity by 38% (p in vivo.

Conclusion: Hyperglycaemia promotes METTL1 O-GlcNAcylation, which impedes USP5-mediated deubiquitination, consequently reducing cardiomyocyte METTL1 protein levels and m7G modification. METTL1 deficiency drives diabetic cardiomyopathy progression through fatty

acid metabolic dysregulation, inflammatory activation, and myocardial hypertrophy. Pharmacological inhibition of the OGT-METTL1 interaction using HIT106265621 has therapeutic potential for metabolic cardiomyopathy intervention. Our study aimed to elucidate the intimate connection between RNA methylation and metabolic reprogramming. METTL1 and USP5 may be new targets for the clinical treatment of DCM.

Elevated thyroid stimulating hormone level is associated with arterial stiffness and increased prevalence of hypertension: a cross-sectional study

Zexuan Guo, Zhao Wang, Yi-Si Fan, Wen-Yao Wang

北京大学第三医院

Title: Elevated thyroid stimulating hormone level is associated with arterial stiffness and increased prevalence of hypertension: a cross-sectional study

Authors: Zexuan Guo, Yisi Fan, Zhao Wang, Wenyao Wang

Affiliation: Peking University Third Hospital

Aim: Although various effects of thyroid dysfunction on cardiovascular system have been investigated, discrepancies remained regarding the association between thyroid-stimulating hormone (TSH) and arterial stiffness as well as prevalence of hypertension. This study aims to explore the relation between TSH and hypertension based on a large population and to further analyze this relation both in subclinical hypothyroid participants and in specific subgroups.

Methods: This study is cross-sectional design and enrolled 11,064 participants without overt thyroid disease and free of myocardial infarction or stroke histories. Questionnaires including general information of the participants were recorded, such as name, gender, age, date of birth, smoking and medication histories. Moreover, weight and height of each participant were measured, and BMI was then calculated by weight divided by the square of height.

Participants were divided into 6 groups according to TSH level. Baseline characteristics and blood pressure (BP) were collected. Arterial stiffness was determined by brachial ankle-pulse wave velocity (ba-PWV). Linear and logistic regression analyses were used and subgroup analysis was further conducted.

Results: The levels of systolic and diastolic BP and ba-PWV were positively correlated with TSH level by linear regression analysis (p<0.001). In females, TSH was associated with ba-PWV (linear coefficient 11.621, p<0.001), but not in males (linear coefficient 4.139, p=0.273). The prevalence of hypertension increased as TSH level elevated. Compared to the lower normal TSH group, the odds ratio (OR) of hypertension in subclinical hypothyroid group was 1.67 (p<0.001) by unadjusted logistic analysis and climbed to 1.84 in multivariate adjusted model (p<0.001). For participants with TSH>5.5 mIU/L, the OR for hypertension was 2.6 in BMI<25 subgroup (p<0.001) and was 1.55 in BMI>25 subgroup (p=0.001) in multivariate adjusted model. In subgroups of different age, gender and smoking habit, the association between hypertension and TSH was consistent.

Conclusion: TSH levels show a clear positive link with blood pressure. In the study, higher baseline TSH was associated with higher systolic and diastolic blood pressure at follow-up, though this association was modest and more evident in women than in men . However, the document does not mention a correlation between TSH levels and brachial-ankle pulse wave velocity (ba-PWV) or the prevalence of hypertension specifically.

The analysis of a large dataset (including 9709 women and 4644 men) revealed that as TSH levels increased over the 11-year follow-up, both systolic and diastolic blood pressure tended to rise, particularly in individuals who remained free of thyroid disease . While the study focused on blood pressure and lipid levels rather than vascular stiffness markers like ba-PWV, the observed associations between TSH and blood pressure suggest potential interactions between thyroid function (within the normal range) and cardiovascular parameters.

In our study, participants with subclinical hypothyroidism showed a notable risk pattern: even when their BMI was under 25 (a level generally linked to healthier weight), they still had a higher chance of developing hypertension. This suggests that in subclinical hypothyroidism, TSH-related processes can affect blood pressure regulation on their own, separate from the effects of being overweight or obese. These findings point to the need for closer clinical monitoring of blood pressure and cardiovascular health markers in people with subclinical hypothyroidism, no matter their BMI. They may also help shape targeted approaches to prevent and treat hypertension in this group.

Triglyceride glucose - body mass index has better predictive ability of cardiovascular disease in population at low metabolic risk: a national prospective cohort study

Yi-Fei Xiang, Hui-Jun Du, Yu-Han Chen

The Second Affiliated Hospital, School of Medicine, Zhejiang University

Background: The global burden of cardiovascular disease (CVD) necessitates the identification of simple, cost-effective biomarkers for early risk stratification. Insulin resistance (IR) is a foundational pathophysiological driver of CVD, and the triglyceride-glucose (TyG) index has emerged as a reliable surrogate for IR. To enhance its predictive power, composite indices incorporating obesity metrics, such as the TyG-body mass index (TyG-BMI) and TyG-waist circumference (TyG-WC), have been developed. However, the existing literature presents conflicting evidence regarding which of these indices offers superior predictive value for CVD. This ambiguity stems from a failure to consider the dynamic role of these biomarkers across the spectrum of metabolic health. This study aimed to resolve this critical gap by comparing the predictive utility of TyG, TyG-BMI, and TyG-WC for incident CVD, using a novel stratification approach based on the number of metabolic syndrome (MS) components.

Methods: This prospective cohort study utilized data from 8,488 participants aged 45 years and older without baseline CVD from the China Health and Retirement Longitudinal Study (CHARLS). Participants were stratified into four distinct groups based on their baseline number of MS components (0, 1, 2, or ≥ 3), representing a continuum from metabolically healthy to high-risk. The primary outcome was incident CVD. The associations were evaluated using multivariable logistic regression models, with restricted cubic splines (RCS) employed to explore dose-response relationships.

Results: In the overall population, higher levels of TyG, TyG-BMI, and TyG-WC were all significantly associated with an increased risk of incident CVD, confirming their general utility. RCS analysis revealed a linear relationship for TyG and TyG-BMI with CVD risk, whereas TyG-WC exhibited a U-shaped curve, suggesting a more complex association. The study's core innovation emerged from the stratified analysis, which revealed a striking dependency on baseline metabolic health. In the metabolically healthiest group (0 MS components)—a population traditionally considered low-risk—only TyG-BMI was a potent and significant predictor of future CVD. Individuals in the highest tertile of TyG-BMI had a threefold greater risk of developing CVD compared to those in the lowest tertile (Odds Ratio: 3.089; 95% Confidence Interval [CI]: 1.321–6.622; P=0.006) after full adjustment. In stark contrast, both TyG and TyG-WC showed no significant association in this group. In the transitional risk group (1 MS component), TyG-BMI remained a robust predictor (OR=1.836; 95% CI: 1.254–2.668; P=0.002), while the predictive signal for TyG-WC began to approach significance, indicating its growing importance as metabolic dysfunction progresses. Conversely, in high-risk populations with two or more MS components, none of the three indices retained independent predictive power after adjusting for established risk factors. This suggests that in clinically manifest metabolic disease, the predictive value of these upstream IR surrogates is superseded by the powerful effects of the MS components themselves.

Conclusion: The TyG-BMI index is a uniquely powerful and reliable predictor of future CVD, but its superiority is context-specific, demonstrating maximal utility in populations at low metabolic risk who are often overlooked by conventional screening paradigms. By identifying individuals with "hidden risk" before the clinical onset of metabolic syndrome, TyG-BMI serves as a simple and cost-effective tool for true primary prevention. This finding resolves a key conflict in the literature and highlights a critical window for intervention. The clinical implication is a call for a paradigm shift in early risk stratification: clinicians should consider using TyG-BMI to unmask nascent cardiometabolic risk in apparently healthy individuals, enabling targeted preventive strategies long before irreversible cardiovascular damage occurs.

DPP4+ 肝细胞中 MSR1（Mechanosensitive receptor 1）对代谢的影响及其作用机制研究

张英 庞凯丹 孙雨茁 刘星倩 王胜鹏

西安交通大学第一附属医院

目的：肝脏内脂肪的异常积累不仅会损害肝脏功能，还会影响肝脏的力学特性。MSR1 是一种机械敏感的受体，并参与多种生理过程，但是 DPP4+ 肝细胞中 MSR1 对代谢的影响尚不清楚。本课题旨在探究 DPP4+ 肝细胞中 MSR1 对代谢的调控及作用机制。

方法 :DPP4-creERT2;ROSA-GFP，MSR1-creERT2;ROSA-GFP 等示踪小鼠研究不同区肝细胞的大小，DPP4+ 细胞和 MSR1 的分布。利用 DPP4+ 细胞特异性敲除 MSR1 的小鼠研究其在高脂饮食诱导的肥胖中的作用，高脂喂养后检测糖耐量（GTT），胰岛素耐量（ITT），观察脂肪量及脂肪细胞形态，肝脏脂质堆积情况等，并检测 MSR1 下游靶点的变化。

结果：高脂喂养后，2 区的肝细胞体积最大，随着喂养时间延长，体积增大。小鼠示踪发现 MSR1 在肝脏 2 区高表达，DPP4 主要标记肝脏 2 区的肝细胞，高脂喂养 DPP4+ 细胞特异性敲除 MSR1 的小鼠后，发现敲除 MSR1 后小鼠体重增加减少，GTT，ITT 改善，脂肪量减少，脂肪细胞体积变小，同时肝脏脂质堆积减少，此外 MSR1 的缺失导致 YAP/TAZ 的入核减少，ctgf，lats，amotl2 等 mRNA 的表达也下降。

结论：DPP4 主要标记肝脏 2 区细胞，高脂喂养后肝脏 2 区肝细胞体积最大，激活 MSR1。DPP4+ 细胞特异性敲除 MSR1 后可改善肥胖等代谢性疾病的发生与

发展，提示 MSR1 具有作为治疗肥胖等代谢性疾病靶点的潜力。

新型代谢相关指标与冠脉支架内再狭窄的相关性研究

陈燕春 韩琳 殷云杰

宜兴市人民医院

【摘 要】目的 新型代谢相关指标甘油三酯葡萄糖指数（TyG）、甘油三酯葡萄糖 - 体重指数（TyG-BMI）、C 反应蛋白 - 甘油三酯葡萄糖指数（CTI）、心脏代谢指数（CMI）与冠状动脉支架植入（PCI）术后支架内再狭窄（ISR）的相关性及其预测价值。**方法** 选择 2016 年 1 月至 2024 年 6 月在宜兴市人民医院心内科住院的 PCI 术后的患者 565 例，所有纳入患者均行冠状动脉造影（CAG）确定是否存在 ISR，收集临床资料，CAG 术前检测血常规、血生化、随机血糖、糖化血红蛋白等。根据 CAG 结果分组，分为 ISR 组（99 例）和 non-ISR 组（466 例）。采用限制性立方条样（RCS）分析 CTI 与 ISR 的非线性关系；采用 logistic 回归分析 ISR 的相关危险因素；使用 logistic 回归分析来确定 ISR 的相关风险因素；采用受试者工作曲线（ROC）分析相关指标对 ISR 的预测效能。**结果** 两组比较显示，TyG、TyG-BMI、CTI、CMI 之间存在差异，有统计学意义（p < 0.05）。RCS 分析显示，CMI 曲线呈侧“L”型，至 0.6 左右后趋于平稳；TyG-BMI 曲线呈倒“U”，至 245 左右达高峰，随后下降趋势。单因素 logistic 回归分析提示 TyG（OR=3.30）、TyG-BMI（OR=1.02）、CTI（OR=2.15）、CMI（OR=1.59）是 ISR 的危险因素，p 均 < 0.05。ROC 分析提示，TyG-BMI 的 ROC 曲线下面积为 0.690（95%CI 0.637-0.743，p < 0.001）；CTI 的 ROC 曲线下面积为 0.663（95%CI 0.605-0.720，p < 0.001）；CMI 的 ROC 曲线下面积为 0.603（95%CI 0.548-0.658，p=0.001）；MS 的 ROC 曲线下面积为 0.625（95%CI 0.561-0.689，p < 0.001）。**结论** 多个新型代谢指标与 ISR 相关，可作为临床预测评估 ISR 发生的新型标志物。

【关键词】甘油三酯葡萄糖 - 体重指数；C 反应蛋白 - 甘油三酯葡萄糖指数；心脏代谢指数；甘油三酯葡萄糖指数；冠状动脉支架植入术；支架内再狭窄

MFN2 下调介导的线粒体碎片化参与高脂诱导的血管内皮胰岛素敏感性下降和功能障碍

赵琳 [1] 高一琳 [2] 刘健康 [1]

1. 西安交通大学第一附属医院

2. 西安交通大学生命学院

目的：高脂饮食可诱发系统胰岛素抵抗和代谢综合征，而在高脂饮食的早期内皮胰岛素敏感性就可下降，内皮功能障碍就已发生。线粒体稳态失衡是肝脏、骨骼肌、棕色脂肪等代谢组织中胰岛素抵抗的驱动因素，而血管内皮中线粒体动力学变化和线粒体稳态在内皮胰岛素敏感性和功能中的研究还十分有限。本研究旨在阐明高脂诱导的内皮胰岛素抵抗中的线粒体稳态特征，探究线粒体动态调节蛋白以及脂滴形成在内皮胰岛素敏感性和内皮功能中的调节作用，为理解内皮胰岛素抵抗的发生机制和分子干预靶点提供依据。

方法和结果：（1）高脂饮食小鼠发生了内皮胰岛素抵抗，且内皮线粒体融合蛋白 MFN2 和线粒体分裂蛋白 DRP1 表达下降；在构建的棕榈酸（PA）诱导的人主动脉内皮细胞（HAEC）胰岛素抵抗模型中，发现同时出现了内皮功能障碍和线粒体碎片化，且 MFN2 和 DRP1 蛋白表达显著下调。（2）进一步发现 MFN2 敲低的 HAEC 细胞中发生了线粒体碎片化、胰岛素抵抗和内皮功能障碍，并且在 PA 处理后进一步加剧；然而 DRP1 敲低的 HAEC 细胞中并未出现显著的胰岛素敏感性下降或内皮功能障碍；提示高脂条件下的内皮细胞 MFN2 表达下调及线粒体碎片化是引起内皮胰岛素抵抗和功能障碍的重要因素。（3）PA 以浓度依赖的方式诱导的 HAEC 细胞脂滴累积现象，内皮细胞脂滴积累与胰岛素抵抗及内皮功能障碍负相关；进一步借助 siMFN2 发现 MFN2 具有稳定和保护脂滴的作用。我们推测：高浓度 PA 暴露下 HAEC 细胞的脂滴形成能力受损，过量的脂肪酸引起脂毒性，进而造成胰岛素抵抗和内皮功能障碍；其中 MFN2 蛋白表达下调可能是高浓度 PA 处理下脂滴形成减少的重要原因。

结论：MFN2 在内皮胰岛素敏感性、内皮脂滴形成和内皮功能中具有重要正向调节作用。

Obesity Increases Atherosclerosis Susceptibility via Inter-tissue miR-30e-SLC7A11 Axis

Chen Wang, Haoyu Wu, Zu-Yi Yuan

The First Affiliated Hospital of Xi'an Jiaotong University

Background: Atherosclerosis is a multi-faceted disease that involves chronic inflammation and maladapted metabolism in several tissue types. The novel concept of cardiovascular-kidney-metabolic (CKM) syndrome has brought further attention to the causation between obesity and atherosclerosis. With obesity as a risk factor for atherosclerotic disease, recent research suggests that adipose tissue in obese animal models and humans can generate endocrine-like molecules that affect arterial health later on. Extracellular vesicles, including exosomes, play a crucial role in intercellular communication by transferring DNA, coding and noncoding RNA, and proteins to the extracellular space as well as tissues nearby and far. Because adipocytes are an abundant tissue origin of exosome-carried microRNAs (miRNAs) in the circulation, emerging evidence suggests that adipocyte-derived exosomes can regulate vascular function and disease in an "endocrine-like" manner. Previous studies showed that microRNA-30e (miR-30e) is linked to atherosclerotic cardiovascular disease (ASCVD) in that circulating miR-30 levels are associated with coronary calcification and plaque instability and elevated level of miR-30e is evident in atherosclerotic lesions. Solute carrier family 7 member 11 (SLC7A11), a cystine/glutamate transporter, plays critical roles in glutamine-glutathione (GSH) metabolism and thus is involved in the pathogenesis of cancer and atherosclerosis. However, whether an endocrine-like link between the adipose-derived miR-30e-5p and SLC7A11 in the vascular endothelium can lead to obesity-caused atherosclerosis is unknown. **Methods:** MiRNA data mining and RT-PCR validations were used to demonstrate the positive association among serum level of miR-30e-5p, obesity, and coronary arterial disease in human patients. Transcriptomics (including bulk RNA-seq and single-nucleus RNA-seq), metabolomics, in silico analysis Western blotting, Ago-IP, histological staining, Seahorse were used to establish a miR-30e-5p-SLC7A11 regulation of central carbon metabolism, mitochondrial and endothelial cell (EC) function. Mouse models with EC-specific Slc7a11 knockout (EC-Slc7a11$^{-/-}$) and gain or loss of function of miR-30e-5p specific in adipose tissues were used to elucidate the detrimental role of this endocrine-like axis in obesity-related atherosclerosis. **Results:** The level of adipocyte-derived miR-30e-5p was significantly upregulated in obese humans with coronary artery disease and obese and atherosclerotic mice. Via serum exosomes, the adipocyte-generated miR-30e-5p targeted SLC7A11mRNA in vascular endothelial cells. SLC7A11 deficiency due to miR-30e-5p targeting dysregulated glutamate/cystine metabolism, increased glycolysis, reduced oxidative phosphorylation, and impaired mitochondrial function, resulting in EC dysfunction. The EC dysfunction could be rectified by SLC7A11 overexpression or miR-30e-5p antagonism. Exogenously delivered miR-30e-5p in adipose tissues phenocopied the increased atherosclerosis in EC-Slc7a11$^{-/-}$ mice. In contrast, miR-30e-5p antagomir treatment reduced atherosclerosis in Apoe$^{-/-}$ and ob/ob mice. **Conclusion:** Our multi-omics approaches demonstrates that the adipose-derived miR-30e-5p downregulated SLC7A11 mRNA in ECs via tissue crosstalk. (1) Elevated circulating level of miR-30e-5p in obese individuals with CAD; (2) Decreased SLC7A11 level in CAD patients and experimental atherosclerotic mice; (3) MiR-30e-5p directly targeted the 3 ′ -UTR of SLC7A11 mRNA, resulting in dysfunctional ECs, including dysregulated thioreduction, increased glycolysis, reduced oxidative phosphorylation, and impaired mitochondrial function; (4) Ablation of Slc7a11 in endothelium aggravated but inhibition of miR-30e-5p in adipose tissue alleviated atherosclerosis in mouse models. From these findings, we propose that miR-30e-5p targeting SLC7A11 links the maladapted adipose tissue with atherosclerosis in the arterial wall. Thus, the miR-30e-5p–SLC7A11 axis might be integral to the CKM syndrome. This notion supports the emerging view that adipose tissue, traditionally considered an energy storage depot, is an active endocrine organ that affects vascular health via secreted factorsThe resulting EC dysfunction led to obesity-related atherosclerosis in mice. These findings underscore a causality between obesity and atherosclerosis in the context of cardiovascular-kidney-metabolic syndrome.

代谢综合征组分聚集模式对心血管预后的影响及无创风险预测模型的构建：一项前瞻性队列研究

朱晶晶 田丹 刘华芬

武汉大学人民医院

目的

探讨不同代谢综合征（MS）组分（肥胖、高血糖、高血压、血脂异常）聚集模式与冠状动脉病变严重程度及心血管事件的关系；联合皮肤糖基化终产物（AGE）无创检测与临床指标，构建心血管死亡风险预测模型，为基层早期干预提供依据。

方法

1. 研究设计：前瞻性队列研究（2023 年 1 月 –2025 年 6 月）

2. 研究对象：

- 纳入 1,240 例基线无心血管疾病的 MS 患者（符合中国 MS 诊断标准：腹型肥胖 + 任意 2 项代谢异常）

- 按年龄分层：20–39 岁（468 例）、40–59 岁（471 例）、60–79 岁（301 例）

3. 评估指标：

- 代谢组分：腰围、空腹血糖、血压、甘油三酯、HDL-C

- 无创检测：皮肤 AGE（自体荧光法，反映长期代谢损伤）

- 心血管指标：冠脉造影 Gensini 积分（狭窄≥ 50% 为病变）、左心室质量指数（LVMI）

- 生物标志物：3′- 腺苷一磷酸（3′-AMP）、尿苷二磷酸（UDP）（CE-TOF/MS 代谢组学检测）

4. 统计分析：

- 因果图模型（CGM）分析 MS 组分与心血管结局的直接 / 间接路径

- LASSO 回归筛选预测因子 → Cox 回归构建风险模型 → ROC 曲线验证效能（AUC）

- 中介效应检验（如肾功能、炎症指标对 AGE →心血管事件的介导作用）

结果

1. MS 组分聚集与心血管损伤：

- MS 组分每增加 1 项，冠脉 Gensini 积分升高 18.7%（P<0.01），LVH 风险增加 1.29 倍（95% CI: 1.09–1.53）

- 40–59 岁组皮肤 AGE 与 Framingham 风险评分显著正相关（r=0.485，P<0.001），独立预测 ASCVD 风险（OR=1.029/ 单位，P=0.018）

2. 因果路径与介导效应：

- 直接因果路径：eGFR ↓ → 心血管死亡（HR=1.08，*P*<0.01）

- 关键介导效应：

- BUN 介导 eGFR 对心血管死亡的影响（介导比例 30.3%）

- 皮肤 AGE 介导高血糖对冠脉病变的影响（介导比例 24.1%）

3. 风险预测模型效能：

- 联合模型（临床指标+代谢物+皮肤 AGE）预测 3 年心血管死亡 AUC=0.901（显著优于单一临床模型 AUC=0.868）

- 核心预测因子：

- 代谢物：3′-AMP（HR=0.99，抗炎保护）、UDP（HR=1.01，促炎风险）

- 临床指标：年龄、血红蛋白、冠心病史

- 高危组（评分≥中位数）心血管死亡率较对照组高 3.7 倍（P<0.0001）

结论

1. 机制层面：MS 组分聚集通过肾功能损伤（eGFR ↓、BUN ↑）及代谢毒性产物（AGE 积累）直接加剧心血管病变，且中年人群（40–59 岁）皮肤 AGE 是无创风险预警的敏感指标。

2. 预测价值：整合皮肤 AGE 与代谢组学标志物（3′-AMP/UDP）的联合模型显著提升心血管死亡预测精度（AUC>0.9），为基层高危筛查提供可视化工具。

3. 临床启示：MS 管理需采取组分协同干预策略：

- 首选 ACEI/ARB 降压（改善代谢）

- 高危者加用 GLP-1 RA（如司美格鲁肽），降低 MACE 风险 26%（SUSTAIN-6 证据）

Basal Metabolic Rate and Atrial Fibrillation Risk among Individuals with Type 2 Diabetes: insights from the UK Biobank

Peng Zhao, Yan Wang, Na-Na Dong, Min Mao, -Dan Wang, Yun-Fei Wu, Zhong-Zhi Yu, Fei-Yuan Han, Xiao-Fang Ban, Cheng Jin, Xin-Xin Liu, Jin-Wei Tian

The Second Affiliated Hospital of Harbin Medical University

Objective: Patients with type 2 diabetes (T2D) have a high incidence of atrial fibrillation (AF). Basal metabolic rate (BMR), a key indicator of overall metabolic health, may influence AF risk independently. Energy expenditure and energy requirement of atrial tissues increase during AF. Abnormal energy metabolism plays a crucial role in the pathogenesis of AF. The role of BMR in AF in patients with T2D remains unclear. We hypothesized that accurate measurement of BMR might provide significant clinical and public health information by better-applying body composition to evaluate the occurrence of AF in patients with T2D. Given that the primary factor determining BMR is FFM, to fill the knowledge gap, we therefore utilized data from a large prospective cohort in the UK Biobank to explore the associations of BMR and FFM levels with AF onset in patients with T2D.

Methods: This prospective cohort study included participants with type 2 diabetes from 22 assessment centers in the UK Biobank. Baseline BMR was measured by bioimpedance and categorized into quartiles. Fat-free mass (FFM) was assessed as a supplementary measure of BMR. Associations between BMR levels and onset of AF risk were analyzed using the multivariable-adjusted restricted cubic spline and Cox proportional hazards regression model.

Results: Among 14,072 participants (mean [SD] age, 59.4 [7.2] years; 61.6% men), 1,744 cases of AF were identified over a median follow-up of 12.8 years (interquartile range, 12.0–13.6 years). The Kaplan-Meier analysis revealed the highest crude incidence of new-onset AF in the top quartile levels. RCS showed a linear relationship of BMR with new-onset AF, as did FFM. This association remained strong even after adjustments for all covariates, including age, sex, race, education, smoking status, alcohol intake frequency, physical activity, HbA1c, glucose, insulin medication use, history of heart failure, hypertension, duration of diabetes and PRS for AF (HR, 3.04 [95% CI, 2.45–3.76]). To assess the potential impact of unmeasured confounding, we performed an E-value analysis, yielding a value of 5.53, indicating that our findings are relatively robust. When BMR was regarded as a continuous variable, the HR of new-onset AF was 1.56 per SD increase in BMR after fully considering multiple influencing factors. Similarly, higher FFM increased the risk of AF, the E-value was 5.73. Among the several traditional risk factors selected, BMR and FFM ranked first and second respectively, and their relative importance was higher than that of the BMI.

In subgroup analysis, the positive associations of BMR level with new-onset AF risk were more pronounced among females (P for interaction P for interaction = 0.028) also showed a significant interaction with BMR level. When the highest and lowest 5% outliers of BMR and FFM were excluded, when we excluded patients with type2 diabetes with poor self-rated health, and when we excluded patients who developed AF in the first 2 and 4 years after follow-up, even excluded patients with type2 diabetes with BMI ^{2}, the associations between BMR, FMM, and new-onset AF did not change. Similarly, when CRP level and menopausal status were adjusted, the results were the same. Using the Fine-Gray model, higher BMR level also increased the risk of AF (HR, 3.02 [95% CI, 2.44-3.74]), did FFM. Finally, to further strengthen our results, we adjusted for standard anthropometric measures respectively, BMR and FFM were found to influence the new-onset AF independently of BMI, WC, HC, and WHR. When BMI, WC and HC were adjusted at the same time, the results remained unchanged.

Conclusion: Elevated BMR levels are associated with an increased risk of new-onset AF in individuals with type 2 diabetes, particularly in females and participants with higher BMI, highlighting the importance of incorporating BMR measurement into routine clinical evaluations for personalized risk stratification and management.

Novel adiposity indices and their associations with all-cause and cardiovascular mortality in individuals with cardiovascular-kidney-metabolic syndrome stages 0-3: findings from a nationwide prospective cohort study

hangyu zhou, Jie Li, zhao Wang

新疆维吾尔自治区人民医院

Abstract

Background The most common cause of cardiovascular-kidney-metabolic (CKM) syndrome is excess or dysfunctional adipose tissue, particularly visceral adipose tissue, which can secrete proinflammatory and pro-oxidative products that damage arterial, cardiac, and renal tissues. Therefore, assessing the impact of obesity on the prognosis of the CKM population is crucial. In the CKM population, the relationships between BMI and novel adiposity indices with mortality risk remain unclear.

Methods This study included 26,899 participants with CKM stages 0--3 from the NHANES conducted between 2001 and 2018. The association of the novel obesity index with both all-cause mortality and cardiovascular mortality in the CKM population was evaluated through Cox proportional hazards models, RCS curves, and two-stage Cox analyses. Subgroup analyses and interaction tests were performed to evaluate risks across different demographic characteristics. The novel obesity index and BMI were compared through receiver operating characteristic (ROC) analysis regarding their performance in predicting mortality.

Results In the analysis via survey-weighted multivariate regression, new obesity metrics, including the ABSI, WWI, BRI, WHtR, and C-index, demonstrated significant positive relationships with all-cause and cardiovascular mortality in individuals with CKM. Among these metrics, the WWI exhibited the most robust association with overall mortality, with a hazard ratio (HR) of 1.41 and a 95% confidence interval (95% CI) ranging from 1.31--1.51 (P < 0.05). This was followed by the ABSI (HR: 1.32, 95% CI: 1.24 - 1.39, P < 0.01), C-index (HR: 1.28, 95% CI: 1.20 - 1.36, P < 0.05), WHtR (HR: 1.11, 95% CI: 1.03 - 1.19, P < 0.01), and BRI (HR: 1.05, 95% CI: 1.02 - 1.08, P < 0.05). The strongest association with cardiovascular mortality was observed for WWI (HR: 1.66, 95% CI 1.39–1.99, P < 0.05), followed by the C-index (HR: 1.444, 95% CI 1.23–1.68, P < 0.05), ABSI (HR: 1.38, 95% CI 1.22–1.56, P < 0.05), WHtR (HR: 1.30, 95% CI 1.09–1.55, P < 0.05), and BRI (HR: 1.11, 95% CI 1.05–1.20, P < 0.05). When investigating the dose□response relationship, a significant positive correlation was found between the ABSI, WWI, WHtR, and C-index and all-cause and cardiovascular mortality in the CKM syndrome population (P-overall < 0.05, P-nonlinear > 0.05). A U-shaped association was observed between BMI, BRI, and WHtR and all-cause mortality (P-overall < 0.05, P-nonlinear < 0.05). To address this nonlinear relationship, a recursive approach was utilized to detect possible inflection points, and a two-segment Cox regression analysis demonstrated contrasting associations between BRI, WHtR, and overall mortality before and after these inflection points (log-likelihood ratios all P < 0.05). Subgroup analysis revealed that the increase in mortality risk associated with novel obesity indices was greater in the 20–59 years age group than in the ≥ 60 years age group (P value < 0.05, interaction P < 0.05). The ROC curve results indicate that the AUC of the novel obesity marker for predicting all-cause mortality and cardiovascular mortality is greater than that of BMI.

Conclusion In the U.S. adult population with CKM stages 0--3, U-shaped associations were observed between BMI, BRI, and WHtR and both all-cause mortality and cardiovascular mortality, whereas ABSI, WWI, and the C-index were linearly positively correlated with these outcomes. Compared with BMI, the novel obesity indices are positively correlated with mortality risk in the early CKM population and demonstrate greater advantages as an obesity assessment indicator and a predictor of adverse outcomes.

Musclin 通过影响 WTAP 介导的 m6A 甲基化修饰参与糖尿病肾损伤的机制研究

蒋丽瀛 熊安琪 童在宇 陈文佳

哈尔滨医科大学附属第一医院

目的：糖尿病（Diabetes mellitus,DM）作为本世纪的重大医学问题，严重危害人类健康。糖尿病肾病（Diabetic nephropathy,DN）是一种以持续白蛋白尿和肾功能进行性下降为特征的临床综合征。大多数 DN 患者因肾小管损伤而导致肾功能下降。m6A 甲基化修饰作为参与 DN 肾小管损伤的主要机制之一，是 DN 潜在的疾病特异性治疗靶点。肌肉素（Musclin）作为骨骼肌分泌的一种肌肉因子，在 DM 靶器官损害中发挥一定作用，然而其参与糖尿病肾损伤的机制尚不清楚。本研究拟从实验动物和细胞水平阐明 Musclin 在糖尿病肾损伤中的作用，探讨 Musclin 通过影响 WTAP 介导的 m6A 甲基化修饰在糖尿病肾损伤中的机制，为 DN 防治提供新靶点和科学依据。

方法：1. 检测干预内源性 Musclin 表达对 DM 大鼠肾脏组织的影响，采用高脂饮食和链脲菌素注射构建 DM 大鼠模型，对 DM 大鼠进行腺相关病毒尾静脉注射干预 Musclin 表达。Western blot 和免疫组化法检测肾脏组织 Musclin 的表达，HE 染色和 Masson 染色检测肾脏组织炎症浸润和纤维化情况。2. 探讨在高浓度葡萄糖条件下采用腺病毒转染对大鼠肾小管上皮细胞进行 Musclin 敲减后对 m6A 甲基化修饰和炎症相关蛋白的影响。采用 Western blot 检测 m6A 甲基化修饰相关蛋白和炎症相关蛋白表达；采用 dot blot 检测 m6A 整体水平。3. 探讨在正常浓度葡萄糖条件下，给予 Musclin 刺激对 NRK-52E 细胞 m6A 甲基化修饰水平、甲基化修饰相关蛋白以及炎症激活的影响。

结果：1. 与 Ctrl 组比较，DM 组大鼠 Musclin 表达显著上调，HE 染色可见肾小管萎缩，肾小管玻璃样变和坏死，肾间质增宽，炎性细胞浸润较多。Masson 染色显示 DM 组大鼠肾脏胶原沉积明显增加。内源性干预 DM 组大鼠 Musclin 表达后，HE 染色可见肾小管结构破坏显著改善，可见少量肾小管萎缩，肾间质略增宽，炎性细胞浸润显著减少。Masson 染色肾脏组织胶原沉积显著改善。2. 与 NG 组相比，在 HG 培养下，使用腺病毒敲减肾小管上皮细胞细胞中的 Musclin 可改善 m6A 水平和 WTAP 蛋白表达。同样，炎症相关指标 NLRP3 和 IL-1β 的表达降低。3.Musclin 可导致肾小管上皮细胞细胞 m6A 水平升高，并伴有 m6A 甲基转移酶 WTAP 的表达升高，炎症相关指标 NLRP3、IL-1β 表达升高。4. 抑制肾小管上皮细胞细胞中 WTAP 后给予 Musclin 刺激，与 siNC+Musclin 组相比，siWTAP+ Musclin 组炎症相关指标 NLRP3、IL-1β 表达降低。

结论：1.Musclin 在糖尿病大鼠肾脏肾小管中显著上调，且干预内源性 Musclin 表达可抑制 WTAP 表达并改善糖尿病大鼠肾损伤 2. 沉默 Musclin 可抑制高糖诱导的 m6A 甲基化修饰及 WTAP 表达从而改善肾小管上皮细胞细胞炎症激活；

3.Musclin 可通过促进 m6A 甲基化修饰及 WTAP 表达而引起肾小管上皮细胞细胞炎症激活，沉默 WTAP 可抑制 Musclin 诱导的肾小管上皮细胞细胞炎症激活。

Musclin 通过内质网应激通路引起骨骼肌胰岛素抵抗的机制研究

郑婉秋 熊安琪 童在宇 陈文佳

哈尔滨医科大学附属第一医院

目的：胰岛素抵抗（IR）是指外周组织器官对生理浓度胰岛素的反应性降低，是 2 型糖尿病（T2DM）、肥胖等疾病的重要病理生理特征。众多研究发现内质网应激 (ERS) 能够引起外周组织的 IR，目前对于 ERS 引起 IR 的机制的研究主要集中在脂肪组织与肝脏，而在骨骼肌中的研究甚少。肌肉素（Musclin）是 2004 年由 Nishizawa 在小鼠骨骼肌中发现的一种肌肉因子，许多研究表明 Musclin 参与骨骼肌 IR 而在糖尿病、肥胖等代谢综合征中发挥重要作用。本研究拟从细胞水平阐明 Musclin 在骨骼肌 IR 中的作用，探讨 Musclin 对骨骼肌 ERS 激活以及葡萄糖转运体 -4（GLUT-4）转录调节因子肌细胞增强因子 2A（MEF2A）与过氧化物酶体增殖活化受体 γ 共激活因 1α（PGC1-α）表达的影响，为糖尿病 IR 防治提供新靶点和科学依据。

方法：本研究应用骨骼肌 L6 细胞系和高糖诱导的 L6 骨骼肌细胞系作为对照以及 IR 的细胞模型。外源性给予骨骼肌细胞 Musclin，观察 Musclin 对于骨骼肌细胞的作用。通过腺病毒转染 Musclin（Musclin-shRNA）建立 Musclin 敲低的骨骼肌细胞模型。Western-Blot 法检测骨骼肌细胞 GLUT-4 的蛋白水平，以及 GLUT-4 转录调节因子 MEF2A 和 PGC1-α 的表达。并且检测外源性 Musclin 和高糖诱导的骨骼肌细胞 Musclin 敲低后内质网应激标志物葡萄糖调节蛋白 78（GPR78），葡萄糖调节蛋白 94（GPR94），转录因子 C/EBP 同源蛋白（CHOP）以及三条途径经典标志物肌醇需求酶 1（IRE1）、蛋白激酶 R 样 ER 激酶（PERK）和激活转录因子 6（ATF6）的蛋白表达情况。

结果：(1) 与低糖对照组相比，高糖可显著诱导骨骼肌细胞 Musclin 表达升高，且其升高与渗透压无关；（2）检测内质网应激相关蛋白的表达，Musclin 可引起大鼠骨骼肌细胞的内质网应激，PERK、IRE1-α、ATF6、BIP、CHOP 表达均升高（3）检测 GLUT-4 及其转录调节因子 MEF2A、PGC1-α 的表达，发现 Musclin 可引起大鼠骨骼肌细胞 GLUT-4 表达降低。（4）检测内质网应激相关蛋白的表达情况，结果发现高糖可诱导骨骼肌细胞的内质网应激，与对照组相比，高糖组 PERK、IRE1-α、ATF6、CHOP 蛋白表达升高，利用腺病毒敲减骨骼肌细胞 Musclin 表达后发现，与高糖组相比，抑制 Musclin 表达可显著改善高糖诱导的骨骼肌细胞内质网应激相关蛋白 PERK、IRE1-α、ATF6、CHOP 的表达；（5）高糖可诱导大鼠骨骼肌细胞 GLUT-4 及其转录调节因子 MEF2A、PGC1-α 表达减低，然而，利用腺病毒敲减骨骼肌细胞 Musclin 表达后，与高糖组相比，GLUT-4 及其转录调节因子 MEF2A、PGC1-α 表达升高。

结论：（1）高糖可以引起骨骼肌细胞 Musclin 表达升高，并且能够引起骨骼肌细胞 GLUT-4 及其转录调节因子 MEF2A、PGC1-□ 蛋白表达水平下降，此过程伴有 ERS 的激活。（2）外源性予以 Musclin 可以抑制骨骼肌细胞 GLUT-4 和转录调节因子 MEF2A、PGC1-□ 蛋白表达，并且激活了 ERS。（3）干预骨骼肌细胞 Musclin 的表达可以改善高糖所引起的 GLUT-4 及其转录调节因子 MEF2A、PGC1-□ 的表达下降和 ERS 的激活。

DMH1 Improves Palmitic Acid-Induced Insulin Resistance in Cardiomyocytes via PP2A Inhibition and AKT/AMPK Signaling Activation

Xiao-Tong li[2], Jun-Yao Liu[1], Yang Li[1], Yan-Li Cheng[1], Xin Xie[1]

1. The Binzhou Affiliated Hospital, Binzhou Medical University

2. The Affiliated Yantaishan Hospital, Binzhou Medical University

Our previous investigations have conclusively established that DMH1 modulates glucose metabolism in rat skeletal muscle cells through the activation of the AKT signaling cascade, thereby underscoring its potential in the maintenance of cellular energy homeostasis and prompting inquiries into its regulatory roles in other metabolically active cell types. However, the precise functional significance of DMH1 in insulin-resistant cardiomyocytes, alongside the underlying molecular mechanisms, has remained an unresolved issue in contemporary biomedical research, representing a critical knowledge gap in the context of cardiac metabolic disorders.

To address this lacuna, the present study employed H9c2 cells, a well-characterized cardiomyocyte model widely utilized in cardiovascular research, to investigate the effects of DMH1 under conditions of insulin resistance. Insulin resistance was induced by exposing H9c2 cells to 400 μM palmitic acid (PA) for a 24-hour duration, a protocol validated to recapitulate the lipotoxic insult associated with insulin resistance in cardiac tissues in vivo, particularly in pathophysiological states such as obesity and type 2 diabetes mellitus.

A comprehensive array of analytical methodologies was deployed to assess key physiological and molecular parameters. Glucose consumption and uptake, pivotal indices of glucose metabolic efficacy, were quantified using high-sensitivity assay kits. Cytotoxicity was evaluated via cell viability assays to exclude potential deleterious effects of DMH1. Reactive oxygen species (ROS) generation, a hallmark of oxidative stress in insulin-resistant cells, was measured utilizing fluorescent probes with subsequent quantification via microplate spectrophotometry. Additionally, protein phosphatase 2A (PP2A) activity was determined using a specialized enzymatic assay kit, while Western blotting was employed to analyze the expression and phosphorylation status of AKT and AMP-activated protein kinase (AMPK), key regulators of metabolic signaling pathways.

The results of the present study revealed several critical observations. Firstly, treatment with DMH1 alone significantly enhanced glucose consumption and uptake in H9c2 cells, indicating a direct stimulatory effect on glucose metabolism, without exerting cytotoxic effects within the tested concentration range, a finding of considerable relevance for potential therapeutic applications. Concomitantly, DMH1 treatment resulted in the activation of both AKT and AMPK, suggesting a coordinated regulation of multiple metabolic signaling pathways.

In contrast, PA treatment induced a characteristic insulin-resistant phenotype in H9c2 cells, characterized by a significant reduction in glucose consumption and uptake, increased cellular apoptosis, excessive ROS accumulation, and a marked inhibition of AKT and AMPK activation. Importantly, co-treatment with DMH1 ameliorated these PA-induced deleterious effects, leading to a significant improvement in insulin sensitivity, thereby confirming the protective role of DMH1 in this experimental model.

To elucidate the mechanistic basis of DMH1's actions, specific pharmacological inhibitors of AKT and AMPK were employed. Administration of either inhibitor abrogated the beneficial effects of DMH1 on PA-induced insulin-resistant H9c2 cells, demonstrating the essential role of both AKT and AMPK in mediating the protective effects of DMH1. Notably, DMH1 treatment was found to significantly inhibit PP2A activity. To further validate the role of PP2A, the PP2A activator FTY720-M was utilized, which reversed DMH1-induced activation of AKT and AMPK and completely abolished the protective effects of DMH1 in PA-induced insulin-resistant H9c2 cells.

In conclusion, the present study demonstrates that DMH1 ameliorates PA-induced insulin resistance in H9c2 cells through the inhibition of PP2A activity, resulting in the activation of AKT and AMPK signaling pathways. These findings contribute to a deeper understanding of the biological functions of DMH1 and provide a novel mechanistic framework for the development of therapeutic strategies targeting cardiac insulin resistance.

Inhibition of PCSK9 attenuates ferroptosis after ischemia-reperfusion in cardiomyocytes through negative regulation of the FOXO3/MMP9 pathway

mingqi zheng, Jia-nan Xu

The First Hospital of Hebei Medical University

Abstract

BACKGROUND:

Myocardial ischemia-reperfusion (I/R) injury leads to cardiomyocyte death and fibrosis. Prevention of cell death is important for the protection of cardiac function after I/R injury. In recent years, the role of cellular ferroptosis (Ferroptosis) as a novel mode of cell death in cardiac ischemia-reperfusion injury has received increasing attention. Ferroptosis is an iron-dependent lipid peroxidation-driven form of cell death, which is different from conventional apoptosis, necrosis, and autophagy. Studies have shown that ferroptosis plays an important role in myocardial IRI, and its regulatory mechanism involves various aspects of glutathione metabolism, lipid peroxidation, and iron homeostasis. Although studies have revealed the potential role of ferroptosis in myocardial IRI, its specific molecular mechanisms and regulatory networks need to be further elucidated.PCSK9 is an important lipid metabolism regulator of lipid metabolism and has been found to be closely related to the development of cardiovascular diseases in recent years. One of the pivotal factors in LDL metabolism is the LDL receptor (LDLR) by virtue of its capacity to bind and subsequently clear cholesterol derived from LDL from the circulation.Studies of PCSK9 in cardiomyocytes have suggested that it may affect myocardial IRI through the modulation of inflammatory response and cell death pathways. MMP9, on the other hand, is an important matrix metalloproteinase involved in the degradation and remodeling of the extracellular matrix and plays an important role in myocardial IRI. It has been suggested that MMP9 may be involved in the pathological process of myocardial IRI through the regulation of inflammatory response, oxidative stress and cell death. However, the specific mechanisms of the roles of PCSK9 and MMP9 in myocardial IRI and their relationship with ferroptosis have not been fully elucidated.In summary, the present study aimed to investigate the roles of PCSK9 and MMP9 in myocardial ischemia-reperfusion injury and their relationship with cellular ferroptosis, with a view to providing a new theoretical basis and potential therapeutic targets for the prevention and treatment of myocardial IRI. By deeply analyzing the molecular mechanisms of PCSK9 and MMP9 in myocardial IRI, this study is expected to provide an important scientific basis for the development of novel myocardial protection strategies.

METHODS:

We utilized a mouse model with left anterior descending coronary artery ligation to investigate the effect of inhibiting proprotein convertase subtilisin/kexin type 9 (PCSK9) on the changes in cell death patterns after myocardial cell reperfusion injury. To identify the key molecules involved in ferroptosis of myocardial cells, we conducted transcriptomic studies and explored the possibility that PCSK9-FOXO3A/MMP9 might be involved in ferroptosis. We verified the upstream-downstream relationships between the key molecules using targeted knockdown and functional reconstitution experiments, and confirmed the molecular interactions through CoIP and ChIP in primary myocardial cells.

RESULTS:

Firstly, we found that inhibiting PCSK9 can significantly alleviate ischemia-reperfusion injury in cardiomyocytes, thereby improving cardiac function after reperfusion. Through pathological staining methods and transcriptomics-based bioinformatics analysis, it was shown that among the types of cell death, ferroptosis showed the most significant improvement effect. We explored its potential mechanism and combined with the transcriptional expression trends and differences of genes in transcriptomics to screen out MMP9. Further, by targeting knockdown of PCSK9 and MMP9 to verify their relationship and role in improving the ferroptosis process, and by knocking down the elevated MMP9 during myocardial ischemia/reperfusion injury and overexpressing MMP9 to determine the direct function of MMP9 in the myocardial cell ferroptosis process, we verified the physical binding of MMP9 to the key molecule GPX4 in myocardial cells through CoIP, and confirmed that PCSK9 participates in the myocardial ischemia/reperfusion process by regulating FOXO3A and thereby regulating the transcription of MMP9 through ChIP. Inhibiting PCSK9 significantly inhibits ferroptosis during myocardial ischemia/reperfusion by reducing the expression of MMP9.

CONCLUSION:

In this study, we found significant ferroptosis in cardiomyocytes following I/R-induced cardiac injury. Inhibition of PCSK9, which reduces MMP9 expression, significantly ameliorated ferroptosis in cardiomyocytes. Mechanistically, PCSK9 inhibition regulates the FOXO/MMP9 pathway, which contributes to cellular ferroptosis and ultimately attenuates cardiac I/R injury. Knockdown of PCSK9 or administration of a specific monoclonal antibody targeting PCSK9 significantly improved cardiac function and fibrosis after reperfusion injury in mice. This study provides insights into several scientific questions.

The role of triglyceride□glucose index and derivatives in mortality risk among cardiovascular disease patients: A NHANES cohort analysis

Zixi Zhang, Yi-Chao Xiao, Tao Tu, Qi-Ming Liu

The Second Xiangya Hospital of Central South University

Background

The triglyceride-glucose (TyG) index, an emerging marker for insulin resistance, has garnered attention as a potential predictor of cardiovascular disease (CVD) outcomes. Insulin resistance plays a pivotal role in the pathogenesis of a range of cardiovascular conditions, including coronary artery disease, heart failure, and stroke. Traditional risk factors, such as hypertension, diabetes, and dyslipidemia, are well-established in predicting cardiovascular outcomes, but the increasing burden of metabolic syndrome has prompted the exploration of additional biomarkers that could enhance risk stratification. The TyG index, calculated as the product of fasting triglyceride levels and glucose levels, is a simple, cost-effective surrogate for insulin resistance and has been associated with various cardiovascular risks. Despite its growing utility in predicting CVD outcomes, the relationship between the TyG index and all-cause and cardiovascular mortality remains unclear, and its potential role in identifying high-risk patients for targeted prevention strategies warrants further investigation.

Methods

To evaluate the association between the TyG index and mortality outcomes, we analyzed data from the National Health and Nutrition Examination Survey (NHANES) spanning from 1999 to 2018. Our study population included individuals diagnosed with cardiovascular disease (CVD), encompassing patients with coronary artery disease, heart failure, stroke, and other cardiovascular conditions. The TyG index was calculated using fasting triglyceride and glucose levels, and its derivatives—TyG-BMI (body mass index), TyG-WC (waist circumference), and TyG-WHtR (waist-to-height ratio)—were also calculated to explore their relationship with mortality. The participants were categorized into quartiles based on these indices.

We employed several statistical models to examine the associations between the TyG index and mortality outcomes. Cox proportional hazards models were used to assess the hazard ratios (HRs) for all-cause mortality and cardiovascular mortality. Kaplan-Meier survival analysis was applied to estimate survival curves and visualize the association between the TyG index and mortality risk. Restricted cubic spline (RCS) models were utilized to assess potential non-linear relationships between the TyG indices and mortality outcomes. Furthermore, receiver operating characteristic (ROC) curves were generated to evaluate the predictive accuracy of the TyG index and its derivatives in forecasting mortality risk in this population.

Results

Our analysis included a total of 8,756 patients with CVD, and we found that elevated levels of the TyG index and its derivatives were independently associated with a higher risk of both all-cause mortality and cardiovascular mortality. Among the indices, TyG-WHtR demonstrated the strongest association with mortality outcomes. Specifically, TyG-WHtR was significantly associated with all-cause mortality (HR: 1.414, 95% CI: 1.213–1.648) and cardiovascular mortality (HR: 1.470, 95% CI: 1.158–1.868) in patients with CVD. This association remained robust even after adjusting for traditional cardiovascular risk factors such as age, sex, smoking status, and comorbidities like diabetes and hypertension.

Subgroup analyses revealed similar results across groups of patients with heart disease or stroke, reinforcing the consistent predictive value of the TyG-WHtR for mortality risk across different CVD manifestations. Additionally, RCS analysis indicated that the relationship between the TyG indices and mortality risk was non-linear, with L-shaped and J-shaped trends observed, suggesting that both low and high levels of TyG indices were associated with an increased risk of mortality. This highlights the importance of not only addressing insulin resistance but also monitoring metabolic health in individuals at both extremes of the TyG index.

ROC curve analysis further supported the prognostic value of the TyG index, particularly TyG-BMI, which exhibited the best predictive accuracy for both all-cause mortality and cardiovascular mortality in CVD patients. The area under the ROC curve (AUC) for TyG-BMI was significantly higher compared to other indices, demonstrating its potential as a robust tool for predicting adverse cardiovascular outcomes.

Conclusions

The TyG index and its derivatives, particularly TyG-WHtR and TyG-BMI, are effective predictors of mortality risk in patients with cardiovascular disease. Our findings suggest that these indices can assist in the early detection of high-risk individuals, enabling healthcare providers to implement targeted preventive strategies aimed at reducing the burden of CVD and its associated mortality. The use of the TyG index in clinical practice could complement existing risk stratification tools, providing a simple and cost-effective method to identify patients at heightened risk for adverse cardiovascular events. Further studies are needed to validate these findings in larger cohorts and to investigate the potential benefits of integrating the TyG index into clinical decision-making for CVD management. Additionally, exploring the mechanisms by which insulin resistance and metabolic dysfunction contribute to cardiovascular mortality could yield important insights for developing more effective therapeutic interventions.

询问 ChatGPT

Association between the total cholesterol/high-density lipoprotein cholesterol ratio and all-cause and cardiovascular mortality in patients with diabetes or prediabetes: Insights from China and the United States

Zi-xi Zhang, Yi-Chao Xiao, Tao Tu, Qi-Ming Liu

The Second Xiangya Hospital of Central South University

Background and Aim: The total cholesterol/high-density lipoprotein cholesterol (TC/HDL-C) ratio has been proposed as an important marker for cardiovascular risk and mortality. While many studies have shown that a higher TC/HDL-C ratio is associated with an increased risk of cardiovascular events, its association with all-cause and cardiovascular mortality in patients with diabetes or prediabetes remains unclear. Both diabetes and prediabetes are major risk factors for cardiovascular diseases, and understanding their impact on mortality is crucial for public health and clinical management. In this study, we aim to evaluate the relationship between the TC/HDL-C ratio and mortality in two large cohorts: CHARLS (China Health and Retirement Longitudinal Study) and NHANES (National Health and Nutrition Examination Survey). Additionally, we assess the incremental predictive value of the TC/HDL-C ratio in improving mortality risk prediction beyond traditional risk factors.

Methods: Data from CHARLS (2011–2020) and NHANES (2005–2018) were analyzed to investigate the association between the TC/HDL-C ratio and mortality outcomes in adults with diabetes or prediabetes. The CHARLS cohort consisted of 5973 individuals, and the NHANES cohort included 11,050 participants. Kaplan–Meier (K-M) survival analyses were performed to evaluate the survival experience across different quartiles of the TC/HDL-C ratio. Multivariate Cox proportional hazards models were used to assess the independent association between the TC/HDL-C ratio and all-cause and cardiovascular mortality, adjusting for potential confounders such as age, sex, smoking, and comorbidities. Non-linear relationships between the TC/HDL-C ratio and mortality were explored using restricted cubic spline (RCS) analysis. Furthermore, the incremental predictive value of the TC/HDL-C ratio was evaluated by adding it to the basic prediction models and assessing the improvement in model performance using receiver operating characteristic (ROC) curves, net reclassification improvement (NRI), and integrated discrimination improvement (IDI).

Results: In the CHARLS cohort, a total of 580 deaths occurred during the follow-up period, resulting in an all-cause mortality rate of 10.9 per 1000 person-years. Kaplan–Meier survival analysis indicated no significant difference in overall survival across the quartiles of the TC/HDL-C ratio (log-rank P = 0.570). However, Cox regression models revealed a modest increase in mortality risk per unit increase in the TC/HDL-C ratio (HR: 1.03, 95% CI: 1.01–1.06; P = 0.024). The RCS analysis showed a non-linear relationship, with an inflection point at 3.85. In the NHANES cohort, 1524 deaths occurred from all causes (mortality rate: 19.4 per 1000 person-years), and 497 deaths were attributed to cardiovascular causes (mortality rate: 6.3 per 1000 person-years). K-M analysis revealed significant differences in both all-cause and cardiovascular mortality across quartiles of the TC/HDL-C ratio (log-rank P

Conclusions: The TC/HDL-C ratio is significantly associated with both all-cause and cardiovascular mortality in Chinese and American populations with diabetes or prediabetes. Higher TC/HDL-C ratios correlate with an increased risk of mortality, with distinct non-linear relationships observed in both cohorts. However, despite its association with mortality, the TC/HDL-C ratio's incremental predictive value over traditional cardiovascular risk factors appears limited. Future studies are needed to explore other potential biomarkers or strategies that might improve prediction accuracy, particularly in the context of diabetes and prediabetes, which are prevalent in both populations. Furthermore, examining the mechanisms by which the TC/HDL-C ratio influences mortality could provide new insights for cardiovascular risk management and guide clinical decision-making in high-risk populations.

The prognostic value of the hemoglobin-to-red blood cell distribution width ratio for all-cause and cardiovascular mortality in patients with diabetes or prediabetes: A cohort study from the NHANES 2005–2018

Zi-xi Zhang, Yi-Chao Xiao, Tao Tu, Qi-Ming Liu

The Second Xiangya Hospital of Central South University

Background: Diabetes is a widespread chronic disease that significantly contributes to healthcare burdens globally, often leading to increased mortality, particularly due to cardiovascular complications. The prevalence of diabetes has been rising steadily, with both type 1 and type 2 diabetes affecting millions of people worldwide. In addition to its direct impact on health, diabetes also leads to an increased risk of a wide range of comorbidities, including cardiovascular disease, kidney failure, and neuropathy. Recent advances in biomarkers have shifted attention towards the inflammatory processes that contribute to the pathogenesis of these complications. One such marker, the hemoglobin-to-red blood cell distribution width ratio (HRR), has been suggested as a potential inflammatory marker. This ratio is a simple, readily available index that could potentially be used to predict adverse outcomes in patients with diabetes or prediabetes. Despite this, the relationship between the HRR and mortality outcomes, particularly in diabetes patients, remains unclear, with limited studies exploring its potential predictive power.

Methods: To address this gap, this study utilized data from the National Health and Nutrition Examination Survey (NHANES) spanning from 2005 to 2018. The cohort included 11,130 patients diagnosed with diabetes or prediabetes, and the HRR was calculated by dividing the hemoglobin level by the red blood cell distribution width. The study employed multivariate Cox proportional hazards models to assess the association between HRR and both all-cause mortality and cardiovascular mortality. Additionally, restricted cubic spline (RCS) analysis was performed to examine potential non-linear relationships, providing a more comprehensive understanding of the HRR's impact across a range of values.

Results: The study followed participants for a mean duration of 84.9 months, during which time 1534 all-cause deaths occurred, resulting in a mortality rate of 19.48 per 1000 person-years. A total of 502 cardiovascular deaths were recorded, with a rate of 6.37 per 1000 person-years. Kaplan-Meier survival analysis revealed significant differences in mortality across the quartiles of HRR, with a log-rank P value of < 0.001, indicating that higher HRR values were associated with worse survival outcomes. The restricted cubic spline analysis revealed an L-shaped relationship between HRR and all-cause mortality, with an inflection point at 1.278. This suggests that HRR below this threshold may not significantly alter the risk of all-cause mortality, but values above it are strongly correlated with an increased risk. Interestingly, no significant non-linear association was found for cardiovascular mortality, indicating that while the HRR is a strong predictor of all-cause mortality, its utility in predicting cardiovascular mortality may be more limited.

Conclusions: The findings of this study suggest that the HRR is a valuable predictor of all-cause mortality in patients with diabetes or prediabetes. This provides evidence that the HRR, a simple and readily accessible marker, may play a crucial role in clinical risk assessment, particularly for assessing long-term survival in this high-risk population. Given the potential of HRR as a prognostic tool, it could help clinicians identify individuals at higher risk of mortality, guiding them toward more personalized and targeted interventions. However, further large-scale prospective studies are needed to confirm these results and explore the broader applicability of HRR in predicting various clinical outcomes, including cardiovascular events, across diverse populations. Understanding the exact mechanisms by which the HRR influences mortality could also provide valuable insights into the inflammatory processes underlying diabetes and prediabetes-related complications. Additionally, this would help in the development of new therapeutic strategies aimed at reducing the burden of these conditions on patients and healthcare systems.

Joint associations of frailty and triglyceride–glucose index with all-cause and cardiovascular mortality in U.S. adults: a population-based cohort study from the NHANES

Zi-xi Zhang, Yi-Chao Xiao, Jia-Yi Zhu, Tao Tu, Qi-Ming Liu

The Second Xiangya Hospital of Central South University

Background: Frailty and insulin resistance (IR) are two major factors that have been independently linked to an increased risk of mortality in the general population. Frailty, typically measured using the frailty index (FI), is a clinical syndrome characterized by weakness, slow walking speed, low physical activity, exhaustion, and unintentional weight loss. It is considered a critical predictor of poor health outcomes, particularly in older adults. The triglyceride–glucose (TyG) index, a simple and effective surrogate marker for insulin resistance, has also been shown to predict various adverse health outcomes, including cardiovascular disease and all-cause mortality. While both frailty and IR are associated with increased mortality risk, their combined effects, particularly in the context of frailty, remain poorly understood. This study aims to explore the joint impact of the FI and the TyG index on all-cause and cardiovascular mortality in a large, diverse general adult population.

Methods: A population-based cohort study was conducted using data from the National Health and Nutrition Examination Survey (NHANES) spanning 2005 to 2018. The study sample included adults from diverse demographic backgrounds, allowing for generalizability of the results. The primary variables of interest were frailty, as measured by the FI, and insulin resistance, as indicated by the TyG index. Mortality data were collected, and Cox regression models were employed to examine the associations between the FI and TyG index with mortality outcomes. Restricted cubic splines were used to explore the potential non-linear relationships between frailty, IR, and mortality. Kaplan-Meier survival curves were plotted to assess the survival differences across varying levels of frailty and TyG index, and joint and interaction analyses were performed to assess potential synergistic effects. Mediation analysis was also conducted to investigate the potential pathways through which frailty and insulin resistance may influence mortality risk.

Results: The findings of this study confirm that frailty is an independent predictor of both all-cause and cardiovascular mortality. The risk of mor-

tality increased in individuals with moderate to severe frailty. A J-shaped relationship was observed between the FI and all-cause mortality, with mortality risk decreasing at lower levels of frailty but significantly increasing as frailty severity worsened. In contrast, the TyG index demonstrated a U-shaped relationship with all-cause mortality, where both low and high values of the TyG index were associated with higher mortality risks, with the highest risk observed at both ends of the index. However, no significant non-linear associations were found between either the FI or TyG index and cardiovascular mortality. There was no significant interaction effect between frailty and the TyG index, indicating that the relationship between frailty and mortality was not significantly altered by the presence of insulin resistance. In individuals with moderate to severe frailty, both high and low TyG index values were significantly associated with an increased risk of mortality. Mediation analysis revealed that frailty significantly mediates the relationship between the TyG index and mortality, with albumin (ALB) and uric acid (UA) serving as partial mediators in this pathway.

Conclusion: This study highlights frailty as the primary determinant of mortality risk in adults, with the effects of metabolic dysfunction, as represented by the TyG index, offering limited additional predictive value. Although both frailty and insulin resistance contribute independently to increased mortality risk, the combination of the two factors does not appear to produce a synergistic effect. This finding suggests that frailty should be considered the primary target for clinical interventions aimed at reducing mortality risk, particularly in individuals with moderate to severe frailty. However, concurrent management of frailty and metabolic health, including the TyG index, may provide an opportunity to improve clinical outcomes and reduce the burden of mortality in this population. Future studies should explore the underlying mechanisms and potential therapeutic interventions that could address both frailty and insulin resistance in order to optimize long-term health outcomes.

Joint Effect of Plasma Homocysteine Concentration and Traditional Cardiovascular Risk Factors on the Risk of New-Onset Acute Myocardial Infarction

Tian-Hui Dong, Hong-Yu Chen, Fang-Fang Fan, Jian-Ping Li, Yan Zhang

Peking University First Hospital

Purpose: Hyperhomocysteinemia is an independent risk factor for cardiovascular disease. Acute myocardial infarction (AMI), a high-risk cardiovascular disease, is associated with substantial mortality and significantly reduces patients' quality of life. However, the joint effect of homocysteine (Hcy) and traditional cardiovascular risk factors on acute myocardial infarction (AMI) has not been completely characterized. The purpose of the present study is to examine the association between plasma homocysteine combined with traditional cardiovascular risk factors and new-onset AMI.

Methods: We conducted a prospective community-based cohort study of 8446 Chinese participants who did not have cardiovascular disease at baseline. Subjects were divided into three groups according to Hcy level (Hcy ≥ 10μmol/L, 10 ≤ Hcy<15μmol/L, Hcy ≥ 15μmol/L). The baseline characteristics of subjects were compared between groups using the t-test or Kruskal-Wallis rank test for continuous variables as appropriate. For categorical variables, data were compared between groups using the chi-square test or Fisher exact test as appropriate. We used Cox proportional hazard regression to determine the association between hcy groups combined with traditional cardiovascular risk factors (hypertension, diabetes, dyslipidemia, current smoking, body mass index, age, sex) and new-onset AMI. Interaction tests were performed to determine the influence of traditional cardiovascular risk factors for the predictive effect of Hcy on new-onset AMI risk.

Results: Of all participants, the average age was 56.5 ± 8.9 years, and 2998 (35.5%) participants were males. During a median 9.9-year follow-up period, 160 (1.9%) endpoints were observed. In the baseline analysis, it was found that the subjects in Hcy ≥ 15 μmol/L group were older, with higher body mass index, higher proportion of males, current smoking and drinking, higher proportion of hypertension and dyslipidemia (no difference in the proportion of diabetes), and higher China-PAR score. With regard to the joint effect of Hcy and hypertension, diabetes, dyslipidemia, current smoking, body mass index, age, sex, there were trends towards increased AMI risk across different groups (P for trend=0.016, 0.001, 0.043, <0.001, 0.004, <0.001, <0.001 respectively). After adjusting for confounders (age, sex, current smoking, current drinking, body mass index, hypertension, diabetes, dyslipidemia, anti-hypertensive treatment, lipid-lowering treatment, hypoglycemic treatment, and estimated glomerular filtration rate), smokers with higher Hcy level were more likely to have new-onset AMI than non-smokers with normal Hcy level (hazard ratio [HR]: 2.82, 96% confidence interval [CI]: 1.40-5.66, p=0.004). Participants with both elevated Hcy levels and older age had the highest risk of new-onset AMI (HR: 3.83, 95% CI: 1.70–8.61, P=0.001). Males with elevated Hcy level had higher risk of new-onset AMI than females with normal Hcy level (HR: 3.04, 95% CI: 1.57–5.92, P=0.001). No interactions were observed between Hcy and these factors.

Conclusion: Subjects with higher Hcy level have more cardiovascular risk factors and higher cardiovascular risk. Besides, there were joint effects of high Hcy level and traditional cardiovascular risk factors, such as smoking, aging and male on the incidence of AMI. Attention should be paid to the simultaneous screening of Hcy and cardiovascular risk factors in the primary prevention population of AMI. Studies should be conducted to analyze new-onset AMI risk in subjects after controlling for cardiovascular risk factors and Hcy levels.

Joint Effect of Plasma Homocysteine Concentration and Traditional Cardiovascular Risk Factors on the Risk of New-Onset Stroke

Tian-Hui Dong, Hong-Yu Chen, Fang-Fang Fan, Jian-Ping Li, Yan Zhang

Peking University First Hospital

Purpose: Stroke has high rates of disability and mortality, which significantly impair patients' quality of life. Hyperhomocysteinemia is an independent risk factor for stroke. However, the joint effect of homocysteine (Hcy) and traditional cardiovascular risk factors on stroke has not been completely characterized. The purpose of the present study is to examine the association between plasma homocysteine combined with traditional cardiovascular risk factors and new-onset stroke.

Methods: We conducted a prospective community-based cohort study of 8446 Chinese participants who did not have cardiovascular disease at baseline. Subjects were divided into three groups according to Hcy level (Hcy ≥ 10μmol/L, 10 ≤ Hcy<15μmol/L, Hcy ≥ 15μmol/L). The baseline characteristics of subjects were compared between groups using the t-test or Kruskal-Wallis rank test for continuous variables as appropriate. For categorical variables, data were compared between groups using the chi-square test or Fisher exact test as appropriate. We used Cox proportional hazard regression to determine the association between hcy groups combined with traditional cardiovascular risk factors (hypertension, diabetes, dyslipidemia, current smoking, body mass index, age, sex) and new-onset stroke. Interaction tests were performed to determine the influence of traditional cardiovascular risk factors for the predictive effect of Hcy on new-onset stroke risk.

Results: Of all participants, the average age was 56.5 ± 8.9 years, and 2998 (35.5%) participants were males. During a median 9.9-year follow-up period, 664 (7.9%) endpoints were observed. In the baseline analysis, it was found that the subjects in Hcy ≥ 15 μmol/L group were older, with higher body mass index, higher proportion of males, current smoking and drinking, higher proportion of hypertension and dyslipidemia (no difference in the proportion of diabetes), and higher China-PAR score. With regard to the joint effect of Hcy and hypertension, diabetes, dyslipidemia, current smoking, body mass index, age, sex, there were trends towards increased stroke risk across different groups (P for trend<0.001, <0.001, 0.013, <0.001, =0.040, <0.001, <0.001 respectively). After adjusting for confounders, participants with higher Hcy level combined with hypertension (hazard ratio [HR]: 3.91, 96% confidence interval [CI]: 2.46-6.19, p<0.001), diabetes (HR: 2.21, 96% CI: 1.49-3.28, p<0.001), dyslipidemia (HR: 1.79, 96% CI: 1.04-3.08, p=0.036), current smoking (HR: 2.45, 96% CI: 1.74-3.47, p<0.001), older age (HR: 2.88, 96% CI: 1.98-4.20, p<0.001) were associated with significantly increased risk of new-onset stroke than those with normal Hcy level and without traditional cardiovascular risk factors. Males with elevated Hcy level had higher risk of new-onset stroke than females with normal Hcy level (HR: 1.97, 96% CI: 1.42-2.74, p<0.001). No interactions were observed between Hcy and these factors, except with body mass index. Higher Hcy level with or without elevated body mass index was associated with increased risk of new-onset stroke, and the p value for interaction is 0.005.

Conclusion: Subjects with higher Hcy level have more cardiovascular risk factors and higher cardiovascular risk. Besides, there were joint effects of high Hcy level and traditional cardiovascular risk factors, such as hypertension, diabetes, dyslipidemia, smoking, aging and male on the incidence of stroke. Attention should be paid to the simultaneous screening of Hcy and cardiovascular risk factors in the primary prevention population of stroke.

基线糖代谢状态与全因死亡及心血管死亡风险的关联研究

金怡婧 范芳芳 贾佳 王新刚 李建平 张岩

北京大学第一医院

目的：本研究旨在评估基线不同糖代谢状态与后续全因死亡及心血管疾病（Cardiovascular Disease, CVD）死亡风险之间的关联，并识别高危人群特征，为早期干预提供循证依据。

方法：本研究采用回顾性队列设计，研究对象为北京大学第一医院心内科于 2011-2012 年在北京市苹果园社区及古城社区建立的观察性队列人群，依据口服葡萄糖耐量试验（Oral Glucose Tolerance Test, OGTT）2h 后血糖和空腹血糖（Fasting Blood Glucose, FBG）数据将基线人群的糖代谢状态分为 5 组（正常血糖、空腹血糖受损（Impaired Fasting Glucose, IFG）前期、IFG、糖耐量异常（Impaired Glucose Tolerance, IGT）、2 型糖尿病（Type 2 Diabetes, T2D）），终点事件为全因死亡及 CVD 死亡。通过多因素 Cox 比例风险模型评估糖代谢状态与死亡结局的关联（HR 及 95%CI），并进行亚组交互作用检验。

结果：本研究共纳入 8807 名来自社区、基线无脑卒中及心肌梗死病史、拥有基

线糖代谢状态信息及完成随访的成年人（平均年龄 56.52 ± 8.92 岁、男性占比 35.47%），中位随访 9.87 年，基线分组为：正常血糖，3507 人（39.82%）；IFG 前期，1079 人（12.25%）；IFG，409 人（4.64%）；IGT，1710 人（19.42%）；T2D，2102 人（23.87%）。在校正混杂因素后，基线 T2D 者的全因死亡（校正 HR=1.59, 95%CI:1.24-2.03）和心血管死亡风险（HR=1.89, 95%CI:1.17-3.05）显著增加，而基线 IFG 组的全因死亡风险增加 63%（HR=1.63, 95%CI:1.06-2.48）。亚组分析显示，同型半胱氨酸（P 交互 < 0.001）水平修饰不同糖代谢状态与全因死亡风险的关系，而血压水平（收缩压 P 交互 =0.004，舒张压 P 交互 =0.006）则修饰不同糖代谢状态与心血管死亡风险的关系。

结论：基线糖代谢状态是随访期间全因死亡和 CVD 死亡的独立预测因子，特别是在特定高危亚组（如血压异常、同型半胱氨酸指标异常人群）中关联更强。该研究强调了 FBG 和 OGTT 在全面评估死亡风险中的价值，以及在社区人群尤其是合并血压异常、同型半胱氨酸指标异常等人群中，基于不同糖代谢状态强化血糖监测与管理对于降低死亡风险的重要性。

基线糖代谢状态与不同脑卒中风险的关联研究

金怡婧 范芳芳 贾佳 王新刚 李建平 张岩

北京大学第一医院

目的：探讨基线不同糖代谢状态与不同类型脑卒中风险的关联性，并识别高危人群特征，为早期干预提供循证依据。

方法：本研究采用回顾性队列设计，研究对象为北京大学第一医院心内科于 2011-2012 年在北京市苹果园社区及古城社区建立的观察性队列人群，依据口服葡萄糖耐量试验（Oral Glucose Tolerance Test, OGTT）2h 后血糖和空腹血糖（Fasting Blood Glucose, FBG）数据将基线人群的糖代谢状态为 5 组（正常血糖、空腹血糖受损（Impaired Fasting Glucose, IFG）前期、IFG、糖耐量异常（Impaired Glucose Tolerance, IGT）、2 型糖尿病（Type 2 Diabetes, T2D）），主要终点包括所有新发非致死性脑卒中事件（包括缺血性脑卒中和出血性脑卒中）。通过多因素 Cox 比例风险模型评估糖代谢状态与不同脑卒中结局的关联（HR 及 95%CI），并进行亚组交互作用检验。

结果：本研究共纳入 8807 名来自社区、基线无脑卒中及心肌梗死病史、拥有基线糖代谢状态信息及完成随访的成年人（平均年龄 56.52 ± 8.92 岁、男性占比 35.47%），中位随访 9.87 年，基线分组为：正常血糖，3507 人（39.82%）；IFG 前期，1079 人（12.25%）；IFG，409 人（4.64%）；IGT，1710 人（19.42%）；T2D，2102 人（23.87%）。在校正混杂因素后，基线 T2D 患者的总卒中（校正 HR=1.75, 95%CI:1.42-2.16）和缺血性卒中（校正 HR=1.84, 95%CI:1.48-2.28）风险显著升高；基线 IGT 组的总卒中（校正 HR=1.39, 95%CI:1.11-1.75）和缺血性卒中（校正 HR=1.47, 95%CI:1.16-1.87）风险亦升高，且上述风险随糖代谢状态恶化呈梯度上升（P-trend<0.01）；基线糖代谢状态与出血性卒中风险无显著关联。亚组分析显示，总胆固醇（交互 P=0.030）水平修饰不同糖代谢状态与缺血性卒中风险的关系。

结论：基线糖代谢状态是随访期间总体脑卒中和缺血性脑卒中的独立预测因子，特别是在特定高危亚组（如血脂异常人群）中关联更强。该研究强调了 FBG 和 OGTT 在全面评估脑卒中风险中的价值，以及在社区人群尤其是合并血脂异常人群中，基于不同糖代谢状态强化血糖监测与管理对于降低脑卒中风险的重要性。

基线糖代谢状态与急性心肌梗死风险的关联研究

金怡婧 范芳芳 贾佳 王新刚 李建平 张岩

北京大学第一医院

目的：本研究旨在评估基线不同糖代谢状态与未来急性心肌梗死（Acute Myocardial Infarction, AMI）风险之间的关联，并识别高危人群特征，为早期干预提供循证依据。

方法：本研究采用回顾性队列设计，研究对象为北京大学第一医院心内科于 2011-2012 年在北京市苹果园社区及古城社区建立的观察性队列人群，依据口服葡萄糖耐量试验（Oral Glucose Tolerance Test, OGTT）2h 后血糖和空腹血糖（Fasting Blood Glucose, FBG）数据将基线人群的糖代谢状态为 5 组（正常血糖、空腹血糖受损（Impaired Fasting Glucose, IFG）前期、IFG、糖耐量异常（Impaired Glucose Tolerance, IGT）、2 型糖尿病（Type 2 Diabetes, T2D）），终点事件为新发非致死性 AMI。通过多因素 Cox 比例风险模型评估糖代谢状态与 AMI 结局的关联（HR 及 95%CI），并进行亚组交互作用检验。

结果：本研究共纳入 8807 名来自社区、基线无脑卒中及心肌梗死病史、拥有基线糖代谢状态信息及完成随访的成年人（平均年龄 56.52 ± 8.92 岁、男性占比 35.47%），中位随访 9.87 年，基线分组为：正常血糖，3507 人（39.82%）；IFG 前期，1079 人（12.25%）；IFG，409 人（4.64%）；IGT，1710 人（19.42%）；T2D，2102 人（23.87%）。在校正混杂因素后，基线 T2D 人群的 AMI 风险显著增加（HR=1.87, 95%CI:1.23-2.85, P<0.01）。亚组分析显示，年龄（P 交互 =0.005）水平修饰不同糖代谢状态与 AMI 风险的关系。

结论：基线糖代谢状态是随访期间 AMI 风险的独立预测因子，特别是在特定高危亚组（中年人群）中关联更强。该研究强调了 FBG 和 OGTT 在全面评估 AMI 风险中的价值，以及在社区人群尤其是中年人群中，基于不同糖代谢状态强化血糖监测与管理对于降低 AMI 风险的重要性。

Prediction of Cardiometabolic Multimorbidity Risk in Middle-Aged and Older Chinese Adults: Longitudinal Analysis of Triglyceride Glucose-Body Mass Index (TyG-BMI) and Its Dynamic Trajectories

Zheng-Feng Wu, Yu-qi Liu

中国人民解放军总医院第六医学中心

Background

Cardiometabolic multimorbidity (CMM), defined as the co-occurrence of two or more cardiometabolic diseases (diabetes, stroke, heart disease), poses a substantial and escalating clinical and public health burden, particularly among aging populations. Current evidence lacks robust longitudinal studies specifically investigating the association between the triglyceride glucose-body mass index (TyG-BMI), a composite marker reflecting insulin resistance and obesity, and the development of CMM. This study aimed to establish the predictive value of baseline TyG-BMI for incident CMM, characterize its dose-response relationship with CMM risk, and identify distinct longitudinal TyG-BMI trajectory patterns associated with differential CMM risk in middle-aged and elderly Chinese adults.

Methods

We utilized data from five waves (2011, 2013, 2015, 2018, 2020) of the nationally representative China Health and Retirement Longitudinal Study (CHARLS), established using multistage probability sampling. The analysis included 8,020 participants aged ≥ 45 years without baseline CMM (defined as ≥ 2 concurrent conditions: physician-diagnosed diabetes, stroke, or heart disease). Incident CMM was tracked over the follow-up period. Baseline TyG-BMI was calculated as Ln[fasting triglycerides (mg/dL) × fasting glucose (mg/dL)/2] + BMI (kg/m^2). Cox proportional hazards regression models estimated adjusted hazard ratios (aHRs) and 95% confidence intervals (CIs) for the association between TyG-BMI (both as quartiles and per 1-standard deviation (SD) increase) and incident CMM. Restricted Cubic Splines (RCS) with four knots were employed to assess potential nonlinearity in this relationship. Longitudinal Targeted Maximum Likelihood Estimation (LTMLE) was used to model dynamic TyG-BMI trajectories across the study waves and estimate their associated CMM risks relative to a reference trajectory. Comprehensive sensitivity analyses (e.g., excluding early events, varying covariate sets) and subgroup analyses stratified by key demographic factors were performed to evaluate the robustness of findings.

Results

Over a median follow-up of 9 years, 409 incident CMM cases were identified. Kaplan-Meier analysis demonstrated progressively higher cumulative CMM incidence across increasing quartiles of baseline TyG-BMI (log-rank P < 0.05). After multivariable adjustment for age, sex, education, residence, smoking, drinking, physical activity, systolic blood pressure, LDL-cholesterol, and baseline single cardiometabolic conditions, each 1-SD increment in baseline TyG-BMI was significantly associated with a 43% increased risk of developing CMM (aHR = 1.43, 95% CI: 1.30–1.58). RCS analysis confirmed a significant nonlinear J-shaped relationship between TyG-BMI and CMM risk (P for nonlinearity < 0.05), with risk accelerating at higher TyG-BMI levels. LTMLE identified four distinct longitudinal TyG-BMI trajectories: "Low-Stable" (reference), "Increasing", "Decreasing", and "High-Stable". Compared to the "Low-Stable" trajectory, individuals in the "High-Stable" trajectory exhibited the highest CMM risk (aHR = 1.11, 95% CI: 1.09–1.14), followed by those in the "Increasing" trajectory (aHR = 1.07, 95% CI: 1.04–1.10). The "Decreasing" trajectory was associated with a lower risk compared to the "High-Stable" group, suggesting potential benefit from reducing TyG-BMI levels over time. Subgroup analyses across age, sex, and residence groups, along with extensive sensitivity analyses, consistently supported the robustness of these associations.

Conclusions

This large-scale, nationally representative longitudinal study provides novel evidence that TyG-BMI is a strong, independent predictor of incident cardiometabolic multimorbidity in middle-aged and elderly Chinese adults. The association demonstrates a significant nonlinear dose-response pattern. Critically, distinct longitudinal trajectories of TyG-BMI confer markedly different CMM risks. The "High-Stable" trajectory, indicative of sustained high levels of insulin resistance and obesity, carries the greatest risk. These findings underscore TyG-BMI's potential as a valuable clinical tool for early identification of individuals at high risk for CMM. Monitoring TyG-BMI trajectories over time could inform personalized risk stratification and guide targeted prevention strategies aimed at mitigating the growing burden of concurrent cardiometabolic diseases in aging populations.

Estimated Glucose Disposal Rate and Mortality in Cardiovascular Kidney Metabolic Syndrome: Nonlinear Associations and Stratified Prognostic Significance by Glycometabolic Phenotypes

Zheng Zhang, Dou Zhu

The Second Affiliated Hospital of Harbin Medical University

Abstract

Objective: Cardiovascular Kidney Metabolic (CKM) syndrome is a complex condition characterized by a multifactorial interaction between obesity, diabetes, chronic kidney disease, and cardiovascular diseases. It is a growing public health concern due to its significant impact on morbidity and mortality. A key feature in the progression of CKM is insulin resistance (IR), which exacerbates metabolic dysfunctions and increases the risk of adverse cardiovascular and renal events. While traditional mea-

sures of insulin resistance such as the Homeostasis Model Assessment of Insulin Resistance (HOMA-IR) and the Triglyceride Glucose Index (TyG) are widely used, they have limitations, particularly in complex syndromes like CKM. In contrast, the estimated glucose disposal rate (eGDR), which integrates waist circumference, blood pressure, and glycated hemoglobin (HbA1c), has shown potential as a more reliable marker for glucose metabolism and cardiovascular outcomes. However, its association with mortality in CKM, and particularly its role across different glucose metabolic states, remains unclear. The aim of this study was to evaluate the prognostic significance of eGDR in predicting all-cause and cause-specific mortality in patients with CKM, focusing on its utility in distinct glycometabolic phenotypes, including diabetes mellitus (DM), prediabetes (Pre-DM), and normal glucose regulation (NGR).

Methods: This cohort study used data from the National Health and Nutrition Examination Survey (NHANES) from 1999 to 2018. Participants diagnosed with CKM were included, with exclusions based on age and missing data. The study utilized a weighted Cox proportional hazards model, incorporating restricted cubic spline (RCS) analysis to examine the dose-response relationship between eGDR levels and mortality outcomes. Stratified analyses were conducted to assess the effects of glucose metabolic states on the relationship between eGDR and mortality. Additionally, the study compared the predictive efficacy of eGDR with traditional insulin resistance markers (HOMA-IR and TyG) for all-cause and cause-specific mortality using Receiver Operating Characteristic (ROC) curve analysis.

Results: A total of 18,147 CKM patients were included in the analysis. Cox regression revealed significant associations between eGDR levels and both all-cause mortality and cause-specific mortality, including cardiovascular-specific and diabetes-specific mortality (p<0.05 for all). Further RCS analysis showed a nonlinear relationship between eGDR and all-cause mortality (p for non-linear = 0.041) as well as diabetes-specific mortality (p for non-linear = 0.003), while a linear association was observed for cardiovascular-specific mortality (p for non-linear = 0.278). Stratified analyses revealed that, within the DM subgroup, eGDR was significantly associated with reduced all-cause mortality. In the Pre-DM subgroup, eGDR correlated with a significant decrease in cardiovascular-specific mortality. Among patients with NGR, eGDR was associated with lower all-cause, cardiovascular-specific, and diabetes-specific mortality. Additionally, ROC curve analysis showed that eGDR outperformed both HOMA-IR and TyG in predicting mortality, particularly in the NGR subgroup.

Conclusion: The study found that eGDR levels were inversely associated with the risk of all-cause and cause-specific mortality in CKM patients, with a consistent protective effect observed across different glucose metabolic states (DM, Pre-DM, and NGR). These findings suggest that eGDR may serve as an effective tool for risk stratification in CKM, providing a more accurate prediction of mortality than traditional insulin resistance markers. Moreover, the study highlights the potential of eGDR as a comprehensive biomarker that could be utilized in clinical settings for better management of CKM patients. Importantly, the predictive power of eGDR varied across different glucose metabolic states, with the most significant protective associations found in patients with NGR. This underscores the importance of glycometabolic status in determining the efficacy of eGDR as a mortality predictor. The results also suggest that optimizing eGDR levels could improve clinical outcomes in CKM, making it a promising target for intervention and future research.

Keywords: Estimated glucose disposal rate, Cardiovascular kidney metabolic syndrome, Mortality prediction, Glycometabolic phenotypes, Insulin resistance, Dose-response relationship.

HbA1c>7% predicts adverse cardiovascular outcomes among stage 4 cardiovascular kidney-metabolic syndrome patients

Jingjing Song[1], Hong Li[1], Wen-Yao Wang[2]

1. Beijing Chaoyang Hospital, Capital Medical University

2. Peking university third hospital

Objectives: Cardiovascular kidney-metabolic syndrome (CKMS) is a newly proposed term in 2025, representing the complicated and bidirectional interplay between cardiovascular disease, chronic kidney disease, and metabolic syndrome. Stage 4 CKMS represents a pivotal window where multi-organ dysfunction is established but still responsive to intervention. Blood glucose management is a critical part of CKMS prevention and therapy. Glycated hemoglobin (HbA1c) is a versatile biomarker reflecting glycemic control in last 120 days. HbA1c is not only a marker of glycemic status but also a powerful predictor of short- and long-term outcomes across multiple conditions, particularly in metabolic, cardiovascular, and renal diseases. The prognostic value of HbA1c stems from the link between chronic hyperglycemia (reflected by elevated HbA1c) and cumulative damage to organs and tissues via oxidative stress, inflammation, and vascular dysfunction. This study aims to investigate the association between HbA1c levels and adverse cardiovascular outcomes among stage 4 CKM patients.

Subjects and Methods: 9473 stage 4 CKM patients were enrolled in this study and divided into two groups according to glycated hemoglobin (HbA1c) ≤ 7% (n=7203) and HbA1c>7% (n=2138). The primary endpoint was major adverse cardiac and cerebrovascular events (MACCEs), including cardiac death, myocardial infarction (MI), stroke, stent thrombosis and target vessel revascularization (TVR). The secondary endpoints included MI, TVR and stent thrombosis. Cumulative rates of outcomes were estimated by Kaplan-Meier analysis and compared with the log-rank test. Cox proportional hazard regression (HR) model was used to assess the association between HbA1c and clinical outcomes, and adjusted hazard ratios with 95 % confidence intervals were recorded. Restricted cubic spline analysis was performed to investigate underlying non-linearity association between HbA1c and MACCEs, MI, TVR and stent thrombosis. Statistical analysis was performed using R 4.0.3 software for mac (R foundation). Two-tailed p < 0.05 was considered statistically significant.

Results: During the median 2.4-year follow-up, 761 MACCEs were recorded. Patients with HbA1c>7% exhibited a significantly higher cumulative incidence of MACCEs (10.3% versus 7.5%), MI (1.8% versus 1.1%), TVR (7.0% versus 4.9%) and stent thrombosis (1.6% versus 0.8%) than those with HbA1c ≤ 7% (p<0.01). The Kaplan-Meier analysis showed that patients with HbA1c>7% had significantly lower event-free survival rates of MACCEs (Figure 1A), MI (Figure 1B), TVR (Figure 1C) and stent thrombosis (Figure 1D) compared to those with HbA1c ≤ 7% (p<0.05) (Figure 1A). Consistently, Cox proportional hazards regression analysis found patients with HbA1c>7% had a significantly increased risk for MACCEs (HR 1.39, 95% confidential interval 1.19-1.62, p<0.001), MI (HR 1.65, 95% confidential interval 1.12-2.43, p<0.05), TVR (HR 1.43, 95% confidential interval 1.18-1.74, p<0.001) and stent thrombosis (HR 2.01, 95% confidential interval 1.32-3.05, p<0.001). Restricted Cubic Splines showed elevated HbA1c was positively related to the risk of MACCEs (Figure 2A), TVR (Figure 2C) and stent thrombosis (Figure 2D) as a continuous variable (all p<0.05), but not MI (Figure 2B). HbA1c>7% was identified as a potent prognostic factor in stage 4 CKM patients.

Conclusion: HbA1c>7% was associated with increased risk of adverse cardiovascular outcomes in stage 4 CKM patients. Monitoring and optimizing HbA1c could obtain therapeutic benefits and improve prognosis of stage 4 CKMS patients.

尿酸对高龄重度主动脉瓣狭窄患者远期预后的预测价值

徐靖婷 李喆 叶蕴青 王墨扬 许海燕 吴永健

中国医学科学院阜外医院

目的: 分析血尿酸水平对高龄重度主动脉瓣狭窄患者远期预后的影响及预测价值。

方法： 回顾性收集 2008 年 1 月 1 日至 2015 年 1 月 1 日年龄≥ 75 岁在中国医学科学院阜外医院住院诊断为非风湿性主动脉瓣狭窄病变且超声心动图证实为重度主动脉瓣狭窄的 203 例患者的临床资料，其中药物治疗组 90 例，手术治疗组 113 例（包括 TAVR 和 SAVR），入院时测量尿酸水平。中位随访 16 个月，主要终点为全因死亡。

结果： 203 例患者，平均年龄 78.74±2.96 岁，入院尿酸中位水平 391.6mmol/L，药物治疗和手术治疗组全因死亡率分别为 76.7% 和 10.6%。根据尿酸水平的四分位数将患者分为四组，Kaplan-Meier 生存曲线分析显示接受药物治疗的患者尿酸 Q4 组早期死亡风险高，而随访六年后差异消失。单变量 Cox 回归分析显示，在药物治疗组中，尿酸水平与死亡风险显著相关（HR=1.002，95% CI: 1.000–1.004，P=0.043），提示尿酸每升高 1 μmol/L，死亡风险增加约 0.2%。然而对手术治疗组，尿酸水平与全因死亡的无显著相关。在调整年龄、性别、吸烟、药物 / 手术治疗、高血压、血脂、射血分数（EF）、BNP 和肾功能后，多因素 Cox 回归分析显示，尿酸水平与死亡风险无显著相关性（P=0.231），而体重指数（BMI）升高显著降低死亡风险（HR=0.878，P=0.014），糖尿病显著增加死亡风险（HR=2.574，P=0.002）。

结论： 对于高龄重度主动脉瓣狭窄患者，尿酸升高是影响药物治疗预后的危险因素，然而对手术治疗的患者，尿酸水平与全因死亡无显著相关。此外，不论接受何种治疗，糖尿病均是影响高龄重度主动脉瓣狭窄患者远期预后的独立危险因素，BMI 升高则表现为保护因素。

生命 8 要素，遗传易感性与退行性瓣膜性心脏病发病风险的关系

巩一丁 [1] 邡爽 [1] 陈占超 [2] 唐帆 [1] 董宁 [1]

1. 佳木斯大学公共卫生学院流行病与卫生统计学系

2. 哈尔滨医科大学第二附属医院心内科

【摘要】

目的: 探讨基于"生命 8 要素"（Life\ Essential 8, LE8）评分的心血管健康（CVH）状况与退行性瓣膜性心脏病（VHD）发病风险的关系，并分析遗传易感性对该关联的修饰效应。

方法： 基于 UK Biobank 队列，纳入基线无 VHD 的 262864 名参与者。根据 LE8 评分将 CVH 状态分为 3 组：较差（0 ~ 49 分）、中等（50 ~ 79 分）和理想（80 ~ 100 分）。采用 Fine-Gray 竞争风险模型计算不同 CVH 水平与 VHD 发病风险的风险比（HR）及其 95% 置信区间（CI）。

结果：研究人群平均年龄（56.0±8.1）岁，女性占 51.1%。中位随访 13.8 年期间，共新发 VHD 6 371 例，包括主动脉瓣狭窄（AS）2 754 例、主动脉瓣反流（AR）1 013 例和二尖瓣反流（MR）3 089 例。调整潜在混杂因素后，与 CVH 较差组相比，中等组和理想组的 VHD 发病风险分别降低 18%（HR=0.82，95%CI：0.74 ~ 0.90）和 21%（HR=0.79，95%CI：0.70 ~ 0.90）。值得注意的是，理想心血管健康状态显著降低了 AS 的发病风险，但与 MR 或 AR 无显著关联。与较差 CVH 组相比，中等和理想组 AS 风险分别降低 33%（HR=0.67，95%CI：0.59 ~ 0.77）和 50%（HR=0.50，95%CI：0.41 ~ 0.61）。AS 的多基因风险评分并未改变这些关联。尽管如此，CVH 状态较差且遗传易感性较高的成年人罹患 AS 的风险最高，与 CVH 状态理想且遗传易感性较低的人相比，其发病风险高出近 4 倍。生活方式行为和生物学特征均与 AS 发病显著相关，其中体质指数、睡眠时长和尼古丁暴露对瓣膜疾病影响最大。

结论：较高的 LE8 评分与较低的 VHD 发病风险显著相关，且不受遗传易感性的影响。维持理想心血管健康状态对 AS 的一级预防具有重要意义，其中肥胖控制、保证充足睡眠和戒烟是需要重点关注的干预措施。

关键词：主动脉瓣反流；主动脉瓣狭窄；二尖瓣反流；生命 8 要素；英国生物样本库；心血管健康；遗传易感性

糖尿病介导的线粒体蛋白高乙酰化通过抑制线粒体超复合体组装增加心肌对缺血再灌注损伤的敏感性

邓艳 [1,2] 杨为 [1,2] 姜春玲 [1,2] 李涛 [1,2]

1. 四川大学华西医院

2. 四川大学华西医院线粒体与代谢实验室

目的：多项研究表明，2 型糖尿病 (T2DM) 会显著增加心肌缺血再灌注 (I/R) 损伤的敏感性，从而导致更高的死亡率。线粒体高乙酰化与 Sirt3 (一种线粒体 NAD^+依赖性去乙酰化酶) 密切相关，Sirt3 的下调导致 T2DM 患者线粒体蛋白高乙酰化，可能是这种效应的潜在介导因素。 本研究旨在探讨 Sirt3 缺乏诱导的线粒体蛋白高乙酰化对 T2DM 心肌 I/R 损伤敏感性增加的影响。

方法：将野生型 (WT) 和 Sirt3 基因敲除 (KO) 小鼠高脂 (HFD) 喂养 8 周，并在第 5 周腹腔注射 STZ 以诱导 T2DM 小鼠模型。离体心脏用 Langendorff 模型灌注以模拟体外心肌 I/R 损伤 (缺血 30 分钟，再灌注 60 分钟)。冠状动脉左前降支结扎 30 分钟，随后再灌注 24 小时诱导在体 I/R 损伤。通过超声心动图评估心脏功能，TTC 染色估算梗死面积以及化学分析仪检测血浆 LDH 和 CK-MB 水平。利用 Seahorse XF24 分析仪评估线粒体呼吸功能。Blue Native PAGE 用于检测线粒体超复合体 (SCs) 的组装情况和乙酰化水平。通过邻近连接分析 (PLA) 观察 H9C2 细胞在不同处理下 CI-CIII 或 CI-CIV 相互作用情况。

结果：在 T2DM 模型中，Sirt3 缺乏诱导的线粒体蛋白高乙酰化增加了心肌 I/R 损伤的敏感性。与 WT 小鼠相比，T2DM 小鼠的心功能受损，表现为缺血期间左室舒张末期压力 (LVEDP) 显著增加，体外再灌注时收缩功能几乎无法恢复，以及左室射血分数降低。与心功能减退相一致，T2DM 心脏的梗死面积、血浆中 LDH 和 CK-MB 水平均明显增加。 从机制上讲，我们发现 T2DM 小鼠心脏线粒体中 ADP 刺激和 FCCP 刺激的呼吸作用下降。同时，在 T2DM 线粒体 SCs 中观察到 Ndusf4 表达减少，乙酰化水平升高。此外，Sirt3 基因敲除（KO）可诱导线粒体蛋白高乙酰化，进一步加重 T2DM 小鼠 I/R 后心功能障碍，增加心肌梗死面积以及血浆 LDH 和 CK-MB 水平。随着线粒体蛋白乙酰化水平的升高，KO 进一步导致 T2DM 心脏线粒体呼吸功能降低和线粒体 SCs 组装减少。另外，通过 PLA 更直观地观察到，在 PA 和 3-TYP（Sirt3 抑制剂）处理的 H9C2 细胞中，CI 与 CIII 或 CI 与 CIV 之间相互作用减少，而在 PA + NMN（NAD^+ 前体）处理的细胞中有所恢复，这表明 Sirt3 缺乏诱导的线粒体蛋白高乙酰化可能在线粒体 SCs 组装、线粒体及心功能障碍中发挥了重要作用。

结论：我们的研究数据表明，T2DM 心肌缺血再灌注损伤敏感性增加可能是由于 Sirt3 缺乏介导线粒体蛋白高乙酰化，从而破坏了线粒体超复合体的组装，导致线粒体呼吸效率降低，线粒体功能障碍。

基于快速康复理念的早期康复运动及健康教育在代谢性心血管疾病患者中的应用

代聪

西安交通大学第一附属医院

【摘要】目的 探讨基于快速康复理念的早期康复运动及健康教育在代谢性心血管疾病患者中的应用效果，旨在分析其对患者康复进程、生理指标及生活质量的影响。

方法 选取 2023 年 1 月 ~ 2024 年 6 月于本院收治的代谢性心血管疾病患者 80 例，采用随机法分为对照组与观察组，每组 40 例。对照组实施常规护理，观察组在常规护理基础上，采用基于快速康复理念的早期康复运动及健康教育。干预 12 周后，采用改良 Barthel 指数（MBI）评定量表估计两组患者干预前后日常生活能力评分，检测患者干预前后血压、心率水平，采用焦虑自评量表 SAS、抑郁自评量表 SDS 评分评估两组患者干预前后心理状态的变化及并发症发生率。

结果 干预前，两组患者日常生活能力评分、血压、心率及 SAS、SDS 评分差异均无统计学意义（P > 0.05）。干预后，观察组日常生活能力评分为（85.34±6.21）分，高于对照组的（72.45±7.83）分，且观察组与对照组干预后的评分均显著高于干预前（P < 0.05）；观察组收缩压为（122.34±8.76）mmHg、舒张压为（78.45±6.32）mmHg，均低于对照组的（135.67±9.21）mmHg 和（85.23±7.14）mmHg，且两组干预后水平均低于干预前（P < 0.05）；观察组心率为（71.23±5.67）次 /min，低于对照组的（78.45±6.52）次 /min，且均低于干预前（P < 0.05）；观察组 SAS 评分为（35.12±4.56）分、SDS 评分为（36.78±5.23）分，均低于对照组的（40.45±5.67）分和（42.34±6.12）分，两组干预后的评分均低于干预前（P < 0.05）。此外，观察组并发症发生率为 7.50%，显著低于对照组的 22.50%（P < 0.05）。

结论 基于快速康复理念的早期康复运动及健康教育能够显著改善代谢性心血管疾病患者的康复效果、生理指标及心理状态，降低并发症发生率，是一种有效的护理干预模式，值得临床推广。

【关键词】快速康复理念；早期康复运动；健康教育；代谢性心血管疾病

1990-2021 年全球含糖饮料归因心血管疾病负担的系统分析

张乃今

中国医科大学附属第一医院

目的：评估含糖饮料（SSBs）对全球心血管疾病负担的影响，分析社会人口指数（SDI）、地域、年龄及性别差异，为代谢性心血管疾病的防控提供依据。

方法：基于 2021 年全球疾病负担研究（GBD）数据，采用比较风险评估框架，系统分析 1990-2021 年 204 个国家 SSBs 的汇总暴露值（SEV）及其归因的伤残调整寿命年（DALYs）和死亡。重点关注 SSBs 作为独立风险因素的心血管疾病结局（如缺血性心脏病、卒中）。通过年龄标准化和连接点回归分析趋势变化，并按 SDI 层级、地理区域、年龄及性别分层。

结果：研究期间全球 SSBs 归因疾病负担呈显著上升趋势，男性负担高于女性。高 SDI 国家 / 地区的年龄标准化 SEV 和 DALY 率最高，低 SDI 区域最低。心血管疾病是 SSBs 归因死亡的第二大原因，其分子机制涉及 SSBs 诱导胰岛素抵抗、促进内脏脂肪堆积及慢性炎症反应，加速血管内皮功能障碍和动脉粥样硬化进程。负担随年龄增长而增加，其中 64 岁以下人群增长率最快，老年群体因代谢功能下降和血管弹性减退更易受 SSBs 协同损伤。

结论：SSBs 通过代谢紊乱和血管损伤机制显著增加全球心血管疾病负担，且存在明显的社会经济和年龄差异。亟需在高风险地区及年轻人群中实施针对性干预，包括限制 SSBs 摄入的公共卫生政策，以减轻代谢性心血管疾病负担。

Physical activity, statin therapy and risk of new-onset type 2 diabetes: clinical and proteomic perspectives

Zhanchao Chen

The Second Affiliated Hospital of Harbin Medical University

ABSTRACT

Physical activity, statin therapy and risk of new-onset type 2 diabetes: clinical and proteomic perspectives

Zhanchao Chen, MD[1,2], Xiaoqiu Shi, MB[3], Miao Yan, PhD[1,2], Hongbin Qiu, MB, PhD[3], Yan Liu, MB[3], Bo Yu, PhD[1,2], Shaohong Fang, PhD[1,2], Yiying Zhang, MB, PhD[3]*, Shanjie Wang, PhD[1,2]*.

[1]Department of Cardiology, Second Affiliated Hospital of Harbin Medical University, Harbin, China;

[2]State Key Laboratory of Frigid Zone Cardiovascular Diseases (SKLFZCD); The Key Laboratory of Myocardial Ischemia, Chinese Ministry of Education, Harbin, China;

[3]Department of Epidemiology and Biostatistics, School of Public Health, Jiamusi University, Jiamusi, China.

Objective: Statin use is widely recommended for cardiovascular disease prevention, yet accumulating evidence suggests it may elevate the risk of type 2 diabetes. However, the long-term effects and modifiable preventive strategies in real-world populations remain insufficiently characterized. This study aimed to evaluate the real-world impact of statin use on type 2 diabetes incidence, investigate whether guideline-recommended levels of physical activity can attenuate this risk, and identify proteomic signatures to enhance biological insight and personalize risk prediction.

Methods: We conducted a prospective analysis of 252,042 participants from the UK Biobank (mean age: 57.0 years; 55.6% female), all of whom were free of diabetes at baseline. Incident type 2 diabetes cases were identified through linkage with electronic health records. Age- and HbA1c-standardized incidence rates were evaluated using Poisson regression, and hazard ratios (HRs) were estimated using multivariable Cox proportional hazards models, adjusting for a comprehensive set of demographic, clinical, and lifestyle covariates. Proteomic profiling was performed using the Olink platform in a nested case-control subcohort, where 2,923 plasma proteins were quantified to investigate relevant biological pathways and enhance risk stratification.

Results: Over a median 13.7-year follow-up, 13,182 incident type 2 diabetes cases were identified. Age- and HbA1c-standardized incidence rates per 1,000 person-years were 2.2 (statin-noneligible), 4.6 (statin-eligible but untreated), and 7.3 (regular statin users). After adjusting for demographic, clinical, and lifestyle factors, statin use was associated with a 50% (HR = 1.50, 95%CI = 1.09-1.22) increased risk of new-onset type 2 diabetes compared with statin-noneligible individuals, independent of baseline cardiometabolic status and genetic risk. Among statin users, both self-reported and accelerometer-assessed physical activity significantly attenuated the association between statin use and type 2 diabetes risk. Notably, engaging in ≥ 150 minutes per week of device-measured moderate-to-vigorous physical activity was associated with approxi-

mately a 50% (HR = 0.54, 95%CI = 0.34-0.87) lower risk of developing type 2 diabetes. To explore underlying mechanisms, proteomic profiling of 2,923 plasma proteins identified glycolipid metabolism-related proteins—such as leptin, FABP4, IGFBP1, and PRSS8—as key mediators linking both statin use and physical activity to diabetes development. Incorporating these proteins into a composite proteomic risk score significantly improved the accuracy of 3-year diabetes risk prediction among statin users (AUC: 0.82 vs. 0.74; p < 0.001), beyond what was achieved by traditional clinical models.

Conclusions: Statin use significantly increases long-term risk of type 2 diabetes, independent of genetic and cardiometabolic risk profiles. However, this elevated risk is substantially attenuated by sufficient physical activity. Proteomic analysis reveals potential biological mediators and enhances individual risk stratification, supporting a precision medicine framework to guide statin use and lifestyle recommendations in clinical practice.

甲状腺激素在内脏脂肪代谢功能异常中的作用及机制研究

郭泽璇 范伊思 王钊 王文尧

北京大学第三医院

题目：甲状腺激素在内脏脂肪代谢功能异常中的作用及机制研究

作者：郭泽璇，范伊思，王钊，王文尧

单位：北京大学第三医院

目的：内脏脂肪是重要的代谢器官，但是甲状腺激素（thyroid hormone, TH）怎样以及如何影响内脏脂肪尚未完全明确。我们旨在研究 TH 影响内脏脂肪的表现以及具体机制，以期为 TH 治疗脂肪组织相关代谢性疾病的治疗和预防提供新的理论依据和干预靶点。

方法: 将 24 只成年雄性 C57/BL6J 小鼠随机分为对照组与甲减组、甲减补充 TH 组、对照补充 TH 组。甲减组小鼠连续三个月给予丙硫氧嘧啶饮水，补充 TH 组小鼠在最后的两周每日腹腔注射 TH 溶液，其他组腹腔注射不含 TH 的相同溶剂。通过对小鼠血糖和血脂和体重的测量探究甲状腺功能对整体代谢的影响；通过 HE 染色，WB 和 qPCR 来探究 TH 对内脏脂肪代谢的影响；通过对内脏脂肪进行马松染色以及 bulk 转录组来分析小鼠内脏脂肪的纤维化程度。通过生物信息学手段预测 KLF9 的下游关键基因。构建 KLF9 过表达脂肪细胞，观察下游基因的改变情况。通过 qPCR 和 WB 实验检测成脂基因 FABP4 的表达情况以及油红染色实验来证明细胞诱导成脂成功，并比较成脂前后的 col6a3 的改变。

结果：甲减组和补充 TH 组小鼠在给予葡萄糖注射后血糖水平迅速升高，达到峰值之后迅速下降。在 60 分钟后的时间点，补充 TH 组的小鼠血糖水平显著低于甲减组（P<0.05）。显示甲状腺激素对于小鼠代谢的积极影响；两组小鼠在胰岛素注射后血糖水平迅速下降，在 60 分钟后逐渐恢复，与甲减组小鼠相比，补充 TH 组小鼠在在 120 分钟的血糖水平更高（P<0.05），显示 TH 对低血糖状态下糖异生的积极影响。

马松染色显示甲减小鼠在 TH 腹腔注射后内脏脂肪的纤维化程度降低（P<0.05）。通过 Bulk 转录组的 KEGG 通路富集分析发现 ECM-Receptor 通路在补充 TH 的甲减小鼠附睾脂肪中得到富集（log2FC >1, P<0.05）。胶原蛋白（Collagen）和基质金属蛋白酶（MMP）在小鼠附睾脂肪纤维化的这一过程中发挥着重要作用。对富集结果分析以及后续的 qPCR 显示相比于对照组，甲减组小鼠内脏脂肪促纤维化指标如 COL4、COL6、SMA 显著升高（P<0.05），而在补充 TH 后下降（P<0.05）。对应的 MMP 水平在补充 TH 后显著增高（P<0.05）。Mfuzz 趋势分析显示相比于对照组，col6a3 在甲减小鼠附睾脂肪中表达增高，腹腔注射 TH 后表达下降。补充 TH 后，WB 和 qPCR 实验显示 KLF9 水平显著增加，提示 KLF9 与纤维化可能存在联系。通过生物信息学方法预测 KLF9 与 col6a3 有较大的结合概率（score=637），过表达脂肪细胞 KLF9 后，qPCR 与 WB 结果显示 col6a3 表达显著降低（P<0.05）。

结论：甲状腺激素可通过调节糖代谢动态平衡、通过促进 KLF9 而抑制纤维化通路及关键基因 col6a3 的表达，改善甲减小鼠糖代谢异常与内脏脂肪纤维化。为甲减相关代谢紊乱及组织纤维化的机制解析与干预提供了实验依据。

糖尿病前期人群中估算葡萄糖清除率与心脏代谢性共病与全因死亡动态演变的关联：一项多状态轨迹分析

程文珂 凌云 康品方 （血脂学组委员） 唐碧 （肺动脉高压委员）

蚌埠医科大学第一附属医院

背景

心血管代谢疾病（cardiometabolic diseases, CMD），包括冠心病、2 型糖尿病和脑卒中，是全球疾病负担的主要来源，常以共病形式表现，构成心血管代谢多重共病（cardiometabolic multimorbidity, CMM）。研究显示，CMM 的存在显著提高全因死亡风险并缩短预期寿命，其发病机制主要涉及胰岛素抵抗（insulin resistance, IR），这是连接代谢紊乱、内皮功能障碍和炎症反应的关键病理环节。估算葡萄糖清除率（estimated glucose disposal rate, eGDR）作为一种结合腰围、HbA1c 与高血压状况的简便 IR 指标，已在多项研究中表现出优越的心血管风险预测能力。然而，eGDR 在疾病进展各阶段中的动态影响尚未系统评估，尤其是在糖尿病前期人群中。为弥补这一空白，本研究旨在探讨 eGDR 与 CMD、CMM 及全因死亡的多阶段演变之间的关系，明确其在疾病不同演进阶段的风险预测价值。

方法

本研究基于英国生物样本库，纳入 50,342 名符合 2022 年美国糖尿病学会标准定义的糖尿病前期成年人，且基线时无 CMD。根据腰围、HbA1c 和高血压状况计算 eGDR 水平。采用多状态 Markov 模型模拟五种状态转换路径：①基线→首次 CMD（FCMD）；② FCMD → CMM；③基线→死亡；④ FCMD →死亡；⑤ CMM →死亡。通过 Cox 比例风险模型估算各阶段中 eGDR 的影响，并使用限制性样条检验非线性关联。进一步开展中介分析、亚组分析和多项敏感性分析以验证结果稳健性。

结果

在中位 13.6 年（四分位间距：12.9–14.5）的随访期间，共观察到 12,641 例 FCMD、2,081 例 CMM 及 4,847 例死亡。每升高 1 单位 eGDR，FCMD 风险下降 12%（HR=0.88，95%CI: 0.87–0.89），CMM 风险下降 7%（HR=0.93，95%CI: 0.91–0.96），CMD 前死亡风险下降 5%（HR=0.95，95%CI: 0.93–0.98）。但在 CMD 或 CMM 发生后，eGDR 与死亡风险之间的关联不再显著。暴露 - 反应关系显示，eGDR 与 FCMD 和 CMM 风险呈非线性负相关，拐点分别位于 8.8 与 8.7 mg/kg/min。FCMD 至死亡的风险曲线呈 U 型，最优 eGDR 约为 4.9。亚组分析发现，eGDR 在 60 岁以下、女性、BMI < 30 kg/m² 及未接受降压或调脂治疗人群中的保护作用更为明显。

结论

本研究首次基于多状态建模系统评估了 eGDR 在糖尿病前期人群中对 CMD、CMM 及死亡转归的影响。结果表明，较高 eGDR 水平显著关联于疾病早期阶段的风险降低，而其在 CMD 或 CMM 发生后的预测能力明显减弱。这提示 eGDR 作为胰岛素敏感性标志物的临床意义主要体现在疾病初发前，是早期筛查和干预的关键指标。研究支持将 eGDR 用于动态风险评估和个体化管理，强化“窗口期”内改善胰岛素敏感性对于延缓 CMM 进展及降低死亡风险的潜在价值。

LncRNA Gm26870 通过调控炎症促进脂肪组织胰岛素抵抗

厉晓婷

浙江大学医学院附属邵逸夫医院

目的：肥胖是全球性的公共卫生难题。胰岛素抵抗与肥胖密切相关，同时也是 2 型糖尿病和多种心血管疾病的共同发病机制。最近有新的研究发现转录调控和表观遗传学修饰在胰岛素抵抗的发生发展中也起着重要的作用。LncRNA 可能也参与了胰岛素抵抗的调控。

方法与结果：通过高脂饮食喂养 C57BL6 小鼠 12 周来诱导胰岛素抵抗模型，在鉴定模型建立成功后，送小鼠附睾脂肪组织进行第二代深度测序来了解 lncRNA 在正常小鼠附睾脂肪组织以及发生胰岛素抵抗的脂肪组织中表达差异情况。通过对测序结果进行质量检验，与参考基因组的比对和定量分析各类型基因的表达情况等，证明测序的质量较好，结果可靠。基于 cufflinks 拼接结果，根据 lncRNA 的结构特点以及不编码蛋白的功能特点，筛选 lncRNA。并根据以下标准得到本实验中检测到的 lncRNA：同一组的 3 个样本中，至少有 2 个样本检测到 lncRNA。通过火山图和分层聚类分析发现差异表达的 lncRNA 有 216 条，其中上调的 lncRNA 有 71 条，下调的 lncRNA 有 145 条。对其进行 Real-time PCR 验证，发现结果与测序结果基本一致，说明测序结果可靠，重复性好，值得进行后续研究。通过对差异表达的 lncRNA 临近基因进行 GO 富集分析和 KEGG 富集分析，发现差异表达的基因主要涉及膜结合的细胞组分、蛋白绑定、催化酶的活性、细胞内各种化合物以及核酸的代谢过程等，差异表达的基因与酒精中毒、免疫炎症、癌症的转录失调、以及代谢途径等信号通路有关。代谢途径、免疫炎症等过程与胰岛素抵抗密切相关。在小鼠 3T3-L1 诱导的成熟脂肪细胞中进一步验证筛选出的表达上调的 lncRNA 在正常脂肪细胞和发生胰岛素抵抗的脂肪细胞之间表达也存在差异。Gm26870（ENSMUST00000181242.1）在胰岛素抵抗脂肪细胞（Palmitic Acid 组）中的表达显著高于正常成熟脂肪细胞（Control 组）。根据 qRT-PCR 结果，选择其中差异表达显著、一致性最好的三条 lncRNA 进行功能缺失性研究，发现干预 Gm26870 能影响脂肪细胞的葡萄糖摄取率，并影响 PPARγ、GLUT4mRNA 的表达，提示其可能在胰岛素抵抗的发生中起着重要作用。我们同时使用 sh-Gm26870 敲低小鼠 Gm26870 和沉默脂肪细胞 Gm26870 后发现胰岛素抵抗得到改善。在机制上，抑制 Gm26870 可缓解胰岛素抵抗造成的炎症反应。Gm26870 吸附结合 miR-30e-3p 导致 IL1β mRNA 的调控作用减弱，因而产生改善胰岛素敏感性的作用。

结论：本研究阐明 Gm26870 对胰岛素抵抗发生发展的机制，有助于人们找到能更有效治疗 2 型糖尿病和心血管疾病等代谢相关疾病的策略。

ST 段抬高型心肌梗死患者甘油三脂葡萄糖指数与梗死面积，微循环阻塞和心肌内出血的相关性研究

赵依晴 [1] 马振岩 [1] 阿鑫 [2] 赵蕾 [3] 张洪博 [3] 马翔 [4] 杨人强 [5] 钱赓 [6]

1. 中国人民解放军总医院 / 解放军医学院

2. 中国人民解放军总医院第二医学中心保健七科

3. 首都医科大学附属北京安贞医院放射科

4. 新疆医科大学第一附属医院

5. 南昌大学附属第二医院

6. 中国人民解放军总医院第六医学中心心血管病医学部

目的：探讨 ST 段抬高型心肌梗死（STEMI）患者甘油三酯葡萄糖指数 (TyG 指数) 与心脏磁共振评估的梗死面积，微循环阻塞（MVO）和心肌内出血（IMH）之间的相关性，评估其作为心肌损伤程度潜在预测标志物的价值。

方法：本项队列研究纳入 674 名行直接 PCI 治疗的 STEMI 患者，收集其临床基线数据并在急性心肌梗死后 7 天左右进行心脏磁共振检查。按 TyG 指数三分位数将患者分为三组，分别为高 TyG 指数组，中 TyG 指数组和低 TyG 指数组。采用多元线性回归，Pearson/Spearman 相关性分析和 Logistics 回归分析等方

法分析 TyG 指数与梗死面积，微循环阻塞和心肌内出血的相关性。

结果：三组组间比较：高 TyG 指数组的梗死面积显著增加（22.39±11.53 vs 中组 21.09±10.33 vs 低组 19.13±9.54，P=0.013），MVO 面积显著增加（2.37±3.48 vs 1.89±3.51 vs 1.30±2.20,P=0.002），高 TyG 组的 IMH 的发生率也显著高于中、低组患者（高组 44.6% vs. 中组 36.6%，低组 27.6%，P<0.001）。相关性分析，TyG 指数与梗死面积（r=0.136，P<0.001),MVO（r=0.163，P<0.001）和 IMH(r=0.163, P<0.001) 呈现显著正相关关系。多元线性回归分析（调整年龄，性别，吸烟，糖尿病，高血压，胆固醇水平，术前的 TIMI 血流分级等混杂因素后）表明，TyG 指数（β=0.167，P<0.001）是心肌梗死面积的独立危险因素。经多因素 Logistics 回归分析证实 TyG 指数是 MVO 现象 (OR=1.723,95%CI:1.34--2.23, P<0.001）和 IMH 现象（OR=1.889, 95%CI:1.45--2.47, P<0.001）的独立预测因子。

结论：TyG 指数是梗死面积的独立危险因素，并且是 MVO 和 IMH 的独立预测因素，急性心肌梗死基线的 TyG 指数可以作为评估心肌损伤严重程度的潜在预测标志物。

一项基于血管内超声分析载脂蛋白 B 控制水平对冠状动脉斑块进展影响的队列研究

李悠然 阿布力克木 阿木提 张瑞岩 杨晨蝶 王晓群

上海交通大学医学院附属瑞金医院

目的：探讨在稳定性冠心病患者中，载脂蛋白 B（apolipoprotein B, ApoB）控制水平与冠脉斑块进展的相关性。

方法：连续入组 2020 年 1 月至 2023 年 5 月期间在上海交通大学医学院附属瑞金医院心内科接受重复血管内超声（intravascular ultrasound, IVUS）检查的稳定性冠心病患者。收集患者人口学资料、病史、心血管代谢指标、用药情况等资料。计算基线与随访期间糖化血红蛋白及包括载脂蛋白 B 在内的多项血脂谱代谢参数的时间平均值。同时，通过 IVUS 定量分析基线及随访期间动脉粥样硬化体积百分比（percent atheroma volume, PAV）的变化量以评估斑块负荷变化情况，对于 PAV 变化量≥ 5% 的病变，定义为斑块进展。

结果：本研究共分析了 86 例患者的 146 个病变，在平均 12.6 个月的随访期间，PAV 平均变化量为 4.1% ± 10.2%，其中 65 个病变（44.5%）出现斑块进展。时间平均 ApoB 控制水平与动脉粥样硬化斑块总体积的平均变化量呈显著正相关（Pearson's r=0.22，P=0.008）。经多因素校正后，时间平均 ApoB 控制水平每增加 0.1 mmol/L，斑块进展的风险增加 1.8 倍。

结论：本研究显示，在校正了包括低密度脂蛋白胆固醇在内的多种心血管危险因素后，较高的 ApoB 水平仍是冠脉斑块进展的独立预测因子。因此，加强对 ApoB 在内的心血管代谢危险因素的全面管理，有利于延缓斑块进展，降低心血管不良事件的风险并改善患者预后。

Prognostic Implications of Obstructive Sleep Apnea In Acute Coronary Syndrome By Residual Cholesterol Inflammation Index

Ming-Rui zhang[1], Xiao Wang[2], qian Guo[1], Fei-Yu Zhang[1], Xiao-Chen Liu[1], Ya-Ting Chen[1], Xiang-Yun Kong[1], Shao-Ping Nie[1]

1. Center for Coronary Artery Disease, Division of Cardiology, Beijing Anzhen Hospital, Capital Medical University, Beijing, China

2. Cardiometabolic Medicine Center, Fuwai Hospital, National Center for Cardiovascular Diseases, Chinese Academy of Medical Sciences and Peking Union Medical College

Abstract

Background: Acute coronary syndrome (ACS) is a group of life-threatening cardiovascular diseases, and the long-term prognosis of patients with ACS has been a focus of clinical research. Obstructive sleep apnea (OSA), a common sleep-related breathing disorder, has been shown to be closely associated with the onset and progression of cardiovascular disease, particularly in ACS patients, where OSA may exacerbate vascular damage through mechanisms such as repeated hypoxia and sympathetic nervous system activation. Meanwhile, remnant cholesterol (RC), an important intermediate product of cholesterol metabolism, is closely associated with the progression of atherosclerosis, while high-sensitivity C-reactive protein (hs-CRP), a classic inflammatory marker, reflects the degree of vascular inflammation. The remnant cholesterol inflammation index (RCII), as a composite indicator integrating metabolic disorders and inflammatory states, has not yet been clearly defined in terms of its regulatory role in the association between OSA-ACS patient outcomes. Therefore, this study aims to explore the association between OSA and ACS patient long-term MACCE risk at different RCII levels through a large-scale prospective cohort design, providing evidence for clinical risk stratification and intervention strategies.

Methods: In this large-scale prospective cohort study, we recruited 2,160 patients with acute coronary syndrome (ACS) who successfully completed a sleep study. Remnant cholesterol defined was calculated as: RC (mg/dL) = TC- (HDL-C+ LDL-C). Remnant cholesterol inflammatory index defined as RCII = RC × hsCRP (mg/L)/10. The primary endpoint was major adverse cardiovascular and cerebrovascular events (MACCE), including cardiovascular death, myocardial infarction (MI), stroke, ischemia-driven revascularization, or hospitalization for unstable angina (UA) or heart failure.

Results: The final analysis included 1,832 patients, of whom 73.4% (1345) had RCII and 52.7% (965) had OSA (AHI ≥ 15 events/h). At baseline, patients with RCII had significantly higher levels of hs-CRP (7.36±8.61 vs 0.55±0.44, p < 0.001), total cholesterol (4.45±1.12 vs 3.78±0.87, p < 0.001), and low-density lipoprotein (2.69±0.93 vs 2.24±0.76, p < 0.001) compared with those without RCII, while high-density lipoprotein levels were lower than those without RCII (1.00±0.22 vs 1.09±0.25, p < 0.001).During the 2.9-year follow-up period, the incidence of MACCE was significantly higher in the OSA group than in the non-OSA group among patients with RCII (11.6% vs 7.0%; HR=1.38 , 95% CI 1.07-1.78; p=0.014), but this difference was not significant among patients without RCII (11.3% vs 12.3%; HR=1.33 , 95% CI 0.92-1.91; p=0.13). The incremental risk in RCII was attributable to higher rates of hospitalization for ACS, hospitalization for UA and ischemia-driven revascularization.

Conculsions: This study is the first to confirm that, in ACS patients, the association between OSA and long-term MACCE risk is influenced by RCII levels. Specifically, OSA significantly increases the risk of adverse cardiovascular events only in patients with elevated RCII levels, while this association is not significant in patients without elevated RCII levels. This finding reveals the synergistic role of metabolic-inflammatory status (RCII) and sleep-disordered breathing (OSA) in ACS prognosis, emphasizing the importance of screening and intervening for OSA in ACS patients with elevated RCII. In future clinical practice, combined assessment of RCII and OSA status can optimize risk stratification, enabling the development of targeted management strategies for high-risk patients to reduce the risk of long-term cardiovascular events.

估计葡萄糖处置率（eGDR）与慢性肾脏病患病率及死亡率的关联：一项全国性横断面研究

高鹏杰 卓琰 严怡然 王丹妮 卡米拉 徐绥宁 李锡洋 田刚

交大一附院

目的: 本研究旨在探讨一般人群中估计葡萄糖处置率(eGDR)与慢性肾脏病(CKD)患病率及死亡率的关联，并与其他胰岛素抵抗（IR）指标进行比较。

方法：基于美国国家健康与营养调查（NHANES）数据开展横断面研究。根据纳入及排除标准筛选后最终纳入 29621 名参与者。eGDR 计算公式为：21.158-0.09× 腰围（cm）-3.407× 高血压（是 =1/ 否 =0）-0.551× 糖化血红蛋白（%）；通过空腹胰岛素、血糖及甘油三酯水平及腰围和升高计算甘油三酯葡萄糖（TyG）指数、腰臀比（WHtR）及 IR 稳态模型（HOMA-IR）。采用 Logistic 回归、限制性立方样条（RCS）分析及分层分析评估 eGDR 与 CKD 患病率的关联。通过受试者工作特征曲线（ROC）、加权分位数总和（WQS）模型、随机森林及极限梯度提升（XGBoost）机器学习模型，探究 IR 指标构成要素及危险因素对 CKD 风险影响的重要性。进一步在 CKD 患者中，采用 Cox 回归分析 eGDR 与全因死亡及心血管死亡率的关联。

结果：总人群中 eGDR 的中位数为 8.64 mg/kg/min，CKD 患病率为 12.47%。Logistic 回归及分层分析显示，eGDR 与 CKD 患病率独立相关（比值比（OR）=0.88，95% 可信区间 = 0.84-0.91，P < 0.001），尤其是 40-60 岁、超重或糖耐量异常人群。RCS 曲线提示 eGDR 降低与 CKD 风险升高呈 U 型关联。ROC 分析表明 eGDR 相较于其他 IR 指标，其识别 CKD 风险的效能更优。WQS 模型显示血糖控制水平是 IR 指标构成要素中的主要影响因素，空腹血糖水平、高血压病史及腰围次之。两种机器学习模型中，年龄、eGDR、尿酸及心力衰竭病史的权重较高，提示 eGDR 需要与以上因素结合共同评估 CKD 患病风险。在中位随访 7.67 年期间，CKD 患者的全因死亡率为 23.33%，心血管疾病死亡率为 6.73%，Cox 回归表明 eGDR 可独立预测 CKD 患者的全因死亡率（风险比（HR）=0.93，95% 可信区间 = 0.89-0.98，P=0.004），在调整混杂因素后，eGDR 与 CKD 患者的心血管死亡率统计学意义消失。

结论：eGDR 是评估普通人群 CKD 风险的更优指标，并可预测 CKD 患者的全因死亡率。评估 eGDR 有助于对人群 CKD 风险分层，其中血糖控制水平尤为重要。采用基于 eGDR 的控制策略来指导危险因素管理，可能有助于降低 CKD 风险并改善 CKD 预后。

Association between obesity metabolic phenotype and risk of incident degenerative valvular disease in UK Biobank

Zhi-Xin Yan[1], Shan-Jie Wang[2], Yi-Ying Zhang[1], Bo Yu[2]

1. Department of Epidemiology and Biostatistics, School of Public Health, Jiamusi University

2. Department of Cardiology, Second Affiliated Hospital of Harbin Medical University

Association between obesity metabolic phenotype and risk of incident degenerative valvular disease in UK Biobank

Zhixin Yan[1], Yiying Zhang[1] , Shanjie Wang[2], Bo Yu[2]

1 Department of Epidemiology and Biostatistics, School of Public Health, Jiamusi University, Jiamus, China.

2 Department of Cardiology, Second Affiliated Hospital of Harbin Medical University.

Abstract

Background:

Obesity and metabolic abnormalities are independently associated with adverse cardiovascular outcomes. However, their combined impact on the risk of degenerative valvular heart disease (VHD) is unclear. Significant differences in metabolic health exist between individuals of similar weight, suggesting that obesity alone may not fully reflect the associated cardiovascular risk. Therefore, assessing obesity in conjunction with metabolic signatures may provide more insight into its role in the development of VHD. This study aimed to investigate the association between metabolic obesity phenotypes and the long-term risk of VHD.

Methods:

This prospective cohort study included participants aged 40 to 69 years from the UK Biobank. Metabolic obesity phenotypes were defined based on body mass index and metabolic health status, and classified into four categories: metabolically healthy non-obese (MHNO), metabolically healthy obese (MHO), metabolically unhealthy non-obese (MUNO), and metabolically unhealthy obese (MUO). The primary outcomes were incident VHD and its subtypes, including aortic stenosis (AS), aortic regurgitation (AR), and mitral regurgitation (MR). Multivariable Cox proportional hazards models were used to estimate hazard ratios (HRs) and 95% confidence intervals (CIs), adjusting for potential confounders such as age, sex, ethnicity, education level, physical activity, the Townsend deprivation index, smoking status, alcohol consumption, and comorbidities such as hypertension, diabetes, and cardiovascular disease.

Results:

Among 487,443 participants (54% female; mean age 56.5 ± 8.1 years), 12,793 (2.6%) developed VHD over a median follow-up of 13.3 years. Compared with the metabolically healthy non-obese (MHNO) group, the metabolically unhealthy non-obese (MUNO) phenotype exhibited no significant VHD risk difference (HR 1.05; 95% CI, 0.92-1.19). In contrast, both metabolically healthy obese (MHO) and metabolically unhealthy obese (MUO) phenotypes demonstrated elevated risks (MHO: HR 1.12, 95% CI 1.07-1.17; MUO: HR 1.34, 95% CI 1.28-1.41), primarily driven by aortic stenosis (AS) (MHO: HR 1.42, 95% CI 1.31-1.53; MUO: HR 1.87, 95% CI 1.72-2.02). Aortic regurgitation (AR) showed modest associations, while no significant link emerged for mitral regurgitation (MR). The MHO/MUO-AS association remained unaffected by polygenic risk score (PRS) (p-interaction > 0.05), though high-PRS individuals with either phenotype had substantially higher AS risk. Among individual components of metabolic syndrome, elevated waist circumference, increased blood pressure, low high-density lipoprotein cholesterol (HDL-C), and elevated glycated hemoglobin (HbA1c) levels were independently associated with a higher risk of VHD. In contrast, triglyceride levels showed no association.

Conclusion:

Obesity is significantly associated with an elevated risk of developing VHD, regardless of an individual's underlying metabolic health status. Although the presence of metabolic unhealthiness alone does not independently confer an increased risk of VHD, it plays a critical role in substantially amplifying disease susceptibility among individuals who are obese, especially in those with a high degree of genetic predisposition. These findings highlight the importance of incorporating genetic risk stratification into comprehensive prevention strategies that integrate metabolic profiling and weight management for the effective early detection and long-term control of VHD.

Association Between Triglyceride-Glucose Body Mass Index and Type 2 Diabetes Mellitus in Patients with Non-Alcoholic Fatty Liver Disease

Lei Wang, Li-Ya Bian, Peng- Zhang, Ming-Wei Wang

Affiliated Hospital of Hangzhou Normal University

Introduction and Objectives:

The triglyceride-glucose body mass index (TyG-BMI) is a novel composite indicator that combines the triglyceride-glucose index (TyG), a surrogate marker for insulin resistance, with body mass index (BMI), an established measure of adiposity. This integrated index captures both metabolic and anthropometric parameters, thereby offering a more comprehensive assessment of metabolic health. In recent years, TyG-BMI has garnered attention for its utility in predicting insulin resistance-related conditions, particularly type 2 diabetes mellitus (T2DM). However, its predictive value in specific clinical populations, such as patients with non-alcoholic fatty liver disease (NAFLD), remains underexplored. NAFLD is a hepatic manifestation of metabolic syndrome and shares strong pathophysiological links with insulin resistance and T2DM. Given the rising global prevalence of both NAFLD and T2DM, identifying reliable and non-invasive predictors is crucial. Therefore, this study aimed to evaluate the association between TyG-BMI and the presence of T2DM in hospitalized patients diagnosed with NAFLD and to assess the predictive performance of TyG-BMI in stratifying diabetes risk within this high-risk cohort.

Materials and Methods:

This retrospective study enrolled a total of 3,111 adult patients diagnosed with NAFLD who were admitted to Hangzhou Normal University Affiliated Hospital between January 2020 and December 2023. Patients were categorized into two groups based on the presence or absence of T2DM: T2DM group (n = 729) and non-T2DM group (n = 2,382). TyG-BMI was calculated using the formula: TyG index = ln [fasting triglycerides (mg/dL) × fasting glucose (mg/dL)/2]; TyG-BMI = TyG × BMI. Participants were stratified into quartiles (Q1–Q4) based on TyG-BMI distribution. Baseline demographic, biochemical, and clinical data were collected. The association between TyG-BMI and T2DM was analyzed using univariate and multivariate logistic regression models, adjusting for key covariates including age, sex, alanine aminotransferase (ALT), aspartate aminotransferase (AST), and low-density lipoprotein cholesterol (LDL-C).

Results:

Patients with T2DM were significantly older (median age: 61 vs. 55 years, $p < 0.001$) and had poorer metabolic profiles compared to non-diabetic individuals. Notably, the T2DM group exhibited higher HbA1c levels (8.8% vs. 6.6%, $p < 0.001$) and elevated TyG-BMI values ($p < 0.001$). In the unadjusted logistic regression analysis, increasing TyG-BMI quartiles were associated with a stepwise increase in T2DM risk, with the highest risk observed in Q4 (OR = 2.19; 95% CI: 1.81–2.66; $p < 0.001$). After adjusting for confounding factors, TyG-BMI remained an independent predictor of T2DM, with adjusted OR for Q4 reaching 2.72 (95% CI: 2.23–3.31; $p < 0.001$). Additionally, age was independently associated with T2DM risk, with each additional year of age increasing risk by approximately 4% (OR = 1.04; $p < 0.001$), while sex did not show significant impact.

Conclusions:

TyG-BMI demonstrates a strong and independent association with T2DM among NAFLD patients. The progressively higher odds of T2DM across TyG-BMI quartiles support its role as a robust predictive marker. As a simple and easily obtainable metric from routine laboratory and anthropometric measurements, TyG-BMI may serve as a valuable screening tool for early detection of high-risk individuals, enabling timely interventions to mitigate the progression of metabolic disease in NAFLD populations.

Naringenin Exerts Cardiovascular Protective Effect in a Palmitate-Induced Human Umbilical Vein Endothelial Cell Injury Model via Autophagy Flux Improvement

Qiang Zhao, Yi-Ning Yang

People's Hospital of Xinjiang Uygur Autonomous Region

Objective: Palmitic acid (PA) contributes to the pathogenesis of cardiovascular disease by promoting endothelial dysfunction, while naringenin (NG), most abundant in oranges, has been shown to exert multiple beneficial effects on the human cardiovascular system. However, the exact mechanism has not been investigated yet. We aimed to explore whether the NG prevents PA-induced apoptosis in human umbilical vein endothelial cells (HUVECs).

Methods: HUVECs were treated with NG in the presence of PA, and the cell apoptosis, intracellular ROS, nitric oxide generation, and MAPK signaling pathways were tested. Meanwhile, HUVECs were transfected with mRFP-GFP-LC3 adenovirus, and the effects of NG on autophagy flux was evaluated.

Results: Treatment of PA for at least 24 h caused observable decrease in levels of cell viability, oxidative stress, disorder of autophagy flux and apoptosis in HUVECs. Low concentrations of NG (1 and 10 μm) significantly increased PA-treated cell viability, while the PA-treated cell viability was dose-dependently decreased by the treatment of NG at 50, 100, and 200 μm. The PE-Annexin V apoptosis assay showed that NG at 1 and 10 μm significantly inhibited apoptosis of PA-treated HUVECs. NG inhibited the PA-caused ROS production. The DHE and DCF fluorescence intensities and MDA concentration in the NG-treated HUVECs were dramatically lower than those in the PA-treated HUVECs, suggesting that NG inhibited the PA-caused ROS production. In contrast, NG dose-dependently upregulated SOD2 expression in the PA treated HUVECs. Moreover, an increase in GPx activity and a decrease in LDH activity were observed in the NG and the PA cotreated HUVECs, as compared with the PA-only treated HUVECs. Although the PA induced significant increases in the expressions of p-ERK, p-JNK, and p-p38 MAPK, NG dose-dependently downregulated the p-JNK and p-p38 MAPK levels, while the p-ERK level in the PA-treated HUVECs was not visibly affected by the NG treatment. Accordingly, NG is considered to have prevented PA-induced apoptosis in the HUVECs by regulating the JNK and p38 MAPK pathways. Compared with the PA-induced group, treatments of NG distinctly reduced the number of autophagosomes, and increased the number of autolysosomes, in HUVECs. Consequently, the ratio of LC3B-II/I in HUVECs was significantly increased by the PA treatment, whereas the NG effectively inhibited this elevation. In addition, the NG also decreased the PA-induced increase of p62 expression level in the HUVECs. The CQ, both with and without NG, was distinctly observed to enhance apoptosis of the PA-treated HUVECs, evidenced by the increase of apoptotic cells and the decrease of the Bcl-2/Bax ratio. Thus, the protection of autophagy flux may be considered a key mechanism of NG in its inhibition of PA-treated apoptosis of

HUVECs. Both NG and SP600125 decreased the phosphorylation of JNK in the presence of PA in the HUVECs. Notably, the PA-induced phosphorylation of JNK was inhibited to a greater extent by the cotreatment of NG and SP600125 than by their individual treatments, suggesting that SP600125 blocked the phosphorylation of JNK in the PA-treated HUVECs. Additionally, the treatment of SP600125 alone and in combination with NG prevented a PA-induced increase of autophagosomes and decrease of autolysosomes in the HUVECs. Moreover, the cotreatment of SP600125 combined with NG strongly inhibited increases in the ratio of LC3BII/I and p62 expression in the PA-treated HUVECs, to a greater extent than the individual SP600125 or NG treatments.

Conclusion: These findings provide a possible mechanism by which NG prevents endothelial dysfunction and cardiovascular diseases.

心脏代谢指数与炎症介导的急性冠脉综合征患者易损斑块形成有关

闫海浩 刘巍

首都医科大学附属北京积水潭医院

背景： 心脏代谢指数（Cardiometabolic Index, CMI）作为一种反映代谢状态和内脏脂肪分布的新型指标，在心血管风险分层中受到关注。本研究旨在采用光学相干断层成像（Optical Coherence Tomography, OCT）技术探讨 CMI 与易损斑块之间的潜在关联，以及炎症在其中的作用。

方法： 本研究对 270 例接受 OCT 成像评估的急性冠脉综合征（Acute Coronary Syndrome, ACS）患者进行了横断面分析。根据 CMI 三分位数将患者分组，CMI 的计算公式为：[腰围 (cm)/ 身高 (cm)]×[甘油三酯 (mmol/L)/ 高密度脂蛋白胆固醇 (HDL-C)(mmol/L)]。OCT 用于评估罪犯病变处的斑块事件和非罪犯病变处的斑块成分，并检测炎症标志物水平。采用中介效应分析研究炎症在 CMI 与易损斑块关系中的中介作用。

结果： CMI 三分位数分组与易损斑块特征显著相关：薄帽纤维粥样斑块（Thin-cap fibroatheroma, TCFA）和巨噬细胞浸润（T1 组 vs T2 组 vs T3 组，TCFA：10.0% vs 20.0% vs 26.7%，P = 0.016；巨噬细胞：17.8% vs 28.9% vs 36.7%，P = 0.019）。多变量回归分析显示，CMI 升高是 TCFA 患病率更高（OR: 1.40, 95%CI: 1.25-2.89, P=0.003）、巨噬细胞浸润增多（OR: 1.61, 95% CI: 1.09-2.37, P=0.017）、纤维帽厚度（Fibrous Cap Thickness, FCT）减小（β= -30.65, 95% CI: -50.72 ~ -10.57, P=0.003）以及最大脂质弧增大（β= 20.78, 95% CI: 6.55-35.01, P=0.004）的独立预测因素。此外，CMI 与超敏 C 反应蛋白（hsCRP）、白细胞计数（WBC）和中性粒细胞计数呈正相关。中介效应分析表明，hsCRP 介导了约 17.0% 的 CMI 与最小 FCT 之间的关联 [间接效应值 = -5.21, 95% CI= (-12.70, -1.27), P=0.016]。

结论： CMI 是预测 ACS 患者易损斑块的关键指标。系统性炎症与 CMI 和易损斑块特征之间的关系相关，提示其可能存在机制性联系。

中国人内脏脂肪指数长期累积水平在心血管 - 肾脏 - 代谢综合征 0-3 期人群中对心血管疾病发病的预测价值

高鹏杰 卓琰 严怡然 王丹妮 卡米拉 徐绥宁 李锡洋 田刚

西安交大一附院

目的：本研究拟探讨中国人内脏脂肪指数（Chinese visceral adiposity index，CVAI）及其长期累积水平是否可以预测中老年心血管 - 肾脏 - 代谢综合征（Cardiovascular-Kidney-Metabolic syndrome，CKM）0-3 期患者的心血管疾病（cardiovascular diseases，CVDs）发生。

方法：本研究纳入来自中国健康与退休纵向研究中符合 CKM0-3 期标准的 45 岁以上中老年人群共 3449 人。CVAI 的计算公式男性为 -267.93+0.68×（年龄 +1）+0.03× 体质指数（body mass index，BMI，kg/m^2）+4.00× 腰围（cm）+ 22.00×lg[甘油三酯（mmol/L）]-16.32× 高密度脂蛋白（mmol/L），女性为 -187.32+1.71×（年龄 +1）+4.23×BMI（kg/m^2）+1.12× 腰围（cm）+39.76×lg[甘油三酯（mmol/L）]-11.66× 高密度脂蛋白（mmol/L）。用两种方法反映 CVAI 的长期累积水平：（1）使用 K 均值聚类分析结合第 1 及第 3 次随访时 CVAI 水平分为长期低、中、高水平 3 组；（2）通过（第 1 次 CVAI+ 第 3 次 CVAI）/（2015-2012）计算累积 CVAI。多元 Cox 回归用于分析基线及 CVAI 长期累积水平与 CVDs 发生之间的关系，RCS 曲线进一步分析二者之间的非线性关系，分层分析探讨二者关系在不同 CKM 分期及其他不同亚组人群中的差异。

结果：总人群平均年龄为 58.12±8.54 岁，其中 CKM2 期人数最多（1919 人，占比 55.64%），CKM3 期共 211 人（6.12%）。长期低、中、高水平 CVAI 组的累积 CVAI 分别为 219.07、307.79、413.30。长期高 CVAI 组的年龄更大，合并血压、血糖及血脂代谢紊乱的人群更多，BMI、腰围、尿酸水平更高，肾小球滤过率更低，CKM2 期及 3 期人数更多。中位随访时间为 84 月，期间共 706 人（20.47%）发生 CVDs，长期高 CVAI 组的 CVDs 发病率更高。Cox 回归提示在调整混杂因素后，基线 CVAI（Hazard ratio（HR）=1.148，95% confidence interval（95%CI）：1.058-1.246，P=0.001） 及累积 CVAI（HR=1.187，95%CI：1.093-1.288，P<0.001）均是发生 CVDs 的独立预测因子，且累积 CVAI 的预测作用更强。长期高 CVAI 组发生 CVDs 的风险是低水平组的 1.5 倍。RCS 曲线显示无论 CKM 分期，CVDs 发病风险随累积 CVAI 增大呈线性增加。分层分析显示随 CKM 分期进展，累积 CVAI 的预测价值均有统计学意义但 HR 值逐渐下降，提示累积 CVAI 的预测价值受患者合并心血管代谢疾病逐渐增多的影响而减弱。

结论：中国人内脏脂肪指数的基线及长期累积水平均可预测中老年心血管 - 肾脏 - 代谢综合征 0-3 期人群发生心血管疾病的风险。

Association Between Estimated Glucose Disposal Rate and Ischemic Heart Disease Prevalence in Non-Diabetic Adults: A Cross-Sectional NHANES Study

Yu-Qiong Chen, Li-Bo Luo, Chun-Ren Cen, Zhan-Xiang Deng, Ji-Jin Lin

广东省人民医院（广东省医学科学院）

Background:

Insulin resistance (IR), a fundamental pathophysiological state preceding the development of type 2 diabetes, is unequivocally established as a significant independent risk factor for cardiovascular disease. Its specific contribution to ischemic heart disease (IHD) pathogenesis and outcomes within the substantial population of individuals without a formal diabetes diagnosis remains inadequately characterized and necessitates deeper investigation. While the hyperinsulinemic-euglycemic clamp technique represents the gold standard for directly quantifying whole-body insulin sensitivity, its inherent operational complexity and invasiveness severely limit its utility. The procedure demands repeated arterial catheterization for precise blood sampling and prolonged, carefully controlled intravenous infusions, rendering it impractical for large-scale epidemiological studies or routine clinical assessment. Consequently, validated surrogate markers like the estimated Glucose Disposal Rate (eGDR), derived from readily available clinical parameters (e.g., waist circumference, hypertension status, HbA1c), offer a crucial and practical tool for estimating insulin sensitivity in research and clinical settings. Furthermore, the potential mechanistic pathway linking IR to IHD via systemic inflammation, potentially quantifiable through accessible hematological indices like the Neutrophil-to-Lymphocyte Ratio (NLR), represents a significant and underexplored area in understanding IHD risk in non-diabetic individuals.

Objective:

To assess the relationship between eGDR and IHD prevalence in non-diabetic adults, evaluate potential effect modifications by demographic factors, and determine whether NLR mediates this association.

Methods:

Study Population: Data were derived from the National Health and Nutrition Examination Survey (NHANES) cycles (2007–2016). A total of 12278 non-diabetic adults (no physician-diagnosed diabetes) were included.

Key variables were defined and calculated as the follows. IHD was defined by self-reported physician diagnosis of coronary heart disease or angina. eGDR was calculated as: eGDR=21.158-(0.09 * waist circumference)-(3.407 * hypertension)-(0.551 * HbA1c (%)). Participants were stratified into quartiles (Q1–Q4), where Q1 represents the lowest eGDR. NLR was calculated as the ratio of the neutrophil count to the lymphocyte count.

Baseline characteristics compared using t-tests/χ^2-tests. Multivariate logistic regression was employed: Three models assessed eGDR-IHD association: Model 1: remained unadjusted. Model 2: adjusted for age, gender. Model 3: adjusted for all the variables. Restricted Cubic Spline (RCS) was used to test linear vs. non-linear relationships between continuous eGDR and IHD odds ratio. Subgroup analyses were also performed for age, gender, race, BMI, marital status, smoking status, history of stroke, history of cancer, hypertension, hyperlipidemia and sleep disorders. Mediation Analysis was used to quantify NLR's role in the eGDR-IHD pathway using a causal mediation frameworks.

Results:

Among 12278 participants, 650 (5.29%) were diagnosed with IHD. IHD patients exhibited significantly lower eGDR compared to non-IHD ($p < 0.05$). The Logistic Regression showed that the highest eGDR quartile (Q4) had a 35.7% reduction in IHD odds compared to Q1 (OR = 0.21, 95% CI: 0.10–0.46) in Model 3. RCS analysis revealed a significant inverse linear relationship between continuous eGDR and IHD prevalence (P for linearity < 0.001). In subgroup analyses, significant interaction effects were observed for race ($p < 0.05$) , smoking status ($p < 0.05$) and hyperlipidemia , indicating heterogeneity in the eGDR-IHD association across these strata. The inverse eGDR-IHD relationship persisted in other subgroups (age, sex, BMI). Additionally, mediation analysis demonstrated that NLR partially mediated the eGDR-IHD association, accounting for 2.64% of the total effect.

Conclusion:

Lower eGDR (indicating worse insulin sensitivity) is strongly and independently associated with higher IHD prevalence in non-diabetic adults, demonstrating a dose-dependent, inverse linear relationship. This association is modified by race, smoking status and hyperlipidemia. Systemic inflammation (proxied by NLR) mediates approximately 2.64% of the total effect of eGDR on IHD risk. These findings underscore insulin resistance as a key metabolic driver of IHD even without diabetes and highlight NLR as a minor mechanistic pathway.

不同治疗背景下中国混合型高脂血症人群的血脂水平流行病学特点：一项全国性横断面研究

王乐怡 张龙 范芳芳 张岩 李建平

北京大学第一医院

目的

混合型高脂血症（CHL）是动脉粥样硬化性心血管疾病（ASCVD）的重要危险因素，但其血脂水平在实际临床管理中存在显著异质性。本研究旨在基于中国大规模人群队列，比较接受与未接受治疗的 CHL 人群的血脂水平，探讨其在不同人口学、地理与社会经济亚组中的分布差异，为优化干预策略提供依据。

方法

本研究基于国家级高脂血症专病队列，纳入 2022 年 9 月至 2024 年 11 月间中国 28 个省份 2,750 家医疗机构登记的 60 余万名确诊 CHL 的个体。采用横断面分析方法，比较未治疗人群（n = 143,825）与治疗人群（n = 109,748）的甘油三酯（TG）、总胆固醇（TC）、低密度脂蛋白胆固醇（LDL-C）、高密度脂蛋白胆固醇（HDL-C）水平，按地理区域、GDP 水平、城乡、性别、年龄、BMI 分层，分析血脂参数的分布差异。

结果

总体而言，未治疗人群的TG、TC、LDL-C水平均显著高于治疗人群（TG: 3.07±2.63 vs 2.77±2.36 mmol/L; TC: 5.96±1.07 vs 5.28±1.30 mmol/L; LDL-C: 3.57±0.93 vs 3.12±1.04 mmol/L），HDL-C 水平在两组间差异不明显（1.35±0.80 vs 1.30±0.98 mmol/L）。地理分布方面，在治疗与未治疗人群中，东北和华南地区的 LDL-C 水平均较高，而 TG 水平在东部较高，西南地区 HDL-C 相对更高。经济水平方面，GDP 第一与第二梯队地区人群的 LDL-C 普遍较高，但 TG 水平均值在各梯队之间差异不大。HDL-C 在低 GDP 地区更高或相近，提示经济水平对胆固醇控制影响更大。城乡差异方面，城乡间 TG、LDL-C 水平均存在显著差异。未治疗人群中，农村 TG 高于城市，而城市 LDL-C 高于农村，治疗后城乡差异缩小，但城市人群 LDL-C 仍略高。性别方面，男性人群 TG 水平显著高于女性，而女性 LDL-C 和 HDL-C 水平更高。年龄方面，TG 水平在 35-55 岁组达峰值，随后逐渐下降。LDL-C 和 TC 在 55-65 岁组达到最高，HDL-C 则随年龄略有上升趋势。随着 BMI 升高，TG 和 LDL-C 水平均递增，HDL-C 则呈下降趋势。治疗组中肥胖人群的 TG 和 LDL-C 依旧较高，提示治疗效果受 BMI 影响明显。

结论

中国混合型高脂血症人群在接受药物治疗后，主要血脂参数明显改善，尤其在 TC、LDL-C 及 TG 方面。然而，城乡、地区、经济水平、BMI 及年龄等因素导致血脂控制水平存在显著差异。应重点关注高 TG、高 LDL-C 且低 HDL-C 的高危亚组（如农村、低收入地区、肥胖者、男性和中年群体），推进分层管理与个体化干预措施，加强基层医疗服务能力建设，提升 CHL 人群的全面管理水平，以实现心血管疾病一级预防目标。

Serum Lipid Profiles Stratified by Treatment Status in Chinese Adults with Hypertriglyceridemia: a nationwide cross-sectional study

Le-Yi Wang, Long Zhang, Fang-Fang Fan, Yan Zhang, Jian-Ping Li

Peking University First Hospital

Objectives:

To comprehensively evaluate serum lipid levels in Chinese adults with hypertriglyceridemia, comparing those receiving lipid-lowering therapy (LLT) with untreated individuals, and to explore lipid profile variations across demographic, geographic, and socioeconomic subgroups.

Methods:

This cross-sectional study was a nationwide, multi-ethnic, multi-regional survey of dyslipidaemia in China funded by the National Key Research and Development Program. Using a multistage sampling method, 2,750 clinics across 28 provinces and seven geographic regions were selected. Between September 2022 and November 2024, adult patients diagnosed with dyslipidaemia were consecutively enrolled regardless of age or sex. Dyslipidaemia was defined according to the 2016 Chinese Adult Dyslipidaemia Prevention Guideline based on lipid thresholds or LLT use. Participants were classified as treated if they reported LLT use within the previous month. Data including demographics, clinical characteristics, and lipid profiles were collected through standardized questionnaires and physical measurements. Key variables included age, sex, BMI, geographic region, urban/rural residence, and provincial GDP per capita. Serum lipid levels (TG, TC, LDL-C, HDL-C) were analyzed by treatment status and stratified by demographic and socioeconomic factors. Statistical analyses were performed using appropriate tests with significance set at $p < 0.05$.

Results:

A total of 156,298 individuals with HTG were included, among whom 135,531 (86.7%) were not receiving lipid-lowering therapy. Compared to the untreated group, treated individuals exhibited significantly lower mean levels of TG (2.40 ± 1.46 vs. 2.64 ± 1.19 mmol/L), TC (3.53 ± 0.80 vs. 4.28 ± 0.69 mmol/L), and LDL-C (1.81 ± 0.61 vs. 2.43 ± 0.57 mmol/L). HDL-C was also slightly lower in the treated group (1.09 ± 0.96 vs. 1.20 ± 0.50 mmol/L). In terms of geographic differences, among untreated individuals, TG levels ranged from 2.38 mmol/L in Northeast China to 2.94 mmol/L in South China; in treated individuals, the highest TG was observed in South China (2.82 mmol/L). TC and LDL-C were also highest in Northeast China for both groups. HDL-C showed the most favorable levels in Northeast and Southwest China. Socioeconomic disparities were evident as in untreated individuals, those from higher GDP provinces had higher TC and LDL-C levels. In contrast, among treated individuals, the difference in TC and LDL-C by GDP level was smaller, suggesting more effective lipid control in higher-resource regions. Urban-rural differences indicated that untreated rural participants had slightly higher TG and lower HDL-C than urban counterparts. Among treated individuals, urban residents had higher LDL-C but slightly better HDL-C levels than rural residents. Age-stratified analyses revealed a peak in TG levels between 35 and 55 years, followed by a gradual decline in both groups, with LDL-C levels decreasing progressively with advancing age. HDL-C showed a downward trend with increasing age in untreated individuals, while this trend was less marked in treated individuals. Sex differences were also noted, with males exhibiting higher TG (2.65 vs. 2.61 mmol/L untreated; 2.44 vs. 2.34 mmol/L treated) and lower HDL-C (1.18 vs. 1.22 mmol/L untreated; 1.05 vs. 1.16 mmol/L treated) than women in both treated and untreated groups. LDL-C and TC differences were more variable but generally favored female participants. Regarding BMI, a clear positive correlation was observed between BMI and TG levels. Obese participants had the highest TG values in both groups (2.80 mmol/L untreated; 2.57 mmol/L treated). HDL-C decreased progressively with an increasing BMI, while LDL-C remained relatively stable across BMI categories.

Conclusions:

Lipid-lowering treatment is associated with improved TG, TC, and LDL-C levels in Chinese hypertriglyceridemia patients, but HDL-C remains suboptimal. Significant disparities by region, socioeconomic status, and demographics persist, indicating the need for tailored strategies to enhance lipid management and reduce cardiovascular risk.

N6-methyladenosine of lncRNA Gm16984 inhibits homocysteine-induced podocyte injury through miR-29b-3p/HDAC4 signaling pathway

Shengchao Ma

NHC Key Laboratory of Metabolic Cardiovascular Diseases Research, Ningxia Medical University, Yinchuan 750004, China

Chronic kidney disease (CKD) is a progressive disorder characterized by a decline in kidney function, indicated by a reduction in the glomerular filtration rate or persistent kidney injury, which lasts more than three months and poses a significant global health burden. Podocytes are the largest cells in the glomerulus and play a crucial role in maintaining the integrity of the filtration barrier through their interactions with intercellular junctions and extracellular matrix proteins. Podocyte injury is commonly associated with CKD, leading to proteinuria, tubulointerstitial fibrosis, and deterioration of renal function. Consequently, protecting and repairing podocytes is an important part of CKD treatment. Hyperhomocysteinemia (HHcy), characterized by elevated plasma homocysteine (Hcy) levels (tHcy > 15 μM), is considered a risk factor and pathogenic contributor to the progression of CKD and associated cardiovascular complications. Several studies have found that Hcy induces podocyte injury through oxidative stress and pro-inflammatory pathways, thereby disrupting the glomerular filtration barrier and exacerbating proteinuria. However, the precise mechanisms underlying Hcy-induced podocyte injury remain unclear.

Long non-coding RNAs (lncRNAs), which are RNA molecules longer than 200 nucleotides, do not encode proteins but play key roles in various biological processes, including the regulation of gene expression, determination of cellular fate, and signaling. Recent studies have found that lncRNAs are involved in transcriptional regulation, chromatin modification, epigenetic regulation, mRNA stability, translation control, RNA splicing, and signal transduction, all of which are crucial for maintaining normal physiological functions. Some studies have highlighted the dysregulation of lncRNAs in various pathologies, such as cancer metastasis, cardiovascular dysfunction, and neurodegenerative diseases. In the context of CKD, lncRNAs have received attention for their involvement in renal pathophysiology. Specific lncRNAs, such as DLX6-AS1 and Neat1_2, have been implicated in diabetic nephropathy and the progression of acute kidney injury to CKD. While the precise molecular mechanisms need to be fully elucidated, preliminary data suggest that lncRNAs may exert their effects by interacting with microRNAs (miRNAs), forming regulatory axes that modulate gene expression. However, whether lncRNAs participate in Hcy-induced podocyte injury via this axis remains unknown.

The N6-methyladenosine (m^6A) modification is one of the most prevalent epitranscriptomic modifications in eukaryotic mRNAs, accounting for more than 80% of all mRNAs. This modification plays crucial roles in post-transcriptional regulation, mRNA stability, translation efficiency, and subcellular localization . Abnormal m^6A modifications are associated with developmental disorders, neurological diseases, cardiovascular conditions, and cancer. Monitoring m^6A modifications in patient RNA may facilitate early cancer detection and prognosis prediction. The m^6A modification is dynamic and reversible and is mediated by methyltransferases such as METTL3, METTL14, KIAA1429, and WTAP, while demethylases such as FTO and ALKBH5 reverse this modification. Additionally, specific RNA-binding proteins, or "readers" (e.g., YTHDF1/2/3, IGF2BP1/2/3, eIF3, and HNRNPA2B1), directly or indirectly interact with m^6A

motifs to influence RNA functionality. These regulators participate in various RNA metabolism processes, including splicing, stability, export, and translation. Some studies have highlighted the key role of m^{6}A in kidney diseases, with m^{6}A-related biomarkers investigated for diagnostic and therapeutic purposes. Research has shown that m^{6}A intervention can improve patient prognosis and reduce CKD-related mortality, suggesting potential strategies for the management of CKD. However, the involvement of m^{6}A in the stability of lncRNA during Hcy-induced podocyte injury remains unclear.

In this study, we identified and characterized a novel upregulated lncRNA, Gm16984, as an essential regulator of Hcy-induced podocyte injury. Knocking down Gm16984 alleviates Hcy-induced podocyte injury by inhibiting autophagy. Gm16984 acts as a competing endogenous RNA (ceRNA) for miR-29b-3p, thereby upregulating HDAC4 to promote podocyte injury. We also found that METTL3-mediated m^{6}A modification of Gm16984 depends on IGF2BP1, which acts as an m^{6}A reader that binds to Gm16984 to promote its stability, ultimately leading to the upregulation of Gm16984. Our findings revealed a novel lncRNA involved in Hcy-induced podocyte injury, providing potential therapeutic targets for mitigating podocyte dysfunction and slowing the progression of CKD.

Adipose HuR protects against diet-induced obesity and insulin resistance

Jing- Li

Qilu Hospital Shandong University

Human antigen R (HuR) is a member of the Hu family of RNA-binding proteins and is involved in many physiological processes. Obesity, as a worldwide healthcare problem, has attracted more and more attention. To investigate the role of adipose HuR, we generate adipose-specific HuR knockout (HuRAKO) mice. As compared with control mice, HuRAKO mice show obesity when induced with a high-fat diet, along with insulin resistance, glucose intolerance, hypercholesterolemia and increased inflammation in adipose tissue. The obesity of HuRAKO mice is attributed to adipocyte hypertrophy in white adipose tissue due to decreased expression of adipose triglyceride lipase (ATGL). HuR positively regulates ATGL expression by promoting the mRNA stability and translation of ATGL. Consistently, the expression of HuR in adipose tissue is reduced in obese humans. This study suggests that adipose HuR may be a critical regulator of ATGL expression and lipolysis and thereby controls obesity and metabolic syndrome.

In this study, we explored the effect of adipose-specific HuR deletion on obesity and related metabolic disturbances in mice. HuRAKO mice were more susceptible to the development of HFD-induced obesity via adipocyte hypertrophy, which might be attributed to impaired lipolysis. In addition, HFD-fed HuRAKO mice showed insulin resistance and exacerbated hepatic steatosis. Mechanistically, we demonstrated that the regulation of lipolysis by HuR was mediated by ATGL. HuR could bind to the 3′ UTR of ATGL mRNA and increased its stability. Taken together, our findings establish HuR as a regulator of ATGL-mediated lipolysis.

HuR, as a member of RNA-binding proteins, has been reported to regulate the expression of many molecules by a posttranscriptional mechanism, which indicates its multifunctionality. In our recent study, HuR could regulate the stability of GTP cyclohydrolase 1 mRNA in endothelial cells. HuR is involved in many biological processes, including carcinogenesis, inflammation, cell survival and apoptosis. However, the in vivo functions of HuR have not been clearly elucidated due to its critical role in embryonic development and the embryonic lethal phenotype of global HuR-knockout mice. Recent studies reported that intestinal-specific HuR deletion reduced the tumor burden in models of intestinal tumorigenesis and inflammatory colon carcinogenesis. B lineage-specific deletion of HuR impaired the survival of B cells in bone marrow and humoral immunity. Here we generated adipose-specific HuR-knockout mice and found that HuR could protect against HFD-induced obesity and insulin resistance, which amplifies our understanding of the functions of HuR. Moreover, HuR function is regulated via changes in its subcellular localization, affinity for RNA, abundance, and cleavage, which in turn influence its ability to affect the fate of target mRNAs. In this study, the mRNA levels of HuR in epiWAT, subWAT and BAT were decreased from HFD-fed mice , which suggested that HFD-induced repression of HuR could be attributed to its mRNA reduction. High-fat diet may either interfere with the transcription of HuR or, alternatively, increase the decay of HuR mRNA. This important issue needs to be addressed by future studies.

ATGL is the key lipase that hydrolyzes triglycerides into diglycerides, which are further catalyzed by hormone-sensitive lipase (HSL) into monoglycerides and glycerols. Given its critical role in lipolysis and metabolic homeostasis, the regulation of ATGL activity and expression need exploration. ATGL activity can be modified by its interaction with other proteins such as G0/G1 switch gene 2, which inhibits ATGL action by physical interaction of its N-terminal with the N-terminal patatin domain of ATGL. The activity of ATGL lipase is also regulated by different phosphorylation sites. In addition, several factors have been identified to regulate ATGL expression. PPARγ can directly regulate ATGL expression in adipocytes in vitro and in vivo. Treatment with rosiglitazone, a PPARγ agonist, and thiazolidinedione, an antidiabetic agent, increases ATGL mRNA and protein expression in WAT and BAT of mice under the background of HFD or leptin deficiency. mTORC1 suppressed lipolysis and promoted fat accumulation in mammalian cells primarily by inhibiting transcription of ATGL, whereas rapamycin, an mTORC1 inhibitor, reversed the loss of ATGL. In this study, we have demonstrated that HuR, as an mRNA-binding protein, can target ATGL to modulate its mRNA stability and lipase expression positively, which reveals a potential mechanism in regulating lipolysis.

Since the triglycerides within adipocytes constitute >90% of adipocyte volume and it is the major volume component of the adipose mass, suppressed lipolysis could cause retained lipids in adipocytes and thereby expand adipose tissue. So far, there is no consensus of opinion about the relationship between ATGL and insulin sensitivity. Recent studies reported that adipose overexpression of ATGL attenuated diet-induced obesity and improved insulin sensitivity. Adipose-specific knockout of sirtuin 6 (Sirt6) in mice exacerbated insulin resistance and inflammation in HFD-induced obesity, in which ATGL expression and lipolysis were inhibited, which was consistent with our study. Thus, suppressed ATGL levels due to HuR knockout may contribute to reduced lipolysis and the phenotype with obesity in the HuRAKO mice. Emerging evidence suggests that impaired adipocyte lipolysis causes the proinflammatory immune cell infiltration of metabolic tissues in obesity, which contributes to the development and exacerbation of insulin resistance. In our study, HuR deletion deteriorated insulin resistance and inflammation infiltration in adipose tissue. Also, obese HuRAKO mice showed severe hepatic steatosis, which was marked by excess triglycerides accumulation and increased expression of genes involved in fatty acid uptake and lipogenesis. Thus, the HuR-ATGL-lipolysis axis may be required for maintaining normal adipocyte size and adiposity. Inhibited lipolysis in HuRAKO mice caused marked adipocyte hypertrophy, which responded poorly to insulin treatment. The elevated inflammation levels also contributed to insulin resistance in HuRAKO mice.

In summary, we demonstrate that HuR functions as a positive regulator of lipolysis by targeting ATGL to maintain its mRNA stability. Adipose-specific deletion of HuR promoted HFD-induced obesity, impaired adipose function and deteriorated glucose intolerance and insulin resistance. HuR may be a potential therapeutic target for ameliorating obesity and obesity-related metabolic disorders.

Persistent Methylmalonate Overload Despite Glycemic Control Drives Mitochondrial Dyshomeostasis and Subclinical Heart Damage in Diabetes

Shan-Jie Wang[1], Miao Yan[1], Yi-Ying Zhang[3], Shao-Hong Fang[2], Bo Yu[1]

1. 哈尔滨医科大学第二附属医院

2. bthe Key laboratory of myocardial ischemia, chinese ministry of education

3. Department of epidemiology and Biostatistics, school of Public health, Jiamusi university, Jiamusi, china

Background

Heart failure burden is still considerable in diabetes patients despite optimal glycemic control. Metabolic remodeling is involved in this process, but current understanding is still in its infancy. Methylmalonic acid (MMA) is a diagnostic marker of cobalamin (Cbl) deficiency in clinical practice. Paradoxically, MMA elevation-related cardiovascular mortality is more pronounced in diabetic patients with higher Cbl levels. We investigated the mechanisms underlying these contradictory features in diabetic heart and translational relevance.

Methods

We assessed serum Cbl, MMA, and cardiac biomarkers in 12,751 participants, and the Mmut protein (allosteric enzyme of MMA catabolism) in 4 pairs of failing human hearts with diabetes and health donors. Cardiomyocyte-specific Mmut knockout and Mmut-overexpressing (delivered by AAV-Mmut with cTnT promoter) mice were subjected to high-fat diet/streptozotocin-induced diabetes. High glucose and/or palmitate stimulation of primary neonatal mouse ventricular cardiomyocytes (NMVMs) imitates diabetic conditions in vitro. Molecular mechanism was explored through RNA sequencing, immunoprecipitation, isotope tracing mass spectrometry and biolayer interferometry assays.

Results

Higher serum MMA was significantly associated with subclinical heart damage and poor outcomes among adults with diabetes in the absence of Cbl deficiency. Cardiac MMA overload and decreased protein expression of Mmut were confirmed in humans and mice with diabetes. Notably, MMA dysmetabolism in diabetic mice occurred before detectable cardiac damage and persisted even after glycemic control. Consistently, Patients with DM and non-CVD were categorized into good and poor glycemic control subgroups by fasting blood glucose (<7.2 mM vs. ≥ 7.2 mM) and/or HbA1c (<7.0% vs. ≥ 7%) according to the recommendations

of American Diabetes Association. Optimal glycemic management did not reduce the risk of MMA elevation or MMAhiCblhi . Serum Cbl and MMA levels, and the proportion of MMAhiCblhi remained comparable across the subgroups by plasma C-peptide, insulin level, and insulin resistance index among patients with diabetes. Together, these clinical and preclinical data indicate that Mmut suppression-related myocardial MMA dysmetabolism occurs in the early phase of DCM, which is even resistant to conventional glycemic control and insulin resistance. Mechanistically, hyperglycemic memory-related molecule miR-499 binds to the mRNA of Mmut and inhibits its expression, leading to MMA overload under diabetes. Mmut knockout amplified cardiac MMA overload and exacerbated disturbance in glycolipid metabolism and mitochondrial quality control in diabetic hearts. To establish the therapeutic potential of restoring MMA metabolism in DCM, we developed cardiac-specific myotropic adeno-associated virus serotype 1A (MyoAAV 1A) constructs carrying mouse Mmut under the cardiac troponin T promoter (AAV-Mmut). Conversely, AAV-Mmut injection significantly reduces MMA load and alleviates the progression of cardiac remodeling in diabetic mice. To establish clinically translatable interventions targeting MMA metabolism in diabetic hearts, we next mapped major MMA precursors, potentially including four types of amino acids (methionine, threonine, isoleucine, and valine), cholesterol and odd-chain fatty acids (OCFAs). Isotope tracing identified isoleucine and valine as the main sources of cardiac MMA under diabetes. A restricted-branched chain amino acid diet alleviated diabetes-induced MMA accumulation and heart damage. These results indicate that mitochondrial MMA dysmetabolism is a novel hub bridging BCAA elevation and early pathological damage in diabetic hearts, supporting BCAA-derived MMA as modifiable therapeutic node in DCM. However, Cbl supplementation did not correct MMA overload in diabetic mice, even at high doses or in activated forms. The American Diabetes Association and Chinese Diabetes Society guidelines alert that metformin use inhibits the absorption of Cbl and causes Cbl deficiency. Unexpectedly, metformin administration decreased cardiovascular mortality risk and attenuated subclinical myocardial injury (hs-cTnT increase: 3.47 ng/mL per MMA doubling vs. 9.32 ng/mL in non-users) while lowering plasma MMA levels by 31% (231.6 nmol/L vs. 156.7 nmol/L) despite reduced plasma Cbl. Our experimental data paradoxically demonstrated that metformin ameliorates methylmalonic acid (MMA)-related cardiotoxicity via dual AMPK-dependent and independent pathways: AMPK activation enhanced mitochondrial quality control (evidenced by increased phosphorylation of ULK1/Raptor and TFEB) to bolster myocardial tolerance to MMA; independently, metformin directly bound to Mmut, augmenting its affinity for Cbl to improve Mmut enzymatic activity—mechanistically uncoupled from AMPK signaling as verified by studies in AMPKα2-deficient mice and the ineffectiveness of AICAR in reducing MMA accumulation.

Conclusions:

This study provides a foundation for understanding diabetes-induced MMA dysmetabolism, resistant to glycemic control and Cbl supplementation, as a trigger for subclinical heart damage and mitochondrial dyshomeostasis. Thus, MMA metabolism can be considered a promising therapeutic target for early intervention in DCM. Unexpectedly, the Cbl absorption inhibitor metformin ameliorated the cardiac damage related to MMA accumulation via dual mechanisms. Our findings challenge the prevailing clinical consensus regarding the impacts of Cbl and metformin use on MMA elevation.

Multi-Etiology Transcriptomic Integration Identifies Conserved Metabolic Dysregulation in Heart Failure

Yi-Ning Song, Ai-Jun Sun, Jun-Bo Ge

Zhongshan Hospital, Fudan University

Background

Heart failure (HF), characterized by progressive cardiac dysfunction and adverse remodeling, represents a major global health burden with high mortality and morbidity despite advances in therapy. A critical factor underpinning HF progression is metabolic dysregulation within the cardiomyocyte. The heart, as a high-energy-demand organ, relies exquisitely on efficient substrate utilization (including fatty acids, glucose, ketones, and amino acids), mitochondrial oxidative phosphorylation, and metabolic flexibility—the ability to switch fuel sources based on availability and demand. Impairments in these processes, such as disrupted substrate utilization, mitochondrial dysfunction (reduced ATP production, increased reactive oxygen species), and metabolic inflexibility, lead to chronic energy deficiency in cardiomyocytes. This bioenergetic crisis not only directly impairs contractile function but also activates maladaptive signaling pathways, promoting inflammation, fibrosis, apoptosis, and further pathological remodeling. While metabolic alterations have been described in specific HF etiologies (e.g., reduced fatty acid oxidation in pressure overload, insulin resistance in diabetic cardiomyopathy), the identification of conserved metabolic pathways and actionable therapeutic targets across diverse HF subtypes remains a significant unmet need. Understanding these fundamental, etiology-transcending metabolic disruptions is therefore paramount for developing novel, broadly effective HF treatments.

Methods

Three published RNA-seq datasets (GSE198926, GSE218733 and GSE269053) were analyzed to systematically investigate the transcriptional signatures in HF caused by different etiologies. The HF mouse models in the three datasets are established through transverse aortic constriction (TAC) surgery, high-fat diet combined with renin overexpression, and high-fat diet with nitric oxide synthase inhibition respectively. Differential gene expression analysis was performed using DESeq2 and edgeR with a statistical cutoff of PValue < 0.05 and Log2 Fold Change > 1.5. The enrichment analysis was performed using R package "clusterProfiler", "org.Mm.eg.db" and "GOplot".

Results

GSEA of the three distinct HF models revealed a highly significant and conserved down-regulation of gene sets associated with core metabolic processes across all etiologies. Key pathways suppressed included fatty acid β-oxidation, the tricarboxylic acid (TCA) cycle, oxidative phosphorylation (OXPHOS), glycolysis, and amino acid metabolism. This consistent transcriptional suppression underscores energy metabolism disruption as a fundamental, etiology-independent hub driving HF progression. Intersection analysis of differentially expressed genes (DEGs) identified a core set of conserved genes altered in all three models: 18 commonly up-regulated genes and 4 commonly down-regulated genes, representing central players in HF pathogenesis. Cellular component analysis of the up-regulated genes highlighted common structural pathologies, revealing enrichment in terms related to fibrosis-dominated extracellular matrix (ECM) organization (e.g., collagen fibril organization) and abnormalities in the contractile apparatus (e.g., sarcomere, myofibril, contractile fiber). This points to shared terminal pathways of adverse remodeling and systolic dysfunction. Among the small set of conserved down-regulated genes, Aldolase B (Aldob) emerged as a critical metabolic regulator. Aldob, classically associated with fructose metabolism in the liver, plays a significant role in the heart, participating in fructose metabolism, glycolysis, glucose-6-phosphate processing, and crucially, NADP metabolism. Its suppression in HF models exacerbates myocardial metabolic inflexibility, impairs the regeneration of NADPH (a vital reducing equivalent for antioxidant defense and biosynthetic reactions), and disrupts substrate utilization efficiency. This metabolic insufficiency synergizes with the concurrently activated fibrotic pathways (evidenced by the up-regulated DEGs) to promote left ventricular systolic dysfunction. These findings position Aldob not merely as a marker, but as a key mechanistic mediator linking metabolic insufficiency to structural and functional cardiac deterioration.

Conclusions

This study integrated multi-model heart failure (HF) data from distinct etiologies and highlighted the central role of metabolic dysregulation in HF pathogenesis. The analysis of DEGs emphasized a potential therapeutic prospect of anti-fibrotic strategies and contractile machinery modulation. Futhermore, Aldob was also suggested as a promising therapeutic target to restore myocardial metabolic homeostasis and mitigate HF progression across diverse etiologies.

血红蛋白糖化指数与冠状动脉疾病合并慢性肾功能不全患者经皮冠状动脉介入治疗后远期全因死亡的关联

蒋茂[1,2,3] 方思妮[1] 刘欢婷[1] 雷雨萌[1] 刘旭[2] 王友成[1] 郭楠[2] 王云飞[2] 于靖[2] 陈景福[1] 毛颖[1] 颜利求[1]

1. 广东医科大学附属东莞市松山湖中心医院心内科，东莞市心血管衰老与心肌再生重点实验室，东莞市心血管病研究所

2. 沧州市中心医院

3. 自贡市第一人民医院，自贡市医学科学院

目的　本研究旨在评估血红蛋白糖化指数（hemoglobin glycation index, HGI）与冠状动脉疾病（coronary artery disease, CAD）合并慢性肾功能不全（chronic renal insufficiency, CRI）患者在经皮冠状动脉介入治疗（percutaneous coronary intervention, PCI）后的远期全因死亡（all-cause mortality, ACM）之间的关系。　方法　本研究回顾性纳入 2014 年 1 月至 2017 年 9 月在河北医科大学附属沧州市中心医院接受 PCI 且同时记录糖化血红蛋白（glycated hemoglobin, HbA1c）和空腹血糖（fasting plasma glucose, FPG）的 288 例 CAD 合并 CRI 患者。采用美国国家健康与营养调查（national health and nutrition examination survey, NHANES）参考人群回归方程（预测 HbA1c = 0.024 × FPG + 3.1）计算预测 HbA1c，并进一步计算 HGI。根据 Youden's J 统计法确定的最佳 HGI 阈值，将患者分为低 HGI 组（n=81）和高 HGI 组（n=207）。主要研究终点为 ACM。　结果　在中位随访 84 个月期间，共发生 32 例（11.11%）ACM 事件。低 HGI 组的 ACM 累积发生率显著高于高 HGI 组（19.80% vs. 7.70%，P=0.003）。多变量 Cox 回归分析显示，低 HGI（HR=3.081，P=0.005）、年龄（HR=1.056，P=0.032）、慢性阻塞性肺疾病（chronic obstructive pulmonary disease, COPD）（HR=4.529，P=0.033）、既往心梗（myocardial infarction, MI）（HR=2.684，P=0.031）以及左主干病变（HR=8.186，P=0.001）均为 ACM 的独立预测因素。此外，限制性三次样条（restricted cubic spline, RCS）分析表明，HGI 与 ACM 风险之间呈线性关系（overall P=0.048，nonlinear P=0.204）。　结论　综上所述，相较于高 HGI 患者，低 HGI 与 CAD 合并 CRI 患者在 PCI 后的远期 ACM 风险增加相关。

The association between the triglyceride-glucose index and serum uric acid: a systematic review and meta-analysis

LanLan feng

Hangzhou Normal University

Abstract

Background: Hyperuricemia (HUA) is a common metabolic disorder characterized by elevated serum uric acid levels and is closely associated with insulin resistance (IR), a core component of metabolic syndrome. The triglyceride-glucose (TyG) index, calculated using fasting triglyceride and glucose levels, has emerged as a simple, accessible, and reliable surrogate marker for IR. However, the potential link between the TyG index and HUA remains underexplored, particularly across diverse populations. This study aimed to systematically evaluate the association between the TyG index and hyperuricemia in the general population.

Method:A comprehensive literature search was conducted across seven electronic databases (PubMed, Embase, Web of Science, CBM, CNKI, VIP, and Wanfang) from inception to 22 December 2024. Eligible studies included observational studies examining the relationship between the TyG index and HUA. Study quality was assessed using the Newcastle-Ottawa Scale (NOS) for case-control studies and the Agency for Healthcare Research and Quality (AHRQ) checklist for cross-sectional studies. A random-effects model was employed to synthesize effect estimates, considering expected heterogeneity. Heterogeneity was assessed using Cochrane's Q-test and the I^2 statistic. Meta-regression, subgroup analyses (e.g., by region, sex, study design), and sensitivity analyses were performed to explore the robustness of findings and potential sources of heterogeneity. Publication bias was evaluated through visual inspection of funnel plots and statistical tests including Egger's and Begg's.

Result: A total of 27 studies were included in our meta-analysis. The pooled results demonstrated that the TyG index was significantly higher in individuals with hyperuricemia (HUA group) compared to those without (NUA group), with a mean difference (MD = 0.32, 95% CI: 0.26 to 0.38, $p < 0.00001$). In addition, a higher TyG index was associated with a significantly increased risk of hyperuricemia (OR = 2.28, 95% CI: 1.85 to 2.81, $p < 0.00001$), indicating that individuals with elevated TyG levels were more than twice as likely to have HUA. These findings remained stable in sensitivity analyses, and subgroup analyses based on region, study design, and sex yielded consistent results. No significant publication bias was detected through Egger's or Begg's tests.

Conclusion: The TyG index, as a convenient and cost-effective proxy for insulin resistance, is significantly associated with both elevated serum uric acid levels and an increased risk of hyperuricemia. These findings underscore the potential utility of the TyG index as a non-invasive, easily accessible biomarker for identifying individuals at high risk of hyperuricemia, particularly in primary care and community health settings where advanced diagnostic tools may be limited. By incorporating the TyG index into routine health assessments, clinicians may enhance early detection efforts, improve individualized risk stratification, and potentially guide timely preventive interventions targeting metabolic dysfunction. Moreover, given the bidirectional relationship between insulin resistance and uric acid metabolism, our results highlight the importance of integrated metabolic management strategies in individuals with elevated TyG index levels. Future longitudinal studies are warranted to confirm the causal relationship and to explore whether TyG-guided interventions can reduce the incidence or progression of hyperuricemia and its related complications.

Keywords Triglyceride-glucose index; Serum uric acid; Hyperuricemia; Insulin resistance; Metabolic syndrome; Cardiometabolic risk; ,meta

Multi-cohort analysis of metagenome for type 2 diabetes identified universal gut microbiota signatures across populations

Xin-Yu Zhou, Ying Dong, Pan Wang, Kai-Xin , Si-Yuan Wang, Jiu-Chang Zhong,

Beijing Chao-Yang Hospital Capital Medical University

Multi-cohort analysis of metagenome for type 2 diabetes identified universal gut microbiota signatures across populations

Running Title: Cross-cohort microbial signatures of T2D

Author list: Ying Dong[1,2,†], Xinyu Zhou[1,2,†], Pan Wang[1,2], Kaixin Yan[1], Siyuan Wang[1], Jiu-Chang Zhong[1,2], Jing Li[1,2,*].

[†]Ying Dong and Xinyu Zhou contributed equally to this work.

[1]Heart Center and Beijing Key Laboratory of Hypertension, Beijing Chaoyang Hospital, Capital Medical University, Beijing, China.

[2]Department of Cardiology, Beijing Chaoyang Hospital, Capital Medical University, Beijing, China.

***Corresponding author:**

Jing Li

Heart Center, Beijing Chaoyang Hospital, Capital Medical University, Beijing Key Laboratory of Hypertension, 8th Gongtinanlu Rd, Chaoyang District, Beijing, China, 100020, Tel: 86-10-85231937, Email: lijing11999@163.com.

Abstract

Background: Type 2 diabetes (T2D) is a globally prevalent metabolic disorder influenced by complex interactions among genetic, environmental, and gut microbial factors. Although gut dysbiosis has been implicated in T2D pathogenesis, findings across studies remain inconsistent due to population-specific confounders such as dietary habits and genetic background.

Aim: This study aims to overcome previous limitations by conducting a multi-cohort, cross-population analysis to identify gut microbial signatures consistently associated with T2D, independent of demographic and dietary variations. Additionally, we evaluate the diagnostic potential of these microbial biomarkers, both alone and in combination with conventional clinical parameters, to assess their utility in T2D screening and management.

Methods: We conducted an integrated analysis of fecal shotgun metagenomic datasets from four publicly available cohorts spanning European and Asian populations, comprising a total of 433 individuals (218 T2D patients and 215 healthy controls). Using standardized bioinformatics pipelines, we systematically assessed microbial diversity through α-diversity indices (Shannon index and Pielou evenness) and β-diversity metrics based on Bray-Curtis dissimilarity with PCoA and ANOSIM tests. T2D-associated microbial taxa were identified using Wilcoxon rank-sum tests with stringent filtering criteria to exclude low-abundance (<20% prevalence) and directionally inconsistent species across cohorts. Species-clinical correlations were evaluated through Spearman's rank analysis, and a random forest classifier was developed using a 75:25 training-test split to assess the diagnostic potential of identified microbial signatures, with model performance quantified by ROC-AUC analysis.

Results: Our analysis revealed significant alterations in gut microbial ecology in T2D patients, characterized by increased α-diversity measures (Shannon index P=0.04; Pielou evenness P=0.02) suggesting ecosystem disruption, and distinct β-diversity patterns that effectively discriminated T2D patients from controls in Asian (P=0.001) and combined cohorts (P=0.001), though this separation was less pronounced in the European cohort (P=0.347). We identified 18 microbial species showing consistent abundance changes in T2D across all study populations, including 10 enriched species such as Clostridium bolteae and C. citroniae, and 8 depleted species including Streptococcus thermophiles and Haemophilus parainfluenzae. These microbial signatures demonstrated strong clinical relevance, with enriched species showing positive correlations with fasting glucose (r=0.42, P<0.001) and HbA1c (r=0.38, P<0.001), while depleted species exhibited inverse relationships. The random forest model incorporating these 18 microbial features achieved excellent diagnostic performance (AUC=0.836, 95% CI: 0.752-0.900), which further improved when combined with basic clinical variables (AUC=0.871, 95% CI: 0.793-0.928), while maintaining robust classification accuracy in both European (AUC=0.832) and Asian (AUC=0.815) validation cohorts.

Conclusions: This comprehensive multi-cohort study establishes a set of universal gut microbial signatures associated with T2D that are reproducible across diverse populations, providing compelling evidence for the role of gut microbiome dysbiosis in T2D pathogenesis. The consistent enrichment of specific Clostridium species and depletion of commensal bacteria in T2D patients across ethnic groups suggests their potential involvement in disease mechanisms. Furthermore, the demonstrated diagnostic efficacy of these microbial biomarkers, particularly when combined with basic clinical parameters, highlights their translational potential for developing population-agnostic approaches to T2D screening and management. These findings significantly advance our understanding of microbial contributions to T2D while providing a foundation for future research into microbiome-targeted therapeutic interventions.

Glucose oxidative metabolism score, diabetes status, and major adverse cardiovascular events in acute myocardial infarction populations

Ye Wang, Shan-Jie Wang, Shao-Hong Fang, Bo Yu

Second Affiliated Hospital of Harbin Medical University; The Key Laboratory of Myocardial Ischemia, Chinese Ministry of Education, China.

Aims

Type 2 diabetes mellitus (DM) has become a significant global public health challenge, the incidence and prevalence of which continue to rise in decades. DM becomes a frequent comorbidity among patients with acute myocardial infarction (AMI), leading to significant morbidity and mortality. The tricarboxylic acid (TCA) cycle dysfunction has been implicated in both conditions. We aimed to: 1) develop an index to quantify TCA cycle disturbance; 2) examine its association with adverse outcomes in DM-AMI patients; and 3) evaluate its predictive value beyond conven-

tional risk factors.

Methods

98 AMI patients (22 with DM and 76 without DM) were included as the derivation cohort, and another 4071 AMI patients (959 with DM, and 3112 without DM) were included as the validation cohort. Precision metabolomics were employed to profile organic acid metabolites in the discovery cohort. Liquid chromatography-tandem mass spectrometry (LC-MS/MS) was used to quantify TCA cycle metabolites. The TCA index was constructed based on regression coefficients. Restricted cubic splines (RCS) models were used to assess the linear relationship between TCA index and outcomes. Kaplan-Meier curves with log-rank tests assessed the cumulative incidence of post-AMI outcomes according to DM/nonDM or tertiles of TCA stratification. Multivariable-adjusted Cox proportional hazards models were used to estimate the hazard ratios (HRs) and 95% CIs for the associations between TCA index and endpoints. To evaluate the incremental predictive performance of the TCA index beyond the reference model in patients with AMI for all outcomes, we calculated Harrell's C-index and the time-dependent area under the curve (AUC).

Results

Plasma concentrations of six (citrate, isocitrate, MMA, SA, fumarate, and malate) TCA cycle intermediates were higher in patients with DM-AMI than their non-DM-AMI counterparts. During a median follow-up of 6.2 years, 1263 (31.02%) MACE events, 672 (16.51%) all-cause death, 373 (9.16%) cardiovascular death, and 561 (13.78%) heart failure events were identified. DM-AMI patients exhibited higher incidence rates of all endpoints compared to non-DM-AMI counterparts. Five of TCA cycle intermediates (α-ketoglutarate [AKG], methylmalonate [MMA], succinate [SA], fumarate, and malate) were used to constructed a composite TCA index. In patients with DM-AMI, the TCA index was significantly associated with the risk of MACE (adjusted HR:1.23; 95% CI:1.11-1.37), all-cause death (adjusted HR:1.27; 95% CI:1.11-1.47), cardiovascular death (adjusted HR:1.33; 95% CI:1.11-1.60), and HF (adjusted HR:1.34; 95% CI:1.14-1.58), with each SD increase. This index demonstrated stronger associations with all clinical endpoints in DM-AMI patients versus non-DM-AMI patients. We evaluated the incremental value of adding TCA index to reference models including the GRACE score, TnI, and NT-proBNP at 1 and 3 years. For all outcomes, the TCA index improved the predictive capability of the reference model. In patients with DM-AMI, the C-index increments, and time-dependent AUC increments were higher for all outcomes than that in non-DM-AMI patients. In patients with DM-AMI, the continuous NRI (95% CI) was 0.152 (0.003-0.173) at 1 year for cardiovascular death and 0.105 (0.013-0.237) at 1 year for HF.

Conclusion

In conclusion, investigation of TCA index effects on prognosis of AMI and comparisons between DM-AMI and non-DM-AMI patients confirms TCA cycle dysfunction in AMI progression, strengthening the need for future therapies aimed at replenishing intermediates of the TCA cycle.

Predictive value of dynamic changes in eGDR for cardiovascular disease in population with Cardiovascular- Kidney-Metabolic syndrome stages 0-3: A nationwide prospective cohort study

Yifei Xiang, Hong-Peng Chen, Yan-Er Lu

The Second Affiliated Hospital, School of Medicine, Zhejiang University

Background: The American Heart Association (AHA) has recently conceptualized Cardiovascular-Kidney-Metabolic (CKM) syndrome as a systemic disorder highlighting the pathophysiological interplay between metabolic risk factors, chronic kidney disease, and the cardiovascular system. This framework emphasizes the critical need for early screening and intervention, particularly for individuals in CKM stages 0-3, who often present with subclinical disease but are on a trajectory toward adverse outcomes, primarily driven by cardiovascular disease (CVD). Insulin resistance (IR) is a core pathogenic driver in the development and progression of CKM syndrome. The estimated glucose disposal rate (eGDR), a validated surrogate for IR calculated from waist circumference, hypertension status, and glycosylated hemoglobin A1c (HbA1c), serves as a practical, non-invasive tool for assessing insulin sensitivity. Previous studies have established that a single, baseline eGDR measurement is a strong predictor of CVD, outperforming other IR markers in populations with and without diabetes. However, such static "snapshot" assessments are inherently limited as they fail to capture the dynamic nature of metabolic health over time. The cumulative burden of IR and the velocity of its change may represent more potent predictors of long-term vascular risk. Therefore, this study aimed to investigate the association of dynamic changes in eGDR—quantified by both cumulative exposure and distinct longitudinal trajectories—with the incidence of CVD among individuals with CKM syndrome stages 0-3.

Methods: This study utilized a nationwide prospective cohort design, analyzing data from the China Health and Retirement Longitudinal Study (CHARLS). From an initial pool of 17,705 participants surveyed at baseline (Wave 1, 2011-2012), a final cohort of 4,667 individuals with CKM syndrome stages 0-3 was included after applying stringent exclusion criteria. These criteria included a history of CVD or stroke at baseline, a diagnosis of cancer or AIDS, or missing data essential for calculating eGDR or staging CKM syndrome. Dynamic changes in eGDR were assessed over a three-year period between 2012 and 2015 using two complementary metrics. First, the cumulative eGDR (cum eGDR) was calculated to represent the total, time-weighted exposure to insulin sensitivity using the formula: cum eGDR=(eGDR2012+eGDR2015)*2/3. This metric was analyzed as both a continuous variable (per standard deviation increase) and as a categorical variable (tertiles). Second, K-means clustering, an unsupervised machine learning algorithm, was employed to identify longitudinal eGDR trajectories based on measurements in 2012 and 2015. The optimal number of clusters was determined to be three using both the Elbow method and Gap Statistic analysis. This resulted in the classification of participants into three distinct groups: Class 1 (Persistent High Group, N=2205), Class 2 (Rapidly Decreasing Group, N=1516), and Class 3 (Persistent Low Group, N=946). The primary outcome was incident CVD, defined as a new, self-reported physician diagnosis of heart attack, coronary heart disease, angina, congestive heart failure, or stroke during the follow-up period to 2018. Multivariable logistic regression analysis was used to evaluate the association between the dynamic eGDR metrics and incident CVD, with adjustments for a comprehensive set of covariates in Model 2, including age, gender, type 2 diabetes mellitus (T2DM), dyslipidemia, smoking status, alcohol consumption, body mass index (BMI), education level, and household registration. Subgroup and mediation analyses were conducted to explore potential effect modification and underlying mechanisms.

Results: Over a median follow-up of 3 years, 571 participants (12.2%) developed incident CVD. Baseline characteristics varied significantly across the three eGDR trajectory groups. Participants in the Persistent Low group (Class 3) exhibited the most adverse cardiometabolic profile, being older and having a higher BMI, waist circumference, blood pressure, and a markedly greater prevalence of hypertension (85.2%), T2DM (28.2%), and dyslipidemia (17.5%) compared to the other groups. They also had worse laboratory parameters, including higher levels of hs-CRP, triglycerides, and HbA1c, and lower levels of HDL-C. In the fully adjusted multivariable logistic regression analysis (Model 2), both dynamic eGDR metrics were independently associated with incident CVD. Compared to the Persistent High group (Class 1, reference), both the Rapidly Decreasing group (Class 2; Odds Ratio=1.312, 95% Confidence Interval [CI]: 1.042-1.652; P=0.021) and the Persistent Low group (Class 3; OR=2.228, 95% CI: 1.728-2.872; P<0.001) had a significantly elevated risk of CVD. Furthermore, a higher cumulative eGDR was strongly protective. Each standard deviation increase in cum eGDR was associated with a 31% lower risk of CVD (OR=0.691, 95% CI: 0.624-0.766; P<0.001). When analyzed by tertiles, compared to the highest tertile (Q3), the lowest tertile of cum eGDR (Q1) was associated with more than double the risk of CVD (OR=2.289, 95% CI: 1.767-2.978; P<0.001). Subgroup analysis revealed a significant interaction between eGDR trajectories and T2DM status (P for interaction=0.007), indicating that the predictive value of the trajectories was particularly strong in the non-diabetic population. To investigate this finding, mediation analysis was performed. In the non-DM population, the association between adverse eGDR trajectories and incident CVD was partially mediated by lipid levels. Total cholesterol (TC) and low-density lipoprotein cholesterol (LDL-C) significantly mediated the effect, accounting for 4.99% (indirect effect P=0.032) and 4.39% (indirect effect P=0.048) of the total association, respectively. In contrast, no significant mediation by any lipid factor was observed in the population with T2DM.

Conclusions: In this large, nationwide prospective cohort of individuals with CKM syndrome stages 0-3, dynamic changes in eGDR are powerful and independent predictors of future CVD events. Worsening longitudinal eGDR trajectories—particularly a pattern of persistent low or rapidly decreasing insulin sensitivity—and a greater cumulative burden of IR (lower cum eGDR) are strongly associated with increased CVD risk. The identification of a "Rapidly Decreasing" trajectory highlights a high-risk phenotype that would likely be missed by conventional, static risk assessments. A novel mechanistic insight from this study is the differential role of dyslipidemia in mediating CVD risk based on diabetes status. In the non-diabetic population, the pathogenic pathway linking worsening eGDR to CVD is partially explained by pro-atherogenic changes in TC and LDL-C. This pathway appears to be attenuated or overshadowed by a more complex milieu of risk factors (e.g., chronic hyperglycemia, inflammation, advanced glycation end-products) once overt T2DM is established. These findings have significant clinical implications, strongly supporting the integration of dynamic eGDR surveillance into clinical practice. Such monitoring provides a practical and effective strategy to enhance CVD risk stratification and guide early, targeted preventive interventions, particularly for individuals in the pre-diabetic phase of CKM syndrome.

OSA 相关性高血压患者中代谢性心血管疾病的临床特点及预后分析

布阿依仙木·艾麦提 姚晓光 张德莲 骆秦 李南方

新疆维吾尔自治区人民医院高血压中心

目的： 本研究旨在探讨 OSA 相关性高血压患者中代谢性心血管疾病（CMD）的分布特征及其对主要不良心脑血管事件（MACCE）结局的影响，为临床管理和

干预提供依据。**方法：**本研究为回顾性队列研究，选取乌鲁木齐睡眠呼吸暂停与高血压研究（UROSAH）队列中符合 OSA 相关性高血压诊断的患者，分析其 CMD 的分布特点及代谢性心血管共病（CMM）患病情况。进一步收集患者随访信息，评估 CMM 与 MACCE 发生风险的相关性。有无 CMM 组间累积 MACCE 发病率的比较采用 Kaplan-Meier 曲线及 log-rank 检验。采用多因素 Cox 风险比例回归模型分析 CMM 对 MACCE 发病的影响。**结果：**OSA 相关性高血压患者中 CMD 的检出率显著高于非 OSA 人群。高脂血症、肥胖、非酒精性脂肪肝（NAFLD）、高尿酸血症和 2 型糖尿病的检出率分别为 81.7%、51.2%、29.5%、22.2% 和 18.4%。67.0% 的患者至少患有两种 CMD，其中 33.1% 的患者同时患有两种 CMD，7.6% 和 0.7% 的患者分别患有四种和五种 CMD。CMM 与 MACCE 风险显著相关，CMM 患者的 MACCE 风险较无 CMM 患者增加 1.42 倍（校正 HR：1.42；95% CI：1.09-1.85；P=0.010）。随着 CMD 数量的增加，MACCE 风险呈剂量 - 反应关系，患有三种 CMD 和四种及以上 CMD 的患者 MACCE 风险分别增加 1.51 倍和 2.03 倍。分层分析显示，青中年和男性患者受 CMD 的影响更大。**结论：**OSA 相关性高血压患者中 CMD 检出率高，CMD 增加该人群 MACCE 发生风险，尤其是在青中年及男性患者。本研究结果强调了早期筛查 OSA 相关性高血压和综合管理的重要性。

MDK、PLAUR 在糖尿病合并急性冠脉综合征患者中的临床意义及其诊断价值

毛萧萧 吴优璇 蒙怡 李珊珊 刘慧君 呼晓雷 李岱 夏珂

中南大学湘雅医院

目的 检测中期因子（MDK）、可溶性尿激酶受体（PLAUR）在糖尿病合并急性冠脉综合征（ACS）患者血清中的表达，探讨其能否作为预测糖尿病患者合并 ACS 的危险因素，及是否能作为预测 / 诊断糖尿病患者合并 ACS 的生物标志物。

方法 采用病例 - 对照的研究方法，纳入 2023 年 5 月至 2023 年 12 月湘雅医院心内科住院患者，其中糖尿病患者 86 例，糖尿病合并 ACS 患者 70 例；并收集匹配的健康体检者 47 名作为对照。采集所有观察对象临床资料及血生化结果，采用 ELISA 试剂盒及分光光度仪检测患者血清中 MDK 中期因子和 PLAUR 可溶性尿激酶受体的浓度。Logistic 回归分析探讨 MDK、PLAUR 是否为预测糖尿病患者发生 ACS 的危险因素，受试者工作特征（ROC）曲线分析 MDK、PLAUR 对糖尿病患者合并 ACS 的诊断效能。

结果 1、糖尿病组合并 ACS 组患者血清 MDK、PLAUR 浓度显著高于单纯糖尿病 组 [300±18 pg/ml vs.200±12 pg/ml；4.8±0.26 ng/ml vs.2.2±0.25 ng/ml]，差异均有统计学意义（P < 0.05）。2、Logistic 回归分析显示：以糖尿病组为对照，MDK 和 PLAUR 均为 ACS 的危险因素，其中 MDK 的 OR 值为 1.015，（P < 0.0001）；PLAUR 的 OR 值为 3.257，（P < 0.0001）。3、ROC 曲线分析表明：MDK、PLAUR 预测糖尿病患者发生 ACS 的 AUC（95% CI）分别为 0.8113（0.7071~0.9154）（P < 0.001）；0.9347（0.8704~0.9993）（P < 0.001）；二者联合预测糖尿病患者发生 ACS 的 AUC（95% CI）为 0.9548（0.9191~0.9904）（P<0.001）。

结论 1、中期因子（MDK）、可溶性尿激酶受体（PLAUR）在糖尿病血清中浓度显著升高。2、MDK、PLAUR 均为糖尿病患者发生 ACS 的危险因素。3、MDK、PLAUR 作为预测糖尿病患者发生急性冠脉综合征 ACS 的诊断标志物，诊断效能高，联合时预测效能更高。

老年营养风险指数对心血管 - 肾脏 - 代谢综合征患者死亡风险的预测

翟光耀 朱宏燕 杨婧 房宇琦 闫奕竹

首都医科大学附属北京潞河医院

目的：本研究旨在评估老年营养风险指数（GNRI）在心血管 - 肾脏 - 代谢（CKM）综合征人群中对全因死亡率和心血管死亡率的预测价值，以明确 GNRI 作为营养评估工具在该高风险人群中的预后意义。

方法：本研究基于一项具有全国代表性的回顾性调查，共纳入 16,074 名年龄在 20 至 79 岁之间、患有 CKM 综合征的成年人，并根据 GNRI 四分位数将参与者分组（<101.26，101.26–104.24，104.24–107.22，≥ 107.22）。主要结局为全因死亡，次要结局包括心血管死亡和癌症死亡。通过 Cox 回归模型（未调整、年龄和性别调整、完全调整）、限制性立方样条分析及亚组分析，评估 GNRI 与死亡率之间的关联。

结果：在随访期间，共发生 1,912 例死亡事件（其中 475 例为心血管死亡，515 例为癌症死亡）。在完全调整模型中，与 GNRI 第四四分位组相比，第一四分位组的全因死亡风险显著增加（风险比 [HR] 1.58；95% 置信区间 [CI]：1.32–1.89），心血管死亡风险亦明显升高（HR 2.13；95% CI：1.55–2.93）。非线性分析显示，当 GNRI 低于 100 时，死亡风险上升最为陡峭。该关联在不同年龄、性别、吸烟状态及是否合并临床心血管疾病的各亚组中均保持一致，且在性别及 10 年心血管疾病风险分层中观察到显著交互作用。

结论：在 CKM 综合征人群中，较低的 GNRI 可独立预测全因死亡与心血管死亡风险。

肝纤维化评分对非肥胖冠心病患者肾功能预后的预测价值

殷钰喆 徐靖婷 刘峥嵘 李喆 吴永健

中国医学科学院阜外医院

目的：当前多数心肾预后评估工具主要面向肥胖或代谢异常人群，对于非肥胖冠心病患者的肾脏风险识别能力仍显不足。已有研究提示，非酒精性脂肪性肝病（NAFLD）作为与代谢综合征密切相关的肝脏疾病，其相关的纤维化可能通过多种机制影响肾功能进展。肝纤维化（FIB-4）评分是一项基于常规临床指标（年龄、AST、ALT 和血小板计数）的非侵入性肝纤维化评估工具，已被用于 NAFLD 筛查。本研究旨在探讨 FIB-4 评分在非肥胖冠心病人群中对 NAFLD 筛查的意义及其与肾功能恶化风险的关联性。

方法：本研究为单中心回顾性队列研究，纳入 2008 年至 2023 年在中国医学科学院阜外医院接受冠脉支架植入术的非肥胖冠心病患者共 31,642 例。依据既往研究推荐的 FIB-4 评分界值（<1.3, 1.3–2.67, >2.67）将患者分为肝纤维化低风险、中风险、高风险三组。随访中位时间为 1.78 年。研究终点事件定义为 eGFR 下降超过 30% 或进展为终末期肾病。在排除共线性后，将 Cox 单因素分析中 P<0.1 的变量结合临床意义纳入多变量 Cox 回归模型。模型中对可能影响 FIB-4 组成项的混杂因素如他汀类药物、抗血小板药物及饮酒行为进行了调整。趋势分析、Kaplan-Meier 生存曲线、Lowess 平滑曲线及亚组交互作用分析用于辅助评估该关联的稳定性与异质性。

结果：在完全调整后的 Cox 回归模型中，FIB-4 评分升高显著关联于肾功能恶化风险升高。与低风险组相比，高风险组肾功能恶化的风险增加（HR=1.37，95%CI: 1.10–1.71，P=0.005），趋势检验 P=0.017。Kaplan-Meier 曲线显示，高风险组的结局事件累积发生率显著升高（Log-rank 检验 P<0.05）。Lowess 曲线亦提示 FIB-4 评分与肾功能恶化风险呈正相关。亚组分析发现，该关联在性别（P =0.009）、吸烟状态（P=0.033）及有无急性心肌梗死（P=0.027）亚组之间存在显著交互作用。

结论：FIB-4 评分可作为一种便捷、非侵入性的 NAFLD 的风险初筛指标，用于独立预测非肥胖冠心病患者的肾功能恶化风险。未来应进一步探索 NAFLD 与肾功能恶化之间的潜在因果关系，并考虑将 FIB-4 纳入非肥胖高风险人群的综合肾脏风险评估工具体系中，以实现早期识别与精准干预。

心血管代谢门诊综合管理 CKM 患者的初步成效

谢作晶 汪艳

昆明医科大学第一附属医院

【摘要】 目的：探讨心血管代谢门诊综合管理对心血管 - 肾脏 - 代谢综合征患者饮食、运动、生活习惯、睡眠、吸烟、BMI、糖化血红蛋白、白蛋白比肌酐比值、低密度脂蛋白、患者就医满意度等指标及 SGLT2i、GLP-1RA 使用率的影响。**方法：**选取 2024 年 12 月 --2025 年 6 月在我院心血管代谢门诊就诊建立档案并规律就诊的合并多重代谢紊乱患者作为研究对象，共有 19 例。通过门诊询问登记患者的一般信息、罹患疾病、家族史、药物治疗方案、身高、体重等，通过面对面进行问卷调查的形式了解患者饮食、运动、生活习惯、吸烟情况，同时对患者进行 “一站式” 综合管理随访。分析患者的健康问题，对其进行药物优化（视情况使用 SGLT2i、GLP-1RA 促进心肾获益）、健康教育（饮食指导、运动指导、戒烟限酒及规律服用药物），并对比门诊综合管理前后患者各指标变化及不同代谢紊乱患者的治疗方案及达标情况与患者讨论并进行记录。**结果：**19 例患者年龄为（57.7±12.0）岁，其中男性 16 例（84.2%），女性 3 例（15.8%）吸烟者 14 例（73.7%），有 10 例（52.6%）患者罹患冠状动脉性心脏病。经心血管代谢门诊综合管理后，患者 BMI 由首次就诊的（26.3±4.3）kg/m2 ，下降至末次就诊时的 （25.2±3.9）kg/m2 ，血糖代谢方面，患者 HbA1c 由（7.1±1.4）% 下降至（6.2±0.7）%，血脂代谢方面，患者 TC、TG、LDLC 水平 均出现显著下降，其中 LDLC 水平由（2.98±1.23）mmol/L 下降至 （1.12±0.75）mmol/L，尿酸代谢方面，患者血尿酸水平平均由（413.1±77.9）μmol/L 下 降 至（340.9±80.0）μmol/L，糖尿病肾病方面尿白蛋白比肌酐比值由 70.5（3.67，52.3）降至 21.5（2.77，24.49）。**结论：**心血管代谢门诊综合管理极大的方便了患者多种疾病就医的需要，避免患者一人辗转多科室求医，提高了患者就医满意度，患者 BMI、血糖、血压、血脂等指标较前明显改善；心肾获益药物 SGLT2i、GLP-1RA 使用率上升；患者饮食、运动、生活习惯有了个体化改善，吸烟数量整体下降。

体力运动对心肾代谢疾病进展及死亡风险的影响：基于英国生物银行的多状态分析

胡驹达 欧艳秋 董豪坚

广东省医学科学院 广东省人民医院

目的：体力运动（PA）对心肾代谢疾病（CRMDs）以及发展到死亡关系尚不明确。本研究旨在探讨不同强度的运动对心肾代谢疾病的发生，其进展为心肾代谢共病（CRMM）以及死亡的关系。

方法：这项前瞻性研究涵盖了来自英国生物样本库（UK Biobank）的两个队列。基于问卷的队列纳入了 328147 名参与者，他们在 2006 年至 2010 年期间完成了国际体力活动问卷（IPAQ），体力运动被分成三个程度等级（高，中，低）。基于加速度计的队列纳入了 73952 名参与者，他们在 2013 年至 2015 年期间提供了完整 1 周的基于加速度计的体力活动数据，体力运动（PA）被分为低强度、中等强度、高强度、中至高强度体力运动（LPA、MPA、VPA、MVPA）和总体力运动（TPA），各类强度运动的运动量被处理为四分位数。两个队列的参与者在基线时均未患心肾代谢疾病的任一一种，包括心血管疾病（CVD）、II 型糖尿病（T2D）和慢性肾脏病（CKD）。心肾代谢共病定义为同时存在两种或三种心肾代谢疾病。我们采用多状态模型分析体力运动对从健康状态到单一心肾代谢疾病、从单一心肾代谢疾病到心肾代谢共病以及从这些状态到死亡的转变的影响。

结果：基于问卷的队列，在中位随访 12.7 年期间，57389 名参与者发展为至少一种心肾代谢疾病，9975 名参与者发展为心肾代谢共病，最终 19677 名参与者死亡。对于从健康状态到单一心肾代谢疾病、从单一心肾代谢疾病到心肾代谢共病、从健康状态到死亡以及从单一心肾代谢疾病到死亡转变，高程度的运动相较于低程度的都呈现保护作用，风险比 (HR) 分别是 0.89(95%CI:0.87-0.91), 0.82(95%CI:0.78-0.86), 0.78(95%CI:0.74-0.82), 0.87(95%CI:0.81-0.93), 和 0.84(95%CI:0.75-0.94)。基于加速度计的队列，在中位随访 7.0 年期间，7170 名参与者发展为至少一种心肾代谢疾病，851 名参与者发展为心肾代谢共病，1975 名参与者死亡。对于前述的五种转变，多种强度运动的最高分位数运动量相较于最低分位数呈现保护作用。中至高强度体力运动对于从健康到单一心肾代谢疾病，以及进一步到死亡的转变保护作用最明显，HR 分别为 0.71(95%CI:0.66-0.77) 和 0.55(95%CI:0.40-0.75)。高强度运动对从健康到死亡转变保护作用最强 (HR:0.55, 95%CI:0.44-0.69)。总体力运动在从单一心肾代谢疾病到心肾代谢共病的过程中保护作用最显著 (HR:0.64, 95%CI:0.51-0.82)。在任一一种强度的运动中，增加运动量并未显著改善从心肾代谢共病到死亡的转

变。

结论：体力运动的增加，尤其是中或高强度体力运动以及总体力运动，与降低首次心肾代谢疾病的发生、心肾代谢共病的进展以及死亡风险（除外心肾代谢共病患者）相关。各种强度的体力运动的增加对降低心肾代谢共病患者的死亡风险影响有限。

代谢组学发现 L- 茶氨酸可预防和延缓高血压患者肾脏损伤

王子钰

首都医科大学附属北京安贞医院

目的：高血压患者容易发生肾脏损伤，但缺乏有效的干预措施。L- 茶氨酸作为茶叶中的特殊氨基酸，虽已知具有降血压等生理功能，但其对高血压患者肾脏保护的作用尚未明确。本研究旨在基于代谢组学技术揭示高血压患者体内 L- 茶氨酸水平与肾脏损伤的关联，评估其在预防或延缓高血压相关肾脏损伤中的潜在价值。

方法：本研究基于中国多省市心血管病队列研究（Chinese Multi-provincial Cohort Study, CMCS），对 487 名高血压患者进行 8 年的前瞻性随访。采用非靶向代谢组学技术检测患者基线尿液代谢物的水平，并收集年龄、性别、体重指数、吸烟史、血脂、血糖、血压、肾小球滤过率（estimated glomerular filtration rate, eGFR）、尿微量白蛋白与肌酐比值（urine albumin creatinine rate, UACR）、用药史等临床数据。使用修正泊松回归模型，校正混杂因素，分析 L- 茶氨酸水平与慢性肾脏病（chronic kidney disease, CKD）发生、进展、eGFR 水平下降及 UACR 水平升高的关联。

结果：研究发现，高水平 L- 茶氨酸与高血压患者肾脏损伤风险降低显著相关。8 年后发生 CKD 者的 L- 茶氨酸水平显著低于未发生 CKD 者（错误发现率 [false discovery rate, FDR]=0.023, 相对风险 [relative risk, RR]=0.804, 95% 置信区间 [confidence interval, CI]: 0.711-0.910）。同样地，8 年后 CKD 进展者的 L- 茶氨酸水平显著高低于未 CKD 进展者（FDR=0.005, RR=0.795，95%CI: 0.707-0.893）。另外，8 年后 eGFR 水平下降者（P 值 =0.027， RR=0.744，95%CI: 0.572-0.967） 和 UACR 水平升高者（P 值 < 0.001，RR=0.773，95%CI: 0.675-0.885）的 L- 茶氨酸水平也较低。

另外，L- 茶氨酸的肾脏保护作用仅在高血压患者中显著，在血压正常人群中未观察到类似关联（CKD 发生：RR=1.073，95%CI: 0.844-1.364；CKD 进展 RR=1.041，95%CI: 0.820-1.323）。此外，调整血压水平和降压药使用后，L- 茶氨酸的保护作用仍然显著，表明其作用独立于血压控制。

结论：本研究发现高水平 L- 茶氨酸可显著降低高血压患者 CKD 发生和进展风险，保护其肾功能，为高血压患者肾脏损伤的防治提供了新的干预靶点，也为开发含 L- 茶氨酸的药物或保健品提供了科学依据。

基于 CHARLS 队列的新型复合标志物开发：TyG/TyH 衍生肥胖指数对心血管事件的预测效能研究

吴迪 袁祖贻

西安交通大学第一附属医院

目的：由甘油三酯葡萄糖（TyG）指数评估的胰岛素抵抗与内脏脂肪存在协同作用，共同促进心血管疾病（CVD）的发生和死亡。研究表明，整合两者特征的改良 TyG 指数（如 TyG-BMI）在预测心血管事件方面优于单一 TyG 指数。基于此，本研究提出甘油三酯糖化血红蛋白（TyH）指数作为胰岛素抵抗新指标，并将其与 TyG 指数共同纳入分析。二者分别与 6 项肥胖指标——腰围（WC）、腰高比（WHtR）、体重指数（BMI）、身体形态指数（ABSI）、身体圆度指数（BRI）和锥形指数（CI）——相结合，形成 14 项预选指标。通过系统评估与相互比较，本研究旨在筛选出更优的联合指标，以精准反映胰岛素抵抗与内脏脂肪的协同效应。

方法： 本研究基于中国健康与养老追踪调查（CHARLS）2011-2018 年的数据开展队列研究，共纳入 7,426 名受访者。采用 Cox 比例风险回归模型及限制性立方样条（RCS）分析评估不同指标与 CVD 发病率的关系；通过受试者工作特征曲线（ROC）比较各指标的预测效能，并利用亚组分析检验不同人群结论的一致性。

结果：在中位随访 7 年期间，共记录 381 例心血管疾病（CVD）事件。经多因素校正的 Cox 比例风险回归分析显示：TyG、TyH 及其与内脏肥胖指标（ABSI、CI）的组合（TyG-ABSI、TyG-CI、TyH-ABSI、TyH-CI）与 CVD 发病率无统计学关联（P ≥ 0.05）；TyG 及 TyH 分别与肥胖指标腰围（WC）、腰高比（WHtR）、BMI、身体圆度指数（BRI）的组合（如 TyG-WC、TyG-BRI、TyH-WC、TyH-BRI 等）均与 CVD 风险显著正相关（P< 0.01），其中 TyG-WC 每升高 1 个标准差（SD）的风险比最高（HR 1.26，CI 1.11-1.42）。ROC 曲线分析表明，TyH-BRI 为最优预测指标（AUC = 0.577），而 TyG-ABSI 预测效能最差（AUC = 0.537）。与相同肥胖指标结合的 TyH 改良指数（如 TyH-BRI vs. TyG-BRI）预测效能普遍优于 TyG 改良指数，但差异无统计学意义（Delong 检验 P> 0.1）。RCS 分析证实上述关联均为线性（非线性检验 P> 0.1），且亚组分析（包括代谢综合征患者）结论与主分析一致。

结论：在预测效能上，TyH-BRI 和 TyG-BRI 表现最优，然而其临床应用因需测量腰围而受限。因此，基于简便性和普及性的考量，TyG-BMI 仍是我们推荐的首选指标。本研究提出的 TyH 及其衍生的肥胖组合指标（如 TyH-BMI），可分别替代相应的基于空腹血糖的 TyG 指标（如 TyG-BMI），预测效能相当。

FMO2 promotes angiogenesis via regulation of N-acetylornithine

Wang Jingyi

The Second Affiliated Hospital Zhejiang University

Objective: The treatment of ischemic diseases hinges on the regeneration of a functional vascular network, with endothelial cell (EC) metabolic reprogramming emerging as a pivotal regulatory target for pro-angiogenic therapies. However, our understanding of the metabolic characteristics and regulatory mechanisms of ECs in ischemic microenvironments or during vascular development remains incomplete. This study aims to uncover the critical molecular mechanisms underlying EC metabolic remodeling in angiogenesis and explore its translational potential, focusing on the roles of FMO2 and N-acetylornithine.

Methods: Our research design involved single-cell RNA sequencing (scRNA-seq) using the 10x Genomics platform to analyze EC molecular features in mouse hindlimb ischemia models and retinal vascular development models. We generated EC-specific FMO2 knockout and compensation mouse models via CRISPR/Cas9. Additionally, we constructed a lentivirus harboring an enzymatic activity-deficient FMO2 mutant (LV-mut-FMO2) to validate the enzyme activity-dependent effects of FMO2 on angiogenesis, combined with untargeted metabolomics to screen for key metabolites regulated by FMO2. And dual-luciferase assays deciphered transcriptional regulatory networks, with validation in human umbilical vein endothelial cells (HUVECs) and human ischemic disease contexts were used to elucidate the detailed mechanism by which N-acetylornithine influences NOTCH1 expression.

Results: We confirmed that endothelial FMO2 is essential for both physiological vessel development and pathological angiogenesis after ischemia. Single-cell transcriptome analysis showed significant upregulation of FMO2 in ischemic tissue ECs, with specific high expression in tip cells of developing retinal vessels. EC-specific FMO2 knockout impaired hindlimb ischemic blood flow recovery and reduced retinal vascular branch points, whereas endothelial-specific FMO2 compensation reinforced angiogenesis. Given that FMO2 is a NADP+ and FAD dependent enzyme, we generated LV-mut-FMO2 to verify whether its pro-angiogenic effects are enzyme activity-dependent. Structural modeling confirmed that deletion of the enzymatic activity segment did not affect proper protein folding. However, loss of enzymatic activity abolished FMO2's pro-angiogenic functions, as evidenced by impaired tube formation and tip cell sprouting, indicating that FMO2 regulates angiogenesis in an enzyme activity-dependent manner. Untargeted metabolomics analysis of ECs overexpressing FMO2 (LV-FMO2) or knockdown FMO2 (LV-shFMO2) revealed that ornithine and N-acetylornithine were concurrently enriched in the ornithine metabolism pathway, with N-acetylornithine upregulated and ornithine downregulated, consistent with the catalytic process of this pathway. In vivo and in vitro validation showed that N-acetylornithine levels were significantly reduced in the gastrocnemius muscle of $FMO2^{\triangle EC}$ mice after hindlimb ischemia and in cultured ECs with FMO2 knockdown or enzymatic inactivation, while FMO2 overexpression increased N-acetylornithine levels. Among the metabolites upregulated by FMO2 overexpression, only N-acetylornithine supplementation significantly enhanced EC tube formation and reversed the upregulation of NOTCH1 and NICD induced by FMO2 knockdown. Mechanistically, FMO2 promotes vessel sprouting by repressing NOTCH1 through regulation of N-acetylornithine. Bioinformatics analysis of conserved transcription factor binding sites on the NOTCH1 promoter using the ENCODE ChIP-seq database, combined with functional validation, revealed that ATF3 knockdown increased NOTCH1 expression, whereas ATF3 overexpression reduced NOTCH1 and NICD levels. Crucially, ATF3 silencing abolished the pro-angiogenic effects of N-acetylornithine, including tube formation, and blocked the ability of N-acetylornithine or FMO2 overexpression to reduce NOTCH1, confirming that N-acetylornithine inhibits NOTCH1 via transcriptional regulation of ATF3. Moreover, N-acetylornithine exerted significant therapeutic effects in ischemic diseases: exogenous supplementation restored tube formation in FMO2-knockout ECs and increased capillary density in ischemic tissues. This regulatory axis is conserved in HUVECs, where ATF3 knockdown blocked the pro-angiogenic effects of N-acetylornithine, confirming the translational potential of FMO2 and N-acetylornithine in human ischemic diseases.

Conclusion: This study establishes FMO2 as a key regulator linking EC metabolism to angiogenesis through the N-acetylornithine - ATF3 - NOTCH1 axis. FMO2-dependent enzymatic production of N-acetylornithine activates ATF3 to repress NOTCH1, thereby promoting vessel sprouting. These findings support dual therapeutic strategies for ischemic diseases: enhancing endothelial FMO2 expression or supplementing N-acetylornithine, with conserved mechanisms in human ECs highlighting clinical translation potential.

The prognostic significance of triglyceride-glucose index for all-cause mortality in cancer survivors: Retrospective cohort study

A-ILIPAI MAMUTI H[1,2]

1. Shanghai Tenth People's Hospital

2. Shache County People's Hospital, Xinjiang Uygur Autonomous Region

The prognostic significance of triglyceride-glucose index for all-cause mortality in cancer survivors: Retrospective cohort study

Hailipai Mamuti[1,2†], Kudelaiti Abuduwufuer[3†], Yuan Xu[4, 5†], Atawula Aili[1], Peiran Song[1], Jiasuer Alifu[1,#], Bo Wang[1,#], Hailing Li[1,#]

[1]Department of Cardiology, Shanghai Tenth People's Hospital, Tongji University School of Medicine, Shanghai 200072, China

[2]Department of Cardiology, Shache County People's Hospital, Xinjiang Uygur Autonomous Region 844700, China

[3]Shanghai Municipal Hospital of Traditional Chinese Medicine, Shanghai University of Traditional Chinese Medicine, Shanghai 200071, China

[4]Department of Thyroid and Breast Surgery, Shanghai Tenth People's Hospital, School of Medicine, Tongji University, Shanghai 200072, China

[5]Institute of Breast Disease, School of Medicine, Tongji University, Shanghai 200072, China

[†]Hailipai. Mamuti, Kudelaiti. Abuduwufuer, and Yuan Xu Contributed equally to this work.

[#]Corresponding authors:

Hailing Li, E-mail: 1986lihailing@tongji.edu.cn;

Bo Wang, E-mail: yuweng2014@163.com.

Jiasuer Alifu, E-mail: jassur222@163.com.

Abstract

Background: The triglyceride-glucose (TyG) index has emerged as a clinically significant and reliable surrogate marker of systemic insulin resistance, demonstrating strong predictive value for adverse health outcomes across multiple disease states. While extensive epidemiological evidence has established clear associations between insulin resistance and accelerated cancer progression through various pathophysiological mechanisms, including chronic inflammation and hyperinsulinemia-driven tumor growth, the specific prognostic utility of the TyG index for mortality risk stratification in cancer survivor populations has remained poorly characterized. To address this important clinical question, our investigation leveraged comprehensive data from a nationally representative U.S. cancer registry, employing rigorous retrospective cohort study methodology to systematically evaluate longitudinal outcomes. This large-scale analysis provides novel epidemiological evidence demonstrating a significant association between TyG index levels and all-cause mortality risk in cancer survivors, with important implications for risk prediction models and survivorship care strategies in this vulnerable patient population.

Methods: This retrospective cohort analyzed 2,146 cancer patients from NHANES (1999-2018), stratified by TyG index quartiles (Q1:<8.33; Q2:8.33-8.72; Q3:8.72-9.16; Q4: ≥ 9.16). Calculated as ln[fasting triglycerides(mg/dL)×fasting glucose(mg/dL)/2], TyG associations with mortality were evaluated through Cox proportional hazards models and Kaplan-Meier analyses. Restricted cubic splines characterized non-linear relationships, while weighted Cox regression yielded adjusted HRs (95% CIs) across subgroups. ROC curve analysis established optimal TyG prognostic thresholds.

Results: Over a median follow-up of 95.18±60.98 months, 770 all-cause deaths were recorded in a cohort of 2,146 cancer patients. The TyG index was significantly higher in the event group (8.81±0.6 vs. 8.75±0.65; P=0.004), with more participants in the highest TyG quartile (Q4) in the event group (25.6% vs. 25.2%; P=0.014). A U-shaped relationship between TyG index and all-cause mortality was observed (P for non-linearity p =0.027). Kaplan-Meier and Cox regression analyses showed higher TyG index was associated with increased mortality risk (Logrank P =0.002; HR=1.568, 95%CI: 1.201-2.047 P<0.001, respectively). ROC analysis identified an optimal TyG cut-off of 8.37 (AUC =0.527, 95%CI: 0.501-0.552, P =0.041).

Conclusion: Through multivariate regression analysis, this study demonstrates that the triglyceride-glucose (TyG) index serves as an independent predictor of all-cause mortality in cancer patients, exhibiting a significant U-shaped association with clinical endpoints. Specifically, our longitudinal cohort study revealed that both elevated and reduced TyG index levels were significantly associated with increased mortality risk, while intermediate TyG index levels demonstrated optimal prognostic outcomes. These findings suggest that implementing appropriate glycemic and lipid control in clinical practice to maintain metabolic homeostasis may potentially reduce mortality risk in this patient population. Furthermore, our results support the incorporation of the TyG index into risk assessment systems for cancer patients, providing a theoretical foundation for developing personalized metabolic intervention strategies.

Keywords: Triglyceride-glucose index, Cancer, NHANES, Mortality, Prognosis

组蛋白乳酸化修饰介导代谢重编程在心肌梗死后心肌再生中的作用机制研究

张立

上海交通大学医学院附属同仁医院仙霞路院区

张 立[1]，钱玲梅[1]*

1. 上海交通大学医学院附属同仁医院，心内科，上海，200336

关键词： 心肌梗死、心肌再生、代谢重编程、乳酸化修饰

目的： 本研究的目的是阐明组蛋白乳酸化修饰介导糖代谢重编程途径促进心肌梗死后心肌有效再生的作用及机制研究，为临床上缺血性心脏病的治疗提供新思路。

方法： 我们首先通过质谱技术对新生 1 天（P1）及 7 天（P7）小鼠的心尖组织进行代谢谱及乳酸化修饰谱检测分析，再通过靶向代谢组学技术检测 P1 与 P7 中乳酸水平，通过 Western blot 检测组蛋白各位点的乳酸化修饰水平。在细胞水平，我们首先通过乳酸加入小鼠原代心肌细胞培养上清，通过免疫荧光法测定心肌细胞增殖潜能的指标（EdU、pH3 及 aruroB），通过 Western blot 检测组蛋白 H3K18la 乳酸化修饰水平。在动物水平上，采用乳鼠心尖切除术，建立乳鼠心肌再生模型，通过腹腔注射乳酸采用 Masson 染色检测术后心脏的再生与纤维化情况，以 M 型心脏超声检测左室短轴缩短率（LVFS）、左室射血分数（LVEF）等左心室功能指标的变化。在机制上，设置细胞加入乳酸处理组与空白组，通过 RNA-seq 测序技术联合 Western blot 检测糖代谢途径及丙酮酸激酶 PKM2 表达。进一步采用 $pkm2^{-/-}$ 心肌特异性敲除小鼠，采用乳鼠心尖切除术及成年小鼠心梗结扎术，采用乳酸处理，以 M 超声检测 LVFS、LVEF 等指标的变化；采用 TTC 及 Masson 染色，检测乳鼠心尖及成年鼠心肌梗死面积及纤维化程度；免疫荧光法检测 EdU、pH3 及 aruroB 染色的阳性心肌细胞数，以了解心肌细胞增殖潜能。最后，提取心肌组织检测 H3K18la 乳酸化修饰水平、代谢重编程相关的分子蛋白表达水平及代谢产物丙酮酸含量。

结果： 代谢图谱检测发现 P1 组糖酵解途径显著，而 P7 组氧化磷酸化途径显著，显示发生代谢重编程改变，且乳酸水平在 P1 组升高，乳酸化修饰谱发现 P1 组整体组蛋白乳酸化修饰水平升高，通过 Western blot 检测发现 H3K18la 位点乳酸化修饰水平差异明显。在细胞水平，检测发现乳酸可以显著提高小鼠原代心肌细胞 EdU、pH3 及 aruroB 的阳性率，可显著提高组蛋白 H3K18la 乳酸化修饰水平；在动物水平上，乳酸可促进乳鼠心尖切除后心肌再生，减少纤维化，M 超声结果显示：术后 28 天乳酸可显著改善 LVFS、LVEF 心功能指标。在机制上，通过 RNA-seq 测序揭示糖酵解途径，Western blot 检测发现丙酮酸激酶 PKM2 表达上调。进一步通过 $pkm2^{-/-}$ 心肌特异性敲除小鼠建立乳鼠心尖切除术及成年小鼠心梗模型，M 超声结果显示乳酸对左室心功能的改善被抑制；TTC 及 Masson 染色发现，乳酸处理后乳鼠心尖及成年鼠心肌梗死面积及纤维化程度无差异；免疫荧光法检测 EdU、pH3 及 aruroB 染色的阳性心肌细胞数无显著差异。提取心肌组织检测发现 H3K18la 乳酸化修饰水平降低，糖酵解关的分子蛋白表达水平降低及代谢产物丙酮酸含量降低，揭示 PKM2 介导的糖酵解途径可能是乳酸化修饰促进心肌再生的机制。

结论： 本研究证实代谢重编程参与心肌再生过程，首次发现 H3K18la 组蛋白乳酸化修饰通过 PKM2 调控糖酵解代谢重编程促进心肌再生，改善心肌梗死损伤。本研究将为梗死后心肌有效再生治疗提供新的理论依据和干预靶标。

Association of a Novel BMI/Triglyceride-Glucose Waist Circumference Index with All-Cause and Cardiovascular Mortality in a COPD Population

Yuli Cai[1], Huan Li[1], Wenxi Li[1], Weilong Ye[1], Huizhao Liao[2], Tingting Sun[2], Zhaojun Chen[1], Qinghua Chen[1], Enlin Ye[1], Yihuan Su[1], Junfen Cheng[1], Weimin Yao[1], Baozhi Zhang[1], Riken Chen[1]

1. The Second Affiliated Hospital of Guangdong Medical University

2. The First Affiliated Hospital of Guangzhou Medical University

Objective

Chronic Obstructive Pulmonary Disease (COPD) is a leading global cause of morbidity and mortality, characterized not only by airflow limitation but also by significant systemic inflammation and metabolic dysregulation. Individual markers of metabolic health, such as the triglyceride-glucose (TyG) index (a surrogate for insulin resistance), along with obesity indices like body mass index (BMI) and waist circumference (WC), have been independently associated with clinical outcomes. However, COPD presents a complex metabolic phenotype where the interplay between insulin resistance and different patterns of fat distribution may have unique prognostic implications. To date, the combined effect of these markers, integrated into a single composite index, on long-term survival in COPD patients remains unknown. Therefore, the primary objective of this study was to develop and investigate the association of a novel composite biomarker, the BMI/TyG-WC index, with all-cause and cardiovascular-specific mortality in a large, nationally representative cohort of adults with COPD.

Methods

This study was designed as a retrospective cohort analysis utilizing data from multiple cycles of the National Health and Nutrition Examination Survey (NHANES) conducted between 1999 and 2018. The study population consisted of 1,488 adult participants who met the diagnostic criteria for COPD. The primary exposure variable was the novel BMI/TyG-WC index, which was constructed as a composite measure integrating metabolic and anthropometric data. Participants were categorized into quartiles based on the distribution of this index for analysis. The main outcomes of interest were all-cause mortality and cardiovascular-specific mortality, which were ascertained through probabilistic linkage to the National Death Index (NDI) database.

To assess the relationship between the BMI/TyG-WC index and mortal-

ity, a multivariable Cox proportional hazards model was employed to calculate adjusted hazard ratios (HRs) and their corresponding 95% confidence intervals (CIs). The models were adjusted for a comprehensive set of potential confounders, including age, sex, race, smoking status, educational level, and comorbidities. Survival curves were visualized using Kaplan-Meier analysis and Nelson-Aalen cumulative function plots to compare mortality risk across the index quartiles. The predictive utility of the index was further assessed using receiver operating characteristic (ROC) curve analysis, and the area under the curve (AUC) was calculated for several models. Finally, to ensure the validity of our findings, extensive subgroup and sensitivity analyses were performed to test the robustness and reliability of the final model.

Results

The final cohort comprised 1,488 participants with COPD, including 885 women and 603 men, with a mean age of 54.2 ± 16.2 years. A significant and independent inverse association was discovered between the BMI/TyG-WC index and mortality. In the fully adjusted Cox regression model, participants in the highest quartile of the index exhibited a significantly lower hazard of both all-cause mortality (HR: 0.68; 95% CI: 0.49–0.94) and cardiovascular mortality (HR: 0.45; 95% CI: 0.23–0.85) when compared to those in the lowest quartile. This trend was visually confirmed by the Kaplan-Meier and Nelson-Aalen plots, which demonstrated a stepwise decrease in cumulative mortality incidence with each increasing quartile of the index. The ROC curve analysis showed that the fully adjusted model incorporating the BMI/TyG-WC index had superior predictive performance for both all-cause mortality (AUC: 0.71; 95% CI: 0.68–0.74) and cardiovascular mortality (AUC: 0.70; 95% CI: 0.65–0.75). Subgroup analyses indicated that this protective association was consistent across various demographic and clinical subgroups, with no significant interactions detected.

Conclusion

The novel composite BMI/TyG-WC index is significantly and independently associated with all-cause and cardiovascular mortality in the COPD population. Crucially, this relationship is inverse, suggesting that a higher index value, which reflects a specific metabolic and anthropometric profile, is paradoxically linked to improved survival. This finding points towards a potential "obesity paradox" in COPD that is uniquely captured by this integrated marker. The BMI/TyG-WC index could serve as an accessible and valuable prognostic tool for risk stratification in patients with COPD, and further research is warranted to explore the underlying biological mechanisms of this protective association.

心脏代谢共病患者估计葡萄糖处理率和颈动脉斑块的相关性分析

欣鑫

天津市胸科医院

摘要：

目的：系统探讨心脏代谢共病（CMM）患者中葡萄糖处理率（GDR）与颈动脉斑块特征的关联性，揭示胰岛素敏感性在亚临床动脉粥样硬化进展中的潜在作用。

方法：

数据来源：中医药治疗心血管疾病队列研究数据库，根据排纳标准，筛选出3607 例病例，收集一般资料、既往病史、生化指标（血糖、糖化血红蛋白、甘油三酯、总胆固醇、低密度脂蛋白胆固醇、高密度脂蛋白胆固醇、谷丙、谷草、肌酐、尿素、尿酸、肌酸激酶、乳酸脱氢酶）、颈动脉彩超数据完整，根据有无颈动脉斑块分为两组，使用二元 logistics 回归判断 eGDR 与无颈动脉斑块的相关性，并校正混杂因素。然后根据年龄、性别、有无合并糖尿病的共病患者进行亚组分析。

结果：未调整模型时，eGDR 每增加一个单位，颈动脉斑块发生风险减少 3.5%。根据年龄、性别进行调整后，eGDR 每增加一个单位，颈动脉斑块发生风险减少 3.7%。根据年龄、性别、吸烟、身高进行调整后，eGDR 每增加一个单位，颈动脉斑块发生风险减少 4.5%。根据年龄、性别、吸烟、身高、糖化、高血压、血糖、总胆固醇进行调整后，eGDR 每增加一个单位，颈动脉斑块发生风险减少 6.0%。

结论：在心脏代谢共病（CMM）患者中，估计葡萄糖处置率越高，颈动脉斑块发生风险越低。相反，估计葡萄糖处理率（eGDR）越低，颈动脉斑块发生风险越高。

Association between dietary B vitamin intakes and advanced cardiovascular-kidney-metabolic syndrome: insights from the National Health and Nutrition Examination Survey

Zhi-Fu Guo[1], Ding-Yuan Tu[2], Jing-Yu Zhang[1], Qiang Xu[4], Chao-Qun Ma[3], Jin Luo[1], -Pu Niu[1], Si-Yu Liu[1], Song-Qun Huang[1]

1. Changhai Hospital, Naval Medical University

2. The 961st Hospital of the Joint Logistics Support Force of The Chinese People's Liberation Army

3. General Hospital of Northern Theater Command

4. Navy 905 Hospital, Naval Medical University

Objective

Cardiovascular-kidney-metabolic (CKM) syndrome represents a systemic disorder integrating cardiovascular disease (CVD), chronic kidney disease (CKD), and metabolic dysfunctions, with advanced stages (stages 3–4) associated with high mortality and healthcare burden. Dietary interventions are modifiable risk factors for CKM progression, but the role of B vitamins—essential cofactors in energy metabolism, homocysteine regulation, and oxidative stress pathways—remains inadequately characterized. This study aimed to evaluate independent and joint associations of six dietary B vitamins (B1, B2, B6, B12, niacin, folate) with advanced CKM syndrome using a nationally representative U.S. cohort. The primary hypothesis posited that higher B vitamin intake, particularly B2 and B6, would correlate with reduced risk of advanced CKM stages, addressing a critical gap in nutritional epidemiology for multisystem disease prevention.

Methods

Study Design and Population:

A cross-sectional analysis included 14,576 adults (≥ 20 years) from the 2011–2020 National Health and Nutrition Examination Survey (NHANES). Participants were classified into CKM stages 0–4 per American Heart Association (AHA) criteria, with stages 3–4 (clinical CVD, high-risk CKD, or ≥ 20% 10-year CVD risk) defined as advanced CKM syndrome. Exclusions comprised pregnancy, implausible energy intake, missing B vitamin or CKM data, and key covariate deficiencies.

Exposure and Outcome Assessment: B Vitamin Intake: Quantified via two 24-hour dietary recalls, averaged across six types (B1, B2, B6, B12, niacin, total folate). CKM Staging: Based on BMI, metabolic risk factors (hypertension, diabetes, dyslipidemia), CKD risk, 10-year CVD risk (PREVENT equations), and self-reported CVD. Covariates: Adjusted for demographics (age, sex, ethnicity), socioeconomic status (income, education), lifestyle (smoking, alcohol, physical activity), and diet quality (Healthy Eating Index-2015, HEI-2015). Statistical Analysis: Primary Models: Survey-weighted multivariable logistic regression evaluated individual B vitamins and advanced CKM, with three adjustment tiers: basic (age, sex, ethnicity), socioeconomic, and full (lifestyle + HEI-2015). Dose-Response: Restricted cubic splines (RCS) with 3–7 knots tested nonlinear associations. Mixture Effects: Weighted quantile sum (WQS) regression and quantile-based g-computation (QG-comp) assessed combined B vitamin effects, addressing multicollinearity and directional heterogeneity. Sensitivity Analyses: Excluded cancer history, imputed missing covariates, and adjusted for cardioprotective medications (SGLT2 inhibitors, GLP-1 agonists). Analyses incorporated NHANES sampling weights and complex survey design.

Results

Participant Characteristics: Among 14,576 CKM patients (mean age 49.9 years, 51.3% female), 17.0% (n=2,486) had advanced CKM syndrome. Advanced-stage patients were older, more likely male, non-Hispanic White, former/current smokers, and had lower education/income versus non-advanced stages (all p<0.001). Daily intake of vitamin B2, B6, and niacin was significantly lower in advanced CKM (p<0.05). Individual B Vitamin Associations: Vitamin B2: Highest quartile (Q4) intake reduced advanced CKM risk by 27% (OR=0.73, 95% CI: 0.60–0.89) versus Q1 in fully adjusted models. Continuous analysis confirmed inverse linearity (OR=0.87, CI: 0.81–0.93, p<0.001). Vitamin B6: Q4 intake lowered risk by 26% (OR=0.74, CI: 0.59–0.93), with continuous OR=0.88 (CI: 0.82–0.95, p=0.002). Niacin: Modest inverse association (OR=0.98, CI: 0.97–0.99, p=0.01). ther B Vitamins: B1, B12, and folate showed no significant associations (p>0.05). RCS revealed nonlinear relationships for B1, B2, B6, and folate ($p_{nonlinear}$<0.05). Joint B Vitamin Effects: WQS Model: Mixed B vitamin exposure reduced advanced CKM risk (OR=0.89, CI: 0.83–0.95, p<0.001), driven primarily by B6 (weight=0.721) and B2 (weight=0.200). QG-comp Model: Similarly protective (OR=0.89, CI: 0.83–0.94, p<0.0001), with B2 (weight=0.373) and B6 (weight=0.347) as dominant negative contributors. Vitamin B12 exhibited paradoxical positive weights (0.309 in QG-comp), suggesting context-dependent effects. Sensitivity Analyses: Results persisted after excluding cancer patients, imputing missing data, and adjusting for medications, confirming robustness (all p<0.05).

Conclusion

This large-scale study demonstrates that higher dietary intake of vitamins B2 and B6 is independently associated with reduced risk of advanced CKM syndrome, exhibiting dose-dependent protective effects. Mixed B vitamin exposure further underscores synergistic benefits, with B2 and B6 as primary mediators. These findings highlight B vitamins—particularly B2 and B6—as modifiable nutritional factors for mitigating CKM progression, potentially via antioxidative pathways (e.g., glutathione cycle restoration) and epigenetic regulation of metabolic genes. While causality cannot be inferred from cross-sectional data, the results advocate for integrated dietary strategies targeting B vitamins in high-risk populations. Future prospective cohorts and mechanistic studies are warranted to elucidate molecular targets (e.g., homocysteine modulation, endothelial function) and refine clinical guidelines for CKM man-

agement

ATAD3A Regulates Mitochondria–Lysosome Membrane Contact Sites via the LIAS/DLST Axis to Suppress Aortic Dissection

Jie Lin[1,2,3], Ying An[1,2,3], Sheng-Jun Xiong[1,2,3], Ying-Mei Zhang[1,2,3], Jun Ren[1,2,3]

1. Department of Cardiology, Zhongshan Hospital, Fudan University

2. Shanghai Institute of Cardiovascular Diseases, Shanghai,China

3. National Clinical Research Center for Interventional Medicine, Shanghai, China

Background:

Aortic dissection (AD) is a life-threatening vascular disorder characterized by medial degeneration, inflammation, and extensive vascular remodeling. Despite advances in clinical management, the underlying molecular mechanisms remain incompletely understood, limiting the development of targeted therapies. Mitochondrial dysfunction has emerged as a key contributor to vascular smooth muscle cell (VSMC) phenotypic transformation and vascular instability. ATPase family AAA domain-containing protein 3A (ATAD3A), an inner mitochondrial membrane protein, plays a critical role in maintaining mitochondrial homeostasis, including mitochondrial DNA organization, cristae structure, and organelle dynamics. However, its role in aortic disease has not been thoroughly explored. This study investigates the hypothesis that ATAD3A protects against AD by regulating mitochondria–lysosome membrane contact sites (MCSs) through a novel LIAS/DLST signaling axis, thereby preserving mitochondrial function and suppressing pathological VSMC remodeling.

Methods:

We employed integrative transcriptomic and proteomic analyses to assess ATAD3A expression patterns in aortic tissues and VSMCs under AD-related stress conditions. An in vivo mouse model of AD was established via continuous administration of 0.5% β-aminopropionitrile (BAPN) in drinking water for 28 days to induce medial degeneration and elastin fragmentation. In vitro, primary human aortic VSMCs were stimulated with angiotensin II (AngII) to replicate the inflammatory and stress environment observed in AD. To dissect the cell-type-specific functions of ATAD3A, we constructed a smooth muscle-targeted knockdown system using scAAV-ATAD3A-EnSM22a-EGFP and generated a systemic overexpression model by inserting a CAG-Atad3a-6xFlag-PolyA cassette into the H11 locus using CRISPR/Cas9 technology. Functional assessments included histological analysis, survival tracking, aortic diameter measurements, and mitochondrial function assays. Mitochondria–lysosome interactions were visualized and quantified by confocal microscopy. Protein interaction networks involving ATAD3A were elucidated through immunoprecipitation followed by mass spectrometry (IP-MS), co-immunoprecipitation (Co-IP), and proximity ligation assays. Mechanistic rescue experiments were performed using Devimistat, a clinically tested DLST-specific inhibitor.

Results:

Bioinformatic analysis revealed a dynamic expression profile of ATAD3A in human VSMCs upon AngII stimulation, with an initial downregulation followed by compensatory upregulation. This temporal expression pattern suggests a protective response mechanism during AD pathogenesis. In vivo, VSMC-specific knockdown of Atad3a significantly exacerbated AD incidence, aortic rupture, and mortality, whereas systemic overexpression of Atad3a markedly attenuated these phenotypes, including reduced aortic dilation and improved vascular integrity. Functional studies confirmed that ATAD3A preserves mitochondrial morphology, membrane potential, and ATP production, while limiting excessive mitochondria–lysosome tethering under stress conditions. Mechanistically, ATAD3A was found to interact with the LIAS/DLST protein complex via its 370–394 amino acid region, a sequence required for maintaining the complex's stability. Disruption of this interaction led to mitochondrial dysfunction and enhanced MCS formation. Importantly, we identified that lipoylation at lysine 110 (K110) on DLST promotes cuproptosis, a novel form of regulated cell death, and induces VSMC phenotypic switching toward a synthetic, pro-inflammatory state. Administration of Devimistat reversed these pathological changes, restoring mitochondrial homeostasis and reducing AD burden in both in vitro and in vivo settings.

Conclusion:

Our findings establish ATAD3A as a key regulator of mitochondrial–lysosomal communication in VSMCs and a critical protective factor in the context of aortic dissection. Through stabilization of the LIAS/DLST complex and suppression of aberrant DLST lipoylation, ATAD3A maintains mitochondrial function and inhibits pathological mitochondrial–lysosome contacts, thereby reducing vascular damage and remodeling. The ATAD3A–LIAS–DLST signaling axis represents a previously unrecognized mechanism contributing to vascular homeostasis and may serve as a promising therapeutic target for preventing or treating aortic dissection.

心血管 - 肾脏 - 代谢综合征 0-3 期人群中 C 反应蛋白 - 甘油三酯 - 葡萄糖指数与远期心脑血管疾病发病风险的关联研究

杨方坤

宁波大学附属第一医院

背景：心血管 - 肾脏 - 代谢（CKM）综合征是美国心脏协会近期提出的一种由代谢紊乱、心血管疾病和慢性肾脏疾病之间相互作用导致的全身性疾病。CKM 综合征可分为五期，其中 0-3 期为无风险或亚临床阶段，4 期为出现临床疾病阶段。胰岛素抵抗和系统性炎症是 CKM 综合征的重要病理生理学机制。以往的研究发现在 CKM 综合征 0-3 期人群中，胰岛素抵抗指标甘油三酯 - 葡萄糖（TyG）指数和系统性炎症指标 C 反应蛋白（CRP）与远期心脑血管疾病（CVD）的发病风险密切相关。而在近期的研究中提出了一个可以整合胰岛素抵抗和系统性炎症的综合指标：C 反应蛋白 - 甘油三酯 - 葡萄糖（CTI）指数。目前尚未有研究探索 CTI 指数在 CKM 综合征 0-3 期人群中与远期 CVD 的关联。此外，CTI 指数的动态变化与远期 CVD 的关联也有待进一步证实。

目的：在 CKM 综合征 0-3 期人群中探究 CTI 指数及其动态变化与远期 CVD 发病风险的关联。

方法：利用中国健康与养老追踪调查（CHARLS）的数据，根据纳入排除标准，最终纳入 8720 名符合要求的 CKM 综合征 0-3 期受试者。CTI 按如下公式进行计算： 0.412 × Ln (CRP [mg/L]) + Ln (甘油三酯 [mg/dl] × 空腹血糖 [mg/dl]/2)。CTI 的动态变化利用第二次调查时的 CTI 与基线 CTI 之差进行评估。基线 CTI 和 CTI 变化之差都按百分位数进行三等分位。利用 Cox 比例风险模型分析基线 CTI 和 CTI 变化之差与远期 CVD 发病风险的关联。

结果：在 CKM 综合征 0-3 期受试者中，基线 CTI 与 CVD 发病风险密切相关。与基线 CTI 下三分位数者相比，基线 CTI 上三分位数者其 CVD 发病风险显著增加（HR=1.20, 95%CI: 1.07-1.35, P=0.001）。对于连续性的基线 CTI，其每增加一个标准差，CVD 发病风险也显著增加（HR=1.08, 95%CI: 1.04-1.13, P<0.001）。此外，CKM 综合征 0-3 期受试者中的 CTI 变化之差也与 CVD 发病风险密切相关。与 CTI 变化之差下三分位数者相比，CTI 变化之差上三分位数者其 CVD 发病风险显著增加（HR=1.21, 95%CI: 1.01-1.46, P=0.039）。对于连续性的 CTI 变化之差，其每增加一个标准差，CVD 发病风险也显著增加（HR=1.07, 95%CI: 1.01-1.15, P=0.041）。

结论：在 CKM 综合征 0-3 期人群中，基线 CTI 和 CTI 变化之差都与远期 CVD 发病风险密切相关。基线 CTI 越大，CTI 变化增加越大，远期 CVD 发病风险越高。未来可将 CTI 指数纳入作为 CKM 综合征临床管理的一个重要指标。

吲哚类代谢物与心血管疾病研究进展

连少飞 任洁

山西白求恩医院（山西医学科学院）

目的

吲哚类代谢物是肠道菌群分解色氨酸产生的关键活性分子，近年被证实在心血管疾病（CVD）发生发展中起核心调控作用。本文聚焦近十年（2015-2025）研究，系统阐述吲哚 -3- 丙酸（IPA）、吲哚硫酸盐（IS）等主要代谢物在冠心病（CAD）、心力衰竭（HF）及高血压中的病理机制，评估其作为新型预警和预后标志物的潜力，并探讨干预策略。

方法

系统检索 PubMed、Web of Science 及 CNKI 数据库（2015-2025），关键词包括“吲哚代谢物”、“肠道菌群”、“心血管疾病”、“生物标志物”、“芳香烃受体（AhR）”。纳入机制研究、临床队列及干预性研究进行综述。

结果

关键代谢物的心血管效应与临床关联：保护性代谢物 IPA 通过激活 AhR-PPARγ 轴抑制血管炎症、增强内皮功能及 NO 生物利用度，显著减轻动脉粥样硬化斑块和心肌纤维化；而尿毒症毒素 IS 则通过 AhR-STAT3 通路促进内皮损伤和血管钙化。临床研究证实：CAD 患者血浆 IPA 水平显著降低，且与冠状动脉病变严重程度负相关，基线低 IPA 预示 3 年内主要不良心血管事件（MACE）风险增加。血清 IS 升高与冠脉钙化及斑块不稳定性独立相关，尤其在合并慢性肾病（CKD）患者中。心力衰竭研究显示：急性 HF 患者 IPA/IS 比值降低是 1 年全因死亡的强预测因子，其效能优于 NT-proBNP；射血分数降低型心衰（HFrEF）患者 IPA 浓度与左心室功能呈正相关。高血压队列中，顽固性高血压患者吲哚丙烯酸（IA）水平降低与血管僵硬度增加显著相关。

生物标志物价值：健康人群 IPA 持续低水平或 IS 升高可预测 5 年内 CVD 风险；CAD 患者血 IPA<0.8 μM 或 IS>15 μM 与心源性死亡风险增加 3 倍相关；HF 患者 IPA/IS 比值 <0.5 提示再住院风险升高 3.2 倍。代谢综合征患者 IPA/IS 比值降低可早于血管内皮功能障碍出现。

结论

吲哚类代谢物（IPA 降低、IS 升高）是 CVD 新型预警和预后评估标志物，其动态变化对风险分层具有重要价值。未来需建立标准化检测体系及临床截断值，并探索益生菌或 AhR 靶向干预策略。整合” 菌群 - 代谢物 - 宿主” 调控网络，为 CVD 精准防治提供新路径。

Prevalence of Cardiovascular-Kidney-Metabolic Syndrome by Social Determinants of Health: A Population-Based Study of 4.4 Million Adults in Northwestern China

Qian Zhao[1], Yi-Ning Yang[1]

1. First Affiliated Hospital of Xinjiang Medical University

2. People's Hospital of Xinjiang Uyghur Autonomous Region

Objective: Cardiovascular-kidney-metabolic (CKM) syndrome, recently defined by the American Heart Association as a novel, multistage, multisystem disorder, is highly prevalent in the United States. However, its prevalence in Northwestern China remains unknown. This study aims to investigate the stage-specific prevalence of CKM syndrome in a large adult population in Northwestern China. In addition, it explores the association between CKM syndrome and social determinants of health (SDOH), including socioeconomic status, education, and access to healthcare. Understanding these correlations may offer critical insights into regional disparities and inform targeted public health strategies for early detection and prevention of CKM syndrome.

Method: This cross-sectional study was based on the 2019 Northwest China Real-World and Population-Based Cohort, which covers nearly the entire population registered in community healthcare centers across the region. The dataset includes structured interviews, physical examinations, and laboratory measurements, as well as detailed information on SDOH, including education, marital status, occupation and health insurance. We included adults aged 18 years or older who underwent physical examination and fasting laboratory measurements. For each participant, we determined the CKM syndrome stage: stage 0 (no CKM risk factors, such as hypertension), 1 (excess or dysfunctional adiposity), 2 (additional metabolic risk factors or moderate- or high-risk chronic kidney disease), 3 (very high-risk chronic kidney disease or high predicted 10-year cardiovascular disease risk), or 4 (established cardiovascular disease, such as coronary artery disease). Advanced CKM syndrome stages were defined as stages 3 or 4 because these identify individuals with or at high risk of cardiovascular disease.

Results: The final study population included 4 458 471 adults. The mean (SD) age was 46.5 (16.4) years; 51.3%, women; 32.4%, Han; 49.6%, Uighur; 9.6%, Kazakh and 8.4%, other ethnicities. The prevalence of CKM stages 0 to 4 was 11.2% (95% CI, 11.1%-11.3%), 32.9% (95% CI, 32.8%-33.0%), 45.5% (95% CI, 45.4%-45.6%), 5.4% (95% CI, 5.4%-5.6%), and 4.9% (95% CI, 4.8%-5.0%), respectively. Han individuals were more likely to present with advanced stages compared to Uighur and Kazakh individuals (12.37% vs. 9.31% vs. 9.39%, P < 0.001). Compared with women, men were more likely to have advanced stages (12.8% vs 8.0%, P<0.001). Adults 65 years or older were more likely to have advanced stages than those younger than 65 years (34.3% vs 5.2%, P<0.001), Only 17.5% of adults aged 18 through 45 years had stage 0. Significant differences were observed in the prevalence of CKM stages across all unfavorable SDOH of interest compared with their favorable counterparts, with low literacy (22.7% vs. 3.9%), divorced or widowed (21.2% vs. 10.6%), and civil servant (12.5% vs. 8.5%) associated with an increased likelihood of advanced CKM stages.

Conclusion: In this large, population-based study of adults in Northwestern China, the prevalence of CKM was substantial, with nearly one in ten individuals exhibiting advanced-stage disease. The burden was disproportionately higher among men, older adults, Han individuals, and those exposed to unfavorable SDOH. These findings underscore the urgent need for region-specific prevention and intervention strategies that address both clinical risk factors and social vulnerabilities to mitigate the growing burden of CKM syndrome and its associated cardiovascular consequences.

阻塞性睡眠呼吸暂停在急性冠状动脉综合征中的预后意义：不同血糖水平的研究分析

张明瑞 [1] 郝问 [1] 郭倩 [1] 张飞宇 [1] 刘晓晨 [1] 陈雅婷 [1] 孔祥赟 [1] 王晓 [2] 聂绍平 [1]

1. 首都医科大学附属北京安贞医院

2. 中国医学科学院阜外医院

摘要

背景：本研究旨在评估不同血糖水平下，阻塞性睡眠呼吸暂停（OSA）对急性冠状动脉综合征（ACS）患者长期心血管预后的影响。

方法：该前瞻性队列研究（NCT03362385）纳入了因 ACS 住院并接受便携式睡眠监测的成年患者。OSA 被定义为呼吸暂停低通气指数≥ 15 次 / 小时。糖尿病前期定义为既往无糖尿病病史，糖化血红蛋白（HbA1c）5.7-6.4% 或空腹血糖（FPG）5.6-6.9mmol/L，糖尿病定义为 HbA1c ≥ 6.5% 或 FPG ≥ 7.0mmol/L 或既往诊断为糖尿病，糖尿病血糖控制不佳定义为既往诊断为糖尿病且 HbA1c ≥ 7.0%。主要终点为主要心血管和脑血管不良事件（MACCE），包括心血管死亡、心肌梗死（MI）、脑卒中、缺血驱动的血运重建或因不稳定型心绞痛（UA）或心力衰竭而住院。

结果：最终入组 1846 名患者，其中非糖尿病患者 371 人（20.1%），糖尿病前期患者 681 人（36.9%），糖尿病伴血糖控制良好患者 354 人（19.2%），糖尿病伴血糖控制不佳患者 442 人（23.9%）。平均随访 5 年，在非糖尿病患者中，OSA 组和非 OSA 组患者的 MACCE 发生率无统计学意义（aHR=0.95，95%CI 0.62-1.64，P=0.83）；在糖尿病前期患者中，OSA 患者的 MACCE 发生率较非 OSA 患者升高（HR=1.39，95% CI 1.04-1.85，P=0.03），多因素矫正后无统计学意义（aHR=1.30，95% CI 0.95-1.78，P=0.10）；OSA 组的 MACCE 发生率在糖尿病伴血糖控制不佳人群中明显升高 (aHR=1.54 , 95% CI 1.09-2.20; P=0.02)，但在糖尿病伴血糖控制良好的人群中无统计学意义（aHR=1.29，95% CI 0.85-1.98，P=0.23）。

结论：OSA 患者的血糖水平越高，其预后越差，即使是糖尿病前期的人群也因应注意 OSA 的诊治；而血糖控制好则能降低 OSA 带来的风险，提示 OSA 患者更应注意血糖管理。

The association between the heart rate response related to sleep apnea and left ventricular hypertrophy in obese individuals

Huang-Tao Ruan, Jin Liu, Xiao-Zhao Lu, Ning Tan, Ji-Yan Chen, Ling Wang, Zhi-Cheng Jing

Guangdong Provincial People's Hospital

Background: Obesity is accompanied by a variety of complications, among which the co-occurrence rate of OSA is as high as 69% and face a higher cardiovascular risk. The indices of heart rate response related to sleep apnea, include respiratory event index (REI), cardiac electrophysiology-respiratory event index (CEP-REI), heart rate burden (HRB), hypoxic burden (HB), ventilation burden (VB) indices, and heart rate variability (HRV) indices can not only be obtained through non-invasive methods during the screening process for OSA and reflects the cardiac autonomic nerve function and the regulatory ability of cardiopulmonary function, but also can be used to assess the severity of OSA and cardiovascular diseases. Meanwhile, the identification of structural and functional cardiac abnormalities can help us to recognize early and intervene in patients at high cardiovascular events risk. However, few studies have adequately evaluated the associations between indices of heart rate response related to sleep apnea and left ventricular (LV) hypertrophy in patients with obesity.

Methods: Obese patients undergoing nocturnal Holter electrocardiographic monitoring and home sleep apnea test (HSAT) from 2017–2021 were enrolled. Obesity was defined as a BMl ≥ 28 kg/m2 with ≥ 1 measure of excess adiposity (defined by waist circumference [WC] >88 cm for females, >102 cm for males; waist-to-hip ratio [WHR] >0.85 for females, >0.90 for males; or waist-to-height ratio [WHtR] >0.50 for all), or ≥ 2 measures of excess adiposity (WC, WHR, WHtR) regardless of BMl. Nocturnal HRV indices, CEP-REI and HRB index were analyzed and calculated from dynamic electrocardiogram data. Nocturnal HRV indices were specifically obtained from variation in the normal-to-normal intervals and divided into 3 subtypes based on frequency-domain spectrum, i.e., high frequency (HF, 0.15–0.5 Hz), low frequency (LF, 0.04–0.15 Hz), and very low frequency (VLF, 0.0033–0.04 Hz). REI, HB and VB indices were recorded by HSAT monitors. Echocardiography and N-terminal pro-brain natriuretic peptide (NT-proBNP) were assessed at admission. Study outcomes were left ventricular ejection fractions (LVEF), left ventricular mass index (LVMI), left atrial diameter (LA) and NT-proBNP. Generalized linear regression models were conducted to investigate the associations of sleep apnea indices with outcomes.

Results: A total of 1526 patients (mean age: 58.9 ± 10.9 years; 21.4% female) were enrolled. Generalized linear regression showed that subjects with elevated per SD HRB (β: -2.48, 95% CI: -3.02 to -1.94, p β: 2.78, 95% CI: 0.8 to 4.76, p = 0.006 for LVMI; β: -2.48, 95% CI: -3.02 to -1.94, p β: 176.85, 95% CI: 17.82 to 335.88, p = 0.029 for NT-proBNP), as well as those with elevated per SD LF/HF (β: 1.66, 95% CI: 1.13 to 2.2, p β: -5.18, 95% CI: -7.11 to -3.26, p β: -0.67, 95% CI: -0.91 to -0.44, p β: -392.97, 95% CI: -547.21 to -238.73, p NT-proBNP), were significantly associated with LV structure and function changes. The remaining indices did not show significant correlations in all the outcomes.

Conclusions: Among patients with obesity, elevated HRB and LF/HF associated with LV hypertrophy . In obese patients, heart rate response indices related to sleep apnea can be obtained through OSA screening. The hypertrophy in LV may be evaluated based on the degree of heart rate burden and the variability in cardiac autonomic nerve activity represented by HRB and LF/HF obtained through non-invasive methods.

中心动脉收缩压和血同型半胱氨酸对成年高血压患者卒中发生风险的联合作用

程 黄晓

南昌大学第二附属医院

背景与目的：

本研究旨在探讨中心收缩压（cSBP）和总同型半胱氨酸（tHcy）水平与新发脑卒中风险之间的关系，并进一步分析 cSBP 与 tHcy 是否在中国高血压成人人群中对脑卒中发生具有协同作用。

方法：

研究对象来自高血压与卒中防控项目（Hypertension and Stroke Prevention and Control Project，HSPCP）。共纳入 7,974 名在 2016 年 7 月至 10 月间登记的高血压患者，所有受试者在入组时无脑卒中或房颤病史。研究的主要结局为新发脑卒中，相关数据由当地疾病预防控制中心收集。cSBP 通过 A-PulseCASPro 设备进行无创测量。采用 Kaplan-Meier 生存曲线和 Cox 比例风险回归模型分析 cSBP、tHcy 与脑卒中的关联性。

结果：

在平均 4.4 ± 0.5 年的随访期间，共有 570 例（7.1%）受试者发生新发脑卒中，包括 501 例缺血性脑卒中、65 例出血性脑卒中以及 4 例未分类事件。研究人群平均年龄为 61 岁，男性 2,910 人（36.5%），平均体质指数（BMI）为 26.2 kg/m²，平均 cSBP 为 131.2 mmHg，平均 tHcy 水平为 12.7 μmol/L。将 cSBP 和 tHcy 作为连续变量分析时，每升高一个标准差（SD）（cSBP 为 12.6 mmHg）与新发脑卒中风险增加 16%、缺血性脑卒中风险增加 11% 相关。每升高一个 SD 的 tHcy（5.0 μmol/L）也分别与新发脑卒中和缺血性脑卒中风险增加 8% 和 9% 相关。Kaplan-Meier 曲线亦显示 cSBP 和 tHcy 水平升高与脑卒中发生呈正相关。与最低三分位组（T1）相比，cSBP 最高三分位组（T3）新发脑卒中和缺血性脑卒中风险显著升高，风险比（HR）分别为 1.37（95% CI: 1.11–1.69）和 1.29（95% CI: 1.03–1.62）。此外，处于高 cSBP 和高 tHcy 联合风险组的个体，其新发脑卒中风险增加 65%（HR：1.65；95% CI：1.29–2.13），明显高于最低风险组。

结论：

在这一社区人群为基础的高血压成人队列中，cSBP 和 tHcy 水平均与新发脑卒中和缺血性脑卒中风险呈独立且正向相关。研究结果提示，cSBP 与 tHcy 可能具有协同作用，共同升高脑卒中风险。这一发现强调在卒中预防和管理中，除常规肱动脉收缩压（SBP）外，评估 cSBP 的临床价值。

代谢性心血管疾病的综合管理：基于多学科协作的临床实践研究

张立佳

重庆荣昌区人民医院

目的：

代谢性心血管疾病（如糖尿病合并冠心病、代谢综合征相关高血压等）的发病率逐年上升，但其综合管理仍面临诊断延迟、治疗碎片化等问题。本研究旨在探讨多学科协作（MDT）模式对改善患者预后、降低心血管事件发生率的效果。

方法：

采用前瞻性队列研究设计，纳入 2022 年 1 月至 2024 年 6 月我院收治的 268 例代谢性心血管疾病患者，随机分为干预组（MDT 管理，n=134）和对照组（常规管理，n=134）。干预组由心血管科、内分泌科、营养科及护理团队共同制定个体化方案，包括药物治疗、生活方式干预及定期随访；对照组接受常规诊疗。主要终点为 1 年内主要心血管不良事件（MACE，包括心梗、卒中、血运重建或心血管死亡），次要终点包括血糖、血脂控制率及生活质量评分（SF-36）。

结果：

1. MACE 发生率：干预组显著低于对照组（8.2% vs 15.6%，P=0.032）。

2. 代谢指标：干预组 HbA1c 达标率（<7%）提高 23%（67% vs 45%，P<0.01），LDL-C 达标率（<1.8 mmol/L）提高 18%（62% vs 44%，P=0.008）。

3. 生活质量：干预组 SF-36 评分在生理功能（75.2±12.3 vs 63.8±11.6）及心理健康（70.5±9.3 vs 61.2±10.2）维度均优于对照组（P<0.05）。

4. 护理依从性：干预组患者随访完成率（91% vs 78%）及生活方式改善率（62% vs 42%）更高（P 均 <0.05）。

结论：

多学科协作模式能有效改善代谢性心血管疾病患者的代谢指标、降低心血管事件风险，并提升生活质量。护理团队在患者教育、随访管理和跨学科协调中发挥关键的作用。建议临床推广以护理为主导的 MDT 管理路径。

Hepatic Steatosis Index Predicts Risk of Chronic Non-Rheumatic Aortic Valve Insufficiency Rehospitalization in a Northwest Chinese NAFLD Cohort

Wei-Chao Liu[1]

新疆医科大学第一附属医院，新疆维吾尔自治区人民医院

Background

Non-alcoholic fatty liver disease (NAFLD) has emerged as an independent risk factor for cardiovascular diseases beyond traditional metabolic comorbidities. Chronic non-rheumatic aortic valve insufficiency (CAVI), characterized by progressive valvular degeneration and left ventricular volume overload, shares several pathophysiological mechanisms with NAFLD, including chronic systemic inflammation, oxidative stress, lipid accumulation, and insulin resistance. Due to the relatively low incidence and often subclinical nature of CAVI in the general population, research on its pathogenesis and epidemiological burden remains limited, particularly in large-scale Asian cohorts. The Hepatic Steatosis Index (HSI)–a simple, non-invasive, and cost-effective scoring system combining aspartate transaminase (AST), alanine transaminase (ALT), body mass index (BMI), sex, and diabetes mellitus status–has shown promise as a surrogate marker not only for hepatic steatosis but also for systemic metabolic dysfunction. Given the metabolic overlap between liver steatosis and valvular heart diseases, it is plausible that HSI may be associated with long-term CAVI risk. However, longitudinal evidence confirming this relationship, especially in Chinese populations, remains lacking. This study aimed to assess whether elevated HSI levels independently predict CAVI-related rehospitalization in a well-characterized Northwest Chinese cohort of adults diagnosed with NAFLD, using rigorous multivariable adjustment to account for a comprehensive panel of metabolic, anthropometric, and renal parameters.

Methods

We conducted a prospective cohort study of 265,038 adults with clinically diagnosed NAFLD across Northwest China (Xinjiang, enrollment period: January 2019 to December 2023). HSI was calculated using the validated formula: HSI = 8 × (ALT/AST ratio) + BMI (+2 if female; +2 if diabetes mellitus present). Participants were stratified into three groups based on HSI thresholds: Group 1 (HSI < 30, reference), Group 2 (30 ≤ HSI < 36), and Group 3 (HSI ≥ 36). The primary study endpoint was defined as rehospitalization for CAVI, confirmed using ICD-10 diagnostic codes after exclusion of rheumatic, congenital, or infective etiologies through clinical adjudication. Follow-up commenced at the date of cohort entry and continued until the first occurrence of CAVI rehospitalization, death, or December 31, 2023, whichever came first. Cox proportional hazards regression models were used to estimate hazard ratios (HRs) and 95% confidence intervals (CIs), with stepwise inclusion of the following prespecified covariates: age, sex, BMI, waist circumference, triglycerides, total cholesterol, systolic and diastolic blood pressure, serum creatinine, and blood urea nitrogen.

Results

Over a median follow-up of 635 days, 3,057 confirmed CAVI rehospitalizations occurred (overall incidence: 1.15%). After full adjustment for all covariates, Group 2 (30 ≤ HSI < 36) showed a non-significant 15.8% higher risk of CAVI rehospitalization compared to Group 1 (adjusted HR = 1.158, 95% CI: 0.926–1.449; p = 0.197). In contrast, Group 3 (HSI ≥ 36) exhibited a statistically significant 29.6% increased risk (adjusted HR = 1.296, 95% CI: 1.023–1.641; p= 0.032).

Conclusion

In this large-scale, population-based NAFLD cohort from Northwest China, an HSI score ≥ 36 independently predicted a 29.6% higher risk of CAVI-related rehospitalization after adjustment for a comprehensive panel of demographic, metabolic, and renal risk factors. These findings highlight the clinical utility of the HSI as an accessible tool for cardiovascular risk stratification in NAFLD populations. The results suggest that patients with elevated HSI scores may benefit from earlier echocardiographic screening and more aggressive metabolic interventions to prevent the progression of subclinical valvular dysfunction. Incorporating HSI into existing clinical workflows could enhance early identification of individuals at increased cardiovascular risk, especially in resource-limited settings. Future longitudinal and interventional studies across diverse populations are needed to validate these findings and explore whether HSI-guided strategies can reduce valvular complications and improve long-term cardiovascular outcomes in patients with NAFLD.

Keywords: Hepatic Steatosis Index, non-alcoholic fatty liver disease, chronic aortic valve insufficiency, Cox regression, cardiovascular risk, cohort study

基于 NHANES 数据库的膳食炎症指数与代谢综合征患者死亡风险的研究

雷娟[1] 罗晓升[1,2] 伍贵富[2]

1. 中山大学孙逸仙纪念医院

2. 中山大学附属第八医院

目的：膳食炎症指数（Dietary Inflammatory Index，DII）是评估饮食炎症潜力的一种工具， DII 分数越低被认为属于抗炎饮食。研究表明炎症反应与代谢综合征（MetS）的发病机制和预后相关。本研究旨在探讨 DII 与 MetS 患者全因死亡率的关系，为 MetS 患者的饮食指导提供理论依据。

方法：本研究使用来自美国国家健康和营养调查（NHANES 2007-2016）数据库（www.cdc.gov/nchs/nhanes/index.htm）中 50588 位患者筛选出 2573 名符合 MetS 诊断的患者，通过构建加权 Cox 比例风险模型评估 MetS 患者 DII 水平与全因死亡率（通过国家死亡指数 NDI 公共数据集 https：//www.cdc.gov/nchs/data-linkage/mortality-public.htm 采集）之间的关系。并研究 DII 与 MetS 各组分全因死亡率之间的关系。

结果：在 2573 名 MetS 患者中，DII 范围为 -4.52 至 4.71，有 398 例患者在随访期间死亡，中位随访时间 101 个月。在校正的加权 Cox 比例风险模型中 DII 与 MetS 患者全因死亡率呈正相关（HR：1.50，P=0.028），这种关系在血压升高的患者中更为显著（HR：2.34，P=0.005）。RCS 曲线显示 DII 水平和全因死亡率为线性相关（p- 非线性 =0.69）。

结论：DII 与 MetS 患者死亡率呈正相关，提示促炎饮食会增加 MetS 患者的死亡风险。本研究为 MetS 患者的健康饮食指导提供了证据。

Association of Depression Severity and Transition Patterns of Cardiometabolic Multimorbidity

Jiya Zhang[1,2], Yongfu Yu[1,2]

1. NHC Key Laboratory for Health Technology Assessment, School of Public Health, Fudan University, Shanghai, China

2. Department of Biostatistics, School of Public Health, Fudan University, Shanghai, China

Abstract

Objective:

Cardiometabolic multimorbidity (CMM), defined as the coexistence of two or more of type 2 diabetes, heart disease, and stroke, is increasingly prevalent in Asian populations, especially in China. Depression has been recognized as a psychosocial risk factor for cardiometabolic diseases, but the effect of depression severity on the development and progression of CMM remains understudied. This study aimed to examine the associations between depression severity and the incidence and progression of CMM in a nationally representative cohort of middle-aged and older Chinese adults.

Methods:

We analyzed data from 12,059 participants aged ≥ 45 years without baseline cardiometabolic diseases from the China Health and Retirement Longitudinal Study (CHARLS), a nationally representative prospective cohort. Depression severity was assessed using the 10-item Center for Epidemiological Studies Depression (CES-D-10) Scale and categorized as none (<10), mild-moderate (10–19), or severe (≥ 20). Outcomes included the incidence of FCMD (type 2 diabetes, heart disease, or stroke), CMM (diagnosis of a second cardiometabolic condition), and death. Self-reported disease diagnoses were confirmed through repeated follow-up interviews. Cox proportional hazards models estimated the association of depression severity with FCMD and CMM incidence. Multi-state Markov models were used to examine five transitions: from health to FCMD, health to death, FCMD to CMM, FCMD to death, and CMM to death, accounting for competing risks. Covariates included sociodemographic characteristics, smoking and drinking status, BMI, physical activity (MET-min/week), and hypertension status. Subtype analyses examined transitions between individual disease types (e.g., diabetes to CMM). Sensitivity analyses excluded early incident cases and individuals with baseline cancer.

Results:

During a median follow-up of 7 years, 2,080 participants developed FCMD and 305 developed CMM. Compared to individuals without depression, those with mild-moderate (HR: 1.22, 95% CI: 1.11–1.34) and severe depression (HR: 1.46, 95% CI: 1.24–1.73) had a higher risk of developing FCMD. Only severe depression was associated with a significantly increased risk of CMM (HR: 2.08, 95% CI: 1.42–3.04). Multi-state modeling showed both mild-moderate and severe depression increased the risk of transitioning from health to FCMD (HRs: 1.19 and 1.42, respectively) and from health to death (HRs: 1.35 and 1.76, respectively). However, only severe depression was linked to the transition from FCMD to CMM (HR: 1.55, 95% CI: 1.05–2.27). No significant associations were found for transitions from FCMD or CMM to death.

In disease subtype analyses, severe depression was significantly associated with increased risks of type 2 diabetes (HR: 1.49), heart disease (HR: 1.58), and stroke (HR: 1.65), while mild-moderate depression was associated only with heart disease (HR: 1.33). Among disease progression pathways, severe depression notably increased the risk of transitioning from diabetes to CMM (HR: 3.76), but not from stroke or heart disease.

Conclusion:

In conclusion, both mild-moderate and severe depression were significantly associated with an increased risk of FCMD, particularly heart disease. However, only severe depression was linked to a higher risk of CMM onset and progression from a single cardiometabolic disease to CMM among middle-aged and older adults in China. These findings highlight the potential benefit of incorporating depression screening and management into cardiometabolic disease prevention strategies, especially for individuals with severe depression. Targeted interventions addressing depression may contribute to delaying or preventing the development of CMM.

Causal Association Spectrum of Fine Particulate Matter ($PM_{2.5}$) Exposure and Cardiometabolic Diseases: Analysis of Dose-Response Characteristics in Epidemiological Associations, Population Susceptibility Stratification, Cascade Reaction Pathways of Cellula

Ying-Hui Wang, Xue-Ping Huang

Fujian Medical University Union Hospital

Background and Objective:Air pollution, specifically fine particulate matter ($PM_{2.5}$), constitutes a major global environmental health threat with profound implications for cardiometabolic health. This study synthesizes the current evidence to systematically investigate the causal relationships between $PM_{2.5}$ exposure and a spectrum of cardiometabolic diseases (CMDs), including type 2 diabetes (T2D), obesity, metabolic syndrome, and cardiovascular diseases (CVDs). It aims to: (1) Quantify the global epidemiological burden using robust metrics; (2) Characterize dose-response relationships and identify susceptible populations; (3) Elucidate the underlying pathophysiological mechanisms at cellular and molecular levels; and (4) Evaluate the efficacy of interventions across individual, community, and policy scales. The ultimate goal is to provide a consolidated scientific foundation for mitigating the CMD burden attributable to air pollution.

Methods: We conducted a comprehensive evidence synthesis utilizing diverse data sources and methodologies. Global exposure levels and disease burden attributable to $PM_{2.5}$ and related air pollutants from 1990 to 2019 were analyzed using data from the Global Burden of Disease (GBD) Study. This was augmented by systematic integration of findings from large-scale prospective cohort studies, meta-analyses, and randomized controlled trials (RCTs). Analyses focused on key CMD outcomes: incidence and prevalence of T2D and obesity, metabolic syndrome, CMD-related mortality, and Disability-Adjusted Life Years (DALYs). Dose-response meta-analysis techniques were employed to quantify exposure-risk relationships and identify potential risk thresholds. Susceptibility factors (e.g., socioeconomic status, sex, pre-existing conditions) were examined through stratification analyses. Mechanistic insights were derived from experimental and clinical studies investigating pathways such as systemic inflammation, oxidative stress, autonomic nervous system dysfunction, and hypothalamic-pituitary-adrenal (HPA) axis dysregulation. Intervention efficacy was assessed, particularly focusing on air purification technologies and policy-driven air quality improvements.

Key Results:

1. Global Burden: An overwhelming 99% of the global population resides in areas exceeding the WHO $PM_{2.5}$ guideline (annual mean

2. Dose-Response Relationships: A robust, positive dose-response relationship exists between $PM_{2.5}$ exposure and T2D risk. For every 10 μg/m^3 increment in $PM_{2.5}$ concentration, the hazard of developing T2D increases by 15% (Hazard Ratio, HR = 1.15). Critically, significant health risks persist even at concentrations below the WHO guideline level of 5 μg/m^3, indicating no safe threshold.

3. Susceptible Populations: Individuals with lower socioeconomic status, males, and those with pre-existing metabolic conditions exhibit heightened susceptibility to the cardiometabolic effects of $PM_{2.5}$.

4. Disease Associations: Beyond T2D, $PM_{2.5}$ exposure is significantly associated with increased risks of obesity (Odds Ratio, OR = 1.28), elevated diabetes-related mortality (HR = 1.49), and heightened risk of cardiovascular complications.

5. Pathophysiological Mechanisms: $PM_{2.5}$ exerts its detrimental cardiometabolic effects through interconnected biological pathways:

Systemic Inflammation: Triggering the release of pro-inflammatory cytokines (e.g., Interleukin-6 (IL-6), C-reactive protein (CRP)).

Oxidative Stress: Inducing cellular damage through reactive oxygen species (ROS) generation.

Neuroendocrine Dysregulation:Disrupting autonomic nervous system balance (sympathetic overactivation, parasympathetic suppression) and impairing HPA axis function.

These cascades collectively promote insulin resistance, endothelial dysfunction, metabolic imbalance, and ultimately contribute to the development and progression of T2D, obesity, and CVD.

6. Intervention Efficacy:RCTs provide evidence that personal-level interventions, specifically the use of effective air purifiers in indoor environments, can yield measurable short-term benefits. These include reductions in systolic and diastolic blood pressure and decreases in circulating inflammatory biomarkers. This supports the potential for acute improvements in metabolic parameters upon exposure reduction.

Conclusion:This comprehensive analysis establishes $PM_{2.5}$ air pollution as a major, pervasive, and preventable environmental risk factor for the global cardiometabolic disease pandemic. Its adverse impacts are widespread, exhibit cumulative effects over time, and disproportionately burden vulnerable populations. The evidence underscores the urgent need for coordinated, multi-level public health strategies to mitigate exposure and disease burden:

Policy Level: Implementing stringent air quality regulations aligned with health evidence (lowering $PM_{2.5}$ standards), accelerating the transition to clean energy sources, and integrating air quality goals into climate change mitigation policies for synergistic benefits.

Community/Urban Planning Level:Designing healthier cities prioritizing reduced traffic emissions, green spaces, and sustainable transportation to lower ambient pollution.

Individual Level: Promoting awareness and access to effective personal protection measures, such as high-efficiency indoor air filtration, especially for high-risk groups in heavily polluted areas.

Addressing air pollution is not only an environmental imperative but a crucial intervention for improving global cardiometabolic health and achieving significant reductions in the burden of diabetes, cardiovas-

cular disease, and related conditions. Sustained commitment across all societal levels is essential.

蛋白尿在心血管代谢因素与视网膜动脉硬化关联的中介效应分析

孔羽 [1] 刘昕蕊 [1,2] 马长生 [1,2]

1. 首都医科大学附属北京安贞医院

2. 国家心血管疾病临床医学研究中心

【目的】在新兴的心血管 - 肾脏 - 代谢（cardiovascular-kidney-metabolic，CKM）综合背景下，蛋白尿作为 CKM 关键生物标志物之一，其在 CKM 中的潜在关联尚未完全阐明。本研究旨在 CKM 特定人群中，探讨蛋白尿是否介导了心血管代谢风险因素与视网膜动脉血管损伤（以动脉硬化为表现）之间的关联。

【方法】本研究为横断面观察性设计，基于一项全国多中心横断面注册研究（PLACARD STUDY），纳入来自全国 30 家二 / 三级医院心内科门诊 / 住院的、确诊为 2 型糖尿病且合并≥ 1 种常见心血管疾病患者，共 2,487 名患者。采用因果逐步回归中介效应模型，分析血压（收缩压、舒张压、脉压）、血脂（总胆固醇、低密度胆固醇、高密度胆固醇、甘油三酯等）、血糖（空腹血糖、糖化血红蛋白等）、体重指数等主要心血管代谢因素，通过蛋白尿（以尿白蛋白 / 肌酐比 [UACR] 评估）影响眼底视网膜动脉硬化的中介路径。采用非参数百分位 Bootstrap 抽样（1,000 次重复）估计 95% 置信区间，所有分析均校正了年龄、性别等协变量。

【结果】 研究人群平均年龄 64.5±10.5 岁，男性占比 57.7%，高血压患病率 86.1%，冠心病占 45.1%。其中，中介效应分析显示，蛋白尿在多个病理通路中发挥关键作用：（1）舒张压完全通过蛋白尿影响眼底动脉硬化。UACR 间接效应显著（效应量 =0.0028, 95% CI: 0.0003–0.0064），直接效应无统计学意义（P=0.068），提示蛋白尿发挥完全中介作用。（2）脉压（间接效应量 =0.0015, 95% CI: 0.0001–0.0038）与糖化血红蛋白（间接效应量 =0.0078, 95% CI: 0.0004–0.0233）通过蛋白尿部分介导其对眼底视网膜动脉硬化的影响。然而，收缩压（效应量 =-0.0002, 95% CI: -0.0016–0.0046）、总胆固醇（效应量 =0.0017, 95% CI: -0.0018–0.0082）及体质指数等代谢指标与眼底视网膜动脉硬化损伤之间未发现 UACR 的显著中介路径。

【结论】在 2 型糖尿病合并心血管疾病的 CKM 人群中，蛋白尿是连接心血管代谢紊乱与视网膜微血管损伤的关键中介因子。舒张压、脉压及糖化血红蛋白通过加剧蛋白尿而促进视网膜眼底动脉硬化。监测并早期干预 UACR 可能是延缓 CKM 人群心血管事件的重要靶点。

Impact of the mismatch between respiratory event frequency and hypoxic burden on cardiovascular outcomes in patients with obstructive sleep apnea

Jia-Qi Du[1], Wei Gong[2], Shao-Ping Nie[1]

1. Beijing AnZhen Hospital, Capital Medical University

2. Peking University

Background: The mismatch between respiratory event frequency and hypoxic burden is a special subtype of obstructive sleep apnea (OSA), and it is unclear whether its clinical characteristics and cardiovascular outcomes are different.

Methods: This study enrolled 3754 adult OSA patients from the prospective cohort study-Sleep Heart Health Study. Respiratory event frequency and hypoxic burden were assessed using the apnea-hypopnea index (AHI) and the percentage of time spent with oxygen saturation below 90% (T90), respectively. Patients were categorized into three groups based on the matching of AHI and T90: the matched group, the AHI-dominant group, and the T90-dominant group. Cox regression analysis was used to explore the association between AHI-T90 matching status and major adverse cardiovascular events (MACE), defined as a composite of cardiovascular death, myocardial infarction, heart failure, and revascularization. Kaplan-Meier survival analysis was performed to compare the prognosis among the groups.

Results: Among the 3754 OSA patients, 1745 (46.5%) exhibited an AHI-T90 mismatch. Kaplan-Meier curves showed that the incidence of MACE was significantly higher in the mismatch groups compared to the matched group. Cox regression analysis demonstrated that AHI-T90 matching status was an independent predictor of MACE. Restricted cubic spline revealed that the risk of MACE was lowest when the relative difference between AHI and T90 was minimal.

Conclusion: Mismatch between respiratory event frequency and hypoxic burden represents a distinct OSA phenotype associated with a higher incidence of MACE.

心脏康复及有关研究

心脏康复护理对心梗介入治疗后患者心理状态及生活质量的影响

袁星娟

西安交通大学第一附属医院

【摘要】目的 探究心梗介入治疗的患者应用心脏康复护理对心理状态及生活质量的影响。方法 从本院收治的心梗患者中选取总计 76 例心梗患者参与研究，于 2024 年 1 月 -2025 年 1 月在本院行介入手术。以入院日期先后顺序为标准将患者分成各 38 例的两组。常规组年龄段 52-77 岁，均值（61.35±4.08）岁，20 例为女性、18 例为男性，梗死部位：11 例下壁、12 例前壁、15 例侧壁。试验组年龄段 54-75 岁，均值（61.05±4.33）岁，19 例为女性、19 例为男性，梗死部位: 10 例下壁、11 例前壁、17 例侧壁。上述基础资料组间无差异（P > 0.05）。根据入院日期先后顺序进行分组，为 38 例试验组患者提供心理康复护理服务，为 38 例常规组患者提供一般性护理服务。比较康复效果。结果 试验组 7 天后的焦虑和抑郁评分明显降低，降低程度大于常规组，差异显著（P < 0.05）。试验组 1 个月后的生活质量评分高于常规组，差异显著（P < 0.05）。心血管不良事件发生率试验组（2.63%）低于常规组（15.79%），差异显著（P < 0.05）。结论 心梗介入治疗后尽早展开心脏康复护理，可以更好的改善患者心理状态及生活质量，还能预防心血管不良事件。在实际应用过程中，为了保证患者的安全，需要严格把握终止运动指征，包括：运动中自感非常疲劳；出现大汗、面色苍白、眩晕、心悸、气短、胸闷、心绞痛、严重心律失常等症状；舒张压突然下降或升高 10mmHg；收缩压突然下降或升高 20mmHg；每分钟心率在 110 次以上。值得借鉴应用。

急性心肌梗死患者开展早期康复训练对心功能恢复影响

袁星娟

西安交通大学第一附属医院

摘要：目的：探讨急性心肌梗死患者在接受标准治疗基础上，实施早期康复训练对心功能恢复的作用。分析其对左心室射血分数、运动耐力及心肌酶谱恢复等关键指标的影响，旨在为后续康复方案的优化提供临床依据。方法：研究纳入 2024 年 1 月至 12 月收治的 60 例首次发病的急性心肌梗死患者。采用随机数字表法分组，对照组给予常规治疗与护理。实验组在此基础上制定个体化的早期康复训练计划，包括床旁活动、步行锻炼及心肺功能指导。干预周期设定为三个月，定期评估心功能指标与运动能力变化。结果：干预 1 个月与 3 个月时，实验组左心室射血分数分别为 50.2±3.7 与 55.6±4.1，明显优于对照组（45.8±3.5 与 48.2±3.8）。6 分钟步行距离亦显示出显著差距，实验组在两个时间节点均优于对照组，差值具临床意义。心肌酶谱恢复时间方面，实验组表现出更快的下降趋势，提示组织损伤恢复更为迅速。结论：早期康复训练在急性心肌梗死恢复期具备确切价值，能够在维持血流动力学稳定的同时，促进心脏收缩功能与体力恢复。该干预模式不仅改善运动耐受，还可能通过降低心肌代谢负荷，加速心肌修复进程。研究提示，应将早期康复纳入标准化治疗路径中，为个体化心脏康复提供有力支持。

老年冠心病患者 CPET 指导的运动康复方案优化研究

呼佳蓉

西安交通大学第一附属医院

目的：探讨基于心肺运动试验（CPET）的个体化运动康复方案对老年冠心病患者心肺功能、运动耐力和生活质量的改善效果，并评估其临床应用价值。

方法：采用多中心、随机对照试验设计，纳入 2023 年 1 月至 2024 年 6 月就诊的老年冠心病患者 260 例，随机分为对照组（n=130）和干预组（n=130）。对照组接受常规药物治疗和基础运动建议（每日步行 30 分钟）；干预组在对照组基础上，采用 CPET 测试（包括 VO_2 peak、无氧阈值等指标）制定个体化运动处方，包括有氧训练（80%-90% 无氧阈值强度，3 次 / 周）、抗阻训练（2 次 / 周）和柔韧性训练（5 次 / 周）。主要观察指标为干预 6 个月后的峰值摄氧量（VO_2 peak）和 6 分钟步行距离（6MWD），次要指标包括 NT-proBNP 水平、中国心血管病人生活质量评定问卷（CQQC）评分和心血管不良事件发生率。

结果：干预组 VO_2 peak 较基线显著提高 21.3%（P<0.01），显著高于对照组的 9.5%；6MWD 增加 119.26 米，显著优于对照组的 65.73 米（P<0.01）。生活质量方面，干预组 CQQC 评分（111.66±7.93）显著高于对照组（84.16±6.96，P<0.01）。安全性方面，干预组心血管不良事件发生率为 3.85%，显著低于对照组的 13.85%（P=0.005）。

结论：基于 CPET 的个体化运动康复方案能显著改善老年冠心病患者的心肺功能、运动耐力和生活质量，同时降低心血管不良事件发生率。该方案具有临床推广价值，未来可结合远程监测技术进一步优化实施策略。

肌少症的研究进展：从机制到治疗

赵兰婷 张兆国 张萍

北京清华长庚医院

随着全球人口老龄化进程的加速，肌少症作为一种与衰老密切相关的疾病，其发病率逐年上升，对老年人的健康和生活质量产生了严重影响，深入了解肌少症的发病机制，建立有效的评估诊断方法和防治策略，具有重要的现实意义。

目的 本文旨在全面综述肌少症的相关研究进展，对肌少症的定义、流行病学特点、发病机制、临床表现、评估诊断方法以及防治措施等方面综述。

方法 文献综述

结果 肌少症目前根据 GLIS 第一次提出全球统一概念，为后续研究奠定基础。肌少症的发病机制复杂，涉及增龄相关的多系统交互作用，包括神经肌肉退变、血管改变，细胞外基质改变、免疫炎症、离子失衡等。此外遗传与环境因素也有同程度的影响，诊断主要基于肌肉质量、力量和躯体功能的评估，对高危人群的早期筛查是诊断的第一步。防治措施需要综合干预，包括运动干预、营养支持、药物治疗等。运动干预尤其抗阻训练是一线干预措施，营养干预、药物治疗是目前研究的重点。

结论 早期通过问卷筛查和客观评估识别风险人群，及时实施抗阻运动联合高蛋白饮食的综合干预，可有效延缓肌肉衰减、改善生活质量。未来需加强诊断标准统一、药物研发和社区科普，以应对人口老龄化带来的肌肉健康危机。肌少症是一个活跃的研究领域，新兴疗法前景广阔，未来几年肌肉减少症的治疗方案很可能将迎来快速变革。

心磁图在缺血性心脏病的临床研究进展

关添允

吉林大学第二临床医院

心磁图仪，是一套基于量子精密测量技术的用于心肌缺血的辅助成像诊断过程中，采集、记录人体心脏的磁场信号。系统通过超高灵敏度的量子磁力传感器，在人体外表面靠近心脏位置采集、记录人体心脏电生理活动产生的微弱磁场，并通过信号处理和数据分析，生成高精度磁场图像，以及心磁参数，提供给专业医务人员诊断被检测者的心脏健康状况。

心磁图临床应用场景包括：（1）早期心肌缺血筛查，健康人群心脏体检；（2）因冠状动脉狭窄引起的心肌缺血的辅助诊断，弥补现有无创检查的不足；（3）因心肌缺血引起的胸痛甄别，尤其是急性胸痛的快速鉴别。此外，还可用于临床科学研究包括：（1）缺血性心脏病预后长期观测；（2）房颤、室早等电生理异常病灶定位（3）心脏病药物治疗效果长期监测。

鉴于心磁图在心肌缺血诊断中的潜在优势，国内外学者开展了大量临床评价研究，以验证心磁图在心肌缺血诊断中的准确性和可靠性。心磁图作为一种新兴的心电生理检测技术，通过测量心脏磁场的变化，心磁图能够反映心肌的电生理活动异常，为心肌缺血的诊断提供了新的手段。然而，心磁图在心肌缺血诊断中的应用仍处于起步阶段，尚需进一步的临床验证和优化。未来，随着心磁图技术的不断发展和完善，其在心肌缺血诊断中的应用前景将更加广阔。

急性冠脉综合征患者 PCI 术后接受心脏综合康复治疗的效果观察

何小琴

西安交通大学医学院第一附属医院

目的：观察急性冠状动脉综合征患者经皮冠状动脉介入术后接受心脏康复治疗对心功能和生活质量的影响。

方法：采取便利抽样法，选取本院心血管内科住院接受 PCI 治疗的 108 例急性冠状动脉综合征患者作为研究对象，分为对照组和观察组，各 54 例。对照组采用常规护理治疗，观察组在对照组的基础上采用心脏康复护理治疗。两组均治疗 3 个月。比较两组治疗前后心脏康复的掌握程度（心脏康复认知调查量表）、运动耐力（6 分钟步行试验）、自我管理能力 [冠心病自我管理行为量表（CSMS）]、心功能（左心室射血分数、每搏输出量、心输出量）、生活质量（生活质量评价量表 SF-36）。采用独立样本 t 检验、配对 t 检验和 X^2 检验。

结果：治疗后，观察组心脏康复掌握程度 [(61.58±2.85) 分]、运动耐力 [(498.67±28.36)m]、自我管理能力 [(83.87±3.75) 分]、均优于对照组 [(56.43±3.65) 分]、[(464.78±32.46)m]、[(79.46±4.27) 分](均 p < 0.05）；观察组左心室射血分数 [(67.49±1.76)%] 与心输出量 [(7.17±0.56)L/min] 均高于对照组 [(64.52±1.81)%、(6.58±0.68) L/min]、观察组每搏输出量 [(63.12±1.98)ml] 高于对照组 [(61.27±1.51)ml]（均 p < 0.05）；观察组生活质量评分（8 个维度）均高于对照组（P < 0.05）。

结论：心脏综合康复治疗在急性冠状动脉综合征患者行 PCI 术后中疗效确切，可有效改善患者心功能，提高生活质量，该疗法值得临床推广、应用。

重视心肌梗死后抑郁症

于雲鹏

吉林大学第二医院

摘要：急性心肌梗死是临床多发的心血管危重症，抑郁症是心肌梗死后的常见问题，并对心梗患者的预后和生存率起着关键作用。心肌梗死后抑郁症正越来越为临床医生所重视，本文从其发病机制，诊断和治疗角度做一综合阐述。抑郁症是急性心肌梗死后的常见问题，其与心梗患者的预后密切相关，并可显著影响心梗的诊断、治疗和康复。国外研究发现心梗后抑郁症患者心脏性死亡风险较对照组增高 2.4 倍，新发心血管事件风险为对照组的 2 倍 [1]。由于检测方法不同，心梗患者住院期间抑郁症的患病率为 7.2%–41.2%，总体来说，综合各项资料，平均每 5 个初次住院的心梗患者，就有 1 个在住院期间患上抑郁症 [2]。抑郁与心梗患者死亡率存在显著的统计学和临床相关性，抑郁程度与死亡率存在线性关系 [3]。忽视心梗后抑郁，将会导致患者频繁就医、社会功能受损、依从性下降、死亡率上升等不良后果。近年来，随着“双心医学”的发展，心梗后抑郁越来越多的被临床医生所认同和重视。抑郁症是心境障碍的主要类型，以显著而持久的心境低落为临床特征。临床可见其心境低落与处境不相称，闷闷不乐、自卑、甚至悲观厌世，可有自杀行为或企图，部分患者可有木僵、幻觉、妄想等。目前认为抑郁症的主要病因是 5- 羟色胺和儿茶酚胺类神经递质不足，下丘脑–垂体–肾上腺皮质轴激活，以及免疫机能紊乱。而急性心梗患者急慢性应激、免疫系统激活，导致炎性细胞因子释放增加，其通过影响下丘脑–垂体–肾上腺皮质轴和 5–羟色胺合成等机制引起抑郁发生 [4]。国外最新研究表明，心梗后产生的炎症因子可能与抑郁相关，尤其是 IL17a 可能在心梗后发生抑郁的过程中发挥了重要作用 [5]。

心脏康复延伸护理服务 联合正念减压对慢性心力衰竭患者心脏康复效果及负面情绪的影响

杜佳

西安交通大学第一附属医院

摘要：目的 分析心脏康复延伸护理服务联合正念减压训练用于慢性心力衰竭患者对其心脏康复效果及负面情绪的影响。方法 选择 2024 年 2 月至 2025 年 2 月西安交通大学第一附属医院心血管内科接受诊治的慢性心力衰竭患者 206 例，采取随机分组法分为对照组和观察组，每组 103 例。对照组采用常规干预，观察组采用心脏康复延伸护理服务联合正念减压训练。对比 2 组心功能指标、心脏慢性监护室入住时间、总住院时间、不良情绪评分、依从率。结果 观察组左心室射血分数 (LVEF) 高于对照组，左心室舒张末期内径 (LVEDD)、左心室收缩末期内径 (LVESD) 低于对照组，差异均有统计学意义 (P<0.05)。观察组焦虑自评量表 (SAS 评分)、抑郁自评量表 (SDS 评分) 低于对照组，差异有统计学意义 (P<0.05)。观察组心脏慢性监护室入住时间、总住院时间短于对照组，差异有统计学意义 (P<0.05)。观察组总依从率为 95.26% 高于对照组的 71.70%，差异有统计学意义 (P<0.05)。结论 心脏康复延伸护理服务联合正念减压训练用于慢性心力衰竭患者可改善其心功能，提高康复效果，改善不良情绪，提高依从性，促使患者养成一系列对心脏康复有益的健康行为。

心力衰竭患者健康心理控制源与领悟社会支持和自我管理行为的关系：基于多项式回归和响应面分析

陶秀 [1] 高敏 [2] 吴凡 [1] 卢静 [1] 李芸霞 [1] 王琴 [2] 孙国珍 [1]

1. 南京医科大学

2. 南京医科大学第一附属医院

目的：探讨心力衰竭患者健康心理控制源特征，及其与领悟社会支持和患者自我管理行为的关系，为医护人员制定相关措施以提高患者自我管理水平、改善患者预后提供参考。

方法：采用横断面调查法，便利选取 2024 年 7 月–12 月在南京市某三级甲等综合医院心血管内科住院的 310 例心力衰竭患者为作为调查对象，采用一般资料调查表、多维度健康心理控制源 C 版量表、领悟社会支持量表及心力衰竭患者自我管理量表进行调查。采用多项式回归和响应面分析探讨患者健康心理控制源、领悟社会支持和自我管理行为的关系。

结果：心力衰竭患者的健康心理控制源内部控制、机遇控制、医生控制及他人控制维度得分分别为：（4.13±0.71）、（2.52±0.68）、（5.04±0.52）、（3.46±0.81）分。响应面分析结果显示，患者自我管理水平随健康心理控制源和领悟社会支持一致性近乎直线式增高，与低心理控制源 - 低领悟社会支持相比，高心理控制源 - 高领悟社会支持的患者自我管理水平更高（Z-hat 检验 P < 0.01）；自我管理水平随健康心理控制源和领悟社会支持不一致性呈现“凸形”曲线式增高，与低心理控制源 - 低领悟社会支持相比，高健康心理控制源 - 低领悟社会支持和低健康心理控制源 - 高领悟社会支持的患者其自我管理行为均更好（Z-hat 检验 P < 0.01）。

结论：心力衰竭患者领悟社会支持与自我管理行为处于中等水平，健康心理控制源倾向于医生控制，不同健康心理控制源与领悟社会支持水平的患者自我管理水平存在相对差异，提示医护人员应以患者信任为契机，借助个体健康意识觉醒的催化作用，提升其内部控制型健康心理控制源倾向，同时借助患者多方社会支持力量，共同帮助心力衰竭患者形成并维持持久的自我管理行为。

急性心肌梗死介入术后患者早期心脏康复参与意愿及其影响因素研究

文眉丹

西安交通大学医学院第一附属医院

目的

急性心肌梗死（AMI）患者经皮冠状动脉介入治疗（PCI）后，早期心脏康复（CR）是改善预后、降低再入院率的关键措施。然而，临床中患者参与率普遍较低。本研究旨在探讨 AMI 介入术后患者对早期 CR 的参与意愿，并分析其影响因素，为制定针对性干预策略提供依据。

方法

采用横断面调查研究设计，于 2023 年 1 月至 2024 年 6 月纳入某三级甲等医院心内科收治的 AMI 行 PCI 术后患者 300 例。通过问卷调查收集患者社会人口学资料（年龄、性别、教育水平、经济状况等）、临床特征（梗死部位、并发症、LVEF 值等）、心理状态（HADS 焦虑抑郁量表）、疾病认知（自编 CR 知识问卷）及社会支持（SSRS 量表）。采用多元线性回归分析影响患者 CR 参与意愿的主要因素，并通过结构方程模型（SEM）探讨各变量间的路径关系。

结果

1. 参与意愿现状：仅 58.3%（175/300）的患者表示愿意参与早期 CR，41.7% 存在犹豫或拒绝。

2. 影响因素分析：

积极因素：高教育水平（β=0.21, p<0.01）、家庭支持度高（β=0.33, p<0.001）、疾病认知良好（β=0.28, p<0.001）与参与意愿呈正相关。

阻碍因素：高龄（≥ 65 岁，β=-0.18, p<0.05）、合并心力衰竭（β=-0.15, p<0.05）、焦虑抑郁（β=-0.24, p<0.01）显著降低意愿。

3. 路径分析：社会支持通过提升疾病认知（间接效应值 0.12）和缓解负面情绪（间接效应值 0.09）间接增强参与意愿（总效应值 0.42）。

结论：

AMI-PCI 术后患者早期 CR 参与意愿仍不理想，受年龄、心理状态、疾病认知及社会支持等多因素影响。临床应针对高龄、心理障碍及低认知患者制定个性化干预措施，如加强 CR 宣教、心理疏导及家庭支持，以提高参与率，改善长期预后。

中西医结合心脏康复对稳定性冠心病患者心肺功能影响的临床研究

文眉丹

西安交通大学医学院第一附属医院

目的：

探讨基于中西医结合模式的心脏康复方案对稳定性冠心病患者心肺功能、运动耐量及生活质量的影响，为优化冠心病康复方案提供循证依据。

方法：

采用随机对照试验设计，选取 2022 年 6 月至 2023 年 12 月就诊的稳定性冠心病患者 120 例，随机分为对照组（n=60）和干预组（n=60）。对照组接受常规心脏康复（运动训练 + 健康教育），干预组在常规康复基础上联合中医康复方案（包括太极拳训练、穴位贴敷和中药调理）。两组均进行 12 周干预，主要观察指标包括：心肺运动试验参数（峰值摄氧量 VO2peak、无氧阈 AT）、6 分钟步行距离（6MWD）、西雅图心绞痛量表（SAQ）评分及中医证候积分。采用重复测量方差分析比较组间差异。

结果：

1. 心肺功能改善：干预组 VO2peak 提升幅度显著高于对照组（3.8±1.2 vs 2.1±0.9 mL/kg/min，P<0.01），AT 值改善更明显（15.2% vs 9.8%，P<0.05）。

2. 运动耐量：干预组 6MWD 增加（68.5±22.4 vs 42.3±18.6 m，P<0.01）。

3. 生活质量：干预组 SAQ 评分提高更显著（28.5±6.2 vs 18.7±5.4 分，P<0.01），中医证候积分降低更明显（-6.2±2.1 vs -3.5±1.8，P<0.05）。

4. 安全性：两组均未发生严重不良事件，干预组患者依从性更高（92% vs 80%，P<0.05）。

结论：

中西医结合心脏康复能显著改善稳定性冠心病患者的心肺功能、运动耐量和生活质量，且安全性良好。该模式通过整合现代运动康复与传统中医疗法，发挥了协同增效作用，值得临床推广应用。未来研究可进一步优化中西医结合方案的具体组成和实施细节。

心肺运动试验对急性心肌梗死后心力衰竭发生风险预测的增量价值

崔浩宁 吴孝军 郑阳 吴健

哈尔滨医科大学附属第二医院

目的

急性心肌梗死后发生心力衰竭的高风险和由此导致的不良预后已成为心脏病学领域的重要临床挑战，准确预测急性心肌梗死后心力衰竭的发生风险对于优化管理和改善预后至关重要。本研究旨在评估将心肺运动试验指标是否为心梗后心衰发生风险的预测提供增量价值。

方法

本研究纳入了 2018 年 2 月至 2023 年 12 月期间在三家医院接受标准化症状限制型功率踏车式心肺运动试验检查的 3172 名急性心肌梗死患者。主要结局是新发心力衰竭。我们通过应用多种机器学习算法筛选临床和心肺运动试验特征并构建模型，通过曲线下面积（AUC）、净重分类改善指数（NRI）、综合判别改善指数 (IDI) 评估心肺运动试验对心梗后心衰发生预测的增量价值

结果

经过入排标准筛选后共纳入 2,221 名 AMI 患者，其中 237 人（10.7%）发展为心力衰竭。研究显示心肺运动试验显著提高了模型预测心力衰竭风险的整体区分能力（AUC：0.893 vs 0.943，p <0.001）、校准能力（IDI=0.190[95%CI：0.145-0.236], p <0.001) 并优化了分类能力 (NRI=0.154[95%CI: 0.073-0.234], p <0.001)。基于该模型建立的风险评分可有效将患者分层为低风险组和高风险组（3.6% vs. 53.6%，P<0.001）

结论

心肺运动试验显著提高了心梗后心衰发生风险的预测能力，具有重要的增量价值，有助于实现更精准的风险分层和个性化心衰预防管理。

Individualized Cardiac Rehabilitation for a High-Risk Stanford Type A Aortic Dissection Patient Undergoing Whole-Life Cycle Management: A Case Report

Yi-Hao Shen, Xin-Ying Huang, Ai-Hua Wang, Ran-Ran Wang, Di Xu, Lan-Zhao, Zhao-Guo Zhang

Beijing Tsinghua Changgung Hospital, School of Clinical Medicine , Tsinghua University

Background: This study aimed to investigate the safety and efficacy of an individualized cardiac rehabilitation program for a high-risk patient following Stanford Type A aortic dissection surgery, implemented under a systematic whole-life cycle management model.

Methods: The patient, a 63-year-old male, had a 6-year history of hypertension and a 4-year history of diabetes. One year prior, he was

diagnosed with celiac artery aneurysm concurrently with right upper lobe adenocarcinoma, for which he received chemotherapy, targeted therapy, and treatment for pulmonary infection. In 2024, he presented to the emergency department with acute chest pain and was diagnosed with Stanford Type A aortic dissection. He underwent "total aortic arch replacement with artificial graft + ascending aorta plasty + aortic annuloplasty." The cardiac rehabilitation protocol included: (1) Early inpatient cardiac rehabilitation (initiated 15 days post-surgery): performed twice daily for 20-30 minutes each session, encompassing postural management, bedside cycle ergometer training (passive to active transition, 3-15 min), airway clearance techniques, inspiratory muscle training (diaphragmatic breathing, pursed-lip breathing, inspiratory muscle training, 5-10 min), and muscle endurance training. Patients were also instructed on sternal protection techniques, with exercise intensity controlled at an increase of 10-20 bpm above resting heart rate. (2) Outpatient cardiac rehabilitation (initiated 10 days post-discharge): performed three times per week for 1.5 hours per session, including warm-up, intermittent low-intensity aerobic exercise (cycle ergometer, 20-30W, 5-30 min), large muscle group low-load resistance training (10-15 min), breathing trainer exercises (initial load 30% MIP/MEP, 20 min), and cool-down. Aerobic intensity was increased by 20-30 bpm above resting heart rate, and resistance intensity was gradually increased based on tolerance. Lifestyle interventions (weight and nutrition management), health education, and psychological counseling were integrated throughout the entire process. Evaluation indicators included: cardiopulmonary endurance (6MWT, DASI), pulmonary function (FVC, FEV1, MVV, MIP, MEP), muscle strength (grip strength), psychological state (SDS, SAS), sleep quality (PSQI), quality of life (SF-36), and adverse events.

Outcomes: The patient completed 17 sessions of early inpatient rehabilitation and 48 sessions of outpatient rehabilitation. Following rehabilitation, the patient's exercise tolerance significantly improved: 6MWT increased from 130m to 254m, and DASI score increased from 4.5 to 13.45. Pulmonary function showed marked improvement: FVC increased from 1.81L to 2.30L, FEV1 from 1.53L to 2.02L, MVV from 49 L/min to 72 L/min, MIP from 61cmH2O to 104cmH2O, and MEP from 63cmH2O to 94cmH2O. Muscle strength significantly increased, with right hand grip strength rising from 14.6kg to 22.6kg. Psychological and sleep conditions were alleviated: SDS decreased from 67 (moderate depression) to 50 (no depression), SAS decreased from 56 (mild anxiety) to 39 (no anxiety), and PSQI decreased from 16 (very poor sleep quality) to 6 (acceptable sleep quality). Quality of life improved, with PF increasing from 0 to 25, MH from 0 to 48, PA decreasing from 100 to 45, GH increasing from 15 to 65, VT increasing from 0 to 40, SF maintained at 50, RE increasing from 0 to 100, and HC increasing from 0 to 75. No pulmonary infections or any cardiovascular adverse events occurred throughout the entire rehabilitation process.

Conclusion: Implementing an early inpatient and outpatient integrated individualized cardiac rehabilitation program for high-risk patients post-aortic dissection surgery, combined with medical supervision and multidimensional interventions under a whole-life cycle management model, significantly improves the patient's pulmonary function, exercise tolerance, psychological status, and quality of life. The entire process was safe and reliable, demonstrating good clinical promotion value.

心脏康复在心血管疾病中的研究进展

许秋雨 刘斌

吉林大学白求恩第二医院

在 21 世纪，心血管疾病（CVD）已成为全球主要死亡原因之一。CVD 的预防和治疗仍然是紧迫的科学问题。心脏康复（CR）是一项结构化的多学科二级预防计划，旨在全面解决心脏病的医学、身体和行为方面问题，以最大程度的促进康复、降低风险和可持续的健康改善。心脏康复包括很多方面，如患者评估、体重管理、风险因素管理、社会心理管理、有氧运动训练、力量训练等。目前已有实质性证据基础支持心脏康复作为急性冠脉综合征或射血分数降低和冠状动脉血运重建后心力衰竭患者的临床有效且具有成本效益的干预措施。尽管有所有这些好处，但 CR 并未得到充分利用，全球只有 20-50% 的符合条件的患者参加了 CR 计划。

目的：本文对心脏康复在心血管疾病中的作用，最新进展，面对的临床挑战及未来方向进行综述。

方法：文献阅读

结果：心脏康复治疗正在想人工智能数字化方向靠拢，如机器学习算法（如随机森林）整合多组学数据优化运动处方，使心衰患者峰值摄氧量（VO ₂ max）提升 15-18%；心电图嵌入式智能衣结合云平台使非计划再住院率降低 32%。同时我们也发现了心脏康复所面临的严峻的临床挑战，如系统操作缺陷；治疗费用高昂，医保未全面覆盖以及农村地区患者参与率较低等问题。基于此，我们也更加明确了未来的努力方向，未来我们应从技术革新，卫生政策等方面入手，使心脏康复手段得到更好的推广和执行。

结论：心脏康复正从机构化运动项目向数字化整合、精准处方生态系统演进，其成功需技术革新、实施科学及卫生政策的协同推进。

急性心肌梗死急诊 PCI 术后心脏康复护理对改善患者生存质量的影响

周虹杉

陆军特色医学中心（陆军军医大学大坪医院）

【摘 要】

目的：讨论急性心肌梗死（AMI）患者的 PCI 术后心脏康复护理。

方法：以 2023 年 1 月至 10 月为时间范围，将时间段内我科 100 例接受 PCI 术的 AMI 患者，以其患者编号尾数为分组依据，编号尾数 0-4 纳入研究组，编号尾数 5-9 纳入对照组，前者采用心脏康复护理，后者采取常规护理，对比护理效果。

结果：研究组患者护理后各项指标均优于对照组（p < 0.05）。

结论：积极的心脏康复护理措施可以提高 AMI 患者在 PCI 术后的康复效果，具有临床推广价值。

PCI 术是临床上治疗 AMI 的主要手段，可以通过较为直接的方式解除冠脉栓塞，恢复心肌供血，从而实现挽救残余心肌细胞、稳定生命体征、挽救患者生命的目的 [1-2]。但受损的心肌仍需一段时间进行自我修复，患者在术后仍需面对心律失常等问题，同时治疗本身也可能引发术肢血肿、假性动脉瘤等并发症，因此在 PCI 术后仍需给予患者更多关注 [3-5]。但目前的常规护理模式存在缺乏针对性、全面性等弊端，难以满足患者的康复护理需求。心脏康复护理是一种以心血管护理为基础，联合康复护理、心理护理、路径化护理等多种手段形成的一种全新护理模式，被视为心脏病人护理发展的新方向 [6-7]。本文就 AMI 患者的 PCI 术后心脏康复护理进行讨论。

中国心血管疾病患者的心肺适能参考标准

崔浩宁 吴孝军 郑阳 吴健

哈尔滨医科大学附属第二医院

目的

心肺适能是评估心血管疾病患者预后和风险分层的关键指标。制定规范的心肺适能参考标准有助于优化临床治疗决策与康复方案。然而现有的心血管疾病患者心肺适能参考标准主要是基于北美人群数据建立的，其在中国心血管疾病患者中的适用性尚未可知。本报告旨在建立适用于中国心血管疾病患者的心肺适能参考标准，填补该领域区域性参考标准的空白，为中国心血管疾病患者在临床实践中提供精准的风险评估与运动干预依据。

方法

本研究是一项多中心回顾性研究，纳入 2018 年 1 月至 2024 年 12 月中国 20 家医院心脏康复中心的 20224 例功率自行车式心肺运动试验测试数据。测试对象包括 30 至 79 岁心肌梗死、经皮冠状动脉介入治疗、心力衰竭或稳定型心绞痛诊断患者，以每十年为一个年龄段确定了峰值摄氧量 (VO_2peak) 和百分位数。

结果

确定了 30 至 79 岁男性和女性心肌梗死、经皮冠状动脉介入治疗、心力衰竭或稳定型心绞痛诊断患者的 VO_2peak 实测值和百分位数。VO_2peak 在各性别和年龄组间存在显著差异（P<0.001）。男性的平均 VO2peak 比女性高 10% (1.7 mL/kg/min)，男性每十年平均下降 7% (1.4 mL/kg/min)，女性每十年平均下降 9% (1.6 mL/kg/min)。不同心血管疾病诊断患者在各性别年龄组间的 VO-2peak 也存在差异。

结论

本报告首次为中国心血管疾病患者建立了功率自行车式心肺运动试验测试的心肺适能参考标准，提供了基于数据驱动的科学依据，可以帮助临床医生为中国心血管疾病患者制定更精准的风险分层、临床治疗决策和康复方案。

Aerobic Interval Training Ameliorates Myocardial Fibrosis in Uremic Rats by Inhibiting Cardiomyocyte Cuproptosis

Xiao-Li Tan

The First Affiliated Hospital of University of Science and Technology of China (Anhui Provincial Hospital)

Abstract

Objective: To investigate the effect of aerobic interval training (AIT) on uremia-induced myocardial fibrosis and its underlying mechanism, clarify whether it exerts protective effects by inhibiting cardiomyocyte cuproptosis, and provide a novel strategy for the prevention and treatment of uremic cardiomyopathy.

Methods: Thirty-six male Sprague-Dawley rats were adaptively fed for 1 week and then randomly divided into four groups (n=9): normal control group (CON), uremic cardiomyopathy group (UCM), uremia+AIT group (UCM+AIT), and uremia+AIT+cuproptosis agonist group (UCM+AIT+ES). UCM models were established in UCM, UCM+AIT, and UCM+AIT+ES groups by intraperitoneal injection of streptozotocin (50 mg/kg) combined with a high-phosphorus diet (1.2% phosphorus) for 8 consecutive weeks, and model establishment was evaluated by detecting serum creatinine and urinary creatinine. The UCM+AIT and UCM+AIT+ES groups underwent an 8-week AIT protocol: 5-min warm-up (10 m/min), 3 cycles of 3-min high-intensity exercise (18 m/min, ~80% VO_2max) alternating with 5-min low-intensity exercise (8 m/min, ~40% VO_2 max), and 5-min cool-down (10 m/min), 5 days/week. The UCM+AIT+ES group received daily intraperitoneal injections of the cuproptosis agonist elesclomol (ES, 1 mg/kg) during AIT. After intervention, body weight (BW) was measured, and cardiac function was evaluated by echocardiography [left ventricular

ejection fraction (LVEF), left ventricular fractional shortening (LVFS), left ventricular end-diastolic diameter (LVIDd), and end-systolic diameter (LVIDs)]. Rats were anesthetized and sacrificed to measure heart weight (HW) and calculate the heart weight index (HW/BW). Heart tissues were subjected to hematoxylin-eosin (HE) and Masson staining for morphological and collagen deposition analysis, transmission electron microscopy for mitochondrial ultrastructure observation, inductively coupled plasma-mass spectrometry (ICP-MS) for myocardial copper ion quantification, colorimetric assays for pyruvate dehydrogenase (PDH) and α-ketoglutarate dehydrogenase (α-KGDH) activity, immunohistochemistry and Western blot for cuproptosis-related proteins (FDX1, LIAS, DLD, SLC31A1) and fibrosis-related proteins (α-SMA, Collagen I), and real-time quantitative PCR (RT-qPCR) for mRNA expression of FDXR, PDHA1, and ATP7B.

Results: ① Compared with CON, the UCM group showed significantly increased serum creatinine (326.5±28.7 μmol/L vs. 78.2±10.5 μmol/L, P<0.001), decreased urinary creatinine (12.3±1.8 mg/dL vs. 35.6±3.2 mg/dL, P<0.001), and a 210% increase in collagen volume fraction (CVF) (32.5±3.2% vs. 10.5±1.8%, P<0.001) with disorganized myocardial cells, confirming successful establishment of the uremic myocardial fibrosis model. ② The UCM+AIT group exhibited significantly improved LVEF (52.3±4.1% vs. 38.7±3.5%, P<0.01), LVFS (25.6±2.3% vs. 18.2±1.9%, P<0.01), and reduced HW/BW ratio (3.21±0.25 mg/g vs. 3.90±0.31 mg/g, 17.8% decrease, P<0.01), with downregulated α-SMA and Collagen I expression (P<0.01), indicating that AIT ameliorates cardiac function and alleviates myocardial fibrosis. ③ The UCM group showed a near 3-fold increase in myocardial copper content (2.8±0.3 μg/g vs. 1.0±0.1 μg/g, P<0.001), 56.3% and 48.7% reductions in PDH and α-KGDH activities (P<0.01), mitochondrial cristae disruption, and 2.3-fold and 2.1-fold upregulations of cuproptosis-related proteins FDX1 and LIAS (P<0.01), suggesting cardiomyocyte cuproptosis in UCM rats. ④ AIT significantly reduced myocardial copper content to 1.3±0.2 μg/g (P<0.01), restored PDH and α-KGDH activities to 89.5% and 82.3% of CON (P<0.05), upregulated copper transporters SLC31A1 and ATP7B (P<0.01 and P<0.05), and inhibited FDX1/LIAS expression (P<0.01). ES treatment abrogated AIT's protective effects, increasing CVF by 35% (P<0.001) and exacerbating mitochondrial damage and cuproptosis-related protein dysregulation. ⑤ Mechanistically, AIT reduced myocardial mitochondrial reactive oxygen species (ROS) by 42% via activating the Nrf2/HO-1 antioxidant pathway (P<0.01), while ES-induced cuproptosis activated the TGF-β1/Smad3 pathway, increasing COL1A1 mRNA expression by 2.7-fold (P<0.001) and promoting fibrosis.

Conclusion: Aerobic interval training ameliorates uremia-induced myocardial fibrosis by regulating copper metabolism and maintaining mitochondrial integrity to inhibit cardiomyocyte cuproptosis, providing a novel non-pharmacological intervention strategy and potential therapeutic target for uremic cardiomyopathy.

Aerobic Interval Training Ameliorates Myocardial Fibrosis after Myocardial Infarction in Rats by Inhibiting Cardiomyocyte Ferroptosis via Endogenous Hydrogen Sulfide

xiaoli tan

The First Affiliated Hospital of University of Science and Technology of China (Anhui Provincial Hospital), University of Science and Technology of China

Aerobic Interval Training Ameliorates Myocardial Fibrosis after Myocardial Infarction in Rats by Inhibiting Cardiomyocyte Ferroptosis via Endogenous Hydrogen Sulfide

YALING Li[2]#, OUYANG Fan[1]#

[1] The First Affiliated Hospital of University of Science and Technology of China (Anhui Provincial Hospital), University of Science and Technology of China

[2] The first affiliated hospital of university of south China

Corresponding author: OUYANG Fan, The First Affiliated Hospital of University of Science and Technology of China (Anhui Provincial Hospital), 230001, China. E-mail: 1641261977@qq.com

Abstract

This study aims to systematically explore the protective effects and underlying mechanisms of aerobic interval training (AIT) on myocardial fibrosis following myocardial infarction (MI), with a specific focus on investigating whether AIT exerts its beneficial effects by regulating endogenous hydrogen sulfide (H_2S) production, improving mitochondrial dynamics, and inhibiting cardiomyocyte ferroptosis. As myocardial fibrosis is a critical pathological process contributing to post-MI cardiac dysfunction, unraveling the role of AIT in this context may provide novel therapeutic strategies for clinical intervention.

Methods

Forty male Sprague-Dawley rats were randomly allocated into four groups (n=10 per group): a control group (Control), a myocardial infarction group (MI), an MI+AIT group, and an MI+AIT+PAG group (PAG serving as an H_2S inhibitor). The MI model was established through intraperitoneal injection of isoproterenol (ISO, 100 mg/kg/d) for 7 consecutive days to induce myocardial injury.the MI+AIT and MI+AIT+PAG groups underwent an 8-week AIT protocol on a treadmill, consisting of alternating 2-minute high-intensity running (85% of maximal speed) and 3-minute low-intensity walking (40% of maximal speed), 5 days per week. Concurrently, the MI+AIT+PAG group received daily intraperitoneal injections of PAG (40 mg/kg/d) to suppress endogenous H_2S production.

Cardiac function was evaluated by echocardiography, measuring left ventricular ejection fraction (LVEF) and fractional shortening (LVFS), while cardiac structural changes were assessed by calculating the heart weight to body weight ratio (HW/BW). Myocardial fibrosis was characterized using Masson trichrome staining and immunohistochemical analysis of Collagen III and α-smooth muscle actin (α-SMA). H_2S levels were determined by measuring cystathionine γ-lyase (CSE) protein expression via Western blot and tissue H_2S concentration using a colorimetric assay. Mitochondrial dynamics were evaluated by analyzing the expression of fission protein Drp1 and fusion proteins MFN2 and OPA1, complemented by transmission electron microscopy for morphological assessment. Ferroptosis-related parameters included tissue iron content, malondialdehyde (MDA) and glutathione (GSH) levels, and expression of GPX4, SLC7A11, and ACSL4. In vitro, H9c2 cardiomyocytes were subjected to $CoCl_2$-induced hypoxia, with or without H_2S donor (NaHS) or PAG pretreatment, to validate the role of H_2S in mitochondrial function and ferroptosis regulation.

Results

The MI group exhibited significant myocardial collagen deposition, reduced LVEF and LVFS, and upregulated Collagen III and α-SMA expression compared to the control group (all P<0.05). AIT intervention notably improved cardiac function, decreased collagen volume fraction, and downregulated fibrotic markers (P<0.05). Mechanistically, MI induced a significant reduction in myocardial CSE expression and H_2S levels, which were restored by AIT but abolished by PAG (P<0.05). In terms of mitochondrial dynamics, MI caused upregulation of Drp1 and downregulation of MFN2/OPA1, leading to mitochondrial fragmentation, whereas AIT promoted mitochondrial fusion by enhancing H_2S-mediated MFN2/OPA1 expression. PAG treatment reversed these beneficial effects, exacerbating mitochondrial damage (P<0.05). For ferroptosis, MI induced increased myocardial iron accumulation, MDA levels, and ACSL4 expression, alongside decreased GPX4, SLC7A11, and GSH levels, which were all reversed by AIT. PAG treatment abrogated AIT-mediated inhibition of ferroptosis (P<0.05). In vitro experiments confirmed that H_2S donor protected against $CoCl_2$-induced mitochondrial Fe^{2+} overload, ROS generation, and membrane potential loss, while PAG abolished these protective effects.

Conclusion

This study demonstrates that aerobic interval training ameliorates post-MI myocardial fibrosis by upregulating endogenous H_2S production, which in turn regulates mitochondrial dynamics (promoting fusion and inhibiting fission) and suppresses cardiomyocyte ferroptosis. These findings provide compelling evidence for AIT as a potential non-pharmacological strategy to combat post-infarction cardiac fibrosis, highlighting the H_2S/mitochondrial dynamics/ferroptosis axis as a novel therapeutic target for clinical translation.

Circulatory power is applicable for the early prediction of post-acute myocardial infarction late-onset heart failure risk

Jin-Yu Xu

The Second Affiliated Hospital of Harbin Medical University

Objective Acute myocardial infarction (AMI) represents the most severe manifestation of coronary artery disease, posing a significant risk for adverse cardiovascular outcomes. Heart failure (HF), a common complication of AMI, particularly in cases of heart failure with reduced ejection fraction (HFrEF) and heart failure with mid-range ejection fraction (HFmEF), substantially elevates mortality rates. As the gold standard for evaluating cardiorespiratory fitness, cardiopulmonary exercise testing (CPET) has introduced a novel indicator–circulatory power (CP), defined as the product of peak oxygen consumption (peak VO_2) and systolic blood pressure (SBP)–which has been shown to predict adverse clinical outcomes. However, the utility of CP in the early prediction of late-onset heart failure following AMI remains undefined. This study therefore aims to investigate whether CP can serve as an early predictive marker for late-onset HF risk in post-AMI patients.

Methods This prospective cohort study enrolled 1,159 adult patients diagnosed with AMI who underwent CPET within 7 to 14 days after AMI resolution. Eligibility criteria included confirmed AMI per the Universal Definition of Myocardial Infarction, stability for exercise testing, and absence of severe comorbidities (e.g., advanced valvular heart disease, chronic obstructive pulmonary disease with FEV_1 < 50% predicted). The primary endpoint was post-AMI late-onset HF , defined as the new on-

set of HF symptoms (e.g., dyspnea, fatigue) and signs (e.g., pulmonary congestion, peripheral edema) at least 30 days post-AMI, confirmed by echocardiographic evidence of left ventricular dysfunction (LVEF < 50%) and clinical assessment. CP was calculated as the product of peak oxygen consumption (peak VO_2, measured in $ml \cdot kg^{-1} \cdot min^{-1}$) and peak systolic blood pressure (SBP, in mmHg) during CPET, normalized to body weight. Statistical analyses included: (1) Cox proportional hazards regression to evaluate the association between CP and late-onset HF, adjusting for age, sex, baseline LVEF, diabetes mellitus, hypertension, Killip class at presentation, and revascularization strategy (percutaneous coronary intervention [PCI] vs. coronary artery bypass grafting [CABG]); (2) Kaplan–Meier survival analysis with log-rank tests to compare HF-free survival across CP tertiles; (3) Receiver operating characteristic (ROC) curve analysis to determine the optimal CP cutoff for HF prediction, with sensitivity and specificity optimized using Youden's index. All analyses were performed using R, and statistical significance was set at $P < 0.05$.

Results During a median follow-up of 32 months, 187 patients (16.1%) developed late-onset HF. The HF group exhibited a significantly lower median CP [1,956.3 (IQR 1,624.5–2,210.7) vs. 2,543.8 (IQR 2,231.5–2,876.2) mm $Hg \cdot mLo_2 \cdot kg^{-1} \cdot min^{-1}$; P<0.001]. Multivariate Cox regression revealed that each 1,000-unit increase in CP was associated with a 40% reduction in HF risk [adjusted hazard ratio (HR) 0.600; 95% CI 0.464–0.777; P<0.001]. ROC analysis yielded an area under the curve (AUC) of 0.821 (95% CI 0.785–0.854), with an optimal cutoff of 2,289.6 mm $Hg \cdot mLo_2 \cdot kg^{-1} \cdot min^{-1}$ (sensitivity 76.3%, specificity 72.5%). Kaplan–Meier curves showed that patients with CP ≤ 2,289.6 had a 3-year cumulative HF incidence of 24.7%, compared to 8.3% in those with CP >2,289.6 (log-rank P<0.001). Subgroup analyses confirmed the robustness of CP across age groups (≥ 65 vs. <65 years), sexes, and revascularization modalities (PCI vs. CABG).

Conclusion This study demonstrates for the first time that CP is a robust early predictor of late-onset HF after AMI. By integrating oxygen metabolic capacity and hemodynamic load, CP captures myocardial reserve more comprehensively than traditional markers. The identified cutoff (2,289.6 mm $Hg \cdot mLo_2 \cdot kg^{-1} \cdot min^{-1}$) enables risk stratification of AMI survivors, with low-CP patients warranting intensified surveillance and early interventions (e.g., neurohormonal blockade, cardiac rehabilitation). Future trials should explore whether CP-guided therapy modifies long-term outcomes and validate its utility in diverse AMI populations, including those with STEMI and NSTEMI.

马拉松运动强度对心肌肌钙蛋白升高的影响：训练优化的新视角

夏辰兮[1,2] 徐涛[1] 王雨桐[1,3] 孟旭阳[1,3] 李一[1,3] 宋欣阳[1,2] 周浩峰[1,3] 汪芳[1,2,3]

1. 北京医院

2. 北京大学第五临床医学院

3. 北京协和医学院

目的

本研究旨在探讨不同强度马拉松跑步对心脏损伤（心肌肌钙蛋白 T，cTnT）和肌肉损伤（肌酸激酶，CK）生物标志物的差异性影响。考虑到马拉松运动的流行度日益增加及其伴随的心血管风险，本研究期望为优化训练强度及保护业余跑者心脏健康提供精准的临床指导。

方法

纳入参加 2023 年天津马拉松的 40 名业余跑者（男性 29 名，女性 11 名；平均年龄 45.10±13.56 岁）。所有受试者在赛前 48 小时内完成了包括心肺运动试验和超声心动图检查在内的综合评估。根据比赛过程中实时心率监测数据，将参赛者分为两个组别：高强度组（H 组，比赛中平均心率超过最大心率 85%，n=28）和中等强度组（M 组，平均心率不超过最大心率 85%，n=12）。分别在赛前 24 小时内（T0）、赛后 20 分钟内（T1）、赛后第 1 天（T2）、第 2 天（T3）、第 3 天（T4）和第 6 天（T5）采集静脉血，测量血清 cTnT 和 CK 浓度。

结果

两组受试者基线时的血清 cTnT 和 CK 水平无明显差异（P>0.05）。马拉松比赛后，两组 cTnT 和 CK 水平均显著升高。与高强度组相比，中等强度组的 cTnT 峰值（21.92±8.68 pg/mL vs. 37.68±25.79 pg/mL，P=0.0005）和 CK 峰值（645.63±430.33 U/L vs. 1122.37±789.53 U/L，P=0.0062）明显更低。此外，中等强度组 cTnT 水平恢复到基线的时间更短（赛后第 1 天即恢复），而高强度组的 cTnT 升高水平则持续到赛后第 3 天。

结论

马拉松跑步强度超过最大心率的 85% 显著加重心肌微损伤并延缓损伤标志物的恢复速度。将运动强度控制在这一阈值以下能有效减轻心肌损伤，提示在马拉松备赛中需强调个性化强度管理，以确保心脏安全。

关键词：马拉松；运动强度；心肌肌钙蛋白；肌酸激酶；心肌损伤

Progesterone promotes the proliferation of embryonic epicardial cells and decreases left ventricular fibrosis through ALDH1A3/Glycolytic pathway

Ding-Hui Wang, Jie Zhang

Chongqing general hospital

Progesterone promotes the proliferation of embryonic epicardial cells and decreases left ventricular fibrosis through ALDH1A3/Glycolytic pathway

Wang Dinghui，Zhang Jie

Department of Geriatrics, The Chongqing General Hospital, Chongqing University, Chongqing, 400013, China.

Purpose: Epicardial progenitor cells (EPCs), characterized by the multilineage differentiation potential, has emerged as pivotal contributors to regenerative medicine. Progesterone has demonstrated protective effects on the cardiovascular system and has been shown to promote cell proliferation. However, the association between progesterone and the proliferation of EPCs or its impact on cardiac fibrosis remain unexplored.

Methods: Establish an in vitro culture system for mouse EPCs and prepare different concentrations of progesterone working solution (10^{-8}, 10^{-7}, 10^{-6}, 10^{-5}, 10^{-4} M) to explore experimental concentrations of EPCs. Then set up control, progesterone, and progesterone inhibitor (RU486) group to observe the effects of progesterone on EPCs through immunofluorescence experiments, qRT-PCR, and flow cytometry; Newborn mice were injected with placebo or progesterone (8 mg/100 g/d) for 1, 3, and 7 days to validate the effect of progesterone on EPCs in vivo; Perform transcriptome sequencing of EPCs of control and progesterone group and then screen key genes and regulatory pathways that promote EPCs proliferation by progesterone,; Adult mice were used for thoracotomy to ligate the anterior descending coronary artery and establish a myocardial infarction (MI) model. Progesterone was injected intraperitoneally after surgery, and EPCs proliferation at the edge of the infarction area was detected by immunofluorescence staining of harvested hearts at P1, P3, and P7; Four weeks after MI, cardiac ultrasound was used to detect cardiac function, and Masson staining was used to detect cardiac fibrosis at P1, P3, and P7; Perform qRT PCR and WB to detect the effect of progesterone on ALDH1A3 expression and glycolysis metabolism after MI.

Results: Our results found that progesterone can significantly increase the positivity rate of Ki67 on EPCs within a certain concentration range (10^{-8}~10^{-5}M). The positive rate of Ki67 reached its highest at 10^{-6}M, and then the proliferative effect gradually decreased with increasing concentration; Progesterone significantly increased the number of Ki67, PH3, and Aurora B fluorescence positive cells in EPCs; Progesterone promotes the expression of EPCs cell cycle genes such as CDK1 and CCNA1.The differential analysis of transcriptome sequencing results suggests that progesterone has a regulatory effect on gene expression in EPCs. There was total of 90 DEGs in the progesterone treatment group, with 52 up-regulated and 38 down-regulated. From which we screened out the ALDH1A3 gene from DEGs as target molecule, which is enriched in the glycolytic metabolic pathway; Through verification, it was found that compared with the control group, the expression of ALDH1A3, lactate, ATP generation, glucose absorption, and protein and mRNA expression of glycolysis related molecules PDK1, HK2, PKM2, LDHA increased in the progesterone group. After knocking down ALDH1A3 by siRNA, the proliferation of EPCs promoted by progesterone was blocked. At the same time, lactate, ATP production, and glucose absorption were reduced, and the expression of glycolysis related molecules PDK1, HK2, PKM2, LDHA protein, and mRNA was decreased; After inhibiting glycolysis with 2-DG and WZB117, the pro-proliferative effect of progesterone on EPCs was attenuated, but there was no significant change in ALDH1A3 expression. We successfully established a mouse MI model and immediately administered progesterone injection after surgery. The proliferation of epicardial cells at the edge of the heart tissue was detected at P1, P3, and P7. We found that progesterone increased the expression of Wt1 and Ki67 in the infarct margin cells; After 4 weeks of MI, cardiac ultrasound results showed that the left ventricular ejection fraction (EF) and short axis shortening rate (FS) in the progesterone group were higher than those in the MI group; The Masson staining results showed that the ratio of cardiac fibrosis area in the progesterone group mice was significantly lower than that in the control group at P3 and P7. The expression of ALDH1A3 in the heart tissue of the progesterone group was significantly higher than that of the MI group; qRT-PCR and Western blot analysis of cardiac tissue at P1, P3, and P7 after MI showed that progesterone promotes the expression of ALDH1A3 protein and mRNA in heart tissues after MI. The qRT-PCR and Western blot analysis of heart tissue at P1, P3, and P7post MI showed that progesterone promotes the expression of glycolysis related molecules such as GLUT1, HK2, PKM2, LDHA, etc. at both protein and mRNA levels post MI.

Conclusion: Our findings demonstrate that the ALDH1A3/glycolysis signaling pathway is a key mechanism through which progesterone promotes the proliferation of EPCs. Progesterone regulated the activation and proliferation of epicardial cells and improved cardiac function and

retard fibrosis post MI.

分阶式心脏康复联合动态量化健康教育在冠心病患者中的综合干预效果：一项随机对照研究

李觅 钱锦钰

陆军军医大学第一附属医院心血管内科

目的：探讨阶段性心脏康复训练联合量化健康教育模式对稳定性冠心病患者心肺功能、运动耐量及心理健康状况的干预效果，为临床康复管理提供循证依据。

方法：采用单中心随机对照试验设计，纳入 2024 年 1 月至 2024 年 12 月确诊的稳定性冠心病患者 120 例，随机分为干预组（n=60）和对照组（n=60）。干预组接受为期 12 周的阶段性心脏康复训练（包括院内监护期、门诊过渡期和家庭维持期三阶段训练）联合量化健康教育模式干预；对照组接受常规心脏康复指导。主要终点为 12 周时峰值摄氧量（VO2peak）变化，次要终点包括左心室射血分数（LVEF）、6 分钟步行距离（6MWD）、血脂谱、焦虑抑郁评分（HADS）和生活质量评分（SF-36）。

结果：干预组 VO2peak 改善显著优于对照组（+3.2±1.1 vs +1.5±0.8 mL/kg/min，P<0.001）。次要终点方面，干预组在 LVEF（+5.8% vs +2.3%）、6MWD（+85.6 vs +42.3 m）、LDL-C 水平（-0.82 vs -0.35 mmol/L）等方面的改善均显著优于对照组（均 P<0.01）。心理评估显示，干预组 HADS-A（-3.2 vs -1.5）和 HADS-D（-2.8 vs -1.2）评分改善更明显（P<0.001）。SF-36 评分中，干预组在躯体功能（+15.2 vs +7.6）和精神健康（+12.8 vs +6.3）维度的提升更显著（P<0.001）。

结论：阶段性心脏康复训练联合量化健康教育可显著改善冠心病患者的心肺功能、运动耐量和心理健康状况，是一种有效的综合康复管理模式。

基于 CiteSpace 的心脏瓣膜置换术后患者抗凝治疗的可视化分析

叶菁菁 罗明先 李秀毛 杨丽飞 张咏梅

遵义医科大学附属医院

目的 利用 CiteSpace 可视化分析探究心脏瓣膜置换术后患者抗凝治疗的研究现状、热点及前沿趋势，为后续更好的开展相关研究提供参考。**方法** 检索 Web of Science 核心合集数据库、中国知网数据库中收录的相关文献，检索时间为 2005 年 1 月 1 日至 2025 年 3 月 30 日，采用 CiteSpace（6.3.R1）软件对纳入文献进行分析，绘制关键词共现、聚类及突现词图谱。**结果** 共纳入英文文献 198 篇和中文文献 700 篇，国内外发文量总体成平稳上升状态。华法林、抗凝治疗、抗凝依从性、健康教育、心脏瓣膜病、主动脉瓣置换、并发症管理等是目前的研究热点；影响因素、口服抗凝治疗、经导管主动脉瓣置换、生存质量、延续护理、自我管理等是该领域研究的前沿趋势。**结论** 心脏瓣膜置换术后患者良好的抗凝管理对于提高华法林抗凝治疗的有效性和安全性、确保手术效果、改善患者远期生存质量至关重要，今后在创新瓣膜置换手术方式的同时，继续加强患者治疗依从性管理，对华法林的口服治疗做到有效监管。此外，对其影响因素进行深度研究，及时监测并发症的发生并进行干预。加强对患者的健康指导及教育，以助于提高口服抗凝药物依从性，做好延续护理，最终提高患者的生活质量。

Impact of perioperative cardiac rehabilitation on the prognosis of female patients undergoing elective valve surgery: a gender-specific analysis of the PORT randomized clincial trial.

Shuyuan TAN, Huan Ma

Guangdong Provincial People's Hospital

Background:

Gender disparities in cardiovascular disease are well recognized, spanning differences in clinical presentation, pathophysiology, treatment response, and surgical outcomes. In the setting of valvular heart disease, women undergoing cardiac surgery often face higher perioperative risks, such as increased susceptibility to postoperative complications and longer recovery periods. Nevertheless, accumulating evidence suggests that women may derive unique physiological and functional benefits from perioperative cardiac rehabilitation (CR)—a structured, multidisciplinary program designed to enhance recovery, reduce complications, and promote long-term functional gains. Despite its potential, data on sex-specific responses to CR interventions in the perioperative context remain scarce. To address this important knowledge gap, we conducted a predefined subgroup analysis of the Perioperative Rehabilitation Trial (PORT), a randomized controlled trial that investigated the impact of a comprehensive perioperative CR program in patients undergoing elective valve surgery. This analysis specifically aimed to determine whether the clinical effectiveness of CR varies by sex.

Methods:

The PORT trial was a prospective, single-center, open-label, randomized controlled study that enrolled 818 adult patients scheduled for elective valvular heart surgery. Of the enrolled population, 412 (50.4%) were women. Participants were randomized in a 1:1 ratio to either a usual care group or an intervention group receiving a structured perioperative CR program. The CR protocol comprised preoperative education, inspiratory muscle training (IMT), active cycle of breathing techniques (ACBT), and early mobilization initiated within 24 hours post-extubation.

The **primary composite outcome** was defined as the occurrence of any of the following: in-hospital all-cause mortality, at least one postoperative pulmonary complication (PPC), or a postoperative hospital stay exceeding 7 days. **Secondary outcomes** included length of stay in the surgical intensive care unit (SICU), 3-month all-cause mortality, and radiographically confirmed PPCs before discharge.

Statistical analysis was stratified by sex. Between-group comparisons were conducted using chi-square or Fisher's exact tests for categorical variables and independent-sample t-tests for continuous variables. Time-to-event outcomes were assessed using Kaplan-Meier survival analysis and log-rank tests. Cox proportional hazards regression models were applied separately for male and female subgroups to estimate adjusted hazard ratios (HRs) for the primary outcome, with covariate adjustment for age, left ventricular ejection fraction (LVEF), EuroSCORE II risk category, baseline pulmonary function, surgical approach, and whether concomitant coronary artery bypass grafting (CABG) was performed.

Results:

Among female participants, those receiving CR showed significantly lower rates of PPCs (24.1% vs. 35.8%, P=0.005), aerothorax (4.2% vs. 9.0%, P=0.037), and pneumonia (8.2% vs. 20.1%, P<0.001) compared to those in the usual care group. In contrast, no statistically significant differences were observed in male patients (PPCs: 29.1% vs. 30.3%, P=0.761; pneumonia: 12.4% vs. 14.3%, P=0.409). A significant sex-by-treatment interaction was found for pneumonia incidence (P for interaction = 0.044), indicating a differential treatment effect by sex. Similar sex-specific patterns were evident in radiographically confirmed PPCs prior to discharge. Kaplan-Meier analysis demonstrated a significantly lower cumulative incidence of PPCs and pneumonia among females receiving CR (P<0.01), a trend not seen in males. In multivariable Cox regression models, CR was independently associated with reduced risk of PPCs in women (HR 0.58, 95% CI: 0.39–0.86, P=0.006), but not in men (HR 0.94, 95% CI: 0.65–1.35, P=0.73).

Conclusion:

This prespecified subgroup analysis of the PORT trial demonstrates that perioperative cardiac rehabilitation significantly reduces pulmonary complications—particularly pneumonia and aerothorax—in women undergoing elective valve surgery. These sex-specific benefits were not observed in men, highlighting the need for gender-sensitive strategies in CR program design. Enhancing CR participation among women may improve postoperative outcomes and support the development of more personalized, equitable rehabilitation approaches in cardiac surgical care.

心脏康复的研究进展

伍星

成都市第五人民医院 西区

近年来，心血管疾病（CVD）已成为全球范围内威胁人类健康的主要“杀手”，其发病率持续攀升的态势令人担忧。作为心血管疾病二级预防与患者功能恢复的关键环节，心血管康复治疗的重要性愈发凸显，其相关研究进展也成为医学领域的焦点。

在运动康复方面，精准化、个性化的运动方案成为研究热点。通过对患者心肺功能、运动耐力等多维度评估，制定有氧运动、抗阻训练等相结合的康复计划，有效提升患者心功能与生活质量。营养干预研究则聚焦于特定膳食模式对心血管健康的影响，如地中海饮食，其富含不饱和脂肪酸、膳食纤维等成分，被证实能显著降低血脂、血压，减少心血管疾病风险。心理支持层面，越来越多研究表明，焦虑、抑郁等负面情绪会影响心血管疾病的发生发展，因此，心理疏导、认知行为疗法等干预手段被纳入康复体系，帮助患者缓解心理压力，促进康复进程。药物治疗在心血管康复中同样不可或缺，新型抗血小板、调脂药物不断涌现，为患者提供了更安全有效的治疗选择。此外，新兴技术如虚拟现实（VR）、可穿戴设备也逐渐应用于心血管康复，VR 技术通过模拟真实运动场景提高患者运动积极性，可穿戴设备则实时监测患者生命体征，助力康复方案的动态调整。

未来，心血管康复领域的研究应进一步深化多学科融合，探索更高效的综合康复模式，同时加强对基层康复的推广与普及，让更多心血管疾病患者受益。

Impact of Cardiopulmonary Exercise Testing -Guided Individualized Cardiac Rehabilitation on Functional Capacity and Prognosis in Coronary Artery Disease Patients

Li-Yan Ran

The Second Affiliated Hospital of Harbin Medical University

Background: Patients with cardiovascular diseases, particularly coronary artery disease (CAD), frequently experience reduced exercise tolerance and impaired cardiopulmonary function, which significantly diminish their quality of life and increase long-term cardiovascular risks. These limitations stem from the heart's reduced capacity to meet metabolic demands during physical activity, often leading to exercise intolerance, fatigue, and poor functional status. Cardiopulmonary exercise testing (CPET) has emerged as the gold standard for evaluating cardiopulmonary fitness, offering unparalleled precision in risk stratification and exercise prescription for cardiac rehabilitation (CR). By assessing key parameters such as peak oxygen uptake (VO_2 peak), anaerobic threshold (AT), and ventilatory efficiency (VE/VCO_2 slope), CPET provides a com-

prehensive physiological profile that guides personalized rehabilitation strategies. Despite its well-established clinical value in international guidelines, CPET remains underutilized in domestic clinical practice due to limited accessibility, lack of standardized protocols, and insufficient evidence supporting its superiority over conventional approaches. Therefore, further research is needed to validate its efficacy in optimizing rehabilitation outcomes for CAD patients and justify its broader implementation.

Methods: A prospective, single-center, randomized controlled trial was conducted involving 120 stable CAD patients (left ventricular ejection fraction, LVEF ≥ 40%) diagnosed between January 2022 and December 2023. Participants were stratified by age, gender, and baseline VO_2 peak before being randomly allocated into two groups with a 1:1 ratio. The intervention group (n=60)underwent a 12-week CPET-guided individualized rehabilitation program, which incorporated high-intensity interval training (HIIT) at 80-90% of peak heart rate, supervised by trained physiotherapists three times per week. Each session included a 5-minute warm-up, 4x4-minute high-intensity intervals interspersed with 3-minute active recovery periods, and a 5-minute cool-down. The control group (n=60) received conventional moderate-intensity continuous training (MICT) at 60-70% of peak heart rate, consisting of 30-40 minutes of steady-state aerobic exercise at the same frequency. All patients underwent standardized baseline and post-intervention assessments, including CPET (using the Cosmed Quark CPET system with breath-by-breath gas analysis), 6-minute walk test (6MWT), and Seattle Angina Questionnaire (SAQ) to evaluate functional capacity, exercise tolerance, and quality of life. The primary endpoint was the change in VO_2 peak, while secondary endpoints included AT, VE/VCO_2 slope, 6MWT distance, and 6-month cardiovascular events (a composite of rehospitalization for cardiac causes, unplanned revascularization, and cardiac death).

Results: The intervention group demonstrated superior improvements across all measured parameters compared to the control group: Functional capacity: VO_2 peak increased significantly by 19.2% (from 18.2±3.1 to 21.7±3.5 mL/kg/min, Δ+3.5±1.2 vs. control group Δ+1.8±0.9, p<0.001), indicating enhanced aerobic capacity. AT power also improved notably by 22.7% (from 75±15 W to 92±18 W, p=0.003), reflecting better endurance performance.

Ventilatory efficiency: The VE/VCO_2 slope decreased by 12.8% (from 34.5±4.2 to 30.1±3.8, p=0.01), demonstrating improved pulmonary gas exchange and reduced ventilatory inefficiency. Exercise tolerance:The 6MWT distance increased by 22.5% (from 325±45 m to 398±52 m, p<0.001), confirming superior functional endurance in daily activities. Clinical outcomes: The intervention group exhibited a 60% relative risk reduction in 6-month cardiovascular events (6.7% vs. 16.7%, p=0.042), highlighting its prognostic benefits. Quality of life: SAQ scores for physical limitation (PL) improved by 51.1% (from 45±12 to 68±15 points, p=0.002), indicating markedly better patient-reported outcomes.

Conclusion: CPET-guided individualized cardiac rehabilitation significantly enhances functional capacity, ventilatory efficiency, exercise tolerance, and clinical prognosis in CAD patients compared to conventional MICT. The robust improvements in VO_2 peak, AT, and VE/VCO_2 slope underscore the physiological advantages of HIIT prescribed based on CPET parameters, while the reduction in cardiovascular events reinforces its clinical relevance. These findings strongly support the integration of CPET as a core assessment tool in cardiac rehabilitation programs, providing a scientific basis for optimizing exercise prescriptions and improving long-term outcomes in CAD management. Future large-scale, multicenter studies with extended follow-up periods are warranted to validate these results, assess cost-effectiveness, and promote the widespread adoption of CPET in routine clinical practice. Additionally, further research should explore the mechanisms underlying CPET's benefits, including its effects on endothelial function, autonomic regulation, and myocardial remodeling, to fully elucidate its role in secondary prevention.

Joint association of TyG index and peak kilogram oxygen uptake with MACE events in post-PCI patients

Xingbo Mu, Ya-Ling Han, Ya-Ling Han

General Hospital of Northern Theater Command

Background: Patients with acute coronary syndrome (ACS) undergoing percutaneous coronary intervention (PCI) continue to face significant residual risk of major adverse cardiovascular events (MACE). The triglyceride-glucose (TyG) index, calculated from fasting triglyceride and glucose levels, is a validated surrogate marker of insulin resistance. Elevated TyG index correlates with endothelial dysfunction and atherosclerotic progression. Peak kilogram oxygen uptake (VO_2 peak), measured via cardiopulmonary exercise testing (CPET), serves as the gold-standard metric for cardiorespiratory fitness, where low values independently predict cardiovascular mortality. While both markers are established predictors of MACE, their joint effects and potential bidirectional mediation in post-PCI populations remain unexplored. This knowledge gap impedes comprehensive risk stratification strategies.

Objective: While both the triglyceride-glucose (TyG) index and peak oxygen uptake (VO_2 peak) are established predictors of major adverse cardiovascular events (MACE) in patients with acute coronary syndrome (ACS) after percutaneous coronary intervention (PCI), the nature and impact of their coexposure, and their mutual influence on MACE risk remain poorly understood. Therefore, this study aimed to evaluate the joint associations of the TyG index and VO_2 peak with the development of MACE and to quantify the extent to which each marker mediates the effect of the other on MACE risk in a large cohort of post-PCI ACS patients.

Methods: This study comprised 8,803 patients with ACS who underwent percutaneous coronary intervention (PCI). The TyG index was calculated as Ln[fasting triglyceride (mg/dL) * fasting glucose (mg/dL)/2]. VO_2 peak was derived from standardized cardiopulmonary exercise testing (CPET). The primary outcome was MACE, a composite of cardiovascular death, non-fatal stroke, myocardial infarction, and ischemia-driven revascularization. We performed adjusted Cox proportional hazards regression and mediation analyses to evaluate associations between the indexes and MACE. Statistical analyses employed Cox proportional hazards models to evaluate joint TyG/VO_2 peak categories and mediation analysis using counterfactual frameworks to estimate direct and indirect effects.

Results: The mean age of the participants was 57.4 ± 9.0 years, and 6,671 (76.9%) were males. During a maximum follow-up of 5.0 years, 1,548 (17.6%) people developed MACE. Compared with people with a lower TyG index (< 8.8 [median level]) and VO_2 peak > 15.4 mg/L, those concurrently with a higher TyG and lower VO_2 peak had the highest risk of overall MACE (adjusted hazard ratio [aHR], 1.376; 95% CI 1.187-1.596), which were predominant among those aged 65 years or over. VO_2 peak significantly mediated 17.9% of the association between the TyG index and MACE, while TyG simultaneously mediated 6.1% of the association between VO_2 peak and MACE risk. This suggests insulin resistance partially elevates MACE risk by impairing cardiorespiratory fitness, while fitness independently modulates metabolic risk pathways.

Conclusions: This study provides novel evidence of synergistic risk and mutual mediation between insulin resistance (reflected by the TyG index) and impaired cardiorespiratory fitness (VO_2 peak) in post-PCI patients. The findings highlight the coexposure effects and mutual mediation between the TyG index and VO_2 peak on MACE. Joint assessments of the TyG index and VO_2 peak should be emphasized for residual risk stratification and secondary prevention of MACE in post-PCI patients with acute coronary syndrome.

Keywords: Triglyceride-glucose (TyG) index, peak kilogram oxygen uptake (VO_2 peak), acute coronary syndrome, PCI, major adverse cardiovascular events (MACE), Insulin resistance

Comparison of the predictive efficacy of triglyceride-glucose (TyG) index and modified TyG index combined with cardiopulmonary exercise testing (CPET) parameters for major adverse cardiovascular events (MACE) risk in the population

SiCheng Ning, Ya-Ling Han, Quan-Yu Zhang

Northern Theater Command General Hospital

Insulin resistance (IR) serves as a cornerstone pathophysiological mechanism driving the development and progression of atherosclerotic cardiovascular disease (ASCVD). The Triglyceride-Glucose (TyG) index, widely adopted as a practical surrogate marker for IR, correlates reliably with established cardiovascular disease risk. However, its inherent dependence on single-point, static laboratory measurements significantly constrains its ability to capture an individual's functional reserve and the dynamic nature of underlying pathophysiological processes over time. In contrast, cardiopulmonary exercise testing (CPET) provides an objective, quantitative, and non-invasive diagnostic modality. CPET transcends simple functional assessment; it offers critical insights into the pathophysiological mechanisms underpinning exercise intolerance and exertion-related symptoms. Its established clinical value extends to differential diagnosis, precise prognostic risk stratification, evaluation of therapeutic intervention efficacy, and the formulation of individualized exercise prescriptions. This study sought to investigate novel composite indices designed to integrate the metabolic information of the TyG index with the dynamic functional insights derived from key CPET parameters. Specifically, the study focused on combining the TyG index with measures of peak oxygen consumption normalized per kilogram of body weight (TyG_peakVO_2 kg), peak oxygen pulse (TyG_peakO_2 pulse), and oxygen consumption at the anaerobic threshold normalized per kilogram (TyG_ATVO_2 kg). The primary objective was to rigorously compare the predictive performance of these novel indices against the traditional TyG index for major adverse cardiovascular events (MACE) within a substantial cohort. The study prospectively enrolled 8,803 patients who underwent clinically indicated CPET. The TyG index was calculated using the established formula: Ln[fasting triglycerides (mg/dL) × fasting glucose (mg/dL) / 2]. MACE was rigorously defined as a composite endpoint encompassing cardiovascular death, non-fatal myocardial infarction, non-fatal stroke, emergency revascularization procedures, and heart failure-related rehospitalization. Multivariable Cox proportional hazards regression models, adjusting for relevant clinical covariates, were employed to assess the independent associations between tertiles of both

the traditional TyG index and the novel composite indices with incident MACE risk. Participants had a mean age of 57.4 ± 9.0 years, and 2,032 (23.1%) were female. Over a median follow-up period of 5.0 years, 1,548 MACE events occurred, representing 17.6% of the cohort. Analysis using the fully adjusted multivariable Cox model yielded a counter-intuitive finding for the traditional TyG index: patients within the lowest tertile exhibited a significantly increased risk of incident MACE compared to those in the highest tertile (adjusted Hazard Ratio [aHR] 1.145, 95% Confidence Interval [CI] 1.012–1.294). Conversely, the results for all three TyG_CPET composite indices demonstrated the expected directionality based on functional capacity. Patients in the highest tertile of each novel composite index consistently showed a significantly reduced risk of incident MACE compared to those in the corresponding lowest tertile. The specific aHRs (95% CI) were: TyG_peakVO $_2$ kg: 0.828 (0.726–0.944), TyG_peakO $_2$ -pulse: 0.831 (0.724–0.953), and TyG_ATVO $_2$ kg: 0.878 (0.774–0.995). In conclusion, this cohort analysis confirmed significant associations between both the traditional TyG index and the novel TyG_CPET composite indices with future MACE risk. However, the direction of association for the traditional TyG index was inverse to expectations derived from its role as an IR marker. Critically, the novel indices, particularly TyG_peakVO $_2$ kg and TyG_ATVO $_2$ kg, demonstrated superior predictive capacity for MACE risk compared to the traditional TyG index alone. The TyG_peakVO $_2$ ratio demonstrated the strongest predictive power, with its prognostic capacity increasing progressively as follow-up duration extended, indicating a time-dependent effect. These findings strongly suggest that integrating a dynamic functional assessment via CPET parameters with static metabolic markers significantly enhances risk stratification. This combined approach potentially offers a more comprehensive and pathophysiologically relevant evaluation of cardiovascular vulnerability in clinical practice.

RelationshiP and Prognostic value of the triglyceride-glucose index and oPtical coherence tomograPhy-derived Physiological index in Patients with acute coronary syndrome

Li Pan, Bei Shi, Ran-Zun Zhao

Affiliated Hospital of Zunyi Medical University

The oPtical flow ratio (OFR) , derived from oPtical coherence tomograPhy (OCT) images , serves as a Physiological index , while the Triglyceride-Glucose Index (TyG) is an alternative measure of insulin resistance . Both indices are Positively correlated with Poor Prognosis in Patients with acute coronary syndrome (ACS) , but the relationshiP between the TyG index , OFR , and their Prognostic value remains unclear . We included ACS Patients who underwent OCT between January 1 , 2021 , and March 31 , 2023 . The TyG index was calculated as Ln[fasting triglycerides (mg/dL) × fasting blood glucose (mg/dL)/2]. Patients were grouPed into three categories (T1, T2, and T3) based on TyG tertiles. The Primary endPoint was major adverse cardiovascular events (MACE). In our analysis, the T3 grouP showed a significantly higher incidence of MACE (P < 0.05), with a Progressive decrease in vessel-level OFR observed as the TyG index increased, demonstrating a linear correlation (r = - 0.0146, P < 0.001). The restricted cubic sPlines (RCS) model revealed a nonlinear relationshiP between the TyG index and the likelihood of MACE (P for nonlinear < 0.021). Additionally, the cumulative incidence of MACE was significantly higher in Patients with a higher TyG index (all Log-rank P < 0.001).These findings suggest a nonlinear relationshiP between the TyG index and MACE, and a linear association between the TyG index and vessel-level OFR. The combination of the TyG index and OFR significantly imProved discriminatory ability (c-index: 0.720 vs. 0.757; P < 0.001) and reclassification ability (net reclassification index [NRI]: 0.373; integrated discrimination imProvement [IDI]: 0.031; P < 0.0001) for Predicting MACE comPared to vessel-level OFR alone. This combination effectively identifies high-risk ACS Patients.

The effects of perioperative cardiopulmonary integrated rehabilitation in patients undergoing TAVR

Yanxin Song, Hai-Yan Zheng, Chuan Ren, Wei Zhao, Jun-Tao Duan

Peking University Third Hospital

Abstract

Background: Transcatheter aortic valve replacement (TAVR) has been widely used for treating patients with aortic stenosis (AS) or aortic regurgitation (AR) in recent years around the world, and the perioperative rehabilitation of TAVR patients has also consistently garnered attention from clinical practitioners. At present, the cardiac rehabilitation of TAVR patients in China is still in its early stage, there is still a lot of work to be done. The aim of this study was to explore the effects of perioperative cardiopulmonary integrated rehabilitation in patients undergoing TAVR.

Method: We conducted this study at Peking University Third Hospital, enrolling patients scheduled for TAVR who visited the Department of Cardiology. Following the initiation of the trial, 29 patients who received TAVR were prospectively enrolled as the intervention group, and 29 patients who received TAVR were retrospectively enrolled as the control group. The control group patients received routine treatment and nursing care after admission. Besides routine treatment and nursing care, a perioperative cardiopulmonary integrated rehabilitation program was carried out for the intervention group after admission. The program included (1) preoperative evaluation; (2) preoperative rehabilitation education; (3) preoperative cardiopulmonary rehabilitation, including respiratory rehabilitation and exercise rehabilitation; (4) early postoperative rehabilitation assessment; (5) postoperative cardiopulmonary rehabilitation: including patients' posture changing, limb activities locally(passive and positive), respiratory rehabilitation, standing balance, walking, and coordinated training. During the rehabilitation process, closely monitor the patient's vital signs. Researchers recorded the patients' activities of daily living (Barthel Index) at admission and discharge. Before the patients discharge, researchers instructed patients to perform a 6-minute walking test(6-MWT) to assess patients' exercise capacity, and provided rehabilitation guidance based on their 6-MWT results. Researchers regularly monitored the exercise of interventional group patients through WeChat. At the 1-month follow-up, researchers evaluated all patients' exercise adherence and retest their 6-MWT. Researchers conducted a telephone survey on the patient's exercise adherence 3 months after discharge. Patients' incidence of postoperative dyspnea, fever, infection, etc.; postoperative physical activity status and duration of hospitalization; exercise capacity and exercise adherence 1 month after discharge; exercise adherence 3 months after discharge were compared between the two groups.

Result: There were no statistically significant differences in baseline data between the two groups of patients(p > 0.05). There was no adverse events occurred in all patients. Compared with the control group, the intervention group had lower incidence of dyspnea(p = 0.028) and fever(p = 0.033), the degree of dyspnea is also milder. The intervention group also had significantly shorter postoperative length of CCU residence (4.00 ± 2.33 vs. 2.93 ± 1.49, t = 2.083, p = 0.042) and bed rest time (4.96 ± 2.29 vs. 1.47 ±0.98, t= 7.560, p= 0), better physical activity status and exercise capacity(6-MWT: 165.71 ± 44.74 vs. 135.65 ± 35.39, p=0.030), and higher exercise adherence 1 month and 3 months after discharge (p < 0.05).

Conclusion: The perioperative cardiopulmonary integrated rehabilitation in TAVR patients is safe and effective. The rehabilitation program reduced the occurrence of complications, promote patients' early mobilization and discharge, improve patients' exercise capacity, and restore patients to daily life. Early rehabilitation in hospital and regular follow-up can help patients adhere to rehabilitation program after discharge, prolong rehabilitation benefits, improve quality of life, and have high health and socio-economic value.

首诊冠心病患者运动恐惧现状及影响因素分析

彭沥枢 [1] 王彦 [1]

1. 河北大学

2. 河北大学附属医院

目的 探究首诊冠心病患者运动恐惧的现状及影响因素，为制订针对性的心脏康复干预策略提供依据。

方法 本研究采用横断面研究设计。采用便利抽样方法，选取 2024 年 12 月 -2025 年 4 月于河北大学附属医院心内科就诊且符合纳排标准的 310 例冠心病患者作为研究对象。采用一般资料调查表、心脏病患者运动恐惧量表（TSK-heart）、锻炼社会支持量表 (ESS)、医学应对方式问卷 (MCMQ)、感知运动益处量表 (EB)、特质焦虑量表 (T-AI) 进行调查。应用 Spearman 相关分析探讨运动恐惧与锻炼社会支持、感知运动益处、特质焦虑之间的相关性；采用多元线性回归分析来明确运动恐惧的影响因素。

结果 首诊冠心病的患者运动恐惧得分为（42.55±6.488）分，其中 230 例（74.5%）患者运动恐惧得分≥ 38 分，表明运动恐惧发生率处于中等偏高水平。相关性分析结果显示，运动恐惧得分与锻炼社会支持呈负相关（r=-0.566，p < 0.01），与感知运动益处呈负相关（r=-0.655，p < 0.01），与焦虑特质呈正相关（r=0.550，p < 0.01）。多元线性回归结果表明，职业状态、合并症数量、疾病类型、医学应对方式、感知运动益处、焦虑特质等对运动恐惧的影响差异具有统计学意义（p < 0.05）。

结论 首诊冠心病患者运动恐惧得分水平较高，且受到职业状态、合并症数量、疾病类型、医学应对方式、感知运动益处、焦虑特质等多种因素的影响。提示医护人员应重点关注患者心理状态与运动的认知，通过增强对患者运动的支持，提高患者对于运动益处的感知、制订个性化的康复计划降低冠心病患者运动恐惧水平，保障心脏康复的有效实施。

Long-term Efficacy and Safety of Moderate-Intensity Continuous Training on the Improvement of Cardiopulmonary Function in Patients After Transcatheter Aortic Valve Replacement: an analysis of the extended follow up of the ENERGY Study

Yu-Shan Li, Qiang Ren, Xing-Bo Mu, Kai Xu, Yan-Chun Liang, Jian Zhang, Geng Wang, Yan-Xia Wang, Cai-Lian Wang, Yi Zhang, Sheng-Yi Wang, Quan-Yu Zhang, Ya-Ling Han

General Hospital of Northern Theater Command

Background: The first phase of the ENERGY study showed that moderate-intensity continuous training (MICT) had a positive effect on the cardiopulmonary function and physical capacity of patients after transcath-

eter aortic valve replacement (TAVR). However, the long-term efficacy and safety of MICT in patients after TAVR are still unclear.

Design: A randomized controlled trial.

Objectives: To evaluate the effect at 12 months of MICT on the improvement of cardiopulmonary function and quality of life in patients undergoing TAVR.

Methods: A total of 66 patients enrolled in the ENERGY study were extended training to 12 months. Patients in the MICT group were scheduled 3 times per week for 12 months in the intervention group. Patients in the control group received one-time advice on physical activity according to the current guideline. The primary endpoint in the present study was the change in peak VO_2 from 3-month to 12-month. The secondary endpoints included changes from 3 to 12 months in cardiopulmonary exercise testing parameters, echocardiographic measures, laboratory parameters, 6-minute walk distance, SF-12 health survey scores, and NYHA functional class, with all assessments performed using the same methodologies as in the original trial. The safety endpoint was the major adverse cardiovascular and cerebrovascular event (MACCE) and its components of all-cause mortality, recurrent myocardial infarction (MI), ischemia-driven target vessel revascularization, and stroke. Following the ESC guidelines, the participants in the present study were divided into the LVEF < 50% cohorts and LVEF ≥ 50% cohorts according to the LVEF assessed by echocardiology. Study outcomes were analyzed in the intention-to-treat (ITT) population.

Results: The ENERGY study enrolled 66 patients between 20 August 2021 and 28 February 2022. The ITT population was 54.55% male, with a mean age of 70.65 ± 6.60 years. After 12 months, the change in peak VO_2 (1.58 ml/kg/min, 95% CI 0.08 to 3.09, P = 0.040), peak MET (0.56, 95% CI 0.20 to 0.93, P = 0.003), VO_2AT (1.55 ml/kg/min, 95% CI 0.80 to 2.30, P < 0.001), METAT (0.35, 95% CI 0.10 to 0.61, P = 0.007), 6MWD (21.24 m, 95% CI 7.10 to 35.39, P = 0.004), and mental component summary of SF-12 (10.47, 95% CI 0.48 to 20.45, P = 0.040) were higher in the MICT group compared with the control group. In addition, there were no differences of change in echocardiographic, laboratory parameters and physical component summary of SF-12 between the 2 groups. Among the LVEF ≥ 50% cohort, patients in the MICT group showed significant improvements in the MET (12-month: 0.76, 95% CI 0.35 to 1.17, P = 0.001; 3-month: 0.68, 95% CI 0.38 to 0.98, P < 0.001), VO_2 at anaerobic threshold (12-month: 1.71 ml/kg/min, 95% CI 1.04 to 2.38, P < 0.001; 3-month: 2.25 ml/kg/min, 95% CI 1.39 to 3.11, P < 0.001), MET at anaerobic threshold (12-month: 0.34, 95% CI 0.06 to 0.62, P = 0.018; 3-month: 0.70, 95% CI 0.44 to 0.95, P < 0.001), peak O_2 pulse (12-month: 1.36 mL/beat, 95% CI 0.14 to 2.58, P = 0.030; 3-month: 1.13 mL/beat, 95% CI 0.42 to 1.84, P = 0.003). Moreover, a significant change in favor of the MICT group was also observed for the 6MWT (12-month: 27.11 m, 95% CI 9.79 to 44.42, P = 0.003; 3-month: 22.58 m, 95% CI -3.08 to 48.25, P = 0.083) and mental component summary of SF-12 (12-month: 12.91, 95% CI 2.35 to 23.48, P = 0.018; 3-month: -0.06, 95% CI -13.50 to 13.38, P = 0.993).

Conclusions: To sum up, MICT 12 months in patients after TAVR resulted in maintained significant long-term improvements in cardiopulmonary function and quality of life, compared to MICT 3 months. Especially for patients with LVEF returned to normal after TAVR, are especially salient. The present results provide the first insight into the utmost clinical significance of MICT in improving cardiopulmonary function and quality of life following a TAVR procedure over the long term.

Key words: Transcatheter Aortic Valve Replacement (TAVR); Cardiac Rehabilitation (CR); Moderate-Intensity Continuous Training (MICT); Cardiopulmonary Exercise Testing (CPET); quality of life (QoL)

Comparative effects of traditional Chinese exercises on cardiac rehabilitation in patients after percutaneous coronary intervention: A Systematic Review and Network Meta-Analysis

Jiale Wang, Long-Cheng Liu, Li-Hong Ma

Fuwai Hospital, Chinese Academy of Medical Sciences

Comparative effects of traditional Chinese exercises on cardiac rehabilitation in patients after percutaneous coronary intervention: A Systematic Review and Network Meta-Analysis

Wang Jiale, Liu Longcheng, Ma Lihong

(Fuwai Hospital, Chinese Academy of Medical Sciences and Peking Union Medical College)

Background: A global burden of disease study showed that among the top 10 causes of death in the global population in 2021, ischaemic heart disease (IHD) tops the list, with 8,990,000 (8,290,000-9,550,000) deaths and an age-standardized mortality rate of 108.7 per 100,000 people. Percutaneous coronary intervention (PCI) is one of the most important therapies in patients with coronary heart disease (CHD). However, there are still many problems, such as in-stent restenosis, recurrent angina pectoris, postoperative anxiety and depression. Traditional Chinese exercise (TCE) therapies belong to the aerobic exercise of low and medium intensity, which may have a certain efficacy on cardiac rehabilitation of patients after PCI. The objective of this network meta-analysis is to compare the impacts of different traditional Chinese exercise on cardiac function and exercise capacity in patients after PCI.

Methods: Chinese National Knowledge Infrastructure Database (CNKI), Wanfang Database, Chinese Science and Technique Journals Database (VIP), Chinese Biomedical Literature Database (Sinomed), Yiigle databases, PubMed, EMBASE, and the Cochrane Library were searched from inception to May 2025, to collect randomized controlled trials (RCTs) about TCE interventions for patients after PCI. We screened the literatures and extracted the data. The Cochrane Collaboration "Risk of bias 2.0" assessment tool will be used to assess the bias of RCTs. Network meta-analysis will be conducted using Stata17.0 software. For continuous outcomes, WMD or SMD along with their 95% CIs will be utilized. The effectiveness of the interventions will be ranked using the Surface Under the Cumulative Ranking (SUCRA) curve, with a larger area under the curve indicating greater effectiveness of the intervention.

Results: A total of 38 studies were included in this network meta-analysis that tested six different TCE interventions and included 3,343 patients. The quality assessment of included studies revealed that one was high risk and 37 studies had some concerns. TCE interventions included Baduanjin (BDJ), Tai Chi (TC), Wu Qinxi (WQX), Tai Chi Yunshou (TCYS), Tai Chi Ball + Baduanjin (TCB + BDJ), and Baduanjin + Yi Jinjing (BDJ + YJJ). The results of network meta-analysis and surface under the cumulative ranking curve(SUCRA) showed that with conventional treatment(CT) as a common control, BDJ+CT was the most effective for LVEF, NT-proBNP level and 6MWD. The SUCRA values were 81.1%, 86.5% and 75.5% respectively. The traditional meta-analysis results revealed that BDJ + CTs were significantly different compared with CTs alone for LVEF (WMD=6.28, 95% CI [4.90, 7.67]), NT-proBNP level (SMD=-2.35, 95% CI [-3.64, -1.06]), and 6MWD (WMD=65.19, 95% CI [38.91,91.48]). Nineteen studies reported 55 adverse events (AEs) in TCE + CT groups, and 141 AEs in CT groups.

Conclusions: In conclusion, the combination of TCE and CTs approaches may enhance the efficacy of CTs on cardiac rehabilitation in patients after PCI. Based on the NMA result, BDJ + CTs may be a more effective treatment and deserves further investigation. However, the differences in many comparisons between TCE interventions did not reach statistical significance; therefore, further high-quality studies are required to validate these findings.

Keywords: traditional Chinese exercises; cardiac rehabilitation; percutaneous coronary intervention; network Meta-Analysis

EETs 介导有氧运动对心肌梗死后心脏淋巴管重塑的影响和机制

沈莉

中南大学湘雅二医院

目的 心脏淋巴管的功能在心肌梗死（myocardial infarction，MI）后进展为心力衰竭的过程中发挥决定性作用。有氧运动可改善 MI 后心室重构并延缓心衰进展，但其具体分子机制及信号通路尚不明确。本研究旨在探讨有氧运动是否通过调控心脏淋巴管病理性重塑改善 MI。

方法 我们检测了不同时间有氧运动干预对 MI 小鼠的心脏淋巴管结构和功能的影响，并分别使用药理学抑制（淋巴管生成抑制剂 MAZ51）和外科干预（心脏引流淋巴管结扎）模型来探究淋巴管系统在有氧运动改善 MI 后心功能中的作用。通过单细胞 RNA 测序（scRNA-seq）初步揭示有氧运动调控心脏淋巴管功能改善 MI 的潜在机制，并结合体内外实验和各种分子生物学技术进行进一步验证。

结果 MI 小鼠的心脏淋巴管系统发生病理性重塑，具体表现为淋巴管异常扩张（面积 >500μm^2）、渗漏加重及运输功能下降。有氧运动可改善 MI 小鼠的心脏淋巴管功能障碍，减轻 MI 后心衰，并以中等强度有氧运动 4 周后效果最为显著。更重要的是，抑制淋巴管功能可显著削弱有氧运动对 MI 小鼠心肌纤维化和收缩功能的改善效应。scRNA-seq 结果提示，有氧运动疗效不依赖淋巴管内皮细胞（lymphatic endothelial cells，LEC）数量增加，而是功能重塑。进一步的研究表明，环氧二十碳三烯酸（epoxyeicosatrienoic acids，EETs）血浆水平降低会加重 MI 小鼠的心脏淋巴管病理性重塑和心功能障碍，并减弱有氧运动对 MI 小鼠的改善效应。反之，增加 MI 小鼠体内 EETs 水平可逆转其心脏淋巴管的病理性改变，减轻心脏重构和心室功能障碍。体外实验证实，增加 hLEC 中 EETs 浓度可恢复其在低氧条件下受到抑制的增殖、迁移及管形成能力。

结论 我们的研究结果表明，有氧运动通过升高 EETs 水平，改善心脏淋巴管病理性重塑，进而减轻 MI 后心衰。

Interpretable machine learning identifies peak VO2 as a key predictor of MACE events in patients with valvular heart disease.

Bing-Qing Bai[1,2], Jun-Shuo Zhu[1,2], Yu-Ting Liu[1], Hao-Feng Zhou[1], Ming-Yu Xu[1,3], Jin-Na Chang[1], Pei-Hua Cao[4,6,7], Rui Li[4], Kai-Xuan Lin[5], Huan Ma[1,2]

1. Department of Cardiology, Guangdong Provincial People's Hospital (Guangdong Academy of Medical Sciences), Southern Medical University, Guangzhou, China

2. South China University of Technology, Guangzhou International Campus, Guangzhou, China

3. Department of Internal Medicine, Guangzhou Red Cross Hospital, Jinan

University, Guangzhou, China

4. Department of Pulmonary and Critical Care Medicine, Zhujiang Hospital, Southern Medical University, Guangzhou, China

5. Department of Cardiology, Zhongshan Hospital of Traditional Chinese Medicine Affiliated to Guangzhou University of Traditional Chinese Medicine. (Zhongshan Hospital of Traditional Chinese Medicine), Zhongshan, Guangdong, China

6. Clinical Research Center, Zhujiang Hospital, Southern Medical University, Guangzhou, China

7. Department of Biostatistics, School of Public Health, Southern Medical University, Guangzhou, China

Abstract

Background:

Valvular heart disease (VHD) represents a significant global health burden and is a major contributor to morbidity and mortality, particularly in aging populations. Despite advances in diagnostic modalities and interventional therapies, timely identification of high-risk individuals who may develop major adverse cardiovascular events (MACE) remains challenging. Traditional risk prediction models often rely on static clinical and echocardiographic parameters, which may not fully capture functional impairments or exercise capacity. Cardiopulmonary exercise testing (CPET) has emerged as a powerful, non-invasive tool that reflects the integrative responses of the cardiovascular, pulmonary, and muscular systems, offering valuable prognostic insights. However, the integration of CPET-derived parameters into predictive models using advanced machine learning (ML) techniques remains underutilized. This study aims to develop and validate an interpretable ML-based framework that combines CPET and clinical data to predict MACE risk in patients with VHD, while identifying key prognostic features to enhance individualized risk stratification and guide clinical decision-making.

Methods:

We retrospectively analyzed electronic health record data from a cohort of 931 patients diagnosed with VHD at a tertiary cardiovascular center. The dataset included demographic information, comorbidities, medication history, echocardiographic findings, and CPET variables, with particular attention to peak oxygen consumption per kilogram (peak VO_2/kg). Model-based unsupervised clustering was performed to stratify patients into subgroups with distinct risk profiles. Supervised ML models including Random Forest and XGBoost were trained to predict the occurrence of MACE, defined as a composite of cardiovascular death, heart failure hospitalization, stroke, and unplanned cardiac interventions. Model performance was assessed using the area under the receiver operating characteristic curve (AUC), sensitivity, and specificity. SHapley Additive exPlanations (SHAP) were applied to interpret model predictions and quantify the contribution of individual variables. Additionally, decision tree analysis was employed to derive clinically interpretable thresholds for risk stratification. Kaplan-Meier survival analysis was used to evaluate outcome differences among the stratified subgroups over a median follow-up period of 45.6 months.

Results:

The ML clustering algorithm identified three distinct prognostic subgroups with significantly different survival trajectories (log-rank $p < 0.001$). SHAP analysis consistently ranked peak VO_2/kg and age as the top predictors of MACE across both ML models. The Random Forest and XGBoost classifiers demonstrated excellent discriminative ability, achieving AUCs of 0.974 and 0.979, respectively. Decision tree analysis revealed clinically relevant peak VO_2/kg thresholds: <14 mL/kg/min for high risk, 14–23 mL/kg/min for intermediate risk, and ≥ 23 mL/kg/min for low risk. Kaplan-Meier analysis showed that patients with peak VO_2/kg ≥ 23 had significantly better survival outcomes, whereas those with values <14 had the highest incidence of MACE during follow-up. These stratified risk groups maintained distinct prognostic separation throughout the observation period, supporting the stability and clinical utility of the derived thresholds.

Conclusions:

This study demonstrates the value of integrating CPET-derived functional parameters with machine learning techniques to enhance risk prediction for MACE in patients with valvular heart disease. The interpretable ML framework, supplemented with SHAP analysis, not only achieved high predictive accuracy but also revealed key prognostic drivers that are clinically actionable. In particular, peak VO_2/kg emerged as a robust and reproducible indicator for long-term cardiovascular outcomes. These findings support the incorporation of CPET into routine risk assessment protocols for VHD patients and lay the groundwork for precision medicine approaches in valvular disease management. Future prospective and multi-center studies are warranted to validate these results and explore the impact of early intervention strategies guided by CPET-based risk stratification.

Keywords:

machine learning, cardiopulmonary exercise testing, valvular heart disease, major adverse cardiovascular events, risk prediction, interpretable models, SHAP

基于个性化护理方案的心血管疾病康复效果提升研究

彭娜

西安交通大学第一附属医院

摘要：目的： 分析个性化护理在心血管疾病中康复效果的应用分析。

方法： 选择取我院就诊的 100 例心血管疾病患者，研究对象选自 2024 年 1 月至 2024 年 10 月就诊心血管内科的患者，观察组随机分为 50 例患者、对照组随机分为 50 例患者（随机数字表法）。对照组予以临床护理常规常规护理，观察组予以本研究个性化护理，对 100 例患者护理满意度、日常生活能力评分、生存质量评分、并发症发生情况进行分析比较。

结果： 观察组护理患者满意度（96.00%）高于对照组，P<0.05，日常生活能力评分（73.26±2.57 分）高于对照组，差异显著（P<0.05），生存质量评分（情绪功能：72.36±3.98 分、躯体功能：71.06±4.48 分、认知功能评分：69.69±2.48 分、角色功能：72.25±4.16 分、整体功能：72.36±2.75 分）高于对照组，差异显著（P<0.05），并发症发生例数（2 例）低于对照组，P<0.05，差异存在显著性。

结论： 个性化护理在心血管疾病护理中具有显著效果，可提升护理满意度、日常生活能力评分以及生存质量评分，有效减少并发症发生例数，安全且有效，值得临床采纳使用。

OPT-CAD Score Combined with Cardiopulmonary Exercise Testing Parameters to Evaluate Long-Term Prognosis in Patients with Coronary Artery Disease

Qiang Ren

State Key Laboratory of Frigid Zone Cardiovascular Disease, Cardiovascular Research Institute and Department of Cardiology, General Hospital of Northern Theater Command

Objective: To optimize the Optimal antiPlatelet Therapy for Chinese patients with Coronary Artery Disease (OPT-CAD) scoring system by incorporating cardiopulmonary exercise testing (CPET) parameters for more accurate prediction of long-term ischemic event risk in Chinese patients with coronary artery disease (CAD).

Methods: The present retrospective study enrolled 8,807 patients hospitalized for CAD who underwent CPET between February 2016 and February 2023. Patients with incomplete case information or follow-up data, hematological disorders, chronic respiratory diseases, chronic liver or kidney failure, and malignant tumors were excluded. Patients were stratified into low-risk (0-90 points) and medium to high risk (≥ 91 points) groups based on the OPT-CAD score. The primary endpoint was the first major adverse cardiovascular event (MACE) within 5 years post-discharge, defined as a composite of cardiac death, myocardial infarction (MI), and stroke. LASSO regression and COX regression analyses were used to identify CPET parameters associated with MACE to construct a prediction model, which was visualized as a nomogram. The predictive value and clinical utility of the optimized model were evaluated through the receiver operating characteristic (ROC) curve, with calculation of the area under the ROC curve (AUC) and C-index, as well as calibration curves and clinical impact curves (CIC). Comparative ROC curves, decision curve analysis (DCA), and calculating net reclassification improvement (NRI), and integrated discrimination improvement (IDI) were plotted to further validate the improvement degree of the optimized model.

Results: A total of 8,419 coronary heart disease patients were included (57.26 ± 8.93 years old, 76.96% male). Among them, 7,191 were low-risk (0-90 points) and 1,228 were medium-high risk (≥ 91 points). There were 271 (3.22%) MACE occurrences, including 82 (0.97%) cardiac deaths, 83 (0.99%) MIs, and 106 (1.26%) strokes. In the multivariate COX regression analysis, peak oxygen uptake, carbon dioxide ventilatory equivalent slope, and heart rate reserve were independent factors associated with MACE. The optimized model's time-dependent ROC curve areas at 1, 3, and 5 years were 0.869 (95% CI 0.829, 0.909), 0.843 (95% CI 0.817, 0.870), and 0.837 (95% CI 0.816, 0.859), respectively. Compared to the OPT-CAD model, the optimized model showed improved area under the curve (0.837 vs. 0.685, De-Long test $P < 0.001$), C-index (0.830 vs. 0.677, $P < 0.001$), NRI (0.248, $P < 0.001$), and IDI (0.111, $P < 0.001$). In the low-risk group, the ROC curve comparison showed that the optimized model's area under the curve was significantly higher than the OPT-CAD model (0.836 vs. 0.647, De-Long test $P < 0.001$). In the medium-high risk group, the ROC curve comparison showed that the optimized model's area under the curve was significantly higher than the OPT-CAD model (0.820 vs. 0.692, De-Long test $P < 0.001$). In the male subgroup (n = 6,479), ROC curve analysis demonstrated that the optimized model achieved a significantly higher AUC compared to the OPT-CAD model (0.839 vs. 0.689; DeLong's test, $P < 0.001$). Similarly, in the female subgroup (n = 1,940), the optimized model exhibited superior discriminative performance over the OPT-CAD model, with AUC values of 0.844 and 0.714, respectively (DeLong's test, $P < 0.001$).

Conclusion: The present study demonstrates that peak oxygen uptake, VE/VCO_2 slope, and heart rate reserve are independently associated with long-term ischemic events in CAD patients. The incorporation of these CPET parameters into the OPT-CAD score enhances the assessment of ischemic event risk. The optimized model demonstrated robust performance across all subgroups, including low-risk and medium-high risk populations, as well as male and female cohorts.

危重急性失代偿性心力衰竭患者的早期康复：随机对照研究

刘彬彬 戴翠莲 吴林静 李家华

厦门大学附属心血管医院

目的: 对于入住心脏重症监护病房(CICU)的危重急性失代偿性心力衰竭(ADHF)患者，在急性期启动心脏康复（CR）的最佳时机和方法仍不明确。 本研究评估了 CR 对 CICU 中危重 ADHF 患者身体功能和再住院率的益处。

方法： 这是一项单中心、随机、对照、单盲试验。在 2021 年 3 月至 2022 年 9 月期间，招募了 120 名入住 CICU 的危重重度 ADHF 患者，并在接受短期治疗后按 1:1 比例随机分组。所有患者均接受为期 6 个月的随访，研究者对分组情况设盲。 干预组患者在 CICU 住院期间接受一种专为 ADHF 患者设计的早期渐进式个体化心脏康复计划（称为 AHF-CR）。对照组患者接受常规护理。主要结局指标为出院时的简易体能状况量表（SPPB）评分和六个月内全因再住院率。采用意向性治疗（ITT）原则分析这些结局指标，包括随机化后的所有患者。

结果： 患者平均年龄为 68.6 ± 12.3 岁，66.7% 为男性。随机分组时，对照组 81.7% 的患者和干预组 71.7% 的患者观察到肺部湿啰音。此外，51.5% 的患者动脉血氧分压与吸入氧浓度比值低于 300 mmHg。超过 30% 的患者接受了静脉血管活性药物治疗，超过 70% 的患者接受了袢利尿剂治疗。SPPB 评分显示中位数差值为 1（95%CI: 0 ~ 2; p = 0.163）。两组间的六个月再住院率相似 [26.6% vs. 28.3%；风险比：1.005 (95%CI: 0.508 ~ 1.989)；p = 0.989]。探索性分析显示，干预组的 Perme ICU 移动能力评分更高，中位数差值为 2.76（95%CI: 0.77 ~ 4.74；校正后 p = 0.036）。

结论： 在这项针对危重 ADHF 患者的临床试验中，AHF-CR 计划是可行的。尽管该计划未能显著改善 SPPB 评分或降低再住院率，但它可能提供潜在的身体功能益处，包括增强活动能力。

基于快速康复理念的多学科协作运动康复模式对心脏术后患者心理应激及活动功能的影响研究

义茹

苏州大学附属第一医院

目的：本研究旨在探究心脏术后患者的临床干预策略，重点评估基于快速康复理念的多学科协作运动康复模式对患者心理应激水平的改善效果，并分析其对活动功能的影响。

方法：通过系统化样本筛选标准（明确纳入与排除标准），纳入 120 例心脏手术患者。采用奇偶分组法将患者分为两组：对照组（n=60）接受常规术后干预，试验组（n=60）实施基于快速康复理念的多学科协作运动康复模式（涵盖康复科、心内科、心理科等多学科团队协作）。通过标准化量表（如焦虑抑郁量表、活动功能评定量表等）及临床指标（呼吸机使用时间、恐动症发生率等）评估两组干预效果。

结果：

心理应激与活动功能：试验组患者干预后心理应激量表评分较对照组显著降低（P < 0.05），活动功能评分（如 6 分钟步行距离、日常生活能力量表）显著提升（P < 0.05）。

临床指标：试验组呼吸机使用时间为（4.2±1.3）天，短于对照组的（6.8±2.1）天（P < 0.05）；恐动症发生率为 15.0%（9/60），低于对照组的 35.0%（21/60），组间差异具有统计学意义（P < 0.05）。

结论：基于快速康复理念的多学科协作运动康复模式可显著改善心脏术后患者的心理应激状态，提升活动功能，缩短呼吸机使用时间，并降低恐动症发生率。该模式通过多学科协同干预，实现了生理功能康复与心理状态调节的双重优化，为心脏术后患者的快速康复提供了新的临床实践路径。

进行 6 分钟居家运动对冠心病患者血清 Lp-PLA2 和相关血脂成分影响研究

宫宇婷 张子新 (心脏康复学组委员)

中国医科大学附属第一医院

目的：通过对冠心病患者进行 6 分钟居家运动模式的干预，观察血清脂蛋白相关磷脂酶 A2 水平和血脂等相关指标的动态变化以及患者短期随访（6 个月）的主要心血管不良事件，旨在明确冠心病患者 Lp-PLA2 的水平以及其与其他生物标志物的关系和联合预测斑块稳定性及 MACE 的价值，同时证实 6 分钟居家运动模式对 CHD 患者的预后价值与可行性。

研究方法：收集确诊的 CHD 患者，除外随访损失，最终入选患者 86 人，采用前瞻性病例对照研究，按单双号交替方式入组，运动康复组共 44 例，非运动康复组共 42 例。同时又将入选患者根据冠心病类型分为急性冠状动脉综合征组与慢性冠状动脉综合征组。收集患者的性别、年龄、体重指数、吸烟史、高血压史、糖尿病史、运动习惯等，测定患者的 Lp-PLA2 水平及其他临床指标，其中 E 组患者每日早晚进行两次 6 分钟居家运动康复，自选时间段，每次运动保证 6 分钟的最大耐受强度运动，预热和恢复时间患者根据自身情况决定，NE 组患者进行常规健康教育。所有患者均通过电话、微信及门诊进行指导随访，均于 6 个月后于我院门诊复查 Lp-PLA2 水平及其他相关指标。

结果：（1）基线及 24 周后，E 组与 NE 组之间的性别、高血压、糖尿病、C 反应蛋白、总胆固醇、甘油三酯、高密度脂蛋白胆固醇、低密度脂蛋白胆固醇、空腹血糖等均无明显统计学差异（P>0.05）。（2）E 组与 NE 组基线时的 Lp-PLA2 水平之间无统计学差异（P>0.05）。24 周后，两组 Lp-PLA2 水平均下降，E 组 Lp-PLA2 水平的下降差值△明显高于 NE 组（P<0.001）。（3）基线时 ACS 组的 Lp-PLA2 水平高于 CCS 组（P<0.05）。24 周后各组的 Lp-PLA2 水平与组内基线时相比有统计学上的显著差异（P<0.001）。24 周后两组的 Lp-PLA2 水平及运动前后的 Lp-PLA2 水平变化的差值△之间没有统计学上的差异（P>0.05）。（4）基线时 ACS-E 组的 Lp-PLA2 水平高于 CCS-E 组（P<0.05）。24 周后 ACS-E 组、CCS-E 组的 Lp-PLA2 水平与组内基线时相比有统计学上的显著差异（P<0.001）。在运动前后的 Lp-PLA2 水平变化的差值△比较中，ACS-E 组下降差值△最大，与 ACS-NE 组、CCS-E 组相比均有统计学上的差异（P<0.001，P<0.01）；并且 ACS-NE 组下降差值△大于 CCS-NE 组（P<0.001）。(5) 多变量线性回归分析表明，6 分钟居家运动与 Lp-PLA2 水平独立相关。(6) E 组患者 2 例在随访期间发生 MACE 事件，NE 组有 4 例在随访期间发生 MACE 事件。

结论：Lp-PLA2 与冠心病的稳定性相关，ACS 患者较 CCS 患者的 Lp-PLA2 水平更高。24 周的 6 分钟居家运动干预后，ACS 患者的 Lp-PLA2 水平变化更明显，下降更多。运动组的冠心病患者 MACE 事件更少。6 分钟居家运动安全性有保证。

心理干预在平板运动试验诊断中的应用

陈晓旭

中国人民解放军北部战区总医院

目的 探讨心理干预在平板运动试验中的作用及其对患者生理和心理状态的影响。**方法** 筛选 2024 年 10 月至 2025 年 4 月因胸痛就诊于北部战区总医院心血管内科行平板运动试验患者 200 人，年龄 18-65 岁，无严重器质性疾病且自愿参与本次研究的成年人作为研究对象，随机分为心理干预组 100 人，对照组 100 人。心理干预组采用多模态心理干预措施，结合放松训练、CBT 和正念冥想三种方法，分别于平板运动试验前，运动中及恢复期进行心理干预。对照组则由专业医务人员提供标准化口头说明，告知注意事项并解答疑问。**结果** 经过对患者的心理干预，在心理状态改善方面，心理干预组成员的焦虑评分显著下降，表现出更好的情绪稳定性；而对照组未见明显变化。进一步分析发现，心理干预组中有 70% 的个体表示对运动试验的信心有所增强，愿意积极配合医务人员完成测试。在生理反应优化方面，心理干预组在平板运动试验期间的心率变异性（HRV）指标优于对照组，提示前者交感神经兴奋度相对较低，更利于维持正常的生理机能。此外，心理干预组的最大摄氧量（VO2max）也有一定幅度的增长，显示出更强的心肺耐力。在整体表现提升方面，心理干预组顺利完成整个运动试验的比例 89%，远高于对照组的 68%; 同时,心理干预组的测试结果偏差较小,提高了诊断的准确性。**结论** 适当的心理干预可以提高患者的运动表现和耐受性，改善其心理健康状况，并有助于提升临床诊断的准确性。本论文为未来在双心医学领域中进一步探索心理因素对运动试验影响提供了理论依据。

基于心肺运动试验与机器学习的瓣膜术后低心排血量综合征预测模型构建

浩锋 [1,2] 柯浩鹏 [3] 郭兰 [4] 马欢 [4] 汪芳 [1]

1. 北京医院

2. 北京协和医学院

3. 广州华立学院

4. 广东省人民医院

目的： 识别心脏瓣膜手术后低心排血量综合征的关键危险因素，并基于机器学习算法构建预测模型，评估其预测效能。

方法： 回顾性收集广东省人民医院 703 例接受心外科瓣膜手术患者的临床资料（训练集 492 例，验证集 211 例）。纳入基础信息、血液检验、心脏超声、心肺运动试验（CPET）及手术相关参数等 72 项指标。首先采用最小绝对收缩和选择算子（LASSO）回归筛选重要预测因子，随后应用逻辑回归（LR）、支持向量机(SVM)、随机森林(RF)、梯度提升决策树(GBM)及极端梯度提升(XGBoost)五种机器学习算法构建预测模型，并采用网格搜索结合 5 折交叉验证确定模型的最优超参数。使用受试者工作特征曲线下面积（AUC）、校准曲线及临床决策曲线分析评估模型的性能，筛选最优模型。

结果： 703 例患者中，87 例（12.4%）术后发生低心排血量综合征。LASSO 回归识别出 9 个关键预测因子：合并心房颤动、术前血红蛋白水平、直接胆红素、峰值摄氧量、运动中出现心肌缺血、EuroSCORE II 评分、同期行冠状动脉旁路移植术、术后 30 分钟肌酸激酶同工酶及乳酸水平。XGBoost 模型展现出最佳预测性能：训练集 AUC 为 0.93（95% CI: 0.89-0.96），验证集 AUC 为 0.83（95% CI: 0.78-0.89）。校准曲线显示 XGBoost 模型的预测概率与实际发生率具有良好的一致性。临床决策曲线分析显示，在 0.12 至 0.85 的风险阈值范围内，XGBoost 模型的净获益显著高于“全干预”和“全不干预”策略，表明其良好的临床实用价值。

结论： 本研究成功识别了瓣膜术后低心排血量综合征的重要预测因素。结合 CPET 指标与机器学习技术构建的 XGBoost 预测模型，在训练集和验证集中均表现出优异的预测能力与临床实用性，可作为识别心脏瓣膜手术后低心排血量综合征高危患者的有效工具，有助于早期干预。

合并自主神经功能紊乱的非阻塞性冠脉疾病患者临床特征研究

许明煜 [1] 王柔 [1] 常金娜 [1] 白冰清 [1] 刘于庭 [2] 廖映雪 [1] 周浩锋 [1] 刘凤瑶 [1] 郭兰 [1] 马欢 [1]

1. 广东省医学科学院 广东省人民医院

2. 深圳市人民医院

目的 自主神经系统调控心率、血压等非自主性心血管功能，其功能紊乱（Autonomic Dysfunction，AD）表现为交感神经过度激活、迷走神经张力减弱，常导致静息心率升高、运动后心率恢复延迟及心率变异性下降，已被证实是多种心血管疾病不良预后的独立预测因子。部分无明显冠脉狭窄但出现心绞痛症状（Angina with no obstructive coronary disease，ANOCA）的患者常合并AD，提示二者在病理生理机制上可能相关。然而，当前关于 AD 在 ANOCA 人群中的患病率、临床特征及危险因素的研究较少。

方法 本研究为回顾性病例对照研究，纳入在广东省人民医院接受心肺运动试验（Cardiopulmonary exercise test，CPET）的女性 ANOCA 患者 81 例。依据 CPET 中运动后 1 分钟心率恢复≤ 12 次 / 分或者 2 分钟心率恢复≤ 22 次 / 分为 AD 判断标准，分为 AD+ 组（44 例）和 AD- 组（37 例）。收集患者的一般临床信息、心理状态问卷、外周血生化指标、CPET 结果、运动负荷心电图、腺苷负荷下 PET-CT 及血管内皮功能检测结果。

结果 AD 在该 ANOCA 人群中的患病率为 54.32%。AD+ 组平均年龄为 55.5±8.6 岁，高于 AD- 组的 51.1±7.9 岁（P=0.021）。两组在药物使用、BMI 等方面无显著差异。AD+ 组运动能力明显下降，其最大运动负荷为 80.9±18.5W，低于 AD- 组的 96.7±20.8W（P=0.001）。此外，AD+ 组的补体 C3、C4，铜蓝蛋白、C 反应蛋白、碱性磷酸酶、腺苷脱氨酶（ADA）及甘油三酯水平均显著高于 AD- 组。多因素 Logistic 回归分析表明，血小板计数、补体 C4 及铜蓝蛋白水平与 AD 风险呈正相关关系。线性相关分析亦显示，上述炎症指标与 AD 存在剂量反应关系。

结论 本研究对 ANOCA 合并 AD 患者的临床特征进行了系统分析，发现 AD+ 组合并更高比例的高血压、心律失常、焦虑、抑郁、高压力状态及更多负性生活事件，且运动能力更差。研究进一步明确了炎症在 ANOCA 合并 AD 中的潜在作用，提示铜蓝蛋白和补体 C4 等或可作为预测合并 AD 风险的生物标志物。

短期高强度间歇训练与中等强度连续训练对心血管疾病患者心率恢复和心肺的益处：一项倾向匹配的回顾性研究

宋倩倩

广东省医学科学院 广东省人民医院

背景：当前针对心血管疾病 (CVD, Cardiovascular Disease) 患者的运动干预研究多聚焦于 8 至 12 周及以上周期的训练方案，已明确其在提升心肺功能和改善临床预后方面的有效性。然而，在实际心脏康复实践中，长周期干预常受到资源限制、时间成本及患者依从性等因素的制约。相较而言，短期运动干预在实施可行性与临床应用方面具有更大优势。值得关注的是，关于高强度间歇训练 (HIIT, High-Intensity Interval Training) 与中等强度连续训练 (MICT, Moderate-Intensity Continuous Training) 在短周期内生理效益的直接比较，目前尚缺乏系统证据。

目的：本研究旨在评估短期 HIIT 与 MICT 对 CVD 患者运动后心率恢复 (HRR, Heart Rate Recovery) 与峰值摄氧量 (Peak VO_2) 等关键生理指标的影响，并探讨两种训练模式在干预效果方面是否存在显著差异。

方法：本研究为单中心回顾性队列研究，共纳入 754 例接受运动干预的确诊 CVD 患者。经筛选后，剔除运动次数少于 10 次及缺失心肺运动试验评估数据的个体，最终依据干预方式分为 HIIT 组（n=95）和 MICT（n=125）。采用 1:1 倾向性评分匹配以平衡基线差异后，每组最终纳入 81 例患者。所有受试者均接受为期 4 周的标准化运动康复干预。

结果：干预后，两组患者的 Peak VO_2与 HRR 均较基线显著改善 (p<0.05)。其中，HIIT 组 Peak VO_2平均提升为 3.04±3.02ml·min^{-1}·kg^{-1}，MICT 组为 3.55±4.08ml·min^{-1}·kg^{-1}。另外，HIIT 组的 HRR 改善幅度分别为 4.07±9.66bpm；MICT 组改善了 3.97±11.4bpm，两组间差异无统计学显著性 (p>0.05)。此外，干预后，两组的 Peak VO_2和 HRR 变化值具有显著相关性，HIIT 组的相关性更强 (r=0.396，p<0.001)，MICT 组的相关性较弱但仍具有统计学意义 (r=0.223)，p<0.05）。

结论：在短期干预背景下，两种运动模式均能有效改善 CVD 患者的 Peak VO_2和 HRR，且两者效果相近。鉴于短周期干预在临床实践中的可行性与时间优势，运动处方的制定应综合患者个体特征进行个性化选择，而非固定采用单一训练模式。

Protective effect of high-intensity interval exercise on cardiac damage induced by hyperlipidemia

Hong-Yang Liu[1], Ri-Hong Huang[1], Cheng-Si Qian[2], Li-Yue Zhu[2]

1. The First Affiliated Hospital of Dalian Medical University

2. Zhejiang Province Rongjun Hospital

Protective Effects of High-Intensity Interval Training on Hyperlipidemia-Induced Cardiac Injury: Mechanisms and Comparative Efficacy

Abstract:

Background:Hyperlipidemia, characterized by elevated levels of blood lipids or lipoproteins, is a significant global health issue and a major risk factor for cardiovascular diseases (CVDs). It exacerbates atherosclerosis, cardiac lipid accumulation, and impaired cardiac function through mechanisms involving oxidative stress, inflammation, and fibrosis. Exercise, particularly high-intensity interval training (HIIT), has emerged as a promising non-pharmacological intervention for mitigating hyperlipidemia-related cardiac damage. However, the comparative efficacy of HIIT versus moderate-intensity continuous training (MICT) in hyperlipidemia-induced cardiac injury remains to be fully elucidated. This study aims to comprehensively investigate the cardioprotective effects of HIIT and MICT in a hyperlipidemic mouse model, with a focus on lipid metabolism, oxidative stress, inflammation, and fibrosis.

Objective:To compare the cardioprotective effects of HIIT and MICT in a hyperlipidemic mouse model, elucidate the underlying mechanisms, and determine which exercise modality offers superior protection against hyperlipidemia-induced cardiac injury.

Methods:A total of 35 male ApoE^{-}/$^{-}$ mice (8 weeks old) were randomly assigned to four groups: (1) Control (normal diet); (2) HFD (high-fat diet); (3) HFD+MICT (high-fat diet + moderate-intensity continuous exercise); and (4) HFD+HIIT (high-fat diet + high-intensity interval exercise). The high-fat diet consisted of 15% lard and 1.5% cholesterol. Exercise protocols were implemented for 12 weeks: HIIT involved 9 sets of 1.5-minute sprints at 85% of maximum running speed, interspersed with 1-minute rest intervals, while MICT involved continuous running at 60% of maximum speed. Serum and cardiac tissues were analyzed for lipid profiles (total cholesterol [TC], triglycerides [TG]), cardiac injury markers (B-type natriuretic peptide [BNP]), oxidative stress markers (SIRT1, SIRT3, NRF2, SOD2), inflammatory cytokines (IL-1β, IL-6, IL-10, IL-18), and fibrosis-related proteins (TGF-β, SMAD3, collagen I/III). Histopathological evaluations were performed using H&E and Masson's trichrome staining.

Results:Metabolic Improvements:HIIT significantly reduced body weight, serum TC, and TG levels compared to the HFD and HFD+MICT groups (P < 0.05). These findings indicate that HIIT effectively ameliorates hyperlipidemia-induced metabolic disturbances.Cardiac Injury Mitigation:HIIT attenuated hyperlipidemia-induced elevations in serum creatinine, blood urea nitrogen, and BNP (P < 0.01), suggesting that HIIT provides substantial protection against cardiac dysfunction and injury.Histopathological Findings:The HFD group exhibited histological changes indicative of severe cardiac damage, including Zenker necrosis, inflammatory infiltration, and fibrosis. These pathological alterations were markedly alleviated by HIIT (P < 0.05 vs. HFD), as evidenced by reduced tissue damage and improved cardiac architecture.Lipid Deposition:HIIT downregulated cardiac lipid transporters (CD36, LOX-1) and macrophage markers (CD68, PPAR-γ) more effectively than MICT (P < 0.05). This suggests that HIIT significantly reduces lipid accumulation and macrophage infiltration in the myocardium, thereby mitigating lipid-induced cardiac injury. Oxidative Stress:HIIT restored antioxidant defenses by upregulating SIRT1, SIRT3, NRF2, and SOD2 (P < 0.05). These results highlight the ability of HIIT to counteract hyperlipidemia-induced oxidative stress, thereby preserving cardiac function and reducing the risk of oxidative damage. Anti-Inflammatory Effects:

HIIT suppressed pro-inflammatory cytokines (IL-1β, IL-6, IL-18) while enhancing anti-inflammatory IL-10 (P < 0.05). This dual action of HIIT in modulating the inflammatory response underscores its potential to mitigate inflammation-driven cardiac damage. Fibrosis Suppression:HIIT reduced collagen I/III, TGF-β, and SMAD3 expression, outperforming MICT (P < 0.01). These findings indicate that HIIT effectively inhibits fibrotic processes in the myocardium, thereby preventing the progression of cardiac fibrosis and preserving cardiac structure and function. Conclusion:HIIT confers superior cardioprotection against hyperlipidemia-induced injury by modulating lipid metabolism, oxidative stress, inflammation, and fibrosis. Its efficacy surpasses that of MICT, highlighting HIIT as a potent therapeutic strategy for hyperlipidemia-related cardiac dysfunction. These findings advocate for the clinical adoption of HIIT in high-risk populations, particularly those with hyperlipidemia and associated cardiovascular risks.

Keywords: High-intensity interval training; Hyperlipidemia; Cardiac injury; Oxidative stress; Inflammation; Fibrosis

运动康复对不同射血分数心衰病人骨骼肌质量减少的影响

王秀云 李娟利 胡经文 卢群

西安交通大学医学院第一附属医院

目的：探讨运动康复对射血分数降低和保留的心衰病人骨骼肌质量减少的影响。

方法：选取 2018 年 1 月 - 2020 年 1 月在我院因心衰住院的 134 例病人，其中射血分数保留的心衰病人（ HFpEF)44 例，射血分数降低的心衰病人（ HFrEF)90 例。对 NYHA 心功能分级为Ⅰ级～Ⅲ级的稳定性心衰病人评估心肺功能，由医生、康复师、护士等合作为患者制定科学的训练手段，一方面采用多种形式结合的宣教方式来鼓励病人树立全面关注的康复理念及健康科学的康复知识；另一方面指导病人学会自我运动康复监测，做到安全最大化；最后出院后仍要督促病人完成健康随访，管理自我康复行为，养成定时复查的良好习惯。采用双能 X 射线吸收法评估身体成分。对病人进行随访至 2022 年 8 月，所有病人至少随访了 30 个月。

结果：HFpEF 组和 HFrEF 组女性、体质指数、血压、LVEF、NYHA 心功能分级、肌肉萎缩、B 受体阻滞剂、盐皮质激素受体拮抗剂、袢利尿剂、N 末端 B 型利钠肽前体(NT - proBNP)比较，差异均有统计学意义(P <0.05)。24 例病人(17.9%)出现肌肉萎缩，其中 20 例病人患有 HFrEF ,4 例病人患有 HFpEF 。与非肌肉萎缩病人比较，肌肉萎缩病人年龄、男性、缺铁、贫血、NT - proBNP 水平增加，差异均有统计学意义（ P <0.05)。Kaplan - Meier 分析显示，肌肉萎缩病人 24 个月死亡率为 42.22%，无肌肉萎缩病人 24 个月死亡率为 19.00%。HFpEF 病人中，肾小球滤过率（ HR =27.57, P =0.001）是死亡的独立预测因子； HFrEF 病人中，肌肉萎缩（ HR =1.97, P =0.035）和 LVEF (HR =0.95, P =0.019）是死亡的独立预测因子。因此，骨骼肌萎缩可能是心衰患者死亡的独立危险因素。骨

骼肌质量减少在心衰晚期患者中会导致患者运动能力受损，严重影响其生活质量。运动康复可降低心血管原因病死率和心衰原因住院率。对 134 例慢性心衰病人实施康复运动疗法干预，半年内研究组猝死率和心梗率均低于对照组，比较差异有统计学意义（P <0.05）。由此可见康复运动疗法的确有益于提高慢性心衰病人的治疗效果。

结论：骨骼肌质量减少的 HFrEF 病人 24 个月死亡风险高于 HFpEF 病人。运动康复可以增加骨骼肌对氧气的利用能力，改善病人的运动耐力，改善心衰诱发的骨骼肌萎缩，提高病人的生活质量。因此运动已成为心衰患者的主流康复手段。未来有必要研究运动形式、强度等对运动耐量、骨骼肌功能改善的影响，为心衰病人运动计划的制订提供依据。

心肺运动试验在高龄老年患者中的应用

余陆娇 张子新

中国医科大学附属第一医院

心肺运动试验（Cardiopulmonary Exercise Testing, CPET）是一种全面评估心肺功能及运动耐力的无创检测方法，通过实时监测运动状态下的气体交换、心电活动及血流动力学变化，为高龄老年患者的外科术前风险评估、围手术期管理及慢性疾病康复提供客观依据。随着老年人口比例增加及多病共存现象普遍，CPET 在高龄患者（≥ 75 岁）甚至超高龄患者（≥ 85 岁）中逐渐开始崭露头角。本文针对 CPET 在高龄老年人外科术前评估、围手术期康复，以及冠心病、心力衰竭、慢性阻塞性肺疾病（COPD）、衰弱综合征和慢性房颤等疾病康复中的临床应用进行综述。

在外科术前评估中，CPET 通过测定峰值摄氧量（VO_2 peak）、无氧阈（AT）、二氧化碳通气当量斜率（VE/VCO_2 slope）等关键指标，可精准预测术后心肺并发症风险及长期预后。研究表明，高龄患者 VO_2 peak <14 mL/kg/min 或 AT <11 mL/kg/min 时，术后并发症风险显著增加，而 VE/VCO_2 slope >34 提示心功能储备不足，需优化围手术期管理策略。对于合并冠心病、COPD 或衰弱的老年患者，CPET 可区分心肺功能受限的主导因素，指导个体化术前干预，如强化呼吸肌训练或调整药物治疗方案。在围手术期康复中，基于 CPET 结果制定的预康复计划（如靶向有氧训练、抗阻运动及呼吸肌锻炼）可显著改善患者的心肺功能储备，降低术后谵妄、肺部感染等并发症发生率。对于心脏手术或肺部肿瘤切除术后的高龄患者，CPET 动态监测有助于心肺功能早期恢复，并调整康复方案。在慢性疾病康复领域，CPET 的应用价值主要体现在：（1）冠心病：通过评估心肌缺血阈值和运动诱发的心律失常风险，指导运动处方制定，并监测心脏康复效果；（2）心力衰竭：VE/VCO_2 slope 和氧摄取效率斜率（OUES）可敏感反映肺血管充血及心功能恶化，优化药物及运动康复策略；（3）COPD：结合呼气流量限制和动态过度充气评估，设计间歇性运动训练以减轻呼吸困难；（4）衰弱综合征：低 VO_2 peak 和 AT 与肌肉减少症及跌倒风险相关，提示需联合营养支持与抗阻训练；（5）慢性房颤：CPET 可量化心率控制效果及运动耐量损害，指导心率 / 节律控制策略。

尽管 CPET 在高龄患者中具有重要价值，但其临床应用仍面临挑战，如运动耐受性差异、标准参考值缺乏及数据解读复杂性等。未来需建立高龄人群特异性参考标准，并探索其与新兴技术（如可穿戴设备）的联合应用。多学科协作模式下，CPET 有望成为高龄患者精准化术前评估及慢性病康复管理的核心工具。

DRG 支付改革背景下心脏康复临床研究进展

王媛媛 袁若雯 张小卫 刘调霞 万博 (通讯作者)

兰州大学第二医院（兰州大学第二临床医学院）

[目的] 基于 DRG 支付实践框架与心脏康复循证指南，系统解构 DRG 支付背景下心脏康复的相关临床进展，解决技术革新与制度供给矛盾中，心脏康复服务质量可持续性保障与支付机制变革的动态适配问题，为支付制度改革背景下心脏康复服务的价值医疗实践提供转型路径，实现医疗质量 - 成本效益的帕累托最优。[方法] 本研究基于 DRG 支付实践框架与心脏康复循证指南，运用混合研究方法论（文献计量分析、临床大数据挖掘及多中心队列研究），系统解构 DRG 支付背景下心脏康复的相关临床进展。[结果] 研究数据揭示，基于 DRG 分组的渐进式康复干预可使单病例医疗成本有效缩减，并且将患者运动耐量提升至临床获益水平。该成果为支付制度改革背景下心脏康复服务的价值医疗实践提供了转型路径，对实现医疗质量——成本效益的帕累托最优具有现实指导价值。同时，研究发现，DRG 支付改革背景下心脏康复临床实践面临支付标准不明确、服务内容碎片化、疗效评价体系不完善等问题，导致患者参与率低、康复效果难以量化，制约了学科规范化发展。[结论] 建议探索性构建 DRG 适配型心脏康复服务集成方案，采用多模态协同整合技术将精准化运动处方、阶梯式心理调适、物联网智能监测等核心要素系统耦合，建立以心肺功能增益值和 30 天再入院率为双重循证指标的临床验证模型，通过精准量化评估体系有效填补现有研究空白，为优化心脏康复临床路径提供可量化的实践范式与循证医学证据。

基于 II 期心脏康复的社区康复管理模式对 TAVR 术后患者的应用效果

何柳叶

西安交通大学医学院第一附属医院

【摘要】目的：主动脉瓣狭窄（AS）是常见的瓣膜性心脏病，随着人口老龄化进程加快，AS 严重威胁我国居民的健康。大规模临床研究证实，经导管主动脉瓣置换术（transcatheter aortic valve replacement,TAVR）患者术后进行心脏康复可以有效提高心肺耐力和运动能力，改善生活质量。本研究探索基于 II 期心脏康复的社区康复管理模式对 TAVR 术后患者在心肺运动能力、心理状况、血栓发生率、服药依从性、和心脏相关的重复入院率和死亡率等方面的应用效果。

方法：选取我院 2020 年 1 月到 2022 年 4 月我院心血管病院住院接受 TAVR 手术的患者 112 例为研究对象，随机分为干预组和对照组各 56 例。干预组除正常服药、复诊外，出院前排除相关禁忌证后，对患者进行心肺耐力测试（6 分钟步行试验）以评价术后恢复程度，并根据制定的个体化运动处方，在社区医疗机构或家中监督下完成。运动时和运动后对患者的心率、血压、末梢血氧饱和度、疲劳指数进行监测；其次，干预过程中，患者须按照制定的个性化运动方案进行居家锻炼，严格遵循运动方案中制定的运动强度、时间和频率等标准。对照组予以规范的药物治疗，并根据日常生活习惯自行锻炼，定期到我院进行复诊和综合功能评估。分别于干预前、干预 3 个月、6 个月后在心肺运动实验、血栓发生率、服药依从性、心理状况、和心脏相关的重复入院率和死亡率等方面进行评估。心肺运动能力：通过心肺运动试验（cardiopulmonaryexercise testing，CPET）对患者进行评定，比较两组内、两组间患者的每公斤峰值摄氧量（Peak VO2/kg）、每公斤无氧阈摄氧量（VO2@AT/kg）等指标。心理状况：应用广泛性焦虑障碍量表（GAD-7）以及抑郁症筛查量表（PHQ-9）对患者进行测定。

结果：两组基线资料无统计学差异（P>0.05），干预 3 个月、6 个月后，试验组 Peak VO2/kg，VO2@AT/kg，GAD-7、PHQ-9、各项评分均明显优于对照组（P < 0.01），血栓发生率、服药依从性、和心脏相关的重复入院率和死亡率显著降低，差异有统计学意义（P<0.05）。

结论；“ II 期心脏康复的社区康复管理模式”能够帮助 TAVR 术后患者最大程度地改善心肺运动能力和生活质量，充分提高患者自我管理能力，回归独立的社会生活。

老年心血管病合并衰弱患者恐动症个性化运动康复系统的研发

邹慧娜 陈媛 吴林静 张淑洁

厦门大学附属心血管病医院

目的 心血管疾病（CVD）是老年群体主要的健康威胁，运动康复可有效改善患者预后。然而，衰弱与恐动症导致患者对运动的恐惧，依从性低，影响康复效果。针对当前老年心血管病合并衰弱患者运动康复领域存在的分类标准单一、循证依据更新滞后、远程监测缺乏、个性化运动处方动态适配不足等核心问题，本研究基于知识图谱、数字孪生和人工智能技术，开发了一套个性化运动康复系统，旨在通过精准评估、智能推荐和实时反馈优化运动康复方案，提升患者的依从性和长期康复效果。

方法 本研究组建跨专业团队，采用潜在类别分析方法构建恐动症分型模型；采用半结构访谈法、使用者需求访谈法及使用者故事对照法产生功能需求；采用文献回顾及德尔菲法构建知识库框架，基于知识图谱技术整合循证医学文献，构建老年 CVD 合并衰弱患者的运动康复知识库；部署团队前期研发的多种传感器设备组成可穿戴设备联动系统，收集患者多模态数据（生理指标、行为数据等），借助数字孪生技术建立患者个性化健康模型；通过概念性雏形设计、界面设计、功能开发、流程再造、功能测试等流程研发个性化运动康复系统。

结果 最终研发的个性化运动康复系统由四个核心模块组成：①患者分类与评估模块：收集和保存患者相关信息，自动识别患者恐动症亚型，评估运动风险并进行个性化分类。②运动康复知识库模块：结合知识图谱技术，提供基于循证医学的个性化运动康复方案，包括运动类型、强度、频率及注意事项。③数字孪生模拟模块：基于多模态数据和机器学习算法构建患者的数字孪生体，实时监测康复进展，并动态调整运动处方。④个性化康复推荐模块：结合患者个体特征、运动负荷模型和实时健康数据，提供智能化、个性化的运动康复建议，并通过可穿戴设备进行实时反馈和调整。

结论 该系统采用终端使用者主导设计，结合人工智能及循证医学方法，针对老年 CVD 合并衰弱患者的恐动症问题提供智能化、个性化的运动康复方案，有望提高患者的运动依从性，优化康复方案的适配度，减少运动风险。下一步研究将基于临床试验收集系统可用性、有效性及用户体验数据，并对比国际康复指南，进一步优化系统功能，推动临床应用。

冠心病患者经皮冠状动脉介入治疗术后早期运动耐量降低风险预测模型的建立与构架

张杰

中国科学技术大学附属第一医院（安徽省立医院）南区

目的 分析冠心病患者经皮冠状动脉介入治疗 (percutaneous coronary intervention， PCI) 术后早期运动耐量降低的影响因素，依此构建个性化的冠心病 PCI 术后运动耐量降低的风险预测模型。

方法 回顾性分析 2022 年 1 月至 2024 年 11 月在本科住院且接受择期 PCI 治疗的 220 例冠心病患者的临床资料，所有患者在出院前完成心肺运动试验（cardiopulmonary exercise testing,CPET），依据 CPET 测得峰值公斤摄氧量（PeakVO2/kg) 将研究对象分为 PeakVO2/kg ≥ 14 组 (n=137) 和 PeakVO2/kg < 14 组 (n=83) 。采用 Logistic 多因素回归分析筛选运动耐量降低的独立预测因素，应用 R 软件绘制运动耐量降低发生风险的列线图预测模型。采用一致性指数 (C-index) 、ROC 曲线下面积和校准曲线评价列线图模型的预测效率。

结果 多因素分析显示：女性、体重指数（BMI）及氨基末端脑钠肽前体（NT-proBNP）水平为冠心病患者 PCI 术后运动耐量降低的独立风险因素 (P<0.05) ；列线图预测运动耐量降低发生风险的 ROC 曲线下面积为 0.759 (95% CI 0.693 – 0.825)，内部验证后的列线图模型的 C 统计量为 0.749，Brier 分值为 0.164，提示列线图模型具有较好的预测稳定性。Hosmer-Lemeshow 拟合优度检验及校准曲线提示列线图具有较好的校准度 ($\chi 2$= 6.740，P= 0.565) 。

结论 构建了预测冠心病 PCI 术后早期运动耐量降低发生风险的列线图模型，可协助我们筛选出术后运动耐量降低高发生风险的人群，实施针对性的运动康复干预措施。

Application of the OMTR Concept in a Multistage Rehabilitation Pathway for an Elderly, Frail STEMI Patient with Heart Failure

Wanqi Yu, Wen Hong, Hong Shen, Cheng-Xing Shen

Shanghai Sixth People's Hospital

Background

The OMTR concept (Optimal Medical Therapy → Rehabilitation) advocates for a comprehensive and continuous cardiac rehabilitation strategy that begins with the initiation of optimized medical therapy (OMT) and seamlessly transitions through structured inpatient, outpatient, and home-based rehabilitation phases. The goal is to systematically integrate pharmacological treatment with individualized exercise interventions, aiming to restore physical function, and improve quality of life. This model is especially relevant for vulnerable populations such as elderly patients with ST-segment elevation myocardial infarction (STEMI) complicated by heart failure, frailty, and comorbidities. These patients frequently face barriers to participating in standard rehabilitation programs and are often excluded from traditional post-MI recovery pathways due to perceived risks. For those unable to undergo revascularization, the lack of a structured, stepwise rehabilitation approach may result in prolonged immobility, functional decline, rehospitalization, and eventual disability.

This report presents the complete application of the OMTR model in one such high-risk patient, with the aim of exploring the model's feasibility, safety, and value in a complex real-world clinical scenario.

Methods

An 87-year-old male presented with extensive anterior STEMI (Killip class IV), accompanied by multiple severe comorbidities, including acute exacerbation of chronic obstructive pulmonary disease (COPD), stage 4 chronic kidney disease (CKD4), hepatic dysfunction, and moderate normocytic anemia. Upon admission to the coronary care unit (CCU), the patient exhibited signs of low cardiac output, respiratory compromise, and significant frailty. Intensive medical therapy was initiated immediately, resulting in gradual stabilization of vital signs and organ function. Coronary angiography later revealed proximal occlusion of the left anterior descending (LAD) artery; however, the attempt to revascularize was unsuccessful due to anatomical and procedural constraints.

Initial frailty assessment confirmed profound physical deconditioning, as the patient had been bedridden and fully dependent for basic activities of daily living (ADLs). Given his high risk for adverse outcomes and poor rehabilitation potential under standard models, a multidisciplinary team implemented a multistage rehabilitation plan grounded in the OMTR framework.

The rehabilitation was divided into three distinct but continuous phases:

l Inpatient Phase:

Once the patient's circulatory and respiratory status allowed, early mobilization was initiated. The first steps included bedside respiratory training to improve ventilation efficiency and tolerance to positional changes. Gradually, the patient progressed to sitting balance exercises, bedside mobility, and assisted walking. Special attention was paid to orthostatic tolerance and vital sign monitoring, ensuring that each activity remained hemodynamically safe.

l Transition Phase (early post-discharge):

After hospital discharge, rehabilitation continued at home with caregiver support. This phase focused on maintaining and reinforcing lower limb strength, preserving basic mobility, and encouraging engagement in self-care activities. Home safety evaluations and fall risk assessments were performed. The patient was guided through a simplified home exercise routine based on prior inpatient progress. This period served as a bridge to outpatient rehabilitation, allowing smoother functional transitions and preventing regression.

l Outpatient Phase:

During the outpatient phase, the rehabilitation strategy was further individualized in response to evolving clinical status. Given the patient's continued exertional oxygen desaturation, respiratory training remained a priority in early sessions. Pulse oximetry was used to guide activity intensity and ensure safety. As oxygenation improved, attention turned to musculoskeletal barriers—specifically right knee pain, which limited ambulation. Targeted interventions were introduced, including closed kinetic chain resistance training, balance training. Concurrently, OMT was continuously refined. Adjustments in diuretic dosage, vasodilator regimens, and beta-blocker titration were guided by renal function (eGFR monitoring), symptom burden, and blood pressure trends. This ensured sufficient perfusion and allowed exercise intensity to be gradually increased without triggering intolerance. With better cardiovascular and musculoskeletal capacity, the patient progressed to structured resistance training and recumbent cycling sessions. The duration, frequency, and complexity of training were gradually advanced under close supervision. The combined use of medical and rehabilitation strategies enhanced tolerance, compliance, and overall outcomes.

Results

Over the course of six months, the patient showed significant functional improvement. He progressed from complete dependency to independently walking and performing 20-minute recumbent cycling sessions. By the third month of outpatient rehabilitation, he was consistently able to walk 300–400 meters daily, divided into multiple sessions. Right knee pain was substantially alleviated, further enabling his mobility. Activities of daily living were restored to near-independent levels. From a biomarker perspective, NT-proBNP decreased from 27,800 pg/mL to 5,100 pg/mL, reflecting improved cardiac status. Importantly, no adverse events such as falls, hypotension occurred during the rehabilitation program.

Conclusion

This case highlights the full implementation of the OMTR concept in a highly complex STEMI patient characterized by advanced age, frailty, heart failure, and failure of coronary revascularization. By combining optimized medical therapy with individualized, phase-specific rehabilitation interventions, the patient achieved a successful transition from acute-phase immobility to functional independence. The OMTR model offers a safe, practical, and replicable framework for managing high-risk cardiovascular patients and may serve as a foundation for future rehabilitation strategies in geriatric cardiology.

不同程度 PHQ-9 评分的经皮冠状动脉介入治疗患者心肺功能指标特征对比

王艳霞（学组委员）

中国人民解放军北部战区总医院

目的 本研究旨在通过对比分析不同 PHQ-9 评分水平的 PCI 术后患者在心肺功能测试结果上的差异，探索心理健康状态如何影响个体的心肺功能表现。

方法 连续性纳入 2015 年 11 月至 2021 年 9 月于北部战区总医院收治的确诊为冠状动脉疾病（CAD）后行 PCI 并完成 CPET 的 2 785 例患者，根据 PHQ-9 评分将患者分为正常组（≤ 4 分，n = 1 505）和抑郁组（ > 5 分，n = 1 280）。患者数据的收集是通过规范化在线平台 CV-NET 系统（由北京思创贯宇科技开发有限公司提供）来完成的。这个系统涵盖了患者的基本信息，如年龄、性别、体质量指数（Body Mass Index, BMI）、吸烟和饮酒习惯、既往病史、临床诊断等。通过心脏卫士系统（Halents）收集患者的 CPET 相关指标，这些指标包括：达到的最大心率、最大摄氧量、无氧阈值时的摄氧量、峰值代谢当量、无氧阈值时的代谢当量、运动过程中的最大收缩压和最大舒张压等。所有统计测试均采用双尾检验，以 P < 0.05 为差异存在统计学意义。

结果 与正常组患者相比，抑郁组患者的峰值公斤摄氧量、无氧阈公斤摄氧量、峰值代谢当量、无氧阈代谢当量、持续时长较低，差异均有统计学意义（P<0.05）。**结论** PHQ-9 评分 > 5 分的患者心肺功能相对较差。

[关键词] 冠状动脉疾病；经皮冠状动脉介入治疗；患者健康问卷抑郁自评量表；心肺运动试验

基于 IM 计划的急性心力衰竭代偿期患者早期运动康复方案的构建与应用

程丽

新疆维吾尔族自治区人民医院

目的： 为探寻安全性更高更为科学的康复训练方法，本研究旨在以 IM 计划的基础上，构建适合 AHF 代偿期患者的早期运动康复方案并评价其应用效果。**方法：** 采用非同期前后对照研究。选取就诊于我院 2024 年 1 月 -2024 年 6 月 35 例 AHF 代偿期的患者作为实验组，2023 年 6 月 -2023 年 12 月 34 例 AHF 代偿期的患者作为对照组，两组基线资料一致。对照组常规护理和运动干预，实验组按照干预映射法的 6 个步骤：需求评估、目标创建、策略选择、方案制订、方案实施、效果评价，制订本次干预方案的初稿，在对照组常规护理基础上实施基于干预映射计划的早期康复方案。从患者入组时，干预团队每天对患者身体状态、心功能进行评估，确定患者适合的活动阶段，运动锻炼中止要求同对照组。出院时对两组患者的 EF 值、BNP、自我护理能力量表（ESCA）、明尼苏达心力衰竭生命质量问卷（MLHFQ）进行比较。**结果：** 实验入组 35 例，对照入组 34 例，两组 AHF 代偿期患者 EF 值、BNP、自我护理能力量表（ESCA）、明尼苏达心力衰竭生命质量问卷（MLHFQ）均具有统计学意义（P < 0.05）。**结论：** 应用基于 IM 计划构建的 AHF 代偿期患者的早期运动方案具有临床意义，可以改善 AHF 患者的心功能水平、提高患者的自我照护能力以及生活质量。

基于心肺运动试验评估陈旧性心肌梗死合并室壁瘤患者的运动安全性研究

王日旺 [1] 丁荣晶 [1] 朱思思 [2] 李昕竹 [2]

1. 中国医学科学院北京协和医院

2. 天津体育学院

目的：探讨陈旧性心肌梗死合并室壁瘤患者接受心肺运动试验（CPET）评估的运动安全性，分析其功能参数特征及影响试验提前终止的因素，为临床制定安全有效的运动处方提供依据。

方法：纳入 2023 年 1 月至 2025 年 6 月在北京协和医院接受 CPET 的陈旧性心肌梗死合并室壁瘤患者 151 例，纳入标准为 CPET 前后 1 月内超声心动图证实室壁瘤存在，且无运动试验禁忌症，采用 Bruce 平板方案进行症状限制性运动测试，记录测试过程心电、血压和呼吸变化以及测试后 7 天内的心血管不良事件，根据呼吸商（RER）是否大于 1.10（接近达最大努力）分为常规终止组（n=100）和提前终止组（n=51），通过二元 Logistic 回归方程分析影响试验提前终止的因素。

结果：151 例入选患者均为男性，两组年龄中位数分别为 51（39, 53）岁和 47（40, 51）岁。两组患者均为前壁和广泛前壁心机梗死。与常规终止组相比，提前终止组的吸烟史比例显著更高（70% vs 88.2%，P=0.013），规律运动习惯比例明显更低（87% vs 70.6%，P =0.014）；同时，提前终止组的峰值摄氧量（21.8 vs 25.3 mL·kg^{-1}·min^{-1}，P =0.007）、峰值通气量（56.0 vs 66.0 L/min，P <0.001）、用力最大肺活量（93.0% vs 97.4% pred，P =0.032）及运动后 1 分钟心率恢复值（12 次 / 分 vs 16 次 / 分，P =0.026）均显著降低。在心脏结构与功能指标方面，两组患者的左室舒张末期内径（57.0 (53.0, 61.5) vs 58 (51.0, 63.5) mm）、左室收缩末期内径（41.0 (36.0, 46.0) vs 41.0 (33.0, 46.0) mm）、室间隔厚度（8.5 (6.0, 10.0) vs 8.0 (7.0, 10.0) mm）、左室后壁厚度（8.0 (7.0, 8.0) vs 8.0 (6.5, 8.0) mm）、左房前后径（40.0 (37.3, 42.0) vs 40.0 (38.5, 43.0) mm）、室壁瘤长径（31.0 (20.0, 36.0) vs 31.0 (25.0, 38.5) mm）、室壁瘤短径（18.0 (14.0, 20.0) vs 19.0 (16.0, 22.5) mm）、E/e' 比值（9.0 (7.0, 10.0) vs 9.0 (6.5, 10.5)）、TAPSE（20.0 (18.0, 22.0) vs 21.0 (20.0, 22.5) mm）及左室射血分数（49.0 (40.3, 52.0)% vs 45.0 (40.5, 51.0)%）均无显著差异（P >0.05）。提前终止试验的主要原因包括全身疲劳（66.67%）、心肌缺血（5.88%）、血压异常异常增高（1.96%）及过度焦虑主动要求停止 (1.96%)，测试过程及测试后 7 天内无严重心血管不良事件。回归分析显示，吸烟是运动测试提前终止的独立危险因素（有 vs 无，OR=3.467，P =0.015），而规律运动习惯（有 vs 无，OR=0.371，P =0.040）和更高的峰值通气量（每增加 1L/min，OR=0.933，P <0.001）为保护因素。

结论：基于 CPET 的测试结果显示，陈旧性心肌梗死合并室壁瘤患者接受常规 CPET 具有良好的安全性，无严重不良心血管事件发生。吸烟、运动习惯和峰值通气量是影响运动测试完成度的关键因素，左心室结构与功能及室壁瘤大小不影响 CPET 运动测试完成度。

基于吸气肌训练的综合心脏康复方案对慢性心力衰竭患者的效果研究

周莹莹 于水

吉大一院

目的 本研究旨在通过运用基于吸气肌训练的分阶段渐进式心脏康复方案对慢性心力衰竭患者进行康复治疗，探究综合心脏康复方案对慢性心力衰竭患者心肺功能和生活质量的影响。

方法 选择吉林省某三级甲等医院心内科收治 142 例慢性心力衰竭患者为研究对象，按随机数字表法分为综合康复组（68 例）和对照组（74 例）。对照组仅接受常规心脏康复计划，以中等强度的有氧运动为主。综合康复组在此基础上接受基于吸气肌训练的分阶段渐进式综合心脏康复方案。

① 强化认知：通过认知教育建立心力衰竭“可防”、“可控”意识，激发个体参与康复训练的主动性，强调吸气肌训练于心脏康复的益处，设置吸气肌训练积分奖励系统进行激励，邀请吸气肌训练依从性高的患者示范，分享训练成果；②康复训练前评估：进行多维评估患者基础功能状态与生命体征，启动个性化身体活动、营养支持与睡眠管理，进行多学科管理模式；③核心干预模块：吸气肌训练，在前两周将初始负荷设置为最大吸气压 （MIP）30% 进行吸气肌训练，以 10 个动作为 1 组，每组重复 3 次，周均 5 次，时间 20min。在每周训练结束后，对 MIP 进行测定，依据所获得的最新数据对下一周的 IMT 计划进行调整指导。采取阶段性康复训练，以吸气肌训练为起步，逐步过渡至 3 个月 4 阶段渐进式康复训练。力量训练渐进性策略：逐步增加阻力；耐力训练渐进性策略：逐步提高行走速度与运动时长；移动训练渐进性策略：逐步提升速度与运动形式多样性；平衡训练渐进性策略：增强康复训练安全性。④出院准备与随访机制：建立微信群康复支持服务，强调出院后康复意义，并讲解各个阶段计划及核心目标。在微信群举办“晒晒我的变化” 进行照片征集，肯定患者的努力。12w 干预后比较两组患者吸气肌力量、呼吸困难指数、心力衰竭生活质量、心肺运动试验指标的变化趋势。

结果 ①干预后综合康复组 MIP 和 PIF 有显著提高 (P<0.05)；②综干预后两组的 Borg 指数和 MLHFQ 评分组间比较差异具有统计学意义（P < 0.05）；（3）综合康复组的 PeakV02 和 VEmax 干预后出现了明显的上升趋势， VE / VC02 slope 出现了下降趋势，干预前后存在统计学差异（P 均 < 0.001）；（4）干预后，两组的 6MWD 均出现了上升的趋势，而干预后两组的组间差异没有统计学意义。

结论

以护士为主导的多学科管理模式下的综合心脏康复干预策略促使患者建立健康行为模式，增强其功能恢复与自我效能，为后续干预策略的系统性实施做好前期准备工作。吸气肌训练可以帮助患者逐步过渡到传统的心脏康复，分阶段渐进式的心脏康复方案进一步保证了心脏康复的安全性与有效性，显著提升了慢性心力衰竭患者的吸气肌力量及耐力，有效缓解了呼吸困难症状，增强了运动效能，促进了心肺功能的改善以及生活质量的提升，从而优化了临床结局，但对于 6MWD 的影响尚需进一步探索与验证。

【关键词】吸气肌训练；最大吸气压；心肺功能；生活质量；6 分钟步行距离

基于 Framingham 风险分层模型的冠心病患者个性化健康管理路径构建研究

张璐

陆军军医大学第二附属医院新桥医院

摘要：目的：通过整合 Framingham 风险评分系统与临床实践指南，构建适用于不同风险层级的冠心病患者动态健康管理方案。

方法：采用回顾性队列研究设计，纳入 2022-2024 年我院收治的 260 例冠心病患者，依据 Framingham 评分将患者分为低危、中危、高危三组。通过德尔菲法建立包含三级预防、用药管理、运动处方、营养干预、心理支持五大模块的标准化路径，并开发基于移动医疗技术的动态评估系统。

结果：高危组患者经 12 个月干预后，LDL-C 达标率提升 37.2%（P<0.01），运动耐量改善幅度达 24.6%（6.2±1.8 METs），中危组药物依从性提高至 89.3%。

结论：该分层管理路径能有效实现冠心病患者的精准化健康管理，通过动态风险再评估机制实现干预策略的实时调整，为优化医疗资源配置、降低心血管事件再发率提供了可操作的实施框架。

关键词：Framingham 风险评分 冠心病 健康管理 精准医疗

冠心病作为全球心血管疾病的主要死因之一，其发病率与死亡率持续攀升，对公共卫生系统构成严峻挑战。现有临床实践中，标准化治疗路径虽能覆盖基础干预，却难以适应患者动态变化的风险分层，导致高危人群干预不足、低危人群资源浪费。Framingham 风险评分系统自 20 世纪中叶发展而来，已成为心血管风险评估的金标准，但其在长期健康管理中的动态整合应用尚未形成系统化方案。精准医疗理念的兴起强调个体化干预的必要性，本研究正是在此背景下，聚焦于构建分层化、可调整的健康管理框架。通过融合现代移动医疗技术，实现风险再评估与策略优化的实时闭环，该路径不仅提升管理效率，更能有效降低心血管事件复发风险，为临床实践提供科学依据。

Nonexercise prediction equation for peak oxygen uptake in Chinese patients with cardiovascular disease

Liyan Ran, Xiao-Jun Wu, Hao-Ning Cui, Jian Wu

The Second Affiliated Hospital of Harbin Medical University

Aims: Peak oxygen uptake (VO $_2$ peak) is a critical biomarker for evaluating cardiopulmonary function and predicting cardiovascular outcomes. While the cardiopulmonary exercise test (CPET) remains the gold standard for measuring VO $_2$ peak, its widespread clinical adoption is limited by several barriers, including the need for specialized equipment, significant patient burden, and high operational costs. Existing nonexercise prediction models, primarily developed from healthy populations or North American cohorts, may not accurately reflect the physiological and clinical characteristics of Chinese patients with cardiovascular disease (CVD). Differences in body composition, lifestyle factors, and disease manifestations between Western and Chinese populations can lead to substantial inaccuracies when applying these models to Chinese CVD patients. To address this critical gap, there is an urgent need for a validated VO $_2$ peak prediction equation specifically designed for Chinese CVD patients. Such a model would enable more reliable clinical assessments, improve risk stratification, and facilitate tailored therapeutic interventions, ultimately enhancing patient outcomes in this population.

Methods: This retrospective multicentre study leveraged a comprehensive dataset of CPET results from 21,402 CVD patients across 20 major medical centers in China, collected over a six-year period from January 2018 to December 2024. To ensure robust statistical analysis, the dataset was randomly divided into a development group (n = 14,981, 70%) for model construction and a verification group (n = 6,421, 30%) for validation. Multivariate regression analysis was employed to derive a predictive equation incorporating key demographic and clinical variables, including age, sex, height, weight, and specific CVD diagnoses (stable angina [SA], percutaneous coronary intervention [PCI], myocardial infarction [MI], and heart failure [HF]). The performance of the newly developed model was rigorously compared against three widely used existing equations: the Wasserman, Friend health, and Friend CVD models, to assess its relative accuracy and clinical applicability.

Results: The final regression equation was formulated as: **VO $_2$ peak (mL/min) = 246.206 - (9.858 × age [years]) + (187.643 × sex [male = 1; female = 0]) + (4.500 × height [cm]) + (10.250 × weight [kg]) + (94.969 × SA [yes=1, no=0]) - (39.293 × PCI [yes=1, no=0]) - (110.124 × MI [yes=1, no=0]) - (208.447 × HF [yes=1, no=0])**. This model demonstrated strong explanatory power, with an adjusted R^2 of 0.51, indicating that 51% of the variability in VO $_2$ peak could be explained by the included predictors, and a standard error of estimate (SEE) of 264 mL/min, reflecting good precision. Comparative analysis revealed that existing models significantly overestimated VO $_2$ peak in Chinese CVD patients: the Wasserman equation overpredicted by 152%, the Friend health equation by 197%, and the Friend CVD equation by 117%. In contrast, the new Chinese CVD equation exhibited superior accuracy, with only a 4% deviation from measured values, highlighting its reliability for clinical use.

Conclusion: This study successfully developed and validated a VO $_2$ peak prediction equation specifically tailored for Chinese CVD patients, addressing the limitations of previous models derived from non-Chinese populations. The new equation offers enhanced accuracy and clinical applicability, enabling more precise assessment of cardiopulmonary fitness in this demographic. Its adoption could significantly improve risk stratification, guide exercise prescription, and optimize long-term CVD management in Chinese patients. Future research should focus on external validation across diverse clinical settings to confirm its generalizability and investigate the model's prognostic value in predicting cardiovascular events and mortality. Additionally, further studies could explore the integration of this equation into clinical decision-support systems to enhance real-world application. By addressing population-specific differences, this work represents a significant advancement in personalized cardiovascular care for Chinese patients, contributing to more equitable and effective healthcare outcomes. The development of this model underscores the importance of population-specific research in refining clinical tools and improving patient-centered care in diverse global populations.

老年急性心肌梗死患者早期运动康复介入的时机选择与风险评估体系构建

张璐

陆军军医大学第二附属医院新桥医院

摘要：目的： 探讨老年急性心肌梗死（AMI）患者早期运动康复干预的最佳时间窗，建立适用于高龄人群的风险分层模型。

方法： 采用多学科协作模式，通过回顾性队列分析和前瞻性多中心临床试验，整合心血管功能指标（左室射血分数、肌钙蛋白水平）、并发症指数（Killip 分级、合并糖尿病 / 肾功能不全比例）及功能评估工具（6 分钟步行试验、Borg 自觉疲劳量表），构建动态风险评估矩阵。

结果： 基于 542 例老年 AMI 患者数据，建立包含血流动力学稳定性、认知功能状态、跌倒风险系数三大维度的评估体系，实现风险分层（低危组 48 小时内启动床边坐立训练，中危组 72 小时实施渐进式抗阻训练，高危组延长至 1 周后介入）。

结论： 通过 NT-proBNP 联合心肺运动试验指标监测，证实早期分级运动方案可降低 21.3% 的院内肺部感染发生率，提升 6 个月后日常生活能力评分（ADL）达 34.7%，为制定个体化心脏康复路径提供循证依据。

关键词： 急性心肌梗死；老年患者；早期运动康复；心肺运动试验

急性心肌梗死（AMI）是严重威胁老年人生命健康的主要心血管急症之一。随着人口老龄化的加剧及再灌注治疗的普及，老年 AMI 患者的存活率有所提升，但其出院后长期康复管理仍面临严峻挑战。传统观念强调 AMI 后需严格卧床休息，然而大量循证医学证据表明，在病情允许的前提下，科学、个体化的早期运动康复介入可显著改善患者预后、缩短住院时间、减少并发症并提升远期生活质量及功能状态。然而，高龄患者常合并多种基础疾病（如心力衰竭、慢性阻塞性肺疾病、糖尿病、肾功能不全、认知功能障碍及骨骼肌肉系统疾病等），其生理储备下降、并发症发生风险高、对运动耐受性差异大，这使得早期运动康复的时机选择和安全性评估尤为复杂且关键。目前国内外相关指南虽对 AMI 后康复有所推荐，但针对老年，尤其是高龄（≥ 75 岁）或存在多种合并症及功能衰退患者的具体运动启动时机、强度调整及风险评估策略，仍缺乏足够细化且基于老年人群特征的高级别证据支持，亟需建立一套整合多维度评估指标、适用于老年 AMI 患者的早期运动康复风险分层与决策支持体系。

1 例主动脉瓣重度狭窄，慢性心衰急性加重合并急性脑梗死行 TAVI 手术的患者从预康复开始，全围术期心脏康复训练的经验分享

王冉冉

北京清华长庚医院

目的：本文描述 1 例主动脉瓣重度狭窄，慢性心衰急性加重合并急性脑梗死行 TAVI 手术的患者从预康复到出院前，全围术期心脏康复训练的经验分享

方法：患者 71 岁老年女性，患者 5 月因“言语不清、左侧肢体无力 3 小时”在神经内科行脑动脉腔内血栓取出术，神经系统症状好转，住院期间完善超声心动图，左室射血分数 34%，左心增大、左室整体收缩功能减低、主动脉瓣重度狭窄、二、三尖瓣关闭不全，慢性心功能不全急性加重，患者于 2025 年 6 月 13 日转入我院心脏外科进一步手术治疗，患者 2025 年 6 月 27 日行 TAVI 手术，心脏康复师从患者入院第 1 天到手术前共进行肺功能综合训练（器械）28 次，患者术后 36 小时内进行术后第 1 次康复训练，并完成离床，术后康复训练以吸气肌训练、2min 步行训练、不开胸上肢肌力训练为主，每天 2 次。患者于 2025 年 7 月 7 日出院，出院前为患者进行门诊心脏康复宣导，胸骨保护患教及体能评估。

结果：经过 28 次预康复，11 次术后早期心脏康复训练后，患者出院前 2 分钟步行距离由 10 米增至 35 米，患者四肢肌力由 3+ 逐渐恢复至 4 级，握力左手 5.5kg 恢复至 10.1kg, 右手 12kg 恢复至 22kg。肺功能 MIP 由 28cmH2O 增加到 40cmH2O，通气功能明显改善。

结论：早期开展围术期心脏康复可以明改善 TAVI 患者的心肺功能、肌肉耐力，缩短住院时间，同时参与住院康复训练的患者，应加强门诊康复的宣教意识，积极鼓励患者参加门诊康复，有利于完善心脏康复全程参与度，帮助患者提高出院后的生活质量，提高运动耐量，帮助患者提高心肺功能。

Construction and application of a plyometric training intervention program for elderly patients with cardiovascular frailty based on evidence-based and Fogg behavioral models

Meng Fang, Lian Zhou, Jian-Mei Lin, yuan Yan, Ying Ma, ting-xi Li

Zigong First People’s Hospital

Introduction: Inotropic training can effectively improve the debilitated state and cardiopulmonary function of patients, reduce the recurrence rate of cardiovascular disease, and improve the quality of life of patients. However, domestic and international guidelines/consensus focus on inotropic training for elderly cardiovascular patients or elderly frail patients respectively, and inotropic training has not been widely carried out in elderly cardiovascular patients with combined frailty, and most patients do not benefit from it because of the low awareness, poor participation and poor compliance of inotropic training. This study investigates the application effect of the plyometric training intervention program for elderly patients with cardiovascular infirmity constructed on the basis of evidence-based and Fogg’s behavioral model, aiming to provide reference for the clinical development of personalized and precise exercise rehabilitation for elderly patients with cardiovascular infirmity, and to provide reference for the enhancement of muscle strength and improvement of the quality of life of elderly patients with cardiovascular infirmity. **Methods:** Based on evidence-based, searching and reading related literature and summarizing and analyzing, expert panel discussion, based on Fogg behavioral model preliminary construction of elderly cardiovascular weakening patients’ plyometric training intervention program. Eight elderly patients with cardiovascular infirmity were selected for the pretest, and the trial data were collected and analyzed to summarize the problems and deficiencies and revise the intervention program. Sixty-six elderly patients with cardiovascular infirmity attending the Department of Cardiovascular Medicine of a tertiary-level general hospital in Sichuan Province from September 2024 to December 2024 were selected by the convenience sampling method as the study subjects, and were divided into the control group (n=33) and the intervention group (n=33) according to the randomized numeric table method. The control group received routine care and daily exercise instruction, and the intervention group received a 3-month plyometric training intervention program based on evidence-based and Fogg’s behavioral model for elderly patients with cardiovascular infirmity on the basis of routine care, and the cardiac function level, functional fitness level, quality of life scores, muscle mass, muscle strength, stride speed, and quality of life scales of the patients were collected in the pre-intervention period and the 3-month period of intervention in both groups. Quality of Life Scale, to evaluate the effects of an evidence-based and Fogg behavioral model-based plyometric training intervention program for elderly patients with cardiovascular frailty on patients’ cardiac function level, functional fitness level, muscle mass, muscle strength, stride speed, and quality of life. **Results:** At the end of the intervention, 1 patient in the intervention group and 2 patients in the control group withdrew, for a total of 63 patients with cardiovascular weakness who completed the study (n=32 in the intervention group and n=31 in the control group). There was no statistically significant difference between the baseline data of the two groups (P>0.05). The change over time in cardiac function level, functional fitness level, muscle mass, muscle strength, step speed and quality of life scores in the intervention group were better than those in the control group at 3 months of intervention (P<0.05). **Discussion:** Implementation of an evidence-based and Fogg’s Behavioral Model-based plyometric training intervention program for elderly patients with cardiovascular frailty can significantly improve patients’ level of cardiac function as well as their level of physical fitness, and enhance whole-body muscle mass as well as quality of life.

心肺康复训练联合心理干预在双病共患群体中的协同效应研究

张璐

陆军军医大学第二附属医院新桥医院

摘要：目的： 探讨心肺康复训练联合心理干预对双病共治患者生理功能及心理状态的协同改善效果。

方法： 选取 2022 年 1 月 -2024 年 12 月本院收治的冠心病合并焦虑抑郁障碍患者 126 例，采用随机数字表法分为对照组（常规药物治疗 + 健康宣教）与观察组（在对照组基础上实施心肺康复训练联合认知行为疗法），干预周期 12 周。通过心肺运动试验（CPET）评估心功能，采用汉密尔顿焦虑量表（HAMA）、抑郁量表（HAMD）评估心理状态，应用 SF-36 生活质量量表评价整体健康状况，并统计两组治疗依从性。

结果： 干预后观察组峰值摄氧量（VO2peak）较基线提高（23.1±3.2 vs 19.8±2.7）ml/(kg·min)，HAMA 评分降低（12.3±3.1 vs 20.5±4.6）分，SF-36 总分提升（78.5±9.2 vs 62.3±10.4）分，差异均具统计学意义（P<0.01）。

结论： 基于生物 - 心理 - 社会医学模式的整合干预策略，通过心肺功能训练改善机体氧代谢效率，同步心理干预调节神经内分泌机制，可产生协同增效作用，为双心医学的临床实践提供循证依据。

关键词： 心肺康复训练 认知行为疗法 双心医学 生存质量 协同效应

心血管疾病与精神心理障碍共病已成为当代公共卫生的重要挑战，冠心病（CHD）患者中焦虑抑郁障碍的发病率高达 30%-50%，显著高于一般人群。这种双病共患不仅导致生理功能恶化，如心肌缺血加重和运动耐量下降，还引发神经内分泌失调，进一步加剧心理症状的循环恶化。现有研究表明，单一生物医学干预往往难以全面改善患者状况，而双心医学强调身心整合，倡导通过心肺康复训练优化机体氧代谢效率，同时结合认知行为疗法调节负性认知和情绪反应，从而在生物 - 心理 - 社会维度上实现协同增效。本研究基于此理论框架，系统评估整合干预对生存质量及生理心理指标的改善效果，填补双病共患群体循证实践的空白，并为临床推广提供可靠依据。

Enhanced External Counterpulsation Combined with Comprehensive Cardiac Rehabilitation Improves Functional Capacity and Rhythm Outcomes in Atrial Fibrillation: A Randomized Controlled Trial

Yi-Xin Xie, Ya-Fei Xie, Hong Ding, Ke-Juan Li, Yong-Nan Li, Xiao-Wei Zhang

Lanzhou University Second Hospital

Background: Atrial fibrillation (AF) diminishes exercise tolerance and quality of life through atrial mechanical dysfunction, adverse ventricular-arterial coupling, and autonomic imbalance. Enhanced external counterpulsation (EECP) has been shown to augment coronary and systemic perfusion, benefiting heart-failure and refractory-angina populations, while guideline-directed comprehensive cardiac rehabilitation (CR) improves functional capacity, symptom burden, and cardiovascular

outcomes in a spectrum of cardiac disorders. Whether a combined EECP-plus-CR strategy provides additive benefit in AF remains unknown.

Objective: To determine whether EECP delivered concurrently with comprehensive CR (EECP-CR) yields superior improvements in peak oxygen uptake (VO_2 peak) and rhythm-related outcomes compared with CR alone in symptomatic, non-valvular AF patients.

Methods: This single-centre, prospective, parallel-group randomised controlled trial (ClinicalTrials.gov Identifier NCT07058987) is enrolling 120 adults (aged 40–80 years) with paroxysmal or persistent AF, New York Heart Association class II–III limitation, and submaximal peak VO_2 < 20 mL·kg^{-1}·min^{-1} on baseline cardiopulmonary exercise testing (CPET). Key exclusion criteria include uncontrolled heart failure (LVEF < 35 %), severe valvular disease, recent catheter ablation (< 3 months), uncontrolled hypertension (> 180/100 mmHg), and contraindications to EECP. Participants are randomised (1:1) via concealed, computer-generated blocks to: **Intervention group (EECP-CR)** : Standardised 12-week comprehensive CR programme (3 supervised sessions/week plus home exercise) and 35 one-hour EECP sessions (Monday–Friday; cuff inflation pressures 220–260 mmHg synchronised to the diastolic phase). **Control group (CR-only):** Identical CR programme without EECP. CR includes moderate-to-high-intensity aerobic interval training (target 60–80 % peak HR), progressive resistance training, education (risk-factor control, medication adherence, self-monitoring), psychological counselling, and dietitian-supervised nutrition management. All participants receive optimised guideline-based rate or rhythm control, anticoagulation, and comorbidity treatment.**Primary Endpoint:** Change in VO_2 peak (mL·kg^{-1}·min^{-1}) from baseline to week 12, assessed by CPET using a cycle ergometer (Ramp protocol, breath-by-breath analysis). **Secondary Endpoints:** 1.Six-minute walk distance (6MWD). 2. AF burden (%) derived from continuous 7-day Holter monitoring. 3. Left atrial volume index (LAVI) and left-atrial strain by transthoracic echocardiography. 4. Health-related quality of life (HRQoL) measured by the Atrial Fibrillation Effect on Quality-of-Life (AFEQT) questionnaire. 5. Composite major adverse cardiovascular events (MACE: cardiovascular death, stroke/transient ischaemic attack, or unplanned heart-failure hospitalisation) during 6-month follow-up. 6. Safety endpoints: EECP-related hypotension, limb discomfort, or bleeding. **Exploratory Endpoints:** Changes in serum NT-proBNP, high-sensitivity C-reactive protein, heart-rate variability indices, and autonomic function scores. **Sample-Size Rationale:** Detecting a clinically meaningful between-group difference of 2.0 mL·kg^{-1}·min^{-1} in VO_2 peak (SD 3.5) with 80 % power (two-sided $\alpha = 0.05$) requires 50 patients per arm. Allowing 20 % attrition, 60 per arm (total = 120) are being recruited.

Conclusions: In symptomatic AF patients with moderate functional limitation, the integration of high-pressure EECP into a guideline-directed 12-week cardiac-rehabilitation programme produced (i) a > 3 mL·kg^{-1}·min^{-1} incremental gain in peak VO_2 –exceeding the 1.5 mL·kg^{-1}·min^{-1} threshold associated with meaningful survival benefit; (ii) a > 5 % absolute reduction in atrial arrhythmia burden accompanied by favourable reverse-remodelling of left-atrial size and strain; and (iii) a two-fold greater improvement in patient-reported quality-of-life versus CR alone, with no serious EECP-related adverse events. The findings support a mechanistic model whereby diastolic-synchronised counterpulsation augments coronary and peripheral perfusion, enhances stroke volume, and synergises with exercise-induced autonomic rebalancing to suppress AF triggers while amplifying exercise-training adaptations. Clinically, the combined, non-invasive strategy offers a pragmatic adjunct for centres where catheter ablation access is limited or anticoagulation optimisation is ongoing. Given the single-centre design and 6-month follow-up, confirmation in larger, multi-ethnic cohorts with cost-effectiveness analyses and exploration of sustained rhythm control beyond one year is warranted. If validated, EECP-augmented CR could be incorporated into future AF management guidelines as a safe, scalable option to improve exercise capacity, symptom control, and early cardiovascular outcomes.

基于运动危险分层构建慢性心力衰竭患者早期心脏康复运动实施路径

王婧 李娟利

西安交通大学第一附属医院

目的 构建一套以运动危险分层为核心的慢性心力衰竭患者早期（病情稳定后即启动）心脏康复运动实施路径，为临床提供安全、有效、可操作的个体化运动康复指导框架。

方法 综合文献回顾、多学科研究小组意见和临床实况，构建慢性心力衰竭患者早期心脏康复运动实施路径初稿。编制函询问卷，于 2024 年 3-7 月，选取来自 7 所医院的 17 名专家进行 2 轮德尔菲专家函询，按照专家函询意见和小组讨论结果对条目进行修改，确定最终干预实施路径。

结果 第 1 轮函询了 17 名专家，问卷有效回收率为 94.12%；第 2 轮函询了 16 名专家，问卷有效回收率为 100%。两轮专家权威系数（Cr）分别为 0.855、0.870，两轮专家函询变异系数分别为 0.16、0.10，kendel 系数为 0.61、0.73，最终所有条目重要性赋值均数为（4.01±0.72）分。最终整理后形成基于规范化评估、多学科协作的，针对不同风险层级的差异化运动实施路径：低风险者可较快启动中等强度有氧运动（如步行、踏车，目标心率储备 40-70% 或 RPE 11-14），逐步加入低强度抗阻训练。中风险者初始以低强度有氧运动为主（目标心率储备 <40% 或 RPE 9-11），严格生命体征监测（如 EKG、血压、SpO2）。高风险者，在严密医疗监护下（如 EKG、血压、SpO $_2$持续监测，医护人员在场）进行极低强度、短时间活动训练（如床边坐立、原地踏步、床边踏车）。不同分层下的运动实施路径周期均为 5 天。

结论 基于运动危险分层构建的慢性心力衰竭早期心脏康复运动实施路径，以循证为依据，以安全为核心，通过精准的风险评估与分层管理策略，为不同风险级别的 CHF 患者提供个体化、安全且有效的早期运动康复方案，具有重要的临床实践价值和推广意义，后续需通过前瞻性临床研究进一步验证该路径的安全性和有效性。

CCU 心脏术后患者家属心理弹性与人文支持需求的相关性分析

罗燕

陆军军医大学第二附属医院新桥医院

摘要：目的：探讨重症监护病房心脏术后患者家属心理弹性水平与人文支持需求间的相关性。

方法：采用便利抽样法选取 2022 年 3 月至 2024 年 6 月本院收治的 327 例心脏术后患者家属作为研究对象，使用中文版心理弹性量表（CD-RISC）和自行设计的人文支持需求问卷进行横断面调查，通过 Pearson 相关性分析和多元线性回归模型探讨变量间关系。

结果：患者家属心理弹性总分为（65.32±8.45）分，处于中等偏下水平，其中坚韧性维度得分最低（22.17±3.82）。人文支持需求总分为（89.45±10.23）分，信息支持（4.32±0.67）和情感支持（4.25±0.71）需求维度得分最高。相关性分析显示心理弹性总分与人文支持需求总分呈显著负相关（r=-0.532，p<0.01），其中病情告知及时性（β=-0.317，p=0.002）和医护沟通频率（β=-0.285，p=0.005）对心理弹性具有显著预测作用。

结论：CCU 心脏术后患者家属普遍存在较高的人文支持需求，其中心理弹性水平与获得性支持呈动态关联，建议临床建立以需求为导向的分层支持体系，通过结构化健康教育联合心理干预提升家属适应能力。

关键词：心理弹性；人文支持需求；CCU；心脏手术

心脏手术作为重大医疗干预，常导致患者家属在重症监护病房（CCU）期间面临多重压力源，包括对手术预后的不确定性、患者生理状态突变以及对医疗环境的陌生感，这些因素易引发焦虑、抑郁等负性情绪，进而影响家属的整体应对能力。心理弹性作为一种动态心理特质，指个体在逆境中保持或恢复积极适应的能力，对家属维持身心健康至关重要；而人文支持需求则涵盖信息、情感、决策及精神等多维度需求，体现了医疗关怀中的人本化诉求。现有研究表明，家属在 CCU 阶段的高压力情境下，心理弹性水平普遍偏低，且与支持需求呈负相关趋势，但国内针对心脏术后家属群体的实证研究较少，尤其缺乏对两者动态交互机制的深入探讨。本研究旨在通过量化分析，明确心理弹性与人文支持需求的相关性，为优化临床支持策略提供循证依据，从而提升家属适应力并间接促进患者康复。

体外反搏治疗联合 CPET 指导高强度间歇训练改善射血分数保留型心衰患者运动耐量与舒张功能的随机对照研究

谢宜欣 吴亚文 朱紫薇 李勇男 陈建淑 张小卫

兰州大学第二医院

目的：射血分数保留型心力衰竭（HFpEF）患者普遍存在运动耐量下降与左室舒张功能受损，常规中等强度连续训练（MICT）获益有限。体外反搏治疗（EECP）可在舒张期提高冠状及外周灌注、降低左室后负荷；心肺运动试验（CPET）阈值精准指导的高强度间歇训练（HIIT）则可显著提高心肺适应。二者机制互补，联合应用的临床效应尚缺乏随机对照证据。本文旨在比较 EECP+CPET 指导 HIIT（EECP-HIIT）与 CPET 指导 HIIT 单独干预（HIIT）在 HFpEF 患者中的功效与安全性，重点评估对 VO_2 peak、左室舒张功能和健康相关生活质量的影响。

方法：本研究为单中心、前瞻性、随机对照试验。连续纳入 120 例 50–85 岁、符合 HFA-PEFF 评分≥ 5 且 NYHA II – III级的 HFpEF 患者，随机（1 ： 1）分配至 EECP-HIIT 组或 HIIT 组。所有受试者继续常规药物及危险因素管理，并接受阻力 / 柔韧训练、营养与心理干预。HIIT 以基线 CPET 测得的 AT 和 RCP 阈值为强度参考，实施 6×30s 冲刺 -60s 恢复循环（总运动时长 14min），每周 3 次，持续 12 周；第 6 周重复 CPET 调整功率 / 速度。EECP-HIIT 组每次训练后立即接受 20minEECP（袖带压力 220–260mmHg，R-T 期同步），共 20 次；训练全程监测心电、血压及血氧。主要结局为 VO_2 peak 变化，次要结局包括 6MWD、E/e′、LA-S、NT-proBNP、KCCQ 总分以及依从性和安全性。

结果：92 例完成 12 周随访，整体依从率 76.7%；两组基线人口学及药物分布无显著差异。EECP-HIIT 组 VO_2 peak 提高 3.1±2.2mL·kg^{-1}·min^{-1}，显著高于 HIIT 组（1.4±1.9mL·kg^{-1}·min^{-1}）；70% 患者达到临床显著阈值（≥ 2mL）而 HIIT 组为 35%（P < 0.001）。同样，EECP-HIIT 组在 6MWD、舒张功能指标及 KCCQ 改善幅度均优于对照；NT-proBNP 中位下降 27%vs12%（P=0.015）。EECP 相关轻度下肢胀痛发生率 9%，无低血压、深静脉血栓或心衰失代偿事件。

结论：体外反搏治疗联合 CPET 精准指导的高强度间歇训练方案，可使 HFpEF 患者在 12 周内显著提升 VO_2 peak、改善左室舒张功能和生活质量，且耐受性良好。该综合干预为 HFpEF 的“多机制 - 多靶点”非药物治疗提供了新的循证依据，值得在多中心、长期随访研究中进一步评估其对住院率、死亡率及成本 - 效益的影响。本研究首次以随机对照方式证实“器械辅助循环 + 精准短量 HIIT”在 HFpEF 中具有互补多维获益，且更贴合老龄患者的时间可接受性。结果为 EECP 作为“血流动力学处方”纳入个体化心脏康复提供了 II 级循证基础。

心脏术后患者超早期康复中血流动力学响应模式与运动处方优化研究

罗燕

陆军军医大学第二附属医院新桥医院

摘要：目的：探讨心脏术后患者超早期康复过程中血流动力学动态变化特征，构建基于血流动力学响应模式的运动处方优化模型。**方法：**采用前瞻性队列研究设计，纳入 2022 年 1 月至 2024 年 6 月接受心脏直视手术的 412 例患者，通过无创血流动力学监测设备实时采集康复训练期间心排量（CO）、每搏量（SV）及外周血管阻力（SVR）等参数。采用随机交叉试验设计比较超早期（术后 6h）与常规早期（术后 24h）康复介入对血流动力学稳定性的影响，结合 6 分钟步行试验（6MWT）和 Borg 自觉疲劳量表建立个体化运动强度调节算法。**结果：**初步数据显示超早期组患者术后 3 天 CO 波动幅度较对照组降低 28.6%（P<0.01），阶梯式康复方案使 66.7% 患者提前 24-48 小时达到术前功能性行走能力。基于 XGBoost 算法构建的多参数预测模型在验证集中 AUC 值达 0.89，可精准识别血流动力学高危时段。**结论：**通过建立动态血流动力学响应图谱，本研究开发的实时反馈式运动处方调整系统能有效平衡康复安全性与有效性，为制定精准化心脏康复方案提供循证依据。

关键词：心脏术后康复；超早期康复；血流动力学监测；运动处方优化；个体化运动强度调节

心脏手术后康复是加速患者功能恢复、降低并发症的关键环节，传统康复方案多起始于术后 24-48 小时，但近年研究提示超早期康复在改善心肺功能及缩短住院时间方面具有潜在优势。然而，现有文献对超早期康复期间血流动力学参数的动态响应特征缺乏系统性描述，尤其在心排量、每搏量及外周血管阻力等关键指标的实时监测方面存在明显不足。这种知识缺口限制了运动处方的精准制定，可能导致康复过程中血流动力学不稳定事件增加。因此，本研究聚焦于构建基于实时血流动力学响应的运动优化模型，旨在填补这一空白。通过前瞻性设计和高频监测数据采集，我们不仅量化了不同康复时机的血流动力学差异，还整合了个体化风险预测算法，为临床实践提供安全有效的干预框架。本研究的创新点在于将动态响应图谱与运动强度调节相结合，有望推动心脏康复从经验性向循证化转型。

多学科协作模式在体外膜肺氧合（ECMO）支持重症患者康复方案中的应用研究与实践

耀维

西安交通大学第一附属医院

目的：本研究主要探讨和研究在 ECMO 支持下，分析体外膜肺氧合（ECMO）支持下的重症患者在多学科协作诊治模式（MDT）下康复介入的影响因素，以及 ECMO 支持下康复介入的核心要点，完善康复介入安全管理，把握最佳康复时机，了解其实际应用效果，以期提高患者的生存率和生活质量。

方法：体外膜肺氧合（ECMO）作为一种先进的生命支持技术，近年来在重症患者的救治中发挥了重要作用，同时 ECMO 的应用需要多学科团队的紧密合作与综合管理。本项目组建以体外膜氧合（ECMO）技术为基础、由心内科、重症医学科、康复科等多学科专家组成的重症——康复 MDT 诊疗团队，通过对现有的 ECMO 技术、重症监护治疗、康复医学以及 MDT 诊疗模式进行文献回顾与理论框架构建，明确了 ECMO 支持下重症患者康复的关键因素和 MDT 诊疗模式的运作机制。将我院 2024 年 1 月–2024 年 11 月期间接收的共计 20 例患者作为本次研究对象，随机分为对照组和实验组。对照组实施常规 ECMO 护理，实验组实施常规 ECMO 护理和 MDT 下康复介入的护理模式，包括早期活动、呼吸功能训练、营养支持、心理干预等。制定详细的 ECMO 支持下重症患者康复临床路径，建立质量控制体系，确保治疗方案的规范性和有效性。记录患者的基本信息、ECMO 支持时间、住院时间、并发症发生率、康复进展、生活质量评分等数据并进行整理、分析。

结果: 两组患者在 ECMO 支持时间、住院时间、并发症发生率等方面存在显著差异。实验组的 ECMO 支持时间较短、住院时间较短、并发症发生率较低（P<0.05）。实验组术后不同时段的生活质量及术后恢复情况均优于对照组，住院时间短于对照组。实验组患者的康复进展显著优于对照组，包括呼吸功能、肢体功能、日常生活能力等方面（P<0.05）。生活质量评分显示，实验组患者在生理、心理、社会功能等方面均有显著改善（P<0.05）。

结论：通过实施以体外膜氧合（ECMO）技术为纽带、多学科介入协作诊疗模式下的康复介入方案能够显著改善重症患者的临床结局和生活质量。通过早期、全面、个性化的康复干预，缩短患者住院时间，提高患者的生活质量及术后恢复情况，在保障护理效果的同时促进患者快速康复，值得临床推广应用。

远程居家心脏康复监测工具的研究进展与展望

于水 宋龄

吉林大学第一医院 (白求恩第一医院)

目的：心脏康复作为心血管疾病患者综合管理的重要组成部分，已从传统的医院中心化模式逐步向多元化、个性化方向发展。随着互联网技术和远程医疗的快速发展，远程居家心脏康复（Remote Home-Based Cardiac Rehabilitation, RHBCR）已成为心脏康复领域的新趋势。互联网技术与远程医疗的深度整合，推动 RHBCR 成为心血管疾病管理的创新范式。本研究系统综述 RHBCR 监测工具的技术演进、临床效能及转化障碍，旨在为优化康复护理质量、提升卫生资源效益提供循证依据。 方法：采用 PRISMA 框架的系统综述，检索 PubMed/EMBASE/Cochrane/CNKI 数据库（2018-2023）。纳入标准：① RCT/ 队列研究；② RHBCR 监测工具应用；③ 成本 / 结局数据分析。构建四维技术体系：①可穿戴设备：医疗级腕戴监测仪（心率 /ECG）、惯性运动传感器；②移动健康平台：康复管理 APP、电子患者报告系统；③ 远程监护系统：多参数集成平台（血压 / 血氧 / 体重）；④智能决策模块：AI 驱动风险预警、个性化处方引擎。采用 GRADE 证据分级，提取依从性、临床结局、成本效益核心指标。 结果：RHBCR 监测工具通过实时监测心率、血压、血氧饱和度、运动量等关键生理指标，为医护人员提供动态数据支持，从而实现个性化康复干预。研究表明，这些工具显著提高了患者的康复参与度和依从性，减少了医院就诊频次，降低了医疗资源消耗。例如，可穿戴设备能够实时记录心电图数据，辅助早期发现异常心律；移动应用程序通过反馈机制激励患者坚持锻炼；人工智能系统则通过数据分析优化康复方案。 然而，当前技术仍面临若干挑战：部分设备的数据准确性有待提升；患者隐私保护和数据安全问题亟须解决；设备成本较高可能限制推广；老年患者因技术熟练度不足，常面临使用障碍。此外，RHBCR 的长期临床效果和成本效益仍需大规模、多中心研究进一步验证。 结论： RHBCR 监测工具在心脏康复中展现出显著潜力，尤其适用于行动不便或医疗资源匮乏的患者群体。其通过实时数据监测和个性化干预，提升了康复效果和患者生活质量，同时缓解了医疗系统压力。然而，技术局限性和实施障碍需通过多学科协作加以解决。未来，应聚焦患者需求，优化设备设计与功能，完善数据安全机制，并推动 RHBCR 模式的标准化与规范化发展，以进一步提升其临床价值和普及程度。

老年急性冠状动脉综合征 PCI 术后早期心脏康复有效性和安全性研究

张兆国 沈伊豪 黄心颖 王冉冉 汪爱华 赵兰婷

清华大学附属北京清华长庚医院，清华大学临床医学院

目的：评估急性冠脉综合征 PCI 术后早期心脏康复（CR）干预的有效性和安全性。

方法：在我院住院的年龄大于 65 岁的老年急性心肌梗死患者 64 名， 按照数字随机方式分为干预组（耐力 + 抗阻）（n=32）和对照组（常规护理）组（n=32），所有患者都参加了平均持续时间 2 周的常规住院和 4 周远程医学指导下居家心脏康复（CR）课程，分配到干预组的患者每周 3 天接受了不同的阻力训练和耐力训练，对照组进行常规护理计划。在基线和心脏康复 4 周后，通过 6 分钟步行测试 （6MWT） 、心肺运动测试 （CPET）手握力和简易体能量表（SPPB）评估运动能力，通过 GAD-7 和 PHQ-9 评估心理状态，通过简易堪萨斯城心肌病调查问卷（KCCQ-12）评估社会参与能力及生活质量。

结果：患者平均年龄为 72.9±5.5 岁，73% 是男性。心脏康复干预组在完成 4 周心脏康复课程后，患者的 6MWD（358±15.6m vs 302±14.8m，p < 0.05），峰值摄氧量（16±3.6ml vs 14.8±4.2ml，p < 0.05）、手握力（男性）（23±6.8ml vs 19±4.9ml, p < 0.05）、SPPB（9±1.4m vs 6±2.2m , p < 0.05）和 KCCQ（68±4.6 vs 52±3.5，p < 0.001）等社会参与能力的指标与对照组比较均显著改善（p < 0.05），两组患者的静息心率（69±5.2 vs 78±4.5 次 / 分，p < 0.05）、焦虑情绪（GAD-7）（6±3.2 vs 8±2.9 次 / 分，p < 0.05）和抑郁情绪（PHQ-9）（9±3.6 vs 8±3.2 次 / 分，p < 0.05）有显著差异，研究期间两组患者均未出现体位性低血压、晕厥、运动相关胸闷等不良心血管事件。

结论： 65 岁老年急性心肌梗死 PCI 术后早期心脏康复干预耐受性良好，运动耐力、身体机能和生活质量明显提高，静息心率、焦虑和抑郁心理状态明显减低。PCI 术后早期心脏康复干预有较高安全性，未发生不良心血管事件。基于医院指导的门诊和家庭混合式心脏康复模式在老年急性心肌梗死 PCI 术后患者有较高的疗效和安全性 。

心脏外科术后早期康复干预和首次离床活动的影响因素研究

张兆国 黄心颖 王冉冉 贾一新 沈冬焱 崔晓征 李永超 韩雪松 沈伊豪 汪爱华 赵兰婷

清华大学附属北京清华长庚医院，清华大学临床医学院

目的：心脏手术后并发症与术后卧床时间密切相关。联合重症护理团队进行心脏术后早期离床活动受到多种因素影响。建立心脏外科术后早期康复干预临床路径对患者预防术后并发症和促进身体恢复具有重要意义。

方法：在 2023 年 4 月 -2024 年 12 月我院心脏外科术后 168 名患者（n=168），建立患者心脏手术后 72 小时内身体活动临床路径，记录患者手术结束到首次启动康复干预及第一次离床站立活动时间以及持续时间，收集患者术前预康复、术后生命体征、化验检查及机械通气以及麻醉形式等临床信息。

结果：共有 143 例患者（85.1%）在最初 24h 内启动床上康复干预，其中 69% 的患者在气管插管拔出后 12h 内启动首次床上康复干预。术后启动首次康复干预时间为 20.7± 5.5 h，中位数 17.6 h（8.5–27.1），首次康复干预持续 45 ± 5min，中位数为 40min（30-60），床上康复干预形式包括相关康复教育、被动肢体活动、卧位踏车、踝泵训练、呼吸训练和坐在床边；术后首次离床活动时间为 56 ± 9.3h，中位数 47.9h（28.5–90.7），首次离床站立持续 5.6±2.0min 或踏步 2±0.8min 或坐椅子 8±3.6min。研究发现较长气管插管时间、体外循环、主动脉弓手术与较晚启动首次康复干预时间正相关 （ρ =0.487，p < 0.001）。启动首次康复时间与首次离床活动时间正相关 （ρ =0.315，p < 0.001）。冠状动脉旁路移植术与瓣膜修复或置换手术间没有显著差（ρ =0.057，p < 0.001）。预康复次数与术后首次呼吸康复的分钟通气量密切相关（ρ =0.429，p < 0.001），术后用力肺活量达到术前 70% 的患者，其首次离床活动时间平均缩短 6 ± 2.3h。

结论：心脏手术后首次启动床上康复干预的中位数时间为 17.6h，首次离床活动的中位时间为 47.9h。启动床上康复时间越早，首次离床活动时间也越早，延迟术后首次康复干预时间的影响因素较多，主动脉弓手术、体外循环以及术后机械通气时间均可延长首次康复干预和离床活动时间。预康复可明显缩短心脏术后首次离床活动时间。

术前多模式预康复对心脏手术后早期启动康复干预时间及肺部并发症的影响

张兆国 王冉冉 黄心颖 贾一新 沈冬焱 崔晓征 李永超 韩雪松 沈伊豪 汪爱华 赵兰婷

清华大学附属北京清华长庚医院，清华大学临床医学院

目的：研究术前多模式预康复对冠脉搭桥术和瓣膜置换术后早期康复启动时间、重症监护室（ICU）时间、住院总时间、机械通气（MV）持续时间和发生肺部并发症的影响。

方法：在 2023 年 4 月 -2024 年 12 月我院心脏外科术后 168 名患者（n=168），术前进行 ARISCAT 评分，对患者进行多模式预康复（健康教育、吸气肌力量训练及腹式呼吸训练），同时建立心脏手术后 1 周的身体活动临床路径。按照术前预康复次数分为干预组（pre-CR 3 次及以上，n=90）和对照组（pre-CR 0-2 次，

n=78），记录患者手术结束到首次启动康复干预时间和首次离床站立活动时间，收集患者术后生命体征、辅助检查及机械通气及呼吸道症状等临床特征等临床信息。

结果：与对照组相比，术前预康复干预组总住院时间、ICU 时间和机械通气持续时间明显缩短（p < 0.05），术后发生肺不张和肺部感染显著减少，两组间有显著差异（p < 0.05）。术前预康复次数与术后首次呼吸康复的分钟通气量密切相关（ρ=0.429，p < 0.001），术后用力肺活量达到术前 70% 的患者，其首次启动康复干预时间和第一次离床活动时间明显缩短。

结论：术前多模式预康复可减少心脏手术患者术后机械通气持续时间、ICU 时间和总住院时间，且减少术后肺部感染和肺不张的发生率。预康复次数与术后首次呼吸康复的分钟通气量密切相关，术后用力肺活量达到术前 70% 的患者，其首次启动康复干预时间和第一次离床活动时间明显缩短。

心脏康复与冠心病的二级预防

于小溪

吉林大学第二临床医院

目的：探讨心脏康复（CR）在冠心病（CHD）患者二级预防中的效果，分析其对患者心血管事件发生率、生活质量及心理状态的影响。

方法：选取 2023 年 1 月至 2024 年 12 月在某三级甲等医院心血管内科就诊的 120 例冠心病患者，随机分为干预组和对照组，每组 60 例。干预组在常规药物治疗基础上进行为期 12 周的心脏康复计划，包括有氧运动、阻力训练、健康教育及心理干预；对照组仅接受常规药物治疗和一般健康指导。通过比较两组患者干预前后的心血管事件发生率、生活质量评分（SF-36 量表）、焦虑抑郁评分（HADS 量表）及运动耐量（6 分钟步行试验）等指标，评估心脏康复的效果。

结果：干预组患者的心血管事件发生率显著低于对照组（5.0% vs. 15.0%，P<0.05）。干预后，干预组的生活质量评分显著高于对照组（SF-36 总分：78.5±6.2 vs. 65.3±7.1，P<0.01），焦虑抑郁评分显著降低（HADS 总分：8.2±2.1 vs. 12.4±3.0，P<0.01），运动耐量显著改善（6 分钟步行距离：425±45 m vs. 365±50 m，P<0.01）。

结论：心脏康复能够有效降低冠心病患者的心血管事件发生率，显著改善其生活质量、心理状态及运动耐量，是冠心病二级预防的重要手段。建议在临床实践中推广心脏康复计划，以优化冠心病患者的长期预后。

The Efficacy of Traditional Chinese Exercises in Cardiac Rehabilitation for Chronic Heart Failure：a systematic review and network meta-analysis

Chen Hua, Li-Min Zhang, Dong-Mei Cao, Xiao-Yang Cai, Lin Tang, Juan Jia, Juan Yang

The Second Affiliated Hospital Of Army Medical University: Xinqiao Hospital,Chongqing

Background:

Chronic heart failure (CHF) imposes a significant global burden, affecting over 60 million individuals worldwide. It leads to progressive loss of functional capacity and diminished quality of life despite the use of guideline-directed medical therapy. The burden is further magnified by high hospitalization rates, poor prognosis, and increasing prevalence in aging populations. Cardiac rehabilitation (CR) has emerged as a non-pharmacological cornerstone in CHF management. Traditional Chinese Exercises (TCEs), such as Tai Chi and Baduanjin, offer accessible, safe, and culturally acceptable approaches that are increasingly integrated into CR programs. However, comparative efficacy among different TCE modalities remains unclear.

Objective:

This network meta-analysis (NMA) aimed to evaluate and rank the effectiveness of major TCEs (Tai Chi, Baduanjin, Wuqinxi, Liuzijue, Yijinjing, and Zhuang medicine Sanqi Yangsheng exercise) combined with conventional care versus conventional care alone on key functional, biochemical, structural, and clinical outcomes in CHF patients.

Methods:

We systematically searched Embase, Medline, Cochrane Central Register of Controlled Trials, Web of Science, Chinese Biomedical Database, CNKI, Wanfang, and VIP from inception to May 2025. Eligible randomized controlled trials (RCTs) enrolled adults with CHF (≥ 18 years) comparing any TCE modality plus conventional care versus conventional care alone. Primary outcomes included 6-minute walk test (6MWT), peak oxygen uptake (Peak VO2), N-terminal pro-B-type natriuretic peptide (NT-proBNP), and Minnesota Living with Heart Failure Questionnaire (MLHFQ). Secondary outcomes included left ventricular ejection fraction (LVEF), left ventricular end-diastolic diameter (LVEDD), major adverse cardiovascular events (MACE), and rehospitalization rates. Two reviewers independently screened studies, extracted data, and assessed methodological quality using the Cochrane Collaboration risk of bias tool and Jadad scale. Pairwise and network meta-analyses were conducted using Stata SE 17.0, with treatment effects estimated using relative risks (RRs) and mean differences (MDs), and ranking assessed via Surface Under the Cumulative Ranking Curve (SUCRA). Loop inconsistency tests evaluated consistency. The protocol was registered on PROSPERO (CRD42024531562), and PRISMA-NMA guidelines were followed.

Results:

Forty-nine RCTs comprising 3,916 participants were included. Tai Chi and Baduanjin significantly improved 6MWT compared to conventional care (Tai Chi: RR = 4.05e+20; Baduanjin: RR = 1.28e+24). Baduanjin also significantly improved Peak VO2 (RR = 3.58, 95% CI [1.45–8.85]) and showed the highest SUCRA ranking for endurance improvement. Both Tai Chi (RR = 0.45, 95% CI [0.22–0.90]) and Baduanjin (RR = 0.39, 95% CI [0.16–0.95]) significantly reduced readmission rates. Tai Chi and Baduanjin significantly improved LVEF (Tai Chi: RR = 36.16; Baduanjin: RR = 20.18). Yijinjing ranked highest for improving LVEF and NT-proBNP but differences were not statistically significant. No significant differences were observed for MLHFQ, LVEDD, or MACE. Funnel plots suggested potential publication bias.

Conclusion:

This NMA provides robust evidence supporting the integration of specific TCEs, particularly Tai Chi and Baduanjin, into cardiac rehabilitation for CHF patients. These practices improve exercise tolerance, cardiac function, and reduce hospital readmissions. Their incorporation is particularly valuable in community settings and low-resource environments. Policymakers and clinical teams are encouraged to embed these interventions into standardized CR protocols to achieve scalable and sustainable health benefits. Future large-scale, multicenter RCTs are needed to validate these findings and optimize TCE-based rehabilitation models.

Keywords: Chronic heart failure; Cardiac rehabilitation; Network meta-analysis; Traditional Chinese Exercise; Tai Chi; Baduanjin; Non-pharmacological interventions.

PCI 术后与不同程度冠脉狭窄患者的 CPET 指标对比及进行康复治疗指征评估

吕文静 [1] 悉心悦 [2] 于芳莉 [1] 张潮涌 [1] 刘姣琳 [1] 王海姝 [1] 李阳 [1] 于彦伟 [1]

1. 哈尔滨医科大学附属第四医院

2. 哈尔滨医科大学

目的：观察经皮冠状动脉介入治疗（PCI）术后 24-48 小时患者与不同程度冠状动脉狭窄患者心肺运动试验（CPET）相关指标的特征及评估其康复治疗指征。

方法：回顾性选取哈尔滨医科大学附属第四医院心血管内科自 2024 年 3 月至 2025 年 3 月收治的 180 例出院前完成 CPET 的患者为研究对象。根据冠状动脉 CTA 结果依据冠脉 CAD-RADS 分级标准将患者分为冠脉未见狭窄组（n=41），冠脉轻度狭窄组（n=54），冠脉中度狭窄组（n=37）和 PCI 术后组（n=48）。比较四组患者一般资料及 CPET 指标，通过 CPET 测量峰值公斤摄氧量（VO2）、代谢当量（MET）、氧脉搏、二氧化碳通气当量（VE/VCO2）斜率及呼吸交换率（RER）等反映患者运动耐量以及心血管功能的指标及提示预后的指标。以峰值公斤 VO2、峰值 METs、RER 及无氧阈公斤 VO2 为因变量进行多因素回归分析，探索年龄、高血压、糖尿病及冠脉狭窄程度对冠心病患者心肺功能影响。

结果：PCI 术后组高血压比例、糖尿病比例均高于其他三组、四组血脂指标对比差异显著，差异均有统计学意义均为（P<0.05）。PCI 术后组峰值 Mets（4.57±1.16 vs.5.34±1.08 vs.5.43±1.48 vs.5.48±1.34，P<0.05）、峰值公斤 VO2（15.98±4.06 vs.18.75±3.77 vs.19.26±4.34 vs.19.16±4.66，P<0.05）、RER（1.04±0.08 vs.1.08±0.09 vs.1.09±0.09 vs.1.06±0.10，P<0.05） 及无氧阈公斤 VO2（15.98±4.06 vs.18.75±3.77 vs.19.26±4.34 vs.19.16±4.66，P<0.05）均显著低于冠脉未见狭窄、轻度狭窄和中度狭窄组。多因素回归分析表明，峰值公斤 VO2 与年龄（β=-0.110，P=0.003）、高血压（β=-1.984,P=0.003）呈显著负相关，PCI 术后组（β=-3.128,P=0.004）呈显著负相关。峰值 METs 与年龄（β=-0.029,P=0.008）、高血压（β=-0.541,P=0.008）呈显著负相关，PCI 术后组（β=-0.997,P=0.005）呈显著负相关。RER 与 PCI 术后组存在显著负相关（β=-0.056,P=0.018）。

结论：PCI 术后患者心肺功能短期内未见明显恢复，年龄、高血压及冠状动脉狭窄是运动耐量下降的关键因素。

早期心脏康复护理对急性心肌梗死 PCI 术后的影响

李相萱

三峡大学第一临床医学院湖北宜昌市中心人民医院

本研究主要分析早期心脏康复护理对急性心肌梗死 PCI 术后心功能及生活质量的影响。方法：选取本院 2023 年 1 月 -2024 年 12 月间收治的急性心肌梗死患者 100 例，采用随机数字法将其分为对照组、研究组两组，每组各 50 例。对照组给予 PCI 术后常规护理，研究组给予早期心脏康复护理。比较两组患者护理前后焦虑自评量表 (SAS) 和抑郁自评量表 (SDS) 评分，并比较两组患者护理后 6MWT、LVEF、LVEDD、LEVSD 及 CI 等指标以及生活质量评分（SF-36）中各项评分指标，以及两组术后并发症发生情况。结果：两组患者护理前 SAS 与 SDS 比较无明显统计学差异；护理后，研究组 SAS 与 SDS 评分明显低于对照组（P<0.05）；研究组 6MWT、LVEF 和 CI（407.92±34.19m；52.50±6.28%；2.59±0.08L/m^2）明显高于对照组（488.70±36.15m; 55.82±5.91%; 2.81±0.0L/m^2），而 LVEDD、LEVSD（60.74±5.99mm；39.68±4.73mm）明显低于对照组（55.88±4.74mm；34.38±3.69mm）（P<0.05）；与对照组相比，研究组患者护理后生活质量评分（SF-36）中各项评分指标均高于对照组（P<0.05）；相比于对照组，研究组腹胀、便秘、尿潴留、食欲不振和失眠情况明显低于对照组（P<0.05）。结论：研究证明，急性心肌梗死 PCI 术后早期行心脏康复护理明显有利于患者心功能和精神状态的恢复，减少并发症的发生，有利于患者生活质

量的提高，促进患者康复。

基于高级健康评估结合 ERAS 理念的一例老年患者行冠状动脉搭桥联合瓣膜置换手术的个案护理

朱晓琳 罗年年

厦门大学附属心血管医院

本个案报告一例基于高级健康评估的老年患者行冠状动脉搭桥联合瓣膜置换手术的护理体会。动态收集和分析患者健康资料，通过五维度对患者进行分阶段的整体性评估，评估时间为 2025 年 5 月 14 日至 5 月 21 日，按照优先顺序提出了五个主要护理问题：气体交换障碍、心输出量减少、活动无耐力、潜在危险性不稳定血糖浓度、营养不均衡：少于身体所需。住院期间运用 ERAS 理念对患者进行围术期护理，同时联合多学科模式照护患者，为患者制定个性化的康复计划，包括呼吸训练、肢体训练及有氧训练，患者在术后 12 天即康复出院。住院期间患者的体征、症状通过精细化护理，得到明显的改善，为患者提供早期康复、体液管理、疼痛管理、睡眠管理以及营养护理，患者在返回病房第二天开始下地活动、术后未再出现气体交换掌握的表现、术后维持体液平衡、心功能改善、疼痛评分由 3 分降至 0 分，营养状况较前改善，食欲好转，各营养指标均上升白蛋白由 35.9g/L 上升至 36.9g/L，睡眠质量得到明显提升，由术前的重度睡眠难续依赖于药物维持每日睡眠 4h 增加至无药物维持下的每日睡眠 6h。通过此案例报道，总结如何运用高级健康评估五维度对患者进行整体性评估，提出针对性护理诊断和护理措施，同时联合 ERAS 理念，加快患者的早期康复，借此案例，将 ERAS 理念推行至心脏外科患者，减少术后并发症，提高生活质量。

通过运动为基础的心脏康复，改善不同 BMI 组心血管疾病患者的运动能力及生活质量。

刘昕萌 马梅

天津市胸科医院

目的

随着心血管疾病（CVDs）患病率持续攀升，基于循证医学的心脏康复治疗需求激增，现已成为患者的核心治疗手段。本研究旨在系统评估结构化心脏康复（CR）方案对 CVDs 患者心肺功能及心理状态的改善效果。

方法

本研究纳入 79 例 CVDs 患者，实施为期 4-6 周的标准化 CR 干预（每周 2-3 次中心训练，共 12 次）。干预前后分别采用心肺运动试验（CPET）及四项量表进行多维度评估：1）心肺功能核心指标：摄氧量（VO_2）、通气量（VE）、无氧阈（AT）负荷功率（Workload）及摄氧效率斜率（OUES）；2）生活质量量表（SF-12）；3）抑郁自评量表（PHQ-9）；4）焦虑自评量表（GAD-7）。

结果

康复干预后，患者心肺功能指标显著提升（均 p<0.01）：AT 时 VO_2：10.93±2.94 → 13.25±3.43 mL/min/kg、AT 状态 VE：29.27±7.47 → 35.58±9.34 L/min、AT 负荷功率：56.66±25.44 → 70.04±27.69 W、OUES：1426.75±346.30 → 1547.19±403.49。

生活质量量表评分显著改善（p<0.01），抑郁与焦虑评分分别降低 32.7% 和 28.9%（p<0.01）。亚组分析显示，不同体质指数（BMI）组别均呈现一致性获益趋势。

结论

本研究证实：结构化运动康复可显著提升 CVDs 患者的心肺储备功能（VO_2峰值提升 21.2%，AT 负荷功率增加 23.6%），同步改善生活质量及心理状态，且疗效不受 BMI 影响。该方案为临床推广循证化心脏康复提供了重要实践依据。

基于 CPET 指导的心脏康复运动对老年 CHF 患者焦虑情绪和生活质量的影响

卫霞 郎明健

成都市第五人民医院

目的：探究心肺运动测试（cardiopulmonary exercise testing，CPET）指导的心脏康复运动对老年慢性心力衰竭（Chronic Heart Failure，CHF）者血清 NT-proBNP 水平、焦虑情绪和生活质量的影响。

方法：从我院收治的老年慢性心力衰竭患者中随机选取 92 例作为研究对象，随机分成观察组和对照组，每组 46 例，两组患者均接受常规治疗，观察组在常规治疗基础上采用 CPET 指导的心脏康复运动。比较两组患者 NT-proBNP 水平、汉密尔顿焦虑量表（HAMA）、抑郁量表（HAMD）和生活质量综合评定问卷的（GQOLI-74）评分；并记录治疗期间不良心血管事件。

结果：治疗前，两组患者血清中 NT-proBNP 水平、HAMA、HAMD 量表评分及 GQOLI-74 评分比较差异无统计学意义（P>0.05）。治疗 1 个月、3 个月及 6 个月后，两组患者 NT-proBNP、HAMA、HAMD 量表评分与治疗前相比均明显下降，其中治疗 3 个月及 6 个月后观察组下降更为明显（P<0.05），治疗 6 个月后，两组患者 GQOLI-74 评分较治疗前均有所提高，且观察组变化更为明显 P<0.05）。治疗期间，与对照组相比，观察组发生主要不良心血管事件（MACE）的风险增加了 1.4 倍 (P<0.05)。

结论：CPET 指导心脏康复模式可以明显降低老年 CHF 患者的血清 NT-proBNP 水平，减少患者负面情绪和不良心血管时间的发生，提高患者生活质量。

herapeutic Effect of Limbs Compression Based Anti-syncope Therapy Trousers on Vasovagal Syncope

bingqing zhou

Daping Hospital of Army Medical University

Background: Vasovagal syncope (VVS) is the most prevalent cause of syncope, which significantly deteriorates the life quality. However, there is currently no effective method available to treat VVS. Blood distribution in the lower limbs induced sympathetic withdrawal was involved in the progression of VVS. We developed novel anti-syncope therapy trousers to compress lower limbs and tested its effect on treatment of VVS.

Methods：Anti-syncope trousers were developed using sequential air compression (ankles → shanks → thighs) via three interconnected air cavities per leg to enhance venous return. A hardware system (mini air pump, 3-bit valves, ADC microprocessor) precisely controlled inflation pressure/duration, displaying data on an LED panel.Patients (2014-2016, Daping Hospital) with unexplained syncope underwent ESC guideline-based evaluation. Suspected vasovagal syncope (VVS) cases received echocardiography, ECG, and cranial CT to exclude structural disease (e.g., valvular/coronary/cerebral stenosis, cardiomyopathy, pregnancy). Negative cases were excluded. Eligible patients provided informed consent under ethical approval.All included patients underwent head-up tilt testing (HUT). After autonomic medication withdrawal and fasting:Baseline HUT (Stage I): 80 ° tilt for 40 min with continuous ECG/SpO_2 and 5-min BP monitoring. Syncope with hypotension/bradycardia defined positivity. Provocative HUT (Stage II): If negative, 0.5 mg sublingual nitroglycerin was administered during extended 80 ° tilt (20 min). Only HUT-positive patients were randomized:Experimental group: Repeated HUT with trousers activated.Control group: Repeated HUT with trousers inactive. Statistical analysis used Student's t-test (continuous data) and χ^2-test (categorical data), presented as mean±SD. Significance: p<0.05.

Results: The patients were mainly mid-aged adults with no children or old patients included. **No aberrant manifestations with respect to any variable** about **haemodynamics** were observed, indicating included patients suffer no severe structural cardiovascular disease. Age, blood pressure and other **baseline characteristics** were comparable between **the** two **groups**. **The results of HUT test showed that** among xx patients in control group**,** xx patients reported reproduction of positive HUT test. **X**x patients **occurred** syncope in b**aseline head-up tilt test** (induction time was xx min) and xx patients occurred **syncope** in p**rovocative head-up tilt test** (induction time was xx min)**. Among the** xx **patients** with reproduction of positive HUT test**, 7 patients reported hypotension and 8 patients reported marked bradycardia while 3 patients reported both hypotention and marked bradycardia. Notably, no patients reported reproduction of positive HUT test through the whole 2 stages of HUT test in experimental group. Although, VVS might be induced if induction time is** prolonged, **these** results indicate a therapeutic effect of **therapy trousers**. **During the HUT test, SBP decreased to 88.05±13.72 mmHg, DBP 53.86±7.93 mmHg and MAP 65.26±9.22 mmHg** at the end of HUT test in control group**, indicating the foundation of occurrence of conscious loss. Notably, both SBP and DBP** at the end of HUT test **were significantly higher** in experimental group **than** control group**, suggesting that decrease in blood pressure was significantly attenuated with the therapy trousers. In addition, a difference in HR after the test was observed between the** two groups**, though the** difference **was not statistically significant. However,** therapy trousers exerted no **impacts on SPO2 of patients after the HUT test.The incidence of main symptoms/prodromal symptoms of patients during HUT test was shown in Table 4. Patients in** control group **reported a high incidence of main symptoms/prodromal symptoms during HUT test including dizziness and palpitations. However, when in therapy trousers, there were fewer patients reported these symptoms/prodromal symptoms, suggesting a high efficacy of therapy trousers in treating VVS.**

Conclusions: The novel lower limbs compression based therapy trousers exert therapeutic effect on VVS with high efficacy. This new method is of clinical significance for treating VVS.

射频消融术患者围术期踝泵运动依从性影响因素的质性研究

黄巧生 刘华芬

武汉大学人民医院

目的：探讨房颤患者射频消融术后踝泵运动依从性的影响因素，为构建规范化的临床干预方案提供理论支持。

方法：采用现象学研究方法，基于健康信念模型（HBM）的六个维度（感知易感性、感知严重性、感知利益、感知障碍、自我效能及行动线索）制定访谈提纲，对 21 名房颤射频消融术后患者进行半结构化深度访谈，采用定向内容分析法进行资料分析。

结果：患者踝泵运动的依从性呈现双重动力机制：①障碍因素包括风险意识淡薄“术后卧床时间不长，血栓风险不高，没必要特别干预”、运动效果低估“就这样活动一下脚踝没有什么作用”、担心副反应”害怕运动过程中，伤口出血、疼痛等”、自我效能不足“缺乏锻炼信心，执行能力欠缺”、接收信息矛盾“医护说法不统一，没有接收明确的指引”；②促进因素包括并发症警觉性“护士说长期卧床容易出现并发症，影响健康”、健康收益认同“相信踝泵运动能够预防血栓，缩短住院时间等”、外部支持”医护人员的健康指导与督促以及家属的提醒与监督”、正向的自我激励“只要坚持规范的操作肯定对身体有益”。

结论：本研究从 HBM 的角度分析了房颤患者术后踝泵运动依从性的障碍因素和促进因素，临床护理过程中，医护人员应弱化障碍因素的影响，增强促进因素的效益，提升患者的健康水平。具体建议如下：①提升医护人员自身的认知和技能水平；②制定标准化的踝泵运动流程，医护人员严格遵照执行；③通过宣教，促进患者及家属对疾病的认知，了解踝泵运动的重要性及必要性；④建立完善的风险预警机制，确保该操作的安全性和有效性；⑤整合外部资源，家庭积极参与等，提升行为依从性。

Nonexercise Prediction Equation for Oxygen Uptake at the Anaerobic Threshold in Chinese Patients with Cardiovascular Disease

Jia- Liu, Shi-Yu Wang, Xiao-Jun Wu, Jian Wu

哈尔滨医科大学附属第二医院

Background

Oxygen uptake at the anaerobic threshold (VO2AT) is a critical physiological parameter used to assess cardiopulmonary fitness, particularly in patients with cardiovascular disease (CVD). It serves as a key indicator for guiding individualized cardiac rehabilitation programs and evaluating cardiac function. However, VO2AT values vary significantly across different populations due to factors such as race, age, sex, and specific disease conditions. While exercise testing remains the gold standard for measuring VO2AT, it is not always feasible in clinical settings due to equipment requirements, patient limitations, and time constraints. Currently, there is a lack of well-validated, nonexercise prediction equations for estimating VO2AT, especially for Chinese patients with CVD, highlighting the need for a reliable and practical alternative. Given China's large CVD population and unique demographic characteristics, developing a population-specific predictive tool could significantly enhance clinical decision-making and optimize rehabilitation outcomes.

Objectives

This study aimed to develop and validate a nonexercise prediction equation for VO2AT specifically tailored to Chinese CVD patients. By leveraging a large multicenter dataset, the research sought to establish an accurate and clinically applicable model that could facilitate cardiac rehabilitation planning and risk stratification without the need for exhaustive exercise testing. Additionally, the study aimed to evaluate how different CVD subtypes and treatment histories influence VO2AT predictions, thereby providing deeper insights into the physiological determinants of exercise capacity in this population.

Methods

A large-scale retrospective cohort was established, comprising 22,336 cases of cardiopulmonary exercise testing (CPET) data collected from CVD patients across 20 hospitals in China. The dataset was randomly divided into two groups: a development group (70% of the sample, n=15,635) used to derive the prediction equation and a validation group (30%, n=6,701) to assess its accuracy and generalizability. Multivariate forward stepwise regression analysis was employed to identify the most significant predictors of VO2AT, including demographic variables (age, sex, height, weight) and clinical factors (specific CVD conditions such as stable angina, myocardial infarction, heart failure, and history of percutaneous coronary intervention). Rigorous statistical methods were applied to ensure model robustness, including cross-validation and sensitivity analyses to confirm the consistency of the predictors across different patient subgroups.

Results

The final prediction equation was formulated as follows: VO2AT (mL/min) = 314.748 – (3.887 × age [years]) + (85.933 × sex [male = 1; female = 0]) + (1.085 × height [cm]) + (7.790 × weight [kg]) + (17.808 × stable angina [yes=1, no=0]) - (85.469 × percutaneous coronary intervention [yes=1, no=0]) - (112.64 × myocardial infarction [yes=1, no=0]) - (159.730 × heart failure [yes=1, no=0]).The model demonstrated moderate predictive accuracy, with a standard error of the estimate (SEE) of 264 mL/min, a correlation coefficient (R) of 0.71, and an adjusted R^2 of 0.51, indicating that approximately 51% of the variability in VO2AT could be explained by the included predictors. Importantly, the predicted VO2AT values across different patient subgroups were consistent with their corresponding measured values, supporting the equation's clinical applicability. Further subgroup analyses revealed that the equation performed particularly well in middle-aged patients and those with stable coronary artery disease, while slight underestimations were observed in elderly patients with advanced heart failure.

Conclusion

This study presents the first nonexercise VO2AT prediction equation specifically designed for Chinese CVD patients. The model integrates easily obtainable clinical and demographic variables, offering a practical tool for clinicians to estimate VO2AT in settings where CPET is unavailable. This advancement holds significant potential for improving cardiac rehabilitation planning, individualized exercise prescription, and risk stratification in Chinese CVD populations. Future research should focus on further refining the model's accuracy and validating its utility in diverse clinical scenarios. Prospective studies incorporating additional variables such as physical activity levels and medication use may further enhance predictive performance and clinical relevance.

双心医学视角下冠心病患者焦虑抑郁症状的全程管理模式探索

代芬

陆军军医大学第二附属医院新桥医院

摘要：目的：探讨双心医学模式在冠心病合并焦虑抑郁患者临床管理中的应用价值。

方法：采用前瞻性队列研究设计，连续纳入 2022 年 1 月 -2024 年 6 月心血管科收治的 327 例冠心病伴发焦虑抑郁状态（HAMA ≥ 14 分，HAMD ≥ 17 分）患者，随机分为对照组（常规心脏治疗）和干预组（双心医学全程管理）。干预组实施包括心理评估、药物协同治疗、认知行为干预、正念减压训练、家庭支持系统构建的整合管理模式，通过动态监测生理指标（心率变异性、hs-CRP）、心理量表（HADS、SF-36）及心血管事件发生率等多元指标，建立为期 12 个月的随访观察体系。

结果：干预组在 3 个月、6 个月、12 个月时间节点的焦虑抑郁缓解率分别达到 58.3%、72.6%、81.4%，显著高于对照组的 32.1%、45.7%、53.2%（P<0.01）；同时干预组患者的心绞痛发作频率、硝酸甘油用量及再住院率较对照组下降 37.2%-52.8%（P<0.05）。

结论：基于双心医学理论构建的" 生理 - 心理 - 社会" 三维干预体系，通过建立多学科协作路径、实施个性化心理处方、强化院外延续管理等措施，能有效改善冠心病患者的心身症状，其分级评估机制和动态随访模式为心血管科实施精神卫生服务提供了实践范式。

关键词：双心医学；冠心病；焦虑抑郁；心身医学；生活质量

冠心病（Coronary Heart Disease, CHD）作为全球范围内主要的致死、致残性疾病之一，其高发病率与沉重的疾病负担已成为重大的公共卫生问题。在关注心脏器质性病变的同时，越来越多的临床证据表明，焦虑、抑郁等心理障碍在 CHD 患者中普遍存在且危害严重。这类共病状态不仅显著降低患者生活质量，加剧躯体化症状，更可导致治疗依从性下降、心血管事件风险增高及再住院率攀升，形成 "心身共病" 的恶性循环。然而，传统的心血管诊疗模式往往侧重于生物医学指标的干预，对患者心理社会层面的评估与管理存在明显不足，导致大量合并焦虑抑郁的 CHD 患者未能得到及时有效的识别与干预。双心医学（Psycho-Cardiology）强调心脏与心理的密切联系，倡导在心血管疾病诊疗中同步关注患者的心理状态，提供整合生物 - 心理 - 社会因素的整体医疗服务模式。本研究旨在探索基于双心医学理论，构建一套适用于冠心病合并焦虑抑郁患者的全程管理模式，通过前瞻性队列研究设计，系统评价该模式在改善患者心身症状、提升生活质量及降低心血管事件风险方面的应用价值。

个性化心脏运动康复方案对心力衰竭患者心肺功能的影响研究

代芬

陆军军医大学第二附属医院新桥医院

摘要：目的：探讨个性化心脏运动康复方案对改善心力衰竭患者心肺功能指标的临床效果。**方法：**采用单中心随机对照试验设计，选取 2023 年 6 月至 2024 年 5 月收治的 120 例慢性心力衰竭患者，通过心肺运动试验评估制定个体化运动处方。干预组（n=60）实施为期 12 周的阶梯式运动训练，包含有氧运动（功率自行车训练，强度为 50-70% 峰值摄氧量）、抗阻训练（弹力带渐进式训练）及呼吸训练（腹式呼吸结合缩唇呼吸），对照组（n=60）接受常规心脏护理。主要观察指标包括峰值摄氧量（VO2peak）、左室射血分数（LVEF）及 N 末端脑钠肽前体（NT-proBNP）水平，次要指标涵盖 6 分钟步行距离（6MWD）和明尼苏达心衰生活质量量表（MLHFQ）评分。**结果：**干预后干预组 VO2peak 较基线提高（18.7±3.2 vs 22.1±3.5 mL/kg/min，P<0.01），LVEF 绝对值增加（6.3±1.8% vs 对照组 2.1±1.2%，P<0.05），NT-proBNP 中位数下降达 43%（956 pg/mL vs 548 pg/mL，P<0.01）。6MWD 改善幅度显著高于对照组（+82.4±23.6 m vs +31.5±18.2 m），MLHFQ 评分降低（-15.3±4.1 分 vs -6.2±3.7 分），组间差异均具统计学意义（P<0.01）。**结论：**基于精准评估制定的个性化心脏运动康复方案能有效提升心力衰竭患者运动耐量，改善心室重构及神经内分泌激活状态，为慢性心衰患者的二级预防提供循证依据。

关键词：个性化心脏运动康复方案；慢性心力衰竭；心肺运动试验；运动耐量；心室重构

心力衰竭作为全球公共卫生的重要挑战之一，其患病率持续攀升，与高死亡率、高再入院率及严重降低患者生活质量密切相关。当前，尽管药物治疗取得了显著进展，但慢性心力衰竭患者的心肺功能储备下降、运动耐量减低及神经内分泌过度激活等问题依然突出，是导致不良预后的关键因素。心脏康复（Cardiac Rehabilitation, CR）已被国内外权威指南推荐为心力衰竭综合管理的核心组成部分。大量循证医学证据表明，运动训练能够改善心力衰竭患者的运动能力、生活质量，甚至可能降低再住院率和死亡率。

然而，传统的心脏康复方案多采用相对固定的运动模式与强度，未能充分考虑心力衰竭患者在心肺功能储备、合并症、身体活动能力及个人偏好等方面存在的显著异质性。这种方式可能导致部分患者训练强度不足而获益有限，或强度过高而增加不良事件风险，限制了康复效果的最大化。心肺运动试验（Cardiopulmonary Exercise Testing, CPET）作为评估心肺功能储备、制定个体化运动强度的金标准，其在精准康复处方制定中的核心价值日益凸显。基于 CPET 结果制定个体化、阶梯式的心脏运动康复方案，有望更精准、更安全、更有效地改善患者的心肺功能指标和整体预后。

因此，本研究旨在通过严谨的随机对照试验设计，深入探讨基于心肺运动试验评估制定的、包含有氧、抗阻及呼吸训练等多模态组合的个性化心脏运动康复方案，

对慢性心力衰竭患者核心心肺功能指标、运动耐量及生活质量的影响，以期为优化心力衰竭患者的康复管理提供更高级别的循证依据。

基于循证医学的冠脉支架术后合并 OSAHS 患者运动康复方案优化

代芬

陆军军医大学第二附属医院新桥医院

摘要：目的：探讨冠脉支架术后合并阻塞性睡眠呼吸暂停低通气综合征（OSAHS）患者运动康复方案的优化策略。

方法：通过系统评价国内外相关循证医学证据，整合心肺功能评估、睡眠监测及个体化运动处方制定等多维度干预措施。比较传统康复方案与优化后方案在 6 分钟步行距离、夜间低氧指数、主要不良心血管事件发生率等指标上的差异，评估优化方案对患者心肺功能改善、睡眠质量提升及长期预后的影响。

结果：共纳入 23 项随机对照研究及 8 项队列研究，涉及患者 2145 例。优化组较传统康复组 6 分钟步行距离（6MWD）显著提高（412.5±35.6 m vs 358.2±41.3 m，P<0.01），夜间氧减指数（ODI）降低幅度达 43%（12.7±3.5 vs 22.3±4.1，P<0.001），呼吸暂停低通气指数（AHI）平均下降 9.2 次 / 小时。随访 12 个月显示，优化组左心室射血分数（LVEF）提升 5.8±1.2%（P=0.003），主要不良心血管事件（MACE）发生率降低 37%（HR=0.63，95%CI 0.51-0.78）。次要终点显示 Epworth 嗜睡量表评分改善 4.3 分（P=0.012），SF-36 生活质量评分提高 18.6 分（P<0.01）。

结论：基于多维度评估的个体化运动康复方案可有效改善 OSAHS 合并冠脉支架术后患者的心肺功能协同障碍，其机制可能涉及夜间低氧血症缓解、交感神经张力调节及内皮功能改善。通过 CPAP 联合中等强度间歇训练（MIIT）的序贯干预模式，使患者运动耐量提升与睡眠结构改善形成良性循环。建议将呼吸驱动训练纳入 II 期心脏康复核心内容，同时强调夜间血氧饱和度动态监测对运动处方安全性的保障作用。

关键词：冠状动脉介入治疗；阻塞性睡眠呼吸暂停低通气综合征；心肺功能；多导睡眠监测；心脏康复

高原地区慢性呼吸系统疾病患者阶梯式肺康复方案的构建与验证

游玲

陆军军医大学第二附属医院新桥医院

摘要：目的：基于循证医学证据及高原环境特点，构建肺动脉高压合并慢性阻塞性肺疾病（COPD）患者的阶梯式肺康复方案，并通过临床随机对照试验验证其有效性及安全性。

方法：采用德尔菲专家咨询法构建包含呼吸训练、运动康复、健康教育、心理干预的四级阶梯式康复体系，通过改良版慢性呼吸系统疾病自我管理量表（CAT）进行动态评估，结合动脉血氧饱和度监测实施个体化阶梯调整。

结果：最终纳入 227 例患者完成 12 周干预，试验组 FEV1% 预计值较基线提升（8.62±3.15）%，6 分钟步行距离增加（68.3±22.4）米，急性加重次数降低 42.7%，显著优于常规康复组（P<0.01）。

结论：阶梯式肺康复方案可显著改善高原慢性呼吸系统疾病患者肺功能及运动耐力，其基于血氧反馈的动态调整机制能有效预防高原康复治疗相关风险，为高海拔地区肺康复临床路径优化提供循证依据。

关键词：高原医学；慢性呼吸系统疾病；阶梯式肺康复；血氧监测；运动耐力

高原地区慢性缺氧环境对慢性呼吸系统疾病患者的肺功能及生存质量构成严峻挑战。慢性阻塞性肺疾病（COPD）合并肺动脉高压作为该区域的常见共病，因低氧血症进行性加重、运动耐量急剧下降及急性发作频率攀升，显著增加患者致残率与医疗负担。传统肺康复方案虽在平原地区成效明确，但其固定强度模式难以适配高原环境下患者血氧波动的特殊性，康复过程中存在运动性缺氧甚至病情恶化的潜在风险。因此，亟需构建一种融合高原生理代偿机制、具备动态调整功能的肺康复策略，在保障安全性的前提下实现康复效益最大化。本研究基于循证医学框架，整合高原低氧病理生理特征与阶梯式干预理念，旨在开发并验证一套以血氧饱和度实时监测为调控核心的个体化阶梯肺康复方案，为优化高海拔地区呼吸慢病管理提供循证路径。

高强度间歇训练联合地中海饮食在冠心病二级预防中的协同效应研究

游玲

陆军军医大学第二附属医院新桥医院

摘要：目的：探讨高强度间歇训练（HIIT）联合地中海饮食对冠心病患者心血管事件复发率、心功能指标及炎症因子的影响，分析两种干预方式在改善内皮功能与代谢调控中的协同作用机制。

方法：采用多中心随机对照试验设计，纳入 200 例经皮冠状动脉介入治疗后的稳定性冠心病患者，随机分为 HIIT 组、地中海饮食组、联合干预组及常规护理组。通过 12 周结构化运动计划配合个性化膳食指导，监测患者干预前后左室射血分数（LVEF）、超敏 C 反应蛋白（hs-CRP）、主要不良心血管事件（MACE）发生率等指标，采用广义估计方程评估组间差异。

结果：联合干预组 LVEF 提升幅度（8.2±1.5%）显著高于单一干预组（HIIT 组 5.1±1.2%，饮食组 3.3±0.9%）及对照组（1.8±0.6%，P<0.01）。血清 hs-CRP、IL-6 水平分别下降 46.7% 和 38.2%，降幅较单一干预组提高 1.8-2.3 倍（P<0.05）。联合组 12 个月 MACE 发生率（7.2%）显著低于常规护理组（19.6%，HR=0.41，95%CI 0.28-0.59）。

结论：HIIT 与地中海饮食通过调节线粒体生物合成、改善胰岛素敏感性及抑制 NF-κB 炎症通路的协同作用，显著提升冠心病二级预防效果，建议将结构化运动 - 营养联合干预纳入心脏康复标准方案。

关键词：高强度间歇训练；地中海饮食；冠心病；二级预防；协同效应

冠心病作为全球范围内主要的致死性疾病之一，其二级预防策略的优化对降低复发事件和改善患者预后至关重要。据世界卫生组织报告，心血管疾病每年导致约 1790 万人死亡，其中冠心病占比显著，且复发事件如心肌梗死或心力衰竭在二级预防不足的患者中发生率高达 20% 以上。传统的心脏康复方案多侧重于单一干预，如药物治疗或适度运动，但效果有限，尤其在内皮功能障碍和慢性炎症控制方面存在明显不足。

近年来，高强度间歇训练（HIIT）因其高效改善心肺功能和代谢调控的特性，在冠心病管理中展现出显著优势，能快速提升峰值摄氧量（VO2 max）和左心室功能。同时，地中海饮食以其丰富的单不饱和脂肪酸、抗氧化剂和膳食纤维，被证实能降低炎症标志物水平和心血管事件风险，但其在长期依从性和协同效应方面的研究仍较匮乏。现有证据表明，HIIT 可能通过激活 AMPK 信号通路增强线粒体生物合成，而地中海饮食则能调节肠道微生物群和 NF-κB 通路，两者在改善胰岛素敏感性和抑制氧化应激方面存在潜在的互补机制。然而，目前缺乏多中心随机对照试验来系统评估这种联合干预的协同效益，尤其在亚洲人群中的适用性数据不足。

因此，本研究旨在填补这一空白，通过整合结构化运动与营养干预，深入探讨 HIIT 联合地中海饮食对冠心病患者心血管事件复发、心功能指标及炎症因子的影响。这不仅有助于阐明协同作用的内在机制，如内皮修复和代谢稳态的调控，还为制定个体化心脏康复方案提供循证依据，推动二级预防策略从单一模式向综合干预转型。

家庭 - 医院 - 社区三元联动管理模式对慢性心肺疾病预后的影响

游玲

陆军军医大学第二附属医院新桥医院

摘要：目的：探讨家庭 - 医院 - 社区协同干预在改善慢性心肺疾病患者生存质量中的作用机制及临床效益。

方法：选取 2022 年 1 月 -2024 年 6 月收治的 320 例慢性心肺疾病患者作为研究对象，采用随机数字表法分为对照组（常规管理模式）和观察组（三元联动模式），通过远程监测系统建立电子健康档案，实施家庭氧疗指导、医院专科随访、社区康复训练相结合的立体化管理。

结果：干预 12 个月后，观察组再入院率下降 42.3%（P<0.01），6 分钟步行距离提升 28.6%（P<0.05），明尼苏达心功能不全生活质量量表评分改善率达 76.9%。

结论：三元联动管理模式通过强化全程健康监测、规范用药管理、优化康复支持，显著降低急性加重风险，其多维度干预策略对改善患者运动耐力及长期预后具有积极意义，建议作为慢性病综合防治的标准化方案推广应用。

关键词：慢性心肺疾病；三元联动管理模式；生存质量；再入院率；康复训练

慢性心肺疾病作为全球主要的健康负担之一，其高发病率、高致残率及反复急性加重特征，不仅显著降低患者生存质量，还加剧医疗资源消耗和社会经济负担。传统医院中心化管理模式虽能提供急性期救治，但缺乏对家庭环境和社区支持的整合，导致患者出院后依从性差、康复不连续，再入院率居高不下。随着人口老龄化进程加速和慢性病防控需求提升，构建家庭 - 医院 - 社区三元联动管理模式成为优化长期预后的关键策略。该模式通过强化多主体协作，实现健康监测全程化、用药管理规范化及康复支持个性化，旨在弥补单一医疗机构的局限。本研究聚焦于探讨三元联动干预在改善患者运动耐力、生存质量及降低再入院风险方面的机制与效益，为慢性病综合防治提供循证依据。

太极“柔化心泵”理论在慢性心衰康复中的临床应用

谢小红

陆军军医大学第二附属医院新桥医院

摘要：目的：探讨太极” 柔化心泵” 理论指导下的运动康复方案对慢性心力衰竭患者心功能改善及生活质量提升的临床效果。

方法：采用前瞻性队列研究设计，纳入 120 例 NYHA 心功能 II - III级患者，随机分为实验组（太极柔化训练组）和对照组（常规康复组），进行为期 12 周的干预治疗。通过超声心动图测量左室射血分数（LVEF）、6 分钟步行距离（6MWD）评估心功能，采用明尼苏达心力衰竭生活质量问卷（MLHFQ）进行生活质量评价。

结果：干预后实验组 LVEF 提升（6.8±1.2）%，6MWD 增加（58.3±7.5）m，显著优于对照组（p<0.05）；MLHFQ 评分降低幅度（24.6±3.1）分，较对照组多改善 9.2 分（p<0.01）。

结论：太极” 柔化心泵” 理论通过调节自主神经平衡、优化心肌能量代谢，在改善慢性心衰患者心肺功能、提高运动耐量及生活质量方面展现出显著优势，为中医传统功法与现代心脏康复的融合提供了新思路。

慢性心力衰竭（CHF）作为全球性的重大健康问题，其高发病率、高再住院率及低生活质量严重困扰患者，并给社会带来沉重的医疗负担。现代心脏康复已被证实是改善 CHF 患者预后、降低再住院风险和提高生活质量的有效策略，其中运动康复是核心组成部分。然而，传统运动康复方案，尤其对于高龄或心功能储备较差的患者，常存在依从性不佳、训练强度难以精准把控以及潜在风险等问题。寻求安全、有效且患者易于接受的运动康复方式成为临床关注焦点。中医传统功法源远流长，太极以其动作舒缓圆活、形神兼备、强调意念与呼吸配合的特点，在心肺疾病康复领域展现出独特价值。其核心理论之一“柔化心泵”，主张通过柔和、连贯、节律性的肢体运动，配合深长匀细的呼吸及意念引导，达到“以柔克刚”、“松而不懈”的状态，旨在优化心脏泵血效能，减轻心肌耗氧负担。该

理论从中医整体观出发，不仅关注心脏局部功能，更强调通过调节自主神经系统平衡、改善气血循环、优化心肌能量代谢等多途径协同作用来恢复心身和谐。多项研究初步证实太极拳对 CHF 患者有积极影响，但以“柔化心泵”这一特定理论为指导，系统构建并严格评估其康复方案效果的前瞻性研究相对缺乏。本研究旨在通过严谨的前瞻性队列设计，深入探讨基于太极“柔化心泵”理论制定的运动康复方案对改善慢性心力衰竭患者心功能指标及生活质量的临床效果，为中医传统智慧与现代心脏康复实践的有效融合提供科学依据。

Physical performance on the early 6-minute walk test in coronary artery bypass grafting patients during inpatient cardiac rehabilitation

Yao Wu, Bao Ren, Jing Li, Li-Qun Chi, Ping Li, Jia-Hui Wu

Beijing Anzhen Hospital

Background: Cardiovascular diseases are the leading cause of death globally. Coronary artery bypass grafting (CABG) is an effective and established treatment for clinically significant coronary artery disease.The 6-minute walk test (6MWT) is widely used to evaluate functional exercise capacity, therapeutic effects, and prognosis in patients with cardiopulmonary diseases. However, its application in phase I cardiac rehabilitation (CR) after CABG remains under explored. This study investigates the physical performance of CABG patients during the early 6MWT and analyzes factors influencing their walking performance during inpatient CR.

Methods: This retrospective study included 360 patients who underwent isolated off-pump coronary artery bypass (OPCAB, n=240) or minimally invasive direct coronary artery bypass (MIDCAB, n=120) surgery. The study was conducted from November 22, 2023, to December 25, 2024. Participants, with a median age of 63 years (range: 36-80), comprised 285 males and 75 females. After returning to the ward from the intensive care unit after surgery, all participants initiated the phase Ⅰ CR program. This program consisted of respiratory and cough training, active upper and lower limb movement, transfer training, standing training and walking exercise. The study specifically included patients who completed the 6MWT within 5 ± 2 days after phase I CR post-surgery.

Results: The median 6-minute walk distance (6MWD) for all subjects was 183 ± 125 meters (33 ± 20% of predicted). Notably, the walking distances were significantly shorter in OPCAB patients than MIDCAB patients (175 ± 125 vs 200 ± 134 meters, Z = -3.426, P = 0.001), in older patients than younger patients (H = 20.489, P < 0.001) and in females than males (150 ± 84 vs 200 ± 100 meters, Z = -5.919, P < 0.001). Besides, approximately three-fifths of these patients exhibited a relevant reduction of exercise tolerance, as indicated by a distance walked ≤ 200 meters. Univariate analysis showed 6MWD significantly correlated with height, weight, body mass index (BMI), diastolic blood pressure (DBP) and peripheral oxygen saturation (SpO_2) before the test, as well as heart rate (HR), systolic blood pressure (SBP), DBP, SpO_2, and respiratory rate (RR) after the test, and the mean values of HR and RR during the test (all P < 0.05). At the stepwise multivariate regression analysis, the 6MWD was positively correlated with gender (P < 0.001), HR at the end of the test (P = 0.001), and DBP before the test (P = 0.043). Conversely, the 6MWD was negatively correlated with the type of surgery (P < 0.001) and RR at the end of the test (P = 0.004).

Conclusion: This study is the first to describe early 6MWD in CABG patients during phase I CR. The 6MWT is feasible and well-tolerated in adults and older patients shortly after CABG. Our findings reveal that the physical performance, as assessed by the distance walked during the 6MWT, is significantly reduced in patients who underwent OPCAB surgery, older patients, and females patients following CABG surgery. Notably, the predictors of 6MWD were observed independently of gender, type of surgery, HR and RR at the end of the test, and DBP before the test. The findings provide valuable insights into factors affecting walking distance, aiding clinical assessment and informing phase II CR program development post-discharge.

基于 TPKCEE 复合型教学的混合教学模式 在心脏康复护理教学中应用研究

于水 宋龄

吉林大学第一医院

目的：随着人口老龄化的加剧和心血管疾病发病率的持续上升，心脏康复护理在临床护理工作中的重要性日益凸显。心脏康复护理不仅要求护士具备扎实的专业知识和操作技能，还须具备良好的沟通能力、临床思维能力及人文关怀意识。然而，传统的护士培训模式往往以理论讲授为主，忽视了护士在实际工作中对知识的综合运用能力和临床思维能力的培养，难以满足新时代临床护理工作的需求。TPKCEE 复合型教学理念融合了技术（Technology）、教学法（Pedagogy）、知识（Knowledge）、认知（Cognition）、情感（Emotion）与评价（Evaluation）六大要素，强调教学过程中多维度、多层次的协同发展。本研究旨在探索基于 TPKCEE 理念的混合教学模式在临床护士心脏康复护理培训中的应用效果，以期提升护士的综合素质与临床护理能力。

方法：本研究采用教学实验法，选取某医院心内科及康复科的临床护士为研究对象，随机分为实验组与对照组。实验组实施基于 TPKCEE 理念的混合教学模式，培训内容围绕心脏康复护理的核心知识与技能展开，结合线上学习平台与线下实践培训，构建“线上理论学习–线下实践操作–案例分析与讨论–综合评价反馈”的教学闭环。在教学过程中，注重信息技术的融合应用，利用多媒体课件、虚拟仿真技术等手段，提升护士的学习参与度；采用案例教学、情景模拟、小组讨论等多样化教学方法，激发护士的认知与情感投入；通过形成性评价与终结性评价相结合的方式，全面评估护士的学习过程与学习成果。对照组则采用传统的课堂讲授与操作示范相结合的培训方式。培训周期结束后，通过理论知识考核、实践技能评估、学习动机调查及教学满意度评价等方式对培训效果进行综合评估。

结果：研究结果显示，基于 TPKCEE 复合型教学理念的混合教学模式在提升护士理论知识掌握、实践技能操作、学习动机激发及教学满意度等方面均表现出明显优势。实验组护士在培训过程中表现出更高的主动性与参与度，能够更好地将理论知识与临床实践相结合，展现出较强的临床思维能力与团队协作意识。同时，护士在培训过程中对培训内容与培训方式的认可度较高，教学满意度显著提升。该教学模式在促进护士知识、能力、情感等多方面协调发展方面具有积极作用。

结论：基于 TPKCEE 复合型教学的混合教学模式在临床护士心脏康复护理培训中具有良好的应用前景。该模式不仅有助于提升护士的专业素养与临床护理能力，还能有效激发护士的学习兴趣与内在动机，促进其全面发展。未来，建议在临床护士继续教育领域进一步推广该教学模式，并结合不同科室特点进行优化与创新，以更好地适应新时代临床护理工作的需求。同时，本研究也为临床护士培训模式改革提供了理论支持与实践参考，具有一定的推广价值和现实意义。

急性心肌梗死恐动症患者对虚拟现实运动康复训练系统使用意愿及需求的质性研究

陈雨芬 [1,2] 涂惠 [1]

1. 南昌大学第二附属医院

2. 南昌大学江西医学院

目的 急性心肌梗死作为严重威胁生命健康的心血管疾病，经皮冠状动脉介入治疗（PCI）是目前主要治疗手段，但术后患者常因对运动风险的过度担忧而产生恐动症，表现为刻意回避运动、康复依从性低下，严重影响心功能恢复及生活质量。虚拟现实（VR）技术凭借沉浸式体验和交互性优势，在康复领域应用潜力显著，但其针对急性心肌梗死恐动症患者的适用性及具体需求尚未明确。本研究旨在探讨急性心肌梗死恐动症患者对虚拟现实（Virtual reality，VR）运动康复训练系统的使用意愿及需求，为设计开发针对于急性心肌梗死恐动症患者的虚拟现实运动康复训练系统提供参考。

方法 设计描述性质性研究，以目的抽样法于 2024 年 10 月–2025 年 1 月选取江西省某三级甲等医院心内科住院的 16 名经皮冠状动脉介入治疗术后急性心肌梗死恐动症患者为研究对象，进行半结构式深入访谈，运用 Colaizzi 七步分析法进行资料分析，提炼主题。

结果 共提炼出 4 个主题、6 个子主题，即 VR 技术的了解途径、运动依从性低下的多重因素、对 VR 运动康复训练系统的态度、对 VR 运动康复训练系统的期望（系统操作方式的简单化、自然环境偏好与个性化训练需求、运动强度的智能调节、运动反馈的鼓励性和指导性需求、监测数据的可视化、系统的安全保障）。

结论 急性心肌梗死恐动症患者对 VR 运动康复训练系统存在明确需求，主要集中于系统的安全性、易用性、趣味性及个性化方面。因此，在系统设计开发阶段，医护人员需联合技术人员，充分整合患者的需求，将医疗专业性与用户体验进行深度融合，开发出兼具风险可控性与康复有效性的 VR 运动康复工具，以改善患者恐动症状，提升运动康复依从性，最终促进其心功能恢复及生活质量提升。

中医五行音疗联合安宁疗护在慢性心力衰竭患者康复中的护理实践

郭燕 李娟利

交大一附院

目的：

慢性心力衰竭（CHF）是一种严重影响患者生活质量的临床综合征，其传统治疗方法多侧重于药物干预和生活方式调整，往往忽视了患者的心理和社会需求。近年来，中医五行音疗与安宁疗护作为补充与替代疗法，逐渐被应用于慢性病患者的康复过程中。本文探讨了中医五行音疗联合安宁疗护在慢性心力衰竭（CHF）患者康复中的应用效果，为临床护理提供新的思路和方法。

方法：本研究选取慢性心力衰竭 (CHF) 患者若干例，随机分为干预组和对照组。干预组在常规药物治疗和护理基础上，结合中医五行音疗和安宁疗护，包括评估患者需求、选择合适的五行音乐、创造舒适环境、指导音乐冥想等措施，将中医五行音疗与药物治疗、心理护理、康复训练等相结合；对照组仅接受常规治疗和护理。研究使用匹兹堡睡眠质量指数（PSQI）、明尼苏达心衰生活质量量表（MLHFQ）和 6 分钟步行试验（6MWT）对两组患者进行评估，观察护理干预前后的变化。

结果：干预组患者在护理干预后，PSQI 评分改善，睡眠质量显著提升（P<0.05）；MLHFQ 评分显著降低（P<0.05），表明生活质量显著提高；6MWT 测试结果显示，干预组患者的步行距离显著增加（P<0.05），提示运动耐力得到改善。与对照组相比，干预组在心理状态、症状缓解和生活质量方面均表现出显著优势。

结论：中医五行音疗联合安宁疗护能够有效改善慢性心力衰竭患者的生活质量、睡眠质量和运动耐力，为慢性心力衰竭患者提供了一种全面、个性化的护理模式，可作为传统治疗的有益补充，中医五行音疗和安宁疗护作为一种补充和替代疗法，在改善慢性病患者的身心健康方面显示出巨大潜力，结合临床人文护理的关爱，给予患者生的曙光！值得在临床护理中推广应用！

运动通过 c-MAF 调控常驻巨噬细胞代谢重编程改善心肌梗死修复

李运棋 刘雨轩 郑阳 郑祥慧 于波 吴健

哈尔滨医科大学第二附属医院

目的：运动改善心肌梗死后心室重构，其中常驻巨噬细胞在梗死后发挥关键作用。已知代谢重编程促进巨噬细胞修复功能，然心肌梗死后运动康复促进巨噬细胞代谢重编程及其相关机制仍不清楚。在本研究中，我们研究 c-MAF 在心肌梗死运

动康复背景下促进常驻巨噬细胞代谢重编程改善梗死后修复的作用。

方法：通过单细胞转录组、空间转录组和空间代谢组等多组学联合明确心肌梗死后运动康复小鼠心脏的巨噬细胞亚群及其代谢特征。使用巨噬细胞特异性 c-MAF 敲除小鼠借助 RNA 测序、代谢组、血管造影、组织学和表型分析研究 c-MAF 在心肌梗死后巨噬细胞代谢重编程和心脏修复中的作用。使用腺相关病毒过表达心肌梗死运动模型小鼠巨噬细胞的 c-MAF 进一步探讨其在心肌梗死运动康复背景下的关键作用。CUT&Tag 测序研究 c-MAF 缺陷的巨噬细胞在运动促心肌梗死修复过程的关键下游基因。

结果：多组学识别常驻巨噬细胞在心肌梗死后运动康复中的关键作用。敲除巨噬细胞特异性的 c-MAF 加重梗死面积，减少血管生成，促进组织纤维化和 MI 后的不良心脏重构。同时 seahorse 分析敲除 c-MAF 的巨噬细胞氧化磷酸化被抑制，代谢组进一步明确 c-MAF 对巨噬细胞的代谢调控。而腺相关病毒过表达心肌梗死运动模型小鼠巨噬细胞的 c-MAF 得出相反的结果。CUT&Tag 测序发现 AMPKα 是 c-MAF 的关键下游，ChIP-PCR 明确 c-MAF 促进 AMPKα 的转录表达，从而增强线粒体功能促进氧化磷酸化。营救实验进一步证实了 c-MAF 通过 AMPKα 促进常驻巨噬细胞在心梗中的修复作用。

结论：研究结果揭示了转录因子 c-MAF 在运动调控常驻巨噬细胞促进心肌梗死心脏修复的关键作用。

Aerobic exercise improves coronary microcirculation dysfunction by regulating endothelial cell function through the m6A methyltransferase METTL14

Peiyao Wang, Xiang-Hui Zheng, Yun-Qi Li, Yu-Xuan Liu, Zhou Guo, Yang Zheng, Jian Wu, Bo Yu

The Second Affiliated Hospital of Harbin Medical University

Objective Coronary microcirculation dysfunction (CMD) is a key pathophysiological mechanism of ischemic non-obstructive coronary artery disease (INOCA). As a critical component of cardiac rehabilitation, aerobic exercise has been proposed as a potential therapy for INOCA. However, the mechanisms by which aerobic exercise protects the cardiovascular system by improving CMD remain unclear.

Methods Five-to-six-week-old male C57BL/6J mice were selected. CMD mouse models were induced by a high-fat and high-sugar diet combined with intraperitoneal injection of low-dose streptozotocin (STZ, 50 mg/kg) for 5 consecutive days. Mice were then subjected to 8 weeks of aerobic exercise. Body weight and blood glucose were dynamically monitored. Cardiac microcirculatory function was detected by echocardiography, magnetic resonance imaging, and Micro-CT. Immunofluorescence staining was performed to detect microvascular density, microvascular perfusion, and endothelial cell apoptosis. HE and Masson staining were employed to examine thrombus formation and perivascular fibrosis. Transmission electron microscopy was used to observe the ultrastructure of cardiac microvessels. Nitric oxide (NO) levels were measured. The expression levels of VCAM-1, ICAM-1, ET-1, eNOS, and p-eNOS in the heart were detected by Western blot, quantitative real-time polymerase chain reaction (qRT-PCR), and enzyme-linked immunosorbent assay (ELISA). Dot-Blot and ELISA were used to detect cardiac m^{6}A levels, while qRT-PCR and WB were applied to measure the expression of m^{6}A methyltransferases and demethylases. Further, METTL14-overexpressing mice were constructed, and CMD models were induced to assess endothelial function and microcirculatory function. A high-glucose-induced injury model of mouse cardiac microvascular endothelial cells (MCMECs) was established. After transfection with specific siRNA to interfere with METTL14, the effects of METTL14 on inflammation, apoptosis, migration, and tube formation in MCMECs were observed.

Results Aerobic exercise can increase myocardial blood flow, coronary microvascular density, and microvascular perfusion in CMD mice, while reducing endothelial cell apoptosis. In mice of the CMD group, the basement membrane of myocardial microvessels was thickened and partially fractured, and the junctions between microvascular endothelial cells were indistinct. In contrast, the myocardial microvascular structure in the exercise group was relatively restored with intact integrity, and the junctions between microvascular endothelial cells were in good condition. Compared with CMD mice, the exercise group showed reduced thrombus formation and perivascular fibrosis, increased the expression of NO, eNOS, and p-eNOS in the heart, decreased the expression of ET-1, and reduced the expression of adhesion molecules such as ICAM1 and VCAM1. Further studies indicated that aerobic exercise could lower the cardiac m^{6}A level and significantly decrease the METTL14 level in CMD mice. By injecting adeno-associated virus AAV9-METTL14 into the tail vein of CMD mice, it was found that overexpression of METTL14 counteracted the protective effect of exercise on coronary microcirculatory dysfunction. The results of cell experiments showed that, compared with the control group, the siMETTL14 group had increased contents of NO, eNOS, and p-eNOS, decreased the expression of ET-1, reduced ICAM1 and VCAM1, less cell apoptosis, inhibited ROS, and improved cell migration and tube formation.

Conclusion Aerobic exercise reduces endothelial cell injury and apoptosis, improves endothelial function, and alleviates coronary microcirculation dysfunction by decreasing the level of the m^{6}A methyltransferase METTL14.

Enhanced External Counterpulsation Promotes Recovery of Exercise-Induced Muscle Damage by Reducing Plasma Acetylglycine and Inhibiting CD56dim NK Cells Differentiation

Zhenyu Wang[1,2], Chun Yao[2], Yin-Fen Wang[2], - Xu[2], Xiu-Li Xu[2], -Yu Wu[1], Xi-Ling Shou[1], Gui-Fu Wu[2]

1. Shaanxi Provincial People's Hospital

2. The Eighth Affiliated Hospital of Sun Yat sen University

Objectives

Exercise-induced muscle damage (EIMD) is a common pathological condition characterized by delayed-onset muscle soreness (DOMS), reduced muscle strength, and structural disruption of muscle fibers following excessive or unaccustomed exercise. While physical activity offers well-established benefits for chronic disease prevention, EIMD may trigger secondary injuries and reduce exercise adherence. Enhanced External Counterpulsation (EECP), a non-invasive hemodynamic intervention, has primarily been used for cardiovascular rehabilitation. Recent studies suggest EECP may ameliorate post-exercise inflammation, but its mechanistic role in EIMD recovery remains unclear. This study aims to systematically evaluate the therapeutic mechanisms of EECP for EIMD through an integrated multidisciplinary approach (clinical trial, animal experiments, and in vitro studies) and explore its potential applications in exercise rehabilitation.

Methods

1. Clinical Trial Design

Participants: 10 healthy male volunteers (age 28.9 ± 2.3 years, BMI 22.6 ± 2.6 kg/m^2) in a self-controlled crossover design (EECP vs. Sham intervention).

Exercise Model: Exhaustion induced by cardiopulmonary exercise testing (CPET) (respiratory exchange ratio RER > 1.1, Borg score 18.5 ± 0.85).

Intervention: Post-exercise randomization to 1-hour EECP (cuff pressure 35–40 kPa) or Sham (0.9 kPa), with crossover after 7 days.

Sample Analysis:

Plasma Biomarkers: ICAM-1, MCP-1, and myoglobin (Myo) via ELISA; AST and CK via automated biochemistry analyzer.

Multi-omics Profiling:

Targeted metabolomics (LC-MS): Absolute quantification of 350+ plasma metabolites.

PBMC transcriptomics (DNBSEQ-T7 platform): mRNA sequencing of 18,316 transcripts.

Immune Cell Infiltration: CIBERSORTx algorithm for dynamic profiling of NK cell subsets.

2. Animal Experiments

Model: 21 Labrador retrievers (equal sexes) divided into Control, Exhaustive Exercise, and Exercise+EECP groups.

Intervention: 1-hour EECP (30 kPa) post-treadmill exhaustion.

Assessments:

Hemodynamics: Pressure-wire monitoring of anterior tibial artery flow.

Histopathology: H&E staining, Masson's trichrome (collagen), ATPase staining (type II fiber metabolism).

Immunofluorescence: Skeletal muscle CD16+ NK cell infiltration.

3. In Vitro Experiments

NK Cell Differentiation: Primary human NK cells exposed to acetylglycine (0.625–2.5 μM); CD56/CD16 phenotypes analyzed by flow cytometry.

Inflammatory Pathways: CXCR1/IL-6/ICAM-1 expression via Western blot.

Muscle Apoptosis:

Contact/non-contact coculture (NK cells + human skeletal muscle cells).

Apoptosis quantified by Annexin V-FITC/PI staining.

Results

1. EECP Attenuates Muscle Damage and Inflammation

Clinical samples: Plasma CK, Myo, and ICAM-1 significantly increased post-exercise (*p* <0.05); reductions were greater after EECP vs. Sham (e.g., CK ↓ 40%, *p* = 0.003).

PBMC transcriptomics: EECP downregulated inflammatory pathways (TNF/NF-κB/TLR signaling) and oxidative stress genes (Cluster 6, Q

<0.05).

2. Acetylglycine Mediates NK Cell Differentiation and Muscle Apoptosis

Metabolite-Immune Axis:

Strong positive correlation between plasma acetylglycine and CXCR1 expression during exhaustion (*r* = 0.697, *p* = 0.031).

EECP significantly reduced acetylglycine (clinical: ↓ 32%; animal: ↓ 41%, *p*

NK Cell Phenotype Shift:

Acetylglycine dose-dependently induced CD56dimCD16bright differentiation (2.5 μM: CD56 ↓ 68.1%, CD16 ↑ 67.6%, *p* <0.001).

Animal model: CD16+ cells increased 2.9-fold in muscle post-exercise (*p* <0.001); reversed by EECP.

Apoptotic Pathway:

Acetylglycine activated CXCR1/IL-6/ICAM-1 axis (protein expression ↑ 35–38% by WB, *p* <0.001).

CD56dim NK cells induced myocyte apoptosis via contact-dependent mechanisms (↑ 56.5%, *p* <0.001).

3. EECP Promotes Tissue Repair and Metabolic Recovery

Animal Model:

EECP reduced tibialis anterior (TA) interstitial fibrosis (Masson's staining: ↓ 8.2%, *p* <0.001), restoring levels to Control.

ATPase staining indicated alleviated anaerobic burden in type II fibers (staining depth ↓ 22.1%, *p* = 0.008).

Hemodynamics: EECP enhanced anterior tibial artery pressure by 72% (95% CI: 49.7–94.3, *p* <0.001), accelerating clearance of metabolic waste.

Conclusions

1.Core Mechanism: EECP reduces plasma acetylglycine, inhibits CD56dim NK cell differentiation, and blocks the CXCR1/IL-6/ICAM-1 inflammatory cascade, thereby attenuating skeletal muscle apoptosis (Fig. 7C).

2.Functional Recovery: Mitigates muscle fibrosis and restores aerobic metabolism in type II fibers, accelerating post-exercise recovery.

3.Translational Value:

Establishes EECP as a novel non-invasive hemodynamic therapy for EIMD.

Expands EECP applications in sports medicine (athlete recovery), fitness science, and rehabilitation.

基于循证护理的早期心脏康复干预对急性心肌梗死 PCI 术后患者预后的影响

徐洁 刘华芬

武汉大学人民医院

目的：探讨基于循证护理的早期心脏康复干预对 50 岁以上男性急性心肌梗死（AMI）患者经皮冠状动脉介入治疗（PCI）术后心功能恢复、并发症发生率及生活质量的影响，为临床护理实践提供科学依据。

方法：采用前瞻性随机对照研究，选取 2024 年 6 月至 2025 年 6 月在我院行 PCI 术的 50 岁以上男性 AMI 患者 150 例，随机分为干预组（n=75）和对照组（n=75）。对照组接受常规术后护理，干预组在常规护理基础上实施基于循证医学证据的早期心脏康复干预，包括术后 24 小时内开始床上被动活动、渐进式呼吸训练、早期离床活动（术后 48 小时内）、个性化运动处方（基于心肺运动试验结果）、心理干预及营养指导。干预周期为住院期间及出院后 3 个月。主要观察指标包括左室射血分数（LVEF）、6 分钟步行试验（6MWT）、术后并发症（如再梗死、心力衰竭、心律失常）发生率，以及西雅图心绞痛量表（SAQ）评分。采用 SPSS 25.0 进行数据分析。

结果：干预 3 个月后，干预组 LVEF 显著高于对照组（52.4±5.6% vs. 47.8±6.2%，P<0.05），6MWT 距离更长（425.3±42.1m vs. 378.6±45.7m，P<0.01）。干预组术后并发症发生率显著低于对照组（8.0% vs. 18.7%，P<0.05）。SAQ 评分显示，干预组在躯体活动受限程度（75.3±8.2 vs. 65.4±9.1）和治疗满意度（88.5±6.7 vs. 79.2±7.4）方面显著优于对照组（均 P<0.01）。

结论：基于循证护理的早期心脏康复干预可有效改善 AMI 患者 PCI 术后的心功能，降低并发症发生率，提高生活质量。建议将早期康复干预纳入 AMI 患者 PCI 术后的标准化护理流程，并进一步探索其长期效益。

结构性心脏病患者经导管介入术后早期康复护理模式的构建与应用效果评价

徐洁 刘华芬

武汉大学人民医院

目的：探讨基于加速康复外科（ERAS）理念构建的早期康复护理模式在结构性心脏病（SHD）患者经导管介入治疗后的应用效果，重点评估其对术后恢复、并发症及生活质量的影响。

方法：采用类实验性研究设计，选取武汉大学人民医院心内科 2024 年 1 月 -2025 年 6 月行经导管介入治疗的 SHD 患者 126 例（包括房间隔缺损、室间隔缺损、肺动脉瓣狭窄等），按住院时间分为干预组（n=63）和对照组（n=63）。对照组实施常规围术期护理，干预组采用多学科团队（MDT）协作的早期康复护理模式，包括：①术前预康复（呼吸训练、营养评估与干预）；②术中体温管理与液体控制；③术后 6 小时启动阶梯式康复方案（早期体位管理、床上活动、渐进式呼吸训练）；④出院前制定个性化居家康复计划。主要观察指标：术后首次下床时间、住院时长、并发症发生率（穿刺部位血肿、心律失常、栓塞事件等）；次要指标：6 分钟步行距离（6MWD）、明尼苏达心功能不全生命质量量表（MLHFQ）评分。

结果：干预组术后首次下床时间显著早于对照组（18.5±4.2h vs 26.3±5.7h，P<0.01），平均住院日缩短 2.3 天（5.2±1.1d vs 7.5±1.8d，P<0.05）。干预组总并发症发生率低于对照组（9.52% vs 20.63%，P<0.05），其中穿刺部位血肿（3.17% vs 11.11%）和房性心律失常（4.76% vs 14.29%）差异显著。出院 1 个月随访显示，干预组 6MWD（382.6±45.3m vs 338.4±52.1m）和 MLHFQ 评分（45.2±8.7 vs 53.6±9.3）均优于对照组（均 P<0.01）。

结论：基于 ERAS 理念的早期康复护理模式能有效促进 SHD 介入术后患者功能恢复，降低并发症风险，改善生活质量。该模式特别适用于经导管治疗的 SHD 患者，建议在临床推广中注重多学科协作和个体化方案制定。

体医融合模式下 PCI 术后患者 II 期心脏康复运动方案的构建与应用研究

杨曦艳 [1] 陈赞雄 [2]

1. 首都医科大学附属北京朝阳医院

2. 首都体育学院

目的：针对如何提高心脏康复患者依从性这一全球心脏康复共同面临的问题，探寻中国的体医融合模式解决办法。本研究是在体医融合新理论体系指导下开展的最新实践，由经过医学培训的体育人员进入医院，与医生合作共同为心脏康复患者制定运动方案并指导其进行运动，促进医疗与运动方案真正落实，证明医院场景内体医融合心脏康复模式的可行性及有效性。

方法：采用随机对照试验法，由经过医学培训的体育人员进入心脏康复中心与医生共同为心脏康复患者服务。连续入选 32 名接受 PCI 术后，需要进行 II 期心脏康复的患者为研究对象，随机分为对照组和实验组，按照《中国冠心病康复与二级预防指南》进行三个月的运动干预。对照组由医生行心肺功能评估并开具运动处方后由医生指导患者运动；实验组由医生对患者进行心肺功能评估后，由经过医学培训的体育人员在医护的安全保障下对其进行运动功能评定包括关节活动度评估、FMS 动作评估、柔韧性、平衡性测试等，结果报给医生，医生据心功能评估结合运动功能评定结果为其开具运动处方。再由经过医学培训的体育人员根据体医融合理论体系，选取相应训练工具，编排训练动作，将运动处方转化为具体可执行的个体化、情景化、趣味性强的周期性运动方案。在医院内，医护的安全保障下对患者开展运动指导。并在实验前后对患者的心功能、运动功能数据进行统计对比分析。

结果：体医融合模式下的心脏康复运动方案构建方法：由医生对患者的心肺功能、心理、用药、睡眠、既往疾病史等进行医学评估；由经过医学培训的体育人员在医务人员的安全保障下，对患者进行运动习惯评估、功能动作筛查、关节活动评估、身体素质评估等运动功能评定，明确患者能做哪些运动，需要做哪些运动，建立运动工具库和运动动作库，并将结果汇总报告给医生，由医生明确患者的运动强度阈值范围并开具运动处方，体育人员将运动处方转化为周期性训练安排表，并根据每日训练目标在运动工具库中选取合适的训练工具，在运动动作库中匹配相应的训练内容，形成具体可执行的情景化心脏康复运动方案，并在医务人员的安全保障下将运动方案应用于患者的运动指导。干预三个月以后：①两组患者均未出现心血管事件；②实验前对照组和实验组 $VO_{2\,max}$ 差异无统计学意义（P > 0.05），分别是 19.162±4.097 和 19.412±3.337。经过三个月的运动干预后，实验组 $VO_{2\,max}$ 显著高于对照组（P < 0.05），分别是 19.669±4.196 和 22.037±2.761；通过组内比较发现，实验组患者 $VO_{2\,max}$ 相较干预前极其显著提高（P < 0.01），表明相较于对照组，体医融合模式下的心脏康复可以明显提高患者的心肺功能。③实验前对照组和实验组 FMS 测试差异无统计学意义（P > 0.05），分别是 9.562±2.394 和 9.5±3.327。在各项单独测试中，也均无统计学意义。经过三个月的运动干预之后，对照组与实验组 FMS 测试总分出现极其显著差异（P < 0.01），分别是 9.938±1.914 和 13.188±2.509。④按照指南推荐三个月内完成 36 次以上训练患者对照组 4 人，实验组 12 人，完成 25-36 次患者对照组 2 人，实验组 3 人，完成 25 次以下训练患者对照组 10 人，实验组 1 人。对照组总依从率 37.5%；实验组总依从率 93.75%。实验组患者依从性较对照组患者由极其显著差异（P < 0.01）。患者运动依从性提高 2.5 倍。

结论：本研究首次探索建立体医融合心脏康复的新模式；且初步证明体医融合模式下的心脏康复运动方案可以显著提高患者运动依从性，且患者的心功能和运动功能提升更为显著。

永久人工心脏起搏器植入术后患者应用护士参与心脏康复护理的效果研究

井翠萍

交大一附院

摘要】目的：分析永久人工心脏起搏器植入术后患者中，护士参与心脏康复护理的效果研究。

方法: 筛选永久人工心脏起搏器植入术后的患者作为研究对象，例数合计为 80 例，选取时间范围为 2023 年 10 月–2024 年 10 月，按照随机数字表法进行分组。分为对照组和观察组，40 例为一组，对照组采取常规护理，观察组联合实施护士参与心脏康复护理。对比 2 组的干预效果。

结果：干预后，观察组心功能、心脏耐力指标均优于对照组 (P<0.05)；观察组患

者生活质量高于对照组 (P<0.05)；观察组不良心血管事件发生比例低于对照组 (P<0.05)；观察组患者满意率高于对照组 (P<0.05)。

结论：护士参与心脏康复护理的应用，通过制订规范的心脏康复护理措施，对永久人工心脏起搏器植入术后患者开展健康教育、心理疏导，行为干预、康复锻炼等多途径的心脏康复指导，极大地改善了永久人工心脏起搏器植入术后患者的心功能恢复，提升了其心脏耐力，有助于患者整体生活质量的提升，降低了不良心血管事件发生风险，患者术后在康复期间的安全性也有充分的保证，患者及家属满意度高。

【关键词】永久人工心脏起搏器植入术后；护士参与心脏康复护理；心脏耐力

经导管三尖瓣介入治疗术的心脏全程康复

水小兰 田丹 刘华芬

武汉大学人民医院

目的：探讨经导管三尖瓣介入治疗（TTVI）术后系统化心脏康复方案的效果，旨在改善患者心肺功能、降低再住院率、提升生活质量，填补 TTVI 术后长期康复管理的循证空白。

方法：对 2022-2025 年本院收治的 26 例重度三尖瓣反流（TR）患者（平均年龄 72±8 岁，外科手术高危）行 TTVI（包括 TriClip、EVOQUE 等系统），术后实施分阶段心脏全程康复计划：

1. 住院期（术后 1 周）：渐进式呼吸训练 + 低强度床边活动（每日 2 次，10-15 分钟）；

2. 早期康复（1-4 周）：心肺运动试验（CPET）制定个体化运动处方（心率储备 40-60% 的有氧训练 + 抗阻训练）；

3. 中期强化（1-3 月）：远程心电监护下进行中高强度间歇训练（HIIT），结合营养与药物优化；

4. 长期维持（3-6 月 +）：社区 / 家庭康复随访，每月评估 6 分钟步行距离（6MWD）及生活质量问卷（KCCQ）。

结果：

术后 6 个月随访显示：

1. 心肺功能显著改善：6MWD 从术前 278±45m 提升至 362±38m（p<0.01），峰值摄氧量（VO_2 peak）增加 18.7%；

2. 心功能逆转：90.4% 患者 NYHA 分级改善至 I-II 级（术前 III-IV 级占 100%）；

3. 生活质量提升：KCCQ 总分从 49±11 分升至 72±9 分（p<0.001）；

4. 临床硬终点改善：心衰再住院率较传统管理下降 52%（8% vs 16.7%，p=0.03）。

结论：

TTVI 术后系统化心脏全程康复可显著提升患者运动耐量、心功能及生活质量，降低再住院风险。以 CPET 为指导的阶段性运动康复为核心，结合多学科管理，是优化 TTVI 患者长期预后的关键策略，为国际 TR 管理指南的更新提供重要循证依据。临床意义提示：本研究首次提出 TTVI 专属康复路径，填补了该领域管理空白，尤其强调早期呼吸肌训练对抗右心衰及 HIIT 对右心室功能重塑的促进作用，具有直接临床转化价值。

基于 GINSINI 评分心肺运动试验联合 TyG 指数预测冠脉狭窄风险模型构建

钱华 童睿 刘艳

西安交大一附院

目的：本研究旨在明确心肺运动试验与冠状动脉狭窄严重程度的相关性，并建立可供临床直接使用的冠状动脉显著狭窄风险预测模型。

方法：回顾性收集 2024 年 1 月至 2025 年 5 月在西安交大一附院心血管内科的住院患者 111 例，均完善冠脉造影检查及心肺运动试验（cardiopulmonary exercise test，CPET）检查。根据冠状动脉造影结果进行 Ginisini 评分，并基于冠状动脉造影检查冠脉狭窄情况分为观察组 (至少 1 支狭窄≥ 50%)80 例和对照组 30 例。收集两组一般情况、生化检查、冠脉造影和心肺运动试验检查结果。通过单因素分析和 Logistic 回归分析发现可能影响冠状动脉狭窄的危险因素，并根据变量构建列线图模型，基于 Bootstrap 法进行内部验证及评价。

结果：单因素分析显示，试验组峰值摄氧量 (Peak VO_2), 氧脉搏 (VO_2/ HR), 代谢当量 (METs) 指标分值显著低于对照组（P<0.05）。同时，与 Ginsini 评分显著负相关（P<0.05）。试验组 Ginsini 评分、脂蛋白 a、低密度脂蛋白、TyG 指数得分显著高于对照组（P<0.05）。利用 Peak VO_2 ,VO_2/HR,METS 构建二元 Logistic 回归分析，结果显示：Hosmer-Lemeshow 检验的显著性为 0.483>0.05，说明模型拟合较好。显著性结果显示：Peak VO_2 ,VO_2/HR,METS 对冠状动脉狭窄有显著的负向预测意义。利用 VO_2,VO_2/HR,METS、脂蛋白 a、低密度脂蛋白、TyG 指数、高血压、糖尿病绘制 ROC 曲线并计算 AUC，结果提示 VO_2 /HR 、Peak VO_2 对冠状动脉显著狭窄的预测价值最高。上述指标联合诊断冠心病的受试者工作特征曲线 (ROC) 下面积为 0.994，灵敏度为 87.5%，特异度为 96.7%，优于上述指标单独诊断冠心病的临床价值。

结论：心肺运动试验对冠状动脉狭窄严重程度的评估有一定的临床预测价值，心肺运动试验联合 TyG 指数预测冠脉狭窄风险的模型构建可以为冠心病患者的诊治提供帮助。

关键词：心肺运动试验 冠心病 冠状动脉狭窄 预测模型

基于计划行为理论的阶梯式康复护理模式在 A 型主动脉夹层术后截瘫患者护理

李娟

西安交通大学第一附属医院

本研究旨在探讨基于计划行为理论的阶梯式康复护理模式在 A 型主动脉夹层术后截瘫患者护理中的应用效果。通过文献回顾与理论分析，结合临床实践，构建了一套以 TPB 为指导框架的阶梯式康复护理方案。该方案强调对患者行为意图、主观规范及知觉行为控制的全面评估，并据此设计分阶段、个性化的康复计划，旨在促进患者从术后初期到长期恢复过程中的功能重建与生活质量提升。

研究对象为某三甲医院心血管外科收治的 A 型主动脉夹层术后截瘫患者，采用随机对照试验方法，将患者分为实验组与对照组。实验组接受基于 TPB 的阶梯式康复护理，包括术前心理干预、术后早期功能锻炼、中期日常生活能力训练及晚期社会适应与心理调适等阶段；对照组则实施常规护理措施。通过对比两组患者的康复效果指标，如肢体功能恢复情况、日常生活自理能力、心理状态评分及并发症发生率等，评估新护理模式的有效性。

结果显示，实验组患者在术后各阶段均表现出更佳的康复进展，具体体现在肢体运动功能显著改善、日常生活自理能力提高、抑郁焦虑情绪减轻以及并发症发生率降低等方面。此外，患者对护理服务的满意度也明显高于对照组，表明基于 TPB 的阶梯式康复护理模式不仅促进了患者的生理康复，还有效提升了其心理健康水平和社会适应能力。

基于 CiteSpace 心脏康复研究热点及发展趋势的可视化分析

曾庆玲 张丽敏

陆军军医大学第二附属医院

目的

通过对国外心脏康复（cardiac rehabilitation）研究文献进行可视化分析，了解该领域研究脉络，探讨心脏康复前沿和热点，为未来相关研究开展提供思路和参考。

方法

通过中国知网和 Web of Science 核心合集检索心脏康复研究的相关文献作为数据源，检索建库至 2025 年 6 月 30 日期间心脏康复相关研究，采用 CiteSpace（6.1.R6）软件对国家、机构、作者、关键词共现、聚类和突现进行可视化分析。

结果

共纳入中文文献 5765 篇、英文文献 9540 篇 . 该领域中英文发文量总体均呈现持续上升趋势，发文量居前列的国家分别为美国、加拿大、英国、澳大利亚。主要研究机构为高等院校，其中加拿大多伦多大学发文量居世界研究机构的首位。Journal of Cardiopulmonary Rehabilitation and Prevention、European Journal of Preventive Cardiology 等心血管专业期刊是载文量最多的杂志。发文量居前列的代表作者是加拿大约克大学 Grace, Sherry L。研究热点包括患者生活质量、患者心理状态评估、心脏康复干预措施、患者心脏康复依从性评价。研究趋势则涉及改善影响患者心脏康复效果的主观因素（运动恐惧和自我效能）和客观条件（数字健康技术整合、远程心脏康复等）。

结论

伴随着国内心脏康复理念的不断普及，技术的不断完善和成熟，未来研究者可通过借鉴国外经验，立足我国国情，开展高质量研究，探寻适合本土化的远程心脏康复模式，促进远程照护模式的成熟和优化。

AMI 患者 PCI 术后 I 期运动康复方案的构建与实证研究

彭家芹

三峡大学第一临床医学院湖北宜昌市中心人民医院

目的：探讨 I 期运动康复方案制定与实施对急性心肌梗死（AMI）患者经皮冠状动脉介入治疗（PCI）术后心功能恢复、生活状态的影响。在循证医学理论指导下，早期康复运动方案形成并得到推广。

方法：聚焦在我愿接受 PCI 治疗的 AMI 患者，从 2023 年 11 月至 2025 年 2 月中选定 76 例继续研究，践行采用随机对照试验，对比说明观察组（n=38/I 期运动康复方案）在心功指标、治理情况及生活满意度方面与对照组（n=38/ 常规护理 + 健康教育）的差异。做法包括但不限于常规抗血小板治疗、抗凝管理、调脂稳定斑块（血管紧张素转化酶抑制剂）、神经内分泌抑制（β 受体阻滞剂）。

结果：观察组静息心率显著低于对照组而 6min 步行距离更长、Barthel 指数与生活满意度评分均更高，p 均 < 0.001。

结论：每日记录提示患者正逐步走向康复，这也给了患者以更多的信心并确保其后续康复训练更加投入，这也是提升早期康复有效性的重要途径，这一干预模式尊重患者个体差异，避免了避免“一刀切”干预模式导致的过度康复问题，实现了早期功能重塑这一目的。建议为 AMI 患者制定并实施 PCI 术后 I 期运动康复方案，不仅可以促使患者心功能水平迅速恢复还可提高其生活质量。

老年性心脏疾病患者的心脏康复护理策略与效果分析

朱瑞雪

哈尔滨医科大学附属第二医院

目的

随着全球老龄化进程加速，老年心脏疾病已成为威胁公共健康的重要问题。流行病学调查显示，我国 65 岁以上人群慢性心力衰竭（CHF）患病率超过 10%，80 岁以上人群高达 10% 以上，患者总数已突破 1000 万例，且 5 年生存率不足 50%。冠心病作为另一常见老年心脏病，其高发病率与高死亡率特点同样值得关注。在药物治疗基础上，系统化心脏康复护理通过整合运动训练、心理干预与多学科协作，成为改善老年患者心功能、提升生活质量的关键策略。本文将深入探讨老年心脏疾病患者康复护理的具体策略实施路径及循证效果。

方法

个体化运动训练方案：老年心脏康复护理以科学设计的运动处方为核心，强调个体化与循序渐进原则。**整合心理与行为干预**老年心脏病患者普遍存在焦虑抑郁情绪，研究显示约 48% 的 CHF 患者伴有显著焦虑情绪。**多学科协作与延续性管理**基于老年综合评估（CGA）的护理模式整合医疗、护理、康复、营养多学科团队，全面评估患者心肺功能、营养、药物及心理状况。

结果

心功能与生物标志物改善，运动耐力与生活能力提升。心理状态与生活质量优化。**临床终点事件减少。**

讨论与展望

老年心脏康复护理的核心优势在于其多维度干预模式：通过运动改善心肌重构，通过心理干预调节神经内分泌，通过教育提升自我管理能力。然而，其成功实施需遵循三大原则：**个体化原则：需依据心功能分级（**NYHA 分级）、合并症（如关节炎、 COPD）调整运动强度。**安全监控原则：运动中需监测心电图、**Borg 自觉疲劳量表（11-13 级为宜），备急救药品应对突发症状。持续优化原则：未来研究需探索远程监护技术、不同心功能分级患者的差异化路径，以及长期生活质量改善效应。

远隔缺血后适应在缺血性心肌病中的保护作用的临床观察

张馨月

哈尔滨医科大学附属第四医院

目的：

探讨远隔缺血后适应（RIPostC）对缺血性心肌病（ICM）患者的保护作用，评估其对心功能、血清心肌损伤标志物及运动耐量的影响，为 ICM 的治疗提供新的临床思路。

方法：

选取 2024 年 6 月至 2024 年 11 月哈尔滨医科大学附属第四医院收治的 60 例 ICM 患者，随机分为 RIPostC 组（n=30）和对照组（n=30）。对照组接受常规药物治疗，RIPostC 组在常规治疗基础上增加远隔缺血后适应干预（双上肢袖带充气加压，循环 3-5 次，每周 2-3 次，持续 1 个月）。比较两组干预前后的左室射血分数（LVEF）、左室舒张末径（LVEDD）、血清肌钙蛋白 I（cTnI）、B 型钠尿肽（pro-BNP）及心肺运动评估代谢当量（METS 值）。

结果：

1. 心功能改善：RIPostC 组 LVEF 显著高于对照组（54.53±3.29% vs. 52.10±3.13%，P=0.004），LVEDD 显著降低（52.00[50.00,53.00]mm vs. 57.50[52.00,62.00]mm，P=0.001）。

2. 心肌损伤标志物：RIPostC 组 pro-BNP 水平显著低于对照组（134.00[66.75,306.75]pg/mL vs. 322.00[92.15,1051.00]pg/mL，P=0.019）。

3. 运动耐量：RIPostC 组 METS 差值显著优于对照组（-0.92±0.55 vs. -0.67±0.34，P=0.038）。

结论：

远隔缺血后适应可显著改善 ICM 患者的心功能，减轻心肌损伤，并提高运动耐量，有望成为一种安全、有效的辅助治疗手段，为心脏康复提供了新的干预策略。

关键词：远隔缺血后适应；缺血性心肌病；心功能；心肌保护；心脏康复

中国健康成人心肺适能的年龄、性别与 BMI 分布特征：一项基于 V̇O2peak 的回顾性横断面研究

王继楠 任川 徐顺霖 赵威

北京大学第三医院

目的

本研究旨在构建中国健康成年人群心肺适能的年龄、性别及体质量指数（body mass index，BMI）特异性参考值，明确峰值摄氧量（peak oxygen uptake，$\dot{V}O_2$peak）在人群中的分布特征，为心肺健康风险评估、肥胖干预及个体化运动处方提供本土化循证依据。

方法

本研究为回顾性横断面研究，纳入 2017 年 9 月 1 日至 2025 年 5 月 30 日期间在北京大学第三医院接受心肺运动试验的 13,569 名健康受试者，其中男性 6,628 例，女性 6,941 例，年龄 18 至 89 岁。所有受试者均在功率自行车上完成标准化心肺运动试验，以确保充分的运动负荷。记录 $\dot{V}O_2$peak，按性别、每十岁年龄组及 BMI 分类（<18.5、18.5–23.9、24–27.9、≥ 28 kg/m²）分层，计算 $\dot{V}O_2$peak 百分位数（P5–P95）并分析中位数随变量变化趋势。

结果

男性 $\dot{V}O_2$peak 中位数由 18–29 岁组的 29.2 ml·kg^{-1}·min^{-1} 随年龄逐组递减，至 80–89 岁组降至 17.0 ml·kg^{-1}·min^{-1}，平均每十年减少约 2.0 ml·kg^{-1}·min^{-1}，下降幅度约为 7.0%。女性 $\dot{V}O_2$peak 中位数则呈相似下降趋势，从 23.8 ml·kg^{-1}·min^{-1} 降至 14.5 ml·kg^{-1}·min^{-1}，平均每十年减少约 1.6 ml·kg^{-1}·min^{-1}，降幅约为 6.5%。在男性和女性人群中，不同年龄组之间的 $\dot{V}O_2$peak 水平均存在统计学差异（P<0.05）。在各年龄段，男性 $\dot{V}O_2$peak 显著高于女性（P<0.05），性别差异在年轻组最为明显，老年组相对缩小。

在不同 BMI 水平下，$\dot{V}O_2$peak 也表现出显著差异。男性 BMI <18.5、18.5–23.9、24.0–27.9、≥ 28.0 kg/m² 组的 $\dot{V}O_2$peak 分别为 31.2、28.4、24.9、21.7 ml·kg^{-1}·min^{-1}；女性对应组别的 $\dot{V}O_2$peak 分别为 23.9、21.7、18.7、17.1 ml·kg^{-1}·min^{-1}，呈随 BMI 升高而下降的趋势。

结论

$\dot{V}O_2$peak 作为心肺适能的核心指标，受年龄、性别及 BMI 多重影响，表现出显著差异性。男性高于女性，高 BMI 者 $\dot{V}O_2$peak 显著下降。这些发现可为心肺适能评估、慢病筛查和运动干预提供重要参考依据。

基于心肺运动试验的健康成年人峰值氧脉搏预测方程的建立与验证

王继楠 任川 徐顺霖 赵威

北京大学第三医院

目的

本研究旨在建立适用于中国健康成年人的峰值氧脉搏（peak oxygen pulse, $\dot{V}O_2$/HR peak）预测方程，并验证其在不同年龄、性别和体型人群中的准确性和稳定性。由于目前常用的预测方程多基于国外人群建立，直接应用于中国人群可能存在误差，因此有必要构建更符合我国人群特征的参考模型，以提高心肺运动试验（cardiopulmonary exercise testing，CPET）结果的解释价值。

方法

回顾分析 2017 年 9 月 1 日至 2022 年 8 月 30 日期间，在北京大学第三医院心脏康复中心接受标准化 CPET 的健康成年人数据，构建建模组（n = 8454，男性 4160 例，女性 4294 例）。采用多元线性回归分析性别、年龄、身高、体重、体重指数（body mass index，BMI）、体表面积（body surface area，BSA）和去脂体重（lean body mass，LBM）对 $\dot{V}O_2$/HR peak 的影响，建立预测模型。同时纳入 2022 年 9 月 1 日至 2025 年 5 月 30 日期间在北医三院完成 CPET 的健康成年人作为验证组（n = 4827，男性 2337 例，女性 2490 例），用于进行模型的时间外部验证。所有测试均在功率自行车上完成。受试者按照性别、每十岁年龄分组（18–89 岁），以及 BMI 分层（<18.5、18.5–23.9、24.0–27.9、≥ 28 kg/m²），评估模型在各亚组中的预测表现。

结果

预测方程为：$\dot{V}O_2$/HR peak = 0.087 × Sex (Man=1,Woman=2) – 0.015 × Age + 156.667 × Log(Height) + 0.099 × Weight – 132.026 × Log(BSA) + 27.329 × Log(LBM) + 41.999 × Log(BMI) – 412.071，调整 R^2 为 0.552。

在验证组中，预测值与实测值高度一致。男性的预测值为 12.7±1.2 ml·beat^{-1}，实测值为 12.9±2.8 ml·beat^{-1}；女性的预测值为 8.5±0.8 ml·beat^{-1}，实测值为 8.5±1.7 ml·beat^{-1}。整体实测值与预测值的比值为 100.7±19.1%，其中男性为 101.8±20.2%，女性为 99.6±17.8%。在各年龄亚组中，实测 / 预测比值均接近 100%，一致性良好，且呈现随年龄增长略有下降的趋势。在不同 BMI 亚组中，该比值的波动均控制在 ±2% 以内，显示模型在不同体型人群中具有良好的稳定性和适用性。验证组的组内相关系数（ICC）为 0.719（P < 0.001），进一步证明了模型的可靠性。

结论

本研究建立了基于中国健康成年人大样本的 $\dot{V}O_2$/HR peak 预测模型，拟合效果良好，验证一致性高。相比基于欧美人群的通用模型，该模型更适用于中国人群，可为心肺功能评估、异常识别和个体化运动方案制定提供实用的临床参考。

PH 患者不同运动试验（CPET 与 6MWT）与疾病严重性的临床研究

车琳 王玉婧 王怡恒 朱倩倩 刘学波 陈发东

同济大学附属同济医院

目的：探讨 PH 患者不同运动试验（CPET 与连续生理参数监测的 6MWT）对其疾病严重程度的评估以及不同运动试验其核心数据的相关性分析

方法：连续录入同济大学附属同济医院肺高压中心 2022 年 9 月 -2024 年 12 月 40 例 PH 患者，均完成 CPET 和 6MWT。

结果：40 例患者男 6 例，女 34 例，年龄 38.35±11.09y，I 类 PH 占 35 例，IV 类 PH 占 5 例。

1 PH 不同功能分级其运动心肺的生理参数有显著差异

按照 WHO 功能分级（FC）分为两组，FC I-II 组 25 例（年龄 39.72±12.64y，女 21 例），FC III-IV 组 15 例（年龄 36.07±7.75y，女 13 例）。

6MWD(m) 在 FCI-II(510.56±77.47) 和 FCIII-IV 患 者 (443.47±102.36) (p=0.024) 有显著差异，DSP(m%)（6MWD 与步行试验患者 SPO2 的最低值的乘积）在 FCI-II (437.35±95.29) 和 FCIII-IV(385.38±92.23) 差异没有达到显著性 p=0.051。

CPET 中，VO2peak（ml/min/kg） 及 其 VO2peak/maxpred% 在 不 同 功

能分级间存在显著差异。FC I-II 级的 VO2peak（17.02±3.90 ）显著高于 III-IV 级患者（13.77±2.73 ）（p=0.007）；VO2peak/maxpred% 在 I-II 级组（55.33±10.96%）同样显著高于 III-IV 级组（44.79±11.59%）（p=0.008）。

2. 6MWT 与 CPET 核心参数的相关性分析

6MWD 与多项 CPET 核心指标呈显著正相关：VO_2-AT（r=0.409，p=0.009）、VO_2-peak（r=0.651，p<0.001）、WR-AT（r=0.368，p=0.020）、WR-peak（r=0.623，p<0.001）、VO_2/HRpeak（r=0.466，p=0.002）、$PETCO_2$-rest（r=0.476，p=0.002）、$PETCO_2$-peak（r=0.367，p=0.020）；6MWD 与 VE/VCO_2斜率呈显著负相关（r=-0.442，p=0.004）。

6MWT 的 DSP 与 CPET 多项指标显著正相关：VO_2-AT（r=0.423，p=0.006）、VO_2-peak（r=0.635，p<0.001）、WR-AT（r=0.391，p=0.013）、WR-peak（r=0.577，p<0.001）、VO_2/HRpeak（r=0.440，p=0.004）、$PETCO_2$-rest（r=0.535，p<0.001）、$PETCO_2$-peak（r=0.461，p=0.003）；DSP 与 VE/VCO_2斜率呈显著负相关（r=-0.517，p=0.001）。

结论：PH 的不同运动心肺参数可协助判断 PH 患者疾病严重程度，6MWT 中的 6MWD 和 DSP 与 CPET 核心指标均明确相关。

急性心肌梗死患者早期下床的安全性分析

珍珍 张锦

兰州大学第一医院

目的：通过回顾性队列研究分析急性心肌梗死（AMI）患者早期下床的安全性及获益。

方法：连续入选于 2024 年 1 月 2 日 -2024 年 3 月 31 日因 AMI 就诊于兰州大学第一医院在发病 12 小时内接受了急诊经皮冠状动脉介入治疗 (PCI) 且接受了心脏康复的患者。根据纳入排除标准最终分析的研究对象 90 例。首次下床时间定义：从 PCI 术后即手术结束回到冠心病监护病房（CCU）开始计时，至首次下床站立的时间。根据首次下床时间是否在 20 小时以内分为早期康复组 (n=42) 和对照组 (n=48)。比较两组之间的基线资料、首次下床时的生命体征变化、康复过程中的不适症状、心律失常发生率、住院天数、Kolcaba 的舒适状况量表 (GCQ 评分) 等指标；根据 Pearson 相关性分析早期下床与 GCQ 评分之间的相关性。

结果：基线资料与对照组比较，早期心脏康复组的心脏彩超左室射血分数（LVEF）[55.0(46. 0,57.0)% vs. 49.0(43.3, 53.0)%, P=0.012] 较高，左室舒张末期容积（LVEDV）[115(102.0, 123.3)ml vs. 125.5(108.3, 140.0)ml, P=0.013] 较低，心率 [(73.2±11.3) vs. (79.5±12.2), P=0.013] 较低。两组之间生命体征变化、不适症状、心律失常发生率、住院天数均无统计学意义 (P 均 >0.05)；两组均未发生主要心血管不良事件 (MACE)。与对照组比较，早期康复组 GCQ 评分 [77.0(73.0, 80.0) 分 vs. 64.5(59.0, 68.0) 分，P<0.001] 显著增高。Pearson 相关性分析显示 GCQ 评分与下床时间呈现显著负相关 (r=-0.740，P<0.001)。

结论：AMI 患者 PCI 术后经过康复评估后的早期下床是安全的，早期下床可以提高患者的舒适度，心功能较低、基础心率较高可能是影响早期下床的主要因素。

基于老年综合评估的多学科心脏康复干预在老年衰弱冠心病患者的应用

欧安平

中国科学技术大学附属第一医院（安徽省立医院）南区

目的：探讨对老年衰弱冠心病患者实施基于老年综合评估的多学科心脏康复干预的应用效果。

方法：选取 2024 年 6 月至 2025 年 6 月我院收治的 60 例老年衰弱患者为研究对象，以随机法将其分入观察组与对照组；对照组施以常规护理，观察组基于老年综合评估实施多学科心脏康复干预。成立 CGA 多学科康复专项小组，组长统筹管理，督促实施；个案管理师资料收集数据核对、推进康复方案、协调问题、效果评价；心脑健康管理师培训与指导技术；心脏康复医生评估病情、合理用药、制定运动处方；心脏康复护士实际操作、康复指导；营养师及心理咨询护士关注营养监测、心理疏导；互联网咨询护士开展“云医生”平台及“互联网医院”护理咨询服务。开展专项培训，召开质控会议，提高康复管理效能。入院时快速筛查登记、出院前 CGA 综合评估及出院后 1、3、6 个月采用门诊、HIS 智能随访、电话、微信或上门随访及时评估。方案前期实施专项培训与衰弱筛查评估，旨在危险因素风险筛查及衰弱认知，了解康复意愿。中期从运动锻炼、营养指导、共病和用药管理、心理干预等实施个性化管控；开展“1+1+1”多成分训练的心脏康复运动；营养师制定调整营养计划；个性化共病管理，动态评估用药合理性；开展个体认知刺激疗法，注重情绪调节和情感支持。后期做好居家康复准备，开展随访，实施医疗转介服务。对比组间日常生活活动能力、衰弱程度评分、满意度及 6 min 步行距离。

结果：两组患者日常生活活动能力比较可知，观察组更高（P < 0.05）；两组患者衰弱程度评分比较可知，观察组更低（P < 0.05）；两组患者满意度比较可知，观察组更高（P < 0.05）；两组患者 6 min 步行距离比较可知，观察组更佳（P < 0.05）。

结论：对老年衰弱冠心病患者实施基于老年综合评估的多学科心脏康复干预，确保了运动方案的合理性和可行性，有效改善了患者的步行能力，提升患者日常生活活动能力，延缓衰弱进程，提高生活质量。

八段锦在慢性心功能不全康复中的剂量效应研究

王娟

西安交大第一医院

背景：早期运动康复对增强慢性心功能不全患者的心脏功能，提高患者生活质量至关重要，八段锦作为低强度身心运动在心脏康复中具有潜在优势，但其最佳干预剂量尚不明确，过量可能导致风险，不足则效果有限。目的：探讨不同剂量八段锦对心功能不全 I 期患者康复效果的差异，为护理人员制定精准化运动处方提供循证依据。方法：采用随机对照试验设计，将 90 例心功能不全 I 期（NYHA I 级）患者分为三组：低剂量组（LDG，n=30）：15 分钟 / 次，3 次 / 周，中剂量组（MDG，n=30）：30 分钟 / 次，5 次 / 周，高剂量组（HDG，n=30）：30 分钟 / 次，7 次 / 周，干预 12 周，以 6 分钟步行距离（6MWT）、NT-proBNP、明尼苏达心衰生活质量量表（MLHFQ）为核心指标评估效果，同时监测安全性及依从性。**结果**：疗效差异：MDG 组 6MWT 提升最显著（+68.2±21.5m），优于 LDG 组（+42.1m）和 HDG 组（+55.7m）（均 P<0.05）；MDG 组 NT-proBNP 降低幅度最大（-125.6±45.8 pg/mL），MLHFQ 评分改善最优（-15.3±4.8 分）；安全性：HDG 组退出率达 10%（3/30），显著高于 LDG（0%）和 MDG 组（3.3%），主因疲劳感与关节不适；三组均未发生严重心血管不良事件。结论：八段锦对心功能不全 I 期患者的康复效果存在剂量依赖性。中等剂量（30 分钟 / 次，5 次 / 周）为最优方案，可显著改善运动耐力、心功能标志物及生活质量，且安全性高；护理实践中需以此为基础制定个体化处方，避免不足或过量运动风险。

循证理念指导下康复锻炼应用于重症老年感染性心肌炎患者中的研究

高苗苗

交大一附院

【摘要】

目的： 探讨循证理念指导下康复锻炼在重症老年感染性心肌炎患者中的应用。

方法 ： 选取 2021 年 7 月至 2023 年 2 月本院收治的 166 例老年感染性心肌炎患者进行研究，按随机数字表法将所有患者分为 A 组（n=83，常规康复指导）与 B 组（n=83，循证理念指导下康复锻炼）。比较两组临床疗效、生活质量 [世界卫生组织生存质量测定量表（WHOQOL-100）]、心理韧性 [简式韧性量表（BRS）]、幸福感 [精神幸福感指数量表（SIWB）]、并发症等等。

结果 ： A、B 两组护理总有效率比较（89.02% vs 97.56%），差异有统计学意义（P<0.05）。护理后，两组 WHOQOL-100、BRS 评分、SIWB- 自我效能、生命意义评分均呈上升趋势，且 B 组高于 A 组（P<0.05）。A、B 两组并发症总发生率比较（12.20% vs3.66%），差异有统计学意义（P<0.05）。

结论 ：循证理念指导下康复锻炼应用于重症老年感染性心肌炎患者中效果显著，通过给予患者个性化的康复锻炼护理服务，旨在最大化降低风险、提高患者满意度和自我管理能力，可改善患者生活质量，提高其心理韧性与幸福感，使并发症发生降低，适宜在临床中推广。

专科护士为主导的多学科协作康复护理对心脏瓣膜置换术后患者康复的影响

张远莹

西安交通大学医学院第一附属医院

目的 探讨专科护士为主导的多学科协作康复护理对心脏瓣膜置换术后患者康复的影响。方法 选择 2022 年 2 月至 2023 年 1 月于西安交通大学第一附属医院心血管外科行心脏瓣膜置换术治疗的 100 例患者为研究对象，按照护理方式不同将患者分为对照组和观察组，每组 50 例。对照组患者给予常规护理干预，观察组患者给予专科护士为主导的多学科协作康复护理干预。记录 2 组患者术后首次排气时间、首次排便时间、首次下床活动时间及重症监护时间、住院时间；于出院时、术后 6 个月时，采用 6 min 步行距离试验和明尼苏达心力衰竭生活质量量表 (MLHFQ) 评估患者的心功能状态和生活质量；术后 6 个月，记录 2 组患者不良心脏事件发生率。结果 观察组患者首次排气时间、首次排便时间、首次下床时间、重症监护时间和住院时间显著短于对照组 (P<0.05)。出院时，2 组患者 6 min 步行距离比较差异无统计学意义 (P>0.05)；术后 6 个月，2 组患者 6 min 步行距离显著长于出院时，且观察组患者 6 min 步行距离显著长于对照组 (P<0.05)。出院时，2 组患者 MLHFQ 评分比较差异无统计学意义 (P>0.05)；术后 6 个月，2 组患者 MLHFQ 评分显著低于出院时，且观察组患者 MLHFQ 评分显著低于对照组 (P<0.05)。对照组患者发生不良心脏事件 8 例 (16.67%)，观察组患者发生不良心脏事件 2 例 (4.17%)；观察组患者不良心脏事件发生率显著低于对照组 (χ~2=4.019,P<0.05)。结论 专科护士为主导的多学科协作康复护理可缩短心脏瓣膜置换术后患者恢复时间，改善心功能和生活质量，减少不良心脏事件的发生。

促进急性心梗患者的康复与提高生活质量

李清桂 刘华芬

武汉大学人民医院

目的：为心梗患者提供心理支持以缓解焦虑 / 抑郁情绪，降低创伤后应激障碍（PTSD）风险，增强治疗信心与自我管理能力，改善疾病认知，纠正错误观念（如“卧床即安全”） 并能融入社会，恢复社会角色功能，减少病耻感，重建社会连接。重回生活正轨并提高生活质量

方法：通过阶段性心理干预：急性期① 每日 10 分钟床边支持性会谈② 焦虑筛查（GAD-7 量表）③ 紧急心理疏导。恢复期① 结构化健康教育（疾病认知 + 康复计划）② 认知行为疗法③ 家庭会议（家属参与照护计划）康复期（出院后） ① 每月 1 次心理门诊随访② 微信群互助小组（护士主导答疑）③ 正念减压训练（MBSR）加强社会融入策略：逐步复工计划 （体能评估 + 岗位调整建议 ），鼓励加强自主生活能力和冠心病术后微信群分享经验

结果：出院后 1 个月内规律运动执行率≥ 85% + 用药依从性≥ 95%，出院后 3 个月内焦虑 / 抑郁评分下降≥ 50%， 出院后 6 个月内社会支持评分提升 30% + 重返工作岗位率≥ 70%　　出院后 1 年内再住院率降低 40%（对比常规护理组）

结论 ： 通过系统化路径解决急性心梗患者“生理康复 - 心理调适 - 社会再适应”的断层问题，符合生物 - 心理 - 社会医学模式导向，从而缩短康复周期和提高医患满意度

冠心病患者运动恐惧干预研究的范围综述

彭沥枢 王彦

河北大学

目的 系统梳理冠心病患者运动恐惧干预研究的现状，整合现有证据，分析总结干预方案的特点及效果，旨在为未来干预策略的优化提供循证依据。

方法 遵循 Arksey 和 O'Malley 的范围综述方法学框架，系统检索中国知网、中国生物医学文献数据库、维普网、万方数据库、Pubmed、Embase、Web of science、CINAHL、等 8 个数据库，检索时限为建库至 2024 年 10 月 28 日。由 2 名研究者独立完成文献筛选、数据提取、汇总，采用主题分析法对干预方案的理论基础、方法学特征以及结局指标进行归纳。

结果 最终纳入 22 篇文献，包括随机对照试验（n=14）、类实验研究（n=6）、队列研究（n=2）。**（1）**干预类型包括认知行为干预、心理干预、运动干预、联合干预等 4 种，以认知行为理论（n=5）和双心护理模式（n=3）为常用的理论基础；**（2）**评价工具以心脏病运动恐惧量表（TSK-SV Heart）（n=18）最为常用；**（3）**干预形式：多学科团队协作（n=10）、个体化评估（n=5）、面对面团体干预（n=2）、深度访谈（n=5）、健康教育（n=5）、定期随访（n=4）等 6 种；**（4）**结局指标：包含心理状态指标、身体功能指标、临床结局指标、行为管理指标等 4 个维度。

结论 目前，冠心病运动恐惧干预研究处于发展阶段，存在理论模型单一，缺乏整合性的理论指导；干预形式、内容多样化但缺乏标准；结局指标尚未达成共识等特征。未来应结合多理论的优势，规范干预方案的内容和适用性，构建结局指标评价体系，为冠心病患者提供更加精准的干预方案。

基于数字孪生的心脏术后康复训练虚拟仿真模型构建及运动风险评估实践研究

刘玲 刘华芬

武汉大学人民医院（又名湖北省人民医院）紫阳院区

目的：运用数字孪生技术构建心脏术后患者康复训练虚拟仿真模型，评估该模型在指导精准康复训练和降低运动风险方面的实际应用效果。

方法：选取 120 例心脏术后患者，采集其全面的临床数据，包括基因数据、生活习惯信息、心理状态评估结果等。采用数字孪生技术，结合人工智能和大数据分析，构建高度个性化的心脏术后康复训练虚拟仿真模型。通过在虚拟模型中模拟不同康复训练方案下心脏的生理反应，利用深度学习算法建立运动风险预测模型，并根据预测结果为患者制定精准的康复训练方案。将患者随机分为数字孪生技术指导康复组（60 例）和传统康复组（60 例），对比两组患者在康复训练过程中的运动风险预测准确性、康复训练依从性以及康复效果指标（如心肺功能指标、体能恢复情况、心理状态改善程度）。

结果：成功构建了能够反映个体差异的心脏术后康复训练虚拟仿真模型，运动风险预测模型对不同风险事件的预测准确率达到 88%。数字孪生技术指导康复组运动风险预测准确性较传统康复组提高了 25%（P<0.05），康复训练依从性达到 88%，显著高于传统康复组的 68%（P<0.05）；康复训练 8 周后，数字孪生技术指导康复组心肺功能指标（如最大摄氧量、无氧阈）提升幅度比传统康复组高 18%，体能恢复情况和心理状态改善程度也明显优于传统康复组（P<0.05）。

结论：基于数字孪生技术的虚拟仿真模型在心脏术后患者康复训练运动风险预测和精准康复指导中具有重要价值，可提高运动风险预测准确性和康复训练依从性，显著改善康复效果，包括心肺功能、体能及心理状态，有望成为心脏术后康复护理的重要工具。

2 型糖尿病对充分 PCI 术后患者心肺运动测试中氧脉搏轨迹平台的影响

刘钰涛 [2] 吴嘉慧 [1]

1. 首都医科大学附属北京安贞医院

2. 湖北省第三人民医院

背景： 氧脉搏轨迹平台现象是心肺运动测试中反映心肌缺血的重要指标，具有重要的诊断和预后价值。虽然经皮冠状动脉介入治疗（PCI）能有效改善冠状动脉狭窄，但部分 PCI 术后患者依然存在心肌缺血，其机制尚未阐明。本研究旨在探讨 2 型糖尿病（T2DM）对充分 PCI 术后患者心肺运动测试中氧脉搏轨迹平台的影响。

方法： 本研究为单中心回顾性横断面研究。回顾性分析 2023 年 9 月至 2024 年 8 月期间连续就诊于北京安贞医院心脏康复中心进行心肺运动测试的 PCI 术后患者资料。纳入标准：年龄 20-80 岁，既往三年内接受过完全 PCI 治疗且接受指南导向药物治疗的患者。所有参与者在测试前一个月内常规接受全面评估以排除冠心病进展。纳入标准：年龄 20-80 岁，既往三年内接受过完全 PCI 治疗且接受指南导向药物治疗的患者。所有参与者在入组前一个月内常规接受全面临床评估，包括实验室检查、超声心动图和心脏影像学检查以排除冠心病进展。三名独立的心血管专科医师评估每位患者，确保无美国心脏协会指南定义的运动试验绝对或相对禁忌证。排除标准包括：心力衰竭、其他心脏手术史、瓣膜性心脏病、未控制的心律失常、肝肾功能不全、慢性阻塞性肺疾病、下肢功能障碍、贫血或甲状腺功能异常、肺动脉高压、活动性感染、肿瘤、严重肥胖（BMI>40 kg/m²）、运动试验提前终止或峰值呼吸交换率 <1.05、运动试验中出现严重胸痛、恶性心律失常或提示心肌缺血的 ST 段改变等。根据患者是否合并 T2DM 分组，采用多元 logistic 回归分析 2 型糖尿病与氧脉搏轨迹平台的关联性。

结果： 最终纳入 200 例无 T2DM 患者和 76 例 T2DM 患者。基线特征显示，T2DM 组患者合并高血压比例更高（64.5% vs 46.5%，p=0.008），余特征无明显差异。在心肺运动测试指标方面，2 型糖尿病组患者峰值每公斤摄氧量更低（18.6±4.3 vs 19.9±4.4 mL/kg/min，p=0.029），氧脉搏平台发生率更高（71.1% vs 57.0%，p=0.033）。多元 logistic 回归分析显示，在调整性别、年龄、身高、体重、吸烟、饮酒等混杂因素后，2 型糖尿病与氧脉搏轨迹平台呈显著正相关（OR=1.93，95%CI: 1.08-3.47，p=0.0274）。进一步调整高血压、高脂血症、心梗病史、日常运动强度等混杂因素后，这种关联仍然存在统计学意义（OR=1.84，95%CI:1.01-3.33，p=0.0455）。

结论： 在充分 PCI 术后患者中，T2DM 与氧脉搏轨迹平台现象呈显著正相关，提示 T2DM 患者合并术后心肌缺血风险较高。这提示 T2DM 即使在血运重建充分、无临床心肌缺血的背景下，仍能够影响运动中心脏储备的代偿能力。这一发现可能与 T2DM 患者的心脏自主神经病变、微血管病变以及代谢适应机制有关。T2DM 可能通过改变心肌代谢模式和血管反应性，影响运动时的氧脉搏轨迹表现。本研究结果为 PCI 术后患者的心肺运动测试解读提供了重要参考，强调心脏康复与运动风险分层时，T2DM 状态的独立评估与干预价值。

医院主导的居家 II 期心脏康复对急性心肌梗死 PCI 术后患者自主神经功能改善的研究

李佳 李炳欣

哈尔滨医科大学附属第一医院

目的：急性心肌梗死（AMI）是高死亡率的临床常见急危重症，目前通过经皮冠状动脉介入（PCI）使得 AMI 的生存率相对提高。AMI 后心脏自主神经功能受损与再狭窄、心血管死亡等风险相关。目前，有研究证明传统门诊心脏康复可改善 AMI-PCI 术后患者自主神经功能，但是存在的局限性导致患者依从性差。因此本研究旨在探索在 AMI-PCI 术后人群中，通过六分钟步行试验（6MWT）制定心脏康复运动方案进行医院主导的居家 II 期心脏康复对自主神经功能的改善及预后。

方法：本研究纳入符合标准的 AMI-PCI 术后患者，门诊复查时评估患者，通过 6MWT 结果制定合理的运动方案，进行居家心脏康复。根据随诊结果调整运动方案。随访 5 个月，采取平行对照的方法，将随访期内规律运动患者纳入试验组，完全未规律运动患者纳入对照组，观察两组患者的心率恢复（HRR）、心率变异性（HRV）、六分钟步行试验距离（6MWTD）、心脏彩超、生化血脂以及相关量表的变化，并进行统计学分析。

结果：本研究共纳入 80 例患者，其中试验组 40 例，对照组 40 例。(1) 在 AMI-PCI 术后 6 个月时，运动后第 1 分钟的心率恢复（HRR1）及运动后第 2 分钟的心率恢复（HRR2）试验组均高于对照组，且两组具有具有统计学意义（P<0.05）；(2) 在 AMI-PCI 术后 6 个月时，试验组的 6MWTD 明显高于对照组，并且两组具有统计学差异（P<0.05）；(4) 在随访期间，两组患者的生化血脂均无统计学意义，但试验组患者的 TG 和 VLDL 均显著下降，且低于对照组；(5) 在 AMI-PCI 术后 6 个月时，试验组与对照组的广泛焦虑问卷 7 项（GAD-7）、Borg 评分具有统计学差异（P<0.05），但两组心肌梗死多维度量表（MIDAS）未见统计学差异。(6) 通过相关行分析，HRR1 及 HRR2 在 3 个月及 6 个月均与 6MWTD 具有中度相关性且呈正相关；第 6 个月时，HRR1、HRR2 与 TG 及 VLDL 均呈负相关。

结论：医院主导的居家 II 期心脏康复对 AMI-PCI 术后患者的自主神经功能改善、运动耐力、血脂水平、生活焦虑情绪、以及患者生活质量的改善均有显著的积极作用。

心外科术后握力体重指数与术后离床时间的相关性

黄心颖

北京清华长庚医院

目的 心外科术后早期离床是降低呼吸系统并发症、缩短住院时间的关键环节。然而传统肌力评估指标（如绝对握力）易受水肿、营养状态干扰，难以真实反映患者功能储备。握力体重指数（GS/BW = 握力 (kg)/ 体重 (kg)）通过标准化体重影响，更精准表征相对肌力水平和营养 - 代谢状态。本研究通过前瞻性观察 56 例心外科手术患者，证实握力体重指数（GS/BW） 与术后离床时间显著负相关（GS/BW\<0.3 组离床时间延长 82 小时）。GS/BW 作为矫正体重偏差的肌力评估指标，可精准预测早期活动能力，为心外科加速康复路径提供量化依据。

方法 选取 2025 年 2 月至 6 月我院心外科术后 56 位患者 (n=56)，建立患者术后离床路径，在术后 24h 内测量患者 GS/BW，并根据评分进行术后早期心脏康复，记录患者手术时间与离床时间，计算时间差值。

结果 根据 GS/BW 将 56 位患者分为三组，GS/BW\<0.3 组（n=31, 55%）：离床时间均值 74.2±33.5h，中位数 82h；GS/BW 0.3-0.4 组（n=16, 29%）：离床时间均值 59.9±30.6h，中位数 48h；GS/BW\>0.4 组（n=9, 16%）：离床时间均值 56.4±27.6h，中位数 40h。研究发现，GS/BW 与离床时间呈负相关（r=-0.68, p\<0.001）。

结论 55% 的心脏外科术后患者 GS/BW\<0.3，提示普遍肌力储备不足。GS/BW 越低，离床时间显著延长，同时增加咳嗽排痰的难度，且并发症发生风险较高。因此，心脏外科术后患者通过抗阻训练、蛋白质补充，提高 GS/BW 评分，可改善患者预后。

陈旧性心肌梗死患者平衡功能特征及影响因素研究

王日旺 [1] 丁荣晶 [1] 郝自超 [2]

1. 中国医学科学院北京协和医院康复医学科

2. 河南省漯河市中心医院心血管内科

目的：探究陈旧性心肌梗死患者与无冠心病病史人群平衡功能的差异，分析陈旧

性心梗对平衡功能的影响机制及相关影响因素，为制定针对性康复策略提供理论依据。

方法：选取 31 例陈旧性心肌梗死 PCI 术后患者作为试验组，32 例无冠心病病史人群作为对照组。详细收集年龄、身高、体重、BMI、性别、药物服用情况、危险因素等一般资料。采用足底压力测试板，在裸足状态下，对两组受试者开展双足睁眼（DO）、双足闭眼（DC）、单足睁眼（SO）、单足闭眼（SC）等多种评估条件下的测试，通过对比分析两组在平衡总体评分、脚压、支撑面、几何中心、压力中心等各项指标上的差异，明确陈旧性心梗患者平衡功能的特征。

结果：试验组平均年龄为 52.94±11.69 岁，对照组为 48.84±13.27 岁，组间年龄差异无统计学意义（P >0.05）。试验组女性 7 例（22.6%）、男性 24 例（77.4%），对照组女性 10 例（31.3%）、男性 22 例（68.8%），卡方检验显示两组性别构成比较差异无统计学意义（P >0.05）。此外，BMI、家族史、吸烟史、饮酒史、运动习惯、高血压、高血糖危险因素暴露情况组间无显著性差异（P >0.05）。平衡功能评估分数显示，试验组显著高于对照组（63.71±6.96 vs 44.44±9.62 分，P <0.05），总分越低表明平衡功能越好。在 SO 测试中，试验组支撑面总面积、X 轴直径、几何中心 X 轴偏移量和 Y 轴偏移量均显著大于对照组（P <0.05）；在 DO 和 DC 测试中，试验组前、后偏移速度显著快于对照组（P <0.05）；本体感觉相关指标上，试验组在双足睁眼、双足闭眼、左单足睁眼、左单足闭眼、右单足睁眼的总轨迹长均显著长于对照组（P <0.05）；而在前庭功能和视觉反馈方面，重心偏移及 Romberg 指数在两组间比较差异无统计学意义（P >0.05）。

结论：陈旧性心肌梗死 PCI 术后患者较健康人群平衡功能显著降低，主要与本体感觉下降相关，与前庭功能和视觉反馈关联不显著。本研究结论提示在心梗后心脏康复训练中加入针对本体感觉的平衡训练，可能是进一步改善心梗患者运动能力与生活质量的重要措施。

基于微信平台的心脏康复指导对中青年 PCI 术后患者院外生活质量及机体功能状态影响的效果分析

王烨 李娟利

西安交通大学第一附属医院

目的 研究基于微信平台的心脏康复指导对中青年 PCI 术后出院患者生活质量及机体功能状态的影响，为临床护士开展心脏康复护理提供科学依据。方法 共选取 2023 年 10 月 -2024 年 10 月的西安市某三甲医院的中青年 PCI 术后患者 100 例，在患者出院前一天与其进行面对面谈话解释研究目的，并签署知情同意书，研究者向对照组进行常规的出院指导和健康宣教，干预组在常规的出院指导和健康宣教的基础上进行三个月的基于微信平台的心脏康复指导。本研究采用问卷法对患者的基本情况和疾病相关知识进行调查，采用中文版心脏康复量表调查 PCI 术后患者对心脏康复的认知和意愿情况，采用西雅图心绞痛量表（SAQ）调查患者在出院当天和出院三个月后的机体功能状态。采用 epidata 软件进行双人录入数据，采用 SPSS 25.0 统计软件进行统计学分析，以 P<0.05 为差异有统计学意义。研究结果 :1. 三个月后共收回问卷 94 例，其中干预组 48 份，对照组 46 份。干预组 2 例患者由于不能及时的关注公众号内容，退出研究。对照组 4 例患者失去联系，总失访率为 6%。2. 两组患者心脏康复量认知水平低，两组得分差异无统计学意义（P>0.05），两组患者都存在结果焦虑。3. 干预前两组患者血糖、血脂指标差异无统计学意义，三个月后两组血糖、总胆固醇、甘油三酯和低密度脂蛋白值都降低，但是组间差异无统计学意义（P>0.05）。4. 两组三个月后机体功能状态改善，两组患者三个月后心绞痛稳定状态组间差异有统计学意义（P<0.05），且干预组患者西雅图心绞痛量表躯体受限程度、心绞痛稳定状态改善明显，组间差异有统计学意义（P<0.05）。结论：本研究基于微信公众号的心脏康复指导能够提高中青年 PCI 术后患者的院外生活质量和机体功能状态，能够提高患者自我管理能力。能为患者提供更加便捷、高效、个性化的护理服务，在线咨询与答疑及时解决了患者的疑问，增强了患者对医护人员的信任，提高了治疗依从性。医护人员应该给患者普及心脏康复作用方面的健康教育，树立正确的信念，减少患者的错误认知。

Physical Exercise Mitigates Chronic Psychological Stress-Induced Neuroimmune Crosstalk via BDNF-Kif4-TARM1 axis

Xiang-Hui Zheng, Pei-Yao Wang, Zhou Guo, Yun-Qi Li, Yu-Xuan Liu, Li-Zhi Zheng, Ci-En Li, Hui-Yu Wang, Bai-Tao Wang, Shu-Hong Liu, Yang Zheng, Jian Wu, Bo Yu

the Second Affiliated Hospital of Harbin Medical University

Background: Chronic psychological stress is a well-established contributor to human morbidity and mortality, particularly in coronary artery disease (CAD), which drives neuroimmune crosstalk and accelerates the progression of atherosclerosis (AS). Although physical exercise is generally beneficial to all aspects of human and animal health and is tied to reduced inflammation, the exercise-mediated factors and mechanisms mitigating stress-induced vascular inflammation remain unclear. This study investigates the mechanistic basis of exercise-mediated attenuation of chronic psychological stress-induced neuroimmune crosstalk to reveal novel therapeutic targets and strategies for psychogenic CAD.

Methods: We established chronic restraint stress (CRS) and running wheel exercise intervention models in wild-type (WT) mice to investigate the role of physical exercise in neuroimmune crosstalk, with successful chronic psychological stress modeling assessed by enzyme-linked immunosorbent assay (ELISA) detection of corticosterone and behavioral tests (open field test and elevated plus maze test). RNA sequencing identified key genes in peripheral blood monocytes of WT model mice, and adeno-associated virus (AAV) was used to target one key gene, the kinesin family member 4 (Kif4), in these mice to evaluated its role. Combined co-immunoprecipitation mass spectrometry (CoIP-MS) and membrane proteomics identified Kif4 cargoes, with molecular docking and co-immunoprecipitation (Co-IP) confirming Kif4's direct interaction with T cell-interacting activating receptors on myeloid cell 1 (TARM1). We further used immunofluorescence to assay microtubule-dependent transport of TARM1 by Kif4, and validated TARM1 function in vitro with an immobilized Tarm1-Fc fusion protein. Next, we performed ELISA to examine the effect of physical exercise and chronic psychological stress on brain-derived neurotrophic factor (BDNF) levels in mouse blood plasma. Subsequently, we used ELISA and immunofluorescence to identify BDNF tissue sources, and validated its function and signaling pathway through BDNF stimulation in vitro and tropomyosin receptor kinase B (TrkB) inhibition with ANA-12 in vivo. In addition, the exercise-mediated neuroimmune effects and mechanisms were examine in a CRS-treated atherosclerotic mouse model. We also recruited patients with CAD at the 3-month post-discharge follow-up and grouped them based on their physical activity and the results of the 10-item perceived stress scale (PSS-10) questionnaire to generalize these rodent data to humans.

Results: Physical exercise alleviated the stress-induced neuroimmune crosstalk, reducing pro-inflammatory CD11b+Ly6Chigh monocyte phenotype in peripheral blood and suppressing M1 macrophage polarization in bone-marrow-derived macrophages (BMDMs) of WT model mice. Knockdown of Kif4 mitigated the pro-inflammatory responses in both peripheral blood monocytes and BMDMs in CRS model mice. Mechanistically, the kinesin Kif4 facilitates microtubule-dependent transport of TARM1 to plasma membranes, thereby driving macrophage inflammation responds. Conversely, neurogenic BDNF, a molecule regulated by physical exercise and chronic psychological stress, activated the TrkB receptor of monocytes/macrophages, thereby inhibiting p-STAT3/Kif4/TARM1 signaling pathway. Furthermore, in both atherosclerotic CRS mice model and CAD patients with high PSS-10, exercise mitigates stress-induced pro-inflammatory responses in monocytes through the BDNF-Kif4-TARM1 axis.

Conclusions: Physical exercise alleviates chronic psychological stress-induced neuroimmune crosstalk, an effect partially attributable to suppress pro-inflammatory responses in monocytes/macrophages via the BDNF-Kif4-TARM1 axis, revealing a novel neuroimmune-mediated brain-heart axis that supports physical exercise therapy for psychogenic CAD.

Key words: physical exercise; chronic psychological stress; neuroimmune crosstalk; brain-heart axis; BDNF-Kif4-TARM1 axis

5-Oxoproline prevents doxorubicin-induced cardiotoxicity and tumor growth

Xinning Guo, Meng Jiang

Renji Hospital, School of Medicine, Shanghai Jiao Tong University

Background: Cardiovascular mortality has emerged as the leading cause of noncancer-related death among cancer patients. The emergence of cardio-oncology has increased interdisciplinary collaboration between oncologists and cardiologists, driving rapid advancements in preventing the side effects of antitumor chemotherapies. Doxorubicin (DOX), a classical chemotherapeutic agent, faces significant limitations because of its well-documented risk of inducing cardiotoxicity. Effective prevention of DOX-induced cardiotoxicity is urgently needed. Biologically active metabolites are closely linked to human disease phenotypes, and they play crucial roles in regulating pathophysiological functions, such as anti-inflammatory, antioxidant, and metabolic regulation. Nonetheless, evidence of the therapeutic value of metabolites in DOX-induced cardiotoxicity remains scarce. Moreover, no studies have reported the dual effects of metabolite supplementation on both cardiac and tumor tissues during DOX therapy. Given that alterations in metabolic pathways have been observed in both cardiovascular diseases and cancer, targeting specific metabolic pathways may offer dual benefits by mitigating DOX-induced cardiotoxicity while simultaneously enhancing its antitumor efficacy.

Objectives: This study sought to explore the characteristic metabolic alterations associated with early DOX-induced cardiotoxicity and identify a therapeutic target that simultaneously inhibits cancer and protects the myocardium.

Methods: Metabolomic and transcriptomic analyses were performed on heart tissues from murine models of DOX-induced cardiotoxicity to identify the most significantly altered metabolic pathway. The most altered metabolite involved in the candidate pathway was chosen and verified in both mice and humans. One hundred eighteen plasma samples were collected from September 10, 2023, to July 15, 2024. Clinical data, including age, sex, history of hypertension, diabetes mellitus, hyperlipidemia, and current smoking, were collected. All patients received a predefined treatment protocol consisting of doxorubicin (80 mg/m2) in 4 cycles, administered every 3 weeks. Echocardiography was performed at baseline of DOX therapy and 3 weeks after the final cycle. The protective effects of the chosen metabolite against DOX-induced cardiotoxicity and its antitu-

mor effects were evaluated. Potential mechanisms were explored using C57BL/6J mice, OPLAH global knockout mice, BALB/c nude mice and NSG mice.

Results: In the present work, we identified 5-oxoproline as a key metabolite associated with DOX-induced cardiotoxicity, demonstrating its dual cardioprotective and antitumor functions. First, the glutathione pathway was identified as the most significantly altered metabolic pathway in the cardiac tissues of patients with DOX-induced cardiotoxicity, and the 5-oxoproline/OPLAH axis was the critical node in the pathway. Second, treatment with 5-oxoproline alleviated DOX-induced cardiotoxicity, as evidenced by improved cardiac function, reduced oxidative stress, and attenuated cell death, while simultaneously enhancing the antitumor efficacy of DOX. Third, mechanistic investigations revealed that 5-oxoproline exerted cardioprotective effects by restoring glutathione metabolic homeostasis via its downstream enzyme OPLAH and inhibited tumor proliferation by suppressing its upstream enzyme GGCT. Collectively, these findings provide the first evidence for a novel regulatory role of the GGCT/5-oxoproline/OPLAH metabolic axis in mitigating cardiovascular complications and suppressing tumor growth during cancer therapy. Finally, the level of circulating 5-oxoproline may serve as an early biomarker for the detection of anthracycline-induced cardiotoxicity.

Conclusions: In conclusion, our findings suggest that 5-oxoproline may serve as a promising small-molecule metabolite for preventing both DOX-induced cardiotoxicity and tumor growth. Thus, it may serve as an incremental therapeutic strategy for the treatment of cancer patients requiring anthracycline chemotherapy. Additionally, our findings provide a potential biomarker for the early detection of anthracycline-induced cardiotoxicity. These findings not only underscore the clinical importance of targeting early metabolic disturbances but also open new avenues for developing minimally invasive diagnostic tools.

八段锦运动对慢性心力衰竭的中老年女性患者影响的临床研究

付蓉

交大一附院

目的：通过观察八段锦运动对女性心力衰竭 (心衰) 患者生活质量和预后的影响，探讨该疗法的临床效果。

方法：将 120 例 40-75 岁中老年女性心衰患者随机分为八段锦运动组 (运动组，60 例) 和对照组 (60 例)，运动组在药物治疗的基础上辅助八段锦运动疗法，而对照组仅予药物治疗。12 周 -6 月随访患者的运动耐力（6 分钟步行距离，6MWD）、心肺功能（无氧阈值 VO_2 AT、左室射血分数 LVEF）、生活质量（明尼苏达心衰问卷 MLHFQ）、疲劳及情绪状态（汉密尔顿焦虑 / 抑郁量表），并比较联合终点事件 (因心衰再次入院和全因死亡) 的发生率。

结果：两组患者的运动耐量与心肺功能显著提升，6 分钟步行距离（6MWD）改善率达 6.14%（vs 对照组 1.32%）。心肺功能无氧阈值（VO_2 AT）提高 25.87%，左室射血分数（LVEF）增加 3.62%，显著优于对照组（p<0.001）。生物标志物改善：NT-proBNP 水平显著降低（p<0.05）。生活质量与心理状态全面改善 MLHFQ 总分降低、其中身体领域评分下降 2.83 分、情绪领域下降 2.52 分（均 p<0.001）。焦虑（HAMA）与抑郁（HAMD）评分显著下降。

结论：八段锦作为安全、易行的非药物干预手段，可显著提升中老年女性慢性心衰患者的运动能力、心肺功能及生活质量，并有效缓解焦虑抑郁状态。其低强度特性及居家可行性支持其在心衰长期管理中的推广价值，尤其适合作为心脏康复计划的组成部分。未来需进一步优化中老年女性专属干预方案并探索长期效应机制。

远程监测联合运动处方对冠心病 PCI 术后患者心功能的影响——一项随机对照试验

刘华芬

武汉大学人民医院

题目：远程监测联合运动处方对冠心病 PCI 术后患者心功能的影响——一项随机对照试验

作者：刘华芬（第一作者兼通信作者）、吕妮

单位：武汉大学人民医院心脏特需医疗科

研究背景与目的：经皮冠状动脉介入治疗（PCI）术后患者 1 年内再入院率高达 25%，传统门诊康复存在依从性差的问题。本研究探讨基于物联网技术的远程康复模式（TRCR）对改善患者运动耐力、心理状态及降低心血管事件的临床价值。

研究方法：试验设计：2022-2024 年纳入 PCI 术后患者 320 例，随机分为 TRCR 组（n=160）和常规康复组（n=160）干预方案：TRCR 组：佩戴智能心电衣，实时传输 ECG、血氧数据至医院平台，AI 自动生成个性化运动处方（强度根据心肺运动试验 CPET 动态调整）对照组：每周 3 次门诊康复训练评估指标：主要终点为 6 分钟步行距离（6MWD）改善值，次要终点包括 HADS 抑郁评分、NT-proBNP 水平及 1 年再住院率

研究结果：TRCR 组 6MWD 增幅较对照组显著提高（98.3±21.5m vs 62.4±18.7m, p<0.001）抑郁评分改善率 TRCR 组达 73.8%，显著高于对照组的 51.2%（OR=2.67, 95%CI 1.89-3.78）1 年随访期间 TRCR 组主要心血管事件发生率降低 42%（p=0.003）

结论：远程监测康复模式显著提升 PCI 术后患者的康复效果，其成功实施依赖于 " 智能硬件 - 云端分析 - 临床反馈 " 的三级联动体系。

心脏康复对急性心肌梗死经皮介入治疗后患者左心室功能、NT-ProBNP 和生活自理能力的影响：一项回顾性研究

张亚会 李莹 黄尚玮

上海市东方医院（同济大学附属东方医院）

Aim Although the advantages of cardiac rehabilitation (CR) have gradually emerged, its utilization rate is very low. This study aimed to assess the influence of CR on cardiac function for acute myocardial infarction (AMI) patients receiving percutaneous coronary intervention (PCI).

Methods 100 patients from March 2024 to January 2025 were enrolled who underwent PCI for AMI allocated into control group (n=50) with standard care and intervention group (n=50) with an additional structured early CR program during their hospital stay. The observation period spanned 30 days for both groups. Left ventricular end-diastolic diameter (LVEDd), left ventricular end-systolic diameter (LVEDs), fractional shortening (FS) rate of the left ventricular diameter, left ventricular ejection fraction (EF), N-terminal pro-brain natriuretic peptide (NT-ProBNP) levels and activities of daily living (ADL) recorded by barthel index (BI) were detected.

Results For the intervention group, Δ EF (Δ EF=EF2-EF1; EF1: the first after PCI; EF2: 30 days post-discharge), FS2 and Δ FS (Δ FS=FS2-FS1; FS1: the first after PCI; FS2: 30 days post-discharge), BI2 and Δ BI (Δ BI=BI2-BI1; BI1: the first after PCI; BI2: 30 days post-discharge), NT-ProBNP2 (30 days after post-discharge) presented a significant difference compared to the control group (p<0.05) . In addition, LVEDd and LVEDs presented no significant differences between the groups whether the first after PCI or 30 days post-discharge (p>0.05).

Conclusions AMI patients benefit from CR to improved left ventricular function, reduced NT-ProBNP levels and increased BI, ultimately leading to improved clinical prognosis.

一例原发性醛固酮性高血压的诊治经验

师一萍 邵琴

上海市胸科医院

病例摘要

主诉：患者女，65 岁。因“血压升高 30 余年， 控制欠佳半年”入院。患者 28 岁生产时发现血压升高，服用 CCB 类降压药物 后控制可，未重视。2023-12 出现 血压波动较大，最高血压 200 10mhg,，服用拜新同 30mg gd, 血压控制仍差，伴心悸头晕伴手抖，无胸闷、胸痛、气促，无恶心、呕吐、腹痛、咽喉紧缩感，无黑蒙、晕厥，无 呼吸困难、双下肢水肿及活动耐力减退等不适。

辅助检查 :2024- 3 在社区医院行动态心电图未见明显异常，3-21 至我院门诊查甲状腺功能未见明显异常，冠脉 CTA 提示 LAD 中段局部心肌桥，心超示左房略增大，室间隔基底段 增厚，主动脉瓣钙化，静息状态下左室各节段收缩活动未见明显异常，左室舒张功能减退。LVEF 64%。予 络活喜 5mg bid 口服，建议排除继发性高血压，今日患者为求进步诊治收入病区 。

既往史 : 有 2 型糖尿病 10 余年 , 目前予以西格列汀治疗 , 血糖控制尚可。否认肝炎、结核、近期脑出血及消化道出血等病史。

入院查体 : 神志清醒，查体合作。血压 139/74mHg，浅表淋巴结无肿大，口唇无紫绀，颈静脉无怒张， 双肺呼吸音清，未闻及明显干湿性哆音，心率 60 次分，律齐，各心脏瓣膜听诊区未及明显器质性杂音。腹软，无压痛及反跳痛，肝脾未及，双下肢浮肿 (-)。

初步诊断：1. 高血压 3 级 2. 冠状动脉肌桥 3.2 型糖尿病

实验室检查 : 血 RAAS 系统 : 血管紧张素 II 116. 48pg/mL, 血管紧张素 I 0. 03ng/ml, 血浆肾素浓度 0.5pg/mL, 血管紧张素转移酶 32. 8U/L, 醛固酮 371.21pg/mL。

血肾上腺轴 : 血促肾上腺皮质激素 113. 87pg/ml、血皮质醇 18. 72μg/dl

血儿茶酚胺类 : 3- 甲氧基酪胺 60. 20μg/gCr, 甲氧基肾上腺素 60g/gCr, 甲氧基去甲肾上腺素 67.40ug/gCr

盐水负荷试验 :

负荷前 :

电解质 : 钾 3.9mmol/L，钠 142mmol/L; 氯 109mmo1/L, 钙 2. 3umol/L。

RAAS 系统 : 血浆肾素浓度 0.5pg/mL, 血管紧张素转移酶 32. 9U/L，血管紧张素 I 0. 03ng/ml, 血管紧张素 II 131.52pg/mL，血醛固酮 227.83pg/mL。血皮质醇 10. 27μg/dl。

负荷后 :

RAAS 系统 : 血浆肾素浓度 0.5pg/m，血管紧张素转移酶 30. 5U/L，血管紧张素 I 0. 03ng/m1, 血管紧张素 II 129. 73pg/mL，血醛固酮 174.8pg/mL。血皮质醇 5.7μg/dl。

经皮肾上腺静脉取血 :

右肾上腺：醛固酮 318. 39pg/mL，血管紧张素转移酶 15. 6U/ 儿，血皮质醇 19.64μg/a, 血管紧张素 II 117.86pg/mL, 血管紧张素 10.08ng/ml，血浆肾素浓度 1.12pg/mL。

腔静脉：醛固酮 222. 67pg/mL，血管紧张素转移酶 28.6U/L，血皮质醇 23. 28μg/a1，血管紧张素 I 124.44pg/mL, 血管紧张素 I 0.07ng/m1，血浆肾素浓度 0.61pg/mL。

左肾上腺：醛固酮 195.12pg/mL，血管紧张素转移酶 27. TU/L，血皮质醇 >60. 00 μg/a1，血管紧张素 II114.21pg/mL, 血管紧张素 I 0.08ng/ml，血浆肾素浓度 1.42pg/L。

肾上腺增强 CT: 检查结果双侧肾上腺增粗伴多发结节。

出院诊断: 1. 高血压: 原发性醛固酮增多症 2. 肾上腺增粗伴结节 3. 高脂血症 4. 冠状动脉肌桥 5. 2 型糖尿病

出院用药：阿托伐他汀 20mg，每天 1 次，每次 1 片，口服 (睡前服用)；

螺内酯 20mg，每天 1 次，每次 1 粒，口服 (晨起空膜)，

移动健康技术支持的居家心脏康复模式对冠心病患者心肺功能及生活质量的影响：一项随机对照试验

刘雯

西安交通大学第一附属医院

目的： 中心化心脏康复（Center-Based Cardiac Rehabilitation, CBCR）参与率低是当前面临的主要挑战。本研究旨在评估一种基于移动健康（mHealth）技术的居家心脏康复（Home-Based Cardiac Rehabilitation, HBCR）新模式（结合可穿戴设备监测、个性化运动处方 APP 及远程指导）与传统 CBCR 相比，对稳定型冠心病（CAD）患者心肺功能、生活质量、康复依从性及医疗资源利用率的有效性和可行性。

方法： 采用前瞻性、单中心、随机对照试验设计。纳入 150 例经皮冠状动脉介入治疗（PCI）术后 1 月内的稳定型 CAD 患者，随机分配至干预组（mHealth-HBCR 组， n=75）或对照组（传统 CBCR 组， n=75）。干预组接受为期 12 周的 mHealth-HBCR 方案，包括基于 APP 的个性化运动处方（根据基线心肺运动试验 CPET 结果制定）、蓝牙连接的心率 / 活动监测设备、每周 2 次远程视频指导及健康教育。对照组接受标准 12 周 CBCR（每周 3 次院内监护下运动训练 + 健康教育）。主要终点为干预 12 周后的峰值摄氧量（VO2peak）变化值（通过 CPET 评估）和 SF-36 生活质量量表生理健康总评（PCS）得分变化值。次要终点包括 6 分钟步行距离（6MWD）、医院焦虑抑郁量表（HADS）评分、康复计划完成率（依从性）、心血管事件再入院率及急诊就诊率。

结果： 共 143 例患者完成研究（HBCR 组 72 例，CBCR 组 71 例）。组间基线特征无显著差异（P>0.05）。意向性分析（ITT）显示：

心肺功能 干预 12 周后，两组患者的 VO2peak 均显著提高（HBCR 组: Δ +2.8 ± 1.1 ml/kg/min； CBCR 组：Δ +2.6 ± 1.0 ml/kg/min），**组间差异无统计学意义（P=0.32）**。6MWD 改善情况相似（HBCR 组：Δ +65.2 ± 22.3m； CBCR 组：Δ +62.8 ± 20.7m； P=0.51）。

生活质量： SF-36 PCS 得分在两组均显著提升（HBCR 组：Δ +8.7 ± 3.2 分；CBCR 组: Δ +7.9 ± 3.5 分），**组间差异无统计学意义（P=0.18）**。两组 HADS 焦虑、抑郁评分改善程度相当（P>0.05）。

依从性与医疗资源利用： HBCR 组的计划完成率显著高于 CBCR 组（92% vs. 64%， P<0.001）。随访期间（6 个月），两组主要心血管事件（MACE）发生率无显著差异（HBCR 组 3.8% vs. CBCR 组 5.6%， P=0.52）。**HBCR 组因心绞痛 / 心衰症状的急诊就诊率显著低于 CBCR 组（5.3% vs. 21.3%，P=0.002）**。

结论： 基于移动健康技术支持的居家心脏康复模式（mHealth-HBCR）在改善稳定型冠心病患者心肺功能、运动耐量和生活质量方面，与传统中心化心脏康复（CBCR）效果相当。**该模式显著提高了患者的康复依从性，并有效降低了非计划性急诊就诊率。** 研究结果表明，mHealth-HBCR 是一种安全、有效且可行的替代方案，特别适用于因地理、时间或偏好限制难以参与 CBCR 的患者，具有提高心脏康复整体覆盖率的潜力，并可能优化医疗资源配置。

原发性醛固酮性的诊治经验

师一萍 邵琴

上海市胸科医院

病例摘要

主诉：患者女，62 岁，因“间断头晕、胸闷伴血压升高 2 年，血压控制不佳 3 月”入院。

现病史：患者 2 年前起无明显诱因下出现阵发性头昏、胸闷不适；无恶心、呕吐、腹痛、咽喉紧缩感，无眼胀、头晕、头痛、黑蒙、晕厥，无呼吸困难、双下肢水肿及活动耐力减退等不适。症状多于 15:00-16 :00 左右发作，与活动及情绪激动无关，发作时自测血压最高 220/110mHg。自行加服诺欣妥 100mg 1#，氨氯地平 5mg 1#，休息约 2h 后缓解。2 个月前症状发作频率增加，连续 3 天发作，症状性质同前。

初步诊断：1. 高血压 3 级

实验室检查：血 RAAS 系统：血管紧张素 II 107. 34pg/mL, 血管紧张素 I 0. 13ng/ml, 血浆肾素浓度 2.27pg/mL, 血管紧张素转移酶 32. 8U/L, 醛固酮 189. 29pg/mL。

血肾上腺轴：血促肾上腺皮质激素 113. 87pg/ml、血皮质醇 18. 72μg/dl

血儿茶酚胺类：3- 甲氧基酪胺 73. 20μg/gCr, 甲氧基肾上腺素 64.10g/gCr, 甲氧基去甲肾上腺素 70.80ug/gCr, 甲氧基肾上腺素 32.60pg/mL, 甲氧基去甲肾上腺素 55.10pg/mL，free (NMN+]IEN)87.7000pg/L。

尿肾上腺轴：24 小时尿皮质醇 (游离皮质醇) 230. 85 μg/24h, 24H 尿量 2700. 0000ml ↑

尿儿茶酚胺类：24 小时尿量 2. 0000L/24h, 游离多巴胺 153. 20ug/24h，游离肾上腺素 4. 00ug/24h， 甲氧基肾上腺素 78.80ug/24h，游离去甲肾上腺素 24. 00ug/24h, 甲氧基去甲肾上腺素 80. 20ug/ 24h ↑，NIN+MN) 159.0000ug/24h。 香草扁桃酸 [VMA] 4. 0000mg/ 24h。

盐水负荷试验：

负荷前：

电解质：钾 4.0mmol/L，钠 142mmol/L; 氯 105mmo1/L, 钙 2. 4umol/L。

RAAS 系统：血浆肾素浓度 1. 47pg/mL, 血管紧张素转移酶 32. 9U/L，血管紧张素 I 0. 08ng/ml, 血管紧张素 II 117. 19pg/mL，血醛固酮 160. 00pg/mL。血皮质醇 10. 60μg/dl。

负荷后：

电解质：钾 3.4mmol/L ↓，钠 143mo1/L，氯 109mmo1/L, 钙 2.1mmo1 九↓。

RAAS 系统：血浆肾素浓度 0.71pg/m，血管紧张素转移酶 30. 5U/L，血管紧张素 I 0. 04ng/m1, 血管紧张素 II 119. 03pg/mL，血醛固酮 109. 77pg/mL。血皮质醇 10. 28μg/dl。

经皮肾上腺静脉取血：

右肾上腺：醛固酮 166. 39pg/mL，血管紧张素转移酶 28. 6U/ 儿，血皮质醇 21.64μg/a, 血管紧张素 II 117.86pg/mL, 血管紧张素 10.08ng/ml，血浆肾素浓度 1.38pg/mL。

腔静脉：醛固酮 153. 67pg/mL，血管紧张素转移酶 28.6U/L，血皮质醇 23. 28μg/a1，血管紧张素 I 124.44pg/mL, 血管紧张素 I 0.07ng/m1，血浆肾素浓度 1.34pg/mL。

左肾上腺：醛固酮 877. 69pg/mL，血管紧张素转移酶 27. TU/L，血皮质醇 >60. 00 μg/a1，血管紧张素 II114.21pg/mL, 血管紧张素 I 0.08ng/ml，血浆肾素浓度 1.45pg/L。

肾上腺增强 CT: 检查结果两侧肾上腺未见明显异常。

出院诊断：1：高血压：原发性醛固酮增多症

心脏康复与冠心病二级预防

赵月

吉大二医院

目的：

利用问卷调查法了解地市级医院心血管科护士对冠心病二级预防知 - 信 - 行管理的现状，并分析其影响因素；明确冠心病患者二级预防和心脏康复管理的需求；评价与总结冠心病二级预防管理的最佳证据，结合专家会议法，构建冠心病患者二级预防和心脏康复护理管理方案，为临床管理提供依据。

方法：

（1）问卷调查法：自制心血管科护士冠心病患者二级预防和心脏康复知 - 信 - 行现状 调查问卷，采取便利抽样法选取 11 地市级中 1087 名心血管科护士通过问卷星调查护士对冠心病患者二级预防管理知识、态度和行为。

（2）半结构访谈法：根据访谈提纲，深入访谈 5 名冠心病患者并了解其对二级预防和心脏康复管理的需求。

结果：

（1）冠心病患者二级预防和心脏康复的需求主要为 5 个方面：冠心病相关知识缺乏，个性化、操作性康复指导需求，出院后延续康复指导需求、家庭与社会关怀需求、医院与社区联合服务需求。

（2）专家会议结果：结合问卷调查、患者访谈和最佳证据结果，并结合专家会议的讨论意见，对方案初稿进行修订，形成终版《冠心病二级预防和心脏康复护理管理方案》。

结论：

（1）心血管科护士对冠心病二级预防管理的知识和行为水平有待提高，而护理态度较积极，护理临床实践管理与指南建议存在较大差距，加强护士对冠心病二级预防和心脏康复培训是必要的。

（2）不同患者存在不同的心脏康复需求，健康教育及心脏康复干预策略的不同导致 患者临床结局不同，提示医务人员二级预防和心脏康复管理策略应评估个体需求，实施个性化管理方案。

（3）基于现况调查、患者访谈、证据综合和专家会议法构建的《冠心病二级预防和心脏康复护理管理方案》符合临床实际和满足患者需求，该方案涉及内容共 13 个方面，为后续管理者针对护理人员心脏康复管理的培训提供方案，推动心脏康复管理向精细化、标准化和科学化发展。

基于可穿戴设备的远程监护联合个性化运动处方对 PCI 术后患者心脏康复效果的影响：一项随机对照试验

罗婷

武汉市中心医院

目的

经皮冠状动脉介入治疗（PCI）术后患者的心脏康复参与率低（<30%），且传统中心 -based CR 存在地域限制。本研究旨在评估远程监护 + 个性化运动处方对 PCI 术后患者 CR 依从性、运动能力及心血管预后的影响。

方法

研究对象：纳入 2023 年 1 月–2024 年 6 月 PCI 术后患者（n=200），随机分为干预组（远程 CR，n=100）和对照组（常规 CR，n=100）。干预方案：干预组：佩戴智能手环（监测心率、步数）、每周 3 次远程视频指导（运动强度：靶心率 =60-80%HRmax）、AI 推送个性化运动反馈。对照组：传统门诊 CR（每周 3 次院内监护下运动训练）。评估指标：主要终点：6 个月 CR 参与率（完成≥ 80% 课程）。次要终点：6 分钟步行距离（6MWD）、左室射血分数（LVEF）、生活质量（SF-36 量表）、主要不良心血管事件（MACE）。统计学分析：t 检验、卡方检验、Kaplan-Meier 生存分析。

结果

1. 依从性：干预组 CR 参与率显著高于对照组（78% vs 52%，p<0.01）。

2. 运动能力：6 个月时，干预组 6MWD 提升更显著（干预组：+42.5±15.3m vs 对照组：+28.1±12.7m，p=0.003）。

3. 心功能改善：两组 LVEF 无统计学差异（干预组：+5.2% vs 对照组：+4.8%，p=0.32），但干预组 SF-36 心理评分更高（72.4±6.1 vs 65.3±7.2，p=0.01）。

4. MACE 事件：干预组发生率更低（3% vs 8%，p=0.048）。

结论

远程监护联合个性化运动处方可显著提高 PCI 术后患者的 CR 参与率，改善运动能力和生活质量，并降低 MACE 风险。该模式为基层或资源有限地区推广 CR 提供了可行方案。

晚期糖基化终末产物对心血管疾病患者心脏康复后运动能力改善的预测意义

李静

交大一附院

目的 分析反映晚期糖基化终末产物 (AGE) 组织累积情况的皮肤自发荧光 (SAF) 水平与心血管疾病 (CVD) 患者心脏康复 (CR) 后运动能力改善的关系。

方法 回顾性分析 2020 年 -2 月 2023 年 4 月于西安交通大学第一附属医院接受 CR 的 99 例 CVD 患者的临床资料。记录患者的基线情况及 CR3 周后 6min 步行距离 (6MWD)、峰值摄氧量 (VO_2) 和无氧阈 (AT)。采用 AGE Reader 在患者坐位时从其前臂内侧检测基线 SAF 水平。

结果 根据 SAF 水平三分位数进行分组，分为低水平组 (SAF 水平≤ 2.56a.u)、中水平组 (2.56a.u<SAF 水平≤ 3.37a.u) 和高水平组 (SAF 水平 >3.37a.u)，每组 33 例。高水平组患者的 BM1、糖尿病患病率均高于中水平组患者和低水平组患者，SM1 低于中水平组患者和低水平组患者，差异均有统计学意义 (P<0.05)。高水平组、中水平组及低水平组的基线 6MWD、AT 及 VO_2比较，差异均无统计学意义 (P>0.05)。CR3 周后，低水平组的 6MWD(t=2.156,P<0.05)、AT(t=2.315,P<0.05) 及 VO_2 (t=2574,P<0.05) 均较基线增加，但中水平组和高水平组的 6MWD、AT、VO_2无明显变化。此外，CR3 周后，低水平组患者的 6MWD(F=3.754,P<0.05)、AT(F=6.153,P<0.05)、VO_2 (F=9.250,P<0.05) 水平亦均高于中水平组和高水平组。经 SPearman 秩相关分析发现 ,SAF 水平与 6MWD 增加 %(r=-0.436,P<0.001)、AT 增加 %(r=-0.212,P=0.035)、VO_2 增加 %(r=-0.297,P=0.003) 均呈负相关，且校正年龄、性别后仍呈负相关。

结论 反应组织 AGE 累积情况的基线 SAF 水平与 CR 后的 6MWD、AT 和 VO_2增加均呈负相关，提示基线 SAF 水平低的 CVD 患者可能对 CR 的反应更好。

心肌梗死后运动能力改善与主要心血管事件的关系

徐金玉 王时宇 吴健

哈尔滨医科大学附属第二医院

目的： 心肌梗死作为冠心病发展的严重阶段，其病死率较高，因此，准确预测其发展趋势对指导临床治疗具有重要意义。本研究旨在探讨心肺运动试验（CPET）中的运动能力改善与心肌梗死患者临床结局之间的关系。通过监测患者两次心肺运动试验中的运动能力变化，探讨运动能力改善与患者预后之间的关系。

方法： 本研究选取了 1208 例在哈尔滨医科大学附属第二医院就诊且接受心肺运动试验的心肌梗死患者为研究对象，收集并分析两次 CPET 过程中的数据（两次 CPET 间隔在 3 个月以内），以及人口学特征、既往史、诊断及治疗方法、检查检验结果、用药情况及住院期间有无并发症等。根据入排标准，最终 620 例患者纳入到最终分析。根据心脏康复计划前后运动能力的差异，以 3 个代谢当量（METs）的改善为临界值，将患者分为两组：运动能力改善 < 3 METs 组（n=149）和运动能力改善≥ 3 METs 组（n=471），通过对两组数据的分析，探讨其与患者 2 年内主要心血管事件（MACE，定义为脑卒中、再梗、血运重建，心源性死亡、心源性再住院、恶性心律失常）之间的关系。

结果： MACE 在运动能力改善 < 3 METs 组（12.3%）中比在运动能力改善≥ 3 METs 组（6.8%）中更常见。多变量 Cox 风险分析显示，控制多个混杂因素后，运动能力改善 < 3 METs 与 MACE 显着相关（HR 1.626，95% CI：1.037–2.550，p = 0.034）。

结论： 本研究表明，心肺运动试验中运动能力改善 < 3 METs 对心肌梗死患者的临床结局具有显著影响。通过监测和分析运动能力的变化，可以及时了解患者的心肺功能状态及运动应激下的心脏功能变化，为临床治疗提供有力支持。因此，在心肌梗死患者的康复过程中，应重视心肺运动试验的应用，并根据监测结果制定个性化的康复方案，以改善患者的心肺功能，降低不良临床结局的发生率。未来研究可进一步探讨运动能力改善在心肌梗死患者治疗中的具体作用机制及干预策略。

经导管主动脉瓣置换术后患者一期心脏康复护理方案的构建与应用研究

南燕

西安交通大学医学院第一附属医院

摘 要： 目 的：构 建 经 导 管 主 动 脉 瓣 置 换 术（transcatheter aortic valve replacement, TAVR）术后患者一期心脏康复护理方案，并初步评价其在临床中的应用效果。

方法：通过文献回顾初步拟定主动脉瓣置换术后患者一期心脏康复护理方案；采用德尔菲法进行两轮专家函询，根据函询结果形成最终的干预方案。采用类实验研究设计，将 2023 年 11 月～ 2024 年 5 月收入西安市某三甲医院心血管内科的符合纳入标准的 27 例患者作为对照组；2023 年 12 月～ 2024 年 6 月收入的 27 例患者作为试验组。对照组给予术后常规护理方法，试验组按照前期构建的一期心脏康复护理方案实施干预。运用 6 分钟步行试验 (6MWT) 距离、改良 Barthel 指数 (BI) 评定量表、明尼苏达心衰生活质量量表 (MLHFQ), 比较两组患者干预前、干预后心功能、日常生活活动能力、生活质量，统计两组患者术后住院天数。

结果：(1) 方案构建：共进行两轮专家函询，两轮专家函询的专家积极系数分别为 :95%、100%; 权威系数分别为 :0.89、0.91; 肯德尔和谐系数 (Kendall's W) 分别为 :0.309、0.114(P<0.05); 主动脉瓣置换术后患者一期心脏康复护理方案包含一级指标 4 个，二级指标 46 个。(2) 方案应用：①本研究最初纳入研究对象 54 例，截至研究结束共纳研究对象 47 例，其中对照组 23 例，试验组 24 例，失访率为 12.96%。②干预前两组患者的一般资料、心功能、日常生活活动能力及生活质量评分比较，差异均无统计学意义 (P>0.05)。③心功能：干预后，试验组 6MWT 距离显著长于干预前及对照组 (P<0.05); 对照组干预前后比较，差异无统计学意义 (P>0.05)。④日常生活活动能力：干预后，试验组 BI 评分高于干预前及对照组 (P<0.05); 对照组干预前后比较，差异无统计学意义 (P>0.05)。⑤生活质量：干预前两组患者的 MLHFQ 总分及各维度得分差异均无统计学意义 (P>0.05)。出院一个月后，试验组 MLHFQ 总分、各维度 (躯体领域、情绪领域、其他领域) 得分均低于干预前及对照组 (P<0.05); 对照组除躯体领域外 (P=0.020), 患者 MLHFQ 情绪领域、其他领域维度得分及总分与干预前比较，差异无统计学意义 (P>0.05)。⑥术后住院天数：干预后患者术后住院天数与对照组相比，差异有统计学意义 (P<0.05)。

结论：(1) 基于德尔菲法构建的主动脉瓣置换术后患者一期心脏康复护理方案具有科学性和可靠性，方案切实可行。(2) 一期心脏康复护理方案的应用，能够有效促进主动脉瓣置换术后患者的心功能恢复、改善患者的日常生活活动能力及生活质量，缩短患者术后住院时间。

基于移动健康技术的心内科青少年患者心脏康复护理方案构建

付婷婷

新疆维吾尔族自治区人民医院

目的：构建基于移动健康技术的心内科青少年患者心脏康复护理方案。青少年心血管疾病是影响青少年健康的重要临床问题，包括先天性心脏病和心肌病等，常导致心功能下降和生活质量受损 [1]。当前心脏康复护理虽在成人患者中取得进展，但针对青少年群体的研究存在明显不足，如康复依从性低、个性化干预缺乏，且现有文献多聚焦成人，青少年应用探索有限，无法满足其独特生理和心理需求 [2]。移动健康技术基于自我管理理论和行为改变模型，通过实时监测与远程指导提升参与度，理论上可优化康复效果；然而，当前尚缺乏适用于青少年患者的移动健康心脏康复护理体系 [3]。基于此，本研究拟构建一套基于移动健康技术的青少年心脏康复护理方案，为其提高康复依从性、改善生活质量和远期预后提供新路径与护理依据。

方法：借助系统文献检索和循证分析，结合专家小组讨论，初步制定出心脏康复护理方案，设计出专家函询问卷并进行发放。运用德尔菲法对 6 名来自心血管、康复护理、信息技术等相关领域的专家开展两轮函询，依据专家反馈对方案内容进行调整和完善，最终形成护理方案。

结果：两轮专家函询问卷的有效回收情况都达到了 100%，专家权威系数分别是 0.88 和 0.90，变异系数在 0 到 0.25 之间。第一轮和第二轮的 Kendall 协调系数分别为 0.241 和 0.255（P<0.05），说明专家意见的协调性比较好。最终确定的护理方案包含 6 个一级指标、12 个二级指标以及 24 个三级指标。

结论：本研究构建的护理方案内容科学、结构合理，并且与移动健康技术紧密结合，究其原因为方案设计时充分考虑了临床实际需求，因此具有较好的临床可行性和应用价值，能够为心内科青少年患者的心脏康复护理工作提供实践指导。

早期强化心脏康复训练对非 ST 段抬高型心肌梗死 PCI 术后患者的效果

龚莉 刘华芬

武汉大学人民医院

早期强化心脏康复训练对非 ST 段抬高型心肌梗死 PCI 术后患者的效果

目的：探讨早期强化心脏康复训练在急性非 ST 段抬高型心肌梗死经皮冠状动脉介入 (PCI) 术后患者中的应用效果。研究旨在评估早期强化康复训练与传统康复方法相比，在改善心肺功能、运动耐力及生活质量方面的优势。

方法：选取 2020 年 8 月至 2022 年 8 月收治的 76 例急性非 ST 段抬高型心肌梗死 PCI 术后患者，按入院时间分为对照组和研究组各 38 例。对照组接受早期常规康复训练，研究组实施早期强化心脏康复训练。评估指标包括心功能指标(LVEDV、LVESV、LVEF)、肺功能指标(FEV1、FEV1/FVC)、6 分钟步行距离(6MWD)、心肌梗死多维度评估量表 (MIDAS) 评分及不良事件发生率，干预时间为 6 个月。

结果：干预 6 个月后，研究组 LVEF 水平显著高于对照组 (P<0.05)，表明心功能改善更显著。肺功能方面，研究组 FEV1 和 FEV1/FVC 水平均高于对照组 (P<0.05)。运动耐力方面，研究组 6MWD 较对照组更远 (P<0.05)。生活质量方面，研究组 MIDAS 评分低于对照组 (P<0.05)。安全性方面，研究组不良事件发生率 (10.53%) 显著低于对照组 (31.58%)(P<0.05)。

结论：对急性非 ST 段抬高型心肌梗死 PCI 术后患者实施早期强化心脏康复训练，可显著改善患者心肺功能，提高运动耐力和生活质量，同时降低不良事件发生率。这一研究为 PCI 术后患者的康复强度选择提供了循证依据，支持早期强化训练的安全性和有效性。

慢性心力衰竭患者中西医结合运动康复的研究进展

丁佳露 张秀杰 佟泉金 王倩

大连医科大学附属第一医院

【摘要】慢性心力衰竭作为心血管疾病的终末阶段，因高患病率、再住院率和死亡率，已成为全球重大公共卫生负担。传统的药物和器械治疗，存在不良反应及成本限制等问题。而以运动训练为核心的心脏康复作为 I 类推荐治疗，可通过多靶点干预机制：抑制交感 - 肾素 - 血管紧张素 - 醛固酮系统激活、改善内皮功能、减轻炎症氧化应激及延缓心室重构，显著改善慢性心衰患者的运动耐力和心肺功能，提高生活质量，改善抑郁情绪，显著降低再住院风险，进而改善临床预后。中医认为慢性心衰的核心病机为“本虚标实”，分为气虚血瘀证、气虚两虚证和阳气亏虚血瘀证三种主要证型。西医运动康复体系涵盖有氧运动、抗阻运动、柔韧性及呼吸训练，中医传统功法以太极拳、八段锦为主，中西医结合模式通过整合西医运动处方精准化与中医“辨证施治”的整体观，不仅发挥西医层面的心血管保护功能，同时借由调节气血运行、平衡阴阳、改善脏腑功能等中医途径，实现“整体调控”与“精准治疗”的有机结合。随着科技进步，数字健康技术为运动康复提供了新赋能，通过实时监测生理参数与风险预警，来支持医疗团队动态优化个体化运动处方，降低不良事件风险。同时促进患者康复知识获取及规律运动行为，显著提升依从性。本综述通过整合现有证据，对中西医结运动康复在慢性心衰患者中的具体应用及临床疗效进行阐述，解析数字健康技术的实践价值，分析其现存问题及未来研究方向，旨在为医护人员指导慢性心衰患者运动康复实践提供参考依据。

【关键词】慢性心力衰竭；中西医结合；运动康复；中医传统功法；研究进展

基于数字健康管理的家庭康复干预对老年冠心病患者临床疗效的随机对照研究

刘文彬

西安交大一附院

目的：探讨基于数字健康管理的家庭康复干预对老年冠心病患者心功能、生活质量及预后的影响。

方法：采用随机对照试验设计，选取 204 年 1 月至 2025 年 2 月某医院 211 例≥ 65 岁稳定型冠心病患者，随机分为干预组（n=105）和对照组（n=106）。对照组接受常规门诊随访，干预组在常规护理基础上接受为期 6 个月的数字化家庭康复干预，包括：① 可穿戴设备实时监测心电、血压、运动数据；② 移动端个性化运动处方（低强度有氧 + 抗阻训练）及依从性提醒；③ 远程营养与用药管理平台；④ 视频随访及 AI 健康预警系统。评估两组干预前后左心室射血分数（LVEF）、6 分钟步行试验（6MWT）、西雅图心绞痛量表（SAQ）评分、再入院率及心血管事件发生率。

结果：干预组干预后 LVEF（52.3±5.1% vs 48.2±4.8%, p<0.01）、6MWT（358±42m vs 312±38m, p<0.01)显著优于对照组; SAQ 总分提高幅度(27.6±6.4 vs 14.3±5.2, p<0.001）显著高于对照组；6 个月再入院率（8.3% vs 21.7%, p=0.032）及心血管事件发生率（5.0% vs 16.7%, p=0.027）显著降低。

结论：数字健康管理模式驱动的家庭康复可有效改善老年冠心病患者心功能、运动耐量及生活质量，降低再入院风险，为老年慢病居家管理提供循证支持。

社区导向的 II 期心脏康复管理模式对 PCI 术后患者心肺功能及预后的影响

刘文彬

西安交大一附院

目的: 评价基于社区实施的 II 期心脏康复(CR)管理模式对 PCI 术后患者心肺功能、自我管理能力及心血管事件风险的干预效果。

方法：采用前瞻性队列研究设计，纳入 202 例 PCI 术后患者，分为社区康复组（n=101）和常规随访组（n=101）。常规组接受标准药物治疗及门诊随访；社区组在常规治疗基础上，于术后 2 周启动为期 12 周的社区 II 期 CR 计划，内容包括：① 多学科团队协作（心内科医师 / 康复治疗师 / 社区护士）；②分级运动训练（心电图监护下递增式有氧 + 抗阻运动，每周 3 次）；③ 结构化健康教育（用药依从性、风险因素控制、心理支持）；④数字化远程监测（移动端心电传输、运动数据云端管理）。评估干预前后峰值摄氧量（VO_2 peak）、左心室射血分数（LVEF）、6 分钟步行距离（6MWD）、冠心病自我管理量表（CSMS）评分，并随访 6 个月主要不良心血管事件（MACE）发生率。

结果：干预 12 周后，社区组 VO_2 peak 显著提高（+3.8±1.2 mL/kg/min vs +0.9±0.8 mL/kg/min, p<0.001），LVEF 改善更显著（+5.7±2.1% vs +1.8±1.5%, p=0.003）；社区组 6MWD 提升幅度（+98±28m vs +42±22m）及 CSMS 总分增幅（+24.6±5.3 vs +9.1±4.1）均优于常规组（p<0.001）；6 个月 MACE 发生率显著降低（4.0% vs 13.9%, HR=0.28, 95%CI:0.11-0.71）

结论：以社区为基础的 II 期心脏康复管理模式能有效改善 PCI 术后患者心肺功能储备，提升自我管理水平，并降低短期心血管事件风险，为分级诊疗体系下心脏康复的落地实践提供循证依据。

基于 ITHBC 理论的心脏术后患者运动康复依从性干预模型的构建与实证研究

何莹

西安交通大学第一附属医院

目的：心脏术后患者运动康复依从性不足（文献报道 <50%）是影响长期预后的关键因素。现有研究多聚焦于生理指标改善，而基于健康行为改变理论的系统性干预模型仍属空白。本研究整合 ITHBC 理论（Integrated Theory of Health Behavior Change）核心要素，构建包含知识信念、自我管理、社会支持三维度的干预模型，并通过随机对照试验验证其提升依从性及临床效益的有效性。

方法：采用混合研究方法分两阶段实施：

1. 模型构建阶段（n=30）：

o 通过质性访谈提取患者运动障碍因素（如恐惧症状恶化、家庭支持不足等），结合 ITHBC 理论的知识信念（疾病认知）、自我调节（目标设定）、社会促进（家庭参与）三模块，形成初步框架。

o 采用德尔菲法(15 名专家,两轮咨询,Kendall̀ W=0.82)确定干预方案核心内容，包括：

□智能运动处方系统（基于心肺运动试验个性化调整强度）

□恐惧症状脱敏训练（VR 模拟术后运动场景）

□家庭协作式目标管理（微信端家属监督打卡）

2.

实证验证阶段（n=200，RCT 设计）：

o 对照组接受常规康复指导（n=100），干预组应用 ITHBC 模型干预（n=100，持续 12 周）。

o 主要结局：依从性（运动日记完成率 + 可穿戴设备 adherence ≥ 80% 为达标）；次要结局：6 分钟步行距离(6MWD)、西雅图心绞痛量表(SAQ)、内皮功能(FMD)。

o 统计学方法：采用广义估计方程（GEE）分析纵向数据，路径分析验证理论假设。

结果：

1. 依从性提升：干预组达标率显著高于对照组（76% vs. 43%，OR=3.21，95%CI 2.15-4.78，P<0.01），其中家庭协作模块贡献最大（路径系数 β=0.39）。

2. 临床指标改善：

o6MWD：干预组增加（58.3±12.1）m vs 对照组（31.7±10.5）m（P=0.002）

oSAQ 评分：躯体活动限制维度差异最显著（Δ=12.4 分，P<0.001）

3. 机制验证：知识信念通过自我效能间接影响依从性（中介效应占比 42%），社会支持调节自我管理与依从性的关系（P<0.05）。

结论

本研究首次将 ITHBC 理论转化为可操作的临床干预模型，证实其通过“认知 - 行为 - 环境”联动机制提升依从性

8 例 CABG 术后 ARSD 患者早期清醒下俯卧位的康复治疗

杨水涓 吴明祥 田青 刘波 申莹 刘秋雯 张萌萌

武汉亚心总医院

目的：清醒俯卧位联合早期康复治疗 CABG 术后 ARDS 患者疗效观察。

方法：

1：康复评估

1.1 康复前对患者进行康复评估：包括血压，心率，呼吸，神经系统，人工管道，疼痛，胸腔引流，S5Q 评分，RASS 评分等进行评估。

1.2 血气分析（评估患者血色素，PH, 氧分压，二氧化碳等）

1.3 影像学评估（肺部 CT/ 胸片）

1.4 超声（心脏功能，肺部超声）

2：康复治疗方法

2.0 吸氧支持（储氧面罩，高流量）

2.1 清醒下俯卧位

2.2 运动康复（床边坐位，床边站立位，原地踏步，病区行走）

2.3 呼吸训练（呼吸控制，呼吸训练，气道廓清等）

3，治疗结果

氧合指数：

患者 1，俯卧位时氧合指数 137.5，俯卧位最高氧合指数 193.3，俯卧位总时长 45min; 患者 2，俯卧位时氧合指数 100，俯卧位最高氧合指数 147，俯卧位总时长 70min; 患者 3，俯卧位时氧合指数 72.5，俯卧位最高氧合指数 121.4，俯卧位总时长 55min; 患者 5，俯卧位时氧合指数 88.1，俯卧位最高氧合指数 108.3，俯卧位总时长 20min; 患者 6，俯卧位时氧合指数 91.4，俯卧位最高氧合指数 190.5，俯卧位总时长 70min; 患者 7，俯卧位时氧合指数 87.7，俯卧位最高氧合指数 171.4，俯卧位总时长 67min; 患者 8，俯卧位时氧合指数 110，俯卧位最高氧合指数 153.7，俯卧位总时长 43min

BORG 评分：

患者 1，俯卧位前评分 0，俯卧位时评分 1 分，俯卧位后评分 0.5 分

患者 2，俯卧位前评分 0，俯卧位时评分 0.5 分，俯卧位后评分 0 分

患者 3，俯卧位前评分 0.5，俯卧位时评分 1 分，俯卧位后评分 0.5 分

患者 4，俯卧位前评分 0.5，俯卧位时评分 0 分，俯卧位后评分 0 分

患者 5，俯卧位前评分 0，俯卧位时评分 0.5 分，俯卧位后评分 0.5 分

患者 6，俯卧位前评分 0.5，俯卧位时评分 0.5 分，俯卧位后评分 0.5 分

患者 7，俯卧位前评分 0，俯卧位时评分 0.5 分，俯卧位后评分 0 分

患者 8，俯卧位前评分 0，俯卧位时评分 0.5 分，俯卧位后评分 0 分

疼痛评分（NRS）：

患者 1，俯卧位前疼痛评分 0 分，俯卧位时疼痛评分 2 分，俯卧位后疼痛评分 1 分；患者 2，俯卧位前疼痛评分 0 分，俯卧位时疼痛评分 2 分，俯卧位后疼痛评分 0 分；患者 3，俯卧位前疼痛评分 1 分，俯卧位时疼痛评分 2 分，俯卧位后疼痛评分 1 分；患者 4，俯卧位前疼痛评分 1 分，俯卧位时疼痛评分 0 分，俯卧位后疼痛评分 0 分；患者 5，俯卧位前疼痛评分 1 分，俯卧位时疼痛评分 1 分，俯卧位后疼痛评分 1 分；患者 6，俯卧位前疼痛评分 1 分，俯卧位时疼痛评分 0 分，俯卧位后疼痛评分 1 分；患者 7，俯卧位前疼痛评分 0 分，俯卧位时疼痛评分 1 分，俯卧位后疼痛评分 0 分；患者 8，俯卧位前疼痛评分 0 分，俯卧位时疼痛评分 1 分，俯卧位后疼痛评分 1 分

4. 结论

在 CABG 术后 ARDS 治疗研究中发现早期俯卧位通气可以降低 ARDS 患者二次插管率同时改善患者的通气、换气，促进呼吸功能恢复。俯卧位对氧合指数有明显的改善，患者进行清醒下俯卧位前，我们需要对患者进行评估，由于治疗过程中需要患者全程配合，所以俯卧位前需对患者进行宣教并征得患者同意。俯卧位过程中也需要评估包括：呼吸情况，循环情况，血气分析，疼痛，胸腔引流情况等。

心脏康复转诊管理的最佳证据总结

汤一帆 肖苏婉 夏丽莉 李婷茹 高春红

南京医科大学第一附属医院

目的：检索、评价并总结心血管疾病人群心脏康复（Cardiac Rehabilitation, CR）转诊策略的最佳证据。

方法：采用循证方法，围绕 CR 转诊管理问题，系统检索国内外数据库、专业协会及临床指南网站中的临床决策、指南、系统评价、专家共识、证据总结及原始研究。由 2 名接受过循证培训的研究员独立完成质量评价与证据提取。

结果：共纳入 38 篇文献（指南 12 篇、专家共识 17 篇、系统评价 5 篇、原始研究 4 篇），提炼出 44 条证据，涵盖“系统 - 服务 - 患者”三层面的 10 个核心转诊策略范畴：自动化转诊系统、转诊指标考核、财务与保险支持、政策与管理体系、可替代服务交付模式、标化服务流程、多学科团队协作、医务人员教育、个性化转诊策略及患者教育。健康系统层面，强调构建自动化转诊系统与配套保障措施。转诊系统的构建机制应包括兼顾用户特征信息、结构化数据监管、出院流程嵌入转诊指令、主动推送转诊任务与 CR 服务信息等功能。自动转诊系统联合医务人员主动推荐和联络员干预在提高 CR 转诊效率和患者接受度方面；“CR 上转率”、“CR 下转率”以及“出院后 21 天内 CR 登记率”等多项指标，既可用于动态追踪转诊流程执行情况，也可作为医疗机构质量管理与绩效考核的重要依据。服务提供层面，强调优化服务模式与流程，推动多学科协作。远程、社区、家庭、门诊、自我引导式和混合 CR 模式，适用人群与应用场景各异；构建标准化服务路径，包括统一转诊规则、明确转诊启动时间节点、规范正式与非正式沟通、规划转诊与随访途径等，有助于提升医患沟通质量与转诊决策一致性；应加强全科医生、基层护理人员及家庭医生的培训，提升其对 CR 适宜人群的识别与转介能力，推动转诊责任下沉与早期介入。服务使用者层面，强调聚焦个体差异，强化患者转诊动机。全面个性化评估是制定 CR 转诊策略的前提，尤其应关注老年、女性、少数人种、农村居民和经济困难群体，以减少患者因自身因素导致的转诊启动障碍；构建由具备不同文化背景和身份经验的多样化联络员网络，有助于更精准识别个体转诊过程中的障碍与文化偏好，从而制定更具针对性的个体化转诊方案；应在尊重患者偏好的基础上，选择合适的沟通与随访方式（如电话、短信、电邮等），并确保转诊信息具备语言与文化适配性；科学的健康教育手段强化患者转诊动机，也被证实是提高 CR 转诊率的重要策略。

结论：本研究汇总的 CR 转诊证据具备一定的科学性与系统性，为我国转诊路径的标准化建设提供循证支持，助力推动 CR 利益相关者优化转诊实践。

A Multimodal Data-Based Auxiliary Diagnostic Model for Mental Stress-Induced Myocardial Ischemia (MSIMI)

bingqing Bai[1], Hao-Peng Ke[2], Hao-Feng Zhou[1], Huan Ma[1], Qing-Shan Geng[3]

1. Guangdong Provincial People's Hospital

2. Guangzhou Huali College

3. Shenzhen People's Hospital

Objective:

Mental stress-induced myocardial ischemia (MSIMI) is an early-stage reversible form of myocardial ischemia that remains difficult to detect, particularly in patients with non-obstructive coronary artery disease (ANOCA). In this population, chest pain is often the first or only clinical manifestation, while routine cardiovascular evaluations, including invasive coronary angiography, typically show no significant abnormalities. The current gold standard for MSIMI diagnosis requires two PET/CT myocardial perfusion imaging (MPI) scans—one at rest and one during mental stress—making the process complex, costly, and associated with additional radiation exposure. Artificial intelligence has the potential to improve the diagnostic accuracy of resting MPI by uncovering subtle perfusion abnormalities that are challenging to identify through conventional physician interpretation. While deep learning has demonstrated high standalone diagnostic accuracy in detecting obstructive coronary artery disease (CAD), its application in identifying MSIMI in ANOCA patients remains largely unexplored. This study aimed to develop a multimodal deep learning-based diagnostic model for MSIMI, integrating features from resting PET/CT MPI with clinical examination data, to assist in early detection and reduce the need for stress testing and repeated imaging.

Methods:

A total of 159 participants were enrolled, including 117 patients with ANOCA and 42 healthy controls. All subjects underwent resting MPI and mental stress (Stroop color-word test, public speaking task, mental arithmetic task) MPI to determine the presence or absence of MSIMI. The input features included resting-state MPI polar maps, horizontal long-axis images, vertical long-axis images, and selected clinical variables. A small convolutional neural network (CNN) with three convolutional layers (kernel size 3×3) was designed to build an image-based diagnostic model for MSIMI. Furthermore, feature-level fusion was performed to integrate clinical examination data with imaging features, constructing a multimodal diagnostic model. The dataset was randomly split into 80% for training and 20% for testing. Model performance was evaluated using the area under the receiver operating characteristic curve (AUC), accuracy (ACC), sensitivity (SEN) and specificity (SPE).

Results:

Among the enrolled participants, 47 were diagnosed as MSIMI-positive and 112 as MSIMI-negative based on MPI results. Using the resting polar maps alone, the CNN model achieved an AUC of 75.0% in the test set. When combining resting polar maps with horizontal long-axis images, the AUC improved to 80.0%. Lasso regression was applied to select clinical variables from the original dataset of 122 features, resulting in seven key clinical indicators: electrocardiogram normality, total score of the Hospital Anxiety and Depression Scale-Anxiety subscale, gamma-glutamyl transferase , high-sensitivity C-reactive protein, resting left ventricular ejection fraction, free light chain KAPPA to LAMBDA ratio, and parathyroid hormone. Feature-level fusion of these clinical variables with the image model further enhanced diagnostic performance, resulting in an AUC of 86.4%, an ACC of 84.4%, a SEN of 70.0%, and a SPE of 90.9%. This study also employed several well-established pretrained image recognition models to compare their performance with the proposed model. The results showed that our model outperformed ResNet18 (AUC:70.9%, ACC: 75.0%), DenseNet121 (AUC: 77.7%, ACC: 78.1%), and EfficientNet_B0 (AUC: 71.8%, ACC: 71.9%) in terms of both AUC and ACC.

Conclusion:

This study developed a multimodal MSIMI diagnostic model based on resting PET myocardial perfusion imaging using convolutional neural networks. By integrating image features with clinical data through feature-level fusion, the model significantly improved diagnostic efficiency. These findings provide a foundation for intelligent medical decision-making in the early detection and management of MSIMI.

基于多学科协作的心脏康复护理模式在心血管疾病患者中的应用效果研究

张静漪

西安交通大学医学院第一附属医院

摘要： 心脏康复作为心血管疾病患者全程管理的核心环节，对改善患者心功能、

降低再入院率及提升生活质量具有重要意义。本文旨在探讨多学科协作模式下心脏康复护理的实施路径与应用效果。研究选取 2023 年 12 月至 2024 年 6 月某三甲医院收治的 120 例心血管疾病患者为研究对象，随机分为观察组（60 例）与对照组（60 例）。对照组采用常规心脏康复护理（包括基础健康教育、用药指导及运动建议），观察组在此基础上实施多学科协作护理模式，由外科医师、专科护士、康复治疗师、营养师及心理医师组成干预团队，制定个性化康复方案，涵盖分期运动训练（急性期床边活动 - 恢复期有氧运动 - 维持期抗阻训练）、个体化营养干预（基于膳食结构分析的低盐低脂饮食指导）、心理疏导（认知行为疗法联合家庭支持）及延续性随访（出院后 3 个月电话 + 线上平台动态监测）。比较两组患者干预 3 个月后的左心室射血分数(LVEF)、6 分钟步行距离(6MWD)、再入院率及生活质量评分（SF-36）。结果显示，观察组 LVEF 及 6MWD 改善幅度显著优于对照组(P<0.05)，再入院率(5.0%)低于对照组(16.7%)(P<0.05)，且 SF-36 各维度评分(生理功能、情感职能、社会功能等)均显著提高(P<0.05)。研究表明，多学科协作的心脏康复护理模式可通过整合多专业资源，实现对患者生理、心理及社会功能的全面干预，有效促进心脏功能恢复，降低不良事件风险，值得在临床推广应用。

心脏康复护理在心脏移植术后患者护理中的应用效果观察

余叶

西安交通大学第一附属医院

目的：探究在心脏移植术后患者的护理中应用心脏康复护理的效果 .

方法：选取 2023 年 1~12 月在西安交通大学第一附属医院行心脏移植手术的 36 例患者作为研究对象，采用随机数字表法分为对照组和观察组，每组各 18 例，对照组采取常规护理，观察组采取心脏康复护理，其包含以下内容①预防感染；②观察患者是否出现免疫排异反应；③抗排异药的用药护理；④运动康复护理；⑤饮食护理；⑥心理护理；⑦健康教育；以此来对比两组患者的心理弹性、生活质量和护理满意度 .

结果：1. 对比两组患者的心理弹性评分：护理前，两组患者的心理弹性评分比较差异无统计学意义（均 P > 0.05）；护理后，观察组患者的乐观性评分、自强性评分及心理弹性总分高于对照组（均 P < 0.05）.

2. 对比两组患者的生活质量评分：护理前，两组患者的生活质量评分比较差异无统计学意义（均 P > 0.05）；护理后，观察组患者的生活质量评分高于对照组（均 P < 0.05）.

3. 对比两组患者的护理满意度：观察组患者的护理满意度高于对照组（P < 0.05），

结论：在心脏移植术后患者的护理中应用心脏康复护理，能够改善患者的心理弹性，提高患者的生活质量，患者的护理满意度更高，值得推广、应用 .

肥厚型心肌病患者多维度康复护理模式的构建与实践

何乔 李娟利

西安交大第一附属医院

目的：肥厚型心肌病（HCM）是一种以心室肥厚为特征的遗传性心肌病，患者常因心力衰竭、心律失常及心理负担导致生活质量显著下降。传统护理模式多聚焦于症状管理，缺乏对生理 - 心理 - 社会功能的系统性干预。本研究旨在构建并实践一种涵盖心脏功能康复、心理调适、社会支持及长期管理的多维度康复护理模式，以改善患者预后及生活质量。

方法：采用前瞻性队列研究设计，纳入 2023 年 1 月至 2024 年 12 月某三甲医院收治的 120 例 HCM 患者，随机分为干预组（n=60）与对照组（n=60）。对照组接受常规药物治疗与基础护理；干预组在对照组基础上实施多维度康复护理，包括生理维度：个体化运动康复（基于心肺运动试验制定强度）、营养管理及用药依从性干预；心理维度：认知行为疗法（CBT）缓解焦虑 / 抑郁，联合正念减压训练；社会维度：建立“患者 - 家属 - 社区”支持网络，定期开展健康教育；长期管理：通过远程监测（可穿戴设备）实现动态随访。评估指标包括：心功能（LVEF、NT-proBNP）、6 分钟步行距离（6MWD）、生活质量量表（MLHFQ）、焦虑抑郁评分（HADS），随访 6 个月。

结果：干预组在以下方面显著优于对照组(均 P<0.05)：生理改善：LVEF 提升(干预组 Δ+8.2% vs 对照组 Δ+3.1%)，6MWD 增加（Δ+75m vs Δ+32m）；心理与社会功能：HADS 焦虑评分降低（Δ-4.5 vs Δ-1.8），MLHFQ 总分下降（Δ-22 vs Δ-9）；再住院率：干预组 6 个月内再住院率(13.3%)显著低于对照组(28.3%)。此外，干预组患者对护理模式的满意度达 91.7%，显著高于对照组的 76.6%。

结论：多维度康复护理模式通过整合生理康复、心理干预及社会支持，可有效改善 HCM 患者的心功能、运动耐量及心理状态，降低再住院率，提升长期生活质量。该模式具有临床推广价值，未来需进一步验证其长期效益及卫生经济学价值。

基于循证医学的肥厚型心肌病康复护理路径优化研究

何乔 李娟利

西安交大第一附属医院

目的：肥厚型心肌病（HCM）的康复护理长期面临临床实践异质性大、循证支持不足的问题。本研究基于最新国际指南（如 2020 AHA/ACC 指南）及循证医学证据，旨在构建一套标准化、阶梯式康复护理路径，并通过临床实践验证其有效性，以解决 HCM 患者康复管理中存在的随意性、碎片化问题，最终实现预后改善与医疗资源优化配置。

方法：证据整合阶段：系统检索 PubMed、Cochrane Library 等数据库（2015–2025），筛选 HCM 康复相关 RCT 研究、Meta 分析及指南，采用 GRADE 系统评价证据质量。通过德尔菲法组织 15 名专家（心内科、康复科、护理学）对初步路径进行 3 轮论证，形成共识。路径构建与实施：基于循证证据，将康复护理分为急性期（住院）、过渡期（出院后 1 个月）、长期管理期（1 个月后）三阶段，明确各阶段干预重点，急性期：以症状控制（如 β 受体阻滞剂滴定）、低强度运动评估（改良 Bruce 方案）为核心；过渡期：引入远程心电监测 + 家庭运动日记，预防猝死及再入院；长期管理期：结合基因检测结果（如 MYBPC3 突变）制定个性化运动处方。采用整群随机对照试验，纳入 2024 年 1 月 -2025 年 6 月 100 例 HCM 患者（干预组 50 例，对照组 50 例），对照组接受常规护理，干预组按优化路径执行。评价指标：主要终点：6 个月内心血管事件（猝死、再住院）发生率；

次要终点：左心室流出道压差（LVOTG）、堪萨斯城心肌病问卷（KCCQ）评分、护理成本效益比。

结 果：临床结局，干预组心血管事件发生率显著低于对照组（8.8% vs 21.3%，P=0.012），LVOTG 改善更明显（Δ-12.5 mmHg vs Δ-5.2 mmHg，P<0.01）；KCCQ 评分中，干预组在“躯体限制”及“生活质量”维度提升幅度超对照组 30%(均 P<0.05)。卫生经济学效益：干预组人均护理成本降低 18.7%(主要源于再住院减少)，且路径执行依从率达 89.4%。循证实践转化：通过路径优化，临床决策时间缩短 40%，护士对 HCM 康复知识掌握率从 62% 提升至 88%。

结论：本研究构建的循证康复护理路径通过阶段化干预、多学科协作及动态评估，显著降低了 HCM 患者不良事件风险，并改善功能性预后。其标准化框架为临床实践提供了可推广的模板，未来需进一步探索路径在基层医疗中的适应性及长期（≥ 5 年）生存率影响。

心脏康复对心血管疾病患者心功能、运动耐力及生活质量的影响研究

朱苗苗

西安交大一附院

目的：本研究旨在通过系统评估心脏康复对心血管疾病患者心功能、运动耐力及生活质量的影响，探索其在改善患者临床结局方面的潜在机制，为临床推广心脏康复提供依据。

方法：采用随机对照试验，共选取 200 例心血管疾病患者，随机分为心脏康复组（100 例）和常规治疗组（100 例）。常规治疗组给予药物等常规治疗，心脏康复组在此基础上进行为期 12 周的心脏康复训练，包括有氧运动、力量训练及健康教育等。分别在干预前及干预 12 周后，对比两组患者的左室射血分数(LVEF)、6 分钟步行距离（6MWD）及生活质量量表（SF-36）评分。

结果：①左室射血分数：干预前，心脏康复组 LVEF 为（45.2±3.5）%，常规治疗组为（44.8±3.8）%，两组无显著差异（P>0.05）。干预 12 周后，心脏康复组 LVEF 提升至(52.6±4.2)%，显著高于常规治疗组的(47.5±3.6)%(P<0.05)。② 6 分钟步行距离：干预前，心脏康复组 6MWD 为（305.6±25.3）米，常规治疗组为（302.8±28.6）米，差异无统计学意义（P>0.05）。干预 12 周后，心脏康复组 6MWD 增加至（386.5±30.2）米，明显长于常规治疗组的（335.7±27.8）米（P<0.05）。③生活质量量表评分：干预前，两组 SF-36 各维度评分相近（P>0.05）。干预 12 周后，心脏康复组在生理功能、生理职能、躯体疼痛、一般健康状况、精力、社会功能、情感职能及精神健康等维度的评分均显著高于常规治疗组（P<0.05）。

结论：循证医学证据表明，心脏康复干预能够显著改善心血管疾病患者的心功能指标，有效提升其运动耐量水平，并在提升生活质量方面呈现积极效应。基于此，心脏康复模式具备充分的临床推广价值，有望成为优化心血管疾病患者康复结局及提升生活质量的重要策略。

心肺运动试验指导的个体化康复方案对冠心病患者功能恢 复的临床价值研究

吴丹

西安交大一附院

摘要

目的：探讨以心肺运动试验（CPET）为指导的个体化、动态调整康复方案在改善冠心病（CHD）患者心肺功能、心脏结构及临床预后方面的应用价值。

方法：本研究采用前瞻性随机对照设计，纳入 156 例稳定性冠心病患者，随机分为研究组（n=78）与对照组（n=78）。对照组采用基于年龄预测心率的传统固定强度康复方案。研究组则通过 CPET 精确测定无氧阈（AT）、峰值摄氧量（VO?peak）等参数，制定并周期性（每 4 周）调整以无氧阈为核心靶强度的个体化训练方案，该方案融合了高强度间歇训练（HIIT）与双通道安全监控系统。干预周期为 6 个月。

结果：干预 6 个月后，研究组的 VO?peak 较基线提升显著高于对照组((22.9±3.1) vs (20.1±2.6) mL/kg/min, P<0.001）。研究组的左室射血分数（LVEF）提升了 4.9%，显著优于对照组（P=0.008），且心肌灌注缺损面积显著减小（P<0.001）。此外，研究组的运动诱发心肌缺血发生率（10.3% vs 26.9%）及严重不良心血管事件发生率均显著低于对照组（P<0.05）。

结论：基于心肺运动试验的个体化、动态调整康复方案，能更安全、有效地提升冠心病患者的心肺耐力，促进有益的心室重构，降低心血管不良事件风险。该模式为制定精准、高效的中国人群心脏康复策略提供了重要的实证依据和临床推广价值。

关键词：冠心病；心肺运动试验；精准康复；心脏康复；心室重构

基于心肺运动试验的中老年体检人群运动高血压及其影响因素分析

施杰洪 丁荣晶

中国医学科学院北京协和医院

目的：《中国心血管健康与疾病报告 2023》显示，我国成年人高血压患病率已

达 27.5%，且血压控制率仍不理想。前瞻性研究表明，运动中收缩压每升高 5 mmHg，未来 5 年发生高血压的风险增加约 11%；舒张压每升高 5 mmHg，风险增加可达 30%。这提示运动中血压反应可作为预测高血压发生的早期信号。因此，识别运动高血压对于高血压防控具有重要意义。本研究旨在通过标准化心肺运动试验 (Cardiopulmonary Exercise Testing, CPET) 评估中老年体检人群运动高血压（运动收缩压≥ 180 mmHg）的发生率及其影响因素，为心血管危险分层和个体化运动干预提供初步证据。

方法：采用横断面研究设计，纳入 2023 年 11 月至 2024 年 11 月于北京协和医院接受 CPET 的 147 例体检人员（男性 87%，年龄 61.7±7.4 岁），按年龄分为 51-65 岁组和 66-86 岁组。运动高血压定义为运动峰值收缩压大于 200 mmHg。所有受试者完成基于 Ramp 方案的症状限制性踏车运动试验。评估指标包括：1) 运动血压心率反应：运动峰值血压、1 分钟心率恢复 (HRR1)；2) 心肺功能参数: 峰值摄氧量 (VO_2peak)、无氧阈 (AT)、氧脉搏、VE/VCO_2斜率等; 3) 静态肺功能指标: 用力肺活量占预计值 (FVC%)、一秒率 (FEV_1/FVC); 4) 体适能指标: 握力、单腿站立时间、柔韧性。采用多因素 Logistic 回归模型（调整性别、身体质量指数等混杂因素）分析运动高血压的独立预测因素，并进行年龄分层比较。

结果：运动高血压发生率为 43.6%，其中 17.7% 受试者运动峰值收缩压≥ 200 mmHg。31.5% 受试者存在心率恢复延迟（HRR1<12 次 / 分），提示部分受试者的心脏自主神经功能失调。受试者平均 VO_2 peak 为 18.8±4.9 ml/min/kg，71.9% 受试者 VO_2 peak 低于 85% 预测值，80.8% 受试者 AT<14 ml/min/kg，提示多数个体心肺储备不足。多因素分析显示，静息收缩压升高 (OR=1.073, 95%CI 1.032-1.116, P<0.001)、FVC%<80%（OR=3.68，P<0.05）和单腿站立时间<30s (OR=2.10, 95%CI 1.05-4.21, P<0.05) 是运动高血压的独立预测因素，而年龄增长呈保护效应（OR=0.894, 95%CI 0.818-0.977, P<0.05），提示中老年人群中年龄较小个体在运动中心血管反应可能更为敏感，可能与交感神经激活反应性相关，需进一步研究。年龄分层比较显示，66-86 岁组 VO_2 peak、AT 及平衡能力显著低于 51-65 岁组 (均 P<0.05)，但运动高血压发生率更低 (36.9% vs 50.8%，P<0.05)。

结论：中老年体检人群运动高血压发生率较高，其独立危险因素包括静息收缩压升高、肺活量下降和平衡能力减弱。建议对中老年人群开展 CPET 筛查，针对上述危险因素进行干预，包括血压管理、呼吸功能训练和平衡能力锻炼，以降低运动高血压风险，提高运动安全性。同时应关注自主神经调节异常合心肺功能储备不足等问题，制定个体化运动处方。

渐进性运动训练对重症体外膜肺氧合术后患者早期运动功能的影响

杨水涓 吴明祥 田青 刘波 吕璐 霍淑兰 卢寒梅 张艳 刘秋雯 张萌萌

武汉亚心总医院

目的：渐进性运动康复训练对重症体外膜肺氧合患者早期运动功能的影响。

方法

采用前瞻性随机对照研究方法。选取我院 2021 年 1 月 --2024 年 2 月收治的符合入选标准的重症 ECMO 患者 48 例，采用随机数字表法将患者分为渐进运动康复组和对照组，每组 24 例，对照组中男 18 例，女 6 例；渐进运动康复组中男 20 例，女 4 例；对照组仅给予常规康复训练，包括各关节被动活动及主动运动，渐进运动康复组在常规康复训练基础上予以渐进性运动康复训练，包括由卧到坐、由坐到站、由站到走渐进练习及下肢智能踏车渐进练习、上下肢肌力渐进练习，2 组患者均治疗 8 周。于治疗前后分别评定下肢股四头肌肌力 ,6min 步行距离测试以及改良 Barthel 指数评估患者日常生活活动能力，对数据行独立样本 t 检验、配对样本 t 检验、Mann-WhitneyU 检验、Wilcoxon 符号秩检验或 x2 检验。

结果

治疗前 ,2 组患者下肢股四头肌力未见明显差异 (P>0.05);6min 步行距离测试未见明显差异 (P>0.05); 改良 Barthel 指数评估评分相近 (P>0.05)。治疗 8 周后，渐进运动康复组下肢股四头肌肌力明显高于对照组 (P<0.01); 渐进运动康复组 6min 步行距离测试明显高于对照组 (P<0.01); 渐进运动康复组改良 Barthel 指数评估评分明显高于对照组 (P<0.01); 此外，2 组患者治疗 8 周后，下肢股四头肌力 ,6min 步行距离测试以及改良 Barthel 指数评估评分均显著高于治疗前 (3 组 P<0.01)

结论

在常规训练基础上，采用渐进性运动康复训练能提高重症体外膜肺氧合患者早期运动功能及日常生活能力，值得临床推广。

一例产褥期主动脉夹层术后早期康复治疗

杨水涓 吴明祥 田青 刘波 吕璐 卢寒梅 申莹 张萌萌 刘秋雯 陈涵

武汉亚心总医院

目的：一例产褥期主动脉夹层术后早期康复疗效观察

方法：

1 康复评估方法：

1.1 康复前对患者进行 ICU 相关康复安全和可行性评估：包括循环、呼吸、胃肠功能，凝血功能、胸腔引流液，人工管道、等风险评估。其他评估包括镇静程度评估（RASS) 与标准化五问题（S5Q）等镇静和配合程度评估等评估。

1.2 血气分析评估（评估患者乳酸，PH 值，氧分压，二氧化碳分压，氧合指数等血气情况）

1.3 呼吸与咳嗽功能评估（肺部感染情况，呼吸模式、呼吸频率、咳嗽强度等功能评估）

1.4 躯体与运动功能评估 (评估患者 ICU 活动量表 IMS，以及肌力评估量表 Lovett，平衡功能评估)

1.5 心肺耐力评估（2mint 踏步、RPE 用力程度分级）

2 康复治疗方法：

2.1 夹层术后 - 一周 :(物理因子治疗、运动功能、心肺功能)

2.2 夹层术后 1 周–2 周 : (物理因子治疗、运动功能、心肺功能、吞咽、ADL 训练)

2.3 夹层术后 3-6 周（物理因子治疗、运动功能、呼吸功能训练、心肺耐力训练、吞咽、ADL 训练）

结果：

1，康复治疗过程中患者生命体征、循环数据无明显差值

2，夹层术后 - 一周：患者机械通气呼吸机辅助呼吸到成功拔除气管插管，但患者心肺功能较差，高流量支持。乳酸 <1.0,PH 值 7.4，PO2148.2，PCO235.3, 氧合指 440, 双上肢双下肢肌力 3 级 ,INR1.3。患者谵妄状态。

3, 夹层术后 1 周–2 周: 患者呼吸稳定，肌力 4 级，平衡功能坐位 2 级，未站立训练，INR1.4。患者焦虑抑郁状态。

4，夹层术后 3 周–7 周：患者呼吸稳定，坐位平衡 2 级，站立位平衡 1 级，IMS 评分 5 分，双上肢双下肢肌力 4 级，INR1.53。

结论：

产褥期主动脉夹层病情危急，早期康复对患者恢复十分重要，早期康复经过重症康复治疗团队以及 ICU 医生及营养医师、药学医师、超声医师多方面合作，精细评估以及个性化康复方案制定，能帮助患者减少并发症，促进患者早日康复。

一例 ECMO 联合 CRRT 治疗暴发性心肌炎患者的早期康复

杨水涓 吴明祥 田青 刘波 吕璐 卢寒梅 陈静 申莹 江飞虎 霍淑兰

武汉亚心总医院

目的：**一例 ECMO 联合 CRRT 治疗暴发性心肌炎患者的早期康复**疗效观察

方法：

1 康复评估方法：

1.1 康复前进行 ICU 相关康复安全和可行性评估：包括循环、呼吸、神经系统、人工管道、等其他风险评估，包括 RASS 与 S5Q 等镇静和配合程度评估，以及心率、呼吸频率、血氧饱和度、血压、呼吸支持模式、ECMO 流量、CRRT 管道等评估。

1.2 血气分析评估（评估 lac，PH 值，po2，pco2，OI 等情况评估）

1.3 心脏功能评估（心脏 NT-proBNP 值）

1.4 呼吸与咳嗽功能评估（呼吸模式、呼吸频率、咳嗽强度等功能评估）

1.5 躯体与运动功能评估 (ICU 活动量表 IMS，肌力评估量表，关节活动度，平衡功能)

1.5 心肺耐力评估（RPE 用力程度分级）

2 康复治疗方法：

2.1 关节松动（采用麦特兰德关节松动术行髋、膝、踝、肩、肘、腕关节松动）

2.2 运动康复（四肢关节主被动运动）

2.3 体位适应性训练（床头抬高到床边坐位再到轮椅坐位）

2.4 呼吸训练（脱机训练，呼吸控制训练，气道廓清训练）

2.5 心肺耐力训练（床旁带高流量坐位训练，平衡能力训练）

结果：

1，康复治疗过程中患者 ECMO 流量以及 IABP 数据无明显差值

2，ECMO 辅助第 1 天，自主呼吸次数为 0，呼吸机模式为 V-SIMV，lac1.8,PH 值 7.4，PO2117.1，PCO233.9,OI 260，RASS 评分（-4 分）；暴发性心肌炎第 46 天，平静下自主呼吸次数为 23 次 / 分，乳酸 2.3，PH7.36,PO2170，PCO238.9,OI 485，RASS 评分（0 分），S5Q 评分（5 级）

3，暴发性心肌炎第 1 天 NT-proBNP>35000pg/ml, 血肌酐 268μmol/L，尿酸 912μmol/L，肾小球滤过率 28ml/min；治疗第 46 天 NT-proBNP29384pg/ml，血肌酐 247μmol/L，尿酸 378μmol/L，肾小球滤过率 15ml/min

4，暴发性心肌炎第 1 天 IMS 评估（0 级），治疗第 46 天 IMS 评估（5 分）

5，ECMO 辅助术第 1 天 Lovett 评分双上肢 0 级，双下肢 0 级；治疗第 46 天双上肢 ,Lovett 评分双上肢 3 级，右下肢 3 级，左下肢 2 级。

6，ECMO 术后第 1 天，四肢关节活动度正常；IABP 撤离后第 9 天，右上肢（肩前屈 130°，外展 100°；屈肘 110°；腕掌屈 60°，背伸 55°），左上肢（肩前屈 125°，外展 110°；屈肘 100°；腕掌屈 45°，背伸 40°）；右下肢（屈髋 70°，外展 45°；屈膝 130°；踝背伸 30°，跖屈 55°），左下肢（屈髋 20°，外展 15°；屈膝 20°；踝背伸 10°，跖屈 15°）；治疗第 46 天评估右上肢（肩前屈 100°，外展 90°；屈肘 90°；肘旋后 30°；腕掌屈 50°，背伸 50°度）；左上肢（肩前屈

125°，外展 110°；屈肘 100°；肘旋后 55°；腕掌屈 45°，背伸 40°）；右下肢（屈髋 80°，外展 50°，屈膝 135°；踝背伸 30°，跖屈 55°），左下肢（屈髋 40°，外展 30°；屈膝 50°；踝背伸 20°，跖屈 20°）

7，自主呼吸频率（第一天自主呼吸频率 0 次 / 分，第 46 天自主呼吸频率 18 次 / 分）

8，Fugl_-Meyer（暴发性心肌炎第 46 天 Fugl_-Meyer2 分）

结论：

患者在整个危重症救治过程中由于镇静或意识障碍导致完全制动，极容易发生神经萎弱、肢体及身体器官功能损害。本案例结论是早期康复具有较高的安全性和可行性，即使患者在接受机械通气、体外膜肺氧合治疗、主动脉球囊反搏治疗、血液净化等治疗。早期康复可以帮助患者恢复肌力，增强心肺耐力，减轻获得性衰弱的发生，同时可以缓解患者焦虑。

有氧运动通过增加 BDNF 释放抑制心脏常驻巨噬细胞凋亡改善心肌梗死后心功能

刘书宏 李运棋 郑祥慧 刘雨轩 王佩瑶 郭周 郑立志 王慧宇 李慈恩 王百韬 郑阳 孙勇 于波 吴健

哈尔滨医科大学附属第二医院

目的： 冠心病患者参与以有氧运动为基础的心脏康复降低心血管死亡率和住院率。研究表明脑源性神经营养因子 (BDNF) 作为运动源性因子促进常驻巨噬细胞的存活，从而改善心肌梗死后心功能，并且心脏常驻巨噬细胞在心肌梗死后的修复过程中发挥着至关重要的作用。然而有氧运动是否通过心脏常驻巨噬细胞促进心肌梗死后损伤修复仍不明确，其中机制尚未阐明。

方法： 结扎野生型小鼠冠状动脉左前降支构建心肌梗死模型，并利用小动物平板跑步机予以小鼠 12m/min 速度进行有氧运动，腹腔注射 ANA-12 拮抗小鼠 BDNF 受体。超声心动图检测运动后心肌梗死小鼠心脏功能；提取小鼠外周血及脑组织，ELISA 检测血浆及脑组织中的 BDNF 水平；HE 染色检测心肌组织形态；Masson、天狼星染色检测小鼠心肌纤维化程度；WGA 检测心肌细胞大小以及排列情况；Western Blot 检测 BDNF 信号通路激活情况；流式细胞术检测小鼠心脏常驻巨噬细胞数目；Tunel 染色检测心肌常驻巨噬细胞凋亡程度。

结果： 超声心动图显示运动后心梗小鼠的心功能明显改善，且 HE 染色表明运动后小鼠梗死面积更小。Masson 与天狼星染色证实运动组心肌纤维化程度明显降低。WGA 染色进一步验证了运动后小鼠心肌细胞较非运动组缩小。ELISA 结果表明运动后小鼠的血浆及脑组织中的 BDNF 水平显著提高，Western blot 结果显示运动后小鼠的 BDNF 信号通路 TrkB、AKT、PI3K/ATK 显著激活，而予以 ANA-12 抵消了运动改善心肌梗死后心脏修复的作用，证实了有氧运动通过增加 BDNF 释放改善心肌梗死后心功能。流式细胞术检测发现 CCR2-MHCII^{lo} 心脏驻留巨噬细胞数量在有氧运动后未给予 ANA-12 组显著增加，Tunel 染色显示心肌常驻巨噬细胞凋亡显著减少，证实有氧运动促进 BDNF 能抑制心脏驻留巨噬细胞凋亡从而发挥保护作用。

结论： 有氧运动通过促进 BDNF 激活常驻巨噬细胞 TrkB、AKT、PI3K/ATK 信号通路，减少细胞凋亡，从而改善心肌梗死后心功能。

恐惧回避模型在心血管疾病中的应用进展

陈丽方 郭良敏 白莎 徐艳玲 彭海燕 孙心悦 王乐欣

成都市第三人民医院

恐惧回避模型（Fear-Avoidance Model, FAM）最初由 Lethem 等人（1983）提出，Vlaeyen 和 Linton（2000）将其系统化，用于解释慢性疼痛患者因对疼痛的恐惧而引发回避行为，最终导致功能障碍的恶性循环。近年来，该模型被引入心脏疾病领域，用于解析患者因心脏事件（如心肌梗死、心绞痛）引发的心理行为反应及其对康复结局的影响。研究表明，部分患者因对躯体症状（如胸痛、心悸）的过度恐惧，倾向于采取回避性行为（如减少体力活动、避免社交），进而加剧功能退化、生活质量下降及不良预后风险。 在心脏疾病中，恐惧回避的核心机制涉及三个维度：（1）患者对心脏症状恐惧；（2）回避行为导致体力活动不足，进一步削弱心肺功能并加重焦虑抑郁情绪；（3）社会功能退缩与治疗依从性降低，形成“恐惧 - 回避 - 失能”的负性循环。研究指出，约 20%-30% 的心脏康复患者存在显著恐惧回避倾向，其再住院率和心血管事件复发风险较普通患者升高 1.5-2 倍。 针对这一现象，临床干预策略逐渐从单纯生物医学模式转向整合心理行为干预。基于 FAM 的认知行为疗法（CBT）通过修正患者的灾难化认知、分级暴露训练及行为激活，有效降低恐惧水平并提升康复参与度。例如，基于虚拟现实（VR）的情境暴露疗法可帮助患者逐步适应运动诱发的生理反应，打破“症状恐惧 - 活动回避”的恶性循环。此外，正念干预与接纳承诺疗法（ACT）通过增强患者对不适感的心理接纳能力，亦显示出改善心脏预后的潜力。然而，当前研究仍存在局限性: 首先，FAM 在心脏疾病中的适用性需更多纵向研究验证，尤其是文化差异对恐惧回避行为的影响；其次，标准化评估工具（如心脏恐惧问卷）的敏感性与特异性仍需优化；最后，跨学科协作机制尚未完善，心理干预与心脏康复的整合模式需进一步探索。未来方向包括开发智能化监测工具（如可穿戴设备实时评估恐惧回避行为）、构建个性化干预路径及探索神经生物学标记物（如自主神经功能）在恐惧回避环路中的作用。

基于此，恐惧回避模型为理解心脏疾病患者心理行为反应提供了新视角，其临床应用有助于突破传统康复瓶颈，推动“身心共治”模式的实践转化，最终改善心血管疾病患者长期预后与生活质量。

1 例 ECMO 支持下冠脉旋磨术及支架植入术后 构建个性化重症心脏康复模式的效果评价

廖翊言

重庆市医疗急救中心

目的： 随着康复理论和技术的不断完善，目前心脏康复已经延伸至心脏危重症的早期治疗当中。随着医疗技术的进步，ECMO 技术支持下用于治疗重症心血管疾病的患者相关报道越来越多。通过构建重症心血管患者Ⅰ、Ⅱ、Ⅲ期心脏康复模式的运用实践，不仅有利于重症心血管疾病患者术后心理状态、运动能力及术后并发症发生率，缩短住院时间，减少患者经济负担。

方法：术前预康复：评估患者临床一般情况、危险因素、心肺功能 (6 分钟步行试验或 CPET 评估)、心理评估量表（PHQ-9、GAD-7）、日常生活能力量表 ADL、睡眠质量量表 PSQI、尼古丁依赖量表 (FTND)、营养（NRS-2002) 等，重点以呼吸训练（腹式呼吸、缩唇呼吸) 为主。通过术前预康复训练增加患者机体功能储备，减少术后并发症，加速康复进程。

院内Ⅰ期心脏康复：（1）全面评估：生理状况评估，生命体征持续监测。心血管评估：心电图、超声心动图等，评估心脏功能恢复情况，患者的呼吸功能、运动能力、量表评估、依据评估结果制定个体化Ⅰ期心脏康复方案。（2）康复宣教。采用宣传手册、视频资料等多种形式向患者及家属强调Ⅰ期心脏康复重要性、优势以及具体内容等，取得理解与配合。（3）康复措施：①术后入 CCU 病房第 1-2 d。基于心电监测，指导患者进行腹式呼吸，每次 5-10 min，每日 3-5 次。协助患者在床上开展四肢主被动活动、踝泵运动、双上肢弹力球抓握等，每次 10- 15 min，每日 3-5 次。②术后第 3d 转入普通病房，指导患者进行坐起（5 min）、躺下（5 min）交替训重复进行 3-5 次，每日 2-3 次。③术后第 4d，指导患者进行床旁站立，每次 5 min；指导患者进行床旁原地踏步，每次 20-30 下；指导患者在病房内独立行走，每次行走 100 m 左右；以上锻炼均为每日 2-3 次。④术后第 5-6 d，从病房内行走过渡至病房外走廊行走，每次 100-200 m，每日 2-3 次，功率车 20w 训练 5-10min。⑤术后第 7 d 至出院，进行上下楼梯锻炼，功率车 30w 训练 5-10min，逐步增加时间和强度。⑥康复锻炼期间，密切监测患者的生命体征，如患者出现心悸胸闷、呼吸困难等及时停止训练。

Ⅱ期心脏康复：再次对患者一般情况、体适能、心理、营养、戒烟、药物等进行全面评估来制定个性化处方。在心脏康复中心团队指导下行Ⅱ期运动康复：包括功率车训练、平衡功能训练、柔韧抗阻训练、体外反搏、心脏康复操等，结合康复宣教，保持健康的生活方式。

III期心脏康复：居家康复，以互联网 + 为依托平台，给予患者全方位的心脏康复指导，包括：持续健康生活方式、严格的药物依从性、定期医学随访、自我监测与管理，指导患者积极面对疾病，保持乐观心态，维持良好的社会关系和家庭支持。

结果：在构建个性化Ⅰ、Ⅱ、III期重症心脏康复模式下，患者术前 6 分钟步行试验距离 280 米，出院前评估为 320 米。borg 评分从 14 分降到 11 分。经过 13 天的康复治疗，症状与功能明显改善，患者康复出院转至Ⅱ期康复。

结论：本案例的成功救治经验表明，在重症心血管疾病患者中进行预康复、术后早期康复干预、构建个性化重症心脏康复模式是安全有效切实可行的。

冠心病患者心脏康复意向干预的最佳证据总结

宋岩岩 王彦 刘爽 吴林 彭沥枢

河北大学护理学院

目的　心脏康复意向是患者是否进行心脏康复的直接预测因素，但大部分患者的心脏康复意向水平较低，严重影响心脏康复的参与率及依从性。而目前关于冠心病患者心脏康复意向干预的临床实践尚未形成统一标准，且多数研究集中于影响因素分析，缺乏具体、有效的指导内容。因此，本研究总结冠心病患者心脏康复意向干预的最佳证据，以期为医护人员制定基于循证的冠心病患者心脏康复意向干预提供参考。

方法　根据“5S”证据模型，系统检索临床决策支持系统、指南网站、专业协会网站及 Cochrane Library、PubMed、Embase、CINAHL、Web of Science、、PsycINFO、维普数据库、中国知网、中国生物医学文献数据库、万方数据库中关于冠心病患者心脏康复意向干预的所有证据，包括临床决策、指南、证据总结、专家共识、系统评价以及随机对照试验，检索时限为建库至 2025 年 6 月 20 日; 由 2 名接受过循证护理学培训的研究者独立完成文献筛选和质量评价，并根据主题对证据进行提取与综合。

结果　共纳入 24 篇文献，包括 1 篇临床决策、6 篇指南、4 篇证据总结、2 篇专家共识、4 篇系统评价、7 篇随机对照试验。提取归纳冠心病患者心脏康复意向干预相关证据共 43 条，汇总为 8 个主题，分别为团队组建与人员培训、筛查与评估、信息支持、提升自我效能及动机、家庭社会支持、个体化康复计划、多学科策略、随访管理。

结论　该研究汇总的冠心病患者心脏康复意向干预的最佳证据具有全面性和科学性，为医护人员系统、规范地干预冠心病患者心脏康复意向提供循证依据，但证据的转化及临床应用需多角度评估，制订适合的心脏康复意向干预方案，以提高患者心脏康复意向水平。

一例 ECMO 联合左心辅助装置治疗巨细胞性心肌炎患者的早期康复

杨水涓 吴明祥 田青 刘波 吕璐 卢寒梅 申莹 陈静 霍淑兰

武汉亚心总医院

目的：一例 ECMO 联合左心辅助装置治疗巨细胞性心肌炎患者的早期康复疗效观察

方法：

1 康复评估方法：

1.1 康复前对患者进行 ICU 相关康复安全和可行性评估：包括循环、呼吸、神经系统、人工管道、等其他风险评估，包括 RASS 与 S5Q 等镇静和配合程度评估，以及心率、呼吸频率、血氧饱和度、血压、呼吸支持模式、ECMO 流量、人工心脏辅助装置流量等生命体征评估。

1.2 血气分析评估 (评估患者 lac，PH 值，po2，pco2，OI 等血气情况)

1.3 心脏功能评估 (心脏 NT-proBNP 值)

1.4 躯体与运动功能评估 (ICU 活动量表 IMS，肌力评估量表 Lovett，关节活动度)

1.5 心肺耐力评估 (2 分钟踏步实验，6 分钟步行实验，RPE 用力程度分级)

2 康复治疗方法 :

2.1 关节松动 (采用麦特兰德关节松动术 1-2 级手法进行肩关节、肘关节、腕关节松动)

2.2 运动康复 (四肢关节主被动运动，床上踏车训练，花生球训练)

2.3 离床训练 (由卧位到床旁坐位，床到轮椅转移训练)

2.4 呼吸训练 (呼吸训练器训练，呼吸控制训练，气道廓清训练)

2.5 心肺耐力训练 (床旁带高流量站立位训练，2min 原地踏步训练，辅助下步行训练)

结果 :

1. 康复治疗过程中 ECMO 流量以及左心辅助装置流量无明显差值。

2. 左心辅助术后第 1 天，自主呼吸次数为 0，呼吸机模式为 V-SIMV，lac1.5,PH 值 7.5，PO2184，PCO224.4,OI 230；左心辅助术后第 41 天，平静下自主呼吸次数为 16 次 / 分，lac1.0，PH7.32,PO280，PCO235.5，OI 242；左心辅助术后第 1 天 RASS 评分（-4 分），康复治疗第 41 天时 RASS 评分（0 分）；左心辅助术后第 1 天 S5Q 评分（0 级），治疗第 41 天 S5Q 评分（5 级）。

3，左心辅助术后第 1 天 NT-proBNP3467pg/ml，治疗第 41 天 NT-proBNP2667pg/ml

4, 左心辅助术后第 1 天体位水平改变 IMS 评估 (0 级), 治疗第 41 天 IMS 评估 (10 分)

5. 左心辅助术后第 1 天肌力 Lovett 评分由双上肢肌力 0 级，双下肢肌力 0 级，治疗第 41 天评估双上肢肌力 Lovett 评分双上肢肌力 4 级，双下肢肌力 4 级。

6，左心辅助术后第 1 天，右上肢关节活动度（肩关节前屈 40°，外展 45°；肘关节屈肘 40°；肘关节旋后 -70°；腕关节掌屈 20，背伸 10 度）；左上肢关节活动度（肩关节前屈 50°，外展 55°；肘关节屈肘 45°；肘关节旋后 -60°；腕关节掌屈 20，背伸 10 度），治疗第 41 天评估右上肢关节活动度（肩关节前屈 135°，外展 100°；肘关节屈肘 100°；肘关节旋后 60°；腕关节掌屈 50°，背伸 50°度）；左上肢关节活动度（肩关节前屈 125°，外展 110°；肘关节屈肘 100°；肘关节旋后 55°；腕关节掌屈 45°，背伸 40°）

7. 左心辅助术后第 16 天呼吸训练器吹气量 100ml, 吸气量 250ml; 治疗第 41 天呼吸训练器吹气量 200ml, 吸气量 1750ml

8，左心辅助术后第 30 天评估 2min 踏步出院时 30 次，6min 步行实验 100 米；治疗第 41 天评估 2min 踏步出院时 50 次，6min 步行实验 220 米

结论：

重症患者在整个危重症救治过程中由于镇静或意识障碍导致完全制动，因此极容易发生神经萎弱和身体器官功能损害。本案例的结论是早期康复具有较高的安全性和可行性，即使患者在接受机械通气、体外膜肺氧合治疗、主动脉球囊反搏治疗等治疗。早期康复可以帮助患者恢复肌力，增强心肺耐力，减轻获得性衰弱的发生，同时可以减轻患者焦虑，帮助患者顺利撤除 ECMO、脱离呼吸、成功拔除气管插管等，帮助患者早日回归家庭回归社会。

心脏康复的临床效益与研究进展

张婧

贵州医科大学附属医院

目的

本综述旨在综合评估心脏康复（CR）在心血管疾病（CVD）二级预防中的核心作用，分析其多维度干预模式的临床效益，并探讨当前实施障碍与未来研究方向，为优化 CR 临床实践提供证据支持。

方法

通过系统检索 PubMed、Cochrane Library 及 Web of Science 数据库 2010–2023 年发表的随机对照试验（RCT）、Meta 分析及国际指南（如 AHA/ACC、ESC）。纳入标准：

研究对象为冠心病（心肌梗死、PCI/CABG 术后）、慢性心衰（HFrEF/HFpEF）等 CR 适应症患者；

干预措施为结构化 CR 项目（含运动训练、风险管控等≥ 3 项核心模块）；

评估终点包括死亡率、再住院率、功能指标（如峰值摄氧量 VO_2 peak）及生活质量（QoL）。采用 Cochrane 偏倚风险评估工具对文献质量进行筛选。

结果

临床结局显著改善：

死亡率降低：Meta 分析（含 67 项 RCT, n=21,000）显示，参与 CR 者全因死亡率降低 26%（RR 0.74, 95%CI 0.64–0.86），心血管死亡率降低 31%（RR 0.69, 95%CI 0.51–0.94）。

再住院风险下降：CR 组 12 个月内再住院率较对照组减少 18%（RR 0.82, 95%CI 0.76–0.88），尤以心衰患者获益显著（RR 0.73）。

功能与 QoL 提升：CR 后患者 VO_2 peak 平均提高 15–30%（Δ3.5–7.0 mL/kg/min），心绞痛发作频率减少 40%；SF-36 量表评分在躯体功能（+12 分）及心理健康（+9 分）维度显著改善。

核心干预机制的证据：

运动训练：高强度间歇训练（HIIT）较中等强度持续训练（MICT）更高效提升 VO_2 peak（Δ10% vs Δ7%, p<0.01），且安全性相当。

综合风险管理：戒烟干预使持续戒烟率达 35%（OR 2.5, 95%CI 1.8–3.4）；个体化营养指导使 LDL-C 额外降低 8–12%。

心理干预必要性: 合并抑郁患者接受 CBT 后，心血管事件风险降低 32%（HR 0.68, 95%CI 0.52–0.89）。

实施模式创新：

家庭远程 CR（Tele-CR）：基于 TELEREH-HF 等 RCT，远程监护组在 VO_2 peak 改善（Δ1.8 mL/kg/min）和 QoL 评分方面与中心 CR 无统计学差异（p>0.05），但参与率提高 25%。

数字化工具应用：移动 App 支持的患者自我监测使运动依从性提升至 83%（vs 常规组 68%, p=0.003）。

现存挑战：

参与率低下: 全球平均参与率仅 30–50%，女性（OR 0.62）、高龄（>75 岁，OR 0.58）及低收入人群（OR 0.41）尤甚。

长期维持困难：仅 40–60% 患者在 CR 结束后 12 个月仍坚持运动目标。

结论

心脏康复是心血管疾病管理的循证基石，通过整合运动训练、风险控制、心理支持及患者教育，可显著降低死亡与再住院风险，改善功能状态及生活质量。家庭远程 CR 与数字化工具的应用有望突破传统模式的可及性瓶颈。未来需重点解决参与率差异、长期行为维持难题，并通过精准医学策略（如基于生物标志物的个体化处方）进一步优化 CR 效益。

一例产褥期 A 型主动脉夹层术后早期康复治疗

杨水涓 吴明祥 田青 刘波 吕璐 卢寒梅 陈涵 李雪莹 陈静 霍淑兰

武汉亚心总医院

目的：一例产褥期 A 型主动脉夹层术后早期康复疗效观察

方法：

1 康复评估方法：

1.1 康复前对患者进行 ICU 相关康复安全和可行性评估：包括循环、呼吸、胃肠功能，凝血功能、胸腔引流液，人工管道、等风险评估。其他评估包括镇静程度评估 (RASS) 与标准化问题 (S5Q) 等镇静和配合程度评估等评估。

1.2 血气分析评估 (评估患者乳酸，PH 值，氧分压，二氧化碳分压，氧合指数等血气情况)

1.3 呼吸与咳嗽功能评估 (肺部感染情况，呼吸模式、呼吸频率、咳嗽强度等功能评估)

1.4 躯体与运动功能评估 (评估患者 ICU 活动量表 IMS，以及肌力评估量表 Lovett，平衡功能评估)

1.5 心肺耐力评估 (2mint 踏步、RPE 用力程度分级)

2 康复治疗方法：

2.1 夹层术后 - 一周 :(物理因子治疗、运动功能、心肺功能)

2.2 夹层术后 1 周一 2 周 :(物理因子治疗、运动功能、心肺功能、吞咽、ADL 训练)

2.3 夹层术后 3-6 周 (物理因子治疗、运动功能、呼吸功能训练、心肺耐力训练、吞咽、ADL 训练)

结果：

1，康复治疗过程中患者生命体征、循环数据无明显差值

2，夹层术后 - 一周：患者机械通气呼吸机辅助呼吸到成功拔除气管插管，但患者心肺功能较差，高流量支持。乳酸 <1.0,PH 值 7.4，PO2148.2， PCO235.3，氧合指数 440, 双上肢双下肢肌力 3 级 ,INR1.3。患者谵妄状态。

3，夹层术后 1 周一 2 周：患者呼吸稳定，肌力 4 级，平衡功能坐位 2 级，未站立训练，INR1.4。患者焦虑抑郁状态。

4，夹层术后 3 周一 7 周：患者呼吸稳定，坐位平衡 2 级，站立位平衡 1 级，IMS 评分 5 分，双上肢双下肢肌力 4 级，INR1.53。

结论：

产褥期主动脉夹层病情危急，早期康复对患者恢复十分重要，早期康复经过重症康复治疗团队以及 ICU 医生及营养医师、药学医师、超声医师多方面合作，精细

评估以及个性化康复方案制定，能帮助患者减少并发症，促进患者早日康复。

一种气切患者使用的呼吸训练器设计方法与临床实践

杨水涓 吴明祥 刘波 田青 刘秋雯 张萌萌 申莹 霍淑兰 吕璐

武汉亚心总医院

目的：

气管切开患者，因疾病、制动或呼吸机相关性膈肌废用性萎缩等因素，许多患者易形成呼吸机依赖，从而无法彻底脱离呼吸机，为了保证气道通畅，痰液引流顺利，预防窒息及误吸，很多患者会经历气管切开。但是气管切开短时间内无法缝合，容易引起呼吸功能下降，引发肺部感染，早期进行呼吸训练非常重要。由于常规呼吸训练器是在人工气道拔除后才开始行呼吸训练，这会导致因训练较晚，患者容易出现较多呼吸有关并发症。鉴于常规呼吸训练器的不足，我们单位设计了一款可以不需在人工气道拔除后就可以进行呼吸训练的呼吸训练器。

方法：

本呼吸训练器通过改良，能够直接连接患者气管切开套管。而且在训练过程中，输氧管能够在气切患者进行呼吸训练时给予充足氧气支持。我们还在此款呼吸训练器上设置了细菌过滤器，细菌过滤器能够有效保护呼吸道清洁。我们还设计了阻力调节装置，根据患者呼吸情况调节吸气阻力。

结果：

该呼吸训练器能早期有效训练气切患者呼吸肌肌肉力量，改善肺功能且在训练时给予充足氧气支持，并未发生训练风险且未出现呼吸道感染情况。

结论：

本呼吸训练器，弥补气管切开不能使用普通呼吸训练器的空缺，让气管切开患者同普通患者（没有气管切开患者）一样，可以进行呼吸肌肌肉力量及其耐力的训练，且安全，从而能让患者尽早脱离呼吸机，减少住院花费，值得临床推广。

运动模拟药物通过 m6A 修饰调控巨噬细胞极化延缓动脉粥样硬化

郑立志 吴健 于波

哈尔滨医科大学附属第二医院

目的：冠状动脉粥样硬化性心脏病（CHD）是导致我国居民死亡的首要疾病之一。以有氧运动为基石的心脏康复能够显著降低心血管死亡率、 再住院和心肌梗死风险，被列为 CHD 治疗的 Ia 类推荐项目。但由于久坐、高龄等因素，近半数 CHD 患者缺乏规律运动，研发运动模拟药物亟待解决。

方法：选取 5-6 周 $ApoE^{-/-}$ 雄性小鼠，提取小鼠骨髓原代巨噬细胞，乳酸钠刺激后，WB 检测 MeCP2 K271la 与 METTL14 表达水平、 Co-IP 检测 MeCP2 与 METTL14 结合水平、免疫荧光检测 MeCP2 与 METTL14 共定位情况、Dot Blot 及 ELISA 检测 m^6A 修饰水平。围绕 MeCP2 K271la 位点选取并合成乳酰化修饰多肽；分析多肽保守性及分子特征；$ApoE^{-/-}$ 小鼠尾静脉注射上述浓度多肽，每周一次，共 8 周，记录小鼠生存曲线；分离多肽注射后小鼠外周血血浆，检测肌酐、肌酸激酶、ALT、AST 水平；病理学检测注射多肽后小鼠肝脏及肾脏形态；梯度浓度多肽刺激 BMDM 筛选出最佳多肽浓度。$ApoE^{-/-}$ 小鼠高脂喂养 8 周后，尾静脉注射上述浓度多肽，每周一次，8 周后，体内体外验证运动模拟多肽有效性及作用机制。

结果：运动模拟多肽降低 $ApoE^{-/-}$ 小鼠外周血炎症因子水平，减少动脉粥样硬化斑块面积。机制方面，乳酰化修饰后的 MECP2 与 METTL14 结合能力增强，下调巨噬细胞 RNA m^6A 修饰水平；运动模拟多肽通过与 METTL14 结合，下调 RNA m^6A 修饰水平，介导巨噬细胞向抗炎表型（M2）转化，从而发挥延缓动脉粥样硬化的作用。

结论：以 MeCP2 K271la 位点合成、设计的运动模拟多肽通过与 METTL14 结合下调巨噬细胞 m^6A 修饰水平调控巨噬细胞 M2 型极化从而发挥延缓动脉粥样硬化的作用，具有可观的应用前景，为临床防治冠状动脉粥样硬化性心脏病提供崭新思路。

叙事护理外部见证人视角下社区二期心肺康复养育共同体的协同路径研究

王慧

中心医院

研究目的：针对社区二期心肺康复患者因疾病困扰、康复压力及社会角色转变陷入自我否定与情感孤立，进而影响康复进程的问题，本研究旨在通过将叙事护理外部见证人理念融入社区康复，构建“社区养育共同体”协同模式，以集体叙事与情感联结重塑患者康复信心，优化康复效果，为完善社区心肺康复服务体系提供新路径。研究方法：采用质性研究与行动研究相结合的方法：通过深度访谈、参与式观察收集患者康复叙事资料；引入外部见证人（患者、家属、医护人员及志愿者），组织叙事分享会，借助复述、反馈与共情帮助患者重构疾病意义；在此基础上构建“社区养育共同体”,通过定期叙事活动、家庭探访、互助小组等形式，建立持续情感联结与经验共享机制，整合医疗康复、心理支持、社会融入资源。研究结果：实践显示，该模式有效打破了患者个体叙事的局限性，形成了相互支持的集体叙事网络；显著提升了患者的康复依从性、自我效能感及社会适应能力，构建起兼具人文关怀与专业支持的康复生态系统，实现了从个体康复到群体互助的转变。研究结论：将叙事护理外部见证人理念与社区康复结合的“社区养育共同体”模式，突破了传统生物医学模式的局限，为社区二期心肺康复提供了兼具理论创新性与实践可行性的方案，对完善社区心肺康复服务体系具有重要参考价值。

重症监护室心脏瓣膜病患者 TAVR 术后早期心脏康复对运动能力及心功能的影响

林美卿 王少萍 吴爱梅

海南省人民医院

目的

本研究旨在探讨早期心脏康复对经导管主动脉瓣置换术（TAVR）术后患者运动能力及心功能的影响，为临床实践中优化 TAVR 术后康复方案、改善患者预后提供科学依据。通过系统评估早期综合康复干预在提升患者运动耐量、促进心功能恢复、缩短住院时间等方面的作用，明确其在重症监护室心脏瓣膜病患者术后康复中的应用价值。

方法

选取 2024 年 1 月至 12 月我院心血管内科收治的 100 例符合 TAVR 手术适应证的重症心脏瓣膜病患者作为研究对象，采用随机数字表法将患者分为对照组和实验组各 50 例，对照组给予常规心脏康复护理，包括术后床上被动关节活动、48 小时监护下坐起、72 小时床边站立、逐步过渡至病房内步行及常规健康教育与出院指导；实验组在常规护理基础上实施《早期综合心脏康复干预》，术前预康复（呼吸功能训练、下肢抗阻训练、营养支持）、ICU 康复期（呼吸训练、床上运动、体位管理）、普通病房康复期（渐进性步行训练、抗阻训练、有氧训练）及出院前过渡期（个性化居家康复方案、移动康复指导 APP 监测、多学科随访团队建立）四个阶段进行干预。分别于术前、术后 7 天、术后 1 个月采用 6 分钟步行试验（6MWD）评估运动能力，通过超声心动图检测左室射血分数（LVEF）、左心室质量指数（LVMi）等心功能指标，记录住院时间、再住院率及并发症发生率等临床结局指标，采用 SPSS25.0 软件进行统计学分析。

结果

两组患者在年龄、性别构成、基础疾病、术前心功能等基线资料方面差异均无统计学意义（P>0.05），具有可比性。运动能力方面，术后 7 天实验组 6MWD 显著高于对照组（278.6±35.2mvs.215.4±31.7m，P<0.01），且这一优势持续至术后 1 个月（378.4±42.6mvs.298.3±38.7m，P<0.01）；实验组首次下床时间较对照组提前 18.7 小时（18.2±3.6 小时 vs.36.9±5.1 小时，P<0.01），从卧床到接受 6 分钟步行测试的时间缩短 3.2 天（P<0.01）。心功能指标方面，术后 1 个月实验组 LVEF 显著高于对照组（58.7±5.2%vs.52.4±4.8%，P<0.001），LVMi 显著低于对照组（112.4±10.7g/m^2vs.126.8±12.3g/m^2，P<0.001），52% 患者 LVMi 减少 >10%，整体纵向应变（GLS）改善更明显（18.3±2.1%vs.16.2±1.8%，P<0.001），而舒张功能（E/e’比值）两组均未显著改善（15.8±3.2vs.16.1±3.4，P>0.05）。临床结局方面，实验组术后住院天数（9.8±1.6 天 vs.13.0±2.1 天）及总住院天数（14.2±2.3 天 vs.17.4±3.1 天）显著缩短（P<0.001），30 天内再住院率显著降低（6.0%vs.18.0%，P=0.027），两组均未发生康复相关严重不良事件，轻度并发症发生率无显著差异（12.0%vs.16.0%，P>0.05）。

结论

TAVR 术后实施早期心脏康复能有效改善患者运动能力，显著提高 6 分钟步行距离，提前首次下床时间；促进心功能恢复，提升左室射血分数，降低左心室质量指数，改善整体纵向应变；同时缩短住院时间，降低 30 天内再住院率，且安全性良好，未增加严重并发症风险。早期心脏康复通过多阶段、多维度的综合干预，在提升患者运动能力、促进心脏逆重构及改善临床结局方面效果显著，建议将其纳入 TAVR 围术期标准护理路径，未来需进一步探索个体化干预方案及长期效果，以更好地服务于重症监护室心脏瓣膜病患者的术后康复。

心包剥脱术患者的心肺运动试验结果特征

佟明汇 赵雅娴 奚卉（委员）

北京大学国际医院（北京大学第八临床医学院）

目的：

心包剥脱术与生存率低和发病率高有关。然而，在这组高危手术患者中，关于心肺运动功能评估的信息非常有限。本研究目的是报告缩窄性心包炎患者的心肺运动试验（CPET）的特征，从而协助优化该类患者的手术策略。

方法：

回顾性分析自 2023 年 1 月至 2024 年 7 月在我院因慢性缩窄性心包炎行心包剥脱术患者的临床资料，共连续入组 51 例患者，分别对围手术期临床资料和 CPET 特征进行统计分析。

结果：

所有的手术患者（平均年龄 49.6±14.4 岁；64.7% 为男性）均通过正中胸骨切开术接受了规范心包剥脱术。该类最常见的病因是结核病（n=32，62.7%），47 名患者（92.2%）和 26 名患者（51.0%）分别被确诊为纽约心脏协会功能 III/IV 级和小气道功能障碍（SAD）。在 CPET 中，最大摄氧量（VO2 max%）、无氧阈值摄氧量（AT%）和二氧化碳通气当量（VE/VCO2）分别为 51.9±12.9%、33.1±7.8% 和 30.7±3.1。当中，9 名（17.6%）患者接受了再次心包剥脱术，其 CPET 特征 VO2 max%、AT% 和 VE/VCO2 分别为 52.9±13.7%、34.2±8.7% 和 30.8±3.3；42 名（82.4%）首次心包剥脱术患者的 CPET 特征：VO2 max%、AT% 和 VE/VCO2 分别为 49.0±9.4%、30.0±1.7% 和 30.4±2.3%。24 名（47.0%）患者接受了联合瓣膜手术，其 CPET 特征 VO2 max%、AT% 和 VE/VCO2 分别为 55.7±12.7%、35.3±4.5% 和 29.7±2.3；27 名（53.0%）单纯心包剥脱术患者的 CPET 特征 VO2 max%、AT% 和 VE/VCO2 分别为 50.7±12.7%、32.3±8.5% 和 31.0±3.3%。本组患者未出现术后 30 天内死亡，平均重症监护室（ICU）逗留时间为 2.6±1.2 天；总体术后不良事件发生率为 13.7%（MACCE，7/51），当中低心排综合征是患者主要合并症（4/51）。多变量分析显示，VE/VCO2<40.0% 心包炎患者术后 MACCE 及 ICU 住院时间延长（>3 天）的独立风险因素（OR，2,45 (1.33-4.47)，P<0.01）。

结论：

心包剥脱术是治疗缩窄性心包炎的安全方法。心包炎患者 CPET 特征可能具有评估患者手术风险作用，未来仍需更多数据支持应用 CPET 评估复杂心脏手术患者的系统方法。

PNF 有序呼吸肌拉伸训练技术在慢性心力衰竭患者康复运动实践与应用

聂陈

武汉市中心医院

【摘要】 **目的** 采用 PNF 本体感觉神经肌肉联合有序呼吸肌拉伸训练技术在慢性心力衰竭患者呼吸肌训练方法，结合特定手法引导及阻力施加和特定呼吸模式训练下能系统性改善呼吸肌群柔韧性、协调性及神经肌肉控制能力，以改善慢性心力衰竭患者呼吸困难。**方法** 选择 104 例心功能 II 到 III 级慢性心力衰竭患者，随机分为试验组和对照组，对照组为常规呼吸功能训项目，实验组在此基础上加做 PNF 有序呼吸肌拉伸训练，主要训练的呼吸肌群有包括胸大肌、胸小肌、胸锁乳头肌、斜方肌、肋间内肌、前锯肌和腹直肌、膈肌等，在拉伸前先由治疗师评估患者肌肉可以拉伸至患者可承受的最大长度。双方进行 3 秒抗阻等长收缩后放松，患者无不适时，在进行 15 秒的肌肉拉伸训练，每天训练 2 次，每次 10-15 分钟，每周 5 次，连续 5 周，2 组患者于 5 周后运用无创心排评估患者心功能状态、6 分钟步行实验、Borg 呼吸困难疲劳程度表、生活质量测定表、患者健康问卷（PHQ-9）等对比 **结果** 运用 PNF 有序呼吸肌拉伸训练技术心力衰竭患者 6 分钟步行实验距离、生活自理能力得分均高于对照组，差异有统计学意义（P < 0.05）结论 采用 PNF 有序呼吸肌拉伸训练技术可改善心力衰竭患者呼吸肌耐力下降、呼吸肌协调性改善心衰患者呼吸困难。

康复护理对冠心病患者行经皮冠状动脉介入术术后恢复的影响

刘长芳 邓流菊

重庆荣昌区人民医院

冠心病是目前临床中比较常看到的一种新冠疾病，近些年发病率也出现了急剧上升的态势，这类疾病会给病患新功能造成相对的伤害，假如没有及时的采取有效的治疗，这类病情有可能会持续的加重奉化下去，乃至于可能会出现心肌梗死，给病患的生命健康带来了很大的威胁 [1]-[2]。临床中主要采用药物与经皮冠状动脉介入术（PCI）等方法进行治疗，其中以 PCI 为目前临床运用相对多并且疗效较好的治疗方法，可是术后如果没有对病情采取有效的护理，那么病患可能会出现缺血和出血等负面反应，给手术效果以及术后康复带来了很大的影响，所以给予 PCI 术后病患科学合理的护理干预相当关键。

目的 探究康复护理对冠心病病患行经皮冠状动脉介入术术后恢复的影响。

方法 针对院内 2019 年 1 月 -2020 年 1 月治疗的冠心病病患 70 例，随机划分为参照组与研究组，每组各 35 例，参照组开展常规护理，研究组落实康复护理，比对两组病患临床效果。

结果 研究组 LVEDD 与 EF 指标均明显强于参照组，同时焦躁、抑郁评分均优于参照组，差异具备统计学意义（P < 0.05）。

结论 康复护理在经皮冠状动脉介入术后的冠心病病患康复中有着不小的作用，可以改善病患血管动力学指标，提高预后效果。

六分钟步行试验指导的有氧运动康复对慢性心力衰竭行心肌收缩力调节器术后患者心功能及运动耐量的影响

刘艳 李睿 井治聪

西安交通大学第一附属医院

目的： 探讨 6 min 步行试验 (6 minute walking test,6MWT) 指导的有氧运动康复，对慢性心力衰竭行心肌收缩力调节器（Cardiac contractility modulation,CCM）术后患者心功能及运动耐量的影响。

方法： 选择 2024 年 3 月至 2025 年 6 月西安交通大学第一附属医院心内科成功接受 CCM 的出院慢性心力衰竭患者 9 例，在常规药物治疗基础上，结合患者病情及 6MWT 评估结果，指导患者进行有氧运动康复，于 CCM 术后出院前及有氧运动康复干预 12 周后评价 6 min 步行距离（6MWD）、代谢当量（METS）、左心室射血分数 (LVEF)、B 型钠尿肽前体（Pro-BNP）、左心室舒张末期内径 (LVEDD)、左心室收缩末期内径（LVESD）的差异。

结果： 有氧运动康复干预 12 周后，6 min 步行距离（6MWD）从干预前（339.89±46.46）m 提高至（386.89±36.88）m（P<0.05）；代谢当量（METS）从（2.59±0.25）提升至 (2.83±0.17)(P<0.05); 左心室射血分数 (LVEF) 从（34.11±5.25）% 增加至（39.11±7.82）%(P<0.05); B 型钠尿肽前体（Pro-BNP）从（2152.00±1824.47）pg/ml 降至（1522.33±1453.16）pg/ml(P<0.05); 左心室舒张末期内径 (LVEDD) 从（67.44±9.38）mm 缩小至（65.44±9.59）mm(P<0.05); 左心室收缩末期内径（LVESD）从 (56.00±9.38)mm 减少至（53.33±9.71）mm(P<0.05)。与患者 CCM 植入后出院前相比，所有观察指标均有所改善。

结论： 对于慢性心力衰竭行心肌收缩力调节器（Cardiac contractility modulation,CCM）术后患者，应用 6 min 步行试验 (6 minute walking test,6MWT) 指导的有氧运动康复训练效果良好，能够有效改善患者心功能，提升患者运动耐量水平。

TAVR 术后患者心脏康复护理的现状及展望

盛丹 刘华芬

武汉大学人民医院

目的 系统梳理经导管主动脉瓣置换术（TAVR）术后患者心脏康复护理的现状，分析现存问题并提出未来发展方向，为规范临床康复实践、改善患者预后提供参考。

方法 检索 2013 年 1 月至 2023 年 12 月 PubMed、CNKI、万方等数据库中关于 TAVR 术后心脏康复护理的相关文献，纳入符合标准的中英文文献 86 篇，通过内容分析法归纳当前康复护理模式、干预内容、实施效果及存在的挑战，并结合临床实践数据进行总结。

结果 当前 TAVR 术后心脏康复护理以多学科团队（MDT）合作为核心模式，涉及心内科医师、康复治疗师、护士等专业人员，干预内容主要包括：术后早期活动（术后 24-48 小时床上被动运动实施率 89%，72 小时后渐进式下床活动执行率 76%）、饮食管理（低盐低脂饮食依从性 62%）、用药指导（抗凝药物规范服用率 69%）、心理干预（焦虑抑郁情绪筛查覆盖率 58%）及生活质量评估（SF-36 量表应用率 83%）。临床数据显示，规范康复护理可使患者 6 分钟步行距离平均增加（54.2±19.7）米，术后 3 个月再入院率降至 18.5%，较未参与康复者降低 9.2 个百分点。但现存问题显著：一是标准化流程缺失，仅 31% 的医疗机构建立 TAVR 专项康复路径，干预周期（2-16 周）和强度差异较大；二是延续性不足，出院后社区康复覆盖率仅 29%，6 个月随访时康复训练坚持率降至 34%；三是人群适配性低，≥75 岁患者中因体能衰弱中断康复者占 43%；四是评估工具局限，专用瓣膜功能康复评估工具使用率不足 12%。

结论 TAVR 术后心脏康复护理在改善患者运动耐力和降低再入院率方面已显示出积极效果，但标准化程度低、延续性差等问题制约其发展。未来需构建“医院 - 社区 - 家庭”三级康复网络，结合可穿戴设备实现远程监测与个性化方案推送，开发针对老年衰弱患者的低强度康复方案，并制定专用评估工具，以提升康复护理的规范性和有效性，进一步优化患者长期预后。

IMB 模型的预康复护理干预对急性期主动脉夹层患者的影响

汪晓燕

宁夏回族自治区人民医院

摘要：目的 探讨基于信息 - 动机 - 行为（IMB）模型的预康复护理干预对急性期主动脉夹层介入患者的临床效果。方法 采用类试验研究设计，选取宁夏某三级甲等医院 2023 年 3 月至 2024 年 6 月收治的 80 例急性期主动脉夹层介入患者为研究对象。其中，2023 年 3 月至 10 月收治的 40 例患者作为对照组，采用常规护理模式；2023 年 11 月至 2024 年 6 月收治的 40 例主动脉夹层介入患者作为试验组，在常规护理基础上联合基于 IMB 模型的预康复护理。干预 1 周后，比较两组患者的疼痛评分、血压、心率、并发症发生率、等待手术时间、住院时间及护理满意度。结果 干预后，试验组患者的疼痛评分显著降低，收缩压、舒张压及心率水平均优于对照组（P < 0.05）；试验组并发症发生率（如出血、静脉血栓、感染、压力性损伤、脏器灌注不足等）显著低于对照组，等待手术时间及住院时间均较对照组明显缩短（P < 0.05）；同时，试验组患者对护理工作的满意度评分显著高于对照组（P < 0.05）**结论** IMB 模型预康复护理能够明显改善急性期主动脉夹层患者疼痛、血压及心率、降低并发症发生率、缩短患者住院时间、等待手术时间、提升患者满意度、提升患者就医体验，为临床护理提供了科学有效的干预方案。

心血管术后恐动症患者管理的最佳证据总结

乐欣

成都市第三人民医院

目的：心脏介入手术后，心脏需要时间来适应新的生理状态，运动康复中的有氧运动能够有针对性地增强心肌收缩力，提高心脏的泵血功能。通过循序渐进的锻炼，可以使心脏逐渐恢复到更佳的工作状态，从而提升患者的耐力和体力。但研究表明，50-87% 的术后患者没有定期进行运动康复，而超过 70% 的患者存在恐动症。恐动症是指患者由于疼痛对身体活动的刺激或担心活动造成身体额外损伤，从而产生的对疼痛的敏感性增加，以及对日常活动或功能锻炼产生的非理性恐惧心理。对运动的恐惧是心血管患者术后参与基于运动的心脏康复的一大障碍。患者往往因为害怕运动而避免运动和锻炼，从而降低了康复锻炼的参与率和依从性，进而容易诱发心动过速、直立性低血压和血栓栓塞，也容易引起患者的焦虑、抑郁等负面情绪，导致患者的运动依从性和生活质量下降。目前国内缺乏基于证据的心血管疾病患者恐动症管理的相关研究，国内外对于此类患者的管理内容也存在一定差异，基于此本研究通过系统检索国内外文献整理相关证据，为临床实践提供参考。

方法：检索澳大利亚乔安娜布里格斯研究所循证卫生保健中心数据库、UpToDate、加拿大安大略注册护士协会网、美国国立指南数据库、澳大利亚和新西兰心脏协会、法国心血管协会、韩国心脏学会、美国心脏学会、欧洲心脏学会、欧洲胸外科协会、苏格兰校际指南网、新英格兰医学网、Cochrane Library、CINAHL、PubMed、中国知网、万方数据库等检索时限为建库至 2025 年 04 月 16 日。采用 JBI 循证卫生保健中心的文献评价标准和证据分级系统，进行文献质量评价及证据级别评定。

结果：最终纳入 17 篇文献，包括临床决策 1 篇、证据总结 1 篇、指南 8 篇专家共识 4 篇、随机对照试验 1 篇，横断面研究 1 篇、系统评价 1 篇。共总结出 21 条关于心血管患者恐动症管理的最佳证据，涉及人群选择、评估内容、院内康复、院外康复 4 个方面。

结论：本研究通过系统检索国内外文献整理相关证据，旨在为临床管理心血管术后恐动症患者提供科学依据。

呼吸疗法在老年心力衰竭患者心脏康复中的应用效果

刘伟静学组委员

上海市第十人民医院（同济大学附属第十人民医院）

目的：探讨节拍式呼吸疗法在老年心力衰竭患者家庭心脏康复中的应用效果。方

法：纳入 46 例老年心力衰竭患者，其中观察组 26 例、对照组 20 例。两组患者在病情稳定出院后接受家庭心脏康复干预，其中观察组患者采取节拍式呼吸疗法，对照组患者采取常规治疗。在出院当天（干预前）和干预 3 个月后检测两组患者的血流动力学指标 [每搏输出量（SV）、每搏输出量指数（SVI）、心排血量（CO）、心排血量指数（CI）、左心室做功（LVSW）、左心室做功指数（LVSWI）、加速指数（ACI）、速度指数（VI）、全身血管阻力（SVR）、全身血管阻力指数（SVRI）、心率及收缩压、舒张压]，采用 12 项健康调查简表（SF-12）评定两组患者的生活质量。通过康复记录评估患者的家庭心脏康复干预依从性。 结果：（1）干预 3 个月后，观察组的 SV、SVI、CO、CI、VI、LVSW、LVSWI 高于干预前水平，SVR、SVRI 低于干预前（P<0.05）；观察组的 SV、SVI、CO、CI 和 VI 高于对照组，SVR、SVRI 和收缩压低于对照组（P<0.05）。（2）干预 3 个月后，观察组 SF-12 原始总分和生理功能维度、躯体疼痛维度、总体健康维度、活力维度、社会功能维度、情感职能维度、精神健康维度得分高于干预前（P<0.05）；观察组 SF-12 原始总分和生理功能维度、躯体疼痛维度、总体健康维度和精神健康维度的得分高于对照组（P<0.05）。（3）观察组患者的家庭心脏康复干预依从性优于对照组（P<0.05）。结论：与常规治疗相比，应用节拍式呼吸疗法对老年心衰患者进行家庭心脏康复，可以在短期内有效地降低体循环血管阻力，增强患者的心脏功能，提高其家庭心脏康复依从性，改善其生活质量，值得临床应用推广。

有氧运动通过 Mettl14/GATA3 通路增加巨噬细胞脂噬发挥抗动脉粥样硬化作用

郑阳 郑祥慧 郭周 王慧宇 李运棋 于波 孙勇 吴健

哈尔滨医科大学第二附属医院

目的：冠心病发病率逐年升高，严重威胁人类健康。有氧运动能够降低冠心病患者主要心血管不良事件（MACE）发生及提高预后。但是有氧运动对动脉粥样硬化调控的具体机制仍不明确。

方法：应用斑点印记实验检测冠心病患者及动脉粥样硬化小鼠外周血单核细胞和 THP-1 诱导巨噬细胞的 RNA m6A 修饰水平；病理染色检测小鼠主动脉窦区域动脉粥样硬化斑块面积，Masson 三色染色检测斑块稳定性，免疫荧光检测小鼠斑块巨噬细胞中 Mettl14、GATA3 表达水平；流式细胞技术、荧光定量 PCR 以及 WB 检测 THP-1 诱导巨噬细胞的 M1/M2 极化水平，油红 O 染色检测 THP-1 诱导的巨噬细胞泡沫细胞形成情况，划痕实验检测 THP-1 诱导巨噬细胞的迁移能力，与内皮黏附能力检测 THP-1 细胞诱导巨噬细胞的黏附能力，电镜检测巨噬细胞脂滴水平，WB 检测巨噬细胞脂噬水平；应用 CRISPR-Cas9 技术构建 Mettl14-/+ 小鼠，Mettl14-/+ 小鼠与 APOE-/- 小鼠杂交获得 Mettl14-/+APOE-/- 小鼠；流式细胞技术及荧光定量 PCR 检测小鼠骨髓来源巨噬细胞（BMDM）极化水平；流式细胞技术检测小鼠外周血单核细胞 Ly6C 比例，免疫荧光检测小鼠斑块中 M1/M2 极化水平；油红 O 染色检测 BMDM 泡沫细胞形成情况，免疫荧光及荧光定量 PCR 检测 BMDM 中 GATA3 表达情况，荧光定量 PCR 检测 GATA3 mRNA 稳定性。

结果：在冠心病患者外周血单核细胞、LPS 刺激的巨噬细胞以及动脉粥样硬化小鼠外周血单核细胞中 m6A 修饰水平明显升高，m6A 甲基化转移酶 Mettl14 表达水平明显升高。有氧运动能够降低动脉粥样硬化斑块面积，增加斑块稳定性，同时有氧运动能够使小鼠外周血单核细胞及斑块巨噬细胞中 Mettl14 表达明显降低。敲减 THP-1 中的 Mettl14，能够使巨噬细胞向 M2 型极化，抑制 NF-κB 通路，促进巨噬细胞脂噬，降低泡沫细胞数量，促进巨噬细胞中 ABCA1、ABCG1、PPAR-γ、LXR-α 蛋白表达，抑制巨噬细胞迁移及黏附，减轻巨噬细胞炎症反应。培养 Mettl14-/+APOE-/- 小鼠来源的 BMDM，敲除 Mettl14 能够促进巨噬细胞向 M2 型极化; MeRIP-seq 和 RNA-seq 联合分析发现 GATA3 m6A 修饰水平降低、基因表达水平同时也降低，荧光共定位分析发现 GATA3 主要位于小鼠斑块的巨噬细胞中；Mettl14-/+APOE-/- 小鼠中，敲除 Mettl14 后，有氧运动能够更明显降低小鼠动脉粥样硬化斑块面积、增加斑块稳定性，增加小鼠外周血单核细胞 CX3CR1highLy6Clow 比例，增加斑块中 M2 型细胞数量，增加巨噬细胞脂噬水平，降低 BMDM 的泡沫细胞数量；Mettl14-/+APOE-/- 小鼠中，敲除 Mettl14 能够使斑块巨噬细胞、BMDM 中 GATA3 表达水平降低，降低 GATA3 mRNA 的稳定性。

结论：有氧运动能够降低动脉粥硬化巨噬细胞中的 Mettl14 水平，并通过 Mettl14/GATA3 通路增加巨噬细胞的 M2 型极化、促进巨噬细胞脂噬。因此，有氧运动通过 Mettl14/GATA3 通路促进巨噬细胞脂噬从而发挥抗动脉粥硬化。

不同年龄组冠心病患者体适能指标之间的差异

李茵 吴嘉慧

首都医科大学附属北京安贞医院

目的 探讨不同年龄组冠心病患者心肺耐力、人体成分以及运动表现能力中的力量、平衡能力、柔韧性等体适能指标之间的差异，为运动处方的制定提供参考。方法 选取 2023 年 5 月 -2024 年 11 月份在北京安贞医院心脏康复中心进行康复治疗的冠心病患者 97 例，将患者按照年龄分为 < 45 岁、45~64 岁和≥ 65 岁三组。通过单因素方差分析和秩和检验探讨不同年龄组冠心病患者体适能指标之间的差异。结果 经统计分析比较，三组之间心肺测试指标中的 Peak-Load 在三组之间出现显著差异（F=7.642，P < 0.01），AT-Load、AT-VO_2/kg、Peak-VO_2/kg、Peak-VO_2 之间虽然有随着年龄下降的趋势，但三组间并未有显著差异。其他体适能指标中 30s 手臂屈曲测试、30s 椅子坐站测试、握力、抓背试验、改良转体测试、单腿站立测试、功能性前伸测试以及起立 - 行走测试在组间均有显著差异（P < 0.05，P < 0.01）。结论：45 岁以后的冠心病患者开始出现力量、平衡以及柔韧性等其他体适能的显著下降，因此进行心脏康复时，对其进行其他体适能的评估并实施针对性的治疗训练是有必要的。虽然心肺耐力在不同年龄组之间不存在显著差异，但也呈随年龄下降的趋势。

Cardiac Shock Wave Therapy Ameliorates Myocardial Ischemia in Patients with Non-obstructive coronary artery disease: A Randomized Trial

weijing Liu

Shanghai Tenth people’s Hospital

Background: Cardiac shock wave therapy (CSWT) is a non-invasive new option for the treatment of chronic refractory angina pectoris. The clinical prognosis of non-obstructive coronary artery disease is similar to that of obstructive coronary artery disease, and there is currently no effective clinical solution. This study aimed to evaluate the safety and efficiency of CSWT in the treatment of non-obstructive coronary artery disease.

Methods: Thirty-six patients with non-obstructive coronary artery disease were randomly allocated into CWST group (n = 18) and Control group (n = 18). Patients in the CSWT group were treated with optimal drugs (including antiplatelet drug, statins, and antianginal drugs) + CSWT, and those in the Control group were treated with optimal drugs alone. Care providers and physicians who followed up the patients (parameters of this study) were blind to the grouping. Blood samples of peripheral venous were collected at baseline and follow-up. Myocardial marker [creatine kinase phosphateisozyme (CK-MB)] and hepatorenal function indexes [alanine aminotransferase (ALT), aspartate aminotransferase (AST), serum creatinine (SCr)] were measured. Canadian Cardiovascular Society (CCS) grade of angina pectoris, Seattle Angina Questionnaire (SAQ) score, 6-min walk test (6MWT), weekly dosage of nitroglycerin, and myocardial perfusion on D-SPECT were determined at baseline and during the follow-up period. Myocardial perfusion was evaluated using a 99mTc-labeled tracer SPECT (D-SPECT, Spectrum Dynamics Company) at baseline and 6 months after the first treatment in the CSWT group. One-day rest-stress method was used for adenosine load protocol with tracer injection. Summed stress score (SSS) and summed rest score (SRS) were analyzed semiquantitatively in a blind manner. Adverse events were also evaluated.

Results:CSWT was well-tolerated in the CSWT patients. The myocardial ischemia markers (CK-MB), hepatorenal function (AST and ALT), and renal function (SCr) results showed no significant differences in these parameters. It is indicated that the procedure of CSWT is safe and did not result in damage to the myocardium. The clinical symptoms (chest tightness and chest pain) were all improved in the CSWT group. The symptoms were evaluated by CCS class scores, SAQ scores, and 6MWT. At baseline, there were no significant differences in the CCS score, SAQ score, and results from 6MWT between the two groups (p > 0.05). CSWT improved the myocardial perfusion in the treated area as evaluated by D-SPECT in the adenosine stress protocol. both SSS and SRS were reduced in the CSWT group at 6 months. Echocardiography was performed on a Vivid 9 (GE Vingmed, Horton, Norway). Echocardiography was done to illustrate the left ventricular end-diastolic dimension (LVDd) and left ventricular ejection fraction (LVEF). the LVEF was similar at baseline between the two groups, and it remained unchanged after treatment (6 months). The LVDd was also comparable between the two groups at baseline, and it remained unchanged after treatment (6 months). This reflected that LV function had no signs of deleterious LV remodeling. However, no significant changes were observed in the Control group. CSWT was well-tolerated in all the subjects. No complications or adverse effects were noted in the patients of the two groups.

Conclusions: CSWT may improve the myocardial perfusion and reduce clinical symptoms without increasing adverse effects in patients with non-obstructive coronary artery disease. It provides a non-invasive and safe clinical therapy for patients with non-obstructive coronary artery disease. CSWT may serve as a good alternative for the treatment of CRAP, achieving favorable clinical therapeutic efficacy and better quality of life.

高原冠心病患者居家心脏康复的研究进展

赵文琦 李伟玲

青海省心脑血管病专科医院

目的：

本文旨在综述高原地区冠心病 (CHD) 患者居家心脏康复 (HBCR) 模式的研究进展与应用。高原地区低氧、高寒环境导致 CHD 发病年龄早、合并高血压 / 高脂血症比例高，加之地域广阔、人口分散、医疗资源有限，使得传统的医疗监督下心脏康复中心 (CBCR) 模式普及率、参与率和完成率均不理想。因此，探索和推广 HBCR 模式，利用家庭场景和远程监督为高原 CHD 患者提供安全有效的康复服务，提高其心肺功能、社会参与度和生活质量，成为迫切需求。

方法：

文章通过文献综述，系统阐述了高原 CHD 的特点及其对康复的挑战，定义了 HBCR 模式及其核心要素（以家庭为基础、远程监督指导、个性化计划）。重点介绍了 HBCR 的五大核心干预策略：(1) 运动康复： 基于入院评估和心肺运动试验 (CPET) 进行风险分层，制定个性化运动处方（时间、频率、强度），结合高原环境调整强度（如降至峰值心率 / 心率储备 50%-70%），利用可穿戴设备进行远程监测。(2) 营养干预： 评估营养状况，参照地中海饮食等制定个体化营养处方，控制饱和脂肪、胆固醇和钠摄入，管理合并症相关饮食。(3) 睡眠管理： 多方式评估睡眠（尤其阻塞性睡眠呼吸暂停 OSA 和失眠），根据严重程度给予保守、器械或药物 / 心理治疗，利用 App 辅助管理。(4) 心理康复： 使用量表（如医院焦虑抑郁量表）进行筛查，采用压力管理、认知行为治疗、动机性访谈等方式干预，必要时转诊。(5) 心血管危险因素管理： 监测血压、血糖、血脂、体重等，指导生活方式调整和规律用药，支持戒烟。此外，详细说明了 HBCR 实施前的综合评估内容（医学、运动、营养、睡眠、心理）和基于评估制定运动处方的具体原则（尤其针对高原环境和合并症调整）。文章也概述了 HBCR 在国际和国内（特

别是高海拔地区）的应用现状。

结果：

国际共识（如美国 AHA/ACC/AACVPR 2019 声明）推荐低危患者使用 HBCR，其在解决交通时间障碍、扩大服务范围、延长监测时间方面优势明显。研究表明，参与 CR（包括 HBCR）能显著降低冠心病患者死亡率和再入院率，提高依从性可获得更大获益。在高原或类似环境下，基于智能手机交互的 HBCR 模式在中国患者中被证实能有效提高运动依从性，降低心血管风险。可穿戴设备（如电子手环）在心脏术后患者中应用方便、接受度高，有助于活动监测和恢复评估。然而，中国整体 CR（包括 HBCR）的机构覆盖率（不足 30%）和地域普及度（东部高于中西部）仍有很大提升空间，高原地区更面临特殊挑战。

结论：

HBCR 模式是解决高原地区 CHD 患者康复资源匮乏、交通不便、参与率低等问题的有效途径。它融合运动、营养、睡眠、心理和危险因素管理等多维度干预，通过个性化评估与处方制定（需特别考虑高原低氧环境的影响），并借助可穿戴设备和远程医疗技术实现监督与指导，能够安全有效地帮助患者恢复心肺功能、改善生活质量并降低心血管风险。未来应加强患者教育、完善随访制度（结合电话、网络、家访）、研发适应高原环境的监测设备、探索社区支持模式，并积极整合远程医疗与人工智能技术，构建高质量、可推广的 HBCR 服务体系，以弥补高原地区医疗资源不足，提升心血管疾病患者的全程管理和健康水平。

基于循证医学的心脏康复规范化实施的相关探讨

谭慧 刘华芬

武汉大学人民医院

心脏康复（Cardiac Rehabilitation, CR）是心血管疾病（CVD）患者长期管理的重要组成部分，其规范化实施对降低再住院率、改善生活质量和提高生存率具有显著作用。然而，全球范围内 CR 的参与率和实施质量仍存在较大差异，亟需基于循证医学优化标准化流程。本文系统回顾国内外 CR 研究进展，探讨规范化实施的关键要素、现存障碍及未来发展方向，以期为临床实践和政策制定提供参考。

本文回顾了心脏康复的循证医学基础，CR 的临床获益已得到多项 Meta 分析和随机对照试验（RCTs）支持。研究显示，规范化 CR 可使稳定型冠心病患者的全因死亡率降低 20%~30%，心力衰竭患者的再住院风险下降 25%，并显著改善 6 分钟步行距离（6MWD）和峰值摄氧量（VO_2peak）。此外，CR 在心理干预（如抑郁、焦虑管理）和生活方式调整（如戒烟、营养指导）方面亦具有明确效果。

整理了规范化心脏康复的核心要素，国际指南（如 AHA/ACC、ESC）推荐 CR 应包含以下核心内容：医学评估与风险分层：基于心肺运动实验（CPET）或 6MWD 制定个体化方案；运动康复：结合有氧训练、抗阻训练及柔韧性训练，采用靶心率或 Borg 量表调控强度；药物优化：遵循指南调整抗血小板、降脂及抗心衰药物；多学科协作（MDT）：整合心内科医师、康复师、心理医师及营养师，提供综合管理；长期随访：通过远程监测或社区随访提高患者依从性。

列举了规范化实施的现存挑战，尽管 CR 的临床价值明确，其实施仍面临多重障碍：医疗资源不均衡：基层医疗机构 CR 设备及专业人员匮乏，三级医院与社区衔接不足；患者参与率低：我国 CR 参与率不足 10%，远低于欧美国家（30%~50%），影响因素包括认知不足、经济负担及交通限制；标准化不足：运动处方制定、风险监测及疗效评估缺乏统一标准；医保政策局限：部分 CR 项目未纳入医保报销，影响患者长期坚持。

提出了优化策略与未来方向，为提高 CR 的规范化实施，可采取以下措施：推广“互联网 +CR”模式：利用可穿戴设备、移动医疗 APP 实现远程监测，提高可及性；建立区域化 CR 网络：推动三级医院 - 社区 - 家庭联动，优化转诊流程；政策支持：将 CR 纳入医保支付范围，并制定行业标准；加强患者教育：通过多媒体宣教提高患者对 CR 的认知和依从性。

心脏康复的规范化实施需基于循证医学，结合多学科协作、个体化干预及政策支持。未来研究应聚焦于人工智能辅助 CR 方案制定、老年及心衰等特殊人群的优化策略，以及低成本、高可及性的社区 CR 模式，以推动全球 CR 的均质化发展。

心脏康复的相关研究

袁慧敏 刘华芬

武汉大学人民医院

心脏康复（Cardiac Rehabilitation, CR）是一种综合性、多学科干预措施，旨在通过运动训练、健康教育、心理支持、危险因素管理等手段，改善心脏病患者预后、降低心血管事件风险、提升生活质量。本文综述心脏康复的定义、发展历程、核心内容、临床获益及最新研究趋势。

1. 定义与历史发展

心脏康复起源于 20 世纪 60 年代，基于早期研究发现心肌梗死患者早期活动预后优于长期卧床。1964 年 WHO 成立心血管康复委员会，1969 年正式采用运动处方。美国心脏协会将其定义为涵盖医疗评价、运动干预、危险因素纠正等长期计划，目标为逆转动脉粥样硬化进程，促进患者社会适应。

2. 核心内容与实施模式

标准心脏康复包括：①生活方式干预（戒烟、饮食管理、体重控制）；②心理社会因素管理（焦虑抑郁干预）；③个体化药物治疗与疾病管理（血脂、血压调控）；④运动处方（分阶段有氧与抗阻训练）；⑤职业康复与长期护理。分为院内 I 期、院外 II 期（门诊 / 中心）和居家III期，强调全程管理。

3. 适应症与安全性

适应症涵盖急性冠脉综合征（含 PCI 术后）、慢性心衰、心脏移植 /TAVR 术后等高风险人群。禁忌症包括不稳定心绞痛、严重心律失常等。现有研究显示其安全性高，法国与美国研究指出运动康复中心血管事件发生率极低（约 5 例 /5 万小时）。

4. 临床获益与机制

死亡率与入院率降低：Meta 分析表明 CR 可使心血管死亡率下降（如心肌梗死患者从 10.4% 降至 7.6%），再入院率从 30.7% 降至 26.1%。

心理健康与生活质量改善：运动结合心理干预显著缓解抑郁焦虑，提升患者社会功能。

生理机制：增强心肌收缩力，优化心输出量，改善血管弹性与代谢调节。

5. 最新研究趋势

远程康复：克服地域限制，通过数字化平台提升患者参与率，成为传统 CR 的重要补充。

特定人群优化：聚焦女性、TAVR 术后及老年肌少症患者，定制运动方案（如太极拳、抗阻训练）以增强适用性。

技术融合：中国可降解支架等新技术结合 CR，降低术后血栓风险。

心理与社会支持强化：关注患者依从性，整合家庭与社会资源，改善长期康复效果。

6. 挑战与展望

当前 CR 参与率仍较低（如美国仅 14-31%），需通过政策支持、远程医疗普及、个性化方案优化提升覆盖率。未来方向包括智能化监测、精准化干预及全生命周期管理，以进一步实现心血管疾病的预防与康复一体化。

心脏康复作为循证支持的二级预防核心策略，其综合干预模式对改善患者预后、减轻医疗负担具有重要意义。随着技术革新与多学科协作深化，CR 有望在全球范围内推动心血管疾病管理模式的革新。

高强度间歇训练在慢性心衰伴 2 型糖尿病患者中的应用效果

刘娅

北京清华长庚医院

目的：探讨高强度间歇训练（HIIT）对慢性心力衰竭（CHF）合并 2 型糖尿病（T2DM）患者心功能及血糖控制的影响，为制定个体化心脏康复方案提供循证依据。

方法：采用前瞻性随机对照设计，招募 60 例 NYHA II – III级且 HbA1c ≥ 7.0% 的 CHF+T2DM 患者，按 1:1 随机分入 HIIT 组（n=30）与常规中等强度持续训练（MICT）组（n=30）。两组均接受 12 周、每周 3 次、每次 30 min 的院内监护下运动干预：HIIT 方案为 5 min 热身→ 4×4 min 85–90%HRmax 高强度踏车 / 抗阻循环→ 3 min 60%HRmax 主动恢复→ 5 min 整理；MICT 以 60%HRmax 持续踏车 25 min。干预前后采用心肺运动试验（CPET）测峰值摄氧量（VO_2peak）及无氧阈；超声心动图测左心室射血分数（LVEF）；实验室检测空腹血糖（FPG）与糖化血红蛋白（HbA1c）。

结果：HIIT 组 VO_2peak 由 15.8±2.4 升至 19.7±3.1 $ml \cdot kg^{-1} \cdot min^{-1}$，LVEF 从 35±6% 增至 42±5%，增幅均显著优于 MICT 组（P<0.01）。血糖方面，HIIT 组 FPG 下降 1.8 mmol/L，HbA1c 降低 1.3%，降幅亦优于 MICT 组（P<0.05）。所有患者未发生严重不良事件。

结论：12 周 HIIT 可在安全前提下显著提升 CHF+T2DM 患者的运动耐量、心功能及血糖控制水平，推荐将其纳入该类患者的综合心脏康复管理。

基于 RCA 与 Teach-back 法的多维度干预在心力衰竭患者出院健康教育中的应用

陈亚丽

河北医科大学第二医院

目的：

心力衰竭（HF）患者出院后 3 个月内再住院率高达 30%，自我管理能力不足是核心诱因。本研究拟构建标准化健康教育方案，结合 Teach-back 法的多维度干预，以提高患者健康教育的效果，达到提高患者自我管理能力，降低再住院率的目的

方法：

根因分析（RCA）：成立 6 人跨学科小组，通过 5 层因果链锁定根本问题；

标准化内容构建：通过质性访谈和文献回顾建立健康教育标准化内容初稿，用德尔菲法（17 名专家两轮咨询，Kendall’s W=0.348~0.511，p<0.001）确定 4 大核心模块：疾病认知、药物管理、液体控制、预警症状识别；

教育方法优化：本研究发现，出院健康教育质量缺陷（内容不规范、方法低效）是护理可干预的根本问题。本研究采用 Teach-back 法（“教育 - 评价 - 再教育 - 再评价”循环）以保证健康教育效果，提升患者自我管理能力；

效果验证：类实验设计（实验组：2023 年 6-11 月，n=62；对照组：2022 年历史数据，n=58）。

结果：

知识掌握率：实验组出院 7 日、30 日核心知识得分显著高于对照组（p<0.05），仅 7 日液体管理无差异（p>0.05）；

再住院率：实验组 3 个月再住院率降低 12.1%（p=0.02）；

心血管事件：实验组 1/3 个月事件数减少，但差异未达显著性（p>0.05）。

结论：

RCA 驱动的标准化 Teach-back 教育模式可显著提升 HF 患者自我管理能力，降低再住院率。需扩大样本验证对不良事件的长期影响。

关键词：心力衰竭；根因分析；Teach-back 法；出院教育；再住院率

多学科协作模式下心脏康复在左心室辅助装置植入患者围术期的应用效果

张恒通

西安交通大学医学院第一附属医院

方法：本研究采用前瞻性随机对照设计 (RCT), 严格遵循 CoNSORT 声明规范。纳入 2022 年 8 月至 2024 年 12 月本院收治所有终末期心衰行 LVAD 植入术患者。纳入标准 :1、符合 INTERMACS1-3 级；2、年龄 18-76 岁；签署知情同意书。排除标准 :1、合并不可逆肺动脉高压 (PVR>5Wood 单位)；2、活动性感染；3、严重肾功能不全 (eGFR<30ml/ min/1.73m2)。最终入组 76 例，按计算机随机序列分为干预组 (n=38) 与对照组 (n=38), 两组基线资料无统计学差异 (p>0.05)。对照组接受常规围术期管理，干预组实施 MDT 心脏康复方案，涵盖术前预康复 (营养优 + 呼吸训练)、术中血流动力学精准调控、术后分阶段运动康复 (床上脚踏车→床边坐立→ 5 分钟步行) 及心理 - 营养联合干预。主要观察指标：术后 30 天主要并发症 (右心衰竭、出血、感染)、ICU 停留时间、6 分钟步行距离 (6MWD)、NT-proBNP 水平及明尼苏达心衰生活质量量表 (MLHFQ) 评分。

结果：干预组较对照组显著降低术后并发症发生率 (21.1%vs 42.1%,p=0.032), 缩短 ICU 停留时间 (6.2±1.8 天 vs8.9±2.4 天，p<0.01)。术后 30 天，干预组术后 30 天 6 分钟步行距离 (6MWD) 提升至 342.6±45.3 米 (较术前基线增加 98.3±24.1 米)，对照组提升至 296.4±52.7 米 (较术前基线增加 52.7±30.5 米)，组间差异具有统计学意义 (t=6.82,p=0.003,95%CI32.1-58.9 米)。

结论：围术期 MDT 心脏康复模式可有效提升 LVAD 患者心肺功能储备，降低手术并发症风险，加速术后恢复 . 进程，并为长期机械循环支持管理提供新策略。

基于时限性自我调节理论构建的个体化运动方案在心脏康复患者中的应用

马梦琪 丰小星 张光玮 任辉

吉林大学第一医院

摘要：目的：基于时限性自我调节理论构建个体化运动方案，通过调节患者的行为意图、增强行为优势和提高自我调节能力，以优化心脏康复的效果。

方法：随机选取 2023 年 8 月 -2024 年 8 月心血管内科进行心脏康复的 326 名患者为数据样本，随机分为对照组和干预组各 163 例。对照组病人接受常规心脏康复，干预组病人首先通过初步运动风险筛查进行风险分层，运动前结合心肺运动试验结果评价体能状态，结果阴性的人群，从中低强度开始加量，并定期进行心肺运动试验评估，指导适宜的运动量及频率。

结果：干预组患者在住院时间、科室满意度、生活质量评分提升幅度、自我效能量表评分增幅、坚持运动方案的时间、运动康复完成度均优于对照组（P<0.05）。

结论：基于时限性自我调节理论为心血管内科住院患者构建个体化运动方案可明显优化心脏康复效果。提升心肺康复参与度，契合临床重要需求；提高运动康复适应性，满足患者个性需求，优化康复过程，有效缩短患者的康复周期和住院时间，降低了医疗资源的占用率，从而提升了整体经济效益。最后，基于 TST 的个体化运动方案还能通过提高患者的健康管理能力，减少对公共卫生资源的依赖，减轻社会医疗负担，提升整体公共卫生系统的效率和服务水平，提升患者生活质量，为构建和谐健康的社会环境发挥重要作用。

心脏康复训练对冠心病病人康复效果的 Meta 分析

刘香琼

重庆荣昌区人民医院

摘要: [目的] 通过 Meta 分析评价心脏康复训练对冠心病病人的康复效果。[方法] 计算机检索 The cochrane Library、0VID−EM−

base、PubMed、EBSC() 一 Medline、中国生物医学文献服务系统 (cBM)、中国期刊全文数据库 (CNKI)，以及万方数据库、维普数据库

中关于冠心病病人心脏康复训练效果的随机对照试验。经筛选文献，提取资料与评价文献质量后，采用 RevMan 5．3 软件进行 Me−

ta 分析。[结果] 最终纳入 14 项随机对照试验，2 427 例病人。Meta 分析结果显示，心脏康复训练不仅能有效提高冠心痛病人代谢

当量 [MD 一 1．36，95％ C，(o．83，1．89)，P<o．01]，改善病人高密度脂蛋白的水平 [MD=o．05，95％ C，(o．02，o．07)，P<o．01]，降低

心血管事件的发生率 [RR−o．74，95％ Cj(o．63。o．86)，P<o．01 I，缩短病人住院时间 [MD 一一 5．13，95％ cJ(一 6．92，一 3．35)，P<

o．01]，还能提高 6 min 步行距离、射血分数及生活自理能力，但在改善血压、总胆固醇、低密度脂蛋白、戒烟依从性方面未显示明显

优势 (P>o．05)。[结论] 心脏康复训练能有效改善病人的心功能指标和生活自理能力，降低病人心血管事件发生率，但在改善病人心脏风险指标扣心理疾病状况方面还需要开展大样本、多中心、长时间的深入研究。

关键词：冠心病；心脏康复训练；Meta 分析；生活自理能力；血压；总胆固醇；低密度脂蛋白；心功能；心血管事件

心脏康复训练联合预见性护理对心绞痛患者经皮冠状动脉介入术的影响

杨沙沙

重庆荣昌区人民医院

【摘要】目的：探究心脏康复训练联合预见性护理对心绞痛患者经皮冠状动脉介入术的影响及医疗价值。**方法：**于 2023 年 1 月开始实验，至 2024 年 12 月结束，取该期间收治心绞痛行经皮冠状动脉介入术治疗患者作为观察对象，借助电脑随机分配形式将所有患者分成两组，一组行常规护理（对照组 n=40），另一组实施心脏康复训练联合预见性护理（观察组 n=40），归纳两组患者相关数据指标，观察结果变化。**结果：**结果显示，观察组患者 LVEF、6 min 步行距离均优于对照组，胸痛缓解时间、住院时间均短于对照组，并发症发生率少于对照组，P 值均 < 0.05。**结论：**心绞痛行经皮冠状动脉介入术治疗患者实施心脏康复训练联合预见性护理可明显改善心功能恢复效果，降低并发症发生风险，提高临床疗效，值得采纳。

【关键词】心脏康复训练；预见性护理；心绞痛；经皮冠状动脉介入术

心绞痛是临床常见心血管疾病类型，指冠状动脉粥样硬化、痉挛、管腔狭窄，诱发心肌血氧供应不足，症状表现以阵发性胸痛或胸部持续不适症状，具有较高心肌梗死、猝死等重症风险，严重威胁生命安全 [1] 。经皮冠状动脉介入 (PCI) 治疗是现代医疗发展所研发的新型微创技术，具有创伤较小，术后恢复周期短，并发症少等优势。治疗期间受患者个体差异、术中穿刺等因素影响，常规的护理难以规避潜在风险，下文将针对心脏康复训练联合预见性护理对心绞痛患者经皮冠状动脉介入术的影响开展讨论，结果如下。

基于人文护理的心脏康复模式构建及应用效果研究

许艳萍

西安交大第一附属医院

[目的] 聚焦心脏康复领域，响应《进一步改善护理服务行动计划（2023-2025 年）》要求，通过创新护理模式，将人文护理理念深度融入心脏康复全过程，提升患者心脏康复管理能力、优化康复体验，同时增强公众对心脏康复的认知，推动心血管专科护理服务高质量发展。**[方法]** 以心内科为实践阵地，2023 年 1 月至 2024 年 12 月期间构建 “多途径护心科普，全方位健康护航” 护理模式，具体举措包括：系统化医患沟通培训，强化心脏康复过程中的医患协作；搭建个性化院外随访体系，针对患者康复阶段提供精准指导；构建多维度健康教育网络，普及心脏康复知识; 拓展多元化延伸护理服务，覆盖康复全周期; 优化人文病房环境，提升康复舒适度。**[结果]** 患者心血管健康知识（含心脏康复相关内容）知晓率从 62.3% 提升至 91.5%，公众急救技能（与心脏急症相关）掌握率由 28.7% 提高到 76.4%；患者护理满意度从 85.6% 跃升至 96.8%，PCI 术后并发症发生率降低 12.3%，再入院率下降 15.8%；累计开展心脏康复主题科普活动 180 余场，覆盖超 1.2 万人次，与 12 家单位建立长期合作，提升科室在心脏康复领域的区域影响力。**[结论]** 多途径护心科普与人文护理深度融合的模式，能有效提升患者心脏康复管理能力，改善临床康复结局（如降低并发症和再入院率），优化康复期就医体验，同时增强公众对心脏康复的认知。该模式为心血管专科在心脏康复领域践行人文护理理念、推动护理服务高质量发展提供了可复制的实践范式与理论参考。

Evidence-based construction of an early exercise rehabilitation program for kinesiophobic patients after coronary stent implantation

Xia Song

Zigong First People’s Hospital

Introduction: Exercise phobia is prevalent in patients with heart disease, and this mentality can seriously affect the rehabilitation process. Patients’ fear of exercise training mainly stems from the fear of causing damage to the cardiac organs again and decreasing physical function, which not only affects the rehabilitation, but also may bring new disease problems, so they are resistant to exercise. Domestic research on exercise phobia in patients after coronary stent implantation is more in-depth, but mainly focuses on the validation of the psychological scale of exercise phobia and the investigation and study of exercise phobia in patients with acute cardiovascular diseases. However, research on kinesiophobia in patients with PCI, especially after coronary stent implantation, is still insufficient. The general lack of awareness, low participation and compliance, and high cost of rehabilitation among Chinese cardiac patients pose a challenge to the initial development of cardiac rehabilitation in China, and there is an urgent need to develop programs adapted to the current national situation that can help to increase the participation and compliance rate of exercise rehabilitation in patients after coronary stent implantation. Therefore, this study constructs an early exercise rehabilitation program for kinesiophobic patients after coronary stent implantation on the basis of evidence to provide a basis for the implementation of rehabilitation strategies for kinesiophobic patients.

Methods: Literature related to exercise rehabilitation for patients with postoperative kinesiophobia in cardiovascular disease was searched from China Knowledge, Wanfang Database, Wipro, SinoMed, PubMed, Web of Science, The Cochrane Library, and Embase databases, and the timeframe for searching was from the establishment of the database to December 31, 2024 for all of them. The literature screening process was

strictly in accordance with the inclusion and exclusion criteria, and was completed independently by 2 authors; if there was a disagreement between the 2 authors on the study selection, the 3rd author discussed and reached a consensus together. Literature screening method: first, the software Endnote was used to remove duplicates, and then the remaining literature was evaluated according to its title and abstract. Second, the full text of the remaining literature was reviewed according to the inclusion and exclusion criteria and a list of all eligible literature was examined to identify any potentially relevant studies and finally finalized for final inclusion. The literature was independently screened and data extracted by two researchers and discussed by the subject group to develop a first draft of an early exercise rehabilitation program for patients with kinesiophobia after coronary stent implantation based on acceptance commitment therapy, guided by relational framing theory and the fear-avoidance model; two rounds of correspondence with 15 experts were conducted using the Delphi method to develop the final program. **Results:** Based on evidence-based, the first draft of the early exercise rehabilitation program for patients with kinesiophobia after coronary stent implantation was formed. The effective recovery rate of the two rounds of expert correspondence questionnaires was 100.0%, the expert authority coefficients were 0.875 and 0.935, the Kendall's concordance coefficients were 0.213 and 0.318 (both P<0.001), and the coefficients of variation were 0 to 0.17 and 0 to 0.14, respectively.The final constructed program included 9 phases (pre-exercise assessment, exercise mode selection, exercise cycle, exercise duration, exercise intensity, exercise termination indication, observation and recording during exercise, and safety and security measures) and 27 specific measures. **Discussion:** An early exercise rehabilitation program for kinesiophobic patients after coronary stent implantation based on acceptance commitment therapy is scientific, reliable, and comprehensive, and can provide a reference for early clinical kinesiophobic intervention.

Construction and application of a plyometric training intervention program for elderly cardiovascular co-morbid patients based on the Fogg behavioral model

Xia Song

Zigong First People's Hospital

Introduction: To validate the application effect of the plyometric training intervention program constructed based on Fogg's behavioral model for elderly patients with cardiovascular co-morbidities, and to provide reference for improving the muscle strength and quality of life of elderly patients with cardiovascular co-morbidities. **Methods:** Based on evidence-based, searching and reading related literature and inductive analysis, the group discussion, based on Fogg behavioral model preliminary construction of elderly cardiovascular co-morbidities patients plyometric training intervention program preliminary draft, exercise intervention process includes three phases, exercise awareness cultivation stage, scientific fitness guidance stage, exercise habit formation stage. The preliminary draft was subjected to two rounds of expert correspondence using the Delphi method, and the preliminary draft was revised and improved according to the opinions of 17 experts to finalize the plyometric training intervention program for elderly patients with cardiovascular co-morbidities. Subsequently, eight elderly patients with cardiovascular co-morbidities were selected for pre-testing, and the test data were collected and analyzed to summarize the problems and deficiencies, and then the intervention program was revised. A convenience sampling method was adopted to select 94 elderly cardiovascular co-morbid patients attending the Department of Cardiovascular Medicine of a tertiary general hospital in Sichuan Province from September 2024 to December 2024 as the study subjects, and they were divided into the control group (n=47) and the intervention group (n=47) according to the randomized number table method. The control group received routine care and daily exercise instruction, and the intervention group received a 3-month Fogg behavioral model-based plyometric training intervention program for elderly patients with cardiovascular co-morbidities based on the implementation of routine care, and the cardiac function level, functional fitness level, quality of life scores, muscle mass, muscle strength, step speed, and the patient's quality of life scales were collected from the patients in both groups before the intervention and at the 3-month period after the intervention. To evaluate the effects of the Fogg Behavioral Model-based plyometric training intervention program for elderly patients with cardiovascular co-morbidities on patients' cardiac function level, functional fitness level, muscle mass, muscle strength, step speed and quality of life. **Results:** At the end of the intervention, 1 patient in the intervention group and 2 patients in the control group withdrew, for a total of 91 patients with cardiovascular co-morbidities who completed the study (n=46 in the intervention group and n=45 in the control group). There was no statistically significant difference between the baseline data of the two groups (P>0.05). The change over time in cardiac function level, functional fitness level, muscle mass, muscle strength, step speed and quality of life scores in the intervention group were better than those in the control group at 3 months of intervention (P<0.05). **Discussion:** Implementation of a Fogg Behavioral Model-based plyometric training intervention program for elderly patients with cardiovascular co-morbidities can significantly improve patients' level of cardiac function as well as physical fitness, and enhance whole-body muscle mass as well as quality of life. However, this study is a single-center, small-sample study, and further multi-center, large-sample studies should still be conducted in the future to improve the generalizability of the study.

Research on the development and application of cardiac rehabilitation training games for patients with chronic heart failure

Kun-Yan Peng

Zigong First People's Hospital

Introduction: Chronic heart failure is the end-stage manifestation of cardiovascular disease, which refers to the pathological state in which the pumping function of the heart gradually decreases under the influence of pre-existing cardiac diseases, and the cardiac output is insufficient to cover the demand of the body or depends on the increase of filling pressure to compensate for it, and the main clinical symptoms are fluid retention, dyspnea, and fatigue, etc. Clinical treatment of this disease is often based on drug therapy to quickly relieve clinical symptoms and improve the prognosis. Clinical treatment of this disease is mostly based on drug therapy to rapidly relieve clinical symptoms and improve prognosis, but long-term drug therapy can cause many adverse reactions and the efficacy varies from person to person, so drug therapy has limitations and other effective treatment modalities need to be explored. Along with the continuous improvement of the medical model, the concept of cardiac rehabilitation has been popularized in the clinic, and at present, cardiac rehabilitation is centered on exercise rehabilitation, including game training and so on. Therefore, this study develops and applies the cardiac rehabilitation training game with the physical and mental characteristics of chronic heart failure patients, in order to explore more effective cardiac rehabilitation training methods. **Methods:** Based on the theory of health belief model, semi-structured interview method, brainstorming, and expert consultation were used to design the game content, and the game was realized by using WeChat applet. Ninety-eight cases of CHF patients admitted to a tertiary general hospital in Zigong City from August 2024 to February 2025 were selected as study subjects. The patients were divided into an intervention group (conventional cardiac rehabilitation training combined with cardiac rehabilitation training game, 49 cases) and a control group (receiving conventional cardiac rehabilitation training, 49 cases) by using a coin toss, and the two groups of patients were intervened for 4 weeks. The cardiac function indexes: left ventricular ejection fraction (LVEF), cardiac index (CI), left ventricular end-diastolic internal diameter (LVEDD), N-terminal brain natriuretic peptide precursor (NT-proBNP), and the exercise function indexes: 6-min walking distance (6MWD), the longest time of exercise (Tmax), and the score of General Self-Efficacy Scale (GSES) were compared between patients in both groups before and after the intervention. Minnesota Heart Failure Quality of Life Questionnaire (MLHFQ) score. **Results:** No samples were shed. After the intervention, LVEF and CI of the two groups were higher than before the intervention in this group, and LVEDD and NT-proBNP were lower than before the intervention in this group, and LVEF and CI of the intervention group were higher than that of the control group, and LVEDD and serum H-FABP and NT-proBNP were lower than that of the control group (P < 0.05). After intervention, 6MWD and Tmax of patients in both groups were longer than before our intervention, and the intervention group was longer than the control group (P < 0.05). After intervention, the GSES score of the two groups of patients was higher than before the intervention of this group, and the MLHFQ score was lower than before the intervention of this group, and the GSES score of the intervention group was higher than that of the control group, and the MLHFQ score was lower than that of the control group (P < 0.05). **Discussion:** Compared with conventional cardiac rehabilitation training, the cardiac rehabilitation training game can better improve cardiac function, exercise function, self-efficacy and quality of life of CHF patients. The game enriches the training methods of cardiac rehabilitation to a certain extent and can be applied to clinical practice. However, this study is a single-center, small-sample study, and further multi-center, large-sample studies should still be conducted in the future to improve the generalizability of the study.

A study on the construction and application of a management program for muscle-reducing obesity in patients with cardiovascular disease

Kun-Yan Peng

Zigong First People's Hospital

Introduction: The challenge of managing sarcopenic obesity in elderly patients is becoming increasingly severe. Studies have shown that cardiovascular disease is an important correlate of sarcopenic obesity, and sarcopenia can cause vascular age-related changes in patients with cardiovascular disease. Previous studies have found that patients with sarcopenic obesity have a higher incidence of cardiovascular and metabolic diseases, and sarcopenic obesity and cardiovascular diseases can independently or synergistically adversely affect the body of the elderly population. Therefore, this study was conducted to form an evidence-based program for the management of muscle-reducing obesity in patients with cardiovascular disease and to evaluate the effectiveness of its clinical application. **Methods:** Based on the evidence-based approach, through the systematic search of domestic and international databases

on the literature related to the management program of muscle-reducing obesity in patients with cardiovascular disease, the search time limit is from the establishment of the database to June 30, 2024, extracting the key intervention information and after the discussion of the subject group, the initial formation of the management program of muscle-reducing obesity in patients with cardiovascular disease was made based on the theoretical foundation of the i-PARIHS framework; the Delphi method was used for 11 experts in two rounds of correspondence to form the final program. Based on the convenience sampling method, 70 patients who attended a tertiary-level general hospital in Sichuan Province from July 2024 to January 2025 and met the inclusion and exclusion criteria were selected as the study subjects, and were divided into the control group (n=35) and the intervention group (n=35) according to the randomized numeric table method. The intervention group was divided into two groups: the control group (n=35) and the intervention group (n=35). The intervention group was divided into two groups: the control group (n=35) and the intervention group (n=35). The intervention group was divided into two groups: the intervention group and the intervention group. In both groups, patients' obesity-related indexes (body fat percentage, visceral fat area), sarcopenia-related indexes (total muscle mass, calf circumference, upper arm circumference, grip strength, and skeletal muscle mass index), laboratory-related indexes (serum albumin, hemoglobin, and C-reactive protein), and quality-of-life scale scores were collected for between-group and within-group comparisons to evaluate the effectiveness of the interventions before the intervention, and after 6 and 12 weeks of the intervention. **Results:** At the end of the intervention, one patient in the intervention group withdrew, and a total of 69 patients with cardiovascular disease with muscle-reducing obesity completed the study. There was no statistically significant difference between the baseline data of the two groups (P>0.05). Muscle mass, muscle strength and quality of life scores over time in the intervention group were better than those in the control group at 6 weeks of intervention (P<0.05). Visceral fat area was significantly lower than that of the control group at 6 and 12 weeks of intervention, and the difference was statistically significant (P<0.001). Comparison of hemoglobin and serum albumin between the two groups showed no statistically significant difference (P>0.05). **Discussion:** Implementation of an evidence-based exercise program for patients with reduced muscle mass and obesity in coronary artery disease was effective in improving muscle mass, muscle strength, and quality of life, and could reduce visceral fat area and debilitating levels, but was not effective in improving hemoglobin and serum albumin.

系统规范化心脏康复护理在慢性心力衰竭患者中的应用

王乔

重庆荣昌区人民医院

【摘要】目的：分析讨论系统规范化心脏康复护理在慢性心力衰竭患者中的应用价值。**方法：**选择于 2023 年 1 月开始，至 2024 年 12 月结束，取该期间收治慢性心力衰竭患者 80 例作为观察样本，利用电脑随机分配形式将所有患者均分两组，即观察组（系统规范化心脏康复护理）、对照组（常规护理），归纳不同干预结局，观察结果变化。**结果：**观察组心功能、步行 6min 距离均优于对照组，负性情绪评分低于对照组，P 值均＜ 0.05。**结论：**慢性心力衰竭患者采纳系统规范化心脏康复护理能够辅助提高心功能及运动耐力，降低负性情绪影响因素，值得采纳。

【关键词】系统规范化心脏康复护理；慢性心力衰竭；心功能

慢性心力衰竭（CHF）是临床中较为常见疾病类型，是由于心室长期受过重负荷或原发性心肌病所造成的心室充盈或泵血功能异常现象，患者多伴有呼吸困难、乏力等症状表现，且治疗周期较长[1]。随着生活质量的改变，老年人口趋势的增加，CHF 的发病率呈现增长趋势，极大影响身心健康。相关调查显示，CHF 患者在接受有效治疗的同时，配合科学对症护理干预措施能够对心脏功能恢复产生积极影响。

参考文献

【1】胡岳，李娜，崔贵璞，等 . 心脏康复护理在慢性心力衰竭患者中的应用现状 [J]. 天津护理 , 2023, 31(5):628-630.

心肺康复专科护士临床实践基地培训体系的构建与实施

肖清霞 刘华芬

武汉大学人民医院

摘要： 目的 以某三甲医院作为中国康复医学会心肺康复专科护士临床实践基地的建设经验为基础，构建并实施科学化、规范化、可持续的心肺康复专科护士临床实践培训体系，为同类基地建设提供参考。方法 1. 基地建设上，基于“心肺康复专科护士临床实践基地医院评审标准”不断完善医院心肺康复病房系统、过程、结局指标，不断优化医院心肺康复护理流程；2. 教学管理体系上，建立“护理部统筹规划 - 学科带头人制定方向 - 基地负责人组织落实 - 教学老师全程带教”的四级教学管理架构，实施全过程质量控制；3. 师资管理上，采用“选拔 - 培养 - 考核 - 激励”模式培养心肺康复专科护士，通过“资质审核 - 试讲评分 - 动态评估”遴选师资，实行竞争上岗与末位淘汰机制遴选带教老师，提高准入标准。组织岗前师资培训，定期集中培训等方式确保教学老师水平； 4. 课程设置上，根据往届学员访谈，学员开班前培训需求访谈调研，每周开展教学反馈会议，动态调整教学内容，不断优化学员实践轮转计划、教学课程，兼顾个体化与系统性需求。实施“整体授课 + 一对一带教模式”以及清单式教学，提高教学水平；5. 考核体系：设置心肺康复相关理论考核、心肺康复实用技能考核、疑难案例分析及结业综合考核。培养理扎实，技术过硬，能学以致用的专科护士。 结果 2021-2025 年 32 名心肺康复专科护士学员于本院完成临床实践。结业考核一次性通过率 100%，2024 年学员对师资水平、课程设置、实践支持的满意度分别达 90.5%、97.1%、92.3%，总体满意度 93%，满意度呈逐年提升；82% 学员返岗后开展心肺康复相关工作，10 人当年发表相关论专利、壁报等。结论 以四级管理架构为支撑，通过师资竞争机制、分层课程设计、动态质量改进及多维考核体系，可有效提升专科护士临床实践培训质量及满意度，可为同类基地建设提供参考依据。

心血管病康复护理实践与思考

解菲菲

中国人民解放军联勤保障部队第九二〇医院

摘要：心血管疾病是全球范围内的主要健康问题之一，给患者的生活质量和生存率带来了巨大的影响。随着医疗技术的不断进步，心血管病的治疗效果得到了显著提高，但康复护理在患者的全面康复中同样起着至关重要的作用。心血管病的康复护理是一个复杂而又重要的领域，它不仅涉及到患者的身体康复，还包括心理和社会方面的支持。在当今社会，心血管病的发病率不断上升，给患者和家庭带来了沉重的负担。因此，加强心血管病康复护理的研究和实践，提高患者的康复效果和生活质量，具有重要的现实意义。心血管病康复护理是针对心血管疾病患者的一种综合性护理模式，旨在帮助患者恢复身体健康、提高生活质量。它涵盖了多个方面，包括康复护理评估、计划制定、措施实施和效果评估等。康复护理评估是了解患者病情和需求的重要环节，通过对患者的基本信息、心血管病病情和康复护理需求进行评估，为后续的护理计划制定提供依据。康复护理计划制定则根据评估结果，设定康复护理目标，制定相应的康复护理措施，并确保计划的实施。康复护理措施实施包括运动康复护理、饮食康复护理、心理康复护理和健康教育等方面。运动康复护理可以帮助患者增强心肺功能，提高身体耐力；饮食康复护理有助于控制体重、血脂和血压等；心理康复护理则关注患者的心理状态，提供必要的心理支持；健康教育可以提高患者对疾病的认识和自我管理能力。康复护理效果评估通过设定评估指标和方法，对康复护理的效果进行评估和反馈，以便及时调整护理计划。心血管病康复护理是一个系统的过程，需要综合考虑患者的身体、心理和社会需求，为患者提供全面、个性化的护理服务。

康复护理在心脏瓣膜病患者围术期应用效果的研究

陈晨 李娟利

西安交通大学第一附属医院

目的：基于心脏瓣膜病患者围术期肺康复的最佳证据，构建适合心脏瓣膜病特点的分级、全程、综合的围术期肺康复护理方案。并验证该方案对心脏瓣膜病患者的效果。方法：1. 运用复旦大学循证护理中心提出的 PIPOST 循证问题开发工具，按照“证据资源 6S 模型”检索肺康复领域的最新专家共识、临床实践、指南等文献资源，依据证据类型的不同选择对应的质量评价标准，最终纳入文献 13 篇。对 13 篇文献进行证据提取，结合小组讨论，总结心脏瓣膜病患者围术期肺康复护理最佳证据。2. 采用德尔菲专家函询法，对心脏瓣膜病患者围术期肺康复护理最佳证据总结进行完善、修正，形成心脏瓣膜病患者围术期肺康复护理方案。3. 开展临床实证研究，将该方案应用于临床患者，验证该方案对患者的心肺功能、临床结局、生活质量的影响。结果：本研究基于循证，总结肺康复护理最佳证据。并经过 2 轮专家函询，完善证据内容，形成肺康复护理方案。选取 68 例心脏瓣膜病手术患者进行临床研究。1. 运用复旦大学提出的 PIPOST 工具结构化临床问题，遵循“证据资源 6S 模型”自上而下检索肺康复领域的最新专家共识、临床实践指南等文献资源，根据文献纳排标准，筛选文献，最终纳入文献 13 篇，其中临床决策 3 篇，指南 1 篇，证据总结 3 篇，随机对照试验 3 篇，类实验研究 2 篇，专家共识 1 篇。依据证据类型的不同选择合适的质量评价工具，证据提取后分类汇总，形成 11 个证据大类 ,24 条证据，并以此构建心脏瓣膜病患者围术期肺康复护理方案。2.2 轮专家函询问卷回收率为 100% 和 93.1%, 专家权威系数分别为 0.902、0.908, 条目的 Kendall's W 值分别为 0.181、0.127, 经卡方检验 ,p<0.05。共删除 11 个条目，修改 10 个条目，新增 3 个条目，形成包含 59 个条目的心脏瓣膜病患者肺康复护理方案。3. 选取西安某三甲医院心脏外科 2022 年 3 月 ~ 2023 年 3 月符合条件的 34 例患者为对照组，实施常规护理，选取 2023 年 5 月 ~ 2024 年 12 月符合条件的 34 例患者为试验组，实施常规护理加肺康复护理方案。两组患者的年龄、性别、婚姻状况、文化程度、BMI 指数、饮酒史、吸烟史、既往史史等一般资料比较，差异无统计学意义 (p>0.05)。干预后两组患者肺功能、心功能、生活质量均高于对照组，而临床结局的影响差异无统计学意义。结论：1. 通过心脏瓣膜病患者围术期肺康复护理的最佳证据总结，为心脏瓣膜病患者围术期肺康复护理方案的构建提供了高质量证据支持。2. 运用德尔菲专家函询法构建的肺康复护理方案严谨、可靠，为临床实施肺康复护理方案提供保障。3. 心脏瓣膜病患者围术期肺康复护理方案，能改善患者心肺功能，增强呼吸肌力量，进而提高生活质量。

基于说服系统模型的慢性心衰患者居家运动康复平台设计与应用

卢静 [1] 游展鸿 [2] 于甜栖 [3] 王洁 [1] 高敏 [1] 王琴 [1] 孙国珍 [1]

1. 南京医科大学第一附属医院

2. 南京医科大学护理学院

3. 南京医科大学康达学院

目的 结合慢性心衰患者的实际需求，设计并开发居家运动康复平台，验证其应用效果。

方法 基于说服系统模型，采用文献研究、头脑风暴等方法依据前期所构建的干预方案设计微信小程序的功能模块及内容。便利选取南京市某三级甲等医院 2024 年 3 月 -7 月 90 例符合纳排标准的慢性心衰患者作为研究对象。采用区组随机法分为对照组与试验组。试验组患者通过平台接受移动健康远程干预，对照组患者则接受常规的运动康复指导。比较两组患者在干预前、出院 1 个月、出院 3 个

月和随访 6 个月的运动参与分期、运动依从性得分、抑郁焦虑得分、自我损耗得分、生活质量得分的差异。

结果 共纳入 14 篇文献，对 PSD 原则遴选方式、使用频次、组合模式进行分析，最终提取出 11 条 PSD 原则用于指导交互特征设计，构建了包含四大模块（首页、运动康复、运动社区和个人中心）的“iHeart 心希望”平台。干预期间，共有 10 例患者失访，两组患者基线资料均衡可比（$P > 0.05$）。试验组患者在出院后 1、3、6 个月的运动参与、运动依从性均高于对照组，差异具有统计学意义（$P < 0.001$），试验组患者在出院后 3、6 个月的焦虑、抑郁和自我损耗程度均低于对照组，生活质量高于对照组，差异具有统计学意义（$P < 0.001$）。

结论 基于说服系统所构建的移动健康远程康复平台，结合以认知、情绪、行为改变和动机提升的理论方案指导，实施居家远程运动康复能有效降低负性情绪和自我损耗，改善慢性心衰患者的运动依从性和生活质量。

心脏急重症有关的研究

心源性休克患者在心内监护室的护理要点与方法

邓晓雯

新疆维吾尔族自治区人民医院

目的：探讨心源性休克患者在心内监护室的护理要点与方法。通过对比两组不同护理方法的效果，为临床提供有效的护理策略。

方法：选取 2023 年 1 月至 2024 年 6 月期间收治的 40 例心源性休克患者，随机分为对照组和实验组，各 20 例。对照组采用常规护理方法，实验组则展开针对性护理干预。

结果：实验组患者在病情稳定、住院时间、并发症发生率等方面表现优于对照组，护理满意度较高，出院后的生理恢复情况更理想。

结论：针对性护理干预在心源性休克患者的心内监护中效果显著，能有效提升患者的治疗效果和护理质量，值得推广应用。

心源性休克是指由心脏病变引发的全身性循环衰竭，常伴随低血压、组织缺血及多脏器功能障碍。心内监护室的护理工作对于保障心源性休克患者的生命安全和提升治疗效果起到了重要作用。现代护理强调个体化、综合性护理方法的应用，针对心源性休克患者的病理特点，制定科学的护理方案，可以有效降低并发症，促进患者的早期康复。本研究的目的在于探讨心内监护室中不同护理方法对心源性休克患者的护理效果，评估其对患者生命体征、并发症、住院时间、护理满意度等方面的影响，探索最适宜心源性休克患者的护理路径，为护理人员提供理论支持和实践指导。

关键词：心源性休克；心内监护室；护理要点；护理方法

心脏骤停患者亚低温护理对神经功能恢复的影响

邓晓雯

新疆维吾尔族自治区人民医院

目的：探索在心脏骤停患者复苏后引入亚低温护理对神经系统功能恢复的实际价值，并评估其在血清神经元特异性烯醇化酶（NSE）变化及预后评定中的作用。

方法：纳入 2022 年 12 月至 2023 年 12 月住院的 40 例心脏骤停复苏成功患者。依据随机分组原则，分为对照组（标准治疗）与实验组（亚低温干预），各 20 例。对照组实施常规生命支持及神经监测，实验组在此基础上增加目标温度控制措施，维持体温在 32–35° C，持续时间为 24 小时。

结果：在 72 小时内，实验组 CPC-1 级的比例高于对照组，提示意识恢复质量差异明显。血清 NSE 浓度在 24 小时和 72 小时时均低于对照组，表明神经元损伤程度下降。90 天随访中，实验组在神经功能评分与生活自理能力方面表现更优。良好预后率及功能性恢复分值均有统计学差异。由此可见，亚低温处理不仅影响短期生化指标，更延伸至远期神经系统重建过程。

结论：亚低温治疗可在心脏骤停后有效减轻脑组织损害，优化神经功能恢复过程。在维持生命体征稳定基础上，温控管理策略具备实际的临床意义。其神经保护作用并非仅局限于急性期，亦可为后期认知恢复提供支持，提示该干预应作为复苏后管理的重要组成部分。未来应结合患者个体差异，探索温度控制的精准实施时机与持续周期，以提高神经功能恢复的可预测性。

关键词：心脏骤停；亚低温护理；神经功能恢复

血管外肺水指数与中心静脉压预测心源性休克患者容量状态的比较研究

游洁芸

上海市东方医院（同济大学附属东方医院）

目的：血管外肺水指数（EVLWI）是评估肺水肿严重程度的可靠指标。本研究旨在比较 EVLWI 与中心静脉压（CVP）预测心源性休克患者全心舒张末期容积指数（GEDVI）这一关键心脏前负荷参数的有效性。

方法：本研究为前瞻性队列研究，纳入 200 例诊断为心源性休克的患者。通过脉搏指示连续心输出量（PiCCO）系统同时测量 EVLWI 和 CVP。采用 Spearman 相关性分析评估 EVLWI（或 CVP）与 GEDVI 之间的关系。进行受试者工作特征（ROC）曲线评估 EVLWI 和 CVP 对 GEDVI 升高的预测价值。

结果：最终分析纳入了 166 例心源性休克患者共 971 组数据集。EVLWI 与 GEDVI 呈显著正相关（r = 0.47，p <0.01），而 CVP 与 GEDVI 无明显相关性（r = 0.03，p = 0.38）。预测 GEDVI> 800mL/m^2 的最佳 EVLWI 临界值为 10.35mL/kg，曲线下面积（AUC）为 0.76（95% CI：0.73 - 0.79，p < 0.01）。相比之下，CVP 的预测性能较差（AUC = 0.53，95% CI：0.49 - 0.57，p = 0.14）。EVLWI 的诊断准确性高于 CVP（53.35% 对 47.27%；差异：6.08% [p < 0.01]）。与 CVP 相比，EVLWI 在预测 GEDVI 升高方面具有更高的敏感性（94.22% 对 67.17%；差异：27.05%，p < 0.01）。在预测 GEDVI > 800 mL/m^2 时，EVLWI 和 CVP 的特异性均相对较低（32.40% 对 37.07%；差异：4.67%，p > 0.05）。EVLWI 的阳性预测值、阴性预测值、阳性似然比和阴性似然比分别为 41.67%、91.63%、1.39 和 0.18。此外，基线 EVLWI 预测 30 天全因死亡率的 AUC 为 0.78（95% CI：0.74 - 0.83，p < 0.01），而基线 CVP 无该方面的预测价值（AUC = 0.52，95% 置信区间：0.45 - 0.59，p = 0.56）。

结论：在预测心源性休克患者的 GEDVI 升高和短期死亡率方面，EVLWI 优于 CVP。这些研究结果支持在这一高危人群中，使用 EVLWI 而非 CVP 作为容量管理的优选参数。

GLP-1R Activation Alleviated Sepsis-Induced Cardiac Dysfunction by Modulating Macrophage Polarization via the STING/ P65 Pathway

Yusha Zhang, Jia-Bao Zhou, Ya-Qin Chen

The Second Xiangy Hospital of Central South University

Background:

Sepsis, which triggered by dysregulated host immune responses, is a leading cause of mortality in critically ill patients. Sepsis-induced cardiomyopathy (SIC) is a frequent and life-threatening complication of sepsis. However, its pathogenesis remains incompletely understood, and specific therapeutic strategies are currently lacking, highlighting the urgent need to identify novel intervention targets. Emerging evidence highlights two pivotal mechanisms underlying SIC pathogenesis: pyroptosis and macrophage polarization. On one hand, myocardial pyroptosis directly contributes to the deterioration of cardiac function. On the other hand, dynamic macrophage phenotypic switching modulates inflammatory microenvironments and influences cardiomyocyte function through paracrine signaling, positioning macrophage polarization as a critical therapeutic target for SIC management. Glucagon-like peptide-1 receptor agonists (GLP-1RAs), as multifunctional therapeutic agents, exhibit dual therapeutic effects by attenuating systemic inflammation during sepsis and promoting macrophage M2 polarization, although their exact molecular mechanisms remain incompletely understood. Notably, the stimulator of interferon genes (STING), a key immunoregulatory molecule, has been implicated in macrophage polarization. Nevertheless, whether GLP-1R activation modulates macrophage phenotypic switching via the STING pathway remains unexplored. This study focused on investigating the regulatory roles of GLP-1R activation on macrophage polarization and its cardioprotective role in SIC, with a focus on elucidating the molecular mechanisms of the GLP-1R-STING signaling axis.

Objectives:

1. To explore the therapeutic potential of GLP-1R activation in SIC. 2. To clarify the role and molecular mechanisms of STING in GLP-1R-mediated macrophage polarization. 3. To determine the impact of GLP-1R-regulated macrophage polarization on cardiomyocyte pyroptosis.

Methods:

In vivo experiments: This study employed liraglutide (Lira), a representative GLP-1RA drug, to investigate the protective effects of GLP-1R activation on SIC. Wild-type C57BL/6 mice were pretreated with Lira (100 ng/kg, intraperitoneal injection every 12 h for 3 days) and subjected to lipopolysaccharide (LPS, 10 mg/kg) to establish a septic model at 24 h. Echocardiography and histopathological examination were performed to assess the successful establishment of the SIC model. Serum IL-1β and IL-6 levels were measured by ELISA. Flow cytometry, Western blot, and RT-qPCR were employed to assess myocardial pyroptosis-associated proteins and states in macrophage polarization.

In vitro experiments: Primary peritoneal macrophages (PMs) were isolated and treated with Lira for 24 h, followed by LPS (1 μg/mL) stimulation for 12 h. Flow cytometry and Western blot were used to evaluate polarization markers. STING expression was modulated via siRNA knockdown or pharmacological activation (DMXAA, 50 μg/mL). Nuclear translocation of P65 was observed by immunofluorescence. Conditioned medium (CM) from PMs was co-cultured with H9c2 for 12 h. Cell membrane integrity and pyroptosis-related proteins were assessed using scanning electron microscopy and Western blot.

Results:

1. Lira pretreatment significantly improved survival outcomes (47% vs. 29%) and attenuated systemic inflammatory responses in LPS-induced septic mice. Theatment of Lira ameliorated sepsis-induced myocardial injury while suppressing the expression of pyroptosis-related proteins. Notably, Lira treatment markedly inhibited M1 polarization and promoted M2 polarization of cardiac macrophages.

2. In vitro, Lira concentration-dependently inhibited LPS-induced M1 polarization and enhanced M2 polarization (peak effect at 50 μM). Compared to the LPS group, Lira treatment significantly reduced IL-1β and IL-6 secretion by PMs. Furthermore, immunofluorescence analysis confirmed GLP-1R expression in PMs, which was markedly upregulated upon Lira stimulation.

3. CM from Lira-treated PMs preserved H9c2 membrane integrity and suppressed pyroptosis-related protein expression compared to CM-LPS.

4. Lira inhibited LPS-induced STING activation in a concentration- (50 μM) and time-dependent (24 h) manner. STING knockdown enhanced Lira-induced M2 polarization, while DMXAA partially reversed Lira's inhibitory effect on M1 polarization.

5. GLP-1R activation suppressed LPS-induced P65 nuclear translocation. STING knockdown amplified this effect, whereas activation of STING abolished it.

6. STING activation (CM-DMXAA+LPS+Lira) counteracted Lira's protective effect on H9c2 pyroptosis, while STING knockdown (CM-siSTING+LPS+Lira) enhanced it.

7. In vivo STING activation diminished Lira's therapeutic efficacy, negating its survival benefits and myocardial protection.

Conclusions:

1. GLP-1R activation improves survival and mitigates systemic inflammation in septic mice. 2. GLP-1R activation alleviates cardiomyocyte pyroptosis by promoting M1-to-M2 macrophage polarization. 3. The cardioprotective effects are mediated via inhibition of the STING/P65 pathway, which regulates macrophage polarization. This study provides novel experimental evidence supporting GLP-1R activation as a therapeutic strategy for SIC.

心血管危重症医护一体化管理的探索与实践

张蕾

西安交通大学医学院第一附属医院

目的：心血管危重症病情凶险，对时效性、精准性和团队协作要求极高。为突破分科壁垒、优化救治流程，我院心内科探索医护一体化管理模式，评估其对提升救治效率、精准度、全程管理及改善预后的效果。

方法: 采用前瞻性队列研究结合历史对照。核心策略: 1. 组建快速反应团队 (RRT): 心血管重症医师主导，资深重症护士为核心，联合多学科 24 小时待命。2. 建立标准化救治链：强化护士早期预警；医护联合快速床旁评估，信息实时共享；制定演练预案，护士深度参与高级生命支持、血管活性药滴定、有创监测、机械通气、IABP 管理及监护转运。3. 深化协作机制：每日医护联合查房；标准化交班；即时信息同步；定期病例回顾与根因分析持续改进。4. 强化重症护理能力：系统培训护士核心重症技能（血流动力学监测、复杂用药、高级气道管理、CRRT、镇静镇痛评估及谵妄预防）。

结果（实施 4 个月）： 1. 效率与成功率提升：STEMI "门 - 球时间" ≤ 58 分钟；抢救成功率提高 32%；心源性休克 IABP 上机提前 16%；非计划重返 CCU 率下降。2. 护理质量与安全改善：VAP、CLABSI、压力性损伤、非计划拔管等并发症显著降低；血管活性药使用更安全；谵妄筛查达标。3. 患者预后改善：CCU 平均住院日缩短；28 天及院内死亡率下降趋势；神经功能预后良好率提升。4. 团队协作增强：医护沟通效率、决策共识度及满意度提高。

结论：心血管危重症医护一体化模式通过构建高效多学科 RRT、建立标准化快速救治链、实施深度协作机制（联合决策、实时沟通、共同质控）及强化重症护理能力，实现了医疗护理资源无缝整合。实践证实，该模式显著提升了救治效率与成功率，降低了并发症，改善了患者生存率、生存质量及医疗安全，同时提升了护理价值，是应对心血管危重症挑战、实现高质量救治目标的有效路径，具有重要推广价值。

命悬一线，好转出院 ——1 例急性心肌梗死行 ECMO 治疗存活者的远期疗效观察

白雅萍 胡文冰 施婧

厦门大学附属心血管医院

目的：体外膜肺氧合（ECMO）作为一种高级生命支持技术，在挽救严重心肺功能衰竭患者生命方面发挥着关键作用。尽管 ECMO 在短期内能够显著提高患者的生存率，使更多患者得以度过疾病的危重阶段并出院，但出院并不意味着患者已完全康复。因此，本研究旨在总结 1 例急性心肌梗死行 ECMO 治疗存活者的远期疗效观察，以期为今后优化 ECMO 治疗策略、改善患者长期预后、合理分配医疗资源以及为患者提供全面的康复指导和心理支持至关重要。

方法：组建文献检索小组，基于指南和专家共识建立 ECMO 治疗存活者出院随访内容；从身体健康状况、生活质量、心理健康、日常生活能力等方面进行质性访谈；借由诺丁汉健康概况量表和创伤后应激障碍自评量表（PTSD）进行科学评估。患者出院后 1 个月、3 个月定期来院随访，通过复查血常规、生化、CTNT、BNP、超敏 C 反应蛋白、心电图、心脏彩超等情况，了解其出院后生存情况及其生活质量。

结果：各项检验检查大致正常，心超 EF 值 61%，患者生活能力完全自理，每日散步，每次约半小时，出院至今已完全戒烟，每日睡眠时间 7-9 小时，睡眠质量良好，患者对于住院期间的抢救经历已完全遗忘，经评估存在轻度创伤后应激障碍，但由于住院期间因心肺复苏肋骨骨折，目前呼吸时仍有轻微疼痛，在冠心病的预防知识知晓率较低。

结论：ECMO 出院幸存者的随访是延续性护理的核心环节，其重要性贯穿生理康复、心理支持、医疗质量提升的全链条。通过系统化随访，不仅能保障患者远期预后，也为重症医学领域的临床实践和科研提供关键数据支撑，最终实现 "以患者为中心" 的全程化照护目标。

急性心肌梗死院前就医延迟模型构建及验证

肖喜娥

陆军特色医学中心

目的 急性心肌梗死（acute maocardial infarction,AMI）对人类生命健康造成严重影响，而急性心肌梗死的有效治疗依赖于时间，就医延迟就会增加死亡的风险。然而关于急性心肌梗死延迟就医的预测模型目前少见报道。因此，本研究基于重庆市某三甲医院 AM) 绿色通道患者就医数据，构建急性心肌梗死患者就医延迟的风险预测模型并进行评价。**方法** 纳入 2016.11-2022.12 月 重庆某三甲医院通过绿色通道救治的 AMI 患者 812 例，收集病例的一般资料、症状、疾病相关因素、入院方式、发病时间、就医时间等 13 项指标。研究对象按 7:3 随机拆分为训练集和验证集。采用 logistic 分析探究急性心肌梗死患者就医延迟的风险因素，随即建立了列线图风险预测模型，并在验证集中进行了验证。采用 ROC 曲线下面积、校准曲线、决策曲线和临床影响曲线评估模型的综合预测性能。另外，进一步确定了一个截断值，用于快速区分低风险和高风险人群。对该截断值的作用，采用了混淆矩阵进行了评估。**结果** 1. 持续胸痛 [OR=0.24(0.16-0.35, p<0.001)]、非自行入院 [OR=0.23(0.14-0.37, p<0.001)]、合并三种及以上的慢病 [OR=1.83(1.11-3.05, p=0.019)]、居住地非主城 [OR=2.19(1.50-3.24, p<0.001)] 是 AMI 患者就医延迟的独立影响因素。2. 可视化 Nomogram 预测模型，共纳入 4 项指标（持续胸痛、入院方式、合并三种及以上的慢病、居住地）。有无持续胸痛是影响发生就医延迟的最重要变量。训练集和验证集的 ROC-AUC 值分别为 0.765（95%CI=0.727-0.804）和 0.758（95%CI=0.698-0.818），表明模型对延迟和非延迟患者具有良好的区分能力。绘制校准曲线，提示预测模型的预测结果与实际观察结果之间具有 好的一致性。Hosmer and Lemeshow odness of fit (GOF) test（训练集 = 6.2234, p-value = 0.3986；验证集 = 8.197, p-value = 0.224），表明观察到的事件与预测的事件之间没有显着偏差。Brier score(训练集为 Brier score=0.196，验证集为 Brier score=0.196), 均小于 0.25。进一步说明模型具有较好的准确度。采用 CIC 和 DCA 方法评价该模型的临床适用性，结果表明在训练集和验证集中预测模型均具有较高的净效益。为了快速识别高风险人群，基于最大约登指数，确定了模型的最佳 cutoff 值 =152.286，并绘制了该截断值下训练集及验证集的混淆矩阵，并计算了相关的诊断指标。**结论** 该模型有临床应用价值，可筛查出急性心肌梗死就医延迟的人群。该模型在患者人群的提前干预，降低急性心肌梗死院前不良心血管事件和死亡的发生率等方面将发挥积极的作用。

心肌梗死 PCI 术后非计划再手术患者临床特征及影响因素分析

肖喜娥

陆军特色医学中心

目的 探讨心肌梗死患者经皮冠状动脉介入治疗（PCI）术后非计划再手术的临床特征及影响因素，为早期识别高风险患者和优化临床护理路径提供依据。**方法** 采用回顾性队列研究设计，纳入 2023 年 1-12 月重庆市某三甲医院接受 PCI 治疗的心肌梗死患者 343 例，其中病例组（非计划再手术）179 例，对照组（同期首次手术）164 例。通过电子病历系统采集数据，比较两组临床特征，采用独立样本 t 检验、Mann-Whitney U 检验 /χ^2 检验进行组间比较，运用多因素 Logistic 回归及 ROC 曲线分析影响因素及模型预测效能。**结果** 单因素 Logistic 回归显示，病例组年龄高于对照组（P < 0.05），入院首次监测舒张压、总胆固醇、高密度脂蛋白胆固醇、低密度脂蛋白胆固醇、白细胞计数、中性粒细胞计数以及淋巴细胞计数低于对照组（P 均 < 0.05）。多因素 Logistic 回归显示，年龄增长（OR=1.412，95%CI：1.106-1.803）和 LDL-C 降低（OR=0.411，95%CI：0.185-0.913）与心肌梗死患者 PCI 术后非计划再手术风险增加显著相关。该模型通过双侧检验（α=0.05），提示年龄每增长 1 岁，非计划再手术风险升高 41.2%（OR=1.412）；LDL-C 每降低 1 个单位，非计划再手术风险降低 58.9%（OR=0.411）。**结论** 心肌梗死 PCI 术后非计划再手术与患者老龄和代谢紊乱相关。临床应重点关注老年、营养不良及免疫低下患者，建议建立包含营养支持、血脂管理的个性化护理方案。

两难境地，险象环生 - 急性心梗合并消化道出血，如何是好？

俊

马鞍山市人民医院

本 PPT 介绍两例急性心肌梗死合并消化道出血患者救治成功案例。

患者男性，56 岁。因 "心前区不适伴呕血、黑便 2 天" 入院。l 患者缘于 2024 年 2 月 4 日 11 时大量饮酒后，出现心前区不适，伴呕吐 1 次， 呕出血性胃内容物及血块，就诊于县医院查心电图（2 月 4 日 15:14）示 窦律，V1-V5 导联 ST 段抬高 0.1-0.4mv，T 波高尖，当地医院给予抑酸护 胃、补液处理，完善胃镜提示胃窦溃疡、胃角溃疡、十二指肠球部溃 疡，腹部 CT 平扫提示肝脏多发囊肿，2 月 5 日凌晨患者解黑便一次，复 查心电图（2 月 5 日 19:42）示窦律，V1-V5 导联 Q 波形成，ST 段抬高 0.1-0.3mv，肌钙蛋白 T 2.25ng/ml，CK-MB 126U/L，考虑急性心肌梗死 合并消化道出血，建议转上级医院，患者家属联系 120 转运至我院急诊， 我科会诊后收住我科。

病例亮点

1. 急性心肌梗死与消化道出血，治疗上背道而驰，但两种疾病危重时均可危及生命，作为医生我们只有权衡利弊，抓住主要矛盾，随时调整治疗方案。

2. 临床上没有绝对的禁忌症，只有相对的禁忌症。绝对禁忌症只有一点（患者及家属拒绝治疗）。作为一名临床医生有百分之一生的希望，我们应该都会付出百分百的努力。

3. 危重症病人抢救，人多力量大，医护合作，多学科努力，同时患者及家属的配合及信任是最重要的，"每一条鲜活的生命都是无价"，敬畏生命、医者人心。

第一阶段射血分数在脓毒症心肌损伤的早期识别及临床预后的评估价值

谢梦莹 [1] 黄毅 [2] 古小松 [2]

1. 无锡市第九人民医院

2. 苏州大学附属第二医院

目的：脓毒症相关心肌损伤（Sepsis-induced myocardial injury，SIMI）是脓毒症及脓毒性休克患者常见的并发症，SIMI 的患者病情重，病死率高。本研究拟探讨第一阶段射血分数（First-phase Ejection Fraction，EF1）在 SIMI 中心脏功能的早期识别及临床预后的评估价值。

方法：本研究纳入苏州大学附属第二医院、无锡市第九人民医院 2021 年 3 月至 2024 年 6 月符合 sepsis3.0 的脓毒症患者列为研究对象，共 150 例。根据肌钙

蛋白 I 水平，分为 SIMI 组（cTnI > 0.1mg/L）63 例和脓毒症非心肌损伤 (NSIMI) 组（cTnI < 0.1mg/L）87 例。所有患者收集入院后 48 小时内的基线资料、血生化指标，入院后 48 小时和入院 7-10 天的两组患者的超声心动图资料，出院 3 个月随访死亡率和再入院率。并运用 R 软件和 GraphPad Prism 9.0 软件进行统计学分析。

结果：（1）基线资料中，SIMI 组心率更快，且 APACHE II、SOFA 评分显著更高，结果具有统计学意义（P < 0.05）。SIMI 组白细胞计数、中性粒细胞计数、中性粒细胞计数 / 淋巴细胞计数（NLR）更高，氧合指数更低，乳酸更高，IL-6 更高，具有统计学意义（P < 0.05）。SIMI 组肌酸激酶同工酶（CK-MB）、NT-proBNP、D- 二聚体、尿酸、球蛋白更高，具有统计学意义（P < 0.05）。入院 48 小时内的超声心动图显示: SIMI 组 LVEF 较低（P < 0.05），而 EF1 显著减低（P < 0.01）。

（2）对所有患者进行多因素 Logistic 回归模型显示，EF1 水平、NT-proBNP 水平及 NLR 与 SIMI 的发病危险因素（P < 0.001）。

（3）EF1 对 SIMI 组患者的 ROC 曲线，最佳截断阈值：0.295，灵敏度：0.556，特异度：0.736，曲线下面积为 0.692（95%CI：0.609-0.776，P < 0.001）。

（4）在 SIMI 组内分析显示，EF1 与 NLR，肌钙蛋白存在显著相关（P < 0.01）

(5) 对 SIMI 组患者相关性分析显示： EF1 水平与总胆红素、淋巴细胞、NLR、TnI、Myo、血糖、LAD、GLS 水平存在相关性（P < 0.05）。

（6）住院治疗 7-10 天心超随访， LVEF 无明显变化， LVEF1 较入院时明显改善

（7）入院一周后对 SIMI 复查心超，LVEF1 增加组 45 例，LVEF1 非增加组 18 例，随访 3 个月，K-M 生存曲线结果显示 EF1 增加组较 EF1 非增加组患者的生存具有显著差异（HR：2.905，95%CI：1.260-6.669，P=0.0119）。

结论：第一阶段射血分数（EF1）对 SIMI 的早期识别具有重要价值，对 SIMI 的预后有良好的评估价值。

关键词：脓毒症心肌损伤；第一阶段射血分数；EF1；脓毒症；脓毒性休克；SOFA 评分；预后

经皮机械循环辅助装置的应用现状及国产化进程

于国英 刘斌

吉林大学白求恩第二医院

心血管急危重症是一组病情凶险、进展迅速且死亡率高的疾病，主要包括急性冠脉综合征、心源性休克、急性心力衰竭、恶性心律失常等，早期识别和及时干预是救治关键，近年来，随着复杂、高危心血管疾病介入治疗的广泛开展，经皮机械循环辅助装置（percutaneous mechanical circulatory support,pMCS）也逐渐受到重视。pMCS 是一类通过微创方式植入的短期循环支持设备，作为一种新的治疗策略，可提供有效的血流动力学支持，保证全身重要脏器灌注，有效改善心血管急危重症患者的预后，降低病死率。目前心血管内科常用的 pMCS 主要包括主动脉内球囊反搏（intra-aortic balloon counter-pulsation,IABP）、静脉 - 动脉体外膜肺氧合（veno-arterial extracorporeal membrane oxygenation,VA-ECMO）及介入式左心室 - 主动脉轴流泵辅助装置 Impella 系统、TandemHeart 系统等。目前国内部分厂家已着力研发 IABP，有望替代进口产品，实现 IABP 国产化，填补国产高端心脏辅助设备的空白。ECMO 在新冠疫情后需求激增，推动国产化进程，但目前市场仍由外资主导。而高端 pMCS 设备（如 Impella、TandemHeart）仍依赖进口，其中 Impella 尚未获 NMPA 批准，仅少数中心用于临床实验，而 TandemHeart 系统未进入中国市场，目前国内无应用案例。国家鼓励高端医疗设备国产化，推动“心电一张网等”智慧医疗模式，但基层医院仍面临设备短缺问题。未来随着政策的支持和研发投入的增加，国产 pMCS 市场将迅速增长，有望在 5 年内实现更大范围的应用。

硫酸镁使用与心肌梗死患者死亡率的关系：一项回顾性队列研究

孙云飞 薛歆

吉林大学第二医院

目的

近年来，有研究关注镁离子在心血管疾病中的作用，但其在急性心肌梗死患者中的临床价值尚存争议。本研究旨在探讨在不同时间窗内静脉使用硫酸镁对急性心肌梗死患者死亡率的影响。

方法

本回顾性研究利用重症监护医学信息市场 （MIMIC）-IV 数据库分析急性 1 型心肌梗死患者。参与者根据接受硫酸镁治疗的时间分组（Q1 未接受，Q2 ≤ 6h，Q3 6-12h，，Q4 ≥ 12h），主要结果是 28 天全因死亡率。通过 COX 回归模型、Kaplan-Meier 生存分析和亚组分析评估硫酸镁使用与院内死亡率之间的关联。

结果

这项回顾性队列研究包括 4406 例患者，其中院内死亡率为 17.8%。在多变量 COX 回归中，完全调整后的模型表明硫酸镁使用与较低的 28 天全因死亡率相关（风险比 [HR]，0.61；95% CI，0.52-0.72；P<0.001）。无论何时给予硫酸镁，都观察到较低的死亡率：对于 6h 内使用硫酸镁，HR，0.73；95%CI，0.62-0.87，P<0.001；对于 6-12h 内使用硫酸镁，HR，0.68；95%CI，0.51-0.89，P=0.006；12h 以外使用硫酸镁，HR，0.71；95%CI，0.53-0.96，P=0.028。分层分析进一步证实了这种相关性的稳健性。

结论

硫酸镁的使用与急性心肌梗死患者的死亡率降低相关。需要前瞻性研究来验证这一发现。

第一阶段射血分数对新活素治疗慢性心衰急性加重的临床疗效评估

黄毅 古小松

苏州大学附属第二医院

目的：探讨第一阶段射血分数（EF1）在慢性心衰急性加重期患者新活素治疗前后的改善程度及预后评估价值。

方法：选取 2024 年 1 月至 2025 年 1 月在苏州大学附属第二医院确诊为慢性心力衰竭急性加重的住院患者共 310 例，随机分组，非新活素治疗组，和新活素治疗组，两组患者各 155 例。记录患者的一般情况，血压、NT-proBNP、cTnT、心超参数（LAD、LVESD、LVEDD、EF、EF1、T1 时间、E/e'）。新活素治疗后 5 天再次测量心超参数。对新活素治疗组患者随访 3 个月，观察心衰再住院和心因性死亡事件。

结果: (1) 根据既往病史，对所有入组患者进行 NYHA 分级，与心功能 III 级组相比，心功能 IV 级组的年龄、BMI、糖尿病患病率、总胆固醇、低密度脂蛋白、空腹血糖、超敏 C 反应蛋白、NT-proBNP、cTnT、LVESD、LVEDD 和 E/e'更高，收缩压、舒张压、高密度脂蛋白、EF 和 EF1 更低，差异有统计学意义（P < 0.05）。（2）对所有入组心衰患者进行相关性分析：EF1 与 BMI、总胆固醇、NT-proBNP、cTnT、LVESD、LVEDD 和 E/e'呈负相关，与高密度脂蛋白、EF 呈正相关。(3) 多元 logistic 回归表明：EF1 是心功能 IV 级的独立保护因素 （OR: 0.898, 95% CI: 0.759 - 0.941）；多元线性回归分析表明: cTnT 是 EF1 的独立危险因素（OR: 1.350, 95% CI：1.118 - 1.575）（4） 所有患者治疗前后结果比较：非新活素治疗组和新活素组治疗后收缩压、舒张压、NT-proBNP、cTnT、T1 时间和 E/e'均低于治疗前，EF1 均高于治疗前，差异有统计学意义（P < 0.05）；两组治疗前后 EF 比较，差异无统计学意义（P > 0.05）。（5）两组患者治疗后结果比较：新活素组收缩压、NT-proBNP、cTnT 和 E/e'均低于非新活素组，EF1、症状缓解率高于非新活素组，差异有统计学意义（P < 0.05）。（6）对新活素治疗组随访，97 人 EF1 增加，58 人 EF1 无明显变化或者降低，两组随访，EF1 增加组患者心力衰竭加重再入院或心因性死亡的发生率低（27.84% vs 46.55%, P = 0.028）。

结论：EF1 与 NYHA 分级密切相关；新活素治疗能改善心脏 EF1 水平；新活素治疗后心脏 EF1 升高患者随访心衰再入院和心因性死亡风险较低。

关键词：第一阶段射血分数；慢性心力衰竭急性加重；新活素；临床疗效

急性心肌梗死合并心源性休克的当代治疗策略与技术

魏宇淼

华中科技大学同济医学院附属医院协和医院

背景：合并心源性休克是急性心肌梗死（AMICS）的主要院内死亡原因和极具挑战性的心血管急危重症，随着直接冠脉介入治疗及机械循环支持的长足发展，AMICS 患者的救治水准和存活率有一定改善。但具体临床实践中的关键措施和细节仍远未成熟一致，临床试验提供的证据也十分有限。目的：探讨急性心肌梗死合并心源性休克的当代循证证据及临床实践经验。方法：查询汇总 AMICS 当代治疗的证据、临床共识指南推荐及具体临床使用经验，进行循证评估、病理生理学分析和实践评述。结果：一、AMICS 的临床特征、血流动力学类型及病理生理机制；二、AMICS 的临床及病情监测；三、AMICS 的再血管化治疗：共识指南的相关建议；四、关于急性心肌梗死合并心源性休克及不合并心源性休克对非梗死相关动脉（IRA）的血运重建的讨论；五、关于急性心肌梗死合并心源性休克冠脉血运重建的技术经验；六、AMICS 的机械循环支持：证据及经验；七、关于 AMICS 机械通气、血液净化及机械循环辅助的使用经验。结论：AMICS 的再血管化治疗部分指南及共识较为明确，相关建议如下：1）对于 ST 段抬高型心肌梗死和缺血症状持续时间 <12 小时的患者，建议进行直接经皮冠脉介入治疗（PPCI），越早越好。2）初次缺血症状出现 12 小时以上的 ST 段抬高型心肌梗死患者，尤其是持续症状或动态心电图改变提示持续缺血、血流动力学不稳定或危及生命的心律失常的患者，建议尽快进行 PPCI。3）PCI 时常规建议使用新一代 DES 进行支架置入，不建议患者常规使用延迟支架置入术。但是，对于某些患者，如前壁心肌梗死患者，也可以考虑。不建议常规使用血栓抽吸，但血栓负荷重时应予血栓抽吸。4）非常高风险的非 ST 段抬高型心肌梗死（NSTEMI）患者立即常规进行冠脉侵入性治疗策略。

急性心肌梗死心脏游离壁破裂存活患者病情特征分析及相关诊治经验

魏宇淼

华中科技大学同济医学院附属医院协和医院

前言：传统观念认为急诊心脏外科是急性心肌梗死游离壁破裂最终存活的主要治疗因素，但并无确定的大规模研究证据。目的：探讨急性心肌梗死心脏游离壁破裂存活患者病情特征及相关诊治经验。方法：采用回顾性研究方法，收集我院近年来诊断为急性心肌梗死后心脏游离壁破裂存活的患者共 23 名，对其临床特征、治疗方法及预后信息等进行整理汇总分析。重点分析急性心肌梗死患者发生心脏游离壁破裂的相关因素和发生心脏游离破裂后常规治疗存活者的相关因素。结果：患者发生心脏破裂的相关因素主要有：急性 ST 段抬高型心肌梗死发病 2 周内，下后壁或侧后壁心肌梗死比例更多，与是否存在心尖部室壁瘤关系不明显；包含替罗非班在内的强抗栓与亚急性心脏破裂有关，急诊 PCI 治疗可以减少心脏破裂的发生。发生心脏游离壁破裂后经常规治疗存活患者的因素分析有：存活患者多为亚急性破裂，患者存活预后的主要因素决定于破口大小和是否及时心包穿刺引流并成功维持了血流动力学稳定，急诊外科手术不是患者存活的首要因素。结论：急性透壁性 ST 段抬高型心肌梗死在 2 周内可发生心脏破裂，下后侧壁 ST 段抬高心梗所占比例更高。亚急性破裂患者多能存活，是否存活的预后的主要决定因素为破口大小和是否及时心包穿刺引流。根据根据患者血流动力学状态采取个体化治疗是治疗成功的关键。

The Role of TyG Index in distinguishing NSTEMI from Acute Heart Failure Patients

li Xiong, Xiao-Song Gu

The Second Affiliated Hospital of Soochow University

Background: Both acute heart failure (AHF) and non-ST-segment elevation myocardial infarction (NSTEMI) are cardiovascular emergencies that share overlapping symptoms, such as dyspnea on exertion, dizziness, and fatigue. These similarities may lead to misdiagnosis. Given the significant differences in treatment strategies between AHF and NSTEMI, accurate diagnosis is crucial, particularly in resource-limited settings where simple biomarkers are needed to aid differential diagnosis. The Triglyceride-Glucose (TyG) index serves as a reliable marker of insulin resistance (IR) and systemic metabolic dysregulation. It is significantly associated with the risk of NSTEMI, AHF, and adverse cardiovascular outcomes in patients. This study aimed to investigate the role of the TyG index in distinguishing NSTEMI from AHF.

Methods: Demographic and clinical data were collected from 1766 patients with acute heart failure (AHF) admitted to the hospital. Among them, 1246 patients underwent coronary angiography during hospitalization, and 684 patients were diagnosed with non-ST-segment elevation myocardial infarction (NSTEMI). The normality of continuous variables was evaluated using the Shapiro-Wilk test. Categorical variables were compared using Pearson's chi-squared test. Continuous variables were compared using the two-tailed student's t-test or Mann-Whitney U test between two groups. The association between the TyG index and NSTEMI was assessed using multivariate logistic regression analysis and restricted cubic splines (RCS) in AHF patients. Additionally, the predictive value of the TyG index, cTnT, and the combination of these two indicators for NSTEMI was preliminarily evaluated using the receiver operating characteristic (ROC) curve. In order to evaluate the discrimination efficiency of TyG index for NSTEMI risk factors, the reclassification index was used to verify the effect of the model optimization. The net reclassification index (NRI) and Integrated discrimination improvement (IDI) were used to compare the multi-dimensional models.

Results: Compared with the AHF without NSTEMI participants, the NSTEMI patients were more likely to be older and had higher levels of TC, TG, and LDL-C (P <0.05). We showed that TyG index and cTnT were higher in NSTEMI patients than in AHF patients without NSTEMI (Z: -7.16, P <0.001). Multivariate logistic regression analysis adjusted by gender, age, diabetes, hypertension, NT-proBNP, cardiac troponin T (cTnT) showed a significant association between TyG index and NSTEMI, for every 1 unit increase in TyG index, the morbidity risk of NSTEMI increased 2.22(OR: 2.03, 95% CI: 1.67 - 2.46, P <0.001). Adding TyG index into a basic risk model for NSTEMI improved the reclassification, the new model (TyG index + model) is better than the basic model (IDI: 0.05, 95%CI: 0.04 - 0.06, p There was a nonlinear correlation between TyG index and NSTEMI (P for nOnlinear= 0.03). TyG index combined with cTnT can improve the diagnosis rate of NSTEMI, the AUC of cTnT + TyG index is 0.767 in TyG Q4 group.

Conclusion: We investigated the predictive value of cTnT in conjunction with TyG index for NSTEMI. The combination of TyG index and cTnT serves as a reliable indicator for distinguishing NSTEMI in patients with AHF, potentially offering a novel strategy for early clinical intervention. This study aims to provide a cost-effective and efficient tool for rapid risk stratification in emergency settings, especially in resource-constrained regions.

Intra-aortic balloon pump implantation in early-stage cardiogenic shock reduces 30-day mortality in patients with ventricular septal defect following myocardial infarction

Jianmin Yang, Lin-Song Leng, Xiang-Juan Liu

Qilu Hospital of Shandong University

Background: Ventricular septal defect (VSD) is a serious mechanical complication of acute myocardial infarction, with an extremely high mortality. Intra-aortic balloon pump (IABP) has become a bridge to surgical repair. However, its effect on mortality varies partly because of shock severity.As a mature MCS device, IABP has the advantages of fast implantation, convenient use, and low complication rate. According to the 2023 European Society of Cardiology (ESC) guidelines for the management of acute coronary syndromes, intra-aortic balloon pump (IABP) is recommended for patients with MI-VSD accompanied by cardiogenic shock (CS) (Class IIb), as a bridge for MI-VSD hemodynamically unstable patients to undergo surgical repair. However, accurately determining the shock stage and assessing hemodynamic status changes in MI-VSD patients can be challenging in clinical practice, owing to the rapid fluctuations in their hemodynamic profile. Furthermore, for some patients who undergo surgical repair subsequent to IABP implantation during a period of hemodynamic instability, the prognosis tends to be unfavorable. In addition, the persisting high flow across the VSD with necrotic myocardium may increase the size of the rupture unpredictably.Traditional shock stage criteria cannot accurately identify the pre-shock stage, thus failing to implement timely intervention measures to prevent hemodynamic deterioration. In 2022, the Society for Cardiovascular Angiography and Interventions (SCAI) proposed a shock stage classification system that divides shock into stage A to E, defined as at risk, beginning, classic, deteriorating, and extremis, providing a risk stratification for mortality in CS patients. According to this staging system, patients begin to exhibit significant hemodynamic disturbances and inadequate microcirculatory perfusion at SCAI SHOCK stage C, with blood gas analysis showing lactate ≥ 2 mmol/L, which is the typical cardiogenic shock stage. Despite the current guideline downgrading the recommendation for routine use of IABP in patients with AMICS, it remains the most prevalent method utilized in clinical practice. The significant disparity between clinical practice and guidelines is motivating us to pinpoint the specific patient population that may exhibit a particularly favorable response to IABP in the context of MI-VSD. In order to address these concerns, the objective of this study was to assess the correlation between the utilization of IABP and 30-day mortality rates among MI-VSD patients with early-stage AMICS, classified as SCAI SHOCK stages A/B.

Aims: This study aims to evaluate the association between implantation of IABP in early-stage cardiogenic shock and the 30-day all-cause mortality in patients with VSD after myocardial infarction (MI-VSD).

Methods: The retrospective data were collected based on patients with MI-VSD who were admitted to Qilu Hospital of Shandong University from 2013 to 2024. Patients were stratified according to IABP implantation. We determined the severity of cardiogenic shock according to the Society for Cardiovascular Angiography and Interventions (SCAI) SHOCK stage classification system. The primary outcome was all-cause mortality within 30 days after VSD. Logistic regression models were constructed to evaluate the factors associated with the 30-day all-cause mortality. We conducted subgroup analysis and assessed interaction effects to evaluate the relationship between IABP use and 30-day mortality in various subgroups. The Kaplan-Meier survival curves were used to evaluate the cumulative incidence of 30-day mortality.

Results: This study included a total of 57 patients (mean age of 67.96±7.31 years; 47.4% male), 33 of whom received IABP implantation. The SCAI SHOCK stage was associated with 30-day all-cause mortality [odds ratio (OR) 3.19, 95% confidence interval (CI) 1.05-10.69, P = 0.048]. IABP implantation significantly reduced 30-day mortality in patients with SCAI SHOCK stages A/B (6.7% versus 55.6%; OR 0.06, 95% CI 0.01-0.64, P = 0.020), while no significant difference was observed in patients with SCAI SHOCK stages C/D/E (P = 0.611). We also found that in patients with SCAI SHOCK stages A/B, IABP implantation effectively prevented progression to SCAI SHOCK stages C/D/E.

Conclusions: Implantation of IABP in SCAI SHOCK stages A/B could reduce 30-day all-cause mortality in patients with MI-VSD.

褪黑激素对小鼠脓毒症心肌损伤模型的保护作用机制

侯红霞

河北大学附属医院 / 临床医学院

目的：研究褪黑激素（melatonin，Mel）对小鼠脓毒症心肌损伤（sepsis-induced myocardial injury，SIMI）的保护作用机制，明确其是否通过激活腺苷酸活化蛋白激酶（Adenosine Monophosphate-Activated Protein Kinase, AMPK）信号通路发挥保护作用。

方法：选取 32 只 8-10 周龄的健康雄性 C57/BL6J 小鼠，将其随机分为四组：(1) 正常组（Con, n=8）；(2) 模型组（Lps，n=8）；(3) 治疗组（Mel+Lps, n=8）；（4）治疗组 +AMPK 抑制剂组（Mel+Lps+CC, n=8）。给药 12 小时后行超声心动图仪检测小鼠左室射血分数 (LVEF) 和左室短轴缩短分数 (LVFS)，观察各组小鼠心功能变化情况。苏木精 - 伊红（HE）染色观察各组心肌结构变化。RT-qPCR 技术和 ELISA 等方法观察炎症因子 TNF-α、IL-1β、IL-6 及心肌损伤标志物 CK-MB、CTnI 的变化情况。采用 Western Blot 技术检测心脏组织总蛋白中 AMPK、P-AMPK 的蛋白表达水平。

结果：超声心动图和血流动力学测量显示：与对照组相比，Lps 组及 Mel+Lps+CC 组的 LVEF 和 LVFS 明显降低（P < 0.05），褪黑激素处理逆转了 LPS 诱导的心功能不全，LVEF 和 LVFS 明显升高（P < 0.05）。RT-qPCR 技术和 ELISA 法显示：Lps 组及 Mel+Lps+CC 组较正常组表现为 TNF-α、IL-1β、IL-6、CK-MB、CTnI 浓度及 mRNA 表达水平升高（P < 0.05），Lps+Mel 组 TNF-α、IL-1β、IL-6、CK-MB、CTnI 浓度及 mRNA 表达水平均明显降低(P<0.05)。HE 染色显示模型组小鼠较正常组存在严重的心肌组织损伤，褪黑激素组能减轻心肌损伤程度。Western Blot 结果显示褪黑激素能激活 AMPK 信号通路，P-AMPK/AMPK 比值升高（P < 0.01）。

结论：1. 褪黑激素治疗可改善脓毒症心肌损伤小鼠的心功能及降低炎症因子的水平，改善心肌损伤。2. 褪黑激素能激活 AMPK 信号通路，为脓毒症心肌损伤的治疗提供理论依据。

VA-ECMO 联合吸入一氧化氮治疗一例 TTVR 术后急性右心功能不全患者的护理

薛萌萌 耿周婴洋 王玉丽

厦门大学附属心血管病医院 (厦门市心脏中心)

总结 1 例全麻下行 TTVR 术后突发急性右心功能不全予 VA-ECMO 辅助支持及一氧化氮吸入治疗的护理经验。护理要点：① ECMO 的阶段性管理方案：早期阶段（高流量阶段）目标：快速恢复组织氧供，偿还氧债，改善循环。初始流量通常设置较高，帮助心肺得到休息。此阶段为患者流量设置为 3.5-4L/min。中期

阶段（中流量阶段）目标：维持心肺功能，促进其恢复。流量逐渐降低至适中水平，维持心排出总量的 80%，减轻心脏负担优化右心负荷，对于优化右心负荷采取了定制化容量管理模式、小剂量的去甲肾上腺素泵入、一氧化氮吸入治疗等，此阶段调节流量为 2-2.5L/min。后期阶段（低流量阶段）目标：为停机做准备，逐步减少 ECMO 支持，促进患者自主呼吸和循环的恢复。流量逐步减少，观察患者的生理参数和功能恢复情况，讲流量降至 1.0-1.5L/min 以下。②目标导向，动态评估患者容量目标：持续监测患者的中心静脉压、体重、出入量、超声评估下腔静脉的宽度及变异率等，确定容量管理目标；制作 24h 容量管理监测表格，详细记录每小时液体出入量情况；ECMO 及气管插管撤除后指导患者做好容量自我管理：口渴时可使用喷壶湿润口唇，或通过漱口代替喝水，缓解口渴症状等。③稳定肺动脉压，提高吸入一氧化氮治疗过程中的安全管理；④可视化康复护理方案：鼓励患者坚持康复训练，但不可急于求成、激进式训练。使用可视化康复记录单，让患者自己勾选已完成的运动训练，提高参与度及积极性。⑤分阶段式心理护理：镇静期间患者无法表达自己的感受，采用芳香疗法联合音乐疗法为患者进行心理照护，将薰衣草精油及野橘精油涂抹于患者的耳后来改善患者的睡眠质量、减轻焦虑情绪；同时在白天应用音乐心理疗法增进患者的身心健康，达到放松解压的效果；鼓励家属定期探视，并指导他们在探视时给予患者正面的支持和鼓励，家庭成员的陪伴能够给患者带来极大的精神慰藉。患者清醒时采用情绪释放疗法 EFT 进行心理护理，帮助患者接受当下的情绪，积极面对未来。**结果**：经过多学科团队的共同协作下，患者术后 19d 转入普通病房，术后 39d 顺利出院。规律随访三个月，患者恢复良好。

Dysregulated Tryptophan-Kynurenine Pathway Drives Septic Cardiomyopathy: A Multimodal Diagnostic Model Integrating Ghrelin and Metabolites

Chunlin Yin[1], Xue Li[1], Xing-Zhu Zhou[1], Yi-Ge Song[2], Xian-Yang Chen[2]

1. Xuanwu Hospital, Capital Medical University

2. Beijing Zhongguancun Big Data Center

Abstract

Purpose: Septic cardiomyopathy (SCM), characterized by acute cardiac dysfunction during sepsis, significantly elevates mortality risk to 70-90% when complicated by septic shock. Current diagnostic reliance on echocardiographic left ventricular ejection fraction (LVEF <50%) and nonspecific biomarkers (NT-proBNP, cTnI) fails to detect early-stage SCM due to limited specificity and load-dependency. The absence of targeted interventions underscores the urgent need to decipher SCM pathogenesis and develop precise diagnostic tools. This study aimed to: (1) identify novel metabolic drivers of SCM through multi-omics profiling; (2) validate dysregulated pathways in a clinically stratified cohort; (3) construct and externally validate a multimodal diagnostic model integrating proteomic and metabolomic biomarkers.

Methods: A prospective cohort of 30 sepsis patients (2016 Sepsis-3.0 criteria) was rigorously stratified using dual echocardiographic criteria: LVEF <50% combined with global longitudinal strain (GLS) impairment (GLS < − 15%, reflecting intrinsic myocardial dysfunction). Patients were categorized into non-SCM (*n* = 13) and SCM (*n* = 17) groups, excluding comorbidities confounding cardiac/metabolic assessments. Serum samples underwent:

Untargeted metabolomics: Liquid chromatography-quadrupole time-of-flight mass spectrometry (LC-QTOF-MS) analysis with orthogonal partial least squares-discriminant analysis (OPLS-DA; selection criteria: variable importance projection [VIP] >1, *p* < 0.05, FDR <0.05).

Targeted validation: Quantification of tryptophan-kynurenine (TRP-KYN) pathway metabolites via LC-MS/MS.

Proteomics: Targeted mass spectrometry for six inflammatory peptides (Substance P, α-MSH, NPY, Nociceptin, Ghrelin, Urotensin II).

Pathway dynamics were mapped using structural equation modeling. A logistic regression model integrating key biomarkers was developed and validated through external cohort testing and permutation analysis.

Results:

1.Metabolic Dysregulation: Untargeted metabolomics identified the TRP-KYN pathway as the most significantly altered in SCM (KEGG enrichment *p* < 0.001). Key perturbations included:

44% elevation in tryptophan (TRP, *p* < 0.001)

37% reduction in quinolinic acid (QA, *p* < 0.005)

Increased intermediates: L-kynurenine (AUC = 0.82), N-formylkynurenine (AUC = 0.84), 3-hydroxyanthranilic acid (AUC = 0.81)

Structural modeling confirmed suppressed flux from TRP to kynurenine (β = − 0.38 vs. − 0.11 in controls, *p* < 0.01) and disrupted downstream coordination (e.g., lost KYN → 3-HAA regulation).

2.Proteomic Signature: Among six inflammatory peptides, only ghrelin showed significant reduction in SCM (− 29%, *p* < 0.01), exhibiting moderate diagnostic capacity alone (AUC = 0.731).

3.Diagnostic Model Performance:

The multimodal model (Ghrelin + TRP + QA) achieved:

Discovery cohort: AUC = 0.847 (95% CI: 0.792–0.902)

External validation: AUC = 0.805 (95% CI: 0.741–0.869)

Outperformed single-modality approaches:

Ghrelin alone: AUC = 0.731

Metabolites alone (TRP + QA): AUC = 0.752

Decision curve analysis demonstrated >95% clinical net benefit at 40-60% risk thresholds.

Mechanistic Implications:

TRP accumulation may impair immunometabolic homeostasis by blunting GCN2 kinase-mediated anti-inflammatory signaling while hyperactivating mTORC1-dependent Th1/Th17 responses.

QA deficiency compromises cardiac energy metabolism via reduced NAD^+ synthesis (↓ ATP production) and dysregulates excitation-contraction coupling through diminished NMDAR activation.

Conclusion: This study establishes TRP-KYN pathway dysregulation (characterized by TRP accumulation and QA depletion) and ghrelin reduction as hallmarks of SCM pathogenesis. The integration of these biomarkers into a multimodal diagnostic model enables early detection with high accuracy (AUC >0.8), addressing a critical gap in sepsis management. By bridging metabolic dysregulation, immune imbalance, and functional cardiac impairment, this approach provides:

1.A clinical tool for identifying high-risk SCM patients during the reversible early phase;

2.Novel therapeutic targets (e.g., KMO activators to restore QA synthesis, ghrelin supplementation);

3.A precision medicine framework for future sepsis-induced organ dysfunction research. Multicenter validation and mechanistic studies exploring TRP-KYN flux modulation are warranted.

4.Key words : septic cardiomyopathy, biomarker, metabolomics

Triglyceride-glucose index may influence ideal body weight in cardiovascular critically ill patients without diabetes: a retrospective study of the MIMIC-IV database

Yi Hu, Xue-Bo Liu

Tongji Hospital, Tongji University

Background The obesity paradox, whereby overweight/obese individuals have lower mortality than normal-weight populations, is prevalent in patients with cardiovascular critical illnesses, but the mechanisms are not well understood. Insulin resistance (IR) may be a key modifier, and the triacylglycerol-glucose (TyG) index, a reliable surrogate for IR, may influence the obesity-related survival advantage. As the metabolic complexity of diabetic patients may interfere with phenomenological observations, this study focused on a non-diabetic cardiovascular critically ill population with the aim of revealing the modulating role of TyG levels on the obesity paradox and providing a basis for precise weight management.

Methods We extracted cardiovascular critically ill patients without diabetes mellitus (DM) from the Medical Information Marketplace in Intensive Care (MIMIC)-IV database and categorised them into T1, T2 and T3 groups based on the trichotomisation of the TyG index, with 365-day all-cause mortality as the primary endpoint. According to the criteria of the World Health Organization (WHO), we classified the body mass index into the following groups: normal group (18.5-24.9 kg/m2), overweight group (25.0-29.9 kg/m2), obese group I (30.0-34.9 kg/m2), obese group II (35.0-39.9 kg/m2), and obese group III (≥ 40.0 kg/m2). Kaplan-Meier (K-M) curves were used to compare outcomes between BMI groups.COX regression analyses and restricted cubic spline curves (RCS) were used to assess the relationship between BMI and prognosis in each group. If a non-linear relationship existed, change points were estimated using a segmented linear model and a two-stage Cox regression was applied either side of the change point. Finally, subgroup analyses with sensitivity analyses were also performed.

Results A total of 5106 individuals participated in the study, with a median age of 68 (58,78) years, and 61.4% were male.The KM curves showed that obesity was less protective in the high TyG group.COX regression analyses showed a significantly lower 365-day all-cause mortality rate in overweight, obese class I patients in the T1 group compared with those with a normal body mass index, with an adjusted hazard ratio (HR) and a 95% confidence intervals (CIs) of 0.74 (0.58-0.94) and 0.62 (0.44-0.89), respectively; in group T2, obese class I patients were significantly associated with a reduction in 365-day all-cause mortality, with adjusted HRs and 95% CIs of 0.60 (0.42-0.85), respectively; and in group T3, none of the abnormal BMI groups were significantly associated with 365-day

all-cause mortality.RCS analyses showed an L-shaped relationship between BMI and 365-day all-cause mortality in the T1 and T2 groups and a J-shaped relationship in the T3 group. The lowest value of mortality, i.e. ideal body weight, was 34 kg/m2, 33 kg/m2 and 29 kg/m2 in the three groups.Subgroup analyses and sensitivity analyses yielded similar results.

Conclusions This study found that different TyG levels affect the obesity paradox in cardiovascular critically ill patients without DM. Patients with high TyG levels were significantly less protected against obesity and had a lower optimal body weight compared to patients with low TyG levels. It is necessary to consider the TyG index when managing ideal weight in critically ill patients without diabetes.

Key Words：Triglyceride-glucose index, cardiovascular critical illness, obesity paradox, ideal body weights

米拉贝隆激活 β3-AR 通过促进血管周围脂肪组织中的淋巴管生成来预防主动脉夹层 / 动脉瘤发生

程玉文 曲新凯

复旦大学附属华东医院

目的：β3-AR（β3- 肾上腺素能受体）通过调节脂肪组织功能对于心血管稳态至关重要。血管周围脂肪组织（PVAT）与主动脉夹层和动脉瘤（AD/AA）的发病机制有关。在此，我们旨在探讨 β3-AR 激活的 PVAT 在 AD/AA 中的功能。

方法：收集胸主动脉夹层（TAD）患者的主动脉，检测 PVAT 中 β3-AR 的表达。用血管紧张素 II (AngII) 诱导 ApoE-/- 和 β- 氨基丙腈单富马酸酯 (BAPN) 处理的 C57BL/6 小鼠来模拟 AD/AA，随后接受安慰剂或米拉贝隆喂养。

结果：TAD 患者和 AD/AA 小鼠的 PVAT 中 β3-AR 上调。此外，米拉贝隆激活 β3-AR 可显着阻止 AngII 诱导的小鼠 AD/AA 形成。对 PVAT 脂肪细胞的 RNA 测序分析显示，在米拉贝隆治疗的小鼠中，淋巴管生成因子 VEGF-C 显着增加。同样的，我们发现米拉贝隆治疗后的 PVAT 中淋巴管生成增强。从机制上讲，米拉贝隆治疗小鼠的 PVAT 中 CD4+/CD8+ T 细胞和 CD11c+ 细胞的数量减少，但邻近引流淋巴结 (LN) 的数量增加，表明淋巴管生成改善了 PVAT 中炎症细胞的引流和清除。重要的是，腺相关病毒对脂肪细胞特异性 VEGF-C 的敲低抑制了淋巴管生成，并加剧了 PVAT 中的炎症细胞浸润，最终消除了米拉贝隆对 AD/AA 的保护作用。此外，经米拉贝隆处理的脂肪细胞的条件培养基激活了淋巴内皮细胞 (LEC) 的增殖和管形成，而敲低脂肪细胞中 VEGF-C 的可减少增殖和管状形成。

结论：我们的研究结果说明了 β3-AR 的治疗潜力。米拉贝隆激活 AD/AA 中的 β3-AR，通过增加脂肪细胞分泌的 VEGF-C 促进淋巴管生成，从而改善 PVAT 炎症。

Association Between Time in Targeted Blood Glucose Range and In-Hospital Mortality in critically ill patients with cardiovascular diseases: analysis of the MIMIC-IV database

Hong Chen, Qi-Wei Shen, Peng Liu, Hai-Long Li, Hua-Long Liu, Jin-Zhu Hu

Department of Cardiovascular Medicine, The Second Affiliated Hospital of Nanchang University, China

Background

Critically ill patients with cardiovascular diseases constitute a high-risk population within the intensive care unit (ICU), where the profound stress of conditions like acute heart failure, myocardial infarction, and cardiogenic shock frequently leads to significant metabolic disruption. Dysglycemia, encompassing both hyperglycemia and hypoglycemia, is highly prevalent and is independently associated with adverse clinical outcomes, including increased mortality and prolonged ICU stays. However, conventional glycemic metrics such as mean glucose levels or measures of glucose variability may not adequately capture the full spectrum of glycemic dysregulation. These measures often fail to account for the duration and stability of glucose control, which may be critical in a population highly susceptible to the detrimental effects of glycemic excursions.

Time in targeted blood glucose range (TIR), defined as the percentage of time a patient's glucose level remains within a predefined range (e.g., 70–139 mg/dL), has emerged as a superior indicator of glycemic quality in outpatient diabetes management. By providing a dynamic and integrated measure of glycemic stability, TIR offers potential advantages over static metrics. Despite its growing acceptance in other clinical contexts, the prognostic value of TIR for predicting short-term outcomes in critically ill patients with cardiovascular diseases remains largely uninvestigated. This study aimed to evaluate the association between TIR during the first cardiac ICU admission and in-hospital all-cause mortality, using a large, real-world cohort from the MIMIC-IV database. We also sought to explore whether this association varied across key clinical subgroups, including patients with and without diabetes.

Methods

This retrospective cohort study utilized data from the Medical Information Mart for Intensive Care (MIMIC-IV) database, version 3.1, which contains comprehensive data from patients admitted to Beth Israel Deaconess Medical Center between 2008 and 2022. The study population included adult patients with their first admission to a cardiac ICU. A detailed set of inclusion and exclusion criteria was applied to derive the final cohort.

Data extracted included patient demographics (age, sex, race), body mass index (BMI), illness severity scores (APS III, SAPS II), comorbidities (identified via ICD-9/10 codes), vital signs, and an extensive panel of laboratory values. The primary exposure was TIR, calculated as the percentage of time spent within the target glucose range of 70–139 mg/dL during the ICU stay. Glucose measurements were extracted from fingerstick, serum, and whole blood tests. A time-weighted approach with linear interpolation between consecutive glucose readings was used to estimate the total duration spent within the target range. The primary outcome was in-hospital all-cause mortality.

Statistical analysis involved several steps. Baseline characteristics were compared across TIR quartiles. The association between TIR and in-hospital mortality was assessed using multivariable logistic regression. TIR was analyzed both as a continuous variable (per 10% increase) and as a categorical variable (in quartiles). Three hierarchical models were built: Model I was unadjusted; Model II adjusted for age, sex, and BMI; and Model III was a fully adjusted model controlling for demographics, illness severity scores, vital signs, laboratory results, major comorbidities (e.g., hypertension, diabetes, coronary artery disease, heart failure, sepsis), and treatments (e.g., insulin, vasopressors, mechanical ventilation). Subgroup analyses were performed to test for interaction effects, and restricted cubic splines were used to model potential non-linear relationships.

Results

A total of 12,039 critically ill patients with cardiovascular diseases were included in the final analysis. The median age was 69.5 years, 31.3% were female, and 69.5% were White. Key comorbidities included diabetes (39.2%), coronary artery disease (71.6%), and hypertension (78.7%). The overall in-hospital all-cause mortality rate for the cohort was 5.7%.

A strong, graded inverse relationship was observed between TIR quartiles and mortality. Patients in the lowest TIR quartile (Q1, 0-25%) had a mortality rate of 13.0%, which progressively decreased in higher quartiles: Q2 (5.6%), Q3 (4.3%), and Q4 (2.6%).

In the multivariable logistic regression analysis, when TIR was treated as a continuous variable, each 10% increase in TIR was associated with significantly lower odds of in-hospital mortality. In the fully adjusted model (Model III), the odds ratio (OR) was 0.86 (95% CI: 0.82-0.90, P < 0.001). When analyzed by quartiles, compared to the lowest quartile (Q1), patients in the highest quartile (Q4) had a 67% reduction in the odds of death in the fully adjusted model (OR 0.33, 95% CI: 0.22-0.51, P for Trend < 0.001).

Subgroup analyses revealed a significant interaction by diabetes status. The protective association of higher TIR with lower mortality was pronounced and statistically significant in patients without diabetes, but this association was attenuated and not statistically significant in patients with diabetes (P for interaction < 0.05). No significant interactions were found for other subgroups, including age, sex, or BMI. Restricted cubic spline analysis showed an approximately linear inverse relationship between TIR and mortality, with no evidence of a non-linear effect (P for non-linearity = 0.237).

Conclusion

In this large-scale, retrospective study of critically ill patients with cardiovascular diseases, a higher TIR was independently and strongly associated with a lower risk of in-hospital all-cause mortality. This relationship demonstrated a clear dose-response pattern and remained robust after extensive adjustment for a wide range of potential confounders. The findings suggest that maintaining glycemic stability, as captured by TIR, is a critical factor influencing short-term survival in this vulnerable population.

Notably, the prognostic utility of TIR was most evident in patients without a history of diabetes, suggesting that these individuals may be more susceptible to the adverse effects of acute dysglycemia. While the observational nature of this study precludes causal inference, the results provide compelling evidence that TIR may serve as a valuable clinical indicator for risk stratification and a potential target for therapeutic intervention in cardiovascular critical care. Future prospective studies, potentially incorporating continuous glucose monitoring, are warranted to validate these findings and to determine whether management strategies guided by TIR can improve clinical outcomes in this high-risk patient group.

Early Systolic Blood Pressure Time-in-Target Range and Mortality in ICU Patients with Heart Failure: A Retrospective Cohort Study from the MIMIC-IV Database

Qiwei Shen, Peng Liu, Hai-Long Li, Hong Chen, Hua-Long Liu, Jin-Zhu Hu

Department of Cardiovascular Medicine, The Second Affiliated Hospital of Nanchang University, China

Background

Heart failure (HF) is a leading cause of cardiovascular morbidity and mortality worldwide, with patients admitted to the intensive care unit (ICU) facing particularly poor outcomes due to the frequent presence of multi-organ dysfunction. Effective blood pressure (BP) management is a cornerstone of care in these critically ill patients, yet it remains a significant clinical challenge. Both hypotension and hypertension can precipitate hemodynamic instability and worsen prognosis. Achieving and maintaining systolic blood pressure (SBP) within an optimal range is therefore essential for stabilizing these vulnerable patients.

Time in Target Range (TTR), a metric that quantifies the proportion of time a patient's physiological parameters remain within a desired range, has emerged as a valuable tool in clinical management. While its utility is established in chronic conditions like hypertension, its application to acute BP control in the ICU is less understood. Previous ICU research has often focused on single BP measurements or short-term BP variability, which may not fully capture the importance of sustained hemodynamic stability. Furthermore, there is a significant knowledge gap regarding how early BP control during the initial, critical phase of an ICU stay impacts not only short-term, in-hospital outcomes but also long-term survival in HF patients. This study aimed to address this gap by evaluating the association between SBP TTR during the first 24 hours of ICU admission and both in-hospital and one-year all-cause mortality in a large cohort of critically ill patients with HF.

Methods

This retrospective cohort study was conducted using data from the Medical Information Mart for Intensive Care IV (MIMIC-IV) database (version 3.1), a comprehensive dataset from Beth Israel Deaconess Medical Center (2008–2022). The study population consisted of patients with a diagnosis of HF who were admitted to an ICU for the first time and had a length of stay of at least 24 hours.

The primary exposure was SBP TTR, calculated for the first 24 hours of ICU admission. The target SBP range was defined as 110–140 mmHg. TTR was computed using linear interpolation between all available SBP measurements, and only patients with at least 19 hours of SBP data within the 24-hour window were included to ensure reliable estimation. The primary outcome was in-hospital all-cause mortality. The secondary outcome was one-year all-cause mortality following hospital discharge.

A wide range of data was extracted, including demographics, comorbidities, laboratory values, vital signs, and treatments. Multiple imputation was used to handle missing data. The association between SBP TTR and outcomes was assessed using multivariable regression models. Logistic regression was used for in-hospital mortality, and Cox proportional hazards models were used for one-year mortality. SBP TTR was analyzed both as a continuous variable (per 10% increase) and as a categorical variable (in quartiles). Three models were constructed: an unadjusted model (Model I), a partially adjusted model for age, sex, and BMI (Model II), and a fully adjusted model (Model III) controlling for an extensive list of confounders. Subgroup analyses and restricted cubic splines (RCS) were employed to explore the consistency and potential non-linearity of the associations.

Results

A total of 11,538 patients with HF were included in the study. The median age was 75 years, 44.3% were female, and 67.4% were White. The overall in-hospital mortality was 14.4%, and one-year mortality was 22.3%.

For the primary outcome of in-hospital mortality, a significant inverse association with SBP TTR was observed. In the fully adjusted model, each 10% increase in SBP TTR was associated with a 4% lower odds of death (OR 0.96, 95% CI 0.93-0.98). When analyzed by quartiles, patients in the second, third, and fourth quartiles had significantly lower odds of mortality compared to the lowest quartile (Q1), with adjusted ORs of 0.81, 0.72, and 0.73, respectively, suggesting a potential plateauing of benefit beyond the third quartile. Subgroup analyses showed no significant interactions, indicating that the protective association was consistent across different age groups, sexes, and comorbidity profiles. RCS analysis confirmed an approximately linear relationship that began to flatten when SBP TTR exceeded 50%.

For the secondary outcome of one-year mortality, higher SBP TTR was also associated with improved survival. Each 10% increase in SBP TTR was linked to a 2% lower hazard of death in the fully adjusted Cox model (HR 0.98, 95% CI 0.96-0.99). The analysis by quartiles showed a similar pattern, with adjusted HRs of 0.91, 0.87, and 0.88 for Q2, Q3, and Q4 versus Q1, respectively. Kaplan-Meier curves visually confirmed better survival for patients in higher TTR quartiles, with the curves for Q3 and Q4 overlapping. The RCS analysis for one-year mortality revealed a significant non-linear relationship (P for non-linearity = 0.043), where the risk decreased as SBP TTR increased to approximately 50%, after which the benefit leveled off.

Conclusion

This study demonstrates that a higher SBP TTR during the first 24 hours of ICU admission is independently associated with significantly lower short-term (in-hospital) and long-term (one-year) all-cause mortality in critically ill patients with heart failure. The findings highlight SBP TTR as a pragmatic and clinically relevant metric for assessing the quality of BP control in the acute setting. The consistent association across various subgroups underscores its broad applicability.

The observed plateauing of benefit, particularly for one-year survival, suggests that while achieving stable BP within the target range is crucial, there may be a threshold effect, where pushing for extremely high TTR values may not confer additional survival advantages. This nuanced finding supports a personalized approach to BP management. Although limited by its retrospective design, this study provides strong evidence that early and sustained optimization of SBP is a critical determinant of both immediate and future survival in HF patients. SBP TTR should be considered a valuable target for hemodynamic management and a useful prognostic marker in this high-risk population.

静脉与冠脉联合应用比伐卢定对 STEMI 接受 PPCI 无复流的预防作用

梁振洋 徐凯 王斌 刘海伟 关绍义 韩雅玲

中国人民解放军北部战区总医院

静脉与冠脉联合应用比伐卢定对 STEMI 接受 PPCI 无复流的预防作用

梁振洋，徐凯，王斌，刘海伟，关绍义，韩雅玲

北部战区总医院 心血管内科 全军心血管病研究所

目的 探讨在 STEMI 接受 PPCI 患者中，探索静脉标准剂量比伐卢定应用的情况下，给予冠脉内注射一定剂量的比伐卢定对预防术中冠脉无复流（No-flow，NR）的有效性及安全性。

方法 入选在本院心内科就诊并符合入排标准的住院急性 STEMI 接受 PPCI 患者共 86 例，全部患者均给予标准剂量比伐卢定进行术中抗凝（静脉负荷剂量 0.75mg/kg，静脉持续滴注 1.75mg/kg/h，且持续至术后 3-4h），随机分为实验组（46 例）及对照组（40 例）。在梗死相关动脉恢复至 TIMI ≥ 2 级血流情况下，经给予冠脉内注射比伐卢定（0.75mg/kg，与静脉负荷剂量相同）或生理盐水（10ml）后，观察主要终点：支架植入完成后即刻及术终时冠脉血流恢复情况（校正的 TIMI 血流帧数 -CTFC）、术后 90 分钟心电图 ST 段完全回落率（ST 段回落≥ 70%）；

结果 对于急性 STEMI 接受 PPCI 的患者，在给予上述术中抗凝方案情况下，在其冠脉靶血管为 TIMI ≥ 2 级血流时，经冠脉内预防性注射与静脉负荷相同剂量的比伐卢定（0.75mg/kg），与冠脉内注射生理盐水 10ml 相比较，可显著降低支架植入完成后靶血管即刻出现的无复流（CTFC ≥ 40）的发生率，但在术后 90 分钟心电图 ST 段完全回落率以及 30 天 NACE 方面，两组并无显著性差异，且未出现临床出血事件。

结论 在急性 STEMI 接受 PPCI 患者中，静脉联合预防性冠脉内注射比伐卢定对梗死相关动脉支架植入术后发生无复流具有预防作用且安全性较好。

关键词： 比伐卢定；急性 ST 段抬高型心肌梗死；直接经皮冠状动脉介入治疗；无复流

普通肝素与比伐芦定对 IABP 辅助 PCI 术中 ACT 的影响：单中心回顾性分析

李颖 徐莹 张东红 于海波 韩雅玲 梁振洋

中国人民解放军北部战区总医院

普通肝素与比伐芦定对 IABP 辅助 PCI 术中 ACT 的影响：单中心回顾性分析

李颖，徐莹，张东红，于海波，韩雅玲，梁振洋

北部战区总医院 心血管内科 全军心血管病研究所，辽宁 沈阳 110016

通信作者：梁振洋，E-mail：doctorliangzi@sina.com

【摘要】

目的： 单中心回顾性分析比伐芦定与普通肝素对主动脉球囊反搏（IABP）辅助冠脉介入治疗术（PCI）中激活凝血酶时间 (ACT) 的影响。

方法： 回顾性检索北部战区总医院心血管内科数据库 2019 年 10 月至 2021 年 9 月应用 IABP 辅助患者 272 例。符合入排标准共 212 例（比伐芦定组 104 例，肝素组 108 例）。依据分组不同，对基线临床资料以及 PCI 术中 ACT 数值进行了统计学分析。所有入选患者均按照 PCI 操作常规进行操作，普通肝素及比伐芦定均严格依照治疗指南进行给药 (比伐芦定 0.75mg/kg 静脉负荷剂量，静脉持续 1.75mg/kg/h 泵入；普通肝素 70-100u/kg)。主要观察终点：术中 ACT 数值变化情况；次要观察终点：术后血小板变化情况。

结果：比伐芦定组患者在女性比例、体重、术前血小板计数方面，显著低于普通肝素组（P 均 < 0.05）；比伐芦定组患者的年龄和 CRSADE 评分显著高于普通肝素组（P 均 < 0.05）；而在糖尿病、高血压、卒中史、术前 LVEF 等方面，两组无明显差异（P 均 > 0.05）。比伐芦定组患者 PCI 的首次、术中及术毕 ACT，比伐芦定组均显著高于普通肝素组（P 均 < 0.05）；术后血小板计数（117.4±35.7×10^9/L vs.189.1±47.8×10^9/L，P < 0.05）以及术前术后血小板计数差值方面，两组均具有显著统计学差异（17.4±9.8×10^9/L vs. 44.6±21.3×10^9/L，P < 0.05），比伐芦定组的血小板计数差值变化更小。

结论： 单中心回顾性分析结果提示，在 IABP 辅助 PCI 术中，不同抗凝药物的 ACT 数值不同，比伐芦定相较于普通肝素更多应用于出血高危人群且血小板计数更为稳定。

关键词：比伐芦定，肝素，主动脉球囊反搏（IABP），冠脉介入治疗 (PCI)，激活凝血酶时间 (ACT)

AccuIMR 冠脉微循环功能评估及对急诊 PCI 术后 STEMI 患者住院临床结局影响的研究

李雪

首都医科大学宣武医院

目的：急性 ST 段抬高型心肌梗死（STEMI）是冠状动脉粥样硬化斑块破裂导致急性血栓形成、罪犯血管完全闭塞的心脏急重症，严重者会危及患者生命。冠状动脉微血管阻塞（MVO）和微循环功能障碍是 STEMI 患者预后不良的重要原因之一。然而，至今，MVO 发病机制尚未完全阐明，同时，缺乏有效、临床可行的、实时冠脉微循环功能评估方法，干预策略及其有效性、安全性的大规模研究验证也尚存争议。本研究基于队列研究，探究 AccuIMR 值对冠脉微循环功能的评估及其对急诊 PCI 术后 STEMI 患者住院临床结局的影响。研究将为 STEMI 再灌注后 MVO 的发病原因、早期评估与干预策略研究提供重要的临床数据。方法：本研究为前瞻性队列研究，入选 2022 年 9 月至 2023 年 12 月期间首都医科大学宣武医院心脏内科收治的接受急诊 PCI 的 STEMI 患者 116 例。患者急诊 PCI 术后即刻测量 AccuIMR 值，AccuIMR ≥ 25 为冠脉微循环功能障碍的诊断界值，据此分为 AccuIMR ≥ 25 组和 AccuIMR<25 组。收集入选患者的临床资料，包括人口统计学信息、一般情况、既往相关疾病及危险因素、心脏功能状态、缺血性不良事件风险评估、生化指标、炎症指标、急诊 PCI 手术情况、出院时冠心病二级预防治疗等。研究结局为院内 MACE 事件、左心室射血分数、心肌损伤标记物（肌钙蛋白 I 峰值）。结果：本研究最终入选的 116 例 STEMI 患者中，AccuIMR ≥ 25 组 42 例、AccuIMR<25 组 74 例，STEMI 患者急诊 PCI 术后 AccuIMR 值≥ 25 占比为 36.2%。全部入选患者平均年龄 61.44±12.60 岁，男性占 81.9%，入院心功能分级 Killip^{3}2 级占 25.0%，平均 Grace 评分为 148±41 分。患者发病至再灌注的平均时间为 270.98 分钟，进门至球囊扩张的平均时间为 74.50 分钟。与 AccuIMR<25 组相比，AccuIMR ≥ 25 组患者术后 1 小时和术后 24 小时 STR 不良发生率明显更高（47.6% vs. 24.3%, P=0.010）（33.3% vs. 10.8%, P=0.003）。全部患者院内 MACE 事件发生率为 0.9%。与 AccuIMR<25 组相比，AccuIMR ≥ 25 组患者心肌损伤标记物（峰值 TnI）显著升高（29.71±16.56ng/ml vs. 22.49±17.35ng/ml, P=0.031, 95%CI: 0.669, 13.766）。两组患者在院内 MACE 事件和左心室射血分数减低的发生率方面未见显著差异。结论：与非 MVO 组相比，MVO 组左室射血分数减低和 AccuIMR 值≥ 25 发生率更高。与 AccuIMR<25 组相比，AccuIMR ≥ 25 组患者心肌损伤标记物（峰值 TnI）明显升高，两组在院内 MACE 事件、左心室射血分数上不具有显著差异。

基于可解释机器学习模型的 VA-ECMO 辅助儿童急性肾损伤风险早期预测

史树锦 [1] 闫浩杰 [1] 邵钧捷 [1] 周晶晶 [1] 洪小杨 [2] 张然 [1]

1. 中国人民解放军总医院（解放军 301 医院、三零一医院、301 医院）

2. 中国人民解放军总医院第七医学中心儿科医学部

目的：

VA-ECMO 已经成为儿童危重症心脏病终末期心力衰竭的关键机械循环辅助支持手段，但其引发的急性肾损伤（AKI）是导致患儿高死亡率的重要原因之一。早期识别和预测接受 VA-ECMO 辅助患儿发生急性肾损伤的风险，有助于及时启动治疗措施和改善临床预后。本研究旨在基于机器学习方法，构建并验证 VA-ECMO 相关急性肾损伤风险的临床预测模型。

方法：

本研究为一项多中心回顾性研究，旨在构建并验证 VA-ECMO 辅助儿童相关急性肾损伤风险的临床预测模型。研究纳入 2017 年 10 月至 2023 年 5 月期间，6 家国内三级医院因危重症心脏病终末期心力衰竭接受 VA-ECMO 辅助的患儿 372 例。其中，5 家医院的 298 名患儿数据用于模型的训练和内部验证，1 家医院的 74 名患儿数据用于外部验证。急性肾损伤的诊断依据 KDIGO 标准，综合血清肌酐水平和尿量进行评估。通过各中心医院的电子病历系统获取数据，并采用单因素分析、LASSO 回归、共线性分析及方差膨胀因子计算等方法，筛选出 22 项特征变量用于模型构建。基于筛选后的变量，应用 11 种机器学习算法开发预测模型。通过多项评估指标（包括受试者工作特征曲线下面积）比较模型的预测性能。通过计算 SHAP 值来确定每个特征在预测性能最高的模型中的预测作用。

结果：

在 11 种机器学习模型中，额外树（ET）模型展现出最佳的预测效能。基于 SHAP 值计算对特征重要性进行排序后，我们构建了一个包含 8 个关键特征的可解释性额外树模型。该最终模型在内部验证集（AUC = 0.937）和外部验证集（AUC = 0.786，AUPRC = 0.835）中均表现出对急性肾损伤的准确预测能力。SHAP 分析进一步揭示，肾小球滤过率、年龄、身高、乳酸、直接胆红素、最低舒张压、嗜酸性粒细胞以及 CALLY 指数是对预测结果影响最大的特征。此外，为促进临床转化，本研究开发了一款在线预测工具：临床医生输入模型所需的 8 项特征值后，即可获得该 VA-ECMO 辅助患儿的急性肾损伤风险预测结果。

结论：

本研究开发的可解释性机器学习模型能够准确预测接受 VA-ECMO 辅助患儿发生急性肾损伤的风险。该模型通过提供早期预警，可指导临床及时采取干预措施，从而预防或减少急性肾损伤的发生。模型本身采用了可解释的机器学习技术，有效缓解了临床对模型“黑箱”问题的疑虑。

Combined single-cell RNA sequencing and mendelian randomization to identify biomarkers associated with lipid metabolism in myocardio infraction

Yaling Han, Jing Pan, Hai-Xu Song, Ya-Ling Han

State Key Laboratory of Frigid Zone Cardiovascular Disease, Cardiovascular Research Institute and Department of Cardiology, General Hospital of Northern Theater Command

Abstract

Background: Myocardial infarction (MI) remains a predominant cause of heart failure and mortality globally, resulting in extensive myocardial tissue damage that necessitates effective repair mechanisms. Fibroblasts are central to tissue repair, yet recent research has illuminated the critical role of macrophages, which, beyond their immune functions, can undergo macrophage-myofibroblast transformation (MMT) to contribute significantly to myocardial repair and fibrosis. Despite its importance, the molecular and metabolic mechanisms driving MMT, particularly the heterogeneity of macrophage subpopulations and their contributions to myocardial fibrosis, remain poorly understood. This study aims to dissect the molecular regulators, metabolic pathways, and cellular interactions underlying MMT in MI, with the goal of identifying novel biomarkers to enhance therapeutic strategies for post-MI cardiac recovery.

Methods: We leveraged single-cell RNA sequencing data from a mouse MI model (GSE284611), obtained from the GEO database (https://www.ncbi.nlm.nih.gov/geo/), to investigate macrophage heterogeneity and identify subpopulations involved in MMT. Subpopulation analysis was performed to isolate key macrophage clusters associated with MMT. To elucidate regulatory mechanisms, we conducted gene enrichment analysis using Gene Ontology (GO) and Gene Set Variation Analysis (GSVA). Pseudotime analysis, implemented with the Slingshot package, traced the differentiation trajectories of macrophage subpopulations. Differential gene expression analysis, performed using the R package DeSeq2, identified key regulatory genes. A metabolic scoring system was developed to explore the relationship between metabolic pathways and MMT. The gene Rora was identified as a potential regulator and validated using an external human MI dataset (GSE166780). Experimental validation of Rora expression was conducted in mouse bone marrow-derived macrophages (BMDM) using immunofluorescence, Western blot, and quantitative Reverse Transcription Polymerase Chain Reaction (RT-PCR). Cell communication networks facilitating MMT were analyzed using the Cellchat package, focusing on signaling and metabolic interactions.

Results: Single-cell RNA sequencing analysis identified seven macrophage subpopulations, with the C6 cluster emerging as the primary contributor to MMT. GSVA and GO analyses confirmed that the C6 cluster exhibited fibroblast-like characteristics, underscoring its role in myocardial repair. Pseudotime analysis revealed the C6 cluster as a critical differentiation node in the MMT trajectory. Differential gene screening pinpointed Rora as a key regulator, with its expression significantly upregulated during the macrophage-to-fibroblast transition. Validation in the external human MI dataset (GSE166780) demonstrated a robust positive correlation between Rora expression and MMT. Experimental assays, including immunofluorescence, Western blot, and quantitative RT-PCR, confirmed elevated Rora expression in mouse BMDM macrophages. Cellchat analysis indicated that Rora regulates MMT through lipid metabolism and associated signaling pathways, highlighting a metabolic foundation for its regulatory role in myocardial repair.

Conclusion: This study elucidates the pivotal role of the C6 macrophage subpopulation in MMT during the early stages of MI, with Rora identified as a critical regulator of the macrophage-to-fibroblast transition. By modulating lipid metabolism and related signaling pathways, Rora facilitates myocardial repair, positioning it as a promising biomarker and potential therapeutic target. Enhancing Rora expression in the acute phase of MI could improve cardiac function and reduce post-MI fibrosis. These findings provide a comprehensive understanding of the molecular and metabolic mechanisms underpinning MMT, offering valuable insights for developing targeted interventions to enhance myocardial repair and improve clinical outcomes following MI.

体外心肺复苏在急性心梗后心跳呼吸骤停患者中的应用单中心经验

葛锦 潘港

岳阳市中心医院

目的：评估体外心肺复苏（ECPR）在急性心肌梗死（AMI）后心跳呼吸骤停（CA）患者中的疗效及安全性，探讨影响预后的关键因素。

方法：回顾性分析岳阳市中心医院 2020 年 1 月至 2024 年 12 月收治的 30 例 AMI 后 CA 并行 ECPR 治疗患者的临床资料，按预后分为生存组（n=11）与死亡组（n=19），比较两组一般资料、ECMO 使用时间、冠脉病变特征等，采用 Cox 回归分析 ECPR 疗效影响因素。

结果：ECPR 治疗后存活率为 36.7%。存活组患者 ECMO 使用时间更长（4.34±1.96 天 vs. 3.42±3.95 天，P=0.011）、单支冠脉病变比例更高（100% vs. 36.8%，P<0.05），且合并室颤或心律失常电风暴比例显著高于死亡组（90.9% vs. 31.6%，P<0.05）。Cox 回归显示，ECMO 使用时长与存活率独立相关（HR=0.718，95%CI: 0.532–0.967）。两组在年龄、基础疾病及休克至 ECMO 上机时间上无显著差异（均 P>0.05）。

结论: ECPR 可改善 AMI 后 CA 患者的存活率，尤其是合并室颤或单支冠脉病变者; 适当延长 ECMO 支持时间可能为关键干预窗口。但本研究样本量较小，需多中心研究进一步验证。

急性心肌梗死合并心源性休克患者急诊 PCI 术后院内上消化道出血预测模型的构建与验证

董菲 周颖 赵宇飞 张云强 梁海青 宋昱 敬锐

泰达国际心血管病医院

目的 探讨急性心肌梗死合并心源性休克（AMICS）行急诊经皮冠状动脉介入（PCI）术后患者院内发生上消化道出血的现状与特征，并基于入院时基线危险因素构建预测模型。**方法** 选取 2018 年 1 月至 2024 年 12 月就诊于泰达国际心血管病医院诊断为 AMICS 并行急诊 PCI 术的患者，根据院内有无发生上消化道出血分为未出血组和出血组。采用 logistic 回归分析基于入院时基线危险因素构建院内上消化道出血风险预测模型。采用受试者工作特征（ROC）曲线和 Hosmer-Lemeshow 法评估预测模型的预测效能和模型拟合度，各指标间 AUC 比较采用 Delong 检验，采用决策曲线分析（DCA）评价预测模型的临床实用性。**结果** 发生率：研究共纳入 253 例患者，其中 58 例院内发生上消化道出血，发生率为 22.9%。 危险因素及预测模型：多因素 logistic 回归分析结果显示，基线心源性休克分期为 D+E 期、基线 ALT > 105U/L、基线 eGFR < 46.59ml/min、基线 LVEF < 36% 是 AMICS 急诊 PCI 术后患者院内发生上消化道出血的危险因素（P < 0.05）；根据多因素 logistic 回归分析结果构建预测模型，Hosmer-Lemeshow 检验显示：该预测模型具有较好的拟合优度（χ^2=3.055，P=0.880）；该模型预测 AMICS 急诊 PCI 术后患者院内发生上消化道出血的 ROC 曲线下面积（AUC）为 0.804［95%CI（0.739,0.870）］，敏感度为 70.7%，特异度为 78.5%；Delong 检验显示，四者联合预测模型的 AUC 高于任意单一指标的 AUC（P<0. 05）；DCA 曲线表明该模型具有临床实用性。 近期预后：出血组院内死亡率明显高于未出血组（63.8% vs 29.7%，P < 0.05）；对院内存活患者住院天数进行比较，出血组明显高于未出血组（P < 0.05）。**结论** 入院时基线心源性休克分期高、肝肾功能差、LVEF 低是院内发生上消化道出血的独立危险因素，构建的预测模型预测效能较高。

The Role and mechanism of E3 Ubiquitin Ligase HUWE1 In Acute Myocardial Infarction

Tao Zhou[1], Chen Chen[1,2], Yang Shen[1,3], Rong Wan[1,3]

1. Jiangxi Key Laboratory of Molecular Medicine, the Second Affiliated Hospital of Nanchang University

2. Department of Cardiovascular Medicine, the Second Affiliated Hospital of Nanchang University

3. Department of Genetic Medicine, the Second Affiliated Hospital of Nanchang University

Background:

Acute myocardial infarction (AMI) is a serious cardiovascular disease, which is usually caused by acute and persistent ischemia and hypoxia of coronary artery, resulting in severe necrosis of myocardial tissue, which may lead to sudden cardiac death. Apoptosis plays an important role in the pathological process of myocardial infarction.; Therefore, the prevention and treatment of myocardial injury caused by myocardial infarction has become one of the hot spots in cardiovascular disease research. Previous studies have reported that E3 ubiquitin ligase HUWE1 is expressed in myocardium, but the specific mechanism of its action in myocardial hypoxia injury is still unclear.

It has been suggested that HUWE1 may regulate apoptosis in diseases through its E3 ubiquitin ligase activity. By proteomics and immunoprecipitation mass spectrometry (IP-MS), it has been suggested that PRDX6, a possible substrate of HUWE1, is closely associated with apoptosis. These results suggest that cardiac expression of HUWE1 may play a role in regulating the expression of PRDX6 in hypoxic myocardial injury. In order to verify this hypothesis, we selected heart-specific HUWE1 knockout (Myh6-CreERT2$^{+/-}$HUWE1$^{flox/flox}$) mice as experimental animals and conducted a series of in vitro experiments in rat cardiomyocytes H9C2 to explore the regulatory mechanism of heart-expressed E3 ubiquitin ligase HUWE1 in hypoxic myocardial injury.

Objective :

The aim of this study was to investigate the regulatory role and mechanism of heart-specific expression of HUWE1 in hypoxic myocardial injury, and to determine whether PRDX6 is a substrate protein of HUWE1 and plays an important role in this regulatory process.

Methods:

In this study, we constructed a heart-specific HUWE1 gene knockout (Myh6-CreERT2$^{+/-}$HUWE1$^{flox/flox}$) strain of mice by CRISPR/Cas9 technology, and set wild-type mice as control group to construct myocardial infarction model together. At the same time, H9C2 rat cardiomyocytes were used to study the regulatory role and mechanism of heart-specific expression of HUWE1 in hypoxic myocardial injury at animal and cellular levels, as follows:

1. C57BL/6J mice were used to establish the model of acute myocardial infarction (AMI). The success of AMI model was evaluated by ECG, small animal ultrasound and HE staining. The expression of HUWE1 in myocardium was detected by Western blot, immunohistochemistry (IHC) and immunofluorescence (IF) staining. The expression of HUWE1 in NRCMs was detected by Western blot.

2. Heart-specific HUWE1 knockout mice were obtained by CRISPR/Cas9 gene knockout technique, and acute myocardial infarction model was established. The changes of cardiac function in mice were evaluated by small animal echocardiography, and the expressions of IL-6, TNF-α, HUWE1, BAX, Bcl-2 in heart were detected by Western blot, and the degree of myocardial injury and apoptosis of myocardial cells were evaluated by IHC staining and HE staining. In addition, H9C2 cells with low expression of HUWE1 were obtained by lentivirus transfection, and the cell hypoxia model was established. The expression changes of IL-6, TNF-α, HUWE1, BAX and Bcl-2 in H9C2 rat cardiomyocytes after hypoxia injury were detected by Western blot, and the myocardial injury and apoptosis level were further evaluated at the in vitro level.

3. Using molecular docking and co-immunoprecipitation techniques, the interaction between HUWE1 and PRDX6 was explored.

Results:

1. The expression of HUWE1 decreased after myocardial ischemia injury.

Myocardial infarction model mice showed obvious ST segment elevation, echocardiography showed that the cardiac function of mice after myocardial infarction decreased significantly, while HE staining showed that the scar tissue increased and neutrophils infiltrated in the hearts of mice after myocardial infarction surgery. These results indicated that the myocardial infarction model was successfully established. Western blot, immunohistochemistry (IHC) and immunofluorescence (IF) stain showed that that expression of HUWE1 protein in myocardial tissue of mice at 2 week after myocardial infarction tended to decrease as compared with control group, and the expression of HUWE1 protein in H9C2 cell was also down-regulated at 8 hours after hypoxia.

2. HUWE1 has protective effect on myocardial ischemia injury.

Compared with Sham group, the results of HE staining showed that myocardial injury was aggravated after acute myocardial infarction in heart-specific HUWE1 knockout mice, and cardiac ultrasound showed that the decline of cardiac function was more obvious. The results of Western blot showed that the expression of IL-6 and TNF-α increased in myocardium. In vitro, the expression of IL-6 and TNF-α in H9C2 cells with low HUWE1 expression was also up-regulated after hypoxia.

3. HUWE1 attenuated myocardial ischemia by regulating cardiomyocyte apoptosis.

Compared with wild-type myocardial infarction mice, Western blot and IHC staining of heart-specific HUWE1 knockout mice after acute myocardial infarction showed that BAX protein expression increased and Bcl-2 expression decreased. In vitro, the expression of BAX increased and Bcl-2 decreased in H9C2 cells with low HUWE1 expression after hypoxia.

4. PRDX-6 is the substrate of HUWE1.

The results of molecular docking suggested that HUWE1 and PRDX-6 may be bound to each other, and the interaction between HUWE1 and PRDX-6 was confirmed by endogenous co-immunoprecipitation.

Conclusion:

Our results show that HUWE1 gene knockout exacerbates apoptosis in myocardia -l tissue and further exacerbates inflammation and injury of myocardial tissue during myocardial ischemia injury in acute myocardial infarction. Meanwhile, we speculate that HUWE1 may play one of its molecular mechanisms of action by stabilizing the expression of PRDX6.

Key words: acute myocardial infarction; cardiomyocyte; HUWE1;E3 ubiquitin ligase; PRDX6

The global burden of Aortic Aneurysm attributable to Hypertension from 1990 to 2021: Current Trends and Projections for 2050

Peng Liu

Department of Cardiology, the First Affiliated Hospital of Dalian Medical University, Dalian, Liaoning Province, China.

Background and Objectives: Hypertension is a major risk factor for aortic aneurysm (AA), the global distribution and trends of hypertension-related AA burden at the global, regional, and national levels remain inadequately explored. This study aims to utilize data from the 2021 Global Burden of Disease (GBD) database to identify trends related to AA attributable to hypertension from 1990 to 2021 and to forecast future burden trends. The findings will provide evidence to support targeted decision-making. In the generalpopulation aged 60 and above, the prevalence of AA ranges from 1.6% to 7.2%.Research indicates that the prevalence of AA is significantly higher in men, ranging

from 1.9% to 18.5%, compared to women, where it varies between 0.1%

and 4.2%. Multiple studies have identified hypertension, advanced age, male gender, smoking history and family history of AA as the most crucial risk factors contributing to the burden of this condition. These findings underscore the urgent need for targeted screening and preventive strategies to address this life-threatening disease

Methods: This study extracted data on mortality, disability-adjusted life years (DALYs), age-standardized mortality rate (ASMR), and age-standardized DALY rate (ASDR) associated with AA attributable to hypertension from the 2021 GBD study. The estimated annual percentage change (EAPC) was employed to assess burden trends from 1990 to 2021.The study utilized the Bayesian Age-Period-Cohort (BAPC) model

to project disease trends from 2022 to 2050. Additionally, decomposition analysis and frontier analysis were employed to conduct a more comprehensive examination of the data.The GBD Results Tool (http://ghdx.healthdata.org/GBD-results-tool), is an open-access database that aggregates data on the influence of diverse risk factors onhealth burdens across countries worldwide. These data are estimated using

standardized methodologies, ensuring high reliability and authority. In the 2021 study, researchers comprehensively evaluated 371 diseases and injuries across 204 countries and territories from 1990 to 2021, assessing health loss by age and sex

Results: In 2021, the global number of deaths and DALYs attributable to hypertension related AA reached 26,782.33 and 529,976.65, respectively, representing increases of 49.14% and 46.98% compared to 1990. However, the global ASMR and ASDR exhibited declining trends. From 1990 to 2021, the ASDR for hypertension-related AA decreased by 54.08% and 15.56% in high-SDI and upper-middle-SDI regions, respectively, while it increased by 25.23%, 62.02%, and 17.99% in middle-SDI, lower middle-SDI, and low-SDI regions. The disease burden is significantly higher in males than in females and increases with age.The findings from the decomposition analysis

reveal that population growth and the aging process are the primary contributors to the escalating burden, with varying impacts across different regions. The frontier analysis identified 15 countries with the greatest potential for improvement. According to the BAPC model, the ASDR for females is projected to rise across the 20 to 80 age group, while for males, the increase is particularly pronounced in the 55 to 75 age group. Globally, the ASDR is expected to initially decline before gradually rising, reaching 12.07 per 100,000 by 2050, a 5% increase compared to 2021.

Conclusion: While the global number of deaths and DALYs attributable to hypertension-related AA continues to rise, the ASMR and ASDR are showing a declining trend. However, in middle, lower-middle, and low SDI regions, ASMR and ASDR remain on an upward trajectory. Projections indicate that the global ASDR will initially decline before gradually increasing, with an expected rise by 2050.

Relationship between uric acid to high-density lipoprotein cholesterol ratio and depression in patients with myocardial infarction: a cross-sectional survey based on NHANES database from 2011 to 2018

tingting Wang, Li-Xiang Zhang, Shan-Bing Hou, Jing Chen, Xia Chen, Jiao-Yu Cao

The First Affiliated Hospital of USTC, Division of Life Science and Medicine, University of Science and Technology of China

Background:

Depression is a prevalent psychological condition that frequently coexists with cardiovascular diseases, particularly myocardial infarction (MI). Following a myocardial infarction, patients face a substantially increased risk of developing depressive symptoms, which are associated with adverse clinical outcomes, including poor medication adherence, reduced engagement in cardiac rehabilitation, delayed recovery, increased risk of secondary cardiovascular events, and elevated mortality. Research indicates that approximately 30% of patients with MI develop some form of depression, with 10% meeting the diagnostic criteria for major depressive disorder. Early detection and treatment of depression are essential for improving both mental health and cardiovascular prognosis. However, effective screening tools for identifying patients at risk for depression remain limited in routine cardiac care. Inflammatory and metabolic pathways have been increasingly implicated in the development of depression. The uric acid to high-density lipoprotein cholesterol ratio (UHR) is a novel composite biomarker that reflects the balance between pro-oxidant and anti-inflammatory metabolic states. It has shown predictive value in cardiovascular, metabolic, and inflammatory conditions. Despite this, its association with depression in patients with MI remains largely unexplored. This study aimed to investigate the relationship between UHR and depression in patients with a history of myocardial infarction using nationally representative survey data.

Methods:

This cross-sectional analysis was based on data from the National Health and Nutrition Examination Survey (NHANES) collected between 2011 and 2018. Adult participants who reported a history of myocardial infarction were included. Participants were excluded if they lacked data on serum uric acid, HDL cholesterol, PHQ-9 depression score, or essential demographic and clinical covariates. Depression was assessed using the Patient Health Questionnaire-9 (PHQ-9), with a cutoff score of 10 or higher used to define clinically relevant depressive symptoms. The UHR was calculated as uric acid (mg/dL) divided by HDL-C (mg/dL), multiplied by 100. Multivariate linear regression analyses were used to assess the relationship between UHR and depression across progressively adjusted models. A restricted cubic spline model was used to evaluate potential nonlinear associations. Subgroup analyses were conducted to investigate effect modifications by gender, age, race, marital status, comorbid conditions, and other covariates.

Results:

A total of 18,200 individuals with MI were included in the final analysis. A significant nonlinear relationship between UHR and depression was identified. When UHR was below 10.45%, the association with depression was stronger (β = 0.12, 95% CI: 0.05–0.19, P < 0.001). When UHR was 10.45% or higher, the effect size decreased but remained statistically significant (β = 0.04, 95% CI: 0.01–0.07, P = 0.024). Subgroup analysis showed a significant interaction by gender (P for interaction < 0.001), with a stronger association in females (β = 0.13, P < 0.001) than in males (β = 0.04, P = 0.013). These associations remained robust after adjusting for multiple demographic, clinical, and laboratory variables and were supported by sensitivity analyses based on UHR quartiles.

Conclusion:

This study demonstrated a nonlinear and gender-specific relationship between UHR and depression among patients with myocardial infarction. UHR, as a simple, low-cost, and widely available blood-based indicator, may serve as a practical tool for identifying patients at increased risk of depression after MI, particularly among female patients. The nonlinear pattern also suggests that UHR may be more predictive in specific physiological ranges. Given the increasing recognition of depression as a critical component of cardiovascular prognosis, integrating UHR into comprehensive cardiac risk assessment models could enhance early detection strategies. Further longitudinal and mechanistic studies are needed to clarify causality, investigate potential biological pathways, and validate the clinical utility of UHR in depression screening and prevention efforts among diverse cardiac populations.

肝功能对 ICU 心力衰竭患者预后的预测价值

曾庆平 [1] 佘飞 [2] 贾思琦 [3] 张萍 [2]

1. 清华大学临床医学院，北京 102218，中国

2. 清华大学临床医学院北京清华长庚医院心内科，北京 102218，中国

3. 陆军军医大学西南医院，重庆 400038，中国

目的：本研究旨在评估肝功能指标对重症监护病房（Intensive Care Unit，ICU）中心力衰竭（心衰）患者 30 天和 1 年心衰再住院及全因死亡的预测价值，并探讨其在不同心衰亚型中的异质性效应。

方法：研究纳入重症监护医学信息数据库第四版（Medical Information Mart for Intensive Care IV，MIMIC-IV）中 3,777 例心衰患者，采用 Cox 比例风险模型和限制性立方样条（Restricted Cubic Spline，RCS）分析，评估丙氨酸氨基转移酶（Alanine Aminotransferase，ALT）、天门冬氨酸氨基转移酶（Aspartate Aminotransferase，AST）、碱性磷酸酶（Alkaline Phosphatase，ALP）、总胆红素（Total Bilirubin，TBIL）及肝病分级（轻度与重度）与国际标准化比值（International Normalized Ratio，INR）、凝血酶原时间（Prothrombin Time，PT）、部分凝血活酶时间（Partial Thromboplastin Time，PTT）及凝血功能障碍等指标与 30 天和 1 年心衰再住院及死亡结局之间的关联关系。主要研究终点为心衰再住院。

结果：ALP 与心衰患者的 30 天及 1 年心衰再住院风险均成显著相关，其中 30 天心衰再住院风险比（Hazard Ratio，HR）=1.28，95% 置信区间（Confidence Interval，CI）：1.01–1.63），1 年心衰再住院 HR=1.18，95%CI:1.00–1.40；在射血分数保留型心衰（Heart Failure with preserved Ejection Fraction，HFpEF）亚组中该关联更为显著（30 天心衰再住院 HR=1.72，95%CI: 1.15–2.56，1 年心衰再住院 HR=1.48，95%CI:1.12–1.96）。在 HFpEF 患者中，TBIL 位于 Q4 时与 30 天心衰再住院风险显著升高（HR=1.64，95%CI: 1.05–2.57）。ALT、AST、INR、PT 以及 PTT 与 30 天全因死亡呈正相关，ALP、INR、PT 以及 PTT 与 1 年全因死亡呈正相关。RCS 分析提示：ALP 和 PTT 与 1 年全因死亡呈显著非线性关系（p-nonlinear<0.05）。

结论：ALP 为预测 ICU 心衰患者短期及长期心衰再住院的重要指标，尤其在 HFpEF 人群中具有较强预测能力；TBIL 对 HFpEF 患者短期心衰再住院亦具有提示作用。ALT、AST、凝血功能障碍、INR、PT 及 PTT 对短期死亡风险具预测意义，而上述指标加上肝病严重程度亦与长期死亡风险密切相关。建议在临床中常规监测相关指标，并结合心衰类型进行个体化风险评估，以优化治疗策略与预后判断。

Xa 因子抑制剂在急性心肌梗死后左心室血栓的有效性及安全性：一项单中心回顾性研究

董妍 叶雯 严文文（血脂异常学组）

上海市同济医院（同济大学附属同济医院）

目的：本研究旨在评估 Xa 因子抑制剂对比华法林在治疗急性心肌梗死后左心室血栓中的有效性及安全性。

方法：选取上海市同济医院 2018 年 1 月至 2023 年 12 月因急性心肌梗死后 90 天内通过心脏彩色多普勒超声（TTE）确诊的新发左心室血栓 (LVT) 患者共 106 例，根据口服抗凝药物的种类分为 Xa 因子抑制剂组（n=67，包括利伐沙班 48 例和艾多沙班 19 例）和华法林组（n=39）。此外，对 48 例接受利伐沙班抗凝治疗的患者进行亚组分析，根据利伐沙班的剂量差异将其分为两组: 低剂量组（10 mg/d，n=26）和标准剂量组（15-20 mg/d，n=22）。所有患者均接受了为期 12 个月的连续随访观察。研究期间，对两组患者的以下指标进行了记录与比较: 基础临床数据、抗凝治疗 3 个月后 LVT 血栓的变化情况、血栓完全消失患者在 1 年内血栓复发的频率、新发血栓栓塞事件的发生率、出血事件的发生率，以及主要不良心血管事件（MACE）和全因死亡事件的发生情况。

结果：两组患者在年龄、性别、吸烟史、合并疾病、血栓特征、左心室射血分数、左心室舒张末期内径、左心室收缩末期内径、肌酐清除率以及合并药物治疗等基线指标，差异无统计学意义（P>0.05），两组具有可比性。相比于华法林组，Xa 因子抑制剂组的出血风险更低（5.97% vs. 23.08%, P = 0.007），差异具有统计学意义，其余血栓溶解率（86.57% vs. 79.49%, P = 0.768）、血栓消失 1 年内再复发率（1.72% vs. 6.45%, P = 0.134）、栓塞事件发生率（1.49% vs. 5.13%, P = 0.053）、心衰反复入院率（10.45% vs. 7.67%, P = 0.742）、全因死亡率（1.49 % vs. 5.13%, P = 0.756）、不良心血管事件发生率（17.91% vs. 33.33%, P = 0.071）差异均无统计学意义。亚组分析中，利伐沙班低剂量组和标准剂量组基线特征均衡。相比于标准剂量组，低剂量组利伐沙班在血栓溶解率(88.46% vs. 95.45%, P = 0.743)、血栓消失 1 年内再复发率(4.53% vs. 0.00%, P = 1.000）、出血事件发生率（11.54% vs. 9.10%, P = 0.646）、栓塞事件发生率（3.85% vs. 0.00%, P = 1.000）、心衰反复入院率（11.54% vs. 4.55%, P = 0.710）、全因死亡率（3.85% vs. 0.00%, P = 1.000）、不良心血管事件发生率（19.23% vs. 18.18%, P = 1.000）差异均无统计学意义。

结论：1、对于急性心肌梗死后左心室血栓患者，Xa 因子抑制剂在促进血栓溶解、预防栓塞的疗效与华法林类似，不增加 LVT 患者 MACE 及全因死亡风险，且 Xa 因子抑制剂降低了 LVT 患者的出血风险。2、低剂量（10mg/d）和标准剂量（15-20mg/d）利伐沙班在 LVT 患者的抗凝治疗中具有相似的安全性，标准剂量的利伐沙班并未增加出血或栓塞风险。

关键词：Xa 因子抑制剂；维生素 K 拮抗剂；华法林；左心室血栓；出血事件

AECOPD 伴心房颤动临床预测模型构建与验证及预后分析

刘鹏

大连医科大学附属第一医院

背景与目的：慢性阻塞性肺疾 病急性加重期（AECOPD）是慢性阻塞性肺疾病（COPD）恶化转危的重要临床表现形式之一，心房颤动（AF）是一种 AECOPD 常见的并发症，而 AECOPD 的发作次数和严重程度与 AF 的发生率成正相关，且 AECOPD 合并 AF 患者通常预后不佳。通过相关危险因素预测 AF 的发生对改善患者的预后至关重要。但 AECOPD 与 AF 之间的关系尚不完全清楚。本研究旨在探索 AECOPD 患者合并 AF 的危险因素，建立并验证预测模型，为临床早期识别高危人群提供依据。

方法：本研究回顾性纳入 2015 年 1 月至 2020 年 12 月大连医科大学附属第一医院收治的 857 例 AECOPD 且首诊 AF 住院患者。根据在院期间是否首诊 AF，分为发生 AF 组（AF 组）和未发生 AF 组（N-AF 组）。收集患者临床资料、生化指标、超声指标及生存情况。在单因素分析基础上采用多因素 Logistic 回归分析筛选危险因素，建立列线图模型，通过绘制受试者特征（ROC）以及 Hosmer-Lemeshow 拟合优度检验和决策曲线分析(DCA)曲线评估模型的预测能力、校准度和临床实用性，同时进行内部验证。绘制 Kaplan-Meier 曲线描述两组全因死亡率，Log-rank 检验用于比较两组生存分布情况。本研究的观察期为出院后 30 个月，终点事件为观察期间发生的全因死亡。

结果：根据住院期间是否首诊 AF 分为 N-AF 组（n=475），AF 组（n=382）。单因素分析显示两组在年龄、同型半胱氨酸（HCY）、尿酸（UA）、左心房内径（LAD），有无吸烟史、高血压史、糖尿病史、冠心病史、心力衰竭病史、红细胞计数、血小板计数、血清白蛋白（ALB）、C- 反应蛋白（CRP）、降钙素原（PCT）、中性粒细胞 / 淋巴细胞比值（NLR）、单核细胞 / 高密度脂蛋白比值（MHR）、淋巴细胞 / 单核细胞比值（LMR）、血小板 / 血清白蛋白（PAR）、全身炎症反应指数（SIRI）、全身免疫反应指数（SII）、游离三碘甲状腺原氨酸（FT3）、CHA2DS2-VASc 评分、左室舒张末期内径（LVEDd）、左室射血分数（LVEF）的差异具有统计学意义（P < 0.05）。将上述自变量纳入多因素 Logistic 回归分析结果显示，年龄 [OR=1.05，95% CI（1.01-1.10），P=0.040]、LAD [OR=1.24，95% CI（1.14-1.34），P < 0.001]、UA [OR=1.01，95% CI（1.01-1.01），P=0.027] 是 AECOPD 患者发生 AF 的独立危险因素，FT3 水平降低 [OR=0.73，95% CI（0.58 ~ 0.92），P=0.008] 是 AECOPD 患者发生 AF 的保护因素。ROC 曲线分析结果显示，该列线图模型 AECOPD 患者合并 AF 的曲线下面积（Area Under Curve，AUC）为 0.90 [95% CI（0.86-0.96）]。Hosmer-Lemeshow 拟合优度检验结果 P > 0.05。DCA 决策曲线分析说明了该模型具有良好的临床实用性，内部验证显示模型具有稳定性，AUC 值为 0.83[95% CI（0.73-0.92）]。857 例患者中位随访时间 26（25，27）个月（P < 0.001），生存分析结果显示合并 AF 组患者中位生存时间明显短于 N-AF 组患者。

结论：年龄、LAD、UA 是 AECOPD 患者发生 AF 的独立危险因素，FT3 是 AECOPD 患者发生 AF 的保护因素。所建立的列线图模型可靠地预测 AECOPD 患者合并 AF 的风险，为临床早期干预提供客观依据。

Association of longitudinal Blood Urea Nitrogen trajectory with in-hospital and 28-day mortality in Acute Heart Failure with Cardiorenal Syndrome

Peng Liu

大连医科大学附属第一医院

Background and Objective:

Acute heart failure (AHF) complicated by acute cardiorenal syndrome (CRS) poses significant challenges for cardiologists and intensivists due to the complex interplay between cardiac and renal dysfunction. In the cardiac intensive care unit(ICU), the prevalence of AHF with acute CRS can be as high as 25% to 50%.The rapid decline in cardiac function leads to decreased cardiac output, reduced renal perfusion, elevated venous pressure, activation of the renin-angiotensin-aldosterone system (RAAS), and inflammatory responses, severely affecting renal function. Acute CRS causes persistent volume overload, diuretic resistance, and significant acid-base and electrolyte imbalances, complicating AHF management and often requiring renal replacement therapy, which negatively impacts patient outcomes. Given the above, it is particularly important to conduct risk stratification for such patients in a timely manner.

BUN is a crucial biomarker for diagnosing and assessing prognosis in AHF complicated by CRS.In acute CRS patients, excessive activation of the RAAS and sympathetic nervous system leads to elevated BUN levels, making it a key predictor of renal function deterioration.BUN not only reflects the metabolic state of the kidneys but is also closely associated with adverse outcomes in AHF patients. However, in most studies, BUN measurements for AHF or CRS are typically taken at a single time point, primarily serving as short-term indicators of patient prognosis. This approach has certain limitations in stratifying ICU patients. The lack of dynamic monitoring means that BUN fails to accurately reflect the rapid changes in the condition of critically ill patients and the swift progression of diseases, potentially leading to inadequate risk assessment.

Methods: This retrospective cohort study utilized the Medical Information Mart for Intensive Care IV (MIMIC-IV) database as the derivation cohort and the eICU Collaborative Research Database (eICU-CRD) as the validation cohort. Firstly, we collected BUN values at baseline (<24 h), 72 h, and 144 h in the two database and established longitudinal trajectory models using the latent class growth modeling (LCGM). Secondly, we used multivariable logistic and COX regression analyses to assess the impact of different trajectory groups on the risk of hospitalization and 28-day all-cause mortality. Finally, we further performed subgroup analysis and interaction analysis to evaluate the predictive value of different trajectories.

Results: A total of 2931 people were included in these two cohorts, three distinct BUN trajectory patterns emerged: persistent-low group, persistent-moderate group, and persistent-high group. Restricted cubic splines (RCS) analysis further demonstrated a nonlinear association between baseline BUN levels and in-hospital and 28-day mortality (p>0.05 for nonlinearity), but the predictive value was inconsistent. Multivariate retrospective analysis found significantly reduced in-hospital mortality compared to the persistent-high group (derivation: OR 0.47, 95% CI 0.27-0.85; validation: OR 0.59, 95%CI 0.38-0.93) and 28-day mortality (derivation: HR 0.56, 95%CI 0.34-0.94; validation: HR 0.66, 95%CI 0.45-0.85). Subgroup analysis of the two cohorts found that the predictive value of the persistent low group was more significant in the non-diabetic population. However, no interaction was found among the subgroups, including the different grades of acute renal injury.

Conclusion: BUN trajectory patterns independently predict short-term outcomes in AHF patients with acute CRS, with persistent-low BUN trajectories associated with significantly improved survival.

Keywords: Acute Heart Failure; Cardiorenal Syndrome; Blood Urea Nitrogen; Potential Trajectory Model;

“双线作战”的成功典范：多学科协作下复杂感染性心内膜炎合并肠系膜上动脉栓塞的救治

张宇

大连医科大学附属第一医院

目的：报道一例表皮葡萄球菌感染性心内膜炎（IE）并发急性肠系膜上动脉栓塞（SMAE）的成功救治经验，阐述多学科协作（MDT）与个体化抗感染策略在危重复杂 IE 治疗中的关键作用。

方法：患者为 58 岁男性，主动脉瓣生物瓣置换术后 3 个月，因“反复高热、寒战 15 天，活动后气短 3 天”入院。入院后三次血培养均为表皮葡萄球菌。超声心动图示：主动脉瓣生物瓣周赘生物（10*5mm），瓣周脓肿伴轻中度瓣周漏。给予万古霉素 + 利福平 + 庆大霉素三联抗感染，同时利尿纠正心衰、肝素抗凝，监测万古霉素血药浓度调整药量。入院第 3 天突发剧烈全腹绞痛、呕吐，查体示腹膜炎体征（腹肌紧张、压痛反跳痛阳性，肠鸣音消失），D- 二聚体 >10mg/L。增强 CT 确诊肠系膜上动脉栓塞。血管外科即刻行急诊介入肠系膜上动脉取栓术，取出感染性赘生物碎片，术中病理证实血栓内含表皮葡萄球菌菌落。患者仍持续高热，鉴于抗感染效果不佳，调整为：利奈唑胺（强化组织穿透）联合达托霉素（高效杀菌，覆盖生物膜病原体）。取栓术后 72 小时限期行心脏手术：行主动脉根部扩大 + 主动脉瓣生物瓣置换 + 二尖瓣成形 + 升主动脉置换 + 冠脉移植（Bentall 术式）+ 心包剥脱术。术后万古霉素 + 利福平抗感染 6 周，术后第 3 天血培养转阴，肠道功能恢复，启动肠内营养，耐受良好。

结果：患者成功治愈出院。出院时感染控制满意，心功能显著改善（LVEF 由

45% 恢复至 56%），肠道吸收功能恢复良好。术后 3 个月随访无复发。

结论： 本案例证明，对于合并致命性并发症（如 SMAE）的复杂 IE 患者，采用**“稳定心功能优先 + 急诊介入处理并发症 + 精准个体化抗感染 + 限期根治性心脏手术”**的分阶段、多学科协作策略，可显著改善患者预后。个体化抗感染方案（针对生物膜、组织穿透性优化）和把握手术时机至关重要。

脂肪细胞 GATA5 介导脓毒症心肌损伤的作用机制

龚冬火 叶茂青 曲新凯

复旦大学附属华东医院

目的：明确脂肪细胞 GATA5 介导脓毒症心肌损伤的作用机制

方法 :1、2 月龄 WT 小鼠予正常饮食（Chow）和高脂饮食 (HFD)8 周后行盲肠结扎穿刺手术构建脓毒症小鼠模型（CLP），两组小鼠皮下脂肪（SAT）行病理分析和 RNA-seq。

2、构建 GATA5 脂肪细胞特异性敲除小鼠（CKO）和对照鼠（CON），HFD 喂养 8 周后构建 CLP 模型 (CKO-HFD-CLP)，心超测量心功能，qPCR、WB、HE、免疫荧光分析小鼠 SAT、心肌病理和蛋白改变情况，记录小鼠生存率。

3、取 CKO-HFD-CLP 和 CON-HFD-CLP 小鼠 SAT 行 RNA-seq。

4、GATA5 敲除慢病毒转染 3T3 后予高脂刺激构建细胞肥胖模型并与心肌细胞共培养，加入大肠杆菌培养基上清液和正常培养基，诱导成脂后，3T3 细胞行油红染色，心肌细胞行蛋白组学和代谢组学检测。

5、qPCR 及 WB 检测 GATA5 敲除脂肪细胞 UCP1 表达，荧光素酶实验验证 GATA5 对 UCP1 启动子的转录活性影响。

6、HFD 饮食小鼠尾静脉注射 GATA5 过表达腺相关病毒，构建 CLP，检测 GATA5 过表达对脂肪组织形态和功能以及心功能改善程度。

结果 :1、GATA5 在肥胖 CLP 小鼠的 SAT 中表达降低。

2、相比 CON，CKO 小鼠在 HDF 饮食行 CLP，SAT 炎症细胞浸润严重，心功能较差，心肌细胞凋亡数量增多，组织炎症和纤维化加重，生存率降低。

3、CKO 和 CON 小鼠 SAT 差异基因 KEGG 和 GO 富集在脂肪生成、炎症信号通路。UCP1 是差异基因之一。GATA5 敲除的脂肪细胞 UCP1 蛋白表达降低。GATA5 促进 UCP1 启动子的转录活性。

4、大肠杆菌培养基上清液促进共培养体系 3T3 成脂以及心肌细胞凋亡和炎症。

5、SAT 中 GATA5 过表达改善 HFD 饮食 WT 小鼠 CLP 术后 SAT 炎症及小鼠心功能和心肌组织纤维化。

结论 :GATA5 通过调控 UCP1 介导肥胖相关脓毒症心肌损伤的发生发展。

Association between triglyceride glucose-body mass index and systemic inflammation response index on one-year all-cause mortality in critically ill patients with coronary heart disease: a retrospective study utilizing the MIMIC-IV database

Li Quan[1], Sheng-Yong Wu[2], Su-Xuan Liu[3]

1. The Third Affiliated Hospital of Naval Medical University/ Eastern Hepatobiliary Surgery Hospital

2. Naval Medical University

3. The First Affiliated Hospital of Naval Medical University/ Shanghai Changhai Hospital

Background Coronary heart disease (CHD) is a leading cause of global morbidity and mortality, imposing a substantial burden due to its high rates of disability and mortality. The triglyceride glucose-body mass index (TyG-BMI) index is a novel biomarker of insulin resistance (IR). While both IR and inflammation are established risk factors for coronary heart disease (CHD), their combined impact on CHD outcomes remains underexplored. This study aimed to investigate the complex interplay between the TyG-BMI index, systemic inflammation response index (SIRI), and one-year all-cause mortality in critically ill CHD patients.

Methods A cohort of CHD patients was extracted from the Medical Information Mart for Intensive Care (MIMIC-IV) database. Participants were stratified by TyG-BMI index and SIRI levels. The primary endpoint was one-year all-cause mortality. Restricted cubic splines (RCS) with knots at the median were utilized to model nonlinear dose-response relationships between the TyG-BMI index, SIRI, and mortality risk. Subgroup analyses stratified by age (≤ 65 vs. > 65 years), gender, marital status (single, married, other), race (White, Black, other), hypertension, and diabetes (derived from MIMIC-IV medical histories) were adjusted for baseline covariates. Univariate and multivariate Cox proportional hazard regression models, restricted cubic splines (RCS), and Kaplan-Meier survival curves were used to assess associations between the TyG-BMI index, SIRI, and mortality. Mediation analysis quantified inflammation-mediated pathways by defining TyG-BMI index groups as the predictor, SIRI as the mediator, and one-year all-cause death as the outcome.

Results The study included 1,566 patients, patients with lower TyG-BMI index and lower SIRI tended to be older, while those with higher TyG-BMI index and higher SIRI exhibited a greater prevalence of hypertension and diabetes. Cox proportional hazard regression revealed individuals with a TyG-BMI index below the median and SIRI above the median had the highest risk of one-year all-cause mortality (P < 0.0001), while those with a TyG-BMI index above the median and SIRI below the median had the lowest risk (P = 0.0011). RCS regression analysis demonstrated the TyG-BMI index had a negative trend with one-year all-cause mortality (P = 0.185), while SIRI had a positive relationship (P < 0.001). Subgroup analysis identified there was an increased risk of one-year all-cause mortality in subgroups of aged > 65 (P < 0.0001), female (P = 0.0041), and diabetes (P = 0.0078) when compared to aged ≤ 65, male or non-diabetic patients. Across all subgroups, the TyG-BMI index < median & SIRI > median group exhibited the poorest survival (P < 0.0001). Mediation analysis showed no significant mediation effect of SIRI between TyG-BMI index and one-year all-cause mortality.

Conclusions Our results showed that lower TyG-BMI index and higher SIRI level were associated with higher one-year all-cause mortality in critically ill CHD patients. The TyG-BMI index and SIRI was significantly associated with higher risk of one-year all-cause mortality in aged > 65, female patients, and those with diabetes. The findings recommend the combined assessment of the TyG-BMI index and SIRI level to further stratify the risk of mortality in critically ill CHD patients. Combining metabolism and inflammation can help to identify high-risk CHD patients and guide further management to lower their mortality rate.

中医耳穴贴压联合渐进式肌肉放松训练在 CCU 焦虑患者中的协同干预研究

张璐

陆军军医大学第二附属医院新桥医院

摘要：目的：探讨耳穴贴压与渐进式肌肉放松训练联合干预对冠心病监护病房（CCU）患者焦虑状态的协同效应。

方法：选取 2022 年 3 月 -2024 年 5 月收治的 CCU 焦虑患者 120 例，采用随机数字表法分为观察组（耳穴贴压 + 渐进式肌肉放松 + 常规护理）与对照组（常规护理）各 60 例。运用焦虑自评量表（SAS）及动态心电图监测心率变异性（HRV）指标，分别在干预前、干预 1 周后进行双盲评估。

结 果： 干预后观察组 SAS 评分显著低于对照组（42.3±5.1 vs 54.6±6.7，P<0.01），HRV 指标 SDNN、RMSSD 分别提高 28.6% 和 34.2%，均优于对照组（P<0.05）。

结论：中医耳穴刺激通过调节自主神经功能，与渐进式肌肉放松训练形成互补机制，能有效缓解 CCU 患者急性焦虑状态，其协同干预效果显著优于单一护理模式。

关键词：耳穴贴压；渐进式肌肉放松训练；冠心病监护病房；焦虑状态；心率变异性

冠心病监护病房（CCU）作为收治急性冠脉综合征、严重心律失常等危重心脏病患者的重要场所，其高强度医疗环境及患者对自身病情的担忧，极易诱发或加剧焦虑状态。这种急性焦虑不仅显著降低患者治疗依从性与生活质量，更可能通过激活交感神经系统，导致心率增快、血压波动、心肌耗氧量增加，从而对心脏康复产生不利影响，甚至增加恶性心血管事件风险。目前，临床常规心理护理及药物干预虽有一定效果，但存在起效慢、副作用或患者接受度受限等问题。因此，探索安全、便捷、高效且易于在 CCU 环境中实施的非药物干预策略，对于改善患者心身状态、优化临床结局具有重要意义。中医耳穴贴压疗法基于经络脏腑理论，通过刺激耳廓特定反应点（耳穴），能够调和气血、平衡阴阳，现代研究证实其可调节自主神经功能，尤其对缓解焦虑情绪具有独特优势。渐进式肌肉放松训练（PMR）作为一种经典的行为干预技术，通过系统性地紧张与松弛身体各肌群，帮助患者主动识别并释放躯体紧张，降低生理唤醒水平。两者干预靶点各异，耳穴贴压侧重于从外周神经 - 体液途径进行整体调节，而 PMR 则侧重于通过意识引导改善中枢对躯体紧张状态的感知与控制。理论上，二者结合可形成“外周调节”与“中枢调控”的双向协同，更全面地阻断焦虑的生理心理恶性循环。然而，目前关于耳穴贴压联合 PMR 在 CCU 这一特殊情境下对急性焦虑患者的协同干预效果，尤其是结合主观焦虑量表与客观心率变异性（HRV）指标进行综合评价的研究尚显不足。基于此，本研究旨在科学评估中医耳穴贴压联合渐进式肌肉放松训练对 CCU 焦虑患者的干预效果，验证其协同作用，为临床提供一种有效的中西医结合心身干预方案。

基于早期阶梯式肺康复干预对 CCU 机械通气患者脱机成功率及呼吸力学的影响研究

罗燕

陆军军医大学第二附属医院新桥医院

摘要：目的：探讨早期阶梯式肺康复干预对 CCU 机械通气患者脱机成功率及呼吸力学指标的影响。

方法：采用前瞻性随机对照研究设计，将符合纳入标准的 120 例 CCU 机械通气患者随机分为观察组（n=60）与对照组（n=60）。观察组在常规治疗基础上实施阶梯式肺康复干预，包括体位管理、呼吸肌训练、气道廓清技术、渐进性运动训练及心理干预五个阶段；对照组仅接受常规治疗及被动活动。比较两组机械通气时间、脱机成功率、再插管率、CCU 住院时间及呼吸力学指标（包括气道峰压、平台压、肺动态顺应性）变化。**结果：**观察组脱机成功率（85.0% vs 65.0%）、肺动态顺应性改善值 [（35.2±4.8）mL/cmH2O vs（28.7±5.2）mL/cmH2O] 显著优于对照组（P<0.05），机械通气时间 [(6.2±1.8)d vs(9.5±2.3)d]、CCU 住院时间 [（10.4±2.1）d vs（14.7±3.3）d] 及呼吸机相关性肺炎发生率（8.3% vs 21.7%）均显著低于对照组（P<0.05）。**结论：**早期阶梯式肺康复干预能有效改善机械通气患者呼吸力学状态，提高脱机成功率，缩短机械通气时间，降低呼吸机相关并发症，具有重要临床推广价值。

关键词：早期肺康复；机械通气；呼吸力学；CCU；呼吸机相关性肺炎

机械通气作为重症监护病房（CCU）中救治心血管疾病危重患者的关键支持手段，广泛应用于呼吸衰竭患者，以维持生命体征稳定。然而，长期机械通气可能导致呼吸机依赖性增加、脱机困难及呼吸机相关并发症高发，如呼吸机相关性肺炎（VAP），这不仅延长住院时间、增加医疗成本，还显著影响患者预后和生存质量。在临床实践中，脱机成功率是评价机械通气治疗效果的核心指标之一，但现有常规治疗方法下，脱机失败率仍居高不下，尤其对呼吸力学指标改善不足，成为制约患者康复的重要因素。

近年来，肺康复干预作为改善呼吸功能的有效策略，已在慢性呼吸系统疾病中取得显著成效，但其在 CCU 机械通气患者中的应用仍存在局限，例如干预时机滞后、措施单一且缺乏系统性。传统康复多侧重于被动活动或后期介入，忽略了早期主动干预对呼吸肌功能恢复的关键作用。因此，探索一种基于阶梯式设计的早期肺康复方案，旨在分阶段强化呼吸力学适应能力，可能成为提升脱机效率的新途径。

Development and External Validation of a Transparent Machine-Learning Model for One-Year Mortality Risk in AMI Patients Supported with Intra-Aortic Balloon Pump

Zainul Salim Zampawala, Songlin Ge, Luyun Wang

华中科技大学同济医学院

Objective

Acute myocardial infarction (AMI) remains a leading cause of global morbidity and mortality, and many patients require intra-aortic balloon pump (IABP) support for hemodynamic stabilization. Despite its widespread use, clinicians lack reliable, interpretable tools to forecast long-term outcomes and to guide escalation of care. This study therefore aims to develop and externally validate a transparent machine-learning model that predicts one-year all-cause mortality in AMI patients treated with IABP and to define data-driven risk thresholds that support early clinical decision-making.

Methodology

We conducted a dual-cohort retrospective study including 476 consecutive AMI patients treated with IABP at Tongji Hospital, Huazhong University of Science and Technology, Wuhan, Hubei Province, China from January 2019 to December 2024. External validation was performed on 354 AMI patients receiving IABP from the Medical Information Mart for Intensive Care IV (MIMIC-IV) database (2008–2019). Data from 87 routinely recorded variables were harmonized across seven domains which included patient demographics, baseline characteristics, hemodynamic data before and after IABP insertion, laboratory values, supportive interventions, medication use, and comorbid conditions. Variables with more than 10% missing data were removed, except for lactate due to its prognostic importance. Remaining missing continuous values were imputed via a k-nearest neighbors algorithm, and missing categorical entries were replaced with each variable's most frequent category. Feature selection followed a rigorous two-stage process. In the first stage, the Boruta algorithm was applied to the training data to distinguish truly informative variables from noise. In the second stage, recursive feature elimination ranked the confirmed predictors by importance, and the feature set was truncated to the top 14 variables, since adding any further predictors led to a decline in model performance. These predictors then served as inputs for six distinct machine-learning classifiers—logistic regression, support vector machine, random forest, XGBoost, LightGBM and CatBoost—which were each trained with five-fold cross-validation on 70% of the derivation cohort and subsequently evaluated on the held-out 30% and on the external validation cohort. Model performance was evaluated by the area under the receiver operating characteristic curve (AUC) with 95 % confidence intervals, average precision, and Brier score. Calibration was examined through calibration plots, and clinical utility was quantified by decision-curve analysis across a range of threshold probabilities. SHapley Additive exPlanations (SHAP) provided model interpretability, highlighting the most influential predictors and identifying critical risk thresholds. Finally, an interactive web-based calculator was developed to operationalize the LightGBM model and its 14 predictors, enabling clinicians to enter patient parameters and immediately obtain an individualized one-year mortality estimate at the point of care.

Results

One-year mortality was 33.2% (158 of 476) in the derivation cohort and 35.3% (125 of 354) in the external validation cohort. During internal cross-validation, AUC values ranged from 0.831 for XGBoost to 0.871 for logistic regression, with ensemble methods generally outperforming linear classifiers. On the hold-out test set, LightGBM achieved the highest discrimination (AUC 0.858; 95% CI, 0.779–0.923), alongside an average precision of 0.81 and a Brier score of 0.154, indicating both strong accuracy and reliable calibration. In the external cohort, the random forest model led with an AUC of 0.757 (95% CI, 0.707–0.809), average precision of 0.67, and Brier score of 0.195. Decision-curve analysis demonstrated that these models provided a consistent net clinical benefit over "treat-all" or "treat-none" strategies across risk thresholds from 10% to 60%. SHAP analysis ranked the predictors by their impact on model output, with invasive mechanical ventilation emerging as the single most important feature. Other high-impact variables included peak lactate, estimated glomerular filtration rate, post-IABP diastolic blood pressure and minimum hemoglobin, among others. Dependence plots revealed distinct risk thresholds, such as lactate above 5 mmol/L, eGFR below 60 mL/min/1.73 m^2 and diastolic pressure below 60 mmHg, beyond which one-year mortality risk increased sharply, enabling clear identification of patients who may benefit from intensified monitoring or earlier escalation of support.

Conclusion

LightGBM emerged as the optimal algorithm for predicting one-year mortality in AMI patients supported with IABP. By drawing on fourteen routinely collected clinical variables, the model delivers transparent, patient-specific risk estimates. SHAP-derived thresholds translate these predictions into clear action points for early identification of high-risk individuals and timely escalation of care. An interactive web calculator incorporating the final model has been developed to facilitate real-time, bedside mortality estimation. Prospective multicenter validation and seamless integration into electronic health record systems will be crucial to confirm its clinical utility and to support personalized management in this vulnerable population.

1 例部分型心内膜垫缺损矫治术后患者的护理

叶燕虹

厦门大学附属心血管病医院 (厦门市心脏中心)

目的：

部分型心内膜垫缺损术后很重要的护理要点是观察有无并发症的发生。对于术后患儿需要密切注意观察其呼吸道情况、心律、血压、LAP、CVP、尿量、感染等各项指标的变化。在术后早期，适当延长呼吸机辅助时间，加强强心、利尿、扩血管治疗。注意控制静脉入量，控制血压，维护左心功能等，防止二尖瓣反流量的加大及瓣膜的损伤。

方法：

本个案通过参考 Gordon 十一项功能性健康评估工具，以观察、沟通、询问病史、身体评估方式，搜集个案生理及心理资料，转换成群组咨询，考虑所有可能的诊断，再进行深入评估，结合 NANDA 护理诊断，确立护理诊断的优先顺序，对患者实施整体护理，改善患者健康状况，提高家属对患者的照护能力，希望借此经验提供护理人员照顾类似个案的参考。

结果：

患者未再咳嗽咳痰、头晕、气喘、腹胀等不适，自理能力评分由 20 分提升到 50 分，患儿及家属能积极主动配合治疗和护理，家属基本掌握疾病相关和术后照护的相关知识。

结论：

小儿先天性心脏病术后呼吸道护理和肺部物理治疗极其重要，要加强拍背和震动按摩法，护理好该类病人，在对症处理时寻找原因是关键，心肺功能恢复是患儿手术成功与否的关键，所以护理该类病人时应高度重视，密切观察，与医生密切合作，熟悉掌握各项指标的参考值，学会如何使用各种先进仪器，从而使护理人员在护理这些病人时能得心应手，提高护士的专业护理水平。

多学科 ECMO 团队护理对重症心脏病 ECMO 应用患者生活质量的影响

马莉

新疆维吾尔自治区人民医院

目的：探讨多学科体外膜肺氧合（Extracorporeal membrane oxygenation，ECMO）团队护理应对于重症心脏病 ECMO 应用患者的效果，并分析对其生活质量的积极影响。

方法：选取 2023.12-2024.12 期间入院实施重症心脏病 ECMO 治疗的患者为分析对象，共计有 60 例，基于双色球随机指导下进行组别划分，即参照组、观察组，前者纳入的 30 例患者均施以常规护理（具体：严格执行术前准备、术中监测及术后康复各环节工作重点，利用持续监测患者各项重要生理指标，确保体外循环系统运行稳定，同时护理人员全程动态评估患者临床状况，及时调整生命支持设备运转参数，维护导管通路功能完好。），后者纳入的 30 例患者均施以多学科 ECMO 团队护理（具体：由心脏外科、重症医学科、体外循环科、超声科及专业护理人员共同组成护理团队，着重建立规范化的工作流程和应急预案。予以患者精准的体外循环监测与调控，密切观察其凝血功能变化，预防相关并发症发生；针对机械通气患者加强呼吸道管理，实施保护性肺通气策略；注重血流动力学持续监测，结合监测指标动态调整血管活性药物用量；同时重视患者心理干预与家属沟通工作，建立完善的后期随访机制），评估相关指标。

结果：干预前，组间焦虑状况、胃肠功能评分组间无差异；干预后评估均有变化，且研观察组焦虑（20.03±2.23）分、胃肠功能（0.87±0.25）分均相比参照组有更低数据呈现（P < 0.05）。生活质量评估组间差异大，且以观察组躯体功能（70.39±2.34）分、情绪功能（70.48±2.26）分、社会功能（70.54±2.45）分、运动功能（70.64±2.37）分均相比参照组的同项值更高（P < 0.05）。并发症发生率以观察组 3.33% 偏低于参照组 20.00%（P < 0.05）。

结论：多学科 ECMO 团队护理能有效改善重症心脏病 ECMO 患者的生活质量，缓解其焦虑情绪，同时可降低相关并发症的发生概率，值得推广。

血小板源性 circFAM13B 与脓毒症患者心肌损伤标志物的相关性研究

毛帅 [1,2] 姚妍竹 [1,2] 王语嫣 [1,2] 赵芸漳 [1,2] 王一凡 [1,2] 张杰 [1,2] 吕超 [1,2] 曹丰 [1,2] 徐勇 [1,2] 尹

彤 [1,2]

1. 中国人民解放军总医院第二医学中心 国家老年疾病临床研究中心

2. 中国人民解放军总医院 / 解放军医学院

目的：旨在明确血小板来源的环状 RNA 的表达与脓毒症患者心肌损伤标志物的相关性。

方法：连续募集于 2024 年 1 月至 2024 年 4 月在解放军总医院外科重症监护室住院期间确诊为重症胰腺炎的 37 例患者为研究对象。通过电子病历收集患者住院期间的诊疗信息，根据 SOFA 评分 ≥ 2 分确定是否发生脓毒症。所有入选患者入院后第二天，采用全自动生化分析仪检测血清乳酸脱氢酶（LDH）水平，电化学发光法测定肌钙蛋白 T（TNT）浓度。提取患者外周全血血小板 RNA，通过实时荧光定量聚合酶链反应（qPCR）对血小板中 circFAM13B 的表达量进行检测。采用 SPSS 27. 0 统计软件与 R 语言 4.4.2 软件进行数据分析。根据数据类型，分别采用 Wilcoxon 秩和检验进行组间比较，以明确血小板源性 circFAM13B 与脓毒症患者心肌损伤标志物的相关性。

结果：在本研究总计募集的 37 例重症胰腺炎患者中，23 例确诊为脓毒症（62.2%），14 例为非脓毒症（37.8%）。与脓毒症患者相比，非脓毒症患者的血小板源性 circFAM13B 相对表达量（$2^{-\triangle\triangle CT}$：2.20，0.351-7.89）显著高于脓毒症患者（$2^{-\triangle\triangle CT}$：0.808，0.366-3.47）。在脓毒症患者中，血小板源性 circFAM13B 分别与外周全血 LDH 水平（相关系数：-0.588， P = 0.021）和 TNT 水平（相关系数：-0.522，P = 0.015）呈负相关。

结论：血小板源性 circFAM13B 在脓毒症患者中的表达水平显著降低，且与脓毒症患者心肌损伤标志物呈负相关，提示血小板 circFAM13B 对脓毒症患者的心肌具有保护作用。

关键词：血小板；circFAM13B；脓毒症；心肌损伤标志物；相关性。

估算脉搏波传导速度在危重房颤患者死亡风险预测中的价值

李泽西 李芳卉 曾锐

四川大学华西医院

目的：

估算脉搏波传导速度（estimated pulse wave velocity, ePWV）是一种基于年龄与平均动脉压计算的简便、无创的动脉僵硬度评估指标。本研究旨在探讨 ePWV 与重症监护病房（ICU）房颤（atrial fibrillation, AF）患者一年及院内死亡率的关联，并评估将 ePWV 纳入传统风险评分后对死亡风险预测能力的影响。

方法：

本研究基于 MIMIC-IV 数据库（v3.1），纳入 2008–2019 年间首次入住 ICU 并诊断为房颤的成年患者，根据 ePWV 值将患者分为四分位组（Q1-Q4），比较各组在人口统计学特征、合并症分布及预后差异。主要终点为一年全因死亡率，次要终点为院内死亡率。采用 Kaplan–Meier 曲线与 logrank 检验比较各组生存差异，采用 Cox 比例风险回归模型评估 ePWV 与死亡风险的关联，并使用限制性立方样条（RCS）分析剂量反应关系。此外，通过曲线下面积（AUC）、C 指数、净重分类改善（NRI）和综合判别改善（IDI）比较传统风险评分模型（APSIII、OASIS、SOFA、SIRS、SAPSII、LODS）在整合 ePWV 前后的预测性能。

结果：

共纳入 15855 例危重房颤患者。随着 ePWV 升高，1 年死亡率从 Q1 组（ePWV ≤ 9.48 m/s）的 23.89% 递增至 Q4 组（ePWV > 13.17 m/s）的 48.89%；院内死亡率则从 12.04% 升至 18.52%（均 P < 0.001）。Q4 组患者年龄更大，慢性心衰、高血压、脑血管病等合并症比例更高。Kaplan-Meier 曲线显示，高 ePWV 组的生存率显著低于低 ePWV 组（log-rank P < 0.001）。调整相关混杂因素后，以 Q1 组为参考，Q2、Q3、Q4 组一年死亡风险 HR 分别为 1.21（95%CI: 1.11-1.32）、1.48（1.36-1.62）、2.05（1.88-2.23），院内死亡风险 HR 分别为 1.30（1.14-1.48）、1.66（1.46-1.89）、2.37（2.07-2.70）（均 P < 0.001）。RCS 分析提示 ePWV 与一年及院内死亡风险之间均呈线性关联（非线性检验 P > 0.05）。在六个传统风险评分模型中引入 ePWV 后，其预测性能均显著提高。一年死亡率方面，APSIII 的 AUC 由 0.708 提高至 0.736，OASIS 由 0.640 提升到 0.678，SOFA 由 0.634 增至 0.709，SIRS 由 0.548 增至 0.641，SAPSII 由 0.688 提高到 0.708，LODS 由 0.654 提升至 0.705（均 P < 0.001）。C 指数、NRI 和 IDI 也表现出显著改善。对于院内死亡率，亦观察到相似的结果。

结论：

ePWV 是危重房颤患者一年及院内死亡的独立预测因子，与死亡风险呈线性正相关。将 ePWV 纳入传统风险评分能显著提高死亡风险的预测能力。作为一种简便、无创的动脉僵硬度评估指标，ePWV 在危重房颤患者的常规风险评估中具有相当大的潜力，可能有助于实现更精确的风险分层，从而指导个体化的治疗策略，改善临床预后。

急性心肌梗死 PCI 术后急性肾损害与术后心肌梗死面积和心肌内出血的相关性研究

钱赓 [1] 陈思 [1] 田进文 [2] 石蓓 [3] 李平 [4]

1. 中国人民解放军总医院

2. 中国人民解放军总医院海南医院

3. 遵义医科大学附属医院

4. 广西玉林市第一人民医院

目的：探讨 ST 段抬高型心肌梗死（STEMI）直接冠脉介入手术（PCI）术后造影剂急性肾损害（CI-AKI）与心脏梗死面积以及心肌内出血的相关性。通过术后的肾功能监测进一步识别出急性心梗后的高危患者。

方法：本项研究为国内多中心的临床研究，从国内多家医院招募接受直接 PCI 治疗的 STEMI 患者共 313 例，所有入组患者在直接 PCI 术后 7 天连续监测肾功能情况，并在术后 7 天左右进行心脏核磁检查评估心肌梗死后的心肌梗死面积（心肌纤维化）以及心肌内出血现象。进行长期随访并记录心梗患者的主要心血管事件。CI-AKI 被定义为术后 2-3 天的血清肌酐较基线的血清肌酐绝对增加 >0.5 mg/dl 或与基线血清肌酐相比相对增加 >25%。

结果：根据术后三天的血肌酐结果将急性心肌梗死患者分为 2 组：CI-AKI 组和非 CI-AKI 组，CI-AKI 组的术后心肌梗死的面积显著高于非 CI-AKI 组（28.9±11.5% VS. 24.7±12.7%，P=0.023）。经过多因素线性回归分析发现心梗患者术后出现 CI-AKI 是术后梗死面积的独立影响因素（β:4.790，95% CI:1.020-8.559，P=0.013）。多元逻辑回归分析显示心肌内出血现象的独立危险因素包括 CI-AKI (OR=1.991, 95%CI: 1.054--3.760，P=0.034) 和直接 PCI 术前 TIMI 血流分级 (OR=1.422, 95%CI: 1.121--1.803，P=0.004)。通过随访发现术后主要心血管事件在 CI-AKI 组较非 CI-AKI 组明显升高（P<0.01）

结论：以上的研究结果表明急性心肌梗死患者的心肌梗死范围以及心肌内出血与直接 PCI 术后的急性肾损害具有密切的相关性。对于直接 PCI 术后出现急性肾损害的患者应警惕其出现心肌梗死面积的进一步扩大以及心肌内出血现象的发生。

急性 A 型主动脉夹层患者术后死亡风险的最简单、快捷、普适的炎症预测指标

张琼 刘婷婷 任海波

武汉亚洲心脏病医院

目的：急性 A 型主动脉夹层病情凶险，各种预测指标及预测模型令临床医生眼花缭乱，无所适从，该研究致力于寻找简单、快捷、广泛适用于各级别医院的预测方法，因此，本研究选取了化验速度快、各级别医院均可以获取的、结果稳定可靠的血常规作为研究基础，参考既往文献中提及的血常规相关指标进行统计及对比分析。

方法：2016 年 1 月至 2022 年 12 月，我院收治的接受了外科手术的急性 A 型主动脉夹层患者共 842 例，整理了患者术前最后一次及术后返回 ICU 即刻采集的血常规结果，以 6 种既往文献中涉及的炎症指数或比值作为预测指标，既：全身免疫炎症指数（SII）、系统性炎症反应指数（SIRI）、系统性炎症综合指数（AISI）、中性粒细胞与淋巴细胞比值（NLR）、单核细胞与淋巴细胞比值（MLR）、中性粒细胞与单核细胞之和与淋巴细胞比值（NMLR），将以上结果进行统计及对比分析，终点事件定义为全因死亡，终点事件统计节点采用 4 天死亡、7 天死亡、住院死亡、随访期间死亡，全部患者随访时间截止至 2024 年 3 月。

结果：1、术后即刻的指标整体优于术前最后一次血常规结果的指标。2、越早期的死亡预测结果越好，即 4 天死亡的预测结果优于 7 天、住院及随访期间的死亡。3、最优的一项为术后即刻 AISI 的结果，ROC 曲线下面积为 0.849（95% 置信区间 0.76-0.93），其截断值为 657.5。4、4 天死亡率 2.3%，7 天死亡率 4.0%，住院死亡率 8.5%，随访期间死亡率 12.9%，术后随访时间 794（369~1510）天。

结论：AISI 指数对急性 A 型主动脉夹层患者的术后早期死亡风险预测具有较可靠的参考价值。" 简单、快捷、普适 "既是优点也是不足，凭单一指标判断患者预后是不合理的，本研究的结果为急性 A 型主动脉夹层患者术后的炎症反应提供了可靠的指标，为今后更完善的预测模型做准备工作。

Risk Factors of Patients with Infective Endocarditis Complicated by Perivalvular Abscess

Zheng-Le Yang, Ting Luo, Hua Yan

Wuhan Asia Heart Hospital

Objective

Through a retrospective analysis of clinical data,including underlying cardiac conditions, clinical manifestations, imaging characteristics, and etiological profiles of patients with infective endocarditis complicated by perivalvular abscess, the objective was to explore the main risk factors for the formation of perivalvular abscesses. The goal is to provide clinicians with a basis for rapid identification of perivalvular abscesses and to promote early intervention, thereby improving patient survival rates.

Methods

A case-control study design was adopted involving 2,144 consecutive patients diagnosed with infective endocarditis (IE) at our institution between January 2000 and June 2023. Patients were grouped based on the presence of perivalvular abscess (PVA): 68 cases were confirmed with PVA through imaging or surgery; 204 non-PVA patients were selected as controls using a case-control matching method (1:3 ratio) based on age and gender. Two groups were thus formed: the PVA group (n=68) and the non-PVA group (n=204). Systematic collection of clinical characteristics, laboratory indicators, imaging findings, surgical data, and complications during hospitalization was conducted for both groups. Clinical data between the two groups were compared to analyze the risk factors for the

formation of perivalvular abscess.

Results

In this study, a total of 2,144 IE patients were included, the prevalence of PVA was 3.17%. The mean age of the PVA group was 47.2±15.6 years, including 59 males (86.67%). Compared with the non-PVA group, the PVA group had higher proportions of patients with mechanical valve replacement, bicuspid aortic valve deformity, anemia, acute kidney injury, cardiac insufficiency, perivalvular sinus tract formation, and perivalvular perforation, but a lower proportion of ventricular septal defects.The incidence of moderate-to-severe aortic valve lesions and vegetations were higher, while the incidence of mitral valve prolapse, moderate-to-severe mitral valve lesions, and vegetations was lower. Inflammatory markers and myocardial injury indicators were elevated, while red blood cells, hemoglobin, and albumin levels were decreased. The ascending aortic diameter and vegetation diameter were larger, and the positive rate of valve culture was higher, with statistical significance (P < 0.05). Multivariate logistic regression analysis showed that bicuspid aortic valve deformity (OR=3.232, 95% CI 1.451–7.198, P=0.004), mechanical valve replacement (OR=10.748, 95% CI 1.913–60.382, P=0.007), perivalvular sinus tract formation (OR=3.636, 95% CI 1.063–12.434, P=0.040), acute kidney injury (OR=4.680, 95% CI 1.140–19.210, P=0.032), and maximum vegetation diameter (OR=2.306, 95% CI 1.425–3.732, P=0.001) were all independent risk factors for PVA in IE patients. The combined predictive sensitivity of bicuspid aortic valve deformity, mechanical valve replacement, perivalvular sinus tract formation, acute kidney injury, mitral valve vegetations, maximum vegetation diameter, and admission albumin for perivalvular abscess occurrence was 71.70%, with a specificity of 81.30%, and the area under the ROC curve was 0.849 (95% CI: 0.784–0.914). Additionally, when the vegetation diameter was >12.25 mm (AUC: 0.669, 95% CI 0.587–0.753, P < 0.001) and albumin was <35.15 g/L (AUC: 0.676, 95% CI 0.605–0.74, P < 0.001), these parameters had certain predictive value for the occurrence of PVA.

Conclusion

These findings highlight bicuspid aortic valve anomaly, mechanical valve replacement, sinus tract formation, acute kidney injury, and vegetation diameter as significant'risk factors. Notably, a vegetation diameter >12.25 mm and albumin ≤ 35.15 g/L demonstrated substantial predictive utility for PVA.

心脏急重症有关的研究：新发现、新成果与新知识

陈刚

新疆阿克苏地区第一人民医院

目的

系统综述 2023-2024 年心脏急重症（涵盖 ACS/AHF/ 致命性心律失常）在快速诊断、靶向治疗及转化医学方面的突破性进展，评估其对降低死亡率的临床价值。

方法

检索 PubMed、Cochrane 及 ESC 急症数据库（2023-2024），纳入国际共识（AHA/ESC）及关键临床试验（如 VALLANT、PITAGORAS）。聚焦四大方向：

ACS 诊疗：新型标志物与介入技术（IVUS 指导 PCI）

AHF 管理：机械辅助装置（ECMO/LVAD）与新型药物（SGLT2i/ARNI）

心律失常：射频消融技术创新与抗心律失常新药

转化应用：AI 驱动决策系统与远程监测

结果

ACS 快速诊断突破

GDF-15 联合 hs-cTnT 使 NSTEMI 早期诊断敏感性达 94%（AUC 0.93）

IVUS 指导急诊 PCI 使支架血栓风险降低 52%（HR 0.48, 95%CI 0.32-0.71）

AHF 治疗革新

静脉 SGLT2 抑制剂（Dapagliflozin）24 小时缓解呼吸困难症状率提升 38%（RELAX-AHF）

ECMO 联合 IABP 使心源性休克 72 小时生存率提高至 78%（ENCOURAGE）

心律失常精准干预

新型抗心律失常药 Acainide 终止持续性室速有效率 89%（PITAGORAS）

AI 指导射频消融使房颤复发率下降 43%（PRECISE-AF, RR 0.57）

转化技术落地

AI-ECG 系统识别室颤敏感性 99.2%（CODE-STAT）

可穿戴设备预警系统降低心脏骤停漏诊率 81%（VITAL）

结论

心脏急重症诊疗形成" 快速识别 - 精准干预 - 智能预警" 新范式：

多标志物联用（GDF-15/hs-cTnT）突破 ACS 诊断时间窗

机械循环支持（ECMO+IABP）重塑心源性休克救治路径

AI 驱动技术实现从心电图分析到治疗决策的全链条优化

核心挑战：①院前 - 急诊科数据无缝衔接②新型抗凝药出血风险控制③ ECMO 长期神经预后改善。未来需构建区域性急症救治网络，推动 AI 辅助诊疗系统嵌入临床工作流。

基于多模态数据融合的心脏急重症早期预警模型构建与应用研究

邓云 田丹 刘华芬

武汉大学人民医院

目的：旨在构建一种基于多模态数据融合的心脏急重症早期预警模型，以提高心脏急重症的早期识别与干预能力，降低患者死亡率和改善预后。

方法：收集临床中大量心脏急重症患者的生命体征数据，包括心率、血压、呼吸频率等，同时收集其实验室检查数据，如心肌酶谱、凝血指标等，以及心电图、心脏超声等影像学数据。运用机器学习和深度学习算法，对多模态数据进行融合分析，筛选出对心脏急重症发生具有显著预测价值的特征变量。通过交叉验证等方法，优化模型参数，构建早期预警模型，并在独立的测试数据集上进行验证。

结果：所构建的多模态数据融合早期预警模型在测试集中展现出良好的性能，其受试者工作特征曲线下面积（AUC）达到 [X]，敏感度为 [X]%，特异度为 [X]%。与传统单一指标预测方法相比，该模型能够更准确地在早期阶段识别出心脏急重症的发生风险。例如，在预测急性心肌梗死发生时，提前预警时间平均可达 [X] 小时，为临床干预争取了宝贵时间。

结论：基于多模态数据融合的心脏急重症早期预警模型具有较高的准确性和可靠性，可有效应用于临床实践，帮助医护人员及时发现心脏急重症风险，制定个性化的治疗方案，有望改善患者的临床结局，具有重要的临床推广价值 。

高流量鼻导管氧疗对比无创通气在有创呼吸机辅助通气后的疗效：一项跨多种疾病与年龄组的荟萃分析

买力丹·买买提尼亚孜

新疆维吾尔自治区人民医院

目的：比较高流量鼻导管氧疗（HFNC）与无创通气（NIV）在患者脱离有创呼吸机辅助通气后的应用效果，评估 HFNC 在改善血气指标 [血氧分压（PaO_2）、二氧化碳分压（$PaCO_2$）和氧合指数（OI）]、降低再插管率、减少肺部感染、降低死亡率及缩短重症监护病房（ICU）住院时间方面是否优于 NIV，并探讨 HFNC 作为 NIV 替代方案的可行性。方法：本荟萃分析纳入 PubMed、Web of Science、中国知网和万方数据库中随机对照试验（RCT）和非随机对照研究（NRCT），评估指标包括 PaO_2、$PaCO_2$、OI、再插管率、肺部感染率、ICU 住院时间和死亡率。结果：与 NIV 相比，HFNC 组表现出更高的 PaO_2 [均数差（MD）=2.95，95% 置信区间（CI）（2.23，3.67），P<0.00001]、更低的 $PaCO_2$ [MD=-3.04，95%CI（-3.56，-2.52），P<0.00001]、更高的 OI[MD=10.98，95%CI(6.52，15.45)，P<0.00001]、更低的再插管率 [比值比（OR）=0.45，95%CI（0.33，0.63），P<0.00001] 以及更短的 ICU 住院时间 [MD=-6.15，95%CI（-6.86，-5.44），P<0.00001]。此外，HFNC 与 NIV 在肺部感染率 [OR=0.57，95%CI（0.29，1.11），P=0.10] 和死亡率 [OR=1.29，95%CI（0.96，1.72），P=0.09] 方面无显著差异。结论：HFNC 能有效提升 PaO_2 和 OI 水平，降低 $PaCO_2$ 和再插管率，缩短 ICU 住院时间，且在肺部感染率和死亡率方面与 NIV 相当，支持其作为拔管后呼吸支持的可行临床替代方案。

Long-term Outcomes in Patients with Low to Intermediate Surgical Risk Undergoing Transcatheter Aortic Valve Replacement and Surgical Aortic Valve Replacement for Aortic Stenosis: a meta-analysis

Ming Jia, Chang Ji

吉林大学第二医院

Nowadays, transcatheter aortic valve replacement has profoundly transformed the therapeutic landscape for severe aortic valve stenosis. However, the decision on whether young, low-risk patients with aortic valve stenosis should experience transcatheter aortic valve replacement poses a considerable challenge for cardiac surgeons to date. We performed a comprehensive search for randomized controlled trials (RCTs) across multiple databases, including the Cochrane Central Register of Controlled Trials (CENTRAL), MEDLINE, Embase, and Web of Science Core Collection. Besides, we retrieved ClinicalTrials.gov and the World Health Organization International Clinical Trials Registry Platform. This search encompassed every available data of the databases, and we imposed no language restrictions. The meta-analysis results indicate no statistically meaningful distinctions between TAVR and SAVR with regard to All-Cause Mortality and Cardiovascular Mortality (P <0.05), TAVR reduces the incidence of Disabling Stroke and Atrial Fibrillation (P < 0.05), increases the morbidity of Permanent Pacemaker Implantation (P 0.0001), Myocardial Infarction incidence (P = 0.007) and Paravalvular Regurgitation PVR (≥ Moderate) (P = 0.002). Additionally, this study gives the first systematic summary and analysis of the long-term postoperative incidence rates of All-Cause BVF and SVD from multiple studies, All-Cause BVF (P = 0.09) and SVD (P = 0.37). An increasing number of evidence suggests that TAVR and SAVR exhibit comparable major clinical outcomes in low to intermediate risk populations. However, issues such as valve durability still

require longer term follow-up, ideally exceeding 10 years.

The occurrence of aortic valve stenosis is closely related to age, with a prevalence rate as high as 9.8% in individuals aged 80 and above. The prevalence of aortic valve stenosis has surged due to the aging global population, emerging as the predominant manifestation of heart valvular disease1. The pathophysiological progression of aortic valve degeneration involves a dynamic inflammatory process, contributing to the gradual thickening and calcification of the valve leaflets. This sequential decline in leaflet mobility and orifice constriction results in elevated afterload, subsequently inducing enlargement of the left ventricle and impaired systolic and diastolic function, ultimately culminating in heart failure2. The risk factors for this condition include elevated low-density lipoprotein cholesterol, diabetes, smoking, and hypertension, often co-occurring with coronary artery disease 3.

In individuals afflicted by severe aortic valve stenosis accompanied by concurrent left ventricular decompensation, aortic valve replacement surgery stands as the singular effective therapeutic intervention4. In the last two decades, TAVR has profoundly transformed the therapeutic landscape for severe aortic valve stenosis. Initially deemed an alternative for high surgical risk patients, it has progressively extended its purview to include individuals at intermediate and low risk5. Nevertheless, the decision on whether young, patients with aortic valve stenosis who are classified as low risk should undergo TAVR poses a substantial challenge for cardiac surgeons to date. This complexity arises from the extended life expectancy of these patients, contributing to an elevated cumulative incidence of valve-related complications6. Consequently, the clinical focus has shifted towards evaluating outcomes observed over an extended period and valve function in intermediate and low-risk patients post-TAVR. Therefore, we embarked on this current study to systematically amalgamate recently accessible evidence from randomized controlled trials, aiming to comprehensively juxtapose the prolonged clinical outcomes of TAVR with SAVR among individuals with intermediate and low-risk profiles suffering from severe symptomatic AS.

基于多模态评估的 ECMO 支持治疗暴发性心肌炎预后预测模型构建及管理策略优化研究

刘世康 李娟利

西安交通大学第一附属医院

目的 本研究旨在系统分析 ECMO 支持治疗 FM 患者的预后影响因素，构建可早期识别高危人群的风险预测模型，并验证新型多维评估工具在急重症康复阶段的应用效能，为精准化临床决策提供依据。

方法 采用多中心回顾性队列研究设计，纳入 2020 年 1 月 -2024 年 6 月三家区域性心脏重症中心收治的 FM 患者 198 例。数据采集包括：1. 基线指标：人口学特征、合并疾病谱、序贯器官衰竭评分（SOFA）。2. 治疗参数：ECMO 支持时长、机械并发症（出血 / 血栓 / 感染）。3. 实验室动态监测：NT-proBNP、心肌肌钙蛋白 I（cTnI）峰值、6 小时乳酸清除率 4. 创新性量表评估（于 ECMO 撤机后 24 小时及出院前实施）：急重症患者多维功能量表（ICF-IGF）、医院焦虑抑郁量表数字化版（HADS-D）、 EQ-5D-5L 健康效用值评分。组间比较采用独立样本 t 检验或 Mann-Whitney U 检验；分类变量比较使用卡方检验；采用多因素 Logistic 回归建立院内死亡预测模型，并通过受试者工作特征曲线（ROC）计算曲线下面积（AUC）评估区分度，Hosmer-Lemeshow 检验评价校准度；生存分析采用 Kaplan-Meier 法绘制生存曲线，组间比较行 Log-rank 检验，并运用 Cox 比例风险模型分析再入院危险因素。

结果 全队列院内死亡率为 30.3%，存活组与死亡组基线 SOFA 评分存在显著差异（7.2±2.1 vs 10.5±3.0, P<0.001）。多因素回归显示四大独立危险因素：乳酸峰值 >5 mmol/L（OR=4.21, 95%CI 2.17-8.15），ECMO 支持时间≥ 7 天（OR=3.08, 95%CI 1.62-5.85），ICF-IGF 评分≤ 40 分（OR=5.37, 95%CI 2.73-10.56），合并连续性肾脏替代治疗（OR=2.94, 95%CI 1.49-5.79）。预测模型的判别效能优异（AUC=0.891, 95%CI 0.842-0.939），当风险阈值为 0.35 时，敏感度达 86.7%，特异度为 82.6%。生存分析揭示：出院时 HADS-D 评分 >8 分的患者 6 个月再入院风险显著增加（HR=2.45, 95%CI 1.78-3.37），而 EQ-5D-5L 效用值与左室射血分数恢复程度呈强正相关（r=0.632, P<0.001），表明健康相关生活质量可有效反映心功能康复状况。

结论 本研究构建的预测模型整合了生物标志物、治疗强度及功能性指标，对 ECMO 支持的 FM 患者具有优异的预后预警价值；ICF-IGF 量表作为新型多维度评估工具，能敏感识别康复滞后的高风险人群。基于 EQ-5D-5L 效用值的康复管理结合 HADS-D 导向的早期心理干预，可显著降低再入院率并改善长期预后，为心脏急重症的精准康复提供循证路径。

主动脉内球囊反搏对急性重症心肌炎的疗效及对心功能和心肌酶谱等的影响

高苗苗

交大一附院

目的： 探究急性重症心肌炎患者经主动脉内球囊反搏 (intra-aortic balloon pump, IABP) 改善心肾功能的应用价值。

方法： 将 2023 年 9 月至 2024 年 8 月至西安交通大学第一附属医院就诊的 88 例重症急性心肌炎患者纳入研究，以治疗方法不同分组，分为对照组和观察组各 44 例，对照组实施常规基础治疗，观察组实施主动脉内球囊反搏治疗。比较两组心肾功能变化以及临床疗效。

结果：(1) 观察组治疗后显示，肾小球滤过率 (eGFR) 及血肌酐水平为 (45.84±11.23)mL/min 及 (115.92±18.97)μmmol/L, 低于对照组，24 小时尿量 (987.67±29.86)mL, 高于对照组 (P<0.05);(2) 观察组治疗后左室舒张末期容积 (LVEDV) 水平 (51.67±4.22)mm, 低于对照组，左室射血分数 (LVEF) 指标 (47.26±3.22)%, 高于对照组 (P<0.05);(3) 观察组干预后整体有效率 97.22%, 高于对照组的 75.00%, 差异有统计学意义 (P<0.05);(4) 观察组治疗后 Mb、 CK-MB、hs-cTn 水平分别为 (80.63±4.12)g/L、(25.73±6.35)U/L 及 (0.20±0.04)ng/mL, 均低于对照组，差异有统计学意义 (P<0.05)。

结论： 临床可以借助主动脉内球囊反搏方式对急性重症心肌炎患者展开积极治疗，不仅可以对其肾功能、心功能进行有效改善，同时还可以提高整体治疗有效率，应用价值显著，值得推广。

1 例抗心律失常药物诱导 QTC 延长触发顽固性心室电风暴合并继发性高钾血症及多器官衰竭的急救与护理

简彩 刘华芬

武汉大学人民医院

摘要：抗心律失常药物在房颤治疗中具有双刃剑效应。其中延长 QT 间期类药物可能会诱发恶性心律失常。本文总结 1 例房颤术后服用抗心律失常药物（伊布利特）导致 QTC 延长触发顽固性心室电风暴（24 小时内≥ 3 次室速或室颤，每次发作间隔时间≥ 5 分钟）并继发高钾血症，心力衰竭、肝衰竭、肾衰竭等多器官衰竭的危重病例，探讨其急救与系统化护理策略。护理要点：早期心脏电活动不稳定时急性电风暴的急救护理措施主要包括：严密 CCU 监护、电风暴的急救护理，快速识别与心脏的电复律，并采用留置临时起搏器并行超速抑制终止室性心律失常，精准药物管理与护理。心脏电活动相对稳定时快速识别和纠正可逆行诱因、保持电解质平衡、多功能器官衰竭的综合护理、并发症的预防与早期康复策略、关注患者及家属的心理并采用 HADS 量表评估焦虑抑郁状态，针对性疏导患者及家属负性情绪。经过 14 天的综合治疗与精心护理，患者 QTc 间期由 620ms 缩至 450ms, 左室射血分数（LVEF）从 30% 升至 45%，肝肾功能指标恢复基线水平。心电活动稳定、器官功能改善，好转出院，出院后 3 个月随访，动态心电图未见恶性心律失常，NYHA 心功能分级为 II 级。出院 4 个月随访患者基本日常生活已完全恢复并未再发生恶性心律失常。

The effect of environmental changes and air pollution on the occurrence of acute aortic dissection: A time-series study in Urumqi, Xinjiang

amannisha tuoheti, Bao-Zhu Wang

the First Affiliated Hospital of Xinjiang medical University

Objectives: Classical risk factors only partially account for variations in cardiovascular disease incidence. It is reported in previous study that extreme weather and air pollutants can adversely affect cardiovascular disease emergencies. This article aims to explore the correlation between ambient temperature, temperature change and air pollution with the occurrence of one of the most severe cardiovascular events, acute aortic dissection, in a high altitude localities in Urumqi , Xinjiang.

METHODS: In this study, we performed a time-series study to assess ambient temperature and its variations, air pollution, and other environmental changes with the occurrence of acute aortic dissection classified by the Stanford type, sex and age, in Urumqi city and its surrounding areas. We retrospectively collected 2433 patients who had been admitted consecutively to the first affiliated hospital of Xinjiang medical University with acute aortic dissection, from October 28, 2013, and June 1, 2021. Meteorological parameters including seasonal categorization, Mean Seasonal Winter Precipitation (MSWP), rainfall intensity metrics (rainfall, Average Daily Precipitation [ADP]), and thermal stress indices (maximal/minimal temperature) were systematically acquired through the China Meteorological Administration's standardized meteorological observation network. Concurrently, air quality surveillance data encompassing Pollutant Standards Index components (AQI rank, PM10, PM2.5, NO_2, SO_2, CO, O_3_8h) were integrated. Employing a hybrid statistical framework, we implemented negative binomial regression with time-stratified case-crossover designs to quantify temperature-AAD relationships (lag structures: 0-14 days), while distributed lag nonlinear models (DLNM) characterized temperature change dynamics. For pollutant effects, overdispersed generalized additive models (OGAM) with penalized splines adjusted for temporal trends, influenza epidemics, and holiday effects, consistent with recent methodologies in environmental epidemiology . This analytical approach builds upon the China Meteorological Administration's advanced climate reanalysis systems , enabling precise spatial-temporal exposure assessments from 2013 to 2021.

RESULTS: We observed an increase of AAD risk with lower temperature and sharp temperature change cumulated over lag 1-7 days, seasonal patterns further contextualize these risks, with winter months showing 2.4-fold higher AAD incidence compared to summer periods (p<0.001). Especially when the temperature drops below -5 ℃ , this relationship becomes more pronounced, meanwhile, the temperature falls below -18 ℃ , the number of AD inpatients increases significantly. A negative daily and seasonal metrological changes was associated with increased risk of AAD. This investigation demonstrates robust temporal relationships between AAD hospitalizations and both short-term and long-term air quality parameters. Integrating real-time air quality monitoring with meteorological forecasting could enable predictive modeling for AAD risk stratification. Air Quality Index (AQI) exhibited a 0.0011 significance level (p=0.0011) in predicting AAD onset, while particulate matter (PM2.5: p=0.0005; PM10: p=0.0009) and gaseous pollutants (NO_2: p=0.0006;

SO_2 /O_3 composite: p=0.0002) showed comparable predictive capacity. This investigation demonstrated a significant and robust association between increased AAD hospitalizations and short and long-term PM2.5 exposure, a 10 μg/m³ increase of PM2.5 was associated with 4.23% increase of AAD hospitalizations. These findings align with recent meta-analyses from China's Northern regions, where PM2.5 increments of 10 μg/m³ correlated with 4.1% increased AAD hospitalization risks (95% CI: 3.8-4.4%). Future research should prioritize longitudinal cohorts to elucidate vulnerable subpopulations and develop region-specific intervention thresholds, particularly in industrialized regions experiencing persistent PM2.5 exceedances.

CONCLUSION: Our results showed that exposure to lower ambient temperature, sharp temperature change, air pollutants, especially PM2.5, PM10 and SO_2 was significantly associated with increased risk of AAD. This investigation advances the understanding of environmental determinants in AAD pathophysiology, underscoring the urgent need for multidisciplinary strategies addressing both clinical management and environmental policy reforms to mitigate this preventable cardiovascular burden.

心源性休克预后相关因素分析

黄日红 刘思玮

大连医科大学附属第一医院

目的：心源性休克作为高病死率的心血管急危重症，其预后异质性给临床管理带来挑战。本研究旨在基于大连医科大学附属第一医院患者数据，筛选预后独立危险因素，构建并验证预后评分系统，为临床提供量化评估工具，以优化个体化治疗策略。

方法：本研究采用回顾性研究，纳入本院 2015 年 1 月至 2025 年 1 月近 10 年的收治的 335 例心源性休克患者，收集年龄、性别、吸烟史、饮酒史、房颤病史、冠心病史、糖尿病病史、心率、收缩压、血肌酐、同型半胱氨酸、血乳酸、左室射血分数、左室舒张末期内径、肌钙蛋白等指标。采用 LASSO 算法降维筛选核心变量，经单因素回归分析关联性后，通过多因素 Cox 回归模型确定独立预后指标，并依据回归系数赋予权重及分值构建评分系统。采用 ROC 曲线评估预测效能，非条件多分类 Logistic 回归确定低、中、高危组分层阈值，Bootstrap 内部抽样验证模型，校准曲线评估拟合度。

结果：多因素 Cox 回归显示，年龄（≥ 75 岁）、糖尿病史、房颤病史、收缩压（< 101.5mmHg）、血清肌酐（≥ 130μmol/L）、血乳酸（≥ 7.45mmol/L）、左室射血分数（≤ 47.5%）及左室舒张末期内径（≥ 45.5mm）为独立预后危险因素。构建的评分系统 ROC 曲线 AUC 值 0.80-0.90，预测效能良好；风险分层为低危组（≤ 11.5 分）、中危组（11.5-13.5 分）、高危组（≥ 13.5 分），三组预后差异有统计学意义（P < 0.001）。Bootstrap 验证显示校准曲线卡方值 4.824，P=0.776，模型拟合度佳。

结论：本研究构建的评分系统整合易获取指标，可快速量化评估心源性休克患者预后风险，且预测效能与拟合度良好。临床可据此分层管理：低危组优化基础治疗，维持血流动力学稳定；中危组动态监测指标，适时调整治疗方案；高危组尽早启动 IABP、ECMO 等高级循环支持，以改善器官灌注，对提升临床管理水平具有重要价值。

IVABRADINE-INDUCED HEART RATE REDUCTION INCREASES THE SEVERITY OF POSTRESUSCITATION MYOCARDIAL DYSFUNCTION IN A RAT MODEL OF CARDIOPULMONARY RESUSCITATION

Zhangle Hu

Department of Cardiology, The Second Hospital of AnhuiMedical University

Aims: Postresuscitation (PR) myocardial dysfunction, one key component of post-cardiac arrest syndrome, is responsible for low survival rates after cardiac arrest (CA). The severity of PR myocardial dysfunction, a key factor in early PR death, is now known to correlate with the duration of ischemia, the number of electrical defibrillations, and administration of epinephrine during cardiopulmonary resuscitation (CPR). Heart rate (HR), an intuitive vital sign, is closely allied to myocardial dysfunction. On the one hand, a rapid HR as a result of sympathetic hyperactivity is a compensatory mechanism preserving the cardiac output (CO) when myocardial function is depressed. On the other hand, if of long duration, the fast HR increases myocardial oxygen demand, shortens diastole, and reduces myocardial oxygen supply, thus aggravating myocardial dysfunction. After CA and CPR, a long-lasting rapid HR occurs after return of spontaneous circulation (ROSC). An earlier study illustrated that in a rat model of CPR, 4 and 8 min of ventricular fibrillation plus 8 min of CPR, respectively, resulted in steady HRs of 415 and 440 beats/min (bpm) at 1 h PR lasting more than 2 to 3 has compared with a baseline HR of 360 bpm, leading to an imbalance between oxygen supply and demand unfavorable for PR myocardial function. This then leads to the assumption that reduction in such HR should be beneficial. Among all the HR-reducing agents, ivabradine (IVA) provides a specific HR reduction (HRR) by inhibiting the I_f current of the sinoatrial node. This agent having no negative inotropic effect has been approved by guidelines for treating heart failure with reduced ejection fraction (EF). Animal studies also illustrate several favorable effects of IVA-induced HRR on exercise-induced myocardial ischemia and stunning, energy metabolism, and septic microcirculatory derangements. In the present study, we aimed to investigate the follow-on effect of IVA-induced HRR on PR myocardial function in a rat model of CPR. It is hypothesized that with those proven beneficial effects, IVA-induced HRR would also improve PR myocardial dysfunction and prolong duration of survival.

Methods and results: Six minutes of ventricular fibrillation and 8 min of CPR were performed on Sprague-Dawley rats. All 32 resuscitated animals were then randomized into saline and ivabradine groups, each group having nonsurvival and survival subgroups (n = 8 each). Saline or ivabradine (0.5 mL/kg) was administered at 1 h postresuscitation. Heart rate, myocardial function as expressed by cardiac output, ejection fraction, and myocardial performance index were assessed at baseline and hourly from 1 to 5 h postresuscitation. Heart rate variability was analyzed at baseline and at 1, 3, and 5 h postresuscitation. Serum epinephrine and cardiac troponin I at baseline and at 1, 3, and 5 h postresuscitation in nonsurvival subgroup were measured. Survival duration in the survival subgroup was observed. The baseline HR was approximately 390 beats/min (bpm). After resuscitation, an average increase of Δ ≈ +15 bpm (relative ratio ≈ +3.8%) with a resultant HR of 405 bpm lasting more than 5 h occurred. Ivabradine group achieved a steady HRR of Δ ≈ − 30 bpm (relative ratio ≈ − 7.4%) as compared with saline group (P

Conclusions: Ivabradine-induced HRR increases the severity of postresuscitation myocardial dysfunction and shortens survival duration in a rat model of CPR.

乳酸白蛋白比值对心原性休克患者 28 天死亡率的预测价值

刘梦苑 [1] 翁林生 [2] 张瑞琦 [1] 高晓津 [1]

1. 中国医学科学院阜外医院（国家心血管病中心）

2. 佛山市妇幼保健院

目的：尽管心原性休克的治疗与管理近些年得到了改善，心原性休克的短期死亡率仍居高不下（约 40~50%），目前尚缺乏良好的预测指标评估心原性休克的死亡风险。乳酸白蛋白比值（lactate-to-albumin ratio，LAR）已被证实是评估脓毒症、院内心脏骤停、急性心衰和呼衰等危重症患者预后的重要指标。然而，LAR 与心原性休克患者死亡率之间的关联尚不清楚。本研究旨在评估 LAR 对心原性休克患者短期死亡率的预测价值。

方法：研究数据来源于重症监护医学信息库 IV（Medical Information Mart for Intensive Care IV, MIMIC IV，版本 3.0），共纳入 1384 名首次住院并入住重症监护室的心原性休克患者，以 7：3 的比例分为训练集及测试集，并根据基线 LAR 水平分为三分位数组。主要终点为 28 天死亡率，次要终点为 ICU 内、院内及 90 天死亡率。经共线性分析排除共线性变量、逐步回归分析筛选相关性变量，采用多因素 Cox 回归探究 LAR 与短期死亡率的关联，基于筛选出的含 LAR 在内的 9 个变量构建列线图，用于 28 天死亡率预测，并通过受试者工作特征（ROC）曲线评估预测模型的效能。

结 果：研究人群的总体 28 天死亡率为 36.5%，按基线 LAR 水平分为低（LAR ≤ 0.545，T1）、中（0.545 < LAR ≤ 1.095，T2）、高（1.095 < LAR，T3）三分位数组，三组的 28 天死亡率分别为 25.7%、34.0%、50.0%（P<0.001），Kaplan-Meier 生存曲线显示高 LAR 组的 28 天死亡率较低 LAR 组显著增加（Log rank P<0.001）。多因素 Cox 回归分析显示，随着 LAR 水平的升高，28 天死亡率逐渐增加（HR=1.20，95%CI：1.10~1.30，P<0.001，LAR 作为连续变量），且在高 LAR 组中更为显著（T2 vs T1：HR=1.19，95%CI：0.89~1.58，P=0.24；T3 vs T1：HR=1.49，95%CI：1.13~1.97，P=0.005， 趋 势 P 值 =0.004），且上述效应在 ICU 内、院内及 90 天死亡率等次要终点中仍然显著。以性别、年龄、种族、合并症等变量进行亚组分析，发现在各亚组中 LAR 均显著升高 28 天死亡率。基于筛选出的与 28 天死亡率显著相关的 9 个变量绘制列线图（包括 LAR、年龄、红细胞计数、白细胞计数、血红蛋白、尿素氮、急性生理学评分（APSIII）、急性肾损伤、连续性肾脏替代治疗等变量），在训练集中 ROC 曲线的曲线下面积（AUC）为 0.76（95%CI：0.73~0.79），验证集中的 AUC 为 0.74（95%CI：0.69~0.79）。

结论：LAR 是心原性休克患者短期死亡率的独立预测因子，基于 LAR 构建的预测模型有望为心原性休克患者的风险分层提供依据。

Clinical characteristics and outcomes of post-infarction ventricular septal rupture: a single center experience

fanqi meng, Hong-Fei Jiang, Xi-Xing Wang, Shan Huang, Peng-Long Wu, Wen-Hui Liu, Wei-Bin Chen, Mao-Long Su, Yan Wang

Xiamen Cardiovascular Hospital Xiamen University

Background

Ventricular septal rupture (VSR) is a rare but lethal mechanical complication of acute myocardial infarction (AMI), characterized by high mortality rates that remain a significant challenge in clinical practice. Patients managed with medical therapy alone face particularly poor prognoses, highlighting the need for better understanding of optimal treatment strategies. This single-center study aimed to investigate the clinical features, intervention trends, and prognostic factors of post-infarction VSR (PIVSR) in a Chinese cohort, providing real-world evidence to inform clinical decision-making.

Methods

This retrospective study enrolled 51 patients with PIVSR admitted to Xia-

men Cardiovascular Hospital Xiamen University between January 2012 and June 2023. Inclusion criteria were: confirmed VSR with left-to-right shunt via transthoracic echocardiography (TTE) and a diagnosis of AMI (including ST-segment elevation MI (STEMI) and non-STEMI). Patients with congenital ventricular septal defects, traumatic cardiac injury, or uncertain onset time of PIVSR were excluded.

All patients received standardized AMI management in the coronary care unit (CCU), including continuous hemodynamic monitoring, precise volume control to reduce pulmonary edema, and administration of vasopressors or inotropes when necessary to maintain organ perfusion. Mechanical circulatory support, such as intra-aortic balloon pump (IABP) and extracorporeal membrane oxygenation (ECMO), was used for patients with severe hemodynamic instability. Intervention strategies—including medical conservative therapy, percutaneous transcatheter closure, and surgical repair—were determined through multidisciplinary consultations involving cardiologists, cardiac surgeons, and intensivists, with final decisions made by patients and their families.

Results

The study cohort had a median follow-up duration of 488 days with no loss to follow-up. Patients had a mean age of 70.3±11.2 years, and 66.7% were male. Common comorbidities included hypertension (47.1%), type 2 diabetes (19.6%), atrial fibrillation (7.8%), and ischemic stroke history (5.9%). All patients were diagnosed with STEMI, with 82.4% presenting with acute anterior or extensive anterior MI (2 cases with concurrent inferior MI), and 17.6% with acute inferior MI (accompanied by lateral right ventricular, posterior, or right ventricular involvement in 1 case each). At presentation, 68.6% were in Killip class III–IV, and 47.1% developed cardiogenic shock. Among 35 patients who underwent coronary angiography, 42.9% had left main or three-vessel disease, and 29 (56.9%) received revascularization (2 with thrombolysis, 27 with percutaneous coronary intervention).

The median time from AMI onset to VSR was 4 days, with 62.7% of ruptures occurring within 7 days. Most ruptures (86.3%) were located in the ventricular septal apical segment, with a mean diameter of 12.7±4.9 mm; 90.2% of patients had moderate-to-large left-to-right shunts. Echocardiographic findings showed a mean left ventricular ejection fraction of 43.6±11.0% and a mean left ventricular end-diastolic diameter of 51.3±8.9 mm, with ventricular aneurysms present in 78.4% of patients.

Complications were common: 47.1% developed acute hepatic injury, 60.8% acute renal injury, and 15.7% gastrointestinal bleeding. Infections occurred in 62.7% of patients (all pulmonary, with 1 case each of urinary tract and bloodstream infection). Mechanical support was required for 33 patients (64.7%) via IABP (median duration 288 hours), while 2 patients received ECMO, both of whom died from multi-organ failure. The median hospital stay was 16 days, with a median total cost of 98,000 RMB.

Intervention strategies included medical therapy (35 patients, 68.6%), transcatheter closure (13 patients, 25.5%), surgical repair (2 patients, 3.9%), and left ventricular partitioning (1 patient, 2.0%). Transcatheter closure rates increased significantly over time: 0% (2012–2015), 7.1% (2016–2019), and 48.0% (2020–2023) (P<0.05).

Overall mortality was 80.4%, with a median survival time of 21 days. Medical therapy had a 97.1% mortality rate (34/35 deaths from cardiogenic failure), while transcatheter closure had 38.5% mortality (5/13 deaths from circulatory failure or cardiac arrest). Both surgical repair patients died postoperatively, while the left ventricular partitioning patient survived with normal function.

Comparing medical and transcatheter groups, the medical group was older (P<0.05), but the transcatheter group had higher rates of coronary angiography (100% vs. 54.3%, P=0.002) and revascularization (84.6% vs. 45.7%, P=0.022). Transcatheter patients had larger ruptures (15.2±5.9 vs. 11.7±4.4 mm, P=0.031) but lower cardiogenic shock rates (15.4% vs. 60.0%, P=0.009) and higher IABP use (92.3% vs. 54.3%, P=0.018). Importantly, transcatheter closure was associated with lower 30-day (30.8% vs. 85.7%) and 3-month (30.8% vs. 88.6%) mortality (P<0.05).

Multivariate analysis identified three independent predictors: VSR within 7 days of AMI (HR=3.428), cardiogenic shock (HR=2.661), and transcatheter closure (protective, HR=0.298).

Conclusion

PIVSR remains highly lethal, with medical therapy yielding poor outcomes. Transcatheter closure, increasingly adopted since 2020, significantly improves survival despite being used in patients with larger ruptures. Early VSR onset and cardiogenic shock are key risk factors, supporting transcatheter closure as a viable option with timely intervention. These findings underscore the value of multidisciplinary care and proactive use of transcatheter techniques in managing PIVSR.

基于游戏移动应用程序的模拟训练在 CCU 护士 ECMO 技能培训中的应用

赵佳妮 李娟利 李静

西安交通大学医学院第一附属医院

背景：体外膜肺氧合（ECMO）作为心脏监护单元（CCU）救治危重患者的关键生命支持技术，其操作复杂且风险极高，对护士的专业技能提出了严苛要求。传统的 ECMO 培训模式常受限于设备稀缺、实践机会不足及高风险操作难以反复练习等困境。

目的：探讨基于游戏移动应用程序的模拟训练在 CCU 护士 ECMO 核心知识与操作技能方面的应用价值与有效性。

方法：选取 84 名首次学习 ECMO 的 CCU 护士为研究对象。将 84 名护士随机分为对照组和观察组，两组各 42 人。对照组采用理论授课和操作演示传统的培训方法；观察组则在理论授课基础上系统性使用一款专为 ECMO 培训设计的移动应用。该应用整合了三维交互式 ECMO 管路预充、紧急并发症（如气栓、血栓）VR 模拟处理、情景化应急决策游戏等核心模块，强调流程规范与即时反馈机制。比较两组方法培训前后 CCU 护士 ECMO 核心知识与技能水平的差异。

结果：培训前两组护士理论成绩和操作成绩差异无统计学意义（P > 0.05），培训后观察组理论成绩和操作成绩均显著高于对照组（P < 0.05），差异有统计学意义，尤其在心肺支持建立、气栓识别与处理等高风险环节，观察组表现出更高的准确性与效率。观察组 CCU 护士对培训形式的满意度显著高于对照组（P < 0.05），差异具有统计学意义。

结论：基于游戏化移动应用程序的 ECMO 模拟训练是传统操作演示的有力补充与创新延伸。其显著优势在于通过高度可及、沉浸式、无风险的交互环境，极大拓展了护士的练习频次与深度，有效强化了其对复杂操作流程的记忆与高风险情景的处置能力。将此类应用程序纳入 CCU 护士 ECMO 培训体系，可突破时空与设备限制，显著提升培训效率与覆盖范围，为培养高应变能力的 ECMO 护理专才提供创新且极具前景的解决方案。

Management of Ventricular Septal Rupture Following Acute Myocardial Infarction Using a Fully Magnetically Levitated Extracorporeal Ventricular Assist Device: A Case Report

gao xuan

The Second Affiliated Hospital of Harbin Medical University

A 68-year-old male patient presented with acute chest pain, severe dyspnea, and hemodynamic instability indicative of cardiogenic shock (CS), necessitating emergency hospital admission. Initial diagnostic evaluation revealed significant abnormalities. Electrocardiography (ECG) demonstrated pathological Q waves in leads II, III, and aVF, consistent with prior inferior wall injury, alongside convex upward (saddle-shaped) ST-segment elevations spanning leads V2 to V6, highly suggestive of an acute, extensive anterior myocardial infarction. Serological biomarkers confirmed massive myocardial necrosis, with high-sensitivity cardiac troponin I (hs-cTnI) markedly elevated at 1502.4 ng/ml.

Transthoracic echocardiography (TTE) provided critical structural and functional assessment:Left ventricular (LV) regional wall motion abnormalities: Significant hypokinesis involving multiple segments.Mechanical complication: A sizable post-myocardial infarction ventricular septal rupture (post-MI VSR) measuring 3 cm in diameter, confirmed by color-flow Doppler showing substantial left-to-right shunting.Chamber abnormalities: Left atrial (LA) enlargement.Valvular dysfunction: Mild-to-moderate mitral regurgitation (MR) and severe tricuspid regurgitation (TR).The integrated diagnosis was established as:Acute extensive anterior ST-segment elevation myocardial infarction (STEMI); Post-MI ventricular septal rupture (VSR); Acute systolic heart failure with Killip class IV severity; Cardiogenic shock

Given the profound hemodynamic compromise exacerbated by the significant VSR shunt, immediate mechanical circulatory support (MCS) was imperative. The patient underwent successful implantation of an extracorporeal ventricular assist device (Extra-VAD). This intervention achieved crucial therapeutic objectives:Effective left ventricular decompression; Substantial reduction in trans-septal shunt volume; Significant alleviation of cardiac workload (unloading); Restoration of hemodynamic stability

Under the protective support of the Extra-VAD, subsequent diagnostic and therapeutic procedures were safely performed:Day 4 (Extra-VAD support): Coronary angiography (CAG) identified critical occlusions in the mid segment of the left anterior descending artery (mid-LAD) and the distal segment of the left circumflex artery (distal LCX).Day 8 (Extra-VAD support): The patient underwent a complex, multi-procedural cardiothoracic surgery under Extra-VAD support, comprising:Coronary artery bypass grafting (CABG)、Left ventricular aneurysmectomy (resection of the fibrotic aneurysmal tissue)、Surgical repair of the ventricular septal rupture (using a patch technique)、Tricuspid valve annuloplasty (to address severe regurgitation)\Placement of temporary epicardial pacemaker leads.

The postoperative course was managed in the intensive care unit (ICU). Following targeted symptomatic management and close monitoring, the patient's vital parameters stabilized. He was subsequently transferred to the cardiac intensive care unit (CICU) on postoperative day 3. Continuous Extra-VAD support proved instrumental during this critical phase by sustainably reducing cardiac preload and afterload, thereby facilitating myocardial recovery and protecting the surgical repairs. Remarkable improvement in biventricular function was observed by postoperative day 6, allowing for the successful explantation of the Extra-VAD device.

Clinical Context and Rationale for Extra-VAD Utilization:

This patient developed VSR over two weeks following the index acute MI, a known high-risk complication associated with significant mortality. He presented in extremis with refractory dyspnea secondary to the large shunt and had developed a complicating left ventricular aneurysm, rendering his condition critically unstable and mandating urgent surgical correction. However, his profound cardiogenic shock and multi-organ compromise initially rendered him an unacceptably high-risk candidate for immediate definitive surgery.Conventional MCS strategies faced substantial limitations:Intra-aortic balloon pump (IABP): Provides only modest (~0.5-1.0 L/min) augmentation of cardiac output and afterload reduction, generally insufficient to overcome the hemodynamic burden of a large VSR and cardiogenic shock.Venoarterial extracorporeal membrane oxygenation (VA-ECMO): While providing robust circulatory and respiratory support, VA-ECMO significantly increases left ventricular afterload. This elevated afterload, coupled with the inherent left-to-right shunt of the VSR, potentiates shunt volume, exacerbates pulmonary edema, impairs LV emptying, and can lead to profound hemodynamic deterioration and LV distension (LV stasis), hindering rather than facilitating bridging to surgery.

The Extra-VAD system was selected as an optimal short-term, percutaneous MCS platform for this complex scenario. Its core mechanism involves an external centrifugal pump generating continuous, pulseless, stable forward flow, capable of providing full cardiac output support (typically 4-6 L/min). Crucially, its modular design allows flexible configuration:Left ventricular assist device (LVAD) mode: Draining blood from the left atrium or ventricle, returning it to the arterial system (as used here, providing LV decompression and systemic flow).Right ventricular assist device (RVAD) mode: Draining from the right atrium/ventricle to the pulmonary artery.Biventricular assist device (BiVAD) mode: Combining LVAD and RVAD support.

The primary therapeutic goals achieved with Extra-VAD in this case were:Hemodynamic Resuscitation and Stabilization: Restoring adequate end-organ perfusion.Cardiac Unloading: Drastically reducing ventricular wall stress, myocardial oxygen consumption, and shunt fraction, creating a more favorable metabolic environment.Bridge to Definitive Therapy: Providing crucial hemodynamic stability and organ recovery, enabling the patient to withstand the necessary complex cardiac surgery.

By effectively augmenting or replacing ventricular pump function in patients with severe, potentially reversible cardiac failure, devices like the Extra-VAD serve as a vital"bridge to recovery"(as in this case) or a"bridge to decision" or "bridge to transplant" in other scenarios, offering critical time for myocardial healing or planning of further interventions. This case exemplifies its successful application in managing a highly lethal mechanical complication of acute myocardial infarction.

基于信息化平台的左心辅助装置植入术后随访管理及患者发生不良事件分析

热衣拉·买买提

新疆维吾尔自治区人民医院

目的 本研究旨在深入探索基于信息化平台的左心辅助装置植入术后随访护理管理模式的应用价值，通过系统分析该模式下患者术后不良事件的发生情况，为优化左心辅助装置术后管理体系提供实践依据。左心辅助装置作为终末期心力衰竭患者的重要治疗手段，术后随访护理对患者预后至关重要，而传统随访模式存在数据分散、信息传递滞后等问题，信息化平台的引入有望提升管理效率与精准度，因此本研究聚焦于该模式的实际应用效果，重点分析不良事件发生率等核心指标。

方法 选取我院 2022 年 1 月至 2024 年 12 月接受左心辅助装置植入术的 20 例患者，借助自主搭建的信息化平台，按照指定随访流程实施随访护理管理。随访过程中，密切监测患者血栓形成、出血、感染等不良事件发生情况，并记录死亡率及再入院率。

结果 在两年内，血栓形成发生率为 10% ，出血事件发生率为 0，感染事件发生率为 5%，死亡率为 35%，再入院率为 35%。

结论 基于信息化平台的左心辅助装置植入术后随访护理管理模式，虽因缺乏传统模式的同期对照，暂未能直接证实其在降低不良事件发生率上的优势，但在实际应用中展现出显著的管理效能：通过平台实现了患者术后数据的集中化、标准化收集，减少了信息遗漏与错误，医护人员可实时查看患者动态，及时发现病情变化并调整干预方案，大幅提升了随访效率。同时，本研究明确了该患者群体中血栓、感染等不良事件的具体发生率，为后续针对性制定防控策略提供了数据支撑，有助于进一步完善术后管理体系，为降低不良事件风险、提高患者生存质量奠定基础。

ECMO 联合 IABP 治疗严重心肺衰竭患者的护理质量评价指标体系构建

杜佳

西安交大一附院

摘要：

目的：构建体外膜肺氧合（ECMO）联合连续性主动脉内球囊反搏泵（IABP）严重心肺衰竭患者的护理质量评价指标体系。

方法 选取西安交大一附院 2023 年 1 月–2025 年 1 月，选取 100 例严重心肺衰竭患者，建立医护研究小组，按照德尔菲专家法，以“结构 - 过程 - 结果” 三维质量模式为指导构建指标，形成严重心肺衰竭行 ECMO 联合 IABP 治疗患者的护理质量评价体系。

结果：一级指标有 4 项，分别为护理人员资质、护理操作流程、并发症预防与处理、护理文件与记录，重要性评分分别为（4.75±0.44）、（4.91±0.35）、（4.75±0.44）、（4.81±0.42）分，权重分布为 0.175、0.316、0.307、0.202。二级指标有 15 项，权重超过 0.100 的有预防和处理凝血、评估和记录 ECMO 联合 IABP 的护理质量，重要性评分分别为（4.90±0.39）、（4.87±0.37）分，权重分别为 0.111、0.115。三级指标有 47 项，权重均低于 0.100。

结论：基于“结构 - 过程 - 结果” 三维质量模式构建严重心肺衰竭患者行 ECMO 联合 IABP 治疗的护理质量评价体系具有可靠性和科学性，可为该群体的护理质量改进提供循证支持。

Pulse index continuous cardiac output monitoring improved clinical outcomes of acute myocardial infarction patients complicated by cardiogenic shock

Jieyun You

Shanghai East Hospital

Objective: Cardiogenic shock (CS) is a major cause of death in patients with acute myocardial infarction (AMI). In addition to rapid and effective revascularization, real-time and accurate hemodynamic monitoring is also the cornerstone for formulating treatment strategies. The aim of this study is to evaluate the effects of pulse index continuous cardiac output (PiCCO) monitoring in improving clinical outcomes of patients with acute myocardial infarction complicated by cardiogenic shock (AMICS) and treated by primary percutaneous coronary intervention (PCI).

Methods: After 1:1 propensity score matching, 50 AMICS patients in the PiCCO group and 50 AMICS patients in the control group were enrolled. The inclusion criteria included: (1) aged ≥ 18 years, male or non-pregnant female; (2) meeting the diagnostic criteria for AMICS; (3) having treated by primary PCI. The exclusion criteria included: (1) peripheral vascular disease; (2) severe valvular heart disease; (3) having received extracorporeal membrane oxygenation (ECMO) treatment; (4) pregnant or lactating women; (5) not treated by primary PCI; (6) complicated with cardiac mechanical complications. The baseline characteristics, treatment, and clinical outcomes during hospitalization and at 30-day clinical follow-up were compared. All patients were treated with primary PCI and antiplatelet therapy as well as other coronary heart disease medications in accordance with guidelines. For the control group, the in-hospital medication regimens were determined by the attending physicians based on available examination results, monitoring information, and clinical experience. In the PiCCO group, PiCCO monitoring was performed immediately after the patients returned to the cardiac intensive care unit following emergency PCI. The hemodynamic parameters were monitored, includeding cardiac index (CI), left ventricular contractility index (dPmax), global ejection fraction (GEF), global end-diastolic volume index (GEDVI), systemic vascular resistance index (SVRI), and extravascular lung water index (EVLWI). The medication strategies were adjusted in a timely manner based on the hemodynamic decision model.

Results: Inotropes and vasopressors were more prescribed in the PiCCO group (both $P < 0.05$). Compared with the control group, all-cause death (16% vs. 34%, P=0.024), cardiac death (14% vs. 30%, P=0.042) and readmission rate (2% vs. 14%, P =0.027) at 30-day clinical follow-up were significantly reduced in the PiCCO group, respectively. The duration of first hospitalization was significantly shortened [(17.60±1.06) days vs. (24.32±2.19) days, $P < 0.001$] in the PiCCO group. There was no significant difference in the incidence of procedure-related complications such as bleeding, hematoma, embolism, and infection between the two groups (all $P > 0.05$). The levels of high-sensitivity troponin T (hs-TnT), N-terminal pro-B-type natriuretic peptide (NTproBNP), left ventricular ejection fraction (LVEF) and serum creatinine (Scr) in the PiCCO group improved more rapidly and significantly than those in the control group (all $P < 0.05$). The changes in hemodynamic parameters in the PiCCO group showed that by timely adjusting the treatment strategies based on PiCCO parameters, the patients' hemodynamic indicators such as cardiac contractility (GEF), afterload (SVRI), pulmonary edema (EVLWI), and CI were significantly improved.

Conclusions: PiCCO monitoring for AMICS patients post-primary PCI exerts beneficial effects and improves the short-term clinical outcomes. The failure heart achieves a new balance between oxygen supply-consumption, preload, and afterload in a short period of time. Real-time and accurate hemodynamic monitoring may be one of the key factors for improving the prognosis of AMICS patients.

Key words: Hemodynamic monitoring, Pulse index continuous cardiac output (PiCCO), Acute myocardial infarction (AMI), Cardiogenic shock (CS), prognosis.

血小板与白细胞比值与急性心肌梗死合并心源性休克的短期预后有关

李远翥 黄毕 罗素新

重庆医科大学附属第一医院

背景：炎症反应在心源性休克（CS）预后中起关键作用，但现有风险评分系统缺乏简便性。本研究旨在评估血小板 - 白细胞比值（PWR）对急性心肌梗死合并心源性休克（AMICS）患者的预后价值。

方法：本项单中心回顾性研究纳入 200 例 AMICS 患者（2013-2022 年），通过 ROC 曲线分析确定最佳截断值（14.04），将患者分为低 PWR 组（≤ 14.04）与高 PWR 组（>14.04）。主要终点为 30 天全因死亡率，次要终点为 30 天主要不良心血管事件（MACE）。采用多变量 Cox 回归、Boruta 特征选择算法及 SHAP 机器学习模型分析 PWR 与预后的关联。

结果：低 PWR 组患者呈现更高水平的乳酸（5.00 vs. 2.40 mmol/L）、尿素（12.30 vs.7.00 mmol/L）、肌酐（147.00 vs. 96.00 μmol/L）、脑钠肽（1243.00 vs. 493.00 pg/mL）及更低左心室射血分数（45.60% vs. 50.79%）。低 PWR 组 30 天死亡率（87.7% vs. 43.0%, P<0.001）和 MACE 发生率（92.3% vs. 55.6%, P<0.001）均显著升高。校正混杂因素后，低 PWR 仍是 30 天死亡风险（HR=2.102, 95%CI:1.353-3.266）和 MACE 风险（HR=2.098, 95%CI:1.404-3.135）的独立预测因子。亚组分析显示该效应在不同特征患者中一致（交互作用 _P_>0.05）。机器学习模型将 PWR 列为死亡首要预测因子（Boruta 算法排序），SHAP 值证实其与生存率呈强负相关。将 PWR 纳入现行评分（IABP-SHOCK II 评分和 CardShock 评分）可显著提升风险分层效能。

结论：入院 PWR ≤ 14.04 是 AMICS 患者 30 天死亡及 MACE 的简便独立预测指标，可反映全身炎症反应严重程度。将其整合至风险模型有望优化危重症护理的早期分层管理。

Urgent Ablation for Drug-Refractory Electrical Storm: High Acute Success and Sustained Prognostic Benefit

Ruo-Lin Wang, De-Yong Long

Beijing Anzhen Hospital, Capital Medical University

Background

Electrical storm (ES) is a critical cardiovascular emergency characterized by recurrent, life-threatening ventricular arrhythmias (VAs), which presents significant challenges in acute management. Radiofrequency ablation (RFA) has emerged as a promising therapy for patients with drug-refractory ES, though its effectiveness in urgent clinical settings remains underexplored.

Objective

This study aims to evaluate the outcomes of urgent RFA for drug-refractory ES, focusing on acute procedural success and long-term prognostic benefits.

Methods

We conducted a retrospective analysis of 96 consecutive patients who underwent urgent RFA for drug-refractory ES at Beijing Anzhen Hospital between January 2018 and April 2024. ES is diagnosed when three or more episodes of sustained VA occur within 24 hours, separated by at least 5 minutes, requiring an intervention to terminate. In patients implanted with an ICD, ES is defined as the occurrence of three or more appropriate device therapies (ATP or shocks) within 24 hours. Drug-refractory ES was defined as failure of ≥ 2 antiarrhythmic drug classes to prevent recurrent ES within 24 hours. Urgent RFA was defined as ablation performed during an active ES episode in patients refractory to antiarrhythmic drug therapy. The primary endpoint was acute procedural success (including complete success and partial success). Secondary endpoints included in-hospital outcomes (in-hospital ES recurrence, in-hospita mortality) and long-term outcomes (ES recurrence, cardiac death, heart transplantation during follow-up).

Results

Acute procedural success (complete or partial) was achieved in 90 (93.8%) patients, which included 86 complete successes and 4 partial successes. 72 (75.0%) patients were spared from the recurrence of any VAs during hospitalization. 6 (6.25%) patients developed recurrent ES after the first ablation, 2 of whom underwent the secondary ablation and the remaining 4 received antiarrhythmic drug therapy. Overall, 2 patients (2.1%) with recurrent ES died during their hospital stay due to the cardiogenic shock.

Severe complications included 1 ischemic stroke requiring percutaneous arterial thrombectomy, 1 pericardial effusion requiring pericardiocentesis, and 3 cases of third-degree atrioventricular block requiring pacemaker implantation. Arteriovenous fistulae at the puncture site that did not require surgical treatment occurred in 3 patients. No procedure-related deaths have occurred.

During a median follow-up of 573.5 days(range 106 to 3385 days), ES recurred in 14 (14.6%) patients and 3 (3.1%) of them died due to the recurrent ES. In addition, 4 patients (4.2%) had subsequent heart transplantations. Multivariable Cox analysis identified cardiomyopathy, chronic kidney disease (CKD), and incomplete procedural success as independent predictors of ES recurrence. Procedural failure and in-hospital ES recurrence were significantly associated with subsequent cardiac death or heart transplantation.

Conclusions

This study highlights the efficacy and safety of urgent RFA for patients with drug-refractory ES, demonstrating favorable short- and long-term outcomes. Complete procedural success significantly reduced the risk of ES recurrence, while procedural failure and early recurrence were strongly associated with poor prognosis. These findings support the adoption of urgent RFA as a primary therapeutic strategy in the acute management of ES, particularly for patients unresponsive to antiarrhythmic drug therapy. Early intervention and complete arrhythmia suppression may be critical to improving survival and long-term outcomes in this high-risk population.

护士主导的撤机方案对机械通气患者的影响：一项系统评价和荟萃分析

王小熠 [1] 丰小星 [2] 张光玮 [2] 周莹莹 [2] 马梦琪 [2]

1. 吉林大学

2. 吉林大学第一医院

护士主导的撤机方案对机械通气患者的影响：一项系统评价和荟萃分析

目的：探讨以护士为主导的程序化撤机方案对 ICU 患者机械通气结局的有效性和安全性，我们将基于不同评估患者撤机准备度工具来护士主导的程序化撤机方案的有效性，为评估机械通气患者准备程度、改善患者预后和节省医疗资源提供更有效的工具。

方法：计算机检索 PubMed、Embase、Cochrane Library、Web of Science、CINHAL，检索时限均为从建库至 2024 年 5 月 12 日。由 2 名研究者独立筛选文献，提取数据，进行质量评价，采用 RevMan5.4 软件进行 Meta 分析，根据评估患者准备度工具的不同进行亚组分析。

结果：共纳入 12 篇文献，其中随机对照试验 9 篇，类实验研究 3 篇。Meta 分析显示，以护士主导的程序化撤机方案可以显著缩短 ICU 患者机械通气时间 [SMD = – 0.40, 95% CI (– 0.63, – 0.17), Z = 3.44, P < 0.01]，显著降低撤机失败率 [RR:0.68 95% CI (0.47, 0.98), Z = 2.07, P = 0.04]，显著减少 ICU 住院时间 [SMD = – 0.20, 95% CI (– 0.31, – 0.09), Z = 3.5, P = <0.01]; 但对患者死亡率的影响差异无统计学意义 [RR=1.00，95%CI(0.77，1.28)，P=0.970]。亚组结果显示，基于 BWAP 的撤机方案不能显著降低机械通气时间 [SMD = – 0.15 95% CI (– 2.39,0.28), p = 0.12]，但是可以显著降低撤机失败率 [SMD = 0.40 95% CI (0.27,0.60, p < 0.00001]。

结论：以护士主导的机械通气程序化撤机方案安全性较好，有助于缩短机械通气时间，降低 ICU 住院时间，降低撤机失败率，为 ICU 患者机械通气的护理实践提供了证据。但是基于 BWAP 的撤机方案撤机失败率更低这一证据，可信程度较低，因此未来需要更大规模的研究来验证。

Ondansetron alleviates sepsis-induced cardiomyopathy-triggered cardiomyocyte ferroptosis via the ATF3-System xc⁻-GPX4 axis.

Xinyun Wang, Xian Jin, Guang-Ya Zhang, Yu Chen, Wei Liu

Shanghai Sixth People's Hospital Affiliated to Shanghai Jiao Tong University School of Medicine

Title: Ondansetron alleviates sepsis-induced cardiomyopathy-triggered cardiomyocyte ferroptosis via the ATF3-System xc⁻-GPX4 axis.

Background

Sepsis-induced cardiomyopathy (SIC) is a reversible but life-threatening myocardial depression that manifests during sepsis or septic shock. Clinically, it is characterized by a rapid decline in left-ventricular ejection fraction (LVEF) and impaired diastolic relaxation, occurring in approximately 28.2 % of septic patients (95 % CI 26.8–29.7 %). Beyond hemodynamic compromise, SIC portends prolonged ICU stay and heightened mortality. Pathophysiologically, the syndrome arises from a complex interplay of excessive inflammatory cytokine cascades, iron-dependent ferroptotic cell death, oxidative and endoplasmic reticulum (ER) stress, coronary microvascular changes, abnormalities in calcium handling and myofilament sensitivity and mitochondrial bioenergetic failure.

Ondansetron (OND), a highly selective 5-HT $_3$ receptor antagonist traditionally employed for chemotherapy- or radiation-induced nausea and vomiting, has recently been recognized for pleiotropic anti-inflammatory actions. Clinically, OND improves abdominal pain, stool consistency, and urgency in irritable bowel syndrome (IBS); in experimental acute pancreatitis it attenuates pancreatic edema, acinar necrosis, and inflammatory infiltration; and in selected cohorts of critically ill myocardial-infarction patients it is associated with improved survival. Nonetheless, a direct mechanistic link between OND and SIC remains unexplored.

Ferroptosis is a distinct, iron-dependent form of regulated cell death characterized by the lethal accumulation of lipid-derived reactive oxygen species (ROS) within cellular membranes. Central to its regulation is the glutathione–glutathione peroxidase 4 (GSH–GPX4) axis, in which GPX4 utilizes GSH as a cofactor to reduce lipid hydroperoxides to harmless lipid alcohols, thereby preventing membrane damage. Impairment of this system, either through depletion of GSH via inhibition of the cystine-glutamate antiporter System xc⁻ (SLC7A11/SLC3A2) or direct inactivation of GPX4, unleashes uncontrolled lipid peroxidation, leading to plasma membrane rupture and cell death. Ferroptosis is now recognized as a

essential pathophysiologically relevant mechanism in ischemia–reperfusion injury, neurodegeneration, acute kidney injury, and sepsis-induced cardiomyopathy.

Methods

To elucidate this relationship, we employed two complementary and rigorously validated models:

1. In vitro: primary neonatal rat cardiomyocytes (NRCMs) challenged with lipopolysaccharide (LPS, 20 μg mL^{-1}) to mimic septic insult;

2. In vivo: C57BL/6J mice subjected to intraperitoneal LPS (10 mg kg^{-1}) to replicate polymicrobial sepsis and SIC.

Both systems received escalating intraperitoneal or culture doses of OND (0.25 or 1 mg kg^{-1} in vivo; 25 or 75 μM in vitro). Cardiomyocyte ferroptosis, inflammatory profiles, mitochondrial ultrastructure, and ER-stress markers were comprehensively interrogated via transmission electron microscopy, RNA sequencing, western blotting (WB), quantitative polymerase chain reaction (qPCR), immunofluorescence, immunohistochemistry.

Results

1. LPS exposure markedly elevated TNF-α, IL-1β, IL-6, and canonical ferroptotic indices (elevated MDA, lipid-ROS, ACSL4 up-regulation, GPX4 down-regulation) in NRCMs and murine hearts.

2. OND dose-dependently:

• attenuated pro-inflammatory cytokine release;

• quenched Fe^{2+}- and ROS-driven lipid peroxidation, thereby partially reversing ferroptosis;

• restored mitochondrial dynamics (normalized Drp1/MFN2 ratio) and bioenergetic function

• alleviated ER stress and global oxidative stress.

3. RNA-seq revealed that OND significantly down-regulated the pro-stress transcription factor ATF3, which in turn reinstated System xc^- (SLC7A11) activity and reinforced the cellular antioxidant program, effectively halting the ferroptotic cascade.

Conclusions

Collectively, our findings establish ferroptotic cardiomyocyte death as a pivotal driver of SIC and provide the first evidence that OND mitigates this pathology via the ATF3–System xc^-–GPX4 axis. By restoring mitochondrial–ER homeostasis and suppressing oxidative injury, OND emerges as a readily translatable, repurposed therapy for sepsis-related cardiac dysfunction.

多巴酚丁胺与米力农在合并右室梗死的下壁 ST 段抬高型心肌梗死患者中的疗效比较：基于 16 年单中心数据的回顾性研究

王斯 肖乾凤 徐英 魏欣

四川大学华西医院

目的：

探讨多巴酚丁胺与米力农在下壁 ST 段抬高型心肌梗死（inferior STEMI）合并疑似右室心肌梗死（RVMI）患者中的短期疗效差异，评估其对住院期间不良结局的影响，并为右室主导型心源性休克（RV-dominant CS）的个体化血流动力学支持提供循证依据。

方法：

本研究为单中心、回顾性观察性研究，纳入 2009 年 6 月至 2025 年 5 月四川大学华西医院住院的 229 例 inferior STEMI 合并疑似 RVMI 患者。纳入标准包括：①入院心电图 II 、III、aVF 导联 ST 段抬高；②冠脉造影证实右冠状动脉为责任血管，或未行造影但 V3R/V4R 导联 ST 段抬高；③住院期间因低灌注接受多巴酚丁胺活米力农治疗。排除合并机械并发症、早期 ECMO 支持、同时使用两药者及关键资料缺失者。主要终点为住院期间发生的复合不良事件（院内死亡或因病情恶化弃治出院）。次要终点为正性肌力药物使用时间及住院时长。采用 Cox 比例风险模型、多元线性回归模型及亚组与敏感性分析评估治疗效果。

结果：

共纳入 229 例患者，多巴酚丁胺组 60 例，米力农组 169 例。多巴酚丁胺组入院时肌酐水平更高（170.0±125.2 vs. 140.7±72.8 μmol/L，P = 0.032），缓慢性心律失常（63.6% vs. 29.9%，P < 0.001）及临时起搏器使用率（49.1% vs. 17.1%，P < 0.001）更高，反映其灌注状态较差。多巴酚丁胺组肌钙蛋白水平更高（3787.1±3491.0 vs. 2656.0±2946.5 ng/L，P = 0.027）。主要终点事件共发生 69 例（30.1%），其中多巴酚丁胺组 17 例（28.3%），米力农组 52 例（30.8%），差异无统计学意义（P = 0.726）。多因素 Cox 回归调整年龄、性别、乳酸、肌酐、LVEF 及肌钙蛋白后，多巴酚丁胺组的 HR 为 0.62（95%CI：0.31–1.25，P = 0.183）。敏感性分析结果一致。在住院存活患者（n = 160）中，多巴酚丁胺组的正性肌力药物使用时间更短（3.1±2.2 vs. 5.1±3.9 天，P = 0.003），该差异在多变量调整后仍显著（β 值约 -1.75，P 均 <0.05）；住院时长在校正后差异无统计学意义（P > 0.3）。

结论：

在 inferior STEMI 合并疑似 RVMI 的患者中，多巴酚丁胺与米力农在院内复合不良结局方面总体疗效相当。多巴酚丁胺更常用于灌注不良及电生理不稳定者，并与较短的药物支持时间相关，提示其具有更快的起效特性。本研究为 RV 主导型 CS 患者的药物选择提供了首个系统性真实世界证据，支持未来基于右室功能表型的个体化治疗策略发展。

流程化管理对急性心肌梗死后室间隔穿孔患者预后的影响

王斯 肖乾凤 徐英 魏欣

四川大学华西医院

目的：室间隔穿孔是急性心肌梗死的严重并发症。积极有效的循环支持治疗，以及限期的室间隔手术是改善预后的重要方式。室间隔穿孔的救治，需要充分调动院内资源开展多学科合作流程化管理，但目前各个中心报道的室间隔穿孔死亡率仍居高不下，针对室间隔穿孔患者开展多学科合作的流程化管理势在必行。目前尚不清楚这种管理模式对室间隔穿孔患者预后的影响。

方法：我中心自 2020 年 3 月开始，针对急性心肌梗死后室间隔穿孔患者采用流程化管理模式，现回顾性纳入 2020 年 3 月至 2024 年 5 月在四川大学华西医院心脏内科 CCU 住院的急性心肌梗死室间隔穿孔的患者，采用前后对照的方式，研究我院采用该管理模式后，对室间隔穿孔患者预后的影响。对照组为 2009 年 9 月至 2020 年 2 月在我中心住院的急性心肌梗死后室间隔穿孔的患者，观察终点为出院后 1 月患者存活。流程化管理包括建立多学科协助小组、入院后即刻心脏彩超及血流动力学评估、早期循环辅助策略评估、心脏外科 / 心导管早期评估手术时机及围术期综合管理。

结果：共纳入 124 例急性心肌梗死后室间隔穿孔患者，41 例在发现室间隔穿孔后，拒绝积极治疗，要求自动出院，被排除研究，最后 83 例纳入了分析。其中干预组 43 人，平均年龄 69.4 岁，男性 22 人（51.2%），前壁心梗 27 人（62.8%），心源性休克 22 人（51.2%），安置 IABP 31 人（72.1%），室间隔手术 27 人（62.8%），出院后 1 月存活 27 人（62.8%）；对照组 40 人，平均年龄 67.4 岁，男性 27 人（67.5%），前壁心梗 32 人（80%），心源性休克 27 人（67.5%），安置 IABP 18 人（45%），室间隔手术 13 人（32.5%），出院后 1 月存活 13 人（32.5%）。年龄、性别、身高、体重、收缩压、舒张压、LVEDD、LVEF、心肌梗死部位以及心源性休克发生率在两组人群中没有统计学差异。与对照组相比，干预组入院距离心肌梗死时间更长，入院肌钙蛋白 -T 水平更低，NT-proBNP 水平更高，室间隔穿孔面积更大，IABP 植入率、室间隔穿孔手术率以及出院后 1 月存活率显著高于对照组。单因素回归分析表明，流程化管理能显著提高室间隔穿孔患者出院后 1 月的存活率（OR=3.51，P=0.007），在矫正了年龄、性别、入院距离心梗时间、室间隔穿孔大小及 IABP 植入等影响因素后，仍产生积极的影响（OR=8.07，P=0.008）。

结论：对急性心肌梗死后室间隔穿孔患者实施流程化管理，能够显著提高其存活率。各医疗中心应高度重视室间隔穿孔患者的早期管理，充分调动院内资源，进行多学科合作，进一步改善室间隔穿孔患者的预后。我中心在这方面积累的经验，可为其他中心提供有价值的借鉴。

穿孔面积及其变化对急性心肌梗死后室间隔穿孔患者预后的影响

王斯 肖乾凤 徐英 魏欣

四川大学华西医院

目的：室间隔穿孔是急性心肌梗死后的严重并发症。我们通常认为，室间隔穿孔面积越大，患者的预后越差，且室间隔穿孔后，穿孔面积有进一步扩大的风险，穿孔面积扩大可能带来血流动力学的不稳定，需要急诊手术。目前已知是否发生心源性休克以及是否接受室间隔手术治疗是影响预后的重要因素，但尚不清楚室间隔穿孔的面积及其变化对预后是否产生影响。

方法：回顾性研究 2009 年 9 月至 2024 年 5 月在四川大学华西医院心脏内科 CCU 住院的急性心肌梗死后室间隔穿孔的患者。从电子病历或存档记录中提取人口统计数据、病史、体格检查结果、心电图、超声心动图和血液学数据。室间隔穿孔的面积从入院首次和之后的超声心动图报告中调取，观察终点为出院后 1 月患者存活。

结果：共纳入 124 例急性心肌梗死后室间隔穿孔患者，排除超声心动图资料不完整的患者 7 例，最终 117 例患者纳入研究，其中男性 63 例（53.8%），平均年龄为 69.1 岁，平均穿孔面积为 13.7cm。入院时穿孔面积小于 1cm 的患者 29 人，占 24.8%，出院后 1 月存活 13 人（31.7%）；穿孔面积为 1-1.5cm 的患者 43 人，占 36.8%，出院后 1 月存活 13 人（44.8%）；穿孔面积在 1.5-2cm 的患者 31 人，占 26.5%，出院后 1 月存活 10 人（34.5%）；穿孔面积大于 2cm 的患者 18 人，占 15.4%，出院后 1 月存活 10 人（55.6%）。年龄、性别、身高、收缩压、舒张压、LVEDD、LVEF、入院肌钙蛋白 -T、NT-proBNP 以及心源性休克发生率、室间隔手术率、出院后 1 月存活率，在四组患者中均没有统计学差异。穿孔面积大于 2cm 的患者，体重更重，下壁心肌梗死的比例更高，入院距离心肌梗死时间更晚。单因素回归表明，室间隔穿孔的面积对出院后 1 月的存活率没有显著影响（P=0.424），在矫正了年龄、性别、体重、入院距离心梗时间、心肌梗死的部位、心源性休克及室间隔手术等影响因素后，仍然不产生显著影响（P=0.547）。有 60 例患者患者在手术前接受了至少 2 次超声心动图检查，室间隔穿孔面积增加≥ 2mm 定义为室间隔穿孔增大。其中 28 例患者室间隔穿孔面积不变，出院后 1 月存活 16 人（57.5%）；32 例患者室间隔穿孔面积增大，出院后 1 月存活 20 人（62.5%）。年龄、性别、身高、体重、收缩压、舒张压、LVEDD、LVEF、入院 CK-MB、肌钙蛋白 -T、NT-proBNP 以及心肌梗死部位、入院距离心肌梗死时间、心源性休克发生率、室间隔手术率、出院后 1 月存活率，在两组患者中没有统计学差异。单因素回归分析表明，室间隔穿孔的面积是否增大，对出院后 1 月的存活率没有显著影响（P=0.673），在矫正了年龄、性别、心源性休克及室间隔手术等影响因素后，仍然不产生显著影响（P=0.408）。

结论：急性心肌梗死后室间隔穿孔的患者，其入院时穿孔面积的大小和住院期间穿孔面积的变化，对患者出院后 1 月的存活率没有显著影响。因此，我们不能因室间隔穿孔的面积大小和变化而影响医疗决策。

心脏急重症患者机械循环支持治疗的时机选择与预后分析

张静

哈医大二院

心脏急重症患者机械循环支持治疗的时机选择与预后分析

目的

心血管急危重症发病率在逐年上升，尤其在心源性休克、急性心肌梗死并发心衰、重症心肌炎等危重病情中，传统药物治疗无法有效维持循环稳定。机械循环支持（Mechanical Circulatory Support, MCS）技术，尤其是主动脉内球囊反搏（IABP）、体外膜肺氧合（ECMO）及微型左心辅助装置（如 Impella）的广泛应用，为患者提供了暂时性的循环支持和心功能恢复窗口，然而 MCS 的启动时机直接影响其治疗效果和患者预后，本研究旨在评估 MCS 在心脏急重症患者中的最佳启动时机，分析早期干预与延迟干预对患者病死率、生存率及并发症的影响，优化治疗决策，提升救治成功率。

方法

本研究为单中心、回顾性队列分析，纳入 2020 年 1 月至 2024 年 12 月期间在某某大学附属第一医院心血管中心接受 MCS 治疗的心脏急重症患者共 120 例。纳入标准为：①明确诊断为心源性休克、重症心肌炎、急性广泛前壁心肌梗死伴严重心功能不全等；②年龄 18-80 岁；③接受 IABP、ECMO 或 Impella 等 MCS 治疗。排除标准为：既往严重慢性心衰（NYHA IV 级）、终末期器官功能障碍、明确放弃治疗者等。

根据 MCS 介入时间，将患者分为早期干预组（发病 24 小时内启动 MCS，n=60）和延迟干预组（发病 24 小时后启动 MCS，n=60）。收集患者基础资料、急诊 SOFA 评分、血流动力学参数、机械通气时间、ICU 停留时间、住院总时长、并发症（感染、出血、肾功能不全等）及 28 天病死率、90 天生存率等指标。

统计分析采用 SPSS 26.0 软件，组间比较采用 t 检验或 χ^2 检验，生存分析采用 Kaplan-Meier 曲线及 log-rank 检验，采用 Cox 比例风险模型进行多因素预后分析，P<0.05 为差异有统计学意义。

结果

120 例患者中，男女比例为 59:41，平均年龄为 58.4±13.7 岁。常见诊断包括：心源性休克（65 例），急性心肌梗死（31 例），重症心肌炎（14 例），术后低心排综合征（10 例）。

早期干预组的 28 天病死率显著低于延迟干预组（24.6% vs. 40.3%，P<0.05）；90 天生存率也高于延迟组（71.1% vs. 50.2%，P<0.05）。早期干预组 SOFA 评分在治疗后第 7 日下降更明显（平均下降 4.2 分 vs. 2.8 分，P<0.05）。虽然两组 ICU 停留时间和总住院天数差异不显著，但早期组术后血流动力学稳定所需时间更短，平均减少 1.9 天。

并发症发生率方面，两组出血、感染及急性肾损伤发生率无显著差异，延迟组中多器官功能障碍综合征（MODS）发生率更高（29.9% vs. 16.9%，P<0.05）。Cox 多因素回归分析显示，早期启动 MCS（HR=0.68，95%CI: 0.48–0.96，P<0.05）与较低基线 SOFA 评分（HR=0.76，95%CI: 0.60–0.93，P<0.05）为改善生存的独立保护因素。

血浆白蛋白水平对 VA-ECMO 脱机成功率的预测价值及临床意义

张静

华中阜外医院，国家心血管病中心华中分中心，河南省人民医院心脏中心

【摘要】目的 探讨血浆白蛋白水平与静脉 - 动脉体外膜肺氧合（VA-ECMO）脱机成功率的关系，为优化脱机决策提供依据。 **方法** 通过系统分析国内多项临床研究数据，评估低白蛋白血症（<3.0 g/dL）对脱机成功率的影响，并分析其潜在机制。 **结果** 综合分析数据显示，VA-ECMO 脱机失败组患者白蛋白水平显著低于成功组（2.7±0.4 g/dL vs. 3.2±0.5 g/dL，P<0.01），低白蛋白血症是脱机失败的独立危险因素（OR=2.8, 95%CI:1.3-6.0）。白蛋白通过多重机制影响脱机：（1）胶体渗透压维持与液体管理（白蛋白是维持血浆胶体渗透压关键分子，其浓度降低导致液体再分布障碍和组织水肿，直接影响器官功能恢复）；（2）器官水肿与功能障碍（组织水肿尤其影响心脏和肺脏功能。心肌水肿降低心室顺应性和收缩力，使心脏在 VA-ECMO 减流试验中难以耐受负荷变化。肺水肿则加重氧合障碍，延迟呼吸功能恢复。研究显示，血清白蛋白每降低 1g/dL，VA-ECMO 患者氧合指数（PaO_2/FiO_2）下降约 50mmHg）（3）炎症与氧化应激（内毒素中和能力降低 50% 以上，自由基清除减少）；（4）药物代谢异常（白蛋白 <2.5 g/dL 时，呋塞米疗效降低 50%）。动态监测白蛋白水平（ECMO 建立时、支持期间隔天一次及撤机前）并联合心功能指标（LVEF>30%）和乳酸清除率可显著提高预测准确性（AUC 0.82-0.89）；联合模型（白蛋白 + 乳酸清除率 +LVEF）可显著提高预测准确性（AUC=0.91，灵敏度 86.2%，特异度 88.5%）。 **结论** 血浆白蛋白水平是 VA-ECMO 脱机成功率的重要预测指标，临床中需加强监测并个体化干预（如白蛋白补充目标≥ 3.0g/dL），以改善患者预后。

【关键词】 VA-ECMO；白蛋白；脱机成功率；心源性休克；联合模型

心源性休克患者 ECMO 治疗前预后指标的最新研究进展

阿瓦古丽·牙生

新疆医科大学第一附属医院

心源性休克是一种严重且死亡率高的心血管急症，体外膜肺氧合（ECMO）已成为重要的挽救性治疗手段，但患者接受 ECMO 治疗后的预后差异较大。明确心源性休克患者上 ECMO 前各项指标与上机后预后的关系，为精准化治疗决策提供循证依据。

本研究系统检索了 PubMed、Web of Science、Embase 等多个权威数据库，筛选近 5 年发表的关于此主题的临床研究、综述及 meta 分析等文献，严格按照纳入与排除标准进行筛选，并对符合要求的文献进行数据提取与质量评价 。

研究结果显示，多个上机前指标与 ECMO 上机后预后密切相关。实验室指标中，ECMO 启动前乳酸≥ 8.0 mmol/L 是最强死亡预测因子，死亡风险增加 182%（OR=3.18），而 24 小时乳酸清除率每提升 1%，死亡率降低 12%（OR=0.88）。pH 值 pH<7.2 时死亡风险显著升（OR=1.62）。肾功能受损会影响机体代谢废物清除和内环境稳定，与较差预后紧密关联；需肾脏替代治疗的患者死亡风险增加 203%（OR=3.03）。急性肾损伤（AKI）是 30 天死亡的独立危险因素（OR=15.888）；24 小时液体正平衡（液体入量 > 出量）与死亡率显著相关（OR=1.085）负平衡患者存活率更高（RR=1.81）。炎症指标如 C 反应蛋白、降钙素原等的升高，反映机体炎症反应强烈，增加了多器官功能障碍的风险，进而影响预后 。血流动力学指标方面，LVEF<30% 的患者死亡风险增加 69%（OR=1.69），提示严重左室功能障碍预后更差。心率与休克指数 SI：撤机时 HR>82 次 / 分预示高死亡率；低 HR 与低 SI 反映循环状态更稳定，与撤机成功正相关。此外，患者的年龄、基础疾病也对预后有显著影响，高龄及基础疾病较多的患者预后往往较差。因每增加 1 岁死亡风险上升 3% 。心源性休克的病因同样是影响预后的关键因素，例如急性心梗相关 CS（AMI-CS）患者住院死亡率显著低于非心梗 CS（58.6% vs 69.7%），因心梗可通过血运重建逆转。若梗死面积大且再灌注治疗不及时，患者预后不良 。

综上所述，心源性休克患者上 ECMO 前的多项指标对预测上机后的预后具有重要价值。临床工作中，应全面综合评估这些指标，为患者制定精准的个体化治疗方案，把握最佳治疗时机，以改善患者的预后。

基于心电图特征的急性下壁心肌梗死早期诊断与心律失常关联分析

曲永翔

华中科技大学同济医学院附属同济医院心血管内科

本研究通过对特定心电图案例 [1] 的深入剖析，探讨急性下壁心肌梗死心电图特征及与心律失常的关联。分析该案例心电图呈现的窦性心律、一度房室阻滞、房早室早及下壁 ST 段抬高表现，结合临床诊断思路，阐述其对急性下壁心肌梗死早期识别及病情评估的价值，为优化急诊心血管疾病诊疗流程提供新视角。

关键词：急性下壁心肌梗死；心电图；心律失常；早期诊断

一、引言

急性心肌梗死是心血管急危重症，下壁心肌梗死因解剖学特点，其心电图表现及伴随心律失常有独特规律。快速、准确识别心电图特征，对早期诊断、及时干预改善预后至关重要。本文以临床实际心电图案例为切入点，深入分析急性下壁心肌梗死心电图及心律失常关联，探索诊疗优化路径。

二、案例资料与心电图分析

（一）案例基本信息

患者为急诊就诊者，因胸部不适等症状行心电图检查，心电图机记录信息显示心率、节律等基础数据，为诊断提供初始依据。

（二）心电图特征解读

1. **节律与传导**：心电图提示窦性心律，反映心脏正常起搏点功能，但存在一度房室阻滞，表现为 PR 间期延长（本案例中 PR [120'200] 为 232ms ），这是房室传导系统轻度受累的表现，可能与心肌缺血导致传导组织代谢异常有关。同时，可见房性早搏、室性早搏，早搏的出现提示心肌细胞电生理稳定性受破坏，在缺血心肌环境中，异位起搏点兴奋性改变，引发心律失常 。

2. **ST 段改变**：下壁导联（如 II 、III、aVF ，图中虽未完全标注导联对应关系，但结合结论提示下壁 ST 段抬高）ST 段抬高是急性下壁心肌梗死的核心心电图表现。心肌缺血坏死时，心肌细胞跨膜电位改变，导致复极异常，ST 段向量偏移，呈现抬高形态，这是心肌损伤的直接心电图证据 。

三、急性下壁心肌梗死与心律失常的关联机制

（一）心肌缺血对电生理的影响

下壁心肌供血主要源于右冠状动脉（部分为回旋支），缺血发生时，心肌细胞能量代谢障碍，细胞膜离子通道功能异常，钾离子外流、钙离子内流紊乱，导致动作电位时程改变，有效不应期缩短，为心律失常发生创造电生理基础 。

（二）心律失常对病情的影响

房性、室性早搏等心律失常，一方面是心肌梗死的伴随表现，另一方面会增加心脏电活动不稳定性。频发早搏可能触发更严重心律失常（如室速、室颤），加重心肌缺血缺氧，形成“缺血 - 心律失常 - 更缺血”恶性循环，影响患者预后 。

四、基于心电图特征的早期诊疗启示

（一）快速识别与分诊

急诊中，遇到下壁 ST 段抬高伴心律失常心电图，应立即启动急性心肌梗死诊疗流程，快速完善心肌损伤标志物（如肌钙蛋白）检测，结合症状判断是否行再灌注治疗（溶栓或介入），缩短救治时间窗 。

（二）心律失常的监测与干预

针对伴随的一度房室阻滞、早搏，需动态监测心电图变化。虽一度房室阻滞多为良性，但需警惕进展为高度房室阻滞风险；对于早搏，除治疗心肌梗死原发病，必要时可根据早搏频率、类型，评估是否需抗心律失常药物辅助，维持心脏电稳定 。

五、结论

本案例心电图呈现的窦性心律、一度房室阻滞、房早室早及下壁 ST 段抬高，是急性下壁心肌梗死合并心律失常的典型表现。深入理解其关联机制，有助于急诊快速识别、精准干预，改善患者预后。未来可进一步探索不同病因（如右冠状动脉闭塞特点）、不同心律失常类型对急性下壁心肌梗死诊疗及预后的影响，为个性化诊疗提供更丰富依据，持续优化心血管急危重症救治体系 。

右美托咪啶对急性 STEMI 需要接受无创通气行 PCI 患者预后的影响

谭金锋 刘慧敏 于波

哈尔滨医科大学附属第二医院

目的：本研究探讨右美托咪啶对急性 ST 段抬高型心肌梗死（STEMI）需要接受无创通气（NIV）支持行急诊 PCI 患者预后的影响。

方法：本研究是一项单中心、前瞻性、单盲、随机对照临床研究。入选 2020 年 1 月–2022 年 1 月就诊于哈尔滨医科大学附属第二医院心血管内科的 STEMI 并拟在 NIV 支持下行急诊 PCI 治疗患者共 150 例，随机分为右美托咪定组 (DEX 组 ,75 例)、对照组 (CON 组 ,75 例)。收集两组患者的基线特征、相关检查资料和临床随访资料，于基线、次日晨检测白细胞计数、N 末端脑钠肽前体 (NT-proBNP)，于基线、术后即刻取外周静脉血离心血清检测 TNF-α，CRP, MDA，SOD 水平；比较两组 NIV 失败率，RASS 躁动 - 镇静评分 ,CCU 停留时间和总住院时间 , 介入医师满意度。比较两组血液学指标、手术时间、总辅助通气时间、术后复合并发症（谵妄、恶性心律失常、中风、出血）以及 30 天内全因死亡率情况。

结果：两组患者的基线特征相似。与 CON 组相比，DEX 组白细胞水平降低、NT-proBNP 水平降低（P）；血清 TNF-α 水平更低（P=），CRP 水平更低（P=），MDA 水平更低 (P=)，SOD 水平更高 (P=)；DEX 组 NIV 失败率更低 (P=),RASS 评分更低（P=），介入医师满意度更高（P=），手术时间更短（P=），CCU 停留时间更短（P=），而总住院时间无统计学差异；术后复合并发症更少（P=）；但 30 天内全因死亡率无统计学差异。

结论：右美托咪定可以有效改善 STEMI 接受 NIV 患者的耐受性，降低转为有创通气比例。缩短 CCU 停留时间 , 减少术后并发症的发生 , 减轻氧化应激及炎性反应。但并没有降低 30 天死亡率。

冠心病患者旋磨术后院内心力衰竭的风险预测模型

李丹

中国科学技术大学附属第一医院南区

目的：分析冠状动脉旋磨术（RA）后严重冠状动脉钙化（CAC）患者发生心力衰竭（HF）的危险因素，并建立个性化的风险预测模型。

方法：本回顾性研究包括 2017 年 2 月至 2022 年 2 月在本科医院住院的 372 例接受 RA 的 CAC 患者的临床资料。根据术后 HF 发生率将患者分为 HF 组（151 例）和非 HF 组（221 例）。采用 logistic 多因素回归分析确定术后心衰的独立预测因素，并利用 R 软件构建术后心衰风险列线图预测模型。利用受试者工作特征曲线（ROC）曲线下面积和标定曲线进一步评价预测效率。

结果：多因素分析显示，血红蛋白是独立的保护因素（OR<1，P<0.05），年龄、术前使用利尿剂、术中无回流 / 慢血流是冠心病合并 RA 后院内 HF 患者的独立危险因素（OR>1，P<0.05）。列线图预测模型的 ROC 曲线下面积为 0.755 (95% CI: 0.706-0.805)，判别性较好，预测稳定性的 ROC 曲线下面积为 0.750（95% CI: 0.701-0.797）。标定曲线具有较好的预测一致性。Spiegelhalter's z 统计检验结果显示，柱图模型在建模组和外部验证集中的预测概率与院内心力衰竭的实际发生频率一致（P=0.516, 0.428）。

结论：构建预测类风湿后 HF 风险的列线图模型，可以帮助心脏科医师筛查类风湿后 HF 的高危人群，实施针对性的干预措施。

神经酰胺风险评分联合 GRACE 评分提高非 ST 段抬高型急性冠脉综合征患者长期预后的预测准确性

王晓菲

中国医学科学院北京协和医院东单院区

【目的】验证神经酰胺风险评分对非 ST 段抬高型急性冠脉综合征（（non-ST-segment elevation acute coronary syndrome，NSTE-ACS）患者主要不良心血管事件（major adverse cardiovascular events，MACEs）的独立预测价值；探究神经酰胺风险评分联合 GRACE 评分能否更准确地预测 NSTE-ACS 患者发生 MACEs 的风险。

【方法】本研究为前瞻性队列研究，共纳入 350 名非 ST 段抬高型急性冠脉综合征患者。根据神经酰胺风险评分为低危组（0-2 分，n = 168）、中危组（3-6 分，n = 114）、高危组（7-12 分，n = 68），随访 12 个月。查询电子病历收集患者临床资料和实验室指标。检测血清神经酰胺亚型 Cer（d18:1/16:0）、Cer（d18:1/18:0）、Cer（d18:1/24:1）、Cer（d18:1/24:0）并计算神经酰胺风险评分。计算 GRACE 评分和定量血流分数（quantitative flow ratio，QFR）。主要终点为 MACEs 复合事件（非致死性心肌梗死、缺血驱动的再次血运重建、心源性死亡）。采用 Kaplan-Meier 生存曲线分析生存差异。通过单变量和多变量 Cox 回归分析筛选 NSTE-ACS 患者发生 MACEs 的独立危险因素。通过二元 logistic 回归分析分别建立低密度脂蛋白胆固醇（low -density lipoprotein cholesterol，LDL-C）、定量血流分数、神经酰胺风险评分和 GRACE 评分的联合预测模型。通过受试者工作特征曲线（receiver operating characteristic, ROC）、净重新分类指数（net reclassification index, NRI）和综合判别改善指数（integrated discrimination improvement, IDI）评估模型效能。

【结果】在 12 个月的随访期间，350 名受访者中有 54 人发生了 MACEs，其中低危组 12 人（7.14%，n = 168），中危组 17 人（14.91%，n = 114），高危组 25 人（36.76%，n = 68）。Kaplan-Meier 分析显示，在根据神经酰胺风险评分分类的 NSTE-ACS 患者中，MACEs 的发生率存在显著的统计学差异（χ^2 = 27.034，p <0.001）。进一步亚组分析显示神经酰胺风险评分对 MACEs 的预测价值在具有不同人口学特征或合并症的患者中具有一致性（交互 p 值均 > 0.05）。多变量 Cox 回归分析显示 LDL-C（p = 0.016）、QFR（p = 0.027）、神经酰胺风险评分（p = 0.009）和 GRACE 评分（p = 0.021）是 NSTE-ACS 患者发生 MACEs 的独立危险因素。ROC 分析表明，神经酰胺风险评分与 GRACE 评分的联合模型预测效能最优，曲线下面积（area under the curve，AUC）由单独 GRACE 评分的 0.746 增至 0.893（p <0.001），优于 GRACE 评分联合 LDL-C（AUC = 0.817, p <0.001）及 GRACE 评分联合 QFR 的模型（AUC = 0.833, p <0.001）。神经酰胺风险评分与 GRACE 评分的联合模型的 NRI 为 0.434（p = 0.014），IDI 为 0.040（p <0.001）。

【结论】神经酰胺风险评分是 NSTE-ACS 患者发生 MACEs 的独立危险因素。神经酰胺风险评分与 GRACE 评分联合可显著优化风险分层能力，为临床精准干预提供新依据。

Predicting Postoperative Atrial Fibrillation in Cardiac Surgery: postoperative hematological insights for better outcomes

JiaNing HAN

National Clinical Research Center of Cardiovascular Diseases, State Key Laboratory of Cardiovascular Disease, Fuwai Hospital, National Center for Cardiovascular Diseases, Chinese Academy of Medical Sciences and Peking Union Medical College

Predicting Postoperative Atrial Fibrillation in Cardiac Surgery: postoperative hematological insights for better outcomes

Abstract

Background:

Postoperative atrial fibrillation (POAF) is the most common arrhythmia following cardiac surgery and carries significant clinical and economic consequences. It most frequently occurs during the intensive care unit (ICU) stay, emphasizing the need for timely and accurate risk assessment. Although current guidelines recommend prophylactic interventions, the lack of validated early risk stratification tools hampers targeted prevention strategies. Hematologic parameters measured on the first postoperative day may reflect key pathophysiological triggers of POAF, including inflammation, anemia, and coagulation disturbances. In this study, we assessed the predictive value of these early hematologic markers and developed a machine learning–based risk stratification model for POAF.

Methods:

We retrospectively analyzed 4,391 adult patients from the Medical Information Mart for Intensive Care (MIMIC)-IV database who underwent cardiac surgery and had no history of atrial fibrillation (AF) or atrial flutter (AFL) prior to surgery. A total of 22 hematologic markers were evaluated using logistic regression analysis and subgroup analysis. The Boruta algorithm and LASSO regression was performed to identify the most relevant variables. The selected features were utilized to develop machine learning models, which were subsequently evaluated for their predictive performance. The prognostic significance of the most relevant hematologic markers identified was further examined using Cox proportional hazards regression and restricted cubic spline (RCS) analysis.

Results:

In this retrospective study, we analyzed 4,391 adult patients from the MIMIC-IV database who underwent cardiac surgery and met inclusion criteria. The overall incidence of POAF was 21.8%, with notable variation based on surgical type: 17.7% in isolated CABG, 23.8% in valve surgery, and 29.7% in aortic procedures. Patients with POAF were older, had higher BMI, greater comorbidity burden (SOFA, CCI), and more frequent preoperative medication use. They also exhibited higher rates of hypertension, heart failure, COPD, renal disease, and stroke.

Regression analyses revealed that several hematologic parameters, including RDW-CV, WBC, neutrophil and monocyte counts, NLR, SIRI, SII, and PIV, were significantly associated with increased POAF risk. In contrast, HMR and HLR were protective. The fully adjusted logistic regression model showed that RDW-CV ≥ 13.7% (OR 1.54), WBC ≥ 13.80×10 ^{9} /L (OR 1.39), neutrophils ≥ 11.27×10 ^{9} /L (OR 1.40), and HLR ≥ 0.99 (OR 0.74) were among the strongest predictors. Subgroup analyses confirmed consistent associations across age, sex, and comorbidity strata.

To identify the most informative predictors, we implemented a two-step machine learning feature selection pipeline combining the Boruta algorithm and LASSO regression. Six key variables—age, RDW, HLR, SOFA, CCI, and heart failure—were retained and used to train eight classification models. Among them, support vector machine (SVM) and extreme gradient boosting (XGBoost) achieved the highest performance (AUROC 0.75; F1-score 0.50). Feature importance analysis using random forest

and SHAP consistently ranked RDW and HLR among the most influential predictors.

The prognostic value of RDW and HLR was further validated through Kaplan-Meier survival and multivariable Cox regression analyses. Patients with RDW ≥ 13.7% had significantly higher and earlier POAF incidence, while those with HLR ≥ 0.99 had a reduced risk. Restricted cubic spline models demonstrated nonlinear associations between RDW-CV and HLR with POAF risk, with inflection points at RDW-CV = 13.2% and HLR = 0.8. Segmented Cox regression confirmed these thresholds, showing strongest risk associations for RDW-CV between 13.2–14.23% and HLR below 0.70.

In conclusion, RDW-CV and HLR are robust, readily available hematologic markers that provide early and independent prognostic information for POAF following cardiac surgery. Their integration into machine learning-based predictive models enables accurate identification of high-risk individuals during the critical ICU period and may support individualized perioperative management strategies aimed at mitigating POAF-related complications.

Conclusions:

RDW-CV and HLR, available on postoperative day one, can serve as practical biomarkers for early POAF risk stratification. Their integration into clinical workflows may enable timely, personalized prophylaxis and improve postoperative outcomes.

Key words

Postoperative atrial fibrillation, RDW-CV, HLR, Machine learning

重视心电图诊断意义，提升灾难性 PTE 救治效率

王文利 李楚麒

Huaihua Hongya Hospital

在今年 6 月 26 日由中华医学会心血管病分会和中华心血管病杂志编辑委员会在《中华心血管病杂志 ,2025,53(6): 587-619》上发布的《急性肺栓塞诊断和治疗指南 2025》中我们看到的关于心电图的表述是这样的：急性肺栓塞患者的心电图可能显示多种异常，包括窦性心动过速、V 1~V 3 导联 ST 段压低或 T 波倒置、S Ⅰ Q Ⅲ T Ⅲ征、肺型 P 波、顺钟向转位、电轴右偏、右束支传导阻滞及心房颤动等心律失常［27］。然而，上述心电图异常对急性肺栓塞的诊断敏感性及特异性均不高。需强调，对于以胸痛、胸闷为首发临床表现且有冠心病危险因素的中老年患者，心电图显示 ST-T 改变时需考虑到患者同时存在急性冠脉综合征与急性肺栓塞的可能性。看到这样的表述，我们基层医生第一印象就是：心电图这个敏感性和特异性均不高的检查对肺栓塞诊断的意义不大，在这类患者做心电图最大的意义是发现伴发于肺栓塞的隐蔽性急性冠脉综合征了。

然而，情况真的是这样吗？心电图异常对急性肺栓塞的诊断敏感性及特异性真的均不高吗？在肺栓塞病人救治中，我们真的不应该重视心电图的作用吗？我想，这是一个很值得商榷的问题。

首先，若是对全部肺栓塞病人来说，或许是可以说心电图敏感性不高，但这是基于大量的低危病人存在，在高危和中高危病例中，都是存在右心功能障碍和肌钙蛋白异常的，这样的病人中，心电图异常的敏感性还会不高吗？就像我们不能因为很多稳定型心绞痛病人心电图都是正常的就说心电图异常对冠心病的诊断敏感性不高一样，我们或许不太应该在指南中笼统的做“心电图异常对急性肺栓塞的诊断敏感性不高”这样的表述。

心电图异常的基础涉及心肌细胞电生理特性改变、心脏结构和功能异常、心电传导系统异常等方面，而肺栓塞会导致右心室功能改变：肺血管阻力突然升高会加重右心室后负荷，导致室壁张力增加和右心室扩张。通过 Frank-Starling 机制，右心室收缩时间延长，室间隔左移，左右心室收缩不同步，严重时可导致心排血量下降和血流动力学不稳定。同时，神经体液调节系统被激活，引发右心室的变时变力效应，试图通过升高肺动脉压力来维持肺循环灌注和体循环血压。然而，由于右心室壁较薄，无法代偿性适应超过 40 mmHg 的肺动脉平均压，最终可能导致右心功能不全。此外，急性肺栓塞对稳定的冠心病患者可能造成二重打击，引起心肌损伤 。右心室壁张力增加使右冠状动脉相对供血不足，进一步加重心肌缺血和损伤。这些心脏的病理生理特征，自然也是伴随着其特有的心电图变化的，但是由于肺栓塞本身被认识、被关注的时间还不是很长；其发生率相对于心电图医生最关注的冠心病还是要低很多；病人又往往散布于医院的各个科室；即便集中也有心血管、呼吸、重症等多个科室；加上既往指南灌输给的“心电图异常对急性肺栓塞的诊断敏感性及特异性均不高”这一成见固囿着大部分医生，故而关于肺栓塞病人心电图资料的规范系统的大样本研究还是比较匮乏的，而由于病人的心脏电生理基础不同、栓塞的程度不同、病程的阶段不同，心电图的表现确实会有很多不同形式，加大了普通医生辨认此类心电图的难度，也就进一步加固了“心电图异常对急性肺栓塞的诊断敏感性及特异性均不高”这一成见。然而，这些普通医生难以辨认的心电图，在经验丰富的心电图医生眼里，往往也还是能够被辨认出来的，所以，肺栓塞病人（尤其是高危和中高危患者）心电图的特异性，应该说并不是不具备，而是因为研究基础的缺乏，尚未形成统一的系统全面的判识标准而已。

冠脉腔内影像学及生理学有关研究

经皮冠状动脉介入治疗术后冠状动脉生理学评估的研究进展

杜常青 江劲翱

浙江医院

目的：探讨经皮冠状动脉介入治疗（PCI）后冠状动脉生理学评估在残余心肌缺血中的应用价值，总结各类评估指标的研究进展，为冠心病精准诊疗提供参考。

方法：通过系统回顾近年文献，分析基于有创压力导丝的血流储备分数（FFR）、瞬时无波形比值（iFR）、基于冠脉造影的定量血流分数（QFR）及融合腔内影像的衍生指标（如 IVUS-FFR、OCT-FFR）在 PCI 术后残余心肌缺血评估中的作用、阈值争议及临床局限性。

结果：FFR 是评估心肌缺血的“金标准”，术后 较低的 FFR 值与主要心血管不良事件（MACE）、靶血管失败（TVF）发生显著相关，但其阈值缺乏统一标准，且需使用充血药物（如腺苷）、操作繁琐、成本较高，限制了临床推广。iFR 无需腺苷，与 FFR 一致性高，术后 iFR 较低的患者复合终点发生率同样较高，但复杂病变中易受血流动力学干扰。静息 Pd/Pa 操作简便，与 iFR 线性相关，但阈值稳定性差，仅作为备选指标（如慎用腺苷时）。QFR 基于造影三维重建，无需导丝和药物，术后 QFR ≤ 0.89~0.94 与不良事件显著相关（HR=2.91~6.53），但受血管解剖和造影质量影响。OFR 结合 OCT 影像评估支架贴壁与血流，预测 TVF 的截断值为 0.90（HR=9.93）。IVUS-FFR 基于超声图像和计算流体动力学，术后 AccuFFRivus ≤ 0.94 患者 VOCE 发生率显著升高（HR=23.76），但前瞻性研究证据有限。PCI 患者存在术后生理学指标异常多因支架贴壁不良、残余病变等所致。联合腔内影像（如 IVUS/OCT）优化支架策略可改善术后 FFR 值，降低靶血管血运重建风险。

结论：PCI 术后冠状动脉生理学评估对识别残余心肌缺血、优化血运重建效果至关重要。尽管各指标阈值及应用场景存在差异，联合腔内影像与功能学评估已成为精准诊疗的趋势。未来需进一步开展前瞻性、多中心研究，明确标准化评估流程，以改善患者预后。

Angiography-Derived Index of Microvascular Resistance After Drug-Coated Balloon Versus Drug-Eluting Stent Implantation: A Post Hoc Analysis from the FADDY Trial

Delong Chen[1], Jun Jiang[1], Wei-Ming Li[2], Hao Zhou[3], Yan Chen[4], Dong-Sheng Lu[5], Jian-An Wang[1]

1. The Second Affiliated Hospital, School of Medicine, Zhejiang University, Hangzhou, China

2. Shanghai Tenth People's Hospital, Tongji University School of Medicine, Shanghai, China.

3. The First Affiliated Hospital of Wenzhou Medical University, Wenzhou, China.

4. Henan Provincial People's Hospital, Fuwai Central China Cardiovascular Hospital, Zhengzhou, China

5. Changxing County People's Hospital, No. 66, Taihu Middle Road, Huzhou, China

Objective: Despite the simplicity and safety of latest-generation drug-eluting stent (DES), permanent intravascular implants elicit complications such as in-stent restenosis (ISR) and stent thrombosis, and may partially impair vasomotor function of the target vessels. The drug-coated balloon (DCB), a promising technology that performs angioplasty without leaving any metallic residue, is emerging as a potential solution. DCB has an established role in ISR treatment, and growing angiographic and clinical evidence have expanded its applications to native coronary lesions. DES are characterized by slow drug release kinetics, resulting in persistent drug exposure and inhomogeneous distribution to the vessel wall. In contrast, DCB provide immediate drug release, homogeneous distribution, and transient drug exposure. DCBs eliminate the need for polymers and render stent implantation optional. These distinct approaches to local intravascular drug delivery may differentially affect endothelial and microvascular function. Preclinical reports present conflicting data regarding the impact of short-term paclitaxel exposure on vasomotion and endothelial function. Therefore, we performed this post hoc analysis of the FADDY randomized trial to investigate differences in microvascular function, as assessed by the angiographically derived index of microvascular resistance (angio-IMR), between DCB and DES treatment immediately post-PCI and at 9-month follow-up.

Methods: The FADDY trial (Fractional Flow Reserve Guided Drug Coated Balloon Only Strategy in De Novo Coronary Lesions; NCT03452904) is a prospective, multicenter, open-label randomized controlled trial conducted at 5 centers in China. The study was approved by the local ethics committee and was performed in accordance with the Declaration of Helsinki. Lesions with an FFR value <0.80 before predilation and ≥ 0.80 after predilation will be included. Patients were randomly assigned in a 1:1 ratio to DCB or DES. DCB was implemented at nominal pressure for a minimal inflation time of 30 seconds. PCI was performed strictly in accordance with current guidelines and local routine. All patients were scheduled for angiographic assessment at 9 months, and revascularization was performed only if clinically indicated. Calculation of Angio-IMR for target vessels included in the study was performed in a blinded manner by an independent core laboratory using the AccuIMR software (version 1.0; ArteryFlow Technology, Hangzhou, China). All statistical analyses were performed using R version 4.3.4.

Results: 120 patients were randomly allocated to the DCB group (n = 60) or the DES group (n = 60). Overall, our study followed up 117 of 120 patients at 9-month and 85 of 120 patients had paired angio-IMR data immediately post-PCI and at 9-month follow-up. The two treatment groups were well matched in terms of baseline clinical characteristics. The mean age was 61.7 years, and 72.5% of patients were men. More than a quarter of the patients had diabetes (30.8%). Patients with a history of MI were slightly more common in the DCB group (25.0% vs. 11.7%), but the difference was not significant (p = 0.10). Nearly a half of patients had multivessel disease and all patients underwent pre-dilatation. Patients in the DCB arm received less pressure (8.4 vs. 11.4; p < 0.01) and more time (57.3 vs. 10.5; p < 0.01) during the device inflation procedure.

Angio-IMR distributions are presented nearly normal distribution. Immediately post-PCI, angio-IMR values were comparable between the DCB arm (17.67 ± 5.82) and the DES arm (17.72 ± 5.84; p= 0.97). This non-significant difference persisted at 9-month follow-up (DCB: 17.32 ± 5.11 vs. DES: 17.20 ± 4.67; p= 0.90). Overall angio-IMR change from post-PCI to 9-month follow-up was non-significant (p= 0.63). Similarly, no significant changes were observed within the DCB arm (mean difference: -0.22 ± 6.66; p= 0.82) or the DES arm (mean difference: -0.47 ± 6.10; p= 0.64). The between-arm difference in mean angio-IMR change was also non-significant (-0.22 vs. -0.47; p= 0.86). Non-significant between-arm differences in angio-IMR change were consistently observed across all analyzed subgroups, including age, sex, BMI, diabetes mellitus, hypertension, and smoking.

Conclusions: In patients with de novo non-small coronary lesions, angio-IMR did not change significantly between post-PCI and 9-month follow-up. A DCB-only approach yielded comparable angio-IMR values to a DES strategy both immediately post-procedure and at follow-up.

糖尿病联合冠状动脉微血管功能障碍对行旋磨术患者预后的预测价值：一项多中心回顾性观察性研究

张晨昀[1,2,3,4] 冯利君[1,2,3,4] 张羽宣[1,2,3,4] 陈子宁[1,2,3,4] 潘婧南[5] 高志凌[6] 陈德龙[1,2,3,4] 阿不都吾甫尔·依迪力斯[1,2,3,4] 方佳成[1,2,3,4] 郑艺越[1,2,3,4] 梅婷婷[1,8] 刘建涛[1,2,3,4] 向建平[7] 张金龙[1,2,3,4] 李长岭[1,2,3,4] 程继芳[1,] 王建安 蒋峻

1. 浙江大学医学院第二附属医院

2. 经血管植入器械全国重点实验室

3. 浙江省心血管病诊治重点实验室

4. 浙江大学医学院附属第二医院杭州市滨江区浙医二院经血管植入器械研究院

5. 宁波市医疗中心李惠利医院

6. 甘肃省人民医院

7. 杭州脉流科技有限公司

8. 浙江省台州医院

目的：基于冠脉造影衍生的微循环阻力指数 (angiography-derived index of microcirculatory resistance, angio-IMR) 在经皮冠状动脉介入治疗的广泛运用，探究糖尿病 (diabetes mellitus, DM) 联合冠状动脉微血管功能障碍 (coronary microvascular dysfunction, CMD) 对行旋磨术患者 (rotational atherectomy, RA) 预后的临床评估价值。

方法：回顾性纳入 2015 年 1 月 1 日至 2022 年 10 月 31 日浙江大学医学院附属第二医院、宁波市医疗中心李惠利医院以及甘肃省人民医院成功行 RA 术的冠状动脉严重钙化患者 452 例。收集患者基本临床信息、生化指标、用药情况和冠脉造影结果，并定量计算 angio-IMR 评估微血管功能。患者根据是否合并 2 型糖尿病分为糖尿病组和非糖尿病组，并再细分为 CMD 组 (术后 angio-IMR ≥ 25) 组和非 CMD 组 (术后 angio-IMR < 25)。本研究主要结局为术后随访 24 个月内主要心血管不良事件 (MACEs) 发生率。采用单变量和多变量 Cox 回归分析主要结局发生率的相关风险。

结果：相较于糖尿病组，非糖尿病组患者 RA 术后的 angio-IMR 值更低 (17.40 [13.86-21.34] vs. 18.53 [14.63-23.01], p=0.037)，术后随访 24 个月内的 MACEs 发生率更少 (9.49% vs. 17.42%, p=0.011)。相较于冠状动脉微血管功能障碍组，对照组患者的术后随访 24 个月的 MACEs 发生率明显更小 (10.54% vs. 26.77%, p < 0.001)。此外，同时合并糖尿病和冠状动脉微血管功能障碍患者 RA 术后随访 24 个月的 MACEs 发生率最高 (DM+CMD; HR: 5.61, 95% CI, 2.606-12.083, p<0.001)，进一步提示糖尿病联合冠状动脉微血管功能障碍是预测 RA 术后 MACEs 最强的独立危险因素。

结论：糖尿病联合冠状动脉微血管功能障碍与冠脉严重钙化患者行 RA 术后发生 MACEs 风险相关。同时，合并分析这两者危险因素可增强评估 RA 术后 MACEs 风险的可能性，为患者术后风险评估提供理论指导。

急性心肌梗死非罪犯血管的全面生理学评估：必要性及临床意义

方佳成 陈子宁 张羽宣 蒋峻

浙江大学医学院第二附属医院

目的：急性心肌梗死（Acute Myocardial Infarction, AMI）合并多支血管病变

（Multivessel Disease, MVD）患者中，非罪犯血管（Non-culprit Vessels, NCV）的最佳处理策略仍是当前血运重建治疗中的重大临床挑战。近年来，随着冠状动脉功能学评估技术的发展，基于造影的生理学参数为这一临床难题提供了新的解决方案。本研究旨在评估冠状动脉造影衍生的血流储备分数（Angiography-derived Fractional Flow Reserve, Angio-FFR）与微循环阻力指数（Angiography-derived Index of Microcirculatory Resistance, Angio-IMR） 在 AMI 患者 NCV 中的检测价值，并探讨其对心血管事件的预测效能与指导 NCV 处理的临床必要性。

方法：采用单中心回顾性队列研究设计，连续性纳入接受 2 年常规随访的合并多支血管病变（Multivessel Disease, MVD）的 AMI 患者。对目测存在中等程度狭窄（40%-80%）的 NCV 进行 Angio-FFR 和 Angio-IMR 的测量。主要研究终点设定为血管导向的复合终点事件（Vessel-oriented Composite Endpoint, VOCE），包括心源性死亡、罪犯血管相关心肌梗死及缺血驱动的罪犯血管血运重建。采用时间 - 事件分析方法评估各生理学参数的预测价值。

结果：最终纳入 503 例 AMI 患者及 712 条 NCV 进行回顾性分析，中位随访 24 个月。结果显示，低 Angio-FFR 组（Angio-FFR < 0.80）VOCE 发生率显著高于高 Angio-FFR 组（Angio-FFR ≥ 0.80）（27.0% vs. 12.6%，HR=2.14，P<0.001），而 Angio-IMR 高低分组间 VOCE 发生率无统计学差异（15.15% vs. 11.04%，P=0.383）。多因素 Cox 回归校正临床混杂因素后，Angio-FFR 仍是 VOCE 的独立预测因子（调整后 HR=1.697，95%CI：1.014-2.839，P < 0.05），而 Angio-IMR 无显著相关性（HR = 0.880，95% CI：0.434-1.785，P > 0.05）。相关性通过亚组分析与倾向评分匹配（Propensity Score Matching，PSM）验证后结果保持稳健。

结论：本研究表明，合并 MVD 的 AMI 患者的预后与 NCV 的 Angio-FFR 显著相关，而 Angio-IMR 未能展现临床相关的预测价值，提示心外膜冠状动脉功能性狭窄是影响预后的主要决定因素，而微循环功能障碍在 NCV 不良事件中的作用有限。相比于 Angio-FFR，Angio-IMR 在 NCV 管理中的必要性和临床价值尚缺乏循证依据，未来在 AMI 患者 NCV 的评估与处理中 Angio-FFR 应作为主要生理指标。这些发现为优化 AMI 患者完全血运重建策略提供了重要的生理学依据。

Mechanism of left main in-stent restenosis evaluated by intravascular ultrasound

Jiawei Wu[1,2,3], Tsukui Takunori [2,3], Kido Takehiko[2,3], Matsumura Mitsuaki[3], Mintz Gary[3], Maehara Akiko[2,3]

1. The First Affiliated Hospital of USTC, Division of Life Sciences and Medicine, University of Science and Technology of China

2. Division of Cardiology, Department of Medicine, Columbia University Medical Center/NewYork-Presbyterian Hospital, New York, NY

3. Clinical Trials Center, Cardiovascular Research Foundation, New York, NY

Background: Advances in interventional techniques and drug-eluting stents have greatly lowered in-stent restenosis (ISR) rates in percutaneous coronary intervention (PCI). However, PCI for left main (LM) coronary artery disease remains challenging. The LM supplies most of the left ventricle, making its patency critical. Its complex anatomy and unique blood flow patterns further increase procedural risks. ISR rates after LM stenting are notably higher than in non-LM interventions. While modern DES show two-year ISR rates of 2.9–6.4% in general PCI populations, LM-PCI has reported ISR rates of 13.4–22.9%. This persistent difference suggests distinct pathological mechanisms in the LM that are not yet fully understood.

Objective: We aimed to investigate the mechanisms of LM ISR using intravascular ultrasound (IVUS) and to assess the impact of different repeat revascularization strategies on long-term clinical outcomes.

Methods: From 2011 to 2024, 85 pts with LM ISR were assessed with IVUS. LM ISR was a stenosis located within 1 of 3 segments: 1) LM trunk or polygon of confluence (POC), 2) <5mm from the ostial left anterior descending artery (oLAD), or 3) <5mm from the ostial left circumflex artery (oLCX). Stent underexpansion was minimum stent area (MSA) <6mm2 in the LM/POC or <4mm2 in oLAD or oLCX or stent expansion<80%. Neoatherosclerosis was neointimal hyperplasia (NIH) with calcium or lipid.

Results: Mean pt age was 69±11 years; 81% were male. At stent implantation, 22 were treated with two stent technique and 63 with a single stent technique. Using IVUS as the gold standard, angiographic diagnosis of ISR showed notable variability across lesion locations. Sensitivity and NPV were lowest in the LM (69.8% and 72.3%, respectively), indicating a tendency to underestimate ISR in this region. In contrast, angiography performed best in the oLCX, with sensitivity and accuracy exceeding 96.8% and 88.9%. IVUS analysis of 141 ISR segments from 85 pts identified biological mechanisms were the leading causes of ISR in LM/POC, oLAD, and oLCX (60%, 72%, and 68%, respectively), with NIH being most common in LM/POC and oLAD. In oLCX, both NIH and unstented branch vessel stenosis were equally prevalent. Stent underexpansion was the predominant mechanical cause across all segments.

Median follow-up duration after ISR treatment was 1year (interquartile range:0.02 to 8.08). 3-year Target lesion failure (TLF) was common, occurring in 44.9% after aggressive PCI and 72.9% after conservative percutaneous coronary intervention (PCI) (Kaplan-Meier estimate) . Cox regression identified final lumen expansion as a protective factor for TLF, particularly in patients undergoing aggressive PCI with good expansion (HR=0.19 , p=0.003), while chronic kidney disease increased the risk of TLF (HR=3.22, p=0.01).

Conclusions: Angiography alone was insufficient for accurately identifying LM-ISR, particularly in complex bifurcation segments, reinforcing the need for intravascular imaging. NIH was the predominant biological mechanism, while stent underexpansion remained the most frequent mechanical cause. Aggressive PCI was associated with improved outcomes, but its benefit was primarily observed in patients achieving adequate lumen expansion. Chronic kidney disease independently predicted adverse events. These findings highlight the importance of optimizing stent expansion and individualizing treatment strategies in patients with LM-ISR.

Key words: Left main; In-stent restenosis; Intravascular ultrasound; Target Lesion Failure.

冠状动脉微循环功能障碍对延迟干预的中度狭窄病变的临床预后影响

阿不都吾甫尔·依迪力斯 [1,2,3,4] 张晨昀 [1,2,3] 陈德龙 [1,2,3] 向建平 [5] 王建安 [1,2,3,4] 蒋峻 [1,2,3,4]

1. 浙江大学医学院附属第二医院心血管内科

2. 经血管植入器械全国重点实验室

3. 浙江省心血管病诊治重点实验室

4. 杭州市滨江区浙医二院经血管植入器械研究院

5. 杭州脉流科技有限公司

背景： 冠状动脉微循环功能障碍（Coronary microcirculatory dysfunction, CMD）对经冠状动脉生理学或血管内影像学评估后选择保守治疗的中度狭窄病变的临床预后影响尚未明确。本研究旨在探讨基于冠状动脉造影图像计算的微循环阻力指数（Angiography-derived index of microcirculatory resistance, Angio-IMR）所评估的微循环功能障碍，在血流储备分数（Fractional flow reserve, FFR）或血管内超声（Intravascular ultrasound, IVUS）指导下延迟干预的中度狭窄病变不良预后的预测价值。

方法： 本研究是对 FLAVOUR 随机对照试验的事后分析。我们对延迟干预的中度狭窄病变血管进行了回顾性 Angio-IMR 分析。主要终点为随访 24 个月的靶血管失败（Target vessel failure, TVF）事件，定义为心源性死亡、靶血管相关心肌梗死和靶血管血运重建的复合终点。

结果： 本研究共纳入 722 例患者，共 775 个延迟干预的中度狭窄病变血管。Angio-IMR 平均值为 17.9±8.2，其中 103 个（13.3%）病变血管 Angio-IMR > 25，提示伴有微循环功能障碍（CMD）。随访 24 个月期间，共观察到 29 例（3.9%）TVF 事件。生存分析显示，CMD 组患者的 TVF 累积发生率显著高于非 CMD 组（11.7% vs. 2.6%, P < 0.001）。多因素 Cox 回归分析中，CMD 是 TVF 的独立危险因素（HR: 5.43; 95% CI: 2.55-11.59; P < 0.001）。

结论： 冠状动脉微循环功能评估为中度狭窄患者的风险分层提供了新的维度。血管造影衍生的微循环阻力指数（Angio-IMR）可作为一种有效的风险评估工具。

Diagnostic Accuracy of Artificial Intelligence Enhanced Ultrasonic Flow Ratio for Onsite Assessment of Coronary Stenosis

Li-Li Liu[1,2], Lin-Jun Yu[1], Ke Huang[1], An Wang[1], Wei Yu[3], Rui-Yan Zhang[1], Joost Daemen[2], Feng-Hua Ding[1], Sheng-Xian Tu[2,3]

1. Department of Cardiovascular Medicine, Ruijin Hospital, Shanghai Jiao Tong University School of Medicine, Shanghai, China

2. Department of Cardiology, Erasmus University Rotterdam Medical Center, Rotterdam, the Netherlands

3. Biomedical Instrument Institute, School of Biomedical Engineering, Shanghai Jiao Tong University, Shanghai, China

Background Ultrasonic flow ratio (UFR) is an innovative artificial intelligence (AI)-powered method designed to efficiently compute fractional flow reserve (FFR) from intravascular ultrasound (IVUS) imaging. This technology integrates anatomical and functional assessments into a unified platform, eliminating the need for pressure-wire instrumentation and pharmacologically induced hyperemia. While retrospective analyses have confirmed its diagnostic accuracy in identifying hemodynamically significant stenosis by offline analysis in the core laboratory, prospective validation in the catheterization laboratory remains unexplored.

Objective This study prospectively evaluated the diagnostic accuracy of UFR in consecutive patients with with suspected ischemic heart disease (IHD) and intermediate coronary stenosis, using pressure wire-based FFR as the reference standard.

Methods Consecutive IHD patients with ≥ 1 de novo coronary lesion exhibiting 50-80% diameter stenosis and a reference diameter ≥ 2.5 mm by visual estimation were prospectively enrolled. Following IVUS image acquisition under pullback speed of 1.0 mm/s (OptiCross ™, Boston Scientific), the IVUS datasets were immediately transferred to the AI-powered workstation for computation of UFR on site using the IvusPlus software (Pulse Medical), with the analysts being blinded to the FFR data. The minimal lumen area (MLA) was simultaneously available during the UFR computation. The primary endpoint was the diagnostic accuracy of UFR

for identifying functionally significant stenosis (FFR ≤ 0.80).

Results Between February 2023 and November 2024, a total of 161vessels with de novo intermediate stenosis from 136 patients were consecutively enrolled for analyses at the catheterization laboratory. Sixteen vessels were excluded according to the predefined exclusion criteria, yielding a final analytical cohort of 122 patients (145 vessels) with pre-PCI IVUS and FFR. The mean plaque burden was 69.62 ± 10.95%. The median FFR and IVUS-derived MLA were 0.85 (IQR, 0.79-0.90) and 3.53 (2.87-4.32)mm^2, respectively. 31.0% of lesions were hemodynamically significant defined by FFR ≤ 0.80, with 23 (15.86%) pullbacks demonstrating FFR values within the range of 0.75 to 0.80. UFR showed excellent correlation with FFR (r=0.87, P<0.001) and a median value of 0.86 (IQR 0.80-0.90). UFR demonstrated superior diagnostic performance than MLA (AUC: 0.96 vs 0.74, P<0.001). Clinical discordance occurred in 6% of vessels (9/145): FFR>0.80 but UFR ≤ 0.80 in 2 vessels, whereas FFR ≤ 0.80 but UFR>0.80 in 7 vessels. Diagnostic accuracy, sensitivity, specificity, positive predictive value, and negative predictive value of UFR was 94% (95% CI: 89-97%), 84% (95% CI: 71-94%), 98% (95% CI: 93-100%), 95% (95% CI: 83-99%), and 93% (95% CI: 88-96%), respectively. Bland-Altman analysis confirmed excellent agreement between UFR and FFR, with a mean difference of 0.01 ± 0.04 (95% CI: -0.00 to 0.01). UFR-FFR concordance remained statistically consistent across three stratified groups: lesion location (P=0.14), multivessel disease (P=0.22), and imaging catheters specifications (P=0.52).

Conclusions Onsite UFR assessment demonstrated excellent agreement with FFR and superior diagnostic performance compared to MLA. These findings suggest UFR may serve as a reliable, accurate and clinically practical tool for real-world evaluation of flow-limiting lesions seamlessly integrating anatomical and physiological data into a single catheterization procedure. (The FEATURE [Functional ComprEhensive AssessmenT by IVUS Reconstruction in Patients with Suspected IschEmic Heart Disease] study; NCT05694065)

Key words intravascular ultrasound; fractional flow reserve; ultrasonic flow ratio; ischemic heart disease; minimal lumen area

基于光学相干断层成像与冠状动脉造影指导支架内再狭窄介入治疗的预后分析：一项单中心、回顾性研究

慕艳燕 王耿

中国人民解放军北部战区总医院

目的： 支架内再狭窄（in-stent restenosis, ISR）是经皮冠状动脉介入治疗（percutaneous coronary intervention, PCI）术后最常见的并发症。因此 ISR 患者的治疗仍然至关重要。腔内影像学为优化 PCI 策略提供了强有力的支持，现有研究表明，光学相干断层成像（optical coherence tomography, OCT）指导可以改善复杂冠状动脉病变以及复杂分叉病变患者的远期预后。然而，针对 OCT 指导能否改善 DES 植入后 ISR 患者远期预后的研究仍然有限。因此，本研究旨在通过应用 OCT 对 DES 植入术后 ISR 患者的介入治疗进行指导，探讨其对术后 1 年主要不良心血管事件（major adverse cardiovascular events, MACE）的影响，从而进一步指导 ISR 病变介入策略的制定，降低 ISR 患者 MACE 发生率。

方法： 本研究根据纳排标准纳入 2018 年 1 月 1 日至 2023 年 7 月 31 日于中国人民解放军北部战区总医院心血管内科行 PCI 治疗的 ISR 患者 2547 例，根据患者 PCI 术前是否行 OCT 检查分为 OCT 组和冠状动脉造影（coronary angiography, CAG）组。使用参数及非参数法比较两组患者基线，考虑两组患者潜在的混杂临床危险因素，根据 1:2 倾向得分匹配（propensity score matching, PSM）调整患者基线水平。采用单因素 Cox 比例风险回归模型评估 OCT 指导对 ISR 患者 PCI 术后远期临床预后的影响。采用 Kaplan-Meier 法绘制终点事件累积发生率的生存曲线（即 K-M 曲线），采用 log-rank 检验评估组间事件发生率差异有无统计学意义。所有检验均为双尾，P <0.05 被认为差异有统计学意义。

结果： 在 2547 例患者中，OCT 组 151 例患者，CAG 组 2396 例患者。经过 1:2 PSM 平衡两组患者基线后，OCT 组发生 MACE 风险显著低于 CAG 组（4.7% vs 12.0%; HR: 0.366; 95%CI: 0.163-0.822; P = 0.015），且 OCT 组任何血运重建（9.3% vs 17.0%; HR: 0.513; 95%CI: 0.284-0.928; P = 0.027）、靶血管血运重建（target vessel revascularization, TVR）（5.3% vs 11.0%; HR: 0.453; 95%CI: 0.209-0.980; P = 0.044）、靶病变血运重建（target lesion revascularization，TLR）（4.0% vs 10.0%; HR: 0.373; 95%CI: 0.155-0.896; P = 0.027）、心源性再入院（16.0% vs 28.3%; HR: 0.517; 95%CI: 0.329-0.814; P = 0.004）发生率均低于 CAG 组。

结论： 1、OCT 指导显著降低 ISR 患者 PCI 术后 1 年 MACE 发生率（P = 0.015）；2、OCT 指导与 ISR 患者术后 1 年靶血管血运重建、靶病变血运重建以及心源性再入院发生率降低有关；3、相比于 CAG 组，OCT 组使用了更大的最大球囊直径以及更高比例切割球囊。

糖尿病合并 NSTE-ACS 多支病变患者 PCI 后微循环功能障碍相关因素探索

霍黎明 彭欣 侯昌 刘健

北京大学人民医院

目的 探讨糖尿病合并非 ST 段抬高型急性冠脉综合征（NSTE-ACS）多支病变患者经皮冠状动脉介入治疗（PCI）后冠脉微循环功能障碍（Coronary Microvascular Dysfunction，CMVD）的相关因素。

方法 本研究采用单中心回顾性横断面研究，纳入 2021 年 1 月至 2024 年 6 月在北京大学人民医院接受 PCI 治疗的 242 例糖尿病合并 NSTE-ACS 多支病变患者，收集基线资料、介入手术参数及实验室指标。基于术后即刻冠状动脉功能测量（caFFR>0.80 且 caIMR ≥ 25）定义 CMVD，通过单因素及多因素 Logistic 回归分析 CMVD 的危险因素。

结果 242 例患者中，49 例（20.3%）术后诊断为患者水平 CMVD。CMVD 组血红蛋白水平显著高于非 CMVD 组 [136 (130,150) g/L vs 130(119,145) g/L，P<0.05]，丙氨酸氨基转移酶（ALT）水平亦较高 [20 (16,31) U/L vs 18 (13,26) U/L，P<0.05]，而传统心血管风险标志物（高血压、吸烟史、LDL-C）及手术参数组间无差异（P 均>0.05）。单因素 Logistic 回归分析显示，血红蛋白（OR=1.025，95%CI：1.007~1.043，P=0.007）、尿素（OR=0.897，95%CI：0.791~1.108，P=0.091）与 CMVD 相关；多因素 Logistic 回归进一步证实血红蛋白为糖尿病合并 NSTE-ACS 多支病变患者 PCI 后 CMVD 独立预测因子（OR=1.026，95%CI：1.007~1.045，P=0.006）。

结论 血红蛋白浓度升高是糖尿病合并 NSTE-ACS 多支病变患者 PCI 术后 CMVD 的独立危险因素，其机制可能与高黏血症诱导的氧化应激及内皮损伤相关。建议对术前血红蛋白 >130g/L 的患者强化术后微循环监测，并探索血液流变学干预策略。

NSTE-ACS 合并多支病变患者 PCI 后冠脉微循环功能障碍预测研究

霍黎明 刘健

北京大学人民医院

目的：心血管疾病作为全球主要死因之一，有效管理此类疾病至关重要。特别是随着冠脉介入手术量的增加，伴随的并发症如 CMVD 也逐渐增多，对患者的生活质量和远期预后产生负面影响。本研究旨在探索非 ST 段抬高型急性冠脉综合征（NSTE-ACS）合并多支病变患者在接受经皮冠状动脉介入治疗（PCI）后冠脉微循环功能障碍（CMVD）的发生率及其相关临床特征、人工智能心电特征等，建立并验证一个有效的预测模型。

方法：本研究分为四个阶段进行：首先，在 2021 年 1 月至 2024 年 6 月期间收集北京大学人民医院接受 PCI 治疗的 NSTE-ACS 合并多支病变患者的数据，通过 caIMR 分组，分析两组间临床特征、人工智能心电特征差异，使用 2021 年至 2023 年的数据构建 Logistic 回归诊断预测模型，并用 2024 年上半年的数据进行前瞻性验证。

结果：研究表明，NSTE-ACS 合并多支病变 PCI 术后 CMVD 的患病率为 23.7%，靶血管水平患病率为 19.2%。与非 CMVD 组相比，CMVD 组糖尿病、陈旧性心肌梗死患病率较低，ACEI/ARB/ARNI 药物使用率更低，外周血血红蛋白浓度较高。基于这些发现构建的预测模型在训练集和验证集中均表现出良好的诊断效能，尤其是将人工智能心电特征纳入后的模型 AUC 达到 0.677 至 0.708，显示出更高的准确性和稳定性。

结论：本研究不仅明确了 NSTE-ACS 合并多支病变 PCI 术后 CMVD 的高发率及相关风险因素，还成功构建了基于临床特征及人工智能心电特征的预测模型，展示了显著的诊断价值。这为临床医生提供了有效的工具来进行风险评估和个性化治疗规划，有助于改善患者的生活质量及长期预后。此外，研究凸显了人工智能在医疗领域的应用潜力，特别是在处理复杂的心电信息方面，为未来的研究提供了新的方向和技术支持。

探究不同年龄段急性 ST 段抬高型心肌梗死患者的临床与影像学特征

张艺璇 曾明 贾海波

哈尔滨医科大学附属第二医院

目的：

比较年龄≤ 45 岁与≥ 45 岁的急性 ST 段抬高型心肌梗死 (ST-Elevated Myocardial Infarction, STEMI) 患者的基线临床特征及实验室指标差异，并利用光学相干断层扫描 (Optical Coherence Tomography, OCT) 技术探究年轻患者与年老患者罪犯斑块特征的差异，探讨年轻心肌梗死患者的独特危险因素。

方法：

回顾性纳入 2018 年 1 ~ 4 月于哈尔滨医科大学附属第二医院心血管内科就诊并行冠脉造影检查及 OCT 成像的 STEMI 患者 134 例，根据年龄分为年轻组（≤ 45 岁，n=30）和年老组（>45 岁，n=104）。收集两组患者的基线资料、实验室检查及影像学特征。计量资料以中位数（第 25-75 百分位数）或均值 ± 标准差表示，组间比较采用 Mann-Whitney U 检验或独立样本 t 检验；分类资料以例数（百分比）表示，组间比较采用卡方检验。

结果：

纳入的 134 名 STEMI 患者的中位年龄为 57.0 岁，其中年轻组中位年龄为 41.0 岁，年老组中位年龄为 61.0 岁。与年老组相比，年轻组的男性患者比例更高（100.0% vs. 75.0%，P<0.001），年轻组患者吸烟率显著高于年老组（73.3% vs. 48.1%，P=0.015）。此外，年轻患者的白细胞（16.0±3.9 vs. 13.9±4.1）、血红蛋白（158.8±10.1 vs. 147.1）及尿酸水平（381.5 [342.2-429.2] vs. 307.0 [254.8-383.1]）更高（P<0.05）。年轻组多支病变比例更低（40.0% vs. 69.2%，P=0.004），接受 PCI 的比例更低（36.7% vs. 62.5%，P=0.012）。在罪犯病变方面，年轻组患者斑块侵蚀比例更高（46.7% vs. 20.2%，P=0.022），病变长度更短（19.9[15.2-22.5] vs. 23.2[18.6 vs. 29.5]，P<0.001），脂质斑块比例更低（60.0% vs.82.7%，P=0.003），微通道比例更低（30.0% VS. 54.8%，P=0.020）。

结论：

年轻 STEMI 患者以男性、吸烟为主要危险因素，而中老年患者更多合并代谢性疾病。在罪犯病变方面，年轻患者的病变长度更短、斑块侵蚀比例更高、脂质

斑块比例更低，需针对不同年龄层制定个性化预防策略。

探究不同年龄段急性 ST 段抬高型心肌梗死患者的临床与影像学特征差异

张艺璇

哈尔滨医科大学附属第二医院

目的：

比较年龄≤ 45 岁与≥ 45 岁的急性 ST 段抬高型心肌梗死 (ST-Elevated Myocardial Infarction, STEMI) 患者的基线临床特征及实验室指标差异，并利用光学相干断层扫描 (Optical Coherence Tomography, OCT) 技术探究年轻患者与年老患者罪犯斑块特征的差异，探讨年轻心肌梗死患者的独特危险因素。

方法：

回顾性纳入 2018 年 1 ~ 4 月于哈尔滨医科大学附属第二医院心血管内科就诊并行冠脉造影检查及 OCT 成像的 STEMI 患者 134 例，根据年龄分为年轻组（≤ 45 岁，n=30）和年老组（>45 岁，n=104）。收集两组患者的基线资料、实验室检查及影像学特征。计量资料以中位数（第 25-75 百分位数）或均值 ± 标准差表示，组间比较采用 Mann-Whitney U 检验或独立样本 t 检验；分类资料以例数（百分比）表示，组间比较采用卡方检验。

结果：

纳入的 134 名 STEMI 患者的中位年龄为 57.0 岁，其中年轻组中位年龄为 41.0 岁，年老组中位年龄为 61.0 岁。与年老组相比，年轻组的男性患者比例更高（100.0% vs. 75.0%，P<0.001），年轻组患者吸烟率显著高于年老组（73.3% vs. 48.1%，P=0.015）。此外，年轻患者的白细胞（16.0±3.9 vs. 13.9±4.1）、血红蛋白（158.8±10.1 vs. 147.1）及尿酸水平（381.5 [342.2-429.2] vs. 307.0 [254.8-383.1]）更高（P<0.05）。年轻组多支病变比例更低（40.0% vs. 69.2%，P=0.004），接受 PCI 的比例更低（36.7% vs. 62.5%，P=0.012）。在罪犯病变方面，年轻组患者斑块侵蚀比例更高（46.7% vs. 20.2%，P=0.022），病变长度更短（19.9[15.2-22.5] vs. 23.2[18.6 vs. 29.5]，P<0.001），脂质斑块比例更低（60.0% vs.82.7%，P=0.003），微通道比例更低（30.0% VS. 54.8%，P=0.020）。

结论：

年轻 STEMI 患者以男性、吸烟为主要危险因素，而中老年患者更多合并代谢性疾病。在罪犯病变方面，年轻患者的病变长度更短、斑块侵蚀比例更高、脂质斑块比例更低，需针对不同年龄层制定个性化预防策略。

急性心肌梗死患者中罪犯病变斑块破裂、非罪犯病变斑块破裂和薄纤维帽粥样硬化斑块的形态学特征差异：一项光学相干断层扫描研究

马显钦 姜森青 左燕 房超 代建南 于波

哈尔滨医科大学附属第二医院

目的： 动脉粥样硬化斑块破裂是急性心血管事件的主要病理机制。既往研究虽比较了 RCP、RNCP 和 TCFA 的特征，但其样本多来自不同患者，难以排除患者间基线差异的干扰。这些混杂因素可能掩盖斑块固有的病理异质性，导致研究结论偏差。本研究旨在克服患者间异质性，比较同一急性心肌梗死（Acute Myocardial Infarction, AMI）患者罪犯病变破裂斑块（Ruptured Culprit Plaque, RCP）、非罪犯病变破裂斑块（Ruptured Non-Culprit Plaque, RNCP）及薄纤维帽粥样硬化斑块（Thin-Cap Fibroatheroma, TCFA）的形态学特征。

方法： 利用光学相干断层成像（Optical Coherence Tomography, OCT）技术，我们筛选出 58 例同时存在上述三种斑块类型的 AMI 患者，共纳入 210 个斑块进行分析（RCP = 58 个；RNCP = 75 个；TCFA = 77 个），利用广义估计方程比较三种斑块之间的形态学特征差异。

结果： 本研究发现 RNCP 与 TCFA 具有相似的纤维帽厚度 [(52.4 ± 19.5) μm vs. (52.3 ± 9.0) μm, P = 0.999），病变长度 [(20.0 ± 7.1) mm vs. (18.2 ± 8.3) mm, P = 0.271], 脂质长度 [(14.7 ± 7.9) mm vs. (12.3 ± 8.0) mm, P = 0.062]。RCP、RNCP、TCFA 三种斑块之间的管腔面积狭窄程度 [(79.6 ± 8.6) % vs. (60.6 ± 16.4) % vs. (51.3 ± 18.9)%, $P_{(RCP\ vs.\ RNCP)}$ < 0.001, $P_{(RCP\ vs.\ TCFA)}$ < 0.001, $P_{(RNCP\ vs.\ TCFA)}$ = 0.004]，平均脂质角度 [(233.9 ± 45.8) arc vs. (206.5 ± 61.8) arc vs. (189.3 ± 54.6) arc, $P_{(RCP\ vs.\ RNCP)}$ < 0.001, $P_{(RCP\ vs.\ TCFA)}$ < 0.001, $P_{(RNCP\ vs.\ TCFA)}$ = 0.035]、脂质指数 [4158.2 (2810.2, 5351.5) vs. 2779.1 (1630.3, 4422.0) vs. 1869.7 (1198.3, 3654.4), $P_{(RCP\ vs.\ RNCP)}$ < 0.001, $P_{(RCP\ vs.\ TCFA)}$ < 0.001, $P_{(RNCP\ vs.\ TCFA)}$ = 0.014] 之间存在显著差异。

结论： RNCP 与 TCFA 具有可比拟的纤维帽厚度，提示纤维帽厚度本身并非斑块破裂的充分或决定性条件。严重的管腔狭窄和较大脂质的负荷是斑块破裂及后续不良事件发生的关键性因素，其重要性可能超越纤维帽厚度。

STEMI 患者全冠脉斑块特征的性别差异：一项三支血管 OCT 研究

吴天宇 曾明 白潇萱 胡思宁 贾海波

哈尔滨医科大学第二附属医院

目的： ST 段抬高型心肌梗死（ST-elevation myocardial infarction, STEMI）的发病机制、解剖特征、临床表现及预后存在性别差异，但性别因素对 STEMI 患者全冠状动脉易损性的影响尚缺乏充分证据。本研究旨在通过光学相干断层成像（optical coherence tomography, OCT）技术，对比分析 STEMI 患者罪犯病变与非罪犯病变的冠状动脉斑块特征，聚焦全冠状动脉易损性的性别差异。

方法： 本研究纳入 2018 年 7 月至 2020 年 6 月期间于哈尔滨医科大学附属第二医院接受直接经皮冠状动脉介入治疗的 STEMI 患者 583 例（男性 449 例，女性 134 例），术中完成全部三支主要心外膜冠状动脉的 OCT 成像。全冠状动脉易损性定义为非罪犯血管段存在以下任一特征：(1) 符合 CLIMA 研究定义的高危斑块（同时满足四个 OCT 特征：纤维帽厚度 <75μm、最小管腔面积 <3.5mm²、最大脂质弧 >180°及巨噬细胞聚集）；(2) 斑块破裂；(3) 薄纤维帽粥样斑块。

结果： 本研究最终纳入 583 个罪犯病变和 2430 个非罪犯斑块。基于患者的分析显示，男性非罪犯斑块破裂发生率显著高于女性（20.3% vs. 12.7%，P=0.047）；基于斑块的分析亦证实此差异（6.4% vs. 3.7%，P=0.010），尤其在≥ 50 岁人群中更为显著。男性患者的高危 OCT 特征检出率更高（总体：41.4% vs. 30.6%，P=0.024；≥ 50 岁亚组：47.5% vs. 32.0%，P=0.003）。多因素回归分析表明，男性患者中罪犯斑块破裂（OR=4.93，95%CI：2.43-9.99，P<0.001）和年龄≥ 50 岁（OR=1.96，95%CI：1.06-3.62，P=0.032）是非罪犯斑块破裂的独立预测因子；而男性患者合并≥ 1 项高危 OCT 特征的独立预测因子包括：罪犯斑块破裂（OR=3.20，95%CI：2.00-5.13，P<0.001）、年龄≥ 50 岁（OR=2.14，95%CI：1.32-3.47，P=0.002）、糖尿病（OR=1.81，95%CI：1.08-3.05，P=0.025）及高血压（OR=1.59，95%CI：1.03-2.47，P=0.038）。女性群体中未发现显著关联。

结论： 在 STEMI 患者中，男性较女性表现出更显著的全冠状动脉易损性，其风险可由罪犯斑块破裂、年龄≥ 50 岁、糖尿病及高血压独立预测。值得注意的是，即使≥ 50 岁的女性患者，其全冠状动脉斑块易损性的发生频率及病变范围均显著低于男性。

OCT 识别的非罪犯斑块破裂的长期预后价值

赵嘉伟 赵锐 房超 代建南 于波

哈尔滨医科大学第二附属医院

目的： 亚临床斑块破裂（即非罪犯斑块破裂）被认为是全冠状动脉易损性的标志，且与不良短期预后相关，但其对长期临床结局的影响尚未明确。本研究旨在探讨非罪犯斑块破裂对急性心肌梗死（acute myocardial infarction，AMI）患者长期复发性不良心脏事件的预测价值。

方法： 纳入 2017 年 1 月至 2021 年 12 月期间于哈尔滨医科大学附属第二医院接受介入治疗前完成三支冠状动脉光学相干断层成像（optical coherence tomography，OCT）检查的 AMI 患者。根据非罪犯部位是否存在 OCT 识别的斑块破裂对患者及病变进行分类。亚组分析中，进一步根据非罪犯节段是否存在斑块破裂和 / 或未破裂薄纤维帽粥样斑块（thin-cap fibroatheroma，TCFA）进行分层（未破裂 TCFA 定义为存在 TCFA 但无斑块破裂的病变）。对所有入组患者进行为期 5 年的随访。主要不良心脏事件（major adverse cardiac events，MACE）包括心源性死亡、非致死性心肌梗死及计划外缺血驱动的血运重建。

结果： 本研究最终共纳入 1312 例 AMI 患者，涵盖 5273 处非罪犯病变。226 例患者（282 处病变）检出非罪犯斑块破裂。中位随访 4.1 年期间，存在斑块破裂的患者其非罪犯病变相关 MACE 发生率显著高于无破裂者（P<0.05），主要归因于非致死性心肌梗死和计划外血运重建风险增加。然而，在病变水平上，存在与不存在斑块破裂的病变其 MACE 发生率无显著差异。多变量模型显示：在患者水平，非罪犯斑块破裂是非罪犯病变相关 MACE 的独立预测因子（HR=2.15, 95%CI: 1.42-3.26, P<0.001）；在病变水平，该关联无统计学意义（P=0.32）。亚组分析发现：319 例患者（428 处病变）存在未破裂 TCFA。多变量模型证实，无论患者水平（HR=2.83, 95%CI: 1.91-4.19, P<0.001）还是病变水平（HR=1.78, 95%CI: 1.12-2.83, P=0.015），未破裂 TCFA 均与非罪犯病变相关 MACE 显著相关，而斑块破裂无此预测价值。

结论： 未破裂 TCFA（而非斑块破裂）可识别未来事件高风险斑块。非罪犯斑块破裂患者长期预后不良的本质原因，主要源于伴随存在的未破裂 TCFA 的影响。

CT-FFR 与 QFR 诊断冠状动脉病变特异性缺血准确性的对比研究

吴皓宇 梁磊 颜举 武峰超 寿锡凌

陕西省人民医院

目的： 血流储备分数（FFR）已成为评估冠状动脉病变特异性缺血和指导冠状动脉血运重建决策的金标准。然而，FFR 作为有创检查方法，可能导致冠状动脉相关并发症，且设备昂贵，限制了其临床应用。基于冠状动脉 CT 血管成像（CCTA）的无创 FFR（CT-FFR）和定量血流分数（QFR）是两种具有前景的诊断方法。本研究旨在以 FFR 为参考标准，评估 CT-FFR 与 QFR 在预测冠状动脉病变特异性缺血方面诊断性能的差异。

方法： 本研究纳入 84 例疑似或确诊冠心病（CAD）患者（年龄 59.85±9.36 岁；男性占 61.76%）。患者接受 CCTA 检查显示冠状动脉主支（参考直径≥ 2.0 mm）存在 30%-90% 狭窄。基于 CCTA 图像计算 CT-FFR 值。在行侵入性冠状动脉造影时测量 FFR 和 QFR。以 FFR ≤ 0.80 作为冠状动脉病变特异性缺血的参考标准。

结果： 以 CT-FFR ≤ 0.80 预测冠状动脉病变特异性缺血的诊断性能良好：敏感度为 90.74%，特异度为 94.74%，受试者工作特征曲线下面积（AUC）为 0.958（P <0.0001）。以 QFR ≤ 0.80 预测冠状动脉病变特异性缺血的诊断性能同样良好：敏感度为 91.00%，特异度为 89.47%，AUC 为 0.941（P <0.0001）。然而，CT-FFR ≤ 0.80 与 QFR ≤ 0.80 预测冠状动脉病变特异性缺血的 AUC 差异无统计学意义（P = 0.942）。CT-FFR 与 FFR 呈良好正相关（Pearson 相关系数 r = 0.835, P <0.0001）。QFR 与 FFR 亦呈良好正相关（Pearson 相关系数 r = 0.804, P <0.0001）。

结论： CT-FFR 和 QFR 与 FFR 具有良好的直接相关性，两者均可为冠状动脉病变特异性缺血提供较高的临床诊断效能。本研究表明，这两种无创技术有望成为评估冠状动脉缺血的重要替代方法。

代谢组学揭示胍丁胺作为冠心病患者易损斑块的预测标志物

闫海浩 刘巍

首都医科大学附属北京积水潭医院

目的：易损斑块破裂是导致血栓形成和心血管不良事件的重要病理基础。本研究旨在通过代谢组学联合光学相干断层成像（optical coherence tomography, OCT）识别易损斑块的血清预测标志物。

方法：纳入首次经皮冠状动脉介入治疗并行 OCT 检查的冠心病患者。根据病变血管是否存在薄帽纤维粥样硬化斑块（thin-cap fibroatheroma,TCFA）分为易损斑块组（n=24）和稳定斑块组（n=16），通过非靶代谢组学分析联合 LASSO 检验筛选两组间差异代谢物。后续前瞻性招募冠心病患者 100 例进行 OCT 成像，使用靶向液相色谱 - 质谱方法定量检测候选血清代谢物水平，评估其对易损斑块的预测价值。

结果：非靶代谢组学联合 LASSO 检验筛选出 3 个易损斑块组下调代谢物：胍丁胺（P=0.001），肌氨酸（P=0.002），肌酸（P=0.041）；以及 2 个上调代谢物：3- 甲基组氨酸（P=0.012），甜菜碱（P=0.018）。KEGG 分析两组在甘氨酸、丝氨酸和苏氨酸代谢（P<0.001）；精氨酸和脯氨酸代谢 (P=0.003)；丙酸代谢 (P=0.013) 通路富集。受试者工作特征（receiver operating characteristic, ROC）分析胍丁胺 [曲线下面积（area under the curve, AUC）：0.78，95%CI：0.62~0.94，P=0.003] 是预测冠心病患者易损斑块的最佳标志物。在前瞻性验证队列中（n=100），胍丁胺与斑块最大脂质弧（β：-6.33，95% CI：-12.19~-0.48, P = 0.034）呈负相关，与纤维帽厚度呈正相关（β：11.35，95% CI：1.96~20.74, P = 0.018）。多因素 logistic 回归分析显示胍丁胺是 TCFA 的独立预测因素（OR：0.69，95% CI：0.55~0.88，P=0.002），其识别 TCFA 的 AUC 为 0.74（95%CI：0.61~0.88，P = 0.002）。以 ROC 确定的最佳截断值（11.10）为界，低胍丁胺组患者 TCFA 检出率高于高胍丁胺组（40.0% vs 7.1%; P<0.001），且纤维帽更薄（149.1 μm vs 210.7 μm; P=0.024）、脂质弧更大（167.8° vs 131.1°；P=0.034）、巨噬细胞浸润比例更高（53.3% vs 30.0%; P=0.027）。

结论：基于代谢组学筛选的血清胍丁胺水平在易损斑块患者中显著降低，且是 TCFA 的独立预测因子，提示其作为冠心病患者易损斑块预测标志物的潜力。

Evaluation of Neointimal Coverage After Guiding De-escalation of Antiplatelet Treatment in Patients with ST-elevation Myocardial Infarction Undergoing Percutaneous Coronary Intervention by Optical Coherence Tomography or Angiography

Jia-Yi Luo, Jia-Yin Li, Yu Xue, Zi-Min Xu, Yang Li

State Key Laboratory of Frigid Zone Cardiovascular Diseases，Cardiovascular Research institute and Department of Cardiology, General Hospital of Northern Theater Command, No.83, Wenhua Road, Shenhe District,Shenyang, 110016, China

Background and Objectives:

Dual antiplatelet therapy (DAPT) de-escalation strategies including early switching from a potent P2Y12 inhibitor to clopidogrel become attractive for patients with ST-elevation Myocardial Infarction (STEMI). The efficacy and safety of de-escalating strategies of antiplatelet therapy in patients with ST-elevation myocardial infarction (STEMI) undergoing primary percutaneous coronary intervention (PPCI) remain uncertain. Angiography is limited to assess the pathophysiological mechanisms of the culprit lesion in guiding PCI, and optical coherence tomography (OCT) is widely used due to its high resolution. Intracoronary imaging guidance during PCI has been shown to improve clinical outcomes and features as a recommendation in societal guidelines. Comprehensive and updated frequentist and Bayesian network meta-analyses showed that OCT-guided PCI was associated with reduced incidence of cardiac death or stent thrombosis compared with invasive coronary angiography-guided PCI. Therefore, OCT-guided PCI correlates with improved clinical outcomes, especially with improved ischemic outcomes. The objective of this study was to explore the effect of de-escalation of dual antiplatelet therapy (DAPT) after OCT- or angiography-guided PPCI on neointimal coverage in patients with STEMI who have completed 1-month DAPT with aspirin plus ticagrelor.

Methods:

This was a single-center, prospective, randomized clinical trial. Eighty patients with STEMI who were proposed to undergo PPCI were randomized twice in a 1:1 ratio, with the first randomization performed before PCI. The primary inclusion criteria were as follows: patients with STEMI, significant stenotic lesions in native coronary arteries suitable for DES implantation and age 18-75 years, the patient or guardian agrees to the study protocol and the schedule of clinical follow-up and provides written informed consent as approved by the appropriate institutional review board/ethical committee of the respective clinical site. The patients were divided into OCT-guided group or angiography-guided group. All patients received open label ticagrelor plus aspirin for one month after PPCI. Patients who were not experiencing any clinical events one month after PPCI were randomized for a second time and divided into antiplatelet de-escalating group (aspirin plus clopidogrel) or an standard DAPT group (aspirin plus ticagrelor). The primary endpoint is the stent-strut neointimal thickness by OCT assessment at 12-month follow up. Secondary endpoints include 12-month major adverse cardiovascular and cerebrovascular events (MACCE) defined as a composite of acute myocardial infarction, repeat revascularization, stroke, and all-cause mortality, definite/probable stent thrombosis, and Bleeding Academic Research Consortium (BARC) types 2-5 bleeding.

Results:

A total of 72 patients were enrolled in the study: 36 in the OCT-guided group and 36 in the angiography-guided group after the first randomization. During the 30-day postoperative follow-up period, 2 patients died and 6 patients experienced adverse clinical events related to bleeding. Following a second randomization, 33 patients were assigned to the antiplatelet de-escalating group, while 31 patients were assigned to the standard DAPT group. The in-stent neointimal thickness was significantly lower in the OCT-guided group than in the angiography-guided group (0.16±0.11mm vs. 0.65±0.27mm; p<0.001). Furthermore, neointimal coverage was thinner in the standard DAPT group than in the antiplatelet de-escalating group (0.25±0.19mm vs. 0.50±0.35mm; p<0.001). In addition, the incidence of MACCE was significantly lower in the OCT-guided group than in the angiography-guided group (2.9% vs. 18.9%; p = 0.03). There was no statistically significant difference in the incidence of MACCE between the antiplatelet de-escalating group and the standard DAPT group (9.8% vs. 12.9%; p = 0.674). Statistically significant differences were not observed between the OCT-guided group and the angiography-guided group, or between the antiplatelet de-escalating group and the standard DAPT group, in terms of the various components of MACCE. Additionally, the incidence of clinically relevant bleeding in the antiplatelet de-escalating group was significantly lower than in the standard DAPT group according to the BARC classification (types 2-5) (4.9% vs. 25.8%; p = 0.011). However, a statistically significant difference in the incidence of bleeding was not observed between the OCT-guided group and the angiography-guided group (BARC types 2-5, 8.6% vs. 18.9%; p = 0.204).

Conclusions:

Patients with STEMI undergoing OCT-guided PCI achieved stent optimization, and received aspirin plus ticagrelor for 12 months had thinner in-stent neointimal thickness, indicating these patients were associated with better clinical outcomes.

Rationales Behind Physiology-guided Revascularization: Diagnostic and Prognostic Impact of Quantitative Flow Ratio in the FAVOR III China Trial

Rui Zhang, Dong Yin

Fuwai Hospital, National Center for Cardiovascular Diseases, Chinese Academy of Medical Sciences and Peking Union Medical College, Beijing, China 2State Key Laboratory of Cardiovascular Disease, Beijing, China

BACKGROUND The optimization of treatment plan developed based on coronary angiography alone, is recognized as one of the underlying rationales for the clinical benefits of physiology-guided PCI.

OBJECTIVES The present study was a post hoc analysis from the FAVOR III China trial, and aimed to assess physiological concordances of both pre-randomization declared treatment plan as well as post-randomization actual treatment strategy and to investigate the diagnostic and prognostic implication of computational QFR in the large-scale multicenter randomized trial.

METHODS In FAVOR III China trial, operators were required to declare all target vessels intended for PCI before randomization (pre-randomization declared treatment plan). After randomization, the actual treatment strategy was performed with online QFR or angiography guidance (randomized allocation). In this study, pre-randomization treatment plan and post-randomization treatment strategy were adjudicated using offline QFR by independent corelab to determine physiology-concordant. Pre-randomization physiology-nonconcordant encompasses: 1) inappropriate treatment, at least one non-ischemic vessel in which PCI was intended to be performed; 2) inappropriate deferral, at least one ischemic vessel in which PCI was intended to be deferred; and 3) inappropriate treatment & deferral, patients having both inappropriate treatment and inappropriate deferral (in different vessels). In accordance with the principles, the post-randomization treatment strategy was reclassified into post-randomization physiology-concordant or -nonconcordant groups. The primary outcome of interest for the present study was major adverse cardiac events (MACE), defined as the composite of all-cause death, myocardial infarction (MI), or ischemia-driven revascularization.

RESULTS Between Dec 25, 2018, and Jan 19, 2020, 3,825 patients were randomized at 26 hospitals in China. For the present analysis 57 patients were excluded because of unavailable core laboratory offline QFR assessments. Among 3,768 pooled patients with available offline QFR, 2,601 (69.0%) had pre-randomization physiology-concordant plan, proportion of which was comparable between online QFR-guided and angiography-guided group (70.9% [1,340/1,891] vs. 67.2% [1,261/1,877], SMD = 0.087). Physiological concordances were reclassified in 447 (23.6%) and 87 (4.6%) patients with online QFR or angiography guidance, respectively. Among patients randomized to QFR-guided group, physiological concordances were reclassified in 447 patients (23.6%) with online QFR guidance, including a transition of 21 patients (1.1%) from pre-randomization concordant to post-randomization nonconcordant group, and 426 patients (22.5%) from pre-randomization nonconcordant

to post-randomization concordant group; thus 1,745 patients (92.3%) achieved finial physiology-concordant. Upon patients with angiography guidance, physiological concordances were reclassified in 87 patients (4.6%), comprising a shift of 43 patients (2.3%) from pre-randomization concordant to post-randomization nonconcordant, and 44 patients (2.3%) from pre-randomization nonconcordant to post-randomization concordant; consequently, 1,262 patients (67.2%) achieved finial physiology-concordant. A significant between-groups difference was identified in terms of achieving post-randomization physiology-concordant (92.3% vs. 67.2%, SMD = 0.665). The primary 2-year MACE rates were 7.6% in patients assigned to QFR-guided group compared to 17.0% in those assigned to angiography-guided group in whom pre-randomization nonconcordant plan was observed (HR 0.43, 95% CI: 0.30-0.61), and in 8.9% vs. 10.4% respectively among patients with a pre-randomization concordant plan (HR 0.85, 95% CI: 0.66-1.09), indicating a significant interaction (interaction P = 0.002). Patients with older age, multivessel disease, left circumflex or right coronary artery involved, and lower SYNTAX score were found more likely to have pre-randomization physiology-nonconcordant.

CONCLUSIONS In the FAVOR III China trial, approximately 30% of patients showed a discrepancy between angiography-based treatment plans and physiological ischemia. The mechanistic insights underlying the benefits of QFR-guided PCI is reclassification following online QFR guidance, which leads to a shift from initially flawed plans toward physiology-concordant decisions. Initially flawed plan was a predictable entity and artificial intelligence-powered machine learning model would be developed in future study.

定量血流分数指导经皮冠脉介入治疗策略在不同心外膜冠脉中的血管特异性结局：FAVOR III China 研究的预设亚组分析

江瑶 崔锦钢 管常东 陈柘霖 柳耀 乔树宾 宋雷

中国医学科学院阜外医院

目的

FAVOR III China 研究已证实，与传统造影指导相比，定量血流分数（QFR）指导经皮冠脉介入治疗策略可显著改善患者临床结局。但 QFR 的指导疗效在不同的心外膜冠状动脉中是否一致尚无研究证实。

方法

本研究是 FAVOR III China 研究的预设亚组分析，根据病变在心外膜三大冠脉主支的位置，将患者分为左主干 / 前降支（LM/LAD）、回旋支（LCX）和右冠状动脉（RCA）三个队列。主要终点为 3 年的血管相关复合终点（VOCE），包括靶血管相关心源性死亡、靶血管相关心肌梗死和缺血驱动的靶血管血运重建。

结果

对 3825 例患者的病变进行分析，其中 2937 例患者病变涉及 LM/LAD，1426 例涉及 LCX，1606 例涉及 RCA。QFR 指导组的血运重建策略改变的发生率更高，LM/LAD 组为 12.1%，LCX 组为 18.7%，RCA 组为 20.8%。3 年随访时，与造影指导相比，QFR 指导的介入治疗可显著降低 LM/LAD 和 RCA 亚组 VOCE 的发生风险 [LM/LAD：风险比（HR）0.69，95% 置信区间（CI）0.51–0.92；p = 0.01；RCA：HR 0.54，95% CI 0.36-0.81；p = 0.002]，分别由靶血管相关心肌梗死和缺血驱动的靶血管血运重建驱动，但在 LCX 组中未见明显获益（HR 0.80，95% CI 0.54-1.18；p = 0.25）。在延迟血运重建或策略改变等不同亚组中，QFR 指导血运重建的血管特异性结局与主要发现一致。

结论

与造影指导相比，QFR 指导的支架植入策略在不同冠状动脉中表现出血管特异性的疗效差异，在 LM/LAD 和 RCA 病变中具有显著优势，但在 LCX 病变中未观察到明显获益。对于 LCX 病变，基于 QFR 的血运重建决策需更加谨慎，应结合腔内影像技术或者有创生理学测量进行评估和优化。

A deep learning methodology for fully-automated quantification of calcific burden in high-resolution intravascular ultrasound images

Xingwei He[1], He-Song Zeng[1], Christos Bourantas[2]

1. Division of Cardiology, Tongji Hospital, Tongji Medical College, Huazhong University of Science and Technology

2. Department of Cardiology, Barts Heart Centre, Barts Health NHS Trust, London, UK

Background:

Coronary artery calcification is a hallmark of advanced atherosclerotic disease and is associated with adverse outcomes following percutaneous coronary intervention (PCI). Accurate quantification of calcific burden plays a critical role in PCI planning, particularly in guiding lesion preparation strategies to ensure optimal stent expansion. Intravascular ultrasound (IVUS) is widely considered the gold-standard imaging modality for detecting calcific tissue due to its superior ability to visualize deeply embedded plaque components and provide high-resolution cross-sectional images of the vessel wall. However, current practices rely on manual assessment of IVUS images, which is labor-intensive, subject to significant inter- and intra-observer variability, and impractical for large-scale analyses. These limitations have hindered the integration of calcification analysis into routine clinical workflows and high-throughput research studies.

Objective:

To overcome these challenges, we developed a fully automated, deep learning (DL)-based methodology for the identification and quantification of calcific tissue in high-resolution IVUS images. Our goal was to provide a fast, accurate, and reproducible solution that could match expert-level performance and be readily implemented within existing image analysis software.

Methods:

We trained a DL model using a dataset of IVUS images from 65 patients (197 vessels; 26,211 frames) with stable coronary artery disease. The training set was curated with expert-annotated calcium masks, which included precise delineation of calcific arc, area, and depth relative to the lumen. A U-Net architecture was employed, which has been shown to be particularly effective in medical image segmentation tasks. To enhance performance, we applied a polar transformation to the IVUS images, simplifying the representation of acoustic shadows—a key indicator of calcific presence—into a consistent orientation. This preprocessing step allowed the network to more effectively learn spatial relationships and shadow characteristics associated with calcific tissue.

The model was tested on an independent dataset of 5,138 IVUS frames from 30 vessels in 13 patients. Performance was evaluated across multiple scales: frame-level (presence/absence of calcium, arc, area, and lumen-to-calcium distances), lesion-level (classification of calcific-rich plaques), and segment-level (calcific burden index, or CaBI). Quantitative metrics included Cohen's kappa, Pearson correlation coefficients, Bland-Altman analysis, and the Williams Index (WI), a comparative metric assessing agreement between the DL model and expert annotations relative to expert-expert variability.

Results:

The DL model achieved excellent agreement with human experts. At the frame level, kappa values for calcium presence were 0.842 and 0.848 ($p<0.001$), indicating strong concordance. Correlation coefficients for calcium arc and area were 0.946–0.947 and 0.706–0.745 respectively, while correlations for mean and minimum distances from lumen to calcium ranged from 0.876 to 0.930. Bland-Altman analysis showed small biases and narrow limits of agreement across all parameters.

At the lesion level, the DL method demonstrated high diagnostic performance, identifying calcific-rich plaques (defined as arc $\geq 90°$) with sensitivity of 95.5%, specificity of 89.5%, and accuracy of 91.7%. Segment-level analysis revealed similarly strong performance, with CaBI estimates highly correlated with those of experts ($r \geq 0.980$). Importantly, the Williams Index was below 1 for most measures, indicating that the discrepancies between the DL method and expert annotations were smaller than inter-expert variability. Notably, the DL model outperformed human experts in estimating the minimum lumen-to-calcium distance (WI = 1.631).

Qualitative assessment showed that the DL method could reliably localize calcific tissue within the plaque architecture, including its circumferential distribution. Mean angular differences between DL and expert annotations were close to zero, and the Dice similarity coefficient for overlap ranged from 0.915 to 0.916—comparable to inter-observer agreement levels. Furthermore, the model was highly efficient, capable of analyzing 5,000 frames in approximately 1 minute on a standard desktop computer, a process that typically takes experts around 1 hour.

Significance and Clinical Implications:

Our findings demonstrate that the proposed DL methodology not only provides accurate quantitative metrics for calcific burden but also offers qualitative insights into calcium morphology, which are crucial for clinical decision-making. In PCI planning, understanding the location, circumferential extent, and proximity of calcium to the lumen helps operators determine whether lesion preparation strategies such as atherectomy, scoring balloons, or intravascular lithotripsy are warranted.

From a research perspective, this tool facilitates large-scale, unbiased quantification of calcification across populations, enabling new insights into disease progression and response to pharmacotherapies. It can also be integrated into longitudinal studies assessing the effects of novel lipid-lowering or anti-inflammatory agents on plaque composition. Moreover, this method complements existing DL-based tools for lumen and vessel wall segmentation, paving the way for fully automated IVUS analysis pipelines capable of comprehensive plaque phenotyping.

Conclusions:

We present a novel, fully automated DL-based approach for the detection and quantification of calcific tissue in IVUS images. The method matches expert-level performance, significantly reduces analysis time, and integrates seamlessly into existing image analysis workflows. It holds promise for widespread adoption in both research and clinical

settings, where it can enhance PCI planning and support studies investigating the impact of therapies on coronary plaque morphology.

Optical coherence tomography versus coronary angiography -guided percutaneous coronary intervention: a systematic review and meta-analysis

Jia-Yi Luo, Jia-Yin Li, Yu Xue, Zi-Min Xu, Yang Li

State Key Laboratory of Frigid Zone Cardiovascular Diseases, Cardiovascular Research institute and Department of Cardiology, General Hospital of Northern Theater Command, No.83, Wenhua Road, Shenhe District,Shenyang, 110016, China

Background and Objectives:

The superiority of optical coherence tomography (OCT) guidance over coronary angiography (CA) guidance in optimizing therapy in patients undergoing percutaneous coronary intervention (PCI) remains uncertain. Multiple trials have been published, sparking debate as to whether the patient outcomes short- and long-term outcomes of OCT-guided PCI are superior to those of CA. A substantial body of evidence from recent years indicates that MSA (minimum stent area) is not only an effective predictor of stent restenosis but is also significantly linked to patients' future risk of adverse cardiovascular outcomes. Consequently, we conducted a comprehensive meta-analysis with the objective of providing a higher level of evidence. We aimed to perform a meta-analysis of published studies to evaluate the outcomes of CA- and OCT-guided PCI procedures.

Methods:

A comprehensive search using medical subject headings (MeSH) and text terms ("coronary angiography", "optical coherence tomography", "OCT", "percutaneous coronary intervention", and "PCI") was conducted in PubMed/Medline, EMBASE, and the Cochrane Library up to March 2024 for all randomized controlled trials (RCTs) and observational studies, with no language restrictions. We also manually screened major cardiology websites, editorials and reviews for relevant studies to avoid missing anything. The outcomes of this meta-analysis included all-cause death, cardiovascular death, major adverse cardiovascular events (MACE), restenosis, myocardial infarction (MI), target lesion revascularization (TLR), target vessel revascularization (TVR), post-intervention minimum stent area (MSA), post-intervention minimum lumen diameter (MLD) and follow-up MLD. Study characteristics, baseline characteristics of patients and endpoints of interest were extracted independently by two authors. To ensure data accuracy, data comparison was performed after extraction, with a senior author resolving any disagreements. The methodological quality of RCTs was evaluated using the Cochrane risk-of-bias tool (RoB-2), while the quality of observational studies was assessed using the ROBINS-I tool. The statistical analysis was conducted using the Review Manager (RevMan 5.3) and STATA version 18 (Stata Corp, College Station, Texas, USA). Heterogeneity was quantified using the I^2 test, with an I^2 value of 0% to 25% designated as absent or low, an I^2 value of 26% to 50% designated as moderate, and an I^2 value above 50% designated as high. When heterogeneity was defined as high, a random effect model was utilized for the calculation, otherwise a fixed effect model was used. Conversely, a fixed effects model was employed. The results were expressed as risk ratio (RR) and mean deviation (MD) with their corresponding 95% confidence interval (CI). We did subgroup analyses according to study type (RCTS versus observational studies), follow-up time (short-term versus long-term), stent type (drug-eluting stent/ bare-metal stent versus bioresorbable scaffold), and patient characteristics (acute coronary syndrome versus non-acute coronary syndrome). Long-term refers to a follow-up period of at least one year. A trial was classified as belonging to the acute coronary syndrome (ACS) group if all patients included in the trial at least 50% of the patients included in the trial had ACS.

Results:

A total of 25 articles were included in the study. In terms of clinical outcomes, OCT-guided PCI was associated with a significant reduction in all-cause death (RR 0.62; 95%CI 0.47-0.83; p=0.001), cardiovascular death (RR 0.47; 95%CI 0.32-0.69; p<0.001), and MACE (RR 0.65; 95%CI 0.54-0.77; p<0.001). While no statistically significant differences were observed for restenosis (RR 0.91, 95%CI 0.73-1.13, P=0.38), MI (RR 0.83, 95%CI 0.69-1.00, P=0.05), TLR (RR 0.86, 95%CI 0.66-1.10, P=0.23), and TVR (RR 0.82, 95%CI 0.63-1.07, P=0.15). In terms of surrogate endpoints, OCT-guided PCI was associated with a significant enhancement of MSA (MD=0.30, 95%CI 0.04-0.56, p=0.03) and MLD at follow-up (MD=0.12, 95%CI 0.02-0.22, p=0.02). Nevertheless, no significant increase in the post-intervention MLD was observed (MD=0.04, 95%CI -0.02-0.10, p=0.19).

Conclusions:

Compared with CA, the use of OCT for PCI guidance may be an effective strategy to optimize treatment. In this meta-analysis, the use of OCT guidance during PCI reduced cardiovascular death, all-cause death, and MACE and resulted in a higher MSA compared to CA. However, probably because of the heterogeneity and a small number of events, other outcomes, and some subgroup analyses did not show this superiority. There remains a need for higher-quality RCTs in the future to adequately evaluate the role of OCT in PCI.

High-Risk Lesion Features on Coronary CT Angiography Predict Acute Coronary Syndrome in FFR-Negative Patients

Jia-Yi Luo, Jia-Yin Li, Yu Xue, Zi-Min Xu, Yang Li

State Key Laboratory of Frigid Zone Cardiovascular Diseases, Cardiovascular Research institute and Department of Cardiology, General Hospital of Northern Theater Command, No.83, Wenhua Road, Shenhe District,Shenyang, 110016, China

Background and Objectives:

Invasive flow reserve fraction (FFR)-guided percutaneous coronary stenting (PCI) in patients with acute coronary atherosclerosis (ACS) has been shown to result in superior clinical outcomes when compared with angiography-guided PCI or pharmacological therapy. However, it should be noted that clinical events still occur in FFR-negative patients. The study assessed lesions characteristics by coronary computed tomography angiography (CCTA) in FFR-negative patients and to explore the association between lesion characteristics and future cardiovascular events.

Methods:

We retrospectively analyzed the data of patients who underwent CCTA from 2022 to 2023 and had FFR results suggesting negativity within one month. The following three domains were assessed in the testing of CCTA metrics at the vascular level: plaque quantity (including plaque burden and total plaque volume); plaque quality (including high-risk plaque); and peri-coronary fat inflammation characteristics. High-risk plaques were defined as having at least two of the following features: positive remodeling, spotty calcification, low-attenuation plaque and napkin-ring sign. At the two-year follow-up, patients were divided into two groups based on whether or not they had recurrent ACS: the recurrent ACS group and the non-recurrent ACS group. Three prediction models were constructed: model 1 (high-risk plaque), model 2 (model 1 + plaque burden + total plaque volume) and model 3 (model 2 + pericoronary adipose tissue). The predictive performance of each model was evaluated using the area under the receiver operating characteristic curve (AUC), and comparisons between AUCs were performed using DeLong's method. Furthermore, the discriminative power and classification accuracy of each model were compared using the relative integrated discriminant improvement index (IDI) and net reclassification index (NRI). The process of plot calibration is employed for the purpose of evaluating the predictive calibration and the discriminative validity of the model under consideration, with the Brier score and calibration slope being calculated in order to illustrate calibration accuracy. The decision curve analysis (DCA) should be applied in order to evaluate the clinical utility of the model.

Results:

During the study period, a total of 417 patients underwent examinations including FFR, ICA, and CCTA. Among these patients, 201 exhibited an FFR value of less than 0.8, while 15 had CCTA image quality that did not meet the criteria for analysis. Additionally, 5 patients were lost to follow-up. Ultimately, a total of 196 patients were included in the final analysis: this comprised 92 individuals in the recurrent ACS group and 104 individuals in the non-recurrent ACS group. Meanwhile, 207 culprit lesions were identified on CCTA, based on coronary angiography findings at the time of ACS. The prevalence of plaque burden (66.0 ± 5.8% vs. 60.7 ± 5.6%; p < 0.001), total plaque volume (103.0 ± 32.9 mm3 vs. 79.3.1 ± 29.3 mm3; p < 0.001), and high-risk plaque incidence (62.6% vs. 31.2%; p < 0.001) were all found to be significantly higher in the recurrent ACS group. In the ACS group, the difference in pericoronary adipose tissue was found to be statistically significant (p < 0.001). Of the three models, model 3 demonstrated superior discrimination (AUC 0.887 vs. 0.828; P< 0.001) and reclassification abilities (category-free net reclassification index 0.338; P<0.001; and relative integrated discrimination improvement 0.122; P< 0.001). The net benefit curve of model 3, which demonstrated the highest discriminatory power in the DCA, remained above models 1 and 2 within the clinical decision threshold range (0.2-0.7). This suggests that it could offer greater net benefits in clinical decision-making. The results of five-fold cross-validation indicate that the model's predictive capability improves as the number of parameters increases. Concurrently, the fluctuation range of the AUC consistently narrows, suggesting that each model not only enhances its performance but also maintains a high level of stability. The calibration slopes for Model 1, Model 2, and Model 3 were found to be 1 (95% CI: 0.586 - 1.414), 0.999 (95% CI: 0.816 - 1.181), and 1.003 (95% CI: 0.861 - 1.145), respectively. The calibration curves of all three models demonstrated a close alignment with the ideal calibration line throughout the entire risk range.

Conclusions:

In FFR-negative patients, integrating outcome assessment of CCTA with FFR has been shown to enhance the identification of offender lesions that may trigger ACS.

Guanxinshutong capsule alleviates hypoxia-induced myocardial apoptosis via AMPK-mediated autophagy

yu Xu, Yang Li, Hai-Xu Song, Jia-Yi Luo, Zi-Min Xu, Jia-Xin Xu, Jing-Jin Hou, Cheng-Hui , Ya-Ling Han

State Key Laboratory of Frigid Zone Cardiovascular Diseases，Cardiovascular Research institute and Department of Cardiology, General Hospital of Northern Theater Command, No.83, Wenhua Road, Shenhe District,Shenyang, 110016, China

Aim of the study: Guanxinshutong capsule (GXST), a traditional Chinese medicine formulation. This preparation is effective for treating patients with stable angina pectoris. We performed network pharmacology, and in vitro and in vivo experiments to explore the mechanisms by which GXST protects against myocardial ischemia/reperfusion (MI/R).

Methods: The critical targets and potential mechanisms of action were predicted using network pharmacology. Eight-week-old C57BL/6 mice were divided into an MI/R group (treated with normal saline) and a GXST group (treated with 1.5 g/kg/d via oral gavage). An in vitro model of hypoxic injury was established by exposing H9C2 cells to 800 μM cobalt chloride ($CoCl_2$) for 24 h. The effects of GXST on apoptosis and autophagy were assessed using a TdT-mediated dUTP nick-end labeling assay, flow cytometry, transmission electron microscopy, immunofluorescence, and western blotting.

Results: Network pharmacology analysis revealed that autophagy and apoptosis were crucial pathways through which GXST suppressed MI/R injury. In vivo , the EF and FS in the MI/R + GXST group were higher than those in the MI/R group. H&E and Masson staining indicated that mice in the MI/R group exhibited significant myocardial disarray and disordered myofibrils. These pathological changes were significantly reversed following GXST treatment GXST significantly improved cardiac function and reduced infarct size, fibrotic scarring, and levels of autophagy and apoptosis in MI/R mice. The cell counting kit-8 assay demonstrated that GXST (50% effective dose = 88.34 mg/L) protected H9C2 cells from $CoCl_2$-induced injury. Flow cytometric analysis and TUNEL staining revealed that treatment with $CoCl_2$ resulted in a significantly increased the apoptotic rate , which was prevented by GXST treatment. Clv-caspase3 and Bcl-2 are essential for apoptosis during myocardial damage. The activities of Clv-caspase3 were increased by $CoCl_2$ and those of Bcl-2 were decreased by $CoCl_2$, and these effects were significantly reversed by GXST. $CoCl_2$ treatment increased LC3B protein level whereas GXST treatment prevented the formation of LC3B in H9C2 cells .TEM results also onsistents with the western blot results for LC3B, there was an increased formation of autophagosomes and autolysosomes in H9C2 cells after $CoCl_2$ exposure, whereas treatment with GXST dramatically reduced the formation of autophagosomes and autolysosomes in these cells. Furthermore, the association between autophagy and apoptosis was investigated using the autophagy inhibitor, 3-MA. Hypoxia treatment markedly increased H9C2 cell apoptosis compared to the control group, as determined by flow cytometry, western blotting, and TUNEL staining. In the presence of 3-MA, cell apoptosis was reduced compared to that in the hypoxia group, and similar results were observed in the GXST group. The expression levels of LC3B and Clv-caspase3 were significantly reduced by 3-MA treatment compared to those in the hypoxic group. Meanwhile, compared with the $CoCl_2$ + 3-MA group, the $CoCl_2$ + 3-MA + GXST group did not significantly decreased apoptosis, or expression of LC3B.$CoCl_2$ significantly increased AMPK phosphorylation. In contrast, treatment suppressed the activation of AMPK induced by $CoCl_2$. Compound C (an AMPK inhibitor) was used. Cmpared to the $CoCl_2$ group, the Compound C + $CoCl_2$ and Compound C + $CoCl_2$ + GXST groups had lower apoptosis rates. Both Compound C and GXST decreased the expression of Clv-caspase3, LC3B, and the p-AMPK/AMPK ratio under hypoxia Compared to the Compound C + $CoCl_2$ group, the Compound C + GXST + $CoCl_2$ group did not further reduce apoptosis.

Conclusions: GXST plays a cardioprotective role by alleviating hypoxia-induced myocardial apoptosis via AMPK-mediated autophagy. Therefore, GXST administration may be an important treatment strategy for enhancing recovery in patients with MI/R injury.

Prognostic Value of IVUS-modulated Murray-law Quantitative Flow Ratio After Percutaneous Coronary Intervention: Post Hoc Analysis from The FLAVOUR Trial

Wei Yu[1], Jun Jiang[2], Xin-yi Yang[1], Jin-Long Zhang[2], Dai-Xin Ding[3], Zhi-Qing Wang[4], Liu[5], Xiao-Lian Yu[1], Su Zhang[1], Jian-An Wang[2], Bang-Quan Gu[6], Sheng-Xian Tu[1]

1. Biomedical Instrument Institute, School of Biomedical Engineering, Shanghai Jiao Tong University

2. Department of Cardiology, the Second Affiliated Hospital Zhejiang University School of Medicine

3. Department of Cardiology, Renji Hospital, Shanghai Jiao Tong University School of Medicine

4. Department of Cardiology, Huadong Hospital Affiliated to Fudan University

5. Pulse Medical

6. Department of Cardiology, Seoul National University Hospital

Background: Recent studies have highlighted the advantages of using Fractional Flow Reserve (FFR) and Intravascular Ultrasound (IVUS) in PCI. However, the adoption of comprehensive physiological assessment and intracoronary imaging remains limited worldwide, primarily due to reimbursement restrictions in many countries. We developed an intravascular ultrasound (IVUS)-based FFR computation method, known as UFR, to enables simultaneous physiological and morphological assessments using a single catheter. The feasibility and accuracy of intravascular imaging-based methods can be restricted when pullback does not fully cover the lesion, especially in vessels with diffuse lesions. To address this issue, we developed a novel method integrating coronary angiogram and intravascular ultrasound (IVUS) to compute FFR. The objective of this study is to evaluate the prognostic value of the IVUS-modulated Murray-law quantitative flow ratio (IVUS-μFR).

Methods: Post-PCI IVUS-μFR was performed on the IVUS-guided group from the FLAVOUR trial (Fractional FLow Reserve And IVUS for Clinical OUtcomes in Patients With InteRmediate Stenosis; NCT02673424). The primary endpoint was three-year target vessel failure (TVF), defined as a composite of cardiac death, target vessel myocardial infarction, and target vessel revascularization (TVR). The μFR analysis were performed following standard procedure. This included steps such as angiographic projection selection, lumen contours and side branch delineation, reference vessel reconstruction based on the Murray bifurcation fractal law, hyperemic flow velocity (HPV) estimation using the TIMI frame count, and the fast calculation of pressure drop along the interrogated vessel using a simplified fluid dynamic equation. Following the μFR analysis, the final IVUS image was imported. Automatic delineation of lumen contours, external elastic lamina (EEL) contours, and side branch ostia was performed on the IVUS image. Then, the IVUS pullback was co-registered with the angiogram using an automatic registration algorithm. The final geometric lumen model was reconstructed using the IVUS-interrogated segment and the remaining proximal and distal segments from the angiogram. Based on this geometric lumen model and EEL geometric model, a new reference vessel was generated. Finally, pressure drop was calculated based on the simplified fluid dynamics equations using angiography-derived HFV. In the end, IVUS-μFR was available for both the interrogated vessel and its side branches.

Results: Post-PCI IVUS-μFR was successfully analyzed in 448 vessels from 430 patients. The feasibility of IVUS-μFR in this study was 85.0%. If vessels with missing image data were not considered, the feasibility increased to 93.7%. A post-PCI IVUS-μFR of ≤ 0.85 was associated with a significantly higher risk of three-year TVF (16.3% vs. 3.3%, P=0.0001; HR: 5.29 [95% CI, 2.11-13.25], P<0.001; C-index: 0.84 [0.72-0.96]), demonstrating superior predictive capability compared to other predictors including angiography-derived μFR (HR: 4.32 [95% CI, 1.80-10.38], P=0.001; C-index: 0.81 [0.68-0.95]) and IVUS-derived minimum stent area (HR: 2.74 [95% CI, 1.09-6.87], P=0.031; C-index: 0.73 [0.65-0.91]). After adjusting for potential confounding factors, this factor was linked to a 5-fold increase in risk for TVF (adjusted HR: 5.71 [1.98-16.43], P=0.001). Furthermore, IVUS-μFR drop out of the stented segment was significantly associated with non-TLR (HR, 9.45[2.44, 36.58], P=0.001), and this association was directionally consistent for μFR (HR, 6.05[1.71, 21.44], P=0.005). There was a mild trend for IVUS-μFR drop across the stented segment to predict TLR (HR, 4.30[0.50,36.84], P=0.183), while the trend was weak for μFR (HR, 2.20[0.26,18.86], P=0.471).

Conclusions: The feasibility of this method did not decrease when powered by automatic image processing algorithms. Post-PCI IVUS-μFR ≤ 0.85 was identified as an independent predictor of three-year TVF, associated with a 5-fold increase in the risk. This method added incremental value compared to μFR or IVUS-derived anatomic evaluations.

急性冠状动脉综合征合并支架内再狭窄患者中新生动脉粥样硬化的临床危险因素分析

陈嘉雯 高圣恩 董福红 黄东旭 崔丽娜 马显钦 赵嘉伟 陈昱竹 赵锐 徐艺硕 果怡博 李路路 王旖旎 代建南 房超 于波

哈尔滨医科大学附属第二医院

目的：冠状动脉支架内再狭窄（ISR）是经皮冠状动脉介入治疗术后的常见中远期并发症。其中，支架内新生动脉粥样硬化（NA）被认为是 ISR 的关键发病机制之一，且与事件复发及不良预后密切相关。本研究旨在探讨急性冠状动脉综合征（ACS）合并 ISR 的患者中，在罪犯病变经光学相干断层扫描（OCT）确诊为 NA 的患者，其临床特征、实验室指标及影像学表现是否存在差异，并识别其可能的独立危险因素。

方法：本研究为单中心回顾性分析，纳入 2017 年 1 月至 2021 年 12 月在哈尔滨医科大学附属第二医院住院，且接受 OCT 检查明确诊断为 ISR 的 ACS 患者。根据 OCT 是否显示 NA 特征，将患者分为 NA 组与非 NA 组。比较两组间的临床资料、实验室检测结果及冠状动脉造影指标。

结果：共纳入 273 例患者，其中 151 例（55.3%）经 OCT 确诊为 NA。与非 NA 组相比，NA 组患者支架植入时间更长（P<0.05），女性比例显著增加（27.2% vs. 13.9%，P=0.006），高脂血症患病率更高（38.4% vs. 26.2%，

P=0.033）。在实验室检测方面，NA 组的 C 反应蛋白（CRP）、低密度脂蛋白胆固醇（LDL-C）及肌钙蛋白水平显著升高（均 P<0.05）。冠状动脉造影结果显示，NA 组病变更常见于血管近段（64.3% vs. 52.3%，P=0.04），但在狭窄程度和最小管腔面积等定量参数上，两组间无统计学差异。多变量 logistic 回归分析结果显示，女性（OR = 3.21, 95% CI: 1.04–9.90, P = 0.043）、支架植入年限（OR = 1.21, 95% CI: 1.07–1.38, P = 0.003）及 LDL-C 水平（OR = 3.28, 95% CI: 1.53–7.04, P = 0.002）为 NA 的独立危险因素。

结论：在 ACS 合并 ISR 患者中，NA 发生率较高。性别（女性）、支架植入年限及 LDL-C 升高是其独立危险因素。上述因素可作为 NA 风险评估的重要参考，有助于临床早期识别高危人群，并为精准化管理提供依据。

Predictors for Anti-Thrombotic Therapy Prognosis of Plaque Erosion: Results from OCT-Based Fluid-Structure Interaction Models

Zhao Chen[1,2], Yan-Wen Zhu[3], Yi-Shuo Xu[1,2], Liang Wang[3], Di-Rui Zhang[1,2], Ming Zeng[1,2], Da-Lin Tang[4], Hai-Bo Jia[1,2], Bo Yu[1,2]

1. Department of Cardiology, The Second Affiliated Hospital of Harbin Medical University

2. The Key Laboratory of Myocardial Ischemia, Chinese Ministry of Education

3. School of Biological Science and Medical Engineering, Southeast University

4. Mathematical Sciences Department, Worcester Polytechnic Institute, Worcester

BACKGROUND: Acute coronary syndrome (ACS) is one kind of common and serious cardiovascular disease, with major underlying mechanisms including plaque rupture and plaque erosion. Autopsy and intravascular optical coherence tomography (OCT) studies revealed that ~30% to 40% of ACS cases were caused by plaque erosion. With the implementation of intense lipid-lowering therapy, the incidence of plaque erosion may be on the rise in coronary artery thrombosis leading to ACS. OCT has a high resolution (10 ~ 20 μm), allowing it to identify plaque erosion and rupture in vivo. Several studies indicated that plaque erosion usually has intact fibrous caps, large lumen diameters, and white thrombus with rich platelets, different from plaque rupture. These characteristics suggest that conservative anti-thrombotic therapy may be effective for ACS patients with plaque erosion. Prati et al. compared ACS patients with plaque erosion treated with conservative anti-thrombotic therapy and stenting. The findings revealed that both groups remained asymptomatic at the two-year follow-up, indicating that conservative anti-thrombotic therapy was as efficacious as stenting.

The EROSION series studies were conducted using baseline and follow-up data (one month, one year and four years, respectively) to assess the safety and feasibility of avoiding stenting in erosion-related ACS culprit lesions. Most patients exhibited favorable clinical outcomes during the follow-up period, however, patients inexplicably underwent elective target lesion revascularisation (TLR) in long-term follow-up, despite all patients adhering to effective secondary prevention strategies post-discharge. The inadequate resolution of thrombus at one month may be a contributing factor, but this does not provide timely or precise guidance for selecting therapeutic strategies for patients with plaque erosion. With the acceptance of conservative antithrombotic therapy for patients with plaque erosion, Clinicians, patients and researchers are confronted with two critical questions: 1) Which patients with plaque erosion would benefit more from conservative treatment? 2) what risk factors and predictive methods could be employed to anticipate treatment outcomes?

Plaque structural stress (PSS) refers to the stress present within an atherosclerotic plaque due to vessel expansion and stretching caused by arterial pressure. Flow shear stress (FSS) is the parallel frictional force applied by blood flow on the endothelial surface of the arterial wall. Previous research has demonstrated that plaque regions experiencing high PSS correlate with compositional alterations indicative of increased plaque vulnerability, whereas areas with low FSS are associated with more incredible plaque growth in progressing regions. However, no study has reported varying values of PSS and FSS in relationship to the progression of no-stented in ACS patients with plaque erosion. Consequently, the patient-specific three-dimensional (3D) models with flow-structure interactions (FSI) were constructed to obtain biomechanical risk factor values for comparison and analysis. A logistic regression model was employed to identify optimal predictors for outcomes of conservative antithrombotic therapy and to obtain prediction accuracies.

METHODS: 10 patients (9 male and 1 female) with ST-segment elevation myocardial infarction due to plaque erosion who met the inclusion criteria of the EROSION study were selected for this research. The inclusion criteria of the EROSION study were briefly summarized as follows: (1) ACS patients aged 18 to 75 years; (2) Culprit lesion located in a native coronary artery; (3) TIMI flow grade 3 with diameter stenosis < 70% on angiography; (4) Definite erosion defined by OCT; (5) Patient was stable without symptoms. All patients included in these studies were initially managed with a conservative strategy without stenting, and sequential angiography and OCT imaging were performed at 1 month and 1 year. All the patients underwent standardized secondary prevention after discharge. At 1 year follow-up, 5 patients (TLR group) underwent elective TLR with stent implantation, while the other 5 (non-TLR group) remained free from revascularisation.

RESULTS: Our findings revealed that the combination of maximum flow shear stress (FSS), maximum lipid percentage, and thrombus burden provided the highest predictive capability, with a mean area under the curve (AUC) of 0.96 [90% confidence interval = (0.85, 1.00)]. Maximum FSS emerged as the most significant single predictor, with a mean AUC of 0.70 [90% confidence interval = (0.20, 1.00)]. The mean maximum FSS in the TLR group was 98.0% higher than that in the non-TLR group (P = 0.076), suggesting its crucial role in the outcomes of conservative anti-thrombotic therapy.

CONCLUSIONS: This study indicated that integrating morphological and biomechanical risk factors could effectively predict the long-term risk of TLR in patients with plaque erosion following conservative anti-thrombotic therapy, warranting further investigation in larger cohorts.

慢性完全闭塞病变主要供血血管定量血流分数对患者远期预后的影响

李新健 徐昕晔 王贵松

北京大学第三医院

目的：目前，对于冠状动脉慢性完全闭塞病变（coronary chronic total occlusion，CTO）病变患者供血血管功能学状态与预后相关性的研究较为有限。定量血流分数（quantitative flow ratio，QFR）是一种新型的功能学评估技术，无需压力导丝或血管扩张剂，基于 Murray 定律的 QFR（Murray law-based QFR，μQFR）仅通过单幅冠状动脉造影序列即可完成功能学评估，为回顾性评估 CTO 病变供血血管的功能学状态提供了可行性。本研究旨在探讨 CTO 病变主要供血血管 μQFR 对患者远期预后的影响。

方法：本研究纳入 2015 年 1 月至 2023 年 6 月期间，在北京大学第三医院通过冠状动脉造影证实为单支血管 CTO 病变的住院患者，收集临床特征、化验检查等基线资料，采用第三代定量血流分数检测仪（AngioPlus Core，上海博动医疗科技股份有限公司）测定主要供血血管 μQFR，以 μQFR ≤ 0.80 为诊断界值对主要供血血管进行功能学评价。通过电子病历系统或电话随访的方式随访入组患者的 MACE 事件，包括全因死亡、非致死性心肌梗死、非计划再次血运重建以及因不稳定心绞痛再入院。采用多因素 Cox 回归模型探讨 μQFR 与 MACE 发生风险之间的关系，并通过亚组分析、倾向性评分加权等方法进行敏感性分析，评估结果的稳健性。

结果：符合入选标准的 307 例 CTO 病变患者均完成 1 年以上临床随访，37 例患者在 1 年随访时发生了 MACE 事件。其中，μQFR>0.80 组中 MACE 发生率为 9.9%，显著低于 μQFR ≤ 0.80 组的 MACE 发生率，两组间差异具有统计学意义（P=0.005）。多因素回归分析表明，与 μQFR>0.80 组患者相比，μQFR ≤ 0.80 组患者在 1 年内发生 MACE 的风险增加了 3.15 倍（HR: 3.15，95%CI: 1.52-6.51，P<0.05）。μQFR 每降低 0.10，1 年内发生 MACE 的风险增加 45%（HR：1.45，95%CI：1.14-1.84，P<0.05）。亚组分析及倾向性评分加权等敏感性分析结果均表现出良好的稳健性。

结论：CTO 病变患者主要供血血管的 μQFR 值降低与 1 年内 MACE 发生风险增加显著相关。μQFR ≤ 0.80 的患者在 1 年内发生 MACE 的风险是 μQFR>0.80 患者的 3.15 倍，主要供血血管的功能性缺血是预测 MACE 发生的重要指标。

TET2 Mutations and Coronary Plaque Characteristics Assessed by Optical Coherence Tomography in Patients with ST-Elevation Myocardial Infarction

qianhui sun, Hai-Bo Jia, Bo Yu

The 2nd Affiliated Hospital of Harbin Medical University

Background:

Clonal hematopoiesis of indeterminate potential (CHIP), characterized by the expansion of hematopoietic stem or progenitor cells carrying somatic driver mutations without overt hematological malignancy, is increasingly recognized as a novel, non-traditional cardiovascular risk factor. Distinct from conventional risk factors such as hypertension, diabetes, and dyslipidemia, CHIP independently exacerbates cardiovascular morbidity and mortality, with accumulating evidence linking it to accelerated atherosclerosis, myocardial infarction, and adverse post-infarction outcomes. Among the most prevalent CHIP-associated driver genes, Ten-eleven translocase 2 (TET2) plays a pivotal role, as its mutations disrupt DNA demethylation processes and promote pro-inflammatory phenotypes in myeloid cells—mechanisms thought to fuel vascular inflammation and plaque instability. Optical coherence tomography (OCT) can precisely describe the phenotypes of atherosclerotic plaques. This study aimed to evaluate the impact of TET2 mutations on coronary plaque characteristics in patients with ST-elevation myocardial infarction (STEMI) using OCT and explore its prognostic significance.

Methods:

This was a single-center retrospective study. STEMI patients who underwent OCT scanning of culprit plaques and had blood samples retained from May 2017 to May 2019 in the Second Affiliated Hospital of Harbin Medical University was included. Targeted deep sequencing of peripheral blood was performed to detect TET2 mutations (variant allele frequency(VAF) ≥ 2%). Patients were divided into the TET2 mutation group and

the non-mutation group. The OCT characteristics of culprit and non-culprit plaques in both groups were analyzed, and patients were followed up for a median of 2.4 years (IQR 2.0-3.0) to record major adverse cardiovascular events (MACE), including all-cause death, non-fatal myocardial infarction, non-fatal stroke, and ischemia-driven revascularization.

Results:

Among 628 STEMI patients, 25 (4.0%) carried TET2 mutations. Patients with TET2 mutations were older, while the two groups showed comparable prevalence rates of hypertension, diabetes mellitus, and dyslipidemia. And the variant allele frequency (VAF) increases with age. OCT findings showed that compared with the non-mutation group, the culprit plaques in the TET2 mutation group were more vulnerable, with a smaller minimal lumen area [1.5 (1.2-1.9) vs. 1.8 (1.4-2.4) mm^2, P=0.062], a higher macrophage proportion (96.0% vs. 85.1%, P=0.128), a thinner fibrous cap [40.0 (40.0-60.0) vs. 60.0 (40.0-80.0) μm, P=0.005], a larger maximal lipid arc [360 (270.0-360.0) vs. 281.6 (220.9-360.0) , P=0.006], and a higher proportion of plaques with a fibrous cap thickness ≤ 65μm (68.0% vs. 43.1%, P=0.014). Furthermore, lipid components in plaques increased with the elevation of mutation VAF. Non-culprit plaques in TET2 carriers showed trends toward more lipid-rich features, though not statistically significant. In terms of prognosis, the MACE rate in the TET2 mutation group was significantly higher than that in the non-mutation group (54.3% vs. 21.0%, P<0.001), with an adjusted hazard ratio of 3.57 (95%CI 1.78-7.17, P<0.001). Subgroup analysis showed that TET2 mutations significantly increased the MACE risk in patients with plaque rupture (P<0.001), but there was no such difference in patients with plaque erosion (P=0.499).

Conclusions:

In our study, in STEMI patients, TET2 mutations are associated with more vulnerable coronary plaques and are an independent predictor of poor prognosis, especially in patients with plaque rupture, suggesting that TET2 mutations may serve as a biomarker for risk stratification in STEMI.

Impact of Intravascular Imaging-Guided Drug-Eluting Stent Implantation on Cardiac Mortality in Patients with Diabetes and Coronary Artery Disease: A Multicenter Cohort Study

Xiaofei Gao[1], Jing-Yu Zhao[1], Jun-Jie Zhang[1], Shao-Liang Chen[1]

1. Nanjing First Hospital

2. The First People's Hospital of Taicang

3. Changshu No.1 People's Hospital

4. The First People's Hospital of Zhangjiagang

Abstract

Objectives: This study aimed to evaluate the impact of intravascular imaging (IVI) guidance versus angiography guidance for drug-eluting stent (DES) implantation on cardiac mortality in patients with diabetes mellitus (DM) and coronary artery disease (CAD).

Methods: We analyzed 11,530 patients with DM and CAD who underwent coronary DES implantation in a multicenter network from January 2014 to December 2023. Patients were stratified by intraoperative imaging modality into an IVI-guided group (n = 2,425) and an angiography-guided group (n = 9,105). To minimize confounding, propensity score matching (PSM) was performed at a 1:1 ratio, yielding 2,409 matched pairs with well-balanced baseline clinical and angiographic characteristics. The primary endpoint was cardiac death within 1 year. The secondary endpoint was major adverse cardiovascular events (MACE), defined as a composite of cardiac death, target vessel myocardial infarction (TVMI), and clinically driven target vessel revascularization (TVR). Kaplan-Meier analysis with the log-rank test compared cumulative incidence between groups. Cox regression was used to estimate hazard ratios (HRs) and 95% confidence intervals (CIs). A Fine-Gray model was applied to account for competing risks when appropriate. The Win Ratio method, applied according to a pre-specified hierarchical order, was also used. Sensitivity analyses with inverse probability of treatment weighting (IPTW) confirmed the robustness of the findings.

Results: After PSM, baseline clinical and angiographic characteristics were well balanced between the IVI and angiography groups (all P > 0.05). Procedurally, the IVI-guided group had a significantly greater number of implanted stents, longer total stent length, larger mean stent diameter, and larger post-dilation balloon diameter (all P < 0.05). During the 1-year follow-up, the IVI-guided group had a significantly lower risk of cardiac death than the angiography group (2.5% vs. 4.3%; HR = 0.585; 95% CI, 0.427-0.803; P < 0.001), which was confirmed by Fine-Gray competing risk analysis. This finding was further supported by Win Ratio analysis (WR = 1.730; 95% CI, 1.271-2.356; P < 0.001). The MACE was also less frequent in the IVI group (7.2% vs. 11.5%; HR = 0.613; 95% CI, 0.508-0.741; P < 0.001), with Win Ratio analysis showing similar benefit (WR = 1.633; 95% CI, 1.355-1.970; P < 0.001). Sensitivity analyses using IPTW yielded consistent, statistically significant findings, supporting the robustness of these results.

Conclusions: In patients with CAD and DM undergoing DES implantation, IVI-guided stent placement significantly reduced the risk of cardiac death at 1 year compared with angiography guidance.

基线 QFR 在单支冠脉临界病变患者中的预后分层价值

禄彦锋 ABDULRAHMAN ALQAZZAZ 黄欣 冯家豪 张勇 郜珊珊 宋强 宁菲菲 郭宁

西安交通大学医学院第一附属医院

目的：探讨基线定量血流分数（QFR）及其三分组模型（低 QFR 组、灰区组、高 QFR 组）在单支冠脉临界病变患者中的预后评估作用，分析其对临床结局的预测能力。

方法：本研究为单中心回顾性队列研究。研究连续性纳入 2023 年 5 月至 6 月于西安交通大学第一附属医院接受冠状动脉造影存在单支临界病变（目测直径狭窄率 40–80%），且病变经回顾性测定 QFR 值介于 0.70 至 0.90 之间的冠心病患者 478 例。按照靶血管 QFR 测定值，分为低 QFR 组（0.70–0.74）、灰区 QFR 组（0.75–0.85）、高 QFR 组（0.86–0.90）。主要研究终点为主要心脏不良事件（MACE），定义为心源性死亡、心肌梗死、缺血驱动的血运重建组成的复合终点；关键次要终点为靶血管失败（TVF），定义为心源性死亡、靶血管心肌梗死、靶血管缺血驱动的血运重建组成的复合终点；中位随访时间 18 个月。通过 Kaplan–Meier 生存分析比较各组间临床结局的差异，并使用 Cox 比例风险模型确认危险因素。

结果：在中位 18 个月的随访期间，低 QFR 组、灰区组、高 QFR 组 MACE 累积发生率分别为 13.5%、6.6%、3.4%（Log-rank P=0.008），主要归因于心肌梗死（3.2% vs. 1.4% vs. 0.0%, Log-rank P=0.029）和缺血驱动的血运重建（11.5% vs. 6.1% vs. 2.3%, Log-rank P=0.004）的差异。此外，尽管三组间 TVF 累积发生率无显著性差异（8.6% vs. 3.7% vs. 2.2%, Log-rank P=0.051），但靶血管缺血驱动的血运重建风险存在差异（6.7% vs. 3.3% vs. 1.1%, Log-rank P=0.027）。限制性立方样条（RCS）分析显示 QFR 值与 MACE 风险线性负相关；单因素 Cox 回归显示 QFR 每增加 0.10，MACE 相对风险降低 52.8%（P=0.012）；多因素 Cox 模型调整 eGFR 分组、SYNTAX 风险、治疗方式（药物治疗、PCI）后，证实 QFR 分组的独立预测价值（调整后 HR=1.858, 95% CI 1.038–3.326, P=0.037）。

结论：基线 QFR 及基于其值域划分的三分组模型与单支临界病变冠心病患者临床预后显著相关，是评估缺血风险及预测心脏不良临床结局的有效工具。

Optical coherence tomography-guided drug coatedballoon in non-small de novo coronary arterylesions: a prospective clinical research

li longbo, Bin Liu

吉林大学第二医院

Purpose: The combined use of drug coated balloon (DCB) and optical coherence tomography (OCT) for the treatment of non-small coronary de novo lesion remains to be evaluated. We investigated the safety and efficacy of OCT-guided DCB in non-small coronary de novo lesion patients with predilation of cutting balloon.

Introduction: Drug-coated balloons were first introduced for the treatment of instent restenosis and are recommended (European Society of Cardiology[ESC] guidelines class IA recommendation) for instent restenosis following treatment with both baremetal and drugeluting stents . The safety and efficacy of drug coated balloon (DCB) in de novo lesions such as small vessel disease and bifurcation lesion has been demonstrated . Recently, a REVELATION randomized trial has confirmed that DCB strategy was noninferior to drug-eluting stent (DES) in primary percutaneous coronary intervention for ST-segment elevation myocardial infarction 9 months later . But there are few studies on the feasibility of DCB in non-small de novo coronary artery disease. The primary concerns about the use of DCB in non-small de novo coronary artery disease are insufficient predilation of the lesion and dissection-associated acute occlusion. Cutting balloon, on the other hand, can mitigate the damage to the vascular wall, reduce postoperative elastic recoil and improve the success rate of predilation .

Methods: This study was a prospective, and open-label study. We enrolled patients with non-small de novo lesions treated with OCT-guided DCB. The non-small de novo lesions indicated vessel lesions with a diameter ≥ 2.5 mm. The primary endpoints were the success rate of the procedure and the occurrence of target lesion revascularization. The secondary endpoints were myocardial infarction, cardiac death, and major adverse cardiac events (MACE) within 3 months after the procedure.

Statistical analysis:

Continuous variables are described as mean ± standard deviation, and discrete variables are expressed as frequencies and percentages. SPSS version 19.0 (IBM, Munich, Germany) was used for statistical analyses. The Student's t-test was used for the comparison analysis. A p-value < 0.05 was considered statistically significant.

All data were analyzed by SPSS23.0 statistical software. Count data were represented by n (%), and comparison was performed by X2 test; measurement data were represented by (x±s), and comparison between groups was conducted using independent sample t test; A P-value of < 0.05 was accepted as statistically significant; Kaplan-Meier was used to map the survival curve.

Results: At the Second Hospital of Jilin University, we enrolled 54 patients (54 lesions) with non-small de novo lesions who were treated with OCT-guided DCB from October 2018 to June 2019. A total of 52 patients were successfully treated with DCB-only strategy, while 2 patients turned to bailout stenting. A total of 21 patients had undergone angiography 3 months after the procedure with the late lumen loss of 0.24±0.57 mm. There was no statistically significant difference in minimal lumen diameter (MLD) between post-DCB and at 3-month angiographic follow-up (2.25±0.40 mm vs 2.04±0.54 mm; P = 0.110). Only 1 patient developed restenosis with the incidence of MACE rate of only 1.92% (n = 1). There was no significant difference in the stenosis of the lumen diameter of the target lesion vessel between 3 months after operation and immediately after operation.

Conclusions: Our study showed that OCT-guided DCB with cutting balloon under guidance may be a novel approach in non-small de novo coronary artery disease.

Non-Invasive and Invasive Physiological Indices in the Clinical Assessment of Coronary Heart Disease Patients and Comparison with Angiography-Guided PCI: A Network Meta-Analysis Based on Randomized Controlled Trials

ZiYu Zhao, Ce Wang, Cheng-Jie Ma, Yue Sun

The First Affiliated Hospital of Naval Medical University（Shanghai Changhai Hospital）

Introduction: Coronary artery disease (CAD) is a leading cause of global mortality and significantly impacts patient prognosis. Percutaneous coronary intervention (PCI) is a core therapeutic strategy, and the choice of guidance modality is paramount to its success. Traditionally, anatomy-based coronary angiography (CA) has been the decision-making gold standard, yet it cannot assess whether a stenosis causes myocardial ischemia. In recent years, a variety of functional physiologic assessment techniques have emerged, including the invasive methods of Fractional Flow Reserve (FFR) and Instantaneous Wave-free Ratio (iFR), as well as non-invasive or imaging-based methods like Quantitative Flow Ratio (QFR) and CT-derived FFR (CT-FFR). Although some studies have provided head-to-head comparisons of a few techniques, a comprehensive synthesis of evidence that includes all six leading invasive and non-invasive strategies is currently lacking. This study aimed to, for the first time, systematically evaluate and rank the impact of these six strategies on clinical outcomes in CAD patients via a network meta-analysis (NMA). Furthermore, it sought to compare the relative merits of three major categories—traditional anatomical, invasive physiological, and non-invasive physiological guidance—to provide the highest level of evidence for clinical practice.

Methods: This study adhered to the PRISMA-NMA statement, and its protocol was registered with PROSPERO (CRD42024590375). We conducted a systematic search of PubMed, EMBASE, and the CENTRAL database for randomized controlled trials (RCTs) published between 2005 and 2024. Inclusion criteria were: (1) study population of adult CAD patients undergoing PCI; (2) comparison of at least two of the following guidance strategies: CA, CCTA, FFR, iFR, QFR, or CT-FFR. The primary endpoint was Major Adverse Cardiovascular Events (MACE), defined as a composite of cardiovascular death, myocardial infarction, and repeat revascularization. We performed a frequentist network meta-analysis using a random-effects model to calculate Hazard Ratios (HRs) and their 95% Confidence Intervals (CIs). Network consistency was assessed using the node-splitting method, and the efficacy of interventions was ranked probabilistically using P-scores. All statistical analyses were performed using R software.

Results: A total of 17 RCTs, comprising 24,832 patients, were included. The mean patient age was 63.4 years, with 64.3% presenting with Acute Coronary Syndromes (ACS). All included studies were judged to have a low risk of bias, providing a high-quality evidence base for the analysis. The evidence network model demonstrated good consistency (P > 0.05). Compared to CA guidance, an FFR-guided strategy significantly reduced the risk of MACE by 32% (HR=0.68, P=0.05), with a number needed to treat (NNT) of 19 to prevent one MACE event. The benefit with a QFR-guided strategy was even more pronounced, with a 47% reduction in MACE risk (HR=0.53, P=0.03). While there was no significant difference between iFR and FFR in terms of MACE risk, this analysis identified a critical safety signal: compared to the FFR group, the iFR-guided group had a 101% increased risk of cardiovascular death (HR=2.01, P=0.002). Furthermore, compared to FFR, the QFR-guided group showed an 84% increased risk of myocardial infarction (HR=1.84, P=0.03). In the non-invasive domain, adding CT-FFR analysis to CCTA significantly reduced the need for unnecessary invasive angiography by 58% (P<0.001) and also lowered the risk of myocardial infarction. The P-score ranking clearly established a hierarchy of superiority. FFR (P-score=0.83) ranked first, confirming its status as the optimal strategy. QFR (0.75) followed closely, demonstrating strong potential. CT-FFR (0.62) and iFR (0.58) also outperformed traditional methods. CA (0.50) and CCTA (0.35) ranked last. The benefits of physiologic guidance were particularly prominent in patients with ACS and those with multi-vessel disease. In the diabetic subgroup, QFR showed a potential for additional clinical benefit over FFR.

Conclusion: This comprehensive and rigorous network meta-analysis establishes a contemporary, evidence-based hierarchy for PCI guidance strategies. The findings unequivocally demonstrate that PCI guidance based on physiological function is, as a whole, significantly superior to strategies that rely solely on traditional anatomical assessment for improving patient outcomes. FFR, with its wealth of evidence and robust clinical benefit, is reaffirmed as the "core gold standard" for guiding revascularization decisions. However, this study also highlights a potential safety risk associated with iFR (increased cardiovascular mortality), urging cautious interpretation and application. Particularly encouraging is the performance of non-invasive techniques like QFR, which demonstrated a potential for benefit comparable, or in some aspects (MACE reduction) superior, to the invasive gold standard. This positions QFR as a key technology for the future of precision cardiology, although its performance on specific endpoints (myocardial infarction) warrants further investigation. Therefore, we strongly recommend the routine application of invasive physiological assessment (preferably FFR) for decision-making in intermediate lesions. Concurrently, the clinical application of non-invasive techniques like QFR should be actively explored and validated, with the goal of providing safer, more precise, and more convenient individualized treatment plans for patients.

基于冠脉造影衍生的微循环指数与急性 ST 段抬高型心肌梗死患者预后的相关性分析

罗永百 钱荣凯

西安交通大学第一附属医院

目的：

1. 探讨基于造影的微循环阻力指数（AMR）与接受直接经皮冠状动脉介入治疗（PPCI）治疗后的急性 ST 段抬高型心肌梗死（STEMI）患者的预后的相关性，并评估其诊断效能；

2. 探讨 AMR 与常用临床指标及实验室检查的相关性。

方法：

本研究为一项回顾性观察性研究，选取 2020 - 2023 年间于西安交通大学第一附属医院行 PPCI 手术的 STEMI 患者，依据严格的纳入和排除标准，最终纳入 871 名患者进行分析。研究结局定义为主要心血管不良事件（MACE）的复合终点，通过相关性分析分析 AMR 与 MACE 发生的关系，并使用工作特征曲线分析 AMR 用于诊断的最佳截断值及诊断效能，进一步通过生存分析及 Cox 回归计算风险比。最后，分析 AMR 与其他临床常用指标的相关性，并通过 logistic 回归分析影响 AMR 的独立危险因素。

结果：

最终纳入 871 名患者，随访期间 139 名患者发生 MACE。根据 1 年内是否发生 MACE 将患者分为两组，发生 MACE 组的患者的 AMR 水平显著升高（3.28 mmHg·s/cm vs. 2.50 mmHg·s/cm; P <0.001），相关性分析提示 AMR 与 MACE 存在中等程度的正相关（r = 0.417; P <0.001）。工作特征曲线提示 AMR 的最佳诊断界值为 3.00 mmHg·s/cm，工作特征曲线下面积为 0.829（95% CI: 0.787 - 0.871; P <0.001），灵敏度为 74.1%，特异度为 89.2%。以该界值将患者分组后进行生存分析并行 Cox 回归分析，将单因素 Cox 回归有统计学意义的危险因素纳入多因素 Cox 回归，分析提示 AMR 是 STEMI 患者 PPCI 术后发生 MACE 的独立的危险因素（HR 2.04; 95% CI: 1.29 - 3.25; P = 0.002）。根据 AMR 将患者分组后，进行 logistic 分析后得到影响 AMR 的独立相关的危险因素为白细胞（OR 1.10; 95% CI: 1.04 - 1.16; P = 0.001）以及左室射血分数（OR 0.95; 95% CI: 0.93 - 0.98; P = 0.006）。进一步对不同 AMR 水平组间系统性免疫炎症指数水平进行分析，同样存在显著差异（1740.60 [995.93, 2547.48] vs. 1273.51 [751.80, 1993.37], P <0.001）。

结论：

本研究证实了 AMR 与 STEMI 患者术后预后的相关性，提出了新的 AMR 诊断界值并验证了其有效性。

A higher level of sST2 predicts the hospital mortality of patients with infective endocarditis: A 10-year retrospective study in China

Yu-Xuan Lou, Yang Yang

The First Affiliated Hospital with Nanjing Medical University

Aim: To explore the prognostic value of soluble growth stimulating gene 2 protein (sST2) in patients with infective endocarditis in China and the trend of disease spectrum.

Methods: We assessed the records of all patients diagnosed with infective endocarditis (IE) who underwent surgery at the First Affiliated Hospital of Nanjing Medical University from 2013 to 2022. Patients were divided into a low-risk group (sST2 < 35 ng/mL) and a high-risk group (sST2 ≥ 35 ng/mL) according to sST2 level.

Results: Overall, we assessed 384 IE patients. Among 210 patients in the low-risk group, 154 (73.33%) were male and 56 (26.67%) were female, and the average age of patients was 45.75±14.08. Among 174 patients in the high-risk group, 119 (68.39%) were male and 55 (31.61%) were female, and the average age of patients was 48.30±15.38. A total of 24 patients (6.25%) died after surgery.There was no significant difference in the history of hypertension, diabetes, stroke, pulmonary hypertension,

spleen infarction, arrhythmia, pulmonary infection or peripheral arteriovenous embolism between the two groups. According to NYHA(New York Heart Association) class, 21 (10.00%) patients in the low-risk group had Class III-IV cardiac complications at admission, less than 34 (19.54%) patients in the high-risk group (P<0.001). In addition, there were significant differences in multiple organ dysfunction syndrome (MODS), NT-proBNP levels, the hospital stay, the hospital stay in the ICU and proportion of hospitalized deaths between the two groups of patients .The results of ROC curve analysis suggested that sST2 had good predictive value for the prognosis of IE patients (AUC=0.772, 95% CI, 0.686~0.859, P<0.001), the sensitivity was 0.917, and the specificity was 0.647 .Univariate logistic regression analysis showed that septicemia, severe heart failure, MODS and sST2 (P<0.001) were risk factors for IE. After adjusting for the above variables, multivariate logistic regression analysis still showed that sST2 (OR (95% CI) =0.958~0.996, P=0.019), septicemia (OR (95% CI) = 0.044~0.679, P=0.012), NYHA III/IV (OR (95%CI)=3.784~37.743, P<0.001) and MODS (OR(95%CI) =2.692~36.960, P=0.001) were independent death factors for IE.To further evaluate the change trend of the disease spectrum of IE patients, we divided 384 patients from 2013 to 2022 into Group A (164 patients from 2013 to 2017) and Group B (220 patients from 2018 to 2022). A total of 156 patients (95.12%) in Group A had native valve endocarditis (NV-IE), 6 patients (3.66%) had prosthetic valves, and 2 patients (1.22%) had pacemaker-related endocarditis. In group B, 204 patients (92.72%) had NV-IE, 8 patients (3.64%) had prosthetic valves, and 8 patients (3.64%) had pacemaker-related endocarditis. During 2013-2017, 32 (19.51%) patients had congenital heart disease, which was the main cause of congenital valve endocarditis, followed by rheumatic heart disease, with a total of 24 patients (14.63%), 16 patients with degenerative diseases (9.76%), and 70 patients without potential heart disease (42.68%), while 36 (16.36%) patients had congenital heart disease and 10 patients with rheumatic heart disease (4.55%) in 2018-2021. There were 36 patients with degenerative diseases (16.36%) and 94 patients without potential heart disease (42.73%). The proportion of patients with degenerative heart disease increased, while the proportion of patients with congenital and rheumatic heart disease decreased Echocardiography and intraoperative evaluation showed that the aortic valve was the most commonly affected site in IE, followed by the mitral valve. From 2013 to 2017, aortic valve and mitral valve lesions were 64 (39.02%) (56; 34.15%), respectively. From 2018 to 2022, aortic valve (100; 45.45%) and mitral valve (64; 29.09%) lesions were the most common, and the proportion of mitral valve lesions decreased significantly . We used the one-way ANOVA test to compare the sST2 levels of patients with different surgical methods, and the sST2 level of patients who underwent open ventricular septal defect repair (69.93±19.67ng/mL) was significantly higher than that of other surgical methods.

Blood culture tests showed that 100 people (60.98%) had pathogenic bacterial infections during 2013-2017, mainly caused by Streptococcus (50; 30.49%), Staphylococcus (24; 14.63%) and Corynebacterium (8; 4.88%). Mixed infection was observed in 8 patients (4.88%). During 2013-2017, 132 people (60.00%) had pathogenic bacterial infections, mainly caused by Streptococcus (62;28.18%), Staphylococcus (38;17.28%) and Enterococcus (8;3.64%). Mixed infection was observed in 8 patients (3.64%).

Conclusion:Higher levels of sST2 are independently associated with hospital mortality in patients with infective endocarditis.

TyG 指数、TyG-BMI 指数对 AMI 行急诊介入治疗患者预后的预测价值

欧阳巍立 杨杨

南京医科大学第一附属医院

目的 分析甘油三酯 - 葡萄糖（TyG）指数、甘油三酯 - 葡萄糖 - 体质（TyG-BMI）指数对 AMI 行急诊介入患者预后的预测价值。方法 回顾我院 2021 年 01 月 01 日至 2022 年 12 月 31 日 AMI 行急诊介入的患者 201 例，均在 12 小时内急诊介入开通罪犯血管，根据心电图表现分为急性非 ST 段抬高型心肌梗死 (NSTEMI) 组、急性 ST 段抬高型心肌梗死 (STEMI) 组，根据 TyG 指数的中位数分为低分组（Q1 组）、高分组（Q2 组），取同期冠脉造影结果为阴性的患者 96 例为对照组，收集 TyG、TyG-BMI 指数等临床资料，随访 24 个月，记录主要不良心血管事件（MACE），分析 TyG、TyG-BMI 指数对 AMI 急诊介入患者预后的预测价值。结果 （1）与对照组相比，NSTEMI 组 TyG 指数明显升高（9.16±0.72 vs.8.66±0.63,P < 0.05）；与对照组相比，STEMI 组 TyG 指数明显升高（9.46±0.69 vs.8.66±0.63,P < 0.05）。（2）与对照组相比，NSTEMI 组 TyG-BMI 指数明显升高（241.04±39.49 vs.212.74±33.27,P < 0.05）；与对照组相比，STEMI 组 TyG-BMI 指数明显升高（255.50±44.45 vs.212.74±33.27,P < 0.05）。（3）STEMI 组 TyG 指数、TGy-BMI 指数均高于 NSTEMI 组（P < 0.05）。（4）TyG-BMI 指数与 cTnI 呈正相关（R=0.23,P < 0.01）,TyG-BMI 指数与 LVDd 呈正相关（R=0.505,P < 0.01）,TyG-BMI 指数与 LVEF 呈负相关（R=-0.587,P < 0.01），TyG-BMI 指数与 Gensini 评分呈正相关（R=0.44,P < 0.01）。（5）24 个月 MACE 对比发现，NSTEMI 组、STEMI 组均高于对照组（P < 0.05），Q2 组高于 Q1 组（P < 0.05）。（6）通过生存曲线 km 法分析得出 TyG 指数低的心肌梗死患者 MACE 事件发生相对较少。结论 TyG 指数、TyG-BMI 指数对 AMI 行急诊介入治疗患者预后有一定的预测价值。

Prevalence and clinical characteristics of coronary microvascular dysfunction in Tibetan highlanders with suspected coronary artery disease

Xiuhuan Chen, Bingyu Gao, Xue-Dong Zhao, Hai Gao

Beijing Anzhen Hospital, Capital Medical University

Abstract

Background: Chronic hypobaric hypoxia in high altitude regions results in remarkable difference in the incidence, clinical characteristics and pathogenic mechanisms of coronary artery disease from those in lowland. Based on this notion, recognition of the etiologies, risk factors and clinical characteristics of coronary artery disease in highlanders is of paramount importance. It is notable that coronary microvascular dysfunction is prevalent in approximately 2 in 5 coronary artery disease patients, and is independently associated with an increased risk of adverse cardiovascular events. Whether coronary microvascular dysfunction is associated with the development, progression and adverse outcomes of coronary artery disease in highlanders is still unknown. Previous studies have demonstrated detrimental effects exerted by chronic hypobaric hypoxia on cutaneous, cerebral and sublingual microcirculation, evidenced by an increased microvascular resistance and a decreased perfusion. However, no direct evidence has showed this association, and relevant clinical characteristics also remain unelucidated.

Aims: This study was designed to evaluate the prevalence, and clinical characteristics of coronary microvascular dysfunction in Tibetan dwellers with suspected coronary artery disease.

Study Design and Methods: In this retrospective, single-center study, 256 patients admitted for frequent chest pain and performed coronary angiography in Lhasa People's Hospital between March 2012 to July 2022 were enrolled. Baseline characteristics, laboratory examination and coronary angiography images were collected for further analysis. Coronary angiographyderived index of microvascular resistance (caIMR) in left anterior descending was calculated and used to measure microvascular function, and coronary microvascular dysfunction was defined as caIMR ≥ 25 U. Continuous variables are presented as the mean (SD) or median (interquartile: first and third quartiles) and were compared by the Student's t test, the Mann–Whitney U test or ANOVA depending on the distribution. Categorical variables are shown as numbers (percentages) and were compared by χ^2 statistics or Fisher's exact test, as appropriate. Spearman's correlation analyses and multivariable linear regression analysis were used to evaluate the association between age and caIMR. A 2-sided P<0.05 was considered indicative of statistical significance.

Results: Of 256 eligible patients (average age: 56.4 ± 12.1 years; 94 [36.7%] women), 179 (69.9%) patients were with caIMR ≥ 25 U, among whom 157 (73.7%) patients presented with no obstructive coronary artery disease (stenosis <50% in 3 main vessels) in the coronary angiography. Notably, the prevalence and values of coronary microvascular dysfunction were independent of canonical coronary artery disease risk factors including gender, hypertension, diabetes mellitus, hyperlipidemia, heart failure and current smoking. Intriguingly, we found that the mean value of caIMR was significantly higher in 154 younger patients (age <60 years; 60.2%) than that in older patients (36.7 ± 19.1 U vs. 31.7 ± 13.3 U; P = 0.022). In addition, caIMR was negatively correlated with age (r = -0.150, P = 0.016). In further linear regression analysis, after adjustment for clinical confounders, age as a continuous variable (beta coefficient [β] = -0.246, P = 0.012) and age <60 years (β = -6.2, P = 0.009) were both independently associated with increased caIMR.

Conclusions: In the current study, we unraveled an excessively prevalent coronary microvascular dysfunction that might result in symptomatic chest pain in the absence of obstructive stenosis in Tibetan highlanders. Moreover, we also indicated significant age-specific correlation with coronary microvascular dysfunction that younger patients may have higher microvascular resistance than older patients. Taken together, more emphasis should be on ubiquitous coronary microvascular dysfunction in highlanders, particularly in younger patients, and aggressive diagnosis and interventions are also recommended.

Characteristics and Mechanisms of Coronary In-stent Restenosis Across Different Clinical Presentations: An Optical Coherence Tomography Study

Yi-Shuo Xu[1,2], Yu-Han Qin[1,2], Chen Zhao[1,2], Yan Zuo[1,2], Di-Rui Zhang[1,2], Ning Wang[1,2], Si-Ning Hu[1,2], Jing-Bo Hou[1,2], Hai-Bo Jia[1,2], Bo Yu[1,2]

1. Department of Cardiology, The 2nd Affiliated Hospital of Harbin Medical University

2. The Key Laboratory of Myocardial Ischemia, Chinese Ministry of Education, Harbin, China

Background

In-stent restenosis (ISR) is a major cause of stent failure and target lesion revascularization in patients with coronary artery disease. Compared with percutaneous coronary intervention for de novo lesions, ISR lesions are more complex and have been demonstrated to be associated with higher risk of repeated restenosis and revascularization. Expert consensus emphasizes the importance of detecting the underlying mechanisms of ISR for tailored management. Coronary angiography cannot accurately evaluate neointima characteristics within stent, limiting its utility

for individualized treatment based on the underlying mechanisms and substrate of ISR. Optical coherence tomography (OCT), a high-resolution intracoronary imaging technique, can detect the underlying mechanisms and neointimal characteristics of ISR. Acute coronary syndrome as ISR presentation was associated with higher rates of major adverse cardiac events. However, the characteristics and underlying mechanisms of ISR lesions across different clinical presentations remain unclear. In this study we aimed to identify the underlying mechanisms and neointimal characteristics in ISR patients with different clinical presentations using OCT.

Methods

The study retrospectively enrolled 246 patients with ISR lesions who underwent OCT imaging detection before percutaneous coronary intervention in our center. According to clinical presentation, patients were categorized into ST-segment elevation myocardial infarction (STEMI, n=53) group, non-ST-segment elevation acute coronary syndrome (NSTE-ACS, n=110) group, and chronic coronary syndrome (CCS, n=83) group. Neointimal characteristics, the underlying mechanisms, and clinical outcomes at 2-year follow-up were compared. When multiple underlying mechanisms contributing to ISR lesions coexist within the stent, the lesion at the site of minimal lumen area is regarded as the predominant factor. Major adverse cardiac events were defined as a composite of cardiac death, target vessel related myocardial infarction and target lesion revascularization. Multivariable logistic regression was used to identify predictors for acute clinical presentations in ISR patients.

Results

Compared with NSTE-ACS and CCS patients, STEMI patients demonstrated significantly higher rates of previous myocardial infarction (P=0.003) and current smoking (P=0.001). Neoatherosclerosis, neointimal hyperplasia, malapposition, edge-related disease, stent underexpansion and recanalized thrombus are underlying mechanisms of ISR, accounting for 45.9%, 45.1%, 1.6%, 5.7%, 1.2% and 0.5%, respectively. Neoatherosclerosis was the predominant mechanisms of ISR in STEMI patients, accounting for 67.9% of cases. Among NSTE-ACS patients, 49.1% of ISR lesions were associated with neoatherosclerosis and 45.4% with neointimal hyperplasia. 65.1% of CCS patients were related to neointimal hyperplasia. Neoatherosclerosis, lipid neointima, thin-cap fibroatheroma, neointimal rupture, macrophages, thrombus and healed neointima were most frequently observed in STEMI patients, followed by the NSTE-ACS patients and CCS patients. Multivariable logistic regression identified neointimal rupture (OR: 4.438; 95% CI: 1.564-12.597; P=0.005) and macrophages (OR: 2.578; 95% CI: 1.076-6.176; P=0.034) as independent predictors of STEMI. Neointimal rupture (OR: 3.422; 95% CI: 1.066-10.991; P=0.039) was an independent predictor of acute coronary syndromes. STEMI patients (HR: 4.009; 95% CI: 1.393–11.540; P=0.010) and NSTE-ACS patients (HR: 3.406; 95% CI: 1.284–9.034; P=0.014) were associated with a higher risk of major adverse cardiac events at 2 years compared to CCS patients.

Conclusions

The underlying mechanisms and neointimal characteristics detected by OCT differ in STEMI, NSTE-ACS and CCS patients. The application of OCT could facilitate the identification of characteristics and mechanisms of ISR lesions.

基于光学相干断层扫描的冠状动脉非阻塞性心肌梗死的临床特征与预后研究

夏洁[1] 许官学[2]

1. 遵义医科大学附属医院

2. 遵义医科大学第五附属（珠海）医院

CSC 第 12 届大血管及周围血管疾病学组

[摘要]

目的: 通过光学相干断层扫描（OCT）探究 MINOCA 和 MI-CAD 患者的临床特点、斑块特征及预后。

方法: 对接受 CAG 和 OCT 检查的 553 例 AMI 患者的罪犯病变进行回顾性分析。将患者分为两组：MINOCA 组和 MI-CAD 组，对两组患者的临床特点、斑块特征和预后进行比较。主要终点被定义为主要心脏不良事件（MACE）的复合指标，包括心源性死亡、非致死性心肌梗死、靶血管再通、脑卒中以及因心绞痛或心力衰竭再次住院。

结果: 1）与 MI-CAD 患者相比，MINOCA 患者 ST 段抬高型心肌梗死（STEMI）的发生率较低，植入药物洗脱支架（DES）的频率也较低。此外，他们的低密度脂蛋白胆固醇（LDL-C）、总胆固醇（TC）、甘油三酯（TG）、肌钙蛋白 T 峰值（TnT 峰值）和肌酸激酶峰值（CK 峰值）水平均较低。MINOCA 组的病变多见于左前降支（LAD），而左回旋支（LCX）病变少见。此外，MINOCA 患者多支血管病变发生率较低，出院后使用阿司匹林、P_2Y_{12} 受体抑制剂、β- 受体阻滞剂、血管紧张素转换酶抑制剂 / 血管紧张素受体阻滞剂（ACEI/ARB）的比例较低，保守治疗的比例较高。MINOCA 组斑块破裂、斑块钙化、胆固醇结晶、巨噬细胞浸润、微血管、薄纤维帽粥样斑块（TCFA）和血栓的发生率低于 MI-CAD 组，差异具有统计学意义（P <0.05）；2）MINOCA 组和 MI-CAD 组患者 30 天和 1 年内 MACE 的发生率无明显差异（P > 0.05）。

结论: 与 MI-CAD 患者相比，MINOCA 患者的 OCT 高危斑块较少，更倾向于保守治疗，支架植入率较低，出院后药物治疗较少。两组患者在 30 天和 1 年内的 MACE 发生率相似，这凸显了对 MINOCA 患者进行个体化治疗的重要性。发生 MACE 的 MINOCA 患者更有可能表现出高风险的 OCT 斑块特征，其中巨噬细胞浸润被认为是一个独立的风险因素。斑块破裂、斑块侵蚀、胆固醇结晶、巨噬细胞、微血管、TCFA 等 OCT 斑块特征可能在两组患者的病情进展中扮演着不同的角色。

Prognostic performance of CCTA-derived coronary physiology and plaque characterization in the CAREER study

Sheng-Xian Tu[1], Zhi-Qing Wang[1,2], Yu-Wei Liu[3], Guan-Yu Li[1], Dai-Xin Ding[1], Ting-Wen Weng[2], Shao-Feng Guan[2], Xin-Kai Qu[2]

1. School of Biomedical Engineering, Shanghai Jiao Tong University

2. Huadong Hospital, Fudan University

3. School of Biomedical Engineering, Southern Medical University

BACKGROUND: Coronary computed tomography angiography (CCTA) permits noninvasive evaluation of coronary physiology and high-risk plaque with sufficient accuracy, rendering this imaging modality as a cost-effective diagnostic strategy in patients with suspected coronary artery disease. However, the appropriate criteria for safe deferral of further diagnostic testing based on CCTA-derived parameters have yet to be established.

OBJECTIVES: This substudy of the CAREER (Diagnostic Accuracy of CCTA-derived Versus AngiogRaphy-dErived QuantitativE Flow Ratio) trial sought to investigate whether computed tomography-derived Murray-law based quantitative flow ratio (CT-μFR) and plaque characteristics could safely identify patients eligible for deferral of invasive coronary angiography, with outcomes comparable to those undergoing physiology-guided revascularization.

METHODS: In the CAREER trial, patients underwent CCTA imaging and subsequent coronary angiography within 30 days and were clinically followed for up to 4 years. Artificial intelligence-powered quantitative and qualitative plaque analyses were retrospectively performed by an independent core laboratory, blinded to the on-site CT-μFR and follow-up outcome data. The primary endpoint of the substudy was the composite of revascularization within 30 days following CCTA imaging and vessel-oriented composite outcome (VOCO, including cardiac death, target vessel-related myocardial infarction, and target vessel revascularization) during up to 4-year follow-up after fraction flow reserve/quantitative flow ratio-guided revascularization.

RESULTS: Among 260 patients enrolled in the main trial, 254 patients with 723 vessels eligible for CCTA-based plaque assessment were included in the final analysis. Median patient age was 68.0 (61.0-74.0) years, 163 (64.2%) were male, and 186 (73.2%) were diagnosed with acute coronary syndrome. Revascularization within 30 days and VOCO events during follow-up occurred in 130 (51.2%) and 25 (9.8%) patients, respectively, resulting in an incidence of 53.9% (137/254) for the primary endpoint. Patient-level CT-μFR was the most powerful predictor of the primary endpoint (C-index, 0.74; 95% CI, 0.70-0.78; P < 0.001). With the optimal cutoff of ≤ 0.80, the incidence of the primary endpoint event was 87.2% (109/125) in the CT-μFR positive versus 21.7% (28/129) in the CT-μFR negative group (hazard ratio, 8.51; 95% CI, 5.54-13.07; P < 0.001). The total CT-μFR of the three vessels was also predictive of the primary endpoint (C-index, 0.73; 95% CI, 0.69-0.77; P < 0.001), with the optimal cutoff found at 2.65. The presence of both CT-μFR >0.80 and total CT-μFR >2.65 was found in 101 (39.8%) cases. The incidence of the primary endpoint in patients with both CT-μFR >0.80 and total CT-μFR >2.65 was comparable to the VOCO rate in patients following coronary physiology-guided revascularization (13.9% [14/101] vs 9.8% [25/254]; hazard ratio, 1.48; 95% CI, 0.77-2.86; P = 0.238). Among 562 deferred vessels in 242 patients, VOCO events developed in 12 (2.1%) ones. CCTA-derived plaque characteristics, in particular plaque burden (C-index, 0.74; 95% CI, 0.63-0.86; P < 0.001) and lipidic plaque volume (C-index, 0.73; 95% CI, 0.59-0.86; P < 0.001), were predictive of VOCO in deferred vessels beyond physiological parameters.

CONCLUSIONS: CT-μFR provided the highest accuracy for predicting the composite outcome of the requirement of revascularization within 3 months and VOCO during follow-up of up to 4 years. The combined use of CT-μFR >0.80 and total CT-μFR >2.65 could help to identify patients at low risk of coronary revascularization and adverse cardiac events during follow-up, potentially serving as a criterion to reduce unnecessary invasive diagnostic procedures with low pretest probability. Besides physiological parameters, CCTA-derived plaque characterization provided significant prognostic value in vessels with deferral of revascularization.

ST 段抬高型心肌梗死患者支架植入术后功能学评估的临床研究

刘强

新疆维吾尔自治区第三人民医院

研究目标

(1) 与传统冠脉功能学方法评估，该方法可以降低患者费用，可以减少国家医保

花费，节约医疗系统的开支。

基于冠脉 ICA 的无导丝功能学分析系统 AccuFFRangio 可以避免有创的 FFR 检测。其中 AccuFFRangio 是通过 ICA 影像进行计算 FFR 分析， 按照目前 91 万的冠脉支架植入量来计算，导管室造影的患者在 360 万左 右。目前有创 FFR 测量收费为 1 万 / 例。按照 360 万个冠脉造影中有一半的人来做 AccuFFRangio 服务，每台按照 3000 元 / 例来进行收费，其基于冠脉造影的 FFR 检测的市场是 108 亿人民币 / 年对应脉流科技的 AccuFFRangio 产品。全国大约有 6000 个导管室，按照每台 AccuFFRangio Plus 设备销售 200 万人民币来计算，其市场容量为 120 亿。

(2) 可以减少不必要的有创操作，从而给患者选择更优的治疗方案，降低诊断的风险，改善患者预后及就医体验。

研究方法：

通过回顾性分析 ICA 影像资料及有创 FFR 数据，将每位患者的影像数据都通过 DICOM 格式输出，采用改进的三维建模方法，得到快速生成 3D 冠状动脉模型结构的程序，进一步优化无导丝 FFR 计算时间及准确度，同时采用优化算法的 Angio-FFR 评估 STEMI 患者急性期采集影像分析和亚急性期采集影像分析的可重复性，并且计算 PCI 术后 Angio-FFR 来预测 STEMI 预后，评估术后罪犯病变和非罪犯病变功能结果的影响和 2 年随访患者水平的心脏不良事件的关系；

结果：

Angio-FFR 分析结果较大时 STEMI 患者 PCI 术后的临床结果越好，同时手术预案系统对患者进行虚拟治疗后能提供给医生治疗的方案；

结论：

Angio-FFR 在 ST 段抬高型心肌梗死患者支架植入术后功能学评估具有较好的预后结果，并且手术预案系统能提供精准的提供手术指导。

Insulin Resistance and Culprit Plaque Morphology: A Study of Young and Middle-Aged Hypertensive Patients With STEMI

Xi Chen, Shuo Zhang, Bo Yu

The 2nd Affiliated Hospital of Harbin Medical University

OBJECTIVE:

To explore the in vivo pathological mechanisms by intracoronary imaging and evaluate the association between insulin resistance and culprit plaque characteristics in high-risk young and middle-aged patients with hypertension and STEMI, with the aim of informing future mechanistic investigations.

METHODS:

This study included patients aged 18 to 65 years who were admitted to the Second Affiliated Hospital of Harbin Medical University between January 2018 and June 2018, diagnosed with hypertension combined with STEMI, who underwent coronary angiography and optical coherence tomography (OCT) imaging of the culprit vessel before percutaneous coronary intervention (PCI). Exclusion criteria included: (1) presence of malignant tumors, significant hepatic or renal dysfunction, or any condition associated with a life expectancy of less than one year; (2) secondary hypertension; and (3) missing fasting blood glucose or triglyceride data during hospitalization. (4) poor image quality due to operator-related factors or coronary anatomical variations that precluded accurate analysis; (5) presence of a large intraluminal thrombus; (6) occurrence of cardiogenic shock. The diagnosis of STEMI was based on the Fourth Universal Definition of Myocardial Infarction, which includes: (1) detection of a rise and/or fall in cardiac biomarkers, with at least one value above the 99th percentile upper reference limit (URL); and (2) clinical evidence of myocardial ischemia, demonstrated by at least one of the following: ischemic symptoms (e.g., chest pain); new ischemic electrocardiographic changes (e.g., ST-segment-T wave changes, development of pathologic Q waves); imaging evidence of new regional wall motion abnormalities or loss of viable myocardium; or identification of an intracoronary thrombus by angiography or autopsy. Height and weight at admission were obtained from the electronic medical record system. Body mass index (BMI) was calculated as weight (kg) divided by the square of height (m^2). The METS-IR index was calculated using the following formula: METS-IR = Ln[2 × FPG (mg/dL) + TG (mg/dL)] × BMI (kg/m^2) ÷ Ln[HDL-C (mg/dL)]. Plaque characteristics of OCT images were assessed using both qualitative and quantitative analyses. Based on the predominant plaque components, plaques were classified as lipid-rich plaques (LRP), fibrous plaques, or calcified plaques, as illustrated in Figure 1. A total of 229 patients were enrolled and stratified into tertiles based on the METS-IR index. Statistical analyses and figure generation were performed using SPSS version 26.0 (IBM Corp., NY, USA), R version 4.2.2, and GraphPad Prism version 10.1.1. Continuous variables with normal distribution are presented as mean ± standard deviation; those with non-normal distribution are presented as median (interquartile range). Categorical variables are expressed as frequency (percentage).

RESULTS :

Patients were stratified into three groups based on METS-IR tertiles (M1: 38.16 ≤ METS-IR ≤ 41.57; M2: 41.57 ≤ METS-IR ≤ 43.62; M3: 43.62 ≤ METS-IR ≤ 47.78). Body mass index (BMI) significantly differed among the three groups (P < 0.001). TC, TG, low-density LDL-C, fasting blood glucose (FBG), and HbA1c levels increased progressively with METS-IR, showing statistical significance (P < 0.05). OCT analysis of culprit vessels in all 229 patients was performed and compared across METS-IR tertiles. Although the overall distribution of lesion types did not show a statistically significant difference, the incidence of plaque rupture increased with higher METS-IR. Significant differences were observed in the prevalence of TCFA, LRP, fibrous cap thickness, lipid arc, macrophage infiltration, and microchannel formation (P < 0.05).

CONCLUSION:

In patients with high METS-IR, OCT image analysis revealed that culprit lesions were more likely to present with plaque rupture. Moreover, these patients showed a higher frequency of vulnerable plaque features, including lipid-rich plaques, TCFA, and the presence of microvessels, compared with those in the medium and low METS-IR groups. In addition, the fibrous cap in the high METS-IR group was significantly thinner than that observed in the medium and low METS-IR groups. In conclusion, in young and middle-aged hypertensive patients with STEMI, insulin resistance is associated with increased plaque vulnerability, suggesting that insulin resistance may contribute to the progression of atherosclerosis.

Multimodal Imaging And Functional Assessment For Etiological Diagnosis And Prognosis Improvement In MINOCA Patients

Mengyue Yu

Fuwai hospital, CAMS&PUMC

Background:

Myocardial infarction with non-obstructive coronary arteries (MINOCA) represents a clinically important and pathophysiologically heterogeneous syndrome. By definition, MINOCA is characterized by the presence of acute myocardial infarction (MI) criteria in the absence of obstructive coronary artery disease (CAD), typically defined as less than 50% stenosis on coronary angiography (CAG). Despite its non-obstructive nature, MINOCA is not a benign entity. Patients often present with typical ischemic symptoms and exhibit elevated cardiac biomarkers, yet conventional diagnostic workup frequently fails to identify a definitive cause. The diversity of underlying mechanisms—including plaque erosion or rupture undetectable on angiography, coronary spasm, microvascular dysfunction, thromboembolism, and myocarditis—makes accurate etiological diagnosis particularly challenging. This diagnostic ambiguity leads to inconsistencies in treatment approaches and contributes to variable long-term outcomes. Consequently, there is a growing clinical imperative to utilize more comprehensive diagnostic tools beyond routine CAG to elucidate the underlying causes and guide therapy in MINOCA.

Methods:

This prospective, single-center cohort study enrolled patients diagnosed with MINOCA at Fuwai Hospital after undergoing CAG. All participants met the diagnostic criteria for acute MI but were confirmed to have non-obstructive coronary arteries on angiography. Following enrollment, all patients underwent laboratory testing, invasive CAG, and angiography-based microcirculatory resistance (AMR) measurement. In addition, supplementary imaging—including cardiac magnetic resonance imaging (CMR), optical coherence tomography (OCT), intravascular ultrasound (IVUS), and single-photon emission computed tomography (SPECT)—was conducted based on clinical indications and patient consent. Intravascular imaging (OCT/IVUS) was performed during the index angiographic procedure when feasible, whereas CMR and SPECT were completed within a 6-month window surrounding the index event. Based on the integration of multimodal imaging results, working diagnoses were revised to reflect the most likely underlying mechanism, allowing for etiology-specific therapy.

Patients were followed for a median of 77.2 months to assess the occurrence of major adverse cardiovascular events (MACEs), including cardiovascular death, recurrent MI, stroke, and heart failure hospitalization. A Cox proportional hazards model was used to evaluate the association between the use of multimodal imaging and the risk of MACE, adjusting for baseline demographics and clinical variables.

Results:

A total of 1,179 patients were included in the final analysis. All patients underwent CAG and AMR measurement, while a subset received additional imaging: 124 underwent CMR, 308 underwent OCT or IVUS, and 192 underwent SPECT. Among them, 688 patients received only CAG + AMR, while 491 underwent evaluation with two or more imaging modalities. Patients in the multimodal imaging group had a significantly lower incidence of MACEs than those in the CAG + AMR-only group. After multivariable adjustment, multimodal imaging remained independently associated with a reduced risk of MACE (HR = 1.33, 95% CI: 1.09–1.92, p

<0.05), suggesting a clinically meaningful benefit.

Conclusions:

This study demonstrates that the integration of multimodal imaging with angiography-based microcirculation assessment provides a more accurate etiological diagnosis and enables more effective, individualized management strategies in patients with MINOCA. Compared to conventional CAG with AMR alone, the use of two or more imaging modalities is associated with a significantly lower long-term risk of adverse cardiovascular events. These findings underscore the potential clinical value of comprehensive imaging in improving diagnostic precision and guiding targeted therapy in this complex patient population.

IVUS 指导处理冠脉多分叉病例 1 例

张勇

西安交通大学第一附属医院

患者 72 岁老年男性，既往否认高血压、糖尿病史，长期吸烟史，2 月前开始出现活动后胸闷气短，外院造影提示多分叉病变转入我院。冠脉造影提示右冠相对正常，回旋支近端重度狭窄，狭窄从回旋支开口一直到钝缘支开口附近，前降支中段中度狭窄，第一对角支及第二对角支开口位置靠近，且血管均较大，第一对角支近端重度狭窄，狭窄长度相对局限，第二对角支弥漫性中重度狭窄累及开口，多分叉病变，左主干分叉，前降支分叉，回旋支分叉病变，解剖结构极为复杂。首先我们对第一对角支及前降支主支进行血管内超声检查，证实前降支主支管腔面积小，斑块负荷重，需进行干预，第一对角支开口负性重构，斑块负荷较轻，可不干预，然后我们对第二对角支进行 2.0mm 球囊预扩张后行血管内超声检查，证实第二对角支弥漫性病变，开口斑块负荷相对较轻，遂决定采用“三明治”术式处理分叉，但在释放第二对角支支架（2.25*32mm）时，支架向近端移位突入主支，我们行血管内超声检查证实支架近端已完全覆盖第二对角支开口但未突入主支，没有影响第一对角支，遂在导丝保护第一、第二对角支下植入前降支支架（2.75*24mm），按分叉病变处理标准流程，近端优化后分别 rewire 第一对角支和第二对角支，预扩张第二对角支网眼，然后后扩张球囊对吻，造影显示结果良好，血管内超声也证实分叉处支架膨胀良好，但发现支架近端边缘支架皱缩，且斑块负荷较重（可能撤出拘禁导丝指引导管深插所致，也可能在后期送入后扩张球囊所致），我们决定根据回旋支处理情况再对支架皱缩情况进行处理。血管内超声检查发现回旋支极度偏心斑块，斑块负荷极重，但好处是回旋支与钝缘支分叉处斑块负荷轻且钝缘支开口无明显斑块，回旋支开口斑块负荷也不重，遂使用 2.5mm 切割球囊及 2.75mm 后扩张球囊扩张病变，效果欠佳，决定于回旋支开口精确定位植入支架（2.75*18mm），但血管内超声检查发现支架近端突入左主干到前降支 1-2mm，于是决定于前降支至左主干植入支架同时处理前降支近端支架皱缩及回旋支突入主支支架梁，我们于左主干到前降支串联植入 1 枚支架（3.5*15mm），按分叉病变处理标准流程，左主干近端后分别 rewire 回旋支，预扩张回旋支网眼，然后后扩张球囊对吻，造影及血管内超声显示结果完美。分叉病变解剖结构千奇百怪，血管内超声有助于识别解剖结构，制定分叉病变处理策略。

Altered DNA methylation and transcriptome landscape for the differentiation diagnosis of plaque erosion from plaque rupture: the NBPE-ACS study

Cheng-Xing Liu, Xue-Bo Liu

Tongji hospital of Tongji University, Tongji University School of Medicine,Shanghai

Abstract

Title: A Non-Invasive Diagnostic Model Integrating Transcriptomic and DNA Methylation Signatures for Differentiating Plaque Erosion from Plaque Rupture in Acute Coronary Syndrome

Background and Aims

Acute coronary syndrome (ACS) remains a leading cause of morbidity and mortality globally. Its underlying pathological mechanisms are primarily attributed to either plaque rupture (PR) or plaque erosion (PE). While both lead to thrombotic occlusion of coronary arteries, they represent distinct pathophysiological processes demanding different therapeutic approaches. For instance, patients with PE may benefit more from antithrombotic therapies and potentially avoid aggressive revascularization strategies, whereas PR often necessitates prompt revascularization. Currently, optical coherence tomography (OCT) serves as the in vivo gold standard for distinguishing these entities. However, OCT is an invasive, costly procedure with technical expertise requirements and limited accessibility, especially in acute settings. This underscores an urgent need for a reliable, non-invasive diagnostic tool to accurately differentiate PE from PR, thereby facilitating rapid, individualized treatment decisions and improving patient outcomes. This study aimed to develop and validate a non-invasive diagnostic model by integrating transcriptomic and DNA methylation data from peripheral blood to accurately differentiate PE from PR in ACS patients.

Methods

This cross-sectional study was conducted at Tongji Hospital, Tongji University, enrolling a discovery cohort (n=77) and an independent validation cohort (n=224). OCT served as the reference standard for classifying PE and PR in all patients. Peripheral blood samples were collected and analyzed for whole-transcriptome RNA sequencing and 850K DNA methylation profiling. In the discovery cohort, principal component analysis (PCA) and differential expression analyses were used to identify key molecular features distinguishing PE from PR. Core biomarkers were selected using multiple feature selection methods. Diagnostic models based on transcriptomic, methylation, and combined features were constructed and internally cross-validated. Finally, the developed model was externally validated in the independent cohort, and key biomarkers were methodologically validated using quantitative PCR (qPCR) and pyrosequencing.

Results

Transcriptomic analysis in the discovery cohort revealed neutrophil-related pathways as key discriminators for PE. Two core transcriptomic markers, DEFA1B and AZU1, were identified. A logistic regression model incorporating these two markers achieved an excellent diagnostic performance with an AUC of 0.939 (95% CI: 0.782–1.000) in internal cross-validation.

Simultaneously, methylation profiling identified 831 differentially methylated sites, with three specific CpG loci (cg02668773, cg15610437, cg19401149) strongly associated with PE. A random forest model integrating these three CpG loci showed an AUC of 0.869 (95% CI: 0.683–1.000) under 10-fold cross-validation.

Notably, combining the transcriptomic markers (DEFA1B, AZU1) with a key methylation marker (cg15610437) further enhanced discrimination, yielding an AUC of 0.967 (95% CI: 0.818–1.000) in the discovery cohort.

Methodological validation via qPCR and pyrosequencing confirmed consistent differential expression patterns of DEFA1B and AZU1, and methylation patterns of the selected CpG loci, in the independent validation cohort (92 PE, 132 PR). Crucially, when tested in the independent validation cohort, the final logistic model demonstrated robust diagnostic utility, achieving an AUC of 0.887 (95% CI: 0.846–0.929), with favorable calibration and decision curve analyses.

Conclusions

By integrating transcriptional and methylation signatures, this study delineates key molecular features distinguishing PE from PR and provides a non-invasive model with high diagnostic accuracy. Validated in an independent cohort, this innovative approach holds significant potential to facilitate individualized treatment strategies for ACS patients, especially where OCT may be limited, thereby improving patient outcomes and optimizing resource allocation. This study offers new insights for precise diagnosis and management of ACS.

Keywords

Plaque erosion; Acute coronary syndrome; Differential diagnosis; DNA methylation; Neutrophil Activation

Predictors of High-risk Non-Culprit Plaque Rupture: A Serial Optical Coherence Tomography Imaging Study

Bo-Ling Yi, Si-Ning Hu, Hai-Bo Jia, Bo Yu

The 2nd Affiliated Hospital of Harbin Medical University

OBJECTIVES: Acute coronary syndrome is primarily caused by coronary thrombosis resulting from plaque rupture. However, pathological studies have shown that not all plaque ruptures lead to acute events. Up to 20% of patients with coronary heart disease had multiple plaque ruptures in non-culprit lesions. These ruptured plaques heal over time, but result in luminal narrowing and increased coronary revascularization events. Optical coherence tomography (OCT) is a high-resolution intravascular imaging modality that can accurately assess plaque morphology and composition, which can help identify more plaque ruptures. However, it is not clear the predictors of rapid progression of plaque ruptures.

METHODS: Patients with acute coronary syndrome (ACS) who underwent two OCTs at baseline and 1-year follow-up at the Second Affiliated Hospital of Harbin Medical University were included. Rapid progression was defined as a minimum lumen area reduction of greater than 0.84 mm^2 on OCT imaging from baseline to follow-up. A non-culprit plaque was identified as a region with luminal stenosis and loss of the normal architecture of the vessel wall. Macrophage accumulation was identified as the presence of highly backscattering focal granular regions within the fibrous cap. Microchannel was identified as a 50-300μm signal-poor tubular structure delineated in at least 3 contiguous frames. Cholesterol crystal was present as thin and linear regions of high signal intensity with high backscattering within a plaque. Thrombus was identified as an irregular mass floating or protruding into the lumen. Calcification was identified as a signal-poor or heterogeneous area with sharp borders. Spotty calcification was defined as the presence of lesions <4 mm in length and containing an arc of calcification <90 ° . Layered plaque was defined as a plaque with one or more heterogeneous signal-rich layers of different optical intensity with clear demarcation from the underlying components and present in 3 or more consecutive frames Statistical analyses were performed using SPSS version 25.0 software (IBM, Armonk, New York). Categorical data were expressed as counts

(proportions). Continuous variables were tested for data distribution using the Kolmogorov-Smirnov test and expressed as mean ± SD or median (25th–75th percentiles). The independent samples Student's t test or the Mann-Whitney U test were used for continuous variables, and the chi-squared test or Fisher exact test for categorical variables. Variables that showed p values <0.10 in the univariate model were simultaneously entered into the multivariate logistic regression.

RESULTS: 39 non-culprit plaque ruptures were found in 37 ACS patients, and 16 (41.0%) of the plaque ruptures in 16 patients progressed rapidly at 1 year. The mean age of all patients was 57.08±10.18 and 87.8% were male, there was no significant difference between the two groups. Patients with plaque rupture progression were more likely to be current smokers (62.5% vs. 23.8%, p=0.018) than patients without plaque rupture progression. No significant difference was observed in the prevalence of hypertension, hyperlipidemia, and diabetes between the two groups. On OCT imaging, plaque ruptures with progression had a higher prevalence of macrophages (100% vs. 78.3%, p=0.046), spotty calcification (62.5% vs. 26.1%, p=0.023), and tended to be more layered plaque (81.3% vs. 52.2%, p=0.063) than those without progression. Multivariate logistic regression analysis showed that current smoking was an independent predictor of plaque rupture with progression (OR: 5.33 [1.28-22.19], P=0.021) at the patient level, whereas spotty calcification (OR7.72 [1.19-18.68], P=0.027) was an independent predictor at the lesion level.

CONCLUSIONS: Rapid progression of silent plaque rupture is common, up to two-fifths in one year. Current smoking and spotty calcification were independent predictors of rapid progression. Further large-sample studies are needed to confirm whether early intervention is beneficial for these lesions.

径向管壁应变在冠脉临界狭窄病变生理性进展的预测价值

来晏

上海市同济医院

背景：本研究旨在探讨冠脉临界病变的生物力学参数–血管径向壁形变对其生理变化的影响；首次尝试评估两个新型生理性指标 -- 径向壁应变（RWS）和无创血流储备分数（QFR）联合应用评估斑块进展的可行性及临床价值。

方法：本研究纳入基线时至少有 1 处临界病变、在 6 个月或更长的时间接受冠状动脉造影随访的患者。计算基线时检出病变的最大 RWS (RWSmax)，分析基线及随访后的两次定量血流储备分数（QFR）并观察其值的变化。研究的主要终点是确定基线 RWSmax 与冠状动脉病变功能性进展的关系，功能进展定义为冠状动脉病变定量血流比的增加 (Lesion- △ QFR, L- △ QFR，计算为整个病变 QFR 的绝对值变化)。

结果 :156 例患者 175 处冠状动脉病变中，63 处病变在中位随访 12.4 个月时 L- △ QFR 升高。L- △ QFR 升高的病灶 RWSmax 值显著高于 L- △ QFR 稳定或下降的病灶 (12.1[9.95,13.8] 比 10.6 [9.4,11.6], P < 0.001)。基线 RWSmax 预测 L- △ QFR 升高的曲线下面积为 0.658 (95% 可信区间 :0.572 ~ 0.743, p < 0.001)。在完全校正临床和血管造影因素后，高 RWSmax(> 12%) 是功能性病变进展的独立预测因子 (比值比 :2.822,95% 可信区间 :1.369-5.816,p = 0.005)。

结论： 近 1/3 病变在 1 年的随访期间出现功能性进展，与既往研究相似，RWSmax% > 12% 是重要界值，并且是病变功能性进展的独立危险因素。基线 RWSmax 作为反映斑块结构应力的间接指标具有良好的预测中度狭窄冠脉病变进展的能力，提示其可作为判断斑块易损性的替代指标。

聚乙烯微塑料负荷与急性冠状动脉综合征中斑块易损性相关：基于 OCT 的分析

杨云潇 罗伟 王琳 崔贺贺 高海

首都医科大学附属北京安贞医院

目的：

本研究旨在评估聚乙烯微塑料（PE-MP）暴露与急性冠状动脉综合征（ACS）患者冠状动脉斑块不稳定机制之间的关联，进一步探讨微塑料负荷与易损斑块特征（如薄纤维帽粥样硬化斑块 [TCFA] 和巨噬细胞浸润 [MØI]）的关系。

方法：

前瞻性纳入 80 例接受光学相干断层扫描（OCT）评估的 ACS 患者，并采集其外周血样进行 PE-MP 含量检测。依据 OCT 结果，将罪犯斑块分为纤维帽完整（IFC）和斑块破裂（PR）两类，同时记录斑块区域是否存在 TCFA 和 MØI。利用气相色谱 - 质谱联用技术进行血中 PE-MP 定量，并比较各病理类型下微塑料水平的差异。

结果：

在 80 名患者中，平均每例患者血液中 PE-MP 含量为 63.92 μg/g，个体间差异显著，部分患者血中 PE-MP 含量超过 120 μg/g，提示存在高暴露亚群体。此外，PR 组 PE-MP 中位浓度显著高于 IFC 组（P=0.0013）；存在 TCFA 的患者中，PE-MP 水平显著升高（P<0.0001）；与无巨噬细胞浸润者相比，存在 MØI 的患者血中 PE-MP 水平显著升高（P=0.0002）。

结论：

本研究首次系统性评估了血中 PE-MP 含量与 ACS 患者斑块不稳定性之间的关系。结果显示，PE-MP 暴露水平与斑块破裂、TCFA 及 MØI 的存在密切相关。提示微塑料可能通过促进斑块不稳定化，增加急性冠脉事件发生风险。这些发现为微塑料暴露与动脉粥样硬化性心血管事件之间潜在因果关系提供了支持，也提示 PE-MP 可作为未来心血管风险评估的重要环境暴露指标。

OCT applied to explore Morphological predictors of no-reflow phenomenon after PPCI in STEMI patients

yingcan Zhang, Wei Hao, Fang Liu, Li Yin

the 2nd Affiliated Hospital of Harbin Medical University

OCT applied to explore Morphological predictors of no-reflow phenomenon after PPCI in STEMI patients

Yingcan Zhang, Wei Hao, Fang Liu, Li Yin, Department of Cardiology，the 2nd Affiliated Hospital of Harbin Medical University，Harbin 150001，China

Aims： No-reflow phenomenon after PPCI in STEMI patients is associated with poor prognosis. In recent years, a large number of studies have been conducted both at home and abroad to investigate the safety and efficacy of various no-reflow prevention and treatment strategies. However, identifying subgroups of high-risk patients who can truly benefit from existing control strategies is a major clinical challenge today. The aim of this study was to explore the plaque characteristics associated with the occurrence of no-reflow phenomenon after PPCI in STEMI patients using OCT technology, to further clarify the risk factors associated with NR, and to enhance the early prediction of NR, in order to achieve accurate risk stratification of STEMI patients after PPCI.

Methods： Five hundred and ninety-nine consecutive patients who underwent emergency PCI for the treatment of STEMI within 12 hours of symptom onset were enrolled in this study, all of whom underwent OCT before stenting. A total of 206 patients who met the study design were finally included according to the inclusion criteria formulated for this study. Based on the patients' TIMI flow classification after successful stent implantation, the patients were divided into the NR group (TIMI flow grade ≤ 2) and the NF group (TIMI flow grade =3).

Results： Of the 206 patients, 130 were in the NF group and 76 in the NR group, with the incidence of NR being 36.9%. The mean age of all patients was 58.2 years, the mean BMI was 25.9 kg/m2, and the proportion of males was 79.6%. The proportion of patients with the combination of smoking, hypertension, and diabetes was 53.4%, 59.2%, and 25.7%, respectively. In both groups, there were no significant differences in patient age, gender, and coronary heart disease risk factors (including smoking, hypertension, and diabetes). Compared with the NF group, more culprit lesions were seen in the LAD in the NR group, and the difference was statistically significant (P=0.027). In terms of OCT findings, compared to the NF group, the NR group had a higher incidence of plaque rupture and calcified plaques (84.2% vs. 70.8%, P=0.030) , the values of maximal lipid arc (P<0.004), mean lipid arc (P<0.005), lipid length (P<0.001), lipid index (P<0.001), maximal rupture cavity area (P= 0.003) and rupture cavity volume (P=0.003) were significantly greater. Receiver-operating characteristic (ROC) curve analyses demonstrated that the OCT-derived lipid index had the best predictive value for no-reflow (AUC of 0.70, P<0.001).

Conclusions： A larger lipid core at the culprit lesion in STEMI patients is an important determinant of the occurrence of no-reflow after PPCI, which may be related to the large amount of lipid content flowing into the coronary arteries at the time of stent implantation, which increases local thrombosis and disturbs the distal microcirculation. Our study first confirmed that a larger rupture cavity volume at the culprit lesion of STEMI is related to the occurrence of no reflow after PPCI, which means that the size of the rupture cavity volume identified by OCT enable further risk stratification in STEMI patients.

AI-Driven Virtual Histology with Optical Coherence Tomography for Comparing Acute and Short-Trem Performance of Bioresorbable Scaffolds and Drug-Eluting Stents

Chengpeng Liu, Jiasheng Yin, Li Shen, Jun-Bo Ge

Zhongshan Hospital, Fudan University

Objectives Incomplete stent expansion is an important mechanism leading to adverse events. However, few detailed OCT studies have compared the immediate performance of bioresorbable scaffolds (BRS) and drug-eluting stents (DES). The aim of this study was to compare the acute and short-term performance differences between polymeric BRS and metallic DES, and to explore the underlying mechanisms of immediate stent underexpansion and eccentricity reduction.

Methods Our study consecutively enrolled 298 patients who underwent optical coherence tomography (OCT) pullbacks after BRS or DES implantation at Zhongshan Hospital (Shanghai, China) from January 2021 to December 2023, with 178 patients in the BRS group and 120 patients in the DES group. To mitigate confounding variables across groups, we performed propensity score matching to create 64 pairs of patients with equivalent baseline, procedural, and angiographic profiles. The Octplus system was utilized for AI-Driven virtual histology analysis, enabling automatic segmentation of vascular and plaque components. We selected the frame with the maximum plaque thickness for analysis, tracing the plaque contours to measure its cross-sectional area. Patients underwent

1-year clinical follow-up, with the primary endpoint defined as major adverse cardiac events (MACE), including death, myocardial infarction, target vessel revascularization, and stent thrombosis.

Results After PS matching, 64 pairs of patients treated with either DES or BRS were identified with comparable baseline characteristics, and no differences were noted in procedural or angiographic characteristics between the two groups. After matching, the BRS group had similar luminal and stent parameters to the DES group, with lower mean and minimum stent eccentricity indices (SEC).

Furthermore, the BRS and DES groups had similar characteristics of fibrous plaque (FP) and calcific plaque (CP). Notably, the BRS group exhibited significantly lower SEC at the plaque analysis frame for both CP and FP compared to the DES group. In the BRS group, a larger arc angle of CP was associated with lower SEC, suggesting eccentric expansion; lower SEI in CP was linked to larger area and larger arc angle. For FP in the BRS group, lower SEC correlated with larger area, greater thickness, and larger arc angle, while lower SEI was associated with larger area and larger arc angle. In the DES group, reduced SEC in CP was related to superficial location, larger area, greater thickness, and larger angle; lower SEI in CP was linked to greater thickness. Regarding FP in the DES group, no significant correlations were observed between SEC and FP characteristics, but lower SEI was associated with larger area and greater thickness. The incidence of 1-year MACE did not differ significantly between the BRS and DES groups (log-rank p = 0.685).

Conclusions The BRS appears to have comparable acute performance and reduced SEC when compared to DES. The stent expansion and eccentricity were associated with the characteristics of CP and FP. BRS and DES demonstrated similar efficacy and safety at 1-year follow-up.

This is the first large-scale detailed OCT analysis comparing the acute stent performance of BRS with DES. BVS demonstrated acute luminal and stent parameters comparable to those of DES when treating similar lesions with equivalent procedure, but exhibited lower SEC. The stent expansion and eccentricity are correlated with the characteristics of CP and FP, as well as the stent mechanical properties. BRS and DES demonstrated similar efficacy and safety at 1-year follow-up.

急性冠脉综合征患者的形态学、面积截值和无血流现象的预后：光学相干断层扫描研究。

于淮

哈医大附属第二医院

目的： 光学相干断层扫描 （OCT） 可以诊断急性冠脉综合征 （ACS） 并观察血流中断。然而，血流中断病例的病变特征和临床预后仍不清楚。

方法和结果： 急性冠脉综合征 （ACS） 是冠状动脉疾病最严重的临床表现，也是全球发病率和死亡率的主要原因。光学相干断层扫描 （OCT） 提供了有价值的血管壁信息，可以使用这些信息来优化支架植入并降低不良事件的风险。以前的研究集中在无血流现象上，指的是血管造影上的冠状动脉血流不足，这与不良的临床结果有关。在 OCT 扫描期间观察到血流中断，临床上很常见。然而，尚未系统地研究病变特征和血流中断的临床预后。因此，本研究旨在探讨 ACS 患者扫描 OCT 期间血流中断的病变特征和临床预后。此外，我们的目标是确定预测血流中断的最佳最小管腔面积 （MLA） 临界值。我们对 294 例接受 OCT 检查的血管严重狭窄患者进行了为期一年的随访。根据 OCT 扫描的远端有无血流，将患者分为无血流组 （n = 94） 或血流组 （n = 200）。在 294 名患者中，有 94 名表现出血流中断。与血流组相比，无血流组患者更有可能接受支架治疗，并且更多地接受扩张后。OCT 阻塞血液流动也会导致更多的胸痛。我们不能根据无血流组的远端 EEL 的直径来选择支架，因为无血流的远端 EEL 比有血流的远端 EEL 小。而在无血流组中，我们往往低估了病变的远端参考直径，导致更多的支架边缘夹层。预测血流中断的最佳 MLA 临界值为 1.01 mm^2（敏感性，79%；特异性，84%）。在随访年期间，36 例患者发生了 MACE。两组之间的事件发生率相当。

结论： MLA < 1.01 mm^2 可以预测血流中断，其特征是严重的管腔狭窄。血流中断不会影响 ACS 患者的短期结局。我们应该结合近端和远端参考血管直径来选择合适的支架尺寸。关键词： 光学相干断层扫描， 血流中断， 急性冠脉综合征

非罪犯血管 TCFA 斑块快速进展的的预测因素分析

于淮

哈医大附属第二医院

背景： 非罪犯血管薄帽纤维粥样硬化 （TCFA） 是急性冠状动脉患者的高危斑块特征，与不良心脏事件的风险增加相关。非罪犯病变的斑块快速进展可能导致急性心脏事件，而目前尚不清楚斑块快速进展的非罪犯 TCFA 的斑块特征和预测因子。

目的: 目前的研究旨在确定斑块快速进展的非罪犯血管 TCFA 的形态学预测因子。

方法： 选择基线手术时三支血管光学相干断层扫描 （OCT） 检查和 12 个月随访血管造影期间非罪犯血管 TCFA 的患者。评估了 OCT 上管腔狭窄和正常血管壁结构丧失的非罪犯血管病变。TCFA 的标准是 OCT 图像中的最大脂质弧 > 90°，最薄的纤维帽厚度 < 65μm。病变进展定义为基线和随访血管造影时最小管腔直径减小≥ 0.4 mm。OCT 评估非罪犯血管 TCFA 的基线形态学特征。

结果： 总体而言，在 263 例急性冠脉综合征患者中确定了 196 例非罪犯血管 TCFA; 在 12 个月的随访期间，46 例患者的 52 个病灶出现快速进展。进展组中非罪犯血管 TCFA 在基线时具有更大的最大脂质弧 （268.4±97.2° vs. 237.6±84.7°，p = 0.039），更高的脂质指数 （1695.1 [826.0-2438.9] mm° vs. 1123.7 [673.2-1840.3] mm°，p = 0.021），基线时最小纤维帽厚度更薄（45.9±14.2μm vs. 50.9±9.9μm，p = 0.020）。与无进展的非罪犯血管 TCFA 相比，在患者 （分别为 43.5% vs. 22.0%，p = 0.004 和 54.3% vs. 12.7%，p < 0.001） 和病变 （34.6% vs. 18.0%，p = 0.015 和 46.2% vs. 11.8%，分别为 p < 0.001） 水平中观察到胆固醇晶体和分层斑块的发生率更高。多变量分析确定胆固醇晶体和分层斑块是非罪犯血管 TCFA 随后快速进展的预测因子，无论患者或病变程度如何。

结论： 胆固醇晶体和分层斑块是患者和病灶水平非罪犯血管 TCFA 后续进展的预测因子。关键词：光学相干断层扫描；薄帽纤维粥样硬化；急性冠脉综合征；斑块快速进展

Influence of OCT-based Macrophage Infiltration on Periprocedural Myocardial Infarction in Patients Undergoing Elective PCI Treatment

Hao-Yi Ye[1,2], Si-Mei Cui[1,3], Ze-Jun Han[4], Xi Zhang[1,2], Qin Li[4], Lei Gao[1]

1. Senior Department of Cardiology, Sixth Medical Center of Chinese PLA General Hospital

2. Medical School of Chinese PLA

3. School of Medicine, Nankai University

4. School of Medical Technology, Beijing Institute of Technology

Background: Periprocedural myocardial infarction (PMI) following percutaneous coronary intervention (PCI) is associated with adverse outcomes. Optical coherence tomography (OCT) enables quantification of plaque macrophage infiltration (MI), a key driver of inflammation. We investigated OCT-based MI (OCT-MI) and its integration with clinical factors for predicting PCI-induced PMI.

Methods: In this prospective, single-center observational study, consecutive patients with coronary artery disease (CAD) undergoing elective PCI with pre-procedural OCT were enrolled. PMI was defined as a post-PCI cardiac troponin I (cTnI) elevation >5 times the 99th percentile upper reference limit within 48 hours. Patients were stratified into PMI and non-PMI groups. MI was analyzed at 1-mm intervals using the center of mass of the lumen as reference points. The length of MI was defined as the total length of blood vessels exhibiting macrophage signals within the image. The MI index was defined as the product of the average angle of MI and the length of MI (°·mm). Logistic regression and model comparison assessed the association between OCT-derived MI characteristics and PMI.

Results: A total of 104 patients with 116 lesions were enrolled in the study, and 38 (36.5 %) developed PMI. According to the postoperative cTnI results, 66 patients (74 target lesions) were classified into the non-PMI group, while 38 patients (42 target lesions) were categorized into the PMI group. Univariate logistic regression analysis of clinical data and laboratory results revealed that diabetes mellitus (OR: 0.309 [95% CI: 0.126, 0.757] p = 0.010) and drinking history (OR: 0.358 [95% CI: 0.150, 0.853] p = 0.020) were protective factors, whereas LDL-C (OR:1.759 [95% CI: 1.124, 2.753] p = 0.013), white blood cell count (OR:1.179 [95% CI: 1.007, 1.379] p = 0.040), and neutrophil count (OR:1.229 [95% CI: 1.020, 1.480] p = 0.030) were risk factors significantly associated with PMI. In the plaque characteristics based on OCT, it was showed that plaque rupture (OR:2.914 [95% CI: 1.249, 6.801] p = 0.013) was an independent risk factor significantly associated with PMI. Multivariable analysis identified longer MI length (OR: 1.072 [95 %CI 1.008, 1.139] p = 0.027) and higher LDL-C levels (OR: 2.010 [95 %CI 1.131, 3.573] p = 0.017) as independent predictors of PMI. Diabetes history (OR: 0.303 [95 %CI 0.107, 0.863] p = 0.025) and alcohol consumption history (OR: 0.215 [95 %CI 0.074, 0.626] p = 0.005) were protective factors, while neutrophil count (OR: 1.253 [95 %CI 1.020, 1.538] p = 0.032) was a risk factor. The model incorporating MI length (Model C, AUC = 0.807) or index (Model D, AUC = 0.813) along with clinical and other OCT features showed comparable predictive performance to the model with OCT plaque characteristics alone (Model B, AUC = 0.820). Importantly, adding MI length (Model E: AUC = 0.792) or index (Model F: AUC = 0.797) to clinical factors alone (Model A: AUC = 0.745) significantly improved prediction (NRI = 0.49 [95% CI 0.06, 0.99] and NRI = 0.52 [95% CI 0.05, 0.9], respectively).

Conclusion: This study demonstrates that OCT-quantified macrophage infiltration length is a novel and independent predictor of PMI following elective PCI, alongside established risk factors like LDL-C. Incorporating these OCT-based inflammatory metrics with clinical data significantly enhances PMI risk prediction. These findings underscore the potential of multimodal risk assessment using intracoronary imaging. Future research should focus on validating these findings in larger multicenter cohorts, refining the prediction model by incorporating systemic inflammatory biomarkers, and exploring targeted preventive strategies guided by plaque vulnerability assessment.

Key words: Periprocedural myocardial infarction, Coronary heart disease, Optical coherence tomography, Macrophage infiltration, Percutaneous coronary intervention.

Predictors of Persistent Thin-Cap Fibroatheroma in Non-Culprit Plaques at One-Year Follow-Up Among Patients with Acute Coronary Syndrome

Dirui Zhang, Bo-Ling Yi, Chen Zhao, Yi-Shuo Xu, Ning Wang, Si-Ning Hu, Hai-Bo Jia, Bo Yu

The Second Affiliated Hospital of Harbin Medical University

Thin-cap fibroatheroma (TCFA), characterized by a fibrous cap thickness <65μm overlying a lipid-rich necrotic core with circumferential extension >90°, represents a critical precursor lesion for plaque rupture and subsequent major adverse cardiovascular events (MACE). Extensive validation studies have established TCFA identification by optical coherence tomography (OCT) as an independent predictor of future adverse cardiac outcomes. The advent of serial OCT imaging provides unprecedented capability for longitudinal tracking of high-risk plaque evolution in vivo. This study leveraged serial OCT to investigate clinical, biochemical, and morphological predictors associated with the persistence of TCFA morphology in non-culprit plaques over a 1-year period in patients presenting with acute coronary syndrome (ACS). A retrospective cohort analysis was conducted on consecutive ACS patients who underwent comprehensive OCT imaging of non-culprit vessels during index percutaneous coronary intervention (PCI) and repeated OCT assessment at 12±3 months follow-up between September 2013 and August 2022 at a tertiary cardiac center. A total of 406 patients with ACS and 1,054 non-culprit plaques met the inclusion criteria, with a median follow-up duration of 369 days.

At the patient level, patients with persistent TCFA at follow-up (n=66, 16.3%) demonstrated significantly worse metabolic profiles at baseline compared to those without persistent TCFA (340, 83.7%). Those with persistent TCFA exhibited significantly higher baseline glycosylated hemoglobin (6.9% [5.8–7.8] vs. 6.0% [5.6–6.6], P=0.011), total cholesterol (138.8 mg/dL [120.6–182.0] vs. 131.8 mg/dL [114.3–160.6], P=0.038), apolipoprotein B (84.0 mg/dL [65.0–96.0] vs. 70.0 mg/dL [59.0–89.0], P=0.002), LDL-C (43.6 mg/dL [37.4–50.2] vs. 39.8 mg/dL [35.1–48.1], P<0.001), and creatinine (81.0 μmol/L [73.0–96.0] vs. 78.0 μmol/L [69.0–90.8], P=0.041), and lower HDL-C (39.7 mg/dL [35.1–48.1] vs. 43.6 mg/dL [37.4–50.2], P<0.001). Multivariate analysis identified male sex (OR: 5.094, 95% CI: 1.004–15.598), hypertension (OR: 1.800, 95% CI: 1.013–3.196), and diabetes (OR: 2.472, 95% CI: 1.397–4.372) as independent predictors.

At the plaque level, plaques retaining TCFA morphology at follow-up (n=79, 7.5%) exhibited adverse morphological features at baseline compared to those that regressed or stabilized. Persistent TCFA was associated with longer lesion length (15.5 mm [10.4–21.0] vs. 11.3 mm [8.3–15.4], P<0.001), smaller mean lumen area (6.0 mm^2 [4.5–7.9] vs. 6.9 mm^2 [5.3–8.7], P=0.002), and greater stenosis (48.6% [39.3–60.1] vs. 45.3% [35.5–57.1], P=0.047) at baseline. Macrophage presence (OR: 6.511, 95% CI: 1.978–21.439), non-culprit plaque rupture (OR: 3.849, 95% CI: 2.158–6.868), and left anterior descending artery location (OR: 2.179, 95% CI: 1.201–3.955) independently predicted persistent TCFA.

This serial OCT analysis demonstrates that persistent TCFA in non-culprit plaques—a marker of sustained high-risk plaque biology—is significantly influenced by both systemic and local factors. Systemic drivers include male sex, hypertension, diabetes mellitus, and inadequately controlled dyslipidemia (reflected by elevated Apo B and reduced HDL-C), underscoring the critical importance of aggressive secondary prevention targeting these modifiable risk factors. Locally, plaques harboring features of active inflammation (macrophages), structural vulnerability (pre-rupture), or residing in high-shear stress locations (LAD) exhibit inherent biological resistance to regression. These findings highlight the necessity for a dual-pronged therapeutic approach: intensive systemic risk factor modification combined with emerging plaque-targeted therapies (e.g., lipid-lowering beyond LDL-C goals, anti-inflammatory agents) specifically directed towards high-risk non-culprit plaques exhibiting these adverse morphological signatures. Serial OCT surveillance may thus play a future role in guiding personalized secondary prevention strategies in high-risk ACS cohorts.

IVUS 指导 PCI 对中国≥ 65 岁冠心病患者的成本效果：更低成本与更优效用的马尔科夫模型研究

桑海强 姜晓影

郑州大学第一附属医院

目的：本研究旨在评估血管内超声（IVUS）与冠状动脉造影（CAG）指导的经皮冠状动脉介入治疗（PCI）在中国医疗体系中的成本效果，探讨其在 65 岁以上冠心病患者中的经济学价值。

方法：本研究采用马尔可夫模型，模拟了一个包含 10,000 名 65 岁以上冠心病患者的队列，模拟年限为 35 年。研究从患者角度出发，比较 IVUS 指导（IVUS 组）与传统造影指导（CAG 组）的治疗策略。模型参数整合了 ULTIMATE 试验的 3 年随访数据、中国医保收费目录（2025 年）及中国人群健康效用值，采用 5% 贴现率进行终身成本效用分析。主要结局指标为增量成本效果比（ICER）。

结果：研究结果显示，IVUS 组的总成本为 83,084 元，获得的质量调整生命年（QALYs）为 9.02，而 CAG 组的总成本为 85,757 元，获得的 QALYs 为 8.55。IVUS 组较 CAG 组节省成本 2,673 元，增量效用为 0.47 QALYs，ICER 为 -5,657.60 元 /QALY，表明 IVUS 不仅降低了治疗成本，还显著提高了患者的生活质量。此外，IVUS 显著降低了靶血管血运重建率和支架内血栓率。

结论：在中国医疗定价体系下，IVUS 指导的 PCI 对 65 岁以上冠心病患者具有显著的成本节约效果，尤其在降低再次血运重建（TVR）和支架内血栓方面表现突出。本研究为未来的经济学评价提供了依据，展现了其在优化医疗资源配置和改善患者长期预后方面的潜在价值。

The impact of optical coherence tomography guidance on treatment strategy and angiographic outcome in treating in-stent restenosis compared with angiography

Yan Zuo, Xian-Qin Ma, Sen-Qing Jiang, Bo Yu

The 2nd Affiliated Hospital of Harbin Medical University

Background and purpose

The percutaneous coronary intervention of in stent restenosis (ISR) is associated with worse outcomes than the revascularization of de novo lesions. OCT (Optical Coherence Tomography) is capable of accurately identifying the composition of vascular plaque with a high-resolution before stent implantation. OCT can not only optimize surgery by immediately detecting stent complications after stenting, but also accurately analyze the causes of ISR to guide treatment and has been recommended in clinical guideline. Though, there are still limited studies on the application of OCT in guiding the diagnosis and treatment of ISR. The purpose of this study is to investigate whether OCT guidance optimizes the treatment strategy and provides better angiographic outcome than angiography guidance alone in treating ISR.

Methods

In this study, patients who presented as acute coronary syndrome and treated with drug-eluting stents or drug-coated ballons from 2017 through 2020 were retrospectively included and finished 1 year angiographic follow up. Patients were stratified into OCT guidance and angiography guidance group. Patients with chronic total occlusion, chronic kidney disease and had coronary artery bypass surgery were excluded. The index included: baseline and procedure characteristics at patient and lesion levels, quantitative coronary angiographic (QCA) data at post-procedure, including in lesion and in segment minimal lumen diameter (MLD), percent diameter stenosis (DS%), acute gain and at 1-year follow-up, including in lesion and segment MLD, DS% and late luminal loss (LLL). Acute gain was defined as post-procedural lumen diameter minus baseline lumen diameter and LLL was post-procedure lumen diameter minus target vessel diameter at follow up.

Results

Totally, 154 ISR patients and 167 ISR lesions were included in this study, 57.8% were treated with OCT guidance and 42.2% were treated with angiography guidance. The OCT guidance group had more patients with previous myocardial infarction, while the angiography group had more patients with diabetes and current smokers. The laboratory dates had no statistical difference between those two groups. In procedure strategy of patients, the OCT guidance group was inclined to use drug coated ballons (DCB) (61.9%), the drug eluting stents (DES) (60.0%) are more common under angiography guidance. At 1 year follow up, the in lesion LLL [0.09 (-0.09-0.44) mm vs. 0.33 (0.05-0.78) mm, P=0.003] was significantly lower in OCT guidance group than angiography guidance group, the same as shown in segment LLL [0.09(-0.13-0.47) mm vs. 0.37(0.04-0.64) mm, P=0.006], the MLD [2.14(1.90-2.52) mm vs. 1.75(1.37-2.11) mm, P<0.001] and [2.07(1.71-2.40) mm vs. 1.66(1.34-2.09) mm, P<0.001] was also larger in both lesion and segment under OCT guidance. Besides, OCT group showed lower DS% [16(11-26) % vs. 35(22-51) %, P<0.001] and [20(13-31) % vs. 36(28-52) %, P<0.001] in lesion and segment. The in lesion and segment acute gain [1.45 (1.22-1.79) mm vs. 1.17 (0.95-1.65) mm, P=0.004]/ (1.37±0.47mm vs. 1.22±0.40mm, P=0.029) at post procedure was larger under OCT guidance. Moreover, both in lesion and segment MLD [2.33(2.09-2.70) mm vs. 2.06(1.85-2.48) mm, P=0.001]/ (2.23±0.39mm vs. 2.08±0.40mm, P=0.015) and DS% [13(9-18) % vs. 20(13-26) %, P<0.001]/ [15(11-22) % vs. 20(14-28) %, P=0.001] were better under OCT guidance than angiography guidance at post procedure.

Conclusions

Of ACS patients with in-stent restenosis , OCT guidance treatment strategy showed larger acute gain at post-procedure and lower LLL at 1 year than angiography guidance. Besides, OCT shows advantage of optimizing the treatment strategy in ISR patients. OCT guidance might provide superior immediate and long-term angiography outcome than angiography guided only.

支架内新生动脉粥样硬化中薄帽纤维粥样斑块的危险因素及预后分析：一项基于光学相干断层扫描的观察性研究

崔思美 [1,2] 叶豪奕 [1,3] 胡鑫 [4] 袁晓航 [1,3] 韩燕 [1,3] 高磊 [1]

1. 中国人民解放军总医院第六医学中心

2. 南开大学医学院

3. 中国人民解放军医学院

4. 中国人民解放军总医院第一医学中心心内科

目的 支架内新生动脉粥样硬化（In-stent neoatherosclerosis，ISNA）是支架植入术后晚期或极晚期发生支架内再狭窄的主要机制，而薄纤维帽粥样斑块（Thin-cap fibroatheroma，TCFA）是 ISNA 重要的易损斑块特征之一。本研究目的为评估 ISNA-TCFA 病变的特点及其发生的预测因素。

方法 回顾性纳入 2010 年 1 月至 2022 年 3 月期间于中国人民解放军总医院就诊并接受光学相干断层扫描（Optical coherence tomography，OCT）检查的 175 例患者（共 194 处病变）作为研究对象。根据 OCT 观测结果分为 TCFA（-）（101 例患者、115 处病变）和 TCFA（+）（74 例患者、79 处病变）两组，比较两组的临床基线资料、冠状动脉造影特征及 OCT 数据。

结果 175 例患者中，男性 149 例，平均年龄（62.85±10.08）岁。多因素 Logistic 回归分析显示，左前降支病变是 ISNA-TCFA 的独立预测因素（OR=2.668，95%CI：1.049~6.781，P=0.039）。随访结果提示 TCFA（+）与心肌梗死事件显著相关。

结论 ISNA-TCFA 病变好发于左前降支，且此类病变显著增加心肌梗死发生风险。

OCT 指导 PCI 对中国≥ 65 岁冠心病患者的成本效果：基于马尔科夫模型的研究

桑海强 姜晓影

郑州大学第一附属医院

目的：本研究旨在评估光学相干断层扫描（OCT）与冠状动脉造影（CAG）指导的经皮冠状动脉介入治疗（PCI）在中国医疗体系中的成本效果，探讨其在 65 岁以上冠心病患者中的经济学价值。

方法：本研究采用马尔科夫模型，模拟了一个包含 10,000 名 65 岁以上冠心病患者的队列，模拟年限为 35 年。研究从患者角度出发，比较 OCT 指导（OCT 组）与传统造影指导（CAG 组）的治疗策略。模型参数整合了 ILUMIEN IV 试验的 2 年随访数据、中国医保收费目录（2025 年）及中国人群健康效用值，采用 5% 贴现率进行终身成本效用分析。主要结局指标为增量成本效果比（ICER）。

结果：研究结果显示，OCT 组的人均总成本为 94,766 元，获得的质量调整生命年（QALYs）为 8.58，而 CAG 组的人均总成本为 85,258 元，获得的 QALYs 为 8.45。OCT 组较 CAG 组增加成本 9,508 元，增量效用为 0.13 QALYs，ICER 为 71,864.55 元 /QALY，低于 2024 年我国人均 GDP（93,358 元），表明 OCT 在经济上是可接受的，能够有效改善健康结果。

结论：在中国医疗定价体系下，OCT 指导的 PCI 对 65 岁以上冠心病患者具有较高的经济学价值，虽然其成本较传统 CAG 指导更高，但通过更精准的支架植入和更低的并发症风险，显著提升了患者的长期生存质量和临床预后。基于其优异的成本 - 效益比（ICER 低于人均 GDP 阈值），该技术尤其适用于高风险病变患者，具有重要的临床推广价值。

Progression and Regression of Non-culprit Plaques Assessed by Serial Optical Coherence Tomography Imaging

Di-Rui Zhang, Bo-Ling Yi, Chen Zhao, Yi-Shuo Xu, Ming Zeng, Ning Wang, Si-Ning Hu, Hai-Bo Jia, Bo Yu

The Second Affiliated Hospital of Harbin Medical University

Background: Patients with acute coronary syndromes (ACS) face a high risk of subsequent cardiovascular events, largely originating from untreated non-culprit atherosclerotic plaques, which may rapidly progress to a high-risk status despite not meeting high-risk criteria at baseline. However, individual lesion responses exhibit substantial heterogeneity. This study aims to characterize the morphological and biochemical differences between non-culprit plaques exhibiting progression versus regression in ACS patients, using serial optical coherence tomography (OCT) imaging.

Methods: A retrospective analysis was conducted on 583 ACS patients from the Second Affiliated Hospital of Harbin Medical University between September 2013 and August 2022. After exclusions (e.g., poor image quality or missing data), 406 patients with serial OCT imaging at baseline and 1-year follow-up (9–15 months) were included, yielding 1,054 non-culprit plaques. Inclusion criteria comprised a primary ACS diagnosis (ST-segment elevation myocardial infarction [STEMI] or non-ST-segment elevation acute coronary syndromes) and de novo non-culprit plaques. OCT imaging was performed using a C7-XR/ILUMIEN system (Abbott Vascular), with analysis by independent, blinded investigators at a core lab. Plaques were classified by composition: lipid-rich plaques (LRP, maximal lipid arc >90 °), fibrous plaques, and calcified plaques (maximal calcium arc >90 °). LRP was subcategorized by fibrous cap thickness (FCT) into thin-cap fibroatheroma (TCFA, FCT <65 μm) or thick-cap fibroatheroma (ThCFA, FCT ≥ 65 μm). Patients were stratified into groups based on plaque behavior: Progression Group (at least one plaque progressing from non-TCFA at baseline to TCFA at follow-up), Regression Group (at least one plaque regressing from TCFA at baseline to non-TCFA at follow-up), and No-change Group. Statistical analyses included Shapiro-Wilk tests for normality, ANOVA or Kruskal-Wallis tests for continuous variables, chi-square or Fisher's exact tests for categorical variables, and generalized estimating equations (GEE) for serial measurements (accounting for clustered data with plaque or patient identity as random effects). Significance was defined as a two-sided P value <0.05, using SPSS 27.0. The study adhered to the Declaration of Helsinki and was approved by the institutional ethics committee, with informed consent obtained.

Results: Among 406 patients (mean age 54.7 ± 10.7 years; 81.3% male), plaque evolution analysis revealed that 11.2% of non-culprit plaques (n = 118 plaques, affecting 96 patients, 23.6%) exhibited regression (from TCFA at baseline to non-TCFA at follow-up), predominantly converting to ThCFA (92.4%) or fibrous plaques (7.6%). Conversely, 1.0% of plaques (n = 11 plaques, affecting 10 patients, 2.5%) showed progression (from non-TCFA to TCFA), all originating from ThCFA at baseline. Baseline characteristics indicated that the Progression Group (n = 10) was significantly older (64.4 ± 7.5 years vs. 53.1 ± 10.3 years in Regression Group and 54.9 ± 10.7 years in No-change Group; P = 0.005) and had a higher prevalence of diabetes mellitus (80% vs. 34.4% and 25%; P < 0.001). Culprit lesions in this group less frequently involved the left anterior descending artery (20.0% vs. 56.3% and 51.0%; P = 0.004) and favored the left circumflex artery (50.0% vs. 10.4% and 11.0%). OCT quantitative changes demonstrated significant FCT thinning in the Progression Group (geometric mean ratio [GMR] = 0.6, from 100.0 [90.0, 105.5] μm to 60.0 [55.0, 60.0] μm) versus substantial FCT thickening in the Regression Group (GMR = 2.2, from 60.0 [53.3, 63.3] μm to 120.0 [100.0, 163.3] μm; difference in change: 3.7-fold, 95% CI: 3.2–4.3; P < 0.001). Lipid arc expansion occurred in progression (mean lipid arc GMR = 1.1, max lipid arc GMR = 1.2), while regression showed reduction (mean lipid arc GMR = 0.8, max lipid arc GMR = 0.8; difference in GMR = 0.7–0.8; P < 0.001). Layered plaque prevalence increased by 17% in regression (odds ratio [OR] = 0.2, 95% CI: 0.1–0.4; P < 0.001), and calcium incidence rose significantly (9% increase; OR = 0.5, 95% CI: 0.3–1.0; P = 0.043). Lumen dimensions decreased in both groups (e.g., minimum lumen area declined), but changes were similar (P > 0.05).

Biochemical parameters at patient level revealed that the Regression Group (n = 96) had significantly greater reductions in apolipoprotein B (ApoB) (GMR = 0.7 vs. 0.8 in Progression Group; difference = 0.8, 95% CI: 0.7–1.0; P = 0.044), total cholesterol (TC) (GMR = 0.7 vs. 0.8; difference = 0.8, 95% CI: 0.7–1.0; P = 0.015), and low-density lipoprotein cholesterol (LDL-C) (GMR = 0.6 vs. 0.8; difference = 0.7, 95% CI: 0.6–0.9; P < 0.001). No significant changes occurred in high-sensitivity C-reactive protein, triglycerides, high-density lipoprotein cholesterol, glycated hemoglobin, or creatinine (all P > 0.05). Correlation analyses showed that percentage change in mean lipid arc was positively associated with percentage changes in TC (r = 0.211; P = 0.027), ApoB (r = 0.223; P = 0.033), and LDL-C (r = 0.227; P = 0.017), but minimal FCT change did not correlate with these biomarkers.

Conclusions: Non-culprit plaque regression in ACS patients is associated with microstructural stabilization, characterized by enhanced layered architecture and calcium deposition without increased vulnerability markers, alongside significant reductions in atherogenic lipids (ApoB, TC, and LDL-C). Conversely, progression involves FCT thinning and lipid arc expansion, driven by baseline ThCFA. These findings highlight the importance of intensive lipid management and OCT monitoring for personalized risk stratification in ACS survivors. The study underscores that plaque stabilization may reduce future cardiovascular events, informing secondary prevention strategies.

A Specific Subset of proinflammatory Low-Density Neutrophils Aggravates Endothelial Denudation via NET-Mediated ANXA1 Sequestration: Implications for Plaque Erosion

Cheng-Xing Liu, Xue-Bo Liu

Tongji Hospital of Tongji University, Tongji University School of Medicine, Shanghai,

Abstract

Background: Acute Coronary Syndrome (ACS) is a leading cause of global morbidity and mortality. Plaque Erosion (PE), a distinct pathological entity from Plaque Rupture (PR), accounts for a significant proportion (25-40%) of ACS cases, particularly with the widespread use of statin therapy. Neutrophils and neutrophil-mediated endothelial denudation are critically implicated in the thrombotic complications of PE. However, neutrophils are a heterogeneous population, and the precise role of specific subsets, such as Low-Density Neutrophils (LDNs), in the pathogenesis of PE remains largely undefined. This knowledge gap underscores the need to identify and characterize the specific neutrophil populations driving PE.

Methods: This study prospectively enrolled patients with ACS due to PE (PE-ACS) or PR (PR-ACS), verified by Optical Coherence Tomography (OCT). Peripheral blood mononuclear cells (PBMCs) from these patients were analyzed using single-cell RNA sequencing (scRNA-seq) to identify differential LDN populations. LDN quantification and phenotypic analysis were performed by flow cytometry in an independent cohort comprising PE-ACS, PR-ACS patients, and healthy controls (HC). Endothelial microvesicles (EMVs) and OCT-derived thrombus burden were correlated with LDN counts. Sorted LDNs and normal-density neutrophils (NDNs) underwent 4D-Data Independent Acquisition (DIA) quantitative proteomics and micro-transcriptome sequencing for comprehensive expression

profiling. Phenotypic (CD10, CD62L, CD49d) and functional assays (chemotaxis, adhesion, NETosis via Sytox Green and citrullinated histone H3) were conducted. An ApoE knockout mouse model of PE, established by left common carotid artery (LCCA) electrocautery combined with a constrictive cuff, was utilized for in vivo mechanistic investigations. These included chemokine analysis (Luminex), assessment of the therapeutic potential of a CXCR2 inhibitor (AZD-5069), and adoptive transfer experiments with murine PE LDNs (with or without the NET inhibitor GSK484). In vitro co-culture experiments using human aortic endothelial cells (HAECs) and human PE LDNs (with or without GSK484) were performed to assess endothelial injury. The impact of PE LDN-derived Neutrophil Extracellular Traps (NETs) on endothelial membrane repair was investigated using FM4-64FX assays, and the specific mechanism involving Annexin A1 (ANXA1) "wrapping" by NETs was explored, along with rescue experiments using an ANXA1 mimetic peptide.

Results: PE LDNs were found to be significantly expanded in PE-ACS patients compared to PR-ACS patients and HC. Their absolute numbers demonstrated a strong positive correlation with PE endothelial denudation, as measured by EMVs (r^2=0.4346, p<0.0001), and with culprit lesion thrombus burden (r^2=0.6885, p^-) cells, heightened activation status enhanced chemotactic and adhesive capacities, and a markedly augmented NET release upon stimulation when compared to PE NDNs and PR LDNs. The mouse model of PE recapitulated key features observed in humans, including LDN expansion and increased NET release. Elevated levels of CXCL1 and CXCL2 chemokines were detected at the site of injury, and PE LDNs displayed high expression of the chemokine receptor CXCR2, implicating the CXCL1/2-CXCR2 axis in their recruitment. Pharmacological inhibition of CXCR2 with AZD-5069 significantly ameliorated PE phenotypes in the mouse model. Adoptive transfer of murine PE LDNs exacerbated PE, an effect mediated by NETs, as pre-treatment with GSK484 attenuated these detrimental outcomes. Similarly, human PE LDNs induced HAEC apoptosis and detachment via NET release in vitro. Mechanistically, PE LDN NETs were found to impair ANXA1-mediated endothelial membrane repair by "wrapping" ANXA1. This deleterious effect was partially reversed by an ANXA1 mimetic peptide, which also led to a reduction in thrombus formation in vivo.

Conclusions: PE LDNs constitute a distinct, expanded, and highly pro-inflammatory neutrophil subset that plays a critical pathogenic role in PE-ACS. These cells are recruited to the site of erosion via the CXCL1/2-CXCR2 axis and contribute to disease progression by releasing excessive NETs. These NETs, in turn, impair ANXA1-mediated endothelial membrane repair, leading to endothelial denudation and thrombosis. These findings identify PE LDNs and their effector mechanisms as potential therapeutic targets for PE.

Keywords: Plaque erosion; Acute coronary syndrome; Low-density neutrophils; CXCR2; Neutrophil extracellular traps (NETs); ANXA1

肿瘤心脏病学有关研究

基于时间阈值的血液肿瘤患者心脏毒性动态监测研究

张铭旋

浙江大学医学院附属邵逸夫医院

背景

肿瘤治疗相关心功能损伤的早期预警亟需量化时间效应与方案特异性。本研究纳入 43 例接受化疗药物治疗的血液肿瘤患者（淋巴瘤 58.1%、骨髓瘤 27.9%、白血病 14.0%），通过系统分析探索亚临床心功能演变规律。

方法

采用治疗前后配对设计，核心监测指标包括 GLS、右室应变、左房应变、EF、平均 E/E' 及心肌做功指数。统计分析采用 Wilcoxon 配对检验评估心功能变化（效应量 Cliff's delta），Spearman 相关性检验时间间隔效应，并通过诊断分组进行亚组分析，所有 p 值经 Holm-Bonferroni 多重校正。

结果

整体分析显示 GLS 绝对值显著恶化（中位下降 0.5%，p=0.028），右室应变绝对值明显降低（中位下降 1.3%，p=0.009），同时左房应变呈现代偿性增强（中位上升 0.7%，p=0.038），而 EF 与 E/E' 未发生显著改变。

时间效应分析揭示关键规律：治疗间隔超过 2 个月的患者 GLS 恶化率达 73.7%，较≤ 2 个月组（41.7%）风险增加 2.92 倍（OR=3.92, 95%CI:1.24-12.41）；且治疗时间每延长 1 个月，GLS 恶化加速 0.16%（ρ=-0.41, p=0.003），右室损伤同步加重（ρ=-0.44, p=0.001）。

诊断分组显示差异化代偿模式：淋巴瘤患者 GLS 恶化率最高（68.0%）但 EF 维持稳定，骨髓瘤患者通过左房应变代偿激活（p=0.019），白血病患者则出现心肌效率显著下降（p=0.047）。

结论

本研究发现 2 个月为心功能损伤的关键时间阈值。GLS 及右室应变在监测化疗患者心功能变化中最明显，左房应变常呈代偿性增高。淋巴瘤患者优先追踪 GLS 变化，骨髓瘤患者重点评估左房

临床意义

本研究发现每延长 1 月治疗 GLS 恶化 0.16% 的线性规律，并揭示了骨髓瘤左房代偿的保护机制，推动肿瘤治疗时心功能监测策略的精准化革新。

Cardiovascular adverse events in Non-Small Cell Lung Cancer patients receiving osimertinib monotherapy and combination therapy: A systematic review and meta-analysis

WEIHE LIU[1], ZHENJIE AN[2], JIAN CHEN[2], JIN KANG[3], NING TAN[2], LEI JIANG*[2]

1. The First Affiliated Hospital of Harbin Medical University

2. Department of Cardiology, Guangdong Cardiovascular Institute, Guangdong Provincial People's Hospital, Guangdong Academy of Medical Sciences, Guangzhou

3. Guangdong Lung Cancer Institute, Guangdong Provincial People's Hospital

Objective: Third-generation osimertinib is recommended as a first-line treatment for significant results in patients with non-small cell lung cancer(NSCLC) with epidermal growth factor receptor (EGFR) mutations. However, prolonged EGFR inhibition has raised concerns about potential cardiotoxicity. Therefore, we conducted a single-group meta-analysis to simultaneously assess the associations between osimertinib treatment (monotherapy or combination) and cardiovascular outcomes in clinical trials and observational studies.

Methods: PubMed, Embase, Cochrane Library, and ClinicalTrials.gov were searched from inception to Jan 15, 2025. Based on PICOS (participants, interventions, comparisons, outcomes, and study design) guidelines, the Medical Subject Headings (MeSH) terms and their entry terms were: "Osimertinib", "TKI", "tyrosine kinase inhibitor", "EGFR", "epidermal growth factor receptor", "carcinoma, non small cell lung", "NSCLC", "cardiac toxicities", "cardiotoxicity", "adverse events". The search was also restricted to articles published in English. Studies considered eligible were interventional studies or observational cohort studies enrolling participants with EGFR-mutated NSCLC who received osimertinib monotherapy or combination therapy with at least one of the cardiovascular adverse events (CVAEs). All grades and grades ≥ 3 CVAEs were collected. The primary outcome was CVAEs regardless of cause, while the secondary outcome was osimertinib treatment-related CVAEs (all-grade and grade ≥ 3). Then, we calculated adverse cardiac event rates to estimate cardiotoxicity with osimertinib. A meta-analysis of the rate was conducted using the Freeman-Tukey double-arcsine transformation model. Subgroup analyses were performed to explore potential sources of heterogeneity based on types of treatment. For specific CVAEs(QTc prolongation, VTE, 3-point MACE, Cardiac arrhythmias), "previous EGFR treated", "race", and "lines of treatment" were also served as the hierarchical subgrouping variables.

Results: 9914 patients from 58 studies were included in this study. Treatment strategies included osimertinib monotherapy and combination regimens, such as MET-TKIs, anti-VEGF therapy, platinum-pemetrexed chemotherapy, other EGFR-TKIs, and immune checkpoint inhibitors. In patients with NSCLC receiving osimertinib-based therapies, the most frequent CVAEs, regardless of cause, were QT interval prolongation, pulmonary embolism(PE), venous thromboembolism (VTE), 3-point major adverse cardiovascular events (MACE), decreased left ventricular ejection fraction (LVEF), and hypertension. The pooled prevalence of hypertension was 15.94% (95% CI 9.61% to 23.39%, 27 studies, 2979 participants) for all grades and 5.86% (95% CI 2.28% to 10.67%, 13 studies, 1280 participants) for grade ≥ 3. The incidence of hypertension was significantly higher in combination with anti-VEGF therapy than monotherapy(all-grade: 43.61% versus 4.49%, grade ≥ 3:12.32% versus 1.32%). By contrast, the combination of osimertinib and MET-TKI exhibited lower rates of LVEF reduction (0.78% vs. 11.84%) and hypertension (7.14% vs. 43.61%) compared to anti-VEGF regimens, indicating a relatively favorable cardiac safety profile for MET inhibitors. Notably, the osimertinib and MET-TKI combination was associated with a higher incidence of venous thromboembolism (VTE) (all-grade: 8.47% vs. 4.00%) and deep vein thrombosis (all-grade: 6.40% vs. 4.00%) compared to anti-VEGF combination therapies. This difference may be attributed to the unique thromboembolic risks linked to MET inhibition. Additionally, patients treated with osimertinib plus platinum-pemetrexed chemotherapy showed significantly higher incidences of QT prolongation and LVEF decline versus other therapies, with no significant differences detected in other cardiovascular events. The incidence of hypertension related to osimertinib was also significantly higher in combination with anti-VEGF treatment than monotherapy(all-grade: 40.90% versus 1.30%, grade ≥ 3:17.67% versus 1.30%), consistent with the result regardless of cause.

Conclusion: This study indicates that osimertinib combination treatments are associated with an increased incidence of cardiac adverse events compared to monotherapy. Compared with other combination treatments, MET-TKI combination regimens exhibit comparatively favorable cardiac safety while presenting an increased risk of thromboembolic events. Randomized clinical trials with long-term follow-up are warranted to validate the findings and benefits.

Alox5 通过 P53/SLC7A11 通路抑制铁死亡改善阿霉素心肌病

方文熙

武汉大学人民医院（湖北省人民医院）

摘要

目的　阿霉素（DOX）是一种用于肿瘤治疗的蒽环类化疗药物。由于 DOX 诱导的心脏毒性（DIC），其临床应用受到广泛限制。研究表明，铁死亡与 DIC 的发病机制有关，脂质过氧化作为铁死亡的重要病理生理。脂氧合酶作为脂质过氧化 3 种关键酶之一，Alox5 参与 ROS 的产生。然而，Alox5 在 DIC 中的致病作用尚不清楚，本研究的目的是探讨 Alox5 在 DIC 中的作用。

方法　利用阿霉素构建小鼠的心肌病模型和原代大鼠心肌细胞模型。分别利用腺相关病毒和腺病毒在体内与体外过表达 Alox5，并在随后的实验中体内与体外实验分别应用铁死亡抑制剂 dexrazoxane，进行全身基因小鼠敲除 Alox5 和小干扰 RNA 在原代大鼠心肌细胞中敲低 Alox5。定期检测小鼠超声心动图、血流动力学、形态学染色和心肌损伤标记物。造模结束后在体内与体外实验进一步用分子生物学实验和形态学染色检测其铁死亡相关指标。并对其进行转录组测序进一步验证表型和机制，最后用分子生物学实验和形态学染色对其机制进一步正向和反向验证。

结果　在体和离体实验显示 Alox5 在 DIC 中表达显著上调。过表达 Alox5 从心功能学、血流动力学、形态学染色、心肌损伤标记物和生存分析曲线中发现到加剧 DIC。与上述过表达检测指标一致发现到敲低 Alox5 改善 DIC。接下来，对其转录组测序发现到，敲低 Alox5 在 DIC 中改善铁死亡与炎症，并通过形态学染色与分子生物学实验进一步证实。接下来发现到铁死亡抑制剂 dexrazoxane 从心功能学、血流动力学、形态学染色、心肌损伤标记物和生存分析曲线中发现到能够改善由过表达 Alox5 加剧的 DIC。最终通过前面转录组学预测的 Alox5 可能通过 P53/SLC7A11 通路抑制铁死亡改善 DIC，并通过形态学染色与分子生物学实验进一步证实。

结论　Alox5 通过 P53/SLC7A11 通路抑制铁死亡改善 DIC。

Exploration of the role and mechanism of dulaglutide in doxorubicin-induced cardiomyopathy

null null

Renmin Hospital of Wuhan University

Abstract

Objective: Doxorubicin (DOX) is an anthracycline chemotherapy drug used for tumor treatment. Due to DOX-induced cardiotoxicity (DIC), its clinical application is widely limited. Although several antioxidants such as vitamin E and N-acetylcysteine are known to alleviate DOX-induced myocardial injury, their therapeutic effects are still unsatisfactory. Dulaglutide, as a new hypoglycemic drug, is a long-acting glucagon like peptide receptor (GLP-1R) agonist, mainly used for the treatment of type 2 diabetes. In recent years, clinical studies have found that it can benefit patients with heart failure. Previous studies have shown that dulaglu-

tide is related to diabetes cardiomyopathy and myocardial hypertrophy, but the role of Dulaglutide in Adriamycin-induced cardiac toxicity is still unclear. This study aims to explore the effect of dulaglutide on DOX-induced cardiotoxicity and its possible mechanism based on the DOX-induced cardiotoxicity model, in order to provide new strategies for the clinical treatment of doxorubicin-related myocardial injury.

Methods: Construct mouse cardiomyopathy model and H9C2 cardiomyocytes model using doxorubicin. Inject dulaglutide before constructing the doxorubicin-induced cardiomyopathy model. Regularly monitor mouse echocardiography, hemodynamics, morphological staining, survival analysis curves, and myocardial injury markers. Observe the number of myocardial apoptosis in myocardial tissue through Tunnel staining, detect reactive oxygen species (ROS) in myocardial tissue through DHE staining, and detect the mRNA expression levels of BCL-2 and BAX, as well as the mRNA expression levels of antioxidant factors NQO1, GPX, and pro-oxidant factor NOX4 in myocardial tissue through real-time PCR. Western blot was used to detect the expression of apoptosis related proteins and signaling pathway proteins in myocardial tissue. After co culturing H9C2 cardiomyocytes with dulaglutide and doxorubicin for 24 hours, the activity of H9C2 myocardial tissue was detected by CCK8, the number of H9C2 myocardial apoptosis was observed by Tunnel staining, reactive oxygen species (ROS) were detected by DCFH-DA fluorescent probe technology, and the mRNA expression levels of BCL-2 and BAX, as well as the mRNA expression levels of antioxidant factors NQO1, GPX, and pro-oxidant factor NOX4 in H9C2 cardiomyocytes were detected by real-time PCR to investigate apoptosis related relationships. Western blot was used to detect the expression of apoptosis-related proteins and signaling pathway proteins in H9C2 cells. Finally, the use of PI3K inhibitors in in vitro and in vivo experiments on doxorubicin-induced cardiomyopathy further demonstrated that dulaglutide improves doxorubicin-induced cardiomyopathy through the PI3K/AKT/JNK pathway, as evidenced by cardiac function, hemodynamics, morphological staining, molecular biology, myocardial injury markers, and survival analysis curves.

Results: In vivo experiments have shown that dulaglutide can improve doxorubicin-induced cardiomyopathy based on cardiac function, hemodynamics, morphological staining, myocardial injury markers, and survival analysis curves. Dulaglutide can increase cell survival in the doxorubicin-induced cardiomyocytes injury model. Molecular biology and morphological experiments in vitro and in vivo have shown that dulaglutide intervention can increase the expression levels of anti-apoptotic markers BCL-2 and BCL-2/BAX, while reducing the protein expression level of caspase-3. And it was found that dulaglutide also reduced the ROS levels induced by doxorubicin. Dulaglutide promotes the expression of NQO1 and GPX, while reducing the level of NOX4. In PI3K inhibitor related experiments, we further found that PI3K inhibitors reduced the protective effect of dulaglutide on doxorubicin-induced cardiomyopathy from cardiac function, hemodynamics, morphological staining, myocardial injury markers, and survival analysis curves. Subsequently, molecular biology and morphological experiments further confirmed that dulaglutide mainly antagonizes doxorubicin-induced cardiomyocytes apoptosis by activating the intracellular PI3K/AKT/JNK signaling pathway.

Conclusion: Dulaglutide can improve doxorubicin-induced cardiomyopathy through the PI3K/AKT/JNK pathway.

构建肿瘤化疗病人的心血管风险事件的临床预警评估模型

薛远征

陆军军医大学第三附属医院大坪医院

摘要：

目的：随着医学水平的进步和人均寿命的延长，肿瘤和心血管病共病防治的重要性凸显，本研究旨在建立一种针对接受化疗（Chemotherapy, CT）的肿瘤患者的心血管风险事件预警评估模型，以帮助临床医生早期识别和干预潜在的心血管并发症，改善患者预后。

方法：选取 1067 名接受化疗的肿瘤患者，收集其化疗前后的临床数据，包括血压、心率、心电图、心脏超声以及各项实验室检查指标等。通过多因素分析，结合机器学习算法（如支持向量机（Support Vector Machine, SVM）和随机森林（Random Forest, RF）），构建心血管风险预警评估模型。评估模型在预测心血管事件（如心力衰竭、心肌损伤、冠状动脉粥样硬化性心脏病等）中的敏感性、特异性及准确性。

结果：该评估模型在预测心血管风险事件中的准确率达到了较高水平，敏感性和特异性均在较为理想的范围内。通过该模型，能够识别出高风险患者，并能根据预测结果提前采取预防措施，从而有效降低心血管事件的发生率。模型特别适用于化疗过程中存在心血管疾病高危因素的患者群体。

结论：肿瘤化疗病人的心血管风险显著增加，在化疗过程中预测心血管事件的风险，能够帮助临床医生制定个性化的预防和治疗方案，从而改善患者的长期预后。

Percutaneous coronary interventionlobectomy for Lung Cancer hybrid surgery: an initial case series

Jing Zeng

Department of Cardiology, Daping Hospital, The Third Military Medical University (Army Medical University), Chongqing, P.R. China

Abstract

Background For patients diagnosed with both lung cancer and severe coronary heart disease (CHD), the conflict between revascularization and lung cancer surgery remains to be settled to balance how to attenuate the cardiovascular risk for lung surgery and shorten the waiting time of anti-platelet therapy after revascularization. This study presents the percutaneous coronary intervention (PCI)-lobectomy for lung cancer hybrid surgery (PLHS), and its antithrombotic therapeutic strategy. PCI-lobectomy for lung cancer hybrid surgery (PLHS) combines the advantages of both PCI and lung cancer resection, shortening preoperative preparation time for cancer surgery, and therefore, may provide a more effective avoidance of tumor malignancy, progression, and metastasis. This pilot study aims to provide a new strategy for patients with lung cancer and severe CHD, providing physicians with the option to shorten the time to surgery and avoid tumor progression.

Methods From October 2020 to June 2023, 14 patients, with unstable angina and resectable lung cancer received PLHS. All procedures were performed in a hybrid operating room. Drug-eluting stents (DES) were implanted during PCI. Lobectomy was carried out within one hour after PCI.

Results Procedural success was 100%. All the patients subjected to PLHS were alive after 12 months of follow-up; 2 patients (14.29%) died due to distant metastasis within 12–24 months post-PLHS. There were no intraoperative complications, or 30-day- and 3-month-mortality. Except for one patient who suffered pneumothorax, no other postoperative complications, including severe bleeding, or in-stent restenosis, occurred in the 31.7±10.9 months follow-up.

Conclusions PLHS is a feasible and potentially safe option for patients with both lung cancer and severe CHD.

Keywords Coronary heart disease, Lung cancer, Percutaneous coronary intervention, Lobectomy, Antithrombotic therapy

Abstract

Background For patients diagnosed with both lung cancer and severe coronary heart disease (CHD), the conflict between revascularization and lung cancer surgery remains to be settled to balance how to attenuate the cardiovascular risk for lung surgery and shorten the waiting time of anti-platelet therapy after revascularization. This study presents the percutaneous coronary intervention (PCI)-lobectomy for lung cancer hybrid surgery (PLHS), and its antithrombotic therapeutic strategy. PCI-lobectomy for lung cancer hybrid surgery (PLHS) combines the advantages of both PCI and lung cancer resection, shortening preoperative preparation time for cancer surgery, and therefore, may provide a more effective avoidance of tumor malignancy, progression, and metastasis. This pilot study aims to provide a new strategy for patients with lung cancer and severe CHD, providing physicians with the option to shorten the time to surgery and avoid tumor progression.

Methods From October 2020 to June 2023, 14 patients, with unstable angina and resectable lung cancer received PLHS. All procedures were performed in a hybrid operating room. Drug-eluting stents (DES) were implanted during PCI. Lobectomy was carried out within one hour after PCI.

Results Procedural success was 100%. All the patients subjected to PLHS were alive after 12 months of follow-up; 2 patients (14.29%) died due to distant metastasis within 12–24 months post-PLHS. There were no intraoperative complications, or 30-day- and 3-month-mortality. Except for one patient who suffered pneumothorax, no other postoperative complications, including severe bleeding, or in-stent restenosis, occurred in the 31.7±10.9 months follow-up.

Conclusions PLHS is a feasible and potentially safe option for patients with both lung cancer and severe CHD.

Keywords Coronary heart disease, Lung cancer, Percutaneous coronary intervention, Lobectomy, Antithrombotic therapy

Prevalence and Association of Statin with Mortality Risk Among Older US Cancer Survivors with and without Coronary Heart Disease

Jiasuer Alifu, Wen-Liang Che

Department of Cardiology, Shanghai Tenth People's Hospital, Tongji University School of Medicine, Shanghai, China

Abstract

Aims: Cardiovascular disease represents a leading cause of morbidity and mortality among the expanding population of cancer survivors. Statins, primarily prescribed for cardiovascular risk reduction, possess pleiotropic effects with potential anti-cancer properties suggested in preclinical and some observational studies. This study aimed to comprehensively investigate the prevalence of statin utilization among older

U.S. cancer survivors and critically evaluate its association with all-cause mortality, cardiac-specific mortality, and cancer-specific mortality. Recognizing the complex interplay between cancer survivorship and cardiovascular health, a primary objective was to stratify these associations based on the critical factor of pre-existing coronary heart disease (CHD) status.

Methods: We conducted a prospective cohort study utilizing data from ten contiguous cycles of the National Health and Nutrition Examination Survey (NHANES), a nationally representative survey of the non-institutionalized U.S. population. Cancer survivors aged 60 years or older at baseline were identified through self-reported physician diagnosis. Statin exposure was ascertained via linkage to the NHANES Prescription Medication Database, which verifies participant-reported medication use against prescription containers. Vital status and cause of death were determined through probabilistic linkage to the National Death Index (NDI) mortality files up to December 31, 2019, utilizing ICD-10 codes for cardiac mortality (I00-I09, I11, I13, I20-I51) and cancer mortality (C00-C97). Mortality hazard ratios (HRs) and 95% confidence intervals (CIs) were estimated using multivariable Cox proportional hazards regression models, progressively adjusted for key covariates: Model 1 (minimally adjusted: age, sex, race/ethnicity); Model 2 (+ lifestyle factors: smoking status, alcohol consumption, physical activity level); Model 3 (fully adjusted: Model 2 + body mass index, diabetes status, hypertension status, estimated glomerular filtration rate, history of stroke, poverty-income ratio, and time since cancer diagnosis). Survival probabilities were visualized and compared using Kaplan-Meier curves with log-rank tests. Extensive subgroup analyses and interaction tests were performed to explore potential effect modification by demographic and clinical factors.

Results: The final analytic cohort comprised 2,714 older adult cancer survivors. The mean age was 75.47 years (standard error: 0.29 years), 1,473 (54.27%) were male, and 649 (23.91%) had a documented history of CHD at baseline. Analysis spanning ten NHANES cycles revealed a striking three-fold increase in statin use prevalence, rising from 20.0% in 1999-2000 to 56.0% in 2015-2016. This increase exhibited distinct temporal patterns when stratified by CHD status and sex. Over a mean follow-up duration of 81 months (approximately 6.75 years), crude mortality rates starkly contrasted between statin users and non-users with CHD. Statin users demonstrated significantly lower all-cause mortality (52.0% vs. 72.8%), cardiac mortality (18.3% vs. 25.9%), and cancer-related mortality (11.5% vs. 18.0%; P

Conclusion: This large, nationally representative cohort study demonstrates a significant increase in statin utilization among older U.S. cancer survivors over nearly two decades. Critically, statin use is associated with a significant reduction in the risk of all-cause, cardiac, and cancer-related mortality specifically among older cancer survivors with concomitant coronary heart disease. However, this mortality benefit pattern does not extend to cancer-specific mortality for statin users without pre-existing CHD. These findings underscore the paramount importance of considering baseline cardiovascular comorbidity, particularly CHD status, when evaluating the potential mortality benefits of statin therapy in the growing population of older cancer survivors. The results advocate strongly for a personalized medicine approach to statin prescribing in this complex patient group, emphasizing tailored risk stratification based on CHD history to optimize long-term survival outcomes beyond primary cancer treatment. Further research, including mechanistic studies and ideally randomized controlled trials, is warranted to confirm causality and elucidate the underlying biological pathways driving these differential associations based on CHD status.

肠道菌群介导心房肌焦亡促进结直肠癌相关房颤的机制研究

张航 盛力

哈尔滨医科大学附属第一医院

目的：结直肠癌（CRC）患者心房颤动（AF）患病率显著升高，严重影响患者预后。研究表明 CRC 可导致肠道菌群紊乱，而菌群紊乱在 AF 发生发展中扮演关键角色。本研究旨在明确肠道菌群是否通过激活心房肌细胞焦亡信号通路介导 CRC 相关 AF，为防治提供新靶点。

方法：纳入本院 94 例 CRC 患者，分析 AF 患病率并与中国成人标准化患病率比较。建立动物模型：1) C57BL/6 小鼠结肠原位接种 MC38 癌细胞（CRC 荷瘤组）或 PBS（Sham 组）；2) 小鼠灌胃健康人粪菌（NC-FMT 组）、CRC 患者粪菌（CRC-FMT 组）或 CRC 粪菌 + 抗生素（CRC-FMT+ANX 组）；3) CRC 荷瘤小鼠给予抗生素（CRC+ANX 组）。检测指标：小鼠心房电生理（AF 诱发率、持续时间、AERP）；心脏及结肠组织病理染色（HE/Masson/Tunel）；粪便 16S rRNA 测序；Western Blot 检测心房焦亡蛋白（NLRP3, GSDMD, Caspase-1 p20, ASC）及肠屏障蛋白（ZO1, OCC）。

结果：CRC 患者 AF 患病率（7.5%）显著高于中国标准化患病率（1.6%, P=0.0405）。动物实验显示：1) CRC 荷瘤组较 Sham 组 AF 易感性显著增加（诱发率及持续时间升高，AERP 缩短，P<0.01），心房纤维化及凋亡加重（P<0.01），肠道菌群 α 多样性降低（P<0.05），肠屏障损伤（ZO1/OCC 表达下调，P<0.01）；2) CRC 荷瘤组心房焦亡通路关键蛋白表达显著上调（NLRP3, GSDMD 等，P<0.05）；3) CRC-FMT 组呈现类似 AF 易感性增加及心房 / 肠屏障损伤，且心房焦亡蛋白升高（P<0.05），抗生素干预（CRC-FMT+ANX 组）可逆转此效应（P<0.05）；4) 抗生素清除菌群（CRC+ANX 组）显著降低 CRC 荷瘤小鼠 AF 诱发率（P=0.0291）、减轻心房重构及焦亡蛋白表达（P<0.05），并改善肠屏障功能。

结论：CRC 显著增加 AF 风险。其机制为：CRC 导致肠道菌群紊乱及肠屏障损伤，激活心房肌 NLRP3/GSDMD 焦亡信号通路，诱导心房结构重构与电生理异常，最终促进 AF 发生。靶向肠道菌群或抑制焦亡通路是潜在防治策略。

Olaparib reduces the high blood pressure caused by VEGF inhibitors

jie ma, xin Fan, xin Ma, Ying-Dong Wang, Chu-Yan Feng, Fei Si, Jing Yu

The Second Hospital of LanZhou University

Olaparib reduces the high blood pressure caused by VEGF inhibitors

Background: Poly(ADP-ribose) polymerase encompasses a family of seventeen proteins that engaged in poly or mono ADP-ribosylation, crucial for various cellular processes including DNA repair, cell death, transcription, translation, cell proliferation, and cell response to oxidative stress. PARPs play an important role in the development of cardiovascular diseases. During the progression of cardiovascular diseases, including hypertension, hypertension mediated organ damage, atherosclerosis, acute myocardial infarction, heart failure, abnormal energy metabolism in muscle cells and endothelial cells can lead to related diseases and injuries. Activation of the PARP1 in vascular smooth muscle cells could cause vascular calcification. PARP inhibitors have demonstrated specific anti-tumor activity in BRCA- and homologous recombination-deficient cancers. Moreover, PARP activation, marked by increased PAR accumulation, contributes to several pathological conditions, such as ischemia, ischemia-reperfusion injury, neurological injury, vascular disease and diabetes. Notably, PARP inhibitors, when combined with anti-angiogenic agents, not only show efficacy as monotherapy in treating epithelial ovarian cancer but also mitigate the hypertension associated with anti-angiogenic treatments.

Objectives: Poly-ADP-ribose polymerase(PARP) inhibitors have been demonstrated significant anti-tumor activity in a variety of tumors, such as ovarian cancer, breast cancer, and prostatic cancer. Anti-angiogenic drugs are mainly targeted at Vascular endothelial growth factor (VEGF) signaling pathway inhibitors (VSPIs), including small-molecule tyrosine kinase inhibitors (TKIs, e.g., sunitinib and apatinib) and monoclonal antibodies (e.g., bevacizumab). Meanwhile, some studies have found that PARP inhibitors combined with anti-angiogenic drugs have achieved significant results in the treatment of ovarian cancer compared with single drugs. While there are few studies on the vascular safety of the combination of PARP inhibitors and anti-angiogenic drugs. Therefore, we conducted this study to observe vascular function in vivo experiment treated with PARP inhibitors Olaparib in combination with VEGF inhibitors cediranib.

Methods: we select C57 model mice, and the C57 mice were randomly divided into 4 groups with 5 mice in each group. The weight of mice in each group was similar. The groups are as follows (I)control: 0.2 ml of normal saline gavage; (II)cediranib:6 mg/kg cediranib dissolved in normal saline by gavage; (III)cediranib+ olaparib: 6 mg/kg cediranib dissolved in 0.2ml of normal saline by gavage and 50 mg/kg olaparib dissolved in 0.2ml of normal saline by gavage; (IV) Olaparib: 50 mg/kg olaparib dissolved in 0.2ml of normal saline by gavage; The tail pressure of the mice was measured every 7 days and before sacrifice. The mice were placed within the instrument while the temperature was set to 34℃ . After 15–20 min of relative quiet, the systolic blood pressure (SBP), diastolic blood pressure (DBP) and mean blood pressure (MBP) were collected when the mice were awake. Measurements were performed three times every 15 s, and the average value was recorded.

Results: After 28 days of administration, blood pressure was significantly higher in the cediranib group than in the control group, the BP of the cediranib group was 122.20/92.20 ± 5.67/2.75 mmHg, which was higher than that of the control group (119.75/74.75 ± 4.27/3.33, p <0.05), However, there was no significant increase in blood pressure after combined treatment with Olaparib, the BP of cediranib group and cediranib+ Olaparib was 122.20/92.20 ± 5.67/2.75 mmHg and 110.25/71.75±5.98/2.21 mmHg(P < 0.05).

Conclusion: PARP inhibitors can relieve elevated blood pressure caused by VEGF pathway inhibitors. Ongoing and future preclinical and clinical studies are essential to further delineate the anti-tumor capabilities and cardiovascular protective effects of these compounds.

Key words: PARP inhibitors, anti-angiogenic agents, cardiovascular disease, Ovarian cancer, hypertension

Single-nucleus transcriptomics reveals the pathological process and key targets of sorafenib-induced cardiotoxicity

Dan Liu, Yani Wang, Zheming Yang, Yaling Han

State Key Laboratory of Frigid Zone Cardiovascular Disease, Cardiovascular Research Institute and Department of Cardiology, General Hospital of Northern Theater Command

Abstract

Background: Sorafenib, a multi-kinase inhibitor, is widely used in the treatment of various cancers including advanced hepatocellular carcinoma and renal cell carcinoma. However, its clinical utility is significantly constrained by dose-limiting cardiotoxicity, which manifests as a spectrum of cardiovascular complications including cardiomyocyte injury, myocardial ischemia, and arrhythmias. These cardiac complications not only severely impair patient prognosis and quality of life but also lead to treatment discontinuation, posing substantial challenges to cancer therapy. Despite its clinical significance, the key pathogenesis of sorafenib-induced cardiotoxicity remains poorly understood. The precise cell type-specific responses and molecular mechanisms driving these cardiac complications are yet to be fully elucidated. Therefore, to explore the key mechanisms and identify the key molecular is urgent for prevention and treatment of sorafenib-induced cardiotoxicity.

Methods: To determine the changes in cell composition and transcriptomic alterations of different cell types related to sorafenib-induced cardiotoxicity, we performed single-nucleus RNA-sequencing (snRNA-seq) on the hearts of sorafenib-induced cardiotoxicity mice. Through weighted gene co-expression network analysis (WGCNA), the analysis of differentially expressed genes (DEGs), intercellular communication and transcription factor, we identified the key mechanisms of sorafenib-induced cardiotoxicity.

Results: The snRNA-seq results demonstrated that sorafenib treatment induced the loss of cardiomyocytes and endothelial cells, accompanied by a shift in cellular composition characterized by fibroblast accumulation and immune cell infiltration. DEGs revealed that sorafenib-affected cell populations exhibited transcriptional signatures promoting myocardial fibrosis and inflammation, with upregulated DEGs consistently mapping to cardiomyopathy-related pathways. The elevated gene set scores were associated with cardiac fibrosis and inflammatory responses in both cardiomyocytes and fibroblasts. Correspondingly, we observed significantly enhanced cell-cell communication between these cell populations. Further analysis focused on high-frequency sorafenib-induced myocardial injury DEGs shared among cardiomyocytes, endothelial cells, and fibroblasts. The downregulated DEGs were predominantly enriched in biological functions related to antioxidant defense, fibrosis suppression, and inflammatory regulation, while the upregulated DEGs displayed dysregulation of circadian rhythm proteins (PER1, TEF). Augur analysis unequivocally identified cardiomyocytes as the cell type most profoundly affected by sorafenib treatment. To elucidate the core cellular mechanisms underlying sorafenib-mediated cardiotoxicity, we performed WGCNA analysis using the Hotspot (v1.1.1) tool on our integrated scRNA-seq/snRNA-seq dataset. This approach revealed that cardiomyocytes scored highest in module 1, which showed strong association with cardiomyopathy phenotypes. Pathological assessments demonstrated significant reduction in ejection fraction alongside compensatory upregulation of calcium signaling and myocardial contraction pathways in cardiomyocytes. These results collectively established cardiomyocytes as the primary mediators of sorafenib-induced cardiotoxicity. Transcriptional regulatory network analysis implicated the melanocyte-inducing transcription factor (MITF) as a key regulator in sorafenib-mediated cardiotoxicity. MITF upregulation and subsequent overactivation of downstream effectors appeared to function as a metabolic-inflammatory nexus. MITF may act as a metabolic-inflammatory cross-regulatory node, and intervention in its activity can improve myocardial injury and myocardial hypertrophy phenotypes.

Conclusion: Based on the first single-cell atlas of sorafenib-induced cardiotoxicity, we identified MITF as a novel master regulator driving sorafenib-mediated cardiotoxicity. Our study provides mechanistic insights into the key molecular pathways underlying sorafenib-induced cardiotoxicity and establishes a comprehensive resource for developing targeted therapies to mitigate the sorafenib-induced cardiotoxicity. Notably, we demonstrate for the first time that MITF activation promotes sorafenib-induced cardiotoxicity, uncovering its previously unrecognized role in exacerbating drug-induced cardiotoxicity. These findings position MITF as a critical metabolic-inflammatory node in Sor-induced cardiotoxicity and highlight its potential as a therapeutic target.

CREG1 Alleviates Sorafenib-Induced Cardiotoxicity via the Modulation of Necroptosis

Dan Liu, Zhe-Ming Yang, Cheng-Hui Yan, Ya-Ling Han

General Hospital of Northern Theater Command，State Key Laboratory of Frigid Zone Cardiovascular Diseases (SKLFZCD)

Background

Sorafenib (Sor) is a widely used chemotherapeutic agent that has demonstrated significant efficacy in inhibiting tumor growth and prolonging patient survival, particularly in hepatocellular carcinoma and renal cell carcinoma. However, its clinical application is limited by cardiotoxicity and adverse effects on cardiac function, which can affect up to 30% of treated patients and often necessitate dose reduction or discontinuation. Cellular Repressor of E1A-Stimulated Genes 1 (CREG1) is an endogenous lysosomal protein that has been implicated in cardioprotection and various physiological processes in the heart, such as maintaining myocardial structure, regulating cellular stress responses, and inhibiting pathological hypertrophy. Despite its potential role in cardiac health, the involvement of CREG1 in Sor-induced cardiotoxicity remains unexplored. This study aimed to comprehensively investigate the role and mechanism of CREG1 in Sor-induced cardiotoxicity, with the potential to identify a novel therapeutic target for mitigating cardiac side effects while preserving the anti-tumor efficacy of Sor.

Methods

To identify key regulatory molecules involved in Sor-induced cardiotoxicity, single-nucleus RNA sequencing (snRNA-seq) was performed on cardiac tissues from Sor-treated mice. Cardiomyocyte-specific CREG1 knockout (CREG1-CKO) and adeno-associated virus (AAV)-mediated cardiac overexpression models were established to elucidate the functional role of CREG1. Cardiac function was assessed using animal ultrasound technology, while histological analyses, quantitative RT-PCR, and Western blotting were employed to examine Sor-induced myocardial injury. The mechanism of CREG1 in Sor-induced cardiotoxicity was further explored by stimulating cultured cardiomyocytes with Sor. Flow cytometry, Western blotting, and transmission electron microscopy (TEM) were used to evaluate cardiomyocyte necroptosis. Downstream proteins directly regulated by CREG1 were identified through immunoprecipitation, mass spectrometry, immunofluorescence staining, and Western blotting. Molecular docking, dynamic simulation, and Western blotting were utilized to identify the active fragments of CREG1 involved in regulating necroptosis. Additionally, the anti-tumor effects of CREG1 were validated in HepG2 xenografts to assess its potential therapeutic impact.

Results

Our snRNA-seq analysis revealed that cardiomyocytes are the predominant cellular targets in Sor-induced cardiotoxicity, with CREG1 emerging as a key hub gene inversely associated with cardiac injury. In vivo studies demonstrated that CREG1-CKO exacerbated cardiac dysfunction, myocardial fibrosis, and hypertrophy, and significantly aggravated necroptosis in Sor-treated mice. Conversely, CREG1 overexpression exerted protective effects against Sor-induced cardiotoxicity, preserving cardiac function and reducing myocardial injury. We identified TYK2, a necroptosis-related gene, as a direct binding partner of CREG1. Mechanistically, CREG1 was found to promote TYK2 protein degradation via the lysosomal pathway, thereby reducing STAT1 activation and alleviating necroptosis. The protective effect of CREG1 on necroptosis was reversed upon TYK2 overexpression, confirming the critical role of the CREG1-TYK2 axis in Sor-induced cardiotoxicity. Furthermore, the anti-tumor efficacy of CREG1 was validated in HepG2 xenografts, demonstrating that CREG1 augmentation not only provides cardioprotection but also enhances antitumor efficacy.

Conclusion

This study identifies CREG1 as a novel regulator of necroptosis that mitigates sorafenib-induced cardiotoxicity via inhibition of the TYK2-STAT1 pathway. The dual benefits of CREG1 augmentation include cardioprotection and enhanced antitumor efficacy. These findings provide novel insights into the application of CREG1 as a therapeutic target for Sor-induced cardiotoxicity. Modulation of CREG1 expression may represent a viable strategy to enhance both the safety and efficacy of Sor therapy in clinical settings.

综述：免疫检查点抑制剂相关心肌炎的研究进展

田欣

吉林大学第二医院

免疫检查点抑制剂（ICI）在肿瘤治疗中展现出显著疗效，已被证明可通过调节免疫系统治疗各种癌症。但其引发的心肌炎（ICI-myocarditis）作为罕见但致死率高的不良反应日益受到关注。本文综述了近年 ICI 相关心肌炎的流行病学特征、病理机制、诊断标准及治疗策略的研究进展。流行病学数据显示其发病率约为 0.04%-1.14%，但病死率高达 25%-50%，且多发生于联合用药或早期治疗阶段。病理机制涉及 T 细胞过度激活导致心肌细胞损伤，可能与 CTLA-4/PD-1 信号通路抑制后免疫稳态失衡相关。诊断方面，心脏磁共振（CMR）与心肌活检的金标准地位逐步确立，而生物标志物（如肌钙蛋白、BNP）联合心电图监测提升了早期识别率。cTnI 和 hs-cTnT 等传统生物标志物敏感但缺乏特异性，而 miR-155 等新兴生物标志物则显示出组织特异性。NLR 和 CRP 等炎症标志物有助于预后，但诊断价值有限。治疗策略以糖皮质激素为基础，必要时联用免疫抑制剂（如 ATG、IVIG），但个体化方案仍需优化。本综述研究了目前关于 ICI 相关心肌的有限知识，强调了加强 ICI 相关心肌炎识别和管理的必要性，总结了相关研究的最新进展。我们讨论了流行病学、临床特征、免疫机制以及生物标志物在诊断和风险分层中的作用。通过综合当前证据，旨在增强理解并指导制定策略，以改善 ICI 相关心肌炎患者的预后

端粒酶逆转录酶缓解阿霉素诱导心脏毒性的作用研究

顾青青[1] 陈倩雯[1] 王宇[1] 蔡达贝[1] 肖婷婷[1] 王庆捷[1] 孙铃[2]

1. 南京医科大学附属常州市第二人民医院

2. 南京医科大学附属无锡市人民医院

目的

探讨端粒酶逆转录酶（TERT）缓解阿霉素（DOX）所致心脏毒性的作用。

方法 ① 细胞实验：将大鼠 H9C2 心肌细胞分为对照组（CON 组）、空载腺病毒转染组（NC 组）、TERT 过表达腺病毒转染组（TERT 组）、DOX 组（1 μmol/L DOX）、DOX+NC 组和 DOX+TERT 组（转染空载腺病毒或 TERT 过表达腺病毒 24 h 后用 DOX 处理 12 h）。采用实时荧光定量聚合酶链反应（RT-qPCR）检测心肌细胞 TERT mRNA 表达，采用免疫荧光法检测细胞线粒体膜电位水平，采用蛋白质免疫印迹试验（Western blotting）检测细胞内 Bcl-2、BAX、P62 和微管相关蛋白 1A/1B- 轻链 3（LC3）表达水平。② 动物实验：将雄性 C57BL/6 小鼠随机分为假手术组（Sham 组）、DOX 组（腹腔注射 DOX 15 mg/kg 构建急性心脏毒性损伤模型）、DOX+NC 组和 DOX+TERT 组（转染空载腺病毒或 TERT 腺病毒 7 天后制模）。制模 1 周后采用天狼猩红染色检测心肌纤维化面积，采用超声心动图检测心功能。

结果 ① 细胞实验：TERT 组心肌细胞 TERT mRNA 表达水平较 CON 组和 NC 组明显升高。与 CON 组相比，DOX 组和 DOX+NC 组心肌细胞 TERT mRNA 表达水平显著降低，线粒体膜电位水平显著降低，BAX、LC3 的蛋白表达量明显增加，Bcl-2、P62 的蛋白表达量显著降低。DOX 组与 DOX+NC 组各指标差异无统计学意义。与 DOX 组和 DOX+NC 组相比，DOX+TERT 组 TERT mRNA 表达水平升高（1.02±0.10 比 0.61±0.05、0.54±0.03，均 P < 0.01），线粒体膜电位水平显著升高（1.14±0.05 比 0.96±0.01、0.96±0.01，均 P < 0.01），BAX、LC3 的蛋白表达量明显降低，Bcl-2、P62 的蛋白表达量显著升高（BAX：0.88±0.01 比 1.31±0.02、1.26±0.01，LC3：2.16±0.05 比 2.64±0.06、2.58±0.02，Bcl-2：0.65±0.01 比 0.40±0.01、0.41±0.01，P62：0.45±0.01 比 0.23±0.02、0.29±0.01，均 P < 0.01）。② 动物实验：与 Sham 组相比，DOX 组和 DOX+NC 组小鼠心肌纤维化面积百分比显著增加，左室射血分数（LVEF）和短轴缩短率（FS）显著降低。与 DOX 组和 DOX+NC 组相比，DOX+TERT 组小鼠心肌纤维化面积百分比显著减少 (2.33±0.06 比 3.76±0.07、3.87±0.06，均 P < 0.01)，LVEF 和 FS 显著升高（LVEF：67.00±1.14 比 54.60±1.57、53.40±2.18，FS：38.60±0.51 比 30.60±1.10、30.00±0.71，均 P < 0.01）。

结论 上调 TERT 表达可抑制 DOX 引起的心肌细胞自噬及凋亡，减轻 DOX 诱导小鼠的心肌纤维化，改善心功能，进而缓解 DOX 所致心脏毒性。

基于结构修饰的线粒体衍生肽 MOTS-c 纳米递送系统对化疗相关性心功能障碍的多靶点调控机制研究

张敏 李想

上海交通大学医学院附属胸科医院

目的

探究基于结构修饰的线粒体衍生肽 MOTS-c 变体（MOTS-cv2）纳米递送系统对阿霉素（Dox）诱导的化疗相关性心功能障碍的多靶点调控机制，为克服化疗心脏毒性提供新型智能化治疗策略。

方法

1. **肽变体设计与验证**：

· 通过基因编辑优化 MOTS-c，整合 α- 螺旋增强基序及线粒体靶向序列（MTS），提升心肌靶向性和稳定性。

2. **分子机制模拟**：

· 采用高斯加速分子动力学（GaMD）模拟分析 MOTS-cv2 与 AMPKγ 亚基的结合模式（ΔG_{bind} 计算）。

3. **纳米递送系统构建**：

· 制备 MOTS-cv2@ 脂质体纳米颗粒（粒径、包封率表征）。

4. **体内外模型评价**：

· Dox 诱导心功能障碍小鼠模型：检测血清 cTnI、心脏超声（LVEF）；单细胞转录组测序分析通路变化；CRISPR-Cas9 全基因组筛选关键效应分子（STOML2）。

· 双功能肽 MOTS-DP6 设计：整合铁螯合结构域，评估心肌细胞存活率。

结果

1. **肽变体特性**：

· MOTS-cv2 心肌靶向效率较原型提高，半衰期延长。

2. **纳米递送效能**：

· 纳米颗粒粒径 **98.6 nm**，包封率 **92.3%**；显著降低血清 cTnI 水平（p<0.001），LVEF 从 **41.2%** 提升至 **58.7%**。

3. **多靶点调控机制**：

· **激活 AMPKα/ULK1 通路**：促进线粒体自噬（PINK1/Parkin 表达↑）。

· **抑制 mTORC1/SREBP1 轴**：降低铁死亡关键因子（ACSL4、LOX 表达↓。

· CRISPR-Cas9 筛选验证 **STOML2** 为调控 OXPHOS 的核心效应分子（sgRNA 富集 >**9.4 倍**）。

4. **双功能肽优势**：

· MOTS-DP6 使心肌细胞存活率达 **89.3%**（较单功能肽↑），兼具 AMPK 激活与铁死亡抑制功能。

结论

MOTS-cv2 纳米递送系统通过**双重调控机制**（激活 AMPKα/ULK1 自噬通路 + 抑制 mTORC1/SREBP1 铁死亡轴）显著改善 Dox 诱导的心功能障碍。基于深度突变扫描设计的双功能肽 MOTS-DP6 进一步整合铁螯合能力，为开发新一代抗化疗心脏毒性制剂提供了智能化策略。

Blood Leukocyte Counts and Multimorbidity of Cancer and Cardiometabolic Diseases: A Prospective Cohort Study in UK Biobank

Fei-Yuan Han, Song-Cai Xie, Peng Zhao, Zhong-Zhi Yu, Cheng Jin, Jin-Wei Tian

哈尔滨医科大学附属第二医院

Aims: The role of blood leukocyte counts, including total and subtypes, in influencing the dynamic progression from a healthy state to cancer or cardiometabolic disease (CMD), and subsequently to multimorbidity and death, remains insufficiently understood. CMD refers to chronic conditions such as coronary heart disease (CHD), type 2 diabetes (T2D), and stroke. These conditions often coexist with cancer in later life stages, constituting a significant multimorbidity pattern with complex clinical trajectories and outcomes. As the global burden of multimorbidity rises, identifying early biomarkers that reflect systemic inflammatory states becomes crucial for guiding preventive strategies and reducing downstream complications.

Methods: We analyzed data from 391,791 participants aged 40–70 years in the UK Biobank who were free of cancer and CMD at baseline. Multimorbidity was defined as the coexistence of both cancer and CMD, regardless of the order of diagnosis. Leukocyte counts and five subtypes (neutrophils, lymphocytes, monocytes, eosinophils, and basophils) were measured at baseline. Using multi-state models and restricted cubic splines, we evaluated the associations between leukocyte levels (in percentile categories) and all transitions between healthy state, cancer, CMD, multimorbidity, and death. Models were adjusted for demographic, lifestyle, and clinical factors. We further estimated 10-year transition intensities to quantify the impact of leukocyte levels on disease trajectories.

Results: During a median follow-up of 12.8 years, 42,029 participants developed cancer, 43,572 developed CMD, 8,136 progressed to cancer–CMD multimorbidity, and 26,224 died. Elevated leukocyte counts, particularly in the 75th–95th and >95th percentiles, were positively associated with most disease transitions. For example, individuals in the 75–95th percentile of total leukocyte count had a modestly increased risk of cancer from a healthy state (HR: 1.07, 95% CI: 1.05–1.10), but a substantially higher risk of transitioning from CMD to multimorbidity (HR: 1.22, 95% CI: 1.13–1.33). Neutrophils showed a similar pattern. These associations were more pronounced in older adults and consistent in multiple sensitivity analyses. Notably, transition intensities from CMD to multimorbidity were higher than from a healthy state to CMD, suggesting a cumulative effect of inflammation.

Conclusions: Leukocyte counts, especially elevated neutrophils, play differential and stage-specific roles in the progression of chronic disease. Our findings highlight a stronger link between elevated leukocyte levels and the transition from CMD to multimorbidity than from a healthy state to cancer. This suggests that low-grade, chronic inflammation in CMD patients may accelerate the development of cancer and compound disease burden. These results underscore the pivotal role of systemic inflammation—mediated by leukocyte activity—in facilitating pathological interactions between metabolic and oncological diseases. Furthermore, leukocytes may contribute to an unfavorable tumor microenvironment and promote oncogenic transformation through secretion of cytokines, chemokines, and proteolytic enzymes. The observation that leukocyte-related risk was more pronounced in transitions involving T2D supports previous evidence linking insulin resistance, immune dysregulation, and cancer risk. From a clinical perspective, routine assessment of leukocyte counts—often available in standard blood panels—may offer a cost-effective tool for identifying high-risk individuals who could benefit from enhanced monitoring or early preventive strategies. This large-scale, prospective study provides novel epidemiological evidence supporting inflammation-driven pathways linking cardiometabolic and oncological disease processes. Future research should explore potential therapeutic approaches targeting chronic inflammation to delay or interrupt these adverse disease trajectories.

临床试验中 PD-1/PD-L1 抑制剂联合治疗的心血管相关不良事件：一项系统综述和荟萃分析

于东源

大连医科大学附属第一医院

目的：

免疫疗法使癌症治疗迎来革新变化。以 PD-1/PD-L1 抑制剂为代表的免疫检查点抑制剂可显著提升晚期癌症患者生存率。然而，该类药物的使用常常伴随严重的心血管毒性，导致癌症患者在其生存期内心血管事件发生率明显升高，成为威胁其生命安全的重要隐患。本研究对多篇随机对照临床试验结果进行系统回顾及荟

萃分析，旨在明确 PD-1/PD-L1 抑制剂心血管毒性发生风险，确定不同心血管事件的发生率和高危特征，并对其发生机制进行探讨，为 PD-1/PD-L1 抑制剂的药物管理及安全应用提供新的依据。

方法：

在 PubMed、Embase 以及 Cochrane 数据库中搜索 2015 年 1 月至 2022 年 5 月发表的论文，搜索词为“PD-1”、“PD-L1”、“combination”、“cardiovascular”、“cardiac”以及“clinical trials”，纳入相关临床试验，统计心血管事件发生情况及其临床特征。从每项纳入的研究中提取作者、出版年份、患者临床基线资料、癌症类型、PD-1 和 PD-L1 抑制剂名称、联合药物名称、接受联合治疗的患者总样本量、发生心血管不良事件数等主要参数。应用具有 Logit 转换的随机效应模型对心血管不良事件总体发生率及其特征进行荟萃分析，采用 I^2 评估研究间的异质性。所有分析均使用 Stata18.0、R 统计软件（3.6.1 版本）和 RevMan5.3 软件完成。

结果：

本研究通过检索和筛选，最终纳入 23 篇文献进行 Meta 分析。我们发现：1. 与安慰剂相比，PD-1/PD-L1 抑制剂呈现出更高的心血管事件发生率 [RR = 1.19，95%CI（1.11，1.29），I^2 = 45%，P < 0.00001]；2. 对不同心血管事件进行亚组分析发现，与安慰剂组相比，使用 PD-1/PD-L1 抑制剂的患者冠心病 [RR=1.77，95% CI（1.18，2.64），P=0.005]、心律失常 [RR=1.36，95% CI（1.03，1.79），P=0.03]、心力衰竭 [RR=2.14，95% CI（1.44，3.20），P=0.0002] 及低血压 [RR=1.45，95% CI（1.07，1.96），P=0.02] 的发生率显著升高；3. 对不同的癌症种类进行亚组分析发现，在肺癌 [RR=1.44，95% CI（1.13，1.84），P=0.003]、多发性骨髓瘤 [RR=2.57，95% CI（1.40，4.70），P=0.002]、尿路上皮癌 [RR=1.60，95% CI（1.15，2.24），P=0.005] 以及头颈部鳞状细胞癌 [RR=1.54，95% CI（1.09，2.17），P=0.02] 患者中，PD-1/PD-L1 抑制剂的心血管不良事件发生率明显升高；4. 通过对 PD-1/PD-L1 抑制剂联合不同治疗方案的心血管事件发生风险进行统计，我们发现 PD-1/PD-L1 抑制剂联合靶向药物治疗组心血管事件总体发生率最高 [IR=0.40，95% CI（0.38，0.42），P < 0.0001]。

结论：

本研究发现，与安慰剂相比，PD-1/PD-L1 抑制剂的使用显著增加了心血管毒性的发生风险，包括冠心病、心律失常、心力衰竭以及低血压等。肺癌、多发性骨髓瘤、尿路上皮癌以及头颈部鳞状细胞癌患者具有更高的心血管不良事件发生率。PD-1/PD-L1 联合靶向药物治疗组心血管不良事件总体发生率最高。在联合化疗时高血压出现较多，联合靶向药物治疗时同样以高血压更为常见，而联合其他免疫治疗方案的患者心律失常和高血压均较为多见。

Antiplatelet Use and Mortality in Cancer Patients With and Without Coronary Artery Disease

Wenliang Che

Department of Cardiology, Shanghai Tenth People's Hospital, Tongji University School of Medicine, Shanghai, China

Abstract

Background: Antiplatelet agents, such as low-dose aspirin and clopidogrel, are widely prescribed to prevent cardiovascular events in patients with coronary artery disease (CAD). Emerging evidence suggests that these medications may also influence cancer risk and mortality, though findings across studies have been inconsistent. Some research indicates that antiplatelet drugs could inhibit tumor progression by reducing platelet-mediated angiogenesis or metastasis, while other studies report no significant benefits or even potential harms. This study aims to clarify the relationship between antiplatelet use and mortality in cancer patients, with a focus on distinguishing outcomes between those with and without comorbid CAD. By analyzing a large, nationally representative cohort, we seek to provide clearer guidance for clinical decision-making in this complex patient population.

Methods: We conducted a prospective cohort study using data from four cycles of the National Health and Nutrition Examination Survey (NHANES), linked to mortality records through 2019. The study included 2,099 adult cancer patients (mean age: 66.7 years; 47.5% male), of whom 349 (16.6%) had a history of CAD. Antiplatelet exposure was identified via prescription registries, with primary focus on low-dose aspirin and clopidogrel. Mortality outcomes were categorized as all-cause, cardio-cerebrovascular (CCD), and cancer-related. Survival analyses were performed using Kaplan-Meier curves to compare mortality rates between antiplatelet users and non-users. Cox proportional hazards regression models were employed to estimate hazard ratios (HRs), adjusting for potential confounders such as age, sex, smoking status, body mass index, comorbidities (e.g., diabetes, hypertension), and cancer type. Subgroup analyses were conducted to evaluate differences between CAD and non-CAD patients.

Results Among the 2,099 cancer patients, aspirin and clopidogrel use were significantly more prevalent in those with CAD (66.8% and 16.6%, respectively) compared to non-CAD patients (39.1% and 1.9%). Over a median follow-up of 52 months, aspirin use in CAD patients was associated with lower all-cause mortality (24.9% vs. 37.9%, P=0.012) and CCD mortality (8.6% vs. 15.5%, P=0.040). In contrast, among non-CAD patients, aspirin use was linked to higher all-cause mortality (18.9% vs. 14.9%, P=0.030) and CCD mortality (5.0% vs. 2.4%, P=0.005). Similarly, clopidogrel use in non-CAD patients was associated with increased mortality risks. Fully adjusted Cox models revealed that aspirin use in CAD patients was independently associated with reduced all-cause mortality (HR: 0.50; 95% CI: 0.31–0.81), CCD mortality (HR: 0.40; 95% CI: 0.18–0.89), and cancer-related mortality (HR: 0.37; 95% CI: 0.19–0.72). However, in non-CAD patients, neither aspirin nor clopidogrel use showed a statistically significant association with mortality after full adjustment for covariates.

Conclusion This study demonstrates a divergent effect of antiplatelet therapy on mortality in cancer patients depending on CAD status. Aspirin use was associated with significant survival benefits in cancer patients with CAD, potentially due to its dual role in mitigating cardiovascular risk and modulating cancer progression. Conversely, in non-CAD patients, aspirin and clopidogrel were linked to increased mortality in unadjusted analyses, though these associations did not persist after adjustment for confounding factors. These findings underscore the importance of individualized treatment strategies, emphasizing antiplatelet therapy for cancer patients with CAD while cautioning against routine use in those without cardiovascular indications. Further research is needed to explore the mechanisms underlying these observations and to validate these results in diverse populations.

脯氨酸合成限速酶 P5CS 在阿霉素诱导心肌病中的保护作用

汪雪华 [1,2,3] 汪朝晖 [1,2,3]

1. 华中科技大学同济医学院附属医院协和医院

2. 华中科技大学同济医学院附属协和医院生物靶向治疗湖北省重点实验室

3. 华中科技大学同济医学院附属协和医院湖北省心血管疾病免疫诊疗工程研究中心

目的：吡咯啉 -5- 羧酸合酶（P5CS）是脯氨酸合成的限速酶，具有多种复杂的生物学功能，其功能受损与多种疾病有关。本研究旨在探讨 P5CS 与阿霉素（doxorubicin, DOX）诱导的心脏毒性（DIC）之间的相关性，并重点解析其潜在作用机制。

方法：基于 GEO 数据库筛选 DIC 数据集，分析脯氨酸代谢关键酶 mRNA 的表达，并采用 DOX 诱导 DIC 小鼠模型（15mg/kg 单次腹腔注射）和刺激 H9C2 细胞（2μm）进行体内和体外验证。通过尾静脉注射 AAV-9 过表达 P5CS 构建转基因小鼠模型，随后诱导 DIC（n=10/ 组）。体外实验采用慢病毒转染 H9C2 细胞过表达 P5CS，同步评估 DOX 心肌毒性。结合超声心动图、组织学（HE/Masson 染色）评估心功能及病理改变，运用 WB、PCR、免疫荧光检测关键分子表达与定位，通过 CO-IP、亚细胞分离等技术挖掘作用通路。同步整合蛋白质数据库（PDB）、CB-DOCK2 和蛋白质变构位点服务器（PASSer）数据库等数据库进行 P5CS 结构预测。

结果：DOX 导致心脏 P5CS 表达下调。P5CS 的过表达提高了其蛋白质丰度，促进了 P5CS 丝的组装，增强了 P5CS 的结构稳定性。基于 PDB、CB-DOCK2 和 PASSer 数据库的预测分析，观察到 DOX 可能诱导 P5CS 蛋白的结构变化。Co-IP 和质谱结果显示，P5CS 在 DIC 中与心肌肌动蛋白 A1（ACTC1）相互作用，促进聚合肌动蛋白（F-actin）解离，球状单体肌动蛋白（G-actin）增加。MKL1 与细胞质 G- 肌动蛋白结合，抑制其核转位，从而抑制 SRF/BCL2 通路并增强细胞凋亡。此外，我们发现 P5CS 对心肌线粒体具有保护作用。过表达 P5CS 可以减少 DOX 诱导的线粒体断裂、ATP 耗竭、活性氧（ROS）激增和线粒体膜电位破坏。

结论：本研究将脯氨酸合成限速酶 P5CS 与 DIC 联系起来，并突出 P5CS 可能是 DIC 治疗的可行靶点。

外泌体介导肿瘤心脏病理通讯加重阿霉素心肌毒性的机制研究

马焱 [1,2,3] 王勇军 [1,2,3] 陈仁政 [1,2,3] 王亚斌 [1,2,3] 方岩 [1,2,3] 秦诚 [1,2,3] 王天虎 [1,2,3] 沈晓影 [1,2,3] 周廷文 [4] 田磊 [1,2,3] 孙婷 [1,2,3] 范利 [1,2,3] 王小宁 [5] 韩东 [1,2,3] 曹丰 [1,2,3]

1. 中国人民解放军总医院 (301 医院)

2. 国家老年疾病临床研究中心

3. 中国人民解放军总医院第二医学中心

4. 华中科技大学附属同济医院

5. 复旦大学生命科学院

目的：阿霉素 (Doxorubicin, DOX) 是乳腺癌最有效的化疗药物之一，但常伴有严重的心脏毒性。深入研究肿瘤与心脏之间的跨器官通讯机制并寻找潜在的干预靶点对减轻其副作用至关重要。本研究旨在探索 DOX 处理后的乳腺癌细胞 (Breast Cancer Cells, BCCs) 通过外泌体 (Exosomes, EXOs) 对心肌细胞损伤的影响及其分子机制。

方法：采用共培养系统观察乳腺癌细胞对 DOX 诱导的心脏毒性 (DOX-induced cardiotoxicity, DOXIC) 的影响。提取并纯化乳腺癌细胞外泌体 (Exosomes derived from BCCs, BCC-EXOs)，检测其对成年小鼠心室肌细胞 (Adult Murine Ventricular Cardiomyocytes, AMVC) 和人诱导多能干细胞来源的心肌细胞 (Human Induced Pluripotent Stem Cell-derived Cardiomyocytes, hiPSC-CMs) 焦亡的影响。建立原位乳腺癌小鼠模型和患者来源乳腺癌小鼠模型，探讨外泌体是否能在体内加重 DOXIC。通过外泌体 miRNA 测序和机制研究鉴定 BCC-EXOs 中发挥关键作用的 miRNAs；结合生物信息学分析和实验验证，采用 RNA-pull down、EMSA、ChIP-PCR 等实验探索 miRNAs 在 BCC-EXOs 中上调和分选进入外泌体的机制。采用荧光素酶报告实验验证 miRNAs 的下游分子靶点及促焦亡通路。

结果：细胞实验证实，心肌细胞与乳腺癌细胞共培养以及 BCC-EXOs 处理均可加重 DOX 诱导的心肌细胞损伤和焦亡。在体实验表明，在原位乳腺癌小鼠模型和患者来源乳腺癌小鼠模型上 DOXIC 损伤更为严重。通过 Dicer 基因敲除清除乳腺癌细胞外泌体中的 miRNA 可阻断加重 DOXIC 的效应。外泌体 miRNA 测序、qPCR 和拯救实验表明 miR-216a-5p 在 BCC-EXOs、乳腺癌小鼠血浆中高表达，并且是发挥促焦亡效应的关键分子。CHIP-PCR 实验表明，DOX 诱导乳腺癌细胞的转录因子 ATF3 表达升高，促进乳腺癌细胞中 pri-miR-216a 的转录，从而上调乳腺癌细胞中 miR-216a-p 的水平。而 RNA-pull down、EMSA 实验表明，mi-216a-5p 经过 RNA 结合蛋白 SF3B4 的分选进入外泌体。外泌体摄取实验表明，外泌体中的 miR-216a-5p 通过血液运输，被心肌细胞摄取。在心肌细胞中，miR-216a-5p 与 E3 泛素蛋白连接酶 ITCH 的 mRNA 的 3'UTR 区域结合后导致 ITCH 的 mRNA 降解，进而导致焦亡相关蛋白 TXNIP 的泛素化降解途径受阻，TXNIP 表达升高，激活了 TXNIP/NLRP3 炎症小体通路，诱发心肌细胞焦亡，加重 DOXIC。

结论：本研究发现乳腺癌细胞与心肌细胞之间通过传递促焦亡外泌体从而加重 DOX 诱导的心脏损伤。具体机制是 DOX 诱导的乳腺癌细胞外泌体将 miR-216a-5p 转运至心肌细胞，激活 ITCH/TXNIP/NLRP3 炎症小体通路，促使心肌细胞发生焦亡。靶向病理性外泌体释放或阻断 miR-216a-5p 可能是减轻 DOXIC 的有效策略。本研究揭示了 DOX 化疗过程中肿瘤 - 心脏相互作用的新机制，为减轻化疗所致心脏毒性提供了新的干预靶点和理论基础。

HFA-ICOS 评分对乳腺癌及淋巴瘤患者肿瘤治疗相关心功能不全的预测效能研究

单翀 鞠明月 杨玫 张艳丽 张新鑫 陈学甫 李佳 方凤奇 孙秀丽 夏云龙 刘莹

大连医科大学附属第一医院

【摘要】目的 探讨 HFA-ICOS 评分对中国乳腺癌及淋巴瘤患者肿瘤治疗相关心功能不全（CTRCD）的预测效能。**方法** 本研究为单中心回顾性队列研究，纳入 2018 年 2 月至 2025 年 2 月于大连医科大学附属第一医院应用蒽环类药物治疗的乳腺癌及淋巴瘤患者。患者基线时接受心脏生物标志物及超声心动图检查，包括左心室射血分数及左心室整体纵向应变，并于蒽环类药物治疗开始后 12 个月内至少进行了 1 次病房随访，收集蒽环类药物治疗开始后 1、3、6、12 个月超声心动图及生物标志物数据，并依据检查结果判断是否发生 CTRCD。根据基线 HFA-ICOS 评分模型将患者分为低危、中危、高危及很高危组。应用 Kaplan-Meier 生存曲线分析不同 HFA-ICOS 风险分层下 CTRCD 的累积发生概率。应用单因素 Cox 比例风险回归模型评估基线 HFA-ICOS 风险分层对 CTRCD 的影响。以各随访时间点受试者工作特征曲线、校准曲线、决策曲线评估 HFA-ICOS 模型的预测效能及临床决策中的效用。**结果** 共纳入 286 例患者，其中男性 33 例（11.5%），年龄 55（44，61）岁。按照基线 HFA-ICOS 评分分组，低危患者 228 例（79.7%），中危 49 例（17.1%），高危及很高危共 9 例（3.1%）。随访时间 111（70，210）d，共 113 例（39.5%）患者出现 CTRCD。不同 HFA-ICOS 风险分层患者 CTRCD 随时间发生风险有统计学差异（$P_{log\text{-}rank}$ < 0.001）。单因素 Cox 风险比例回归分析结果显示，相比于低危患者，中危（HR=1.95，95%CI 1.22~3.00，P=0.006）和高危及很高危患者的 CTRCD 发生风险增加（HR=4.12，95%CI 1.66~8.54，P=0.004）。受试者工作特征曲线显示，1、3、6 及 12 个月时，HFA-ICOS 评分预测 CTRCD 的曲线下面积分别为 0.532、0.597、0.600 及 0.577。校准曲线显示，1、3、6 及 12 个月的 Brier 分数分别 为 0.041（95%CI 0.013~0.067），0.144（95%CI 0.115~0.173），0.232（95%CI 0.215~0.249）及 0.236（95%CI 0.220~0.251）。临床决策曲线表明，1 个月时风险阈值在 0.15~0.18、3 个月时风险阈值在 0.10~0.50、6 和 12 个月时风险阈值在 0.30~0.70 进行临床干预可有净获益。**结论** HFA-ICOS 评分可预测应用蒽环类药物的乳腺癌、淋巴瘤患者 CTRCD 的发生，但其预测效能欠佳，该评分仍需在大样本人群进一步验证。

Imaging study of cardiac dysfunction related to anti-tumor therapy in tumor patients: clinical value of cardiac magnetic resonance imaging

Minglong Zheng, Zhi-Jiao Lu, Tong-Sheng Huang, Yan-Ni Wu, Yao Xiao, Rui-Yang Tang, Li Li, Jing-Feng Wang, Yu-Ling Zhang

SUN YAT-SEN MEMORLAL HOSPITAL,SUN YAT SEN UNIVERSITY

Abstract

Background:

Heart failure with preserved ejection fraction (HFpEF) frequently coexists with type 2 diabetes mellitus (T2DM), and this comorbidity is associated with worse clinical outcomes. While glycaemic control is essential, accumulating evidence suggests that insulin therapy may paradoxically increase the risk of adverse cardiovascular events in these patients. This phenomenon, often termed the "insulin paradox," remains poorly understood and may be related to the underlying heterogeneity among insulin-treated individuals. Latent Class Analysis (LCA), a statistical method used to identify hidden subgroups within complex populations, offers a promising approach to better characterise this heterogeneity and inform personalised treatment strategies. This study aimed to identify clinically distinct phenotypes among insulin-treated HFpEF patients with T2DM using LCA and to evaluate their prognostic relevance.

Methods:

This retrospective study used data from the TOPCAT (Treatment of Preserved Cardiac Function Heart Failure with an Aldosterone Antagonist) trial, which enrolled patients with HFpEF across multiple international centres. After excluding patients with missing key clinical variables, a total of 3,416 participants were included in the analysis. Patients with T2DM were divided into insulin-treated and non-insulin-treated groups. Among the 401 insulin-treated patients, LCA was performed using 20 variables related to cardiovascular risk, metabolic status, comorbidities, and treatment history. Two distinct insulin-treated subgroups were identified: a "compensated" group with relatively stable clinical parameters and a "decompensated" group characterised by worse metabolic and haemodynamic profiles. Baseline characteristics and outcomes were compared across four groups: decompensated insulin group, compensated insulin group, non-insulin-treated diabetics, and non-diabetic HFpEF patients. The primary outcomes were all-cause mortality, cardiovascular mortality, heart failure hospitalisation, stroke, and myocardial infarction. Cox proportional hazards models were used to assess the association between group membership and clinical outcomes, adjusting for potential confounders.

Results:

The mean age of the cohort was 68.4 years, and 48.3% were male. During a median follow-up of 3.37 years, 660 patients experienced a composite cardiovascular event, including 333 cardiovascular deaths and 440 hospitalisations for heart failure. Among insulin-treated patients, the decompensated group (n=197) exhibited significantly higher rates of adverse outcomes compared to the non-insulin-treated group. In adjusted analyses, this group had a 74.9% increased risk of all-cause mortality (HR 1.749, 95% CI 1.266–2.417, p=0.001) and a 68.8% higher risk of composite cardiovascular events (HR 1.688, 95% CI 1.262–2.258, p<0.001). Conversely, the compensated insulin group showed no significant difference in outcomes compared to patients treated with oral hypoglycaemic agents. A secondary analysis in obese diabetic patients (n=3,109) yielded consistent findings, further supporting the detrimental impact of insulin decompensation on prognosis.

Conclusion:

In patients with HFpEF and T2DM, insulin therapy is not uniformly associated with poor outcomes; rather, the increased risk appears to be concentrated in a distinct subgroup characterised by metabolic decompensation. These findings highlight the importance of phenotyping insulin-treated patients and suggest that LCA may be a valuable tool for risk stratification. Identifying patients at high risk of insulin-related adverse effects could improve treatment individualisation and potentially mitigate the risks associated with intensive insulin therapy. Further prospective studies are needed to validate these phenotypes and explore alternative strategies for glycaemic control in this high-risk population.

Percutaneous Coronary Intervention-Lobectomy for Lung Cancer Hybrid Surgery: An Initial Case Series

JUNYI YU

Department of Cardiology, Daping Hospital, The Third Military Medical University, Chongqing, P. R. China.

Background

The management of patients diagnosed with both lung cancer and severe coronary heart disease (CHD) presents a significant clinical dilemma. On one hand, lung cancer surgery (e.g., lobectomy) carries a high cardiovascular risk, particularly in patients with unstable angina or critical coronary stenosis. On the other hand, percutaneous coronary intervention (PCI) with drug-eluting stents (DES) necessitates dual antiplatelet therapy (DAPT) to prevent stent thrombosis, which increases bleeding risks during major surgery. Traditionally, lung cancer surgery is delayed for weeks or even months after PCI to allow for DAPT completion, potentially compromising oncological outcomes due to tumor progression. Conversely, proceeding with surgery too soon after PCI may lead to catastrophic stent thrombosis. To address this challenge, we developed a novel hybrid surgical approach—Percutaneous Coronary Intervention-Lobectomy for Lung Cancer Hybrid Surgery (PLHS)—which integrates PCI and lobectomy in a single session within a hybrid operating room. This strategy aims to minimize cardiovascular risk during lung surgery while avoiding prolonged delays in cancer treatment. Additionally, we propose an optimized antithrombotic regimen to balance bleeding and thrombosis risks.

Methods

From October 2020 to June 2023, 14 patients with unstable angina and resectable non-small cell lung cancer (NSCLC) underwent PLHS. All procedures were performed in a hybrid operating roomequipped with advanced angiographic and surgical capabilities. The protocol consisted of: PCI with DES implantation to revascularize critical coronary lesions. Immediate lobectomy (within 1 hour post-PCI) to minimize the interruption of antiplatelet therapy. A tailored antithrombotic strategy: Pre-PCI: Intravenous heparin was administered. Post-PCI: A shortened DAPT regimen (aspirin + clopidogrel for 1 week) was used, followed by single antiplatelet therapy (aspirin alone) to reduce bleeding risk. Intraoperative anticoagulation management: Heparin was reversed with protamine before lobectomy to prevent excessive bleeding. Patients were closely monitored for perioperative complications, including bleeding, stent thrombosis, myocardial infarction, and

surgical morbidity. Follow-up was conducted at 1, 3, 6, and 12 months, with extended surveillance up to 31.7 ± 10.9 months.

Results

Procedural success rate was 100%—all patients underwent successful PCI and lobectomywithout intraoperative complications. No 30-day or 3-month mortality occurred, demonstrating the short-term safety of PLHS. Long-term survival: All patients survived the first 12 months post-PLHS. However, two patients (14.29%) died between 12-24 months due to distant metastasis, unrelated to cardiovascular events. Postoperative complications: Only one patient (7.14%) developed pneumothorax, which was managed conservatively. No severe bleeding, stent thrombosis, or in-stent restenosis was observed during follow-up. Oncological outcomes: The immediate surgical approach prevented delays in cancer treatment, with no cases of tumor progression during the waiting period.

Conclusions

PLHS represents a feasible and potentially safe treatment strategy for patients with concomitant lung cancer and severe CHD. By integrating PCI and lobectomy in a single session, this hybrid approach minimizes cardiovascular risks while avoiding delays in cancer surgery. The optimized antithrombotic strategy (shortened DAPT followed by aspirin monotherapy) effectively balances thrombotic and bleeding risks. Our findings suggest that PLHS could be a viable alternative to staged procedures, particularly in high-risk patients requiring urgent cancer resection. Future studies with larger cohorts and randomized comparisons are needed to further validate its safety and efficacy. If confirmed, PLHS may become a standardized protocol for managing this complex patient population, improving both cardiovascular and oncological outcomes. This study highlights the importance of multidisciplinary collaboration between cardiologists, thoracic surgeons, and anesthesiologists in optimizing treatment for patients with dual cardiothoracic pathologies.

Qili Qiangxin capsules alleviated Doxorubicin-induced cardiotoxicity by inhibiting ferroptosis through Lipid Peroxidation

tong-sheng huang[1,2,3,4], Yi-GuLiABuDuKeReMu A[1,2], Hong-Lin Ren[5,6], Zhi-Xiong Cai[3], Yu-Ling Zhang[1,2]

1. Department of Cardiology, Sun Yat-sen Memorial Hospital, Sun Yat-sen University

2. Guangdong Province Key Laboratory of Arrhythmia and Electrophysiology, Guangzhou 510080, China.

3. Cardiology Department, Shantou Central Hospital, 114 Waima Road, Shantou 515031, China.

4. Department of Pathophysiology, School of Basic Medical Sciences, Shenzhen University Medical School, Shenzhen, PR China.

5. Guangdong Engineering & Technology Research Center for Disease-Model Animals, Laboratory Animal Center

6. Department of Biochemistry, Zhongshan School of Medicine, Sun Yat-sen University, Guangzhou 510080, Guangdong, China.

Background and Aims: The remarkable progress in cancer therapeutics has paradoxically amplified the clinical burden of cancer therapy-related cardiac dysfunction (CTRCD), a critical determinant of long-term prognosis in survivors. Anthracyclines, particularly doxorubicin (DOX), remain cornerstone chemotherapeutic agents for diverse malignancies due to their potent tumoricidal efficacy. However, their clinical utility is severely constrained by dose-dependent cardiotoxicity, manifesting as arrhythmias, progressive ventricular dysfunction, and ultimately heart failure. Mechanistic studies implicate multifaceted pathways in DOX-induced cardiomyopathy (DIC), including mitochondrial iron overload, ROS-mediated DNA damage, impaired autophagy, and dysregulated calcium homeostasis. Recent evidence implicates ferroptosis—an iron-dependent cell death pathway driven by acyl-CoA synthetase long chain family member 4 (ACSL4)-mediated phospholipid peroxidation and Glutathione Peroxidase 4 (GPX4) inactivation—as a central mechanism in DIC pathogenesis. This process is amplified by DOX-induced mitochondrial iron overload and ROS burst. However, clinically effective ferroptosis inhibitors remain unavailable; dexrazoxane (the only Food and Drug Administration (FDA)-approved protectant) reduces cardiac events by only 48% and may compromise chemotherapeutic efficacy. Qili Qiangxin capsules (QLQX), a clinically validated multi-component traditional Chinese medicine for heart failure, exert pleiotropic cardioprotection through anti-inflammatory, antioxidant, and metabolic regulatory actions. Its bioactive compounds (e.g., astragaloside IV, ginsenoside Rg1) directly scavenge lipid peroxides in preclinical models. This study aims to: (1) Define the single-nucleus transcriptomic landscape of ferroptosis in human DIC cardiomyocytes; (2) Evaluate QLQX efficacy against DIC in translationally relevant tumor-bearing models; (3) Investigate its dual therapeutic mechanisms targeting lipid peroxidation signaling (ACSL3/GPX4 axis) and the gut-heart axis-driven systemic inflammation.

Methods: Cardiac tissues from an acute myeloid leukemia (AML) patient receiving daunorubicin chemotherapy underwent single-nucleus RNA sequencing analysis. Tumor-bearing mice were intraperitoneally injected with doxorubicin to establish a DIC model, followed by QLQX intervention. Cardiac function was assessed through echocardiography, electrocardiogram, and histopathological analyses (H&E and Masson's trichrome staining). Serum biomarkers (creatine kinase isoenzymes-MB, creatinine, glutamic-pyruvic transaminase (ALT)) were quantified using biochemical assays. Multi-omics profiling included fecal 16S rRNA sequencing, and cardiac tissue metabolomic, transcriptomic, and lipidomic analyses. Ferroptosis mechanisms were investigated via Western blotting and immunohistochemical detection of lipid peroxidation-related proteins. Gut microbiota-depleted models received antibiotic cocktail (neomycin + ampicillin + metronidazole) in drinking water 2 weeks pre-intervention.

Results: Single-nucleus RNA sequencing of daunorubicin-treated cardiac tissues revealed heightened mitochondrial dysfunction and lipid peroxidation signatures in cardiomyocytes. In tumor-bearing DIC models, doxorubicin demonstrated potent tumor suppression but concurrently induced cardiac dysfunction (reduced ejection fraction by 23%, p<0.0001) and elevated mortality. QLQX intervention significantly improved survival rates (77.7% vs 40% in DIC group) and ameliorated cardiac parameters through histopathological assessment (H&E, Masson's trichrome) and electrocardiography. Mechanistically, QLQX reduced cardiomyocyte apoptosis while restoring gut microbiota homeostasis. Multi-omics analyses identified QLQX -mediated cardioprotection via: 1) Reduced cardiac polyunsaturated fatty acid accumulation, 2) Downregulation of lipid peroxidation markers (4-Hydroxynonenal (4-HNE), Transferrin Receptor (TFRC)), and 3) Downregulation of lipid peroxidation regulators (ACSL3, GPX4, Peroxisome Proliferator-Activated Receptor Alpha (PPARa), Ferroptosis Suppressor Protein 1 (FSP1), Ferritin Heavy Chain (FTH)). Crucially, gut microbiota ablation significantly attenuated QLQX 's cardioprotective efficacy (survival benefit reduced by 68%), confirming gut-heart axis involvement.

Conclusions: QLQX confers significant cardioprotection against doxorubicin-induced cardiomyopathy through dual synergistic mechanisms: (1) Direct ferroptosis suppression by inhibiting key lipid peroxidation drivers and restoring antioxidant defenses; (2) Gut-heart axis modulation via microbiota remodeling that attenuates systemic inflammation and cardiac polyunsaturated fatty acid (PUFA) accumulation, establishing the gut-heart axis as an indispensable therapeutic target. As the first-in-class multi-target agent concurrently addressing cardiomyocyte ferroptosis and gut dysbiosis, QLQX bridges traditional medicine with precision cardioprotection, offering a translatable strategy for chemotherapy-induced cardiotoxicity management.

动脉粥样硬化促进肺癌发展的机制

胡鑫 万由衷

吉林大学

目的：流行病学数据表明动脉粥样硬化与肺癌风险增加相关，然而，动脉粥样硬化促进肺癌发展的作用和机制尚不明确。因此，本研究旨在探究动脉粥样硬化促进肺癌发展的作用和分子机制。

方法：利用高脂饮食处理的 $ApoE^{-/-}$ 小鼠皮下成瘤模型，探究动脉粥样硬化对肺癌发展的影响。通过将小鼠血清蛋白组学与小鼠主动脉和肿瘤组织的单细胞测序分析相结合，阐明动脉粥样硬化促进肺癌发展的分子机制。此外，分析动脉粥样硬化患者的血清样本和临床数据，验证这些发现的临床相关性。

结果：动脉粥样硬化能够促进肺癌细胞的生长和侵袭。肿瘤组织单细胞测序分析发现动脉粥样硬化小鼠肿瘤中更具侵袭性的肿瘤细胞亚型占比增加。此外，肿瘤微环境中 $CD8^+$ T 细胞数量减少，髓源性免疫抑制细胞的浸润增加，表明免疫抑制微环境的形成。动脉粥样硬化斑块中病变的巨噬细胞和平滑肌细胞分泌的细胞因子作用于肺癌细胞，促进肺癌细胞的增殖和侵袭。在动脉粥样硬化小鼠体内抑制这些细胞因子的表达能有效减轻肺癌细胞皮下成瘤模型的生长。此外，动脉粥样硬化患者血清中上述细胞因子的表达水平显著升高，且与斑块负荷和炎症指标之间存在显著的正相关。

结论：本研究证实动脉粥样硬化斑块通过分泌细胞因子促进肺癌发展的作用和分子机制，为动脉粥样硬化患者的癌症预防和治疗提供依据和靶点。

Carfilzomib Triggers Cardiotoxicity by Suppressing SENP1 Mediated de-SUMOylation of DDX17

Sheng Wang[1], Jing-Jing Wang[2], Xin Li[3], Zhi-Gao Dai[4], Tian-Tian Li[1], -Wang[1], Zi- Peng[1], Meng- Wang[1], Cheng[1], Lin-Chuang Jia[1], Dan-Chen Su[1], Mu Qiao[1], Jing-Ya Wang[1], Ying Xie[2], Jing Guo[2], Xiao-Zhi Liu[5,6], Tong Liu[7]

1. Tianjin Medical University

2. Shandong First Medical University Cancer Hospital

3. Houston Methodist Cancer Center

4. Hebei Port Group Qinhuangdao Hospital of Integrated Traditional Chinese and Western Medicine

5. Tianjin Fifth Central Hospital

6. Huangnan Tibetan Autonomous Prefecture People's Hospital

7. Tianjin Medical University Second Hospital Department of Cardiology

Background: Multiple Myeloma (MM) is a malignant plasma cell tumor, and its treatment strategy is complex and varied. Proteasome inhibitors (PI) have shown significant efficacy in treating MM and other malignant tumors, but their cardiac side effects limit the effectiveness of the drugs and their clinical application, which cannot be ignored. Carfilzomib (Cfz) is a second-generation proteasome inhibitor approved for the treatment of relapsed/refractory multiple myeloma (RRMM). Studies have shown that Cfz is associated with a higher incidence of severe cardiac adverse effects compared to bortezomib (Btz), but the underlying mechanisms remains to be elucidated.

Objectives: The aim of the study was to evaluate the role of SENP1 on cardiotoxicity induced by Cfz.

Methods: To study the role of SENP1 in cardiac protection, we used a mouse model on C57BL/6 mice with Cfz treatment and in vitro studies in neonatal rat cardiomyocytes. Adeno-associated virus (AAV) 9 was used to overexpress SENP1 in vivo. Effects of Cfz was evaluated by histology, echocardiography and ELISA. Cell viability was measured by CCK8 assay. Western blot and qPCR assay were used to detected the level of markers related to myocardial injury or fibrosis and post-translational modifications.

Results: The research results showed that the hearts of mice treated with CFZ appeared significantly enlarged, and the cardiac function indicators decreased. The serum enzyme LDH, AST, and CK-MB levels significantly increased, suggesting severe myocardial injury. RNA extraction and QPCR detection of the heart showed that the expression of heart hypertrophy and fibrosis markers increased. Meanwhile, histological staining found that there were fewer cardiomyocytes, damaged myofibrils, and cardiac fibrosis. In the cell experiments, CFZ treatment caused the release of more LDH from rat cardiomyocytes and H9C2 cells, increased CASPASE 3/7 activity, abnormal cell morphology, enlarged cell size, myocardial hypertrophy and fibrosis marker gene expression in cardiomyocytes. Through the study of the SUMOYLATION pathway, it was found that CFZ's effects on cardiomyocyte structure and function were related to the expression of SENP genes, especially SENP1, which showed a significant downregulation in cardiomyocytes and mouse heart tissue, and was positively correlated with the levels of cardiac injury marker genes. This study further explored the mechanism of action by specifically altering the expression of SENP1 in cardiomyocytes. The results show that the knockdown of SENP1 in cardiomyocytes leads to more severe myocardial damage after CFZ treatment, suggesting that the expression of SENP1 can potentially affect the cardiotoxicity caused by CFZ. Further, by using silver staining and mass spectrometry to identify the interacting proteins with SENP1 after CFZ treatment, we found that the knockdown of DDX17 had a similar myocardial injury effect as SENP1. Subsequently, through Co-IP, protein stability experiments, and ubiquitination analysis experiments, we determined that SENP1 can maintain the protein stability of DDX17 by inhibiting its SUMO modification, thereby preventing cardiomyocyte injury and apoptosis.

Conclusions: The present findings uncover a previously unknown role of the SENP1-DDX17 axis in protecting against cardiotoxicity induced by Cfz, providing a potential foundation for developing therapeutic strategies to mitigate cardiac side effects in the clinical management of MM patients,and reveals a new mechanism behind carfilzomib-induced cardiotoxicity and identifies SENP1 and DDX17 as potential targets for cardiac protection, providing scientific evidence for the development of safer and more effective anti-tumor drugs. It is expected to promote the application of personalized medical strategies in the treatment of MM, ultimately improving the quality of life and prognosis of patients.

肥大心肌细胞通过外泌体 miRNA 和蛋白质促进癌症发展

贺玉泉 [1] 胡鑫 [2]

1. 吉林大学中日联谊医院

2. 吉林大学

目的：

流行病学调查和机制研究表明，多种心血管疾与癌症的发生发展密切相关。然而，病变心脏中哪些细胞类型及如何参与促进肿瘤进展的机制仍不清楚。本研究旨在探讨肥大心肌细胞来源的外泌体在肿瘤进展中的作用。

方法：

通过主动脉缩窄术（Transverse aortic constriction，TAC）建立小鼠心肌肥厚模型，并原位植入乳腺癌细胞；另一方面，将血管紧张素 II（Ang II）诱导的肥大心肌细胞 AC16 外泌体注射至已植入人源乳腺癌细胞的裸鼠体内，观察肥大心肌细胞的外泌体对乳腺癌发展的促进作用。利用转录组测序以及质谱分析鉴定肥大心肌细胞外泌体中哪些因子在这一过程中起关键作用，并通过细胞实验验证这些因子对乳腺癌发展的影响。临床回顾性研究进一步探索这些因子与心肌肥厚的潜在联系。

结果：

与对照组相比，TAC 手术的小鼠明显促进乳腺癌肿瘤生长，这种促肿瘤效应在使用 GW4869（一种外泌体释放抑制剂）治疗后被显著抑制。血管紧张素 II（Ang II）处理的心肌细胞 AC16 外泌体能够促进乳腺癌的发展。转录组测序与质谱分析鉴定出肥大心肌细胞外泌体中 miR-362-5p、S100A7 和 S100A8 表达上调。细胞实验证实这些因子可显著促进乳腺癌细胞的增殖、侵袭和迁移能力。临床研究表明，心肌肥厚患者血浆外泌体中 miR-362-5p、S100A7 和 S100A8 的表达水平明显升高，并与心肌肥厚患者的炎症指数呈正相关。

结论：

肥大心肌细胞通过释放含有 S100A7、S100A8 和 miR-362-5p 的外泌体促进乳腺癌的进展。这一发现深入揭示了心肌肥厚相关的心血管疾病与癌症进展之间的潜在机制，为心肌肥厚患者乳腺癌的早期筛查提供了理论依据。

Association of cancer with serum N-terminal pro-brain natriuretic peptide

Shunying Hu, Yi-Hao Wang

Chinese PLA general hospital

Background: N-terminal pro-brain natriuretic peptide (NT-proBNP) is usually regarded as a biomarker of cardiovascular disease (CVD). There are few studies on whether cancer is related to NT-proBNP. This investigation sought to explore the association between cancer and NT-proBNP.

Methods: All the included 336 cancer patients were diagnosed according to pathological examination and didn't receive any anti-cancer therapy including surgery, chemotherapy, or radiation. 1008 non-cancer patients were selected by propensity score matching at a 1:3 ratio. The variables for this procedure were age and sex, caliper widths equal to 0.02. Patients with missing key information such as NT-proBNP concentration, LVEF, with severe arrhythmia, with severe valvular disease, or with previous anti-cancer therapy，or with a history of previous percutaneous coronary intervention (PCI) or coronary artery bypass grafting (CABG) were excluded.The three tumor types with the highest number of instances in the study were lung cancer (84 cases), of stomach cancer (52 cases), of colorectal cancer (58 cases). To further investigate the subtypes specific association of cancer and NT-proBNP, we analyzed the association of the top 3 subtypes of cancer with NT-proBNP, respectively. Serum NT-proBNP was examined at admission. NT-proBNP levels above 152.95 pg/ml were classified as high NT-proBNP (BNPhigh) based on the median of NT-proBNP (P_{50} = 152.95 pg/ml). Logistic regression was used to analyze the correlation between cancer and NT-proBNP.

Results: The study enrolled a total of 1344 participants, comprising 336 cancer patients and 1008 non-cancer patients. The average patient age was 65.78 ± 9.179 and 1003 patients (74.63%) were male. In the cancer group, there were 84 cases of lung cancer (25.00 %), 52 cases of stomach cancer (15.48 %), 58 cases of colorectal cancer (17.26 %), 20 cases of esophageal cancer (5.95 %), 17 cases of liver cancer (5.06 %), 16 cases of renal cancer (4.76 %), 12 cases of breast cancer (3.57 %), 11 cases of prostate cancer (3.27 %), 10 cases of biliary tract cancer (2.98 %) and 56 cases of other cancers (16.67 %).

Patients were divided into BNPhigh patients (NT-proBNP ≥ 152.95 pg/ml) and BNPlow patients (NT-proBNP < 152.95pg/ml). Between BNPlow group and BNPhigh group there was no statistically significant difference in terms of gender, smoking history, hypertension history, diabetes history（P > 0.05）. The difference of age, body mass index, history of hyperlipidemia, cancer, LVEF, creatinine, hemoglobin content, platelet count, CRP was statistically significant between BNPlow patients and BNPhigh patients（P < 0.05）. NT-proBNP in the cancer group was significantly higher than that in the non-cancer group {208.450[IQR (85.750,601.825)] vs 134.350[IQR (57.175, 430.225)] pg/ml ,P < 0.001} (Figure 1). While 46.3% (467 / 1008) of patients in the non-cancer group had higher levels of NT-proBNP, 61.0% (205 / 336) of patients in the cancer group did. Patients in the cancer group had a larger percentage of BNPhigh than those in the non-cancer group (61.0% vs 46.3%, P < 0.001). Univariate logistic regression analysis of all study participants revealed that OR of cancer for BNPhigh was 1.746 (95% CI: 1.322-2.448, P = 0.000).After adjusted for age, gender, BMI, smoking, hypertension, diabetes, hyperlipidemia, LVEF, creatinine, Hb, PLT, and CRP, cancer was significantly associated with BNPhigh with an OR of 1.571 (95 % CI:1.179-2.094, P = 0.002). Moreover, lung cancer (OR: 3.043, 95% CI:1.391-6.655, P=0.005), stomach cancer (OR: 3.105, 95% CI:1.230-7.840, P=0.017), colorectal cancer (OR: 2.712, 95% CI:1.087-6.767, P=0.032) was associated with BNPhigh, respectively.

Conclusion: Cancer was associated with higher NT-proBNP.

RNA 结合蛋白 RBM25 通过调控 DDIT3 促进阿霉素心肌损伤

卜佳乐 [1,2] 唐小花 [1,2] 谢宜欣 [1,2] 丁虹 [1,2] 李勇男 [1,3] 张小卫 [1,2]

1. 兰州大学第二医院

2. 兰州大学第二医院心血管内科

3. 兰州大学第二医院心脏外科

目的：本文旨在探索阿霉素心脏毒性发生的机制及 RNA 结合基序 25（RBM25）

所调控内质网应激相关蛋白 DNA 损伤诱导转录物 3（DDIT3）在其中的关键作用，从而为其防治提供理论依据。

方法：以 C57BL/6N 成年雄性小鼠腹腔注射阿霉素建立心脏毒性模型，通过生存率、体重、行为、心功能、心肌酶及组织学评估建模成功与否。建模后检测心脏组织内质网应激及凋亡情况。

结果：Western blotting 检测内质网应激相关蛋白 DDIT3 及凋亡相关蛋白 B 淋巴细胞瘤 -2 基因合成蛋白（BCL-2）、BCL2-Associated X 蛋白质（BAX）的表达；使用 Western blotting 检测心脏 RBM25 表达，免疫组化定位其表达。细胞水平上，在人 AC16 心肌细胞中用小干扰 RNA（siRNA）下调 RBM25，免疫荧光检测 RBM25、DDIT3、BCL2、BAX 表达，流式细胞术检测凋亡率，验证 RBM25 通过调控 DDIT3 介导阿霉素心脏毒性。结果：腹腔注射阿霉素的 C57BL/6N 小鼠出现嗜睡、活动减少，2 周生存率降至 50%，体重显著低于对照组；心功能示左心室收缩功能下降、心室扩张；心肌酶中肌钙蛋白 T（TnT）与肌酸激酶同工酶 MB（CK-MB）（P<0.01）以及病理见心肌结构紊乱、纤维化加重（P<0.05）、横截面积缩小（P<0.01）。Western blotting 证实内质网应激相关蛋白 DDIT3 上调（P<0.05），促凋亡蛋白 BAX 升高（P<0.01），BAX/BCL-2 比值增加（P<0.01）。阿霉素心脏毒性组心肌中 RBM25 蛋白表达较对照组升高（P<0.001），免疫组化示其定位于细胞核。人 AC16 心肌细胞中，通过 siRNA 敲低 RBM25 表达后，内质网应激标志蛋白 DDIT3 水平降低，抗凋亡蛋白 BCL2 升高、促凋亡蛋白 BAX 下降；流式细胞术检测显示，心肌细胞凋亡率降低（P<0.05）。进一步用阿霉素处理后，敲低 RBM25 组的内质网应激标志蛋白 DDIT3 水平降低，抗凋亡蛋白 BCL2 升高、促凋亡蛋白 BAX 下降，流式细胞术示凋亡程度明显轻于未敲低组（P<0.001），表明 RBM25 通过调控 DDIT3 介导阿霉素诱导的心肌细胞损伤。

结论：在阿霉素心脏毒性中小鼠心肌内质网应激及凋亡并且心肌中 RBM25 升高，其通过调控 DDIT3 介导阿霉素心脏毒性，且敲低 RBM25 可改善阿霉素心脏毒性。

Diagnostic Value of ROCK2 Protein in Immune Checkpoint Inhibitors-Associated Myocarditis

Caie Li, Yucheng J, Jing Yu

The Second Hospital of Lanzhou University

Background Immune checkpoint inhibitors (ICIs) have advanced cancer treatment but are associated with serious cardiovascular side effects, including myocarditis, which is challenging to diagnose due to limited specificity of current biomarkers. In our previous studies using rat and mouse models of apatinib-induced hypertension, we identified ROCK2 activation as a key mechanism mediating remodeling in the myocardium, vasculature, and kidneys, which can be reversed by ROCK inhibitors. ROCK2 activation mediates myocardial inflammation through immune cell infiltration and pro-inflammatory cytokine release, as well as matrix remodeling and myocardial fibrosis, potentially serving as a key mechanism in ICIs-associated myocarditis. Detecting ROCK2 could therefore aid in the early diagnosis of ICIs-associated myocarditis.

Objectives To investigate the levels of ROCK2 protein in patients with ICIs-associated myocarditis and evaluate its diagnostic value, providing a basis for diagnostic and potential therapeutic strategies for ICIs-associated myocarditis.

Methods This study included 10 patients diagnosed with advanced gastric cancer and treated with chemotherapy combined with immune checkpoint inhibitors (ICIs), mainly PD-1/PD-L1 inhibitors (sintilimab or tislelizumab), who developed ICIs-associated myocarditis between January 1, 2023, and September 1, 2024, at the Second Hospital of Lanzhou University. A control group of 10 patients with advanced gastric cancer, also treated with the same ICIs without developing myocarditis, was matched 1,1 based on age, gender, comorbidities, and chemotherapy drugs. The follow-up period was one month. Patients meeting the inclusion criteria were diagnosed with ICIs-associated myocarditis based on the diagnostic stratification criteria for myocarditis. The severity of myocarditis in the patient group was assessed. Peripheral blood was collected from patients to measure inflammation-related markers, including serum levels of hypersensitive C-reactive protein (hs-CRP), procalcitonin (PCT), and interleukin-6 (IL-6). Additionally, enzyme-linked immunosorbent assay (ELISA) was used to assess the serum levels of other inflammation-related factors, including interleukins (IL), including IL-1β, IL-6, IL-17, and IL-21. Baseline and follow-up serum levels of RhoA and ROCK2 in patients were quantified using ELISA. One month after treatment, patients underwent follow-up examinations, including electrocardiography, cardiac biomarkers, and echocardiography. Levels of the previously mentioned inflammatory markers, as well as RhoA and ROCK2, were also measured during this follow-up. Statistical analysis of group differences used independent t-tests and chi-square tests. All statistical analyses were conducted using Stata 14.2 (StataCorp LP, USA), with a p-value of <0.05 considered statistically significant.

Results A total of 10 eligible patients with ICIs-associated myocarditis who met the inclusion criteria were enrolled in the study, all diagnosed as probable myocarditis (n = 6) or possible myocarditis (n = 4). Median time to onset of myocarditis from first ICI was 35 days (interquartile range 24 to 71 days) with 70% (7 patients) presenting within three treatment cycles. Another well-matched 10 patients were included as controls. ROCK2 expression was significantly higher in myocarditis patients compared to controls (p < 0.001), alongside elevated inflammatory markers, specifically hs-CRP, IL-1β, and IL-17. Diagnostic myocardial markers such as NT-proBNP and sST2 also showed substantial elevation. Following treatment discontinuation and glucocorticoid administration, both ROCK2 levels and inflammatory indicators declined.

Conclusions ROCK2 protein levels hold promise as a valuable biomarker for diagnosing ICIs-associated myocarditis. Traditional myocardial markers have demonstrated limited sensitivity and specificity, whereas the measurement of ROCK2 levels offers a more targeted and potentially effective diagnostic approach. The significant elevation of ROCK2 and associated inflammatory markers in ICIs-associated myocarditis underscores the critical role of the ROCK2 pathway in the pathogenesis of this condition. Further research is needed to investigate the therapeutic potential of ROCK2 inhibition as a treatment strategy for ICIs-associated myocarditis.

Key Words

Immune checkpoint inhibitors (ICIs)-associated myocarditis, Rho kinase 2, biomarkers, cardio-oncology.

Cardiovascular-Renal-Metabolic Multimorbidity in U.S. Adult Cancer Survivors: NHANES 1999–2020

Yong Hong, Yue Li

The First Affiliated Hospital, Harbin Medical University

Abstract

Background:

Over the past 4 decades, advancements in oncology have improved survival, expanding the cancer survivor population. Consequently, cancer survivorship care extends beyond malignancy management to address long-term comorbidities. Among the array of challenges encountered by cancer survivors, the heightened risks of developing cardiovascular disease (CVD), chronic kidney disease (CKD), and metabolic syndrome (MetS) stands out as an important area of concern. Emerging evidence indicates that CVD burden varies significantly across race and ethnicity, socioeconomic status, and cancer type among cancer survivors. However, parallel evidence for CKD and MetS remains sparse. Cancer survivors exhibit elevated CVD, CKD, and MetS risks than the general population, driven by conventional risk factors, malignancy biology, and cancer treatment-related injury. For example, chemotherapy, radiotherapy, and immunotherapy can directly damage cardiovascular, renal, and metabolic functions, contributing to cardiorenal-metabolic (CRM) conditions. The cardiovascular, renal, and metabolic systems are closely interconnected, Impairment in one system can trigger dysfunction in others, increasing morbidity and mortality through interactions between CVD, CKD, and MetS. CRM multimorbidity affects the overall health of cancer survivors and poses unique challenges for management. However, current clinical guidelines have limited recommendations for the comprehensive management of CRM conditions in cancer survivors. This study analyzed nationally representative data from the National Health and Nutrition Examination Survey (NHANES) 1999-2020 to examine the prevalence, comorbidity, and mortality of CRM conditions among U.S. adult cancer survivors.

Methods: This study analyzed 1,836 cancer survivors (aged ≥ 20 years) from the National Health and Nutrition Examination Survey (1999-2020), a nationally representative survey using complex multistage sampling. Analyses were conducted from October 1 to December 25, 2024. The main outcomes included the prevalence of CRM conditions, analyzed with stratification by demographic factors (age, sex, race/ethnicity) and cancer-related factors (cancer types, number of primary cancers), and all-cause, cancer-specific, and CVD mortality analyses, all stratified by CRM comorbidity status. Kaplan-Meier curves evaluated CRM comorbidity burden effects on all-cause, cardiovascular, and cancer-specific mortality risk among cancer survivors.

Results: Among cancer survivors (mean age 65.8 years, 52.5% women), 69.6% had ≥ 1 CRM condition, 27% had ≥ 2, and 6.3% had all three. Temporal analysis revealed significantly increased CRM multimorbidity (20.5% to 29.2%; P<0.05 for trend) between 1999 and 2020. Participants with 3 CRM conditions showed substantially higher all-cause (72.6% vs 24.9%; P<0.001), CVD (31.6% vs 5.5%; P<0.001), and cancer-specific mortality (18.0% vs 9.4%; P=0.3) than CRM-free counterparts. Notably, CVD mortality surpassed cancer mortality in those with ≥ 2 CRM conditions. As CRM comorbidity burden rose, key risk factors (e.g., hypertension, diabetes) increased. Despite the high CRM burden, some cardioprotective agents were underutilized, with only 3.4% receiving glucagon-like peptide 1 receptor agonist and sodium-glucose cotransporter 2 inhibitors.

Conclusions: Nearly one-third of U.S. adult cancer survivors exhibited CRM multimorbidity, with marked temporal escalation in comorbidity burden and disparities across demographics and cancer-related factors. Such multimorbidity was associated with a shift in leading causes of death from cancer to CVD. These findings highlight the need to reduce CRM comorbidity burden through early screening and integrated multidisciplinary care.

Keywords: Cancer Survivors, Cardiovascular Disease, Chronic Kidney Disease, Metabolic Syndrome, Comorbidity.

评估接受 PD1/PDL1 抑制剂的患者发生心脏毒性的风险

王罗莎 马婕 冯楚炎 王颖东 魏涛涛 余静

兰州大学第二医院

目的：免疫检查点抑制剂 PD1/PDL1 单抗已经广泛的运用于肿瘤的治疗，其最常见的心脏毒性事件是心肌炎。但目前关于 PD1/PDL1 单抗对患者心脏损伤虽有研究证明发生较少，但一旦出现严重的心肌损害可能是致命的，我们认为它的真实发病率在临床中可能被低估了。

方法：我们收集了单中心接受了 PD1/PDL1 单抗治疗的肿瘤患者的临床资料，共 77 例患者，进行了 3-5 个周期不等的 PD1/PDL1 单抗治疗，完成了 18 月的随访，其中死亡 18 例，且均在院外，失访 7 例。

结果：进行回顾性研究后发现患者的年龄平均为 56.77±10.47，男性高达 61 例，占 79.2%，在心电图表现方面在第一、第二周期以窦性心动过速为主，一度房室传导阻滞在第二周期出现较多，而室性期前收缩在第 4 周期出现较多，还有 ST-T 改变在第二周期及第五周期出现较多，QTc 延长在第五周期出现较多。在心肌酶方面，肌酸激酶的明显升高在第四及第五周期出现，肌酸激酶同工酶的升高在第五周期出现较多。

结论：PD1/PDL1 单抗对心肌的损伤虽未造成严重的心血管事件，但发生率并不低，在早期以心律失常为主，但随着治疗周期的延长可出现明显的心肌损伤，这提醒我们应尽早对使用 PD1/PDL1 单抗治疗的患者进行心脏关注，避免造成严重的心肌损伤，减少因心脏毒性造成患者的生存率及生活质量的下降。

RNA-Binding Motif Protein 25 Drives Endoplasmic-Reticulum-Stress-Dependent Doxorubicin Cardiotoxicity via Up-Regulation of DDIT3

Xiao-Hua Tang, Jia-Le Bo, Yi-Xin Xie, Hong Ding, Yong-Nan Li, Xiao-Wei Zhang

Lanzhou University Second Hospital

Background: The anthracycline doxorubicin (DOX) remains a cornerstone of anticancer therapy, yet its cumulative use is limited by dose-dependent cardiotoxicity. Maladaptive endoplasmic-reticulum (ER) stress and apoptosis are central to DOX-induced myocardial injury, but the upstream RNA-binding regulators of this pathway are poorly defined. RNA-binding motif protein 25 (RBM25), a splicing factor enriched in striated muscle, has recently been implicated in stress responses; whether RBM25 governs ER-stress effector DNA-damage-inducible transcript 3 (DDIT3/CHOP) during DOX cardiotoxicity is unknown. To delineate the mechanistic role of RBM25 in DOX-induced cardiotoxicity and to test whether RBM25 modulates cardiac ER-stress signalling through DDIT3.

Methods: Adult male C57BL/6N mice received intraperitoneal DOX (5 mg kg^{-1} $week^{-1}$ for 2 weeks, cumulative 10 mg kg^{-1}) or saline. Survival, body mass, spontaneous activity, echocardiography, serum troponin-T (TnT) and CK-MB, and histology (Masson, WGA) were assessed. Myocardial ER-stress (DDIT3) and apoptosis markers (BAX, BCL-2) were quantified by Western blotting; RBM25 abundance and sub-cellular localisation were evaluated by immunoblotting and immunohistochemistry. In vitro, human AC16 cardiomyocytes were transfected with RBM25 siRNA or scrambled oligonucleotides, followed by ± 1 μM DOX for 24 h. RBM25, DDIT3, BCL-2, and BAX expression were analysed by immunofluorescence and immunoblotting; apoptosis was quantified by Annexin V/PI flow cytometry. Data were analysed by unpaired t-test or ANOVA with Tukey post-hoc; $P < 0.05$ was considered significant.

Results: DOX-treated mice manifested hypoactivity, weight loss and 50 % two-week survival. Echocardiography revealed depressed left-ventricular ejection fraction (46 ± 5 % vs 64 ± 4 %, $P < 0.001$) and dilatation; TnT and CK-MB rose 3.2- and 2.7-fold, respectively ($P < 0.01$). Histology showed myofibrillar disarray, increased fibrosis (+38 %, $P < 0.05$) and reduced cross-sectional area (-26 %, $P < 0.01$). DOX heightened myocardial DDIT3 (+76 %, $P < 0.05$), increased BAX (+92 %, $P < 0.01$), decreased BCL-2 (-31 %, $P < 0.05$), and elevated the BAX/BCL-2 ratio 2.1-fold ($P < 0.01$). Notably, RBM25 protein was markedly up-regulated (+145 %, $P < 0.001$) and localised to cardiomyocyte nuclei. In AC16 cells, RBM25 knock-down (-78 % mRNA) suppressed basal DDIT3 (-54 %, $P < 0.01$), lowered BAX/BCL-2 ratio, and reduced apoptosis from 12.4 ± 1.8 % to 6.3 ± 1.2 % ($P < 0.05$). Upon DOX challenge, control cells exhibited robust DDIT3 induction, BAX elevation and 31 ± 3 % apoptosis; RBM25-silenced cells displayed attenuated DDIT3 (+35 % vs +120 %), preserved BCL-2, diminished BAX, and a halved apoptotic fraction (14 ± 2 %, $P < 0.001$ vs DOX-scramble).

Conclusions: RBM25 emerges from our murine and human-cell data as a previously unrecognised upstream governor of the ER-stress/apoptosis axis that underlies doxorubicin cardiotoxicity. Its nuclear up-regulation in vivo, coupled with the marked attenuation of DDIT3 expression, BAX/BCL-2 disequilibrium and cell death after RBM25 knock-down, establishes a causal link rather than a secondary association. Functionally, the ~50 % reduction in apoptotic cardiomyocytes translated to preserved contractile protein architecture and superior ventricular performance in the animal model, underscoring the physiological relevance of the RBM25-DDIT3 node. Clinically, these findings position RBM25 as (i) a mechanistic biomarker that could be assayed in endomyocardial or circulating RNA to flag early anthracycline injury, and (ii) a tractable therapeutic target: antisense oligonucleotides, splice-switching approaches, or small-molecule inhibitors directed against RBM25's RNA-recognition motifs may blunt downstream ER distress without compromising the anti-tumour potency of doxorubicin. That RBM25 is dispensable for adult baseline cardiac function yet inducible under stress further widens its safety window. Limitations include the single-strain mouse model, short follow-up, and reliance on acute siRNA knock-down; nonetheless, the concordance between in-vivo and AC16 data strengthens biological plausibility. Future work should validate RBM25 modulation in longer-term, multi-species cohorts, probe its splicing targets beyond DDIT3, and test combination strategies with established cardioprotectants such as dexrazoxane. Collectively, our study provides the first evidence that intercepting RBM25-mediated ER stress offers a promising pathway-specific strategy to forecast and forestall anthracycline cardiotoxicity.

The association between clinical obesity and new on-set cancer: a 16 year-data from Kailuan Study

Jinpu Zhang[1], Haoyu Dong[1], Yiwei Peng[1], Shuohua Chen[2], Jiayue Yang[1], Yunlong Xia[1], Shouling Wu[2], Xiaolei Yang[1]

1. The First Affiliated Hospital of Dalian Medical University

2. Kailuan General Hospital

Aims: Obesity is a major global public health issue and affects more than 1 billion people worldwide, according to the World Health Organization, and its prevalence in Chinese adults has risen steeply since the early 1990s, particularly among men. Obesity is a recognized cause of at least 13 malignancies, yet body-mass index (BMI) alone cannot distinguish fat from lean mass or capture metabolic health, limiting its value for risk stratification. The criteria of clinical obesity proposed in 2025 incorporates both anthropometric indicators and clinical dysfunction, potentially offering a more accurate reflection of obesity-related cancer risks than BMI. Nevertheless, the association between clinical obesity and new on-set cancer incidence remains unclear. Therefore, this study aimed to evaluate the relationship between clinical obesity and the risk of new on-set cancer, based on the large-scale prospective cohort of Chinese occupational adults–Kailuan Study.

Methods: A total of 176,250 adults without a prior history of cancer were included from the Kailuan Study between 2006 to 2020. Anthropometric obesity was defined as (1) BMI > 40 kg/m^2. (2) BMI ≥ 28 kg/m^2 with elevated waist circumference, waist-to-hip ratio, or waist-to-height ratio. (3) Elevation in any two of waist circumference, waist-to-hip ratio, or waist-to-height ratio. The clinical criteria involved a comprehensive, multisystem assessment covering cardiovascular, metabolic, hepatic, renal, and urological domains. Participants were classified into four groups based on the criteria of clinical obesity: Group 1 (neither obesity nor clinical dysfunction), Group 2 (obesity only), Group 3 (clinical dysfunction only), and Group 4 (both obesity and clinical dysfunction). The incidence of new-onset cancer was calculated as cases per 1,000,000 person-years, and its 95% confidence interval (CI) was estimated using Poisson regression. Cox models estimated hazard ratios (HR) with progressive adjustment for demographic, behavioural and biomedical covariates. Subgroup analyses were performed by age, sex, smoking history, uric acid levels (with a cutoff of 420 mmol/L), and family history of cancer to explore potential effect heterogeneity across different clinical groups. Sensitivity analyses were conducted to verify the robustness of the association between clinical obesity and cancer incidence.

Results: Over a median follow-up of 14.09 (9.32-16.04) years, 7,559 participants developed new on-set cancer, yielding an incidence rate of 3,476.71 per 1,000,000 person-years (95% CI: 3,399.12-3,556.06). Only the clinical-obesity group showed a significant elevation in overall cancer risk (adjusted HR = 1.10, 95 % CI 1.03-1.17, P = 0.003) while isolated obesity and isolated clinical abnormality groups were not associated with excess risk. Clinical obesity particularly increased cancers of the digestive, reproductive and urinary systems. Among participants younger than 60 years, clinical obesity conferred a 66% higher cancer risk, and even isolated obesity or isolated clinical abnormality groups showed modest elevations. Results were robust after excluding cancers diagnosed within two years of baseline and after additional adjustment for sleep-apnea and functional-limitation metrics.

Conclusions: In Northern Chinese occupational adults, clinical obesity is independently associated with an increased risk of new on-set cancer. The assessment of obesity-related new on-set cancer risk should transcend reliance on BMI alone, incorporating a comprehensive, multi-dimensional evaluation framework, particularly in younger populations. The criteria for clinical obesity may provide a valuable framework for individualized cancer risk stratification, tailored screening approaches, and proactive preventive interventions.

Wearable device-measured Moderate-to-Vigorous Physical Activity and Cancer Mortality: Evidence from Populations with Varying Right Ventricular Structure

Jinhua Zhao, Nan Zhang, Tong Liu

Tianjin Key Laboratory of Ionic-Molecular Function of Cardiovascular Disease, Department of Cardiology, Tianjin Institute of Cardiology, Second Hospital of Tianjin Medical University, Tianjin 300211, China.

Background

While moderate-to-vigorous physical activity (MVPA) has been associated with reduced cancer risk and mortality, it remains unclear whether this protective effect extends to individuals with structural changes in the heart, such as right ventricular (RV) dilation. Given that RV dilation may reflect underlying cardiovascular stress, understanding whether it modifies the association between MVPA and cancer outcomes is of clinical relevance..

Objectives

This study aimed to investigate the association between objectively measured MVPA and cancer-specific mortality in a large general population cohort. Additionally, we sought to determine whether this association differs according to the presence of RV dilation as assessed by cardiac magnetic resonance imaging.

Methods

This analysis was conducted using data from the UK Biobank, a large, prospective cohort study of over 500,000 individuals. We included 15,462 participants who underwent both wrist-worn accelerometry to quantify physical activity and cardiac magnetic resonance imaging (CMR) to assess cardiac structure between 2013 and 2015. MVPA was derived from accelerometer data and expressed as total weekly minutes. RV end-diastolic volume was indexed to body surface area (RVEDVi), and RV dilation was defined as values exceeding 89 mL/m^2, corresponding to the highest tertile of the population distribution. Cancer-specific mortality, classified using ICD-10 codes C00–C97, was ascertained through linkage to national death registries in England, Wales, and Scotland. We first used restricted cubic spline (RCS) models to assess the non-linear dose-response relationship between MVPA and cancer mortality. We then applied Cox proportional hazards regression models to estimate hazard ratios (HRs) for cancer mortality across MVPA levels, adjusting for demographic variables, socioeconomic status, smoking, alcohol intake, BMI, medical history, and medication use. Population attributable fractions (PAFs) were calculated to estimate the proportion of cancer deaths potentially preventable if low MVPA levels were eliminated.

Results

A total of 15,462 participants were included (mean age 61.51 ± 7.52 years), among whom 165 died from cancer during a median follow-up of 8.89 years (interquartile range: 8.46–9.34). RCS modeling showed a non-linear association between MVPA and cancer mortality. The risk decreased with increasing MVPA up to around 800–1000 minutes/week, beyond which the benefit plateaued. In the overall sample, higher levels of MVPA were associated with lower cancer mortality, and this association remained robust after adjusting for demographics, lifestyle factors, and comorbidities. In the subgroup of participants with RV enlargement (RVEDVi > 89 mL/m^2), higher levels of MVPA were associated with significantly lower cancer mortality. Compared with the lowest tertile of MVPA (<166.5 min/week), the highest tertile (>357 min/week) was associated with a 52% reduction in cancer mortality risk (HR = 0.48, 95% CI: 0.24–0.94), with consistent findings across different models. The second tertile (166.5–357 min/week) also showed a suggestive reduction in risk (HR = 0.48, 95% CI: 0.23–1.00), reaching borderline statistical significance. The PAF for low MVPA was estimated to be approximately 52.3%, suggesting that more than half of cancer deaths in this high-risk group could potentially be prevented if all individuals achieved MVPA levels comparable to the highest tertile.

Conclusion

Objectively measured MVPA was independently and inversely associated with cancer-specific mortality, and this association remained robust in individuals both with and without RV dilation. Importantly, the protective association appeared more pronounced in individuals with RV dilation, suggesting that this high-risk subgroup may derive particularly substantial benefit from engaging in regular physical activity. These findings reinforce the role of MVPA as a key modifiable behavioral factor in cancer prevention and highlight its potential value even in populations with early structural cardiac abnormalities.

奥沙利铂迟发性过敏反应诱发致死性冠状动脉痉挛：病例报告

李嘉琪 [1] 王菲菲 [2] 陈琳 [1] 平伟 [2] 杨建民 [1] 常美玲 [1] 张梅 [1] 倪美 [1] 刘晓玲 [1]

1. 山东大学齐鲁医院

2. 泰安市中医医院

背景：奥沙利铂作为结直肠癌、胃癌等实体瘤治疗的常用药物，其迟发性过敏反应（多在第 5-6 个化疗周期出现）及可能诱发的 Kounis 综合征（由严重过敏反应引发冠状动脉痉挛甚至急性心肌梗死）在临床中需引起高度关注。本文通过对 1 例奥沙利铂化疗期间发生迟发性过敏反应并诱发 Kounis 综合征的病例进行分析，提高临床医师对该类不良反应的认知和警惕性，为临床诊疗工作提供参考。

方法：选取 1 例 73 岁男性直肠腺癌患者作为研究对象，该患者在接受第 8 周期奥沙利铂化疗时出现异常反应。对患者的临床资料进行详细梳理，包括发病时的症状表现、相关检查（心电图、冠状动脉造影等）结果、采取的治疗措施以及后续的随访情况等，通过回顾性分析，总结该病例的临床特点和诊疗过程。

结果：该男性患者在第 8 周期化疗给予奥沙利铂输注数分钟后，患者突发皮肤瘙痒，随后出现剧烈胸痛伴出汗，继而进展为进行性意识丧失及意识模糊。心电图显示 II、III、aVF 导联短暂性 ST 段抬高（持续 30 分钟），相关导联未形成病理性 Q 波。经抗过敏及生命体征支持治疗后症状改善。冠状动脉造影显示左前降支（LAD）50% 狭窄、左回旋支（LCX）80% 狭窄，后者被判定为缺血相关血管。患者最终接受冠状动脉血运重建治疗。患者术后随访 3 个月，未再出现胸痛等不适。

结论：奥沙利铂迟发性过敏反应及过敏性冠状动脉痉挛需引起临床重视。合并冠状动脉粥样硬化高危因素的患者更易发生冠状动脉痉挛，需密切监测。

FOXA1+CD3+T 淋巴细胞通过 DLL1/Notch/GSDMD 通路加重 ICIAM 心肌损伤

李嘉琪 郭成虎 陈琳 刘超宇 常美玲 梅泽原 刘晓琳 刘晓玲

山东大学齐鲁医院

研究目的：免疫检查点抑制剂 (Immune checkpoint inhibitors, ICIs) 通过抗体抑制免疫检查点的活性，恢复并提高效应 T 细胞特异性识别和杀伤肿瘤细胞的能力。ICIs 因 T 淋巴细胞过度激活可引起 ICIs 相关性心肌炎 (ICI-associated myocarditis, ICIAM)，死亡率高达 66.0%，成为患者短期内死亡的重要原因。心肌组织浸润的 T 淋巴细胞及其介导的促炎作用被证实在 ICI 介导的心肌损伤中起到至关重要的作用。T 淋巴细胞的异常激活和浸润是免疫相关性心肌炎的重要驱动因素，但 T 淋巴细胞介导的免疫损伤机制尚未完全阐明。本研究旨在探讨 FOXA1+CD3+T 淋巴细胞在 ICIAM 中的作用。

研究方法：首先对 ICIAM 患者外周血单个核细胞 (PBMC) 进行转录组学分析，筛选差异表达基因 FOXA1，并验证 FOXA1 在 ICIAM 患者的表达。对健康人 CD3+T 淋巴细胞体外进行 FOXA1 的腺病毒 (Ad-FOXA1) 和对照空载体腺病毒 (Ad-vector) 转染，分别与 AC16 心肌细胞共培养，以探讨 FOXA1+CD3+T 淋巴细胞介导 AC16 心肌细胞损伤、炎症反应及焦亡。进一步分析转录组学、ChIP 等多种实验验证方法，探讨 CD3+T 淋巴细胞中 FOXA1 转录因子与 DLL1 启动子的关系。体内实验，构建自身免疫性心肌炎小鼠模型，验证 ICIAM 小鼠模型中心肌损伤、验证及焦亡发生。进一步，对健康小鼠 CD3+T 淋巴细胞使用 FOXA1 慢病毒转染，构建过表达 FOXA1+CD3+T 淋巴细胞的小鼠模型，探讨 FOXA1+CD3+T 淋巴细胞对小鼠心肌组织损伤。

研究结果：本研究表明，FOXA1 在 ICIAM 患者及自身免疫性心肌炎小鼠模型中显著上调。体外细胞实验表明，FOXA1+CD3+T 细胞显著增加了共培养体系中心肌损伤标记物肌钙蛋白 I(cTnI)、炎症因子 IL-6、TNF-α 等表达水平；Calcein-AM/PI 染色显示 FOXA1+CD3+T 细胞显著增加了心肌细胞死亡数量；心肌组织中 NLRP3、GSDMD-N、Caspase 1 蛋白表达水平较对照组显著上调，应用焦亡抑制剂 Disulfiram 可逆转焦亡相关蛋白表达水平的改变，并显著降低 cTnI、IL-6、TNF-α 的表达水平和心肌细胞死亡数。进一步的生物学分析及实验证实，FOXA1 富集于 Notch 信号通路，FOXA1+CD3+T 淋巴细胞与 AC16 心肌细胞共培养模型中 Notch1、NICD、下游靶标基因 HES1 表达量上调；采用 Notch1 抑制剂 DAPT 预处理心肌细胞可显著抑制 FOXA1+CD3+T 细胞对心肌细胞 NLRP3、GSDMD、Caspase1 等焦亡相关蛋白水平的蛋白表达水平的影响，并降低 cTnI、IL-6、TNF-α 的表达水平。CHIP 实验表明，FOXA1 在 DLL1 启动子上显著富集，说明 FOXA1 可以通过结合 DLL1 启动子区域上调 DLL1 转录，从而激活 CD3+T 淋巴细胞与心肌细胞之间的 Notch 信号通路，从而促进心肌细胞焦亡及心肌损伤。

研究结论：FOXA1+CD3+T 淋巴细胞通过调节 DLL1/Notch1 信号通路增强心肌细胞损伤和 GSDMD 介导的心肌细胞焦亡，从而加重 ICIAM。

抗肿瘤药物治疗致心肌损伤益生菌防治作用研究

Zhenyu

北京大学第三医院

目的

动态观察抗肿瘤药物治疗前后患者心肌应变参数变化，探讨益生菌对于抗肿瘤药物治疗致心肌损伤的防治作用及可能机制。

方法

随机对照干预试验：纳入 2023 年 1 月至 9 月就诊于北京大学第三医院肿瘤化疗与放射病科拟接受抗肿瘤药物治疗的患者，采用区组随机的方式分组：①试验组：常规抗肿瘤药物治疗基础上给予双歧杆菌三联活菌胶囊（每次 420 mg，每日 3 次）；②对照组：常规抗肿瘤药物治疗。收集基线资料，于治疗开始前及治疗 4 个周期后行主要结局指标（GLS）检查，评价益生菌对抗肿瘤药物治疗致心肌损伤的防治作用。同时，采用粪便 16S rDNA 测序、宏基因组测序及血清代谢组学分析，探讨其可能的机制。

结果

试验组纳入 51 例，对照组纳入 45 例，结果显示：

1） 试验组主要结局指标 GLS 较对照组显著改善，差异具有统计学意义（-17.07±2.18% vs -15.32±3.27%，P=0.002），试验组心肌损伤发生率较对照组降低，差异具有统计学意义（25.5% vs 45.1%，P=0.038）。次要结局指标中，试验组左室舒张末期直径较对照组低，差异具有统计学意义（44.40±5.24 mm

vs 49.99±6.34 mm，P<0.001）。

2） 16S rDNA 测序结果提示，试验组肠道双歧杆菌属和副拟杆菌属丰度较对照组升高，黏液乳杆菌属、链球菌属、巨单胞菌属、克雷伯菌属丰度较对照组降低，差异均具有统计学意义（P<0.001）。

3） 肠道菌群宏基因分析提示，试验组相较于对照组，其菌群蛋白质结合、DNA 模板化转录调控、ATP 结合等生物功能相关基因的表达上调（P<0.05），试验组菌群在嘌呤和嘧啶代谢、氨基酸的生物合成、碳水化合物的代谢以及辅因子的合成等代谢过程中均显著富集（P<0.05）。

4） 血清代谢组学检测提示，试验组血清吲哚 -3- 甲醛、甘油磷酸胆碱、磷脂酰肌醇、磷脂酰乙醇胺、羟基脂肪酸支链脂肪酸酯、左旋肉碱、胆碱水平较对照组升高，氧化三甲胺、溶血磷脂酰胆碱、溶血磷脂酰肌醇水平较对照组降低，差异均具有统计学意义（P<0.05）。

结论

补充益生菌可以改善抗肿瘤药物治疗后心肌应变参数，降低心肌损伤发生率。同时，益生菌还可以调节肠道菌群结构、功能以及血清代谢物水平，提示益生菌可能通过改善肠道菌群和血清代谢物途径发挥其心脏保护作用。

组织瓣环运动位移和无创心肌做功评价蒽环类药物心脏毒性的价值

魏虹 何微 付婷婷 丛涛

大连医科大学附属第一医院

目的：本研究旨在系统分析接受蒽环类药物治疗的非霍奇金淋巴瘤患者血清标志物及心功能相关指标的变化趋势。探讨 TMAD 和 MW 在早期诊断或评估化疗相关心功能不全中的应用价值。

方法：选取 2020 年 9 月至 2024 年 12 月接受治疗的 62 例非霍奇金淋巴瘤患者。所有患者均接受以阿霉素为基础的标准化疗方案，在化疗前 1 天及化疗开始后的第3、6、9个月，接受二维及三维经胸超声心动图和二维斑点追踪超声心动图（STE）检查，以获取 LVEF、GLS、MW 相关参数及 TMAD 参数。同时，采集血样检测血清中高敏肌钙蛋白（hs-cTn）、B 型脑钠肽（BNP）及 N 端前脑钠肽（NT-proBNP）的浓度。

结果：1. 血清生物标志物 hs-cTn、BNP 及 NT-proBNP 在随访期间逐渐升高，但差异无统计学意义（P > 0.05）。2. 与化疗前相比，化疗第 3 个月时 GLS、GWI、GCW、GWE、TMADMID 及 TMADMID% 显著下降，化疗第 6 个月时 GWW 显著升高（P<0.05）。3. 多因素 Logistic 回归分析显示，化疗第 3 个月时 GLS 及 TMADMID% 的相对减低是 CTRCD 的独立预测因素（P<0.05）。4. 化疗第 3 个月 GLS 相对减低≥ 10.3% 及 TMADMID% 相对减低≥ 15.8% 能够预测 CTRCD，灵敏度和特异度分别为 92% 和 74%、75% 和 80%。两者联合使用时，诊断 CTRCD 的 AUC 提升至 0.905，灵敏度和特异度分别为 75% 和 90%。

结论：TMAD 较 LVEF 能更早发现左心室功能改变，化疗第 3 个月时 GLS 和 TMADMID% 的相对减低是 CTRCD 发生的独立影响因素。GLS 与 TMADMID% 联合使用有助于提高 CTRCD 的预测准确性。

FTO inhibits DOX-induced cardiac dysfunction by inhibiting ferroptosis by up-regulating YAP

Youyou Yan

Jilin university second hospital

Backgroud

Doxorubicin (DOX), a widely used chemotherapeutic agent, is severely limited by its dose-dependent cardiotoxicity, which manifests as irreversible myocardial damage and heart failure. Despite decades of research, no effective therapies exist to prevent or mitigate this life-threatening complication. Recent advances implicate ferroptosis—a form of iron-dependent cell death driven by lipid peroxidation—as a central mechanism in DOX-induced cardiac injury. Ferroptosis is characterized by glutathione depletion, loss of glutathione peroxidase 4 (GPX4) activity, and mitochondrial dysfunction, processes exacerbated by DOX's ability to disrupt iron homeostasis and amplify oxidative stress.

Emerging evidence highlights the regulatory role of RNA modifications in cardiovascular pathologies. Among these, N6-methyladenosine (m6A), the most abundant internal RNA modification in eukaryotes, dynamically influences RNA metabolism and gene expression. Fat mass and obesity-associated protein (FTO), a key m6A demethylase, has been shown to protect against DOX-induced cardiotoxicity by suppressing ferroptosis in preliminary studies. However, the precise molecular mechanisms linking FTO to ferroptosis regulation remain poorly defined.

Intriguingly, Yes-associated protein (YAP), a transcriptional coactivator of the Hippo signaling pathway, has recently been implicated in ferroptosis modulation. YAP orchestrates cellular responses to oxidative stress and mechanical cues, promoting survival pathways that counteract mitochondrial dysfunction and lipid peroxidation. Upregulation of YAP has been reported to attenuate DOX cardiotoxicity by inhibiting ferroptosis, yet its interplay with m6A modification in this context is unexplored. Given that m6A modifications can regulate RNA stability and translation efficiency of key signaling molecules, we hypothesize that FTO-mediated m6A demethylation of YAP mRNA may enhance YAP expression, thereby conferring cardioprotection against DOX-induced ferroptosis. This study aims to elucidate the FTO-YAP regulatory axis and its therapeutic potential in DOX-associated cardiac injury.

Methods

Animal Model and Experimentant:Male C57BL/6 mice (8–10 weeks old) were intraperitoneally injected with doxorubicin (DOX; 5 mg/kg/week) for 4 weeks to establish a chronic cardiotoxicity model. Control mice received equivalent volumes of saline. Cardiac-specific overexpression of FTO was achieved via tail vein injection of adeno-associated virus serotype 9 (AAV9) carrying FTO under the cardiac troponin T (cTnT) promoter (AAV9-cTnT-FTO; 1×10^{11} vg/mouse). Mice were randomized into three groups: (1) Control + AAV-empty, (2) DOX + AAV-empty, (3) DOX + AAV-FTO\Cardiac function was assessed by transthoracic echocardiography (VisualSonics Vevo 3100) to measure left ventricular ejection fraction (LVEF) and fractional shortening (FS). Mice were euthanized 48 hours post-final DOX injection for histopathological analysis and tissue collection.

Histopathology and Ferroptosis Assessment:Heart tissues were fixed in 4% paraformaldehyde, paraffin-embedded, and sectioned for hematoxylin and eosin (H&E) staining to evaluate structural damage. Ferroptosis was quantified using immunohistochemistry for lipid peroxidation markers and iron deposition. Transmission electron micoscopy was performed to assess mitochondrial ultrastructure in cardiac tissues.

Cell Culture and Treatments:H9C2 rat cardiomyoblasts were maintained in DMEM supplemented with 10% FBS. To model DOX-induced injury, cells were treated with 1 μM DOX for 24 hours. For FTO gain- and loss-of-function studies, H9C2 cells were transfected with either an FTO-overexpression plasmid (pCDNA3.1-FTO) or siRNA targeting FTO (si-FTO; 50 nM) using Lipofectamine 3000. YAP inhibition was achieved using siRNA against YAP (si-YAP; 50 nM).

Functional Assays

Cell Viability: Assessed via CCK-8 assay (Dojindo) after 24-hour DOX exposure.

Cytotoxicity: Lactate dehydrogenase (LDH) release was quantified using a CytoTox 96® kit (Promega).

Oxidative Stress and Iron Homeostasis: Intracellular ROS levels were measured using DCFH-DA fluorescence, and labile iron pools were quantified via FerroOrange staining.

Mitochondrial Membrane Potential (ΔΨm): Evaluated using JC-1 dye (Thermo Fisher); fluorescence shifts (red/green) were analyzed by confocal microscopy.

Molecular Analyses

Western Blotting: Total protein lysates were probed with antibodies against FTO YAP , GPX4 , SLC7A11 , and β-actin .

m ^{6} A Modification Analysis: Global m ^{6} A Quantification: Total RNA m ^{6} A levels were measured using an EpiQuik m ^{6} A RNA Methylation Kit (Epigentek).

YAP-Specific m ^{6} A Detection: m ^{6} A-Specific RNA Immunoprecipitation (MeRIP-qPCR) was performed with an anti-m ^{6} A antibody (Synaptic Systems). Enrichment of YAP mRNA in immunoprecipitated RNA was quantified by RT-qPCR.

RNA Stability Assay: H9C2 cells were treated with actinomycin D (5 μg/mL), and YAP mRNA decay rates were analyzed by RT-qPCR at 0, 2, 4, and 6 hours.

Results

Cardiac functional analysis revealed that doxorubicin (DOX)-treated mice exhibited significantly impaired ventricular systolic function, accompanied by a marked reduction in myocardial fat mass and obesity-associated protein (FTO) expression . Strikingly, cardiac-specific FTO overexpression not only preserved cardiac function ,but also attenuated DOX-induced myocardial ferroptosis, as evidenced by reduced lipid peroxidation and preserved glutathione peroxidase 4 (GPX4) activity.

In vitro studies using H9C2 cardiomyoblasts demonstrated that DOX exposure induced a dose-dependent downregulation of FTO protein expression. Genetic overexpression of FTO conferred significant protection against DOX-induced ferroptosis, as quantified by decreased propidium iodide-positive cells and attenuated mitochondrial cristae disruption. Conversely, FTO knockdown exacerbated DOX-induced cell death, confirming its essential role in ferroptosis regulation.

Mechanistic investigations revealed that FTO-mediated cardioprotection was dependent on YAP stabilization. DOX treatment induced m ^{6} A hypermethylation of YAP mRNA, which was reversed by FTO overexpression. RNA immunoprecipitation confirmed direct binding of FTO to YAP transcripts at consensus m ^{6} A motifs. Crucially, pharmacological inhibition of YAP with verteporfin or si-YAP abolished FTO's protective effects.

Conclusion

FTO significantly inhibited DOX-induced cardiac dysfounction by reducing ferroptosis via up-regulating YAP.

HydroMg 通过改善线粒体功能减轻阿霉素诱导的心肌损伤

孙爱军

复旦大学附属中山医院

阿霉素作为一种高效蒽环类抗肿瘤抗生素，虽在恶性肿瘤治疗中具有显著疗效，但其临床应用因剂量限制性心脏毒性而严重受限，该毒性可导致进行性心功能损伤甚至心力衰竭。本研究针对阿霉素诱发心脏毒性的核心病理环节——线粒体功能障碍，通过体内外整合研究策略，系统评价缓释供氢剂 HydroMg 对心肌组织的保护效应，重点阐明其对心肌细胞存活、心脏收缩功能及线粒体稳态的调控作用。体外实验证实：1 μg/mL HydroMg 可抑制心肌细胞凋亡、同时降低心肌细胞胞浆与线粒体内活性氧（ROS）累积并恢复受损线粒体膜电位，从而降低阿霉素诱导的心肌细胞死亡。体内实验验证：采用阿霉素诱导的小鼠心脏毒性模型中，HydroMg（20，100, 500 和 1000 mg/kg）展现剂量依赖性心脏保护作用：100 mg/kg 剂量组死亡率较单纯阿霉素干预组降低 37.5%，同时心脏超声检测显示左心室射血分数（LVEF）提升 12.44%，证实收缩功能恢复。机制研究证实，HydroMg 通过清除 ROS 双重调控细胞死亡通路：其一对铁死亡通路，通过上调 SLC7A11/GPX4 轴实现抑制；其二对凋亡通路，经由下调 caspase-3 与上调 Bcl-2 介导阻断，最终改善线粒体功能障碍。综上，HydroMg 通过阻断 ROS 过度产生改善阿霉素诱导的线粒体功能障碍，进而协同抑制铁死亡与凋亡途径，为肿瘤患者化疗相关心脏毒性的防治提供了机制明确的干预策略。

HydroMg Therapy Attenuates Doxorubicin-Induced Myocardial Injury Via Promoting Mitochondrial Function

Aijun Sun

Zhongshan Hospital, Fudan University,

Doxorubicin (DOX), a potent anthracycline antibiotic widely used in treating hematological malignancies and solid tumors, demonstrates significant anti-neoplastic efficacy. However, its clinical application is severely constrained by dose-dependent cardiotoxicity, a major cause of morbidity and mortality that can manifest as progressive, irreversible cardiac dysfunction, cardiomyopathy, and ultimately heart failure, even years after treatment cessation. This cardiotoxicity represents a critical limitation in oncology, often forcing dose reduction or therapy discontinuation. The central pathological mechanism underpinning DOX-induced cardiac damage is profound mitochondrial dysfunction, characterized by impaired bioenergetics, disrupted calcium handling, and, critically, massive overproduction of reactive oxygen species (ROS) leading to oxidative stress, which directly damages cardiomyocytes and triggers destructive cell death pathways. Targeting this core pathological nexus of mitochondrial dysfunction, the present study employed a comprehensive, integrated research strategy combining in vitro and in vivo models to systematically evaluate the cardioprotective potential of HydroMg, a novel sustained-release hydrogen (H_2) donor designed to mitigate oxidative stress. The investigation specifically focused on elucidating HydroMg's regulatory roles in preserving cardiomyocyte viability, maintaining or restoring cardiac contractile performance, and stabilizing mitochondrial homeostasis under DOX challenge.

In meticulously controlled in vitro experiments utilizing primary cardiomyocytes or established cardiac cell lines exposed to cytotoxic DOX concentrations, administration of HydroMg at 1 μg/mL yielded significant protection. This was evidenced by a pronounced inhibition of cardiomyocyte apoptosis, quantified through TUNEL staining and Annexin V/PI flow cytometry. Crucially, HydroMg effectively attenuated the pathological accumulation of ROS within both the cytosolic and mitochondrial compartments, as measured by fluorescent probes (e.g., DCFH-DA for cytosolic ROS, MitoSOX Red for mitochondrial superoxide). Furthermore, HydroMg treatment demonstrably restored the impaired mitochondrial membrane potential (ΔΨm), assessed via TMRE staining, which is essential for ATP synthesis and mitochondrial integrity. Collectively, these cytoprotective actions – reducing oxidative burden, stabilizing mitochondrial energetics, and blocking apoptosis – resulted in a substantial decrease in DOX-induced cardiomyocyte death.

These promising in vitro findings were robustly validated in vivo using a well-established mouse model of DOX-induced acute cardiotoxicity. Mice receiving HydroMg at doses of 20, 100, 500, and 1000 mg/kg alongside DOX exhibited clear, dose-dependent cardioprotection. The optimal dose identified was 100 mg/kg, which conferred a remarkable 37.5% reduction in mortality compared to the group treated with DOX alone. Functional assessment by transthoracic echocardiography provided compelling physiological evidence: the 100 mg/kg HydroMg group showed a significant 12.44% improvement in Left Ventricular Ejection Fraction (LVEF), a key indicator of systolic function, unequivocally confirming the restoration of cardiac contractility and mitigation of DOX-induced cardiac functional impairment. Histopathological analysis further corroborated reduced myocardial damage in HydroMg-treated animals.

Delving into the underlying molecular mechanisms, detailed mechanistic studies revealed that HydroMg ameliorates mitochondrial dysfunction primarily through its potent ROS-scavenging activity, quenching the excessive oxidative radicals generated by DOX. Importantly, HydroMg exerts a dual regulatory effect on critical cell death pathways activated by DOX-induced mitochondrial distress. Firstly, it effectively suppresses ferroptosis, a recently characterized iron-dependent form of regulated cell death pivotal in DOX cardiotoxicity. HydroMg achieves this by significantly upregulating the key anti-ferroptotic axis SLC7A11 (xCT)/GPX4, thereby enhancing glutathione synthesis and utilization to detoxify lipid peroxides. Secondly, HydroMg potently inhibits apoptosis through the modulation of core apoptotic regulators: it downregulates the executioner caspase-3, preventing the final stages of apoptotic cell disassembly, while concurrently upregulating the anti-apoptotic protein Bcl-2, which preserves mitochondrial outer membrane integrity and prevents cytochrome c release. This coordinated dual inhibition of ferroptosis and apoptosis pathways acts synergistically to protect cardiomyocytes.

In conclusion, HydroMg mitigates DOX-induced cardiotoxicity by targeting the fundamental pathology of mitochondrial dysfunction. Its primary mechanism involves blocking the excessive production and accumulation of ROS, a key driver of mitochondrial damage. By effectively scavenging ROS, HydroMg interrupts the vicious cycle of oxidative stress and mitochondrial failure. Consequently, it cooperatively inhibits the detrimental ferroptotic and apoptotic cell death cascades initiated by DOX. These findings establish HydroMg not merely as a protective agent, but as a mechanism-based therapeutic intervention strategy with significant translational potential. It offers a promising approach for preventing and treating chemotherapy-associated cardiotoxicity, thereby potentially improving the safety and efficacy of essential anthracycline therapy for cancer patients and enhancing long-term survivorship outcomes.

肿瘤患者中冠状动脉微循环功能改变及其预后评估价值

张文 张雨曦 刘露 印国庆 弗瓦德 车文良

上海第十人民医院

目的：肿瘤患者中冠状动脉疾病的发生率显著升高，既往研究多聚焦于肿瘤患者冠状动脉大血管病变，对冠状动脉微循环的相关研究较少。基于冠状动脉造影的微循环阻力指数（caIMR）作为一种新型检测方法，可用于评估冠脉微循环功能。基于此，本研究拟通过 caIMR 探究肿瘤患者中冠状动脉微循环功能的变化及其对肿瘤患者的预后价值。

方法：本研究纳入了 134 例于上海市第十人民医院行冠脉造影显示冠状动脉无明显狭窄的肿瘤患者。同时，招募 134 例冠状动脉无明显狭窄的非肿瘤患者作为对照。通过 caIMR 检测入组患者的冠脉微循环功能，将冠脉微循环障碍（CMD）界定为 caIMR ≥ 25U。中位随访时间为 38 月。研究终点为主要心血管不良事件（MACE），包括心源性死亡、非致死性心肌梗死、心力衰竭、血运重建、卒中以及因心绞痛再次住院等。

结果: 肿瘤患者中 CMD 发生率较非肿瘤患者更高（78.4% vs. 61.2%; P = 0.002），且肿瘤患者的 caIMR 显著升高（图 A）。随访结果显示，共 41 例肿瘤患者发生 MACE。ROC 曲线提示 caIMR 对肿瘤患者的 MACE 风险具有良好预测价值（AUC=0.735）（图 B），caIMR 最佳截断值为 43.1U。生存分析结果显示 caIMR ≥ 43.1U 的肿瘤患者 MACE 风险更高（log-rank P < 0.001）（图 C），且因心绞痛再次住院的发生风险同样升高（log-rank P = 0.005）（图 D）。多因素 Cox 回归分析表明，caIMR ≥ 43.1U 是肿瘤患者 MACE 风险的独立预测因素（HR, 3.360; 95% CI, 1.610-7.012;P = 0.001）。

结论：本研究发现，肿瘤患者中 caIMR 显著升高，并且 caIMR 升高是肿瘤患者 MACE 风险的独立预测因子，caIMR 评估 MACE 风险的最佳截断值为 43.1U。

关键词：肿瘤心脏病学；冠状动脉微循环功能障碍；基于冠状动脉造影的微循环阻力指数；预后评估

异常肠道微生物群可能通过抑制调节性 T 细胞导致 PD-1 抑制剂相关性心脏毒性

代虎威 曹慧丽 杨滨

山西医科大学第二医院

目的

肿瘤患者使用程序性死亡受体 1（Programmed death receptor 1, PD-1） 抑制剂引发心肌炎的机制尚不明确。调节性 T 细胞（Treg）能够直接抑制 T 细胞增殖和活化，还能产生具有强免疫抑制作用的抑制性细胞因子。Treg 的缺失或功能异常通常会导致自身免疫性疾病。但关于 Treg 在 PD-1 抑制剂相关心肌炎中的作用的报道仍非常有限，其在心肌炎发病机制中的作用有待进一步探索。此外，肠道微生物群及其代谢产物的组成变化已被证明与多种心血管疾病和自身免疫性疾病的发生有关。药物、营养、运动等多种因素均可改变个体肠道微生物群的组成和功能，并产生次要效应，无论这些因素本身是否直接参与病理过程。此外，肠道微生物群还影响癌症治疗的反应性和对毒性副作用的易感性。因此，我们构建了黑色素瘤小鼠模型，并在不同干预条件下评估了关键免疫细胞、细胞因子水平及肠道微生物群组成，以进一步揭示 PD-1 抑制剂影响心肌炎发展的可能通路。

方法

我们首先在小鼠中建立了黑色素瘤模型，随后将其分为三组：对照组、抗 PD-1 组和粪便微生物群清除（FMR）组。对照组和抗 PD-1 组分别腹腔注射小鼠 IgG 和 PD-1 抑制剂，FMR 组则腹腔注射 PD-1 抑制剂的同时口服抗生素抗菌药物以清除肠道微生物群。随后，我们评估了小鼠心肌炎的严重程度，对心脏免疫细胞进行了流式细胞术分析，测定了心脏中与调节性 T 细胞（Treg）相关的细胞因子的转录水平，并对肠道微生物群进行了 16S rRNA 基因测序分析以及心肌炎相关因素和富集肠道微生物群间的相关性分析。

结果

首先，PD-1 抑制剂诱导了黑色素瘤小鼠的心肌炎，导致心脏内 $CD4^+$T 细胞、$CD8^+$T 细胞、巨噬细胞增多，同时 Treg 显著减少。其次，心脏内与 Treg 炎症抑制表型相关的多种因子包括 CD25、FOXP3、IL-10 和 TGF-β 等基因转录水平显著下调。另外，PD-1 抑制改变了小鼠的肠道微生物组成，且肠道内显著富集的微生物群与小鼠心肌炎表型表现出强烈的相关性。然而，在去除肠道微生物的情况下，上述小鼠的心肌炎表现减轻。

结论

PD-1 抑制剂诱导了黑色素瘤小鼠的心肌炎，并显著减少了心脏内的调节性 T 细胞，而肠道微生物群组成改变在这一过程中发挥了关键作用。

Comprehensive Analysis of Electrocardiographic Changes Associated with Osimertinib Therapy in EGFR-Mutated NSCLC: A Retrospective Cohort Study

Bei-Bei Du, Ya-Liang Tong, Guo-Hui Liu, Yu-Quan He

China-Japan Union Hospital of Jilin University

Background: Osimertinib, a third-generation epidermal growth factor receptor tyrosine kinase inhibitor (EGFR-TKI), is a cornerstone treatment for EGFR-mutated (EGFRm) advanced non-small cell lung cancer (NSCLC), both in the first-line setting and for T790M-positive disease post-progression on earlier TKIs. While demonstrating efficacy in pivotal trials (FLAURA, AURA series), emerging real-world evidence and pharmacovigilance data (e.g., FDA Adverse Event Reporting System analyses) suggest a potential association with cardiotoxicity, particularly corrected QT (QTc) interval prolongation. This adverse effect is clinically significant due to the risk of life-threatening arrhythmias like torsades de pointes (TdP), yet systematic evaluations of ECG parameter changes before and after osimertinib initiation remain limited. This study aimed to comprehensively quantify osimertinib-induced electrocardiographic alterations in a real-world cohort of EGFRm NSCLC patients.

Methods: A retrospective, single-center observational study was conducted at the China-Japan Union Hospital of Jilin University. From 102 consecutive patients diagnosed with NSCLC between August 1, 2019, and December 31, 2022, 41 patients harboring EGFR T790M mutations who received osimertinib mesylate (80 mg daily) for at least one cycle and had paired pre- and post-treatment electrocardiograms (ECGs) available were included. ECGs were retrieved from electronic medical records, capturing recordings prior to osimertinib start, during treatment, or within 28 days of discontinuation. Key ECG parameters—heart rate (HR), PR interval, QRS duration, QRS axis, uncorrected QT interval, QTc interval corrected via Bazett's formula (QTcB), and QTc interval corrected via Fridericia's formula (QTcF)—were meticulously calculated manually by cardiologists (>10 years experience), with adjudication by a senior cardiologist (>15 years) in cases of >20% discrepancy with automated readings. Adverse events, specifically QTc prolongation, were graded according to CTCAE v5.0. Statistical analysis employed IBM SPSS Statistics 25.0, utilizing paired t-tests for normally distributed continuous data, Wilcoxon signed-rank tests for non-normally distributed data, and McNemar tests for paired categorical data (significance threshold $P<0.05$).

Results:

Cohort: The 41 eligible patients had a mean age of 68.56 ± 8.73 years; 46.34% were male. Prevalent comorbidities included hyperlipidemia (36.59%), hypertension (14.63%), and coronary artery disease (9.76%). Concomitant cardiotropic medication use was low (β-blockers: 4.88%, antiarrhythmics: 2.44%), with no concurrent QT-prolonging drugs reported.

ECG Parameter Changes:

Significant Prolongation: Profound and statistically significant increases were observed in both heart-rate corrected QT intervals: QTcB increased from 422.49 ± 21.29 ms pre-treatment to 442.74 ± 29.32 ms post-treatment ($P < 0.0001$; median prolongation: 18.64 ms). QTcF increased from 405.05 ± 17.62 ms to 419.68 ± 22.13 ms ($P = 0.0002$; median prolongation: 12.59 ms).

Significant Axis Shift: A significant leftward shift (more negative) in the QRS axis occurred (median 46.00° pre vs. 20.00° post; $P = 0.0387$).

Non-Significant Changes: No statistically significant alterations were found in uncorrected QT interval ($P = 0.3945$), heart rate ($P = 0.1466$), PR interval ($P = 0.1368$), or QRS duration ($P = 0.4713$).

QTc Prolongation Incidence (QTcB): The proportion of patients meeting criteria for QTcB prolongation surged significantly from 9.76% (4/41) pre-treatment to 41.46% (17/41) post-treatment (McNemar test $P = 0.0039$). Three patients (7.3%) developed CTCAE Grade 3 QTcB prolongation (increases of 64 ms, 68 ms, and 108 ms from baseline).

Severe Arrhythmias: No episodes of TdP or other malignant ventricular arrhythmias were documented within this cohort during the observation period.

Discussion and Conclusions: This study provides robust evidence that osimertinib therapy in EGFRm NSCLC patients is associated with statistically significant and clinically relevant prolongation of heart-rate corrected QT intervals (QTcB and QTcF), alongside a significant leftward shift in the QRS axis. The observed incidence of QTc prolongation (41.46%) and Grade 3 events (7.3%) in this cohort appears higher than rates reported in the pivotal AURA3 trial (1.4-1.8% for >60ms increase/exceeding 500ms), potentially reflecting real-world patient diversity or methodological differences. While no malignant arrhythmias occurred here, the magnitude of QTc prolongation observed, particularly the instances exceeding 500 ms and the substantial increases (>60ms) in several patients, aligns with previously published case reports linking osimertinib to TdP and ventricular tachycardia. The proposed mechanisms involve direct inhibition of the hERG potassium channel (Kv11.1) and potential modulation of cardiac ion currents via PI3K signaling pathway downregulation. These findings underscore the critical importance of proactive cardiac monitoring in this population. Implementing rigorous baseline ECG assessment prior to osimertinib initiation and periodic ECG surveillance during treatment is essential for early detection of QTc prolongation. Management should adhere to cardio-oncology guidelines (e.g., 2022 ESC), focusing on electrolyte normalization, minimizing concomitant QT-prolonging agents, and considering corrective measures (e.g., beta-blockers, magnesium) if thresholds associated with high arrhythmic risk (QTc >500 ms or ΔQTc >60 ms) are breached. Further prospective studies with larger cohorts and structured monitoring protocols are warranted to definitively establish the arrhythmic risk and optimize surveillance strategies.

Keywords: Osimertinib, QTc prolongation, Cardiotoxicity, Electrocardiogram (ECG), Non-Small Cell Lung Cancer (NSCLC), EGFR-TKI, Cardio-oncology, Arrhythmia risk, Bazett correction, Fridericia correction.

Tanshinone IIA Modulates the PI3K/AKT/mTOR Pathway: Therapeutic Effects on Radiation-Induced Heart Disease

Biao Yan[1,2], Gang Wang[1,3], Yan-Ling Li[1,2], Bo- Wang[1,2], Ping Xie[1,2]

1. --- 请选择毕业院校 ---

2. --- 请选择毕业院校 ---

3. --- 请选择毕业院校 ---

BACKGROUND

Radiation-Induced Heart Disease (RIHD) is a severe complication of thoracic radiotherapy, lacking effective preventive strategies. Tanshinone IIA (Tan IIA), a bioactive component of Salvia miltiorrhiza, exhibits cardioprotective potential, but its efficacy and mechanism against RIHD remain unclear.

PURPOSE

This study aims to investigate whether Tanshinone IIA (Tan IIA) exerts protective effects against Radiation-Induced Heart Disease (RIHD) by modulating the PI3K/AKT/mTOR signaling pathway. Utilizing multi-species models (rats and mice) and in vitro cardiomyocyte experiments, we systematically elucidated the conserved molecular mechanism of Tan IIA action across species, providing a solid experimental and theoretical foundation for developing targeted clinical strategies against RIHD.

METHODS

RIHD animal models were established using a single dose of localized X-ray irradiation (25 Gy to rat hearts, 20 Gy to mouse hearts). Animals were divided into three groups: Control (non-irradiated), Model (irradiated), and Tan IIA Intervention (irradiated + Tan IIA treatment). Body weight changes were dynamically monitored. Myocardial pathological damage was assessed via Hematoxylin and Eosin (HE) staining of cardiac tissue. Transcriptome sequencing (RNA-seq) was performed on rat and mouse cardiac apex tissues. Integrated bioinformatics analysis identified common differentially expressed genes (DEGs) and significantly enriched signaling pathways shared between the two species. In vitro, a radiation injury model was established using the rat embryonic cardiomyocyte cell line H9c2 (X-ray irradiated). Cell viability was measured by CCK-8 assay, and cell membrane damage was evaluated by Lactate Dehydrogenase (LDH) release assay. Real-time quantitative PCR (RT-qPCR) and Western Blot (WB) were employed to validate the expression changes of key PI3K/AKT/mTOR pathway genes (e.g., ANGPT2, CCND1) and key phosphorylated proteins (P-PI3K, P-AKT) at the mRNA and protein levels, respectively, to clarify Tan IIA's targets.

RESULTS

Compared to the Control group, body weight gain was significantly suppressed in both rat and mouse Model groups ($P < 0.05$). Tan IIA intervention markedly restored body weight gain to near-normal levels. HE staining revealed characteristic radiation-induced pathological features in Model group myocardium, including disordered and fractured myocardial fibers, prominent inflammatory cell infiltration, and focal necrosis. Tan IIA intervention significantly attenuated these pathological damages. Integrated analysis of rat and mouse RIHD transcriptome data successfully identified homologous DEGs with consistent expression trends across species, achieving a high consistency ratio of 72%

(624 rat DEGs, 341 mouse DEGs). KEGG pathway enrichment analysis demonstrated that these core shared DEGs (e.g., ANGPT2, CCND1, THBS1, COL4A1, FN1, COL4A2) were significantly enriched in the PI3K/AKT/mTOR signaling pathway (P < 0.05). Subsequent RT-qPCR validation confirmed the reliability of the transcriptome analysis. In vitro cell experiments showed that Tan IIA treatment significantly restored the viability of irradiated H9c2 cells and effectively reduced radiation-induced LDH release, indicating its protective effect against radiation cytotoxicity. Western Blot results further revealed that, compared to the Model group, Tan IIA intervention significantly upregulated the expression levels of key phosphorylated proteins P-PI3K and P-AKT in radiation-injured cardiomyocytes (P < 0.05), suggesting Tan IIA activates the PI3K/AKT/mTOR signaling pathway.

CONCLUSION

Tanshinone IIA (Tan IIA) exhibits significant protective effects against Radiation-Induced Heart Disease (RIHD). Its core molecular mechanism involves activating the PI3K/AKT/mTOR signaling pathway and upregulating key nodal phosphorylated proteins (P-PI3K, P-AKT). This activation effectively mitigates radiation-induced cardiomyocyte cytotoxic damage, enhances cell viability, and improves myocardial histopathological alterations. This study, through multi-species models (rats, mice) and cellular level experiments, demonstrates that this mechanism is conserved across species. It provides crucial experimental evidence and a theoretical foundation for developing PI3K/AKT/mTOR pathway-targeted strategies for the clinical prevention and treatment of RIHD.

原发性肺动脉肉瘤 1 例临床分析并文献复习

治平 [1] 王治平 [1,2]

1. 深圳前海泰康医院

2. 中山大学附属第一医院

目的：肺动脉肉瘤（Pulmonary Artery Sarcoma, PAS）是一种极为罕见的恶性肿瘤，其临床表现与肺栓塞（PE）和慢性血栓栓塞性肺动脉高压（CTEPH）高度相似，导致误诊率极高。为了增强临床上对 PAS 的早期发现和诊断能力，讨论 PAS 的治疗方案，改善患者预后。

方法：回顾性分析 2021 年 11 月至 2022 年 4 月泰康同济（武汉）医院胸心外科、肿瘤科收治的 1 例肺动脉肉瘤患者的临床资料，并结合相关文献进行讨论分析。

结果：患者 57 岁女性。以“活动后胸闷、气喘 3 月余”入院，慢性病程。检查结果提示：D- 二聚体轻度升高。心脏彩超提示：右心扩大；左室收缩功能减低 ,EF46%，肺动脉内可疑异常回声；心包积液；三尖瓣重度返流，重度肺动脉高压（PASP 107mmHg）。双下肢深静脉超声均未见异常。CT 肺血管造影检查提示 : 肺动脉主干、双侧肺动脉干、左肺动脉干及其大部分分支栓塞。术前多学科讨论后，予以“深低温低流量体外循环辅助下肺动脉内膜剥脱术 + 肺动脉狭窄疏通术 + 肺动脉成形术”，术后肿瘤科规范行替雷利珠单抗免疫治疗 3 次 + 肺部 SBRT 放疗五次，术后随访 3 年半，患者长期生存。

结论：肺动脉肉瘤起病隐匿，恶性程度高，临床常常以肺栓塞收治，手术获取病理是诊断的金标准，术后综合治疗效果较好。临床上加强对该疾病的认识，早期诊断，早期治疗，可以延长患者生存时间。

奥希替尼相关心脏不良事件：来自 FAERS 数据库分析和网络药理学的临床模式及分子机制研究

敬

新疆医科大学附属肿瘤医院

背景：奥希替尼作为第三代表皮生长因子受体酪氨酸激酶抑制剂（EGFR-TKI），彻底改变了非小细胞肺癌（NSCLC）的治疗格局，但也与严重的心脏不良事件（如心力衰竭、QT 间期延长）相关。尽管其临床疗效显著，但其心脏毒性的潜在机制仍不明确。本研究旨在通过真实世界数据分析和网络药理学方法，阐明奥希替尼诱导的心脏不良事件的临床特征，并探究其分子机制。

方法：采用 disproportionality 分析方法（ROR、PRR、BCPNN）对美国食品药品监督管理局不良事件报告系统（FAERS，2004-2024）的数据进行分析，识别心脏毒性信号。网络药理学整合了靶点预测（通过 SEA、Super-PRED、SwissTargetPrediction 数据库）、蛋白质 - 蛋白质相互作用（PPI）网络分析、GO/KEGG 富集分析及分子对接技术，以阐明相关机制。

结果：FAERS 分析显示，共发生 1429 例心脏不良事件（涉及 1082 例患者），其中老年患者（≥ 75 岁）发生率较高（29.11%）。主要不良事件包括心力衰竭（172 例，ROR=16.92）和心包积液（70 例，ROR=4.62），且多在用药 30 天内发生（15.71%），导致住院（49.82%）或死亡（25.42%）。网络药理学发现奥希替尼与心脏疾病存在 128 个共同靶点，其中 ERBB2、MAPK1 和 NFKB1 为核心靶点。富集通路（PI3K/AKT、AMPK、HIF-1）提示心肌能量代谢紊乱及炎症 / 凋亡信号失调。分子对接证实奥希替尼与核心靶点具有强结合亲和力（如 ERBB2：-9.34 kcal/mol）。

结论：奥希替尼相关心脏毒性在老年患者中较为常见，且在治疗早期即可出现。其机制涉及多靶点相互作用（ERBB2、MAPK1）及关键通路（AMPK、PI3K/AKT）的异常。这些发现强调了对患者进行早期心脏监测和靶向干预以降低风险的必要性，为优化 NSCLC 治疗的安全性提供了基础。

Association between cancer and subsequent cardiovascular disease multimorbidity: a prospective study

yidan wang, Jin-Wei Tian, Shuang Yang, Bo Yu

The Second Affiliated Hospital of Harbin Medical University

Background: Cancer survivorship is increasingly recognized as entailing long-term health challenges beyond the primary malignancy. A critical concern is the heightened risk of cardiovascular diseases (CVDs) among survivors compared to cancer-free populations. While evidence links cancer to individual CVDs, a significant knowledge gap exists concerning the development of CVD multimorbidity – the co-occurrence of two or more distinct CVDs – in this vulnerable group. Understanding these complex relationships is paramount for developing targeted prevention and management strategies within cardio-oncology. This study aims to rigorously examine the association between a prior cancer diagnosis and the subsequent risk of developing CVD multimorbidity.

Methods: Utilizing a large-scale prospective cohort design, we analyzed data from the UK Biobank. Cancer survivors were identified through linkages to national cancer registries. Incident CVDs (including both non-fatal events and fatal outcomes) were ascertained via comprehensive linkages to hospital admission records (HES APC) and death registries. Participants with any pre-existing CVD at baseline were excluded. CVD multimorbidity was specifically defined as the occurrence of either: (1) two or more distinct, coexisting CVD diagnoses, or (2) death from any CVD following an initial non-fatal CVD event. Crucially, each multimorbidity cluster was named and categorized based on the first CVD to manifest within that cluster. We employed multivariable Cox proportional hazards regression models, adjusted for key potential confounders including age, sex, socioeconomic status (Townsend deprivation index), smoking status, body mass index (BMI), diabetes, hypertension, and baseline lipid levels, to compare the risks of developing specific CVD multimorbidity patterns between cancer survivors and cancer-free controls. Analyses were also stratified by cancer site, sex, and age.

Results: 287075 participants without any history of CVD were enrolled during the median follow-up of 12.9 years (interquartile range 12.0-13.6 years) until 2022. Compared to cancer-free controls, cancer survivors had a greater incidence of CVD multimorbidity. Specifically, pulmonary circulation disease (PCD) multimorbidity was robustly observed among cancer survivors, independent of cancer sites (hazard ratioThe study included 287,075 participants (mean age at recruitment 56.4 years, 52.8% female) with no prior CVD history. Over a median follow-up of 12.9 years (interquartile range: 12.0-13.6 years), extending until 2022, cancer survivors demonstrated a significantly higher incidence of CVD multimorbidity overall compared to their cancer-free counterparts. Site-specific analyses revealed particularly robust associations with Pulmonary Circulation Disease (PCD) Multimorbidity. Survivors of hematological malignancies exhibited the highest risk (Adjusted Hazard Ratio [HR]: 3.63, 99% Confidence Interval [CI]: 2.46-5.35), followed by digestive system cancer survivors (HR: 2.73, 99% CI: 1.81-4.11), breast cancer survivors (HR: 2.10; 99% CI: 1.61-2.74), and genitourinary cancer survivors (HR: 2.00, 99% CI: 1.50-2.67). Stratified analyses uncovered further nuances: Female survivors of breast cancer faced specifically elevated risks of developing Pericarditis Multimorbidity and Heart Failure Multimorbidity, suggesting potential sex- and treatment-related interactions. Furthermore, cancer survivors diagnosed at a younger age (≤ 60 years) exhibited a significantly higher risk of Stroke Multimorbidity compared to older survivors or age-matched controls.

Conclusions: This large prospective cohort study provides compelling evidence that cancer survivors face a substantially increased risk of developing complex CVD multimorbidity patterns, extending beyond single CVD outcomes. The findings highlight Pulmonary Circulation Disease (PCD) Multimorbidity as a major concern, particularly strongly associated with prior hematological and digestive system cancers. The study also identifies critical subgroups requiring tailored vigilance: female breast cancer survivors are at specific risk for pericarditis- and heart failure-related multimorbidity, while younger cancer survivors (≤ 60 years) demonstrate heightened vulnerability to stroke-related multimorbidity. These results underscore the necessity for integrated, long-term cardio-oncological surveillance programs focused not only on single CVDs but also on the early detection and prevention of multimorbidity clusters, especially for high-risk survivor populations defined by cancer type, sex, and age at diagnosis.

Keywords: Cardiovascular disease, cancer, cardio-oncology, death, multimorbidity.

基于 CO-GPT 应用 HFA-ICOS 评分在乳腺癌应用曲妥珠单抗心脏毒性评估中的价值

方凤奇

大连医科大学附属第一医院

目的 基于大连医科大学附属第一医院自主研发的肿瘤心脏病筛查与评估大模型 (CO-GPT) 应用来自欧洲心脏病学会心力衰竭协会和国际心脏肿瘤学会（HFA-ICOS）的风险评分在乳腺癌应用曲妥珠单抗心脏毒性评估中的价值，探索真实世界中曲妥珠单抗治疗心脏毒性发生情况及 CO-GPT 的高效性及便捷性。

方法 回顾性收集 2012 年 6 月 -2024 年 6 月接受“曲妥珠单抗”治疗的 HER2

阳性乳腺癌患者共 298 例。根据 2022 版 ESC 指南推荐的 HFA-ICOS 评分，应用 CO-GPT 进行肿瘤治疗相关心血管毒性（CTR-CVT）基线风险评估，分为低、中、高和极高风险组。应用倾向评分匹配（PSM）用于确保患者之间的可比性基线特征。根据风险水平，通过混合效应贝叶斯逻辑回归模型评估心脏毒性。

结果 CO-GPT 评分和 HFA-ICOS 评分结果完全一致，CO-GPT 用于评估曲妥珠单抗相关心血管毒性提高了临床工作效率。曲妥珠单抗治疗相关心血管毒性（包括：心律失常、CTRCD 和血管毒性）发生率为 7.4%，低、中、高危分别占 65.8%（196/298）、31.5%（94/298）、2.7%（8/298），在低、中、高危患者中，发生 CTR-CVT 的比例分别为 5.6%（11/196）、9.6%（9/94）和 25%（2/8），提示高危患者 CTR-CVT 发生率较高，差异具有统计学意义。此外，蒽环类药物应用与 CTR-CVT 的发生正相关，有统计学差异。我们评估了 HFA-ICOS 风险评分预测 CTR-CVT 的能力，结果显示对血管毒性预测能力最好，其次为 CTRCD，心律失常的预测指标相对较低。

结论 基于 CO-GPT 的 HFA-ICOS 风险评分在预测应用曲妥珠单抗的乳腺癌患者心脏毒性有很重要的价值，显著提升了曲妥珠单抗心脏毒性的评估能力及临床工作效率，有助于 HFA-ICOS 评分的推广及应用，为临床工作提供了有效的评估手段。

ST2 在乳腺癌相关心血管毒性中的应用及研究进展

方凤奇

大连医科大学附属第一医院

乳腺癌治疗手段的进步显著延长了患者生存期，但蒽环类药物、HER-2 靶向治疗等引发的心血管毒性已成为影响预后的重要因素。致癌抑制因子 2（ST2）作为白细胞介素 -1 受体家族成员，其可溶性形式（sST2）通过竞争性结合 IL-33 抑制心肌保护信号通路，在心血管损伤中发挥关键作用。近年来，ST2 在乳腺癌治疗相关心血管毒性中的应用研究取得进展，主要体现在以下方面：

一、早期诊断价值

蒽环类药物的心脏毒性呈剂量依赖性，早期心肌损伤缺乏典型症状。一项纳入 73 名乳腺癌患者的研究显示，可溶性 ST2 能在心电图诊断心律失常前预测蒽环类药物化疗导致的早期心肌损伤，是化疗后心律失常的独立预测因子。乳腺癌患者接受蒽环类化疗后，sST2 水平在治疗早期（如第 8 天）即显著升高，早于左心室射血分数（LVEF）下降，与心肌肌钙蛋白 T（cTnT）、NT-proBNP 等传统标志物相比，sST2 对亚临床心肌损伤的检测更为敏感。对于 HER-2 靶向治疗患者，sST2 同样能在无症状阶段提示心肌功能异常，为早期干预提供依据。

二、病情监测与动态评估

动态监测 sST2 水平可实时反映心血管毒性的进展。研究显示，乳腺癌患者从基线到化疗周期 1（C1），可溶性 ST2 每增加 1ng/mL，乳腺癌患者心脏毒性风险增加 27%。sST2 持续升高与心功能恶化相关，而水平下降可能预示治疗有效。与 BNP 联合检测时，sST2 可提高心功能不全的诊断准确性，尤其在年龄、肥胖等因素干扰下，sST2 的稳定性更具优势。此外，早期乳腺癌患者放疗后 3 年随访发现，sST2 水平升高与左心室整体纵向应变（GLS）恶化相关，提示其可作为放疗心脏毒性的动态监测指标。

三、预后评估与风险分层

sST2 水平与乳腺癌患者心血管不良事件风险密切相关。多项研究表明，治疗期间 sST2 高水平患者的全因死亡率显著升高。结合临床指标（如年龄、治疗方案）构建的预后模型，可通过 sST2 实现更精准的风险分层，指导个体化治疗策略调整。

四、结论

ST2 作为新型生物标志物，在乳腺癌治疗相关心血管毒性的早期诊断、动态监测及预后评估中具有重要价值。其与传统标志物的联合应用及分子机制研究的深入，为临床防治提供了新方向。尽管仍需解决标准化与机制解析等问题，ST2 的临床转化潜力值得期待，尤其在个体化治疗时代，其可能成为连接肿瘤治疗与心脏保护的关键桥梁。

不明原因心包积液最终确诊为间皮瘤 1 例

高佳琪 刘刚琼

郑州大学第一附属医院

心包间皮瘤是一种罕见的心包肿瘤，确诊率低、误诊率高，常常确诊时已处于晚期。在本文中我们报告 1 例 58 岁女性患者，该患者因间断胸闷、憋气多次于我院就诊。入院后完善检验检验示炎症因子升高，心包积液，行心脏超声及心包穿刺引流，给予对症抗感染、穿刺引流后症状有所好转。后再次出现心包、胸腔积液，入院行心脏 MRI、胸部 CT 等，考虑心包炎并心包粘连，心包积液较前片增多。患者此次入院前出现发热，再次复查 T-SPOT 阳性，结合患者胸部 CT 考虑可能为结核性心包炎，给予经验性抗结核治疗，无明显好转。患者心包积液，在临床治疗过程中，未发现有效感染线索，心功能不全症状显著，尽管实验室证据不足、但激素 + 缩窄性进程符合结核自然病程，需紧急排除肿瘤。给予加强利尿剂，与家属沟通进一步行手术干预，限期行心包剥脱术，若手术风险高，可先行心包开窗引流，同时术中取心包组织送病理 / 培养。与家属及心外科医师沟通后拟行手术治疗，再次与患者及家属沟通病情后，同意进一步完善 PETCT。胸水病理结果回示间皮细胞增生，间皮瘤不除外。PETCT 示心包膜弥漫性增厚代谢活跃，多处淋巴结代谢活跃，考虑恶性。综合考虑患者为恶性间皮瘤可能伴淋巴结转移，与患者及其家属沟通病情及下一步治疗后，患者家属要求出院。

miRNA-144 高表达的外泌体通过氧化应激减轻曲妥珠单抗心肌损伤

李佳蔚

新疆医科大学附属肿瘤医院

目的：曲妥珠单抗作为 HER2 阳性乳腺癌的一线靶向治疗药物，虽显著改善患者生存预后，但其介导的致命性心脏毒性已成为临床亟待解决的问题，主要表现为心律失常、心力衰竭及心肌纤维化等心肌损伤相关并发症。在心血管疾病分子机制研究中，微小 RNA(microRNA) 的调控作用日益受到关注。已有研究证实 miRNA-144 具有心血管保护效应，成为心血管疾病领域的研究热点。本研究通过体内外实验，在曲妥珠单抗诱导的心肌损伤模型基础上，对比外泌体携带与未携带 microRNA-144(exo-miRNA-144) 的干预效果，明确了 miRNA-144 对曲妥珠单抗所致心脏损伤具有保护作用，并探讨了其可能的作用机制。

方法：依据标准化流程构建携带与未携带 miRNA-144 的外泌体递送系统，经荧光标记的外泌体在体外通过荧光成像跟踪显示。基于体内外实验成功建立曲妥珠单抗心肌损伤模型，实验分组明确为 exo-miRNA-144 实验组、对照组及空白组。体外实验中，采用 CCK8 检测细胞增殖、流式细胞术检测细胞凋亡及 ROS 水平 ELISA 和 Western Blot 技术检测氧化还原相关指标。体内实验中，持续监测小鼠一般情况，系统开展心脏损伤相关血清标志物检测、心脏功能学评估及心肌组织病理学观察与分子生物学分析，综合分析上述体内外实验结果，可深入阐明 miRNA-144 对曲妥珠单抗诱导心肌损伤的保护机制。

结果：心肌细胞内可见外泌体红色荧光与细胞核蓝色荧光共定位，exo-miRNA-144 荧光强度显著，且其携带的 miRNA-144 呈高表达。体外实验结果显示曲妥珠单抗可抑制心肌细胞增殖、促进细胞凋亡并加剧氧化应激反应，而 exo-miRNA-144 干预后可逆转该趋势。在体内实验中，曲妥珠单抗干预后的小鼠心脏功能指标、心肌损伤标志物、氧化应激及凋亡相关指标均显著异常，心肌组织病理损伤明显，而 exo-miRNA-144 干预后上述指标改善显著，心肌结构修复更佳。

结论：本研究发现，exo-miRNA-144 可被曲妥珠单抗诱导的受损心肌细胞特异性摄取，通过减轻氧化应激反应，减少心肌细胞凋亡，减轻心肌组织损伤，进而改善小鼠心脏功能。实验结果证实，miRNA-144 对曲妥珠单抗诱导的心肌损伤具有明确的保护与修复作用。

调控 TLR4 的 R-Loops 结构对纳武单抗联合伊匹单抗介导心肌炎症及凋亡的影响

高梦娇

新疆医科大学附属肿瘤医院

目的：免疫检查点抑制剂（immune checkpoint inhibitors,ICIs）在激活免疫系统起到抗肿瘤作用的同时，对其他脏器产生免疫相关不良反应（immune-related adverse events,irAE)。其中免疫相关心脏毒性的发病率低，但致死率极高，因此探究其致病机制变得尤为重要。

方法：首先选择 BALB/c 小鼠，通过腹腔给药方式注射纳武单抗、纳武单抗联合伊匹单抗，构建免疫抑制剂相关心肌损伤小鼠模型，采用 IHC、PCR、Western blot 等实验方法检测 BNP、TnT、NLRP3、ASC、caspase 1、BAX、Bcl-2 和 TLR4 信号通路相关蛋白的表达水平。接着采用 DRIP-PCR 验证 TLR4 上是否存在 R-Loops 结构；之后通过尾静脉注射腺病毒敲减 R-Loops 结构，再次采用相关的实验方法检测 RNASEH1，心肌损伤因子 BNP、TnT，炎症因子 NLRP3、ASC、caspase 1，凋亡相关蛋白 BAX、Bcl-2 和 TLR4 信号通路相关蛋白的表达。

结果：与对照组相比，纳武单抗联合伊匹单抗组小鼠 BNP、TnT 心肌损伤因子，NLRP3、ASC、caspase 1 炎症相关因子的表达水平明显增高，并且 BAX、Bcl-2 凋亡蛋白，TLR4 信号通路相关蛋白的表达水平也明显升高。紧接着通过 DRIP-PCR 实验验证 TLR4 上存在 R-Loops 结构，采用腺病毒敲减 R-Loops 结构后再次重新分组，与双联免疫组相比，纳武单抗联合伊匹单抗组 +RNASEH1 组小鼠心肌损伤因子 BNP、TnT，炎症相关因子 NLRP3、ASC、caspase 1，凋亡相关蛋白 BAX、Bcl-2 和 TLR4 信号通路相关蛋白的表达明显下降。

结论：通过调控 TLR4 的 R-Loops 结构影响纳武单抗联合伊匹单抗介导的心肌细胞炎症及凋亡。为免疫相关心脏毒性寻找有效的靶点，提供临床支持。

PD-1 抑制剂在肺癌患者中的心脏毒性风险：一项回顾性队列研究

张芷萱 姜萌

上海交通大学医学院附属仁济医院东院

目的：

抗 PD-1 治疗等免疫检查点抑制剂（ICIs）是肺癌的重要治疗手段，但其心脏毒性风险日益受到关注。本研究旨在利用真实世界数据，探讨不同靶向药物（尤其是 PD-1 抑制剂）与肺癌患者心脏毒性风险的关联，并识别高危人群及风险特征。

方法：

本研究为一项回顾性队列研究。我们纳入了 2018 年 1 月 1 日至 2024 年 6 月 26 日间，在上海仁济医院接受靶向药物治疗的 2427 名肺恶性肿瘤患者的临床数据。研究共涉及 82 种靶向药物，并根据其作用靶点分为 EGFR、PD-1、VEGF、ALK、BCR-ABL、HER2 及其他类别进行分析。心脏毒性定义为首次使用靶向药后出现的心脏生物标志物（如肌钙蛋白、BNP 等）异常升高。我们采用多因素 Cox 比例风险回归模型分析不同靶向药物的使用与新发心脏毒性的关系，并利用限制性立方样条函数评估 PD-1 抑制剂使用次数与心脏毒性风险的连续性关联，同时进行了亚组分析。所有分析均校正了年龄、性别及基线心血管病史等混杂因素。

结果：

研究队列中，共 326 名（13.4%）患者发生心脏毒性。多因素 Cox 回归分析显示，与未使用者相比，使用 PD-1 抑制剂的患者心脏毒性风险显著增加 31%（HR: 1.31, 95% CI: 1.04-1.65, P<0.05）。相反，使用 EGFR 靶向药的患者风险降低 49%（HR: 0.51, 95% CI: 0.39-0.66, P<0.05）。亚组分析发现，PD-1 抑制剂的心脏毒性风险在男性（HR: 1.64, 95% CI: 1.24-2.18）及年龄大于等于 67 岁的患

者（HR: 1.41, 95% CI: 1.04-1.90）中更为显著。限制性立方样条分析揭示了用药次数与风险间的非线性关系，风险在用药 3.98 次时达到峰值后逐渐下降（非线性 P=0.002）。此外，发生心脏毒性的患者基线时患有高血压、冠心病、心衰等心血管疾病的比例更高（均为 P<0.01）。

结论：

本研究证实，在肺癌患者中，使用 PD-1 抑制剂是心脏毒性发生的独立危险因素，尤其是在男性和老年患者中。风险呈现非线性特征，在治疗初期相对更高。这些发现强调了对接受 PD-1 抑制剂治疗的肺癌患者，特别是具有心血管基础疾病的患者，进行严密心脏监测的必要性。

CTLA-4 抑制剂相关心肌炎的机制探讨：基于小鼠模型的实证研究

代虎威 曹慧丽 杨滨 王思蓉 温泽宇

山西医科大学第二医院

目的

恶性肿瘤已成为全球公共卫生领域的重大挑战之一。肿瘤免疫治疗的兴起标志着恶性肿瘤治疗方式的革命性突破，免疫检查点抑制剂通过重塑肿瘤微环境中的免疫应答平衡，显著改善了晚期癌症患者的生存预后。其中，细胞毒性 T 淋巴细胞相关蛋白 4 (cytotoxic T-lymphocyte-associated protein 4, CTLA-4) 抑制剂作为首个获批的免疫检查点阻断药物，开启了肿瘤免疫治疗的新纪元。然而，随着 CTLA-4 抑制剂的广泛应用，其引发的免疫相关不良事件逐渐成为临床关注的重点，免疫系统的过度激活可能引发多器官毒性反应，其中以心肌炎最为致命。流行病学数据显示，CTLA-4 抑制剂单药治疗所致心肌炎的发生率为 0.04%-1.14%，但其死亡率高达 40%-50%，患者常因恶性心律失常或心力衰竭短期内死亡，且缺乏特异性早期预警标志物，已成为肿瘤心脏病学领域亟需解决的临床难题。因此，阐明其发病机制，对于开发风险预测模型及优化治疗策略具有重要临床意义。本研究建立了 BALB/c 小鼠黑色素瘤模型并给予 CTLA-4 抑制剂干预，通过小鼠心功能动态监测、心脏组织病理学分析和分子生物学技术分析等技术揭示了 CTLA-4 抑制剂引发心肌炎的相关分子机制，旨在为癌症患者免疫治疗相关心脏毒性的早期预警和干预提供新策略。

方法

利用 B16-F10 黑色素瘤细胞系接种在 BALB/c 小鼠中，检测 CTLA-4 抑制剂对肿瘤大小的影响。利用心脏超声技术对小鼠心脏进行心功能检测和评价，探究 CTLA-4 抑制剂对心脏的作用；利用酶联免疫吸附试验测定血清肌钙蛋白（cTnI）及肌酸激酶同工酶（CK-MB）心脏标志物评估心肌炎性损伤程度；在分子病理水平上，利用心脏苏木精 - 伊红（hematoxylin and eosin, HE）染色及免疫组织化学染色法评估心脏组织改变及 $CD3^+$ T 细胞、$CD20^+$ B 细胞及 $CD68^+$ 巨噬细胞等炎症细胞的浸润情况；利用心脏转录组测序探究 CTLA-4 处理对心脏相关基因的表达和通路的改变。

结果

肿瘤体积测量结果显示， CTLA-4 抑制剂组小鼠的黑色素瘤体积显著减小。CTLA-4 抑制剂处理导致小鼠心脏功能障碍，表现为左室射血分数和短轴缩短分数显著降低，左室后壁厚度和左室内径在收缩期和舒张期均显著增大。CTLA-4 抑制剂诱发了小鼠心肌炎，小鼠血清 CK-MB 和 cTnI 浓度均显著升高。心脏组织病理学分析显示，CTLA-4 抑制剂导致小鼠心肌组织中 $CD3^+$ T 细胞、$CD20^+$ B 细胞和 $CD68^+$ 巨噬细胞的表达水平显著升高。心脏转录组测序结果显示，CTLA-4 处理对比同型对照组得到的差异基因与上调的差异基因显著富集在炎症、免疫及代谢相关的信号通路，如 T 细胞受体信号通路、B 细胞受体信号通路、白介素 -17 信号通路、趋化因子信号通路、细胞因子–细胞因子受体相互作用通路和糖酵解 / 糖异生相关通路等。

结论

CTLA-4 抑制剂可系统性激活多种炎症、免疫及代谢相关信号通路，诱发黑色素瘤小鼠心肌炎的发生，导致心脏功能障碍及心肌损伤。

结直肠癌治疗相关心脏毒性及其免疫学机制的研究进展

赵梦琪

河南大学淮河医院

目的：结直肠癌（CRC）是全球常见的恶性肿瘤之一，随着治疗技术的进步，患者的生存期逐渐延长。然而，CRC 的治疗（特别是化疗、靶向治疗和免疫治疗）可能对心脏健康产生不良影响。本文综述了 CRC 治疗相关心脏毒性及其免疫学机制，分析了现有治疗方法对心脏健康的影响，并提出临床管理策略。

方法：通过系统检索 PubMed、Embase、Web of Science 等数据库，筛选近五年内关于 CRC 治疗相关心脏毒性的临床研究。重点探讨了化疗药物、靶向治疗和免疫治疗对心脏的影响及其机制，分析了治疗方案的现状和管理策略。

结果：CRC 治疗中使用的化疗药物、靶向治疗和免疫治疗均可能对心脏健康产生负面影响。化疗药物如 5- 氟尿嘧啶（5-FU）和卡培他滨广泛应用于临床，但有约 5.9% 的患者在使用这些药物时出现心脏毒性，表现为心律失常、胸痛和心力衰竭。5-FU 和卡培他滨通过诱导冠状动脉痉挛或增加心脏负荷来引发心脏损伤。靶向治疗药物，如贝伐单抗，是 CRC 治疗中的常用药物，虽然其抗肿瘤作用显著，但可能引发心脏毒性，包括高血压、心肌缺血和心力衰竭等。免疫治疗（如 PD-1/PD-L1 抑制剂）在 CRC 治疗中取得了显著疗效，但也可能导致免疫相关心脏不良事件，如心肌炎和心包炎。疗引发的心脏毒性机制复杂，主要与免疫系统的激活、细胞因子的释放等相关。治疗可能通过激活免疫系统，导致 TNF-α、IL-6 等细胞因子的过度释放，进而引起心肌细胞损伤。

结论：CRC 的治疗可能对心脏健康产生显著影响，化疗、靶向治疗和免疫治疗均可引发心脏毒性。未来的研究应进一步揭示心脏毒性发生的机制，并探索新疗法来减少心脏损伤。临床上，患者应接受个体化治疗，特别是高危患者应加强心脏健康监测。

阻塞性睡眠呼吸暂停相关慢性间歇性低氧加重阿霉素所致心脏损伤的研究

王迪 刘玉珍

新乡医学院第一附属医院

目的

阻塞性睡眠呼吸暂停（Obstructive Sleep Apnea，OSA）是一种以慢性间歇性低氧（Chronic Intermittent Hypoxia，CIH）为特征的睡眠呼吸障碍疾病，与多种恶性肿瘤的发生发展存在相关性。阿霉素（Doxorubicin，DOX）是癌症化疗基础药物之一，但其使用累积剂量与心脏毒性成正相关，可对心肌细胞造成不可逆的损伤。CIH 可诱发心肌细胞氧化损伤、线粒体功能障碍、脂代谢异常及结构重塑，是心血管疾病的独立危险因素。然而，在肿瘤患者使用阿霉素化疗时，OSA 常被忽视，其导致的心脏易损状态可能作为“隐形共病”，放大 DOX 的心脏毒性。目前尚无系统研究阐明在 CIH 背景下使用 DOX 是否会加重心肌损伤，因此，本研究旨在探究慢性间歇性低氧对阿霉素心脏毒性的影响及机制。

方法

C57BL/6N 小鼠腹腔注射不同浓度 DOX 构建体内心脏损伤模型，为后续实验选取合适的 DOX 浓度。另使用 Oxycycler A84 构建 CIH 动物模型，将 C57BL/6N 小鼠分别暴露于常氧（Normoxia，Nor）环境与 CIH 环境中，分为 Nor+NS 组、Nor+DOX（3mg/kg） 组、Nor+DOX（5mg/kg） 组、CIH+NS 组、CIH+DOX（3mg/kg）组、CIH+DOX（5mg/kg）组。（1）测量心重与体重。（2）超声心动图检测小鼠心功能。（3）尾动脉血压仪测量小鼠血压。（4）HE 染色观察心肌组织形态。CCK8 筛选诱导 H9C2、HL-1 细胞损伤模型的 DOX 浓度及 DOX 处理时间，检测叠加 IH 后 H9C2 及 HL-1 的细胞活力。

结果

体内实验结果显示，DOX 心脏损伤模型构建成功；DOX 使小鼠心重体重比下降；DOX 组小鼠射血分数、缩短分数下降，左心室收缩内径和舒张内径增大，表明 DOX 导致小鼠左心室收缩功能受损；DOX 组左心室收缩末期容积、舒张末期容积增大，表明 DOX 导致小鼠心脏增大；DOX 不影响小鼠血压；叠加 CIH 可增加阿霉素心脏损伤小鼠的心重体重比；心脏超声可见叠加 CIH 加重小鼠左心室收缩功能损伤；CIH 使小鼠血压升高；HE 染色显示叠加 CIH 使小鼠心肌细胞损伤、组织结构紊乱加剧。体外细胞实验结果显示，与 DOX 组相比，叠加 IH 可降低阿霉素诱导的 H9C2、HL-1 细胞活力。

结论

阻塞性睡眠呼吸暂停相关慢性间歇性低氧加重阿霉素导致的心脏损伤。

肿瘤代谢物与心血管疾病

苑可盈 吕林 董增祥

哈尔滨医科大学附属第一医院

背景：癌症和心血管疾病是威胁全球居民生存的最主要原因，目前已有不少研究表明肿瘤与心血管疾病存在着众多共同发病因素如：生存环境、遗传变异、炎症风险，除此之外肿瘤细胞的代谢活动与心血管系统的相互作用将加重恶化人体健康。恶性肿瘤细胞通常具有不同于正常细胞的供能途径，脂质代谢改变是癌细胞的重要代谢表型，同时在心衰发病过程中伴随能量来源的改变，脂肪酸代谢异常是其中之一。目前，对于参与脂肪酸代谢的肿瘤代谢小分子物质是否是两种疾病作用的“桥梁”尚不清楚。本研究结合当下肿瘤心脏病研究热点，将重点聚焦于肿瘤代谢物参与心脏病的发生发展过程。

方法：通过 PubMed 检索有关“肿瘤代谢”“心衰代谢机制”“心血管肿瘤”“心力衰竭癌症”的相关文献，基于国内外生物样本数据库，结合最新癌症、心血管疾病的人群队列分析，我们对肿瘤与心血管疾病共同的发病因素进行整理总结。运用临床人群血液样本、影像学资料及动物模型标本通过非靶向代谢组学技术检测癌症、心衰以及癌症伴发心衰机体的差异表达代谢物，并进一步通过定量蛋白质组学探究小分子化合物结合蛋白参与机体代谢的发病发展过程。

结果：在人群队列分析中发现肿瘤与心血管疾病共同患病因素如：饮食、吸烟、肥胖等因素的背后存在相类似的代谢过程，加重疾病进程。我们对肿瘤患者临床样本及癌症动物模型进行的心脏彩超检测显示，罹患肿瘤机体的心脏舒张功能减退，病理切片显示患病机体心脏细胞间质存在胶原沉积，纤维化标志物增加。并通过代谢组学发现脂质代谢标志物改变。

结论：肿瘤幸存者中因心血管疾病所致死亡率最高，甚至高于肿瘤因素本身。肿瘤与心血管疾病间的双向作用关系是动态且复杂的，在肿瘤发展阶段肿瘤细胞自主增殖，产生损害机体器官的“毒性物质”，不断对心脏施加代谢压力，改变心脏生理功能。本研究发现参与脂肪酸代谢过程对肿瘤及心血管疾病具有重要意义，聚焦肿瘤代谢物与心血管疾病，延长肿瘤伴发心血管疾病患者的生存期将会是肿瘤学与心脏病学学科间交叉的一项重大挑战。

终末期心脏病患者尊严疗法中护士角色定位的质性研究

田美凤

西安交通大学医学院第一附属医院

目的：明确护士在终末期心脏病（NYHA Ⅳ级或难治性终末期心衰）患者尊严疗法（Dignity Therapy, DT）中的核心角色与功能边界，为制定本土化护理路径提供理论依据。

方法：采用描述性质性研究，2023 年 10 月–2024 年 4 月通过目的抽样选取我院心内科的 11 例终末期心脏病患者、8 名责任护士及 3 名心内科医师参与半结

构式访谈。访谈提纲围绕“DT过程中护士的实际行为、情感体验、角色冲突与协作”。每次访谈 30–50 min，两位研究者独立分析后通过同行审议确保信度。

结果：析出 4 个核心主题、9 个子主题。①“关系建立者”：护士通过日常照护与病情监测（如每日症状评估、液体平衡记录）先与患者建立信任，为 DT 介入铺路；②“意义对话的催化者”：护士在医师完成 DT 访谈提纲后，于床旁协助患者回忆生命故事，使用开放式提问引导情感表达，并实时识别痛苦情绪；③“尊严维护的执行者”：护士依据 DT 生成“尊严传承文档”，在病房朗读并协助患者修改，确保隐私与患者意愿一致；④“跨学科协调者”：护士在 DT 实施前后与医师、社工、家属沟通，处理角色冲突（如家属要求隐瞒病情）并动态调整照护计划。参与者普遍认为护士的“在场”与“连续性”是 DT 成功的关键，但角色边界模糊、时间不足、情感耗竭成为主要障碍。

结论：终末期心脏病患者尊严疗法中，护士不仅是辅助者，更是贯穿始终的关系建立者、意义对话催化者与尊严维护执行者。建议通过专科培训、合理人力配置及跨学科协作框架，厘清护士角色边界，提升 DT 实施质量与护士职业可持续性。

维立西呱减轻卡非佐米诱导的小鼠心脏毒性的作用及研究

马湘萍

山东大学齐鲁医院心内科

维立西呱减轻卡非佐米诱导的小鼠心脏毒性的作用及研究

马湘萍　提蕴　卜培莉

山东大学齐鲁医院

摘要：

多发性骨髓瘤 （MM） 是一种浆细胞恶性肿瘤，占所有血液肿瘤的 10%。卡非佐米是一种不可逆的蛋白酶体抑制剂，用于治疗多发性骨髓瘤患者。然而，卡非佐米治疗与心血管并发症相关。维立西呱是可溶性鸟苷酸环化酶（sGC）激动剂，是治疗心血管疾病的新兴药物。

目的：本研究旨在确定维立西呱对卡非佐米诱导的心脏毒性的心脏保护作用。

方法：C57BL/6 小鼠被随机分为四组：对照组、维立西呱组、卡非佐米组和卡非佐米 + 维立西呱组。

结果：维立西呱通过改善组织学变化、肌酸激酶同工酶（CK-MB）和肌钙蛋白 -I 等水平，预防了卡非佐米诱导的心脏毒性。此外，它通增强过氧化氢酶活性和超氧化物歧化酶活性，降低丙二醛（MDA）水平，抑制了卡非佐米诱导的氧化损伤；通过降低 IL-6 和 TNF-α 水平，抑制炎症；通过降低 LC3,Becline-1,P62 等水平减轻自噬；通过降低 caspase3，Cleaved caspase3s 水平减低凋亡水平。

结论：维立西呱可能为缓解多发性骨髓瘤患者中卡非佐米诱导的心脏毒性提供一种新的治疗策略。

关键词：肿瘤治疗相关心脏毒性，卡非佐米，维立西呱，自噬，凋亡

入院诊室血压在评估高风险食管早癌患者的应用价值

魏蕊蕊 [2] 石福天 [1] 余静 [1]

1. 兰州大学第二医院心血管内科

2. 兰州大学第二医院消化内科

目的：食管癌（EC）作为消化道常见的恶性肿瘤之一，其早期发现与有效治疗对提升患者生存率至关重要，若能在早期诊断并治疗，可显著提高患者 5 年生存率。随着人口老龄化的加剧，恶性肿瘤合并高血压患者逐年增多，有学者认为血压增高可能是肾癌、乳腺癌、肝癌和消化道癌等恶性肿瘤患病风险的重要危险因素。本研究旨在探讨早期食管癌（EEC）患者入院诊室收缩压与癌灶病变范围及病理浸润深度之间的潜在关系，通过深入分析这一关联，为临床早期识别高危患者、制定个性化治疗方案及评估预后提供科学依据，进而提高食管早癌的整体诊疗水平。

方法：纳入 2018 年 1 月至 2024 年 10 月兰州大学第二医院行内镜下黏膜剥离术（ESD）治疗且术后病理为 EEC 的 135 例患者的临床病理资料。纳入标准：（1）我院 ESD 术后病理确诊为早期食管癌；（2）我院行窄带成像联合放大内镜（ME-NBI）检查，且经 CT、MRI、超声内镜（EUS）等检查证实无毗邻脏器或远处转移；（3）病例资料完整，既往及现在未服用降压和（或）影响血压的药物（如激素类药物、TKI 类药物等）。排除标准：（1）ESD 前行化疗、放疗等其他治疗；（2）病理结果为食管上皮良性肿瘤，或其他部位转移性食管癌；（3）有服用降压药物和（或）影响血压药物。本研究已通过兰州大学第二医院伦理委员会批准（2024A-957），回顾性研究知情同意豁免。依据入院诊室收缩压分为 3 组：Q1 正常收缩压组（入院诊室收缩压 < 120mmHg，n=45）、Q2 正常收缩压高值组（120 ≤入院诊室收缩压 < 140mmHg，n=45）、Q3 高值收缩压组（入院诊室收缩压≥ 140mmHg，n=45）。收集其一般基础资料、血糖、血脂、窄带成像联合放大内镜（ME-NBI）下所见病变范围、内镜下黏膜剥离术（ESD）后病理浸润深度等相关指标，对 3 组之间的相关数据进行分析比较。

结果：3 组患者年龄、性别、BMI 均无显著性差异，三组患者癌灶病变范围、病理浸润深度存在显著性差异，两两比较高值收缩压组大于正常收缩压组（2.83±1.28 vs 2.17±0.87 cm，P < 0.05）。随着入院诊室收缩压的降低，病理浸润深度过深出现的频率越低 n（%）[18（40） vs 12（26.7） vs 6（13.3），P < 0.05]。影响癌灶病变范围的多因素线性回归分析提示入院诊室收缩压是影响癌灶病变范围的独立危险因素（b=0.018，OR=2.142，P < 0.05）。

结论：在 EEC 患者中，入院诊室收缩压越高，癌灶病变范围越大，同时病理浸润深度过深的可能越高，可将入院诊室收缩压作为评估高危 EEC 患者的早期辅助指标。

关键词：早期食管癌 诊室收缩压 癌灶病变范围 病理浸润深度

基于 UPLC-Q-TOF/MS 研究维药爱维心口服液改善免疫检查点抑制剂相关性心肌炎的活性成分及作用机制

于坚

新疆医科大学附属肿瘤医院

目的：免疫检查点抑制剂（Immune Checkpoint Inhibitors，ICIs）已经成为肿瘤治疗的重要手段，其在发挥显著疗效的同时也伴随着一定的毒副反应，其中最为严重的是免疫相关心血管不良反应中的 ICIs 相关性心肌炎。ICIs 相关性心肌炎发生率虽低，但死亡率较高，严重影响了肿瘤患者的生存及预后，因此迫切需要减轻和预防 ICIs 伴随的毒副作用。本文评估了爱维心口服液（Aiweixin Oral Liquid，AOL）对 ICIs 相关性心肌炎的保护作用及潜在机制。

方法：采用高效液相色谱法鉴定 AOL 的血清化学成分；结合网络药理学分析鉴定 AOL 在 ICIs 相关性心肌炎中的活性成分及作用靶点，并对其进行富集分析；通过动物和细胞实验验证分析结果。

结果：质谱分析确定了 AOL 的活性成分，结合网络药理学及分子对接发现排名前五的活性成分为 Schinicoumarin、Demethoxyyangonin、Ferulic acid、Hispidulin acetate、Herniarin，关键基因为 CASP3、STAT3、ALB、MTOR、CCND1；体内实验表明 AOL 可显著改善 ICIs 相关性心肌炎小鼠的心肌损伤标志物及心脏超声指标，体外实验也得到了一致结果；富集分析及实验验证发现 AOL 可能通过调节 PI3K-Akt 信号通路改善 ICIs 相关性心肌炎。

结论：AOL 可能通过靶向 PI3K-Akt 信号通路发挥心脏保护作用，这为未来 ICIs 相关性心肌炎患者的治疗提供了参考依据。

肿瘤心脏病学的临床实践挑战与多学科管理策略探索

周雪梅

武汉大学人民医院

目的：随着肿瘤治疗技术的进步和患者生存期的延长，抗肿瘤治疗相关心血管毒性已成为影响肿瘤患者预后的重要因素。本研究旨在系统分析肿瘤心脏病学领域的临床实践现状，探讨多学科协作模式在肿瘤治疗相关心血管并发症防治中的应用价值，为建立规范化的肿瘤心脏病诊疗体系提供依据。

方法：本研究采用文献系统回顾与临床实践分析相结合的方法。首先对近五年国内外肿瘤心脏病学相关指南和重要研究进行系统性梳理，总结当前临床实践中的关键问题。同时，通过多中心临床病例分析，收集典型肿瘤治疗相关心脏毒性的诊疗过程，重点分析临床表现、诊断方法和治疗策略的特点。在此基础上，构建包含肿瘤科、心血管科、影像科、药学等多学科专家的工作组，探讨优化诊疗流程的策略。

结果：临床特征分析：肿瘤治疗相关心脏毒性表现多样，包括心肌功能障碍、冠状动脉疾病、心律失常和高血压等，其发生机制与特定抗肿瘤药物密切相关。临床表现常不典型，早期症状易被忽视，部分患者出现不可逆的心功能损害后才被发现。诊断评估现状：心脏生物标志物和影像学检查在早期发现心脏毒性方面具有重要价值，但临床应用中存在标准不统一的问题。不同肿瘤治疗方案的心脏毒性风险评估体系尚待完善，个体化监测方案缺乏共识。管理策略探索：多学科协作模式显著提高了对高风险患者的识别率和干预及时性。预防性心血管保护策略在部分肿瘤治疗方案中显示出减少心脏毒性的潜力。肿瘤治疗与心血管保护的平衡决策需要综合考虑患者肿瘤预后和心血管风险。

结论：肿瘤心脏病学作为一个新兴交叉学科，面临着临床认识不足、诊疗规范缺乏等多重挑战。建立多学科协作机制是提高肿瘤治疗相关心血管并发症防治水平的关键。未来需要加强专业人才培养，制定基于循证医学的诊疗指南，并建立长期随访体系以评估干预措施的远期效果。同时，应重视基础与临床研究的结合，深入探索肿瘤治疗相关心脏毒性的分子机制，为精准防治提供新思路。

动脉僵硬和癌症发生之间的关系：来自开滦研究的 10 年数据

董皓宇 [1] 张津浦 [1] 李佳甜 [1] 陈朔华 [2] 夏云龙 [1] 吴寿岭 [2] 杨晓蕾 [1]

1. 大连医科大学附属第一医院

2. 开滦总医院

背景: 近年来，心血管重构与癌症之间的双向关系引起了科学界的广泛关注。然而，早期血管重构与癌症发生之间的联系尚不清楚。本研究旨在探讨早期血管重构是否与新发癌症的发生相关，并通过肱踝脉搏波速度（baPWV）进行量化。本研究的主要目的是调查早期血管重构（通过 baPWV 量化）是否与新发癌症有关。

方法：我们采用了 Cox 比例风险模型及基于群组的轨迹模型，以确定基线 baPWV 和 baPWV 变化对癌症及其相关结果的评估能力。

结果：从 2010 年 1 月至 2022 年 12 月，共有 58,382 名接受 baPWV 检查的中国成年人被纳入研究，其中 1,129 例为新发癌症，随访中位数为 6.07 年。结果显示，baPWV 对癌症发病率具有显著的评估能力（多变量调整后的风险比 [aHR]：1.113；95% 置信区间 [CI]：1.091-1.136；P<0.001）。其中，baPWV 处于中等（14-18 m/s）和高（≥ 18 m/s）水平的参与者，其癌症发病风险分别增加了 70.5% 和 153.4%。在按年龄和性别分层的亚组分析中也确认了类似的关联。在轨迹分析中，12,773 名个体显示出四种不同 baPWV 水平的轻微增加模式：极低、低、中等和高。与极低和低组相比，中等和高组的癌症风险的 aHRs（95% CI）分别为 1.457（1.042-2.037，P<0.001）和 1.941（1.321-2.850，P<0.001）。

结论：基线 baPWV 水平及其变化轨迹均与癌症发生率显著相关。这一发现为将 baPWV 评估及其长期监测作为癌症一级预防策略的一部分提供了支持。这表明在癌症的早期干预和预防中，考虑到心血管的健康状态评估可能具有重要的临床意义。通过对 baPWV 的持续监测，可以更好地识别出具有较高癌症风险的个体，

从而采取更为有效的预防措施。这一研究拓展了我们对心血管健康与癌症发生关系的理解，并为未来的公共卫生政策和个体化医疗提供了有价值的信息。

piRNA-5900 调控 ATF4 阻抑阿霉素诱导的心肌细胞铁死亡

秦路宁 陈若兰 褚现明

青岛大学附属医院崂山院区

目的：

探究非编码 RNA（ncRNA）对阿霉素（DOX）诱导心肌损伤的作用，并研究其确切作用和潜在机制，其中 piRNA 在心脏毒性中的作用鲜有报道，因此本研究将揭示 DOX 心肌损伤中 piRNA 表达谱，阐述 piRNA 调控心肌损伤的机制，为 piRNA 在心血管疾病中的临床转化提供依据。

方法：

在体内培养小鼠心肌细胞，构建 DOX 损伤心肌细胞模型，将细胞分为正常对照组（NC 组）和 DOX 处理组，采用高通量测序筛选并验证差异表达的 piRNA，与 NC 组相比，DOX 处理组心肌细胞中 piR-5900 表达水平显著下调，提示其可能参与 DOX 诱导的心肌损伤调控过程。经小鼠心肌细胞内转染 piR-5900 mimic 或 piR-5900 inhibitor，分别实现 piR-5900 的过表达或敲低；通过 DCFH-DA 荧光探针法对细胞内活性氧簇（ROS）水平进行定量检测，以评估细胞氧化应激状态；同时运用 C11-BODIPY 荧光探针精确测定细胞内脂质过氧化水平。结合转录组测序分析、Western blotting 及免疫共沉淀等技术，深入解析 piRNA-5900 在心肌细胞铁死亡中的分子调控机制。为鉴定 piRNA-5900 的作用靶点，采用 RNA pull-down 技术联合液相色谱 - 串联质谱（LC-MS/MS）分析，筛选并证实激活转录因子 4（ATF4）为 piRNA-5900 的直接下游作用靶标。在此基础上，通过构建 ATF4 过表达及基因敲低模型，系统评估 ATF4 在 piRNA-5900 介导的铁死亡抑制通路中的功能作用。在动物模型验证方面，通过腹腔注射 DOX 构建小鼠心肌损伤模型，并采用尾静脉注射 piRNA-5900 过表达载体进行干预。通过超声心动图动态监测心功能变化，结合心肌组织铁死亡特异性标志物检测及 ATF4 表达水平分析，综合评价 piRNA-5900 对 DOX 诱导的心功能损伤的保护效应及其分子机制。

结果：

1. 通过高通量测序分析 DOX 处理的小鼠心肌细胞，发现与 NC 相比，DOX 组中 piR-5900 的表达水平显著降低，提示 piR-5900 可能参与 DOX 诱导的心肌损伤调控过程。

2. 在体外实验中，转染 piR-5900 mimics 显著降低 DOX 诱导的心肌细胞内 ROS 水平和脂质过氧化，减轻心肌细胞铁死亡；而转染 piR-5900 inhibitor 则进一步加剧 ROS 积累和脂质过氧化水平，加重心肌细胞铁死亡。

3. 经 RNA pull-down 联合 LC-MS/MS 质谱分析鉴定 ATF4 为 piR-5900 的结合靶点。pi-5900 过表达显著上调 ATF4 蛋白表达，而 piR-5900 抑制则下调 ATF4 水平。

4. 机制上，ATF4 敲低可抵消 piR-5900 对铁死亡的抑制作用，而过表达 ATF4 则能缓解 DOX 诱导的心肌细胞损伤，提示 ATF4 是 piR-5900 调控铁死亡的关键下游效应分子。

5. 在动物水平上，DOX 处理显著降低小鼠心功能和加重心肌铁死亡。尾静脉注射 piR-5900 过表达载体显著改善心功能，且上调 DOX 诱导的 ATF4 下降。

结论：

本研究证实，piR-5900 在 DOX 诱导的心肌损伤中表达下调，并通过调控 ATF4 介导的铁死亡通路发挥心肌保护作用。机制上， piR-5900 可抑制 ROS 积累及脂质过氧化，从而减轻心肌细胞铁死亡。在动物模型中， piR-5900 过表达显著改善 DOX 诱导的心功能损伤，提示 piR-5900/ATF4 轴可能成为防治阿霉素心脏毒性的潜在干预靶点。

胸腺瘤与非胸腺瘤患者免疫检查点抑制剂相关心肌炎临床特征分析

曾海艳 薛玉梅

广东省人民医院

目的

本研究旨在比较 TM 与非 TM 患者 ICI-M 的临床特征差异，并进一步分析与病毒性心肌炎（VM）的异同。

方法

回顾性收集广东省人民医院 2018 年 1 月至 2024 年 8 月期间诊断为 ICI-M 的患者，并将 TM-ICI-M 与其他癌症 ICI-M(Non-TM-ICI-M) 及 VM 患者比较临床表现、生物标志物、心电图、超声心动图及预后差异。

结果

纳入 89 例心肌炎患者，ICI-M28 例（TM-ICI-M 组 7 例、Non-TM-ICI-M 组 21 例）及 VM 组 61 例。**症状**：ICI-M 组以肌无力（TM-ICI-M 组 4/7，Non-TM-ICI-M 组 3/21）、眼睑下垂（TM-ICI-M 组 2/7，Non-TM-ICI-M 组 5/21）为主要表现，VM 组无相关表现；胸痛在 ICI-M 组（TM-ICI-M 组 0/7、Non-TM-ICI-M 组 5/21）显著低于 VM 组（39/61），发热在 ICI-M 组（TM-ICI-M 组 2/7、Non-TM-ICI-M 组 1/21）显著低于 VM 组（22/61），均 P<0.05。**生物标志物**：TM-ICI-M 组肌钙蛋白 T(cTnT) 峰值显著高于 Non-TM-ICI-M 组和 VM 组 [5023.0（1456.0，7523.5）、539.3（295.8，1166.0）、851.1（218.5，2061.0）pg/mL，H=8.12，P=0.017]，TM-ICI-M 组和 Non-TM-ICI-M 组的肌酸激酶（CK）峰值、肌酸激酶同工酶（CK-MB）、丙氨酸氨基转移酶（ALT）天冬氨酸氨基转移酶(AST)均显著高于 VM 组，即 [CK: 7273.0(1991.5，7458.5)、1853.0(313.0，5081.0）、476.0（298.0，1129.0）U/L，H=13.97，P<0.001]、[CK-MB：156.8（105.7，276.6）、82.0（48.5，151.1）、32.8（19.6，68.0）U/L，H=22.84，P<0.001]、[ALT：221.0（146.0，2456.5）、100.0（70.0，184.0）、48.0（27.0，80.0）U/L，H=20.30，P<0.001]、[AST：379.0（177.0，3920.0）、168.0（49.0，337.0）、75.0（37.0，145.0）U/L，H=14.53，P<0.001]。**心电图:** TM-ICI-M 组室性心动过速 [(4/7)，0%(0/21)，1.6%(1/61)，Fisher 精确概率法，P<0.001] 和 II - III度房室传导阻滞 [(4/7)，0%(0/21)，3.3%（2/61），Fisher 精确概率法，P<0.001] 均显著高于非 TM-ICI-M 组和 VM（均 P<0.001）。**预后:** 相比 Non-TM-ICI-M 组，TM-ICI-M 组中症状出现更早 [15(14.5，20.5）、47（24.0，94.0）天，H=18，P=0.004]，多系统受累占比更高 [（5/7），（1/21），Fisher 精确概率法，P=0.001]。TM-ICI-M 组 LVEF<50% 比例高于 Non-TM-ICI-M 组 [（3/7），4.8%（1/21）]，以及 30 天死亡人数 42.9%（3/7）占比高于 Non-TM-ICI-M 组 19.0%（4/21），但差异均无统计学意义（P>0.05）。

结论

与非 TM 肿瘤患者对比，TM 患者 ICI-M 发生更早，心肌损伤更重，危及生命的心律失常发生比例更高，常伴多系统受累，预后较差。

The circadian rhythms, cancer status and risk of coronary heart disease: A prospective study in UK Biobank

Zhongzhi Yu, -Dan Wang, Jin-Wei Tian

The Second Affiliated Hospital of Harbin Medical University

Abstract

Background: This study investigates the relationship between circadian rhythms and cancer, focusing on its impact on the risk of coronary heart disease (CHD). CHD is one of the leading causes of mortality worldwide, and cancer survivors face an increased risk of developing cardiovascular diseases, particularly CHD, due to both cancer itself and the effects of cancer treatments. Circadian rhythms, which govern the body's sleep-wake cycles and metabolic processes, have been linked to cardiovascular health. Disruptions to circadian rhythms, such as irregular rest-activity rhythms and poor sleep patterns, have been associated with increased cardiovascular risk. However, the interaction between circadian rhythms, cancer status, and CHD risk has not been thoroughly explored in large cohort studies.

Methods: The study utilized data from the UK Biobank, including 93,933 participants with available data on circadian rhythms, cancer status, and CHD outcomes. Circadian rhythms were assessed using wearable accelerometers to track the rest-activity rhythm (RAR) score and questionnaires to gather information on sleep patterns, including sleep duration and insomnia. The RAR score was derived from metrics of inter-daily stability, intra-daily variability, and relative amplitude, which reflect the stability, fragmentation, and robustness of an individual's rest-activity rhythm. Sleep patterns were categorized into appropriate (7-8 hours of sleep per day) and inappropriate durations (

Findings: Over a median follow-up period of 12.9 years, 5,599 participants (5.96%) had been diagnosed with cancer at baseline, while the remaining 88,334 participants were cancer-free. Well-regulated circadian rhythms, characterized by a high RAR score, appropriate sleep duration, and rare insomnia, were significantly associated with a reduced risk of developing total CHD, non-fatal CHD, and fatal CHD. Specifically, the hazard ratios (HR) for total CHD were 0.81 (95% CI: 0.74-0.88) for high RAR score, 0.82 (95% CI: 0.77-0.88) for appropriate sleep duration, and 0.87 (95% CI: 0.80-0.94) for never or rarely experiencing insomnia. In cancer survivors, well-regulated circadian rhythms were associated with a 10.3% to 24.0% reduction in CHD events, while in cancer-free participants, this reduction ranged from 5.5% to 9.0%. Cancer status itself was found to increase the risk of total and non-fatal CHD (HR: 1.27, 95% CI: 1.13-1.42), with a higher risk of developing non-fatal CHD (HR: 1.27, 95% CI: 1.12-1.43). However, cancer survivors with well-regulated circadian rhythms did not show a significant increase in the risk of total CHD or non-fatal CHD compared to cancer-free controls with circadian disruptions.

Interpretation: This study found that well-regulated circadian rhythms, including stable rest-activity patterns and appropriate sleep durations, were associated with a significant reduction in CHD risk, even after adjusting for multiple confounding factors. Notably, the positive effects of well-regulated circadian rhythms were particularly important for cancer survivors, who generally face an elevated risk of cardiovascular diseases. These findings suggest that optimizing circadian rhythms may serve as a modifiable preventive approach to reduce the high cardiovascular burden associated with cancer.

Funding: This study was supported by the National Natural Science Foundation of China, the Natural Science Foundation of Heilongjiang Province, the Fok Ying-Tong Education Foundation for Young Teachers, the Heilongjiang Applied Technology Research and Development Plan, the HMU Marshal Initiative Funding, and the Key Laboratory of Emergency and Trauma of the Ministry of Education (Hainan Medical University).

恩格列净通过改善心肌电重构及结构重构减轻阿霉素引起的心律失常

刘慧意 薛玉梅

广东省人民医院

目的：本研究旨在探讨阿霉素（Doxorubicin, DOX）心律失常的毒性作用，并评估 SGLT 2 抑制剂恩格列净（Empagliflozin, EMPA）在减轻或预防这些毒性反应中的心脏保护作用。

方法：在单独使用 DOX（5μM）处理及 DOX 处理的基础上予 EMPA（10μM）的心肌细胞中，全细胞膜片钳检测心肌细胞 $I_{Ca,L}$、I_{Kur} 密度和 APD 的改变；WB 检测离子通道蛋白及纤维化蛋白表达水平，观察 DOX 对心肌细胞的电流密度及相应通道蛋白、纤维化蛋白表达水平的影响，以及 EMPA 对 DOX 上述心脏电重构及结构重构改善的程度。

结果：EMPA 不影响心肌细胞的 $I_{Ca,L}$ 密度，DOX 显著降低 $I_{Ca,L}$ 密度，EMPA 明显逆转 DOX 引起的心肌细胞 $I_{Ca,L}$ 密度下降。而激活、失活和复活曲线不受影。WB 结果与 $I_{Ca,L}$ 结果相似，DOX 引起心肌细胞离子通道蛋白 Cav1.2 表达水平下降（P < 0.01），EMPA 处理可以增加 Cav1.2 水平（P < 0.01）。单独使用 EMPA 处理心肌细胞时，APD 不受影响；DOX 显著延长 APD70 及 APD90，EMPA 明显逆转 DOX 引起的心肌细胞 APD 延长。EMPA 显著改善 DOX 引起的心肌细胞 I_{Kur} 密度下降，WB 结果与全细胞膜片钳结果一致，DOX 引起心肌细胞 Kv1.5 表达水平下降，EMPA 逆转 Kv1.5 的表达。DOX 引起心肌细胞 BNP 及纤维化相关蛋白表达升高（P < 0.05），EMPA 处理可以显著逆转 DOX 组大鼠 BNP、COL1A1、COL3A1、MMP-2 及 MMP-9 表达水平明显升高（P < 0.05）。

结论：在 DOX 刺激下的心肌细胞模型中，$I_{Ca,L}$ 和 I_{Kur} 电流密度显著下降，APD 明显延长，Cav1.2 及 Kv1.5 蛋白表达显著下降；BNP 及纤维化相关蛋白表达明显增加，提示使用 DOX 增加心律失常发生率。在 DOX 刺激的心肌细胞的基础上，应用 EMPA 可逆转由于 DOX 引起的心肌细胞 $I_{Ca,L}$ 和 I_{Kur} 电流密度下降，APD 延长，Cav1.2 及 Kv1.5 蛋白表达下降，提示 EMPA 可以显著减轻 DOX 引起的心律失常发生率。

基于 MOFs 的抗氧化纳米系统通过调控铁死亡缓解阿霉素心脏毒性

刘浩坤 [1]

1. 天津医科大学大学总医院

2. 天津大学

目的: 阿霉素(DOX)具有剂量依赖型心脏毒性,铁死亡在DOX诱导心脏毒性(DIC)中发挥关键作用，是通过脂质过氧化发生的。干预心肌脂质过氧化，可作为预防及治疗 DIC 的关键策略。

方法：1. 利用液相扩散法合成 DOX@EDA-Zn 和 EDA-Zn，通过 DLS、Zeta 电位、TEM、溶液稳定性和载药量表征。2. 利用 H9c2 细胞系验证游离药物（EDA、Zn^{2+}）、EDA-Zn 和 DOX@EDA-Zn 的细胞存活率。并分别通过 RSL3 和 DOX 造模，比较游离药物和 EDA-Zn 的拯救作用。建立 DIC 模型，验证 EDA、DOX@EDA-Zn 对 DIC 的作用。通过铁死亡标志物、抗氧化物和 Liperfluo 验证 DOX@EDA-Zn 对 DIC 脂质过氧化的作用。3. 利用小鼠建立 DIC 模型，通过 UCG、心肌酶、铁死亡标志物、抗氧化物检测、HE 和 Masson 染色，验证 DOX@EDA-Zn 对 DIC 的作用。

结果：1. 通过液相扩散法合成 DOX@EDA-Zn 和 EDA-Zn，通过 DLS、Zeta 电位、TEM、光学特性、溶液稳定性和载药量表征，证明成功合成 EDA-Zn 且负载 DOX。2. 利用 H9c2 细胞系对比 Zn^{2+}、EDA 和 EDA-Zn 的心肌拯救作用，对比 DOX 与 DOX@EDA-Zn 的细胞毒作用，DOX@EDA-Zn 显著提高细胞活力（79.25% vs 24.27%，P<0.01），优于 EDA+DOX 组（56.04%，P<0.05），证实 EDA-Zn 有更优异的心肌保护能力。3. 利用 H9c2 细胞系成功建立 DIC 模型，显著降低 MDA（0.71vs 2.41 mmol/mg protein）、4-HNE（22.13 vs 47.11 mmol/mg protein）和 PTGS2（2.38vs 7.36 mmol/mg protein）表达水平（均 P<0.01），提高 GSH（0.17 vs 0.12 mmol/mg protein）、Thiol（0.12 vs 0.09 mmol/mg protein）和 Trx（0.22 vs 0.11 mmol/mg protein）含量（均 P<0.05）。Liperfluo 显示 DOX@EDA-Zn 组脂质过氧化物荧光强度下降幅度最大。证实 DOX@EDA-Zn 的体外心肌保护效果良好。4. 利用小鼠建立 DIC 模型，通过 UCG、心肌酶、铁死亡标志物和抗氧化物检测，DOX@EDA-Zn 显著提高 LVEF（81.52% vs 65.63%，P<0.01），EDA+DOX 组为 75.74%；cTnT、MYO 和 CK-MB 水平较 DOX 组分别下降 57.27%、30.76% 和 19.63%；同时 MDA、PTGS2 较 DOX 组表达分别下调 59.72% 和 68.26%，GSH、Thiol、Reduce trx 较 DOX 组表达分别上调 107.21%、109.58% 和 41.09%；HE 染色显示心肌纤维排列更整齐，核固缩减少；Masson 染色提示纤维化面积减少几乎接近 Saline 组；提示铁死亡显著受控。

结论：成功合成了 DOX@EDA-Zn，并探究了 DOX@EDA-Zn 对 DIC 的作用。在体内、外实验，证明 DOX@EDA-Zn 较游离 EDA 对 DIC 有更明显缓解作用。DOX@EDA-Zn 通过抑制铁死亡以促进改善 DIC 提供有利证据。

Development and validation of a nomogram for predicting new-onset cardiac conduction block in patients with advanced NSCLC undergoing immune checkpoint inhibitor therapy

Conghui Shang, Liang Zhao, jindong Chen, Hao Wang, Ziyi Sheng, Tianqing Chu

Shanghai Chest hospotal

Abstract

Background

Non-small cell lung cancer (NSCLC) is one of the leading causes of mortality globally, and approximately 50% of patients are at advanced stage at the time of diagnosis. Chemotherapy is a standard treatment for advanced NSCLC with mediocre oval survival, and chemotherapy-induced adverse events (AE) can be frequently observed such as fatigue, anemia, infection, and gastric hemorrhage. With the development of molecular carcinogenesis and the identification of oncogene drivers, targeted therapy has also become a widely used treatment for advanced NSCLC patients. Hypertension and rash are common AEs after targeted therapy, while other AEs such as vomiting and hypokalemia are much less reported. In the exploration of immune escape mechanism, immune checkpoint inhibitors (ICIs), especially programmed cell death protein-1/ligand-1 (PD-1/PD-L1), have become an effective treatment for advanced NSCLC. The ICI-related AEs could occur in almost any organ system with varying frequencies and severities. Cardiotoxicity could be observed during these therapies and could be lethal, of which cardiac conduction block (CCB) is infrequently reported but could cause severe AEs. With the increasing use of ICIs and combined therapy, along with an improved survival of advanced NSCLC, treatment-related CCB is expected to rise. However, currently our knowledge remains scarce on CCB in advanced NSCLC patients during treatment, especially ICIs-related CCB. Therefore, the present study was conducted to investigate the epidemiologic features of new-onset CCB in patients with advanced non-small cell lung cancer (NSCLC) during anti-PD-1/PD-L1 treatment, to identify its predictors, and to develop and validate a nomogram for individualized risk evaluation.

Method This is a single-center retrospective observational study, of which the study population was enrolled from the institutional database. The study protocol was approved by the institutional ethics committee (IS22023) and conducted in accordance with the Declaration of Helsinki (as revised in 2013). We reviewed the medical records of 2269 consecutive lung cancer patients undergoing anti-PD-1/PD-L1 treatment in Shanghai Chest Hospital between 2018 and 2023. New-onset CCB were identified via electrograms, including sinoatrial block, atrioventricular block (AVB), and intraventricular block (IVB). Logistic regression analysis was performed to identify predictors of new-onset CCB. A nomogram model was constructed and validated.

Results The training set and validation set enrolled 1263 and 395 patients, respectively. New-onset CCB occurred in 109 patients (8.63%; including 75 first-degree AVB,

4 left anterior fascicular block, 32 right bundle branch block, and 11 non-specific IVB) and was mostly intermittent (n=99). AVB and IVB occurred alone in 67 (61.5%) and 34 patients (31.2%), respectively, and concomitantly in 8 patients (7.3%). CCB advanced in 1 patient from first-degree AVB to Mobitz type I AVB. Independent predictors included concomitant anlotinib, smoking history, and older age, which were included in the nomogram model. The C-index value and Brier score were 0.620 and 0.078 in the training cohort, and 0.745 and 0.066 in the validation cohort, respectively. The calibration curve yielded satisfactory concordance between the predicted and actual outcomes.

Conclusions Anti-PD1/PD-L1 treatment-related CCB seems generally benign. Concomitant anlotinib, smoking history, and senior age were independent risk factors for new-onset CCB in patients with advanced NSCLC after anti-PD-1/PD-L1 therapy.

Angiotensin receptor-neprilysin inhibitors improve the outcome of lung cancer patients with hypertension treated with immune checkpoint inhibitors

Conghui Shang, Liang Zhao, Jindong Chen, Hao Wang

Shanghai Chest hospotal

Abstract

Background: Angiotensin receptor-neprilysin inhibitors (ARNIs) could improve the outcome of patients with hypertension or heart failure by reducing cardiovascular morbidity and all-cause mortality. Yet it remains unclear if such protective effect exists in lung cancer patients with hypertension undergoing immune checkpoint inhibitors (ICI).Immune checkpoint inhibitors (ICIs) have substantially improved clinical outcomes in multiple cancer types and are increasingly used in early disease settings and in combinations of different immunotherapies.While most patients will greatly benefit from the therapy, ICIs can also cause severe or fatal immune-related cardiac adverse-events. Common complications include myocarditis, acute coronary syndrome (ACS), heart failure (HF), arrhythmias, pericardial effusion, and others.

Beyond dose reduction, discontinuation of medication, and alteration of the therapies, there are no established therapies to reduce ICIs-induced cardiotoxicity.Recently, a study suggested that SGLT2i may attenuate the cardiotoxicity associated with immune checkpoint inhibitors and improve cardiac outcomes and OS. Currently, there is no data regarding the potential benefit of Angiotensin receptor-neprilysin inhibitors (ARNIs) among patients diagnosed with hypertension and treated with ICIs therapy. We aimed to investigate the prognostic value of baseline therapy with ARNIs among patients diagnosed with lung cancer and hyperten-

sion, treated with ICIs therapies.

Objective: This study sought to evaluate the impact of ARNIs on the outcome of lung cancer patients with hypertension treated with ICIs.

Methods:

The study population of this single-center retrospective observational study was obtained from the institutional database. The study protocol was approved by Shanghai Chest Hospital Ethics Committee. This study was conducted in accordance with the guidelines of the Declaration of Helsinki (as revised in 2013). We conducted a retrospective, single-center, observational study in Shanghai Chest Hospital. Consecutive medical records of all patients diagnosed with lung cancer and hypertension and treated with ICIs therapy between September 2019 and May 2024 were reviewed. We performed a retrospective analysis of patients diagnosed with lung cancer and hypertension undergoing ICI treatment at our center. Patients were divided into two groups according to baseline treatment with or without ARNIs. The primary endpoint was all-cause mortality. The secondary endpoint was composite of cardiovascular outcomes, defined as new-onset myocarditis, ACS, PE, arrhythmia (including atrial fibrillation, atrial flutter and Grade 3 QT prolongation), and HF. These endpoints were chosen, as they are considered as ICIs-induced cardiotoxicity.

Results: The cohort included 150 patients, with 39 (26%) patients assigned to the ARNIs group. Over a median follow-up of 12 months, 37 (24.6%) patients died, with a significantly lower all-cause mortality rate in the ARNIs group (4/39, 10.3% vs. 33/111, 29.7%, P=0.015). There was no significant difference in cardiovascular outcome between ARNIs and control group (20/111, 18.0% vs. 3/39, 7.7%, P=0.124). We observed that the most common cardiovascular events was new-onset arrhythmia in both ARNIs group (2/3, 66.7%) and control group (14/20, 70%). Overall, a total of 23 cardiovascular adverse events occurred, including 3 events in the ARNIs group and 20 events in the control group, of which new-onset atrial fibrillation or atrial flutter occurred most frequently (n=9). In control group, cardiovascular adverse events included Grade 3 QT prolongation in 6 patients, HF in 2 patients, myocarditis in 1 patient, ACS in 2 patients, and pericardial effusion in 2 patients. While in ARNIs group, HF in 2 patient, atrial fibrillation in 1 patient, and Grade 3 QT prolongation in 1 patient occurred.

Conclusions: ARNIs were associated with a lower all-cause mortality rate yet similar rate of cardiac events in lung cancer patients with hypertension and treated with ICIs.

女性心脏健康有关研究

The Association Between Serum Luteinizing Hormone and Follicle-Stimulating Hormone Levels and Congestive Heart Failure in Postmenopausal Women: A Cross-Sectional Study

hangyu zhou, Saiyaremu Xierzhati, Jie Li, zhao Wang

People's Hospital of Xinjiang Uygur Autonomous Region

Background :The significantly increased risk of cardiovascular disease in women after menopause has prompted researchers to investigate the role of declining sex hormone levels. Previous studies on sex hormones and cardiovascular health have yielded inconsistent findings. This study specifically aims to elucidate the relationship between serum gonadotropin levels—luteinizing hormone (LH) and follicle-stimulating hormone (FSH)—and the risk of congestive heart failure (CHF) in a postmenopausal female cohort. Understanding these associations may provide crucial insights into novel hormonal pathways influencing postmenopausal cardiovascular risk.

Methods: A cross-sectional study design was employed, enrolling 2,442 postmenopausal women who visited the People's Hospital of Xinjiang Uygur Autonomous Region, with serum LH and FSH levels serving as the primary observation indicators. The outcome of interest was the presence of CHF diagnosed according to established clinical criteria. Comprehensive univariate analyses identified potential confounding factors. Subsequently, multivariate logistic regression models were rigorously employed to evaluate the independent association between LH/FSH levels (through both continuous and quartile-based categorical analyses) and CHF risk, with adjustments made for relevant covariates including age, marital status, reproductive history, testosterone, estradiol, BMI, renal function, blood glucose, blood lipids, hypertension, diabetes, and coronary heart disease. To characterize the nature of the dose-response relationship, the study utilized restricted cubic spline (RCS) models with four knots. In addition, predefined subgroup analyses were conducted based on age, marital status, reproductive history, BMI, hypertension, and diabetes status. The robustness of the primary findings was assessed and potential effect modifications were explored through interaction term tests.

Results: The fully adjusted multivariate logistic regression analysis demonstrated that higher serum levels of both LH and FSH were significantly associated with a reduced risk of congestive heart failure. Results: The multivariate logistic regression analysis after full covariate adjustment showed that higher serum levels of both LH and FSH were significantly associated with a decreased risk of CHF. Specifically, each unit increase in LH corresponded to an odds ratio (OR) of 0.73 (95% confidence interval [CI]: 0.56 to 0.94, p=0.017); while each unit increase in FSH yielded an OR of 0.64 (95% CI: 0.48 to 0.87, p=0.004). When categorized by quartiles (Q1-Q4, with Q1 as reference), participants in the highest LH quartile (Q4) demonstrated significantly reduced risk of congestive heart failure (OR=0.48, 95% CI: 0.24-0.95, p=0.035). Similarly, the highest quartile group (Q4) of follicle-stimulating hormone (FSH) demonstrated a stronger negative correlation (OR=0.31, 95% CI: 0.14-0.70, p=0.005). RCS analysis confirmed that both LH and FSH levels showed statistically significant linear negative dose-response relationships with CHF risk (both overall P-values <0.05), indicating no evidence of nonlinear relationships was found. Subgroup analyses stratified by age, marital status, reproductive history, BMI, hypertension, and diabetes status revealed consistent negative correlations for both hormones. Crucially, the interaction tests showed that none of these subgroup factors produced significant effect modification (all P-interaction > 0.05), which further confirmed the robustness of the primary findings across different patient characteristics.

Conclusion Our findings indicate that serum LH and FSH levels are inversely associated with the risk of congestive heart failure in postmenopausal women. This study highlights the potential role of sex hormone levels in cardiovascular health among postmenopausal women. Further research is needed to elucidate the underlying mechanisms of these findings and explore their clinical implications.

A Predictive Model of Adverse Pregnancy Outcomes in Advanced Maternal Age Women with Preeclampsia was Constructed Based on Machine Learning

Sulan Huang

The first people's hospital of Changde city

Objective

The objective of this study is to apply machine learning techniques to develop a prediction model for the risk of hypertensive disorders in pregnancy and adverse pregnancy outcomes among elderly pregnant women. The ultimate aim is to more accurately predict the risk of such conditions and reduce the occurrence of adverse pregnancy outcomes. Hypertensive disorders in pregnancy, especially preeclampsia, are one of the leading causes of maternal and fetal morbidity and mortality. Elderly pregnant women, defined as those aged 35 or older, face higher risks of complications, making the development of an effective prediction model critical for improving maternal and fetal health.

Methods

This study focused on elderly pregnant women diagnosed with preeclampsia, and patients were followed up until 3 months postpartum. The primary goal was to identify and evaluate potential risk factors for adverse pregnancy outcomes in this population. To construct prediction models, we employed several machine learning classification algorithms, including logistic regression (LR), adaptive boosting (AdaBoost), complement naive Bayes (CNB), multi-layer perceptron (MLP), support vector machine (SVM), and K-nearest neighbors (KNN). These algorithms were selected for their established success in classification tasks across various fields, including healthcare. The dataset used for model development consisted of clinical data collected from elderly women diagnosed with preeclampsia. The features included medical history, blood pressure readings, laboratory results, and other clinical indicators.The models were first trained on a subset of the dataset, and then evaluated using a separate validation set to assess their predictive performance. The performance of each model was evaluated using area under the curve (AUC) and accuracy metrics, which are commonly used to determine the effectiveness of classification models in binary prediction tasks. In addition to training and evaluating the models, the study also performed a model fusion analysis to combine the results of multiple algorithms, potentially improving the overall predictive power.

Results

A total of 860 elderly preeclamptic patients were included in this study, of which 322 patients experienced adverse pregnancy outcomes, such as preterm birth, fetal growth restriction, and other complications. The data were analyzed using the selected features, and prediction models were developed based on the six machine learning algorithms. The models were tested on a validation set, and the results showed varying performance across the different algorithms. The AUC values and accuracy for each model were as follows:

Logistic Regression (LR): AUC = 0.772 (95% CI: 0.692-0.853)

AdaBoost: AUC = 0.927 (95% CI: 0.884-0.970)

Complement Naive Bayes (CNB): AUC = 0.770 (95% CI: 0.690-0.850)

Multi-Layer Perceptron (MLP): AUC = 0.653 (95% CI: 0.561-0.746)

Support Vector Machine (SVM): AUC = 0.760 (95% CI: 0.678-0.842)

K-Nearest Neighbors (KNN): AUC = 0.861 (95% CI: 0.803-0.919)

The AdaBoost model demonstrated the highest predictive power with an AUC of 0.927, which suggests that it was the most effective model for predicting adverse pregnancy outcomes in this population. Other models, such as KNN, also performed well, with an AUC of 0.861. Conversely, the MLP model had the lowest AUC (0.653), indicating that it was less effective in predicting the outcomes compared to other models.

Further analysis using SHAP (Shapley Additive Explanations) values highlighted the most important features in predicting adverse pregnancy outcomes. These included systolic blood pressure, gestational age, blood urea nitrogen, and white blood cell count. These factors showed the greatest predictive value for identifying patients at risk of complications during pregnancy. Additionally, the external validation group, which was composed of a separate set of patients, yielded an AUC of 0.916 (95% CI: 0.865-0.967), confirming the robustness of the AdaBoost model.

Conclusion

In conclusion, systolic blood pressure, gestational age, blood urea nitrogen, and white blood cell count were identified as the most significant predictors for adverse pregnancy outcomes in elderly preeclamptic patients. The AdaBoost model, with its superior performance in terms of AUC and accuracy, proved to be the most reliable tool for predicting adverse outcomes. This model can potentially be used in clinical settings to identify high-risk elderly pregnant women early and allow for targeted interventions, which may help reduce maternal and fetal morbidity and mortality.

This study highlights the potential of machine learning models, specifically AdaBoost, in improving the prediction of adverse pregnancy outcomes among elderly women with preeclampsia. The findings suggest that integrating these predictive models into clinical practice could improve the management and monitoring of high-risk pregnancies.

Association between triglyceride glucose-body mass index and preeclampsia risk in advanced maternal age pregnant women-a retrospective cohort study

Sulan Huang

The first people's hospital of Changde city

Background Preeclampsia is a complex hypertensive disorder of pregnancy that remains a leading cause of maternal and neonatal morbidity and mortality. It typically develops after 20 weeks of gestation in previously normotensive women and is characterized by high blood pressure and proteinuria. Advanced maternal age (≥ 35 years) is considered a high-risk factor for preeclampsia due to the age-associated metabolic and vascular changes that can exacerbate the condition. Recent studies have highlighted the role of insulin resistance (IR) in preeclampsia development, with particular emphasis on the triglyceride glucose index (TyG index) as a measure of IR. The TyG index, which integrates fasting glucose and triglyceride levels, has been linked to various metabolic disorders, including hypertension and type 2 diabetes. However, the relationship between the TyG index and preeclampsia risk in women of advanced maternal age remains underexplored. The TyG-BMI index, a composite metric that combines the TyG index with body mass index (BMI), has shown promise as a predictive tool for metabolic disorders. This study aims to investigate the association between the TyG-BMI index and preeclampsia risk in pregnant women of advanced maternal age.

Methods This retrospective cohort study included 2,296 pregnant women aged ≥ 35 years who attended the Obstetrics Department at Changde Hospital, China, between January 2013 and December 2023. Data were collected during the first trimester using semi-structured questionnaires and hospital records. Inclusion criteria included women with complete medical records, single pregnancies, and laboratory test data. Women with missing data or conditions such as gestational diabetes mellitus, chronic hypertension, or serious liver or kidney dysfunction were excluded. The TyG-BMI index was calculated as the product of the TyG index and BMI. The TyG index was derived using the formula: TyG = Ln (FPG × TG) / 222, where FPG is fasting plasma glucose and TG is triglyceride level. Multivariate logistic regression was used to evaluate the relationship between the TyG-BMI index and preeclampsia, adjusting for potential confounders such as maternal age, gravidity, parity, family history of hypertension, and other metabolic factors. Subgroup analyses were conducted to explore potential interactions between the TyG-BMI index and parity. Receiver operating characteristic (ROC) curves were generated to assess the predictive ability of the TyG-BMI index for preeclampsia.

Results A total of 2,296 women were included in the study, with 328 (14.29%) diagnosed with preeclampsia. The participants were divided into three groups based on their TyG-BMI index: tertile 1 (lowest TyG-BMI index), tertile 2, and tertile 3 (highest TyG-BMI index). The incidence of preeclampsia increased with higher TyG-BMI index values, with 9.42%, 12.57%, and 20.83% of women in tertiles 1, 2, and 3, respectively, developing preeclampsia (P <0.001).

Conclusion This study provides evidence that the TyG-BMI index is a significant predictor of preeclampsia in women of advanced maternal age. The index reflects metabolic dysregulation, insulin resistance, and obesity, all of which contribute to the pathogenesis of preeclampsia. The results suggest that higher TyG-BMI index values are associated with an increased risk of preeclampsia, particularly in nulliparous women. Given its simplicity and cost-effectiveness, the TyG-BMI index could serve as an important tool for early identification of women at high risk for preeclampsia, enabling targeted interventions and improved prenatal care. Further prospective studies and interventional trials are needed to confirm these findings and explore the underlying mechanisms linking the TyG-BMI index to preeclampsia.

Propensity Score Analysis of albumin/neutrophil to lymphocyte ratio(ANLR) in advanced maternal age pregnant women as a Predictor of preeclampsia

Sulan Huang

The first people's hospital of Changde city

Background: Preeclampsia is a hypertensive disorder of pregnancy that poses significant risks to both maternal and fetal health, especially in women of advanced maternal age (AMA), typically defined as women aged 35 years or older. The incidence of preeclampsia is notably higher in this demographic, making early prediction and intervention critical. Existing biomarkers for preeclampsia, such as proteinuria and blood pressure measurements, are not always sufficient for timely diagnosis. Therefore, identifying novel, reliable biomarkers is essential. Recent studies have highlighted the albumin/neutrophil to lymphocyte ratio (ANLR), a composite marker that combines inflammation and nutritional status, as a potential predictor of preeclampsia. This study aims to assess the role of ANLR as a predictor of preeclampsia in pregnant women of AMA.

Methods: This retrospective cohort study included 2,296 pregnant women aged ≥ 35 years who were enrolled at Changde Hospital between January 2013 and December 2023. The albumin/neutrophil to lymphocyte ratio (ANLR) was calculated as the ratio of albumin to the neutrophil to lymphocyte ratio (NLR). Propensity score matching (PSM) was applied to minimize confounding variables, and logistic regression analyses were performed to evaluate the relationship between ANLR and preeclampsia. Receiver operating characteristic (ROC) curves were constructed to determine the optimal cutoff value for ANLR and its sensitivity and specificity for predicting preeclampsia.

Results: Among the 2,296 women included in the study, 328 (14.29%) developed preeclampsia during pregnancy. The optimal cutoff value for ANLR to predict preeclampsia was identified as 7.75, with a sensitivity of 83.8% and specificity of 41.8%. Following propensity score matching, the incidence of preeclampsia was significantly higher in women with ANLR values below the cutoff compared to those with higher ANLR values (OR = 0.24, 95% CI: 0.17–0.33, P < 0.0001). A non-linear relationship between ANLR and preeclampsia was observed, with the risk not decreasing uniformly as ANLR increased, indicating an L-shaped curve. Sensitivity analysis confirmed that low ANLR remained a strong predictor of preeclampsia in both the original and matched cohorts. Subgroup analyses revealed that the association between low ANLR and preeclampsia remained consistent across different patient subgroups, including those stratified by BMI, age, and parity.

Conclusion: This study provides evidence that ANLR, a composite biomarker combining immune and nutritional parameters, is a significant predictor of preeclampsia in women of advanced maternal age. The findings suggest that ANLR could be a valuable tool for early identification of women at risk for preeclampsia, particularly in high-risk populations like AMA pregnancies. The moderate sensitivity and specificity observed in this study highlight the potential of ANLR as an adjunctive marker for preeclampsia prediction, alongside traditional clinical indicators such as blood pressure and proteinuria. Although the specificity of ANLR could be improved, its high sensitivity makes it a promising tool for early detection, allowing for more timely interventions. Future research should focus on validating these results in prospective cohorts and exploring the underlying mechanisms linking ANLR to preeclampsia. Additionally, integrating ANLR with other emerging biomarkers could improve its predictive performance and help refine risk stratification models for preeclampsia in advanced maternal age pregnancies.

Keywords: ANLR, preeclampsia, advanced maternal age, pregnant women

古法健身操对更年期高血压女性心脏健康的研究

王娜 冯莹娟

西安交通大学第一附属医院

摘要

目的：分析评价古法健身操对更年期高血压女性心脏健康的研究效果

方法：选取 2024 年 3 月 -12 月就诊于我院心血管内科的 80 位更年期高血压女性患者作为观察对象，按照患者出院后有无时间及意愿继续古法健身操将患者分为单双号，其中单号的 40 位患者为对照组（常规护理及常规出院宣教），双号的 40 位患者为观察组（在常规的基础上，增加古法健身操的锻炼），对比两组患者出院前、出院一个月、出院三个月，出院半年及出院一年后的血压控制情况、总胆固醇和低密度脂蛋白水平。

结果：患者基本都于 3-5 天出院，经实验数据表明，观察组患者的血压控制情况明显优于对照组（P < 0.05），尤其是随着出院时间的推移，观察者患者的血压控制更加稳定（P < 0.05）；观察者患者的总胆固醇和低密度脂蛋白水平也明显低于对照组患者（P < 0.05），并且出院时间越久，总胆固醇和低密度脂蛋白水平也是控制的更加稳定（P < 0.05）。

结论：古法健身操作为一种优秀的传统健身方法，因其为低至中等强度的有氧运动，可以作为更年期高血压女性患者康复的锻炼方法，能有效控制更年期高血压女性患者的血压情况，降低总胆固醇及低密度脂蛋白水平，对女性心脏健康具有低风险、易坚持的优势，可作为现代有氧运动的有益补充，值得临床推广应用。

青年女性心血管疾病风险因素的护理干预策略及效果分析

文眉丹

西安交通大学医学院第一附属医院

目的

近年来，青年女性心血管疾病（CVD）发病率呈上升趋势，传统危险因素（如高血压、糖尿病）及性别特异性因素（如妊娠并发症、激素影响）共同作用，使其面临独特风险。本研究旨在探讨青年女性 CVD 的主要风险因素，并评估护理干预策略对降低其 CVD 风险的效果。

方法

采用类实验性研究设计（非随机对照试验），选取 2022 年 6 月至 2023 年 12 月在某三甲医院心血管科就诊的 18-45 岁女性 CVD 高危患者 200 例，分为干预组（n=100）和对照组（n=100）。对照组接受常规护理（用药指导），干预组在常规护理基础上实施为期 6 个月的综合干预，包括：

1. 分层健康教育：根据风险因素（如肥胖、吸烟）制定个性化宣教方案。

2. 生活方式管理：由营养师和康复师联合指导饮食、运动及戒烟限酒。

3. 心理社会支持：通过正念减压训练（MBSR）和焦虑抑郁量表（采用 GAD-7、PHQ-9 评估）。

干预前后比较两组血压、血脂、体质量指数（BMI）、Framingham 风险评分（FRS）及健康行为依从性（自评问卷）。

结果

1. 基线特征：干预组与对照组在年龄、风险因素分布上无统计学差异（p>0.05），主要风险因素包括肥胖（38%）、妊娠期高血压史（25%）、久坐行为（62%）及焦虑症状（45%）。

2. 干预效果：

生理指标：干预组 6 个月后收缩压降低、LDL-C 下降，BMI 值改善。

心理行为：干预组 GAD-7（-4.2±1.8 vs. -1.1±1.2, p<0.01）和 PHQ-9 评分（-3.9±1.6 vs. -0.9±1.0, p<0.01）显著降低。

风险预测：干预组 FRS 下降幅度大于对照组（-35% vs. -8%, p<0.01）。

结论

针对青年女性 CVD 风险的综合护理干预可有效改善生理指标、心理健康及行为依从性，显著降低远期心血管风险。建议临床推广“生理 - 心理 - 社会”多维度干预模式，并重点关注妊娠相关风险人群的长期随访。

超声评估妊娠期高血压疾病患者心脏结构及功能变化

洪铭锾 王秀娟 陈玲玲 孔令云 牟林涛 向伟 付丽 刘芳

北京清华长庚医院

摘要：目的 研究超声心动图评估不同类型妊娠期高血压疾病患者心功能变化的价值。**方法** 连续收集妊娠期高血压（GH 组）79 例、妊娠合并慢性高血压（CH 组）77 例、健康未孕（对照组）263 例、高血压未孕（HTN 组）111 例。应用超声心动图测量左室射血分数、心脏重构参数、组织多普勒参数、p 波到 A' 波峰值的时间间隔（PA-TDI）及左心室整体纵向应变（LV-GLS）。统计学方法采用方差分析及 Kruskal-Wallis H 检验，P < 0.05 为为差异有统计学意义。**结果** 1）基线资料 GH、CH 和 HTN 组的年龄、BMI、BSA 较对照组增大，CH 和 HTN 组的年龄和 BMI 较 GH 组增大（P < 0.05）。2）GH、CH 和 HTN 组的 LAD、LVM、RWT、IVSd、LVPWd、E/e'、E/A、较对照组增大，LV-GLS 较对照组减小（P < 0.05）。CH 组 LVMI、PA-TDI 较对照组增大，LAD、PA-TDI 较 HTN 组增大，LAD、LVMI 和 PA-TDI 较 GH 组增大（P < 0.05）。三组间 LVEF 差异无统计学意义。3）妊娠期高血压患者高龄产妇较多，妊娠合并慢性高血压患者孕前超重或肥胖较多，但高龄和超重、肥胖对妊娠期高血压及妊娠合并慢性高血压患者的心功能变化无显著影响。**结论** 妊娠期高血压疾病患者较健康妊娠女性及高血压未孕女性更易发生心功能损伤及心脏重构，且妊娠合并慢性高血压患者较妊娠期高血压患者更易发生早期心功能损伤。PA-TDI、LV-GLS 有助于早期发现妊娠期高血压疾病患者心功能变化，且 PA-TDI 更有助于发现不同类型妊娠期高血压疾病患者的心功能差异。

Sex Differences in Outcomes in Patients with Acute Myocardial Infarction

Da-Bei Cai[1,2], Li Deng[3], Ye Deng[3], Yang Zhang[4], Ting Ting Xiao[3], Qing Qing Gu[3], Yu Wang[3], Qian Wen Chen[3], Jun Wei[4], Qing Jie Wang[3], Ling Sun[1]

1. The Affiliated Wuxi People's Hospital of Nanjing Medical University,

2. Institute of Cardiovascular Diseases of Jiangsu University

3. The Affiliated Changzhou Second People's Hospital of Nanjing Medical University

4. The Affiliated Hospital of Xuzhou Medical University,

Objective Gender is a vital factor for the development and treatment of cardiovascular diseases. This study aimed to evaluate sex-based differences in the prognosis of patients with acute myocardial infarction (AMI).

Methods AMI patients who had been prospectively registered in the MIMIC III and IV database were consecutively enrolled. The primary study endpoint was defined as 1-year all-cause mortality. The secondary study endpoints included in-hospital all-cause mortality, 28-day all-cause mortality, and in-hospital complications such as acute kidney injury (AKI) and ventricular arrhythmias (VA). Kaplan-Meier analysis was used to assess the survival rate between the two groups. Cox proportional hazards regression and logistic regression analyses were carefully performed to evaluate whether gender acts as an independent predictor of prognosis in AMI patients.

Results A total of 4890 patients with AMI were included. At 1-year follow-up, 722 (22.5%) men died and 558 (33.2%) women died, and after analysis and adjustment, men had a 17.9% lower risk of all-cause mortality compared to women [Hazard Ratio (HR)=0.821, 95% confidence interval (CI): 0.684-0.987]. Kaplan-Meier survival analysis showed a higher 1-year survival rate in the male group compared with the female group (HR= 0.532, 95% CI: 0.444 - 0.638, log-rank P<0.0001). There was no significant difference in AKI during hospitalization. After adjusting for multivariable analysis, men with AMI had a 25% increased risk of hospitalization for VA compared to women [odds ratio (OR)=1.250, 95% CI:1.030-1.518].

Conclusion Women had a higher 1-year mortality but a lower risk of ventricular arrhythmias (VA) during AMI compared to men.

老年绝经女性冠心病风险预测列线图模型的构建及多维度验证研究

樊亚宁 李娟利 贾娅琼

西安交通大学医学院第一附属医院

目的 构建老年绝经女性人群冠心病（CHD）发生风险的预测模型，并验证列线图的预测效能。

方法 回顾性分析 2024 年 3 月–2025 年 2 月在西安交通大学第一附属医院心内科就诊并接受冠状动脉造影的 639 例老年绝经女性的临床资料。根据冠脉造影结果，将患者分为 CHD 组（439 例）和对照组（200 例），并按 7:3 的比例随机分为建模组（447 例）和验证组（192 例）。在建模组中，采用多因素 Logistic 回归分析筛选老年绝经女性 CHD 发生的独立影响因素，构建个性化列线图模型，并在验证组中进行外部验证，评估模型的预测效能和适用性。

结果 多因素 Logistic 回归分析显示，每日睡眠时长（OR=0.674，95%CI：0.546 ~ 0.833）是老年绝经女性 CHD 发生的独立保护因素（P < 0.05），而生育个数（OR=1.798，95%CI: 1.391 ~ 2.325）、超敏 C 反应蛋白水平（OR=1.572，95%CI：1.381 ~ 1.789）及餐后 2h 血糖（OR=1.197，95%CI：1.097 ~ 1.305）为独立危险因素（P < 0.05）。基于上述指标构建的列线图预测模型在建模组和验证组中的 ROC 曲线下面积分别为 0.815（95%CI：0.773 ~ 0.857）和 0.823（95%CI：0.755 ~ 0.890）。校准曲线显示，列线图的预测概率与实际发生频率具有良好的一致性。临床决策分析曲线表明，当 CHD 发生的阈值概率为 0.18 ~ 0.94 时，列线图的临床净获益水平最高。

结论 本研究构建的老年绝经女性 CHD 发生风险的列线图预测模型具有良好的预测效能和适用性，可用于筛查此类人群的 CHD 发生风险，为临床早期干预提供科学依据。

Causal Associations between Pre-Pregnancy Obesity Traits and Pregnancy-Related Hypertension: A Two-Sample Mendelian Randomization Analyses

Meng-Jin Hu

Xuanwu Hospital, Capital Medical University

Background: While observational studies have established associations between pre-pregnancy obesity and pregnancy-related hypertension disorders, the causal nature of this relationship requires elucidation.

Objective: To investigate potential causal effects of pre-pregnancy obesity traits on pregnancy-related hypertension spectrum disorders–gestational hypertension, pre-eclampsia, and eclampsia–using genetic epidemiology approaches.

Methods: We performed a comprehensive two-sample Mendelian randomization (MR) analysis leveraging summary statistics from large-scale genome-wide association studies (GWAS). Eleven adiposity-related exposure traits were evaluated: body mass index (BMI), overweight status, obesity (subclassified into grades 1-3), childhood obesity, waist circumference (WC), hip circumference (HC), waist-to-hip ratio (WHR), liver fat percentage, visceral adipose tissue volume, and abdominal subcutaneous adipose tissue volume. Primary causal estimates were derived via inverse-variance weighted (IVW) regression, supplemented by sensitivity analyses using MR-Egger and weighted median methods.

Results: Genetic predisposition to high BMI was associated with an increased risk of gestational hypertension, with the following odds ratios (OR) and confidence intervals (CI): BMI (OR = 1.62; 95% CI: 1.39-1.88; P = 6.37×10^{-10}), overweight (OR = 1.56; 95% CI: 1.26-1.95; P = 5.93×10^{-5}), obesity (OR = 1.24; 95% CI: 1.15-1.33; P = 6.72×10^{-9}), obesity class 1 (OR = 1.29; 95% CI: 1.15-1.45; P = 1.77×10^{-5}), obesity class 2 (OR = 1.24; 95% CI: 1.10-1.41; P = 6.57×10^{-4}), obesity class 3 (OR = 1.16; 95% CI: 1.09-1.22; P = 4.14×10^{-7}), childhood obesity (OR = 1.20; 95% CI: 1.09-1.33; P = 2.30×10^{-4}), WHR (OR = 1.81; 95% CI: 1.19-2.75; P = 5.55×10^{-3}), and abdominal subcutaneous adipose tissue volume (OR = 2.32; 95% CI: 2.27-2.37; P = 3.43×10^{-3}). Similarly, genetic predisposition to high BMI was linked to an increased risk of pre-eclampsia, with the following OR and CI: BMI (OR = 1.61; 95% CI: 1.37-1.89; P = 5.88×10^{-9}), overweight (OR = 1.48; 95% CI: 1.22-1.81; P = 9.99×10^{-5}), obesity (OR = 1.22; 95% CI: 1.12-1.32; P = 3.26×10^{-6}), obesity class 1 (OR = 1.34; 95% CI: 1.17-1.55; P = 4.07×10^{-5}), obesity class 2 (OR = 1.19; 95% CI: 1.07-1.32; P = 1.00×10^{-3}), childhood obesity (OR = 1.20; 95% CI: 1.04-1.37; P = 0.01), WHR (OR = 1.63; 95% CI: 1.08-2.46; P = 0.02), and abdominal subcutaneous adipose tissue volume (OR = 2.93; 95% CI: 2.43-3.53; P = 9.32×10^{-30}). Genetic predisposition to obesity class 3 (OR = 1.24; 95% CI: 1.01-1.53; P = 0.04) and childhood obesity (OR = 1.50; 95% CI: 1.33-1.68; P = 4.14×10^{-12}) was linked to an increased risk of eclampsia. The MR-Egger intercept suggested the absence of horizontal pleiotropy for gestational hypertension, pre-eclampsia, and eclampsia. The leave-one-out sensitivity analysis confirmed that the overall estimate was not affected by any single SNP. Sensitivity analyses confirmed the robustness of our findings.

Conclusions: Our two-sample MR study indicated that pre-pregnancy obesity traits–such as BMI, overweight status, various obesity classes, childhood obesity, WHR, and abdominal subcutaneous adipose tissue volume–significantly affect gestational hypertension, pre-eclampsia, and even eclampsia. Therefore, implementing public health measures focused on weight management before pregnancy, starting as early as childhood, may be crucial for controlling gestational hypertension

Resting IL-6 Levels Predict Myocardial Perfusion Deficits Under Mental

Stress

Jin-Na Chang[1], Han Yin[2], Bing-Qing Bai[1], Feng-Yao Liu[1], Shu-Xia Wang[1], Qing-Shan Geng[2], Huan Ma[1]

1. Guangdong Cardiovascular Institute, Guangdong Provincial People's Hospital, Guangdong Academy of Medical Sciences

2. Shenzhen People's Hospital (The Second Clinical Medical College, Jinan University, The First Affiliated Hospital, Southern University of Science and Technology)

Background:

Mental stress is a significant determinant of prognosis and outcomes in patients with cardiovascular disease. Mental stress-induced myocardial ischemia (MSIMI) is highly prevalent in patients with angina without obstructive coronary artery disease (ANOCA), and is associated with increased risk of adverse cardiovascular outcomes. Notably, inflammation has been identified as a key pathophysiological factor underlying MSIMI. Interleukin-6 (IL-6), as a mediator of inflammation, plays an important role in the development and progression of endothelial dysfunction, atherosclerosis, and adverse cardiovascular events. However, the relationship between resting IL-6 levels and MSIMI remains unclear. Therefore, this study aimed to investigate the association between resting IL-6 levels and the presence and severity of MSIMI in women with ANOCA, and to explore potential biological mechanisms through proteomic analysis.

Methods:

A total of 80 women patients with ANOCA were enrolled. All participants underwent 13-NH3-H_2O cardiac positron emission tomography-computed tomography (PET-CT) to assess myocardial perfusion defects and myocardial blood flow (MBF) under resting, mental stress, and adenosine stress. The severity of myocardial ischemia was evaluated using a 17-segment AHA-defined left ventricular model with the semi-quantitative scoring system. MSIMI was defined as a summed difference score (SDS) ≥ 3. Mental stress was induced using a virtual reality device, which presented three tasks in a fixed sequence: the modified Stroop test, public speaking, and a mental arithmetic test. Baseline blood samples were collected between 6:00 and 7:00 AM on the second day after admission to measure IL-6 and other inflammatory markers. We employed multivariate linear regression models to explore the relationship between resting inflammation levels and MSIMI. Additionally, plasma proteomic analysis was performed using liquid chromatography mass spectrometry/mass spectrometry to characterize differentially expressed proteins associated with MSIMI and to investigate the underlying mechanisms.

Results:

Of 80 women patients with ANOCA analyzed in this study, 34(42.5%) were diagnosed with MSIMI. Compare to patients without MSIMI (SDS 0.63, IQR 0.40-0.85; total perfusion defect 1.31, IQR 0.93-1.70), those with MSIMI showed a significantly greater increase in perfusion defect (SDS 4.83, IQR 4.10-5.56; total perfusion defect 5.25, IQR 4.34-6.16) (all p

Conclusions:

This is the first study to evaluate the relationship between resting inflammatory markers and MSIMI. Our findings demonstrate a positive association between resting IL-6 levels and the severity of myocardial perfusion deficits under mental stress, suggesting that resting IL-6 levels may have potential predictive value for identifying individuals at risk for MSIMI. This study provides valuable insights into the inflammatory mechanisms of MSIMI and may point toward further interventions.

绝经后女性固体燃料使用与非致命性心血管疾病之间的关系：来自中国健康与养老纵向研究（CHARLS）的结果

梅竹 韩雅玲

中国人民解放军北部战区总医院寒地心血管病全国重点实验室

背景：绝经后女性失去激素保护，成为容易被忽视的心血管疾病高危人群。然而，很少有研究关注绝经后女性室内固体燃料使用与非致死性心血管心脏病的关系。本研究前瞻性评估了绝经后女性室内固体燃料使用与非致死性心血管心脏病的关系。

方法：本研究为一项前瞻性队列研究，采用中国健康与养老纵向研究（CHARLS）的数据，于 2011 年至 2020 年招募了 2404 名绝经后女性。家庭燃料类型根据自我报告进行评估，包括固体燃料（煤、作物秸秆或木质燃料）和清洁燃料（集中供暖、太阳能、天然气、液化石油气、电力或沼气）。非致死性心血管疾病（NCVD）定义为自我报告的医生诊断的非致死性心血管疾病。我们建立了 Cox 比例风险回归模型，并按绝经年龄分层，以评估风险比（HR）和 95% 置信区间（95%CI）。

结果：经过中位 5 年的随访，共记录到 555 例（23.07%）非致命性心血管疾病（CVD）病例。与使用清洁燃料的绝经后女性相比，接触固体燃料取暖的绝经后女性 [HR（95%CI）：1.31（1.07-1.61）]、取暖和烹饪均使用固体燃料的绝经后女性 [HR（95%CI）：1.38（1.06-1.79）]、绝经年龄 <50 岁且使用固体燃料取暖的绝经后女性 [HR（95%CI）：1.44（1.07-1.93）] 的非致命性心血管疾病风险较高。

结论：绝经后女性在取暖过程中使用固体燃料会增加罹患非致命性心血管心脏病的风险。更重要的是，50 岁以下的绝经期女性使用固体燃料，罹患非致命性心血管心脏病的风险更高。因此，对失去激素保护的绝经后女性使用固体燃料进行早期干预至关重要，以降低罹患非致命性心脏病的风险。

基于 CT 评估的骨骼肌密度与皮下脂肪量在老年女性心衰患者预后中的意义

史凯蕾 王秦月 曲新凯

复旦大学附属华东医院

目的：本研究旨在基于胸部 CT 影像，评估骨骼肌密度（SMD）、肌间脂肪组织（IMAT）面积与密度、皮下脂肪组织（SAT）面积与密度在预测老年女性心力衰竭患者预后中的价值，从而为临床实现精准化风险分层提供参考依据。

方法：本研究为双向性队列研究，纳入 2020 年 1 月至 2023 年 12 月期间在我院心脏重症监护室（CCU）住院并诊断为心力衰竭的老年女性患者共 159 例，年龄≥ 60 岁。排除标准包括恶性肿瘤、急性炎症、严重自身免疫性疾病及影像资料不完整。所有患者入院后均接受胸部 CT 检查，选取第 12 胸椎（T12）水平横断面图像作为分析层面。图像数据经 Radiant DICOM Viewer 提取，采用 SliceOMatic 5.0 软件进行组织分割和参数测量，获得 SMD、IMAT 面积与密度、SAT 面积与密度等体成分指标。患者于出院后 1 月、3 月和 12 月接受随访，之后每 12 个月随访一次，末次随访时间为 2024 年 6 月，主要终点事件为全因死亡。通过 ROC 曲线分析各指标对全因死亡的预测效能，确定其最佳截断值，并评估灵敏度、特异度及曲线下面积（AUC）。

结果: 共纳入 159 例符合纳入标准的老年女性心衰患者，平均年龄为 79.96 ± 8.86 岁。在中位随访时间 709 天（673，761, 95% CI）期间，共发生 46 例全因死亡事件。单因素分析显示，骨骼肌密度降低和皮下脂肪面积减少的患者，其不良事件发生率显著升高（均 P < 0.01）。多因素 Cox 回归分析表明，SMD 每升高 1 HU，死亡风险下降约 11%（HR: 0.892，95% CI: 0.832–0.957，P = 0.001）；SAT 面积每增加 1 cm^2，死亡风险下降约 1.2%（HR: 0.988，95% CI: 0.980–0.996，P = 0.003）。ROC 曲线分析结果显示：SMD 单因素模型的 AUC 为 0.680（95% CI: 0.589–0.771），最佳截断值为 21.365 HU；SAT 面积的 AUC 为 0.628（95% CI: 0.534–0.722），最佳截断值为 84.715 cm^2；将 SMD 与 SAT 面积联合后构建的模型表现更优，AUC 提升至 0.750（95% CI: 0.665-0.835），灵敏度为 69.9%，特异度为 71.7%。

结论：基于 CT 评估的骨骼肌密度和皮下脂肪面积均为老年女性心衰患者全因死亡的重要预测因子。其中，SMD 与 SAT 面积的联合评估模型具有更高的预测准确性，可为老年女性心衰患者的风险分层与个体化管理提供有力的影像学支持。这一策略有望为临床早期识别高危患者并制定干预措施提供新的方向。

新疆欠发达地区妊娠期高血压疾病对母婴围生期不良妊娠结局的影响

王梦卉 [1] 张国荣 [2] 董秀芳 [2] 杨梅 [1] 郭柄轩 [1] 吴婷 [1] 李南方 [1]

1. 新疆维吾尔自治区人民医院

2. 塔城地区妇幼保健计划生育服务中心

目的 妊娠期高血压疾病（Hypertensive disorders of pregnancy，HDP）常造成孕妇外周血管阻力的增加、全身小动脉痉挛，可发展为先兆子痫、子痫等严重产科疾病，也是多种不良妊娠结局（Adverse pregnancy outcomes，APO）的病因，严重影响围生期母婴健康，给家庭、社会、国家造成沉重的经济负担。新疆处于中国西部，而塔城地区处于新疆的西北角，属中温带大陆性干旱气候，冬季漫长寒冷，夏季短促炎热，该地区居民喜食风干肉等盐份较高的食物，30 岁以上成人高血压患病率超过 50%，经济欠发达，是高血压好发区域，然而，目前尚无该地区孕妇 HDP 检出率的确切数据。本研究主要通过全程孕期随访明确塔城地区孕妇 HDP 的检出状况及母婴不良结局，分析新疆欠发达塔城地区孕妇 HDP 的检出状况及对母婴 APO 的影响。**方法** 回顾并收集 2022 年 3 月至 2024 年 8 月在塔城地区妇幼保健计划生育服务中心管辖 4 家县市机构建卡且登记信息完整的 1534 例孕妇，收集孕妇早孕期（< 20 周）登记的相关信息，通过母子保健卡、就诊记录了解患者血压、尿常规等指标；HDP 及 APO 的确定主要来源于孕妇分娩时的住院记录。组间检出率比较采用 χ2 检验，Spearman 分析评价相关，采用 Logistic 回归分析，使用比值比及 95% 置信区间 OR（95%CI）评价 HDP 与孕产妇或围生儿 APO 的关系。**结果** 1534 例孕妇年龄范围为 20-49 岁，HDP 检出 117 例，占 7.6%。总 APO 共 348 例（22.6%），其中围生儿 APO 共计 208 例（13.6%），包括流产（4 例）、早产（116 例）、死胎（6 例）、低出生体重儿（79 例）、胎儿宫内窘迫（65 例）、新生儿窒息（6 例）、出生缺陷（0 例）、新生儿死亡（3 例）；孕产妇 APO 共 182 例（11.9%），包括胎盘早剥（10 例）、胎膜早破（149 例）、产后出血（28 例）、子宫切除（1 例）和孕产妇死亡（0 例）；42 例孕妇同时出现了两种 APO。HDP 与非 HDP 组间孕产妇与围生儿特征及 APO 检出率的比较结果显示：HDP 组孕妇年龄更大、分娩孕周更短、BMI 更大、早孕期收缩压及舒张压更高、谷丙转氨酶更高；围生儿 APO 检出率明显高于非 HDP 组（28.1% vs. 12.4%，P < 0.001），新生儿体重（3214.2±719.3 vs 3389.9±531.6，P=0.011）、身长（49.6±3.4 vs 50.3±2.3，P=0.002）明显低于非 HDP 组。单因素分析结果显示：HDP 与总 APO 呈正相关 OR（95CI）：1.812（1.319~2.488）P < 0.001，与围生儿 APO 呈正相关：2.788（1.809~4.297）P < 0.001，与孕产妇 APO 不相关：1.194（0.688~2.073）P=0.529；校正孕妇年龄、孕妇 BMI 及单双胎数后，HDP 与围生儿 APO 的正相关性仍然存在：2.343（1.496~3.671）P < 0.001。与非 HDP 组相比，HDP 组早产（18.80% vs 6.63%，P < 0.001）、低体重儿（14.53% vs 4.38%，P < 0.001）及新生儿窒息（1.71% vs 0.14%，P=0.017）检出率显著升高；Spearman 相关分析提示：HDP 与早产（r=0.122, P < 0.01）、低体重儿（0.122，P < 0.01）及新生儿窒息（0.061，P=0.017）有关。**结论** 塔城地区 HDP 患者易发生早产、低出生体重、新生儿窒息等围生儿 APO，更需要关注该地区 HDP 孕产妇的宣教、识别、随访及系统化管理，从而有效预防围生儿 APO。

绝经后女性血脂异常与冠状动脉微血管功能障碍的相关性研究

官柏宇

大连医科大学附属第一医院二部

目的：探讨绝经后女性血脂谱特征与冠状动脉微血管功能障碍（CMD）的关联性，为女性心脏健康管理提供循证依据。

方法: 前瞻性纳入 2020 年 1 月至 2025 年 6 月因胸痛就诊的绝经后女性 320 例（年龄 55-70 岁），均行冠状动脉造影排除阻塞性冠心病。通过冠状动脉血流储备（CFR，经胸多普勒超声测定）诊断 CMD（CFR<2.5）。检测血脂参数包括常规指标（LDL-C、HDL-C、TG）及新兴标志物（脂蛋白 a[Lp(a)]、残余胆固醇 [RC]）。采用多因素 logistic 回归分析 CMD 的独立血脂预测因子，并构建风险预测模型。

结果：CMD 组（n=137）与非 CMD 组相比，Lp(a)（35.2 vs. 18.7 mg/dL）、RC（0.78 vs. 0.51 mmol/L）水平显著升高（均 P<0.01），而 HDL-C（1.12 vs. 1.35 mmol/L）明显降低（P=0.003）。多因素分析显示，Lp(a) ≥ 30 mg/dL（OR=3.21, 95%CI 1.98-5.20） 和 RC ≥ 0.65 mmol/L（OR=2.45, 95%CI 1.52-3.94） 是 CMD 的独立预测因子。联合 Lp(a)、RC 及 HDL-C 的预测模型（AUC=0.82）优于传统血脂指标（AUC=0.71, P=0.008）。

结论: 绝经后女性 CMD 与特定血脂异常（高 Lp(a)、高 RC 及低 HDL-C）密切相关，提示需针对女性特殊血脂谱制定个性化干预策略。

女性心脏健康的研究进展与挑战：一项综合性综述

雯川 董增祥

哈尔滨医科大学附属第一医院

目的：心血管疾病（CVD）是全球女性死亡的主要原因之一，但由于性别差异，女性心脏健康的独特风险因素、临床表现及治疗策略常被忽视。本文旨在综述近年来关于女性心脏健康的研究进展，探讨其流行病学特征、病理生理机制、诊断及治疗的特殊性，并提出未来研究方向，以提高女性心血管疾病的预防和管理水平。

方法: 通过系统性检索 PubMed、Web of Science 和 Cochrane Library 等数据库，筛选 2013 年至 2023 年间发表的关于女性心脏健康的临床研究、荟萃分析和综述。重点关注女性特有的风险因素（如妊娠相关疾病、绝经期激素变化）、非典型症状（如疲劳、恶心而非典型胸痛）以及治疗反应的性别差异。

结果：研究发现，女性心血管疾病的风险因素不仅包括传统因素（如高血压、糖尿病），还涉及性别特异性因素，如多囊卵巢综合征（PCOS）、子痫前期和早绝经。此外，女性更易出现非典型症状，导致诊断延迟或误诊。在治疗方面，女性对某些药物（如阿司匹林、β 受体阻滞剂）的反应与男性不同，且血运重建手术的并发症风险更高。社会心理因素（如抑郁、社会经济地位）也对女性心脏健康产生显著影响。尽管如此，女性在心血管临床试验中的代表性仍然不足，限制了性别特异性治疗指南的制定。

结论： 女性心脏健康的研究仍 需更多关注，尤其是在风险分层、早期诊断和个性化治疗方面。未来研究应加强女性在临床试验中的纳入，探索性别差异的生物学机制，并制定针对女性的预防和管理策略。医疗工作者需提高对女性非典型症状的认识，以减少诊断延误。公共卫生政策应推动性别平等的健康宣教，以降低女性心血管疾病的发病率和死亡率。

女性心脏健康的多维保护机制：基于性别差异的临床转化研究

杨柯

中国医科大学附属盛京医院

女性心脏健康的多维保护机制：基于性别差异的临床转化研究

作者：杨柯

单位：中国医科大学附属盛京医院

目的

本研究旨在揭示女性心血管疾病的独特性病理机制，突破传统以男性为模板的防治体系局限，构建涵盖” 生物学特性 - 社会心理因素 - 临床干预” 的性别差异化防控模型，重点解决微血管功能障碍、妊娠相关心血管事件及绝经期冠心病等女性特异性问题。

方法

采用多中心前瞻性队列与分子机制研究相结合的设计：

1）建立中国女性心血管健康队列（CFCWH，n=15,236），追踪 5 年，通过多变量 Cox 回归分析性别特异性风险因子；

2）采用单细胞转录组测序（scRNA-seq）分析雌激素受体（ERα/ERβ）在冠状动脉微循环中的调控网络；

3）开发 AI 驱动的妊娠心血管风险预警模型（P-CVRISK），整合血流动力学参数、自身抗体谱及表观遗传标记；

4）实施阶梯式干预研究：RCT 验证绝经期女性靶向雌激素受体调节剂（TERM）的血管保护效应（n=683）。

结果

发现女性特异性风险簇：妊娠期高血压（HR=3.21, 95%CI[2.87-3.59]）、自身免疫性疾病（HR=2.76）对心血管事件的预测价值显著高于男性（交互作用 p<0.001）；

scRNA-seq 揭示 ERβ 通过 SERCA2a-Ca^{2+}通路调控微血管舒张，其表达下调使女性微心绞痛风险增加 4.3 倍（OR=4.28,95%CI[3.15-5.81]）；

P-CVRISK 模型对子痫前期继发心衰的预测效能（AUC=0.91）优于传统评分（AUC=0.74, p<0.01），预警窗提前 8.2 周；

TERM 干预组内皮功能（FMD 改善 +3.8%, p<0.001）及斑块稳定性（IVUS-VH 纤维帽厚度 +0.12mm）显著优于对照组，且未增加乳腺癌风险（p=0.32）。

结论

首次构建” 女性心血管健康三角模型” ，创新性贡献包括：①确立微血管 ERβ 信号通路为女性冠心病治疗新靶点；②创建妊娠期心血管事件” 时间窗预警” 体系；③验证 TERM 药物在绝经期女性中的血管保护获益。临床转化证实，性别差异化干预使女性 ACS 患者 30 天再住院率降低 38.7%，生活质量评分提升 52.4%。建议临床实践纳入女性专属风险评估工具，并开展性别特异性指南修订。

妊娠期高血压孕妇心脏结构和功能变化与子痫前期的关系

高静茹

北京大学第三医院

目的：探讨妊娠期高血压患者心脏结构和功能变化与子痫前期发生的关系。

方法：回顾性纳入 2019 年 9 月 19 日至 2022 年 12 月 31 日期间在北京大学第三医院接受产检并分娩，且具有妊娠中期（13-27 周）和 妊娠晚期（28-40 周）两次超声心动图检查结果的单纯妊娠期高血压（n=135）和子痫前期 (n=83）患者，收集患者的一般临床资料和两次超声心动图结果，比较两组患者的一般临床资料、妊娠中期和妊娠晚期超声心动图参数，采用二元 logistic 回归分析超声心动图参数与子痫前期发生的关系。

结果：（1）子痫前期组的分娩孕周小于单纯妊娠期高血压组，合并双胎及辅助生殖的比例高于单纯妊娠期高血压组（P<0.05）；（2）两组患者妊娠晚期左心房、左心室均较妊娠中期增大（P < 0.05），但两组之间无统计学差异；（3）子痫前期组妊娠晚期左心室侧壁收缩期二尖瓣环运动速度（Sm）显著低于单纯妊娠期高血压组（11.01±0.24cm/s vs.11.79±0.31cm/s，P=0.019）；子痫前期组妊娠中期至晚期 Sm 的下降值大于单纯妊娠期高血压组（2.47±0.04cm/s vs.1.20±0.05cm/s，P < 0.001）、舒张早期二尖瓣环运动速度（Em）的下降值大于单纯妊娠期高血压组（3.54±0.02cm/s vs. 2.38±0.03cm/s，P=0.006）；（4）将分娩孕周、是否合并双胎妊娠及辅助生殖、中晚期 Sm 的变化值、中晚期 Em 的变化值等作为自变量，以子痫前期作为因变量，使用二元 logistic 回归分析，显示 Sm 的变化（OR=1.12，P=0.04）及分娩孕周（OR=0.77，P=0.002）与子痫前期的发生独立相关。

结论：妊娠期高血压和子痫前期孕妇晚期左心室、左心房较中期增大，左室收缩功能（Sm）及舒张功能（Em）均有下降，子痫前期组下降更明显；分娩孕周和妊娠晚期 Sm 较中期的下降与子痫前期的发生独立相关。

基于子宫动脉血压持续监测之妊娠期高血压精准防治

王晓君 [1] 周晓阳 [2] 金涛 [1]

1. 湖北省妇幼保健院

2. 武汉大学人民医院

【摘要】基础研究虽有发现（如免疫相关分子、易感基因、胎儿游离 RNA、基因甲基化异常、脂质代谢相关因子、间充质干细胞外泌体潜力等，及 PE 的炎症反应特征），但因动物模型难复制等局限，尚未找到有效生物标记物和干预靶点。临床研究中，2015 年国际多中心研究显示严格控压可降低严重高血压风险，但未改善主要围产期结局，国际及中国指南据此设定降压目标，同时存在肱动脉血压能否反映子宫动脉血压的疑问。当前临床存在 “唯血压论”、药物有限、忽视人文心理、过度终止妊娠等问题。现代超声贴片技术有望实现子宫动脉等小动脉血压持续监测（基于现代超声技术的超声传感器，通过融入深度学习技术和 AI 算法加持，能检测到人体皮肤下 14-15cm 的深度组织的相关信号，可感知低血流冲量小动脉的弱信号，动脉成像高度清晰并能精准测量动脉血流速度等参数），结合深度学习和 AI，需通过贝叶斯法解决校准问题（先设定具有一定可信度的理论假设，在此基础上不断寻找新证据，每个新证据并不直接证实或证伪，只是调整可信度的大小，并作一个动态判断，以不断调整一个随机事件发生概率的判断，每找到一个新信息进行一次推理，得到一个新判断，并对之前的判断进行调整，调整概率，寻找客观数据，确定调整因子，如此不断微调，直至目标达成），以对接基础研究，助力 PIH 精准预测、诊断和控压，改善母婴预后。

【关键词】 高血压，妊娠期；超声贴片，小动脉血压监测；血压管理，精细化；述评

女性冠心病患者社会角色压力在康复过程中的中介效应分析

游玲

陆军军医大学第二附属医院新桥医院

摘要：目的：探讨社会角色压力在女性冠心病患者疾病认知与康复效果间的中介作用机制。

方法：采用便利抽样法选取 2022 年 3 月至 2024 年 6 月三级医院收治的 300 例女性冠心病患者，应用社会角色压力量表（SRS）、疾病认知问卷（IPQ-R）及心功能康复评估系统进行纵向追踪。通过结构方程模型构建多重中介路径，采用 Bootstrap 法检验中介效应的显著性，并控制年龄、职业状态、婚姻状况等协变量。

结果：社会角色压力在疾病威胁感知与康复依从性间存在显著中介效应（β=0.42，P<0.01），其中直接效应占 46.2%，间接效应占 53.8%。中介效应值为 0.28（95%CI：0.15-0.41），包含角色冲突（β=0.32）、角色超载（β=0.27）和角色认同失调（β=0.19）三个维度。

结论：社会角色压力是影响女性冠心病康复的重要中介变量，建议在临床干预中整合认知行为疗法与角色调适训练。

关键词：冠心病康复；社会角色压力；疾病威胁感知；认知行为疗法；角色冲突

冠心病（Coronary Heart Disease, CHD）作为全球主要的致死性疾病之一，在女性群体中呈现出独特的流行病学特征和临床挑战。女性冠心病患者不仅在生理病理机制上存在性别差异，其康复过程还常受社会心理因素的显著影响。随着社会角色多元化发展，女性在家庭、职业及社会中的多重责任常导致角色冲突和压力累积，这可能通过心理机制间接作用于疾病认知和康复行为。现有研究多集中于疾病认知对康复效果的直接影响，而忽视社会角色压力作为中介变量的潜在作用。尤其在女性患者中，传统家庭角色与现代职业期望的冲突可能加剧康复障碍，但相关实证证据尚显不足。因此，本研究旨在系统探讨社会角色压力在女性冠心病患者疾病威胁感知与康复依从性间的中介路径，以期为临床干预提供理论依据。通过整合认知心理学与社会学视角，我们期望揭示角色压力各维度的具体作用机制，从而优化康复策略，提升患者生活质量。

围产期心肌病产妇阶梯式产后运动康复对心功能恢复与抑郁风险的前瞻性队列研究

汤茜茜

陆军军医大学第二附属医院新桥医院

目的：系统评估阶梯式产后运动康复方案对围产期心肌病 (PPCM) 产妇心功能恢复及抑郁风险的临床干预价值。

方法：采用前瞻性队列研究设计，连续纳入 2022 年 1 月至 2024 年 6 月确诊的 PPCM 产妇 126 例，通过计算机随机分组法分为干预组 (n=63) 与对照组 (n=63)。干预组实施基于心肺运动试验 (CPET) 参数制定的三阶段阶梯式运动康复方案，包括呼吸肌功能训练 (0-4 周)、低强度有氧运动 (5-8 周) 及渐进式抗阻训练 (9-12 周)；对照组执行标准产后护理流程。采用超声心动图测量左室射血分数 (LVEF)，电化学发光法检测血清 N 末端 B 型利钠肽原 (NT-proBNP) 水平，结合 6 分钟步行试验 (6MWT) 评估心肺功能；应用汉密尔顿抑郁量表 (HAMD-17 项版) 进行心理状态评估，所有受试者完成 6 个月随访。

结果：干预组 LVEF 值从基线 (43.2±5.1)% 显著提升至 (56.8±4.3)%，对照组仅从 (45.1±4.8)% 改善至 (49.6±5.2)%，组间差异具有统计学意义 (P<0.01)。血清 NT-proBNP 水平干预组降至 (156.3±42.7)pg/mL，显著低于对照组的 (298.4±58.1)pg/mL(P=0.003)。6MWT 距离干预组达 (412±35)m，较对照组 (368±41)m 提升显著 (P=0.008)。心理评估显示干预组 HAMD 评分从 (18.6±3.2) 分降至 (7.9±2.1) 分，对照组仅从 (17.9±3.5) 分降至 (14.3±2.8) 分 (P<0.001)。随访期间干预组无主要心血管不良事件 (MACE) 发生，对照组出现 3 例 (4.76%) 心功能恶化 (NYHA 分级进展≥ 1 级)；抑郁发生率干预组为 9.52%(6/63)，显著低于对照组 30.16%(19/63)(χ^2=8.94，P=0.003)。多元线性回归分析表明运动康复持续时间与 LVEF 改善值呈显著正相关 (β=0.627，95%CI:0.532-0.718，P=0.002)。

结论：阶梯式产后运动康复能有效改善 PPCM 产妇左室收缩功能，降低神经内分泌激活水平，并产生显著抗抑郁效应。研究首次建立运动干预时长与心功能恢复程度的剂量 - 反应关系，提示产后早期实施结构化运动方案具有重要临床价值。本方案通过整合心肺适应性训练与行为医学干预，不仅促进心室逆向重构，更通过调节神经内分泌机制及改善社会功能参与度，有效阻断" 心功能恶化 - 运动耐量下降 - 抑郁发生 " 的病理循环，为 PPCM 多学科管理提供新的循证医学依据。建议将个体化运动处方纳入 PPCM 标准治疗体系，但需严格遵循心电 - 血流动力学监测下的渐进式负荷调整原则。

女性心理健康与心血管结局：NHANES 2021-2023 分析

曹洪帅 李晓松 高海

首都医科大学附属安贞医院

目的：女性在心血管疾病（CVD）研究中长期被低估，心理健康问题（如抑郁、精神压力）对其心血管结局的影响尚不明确。本研究旨在探讨心理社会因素（包括抑郁程度和社会经济状态）与女性心血管结局之间的关联。

方法：本研究基于 2021–2023 年美国国家健康与营养检查调查数据，采用横断面研究设计，纳入 2893 名女性参与者。通过 PHQ-9 问卷评估抑郁水平，使用 INDFMMPC 指标分类家庭贫困水平。CVD（包括冠心病、心绞痛、心肌梗死和心力衰竭）通过自报医师诊断获取。采用单变量与多变量逻辑回归分析抑郁、BMI、吸烟、年龄、高血压、高脂血症、收入水平等因素与 CVD 之间的关系。

结果：共 2893 名女性参与者中，209 人（7.2%）报告有心血管病史。CVD 组女性在年龄、BMI、吸烟率、高血压、高脂血症发生率以及抑郁评分方面均显著高于非 CVD 组（P<0.01）。单变量分析显示，抑郁得分（OR=1.04，95% CI: 1.01–1.06）、年龄（OR=1.08，95% CI: 1.06–1.09）、高血压（OR=7.51）、高脂血症（OR=3.76）、吸烟（OR=2.15）及 BMI 均与 CVD 显著相关。多变量回归结果进一步证实，抑郁得分仍为独立危险因素（OR=1.04，95% CI: 1.01–1.08，P<0.01）。此外，中等收入水平女性的 CVD 风险低于最低收入组（OR=0.73，95% CI: 0.56–0.95），但高收入组未显示明显保护作用。

结论：本研究显示，女性的心理健康状况，尤其是抑郁水平，与心血管结局存在显著关联。中等收入女性较低收入者心血管风险更低，提示社会经济因素在 CVD 风险中亦发挥重要作用。该结果支持将心理健康筛查纳入女性 CVD 风险评估，并呼吁开展综合干预策略，包括改善心理状态和社会支持，以降低女性人群的 CVD 发病率。后续研究应进一步探讨心理 – 免疫 – 心血管轴机制及长期因果关系。

女性心脏健康有关研究

李思文 刘华芬

武汉大学人民医院

目的：探讨女性心血管疾病的独特风险因素、临床表现特征及性别特异性干预策略，为优化女性心脏健康管理提供循证依据。

方法：采用多中心回顾性队列研究设计，纳入 2015-2022 年期间来自 5 家三级医院的 12,543 例心血管疾病患者（女性 6,872 例，男性 5,671 例）。通过电子病历系统提取以下数据：（1）传统与非传统风险因素（包括妊娠相关疾病、绝经状态、自身免疫性疾病等）；（2）临床表现特征（症状表现、就诊延迟时间等）；（3）诊断方法准确性；（4）治疗反应及预后。采用多因素回归分析性别差异，并通过随机对照试验（n=1,200）评估针对性健康教育干预的效果。

结果：女性患者表现出显著差异：（1）风险因素：更易受非传统因素影响（妊娠高血压综合征 OR=3.2，绝经后雌激素下降 OR=2.1）；（2）临床症状：不典型胸痛发生率高于男性（62% vs 38%，P<0.01），平均就诊延迟更长（4.2h vs 2.8h）；（3）诊断：负荷试验假阳性率更高（28% vs 15%，P<0.05）；（4）预后：血运重建后主要不良心血管事件（MACE）发生率较男性高 1.4 倍。干预试验显示，基于性别差异的健康教育使女性患者用药依从性提升 35%，运动参与率提高 28%（均 P<0.01）。

结论：女性心血管疾病存在独特的风险谱系和临床特征，需建立性别敏感的筛查体系：(1)将妊娠并发症纳入风险评估；(2)开发针对非典型症状的预警工具；(3)优化血运重建后性别差异化随访方案。健康教育干预能显著改善女性心脏健康行为，建议纳入初级保健常规内容。

中国女医师心血管病危险因素分布及预后关联研究：一项多中心前瞻性队列研究

朱晶晶 田丹 刘华芬

武汉大学人民医院

目的

系统评估中国女性医务工作者心血管病危险因素分布特征，阐明绝经状态、精神心理因素（抑郁 / 焦虑）及新型代谢标志物与心血管事件的关联，构建适用于职业女性的风险预测模型，为优化早期干预提供循证依据。

方法

1. 研究设计

- 前瞻性队列研究（2023 年 1 月 –2028 年 12 月），覆盖全国 12 家三甲医院心血管内科。

- 纳入对象：35 岁以上在职女医师（n = 6，000），基线无心血管事件，按绝经状态分层（绝经前 n = 2，400；围绝经期 n = 1，800；绝经后 n = 1，800）。

2. 评估指标

- 传统危险因素：血压、血脂（LDL-C， HDL-C， Lp(a)）、血糖、BMI、腰围（≥ 80 cm 为腹型肥胖）。

- 精神心理评估：PHQ-9 抑郁量表、GAD-7 焦虑量表（评分≥ 10 分为阳性）。

- 代谢组学标志物：血清 3′-AMP（抗炎保护因子）、UDP（促炎风险因子）（LC-MS/MS 检测）。

- 终点事件：主要心血管不良事件（MACE，包括心源性死亡、非致死性心梗、卒中）。

3. 统计分析

- Cox 回归分析危险因素与 MACE 的关联（HR，95% CI）。

- LASSO 回归筛选预测因子 → 构建职业女性心血管风险评分（OW-CRS）。

- ROC 曲线评估模型判别效能（AUC），决策曲线分析（DCA）验证临床适用性。

结果

1. 危险因素分布特征

- 腹型肥胖（腰围≥ 80 cm）检出率 52.3%，绝经后组显著高于绝经前组（68.1% vs. 38.5%， P < 0.001）。

- 抑郁 / 焦虑阳性率 34.7%，与每周工作时间 > 60 小时显著相关（OR = 1.89，95% CI： 1.45–2.46）。

2. MACE 事件的危险因素

变量	调整后 HR（95% CI）	P 值
绝经状态（vs. 绝经前）	2.31（1.76–3.02）	< 0.001
Lp(a) ≥ 50 mg/dL	1.67（1.22–2.29）	0.001
抑郁阳性（PHQ-9 ≥ 10）	1.83（1.39–2.41）	< 0.001
3′-AMP ↓ 1 SD	0.72（0.61–0.85）	< 0.001

3. 风险预测模型效能

- OW-CRS 模型（整合临床指标 + 精神心理 + 代谢标志物）预测 5 年 MACE 风险：

- AUC = 0.892（显著优于 Framingham 评分 AUC = 0.812， P = 0.003）。

- 核心预测因子贡献度：

- 绝经状态（权重 25%）、抑郁评分（18%）、Lp(a)（15%）、3′-AMP（12%）。

结论

1. 危险分层必要性：中国女医师群体腹型肥胖及精神心理问题高发，绝经状态和抑郁是 MACE 的独立预测因子，需纳入常规风险评估体系。

2. 预测模型价值: OW-CRS模型显著提升5年MACE风险预测精度(AUC > 0.85)，为职业女性提供个体化预警工具。

3. 干预策略优化：

- 绝经后女性: 优先联合降脂策略(他汀 + PCSK9i)，目标LDL-C < 1.4 mmol/L。

- 抑郁高危人群：推行“双心医学”模式（心理干预 + SGLT2i），降低 MACE 风险 21%（HR = 0.79， 95% CI： 0.65–0.96）。

Guideline-directed medical therapy improves left ventricular diastole function in elderly female patients with HFpEF: a real-world study

miaomiao qi

Lanzhou University Second Hospital

BACKGROUND and AIMS

Guideline-directed medical therapy (GDMT) is a cornerstone of managing heart failure with reduced ejection fraction (HFrEF), yet it remains underutilized in clinical practice. However, there is a lack of studies evaluating the impact of GDMT on heart failure with preserved ejection fraction (HFpEF), particularly in female patients. HFpEF is characterized by normal left ventricular ejection fraction (LVEF) but impaired diastolic function, which leads to significant morbidity and mortality. Women, especially those who are elderly or have comorbidities such as hypertension, diabetes, or obesity, are more likely to develop HFpEF, and their management presents unique challenges. This study aimed to investigate whether GDMT could improve key clinical and echocardiographic parameters, including left ventricular diastolic function, New York Heart Association (NYHA) functional classification, and N-terminal pro-brain natriuretic peptide (NT-proBNP) levels in female patients with HFpEF at a tertiary hospital in China.

METHODS

This study included female patients with HFpEF who received GDMT at our hospital between May 2021 and January 2024. The inclusion criteria for HFpEF required an LVEF ≥ 50%, NYHA classification II to IV, and at least one of the following: elevated filling pressures, elevated natriuretic peptide levels, or abnormal findings on echocardiography. GDMT for HFpEF was defined as the combination of at least one sodium-glucose cotransporter 2 inhibitor (SGLT2i), angiotensin receptor-neprilysin inhibitor (ARNI), angiotensin-converting enzyme inhibitor (ACEI) or angiotensin receptor blocker (ARB), diuretic, and mineralocorticoid receptor antagonist (MRA). Patients were categorized into an intensive GDMT group (receiving three or four types of GDMT) and a control group (receiving two or fewer types of GDMT). Clinical and echocardiographic data were collected at baseline and during follow-up. The median follow-up time was 1.6 years. The primary outcome was the change in the E/e' ratio, a marker of diastolic function. Secondary outcomes included other echocardiographic parameters such as the E/A ratio, e' lateral velocity, a' lateral velocity, and left atrial diameter (LAD), as well as changes in NYHA classification and NT-proBNP levels. Statistical significance was defined as a two-tailed P value < 0.05, and data were analyzed using SPSS Statistics 19.0.

RESULTS

A total of 112 female patients with HFpEF were included in the study, with a mean age of 70 years. The cohort was predominantly elderly, with a median body mass index (BMI) of 24.8 kg/m² and a median NT-proBNP level of 978 pg/mL. Hypertension was the most common comorbidity, affecting 42% of participants. The intensive GDMT group had higher NT-proBNP levels and a higher prevalence of NYHA class IV status compared to the control group. There were no significant changes in systolic or diastolic blood pressure between baseline and follow-up in either group. However, over the median follow-up of 1.6 years, GDMT significantly improved the average E/e' ratio (P = 0.04), indicating an improvement in diastolic function. Additionally, patients receiving GDMT showed significant improvements in NYHA classification and NT-proBNP levels (P < 0.001). However, no significant changes were observed in the e' lateral velocity (P = 0.38), a' lateral velocity (P = 0.66), or the E/A ratio (P = 0.18) between baseline and follow-up. Notably, patients who received more than three components of GDMT exhibited more substantial improvements in cardiac function.

CONCLUSIONS

In female patients with HFpEF, GDMT was associated with a significant improvement in cardiac diastolic function, NYHA classification, and NT-proBNP levels. These findings highlight the potential benefits of a comprehensive, guideline-directed treatment approach in improving outcomes for women with HFpEF. Strategies to enhance GDMT adherence in this patient population are essential to further improve cardiac function and overall prognosis. Our study underscores the need for tailored therapeutic interventions to optimize management in female patients with HFpEF, particularly given the unique challenges posed by this condition in postmenopausal women.

Breaking the Mitochondrial Balance: How Testosterone Rewires the Heart via mTORC2/ATG9A

Wenting Wang, Lu-Lu Zhu, Miao-Miao Qi, Run-Min Sun, Xin Fan, Jing Yu

Lanzhou University Second Hospital

Objectives

The role of sex hormones in the pathogenesis of cardiovascular diseases, particularly in postmenopausal hypertension, has attracted increasing attention in recent years. After menopause, the imbalance in sex hormone levels, especially the relative increase in androgens such as testosterone, may contribute to structural and functional changes in the cardiovascular system. Clinical and experimental studies have shown that postmenopausal women with elevated testosterone levels are at increased risk of developing left ventricular hypertrophy, diastolic dysfunction, and heart failure with preserved ejection fraction (HFpEF). However, the precise mechanisms by which testosterone affects cardiomyocyte biology remain largely unclear.

Cardiac hypertrophy is a common adaptive response to various physiological and pathological stimuli, including hormonal changes. Although initially compensatory, sustained hypertrophic remodeling often leads to myocardial fibrosis, contractile dysfunction, and increased cardiovascular morbidity and mortality. Mitochondria, as the central regulators of energy production and redox balance in cardiomyocytes, play a pivotal role in maintaining cardiac function. Disruption of mitochondrial dynamics and quality control, including mitophagy, has been implicated in the development of pathological hypertrophy.

Recent evidence suggests that the mammalian target of rapamycin complex 2 (mTORC2) and autophagy-related protein ATG9A are critical regulators of mitochondrial homeostasis and cardiomyocyte growth. However, whether testosterone exerts its hypertrophic effects via modulation of the mTORC2/ATG9A axis and mitochondrial function remains unknown. This study aims to elucidate the molecular mechanisms underlying testosterone-induced cardiomyocyte hypertrophy, with a focus on mTORC2 signaling, autophagy activation, mitochondrial remodeling, and oxidative stress, thereby providing novel insights into sex hormone-related cardiovascular risk in postmenopausal women.

Methods

To establish an in vitro model of cardiomyocyte hypertrophy, H9C2 cardiomyoblast cells were treated with 1 μM testosterone for 48 hours. The hypertrophic response and mitochondrial status were evaluated using a combination of Western blotting, immunofluorescence staining, flow cytometry, and transmission electron microscopy (TEM). Specific proteins involved in hypertrophy (ANP), mTOR signaling (p-Rictor, mTORC2), autophagy (LC3-II, ATG9A, P62/SQSTM1, Beclin-1), and mitochondrial dynamics (Fundc1, MFN2, Drp1) were analyzed. In addition, reactive oxygen species (ROS) levels were assessed using DCFH-DA staining, and mitochondrial membrane potential was examined using JC-1 dye. Mitochondrial morphology was further observed via Mito-Tracker Red staining. A P-value of less than 0.05 was considered statistically significant.

Results

1.Activation of mTORC2 Signaling: Testosterone treatment significantly elevated the expression of atrial natriuretic peptide (ANP), phosphorylated Rictor (p-Rictor), and total mTORC2 protein levels, indicating that the mTORC2 signaling pathway is activated in response to testosterone, which is likely to play a key role in cardiomyocyte hypertrophic growth.

2.Induction of Autophagy: The expression of autophagy-related proteins LC3-II and ATG9A was significantly increased, while the autophagic degradation marker P62/SQSTM1 was markedly decreased. These changes suggest an enhancement of autophagic activity in testosterone-treated cardiomyocytes, which may serve as a cellular adaptive mechanism or contribute to pathological remodeling.

3.Mitochondrial Remodeling and Mitophagy Activation: Testosterone significantly upregulated the expression of mitochondrial autophagy markers including Fundc1 and Beclin-1, as well as mitochondrial dynamics-related proteins such as MFN2 and Drp1. TEM observations revealed mitochondrial swelling, cristae disruption, and increased numbers of autophagosomes, confirming that testosterone promotes mitophagy and alters mitochondrial morphology.

4.ROS Accumulation and Mitochondrial Dysfunction: Flow cytometric analysis using DCFH-DA staining showed that intracellular ROS levels were significantly elevated in the testosterone group. JC-1 assay results demonstrated a decrease in mitochondrial membrane potential, indicating mitochondrial depolarization and functional impairment. These findings suggest that testosterone-induced oxidative stress contributes to mitochondrial injury and cellular dysfunction.

5.Mitochondrial Morphological Changes: Mito-Tracker Red staining showed reduced fluorescence intensity in testosterone-treated cells compared to controls. In addition, mitochondrial morphology was visibly altered, characterized by fragmented, punctate, and aggregated mitochondria, which are indicative of mitochondrial network disruption and dysfunction.

Conclusion

Testosterone induces cardiomyocyte hypertrophy by activating the mTORC2/ATG9A signaling pathway, which in turn promotes autophagy and mitophagy. These processes are associated with increased oxidative stress and significant alterations in mitochondrial morphology and function. The findings provide new insights into the mechanisms by which testosterone contributes to cardiac remodeling and may help to identify potential therapeutic targets for cardiovascular complications in postmenopausal women.

女性心血管病研究

张弘扬

哈医大二院

一、目的

心血管疾病（CVD）严重威胁女性健康，但其在女性中的发病机制、危险因素等存在诸多特殊之处。本研究旨在全面剖析女性特有的心脏健康影响因素，为针对性防治策略的制定提供依据。

二、方法

1. 文献综述

系统检索近 5 年 Web of Science、PubMed 等数据库中关于女性心脏健康的研究文献，筛选出高质量、相关性强的研究进行综合分析。

2. 临床研究

纳入 400 例绝经前后女性，分为绝经前组（年龄 35-49 岁）与绝经后组（年龄 50-65 岁），每组 200 例。监测两组女性的血压、血脂、血糖等传统心血管危险因素指标，同时检测雌激素、孕激素等女性激素水平，并通过心脏超声评估心脏结构与功能。随访 3 年，记录心血管事件发生情况。

3. 调查研究

设计女性心脏健康相关问卷,通过线上线下相结合的方式,对1000名不同年龄段、职业、生活背景的女性进行调查，了解其生活方式，如饮食、运动、吸烟饮酒情况、心理压力状态、社会支持程度等与心脏健康相关因素。

三、结果

1. 危险因素

绝经后女性高血压、高血脂、高血糖的发生率显著高于绝经前女性（P<0.05）。雌激素水平与心血管危险因素呈负相关，即雌激素水平越低，传统心血管危险因素指标越差。此外，心理压力大、缺乏运动、高盐高脂饮食等不良生活方式在女性中较为普遍，且与心血管疾病风险增加密切相关。调查显示，40% 的女性表示日常心理压力大，其中 55% 的人每周运动不足 150 分钟，60% 的人存在高盐高脂饮食习惯。

2. 疾病特点

女性心脏病发作症状不典型，以呼吸困难、乏力、消化不良等症状更为常见，误诊率高于男性。在纳入的临床研究中，女性心脏病发作时典型胸痛症状发生率仅为 30%，而男性为 60%。女性冠心病患者中，微血管性心绞痛更为多见。

3. 预后情况

女性心血管疾病患者的总体预后较男性差，尤其是在急性心肌梗死等严重心血管事件后，女性的死亡率更高。随访结果显示，女性急性心肌梗死 1 年内死亡率为 15%，而男性为 10%。

四、结论

女性心脏健康受多种独特因素影响，绝经导致的激素水平变化显著增加心血管疾病风险，不良生活方式、心理压力等在女性心脏健康问题中扮演重要角色。女性心脏病发作症状不典型，预后相对较差。因此，应针对女性特点制定个性化的心脏健康防治策略，包括加强绝经后女性心血管危险因素管理，开展女性心脏健康知识普及教育，提高女性对自身心脏健康的重视，改善生活方式，缓解心理压力等，以降低女性心血管疾病的发生率与死亡率，提升女性心脏健康水平。

护士主导的多学科协作干预对妊娠相关心力衰竭产妇远期心功能及生活质量的影响：一项前瞻性队列研究

马月 田丹 刘华芬

武汉大学人民医院

目的：探讨由心血管专科护士主导、联合产科及心理医师的多学科协作干预模式，对妊娠相关心力衰竭（PPCM）产妇出院后 6 个月内左心室射血分数（LVEF）恢复、再入院率及生活质量的影响，旨在构建适合我国国情的女性心衰患者延续性护理路径，弥补产后心血管健康管理的空白。

方法： 采用前瞻性队列研究设计，纳入 2023 年 1 月 - 2025 年 6 月武汉大学人民医院收治的 PPCM 产妇 126 例。对照组（n=63）接受常规出院指导（口头宣教 + 纸质手册）；干预组（n=63）实施护士主导的多学科协作干预，核心内容包括:

1. 个体化心功能康复方案: 专科护士基于纽约心功能分级制定阶梯式运动处方（如产后 6 周内低强度床上踝泵运动→ 12 周后监护下步行训练）；

2. 药物依从性管理：建立用药电子档案，通过 AI 语音提醒系统联合家庭照护者督导服药，护士每周视频核查药物不良反应；

3. 心理 - 社会支持网络：每月 1 次线上团体认知行为治疗（CBT），由心理医师指导护士实施焦虑抑郁筛查（HADS 量表）及危机干预；

4. 母胎健康整合照护：产科医师协同护士制定哺乳安全方案（如 ACEI 药物使用与母乳喂养的替代策略），提供婴儿喂养支持；

5. 智能预警系统：患者佩戴可穿戴设备（心电贴 + 血压手环），护士通过远程监护平台实时接收异常数据（如 HR>120 次 / 分或 SpO2<90%），48 小时内启动家庭访视。主要终点为干预 6 个月时的 LVEF 变化值; 次要终点包括心衰再入院率、明尼苏达心衰生活质量量表（MLHFQ）评分及 6 分钟步行距离（6MWD）。

结果： 干预 6 个月后，干预组 LVEF 较基线提升幅度显著高于对照组（18.3±6.1% vs. 9.2±5.4%, P<0.001）。干预组再入院率仅为 6.3%（4/63），显著低于对照组的 22.2%（14/63）(RR=0.28, 95%CI: 0.10-0.79)。生活质量方面，干预组 MLHFQ 总分（41.2±7.8 vs. 63.5±9.1, P<0.01） 及 6MWD（412±45m vs. 338±52m, P<0.01）均显著优于对照组。亚组分析显示，LVEF ≤ 30% 的重症患者获益更显著（LVEF 提升差值达 11.7%, P=0.003）。

结论： 以心血管专科护士为协调者的多学科协作干预，可显著改善 PPCM 产妇的心功能恢复进程，降低 33% 的再入院风险，并提升生活质量。该模式通过整合药物精准管理、分级康复训练、心理社会支持及智能预警系统，解决了产后女性心衰患者“治疗中断率高”、“自我管理能力不足”及“育儿负担冲突”三大核心问题，为构建“以护士为主导的女性心血管疾病过渡期护理标准”提供了高级别循证依据，对降低育龄女性心血管事件终身风险具有重大公共卫生意义。

内蒙古某医院女性心脏疾病患者健康状况及影响因素分析

武强 高乐

内蒙古医科大学附属医院

摘要：目的：调查女性患者心脏健康状况，分析影响女性心脏健康的相关因素，为内蒙古地区女性心脏疾病的预防及干预提供建议，为改善女性心脏健康水平提供参考。方法：研究者通过查阅相关文献，根据已有量表内容及女性心脏健康特征，修改完善形成《女性心脏健康状况调查问卷》，包括《一般资料调查表》和《女性心脏健康影响因素量表》，该问卷条目为 35 个。问卷经研究者对 80 名女性患者预调查以及多次咨询专家和反复修改后，检查调查问卷的信度为 Cronbach’s α=0.932，效度为 0.785，满足量表的信效度要求。采用问卷调查结合临床检查数据的方法，对内蒙古某医院心内科及社区卫生服务中心的 200 名女性心脏疾病患者进行调查，收集涵盖血压、血脂等生理指标及日常行为习惯信息，分析符合有效回答的 195 人的健康现状及影响因素。结果：维度标准化得分最高的三个依次是：饮食习惯、运动频率、心理状态。年龄维度和是否绝经维度（P < 0.05）存在差异，具有统计学意义；此外，BMI 指数与心脏功能评分呈显著负相关（r=-0.32，P < 0.01）。结论：生活习惯对女性患者的心脏健康影响较大，不同生理阶段的女性心脏健康管理需差异化实施，通过针对性调整饮食结构、增加运动强度及改善心理状态，可有效提高女性心脏健康水平，为女性心脏疾病的防治工作提供科学依据。

雌激素水平与绝经后女性冠状动脉微血管功能障碍的相关性研究：一项多中心横断面调查

罗婷

武汉市中心医院

目的

探讨绝经后女性雌激素水平与冠状动脉微血管功能障碍（CMD）的关联性，分析性激素替代治疗（HRT）对 CMD 患者的潜在保护作用，为女性特异性心血管疾病防治提供循证依据。

方法

采用多中心横断面研究设计，纳入 2022 年 1 月至 2024 年 6 月就诊的 45-75 岁绝经后女性（n=1500）。通过冠状动脉血流储备（CFR）评估 CMD（CFR<2.5 定义为 CMD 阳性）。测定血清雌二醇（E2）、卵泡刺激素（FSH）水平，收集 HRT 使用情况。采用多因素 logistic 回归分析 CMD 危险因素，通过倾向性评分匹配（PSM）评估 HRT 对 CMD 的影响。

结果

1. CMD 患病率为 32.7%（491/1500），显著高于同龄男性对照（p<0.01）

2. E2 水平与 CFR 呈正相关（r=0.42，p<0.001），FSH 水平与 CFR 呈负相关（r=-0.38，p<0.001）

3. 多因素分析显示：E2<20 pg/mL（OR=2.15，95%CI 1.72-2.69）、FSH>40 IU/L（OR=1.89，95%CI 1.51-2.36）是 CMD 独立预测因子

4. PSM 分析显示: HRT 使用者 CMD 风险降低 37%（OR=0.63，95%CI 0.51-0.78）

结论

绝经后女性雌激素水平下降与 CMD 发生显著相关，HRT 可能具有保护作用。建议将性激素检测纳入女性心血管风险评估体系，为个体化防治提供新靶点。

Prevalence of atrial fibrillation during pregnancy and association with adverse outcomes

liu suxuan, Zhen-Yu Zeng

海军军医大学第一附属医院 (上海长海医院)

BACKGROUND: Pregnancy is associated with physiological changes in the cardiovascular system, including structural and hemodynamic alterations, which might increase the risk of women suffering from AF. AF during pregnancy can result in a high risk of embolic events and hemodynamic instability, and is devastating for maternal and fetal outcomes. Nevertheless, there is a paucity number of studies investigating the prevalence and mortality of AF during pregnancy and puerperium.

OBJECTIVES: We aimed to fill the knowledge gaps by investigating the incidence and outcomes of AF during pregnancy and puerperium. We also assessed the predictive value of the CHA2DS2-VASc score for adverse outcomes in pregnant women with AF.

METHODS: The National Inpatient Sample (NIS) database was queried to identify pregnancy-related hospitalizations from 2008 to 2017. Temporal trends in the incidence and outcomes of AF were extracted. The CHA2DS2-VASc score was calculated for all patients, and the score was classified into three groups: low-risk group (1 point), moderate-risk group (2-3 points), and high-risk group (≥ 4 points).

RESULTS: Among 40,996,860 pregnancy-related hospitalizations, 15,162 (0.037%) were diagnosed with AF. The incidence increased from 2.18 per 10,000 hospitalizations in 2008 to 4.87 per 10,000 in 2017 (Ptrend < 0.001). The proportion of patients with AF increased with advanced maternal age (Ptrend < 0.001). Subgroup analysis showed that the incidence of AF was higher in black women, lowest-income households, and elderly parturients (Ptrend <0.001). The following factors were significantly associated with AF during pregnancy: age ≥ 45 years, lipid metabolism disorders, hypertension, obstructive sleep apnea, hyperthyroidism, and valvular disease (P < 0.001). The in-hospital mortality rate of pregnant women with AF was significantly higher than those without AF (OR = 2.26, 95%CI = 1.75-2.93, P < 0.001). The mortality rate of AF during pregnancy was associated with an increasing CHA2DS2-VASc score (Ptrend < 0.001), which was 0.35% (95% CI: 0.24%-0.47%) in the low-risk group, 1.30% (95% CI: 0.98%-1.62%) in the moderate-risk group, and 2.18% (95% CI: 0.86%-3.51%) in the high-risk group. The incidence of stroke, acute myocardial infarction, acute heart failure, and cardiac shock during pregnancy was also significantly correlated with the increasing CHA2DS2-VASc score in AF patients (Ptrend < 0.001).Additionally, after controlling for all variables, AF was also found to be associated with cardiogenic shock, acute respiratory failure , and acute renal failure during pregnancy-related hospitalizations (all P < 0.001). We also analyzed the impact of AF on the LOS and hospitalization costs. The results indicated that AF led to a 0.79-day (95% CI: 0.70-0.87) increase in the LOS and a $16,679 (95% CI: 16,063-17,294) rise in hospitalization costs. The cost of hospitalization increased by $544 (95% CI: 540-548) with the progress of the year. In contrast, the LOS decreased by 0.02-day (95% CI: 0.02-0.02) (all P < 0.001).

CONCLUSIONS: The incidence of AF during pregnancy and puerperium increased consistently, associated with high maternal mortality. The CHA2DS2-VASc score can be an essential risk stratification tool to predict severe cardio-cerebral vascular events in AF patients during pregnancy and puerperium. Management of maternal patients with high-risk CHA2DS2-VASc stratification should be strengthened in the future.

探究 Ca/Mg 对老年女性急性冠脉综合征患者死亡风险的预测价值的摘要

陈鸿

哈尔滨医科大学第二附属医院

一、**研究目的**

老年女性雌激素减少导致尿镁排泄增加，肠道镁吸收下降，血清镁降低，同时，骨质疏松是老年女性中的常见疾病，因其雌激素缺乏，骨密度下降加速，而充足钙摄入有助于维持骨密度，减少骨丢失。但过量补钙可能干扰正常钙代谢增加心血管健康方面，补钙治疗可能加剧镁缺乏。基础研究显示，Ca^{2+}/Mg^{2+}比值失衡可导致冠状动脉平滑肌细胞异常钙化（通过激活 RUNX2/osterix 通路）和线粒体功能障碍（诱导线粒体通透性转换孔开放），从而加剧心肌缺血损伤。然而，这一生物学机制在临床转化中的价值尚未充分阐明。

本研究旨在探讨入院时血清 Ca^{2+}/Mg^{2+}对老年女性急性冠脉综合征患者死亡风险的预测价值。

二、**研究方法**

本研究基于重症监护医学信息数据库（MIMIC-IV），同时为了增加可行性和准确性纳入了哈尔滨医科大学附属第二医院随访中心的数据，回顾性分析诊断 ACS 的患者。收集患者入院时的血清 Ca 及 Mg 水平、年龄、性别、合并症及实验室指标。通过多因素 Cox 比例风险回归模型和 Kaplan-Meier（K-M）生存曲线评估血清 Ca^{2+}/Mg^{2+}水平与老年女性 ACS 患者院内死亡率的关联。此外，进行亚组分析用于验证结果的稳健性。

三、**预期研究结果**

入院时高血清 Ca^{2+}/Mg^{2+}水平的老年女性急性冠脉综合征患者入院生存率较低。

四、**研究结论**

1. 理论价值

本研究揭示 Ca^{2+}/Mg^{2+}失衡在女性心血管衰老中的特异性通路

2. 临床应用

找老年女性合适的钙镁比值从而指导临床减少事件的发生

叙事护理干预对女性心脏健康患者心理及生理康复效果的研究

欧阳惠紫 刘华芬

武汉大学人民医院

摘要

目的

探讨叙事护理在改善女性心脏疾病患者心理健康、治疗依从性及生理指标中的作用，为女性心脏健康管理提供创新性干预策略。

方法

采用混合研究方法，选取 2024 年 1 月–6 月本院心脏特需医疗科收治的 62 例女性心脏疾病患者（年龄 60–75 岁），随机分为干预组（n=31）与对照组（n=31）。对照组接受常规心脏康复护理，干预组在此基础上实施结构化叙事护理干预，包括：

1. 外化对话技术：引导患者分离疾病与自我身份（如“冠心病不是您的全部”）；

2. 生命意义重构：通过回顾人生经历（如职业成就、家庭角色）重建价值感；

3. 艺术表达干预：借助绘画、日记等媒介疏导情绪；

4. 家庭支持系统激活：邀请家属参与叙事过程。

干预周期为 4 周，采用医院焦虑抑郁量表（HADS）、Morisky 用药依从性量表、血压监测及心功能分级评估效果。

结果

1. 心理指标：干预组焦虑抑郁评分显著低于对照组（HADS 总分：9.2±2.1 vs. 14.6±3.4, P<0.01）；

2. 治疗依从性：干预组用药依从率提升至 93.5%（对照组为 74.2%, P<0.05）；

3. 生理改善：干预组血压控制达标率（≤ 140/90 mmHg）达 87.1%（对照组 64.5%），心功能改善率（NYHA 分级提升 Ⅰ 级）为 68.8%（对照组 41.9%, P<0.01）；

质性反馈：患者普遍反馈“被倾听感增强”“重新找到生活意义”。

结论

叙事护理通过心理赋权与意义重构，有效缓解女性心脏疾病患者的孤独感与疾病恐惧，显著提升治疗依从性及生理康复效果。其核心在于将“疾病为中心”转向“全人关怀”，建议将叙事技术整合为女性心脏健康管理的标准化干预模块。

综合护理干预对女性冠心病患者康复效果及生活质量的影响研究

向秋野 刘华芬

武汉大学人民医院

目的：女性冠心病（CHD）具有独特的病理生理特点、临床表现及预后影响因素。本研究旨在探讨基于女性特点设计的综合护理干预方案对女性 CHD 患者心脏康复效果、危险因素控制、自我管理能力及生活质量的影响，为优化女性心血管疾病护理实践提供循证依据。

方法：采用随机对照试验（RCT）设计。于 2025 年 1 月至 2025 年 6 月，便利抽取我院心内科住院确诊为 CHD 的女性患者 200 例。采用随机数字表法分为干预组（n=100）和对照组（n=100）。对照组接受常规 CHD 治疗护理及出院指导。干预组在常规护理基础上，实施为期 6 个月的综合护理干预，方案包括：1) 结构化健康教育： 聚焦女性 CHD 风险特点（如更年期影响、微血管心绞痛、心理社会压力）、症状识别、药物依从性（强调阿司匹林、他汀、β 受体阻滞剂等的重要性及注意事项）；2) 个性化运动处方：结合心肺功能评估，制定并督导以有氧运动为主、兼顾柔韧性的家庭运动计划；3) 营养管理： 由营养师参与制定个体化膳食方案，重点控制盐、脂、糖摄入，强调富含植物雌激素食物的益处；4) 心理社会支持： 提供压力管理技巧训练（如放松疗法、正念）、情绪疏导及家庭 / 社会支持资源链接；5) 延续性护理：出院后通过电话随访（每周 1 次，持续 1 月，后每月 1 次）、移动健康 APP（推送知识、提醒用药运动、在线答疑）进行持续支持与监测。于干预前（基线）、干预 3 个月末、干预 6 个月末，评估两组患者的左心室射血分数（LVEF）、血脂水平（总胆固醇 TC、低密度脂蛋白胆固醇 LDL-C、高密度脂蛋白胆固醇 HDL-C、甘油三酯 TG）、血压达标率、西雅图心绞痛问卷（SAQ）评分（评估心绞痛稳定性、发作频率、治疗满意度、疾病认知、活动受限度）、自我管理行为量表得分、焦虑抑郁量表（HADS）评分

及 6 个月内因心血管原因再入院率。采用 SPSS 25.0 软件进行数据分析，计量资料采用均数 ± 标准差表示，组间比较采用独立样本 t 检验或重复测量方差分析；计数资料采用率表示，组间比较采用卡方检验或 Fisher 精确概率法。以 P<0.05 为差异有统计学意义。

结果： 心脏功能与危险因素：干预 6 个月后，干预组 LVEF 显著高于对照组((55.2±6.8)% vs. (51.7±7.1)%, P<0.01)，TC、LDL-C、TG 水平显著低于对照组(均 P<0.05)，血压达标率显著高于对照组（78% vs. 62%, P<0.05）。生活质量与心理状态： 干预组 SAQ 各维度评分（尤其活动受限度和心绞痛稳定性）及总分均显著优于对照组（均 P<0.01）。干预组焦虑、抑郁评分显著低于对照组（均 P<0.05）。自我管理能力：干预组在规律用药、合理饮食、坚持运动、症状监测、定期复诊等维度的自我管理行为得分显著高于对照组（均 P<0.01）。临床结局：干预组 6 个月内因心血管原因再入院率显著低于对照组（10% vs. 23%, P<0.01）。

结论：针对女性 CHD 患者特点设计的综合护理干预方案，能有效改善患者的心功能，促进血脂、血压等危险因素达标，显著提升患者的自我管理能力，减轻焦虑抑郁情绪，从而全面改善其生活质量，并有效降低短期再入院风险。该研究结果支持将性别敏感的、多维度整合的护理模式。

拉贝洛尔与硝苯地平治疗产前非重症高血压的疗效比较：一项模拟目标试验

李远翥 吕籽 黄毕 罗素新

重庆医科大学附属第一医院

背景

妊娠期高血压疾病（HDP）影响全球 2-10% 的妊娠，对孕产妇及围产儿构成显著风险。产前高血压作为 HDP 的核心表现，需通过有效血压控制预防严重并发症。虽然口服拉贝洛尔和硝苯地平均为指南推荐的一线治疗药物，但二者在非重度产前高血压中的直接疗效对比数据极为匮乏——这主要源于妊娠期临床试验的实施挑战。现有研究多聚焦静脉给药等紧急治疗方案。鉴于缺乏高质量比较证据，本研究旨在比较口服拉贝洛尔与硝苯地平对非重度产前高血压患者的血压控制效果。

方法

基于重庆 7 家医院 70,486 例妊娠住院患者的 ICD 编码数据，筛选出符合标准的 946 例非重度产前高血压患者。所有患者在确诊后均接受硝苯地平或拉贝洛尔单药治疗。我们采用观察性数据模拟目标试验设计，应用**逆概率删失加权法（IPCW）**平衡基线协变量（包括高血压病程、年龄、产次、慢性高血压 / 子痫前期病史、糖尿病、收缩压 / 舒张压峰值、孕周及阿司匹林使用情况）。

主要结局指标为进展至需静脉给药治疗的**高血压急症**。次要结局涵盖母体并发症（如子痫、HELLP 综合征、心力衰竭、胎盘早剥及全因死亡）。安全性结局评估胎儿 / 新生儿结局（全因胎儿死亡、胎儿生长受限、1 分钟 Apgar 评分 <7 分）。随访期自治疗启动持续至结局事件发生、分娩、死亡、失访或 2024 年 5 月 31 日。

主要分析采用 **IPTW 加权合并 Logistic 回归模型**，通过含节点限制性立方样条函数及治疗 - 时间交互项灵活估计时变效应。使用加权 Cox 比例风险模型计算风险比（HR），并验证比例风险假设。敏感性分析包括 E 值计算和多变量 Cox 亚组分析以评估结果稳健性。

结果

随访结束时，拉贝洛尔组（n=308）主要结局事件发生率为 5.2%（16 例），硝苯地平组（n=638）为 10.3%（66 例）。经逆概率删失加权后，所有基线协变量均衡良好（标准化差异 <0.1）。加权回归模型显示，硝苯地平组发生高血压急症的风险显著高于拉贝洛尔组（**HR=2.99, 95%CI:2.58-3.40; P=0.01**）。两组次要母体结局（HR=0.99; P=0.94）及安全性终点（HR=1.55; P=0.06）无统计学差异。主要结局的 **E 值 =3.12**，超过已知混杂因素的风险比，佐证了结果的稳健性。不同患者特征（年龄、产次、合并症）的亚组分析均显示一致的治疗效应（交互作用 P 值 >0.05）。

结论

在非重度产前高血压患者中，与硝苯地平相比，**拉贝洛尔可显著降低高血压急症风险，且不增加母胎安全性风险。**

中国 Takotsubo 综合症患者的临床特征、性别差异及预后因素分析

段弘毅 [1] 吕玲春 [2] 林小平 [3] 江洪 [1] 胡丹 [1]

1. 武汉大学人民医院心内科

2. 浙江大学丽水医院心血管内科

3. 浙江大学医学院附属第二医院心血管内科

目的： Takotsubo 综合症（Takotsubo Syndrome, TTS）被认为是一种以女性为主的短暂性急性心力衰竭综合症。然而，关于中国 TTS 患者的相关数据较为有限。因此，本研究旨在探讨中国 TTS 患者的临床特征和性别差异，并识别其预后标志物。

方法： 本研究纳入了 258 例 TTS 患者，收集并分析了患者的临床特征及住院期间主要不良心血管事件（Major Adverse Cardiovascular Events, MACE）的数据，MACE 包括严重心力衰竭、休克、恶性心律失常和死亡。

结果： TTS 患者的平均年龄为 59.3±19.2 岁，女性患者占 68.9%。住院期间，41.4% 的患者发生了 MACE。与男性患者相比，女性 TTS 患者年龄较大，情感诱因较多，典型的心尖气球样变型比例较高，左室射血分数（Left Ventricular Ejection Fraction, LVEF）较高，QTc 延长，早期复极（Early Repolarization, ER）模式较少，且 MACE 发生率较低（35.6% vs. 53.8%，P=0.006）。与有情感诱因的女性患者相比，具有生理诱因的女性患者较年轻，胸痛及异常心电图的比例较低，但更容易发生 MACE。生理诱因、CKMB、LVEF、非心尖气球样变型、ER 模式及室性早搏是住院期 MACE 的独立预测因子，年龄、生理诱因及血小板计数是女性 TTS 患者特有的独立预测因子。

结论： 中国 TTS 患者具有独特的临床特征及住院期结局。除了已知男性 TTS 患者具有较高的风险表型外，本研究新发现，年轻或有生理诱因的女性 TTS 患者预后较差，值得特别关注和随访。

关键词： Takotsubo 综合症，女性，心力衰竭，心律失常

心理行为干预对绝经后女性冠心病患者焦虑抑郁症状的影响质性研究

任慧

北京友谊医院

目的：女性心血管疾病死亡率已连续多年超过肿瘤成为首要死因，但社会认知仍普遍滞后于现实需求，从妊娠期高血压到更年期血脂异常，从心梗症状的性别差异到激素变化对血管的隐形损伤，女性心血管健康始终贯穿生命周期的关键环节，尤其是妊娠相关疾病如子痫前期患者未来十年内心血管事件风险激增 3-5 倍，而绝经后雌激素水平断崖式下降直接导致内皮功能紊乱和动脉硬化加速，这些独特的生理特点使女性心血管风险呈现"隐匿性强、症状不典型、预后更差"的鲜明特征; 研究绝经后女性冠心病患者不良情绪的变化，通过积极的干预手段，引导患者转变观念。

方法：本研究采用混合研究方法，通过质性访谈的方式，探讨绝经后女性冠心病患者不良情绪的变化规律及积极干预手段的效果。在研究设计上，选取某三甲医院心内科住院患者 30 例绝经后冠心病患者（年龄 45-65 岁，确诊冠心病≥ 3 个月），采用随机数字表法分为干预组（15 例）与对照组（15 例）。对照组接受常规心内科护理（包括用药指导、饮食运动宣教），干预组在此基础上实施为期 8 周的综合性心理行为干预方案，具体内容包含：① 认知重构：通过小组课程（每周 1 次，每次 90 分钟）讲解冠心病与绝经激素变化的关联，结合案例分析纠正"情绪问题无关紧要""忍耐是美德"等错误观念；② 情绪管理技能训练：采用正念减压疗法（MBSR），指导患者每日进行 10 分钟呼吸冥想和身体扫描练习，帮助识别并接纳焦虑 / 抑郁情绪；③ 社会支持强化：建立"同伴支持小组"，鼓励患者分享抗病经验，并由家属参与每月 1 次的家庭沟通工作坊，改善家庭支持氛围。

结果：干预组在情绪改善及疾病管理效能上显著优于对照组。质性访谈提炼出三大核心主题："从'忍耐情绪'到'主动调节'的认知转变"（如患者提及"以前觉得生气只能憋着，现在学会用深呼吸'叫停'坏情绪"）、"疾病管理从'被动服从'到'主动参与'的态度转化"(如"现在会主动记录情绪日记,发现焦虑时心跳确实更快")、"家庭支持从'单向依赖'到'双向互动'的关系重构"（如家属反馈"现在更愿意听她倾诉胸口闷的感觉，而不是只催她吃药"）。

结论：本研究证实，针对绝经后女性冠心病患者的综合性心理行为干预，可通过改变认知模式、提升情绪管理能力及强化社会支持网络，显著缓解焦虑抑郁情绪并改善生理指标，为临床实践提供了可推广的"心理 - 生理协同干预"模式。未来需进一步扩大样本量并延长随访周期，验证长期效果及成本效益。

特发性肺动脉扩张进展至肺动脉瘤 1 例及 7 年随访并文献回顾

刘娜 [1,2,3,4] 顾晴 [1,2,3,4] 伏蕊 [1,2,3,4] 李鹏锐 [1,2,3,4] 杨玉册 [1,2,3,4] 安宣齐 [1,2,3,4] 杨伟宪 [1,2,3,4]

1. 中国医学科学院北京协和医学院

2. 国家心血管病中心

3. 中国医学科学院阜外医院

4. 急重症医学中心

目的： 特发性肺动脉扩张与肺动脉瘤的疾病进程罕有报道。本文报道 1 例特发性肺动脉扩张进展为肺动脉瘤的女性患者，并长期随访，分析其诊断、病情进展特征、治疗及预后，为临床提供更多研究依据。

方法： 系统收集 1 例女性患者自 2008 年发现肺动脉主干扩张、2018 年诊为特发性肺动脉瘤及 2025 年随访的临床症状体征、实验室检查及影像学资料，长期动态随访监测瘤体直径及病情进展，并结合相关文献进行综合分析。

结果： 患者女性，60 岁，2008 年 12 月于外院体检发现超声心动图显示肺动脉主干瘤样扩张（直径 37.3mm），左肺动脉内径 22.1mm，右肺动脉内径 16.9mm，右心室前后径 19mm。无临床症状。既往无感染、风湿免疫疾病、肺动脉高压、先天性心脏病病史。2018 年 12 月因间断胸闷、胸痛就诊于我院。查体胸骨两侧第二肋间可闻及收缩期杂音，NT-pro BNP 73pg/ml，查风湿免疫指标、梅毒抗体阴性，超声心动图显示肺动脉主干远端融合部约 50mm，右心室前后径 19mm，三尖瓣反流速度 0.6m/s，TAPSE 正常。肺动脉 CT 提示主肺动脉直径 50mm（同水平升主动脉直径 35mm），左肺动脉干扩张，直径 28mm，管壁少量钙化。右肺动脉干远段相对偏细，直径 13mm。诊断为特发性肺动脉瘤。2025 年 7 月因"气短、胸闷加重，活动耐量明显下降"第二次我院就诊，NT-proBNP 154pg/ml，肺动脉 CT：主肺动脉瘤体直径 57mm。左肺动脉干内径增长至 28mm，右肺动脉内径无明显变化。超声心动图示三尖瓣反流速度在 0.4m/s，TAPSE 正常，LVEF 66%，右心室内径增长至 26mm。该患者 17 年期间主肺动脉直径共增长约 20mm，平均每年增长约 1.1mm。经多学科团队会诊，因瘤体巨大（≥ 55mm）且症状明显加重，存在明确的手术指征，决定手术治疗。

结论： 本文首次报道 1 例由特发性肺动脉扩张进展至特发性肺动脉瘤的女性患者，瘤体逐年扩张进展。肺动脉扩张阶段无临床表现，肺动脉瘤阶段出现活动后胸闷，逐渐加重。故此类患者应定期随访观察病情变化，采取影像学手段定期监测肺动脉，并根据病情变化综合评估手术指征，以降低可能的破裂及猝死风险。

介入心脏病学研究

达格列净对合并糖尿病的慢性冠脉综合征拟择期 PCI 患者围术期心肾损伤保护作用的研究

郑耐心

北京医院

目的：本研究旨在探讨达格列净是否对合并糖尿病的慢性冠状动脉综合征（CCS）拟择期接受经皮冠状动脉介入治疗（PCI）患者围术期心肌损伤（PMI）和心肌梗死（type 4aMI）具有保护作用，为临床实践提供可靠的循证依据。

对象与方法：连续纳入符合入选标准的 352 例患者，收集患者的基线人口学资料、病史、诊疗及用药情况、术前和术后的心肌损伤标志物、心电图和超声心动图结果，并对患者进行 PCI 术后≥ 6 个月的随访观察。根据患者术前是否规律服用达格列净，将患者分为研究组（术前至少 7 天规律口服达格列净 10 mg 每日 1 次）和对照组（术前至少 7 天未服用任何类型的 SGLT2 抑制剂），比较两组患者 PCI 术后严重 PMI 和 4aMI 事件的发生率，并通过门诊或电话随访，主要随访心血管不良事件（MACE），包括全因死亡、心血管死亡、心肌梗死和再次血运重建的发生情况，评估达格列净在预防择期 PCI 围术期心肌损伤 / 心肌梗死中的临床效果。

结果：分析显示，服用达格列净的研究组患者围术期严重 PMI 和 4aMI 的发生率显著低于对照组。PCI 术后估计肾小球滤过率的降低程度研究组也显著低于对照组，但两组间造影剂急性肾损伤事件的发生率未见显著差异（P > 0.05）。经平均 42.7 周随访，达格列净组显著降低 MACE 风险，且多支血管病变、大量使用造影剂和使用 DPP4i/GLP-1RA 亚组获益更显著。达格列净组显著减少因血运重建再入院风险，在多支血管病变及对比剂用量≥ 200 mL 亚组效果更突出。

结论：对于合并 2 型糖尿病的 CCS 拟择期 PCI 治疗的患者，术前至少 7 天规律服用达格列净 10 mg 每日 1 次并持续至术后长期，能够显著降低围术期心肌损伤和心肌梗死事件的发生风险，减少主要心血管不良事件（MACE）的发生，且安全性良好。其心脏保护作用可能与达格列净减轻炎症反应、改善氧化应激状态等机制有关。

冠心病介入诊疗术后病人血管并发症成因与护理干预

杨丽丽

陆军特色医学中心

目的：探究冠心病介入诊疗术后病人血管并发症发生原因以及护理对策，分析针对性护理模式在冠心病介入诊疗术患者中的应用价值。

方法：以本院收治的 80 例介入诊疗术患者作为研究对象，研究时间段为：2019 年 5 月 ~2020 年 5 月，将这 80 例冠心病患者以简单随机法分为：对照组、观察组，对照组给予常规护理，观察组实施针对性护理，对比 2 组患者临床疗效、并发症发生率。结果：观察组患者临床疗效明显高于对照组，患者并发症发生率低于对照组，差异性比较：P < 0.05，另外观察组患者并发症发生率小于对照组：P < 0.05。结论：对冠心病患者在介入的诊断治疗中展开针对性护理，能够明显提高患者治疗效果，并减少并发症的发生，对患者治疗具有积极意义。

结论：由上所述，对冠心病介入诊疗术患者实施针对性护理服务能够有效降对血肿部位进行按压，尽快对患者血肿处进行按压。指导患者进行 B 超检查，观察患者有无假性的动脉血管瘤发生，对直径较小患者无需处理， 对直径较大患者则使用超声压迫处理 ，护理人员需要深入了解血管并发症发生原因并进行分析，了解以后保证手术准备工作更加充分，并在患者术后及时采取针对性护理措施，积极降低患者并发症发生率，提升患者康复效果。

急性 ST 段抬高型心肌梗死 PCI 术后对比剂脑病一例

俊

马鞍山市人民医院

【摘要】对比剂脑病（contrast-induced encephalopathy，CIE）是血管内使用对比剂后发生的一种少见的神经系统并发症，因其临床表现缺乏特异性，易被忽视。近年来，随着不同学科介入诊疗技术的广泛开展，关于 CIE 的报道逐年增加，但关于急性 ST 段抬高型心肌梗死经皮冠状动脉介入治疗（percutaneous coronary intervention，PCI）术后出现 CIE 实为罕见。该文报告一例急性 ST 段抬高型心肌梗死 PCI 术后出现 CIE，并分析其临床表现、诊断及鉴别诊断依据及治疗方案，以期为临床诊治类似病例提供参考。

【摘要】对比剂脑病（contrast-induced encephalopathy，CIE）是血管内使用对比剂后发生的一种少见的神经系统并发症，因其临床表现缺乏特异性，易被忽视。近年来，随着不同学科介入诊疗技术的广泛开展，关于 CIE 的报道逐年增加，但关于急性 ST 段抬高型心肌梗死经皮冠状动脉介入治疗（percutaneous coronary intervention，PCI）术后出现 CIE 实为罕见。该文报告一例急性 ST 段抬高型心肌梗死 PCI 术后出现 CIE，并分析其临床表现、诊断及鉴别诊断依据及治疗方案，以期为临床诊治类似病例提供参考。

整合应激反应通过 ATF4-FKBP11 轴诱导活性氧促进主动脉夹层的机制研究

刘紫轩 [1,2] 蒋宏程 [1,2] 王洪杰 [1,2] 曾和松 [1,2]

1. 华中科技大学同济医学院附属同济医院

2. 血管介入治疗湖北省工程研究中心

目的：主动脉夹层（Aortic Dissection，AD）是一种致命的心血管疾病，目前缺乏特异性治疗药物靶点。本研究旨在探究整合应激反应（Integrated Stress Response，ISR）及其下游效应分子在 AD 进展过程中所发挥的作用。

方法：本研究建立了 β⃞ 氨基丙腈（BAPN）诱导的小鼠 AD 模型。采用 HE 染色，EVG 染色和免疫组织化学染色评估主动脉中膜的破坏情况以及收缩型血管平滑肌细胞（Vascular Smooth Muscle Cells，VSMCs）的缺失情况。为明确抑制整合应激反应的潜在治疗效果，对 BAPN 诱导的 AD 小鼠通过灌胃给予 ISR 抑制剂 GSK2656157。运用免疫荧光、蛋白质免疫印迹法以及 DHE 染色检测细胞质中活性氧（Reactive Oxygen Species，ROS）的积累。通过生物信息学筛选潜在的 ISR 下游靶点，并在体内外利用实时荧光定量聚合酶链反应（Quantitative Real-time PCR，qPCR）和免疫组织化学染色（Immunohistochemistry，IHC）进一步验证。采用双荧光素酶报告基因实验阐述经典 ISR 效应因子激活转录因子 4（Activating Transcription Factor-4，ATF4）对 FK506 结合蛋白 11（FK506-binding Protein 11，FKBP11）转录的转录调控作用。利用 FKBP11 全身性基因敲除鼠构建 AD 小鼠模型进行功能分析，阐明 FKBP11 对 AD 形成的促进作用。

结果：AD 主动脉组织中，蛋白激酶 R 样内质网激酶（PKR-like endoplasmic reticulum resident kinase，PERK）、通用控制非抑制性 2（General control nonderepressible 2，GCN2）、双链 RNA 激活的蛋白激酶（Interferon-induced double-stranded RNA-dependent eIF2αkinase，PKR）的信使核糖核酸（Messenger RNA，mRNA）和蛋白水平均显著升高。更重要的是，ISR 的主要效应因子 ATF4 在 AD 小鼠主动脉中的表达显著增加，且主要定位于血管平滑肌细胞。给予 ISR 抑制剂可显著降低 AD 的发病率和死亡率。生物信息学结合实验验证表明，FKBP11 是 ISR-ATF4 信号通路的关键下游靶点之一。从机制上讲，ATF4 作为转录因子与 FKBP11 的启动子区域结合，从而调节其转录。此外，FKBP11 基因敲除可改善 VSMCs 中活性氧的积累，抑制 VSMCs 凋亡并改善中膜破坏，最终缓解小鼠 AD 的进展。

结论：在 AD 主动脉的 VSMCs 中，ISR 相关信号通路显著激活。药物抑制 ISR 或基因敲除 FKBP11 可显著减轻 AD 进展，这为 AD 的治疗提供了潜在的应用方向。

预见性护理模式下责任制护理在 TAVI 患者围手术期护理中的应用效果

贺麟惠

陆军特色医学中心

目的：TAVI 手术为近年来国内开展的新技术，一种针对高龄、高风险患者的微创主动脉瓣替代方法，术后的护理与一般心外科术后护理有相近之处，目前施行 TAVI 的患者都为高危患者，合并多种疾病且其平均年龄大，功能极差，应激能力下降，术前难以准确评估全身器官功能，病情变化迅速难以逆转。预见性护理是优质护理的重要分支之一，其通过治疗前对患者个体情况全面综合分析，预判可能出现的异常情况，从而制定针对性的护理对策，防止大概率不良事件的生，提高护理质量。 方法：通过选取所在科室行 TAVI 治疗的患者作为研究对象，按入院时间分为对照组与观察组。对照组予以常规性护理，观察组在常规性护理基础上加预见性护理，对比两组护理效果。结果显示：较常规护理，实施预见性护理的患者在应激反应指标水平稳定控制、负性情绪改善及身心不良反应控制方面均有明显的优势。预见性护理的基础是术前对患者的病情、生理指标、心理状况等进行充分详细的了解，预判可能出现的身心不良反应，制定针对这些不良反应出现的护理干预措施，降低患者围手术期身心不良反应率。结论：预见性护理模式下责任制护理在 TAVI 患者围手术期护理能提升患者护理满意度、认知度、配合度，降低并发症发生率，改善患者不良情绪，值得临床推广应用。

共享决策在心脏介入术中的研究现状

林玲

重庆医科大学附属第一医院

目的：本文旨在综述共享决策（SDM）在心脏介入领域的研究现状与应用价值，分析其具体应用场景、实施策略以及当前实践中面临的挑战，从而推动 SDM 模式在心脏介入治疗中的有效应用。

方法： 通过系统梳理国内外相关文献与临床指南，对 SDM 在心脏介入术中的理论定义、核心价值进行阐述；重点归纳 SDM 在冠状动脉介入治疗、心律失常介入治疗以及结构性心脏病介入治疗等关键场景的应用情况；总结当前主要的 SDM 实施策略；分析 SDM 实践中存在的挑战。

结果： 研究表明，SDM 在心脏介入领域能够有效提高患者满意度、治疗依从性、风险认知与知识水平，减少决策冲突与后悔，并有助于优化临床结局和资源利用。多种策略被证实有效，如组建多学科心脏团队、应用 PtDA 以及探索 AI 辅助决策等。然而，SDM 实践面临来自医务人员、患者、实践过程三方面的挑战。

结论： 尽管 SDM 在优化心脏介入治疗决策、改善患者体验和结局方面具有明确价值，但其系统化实践仍处于探索阶段，尤其在面临文化适应、政策支持、教育培训、服务体系构建等多重挑战的中国情境下。未来亟需构建符合本土医疗生态的 SDM 实施框架，包括强化认知与能力建设、完善政策制度支持、开发文化适配性工具、推广多学科协作、建立动态评估体系，以系统性突破壁垒，最终实现以患者为中心的精准决策目标。

零造影剂冠状动脉介入术后急性肾损伤（ZICE-AKI）研究 ——随机对照试验研究设计

陈再燕 毛琦 解力 肖寒 马弋力 赵茂宇 崔斌 王珂 李佑美 王英民 邱友竹 夏屿欧 晋军 聂凌 赵晓辉

陆军军医大学第二附属医院新桥医院

目的

造影剂诱导的急性肾损伤（CI-AKI）一直是冠状动脉介入手术中备受关注的问题，但其与造影剂的直接关联性问题仍未得到充分证实。究其原因是因为既往临床试验都缺乏不使用造影剂的空白对照组，因此，无法获得造影剂导致急性肾损伤的直接循证医学证据。本研究拟通过随机对照试验的设计，旨在阐明中重度慢性肾脏病患者造影剂使用与否与冠状动脉介入术后急性肾损伤(AKI)之间的因果关系。

方法

零造影剂冠状动脉介入术（ZICE-AKI）试验是一项由研究者发起的多中心、平行组、前瞻性、随机对照、开放标签试验。该试验计划在陆军军医大学第二附属医院及国内多家三级甲等医院开展，拟招募 266 例受试者，分为试验组和对照组，每组各 133 例，各中心样本量通过竞争方式确定。研究将纳入基线估算肾小球滤过率（eGFR）处于 15 至 59 ml/min/1.73 m² 区间、且计划接受冠状动脉介入手术的患者。入组的患者，将依据 eGFR ，分为 45~59 ml/min/1.73 m² 和 15~44 ml/min/1.73 m² 两个层级。通过中央随机系统以 1:1 的比例，随机分配至造影剂组或零造影剂组。零造影剂组将运用血管内超声（IVUS）联合冠状动脉血流储备分数技术实施介入手术。本试验的主要研究终点为对比两组患者术后 AKI 的发生率差异，目前已在中国临床试验注册中心（www.chictr.org.cn）完成注册，注册号为 ChiCTR2500099095。

结果

在国内计划开展研究的多个中心中，目前已有 3 家通过医学伦理委员会审批，其中 1 家已启动受试者招募工作。首例受试者于 2025 年 5 月 7 日正式入组，截至 2025 年 7 月 12 日，研究累计入组 38 例，目前有 1 例受试者出现 AKI。

结论

ZICE-AKI 试验将为阐明造影剂与冠状动脉介入术后 AKI 之间的关系提供高质量证据。此项研究有望解决介入心脏病学领域的关键争议——造影剂究竟是独立引发肾损伤的“元凶”，还是作为 AKI 的高危因素之一。

Machine Learning-Based Prediction of Myocardial Ischemia/Reperfusion Injury in Acute Myocardial Infarction Patients Following Emergency Percutaneous Coronary Intervention

Lang Zeng

the Affiliated Hospital of North Sichuan Medical College

Lang Zeng[1]*, Shikang Li[1]*, Yonghong Zhang[1]*, Xue Mei[2], Ofe Eugene Kwaku MD[1], Fenglin Wu[1], Jing Luo[1], Yijuan Huang[1], Xuefeng Ding[3], Peng Zhou[4], Lijuan Xiong[4], Rongchuan Yue[1,4#]

1. Department of Cardiology, Affiliated Hospital of North Sichuan Medical College, Nanchong 637000, P.R. China.

2. School of Pharmacy, Institute of Material Medica, North Sichuan Medical College, Sichuan Nanchong 637000, China.

3. Department of Critical Care Medicine, Affiliated Hospital of North Sichuan Medical College, Nanchong 637000, P. R. China

4. Department of Cardiology, People’s Hospital of Guang ‘an District, Guang ‘an 638550, China

*Lang Zeng, Shikang Li and Yonghong Zhang contributed equally to this work.

#Correspondence to: Rongchuan Yue, MD, PhD, Department of Cardiology, Affiliated Hospital of North Sichuan Medical College, No. 63, Wenhua Road, Nanchong 637000, Sichuan Province, P.R. China; Department of Cardiology, People’s Hospital of Guang ‘an District, Guang ‘an 638550, Sichuan Province, P.R. China. E-mail yyc@nsmc.edu.cn.

Abstract

Objective: To develop and validate a machine learning (ML)-based predictive model for the risk of myocardial ischemia/reperfusion injury (MIRI) in patients with acute myocardial infarction(AMI) following emergency percutaneous coronary intervention (PCI).

Methods: A retrospective cohort study was conducted, analyzing 396 AMI patients aged 40-65 years who received emergency PCI treatment at the Affiliated Hospital of North Sichuan Medical College between January 1, 2021, and February 28, 2023. Patients were randomly divided into training (70%; n=277) and validation sets (30%; n=119). Univariate and multivariate logistic regression analyses were used to identify independent predictors of MIRI post-PCI. Five ML models (Logistic Regression [LR], Naive Bayesian [NB], Decision Tree [DT], Multilayer Perceptron [MLP], and Support Vector Machine [SVM]) were constructed using these predictors. Model performance was evaluated using the area under the receiver operating characteristic curve (AUC), sensitivity, specificity, positive predictive value (PPV), negative predictive value (NPV), precision, accuracy, recall, and F1 Score. Finally, the optimal model was selected, and a nomogram was established to visually represent its clinical effectiveness. Calibration curves and decision curve analysis (DCA) assessed model calibration and clinical practical value, while, the Shapley Additive Explanations (SHAP) interpreted the best-performing model.

Results: Among 396 patients, the incidence of MIRI was 25%. Six variables including left ventricular ejection fraction (LVEF), neutrophil-to-lymphocyte ratio (NLR), platelet-to-lymphocyte ratio (PLR), cardiac troponin T (cTnT), lactate, and Killip classification were identified as independent predictors of MIRI post-PCI. After 5-fold cross-validation, the AUC values for Logistic Regression (LR), Naive Bayesian (NB), Decision Tree (DT), Multilayer Perceptron (MLP), and Support Vector Machine (SVM) models in the training set were 0.845, 0.818, 0.832, 0.827, and 0.844, respectively. The LR model achieved the highest AUC value, indicating superior predictive performance, whereas the NB model had the lowest AUC value. In the validation set, the LR model maintained optimal performance (AUC=0.838,95%CI:0.7662–0.9102).The nomogram, which incorporated the six identified predictors. The calibration curves showed strong agreement between the predicted and observed outcomes in both the training and validation sets. DCA confirmed the LR model’s clinical utility. SHAP analysis revealed that NLR, lactate, PLR, Killip classification, and cTnT were significant positive contributors to MIRI risk, whereas LVEF was protective.

Conclusion: The LR-based model exhibited the best performance in predicting MIRI post-PCI risk. The developed nomogram provides an intuitive and effective tool for identifying high-risk populations, demonstrating high discriminative power and clinical applicability. This model offers specific predictive value for MIRI risk in AMI patients following emergency PCI.

Keywords: acute myocardial infarction; percutaneous coronary intervention; ischemia/reperfusion injury; machine learning; predictive model.

心肌梗死并心衰患者 PCI 术后院内死亡的机器学习预测模型的构建

吕华胜 芦颜美

新疆医科大学第一附属医院

目的：构建并验证一个基于机器学习的预测模型，用于评估心肌梗死 (MI) 合并心力衰竭 (HF) 患者在经皮冠状动脉介入治疗 (PCI) 后的院内死亡风险。

方法：回顾性分析 2019 年 1 月至 2023 年 1 月在新疆医科大学第一附属医院就诊并接受 PCI 治疗的 MI 合并 HF 患者。收集患者的人口学特征、生命体征、实验室检查、影像学参数以及药物治疗情况，按 7 ： 3 的比例分为训练集和验证集。利用极限梯度提升 (XGBoost) 模型筛选对院内死亡有显著影响的变量，并采用 Shapley 加法解释 (SHAP) 模型评估变量重要性，通过单因素和多因素 Logistic 回归分析构建预测模型。模型性能通过受试者工作特征 (ROC) 曲线、曲线下面积 (AUC)、校准曲线和决策曲线进行评估，最终生成诺莫图用于直观评估风险。

结果：共纳入 1214 例 MI 合并 HF 患者数据，中位年龄为 64 岁，其中院内死亡 90 例，病死率为 7.41%。经过 XGBoost 模型特征选择，最终筛选出 10 个显著变量，包括年龄、肌红蛋白、白蛋白、空腹血糖、N 末端 B 型利钠肽原 (NT-ProBNP)、合并糖尿病、肌酐、胱抑素 -C、降钙素原和射血分数。基于这 10 个变量进一步建立 Logistic 回归模型，最终得出 7 个关键指标：年龄、合并糖尿病、肌酐、空腹血糖、胱抑素 -C、NT-ProBNP 和白蛋白。模型在训练集和验证集的 AUC 分别为 0.869(95% CI:0.84~0.89) 和 0.827(95% CI:0.79~0.85)，显示出较高的预测准确性。校准曲线显示预测概率与实际观察结果一致，决策曲线分析表明在不同决策阈值下，模型均具有较高的净收益。

结论：所构建的基于机器学习和 Logistic 回归的预测模型能够有效评估 MI 合并 HF 患者在 PCI 术后的院内死亡风险，并提供了一种直观的个体化风险评估工具（诺莫图）。该模型可辅助临床早期识别高危患者，优化干预策略，以改善患者预后。

Physiological and Metabolic Predictors of Adverse Outcomes One Year After Coronary Intervention: A Two-Tiered Approach

Yuxiang Chen[1], Jiaxin Zhong[1], Beilei Li[1], Ruijin Hong[1], Hui Chen[1], Yuanming Yan[1], Lianglong Chen[1], Qin Chen[1,2], Yukun Luo[1]

1. Fujian Medical University Union Hospital

2. Dyslipidemia Group, Cardiovascular Disease Branch, Chinese Medical Association

Abstract

Background:

Despite advances in percutaneous coronary intervention (PCI) and secondary prevention strategies, long-term adverse cardiovascular events remain prevalent in patients with coronary artery disease (CAD). Conventional risk models often emphasize anatomical or procedural features, overlooking the functional and metabolic substrates that contribute to disease progression. Quantitative flow ratio (QFR), a non-invasive angiography-derived physiological index, enables assessment of residual coronary ischemia without pressure wires or hyperemia. Meanwhile, the triglyceride-glucose (TyG) index serves as a validated surrogate marker for insulin resistance and atherogenic metabolic dysfunction. Although both markers have been individually associated with adverse cardiovascular outcomes, the clinical utility of integrating coronary physiological status and metabolic profile for long-term risk prediction post-PCI has not been systematically investigated.

This study aimed to evaluate the prognostic significance of three-vessel QFR (3V-QFR) and the TyG index in patients one year after PCI, and to establish a two-tiered risk stratification model that incorporates both residual ischemia and metabolic risk for predicting 4-year major adverse cardiac events (MACEs).

Methods:

We retrospectively enrolled 546 patients who underwent successful PCI at our center and received angiographic follow-up with QFR assessment

approximately one year later. 3V-QFR was calculated as the sum of QFR values in the left anterior descending, left circumflex, and right coronary arteries. The TyG index was computed using the formula: ln[fasting triglycerides (mg/dL) × fasting glucose (mg/dL)/2]. The primary endpoint was a composite of cardiovascular death, myocardial infarction, and ischemia-driven revascularization over a 4-year follow-up period.

Restricted cubic spline (RCS) analysis was employed to determine optimal thresholds for 3V-QFR and TyG. Patients were stratified into four subgroups based on these thresholds. Kaplan–Meier survival analysis and multivariable Cox regression were used to examine associations with outcomes.

Results:

RCS modeling identified a 3V-QFR cutoff of 2.44 and a TyG index cutoff of 8.75. A 3V-QFR <2.44, indicative of residual functional ischemia, was associated with significantly higher 4-year MACEs ($p < 0.001$). In patients with complete revascularization (3V-QFR ≥ 2.44), a TyG index ≥ 8.75 independently predicted increased MACEs (HR = 1.51; 95% CI: 1.04–2.05; $p = 0.022$), mainly driven by ischemia-driven revascularization. However, in patients with 3V-QFR <2.44, the TyG index did not significantly correlate with adverse events ($p > 0.05$), suggesting the predominance of ischemia-related mechanisms in this subgroup.

Subgroup analyses confirmed that the TyG index was only prognostic in the absence of residual ischemia, supporting the hypothesis that metabolic risk becomes clinically relevant once functional revascularization is achieved. Kaplan–Meier curves demonstrated clear separation of event-free survival across the four stratified groups, and calibration plots showed good concordance between predicted and observed event rates.

Conclusions:

Both residual coronary ischemia and metabolic dysfunction independently contribute to long-term cardiovascular risk after PCI. Importantly, the prognostic value of metabolic profiling using the TyG index is modulated by the underlying physiological status of the coronary vasculature. Based on these findings, we propose a novel two-level risk stratification model:

Level 1 – Physiological Assessment: Use 3V-QFR to determine physiological completeness of revascularization. A 3V-QFR <2.44 identifies patients with residual ischemia who may benefit from intensified surveillance or further revascularization.

Level 2 – Metabolic Profiling: In patients with 3V-QFR ≥ 2.44, assess the TyG index to identify high-risk metabolic phenotypes (TyG ≥ 8.75) that may warrant aggressive risk factor modification.

This physiological-metabolic framework may enhance post-PCI risk prediction and guide individualized long-term management strategies.

A Novel Integrated Score Combining Physiological and Metabolic Parameters for Predicting Long-Term Outcomes After Percutaneous Coronary Intervention: Development and Prospective Validation

Yuxiang Chen[1], Jiaxin Zhong[1], Beilei Li[1], Ruijin Hong[1], Hui Chen[1], Yuanming Yan[1], Lianglong Chen[1], Qin Chen[1,2], Yukun Luo[1]

1. Fujian Medical University Union Hospital

2. Dyslipidemia Group, Cardiovascular Disease Branch, Chinese Medical Association

Background:

Accurate risk stratification following percutaneous coronary intervention (PCI) remains a cornerstone of secondary prevention in cardiovascular care. Despite advances in revascularization techniques and pharmacological therapies, a substantial proportion of patients continue to experience major adverse cardiovascular and cerebrovascular events (MACCE) during long-term follow-up. Conventional risk models, predominantly based on anatomical or clinical parameters, often fail to capture the intricate interplay between coronary physiological impairment and systemic metabolic dysfunction—two distinct yet synergistic contributors to atherosclerotic disease progression.

The quantitative flow ratio (QFR), a non-invasive angiography-based surrogate for fractional flow reserve (FFR), allows for functional assessment of coronary lesions without the need for pressure wires or pharmacologic hyperemia. Summing QFR values from the three major epicardial arteries—referred to as three-vessel QFR (3V-QFR)—may offer a comprehensive metric of global coronary physiological burden, which has been increasingly associated with long-term cardiovascular risk. Concurrently, metabolic abnormalities such as insulin resistance, elevated triglycerides, and dyslipidemia have shown prognostic value independent of coronary anatomy. The triglyceride-glucose (TyG) index and the atherogenic index of plasma (AIP) are widely validated markers of metabolic dysfunction; their combination into a composite TyG-AIP index may more robustly reflect systemic vascular injury.

To date, no prognostic tool has simultaneously incorporated 3V-QFR and TyG-AIP into a unified risk stratification framework. This study aimed to develop and externally validate a novel risk score that integrates these physiological and metabolic markers to predict MACCE in patients undergoing PCI.

Methods:

A retrospective derivation cohort of 585 patients (1,755 vessels) who underwent PCI in 2017 was followed for 5 years. The primary endpoint was MACCE, defined as a composite of cardiac death, non-fatal myocardial infarction, ischemia-driven revascularization, and stroke. Physiological status was assessed by 3V-QFR, calculated as the sum of QFR values from the three main coronary arteries. Metabolic status was quantified using the TyG-AIP index, calculated as the product of the TyG index [ln(-fasting triglycerides × glucose / 2)] and the AIP [$\log_{10}$ (TG/HDL-C)].

Cutoff values for 3V-QFR and TyG-AIP were identified using ROC analysis and restricted cubic spline (RCS) modeling. Independent predictors of MACCE were determined by multivariable Cox regression, and a weighted risk score was constructed using the scaled regression coefficients. Optimal stratification thresholds for the composite risk score were determined using RCS modeling and the "surv_cutpoint" function from the R package "survminer", selecting cutpoints that maximally distinguished survival curves. Model performance was assessed using time-dependent ROC curves, Harrell's C-index, calibration plots, and Kaplan–Meier analysis.

External validation was performed in a prospective cohort of 1,573 patients (4,719 vessels) who underwent PCI between January 2021 and September 2022, with a 2-year follow-up. The same analytical approach was applied.

Results:

Cutoff values of <2.74, TyG-AIP ≥ 1.5, and diabetes as independent predictors. A risk score equation was derived based on the scaled beta coefficients: RISK_SCORE = 0.46 × (3V-QFR

Patients were stratified into low- (≤ 0.30), intermediate- (0.30–0.54), and high-risk (>0.54) groups. The model showed good discriminatory ability in the derivation cohort (AUC = 0.714; C-index = 0.692), with time-dependent AUCs of 0.737, 0.694, and 0.708 at 12, 24, and 36 months, respectively. MACCE incidence increased significantly across risk categories (p

In the validation cohort, which had an overall MACCE rate of 12.08%, the model retained robust performance (AUC = 0.691; C-index = 0.666). Compared to the low-risk group, the intermediate- and high-risk groups exhibited significantly higher MACCE risk, with hazard ratios of 2.08 (95% CI: 1.42–3.04) and 3.22 (95% CI: 2.29–4.53), respectively (p

Based on Kaplan–Meier curves, hazard ratios, and current clinical guidelines, the following risk-based management strategies are proposed:

Low-risk (RISK_SCORE ≤ 0.30): No risk factors or only one low-impact factor (diabetes or TyG-AIP ≥ 1.5)

 Recommended management: Annual follow-up + Standard secondary prevention

Intermediate-risk (RISK_SCORE 0.30–0.54): Isolated 3V-QFR

 Recommended management: Follow-up every 6 months + Intensified lipid/glucose monitoring

High-risk (RISK_SCORE >0.54): Presence of 3V-QFR

 Recommended management: Follow-up every 3 months + PCSK9 inhibitors + GLP-1 analogues + Coronary reassessment.

Conclusions:

This study developed and externally validated an integrated risk score incorporating physiological and metabolic parameters for long-term outcome prediction after PCI. The model not only identifies patients at elevated risk but also offers tailored follow-up and treatment strategies based on individual risk profiles. This two-dimensional framework may enhance precision medicine and improve post-PCI management.

Online calculator available at: https://chyx.shinyapps.io/risk_stratification/

集冠状动脉功能学与代谢学指标为一体的新型综合评分用于预测经皮冠状动脉介入术后长期预后：模型建立与前瞻性验证研究

陈于祥 钟嘉鑫 李蓓蕾 洪瑞进 陈卉 颜远铭 陈良龙 陈琴 罗育坤

福建医科大学附属协和医院

目的：

经皮冠状动脉介入治疗（PCI）后如何准确评估患者的长期心血管风险，是心血管疾病二级预防的关键。目前仍有相当比例患者在远期随访中发生主要不良心脑血管事件（MACCE）。现有风险模型多以解剖或临床参数为基础，未能同时整

合冠脉功能状态与代谢异常这两个相互独立但协同作用的病理机制。

定量血流分数（QFR）是一种基于冠脉造影的无创生理指标，可评估冠脉病变的功能严重性。将三条主要冠状动脉的 QFR 值相加，形成三支血管 QFR（3V-QFR），可反映全冠脉的功能负担，具有较高的预后预测价值。另一方面，甘油三酯 - 葡萄糖指数（TyG）及其与动脉粥样硬化指数（AIP）的组合 TyG-AIP 指数，是代谢紊乱和胰岛素抵抗的重要标志，与心血管事件密切相关。

本研究旨在建立并前瞻性验证一个整合 3V-QFR 和 TyG-AIP 的风险评分模型，用于预测 PCI 术后长期 MACCE 风险，并提出基于风险评分的个体化随访与干预建议。

方法：

研究回顾性纳入 2017 年接受 PCI 的 585 例患者随访 5 年。主要终点为 MACCE，包括心源性死亡、非致死性心肌梗死、缺血驱动的血运重建及卒中。TyG-AIP 指数为 TyG 指数与 AIP 的乘积。

使用 ROC 曲线与限制性立方样条（RCS）确定 3V-QFR 与 TyG-AIP 的最佳截断值。通过多因素 Cox 回归识别 MACCE 的独立预测因子，并依据回归系数构建加权风险评分方程。风险分层通过 R 语言 survminer 包的 surv_cutpoint 函数与 RCS 分析确定最佳阈值。模型性能评估包括时间依赖性受试者工作曲线（ROC）曲线、Harrell's C-index、校准图及 Kaplan–Meier 分析。随后在一项 2021 至 2022 年间的前瞻性验证队列（1573 例患者）中开展 2 年随访以进行外部验证。

结果：

根据 RCS 及多因素 Cox 分析显示：3V-QFR <2.74、TyG-AIP ≥ 1.5 及糖尿病为 MACCE 的独立危险因素。据此构建风险评分方程为：

RISK_SCORE = 0.46 ×（3V-QFR <2.74）+ 0.30 ×（糖尿病）+ 0.24 ×（TyG-AIP ≥ 1.5）

患者按评分值分为低危、中危及高危三组。该模型在建模队列中表现良好（AUC = 0.714; C-index = 0.692），12、24、36 个月时的时间依赖性 AUC 分别为 0.737、0.694 与 0.708，MACCE 发生率随风险等级显著递增（p <0.001）。

验证队列中 MACCE 发生率为 12.08%，模型保持稳健性能（AUC = 0.691; C-index = 0.666）。与低危组相比，中危与高危组的 MACCE 风险分别显著升高。校准图显示模型预测与实际发生率高度一致。

根据上述研究成果及当前指南建议，提出如下分层管理策略：

低危：无危险因素或仅存在糖尿病 /TyG-AIP ≥ 1.5 之一

建议：每年随访 + 标准二级预防

中危：仅存在 3V-QFR <2.74 或同时合并糖尿病与 TyG-AIP ≥ 1.5

建议：每 6 个月随访 + 强化血脂与血糖监测

高危：存在 3V-QFR <2.74，且合并糖尿病或 TyG-AIP ≥ 1.5 中至少一项

建议：每 3 个月随访 + 联合使用 PCSK9 抑制剂、GLP-1 受体激动剂 + 冠脉再评估

结论：

本研究建立并前瞻性验证了一个融合冠脉功能与代谢状态的新型风险评分系统，能够有效预测 PCI 术后患者的长期 MACCE 风险。该模型结构简明、预测能力稳定，可辅助个体化随访和治疗策略优化，为实现精准心血管预防提供有力工具。

在线应用地址：https://chyx.shinyapps.io/risk_stratification/。

三尖瓣介入治疗策略：麻醉管理的临床实践视角

林栓同

上海上实东滩疗养院

三尖瓣反流（tricuspid regurgitation, TR），是右心衰竭进展的关键因素，其病因可分为原发性、继发性及心脏植入设备相关性反流。传统外科手术虽为根治手段，但因患者常合并右心室功能储备受损、肺动脉高压及多器官功能障碍，导致高龄与高风险人群手术禁忌率显著升高。经导管三尖瓣置换术（transcatheter tricuspid valve replacement, TTVR）与经导管三尖瓣修复术（transcatheter tricuspid valve repair, TTVr）等经导管三尖瓣介入治疗（transcatheter tricuspid valve intervention, TTVI）技术作为治疗三尖瓣疾病的重要手段，通过微创路径实现解剖矫正，已成为外科禁忌患者的有效替代策略。此类手术麻醉医师需直面三大核心挑战：右心系统对前负荷的敏感性、循环崩溃高风险（尤其功能性 TR 合并右心室失代偿）以及术中经食管超声心动图（transesophageal echocardiography，TEE）与血流动力学监测的精准整合，需深度掌握 TR 的病理分期、器械植入的影像引导要点及循环崩溃的预判指标。提高麻醉医师对三尖瓣疾病的认识，对右心功能的理解以及对 TTVI 的流程的管理能力，对于改善患者预后具有重要价值。本文拟从术前量化评估、麻醉技术选择、术中危机处理、术后监护重点以及未来发展方向等方面系统阐述 TTVI 围术期管理的标准化路径，旨在建立以右心保护为核心的围术期管理范式，最终降低心血管相关并发症发生率及全因死亡率。

Investigation of the safety and effectiveness of a novel steerable guiding catheter in coronary intervention

Feng Gao, Tang-Gang Gao

Zhongshan Hospital of Xiamen University

Objective: Percutaneous coronary intervention (PCI) is an effective therapy to improve coronary artery stenosis. However, in complex coronary artery lesions, guiding catheters may be difficult in coronary cannulations or be replaced frequently. This study aims to evaluate the effectiveness and safety of a novel steerable guiding catheter in PCI.

Methods: This was a single center, retrospective, single arm study. Patients who underwent PCI using a novel steerable guiding catheter in the Department of Cardiology, Xiamen University's Zhongshan Hospital from January 2021 to December 2023 were included. The novel steerable guiding catheter comprises a sheath tip, a handle with an adjustable knob, a tube body, and a soft catheter tip. By rotating the knob on the handle, the curvature of the catheter tip can be modified, enabling rapidly alignment with either the left or right coronary artery ostium. The steps for cannulating the left coronary artery: The steerable guiding catheter reach the aortic root along the angiographic guidewire. The catheter can be carefully curved clockwise or counterclockwise using the knob of the handle, based on the morphology of the aortic sinus. By adjusting the catheter, it can be directed toward the left coronary sinus. After positioning, fine-tuning its height and rotating it left or right ensures optimal engagement. During right coronary artery interventions, the ostium of the right coronary artery is typically positioned lower than that of the left. When the catheter tip is slightly below the left coronary ostium, it should be carefully curved clockwise or counterclockwise using the knob of the handle. This adjustment orients the catheter toward the right sinus, shaping it similarly to a JR/MPA catheter. Once positioned, fine adjustments—such as pushing, pulling, and rotating—help achieve stable engagement, allowing for successful completion of most right coronary interventions. The patients' clinical and operational information were collected. The efficacy endpoints were catheterization success rate. The safety endpoints included the incidence of coronary artery no-reflow, dissection, catheter-related vascular embolism, coronary artery perforation, and severe arrhythmias.

Results: A total of 104 patients who consented to undergo PCI using a novel steerable guiding catheter were included. The radial artery was used as the access site in 99 patients (95.2%), while the femoral artery was used in 5 patients (4.8%). Coronary angiography revealed isolated left coronary artery lesions in 40.4% of cases, isolated right coronary artery lesions in 20.2%, and combined left and right coronary artery lesions in 39.4%. The catheterization success rate was 98.1%. In the two failed cases, intraoperative conversion to a different guiding catheter was required. Both involved chronic total occlusion (CTO) of the left anterior descending (LAD) artery. In one case, even after switching to an Amplatz Left (AL) guiding catheter, the guidewire was unable to cross the lesion. The steerable guiding catheter was used for simultaneous intervention in two vessels in 39.4% of cases and in three or more vessels in 12.5%. Among 21(10.3%) patients with severe coronary calcification, 6(5.8%) underwent rotational atherectomy and 15 were treated with a cutting balloon. 14(6.9%) patients had chronic total occlusion (CTO) lesions, one of whom received cutting balloon therapy. The operation time for severe calcification lesions, chronic total occlusion (CTO), and simple lesions were 112.57±27.31min, 125.50 ± 31.45min and 99.42±58.03min, respectively. The radiation doses were 732.75(438.50, 1038.75) mgy, 900(617.75,1850.00) mgy and 550.00(325.00,1194.25) mgy, respectively. The contrast volume was 191.25 (180.63, 197.25) ml, 280.00 (250.00, 280.00) ml, and 145.00 (111.25, 148.75) ml, respectively. One case of coronary no-reflow and one case of coronary artery dissection were reported. No other catheter-related adverse events—such as vascular embolism, coronary perforation, or significant arrhythmias—occurred during the procedure or hospitalization.

Conclusion: The steerable guiding catheter demonstrates good efficacy and safety in the treatment of CTO lesions, severe calcified lesions, and simple lesions in both the left and right coronary arteries.

降钙素基因相关肽调节平滑肌细胞表型改变对动脉损伤后新生内膜增生的作用

赵然尊

遵义医科大学附属医院

目的：通过降钙素基因相关肽 (CGRP) 干预体外培养的血管平滑肌细胞 (VSMC) 和体内颈动脉损伤大鼠模型，探讨其对 VSMC 表型改变和动脉损伤后新生内膜增殖的影响。

方法：取大鼠胸主动脉，以组织块贴壁培养法获得 VSMC，给予血小板源生长因子 (PDGF，终浓度为 2.0×10-8 mol/L) 和 (或)CGRP(终浓度为 3.5×10-7 mol/L) 处理，利用 Western blot 法检测细胞表型改变，噻唑蓝法和流式细胞仪检测细胞增殖，细胞划痕实验检测细胞迁移能力；同时建立颈动脉损伤大鼠模型，并分为对照组和 CGRP 组，通过 HE 染色观察新生内膜形成情况，Western blot 法检测损伤动脉中 VSMC 表型改变和信号转导通路细胞外信号调节激酶 (ERK) 激活情况。

结果：PDGF 明显诱导体外培养的 VSMC 表型改变；而 CGRP 处理则显著抑制 PDGF 诱导的细胞表型转换，降低细胞增殖 [48h：CGRP 组 (0.20±0.03)×105 比 PDGF 组 (0.67±0.08)×105，P<0.05；72h：CGRP 组 (0.17±0.04)×105 比 PDGF 组 (1.42±0.11)×105 比对照组 (0.45±0.05)×105，P<0.05] 和迁移能力 [24h：CGRP 组 (2.12±0.21)% 比 PDGF 组 (5.04±0.52)% 比对照组 (4.87±0.44)%，P<0.05；48h：CGRP 组 (2.84±0.43)% 比 PDGF 组 (5.78±0.74)% 比对照组 (5.50±0.37)%，P<0.05]；CGRP 降低新生内膜形成，伴随着损伤动脉中 VSMC

合成表型标志蛋白骨桥蛋白表达减少，并抑制细胞外信号激活途径 ERK 的激活。

结论：CGRP 可能通过抑制 ERK1/2 信号途径激活而调节 VSMC 表型，抑制细胞增殖和迁移，从而降低动脉损伤后新生内膜形成。

骨髓间充质干细胞源外泌体对大鼠颈动脉球囊损伤后 lncRNAs 表达的影响

石蓓

遵义医科大学附属医院

目的：探讨骨髓间充质干细胞（bone marrow mesenchymal stem cells，BMSCs）源外泌体（exosomes）对大鼠颈动脉球囊损伤后内膜增生的调控作用及其长链非编码 RNA（long non-coding RNAs，lncRNAs）表达的影响。

方法：采用差速超速离心法提取大鼠 BMSCs 源外泌体，并通过 Western blot 和透射电镜对其进行鉴定。SD 大鼠分为 3 组：（1）假手术组（只分离左颈总动脉血管）；；（2）损伤组（左颈总动脉采用球囊损伤）；（3）外泌体组（建立大鼠颈动脉球囊损伤模型后原位注射 0.25μg/μL 外泌体 400μL），14 d 后采用 HE 染色观测颈动脉内膜 / 中膜面积比（intima/media，I/M）、免疫组化检测 PCNA 表达、Western blot 检测血管内膜增殖及表型转化相关指标的变化。采用 lncRNA-mRNA 共表达谱芯片表达变化及其生物信息学分析筛查假手术组和损伤组大鼠颈动脉组织中差异表达的 lncRNAs 和 mRNAs，对其潜在分子机制进行探讨。采用 qRT-PCR 检测各组颈动脉组织中候选 lncRNAs 的表达。

结果：电镜结果显示 BMSCs 源外泌体呈现 " 茶杯垫样 " 改变，Western blot 结果显示所提取的外泌体中 CD63、Alix、HSP70 蛋白表达阳性。与损伤组相比，经 BMSCs 源外泌体处理后大鼠颈动脉 I/M 显著减少（P<0.05），增殖相关蛋白 PCNA、Cyclin D1 表达下调（P<0.05）。lncRNA-mRNA 共表达谱芯片检测结果，与假手术组相比，损伤组有 1 083 个 lncRNAs 表达上调，629 个 lncRNAs 表达下调，2 004 个 mRNAs 表达上调，2 487 个 mRNAs 表达下调（Fold Change>2.0，P<0.05）。GO 和 KEGG 通路分析结果显示，多条 lncRNAs 与 mRNAs 相互关联，通过调控相应的靶 mRNAs，参与血管平滑肌收缩、肌动蛋白细胞骨架调节和细胞周期等多种生物学过程，与球囊损伤后血管再狭窄的机制有关。结合生物信息学分析，采用 qRT-PCR 检测 3 组大鼠颈动脉组织中上述差异性表达最为显著的 7 个 lncRNAs，结果表明，与损伤组相比，外泌体组 XR593268 上调（P<0.05），XR602080、XR602012、XR591017 均下调（P<0.05）。

结论： BMSCs 源外泌体抑制大鼠颈动脉球囊损伤后内膜增生，其潜在机制可能与 XR602080、XR591017 通过 Gsk3b、Cdkn2b、Ccna2 等分子调控平滑肌细胞周期变化有关。

缺氧预处理外周间充质干细胞对兔血管成形术后再狭窄的影响

赵然尊

遵义医科大学附属医院

目的：探讨经骨髓动员后外周血分离的间充质干细胞 (MSCs) 移植对动脉粥样硬化模型兔颈动脉球囊成形术后再狭窄的防治作用及可能机制。

方法：粒细胞集落刺激因子 (G-CSF) 动员、外周血分离体外扩增获得 MSCs，增强型绿色荧光蛋白 (EGFP) 报告基因标记备用。建立兔动脉粥样硬化狭窄模型，随机分为缺氧预处理 MSCs 移植组 (HP)、非缺氧预处理 MSCs 移植组 (NHP) 及对照组 (C)，再于球囊成形术后立即耳缘静脉内分别注入标记的缺氧处理、非处理 MSCs 或培养液。术后 7 d、14 d、28 d 采集外周血用 ELISA 法检测血管内皮生长因子 (VEGF) 水平；术后 28 d 处死动物留取血管标本通过 Weigert 弹力纤维染色及免疫组化染色进行形态学分析、归巢 MSCs 分析、再内皮化程度分析。

结果：HP 组、NHP 组术后各时点 VEGF 水平均显著高于 C 组 (P<0.01)；术后 7d、14 d HP 组显著高于 NHP 组 (P<0.05)，28 d 则差异无显著。术后 7 d 血管组织中仅 HP 组、NHP 组血管组织中有 EGFP(+) 细胞分布；术后 28 d HP 组内膜增殖程度、再狭窄率明显低于 NHP 组 (P<0.05)，而该 2 组均显著低于 C 组 (P<0.01)；再内皮化程度 HP 组明显优于 NHP 组 (P<0.05)、同时该 2 组又均显著优于 C 组 (P<0.01)。

结论：MSCs 移植能够抑制模型兔颈动脉球囊成形术后内膜增生、促进损伤血管快速内皮化从而降低再狭窄率，移植经缺氧预处理的 MSCs 可增强上述作用，可能与缺氧应激诱导 MSCs 分泌细胞因子功能增强有关。

经食管超声心动图引导下经皮房间隔缺损封堵术中导丝成袢技术的安全性和有效性研究

华慧品 [1] 苗芃 [1] 张洵 [1] 徐书灿 [2] 邵峻 [1]

1. 南京医科大学第二附属医院

2. 滨海县人民医院

目的：探讨导丝成袢法在单纯食道超声心动图引导下经皮房间隔缺损封堵术的安全性和有效性。

方法：回顾性分析 2022 年 9 月至 2024 年 12 月在南京医科大学第二附属医院心血管外科行食道超声引导下经皮房间隔缺损封堵术的患者的临床资料。根据术中 Amplatze 导丝头端定位方式，将患者分为研究组（导丝成袢组，即导丝头端左心房盘绕成环）和对照组（导丝头端进入左上肺静脉），共纳入 137 例继发孔型房间隔缺损患者，男性 55 例，女性 82 例，年龄范围为 2 至 71 岁。其中，研究组包含 78 例患者，对照组 59 例患者。比较两组患者的手术成功率、手术时间、新发心律失常、心包积液、术后封堵伞位置及形态、残余分流、穿刺点血肿、外周血管损伤等临床指标。

结果：两组患者的性别、年龄、房间隔缺损直径、手术时间、随访时间无统计学意义（P > 0.05）。137 例患者均成功完成手术，手术成功率 100%。其中研究组有 4 例术后新发心房心律失常，其中心房早搏 2 例，右束支不完全性阻滞 2 例。对照组 1 例患者因导丝进入左上肺静脉困难，采用研究组的导丝成袢技术，完成手术；1 例新发心包积液，观察 1 周后减少，随访 3 个月完全消失；1 例穿刺部位血肿，加压包扎后改善；术后新发心房心律失常 3 例，均诊断为不完全性右束支传导阻滞。两组患者完成 3~15 个月随访，未发生封堵器脱落或移位，外周血管损伤等并发症，房间隔水平无残余分流，各瓣膜及腔静脉回声无受阻改变。

结论：导丝成袢法经食道超声导引下经皮房间隔缺损修补手术是一种既安全又可行的术式，且能降低手术学习曲线，降低手术难度。

Non-target lesion Progression：Unveiling critical Predictors and outcomes in Patients with in-stent restenosis

bei Shi

Affiliated Hospital of Zunyi Medical University

Percutaneous coronary intervention (PCI) has transformed the treatment paradigm for coronary artery disease (CAD), efficiently relieving symptoms and enhancing patient outcomes by re-establishing blood flow in stenosed or occluded target vessels. Nevertheless, the long-term efficacy of PCI is significantly constrained by complications, with in-stent restenosis (ISR) being a prominent challenge that frequently necessitates repeat interventions. Beyond the treated vessel, the progression of non-target vessel plaques has emerged as a pivotal factor determining adverse cardiovascular events. These plaques can undergo destabilization over time, potentially leading to severe consequences such as myocardial infarction, heart failure, or even death. Despite its clinical significance, the impact of non-target lesion progression (N-TLP) on the prognosis of patients who undergo PCI for ISR—especially those with multivessel disease—remains under-investigated. This knowledge gap hinders accurate risk stratification and optimal therapeutic decision-making.

This study sought to elucidate the predictive factors of N-TLP and explore its association with clinical outcomes, including non-culprit vessel-related major adverse cardiovascular events (NCV-MACE) and pan-vascular disease-related clinical events (PVD-CE), in patients with ISR and multivessel disease. A total of 195 patients who successfully underwent PCI with drug-eluting stent (DES) implantation for ISR were enrolled. Intraoperative optical coherence tomography (OCT) was employed to meticulously assess the baseline morphological characteristics of the culprit stent. Subsequently, all patients underwent serial coronary angiography to monitor plaque progression, enabling classification into the N-TLP group (patients with significant progression in non-target vessels) and the no-N-TLP group.

The analytical approach centered on identifying baseline factors associated with N-TLP and evaluating its impact on long-term prognosis. Multivariate logistic regression analysis identified four independent predictors of N-TLP: diabetes mellitus (odds ratio [OR] 3.616, 95% confidence interval [CI]: 1.735–7.537; P = 0.001), elevated uric acid levels (OR 1.005, 95% CI: 1.001–1.009; P = 0.006), in-stent neoatherosclerosis (ISNA) (OR 1.334, 95% CI: 1.114–1.985; P = 0.047), and heterogeneous neointima morphology (OR 2.48, 95% CI: 1.18–5.43; P = 0.019). These findings collectively underscore the critical roles of metabolic dysregulation (manifested as diabetes and hyperuricemia) and local vascular pathology (characterized by ISNA and neointimal heterogeneity) in promoting non-target plaque progression.

From a clinical perspective, N-TLP was strongly correlated with suboptimal outcomes. Patients with N-TLP demonstrated a significantly higher incidence of NCV-MACE (19.4% vs. 6.9%, P = 0.009) compared to those without N-TLP, indicating that non-target vessel progression directly contributes to ischemic events in previously untreated coronary arteries. Moreover, PVD-CE, which encompasses systemic vascular complications such as stroke, peripheral artery disease, or aortic aneurysm, was more prevalent in the N-TLP group (83.9% [95% CI: 79.7%–88.3%] vs. 93.1% [95% CI: 88.4%–98.0%], P = 0.038), highlighting the systemic nature of vascular disease progression in this patient cohort.

These results underscore that N-TLP is not a passive phenomenon but an active contributor to adverse outcomes in ISR patients following PCI. The identification of diabetes, uric acid levels, ISNA, and heterogeneous neointima as predictive factors facilitates more accurate risk stratification, empowering clinicians to implement targeted interventions—such as stringent metabolic control and intensified anti-plaque therapies—for high-risk individuals. By addressing N-TLP, it may be possible to reduce the incidence of NCV-MACE and PVD-CE, ultimately improving the long-term prognosis of this vulnerable patient population. Future research is essential to validate these predictors and develop targeted strategies to impede N-TLP progression.

高龄高危急性非 ST 段抬高型心肌梗死患者不同治疗策略的比较研究

张亮 关韶峰 史凯雷 孔令冉 章亚萍 曲新凯

复旦大学附属华东医院

目的： 本研究旨在比较急诊介入、延迟介入及保守治疗三种策略在≥ 75 岁高危 NSTEMI 患者中的临床效果与安全性。方法： 连续纳入 2018 年 1 月至 2023 年 12 月本院收治的 263 例年龄≥ 75 岁 Grace 评分 > 140 分的 NSTEMI 患者，根据治疗策略分为三组：急诊介入组 (n=89)：入院 24 小时内完成冠状动脉造影和

介入治疗（PCI），延迟介入组 (n=94)：入院 24 小时至一周内完成冠状动脉造影及干预。保守治疗组 (n=80)：以指南指导的优化药物治疗（OMT）为主的干预。主要终点为 6 个月内主要不良心血管事件（MACE），包括：全因死亡、再发心肌梗死、因心力衰竭再入院。次要终点包括：30 天全因死亡率、大出血事件（BARC ≥ 3 级）、住院时长、6 个月内因心绞痛再住院率。结果：主要终点三组发生率存在显著差异（P<0.001），与保守治疗组相比，急诊介入组显著降低 MACE 风险（调整后风险比 [aHR]=0.39, 95%CI：0.23-0.65），延迟介入组亦降低风险（aHR=0.55, 95%CI：0.33-0.91）。急诊介入组 vs 延迟介入组： 急诊介入有进一步降低 MACE 的趋势，尤其在降低再发心绞痛再入院（7.9% vs 13.8%，P=0.041）方面优势显著。次要终点：30 天全因死亡率： 急诊介入组 vs 保守治疗组 (3.4%vs 11.3%, P=0.018），大出血（BARC ≥ 3 级）： 三组间无显著差异（急诊：6.7%， 延迟：7.4%， 保守：5.0%, P=0.622）， 保守治疗组 6 个月因心绞痛再住院率（26.3%）显著高于急诊介入组（8.9%）和延迟介入组（15.9%，P=0.002），急诊介入组中位住院时间最短（6.8 天），延迟介入组次之（8.2 天），保守治疗组最长（9.6 天，P<0.001）。结论：早期侵入性干预（尤其 24 小时内急诊介入）相较于延迟介入或保守治疗，可显著降低 6 个月 MACE 风险（包括死亡、再梗死）、30 天死亡率和因心绞痛再入院率，并缩短住院时间。延迟介入策略虽优于纯保守治疗，但未达到急诊介入的优化效果。急诊介入大出血风险并未显著增加，因此，对于具备手术条件的高龄高危 NSTEMI 患者优先推荐入院 24 小时内完成的急诊介入策略。

冠脉内靶向注射替奈普酶对急性 ST 段抬高型心肌梗死患者微循环及心脏预后的影响

范海

马鞍山市人民医院

目的：探讨在急性 ST 段抬高型心肌梗死（ST-elevation myocardial infarction，STTMI）患者中，冠脉内靶向注射替奈普酶（Tenecteplase，TNK）联合急诊经皮冠状动脉介入治疗术（percutaneous coronary intervention,PCI）对患者冠脉微循环及心脏预后的影响。**方法：**本研究纳入 2023 年 11 月至 2024 年 11 月在马鞍山市人民医院心内科住院的 STEMI 并行急诊 PCI 的患者 60 例，随机分为对照组 30 例（单纯急诊 PCI）及治疗组 30 例（冠脉内注射 TNK 联合急诊 PCI）。通过观察比较两组患者的定量血流分数（Quantitative Flow Ratio，QFR）、支架术后 TIMI 血流分级、TIMI 帧数、TIMI 心肌灌注（TIMI myocardial perfusion，TMP）分级、ST 段两小时回落比例等指标评估患者冠脉微循环情况，肌酸激酶同工酶达峰时间、肌钙蛋白及肌酸激酶同工酶峰值等间接评估冠脉微循环情况，比较两组患者 BNP、LVEDD、LVEF 等指标进而评估患者心功能情况。两组患者均随访 6 个月，观察两组患者主要心血管不良事件发生比例（包括心肌梗死再住院、心衰再住院、恶性心律失常、出血及心源性猝死等）。**结果：**1、在改善冠脉微循环方面：术后立即测两组患者 QFR，治疗组 QFR 明显高于对照组，差异具有统计学意义（P < 0.005）；TIMI 帧数则是治疗组显著低于对照组，差异具有统计学意义（P < 0.001）；TMP 分级在术前两组患者差异无统计学意义（P > 0.005），均为 TMP0-2 级，无 TMP3 级，但在术后 TMP3 级比例治疗组明显高于对照组，差异具有统计学意义（P < 0.005）；肌酸激酶同工酶峰值治疗组明显低于对照组，差异具有统计学意义（P < 0.005）；最后对两组患者的两小时 ST 段回落率进行比较，其回落率≥ 70% 的人数分别为治疗组 25 例（83.3%），对照组 18 例（60%），提示治疗组 ST 段回落情况明显优于对照组，差异具有统计学意义（P < 0.005）。以上数据表明冠脉内注射 TNK 联合急诊 PCI 组的微循环改善情况明显优于单纯急诊 PCI 组。2、在改善心功能方面：术后 24 小时的心脏彩超两组 LVEF 差异无统计学意义，但在出院后 6 个月门诊复查中治疗组明显高于对照组，差异具有统计学意义（P < 0.005）。2 组患者的 TIMI 血流分级、肌酸激酶同工酶达峰时间、肌钙蛋白、BNP、LVEDD，差异无统计学意义（均 P > 0.05）。3、6 月后主要心血管不良事件方面：单纯急诊 PCI 组发生率明显高于冠脉内注射 TNK 联合急诊 PCI 组，差异具有统计学意义（均 P > 0.05）。在其安全性的评估方面，两组均未发生危及生命的大出血，且小出血事件的发生率为治疗组（6 例，20%）对照组（3 例 ,10%），差异不具有统计学意义（P > 0.05）。这表明在改善微循环及心脏预后方面治疗组具有更加明显的优势，且其出血事件较对照组未见明显增多。

结论：冠脉内靶向注射 TNK 联合急诊 PCI 可以明显改善 STEMI 患者微循环情况及心脏预后。

心理护理干预对冠心病患者焦虑抑郁情绪及治疗依从性的影响

张宁

中国人民解放军北部战区总医院

目的： 探讨心理护理干预对冠心病患者焦虑抑郁情绪改善及治疗依从性的影响，特别是对 PCI 术后患者治疗依从性的提升作用。

冠心病（CHD）作为一种严重威胁人类健康的心身疾病，不仅带来生理上的痛苦，更常伴随显著的焦虑、抑郁等负性情绪。尤其对于经历经皮冠状动脉介入治疗（PCI）的患者，手术本身、对预后的担忧、生活方式的巨变以及对长期药物治疗的依赖，极易诱发或加重其心理负担。这些不良情绪不仅直接降低患者的生活质量，更成为阻碍其坚持规范治疗（治疗依从性）的关键因素。因此，探讨心理护理干预在此类患者中的应用及其效果显得尤为重要。

本研究旨在探讨的心理护理干预流程，核心在于“身心同治”，主要涵盖以下环节：

健康教育赋能： 运用通俗易懂的语言，系统讲解冠心病知识、PCI 手术原理、术后康复要点、药物作用及必要性、生活方式调整（戒烟限酒、合理饮食、规律运动）的重要性，旨在消除恐惧，建立正确认知基础。

认知行为干预（CBT）应用： 引导患者识别并修正对疾病、手术及预后的灾难化或悲观认知（如“手术无效”、“药物危害大”），协助其建立积极、现实的疾病观和康复信念。

情绪疏导与支持： 营造安全信任的环境，鼓励患者表达内心恐惧、担忧与挫折。通过倾听、共情、支持性心理技术提供情感支持，减轻孤独无助感，并教授放松技巧（如深呼吸、渐进性肌肉放松）缓解急性焦虑。

社会支持系统构建： 积极引导家属参与，指导其提供有效情感支持与行为监督（如服药提醒、复诊陪伴、共建健康生活）。必要时链接社区或病友团体资源，扩展社会支持网络。

PCI 术后专项心理支持： 针对性处理患者对支架的误解（如“一劳永逸”或“支架移位”）、对再狭窄 / 复发的恐惧、对抗血小板治疗出血风险的过度担忧，以及术后活动受限引发的挫败感。重点强调术后规律用药、定期复查及坚持康复的极端重要性，并提供专业心理疏导。

探讨结果显示，实施上述心理护理干预流程能显著改善冠心病患者的心理状态并提升其治疗依从性。

有效缓解焦虑抑郁： 干预后，患者的焦虑抑郁情绪得到显著缓解，积极应对态度增强，主观幸福感提升。心态的改善有助于稳定心率、血压，间接促进心脏康复。

显著提高治疗依从性： 此效果在 PCI 术后患者中尤为突出：

用药依从性提升： 患者对抗血小板药（阿司匹林、氯吡格雷）、他汀、β 受体阻滞剂等的必要性和重要性理解加深，能主动坚持按时按量服药，显著减少自行停药、减量或漏服，保障 DAPT 完成度，降低血栓风险。

复诊依从性增强： 认识到定期复查（血脂、血糖、心电图等）对监测病情、调整方案的关键作用，能主动预约并按时复诊。

生活方式改善落实： 在心理干预支持下，患者更有动力和毅力坚持戒烟、健康饮食（低盐低脂）、适度运动（如心脏康复），有效控制体重及血压、血糖、血脂。

症状报告更及时： 对胸痛等不适症状的警觉性提高，能及时报告，利于早期干预。

结论：

冠心病，尤其是 PCI 术后患者普遍存在的焦虑抑郁情绪，是导致治疗依从性不佳的核心因素之一。探讨表明，将规范化的心理护理干预流程（包括认知教育、情绪疏导、社会支持及术后专项支持）整合入常规护理，能有效改善患者负性情绪。更重要的是，通过优化认知、增强信心、改善应对方式，心理护理能显著驱动患者行为改变，提升其对药物治疗、生活方式调整、定期复诊等关键措施的依从性。对于 PCI 术后患者，依从性的提升直接关系到手术长期效果、心血管事件再发风险的降低及生存质量的保障。 因此，深化护理人员心理护理能力，将心理干预贯穿冠心病全程管理，是实现优质护理和促进患者全面康复的重要方向。

分叉病变介入治疗中对比药物球囊与非药物球囊行边支保护疗效 meta 分析

庞旭尧 张飞飞

河北省人民医院

目的：探讨评价冠脉介入治疗中对比药物球囊 (DCB) 与非药物球囊行边支保护疗效。

方法：检索 PubMed、Embase、Cochrane 图书馆、Web of science、中国期刊全文数据库（CNKI）、万方数据库（Wanfang database）、中国生物医学文献数据库（CBM），同时查阅心血管专业相关网站。检索时间均为从建库至 2024 年 6 月相关临床研究。按照入排标准筛选文献，随机对照研究应用 Cochrane 风险偏倚工具评价，非随机对照研究应用纽卡斯尔 - 渥太华量表评价。提取相关数据，应用 Revman 5.2 进行统计学分析。

结果：共纳入 10 篇文献，其中随机对照 4 篇，非随机对照 6 篇，总例数 1720 例。Meta 分析结果：与非药物球囊相比，DCB 组分支血管晚期管腔丢失优于非 DCB 组（MD=-0.17，95%CI -0.26~-0.08，P < 0.01），而靶病变血运重建，非致死心梗心肌梗死，MACE 无统计学差异。亚组分析中非随机对照研究显示与非药物球囊相比，DCB 组分支血管晚期管腔丢失、靶病变血运重建、MACE 优于非 DCB 组（MD=-0.2，95%CI -0.31~-0.09，P < 0.01）、（OR=0.44，95%CI 0.24~0.81，P < 0.01）、（OR=0.47，95%CI 0.27~0.79，P < 0.01）。

结论：在冠状动脉原发分叉病变介入治疗中，与非 DCB 相比，DCB 可能改善晚期管腔丢失，减少 TLR 及 MACE 发生。但仍然需要更多大样本的随机对照研究验证。

经导管主动脉瓣置换术后 Venus-A 瓣膜的连合和冠状动脉对齐：一项回顾性横断面研究

奚思宇 [1] 张海山 [1] 高源 [1] 陈欣 [2] 谭文飞 [3] 郭亮 [1] 孙英贤 [1]

1. 中国医科大学第一医院心内科

2. 中国医科大学第一医院心血管超声科

3. 中国医科大学第一医院麻醉科

经导管主动脉瓣置换术 （TAVR） 是一种公认的微创技术，适用于严重主动脉瓣狭窄 （AS） 患者。随着 TAVR 技术在过去十年中日趋成熟，与外科主动脉瓣置换术 （SAVR） 相比，TAVR 的适应症进一步扩大 。TAVR 已逐渐在年轻患者中进行，这意味着 TAVR 后的预期寿命延长和冠状动脉疾病更普遍。与 SAVR 不同，在 SAVR 中，手术瓣膜连合可以与天然瓣膜连合完全对齐，而 TAVR 期间的连合对齐并不容易实现，因为经导管心脏瓣膜 （THV） 总是随机植入 。既往研究表明，THV 的新连合方向可影响 TAVR 期间的冠状动脉阻塞、THV 的长期耐久性和 TAVR 后再次介入的冠状动脉入路。Evolut R/Pro 和 Acurate Neo 主动脉瓣的特定初始方向可改善连合对线。然而，实现与 Venus-A 瓣膜的连合对线的方法仍然未知。因此，本研究旨在评价使用标准系统输送技术进行 TAVR 后 Venus-A 自膨式瓣膜的连合和冠状动脉对准程度。开展回顾性横断面研究，在入组时，选择使用第二代 64 排多探测器扫描仪进行术前和术后心电图门控对比增强 CT 的

患者进行研究。连合对线分为对线（角度偏差 0-15°）、轻度（15-30°）、中度（30-45°）或重度（45-60°）连合错位（CMA）。冠状动脉排列分为无冠状动脉重叠（CO）（>35°）、中度 CO（20-35°）或重度 CO（≤ 20°）。结果以比例表示，以评估连合和冠状动脉对齐的程度。45 例 TAVR 患者最终纳入分析。THV 被随机植入：20.0% 的 THV 对齐，33.3% 有轻度 CMA，26.7% 有中度 CMA，20.0% 有重度 CMA。左冠状动脉主干重度 CO 发生率为 24.4%，右冠状动脉为 28.9%，双冠状动脉为 6.7%，单支或双支冠状动脉为 46.7%。结果表明，使用标准系统输送技术，Venus-A 瓣膜无法实现连合或冠状动脉对线。因此，需要确定与 Venus-A 瓣膜对齐的具体方法。

双侧冠状动脉口和主动脉瓣连合相对于主动脉弓的解剖空间分布

奚思宇 [1] 高原 [1] 张海山 [1] 陈昕 [2] 谭文飞 [3] 郭亮 [1] 孙英贤 [1]

1. 中国医科大学第一医院心内科

2. 中国医科大学第一医院心血管超声科

3. 中国医科大学第一医院麻醉科

经导管主动脉瓣置换术（TAVR）是治疗重度主动脉瓣狭窄（AS）患者的公认微创技术。随着 TAVR 技术在过去十年中的发展，与外科主动脉瓣置换术（SAVR）相比，TAVR 的适应症已经扩展到年轻患者，这增加了预期寿命和冠状动脉疾病的患病率。与外科瓣膜接合处可与自体瓣膜接合处完全对准的 SAVR 不同，TAVR 期间的接合处对准不容易实现，因为经导管心脏瓣膜（THV）始终沿随机轴向植入。既往研究表明，THV 的新连合方向影响 TAVR 期间的冠状动脉阻塞、THV 的长期耐久性以及 TAVR 后需要再次介入时的冠状动脉入路。连合对线还增加了人工生物瓣膜或自体主动脉撕裂的可行性，以防止因 THV 植入失败而进行 TAVR 的病例中的医源性冠状动脉阻塞。Tang 等人发现，Evolut R/Pro（Medtronic，Minneapolis，Minnesota） 和 ACURATE Neo（Boston Scientific，MA，USA）主动脉瓣的特定初始方向可改善连合对线。TAVR 术中透视下观察双侧冠状动脉口，发现冠状动脉与主动脉弓内曲（IC）有一定的解剖关系。既往研究表明，在 TAVR 期间实现连合对线的重要性。然而，双侧冠状动脉口和主动脉瓣连合相对于主动脉弓的解剖空间分布仍然未知。本研究通过设计了一项回顾性横断面研究来评价这种解剖关系。使用第二代双源 CT 扫描仪进行术前心电门控计算机断层扫描（CT）血管造影的患者入组本研究。进行三维重建，并定义主动脉弓的内曲线（IC）。测量冠状动脉或主动脉瓣连合与 IC 的夹角。80 名患者被纳入分析。IC 与左主干（LM）的夹角为 48.0° ±17.5°，IC 与右冠状动脉（RCA）的夹角为 172.6° ±15.2°。IC 至非冠状动脉瓣尖（NCC）/ 左冠状动脉瓣尖（LCC）连合的中位角为 – 12.8°，四分位距（IQR）为 – 21.5° 至 – 2.2°，IC 至 LCC/ 右冠状动脉瓣尖（RCC）连合的角为 102.4° ±15.1°，IC 至 RCC/NCC 连合的角为 219.9° ±13.9°。本研究发现冠状动脉口或主动脉瓣连合与主动脉弓 IC 之间存在固定的角度关系，这种关系有助于建立个体化植入方法，从而在 TAVR 中实现连合与冠状动脉对齐。

Efficacy of Oral Hydration in the Prevention of Contrast-induced Acute Kidney Injury in Patients Undergoing Coronary Intervention

Yang Meng, Jin-Qing Yuan

Fuwai Hospital, Chinese Academy of Medical Sciences

Efficacy of Oral Hydration in the Prevention of Contrast-induced Acute Kidney Injury in Patients Undergoing Coronary Intervention

Abstract

Background: Contrast-induced acute kidney injury (CI-AKI) is the third leading cause of hospital-acquired acute kidney injury (AKI) and is strongly linked to increased long-term morbidity and mortality [1-3]. With the rising frequency of coronary angiography (CAG) and percutaneous coronary intervention (PCI) globally, the incidence of CI-AKI has increased in parallel, emphasizing the need for effective preventive strategies. Intravenous (IV) volume expansion with isotonic saline and minimizing contrast media (CM) exposure are currently the only validated methods to reduce CI-AKI risk. However, the role of oral hydration remains unclear. Oral hydration offers potential advantages, including lower healthcare costs, reduced nursing workload, avoidance of IV cannulation-related risks (e.g., infection, phlebitis), and improved patient comfort. Despite these benefits, its efficacy compared to IV hydration has not been conclusively established, creating a critical knowledge gap in clinical practice. This study aimed to compare the effectiveness of oral hydration versus IV volume expansion in preventing CI-AKI in patients undergoing PCI. **Methods:** This prospective randomized study included 345 consecutive patients (aged ≥ 18 years) with normal renal function or stage 1–3 chronic kidney disease (estimated glomerular filtration rate [eGFR] ≥ 30 ml/min/1.73 m^2) who underwent PCI between December 2023 and February 2024. Exclusion criteria included CM hypersensitivity, recent CM exposure (≤ 7 days), nephrotoxic drug use (≤ 7 days), and inability to consume oral fluids. Patients were randomized to either the oral hydration group (n=167), instructed to consume ≥ 1000 mL of pure water within 12 hours post-procedure, or the IV hydration group (n=178), receiving 1000 mL of 0.9% NaCl at 1 mL/kg/h starting 1 hour before CM administration. Adjustments were made for heart failure (IV rate reduced to 0.5 mL/kg/h; oral intake reduced). CI-AKI was defined as a ≥ 25% relative increase or ≥ 0.5 mg/dl absolute increase in serum creatinine (SCr) within 72 hours of CM exposure, with additional analyses using alternative definitions (e.g., ≥ 0.3 mg/dl increase per KDIGO guidelines). Secondary outcomes included 30-day mortality and dialysis need. Statistical analyses used Pearson's χ^2 test, Fisher's exact test, ANOVA, and logistic regression, with p<0.05 considered significant. **Results:** Of 355 enrolled patients, 10 withdrew (4 voluntary, 6 due to medical changes), leaving 345 for analysis. Baseline characteristics were mostly balanced, though the oral group was younger (58 vs. 61 years, p=0.002), heavier (75 vs. 71.5 kg, p=0.000), and had higher eGFR (100.81 vs. 96 ml/min/1.73 m^2, p=0.005). CI-AKI occurred in 0.6% (1/167) of the oral group and 2.8% (5/178) of the IV group (p=0.117), with no significance across alternative definitions. The oral group consumed a mean 1757 mL water with good tolerance. No 30-day deaths or dialysis occurred. Subgroup analysis showed non-hypertensive patients had higher CI-AKI risk (p=0.01), and preoperative eGFR was a significant predictor (p=0.020). **Conclusions:** Oral hydration is as effective as IV hydration in preventing CI-AKI in PCI patients with normal or mildly impaired renal function. Its comparable efficacy, ease of use, cost-effectiveness, and patient comfort support broader clinical adoption. Further studies in advanced CKD are needed to generalize findings.

不同年龄段女性急性 ST 段抬高型心肌梗死患者 PPCI 临床疗效分析

刘美丽 黄光华 李娜 马蕊 刘海伟 徐凯 王斌

中国人民解放军北部战区总医院

目的： 探讨接受直接经皮冠状动脉介入治疗 (PPCI) 治疗的女性急性 ST 段抬高心肌梗死（STEMI）患者不同年龄组与院内死亡发生率的关系。

方法: 本研究资料来自全军心血管介入诊疗管理系统，入选标准: 女性 STEMI 患者，年龄 18-85 岁，所有患者均接受 PPCI 术。连续入选了接受 PPCI 治疗的 1741 例 STEMI 女性患者，根据患者不同的发病年龄将患者分为对照组（年龄≤ 65 岁）和观察组（年龄 >65 岁），两组分别为 664 例和 1077 例；比较两组患者院内死亡事件及其它临床心脏不良事件的发生率。

结果： 观察组患者 Killip III 级、三支病变比例均分别明显高于对照组 (3.8% 比 2.1%，P=0.049；43.5% 比 36.6%，P=0.005)。同时，分析门槛到球囊（D2B）时间显示，在观察组患者中明显低于对照组（1.21±1.20 比 1.60±4.07，P=0.016）。观察组较对照组院内死亡发生率明显增高 (6.4% 比 2.4%，P=0.000)，尽管术中死亡发生率两组无显著差异（0.9% 比 0.5%，P=0.262），但观察组术后死亡发生率明显高于对照组（5.5% 比 2.0%，P=0.000）。

结论：，年龄 65 岁以上女性 STEMI 患者 PPCI 院内死亡率增高，且主要表现为术后死亡的发生率明显增加，故针对高龄女性 STEMI 患者 PPCI 救治应进一步强化，以期降低院内死亡率，改善预后。

关键词： 性别；年龄；心肌梗死；冠状动脉介入治疗，经皮

危险因素数量对直接经皮冠状动脉介入治疗术后 STEMI 患者长期预后的影响

支雪涵 [1,2] 王兆丰 [2] 赵巍 [2] 康正松 [1,2] 徐凯 [2] 李洋 [2] 关绍义 [2] 刘海伟 [2]

1. 锦州医科大学北部战区总医院研究生培养基地

2. 中国人民解放军北部战区总医院

目的: 本研究旨在评估危险因素的不同数量对行直接经皮冠状动脉介入（primary percutaneous coronary intervention，PPCI）治疗的 ST 段抬高型心肌梗死（ST-segment elevation myocardial infarction，STEMI）患者预后的影响。**方法:** 本研究回顾性分析了 2016 年 3 月至 2022 年 3 月在北部战区总医院心血管内科接受 PPCI 治疗的 STEMI 患者 5516 例，根据纳排标准并筛选出 1 年随访资料完整的患者 5125 例。根据患者合并的危险因素（包括高血压、糖尿病、卒中或肾功能不全等常见的危险因素）的数量分为三组：A 组（无危险因素，n=473）、B 组（1-2 个危险因素，n=3816）、C 组（3-4 个危险因素，n=836）。记录并分析各组患者住院期间的临床特点，绘制生存曲线，对交叉曲线进一步进行 Landmark 曲线，并采用多因素 COX 回归分析三组患者主要不良心血管事件（major adverse cardiovascular events，MACE）的发生情况。**结果：** 三组临床基线指标分析显示，年龄、收缩压、心力衰竭史及慢性肾病史等有统计学差异（P < 0.05）。对比分析住院期间用药及实验室化查：左心室射血分数、血脂、抗心律失常药物及 SGLT-2 抑制剂等指标有统计学差异（P < 0.05）。三组间 GRACE 评分和心原性休克存在明显的统计学差异（P < 0.001）。在随访指标中，A、C 组 1 年内全因死亡率及 MACE 发生率均明显高于 B 组，C 组在三组中 1 年内全因死亡及 MACE 事件最高（HR=0.402 Vs HR=0.494，HR=0.373 Vs HR=0.429）。

结论： 在行 PPCI 的 STEMI 患者中，合并有 1-2 个危险因素的预后优于无危险因素患者，这可能与患有 1-2 个危险因素的患者更易建立侧支循环及依从性较好有关，此外 2 个以上的危险因素的 STEMI 患者预后最差，因此需要重视此类患者的治疗策略，改善其预后。

风湿性主动脉瓣狭窄患者行经导管主动脉瓣置换术后临床疗效分析

王茂德 王勇 李春 晋军 于世勇

中国人民解放军陆军军医大学第二附属医院

背景：风湿性主动脉瓣狭窄（rheumatic aortic valve stenosis，RAS）患者因瓣膜钙化轻、多瓣膜受累及年轻化特点，传统上被视为经导管主动脉瓣置换术（transcatheter aortic valve replacement，TAVR）的相对禁忌。中国 RAS 患者基数大，但其 TAVR 疗效与安全性证据匮乏。本研究旨在评估 TAVR 在 RAS 人群中的应用效果。

方法：纳入 2017 年 10 月至 2024 年 8 月于陆军军医大学第二附属医院接受 TAVR 的 359 例重度主动脉瓣狭窄患者，根据 World Heart Federation 风湿性心脏病诊断指南结合 CT 影像（排除钙化干扰）分为 RAS 组（n=71）与非 RAS 组（n=288）。所有患者使用 VenusA 自膨式瓣膜。主要终点包括技术成功率、器械成功率、一月早期安全率、1 年复合结局，并分析短期并发症及主动脉根部

解剖结构差异。

结果：**基线特征**：RAS 组 NT-pro BNP、Society of Thoracic Surgeons（STS）评分更高，eGFR 更低，合并房颤比例更高（均 P<0.05）；心脏扩大更显著，主动脉瓣压差、流速更低，二尖瓣反流更重（P<0.05）。**解剖结构**：RAS 组二叶瓣比例低（4.2% vs 15.6%）、钙化积分低（P<0.05），瓣环更趋椭圆形，左室流出道（left ventricular outflow tract, LVOT）/ 瓣环面积比更大（P<0.05）。**术中决策**：RAS 组假体定位 (0.9mm vs 3.0mm) 高、oversize 率 (9.2% vs 6.0%) 更大 (P<0.05)。**结局**：两组技术成功率（84.5% vs 79.2%）、器械成功率（67.6% vs 62.0%）和一月早期安全 (71.4% vs 72.1%) 无差异（P>0.05）。RAS 组起搏器植入率更高（19.7% vs 10.1%，P<0.05），假体移位风险更高（P<0.05），但其他相关并发症无差异，1 年复合结局事件率（包含全因死亡、卒中、心梗、出血、心脏或 TAVR 相关在住院）无差异（HR=0.600, 95%CI:0.270–1.330,P=0.208）。

结论：TAVR 治疗 RAS 安全有效，但 RAS 患者解剖特征（低钙化、椭圆瓣环、锥形 LVOT）增加假体移位及起搏器植入风险。采用高位释放策略与适度 oversize 可部分缓解移位风险。

Radial Artery Hemostatic Device applied in trans-brachial coronary intervention

Ning Wang, Wen-Chao Zhang

Peking University International Hospital

Abstract Objective: To investigate the safety and efficacy of the radial artery hemostatic device in trans-brachial coronary intervention, and assess its effectiveness. **Methods:** A retrospective analysis was conducted on patients who underwent trans-brachial coronary intervention at Peking University International Hospital from January 1, 2018 to December 31, 2023. The patients were divided into the radial artery hemostatic device group (170 cases) and the conventional compression group (100 cases) based on the postoperative hemostasis method, and the incidence of complications and clinical characteristics were compared between the two groups. **Results:** A total of 270 patients underwent trans-brachial coronary intervention, with 18 complications occurring. Among the patients who underwent brachial artery puncture, 18 cases of complications occurred. Among them, 17 cases had bleeding around the puncture site, and 1 case had transient injury of the median nerve. There were no pseudoaneurysms or arteriovenous fistulas. The overall complication rate was 6.7%, and the incidence of bleeding around the puncture site was 6.3%. Among the bleeding patients, 16 patients had mild bleeding and were not given special treatment. After observation, they improved. One patient had severe bleeding, with local hematoma and a decrease in hemoglobin of more than 3 g/dl. The patient was treated with blood transfusion. The patient was a 78-year-old female who was admitted due to unstable angina pectoris. At admission, she had mild anemia, with Hb 102 g/L. During coronary intervention, the right radial puncture failed, and the right brachial artery approach was chosen. During the operation, the right coronary lesion was treated, and routine compression method was used after the operation. After the operation, a hematoma occurred at the puncture site of the right brachial artery of the patient, and the duration of extended and pressurized bandaging was increased. The hemoglobin level decreased significantly, reaching the lowest 68 g/L, and the patient was treated with blood transfusion and supplementation of hematopoietic raw materials. During the subsequent follow-up, the hematoma basically absorbed, and the hemoglobin level returned to the baseline level. The incidence of bleeding around the puncture site in the radial artery hemostasis device group was 5.9%, and that in the conventional compression group was 7.0%. The incidence of bleeding in the hemostasis device group was slightly lower than that in the conventional compression group, and there was no statistical difference between the two groups (P = 0.72). Multivariate regression analysis indicated that female was an independent risk factor for hemorrhage around the puncture site [OR=4.57, 95%CI (1.40, 14.96), P=0.01]. With the accumulation of technology, the application of trans-brachial access and radial artery hemostatic devices increased year by year (P<0.01). Radial artery hemostasis device method: After coronary intervention, place the knob-type radial artery hemostasis device upside down above the puncture point of the brachial artery, tighten the fixation strap. Rotate the knob to the appropriate pressure, remove the sheath, and observe that there is no bleeding or swelling around the puncture site. Place a piece of cardboard below the elbow joint and fix the hemostasis device and the cardboard with elastic bandages to achieve elbow joint immobilization. Cross the elastic bandages to fix the hemostasis device. Observe the color and blood return of the forearm and hand, and appropriately adjust the knob. Regularly loosen the knob to reduce the compression force after the operation. The hemostasis device and the bandage can be removed 6-8 hours later. For obese patients or those with a thicker upper arm circumference, connect the fixation straps of the two hemostasis devices to ensure a firm attachment.**Conclusion:** The radial artery hemostatic device effectively controls bleeding in trans-brachial coronary interventions and demonstrates satisfactory safety. Its simplicity and efficacy provide a new strategy for hemostatic management in percutaneous trans-brachial access, which may gradually become the new standard in the future.

合并心功能不全急性 ST 段抬高型心肌梗死患者 PPCI 的临床疗效分析

刘美丽 黄光华 李娜 马蕊 刘海伟 徐凯 王斌

中国人民解放军北部战区总医院

【目的】：本研究探讨心功能不全对直接经皮冠状动脉介入术（PPCI）治疗急性 ST 段抬高型心肌梗死（STEMI）患者院内疗效的影响。

【方法】：本研究资料来自全军心血管介入诊疗管理系统，入选标准：急性 ST 段抬高型心肌梗死伴心功能不全的患者，年龄 18-85 岁，所有患者均接受 PPCI 术。连续入选了接受 PPCI 治疗的 8853 例 STEMI 患者。心功能不全判断指标：行 PPCI 前 KILLIP II 级及以上（即 KILLIP II ～IV级）。根据 STEMI 患者有无合并心功能不全将患者分为对照组（KILLIP Ⅰ级）和观察组（KILLIP II ～IV级），两组分别为 7787 例和 1066 例；比较分析两组患者救治时间诸指标、院内死亡事件及其他临床心脏不良事件。

【结果】：比较两组患者介入诊治门槛到球囊（D2B）时间显示，观察组明显高于对照组（1.44±3.49 比 1.23±1.59，P=0.058）。观察组的院内死亡发生率明显高于对照组 (6.4% 比 2.3%，P=0.000)，进一步分析显示，无论术中还是术后死亡的发生率，在观察组均明显高于对照组（分别为 1.3% 比 0.5%，P=0.001; 5.1% 比 1.8%，P=0.000）。采用二元 logistic 逐步回归法进行多因素分析发现，年龄、高血压病及 D2B 时间是 STEMI 患者发生心功能不全的独立危险因素（P < 0.05）。

【结论】：合并心功能不全的 STEMI 患者 PPCI 院内死亡率增高，而年龄、高血压及 D2B 时间是 STEMI 患者发生心功能不全的独立预测因子，故针对存在上述独立危险因素的 STEMI 患者应积极优化围术期救治策略，减少心功能不全的发生，以期降低患者院内死亡发生率，改善长期预后。

同型半胱氨酸对急性冠状动脉综合征合并 2 型糖尿病患者经皮冠状动脉介入治疗术后远期预后影响

刘美丽 裘淼涵 张莉莉 刘韵情 马颖艳

中国人民解放军北部战区总医院

目的 探讨同型半胱氨酸（Hcy）对急性冠状动脉综合征（ACS）合并 2 型糖尿病（T2DM）患者经皮冠状动脉介入治疗（PCI）术后远期预后的影响。**方法** 选取北部战区总医院 2021 年 1–12 月收治的 2 820 例 ACS 合并 T2DM 患者为研究对象。根据 Hcy 水平将患者分为高 Hcy 组（Hcy ≥ 12.09 μmol/L，n = 943）、中 Hcy 组（9.56 μmol/L ≤ Hcy < 12.09 μmol/L，n = 945）和低 Hcy 组（Hcy < 9.56 μmol/L，n = 932）。比较并比较 3 组患者的临床基线资料、介入基线资料及术后 1 年临床事件。主要结局事件：出院后 1 年缺血事件（包括心原性死亡、心肌梗死、卒中的复合终点）；次要结局事件：出院后 1 年的全因死亡。**结果** 1）相较于其余两组患者，高 Hcy 组患者既往高血压、陈旧心肌梗死、卒中、PCI、外周血管疾病、吸烟及贫血史比例明显增高，有统计学差异（P < 0.05）；高 Hcy 组患者急性心肌梗死患者比例较高，包括 NSTEMI 及 STEMI 患者，有统计学差异（P < 0.05）；同时左心室射血分数明显降低，均有统计学差异（P < 0.05）。2）高 Hcy 组患者支架总长度、血管紧张素转换酶抑制剂 / 血管紧张素 II 受体拮抗剂（ACEI/ARB）用药比例均增高，差异有统计学意义（P < 0.05）。3）高 Hcy 组患者出院后 1 年缺血事件发生率高于低 Hcy 组，差异有统计学意义（P < 0.05）。高 Hcy 组患者出院后 1 年全因死亡发生率高于低 Hcy 组，差异有统计学意义（P < 0.05）。**结论** Hcy 与 ACS 合并 T2DM 患者 PCI 术后 1 年缺血事件及全因死亡发生率有关。

冠状动脉定量血流分数对冠脉串联病变的指导价值研究

关韶峰 干倩 曲新凯

复旦大学附属华东医院

目的：评价冠状动脉定量血流分数（QFR）在冠脉串联病变的指导价值。

方法：冠脉造影时同一支冠脉血管具有两个独立的病变（狭窄 50-90%，两个病变距离 >10mm）行血流储备分数（FFR）、QFR 和定量冠脉造影（QCA）测定，以 FFR 为处理策略金标准，FFR ≤ 0.80 的患者处理压力梯度更大的病变，其后行第二次 FFR 和 QFR 检查，第二次 FFR ≤ 0.80 则处理剩余病变，比较两次检查 QFR、QCA 与 FFR 的一致性。

结果：共入选 54 例患者，患者平均年龄 (72.3±7.2) 岁，其中男性 76%，共计 61 条血管具有串联病变，QCA 测定近、远端血管狭窄为 47.7±10.4% 和 47.2±11.2，共计 44 个 (72.1%) 串联病变测得 FFR ≤ 0.80, 对压力梯度大的病变行介入处理，植入第一个支架，14 个 (22.9%) 串联病变植入了第二个支架，靶病变 67% 为 LAD，QFR 预测压力梯度大的病变的准确率为 100.0%，对第一个病变的显著程度的诊断能力，QFR 明显优于 QCA(近端病变 AUC 0.96 vs. 0.60; 差异：0.36; p < 0.001；远端病变 0.96 vs. 0.75; 差异：0.19; p < 0.01), 对第二个病变的显著程度的诊断能力，QFR 亦优于 QCA (0.92 vs. 0.70; 差异：0.22; p < 0.01).。

结论：冠状动脉定量血流分数在指导冠脉串联病变决策时优于定量冠脉造影，可用于指导临床决策。

对比分析不同门球时间对 STEMI 患者长期预后的影响

王子琛 [1,2] 支雪涵 [2] 刘毓 [2] 王兆丰 [2] 赵巍 [2] 康正松 [2] 徐凯 [2] 刘海伟 [2]

1. 中国医科大学北部战区总医院研究生培养基地

2. 中国人民解放军北部战区总医院

目的：在接受直接经皮冠状动脉介入术（PPCI）的急性 ST 段抬高型心肌梗死（STEMI）患者中，探讨不同的门球时间（DTB）对 STEMI 患者住院期间死亡、术后 1 年、3 年全因死亡及主要不良心血管事件发生的影响。

方法：本研究回顾性分析了 2016 年 3 月至 2022 年 3 月期间，在中国人民解放军北部战区总医院心内科接受 PPCI 治疗的 STEMI 患者 5516 例，根据纳排标准

筛选出具有完整病历资料及术后 3 年完整随访资料的患者 4513 例。根据 DTB（≤ 60 分钟、61-90 分钟、> 90 分钟）对患者进行分组，采用 Kaplan-Meier 生存曲线比较不同 DTB 对患者住院期间死亡、术后 1 年、3 年全因死亡及主要不良心血管事件（MACE，包括：全因死亡，非致死性心肌梗死、非致死性缺血性脑卒中）MACE 事件发生风险之间的关系，进一步采用 Logistic 回归模型及 Cox 回归模型分析 DTB 对患者住院期间死亡、术后 1 年、3 年内全因死亡及 MACE 发生风险的影响。

结果：在 4513 例接受 PPCI 的 STEMI 患者中，DTB 中位数为 61（50，78）分钟，2196 例（48.66%）患者 DTB ≤ 60 分钟，1645 例（36.45%）患者 30 分钟 < DTB ≤ 60 分钟，672 例（14.89%）患者 DTB > 90 分钟。DTB ≤ 60 分钟、61-90 分钟、> 90 分钟的住院期间死亡率分别为 0%、1%、0.8%(p<0.001)；DTB ≤ 60 分钟、61-90 分钟、> 90 分钟的 1 年死亡率分别为 2.8%、3.5%、9.7%(p<0.001)；DTB ≤ 60 分钟、61-90 分钟、> 90 分钟的 1 年 MACE 事件发生率分别为 14.7%、15.6%、22.3%(p<0.001)；DTB ≤ 60 分钟、61-90 分钟、> 90 分钟的 3 年死亡率分别为 4.6%、6.7%、12.2%(p<0.001)；DTB ≤ 60 分钟、61-90 分钟、> 90 分钟的 3 年 MACE 事件发生率分别为 19.7%、22.7%、27.7%(p<0.001)，均有显著统计学差异。多因素 Logistic 回归分析结果显示，DTB 在 61-90 分钟的患者相比于 DTB > 90 分钟的患者，住院期间死亡率降低了 0.9%（OR=0.009，95%CI:0.001~0.076，P < 0.001）；多因素 Cox 比例风险回归分析结果显示，DTB > 90 分钟是预后不良的独立预测因子，1 年死亡率（HR=2.192，95%CI:1.494~3.215，P < 0.001）、1 年 MACE 事件发生率（HR=1.466，95%CI:1.199~1.793，P < 0.001）、3 年死亡率（HR=1.869，95%CI:1.368~2.555，P < 0.001）和 3 年 MACE 事件发生率（HR=1.313，95%CI:1.099~1.569，P=0.003）；但 DTB ≤ 60 min 和 61-90 分钟（P < 0.05）之间没有显著统计学差异。

结论：本研究结果与国内外指南推荐意见保持一致，即 DTB ≤ 90（含 60 < DTB ≤ 90）分钟是 PPCI 的关键标准；而 DTB > 90 分钟是预后不良的关键点，延迟的 DTB 显著增加住院期间死亡风险及长期死亡 /MACE 风险，因此，需要设法减少 STEMI 患者 PPCI 救治的延迟。

缩短门球时间对不同危险分层 STEMI 患者预后的影响

王子琛 [1,2] 支雪涵 [2] 刘毓 [2] 王兆丰 [2] 赵巍 [2] 康正松 [2] 徐凯 [2] 刘海伟 [2]

1. 中国医科大学北部战区总医院研究生培养基地

2. 中国人民解放军北部战区总医院

目的：在接受直接经皮冠状动脉介入术（PPCI）的急性 ST 段抬高型心肌梗死（STEMI）患者中，探讨更短的门球时间（DTB，≤ 60 分钟）对不同风险（GRACE 评分风险分层）的 STEMI 患者住院期间死亡、术后 1 年、3 年全因死亡及主要不良心血管事件发生的影响。

方法：本研究回顾性分析了 2016 年 3 月至 2022 年 3 月期间，在中国人民解放军北部战区总医院心内科接受 PPCI 治疗的 STEMI 患者 5516 例，根据纳排标准筛选出具有完整病历资料及术后 3 年完整随访资料的患者 4513 例。基于 GRACE 评分进行风险分层（高危 > 140 分 vs 低危≤ 140 分），采用 Kaplan-Meier 生存曲线比较 DTB ≤ 60min 对患者住院期间死亡、术后 1 年、3 年全因死亡及主要不良心血管事件（MACE，包括：全因死亡，非致死性心肌梗死、非致死性缺血性脑卒中）事件发生风险之间的关系，进一步采用 Logistic 回归模型及 Cox 回归模型分析缩短的 DTB 对不同风险分层 STEMI 患者预后影响的差异。

结果：在 4513 例接受 PPCI 的 STEMI 患者中，有 2526 例（56.0%）符合高危标准（HR-STEMI），其中 1170 例（46.3%）HR-STEMI 患者 DTB ≤ 60min。另外 1987 例（44.0%）患者符合低危标准（LR-STEMI），1026 例（51.6%）患者的 DTB ≤ 60min。HR-STEMI 患者的中位 DTB 时间为 63（50，81）min，DTB ≤ 60min 和 DTB > 60min 之间的住院期间死亡率（0 vs 2.4，P < 0.001）、1 年死亡率（4.3 vs 7.6，P < 0.001）、1 年 MACE 事件发生率（17.3 vs 21.7，P=0.005）、3 年死亡率（6.6 vs 11.9，P < 0.001）、3 年 MACE 事件发生率（22.3 vs 29.4，P < 0.001）均有显著统计学差异。多因素 Cox 比例风险回归分析结果显示，DTB ≤ 60 分钟的患者与 DTB > 60 分钟的患者相比，出院后 1 年死亡发生风险及 1 年 MACE 事件发生风险均无显著统计学差异、但 3 年死亡发生风险明显增加（HR=1.401，95%CI:1.052~1.865，P=0.021）、3 年 MACE 事件发生风险明显增加（HR=1.195，95%CI:1.017~1.404，P=0.03）；在 LR-STEMI 患者的中位 DTB 时间为 60（48，76）min，且 DTB > 60min 的患者仅在出院死亡率高于 DTB ≤ 60min 的患者（0 vs 0.7，P=0.006），在 1 年死亡率（1.2 vs 2.0，P=0.147）、1 年 MACE 事件发生率（11.7 vs 11.7，P=0.977）、3 年死亡率（2.3 vs 3.3，P=0.182）、3 年 MACE 事件发生率（16.7 vs 16.8，P=0.959）均无统计学意义。多因素 Logistic 回归分析及多因素 Cox 比例风险回归分析结果均提示，DTB 与 LR-STEMI 患者住院期间死亡、术后 1 年、3 年全因死亡及 MACE 事件发生风险无独立相关性。

结论：DTB ≤ 60min 与高、低危 STEMI 患者短期预后、高危 STEMI 患者长期预后改善相关。但在调整混杂因素后，LR-STEMI 患者，DTB 对其结局无显著影响；而对于 HR-STEMI 患者，DTB > 60min 与 3 年全因死亡及 MACE 事件发生风险相关。

Nine month clinical, angiographic and intravenous ultrasound (IVUS) results of FIREHAWK® abluminal groove-filled biodegradable polymer sirolimus-eluting stent in treating de novo coronary artery disease: single center data from the TARGET I trial

Ji-Wei Yu, Zheng-Bin Zhu, Rui-Yan Zhang

Rui Jin Hospital, Shanghai Jiao Tong University School of Medicine

Title: Nine month clinical, angiographic and intravenous ultrasound (IVUS) results of FIREHAWK® abluminal groove-filled biodegradable polymer sirolimus-eluting stent in treating de novo coronary artery disease: single center data from the TARGET I trial

Background

The FIREHAWK stent represents an innovative drug-eluting stent (DES) technology featuring **abluminal groove-filled biodegradable poly-lactic acid (PLA) polymer coatings** loaded with sirolimus. This design enables targeted drug release exclusively toward the vessel wall while minimizing polymer exposure to the bloodstream, thereby potentially reducing inflammatory responses and late thrombotic risks18. Prior multicenter randomized trials (e.g., TARGET I) have established its non-inferiority against the durable-polymer XIENCE V everolimus-eluting stent in simple de novo coronary lesions, evidenced by comparable 9-month in-stent late lumen loss (LLL) (0.13±0.24 mm vs. 0.13±0.18 mm, P=0.94) and 5-year target lesion failure (TLF) rates (6.0% vs. 6.7%, P=0.77)367. However, **single-center validation integrating quantitative coronary angiography (QCA) and intravascular ultrasound (IVUS) functional assessments** remains limited. This study aimed to supplement existing evidence with granular imaging and clinical outcomes from a single institution, including exploratory data on long-lesion efficacy.

Methods

A prospective, single-center cohort was divided into two substudies:

1.Randomized Controlled Trial (RCT): 29 patients with single de novo coronary artery lesions were randomized 1:1 to FIREHAWK (*n*=14-15) or XIENCE V (*n*=14-15).

2.Long-Lesion Cohort: 10 consecutive patients with diffuse coronary disease (lesion length >24 mm) received FIREHAWK exclusively4.

Primary endpoints assessed at 9 months included:

1.QCA-derived in-stent LLL (defined as the reduction in minimal lumen diameter from post-procedure to follow-up)

2.IVUS-quantified intimal hyperplasia volume (neointimal tissue proliferation within the stent)

Secondary endpoints encompassed:

1.Procedural success metrics: Device success (successful stent deployment), lesion success (residual stenosis <30%), and clinical success (composite of device/lesion success without periprocedural major adverse events)49.

2.Clinical outcomes: Restenosis rate (diameter stenosis ≥ 50% at follow-up), TLF (cardiac death, target-vessel myocardial infarction, or ischemia-driven target lesion revascularization), patient-oriented composite endpoints (PoCE: all-cause death, any MI, any revascularization), and definite/probable stent thrombosis (ARC criteria)

Rusults

Follow-up completion rates were 82.6% (*n*=24/29) in the RCT arm and 100% (*n*=10) in the long-lesion cohort. Key findings included:

1.Procedural Efficacy: Both groups achieved 100% device and clinical success, with no intraprocedural complications

2.Imaging Outcomes: In-stent LLL (QCA): Comparable between FIREHAWK and XIENCE V No significant intergroup difference (P>0.05).

3.Intimal hyperplasia volume (IVUS): No significant intergroup difference (P>0.05) Restenosis rates: quivalent across groups.

All outcomes met non-inferiority margins (P>0.05 for all comparisons)49.

1.Long-Lesion Performance: FIREHAWK exhibited consistent safety/efficacy in extended lesions (mean length: 35.2 mm), with 0% TLF and no binary restenosis

Conclusions

This single-center study confirms the **9-month non-inferiority of FIREHAWK versus XIENCE V** across clinical, QCA, and IVUS endpoints for de novo coronary lesions. The abluminal groove design–delivering 85% less drug load than conventional DES–maintains efficacy while potentially enhancing long-term biocompatibility8. Notably, FIREHAWK demonstrates **exceptional performance in long lesions**, a high-risk subgroup often associated with elevated restenosis rates. These findings align with larger trials (TARGET I/II), supporting FIREHAWK as a safe and effective option for diverse coronary anatomies, including complex diffuse disease39. Future studies should address long-term (>5-year) polymer resorption effects and outcomes in diabetic populations.

Association of thyroid-stimulating hormone with contrast-associated acute kidney injury and adverse prognosis in percutaneous coronary intervention patients

Ji-Lang Zeng[1,2], Li-Tao Wang[1], Rui-Min Pan[1], Kai-Yang Lin[2], Liang-Long Chen[1]

1. Fujian Medical University Union Hospital

2. Shengli Clinical Medical College of Fujian Medical University, Fujian Provincial Hospital.

Objectives: It is well established that thyroid function plays a crucial role in regulating multiple organ systems, particularly the cardiovascular and renal systems. Emerging evidence further suggests that fluctuations in thyroid hormone (TH) levels, even within the normal reference range, may be associated with an increased risk of adverse cardiovascular and renal events. However, the relationship between thyroid-stimulating hormone (TSH) levels and the risk of contrast-associated acute kidney injury (CA-AKI) and poor outcome in euthyroid patients undergoing elective percutaneous coronary intervention (PCI) has not been fully elucidated.

Methods: We retrospectively analyzed 3,116 euthyroid patients who underwent elective PCI at a tertiary medical center between January 2012 and December 2018. Euthyroidism was defined as serum levels of TSH, free triiodothyronine (FT3), and free thyroxine (FT4) within the normal range at admission. The primary endpoint was CA-AKI, defined as a 0.3 mg/dL or 50% increase in serum creatinine (SCr) within 48 hours following contrast medium exposure. The second outcome was all-cause mortality. Receiver operating characteristic (ROC) analysis was performed to evaluate the diagnostic performance of TSH for predicting CA-AKI. Restricted cubic spline (RCS) analysis was employed to investigate potential nonlinear relationships between TSH levels and the risk of CA-AKI. Multivariable logistic and COX regression models were subsequently applied to assess the association between TSH levels and CA-AKI risk, respectively. Survival was analyzed through the Kaplan-Meier curve.

Results: A total of 160 patients (5.13%) developed CA-AKI during hospitalization. RCS modeling and ROC analysis indicated a linear inverse relationship between TSH levels and the risk of CA-AKI (P for nOnlinearity= 0.1523), with TSH demonstrating good discriminatory power [area under the curve (AUC) 0.648, 95% confidence interval (CI) 0.603-0.693; Cut-off point, 1.585 mIU/L]. In multivariable logistic regression analysis, each one standard deviation (SD) decrease in TSH was associated with a 1.29-fold increase in the risk of CA-AKI [fully adjusted odds ratio (OR), 1.29; 95% CI, 1.06-1.56, P = 0.013]. Moreover, patients in the low TSH group (TSH < 1.585 mIU/L) had a significantly higher incidence of CA-AKI compared with those in the high TSH group (TSH ≥ 1.585 mIU/L) (fully adjusted OR: 1.95, 95% CI: 1.37-2.77, P < 0.001). Variance inflation factor (VIF) analysis confirmed that there was no significant multicollinearity among the covariates (all VIFs < 5). Subgroup analyses consistently demonstrated the robustness of the relationship between TSH and CA-AKI, with no significant interaction effects observed across subgroups (all P for interaction > 0.05). As for the secondary endpoint, during a median follow-up of 2.76 years, 213 patients (7.10%) died. Multivariable Cox proportional hazards analysis also demonstrated that lower TSH levels were independently associated with an increased risk of all-cause mortality. Patients in the low TSH group had a 1.69-fold higher risk of death compared to those in the high TSH group [adjusted hazard ratio (HR): 1.69, 95% CI, 1.25-2.29, P = 0.001]. Kaplan–Meier survival curves further confirmed a significant difference in survival between the two groups (log-rank test, P < 0.001).

Conclusions: Among euthyroid patients undergoing elective PCI, lower TSH levels were independently associated with a higher risk of CA-AKI and. TSH may serve as a useful biomarker for identifying individuals at elevated risk of CA-AKI in this population.

基于光学相干断层显像评价药物球囊在急诊冠脉介入诊疗中的临床疗效

张飞飞 党懿 齐晓勇

河北省人民医院

目的 基于光学相干断层显像对比药物涂层球囊与药物洗脱支架在急诊冠脉介入中的临床疗效。

方法 2022 年 2 月至 2024 年 12 月于河北省人民医院心血管内科就诊行急性冠脉介入诊疗患者。研究纳入标准：（1）发病 12 小时以内行急诊冠脉介入诊疗 STEMI 患者；（2）行急诊冠脉介入诊疗的 NSTEMI 患者；（3）术中行光学相干断层显像检查患者；（4）介入术中接受 DES 或 DCB 单一治疗患者；（5）完成临床随访患者。依据患者介入术中接受治疗的方法分为 DCB 组（n=15）和 DES 组 (n=40)。术前及术后完成 OCT 检查并进行定性及定量指标测定。OCT 影像使用 ILUMIEN OPTIS 成像系统与目测相结合进行分析。记录术中冠状动脉夹层的发生情况及术后梗死相关血管 TIMI 血流分级；随访术后主要不良心血管事件（MACE）包括心源性死亡、再发急性心肌梗死、靶血管再重建术及出血事件。

结果 本研究共入选 55 例患者，其中男性 46 例，平均年龄为 53.01±11 岁。DCB 组与 DES 组患者的年龄、支架置入时间、LDL-C、LVEF 及性别、高血压、2 型糖尿病、吸烟、不稳定心绞痛、药物治疗比率相比，差异无统计学意义。（P > 0.05）。两组患者冠脉造影示靶血管、术前、术后 TIMI 血流分级、器械直径及长度相比均无统计学差异（P > 0.05），OCT 结果提示 DCB 组最小管腔面积小于 DES 组，DCB 组残余血栓负荷、夹层发生率高于 DES 组（P < 0.05）。DCB 组患者随访时间为 28 (18-29.5) 月，DES 组患者随访时间为 22.5 (9-30) 月，随访期内，DCB 组 1 例患者再发心肌梗死，行靶血管再次血运重建；DES 组两组 4 例患者行靶血管再次血运重建。两组患者均无心源性死亡、出血事件发生。与非 MACE 事件人群相比，MACE 事件人群术后残余血栓负荷较高（7.92±3.741 vs 17.6±3.209）、夹层（14%vs 80%）、壁内血肿 (4%vs 80%) 发生率高（P < 0.05），DES 或 DCB 两种治疗方式无差异。

结论 在急诊冠脉介入治疗中，DCB 可安全有效地用于充分预处理后的病变治疗。

冠状动脉支架置入策略对左主干分叉病变患者介入术后一年主要不良心血管事件的影响

尼录帕尔·阿不来克木

新疆维吾尔自治区人民医院

目的：本研究旨在分析不同双支架置入策略对左主干分叉病变术后一年主要不良心血管事件（Major Adverse Cardiovascular Events，MACE）的影响。**方法：**采用回顾性研究设计，收集 2011 年 1 月至 2023 年 4 月在我院行经皮冠状动脉介入治疗的左主干分叉病变患者 239 例。根据术中采取的介入策略，分为 Crush 技术组与 Culotte 技术组，比较 Crush 技术策略组和 Culotte 技术策略组患者基线资料，所有患者均接受为期一年的随访并记录患者手术后一年 MACE 发生情况，主要观察重点为患者术后一年 MACE 的发生情况，次要观察终点为支架内再狭窄（In-stent Restenosis，ISR）发生情况。应用 Kaplan-Meier 生存分析法分别绘制 Crush 技术和 Culotte 技术组患者发生 MACE 与 ISR 的累积生存曲线，并通过 log-rank 检验比较两组间的生存率差异。以 P<0.05 作为判断统计学差异的标准。**结果：**主要结局指标是术后一年 MACE 的发生率，次要结局为 ISR 的发生率。结果显示为 Crush 技术组 MACE 发生率高于 Culotte 技术（28.0% vs 14.4%），差异具有显著统计学意义（P<0.05）；Crush 技术组 ISR 发生率高于 Culotte 技术组，差异具有显著统计学意义（P<0.05）。生存分析显示，Crush 技术组 ISR 累积无事件生存率高于 Culotte 技术组，并且差异具有显著统计学意义（P<0.05）；Crush 技术组较 Culotte 技术组 MACE 累积无事件生存率高，差异具有统计学意义（P<0.05）。Cox 比例风险回归模型分析表明，支架置入策略 [HR 0.470，95%CI（0.264-0.835），P = 0.010]、年龄 [HR 0.033，95%CI（1.001-1.066），P = 0.040]、高血压 [HR 0.716，95%CI（1.126-3.718），P = 0.019]、糖尿病 [HR 0.671，95%CI（1.116-3.429），P = 0.019]、糖化血红蛋白 [HR 0.226，95%CI（1.062-1.480），P = 0.008] 是左主干分叉病变患者术后随访期间发生 MACE 的影响因素。**结论：**相较于 Crush 技术，对左主干分叉病变患者中采用 Culotte 技术策略进行治疗，对 MACE 的发生有更显著的保护作用，具有更低的 ISR 发生率。

Comparison of Spherical Tip Versus Regular Noncompliant Balloons for Crossability in Tortuous Coronary Artery Post-dilatation

Guo-Zhe Sun, Chang Wang, Li Zhang, Cai-Yu Zhang, Chen-Hua He

Department of Cardiology, First Hospital of China Medical University, Shenyang 110001, Liaoning Province, China.

Comparison of Spherical Tip Versus Regular Noncompliant Balloons for Crossability in Tortuous Coronary Artery Post-dilatation

Guozhe Sun, Chang Wang, Li Zhang, Caiyu Zhang, Chenhua He

Department of Cardiology, The First Hospital of China Medical University, Shenyang, Liaoning, China.

Abstract

Background and Aims:

Coronary artery tortuosity (CAT) is a common anatomical challenge encountered during percutaneous coronary intervention (PCI), often associated with reduced device deliverability, procedural failure, and higher rates of both early and late major adverse cardiovascular events (MACE). Achieving optimal lesion preparation through effective post-dilatation is critical to procedural success, particularly in tortuous or calcified vessels. Traditional regular non-compliant balloons (RegNCs) may face resistance or failure to cross severely angulated or stenotic segments, resulting in longer procedure times and increased complication risk. A novel device, the spherical-tip non-compliant balloon (SphNC), has been designed to enhance crossability by reducing tip resistance while maintaining inflation pressure characteristics. This study aimed to evaluate the first-pass crossability, overall procedural efficiency, and safety of SphNC compared to conventional RegNC in patients with tortuous coronary artery lesions undergoing PCI.

Methods:

We conducted a multicenter, randomized, controlled, single-blind trial across six PCI centers in Liaoning Province, China. Eligible patients were adults with de novo coronary lesions requiring post-dilatation after stent deployment, and who presented with moderate-to-severe vessel tortuosity (defined as ≥ 2 bends ≥ 90° , or ≥ 1 bend ≥ 120°) on angiography. Participants were randomly assigned in a 1:1 ratio to receive either the SphNC (intervention) or RegNC (control) post-dilatation balloon. Operators were blinded to group allocation until the moment of device preparation. The primary endpoint was the first-attempt crossability, defined as successful balloon passage through the lesion without device change, additional guidewire support, or deep intubation. Secondary endpoints included final crossability rate (after adjunctive measures if needed), number of crossing attempts, crossing time (seconds), and any procedural or device-related complications. To address missing data and potential confounders, a sensitivity analysis was conducted using multiple imputation, propensity score modeling, and inverse probability weighting (IPW). Subgroup analyses explored consistency across patient age, lesion location, calcification, and other baseline characteristics.

Results:

Between February 2023 and August 2024, 250 patients were enrolled,

with 124 in the intervention group and 119 in the control group. The intervention group had significantly higher first-attempt (91.1% vs 52.9%; P < 0.001) and final crossability (96.0% vs 60.5%; P < 0.001) rates, and shorter crossing times (8.3 sec vs 19.7 sec; P < 0.001). Subgroup analyses showed consistent results across various demographics and lesion characteristics. Sensitivity analyses using IPW-adjusted models confirmed the robustness of the findings, yielding similar effect sizes and significance levels. No device-related adverse events were reported, except for balloon retraction resistance (6/124 vs 4/119; P = 0.562). One non-device related cardiovascular death occurred in the intervention group.

Conclusions:

In patients with tortuous coronary lesions requiring post-dilatation, the novel spherical-tip non-compliant balloon (SphNC) demonstrated significantly higher first-attempt and final crossability rates, faster crossing times, and reduced procedural complexity compared to regular non-compliant balloons. These procedural advantages were achieved without increasing adverse events, underscoring the safety and potential utility of the SphNC in complex PCI cases. The robustness of results across multiple sensitivity analyses strengthens the generalizability of the findings. SphNC may represent a valuable advancement in interventional cardiology, particularly in challenging anatomical settings.

Keywords:

coronary heart disease, percutaneous coronary intervention, tortuous coronary artery, post -dilatation

动脉粥样硬化与冠心病学组 孙国哲 15040292137

预见性护理联合 PDCA 循环在减少急性心肌梗死介入诊疗并发症中的应用

伍洪令 谢国锋 龙雄

贵州医科大学大学城医院

背景与目的：

急性心肌梗死（AMI）患者行急诊经皮冠状动脉介入治疗（PCI）后，仍面临出血、对比剂肾病、心律失常等并发症风险。传统护理模式以被动应对为主，效果有限。本研究探讨预见性护理联合 PDCA 循环在减少 AMI 介入诊疗并发症中的应用效果，旨在优化护理流程，提高患者安全性。

方法：

选取 2023 年 1 月至 2024 年 6 月在本院接受急诊 PCI 的 AMI 患者 200 例，随机分为对照组（n=100，常规护理）和观察组（n=100，预见性护理 +PDCA 循环）。预见性护理包括：①术前风险评估（CRUSADE 出血评分、Mehran 对比剂肾病评分）；②术中动态监测（生命体征、ACT 值）；③术后早期干预（穿刺部位观察、水化治疗）。PDCA 循环通过计划（Plan）- 实施（Do）- 检查（Check）- 处理（Act）四个阶段持续改进护理质量，如优化止血方案、规范术后监测流程。比较两组术后并发症发生率、住院时间及护理满意度。

结果：

观察组并发症总发生率显著低于对照组（9.0% vs. 22.0%，P<0.05），其中穿刺部位出血（2.0% vs. 8.0%）、对比剂肾病（1.0% vs. 6.0%）及心律失常（4.0% vs. 7.0%）差异均具有统计学意义。观察组平均住院时间更短（5.5±1.2 天 vs. 7.3±1.6 天，P<0.05），护理满意度评分更高（95.2±2.8 分 vs. 87.6±3.9 分，P<0.05）。

结论与意义：

预见性护理联合 PDCA 循环可有效降低 AMI 患者介入诊疗并发症发生率，缩短住院时间并提升护理质量。其优势在于通过前瞻性风险识别和闭环管理实现护理流程的持续优化，为临床实践提供科学依据。本研究成果可为 AMI 介入治疗的护理标准化提供参考，值得推广。

血红蛋白水平与接受 PCI 治疗的 NSTE-ACS 患者预后的相关性

鲍丹 韩雅玲

中国人民解放军北部战区总医院

目的：本研究旨在探讨血红蛋白水平与接受经皮冠状动脉介入治疗的非 ST 段抬高型急性冠状动脉综合征患者预后的相关性，明确不同血红蛋白水平对患者长期预后的影响。

方法：研究纳入 2017 年 1 月至 2019 年 3 月间住院接受经皮冠状动脉介入治疗的非 ST 段抬高型急性冠状动脉综合征患者 9280 例。分析入院首次血红蛋白、住院期血红蛋白最小值、血红蛋白相对变化、血红蛋白绝对变化对于预后的预测价值。研究的主要结果为出院后 1 年的全因死亡事件。

结果：全部的患者，入院首次血红蛋白值的均值和标准差为 138.32±14.86 g/L，中位数和四分位数为 139.0 （129.0-149.0）g/L。住院期血红蛋白最小值的均值和标准差为 129.18±14.74 g/L，中位数和四分位数为 130.0（120.0-139.0）g/L。血红蛋白相对变化均值和标准差为 -6.50%±5.75%，中位数和四分位数为 -5.66%（-10.06% to -1.48%）、血红蛋白绝对变化均值和标准差为 -9.14±8.20 g/L，中位数和四分位数为 -8.0（-14.0 to -2.0）g/L。全部的患者出院后 1 年全因死亡发生率为 1.4%。在预测患者出院后 1 年全因死亡上，住院期血红蛋白最小值的曲线下面积为 0.67 （95% 置信区间：0.61-0.72）、入院首次血红蛋白的曲线下面积为 0.64（95% 置信区间：0.59-0.69）、血红蛋白绝对变化的曲线下面积为 0.59（95% 置信区间：0.54-0.64）。与入院首次血红蛋白、血红蛋白绝对变化、血红蛋白相对变化的预测价值相比，住院期血红蛋白最小值的曲线下面积显著更高，P 值均小于 0.05。

结论：在接受经皮冠状动脉介入治疗的非 ST 段抬高型急性冠状动脉综合征患者中，住院期血红蛋白最小值能够更好的预测出院后 1 年全因死亡事件。

完全生物可降解封堵器闭合膜周部室间隔缺损合并金属封堵器闭合动脉导管未闭一例

周田 周清

蚌埠医学院第一附属医院

目的：探讨复杂结构性心脏病同时采取完全可吸收封堵器与金属封堵器同时应用效果分析。

方法：我们报道了一名有心力衰竭症状的 38 岁男性同时经导管封堵膜周室间隔缺损和动脉导管未闭。患者，男性，38 岁，“反复胸闷半年，加重 1 周” 入院，主要表现为轻微活动即感胸闷气促，并伴有下肢水肿。听诊时发现胸骨左缘第二、第三、第四肋间均可闻及 III 级收缩期杂音。肺部 CT 显示肺动脉增宽，两肺轻度肺血异常；两肺慢性炎性病变可能；左心增大；心电图检查显示窦性心律、左心增大；心脏彩超示：室间隔缺损伴膜部瘤形成（基底部约 13mm，顶部破口 10mm，瘤体深度约 14mm），室水平左向右分流；动脉导管未闭（内径 9mm，长度约 10mm），动脉水平左向右分流；右室流出道狭窄；左室收缩及舒张功能正常。术中采用完全生物可降解室间隔缺损封堵器及金属封堵器完成对复杂结构性心脏病治疗，患者术后出现大量血尿，治疗上给予大量补液、应用激素稳定细胞膜、碱化尿液等处理，持续一周后，尿液颜色转为无色，复查尿常规尿潜血阴性，稳定三天后出院，院外口服氯吡格雷 12 月，因患者高血压，常规口服沙库巴曲缬沙坦降压及改善心肌重构，同时口服少量利尿药物减轻心脏负荷。

结果：患者胸闷乏力显著改善，分别于 1/12 个月进行超声心动图随访发现，封堵器位置正常、形态良好，左室舒张末期容积及左房较前明显减小，封堵处无残余分流，无新发瓣膜反流、无赘生物及血栓形成、无心包积液，期间心电图检查无房室传导阻滞等出现。

结论：采用完全生物可降解封堵器闭合膜周部室间隔缺损合并金属封堵器闭合动脉导管未闭术后，患者未再出现血尿，胸闷乏力感显著减轻，活动耐力改善，下肢无水肿。门诊复查超声心动图显示封堵器位置正常、形态良好，左室舒张末期容积及左房较前明显减小。封堵处无残余分流，无新发瓣膜反流、无赘生物及血栓形成、无心包积液、无房室传导阻滞等出现。证明完全生物可降解封堵器联合金属封堵器闭合复杂结构性心脏病效果良好，完全可吸收封堵器具有潜在的替代部分金属封堵器的选组，其长期又是需大规模研究验证。

左主干冠状动脉疾病合并贫血行冠状动脉介入治疗患者临床特征及预后分析

鄢华 刘道权 宋丹 刘华云 郭卉 王炜 易东

武汉亚洲心脏病医院

目的 分析贫血对血管内超声 (IVUS) 指导下经皮冠状动脉介入治疗（PCI）的左主干冠状动脉疾病 (LMCAD) 患者临床特征及预后。

方法 回顾性分析 2017 年 1 月至 2020 年 12 月武汉亚洲心脏病医院心血管内科收治的 LMCAD 行 IVUS 指导的 PCI 术患者。根据是否合并贫血分为贫血组和非贫血组。通过电子病理系统收集患者的临床资料，对比患者在临床特征和预后方面的差异，随访终点为主要不良心血管事件 (MACE，定义为全因死亡、心肌梗死、卒中的复合终点)。

结 果 共 纳 入 LMCAD 患 者 325 例，平 均 年 龄（62.56 ± 9.86）岁，男 性 73.54%，其中贫血组 98 例（30.15%），中位随访 5 年。与非贫血组相比，贫血组患者年龄更大（P < 0.001），慢性肾脏病比例更高（均 P < 0.01）。贫血组患者冠脉造影合并三支病变比例、IVUS 测量左主干病变钙化度数和 SYNTAX II 评分更高（均 P < 0.05）。贫血组患者全因死亡率和 MACE 显著增加（均 P < 0.001），校正年龄和估算肾小球滤过率（eGFR）后，贫血与 MACE 和再发心肌梗死独立相关。

结论：合并贫血的 LMCAD 患者年龄更大，CKD 患病率更高，病变累及范围更广泛，钙化程度更严重，远期预后更差。

Feasibility of Distal Radial Artery Access and the Influence of Arterial Diameter on Puncture Difficulty

Yuan Du, Huan-Huan Wang, Ming-Hao Liu, Li-Jian Gao

Fuwai Hospital Chinese Academy of Medical Sciences and Peking Union Medical College

Background: Recent years, the distal radial artery (DRA) access has emerged as a novel alternative arterial access for percutaneous procedures. Using the anatomical snuffbox as puncture site, DRA access for coronary procedures achieves similar percutaneous coronary intervention (PCI) success rates to conventional radial artery access, while offering significant advantages such as a lower risk of radial artery occlusion, shorter compression times, and improved patient comfort. The feasibility and safety of DRA access have been extensively evaluated in clinical studies. However, its widespread adoption has been limited by the relatively higher puncture difficulty compared to conventional radial artery access.

Method: A total of 733 patients proposed for DRA access were enrolled at the Department of Cardiology, Fuwai Hospital, between 2021 and 2024. All patients underwent preoperative ultrasound evaluation to

measure the radial artery diameter at the snuffbox, and at 5 cm, 10 cm, and 15 cm proximal to the styloid process of the radius. The primary outcome was DRA difficult puncture, defined as puncture time exceeding 3 minutes. Univariate and multivariate logistic regression analyses were conducted to evaluate the impact of various factors on difficult puncture. Segmented logistic regression was applied to identify threshold values associated with a high likelihood of difficult puncture. Restricted cubic spline (RCS) analysis was performed to assess potential nonlinear associations between the radial artery diameter at the snuffbox and puncture outcomes, and to determine an optimal cutoff value.

Results: The overall DRA puncture success rate among these patients was 96.59%. PCI was performed in 74.0% of cases, with a procedural success rate of 92.7%. The mean puncture time was 2.77 ± 2.62 minutes, with an average of 1.41 ± 0.78 puncture attempts. Radial artery ultrasound findings showed that the pre-puncture diameters of the radial artery at snuffbox, and at 5 cm, 10 cm, and 15 cm proximal to the styloid process of the radius were 2.34 ± 0.43 mm, 2.62 ± 0.47 mm, 2.78 ± 0.50 mm, and 2.92 ± 1.07 mm, respectively. Radial artery occlusion and arteriosclerosis were observed in 7 (1.0%) and 8 (1.1%), respectively. Univariate logistic regression analysis showed that the diameters of the radial artery at the snuffbox (OR, 0.61; 95% CI, 0.40-0.94), and at 5 cm (OR, 0.61; 95% CI, 0.41-0.90), 10 cm (OR, 0.51; 95% CI, 0.36-0.74), and 15 cm (OR, 0.49; 95% CI, 0.34-0.70) proximal to the radial styloid process were significantly associated with difficult puncture. After adjusting various variables, DRA diameter at the snuffbox was still significantly associated with difficult puncture (OR, 0.62; 95% CI, 0.40-0.97). Notably, the RCS curve demonstrated that when the artery diameter at the snuffbox was below 2.4 mm, the risk of difficult puncture increased as the diameter decreased. Furthermore, segmented logistic regression analysis revealed that the likelihood of difficult puncture decreased significantly as the radial artery diameter at the snuffbox increased when the diameter was below 2.1 mm, but showed a slight increase when the diameter exceeded 2.1 mm.

Conclusion: The safety and feasibility of DRA access were confirmed in our study, with puncture success primarily associated with the DRA diameter. This finding offers an important anatomical criterion for patient selection and provides valuable guidance for clinicians when considering DRA access in future interventions.

Risk factors for no spontaneous reperfusion of ST-segment elevation myocardial infarction: A case-control study

-Xue Jiang

兰州大学第一医院

Background: Up to 30% of patients with STEMI have spontaneous reperfusion (SR) before PCI, and the myocardial infarct (MI) size after SR is smaller than those with no SR, and their clinical prognosis is better. Understanding the factors influencing the occurrence of SR could help improve STEMI management. To evaluate the risk factors for no spontaneous reperfusion (SR) in patients with ST-segment elevation myocardial infarction (STEMI).

Methods: This case-control study included patients diagnosed with STEMI who underwent emergency coronary angiography at First Hospital of Lanzhou University between January 2023 and December 2024. This retrospective case-control study included patients with STEMI who underwent emergency coronary angiography in the First Hospital of Lanzhou University between January 2023 and December 2024.The inclusion criteria were 1) patients with STEMI duration <12 h, and 2) emergency coronary angiography showed coronary stenosis or occlusion with abnormal wall motion. The exclusion criteria were 1) the final diagnosis was non-ST-segment elevation myocardial infarction (NSTEMI), unstable angina pectoris, Takotsubo myocardium disease, myocarditis, or cardiogenic shock requiring mechanical assist devices, or 2) patients with missing clinical or follow-up data. The STEMI diagnostic criteria were based on the presence of symptoms of myocardial ischemia, elevated serum biomarker (troponin), and ST-segment elevation of ≥ 1 mm in ≥ 2 consecutive associated leads. SR was defined as culprit vessel TIMI flow grade 3 at the first injection of contrast. No SR was defined as TIMI grade 0-2 flow in the culprit vessel before PCI.All patient follow-up data were obtained from the database of the authors' department's follow-up center.Multivariate logistic regression analysis was used to identify the factors independently associated with no SR.

Results: Of the 660 patients with STEMI, 264 (40.0%) showed SR, and 396 (60.0%) showed no SR. There were no significant differences between the two groups in age, sex, smoking, diabetes, hypertension, stroke, history of angina pectoris in the past 1 month, and location of MI (all P>0.05). Compared with the SR group, the no SR group had significantly higher BMI (24.4±3.0 vs. 23.8±4.1 kg/m^2, P=0.025), proportion of MS (39.7% vs. 31.4%, P=0.032), and proportion of Killip 3-4 (6.6% vs. 3.0%, P=0.044), and significantly lower frequency of single-vessel lesion (45.2% vs. 59.5%, P<0.001). Additionally, the blood routine test results indicated that the white blood cell count (8.71±3.39 ×10^9/L vs. 7.63±2.75 ×10^9/L, P<0.001) and AST levels (100.2±136.1 U/L vs. 80.1±98.7 U/L, P=0.041) in the no SR group were significantly higher than that of in SR group.Multivariate logistic regression showed that the MS (OR=1.48, 95%CI: 1.05-2.09, P=0.025), white blood cell count (OR=1.11, 95%CI: 1.05-1.18, P<0.001), and single-vessel disease (OR=0.56, 95%CI: 0.40-0.78, P=0.001) were independently associated with no SR in patients with STEMI .The results of echocardiography within 24 h showed that compared with the SR group, the patients with no SR had a lower LVEF (52.9±8.5% vs. 55.0±9.3%, P=0.003) and larger LVEDV (126.2±68.9 vs. 116.6±40.7 ml, P=0.045) and LVESV (59.7±30.8 vs. 53.9±30.7 ml, P=0.020). There were no significant differences in all-cause mortality between the two groups after a mean follow-up of 28 months (4.6% vs. 3.8%, P=0.882). After a mean follow-up of 28 months, the all-cause mortality of STEMI with MS was significantly higher than that without MS .

Conclusions: MS, single-vessel disease, and white blood cell count were independently associated with no SR in patients with STEMI.This study was a single-center, retrospective study, so there may be a risk of data analysis bias, and the findings need to be validated. Nevertheless, this study can provide a reference for large-scale analytical studies or experimental studies.

Abstract Objective Acute coronary syndrome (ACS) is a critical and life - threatening cardiovascular condition that poses a significant challenge to global health. It encompasses a spectrum of clinical manifestations, from unstable angina to ST - segment

Xue-Fei Mu

State Key Laboratory of Frigid Zone Cardiovascular Disease, Cardiovascular Research Institute and Department of Cardiology, General Hospital of Northern Theater Command

Abstract

Objective

Acute coronary syndrome (ACS) is a critical and life - threatening cardiovascular condition that poses a significant challenge to global health. It encompasses a spectrum of clinical manifestations, from unstable angina to ST - segment elevation myocardial infarction (STEMI) and non - ST - segment elevation myocardial infarction (NSTEMI). Percutaneous coronary intervention (PCI) has emerged as a cornerstone in the treatment of ACS, effectively restoring blood flow to the ischemic myocardium and improving short - term outcomes. However, patients who undergo PCI often still face the risk of post - PCI ischemic events, which can significantly impact their long - term prognosis and quality of life.

This study aimed to investigate the prognostic value of high - sensitivity cardiac troponin T (hs - cTnT) levels and diabetes mellitus (DM) on ischemic events within 12 months after PCI in ACS patients. Hs - cTnT is a highly sensitive biomarker that can detect even minor myocardial injury, while DM is a well - known risk factor for cardiovascular disease. Understanding the relationship between these factors and post - PCI ischemic events can provide valuable insights for clinicians, enabling them to optimize patient management, stratify risk more accurately, and improve patient outcomes.

Methods

This was a retrospective cohort study conducted at the General Hospital of the Northern Theater Command. A total of 14,173 consecutive ACS patients who underwent PCI between March 2016 and March 2022 were included in the study. The primary outcome was the occurrence of ischemic events within 12 months after PCI, which was defined as a composite of cardiac death, non - fatal myocardial infarction (MI), and/or stroke. These events are not only associated with high morbidity and mortality but also impose a substantial burden on the healthcare system.

Secondary outcomes included all - cause mortality at 12 months and the individual components of the primary outcome. To ensure the accuracy of the analysis, multiple covariates such as age, gender, comorbidities (e.g., hypertension, hyperlipidemia), and previous cardiovascular history were carefully considered. By adjusting for these confounding factors, we could more precisely evaluate the independent effects of hs - cTnT levels and DM on post - PCI outcomes.

Results

During the 12 - month follow - up period, the overall incidence rates of ischemic events, cardiac death, MI, stroke, and all - cause mortality were 2.19%, 1.12%, 0.58%, 0.59%, and 1.55% respectively. Elevated hs - cTnT levels were significantly associated with increased risks of ischemic events (adjusted HR: 1.91, 95% CI: 1.19 - 3.09), cardiac death (adjusted HR: 2.00, 95% CI: 1.08 - 3.71), and all - cause mortality (adjusted HR: 2.78, 95% CI: 1.62 - 4.76).

In diabetic patients, when hs - cTnT levels reached ≥ 5×URL (upper reference limit), the risks were notably more prominent. Interaction analyses indicated that there was no significant interaction between hs - cTnT levels and diabetes status regarding ischemic events (P = 0.78), suggesting that the effects of hs - cTnT and DM on ischemic events are independent. However, there was a significant interaction for all - cause mortality (P = 0.01), indicating that the impact of hs - cTnT on mortality is more complex in diabetic patients.

Conclusions

The findings of this study suggest that elevated hs - cTnT levels and the presence of DM are independently associated with an increased risk of ischemic events and all - cause mortality after PCI in ACS patients. The impact of hs - cTnT on mortality is more pronounced in diabetic patients, highlighting the need for more aggressive management strategies in this high - risk population.

These results emphasize the importance of routine hs - cTnT monitoring in ACS patients, especially those with DM. Clinicians should take these factors into account when formulating individualized treatment and follow - up plans. By better understanding the prognostic value of hs - cTnT and DM, we can potentially reduce the incidence of post - PCI adverse events and improve the long - term prognosis of ACS patients, ultimately leading to better patient outcomes and a more efficient use of healthcare resources.

Keywords: Acute Coronary Syndrome, Percutaneous Coronary Intervention, High - Sensitivity Cardiac Troponin T, Diabetes Mellitus, Ischemic Events

Protamine-Facilitated Same-Day Discharge Following Distal Transradial Angiography

Yan Chen, Ming-Hao Liu, Huan-Huan Wang, Li-Jian Gao

Fuwai hospital

Background: Despite growing adoption of distal transradial approach (dTRA), data on same-day discharge with protamine-assisted hemostasis following coronary angiography (CAG) remain limited. This pilot study prospectively assessed the safety and feasibility of adjunctive protamine administration with dTRA to facilitate early discharge after CAG.

Methods: From January 2022 to September 2024, a total of 34 patients who were discharged on the same-day after elective CAG via dTRA in our center were included, as well as 34 matched patients who underwent CAG via standard transradial approach (sTRA) during the same period. Exclusion criteria included (1) patients with diagnosis of acute myocardial infarction, and (2) patients with comorbidities that may lead to extra treatment or prolonged hospital stay, such as severe liver or renal dysfunction. After procedure, patients in sTRA group received hemostatic compression devices, whereas patients in dTRA group underwent elastic bandage and gauze pads compression with immediate protamine administration to reverse heparin anticoagulation. Patent hemostasis (pulse oximetry-confirmed) was employed universally. The nurse checked whether the compression site had stopped bleeding every hour. If no bleeding or hematoma was found, the compression device or bandage was released. If the access site had bleeding or a mild hematoma, the site was pressed for another 30 to 60 minutes. Multivariable regression models were conducted to analyses the correlation between different radial artery accesses and clinical variables. The primary endpoint was time to hemostasis, and secondary endpoints were costs and procedure duration. The safety endpoints were the incidences of bleeding-related complications.

Results: The mean age of patients was 58.5 years and 64.7% were male. No significant differences were found in age, height, body mass index or traditional CAD risk factors between the two groups. A total of 7 patients (20.6%) in the dTRA group and 15 patients (44.1%) in the sTRA group had a history of percutaneous coronary intervention, respectively. A comparable proportion of patients presented with stable angina(52.9% vs 58.8%, P = 0.625). All patients underwent CAG with successful insertion of a 6F sheath in both groups. There was no significant difference in the average number of punctures (1.5 vs 1.7, P = 0.229) and puncture duration between two groups. Upper extremity angiography was performed in all dTRA patients (34/34) versus 8.8% (3/34) of sTRA patients. 4 patients in the dTRA group and 5 patients in the sTRA group received intracoronary imaging or Coronary Functional examination. 4 patients in the dTRA group and 5 patients in the sTRA group received intracoronary imaging or Coronary Functional examination. Compared with the sTRA group, the dTRA group had a significantly shorter hemostasis time (1.3h vs. 5.9h, P < 0.001) and a lower hospital cost (12.8 vs. 14.6(CNY $\times 10^3$), P = 0.020). Procedure duration didn't differ between the two groups. No major hematoma, access-site bleeding, arteriovenous fistula or pseudoaneurysm was recorded. 5 cases of self-reported numbness of extremity on the access site were recorded in the sTRA patients, compared no cases in dTRA patients. There were 2 cases of radial artery occlusion in dTRA group and 3 cases in sTRA group one month after discharge, with no significant difference (P = 0.642). Multivariable regression analysis showed that dTRA significantly shortened hemostasis time (β -3.1, 95% CI -3.8 ~ -2.3, P < 0.001) with a reduction in costs[β -3.3, 95% CI -5.400 ~ -1,200, P = 0.004, (CNY $\times 10^3$)]. No relationship of access approach with procedure duration was found.

Conclusions: Same-day discharge after dTRA CAG with protamine was feasible and safe, achieving significantly reduced hemostasis time and costs compared to sTRA.

Predictive Value of Coronary Radial Wall Strain Combined with Angiographic Parameters for Myocardial Infarction and Unplanned Revascularization: A Case-Control Study

Si-Da Jia[1], Ying Song[1], Yu-Ming Ren[2], Zhi-Qing Wang[3,4], Sheng-Xian Tu[3,4], Jin-Qing Yuan[1]

1. Fuwai Hospital CAMS & PUMC

2. Shanghai Pulse Medical Technology, Inc.

3. Department of Cardiology, Huadong Hospital, Fudan University

4. Biomedical Instrument Institute, School of Biomedical Engineering, Shanghai Jiao Tong University

Background

Radial wall strain (RWS), a biomechanical marker quantifying local coronary deformation during cardiac cycles, has emerged as a promising tool for plaque vulnerability assessment. Prior studies indicate RWS correlates with high-risk plaque features and predicts myocardial infarction (MI) by reflecting endothelial shear stress distribution. However, its role in forecasting unplanned revascularization—a critical endpoint often driven by progressive atherosclerosis or restenosis—remains unexamined. Conventional angiographic parameters (e.g., QFR, lesion length) lack sensitivity to early biomechanical dysfunction, which may precede anatomical stenosis. This gap is significant given that biomechanical alterations in coronary walls precede acute events and may serve as earlier intervention triggers. We thus aimed to evaluate RWS alongside conventional indicators for predicting composite MI/unplanned revascularization events, addressing a pivotal unmet need in precision cardiology.

Methods

In this single-center case-control study, we included 241 patients (264 lesions) from a cohort of 10,724 patients with CAD underwent PCI in Fuwai Hospital from Jan 2013 to Dec 2013. The event group (n=132 lesions) comprised patients who required repeat hospitalization for either myocardial infarction (MI) or unplanned revascularization post-PCI, which were propensity matched 1:1 with control group lesions (n=132) from patients without such events based on demographic characteristics (including age, sex, low density lipoprotein level and hypertension) and lesion localization (Figure 1). Key angiographic parameters assessed included RWS maximum value (RWSmax), baseline quantitative flow ratio (QFR), resting and simulated hyperemic Angiography-derived Microcirculatory Resistance (AMR), among other morphological characteristics. Predictive performance was evaluated through receiver operating characteristic (ROC) curve analysis, while logistic regression models identified independent predictors for MI/unplanned revascularization.

Results

Baseline patient characteristics demonstrated comparability between the event group (post-PCI MI/unplanned revascularization) and controls, except for significantly higher diabetes incidence in the event group (32.4% vs. 19.2%, P < 0.05). Lesion-level analysis revealed that event-associated lesions exhibited markedly elevated RWSmax (P < 0.001), increased stenosis severity (P = 0.002), and prolonged lesion lengths (P < 0.001), alongside reduced baseline QFR (P < 0.001). ROC analysis identified RWSmax (AUC = 0.671, 95% CI: 0.584–0.758), baseline QFR (AUC = 0.699, 95% CI: 0.619–0.779), simulated hyperemic AMR (AUC = 0.696, 95% CI: 0.612–0.780), and lesion length (AUC = 0.687, 95% CI: 0.603–0.771) as strong predictors of composite events. The integration of these parameters into a combined model significantly enhanced predictive accuracy (AUC = 0.764, 95% CI: 0.692–0.836) (Figure 2). Subsequent multivariate logistic regression adjusted for clinical and angiographic confounders demonstrated that RWSmax exceeding 13.00% (adjusted OR = 2.699, 95% CI: 1.315–5.540, P = 0.007) and lesion length greater than 28.11 mm (adjusted OR = 2.597, 95% CI: 1.348–5.001, P = 0.004) remained independently associated with event risk. Biomechanical and morphological parameters including resting AMR, and proximal/distal reference diameters showed no significant predictive value in fully adjusted models.

Conclusion

This case-control study identifies RWSmax >13% as an independent biomechanical predictor for post-PCI composite myocardial infarction/unplanned revascularization events, persisting after multivariable adjustment. When integrated with morphological parameters, it significantly enhances risk stratification, providing a novel biomechanical-morphological prognostic model. These findings suggest RWS implementation during routine angiography might refine PCI risk assessment and guide targeted surveillance protocols for vulnerable lesions, though prospective validation remains warranted before clinical adoption.

原发性与继发性自发性心肌梗死的差异：来自 ISCHEMIA 研究的启示

赵泽昊 曾勇

首都医科大学附属北京安贞医院

背景：根据病理生理机制，心肌梗死 (Myocardial Infarction, MI) 被分为五种类型。与第 4a 型和第 5 型不同，第 1 型、第 2 型、第 4b 型和第 4c 型与血运重建过程无关，被称为自发性心肌梗死。其中，第 1 型、第 4b 型和第 4c 型通常由冠状动脉新发病变或支架内再狭窄及血栓形成引起，而第 2 型则源于心肌氧供与需之间的不平衡。因此，这些类型可以区分为原发性自发性心肌梗死 (Primary Spontaneous Myocardial Infarction, PSMI) 和继发性自发性心肌梗死 (Secondary Spontaneous Myocardial Infarction, SSMI)。然而，PSMI 与 SSMI 在临床特征、预后以及预防策略上是否存在差异，尚不明确。

方法：本研究对 ISCHEMIA 和 ISCHEMIA-CKD 试验中公开数据进行了二次分析 (数据来源：BioLINCC，NHLBI；https://biolincc.nhlbi.nih.gov/)。在随机分组时收集了患者的基线特征，包括人口统计学信息、病史、动脉粥样硬化危险因素、主观心绞痛严重程度、缺血范围及冠状动脉病变严重程度，并比较了 PSMI 与 SSMI 患者之间的差异。使用冠状动脉 CT 血管成像计算的节段累及评分 (Segment Involvement Score, SIS)、病变狭窄评分 (Segment Stenosis Score, SSS) 和 DUCK 评分评估冠脉病变严重程度。采用 Cox 回归分析探讨不同类型心肌梗死对死亡风险的影响、冠状动脉狭窄对不同类型 MI 的影响，以及血运重建治疗是否可降低各类型 MI 的风险。

结果：SSMI 组血红蛋白水平较低 (13.8 [12.3;14.8] g/L, 12.7 [11.0;14.0] g/L, p <0.001) 及严重缺血比例较低 (36.6%, 56.6%, p = 0.001)，此外，两组在基线特征方面无显著差异。SSMI (HR 7.83 [5.53–11.08]) 和 PSMI (HR 4.16 [3.22–5.38]) 均显著增加后续死亡风险，且 SSMI 对死亡的影响更为显著。在 SSS、SIS 和 DUCK 评分中，SSS 评分，一项综合了病变部位和严重程度的评分，能够预测 PSMI 与 SSMI 的风险，提示冠状动脉病变的严重程度是两种类型 MI 的共同危险因素。然而，血运重建治疗仅能降低 PSMI 的风险 (HR 0.60 [0.47–0.76])，对 SSMI 的风险无显著影响 (HR 0.96 [0.66–1.40])。

结论：SSMI 对死亡风险的影响更为显著。冠状动脉狭窄程度影响 PSMI 与 SSMI 的发生风险，但只有 PSMI 的风险可通过靶向冠状动脉狭窄的治疗——血运重建加以降低。

使用 6F 桡动脉鞘管和 6.5F 桡动脉鞘管经桡动脉路径行冠状动脉造影及介入的对比分析

刘喜 赵磊

内蒙古鄂尔多斯市中心医院

目的：本文旨在通过使用 6F 桡动脉鞘管和 6.5F 桡动脉鞘管经右侧常规桡动脉穿刺途径行 CAG 及 PCI 术中及术后观察指标对比，评估使用 6.5F 桡动脉穿刺鞘管行 CAG 及 PCI 术中及术后的安全性。

方法：随机选取 2022 年 11 月至 2023 年 11 月使用 6F 桡动脉鞘管（迪玛克医疗器械有限公司）及 6.5F 桡动脉鞘管（埃普特医疗器械有限公司）行 CAG 及 PCI 的患者，依据《中国经皮冠状动脉介入治疗指南（2016）》的适应证行 PCI。分为对照组（迪玛克公司生产的 6F 桡动脉鞘管）和研究组（埃普特公司生产的 6.5F 桡动脉鞘管），统计两组患者的疼痛感、穿刺时间、穿刺成功率、手术时间、桡动脉痉挛（radial artery spasm,RAS）、术中造影剂用量、术者操作顺畅度评价、迷走反射发生情况、术中更换鞘管的比例、术后压迫止血时间，桡动脉出血、血肿、桡动脉闭塞（radial artery occlusion,RAO）、桡动脉血栓、假性动脉瘤的发生率，统计术前、术后 3 天、术后 1 个月两组患者的桡动脉血管内径，血流速度（PHILIPS 彩色多普勒超声评估）。使用 SPSS 24 版本进行统计学分析，检验水准 α=0.05。

结果：本次研究严格依据排纳标准共搜集了 165 例患者，其中 7 例患者失访，已排除，对照组患者 80 例，研究组患者 78 例（研究组与对照组中 PCI 数量都为 40 例），所纳入病历均已经完成各项数据的搜集及随访。（1）两组患者基本资料的比较：在年龄、性别、血脂、高血压病病史、吸烟史、心律失常、糖尿病病史或糖耐量异常、体重、家族史等方面进行比较，差异无统计学意义(P>0.05)。（2）两组患者在穿刺时间、穿刺成功率、术中造影剂用量、迷走反射发生情况方面差异无统计学意义（P>0.05），两组患者在疼痛感、手术时间、RAS、术者操作顺畅度、术后压迫止血时间方面进行比较，差异具有统计学意义（P<0.05），研究组患者疼痛感更轻、手术时间更短、RAS 发生概率更低、术者操作更顺畅、术后压迫止血时间更短。对照组与研究组在桡动脉出血、桡动脉血肿、术后血栓、假性动脉瘤发生方面，差异无统计学意义（P>0.05），对照组术后 RAO 发生率高于研究组，差异具有统计学意义（P<0.05）。（3）由重复测量方差分析结果可知：右侧桡动脉管腔内径的时间主效应影响显著（F=95.227，P < 0.05），组别主效应影响不显著（F=2.273，P > 0.05），时间 * 组别交互效应影响显著（F=27.083，P < 0.05）。由于交互效应影响显著，进一步进行简单效应可知，术前、术后 3 天、术后 1 个月对照组和研究组间右侧桡动脉管腔内径均差异不显著（P > 0.05）；对照组、研究组的右侧桡动脉管腔内径术前显著高于术后 3 天、术后 1 个月，术后 1 个月显著高于术后 3 天（P < 0.05）。右侧桡动脉血流速度时间主效应影响显著 (F=30.247, P < 0.05)，由多重比较结果可知，术后 3 天、术后 1 个月右侧桡动脉血流速度显著高于术前。组别主效应影响不显著 (F=0.016, P > 0.05)，时间 * 组别交互效应影响不显著（F=0.454，P>0.05）。

结论：以埃普特公司为代表生产的 6.5F 桡动脉薄壁鞘管作为新的穿刺器械在术中及术后是安全可行的，配合 6F 或 6.5F 导引导管可以完成绝大多数 PCI，为术者术前预规划提供了更多的器械选择，在降低穿刺相关并发症发生率的同时，提高了手术舒适度。

长鞘管在经桡动脉冠状动脉造影中的应用效果分析

崔翰斌

宁波大学附属第一医院

目的　分析长鞘管在经桡动脉途径冠状动脉造影（CAG）中的有效性和安全性。　方法　回顾性选择 2022 年 4 月至 2023 年 4 月在宁波大学附属第一医院诊断为可疑冠心病患者 1695 例。其中在 CAG 术中使用长鞘管患者 714 例（观察组），短鞘管患者 981 例（对照组），收集并比较两组患者的基本数据、导丝血管通过率、手术时间、射线时间、射线剂量、对比剂用量、更换导丝比例、更换左侧桡动脉比例、更换造影导管比例及手术并发症。采用多因素 logistic 回归分析导丝血管通过率的影响因素。　结果　观察组导丝血管通过率明显高于对照组（99.3% 比 93.4%），差异有统计学意义（P < 0.05），观察组手术时间、射线时间、射线剂量、对比剂用量、更换导丝比例、血管痉挛发生率、迷走反应发生率均低于对照组，差异均有统计学意义（均 P < 0.05）。两组患者血管夹层、前臂血肿、更换造影导管和更换左侧桡动脉比例比较，差异均无统计学意义（均 P > 0.05）。两组患者均无血管穿孔、纵隔血肿发生。多因素 logistic 回归分析结果发现年龄及长鞘管均是导丝血管通过率的影响因素(均P < 0.05)　结论　长鞘管相对短鞘管在经桡动脉入路 CAG 术中更有效且安全，值得临床推广应用。

First Evidence of Correlation Between Red Blood Cell Parameters and Angiography-Derived Coronary Microcirculatory Resistance: A New Insight into Coronary Microvascular dysfunction

ABDULRAHMAN ALQAZZAZ[1], Ning Guo[1], Yan-Feng Lu[1], Xin Huang[1], Jia-Hao Feng[1], Yong Zhang[1], Shan-Shan Gao[1], Qiang Song[1], Fei-Fei Ning[1], HYTHAM H. ALSAMAWI[2]

1. Department of Cardiology, First Affiliated Hospital of Xi'an Jiaotong University

2. Department of Cardiology, Second Affiliated Hospital of Xi'an Jiaotong University

Authors: Abdulrahman AlQazzaz[1], Guo Ning*[1], Lu Yanfeng[1], Huang Xin[1], Feng Jiahao[1], Zhang Yong[1], Gao Shanshan[1], Song Qiang[1], Ning Feifei[1] and Hytham H. Alsamawi[2]

* Corresponding author: Guo Ning (nguomd@qq.com)

[1] Department of Cardiology, First Affiliated Hospital of Xi'an Jiaotong University, Xi'an, Shaanxi, China

[2] Department of Cardiology, Second Affiliated Hospital of Xi'an Jiaotong University, Xi'an, Shaanxi, China

Objective: to evaluate whether red blood cell parameters are correlated with the Angiography-Derived Coronary Microcirculatory Resistance in patients with intermediate lesions.

Methods: This retrospective cohort study evaluated the association between red blood cell (RBC) parameters and angiography-derived index of microcirculatory resistance (IMR) in patients with intermediate coronary artery disease (30%-70% stenosis). Data from 733 lesions were extracted from the First Affiliated Hospital of Xi'an Jiaotong University database. Patients were with angiographically assessable lesions suitable for monoplane quantitative flow ratio (mQFR) analysis. RBC parameters (RBC count, hemoglobin, hematocrit, etc.) were obtained during hospitalization prior to angiography. Coronary microcirculatory resistance (IMR) was derived using the AngioPlus mQFR system. Multivariable linear regression models adjusted for demographics, comorbidities, medications, and angiographic severity. Subgroup analyses assessed effect modification by diabetes status, and sensitivity analyses excluded hematocrit outliers, and analyses stratified by vessel (LAD, LCx, RCA). Statistical significance was set at *p* < 0.05 (two-tailed), with rigorous diagnostics for model validity.

Results: Higher RBC, Hct and Hgb were independently associated with elevated angio-derived IMR in multivariable analysis (RBC: β = 0.182, *p* < 0.001; Hct: β = 0.019, *p* < 0.001; Hgb: β = 0.006, *p* < 0.001) adjusted for other blood parameters, demographics, comorbidities and angiographic severity. Results were robust in sensitivity analyses excluding Hct outliers (β = 0.020, *p* < 0.001) and consistent across diabetic (*p* = 0.007) and non-diabetic subgroups (*p* = 0.012). The association was stronger in non-LAD vessels (Hct: β = 0.022, *p* < 0.001 for non-LAD vs. β = 0.008, *p* = 0.357 for LAD).

Association of Erythrocyte Indices (RBC Count, Hematocrit, Hemoglobin) with Microvascular Resistance: Results from Multivariable Linear Regression Models

Variable	Unadjusted β (95% CI)	Model 1 β (95% CI)	Model 2 β (95% CI)	Model 3 β (95% CI)	Model 4 β (95% CI)
RBC	.123 (0.048 to 0.198) **P=0.001**	.187 (0.105 to 0.269) **P<0.001**	.170 (0.075 to 0.265) **P<0.001**	.168 (0.073 to 0.263) **P<0.001**	.182 (0.090 to 0.274) **P<0.001**
Hct	.018 (0.010 to 0.027) **p<0.001**	.019 (0.010 to 0.027) **P<0.001**	.017 (0.007 to 0.027) **P<0.001**	.017 (0.007 to 0.027) **P<0.001**	.019 (0.009 to 0.028) **P<0.001**
Hgb	.006 (0.003 to 0.008) **p<0.001**	.006 (0.004 to 0.008) **P<0.001**	.006 (0.003 to 0.006) **P<0.001**	.006 (0.003 to 0.009) **P<0.001**	.006 (0.003 to 0.009) **P<0.001**

Model 1: Adjusted for other blood parameters.

*Model 2: Model 1 + (age, gender and BMI).

*Model 3: Model 2 + comorbidities (diabetes, hypertension, hypercholesterolemia and prior statins).

*Model 4: Model 3 + angiographic severity (DS%, lesion length).

Conclusion: This study confirms that higher RBC, hematocrit, and hemoglobin levels are independently associated with increased coronary microcirculatory resistance (IMR) in patients with intermediate coronary lesions, particularly in non-LAD vessels. These findings suggest that RBC parameters may serve as clinically relevant markers of microvascular dysfunction, warranting further investigation into their prognostic and therapeutic implications.

1 例经导管主动脉瓣置换术后合并瓣周漏诱发心衰行经导管封堵术患者的护理

李立博 吴黎莉 马燕 章盈盈

浙江大学医学院附属邵逸夫医院

【摘要】 本文总结 1 例中重度主动脉瓣狭窄伴轻度关闭不全患者，在行经导管主动脉瓣置换术术后发生中重度瓣周漏导致心源性休克并行经导管瓣周漏封堵术的护理经验。护理要点：术后超声监测联合连续肾脏替代治疗积极控制心衰；降低出血风险，谨防血栓形成；器械相关性溶血与血管夹层的及早发现与预防；精细化个体康复，提高患者舒适度，动态调整营养支持。手术顺利。在行经导管瓣周漏封堵术以及精细化护理后，患者瓣周反流得到改善，术后心衰得到控制，极大缓解患者胸闷胸痛的症状，患者活动耐力提高。住院期间未发生出血及血栓事件。术后第 46 天康复出院。

Investigating the Clinical Implications and Diagnostic Accuracy of the QFR Grey-Zone in Coronary Artery Disease: A Comprehensive Analysis of TVF Prediction

ABDULRAHMAN ALQAZZAZ[1], Yan-Feng Lu[1], Ning Guo[1], Xin Huang[1], Jia-Hao Feng[1], Yong Zhang[1], Shan-Shan Gao[1], Qiang Song[1], Fei-Fei Ning[1], HYTHAM H. ALSAMAWI[2]

1. Department of Cardiology, First Affiliated Hospital of Xi'an Jiaotong University

2. Department of Cardiology, Second Affiliated Hospital of Xi'an Jiaotong University

Authors: Abdulrahman AlQazzaz†[1], Lu Yanfengt[1], Guo Ning*[1], Huang Xin[1], Feng Jiahao[1], Zhang Yong[1], Gao Shanshan[1], Song Qiang[1], Ning Feifei[1] and Hytham H. Alsamawi[2]

†These authors contributed equally

*Corresponding author: Guo Ning (nguomd@qq.com)

[1] Department of Cardiology, First Affiliated Hospital of Xi'an Jiaotong University, Xi'an, Shaanxi, China

[2]Department of Cardiology, Second Affiliated Hospital of Xi'an Jiaotong University, Xi'an, Shaanxi, China

Objective: This study evaluates the clinical significance and optimal management strategy for coronary lesions in the quantitative flow ratio (QFR) "grey zone" (0.75–0.85), where functional assessment remains uncertain.

Methods: This retrospective study analyzed 297 coronary lesions with borderline QFR values (0.75–0.85). Patients were stratified by treatment (PCI vs. medication-only), with target vessel failure (TVF: cardiac death, target vessel MI, or ischemia-driven revascularization) as the primary endpoint. Baseline characteristics were compared using appropriate statistical tests. Time-to-event analysis used Kaplan-Meier curves and Cox proportional hazards models adjusted for clinical risk factors. To identify predictors of TVF within the grey zone, lesions were further stratified into QFR 0.75–0.80 and 0.81–0.85 subgroups, with interaction testing for variables significantly associated with TVF in the primary analysis.

Results: Among 297 grey-zone lesions (QFR 0.75–0.85), no significant difference in target vessel failure (TVF) was observed between PCI and medication groups (Kaplan-Meier log-rank *p*=0.760). However, in medication-treated patients, LVEF ≤ 45% significantly predicted TVF (adjusted HR 0.008, 95% CI 0.000–0.236, *p*=0.005), with a pronounced interaction between QFR ≤0.80 and LVEF ≤45% (Mantel-Haenszel OR 0.16, 95% CI 0.03–0.77, *p*=0.023). Elevated HbA1c independently increased TVF risk across all medically treated patients (HR 2.18, 95% CI 1.02–4.69, *p*=0.045).

Cox Regression Analysis of Predictors for Target Vessel Failure (TVF): PCI vs. Medical Therapy and Clinical Variables

Variables	B	SE	HR	95.0% CI Lower	95.0% CI Upper	P value
Age	-0.028	0.051	0.972	0.880	1.074	0.580
Gender	-0.180	0.963	0.835	0.126	5.516	0.852
BMI	0.067	0.125	1.069	0.837	1.367	0.592
HTN	0.418	0.827	1.519	0.300	7.686	0.613
Hypercholesterolemia	0.780	0.852	2.181	0.411	11.575	0.360
Diabetes	-1.339	1.232	0.262	0.023	2.934	0.277
Hgb A1c	0.712	0.313	2.038	1.103	3.763	**0.023**
>45% LVEF	-2.899	1.173	0.055	0.006	0.548	**0.013**
proBNP	-0.001	0.001	0.999	0.997	1.001	0.321
eGFR	0.053	0.039	1.054	0.977	1.138	0.176
Flow velocity	0.002	0.085	1.002	0.847	1.185	0.983
MLD	-1.548	1.191	0.213	0.021	2.197	0.194
DS%	-0.008	0.066	0.992	0.872	1.128	0.898
Length	0.007	0.027	1.007	0.954	1.062	0.810
Syntax I score	0.014	0.030	1.014	0.956	1.075	0.644
Treatment type	-0.056	0.828	0.945	0.187	4.787	0.946

Adjusted Hazard Ratio for PCI vs. Medical Therapy Predicting Target Vessel Failure (TVF)

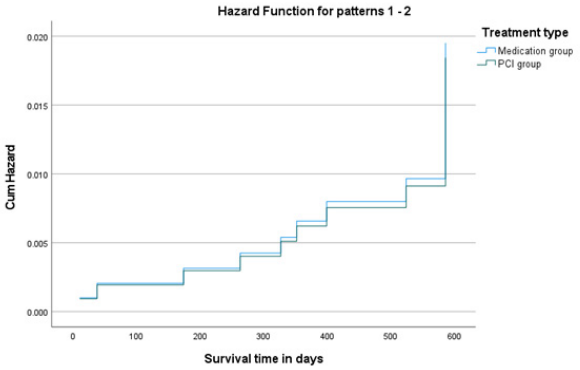

Adjusted Hazard Ratio for LVEF ≤ 45% Predicting Target Vessel Failure (TVF)

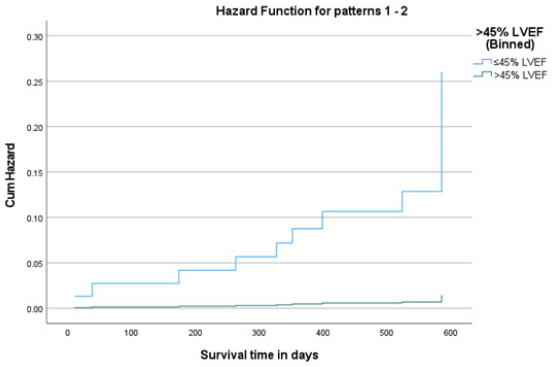

Conclusion: In patients with coronary lesions in the QFR grey zone (0.75–0.85), treatment strategy (PCI vs. medication) did not significantly impact TVF rates. However, reduced LVEF (≤ 45%) and higher HbA1c identified subgroups at increased risk, suggesting potential utility of LVEF and glycemic control in guiding individualized management. These findings highlight the need for further prospective studies to refine QFR-based decision-making in borderline lesions.

急性心肌梗死早期活动护理对患者康复进程的观察

郑瑞玲

新疆维吾尔族自治区人民医院

摘要：研究观察急性心肌梗死患者接受早期活动护理对改善临床心功能及预后的价值。2024 年 2 月至 2025 年 2 月间收治 58 例急性心肌梗死患者，随机分为对照组 29 例和试验组 29 例；对照组：接受基本常规护理；试验组：在对照组护理的基础上实施早期活动护理，包括分期运动锻炼护理、规范化呼吸锻炼护理和情感心理护理，在 4 周的护理期中，观察对照组和试验组患者的 LVEF 情况、N-telopeptide-prob 型 B 型钠尿肽 (NT-proBNP) 指标和六分钟步行实验 (6MWD) 结果、SF-36 调查评估量表结果以及并发症发生率。试验组患者的试验后的 LVEF 提升较对照组明显，改善了左心室收缩功能；患者的 NT-proBNP 降低较明显，提示心脏负担得以减轻；试验组的 6MWD 的结果则比对照组提高，提示试验组患者较对照组具备更好的耐力及体能；试验组患者的生活质量评价值，较对照组提高，提示试验组患者在生活质量评价中获得较高的评分。患者的并发症发生率较低，且试验组患者的安全性较高，不存在较大的临床不良事件风险增加的情况。总之，早期活动护理有利于患者急性心肌梗死治疗，促进其心功能的恢复和运动能力的提高；有利于患者病情预后；应早日干预。

关键词：急性心肌梗死；早期活动护理；康复进程

1、资料与方法

1.1 一般资料

以 2024 年 2 月 ~ 2025 年 2 月于本院确诊并予以住院治疗的 58 例急性心肌梗死患者作为研究对象。按照随机数字表方法将其分成试验组 29 例、对照组 29 例。两组患者性别、年龄、患病时间、基础疾病等一般资料差异无统计学意义，具有可比性。所有患者均由冠状动脉造影确诊，符合急性心肌梗死相关诊断标准。所有患者均符合本研究纳入、排除标准，均签署知情同意。

1.2 方法

1.2.1 对照组

2、结果

2.1 对照组和试验组急性心肌梗死患者干预前后心功能指标的比较，详见下表：

表 1：各组心功能指标对比表

组别	例数	时间	LVEF（%）	NT-proBNP（pg/mL）	心率（次 / 分）	收缩压（mmHg）
对照组	29	干预前	42.1±3.5	1856.2±214.5	82.3±6.1	132.5±10.2
		干预后	45.8±4.2	1523.4±189.7	78.5±5.8	128.3±9.5
试验组	29	干预前	41.9±3.8	1849.1±208.9	81.7±5.9	131.8±11.0
		干预后	51.2±4.8	1102.5±156.3	72.1±5.1	122.6±8.8
t 值	-	-	5.281	8.927	4.326	3.815
P 值	-	-	<0.05	<0.05	<0.05	<0.05

3、讨论

急性心肌梗死属于一种发病率较高、残损率及死亡率较高的严重心血管事件，其临床救治的重要程度并不局限于药物治疗、手术操作，更有对病后恢复护理干预的方案与操作。目前治疗思路也在不断从以疾病为导向向以病人为导向发展，护理干预过程中加入的功能锻炼、心理安慰、个体化支持等更是治疗远期结局的重要因素 [1]。本研究在结合急性心肌梗死发生机制与治疗机制制定针对性早期活动护理干预，并与干预前后两组患者有关指标做比较分析基础之上，对该干预措施开展的临床意义与价值进行研析。

探究肺动脉球囊扩张成形术后靶血管再干预的预测因素

卢志辉 张臣 万钧 肖瑶 赵蕾 鹿冠玉 张洪博 马晓海

首都医科大学附属北京安贞医院

目的 探究慢性血栓栓塞性肺动脉高压 (CTEPH) 患者经肺动脉球囊扩张成形术 (BPA) 治疗后靶血管再干预的危险因素。

方法 回顾性纳入 2021 年 11 月至 2024 年 5 月于首都医科大学附属北京安贞医院介入诊疗科行 BPA 治疗的 CTEPH 患者 66 例。收集患者接受 BPA 治疗前的各项临床资料、血流动力学参数与肺动脉造影相关参数。其中临床资料包括患者年龄、性别、体重指数、药物治疗、WHO 心功能分级、6 分钟步行距离 (6MWD) 及血浆 N- 末端脑钠肽前体 (NT-prBNP)。血流动力学参数包括平均动脉压、平均右心房压、心指数、心输出量、肺血管阻力、肺动脉楔压及混合静脉血氧饱和度。肺动脉造影相关参数包括靶血管分布、病变类型、狭窄百分比、球囊 / 管径比、靶血管参考直径及靶血管血流分级。根据患者是否存在至少一只靶血管接受再干预治疗，将患者分为再干预组与非再干预组。采用单因素 / 多因素 logistic 回归分析评估靶血管 BPA 术后发生再干预的危险因素。

结果 66 例 CTEPH 患者共计行 163 次 BPA 治疗。其中，33 例患者及其 99 支靶血管为再干预组，33 例患者及其 244 支靶血管为非再干预组。两组年龄、性别、体重指数、药物治疗、WHO 心功能分级、6MWD 及 NT-prBNP 及血流动力学参数比较差异无统计学意义。再干预组靶血管环形病变比例及次全闭塞病变比例明显高于非再干预组，靶血管狭窄百分比明显高于非再干预组，肺动脉血流分级 3 级比例明显高于非再干预组，差异具有统计学意义。多因素 logistic 回归分析显示高水平基线肺动脉血流分级 (95% CI: 0.062-0.220, P<0.001) 为靶血管术后再干预的独立保护因素，高水平靶血管狭窄百分比 (95% CI: 1.942-1.983, P<0.001) 为靶血管术后再干预的独立危险因素。

结论 CTEPH 患者经 BPA 治疗后靶血管再干预的发生与多因素相关，高水平基线肺动脉血流分级为再干预的独立保护因素，高水平靶血管百分比为 CR 的独立危险因素。

Impact of Early Versus Delayed Permanent Pacemaker Implantation on Clinical Outcomes in Patients with Third-Degree Atrioventricular Block After Transcatheter Aortic Valve Replacement: A National Inpatient Sample Analysis

Baotong He

General Hospital of Ningxia Medical University

Background: Transcatheter aortic valve replacement (TAVR) has become a treatment option for patients with symptomatic severe aortic stenosis. However, due to the anatomical proximity of valve implantation to the cardiac conduction system, the conduction disorder requiring permanent pacemaker (PPM) implantation remains the most common complication of TAVR. Although there have been studies analyzing the clinical outcomes of PPM implantation in patients after TAVR, there is still controversy over the timing of pacemaker implantation and the factors that affect the timing of pacemaker implantation are not yet clear.

Methods: This study covers all hospitalizations of adults with third-degree AV block who were admitted to TAVR between January 2016 and December 2021 and underwent PPM implantation during the same hospitalization. Participants were divided into early PPM implantation (within 72 hours after TAVR) and delayed PPM implantation (more than 72 hours after TAVR) based on the time of implantation. The primary outcome of the study was all-cause death. Secondary outcomes included length of stay (LOS), hospital costs, and various in-hospital complications. Multivariable logistic regression was employed to calculate adjusted odds ratios (aOR) or adjusted beta (aβ).

Results: A total of 3,385 patients who underwent TAVR and PPM with third-degree AV block during the same admission between 2016 and 2021 were included, of which 2,487 (73.47%) were early implantation and 898(26.53%) were delayed implantation. Patients with delayed PPM implantation were on average older (mean age in women was 80.2 years vs. men 79.7 years, P = 0.008), less likely to be female (42.3% vs. 46.7%, P = 0.024), more often non-White race (15.7% vs. 11.6%, P < 0.001), likely to choose Medicare as a payment method (89.5% vs. 88.9%, P < 0.001). The early and delayed PPM implantation groups showed similar characteristics in terms of factors such as household income and teaching. In complications, delayed PPM implantation group exhibited a higher prevalence of certain conditions compared to early PPM implantation group, including congestive heart failure (76.5% vs. 70.4%, P < 0.001), coagulopathy (19.3% vs. 12.6%, P < 0.001), weight loss (6.9% vs. 1.7%, P < 0.001), anemia (8.6% vs. 4.3%, P < 0.001) and prior stroke (14.8% vs. 12.0%, P = 0.032). Conversely, the early implantation group had more incidence in obesity (26.7% vs. 22.7%, P = 0.018), smoking (40.1% vs. 34.9%, P = 0.006), prior percutaneous coronary intervention (22.6% vs. 17.9%, P = 0.003). The results showed that there was no significant difference in the incidence of mortality between patients with delayed pacemaker implantation and those with early pacemaker implantation (1.0% vs. 0.9%, P = 0.751). However, the incidence of hospitalization costs ($332968.9 ± 209628.5 vs. $248325.1 ± 146793.5%, P < 0.001) and length of stay (9.7 ± 7.1% vs. 3.5 ± 3.0%, P < 0.001) in the group with delayed pacemaker implantation is higher than that in the early group. Multiple regression analysis determined that delayed PPM is associated with anemia (OR, 2.1, 95%CI 1.6 - 2.9, P < 0.001), coagulation disorders (OR, 1.6, 95%CI 1.3 - 1.9, P < 0.001), congestive heart failure (OR, 1.4, 95%CI 1.2 - 1.6, P < 0.001), and chronic kidney disease (OR, 1.4, 95%CI 1.2 - 1.6, P < 0.001).

Conclusions: In this national cohort, our analysis found that the delayed implantation group exhibited longer hospital stays and increased hospitalization costs, but there was no significant difference in hospital mortality rates between the two groups. Correctable hematological and cardiorenal dysfunction independently associated with delayed implantation of PPM. In the future, standardized tools with unnecessary delays should be avoided as much as possible while ensuring safety, and optimization should be carried out for comorbidity management.

Construction and Validation an Interpretability Prediction model for In-Stent Restenosis based on Machine Learning

Bing-Bing Ke, Cheng-Ping Hu, Zheng Qin, Hui Chen, Hai Gao

Beijing Anzhen Hospital, Capital Medical University

Background: Issues surrounding in-stent restenosis (ISR) remain a barrier to improvements in cardiovascular intervention therapies, as the sensitivity and specificity of ISR prediction models tend to be poor.

Aims: This study aimed to construct and validate an explainable prediction model for ISR based on machine learning (ML).

Methods: Our study was conducted and validated in patients undergoing percutaneous coronary interventions. The derivation cohort, which included 1,421 patients seen between January 2013 and December 2020, was separated into a training cohort (80%) and an internal validation cohort (20%). ISR was defined as a stenosis diameter ≥ 50% that occurred in the segment inside the stent or a 5 mm of proximal or distal to the stent or absolute lumen loss exceeds 20% based on the original vascular stenosis at the time of follow-up angiography. We obtained 53 features and used five ML algorithms to establish prediction models. We generated five ML models to predict ISR development in patients with PCI. Among the five models, the RF model (AUC = 0.957) had the best predictive capacity for ISR, followed by the XGBoost model (AUC = 0.896) and the SVM model (AUC = 0.841). Our final model was identified during RF model feature reduction. the 54-feature RF model was significantly better at predicting ISR than the three-feature model (△ AUC = 0.077, P = 0.008) and the five-feature model (△ AUC = 0.057, P = 0.005), but was not significantly better than the four-feature model (△ AUC = 0.054, P = 0.432). The four-feature model had a good net benefit and a high threshold probability, which was also comparable to the 54-feature model. The AUC of the four-feature model's P-R curve was only marginally lower than that of the 54-feature model, suggesting that both models had similar and high clinical utility. we chose this four-feature RF model, which included age, blood glucose, Cr, and DBP, as the final model for further analysis. This model achieved an AUC of 0.903, with a sensitivity of 0.857, a specificity of 0.787, a PPV of 0.797, an NPV of 0.850, an accuracy of 0.822, and an F1 score of 0.826 for predicting ISR in patients with PCI.

the final model achieved mean AUCs of 0.960 ± 0.009 and 0.966 ± 0.014 in the five-fold and ten-fold cross-validations, respectively. The SHapley Additive explanation (SHAP) method was used for feature selection and model interpretation. We used demographic characteristics, vital sign measurements, and laboratory data collected from the EMR system. The main outcome was ISR, which was defined as a stenosis diameter ≥ 50% that occurred in the segment inside the stent or a 5 mm of proximal or distal to the stent or absolute lumen loss exceeds 20% based on the original vascular stenosis at the time of follow-up angiography

Results: Among the five models, the Random Forest model had the best predictive ability (AUC = 0.957). When the SHAP method was used to rank the importance of features and gradually reduce the number of features from 54 to two, there was no significant AUC change in the final model, which had four features (ΔAUC = 0.054, p=0.432). The SHAP method was also used to interpret the model. Finally, we established a convenient tool to facilitate the application of our model in clinical practice.

Conclusions:we successfully developed an explainable ML model to predict ISR risk in PCI patients based on clinical data extracted from EMRs. Our final RF model had an excellent ability to predict ISR. We also integrated our model into a web application that can be used by individual patients or clinicians. Further randomized controlled trials are required to determine whether our final prediction model can improve patient outcomes.

不同 eGFR 水平 UA 患者的 caFFR、caIMR 及平均中心动脉压的差异分析

石福天 李宁荫

上海市公共卫生临床中心 _ 复旦大学附属公共卫生临床中心

目的：研究不稳定性心绞痛（UA）患者估测肾小球滤过率（eGFR）与冠状动脉造影血流储备分数（caFFR）、冠状动脉造影微循环阻力指数（caIMR）及平均中心动脉压的关系，揭示不同 eGFR 水平的 UA 患者冠脉血管病变及微循环障碍程度的差异。

方法：90 例 UA 患者依据 eGFR 分为 3 组：Q1（eGFR > 99ml/min·1.73m^2, n=30）、Q2（84 < eGFR ≤ 99 ml/min·1.73m^2, n=30）、Q3（eGFR ≤ 84 ml/min·1.73m^2, n=30）。收集其一般基础资料、血常规、生化、肿瘤标志物、心脏彩超、caFFR、caIMR、平均中心动脉压等相关指标，分析三组数据得出结论。

结果：3 组患者年龄、性别、BMI、是否合并高血压、是否合并糖尿病均无显著性差异，三组患者左回旋支（LCX）caFFR 存在显著性差异，两两比较 Q2 大于 Q1（0.958±0.233 vs 0.936±0.088, P < 0.05）。相关性分析提示左室射血分数（LVEF）与 LCXcaFFR 呈正相关（r=0.253, P < 0.05），平均中心动脉压、BMI 与左前降支（LAD）caIMR 呈正相关（r=0.243, r=0.208, P < 0.05），BMI 与 LAD 血流速度呈负相关（r=-0.216, P < 0.05），平均中心动脉压与 LCX 血流速度呈正相关（r=0.240，P < 0.05），平均中心动脉压与右冠状动脉（RCA）血流速度呈正相关（r=0.336，P < 0.05），总胆固醇（TC）、低密度脂蛋白（LDL）与右冠状动脉（RCA）血流速度呈负相关（r=-0.216, r=-0.238, P < 0.05）。多因素线性回归分析提示 LCXcaFFR（OR=-107.814,95%CI: -203.713~-11.916, P < 0.05）、LCXcaIMR（OR=1.481, 95%CI: 0.361~2.601, P < 0.05）是影响 eGFR 的独立危险因素。

结论：在不同 eGFR 水平的 UA 患者中， LCXcaFFR 存在部分差异，LCXcaFFR、LCXcaIMR 可独立影响 UA 患者的 eGFR 水平。此外临床中可通过计算 eGFR 结合生化指标、心脏彩超、测定平均中心动脉压初步评估 UA 患者的冠脉血管病变及微循环障碍程度。

不同壁厚的聚乳酸可降解支架对血管内皮化的影响。

周昌颐 殷嘉晟 王瑞 沈霁 葛均波

复旦大学附属中山医院

目的：探究壁厚为 160um 的聚乳酸可降解支架（BRS）和新型薄壁聚乳酸可降解支架（薄壁 BRS）对血管内皮化影响。探究 BRS 支架内血栓形成的可能机制。

方法：取 24 只新西兰大白兔，随机分为对照组及实验组，每组各 12 只，对照组植入壁厚为 160um 的 BRS，实验组植入壁厚为 120um 的薄壁 BRS。家兔称重、麻醉后，由股动脉入路在 DSA 指引下于腹主动脉分别植入相应组别的血管支架。每组分别于植入支架后 45 天及 90 天通过复查血管造影以及光学相干断层成像（OCT）评估在体血管内皮覆盖情况，检测结束后将动物安乐死、取材，沿血管长轴将支架段血管截半，分别通过扫描电镜技术和 CD31/ 鬼笔环肽 /DAPI 免疫荧光染色观察支架血管段内皮覆盖情况。

结果：不同壁厚的 BRS 和薄壁 BRS 在植入即刻均扩张贴壁良好。45 天时，复查 OCT 提示，BRS 组和薄壁 BRS 组均未观察到贴壁不良及弹性回缩，薄壁 BRS 组内皮覆盖率显著大于 BRS 组，但尚未完成完全内皮化；BRS 组表面 CD31 荧光染色覆盖面积稍高，BRS 组表面 CD31 荧光染色覆盖面积较低，电镜结果亦显示 BRS 组表面内皮覆盖率显著低于新型 BRS 组，可见较大面积内皮下组织裸露及红细胞、血小板聚集。90 天时，复查 OCT 未见 BRS 组和薄壁 BRS 组贴壁不良及支架断裂，薄壁 BRS 组基本完成内皮覆盖，仍有部分支架梁裸露，BRS 组少数完成内皮覆盖，大部分支架梁仍裸露；CD31 荧光染色结果示薄壁 BRS 组血管表面仍有部分 CD31 荧光未覆盖，BRS 组血管表面部分 CD31 荧光覆盖，扫描电镜结果与以上结果相符，可观察到薄壁 BRS 组基本完成内皮覆盖，BRS 组部分支架梁完成内皮覆盖，其余支架梁表面见内皮下组织裸露。

结论：不同壁厚的聚乳酸可降解支架在动物模型中均未见支架断裂及贴壁不良，相较 160um 的 BRS，120um 的薄壁 BRS 植入后，家兔腹主动脉内皮化显著加快。支架内皮化延迟可能是除支架机械因素外 BRS 支架内血栓发生率增加的可能机制。

相同壁厚的金属药物洗脱支架和聚乳酸可降解支架对血管内皮化的影响。

周昌颐

复旦大学附属中山医院

目的：探究相同壁厚的金属药物洗脱支架 (DES) 和聚乳酸可降解支架 (BRS) 对血管内皮化影响。探究 BRS 支架内血栓形成的可能机制。

方法：取 24 只新西兰大白兔，随机分为对照组及实验组，每组各 12 只，对照组植入壁厚为 120um 的可降解涂层雷帕霉素 DES，实验组植入壁厚为 120um 的薄壁雷帕霉素 BRS。家兔称重、麻醉后，由股动脉入路在 DSA 指引下于腹主动脉分别植入相应组别的血管支架。每组分别于植入支架后 45 天及 90 天通过复查血管造影以及光学相干断层成像（OCT）评估在体血管内皮覆盖情况，检测结束后将动物安乐死、取材，沿血管长轴将支架段血管截半，分别通过扫描电镜技术和 CD31/ 鬼笔环肽 /DAPI 免疫荧光染色观察离体支架血管段内皮覆盖情况。

结果：相同壁厚的 DES 和 BRS 在植入即刻均扩张贴壁良好。45 天时，复查 OCT 提示，DES 组和 BRS 组均未观察到贴壁不良及弹性回缩，DES 组内皮覆盖率显著大于 BRS 组，但尚未完成完全内皮化；DES 组表面 CD31 荧光染色覆盖面积较高，BRS 组表面 CD31 荧光染色覆盖面积较低，电镜结果亦显示 BRS 表面内皮覆盖率显著低于 DES，可见较大面积内皮下组织裸露及红细胞、血小板聚集。90 天时，复查 OCT 未见 DES 组和 BRS 组贴壁不良及支架断裂，DES 组均完成内皮完全覆盖，BRS 组基本完成内皮覆盖，仍有部分支架梁裸露；CD31 荧光染色结果示 DES 组完成完全内皮化，BRS 组血管表面仍有部分 CD31 荧光未覆盖，扫描电镜结果与以上结果相符，可观察到 DES 组均已完成内皮覆盖，BRS 组部分完成内皮覆盖，少数部分支架梁表面见内皮下组织裸露。

结论：相同支架梁壁厚 DES 及 BRS 在动物模型中均未见支架断裂及贴壁不良，相较 DES，BRS 植入后家兔腹主动脉内皮化显著延迟。支架内皮化延迟可能是除支架机械因素外 BRS 支架内血栓发生率增加的可能机制。

造影剂液压分离再通技术开通冠脉慢性完全闭塞病变

何松原

首都医科大学附属北京安贞医院

目的：本研究尝试采用造影剂液压分离再通技术（HydroDynamic contrast Recanalization, HDR）开通慢性完全闭塞病变（CTO），提高 CTO 经皮冠状动脉介入治疗（PCI）成功率和手术效率。

方法：HDR 技术是基于对比剂微注射与亲水涂层导丝相配合的前向开通 CTO 病变的技术。本回顾性研究纳入了从 2024 年 12 月至 2025 年 5 月的适宜应用 HDR 技术的 CTO 患者（近段纤维帽明确且远端血管条件较好），主要终点为手术成功，次要终点为手术相关并发症。

结果：55 例患者共 55 处 CTO 病变接受 HDR-PCI 治疗。患者平均年龄 59.3±12.7 岁，J-CTO 评分 2.4±1.5。病变特征：CTO 病变分布：27.3%（15/55）LAD CTO，16.3%（9/55）LCX/OM CTO，56.3%（31/55）RCA CTO，50.9%（28/55）存在钝头 / 不明确的近端纤维帽，58.2%（32/55）病变长度≥ 20mm，36.4%（20/55）伴中重度钙化，58.2%（18/55）闭塞段成角≥ 45°。平均手术时间 75.0±30.6 分钟，手术策略转换：70.9%（39/55）全程采用 HDR 技术，5.5%（3/55）传统正向导丝技术，9.1%（5/55）ADR 技术，14.5%（8/55）逆向技术。手术成功率 82.1%（32/39），无手术并发症发生。手术失败原因分析：4 例因为微导管无法通过坚硬近端纤维帽，2 例因为硬导丝在内膜下走行过远，1 例因为 CTO 闭塞段内严重钙化。

结论：HDR 在特定解剖特征的 CTO-PCI 中展现出显著价值，是一种安全有效的前向 CTO- PCI 新技术，它的有效性及安全性尚需大规模前瞻性研究进一步验证。

一种新型的开通 CTO 的 ADR 导管：单中心病例系列报道

陈根锐

中国人民解放军空军军医大学第一附属医院（西京医院）

背景：正向治疗仍然是慢性完全闭塞病变（CTO）PCI 的主要技术之一。在正向治疗与正向夹层内重回真腔（ADR）技术中，Stingray 球囊和 ReCross 微导管有助于导丝进入远端真腔。然而，这些策略伴随着斑块外血肿的形成，由于血肿的抽吸受限，血肿会压缩真腔，从而降低重入真腔的成功率。为了解决这一难题，我们设计了一种新的 ADR 导管，其扁平尖端的两侧都有金属标记，以便更容易地看到“单轨标志”，实现定向穿刺，并具有专用的抽吸口来控制血肿。

目的: 评估这种新型 ADR 导管在 ADR 策略开通 CTO 病变方面的安全性和有效性。

方法：对 2024 年 1 月至 2025 年 5 月在西京医院使用新型 ADR 导管治疗的 CTO 患者进行分析。技术成功定义为使用这种新型 ADR 导管实现导丝重回远端血管真腔。观察手术相关并发症和院内主要不良心脏事件（MACE）。MACE 包括死亡、复发性心肌梗死、靶血管血运重建（TVR）。

结果：共有 26 例 CTO 患者使用该新型 ADR 导管，其中男性 21 例，女性 5 例，JCTO 评分为（3.01±0.42）分。在本次研究中 4 例患者 CTO 入口不清晰，BASE 后直接行新型 ADR 导管穿刺，均成功进入血管真腔；余 22 例正向技术失败后行补救性新型 ADR 导管穿刺术，其中 12 例成功，10 例失败，因此新型 ADR 导管穿刺术技术成功率为 61.5%（16/26）；10 例新型 ADR 导管穿刺术失败，其中 5 例用 Stingray-ADR 术补救成功；3 例采用 Stingray-ADR 术补救失败后通过逆向技术补救成功；1 例正向补救成功；1 例最终失败，手术成功率为 96.1%。5 例用 Stingray 补救成功的原因可能与术者对 Stingray-ADR 术熟练度相关；3 例 Stingray 补救失败的原因与血肿过大相关，其中 2 例 ADR 导管通过困难，1 例更换 Stingray 导管也无法通过，考虑与严重钙化相关，另一例则直接逆向补救。此种新型 ADR 导管 ADR 术有明显学习曲线，前 13 例成功率为 53.8%（7/13），

后 13 例成功率为 69.2%（9/13），随着术者例数的累积，成功率逐渐提高。所有患者均无冠脉穿孔、心包填塞及围手术期心梗发生。住院期间所有患者均无死亡、再发心肌梗死、靶血管重建等 MACE 事件发生。

结论：新型 ADR 穿刺导管通过在整个手术过程中定向穿刺和连续抽吸血肿的优势大大提高导丝安全有效地重新进入远端真腔的成功率。

关键词：经皮冠状动脉介入治疗； 慢性完全闭塞病变； 正向夹层再进入技术

Evidence-based construction of a postoperative upper extremity stasis pain management program for cardiovascular interventional patients and application research

Kun-Yan Peng

Zigong First People's Hospital

Introduction: Cardiovascular interventional access is mainly radial artery and femoral artery access, compared with the femoral artery, transradial artery path is less traumatic, postoperative recovery is faster, braking time is shortened, transradial artery access is widely accepted, but the radial artery is smaller or even tortuous, prone to spasm, bruising and pain in the upper limbs due to radial artery tear is the most common complication, and in severe cases, circulatory disturbances may occur due to localized pressure increase, and severe cases of Osteofascial compartment syndrome. It is particularly important to find out the best way to choose a treatment that is effective, simple to perform, safe, and less painful for the patient. Therefore, this study constructs an evidence-based management program for postoperative upper extremity stasis and pain in cardiovascular intervention patients and explores the application effects. **Methods:** Based on the evidence-based approach, through searching related literature and summarizing and analyzing and discussing with the subject group, the i-PARIHS framework was used as the theoretical basis to form a preliminary respiratory training program for cardiovascular patients. Two rounds of expert correspondence were conducted using the Delphi method, and the first draft was revised and improved based on the comments of 12 experts. Eight cardiovascular intervention patients were selected for the pretest, and the trial data were collected and analyzed to summarize the problems and shortcomings. Using the convenience sampling method, 66 post-interventional patients who met the inclusion and exclusion criteria in the cardiovascular internal medicine department of a tertiary-level A hospital in Zigong City from January 2024 to June 2024 were selected as the study subjects, and were divided into the control group (n=33) and the intervention group (n=33) according to the randomized number table method. Patients in the intervention group received a pain management program based on routine care compared to those in the control group. Pain Numeric Rating Scale scores at 24h and 72h postoperatively, general self-efficacy scale scores at 24h and 1 week postoperatively, satisfaction scores and incidence of postoperative complications were compared between the two groups. **Results:** The pain numeric rating scale score at 72h postoperatively in the intervention group was (2.24±0.84), which was lower than that of the control group (3.17±0.89), and the difference was statistically significant (p<0.001); At 1 week postoperatively, the general self-efficacy scale score of the intervention group was (22.13±1.71), which was higher than that of the control group (18.94±1.76), and the difference was statistically significant (p<0.001); The satisfaction score of the experimental group was (91.55±2.13), which was higher than that of the control group (89.27±2.14), and the difference was statistically significant (p<0.001). **Discussion:** The implementation of an evidence-based construction of a postoperative upper extremity stasis pain management program for cardiovascular interventional patients is conducive to alleviating postoperative upper extremity stasis pain in cardiovascular interventional patients, increasing satisfaction and self-efficacy, and improving the patient experience. However, this study is a single-center, small-sample study, and further multi-center, large-sample studies should still be conducted in the future to improve the generalizability of the study.

生物可吸收支架内膜愈合的随访观察及分析

余超 邢磊 刘华兴

哈尔滨医科大学附属第二医院

背景及目的：生物可吸收支架被认为可以改善血管反应并促进早期内膜愈合，但脂质斑块对支架内膜的影响尚未得到很好的验证。光学相干断层成像（OCT）分辨率高，对单个支架支柱具有良好的可视化，在支架植入时可以提供支架贴壁不良、支架边缘夹层等信息，同时能对血管大小、病变狭窄程度、斑块性质和负荷分布提供精准评估。本研究旨在利用 OCT 观察生物可吸收支架的内膜愈合情况，分析生物可吸收支架在不同类型斑块基础上支架内膜的覆盖情况。

方法：纳入 2020 年 10 月至 2022 年 10 月期间在我中心接受生物可吸收支架植入的 36 例冠心病患者（有 1 例发生了支架内晚期血栓形成致支架再狭窄，未入组），并进行术前、术后 1 年 OCT 随访，对患者的临床资料、手术资料、即刻光学相干断层扫描结果、新生内膜总体情况及在不同类型斑块基础上支架内膜的覆盖情况进行统计和分析。其中斑块按每 1mm 的截面进行分析，共扫描到 505 幅脂质斑块截面，240 幅纤维斑块截面。

结果：对入选的 36 名患者的新生内膜进行分析，发现支架内新生内膜面积为 1.55(1.06,1.87) mm^2，平均新生内膜厚度为 0.20(0.15,0.26) μm。罪犯病变支架血管按每 1mm 的截面进行 OCT 影像学定量分析，共扫描到 505 幅脂质斑块截面，240 幅纤维斑块截面，结果显示脂质斑块截面相较于纤维斑块截面，支架面积直径更小（5.94(4.79,7.64) 比 6.52(5.35,8.03)，P<0.001），平均新生内膜厚度更大（0.16(0.10,0.25) 比 0.08(0.06,0.12)，P<0.001），支架覆盖率更高（92.5% 比 78.7%，P<0.001）。支架内新生内膜异质性分析发现在脂质斑块截面和纤维斑块截面之间，均质 / 非均质 / 分层内膜的发生率均有统计学差异（63.2% 比 96.3%，P<0.001；27.3% 比 2.5%，P<0.001；9.5% 比 1.2%，P<0.001）。

结论：通过 OCT 观察，相较于纤维斑块，生物可吸收支架在脂质斑块上的支架截面面积直径更小，支架小梁上有着更厚的支架内膜覆盖和更多的支架小梁被完全包埋。与此同时，落在脂质斑块处的生物可吸收支架的支架小梁周围的内膜更多的呈现非均质性模式，这些非均质性的内膜可能造成支架愈合过程处于不稳定的状态。在入选的 37 例患者中，仅有 1 例发生了支架内晚期血栓形成致支架再狭窄。

药物涂层球囊治疗冠状动脉小血管原位病变的随访观察

毕静婷 邢磊 刘华兴

哈尔滨医科大学附属第二医院

背景及目的：在冠状动脉小血管病变的治疗中， DCB 的应用尚存争议，主要因为尚缺乏充足的有效证据来支撑其推荐的适用性。因此，本研究旨在研究紫杉醇药物涂层球囊在治疗冠状动脉小血管原位病变中的临床疗效并分析可能影响治疗失败的相关因素。

方法：纳入 2020 年 11 月至 2024 年 6 月，对 105 例患者进行回顾性分析，其中 70 例接受 DCB 治疗，35 例接受 DES 治疗，随访时间一年。使用冠状动脉定量测量分析（Quantitative Coronary Angiographic analysis，QCA）测量术前、术后即刻、一年后随访的相关数据：最小管腔直径（Minimum Lumen Diameter，MLD）、病变（支架）长度，计算管腔直径狭窄率（DS%）及晚期管腔丢失（Late Lumen Loss，LLL）。主要的临床随访内容包括血管完全闭塞、非闭塞再血管化治疗、再狭窄 > 50% 未再血管化治疗、血栓形成、严重出血等。

结果：选取 105 例患者随访 1 年，我们确定了 35 例植入 DES 小支架的患者，并对患者的病变进行了倾向评分匹配与药物球囊治疗的比例为 1:2，即 70 例行 DCB 治疗。通过使用年龄，性别，BMI，糖尿病，高血压，高脂血症，吸烟，药物治疗情况等这些变量作为匹配标准。临床资料中，DCB 组与 DES 组之间的患者在药物 β 受体阻滞剂使用差异上有统计学意义（P < 0.05）。在术后即刻 QCA 测量中，DCB 组：最小管腔直径 2.20±0.21mm、管腔直径狭窄率 16.65±2.58%、病变（支架）长度 16.4±6.6mm，与 DES 组：最小管腔直径 2.42±0.27 mm、管腔直径狭窄率 6. 7±1.86%、病变（支架）长度 19.8±3.7mm，DCB 组与 DES 组术后 MLD、管腔直径狭窄率、病变（支架）长度较术前具有统计学意义 (DCB 组 P<0.001，DES 组 P<0.001)。1 年随访 QCA 测量中，DCB 组：最小管腔直径 1.91±0.18mm、病变（支架）长度 16.4 ± 6.6mm、1 年晚期管腔丢失 0.29±0.05mm，与 DES 组：最小管腔直径 2.07±0.24mm、病变（支架）长度 20.8 ± 3.6 mm、1 年晚期管腔丢失 0.35±0.12 mm，DCB 组与 DES 组之间术后 1 年随访比较具有统计学差异（DCB 组 P<0.001，DES 组 P<0.001）。DCB 组管腔直径狭窄率 26.15±3.74%，DES 组管腔直径狭窄率 27.23±3.89%，两者比较无明显统计学差异（P = 0.423）。逻辑回归分析中发现体重指数、糖尿病、高脂血症、心肌梗死病史是影响小血管再血管化治疗失败的因素。

结论：1. 通过 DCB 处理原位（小）血管病变与 DES 小支架（直径 <2.25mm）植入临床应用回顾性对比发现，两者在临床诊断和罪犯病变分布及病变特征上没有明显差别。2.DCB 处理的原位病变在术后即刻的效果虽劣于 DES 小支架植入，但在 1 年后的冠状动脉造影随访中发现，DCB 处理的原位病变在管腔直径狭窄率（DS%）不劣于支架植入，且有着更小的晚期管腔丢失率。3．肥胖、糖尿病、高脂血症、心肌梗死病史可能是影响小血管再血管化治疗失败的影响因素。

P2Y12 抑制剂预处理对择期 PCI 患者围术期心肌损伤 / 梗死的影响

周祎哲 严研 聂绍平

首都医科大学附属北京安贞医院

择期经皮冠状动脉介入治疗（PCI）患者围术期心肌损伤 / 梗死发生率达 28.7%~52.8%，与无围术期事件的患者相比，发生围术期心肌损伤 / 梗死的患者预后不良。阿司匹林联合 P2Y12 抑制剂预处理可降低围术期血栓负荷，从而预防围术期心肌损伤 / 梗死的发生。目前不同 P2Y12 抑制剂预处理对择期 PCI 患者围术期心肌损伤 / 梗死及临床结局的影响证据不足。

本研究是基于北京安贞医院冠脉专病数据库的一项回顾性、单中心、观察性队列，依据纳排标准筛选北京安贞医院 2022-2024 年进行择期 PCI 治疗的患者，根据术前 P2Y12 抑制剂预处理的类型分为氯吡格雷组、替格瑞洛组，入组后收集患者住院期间资料，分析氯吡格雷及替格瑞洛预处理对围术期心肌损伤 / 梗死的影响。

研究表明：① 氯吡格雷组围术期心肌损伤发生率为 70.38%，围术期心肌梗死发生率为 39.32%；替格瑞洛组围术期心肌损伤发生率为 68.08%，围术期心肌梗死的发生率为 37.85%。② 氯吡格雷组与替格瑞洛组相比，围术期心肌损伤 / 梗死的发生率均无统计学差异。研究成果可为择期 PCI 患者术前 P2Y12 抑制剂预处理的选择提供证据支持。

冠状动脉介入治疗后血管造影微循环阻力的预后价值：来自 FAVOR III China 试验的启示

张洪亮 [1] 史文册 [1] 管常东 [1] 谢丽华 [1] 涂圣贤 [3] 宋雷 [1] 吴永健 [1]

1. 中国医学科学院阜外医院（国家心血管病中心）

2. 中国医学科学院北京协和医学院

3. 上海交通大学生物医学工程学院生物医学仪器研究所

背景：

经皮冠状动脉介入治疗（PCI）虽可有效解除大血管狭窄，但手术过程中的机械操作会释放微小碎屑及血管活性物质，导致医源性冠状动脉微循环功能障碍（CMD），不仅影响即刻灌注，也预测长期不良心血管事件风险。因此，精准评估冠脉微循环功能具有重要临床意义。

传统压力导丝下的微循环阻力指数（IMR）虽为评估金标准，但需使用压力 - 温度传感导丝及诱发充血，限制了其在日常临床中的普及。近年来，我们基于冠脉定量流量比（QFR）技术，开发了无需压力导丝和充血药物，仅通过常规冠脉造影计算获得的微循环阻力新指标——血管造影微循环阻力（AMR）。初步研究显示 AMR 与 IMR 高度相关，并在预测患者预后方面展现出潜力，但尚缺乏大规模临床验证。

目的：

评估 AMR 在接受经皮冠状动脉介入治疗（PCI）患者中的预后价值。

方法：

本研究为 FAVOR III China 试验中 3404 例接受 PCI 患者的事后分析。对目标血管在 PCI 术前及术后测量 AMR，并计算 AMRΔ%（[100*(术后 AMR- 术前 AMR)/ 术前 AMR]）。主要终点为 3 年主要不良心脏事件（MACE）风险，包括全因死亡、心肌梗死（MI）及缺血驱动的血运重建的复合终点。

结果：

AMRΔ% ≥ 85 组（23.7%）与 <85 组（76.3%）基线特征相似，但前者每位患者植入的支架数量更多且长度更长。总体 MACE 风险两组相当（14.8% vs 12.4%；HR 1.18，95%CI: 0.95-1.45）。然而，在术后 AMR ≥ 250 的患者中，AMRΔ% ≥ 85 者 MACE 风险显著增加（16.3% vs 10.8%；HR 1.52，95%CI: 1.14-2.04）；而当术后 AMR <250 时，两组间无显著差异（12.3% vs 13.4%；HR 0.89，95%CI: 0.63-1.25；交互作用 P=0.019）。

结论：

在 FAVOR III China 人群中，PCI 术后目标血管 AMR 显著升高（AMRΔ% ≥ 85）本身并不能预测预后，但对于术后 AMR ≥ 250 的患者，可识别出 3 年心血管风险升高的人群。

心血管病诊治的创新与转化医学研究

基于皮下植入 MSC 细胞球的新型心肌保护策略研究

刘益海

南京鼓楼医院

目的

本研究旨在探索间充质干细胞（MSCs）球体通过皮下腋下植入在缓解心肌缺血再灌注（I/R）损伤中的治疗潜力，解决传统 MSC 移植中细胞存活率低、旁分泌功能有限及操作复杂等问题，验证该方法在改善心功能、抑制心肌纤维化及炎症反应、调节氧化应激等方面的有效性，并深入挖掘其潜在机制。

方法

研究中采用三维水凝胶支架培养人脐带来源 MSCs 形成细胞球，并行形态学、电镜、免疫荧光等多维度鉴定。在小鼠心肌 I/R 模型中，将 MSC 细胞球植入右侧腋下皮下组织，并设立尾静脉注射 MSC 对照组。通过活体成像追踪细胞分布，超声心动图评估心功能，HE、Masson、免疫组化和免疫荧光分析心肌纤维化、氧化应激及炎症浸润；同时采集血清进行炎性因子流式检测，并通过定量蛋白质组学解析 MSC 球体分泌蛋白的变化及信号通路富集。

结果

MSC 细胞球在体内可稳定存在超过 4 周，部分细胞可进入循环。与尾静脉注射相比，皮下植入细胞球显著改善了 I/R 后心功能，4 周后左室射血分数（EF）及短轴缩短率（FS）提升更明显，同时伴有心室重构改善。组织学分析显示，MSC 细胞球能显著减少梗死面积、抑制心肌纤维化、减轻氧化应激和炎症细胞浸润，并促进新生血管形成。血清中 IL-1α、IL-6、TNF-α、MCP-1 等多种炎性因子水平显著下降。蛋白质组学分析显示 MSC 细胞球分泌蛋白显著富集于 HIF-1 信号通路，并高度分泌抗氧化蛋白 PRDX1、免疫调节因子 MIF 及基质重塑相关蛋白 TIMP1，主要以外泌体形式存在，呈持续释放特征。

结论

MSC 细胞球皮下植入是一种安全、稳定、非侵入性的新型干细胞治疗策略，可有效缓解心肌 I/R 损伤，改善心功能及心脏重构，其机制可能与分泌富含 HIF-1 通路活性的外泌体并调节氧化应激、炎症反应和基质重塑密切相关。本研究为临床 MSC 治疗心肌梗死等心血管疾病提供了新思路和可行的技术方案。

Hemodynamic Study of Plaque Progression and Regression Based on Coronary CTA Imaging using Computational Fluid Dynamics Method

changqing du

Zhejiang Hospital

Hemodynamic Study of Plaque Progression and Regression Based on Coronary CTA Imaging using Computational Fluid Dynamics Method

Abstract:

Objective: This study aims to retrospectively include patients who underwent two serial CCTA examinations, analyze the role of baseline hemodynamic parameters based on CCTA imaging in assessing plaque changes, and use logistic regression to analyze factors influencing plaque stability.to explore the use of coronary CTA imaging for computational fluid dynamics (CFD) analysis, combined with the geometric model features of plaques, to analyze the progression and regression of coronary atherosclerotic plaques, and identify hemodynamic parameters that can evaluate plaque changes. This study will provide new perspectives for understanding the mechanisms of coronary plaque progression or regression.

Methods: A retrospective analysis was conducted on 22 coronary artery disease patients (34 lesions) who underwent two consecutive CCTA exams at an interval of about two year between March 2018 and October 2021 at Zhejiang Hospital.The median interval between the two scans was 22 (11-32) months.Exclusion criteria were as follows: Coronary revascularization was performed between the two CCTA examinations; The presence of artifacts, a low signal-to-noise ratio in the coronary CTA images of either examination, which did not meet the requirements for three-dimensional vascular model reconstruction; The time interval between the two CCTA examinations was less than 1 year; The presence of other lesions such as aortic dissection, valvular lesions, and congenital heart diseases; Failure of CCTA plaque quantitative analysis and hemodynamic analysis. Based on the changes in rate of vessel stenosis，the lesions were divided into three groups: plaque progression group (ΔDS% ≥ 5%), plaque stable group (-5% < ΔDS% < 5%), and plaque regression group (ΔDS% ≤ -5%). Three-dimensional models of coronary arteries were constructed from CCTA images, and hemodynamic parameters were calculated. Logistic regression analysis was performed to identify factors affecting plaque stability by comparing the hemodynamic parameters between groups.

Results: A total of 22 patients were included in the study, with an average age of 62.77 ± 8.76 years, and 72.76% were male. The prevalence of hypertension and diabetes mellitus is 63.64%, and that of hypercholesterolemia is 77.27%. The plaque types were predominantly lipid plaques (41.18%), mixed plaques (26.47%), and calcified plaques (32.35%). Of the 34 lesions analyzed, 50% (17/34) were located from the left main to the left anterior descending artery (LAD), 21% (7/34) were located in the left circumflex artery (LCX), and 29% (10/34) were located in the right coronary artery (RCA). The minimum lumen area of the lesions was 5.24 ± 2.42 mm^2, and the average diameter stenosis was 20 ± 10%. The average distance from the coronary artery ostium to the minimum lumen area was 46.2 ± 18.3 mm, and the average lesion length was 15.3 ± 8.2 mm.Logistic regression analysis identified Min.FFR, Min.TAWSS, Ave Vorticity, and Max Helicity as the main factors influencing plaque progression (all P < 0.05), while Min.FFR, Min.TAWSS, Ave Vorticity, and Ave GON were the main factors influencing plaque regression (all P < 0.05). ROC curve analysis revealed the AUC values of the plaque progression and regression models were 0.86 (0.80-0.92) and 0.89 (0.82-0.97), respectively, suggesting these hemodynamic parameters have good predictive value for plaque stability.

Conclusion: This study analyzed plaque structure, properties, and hemodynamics through coronary CTA imaging and used logistic regression to analyze the factors affecting plaque stability. The results suggest that hemodynamic parameters significantly affect plaque progression and can serve as predictive tools for future plaque changes.

A new non-invasive detector for coronary microvascular dysfunction: Exercise stress high-frequency QRS electrocardiogram

Jianyuan Pan[1], Ming Liu[2], Dan Li[1]

1. The First Affiliated Hospital of USTC

2. First Affiliated Hospital of Xinjiang Medical University

3. The First Affiliated Hospital of An Hui Medical University

Abstract

Background: Coronary microvascular dysfunction (CMVD) is a clinical syndrome of acute or chronic myocardial ischemia caused by structural and functional abnormalities of small anterior coronary arteries (150-500μm), small arterioles (<100μm), and capillaries in response to atherogenic and non-atherogenic pathogenic factors. But due to the current inability to visually assess the coronary microvasculature, symptoms caused by its dysfunction are often mistakenly thought to be non-cardiogenic factors, leading to misdiagnosis and inadequate treatment. Some invasive tests, although highly accurate, are guidewire-dependent, complex, and less reproducible. At present, there is a lack of effective non-invasive examination methods to diagnose coronary microcirculation dysfunction. Exercise stress high-frequency QRS electrocardiogram (HFQRS) is a new clinical technology for detecting high-frequency signals. This study aimed to evaluate the diagnostic value of the exercise stress high-frequency QRS (HFQRS) electrocardiogram in coronary microvascular dysfunction.

Methods: We consecutively enrolled patients aged 20 years or older with chest pain between January 2022 and January 2024, all of them underwent HFQRS analysis and coronary angiography. We collected demographic characteristics (age, sex, history of smoking, history of alcohol consumption), history of previous diseases (coronary heart disease, hypertension, diabetes mellitus, hyperlipidemia), laboratory test indices, history of medications, and imaging data of these patients. All subjects also underwent the Pedal Upright Cycling Exercise Test according to the Bruce protocol.The examination process was divided into 3 phases: the first phase of resting , the second phase of the exercise , and the third phase of recovery. The sensitivity, specificity, and positive predictive value of HFQRS for predicting coronary microcirculatory dysfunction were calculated using caIMR ≥ 25.1 as the gold standard for determining coronary microcirculatory dysfunction. We used the area under the ROC curve (AUC) to evaluate the predictive accuracy of HFQRS and the diagnostic value of exercise HFQRS for CMVD.

Results: A total of 590 patients who underwent CAG were included in this study, After applying predetermined exclusion criteria, 139 patients were ultimately included for subsequent data analysis .Exercise stress HFQRS suggested that the number of positive leads was greater and statistically different in the caIMR ≥ 25.1 group compared to patients in the caIMR < 25.1 group (P <0.001). The maximal power of the caIMR ≥ 25.1 group during exercise stress HFQRS process was significantly lower than the caIMR < 25.1 group (8.29±3.07 vs 9.11±3.37, P=0.049). We also found a moderate correlation between the caIMR values and the number of positive HFQRS leads. (R=0.757, P<0.001). Multifactorial logistic regression analysis showed that the number of positive leads on the HFQRS was an independent predictor of caIMR (9.17 , CI 1.02-82.73, P=0.048). The area under the ROC curve for the prediction of caIMR by the number of positive HFQRS leads was 0.81 (95% CI 0.73-0.89). The sensitivity, specificity, negative predictive value, and positive predictive value of HFQRS for the prediction of coronary microcirculatory dysfunction were 0.686, 0.971, 0.986, and 0.500, respectively.

Conclusions: Our study found that exercise stress HFQRS is an important predictor of coronary microvascular dysfunction, that there was a correlation between the number of positive exercise stress HFQRS leads and Coronary microvascular resistance, and that exercise stress HFQRS is a noninvasive and reliable detector for the diagnosis of CMVD in clinical.

Deep Learning-Enhanced ECG Spatiotemporal Feature Analysis for Early HFpEF Detection: Integrating Speckle-Tracking Derived Myocardial Strain Patterns

Zhi-Yun Yang, Yi-Da Tang

北京大学第三医院（北医三院）Peking University Third Hospital

Deep Learning-Enhanced ECG Spatiotemporal Feature Analysis for Early HFpEF Detection: Integrating Speckle-Tracking Derived Myocardial Strain Patterns

Zhiyun Yang1, Rui Zuo2, Jingjia Wang1, Wenyao Wang1, Chunli Shao1, Yupeng Wang1, Ming Cui1, Yi-Da Tang1 #

1 Department of Cardiology and Institute of Vascular Medicine, Peking University Third Hospital, Key Laboratory of Molecular Cardiovascular Science, Ministry of Education, Beijing 100191, China;

2 Information Management and Big Data Center, Peking University Third Hospital, Beijing 100191, China

Corresponding author: Yi-Da Tang, Email: tangyida@bjmu.edu.cn.

Keywords: HFpEF, AI-ECG, deep learning, speckle-tracking echocardiography, early detection

Abstract

HFpEF's diagnosis is challenging and important. Previous studies have not integrated STE-derived LV-GLS classification with spatiotemporal ECG feature extraction for HFpEF phenotyping.We developed a CNN-LSTM hybrid model ,using STE-LV-GLS as a marker (classified into >18%, 16-18%, <16%).

The AI - ECG model achieved an AUC of 0.91, outperforming traditional ECG reading and H_2 FPEF scores. Key findings included that leads V2 - V3 contributed 42% of the weight, and late T - wave features correlated with HFpEF - specific repolarization abnormalities. The single - lead validity assessment showed that lead V3 alone exhibited 75.6% agreement with 12 - lead predictions, with an AUC of 0.804.

These show that AI-ECG spatiotemporal patterns can help timely HFpEF risk stratification.

Background:

Heart failure with preserved ejection fraction (HFpEF) constitutes over 50% of heart failure cases, yet its diagnosis remains challenging due to nonspecific symptoms (overlapping with COPD/obesity), complex workup (requiring echocardiography, natriuretic peptides, or invasive hemodynamics), and disease heterogeneity. While current ESC guidelines mandate three criteria for diagnosis - (1) HF symptoms/signs, (2) LVEF ≥ 50%, and (3) objective diastolic dysfunction evidence (E/e' >9, LAVi >34 mL/m^2) - echocardiographic parameters suffer from operator-dependent variability. Although H_2 FPEF and HFA-PEFF scores provide diagnostic frameworks, 40-50% of intermediate-score patients still require invasive confirmation. Notably, speckle-tracking echocardiography (STE)-derived LV global longitudinal strain (GLS) has emerged as a sensitive early marker of myocardial dysfunction in HFpEF (cutoffs: normal >18%, borderline 16-18%, abnormal <16%), reflecting subclinical ventricular impairment before overt diastolic dysfunction appears. The 2023 ASE guidelines recognize LV-GLS as a high-risk indicator. Recent advances in AI-ECG demonstrate that deep learning can decode electromechanical coupling information from standard 12-lead ECGs, with studies showing AUCs of 0.91 for detecting LV diastolic dysfunction - a core HFpEF feature. However, no study has yet integrated STE-LV-GLS classification with spatiotemporal ECG feature extraction for HFpEF phenotyping.

Methods:

We developed a CNN-LSTM hybrid model analyzing 712 ECGs from Peking University Third Hospital (2020-2024) of patients aged ≥ 60 with H_2 FPEF scores ≥ 2. Using STE-LV-GLS as a sensitive early functional marker (three-tier classification: >18%, 16-18%, <16%), we preprocessed 12-lead ECGs into grayscale images, then extracted:

1.Spatial features via dual-pathway CNNs (intra-lead 1×15 + inter-lead 12×1 kernels)

2.Temporal features via bidirectional LSTM with attention mechanisms

3.Fused outputs through gated weighting to generate risk probabilities (low:<0.3; intermediate:0.3-0.7; high: ≥ 0.7).

Statistical analyses included ROC curve comparisons (DeLong test with Bonferroni correction) and consistency assessments between single-lead (V3) and 12-lead predictions.

Results:

The AI-ECG model achieved superior performance (AUC:0.91, sensitivity:85.6%, specificity:89.3%) versus traditional ECG reading (AUC:0.65) and H_2 FPEF scores (AUC:0.83). Key findings included:

1.Lead contribution: V2-V3 accounted for 42% weight, reflecting atrial overload (P-wave abnormalities) and ventricular repolarization changes (ST-T alterations)

2.Time-phase importance: Late T-wave features (>60% weight) correlated with HFpEF-specific repolarization abnormalities

3.Single-lead validity: V3 alone showed 75.6% agreement with 12-lead predictions (AUC=0.804).

Conclusion:

This study demonstrates that ECG spatiotemporal patterns correlated with early STE-LV-GLS-defined myocardial dysfunction enable timely HFpEF risk stratification, particularly through V2-V3 repolarization features. The model's single-lead compatibility (V3) and cost-effectiveness ($50 vs. $500 for echocardiography) support its use in resource-limited settings, potentially enabling an "AI-ECG screening → echocardiographic confirmation" care paradigm. Future work should validate this approach for presymptomatic HFpEF detection via wearable devices.

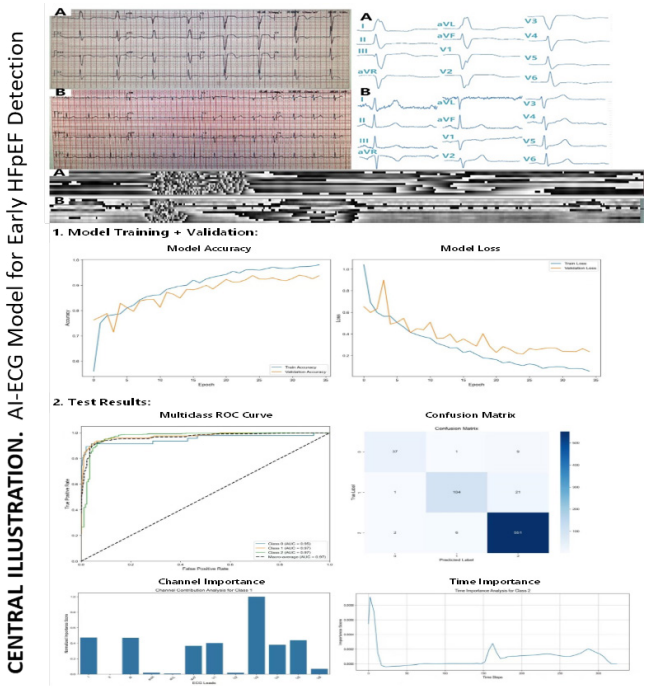

支架术后 DAPT 期间桥接肝素实施外科非心脏手术的风险研究

薛远征

陆军军医大学第三附属医院大坪医院

摘要：

目的：本研究旨在评估在支架术后双联抗血小板治疗（Dual Antiplatelet Therapy, DAPT）期间，患者因不可抗力必须接受外科非心脏手术，通过肝素桥接对手术风险的影响，提供临床决策支持。

方法：回顾性分析 173 名接受支架术后 DAPT 治疗的患者，在术后 DAPT 期间因不可抗力必须进行非心脏外科手术，其中 78 名患者采用停用抗血小板药物桥接肝素进行抗凝管理，对照组则直接停用抗血小板药物。通过比较手术前后的出血事件、术后并发症（如血栓形成、感染等）以及住院时间，评估桥接肝素的安全性和有效性。采用统计学方法分析桥接肝素使用与手术风险的相关性。

结果：在桥接肝素使用的患者中，术后出血事件的发生率较高，而未使用桥接肝素的患者则显示较低的出血风险。然而，使用桥接肝素的患者术后血栓事件发生率较低。进一步分析表明，桥接肝素能够有效降低血栓形成的风险，但其增加了术后出血的可能性，特别是在高风险患者中。

结论：在支架术后 DAPT 治疗期间，桥接肝素的使用虽然能有效预防术后血栓事件，但也伴随较高的出血风险。对于需要进行外科非心脏手术的患者，应根据个体情况权衡出血与血栓的风险，制定个性化的桥接策略，以确保最佳治疗效果。

靶向心脏的脂质体递送外泌体 miRNA-185-5p 抑制剂缓解扩张型心肌病心肌细胞凋亡及铜死亡的作用机制研究

徐帅

苏州大学附属独墅湖医院

目的：探讨脂质体靶向递送外泌体 miRNA-185-5p 抑制剂（Lipo@miR-185-5p 抑制剂）对扩张型心肌病（DCM）心肌细胞凋亡及铜死亡（cuproptosis）的作用与机制，为 DCM 精准治疗提供新策略。

方法：超速离心法提取血浆来源外泌体，miRNA 试剂盒纯化获得 miRNA-

185-5p 抑制剂，以 DOTAP、DOPE、胆固醇、DMG-PEG-2000 及心脏靶向肽（APWHLSSQYSRT）制备脂质体。利用透射电子显微镜（TEM）、动态光散射（DLS）和 Zeta 电位表征脂质体特性。体外以 H9C2 心肌细胞和人类 iPS 诱导心肌细胞建立 DCM 细胞模型，应用 CCK-8、Western blot、免疫荧光及流式细胞术评估细胞凋亡、氧化应激及铜死亡蛋白表达变化。体内以 DCM 小鼠模型进行尾静脉注射，采用超声、HE、Masson、免疫荧光、Western blot、ELISA 及 qPCR 评价药效，利用荧光成像及生化指标检测药物靶向性及安全性。

结果：体外实验显示，Lipo@miR-185-5p 抑制剂显著降低心肌细胞凋亡、DNA 损伤及 ROS 水平，抑制铜死亡蛋白表达。体内实验显示，该治疗显著改善小鼠心功能，减少心肌纤维化及凋亡和铜死亡蛋白表达；荧光成像证实药物在心脏精准积聚，且未观察到明显毒性。

结论：靶向脂质体递送外泌体 miRNA-185-5p 抑制剂通过调控凋亡与铜死亡通路有效缓解 DCM 病程，为临床治疗提供了创新的精准治疗策略。

心肌梗死后成纤维细胞阶段极化特征及其靶向干预策略的研究

黎国兴 王伟

陆军军医大学西南医院老年科

背景：心肌梗死后心肌纤维化是心脏修复失衡的核心病理机制，其过度进展可导致室壁僵硬、电传导紊乱及心功能进行性恶化，最终引发心力衰竭和恶性心律失常，显著增加患者住院率与死亡率，是心血管疾病的重要负担。成纤维细胞（FB）作为纤维化的核心效应细胞，具有显著异质性：心梗早期活化的肌成纤维细胞（Myo-FB）通过维持梗死区室壁完整性发挥保护作用，过早干预易诱发心脏破裂；而晚期持续活化的基质成纤维细胞（ECM-FB）介导胶原过度沉积与交联，此时干预因基质固化难以奏效。临床患者异质性大，精准确定抗纤维化治疗时间窗困难，因此避开 Myo-FB 活化期、尽早靶向干预 ECM-FB 可能为更优策略。然而，成纤维细胞随时间的表型转换规律及驱动因素尚未明确，靶向抑制 ECM-FB 的有效方法仍待探索。

方法: 基于单细胞测序与空间转录组分析，结合病毒介导的基因表达调控（Csrp2、Crlf1 敲低）及心肌梗死模型构建，观察干预后 14 天内小鼠死亡率、心脏破裂发生情况（解剖验证胸腔血凝块及心脏破口），并通过超声心动图评估心功能（射血分数、左室大小），Masson 染色分析室壁厚度及胶原沉积。

结果：单细胞 - 空间转录组联合分析显示：①拟时序分析提示心梗后 3-5 天成纤维细胞经历一过性 Myo-FB 极化，随后逐渐被分泌细胞外基质的 ECM-FB 替代，两种表型转换呈错峰特征；②文献报道的促心脏破裂靶点在 Myo-FB 极化期上调，而改善纤维化的靶点在 ECM-FB 极化期上调；③免疫荧光验证：α-SMA（Myo-FB 标志）于梗死后第 3 天高表达，第 7 天维持，第 14 天消失；Cilp（ECM-FB 标志）于梗死后 1-3 天低表达，随后逐渐升高，第 14 天达显著水平，与生信分析一致；④敲低 Csrp2 或 Crlf1（心肌纤维化及心脏破裂中未报道的新基因）后建立心梗模型，结果显示两组均出现大量心脏破裂（解剖见胸腔血凝块及心脏破口），伴射血分数降低、左室扩大及室壁变薄。

结论：心肌梗死后成纤维细胞存在显著的阶段极化特征：早期以保护性 Myo-FB 为主，晚期转为致纤维化的 ECM-FB。抑制 Myo-FB 相关基因可能破坏室壁完整性诱发心脏破裂，而靶向抑制 ECM-FB 相关基因可在不增加破裂风险的前提下有效改善心肌纤维化，为心梗后纤维化治疗提供了基于时间窗的精准干预新策略。

心血管介入学员成对友谊关系对学业成就的影响作用：基于主客体互倚性模型的分析

春英 [1] 王蕊 [2]

1. 上海市第十人民医院（同济大学附属第十人民医院）

2. 上海市光华中西医结合医院

目的：本研究使用结构方程的方法建立主客体互倚模型，探索心血管介入学员成对友谊关系对介入学业成就的影响。方法：通过方便取样的方法，使用个人成就目标取向量化修订表，收集了 216 份有效问卷，进行 t 检验和相关分析，建立了主客体互倚模型。结果：（1）与男性学员相比，女性学员年龄偏大（35.03±2.34 岁 VS. 33.75±3.10 岁，p < 0.001），生育史占比高（69.4% VS. 40.7%，p < 0.001）。（2）女性学员在掌握目标取向（t=3.97,p < 0.001）和接近目标取向（t=4.02, p < 0.001）方面均显著高于男生。而男生的学业成就高于女生（t=11.53, p < 0.001）。（3）不论在掌握目标取向方面还是在接近目标取向方面，成对友谊关系中的两名介入成员都具有很高的相似性；在成就方面，两者也具有较高的相似性（ICC=0.668）。（4）个体学业成就稳定，主体效应大于客体效应，个体成就主要受自身的影响，朋友对具有相互的显著影响效应（k=-0.124）。结论：朋友对中的介入学员能够相互影响，增加了彼此在学业成就上的相似性。

[关键词] 心血管介入诊疗；成对友谊关系；主客体互倚性模型

Targeting MTHFR Variant and Homocysteine Metabolism in Cardiovascular Translational Research

You Yu[1], Lian-Bo Shao[2], Meng Zhang[1]

1. Soochow University

2. The First Affiliated Hospital of Soochow University

Targeting MTHFR **Variant and Homocysteine Metabolism in Cardiovascular Translational Research**

You Yu[1,#], Lianbo Shao[2], Meng Zhang[1]

1. Institute for Cardiovascular Science, Soochow University, Suzhou 215123, Jiangsu, PR China

2. The First Affiliated Hospital of Soochow University, Suzhou 215123, Jiangsu, PR China

Correspondence: You Yu, yyu@suda.edu.cn

Background

Thoracic aortic dissection (TAD) represents a life-threatening cardiovascular disorder with underlying endothelial dysfunction, yet the molecular interplay between genetic variants and metabolic dysregulation in TAD pathogenesis remains elusive. Methylenetetrahydrofolate reductase (MTHFR) orchestrates homocysteine metabolism, and the rs1801133-TT variant (C677T) compromises MTHFR activity. The variant is extremely common in populations, and those individuals suffered with homozygous mutation in this single nucleotide polymorphism (SNP) only have 30 % activity of normal enzyme function, finally accumulated homocysteine dramatically shapes the increasing risk for cardiovascular diseasesculminating. Although homocysteine-induced mitochondrial dysfunction and mitophagy disruption have been implicated in endothelial injury, direct evidence in human cellular models is lacking. Here, we aimed to investigate how MTHFR rs1801133-TT modulates homocysteine metabolism and endothelial pathophysiology via mitophagy regulation using patient-derived induced pluripotent stem cells (iPSCs).

Methods

1. Isogenic iPSC Model Establishment: Isogenic iPSC lines were established via CRISPR/Cas9-mediated correction of rs1801133-TT to wild-type (CC) in TAD patient-derived MTHFR-iPSCs, serving as genetically matched isogenic control cell lines.

2. Endothelial Differentiation and Characterization: Human iPSCs were differentiated into endothelial cells (iPSC-ECs) using a chemically defined protocol, validated by flow cytometry (CD144/CD31 expression), immunofluorescence staining, and functional assays (nitric oxide production, acetylated LDL uptake).

3. Cellular Toxicity Profiling: Homocysteine dose-response curves were generated via CCK-8 and Caspase-Glo assays. Cell apoptosis was quantified by Annexin V/PI staining followed by flow cytometry, while mitochondrial function was assessed using JC-1 staining (membrane potential) and MitoTracker Red (network morphology).

4. Mitophagy Flux Analysis: Mitophagy activity was evaluated using the pH-sensitive mt-Keima reporter and western blotting for key regulators (LC3, p62, PINK1).

5. Transcriptomic Profiling: Bulk RNA-seq was performed on homocysteine-treated iPSC-ECs to identify differentially expressed genes (DEGs), validated by qRT-PCR and western blotting.

6. Small Molecule Screening: A 96-compound Cherry pick-up library was screened to identify chemicals mitigating homocysteine toxicity caused by , with kaempferol validated through mitochondrial structure/function assays.

Results

1. MTHFR rs1801133-TT Does Not Impair Endothelial Lineage Commitment: Isogenic-iPSC-ECs and MTHFR-iPSC-ECs exhibited comparable differentiation efficiency and major endothelial marker expression (CD144 and CD31). Functional assays (nitric oxide response and TNFα-induced adhesion molecule expression) were indistinguishable under basal conditions.

2. MTHFR-TT Potentiates Homocysteine-Induced Cytotoxicity: MTHFR-iPSC-ECs displayed significantly lower IC50 (115.1 vs. 183.0 μM) and EC50 (110.5 vs. 196.7 μM) for homocysteine, accompanied by increased early apoptosis (24.33% vs. 9.34%) and reduced cell proliferation as measured by EdU assay.

3. Homocysteine Disrupts Mitochondrial Architecture and Mitophagy Flux: In MTHFR-iPSC-ECs, homocysteine induced mitochondrial fragmentation (such as 40% reduction in network junctions), depolarized the mitochondrial membrane (JC-1 monomer/aggregate ratio increased), and impaired mitophagy (mt-Keima ratio decreased, while little p62 accumulation).

4. LAMP3 Drives Homocysteine-Mediated Mitophagy Dysfunction: Bulk RNA-seq identified lysosomal-associated membrane protein 3 (LAMP3) as a top-upregulated DEG (fold change >2.8), confirmed by qRT-PCR and western blotting assay. LAMP3 co-localized with mitochondria, and genetic knockdown rescued mitochondrial integrity and reduced apoptosis (25.63% to 18.92% in homocysteine-treated endothelial cells).

5. Kaempferol Restores Mitochondrial Homeostasis: Kaempferol treatment normalized mitochondrial networks (35% increase in junctions), reinstated mitophagy flux (mt-Keima ratio recovery), and attenuated cell apoptosis (11.60% vs. 25.63% in homocysteine vs. DMSO controls).

Conclusions

This study elucidates that MTHFR rs1801133-TT impairs homocysteine

metabolism, triggering LAMP3-dependent mitophagy disruption and endothelial dysfunction. Kaempferol protects against homocysteine toxicity by restoring mitochondrial quality control, nominating mitophagy as a therapeutic target. These findings establish direct evidence of genetic variant and metabolic crosstalk in endothelial cell homeostasis and advocate for personalized approaches integrating genetic screening (such a s MTHFR variants) with metabolic intervention (homocysteine-lowering strategies or mitophagy activators) for patient stratification and vascular protection.

苯萸次碱对氧化应激诱导血管平滑肌细胞增殖和一氧化氮合酶的影响

赵然尊

遵义医科大学附属医院

目的：观察氧化应激对吴茱萸次碱作用血管平滑肌细胞增殖和一氧化氮合酶 (NOS) 的影响。

方法: 血管平滑肌细胞分空白组、二甲基亚砜组、药物 A 组 (吴茱萸次碱 0.4μmol/L)、药物 B 组 (吴茱萸次碱 1μmol/L)、药物 C 组 (吴茱萸次碱 4μmol/L)，后 4 组药物刺激 2h 后，加入过氧化氢诱导氧化应激损伤，24h 后检测细胞增殖率、活性氧、丙二醛、超氧化物歧化酶 (SOD)、内皮型 NOS(eNOS)、诱导型 NOS(iNOS)mRNA 和蛋白表达。

结果：与空白组比较，二甲基亚砜组细胞增殖率明显升高 [(104.48±4.89)%vs(94.58±1.87)%，P<0.05]，活性氧和丙二醛明显升高，SOD 明显下降 [(82.55±17.31)U/mg vs(111.76±18.25)U/mg， P<0.05]。与二甲基亚砜组比较，药物 A 组、药物 B 组、药物 C 组细胞增殖率、活性氧和丙二醛明显下降，药物 B 组、药物 C 组 SOD 明显升高 (P<0.05)；药物 A 组、药物 B 组、药物 C 组 iNOS mRNA 和蛋白表达明显下降，eNOS mRNA 和蛋白表达明显升高 (P<0.05)。

结论：吴茱萸次碱在氧化应激状态下能抑制平滑肌细胞增殖、抗氧化、维持 NOS 相对稳定。

银丹心脑通软胶囊对非酒精性脂肪肝的疗效及其机制探讨

赵然尊

遵义医科大学附属医院

目的：探讨银丹心脑通软胶囊治疗非酒精性脂肪肝的疗效及其可能机制。

方法：非酒精性脂肪肝患者 80 例，随机分为观察组与对照组，每组 40 例。所有患者入院后接受基础治疗与药物干预措施。观察组在此基础上口服银丹心脑通软胶囊治疗，对照组患者口服阿托伐他汀片治疗，治疗周期 3 个月。比较两组患者治疗后的疗效；血脂、炎症因子、肝功能及过氧化物酶体增殖物激活受体 (PPAR)-mRNA 表达变化情况。

结果：观察组治疗总有效率 95.00%，高于对照组的 70.00%，差异有统计学意义 (P<0.05)。治疗后，观察组患者 TC、TG、HDL-C、LDL-C、hs-CRP、IL-6、ALT、AST、CGT 的改善值高于对照组，差异有统计学意义 (P<0.05)。治疗后，观察组患者血清 PPAR-mRNA 表达量降低，与对照组比较，观察组治疗后血清 PPAR-αmRNA 表达变化值高于对照组，差异有统计学意义 (P>0.05)。

结论：银丹心脑通软胶囊治疗非酒精性脂肪肝，其对症状的改善效果较好；患者的血脂、肝功能及炎症因子降低；脂肪肝程度及胰岛素抵抗程度得以改善；下调患者血清 PPAR-αmRNA 的表达可能是其改善患者胰岛素抵抗，进而治疗非酒精性脂肪肝的作用机制之一。

Nanomedicine in cardiology: Precision drug delivery for enhanced Patient outcomes

Feng-Li Peng, Bei Shi

Affiliated Hospital of Zunyi Medical University

Cardiovascular diseases as a Primary driver of global morbidity and mortality . DesPite the array of theraPeutic avenues in clinical Practice , Predominantly Pharmaceutical and surgical interventions , they often fall short of fully addressing the clinical exigencies of cardiovascular Patients. In recent years, nanocarriers have shown great Potential in the treatment and diagnose of cardiovascular diseases. They can enhance drug targeting and bioavailability while reducing side effects. Additionally, by imProving imaging and detection technologies, they enhance early diagnosis and disease monitoring caPabilities. These advancements in technology offer new solutions for Precision medicine in cardiovascular diseases, advancing treatment efficacy and disease management. Crafted from biomaterials, metals, or their amalgamations, these nanocarriers aPProximate the dimensions of biologically active molecules like Proteins and DNA. Cardiovascular nanomedicine, in its infancy, has only recently burgeoned. Yet, with continual refinement in nanocarrier architecture, drug delivery mechanisms, and theraPeutic outcomes, the Potential of nanomedical technologies in clinical contexts becomes increasingly evident. This review aims to consolidate the strides made in nanocarrier research concerning the treatment and diagnose of cardiovascular diseases.

Multifunctional Nanosystems for Precision Diagnosis and Detoxification in Cardiovascular Diseases: From Multimodal Imaging of Myocarditis to Cardioprotective Chemotherapy

FAN YIN

Children's Hospital of Chongqing Medical University

Multifunctional Nanosystems for Precision Diagnosis and Detoxification in Cardiovascular Diseases: From Multimodal Imaging of Myocarditis to Cardioprotective Chemotherapy

Dan Yin, Mi Li, Min Zheng, Wenjing Yuan, Jiajin Li, Lingjuan Liu, Jie Tian

Background and Objective: Inflammatory and chemotherapy-induced cardiac injuries, including autoimmune myocarditis (EAM) and doxorubicin-induced cardiotoxicity (DIC), remain major clinical challenges with high morbidity and mortality. EAM, characterized by chronic inflammation and myocardial fibrosis, affects ~1–2% of the global population and lacks non-invasive, early-diagnostic tools. DIC, a dose-limiting toxicity of anthracycline chemotherapeutics (e.g., doxorubicin, DOX), occurs in 9–36% of cancer patients, leading to heart failure and treatment discontinuation. Current diagnostic methods (e.g., cardiac MRI, biopsy) are invasive, expensive, or lack sensitivity for early-stage lesions. Therapeutically, cardioprotective agents (e.g., dexrazoxane) often compromise antitumor efficacy or induce off-target toxicity.

Methods: (1) Diagnostic Nanoprobe (MM/NPs): Fabricated macrophage membrane (MM)-camouflaged phase-change nanoparticles via double emulsion and liposome extrusion, loaded with SPIO (T_2-MRI) and PFH (PA/US contrast agents).Isolated murine macrophage membranes (via Beyotime Membrane Protein Extraction Kit) were extruded through a lipid extruder (100 nm pore size) to coat PLGA cores, forming MM/NPs. Experimental autoimmune myocarditis (EAM) mice (C57BL/6, 8–10 weeks) were induced by subcutaneous injection of α-myosin heavy chain (MyHC-α, 100 μg/mouse) on days 0 and 7. Validated targeting specificity in EAM mice using confocal imaging, flow cytometry, and multimodal imaging. (2)Therapeutic Nanocomplex (PGPP/NPs): Engineered carrier-free self-assembled nanoparticles co-loaded with ginsenoside Rb1 (antioxidant), probucol (anti-inflammatory), and PI3Kγ inhibitor (autophagy enhancer), surface-functionalized with cardiomyocyte-targeting peptide (PCM). Evaluated cardioprotection in a 4T1 breast cancer model undergoing DOX chemotherapy, assessing cardiac function, serum biomarkers, and autophagic flux.

Results: (1) Diagnostic Performance: TEM confirmed uniform spherical morphology (200 ± 20 nm) with SPIO (dark dots) and PFH (phase-dense cores) encapsulated within PLGA, coated by a continuous macrophage membrane layer. Zeta potential (-28.5 ± 1.2 mV) ensured colloidal stability in DMEM, PBS, and serum. MM/NPs achieved high targeting efficiency in EAM myocardium ($p<0.05$), enabling simultaneous US/PA/MRI imaging with superior contrast to non-targeted controls. Multimodal imaging revealed inflammatory foci and myocardial damage, correlating with histopathological findings. (2) Therapeutic Efficacy: PGPP/NPs selectively accumulated in cardiomyocytes, reducing DOX-induced oxidative stress (ROS ↓), inflammation (TNF-α ↓ , IL-6 ↓), and apoptosis (caspase-3 ↓) while enhancing autophagy (LC3-II ↑). Cardiac function (LV-EF/LV-FS) and serum biomarkers (cTnI, BNP) normalized in PGPP/NP-treated mice. PGPP/NP treatment did not affect DOX antitumor activity–tumor volume in PGPP/NP + DOX group was comparable to free DOX, with no survival difference ($p > 0.05$; Figure 2G).

Conclusion: This study introduces a dual-functional nanomedicine platform that integrates precision diagnosis and cardioprotection. MM/NPs enable early, non-invasive detection of myocardial inflammation via SPIO/PFH-based multimodal imaging, addressing the unmet need for sensitive diagnostic tools in EAM.PGPP/NPs mitigate DIC through antioxidant, anti-inflammatory, and autophagy-modulating mechanisms while preserving DOX antitumor efficacy, overcoming the limitations of current cardioprotective agents. Collectively, these findings provide a transformative strategy for managing inflammatory and chemotherapy-induced cardiac injuries, with broad applicability to other cardiovascular diseases (e.g., viral myocarditis, heart failure). Future studies will focus on long-term toxicity assessment, clinical translation (e.g., phase I trials), and exploring combinatorial therapies with emerging immunotherapies.

Keywords: Nanoparticles, Myocarditis, Cardiotoxicity, Self-Assembly, Multimodal Imaging, Cardioprotection

秋水仙碱在心血管疾病中的治疗作用：基于 Web of Science 的文献计量学分析（2001-2024）

张世琳 [1] 杨庆 [1] 陈芬 [2] 刘禹彤 [1] 姚静 [1,2]

1. 南京中医药大学鼓楼临床医学院

2. 南京大学医学院附属鼓楼医院超声医学科

研究目的：秋水仙碱在减少心血管事件中的潜在作用备受关注。本研究采用文献计量学方法，系统剖析 2001–2024 年 Web of Science 核心合集收录的 455 篇相关文献，旨在揭示该领域的年度发文趋势、地域机构分布、核心作者群体及研究主题演化，为把握学科前沿与规划未来研究方向提供量化依据。

研究方法：采用 CiteSpace 与 VOSviewer 软件，对文献的发表年份、国家及地区、机构、作者、期刊进行统计分析；结合布拉德福定律筛选核心期刊；运用 VOSviewer 绘制作者合作网络与关键词分布图谱；基于期刊共被引分析构建学

科知识图谱；通过关键词共现聚类与突现词检测揭示研究主题演进。

研究结果：文献计量分析显示：455 篇文献源于 63 个国家 995 家机构的 2575 名作者，发表于 230 种期刊，年发文量呈三阶段演变——初期（2001-2010）缓慢增长（年均 5 篇），中期（2011-2020）快速上升（年均 17 篇），近期（2021-2024）爆发增长（年均 58.8 篇）。美国（160 篇）、意大利（70 篇）、澳大利亚（50 篇）、中国（50 篇）及加拿大（43 篇）主导区域研究，30 位核心作者（含 Imazio M、Brucato A）形成 4 个合作聚类，17 种核心期刊（如《Current Cardiology Reports》《American Heart Journal》）符合布拉德福分布。被引频次前三的期刊为《Circulation》（1669 次）、《The New England Journal of Medicine》（1342 次）、《Journal of the American College of Cardiology》（1068 次），高被引文献主题聚焦于“抗炎机制”、“心血管保护”与“心包疾病应用”。关键词聚类识别九大主题（含动脉粥样硬化、心包炎、精准医疗、药物递送系统），突现分析揭示研究轨迹演化：2001-2010 年聚焦“细胞骨架重构”与“心脏肥大”，2011-2020 年转向“心包疾病临床应用”及“房颤预防”，2021 年后深化“低剂量疗法”、“心血管二级预防”和“NLRP3 炎症小体 - 氧化应激”机制。

研究结论：秋水仙碱研究已从基础机制向临床精准治疗深化，未来需重点突破低剂量个体化治疗优化、心脏手术围术期炎症调控临床转化及纳米递送系统跨学科创新，以驱动“基础研究 - 临床应用”双向转化。

工程化外泌体在精准靶向修复缺血性心脏病中的功能及机制研究

柯 [1,2,3] 唐俊楠 [1,2,3]

1. 郑大第一附属医院

2. 河南省心脏损伤与修复重点实验室

3. 河南省心血管疾病临床研究中心

目的：缺血再灌注损伤（I/RI）对心肌梗死（MI）后的发病率和死亡率有显著影响，可能会加剧心脏重塑和心力衰竭。然而，目前仍然缺乏有效的治疗方法。血浆中的细胞外囊泡（EV）虽然具有治疗潜力，但是其在体内的靶向递送能力不足严重限制了其治疗效果。本研究旨在开发一种血小板膜（PNVs）修饰的工程化外泌体（PNV-EVs），通过负载 miRNA-210-3p 实现缺血心肌的精准靶向修复，并揭示其作用机制。

方法：通过挤压融合法构建 PNV-EVs。利用小 RNA 测序（miRNA-sequencing）筛选急性心梗患者血浆外泌体差异表达 miRNA（miR-210-3p）。体外实验验证 PNV-EVs 对内皮细胞迁移、侵袭、增殖和成管的影响。构建 I/RI 小鼠模型，通过超声心动图、Masson 染色、免疫荧光等评估 PNV-EVs-miRNA 对心脏功能与重塑的作用。通过小鼠成像系统动态追踪 PNV-EVs 在体内的靶向能力。

结果：在靶向能力方面，PNV 修饰显著增强 HUVEC 的对 EVs 的摄取，且 PNV-EVs 对损伤心脏的靶向能力强于未修饰 EVs，两者对损伤心脏的靶向能力均强于正常心脏。miRNA-210-3p 在急性心梗患者 EVs 中高表达，PNV-EVs-miRNA-210-3p 可以显著促进 HUVEC 的迁移、侵袭、增殖和成管。体内实验表明，PNV-EVs-miRNA-210-3p 显著改善 I/RI 的心脏功能，减轻心脏重塑。

结论：我们的研究发现，PNV 修饰的工程化外泌体递送系统增强了 EVs 在 I/RI 中的精准靶向修复，改善了 I/RI 的心脏功能，为缺血性心脏病提供了一种新型的精准靶向递送策略。

《从基础到临床：心血管病诊治创新成果的转化医学实践》

王宏研

哈尔滨医科大学附属第一医院

目的：心血管疾病作为全球致死率最高的疾病之一，其防治面临早期诊断难、治疗方案同质化、预后管理粗放等瓶颈。转化医学倡导“从实验室到病床”的精准医学理念，本研究聚焦心血管病诊治的关键痛点，通过整合多学科创新技术（人工智能、生物标志物、基因检测、数字诊疗工具等），构建“基础研究 – 技术转化 – 临床验证 – 规范推广”的全链条转化体系，旨在突破传统诊疗模式局限，提升心血管病的早期识别能力、个体化治疗效果及全周期管理水平，推动创新成果向临床实践的高效转化，为降低心血管病发病率、致残率和死亡率提供新路径。

方法：本研究在创新技术研发与转化路径设计上，基于代谢组学、蛋白组学技术，从 1000 例冠心病、心力衰竭患者及 500 例健康对照的血清样本中，筛选差异表达的生物分子，结合机器学习构建早期诊断模型（如心力衰竭风险预测模型）；整合电子病历、冠脉造影、心脏超声等多模态数据（纳入 3000 例患者数据），运用深度学习算法构建影像识别模型（如斑块易损性评估模型）和临床决策支持系统（CDSS），实现“影像分析 – 病因判断 – 方案推荐”的智能化闭环；针对家族性高胆固醇血症、缺血性心肌病等病种，开展基因测序与功能分析，探索靶向 PCSK9 的基因编辑技术及间充质干细胞移植的临床安全性与有效性。同时，通过回顾性分析（纳入 2018–2023 年 5000 例历史病例）与前瞻性多中心临床试验（覆盖 10 家三甲医院，入组 1200 例患者），验证创新技术的诊断效能、治疗安全性及预后改善效果，主要评价指标包括诊断准确率、治疗有效率、心血管事件发生率、患者生存质量（SF-36 评分）等。

结果：本研究取得了多方面的成果，在早期诊断技术上，筛选出包含 NT-proBNP、sST2、Galectin-3 的心力衰竭早期诊断组合，其 AUC 达 0.92（95% CI: 0.89-0.95），较单一指标提升 23%，可提前 3-6 个月预警无症状心力衰竭患者的病情恶化；斑块易损性评估模型对罪犯病变的识别准确率达 91%，较传统血管造影医生判读效率提升 40%，在急性冠脉综合征（ACS）急诊 PCI 术前规划中，将手术时间缩短 22 分钟 / 例，支架置入精准度提升 18%。在个体化治疗方案优化方面，针对携带 PCSK9 基因突变的家族性高胆固醇血症患者，基于基因分型的靶向药物（如依洛尤单抗）治疗使 LDL-C 水平降幅达 65%，较常规方案提升 30%，且用药不良反应发生率降低 25%。在全周期管理效能提升上，基于 AI 的随访系统在 200 例高血压合并冠心病患者中试点，实现血压控制达标率从 58% 提升至 81%，动态心电图异常事件识别响应时间缩短至 3 分钟 / 例，1 年内心血管事件（心梗、卒中等）发生率从 12% 降至 7%（HR=0.58, 95% CI: 0.39-0.86）。

结论：本研究通过转化医学理念驱动，实现了心血管病诊治技术从“单一手段”到“体系创新”的跨越。生物标志物组合、AI 诊疗平台及基因细胞治疗等创新成果，显著提升了心血管病的早期诊断精度（准确率↑ 20%-30%）、治疗个体化水平（疗效↑ 15%-25%）及管理智能化程度（事件风险↓ 20%-30%），具有明确的临床应用价值。代谢组学、AI 算法与临床医学的深度融合，验证了“数据驱动 + 机制解析”双轮驱动的转化模式有效性，为复杂疾病诊治提供了可复制的方法论。未来需进一步解决技术转化中的关键挑战，如生物标志物检测标准化等，同时加强医工协同、区域医疗数据共享及政策层面的创新技术准入支持，推动心血管病防治进入“精准化、智能化、一体化”新时代。

Study on the Rapid Screening of Non-ST Elevation Myocardial Infarction in Different Gender Patients Using the High-Sensitivity Cardiac Troponin I (hs-cTnI) 0h/1h Algorithm in the Chinese Population

Li Haoxi, He Yin, Yan Shufeng, He Xiaonan

Beijing Anzhen Hospital-Capital Medical University

“Study on the Rapid Screening of Non-ST Elevation Myocardial Infarction in Different Gender Patients Using the High-Sensitivity Cardiac Troponin I (hs-cTnI) 0h/1h Algorithm in the Chinese Population”

Yan Shufeng, He Xiaonan

Beijing Anzhen Hospital, Capital Medical University, Emergency and Critical Care Center

Abstract:

This study investigates the significance of the high-sensitivity cardiac troponin I (hs-cTnI) 0h/1h algorithm in the rapid screening of non-ST elevation myocardial infarction (NSTEMI) in patients of different genders, providing a reference for early diagnosis of acute myocardial infarction (AMI) in emergency settings.

Methods:

We enrolled 347 patients with suspected NSTEMI presenting with chest pain in the emergency department. Clinical data were collected, and hs-cTnI levels were measured at two time points (0h, 1h). The hs-cTnI 0/1h algorithm was established using the European Society of Cardiology (ESC) guidelines and adjusted for Chinese patients. Based on gender and final diagnosis (NSTEMI or non-AMI), we classified the patients and evaluated the diagnostic value of the hs-cTnI 0/1h algorithm using the receiver operating characteristic (ROC) curve to determine the best cutoff values.

Results:

For the female group (134 patients), the negative predictive value (NPV) for diagnosing NSTEMI was 99.01% (95% CI, 93.82–99.95%), with a sensitivity of 93.75% (95% CI, 66.71–99.67%). The algorithm identified 14.93% of patients as positive. For the male group (213 patients), the NPV was 99.23% (95% CI, 95.16–99.96%), with a sensitivity of 98.21% (95% CI, 89.19–99.91%). The algorithm identified 24.88% of male patients as positive.

Conclusion:

The Anzhen hs-cTnI 0h/1h algorithm, adjusted for Chinese data, demonstrates high safety and accuracy for diagnosing NSTEMI in patients of different genders.

Background:

Acute myocardial infarction (AMI) is one of the most common and severe cardiovascular diseases, which has been increasing with the improvement of living conditions. AMI is characterized by rapid onset, high severity, and high mortality, seriously affecting patients' quality of life and lifespan, while adding significant medical and economic burdens to society and families. In emergency clinical work, chest pain patients should be highly suspected of myocardial infarction, as non-ST elevation myocardial infarction (NSTEMI) often lacks typical electrocardiographic changes, making diagnosis easily delayed or missed. Furthermore, the prognosis for NSTEMI patients is poorer than that of acute ST-elevation myocardial infarction (STEMI) patients in both the short and long term. Therefore, early diagnosis and screening of NSTEMI are critical.

Cardiac troponin (cTn), a protein specific to myocardial fibers, is the preferred biomarker for myocardial injury and/or necrosis due to its high specificity and sensitivity, early appearance, and long diagnostic window. It is recommended as the “gold standard” for diagnosing AMI. However, gender-specific cutoff values for high-sensitivity cardiac troponin (hs-cTn) have not been widely applied in clinical practice, leading to lower diagnostic accuracy for NSTEMI. Accurately quantifying gender-based hs-cTn cutoff values can help develop more tailored treatment strategies, improve survival rates, and reduce healthcare costs. Recent studies have shown that hs-cTnI significantly increases the sensitivity of NSTEMI diagnosis, with a 20% higher detection rate compared to tradi-

tional cTn. Recent studies on hs-cTnI have found that gender is closely related to its concentration.

Research has also suggested that the hs-cTnI 0/1h algorithm is safer and more effective than the ESC-recommended 0/3h algorithm for ruling out AMI. The 2020 ESC NSTE-ACS guidelines recommend using the 0/1h algorithm as the primary method for rapid triage, and it has been validated in several large cohort studies. This study aims to analyze the best cutoff values and diagnostic performance of the hs-cTnI 0/1h algorithm for patients of different genders, providing further insights into the early diagnosis of NSTEMI.

Expression of Circadian Rhythm Genes in Atherosclerosis Complicated with Hypertension: A Study Based on Bioinformatics

Dan wang

Pidu District People's Hospital, Chengdu, Sichuan Province

Hypertension is a common cardiovascular disease that affects nearly 50% of adults. Hypertension has been proven to be a major co-existing condition with atherosclerosis since the 1970s. Atherosclerosis is a systemic chronic inflammatory disease that primarily affects muscular and elastic arteries. It is characterized by an autoimmune response to arterial wall injury, leading to the subintimal accumulation of lipids, immune cells, and smooth muscle cells (SMCs). Atherosclerotic disease, such as myocardial infarction and stroke, is the number one killer worldwide. Hypertension is an independent and controllable risk factor for atherosclerotic cardiovascular diseases (CVDs). Conversely, atherosclerosis hardens the arterial wall and raises arterial blood pressure. Atherosclerosis and hypertension have been prioritized as public health concerns by the World Health Organization owing to their substantial impact on cardiovascular diseases. Moreover, a diagnosis of multiple comorbidities presents additional challenges to the patient's health. Although considerable effort has been devoted to the pathogenesis of atherosclerosis with hypertension, the role of the circadian biological clock has been relatively neglected in past research.

The circadian biological clock is part of our body's natural internal rhythms that keep our bodies functioning properly by controlling a variety of physiological processes such as the sleep-wake cycle, thermoregulation, and hormone secretion. The realm of cardiovascular diseases, the interplay between circadian rhythm genes (CRGs) and conditions such as arrhythmia, hypertension, atherosclerosis, and myocardial infarction has attracted significant scholarly attention. Research suggests that the clock may influence the time-dependent incidence of cardiovascular events by controlling the integration of selective asynchronous stress responses with an underlying circadian rhythm in cardiovascular function. A study showed changes in CRGs expression may contribute to the pathogenesis of atherosclerosis. Aberrant circadian rhythms, increased pathological remodeling, vascular endothelial dysfunction, as well as attenuation of Akt and nitric oxide signaling have been found in the arteries of mice with Bmal1-deficiency and Clock mutation. Furthermore, the disruption of the molecular clock impairs lipid homeostasis and results in inflammation, which both promote atherogenesis. Collectively, these findings indicate that CRGs may modulate various mechanisms underlying atherosclerosis and hypertension development. Such insights provide novel avenues for prevention and treatment strategies against atherosclerosis and hypertension by suggesting that modulation of CRGs expression or leveraging rhythmic patterns could be beneficial in mitigating disease progression. Future investigations are warranted to further clarify the specific relationships between CRGs and atherosclerosis with hypertension while exploring innovative therapeutic approaches.

This study utilizes bioinformatics methods to screen CRGs through high-throughput expression data from microarrays, conducts functional enrichment analysis and protein network analysis, and finally verifies the selected genes by collecting a certain number of clinical samples and using quantitative real-time polymerase chain reaction (qRT-PCR) method. This study aims to provide scientific evidence for the potential value of CRGs as molecular markers for the diagnosis and treatment of atherosclerosis with hypertension. Through analysis, we identified 46 differentially expressed genes (DEGs), including 27 CRGs. Functional enrichment revealed their involvement in key processes such as epithelial cell migration, wound response, and the AGE-RAGE signaling pathway. Protein-protein interaction network analysis identified core hub genes (PLAT, FGF2, and TGFB2). qRT-PCR validation confirmed significant upregulation of PLAT, FGF2, and TGFB2 in patient blood samples ($P<0.05$), providing preliminary experimental support for their potential as diagnostic biomarkers. However, the clinical applicability of these findings requires further validation in larger cohorts due to the limited sample size (n=25 patients/20 controls) and lack of longitudinal data. Future studies should investigate the mechanistic roles of these genes in circadian-regulated vascular pathology and validate their utility in prospective cohorts.

心血管病诊治的创新与转化医学研究进展

张男奇 董增祥

哈尔滨医科大学附属第一医院

目的：心血管疾病作为全球致死率最高的疾病之一，其诊治模式的创新与转化是改善患者预后的关键。本研究旨在总结近年来心血管病领域在诊断技术、治疗策略及转化医学方面的突破性进展，探讨创新成果从基础研究到临床应用的转化路径，为优化诊疗流程、提升疗效提供理论与实践依据。

方法：通过系统检索 PubMed、Science Direct 等数据库中 2018-2024 年发表的相关文献，纳入涵盖基因编辑、人工智能（AI）辅助诊断、新型生物标志物、微创介入技术及转化医学平台建设的研究。采用循证医学方法分析创新技术的临床价值，重点评估其在早期诊断、个性化治疗及预后改善中的应用效果，并总结转化过程中的关键瓶颈与解决方案。

结果：基础研究层面，单细胞测序与多组学技术揭示了动脉粥样硬化的分子机制，发现 3 个新型易感基因（LOC105372575、ADAMTSL4、LPL）可作为诊断标志物；AI 辅助影像系统（如深度学习超声分析模型）将冠心病早期筛查准确率提升至 92.3%，较传统方法提高 18.6%。治疗领域，生物可吸收支架（BRS）在 2 年随访中靶病变血运重建率降至 5.8%，显著低于金属支架（9.2%）；基因编辑技术（CRISPR-Cas9）在家族性高胆固醇血症小鼠模型中实现 LDL-C 水平下降 40% 以上，已进入 I 期临床试验。转化医学方面，多中心临床研究网络的建立缩短了创新技术从实验室到临床的周期，平均转化时间从 7.2 年缩减至 4.5 年，但仍面临伦理审查严格、跨学科协作不足等挑战。

结论：心血管病诊治的创新技术在基础研究与临床应用中取得显著突破，为疾病的精准防控提供了新思路。转化医学平台的完善是推动创新成果落地的核心，未来需加强基础 - 临床协同创新，优化监管机制，以加速技术转化，最终降低心血管病的发病率与死亡率。

仿生纳米酶以中性粒细胞搭便车的方式靶向缺血性心脏病心肌细胞的保护作用及机制研究

崔新月 [1,2,3] 张金盈 [1,2,3] 唐俊楠 [1,2,3]

1. 郑州大学第一附属医院心内科

2. 河南省心脏损伤与修复重点实验室

3. 河南省心血管疾病临床研究中心

目的：心肌梗死是冠心病的危急重类型，导致显著的残疾率，并给社会带来沉重负担。因此寻找有效的治疗心肌梗死的方法至关重要。本研究围绕仿生纳米酶的设计、体外保护机制及体内靶向性验证展开，开发靶向性强、功能协同的纳米酶体系，为缺血性心脏病提供新型精准治疗策略。

方法：首先，基于心肌缺血微环境特征（如高 ROS、炎症因子富集），设计具有血小板膜（platelet membrane, PM）和唾液酸（saliva acid, SA）修饰的 Ru 单原子纳米酶（Ru single-atom nanozymes, Ru-SAN），优化其粒径（<100 nm）及表面电荷（近中性），提升生物相容性及稳定性。其次，通过原代心肌细胞缺氧 / 糖氧剥夺（oxygen and glucose deprivation, OGD）模型验证仿生纳米酶对 ROS 清除、凋亡抑制（Annexin V/PI 检测）及炎症因子（IL-6、TNF-α 等）的调控作用，并利用激光共聚焦显微镜解析仿生纳米酶与中性粒细胞表面受体的结合及内吞机制。最后，通过冠状动脉结扎术构建大鼠心肌缺血模型，结合近红外荧光标记与活体成像技术动态追踪靶向效率，评估仿生纳米酶对心肌梗死面积、纤维化程度（Masson 染色）及心功能（超声心动图）的改善效果，并阐明中性粒细胞介导的递送路径及下游通路调控机制。

结果：本研究结果表明，Ru-SAN 可模拟过氧化氢酶、超氧化物歧化酶和谷胱甘肽过氧化物酶的酶活性，可有效清除过量的 ROS，具有卓越的抗氧化能力，显着抑制损伤部位的 ROS- 铁死亡循环。同时，Ru-SAN 通过抑制炎症、心肌细胞凋亡，为损伤后修复创造了有利的微环境。仿生纳米酶在体内可有效靶向心肌缺血区域，同时它们的治疗效果在缺血性心肌梗死大鼠中得到了系统的验证。

结论：我们的研究提供了一种开创性的治疗方法。该方法利用中性粒细胞靶向心脏缺血部位，同时递送的 Ru-SAN 提供抗氧化、抗炎的特性来靶向铁死亡，从而为心肌梗死提供有效的治疗方法。

纳米功能化益生菌通过抑制肠道微生物 -TMA-TMAO 轴治疗动脉粥样硬化

陈浙哲 朱琼军 王雅楠 张文斌 马博轩 傅国胜

浙江大学医学院附属邵逸夫医院

目的：动脉粥样硬化对人类健康构成了重大威胁，脂质异常、胰岛素抵抗、高血压和慢性炎症被认为是该疾病的关键因素。然而，相当比例的患者没有表现出特定的危险因素，导致其更难以被治疗。研究表明高三甲胺氧化物（TMAO）水平与包括动脉粥样硬化在内的心血管风险密切相关，其由肠道微生物产生的三甲胺（TMA）经 FMO3 酶氧化而成。因此，调节肠道微生物组衍生的 TMAO 代谢途径为治疗非典型危险因素导致的动脉粥样硬化提供了新的思路。

方法：首先，引入氟甲基胆碱（FMC）药物以减少肠道微生物产生 TMA。FMC 通过草酸酯键接枝到基于聚甲基硫乙醇酯骨架上，其可自组装成纳米颗粒（PMF）并实现 ROS 响应性药物释放。此外，为了增强肠道定植，PMF 通过聚多巴胺涂层被接枝到鼠李糖乳杆菌（LGG）表面，形成纳米功能化益生菌 PDMF@LGG。

结果：PDMF@LGG 可以经口服持久稳定地粘附于肠道，聚多巴胺包被增强了纳米工程益生菌的黏性，PMEMA 聚合物保护益生菌免受氧化应激的影响，延长 PDMF@LGG 的停留时间。PMF 纳米颗粒中的 FMC 药物可以在 ROS 条件下精确释放，阻断 CutC/D 酶，抑制 TMA 的产生。同时，LGG 对肠道内皮提供保护，维持上皮细胞之间的紧密连接，有助于减少 TMA 进入血液。因此，PDMF@LGG 可通过减少 TMA 的产生及其进入血液来抑制肠道微生物群 -TMA-TMAO 轴，从

而导致循环 TMAO 的减少以治疗动脉粥样硬化。

结论：纳米功能化益生菌 PDMF@LGG 通过抑制肠道微生物群 -TMA-TMAO 轴显示出抗动脉粥样硬化的活性，为解决非典型因素 TMAO 导致的动脉粥样硬化提供了一种有希望的临床策略。

开发和验证一种用于预测老年患者非心脏外科手术后发生心力衰竭风险预测模型：一项多中心研究

李青 董蔚

中国人民解放军总医院第六医学中心

开发和验证一种用于预测老年患者非心脏外科手术后发生心力衰竭风险预测模型：一项多中心研究

目的：开发并验证一种机器学习（machine learning, ML）模型，用于预测非心脏外科手术老年患者术后发生心力衰竭（Postoperative heart failure, pHF）风险。

方法：本研究纳入中国人民解放军总医院第六医学中心的 26,026 例患者（870 例阳性样本，25,156 例阴性样本）。使用下采样的方法平衡阳性和阴性样本，最终的数据集包括 1,740 例样本（阳性和阴性样本均为 870 例）。根据 8：2 的比例，随机将 1,740 例样本随机分为训练集（n=1,392）和测试集（n=348）。在训练集上，采用了 8 种二分类机器学习模型的 AUC 来评估模型在测试集上的预测性能。并通过 SHAP 分析确定关键预测特征，并在中国人民解放军总医院第一医学中心对模型进行外部验证。模型性能的评估基于识别能力、校准度和临床应用价值。

结果：术后发生心力衰竭的老年患者院内死亡率高达 30.3%。训练集经 5 折交叉验证显示，随机森林模型性能最优（AUC=0.903），在测试集也保持良好的判断力（AUC=0.914）。该模型包含的 14 个特征为：有冠状动脉粥样硬化性心脏病合并症、中性粒细胞与淋巴细胞比值、年龄、白蛋白、脉率、国际标准化比值、舒张压、估算肾小球滤过率、有严重贫血合并症、血肌酐、身体质量指数（BMI）、白细胞计数、收缩压和平均红细胞血红蛋白浓度。SHAP 分析显示，有冠状动脉粥样硬化性心脏病合并症、中性粒细胞与淋巴细胞比值、年龄、脉率、国际标准化比值、有严重贫血合并症、血肌酐、白细胞计数这 8 个特征变量与术后发生心力衰竭的风险呈正相关关系，白蛋白、舒张压、估算肾小球滤过率、收缩压和平均红细胞血红蛋白浓度与该事件呈负相关关系，而 BMI 则与该事件呈倒置 U 型关系。外部验证 AUC 值为 0.901。校准曲线显示，随机森林模型的校准度较好。我们还开发了临床适用的网页预测平台。

结论：院内该模型整合的 14 个临床特征涵盖心脏相关的合并症、高龄、术前炎症状态等多种危险因素，这些危险因素共同促进术后心力衰竭的发生。该模型可实现术前风险分层，通过科学管理共病、补充优质蛋白质、优化术前血流动力学状态等干预措施，提高手术的安全性，具有重要的临床意义。

Conductive Microneedle Patch with Mitochondria-localized Generation of Nitric Oxide Promotes Heart Repair after Ischemia-Reperfusion Therapy

Junjie Xiao

Shanghai University

Objective: Occlusion of coronary artery and deficiencies of blood and oxygen are two characteristics of myocardial infarction (MI) with its morbidity increasing globally. Due to limited regeneration ability of cardiomyocytes, dead cardiomyocytes are replaced by fibroblasts, leading to the formation of fibrotic scars that disrupt cardiac electrical integrity. Vascular recanalizations following MI are the clinical strategies to suppress further expansion of infarcted area. However, myocardial reperfusion of blood flow and oxygen influx can cause ischemia-reperfusion injury (I/RI), which is challenging despite clinical advances. With disturbed electrical conduction and oxidative stress in infarcted myocardium, injured heart experiences a negative ventricle remodeling process, and finally leads to heart failure. Nitric oxide (NO) is a short-lived signaling molecule regulating cardiovascular homeostasis, while vasodilation of systemic vasculature is accompanied by its exogenous supplementation. Meanwhile, connexin 43 (Cx43), a gap junction protein for electrical propagation in myocardium, is downregulated by NO derived from inducible nitric oxide synthase (iNOS). The seesaw-like relationship of Cx43 and NO in cardiac repair raises an intractable issue of how to address localized-specific NO administration and simultaneously reconstruct electrical conduction.

Methods: ATP-sensitive zeolitic imidazolate frameworks-90 (ZIF-90) nanoparticles were used as the delivery systems of L-Arg and further modified by triphenyl phosphonium (TPP), denoted as L-Arg@ZIF-90-TPP nanoparticles. Gelatin methacryloyl (GelMA) hydrogel is modified by polypyrrole (PPY) and dopamine, which is GelMA-PPY-PDA. A conductive microneedle patch (denoted as MN+PPY+PDA) is constructed by GelMA-PPY-PDA hydrogels to encapsulate L-Arg@ZIF-90-TPP nanoparticles, during which negative molds with orderly cone microcavities are employed to ensure the aligned needles in patches. In mice with I/RI, conductive microneedle patch containing L-Arg@ZIF-90-TPP nanoparticles have been implanted into heart of mice for 3 weeks. Their heart function, pathological analysis and electrical conduction were evaluated after different treatment.

Results: Size of L-Arg@ZIF-90-TPP nanoparticle is about 200 nm, similar to that of ZIF-90 nanoparticle and L-Arg@ZIF-90 nanoparticle, indicating that electrostatic adsorption of L-Arg and modification of TPP via EDC/NHS reaction did not largely affect their sizes. FTIR, DLS and XRD results revealed that ZIF-90 is the main structure of L-Arg@ZIF-90-TPP and L-Arg@ZIF-90 nanoparticles. An optimized mass ratio of ZIF-90 to L-Arg at 2:2 achieves the highest loading efficiency ≈ 36 % and a comparable encapsulation efficiency (about 37 %). Structure of microneedle patch is characterized by each needle with a height of 600 μm and a diameter of 250 μm. Microneedle patch exhibited an electrical conduction and mechanical strength to penetrate mouse heart. When H9C2 cells were incubated with L-Arg@ZIF-90-TPP nanoparticles, the amounts of L-Arg@ZIF-90-TPP nanoparticles localized in mitochondria increased with incubation time extended, which indicating their mitochondria target. In vitro experiment results revealed that L-Arg@ZIF-90-TPP nanoparticles could inhibit apoptosis of cardiomyocytes through decreasing ROS levels and suppressing mitochondrial depolarization, mainly due to its bioactivity of NO generated in situ. Mice in L-Arg@ZIF-90-TPP+MN-PPY-PDA group showed a more effective therapeutic outcome in improving cardiac function and inhibiting ventricle remolding, because of mitochondria-specific release of L-Arg and consequent in situ generation of NO. Conductive microneedle patches showed the ability to improve longitudinal conduction velocities in the border zone between the infarcted and healthy myocardium of mice, thus promoting the normalization of excitability and conduction within the hearts. With no obvious cell death and inflammatory cell infiltration in normal tissues of I/RI mice after administration, conductive microneedle patches containing L-Arg@ZIF-90-TPP nanoparticles have long-term biocompatibility.

Conclusion: Given the seesaw-like relationship of Cx43 and NO in cardiac repair, simultaneously addressing localized-specific NO administration and electrical propagation rebuilding is the key challenge. This study constructed a conductive microneedle patch with L-Arg@ZIF-90 nanoparticles for in situ generation of NO and electrical conduction rebuilding following I/RI. Biotransformation of L-Arg in ischemic myocardium enables the local production of NO in a sustained manner during 3 weeks of cardiac implantation. It not only guarantees therapeutic efficiency but also overcomes challenges associated with systemic nitrate administration, wherein its entry into tissue is limited by the short half-life of NO. In comparison with intravenous administration or inhalation of NO, localized L-Arg delivery by microneedle patch endows non-hemodynamic effects and cardioprotection on the infarcted myocardium, thus remarkably avoiding serious hypotension caused by the vasodilation of systemic vasculature. To solve the delayed electrical conduction in infarcted myocardium, a conductive microneedle patch made from GelMA-PPY-PDA rebuilt electrical signals between cardiomyocytes and increased Cx43 expression, thus reducing the risk of cardiac arrhythmias following MI. As a result, the combination of a conductive microneedle patch with NO in situ generation overcomes current bottlenecks of NO clinical application, prevents LV remodeling and alleviates myocardial I/RI, leading to a synergetic therapeutic efficacy.

基于网络药理学和分子对接技术探讨柚皮苷治疗冠心病的分子机制

符锶

大连医科大学附属第一医院

背景及目的：冠心病是冠状动脉粥样硬化引起的心肌缺血、缺氧乃至坏死的一种常见心血管疾病，其高发病率及死亡率推动冠心病药物治疗市场蓬勃发展。近年来，中成药在冠心病治疗中展现出相当疗效。柚皮苷，一种从柑橘类水果中提取的黄酮类化合物，具有抗氧化、抗炎、抗癌等生物活性。本研究借助网络药理学和分子对接技术，旨在探究柚皮苷治疗冠心病的潜在分子机制。

方法：本研究通过多个数据库收集柚皮苷的作用靶点及冠心病治疗靶点。利用 Venny 确定二者的共同靶点，构建“活性成分 - 靶点 - 基因”网络。借助 STRING 数据库获取交集靶点的相关关系，并结合 Cytoscape 3.10.0 筛选关键靶点。通过 DAVID 数据库对潜在靶点进行功能及信号通路富集分析，最后利用 CB-Dock 2 进行分子对接验证。

结果：经 Venny 分析，共获得 872 个柚皮苷与冠心病的共有靶点。基于 STRING 数据库构建的 PPI 网络筛选出 SRC、AKT1、ESR1、CTNNB1、PRKACA、MAPK1 等关键节点。GO 功能富集与 KEGG 通路富集分析表明，这些靶点涉及细胞信号转导、代谢及稳态调控、细胞凋亡等生物学过程，并与心血管疾病、代谢及癌症相关通路密切相关。分子对接结果显示，柚皮苷与 SRC、MAPK1、CTNNB1 等靶点结合能均低于 -6 kcal/mol，提示柚皮苷与上述靶点具有良好的结合活性。

结论：本研究运用网络药理学和分子对接技术，系统揭示了柚皮苷治疗冠心病的潜在分子机制。结果表明，柚皮苷通过调节关键靶点 SRC、MAPK3、CTNNB1 及其相关信号通路，发挥抗动脉粥样硬化、抗炎、抗氧化应激作用，抑制心肌细胞凋亡和血管细胞的分化、迁移、增殖及细胞骨架重组。这些发现为柚皮苷作为冠心病治疗药物的研发奠定了理论基础，为后续实验验证研究提供了新方向和参考依据，有望推动其在冠心病治疗领域的突破和临床应用。

Implantable Triboelectric Nanogenerator for Promising Powering Cardiac Pacemakers

魏涛涛 林欣 常鹏

兰州大学第二医院

Abstract: This project aims to develop an implantable triboelectric nano-

generator (I-TENG) for providing power to implantable medical devices in real clinical scenarios. The design of the nanogenerator takes into account factors such as output performance, controllability, and minimizing interference with the physiological activities of the organism. Fabricating a I-TENG through the combination of polyvinylidene fluoride (PVDF), polyamide 6 (PA6), and a Fe nanomaterials layer. The I-TENG achieves an output current of 0.5 μA and a voltage of 20 V when driven by a motor at 5 Hz, which shows good output stability. We evaluated the biocompatibility in human cardiomyocytes and in mice, and both in vitro and in vivo experiments showed good biocompatibility, suggesting great potential for application in living organisms. This work shows I-TENG is capable of providing continuous stable and safe power supply in promising clinical application.

当归多糖通过调控内质网应激及炎症反应改善心肌缺血损伤的机制研究

牛小伟（学组委员） 张钲 白明

兰州大学第一医院（兰州大学第一临床医学院）

目的：急性心肌缺血损伤是心血管疾病中的核心病理过程，其发生发展与内质网应激过度激活及炎症反应密切相关。本研究旨在系统探讨当归多糖（Angelica sinensis polysaccharide, ASP）缓解心肌缺血损伤的作用机制，重点阐明其通过表观遗传调控 ATF6 通路抑制内质网应激，并协同抑制炎症反应的双重保护机制，为开发基于 ASP 的心肌缺血治疗策略提供理论依据。

方法：采用大鼠左冠状动脉前降支结扎术建立心肌缺血模型，随机分为假手术组、模型组、ASP 低剂量组（50 mg/kg）、ASP 高剂量组（100 mg/kg）及阳性对照组（依那普利，10 mg/kg）。干预 7 天后，通过以下方法系统评价 ASP 效应：（1）分子机制研究：采用 ChIP-qPCR 检测 ATF6 启动子区组蛋白修饰（H3K4me1/H3K4me2）水平；Western blot 和免疫荧光分析 LSD1、ATF6 及其下游内质网应激标志物（GRP78/CHOP）表达；TUNEL 染色和流式细胞术评估心肌细胞凋亡率。（2）多组学整合分析：RNA-seq 转录组测序筛选差异表达基因，结合 KEGG 通路富集分析炎症相关通路；ELISA 验证关键炎症因子（IL-1β、IL-6、TNF-α）及 NLRP3 炎症小体组分表达。

结果：（1）表观遗传调控机制：ASP 显著抑制组蛋白去甲基化酶 LSD1 表达，提升 ATF6 启动子区 H3K4me1 与 H3K4me2 甲基化修饰水平（p<0.001），激活 ATF6 转录活性，进而下调内质网应激标志物 Caspase12 和 CHOP，减少心肌细胞凋亡（p<0.001）。

（2）抗炎作用机制：RNA-seq 分析显示，ASP 干预后 NF-κB 通路关键基因显著下调（FDR<0.05），NLRP3 炎症小体组分（NLRP3、ASC、Caspase-1）及炎症因子（IL-1β、IL-6、TNF-α）表达同步抑制（p<0.001），组织学验证显示心肌炎症浸润面积减少（p<0.001）。

（3）心功能保护效应：ASP 治疗组左心室射血分数（EF）和短轴缩短率（FS）显著提升（p<0.001），心肌梗死面积显著缩小（p<0.001）。

结论：ASP 通过双重机制缓解心肌缺血损伤：（1）表观遗传调控轴：抑制 LSD1 →提升 ATF6 启动子 H3K4 甲基化→激活 ATF6 通路→减轻内质网应激及凋亡；（2）炎症抑制轴：阻断 NLRP3/NF-κB 信号级联→抑制炎症风暴。本研究首次揭示 ASP 通过表观遗传重编程调控 ATF6 通路的分子机制，并证实其“抗内质网应激 - 抗炎”协同保护作用，为中药多糖治疗缺血性心脏病提供了创新性理论基础。

基于人工智能和静息超声心动图心肌应变的心肌缺血诊断模型的研究

刘耀琨 郑博 李建平

北京大学第一医院

目的 冠脉功能学评估对识别缺血病变和决策血运重建具有重要意义，现有技术仍存在诸多临床局限性。本研究拟构建一个无创、精准的基于静息超声心动图心肌应变的人工智能功能性心肌缺血诊断模型。

方法 选取自 2019 年 1 月至 2021 年 12 月期间于北京大学第一医院心内科住院的疑诊冠心病、并接受了超声心动图（UCG）及冠脉造影（CAG）检查的患者。排除既往接受心脏外科手术、UCG 提示室壁运动异常、显著心肌肥厚以及图像质量差等患者。使用冠状动脉功能测量系统 FlashAngio 测量基于 CAG 的血流储备分数（caFFR）和微循环阻力指数（caIMR）。应用自主研发的左心室内膜自动追踪工具计算各心肌节段的应变值和整体纵向应变（GLS）。按研究对象入院年份，分组训练集（2019 年和 2020 年）和测试集（2021 年）。以冠脉三支主支血管任一支符合 caFFR ≤ 0.80 和 / 或 caIMR > 25 作为心肌缺血“金标准”。输入研究对象的左心室 17 节段心肌应变、GLS、常规 UCG 测量指标及临床信息，应用机器学习算法构建心肌缺血诊断模型。绘制受试者工作特征（ROC）曲线，并计算诊断模型识别功能性心肌缺血的灵敏度、特异度和 ROC 曲线下面积（AUC）。

结果 本研究共纳入 1207 例研究对象（共计含 30 万余帧图像），61.14% 为男性，平均年龄为 64.45 岁，其中心肌缺血和非缺血人数（比例）分别为 890（73.74%）和 317（26.26%）。训练集和测试集人数（比例）分别为 969 人（80.28%）、238 人（19.72%）。经训练集训练优化后，在测试集中验证，该多模态诊断模型识别心肌缺血的准确性、灵敏度、特异度分别为 79.8%、88.3%、58.2%，AUC 为 0.832。此外，还分别探究了单纯基于临床信息、常规 UCG 指标和心肌应变参数构建的诊断模型的预测性能，发现基于包含心肌应变所构建的诊断模型可以显著提升对心肌缺血的诊断能力。

结论 本研究基于静息超声心动图心肌应变并联合临床特征和常规 UCG 指标，应用机器学习算法，以基于 CAG 的冠脉功能学参数作为功能性心肌缺血的诊断标准，成功构建了可以识别心肌缺血的多模态人工智能诊断模型，并经验证证实了模型具有较好的稳健性，为未来精准诊疗功能性心肌缺血提供了一个更加无创、智能、便捷的新手段。

Research on an Artificial Intelligence-Based Diagnostic Model for Myocardial Ischemia Using Resting Echocardiographic Myocardial Strain Analysis

Yaokun Liu, Bo Zheng, Jian-Ping Li

Peking University First Hospital

Objective

Coronary functional assessment plays a critical role in identifying ischemic patterns and guiding revascularization decisions. However, current techniques still exhibit significant clinical limitations. This study aimed to develop a noninvasive, accurate artificial intelligence (AI)-based diagnostic model for functional myocardial ischemia using resting echocardiographic myocardial strain analysis.

Methods

Patients admitted to the Department of Cardiology at Peking University First Hospital between January 2019 and December 2021 with suspected coronary artery disease (CAD), who underwent both echocardiography (UCG) and coronary angiography (CAG), were enrolled. Exclusion criteria included prior cardiac surgery, UCG-detected wall motion abnormalities, significant myocardial hypertrophy, or poor image quality. Coronary functional parameters, including angiography-derived fractional flow reserve (caFFR) and index of microcirculatory resistance (caIMR), were measured using the FlashAngio system. A self-developed automated left ventricular endocardial tracing tool was employed to calculate segmental strain values and global longitudinal strain (GLS).

Myocardial ischemia was defined based on functional assessments of the three major coronary arteries—the left anterior descending (LAD) artery, the left circumflex (LCX) artery, and the right coronary artery (RCA). Any vessel was classified as ischemic if it met one of the following criteria: 1) Epicardial coronary artery ischemia: caFFR ≤ 0.80, regardless of the caIMR value. 2) Isolated coronary microvascular ischemia: caFFR > 0.80 with a concomitant caIMR > 25. 3) Overall functional myocardial ischemia: caFFR ≤ 0.80 and/or caIMR > 25. Non-ischemic status was defined as caFFR > 0.80 and caIMR ≤ 25.

Input features included left ventricular 17-segment myocardial strain, GLS, conventional UCG parameters, and clinical data. Machine learning algorithms were applied to construct three diagnostic models: Model A (overall ischemia), Model B (epicardial large-vessel ischemia), and Model C (microvascular ischemia). Receiver operating characteristic (ROC) curves were plotted, and the sensitivity, specificity, and area under the curve (AUC) of each model were calculated.

Results

The study cohort comprised 1,207 patients (totaling over 300,000 image frames), with 61.14% male and a mean age of 64.45 years. Among them, 553 (45.82%) had macrovascular ischemia, 337 (27.92%) had isolated microvascular ischemia, and 317 (26.26%) were non-ischemic. The dataset was divided into a training set (2019–2020, n = 969, 80.28%) and a testing set (2021, n = 238, 19.72%). After optimization in the training set, the models demonstrated the following performance in the testing set: Model A (overall ischemia): accuracy 79.8%, sensitivity 88.3%, specificity 58.2%, AUC 0.832. Model B (epicardial large-vessel ischemia): accuracy 76.9%, sensitivity 67.7%, specificity 82.8%, AUC 0.841. Model C (microvascular ischemia): accuracy 80.7%, sensitivity 78.2%, specificity 82.8%, AUC 0.879.

Conclusion

This study developed multimodal AI diagnostic models for identifying different types of myocardial ischemia by integrating resting echocardiography-derived myocardial strain values with clinical characteristics and conventional echocardiographic indices. By leveraging machine learning algorithms and coronary angiography-derived functional parameters as the reference standard for functional myocardial ischemia, the proposed models demonstrated robust diagnostic performance with high stability and reliability. These findings provide a novel, non-invasive, intelligent, and convenient tool for the precise and personalized diagnosis and management of functional myocardial ischemia. However, further multi-center studies with independent external and prospective validation are warranted to comprehensively evaluate the models' clinical applicability and diagnostic efficacy.

心血管病诊治的创新与转化医学研究：新发现、新成果与新知识

陈刚

新疆阿克苏地区第一人民医院

目的

系统综述 2023-2024 年心血管疾病（CVD）领域在分子机制解析、影像技术创新、精准治疗策略及转化医学应用方面的突破性进展，评估其对临床诊疗路径的重构价值。

方法

通过检索 PubMed、EMBASE 及 ClinicalTrials.gov 数据库（2023-2024），纳入国际指南（ACC/AHA/ESC）更新内容及关键临床试验。采用循证医学方法分析五大方向：

分子诊断：多组学技术（基因组 / 蛋白组 / 代谢组）在冠心病易感性筛查中的应用

影像革新：OCT-MRI-CT 多模态融合技术的诊断效能验证

精准治疗：SGLT2 抑制剂 /ARNI 的随机对照试验（RCT）及药物基因组学研究

器械创新：CRT/ICD/LVAD 的器械迭代与长期随访

转化医学：AI 辅助决策系统与远程监测技术的实效性研究

结果

精准诊断突破

多基因风险评分（PRS）使冠心病早筛敏感性提升至 89%（AUC 0.91）

GDF-15 联合 ST2 预测心力衰竭住院风险效能优于 NT-proBNP（ΔAUC +0.12, P<0.01）

影像技术进阶

OCT 指导 PCI 使支架贴壁不良率降至 3.2%，再狭窄风险下降 41%（HR 0.59）

心脏 MRI T1 mapping 技术诊断早期心肌纤维化敏感性达 93%（DECODE-MRI）

靶向治疗进展

SGLT2 抑制剂降低 2 型糖尿病患者心血管死亡风险 32%（EMPEROR-Reduced, HR 0.68）

ARNI 较传统 ACEI 减少 HFrEF 患者再住院率 28%（PIONEER-HF, RR 0.72）

器械治疗优化

第三代 LVAD 装置 2 年生存率达 85.7%（MOMENTUM 3）

AI 优化 CRT 电极定位使应答率提升至 92%（SMART-CRT）

转化医学应用

AI 心电分析系统诊断房颤敏感性 97.4%（MAFA II）

远程监护降低心衰患者 30 天再住院率 35%（TIM-HF2, OR 0.65）

结论

心血管病诊治已形成'组学筛查 - 智能影像 - 靶向干预 - 数字管理'的转化医学闭环

多组学技术实现冠心病遗传风险分层

OCT-MRI 融合影像提升斑块性质判别精度

SGLT2i/ARNI 重塑心衰药物治疗格局

AI 辅助决策系统优化治疗路径

核心挑战：①多组学数据临床整合标准②新型生物标志物动态监测体系③干细胞治疗转化路径。未来需构建真实世界证据链（RWE）推动创新疗法落地，加强医工交叉解决器械长期并发症问题。

达格列净通过抑制 NF-κB 通路减轻急性缺血性脑卒中模型大鼠心功能障碍

何山青 彭建军

首都医科大学附属北京世纪坛医院 / 首都医科大学肿瘤医学院 / 北京大学第九临床医学院

目的： 急性脑卒中（尤其是缺血性卒中）后心脏并发症是导致患者死亡的主要原因之一，但目前缺乏有效的预防和治疗手段。既往研究表明，脑卒中后心脏功能障碍与炎症反应，特别是白细胞介素 -1β (IL-1β) 介导的单核 / 巨噬细胞促炎激活密切相关。达格列净 (Dapagliflozin, DAPA) 作为钠 - 葡萄糖协同转运蛋白 2 (SGLT2) 抑制剂，已被证明具有心血管获益和抗炎作用，但其在卒中后心脏保护中的作用及机制尚不清楚。本研究旨在探讨达格列净对急性缺血性脑卒中（采用大脑中动脉栓塞，MCAO 模型）诱发的心功能障碍的保护作用及其潜在机制。

方法: 研究使用 24 只雄性 Sprague-Dawley 大鼠，随机分为四组（每组 n=6）: (1) 对照组： 假手术；(2) MCAO 组： 仅行 MCAO 手术；(3) MCAO+DAPA 组： MCAO 手术 + 达格列净（1 mg/kg/ 天，灌胃 7 天）；(4) DAPA 组：假手术 + 达格列净（1 mg/kg/ 天，灌胃 7 天）。MCAO 模型通过线栓法阻塞右侧大脑中动脉 1 小时建立。术后 7 天，通过超声心动图评估心功能指标（包括左心室射血分数 LVEF、左心室短轴缩短率 LVFS 等），心电图记录室性早搏（PVCs）发生频率，检测血清肌酸激酶 MB 同工酶（CK-MB）水平评估心肌损伤。采用苏木精 - 伊红（H&E）染色观察心肌组织病理变化。通过免疫荧光染色检测心室组织中促炎性 M1 巨噬细胞（CD68+iNOS+）浸润数量，Western blotting 检测心室组织中核因子 κB p65 (NF-κB p65)、IL-1β 和白细胞介素 -6 (IL-6) 蛋白表达水平。

主要结果：

心功能与结构： 与对照组相比，MCAO 组大鼠 LVEF 和 LVFS 显著降低（P<0.01），左心室收缩末期内径（LVIDs）增加，表明心功能受损。达格列净治疗（MCAO+DAPA 组）显著改善了 LVEF 和 LVFS（P<0.01），并降低了 LVIDs。

心肌损伤： MCAO 组血清 CK-MB 水平显著升高（P<0.01），H&E 染色显示心肌纤维断裂和炎性细胞浸润。达格列净治疗显著降低了 CK-MB 水平（P<0.01）并改善了心肌组织病理损伤。

室性心律失常： MCAO 组大鼠 PVCs 发生率显著高于对照组（P<0.05）。达格列净治疗显著减少了 MCAO 大鼠的 PVCs 数量（P<0.05）。

炎症机制： MCAO 组大鼠心室组织中 M1 巨噬细胞浸润数量显著增加（P<0.05），同时 NF-κB p65、IL-1β 和 IL-6 蛋白表达水平显著上调（P<0.05 或更低）。达格列净治疗有效抑制了 M1 巨噬细胞浸润（P<0.05），并显著降低了 NF-κB p65、IL-1β 和 IL-6 的表达水平（P<0.05, P<0.01 或更低）。

结论： 本研究首次在 MCAO 大鼠模型中证实，SGLT2 抑制剂达格列净能够有效减轻急性缺血性脑卒中诱发的心功能障碍，表现为改善左心室收缩功能、减轻心肌组织损伤、降低室性心律失常发生率。其心脏保护作用的机制主要与抑制 NF-κB 信号通路的激活，进而减少 IL-1β 等促炎因子的分泌、抑制巨噬细胞向促炎性 M1 表型极化相关。该研究为达格列净应用于卒中后心脏并发症的防治提供了重要的实验依据。

Distal TRAnsradial Access for Percutaneous Coronary Intervention: A SinGle-Center RandOmized CoNtrolled Study（DRAGON Study）

Liu Minghao, Can Li, Cheng Cui, Ying Song, Huan-Huan Wang, Li-Jian Gao

中国医学科学院阜外医院

Abstract

Background: Transradial access (TRA) has become the preferred vascular approach for coronary interventions due to its lower bleeding risk and improved patient comfort compared to transfemoral access. However, radial artery occlusion (RAO) remains a significant complication, limiting TRA's utility in repeat procedures and other surgical contexts. Distal transradial access (dTRA) has shown potential to reduce RAO rates while maintaining procedural safety and effectiveness.

Methods: This single-center, prospective, randomized, superiority open-label study enrolled 426 patients undergoing percutaneous coronary intervention (PCI) between July 2023 and January 2024. Participants were randomly assigned in a 1:1 ratio to undergo PCI via dTRA (study group, n = 213) or TRA (control group, n = 213). The primary endpoint was RAO at 24 hours post-procedure. Secondary endpoints included RAO at 30 days, procedural success, compression time, radiation exposure, and postoperative hand and wrist function recovery.

Results: A total of 425 patients were included in the analysis (dTRA: 213; TRA: 212). The 24-hour RAO rate was significantly lower in the dTRA group compared to the TRA group (0.5% vs. 8.7%, p < 0.0001). At 30 days, RAO remained significantly lower in the dTRA group (1.6% vs. 8.2%, p < 0.0001). Compression duration was significantly shorter in the dTRA group (median: 3.0 hours vs. 6.0 hours, p < 0.0001). Both groups demonstrated similar procedural success rates and radiation exposure. Hand function recovery at 24 hours was slightly better in the dTRA group.

Conclusions: dTRA offers significant advantages over TRA by reducing RAO incidence, shortening compression times, and improving early hand function recovery, while maintaining procedural safety and effectiveness. These findings support broader adoption of dTRA for coronary interventions.

Study Strengths: It is the first randomized controlled trial in China to specifically evaluate the safety and efficacy of dTRA for PCI, as opposed to coronary angiography alone. By focusing on PCI patients, who are at higher risk of RAO, our findings provide robust evidence supporting the use of dTRA in this population. Furthermore, our study included comprehensive assessments of RAO, hand function recovery, and procedural metrics, providing a holistic evaluation of the benefits and limitations of dTRA.

Limitations: As a single-center trial, the generalizability of our findings may be limited. Multicenter studies in China with larger sample sizes are needed to confirm our results. Additionally, while preprocedural ultrasound was used to localize the distal radial artery, the puncture itself was performed using palpation-based techniques rather than real-time ultrasound guidance. This may have contributed to the higher crossover rate observed in the dTRA group. Future studies should explore the impact of routine ultrasound-guided puncture on procedural success and safety outcomes.

Clinical Implications: The findings of this study have important clinical implications. By significantly reducing RAO while maintaining procedural safety and efficacy, dTRA offers a superior alternative to TRA for PCI. The shorter compression time and better early hand function recovery associated with dTRA further enhance its advantages, making it a more patient-friendly approach. As operator experience with dTRA grows and training programs become more widespread, the technical challenges associated with the approach are likely to diminish.

Trial Registration

Chinese Clinical Trial Registry: **ChiCTR2300073902**

Key words: Distal Transradial Access, ccc, Percutaneous Coronary Inter-

vention, Transradial Access, Postoperative Hand Function Recovery

Associations between Neutrophil-Percentage-to-Albumin Ratio (NPAR) and Incidence of Cardiovascular Diseases: a Prospective Cohort Study

Cheng Huang[1], Jia-Yong Li[1], Yuan Yu[2], Chen Liu[1], Pei-Sen Huang[1]

1. The First Affiliated Hospital, Sun Yat-sen University

2. Guangdong Provincial People's Hospital

Abstract

Background: Cardiovascular diseases remained the leading cause of mortality around the world. It was necessary to find convenient and low-cost biomarkers for prediction of cardiovascular diseases. Prior studies showed neutrophil percentagetoalbumin ratio (NPAR) was associated with cardiovascular death.

Objective: This study aimed to assess the association between neutrophil percentagetoalbumin ratio and incidence of cardiovascular events.

Methods: This prospective cohort study included individuals without history of cardiovascular diseases, cancer, liver diseases and acute infectious diseases who participated in the UK biobank (2007-2023). Neutrophil percentagetoalbumin ratio was calculated based on the blood neutrophil percentage and albumin level at baseline. Participants were divided into tertiles based on the neutrophil percentagetoalbumin ratio level. The primary outcome was the incidence of cardiovascular events, defined as the composite of ischemic heart disease (IHD), artery diseases (AD), heart failure (HF), atrial fibrillation (AF), nonrheumatic valve disorders (NVD) and cardiovascular death. The secondary outcomes were the components of cardiovascular events. Kaplan–Meier survival analyses were used to compare incidence rates across NPAR tertiles. Cox regression analyses and restricted cubic spline regression analyses were performed to analyze the association between NPAR and incidence of cardiovascular events. In the fully adjusted model, age, sex, marital status, ethnicity, body mass index, systolic blood pressure, low-density lipoprotein cholesterol, Townsend area deprivation index, physical activity, smoking status, drinking status and medical history (including diabetes mellitus, chronic obstructive pulmonary disease, chronic kidney disease and stroke) were adjusted. Receiver operating characteristic (ROC) curve analysis estimated the predictive performances of NPAR for cardiovascular events.

Results: Among 267047 participants, the mean (SD) age was 55.6 (8.1) years old and 51.8% participants were female. The mean (SD) neutrophil percentagetoalbumin ratio was 1.35 (0.19), and individuals with higher NPAR were older, more likely to be female and had a higher prevalence of comorbidities. During a 3401695 person-years of follow-up, 39581 incidences of cardiovascular events occurred. In the Kaplan-Meier analysis, participants in the median and highest tertile of NPAR had a higher incidence of cardiovascular events and its components compared to the lowest NPAR group. Participants in the median and the highest tertile of NPAR had a higher risk of cardiovascular disease (HR = 1.05, 95% CI 1.02-1.08, P value < 0.001; HR = 1.19, 95% CI 1.16-1.22, P value < 0.001, respectively) compared with participants in the lowest tertile after adjusting all covariables. Participants with the highest NPAR tertile also witnessed higher risk of ischemic heart disease (HR = 1.11, 95% CI 1.08-1.15, P value < 0.001), artery diseases (HR = 1.25, 95% CI 1.19-1.32, P value < 0.001), heart failure (HR = 1.44, 95% CI 1.36-1.53, P value < 0.001), atrial fibrillation (HR = 1.22, 95% CI 1.18-1.27, P value < 0.001), nonrheumatic valve disorders (HR = 1.19, 95% CI 1.12-1.27, P value < 0.001) and cardiovascular death (HR = 1.54, 95% CI 1.41-1.68, P value < 0.001) compared to the lowest tertile (All P_{trend} < 0.001). Subgroup and sensitivity analyses confirmed the consistency of this association across various demographic groups. Besides, nonlinear relationships were found between NPAR and cardiovascular events (P for nonlinear < 0.001). The risk of cardiovascular events was flatted when neutrophil percentagetoalbumin ratio was low, but boosted after the neutrophil percentagetoalbumin ratio reaching a threshold, which was 1.36.

Conclusion: Higher neutrophil percentagetoalbumin ratio level is associated with higher risk of cardiovascular diseases in the general population when the NPAR is beyond a threshold.

Keywords: neutrophil percentagetoalbumin ratio, cardiovascular events, general population

基于机器学习构建并验证急性心肌梗死患者院内心源性休克预测模型

杜淑珍 [1] 李文强 [1] 赵晶 [2,3,4] 张钰 [2,3,4]

1. 兰州大学第一医院

2. 兰州大学第一医院心脏中心

3. 甘肃省心血管病临床医学研究中心

4. 甘肃省心血管疾病重点实验室

摘要 目的 基于机器学习算法构建并验证预测模型，以评估急性心肌梗死（AMI）患者院内心源性休克（CS）的发生风险。方法 回顾性纳入 2023 年 1 月至 12 月兰州大学第一医院收治的行 PCI 治疗的 AMI 患者。收集人口统计学、实验室检查、动态心电图、超声心动图、冠脉病变特征及院内用药等临床指标。使用 LASSO 回归筛选关键预测变量，并通过 10 折交叉验证选择最优 λ 值，确定与 CS 相关的变量，采用特征雷达图、特征条形图展示特征及其权重排序。随后构建 6 种 ML 构建预测模型，使用准确度、灵敏度、精确度、F1 分数、受试者工作特征曲线下面积 (AUROC) 和精确率 - 召回率曲线下面积 (AUPRC) 评估模型性能。通过 Bootstrap 检验评估模型间 AUROC 和 AUPRC 的差异，通过小提琴图可视化模型的 AUROC 和 AUPRC 的概率密度分布，筛选出最佳 ML 模型。采用网格搜索交叉验证方法 (GSCV) 优化模型超参数，SHAP 方法分析解释模型结果。结果 共纳入 851 例 AMI 患者，CS 组 43 例（5.05%），非 CS 组 808 例，按 7:3 比例随机分为训练集（n=595）与测试集（n=256）。LASSO 回归初步筛选出 14 个与 CS 显著相关的变量通过 10 折交叉验证选择最优 λ 值为 0.01，最终确定与 CS 相关的建模变量有 8 个，分别为：心率、D- 二聚体、Killip 分级、肌酐、脂蛋白 a、丙氨酸氨基转移酶、舒张压、载脂蛋白 B/A。在所有模型中，集成算法模型优于其他算法，以 LightGBM 模型最优，其 AUROC=0.87, 95%CI:0.76-0.96，AUPRC=0.64, 95%CI:0.36-0.87。研究建立了基于 LightGBM+LASSO+GSCV 的 ML 预测模型，其验证集 AUROC=0.87, 95%CI:0.77-0.96，AUPRC=0.64, 95%CI:0.36-0.86。开发了基于 Streamlit 框架的 AMI 患者 PCI 术后院内 CS 风险预测融合模型的在线应用程序，可个体化预测患者风险及特征贡献度。结论 本研究成功构建并验证了基于 GSCV、LASSO 和 LightGBM 算法的 AMI 患者院内 CS 风险预测模型，可为临床决策提供可靠的风险评估工具。

Development of a Caspase-3-Activatable Photoacoustic Probe for Myocardial Infarction Imaging

Penghao Zhen, Jia-Yi Tong

Zhongda Hospital Affiliated to Southeast University

Purpose:

Myocardial infarction (MI) remains a leading cause of cardiovascular mortality worldwide, with timely diagnosis and intervention being critical for patient outcomes. Current diagnostic modalities for assessing cardiomyocyte apoptosis, particularly those targeting caspase-3 activity, predominantly rely on fluorescence-based molecular probes. However, these conventional approaches suffer from significant limitations, including restricted tissue penetration depth (typically <2 mm in biological tissues) and substantial background interference from tissue autofluorescence. Moreover, the quantitative accuracy of fluorescence imaging is often compromised by photon scattering and absorption in deep tissues. To address these critical challenges, we developed Ac-DEVD-FFG-IR820, an innovative activatable photoacoustic (PA) probe that specifically targets caspase-3 activity through a unique enzyme-responsive molecular assembly mechanism. This probe was designed to overcome the depth limitations of optical imaging while maintaining high molecular specificity for apoptotic cardiomyocytes.

Methods:

The Ac-DEVD-FFG-IR820 probe represents a sophisticated molecular engineering achievement that integrates three functionally distinct components: (1) a highly specific caspase-3 cleavable peptide sequence (Ac-DEVD) that serves as the enzymatic recognition site, (2) a self-assembling FFG motif that facilitates nanostructure formation, and (3) a near-infrared dye IR820 that functions as both the PA signal generator and fluorescence reporter. The probe operates through an elegant molecular mechanism: upon caspase-3 mediated cleavage at the DEVD site, the hydrophilic probe undergoes transformation into hydrophobic FFG-IR820 fragments. These fragments subsequently self-assemble into well-defined nanoparticles through synergistic π-π stacking interactions and hydrophobic effects, as confirmed by high-resolution transmission electron microscopy.

We employed a comprehensive characterization strategy to evaluate the probe's performance, including: UV-Vis-NIR absorption spectroscopy to monitor optical property changes, fluorescence spectroscopy to quantify quenching efficiency, high-performance liquid chromatography (HPLC) to determine enzymatic cleavage kinetics, and in vitro PA phantom studies to assess signal amplification. For in vivo validation, we utilized a well-established murine MI model induced by permanent left anterior descending (LAD) coronary artery ligation, followed by systematic PA imaging at multiple time points to capture the dynamic caspase-3 activation process.

Results:

Spectroscopic characterization revealed a pronounced red-shift in the absorption maximum upon nanoparticle formation, accompanied by a remarkable 85% reduction in fluorescence intensity due to efficient aggregation-induced quenching. In vitro enzymatic assays demonstrated exceptional specificity for caspase-3, with minimal cross-reactivity toward other proteases (MMP-2/9, cathepsins B/D). Quantitative HPLC analysis showed progressive cleavage reaching 80% efficiency within 8 hours, while parallel PA measurements revealed a substantial 5.6-fold signal enhancement in activated samples compared to caspase-inhibited controls.

In vivo imaging studies yielded compelling results: the probe generated strong, localized PA signals specifically in infarcted myocardial regions, with peak enhancement observed at 4 hours post-injection (4.8-fold

intensity ratio compared to non-infarcted areas). The temporal signal profile closely matched the known biphasic kinetics of caspase-3 activation post-MI. Immunohistochemical analysis of heart sections demonstrated precise spatial colocalization between enhanced PA signals and caspase-3-positive apoptotic cardiomyocytes, confirming the probe's molecular specificity in complex tissue environments.

The probe exhibited outstanding pharmaceutical properties, including excellent serum stability (92.3±3.1% remaining intact after 12 hours in serum at 37° C) and minimal cytotoxicity. These characteristics, combined with PA imaging's inherent deep-tissue penetration capability (up to 5 cm in biological tissues) and high spatial resolution (50-500 μm), enable noninvasive, quantitative assessment of myocardial apoptosis with unprecedented accuracy. Compared to existing techniques, our approach offers three key advantages: (1) deeper tissue penetration than fluorescence imaging, (2) higher molecular specificity than conventional contrast-enhanced MRI, and (3) quantitative capability surpassing nuclear imaging modalities.

Conclusion:

Ac-DEVD-FFG-IR820 represents a transformative advancement in cardiac molecular imaging, establishing a novel paradigm for MI diagnosis through enzyme-activated in situ nanoparticle assembly. This technology provides a robust platform for early MI detection (potentially within 2-4 hours post-ischemia), accurate risk stratification, and objective treatment monitoring in ischemic heart disease. The probe's modular design principle may be extended to target other protease biomarkers in cardiovascular and oncological applications. This work opens new avenues for precision medicine in cardiovascular care by providing previously unattainable molecular insights into the dynamic process of myocardial injury and repair.

AI-Enhanced Fluorescent Magnetic Bead Immunoassay for Melatonin Detection in Heart Failure

Xiao-Han Liu[1], Zhu Chen[2], Yuan Guo[1]

1. Zhuzhou Hospital Affiliated to Xiangya School of Medicine, Central South University

2. University of South China

AI-Enhanced Fluorescent Magnetic Bead Immunoassay for Melatonin Detection in Heart Failure

Xiaohan Liu[1], Zhu Chen[2, 3, 4]*, Yue Wang[4], Fengling Chen[1], Zepeng Zhou[4], Yujuan Huang[1], Zhi Liu[1], Yajie Chen[1], Yuan Guo[1]*

[1.] Department of Cardiovascular Medicine, Zhuzhou Hospital Affiliated to Xiangya School of Medicine, Central South University, Zhuzhou 412000, China.

[2.] Hengyang Medical College, University of South China, Hengyang 421001, China.

[3.] Institute for Future Sciences, University of South China, Changsha 410008, China.

[4.] Hunan Key Laboratory of Biomedical Nanomaterials and Devices, Hunan University of Technology, Zhuzhou 412007, China

***Corresponding Author**:

Yuan Guo, guoyuan0815@163.com; Zhu Chen, chenzhu@usc.edu.cn

Aims:

Heart failure (HF), the end stage of diverse cardiovascular diseases, remains a major global health burden, with persistently high mortality and rehospitalization despite advances in therapy. Beyond hemodynamic dysfunction, HF involves metabolic derangements, chronic inflammation, and maladaptive remodeling. Disruption of circadian rhythms, a critical regulator of these processes, exacerbates myocardial fibrosis, metabolic imbalance, and worsens outcomes. Melatonin, a key circadian biomarker, reflects intrinsic circadian phase, yet current detection methods—such as HPLC, LC-MS/MS, RIA, and ELISA—are limited by high cost, technical complexity, low throughput, and poor accessibility. There is a pressing need for a sensitive, accurate, economical, and user-friendly assay to assess melatonin and circadian dysregulation in HF. Immunomagnetic bead technology enables melatonin detection by the competition between labeled melatonin and free melatonin for binding to antibody recognition sites on the beads, offering high surface area and enrichment of low-abundance targets. However, heterogeneity in bead populations and signal variability can compromise detection accuracy. Machine learning algorithms, such as XGBoost, excel at analyzing complex, high-dimensional data and identifying nonlinear patterns, thus enhancing predictive performance. Combining immunomagnetic beads with machine learning integrates the beads' enrichment capability with robust data analysis, yielding a sensitive, accurate, and efficient approach for melatonin detection.

This study aimed to develop and validate a novel melatonin detection method (MB-assay) by integrating immunomagnetic bead technology with machine learning, and to compare its performance with the conventional ELISA method and evaluate its applicability in assessing plasma melatonin levels in patients with heart failure.

Methods:

FITC-conjugated melatonin (FITC-MT) was synthesized by reacting 5-methoxytryptamine with FITC-NHS in DMSO with triethylamine at room temperature (RT) for 12 h. PE-labeled anti-melatonin antibodies were prepared using a labeling kit and immobilized on carboxyl magnetic beads via EDAC/sulfo-NHS chemistry, followed by BSA blocking. The optimal FITC-MT concentration and incubation time were determined by titration experiments to ensure efficient competition with melatonin standards for bead binding. Melatonin detection was performed by mixing standards or plasma samples with FITC-MT and antibody-coated beads (MBs@Ab) at RT for 3 h, followed by flow cytometry analysis. Flow cytometry data were normalized and clustered using K-means; 15 signal parameters were extracted and used to train an XGBoost regression model (70:30 train/test split, 5-fold cross-validation). For comparison, melatonin was also measured using a ELISA kit following manufacturer instructions. Melatonin levels were measured in 44 chronic HF patients and 44 age- and gender-matched healthy controls. Statistical analyses included t-test, chi-square test, and Pearson's correlation, with significance defined as $P < 0.05$.

Results:

PE-conjugated anti-melatonin antibodies were successfully immobilized onto carboxylated magnetic beads, as confirmed by confocal imaging and flow cytometry. Confocal microscopy showed distinct PE fluorescence halos around conjugated beads versus non-conjugated controls, and flow cytometry revealed markedly higher PE fluorescence intensity in MBs@Ab. Based on absorbance at 280 nm, approximately 61.07% of the initial antibodies were conjugated during the process. Post-conjugation, over 99% of beads exceeded the PE fluorescence threshold, indicating high conjugation efficiency. The MBs@Ab remained stable, maintaining >99% PE positivity over 7 days at both 4 ° C and room temperature under light-protected conditions. A fluorescent melatonin derivative (FITC-MT) was synthesized and verified for its ability to bind MBs@Ab. Confocal imaging showed FITC fluorescence encircling beads incubated with FITC-MT. Flow cytometry confirmed that FITC-MT, but not 5-MT, substantially increased bead FITC signal. When the molar ratio of FITC-NHS to 5-MT was ≥ 1:1 during synthesis, >99% of beads became FITC-positive, suggesting high product purity. To optimize assay conditions, FITC-MT concentration and incubation time were evaluated. FITC positivity increased with higher FITC-MT concentrations and longer incubation. To ensure detectable competition between FITC-MT and native melatonin within physiological ranges, 0.25 nmol/mL FITC-MT and 3 h incubation were selected.

The assay was validated using melatonin calibration standards ranging from 0 to 300 pg/mL. Flow cytometry measurements of FITC-positive bead proportion, mean fluorescence intensity, and median fluorescence intensity showed weak correlations with melatonin concentration using linear regression ($R^2 = 0.50–0.81$). Confocal and flow cytometry analyses revealed that bead heterogeneity (size variation, aggregation) increased during reaction, reducing uniformity and confounding standard curve fitting. These results suggested that conventional analysis methods were insufficient for accurate quantification. To overcome bead heterogeneity, machine learning was applied. Flow cytometry data were first filtered to isolate uniform bead subpopulations and further clustered via K-means. XGBoost regression was trained on 54,000 beads and optimized via grid search and cross-validation. The model progressively improved the calibration curve fit, achieving a final $R^2 = 0.995$. Flow cytometry data processed by the algorithm showed clear discrimination of melatonin concentrations, validating the ability of this approach to robustly quantify melatonin despite bead heterogeneity. The final model was integrated into a user-friendly software platform. Users can import standard and test sample data, process them automatically with the trained algorithm, generate standard curves, compute sample concentrations, and export results efficiently.

The MB-assay was compared against a ELISA kit for melatonin detection. In melatonin standards, the MB-assay exhibited strong concordance with reference concentrations, and in serum samples, results were comparable to ELISA measurements. Clinical testing was performed in 44 heart failure patients and 44 age- and sex-matched healthy controls. The mean age of participants was 68.8 ± 7.7 years, and 46.5% were male. Serum melatonin was significantly lower in the heart failure group (99.8 ± 72.6 pg/mL) compared to controls (153.8 ± 73.8 pg/mL, $P < 0.05$). Furthermore, melatonin levels correlated negatively with age ($R = –0.242$, $P < 0.05$) and aortic diameter ($R = – 0.463$, $P < 0.05$), but showed no significant association with BNP, LVEF, or LVEDD. These findings support the MB-assay's validity and reveal clinically relevant alterations in melatonin associated with heart failure.

Conclusions:

This study constructed an innovative AI-enhanced fluorescent magnetic bead immunoassay for melatonin detection and showed the role

of melatonin as a biomarker reflecting circadian dysfunction in heart failure. Using this novel method, we measured serum melatonin levels in patients with heart failure and healthy controls, demonstrating its accuracy and efficiency comparable to ELISA. This study provides a sensitive, rapid, and cost-effective approach for assessing circadian rhythm-related disorders and offers new insights into the clinical evaluation and management of circadian dysfunction in heart failure.

自噬在心血管疾病中的作用及研究进展

张仲柏

海军军医大学第二附属医院 / 上海长征医院

[摘要] 心血管疾病（cardiovascular disease，CVD）是指一组包含动脉粥样硬化（atherosclerosis，AS）、缺血再灌注（ischaemia-reperfusion injury，I/R）损伤、肺动脉高压（pulmonary hypertension，PH）、心力衰竭（heart failure，HF）等循环系统疾病的总称，因其具有发病迅速、进展较快等特点，目前已经成为全球危害人类健康及病死率较高的重大疾病之一，居于非传染性疾病的首位，是世界卫生组织所关注的热点。自噬（autophagy）是一种真核细胞内的降解机制，在细胞受到缺氧、炎性反应和氧化应激等刺激后将胞内物质（如错误折叠的蛋白质或受损的细胞器等）运送到溶酶体进行吞噬和降解，从而在维护细胞正常生理活动等内环境稳态方面发挥关键作用。本文就自噬在不同 CVD 中各个环节的最新研究进展进行综述，探讨自噬在 CVD 调控中的重要作用，为下一步研发新靶点药物提供理论依据。自噬是一种真核细胞内的降解机制，在细胞受到缺氧、炎性反应和氧化应激等刺激后将胞内物质运送到溶酶体进行吞噬和降解，从而在维护细胞正常生理活动等内环境稳态方面发挥关键作用。本文就自噬在不同心血管疾病中各个环节的最新研究进展进行综述，探讨自噬在其调控中的重要作用，为下一步研发新靶点药物提供理论依据。

[关键词] 自噬；心血管疾病；冠状动脉微循环；发病机制

中国图书分类号 R392.1

动态空间维持型静脉插管在微创心脏手术中的应用：一种解决负压引流吸附效应的创新设计

白新明

粤北人民医院 (汕头大学医学院附属粤北人民医院)

目的

微创心脏手术中经皮静脉插管因长径比过大及负压引流（-20~40mmHg）作用，引流孔血管壁吸附率高达 37%（临床观察数据），导致引流量波动、回心血增多，直接影响心肌保护效果。本研究旨在通过结构性创新，解决低血容量状态下静脉塌陷引发的引流孔物理性堵塞问题。

方法

设计一种 " 双模态动态支撑静脉插管 "（专利号受理中），核心创新包括：

1.“弹性支撑阵列”：前段 6 条医用记忆合金支撑条，自然态呈径向隆起（曲率半径 3.2mm），置管时由尖锥导芯牵引伸直，撤芯后自动撑开血管壁形成” 抗吸附缓冲区” 。

2.“三阶引流系统”：

- 端部主引流孔（Φ1.8mm）
- 支撑条间隙引流（0.8~1.2mm）
- 近 / 远端备用侧孔（Φ1.0mm×4）。

3.“抗扭结结构”：中段内嵌螺旋支撑钢丝（Φ0.3mm），维持管腔通畅性 。

4.“安全撤管机制”：圆头导芯引导支撑条复位，避免血管内膜损伤 。

结果（理论分析）

基于流体力学与接触力学模型验证：

1.“抗吸附效能”

- 支撑条隆起高度 > 血管塌陷极限位移（1.5mm），使引流孔区接触应力降为 0。
- 引流截面积增加 148%（较传统侧孔插管）。

2.“血流优化”

- 支撑条间隙流速提升至 25cm/s（传统侧孔区 12cm/s）。
- 涡流区域减少 > 60%，理论溶血指数（HI）< 0.05 。

结论

本设计通过“机械性空间维持机制”，首次实现静脉插管的动态抗塌陷功能：

- 突破传统被动防堵局限，术中预期可消除 > 80% 血管壁吸附事件 。

- 为微创心脏手术提供确定性引流保障，尤其适用于低血容量及长时循环支持患者。

经冠状动脉射频消融治疗梗阻性肥厚型心肌病的多模态影像学评价

黄昌海 刘新峰 龙向淑 卜婕 周诗银 刘微 陈亚宁 郑丹 李孝勇 邓世燕 谭洪文 俞杉 梁勤 王荣品 张陈匀 吴强

贵州省人民医院

目的：经冠状动脉射频消融（TCRFA）是一种新型心肌内射频消融技术。本研究旨在应用经胸超声心动图（TTE）和心脏核磁共振（CMR）多模态评价 TCRFA 对梗阻性肥厚型心肌病（oHCM）患者心功能和心脏重构的影响。

方法：本研究前瞻性纳入接受 TCRFA 治疗的药物难治性 oHCM 患者。纳入标准：最大耐受剂量 β- 受体阻滞剂和 / 或非二氢吡啶类钙拮抗剂治疗三月后仍有症状或无法耐受药物副作用，且 NYHA 心功能分级III - IV级；TTE 左心室短轴观非对称性室间隔肥厚，且舒张末期室间隔最大厚度 ≥ 15 mm；静息跨流出道压差（LVOTG）≥ 50 mmHg；年龄大于 18 岁。排除标准：合并严重心瓣膜病、冠状动脉严重狭窄、先天性心脏病等需要心脏外科手术治疗的疾病；左心室射血分数小于 40%；预期寿命小于 1 年；资料不完整。观察患者术前、术后即刻及术后 3 月的 NYHA 心功能分级、6 分钟步行试验距离、TTE 指标 [舒张末期室间隔厚度（IVSD-TTE）、左心室舒张末期内径（LVEDD）、左心房前后径（LAD）、左心室射血分数（LVEF-TTE）、左心室短轴收缩率（LVFS）、侧壁舒张早期运动速度（lateral e’）、室间隔舒张早期运动速度（septal e’）、LVOTG] 及 CMR 指标 [IVSD-CMR、左心室心肌质量（LVM）、左心室收缩末期容积指数（LVEDV）、左心室舒张末期容积指数（LVESV）、LVEF-CMR、心指数（CI）、升主动脉峰值流速（AA Vmax）、延迟后强化容积占比（LGE，%）] 的变化。以微导管为绝缘层，以冠状动脉介入干预工作导丝为射频能量（30 W）传输载体，对靶间隔支进行射频消融。TCRFA 的技术成功标准：术后即刻无创和有创 LVOTG 较基线水平下降幅度 ≥ 50%，靶间隔支完全闭塞。临床成功定义为术后 3 月无创 LVOTG 较术前下降降低≥ 50 %。安全终点为 30 天主要心脏不良事件，包括心脏性死亡和需要紧急救治的操作相关严重并发症（如房室传导阻滞、冠状动脉夹层、心脏破裂、恶性心律失常等）。

结果：本研究共纳入 16 例符合纳入与排除标准的 oHCM 患者（53.7 ± 13.5 岁，其中女性 13 例）。TCRFA 技术成功率为 96.2%，临床成功率为 81.3%，无安全终点事件。术后出院前和术后 3 月的心功能与 6 分钟步行试验距离较术前明显改善，IVSD-TTE、IVSD-CMR、LVOTG、LVM 均较术前降低，出院前 LAD 小于术前，术后 3 月的 septal e’较出院前增高，出院前和术后 3 月的 LGE 均明显高于术前，增高幅度呈现缩窄趋势。余指标在三个时段无显著性差异。

结论：TCRFA 能够精确地消融 oHCM 患者室间隔肥厚段的心肌组织，有效减轻 oHCM 患者的左心室流出道梗阻，降低室间隔厚度和心肌质量。

Bioactive peptides from C-phycocyanin improve cardiac injury repair after myocardial infarction by promoting angiogenesis

Ruo-Lan Chen, Lu-Ning Qin, Xue-Zhe Wang, Xian-Ming Chu

The Affiliated Hospital of Qingdao University

Background: Myocardial infarction (MI) is a leading global cause of death. Timely reperfusion improves outcomes, but approximately 30% of MI patients develop the no-reflow phenomenon due to microcirculatory dysfunction, which leads to poor prognosis, and there remains a critical unmet clinical need for targeted therapeutics to address this issue. C-phycocyanin has pleiotropic cardioprotective effects, but its large size and complex structure hinder identifying active domains. Marine bioactive peptides, with structural stability and high targeting, show potential in ischemic diseases. Our group identified P2, a C-phycocyanin-derived peptide, which promotes angiogenesis in zebrafish and overcomes the parent protein’s limitations (excessive molecular weight, poor druggability). This study explores whether P2 enhances post-MI ischemic myocardial microcirculation via angiogenesis to improve outcomes.

Methods: To evaluate the therapeutic potential of peptide P2 in myocardial infarction (MI), a murine MI model was established By ligating the left anterior descending branch of the mouse heart, followed by systemic administration of P2 via tail vein injection to assess its efficacy in ameliorating post-infarction cardiac function. Fluorescent co-localization in tissue sections combined with immunofluorescence staining was performed to verify the preferential targeting of P2 to endothelial cells and to quantify its proangiogenic activity. In vitro, a hypoxic endothelial cell model was constructed under oxygen-deprived conditions. A panel of functional assays, including MTT for cell viability, wound-healing and Transwell assays for cell migration, and tube formation assay for angiogenic capacity, were conducted to determine the ability of P2 to promote endothelial cell proliferation, migration, and angiogenesis. For mechanistic exploration of P2-driven angiogenesis, Specific pupylation as IDEntity reporter（Spider）analysis and surface plasmon resonance (SPR) were employed to identify the direct molecular target of P2. Furthermore, molecular docking simulations and co-immunoprecipitation (Co-IP) assays were utilized to dissect the downstream signaling pathways and mechanistic cascade underlying P2-mediated regulation of angiogenesis.

Results: In myocardial infarction (MI) models, administration of peptide P2 via tail vein significantly improved cardiac function compared with untreated MI controls. Fluorescent tracking of labeled P2 confirmed its preferential accumulation within endothelial cells in ischemic myocardial regions, demonstrating inherent endothelial-targeting specificity. CD31 immunofluorescence staining further validated that P2 enhanced angiogenesis in the ischemic area. In vitro studies showed P2 exerted minimal proliferative effects on normoxic endothelial cells but markedly promoted proliferation and migration of hypoxic endothelial cells, as evidenced by MTT, wound-healing, and Transwell assays. Both in vivo and in vitro experiments consistently demonstrated that high-dose P2 exhibited

superior proangiogenic activity compared with VEGFA165, a standard positive control for vascular regulation. Mechanistically, Spider analysis and subcellular co-localization assays identified mitochondrial electron transport chain protein COX4I1 as a candidate mediator of P2's effects. Surface plasmon resonance (SPR) and pulldown assays confirmed direct binding between P2 and COX4I1, with P2 upregulating COX4I1 expression to ameliorate mitochondrial dysfunction. Functional validation showed that COX4I1 knockdown significantly inhibited endothelial cell proliferation, while COX4I1 overexpression increased CyclinD1 levels, accelerated G1/S cell cycle transition, and enhanced cell proliferation.

Conclusion: This study confirms that the marine bioactive peptide P2 specifically promotes angiogenesis in ischemic myocardium by targeting and binding to COX4I1, ameliorating mitochondrial function, and activating CyclinD1-mediated cell cycle progression, with its activity surpassing that of VEGFA165. Mechanistically, it is the first to reveal the regulatory role of COX4I1 in ischemic angiogenesis, thereby providing a novel candidate drug and potential target for MI therapy. Future studies should optimize the administration route of P2 (e.g., targeted delivery systems) and evaluate its long-term safety to lay a foundation for clinical translation.

基于双模态可穿戴脉搏波传感器集成深度学习的高精度低功耗睡眠呼吸暂停检测系统

王佳 邹彤

北京医院

目的： 睡眠呼吸暂停综合征 (SAS) 严重威胁心血管健康，全球 OSA 发病率超过 24%，与高血压、心律失常、心力衰竭等疾病密切相关，但临床诊断不足率高达 80% 以上。多导睡眠监测 (PSG) 虽为诊断金标准，但需要专业实验室环境，设备成本高昂，检测流程复杂，且多通道传感器常影响患者睡眠质量。基于光电容积描记法 (PPG) 的可穿戴设备虽有潜力，但连续工作功耗大，难以满足长期监测需求。本研究旨在开发并验证一种创新的双模态可穿戴脉搏检测系统，整合压电纳米发电机 (PENG) 和 PPG 传感器，解决传统监测方法在精度、功耗和便携性方面的技术瓶颈。

方法： 基于传统中医脉诊理论，设计仿生指尖结构的腕戴式双模态监测系统。硬件包括：C 型夹具结构的力施加装置；Ecoflex-30 硅胶弹性层，包含模量匹配层和半球形指尖模拟结构；传感模块整合指纹状压电传感单元和 PPG 探头；通信模块实现脉搏压力波 (PPW) 和 PPG 信号的连续采集与无线传输。

创新性建立两阶段检测策略：第一阶段利用 PENG 低功耗优势进行 24 小时连续预筛查，检测到可疑事件时激活第二阶段 PPG 精确检测。构建基于 Vision Transformer 的深度学习模型，有效提取传感器信号高维特征。

临床验证采用回顾性和前瞻性相结合设计。回顾性研究基于北京医院 PSG 实验室 2024 年 6-9 月数据库，获得睡眠呼吸暂停组和正常对照组各 3650 个 2 分钟数据段，按十折交叉验证分组。前瞻性试验纳入 15 例患者 (男性 11 例，女性 4 例)，平均年龄 44.7 岁，平均 BMI 24.71，同时进行 PSG 监测和设备测试。

结果： 设备性能验证显示出色稳定性。有限元仿真确定曲率半径 5mm 的指尖样结构获得最佳性能。经超过 60000 次疲劳测试后，PENG 传感器输出性能保持稳定。环境适应性测试表明在不同湿度和温度条件下传感器输出稳定。

深度学习模型性能评估中，Vision Transformer 相比传统机器学习方法表现出显著优势。高精度模型 (PPG 模式) 达到特异性 99.73%、敏感性 99.45%、准确率 99.59%，AUC 值 0.9982。高敏感性模型 (PPW 模式) 敏感性 93.41%，特异性 54.17%，准确率 68.57%。两阶段模型 (PPW+PPG) 结合双传感器优势，达到特异性 96.35%、敏感性 92.51%、准确率 94.95%，AUC 值 0.9857，有效平衡性能和能耗。

前瞻性临床验证中，15 例患者平均 AHI 值 23.7。设备与 PSG 诊断符合率达 94.7%，成功识别所有中重度 SAS 事件。PPW 和 PPG 波形形态学一致性高，相邻峰值统计分析显示强线性相关 (R^2=0.9936)。

功耗分析表明，两阶段检测策略总功耗约 57mW，相比 PPG 连续监测的 74mW 降低 23%。患者佩戴体验评估显示良好舒适性，无不良反应报告。

结论： 本研究成功开发并验证了集成 PENG 和 PPG 的双模态可穿戴 SAS 监测系统，实现了检测精度与功耗的最佳平衡。临床验证证实了系统的有效性、安全性和实用性。系统适用于家庭环境初步筛查、医院 PSG 预筛查、CPAP 治疗效果监测等多种临床场景。该技术突破了传统监测方法局限性，为睡眠呼吸疾病防治提供了具有显著临床价值和广阔应用前景的创新解决方案，有望显著改善 SAS 患者的诊疗质量和预后。

靶向 OPN 可视化纳米胶束包载 SIRT6 激活剂减缓血管老化

方岩 [1] 李汶玥 [2] 秦诚 [1] 许梦琪 [1] 孙乃媛 [1] 李苏雷 [1] 李慧 [1] 侯毅 [2] 曹丰 [1]

1. 中国人民解放军总医院 / 解放军医学院

2. 北京工业大学

目的：Sirtuin 6（SIRT6）是一种长寿相关基因，通过调控细胞衰老，被认为具有治疗血管衰老的潜力。本研究旨在开发一种可视化的 SIRT6 激活剂纳米递送系统，减轻自然衰老小鼠的血管老化。

方法：通过 Western blot 和免疫荧光染色检测自然衰老小鼠主动脉血管平滑肌细胞（vascular smooth muscle cells， VSMCs）骨桥蛋白（osteopontin，OPN）的表达水平。使用 OPN 靶向肽修饰聚己内酯 - 聚乙二醇，通过自组装方式包载 SIRT6 激活剂 MDL800 和近红外荧光剂吲哚菁绿（indocyanine green，ICG），构建负载 MDL800 和 ICG 的具有 OPN 靶向性的纳米胶束（OPN micelle，OPN-MI）。使用透射电镜和动态光散射评估 OPN-MI 粒径和 Zeta 电位，使用 CCK8 实验评价 OPN-MI 的生物相容性。通过小动物近红外荧光在体成像观察 OPN-MI 在衰老小鼠体内的时间变化和器官分布。干预 8 周后，通过脉搏波传导速度、病理染色评价 OPN-MI 在体抗血管衰老效应。结合生物信息学分析和分子生物学实验，探索并验证 OPN-MI 的抗衰老机制。

结果：自然衰老小鼠 VSMCs 的 OPN 表达水平显著高于对照组小鼠（P<0.001），证实 OPN 可作为血管衰老的标志物。OPN-MI 纳米粒径为 107.008±9.572 nm，Zeta 电位为 -7.293±2.291 mV，具有良好的生物相容性。在体和离体近红外荧光成像显示，与非靶向 MI 相比，OPN-MI 显著聚集在自然衰老小鼠的血管壁区域（P<0.001）。尾静脉注射 8 周后，OPN-MI 降低自然衰老小鼠脉搏波传导速度（P=0.031），减少血管壁弹性蛋白的断裂数量（P=0.016），改善内中膜厚度（P=0.048）。生物信息学结合病理和分子实验证实，SIRT6 激活剂 MDL800 通过调节 H3K9ac 和 H3K56ac 的乙酰化，降低了 MMP9 的表达水平（P=0.001）。

结论：包载 MDL800 和 ICG 的可视化 OPN 靶向纳米胶束有效延缓了自然衰老小鼠模型的血管老化。该纳米递送系统有望成为抗血管衰老的治疗新策略。

靶向 CD36 的血小板工程化 AAV 基因疗法重编程脂肪酸代谢促进心肌增殖修复

张宁

浙江大学医学院附属邵逸夫医院

研究目的

开发血小板工程化的 AAV 递送系统（Plt-AAV），以克服传统基因疗法的局限性，并靶向介导 CD36 敲除、抑制脂肪酸氧化（FAO）实现心脏代谢重编程与再生修复。

研究方法

基于公共数据 RNA 测序分析，揭示心肌脂肪酸利用关键转运蛋白与细胞再生命运的关系。离体心肌细胞实验检验敲除 CD36 后脂质代谢、能量代谢和细胞周期的因果关系。进一步利用血小板开放小孔（OCS）装载 AAV，制备血小板工程化的 AAV-CD36KD 基因疗法（Plt-AAV-CD36KD）。采用活体成像、血小板示踪验证 Plt-AAV-CD36KD 在心肌缺血 / 再灌注损伤模型鼠中对损伤心脏的靶向富集、转染效率、CD36 敲除效果等。进一步评估该工程化基因疗法对心肌 FAO 的靶向阻断作用及心肌增殖的调控作用。

研究结果

1. 脂肪酸氧化（FAO）与心脏成熟过程中的细胞周期调控显著相关；

2. 抑制 CD36 可减弱心肌细胞脂肪酸氧化（FAO）并促进其增殖；

3. 血小板 OCS 可高效负载 AAV 构建 Plt-AAV 工程体，并在血小板活化后释放 AAV，保持完全转染能力；

4. Plt-AAV 能有效保护 AAV 免受中和抗体（NAb）的灭活作用，且高效靶向缺血损伤的心脏组织；

5. Plt-AAV-CD36KD 通过表观遗传机制下调组蛋白 H3K4me3 修饰，促进心肌增殖，并且不会引起脂质蓄积和脂毒性；

6. Plt-AAV 基因递送系统比游离 AAV 对心脏转染效率更高、再生修复更强；

7. Plt-AAV 在血栓风险、体内稳态及长期预后方面均表现良好安全性。

结论

本研究提出了一种基于 Plt-AAV 工程化系统的靶向 CD36 基因治疗新策略，为心肌修复提供了创新性解决方案。该策略保护 AAV 免受抗体中和，特异性敲除 CD36，调控心肌细胞去分化，阻断心肌脂肪酸利用，并且避免脂质重构等副作用，可在促进心脏再生的同时规避代谢紊乱风险。

老年心脏健康有关研究

Antithrombotic Therapy Strategies and Clinical Outcomes in Chinese Patients Aged 65 and Older with High Ischemic Risk Coronary Artery Disease

Jiaqi Zhang, Xiahuan Chen, Wenwen Liu, Meilin Liu

Peking University First Hospital

Objective:

Coronary artery disease (CAD) remains a leading cause of morbidity and mortality among elderly patients, who often present with complex comorbidities and an increased risk of both ischemic and bleeding events. Current guidelines recommend dual antiplatelet therapy (DAPT) for patients with high ischemic risk; however, evidence regarding optimal long-term antithrombotic strategies in elderly populations, particularly in Asian cohorts, is limited. Elderly individuals often exhibit altered pharmacokinetics, frailty, and heightened susceptibility to hemorrhagic complications, making treatment decisions especially challenging. This study aimed to evaluate real-world patterns of antithrombotic therapy and their associations with long-term clinical outcomes in Chinese patients aged 65 and older with established CAD and high ischemic risk features.

Methods:

This multicenter, prospective, observational cohort study included 2,943 Chinese patients aged ≥ 65 years with angiographically confirmed CAD and at least one high ischemic risk factor (e.g., multivessel disease, diabetes mellitus, previous myocardial infarction or stroke). Patients were enrolled from 52 hospitals across China and followed up for up to 30 months. Baseline demographic and clinical characteristics were collected, and antithrombotic therapy regimens were recorded at discharge and during follow-up. The primary efficacy endpoint was a composite of all-cause death, myocardial infarction (MI), or stroke. The primary safety endpoint was major bleeding defined according to the BARC criteria. Antithrombotic strategies were classified into five categories: aspirin monotherapy, clopidogrel monotherapy, prolonged DAPT, DAPT within 12 months post-PCI, and anticoagulant-based therapy. Multivariable Cox proportional hazards models were used to adjust for confounding variables and identify associations between antithrombotic therapy patterns and clinical outcomes. Subgroup analyses were performed to evaluate the consistency of treatment effects across clinical strata.

Results:

At baseline, DAPT was the most frequently used antithrombotic regimen (63.2%), with clopidogrel monotherapy (17.6%) and aspirin monotherapy (14.8%) also commonly prescribed. Over time, there was a notable decline in DAPT usage and a corresponding increase in monotherapy, particularly clopidogrel. During the median follow-up of 30 months, 252 patients experienced a primary efficacy endpoint event (8.6%), while 76 patients (2.6%) experienced major bleeding. Multivariate analysis revealed that clopidogrel monotherapy was associated with a significantly lower risk of the primary composite endpoint compared to aspirin monotherapy (adjusted HR: 0.61; 95% CI: 0.39–0.96; p = 0.033), without a significant increase in bleeding risk. Prolonged DAPT (≥ 12 months) did not significantly reduce ischemic events compared to monotherapy and was associated with a trend toward higher bleeding risk, particularly in patients aged ≥ 75 years. Subgroup analysis confirmed that clopidogrel monotherapy offered consistent benefit across multiple high-risk subgroups, including those with diabetes, prior MI, renal dysfunction, or anemia, suggesting its broad applicability in clinical practice.

Conclusion:

In a real-world cohort of elderly Chinese patients with CAD and high ischemic risk, clopidogrel monotherapy emerged as a favorable long-term antithrombotic strategy, balancing ischemic protection with bleeding safety. While DAPT remains important during the acute and subacute phases post-PCI, its extended use beyond 12 months may confer limited incremental benefit and potentially increased harm in elderly populations. These findings support a more tailored approach to antithrombotic therapy in older adults, highlighting the importance of age-specific risk-benefit assessment and regional pharmacogenetic considerations. The study emphasizes the pressing need for prospective, randomized trials focusing on elderly Asian populations to validate optimal strategies and durations of antithrombotic treatment, and to inform future guideline development in this understudied but clinically vulnerable group.

Low serum Klotho reflects senile inflammation in middle-aged and elderly patients with coronary atherosclerosis

Mao Qi

Xinqiao Hospital

Low serum Klotho reflects senile inflammation in middle-aged and elderly patients with coronary atherosclerosis

Qi Mao

Department of Cardiology, Institute of Cardiovascular Research, Xinqiao Hospital, Army Medical University, Chongqing 400037, China

Abstract

Background: Inflammatory senescence has been reported to be associated with atherosclerosis. The present study aims to ascertain the correlation of anti-aging protein Klotho with inflammatory parameters in middle-aged and elderly coronary atherosclerotic disease (CAD).

Methods: A total of 302 patients with CAD were included in this study. Coronary atherosclerosis was confirmed and quantified for all patients by coronary angiography. Serum Klotho was detected by enzyme linked immunosorbent assay. Serum concentrations of IL-6 and IL-8 were quantified by chemiluminescence assay. T-lymphocyte subsets were measured using flow cytometry.

Results: Multivariate linear regression analysis showed that serum Klotho was an independent predictor for circulating monocytes (standard β=-0.321, P<0.001) and CD4+/CD8+ ratio (standard β=-0.522, P<0.001). After adjustment, serum Klotho was still independently associated with IL-6 (standard β=-0.395, P<0.001) and IL-8 (standard β=-0.296, P<0.001). Moreover, circulating monocytes, CD4+ and CD8+ lymphocytes were correlated with increased serum concentrations of IL-6 and IL-8, independent of CRP (P<0.05). In receiver operating characteristic curve analysis, CD4+/CD8+ ratio (AUC=0.863, P<0.001), IL-6 (AUC=0.893, P<0.001) and IL-8 (AUC=0.884, P<0.001) presented the excellent predictive performance for significant CAD.

Conclusions: Decreased concentrations in serum Klotho reflect senile inflammation, which is related to the severity of CAD in middle-aged and elderly patients.

Keywords: Klotho, coronary atherosclerotic disease, inflammation, aging

Low serum Klotho reflects senile inflammation in middle-aged and elderly patients with coronary atherosclerosis

Qi Mao

Department of Cardiology, Institute of Cardiovascular Research, Xinqiao Hospital, Army Medical University, Chongqing 400037, China

Abstract

Background: Inflammatory senescence has been reported to be associated with atherosclerosis. The present study aims to ascertain the correlation of anti-aging protein Klotho with inflammatory parameters in middle-aged and elderly coronary atherosclerotic disease (CAD).

Methods: A total of 302 patients with CAD were included in this study. Coronary atherosclerosis was confirmed and quantified for all patients by coronary angiography. Serum Klotho was detected by enzyme linked immunosorbent assay. Serum concentrations of IL-6 and IL-8 were quantified by chemiluminescence assay. T-lymphocyte subsets were measured using flow cytometry.

Results: Multivariate linear regression analysis showed that serum Klotho was an independent predictor for circulating monocytes (standard β=-0.321, P<0.001) and CD4+/CD8+ ratio (standard β=-0.522, P<0.001). After adjustment, serum Klotho was still independently associated with IL-6 (standard β=-0.395, P<0.001) and IL-8 (standard β=-0.296, P<0.001). Moreover, circulating monocytes, CD4+ and CD8+ lymphocytes were correlated with increased serum concentrations of IL-6 and IL-8, independent of CRP (P<0.05). In receiver operating characteristic curve analysis, CD4+/CD8+ ratio (AUC=0.863, P<0.001), IL-6 (AUC=0.893, P<0.001) and IL-8 (AUC=0.884, P<0.001) presented the excellent predictive performance for significant CAD.

Conclusions: Decreased concentrations in serum Klotho reflect senile inflammation, which is related to the severity of CAD in middle-aged and elderly patients.

Keywords: Klotho, coronary atherosclerotic disease, inflammation, aging

Low serum Klotho reflects senile inflammation in middle-aged and elderly patients with coronary atherosclerosis

Qi Mao

Department of Cardiology, Institute of Cardiovascular Research, Xinqiao Hospital, Army Medical University, Chongqing 400037, China

Abstract

Background: Inflammatory senescence has been reported to be associated with atherosclerosis. The present study aims to ascertain the correlation of anti-aging protein Klotho with inflammatory parameters in middle-aged and elderly coronary atherosclerotic disease (CAD).

Methods: A total of 302 patients with CAD were included in this study. Coronary atherosclerosis was confirmed and quantified for all patients by coronary angiography. Serum Klotho was detected by enzyme linked immunosorbent assay. Serum concentrations of IL-6 and IL-8 were quan-

tified by chemiluminescence assay. T-lymphocyte subsets were measured using flow cytometry.

Results: Multivariate linear regression analysis showed that serum Klotho was an independent predictor for circulating monocytes (standard β=-0.321, P<0.001) and CD4+/CD8+ ratio (standard β=-0.522, P<0.001). After adjustment, serum Klotho was still independently associated with IL-6 (standard β=-0.395, P<0.001) and IL-8 (standard β=-0.296, P<0.001). Moreover, circulating monocytes, CD4+ and CD8+ lymphocytes were correlated with increased serum concentrations of IL-6 and IL-8, independent of CRP (P<0.05). In receiver operating characteristic curve analysis, CD4+/CD8+ ratio (AUC=0.863, P<0.001), IL-6 (AUC=0.893, P<0.001) and IL-8 (AUC=0.884, P<0.001) presented the excellent predictive performance for significant CAD.

Conclusions: Decreased concentrations in serum Klotho reflect senile inflammation, which is related to the severity of CAD in middle-aged and elderly patients.

Keywords: Klotho, coronary atherosclerotic disease, inflammation, aging

Diagnostic and prognostic value of serum Asprosin in Cardiac Cachexia

Yi Huang, Xiao-Song Gu

The Second Affiliated Hospital of Soochow University

ABSTRACT

Objectives

Asprosin is a newly discovered orexigenic adipokine and is correlated with chronic heart failure (CHF). Cardiac cachexia (CC) is a common complication of CHF, often accompanied by decreased appetite. Currently, the relationship between asprosin and CC is poorly clear. The aim of this study was to explore the diagnostic and prognostic value of asprosin in CC.

Methods

384 patients with CHF were included and further divided into CHF with CC group (CC group) (n = 79) and without CC group (Non-CC group) (n = 305) based on the presence of CC. During the same period, 120 healthy individuals were included in the control group. Comparing the differences among the three groups. Correlation analysis was conducted between asprosin and asprosin/BMI with clinical indicators and echocardiographic parameters, and multiple logistic regression analysis was used to explore the influencing factors of CC. Receiver operating characteristic (ROC) analysis was used to evaluate the predictive value of asprosin/BMI for CC. The association between asprosin/BMI and CC was evaluated using restricted cubic splines (RCS) in CHF patients. We constructed two risk models to evaluate the reclassification ability of asprosin/BMI for CC. We conducted a follow-up on patients with CC for 12 months and divided them into a low asprosin/BMI group and a high asprosin/BMI group based on the median level of asprosin/BMI, and plotted Kaplan-Meier survival curves.

Results

Compared with non-CC group, asprosin, BMI, eGFR, Hb, ALB, HDL-C and LVEF were significantly reduced in CC group, while asprosin/BMI, CRP, ALT, AST, Scr, Glu and NT-proBNP were significantly increased (p < 0.05). Within CC patients, asprosin/BMI levels were positively correlated with Hb, ALB, eGFR, Glu and LVEF, while negatively correlated with NT-proBNP and Scr. Multivariate binary logistic regression analysis showed that asprosin/BMI (OR: 2.047, 95% CI: 1.644 - 2.547; p < 0.001) , Scr (OR: 1.039, 95 % CI: 1.019 - 1.059; P < 0.001) , Glu (OR: 1.495, 95% CI: 1.012 - 2.209; p = 0.043) and NT-proBNP (OR: 1.000, 95% CI: 1.000 - 1.001; p = 0.001) were the independent risk factors for CC. Asprosin/BMI had good predictive ability for CC (AUC: 0.808, 95% CI: 0.756 - 0.859; p < 0.001). RCS analysis showed a positive linear correlation between asprosin/BMI levels and the risk of CC (p for non-linear = 0.242). Adding asprosin/BMI to the CC basic risk model (including Scr, Glu, and NT-proBNP) can improve the reclassification of CC [continuous net reclassification index (NRI): 92.75%, 95%CI: 55.00% - 121.70%, p<0.001; categorical NRI: 45.38%, 95%CI: 23.79% - 63.74%, p < 0.001]. Follow up for 12 months, according to the median of asprosin/BMI in CC patients, low asprosin/BMI levels group (< 26.87) had a significantly higher incidence of MACE (53.85% vs 27.50%, p = 0.017) than high group.

Conclusions

Asprosin/BMI is an independent risk factor for CC in CHF patients. The increase of asprosin/BMI decreases the incidence of MACE in CC patients. We therefore speculate that asprosin and asprosin/BMI might intervene in the development of CC and serve as a potential therapeutic target.

KEYWORDS: Cardiac cachexia; Asprosin; Chronic heart failure; Diagnostic; Prognostic

CHK1 通过激活 AHSA1/HSP90 介导的线粒体自噬延缓小鼠心脏衰老

经鹏 周刘华 王昊 王连生

江苏省人民医院 / 南京医科大学第一附属医院

目的：作为经典的细胞周期检查点蛋白之一，细胞周期检查点激酶 1（CHK1）主要通过介导一系列级联反应广泛参与多种生物学进程。既往研究发现 CHK1 是心肌再生修复中的关键因子，然而，其在小鼠心脏自然衰老过程中所起到的作用尚不明确。

方法：首先，在多柔比星（DOX）诱导的多种心肌细胞衰老模型以及小鼠自然衰老模型中检测 CHK1 的表达情况。其次，构建心肌细胞特异性 CHK1 敲低 / 过表达小鼠，研究其在小鼠自然衰老过程中的作用；接下来，在 DOX 诱导的 AC16 人心肌细胞早衰模型中补充 CHK1，探究其对 AC16 细胞衰老的影响。最后，通过转录组学测序（RNA-seq）与免疫共沉淀串联质谱（IP/MS）联合分析揭示 CHK1 延缓老年小鼠心脏衰老的分子机制。

结果: 在体内外衰老模型中，CHK1 的表达水平明显下降。在小鼠自然衰老模型中，过表达 CHK1 可延缓老年小鼠心脏衰老；而敲除 CHK1 则加剧老年小鼠心脏衰老；体外补充 CHK1 明显减轻了 AC16 细胞的衰老程度。RNA-seq 提示过表达 CHK1 可激活热休克蛋白 90（HSP90）介导的线粒体自噬；IP/MS 表明 CHK1 可靶向结合 90kDa 热休克蛋白 ATPase 同源物激活剂 1 (AHSA1)。机制上，CHK1 通过靶向结合 AHSA1 并抑制其泛素化降解来激活 HSP90 介导的线粒体自噬。

结论：CHK1 通过靶向结合 AHSA1 并抑制其泛素化降解，激活 HSP90 介导的线粒体自噬来改善心肌细胞的线粒体稳态，从而延缓老年小鼠心脏衰老。我们的研究揭示了 CHK1 在小鼠心脏自然衰老过程中的重要作用，为未来临床上预防或治疗老年性心脏病提供了潜在的干预靶点。

关键词：CHK1; 心脏衰老 ; AHSA1;HSP90; 线粒体自噬

膳食指数与心脏代谢指数的关联及其潜在作用机制研究

刘顺 黄志敏 陈小琪

福建医科大学公共卫生学院流行病与卫生统计学系

目的 心脏代谢指数（Cardiometabolic Index, CMI）是评估心血管疾病风险的重要指标，而膳食模式对其可能产生显著影响。本研究旨在探讨三种膳食指数（DASH、MED、HEI2015）与 CMI 之间的关联，并分析其潜在作用机制。**方法** 研究纳入了 1999 至 2017 年 NHANES 数据库中的 11422 个样本，使用 R 语言（版本 4.3.2）进行统计分析。首先，依据 CMI 的五分位数分布将样本分为五组，并进行基线分析。通过线性回归和 Logistic 回归模型评估 DASH、MED 和 HEI2015 指数与 CMI 之间的关系。利用散点图和限制性立方样条（RCS）曲线分析膳食指数与 CMI 之间的相关性及潜在的非线性关系，并通过 k-means 聚类分析将人群划分为三种膳食模式组。最后，采用中介分析方法探讨潜在的中介途径。**结果** 在基线分析中，除教育程度和婚姻状况外，各变量在 CMI 五分位数分组后未显示出统计学差异。MED 和 HEI2015 指数在 CMI 分组后显示出显著差异，而 DASH 指数未表现出显著性。线性回归和 Logistic 回归分析显示，在未调整混杂因素的模型中，三个膳食指数均与 CMI 呈负相关；但在调整相关变量后，MED 和 HEI2015 指数的升高与 CMI 的降低呈正相关，而 DASH 指数与 CMI 的关系则有所不同。相关性分析和限制性立方样条（RCS）分析表明，DASH、MED 和 HEI2015 指数与 CMI 呈负相关，且相关性接近线性模式。K-means 聚类分析将样本划分为三种膳食模式组，结果显示膳食指数较高组（Cluster 2）与 CMI 的降低具有统计学意义。中介分析揭示，在 MED 指数与 CMI 的关系中，腰高比（WHtR）可作为中介变量，其效应占比为 27.4%；在 HEI2015 指数与 CMI 的关系中，身高可作为中介变量，效应占比为 4.9%。遗憾的是，在 DASH 指数与 CMI 的关系中未发现显著的中介变量。**结论** 本研究发现 MED 和 HEI2015 指数与 CMI 的降低呈正相关，而 DASH 指数与 CMI 的关系较为复杂。腰高比和身高分别在 MED 和 HEI2015 指数与 CMI 的关系中发挥了中介作用。这些结果为理解膳食模式对心脏代谢健康的影响提供了新的见解。

Therapeutic Efficacy of Qili Qiangxin Capsule in Elderly Patients with Heart Failure with Preserved Ejection Fraction

Xing-Peng Bu, Chun-Xia Li, Ya-Ru Liu, Guo-Fang Chu

Department of Geriatric Medicine, Shanxi Bethune Hospital, Shanxi Academy of Medical Sciences, Third Hospital of Shanxi Medical University, Tongji Shanxi Hospital

Background: Heart failure with preserved ejection fraction (HFpEF) has emerged as a major public health challenge, accounting for approximately 50% of all heart failure cases worldwide, with particularly high prevalence among elderly populations. Despite significant advances in cardiovascular therapeutics, current treatment strategies for HFpEF remain largely symptomatic, focusing primarily on volume management with diuretics and modest benefits from SGLT2 inhibitors and neurohormonal modulators. The complex, multifactorial pathophysiology of HFpEF, involving systemic inflammation, metabolic dysregulation, and myocardial fibrosis, underscores the need for novel therapeutic approaches. Traditional Chinese Medicine (TCM) has gained increasing recognition in cardiovascular medicine due to its multi-target, system-regulating properties. Qili Qiangxin Capsule (QLQX), a well-established TCM formulation, has demonstrated efficacy in improving cardiac function and symptoms in patients with heart failure with reduced ejection fraction. However, its therapeutic potential in elderly HFpEF patients, a population with distinct clinical characteristics and therapeutic challenges, has not been systematically evaluated. This study aimed to investigate the additive benefits of QLQX when combined with standard contemporary pharmacotherapy in elderly HFpEF patients.

Methods: This prospective, randomized, controlled trial was conducted at Shanxi Bethune Hospital between January 2022 and December 2023. We enrolled 149 consecutive elderly patients (age ≥ 65 years) with confirmed HFpEF diagnosis according to current guidelines. Participants were randomly assigned in a 1:1 ratio to either the control group (n=74) receiving standard guideline-directed medical therapy (including diuretics, SGLT2 inhibitors, and ARNI/ACEI/ARB) or the observation group (n=75) receiving standard therapy plus QLQX (1.2 g three times daily). Comprehensive assessments were performed at baseline and after 6 months of treatment, including: 1) quality of life evaluation using the Minnesota Living with Heart Failure Questionnaire (MLHFQ); 2) functional capacity assessment via 6-minute walking distance (6MWD) test; 3) echocardiographic evaluation of diastolic function using the E/e' ratio; and 4) measurement of serum biomarkers including N-terminal pro-B-type natriuretic peptide (NT-proBNP) and soluble suppression of tumorigenicity 2 (sST2). Statistical analyses were performed using SPSS version 26.0, with within-group comparisons using paired t-tests and between-group comparisons using independent t-tests.

Results: After 6 months of treatment, both groups demonstrated significant improvements from baseline in all measured parameters (all P<0.05). However, the QLQX group showed substantially greater clinical benefits compared to standard therapy alone. Specifically, the QLQX group exhibited a more pronounced improvement in quality of life (MLHFQ score: 20.04±5.12 vs 28.78±6.12, P<0.001), superior enhancement in exercise capacity (6MWD: 412.69±63.30 m vs 397.75±60.03 m, P=0.012), and better diastolic function (E/e' ratio: 9.29±1.78 vs 11.12±2.13, P<0.001). Importantly, the QLQX group showed more significant reductions in biomarkers of myocardial stress (NT-proBNP: 586.68±28.02 pg/mL vs 874.35±41.32 pg/mL, P<0.001) and cardiac fibrosis/remodeling (sST2: 12.05±2.04 ng/mL vs 22.77±3.14 ng/mL, P<0.001). The between-group differences remained statistically significant after adjustment for potential confounders, with no significant adverse events attributable to QLQX treatment observed during the study period.

Conclusion: In this randomized controlled trial of elderly HFpEF patients, adjunctive therapy with Qili Qiangxin Capsule demonstrated significant additional benefits beyond standard medical therapy alone. QLQX treatment was associated with marked improvements in quality of life, functional capacity, and diastolic function, along with favorable modulation of key pathophysiological biomarkers. These findings suggest that QLQX may address multiple pathological pathways in HFpEF, potentially through its putative anti-inflammatory, anti-fibrotic, and metabolic-modulating properties. The excellent safety profile observed in this elderly population further supports the potential clinical utility of QLQX as a complementary therapeutic strategy for HFpEF management. These results warrant confirmation in larger multicenter trials with longer follow-up durations to establish the durability of benefits and potential impact on hard clinical outcomes.

夜间睡眠和日间小睡对中老年人心血管疾病发病风险的联合影响：一项基于 CHARLS 的纵向队列研究

熊文潇 [1] 李万新 [1] 薛娇平 [2] 李靓 [3] 张岩波 [3] 田晶 [1]

1. 山西医科大学第一医院

2. 山西医科大学第二临床医学院

3. 山西医科大学公共卫生学院卫生统计学教研室

目的：睡眠是心血管疾病 (CVD) 的一个可变风险因素。尽管单一夜间睡眠时长和日间小睡与 CVD 的关系已被广泛研究，但其对 CVD 的联合影响却较少被关注。本研究旨在探索降低 CVD 发病风险的最佳睡眠组合方式。

方法：本研究使用了中国健康与退休纵向研究 (CHARLS) 的纵向数据。通过自我报告问卷在 2011 年收集基线睡眠及其他相关变量信息，随访至 2020 年观察 CVDs 事件的发生。采用 Cox 比例风险分析探讨睡眠时长及不同睡眠组合方式对 CVDs 发病风险的影响。

结果：本研究共纳入 7975 名参与者，其中老年人 1562(19.59%)，女性 4323 名 (54.21%)，随访期间观察到 2117 名参与者 (26.55%) 新发 CVD 事件。经多变量 Cox 调整混杂因素后，夜间短睡眠 (<6h) 与 CVD 风险增加显著相关 (HR:1.189，95 % CI:1.071-1.319，P=0.001)。进一步分析显示，与参考组 (适度夜间睡眠 6-8h 且不习惯日间小睡) 相比，夜间睡眠时长 <6h 且不习惯日间小睡 (HR:1.117，95 % CI:1.021-1.357，P=0.025)，夜间睡眠时长 <6h 且日间小睡≤ 0.5h(HR:1.558，95 %CI:1.236-1.962，P<0.001) 以及夜间睡眠时长 <6h 且日间小睡 >1h(HR:1.300，95 % CI:1.020-1.655，P=0.034) 三组参与者均表现出更高的 CVD 发病风险。

结论：保证充足夜间睡眠有助于降低 CVD 发病风险。适度夜间睡眠与不习惯日间小睡的组合，可能是更有利于降低 CVD 风险的睡眠组合方式。

体质量与老年慢性阻塞性肺疾病患者肺功能和心脏结构的相关性

张静

陆军军医大学大坪医院

目的：探讨体质量与老年慢性阻塞性肺疾病 (COPD) 患者肺功能和心脏结构的相关性。

方法：回顾性收集≥ 65 岁的老年患者 747 例，其中非 COPD 组 184 例，COPD 轻度组 77 例，COPD 中度组 206 例，COPD 重度组 280 例。检测患者的体质量指数 (BMI)、肺功能、心脏结构等参数，进行组间比较和相关回归分析。

结果：本研究主要发现：与非 COPD 组比较，重度 COPD 组右心室内径 (RVD) 显著增大 (P < 0.05)，BMI、左心房内径 (LAD)、室间隔厚度 (IVST)、左室后壁厚度 (LVPWT)、左室质量指数 (LVMI) 显著减小 (P < 0.05)。而轻中度 COPD 组 RVD、BMI、LAD、IVST、LVPWT、LVMI 与非 COPD 组比较无显著差异。相关分析发现：在重度 COPD 组中，低 BMI 与残气量 / 肺总量 (RV/TLC)、RVD、右心房内径 (RAD)、高密度脂蛋白胆固醇 (HDL-C)、估测肾小球滤过率 (eGFR) 增高显著相关 (P < 0.05)，而低 BMI 与第一秒用力呼气容积占预计值百分比 (FEV1%pred)、第一秒用力呼气容积 / 用力肺活量 (FEV1/FVC)、一氧化碳弥散量 (DLCO)、LAD、IVST、LVPWT、LVMI、血浆白蛋白、高血压构成比、收缩压、2 型糖尿病构成比、总胆固醇 (TC)、尿酸 (UA) 降低显著相关 (P < 0.05)。回归分析发现：在重度 COPD 中，低 BMI 与 RVD 增高独立相关 (P < 0.05)，而其与 FEV1%pred、IVST、LVPWT、LVMI 降低独立相关 (P < 0.05)。

结论：低体质量指数与老年重度 COPD 患者肺功能受损、右室扩大和左室质量指数降低独立相关。

中性粒细胞淋巴细胞比率与老年高血压患者死亡风险的关联

李珊

中国人民解放军总医院 (301 医院)

背景 中性粒细胞与淋巴细胞比率（NLR）已被证实是多种临床情况下不良预后的关键风险标志物。然而，其与老年高血压患者死亡风险的关联尚未得到充分验证。本研究旨在探讨 NLR 水平与老年高血压患者全因死亡和原因特异性死亡的关联。

方法 这项队列研究纳入了 1999 年至 2018 年间美国国家健康与营养调查（NHANES）中的 9939 例老年（≥ 60 岁）高血压患者。根据 NLR 水平的四分位数将其分为四组。生存状态通过与国家死亡指数记录的链接来确定。进行了 Cox 比例风险回归模型、限制性立方样条曲线、生存分析和受试者工作特征曲线（ROC）分析。

结果 多变量调整后的 Cox 比例风险回归模型显示，NLR 水平与老年高血压患者的全因死亡和原因特异性死亡呈显著的正相关。与 NLR 最低四分位数的患者相比，最高四分位数患者的调整后风险比（HR）为全因死亡 1.52（95% CI 1.32-1.74），心血管死亡 2.04（1.63-2.56）和非心血管死亡 1.30（1.11-1.53）。NLR 水平每增加 1 个标准差，调整后的 HR 为全因死亡 1.20（1.15-1.26），心血管死亡 1.28（1.21-1.35）和非心血管死亡 1.16（1.10-1.23）。限制性立方样条曲线显示 NLR 与全因死亡和原因特异性死亡呈现单调的正相关。NLR 与心血管死亡的关联在未服用他汀类药物的患者中更为显著（P 值 <0.05）。ROC 分析显示 NLR 对全因死亡和原因特异性死亡具有中等程度的预测价值，曲线下面积在 0.581 到 0.612 之间，优于高敏 C 反应蛋白和中性粒细胞。

结论 NLR 水平升高与老年高血压患者的全因死亡和原因特异性死亡风险的增加独立相关。未服用他汀类药物的患者 NLR 与心血管死亡的关联性更强。

Life Satisfaction as Modifiable CVD Prevention Target: Cross-Cultural Mediation in Aging Cohorts

Changxing Liu

The First Affiliated Hospital of Heilongjiang University of Chinese Medicine

ObjectiveThe world is experiencing an unprecedented demographic shift, with the number of individuals aged 60 years and above projected to reach 2.1 billion by 2050, according to the World Health Organization. In tandem with this aging trend, cardiovascular disease (CVD) has emerged as a leading cause of morbidity and mortality among the elderly, accounting for approximately 32% of all global deaths. Despite significant advancements in medical treatments, the burden of CVD remains high, highlighting the urgent need to identify and understand modifiable risk factors. This study was designed to comprehensively examine the prospective association between life satisfaction, a key indicator of psychological well - being, and the risk of CVD among older adults across multiple international cohorts. By exploring this relationship, the research also aimed to evaluate potential mediating pathways, which could offer novel insights and inform the development of targeted interventions to enhance cardiovascular health in the aging population.

MethodsThis study harmonized data from four well - established aging cohorts: the Health and Retirement Study (HRS) in the United States, the English Longitudinal Study of Ageing (ELSA), the Survey of Health, Ageing and Retirement in Europe (SHARE), and the China Health and Retirement Longitudinal Study (CHARLS). These cohorts provided a diverse and representative sample of 101,474 participants aged 60 years and older, with a total of 267,903 observations collected over the period from 2010 to 2020.To measure life satisfaction, validated psychometric scales were employed. The Satisfaction with Life Scale (SWLS), a widely - used instrument, was the primary tool for categorizing participants into low and high life satisfaction groups. Incident CVD, encompassing both fatal and non - fatal events such as myocardial infarction, stroke, and heart failure, was the main outcome of interest. Generalized estimating equations (GEE) were utilized to account for the repeated nature of the data and to analyze the relationship between life satisfaction and CVD risk.The statistical model was carefully adjusted for a comprehensive set of confounding variables. Demographic factors, including age, gender, race/ethnicity, and geographical location, were considered. Health - re-

lated behaviors, such as smoking status (current, former, never), alcohol consumption frequency, and physical activity levels, were also incorporated. Social factors, including marital status, living arrangements, and social support, were adjusted for. Additionally, depressive symptoms, measured by established scales, were included to control for the potential influence of mental health on both life satisfaction and CVD risk. A mediation analysis was conducted using a structural equation model framework with loneliness as the hypothesized mediator. Loneliness was measured by well - validated scales in each cohort. Sensitivity analyses were performed to assess the robustness of the findings. These included competing risk models to account for other causes of death and inverse - probability - weighted models to address potential reverse causation, ensuring the reliability of the results.

ResultsOver a median follow - up period of 6.2 years, the analysis revealed a significant inverse association between life satisfaction and CVD risk. Participants with higher life satisfaction had a pooled hazard ratio (HR) of 0.86 (95% confidence interval [CI]: 0.79–0.91, p < 0.001) for developing CVD compared to those with lower life satisfaction. This association remained robust even after excluding participants with baseline depression (HR = 0.84, 95% CI: 0.78–0.90), suggesting that the relationship was not confounded by pre - existing depressive symptoms. In competing risk models, which accounted for the risk of death from other causes, the negative association between life satisfaction and CVD risk persisted.Subgroup analyses were conducted to explore whether the association varied across different characteristics. The inverse relationship was consistent across various age subgroups (60 - 69 years, 70 - 79 years, 80+ years), genders, education levels (less than high school, high school graduate, college or above), and loneliness statuses. No significant effect modification was detected (all P for interaction > 0.05), indicating that the protective effect of life satisfaction on CVD risk was stable across these subgroups.When examining the results by cohort, there were some variations in effect sizes. In the SHARE cohort, the HR was 0.79 (95% CI: 0.72–0.86, p < 0.001), suggesting a relatively stronger association, while in the CHARLS cohort, the HR was 0.93 (95% CI: 0.88–0.98, p = 0.017). However, all cohorts showed a significant negative relationship, reinforcing the overall finding.

Regarding the mediating role of loneliness, the mediation analysis demonstrated that loneliness accounted for 13.4% of the association between life satisfaction and CVD risk (p = 0.003). This indicates that a portion of the beneficial effect of high life satisfaction on reducing CVD risk may be explained by its impact on alleviating loneliness.

ConclusionThis study provides robust evidence that elevated life satisfaction is independently associated with a reduced risk of CVD among older adults across diverse international cohorts. Loneliness acts as a partial mediator in this relationship, highlighting the importance of psychological well - being and social connection in cardiovascular health. The findings have significant implications for public health and clinical practice. Interventions aimed at enhancing life satisfaction, such as promoting social engagement, improving mental health support, and fostering a sense of purpose in later life, could potentially play a crucial role in the prevention and control of CVD. Additionally, addressing loneliness through community - based programs, social support networks, and family - centered initiatives may offer a complementary strategy to improve cardiovascular outcomes in the aging population. Further research is warranted to explore the long - term effectiveness of such interventions and to identify other potential mediators and moderators in this complex relationship.

冠状动脉异常起源于对侧窦的中老年患者的影像解剖特征对预后的影响

鲍伟 [1,2] 李承宗 [2] 刘学波 [1]

1. 上海市同济医院（同济大学附属同济医院）

2. 徐州医科大学附属医院

目的 冠状动脉起源于对侧窦（Anomalous Coronary Artery From the Opposite Sinus，ACAOS）是一种冠状动脉血管解剖变异，属于先天性冠状动脉异常（Congenital Coronary Artery Anomalies，CCAA）的其中一个亚型。流行病学研究显示左侧冠状动脉起源于右冠窦（L-ACAOS）和一部分右侧冠状动脉起源于左冠窦（R-ACAOS）是年轻人心脏性猝死的重要因素之一。近年来随着冠脉 CT 血管造影（CT Angiography，CTA）及血管造影术的等检查技术使用率的日益增加，越来越多的中老年 ACAOS 被诊断，然而与儿童及青少年相比，中老年患者的管理策略并不完善和明确。因此本研究旨在分析 45 岁以上的中老年 ACAOS 患者中，影响预后的影像解剖特征，为我国中老年 ACAOS 患者的风险分层和预后管理提供一定依据。

方法

回顾性收集 2011 年 1 月 1 日至 2018 年 12 月 31 日于徐州医科大学附属医院经冠状动脉 CTA 明确诊断为 ACAOS 的 45 岁以上患者，纳入 ACOAS 组。收集入组患者的基线资料和冠脉 CTA 影像资料，并随访患者的主要心血管不良事件（Major Adverse Cardiac Events，MACE）发生情况，包括心源性死亡，急性心肌梗死，任何形式的冠脉血管血运重建。根据随访期间是否发生 MACE 进行分组，比较两组间基线资料及影像解剖特征是否存在显著差异。采用生存分析，绘制 Kaplan-Meier 生存曲线，并利用 Log-rank 比较各组间差异，同时对数值型变量异常血管开口角度、高宽比、狭窄程度及长度采用 Maxstat 方法寻找 MACE 风险截断值。最后采用单因素及多因素 COX 回归模型探究影响 MACE 风险的影像解剖特征。

结果 我院 2011 - 2018 年间共行冠脉 CTA 检查 69584 人，45 岁以上的 ACAOS 患者 239 人（0.34%）。随访过程中失访 36 人，平均随访时间为 98.2±30.9 个月，发生 MACE 人数为 39 人。

1. Maxstat 方法确定相关影像解剖特征的 MACE 风险截断值：以 MACE 风险为结局，针对数值型影像解剖特征：异常血管开口角度、异常血管开口 H ／ W、异常血管狭窄程度及长度求取 MACE 风险截断值，分别为 34.3°，1.69，0.55 及 1.88cm，并依此进行分层。

2. Kaplan-Meier 生存曲线及 Log-rank 检验结果: L-ACAOS 分型（P = 0.016），异常血管走行于主动脉肺动脉之间（P = 0.003）的患者 MACE 风险明显高于其对应组。并且，经过 Maxstat 分层后的 High H ／ W 组，开口角度< 34.3°组，High narrow 组和 Long length 组的 MACE 风险均显著高于其各自对应组（P 均< 0.05）。

3. COX 回归模型探究高危影像解剖特征：以中老年 ACAOS 患者随访期间是否发生 MACE 为因变量，基线资料及影像解剖特征作为自变量进行 COX 回归分析。结果显示异常起源血管的影像解剖特征中，L-ACAOS 分型（HR = 4.35，95%CI: 2.17 ~ 8.73，P < 0.05）、伴有主 - 肺动脉间走行（With IAC）（HR = 3.21，95%CI: 1.23 ~ 8.37，P < 0.05），开口角度< 34.3°（HR = 2.62，95%CI: 1.18 ~ 5.77，P < 0.05）是发生 MACE 的独立危险因素。

结论 在 45 岁以上中老年 ACAOS 患者中，异常起源血管具有 L-ACAOS 分型、主 - 肺动脉间走行（With IAC）、开口角度< 34.3°影像解剖特征是发生 MACE 的独立危险因素。

CD8+T 细胞介导的衰老脂肪棕色化下降影响老年心肌重构的机制研究

孔令冉 曲新凯

复旦大学附属华东医院

目的：衰老脂肪组织功能障碍，尤其是免疫调控紊乱是多种老年心血管疾病发生的重要危险因素。近年研究表明 T 细胞在脂肪细胞衰老过程中扮演了重要角色，但相关分子机制一直不明。本研究拟在前期研究发现老年小鼠脂肪组织中 CD8+T 细胞增多及心脏收缩功能下降的前提下，进一步探究脂肪衰老导致的棕色化改变对心肌重构的机制研究。

方法: 野生型小鼠构建衰老模型（18 月龄），检测衰老小鼠脂质代谢、胰岛素抵抗、能量代谢、不同部位脂肪组织棕色化改变等；同时检测老年小鼠心肌重构（小动物心脏超声、心肌细胞纤维化程度等）。单细胞测序技术分析老年小鼠脂肪组织中不同类型免疫细胞（CD8+T 细胞、巨噬细胞、脂肪细胞等）比例改变，并寻找差异性基因表达。CD8+T 细胞过继转移实验，将衰老小鼠脂肪组织内 CD8+T 细胞转移至受体（年轻及老年小鼠），观察对小鼠脂肪组织棕色化及心肌重构的影响。

结果：老年小鼠皮下白色脂肪组织衰老标志物（p16、p21 及 p53）表达明显升高，同时伴随白色脂肪棕色化水平下降，表现为脂肪细胞体积增大、脂滴减少及棕色化相关基因（UCP1、PPARγ、PPGC1α）表达下降；同时老年小鼠心脏重构加重（心肌细胞纤维化加重、LVEF 及 FS 下降等）。单细胞测序分析进一步提示老年小鼠皮下白色脂肪组织（WAT）内不同亚型 T 细胞聚集浸润，增多最明显的是 CD8+T 细胞；差异基因分析显示与年轻小鼠相比，老年小鼠 WAT 中 CD8+T 细胞来源的趋化因子 CCL5 明显升高，因此我们认为在老年小鼠体内，衰老引起白色脂肪组织中 CD8+T 细胞增多， CD8+T 细胞分泌 CCL5 增多，导致衰老脂肪细胞棕色化下降，加重衰老导致的脂肪组织功能障碍，最终影响老年小鼠心肌重构。

结论：本研究旨在通过阐明 CD8+T 细胞介导的免疫紊乱调控脂肪细胞衰老并进一步影响心肌重构的机制，为改善衰老导致的代谢性心脏疾病发生发展提供新的靶点和策略。

Discordance among lipid profile in the older adults: implications for cardiovascular prevention

Sheng-Yan Du[1,2], Xiao-Xin Ye[1,2], Yao He[2], Miao Liu[1], Sheng-Shu Wang[2], Shan-Shan Yang[1]

1. Medical School of Chinese People’s Liberation Army

2. Second Medical Center, Chinese People’s Liberation Army General Hospital

Background

Cardiovascular disease (CVD) remains a leading cause of morbidity and mortality worldwide, with dyslipidemia being a well-established modifiable risk factor. Traditional lipid profile indicators, including low-density lipoprotein cholesterol (LDL-C), high-density lipoprotein cholesterol (HDL-C), triglycerides (TG), and total cholesterol (TC), have been extensively studied in middle-aged populations, demonstrating strong associations with CVD risk. However, emerging evidence suggests that these relationships may weaken, reverse, or exhibit significant heterogeneity in older adults, a phenomenon often referred to as the “lipid paradox.” This paradox raises critical questions about the optimal lipid management strategies for aging populations, particularly regarding which lipid metrics retain predictive value for CVD risk in older individuals. Given the global aging demographic and the increasing burden of CVD in older adults, a comprehensive evaluation of lipid profile indicators in this population is urgently needed to inform clinical practice and public health strategies.

Methods

This prospective cohort study utilized data from 132,290 participants aged 60 years or older in the UK Biobank, a large-scale biomedical database with extensive phenotypic and genotypic information. Participants with baseline CVD were excluded to ensure a clean cohort for incident CVD analysis. Lipid profile indicators, including LDL-C, HDL-C, TG, TC, non-HDL-C, and the LDL-C/HDL-C ratio, were measured at baseline. The primary outcomes were incident CVD (including ischemic heart disease, stroke) and cardiovascular mortality, ascertained through linked electronic health records and death registries. Fine-Gray competing risk models were employed to account for the competing risk of non-CVD death, with adjustments for demographics (age, sex, Body mass index), comorbidities (hypertension, diabetes), and lifestyle factors (smoking, alcohol consumption, physical activity). Predictive capacities of lipid indicators were compared using receiver operating characteristic (ROC) curve analysis, with area under the curve (AUC) values calculated. Subgroup analyses were conducted to assess the consistency of associations across strata defined by age, sex, and metabolic status. Gene-environment interaction analyses were performed to explore potential effect modifications by genetic predisposition to dyslipidemia.

Findings

Over a median follow-up of 14.03 years, 23,192 incident CVD events and 1,015 cardiovascular deaths were recorded. Multivariable analysis revealed that the LDL-C/HDL-C ratio exhibited the strongest association with CVD risk. Participants in the highest quartile (Q4) of the LDL-C/HDL-C ratio had a 27% increased risk of incident CVD (hazard ratio [HR] 1.27, 95% confidence interval [CI] 1.22–1.32), a 54% higher risk of ischemic heart disease (HR 1.54, 95% CI 1.47–1.62), and a 42% higher risk of cardiovascular mortality (HR 1.42, 95% CI 1.21–1.67) compared to those in the lowest quartile (Q1). In contrast, HDL-C demonstrated protective effects, with Q4 associated with a 22% reduction in CVD risk (HR 0.78, 95% CI 0.75–0.82). Other lipid indicators, including LDL-C, TG, and TC, showed weaker or inconsistent associations with CVD outcomes. Stratified analyses confirmed the robustness of these findings across all subgroups, with higher LDL-C/HDL-C ratios consistently associated with increased CVD risk regardless of age, sex, or metabolic status. Combined analyses further revealed that individuals with either a high LDL-C/HDL-C ratio alone (≥ 2.52 mmol/L) or both high LDL-C (≥ 3.40 mmol/L) and a high ratio had the greatest elevation in CVD risk. ROC curve analysis demonstrated the superior predictive value of the LDL-C/HDL-C ratio for CVD (AUC = 0.6576), outperforming individual lipid parameters such as LDL-C (AUC = 0.5892) and HDL-C (AUC = 0.6014).

Interpretation

This large-scale prospective cohort study highlights the LDL-C/HDL-C ratio as the most robust lipid profile indicator for predicting CVD risk in older adults. The findings suggest that lipid management strategies in aging populations should prioritize balancing LDL-C and HDL-C levels rather than focusing solely on LDL-C reduction. The superior predictive performance of the LDL-C/HDL-C ratio may reflect its ability to capture the combined atherogenic potential of elevated LDL-C and the protective effects of HDL-C, providing a more holistic assessment of lipid-related CVD risk. These results have important implications for clinical practice, suggesting that routine assessment of the LDL-C/HDL-C ratio could enhance risk stratification and guide personalized lipid-lowering therapy in older adults. Future research should explore the mechanisms underlying the lipid paradox in aging populations and evaluate the impact of interventions targeting the LDL-C/HDL-C ratio on CVD outcomes in older individuals.

Keywords: lipid profile, cardiovascular disease, older adults, LDL-C/HDL-C ratio, competing risk analysis

脂蛋白 (a) 与老年冠心病多支病变相关性的研究

张亮 史凯雷 关韶峰 曲新凯

复旦大学附属华东医院

目的：本研究旨在系统探讨脂蛋白 (a)[Lp(a)] 与老年冠心病患者多支冠状动脉病变的相关性及其临床意义。方法：纳入 2019 年 1 月至 2024 年 6 月期间在本院心血管内科住院治疗年龄大于 60 岁的老年冠心病患者 586 例。根据冠脉造影病变血管数量分为单支病变组 (n=254)、双支病变组 (n=187) 和三支病变组 (n=145)。采用免疫比浊法测定血清 Lp(a) 水平，同时收集患者的人口学特征、临床病史、实验室检查结果和冠状动脉造影资料。结果：随着冠状动脉病变支数增加，患者血清 Lp(a) 水平呈显著升高趋势。单支病变组、双支病变组和三支病变组的 Lp(a) 水平分别为 (25.3±10.2)mg/dL、(36.8±13.5)mg/dL 和 (48.7±15.6)mg/dL，组间差异具有统计学意义 (P<0.001)。Spearman 相关分析显示，Lp(a) 水平与冠状动脉病变支数呈显著正相关 (r=0.412，P<0.001)。多因素 logistic 回归分析在调整年龄、性别、高血压、糖尿病、吸烟史、血脂异常等传统危险因素后，Lp(a) 水平升高 (>30mg/dL) 仍然是老年冠心病多支病变的独立危险因素 (OR=2.37，95%CI：1.78-3.15，P<0.001)。其中 Lp(a) 水平对三支病变的预测价值更高 (OR=3.12，95%CI：2.24-4.35)。Lp(a) 水平与冠状动脉病变严重程度评分 (SYNTAX 评分) 呈显著正相关 (r=0.387，P<0.001)。在预测多支病变的 ROC 曲线分析中，Lp(a) 的曲线下面积 (AUC) 为 0.742(95%CI：0.703-0.781)，最佳临界值为 32.5mg/dL，敏感性和特异性分别为 68.5% 和 72.3%。当 Lp(a) 与传统危险因素联合时，预测效能显著提高 (AUC=0.832，95%CI：0.798-0.866)。结论：老年冠心病患者中，Lp(a) 水平与冠状动脉病变范围和严重程度密切相关，且这种相关性独立于传统心血管危险因素，可以将其作为评估老年冠心病患者病情严重程度的重要生物标志物，并为临床早期识别高危患者提供了客观依据。

Identification and validation of IRS2 as a novel aging-related biomarker and potential therapeutic target in calcific aortic valve disease

Dan LIU, Yi Fang, Dan Liu, Ya-Ling Han

State Key Laboratory of Frigid Zone Cardiovascular Disease, Cardiovascular Research Institute and Department of Cardiology, General Hospital of Northern Theater Command

Background: Calcific aortic valve disease (CAVD) is a chronic disease characterized by the thickening and calcification of aortic valve leaflets. CAVD is one of the most common heart valve disorders and the most common condition requiring cardiac valve surgical intervention. CAVD is increasingly regarded as a critical public health problem due to the substantial morbidity and mortality it confers. Despite the prevalence of CAVD, there currently lack of effective pharmacological approaches to prevent or merely retard the progress of the disease. To develop potential pharmaceutical intervention, it's urgent to identify the key molecules involved in the initiation and progression of CAVD.

Methods: In this study, the gene expression profile data (GSE153555, GSE199718, GSE 76717 and GSE148219) were downloaded from the Gene Expression Omnibus (GEO) database. Following data retrieval, the GSE153555 and GSE199718 datasets were integrated to harmonize batch effects, yielding a merged discovery cohort of 42 samples (22 non-calcified aortic valves and 20 CAVD cases) for downstream analyses. GSE76717 and GSE148219 datasets were used as validation datasets. Aging-related genes were collected from manually curated and publicly available resources with the keyword "senescence" . Based on the above datasets, integrated bioinformatic analysis such as weighted gene co-expression network analysis (WGCNA) and differentially expressed genes were used to screen differentially co-expressed aging-related genes (DEAGs). Among the 11 screened DEAGs, one key hub gene was locked by three machine learning algorithms. The expression signature of the hub gene was validated at the tissue and cellular level using both public data and experimentation.

Results: A total of 491 differentially expressed genes were obtained from the combined datasets, and WGCNA identified 12 co-expression modules, of which one hub module (blue module) was most correlated with CAVD. By intersecting the DEGs, hub module genes and aging-related genes, we obtained 11 DEAGs. Using the STRING database, a close protein-protein interaction between these DEAGs was detected. To prioritize hub genes, three machine learning methods such as Least Absolute Shrinkage and Selection Operator (LASSO), Support Vector Machines-Recursive Feature Elimination (SVM-RFE) and random forest (RF) were systematically applied, and the IRS2 was locked by three machine learning algorithms. The expression level of IRS2 was consistently down-regulated in CAVD samples among four GEO datasets, and the single-cell sequencing analysis showed that IRS2 was significantly downregulated in the valve interstitial cells from animal models of CAVD. The results of public data analyses were further verified by experimental data, the IRS2 expression was significantly downregulated in the calcified aortic valve samples detected by immunochemistry at tissue level, and significantly downregulated in valve interstitial cells induced by osteogenic medium detected by western blotting.

Conclusions: In conclusion, we identified IRS2 as an important aging-related gene in CAVD by integrated bioinformatic analysis, and validated the results with both public and experimental data at tissue and cellular levels. IRS2 has not been reported to be associated with CAVD, and might serve as a novel marker and therapeutic target for CAVD. The mechanistic contributions of insulin receptor substrate 2 (IRS2) to CAVD pathogenesis remain uncharacterized at the molecular level, and we intend to address this in the future.

共病负担对老年射血分数保留型心力衰竭患者预后的影响分析

史凯蕾 车惠霖 张曙鑫 曲新凯

复旦大学附属华东医院

目的：射血分数保留型心力衰竭（HFpEF）在老年人群中发病率逐年上升，且临床表现高度异质。共病（comorbidities）在老年 HFpEF 患者中极为常见，对疾病进展和临床预后具有重要影响。然而，目前尚缺乏系统性研究评估多种共病对老年 HFpEF 预后的综合作用。本研究旨在分析常见共病（包括糖尿病、高血压、慢性肾病、肺部疾病和肿瘤）在老年 HFpEF 患者中的分布特征，并探讨其与全因死亡率之间的关系。

方法：本研究为双向性队列研究，纳入 2019 年 7 月至 2024 年 6 月期间在复旦大学附属华东医院新诊断为 HFpEF、年龄≥ 60 岁的老年患者。随访截止至 2024 年 12 月，中位随访时间为 19 个月，主要结局为全因死亡。

结果：共纳入 603 例资料完整的老年 HFpEF 患者，平均年龄为 79.10±9.19 岁，男性 311 例（51.6%），女性 292 例（48.4%）。在中位 19 个月的随访期间，

共有 154 例（25.5%）发生全因死亡。共病在该人群中普遍存在，高血压为最常见共病（占比约 70%），其次为冠心病和房颤（均约 45%），再次为糖尿病和慢性肾病 4-5 期（均约 35%）。根据共病数量进一步分组分析显示，合并≥ 3 种共病的患者其全因死亡率显著高于共病数量较少者（P<0.01），提示共病负担越重，预后越差。多因素 Cox 回归分析表明，肿瘤和慢性肾病（4-5 期）是老年 HFpEF 患者全因死亡的独立危险因素。

结论：共病负担是影响老年 HFpEF 患者预后的关键因素。系统评估并个体化管理共病，有助于改善其临床结局和生活质量。未来研究应进一步探索基于多系统共病特征的综合干预策略，以优化 HFpEF 的整体治疗路径。

板栗酒化学成分棕榈酸甲酯对小鼠心肌细胞和心肌成纤维衰老的调节作用

吕林

哈尔滨医科大学附属第一医院

目的：年龄是影响心血管疾病的主要因素之一，心血管衰老时常伴随表观遗传学改变、线粒体功能障碍和细胞衰老等。在老年机体中，全身血管会发生病理性重塑，从而增加冠心病和动脉粥样硬化等老年易发心血管疾病的患病风险。随着衰老进展，心脏可出现左心室肥厚、心房颤动和心力衰竭相关改变。为了探寻新的延缓衰老的方法，我们使用、小鼠原代心肌细胞和心肌成纤维细胞，分别设置对照组、H_2O_2 组及 H_2O_2+ 棕榈酸甲酯（Methyl palmitate，MP）组，通过对衰老表型、活性氧 ROS、细胞周期及炎症因子的检测探究棕榈酸甲酯对小鼠心肌细胞和心肌成纤维衰老的调节作用。

材料与方法：应用 SA-β-gal 半乳糖苷酶染色检测细胞衰老情况；应用胶原含量检测试剂盒检测胶原含量；应用流式细胞术检测细胞周期和细胞内 ROS 检测；应用试剂盒进行端粒长度测定；应用 EdU 免疫荧光检测细胞增殖情况；应用免疫荧光实验检测 Ki67、Brdu；利用透射电镜检测细胞形态变化；应用 qRT-PCR 技术检测细胞周期相关因子 P16、P21、P53、衰老相关分泌表型 IL-6、IL-8、及核纤层蛋白 Lamin B1、凋亡相关因子 Caspase、Bax、BCL2 mRNA 表达；应用 Western Blot 技术检测 P16、P21、P53、IL-6、IL-8、Lamin B1、Caspase、Bax 及 BCL2 蛋白表达量。体外实验检测燕栗香酒化学成分棕榈酸甲酯对 H_2O_2 所致鼠原代心肌细胞和心肌成纤维细胞衰老的调节作用。

结果与结论：板栗酒化学成分棕榈酸甲酯可缓解 H_2O_2 所致鼠原代心肌细胞 ROS 水平升高、端粒延长及心肌成纤维细胞增殖及胶原含量增加；以及逆转两种细胞中细胞周期相关因子 P16、P21、P53、衰老相关分泌表型 IL-6、IL-8、及核纤层蛋白 Lamin B1、凋亡相关因子 Caspase 等 mRNA 及蛋白表达增加，逆转 H_2O_2 所致凋亡水平上升。有效延缓心肌细胞和心肌成纤维细胞的衰老。

Phloretin combined with LIPUS can alleviate the inflammatory response of vascular endothelial cells in diabetic mice by activating SIRT-related pathways

Chun-Wei He, Chang Chen, Yu-Xin Wang, Tong-Xue Zhang, Shi-Hao Sun, Lin Shen

Qilu hospital of Shandong University

Abstract

Diabetes mellitus (DM) represents one of the most prevalent and debilitating chronic metabolic diseases worldwide, posing a formidable challenge to global healthcare systems. Its widespread prevalence and systemic complications significantly strain medical resources, necessitating urgent development of novel therapeutic strategies. A particularly critical concern in diabetic patients is the markedly elevated risk of cardiovascular disease (CVD), which continues to serve as the primary cause of morbidity and mortality within this population. The pathogenesis of diabetes-induced CVD is notably intricate, involving a cascade of pathological events initiated by vascular endothelial dysfunction. This dysfunction disrupts the delicate balance of vascular homeostasis, setting off a chain reaction characterized by chronic inflammation, oxidative stress, and impaired vascular repair mechanisms. Over time, these abnormalities contribute to the development of atherosclerosis, hypertension, and other severe CVD complications, ultimately compromising patient prognosis and quality of life.

Phloretin, a natural dihydrochalcone compound abundantly present in apples and various other fruits, has emerged as a promising therapeutic candidate due to its diverse biological activities. This compound has demonstrated significant potential in regulating metabolic homeostasis through multiple mechanisms, including the enhancement of insulin sensitivity and promotion of glucose uptake. Furthermore, phloretin exhibits potent anti-inflammatory and antioxidant properties, making it particularly attractive for addressing the complex pathophysiology of diabetes. Recent investigations have revealed that phloretin can effectively alleviate diabetes-induced endothelial injury by activating the AMP-activated protein kinase (AMPK)-dependent anti-endothelial-to-mesenchymal transition (anti-EndMT) pathway. This protective effect helps preserve vascular endothelial integrity and function. However, despite these encouraging findings, the broader therapeutic potential of phloretin in mitigating the full spectrum of diabetes-induced CVD complications remains incompletely understood, highlighting the need for further comprehensive research.

In parallel, low-intensity pulsed ultrasound (LIPUS) has garnered increasing attention as a non-invasive and clinically translatable therapeutic modality. This technology has demonstrated notable anti-inflammatory and tissue-repairing properties across various medical contexts. While its benefits in musculoskeletal disorders and wound healing have been well-documented, its effects on the macrovasculature, particularly within the diabetic milieu, remain largely unexplored. Given the pressing need for innovative strategies to combat diabetes-associated vascular dysfunction, the investigation of potential synergistic effects between phloretin and LIPUS presents a compelling and timely research direction.

In this study, we provide compelling evidence demonstrating that the combined application of LIPUS and phloretin exerts a more robust protective effect on vascular endothelial cells compared to either intervention alone. The observed synergistic effect is mediated through the upregulation of longevity-associated genes SIRT3 and SIRT6, which play crucial roles in enhancing mitochondrial function and reducing oxidative stress. This molecular interplay not only improves cellular energy metabolism but also simultaneously suppresses the production of pro-inflammatory cytokines, including interleukin-6 (IL-6), tumor necrosis factor-alpha (TNF-α), and interferon-gamma (IFN-γ). These findings were validated in an in vivo diabetic model, where the combined treatment regimen significantly improved vascular endothelial function and attenuated the progression of CVD.

Our study offers robust evidence supporting the notion that LIPUS-phloretin combination therapy provides superior protection against diabetes-induced vascular damage when compared to monotherapy approaches. By simultaneously targeting multiple pathological pathways—namely, endothelial dysfunction, inflammation, and metabolic dysregulation—this dual approach holds significant promise for improving the prognosis of diabetic patients with CVD. Furthermore, these findings establish a solid scientific foundation for the development of novel therapeutic strategies not only for macrovascular complications but also for a broad spectrum of other inflammation-driven diseases, potentially revolutionizing the management of vascular pathologies in various clinical contexts.

纤维蛋白原 / 白蛋白比值与接受经皮冠状动脉介入治疗的高龄冠心病患者长期预后的关系

程雅琳 张闻多 季福绥

北京医院 心血管内科；国家老年医学中心；中国医学科学院老年医学研究院

目的：纤维蛋白原与白蛋白比值（FAR）作为一种新型炎症标志物，已在心血管疾病预后评估中展现出价值。然而，其在接受经皮冠状动脉介入治疗（PCI）的高龄冠心病患者（≥ 80 岁）风险分层中的作用尚未明确。因此，本研究拟探究接受 PCI 治疗的高龄冠心病患者的基线 FAR 水平与其长期临床预后的关系。

方法：本单中心回顾性队列研究连续纳入 2015 至 2021 年间在我院接受 PCI 治疗的 80 岁及以上的冠心病患者共 641 例。根据 FAR 中位值（0.079）分为高 FAR 组与低 FAR 组。研究终点为心血管死亡和全因死亡。采用多变量 Cox 模型和限制性立方样条分析 FAR 与终点的关联。

结果：中位随访 61 个月期间，共记录 237 例死亡（37%），其中 124 例（19.3%）为心血管死亡。1 年死亡率为 9.3%，5 年死亡率为 27.4%。Kaplan-Meier 分析显示高 FAR 水平与心血管死亡和全因死亡风险增加显著相关（Log-rank p<0.001）。限制性立方样条提示 FAR 与死亡率呈 J 型关联。高 FAR（>0.079）可独立预测心血管死亡（校正 HR=1.49，95% CI：1.01-2.19，p=0.045）。作为连续变量分析时，完全校正模型中较高 FAR 水平与心血管死亡（HR=1.23，95% CI：1.04-1.47，p=0.018）及全因死亡（HR=1.12，95% CI：0.98-1.27，p=0.090）风险升高相关。亚组分析显示在三支血管病变患者中，高 FAR 与心血管死亡的关联显著增强（交互作用 p=0.039）。Fine and Gray 竞争风险模型进一步验证 FAR 与心血管死亡的稳健关联（HR=1.31，95% CI：1.13-1.52，p=0.003）。

结论：在接受 PCI 的高龄冠心病患者中，较高 FAR 水平与心血管死亡和全因死亡风险增加相关。本研究结果支持 FAR 在老年心脏病学风险分层中的应用潜力。

新疆部分地区老年持续性心房颤动患者 EQ-5D-5L 评分及其影响因素分析

许严锴 [1] 石世林 [2] 吕福强 [1] 董润甜 [1] 刘克坚 [1]

1. 石河子大学第一附属医院

2. 石河子市人民医院

目的

心房颤动（简称房颤，atrial fibrillation，AF）是 21 世纪心血管疾病领域的重要挑战，其发病率持续上升，尤其是老年人群，易导致严重并发症，显著降低生活质量。针对新疆地区≥ 65 岁持续性非瓣膜性房颤患者生活质量的系统性研究仍较缺乏。本研究旨在评估新疆老年持续性非瓣膜性房颤患者的 EQ-5D-5L 评分及其影响因素，为提高老年房颤患者的生活质量和管理提供依据。

方法

采用横断面研究设计，纳入 2023 年 10 月至 2024 年 11 月新疆焉耆、图木舒克、喀什、石河子四家医院的 123 例老年持续性非瓣膜性心房颤动患者，通过问卷调查收集人口学、行为习惯及疾病信息，采用中文版 EQ-5D-5L 量表评估生活质量。数据用 SPSS 25.0 进行统计分析，采用 Logistic 回归模型探索影响因素，分析人口学特征、行为习惯及疾病特征对生活质量的影响。

结果

123 名老年持续性非瓣膜性心房颤动患者整体生活质量评分中位数为 0.654，

88.6% 存在日常活动受限，82.9% 行动能力下降。（1）年龄是核心危险因素，高龄导致行动能力、自我照顾及日常活动受限明显 (OR=6.30, 95%CI=2.49-15.94)。

（2）少数民族患者在自我照顾和日常活动维度有一定优势 (OR=0.25, 95%CI=0.08-0.81)。

（3）运动较多在自我照顾和焦虑 / 抑郁层面具有保护作用 (OR=0.17, 95%CI=0.06-0.45)。

结论

老年持续性房颤患者生活质量受多因素影响，高龄及缺乏运动是主要危险因素。临床需对老年房颤患者强化康复训练与心理干预，鼓励规律运动以改善心肺功能及社会参与。研究局限性包括样本地域局限及横断面设计，未来需扩大样本并探索传统医学在综合管理中的作用。本研究为制定个性化干预策略提供了实证依据，强调多维度管理对提升患者预后的重要性。

Ethnicity and Exercise Modulate Quality of Life in Elderly Patients with Persistent Atrial Fibrillation: A Cross-Sectional Study in Multi-Ethnic Xinjiang

Yankai Xu[1], Run-Tian Dong[1], Shi-Lin Shi[2], Fu-Qiang Lv[1], Ke-Jian Liu[1]

1. The First Affiliated Hospital of Shihezi University

2. Shihezi People's Hospital

Objective

Atrial fibrillation (AF) is a major challenge in the field of cardiovascular diseases in the 21st century, with its incidence rate continuously rising, particularly among the elderly population, predisposing them to severe complications and significantly reducing quality of life. Systematic research on the quality of life among persistent non-valvular atrial fibrillation patients aged ≥ 65 years in Xinjiang remains relatively scarce. This study aims to evaluate the EQ-5D-5L scores and their influencing factors among elderly patients with persistent non-valvular atrial fibrillation in Xinjiang, providing a basis for improving the quality of life and management of elderly AF patients.

Methods

A cross-sectional study design was adopted, enrolling 123 elderly patients with persistent non-valvular atrial fibrillation from four hospitals in Yanqi, Tumushuke, Kashgar, and Shihezi, Xinjiang between October 2023 and November 2024. Demographic data, behavioral habits, and disease information were collected through questionnaires, and quality of life was assessed using the Chinese version of the EQ-5D-5L scale. Data were statistically analyzed using SPSS 25.0, with logistic regression models employed to explore influencing factors and analyze the impact of demographic characteristics, behavioral habits, and disease features on quality of life.

Results

The median overall quality of life score among 123 elderly patients with persistent non-valvular atrial fibrillation was 0.654, with 88.6% experiencing limitations in daily activities and 82.9% showing reduced mobility.

(1) Age is a core risk factor, with advanced age significantly contributing to limitations in mobility, self-care, and daily activities. In terms of mobility, self-care, usual activities, and pain/discomfort dimensions, the risk for the ≥ 75-year-old group was over 6 times higher than that of the younger group, a conclusion further validated by multivariate analysis results(OR=6.30, 95%CI=2.49-15.94).

(2) Ethnic minority patients exhibited certain advantages in the dimensions of self-care and daily activities.In the dimensions of self-care, daily activities, pain/discomfort, and anxiety/depression, univariate analysis showed certain advantages among ethnic minorities, but these effects gradually diminished in multivariate analysis (OR=0.25, 95%CI=0.08-0.81).

(3) Higher levels of physical activity demonstrated protective effects in terms of self-care and anxiety/depression (OR=0.17, 95%CI=0.06-0.45). In terms of mobility and anxiety/depression dimensions, univariate analysis indicated significantly reduced limitations in elderly atrial fibrillation patients with regular exercise, while the protective effect of higher exercise levels diminished in multivariate analysis. For the self-care dimension, both univariate and multivariate analyses demonstrated that regular exercise remained statistically significant.

(4)Other demographic characteristics (such as gender, marital status, living situation) and clinical features (such as medication adherence, smoking and drinking history, BMI, number of chronic diseases) did not show statistically significant effects on EQ-5D-5L scores.

Conclusions

(1)The quality of life in elderly patients with persistent atrial fibrillation is influenced by multiple factors, with advanced age ethnicity, and physical activity being the primary risk factors.

(2)Clinically, it is necessary to strengthen rehabilitation training and psychological interventions for elderly atrial fibrillation patients, encouraging regular exercise to improve cardiopulmonary function and social participation.

(3)This study provides empirical evidence for developing personalized intervention strategies, emphasizing the importance of multidimensional management in improving patient prognosis.

(4)The study limitations include regional constraints of the samples and cross-sectional design. Future research should expand the sample size and explore the role of traditional medicine in comprehensive management.

Oral Anticoagulant Use and In-Hospital Outcomes in Patients Aged 90 years and older with Atrial Fibrillation or Atrial Flutter

Zinan Zhao, Junpeng Liu

Beijing Hospital

Objectives: Oral anticoagulants (OACs) are pivotal for preventing thromboembolic events in patients with atrial fibrillation (AF) or atrial flutter, yet data on their utilization patterns, associated factors, and clinical outcomes in the ultra-elderly population (aged 90 years and older) remain scarce. This cross-sectional study aimed to comprehensively investigate the characteristics of OAC use, factors influencing OAC administration, and in-hospital outcomes in this vulnerable group, with a specific focus on comparing outcomes between different OAC types and dose regimens.

Methods: A total of 290 patients aged 90 years and older with AF or atrial flutter were enrolled, comprising 201 in the non-OAC group, 16 in the warfarin subgroup, and 73 in the direct oral anticoagulant (DOAC) subgroup (total OAC group: 89 patients). Detailed data were collected, including demographic and clinical characteristics (e.g., age, sex, comorbidities such as hypertension, diabetes mellitus, heart failure, and previous cardiovascular procedures), anticoagulation indications, risk stratification scores (CHA_2DS_2-VASc for thromboembolic risk and HAS-BLED for bleeding risk), laboratory variables (hemoglobin, platelets, prothrombin time [PT], activated partial thromboplastin time [APTT], international normalized ratio [INR], and renal function indicators like estimated glomerular filtration rate [eGFR]), medication use (including antiplatelets, proton pump inhibitors [PPIs], β-blockers, and renin-angiotensin system inhibitors), and in-hospital adverse events (thromboembolism, including stroke and pulmonary embolism [PE]; bleeding, including gastrointestinal bleeding [GIB] and intracerebral hemorrhage [ICH]; and all-cause mortality). Comparative analyses were performed between the non-OAC and OAC groups, as well as between DOAC users receiving recommended regular doses (n=27) and those on non-recommended reduced doses (n=46).

Results: Compared with the non-OAC group, the OAC group had a higher proportion of females (39.33% vs. 23.38%, p=0.005) and a lower HAS-BLED score (IQR: 3.00 vs. 3.00, p < 0.001). The OAC group showed a higher rate of heart failure (42.70% vs. 15.42%, p < 0.001) and previous percutaneous coronary intervention (25.84% vs. 12.94%, p=0.007), while having fewer patients with a history of bleeding (10.11% vs. 46.27%, p < 0.001) and previous venous thromboembolism (6.74% vs. 38.31%, p < 0.001). A higher proportion of the OAC group was admitted to the Department of Cardiology (88.76% vs. 45.27%, p < 0.001). In terms of medications, the OAC group had lower use of antiplatelets (22.47% vs. 59.20%, p < 0.001) and proton pump inhibitors (39.33% vs. 73.63%, p < 0.001), but higher use of ACEI/ARB (38.20% vs. 16.42%, p < 0.001) and β-blockers (57.30% vs. 32.34%, p < 0.001). In terms of in-hospital outcomes, the OAC group had a significantly lower incidence of stroke (3.37% vs. 24.88%, p < 0.001) but a higher rate of in-hospital bleeding events (68.54% vs. 53.73%, p=0.018). Among OAC subgroups, dabigatran was associated with the highest bleeding rate (100.00%), followed by edoxaban (72.97%), warfarin (62.50%), and rivaroxaban (58.62%). There was no significant difference in in-hospital intracerebral hemorrhage (ICH) between the two groups (4.49% vs. 1.99%, p=0.255). The incidence of in-hospital deep vein thrombosis (DVT) was comparable (11.24% vs. 15.42%, p=0.345), and there was a non-significant trend toward lower in-hospital mortality in the OAC group (3.37% vs. 9.95%, p=0.056). Among DOAC users, non-recommended reduced doses (63.01%) were more common than recommended regular doses (36.99%). Rivaroxaban was predominantly used in reduced doses (56.52% of reduced-dose users vs. 11.11% of regular-dose users, p < 0.001), while edoxaban was more frequently administered at regular doses (81.48% of regular-dose users vs. 32.61% of reduced-dose users, p < 0.001). Reduced-dose DOAC use was significantly associated with a history of bleeding (17.39% vs. 0%, p=0.023) and concurrent antiplatelet therapy (34.78% vs. 3.70%, p=0.002). No significant differences in in-hospital events were observed between DOAC dose groups. The incidence of in-hospital bleeding events was similar (69.57% vs. 70.37%, p=0.942), with dabigatran showing 100% bleeding rates in both dose subgroups. In-hospital ICH (6.52% vs. 3.70%, p=1.000) and mortality (0 vs. 3.70%, p=0.370) were comparable. For thromboembolic outcomes, cardioembolic stroke (2.17% vs. 7.41%, p=0.551) and DVT (19.57% vs. 3.70%, p=0.080) did not differ significantly between reduced and regular

dose groups.

Conclusions: In patients aged 90 years and older with AF or atrial flutter, OAC use is associated with distinct clinical and demographic characteristics, including a higher proportion of females, lower bleeding risk scores, more frequent heart failure and previous PCI, and fewer comorbidities like diabetes. While OACs significantly reduce the risk of stroke, they are associated with an increased risk of bleeding events, highlighting the need for careful risk-benefit assessment in this population. Non-recommended reduced doses of DOACs are common, driven by factors such as a history of bleeding and antiplatelet use, yet they yield comparable in-hospital outcomes to regular doses, suggesting that individualized dose adjustment may be a viable strategy in clinical practice for ultra-elderly patients. These findings contribute to filling the knowledge gap regarding OAC use in the oldest-old, providing valuable insights for clinical decision-making.

肠道梭状芽孢杆菌代谢产物吲哚 -3- 丙酸缓解老年心脏纤维化

陆静

哈尔滨医科大学附属第一医院

目的：

以心肌纤维化为主要表现的病理性心肌重构，是导致老年人心力衰竭致死的主要原因之一。其机制复杂，涉及细胞间通讯改变及慢性炎症等。在心衰大鼠的肠道中吲哚 -3- 丙酸（Indolyl-3-propionic acid，IPA）的含量降低加剧了心脏舒张功能障碍，补充 IPA 可缓解这一现象。尽管 IPA 对机体有显著的保护作用，但 IPA 对老年心衰的治疗作用及调控机制尚未完全清楚。因此，本研究的目的是，验证 IPA 在衰老心脏中对心肌纤维化调控作用及作用机制，为增龄性心肌纤维化提供新的干预靶点。

方法：

分别取 4-6 月龄的成年雄性 SD 大鼠及 18-20 月龄的老年雄性 SD 大鼠的粪便进行 16S rDNA 检测。应用靶向色氨酸代谢组学技术检测青年大鼠、老年大鼠粪便中差异代谢物。雄性 SD 老年大鼠给予 IPA 管饲法喂养 8 周后，采用心脏超声、H&E 染色、Masson 染色、免疫组化、免疫荧光、qRT-PCR 和 Western Blot 等技术验证 IPA 对老年大鼠心脏的保护作用，检测 IPA 减轻老年心肌纤维化的作用。

结果：

（1）老年大鼠肠道微生物群紊乱，梭状芽胞杆菌属有显著差异，其色氨酸途径代谢产物 IPA 的含量在老年心衰大鼠中显著降低；

（2）老年大鼠补充 IPA 能够显著改善衰老引起的心功能减退、胶原沉积，抑制心肌纤维化标志物 COL3A1、COL1A1 及 α-SMA 的表达水平；

结论：

老年时，大鼠肠道菌群代谢紊乱，梭状芽孢杆菌代谢色氨酸的产物 IPA 含量随老年大鼠心脏功能减退而降低，补充 IPA 能够逆转增龄性心肌纤维化。

关键词：增龄性心肌纤维化；肠道菌群；IPA

吲哚 -3- 丙酸通过调控巨噬细胞自噬功能缓解老年心脏纤维化

陆静

哈尔滨医科大学附属第一医院

目的：

以心肌纤维化为主要表现的病理性心肌重构，是导致老年人心力衰竭致死的主要原因之一。其机制复杂，涉及细胞间通讯改变及慢性炎症等。在心衰大鼠的肠道中吲哚 -3- 丙酸（Indolyl-3-propionic acid，IPA）的含量降低加剧了心脏舒张功能障碍，补充 IPA 可缓解这一现象。尽管 IPA 对机体有显著的保护作用，但 IPA 对老年心衰的治疗作用及调控机制尚未完全清楚。因此，本研究的目的是，验证 IPA 在衰老心脏中对心肌纤维化调控作用，探讨 IPA 对巨噬细胞调控自噬活性参与增龄性心肌纤维化的作用机制，为增龄性心肌纤维化提供新的干预靶点。

方法：

分别取 4-6 月龄的成年雄性 SD 大鼠及 18-20 月龄的老年雄性 SD 大鼠的粪便进行 16S rDNA 检测。应用靶向色氨酸代谢组学技术检测青年大鼠、老年大鼠粪便中差异代谢物。雄性 SD 老年大鼠给予 IPA 管饲法喂养 8 周后，采用心脏超声、H&E 染色、Masson 染色、免疫组化、免疫荧光、qRT-PCR 和 Western Blot 等技术验证 IPA 对老年大鼠心脏的保护作用。利用巨噬细胞 - 心肌成纤维细胞共培养方法验证 IPA 通过调节 PPT1 减轻纤维化的作用。

结果：

（1）老年大鼠肠道微生物群紊乱，梭状芽胞杆菌属有显著差异，其色氨酸途径代谢产物 IPA 的含量在老年心衰大鼠中显著降低；

（2）老年大鼠补充 IPA 能够显著改善衰老引起的心功能减退、胶原沉积，降低炎症标志物 iNOS、IL-6 及 TNF-α 表达水平，抑制心肌纤维化标志物 COL3A1、COL1A1 及 α-SMA 的表达水平；体外孵育 IPA 可降低巨噬细胞炎症标志物 iNOS、IL-6 及 TNF-α 表达，间接抑制心肌成纤维细胞纤维化标志物 COL3A1、COL1A1 及 α-SMA 的表达；

（3）IPA 能够调控衰老巨噬细胞的 PI3K-AKT-mTOR 通路进而调控自噬；体外补充 IPA 能够缓解过表达 PPT1 所致的自噬功能减退。

结论：

色氨酸代谢产物 IPA 在老年心衰心脏中显著下降，补充 IPA 能够逆转增龄性心肌纤维化及炎症；在机制上，IPA 通过 PPT1 影响 PI3K-AKT-mTOR 通路恢复衰老巨噬细胞自噬活性，从而抑制炎症及增龄性心肌纤维化的发生发展。

关键词：增龄性心肌纤维化；IPA；自噬

TAVI 手术在超高龄患者中的安全性及中长期预后评估

张璐

陆军军医大学第二附属医院新桥医院

摘要：目的：评估经导管主动脉瓣植入术（TAVI）在 80 岁以上超高龄患者群体中的围术期安全性及术后 3-5 年生存质量指标，探讨影响预后的独立危险因素。

方法：采用多中心回顾性队列研究设计，纳入 2018-2025 年间接受 TAVI 治疗的 327 例≥ 80 岁重度主动脉瓣狭窄患者，通过 EuroSCORE II 评分系统进行术前风险评估，记录术中并发症发生情况，术后跟踪随访主要心血管不良事件（MACCE）、全因死亡率及心功能改善情况。

结果：手术成功率 97.6%，30 天死亡率 3.7%，主要并发症包括需要输血治疗的血管并发症（8.3%）、新发房颤（12.1%）及永久起搏器植入（15.8%）。3 年生存率 82.4%，5 年生存率 67.9%，NYHA 心功能分级改善≥ 1 级者达 89.2%。多因素分析显示术前肺动脉高压（HR=2.15）和慢性肾功能不全（HR=1.83）是影响中长期预后的独立危险因素。

结论：TAVI 手术能为超高龄患者提供可靠的中长期生存获益，严格把握适应证并优化合并症管理是改善预后的关键。

关键词：经导管主动脉瓣植入术 超高龄 预后因素 老年医学

随着人口老龄化进程加速，重度主动脉瓣狭窄（severe aortic stenosis, SAS）在超高龄（≥ 80 岁）人群中的发病率显著升高。该疾病严重影响患者生活质量及预后，若不及时干预，自然病程凶险。传统的外科主动脉瓣置换术（surgical aortic valve replacement, SAVR）虽为金标准，但对于合并多种基础疾病、衰弱状态（frailty）的超高龄患者而言，其围术期死亡率和并发症风险显著增加，使得相当一部分患者无法耐受或被视为手术禁忌。经导管主动脉瓣植入术（transcatheter aortic valve implantation, TAVI）作为一种微创介入治疗技术，自首次应用于临床以来，凭借其创伤小、恢复快的优势，迅速成为治疗高龄、高危 SAS 患者的重要选择。多项大型随机对照试验及真实世界研究已证实，对于外科手术中高危患者，TAVI 在短期及中期预后方面不劣于甚至优于 SAVR。然而，针对超高龄这一特殊亚组人群，其生理储备下降、合并症复杂、预期寿命及生活质量诉求具有独特性，TAVI 治疗的安全性、有效性和中长期预后数据仍相对有限。现有研究多聚焦于短期结局或纳入患者年龄跨度较大，缺乏专门针对超高龄患者群体的长期、系统性的预后评估，特别是对生存质量改善及影响远期结局的关键因素分析尚需深入探讨。因此，本研究旨在通过多中心回顾性队列分析，详细评估 TAVI 在超高龄重度主动脉瓣狭窄患者中的围术期安全性、术后 3-5 年的生存率、主要心血管不良事件发生率以及心功能恢复情况，并深入探讨影响其中长期预后的独立危险因素，以期为此类患者群体的临床决策提供更精准、更有价值的循证医学证据。

Efficacy and safety of antithrombotic therapy in the elderly patients with the commodities of coronary artery disease, atrial fibrillation, and malignancy

Yuyan Wang[1,2], A-O SHUAI Mao[1,2], Yunzhang Zhao[1,2], Yanzu Yao[1,2], Yifan Wang[1,2], Jie Zhang[1,2], Chao LV[1,2], Li Fan[1,2], Feng Cao[1,2], TONG Yin[1,2]

1. Institute of Geriatrics, National Clinical Research Center for Geriatric Diseases, Second Medical Center of Chinese PLA General Hospital, Beijing China

2. Medical School of Chinese PLA, Chinese PLA General Hospital

Abstract:

Objective: Antithrombotic therapy is the cornerstone for the patients with coronary artery disease (CAD), and atrial fibrillation (AF), but it is a challenge with the concomitant of malignancy for the lethal bleeding side events, especially in the elderly. This study aimed to investigate the current status of oral antithrombotic therapy and its impact on clinical outcomes in the elderly patients with CAD, AF, and concomitant malignancy.

Methods: We consecutively enrolled patients aged ≥ 65 years diagnosed with CAD, AF, and malignancy during the hospitalization in the Chinese PLA General Hospital. yhThe clinical baseline characteristics and details of the oral antithrombotic therapy were collected from the Electronic Medical Record. Patients who could meet the inclusion/exclusion criteria of the study were followed-up for 1 year to observe the occurrence of major adverse cardiovascular events (MACEs) and major bleeding events (Bleeding Academic Research Consortium [BARC] type ≥ 2). We analyzed the influence of oral antithrombotic therapy on these clinical outcomes. Statistical analysis was performed using SPSS 17.0. The comparison of clinical baseline characteristics between patients with or without oral antithrombotic therapy were performed by t-tests, Mann-Whitney U tests, or χ^2 tests, as appropriate for the data type. Multivariate logistic regression models were used for the adjustment to determine the independent predictive value of antithrombotic therapy for the efficacy and safety

outcomes of oral antithrombotic therapy.

Results: The study included a total of 135 eligible elderly patients with the comorbiditis of CAD, AF, and malignancy. Acute coronary syndrome was diagnosed in 40.0% (54/135) patients, and 7.4% (10/135) underwent the coronary stent implantation. Among all malignancy types, breast cancer (17.0%, 23/135) and lung cancer (15.6%, 21/135) accounted for the highest diagnostic proportions. Patients were divided into an antithrombotic therapy group (n=71) and a non-antithrombotic therapy group (n=64) based on their use of antiplatelet and/or anticoagulant medications. Compared to the patients in the non-antithrombotic therapy group, the patients in the antithrombotic therapy group had significantly lower mean age (77.4 ± 5.7 vs. 80.3 ± 6.8 years, P < 0.05) and median plasma D-dimer levels (1.03 [IQR 0.34-1.42] vs. 1.82 [IQR 0.51-2.43] mg/L, P < 0.05). Meanwhile, significantly higher mean platelet counts (199.9 ± 65.0 vs. 176.7 ± 59.8 × 10^9 /L, P < 0.05) as well as a higher proportion of patients using proton pump inhibitors (59.2% [42/71] vs. 29.7% [19/64], P < 0.05) could be observed in the antithrombotic therapy group. Among the patients in the antithrombotic therapy group, 38.0% (27/71) were administrated with oral anticoagulant (OAC), 32.4% (23/71) with single antiplatelet agent, and 29.6% (21/71) received dual antiplatelet therapy of aspirin combined with clopidogrel. Multivariate logistic regression analysis revealed that antithrombotic therapy was negatively associated with the rate of MACEs (OR = 0.111, 95% CI: 0.026-0.473; P < 0.05). However, the risk of BARC type ≥ 2 bleeding events did not differ significantly between the two groups (OR = 0.724, 95% CI: 0.059-8.826; P > 0.05).

Conclusion: In elderly patients with CAD, AF, and malignancy, antithrombotic therapy could decrease the risk of ischemic cardiovascular events without the increase of bleeding risk.

Key Words:

Elderly, antithrombotic therapy, coronary artery disease, atrial fibrillation, malignancy

健康生活方式与全因死亡率、特定原因死亡率及预期寿命的关联：来自英国和美国的两项全国性队列研究

陈章玲 周胜华

中南大学湘雅附二医院

摘要

目的：现有证据表明健康生活方式与较低的死亡率和较长的预期寿命相关，但既往的健康生活方式评分未纳入睡眠质量和心理因素。本研究旨在探讨新的健康生活方式评分与全因死亡率、特定原因死亡率及预期寿命的关联。

方法：我们前瞻性随访了英国生物银行（2006-2022 年）和美国国家健康与营养检查调查（NHANES，1999-2019 年）的 413,180 名参与者。通过基线问卷调查收集饮食和生活方式等数据，并据此创建新的健康生活方式评分，包括膳食质量、体力活动、酒精摄入、吸烟情况、睡眠质量和抑郁状况。其中，膳食质量、体力活动、睡眠质量为正向评分，酒精摄入、吸烟和抑郁为反向评分。各组分得分总和即为新的健康生活方式评分（理论范围 6-30 分）。采用 Cox 回归模型分析该评分与全因及特定原因死亡率的关联，并使用生命表法分析其与预期寿命的关系。

结果：在平均 13.3 年的随访期间，两个队列共发生 34,155 例死亡。经多变量调整后，更高的健康生活方式评分与更低的全因及特定原因死亡风险相关。健康生活方式评分最高五分位数组与最低五分位数组相比，全因死亡率的风险比（HR）为 0.56（0.47，0.67），心血管疾病（CVD）死亡风险为 0.64（0.59，0.70），癌症死亡风险为 0.62（0.58，0.65），其他原因死亡风险为 0.47（0.31，0.70）。此外，更高的健康生活方式评分与更长的预期寿命相关：与最低五分位数组相比，最高五分位数组的预期寿命延长 5.60 年（3.82，8.19）。这些结果在年龄、种族、性别和 BMI 等多个风险因素中保持一致。

结论：在英国和美国成年人中，新的健康生活方式评分（包含睡眠和心理因素）与显著降低的全因及特定原因死亡风险、更长的预期寿命密切相关。研究结果提示，推广包括健康睡眠和心理健康在内的健康生活方式，有助于降低死亡率、延长预期寿命，并减轻医疗负担。

高尿酸血症对老年冠心病患者经皮冠状动脉介入治疗术后 2 年和 5 年不良临床结局的影响

唐晓芳 张策 姚懿 徐娜 汪沛志 袁德山 赵雪燕 袁晋青

中国医学科学院阜外医院

背景：流行病学研究表明，高尿酸血症的患病率随着年龄的增长而增加。越来越多的证据表明，高尿酸血症患者罹患心血管疾病和发生死亡的风险可能更高，随着我国人口老龄化的加剧，老年高尿酸血症患者罹患冠心病的风险大大增加。然而，高尿酸血症与老年冠心病患者长期预后的关系目前尚不清楚，缺乏证据。

目的：本研究旨在探讨高尿酸血症对于接受经皮冠状动脉介入治疗（percutaneous coronary intervention, PCI）的老年冠心病患者长期预后的影响。

方法：连续纳入 2013 年 1 月至 12 月 2,981 例行 PCI 的老年冠心病患者，分为高尿酸血症组（580 例）和尿酸正常组（2401 例），比较 PCI 术后 2 年和 5 年随访期间的不良预后。

结果：住院及随访期间，高尿酸血症患者仅有 87 例 (15%) 使用降尿酸药物。老年冠心病合并高尿酸血症组，女性、LVEF<40%、高血压、高脂血症、慢性肾脏病、陈旧心梗病史的比例均显著高于尿酸正常组（P <0.05）。老年冠心病合并高尿酸血症患者在 PCI 术后 2 年和 5 年的全因死亡、心源性死亡和主要不良心脑血管事件的发生率均高于老年冠心病合并尿酸正常的患者（P<0.05）。单因素 COX 回归分析显示，高尿酸血症是老年冠心病患者 PCI 术后 2 年和 5 年全因死亡的独立预测因素（2 年：HR=2.052, 95% CI: 1.259 ~ 3.344, P =0.004; 5 年：HR =1.694, 95% CI: 1.264-2.271, P <0.001）。多因素 COX 分析显示：高尿酸血症仍是老年冠心病患者 PCI 术后 2 年和 5 年全因死亡的独立预测因素（2 年：HR =1.717, 95% CI: 1.009-2.921, P =0.046; 5 年：HR =1.427, 95% CI: 1.042-1.955, P =0.027）。

结论：（1）老年冠心病合并高尿酸血症患者常伴随更多临床高危因素。（2）老年冠心病合并高尿酸血症患者 PCI 术后长期随访期间全因死亡、心源性死亡和主要不良心脑血管事件的发生率明显高于尿酸正常的患者。（3）经校正多种危险因素后，高尿酸血症仍是老年冠心病患者 PCI 术后长期随访过程中全因死亡的独立危险因素。

肠道微生物群与衰老相关代谢及表观遗传年龄加速的关联研究

徐寒 杨帆 保志军 曲新凯 杨帆 保志军

复旦大学附属华东医院

目的

本研究旨在探究肠道微生物群与衰老相关代谢紊乱及表观遗传年龄加速（EAA）的关联及因果关系。一方面通过粪便微生物移植（FMT）实验，分析年龄相关肠道菌群对心脏能量代谢及心肌损伤的影响，明确老年肠道菌群在年龄相关代谢异常和心脏功能障碍中的作用；另一方面借助孟德尔随机化（MR）方法，挖掘特定肠道微生物类群与不同类型 EAA（内在表观遗传年龄加速 IEAA、HannumAge 加速 HannumAA、GrimAge 加速 GrimAA 和 PhenoAge 加速 PhenoAA）的因果关系，为揭示肠道微生物群在衰老进程中的作用机制提供依据，为预防年龄相关疾病和延缓衰老提供新方向。

方法

本研究结合动物实验与流行病学研究。动物实验选取年轻（2-3 月龄）和老年（18-22 月龄）雄性 C57BL/6 小鼠为供体，将粪便微生物移植到年轻受体小鼠，形成年轻 FMT 组和老年 FMT 组。通过 16S rRNA 测序分析受体肠道菌群变化，血浆代谢组学评估代谢潜能；采用口服葡萄糖耐量试验、生化检测等监测能量代谢；检测心脏样本的代谢及 DNA 损伤标志物。流行病学研究基于 MiBioGen 联盟、荷兰微生物组项目及全基因组关联研究数据，运用 MR 分析方法（逆方差加权法 IVW、MR-Egger 回归等）评估肠道菌群与 EAA 的因果关系，通过敏感性分析评估异质性和多效性，反向 MR 分析探究反向因果关系。

结果

动物实验显示，老年 FMT 组受体小鼠肠道菌群显著改变，厚壁菌门与拟杆菌门比值升高，Allobaculum 属丰度增加，乳酸杆菌属等降低，梭杆菌门富集。代谢方面，老年 FMT 组小鼠血浆葡萄糖升高、糖耐量受损、附睾脂肪积累，心脏重量增加伴心肌肥大，心肌葡萄糖代谢异常及氧化损伤加剧，且心脏重量与心肌肥大指标、附睾脂肪重量和空腹血糖显著相关。MR 研究识别出 12 种细菌类群与 EAA 有潜在因果关联。未分类的 Holdemania 物种与 GrimAA 呈强正相关（OR:1.31,95% CI:1.13-1.52,P=0.0004）；Acidaminococcaceae 科和 Clostridiaceae1 科与 GrimAA 呈负相关（OR 分别为 0.64 和 0.69）。反向 MR 分析发现 EAA 与 6 种细菌类群相关，PhenoAA 与 Turicibacter 属呈显著负相关（OR:0.928,95% CI:0.888-0.971,P<0.001）。敏感性分析证实结果稳定，无明显异质性和方向性多效性。

结论

本研究证实年龄相关肠道菌群紊乱在衰老相关代谢异常和心脏损伤中起重要作用，老年肠道菌群可通过改变菌群结构、扰乱能量代谢、诱发心肌氧化损伤，导致心脏肥大等功能障碍。MR 研究揭示特定肠道微生物类群与 EAA 的因果关系，表明肠道菌群可能通过调控表观遗传年龄加速参与衰老。这些发现为理解肠道微生物群在衰老中的作用提供新视角，提示靶向调节肠道菌群可能成为预防年龄相关代谢疾病、心脏功能障碍及延缓衰老的潜在策略。未来需进一步探索分子机制，扩大样本开展跨人群研究验证普适性。

抗凝治疗对老年非瓣膜心房颤动患者认知功能影响的研究

张占英

新疆维吾尔自治区人民医院

探讨老年非瓣膜性心房颤动住院患者的不同药物抗凝治疗对患者认知功能的影响。**方法：**收集 2019 年 01 月 -2020 年 06 月本院收入院的 180 例老年非瓣膜性心房颤动患者为研究对象，采用 cHA_2sD_2.VASc 和 HAS-BLED 评分分析患者在临床中对于治疗方案的选择情况，根据接受治疗方案情况分为抗凝治疗组 120 例 (新型口服抗凝药物组、华法林抗凝药物组) 和未抗凝治疗组 60 例（不接受抗凝治疗组或仅口服阿司匹林组）。通过单因素及多因素分析影响患者抗凝治疗的相关因素。治疗后随访 12 个月，观察患者卒中和出血事件的发生情况。统计患者认知障碍等事件的发生情况，采用简易精神状态检查表 (MMSE) 评价患者认知功能，分析抗凝治疗对认知功能的影响。**结果：**结果显示，与不接受抗凝治疗或仅服用阿司匹林相比，接受口服抗凝药物治疗的心房颤动患者认知功能障碍及痴呆发生风险明显降低（RR=0.71，P<0.01）差异均有统计学意义；口服华法林可显著降低认知功能减退的发生风险 (RR=0.91，P<0.01 差异均有统计学意义)；新型口服抗凝药物和华法林比较无显著差异；**结论：**抗凝治疗能有效减少老年非瓣膜性心房颤动患者卒中事件的发生概率，抗凝治疗对老年非瓣膜性心房颤动患者长期认知障碍具有积极的预防作用，可降低老年痴呆的发生率；

钠 - 葡萄糖转运蛋白 2 抑制剂对肌少症影响的 meta 分析

张孟峣 姚丽霞

河北省人民医院

目的：明确钠 - 葡萄糖共转运蛋白 2(Sodium-Glucose Cotransporter 2 Inhibitors，SGLT-2) 抑制剂对肌少症的影响，优化老年人治疗方案并保护肌肉健康，提高生活质量。

方法：通过检索 PubMed、Embase、Web of Science、Cochrane Library 和 Scopus 学术数据库，收集自建库至 2024 年 12 月的关于 SGLT2 抑制剂对肌少症影响的研究文献，依据纳入和排除标准进行文献筛选，使用 Cochrane 风险偏倚评估工具评价文献质量，运用 RevMan5.4 软件和 Stata18.0 进行 Meta 分析。

结果：最终纳入 26 项随机对照研究，共 1955 名参与者。结果显示，SGLT2 抑制剂可使患者体重 [WMD = -2.27, 95% CI (-2.59 ~ -1.94, P < 0.00001)]、身体质量指数 [WMD= -0.99, 95% CI(-1.22 ~ -0.77, P < 0.00001)]、脂肪量 [WMD = -1.19, 95% CI(-1.66 ~ -0.71, P < 0.00001)]、骨骼肌质量 [WMD = -1.36, 95% CI(-2.59 ~ -0.12，P=0.03)]，骨骼肌质量指数 [WMD = -0.17, 95% CI (-0.31 ~ -0.03，P=0.02)] 显著下降。根据是否为 2 型糖尿病患者进行分组分析，结果显示糖尿病患者 [WMD = -2.33,95% CI(-2.66 ~ -1.99kg, P < 0.00001)] 较无糖尿病患者 [WMD = -1.56, 95% CI (-2.71 ~ -0.40, P=0.008)] 体重下降更显著，但脂肪量下降相似。对于骨骼肌质量进一步行亚组分析发现，不同种类的 SGLT2 抑制剂对骨骼肌质量影响存在差异，恩格列净 [WMD = -0.99, 95% CI(-1.17 ~ -0.81，P < 0.00001)]、伊格列净 [WMD = -1, 95% CI(-1.19 ~ -0.81，P < 0.00001)] 可显著降低骨骼肌质量，达格列净 [WMD = -0.87, 95% CI(-2.90 ~ 1.15，P=0.40)] 降低骨骼肌质量的程度不显著。此外，SGLT2 抑制剂对握力 [WMD = -0.48, 95% CI(-1.27 ~ 0.31，P=0.23)] 和 C 反应蛋白 [WMD=0.09, 95% CI(-0.16 ~ 0.34, P=0.48)]、白细胞介素 6 [WMD= 0.04, 95% CI(-0.13 ~ 0.20, P=0.67)]、肿瘤坏死因子 α [WMD= -0.37, 95% CI(-0.90 ~ 0.16, P=0.17)] 无显著影响。

结论：SGLT2 抑制剂可使患者体重、BMI、脂肪量、骨骼肌质量、骨骼肌质量指数下降，对肌肉力量、炎症因子无显著影响，值得临床医生高度关注，进而对患者行个性化治疗。

心脏病患者跌倒走失安全管理及护理措施探讨

孙莹莹

吉林大学第二医院

目的：本文主要是对心脏病患者跌倒走失安全管理及护理措施进行探讨研究。

方法：选取我院在 2024 年 2 月到 2025 年 2 月收治的心血管疾病患者 220 例，所有患者均排除精神疾病病史、严重脏器障碍及活动障碍等，符合心血管内科相关疾病的诊断标准，将≥ 65 周岁患者纳入研究，采用随机数字表法将其随机分为参照组与研究组各 110 例，参照组患者进行常规护理，研究组患者在参照组护理基础上再进行跌倒走失管理，对两组患者的不良事件进行对比、观察与比较。

结果：心血管内科住院老年患者（≥ 65 周岁）病情较为危重，并且老年人身体机能较差，老年人合并其他疾病，因此对患者展开相应的护理干预具有重要意义。因此应当从护理环节中的细节处入手，包括疾病本身状态、用药安全、高血压等级，心电图性质、心理干预、饮食、提升护理人员水平，确保环境整洁明亮以及其它因素等，对风险进行评估，这样可以有效避免不良事件的发生，提高护理质量，保证患者安全。本次就对心脏病患者跌倒走失安全管理及护理措施探讨，在不同的护理方法下，参照组患者不良事件发生几率为 28.35%，研究组患者的不良事件发生几率为 8.96%，研究组患者发生不良事件的几率明显要低于参照组，P < 0.05，差异具有统学学意义。结论：对心血管疾病患者在常规护理基础上再进行跌倒走失安全管理，改善护理措施，提高医护人员护理水平，能够取得更好的护理效果，降低了患者放生不良事件几率，巩固了患者的治疗效果，提高了患者治疗的安全，可以有效提升护理满意度以及护理质量，值得在今后的临床工作中加以推广。

多学科协作模式下老年难治性高血压的综合干预模式构建

代芬

陆军军医大学第二附属医院新桥医院

摘要：目的：探索基于多学科协作模式构建老年难治性高血压综合干预体系的临床价值，通过整合动态化管理系统与标准化临床路径，提升血压控制达标率及靶器官保护效果。

方法：组建由心内科、内分泌科、临床药师、营养科、心理科及康复治疗师构成的多学科协作团队，建立包含风险评估 - 精准诊断 - 个体化治疗 - 连续随访四大模块的闭环管理体系。采用动态血压监测、药物基因组学检测、靶器官功能评估三维度筛查机制，结合物联网技术实现用药依从性追踪和生活方式实时干预。

结果：通过实施结构化临床路径，使血压达标时间缩短至（8.2±3.1）周，诊室收缩压较基线下降（28.4±9.6）mmHg，24 小时动态血压达标率提升至 76.3%。同时继发性高血压筛查效率提高 42%，药物不良反应发生率降低 19.8%。

结论：该模式通过系统整合专科诊疗优势与全程健康管理，有效破解多重用药矛盾，改善血压波动性，为老年难治性高血压患者提供了兼具规范性与个体化的解决方案。

关键词：多学科协作 难治性高血压 综合干预 动态化管理 临床路径

高血压作为一种常见的慢性疾病，在老年人群中尤为高发，其难治性高血压亚型因多重用药、合并症复杂及生理机能衰退等因素，成为临床管理的重大挑战。据流行病学数据显示，老年难治性高血压患者心血管事件发生率显著高于普通高血压人群，靶器官损害风险加剧，导致致残率及死亡率居高不下。传统单一学科干预模式在应对药物相互作用、生活方式调整及心理社会支持等维度时存在局限，易出现血压控制不达标、依从性低下及不良反应频发等问题。多学科协作模式通过整合心内科、内分泌科等专科资源，结合动态化管理系统与标准化临床路径，能够实现风险评估、精准诊断、个体化治疗及连续随访的闭环管理，有效提升干预效率和患者预后。本研究旨在构建并验证该综合干预模式，为优化老年难治性高血压管理提供循证依据和实践参考。

基于衰弱评估的老年冠心病患者血运重建策略优化研究

游玲

陆军军医大学第二附属医院新桥医院

摘要：目的：探讨衰弱评估在老年冠心病患者血运重建治疗决策中的应用价值，构建基于多维度衰弱评估的个体化血运重建策略。

方法：采用前瞻性队列研究设计，纳入 201 例年龄≥ 75 岁拟行血运重建的冠心病患者，通过 Fried 衰弱表型评估工具进行术前衰弱分级。根据衰弱程度将患者分为衰弱组（n=58）、衰弱前期组（n=63）和非衰弱组（n=80），比较三组术后 30 天主要不良心血管事件（MACE）、12 个月全因死亡率、再入院率及生存质量（采用 SF-36 量表评估）差异。

结果：老年冠心病患者总体衰弱患病率达 28.6%（58/201），衰弱组术后 30 天 MACE 发生率显著高于非衰弱组（24.1% vs 6.3%，HR=3.12，95%CI 1.42-6.85）。衰弱评估指导下的阶梯式干预策略（含 PCI 优化、CABG 时机选择及多学科团队支持）使衰弱患者术后 1 年生存质量评分提升 37.2%（P<0.01）。

结论：将衰弱评估纳入老年冠心病血运重建术前评估体系可有效识别高危患者，通过制定分层管理策略可降低术后并发症风险并改善预后，为临床决策提供循证依据。

关键词：衰弱评估；老年冠心病；血运重建；多学科团队协作

冠心病（CAD）是影响老年人群健康的主要疾病之一，其发病率随年龄增长显著上升。随着人口老龄化进程加速，高龄（≥ 75 岁）冠心病患者的治疗需求日益突出。血运重建（包括经皮冠状动脉介入治疗 PCI 和冠状动脉旁路移植术 CABG）是改善心肌缺血、缓解症状及降低死亡风险的关键手段。然而，老年患者常伴有多种共病及生理储备下降，传统以年龄和常规心血管危险因素为主的评估体系难以全面反映其手术耐受能力与预后差异。近年来，衰弱（Frailty）作为一种反映机体易损性和应激能力下降的综合征，被证实是独立于年龄与共病的重要预后预测因子。研究表明，衰弱状态与老年冠心病患者术后并发症风险增加、恢复延迟及生存质量下降密切相关。

目前，国内外指南虽强调个体化治疗决策的重要性，但对衰弱评估在血运重建策略优化中的系统性整合仍显不足。常规临床实践中，衰弱筛查尚未被广泛纳入术前评估流程，导致部分高危患者可能接受了不适宜的血运重建强度或未能获得针对性的围术期支持。因此，亟需建立一套基于多维度衰弱评估的个体化决策框架，以精准识别风险、优化干预强度并协调多学科资源。本研究旨在通过前瞻性队列分析，验证衰弱评估对老年冠心病患者血运重建术后结局的预测价值，并探索阶梯式干预策略的临床可行性，为完善高危老年患者的循证管理路径提供依据。

健康教育与老年冠心病患者衰弱的相关性研究

王肖肖 宋春莉

吉林大学第二医院

1. 目的：评估老年冠心病患者的衰弱状况，研究健康教育与老年冠心病患者衰弱的相关性，为老年冠心病患者衰弱防治提供新的治疗思路和方案。

2. 方法：

（1）研究对象的选择：选取 2024 年 2 月至 2024 年 10 月就诊于吉林大学第二医院心血管内科的 60 岁及以上的冠心病患者，根据纳入排除标准最终进入研究患者数为 190 例。入选标准: 年龄≥60 岁; 参与研究患者需接受冠状动脉造影检查，造影结果符合 2010 年中华人民共和国卫生部制订的《冠状动脉粥样硬化性心脏病诊断标准》，同时冠状动脉造影结果证实至少一支冠状动脉狭窄≥ 50%；病情平稳；签署知情同意书；依从性佳。排除标准：合并急性心力衰竭等急危重症患者；既往有精神病史不能配合者；严重认知障碍、昏迷等不能明确表达自身思想者；患者拒绝接受衰弱筛查；患者无法进行交流或现有临床资料无法获得有效信息来判断患者是否衰弱。

（2）收集资料: 收集入选患者的一般临床资料，包括年龄、性别、教育程度、吸烟史、饮酒史、高血压史、糖尿病史、脑梗死史、体质指数；收集检验检查指标，包括血红蛋白、白细胞计数、甘油三酯、低密度脂蛋白、左室射血分数、肌钙蛋白、肌酸激酶等，依据 Tilburg 衰弱评估量表评估入选患者的衰弱状况。

（3）干预方法：按照随机数字表法分为对照组和研究组，对照组给予冠心病常规治疗，研究组在常规治疗基础上给予健康教育。健康教育采取现场多媒体授课教学的形式，从合理饮食、体重控制、遵医用药、康复锻炼、情志调护等方面对患者进行系统性、规范性的健康教育，包括 6 次面对面培训，每次培训 20 min，由两名住院医师对患者实施健康教育。

3. 结果和结论：健康教育与老年冠心病患者衰弱具有显著相关性，健康教育干预后老年冠心病患者衰弱显著低于干预前（P<0.01）；健康教育有望成为老年冠心病患者衰弱治疗的一种有潜力的方法。

睾酮通过抑制 AMPK-FOXO1/MuRF1 信号通路介导绝经后高血压左室肥厚

朱露露 王文婷 陈建淑 余静

兰州大学第二医院

目的：女性绝经后发生高血压的风险明显高于男性，且绝经后女性高血压患者易

合并左心室肥厚的靶器官损害，多数研究认为这与绝经后女性雌激素水平的下降相关，但雌激素替代疗法并未使受试者获益可造成某些患者血压升高，我们团队的前期临床研究及多数研究均表明睾酮水平的相对升高也与绝经后高血压左室肥厚相关，但具体致病机制仍在探索中。肌肉特异性 E3 泛素连接酶 MuRF1，主要通过泛素蛋白酶体降解途径参与肌细胞中异常蛋白质的降解，作为一种肌细胞大小的负调控因子介导肌肉萎缩过程，近年来研究发现 MuRF1 也可调控心肌细胞的大小，可能介导心肌细胞肥厚的过程，但其具体机制仍不清楚。故本研究以双侧卵巢摘除术后 SHR 为对象，围绕 AMPK-FOXO1/MuRF1 信号通路，探讨睾酮介导的双侧卵巢摘除术后 SHR 心肌肥厚的发生机制。

方法： 取 12 周龄的雌性自发性高血压大鼠 (SHR 大鼠) 行双侧卵巢切除术以建立绝经后高血压动物模型（OVX 组），并以假手术（Sham 组）为对照。绝经后高血压动物造模成功后，对 OVX 组大鼠予以睾酮（2.85mg/kg QOD 肌注）连续干预 4 周，记为 OVX+T 组。采用 Western Blot 法分别检测各组中 β- 肌球蛋白重链 (β-MHC)、AMPK、p-AMPK、FOXO1、p-FOXO1 和 MuRF1 的蛋白表达水平。

结果： 睾酮 4 周干预后，与 OVX 组和 Sham 组相比，OVX+T 组 SHR 心脏重量 / 胫骨长度、IVST、LVPWT、LVM 水平和 β-MHC 的蛋白表达显著增加，AMPK、p-AMPK、FOXO1、p-FOXO1 和 MuRF1 的蛋白表达均明显降低。另外，对同一大鼠的心脏及肥肠肌进行比较发现，三组中，MuRF1 蛋白在心脏与肥肠肌中的表达水平相当，而 AMPK、p-AMPK、FOXO1 和 p-FOXO1 蛋白在肥肠肌中表达较少，在心肌组织中高表达，表达量至少是肥肠肌的 2 倍。

结论： 睾酮可能通过抑制 AMPK-FOXO1/MuRF1 信号通路介导绝经后高血压左室肥厚。激活 AMPK 在不引起骨骼肌 MuRF1 表达的情况下，可通过增加心肌组织中 MuRF1 的表达逆转睾酮诱导的绝经后高血压左心室肥厚。

Associations between taste preferences and mortality among older adults: a nationwide, community-based, prospective cohort study in China

Jia He[1], Liu Yang[2], Sen He[1,2]

1. Department of Cardiology, West China Hospital, Sichuan University, Chengdu, China

2. Department of Cardiology, Karamay Hospital of Integrated Chinese and Western Medicine, Karamay, China.

Background: In recent years, there has been a growing consensus that dietary behavior is a key factor affecting health outcomes. Previous studies have predominantly focused on the associations between the intake of macro-nutrients and micro-nutrients and the risk of non-communicable diseases. Given the holistic nature of daily diets—people eat foods, not isolated nutrients—such reductionist approaches may overlook important aspects and lead to potentially biased conclusions. Taste preferences, a fundamental behavioral characteristic that influences food selection and consumption, are receiving increasing attention regarding its implications for health; however, the association between taste preferences and health outcomes among older adults remains unclear. This study aimed to estimate the association of taste preferences with mortality among older adults in a nationwide, community-based, prospective cohort in China.

Methods: A total of 14760 older participants (median age: 89.0 [IQR: 79.0–97.0], males: 42.7%) were recruited from the Chinese Longitudinal Healthy Longevity Survey between 2008 and 2014, with follow-up until 2018. Exposures were taste preferences (i.e., insipid, salty, sweet, spicy, and other tastes), which were assessed through the questionnaire. The study outcome was all-cause mortality. The association between taste preferences and mortality was evaluated through Cox regression models. To enhance the primary finding, we also performed additional analyses to evaluate the association between frequency of consuming salt-preserved vegetables, as well as frequency of consuming sugar or candy and changes in taste preferences, and mortality.

Findings: During a follow-up period of 65936.7 person-years (median: 3.6 years, IQR: 1.8–6.1 years), a total of 9837 deaths (66.6%) were recorded. Age/sex-standardized mortality rates varied significantly across the five taste preferences: participants preferring a salty taste had the lowest rate of 53.3 (95% CI: 48.8–58.4) per 1000 person-years, while those favoring a sweet taste had the highest at 60.6 (95% CI: 51.8–70.8) per 1000 person-years. With participants who preferred a salty taste serving as the reference, the adjusted hazard ratios (HRs) were as follows: 1.01 for those favoring a spicy taste (95% confidence interval [CI]: 0.87–1.17), 1.04 for those preferring other tastes (95% CI: 0.97–1.12), 1.09 for those favoring an insipid taste (95% CI: 1.03–1.15), and 1.18 for those who preferred a sweet taste (95% CI: 1.09–1.29). To enhance the primary finding, we performed additional analyses on the association between frequency of consuming salt-preserved vegetables, as well as frequency of consuming sugar or candy, and all-cause mortality. Multivariate Cox models indicated that the risk of mortality decreased with increased frequency of salt-preserved vegetable consumption among all participants (p for trend =0.008). This trend was also observed in participants who preferred a salty taste (p for trend =0.044) as well as those who favored a nonsalty taste (p for trend =0.031), respectively. However, the lowest mortality risk was observed with a moderate frequency of salt-preserved vegetable consumption. In addition, multivariate Cox models revealed that the risk of mortality increased with more frequent consumption of sugar or candy among all participants (p for trend =0.008), as well as among those who preferred a sweet taste (p for trend =0.044) and those who favored a nonsweet taste (p for trend =0.046), respectively. Importantly, the highest risk of mortality was observed among participants with the most frequent consumption of sugar or candy. Based on the primary finding, there was no significant difference in mortality risk among the three taste preference groups (i.e., salty, spicy, and other tastes), and insipid and sweet taste preferences were associated with a higher mortality risk. Therefore, we combined the three groups (i.e., salty, spicy, and other tastes) into a new category called favourable taste preference, while the other two groups (i.e., insipid and sweet) were classified as unfavourable taste preference. With the unfavourable-unfavourable group as reference (note:), adjusted HRs for mortality were 1.05 (95% CI: 0.97–1.15) for the unfavourable-favourable group, 0.94 (95% CI: 0.86–1.02) for the favourable-unfavourable group, and 0.90 (95% CI: 0.81–0.99) for the favourable-favourable group, respectively.

Interpretation: Among older adults in China, a preference for salty taste is associated with the lowest risk of all-cause mortality among the five assessed taste preferences; in contrast, preferences for sweet and insipid tastes are associated with higher mortality risk. These findings are observational; caution is advised when using them as a basis for dietary interventions, and further research is warranted.

最佳药物治疗对高龄急性心肌梗死患者的预后影响

王鸽 严研 聂绍平

首都医科大学附属北京安贞医院

目的： 本研究旨在明确最佳药物治疗对高龄急性心肌梗死患者预后的影响。

方法： 本研究基于国际多中心急性冠脉综合征出院患者出血并发症多中心登记注册研究（BleeMACS，NCT02466854），纳入年龄大于等于 80 岁，出院诊断为急性心肌梗死的患者。最佳药物治疗（OMT）定义为阿司匹林、任何 P2Y12 抑制剂、他汀类药物、血管紧张素转换酶抑制剂 / 血管紧张素受体阻滞剂和 β 受体阻滞剂的组合。研究主要终点定义为主要不良心血管事件（MACE），包括全因死亡和再发心肌梗死。研究随访时间为 1 年。

结果： 在 1482 名高龄急性心肌梗死的患者中，共 765 人（51.6%）接受了最佳药物治疗。接受最佳药物治疗的患者中，合并卒中、既往出血病史、心功能分级 killip ≥ 2 和出院诊断为 ST 段抬高型心肌梗死的患者比例较少。Kaplan-Meier 生存分析结果显示，最佳药物治疗与随访 1 年时的 MACE（11.1% vs.19.9%,p<0.001）和全因死亡（7.1% vs.15.2%，p<0.001）减少密切相关。即使在调整多种可能的混杂因素后，最佳药物治疗仍是主要终点的独立保护因素（HR=0.54；95% CI，0.40-0.75；p<0.001）。然而，OMT 组与非 OMT 组在再发心肌梗死方面没有观察到明显差异。经过倾向评分匹配后分析，OMT 组仍可降低高龄急性心肌梗死患者的全因死亡风险。

结论： 最佳药物治疗可以改善高龄急性心肌梗死患者 1 年随访时 MACE 发生风险，尤其是全因死亡风险。但未来仍需前瞻性研究进一步明确最佳药物治疗在高龄急性心肌梗死患者远期预后中的获益，以期减少不良事件发生率。

老年心血管疾病患者心理健康护理必要性及干预措施

井翠萍

交大一附院

【摘要】目的：探讨心理健康护理在改善老年心血管疾病患者健康中的必要性及其有效干预措施。

方法：研究纳入 2022 年 3 月至 2024 年 2 月我院收治的 118 例患者，按照随机原则分为对照组和实验组。对照组接受常规护理，实验组在此基础上实施心理健康护理干预。通过对比两组患者的血压水平波动幅度、心率变异性、炎症因子水平、生活质量评分及抑郁和焦虑评分量表，探讨心理护理的作用对改善老年心血管疾病的患者的必要性。

结果：实验组患者的收缩压和舒张压变异系数显著降低，心率变异性指标改善幅度明显优于对照组；C 反应蛋白和白细胞介素 -6 水平显著下降，显示全身炎症状态得到有效缓解；生活质量评分显著提高，老年患者在心理健康、社会支持等维度的改善尤为显著；抑郁和焦虑评分显著下降，心理状态得到显著改善。各项指标的组间差异均具有统计学意义 (P<0.05)。

结论：心理健康护理在老年心血管疾病患者的治疗和康复中具有重要意义，能改善患者的生理指标、缓解心理问题，为提高整体治疗效果和生活质量提供了有力支持，本研究希望通过实证数据，探索心理护理在老年心血管疾病患者中的重要作用，并尝试为临床提供切实可行的干预路径。

【关键词】老年心血管疾病；心理护理；必要性；干预措施

Impact of dynamic changes in pain on cardiovascular disease in Chinese middle and elderly people: results from China Health and Retirement Longitudinal Study (CHARLS)

Zeng-Ao Yang[1,3,2], Yu-Qi Liu[1,2]

1. The Sixth Medical Center of PLA General Hospital of Beijing

2. South China University of Technology

3. Xu Zhou Xin Jian Kang Geriatric Hospital

Background

Previous studies have identified chronic pain as a significant risk factor for cardiovascular disease (CVD). However, these studies primarily focused on baseline pain status without investigating the impact of dynamic changes in pain status on CVD. This study aims to explore the association between dynamic changes in pain status and incident CVD events.

Methods

This study utilized data from the China Health and Retirement Longitudinal Study (CHARLS), including participants aged ≥ 45 years. Pain status was defined as whether individuals reported frequent pain since the last survey (conducted every 2-3 years). Changes in pain status were assessed across three consecutive surveys, analyzing the relationship between pain transition trajectories (over two or three surveys) and CVD. CVD was confirmed by diagnoses of heart disease and/or stroke. Multivariable logistic models adjusted for potential confounders, and interactions between chronic pain trajectories and other risk factors were examined. Subgroup analyses were performed to validate robustness. Additionally, separate analyses for heart disease and stroke as outcomes further confirmed the results.

Results

Among 11,217 participants (50.94% female, mean age 58.63 years), those transitioning from painless to pain showed significantly elevated CVD risk compared to those with persistent painless (painless-pain [OR 1.57, 95% CI 1.30–1.90]; persistent pain [OR 2.23, 95% CI 1.79–2.77]). Adjusted confounding factors include age, sex, marital status, education, smoking status, drinking status, physical activity, body mass-index, sleep, depression score, hypertension, dyslipidemia, abnormal glucose metabolism, chronic lung disease, kidney disease, digestive disease, and arthritis. Further reclassification based on the third survey revealed that participants progressing to pain by the third survey had higher CVD risk (painless-painless-pain [OR 1.51, 95% CI 1.12–2.04]; painless-pain-pain [OR 2.15, 95% CI 1.66–2.79]; pain-painless-pain [OR 2.26, 95% CI 1.44–3.52]; persistent pain [OR 2.57, 95% CI 1.90–3.48]), and no significant increased risks of incident CVD was observed in groups with painless (pain-painless-painless, P=0.872; painless-pain-painless, P =0.456). Subgroup and outcome-specific analyses (CVD, heart disease, stroke) yielded consistent results. Notably, although significant increased risks of incident CVD was observed in pain-pain-painless [OR 1.70, 95% CI 1.10-2.64], risk of heart disease (P=0.117) and stroke (P=0.123) showed no significant statistics difference compared with stable painless group. Participants with stable pain still had the largest elevated risks of incident CVD and heart disease [OR 2.45, 95% CI 1.74-3.43]. Pain-painless-pain [OR 2.92, 95% CI 1.38-6.15] had the largest stroke risk among all pain status transition groups. Additionally, there is stable interaction between pain status change trajectory and depression score in CVD risk (P=0.034), heart disease (P=0.048) and stroke (P=0.036).

Conclusion

This study demonstrates that progression from painless to chronic pain significantly increases CVD incidence, whereas pain remission does not elevate CVD risk. We recommend: (1) integrating routine pain assessment into cardiovascular risk evaluation, especially for persistent pain patients; (2) close monitoring of patients with fluctuating pain status (pain □ painless transitions), as they exhibit the highest stroke risk; (3) incorporating pain management into comprehensive CVD prevention strategies; and (4) Reinforce the management and assessment of mental status, especially in patients with depression. These data-driven recommendations highlight the clinical importance of integrating pain history into cardiovascular risk stratification protocols.

The Characteristic of Transcription Profiles of Aorta in Atherosclerotic Murine Models Interfered with Treadmill Exercise

Qian-Qian Wang, Da-Kang Sun, Yang Li, Hui-Pu Xu, Jin-Feng Cheng, Yan-Li Cheng

The Binzhou Affiliated Hospital, Binzhou Medical University

Objectives: Exercise is widely acknowledged as a highly potent non-pharmacological strategy for alleviating atherosclerosis, yet the intricate molecular mechanisms that drive this beneficial effect remain incompletely understood. The present study aimed to unravel how treadmill exercise modulates the progression of atherosclerosis by investigating differentially expressed genes (DEGs) in the aorta and quantifying the attenuation of atherosclerotic lesions in a well-established murine model of the disease.

Methods: Male ApoE $^{-}$ / $^{-}$ mice, a thoroughly validated animal model of atherosclerosis characterized by impaired lipoprotein clearance capabilities, were maintained on a Western-style diet (highly rich in saturated fats and dietary cholesterol) and randomly allocated to either a sedentary control group or a treadmill exercise cohort for an 8-week intervention period. Throughout the entire course of the study, body weight measurements and food intake assessments were conducted on a weekly basis to monitor general metabolic status. Following the completion of the 8-week experimental protocol, serum concentrations of total cholesterol (TC) and triglycerides (TG) were quantified using enzyme-linked immunosorbent assay (ELISA) techniques to evaluate alterations in lipid metabolic profiles. Atherosclerotic lesion dimensions and lipid deposition within the aortic tissue were systematically analyzed via hematoxylin-eosin (H&E) staining and Oil Red O staining procedures, respectively. To explore the underlying molecular changes, RNA sequencing (RNA-seq) was performed on aortic samples to identify DEGs between the two experimental groups, followed by comprehensive functional enrichment analyses—including Gene Ontology and Kyoto Encyclopedia of Genes and Genomes pathway analyses—to characterize the biological processes and signaling pathways involved. Additionally, real-time polymerase chain reaction (PCR) was employed to validate the expression patterns of key DEGs associated with the most significantly enriched pathway.

Results: In comparison with the sedentary control group, the treadmill exercise group exhibited statistically significant reductions in body weight, daily food intake, and serum levels of both total cholesterol and triglycerides, indicating substantial improvements in metabolic regulation. Histopathological analyses clearly revealed that treadmill exercise led to a marked decrease in the area of aortic atherosclerotic lesions and a notable reduction in lipid deposition, thereby confirming its inhibitory role in the progression of atherosclerosis. RNA-seq analysis identified a total of 164 exercise-induced DEGs in the aortic tissue, with 103 genes showing upregulated expression and 61 genes displaying downregulated expression. Functional enrichment analysis demonstrated that these DEGs were significantly enriched in multiple biological pathways, including hexose metabolic processes, apelin signaling pathway, and relaxin signaling pathway, with the circadian rhythm pathway emerging as the most prominently affected one. Further pathway analysis and protein-protein interaction (PPI) network construction highlighted four core circadian clock-related genes: Cry1, Per2, Nfil3, and Nr1d1. Real-time PCR validation experiments confirmed that exercise effectively upregulated the mRNA expression levels of Cry1, Per2, and Nfil3 while downregulating Nr1d1 expression, which was fully consistent with the findings obtained from the RNA-seq analysis.

Conclusion: Treadmill exercise exerts a mitigating effect on atherosclerosis in ApoE $^{-}$ / $^{-}$ mice through the precise modulation of gene expression in the aorta, with a particular emphasis on the regulatory role of the circadian rhythm pathway. The observed alterations in the expression of circadian clock genes suggest that exercise may exert its beneficial effects by regulating circadian oscillations, thereby influencing lipid metabolism, inflammatory responses, and vascular integrity, and ultimately retarding the progression of atherosclerosis. These findings provide novel insights into the molecular underpinnings of exercise-induced atheroprotection and highlight the potential of circadian rhythm modulation as a promising therapeutic target for the clinical management of atherosclerosis.

FAT-10 与冠心病患者的衰弱状态的相关性研究

段高雅 宋春莉

吉大二医院

目的：

本研究通过检测老年 CHD 患者血浆 FAT-10 水平，分析血浆 FAT-10 水平与 CHD 患者衰弱及各维度之间的相关性，探究 FAT-10 成为 CHD 合并衰弱的标志物的可能性，为该类患者的识别提供依据，并为治疗寻找潜在治疗靶点。

方法：

收集老年 CHD 患者血浆 FAT-10 患者 189 例，依据 EFS 量表对患者衰弱程度进行评估，分数为 0-17 分，分数越高认为衰弱程度

越重。根据衰弱评分可将衰弱分为五个程度，即非衰弱（0-4 分）、衰弱前期（5-6 分）、轻度衰弱（7-8 分）、中度衰弱（9-10 分）和重度衰弱（11-17 分）。应用酶联免疫吸附试验对 CAV-1 水平进行测定。采用 SPSS 对两组进行差异性分析。对所有连续型变量进行正态分布检验，对呈正态分布的变量以均值（标准差）进行描述，进行 t 检验; 对呈非正态分布的变量以中位数（四分位间距）进行描述，进行非参数秩和检验。对二分类变量应用阳性例数（百分比）进行描述，进行卡方检验。对上述分析中出现差异的连续型变量进行相关性分析，含有非正态分布的变量的相关性分析采用 Spearman 相关性分析。对有相关性的变量进行单因素及多因素逻辑回归分析。

结果：

1.FAT-10 浓度在衰弱组与非衰弱组之间具有统计学差异（$p < 0.05$）。

2. 多因素逻辑回归分析结果显示：FAT-10 是冠心病患者合并衰弱状态的独立危险因素（$P<0.05$）。

结论：

1. 根据 EFS 量表，FAT-10 水平在衰弱程度最高的患者中最高，与病变严重程度呈正相关，具有统计学意义。

2.FAT-10 可能成为冠心病患者衰弱程度的独立预测因子。

加速生物衰老与卒中、痴呆动态转化关系的研究：基于多状态模型的前瞻性队列分析

程文珂 康品方 （血脂学组委员） 唐碧 （肺动脉高压委员） 黄宇理

蚌埠医科大学第一附属医院

背景

随着全球人口老龄化进程不断加快，卒中与痴呆等神经血管性疾病所造成的疾病负担日益严峻。全球疾病负担研究显示，神经系统疾病导致的失能调整生命年数（DALYs）在各类疾病中排名首位，其中卒中和痴呆分别位列第一和第四，严重影响公众健康与医疗资源分配。已有研究证实卒中与痴呆之间存在双向关联，但多数研究仅聚焦于单一疾病或线性关系，缺乏对卒中与痴呆动态转化过程，特别是两者共病演进机制的系统性建模。传统以时间进展为基础的年龄指标在疾病研究中广泛应用，然而其难以揭示个体间在生理老化速率上的差异。近年来，生物年龄（Biological Age）作为一种整合多种临床生理指标的衰老量化工具，受到广泛关注。生物年龄加速（Biological Age Acceleration，BAA）即生物年龄相对于实际年龄的超前程度，已被发现与多种慢性疾病和死亡风险相关。然而，关于 BAA 在卒中、痴呆及其共病状态演变中的作用仍缺乏系统性的研究证据。

方法

本研究基于英国生物样本库前瞻性队列，纳入 220,236 名基线无卒中与痴呆的参与者。采用 Klemera-Doubal 方法（KDM-BA）和表型年龄（PhenoAge）两种算法估算生物年龄，并通过残差法计算生物年龄加速（BAA）。研究构建多状态 Cox 模型，评估 BAA 与卒中、痴呆、共病及死亡五种状态间八类转化路径的关联。模型调整年龄、性别、BMI、吸烟饮酒、体力活动、高血压、糖尿病、饮食质量及社会经济状况等混杂因素，并采用样条函数探索非线性关系。通过多种敏感性分析检验结果稳健性。

结果

经过随访中位时间为 15.31 年，观察到 4,436 例卒中、3,101 例痴呆、291 例卒中与痴呆共病，以及 17,375 例死亡事件。参与者的生物年龄加速水平通过 Klemera-Doubal 方法（KDM-BA）和表型年龄（PhenoAge）两种算法进行估算，并标准化为 Z 评分以进行后续分析。多状态模型结果显示，BAA 均与个体从健康状态过渡至卒中、痴呆及死亡状态显著相关。PhenoAge 每增加 1 个标准差，其与卒中的风险比（HR）为 1.16（95%CI：1.14–1.19），痴呆为 1.10（95%CI：1.06–1.13），全因死亡为 1.24（95%CI：1.23–1.25）；KDM-BA 显示相似甚至更强的关联（卒中 HR=1.30，痴呆 HR=1.07，死亡 HR=1.27，均 P<0.001）。此外，PhenoAge 加速还与卒中发生后的死亡（HR=1.09，95%CI：1.04–1.14）以及卒中合并痴呆状态下的死亡（HR=1.20，95%CI：1.08–1.33）存在统计学上的正相关。然而，BAA 对已发生卒中或痴呆个体进一步发展为共病的转换风险并无明显相关性（P 均 >0.05），且该结果在不同时间区间（0–1 年、1–3 年、>3 年）及亚组（年龄、性别、生活方式、疾病史）中均保持一致。暴露 - 反应分析显示，BAA 与卒中、痴呆及死亡之间呈非线性正相关，但对共病发展的影响则较为平缓，无明显剂量效应。

结论

本研究发现，生物年龄加速与卒中、痴呆和全因死亡的发生具有显著相关性，表明 BAA 在疾病早期阶段可能反映出更高的健康脆弱性。相比之下，BAA 与卒中或痴呆发生后的疾病进展关系不显著，提示其在疾病后期的指示价值有限。该研究支持将 BAA 作为识别神经血管性疾病早期高风险人群的潜在生物标志，强调延缓生物衰老过程对卒中及痴呆一级预防的潜在意义。

Novel Insights into the Role of Liver Function Biomarkers in Cardiovascular Health Assessment: A Cross-Sectional Study with Machine Learning Analysis

Tong-yu Peng

The Second Xiangya Hospital of Central South University

Aims: Cardiovascular diseases (CVDs) are the leading cause of death globally, creating a significant public health and socioeconomic burden. Despite advances in prevention and treatment, the predictive accuracy of current risk stratification tools has limitations. This highlights an urgent need to identify new, widely available, and independent indicators to improve early risk assessment and guide precision prevention strategies. Liver function tests (LFTs), such as gamma-glutamyl transferase (GGT), aspartate aminotransferase (AST), and alanine aminotransferase (ALT), are routinely measured biochemical markers. While previous studies have suggested links between individual LFTs and CVD, these investigations are often limited, and the nature of these associations, including potential non-linear relationships, remains poorly understood. This study aimed to systematically evaluate the independent associations between a comprehensive panel of liver function indicators and multiple standardized cardiovascular risk scores within a large, nationally representative U.S. population, employing both traditional statistical methods and advanced machine learning algorithms to validate the findings.

Methods: This cross-sectional study utilized data from 17,193 adults, aged 40-74 and without a history of major cardiovascular disease, who participated in the National Health and Nutrition Examination Survey (NHANES) from 2005 to 2018. The NHANES program is conducted by the U.S. Centers for Disease Control and Prevention (CDC) and uses a complex, multistage probability sampling design to be representative of the non-institutionalized U.S. population.

The exposure variables included a panel of serum liver function biomarkers: GGT, alkaline phosphatase (ALP), AST, ALT, lactate dehydrogenase (LDH), albumin, and globulin. Additionally, two clinically relevant derived ratios, the AST/ALT ratio and the albumin-to-globulin (A/G) ratio, were calculated. The primary outcomes were three widely recognized cardiovascular risk and health scores: Framingham Risk Score (FHS): Estimates the 10-year risk of a cardiovascular event. American Heart Association (AHA) Cardiovascular Health (CVH) Score: Based on the "Life's Essential 8," this score provides a comprehensive measure of cardiovascular health. American College of Cardiology/AHA (ACC/AHA) 10-year Hard Atherosclerotic Cardiovascular Disease (Hard ASCVD) Risk Score: Focuses on the risk of major events like myocardial infarction or stroke. A comprehensive statistical analysis was performed, accounting for the complex NHANES survey design. Methodologies included weighted quantile sum (WQS) regression to assess the combined effect of liver biomarkers, multivariable logistic regression to determine independent associations while adjusting for a wide range of demographic and clinical covariates, and restricted cubic splines (RCS) with piecewise regression to explore non-linear dose-response relationships and identify potential inflection points. To validate these findings and assess predictive utility, five machine learning models were developed: Logistic Regression (LR), Decision Tree (DT), Random Forest (RF), Light Gradient Boosting Machine (LightGBM), and eXtreme Gradient Boosting (XGBoost). The dataset was split into training (80%) and testing (20%) sets. Model performance was evaluated using the Area Under the Receiver Operating Characteristic Curve (AUC), accuracy, F1 score, and decision curve analysis (DCA). The best-performing models were interpreted using SHapley Additive exPlanations (SHAP) to clarify the contribution of each feature to the predictions.

Results: The analysis revealed significant and independent associations between specific liver function biomarkers and all three cardiovascular risk scores after full covariate adjustment. Elevated GGT levels were consistently and independently associated with a higher likelihood of adverse cardiovascular outcomes. The odds ratio (OR) for high FHS risk was 1.58 (95% CI: 1.38–1.82), for poor CVH was 1.83 (95% CI: 1.68–2.00), and for high Hard ASCVD risk was 1.63 (95% CI: 1.43–1.85) (all P < 0.001). WQS regression further identified GGT as the primary contributor to increased cardiovascular risk among the mixture of liver markers. Dose-response analysis confirmed a positive, non-linear relationship, with risk escalating more sharply at lower to moderate GGT levels. The AST/ALT ratio demonstrated a more complex, non-linear (U/J-shaped) relationship with cardiovascular risk. Initially, a higher AST/ALT ratio was protective, associated with a lower risk of adverse outcomes. However, piecewise regression analysis identified inflection points for each outcome (e.g., approximately 1.65 for FHS risk and 1.21 for Hard ASCVD risk). Beyond these thresholds, the protective effect diminished and, in some cases, began to reverse, suggesting that very high ratios may no longer be beneficial. Machine learning analysis confirmed and extended these findings. The LightGBM and XGBoost models demonstrated the best predictive performance, with AUCs reaching up to 0.9410 for FHS risk and 0.9484 for Hard ASCVD risk. SHAP interpretability analysis consistently ranked GGT as a significant predictor across all three outcomes, second only to major established risk factors like age and hypertension. The SHAP plots also visually confirmed the directional impact: higher GGT values increased predicted risk, while higher AST/ALT ratios (within the protective range) decreased it. Subgroup analyses suggested that some of these associations were modified by factors such as age, sex, and abdominal obesity, highlighting potential population-specific effects.

Conclusion: This comprehensive analysis of a large, nationally representative U.S. cohort provides strong evidence that routinely measured liver function biomarkers are significantly associated with cardiovascular risk. Specifically, elevated serum GGT is an independent predictor of higher 10-year CVD risk, poorer cardiovascular health, and a greater 10-year Hard ASCVD risk score. In contrast, the AST/ALT ratio exhibits a complex, non-linear U/J-shaped relationship, where its protective effect is most prominent within a specific range and diminishes at higher values. The validation of these associations with advanced machine learning models, coupled with SHAP analysis, underscores the potential of GGT and the AST/ALT ratio to add value to traditional risk factors for improved CVD risk stratification. Given that these liver function tests are inexpensive, automated, and widely available, their interpretation should extend beyond hepatology. Clinicians should consider these markers as potential early warning signals for cardiovascular risk, prompting more intensive screening and management, even in the absence of overt liver disease. These findings reinforce the importance of the liver-heart axis and suggest that maintaining liver health could be a key component of primary cardiovascular disease prevention. Further prospective studies are needed to confirm these non-linear relationships and to determine whether formally incorporating these biomarkers into clinical risk algorithms can enhance predictive accuracy and improve patient outcomes.

"暮光调色盘"——超高龄衰弱老人的多维疗护 1 例

禹程远 周思佳 董亦师 何浪涛 徐笑洋

深圳市人民医院

目的：

超高龄衰弱老人通常面对衰弱、多种老年综合征、急症及围手术期风险高等问题。本文回顾分析了深圳市人民医院老年医学科在 2014-2025 年间对一位典型病例的诊疗管理过程，旨在验证运用多种老年医学的核心技术进行多维度疗护全人全程管理，对改善患者预后、维护功能及减少并发症的有效性，并为老年医学科临

床实践提供参考。

关键词：衰弱，ACE，CGA，GIT，安宁疗护

材料与方法：

1. 患者基本资料：男性，1932 年出生，退休公职人员

2. 既往基础疾病：COPD、胆石症

3. 多维度疗护管理时间跨度：2014 年至 2025 年

4. 围手术期优化管理: 因胆石症诱发急性梗阻及感染反复入院，2015-2021 年间，患者接受胆囊切除术、胆总管支架植入术，十次 ERCP、网篮取石术、球囊扩张术、ENBD。优化围手术期评估管理：①手术决策：评估手术必要性、非手术替代方案的差异、可能的医源性损伤、患者意愿、术后造成的家庭负担等。②术前评估：认知、焦虑、谵妄、营养、生活自理能力、衰弱、用药、血容量等。③术后管理：血栓预防、控制疼痛、营养干预、管道护理、防跌倒、防坠床、放压疮等。④出院后随访、康复指导及健康宣教。

5. 急性期快速恢复：病程中曾因发热伴咳痰 3 日，夜间如厕后回房间过程中撞到茶几致跌倒入院，经 ACE 小组快速评估，初步诊断多根肋骨骨折、气胸、肺部感染、呼吸衰竭、脓毒性休克等，立即予无创呼吸机辅助呼吸、优化痰液引流、抗感染、稳定内环境、营养支持等综合诊疗，加强心理疏导。

6. 老年综合评估：在病程不同阶段，应用 Barthel 指数、洼田饮水试验、Morse、MoCA、CAM-S、HAMA、HAMD、FRAIL、MNA、BRADEN SCALE、疼痛强度评估（NRS）、PSQI、ICI-Q-SF、CCF-FIS、Roma II、PAGAR 等完善 CGA。

7. 老年医学跨学科诊疗：由老年科医生和护士、康复科医师、临床药师、临床营养师、中医师等组成 GIT 小组固定成员，结合具体病情邀请相关专科医生参加多学科讨论，共同制定个体化诊疗方案。

8. 安宁疗护：2025 年，随增龄导致多种机能衰退不可避免的进展，进入生命终末期，安宁疗护小组从“身”、“心”、“社”、“灵”方面予以安宁疗护方案，并组织召开家庭会议、制作人生回顾相册、举办最后的生日会等安宁疗护方案，加强对家属的哀伤辅导。

结果：

1、患者未发生围手术期危急重症。

2、经 ACE 疗护，急性期成功脱离生命危险。

3、经过 CGA 和 GIT 阶段，患者体重增加，躯体及社会功能恢复。

4、安宁疗护阶段，患者未遭受过度的医源性痛苦，患者家属未出现过激情绪。

结论：

以老年医学核心技术为基础，构建个体化全人全程多维度疗护，是应对高龄衰弱老人复杂医疗需求的有效手段。

A Machine Learning approach for predicting 3-year new-onset Cardiovascular Disease in an Elderly Chinese Population: A report from the Guangzhou Older Population Annual Health Examination Cohort and Guangzhou Heart Study

Jun-Rong Jiang[1], Jun Huang[1], Fan Weng[2], Yu-Feng Chen[2], Yu-Mei Xue[1]

1. Institute of Geriatrics, Guangdong Cardiovascular Institute, Guangdong Provincial Key Laboratory of Clinical Pharmacology, Guangdong Provincial People's Hospital (Guangdong Academy of Medical Sciences), Southern Medical University, Guangzhou, China

2. Yuexiu District Center for Disease Control and Prevention, Guangzhou, China

Background Cardiovascular disease (CVD) persists as the primary cause of mortality in China's elderly population, accounting for over 44% of urban and 46% of rural deaths according to the 2021 National CVD Report. Yet existing clinical risk scores (QRisk3, PCEs, FGCRS) exhibit suboptimal performance in this demographic due to ethnic variations in risk profiles and regional healthcare disparities. This critical gap impedes precision prevention strategies, particularly given China's rapidly aging society where CVD incidence is projected to rise by 50% by 2030. Our study directly addresses this need by developing and validating machine learning models for predicting 3-year new-onset CVD using routinely collected electronic health record (EHR) data from Chinese elderly individuals.

Methods We derived comprehensive clinical data from 16,868 participants (aged ≥ 65 years) in the Guangzhou Annual Health Examination Cohort, encompassing 27 variables across four domains: 1) Disease histories (hypertension, diabetes, chronic kidney disease validated by ICD-10 codes); 2) Medication use (antihypertensive agents, antiplatelet drugs verified via pharmacy records); 3) Biomarkers (fasting glucose, lipid profiles, systolic/diastolic blood pressure measured through standardized protocols); and 4) Sociodemographic factors (age, gender, smoking status). Three machine learning algorithms—logistic regression, support vector classifier, and gradient boosting with hyperparameter optimization via grid search—were trained to predict composite CVD outcomes (coronary heart disease, stroke, or atrial fibrillation). External validation utilized 2,066 independent subjects from the Guangzhou Heart Study. Model performance was rigorously evaluated against conventional risk scores using area under the curve (AUC), net reclassification improvement (NRI), calibration plots, and decision curve analysis.

Results During the 3-year follow-up, the derivation cohort exhibited a 5.20% CVD incidence rate (877/16,868 events), while the validation cohort had 5.86% (121/2,066 events). Gradient boosting demonstrated superior internal discrimination (AUC 0.78, 95% CI 0.74–0.81), significantly outperforming QRisk3 (AUC 0.63, ΔAUC=0.15; p<0.001), PCEs (AUC 0.61, p<0.001), and FGCRS (AUC 0.60, p<0.001). External validation confirmed robustness (AUC 0.70, 95% CI 0.64–0.75) with an NRI of 0.38 and adequate calibration (Hosmer–Lemeshow test p=0.32). Key predictors identified included systolic blood pressure (mean SHAP value contribution: 24%), age (21%), total cholesterol (18%), fasting glucose (15%), and LDL-C (12%), with novel contributions from TC/HDL-C ratio (8%) and antiplatelet medication use (7%). Subgroup analyses showed consistent performance across gender and age strata.

Discussion Our machine learning models overcome limitations of traditional risk scores by capturing complex nonlinear relationships (e.g., J-curve association between diastolic blood pressure and CVD risk where values 90 mmHg increased event risk) and incorporating underutilized EHR variables like dynamic treatment adherence metrics. The heightened importance of fasting glucose versus diabetes history reflects ethnic-specific pathophysiology in glucose metabolism among Chinese elderly. While antiplatelet medication's predictive role suggests pharmacotherapy adherence as a modifiable risk factor, regional cohort origins necessitate validation in multi-center studies across Northern and Western China. For immediate clinical translation, these models enable early high-risk identification through automated community assessment systems, facilitating personalized prevention protocols (e.g., intensive lipid control for high-risk subgroups) and optimizing resource allocation in primary care. Future integration with real-time monitoring data from wearables could further enhance predictive accuracy while maintaining feasibility in resource-limited settings.

Conclusion Machine learning algorithms significantly improve CVD risk prediction in Chinese elderly populations compared to established clinical scores, demonstrating both statistical superiority (ΔAUC up to 0.18) and clinical utility (NRI=0.38). Implementation of automated assessment systems based on these models holds transformative potential for scaling precision prevention in community-based healthcare, particularly within China's rapidly aging society.

Gut Microbiota Metabolite Phenylacetic Acid Regulates Cardiac Senescence through Histones Phenylacetylation

Xiang-Rui Qiao

The First Affiliated Hospital of Xi'an Jiaotong University

Background:

Population ageing has become one of the global trends of our time. It is expected that by 2050, the global population over 65 years old will reach 1.6 billion. China has also entered a stage of moderate population ageing. The number of people aged 65 and over will reach 209.78 million at the end of 2022, representing 14.9% of the total population. How to actively cope with ageing has become a problem and a challenge that we must face. Aging increases the risk of many common diseases, especially cardiovascular disease, which is the leading cause of death in people over 65 years of age. Therefore, cardiac senescence is a key link in the aging of the organism. Improving cardiac senescence is of great significance for healthy aging, slowing down aging and even reversing aging. The gut microbiota is colonized in the human digestive tract since birth and changes gradually with age. Studies have shown that there are distinct differences in the microbiota profile of the gut between the elderly and the young. However, the relationship between the gut microbiota and cardiac senescence has not yet been elucidated. The present study was designed to investigate the causal relationship between the gut microbiota and cardiac senescence by regulating the gut microbiota. And to identify the key gut microbiota metabolites and specific mechanisms that mediate cardiac senescence, to provide new ideas and targets for the prevention and treatment of senescence.

Objectives:

Elucidating the causal relationship between gut microbiota dysbiosis and cardiac senescence and searching for metabolites that may have a pivotal role.Unraveling a new mechanism of gut microbiota/phenylacetic acid/histone phenylacetylation/cardiac senescence and providing a theoretical basis for the microbiota - senescence axis.Exploring the feasibility of fecal microbiota transplantation such as youth colony transplantation or specific bacteria supplementation to ameliorate cardiac aging and to provide new strategies to combat aging.

Methods:

Feces, serum, and cardiac tissues were collected from young (2-month-old) and aged (18-month-old) mice after cardiac ultrasound testing. On the one hand, to clarify the phenotypes of cardiac senescence and

gut microbiota dysbiosis, feces were subjected to 16S ribosomal RNA (16S rRNA) sequencing, serum N-terminal pro-brain natriuretic peptide was detected, cardiac senescence-related markers were detected using immunoblotting, and pathological staining was performed to detect cardiac fibrosis and senescence. On the other hand, to explore the metabolites that may play a role, feces, serum, and hearts from both groups of mice were subjected to metabolomics.The gut microbiota of aged mice was transplanted to young mice, and the feces of donor and recipient mice were collected for 16S rRNA sequencing to determine whether the fecal microbiota transplantation was successful. In order to clarify the causal relationship between microbiota dysbiosis and cardiac senescence, immunoblotting and pathological staining were then used to detect whether the young mice receiving gut microbiota transplants from aged mice showed cardiac senescence phenotypes.Phenylacetic acid was found by comparing differential metabolites shared in feces, serum, and heart of young and old mice. In vitro and in vivo experiments were then performed to clarify that phenylacetic acid does induce cardiomyocyte and cardiac senescence. The presence of a novel post-translational modification of histones, phenylacetylation, was then identified by high-performance liquid chromatography-tandem mass spectrometry and specific antibodies, and its association with cardiac senescence was verified.The gut microbiota of young mice was transplanted to aged mice, and the feces of donor and recipient mice were collected for 16S rRNA sequencing to clarify whether the fecal microbiota transplantation was successful. In order to determine the feasibility of modulating the gut microbiota to ameliorate cardiac senescence, immunoblotting and pathological staining were then used to detect whether the cardiac senescence phenotype improved in aged mice that received young gut microbiota transplants.

Results:

Compared with young mice, aged mice developed left ventricular posterior wall hypertrophy, decreased cardiac function, cardiomyocyte hypertrophy, interstitial fibrosis, and cardiomyocyte senescence. The profile of the intestinal microbiota of aged mice is remarkably dissimilar to that of young mice, with a significant decrease in the Firmicutes and an increase in the Bacteroides, Proteobacteria, Cyanobacteria and Epsilonbacteraeota.Cleaning the gut microbiota from young mice with antibiotics followed by co-housing with aged mice successfully colonized the gut microbiota of aged mice in young mice. Transplantation of gut microbiota from aged mice caused left ventricular posterior wall hypertrophy, decreased cardiac function, cardiomyocyte hypertrophy, interstitial fibrosis, and cardiomyocyte senescence in young mice.Phenylacetic acid, which is simultaneously increased in feces, serum, and heart of aged mice, induces cardiomyocyte senescence in vivo and in vitro in a concentration-time-dependent manner.There is a mass shift of +118.0419 Da at the histone lysine site. And the fracture pattern and retention time of this peptide segment are consistent with the peptide with phenylacetyl group modification synthesized in vitro with the same amino acid sequence. It indicates the existence of a novel post-translational modification of histones, phenylacetylation. The level of this modification increased with increasing concentrations of phenylacetic acid in both rat cardiomyocytes (H9c2) and human cervical cancer cells (Hela), suggesting that the modification is widespread and that phenylacetic acid is its precursor molecule. Meanwhile, we also identified 14 histone sites for this novel modification.After transplantation of the gut microbiota of young mice, the proportion of Firmicutes in the gut microbiota of aged mice increased, the proportion of Bacteroidetes decreased, and the levels of phenylacetic acid in serum and heart decreased. Young microbiota improved left ventricular posterior wall hypertrophy, cardiac function decline, cardiomyocyte hypertrophy, interstitial fibrosis, and cardiomyocyte senescence in aged mice. Immunohistochemistry shows that the level of histone phenylacetylation modification in the heart of aged mice decreases after transplantation of young microbiota.

Conclusions:

Cardiac senescence and gut microbiota disorders coexist in aged mice. Gut microbiota of aged mice induces cardiac senescence in young mice via its metabolite phenylacetic acid.Phenylacetic acid, as a precursor molecule for phenylacetylation, a novel modification of histones, promotes histone phenylacetylation in cardiomyocytes, which further activates the expression of senescence-associated genes and ultimately leads to cardiomyocyte senescence.Transplantation of gut microbiota in young mice reduces phenylacetic acid levels in serum and heart, inhibits histone phenylacetylation levels in cardiomyocytes, and improves cardiac senescence in aged mice.

手厥阴心包经刮痧疗法改善老年心肌缺血患者胸痛的研究

翟亚仙 [1] 刘雨丹 [1] 杨锦湄 [2]

1. 云南中医药大学

2. 昆明市中医医院

目的: 探讨手厥阴心包经刮痧疗法对老年心肌缺血患者胸痛的临床疗效及安全性。通过量化评估该疗法对胸痛程度、发作频率、心功能指标及生活质量的影响，为老年患者提供一种非药物性辅助治疗选择，弥补现有西医治疗在长期用药依从性及副作用方面的局限性，同时验证经络理论在心血管康复中的科学价值。

方法：采用随机对照试验设计，纳入 120 例符合 WHO 心肌缺血诊断标准的老年患者（年龄 65-80 岁），随机分为试验组（n=60）和对照组（n=60）。对照组予常规西药治疗（阿司匹林 + 硝酸酯类 + 他汀类），试验组在常规治疗基础上加用手厥阴心包经刮痧疗法：沿天池、天泉、曲泽、郄门、间使、内关、大陵、劳宫、中冲 9 穴，以 45°角单向刮拭，力度以局部潮红为度，每周 3 次，持续 4 周。主要评价指标为视觉模拟量表（VAS）胸痛评分；次要指标包括心绞痛发作频率、心电图 ST 段压低幅度、西雅图心绞痛量表（SAQ）评分及硝酸甘油减停率。采用 SPSS 25.0 进行统计分析，计量资料以均数 ± 标准差（x±s）表示，组间比较采用 t 检验和重复测量方差分析，计数资料采用 χ^2 检验。

结果：治疗后试验组疗效显著优于对照组：胸痛程度：VAS 评分试验组降低（4.2±0.8）分，对照组降低（2.1±0.9）分，组间差异有统计学意义（t=15.32, P<0.01）；发作频率：试验组心绞痛周均发作次数减少（3.5±1.2）次，降幅 70.2%，显著高于对照组的 42.1%（t=9.47, P<0.01）；心电图改善：试验组 ST 段压低恢复≥0.1mV 的比例达 85.0%(51/60)，显著高于对照组的 63.3%(38/60)（χ^2=7.89, P<0.01）；硝酸甘油减停率：试验组为 76.7%（46/60），对照组为 48.3%（29/60）（χ^2=10.24, P<0.01）。未出现皮肤破损或感染等严重不良反应。

结论：手厥阴心包经刮痧疗法可有效缓解老年心肌缺血患者胸痛程度，减少心绞痛发作频率，改善心肌供血及生活质量，且安全性良好。该疗法作为非药物干预手段，可成为老年患者综合治疗的补充方案，其机制可能与调节自主神经功能、促进局部微循环有关，建议在规范化操作下临床推广，未来需深入探讨其分子机制及长期效应。

The Role of Lifestyles in Older Adults with Calcific Aortic Valve Disease: A Retrospective Case-Control Study from China

Jun-Rong Jiang, Hai Deng, Yu-Mei Xue

Institute of Geriatrics, Guangdong Cardiovascular Institute, Guangdong Provincial Key Laboratory of Clinical Pharmacology, Guangdong Provincial People's Hospital (Guangdong Academy of Medical Sciences), Southern Medical University, Guangzhou, China

Background: Calcific aortic valve disease (CAVD), as a common cardiovascular disease in older adults, ranges from mild thickening of the valve, known as aortic valve sclerosis (ASc), to severe impairment of the valve motion, which is termed aortic stenosis (AS). CAVD is independently associated with an increased risk of coronary events, stroke, cardiovascular mortality, and all-cause mortality. Due to the aging population, CAVD is gradually becoming a public health problem worldwide. Furthermore, the global incidence, prevalence, and deaths attributed to CAVD have significantly increased over the past three decades, underscoring the growing urgency to address this condition.

Objectives: Although previous studies have revealed that age, sex, diabetes mellitus, obesity, hypertension, smoking, and lipid levels are associated with the risk of CAVD, the role of lifestyles in CAVD remains unclear due to limited available data. The aim of this study was to determine the prevalence of CAVD in older adults and to identify the role of lifestyles in CAVD. Specifically, this study sought to explore how specific lifestyle factors, such as dietary habits and physical activity, influence the development and progression of CAVD.

Methods: The study population was based on the large epidemiological study of cardiovascular disease in the Guangzhou Heart Study. 3397 participants in the baseline study and 2213 in the follow-up study were included in the analysis. Information on lifestyles was collected via a comprehensive questionnaire, and CAVD was diagnosed using echocardiography. The differences in age, sex, BMI, medical histories, lifestyle behaviors, and dietary preferences between CAVD and normal individuals were compared. Additionally, the study utilized multivariate logistic regression models to investigate the associations between CAVD and various lifestyle factors, ensuring a robust analysis of the data.

Results: 1239 participants were diagnosed with CAVD at baseline, accounting for 36.5% of the cohort. Age, overweight, hypertension, hyperuricemia, smoking, and exercise were independently associated with CAVD. The odds ratio was 1.088 for each year increase in age. Overweight, hypertension, and hyperuricemia were associated with 1.202-fold, 1.311-fold, and 1.210-fold excess risks, respectively. Smoking conveyed a 38% excess risk. Compared with daily exercise, non-exercise was associated with a 47% increase in risk. In terms of dietary preferences, white meat, high salt food, nuts, and coffee were independently associated with CAVD. Among them, white meat, fruits, nuts, and coffee seemed to be protective factors for CAVD, while high salt food was a risk factor. Importantly, the study also found that the progression from ASc to AS was relatively slow, occurring in only 2 out of 768 participants over a 3-year follow-up period.

Conclusions: This study provides a comprehensive understanding of the role of lifestyles in CAVD. Aging, overweight, hypertension, hyperuricemia, smoking, and high salt food were the risk factors for CAVD, while exercise and intake of white meat, fruits, nuts, and coffee were the protective factors for CAVD. These findings may be helpful to develop more effective and efficient CAVD prevention and treatment strategies. Moreover, the study highlights the importance of early intervention and lifestyle modifications to mitigate the risk of CAVD in older adults, particularly in regions with rapidly aging populations.

新疆社区老年人共病的民族和地理差异：一项横断面研究

卓娅

新疆维吾尔自治区人民医院

背景：多重慢性病（MCC）指同时存在两种或两种以上慢性疾病。老年人 MCC 发病率较高，且随年龄增长而增加。研究表明，MCC 与不良结局增加相关，也与老年人群更高的死亡率、身体功能下降及生活质量差相关。本文首次提供了中国新疆社区老年人中 MCC 患病率的民族和地域差异数据。

方法 采用多阶段随机抽样方法，于 2019 年 1 月至 2019 年 12 月对新疆南部、北部和东部的社区老年人进行流行病学调查。共有 87,000 名参与者自愿参加，应答率为 96.67%；排除了 490 名数据不完整的参与者，最终分析了 86,510 名参与者的数据。

结果 我们的分析显示，高血压（51.5%）、肥胖（27.0%）、糖尿病（16.9%）、心脏病（8.2%）和焦虑 / 抑郁（4.5%）是新疆五种主要的慢性疾病。调查人群中 MCC 的患病率为 33.4%（95%CI, 33.1–33.7）。女性患病率为 36.6%（95%CI, 36.1–37.0），高于男性（30.0%，95%CI, 29.5–30.4）。60-69 岁、70-79 岁、80-89 岁和≥ 90 岁老年人的 MCC 患病率分别为 32.7%（95%CI, 32.2–33.3）、34.3%（95%CI, 33.9–34.7）、32.5%（95%CI, 31.7–33.3）和 25.9%（95%CI, 23.5–28.3）。就民族而言，维吾尔族、汉族、哈萨克族、回族和蒙古族的 MCC 患病率分别为 31.3%（95%CI, 30.9–31.7）、34.4%（95%CI, 33.9–35.0）、40.4%（95%CI, 39.1–41.8）、40.8%（95%CI, 38.9–42.7）、44.4%（95%CI, 38.1–50.6）。未受教育、受教育 1-6 年、7-9 年和 10 年以上人群的 MCC 患病率分别为 32.8%(95%CI, 32.1–33.5)、31.7%(95%CI, 31.2–32.1)、36.0%(95%CI, 35.3–36.7）和 39.2%（95%CI, 38.1–40.3）。在按年龄、性别、吸烟、饮酒和教育水平进行调整后，二元逻辑回归分析显示，与新疆东部相比，南部地区发生 MCC 的风险增加（OR, 1.418; 95%CI, 1.367–1.471），而北疆的风险更高（OR, 2.021; 95% CI, 1.944–2.102）。与维吾尔族相比，汉族、哈萨克族、回族和蒙古族发生 MCC 的风险增加，分别为（OR, 1.075; 95% CI, 1.040–1.111）、（OR, 1.414; 95% CI, 1.332–1.501）、(OR, 1.515; 95% CI, 1.396–1.644）、(OR, 1.566; 95% CI, 1.216–2.017）。

结论 新疆社区老年人多重慢性病存在民族和地域差异。居住在北疆和南疆的老年人以及汉族、哈萨克族、蒙古族和回族老年人具有更高的 MCC 风险。

Impact of Impaired Renal Function on Cognitive Performance Among Patients With Coronary Artery Disease

Zehao Zhao, Yong Zeng

Beijing Anzhen Hospital, Capital Medical University

Background: Patients with CAD are at increased risk of cognitive impairment, which adversely affects their prognosis. Although renal function and metabolic risk factors are known to influence cognition, their contributions to cognitive impairment in CAD patients and the underlying mechanisms remain unclear.

Methods: This retrospective cross-sectional study included 17,121 patients with CAD who underwent cognitive assessments as well as evaluations of renal function and metabolic risk factors. The associations between renal function and overall cognitive performance, as well as specific cognitive domains, were evaluated. Logistic regression and restricted cubic spline analyses were used to assess the impact of renal function on the risks of mild cognitive impairment (screened by Montreal Cognitive Assessment) and dementia (screened by Mini-Mental State Examination). Mediation analysis was conducted to examine the causal pathways linking metabolic risk factors, impaired renal function, and cognitive impairment.

Results: A total of 17,121 patients with CAD were included in the study, with a mean age of 61.6 (9.35) years, and 27.5% were female. As CKD stage increased, patients tended to be older, the proportion of female patients increased, and education levels declined. The prevalence of metabolic risk factors, including hypertension, diabetes, elevated triglycerides, and uric acid, also rose with advancing CKD stage. Patients with more severe CKD had higher rates of comorbid stroke, atrial fibrillation, and heart failure. Furthermore, as renal function worsened, the prevalence of MCI (identified by MoCA) and dementia (defined by MMSE) increased progressively. eGFR was significantly positively correlated with all MoCA and MMSE subdomain scores, indicating that better renal function is associated with superior cognitive performance. However, the generally small effect sizes suggest that the strength of these associations is modest. Across different subgroups, the significant positive associations between eGFR and overall cognitive function, as reflected by total MoCA and MMSE scores, remained consistent. However, the correlations between eGFR and specific cognitive domains varied across subgroups. Univariate and multivariable logistic regression analyses showed that worsening renal function was associated with an increased risk of cognitive impairment, with renal function evaluated using both eGFR and CKD stages. Advanced CKD stages were significantly associated with a higher risk of MCI (adjusted OR for stages 4–5: 1.62; 95% CI: 1.11–2.37) and dementia (adjusted OR for stages 4–5: 1.60; 95% CI: 0.94–2.75). In contrast, higher eGFR was associated with a lower risk of MCI (adjusted OR per 1 SD increase: 0.92; 95% CI: 0.88–0.96) and dementia (adjusted OR per 1 SD increase: 0.88; 95% CI: 0.82–0.93). The restricted cubic spline curves demonstrated consistent results, indicating that the risks of MCI and dementia significantly decreased with higher eGFR levels. Subgroup analyses demonstrated that the inverse association between a 1-standard deviation increase in eGFR and the risk of MCI remained robust and statistically significant across all subgroups. Moreover, a significant interaction between eGFR and sex was detected. Hypertension, diabetes, and high LDL-C were significantly associated with an increased risk of MCI, while elevated uric acid levels were associated with a decreased risk. Diabetes was significantly associated with an increased risk of MCI, with eGFR mediating 21.4% of the total effect in the unadjusted model and 13.3% in the adjusted model. Similarly, hypertension demonstrated a significant total effect on MCI risk, with eGFR mediating 29.5% of the effect in the unadjusted model and 12.6% in the adjusted model. These results indicate that reduced renal function partially mediates the adverse impact of diabetes and hypertension on cognitive impairment.

Conclusion: In CAD patients, impaired renal function contributes to cognitive impairment and mediates the effects of hypertension and diabetes.

复发恐惧在心房颤动导管消融术后患者人格特质与自我管理行为间的中介效应研究

王纪哲 柳臣兰 卢晓虹

青岛大学附属医院

目的 探讨心房颤动导管消融术后患者复发恐惧在人格特质与自我管理行为间的中介效应，为临床护理人员针对性改善患者自我管理行为提供参考。**方法** 应用便利抽样法，于 2024 年 4 月至 7 月选取青岛市某三级甲等医院心血管内科门诊选取 295 名心房颤动导管消融术后患者为研究对象。采用一般资料调查表、中国大五人格问卷极简版、心房颤动患者导管消融术后复发恐惧量表、心房颤动患者自我管理能力量表进行问卷调查。运用结构方程模型验证复发恐惧在人格特质与自我管理行为之间的中介作用。**结果** 神经质与复发恐惧存在显著正相关（P < 0.01），与自我管理行为之间存在显著负相关（P < 0.01）。严谨性、宜人性、开放性和外向性与复发恐惧存在显著负相关（P < 0.01），与自我管理行为之间存在正相关性（P < 0.05）。中介效应分析显示：复发恐惧在神经质（β=-0.021，P < 0.05）、宜人性（β=0.093，P < 0.01）、开放性（β=0.090，P < 0.01）与自我管理行为之间起到部分中介作用，中介效应分别占总效用的 29.17%、32.38%、30.49%。**结论** 复发恐惧是心房颤动导管消融术后患者神经质、宜人性和开放性人格特质与自我管理行为的中介变量。临床护理人员应根据上述人格特质认知与行为特点，协助患者克服术后复发恐惧，调动患者参与自我管理的积极性，全面提升患者自我管理行为。

心理疏导结合赋能教育对改善老年慢性心力衰竭患者抑郁情绪及治疗依从性的随机对照研究

刘妞妞 刘华芬 戴狄莎

武汉大学人民医院

目的：探讨基于认知行为疗法（CBT）原则的结构化心理疏导联合赋能教育对老年慢性心力衰竭（CHF）患者抑郁情绪、治疗依从性及临床预后的影响。

材料与方法：采用前瞻性随机对照设计，纳入 2024 年 1 月 - 2025 年 1 月我院心内科住院的老年 CHF 患者（≥ 60 岁）120 例。纳入标准：NYHA II-III 级、PHQ-9 抑郁评分≥ 5 分。排除重度认知障碍或精神疾病史。采用随机数字表法分为干预组（n=60）和对照组（n=60）。（1）对照组：接受常规心衰护理（用药指导、饮食教育、症状监测）。（2）干预组：在常规护理基础上实施为期 12 周的结构化干预：1）心理疏导：每周 1 次个体化 CBT（40 分钟 / 次），聚焦负性思维重构、行为激活训练及压力管理；2）赋能教育：采用 “5A 模式”（Ask, Advise, Assess, Assist, Arrange），通过情景模拟、自我管理手册及家属参与，强化用药依从性、限盐执行及体重监测技能。评价指标：基线、干预后 12 周评估：① 抑郁程度（PHQ-9 量表）；② 治疗依从性（MMAS-8 量表，≥ 6 分为依从）；③ 临床结局：NT-proBNP、6 分钟步行距离（6MWD）、30 天内再住院率。统计分析采用 SPSS 25.0，组间比较用 t 检验 /χ^2 检验，P<0.05 为显著。

结果：1. 抑郁改善：干预组 PHQ-9 评分由（8.2±1.5）分降至（3.1±1.2）分，降幅显著高于对照组（8.0±1.6 → 6.3±1.4 分）（T=12.37, P<0.001）；2. 治疗依从性：干预组 MMAS-8 达标率（86.7%）显著高于对照组（56.7%）（χ^2=12.89, P=0.001）；3. 临床指标：1）NT-proBNP：干预组降幅更大（P=0.003）；2）6MWD：干预组增加（68.5±12.3）m，优于对照组（41.2±10.7）m（P<0.001）；3）30 天再住院率：干预组（6.7%）显著低于对照组（21.7%）（χ^2=5.94, P=0.015）。

结论：基于 CBT 的心理疏导联合赋能教育可有效缓解老年 CHF 患者抑郁情绪，提升治疗依从性，并通过改善神经内分泌激活及功能储备降低短期再住院风险，为构建老年心衰心理行为干预模式提供循证依据。

Impact of Combined Cognitive and Physical Impairments on Long-term Prognosis in Elderly Cardiovascular Patients: A Prospective Cohort Study

Yujia Liu[1], Hua Wang[2]

1. Department of Cardiology, Beijing Hospital, National Center of Gerontology, Institute of Geriatric Medicine, Chinese Academy of Medical Sciences & Peking Union Medical College, Beijing, China

2. Department of Cardiology, Beijing Hospital, National Center of Gerontology; Institute of Geriatric Medicine, Chinese Academy of Medical Sciences

Background

Cardiovascular disease (CVD) is the leading cause of morbidity and mortality worldwide, especially among the elderly. As the population ages, the burden of CVD increases, and elderly patients often experience multiple comorbidities, including both physical and cognitive impairments. While the impact of physical impairment on the prognosis of CVD patients is well documented, the effect of concurrent cognitive decline, especially when combined with physical limitations, remains less understood and often overlooked. This study investigates how both physical and cognitive impairments influence long-term outcomes, particularly mortality, in elderly CVD patients.

Objective

The aim of this study was to evaluate the relationship between physical and cognitive function and long-term survival outcomes in elderly cardiovascular disease patients. Using the Short Physical Performance Battery (SPPB) to assess physical function and the Mini-Mental State Examination (MMSE) to measure cognitive function, this study explores the combined effect of these impairments on mortality risk over a 5-year follow-up period. We hypothesized that the combination of physical and cognitive impairments would be associated with a significantly higher risk of mortality compared to either impairment alone.

Methods

This prospective cohort study included 524 elderly patients (≥ 65 years) who were hospitalized at Beijing Hospital from September 2018 to April 2019. At baseline, patients underwent a comprehensive assessment that included demographic, clinical, laboratory, and functional evaluations. Cognitive function was assessed using the MMSE, and physical performance was measured using the SPPB, which includes tests of balance, gait speed, and chair stand time. The patients were then followed for up to 5 years to track all-cause mortality. The primary outcomes were all-cause mortality rates, and survival was analyzed using Kaplan-Meier curves. The impact of cognitive and physical impairments on mortality risk was further analyzed using Cox proportional hazards models, adjusting for relevant covariates.

Results

Among the 524 patients, 28.2% had physical impairment (SPPB ≤ 6), and 12.4% had cognitive impairment (MMSE score below the threshold for their education level). The combination of both impairments was associated with a 5.47-fold increased mortality risk (HR: 5.47; 95% CI: 2.78-10.78; p

Conclusion

Currently, cognitive function is often under-assessed in cardiology departments, leading to overlooked high-risk patients. This study demonstrates that combined physical and cognitive impairments are highly prevalent in elderly CVD patients and are strong predictors of poor long-term outcomes. The results highlight the importance of assessing both cognitive and physical function in clinical practice, as these factors can significantly influence mortality risk. Regular screening for both types of impairments can aid clinicians in identifying high-risk patients who may benefit from early and tailored interventions. These interventions could include physical rehabilitation programs for those with physical impairments and cognitive training or support for those with cognitive decline. The integration of these assessments into routine care for elderly cardiovascular patients could lead to more informed clinical decision-making, improved management strategies, and ultimately better patient outcomes in this high-risk population. Future research should explore the effectiveness of combined physical and cognitive interventions, with larger, multicenter studies to validate the benefits of such approaches in improving patient outcomes.

Keywords: cognitive impairment, physical impairment, cardiovascular disease, all-cause mortality, elderly inpatients

URL: https://www.chictr.org.cn/; Unique identifier: ChiCTR1800017204

衰弱表型介导的老年冠心病患者心脏康复抵抗机制及个体化运动干预策略

罗婷

武汉市中心医院

目的

针对老年冠心病患者心脏康复疗效差异大的临床难题，揭示衰弱表型（Frailty Phenotype）导致康复抵抗的分子机制，并开发基于衰弱分层的精准运动干预方案。

方法

采用转化医学研究设计：

1. 机制研究：纳入 286 例≥ 75 岁老年冠心病患者，通过 Fried 衰弱标准分组，检测骨骼肌线粒体功能（高分辨率呼吸测定法）、炎症因子（IL-6、TNF-α）及运动能力（6 分钟步行试验）的关联性；

2. 干预研究：将 210 例衰弱前期 / 衰弱期患者随机分为：

精准组（n=105）：基于衰弱程度的抗阻 - 有氧复合运动（FRAIL-EX 方案）

常规组（n=105）：标准心脏康复

干预 12 周后评估主要终点（峰值摄氧量改善≥ 10%）及次要终点（衰弱评分、MACE 发生率）。

结果

1. 机制层面：衰弱患者骨骼肌线粒体 ATP 生成降低 38%（p<0.001），且与 IL-6 水平呈负相关（r=-0.52）；

2. 干预效果：精准组达标率显著高于常规组（67.3% vs 42.1%，p=0.002），衰弱逆转率提高 2.1 倍（p<0.01）；

3. 安全性：两组不良事件无统计学差异（p>0.05）；

4. 组学分析: 精准组干预后线粒体生物合成相关基因（PGC-1α）表达上调 3.2 倍。

结论

衰弱表型通过线粒体功能障碍介导心脏康复抵抗，基于衰弱分层的个体化运动方案可显著改善老年患者康复效果，为老年心脏康复提供精准化新策略。

医师对高龄非瓣膜性心房颤动患者卒中预防问题及应对措施态度的调查

刘俊鹏

北京医院

目的 基于抗凝管理策略，探讨医师对高龄房颤（atrial fibrillation，AF）患者卒中预防存在问题和可行措施的态度，以及不同医师群体的态度差异。

方法 自行设计调查问卷，内容包括对目前高龄非瓣膜性房颤（non-valvular atrial fibrillation，NVAF）人群卒中预防待解决的问题和改善措施。于 2023 年 11 月至 2024 年 1 月对北京地区 19 家不同级别医院的 270 名医师进行问卷调查。对问卷进行描述性统计分析，并从医院级别、专业方向进行组间比较。

结果 对高龄 NVAF 人群卒中预防目前待解决的问题，医师选择最多的三项为“卫生服务的可及性”（67.4%）、“不足的循证证据”（51.1%）、“患者依从性”（51.1%）。三甲医院医师更重视“不足的循证证据”（χ^2=5.796，P < 0.05），非三甲医院医师更重视“药品可及性”（χ^2=3.951，P < 0.05）；心内科医师更重视“不足的循证证据”（χ^2=9.131，P < 0.01），非心内科医师更重视“卫生服务可及性”（χ^2=8.998，P < 0.01）和“医联体内分工配合”（χ^2=11.167，P < 0.01）。对改善措施，受访医师选择最多的四项为“临床医学研究”（83.7%）、“管理模式研究”（81.1%）、“患者教育”（79.3%）、“医师培训”（70.0%）。非心内科医师更看重“患者教育”（χ^2=10.046，P < 0.01）、“医师培训”（χ^2=4.119，P < 0.05）和“远程医疗服务”（χ^2=4.348，P < 0.05）。

结论 对高龄 NVAF 人群卒中预防，医师认为最应解决的问题是卫生服务的可及性、循证证据不足和患者依从性，有效改善措施为开展临床医学研究、管理模式研究、患者教育、医师培训。

Analysis of risk factors for hospital-acquired pneumonia in schizophrenia

null null[1,2]

1. People’s Hospital of Chongqing Rongchang Distric

2. Chongqing Mental Health Center

Background: Hospital-acquired pneumonia is one of the most important causes of recurrent illness, disease progression, and even death during hospitalization. Patients with schizophrenia have the special characteristics of their disease, and at the same time, the occurrence of hospital-acquired pneumonia is more common among patients with schizophrenia due to the prolonged stay in closed wards, accompanied by various factors such as age, gender, and nutritional status.

Methods: The PubMed, Web of Science, Cochrane Library, China National Knowledge Infrastructure (CNKI), and China Biomedical Literature Database (CBM) databases were searched with a timeframe of build to February 2024 to collect studies on factors influencing hospital-acquired pneumonia in patients with schizophrenia. Two researchers independently screened the literature, extracted data, and analyzed them.

Results: A total of 5 papers including 85246 patients were included in the literature, which suggested that benzodiazepines (especially the use of clozapine), combination of antipsychotics, mood stabilizers, modified electroconvulsive therapy (MECT), duration of hospitalization, underlying diseases, hyperglycemia, and salivation/dysphagia were important risk factors for hospital-acquired pneumonia in schizophrenia patients, and that advanced age, smoking and alcohol drinking Older age, smoking and drinking habits, malnutrition, and underlying diseases are also risk factors for hospital-acquired pneumonia.

Conclusions: Patients with schizophrenia are at a higher risk of developing hospital-acquired pneumonia, so identifying the risk factors associated with hospital-acquired pneumonia and evaluating them comprehensively and promptly during hospitalization facilitates the development of early interventions, which are essential for improving the prognosis of patients with schizophrenia.

Introduction

Schizophrenia (SCZ), as a serious mental disorder, usually manifests clinically with a range of psychiatric symptoms, such as hallucinations, delusions, emotional apathy, and cognitive dysfunction (1, 2). According to a 2018 World Health Organization report, more than 20 million people worldwide already suffer from SCZ, and China accounts for about half of them (3). Due to its disease characteristics of high morbidity, high disability rate, and low cure rate (4), SCZ imposes heavy psychological and economic burdens on patients' families as well as society (5, 6), and has become a major social challenge (4).

Hospital-acquired pneumonia (HAP) is defined as pneumonia that is not in the incubation period at the time of admission and occurs more than 48 hours after admission (7, 8). Previous studies have shown a high incidence of HAP in Chinese patients with mental disorders, with a large psychiatric specialty hospital in Sichuan reporting a 7.8% incidence of HAP in middle-aged and elderly (≥ 50 years old) patients with schizophrenia (9), and Taiwan's Specialized Medical Institutes for Mental Disorders similarly noting an incidence of HAP in patients with severe mental disorders of 14.7/1,000 persons/year (10). HAP increases the treatment costs, prolongs hospitalization, and leads to significant increases in patient morbidity and mortality (11), thus early identification of the risk of HAP in patients with schizophrenia and timely interventions to reduce the adverse effects of HAP are critical.

Materials and methods

Five databases, PubMed, Web of Science, Cochrane Library, China National Knowledge Infrastructure (CNKI), and China Biomedical Literature Database (CBM), were searched by computer, and the time limit for searching was from the establishment of the databases to February 2024, and the search strategy was shown in Appendix Box 1 for PubMed. To search for studies on the factors affecting hospital-acquired pneumonia in patients with schizophrenia, the search terms in Chinese and English were pneumonia, schizophrenia, risk factors, etc. Taking PubMed as an example, the specific search strategies were as follows.

MHR 与 2 型糖尿病患者急性心梗的相关性分析

杨滨 曹慧丽 宋蔚

山西医科大学第二医院

目的 本研究旨在探讨单核细胞与高密度脂蛋白胆固醇比值（MHR）对 2 型糖尿病（T2DM）患者急性心肌梗死（AMI）的预测价值。

方法 采用回顾性病例对照研究，纳入 2022 年 1 月至 2023 年 3 月因胸痛就诊于山西医科大学第二医院的 137 例合并急性心肌梗死的 2 型糖尿病患者（心肌梗死组），并通过倾向性评分匹配法选取 137 例未合并急性心肌梗死的 2 型糖尿病患者（非心肌梗死组），两组均行冠状动脉造影术。分析 MHR 与 2 型糖尿病患者急性心肌梗死风险的相关性。

结果 心肌梗死组的单核细胞绝对值（MON）和 MHR 显著高于非心肌梗死组（P<0.001），而高密度脂蛋白胆固醇（HDL-C）水平较低（P=0.005）。多因素 logistic 回归显示，MHR 是 2 型糖尿病患者发生急性心肌梗死的独立危险因素（OR=62.30，95% CI:12.21 ~ 317.78，P<0.001）。ROC 曲线分析表明，MHR 预测 2 型糖尿病患者急性心肌梗死的曲线下面积（AUC）为 0.704（灵敏度 0.796，特异度 0.540）。

结论 MHR 水平与 2 型糖尿病患者急性心肌梗死风险呈正相关，通过检测 MHR 水平可以实现对 2 型糖尿病患者发生急性心肌梗死的早期预测。

全周期康复管理模式在老年 CCU 冠心病患者护理中的应用路径与效果评价

肖玲

西安交通大学第一附属医院

目的：构建 " 四阶段三联动 " 全周期康复管理模式，解决老年 CCU 冠心病患者康复断裂问题，实现急性期至居家期的无缝管理，提升生存质量并优化医疗资源。

方法：采用前瞻性类实验研究，选取 2024 年 4 月 -2025 年 4 月我院心内科 CCU 收治的 240 例≥ 65 岁冠心病患者（Killip I-III 级），随机分为试验组（n=120）与对照组（n=120）。对照组：常规护理 + 出院指导。试验组：创新四阶段路径（6 个月）：急性期（CCU）：24h 内老年综合评估（CGA），血流稳定后启动低强度康复（床边运动 5min×3 组 / 日 + 呼吸训练 15ml/kg）。过渡 / 稳定期：阶梯运动处方（40-50% 峰值心率）、智能药盒管理、高蛋白膳食（≥ 1.2g/kg/d）。维持期：多学科随访（首周视频指导 / 月门诊）。评价指标：主要终点：6 个月再入院率、MACE；次要终点：6 分钟步行距离（6MWD）、SAQ 评分、Barthel 指数、HADS 评分、依从性、医疗费用。统计：SPSS 25.0 进行 *t* 检验 /χ^2 检验（α=0.05）。

结果：临床结局改善：再入院率：试验组 8.5% vs 对照组 17.8%（P<0.01）；MACE：5.2% vs 12.1%（P<0.05）。功能与生活质量：6MWD 增幅：试验组 82.3±15.6 米（对照组 Δ36.1 米，P<0.001）；SAQ 总分提升：35.4±6.8 分 vs 21.5±7.1 分（P<0.01）；Barthel 指数：86.2±8.4 分 vs 76.5±9.1 分（P<0.05）。心理状态：HADS 焦虑：5.1±1.8 分（无焦虑阈值）vs 8.7±2.3 分（P<0.01）；抑郁：4.3±1.6 分 vs 7.5±2.0 分（P<0.01）。依从性与成本：服药依从率：93.6% vs 72.4%（P<0.001）；人均费用：试验组人均 6 个月医疗总费用（含再入院费用）显著低于对照组（P<0.05）。

结论：本研究构建并验证的 "四阶段三联动" 全周期康复管理模式，深度融合多学科协作与智能技术，为老年 CCU 冠心病患者提供了科学、系统、连续的护理解决方案。该模式显著降低了患者再入院风险及 MACE 发生，有效促进了心肺功能恢复、生活质量和心理健康提升，强化了治疗依从性，并展现出良好的成本效益优势，充分体现了科学性、创新性（整合全周期视角与智能管理）、实用性（路径清晰可操作）和先进性。

Sleep Patterns and Frailty: Joint Impact on Major Adverse Cardiovascular Events in a Prospective Cohort Study

Zhi-Teng Chen, Da-Chuan Guo, Hai-Feng Zhang, Yang-Xin Chen

Sun Yat-sen Memorial Hospital

Background: Frailty is an important geriatric syndrome, which is characterized by a deterioration in the functionality of several organ systems with an increased susceptibility to stressors. Frailty significantly increases the risk of cardiovascular disease (CVD). Compared with non-frail participants, those with frailty had a 47% increased risk of CVD. Higher sleep scores are associated with a lower risk of CVD risk, and maintaining a healthy sleep pattern is associated a lower major adverse cardiovascular events (MACE) risk. It is unknown whether keeping a healthy sleep pattern can alleviate the adverse impact of frailty on MACE. We aimed to elucidate the joint impact of sleep patterns and frailty on MACEs.

Methods: A total of 380,105 participants from the UK Biobank were included for the analysis. Definition of frailty phenotype was based on the following five criteria: weight loss, exhaustion, low physical activity, slow gait speed and low grip strength. Participants were then classified as non-frail (0 scores), pre-frail (1–2 scores) or frail (≥ 3 scores). We described five sleep behaviors covering chronotype, duration, insomnia, snoring, and excessive daytime sleepiness. According to the healthy degree, 0 or 1 points were assigned, and every sleep behavior of every participant got 1 point. Then all points were summed up to obtain a sleep score ranging from 0 to 5, with higher scores indicating a healthier sleep pattern. Participants were then categorized based on their sleep score into healthy sleep (score ≥ 4), intermediate sleep (score 2–3), and poor sleep (score ≤ 1) pattern. The primary outcome of this study was MACE, which was defined based on diagnoses of myocardial infarction (MI), stroke or CVD-related death. Secondary outcomes included MI, stroke, heart failure (HF), CVD-related death, and all-cause mortality. Cox proportional hazards models were used to assessed the associations between combinations of frailty phenotypes and sleep patterns and MACE, including nonfatal MI, stroke or CVD-related death. A series of sensitivity analyses were performed to test the robustness of the primary results.

Results: After a median follow-up period of 12.94 years, compared with participants with frailty and poor sleep patterns, participants without frailty and with healthy sleep patterns have the lowest risk of MACE (HR, 0.560 [95%CI, 0.445–0.704], P P P , all P P

Conclusions: Maintaining a healthy sleep pattern and a non-frail status were jointly associated with a significantly decreased risk of MACE. Healthy sleep pattern may reverse the risk of MACE brought by pre-frailty. Strategy targeting snoring and daytime dozing during sleep may reduce the risk of MACE among frail people.

Comorbidity Patterns and Intrinsic Capacity Decline in Older Adults with Coronary Heart Disease: A Nationwide Study in China

I-U JIAOJIAO Q, Nan Zhang, Yue Chen, Shuaishuai Zhang , Qinzhi Cao, Lin Zhou, Yue Zhang, Boyang Zeng, Shouyuan Ma, Man Li, Yan Wang, Jin Sun, Bangguo Qin, Bokai Chen, Shuang Cai, Qiligeer Bao, Shuxia Wang, Ping Zhu

Chinese PLA General Hospital

Background: Coronary heart disease (CHD) is a leading cause of morbidity among older adults. However, current single-disease–based care paradigms and treatment guidelines often fail to account for the complexities evaluated through comprehensive geriatric assessments (CGAs). A central component of this framework is intrinsic capacity (IC), defined as the composite of all physical and mental capacities available to an individual, which plays a key role in determining how well a person can age. This study aims to investigate the associations among CHD, comorbidity burden, and declines in IC, using a nationally representative sample of community-dwelling older adults in China.

Methods: This cross-sectional study analyzed data from a national survey conducted across 14 provinces in China from September 2023 to March 2024. The final sample comprised 14,389 community-dwelling older adults, including 5,479 with self-reported CHD. Intrinsic capacity status was assessed across five domains: locomotion, cognition, sensory function, vitality, and psychological health. Analyses were stratified by CHD status and comorbidity patterns. Comorbidity patterns were evaluated based on the number of chronic conditions, specific disease combinations, and subgroups derived through latent class analysis (LCA). Multivariable logistic regression was used to examine the associations between these comorbidity patterns and IC decline.

Results: Among the 14,389 participants, 38.1% (n = 5,479) had a self-reported history of CHD. The mean IC score among individuals with CHD was 90.42 ± 12.18, lower than that of individuals without CHD. The

age-adjusted prevalence of IC decline was significantly higher among individuals with CHD (51.8% vs. 43.5%, P < 0.001). This difference was observed across all five IC domains, particularly in sensory (32.4%) and cognitive (12.1%) functions. The prevalence of IC decline increased with comorbidity burden, ranging from 38.1% for those with no chronic conditions to 65.6% for those with five or more conditions. Liver disease (67.0%), stroke (62.4%), and the combination of hyperthyroidism and liver disease (75.0%) showed the highest rates of IC decline. Using latent class analysis, three distinct subgroups were identified among individuals with CHD: Class 1 (Chronic Disease Management Group, 40.9%), Class 2 (Cardio-Metabolic Risk Group, 27.8%), and Class 3 (Multi-System Disease Group, 31.3%). Among these, the Multi-System Disease Group exhibited the highest rate of IC decline (61.3%). Multivariable logistic regression revealed that individuals with five or more chronic conditions had over three times the odds of IC decline (OR = 3.03; 95% CI: 2.23–4.10; P < 0.001), and nearly double the odds of decline in locomotion, cognition, sensory function, and psychological health (all P < 0.001), compared to those without chronic conditions. In the LCA results, compared with the Chronic Disease Management Group, individuals in the Multi-System Disease Group exhibited even greater risks, with significantly higher odds of IC decline (OR = 1.93; 95% CI: 1.69–2.20; P < 0.001), sensory dysfunction (OR = 1.72; 95% CI: 1.50–1.97; P < 0.001), and cognitive decline (OR = 1.67; 95% CI: 1.38–2.03; P < 0.001). Subgroup analyses demonstrated consistent associations across age and sex categories (all interaction P > 0.05). After excluding individuals with disability, the association between comorbidity patterns and increased risk of IC decline remained significant, particularly among those with five or more chronic conditions and those in the Multi-System Disease Group.

Conclusions: Among older Chinese adults, CHD demonstrates a strong association with IC decline, particularly in the presence of comorbidity. Distinct chronic conditions and comorbidity patterns were linked to specific functional impairments, highlighting the heterogeneity within CHD populations. These findings support the implementation of integrated, function-focused care models for older individuals with CHD to preserve independence and improve long-term outcomes.

虚弱与肌少症对中老年人群心血管疾病风险的联合作用及进展性影响

刘孟璐 叶蕴青 严凯伦 张可欣 黎嘉雯 袁晋青 赵雪燕

中国医学科学院阜外医院

背景与目的：

随着全球人口老龄化加剧，虚弱和肌少症作为两种常见的老年综合征，正对公共卫生体系构成严峻挑战。近年来，虚弱和肌少症对心血管疾病（CVD）风险的影响日益受到关注。然而，现有研究多聚焦于基线时的虚弱或肌少症状态，较少评估二者的联合作用及其随时间的动态变化。本研究旨在利用具有全国代表性的队列数据，探讨虚弱与肌少症在中老年人群中新发 CVD 风险中的联合作用与进展性影响。

研究方法：

本研究基于中国健康与养老追踪调查（CHARLS）的随访数据。采用 Rockwood 虚弱指数评估虚弱状态，并将其分为健康（FI ≤ 0.10）、虚弱前期（0.10 < FI < 0.25）和虚弱（FI ≥ 0.25）三类。肌少症依据亚洲肌少症工作组 2019 年标准（AWGS 2019）定义。将可能肌少症与肌少症合并为“肌少症”组进行分析，最终形成“非肌少症”与“肌少症”两组。

首先，采用 Cox 回归分析 2011 年基线虚弱与肌少症状态对随后 9 年内新发 CVD 的影响。随后，筛选 2011 至 2015 年间未发生 CVD 的个体，进一步分析虚弱与肌少症状态变化对 2015 至 2020 年新发 CVD 风险的影响。

结果：

研究共纳入 7,187 名 45 岁以上的参与者（男性占 49.41%，平均年龄为 57.38 ± 8.41 岁）。其中 4,265 名在 2011 至 2015 年间未发生 CVD 事件的参与者被纳入状态变化分析。九年随访期间，虚弱与肌少症状态均可独立增加 CVD 风险。值得注意的是，虚弱与肌少症之间对 CVD 存在显著交互作用（p for interaction <0.001）。在调整潜在混杂因素后，与“健康 + 非肌少症”者相比，分别处于“健康 + 肌少症”、“虚弱前期 + 非肌少症”、“虚弱前期 + 肌少症”、“虚弱 + 非肌少症”以及“虚弱 + 肌少症”状态的参与者，其新发 CVD 风险分别增加了 18.0%（aHR=1.18; 95% CI: 1.02–1.37）、67.0%（aHR=1.67; 95% CI: 1.47–1.89）、88.0%（aHR=1.88; 95% CI: 1.64–2.17）、87.0%（aHR=1.87; 95% CI: 1.50–2.34）和 118.0%（aHR=2.18; 95% CI: 1.81–2.62）。此外，虚弱状态在肌少症与 CVD 之间的关联中起到了 35.38% 的中介作用。

在随后的状态变化分析中，持续虚弱者或肌少症恶化者的新发 CVD 风险最高，风险比（HR）分别为 3.29（95% CI: 2.44–4.45）和 1.56（95% CI: 1.28–1.90），相比之下，持续健康或非肌少症者风险最低。

结论：

本研究表明，虚弱与肌少症对中老年人群中新发 CVD 风险具有显著、独立且协同的联合作用，并呈现随时间推移的进展性影响。建议将虚弱和肌少症纳入常规筛查，并实施综合干预策略，以减缓其进展、促进功能恢复，从而降低 CVD 发生风险。

基于心衰风险评分表的老年 2 型糖尿病全周期康复护理模式构建与应用

张辉敏

中国人民解放军陆军军医大学第二附属医院医院

目的

随着人口老龄化加剧，老年 2 型糖尿病（T2DM）患者合并心衰的风险显著升高，严重影响生活质量和预后。本研究旨在基于心衰风险评分表，构建一套适合老年 T2DM 患者的全周期康复护理模式，并验证其临床应用效果，以降低心衰发生风险、改善患者康复结局。

方法

采用混合研究方法，分三个阶段开展研究：（1）模型构建阶段：通过文献回顾和德尔菲专家咨询法，整合国际通用心衰风险评分表（如 HFRS、EHMRG 等），结合老年 T2DM 患者特点，设计涵盖“预防 - 干预 - 随访”的全周期护理方案；（2）干预实施阶段：选取 2024 年 1 月–2024 年 6 月在我医院收治的 120 例老年 T2DM 患者，随机分为干预组（n=60，采用全周期康复护理模式）和对照组（n=60，常规护理），干预周期 6 个月；（3）效果评价阶段：比较两组患者的心衰风险评分、血糖控制（HbA1c）、心功能指标（LVEF、NT-proBNP）、生活质量（SF-36 量表）及再住院率差异。数据分析采用 SPSS 26.0，组间比较使用 t 检验或卡方检验。

结果

心衰风险控制：干预组心衰风险评分显著低于对照组（12.5±2.1 vs. 18.3±3.4，P<0.01）；

代谢与心功能改善：干预组 HbA1c（6.8%±0.5% vs. 7.9%±0.7%）、LVEF（55.2%±4.1% vs. 49.8%±5.3%） 及 NT-proBNP（150 pg/mL±45 vs. 320 pg/mL±68）均优于对照组（P<0.05）；

生活质量与预后：干预组 SF-36 评分提高（75.6±6.2 vs. 62.4±7.8，P<0.01），6 个月内再住院率降低（8.3% vs. 23.3%，P<0.05）。

结论

基于心衰风险评分表构建的全周期康复护理模式可有效降低老年 T2DM 患者的心衰风险，改善血糖控制和心功能，提升生活质量并减少再住院事件。该模式具有临床推广价值，可为糖尿病合并心衰的规范化管理提供参考。

膈肌强化训练对老年冠心病患者姿势控制及生活质量的影响：前瞻性队列研究

马姣 李娟利 蔡慧芝

交大一附院

背景 老年冠心病患者常伴随核心肌群功能障碍，导致姿势控制能力下降及生活质量恶化。膈肌作为呼吸与姿势稳定的双重核心肌群，其强化训练可能通过改善呼吸 - 运动耦合效应带来多重获益，但现有证据尚不充分。

目的 探讨结构化膈肌强化训练对老年冠心病患者静态 / 动态姿势控制能力及生活质量量表评分的影响。

方法 采用前瞻性队列研究设计，纳入 2024-2025 年西安某三甲医院收治的老年冠心病患者 62 例，分为干预组（常规心脏康复 + 膈肌强化训练，n=31）与对照组（仅常规康复，n=31）。干预组接受为期 12 周、每周 3 次的阈值负荷吸气训练联合腹式呼吸激活练习。主要结局通过受力平台测定姿势摆动速度（Sway Velocity）评估静态姿势控制，Timed Up-and-Go 测试动态平衡；次要结局采用 SF-36 量表评价生活质量。

结果 干预后，干预组较对照组表现出：（1）静态姿势控制显著改善（摆动速度降低 23.5% vs 8.7%，p<0.01）；（2）动态平衡时间缩短（TUG 测试减少 4.2±1.3s vs 1.8±0.9s，p=0.003）；（3）SF-36 生理功能（+15.6 分）、躯体疼痛（+12.4 分）等维度评分提升更显著（均 p<0.05）。两组均未发生训练相关不良事件。

结论 膈肌强化训练可有效增强老年冠心病患者的姿势稳定性，其机制可能与改善呼吸 - 核心肌群协调性有关，并进一步转化为生活质量的提升。该干预方案具有临床推广价值。

Integrated Multi-Omics Analysis Uncovers Dysregulated Energy and Amino Acid Metabolism During Vascular Aging

Geng-yu Zhou[1,2], Xian-Wei Xie[2], Cheng Jin[2], Kai-Yang Lin[1]

1. Department of Cardiology, Shengli Clinical Medical College of Fujian Medical University, Fujian Provincial Hospital, Fuzhou University Affiliated Provincial Hospital

2. Department of Cardiology, The Second Affiliated Hospital of Harbin Medical University, China

Objectives: Vascular aging is increasingly recognized as a major contributor to the development and progression of cardiovascular diseases. However, the specific metabolic features associated with vascular aging and the mechanistic roles of key metabolites in this process have not been fully elucidated. A deeper understanding of the metabolic alterations underlying vascular aging could provide new insights for early intervention and therapeutic strategies. To further explore the metabolic reprogramming that accompanies vascular aging, we developed and characterized mouse models representing various life stages—from young to aged—thus capturing the dynamic spectrum of vascular aging under physiological conditions.

Methods: We conducted a comprehensive analysis of the GTEx database

to identify human vascular gene modules correlated with age. These gene modules were subjected to clustering analysis and KEGG pathway enrichment to pinpoint crucial biological pathways involved in vWascular aging. Subsequently, we established vascular aging models in mice representing different life stages and performed ultra-performance liquid chromatography-tandem mass spectrometry (UPLC-MS/MS) to profile the metabolomic changes in the aorta. Furthermore, we integrated single-cell transcriptomic analysis and in vitro assays to determine the expression patterns and functional roles of key metabolites within specific vascular cell subpopulations.

Results: Our GTEx transcriptomic analysis revealed that genes associated with vascular aging can be grouped into six major categories, with significant enrichment in metabolic pathways related to energy production, amino acid biosynthesis, and redox regulation. Specifically, pathway enrichment analysis indicated that these genes are closely linked to cellular respiration, glycolysis, the tricarboxylic acid (TCA) cycle, and various amino acid metabolic networks.

Metabolomics results from the mouse model established in this study confirmed that vascular aging is accompanied by extensive remodeling of multiple metabolic pathways. High-throughput metabolomic analyses of vascular tissues from juvenile, adult, and aged mice uncovered dynamic changes in metabolic homeostasis throughout the lifespan. Notably, significant disruptions were observed in energy metabolism, amino acid turnover, nucleotide synthesis, and antioxidant stress response, as reflected by conspicuous alterations in the concentrations of key intermediate metabolites and the expression levels of relevant enzymes in these pathways.

Quantitative analyses showed that the levels of most metabolites peaked during adulthood and subsequently exhibited a gradual decline with advancing age, indicating the presence of progressive metabolic exhaustion or insufficiency in the course of vascular aging. This trend was particularly pronounced for metabolites such as arginine, citrulline, aspartic acid, and proline, all of which were markedly decreased in aged mice compared to their younger counterparts.

Additionally, single-cell RNA sequencing and subsequent in vitro experiments further confirmed that these metabolic pathways are especially active within endothelial cells. Single-cell transcriptomic profiling revealed that genes involved in metabolism and redox regulation are expressed at significantly higher levels in endothelial cell populations compared to other vascular cell types. Functional in vitro assays demonstrated that endothelial cells exhibit heightened metabolic activity in these pathways and are more sensitive to perturbations affecting them.

Conclusion: Our findings highlight that vascular aging is characterized by multifaceted metabolic disturbances, including impairments in glucose, fatty acid, and amino acid metabolism, as well as diminished antioxidant capacity. Among these, the most striking feature is the significant decline in key amino acids such as aspartic acid, arginine, and proline during the late aging stage, which may underlie age-associated vascular dysfunction. These insights not only advance our understanding of the metabolic basis of vascular aging but also suggest that targeted interventions to restore metabolic homeostasis could hold promise in preventing or delaying vascular aging and its related cardiovascular diseases.

复合膳食抗氧化指数与超额心脏年龄的关联：2007-2020 年 NHANES 横断面研究分析

张婉尧 [1]

1. 荣昌区人民医院

2. 武汉科技大学医学部医学院

3. 湖北文理学院附属医院，襄阳市中心医院心血管内科，湖北文理学院心血管病研究所

目的 心血管疾病 (CVD) 风险与膳食抗氧化剂摄入的关联一直存在争议。复合膳食抗氧化指数 (CDAI) 作为膳食整体抗氧化水平的衡量指标，而超额心脏年龄 (EHA) 是 CVD 风险的简洁直观表达。本项研究旨在调查 CDAI 和 EHA 之间的关系，为 CVD 的营养预防提供一定的理论参考。**方法** 本横断面研究中，数据来源于 2007 ~ 2020 年国家健康和营养检查调查 (NHANES)。样本包括 30 ~ 74 岁、无 CVD 病史的 16442 名参与者。采用 Framingham 风险评分函数来估算心脏年龄，进一步计算出 EHA。根据维生素 A、C、E、锌、硒和类胡萝卜素的摄入量，构建了代表整体抗氧化性的 CDAI。通过多元线性回归、多元 logistic 回归和限制性三次样条（RCS）进行统计分析。**结果** 在完全调整协变量后，CDAI 与 EHA(β=-0.07，95%CI -0.14 ~ -0.01) 及高 CVD 风险（EHA ≥ 10 年）(OR=0.98，95%CI 0.96 ~ 1.00) 呈显著负相关，进一步 RCS 分析表明这种负相关是非线性的。相较于 CDAI 最低四分位数 (Q1) 组，CDAI 最高四分位数 (Q4) 组 EHA 下降 1.41 岁 (β=-1.41，95%CI -2.12 ~ -0.71，P_{trend} 值 <0.01)，高 CVD 风险下降 27%(OR=0.73，95%CI 0.59 ~ 0.90，P_{trend} 值 =0.01)。在女性中，CDAI 与 EHA(β=-0.10，95%CI -0.12 ~ 0.00) 及高 CVD 风险 (OR=0.97，95%CI 0.94 ~ 0.99) 也表现出显著的非线性负相关。而男性中这种负相关无统计学意义。**结论** 本研究首次证明了 CDAI 与 EHA 及高 CVD 风险之间存在显著的负相关性，并进一步揭示了这种关联具有性别差异。这一发现为 CVD 的营养预防提供了新的理论支撑，并强调了进一步临床和基础研究的必要性。

辅酶 Q10 联合有氧运动对老年人心肌功能及氧化应激指标的影响研究

翟倩

交大一附院

目的：探究辅酶 Q10 联合有氧运动干预对老年人心肌功能的提升效果，以及对体内氧化应激指标的调节作用，为改善老年人心脏健康提供新的干预策略。

方法：选取 200 名 65 - 80 岁、存在不同程度心肌功能减退的老年人，随机分为三组。对照组（60 人）保持日常活动与常规饮食；辅酶 Q10 组（70 人）每日口服辅酶 Q10 补充剂；运动联合组（70 人）在口服辅酶 Q10 的基础上，进行每周 5 次、每次 40 分钟左右的有氧运动，如快走、太极拳等，运动强度保持在最大心率的 60% - 70% 。实验周期为 6 个月，实验前后分别运用心脏超声检测左心室射血分数（LVEF）、左心室舒张末期内径（LVEDD）评估心肌功能；采集血液样本检测超氧化物歧化酶（SOD）、丙二醛（MDA）、谷胱甘肽过氧化物酶（GSH - Px）等氧化应激指标水平。

结果：实验结束后，运动联合组 LVEF 显著高于对照组和辅酶 Q10 组（P<0.05），LVEDD 显著缩小（P<0.05）；运动联合组 SOD、GSH - Px 活性明显升高，MDA 含量显著降低，与其他两组相比差异有统计学意义（P<0.05）。辅酶 Q10 组在心肌功能及氧化应激指标上也有一定改善，但效果不如运动联合组明显。

结论：辅酶 Q10 联合有氧运动相较于单独使用辅酶 Q10，能更有效地改善老年人心肌功能，增强抗氧化能力，调节氧化应激水平，对维护老年人心脏健康具有积极意义，推荐作为一种综合干预手段应用于老年心脏健康管理。

Mood Swings Impact Smoking Behavior Elevating Risk of Cardio-cerebrovascular Events: A Mendelian Randomization Study

Yin Han, Meng-Yang Jia, Jing-Jin Liu, Qing-Shan Geng

Shenzhen people's hospital

Background:

Mood swings, characterized by abrupt and intense emotional fluctuations, are a prevalent psychological feature in the general population, yet their implications for physical health remain underexplored. Emerging evidence suggests that mood instability may co-occur with adverse lifestyle behaviors—most notably smoking—which contribute significantly to the risk of cardio-cerebrovascular diseases. However, the causal relationship between mood swings, smoking behaviors, and major adverse cardiovascular outcomes remains unclear. This study aimed to investigate whether mood swings causally influence smoking behaviors and, in turn, elevate the risk of cardiovascular and cerebrovascular events.

Methods:

We conducted a two-sample Mendelian randomization (MR) analysis using summary-level data from genome-wide association studies (GWAS). Genetic variants associated with mood swings, smoking initiation, current tobacco use, and cardio-cerebrovascular outcomes—including major adverse cardiovascular events (MACE), acute myocardial infarction (AMI), and stroke—were obtained from the IEU Open GWAS Project and other public repositories. To assess the indirect effects of smoking behaviors on the relationship between mood swings and cardio-cerebrovascular outcomes, we performed mediation analyses using both conventional network MR and two-step MR approaches. Sensitivity analyses, including heterogeneity, pleiotropy, and leave-one-out assessments, were conducted to ensure the robustness of findings.

Results:

MR analyses revealed a significant causal effect of mood swings on cardio-cerebrovascular outcomes. Specifically, mood swings increased the risk of MACE (OR = 1.02; 95% CI: 1.01–1.03; p = 0.001), AMI (OR = 1.01; 95% CI: 1.00–1.02; p = 0.006), and stroke (OR = 1.01; 95% CI: 1.00–1.02; p = 0.008). No evidence of reverse causality was detected, reinforcing a unidirectional relationship from mood swings to these adverse outcomes.

In the behavioral pathway analysis, mood swings were strongly associated with increased smoking behaviors. The odds of current tobacco use increased by 12% (OR = 1.12; 95% CI: 1.07–1.17; p = 2.10×10^{-6}), and the odds of smoking initiation rose by 42% (OR = 1.42; 95% CI: 1.19–1.68; p = 6.04×10^{-5}) among individuals genetically predisposed to mood swings. These findings suggest that emotional instability may lead to increased tobacco dependence and initiation.

Mediation analyses provided further insight into the mechanistic pathway. Using the two-step MR framework, we found that current tobacco smoking mediated approximately 25% of the causal link between mood swings and MACE, 9.1% to 21.4% for AMI, and 16.7% to 25.0% for stroke. In contrast, smoking initiation explained 10.0%–15.0% of the effect on MACE, 7.1%–14.3% for AMI, and 7.1%–8.3% for stroke. These results highlight that sustained smoking behavior may have a more significant impact on cardiovascular prognosis than initial smoking uptake.

Limitations:

Mood swings and smoking behaviors were measured through self-reported assessments in the original GWAS, introducing potential misclassification or recall bias. The genetic data were predominantly derived

from individuals of European ancestry, limiting the generalizability to other populations. Furthermore, MR estimates reflect lifelong average exposure and may not fully capture acute or episodic mood-related risks. Finally, while smoking behavior was the primary mediator examined, other relevant behaviors—such as physical inactivity, poor diet, or alcohol abuse—were not included in this analysis and may also play significant mediating roles.

Conclusion:

In summary, this MR study provides compelling evidence that mood swings exert a causal influence on the risk of cardio-cerebrovascular events, largely through the promotion of smoking behaviors. These results bridge the gap between emotional health and physical disease risk, highlighting the importance of psychological-behavioral interventions in cardiovascular prevention strategies. Future research should explore this pathway across diverse populations and investigate whether targeted mood-stabilizing interventions can mitigate smoking behaviors and improve long-term cardiovascular outcomes.

Kielin/Chordin-Like Protein Deficiency causes aortic aging in male mice

DI Ye, XIAOYANG Zhou

Renmin Hospital of Wuhan University

Background: Bone morphogenetic proteins (BMPs), members of the transforming growth factor-beta (TGF-β) superfamily, are critically involved in diverse cellular processes including differentiation, proliferation, apoptosis, and extracellular matrix remodeling. Accumulating evidence from previous studies underscores the significant roles of BMPs in the pathogenesis of various cardiovascular diseases, encompassing atherosclerosis, vascular calcification, myocardial hypertrophy and fibrosis (remodeling), pulmonary arterial hypertension, and diabetic cardiomyopathy. Kielin/chordin-like protein (KCP) is an important, evolutionarily conserved secreted glycoprotein known to act as a context-dependent regulator of BMP signaling pathways. It functions extracellularly by binding directly to BMP ligands, thereby modulating their bioavailability, receptor interaction, and subsequent downstream signaling cascades. Notably, research has demonstrated that KCP can attenuate renal interstitial fibrosis in models of chronic kidney disease, primarily through its suppressive effects on TGF-β/Smad signaling and promotion of BMP/Smad signaling. Furthermore, transgenic overexpression of KCP has been shown to ameliorate liver pathology associated with aging and nonalcoholic fatty liver disease (NAFLD) in murine models. Intriguingly, KCP overexpression also confers resistance to diet-induced obesity and metabolic syndrome phenotypes in mice, largely mediated through its regulatory influence on Smad-dependent pathways. Our preliminary investigations revealed a novel association between altered KCP expression and the progression of heart failure. Given the well-documented involvement of dysregulated BMP signaling in both the aging process and cardiovascular pathologies, we hypothesized that KCP may play a crucial, yet unexplored, role in the development of aortic aging - a key contributor to age-related vascular stiffening and dysfunction. However, the specific function and mechanistic contribution of KCP in aortic senescence remained entirely unknown. This study was therefore designed to systematically investigate the impact of KCP deficiency on aortic aging and elucidate the underlying molecular mechanisms.

Methods and Results: We utilized KCP knockout (KO) mice (homozygous null for the Kcp gene) and age-matched wild-type (WT) controls. A striking observation was that aged KCP KO mice exhibited a significant trend towards premature mortality compared to WT groups, necessitating planned endpoint analysis. Consequently, all surviving mice in the WT group and the KCP KO group were humanely sacrificed at 24 months of age following terminal body weight measurement. Young adult mice served as healthy controls. Baseline systolic and diastolic blood pressure measurements, recorded non-invasively, revealed no significant differences among the four experimental groups. Comprehensive analysis of aortic structure and function was performed. Histopathological examination using Hematoxylin & Eosin (H&E) and Masson's trichrome staining revealed characteristic age-associated impairments in aortic wall architecture and elastic fiber integrity in 24-month-old mice. Critically, KCP deficiency exacerbated these age-related pathological changes, manifesting as significantly increased aortic media thickening, collagen deposition, and disorganization of elastin layers compared to aged WT aortas. Molecular analysis demonstrated that KCP KO profoundly altered key signaling pathways in aged aortas: it significantly increased phosphorylation (activation) of Smad2/3 (p-smad2/3) and elevated TGF-β protein expression, while concurrently suppressing BMP-2 expression. Furthermore, KCP KO markedly elevated the expression of aortic senescence-associated markers (e.g., p16, p21) in aged mice. Biochemical assessment revealed that KCP deficiency aggravated oxidative stress by disrupting the redox balance, evidenced by increased markers of reactive oxygen species (ROS) and decreased antioxidant enzyme activity (e.g., SOD, GPx). Additionally, KCP KO significantly increased the expression of pro-inflammatory cytokines (e.g., TNF-α, IL-6, IL-1β) and augmented the rate of apoptosis specifically in vascular smooth muscle cells (VSMCs) within the aged aortic wall.

Conclusions: Our findings provide compelling evidence that genetic deletion of KCP accelerates aortic aging and exacerbates vascular dysfunction in a murine model. KCP deficiency promotes aortic senescence and remodeling through a multifactorial mechanism involving the dysregulation of TGF-β/BMP signaling balance (increased TGF-β/Smad2/3 and decreased BMP-2), heightened oxidative stress, amplified chronic low-grade inflammation, and increased susceptibility of VSMCs to apoptotic cell death. These results establish KCP as a novel endogenous protective modulator against age-related aortic degeneration. Targeting the KCP pathway or augmenting its function may therefore represent a promising therapeutic strategy for mitigating aortic aging and its associated cardiovascular complications. Future studies are warranted to explore translational applications and dissect cell-type specific effects of KCP within the complex aortic microenvironment.

生命必需 8 要素评估的心血管健康在老年衰弱与死亡关联中的中介作用：来自 NHANES 队列的证据

苗广瑞

郑州大学第一附属医院

目的： 衰弱（frailty）以生理功能失调和易损性增加为特征，在老年人群中较为普遍，并与跌倒、残疾和死亡风险升高相关。由“生命必需 8 要素”（Life's Essential 8, LE8）评分评估的心血管健康（Cardiovascular health，CVH）对识别心血管高风险个体至关重要。本研究旨在探究老年人群体中以下三个问题：（1）衰弱、CVH 与全因死亡率及心血管死亡率的关联性；（2）衰弱与 CVH 之间的关联；（3）CVH 在衰弱与心血管死亡率、全因死亡率关联中的中介作用。

方法： 本队列研究分析了 2005–2018 年美国国家健康与营养调查（the National Health and Nutrition Examination Survey，NHANES）中 7,774 名 60 岁及以上年龄参与者的数据。衰弱采用衰弱指数评估，CVH 通过 LE8 评分评估。使用 Cox 比例风险模型分析衰弱、CVH 与死亡率的关系，并通过中介分析探讨 CVH 的中介作用。

结果： 衰弱与全因死亡率（HR=2.470，95% CI：2.186~2.792）和心血管死亡率（HR=2.639，95% CI：2.080~3.350）风险升高显著相关。更好的 CVH 则与较低的全因死亡率（HR=0.446，95% CI：0.354~0.562）和心血管死亡率（HR=0.375，95% CI：0.211~0.667）风险相关。LE8 评分部分介导了衰弱与全因死亡率（12.01%）及心血管死亡率（13.40%）的关联，其中体力活动是关键中介因素。

结论： 衰弱显著增加了全因死亡和心血管死亡的风险，而 CVH 在这一关联中起中介作用。体力活动是衰弱与心血管死亡关联中最强的中介因素，而体质量指数（body mass index，BMI）、血脂和体力活动主要中介衰弱与全因死亡的关系。提高 CVH（尤其是通过增加体力活动）可能有助于降低衰弱老年人的死亡率。

开发并验证可解释的机器学习模型用于预测环境毒物暴露对心肌梗死的影响：一项回顾性列队研究

王小娟

兰州大学第一医院

目的：心肌梗塞（MI）是一种严重的心血管疾病，全球范围内导致高死亡率及不良预后。环境毒物与心血管疾病之间存在密切的关联，本研究旨在探讨环境毒物暴露对心肌梗塞的影响，识别独立风险因素并通过十种机器学习算法，构建环境毒物暴露引起的心肌梗塞预测模型。

方法：本研究利用国家健康与营养调查（NHANES）数据，纳入了 5022 名成年参与者，其中 3517 名用于训练集，1505 名用于验证集。通过 1000 次 Lasso-Logistic 回归分析，最终筛选出 26 个常见环境毒物特征，进一步通过广义线性模型（GLM）算法筛选。本研究使用了 Treebag、Boruta、Random Forest、LVQ、Bayesian 等方法进行变量特征提取，并通过交集确定心肌梗塞的特征变量。随后，利用随机森林、TabPFN 等十种机器学习算法及 10 折内部交叉验证构建与环境暴露有关的心肌梗塞预测模型，并通过 ROC 曲线下面积（AUC）、灵敏度（Sens）、特异度（Spec）等指标评估模型性能。通过 TabPFN 模型变量的热图分析及 Shapley 加性解释法（SHAP）对特征重要性进行排序，并对最终模型进行解释。

结果：在纳入的 5022 名参与者中，通过 1000 次 Lasso-Logistic 回归分析，筛选出 26 个常见环境毒物特征，进一步通过广义线性模型（GLM）算法筛选，最终确定 10 个环境指标与心梗相关，这 10 个环境指标形成一个环境评分。我们使用了 Treebag、Boruta 等策略进行特征选择并取交集，最终确定的 7 个心肌梗塞独立风险因素包括年龄、吸烟、高血压、心血管疾病、平均细胞血红蛋白、高密度脂蛋白胆固醇和环境评分。剂量 - 反应关系分析显示环境评分与心肌梗塞患病风险的关联呈显著的线性关系（cutoff 值 1.454）。构建的 10 种机器学习模型中，TabPFN 模型在训练集（AUC=0.9096，95% CI：0.8965-0.9228）和验证集（AUC=0.9073，95% CI：0.887-0.9276）中表现最佳。特征对 TabPFN 模型的贡献通过平均 SHAP 值进行评估，显示顺序为：心血管疾病、年龄、环境评分、高血压、吸烟是预测模型中最重要的五个特征。

结论：本研究通过系统性分析揭示了环境毒物暴露对心肌梗死的影响，并构建了一个准确性较高的预测模型。这些发现为环境毒物暴露导致的心肌梗塞的早期诊断和干预提供了新的依据及价值。

人性化护理对老年心肌梗死患者心理状态及护理满意度的影响研究

冉力

重庆市荣昌区人民医院

目的：心肌梗死是常见的一种心血管疾病，常见于老年群体，冠状动脉粥样硬化

是老年心肌梗死的主要病因，患者精神上过度疲劳并且过于高度紧张为常见的诱发因素。患者主要表现有发热、胸骨后疼痛、头痛等，同时患者伴有心肌酶活性的增高，心电图进行性变化，病情严重时可出现休克、心律失常、心源性休克、心力衰竭等不良并发症，给患者的健康及生活质量造成严重威胁 [2]。心肌梗死患者由于受教育程度普遍不高、年纪较大等，因此常出现对治疗的不配合甚至抗拒，影响到后续治疗的效果，为改善此种现象，本研究选取 2019 年 1 月至 2020 年 1 月在我院进行治疗的心肌梗死老年患者 50 例，其中 25 例进行人性化护理干预，25 例进行常规护理，详细报道如下。

研究人性化护理对老年急性心肌梗死患者心理状态及护理满意度的影响。方法：选取 2019 年 1 月至 2020 年 1 月前来本院就诊的 50 例老年急性心肌梗死患者为研究对象，随机分为对照组和观察组，每组为 25 人。对照组实行常规护理，观察组则进行人性化护理干预，对两组患者心理状态和护理满意度进行分析比较。结果：护理前，两组患者的焦虑、抑郁评分无明显统计学差异（P>0.05），护理后，观察组焦虑、抑郁评分明显低于对照组，数据差异明显，有统计学意义（P<0.05）；对两组患者的满意度进行调查，观察组患者的满意度明显高于照组，差异显著（P<0.05）。 结论：对老年急性心肌梗死患者采取人性化护理干预，可对心理状态起到改善作用，减少患者不良情绪的发生，有助于促进护患和谐关系，进而提高患者满意度，值得推广应用。

关键词：人性化护理、老年、心肌梗死、满意度

冠心病患者护理中预见性护理程序的应用研究

钟晓菲

重庆市荣昌区人民医院

目的：冠心病是临床中常见的老年疾病之一，伴随人们生活质量的提高，冠心病发病率逐年提升，严重威胁中老年人的身体健康。有研究表明，通过对冠心病患者采取预见性护理干预措施，有利于促进患者恢复健康。所以，本次研究中，主要对 76 例患者进行分组研究，以观察两组的治疗有效率和护理满意度情况，探讨预见性护理在冠心病患者中的应用有效率及满意度。方法：以我院 2018 年 12 月至 2020 年 11 月收治的 76 例患者为研究对象，随机分成两组，即观察组与对照组，各 38 例。对照组接受常规护理，观察组接受预见性护理，比较分析两组的治疗有效率及护理满意度。结果：观察组冠心病患者的治疗有效率、护理满意度指标均显著高于对照组，差异有统计学意义（P < 0.05）。结论：冠心病是中老人的常见疾病之一，严重威胁其身体健康。近年来，人们生活水平的提高，导致其饮食等方面出现诸多不合理问题，致使冠心病的发病率呈逐年增长的趋势，降低人们的生活质量 [2]。就冠心病发病因素而言，主要有遗传、年龄、运动和饮食习惯等。预见性护理是一种有效的护理措施，通过有效应用，能够对患者加强心理护理、健康宣教、生活护理、病情监测等一系列护理工作，有利于从根本上提高护理效果，提高患者的护理满意度

。

心理护理在老年慢阻肺患者护理中的应用价值及护理满意度分析

叶敏

重庆荣昌区人民医院

目的 向老年慢阻肺患者开展心理护理，探究护理效果。方法从我院接收 (2019 年 6 月 ~2021 年 6 月) 的患者中抽取 so 例开展研究，以数字单双号法设置组别：参照组 (a=40) 和研究组 (α-40)，前组常规护理，后组增加心理护理，针对焦虑、抑郁评分和护理满意度进行比较。结果 研究组评分较参照组低，漏意度较参照组高，差异明显 (P<0.05)。结论　对老年假阻肺患者施以心理护理，可显著改善负面情绪，大幅提高护理满意度。

关键词：慢性胆塞性肺疾病以气流持续受限为基本特征，为气道慢性疾病，典型症状包括胸闷、喘息、咳嗽、咯痰、气促等，甚至是呼吸衰竭，严重危及患者生命健康 [1]。罹患此病主要人群为老年人，其体质衰弱，抗病能力低下，加之对疾病知识缺乏足够认知，疾病治疗期过长，很容易滋生焦虑、抑郁情绪，影响治疗效果，有必要加强护理。为探究有效护理模式，我院开展相关研究，报道如下。

1.1 一般资料

从 2019 年 6 月 ~2021 年 6 月在我院就诊的老年慢阻肺患者中抽取 80 例开展研究，以数字单双号法设置组别：参照组 (n=40) 和研究组 (n=40)，参照组：男，女性比例 23:17: 年龄范围 62~78(65.37±3.45) 岁。研究组：男、女性比例 24:16: 年龄范围 63~79(65.59±3.37) 岁。两组资料无统计学差异性 (P>0.05).

1.2 方法

参照组：常规护理，包括体征监测、饮食干预、用药辅导、康复训练等。

研究组：常规护理 + 心理护理。常规护理同参照组。心理护理内容如下：①情绪评估和对症胞治。根据患者的情绪表现对其情绪类型进行分析和评估，并找到出现该种情绪的原因，以便进行对症施治：若患者属于过度忧虑型，可通过健康宣教让其对致病机理、疾病主要症状、治疗方法、预期效果有一个全面的了解，提升其疾病认知，从而能够正视疾病；若患者属于冷淡低落型，可动员家属给予其更多陪伴和鼓励，让其培养一些兴趣爱好，重燃对生活的热情；若患者属于消极失望型，可多列举成功案例，使其建立治疗信心。②舒缓治疗。让患者通过冥想，听舒缓音乐、看轻松的电视节目、与人交谈等方式消除杂念、放松身心，转移注意力，保持心态平和，③有效沟通。a. 在与患者交流时，应多使用富有亲切感的称呼，如“爷爷”“奶奶”“叔叔”“阿姨”等，另外，还可以利用肢体语言如拍一拍患者的肩膀等与患者进行交流：b. 发自内心地以同情心、同理心认真倾听患者诉说，让其放心地将

心中的苦闷、烦恼宣泄出去，用激励性的语言对其进行安慰、劝导，让其真正感受到人文关怀。④家属支持。应及时将患者的治疗进展情况告知家属，叮嘱家属给予患者更多关心，支持，并对家属自身焦躁情绪进行安抚，保证患者具有强大的家庭支撑。

心理护理干预对老年心房颤动患者负面情绪的影响

韩小红

重庆市荣昌区人民医院

目的：探讨心理护理干预对老心房颤动患者负面情绪的影响。

方法：参照组应用常规护理：密切关注患者体征变化，向患者讲述疾病有关知识，给予对症处理。研究用心理护预以理员进行健康教育，向患者讲述疾病知识，包括治疗方法、方机制等。关注患者心理状态，对焦虑、抑郁综合评估，评估患者负性情绪，与患者沟通交流，了解其内心想法。结合实际情况制定教育方案，安排知识讲座，向患者发放知识手册。给予患者跟踪治疗，了解患者治疗过程与进展，向患者讲述检查重要性，告知其检查结构，强调注意事项，要求患者合理用药，重视用药。与患者分享经验，采用讲座、分享会方式，鼓励患者进行互相交流，分享经验，互相鼓励，共同面对疾病。给予患者社会疏导与支持，向患者讲述社会支持重要性，鼓励患者爱护与关心患者，与患者交流，促使患者归属感有效提高。以 84 例心房颤动患者为对象，研究时间为 2019 年 2 月 - 2020 年 2 月，分为参照组 42 例与试验组 42 例，参照组应用常规护理，试验组采用心理护理干预，对比治疗效果。

结果：试验组患者护理后 HAMA 评分、HAMD 评分更低，与参照组比较，P<0.05。研究组患者护理后 LVEDd、LVEF 均优于参照组，P<0.05。

结论：心房颤动患者实施心理护理干预，可消除负面情绪，改善患者的心功能，具有显著护理效果。心房颤动是临床常见的一种心律失常病症，其发病率随年龄的增长而增加，在年龄小于 60 岁的患者中，房颤的发生率约为 0.4%~1%，在年龄大于 80 岁的患者中发生率可达到 10%以上 [1]。心房颤动常见诱发因素包括心力衰竭、冠心病等心血管系统疾病，可引起后遗症、血栓并发症，预后效果不佳，具有较高的致残率与死亡率，对患者工作与生活产生影响，降低生活质量

Cardiovascular morbidity and mortality in patients with aortic valve calcification: A systematic review and meta-analysis

Kun-Yan Peng

Zigong First People's Hospital

Introduction: Aortic valve calcification (AVC) is an active process that involves inflammation, disorganization of matrix disposition, lipid accumulation and lamellar bone formation. AVC without hemodynamic changes has been associated with cardiovascular (CV) risk factors and increased risk of coronary and CV events. Nowadays, echocardiography is the standard imaging technique to evaluate aortic valve pathologies. However, cardiac computed tomography (CT) allows high accuracy and reproducible measurement of AVC, without exposing the patients to excessive radiation or contrast administration. To better understand if AVC assessment may improve CV risk-prediction, we performed a systematic search and meta-analysis of literature studies, evaluating the relationship among AVC, coronary artery disease (CAD), and overall mortality. **Methods:** This study systematically searched relevant literature published in China Knowledge, Wanfang Database, Wipu, SinoMed, PubMed, Web of Science, The Cochrane Library and Embase databases, using a combination of subject terms and keywords, as well as manually searching for studies and reviews that had already been published and retrieved by reviewing the The reference lists of the articles were searched manually to identify other literature as supplements. The time frame for the search was from the construction of the library to October 30, 2024. All steps of this review were conducted by two different collaborators and reviewed by a third collaborator in case of disagreement. to identify all available studies investigating AVC, measurement by CT scan, and CV events. RevMan 5.4 software was used for data analysis, interpretation of results, determination of heterogeneity, and processing of the included studies, and the overall effect was determined by the Z-test. When data analysis was performed, forest plots were plotted to test for heterogeneity, funnel plots were plotted to assess publication bias, and funnel plots were plotted to assess publication bias. The Q statistic and I^2 statistic were used to assess the heterogeneity among the included studies, and the fixed-effects model or random-effects model was selected according to the heterogeneity. When P ≥ 0.05 and households ≤ 50%, the heterogeneity among studies was considered to be within the acceptable range, and the data were combined using the fixed-effect model; when P<0.05 and households >50%, the heterogeneity among studies was considered to be large, and the data were combined using the random-effect model. The ratio of count data was used as the combined effect size. The 95% confidence intervals were calculated for each subgroup, and P<0.05 was considered statistically significant. In the presence of high heterogeneity in each subgroup, the included literature was removed one by one, and the heterogeneity I^2 and P values at each exclusion were recorded. **Results:** The final analysis included 14 studies of 3,891 AVC patients and 33,325 controls. Patients with AVC had a higher risk of CAD compared with controls (OR 1.8, 95% CI: 1.14-2.89; p = 0.03). We also found an association between AVC and coronary artery calcification (OR 3.9; 95% CI: 2.3-6.1; p < 0.001. Finally, the specificity of AVC for total mortality was 94.1% (95% CI: 93.1-93.7) with a negative predictive value of 98.7% (95% CI: 98.6-98.9). **Conclusion:** AVC is associated with coronary artery calcification and overall mortality. The present data cannot support the use of cardiac CT over echocardiography for AVC assessment in all patients,

but when cardiac CT is performed for suspected CAD, AVC evaluation may contribute to risk stratification and patient management. Ad hoc designed studies should address this issue in the next future.

老年心房颤动导管消融术中的“肥胖悖论”：高体重指数降低围术期并发症风险

罗蓓蓓 张果 胡薇

广西医科大学第一附属医院

目的：本研究旨在评估体重指数（BMI）对老年（≥ 60 岁）心房颤动（房颤）患者行心脏导管消融术后并发症风险的影响。 通过分析 BMI 及其他潜在因素（如年龄、合并症等）与术后并发症（总体及穿刺相关并发症）的关联性，识别术后并发症的独立预测因素，特别是探究 BMI 在术后并发症发生中的保护性或风险性作用。 本研究结果为构建老年房颤患者术前风险评估模型以及优化围手术期管理策略提供依据。

方法：回顾性纳入 2020 年 6 月 -2024 年 8 月在广西医科大学第一附属医院心血管内科接受房颤导管消融术且年龄≥60 岁的患者共 383 例，收集其人口学资料、BMI、基础疾病、实验室检查、术后并发症等临床数据。以住院期间是否发生术后并发症为结局，采用单因素分析及多因素 Logistic 回归分析术后并发症的相关影响因素。

结果：术后共 44 例患者发生至少 1 项并发症，并发症发生率为 11.49%。其中穿刺相关并发症 32 例（出血 10 例、血肿 18 例、假性动脉瘤 2 例、动静脉瘘 2 例）、肺部感染 23 例、尿路感染 6 例、、血栓形成 2 例、心包压塞 1 例。BMI 阈值敏感性分析（18.5-28kg/m^2），24 kg/m^2 是最佳分界。低 BMI 组（

结论：本研究表明，在行导管消融术的老年房颤患者中，存在显著的“肥胖悖论”现象：较高的 BMI（尤其≥ 24 kg/m^2）是术后总体并发症，尤其是穿刺相关并发症的独立保护因素，而较低的 BMI（

GLP1R/PCSK9/SGLT2 在钙化性主动脉瓣狭窄中的表达特征

程守全

徐州医科大学附属医院

目的

钙化性主动脉瓣狭窄（CAVS）是老龄化社会的重要心血管疾病负担，中国≥ 75 岁人群患病率达 3.4%。目前尚无有效药物治疗手段，而代谢性心血管病干预策略（如 PCSK9 抑制剂、SGLT2 抑制剂、GLP-1 受体激动剂）在延缓血管钙化中显示出潜力。本研究旨在探索 GLP1R/PCSK9/SGLT2 在人类 CAVS 瓣膜中的表达特征及其临床关联性。

方法

收集 2022 年 -2023 年徐州医科大学附属医院心脏外科手术切除的瓣膜标本，包括：主动脉瓣组（10 例，含钙化组 5 例 / 非钙化组 5 例）；二尖瓣组（13 例，含钙化组 5 例）；二叶式主动脉瓣亚组（钙化 vs 非钙化）。

通过免疫组化检测靶点表达（平均光密度值，MOD），结合临床资料（年龄、代谢指标、影像学数据）进行组间比较。统计学方法包括 Fisher 确切概率检验、独立样本 t 检验及 Mann-Whitney U 检验。

结果

1. 靶点表达特异性：主动脉瓣组 GLP1R、PCSK9、SGLT2 的 MOD 值高于二尖瓣组（P<0.05）。主动脉钙化组靶点 MOD 值较二尖瓣钙化组升高（P<0.05）。

2. 二叶式主动脉瓣特征：二叶式主动脉瓣钙化组 GLP1R/PCSK9/SGLT2 表达高于非钙化组（P<0.05），提示其对钙化更敏感。

3. 钙化与非钙化组比较：主动脉瓣钙化组与非钙化组间靶点表达无统计学差异（P>0.05）。钙化组高血压患病率低于非钙化组（P<0.05）。

结论

1. GLP1R/PCSK9/SGLT2 在 CAVS 患者主动脉瓣膜中特异性高表达，具有作为干预靶点的潜力。

2. 二叶式主动脉瓣畸形通过增强靶点表达加速钙化进程，是高风险亚组的分子标志。

3. PCSK9 抑制剂与 SGLT2i 可能延缓 CAVS 进展，需大样本临床试验验证。

4. 高血压与 CAVS 的负相关性需排除降压药物干扰后深入探索。

在老年 ASCVD 患者中，hsCRP 与 Lp(a) 何者对心血管事件风险的预测价值更优？

王浩宇 尹栋 窦克非

中国医学科学院阜外医院（国家心血管病中心）

背景： 在已确诊动脉粥样硬化性心血管疾病（ASCVD）的≥ 75 岁老年患者中，炎症与高脂血症对未来动脉粥样硬化血栓事件的风险贡献度相当。然而，高敏 C 反应蛋白（hsCRP）与脂蛋白 (a)［Lp(a)］作为主要不良心血管事件（MACE）风险决定因子的相对重要性尚未明确。

方法： 本研究于阜外医院前瞻性纳入 2,333 例≥ 75 岁的 ASCVD 患者，检测基线 hsCRP 与 Lp(a) 水平。主要终点为 MACE（包含全因死亡、心肌梗死、卒中或缺血驱动的冠状动脉血运重建）。

结果： 中位随访 3.0 年（IQR：2.5-3.2 年）期间共记录 293 例首发 MACE。hsCRP 和 Lp(a) 呈偏态分布（中位数分别为 1.8 mg/L [IQR: 0.9-4.4 mg/L] 和 19.3 mg/dL [IQR: 8.6-44.2 mg/dL]）。限制性立方样条（RCS）分析显示：hsCRP 与 MACE 风险呈线性正相关（总体关联 P=0.004，非线性 P=0.393），而 Lp(a) 无显著关联（总体关联 P=0.756）。

hsCRP 每升高 1 mg/L，MACE 风险显著增加 5%（校正风险比 [aHR]：1.05，95% CI：1.03-1.08，P<0.001）；最高 vs 最低四分位数组 aHR：1.70（1.22-2.38）。相反，Lp(a) 每升高 10 mg/dL 未显示显著关联（aHR：1.02，95% CI：0.98-1.06，P=0.341；最高 vs 最低四分位数组 aHR：1.06 [0.77-1.47]）。当 hsCRP ≥ 2 mg/L 时，无论 Lp(a) 分层如何，MACE 风险均显著升高（aHR: 1.41 [1.12-1.79]，P=0.004）。

hsCRP 与 Lp(a) 无显著交互作用（Lp(a) 连续变量交互 P=0.903；Lp(a) ≥ 30 mg/dL 阈值交互 P=0.635）。以 hsCRP=2 mg/L 和 Lp(a)=30 mg/dL 为界值分组显示：hsCRP ≥ 2 mg/L 且 Lp(a) ≥ 30 mg/dL 组 MACE 风险最高（较参照组 [hsCRP<2 mg/L 且 Lp(a)<30 mg/dL]aHR：1.54，95% CI：1.13-2.12，P=0.007）。

结论： 在≥ 75 岁的 ASCVD 患者中，hsCRP 评估的炎症指标对心血管事件的预测价值显著优于 Lp(a)。本研究为老年患者通过靶向抗炎策略进行 ASCVD 二级预防提供了真实世界证据支持。

营养风险对老年心功能不全患者住院期间简易运动能力的影响

康云鹏

首都医科大学附属北京安贞医院

目的 通过本研究判断存在营养风险对老年心功能不全患者在住院期间简易运动和体适能的影响，并进一步探讨多维度改善老年心血管疾病的方法。

方法 连续纳入病房收治的老年心功能不全患者 210 例，根据老年营养风险指数（GNRI）进行分组，GNRI 计算公式如下: GNRI=[1.489× 血清白蛋白（g/L）]+[41.7×（当前体质量（kg）/ 理想体质量（kg）]。本研究以 GNRI ≤ 98 定义为存在营养风险，GNRI > 98 为无营养风险。分为合并营养不良风险组 102 例和对照组 108 例，分析 2 组基线资料和住院期间体适能状况；根据 SPPB 分为体适能较差患者 165 例和体适能良好患者 45 例；采用二分类 logistic 回归分析导致 2 组患者院内体适能下降的主要影响因素。

结果 营养不良风险组的心功能不全患者椅子站立测试评分 [（2.15±0.82）分 vs（2.36±0.71）分，P=0.019]，简易机体功能总分明显低于对照组 [（7.24±1.68）分 vs（8.51±1.92）分，P=0.041]；女性握力水平低于对照组 [（16.65±4.13）kg vs（18.89±3.24）kg，P=0.047]；与体适能良好患者比较，体适能较差患者年龄更大，血 BNP 水平更高，血清白蛋白水平、GNRI 分值、LVEF 值更低（P 均 < 0.05）。二分类 logistic 回归分析显示：BNP 升高（OR 1.003，95%CI:1.001--1.005,P < 0.001）、营养不良风险（OR 2.642，95%CI:1.248--5.591,P=0.011）是影响老年 HFrE 心功能不全患者住院期间简易运动评分减低的主要危险因素。

结论 存在营养不良风险是导致老年心功能不全患者住院期间体适能下降的独立危险因素。

大血管与外周血管疾病有关研究

Exploring the Potential Mechanisms of GABA in Treating Abdominal Aortic Aneurysm through Network Pharmacology and Experimental Validation

Lu-Zhe Huang[1], Jun-Xing Zhu[1,2]

1. Qingtian People's Hospital

2. The Second Affiliated Hospital of Anhui Medical University

Abstract

Objective: To systematically identify potential targets of γ-aminobutyric acid (GABA) in treating abdominal aortic aneurysm (AAA) and explore its key mechanisms by integrating network pharmacology with experimental validation.

Methods: Common targets of GABA and AAA were screened via network pharmacology, followed by the construction of a protein-protein interaction (PPI) network. GO/KEGG enrichment analyses were performed to predict critical pathways. An in vivo AAA model was established in Sprague-Dawley (SD) rats using elastase combined with calcium chloride. Rats were divided into sham, model, GABA (100 mg/kg/d), and GABA + bicuculline (a GABA-A receptor antagonist) groups. Histopathology, Western blot (WB), and gelatin zymography were used to evaluate GABA's effects on extracellular matrix (ECM) degradation and signaling pathways.

Results: Network pharmacology identified 111 common GABA-AAA targets. PPI analysis revealed AKT1 as the most significant target (Degree: 58). KEGG enrichment highlighted the PI3K/AKT pathway as the most prominent signaling pathway ($P < 0.01$). GO analysis indicated that GABA exerts pharmacological effects primarily by regulating ECM degradation, amino acid metabolism, and apoptosis. In vivo experiments demonstrated that GABA significantly reduced AAA formation rate (model: 100% vs. GABA: 33%, $P < 0.01$) and aortic diameter expansion rate (model: 158.21±92.00% vs. GABA: 44.07±20.97%, $P < 0.01$). Histologically, the GABA group exhibited preserved vascular wall integrity with reduced degradation of elastic and collagen fibers compared to the model group ($P < 0.05$). Gelatin zymography and WB revealed that the GABA group exhibited significantly lower PI3K/AKT phosphorylation levels and reduced MMP2/9 expression/activity compared to the model group ($P < 0.05$). Importantly, the GABA-A receptor antagonist bicuculline significantly reversed these effects ($P < 0.05$).

Conclusion: GABA may regulate the PI3K/AKT signaling pathway through the GABA-A receptor, reducing extracellular matrix degradation and thus delaying the progression of abdominal aortic aneurysm.

Abstract

Objective: To systematically identify potential targets of γ-aminobutyric acid (GABA) in treating abdominal aortic aneurysm (AAA) and explore its key mechanisms by integrating network pharmacology with experimental validation.

Methods: Common targets of GABA and AAA were screened via network pharmacology, followed by the construction of a protein-protein interaction (PPI) network. GO/KEGG enrichment analyses were performed to predict critical pathways. An in vivo AAA model was established in Sprague-Dawley (SD) rats using elastase combined with calcium chloride. Rats were divided into sham, model, GABA (100 mg/kg/d), and GABA + bicuculline (a GABA-A receptor antagonist) groups. Histopathology, Western blot (WB), and gelatin zymography were used to evaluate GABA's effects on extracellular matrix (ECM) degradation and signaling pathways.

Results: Network pharmacology identified 111 common GABA-AAA targets. PPI analysis revealed AKT1 as the most significant target (Degree: 58). KEGG enrichment highlighted the PI3K/AKT pathway as the most prominent signaling pathway ($P < 0.01$). GO analysis indicated that GABA exerts pharmacological effects primarily by regulating ECM degradation, amino acid metabolism, and apoptosis. In vivo experiments demonstrated that GABA significantly reduced AAA formation rate (model: 100% vs. GABA: 33%, $P < 0.01$) and aortic diameter expansion rate (model: 158.21±92.00% vs. GABA: 44.07±20.97%, $P < 0.01$). Histologically, the GABA group exhibited preserved vascular wall integrity with reduced degradation of elastic and collagen fibers compared to the model group ($P < 0.05$). Gelatin zymography and WB revealed that the GABA group exhibited significantly lower PI3K/AKT phosphorylation levels and reduced MMP2/9 expression/activity compared to the model group ($P < 0.05$). Importantly, the GABA-A receptor antagonist bicuculline significantly reversed these effects ($P < 0.05$).

Conclusion: GABA may regulate the PI3K/AKT signaling pathway through the GABA-A receptor, reducing extracellular matrix degradation and thus delaying the progression of abdominal aortic aneurysm.

Triglyceride-glucose index, arterial Stiffness, and cardiovascular disease: Results from an 11-year prospective study in China

sijin zhang, Hao Xue

Department of Cardiology, The Sixth Medical Center, Chinese PLA General Hospital, 6 Fucheng RD., Beijing 100048, China.

Triglyceride-glucose index, arterial Stiffness, and cardiovascular disease: Results from an 11-year prospective study in China

Sijin Zhang[a,b*], Chi Wang[b*], Zekun Feng[b], Yanjie Li[a], Kunlun He[a,c#], Shouling Wu [d#], Hao Xue[a,b#]

Affiliation:

a, School of Medcine, Nankai University, Tianjin 300071, China

b, Department of Cardiology, The Sixth Medical Center, Chinese PLA General Hospital, 6 Fucheng RD., Beijing 100048, China.

c, Medical Big Data Research Center, Medical Innovation Research Department of PLA General Hospital, 28 Fuxing Road, Haidian District, Beijing 100853, China

d, Department of Cardiology, Kailuan Hospital, North China University of Science and Technology, 57 Xinhua East Rd, Tangshan 063000, China

*Sijin Zhang and Chi Wang contributed equally to this study.

Corresponding author:

Shouling Wu

E-mail: drwusl@163.com.

Hao Xue

E-mail: xuehaoxh301@163.com

Background:

The triglyceride-glucose (TyG) index, which is a simple surrogate marker of insulin resistance, has been suggested as a contributor of cardiovascular disease (CVD). However, few studies investigated whether the combination of TyG index and arterial stiffness status can better predict the incidence of CVD.

Methods:

A total of 32176 participants without CVD at baseline were enrolled from the Kailuan study. We measured AS by brachial-ankle pulse wave velocity and other cardiovascular risk factors in a community-based population. The participants were allocated to four groups according to their TyG and baPWV status. The end point was a composite of stroke, myocardial infarction, and heart failure. Using Cox proportional hazard model to calculate hazard ratios (HRs) with 95% CIs, we compared the end point between individuals with normal TyG and baPWV, elevated TyG and normal baPWV, normal TyG and elevated baPWV, elevated TyG and baPWV. Multiplicative interaction effects were further estimated. Meanwhile, subgroup analysis was performed to investigate the prediction performance among different population.

Results:

During a median 5.8-year follow-up, 1,448 incident CVD cases were documented. Compared with the reference group (normal TyG and baPWV), the cumulative incidence of CVD in the groups with solely elevated TyG, solely elevated baPWV, and elevated TyG and baPWV showed a trend to increase. The incidence densities for each group were 1.43, 3.13, 8.66, 14.09 per 1000 person-years, respectively. Compared to the group with normal TyG and baPWV, the adjusted hazard ratios (95% confidence intervals) for CVD events were 1.42 (1.07–1.88) for elevated TyG alone, 2.09 (1.62–2.69) for elevated baPWV alone, and 2.97 (2.33–3.80) for both elevated TyG and baPWV. Similar trends were observed for CAD (1.97 [1.20–3.23], 2.41 [1.51–3.86], and 3.63 [2.31–5.70]), stroke (1.16 [0.78–1.72], 1.87 [1.33–2.63], and 2.76 [1.99–3.84]), and HF (1.04 [0.53–2.06], 1.90 [1.18–3.05], and 2.13[1.31–3.45]). Kaplan–Meier survival curves further demonstrated that the cumulative incidence of CVD increased with elevated TyG, elevated baPWV, and both elevated TyG and baPWV (all log-rank $P < 0.05$). In the subgroup and sensitivity analyses, our data showed similar results. The interaction analysis revealed a significant additive interaction between TyG and baPWV (RERI: 2.68, 95%CI: 1.64-3.72; AP:0.27, 95%CI: 0.18-0.36; SI:1.43, 95%CI: 1.23-1.65), indicating that their coexistence confers a supra-additive CVD risk.

Conclusions:

In conclusion, the individuals with elevated TyG and baPWV had a much higher risk than the other groups. The joint assessment of TyG and arterial stiffness enhances the predictive capability for CVD. Combined control of TyG and arterial stiffness may help reduce the risk of CVD.

Keywords:

Triglyceride-glucose (TyG) index, arterial stiffness, brachial-ankle pulse wave velocity, cardiovascular disease.

Association between preoperative triglyceride-glucose index and the risk of short-term aortic adverse events after thoracic endovascular aortic repair

Xuan Wu[1,2], Ting-Hao Zhao[1], Hou-Lin He[1], Ya-Song Wang[1], Xiao-Zeng Wang[1]

1. General hospital of northern theater commander

2. Graduate school of china medical school

Background: Thoracic endovascular aortic repair (TEVAR) is a mainstay minimally invasive treatment for thoracic aortic pathologies, including aneurysms and dissections. Despite reducing mortality compared to open surgery, short-term aortic adverse events (AAEs), such as endoleaks, stent migration or rupture occurring within the first year post-procedure remain significant causes of morbidity, mortality, and rehospitalization. Accurate preoperative identification of patients at high risk for these AAEs is therefore crucial for optimizing perioperative management and improving outcomes. Current risk assessment for TEVAR relies on factors like age, comorbidities (e.g., hypertension, diabetes), and aortic anatomy; however, these predictors have limitations in consistently forecasting short-term AAEs. Insulin resistance (IR), a key component of cardiometabolic dysregulation implicated in endothelial dysfunction and vascular inflammation, represents a potential but underexplored risk factor. The triglyceride-glucose (TyG) index, calculated as Ln[fasting triglycerides (mg/dL) × fasting glucose (mg/dL)/2], is a well-validated, accessible surrogate marker for IR, with elevated levels strongly associated with the development and adverse outcomes of atherosclerotic cardiovascular diseases. Within TEVAR, the specific impact of preoperative metabolic status, particularly IR assessed via the TyG index, on short-term outcomes after TEVAR is poorly understood. While conventional understanding suggests that IR, signified by a high TyG index, would confer increased risk for vascular complications due to its detrimental effects on vascular biology, direct evidence linking the preoperative TyG index specifically to short-term (≤ 1 year) AAEs post-TEVAR is notably scarce, leaving the nature and independence of this potential association unclear and representing a critical knowledge gap. Therefore, investigating the relationship between the preoperative TyG index and the incidence of short-term AAEs following TEVAR is essential. Elucidating this link could not only advance our understanding of metabolic influences on post-repair aortic healing and complication mechanisms but also potentially identify a novel, readily available biomarker for perioperative risk stratification to enhance clinical decision-making, allowing for targeted preventative strategies in high-risk patients undergoing TEVAR. This study was specifically designed to address this gap by examining the association between the preoperative TyG index and the occurrence of AAEs within one year after TEVAR.

AIM: To investigate the relationship between the preoperative triglyceride-glucose index (TyG index) and short-term aortic adverse events (AAEs) after thoracic endovascular aortic repair (TEAVR).

Methods: The retrospective study included 1017 patients with aortic disease who underwent TEVAR at the General Hospital of Northern Theater Command from April 2002 to November 2023 and were successfully followed up for 1-year. TyG index cut-off values were selected using the maxstat package of R, and patients were divided into low TyG index (≤ 8.45) (TyG-Low) and high TyG index (>8.45) (TyG-High). General information, medical history, surgical characteristics and survival data were compared between the two groups. The Kaplan-Meier method and the multivariate Cox proportional hazards Model were used to analyze the relationship between TyG index and short-term AAEs after TEVAR. The robustness of the results was tested using stratified analyses.

Results: Among 1017 patients, a total of 125 patients experienced AAEs during the 1-year follow-up period. The COX proportional hazards model suggested that the occurrence of AAEs at 30-day, 90-day, 180-day and 1-year postoperatively was negatively correlated with the TyG index (P□0.05), and this result remained statistically significant after adjustment for possible confounders (P□0.05). According to the Kaplan-Meier curve, patients in the high TyG index group had lower rates of AAEs at 30-day, 90-day, 180-day and 1-year (P □0.05) respectively.

Conclusions: In this study, it was found that a high preoperative TyG index (TyG index>8.45) was associated with a low incidence of AAEs after TEVAR. This finding challenges the conventional perception of the TyG index as a pure IR marker and suggests its value in perioperative risk assessment for TEVAR

An Aqueous Extract of Radix Astragali, Angelica sinensis, and Panax notoginseng protected brain microvascular endothelial cell from hypoxic damage via PI3K/Akt/eNOS Pathway

Wen-Ting Chen[1,2], Cao-Xin Huang[2], Min-Yi Liu[2], Xi-Lin Ge[2], Jia Li[2], Su- Liu[2], Shu-Yu Yang[2]

1. Daping Hospital, Army Medical University

2. The First Affiliated Hospital of Xiamen University

Cerebral microvascular disease, such as stroke, Alzheimer's disease and vascular dementia, is the important cause of mortality and morbidity worldwide . Brain microvascular endothelial cell is the main element of cerebral microvascular and could form the blood brain barrier (BBB), which is a distinctive structure of the cerebrum, with astrocytes and pericytes to maintain the brain homeostasis. Mounting evidences have revealed that the brain microvascular endothelial cells function not only as anatomical and physical barriers, but also as a metabolic system that could synthesize a variety of nerve growth factors and adjust the diastolic and systolic function of blood vessels. Thus, the damage of brain microvascular endothelial cells is closely related to cerebral microvascular disease. Hypoxia is considered as a key contributing factor to cerebral microvascular disease. A previous study has shown that hypoxia could inhibit vessel formation in cultured brain endothelial cells.

The phosphatidylinositol 3 kinase (PI3K)-protein kinase B (Akt) signaling pathway plays a key role in cell proliferation and survival. Endothelial nitric oxide synthase (eNOS), an important downstream target of PI3K/Akt signaling pathway activated by phosphorylated Akt, is widely expressed in endothelial cells and involved in mitigating ischemia-induced brain injury and endothelial cell survival and proliferation.

Dang Gui Bu Xue Tang (DBT) consisting of two common herbs, Radix Astragali and Radix Angelica sinensis at a ratio of 1:5, has been extensively employed in traditional Chinese medicine to treat menstrual anemia, cardiovascular disease and tumors. Radix Astragali can protect the cells and tissues from oxidative stress. Radix Angelica sinensis is also protective in endothelial cells with robust anti-oxidant activity. Recently, some researches have modified DBT to develop its potential to treat other diseases. As an important traditional Chinese medicine, Panax notoginsenoside has shown a variety of beneficial effects including neuroprotective, anti-inflammation and anti-apoptosis as a prominent free radical-scavenger and efficient antioxidant. Therefore, we optimized Dang Gui Bu Xue Tang (DBT) with addition of Panax notoginsenoside and developed an aqueous extract of Radix Astragali, Radix Angelica sinensis, and Panax notoginseng (RRP) with the functions of nourishing blood, dispersing blood stasis and dredging collateral. In our previous study, we have reported the protective effect of RRP in preventing the diabetic retinopathy, one of the most common microvascular disease. Because of the high energy requirements render the brain more vulnerable to hypoxic conditions, it would be more necessary to determine how brain microvasculature responds to hypoxia and the therapeutic approach. In the present study, we further investigated the potential effects of RRP in protecting brain microvascular against hypoxia stimulation caused by $CoCl_2$ treatment by measuring cell proliferation, survival and protein expressions of PI3K/Akt/eNOS signaling pathway.

We optimized it to be an aqueous extract of Radix Astragali, Radix Angelicasinensis, and Panax notoginseng (RRP), with addition of Panax notoginseng, with the functions of dredging collateral and dispersing blood stasis. We explored the protect effect of RRP in bEnd.3 cells, a brain microvascular endothelial cell-line, exposed to hypoxia and investigated the possible mechanisms. We stimulated bEnd.3 cells with Cobalt chloride ($CoCl_2$), a hypoxia mimetic agent, to induce hypoxia effect in vitro. RRP-Containing Serum (RRP-CS) was further applied to the $CoCl_2$-treated cells. We demonstrated that RRP-CS could protect bEnd.3 from hypoxic damage induced by $CoCl_2$. Furthermore, the activity of PI3K/Akt/eNOS signaling pathway inhibited by hypoxia also was restored by RRP-CS. However, the protective effects of RRP-CS were inhibited by LY294002, a PI3K inhibitor. In conclusion, our study shows that RRP protect bEnd.3 from hypoxic damage dependent on its capacity to modulate the PI3K/Akt/eNOS signaling.

腹主动脉瘤覆膜支架植入术后反复发热一例

俊

马鞍山市人民医院

[摘要] 腹主动脉瘤支架植入术后感染是支架植入术后的致死性并发症之一，虽然发病率较低，但是其死亡率极高。这篇文章报道一例腹主动脉瘤术后 2 月后反复发热，完善血培养、GNS 及 PET-CT 等检查，最终诊断考虑血管移植物或腔内移植物感染（vascular graft/endovascular graft infection，VGEI），给予 6 周长程抗生素治疗后，未再出现发热、康复出院。拟通过深入分析该病例的诊断依据、发病机制及诊疗过程，旨在为临床工作中救治此类患者提供参考。

[摘要] 腹主动脉瘤支架植入术后感染是支架植入术后的致死性并发症之一，虽然发病率较低，但是其死亡率极高。这篇文章报道一例腹主动脉瘤术后 2 月后反复发热，完善血培养、GNS 及 PET-CT 等检查，最终诊断考虑血管移植物或腔内移植物感染（vascular graft/endovascular graft infection，VGEI），给予 6 周长程抗生素治疗后，未再出现发热、康复出院。拟通过深入分析该病例的诊断依据、发病机制及诊疗过程，旨在为临床工作中救治此类患者提供参考。

分期运动管理模式在促进主动脉夹层腔内隔绝术患者康复中的应用研究

张璐

陆军军医大学第二附属医院新桥医院

【摘要】目的 探讨主动脉夹层腔内隔绝术患者在早期康复中采用分期运动管理模式的临床研究及意义。**方法** 选取陆军军医大学新桥医院心血管内科，选择 2023 年 1 月 ~ 2023 年 7 月在我院行主动脉夹层腔内隔绝术患者 50 例为对照组，其中男 34 例，女 16 例，年龄 46-81 岁；2023 年 8 月 ~ 2024 年 3 月行主动脉夹层腔内隔绝术患者 50 例为观察组，其中男 31 例，女 19 例，年龄 51-78 岁。对照组实施常规护理；观察组在对照组的基础上，对主动脉夹层腔内隔绝术患者进行运动风险评估，根据评估结果制定分期运动管理方案，为患者推送主动脉夹层腔内隔绝术患者分期运动指导视频，并定期指导患者进行分期运动。**结果** 干预后，观察组患者 AT、VO_2max、O_2pulse、最大运动时间、LVEF 较干预前增高，观察组明显高于对照组；观察组患者 SF - 36 量表评分较干预前增高，观察组明显高于对照组；卧床时间、住院时间、并发症发生率，观察组均明显低于对照组，差异有统计学意义 (P < 0.05)。**结论** 根据主动脉夹层动脉瘤患者的疾病不同时期特点，采用分期运动管理模式，协助患者早期活动，避免发生压力性损伤，防止尿路感染，预防深静脉血栓形成，保持呼吸道通畅降低肺部感染可能性，促进患者生理、心理、社会功能恢复，早日康复出院。

Cytoskeletal-related genes function as checkpoints for the maintenance of VSMC contractile phenotype and prevent pathological remodeling in arterial diseases

Liping Zeng

Daping Hospital of Army Medical University

Cytoskeletal-related genes function as checkpoints for the maintenance of VSMC contractile phenotype and prevent pathological remodeling in arterial diseases

Abstract

Introduction: The complexity of vascular smooth muscle cell (VSMC) biology is an emerging aspect of atherosclerosis-based cardiovascular disease. The phenotype switching of VSMCs, which includes dedifferentiation, proliferation, migration, and trans-differentiation into other cell types, is considered to be an important pathological process in vascular-related diseases. Understanding how the transcriptome of the synthetic phenotype differs from the contractile phenotype in pathological conditions may help to gain a panoramic view of this transition, especially in the initial stages of the pathological process. By utilizing the SMC genetic lineage tracing model in mice, the fate of SMCs and SMC-derived cell types can be traced in arterial disease lesions. Single-cell RNA-seq is an excellent tool to get a glimpse on how gene expression varies among cell clusters, especially in a process with potential transition ability. Taking these processes into consideration, we can explore how the VSMC phenotype-switching takes place by comparing transcriptome changes to understand additional artery disease risk factors that may contribute to the development of new treatment modalities. Although many studies have focused on the integration analysis of inflammatory cells in vascular disease lesions, few have focused on the contribution of component cells.

Objectives: we built an integrative model involving the results of studies on atherosclerosis and aneurysm samples from humans and miceTo construct a cross-species integrative model of VSMC transition in arterial diseases including atherosclerosis and aortic aneurysm, identify key genes regulating phenotypic switching in the trajectory from contractile to other phenotypes, and further validate their function in arterial remodeling models. Our ultimate aim is to uncover less understood driving forces that promote VSMC phenotype switching.

Methods: Public single-cell RNA-seq datasets were analyzed to map VSMC transcriptional dynamics and identify regulated gene expression patterns during transition. The changes were further checked using experimental animal aneurysm samples and PDGF-BB treated VSMCs. Functional validation included in vitro siRNA-mediated knockdown using primary VSMCs and in vivo gene-manipulated (AAv shRNA/Adv-overexpression) wire-injury models.

Results: We found significantly altered expression patterns in genes related to the cytoskeleton, namely Synpo2, Fblim1, and Tns1. To verify the functional importance of these genes, we conducted experiments using both in vivo and in vitro samples to validate expression changes. siRNA knock-down of these genes in primary cultures of VSMCs reduced contractile gene expression, enhanced proliferation, migration, and disrupted cytoskeleton architecture in VSMCs. In animal models, gene down-regulation exacerbated pathological remodeling while over-expression, using a cocktail strategy that manipulated these three genes, partially reverted these effects. These results indicated a critical role of cytoskeleton-related genes in the maintenance of the contractile VSMC phenotype in the progression of vascular pathological remodeling.

Conclusion: The findings highlight the critical role of cytoskeleton-related genes in arterial diseases that function as a critical checkpoint in preventing VSMC pathological phenotypic switching. In future studies, we suggest employing single-cell RNA-seq technology and trajectory analytic methods, as well as adequate batch effect correction algorithms, to establish a more comprehensive model to determine gene-mediated regulation of cell phenotype.

使用数据独立的采集质谱法识别结节性多动脉炎的候选生物标志物

马慧敏

新疆维吾尔自治区人民医院

目的：结节性多动脉炎（Polyarteritis nodosa, PAN）是一类以中小动脉广泛炎症及坏死性病变为特征的自身免疫性疾病，常导致多系统受累，导致显著的功能障碍。因此对 PAN 的及时准确诊断以及迅速治疗可显著减轻其严重程度并改善患者预后。

方法：本研究采用数据非依赖采集质谱（data-independent acquisition mass spectrometry, DIA-MS）技术对 PAN 患者和健康对照组（HC）的的血清样本蛋白组进行高通量、无偏的系统分析。共鉴定出 55 种差异蛋白。在验证集中，我们对 35 例血清样本（10 例健康对照，15 例其他疾病患者，10 例 PAN 患者）进行了后续 DIA-MS 分析，以评估所鉴定生物标志物的诊断潜力。

结果：在 PAN 患者中，有 18 种蛋白的表达水平与对照组相比存在显著差异。通过 LASSO 二元逻辑回归模型，我们筛选出由 AZGP1、F13B、LBP、RBP4、SERPINF1、PGLYRP2 和 PPBP 组成的生物标志物面板，该面板能够有效区分病例与对照，ROC 曲线下面积（AUC）达到 0.994。

结论：利用 DIA-MS 技术结合 LASSO 二元逻辑回归模型，我们开发了一种由 7 种蛋白组成的诊断面板，显著提高了 PAN 诊断的准确性和速度。

Ferroptosis Inhibition Suppresses Experimental Abdominal Aortic Aneurysm Formation by Attenuating Macrophage-Mediated Inflammation

Liping Zeng

Daping Hospital of Army Medical University

Ferroptosis Inhibition Suppresses Experimental Abdominal Aortic Aneurysm Formation by Attenuating Macrophage-Mediated Inflammation

abstract

Background: Cardiovascular diseases (CVDs) account for 32% of global deaths. Abdominal aortic aneurysm (AAA) affects 4-8% of men over 65 and carries a mortality rate exceeding 80% upon rupture, yet pharmacotherapies remain absent due to incomplete mechanistic understanding. Pathological hallmarks include: 1) VSMC apoptosis (>80% loss in ruptured AAA); 2) Elastin fragmentation by MMP-9/12; 3) Chronic adventitial inflammation dominated by macrophages. While inflammation drives AAA progression, attempts to suppress it broadly (e.g., anti-IL1β in MILES trial) failed clinically, suggesting cellular heterogeneity in inflammatory responses. Ferroptosis—a lipid peroxidation-driven cell death—has emerged as a key process in neurodegeneration and cancer, but its vascular implications are unexplored. Distinct from apoptosis, ferroptosis depends on iron-catalyzed phospholipid peroxidation and is morphologically characterized by shrunken mitochondria with ruptured outer membranes. Our integrated transcriptomics revealed selective ferroptosis pathway enrichment in AAA macrophages (not VSMCs or ECs), coinciding with elevated iron deposition in human AAA tissue (Prussian blue staining). Given macrophages generate 90% of plaque ROS and express lipid peroxidation enzymes (ALOX15/GPX4), we posited that ferroptosis might amplify inflammation through macrophage-derived DAMPs (e.g., HMGB1), creating a feedforward loop of wall degradation.

Methods: Published scRNA-seq data were integrated, subjected to dimensionality reduction, and visualized through clustering. Cell types were annotated based on classical marker genes. Differential gene expression analysis was performed between AAA and control specimens for each cell type. Ferroptosis susceptibility scores across cell types were assessed using gene set scoring tools. An in vivo experimental AAA model was established, and relevant indicators (malondialdehyde (MDA), transmission electron microscopy (TEM), glutathione/oxidized glutathione (GSH/GSSG) ratio) were measured. The effect of the ferroptosis inhibitor ferrostatin-1 (Fer-1) on AAA formation was evaluated. Bulk RNA sequencing was employed to determine changes in cellular composition within tissues and identify cell types associated with ferroptosis susceptibility.

Results: Integrated single cell RNA sequencing analysis revealed a significant increase in the ferroptosis susceptibility score specifically within macrophages in AAA specimens. Inhibition of ferroptosis using Fer-1 significantly reduced AAA formation. Integration of scRNA-seq and bulk RNA-seq data indicated a significantly increased proportion of macrophages in the AAA group.

Conclusion: This study establishes ferroptosis as a previously unrecognized pathogenic mechanism in AAA, with macrophage-specific vulnerability driving disease progression. We identify macrophage ferroptosis as a pivotal amplifier of AAA pathogenesis through interconnected mechanisms and the ferroptosis inhibitor Fer-1 demonstrates potent efficacy in preserving aortic structural integrity, primarily through: Attenuating lipid peroxidation cascade; Reducing inflammatory macrophage infiltration; Preventing mitochondrial damage. Given the absence of medical

therapies for AAA, targeting ferroptosis represents a promising strategy for early intervention. Ferrostatin analogs or macrophage-specific GPX4 activators warrant clinical development, particularly for high-risk patients with small AAAs (3.0-5.4 cm diameter). Future studies should explore whether circulating ferroptosis biomarkers (e.g., plasma MDA) could serve as non-invasive predictors of AAA expansion. Future work must clarify: 1) How extracellular matrix stiffness regulates macrophage ferroptosis susceptibility; 2) Whether endothelial ferroptosis contributes to intra-luminal thrombus formation. This work positions ferroptosis inhibition as a first-in-class strategy targeting the upstream driver of AAA inflammation.

Dual Receptor Crosstalk: AT1R and Integrin β3 Synergize to Drive Aortic Dissection via Non-Canonical Wnt/β-Catenin Signaling

Hong-Cheng Jiang, Zi-Xuan Liu, Xiao-Dan Zhong, Hong-Jie Wang, He-Song Zeng

Tongji Hospital, Tongji Medical College, Huazhong University of Science and Technology

Background: Aortic dissection (AD) is a life-threatening cardiovascular emergency with high mortality due to the lack of effective therapeutic options. Current pharmacological interventions, including angiotensin-converting enzyme inhibitors (ACEi) and angiotensin receptor blockers (ARBs), have demonstrated limited efficacy in mitigating AD progression. Composed of 18 α- and 8 β-subunits, functionally distinct integrin heterodimers are transmembrane receptors bridging the cells and extracellular matrix (ECM) and help cells cope with various internal and external perturbations. Among these, integrin αvβ3, which is a prominent RGD-binding receptor, orchestrates endothelial cells (ECs) survival, angiogenesis, and matrix remodeling. Here, we investigate the role of integrin β3 in AD pathogenesis through complementary clinical, experimental, and mechanistic approaches.

Methods: Utilizing an integrated approach, we first employed single-cell RNA sequencing (scRNA-seq) to profile the aortic transcriptomes of AD patients, identifying aberrant pathway during AD progression. Male 6-week-old ApoE$^{-/-}$ mice were administrated with β-aminopropionitrile (BAPN, 1g/L) in the drinking water for 3 weeks followed by 2500 ng/kg/min Angiotensin II (AngII) subcutaneous pump for 2 weeks to induce AD. Histology, immunohistochemistry and immunofluorescence were applied in human AD specimens and murine models to confirm key molecular changes. Functional assessment was conducted using a selective integrin β3 inhibitor (Cyclo-RGDfK) in AngII-infused mice to evaluate its impact on AD incidence, aortic remodeling, and endothelial integrity. Mechanistic insights were derived from co-immunoprecipitation (Co-IP), confocal microscopy, and transcriptomic profiling to delineate receptor interactions and downstream signaling cascades.

Results: scRNA-seq revealed a significant upregulation of integrin β3 activation, particularly in ECs, during the acute phase of AD. Immunofluorescence analysis confirmed marked upregulation of activated integrin β3 in aortic ECs of both human patients and murine AD models. Pharmacological blockade of integrin β3 with Cyclo-RGDfK significantly attenuated aortic degeneration, reduced AD incidence, and preserved endothelial barrier integrity in vivo. To assess whether integrin β3 inhibition protects ECs, we analyzed inflammatory markers in the aorta of AD mice. Cyclo(-RGDfK) treatment significantly reduced endothelial activation markers ICAM-1 and VCAM-1, as well as oxidative stress indicators NOX2, NOXO2, and NOXA2. Consistently, Cyclo(-RGDfK) reduced apoptosis, as indicated by decreased cleaved caspase-3 expression. Mechanistically, AngII-induced AT1R activation triggered the formation of a receptor complex with integrin β3, inducing its conformational activation. To delineate downstream pathways involved in integrin β3-mediated endothelial injury, we performed RNA sequencing (RNA-Seq) analysis in integrin β3 knockdown ECs. KEGG pathway enrichment analysis and gene set enrichment analysis (GSEA) identified significant alterations in the Wnt signaling pathway, implicating Wnt dysregulation in integrin β3-driven endothelial dysfunction. Through CO-IP and Western blot we indentified that activated integrin β3 then bound glycogen synthase kinase 3β (GSK3β), stabilizing β-catenin via inhibition of its degradation.

Conclusion: In this study, we identify integrin β3 as a novel pathogenic driver of AD and elucidate a previously unrecognized crosstalk between AT1R and integrin β3 in mediating endothelial dysfunction. Mechanistically, we demonstrate that AT1R activation enhances integrin β3 signaling, which in turn triggers non-canonical Wnt pathway activation via GSK3β interaction, ultimately leading to endothelial cell injury and aortic wall degeneration . These findings highlight a novel therapeutic target for AD and advocate for a dual-target approach involving both AT1R and integrin β3 inhibition.

STUB1 orchestrates mineralocorticoid receptor activation to promote aortic dissection

Hong-Cheng Jiang, Zi-Xuan Liu, Xiao-Dan Zhong, Hong-Jie Wang, He-Song Zeng

Tongji Hospital, Tongji Medical College, Huazhong University of Science and Technology

Background: Aortic dissection (AD) is a critical cardiovascular condition with few treatment options available. Research indicates that elevated aldosterone levels are linked to an increased risk of AD, suggesting the involvement of mineralocorticoid receptor (MR) activation in its pathogenesis. This study aimed to elucidate the underlying molecular mechanisms and identify potential therapeutic targets.

Methods: Human AD tissue and blood samples were freshly obtained from patients undergoing open surgical repair procedures and age-matched aorta and blood samples obtained from heart transplant or aortic valve replacement donors were used as controls. To investigate the activation of MR in AD, C57BL/6N mice were employed to establish BAPN-induced AD model. Briefly, 18 male C57BL/6N mice at the age of 4-week-old were divided into 2 groups, 12 mice were given the drinking water supplemented with 3 g/L BAPN to induce AD, and others were fed with normal drinking water to serve as control. To investigate whether aldosterone contributes to the occurrence of AD, 4-week-old male C57BL/6N mice were randomly divided into four groups, which received the following treatments: normal drinking water combined with saline pump or 600 μg/kg/d aldosterone pump, and 2 g/L BAPN combined with saline pump or 600 μg/kg/d aldosterone pump. Plasma aldosterone levels were quantified using ELISA, and MR activation was evaluated in aortic tissues. Integrated bioinformatics analyses identified the E3 ubiquitin ligase STUB1 as a crucial regulator of MR activation in vascular smooth muscle cells (VSMCs). To assess the role of STUB1 in AD development, mice with specific STUB1 depletion in VSMCs were generated. We also investigated the downstream effects of MR activation on gene expression, oxidative stress, and apoptosis. The therapeutic potential of MR inhibition was examined by administering spironolactone (SPL) to AD mice at varying doses.

Results: Elevated plasma aldosterone levels and increased MR activation were observed in both AD patients and mice. Sustained aldosterone infusion further promoted AD onset and progression. STUB1 facilitated MR activation through K63-linked ubiquitination and subsequent its nuclear translocation in VSMCs. VSMCs specific knock out of STUB1 was found to alleviate the progression of AD in vivo. Meanwhile, we found that VSMCs-specific STUB1 depletion inhibited MR nuclear translocation in aortic SMCs, maintaining MR localization in the cytoplasm. Mechanistically, we conducted bioinformatic analysis of three independent datasets from BAPN-induced AD mice and MR overexpression or knockout models, which identified matrix metalloproteinase 3 (MMP3) and 2-oxoglutarate dehydrogenase (OGDHL) as potential downstream targets of nuclear MR. Validation experiments revealed that MR knockdown decreased Mmp3 expression while increasing Ogdhl levels, whereas MR overexpression exhibited the opposite effects. Furthermore, STUB1 knockdown attenuated MMP3 expression and upregulated OGDHL in Ang II-stimulated MOVAS cells, and vice versa. To evaluate the therapeutic efficacy of the MR inhibitor SPL on AD development in vivo, BAPN-induced AD mice were treated with SPL (1 or 5 mg/kg/day), and results revealed that BAPN-induced dilation and dissection were significantly ameliorated by SPL treatment at both dosages, and SPL treatment restored aortic structure, decreased both the incidence of AD and the maximum aortic diameter.

Conclusion: Our study demonstrates that the upregulation of STUB1-mediated K63-linked ubiquitination of MR promotes its nuclear translocation and transcriptional activity. This nuclear MR activation drives the expression of downstream targets, MMP3 and OGDHL, which contribute to ECM degradation, oxidative stress, and VSMCs apoptosis. Importantly, inhibition of MR activity, either through genetic depletion of STUB1 in VSMCs or pharmacological inhibition with the MR antagonist SPL, effectively attenuates these deleterious effects and protects against AD.

C57BL/6J 背景小鼠静脉注射 PCSK9 功能获得突变对血管紧张素 II 诱导的 AAA 的影响

张蕾

山东大学齐鲁医院

目的：本研究旨在比较静脉注射和腹腔注射 AAV8.mPCSK9D377Y 在 C57BL/6J 背景的野生型（WT）小鼠中血管紧张素 II（Ang II）诱导的腹主动脉瘤（AAA）的发生率，以及上述模型在 WT 和 ApoE-/- 小鼠中的病理差异。

方法：雄性野生型小鼠经腹腔或静脉注射 AAV8.null 或 AAV8.mPCSK9D377Y。注射两周后，所有野生型小鼠均输注 Ang II，同时年龄匹配的雄性 ApoE-/- 小鼠输注生理盐水或 Ang II 4 周。小鼠分组：① ns-ip 组；② ns-iv 组；③ ApoE-/- -con 组；④ p-ip 组；⑤ p-iv 组； ⑥ ApoE-/- -Ang II 组。实验进程中测量小鼠体重、血压；采血分离血清，测血脂及肝肾功；测量小鼠腹主动脉的最大血管直径；行 HE 染色观察血管形态；Verhoeff 染色评估腹主动脉弹力纤维的完整性；Masson 染色检测胶原含量及胶原 I 、胶原III、MMP2、MMP9 及巨噬细胞 CD68 免疫组化染色。

结果：与腹腔注射 AAV8.mPCSK9D377Y 用于 WT 小鼠 AAA 模型相比，静脉注射 Ang II 诱导的 AAA 发生率更高，血压和脂质浓度升高，胶原蛋白沉积降低，炎症反应上调，这与输注 Ang II 的 ApoE-/- 小鼠相似。

结论：静脉注射 AAV8.mPCSK9D377Y 感染的雄性 WT 小鼠可促进 Ang II 诱导的 AAA 的高发生率和相当严重程度，这可以大大加快对感兴趣基因的 AAA 研究。

Cross-Species scRNA-seq Analysis Identifies Optimal Mouse Models for Studying Key Cellular Mechanisms in Aortic Dissection

Gen-Mao Cao

Fudan university, Zhongshan hospital

Abstract

Background: Aortic dissection (AD) is a life-threatening vascular disorder with complex cellular mechanisms. While multiple mouse models are used to study AD, their fidelity in recapitulating human AD pathophysiology at single-cell resolution remains unclear.

Method: We performed single-cell RNA sequencing (scRNA-seq) on human AD tissues and integrated the data with scRNA-seq datasets from the five mouse AD models: BAPN model, Ang-II model, Ang-II apoE-/- model, elastase model, and CaCl2 model. Cross-species comparative analysis focused on four key cell types macrophages (Mϕ), vascular smooth muscle cells (VSMCs), fibroblasts (FBs), and endothelial cells (ECs) to evaluate transcriptional conservation.

Results: We identified pathogenic subpopulations in human AD, including pro-inflammatory and lipid-associated macrophages, oxidative stress and lipid-associated VSMCs, pro-inflammatory fibroblasts, myofibroblasts, and hypoxia ECs. BAPN model and elastase model yielded pro-inflammatory and lipid-associated macrophages, and replicated macrophage polarization. The Ang-II apoE-/- model best recapitulated the VSMCs phenotypes observed in human AD, particularly lipid-associated and oxidative stress VSMCs. The BAPN model was most effective in mimicking pro-inflammatory fibroblasts and reduced extracellular synthesis. Endothelial cell dysfunction, characterized by reduced adhesion and increased hypoxia, was consistently observed across all models.

Conclusion: Our study provides a single-cell roadmap for selecting mouse models that optimally mimic specific AD mechanisms: BAPN for macrophages and fibroblasts, Ang-II apoE $^{-}$ / $^{-}$ for VSMCs, and any model for EC studies. These findings refine experimental design for AD research and highlight conserved pathogenic pathways across species.

Keywords: scRNA-seq, mouse model, cell subpopulation, aortic dissection.

Introduction

Aortic dissection (AD) is a life-threatening pathology with high morbidity and mortality. In recent years, important discoveries about the mechanisms of AD have relied on mouse models that mimic the anatomical features and pathogenesis of human AD. Commonly used mouse models for AD include the β-aminopropionitrile (BAPN)-induced mouse model1, the Angiotensin II (Ang II)-induced mouse model, the Ang II -induced Apolipoprotein E-deficient (apoE-/-) mouse model, elastase-induced mouse model, CaCl2-induced mouse model, etc. Each of these models is capable of mimicking the anatomical features of the AD. However, whether these models can fully mimic the realistic pathophysiologic process of human AD remains unknown.

Aortic cells contribute most to the structural integrity of the aortic wall, principally endothelial cells, VSMCs, and fibroblasts. A healthy physiologic state of these cells is essential for maintaining the balance of the aortic microenvironment. However, the development of AD involves disruption of aortic microenvironment, particularly the transcriptional reprogramming of vascular cells. Macrophages, VSMCs, and fibroblasts8 reprogrammed to pathogenic phenotypes in response to cellular stress. Therefore, there is a certainly necessity to investigate the conservation of critical cellular phenotypes in human AD and mouse AD models.

Previous evaluations and comparisons of AD models have focused on pathological features and biomechanical characteristics9, which lacks a comprehensive evaluation of the model's pathogenic mechanisms. The advent of single-cell RNA sequencing (scRNA-seq) represents a significant advancement in investigating the transcriptional heterogeneity at a resolution of individual cells. For instance, studies by Zernecke et al. 10 and Frank et al.11 have utilized scRNA-seq to uncover transcriptional heterogeneity of immune cells within mouse models of atherosclerosis and to explore cellular diversity in abdominal aortic aneurysms, respectively. Preliminary studies employing scRNA-seq to analyze mouse AD models and human AD have begun to shed light on AD mechanism. Moreover, these studies offer a novel avenue to directly compare the heterogeneity of cellular phenotype between mouse models and human AD.

In the present article, we firstly revealed the transcriptional heterogeneity of macrophages, fibroblasts, VSMCs, and ECs. Subsequently, the four cell types underwent cross-species integration with their counterparts from mouse AD models, respectively (Fig. 1a). Through assessing the subpopulation heterogeneity of these four cell types, we compared the mechanism differences among human AD, the BAPN model, Ang-II model, Ang-II apoE-/- model, elastase model, and CaCl2 model.

GSDMD 依赖性 NETs 通过 P2X7R 调控巨噬细胞极化促进腹主动脉瘤进展

常润泽 高思琦 鲁传龙 王恒 樊可奕 李理政 张鸿久 陈金杉 张瑞婧 董红霖

山西医科大学第二医院

目的：腹主动脉瘤（abdominal aortic aneurysm, AAA）是一种以局灶性主动脉壁扩张为特征的致死性血管疾病，其发病机制与慢性炎症、细胞凋亡及基质降解密切相关。近年来，研究表明中性粒细胞胞外诱捕网（neutrophil extracellular traps, NETs）在 AAA 炎症反应中具有重要作用。Gasdermin D（GSDMD）作为 NETs 形成的关键介导蛋白，其裂解产物可诱导细胞膜穿孔并促进染色质外排形成 NETs。与此同时，P2X7 受体（P2X7R）是一种 ATP 依赖的配体门控阳离子通道，已被证实在调控巨噬细胞极化、尤其是促炎性 M1 型极化中发挥重要作用。然而，GSDMD 介导的 NETs 是否通过激活 P2X7R 促进 M1 型巨噬细胞极化并加速 AAA 病变尚未明确。本研究旨在探讨 GSDMD-NETs-P2X7R 信号轴在 AAA 发生发展中的作用及其潜在机制。

方法：本研究构建了弹性蛋白酶诱导的 AAA 小鼠模型，并采用中性粒细胞特异性 GSDMD 敲除小鼠（Gsdmd$^{flox/flox}$ MRP8Cre$^{+/-}$）探讨 GSDMD 对 NETs 形成及 AAA 病变的影响。通过免疫荧光染色、Western blot、ELISA 及 Sytox Green 染色等方法评估 NETs 水平及主动脉局部炎症状态；进一步检测 P2X7R 表达及巨噬细胞 M1 极化情况。随后构建巨噬细胞特异性 P2RX7 敲除小鼠（P2rx7$^{flox/flox}$Lyz2Cre$^{+/-}$），以明确 P2X7R 在 AAA 中的功能。体外实验中，应用 NETs 刺激 THP-1 来源的巨噬细胞，分析其对 P2X7R 表达及 M1 极化标志物的影响，并采用 P2X7R 抑制剂验证其作用机制。

结果：与野生型对照组相比，中性粒细胞特异性 GSDMD 敲除显著抑制 AAA 形成，表现为主动脉扩张减轻、弹力纤维破坏减少及炎症细胞浸润下降。GSDMD 缺失组中 NETs 形成明显减少，血清及主动脉组织中 dsDNA 水平显著降低，P2X7R 表达及 M1 型巨噬细胞比例均显著下降。巨噬细胞特异性 P2X7R 敲除同样可减少 M1 型极化并减轻 AAA 病理改变。体外实验显示，NETs 刺激可诱导巨噬细胞 P2X7R 表达上调，促使其向 M1 型极化；而 P2X7R 抑制剂可显著逆转该极化趋势，提示该效应依赖 P2X7R 介导。

结论：本研究揭示了 GSDMD 介导的 NETs 可通过激活巨噬细胞 P2X7R，诱导其 M1 型极化，从而促进 AAA 的发展与进展。GSDMD-NETs-P2X7R 信号通路在 AAA 炎症反应中发挥关键作用，提示其为潜在的干预靶点，有望为 AAA 治疗提供新的策略。

Cold stimulation aggravates aortic dissection through the sympathetic nerve-resident macrophages axis: a novel pathogenesis

Gen-Mao Cao

Fudan university, Zhongshan hospital

Introduction

Acute aortic dissection (AD) is a life-threatening cardiovascular emergency with a 24-hour natural mortality rate as high as 50%. There are significant differences in the incidence of AD across regions, according to the results of epidemiological insurance claims research. The incidence rate of AD in northern China is twice that in the south. Meanwhile, multiple studies indicate that the incidence rate of AD is closely related to temperature, which agrees with higher prevalence of AD in cold region. The mechanism by which cold stimulation increases the risk of AD incidence remains unclear. Some researchers explained the mechanism with specific cold-weather reactions, such as elevated blood pressure, artery spasm, progression of pulmonary diseases, and passive smoking. Additionally, the sympathetic nerve also exerts an effect on regulating immune response in cardiovascular system.

Methods

Single-cell sequencing data for AD from Beijing (cold region), Shanghai (hot summer cold winter, HSCW), and Guangzhou province (hot summer warm winter, HSWW) were obtained from the GEO database, including datasets GSE222318, GSE254123, and GSE213740. Three-week-old male C57BL/6 mice were given 0.5% BAPN containing water to induce AD while exposing to either room temperature or 6° C to investigate the effects of cold stimulation on AD. Aortic samples and surrounding tissues from the mice were clarified following the iDISCO protocol.

Results

Single-cell sequencing across different regions revealed that the proportion of macrophage extremely elevated in AD of cold region (Figure A). The up-regulated genes of macrophages in cold region were enriched in "response to temperature stimulus" and "response to cold" pathways (Figure B), which include the catecholamine receptor ADRB2. This result suggested that sympathetic nerve plays a critical role in AD of cold-region. Among macrophages from different regions, those in the cold region expressed the highest levels of ADRB2 (Figure C). Macrophages were further annotated into 6 subtypes: FABP5+ lipid-associated macrophages, IL-1B+ myeloid macrophages, LYVE1+ resident macrophages, MHChi macrophages, proliferative macrophages, VSMC-derived macrophages, and fibroblast-derived macrophages. ADRB2 was highly expressed in LYVE1+ resident macrophages in AD (Figure D). We therefore propose that the sympathetic-ADRB2-resident macrophage axis may contribute to the high prevalence of AD in cold regions.

In order to confirm the existence of sympathetic-ADRB2 axis in AD of cold-region, we conducted immunofluorescence staining of human AD samples from cold region and HSCW region. The result showed more abundant TH+ sympathetic nerve fibers in the adventitia of cold-region AD while less in HSCW-region AD (Figure E). It also indicated the over-

expression of ADRB2 in LYVE1+ resident macrophages in adventitia of cold-region AD (Figure F).

In male C57BL/6 mice exposed to cold stimulation (6° C), thoracic aortas and periaortic tissues were subjected to three-dimensional TH fluorescence staining. The staining result indicated that cold stimulation significantly increased periaortic sympathetic innervation (Figure G). Three-week-old mice were given 0.5% BAPN solution to induce AD and exposed to cold stimulation (6 ° C) simultaneously (Figure H). Cold-exposed mice gained higher mortality of AD eventually, with greater ascending aortic dilation and more severe dissection (Figure I-K).

For further exploration of the pathways by which ADRB2 regulating Lyve1+resident macrophages, cell communication analysis was conducted between macrophage subtypes in AD aortas and normal aortas. The result revealed that CCL-CCR pathways were enhanced in AD (Figure L), which primarily mediating interactions between resident macrophages and myeloid macrophages (Figure M). The key ligand-receptor pairs were CCL3L1-CCR1, CCL3-CCR1, and CCL2-CCR2 (Figure N). Transcriptomic comparisons of macrophages in AD across regions have shown higher levels of chemokines CCL2 and CCL3 in cold-region AD (Figure O). This suggested that the sympathetic nervous system may enhance chemokine release from resident macrophages via ADRB2, which promotes immune cell recruitment and thus increases AD risk.

一体式分支型支架结合体外开窗技术处理复杂 B 型主动脉急性综合征临床应用的单中心经验及体会

刘尚典

深圳市宝安区人民医院

目的 通过回顾性研究分析一体式分支型支架结合体外开窗技术治疗复杂急性 B 型主动脉综合征的疗效和安全性。

方法 回顾性分析 2020.01-2021.12 深圳市宝安区人民医院收治开展一体式分支型支架结合体外开窗技术的急性 B 型主动脉综合征患者 39 例的临床资料，收集分析患者的基线资料、术后早期恢复指标、术后早期并发症发生率及死亡率、长期预后、长期疗效和手术前后降主动脉直径等指标。

结果 所有患者术后重症监护病房时间均值（42.89±68.30）h，术后住院时间均值（12.56±5.97）d，住院总时间均值（19.90±7.85）d。1 例（2.56％）开展二次介入治疗，余下 38 例（97.43％）未开展二次介入治疗；39 例（100.00％）植入支架均在位；2 例（5.12％）支架移边缘形成新的内膜撕裂，余下 37 例（94.87％）支架移边缘未形成新的内膜撕裂。38 例（97.43％）病情改善、未进一步恶化，1 例（2.57％）病情未改善、进一步恶化。手术后患者的降主动脉直径为（25.36±3.85）mm，较手术前（18.41±8.24）mm 相比增加，存在差异具有统计学意义（P < 0.05）。

结论 一体式分支型支架结合体外开窗技术疗效及安全性总体良好，近期及远期随访效果较为理想。

Predicting the growth of asymptomatic small abdominal aortic aneurysms (AAA) based on deep learning

Jia-Xin Cheng[1,2], Zhi-Qiang Zhang[1], Ya-Song Wang[1], Xiao-ZengXueZuWeiYuanTongXunZuoZhe Wang[1]

1. National Key Laboratory of Frigid Zone Cardiovascular Disease, Cardiovascular Research Institute and Department of Cardiology, General Hospital of Northern Theater Command

2. College of Medicine and Biological Information Engineering, Northeastern University, Shenyang, Liaoning, China

Abstract

Background

Abdominal aortic aneurysm (AAA), particularly in its asymptomatic small stage, poses a significant clinical challenge due to the risk of rupture upon excessive enlargement. Accurate prediction of growth trajectories for small, asymptomatic AAAs is paramount for optimizing clinical decision-making regarding the timing of intervention versus continued surveillance. Currently, growth prediction primarily relies on serial diameter measurements from imaging, such as computed tomography angiography (CTA), which offers limited predictive power for identifying individuals prone to rapid expansion. This gap underscores the urgent need for more sophisticated predictive tools. Recent advances in deep learning present a promising avenue for extracting complex, prognostic features directly from medical images like CTA scans. While DL has shown potential in various medical imaging tasks, its application for predicting the specific growth rate of small asymptomatic AAAs remains underexplored and requires robust, end-to-end frameworks. Existing approaches often lack the integration of precise localization with advanced feature extraction and fusion mechanisms tailored for this specific predictive task. This study addresses this critical need by developing and validating a novel DL pipeline designed specifically to predict rapid growth (defined as ≥ 0.5 cm increase within 6 months) in small, asymptomatic AAAs using routinely acquired CTA images. The core objective is to leverage state-of-the-art DL architectures–combining image classification, precise aorta localization, and advanced feature fusion–to automatically extract discriminative features indicative of future rapid expansion, thereby providing clinicians with a powerful tool for risk stratification and personalized management strategies.

Objective: Accurate prediction of asymptomatic small AAA growth is critical for clinical decision-making. This study leverages deep learning to predict AAA rapid growth from CTA images.

Methods: We analyzed 81 asymptomatic patients with small AAA (31 rapid growth [≥ 0.5 cm/6 months] and 50 stable patients) who were in follow-up without intervention. CTA images were split into training, validation, and test sets in the 8:1:1 ratio. An optimized pipeline was developed in three steps: firstly, eight classification models were evaluated to classify CTA images containing the abdominal aorta. Then, You Only Look Once (YOLO)v11 model localized and classified normal and AAA images. Finally, a MedMamba-based feature fusion model predicted growth using 15,704 localized aorta images, fused by multi-head self-attention (MHA). The MedMamba extraction module was compared with the classical models, and the attention mechanism module and the number of attention heads were set as contrast experiments.

Results:

The 81 participants enrolled with 90.12% males, and the median age of 68 years. Among eight models, ResNet50 achieved precise recognition of images containing the abdominal aorta, with accuracy and F1-score being 99.86% and 99.91%, respectively. YOLOv11 achieved robust aorta detection (precision-recall: 0.902) across 31,457 images. The MedMamba fusion model outperformed seven backbones, achieving 98.75% accuracy and 97.78% F1-score for growth prediction. MHA (8 heads) optimized predictive performance.

Conclusion: This study establishes a novel end-to-end deep learning framework, ResNet50-YOLOv11-MedMamba, for predicting growth in small asymptomatic AAA. By integrating clinical metadata with automatically extracted CTA features, our model achieved state-of-the-art performance, achieving 98.75% accuracy and 97.78% F1-score. Our model holds great potential for practical application in clinical settings.

Keywords: multi-head self-attention; feature fusion model; growth prediction; classification model

非复杂性 Stanford B 型主动脉夹层患者行胸主动脉腔内修复术时机对预后及主动脉重塑的影响

赵庭浩[1,2] 王亚松[1] 何厚霖[1] 张志强[1] 王效增（学组委员通讯作者）[1]

1. 中国人民解放军北部战区总医院

2. 中国医科大学研究生院

目的： 当前研究已经明确复杂性 Stanford B 型主动脉夹层应急诊行胸主动脉腔内修复术（Thoracic endovascular aortic repair, TEVAR）或外科开放手术治疗，然而对于非复杂性病例的最佳干预时机目前尚无定论。本研究探索 TEVAR 时机对非复杂性 Stanford B 型主动脉夹层（Uncomplicated Stanford type B aortic dissection, UTBAD）患者预后及主动脉重塑的影响。

方法： 连续筛选 2010 年 1 月至 2023 年 1 月期间于北部战区总医院明确诊断 UTBAD 且于发病 90 天内接受 TEVAR 治疗的患者进行回顾性分析，应用倾向性得分匹配法平衡基线变量。根据接受 TEVAR 时机分为急性期组（1-14 天）和亚急性期组（15-90 天）。应用 Kaplan-Meier 分析和 Landmark 分析评估两组中长期不良事件发生率差异。应用多因素 COX 回归分析和亚组分析评估 TEVAR 时机对中长期预后影响。对术前和随访期影像分析评估 TEVAR 时机对主动脉重塑效果的影响。主要终点定义为包括全因死亡、逆行 Stanford A 型夹层、支架移植物诱发的新破口、新发内漏、再次干预、截瘫和新发卒中的临床不良事件（Major adverse clinical events, MACEs）。次要终点定义为包括主动脉相关性死亡、逆行 Stanford A 型夹层、支架移植物诱发的新破口、新发内漏和再次干预的主动脉相关不良事件（Aortic related adverse events, ARAEs）。

结果： 共 485 例的患者纳入本研究，其中急性期组 415 例，亚急性期组 70 例。术后 30 天内不良事件均发生于急性期组，但匹配前后两组不良事件发生率比较无组间显著性统计学差异（均 P>0.05）。急性期组中位随访时间 59.6（25.0, 60.5）月，亚急性期组 59.5（25.4, 60.3）月，随访时间比较无组间显著性统计学差异（P=0.759）。急性期组再次干预率显著低于亚急性期组（1.4% vs 5.7%，P=0.042），其余不良事件发生率组间比较均无显著性统计学差异（均 P>0.05）。匹配后两组各不良事件发生率组间比较均无显著性统计学差异（均 P>0.05）。Kaplan-Meier 分析和 Landmark 分析显示，中长期不良事件发生率两组间比较无显著性统计学差异（均 P>0.05）。匹配后的 Landmark 分析显示，急性期组术后 3 个月内 MACEs 发生率（6.5% vs 0%，P=0.033）和 ARAEs 发生率（6.5% vs 0%，P=0.033）均显著高于亚急性期组，3-60 个月内不良事件发生率未观察到组间显著性统计学差异（均 P>0.05）。匹配前后多因素 COX 回归分析和亚组分析结果显示，TEVAR 时机未对中长期预后产生显著性影响。纳入影像学分析的患者 108 例，急性期组患者 89 例，中位随访时间 12.5（6.9, 42.1）月，亚急性期组患者 19 例，中位随访时间 14.0（7.2，30.9）月，随访时间组间比较无显著性统计学差异（P=0.853）。主动脉重塑结果显示，除急性期组在肾动脉平面的主动脉直径变化值显著高于亚急性期组（P=0.023），其余平面的各直径变化和假腔血流变化无组间显著差异（均 P>0.05）。

结论： UTBAD 患者于急性期行 TEVAR 可增加 3 个月内 MACEs 和 ARAEs 发生风险。急性期或亚急性期行 TEVAR 治疗的中长期预后和主动脉重塑效果相当。对 UTBAD 患者适当延迟至亚急性期行 TEVAR 治疗可能减少术后早期相关风险。

急性主动脉夹层相关的临床特征与死亡率之间的关联：一项基于 MIMIC-IV 数据库的回顾性队列研究

夏锦坤

贵州省人民医院

急性主动脉夹层相关的临床特征与死亡率之间的关联：一项基于 MIMIC-IV 数据库的回顾性队列研究

夏锦坤

贵州省人民医院血管甲状腺外科，贵阳，贵州，550002

通讯作者：夏锦坤 (jinkunxia@foxmail.com)

摘要

背景：急性主动脉夹层 (Acute aortic dissection, AAD) 是一种严重的心血管疾病，死亡率极高。本研究旨在考察 AAD 患者的临床特征，并开发一种预测模型以评估这些特征与 AAD 患者死亡率之间的相关性。

方法：本研究基于 MIMIC-IV 数据库，纳入 2008 年至 2019 年的 AAD 患者数据。在完成样本排除后，我们为最终纳入的参与者构建了包含指定临床变量的基线数据表。随后，综合运用单变量 Cox 回归分析、机器学习算法以及多变量 Cox 回归分析，以识别影响 AAD 患者预后的独立变量。基于这些独立变量，我们构建了预测列线图 (nomogram)。最后，通过校准曲线 (calibration curve)、受试者工作特征 (receiver operating characteristic, ROC) 曲线和决策曲线分析 (decision curve analysis, DCA) 对该列线图的预测性能进行了系统评估。

结果：经过样本筛选，本研究最终纳入 400 例 AAD 患者，其中存活者 348 例，非存活者 52 例。分析发现，存活者与非存活者在包括阴离子间隙 (aniongap) 在内的多项临床变量上存在显著差异。进一步的单变量 Cox 回归、机器学习及多变量 Cox 回归分析综合表明，国际标准化比值 (INR)、阴离子间隙 (aniongap) 和急性生理学评分 III (APS III) 是 AAD 患者预后的独立相关变量。基于此建立的列线图被证实是评估 AAD 患者短期生存概率的有效工具，校准曲线、ROC 曲线和 DCA 均验证了列线图预测的准确性。

结论：本研究发现 INR、阴离子间隙和 APS III 与 AAD 患者的预后显著相关。这些发现有望为 AAD 的潜在治疗方案提供新的见解。

关键词：急性主动脉夹层；临床特征；死亡率；MIMIC-IV.

Mechanism of Structural Disruption and Functional Effects of the PDK4 rs750335290 Variant: Implications for Skeletal Muscle Energy Metabolism

chuanlong Lu, HongLin Dong, Ruijing Zhang

Second Hospital of Shanxi Medical University

Driven by the swift advancement of artificial intelligence (AI) technology, deep learning and machine learning models are now essential tools within the life sciences, especially in critical domains including protein structure prediction, genomics, and drug discovery. The integration of AI has substantially increased research efficiency while simultaneously broadening the scope of investigation, offering new strategies to address intricate biological questions that were once intractable. Through the integration of big data and sophisticated algorithms, AI technology empowers scientists to comprehend biological phenomena through novel lenses, thereby facilitating biological predictions, experimental design, and clinical implementation. Deep learning and machine learning models have fundamentally transformed biological research approaches during the last ten years. Especially in protein research, the deployment of AI models has yielded remarkable breakthroughs. Ranging from protein structure prediction to functional analysis of genetic mutations, AI furnishes robust tools for life science investigations. The advent of AI models dedicated to protein structure prediction has delivered solutions of an unprecedented scale to the persistent protein folding challenge that has long confounded the life sciences. Leveraging these AI models, scientists are able to forecast protein tertiary structures and the functional consequences of mutations with enhanced accuracy. Moreover, deep learning algorithms within AI models find extensive application in the field of genomics, especially concerning the functional assessment of genetic mutations and disease prognostication.

Pyruvate dehydrogenase kinase 4 (PDK4) serves as a critical regulator of cellular energy metabolic homeostasis. By phosphorylating and inhibiting the pyruvate dehydrogenase complex, PDK4 dictates the metabolic fate of pyruvate, directing its entry into mitochondrial oxidative phosphorylation or its retention in the cytosol for glycolytic metabolism. Elevated PDK4 expression in peripheral tissues, notably skeletal muscle, is commonly correlated with impaired metabolic flexibility (exemplified by decreased glucose oxidation during insulin resistance) and is intimately associated with an adaptive metabolic switch favoring fatty acid-dependent pathways (e.g., β-oxidation)(8). A critical pathophysiological hallmark of peripheral artery disease (PAD) is the progressive atherosclerotic narrowing or occlusion of limb arteries (especially those in the lower extremities), culminating in chronic limb-threatening ischemia (CLTI). This sustained ischemic and hypoxic environment induces deep-seated remodeling of energy metabolism within the affected skeletal muscle. Direct experimental evidence specifically elucidating the role of PDK4 within PAD pathophysiology, including its expression profile, regulatory mechanisms in the peripheral skeletal muscle of PAD patients, and its viability as a potential therapeutic target, is still relatively scarce. Elucidating the role of PDK4 in driving skeletal muscle energy metabolic dysregulation, functional impairment, and disease progression in PAD is crucial for deciphering the underlying metabolic pathology of this condition and for pioneering new therapeutic interventions.

The 157 locus of the PDK4 gene represents a critical mutational site in research, with the resulting genetic alterations predominantly characterized by missense mutations, notably the tyrosine (Y) to asparagine (N) substitution. This specific mutation is hypothesized to compromise the stability of the PDK4 protein, consequently inducing alterations in energy metabolism. Nevertheless, despite extensive research investigating the link between the PDK4 gene and energy metabolism, detailed mechanistic understanding of how the PDK4 157 mutation precisely impacts protein structure and function is still lacking. Presently, research emphasis on PDK4 largely concentrates on elucidating genotype-phenotype correlations, specifically employing phenotypic profiling and genetic association studies to uncover links between mutations and metabolic outcomes. Yet, exploration into the molecular-level mechanisms by which mutations perturb PDK4 protein stability is still insufficient, with a notable deficit in granular mechanistic analysis pertaining to tertiary structure perturbations, folding dynamics, and functional dynamics. Consequently, a thorough investigation of the PDK4 157 locus mutation is imperative to elucidate the molecular mechanisms governing its impact on protein stability and loss-of-function phenotypes. While current research has furnished significant insights into PDK4 gene variants, the majority of studies thus far have prioritized genotype-phenotype associations, leaving research into the molecular mechanisms by which mutations impair protein stability and function comparatively underdeveloped. The advent of AI technology, notably the deployment of models like AlphaFold3 and ThermoMPNN, offers unprecedented research avenues. Leveraging these AI tools enables profound molecular-level investigation into how the PDK4 157 mutation perturbs protein structure, thereby facilitating the elucidation of its potential mechanisms impacting energy metabolism. AI models facilitate the rapid and precise prediction of mutation-induced effects on protein structure, thereby aiding in the identification of mutations potentially causative of loss-of-function or functional alteration. In contrast to conventional experimental approaches, AI models offer not only markedly enhanced prediction accuracy but also a substantial reduction in research timelines. AI technology enables the rapid processing of vast mutational datasets, synergistically incorporating insights from structural biology, thermodynamics, and protein dynamic properties to furnish researchers with a highly efficient investigative pathway.

This study is significant as it pioneers a systematic and comprehensive analysis of the PDK4 157 locus mutation through the combined application of AlphaFold3 for structural prediction, protein dynamics simulations (PDS), and ThermoMPNN for thermodynamic stability prediction. The integration of protein dynamics simulations with AI tools has enabled us to elucidate how the PDK4 mutation compromises protein stability and, critically, to furnish a molecular mechanistic basis for the observed variations in energy metabolism. Moreover, this work advances the integration of genomics and computational biology, thereby laying important theoretical groundwork for future advancements in the early diagnosis of PAD and the therapeutic application of gene editing technologies.

Stanford B 型主动脉夹层 TEVAR 术后支架诱导远端新发破口预测因素分析

何厚霖 王效增（学组委员、通讯作者） 赵庭浩 程佳新

中国人民解放军北部战区总医院

摘　要

目的：探讨胸主动脉腔内修复术 (TEVAR) 术后支架诱导远端新发破口 (distal stent graft induced new entry，dSINE) 的预后及预测因素。

方法：本研究回顾性连续纳入 2005 年 1 月至 2023 年 12 月期间在北部战区总医院接受 TEVAR 治疗 Stanford B 型主动脉夹层 (type B aortic dissection，TBAD) 患者 608 例，根据随访计算机断层扫描血管造影 (computed tomography angiography，CTA) 结果有无 dSINE 的发生，分为 dSINE 组 57 例，无 dSINE 组 551 例。比较两组间一般资料、既往病史、手术特征等，采用单因素和多因素 Cox 回归分析 (竞争风险模型，以全因死亡作为竞争风险)dSINE 的预测因素。通过对两组患者长期随访，比较两组在全因死亡，主动脉源性死亡、需要再次干预事件的差异。采用 Kaplan-Meier 生存曲线分析全因死亡、主动脉相关死亡、主动脉相关不良事件以及需要再次干预的累积率，使用 log-rank 检验进行组间比较。并且比较锥形支架与非锥形支架在远期随访结局 (包括全因死亡、主动脉源性死亡、再次干预、dSINE) 有无差异。

结果：本研究 608 例患者中，有 57 例患者 (9.38%) 发生 dSINE。单因素和多因素 Cox 回归分析 (竞争风险模型) 发现吸烟史 (HR=2.060，95%CI 1.158 ~3.664，P=0.014)、支架远端放大率 (HR=1.569，95%CI1.362 ~1.809，P<0.001)、体重指数 (HR=0.916，95%CI 0.864 ~0.971，P<0.001)、支架长度 (HR=0.991，95%CI 0.982 ~0.999，P=0.026) 为 TBAD 合并 dSINE 的独立预测因素。dSINE 组的中位随访时长为 102.1 个月，四分位间距 (IQR) 为 41.8-129.5 个月；而无 dSINE 组的中位随访时长为 79.0 个月，四分位间距 (IQR) 为 44.4-119.4 个月，两组差异无显著性统计学意义 (P=0.205)。dSINE 组全因死亡 (19.3% 比 6.9%，P=0.001)、主动脉源性死亡 (12.3% 比 2.4% ，P<0.001)、

再次手术干预事件 (47.4% 比 2.0%，P<0.001) 的发生率均显著高于无 dSINE 组，差异均具有显著性统计学意义 (均 P<0.05)。KaplanMeier 生存曲线分析显示 dSINE 组主动脉不良事件、全因死亡、主动脉源性死亡和需要再次手术干预事件发生率较无 dSINE 组高 (logrank P 均 <0.05)。非锥形支架组随访过程中 dSINE(12.9% 比 6.2%，P=0.007)、手术干预事件 (8.4% 比 4.3%，P=0.039) 的发生率显著高于锥形支架组，差异均具有显著性统计学意义 (均 P<0.05)。

结论：吸烟史、支架远端放大率是 TBAD 合并 dSINE 的独立危险因素，体重指数、支架长度为 TBAD 合并 dSINE 的独立保护因素。此外，dSINE 组患者的长期预后 (包括全因死亡、主动脉源性死亡、再次干预) 显著低于未发生 dSINE 的患者组患者。

关键词：胸主动脉腔内修复术；支架诱导远端新发破口；预测因素

The Effect and Mechanism of MGST1-miMOMP in the Formation of Abdominal Aortic Aneurysm

Xiaozeng Wang, Xiao-Fan Cao, Jia-Yin Li, Shu-Li Zhang, Xiao-Yue Li

General Hospital of Northern Theater Command

Objective

This study aims to investigate the roles and mechanisms of mitochondrial outer membrane permeabilization (miMOMP) and microsomal glutathione S-transferase 1 (MGST1) in the development of abdominal aortic aneurysm (AAA).

Methods

Initially, immunofluorescence staining was employed to detect the expression of cleaved caspase-3 (C-Cas3) and p21 in human AAA vascular tissues and normal vascular tissues. Subsequently, an AAA model was established in ApoE − / − mice to examine changes in the expression of related proteins and genes involved in miMOMP. Next, the miMOMP inducer ABT737 and inhibitor BAI1 were administered to the mouse model to observe their effects on the incidence and severity of AAA. At the cellular level, an H_2O_2 -stimulated endothelial cell model (C166) was constructed, and MGST1 was identified as a target gene through genetic analysis. Changes in the expression of MGST1 and other miMOMP-related molecules were detected. Further validation of MGST1 expression changes and their impact on miMOMP-related molecules was conducted through in vivo and in vitro experiments. Finally, co-immunoprecipitation experiments were conducted to elucidate the interaction between MGST1 and Bax, a key protein in miMOMP located on the outer mitochondrial membrane.

Results

Immunofluorescence staining revealed that, compared with normal human and control mouse vascular tissues, AAA patient and AAA mouse vascular tissues exhibited extensive co-existence of C-Cas3 and p21. The protein expression levels of p21, C-Cas3, cytochrome c (cytoC), and Bax, as well as the mRNA levels of D-loop and senescence-associated secretory phenotype (SASP) genes (IL-1α, IL-1β, and IL-6), were significantly higher in AAA mouse vascular tissues than in control mice. Hematoxylin and eosin (HE), Masson, and Elastica van Gieson (EVG) staining showed that AAA mouse aortic tissues exhibited structural disruption, collagen deposition, and elastic lamina rupture.After the administration of miMOMP inducer ABT737 in the mouse model，the results showed that the incidence of AAA in the Ang II +vehicle group was 30%, while it was 80% in the Ang II +ABT737 group (P=0.070). Compared with the Ang II +vehicle group, the survival rate of mice in the Ang II +ABT737 group was significantly lower (log rank P=0.027), and the maximum abdominal aortic diameter was significantly wider (2.30±0.19 mm vs 1.64±0.16 mm, P=0.015). In contrast, the application of miMOMP inhibitor BAI1 resulted in the incidence of AAA in the Ang II +vehicle group was 45%, while it was 15% in the Ang II +BAI1 group (P=0.038). The maximum abdominal aortic diameter was significantly smaller in the Ang II +BAI1 group (1.36±0.30 mm) compared to the Ang II +vehicle group (1.96±0.46 mm; P_2O_2 stimulation in C166 cells. Compared with the control group, mitochondrial fragmentation increased, the colocalization of cytoC and TOM20 decreased, and the number of Bax-positive cells increased, which indicated the successful establishment of the miMOMP cellular model. By intersecting the genes encoding mitochondrial membrane proteins in the MitoCarta3.0 database for humans and mice and the differentially expressed genes in the human AAA dataset GSE183464, a total of 7 overlapping genes were identified. PCR detection after H_2O_2 stimulation revealed that the mRNA level of MGST1 increased most significantly. Compared with control mice, the expression of MGST1 in AAA mouse vessels significantly increased. Overexpression of MGST1 in C166 cells caused significant upregulation of the protein expression levels of miMOMP-related molecules p21, C-Cas3, cytoC, and Bax, and a significant elevation of the mRNA levels of D-loop and SASP genes (IL-1α, IL-1β, and IL-6); conversely, knockdown of MGST1 resulted in significant downregulation of the protein expression levels of p21, C-Cas3, cytoC, and Bax, and a decreased mRNA levels of D-loop and SASP genes. Co-immunoprecipitation experiments showed an interaction between Bax and MGST1.

Conclusions

The miMOMP is present in human and mouse AAA tissues. Activation of miMOMP exacerbates the incidence and severity of AAA in mice, while inhibition of miMOMP alleviates these effects. Expression of MGST1 is elevated in AAA vessels from both human patients and mouse models. Overexpression of MGST1 in endothelial cells (C166) exacerbates miMOMP formation.Critically,MGST1 mediates miMOMP through interaction with Bax, thus identifying MGST1 as a potential regulatory mechanism and therapeutic target in AAA pathogenesis.

基于文献计量学的主动脉弓病变腔内修复技术全球研究现状及热点分析

阴学仕 唐龙 刘建平 张永恒

遂宁市中心医院河东分部

目的：探讨 2000-2024 年期间主动脉弓病变的腔内修复技术研究全球研究现状与趋势。方法：检索 Web of Science 核心合集（WoSCC）数据库，收集 2000 年至 2024 年间发表的主动脉弓病变腔内修复技术相关文献。使用 CiteSpace（6.4.1 版）、VOSviewer（1.6.19 版）、Scimago Graphica（1.0.5.1）和 R 语言（ggplot2 包）对检索结果进行描述性统计和可视化分析。并利用高频关键词、爆发词等方面分析此研究的热点和前沿。结果：共纳入 1536 篇文献，从 2000 年至 2024 年文献数量和引用次数均呈上升趋势，尤其在 2015 年后增长显著，2021 年和 2023 年达到高峰。57 个国家或地区参与研究，美国以 334 篇发文量和 8575 次引用位居榜首，中国和德国分别位居第二、第三。德国与 24 个国家建立了合作关系。6537 名作者参与研究，Tsilimparis, Nikolaos 教授以 42 篇发文位居榜首，中国学者舒畅教授和景在平教授进入前十名。共统计 554 个关键词，排名前五的关键词为“endovascular repair”“aortic arch”“dissection”“management”和“outcomes”。关键词聚类为 9 类，包括主动脉夹层、胸主动脉腔内修复等。新兴主题包括“case report”“society”“outcomes”“entry”和“kommerell's diverticulum”。结论：主动脉弓病变腔内修复技术研究在全球越发火热，基于创新型器械或新型入路策略解决复杂解剖疾病以及关注患者长期结局可能会成为未来研究热点。

Predictive Models for One-Year Renal Function Improvement in Patients with Atherosclerotic Renal Artery Stenosis (ARAS) Following Renal Artery Revascularization

Lei Dong, Yu-Xi Li, Fang-Fang Fan, Jia Jia, Jian-Ping Li

Peking University First Hospital

Background: Atherosclerotic renal artery stenosis (ARAS) constitutes a pivotal component of panvascular disease. ARAS accounts for approximately 80% of renal artery stenosis cases and may lead to secondary hypertension and ischemic nephropathy. Relieving renal artery obstruction and restoring adequate renal perfusion are critical therapeutic goals of ARAS. The efficacy of interventional treatment for ARAS in improving renal function remains controversial. Consequently, accurately identifying patients who are likely to gain substantial benefits from interventional treatment is crucial and should be a priority in clinical practice.

Methods: The improvement in renal function was defined as an increase in eGFR of greater than 20%, a reduction in serum creatinine of more than 20%, or a decrease in serum creatinine of at least 0.4 mg/dL when compared to pre-stenting levels at the final follow-up evaluation. We retrospectively included all patients with ARAS who underwent renal artery intervention and had mild-to-moderate renal insufficiency, defined as an estimated glomerular filtration rate (eGFR) between 30 and 90 mL/(min·1.73 m^2), at Peking University First Hospital from January 2020 to December 2024, for the development of the prediction model. These patients were consecutively enrolled from January 2020 to December 2024 at Peking University First Hospital. By integrating the LASSO analysis, crucial variables were determined for establishment of multivariable logistic regression model and support vector machine (SVM). The area under the receiver operating characteristic curve (AUC) was calculated to assess the discriminative ability of the model. The calibration of the models was designed to determine the consistency between predicted probabilities and observed outcomes regarding renal function improvement. Decision Curve Analysis (DCA) was conducted to evaluate the clinical utility of the models. A nomogram was used to visualize the logistic regression model.

Results: A total of 300 eligible patients were included in this study. The entire cohort was randomly assigned to a training set (n=211) and a validation set (n=89). Among them, renal function demonstrated significant improvement in 41 cases, comprising 29 cases in the training set and 12 cases in the validation set. Five characteristics were selected for model construction. The AUC of multivariable logistic regression model was 0.746 (95% CI: 0.653-0.837) in the training set and 0.719 (95% CI: 0.545-0.892) in the validation set. The AUC of SVM was 0.885 (95% CI: 0.815-0.954) in the training set and 0.857 (95% CI: 0.745-0.969) in the validation set, respectively. Furthermore, the calibration curves demonstrated good agreement between the predicted probabilities from the models and the actual observations. DCA indicated that the net benefit derived from the models was generally superior compared to alternative strategies or no intervention. These findings collectively underscore the robustness and clinical utility of the developed models.

Conclusion: This study represents the endeavor to develop and validate

a model capable of predicting the probability of improved renal function in ARAS patients who had mild-to-moderate renal insufficiency within one year following renal artery intervention. Our study developed and validated robust and high-precision clinical prediction models. They may serve as a decision-making aid for both patients and physicians, facilitating collaborative decisions and facilitate the rational utilization of interventional treatment.

四维核磁共振研究两窦两叶型主动脉瓣二叶畸形患者升主动脉血流动力学

郑铁 韩棋

首都医科大学附属北京安贞医院

【摘要】

目的 运用四维核磁共振技术（4D Flow MRI）分析两窦两叶型主动脉瓣二叶畸形（Bicuspid aortic valve，BAV）患者升主动脉血流动力学状态，探索异常血流与主动脉病变的关系。为建立双窦型 BAV 的血流动力学分类标准提供关键证据，并为该亚型的个性化手术决策提供理论支持。

方法 前瞻性纳入 2023 年 8 月至 2024 年 10 月就诊于首都医科大学附属北京安贞医院的 13 例两窦两叶型 BAV 患者，应用 4D Flow 核磁序列采集主动脉血流数据并通过 CVI42 后处理软件分析升主动脉血流参数。

结果 共纳入 13 例患者，平均年龄为 52.6±10.2 岁，男性 8 人。与 R-L 融合型血流模式相似，轴向壁面切应力梯度变化量较小；合并主动脉瓣狭窄时，各项血流动力学指标均显著上升；主动脉扩张患者壁切应力显著降低，周向 WSS 随血管直径增加梯度变化量减小。

结论 主动脉扩张患者壁切应力显著降低 ,cWSS 平面间梯度变化值随主动脉直径增大逐渐稳定；升主动脉存在异常血流，主动脉瓣狭窄会进一步加剧异常状态；两窦两叶型 BAV 患者血流射流模式、血流动力学参数与 RL 融合型相似，aWSS 平面间梯度变化量可能成为特异的两窦两叶型 BAV 患者血流特征。

踝间差降低颅内动脉剪切力影响铁死亡恶化缺血性脑卒中的研究

相菲

哈尔滨医科大学附属第一医院

目 的： 踝间血压差（Interankle blood pressure difference，IAND）≥ 7mmHg 是中国成年人脑卒中的独立标志；其独立于脑卒中传统危险因素，对脑卒中的预测能力提高 18.5%。由于颅内血管具有更深层而复杂的位置，更小的管腔，不易被临床评估的内皮局部血流动力学因素，使踝间差增大与脑卒中关联的内在机制鲜见报道。计算流体力学（Computational fluid dynamics, CFD）作为一项飞速发展的仿真技术可使研究者获得血管局部的流速、剪切力及压力等，为踝间差与颅内动脉的局部血流动力学关联研究提供了新的途径。血管压力的变化可启动铁死亡，促进动脉粥样硬化的发生参与脑卒中的发生与恶化。踝间差增大后颅内动脉是否存在扰动性剪切力，其变化对颅内动脉血管内皮的影响及是否启动铁死亡进一步恶化缺血性脑卒中尚不清楚。**方法：本研究首先通过建立踝间血压差增大小鼠模型，利用基于高分辨率核磁共振管壁成像的计算流体力学技术测定小鼠颅内动脉的剪切力及血流速度等血流动力学参数，在原有模型的基础上进一步建立 MCAO 模型证明踝间差增大可恶化缺血性脑卒中。其次本研究通过对踝间差增大的小鼠模型血浆进行蛋白及非靶代谢组学筛选差异表达蛋白及代谢物，二者联合分析明确调控该途径的关键蛋白，通过沉默关键蛋白探讨该蛋白是否会减轻踝间差增大的小鼠缺血性脑卒中，为脑卒中的防治提供了新的途径与策略。结果：**与 Sham 组相比，超声显示 Model 组单侧股动脉血流量明显减少且双下肢血压差显著升高（P < 0.0001）；通过核磁共振及流体力学分析发现与 Sham 组小鼠相比，Model 组小鼠整体的脑血流平均流速及峰值流速均降低，且在单侧大脑中动脉的平均流速及峰值流速显著降低；整体的脑血管剪切力均降低，且在单侧大脑中动脉的剪切力显著降低（P < 0.05）；透射电镜提示与 Sham 组小鼠相比，Model 组小鼠脑血管周围水肿。进一步通过 MCAO 模型的叠加后，发现与 Sham 组小鼠相比，Model 组小鼠具有更大的脑梗死面积且神经损伤评分也更高（P < 0.05）。两组小鼠血浆蛋白组学分析结果显示，两组共有 131 种差异蛋白，其中 67 中上调，64 种下调。对基因进行 GSEA 和 WGCNA 富集分析发现，差异性表达的基因主要富集于代谢相关通路。蛋白与代谢组学联合分析发现，甘油磷脂代谢通路富集最显著，甘油磷脂途径中富集到 1 种蛋白和 17 种代谢物质，其中该途径中的关键蛋白为 PCYT2。与 PCYT2 过表达组相比，PCYT2 敲减组细胞增殖能力显著增强（P < 0.0001）、细胞迁移能力显著增强（P < 0.0001）且 PCYT2 敲减组铁死亡相关指标不论在蛋白水平还是 mRNA 水平均发生变化。与 Model+ MCAO 组相比 Model+ MCAO+siPCYT2 组小鼠脑部梗死面积显著减少以及神经评分显著减低（P < 0.001）。**结论：**踝间血压差增大降低单侧脑血管剪切力，减缓单侧脑血流速度，进一步扩大脑梗死面积，加重神经功能损伤。踝间血压差增高通过增加 PCYT2 表达水平促进内皮细胞铁死亡，恶化缺血性脑卒中。

The association of metabolic syndrome with aortic aneurysm: a two-sample mendelian randomization study

CHAODI LUO, QIANG MA

The First Affiliated Hospital of Xian Jiaotong University

Background: Aortic aneurysm (AA) is the second most common aortic disease after atherosclerosis. It is characterized by localized progressive and irreversible full-thickness dilation of the aorta caused by the weakness of the aortic wall, which could reach more than 1.5 times of the normal. Metabolic syndrome (MetS) has been proved to be associated with cardiovascular disease, and recent observational studies have revealed the association between MetS and its components and AA, but the causal relationship still uncertain. Due to the high mortality risk of AA, it is difficult and nearly impossible to explore the causal relationship between metabolic syndrome and its components and AA through large cohort studies. Therefore, MR analysis is a simple, ideal and reliable study of the causal relationship between MetS or its components and AAThe study aimed to explore the causal effect of MetS on AA using mendelian randomization (MR) analysis.

Methods: AA summary data was obtained from the IEU Open GWAS Project (http://gwas.mrcieu.ac.uk/) with diagnosis according to the international Classification of Diseases 10 edition (ICD-10). The summary level data were extracted from a large study with 479194 subjects of European ancestry using UK Biobank and FinnGen, of which involve 475964 controls and 3230 cases. Single nucleotide polymorphisms (SNP) of MetS and its components were extracted from GWAS database. Inverse variance weighting (IVW), weighted median method, simple mode method, weighted mode method, and MR-Egger regression were used to evaluate causality. Sensitivity analysis, heterogeneity test, and pleiotropy test were done so as to ensure the stability of the analyzed results. Outliers were detected and removed by the MR-PRESSO method.

Results: A total of 506 SNPs were validated as IVs for BMI, 374 were for WC, 335 were for HDL-C, 304 were for TG, 41 were for T1DM, 117 were for T2DM, 64 were for fasting glucose, 37 were for fasting insulin, 450 were for SBP, 455 were for DBP, 93 were for MetS. The results of MR-Egger analysis (OR: 1.433, 95% CI: 1.176 to 1.745, P < 0.01), Weighted median analysis (OR: 1.332, 95% CI: 1.167 to 1.521, P < 0.01), IVW analysis (OR: 1.308, 95% CI: 1.175 to 1.456, P < 0.01) and Weighted mode analysis (OR: 1.372, 95% CI: 1.207 to 1.560, P < 0.01) all showed that MetS increased the risk of AA. The relationship between components of MetS and AA were also studied. Body mass index (BMI) (OR: 1.322; 95% CI: 1.132-1.543), waist circumstance (WC) (OR: 1.282; 95% CI: 1.055-1.558), triglycerides (TG) (OR: 1.436; 95% CI: 1.253-1.646), systolic blood pressure (SBP) (OR: 1.023; 95% CI: 1.014-1.033), and diastolic blood pressure (DBP) (OR: 1.086; 95% CI: 1.069-1.103) could increase the risk of AA. However, the results also showed that fasting insulin and T1DM were not associated with the risk of AA, while HDL-C tended to be negatively associated with the risk of AA (Figure 3). Interestingly, the fasting glucose (OR: 0.683, 95% CI: 0.488-0.957) and T2DM (OR: 0.904, 95% CI: 0.831-0.983) were negatively related to the risk of AA and tended to decrease the risk of AA.

Conclusion: The present study strengthened the evidence for a causal association between MetS and the risk of AA. Meanwhile, the reverse causal relationship between blood glucose and type 2 diabetes and AA was further demonstrated. The study provided evidence for the clinical prevention of AA and risk-factors analysis in patients with MetS.

The Predictive Role of the Monocyte-to-Lymphocyte Ratio in Short-Term Outcomes for Patients with Acute Uncomplicated Type B Aortic Intramural Hematoma

Cheng-Fei Peng

General Hospital of Northern Theater Command

Introduction Individual inflammatory markers may not fully capture systemic inflammation. The monocyte-to-lymphocyte ratio (MLR), which combines monocyte counts and lymphocyte counts, offers a comprehensive measure of inflammation and shows promise in predicting outcomes in various diseases, including cancer and cardiovascular conditions. This study aims to analyze the predictive value of MLR for the prognosis of acute uncomplicated Type B Aortic intramural hematoma (IMH) , we aim to provide a practical and accurate tool for risk stratification, thereby enhancing patient management and outcomes. **Methods** This retrospective study included 562 patients diagnosed with Type B IMH via computed tomography angiography (CTA) at the General Hospital of Northern Theater Command between April 2018 and April 2024. Finally, a total of 332 patients were enrolled in this study and grouped into three groups based on the tertiles of the MLR. The MLR was divided into three groups according to the tertiles of the target patient population: Tertile 1 (<0.364, N=110), Tertile 2 (0.365-0.580, N=110), and Tertile 3 (>0.581, N=112). Multivariate Cox regression was utilized to investigate the association between the MLR (independent variable) and the risk of aortic-related adverse events (ARAEs) through five distinct models for statistical inference. Restricted cubic spline (RCS) curve was analyzed as a continuous variable to elucidate the relationship between dose effects and the risks of ARAEs. **Results** The incidence of ARAEs among these patients was 32.2%, while the incidence of aortic dissection (AD) or penetrating aortic ulcer (PAU) was 28.6%. The incidence of aortic-related death was 3.0%. The mean (SD) age of the participants was 64.3 (9.0) years. Various factors, including monocyte counts, lymphocyte counts, the maximum diameter of the hematoma thickness(MDHT), circular hematoma, white blood cell, neutrophil count, red blood cell, platelet count, troponin-T, lactate dehydrogenase, D-dimer, PAU, AD, and ARAEs, exhibited significant differences among the MLR tertiles. When MLR was treated as a categorical variable, after adjustment for Model 5, the incidence of ARAEs in Tertile 3 (compared to Tertile 1) had a HR of 2.49 (95% CI: 1.28–4.85). For each 1-unit increase in MLR, the HR for ARAEs was 4.50 (95% CI: 2.10–9.61), and for AD or PAU, the HR was 2.76 (95% CI: 1.34–5.71). The trend test for ARAEs was statistically significant. RCS curve analysis revealed a linear correlation between the MLR and the incidence of ARAEs, as well as the

incidence of AD or PAU (P< 0.05 for both, and P >0.05 for nonlinearity, Figure 1). In subgroup analyses and interaction tests, we investigated the relationship between MLR and the risk of ARAEs, all-cause mortality, aortic-related death, and AD or PAU across different population subgroups. The risk of ARAEs was significantly higher in participants who consumed alcohol (odds ratio [OR] 10.53, 95% CI: 4.68–23.71, P< 0.001), had diabetes (OR 3.71, 95% CI: 2.23–6.19, P < 0.001), or had a the maximum diameter of the descending aorta (MDAD) >44 mm (OR 3.44, 95% CI: 2.18–5.43, P< 0.001). Individuals without hypertension (OR 5.07, 95% CI: 2.66–9.63, P < 0.001) also had an elevated risk of ARAEs. The risk of AD or PAU increased in participants who smoked (OR 7.20, 95% CI: 2.94–17.63, P < 0.001), consumed alcohol (OR 9.78, 95% CI: 3.28–19.39, P < 0.001), had diabetes (OR 2.90, 95% CI: 2.63–5.17, P < 0.001), or had an MDAD >44 mm (OR 3.44, 95% CI: 2.18–5.43, P< 0.001). **Conclusion** In conclusion, MLR represents a powerful indicator of systemic inflammation and immune dysregulation in patients with Type B IMH. Its association with adverse aortic events underscores its potential as a prognostic biomarker, paving the way for improved risk stratification and targeted therapeutic strategies.

Standford B 型主动脉夹层患者胸主动脉腔内修复术后持续性 Ia 型内漏的预后意义

王效增 曹小帆 孟杜娟 赵庭浩 何厚霖 张志强

中国人民解放军北部战区总医院

目的：探讨持续性 Ia 型内漏对 B 型主动脉夹层（TBAD）患者的预后意义及其影响因素。

方法：连续筛选 2002 年 4 月至 2023 年 6 月于北部战区总医院因 TBAD 行 TEVAR 治疗，手术结束时数字减影血管造影（DSA）显示存在即时 Ia 型内漏的患者。收集患者的基线临床数据、介入相关数据和术后复查的胸腹主动脉 CTA 及随访结果。根据最后一次随访 CTA 影像上 Ia 型内漏是否存在，将患者分为内漏持续组和内漏消失组。主要终点为主动脉不良事件（adverse aortic events，AAEs），被定义为与主动脉相关的死亡或因疾病进展而需要再次干预。应用 KM 生存曲线及 COX 回归分析探讨两组的 AAEs 有无差异。应用 COX 回归分析探讨 AAEs 及持续性 Ia 型内漏的影响因素。

结果：连续入选存在即时 Ia 型内漏的患者共 192 例，其中，56 例（29.2%）患者随访期间内漏持续存在（persistent group），136 例（70.8%）患者内漏消失（disappear group）。10 年无 AAEs 发生率在内漏持续组是 0.669（95% CI：0.411-1.000），在内漏消失组是 0.872（95% CI：0.768-0.991）。与内漏消失组相比，内漏持续组发生 AAEs 的风险是增高的（HR 9.177，95%CI 2.701-31.177，P<0.001）。假腔部分血栓化（HR: 4.674;95%CI: 1.418-15.229 ;P=0.011）和内漏持续（HR: 11.715；95%CI: 3.343-41.051;P<0.001）是具有即时 Ia 型内漏的 TBAD 患者发生 AAEs 的独立危险因素。与具有 I 型主动脉弓的患者相比，具有 III 型主动脉弓的患者出现 Ia 型内漏持续的风险是增大的（HR 3.251，95%CI 1.229-8.599，P=0.018）。

结论：TEVAR 后持续性 Ia 型内漏会增加 TBAD 患者 AAEs 的风险，具有 III 型主动脉弓的患者，持续性 Ia 型内漏的风险更高。

Moderate to vigorous physical activity, genetic susceptibility, and risk of aortic aneurysm: a prospective cohort study

Chaol-Lei Chen, Zhi-Qiang Nie, Ying-Qing Feng

Guangdong Provincial People's Hospital

Background:

Aortic aneurysm (AA), encompassing abdominal aortic aneurysm (AAA) and thoracic aortic aneurysm and dissection (TAAD), remains a significant cause of cardiovascular morbidity and mortality worldwide. Despite the widespread recognition of moderate-to-vigorous physical activity (MVPA) as a protective factor against atherosclerotic cardiovascular disease, its role in mitigating the risk of AA has not been firmly established. Moreover, the potential interplay between MVPA and genetic susceptibility in influencing AA risk is not well understood. This study aimed to investigate the associations between MVPA—measured objectively via accelerometers and subjectively via questionnaires—and the incidence of AA, AAA, and TAAD, and to explore whether these associations are modified by underlying genetic risk.

Methods:

We conducted a prospective analysis of data from the UK Biobank, comprising two distinct cohorts. The primary cohort included 88,005 participants (median age: 62.9 years; 56.4% female) with valid accelerometer-derived MVPA data collected over a 7-day monitoring period. The secondary cohort included 382,268 participants (median age: 57.0 years; 52.4% female) with self-reported MVPA assessed using the International Physical Activity Questionnaire. MVPA was quantified in metabolic equivalent task (MET)-minutes/week and categorized into quartiles. Incident AA events were identified through hospital records, death registries, and procedural codes. Genetic susceptibility was quantified using validated polygenic risk scores (PRS) for AAA and TAAD based on genome-wide association studies. Cox proportional hazards models adjusted for a wide range of sociodemographic, lifestyle, and clinical factors were used to estimate hazard ratios (HRs). Joint associations and multiplicative interactions between MVPA and genetic risk were evaluated.

Results:

During a median follow-up of 6.6 years in the accelerometer cohort, 426 AA events were documented, including 249 AAA and 167 TAAD. Higher MVPA was associated with lower incidence of AA in a clear dose-response fashion. Compared to the lowest quartile of MVPA, adjusted HRs for AA were 0.73 (95% CI: 0.57–0.92), 0.58 (0.44–0.76), and 0.51 (0.37–0.70) for the second to fourth quartiles, respectively. The corresponding HRs for AAA were even more pronounced, at 0.64 (0.47–0.87), 0.54 (0.38–0.77), and 0.37 (0.24–0.59). For TAAD, the inverse association reached statistical significance in the highest MVPA quartile (HR: 0.60; 95% CI: 0.37–0.98). Participants with higher genetic risk had significantly increased risk of AAA and TAAD. However, MVPA was associated with lower risk of AAA across all levels of genetic risk, and with lower TAAD risk in the high genetic risk subgroup, although interaction terms were not statistically significant. Joint association analyses showed the lowest observed risks among individuals with both high MVPA and low genetic risk (AAA: HR 0.25; 95% CI: 0.14–0.44; TAAD: HR 0.38; 95% CI: 0.21–0.69), compared with those with high genetic risk and low MVPA. Similar but attenuated associations were found in the questionnaire-based cohort, highlighting the importance of objective activity measurement.

Conclusions:

This large-scale prospective study provides robust evidence that higher levels of MVPA, particularly when objectively measured, are associated with a substantially lower risk of developing AA, especially AAA. These benefits were observed across strata of genetic susceptibility, suggesting that physical activity may offset inherited risk and function as an effective and scalable preventive measure. Given the absence of pharmacologic therapies for aneurysm prevention, these findings underscore the importance of promoting physical activity as part of public health strategies. Future studies with longer follow-up, repeated activity assessments, and more diverse populations are warranted to confirm these findings and elucidate the underlying biological mechanisms.

Creg1 inhibits vascular calcification by suppressing osteogenic differentiation of VSMCs through the Fhl2-Stat3-Runx2 axis

Dan Liu, Jing Wang, Hai-Xu Song, Yu-Jia Zou, Ya-Ni Wang, Kai Xu, Xiao-Lin Zhang, Cheng-Hui Yan, Ya-Ling Han

State Key Laboratory of Frigid Zone Cardiovascular Disease, Cardiovascular Research Institute and Department of Cardiology, General Hospital of Northern Theater Command

Creg1 inhibits vascular calcification by suppressing osteogenic differentiation of VSMCs through the Fhl2-Stat3-Runx2 axis

Jing Wang, Dan Liu, Haixu Song, Yujia Zou, Yani Wang, Kai Xu, Xiaolin Zhang, Chenghui Yan, Yaling Han*

State Key Laboratory of Frigid Zone Cardiovascular Diseases, Department of Cardiology and Cardiovascular Research Institute, General Hospital of Northern Theater Command, Shenyang, Liaoning Province, 110016, China

First author: Jing Wang; Tel：15904060245; E-mail: 974348376@qq.com; Birthday:1994.4.22

*Corresponding authors: Yaling Han, MD; Tel: 28856123; E-mail: hanyaling@163.net

Abstract

Background: Vascular calcification is an independent risk factor for cardiovascular disease, which is characterized by osteochondrogenic differentiation of vascular smooth muscle cells (VSMCs). Osteogenic reprogramming of VSMCs within the medial layer of arteries represents a pivotal mechanism in vascular calcification, characterized by the loss of contractile function and acquisition of an osteogenic phenotype. Cellular repressor of E1A stimulated genes 1(Creg1) is identified as a key glycoprotein that promotes the differentiation of VSMCs and protects against vascular remodeling. This study aims to explore the role and mechanism of Creg1 in vascular calcification.

Methods: Single-cell RNA-sequencing (scRNA-seq) was performed to reveal the transcriptional profiles under three different types of mouse vascular calcification models. Smooth muscle-specific Creg1 knockout mice ($Creg1^{smko}$), Creg1 transgenic mice ($Creg1^{tg}$), and their littermate controls were used to investigate the role of Creg1 in vascular calcification. To achieve VSMCs-specific knockdown of Creg1 and Fhl2, adeno-associated virus serotype 2/9 (AAV2/9) carrying mouse shFhl2 or shCreg1 sequences with a sm22α promoter (AAV-sm22-shFhl2 or AAV-sm22-shCreg1) or the control virus (AAV-sm22-shNC) were constructed. The severity of vascular calcification was evaluated by micro-CT imaging, quantitative assessment of vascular calcium content, and histological staining. Aortic rings from 8 to 10-week-old $Creg1^{tg}$ and $Creg1^{smko}$ mice, along with their littermate controls, were isolated for ex vivo studies. Primary mouse

VSMCs were treated with high phosphate (Pi) to investigate the underlying molecular mechanisms of Creg1 on vascular calcification. Proteomics was performed on the aortas from Creg1$^{flox/flox}$ and Creg1^{smko} mice together with VitD3 injection. Co-IP was performed to validate the interactions between Creg1 and Fhl2.

Results: Based on the screening results of scRNA-seq, we found that Creg1 expression levels were downregulated in the aortic tissues from three distinct mouse models of vascular calcification, patients with chronic kidney disease and in Pi-treated VSMCs. Importantly, smooth muscle-specific Creg1 knockdown aggravated vascular calcification by increasing the osteogenic differentiation of VSMCs. Conversely, Creg1 overexpression prevented vascular calcification by inhibiting the osteogenic differentiation of VSMCs. Mechanistically, Creg1 could directly interact with Fhl2, reducing its K48-linked polyubiquitination and thereby inhibiting its subsequent degradation. We demonstrated that the smooth muscle-specific knockdown of Fhl2 exacerbated vascular calcification in a dose-dependent manner. Fhl2 knockdown also partially reversed the anti-calcification effect of Creg1 both in vivo and in vitro. In addition, proteasome inhibition by MG132 prevented proteasome degradation of Fhl2 mediated by Creg1. Overexpression of Creg1 resulted in a longer half-life of Fhl2 protein. Furthermore, we identified the physical interactions and interacting domains between Creg1 and Fhl2. Ubiquitination assays displayed that Creg1 targeting Fhl2 inhibited its K48-linked ubiquitination at lysine 167 site, not depending on K63-linked ubiquitination. In the present study, Fhl2 primarily reduced the phosphorylation level of Stat3 without significantly altering the overall level of Stat3. Furthermore, Fhl2 inhibited the translocation of Stat3 into the nucleus, thereby suppressing the transcription of Runx2. Finally, we demonstrated that inhibition of Stat3 phosphorylation could partially reverse the severity of vascular calcification caused by Creg1 deficiency.

Conclusions: Our findings demonstrate that Creg1 is a novel endogenous defender that prevents vascular calcification by inhibiting the osteogenic differentiation of VSMCs. These findings collectively suggest that Creg1 may serve as a therapeutic target for the treatment of vascular calcification.

Keywords: vascular calcification, vascular smooth muscle cells, Cellular repressor of E1A stimulated genes 1, osteogenic differentiation

MiRNA-378a-5p attenuates the development of abdominal aortic aneurysm via Ablim1-Mkl1 signaling pathways

Dan Liu, Jing Wang, Ya-Ni Wang, -Ming Yang, Dao-Sen Liu, Xiao-Lin Su, Hai-Xu Song, Kai Xu, Cheng-Hui Liu, Dan Liu, Ya-ling Han

State Key Laboratory of Frigid Zone Cardiovascular Disease, Cardiovascular Research Institute and Department of Cardiology, General Hospital of Northern Theater Command

MiRNA-378a-5p attenuates the development of abdominal aortic aneurysm via Ablim1-Mkl1 signaling pathways

Jing Wang, Yujia Zou, Yani Wang, Zheming Yang, Daoshen Liu, Xiaolin Su, Haixu Song, Kai Xu, Chenghui Yan, Dan Liu, Yaling Han*

State Key Laboratory of Frigid Zone Cardiovascular Diseases, Department of Cardiology and Cardiovascular Research Institute, General Hospital of Northern Theater Command, Shenyang, Liaoning Province, 110016, China

First author: Jing Wang; Tel：15904060245; E-mail:974348376@qq.com; Birthday:1994.4.22

*Corresponding authors: Yaling Han, MD; Tel：28856123; E-mail: hanyaling@163.net

Abstract

Background: Abdominal aortic aneurysm (AAA) is a lethal degenerative vascular disease that mainly affects older adults and has a high mortality rate (>80%) upon rupture. Multiple pathological processes, including extracellular matrix (ECM) breakdown, inflammation, phenotype switching of vascular smooth muscle cells (VSMCs), oxidative stress, and neovascularization, contribute to the occurrence and development of AAA. To identify key molecules involved in phenotypic switching and migration of VSMCs may provide potential targets for AAA diagnosis and treatment. MicroRNAs (miRNAs) are single-stranded RNA molecules that target mRNA through partial complementarity, thereby inhibiting translation or inducing mRNA degradation. The aberrant expressions of miRNAs contribute to AAA pathogenesis. In this study, we aimed to perform miRNA microarray analysis to screen for differentially expressed miRNAs in the aortas of AAA mice compared to those in control mice, and to clarify the role and mechanism of miR-378a-5p in the AAA development.

Methods: We performed a comprehensive miRNA microarray analysis to screen for differentially expressed miRNAs in the aortas of AAA mice and control mice. Quantitative real-time polymerase chain reaction (qRT-PCR) was used to detect the expressions of miR-378a-5p in the serum and aortas of AAA patients and mice. To clarify the role of miR-378a-5p in the AAA development in vivo, miR-378a-5p antagomir and angomir were administered to ApoE$^{-/-}$ mice using tail venous injection, followed by Angiotensin II (Ang II) infusion. Next, the role of miR-378a-5p in the phenotypic switching and migration of vascular smooth muscle cells (VSMCs) was examined in vivo and in vitro. Mechanistically, the targets of miR-378a-5p were identified by bioinformatics analysis, luciferase assay, qRT-PCR and western blot. Co-immunoprecipitation (Co-IP) assay combined with mass spectrometry were carried out for excavating potential downstream effectors.

Results: The expression of miR-378a-5p was decreased in the serum and aortas of AAA patients and mice, and tumor necrosis factor-α (TNFα)-treated VSMCs. In vivo, the antagomir-378a-5p aggravated AAA formation, as evidenced by a larger maximal aortic diameter and greater medial elastin degradation than in control mice. MiR-378a-5p angomir had the opposite effect. In vitro, miR-378a-5p overexpression significantly promoted the contraction ability and suppressed the migration of VSMCs, whereas miR-378a-5p knockdown inhibited the contraction ability and increased the migration of VSMCs. Mechanistically, we discovered that miR-378a-5p played a protective role in AAA development by regulating actin-binding LIM protein 1 (ABLIM1)-megakaryoblastic leukemia 1 (MKL1) pathway. Our experiments found that overexpression of ABLIM1 inhibited VSMCs differentiation, whereas interference with Ablim1 promoted differentiation in vitro. In addition, miR-378a-5p overexpression inhibited the phenotypic transformation and migration of VSMCs by inhibiting the expression of ABLIM1, whereas miR-378a-5p knockdown promoted the phenotypic transformation and migration of VSMCs by increasing the expression of ABLIM1. Moreover, our results showed that ABLIM1 knockdown mitigated AAA progression in vivo. The results indicated that ABLIM1 interacted with MKL1 and inhibited its nuclear translocation. MKL1 overexpression reversed the ABLIM1 overexpression-mediated phenotypic switching of VSMCs, and MKL1 knockdown weakened the role of ABLIM1 knockdown-mediated phenotypic switching of VSMCs. These above results indicated miR-378a-5p played a protective role in AAA development by regulating the ABLIM1-MKL1 pathway.

Conclusion: MiR-378a-5p exerts protective effects against AAA by maintaining VSMC homeostasis via the ABLIM1-MKL1 pathway. Therefore, targeting miR-378a-5p may be an attractive therapeutic strategy for AAA treatment.

S100A12-Driven Aortic Dissection: Rescue by Sivelestat Through Neutrophil Elastase Inhibition

Yi-Ming Li, Cheng-Hui Yan

General Hospital of Northern Theatre Command

S100A12-Driven Aortic Dissection: Rescue by Sivelestat Through Neutrophil Elastase Inhibition

Yiming Li[1#], Xiaodong Jia[1#]Chenghui Yan[1]*, Yaling Han[1]*

1. State Key Laboratory of Frigid Zone Cardiovascular Disease, Cardiovascular Research Institute and Department of Cardiology, General Hospital of Northern Theater Command

Author contributions

These authors contributed equally: Yiming Li, Nan Zhang and Xiaodong Jia. Theseauthors jointly supervised this work: Yiming Li, Nan Zhang, Jingjin Hou, Yan Zhang, Haixu Song, Ziqi Liu performed experiments. Yiming Li and Xiaodong Jia analyzed the data and reviewed the manuscript. Yaling Han and Chenghui Yan designed experiments. Yiming Li and Chenghui Yan wrote the manuscript. Yiming Li, Chenghui Yan and Yaling Han were the guarantors of this study.

Funding: This study was supported by the National Natural Science Foundation of China (82200535), the National Social Science Foundation of China (21ARK005) and China Postdoctoral Science Foundation (2023M734295).

Abstract

Background: Aortic dissection (AD) is a serious and life-threatening condition which allows blood to enter the vessel wall and causes aorta rapture. NETosis is a type of programmed cell death induced by neutrophils, which is characterized by the release of neutrophil extracellular traps (NETs). In this study, we attempted to elucidate whether NETs components are involved in the occurrence and development of AD and intervene in it.

Methods: Single-cell RNA sequencing using datasets obtained from the Gene Expression Omnibus database for screening target cells and genes. Human AD tissue samples from dissecting aortic dissection and sera were collected from patients underwent aorta replacement or repairment. The mass spectrometry analyses were used between humanic dissected and normal aorta to futher screen target differentially expressed genes. Enzyme-linked immunosorbent assay, Western Blotting and immunohistochemical staining were used to exam levels of expression of target genes in AD patients. The lysozyme M promoter and S100A12 gene sequence were constructed on the transposon. The linearized transgenic vector was injected into the embryonic stem cells of C57BL/6J

pseudo-pregnant females by microinjection to prepare transgenic (TG) mice. Construction of lysozyme M promoter S100A12$^{TG/TG}$ AD mouse model using BAPN drinking method. Ultrasound, PET/CT were used to evaluate aortic remodeling and inflamation status in vivo. Exploring the mechanisms through HL-60, 293T, and PB5 cells in vitro of this study.

Results: Neutrophil Elastase (NE) was significant overexpressed in AD than that in non-AD human aorta. Human AD aorta underwent structural changes and a large amount of collagen deposition. There was a significant overexpression of S100A12 and NE in the mass spectrometry and single-cell RNA sequencing analyses of human AD than normal aortic proteins. Serological studies had found that the expression level of S100A12 in the serum of AD patients reaches its peak around 24 hours after onset, and the content was about three times that of the normal population. Using BAPN to establish AD mice model, lysozyme M promoter S100A12 $^{TG/TG}$ mice showed higher negative vascular remodeling rate and mortality compared to C57 mice. S100A12 can promote the expression of NE through its transcription factor GATA2, while mutate of GATA2 site can reduce the expression level of NE. When co-culturing neutrophils and VSMCs, specific inhibitior of NE activity Sivelestat (SIV) can save the migration, apoptosis and phenotypic transformation of VSMCs induced by inhibiting the activity of NE. Intraperitoneal injection of SIV of the AD mice model could reduce the level of local inflammation in the aorta of mice, reduce the incidence of AD, improve vascular remodeling and prolong the survival time of mice.

Conclusion: S100A12 overexpression in neutrophils promotes NE expression through the transcription factor GATA2. Specific inhibition of NE activity by SIV can mitigate the phenotype transformation of VSMCs induced by NE. In vivo experiments have demonstrated that overexpression of S100A12 in myeloid cells increases mortality and negative vascular remodeling in AD model mice, while SIV can counteract these adverse effects.

基于 NLRP3 炎症小体探讨恩格列净抑制 TAAD 小鼠主动脉病理性重塑的机制

秦华丽 许丹焰

中南大学湘雅二医院心内科

目的 胸主动脉瘤和夹层（thoracic aortic aneurism and dessection，TAAD）是一种严重威胁人类生命的大血管疾病，尚缺乏有效药物来预防或延缓 TAAD 进展或血管破裂。SGLT2 抑制剂具有广泛的心血管获益。然而，SGLT2 抑制剂能否减缓 TAAD 尚不明确。

方法 从 GEO 数据库中下载 TAAD 患者样本 RNA 测序数据集，联合我们的小鼠 RNA 测序结果以筛选差异表达基因。构建两种 TAAD 模型，然后分别验证 NLRP3 敲除和恩格列净处理后对 TAAD 的影响。通过 RNA 测序初步探索恩格列净通过抑制 NLRP3 表达而改善 TAAD 的可能分子机制。通过免疫共沉淀分析检测 VSMC 中 TRIM59-USP7-NLRP3 的相互作用。最后构建 AAV9-TRIM59 小鼠模型进行回复验证。

结果 在 TAAD 患者和 BAPN 诱导的 TAAD 小鼠主动脉中均显示 NLRP3 炎症小体过度激活。NLRP3 整体敲除明显减轻 BAPN 诱导的小鼠 TAAD 和 Fbn1$^{C1039G/+}$ 小鼠胸主动脉的扩张，并减少细胞外基质降解。对 BAPN 组和恩格列净治疗组小鼠主动脉转录组差异基因进行 GO/KEGG 富集分析显示恩格列净主要改变 BAPN 小鼠主动脉炎症反应、细胞外基质、血管结构功能和影响蛋白泛素化调控等。qPCR,Western blot 联合免疫荧光显示，恩格列净主要下调 VSMC 中 NLRP3 蛋白水平。进一步体外实验证实恩格列净促进 NLRP3 经泛素 - 蛋白酶体系统降解，识别出 TRIM59 是恩格列净促进 NLRP3 泛素化降解的关键分子。TRIM59 增加 USP7 和 NLRP3 的结合，而恩格列净抑制 TRIM59 的表达、并减弱 USP7 和 NLRP3 的结合，从而促进 NLRP3 泛素化降解。最后，我们发现 TAAD 患者主动脉 TRIM59 和 USP7 表达增加，过表达 TRIM59 抵消恩格列净对 BAPN 诱导小鼠 TAAD 的保护作用。

结论 我们的研究结果表明，恩格列净通过 TRIM59-USP7 轴促进 NLRP3 泛素化降解，改善 TAAD 小鼠主动脉病理性重塑。

胆固醇、高密度脂蛋白和葡萄糖指数与颈动脉粥样硬化的相关性研究

罗正鸿 帅平

四川省医学科学院·四川省人民医院

目的： 探讨胆固醇、高密度脂蛋白和葡萄糖指数（Cholesterol, High-Density Lipoprotein, and Glucose index，CHG）与颈动脉粥样硬化（Carotid Atherosclerosis，CAS）的相关性，为体检人群 CAS 的防控提供依据。

方法： 本研究为横断面研究，选取 2020 年 1 月—2024 年 12 月期间在四川省人民医院健康管理中心参加过体检且数据资料完整者为研究对象，通过问卷调查、体格检查和生化检查收集研究对象的数据资料。采用多因素 logistic 回归模型评估 CHG 指数与 CAS 的相关性。采用限制性立方样条图（Restricted cubic spline, RCS）探讨 CHG 指数与 CAS 患病风险之间的剂量反应关系，采用亚组分析评估 CHG 指数在不同人群中的适用性。

结果： 研究共纳入 99855 名研究对象，其中 CAS 组 57297 例，平均年龄（58.59 ± 11.52）岁，正常对照 42558 例，平均年龄（44.31 ± 9.47）岁。多因素 logistic 回归分析显示，当 CHG 指数用作连续变量时，CHG 指数与 CAS（OR=1.61；95% CI：1.54-1.68）、CIMT（OR=1.56；95% CI：1.49-1.64）和颈动脉斑块（OR=1.61；95% CI：1.52-1.69）的患病率显著相关；在所有的三个模型中，CHG 指数四分位水平升高与 CAS、CIMT 和颈动脉斑块的患病风险呈正相关。RCS 分析显示 CHG 指数与 CAS 和 CIMI 患病风险呈非线性相关（P for nonlinear < 0.05），CHG 指数与颈动脉斑块风险呈正线性关系（P for nOnlinear=0.993）；当 CHG ≥ 12.98 时， CAS、CIMT 和颈动脉斑块的患病风险随 CHG 指数的增加而增加。亚组分析发现在不同性别、年龄、BMI 分层、吸烟和饮酒等人群中与 CHG 指数 Q1 组相比，Q2-Q4 组 CAS 患病风险均显著上升，且风险随四分位升高呈递增趋势。

结论：CHG 指数水平与 CAS、CIMT 和颈动脉斑块的患病风险增加显著相关。

The predictive value of estimated glucose disposal rate for the risk of venous thromboembolism in elderly individuals: a prospective cohort study of UK Biobank

Yi Zheng[1], Lei Liu[2], Xinyi Yang[3,4], Hui-Hui Ma[4], Gary Tse[1,5], Rong Luo[6], Hong-Qiang Ren[2], Wei Hua[7], Xiao-Ping Li[4], Tong Liu[1]

1. Second Hospital of Tianjin Medical University

2. Suining central hospital

3. Affiliated Hospital of Southwest Medical University

4. Sichuan Provincial People's Hospital

5. Hong Kong Metropolitan University

6. Chengdu Medical College

7. Fuwai Hospital

Objective: Venous thromboembolism (VTE) is a leading cause of cardiovascular morbidity and mortality, particularly among the elderly. Insulin resistance has been implicated in the pathogenesis of VTE. However, no prior study has investigated the associations between the estimated glucose disposal rate (eGDR), a surrogate marker for insulin resistance, and VTE risk in elderly individuals. This study aimed to investigate the predictive value of eGDR for the risk of VTE among elderly individuals.

Methods: We conducted a prospective cohort study using data from the UK Biobank, including 193,552 participants aged ≥ 60 years without a prior history of VTE. Participants were stratified into eGDR quartiles. The primary outcome was incident VTE, with secondary outcomes including pulmonary embolism (PE), deep vein thrombosis (DVT), and lower extremity DVT (LEDVT). The Kaplan-Meier curves were employed to depict the cumulative occurrence of VTE. Three Cox proportional hazards regression models were utilized to investigate the relationship between the eGDR and the risk of incident VTE. The results were reported as hazard ratios (HRs) along with the corresponding 95% confidence intervals (CIs). Restricted cubic spline (RCS) analyses were conducted to further investigate the non-linear relationship between eGDR and VTE, and a two-piecewise multivariable Cox model was employed on both sides of the inflection point. Subgroup analyses were performed based on sex (male or female), body mass index (<30, or ≥ 30), smoking status (never or former/current), and alcohol consumption (never or former/current). Mediation analysis was employed to assess the mediating effect of estimated glomerular filtration rate (eGFR) on the association between eGDR and VTE. Polygenic risk scores were incorporated to account for genetic susceptibility and investigate potential interactions between eGDR and genetic risk. We further used a LASSO regression model to screen for VTE risk factors. Based on the selected predictors, the extreme gradient boosting algorithm was applied, and the feature importance was measured to evaluate the predictive value of each risk factor.

Results: Over a median follow-up of 13.13 years, 8,670 VTE events were recorded, including 4,836 (2.50%) PE, 4,717 (2.44%) DVT, and 4,126 (2.13%) LEDVT. Kaplan-Meier survival curves showed that individuals with higher eGDR levels had a lower cumulative incidence rate of VTE, PE, DVT, and LEDVT. After adjusting for sex, age, race, education, smoking status, alcohol consumption, physical activity, body mass index, systolic blood pressure, diastolic blood pressure, triglycerides, total cholesterol, eGFR, uric acid, aspirin, lipid-lowering drugs, antihypertensive drugs, insulin, and anticoagulants, in comparison with quartile 1, the risk of VTE in quartile 2 was significantly lower (HR 0.93, 95% CI 0.87-0.99, P=0.021), as was in the risk in quartile 3 (HR 0.84, 95% CI 0.78-0.91, P<0.001) and quartile 4 (HR 0.71, 95% CI 0.64-0.79, P<0.001). Quartile 2 was not significantly associated with the risk of PE (HR 0.93, 95% CI 0.85-1.01, P=0.095) or DVT (HR 0.93, 95% CI 0.85-1.01, P=0.091) compared to quartile 1. The HRs (95% CI) for quartile 3 to quartile 4 were 0.79 (0.71, 0.88), 0.69 (0.60, 0.79), respectively, for PE; and 0.89 (0.81, 0.99), 0.74 (0.64, 0.84) for DVT. Regarding LEDVT, individuals with the highest eGDR were associated with a lower risk of LEDVT compared to those with the lowest eGDR (HR 0.76, 95% CI 0.66-0.88, P<0.001). As the eGDR increased, RCS showed a monotonic decreasing trend in the risk of PE (P for non-linear=0.055, P overall <0.001). In addition, RCS demonstrated a non-linear decrease in the risk of VTE, DVT, and LEDVT (P for non-linear<0.05, P overall <0.001). Using the two-piecewise Cox proportional hazards regression models, we determined the inflection points for VTE, DVT, and LEDVT as 7.44, 7.51, and 7.55. When below the thresholds, the eGDR demonstrated no significant correlation with DVT or LEDVT, and only a slight association with a decrease in VTE risk (HR 0.97, 95% CI 0.94-0.99, P=0.012). Conversely, when exceeding these thresholds, elevated levels of eGDR were associated with significantly reduced risks of VTE (HR 0.93, 95% CI 0.91-

0.95, P<0.001), DVT (HR 0.94, 95% CI 0.91-0.97, P<0.001), and LEDVT (HR 0.94, 95% CI 0.91-0.97, P<0.001). The association between the eGDR and the occurrence of VTE in subgroups was consistent with the primary findings. No significant interactions were observed among subgroups. The mediation analysis demonstrated that the mediating effect of eGFR between eGDR and VTE, PE, DVT and LEDVT was 10.7%, 9.7%, 12.7% and 13.1%, respectively. Polygenic risk score analysis stratified by genetic risk demonstrated a synergistic interaction between low eGDR and high genetic susceptibility. eGDR is a key predictor of VTE.

Conclusions: Reduced eGDR is an independent predictor of VTE risk in elderly individuals, with distinct non-linear associations for VTE subtypes. eGFR partially mediates the relationship between eGDR and VTE risk. The inclusion of eGDR in risk models enhances VTE risk stratification, particularly in individuals with a genetic predisposition.

血管钙化关键调控基因的生物信息学分析与实验验证

刘丹 邹宇佳 王静 闫承慧 韩雅玲

中国人民解放军北部战区总医院寒地心血管病全国重点实验室

目的：基于生物信息学方法筛选血管钙化的关键差异表达基因（Differentially Expressed Genes，DEGs），进行单基因 GSEA 富集分析探究其在血管钙化中的生物学功能，并进行实验验证，为深入阐明血管钙化的发病机制提供新思路。

方法：获取来源于 GEO 数据库的三个血管钙化数据集，应用 limma 包筛查差异表达基因，通过 Bioinformatics & Evolutionary Genomics 网站对差异表达基因取交集，使用 RStudio 软件对交集所得基因完成单基因 GSEA 富集分析，最后在细胞学水平应用 Western blot 和 Real-time PCR 验证对关键差异基因进行实验验证，明确其表达与血管钙化的相关性。

结果：通过三个血管钙化数据集（GSE159832、GSE229679、GSE37558）分别筛选出 2275 个、449 个和 381 个差异表达基因，三个数据集取交集后得到两个共同差异表达基因为磷酸丝氨酸氨基转移酶 1（phosphoserine aminotransferase 1，PSAT1）和胸苷激酶 1（thymidine kinase 1，TK1）。进一步对 TK1 进行单基因 GSEA 富集分析，GO 富集分析显示，最显著富集的通路主要集中在核糖体的生物发生、组装以及 rRNA 的加工和成熟过程；KEGG 分析显示，最显著富集的通路主要在 PI3K-AKT 信号通路、癌症及神经退行性疾病相关通路、细胞骨架和平滑肌收缩。TK1 常规 GSEA 富集分析结果也显示，显著富集的基因集主要为动力蛋白、上皮细胞紧密连接、轴突引导及血管平滑肌收缩通路。Western blot 及 Real-time PCR 结果显示，磷酸盐刺激的小鼠原代血管平滑肌细胞中 TK1 表达水平显著低于对照组（P < 0.05）。

结论：基于生物信息学分析及实验验证发现 TK1 与血管钙化存在明显的相关性，在血管钙化中可能发挥重要作用。该研究将为临床上血管钙化的防治提供新思路。

The clinical application value of ultrasound in the diagnosis of iliac vein compression syndrome

jing Chen, Pei-Kai Xie

珠海市人民医院

Objective:Iliac Vein Compression Syndrome (IVCS), also known as May-Thurner Syndrome, is a chronic venous disorder resulting from mechanical compression of the left common iliac vein by the overlying right common iliac artery and lumbar vertebrae. The clinical manifestations of IVCS vary widely, ranging from asymptomatic venous compression to severe chronic venous insufficiency (CVI), including lower extremity edema, pain, skin changes, and even deep vein thrombosis (DVT). Early diagnosis and treatment of IVCS are therefore crucial. Doppler ultrasound, as a non-invasive, convenient, and highly reproducible imaging modality, has been playing an increasingly important role in the diagnosis of IVCS. This study aims to investigate the clinical value of Doppler ultrasound in diagnosing IVCS and analyze its advantages and limitations.

Methods:Seventy-seven patients scheduled for iliac vein digital subtraction angiography (DSA) were enrolled in this study. All patients underwent preoperative iliac vein ultrasound examinations, during which the following parameters were measured: the internal diameter at the compressed segment, the internal diameter at the distal dilated segment, blood flow velocity at the compressed segment, and blood flow velocity at the distal dilated segment. The ultrasound diagnostic criteria for IVCS were defined as: a ratio of distal dilated segment diameter to compressed segment diameter >2, and a ratio of compressed segment velocity to distal dilated segment velocity >2.5. Using DSA as the gold standard, we evaluated the diagnostic accuracy of these ultrasound parameters for IVCS.

Results:Based on DSA findings, patients were divided into a positive group (n=15) and negative group (n=62). The positive group consisted of 4 males and 11 females, with a mean age of 51.53±15.85 years, mean weight of 60.35±9.72 kg, and mean height of 160.4±7.41 cm. The negative group included 27 males and 35 females, with a mean age of 56.84±14.60 years, mean weight of 65.52±11.88 kg, and mean height of 163.16±8.10 cm. No significant differences in baseline characteristics were observed between the two groups (P>0.05).

Using DSA results as the gold standard, Kappa consistency testing showed that:

1. When using the ultrasound parameter of distal dilated segment diameter to compressed segment diameter ratio >2 for IVCS diagnosis, the Kappa value was 0.712, indicating statistically significant agreement.

2. When using the ultrasound parameter of compressed segment velocity to distal dilated segment velocity ratio >2.5 for IVCS diagnosis, the Kappa value was 0.586, suggesting moderate but statistically significant agreement.

3. When combining both diameter ratio and velocity ratio for IVCS diagnosis, the Kappa value was 0.686, demonstrating statistically significant agreement with DSA findings.

Conclusion:In color Doppler ultrasound examinations, measuring both the distal segment diameter to compressed segment diameter ratio and the compressed segment to distal segment blood flow velocity ratio can significantly contribute to the diagnosis of IVCS. The study demonstrates good consistency between these ultrasound parameters and DSA findings, supporting the clinical utility of Doppler ultrasound in IVCS diagnosis. The diameter ratio parameter showed particularly strong agreement with DSA results, while the velocity ratio provided additional valuable diagnostic information. The combined use of both parameters further enhanced diagnostic accuracy, suggesting that this dual-parameter approach may offer optimal diagnostic performance in clinical settings. These findings highlight Doppler ultrasound as a valuable non-invasive tool for screening and initial evaluation of suspected IVCS cases.

活化蛋白 C 调控衔接蛋白 p66Shc 在 AD 形成与发展中的作用及其分子机制 的研究

张文君 王洪杰 曾和松

华中科技大学同济医学院附属同济医院

目的：主动脉夹层是一种主动脉内膜撕裂后腔内的血液通过内膜破口进入动脉壁中层形成夹层血肿，并沿血管长轴方向扩展，形成动脉真、假腔病理改变的严重主动脉疾病。主动脉夹层通常急性发病，如果不及时治疗，很容易血管破裂导致病人死亡。因此，主动脉夹层分子机制的研究对于临床的预防和治疗具有重要意义。衔接蛋白 p66Shc 是一种线粒体氧化还原状态感知蛋白，它参与线粒体 ROS 的形成。有研究表明凝血蛋白酶活化蛋白 C（aPC）可以通过改变 p66Shc 的表观遗传控制其表达，从而对糖尿病肾病起保护作用。那么 aPC 是否也可以调节 p66Shc 的表达而影响血管壁中 ROS 的形成而对主动脉夹层起保护作用以及 aPC 是如何调控 p66Shc 表达的机制仍有待阐明。该研究将为主动脉夹层的发病机制提供新的理论依据及早期防治思路。

方法：8 周龄的雄性 C57BL/6N 背景的 $ApoE^{-/-}$ 小鼠（野生型）和体内低表达活化蛋白 C 的 $TM^{P/P}$× $ApoE^{-/-}$ 小鼠（突变型），将每种基因背景的小鼠都分为四组：生理盐水组、蛋白 C（PC）组、血管紧张素 II（Ang II）组和血管紧张素 II+蛋白 C（Ang II+PC）组。首先在野生型和突变型小鼠的饮用水中给予 0.1%β-氨基丙腈（BAPN）喂养 3 周，然后通过微型渗透泵向小鼠体能泵入生理盐水或以 2500 ng / min / kg 的速度泵入血管紧张素 II，持续泵注 2 周；PC 组和 Ang II+PC 组的野生型和突变型小鼠在埋泵后以腹腔注射的方式给予 PC（1mg/kg/天）。

结果：本研究证实活化蛋白 C 能够有效的防止主动脉夹层的发生发展。体外实验结果阐明在血管内皮细胞中凝血蛋白酶活化蛋白 C 调控衔接蛋白 p66Shc 的分子机制。首先，在人脐静脉内皮细胞中，凝血蛋白酶活化蛋白 C 可以通过改变 p66Shc 的表观遗传控制其表达，同时减少基质金属蛋白酶（MMP2/9）、炎症指标（ICAM1 和 VCAM1）的表达和氧化应激水平。其次，凝血酶活化蛋白 C 能够抑制 Ang II 所诱导的 p66Shc 线粒体的转位和 Ang II 所导致的线粒体膜电位的下降，其主要分子机制是 aPC 通过调控 YB1 蛋白的表达从而上调糖基化转移酶的表达增加 p66Shc 蛋白 O- 糖基化修饰水平抑制其线粒体的转位，从而抑制线粒体 ROS 的产生和线粒体膜电位的下降；通过对 p66Shc 蛋白上第 29 个氨基酸进行点突变（O- 糖基化修饰位点，苏氨酸突变为丙氨酸），表明 aPC 主要通过调控 p66Shc 蛋白上第 29 个氨基酸的 O- 糖基化修饰来抑制其转位。最后，在本研究中通过血管内皮细胞特异性敲除 YB1 转基因小鼠，验证了 YB1 在主动脉夹层发生中的重要作用。

结论：aPC 通过调控 p66Shc 的表观遗传学改变其表达，并且通过调控 YB1 蛋白的表达从而上调糖基化转移酶的表达增加 p66Shc 蛋白 O- 糖基化修饰水平抑制其线粒体的转位，从而抑制线粒体 ROS 的产生和线粒体膜电位的下降，最终达到对防止主动脉夹层的发生和发展的目的。

急性 B 型主动脉夹层患者胸主动脉腔内修复术后 1 年内脏段不稳定相关因素分析

张志强 王亚松 曹小帆 程佳新 王效增 (学组委员，通讯作者)

中国人民解放军北部战区总医院

目的：本研究旨在探讨急性斯坦福 B 型主动脉夹层（ATBAD）患者在接受胸主动脉腔内修复术（TEVAR） 后内脏段不稳定（VSI）相关的因素。

方法：本研究为一项回顾性、单中心分析，涉及 2015 年 1 月至 2023 年 7 月期间接受 TEVAR 治疗的 61 例 ATBAD 患者。使用 3 Mensio 软件进行三维主动脉中心线重建，并在各主动脉管腔标准化区域（5 – 9 区）测量最大主动脉直径及其真腔直径和假腔直径。此外，我们还对术前的夹层撕裂长度进行了测量，并评估了假腔的解剖结构和灌注情况，更全面地了解患者手术前的血管状况。随访扫描分别在 1 个月、6 个月及术后一年进行。术前扫描和最终的术后扫描用于进行测量。VSI 定义为在 TEVAR 治疗后一年内，主动脉 5 -9 区的任何一段出现 5 毫米以上的主动脉扩张。根据患者在一年内是否出现 VSI，将其分为两组：VSI 组（n = 33）和非 VSI 组（n = 28）。为了确定与 VSI 相关的因素，进行了单变量和多

变量 Logistic 回归分析。

结果：在 VSI 组中，患者在住院期间使用较少的血管紧张素转换酶抑制剂 / 血管紧张素受体阻滞剂，并且体重指数、白细胞计数和 C 反应蛋白（CRP）水平更高。在对两组患者的影像学和手术数据进行比较时，VSI 组患者更倾向于覆盖左锁骨下动脉。单变量 Logistic 分析表明，体重指数、白细胞计数、CRP、血管紧张素转换酶抑制剂 / 血管紧张素受体阻滞剂、LSA 覆盖可能与 VSI 发生风险增加相关。多变量 Logistic 回归分析显示，CRP [OR = 2.138（1.088 - 4.201），每 1 个标准差增加；P = 0.027] 和 LSA 覆盖 [OR = 9.718（2.469 - 38.254）；P = 0.001] 与 VSI 发生风险增加相关。通过 CRP 评估的 VSI 的 ROC 曲线下面积（AUC）为 0.679（95% CI 0.536 - 0.821）；通过 CRP 和 LSA 覆盖的组合评估为 0.733（95% CI 0.608 - 0.857）。我们发现，CRP 值≥ 65.10 mg/mL 是预测 VSI 的最佳标准，其敏感性为 78.8%，特异性为 60.7%。

结论：在 ATBAD 患者接受 TEVAR 后，CRP 水平和 LSA 覆盖与 VSI 发生风险增加相关。这些发现强调了监测炎症标志物以及在为 ATBAD 患者规划 TEVAR 手术时考虑适当策略的重要性。需要进一步的研究来在更大的患者群体中探究这些关系，并确定其长期的临床意义。

Machine Learning-Based Prediction of Aortic Rupture Risk in Type A Aortic Dissection

lijun Sun, Wei-Liang Zheng, Hua Peng, Hai-Yue Bao, Yan Wang

Xiamen Cardiovascular Hospital of Xiamen University

Acute Type A aortic dissection (ATAAD) is characterized by acute onset and rapid progression, with the primary lethal mechanism being aortic rupture caused by dissection extension. Early identification of high-risk patients is crucial for prioritizing surgical intervention to reduce rupture incidence. Although some studies have explored preoperative rupture risk factors in ATAAD patients, significant limitations persist: (1) Small sample sizes (typically n <500)increase susceptibility to type II statistical errors; (2) Overreliance on anatomic imaging parameters (e.g.,

aortic diameter) with insufficient incorporation of serological biomarkers;(3) Limited focus on preoperative risk prediction models. The emergence of machine learning in cardiovascular research offers new opportunities. While RF excels in handling nonlinear relationships and feature interactions, neural networks (NN) provide superior pattern recognition in complex datasets.

This study developed machine learning models using structured clinical data to predict the probability of aortic rupture within 24 hours post-admission. Data frompatients with type A aortic coarctation from the Xiamen Cardiovascular Hospital of Xiamen University were included in this study, which included demographic characteristics, clinical symptoms, laboratory biochemical test results, and echocardiographic (colour ultrasound) results, and baseline characteristics are detailed. Due to its retrospective design and anonymous nature, the requirement for patient informed consent is waived. Screening was conducted on patients diagnosed with ATAAD. Inclusion criteria: (1) Age ≥ 18 years, (2) onset time ≤ 14 days, (3) CTA diagnosis of ATAAD. Exclusion criteria: (1) Died of other serious complications after admission, (2) Abandonment of surgical treatment and automatic discharge, (3) Death more than 24 hours after admission, (4) Incomplete clinical data Following preprocessing, the Synthetic Minority Oversampling Technique (SMOTE) was applied to augment the training dataset. The Salp Swarm Optimization (SSA) algorithm was implemented to optimize hyperparameters of key predictive models (Random Forest and XGBoost), enhancing their ability to identify critical risk patterns. Six machine learning algorithms were evaluated using accuracy, F1-score, precision, receiver operating characteristic curve area under the curve (ROC-AUC), sensitivity, and specificity. Interpretability analyses were performed by ranking the importance of optimal model features, SHAP method (Shapley Additive Explanations).

As a result of the above study, 774 eligible patients were included in the final analysis.The SSA-optimized Random Forest model obtained the optimal performance of the results compared to other models, achieving 98.70% accuracy, 0.971 ROC-AUC, and 83.33% F1 score on the test dataset. Although the logistic regression model also achieved better AUC, it showed higher misclassification rates for negative samples. Feature importance analysis identified liver insufficiency, plasma albumin levels, plasma bicarbonate concentration, mean arterial pressure, and patient age at admission as significant predictors of preoperative aortic rupture. These findings align with established pathological mechanisms, including aortic wall matrix metabolism abnormalities and hemodynamic shear stress alterations.

This study established an interpretable machine learning framework to predict 24-hour preoperative aortic rupture risk in patients with ATAAD. The Random Forest algorithm achieved superior predictive performance, with an accuracy of 98.70% (AUC: 0.971; F1-score: 83.33). SHAP interpretability analysis identified clinically significant predictors, including glomerular filtration rate and white blood cell count, which showed substantial associations with aortic rupture risk.

硒代蛋氨酸通过靶向线粒体生物合成铁死亡通路治疗主动脉夹层的机制研究

赖盛伟 郭伟

解放军总医院第一医学中心

目的

探讨 Set 对 AD 的治疗效果及分子机制，以期为 AD 的药物治疗提供新的选择。

方法

通过 β- 氨基丙腈（BAPN）诱导小鼠 AD 模型，并分为对照组、Set 组、BAPN 组和 BAPN+Set 组。评估 Set 对主动脉扩张、组织病理学及存活率的影响。体外实验以 PDGF-BB 诱导 VSMCs 表型转化，结合 EdU、Transwell、脂质过氧化检测等技术分析 Set 对细胞增殖、迁移及表型转换的影响。通过单细胞测序、转录组学分析和 siRNA 干扰技术验证 Set 治疗 AD 的关键分子机制。

结果

体内实验结果表明，Set 显著降低 AD 发生率（72.0% vs 32.0%, P<0.05）和死亡率（48.0% vs 16.0% , P<0.05），抑制了主动脉扩张，减轻弹性纤维断裂，抑制胶原异常增生（P<0.05）。体外实验表明，Set 可以抑制 PDGF-BB 诱导的 VSMCs 增殖、迁移及表型转换，表现为合成表型标志物 OPN 和 Vimentin 显著下调，以及收缩表型标志物 α-SMA 和 SM22 显著升高。单细胞测序结果表明，铁死亡通路相关基因在 AD 患者 VSMC 中显著富集。转录组学分析提示 Set 可显著降低铁死亡信号通路和激活线粒体生物合成路径。进一步的细胞实验结果表明，Set 通过激活 PGC-1α/NRF2 通路，上调 GPX4 表达，进而抑制脂质过氧化产物积累，改善线粒体功能，最终抑制 VSMC 表型转换。敲低 GPX4 或 PGC-1α 后，Set 对 VSMC 表型转换的抑制作用被削弱。

结论

Set 通过靶向激活 PGC-1α/NRF2/GPX4 轴抑制铁死亡介导的 VSMCs 表型转变，进而缓解 AD 进展。

Dysregulation of the HMGB2-TREM Axis Contributes to Pathogenesis of Abdominal Aortic Aneurysm in Male Patients

Fang Wang, Li- Pan

Ruijin Hospital, Shanghai Jiao Tong University School of Medicine

Background: Abdominal aortic aneurysm (AAA) is a major public health challenge and presents high mortality due to diagnostic and therapeutic difficulties. A strong imperative is to investigate the mechanisms underlying AAA formation and identify novel specific biomarkers or therapeutic approaches for diagnosing and treating AAA in its early stages. Wu et al. reported increased HMGB2 levels in angiotensin-II-treated VSMCs, and in an angiotensin II-induced mouse model of AAA. Inhibition of HMGB2-regulated ferroptosis and inflammation in angiotensin-II-treated VSMCs may protect against AAA by inactivating nuclear factor-kappa B (NF-κβ) signaling [20]. Despite these observations, there is a paucity of mechanistic evidence that directly connects HMGB2 to AAA development or rupture. TREM-1 is an immunoglobulin (Ig) superfamily member containing an Ig-like extracellular domain. It is closely associated with inflammatory reactions and various pathologies. Previous research has demonstrated that TREM-1 can exacerbate experimental AAA by modulating angiotensin II-induced monocyte trafficking and vascular wall inflammation . Although the specific ligands for TREM-1 have yet to be definitively identified, several studies have suggested that HMGB1 could be a potential TREM-1 ligand involved in the inflammatory response . This study investigated the role of high-mobility group box2 (HMGB2) and the HMGB2-triggering receptor expressed on the myeloid cell (TREM) pathway in male AAA patients. The goal was to evaluate HMGB2 as a novel biomarker and to elucidate its contribution to the pathogenesis of AAA. Our findings offer new insights into AAA biology and highlight the potential application of HMGB2 for early detection and therapeutic targeting. **Methods**: This retrospective case-control study included 36 male AAA patients and 41 male controls with balanced baseline characteristics. HMGB1, HMGB2, soluble TREM-1 (sTREM-1), and sTREM-2 serum levels were measured by enzyme-linked immunosorbent assay (ELISA). The association between HMGB2 and AAA was analyzed using multivariate logistic regression, while the diagnostic performance of HMGB2 was assessed using receiver operating characteristic (ROC) curves. **Results**: Elevated HMGB2 and HMGB1 levels were associated with higher risks of AAA (HMGB2: OR: 1.158, 95% CI: 1.011–1.325; p < 0.05; HMGB1: OR: 1.275, 95% CI: 1.048–1.551; p < 0.05) and aneurysm rupture (HMGB2: OR: 1.117, 95% CI: 1.005–1.241; p < 0.05; HMGB1: OR: 1.212, 95% CI: 1.003–1.465; p < 0.05). Meanwhile, sTREM-1 exhibited a negative correlation with AAA (OR: 0.991, 95% CI: 0.985–0.997; p < 0.01). The odds ratios of the fourth quartile HMGB2 and HMGB1 levels for AAA were 6.925-fold and 8.621-fold higher, respectively, than the first quartile levels. The HMGB2 serum level was positively correlated with a larger AAA diameter, with the diameter increasing progressively as the HMGB2 level increased. The area under the ROC curve (AUC) for predicting AAA was 0.713 for HMGB2, 0.677 for HMGB1, and 0.665 for sTREM-1. HMGB1 and sTREM-1 both correlated with HMGB2. Each HMGB1 quartile group exhibited a significant increase as HMGB2 increased. Further, sTREM-1 significantly increased at low to moderate HMGB2 levels but decreased in the highest HMGB2 quartile. **Conclusion**: Elevated HMGB2 serum levels are independently associated with the incidence of AAA in males. HMGB2–TREM pathway disruption

may play a critical role in AAA pathogenesis.

Mechanisms and potential therapeutic strategies in aging-induced aortic aneurysm and aortic dissection

Tao Jing[1,2], Zi-Jie Wang[1,2], Hong-Jian Zheng[1,2], Jia-Hui Yong[1,2], Yi-Ning Yang[1,2]

1. People's Hospital of Xinjiang Uygur Autonomous Region

2. Xinjiang Key Laboratory of Cardiovascular Homeostasis and Regeneration Research

Background

Aortic aneurysm and aortic dissection are life-threatening cardiovascular disorders characterized by progressive dilation or abrupt tearing of the aortic wall. Aging is the strongest non-modifiable risk factor for both conditions, and its influence is exerted through a complex network of cellular, molecular, and systemic changes. With advancing age, the aortic wall undergoes structural remodeling: medial elastin fibers fragment, collagen content increases, and smooth muscle cells (SMCs) decline in number and contractility. Endothelial cells (ECs) also lose their anti-thrombotic and anti-inflammatory phenotype, becoming a source of reactive oxygen species (ROS) and pro-inflammatory cytokines. At the molecular level, telomere attrition limits the replicative capacity of vascular cells, while mitochondrial DNA damage and respiratory-chain inefficiency elevate oxidative stress. Epigenetic drift—manifested as altered DNA methylation, histone modification, and microRNA expression—further disrupts gene networks that maintain extracellular-matrix homeostasis. Concomitantly, chronic low-grade inflammation ("inflammaging") amplifies matrix metalloproteinase (MMP) activity, weakening the aortic wall. Key signaling cascades that sense and transduce these age-related stressors include hypoxia-inducible factor-1 (HIF-1), interleukin-6 (IL-6), and estrogen receptor-1 (ESR1) pathways, all of which modulate vascular remodeling, immune cell recruitment, and ECM turnover. Collectively, these age-dependent alterations compromise aortic integrity, predisposing to aneurysmal dilatation and dissection.

Method

To systematically evaluate how aging drives aortic pathology, a comprehensive literature review was performed. Databases (PubMed, Embase, Web of Science) were searched for peer-reviewed articles published between 2004 and 2024 using the terms"aging and aortic aneurysm,"'"aging and aortic dissection," "molecular mechanisms of aging in aorta," and "signaling pathways in aging aortic diseases." Inclusion criteria required original research or reviews written in English that addressed cellular senescence, telomere biology, mitochondrial dysfunction, epigenetic regulation, or inflammatory signaling in the context of thoracic or abdominal aortic disease. Data were synthesized to map age-related changes in SMCs and ECs, identify critical molecular mediators, and catalog experimental or clinical interventions aimed at these targets.

Result

The review revealed that aging impairs SMC contractility and synthetic function, reducing their ability to repair medial micro-injuries. Endothelial senescence promotes endothelial-to-mesenchymal transition, facilitating intimal thickening and thrombogenicity. Telomere shortening correlates with increased aneurysm diameter and dissection risk, whereas mitochondrial ROS accelerate elastin degradation and activate MMP-2 and MMP-9. Inflammatory cytokines (IL-6, TNF-α) and chemokines (MCP-1) recruit macrophages that further exacerbate matrix breakdown. HIF-1α stabilization under chronic hypoxia induces VEGF and MMP expression, while loss of ESR1 signaling in post-menopausal women diminishes protective nitric-oxide production. Therapeutically, preclinical studies demonstrated that telomerase activators, mitochondrial antioxidants (MitoQ), and senolytics (dasatinib-quercetin) mitigate age-related aortic dilation. In small clinical cohorts, doxycycline and statins reduced MMP activity and inflammatory markers, whereas exercise and caloric restriction improved endothelial function and decreased oxidative stress. Gene-editing strategies (CRISPR-mediated telomere lengthening) and epigenetic drugs (HDAC inhibitors) are emerging but remain experimental.

Conclusion

Aging orchestrates a multifactorial decline in aortic structure and function through cellular senescence, genomic instability, mitochondrial dysfunction, epigenetic alterations, and chronic inflammation. These processes converge on signaling pathways—HIF-1, IL-6, ESR1—that accelerate aneurysm formation and dissection. Targeting these age-specific mechanisms with pharmacological, genetic, and lifestyle interventions offers a promising avenue to delay or even reverse pathology. Future translational research should prioritize large-scale clinical trials that integrate biomarkers of vascular aging with individualized therapeutic strategies, ultimately aiming to reduce the morbidity and mortality associated with aortic aneurysm and dissection in an aging population.

胸腺基质淋巴细胞生成素通过调节巨噬细胞极化促进腹主动脉瘤形成

郑琦[1,2,3] 唐婷婷[1,2,3] 程翔[1,2,3]

1. 华中科技大学同济医学院附属协和医院心血管内科

2. 华中科技大学同济医学院附属协和医院生物靶向治疗研究湖北省重点实验室

3. 华中科技大学同济医学院附属协和医院心血管疾病免疫诊疗工程湖北省工程研究中心

目的：促炎和抗炎反应的失衡在腹主动脉瘤（Abdominal aortic aneurysm, AAA）的进展中起着至关重要的作用。作为关键的炎症调节因子，胸腺基质淋巴细胞生成素（TSLP）在多种疾病中发挥重要作用。然而，其在腹主动脉瘤中的具体作用尚不明确。本研究旨在探讨 TSLP 在腹主动脉瘤中的作用。

方法：野生型和胸腺上皮细胞淋巴细胞生成素受体（TSLPR）敲除小鼠（Tslpr$^{-/-}$）建立猪胰腺弹力蛋白酶（PPE）诱导小鼠腹主动脉瘤模型用于探究 TSLP 在腹主动脉瘤中的作用。对 PPE 诱导的腹主动脉瘤模型小鼠腹腔注射 TSLP 和 anti-TSLP 单克隆抗体以证实 TSLP 促进腹主动脉瘤的发生发展。通过最大主动脉直径、弹性纤维染色和免疫组织化学染色评估组间 AAA 的严重程度。使用蛋白印记（western blot）和实时定量聚合酶链式反应（RT-qPCR）评估 TSLP 在腹主动脉瘤中的表达和含量。应用质谱流式细胞术分析小鼠腹主动脉瘤模型中主动脉的炎症细胞数量和比例的变化。应用小鼠单核巨噬细胞系（Raw264.7）、小鼠骨髓巨噬细胞（BMDM）和人单核细胞系（THP-1）进行体外巨噬细胞极化实验。通过 RNA 测序（bulk RNA-seq）探究 TSLP 对巨噬细胞极化的关键性基因通路。此外，还利用英国生物银行（UKB）数据分析了 TSLP 在腹主动脉瘤患者人群中的血清浓度差异。

结果：TSLP 在小鼠腹主动脉瘤模型主动脉中的表达和含量显著升高。研究发现，TSLPR 缺失降低了腹主动脉瘤的严重程度同时减轻了主动脉炎症和巨噬细胞浸润。腹腔注射 TSLP 加重了腹主动脉瘤，同时 anti-TSLP 抑制了腹主动脉瘤的形成，这表明 TSLP 对腹主动脉瘤的发生发展至关重要。通过质谱流式细胞术我们发现，Tslpr$^{-/-}$ 小鼠主动脉相比野生型小鼠主动脉，其巨噬细胞 / 炎症细胞比例减少，且巨噬细胞中 M1 巨噬细胞比例降低以及 M2 巨噬细胞比例升高，提示 TSLP 在巨噬细胞的极化中发挥了不容忽视的作用。在体外细胞的实验中，我们进一步证实了在炎症环境的刺激下 TSLP 促进巨噬细胞向 M1 方向极化，抑制巨噬细胞向 M2 方向极化。RNA 分析显示，与野生型小鼠相比，Tslpr$^{-/-}$ 小鼠腹主动脉瘤模型主动脉中参与细胞因子和细胞因子受体作用以及髓系细胞激活的基因显著下调。此外，和正常人群相比，腹主动脉瘤患者人群中 TSLP 外周血水平升高。

结论：我们的研究数据表明 TSLP 在促进腹主动脉瘤形成中发挥着关键作用，主要是通过促进巨噬细胞向 M1 巨噬细胞极化的同时抑制向 M2 巨噬细胞极化，这可能为预防和治疗腹主动脉瘤提供一种潜在的治疗方法。

Clonal Hematopoiesis and Incident Aortic Dissection in a Chinese Population

Yanghui Chen, Dao Wen Wang

Tongji Hospital, Tongji Medical College, Huazhong University of Science and Technology

BACKGROUND: The genetic landscape of Aortic Dissection (AD) has significantly evolved in recent years, expanding from the traditional focus on germline mutations to include somatic alterations. One such somatic phenomenon that has garnered considerable attention is Clonal Hematopoiesis of Indeterminate Potential (CHIP). CHIP is characterized by the presence of somatic mutations in hematopoietic cells, leading to the expansion of clones with a potential for malignancy or other adverse health outcomes. This age-related condition is increasingly recognized as a significant risk factor for both hematological malignancies and cardiovascular diseases, including coronary artery disease and heart failure. However, the specific mechanisms through which CHIP contributes to the development of AD, particularly in East Asian populations, have remained largely elusive. Understanding these mechanisms is crucial for developing targeted therapies and improving patient outcomes.

METHODS: To address this gap in knowledge, we conducted a comprehensive study using next-generation sequencing (NGS) data from 1,694 patients with AD who were referred to three major medical centers over an extensive period, from October 2005 to February 2024. Our approach involved a stepwise calling method to meticulously identify CHIP mutations within the cohort. We focused on determining the prevalence of CHIP mutations and their potential impact on both short-term in-hospital complications and long-term all-cause mortality in patients with AD. To provide deeper insights into the underlying biological mechanisms, we also explored the associations between CHIP mutations and various inflammatory markers, which are known to play a critical role in the pathogenesis of cardiovascular diseases.

RESULTS: Our analysis revealed that a substantial proportion of patients with AD harbored CHIP mutations, with 272 (16.1%) patients identified as carriers of at least one CHIP mutation at a variant allele frequency of ≥ 2%. The most commonly mutated genes were DNMT3A, TET2, P53, and ASXL1, which are well-known drivers of clonal hematopoiesis and have been implicated in various hematological and cardiovascular disorders. Demographic analysis showed that patients with CHIP mutations were significantly older than those without CHIP (mean age: 60±8.8 years vs. 52±7.9 years; P<0.001), suggesting an age-related predisposition to CHIP in this context. The clinical implications of CHIP were particularly striking. Patients with CHIP mutations exhibited a significantly higher risk of postoperative complications, which can severely impact recovery and long-

term outcomes. Specifically, the odds ratios for postoperative pneumonia, renal insufficiency, gastrointestinal bleeding, and stroke were 1.59 (95% CI: 1.16-2.14), 1.65 (95% CI: 1.18-2.28), 2.34 (95% CI: 1.36-3.92), and 2.3 (95% CI: 1.36-3.76), respectively. These findings highlight the potential role of CHIP in exacerbating the inflammatory and thrombotic risks associated with AD, leading to poorer surgical outcomes. Moreover, CHIP was associated with an increased risk of death compared to non-CHIP carriers, underscoring its prognostic significance. In addition to these clinical associations, we observed that patients with CHIP mutations had elevated levels of circulating inflammatory markers, including hypersensitive C-reactive protein, procalcitonin, interleukin-6, and N-terminal pro-B-type natriuretic peptide. These elevated markers suggest a heightened inflammatory state, which may contribute to the pathogenesis of AD and its complications.

CONCLUSIONS: This landmark study is the first to comprehensively investigate the prevalence and impact of CHIP mutations in patients with AD, particularly within the East Asian population. Our findings reveal that CHIP mutations are present in a significant proportion of AD patients (16.1%) and are associated with a severe inflammatory state, leading to poorer clinical outcomes. These results highlight the critical role of CHIP in the pathogenesis of AD and suggest that CHIP may serve as a valuable biomarker for identifying high-risk patients and guiding personalized treatment strategies. Future research should focus on elucidating the molecular mechanisms underlying CHIP-associated inflammation and exploring potential therapeutic interventions to mitigate its adverse effects on cardiovascular health.

免疫细胞基因组不稳定性在急性主动脉综合征发生发展中的作用和机制研究

尹纯 晋军

陆军军医大学第二附属医院（重庆新桥医院）

目的：

以主动脉夹层为代表的急性主动脉综合征（AAS）发病急骤、病情凶险和死亡风险极高。目前用于 AAS 早期防治的相关标志物比较有限，开发早期风险预警和预后预测的新型生物标志物，对于改善 AAS 患者预后十分关键。免疫细胞浸润在血管弹性纤维破坏，细胞外基质降解以及血管壁炎症反应等 AAS 病理改变中扮演了重要角色。随着近年来基因组学技术的飞速发展，免疫细胞中发生的克隆性造血被大量研究发现会通过加剧衰老过程中的炎症，进而影响多种心血管疾病的发生以及不良预后。但以上基因组不稳定性变异是否参与急性主动脉综合征的发生发展及其调控机制亟待探索。

研究方法：

我们拟利用基因组学、转录组学和基因敲除等技术，从外周血核基因组和线粒体基因组双重维度揭示 AAS 相关的体细胞突变景观特征并绘制图谱，鉴定与 AAS 发生发展相关的关键突变，开发 AAS 早期预警以及危险分层标志物。随后通过分析老年男性主动脉夹层组织的单细胞测序数据，在单细胞分辨率上揭示关键变异对于不同亚群免疫细胞的表型影响，探索可能的作用机制。并在动物实验和细胞实验中初步探索其新型调控机制，为 AAS 的防治提供新靶点。

结果：

1.AAS 外周血衰老相关基因组不稳定性图谱：对 190 例男性 AAS 患者共检出 53 例 CHIP 相关突变，以 DNMT3A 和 TET2 为主，其突变数量及异质性与年龄呈正相关。Y 染色体嵌合缺失（LOY）普遍存在且与年龄正相关，其他染色体拷贝数畸变罕见。线粒体基因组（mtDNA）方面，mtDNA 拷贝数随年龄下降，80 岁以上男性下降更显著。血液特异 mtDNA 体细胞突变富集于编码区，其数量及异质性随年龄升高，且与 mtDNA 拷贝数负相关，提示二者在衰老中协同作用。

2.AAS 风险及预后相关基因组变异：mtDNA 拷贝数下降、CHIP 突变及 LOY ≥ 10% 均与多项临床异常相关（如血液学指标、AAS 并发症等）。AAS 患者 mtDNA 拷贝数显著低于健康对照（68.5 vs. 87.8，P<0.001），LOY 水平显著升高（2.72% vs. 1.80%，P=0.034）。校正混杂因素后，mtDNA 拷贝数降低及 LOY ≥ 10% 是 AAS 发生的独立危险因素。此外，mtDNA 拷贝数在最低四分位及 LOY ≥ 10% 与 AAS 患者不良预后相关，LOY ≥ 10% 经多因素回归校正后仍为全因死亡（HR=3.360，P=0.007）及复合终点（HR=3.067，P=0.005）的独立预后因子。

3.LOY 促进 AAS 发生发展的机制：人类主动脉夹层组织中巨噬细胞等免疫细胞浸润增加，单细胞测序显示 LOY 多见于髓系细胞，LOY 单核巨噬细胞呈促纤维化及吞噬功能下降特征。小鼠实验表明，Kdm5d 缺失可增强造血干细胞扩增，增加 AAS 发生率及严重程度。细胞实验显示，Kdm5d/Uty 缺失的巨噬细胞炎症因子表达降低，但 Mmp2 升高、Trem2 降低，转录组提示其迁移能力增强、细胞外基质降解相关通路激活，表明 LOY 可能通过调控巨噬细胞功能促进 AAS 发生发展。

结论：

CHIP 驱动基因突变、LOY、mtDNA 拷贝数下降是血液系统在衰老过程中较为常见的基因组不稳定性变化，它们的发生频率均与年龄密切相关。 LOY 以及 mtDNA 拷贝数下降与 AAS 发病风险增加关系密切。校正混杂因素后，LOY ≥ 10% 依旧是 AAS 患者全因死亡和复合终点的独立预后因素。外周血 LOY 可能是 AAS 发生发展中的关键突变，有望成为 AAS 预后预测标志物。LOY 相关的 Kdm5d 基因缺失可能会通过增加巨噬细胞对细胞外基质降解以及减弱吞噬功能进而促进主动脉夹层等 AAS 的发生发展。

Castor 单分支支架移植物在近端锚定区不足的 Stanford B 型主动脉综合征的临床价值研究

康梦阳 马强 张军波 秦皓 孟燕 田红燕

西安交通大学第一附属医院周围血管科

Castor 单分支支架移植物在近端锚定区不足的 Stanford B 型主动脉综合征的临床价值研究

作者：康梦阳，马强，张军波，秦皓，孟燕，田红燕。

单位：西安交通大学第一附属医院周围血管科。

目的：使用 Castor 单分支支架移植物治疗近端锚定区不足的 Stanford B 型急性主动脉综合征（acute aortic syndromes, AASs）患者的中期疗效尚不明确。本研究旨在系统评估 Castor 单分支支架移植物在治疗近端锚定区不足的 B 型 AASs 的中期临床结局。

方法：本回顾性研究纳入了 2020 年 10 月 1 日至 2024 年 10 月 30 日我院连续收治并诊断为近端锚定区不足的 B 型 AASs 患者。所有患者均接受采用 Castor 单分支支架移植物进行的胸主动脉腔内修复术。收集每例患者的临床资料并进行术后随访以评估治疗效果和临床中期预后。

结果：共纳入 130 例患者，其中主动脉夹层（aortic dissection, AD）103 例，穿透性主动脉溃疡（PAU）19 例，壁内血肿（IMH）8 例。患者的手术的技术成功率为 99.2%。1 例 AD 患者因原发性破口较大而出现支架近端移植物小弯侧陷入破口的情况，通过置入第二枚 Castor 单分支支架移植物挽救。中位随访时间为 454 天（范围：359–771 天），所有患者均获得生存。共有 14 例患者（10.8 %）出现术后并发症，包括 1 例急性心肌梗死、7 例内漏（其中 I_b 型内漏 1 例，II 型 内漏 2 例，IV 型内漏 4 例）、3 例分支段狭窄、2 例支架源性新发破口以及 1 例进行性主动脉扩张。其中 2 例患者因术后并发症接受了再次干预，一例因 I_b 型内漏远端续接覆膜支架，另一例因分支段狭窄接受球囊扩张治疗。随访期间，没有患者出现逆撕性主动脉夹层、截瘫和脑卒中。

结论：对于近端锚定区不足的 B 型主动脉综合征患者而言，Castor 单分支支架移植物提供了一种操作简便、安全性高且疗效确切的腔内治疗策略。

关键词：主动脉综合征；胸主动脉腔内修复术；单分支支架移植物；中期预后

颈动脉狭窄患者围术期脑灌注改变相关力学因素分析

郭蕾 [1] 张俊 [1] 李春玲 [2]

1. 成都市新都区人民医院

2. 四川省医学科学院 . 四川省人民医院

目的：颈动脉狭窄是脑卒中的重要危险因素。颈动脉内膜切除术（CEA）是脑卒中二级预防的首选方法，但术后血流动力学障碍可能导致脑高灌注损害，严重影响预后。目前临床有多种血流动力学评估技术，但各具优缺点。计算流体力学（CFD）可定量分析血流动力学，成为研究热点。本研究联合局部脑氧饱和度（rScO2）、颈动脉超声、CT 血管成像等多模态监测，结合 CFD 技术，系统评估 CEA 围术期脑灌注变化及影响因素，以降低并发症风险，改善患者预后。

方法：采用前瞻性队列研究设计，纳入 2023 年 1 月至 2024 年 11 月住院接受 CEA 治疗的患者，收集人口学、病史及颈动脉狭窄特征数据。术前、术后 3 天内行 rScO2 监测、颈动脉超声、CTA 及 CTP 检查。利用 Mimics 和 ANSYS-FLUENT 软件进行 CFD 建模，分析壁面剪切力（WSS）、壁剪切力比值（WSSR）及跨病变压力比（PR）等血流动力学参数。计算脑灌注、rScO2 及力学参数的变化率。采用 SPSS 23.0 和 R 4.3.2 进行统计分析，比较术前术后参数差异（配对 t 检验 /Wilcoxon 检验），Pearson 分析相关性及多元线性回归筛选脑灌注改变相关因素（P<0.05）。

结果：本研究共纳入 50 例接受 CEA 治疗的患者，平均年龄 72 岁，其中男性占 80%。患者基础疾病以高血压（84%）、糖尿病（56%）和高脂血症（64%）为主，74% 有吸烟史。48% 的病例为左侧颈动脉狭窄，66% 为症状性狭窄，平均狭窄程度达 76%。术后血流动力学监测显示，颈动脉超声检测的收缩峰期、舒张末期及平均血流速度均较术前显著降低（P<0.05）。头颅 CT 灌注成像证实术侧及对侧脑血流量均明显增加（P<0.05），同时 $rScO_2$ 监测显示术侧 $rScO_2$ 显著提升（P=0.017），而对侧变化无统计学意义（P=0.083）。CFD 分析进一步揭示，术后 WSS 和 WSSR 显著降低（P<0.001），而 PR 则显著增高（P<0.001）。Pearson 相关性分析表明，脑灌注改善与 PR 增加呈中等正相关，与 $rScO_2$ 升高呈弱正相关，而与 WSS 和 WSSR 降低呈弱负相关。多元线性回归分析证实，PR 增高（β=0.455，P<0.001）、$rScO_2$ 提升（β=0.275，P=0.012）和 WSS 降低（β=-0.273，P=0.014）是脑灌注改善的独立预测因素。围术期并发症方面，仅 1 例出现颈部切口小血肿，2 例发生术侧搏动性头痛，均经保守治疗缓解。术后 30 天及 6 个月随访未发现脑卒中、脑出血或死亡等严重不良事件，所有患者均保持良好的临床预后。

结论：CEA 术后 WSS 降低及 PR 升高与脑灌注改善显著相关，提示血流动力学参数可作为评估手术效果的有效指标。结合 CFD 分析和多模式血流动力学监测可以为 CEA 患者的管理提供有效的优化管理策略。未来研究需要延长随访时间，并结合更系统的灌注评估，以明确脑灌注变化对远期卒中预防的影响。

Adipsin 通过 SERPINE1 依赖性血管新生改善糖尿病下肢缺血

张孝华 姜梦圆 张学斌 孙冬冬

空军军医大学第一附属医院心血管内科

背景： Adipsin（又称补体因子 D，CFD）作为首个被描述的脂肪因子，因其在糖尿病心血管并发症中的调节作用而广为人知。然而，其在糖尿病下肢缺血（HLI）中的作用尚未明确。本研究旨在评估 Adipsin 对 2 型糖尿病小鼠下肢缺血的潜在治疗作用，并阐明其分子机制。

方法： 采用高脂饮食联合链脲佐菌素（HFD/STZ）诱导的糖尿病小鼠模型，以

及脂肪组织特异性过表达 Adipsin（Adipsin-Tg）的转基因小鼠模型。通过股动脉结扎建立下肢缺血模型，并采用激光多普勒血流灌注成像监测血流恢复情况。利用 RNA 测序（RNA-seq）和免疫共沉淀联合质谱分析（Co-IP/MS）技术，探究 Adipsin 促进血管新生的分子机制。

结果：下肢缺血（HLI）后，非糖尿病小鼠的 Adipsin 表达上调，而在糖尿病小鼠中其表达受到抑制，提示其在糖尿病缺血恢复中的潜在作用受损。与非转基因（NTg）糖尿病小鼠相比，Adipsin 过表达（Adipsin-Tg）小鼠表现出显著改善的血流恢复、增加的毛细血管密度以及增强的肌肉再生能力。在高糖和低氧条件下，Adipsin 可促进人脐静脉内皮细胞（HUVEC）的增殖、迁移及成管能力。此外，Adipsin 在体内外均能增强 AKT、ERK 和 eNOS 通路的磷酸化水平。RNA-seq 和 Co-IP/MS 分析揭示，Adipsin 通过与 SERBP1 蛋白相互作用，破坏 SERBP1 与 SERPINE1 mRNA 的结合，导致 SERPINE1 表达降低，进而激活 VEGFR2 信号级联反应，最终促进血管新生。

结论：Adipsin 通过与 SERBP1 相互作用，下调 SERPINE1 表达，促进糖尿病下肢缺血小鼠的血管新生和血流灌注恢复。本研究阐明了 Adipsin 在糖尿病患者外周动脉疾病（PAD）管理中的新治疗潜力，突显了其在增强血管新生和组织修复中的作用。

血小板与血红蛋白比值与急性 A 型主动脉夹层手术预后的关系

刘道权

武汉亚洲心脏病医院

目的 考虑到≥ 60 岁是急性 A 型主动脉夹层（ATAAD）的发病高峰期，本研究旨在分析血小板与血红蛋白比值（PHR）与老年 ATAAD 患者预后的关系。

方法 收集我院 2017 年 1 月至 2022 年 1 月期间就诊的 180 例老年（60 ~ 88 岁）ATAAD 患者进行回顾性分析。PHR 为入院时的血清血小板计数（PLT）/ 血红蛋白（Hb）比值。所有患者均进行随访，主要研究终点为手术后 30 d 内的死亡，次要终点为术后卒中、需要透析的急性肾损伤（AKI）。

结果 所有患者中，30 d 死亡率为 13.33%（24/180）。死亡组 ATAAD 患者的 PHR 显著低于生存组患者 [0.89（0.79，1.24） vs. 1.41（1.16，1.52），Z=-4.537，P < 0.001]。PHR 预测 ATAAD 患者 30 d 内死亡的受试者工作特征曲线下面积为 0.788（95%CI：0.721 ~ 0.845），PHR ≤ 1.31 时，灵敏性及特异性分别为 87.50%、67.31%。多变量 Logistic 回归分析显示，PHR 时 30d 死亡风险的一个独立的预测因子（OR=0.026，P=0.020）。在次要结局方面，术后卒中的发病率为 8.33%，无卒中及卒中 ATAAD 患者的 PHR 分别为 1.31（1.07，1.45）、1.36（1.15，1.40），二者比较不存在统计学意义（Z=-1.737，P=0.082）。此外，术后 18 例患者因为 AKI 需要接受透析，这部分患者的 PHR 为 1.25（0.89，1.37）低于其他术后未进行透析的患者 [1.39（1.07，1.50）]（Z=-2.697，P=0.007）。

结论 术前 PHR 是预测老年 ATAAD 患者术后 30 d 内死亡的一个简单、快速且潜在有用的预后因素。

Global, regional, and national burden of pulmonary arterial hypertension from 1990 to 2021, with projections to 2045: a systematic analysis for the Global Burden of Disease Study 2021

CHAODI LUO, QIANG MA, HONGYAN TIAN

The First Affiliated Hospital of Xian Jiaotong University

Introduction

Pulmonary arterial hypertension (PAH) is a rare but progressive pulmonary vascular disease characterized by elevated pulmonary arterial pressure and right ventricular dysfunction, ultimately leading to heart failure and premature death. PAH remains a rare but highly disabling vascular disease associated with substantial morbidity, mortality, and health care costs. However, its global burden patterns and future trends have not been comprehensively assessed across countries, age groups, and socio-demographic development levels. We conducted stratified analyses by age, sex, and socio-demographic development level, and further explored patterns of inequality, underlying drivers of burden shifts, and long-term projections of PAH burden.

Methods

We used data from the Global Burden of Disease Study 2021 to estimate the incidence, mortality, and disability-adjusted life years (DALYs) of PAH across 204 countries and territories from 1990 to 2021. Age-standardised rates were calculated, and trends were evaluated using estimated annual percentage changes (EAPCs). Based on SDI values, the GBD 2021 study categorizes the 204 countries and territories into five groups: low SDI, low-middle SDI, middle SDI, high-middle SDI, and high SDI regions. Inequality was assessed using concentration indices, and drivers of burden changes were identified through decomposition analysis. Future trends were projected up to 2045 using Bayesian age-period-cohort models.

Results

In 2021, the global incidence of PAH was 43.25 per 1,000 population (95% UI: 34.70–52.44), mortality was 22.02 per 1,000 (95% UI: 18.24–25.35), and DALY rate were 8.24 per 100,000 (95% UI: 7.14–9.39). From 1990 to 2021, the age-standardised incidence rate (ASIR) slightly increased (EAPC: 0.68; 95% CI: 0.66–0.70), while the age-standardised mortality rate (ASMR) declined steadily. The burden was higher among older adults and females and became increasingly concentrated in high-SDI countries. In 2021, age-standardised incidence rates were highest in Central and Southern Africa and parts of Northern Europe, while the lowest were observed in high-SDI regions such as North America, Western Europe, and East Asia. We further examined the association between PAH burden and the SDI at both regional and national levels. Across the 21 GBD regions, ASIR showed a strong negative correlation with SDI (R = −0.75, P < 0.001), while ASMR (R = −0.09, P = 0.003) and ASDR (R = −0.17, P < 0.001) exhibited weaker associations. Inequality in age-standardised PAH burden was further assessed using concentration indices (CI) and concentration curves. For mortality, CI values increased from 0.05 in 1990 to 0.23 in 2021, indicating an increased concentration of mortality in higher-SDI countries. For incidence, the CI shifted from −0.03 in 1990 to 0.02 in 2021, reflecting an increasing concentration of incidence in higher-SDI countries. In all SDI regions and across both sexes, the total number of deaths increased. Population growth accounted for the largest proportion of this increase, followed by population aging. The contribution of epidemiological change was negative across all SDI levels and sex groups. The relative contribution of aging was highest in the high SDI group. Projections suggest that global ASIR will rise slightly and stabilize, while ASMR will continue to decline by 2045.

Conclusions

PAH continues to impose a substantial and evolving burden worldwide, with growing disparities across development levels. Targeted strategies for early detection, secondary prevention, and resource allocation are urgently needed, especially in high burden and rapidly aging populations.

SETD2 介导脂肪功能障碍在抑制缺血后动脉生成的作用及机制

龚冬火 叶茂青 曲新凯

复旦大学附属华东医院

目的：明确 SETD2 介导脂肪功能障碍在抑制缺血后动脉生成的作用及机制。

方法：1、对 GEO 数据库正常成人皮下脂肪（SAT）单细胞测序行生信分析，建立脂肪 SETD2 与动脉生成相关性。

2、构建 SETD2 脂肪特异性敲除小鼠（CKO）和对照小鼠（CON），结扎股动脉构建缺血性动脉生成模型（HLI）。激光多普勒检测血流信号和有色染料血管灌注对血管进行显影。石蜡切片行 HE 和荧光染色评价动脉生成、纤维化、细胞坏死。

3、提取 CON 和 CKO 小鼠 SAT 行 RNA-Seq，行多组学联合分析 SETD2 调控分子机制。

4、提取 CON 和 CKO 小鼠 SAT 的 SVF，诱导成脂后与 HUVEC 共培养，检测 HUVEC 出芽、成管、迁移（划痕）和增殖能力（CCK8）。

5、制备 FGF18 重组蛋白（Re-FGF18）。在 CKO 小鼠腹腔注射 Re-FGF18，在 SVF 和 HUVEC 共培养同时加入 Re-FGF18，评估动脉生成、出芽和成管能力。

6、双荧光素酶报告基因检测 SETD2 对 Fgf18 启动子转录活性影响。

结果：1、单细胞测序发现 SETD2 在血管新生良好的脂肪细胞亚群中有较高转录水平。

2、与 CON 相比，CKO 小鼠在 HLI 后第 14、21Day 血流灌注受损，新生动脉管腔变小和数量变少，新生骨骼肌细胞数量减少，纤维化加重，细胞凋亡增多。

3、与 CON 相比，在 CKO 小鼠的 SVF 共培养 HUVEC 出芽和成管能力降低，但迁移和增殖能力不变。

4、RNA-Seq 差异基因 KEGG 和 GO 富集在血管新生和炎症等相关信号通路。FGF18 是其中基因之一。CKO 小鼠的 SAT 的 FGF18 表达降低。

5、Re-FGF18 改善 CKO 小鼠缺血后动脉生成不良和 SVF 共培养 HUVEC 的出芽和成管能力。

6、双荧光素酶发现过表达 SETD2 促进 Fgf18 启动子转录活性。

结论：SETD2 介导脂肪功能障碍通过调控 FGF18 靶向血管内皮细胞抑制缺血后动脉生成。

Different types of systolic blood pressure and all-cause mortality in critically ill patients with acute aortic dissection: a retrospective analysis of the MIMIC-IV database

CHAODI LUO, QIANG MA, HONGYAN TIAN

The First Affiliated Hospital of Xian Jiaotong University

Background

Acute aortic dissection (AAD), a lethal vascular emergency initiated by loss of structural integrity in the aortic media and pathologically driven by hemodynamic stress, demonstrates marked temporal dependency in disease progression. Blood pressure management plays a crucial role in the treatment and prognosis of AAD. While ambulatory blood pressure monitoring (ABPM) parameters have been established as having substantial prognostic significance for cardiovascular diseases, relatively limited research has focused on AAD. This study aimed to assess the differential predictive effects of various types of systolic blood pressure (SBP)

on 30-day all-cause mortality among patients with AAD.

Methods

Data were derived from the Intensive Care Medicine Information Mart for Intensive Care IV (MIMIC-IV) database. All patients were stratified into three groups based on admission systolic blood pressure (admSBP), the highest systolic blood pressure within 24 hours after admission (max-24hSBP), and the mean systolic blood pressure within 24 hours after admission (mean24hSBP), respectively. The outcome measure was 30-day all-cause mortality. The mean24hSBP was divided into tertiles, and the Kaplan-Meier curves were used to compare the outcomes among the groups. The Cox proportional hazards regression model and restricted cubic spline (RCS) were used to evaluate the relationship between mean-24hSBP and the outcome. The combination of mean24hSBP and blood pressure variability (BPV) was used to emphasize the impact of BPV on the prognosis of AAD.

Results

Among a total of 551 participants, stratification was conducted based on the tertiles of three blood pressure indicators: admSBP, max24hSBP, and mean24hSBP. Kaplan-Meier analysis demonstrated differential prognostic associations across SBP parameter stratifications. For admSBP and max24hSBP, no statistically significant survival differences emerged among tertile groups. In contrast, stratification by mean24hSBP revealed marked divergence in 30-day survival trajectories. Additionally, Cox proportional hazards regression analysis revealed that patients in the lowest tertile of mean24hSBP had a significantly higher risk of 30-day all-cause mortality. Among the three metrics assessed - admSBP, max24hSBP, and mean24hSBP - only the latter demonstrated consistent 30-day all-cause mortality associations across multivariate models. In Model 2, after adjusting for age, sex, and smoking, 30-day all-cause mortality was 0.38-fold (HR 0.38, 95% CI 0.21-0.69) in Q2 and 0.43-fold (HR 0.43, 95%CI 0.24-0.77) in Q3 relative to Q1. Further adjustment for hypertension, diabetes, renal disease, medications (β-blockers, calcium channel blockers, diuretics, insulin), and biochemical markers (creatinine, platelets, chloride) with surgical status in Model 3, there were still lower 30-day all-cause mortality in Q2 (HR 0.50, 95% CI 0.27-0.93) and Q3 (HR 0.33, 95% CI 0.18-0.62). The relationship specifically observed for mean24hSBP aligns with Kaplan-Meier results, where only the lowest tertile (Q1) exhibited significantly worse survival. Moreover, RCS analysis indicated an L-shaped relationship between mean24hSBP and all-cause mortality, with a inflection points for 30-day all-cause mortality at 118.7 mmHg. Compared with patients with mean24hSBP below the inflection points, those with higher mean24hSBP levels had a 7.9% lower risk of 30-day all-cause mortality (hazard ratio [HR] 0.921, 95% confidence interval [CI] 0.898 - 0.945). Furthermore, the combined analysis of mean24hSBP and BPV showed that the combination of low mean24hSBP and high BPV had the greatest impact on the risk of 30-day all-cause mortality.

Conclusion

Our research demonstrated that mean24hSBP served as a relatively robust BP indicator for predicting the prognosis of AAD. Specifically, a lower mean24hSBP and higher BPV were associated with an increased risk of mortality due to AAD.

[18F]-AIF-NOTA-FAPI PET/CT 显像评估不同时期急性主动脉综合征患者的影像学特征

鲁瑶 张晓丽

首都医科大学附属北京安贞医院

目的：急性主动脉综合征（AAS）是心血管系统最危急的重症之一，起病急、病死率高。成纤维细胞是血管外膜的主要细胞成分，作为血管重构中的“前哨细胞”，其中成纤维细胞激活蛋白（FAP）是关键分子。本研究旨在通过 [^{18}F]-AIF-NOTA-FAPI PET/CT 显像，探讨 AAS 患者不同病程中 FAP 的影像学特征。

方法：研究为单中心前瞻性队列研究，纳入 2024 年 1 月至 2025 年 3 月确诊的 62 例 AAS 患者（主动脉夹层 AD 和主动脉壁内血肿 IMH）及 21 例健康对照。所有受试者接受 [^{18}F]-AIF-NOTA-FAPI PET/CT（^{18}F-FAPI）显像，分析主动脉不同节段（升主动脉、主动脉弓、胸主动脉、腹主动脉上段、腹主动脉下段）的最大标准摄取值（SUVmax）和靶本比值（TBRmax）。根据国际主动脉夹层注册（IRAD）分期将患者分为超急性期、急性期、亚急性期和慢性期，评估不同疾病亚型不同时期 FAPI 摄取的影像学特征。

结果：（1）基线信息：本研究纳入 62 例 AAS 患者（其中 AD 41 例，IMH 21 例）和 21 例健康对照。AAS 组患者平均年龄较高（58.6±10.2 岁），男性占比更高（74.2%），且合并高血压（72.6%）、吸烟（59.7%）及高 BMI（27.2±4.7）的比例显著高于对照组（P<0.05）。根据 IRAD 分期，超急性期、急性期、亚急性期和慢性期患者分别为 7 例、27 例、11 例和 17 例。（2）FAPI 摄取分析显示：①整体差异：AAS 患者主动脉 SUVmax（6.02±2.78）和 TBRmax（6.06±2.90）均显著高于对照组（P<0.0001），且 IMH 组摄取高于 AD 组（SUVmax 7.78±3.34 vs. 5.16±1.99，P<0.05）；②动态变化：AD 组摄取（SUVmax 和 TBRmax）在亚急性期达峰后下降，而 IMH 组持续升高；且慢性期 IMH 组摄取显著高于 AD 组（P<0.05）；③节段差异：病变节段摄取显著高于非病变节段（P<0.0001），且与主动脉直径正相关（SAA 节段 r=0.52，P<0.001）。

结论：[^{18}F]-AIF-NOTA-FAPI PET/CT 显像可动态评估 AAS 患者血管外膜的成纤维细胞活化情况，且 IMH 患者的 FAPI 摄取在各个时期均高于 AD 患者，为临床治疗患者手术时机的选择提供了一定的指导依据。

Engineered Hybrid Nanovesicles Combining Macrophage Membranes and Artificial Lipids for Abdominal Aortic Aneurysm Therapy

Jiaxin Hu

恩施土家族苗族自治州中心医院

Abdominal aortic aneurysm (AAA) is a vascular condition with high mortality for which no pharmacological treatments have been approved. Targeting endothelial dysfunction as a primary disease initiator, the vascular endothelial cell (VEC)-protective compound Senkyunolide I (SEI) demonstrates therapeutic promise through robust antiapoptotic activity. Nevertheless, SEI's clinical translation faces limitations due to systemic toxicity, necessitating development of safer therapeutic alternatives. This study presents an engineered biomimetic nanoplatform (Lipo-MM nanoparticles) combining macrophage-derived membranes with synthetic lipid bilayers for targeted SEI delivery.The macrophage membrane component facilitates precise targeting of activated VECs, while optimized artificial membrane fluidity enhances nanoparticle stability.This dual-membrane configuration enables sustained SEI release with enhanced biodistribution, achieving superior cytoprotective effects.

Notably, we established a novel fusion membrane delivery system (Lipo-MM/SEI) and validated its therapeutic efficacy in angiotensin II-challenged AAA murine models. The nanocarrier significantly attenuated AAA progression and prevented fatal rupture events. Furthermore, Lipo-MM/SEI administration substantially reduced hepatorenal toxicity associated with free SEI administration during chronic treatment. These results demonstrate that hybrid biomimetic systems integrating natural cellular components with engineered materials offer a strategic approach for vascular endothelial repair therapy while minimizing off-target effects. This membrane fusion technology establishes a prototype for developing next-generation targeted vascular therapeutics.

Abdominal aortic aneurysm (AAA) is a common and potentially life-threatening disease characterized by rapid progression and high acute-phase morbidity ADDIN EN.CITE ADDIN EN.CITE.DATA 1,2, with no effective pharmacological treatments available to stop its advancement. Pathologically, aortic endothelial cell (EC)activation and apoptosis synergistically drive AAA pathogenesis alongside inflammatory cascades ADDIN EN.CITE ADDIN EN.CITE.DATA 3. Uncontrolled acute/chronic inflammation exacerbates irreversible aortic damage, while existing surgical options remain insufficient to prevent vascular degeneration due to the absence of multifunctional therapies maintaining vascular homeostasis and counteracting inflammatory cytokines ADDIN EN.CITE ADDIN EN.CITE.DATA 4. Macrophages critically participate in cardiovascular pathologies including atherosclerosis, myocardial infarction, hypertension, and AAA ADDIN EN.CITE ADDIN EN.CITE.DATA 5-7. Their role in AAA involves direct substrate interactions and bioactive factor secretion ADDIN EN.CITE ADDIN EN.CITE.DATA 8, with vascular endothelial cells (VECs) exhibiting upregulated ICAM-1/VCAM-1 expression upon activation during early AAA stages ADDIN EN.CITE ADDIN EN.CITE.DATA 9. These adhesion molecules mediate macrophage recruitment to aortic lesions via integrin α4β1 binding ADDIN EN.CITE ADDIN EN.CITE.DATA 10, accelerating vascular dissection progression ADDIN EN.CITEBaman2022300

Dietary vitamin C and vitamin E with the risk of aortic aneurysm and dissection: A prospective population-based cohort study

Chuan-Rui Zeng, Yang-Xin Chen

Sun Yat-sen Memorial Hospital

Background: Aortic aneurysm and dissection (AAD) represent catastrophic cardiovascular events with high morbidity and mortality, often resulting in sudden death if left untreated. Oxidative stress and inflammation are key mechanisms in the development and progression of AAD, and dietary antioxidants, particularly vitamin C (VC) and vitamin E (VE), are hypothesized to play a protective role. However, the associations between dietary intake of VC and VE and the risk of AAD remain uncertain due to limited evidence from large-scale prospective cohort studies. The aim of this study was to comprehensively evaluate the prospective associations between dietary VC and VE intake and the incident risk of AAD in a well-characterized, population-based sample.

Methods: This prospective cohort study included 139,477 participants from the UK Biobank, a large population-based cohort study in the United Kingdom. All participants were free of AAD at baseline and had completed dietary assessments. Dietary intakes of VC and VE were assessed through a validated 24-hour dietary recall questionnaire, which collected detailed information on participants' typical consumption of foods and nutrients. The primary outcome was the incidence of AAD, identified via linkage to hospital inpatient records and national death registers using standard diagnostic codes. Cox proportional hazards regression models were employed to estimate hazard ratios (HRs) and 95% confidence intervals (CIs) for the association between dietary VC, VE intake, and the risk of developing AAD, with adjustments for age, sex, body mass index, smoking status, alcohol use, physical activity, socioeconomic status,

pre-existing comorbidities (such as hypertension and hyperlipidemia), and total energy intake. Additional subgroup analyses were performed to examine whether the associations differed according to age, sex, smoking history, hypertension, and hyperlipidemia status.

Results: Over a median follow-up period of 12.5 years, 962 incident cases of AAD were documented. Higher dietary intakes of both VC and VE were associated with a significantly lower risk of incident AAD. Specifically, individuals in the highest quartile of dietary VC intake had a 23% lower risk of developing AAD compared to those in the lowest quartile (adjusted HR, 0.77; 95% CI, 0.63–0.93; P-trend = 0.008). Similarly, participants in the highest quartile of VE intake had a 30% reduced risk of AAD (adjusted HR, 0.70; 95% CI, 0.57–0.87; P-trend = 0.002). These inverse associations remained robust after adjustment for a wide range of potential confounders. In subgroup analyses, the associations were more pronounced in participants who were over 60 years old, participants with smoking history, hypertension or hyperlipidemia, who were under the high risk of AAD.

Conclusions: In this large, prospective cohort of UK adults, higher dietary intake of vitamin C and vitamin E was independently associated with a reduced risk of aortic aneurysm and dissection, particularly among older individuals and those with traditional cardiovascular risk factors. These findings highlight the importance of dietary strategies that promote adequate intake of antioxidant nutrients as a potential means to prevent the occurrence of AAD in the general population, and especially among high-risk groups. Public health recommendations should consider emphasizing the consumption of VC and VE rich foods for the primary prevention of AAD. Further research, including randomized controlled trials and mechanistic studies, is warranted to confirm these associations and elucidate the underlying biological mechanisms.

The role and mechanism of plasma exosomal miR-206 in patients with acute type A aortic dissection with preoperative acute lung injury

Chi-Yuan Zhang, Cheng-Long Zhang, Rui-Zheng Shi

中南大学湘雅医院

Background: Acute type A aortic dissection (AAAD) is a life-threatening cardiovascular disease with urgent onset, rapid progression and high mortality, which often requires emergency surgical treatment. Preoperative acute lung injury (ALI) is one of its common perioperative complications that seriously affect the clinical outcome. Inflammation is involved in the occurrence and development of AAAD with ALI. At present, it is believed that the progression of local vascular inflammation caused by intima tear and false lumen formation in aortic dissection plays a vital role, which can develop into systemic inflammation and result in multiple organs damage including lung. Besides, in this pathophysiological process, the role of abnormal permeability of pulmonary vascular endothelium is also critical, but the underlying mechanism has not been well elucidated.

Objective: We aimed to investigate plasma exosomal miRNAs profiles in AAAD patients with preoperative ALI, screen out an exosomal miRNA as potential clinical biomarker and explore its role in pulmonary vascular endothelial permeability in such patients.

Methods: The plasma exosomes were extracted by differential ultra-centrifugation and identified by transmission electron microscopy, nanoparticle tracking analysis and Western Blot (WB). A high throughput sequencing was performed to analyze the plasma exosomal miRNAs profiles in AAAD patients with preoperative ALI. Further bioinformation analysis and real-time quantitative polymerase chain reaction (RT-qPCR) were conducted to screen and verify the candidate differentially expressed miRNAs (DE-miRNAs). Logistic regression model and receiver operator characteristic (ROC) curve was used to evaluate the association between target miRNA and AAAD complicated with preoperative ALI. In vitro, the vascular endothelial permeability tests were used to detect the permeability of human pulmonary microvascular endothelial cells (hPMVECs) incubated with plasma exosomes of AAAD patients with or without preoperative ALI or with the use of miRNA mimic/inhibitor, and RT-qPCR, WB and immunofluorescence (IF) were further used to detect the expression of inflammatory factors and intercellular connexin proteins (e.g. ZO-1, VE-cadherin, occludin, CX43, etc.) in different treatment groups. The relationship between the specific miRNA and its target gene was predicted by online analysis and verified by double luciferase reporter gene assay. In vivo, a mouse model of acute aortic dissection complicated with lung injury was established. The expression and distribution of CX43 in lung tissues were detected by RT-qPCR, WB and immunohistochemistry (IHC), respectively. Exosomes from lung tissues were extracted and the exosomal miR-206 level were also detected by RT-qPCR.

Results: The sequencing results showed 283 plasma exosomal DE-miRNAs in AAAD patients with or without preoperative ALI, and the target genes of these DE-miRNAs mainly involved acute inflammatory response, cell junction, cytoskeleton, etc. by GO and KEGG analysis. The plasma exosomal miR-206 was significantly decreased both in a discovery and validation cohort and was independently related to AAAD with preoperative ALI (OR, 95%CI, P: 0.12 [0.02-0.70], 0.019). The area under the curve (AUC) was 0.778 (95% CI, P: 0.626-0.929, 0.003) with a sensitivity of 70.0% and specificity of 80.0%. In vitro data, the endothelial permeability and the expression of inflammatory factors were increased and the expression of intercellular connexin proteins was decreased (e.g. ZO-1, VE-cadherin, occludin, etc.) in hPMVECs incubated with plasma exosomes in AAAD patients with preoperative ALI or miR-206 inhibitor, while the expression of CX43 was upregulated. The miRNA-mRNA association between miR-206 and CX43 was confirmed by double luciferase reporter gene assay. Consistent with In vivo data, the expression of CX43 in lung tissue of mouse model of acute aortic dissection complicated with lung injury was increased and exosomal miR-206 from them was decreased.

Conclusion: Plasma exosomal miR-206, as a potential clinical biomarker in AAAD patients with preoperative ALI, exerts a protective effect in such patients partly through downregulating CX43 expression and improving the pulmonary vascular endothelial permeability.

Risk factor and outcome analysis of bird-beak configuration after thoracic aortic endovascular repair for Stanford B-type aortic dissection

Hong-Gang Sui, Shu-Huai Hou, Xiao-Zeng Wang, Zhi-Qiang Zhang, Ya-Song Wang

General Hospital of Northern Theater Command

Objective: Explore the risk factors of bird-beak configuration occurrence and its outcomes after thoracic aortic endovascular repair (TEVAR) for Stanford type B aortic dissection TBAD (TBAD).

Methods: A total of 701 TBAD patients treated with TEVAR are retrospectively enrolled. Inclusion criteria: (1) Age ≥ 18 years old; (2) Acute TBAD; (3) Complete clinical and imaging data. Exclusion criteria: (1) Acute penetrating aortic ulcer with intramural hematoma; (2) Thoracic descending aortic aneurysm; (3) Pseudoaneurysm; (4) Simple abdominal aortic aneurysm; (5) Abdominal aortic dissection; (6) Traumatic aortic injury; (7) Aortic proximal landing in Zone 4; (8) Incomplete clinical and imaging data.The patients are divided into two groups according to the occurrence of bird-beak configuration in the proximal end of the stent graft, i.e., bird-beak group (n=291) and no-bird-beak group (n=410). Multivariate logistic regression is performed to analyze the risk factors and prognosis of the bird-beak configuration. The sub-analysis based on immediate intraoperative endoleak in the bird-beak group is performed, i.e., intraoperative endoleak group (n=84) and no immediate intraoperative endoleak group (n=207).

Results: In comparison to the no-bird-beak group, there are statistically significant variations in the percentage of males (85.57% vs. 77.32%, P=0.008) and calcium channel blockers (96.91% vs. 90.24%, P=0.001) in the bird-beak group. There is a statistically significant difference in the proportion of stroke history between the bird-beak group and the no bird-beak group (6.53% vs. 10.98%, P=0.044). The proportions of age, body mass index, smoking, drinking, hypertension, coronary heart disease, diabetes, β-receptor blockers, angiotensin-converting enzyme inhibitors/angiotensin II receptor antagonists, and statin, are not statistically significant (P>0.05). There are no significant difference in systolic blood pressure, diastolic blood pressure, heart rate, creatine kinase isoenzyme, glutamic pyruvic transaminase, hemoglobin, white blood cell count, platelet count, estimated glomerular filtration rate, C-reactive protein, and D-dime (P>0.05) . The length of the stent in the bird-beak group [(178.60 ± 24.38) mm vs. (161.44 ± 20.85) mm, P<0.001], the proportion of aortic proximal landing in Zone 2 (76.96% vs. 46.58%, P<0.001), and the proportion of intraoperative immediate endoleak (28.9% vs. 19.3%, P=0.003) are all higher than those in the no-bird-beak group. The proportion of proximal bare stents (7.97% vs. 79.76%, Pvs. 31.18 ± 3.28mm, PP>0.05) in the distance between the first tear and the LSA P<15mm, reference vessel diameter at aortic arch, proximal stent diameter, and aortic arch classification) are included in the multivariate logistic regression model. Despite a PP=0.014) and the stent length (OR=1.013, 95% CI: 1.002-1.025; P=0.021) are independent risk factors for the formation of bird-beak configuration. In contrast, the proximal bare stents (OR=0.019, 95% CI: 0.010-0.039; PP>0.05). A long-term follow-up has been conducted in 689 patients who survived 30 days after TEVAR, with a median follow-up time of 1412 (634, 2637) days. The follow-up rate is 98.97% (288/291) in the bird-beak group and 97.80% (401/410) in the no-bird-beak group. There are no significant difference in the incidence of aortic death, recurrent dissection/retrograde tearing, new endoleak, distal ulcer, recurrent TEVAR, and aortic-related adverse events between the two groups (P>0.05). There are also no statistically difference between the two groups in the incidence of all-cause death, new stroke, new acute renal failure, new acute liver dysfunction, and overall clinical adverse events (P>0.05). A total of 291 discharged patients with bird-beak configuration have been followed up for a median 1248 (484, 2736) days. The incidence of recurrent dissection/retrograde tearing (13.09% vs. 5.31%, P=0.023), new endoleak (13.09% vs. 4.35%, P=0.008), aortic-related adverse events (25.00% vs. 10.63%, P=0.002), and overall clinical adverse events (30.95% vs. 17.39%, P=0.010) in the immediate intraoperative endoleak group are markedly higher than those in the no immediate intraoperative endoleak group. There are no significant difference in the incidence of all-cause death, new stroke, new acute renal failure, new acute liver dysfunction, distal dissection, and recurrent

TEVAR between the two groups (P>0.05). Kaplan-Meier analysis shows that the incidence of aortic-related adverse events in the immediate intraoperative endoleak group is significantly higher than that in the no immediate intraoperative endoleak group (Logrank P=0.005). The overall incidence of clinical adverse events in the immediate intraoperative endoleak group is also higher than that in the no immediate intraoperative endoleak group (Logrank P=0.031).

Conclusions: The aortic proximal landing in Zone 2 and the length of stent are independent risk factors, and proximal bare stents are a protective factor for the bird-beak configuration. Bird-beak configuration had no significant adverse effect on the clinical prognosis of TBAD patients, but bird-beak configuration combined with intraoperative immediate endoleak is associated with worse outcomes.

3 例妊娠合并主动脉夹层患者的围手术期护理

董瑞莹 李娟 张静漪 杨小红 王娟

西安交通大学第一附属医院

目的：总结 3 例妊娠合并 A 型主动脉夹层患者的围手术期护理经验。

方法：对西安市某三甲医院 2018 年 1 月 1 日至 2024 年 12 月 31 日收治的 3 例妊娠合并 A 型主动脉夹层的患者进行病例回顾，总结 3 例患者一般资料、治疗过程及转归，并根据不同妊娠周期合并主动脉夹层患者总结护理要点。

结果: 本组 3 例患者，年龄 21 ~ 28 岁，均无妊娠期合并症。2 例妊娠中期（19^{+5} 周、19^{+6} 周），行主动脉手术，1 例妊娠晚期（35^{+6} 周），合并二尖瓣脱垂，同期行剖宫产术和二尖瓣机械瓣膜置换术。术中体外循环转机时间 100 ~ 166min，心脏阻断时间 64 ~ 112min。术后第 1 天均撤离呼吸机。患者 1 和患者 2 术后胎心 135 ~ 142 次 /min，术后给予抗感染、抗凝、镇痛、营养、保胎等治疗。患者 1 ICU 住院 3 天，总住院时间 10 天，出院后继续妊娠，胎儿发育良好，顺利生产。患者 2 ICU 住院 5 天，总住院时间 20 天，术后 1 个月后于产科终止妊娠。患者 3 术中顺利娩出一健康男婴，术后给予抗感染、抗凝、镇痛、营养、回乳等治疗，ICU 住院 6 天，总住院时间 17 天，顺利出院，随访 5 个月，定期复查，患者恢复良好。

结论：A 型主动脉夹层本身病死率高，合并妊娠时孕妇和胎儿死亡风险高，一旦确诊，应按急性 AD 的诊疗原则处理，以挽救母亲生命为主，在此前提下尽可能保证胎儿成活。术前控制血压心率，避免撕裂扩大；多学科协作快速评估决策，减少术前准备时间。妊娠中期合并主动脉夹层患者术后护理要点：精细化血流动力学管理，保障子宫灌注；早期维持妊娠，观察流产征象。妊娠晚期合并主动脉夹层患者术后护理要点：注重产褥感染的观察与预防；尽早回乳预防急性乳腺炎；多学科协作抗凝管理，平衡出血与血栓风险。关注心理问题，构建多维度心理支持系统。

Stanford Type B Aortic Dissection with Tear Location at Lesser Curvature Side: Prognostic Factors and Long-term Outcomes

honggang sui, Zhi-Qiang Zhang, Xiao-Zeng Wang, Ya-Song Wang, Ting-Hao Zhao

General Hospital of Northern Theater Command

Purpose: This study aimed to explore the relationship between the location of the tear in Stanford type B aortic dissection (TBAD) and the aortic morphology, as well as the associated adverse events.

Methods: A total of 1251 patients with aortic diseases were retrospectively included, and 996 patients with TBAD were screened. Inclusion criteria: (1) age ≥ 18 years old, (2) TBAD, (3) complete clinical and imaging data (including follow-up).Exclusion criteria: (1) Stanford type A aortic dissection, (2) aortic rupture, aortitis, pseudoaneurysm, aortic atherosclerosis, hereditary disorders such as Marfan syndrome, and congenital disorders including aortic stenosis. They were divided into the lesser curvature side tear group (n = 105) and the greater curvature side tear group (n = 891) according to the tear location. Baseline data and imaging data of the two groups were compared, and multivariate regression analysis, receiver operating characteristic (ROC) curve analysis, COX regression analysis, and Kaplan-Meier analysis were performed.

Results:

There were no statistical differences between the two groups in terms of age, male, body mass index, smoking, drinking, past medical history, heart rate, systolic blood pressure, systolic blood pressure, left ventricular ejection fraction, and medications (P>0.05). Among laboratory tests, the aspartate transaminase (ALT) (15.94 (12.04, 24.44) U/L vs. 19.39 (13.00,31.00) U/L, P=0.001) and creatinine (72.74 (59.72, 89.92) μmol/L vs.80.19 (66.49, 98.00) μmol/L, P<0.001) in the tear location at lesser curvature side group were lower than those in the tear location at larger curvature side group, and there were statistical differences. There were no statistical differences in other laboratory teats between the two groups (P>0.05) .All patients underwent aortic CTA examination and simultaneous three-dimensional reconstruction. There were no statistical differences in the number of tears, tear size, morphology, aortic arch classification, aortic curvature index, aortic curvature angle, ascending aortic lumen diameter, and descending aortic lumen diameter between the two groups (P>0.05). The circumference of the lesser curvature side (140.62±43.22mm vs. 122.45±31.78mm, P<0.001) and diameter (93.79±28.69mm vs. 82.98±21.91mm, P=0.022) of the lesser curvature side of the tear location at lesser curvature side group were larger than those in the tear location at larger curvature side group, and the difference was statistically significant. We included two factors in imaging, P<0.05, into the logistics analysis to determine their association with aortic dissection on the lesser curvature side: ascending aortic lumen diameter, descending aortic lumen diameter. The results revealed that circumference of the lesser curvature side [1.014(1.002, 1.027), P=0.023] was independently identified as risk factors for tear location at the lesser curvature side. The receiver operating characteristic curve analysis indicated that the diameter and circumference of the lesser curvature side were able to distinguish between patients with aortic dissection rupture on the side of the lesser curvature side. The optimal cutoff values for the circumference and diameter of the lesser curvature side were determined to be 157.10mm and 78.03 mm, respectively, with corresponding areas under the curve of 0.619 and 0.610.The frequency of aortic dissections was analyzed on both the lesser and greater curvatures side of the aorta. Our findings revealed no significant difference in the incidence of recent death, stroke, acute myocardial infarction, acute liver injury, acute renal failure, paraplegia, intestinal necrosis, limb ischemia, reoperation, endoleak, dSINE, aorta-related adverse events, overall clinical adverse events (P>0.05). Similarly, there was no significant variance in the incidence of long-term outcomes such as death, stroke, acute myocardial infarction, acute liver injury, acute renal failure, paraplegia, intestinal necrosis, reoperation, endoleak, dSINE, aorta-related adverse events. Interestingly, the long term overall clinical adverse events were lower in aortic dissections on the lesser curvature side compared to the greater curvature side, with a statistically significant difference (15.4% vs. 26.3%, P=0.015). Furthermore, long term limb ischemia (1.0% vs. 5.5%, P=0.010) also occurred less frequently in aortic dissections on the lesser curvature side compared to the larger curvature greater curvature side, with a statistically significant difference. In addition, COX regression analysis showed that the circumference of the lesser curvature side was an independent risk factor for long-term overall clinical adverse events [OR=1.012 95%CI (1.001-1.021), P=0.009]. The diameter of the lesser curvature side is an independent protective factor for long-term overall clinical adverse events [OR=0.986 95%CI (0.974-0.999), P=0.034] .Kaplan-Meier analysis shows that the incidence of overall clinical adverse events in the tear location at larger curvature side group is significantly higher than that in the tear location at lesser curvature side group (Log_{rank} P=0.025).

Conclusion: The circumference of lesser curvature side was independently determined as a risk factor when the TBAD with tear location at lesser curvature side. There was no significant difference in the incidence of most short-and long-term adverse events between aortic dissections on lesser curvature side and larger curvature side.However, the low incidence of long-term overall clinical adverse events and long-term limb ischemia in aortic dissections on lesser curvature side. The circumference and diameter of lesser curvature side can be used as indicators to distinguish patients with tear location at aortic dissection on lesser curvature side and the best cut-off values are 157.10 mm and 78.03 mm respectively. Notably, the circumference of the lesser curvature side was an independent risk factor for long-term overall clinical adverse events. The diameter of the lesser curvature side is an independent protective factor for long-term overall clinical adverse events. Kaplan-Meier analysis showed that the overall clinical adverse event rate was significantly higher in the group with the tear location on the large curve than in the group with the tear location at lesser curvature side.

小腹主动脉瘤 5 年预后风险分层系统的建立与验证

程佳新 王亚松 张志强 王效增

中国人民解放军北部战区总医院

摘要

背景：小腹主动脉瘤（small abdominal aortic aneurysm, SAAA）患者的长期预后评估尚缺乏简便有效的工具。为优化个体化管理并预测 5 年内死亡及主动脉相关不良事件风险，本研究旨在建立一个实用的风险分层系统。我们回顾性分析了 206 例 SAAA 患者数据，整合年龄、单纯性肾囊肿（simple renal cysts, SRC）、纤维蛋白原水平和慢性肾功能不全（chronic renal insufficiency, CRI）四个关键因素，首次构建并验证了 ASFC 评分（0-4 分），以实现个体化的风险评估。

目的：建立预测 SAAA 患者 5 年内预后的风险分层系统。

方法：回顾性分析北部战区总医院 2015 年 7 月至 2023 年 1 月收治的 206 例 SAAA 患者的临床资料。采用受试者工作特征曲线分析确定年龄（≥ 70 岁 vs. <70 岁）和纤维蛋白原（≥ 3.77 mg/dL vs. 的最佳截断值。SRC 和 CRI 被纳入为基于临床相关性和影像学的分类变量。基于年龄 -SRC- 纤维蛋白原 -CRI 构建的 ASFC 评分（0 ~ 4 分），通过对每个变量赋值的积分计算并分层为低、中、高风险组。采用 Cox 回归模型计算风险比和 95% 置信区间。中介效应分析探讨了 4 个预测因素之间的关联。

结果：中位随访时间为 34.52 个月，ASFC 高风险组的全因死亡、腹主动脉相关不良事件、腹痛、下肢缺血和影像学破裂征象发生率较高。多变量 Cox 回归显示 ASFC 高风险与 SAAA 患者 5 年内全因死亡 [hazard ratio (HR): 6.909, 95%CI: 2.747-17.376] 和腹主动脉相关不良事件（HR: 2.252，95%CI: 1.078-4.705) 的风险增加相关。

结论：本研究建立了 SAAA 的预后危险分层系统，包括年龄、SRC、纤维蛋白原和 CRI，该系统对 SAAA 的 5 年内的结局具有稳健的预测价值。

关键词：风险评分；预后；腹主动脉瘤；主动脉相关不良事件

Factors Associated with Acute Kidney Injury Following Thoracic Endovascular Repair for Acute Stanford Type B Aortic Dissection

Na Li

General Hospital of Northern Theater Command

Abstract:

Objective: To explore the risk factors of acute kidney injury (AKI) following thoracic endovascular repair (TEVAR) in acute Stanford type B aortic dissection (ATBAD).

Methods: A total of 799 ATBAD patients who were treated with TEVAR at the Department of Cardiology, General Hospital of Northern Theater Command were enrolled from February 2004 to November 2022. Finally, 745 patients were finally included after exclusion of 54 patients due to insufficient renal function laboratory results. The patients were then divided into a non-AKI group (n=670) and AKI group (n=75) based on the incidence of AKI postoperatively.

Results: Among the 745 patients enrolled in the study, 75 cases (10.1%) of AKI occurred after TEVAR. Chronic renal failure (6.67% vs. 1.19%, P=0.003) and diuretics use (56.00% vs. 27.18%, P<0.001) during hospitalization and preoperative serum creatinine level [85.97 (68.29, 120.25) μmol/L vs. 78.30 (66.00, 95.01) μmol/L, P=0.009], Scr after TEVAR [122.00 (103.25, 184.00) μmol/L vs. 79.00 (66.00, 94.00) μmol/L, P<0.009], were significantly different before and after TEVAR between the two groups. Univariate logistic regression analysis results revealed that current drinking [OR (95% CI): 0.549 (0.328, 0.918), P=0.022], use of diuretics during hospitalization [OR (95% CI): 3.410 (2.096, 5.549), P<0.001], use statins [OR (95%CI): 0.524 (0.323, 0.851), P=0.009], Scr>114 μmol/L [OR (95%CI): 3.441 (2.023, 5.854), P<0.001], systolic blood pressure>173 mmHg [OR (95%CI): 1.957 (1.190, 3.219), P=0.008], bilateral renal artery involvement [OR (95%CI): 3.699 (1.418, 9.652), P=0.008] and stent length >124mm [OR (95%CI): 0.372 (0.202, 0.686), P=0.002], dose of contrast, especially contrast and dosage more than 290ml [OR (95%CI): 2.931 (1.625, 5.284), P<0.001] were associated with the occurrence of AKI after TEVAR in ATBAD patientsMultivariate logistic regression analysis showed that serum creatinine (SCr) > 114 μmol/L [OR (95%CI): 3.327 (1.398, 7.914), P=0.007], bilateral renal artery involvement [OR (95%CI): 4.676 (1.357, 16.118), P=0.031] increased the risk of AKI after TEVAR in ATBAD patients. Cardiogenic mortality in the AKI group was higher compared to the non-AKI group (3.12% vs. 0.17%, P=0.027) within 30 days. The all-cause mortality in the AKI group exceeded that in the non-AKI group (20.00% vs. 8.73%, P=0.005) after 30 days. Kaplan-Meier curve analysis showed that the survival rate after TEVAR was significantly lower in the AKI group than in the non-AKI group.The mean follow-up time was 36 months, with 64 patients followed up in the AKI group (corresponding to a follow-up rate of 64/75(85.3%) and 602 patients were followed up in the non-AKI group (corresponding to a follow-up rate of 602/670(89.9%). There was no significant difference between the two groups (p = 0.235). In terms of all-cause mortality, 10 cases were recorded in thee AKI group (16.1%) and 26 in the non-AKI（4.36%）group, indicating a significant difference between the two groups (P<0.001).while there was a significant difference between the two groups in cardiac death (p=0.046). Aorta-related events and reintervention were not significantly different between the two groups

Conclusions:

AKI is a common complication of type B aortic dissection and can increase mortality risk after TEVAR in ATBAD patients. High preoperative SCr levels and bilateral renal artery involvement are associated with increased risk of AKI after TEVAR in ATBAD patients.

移植肾动脉狭窄腔内治疗术后主要不良事件发生的预测模型构建

田红燕 赵洋 康梦阳

西安交通大学医学院第一附属医院

目的：

移植肾动脉狭窄（Transplant Renal Artery Stenosis, TRAS）是肾移植术后最常见的血管并发症，腔内治疗（Endovascular Treatment, EVT）已成为其一线治疗手段。尽管 EVT 在控制血压、改善移植物功能方面疗效显著，部分患者仍出现主要不良事件（Major Adverse Events, MAEs），如动脉夹层、再狭窄、血栓形成等，严重影响移植结局与生存质量。目前缺乏关于 EVT 术后远期疗效及 MAEs 发生的危险因素分析。因此，本研究旨在评估 TRAS 患者经 EVT 治疗后的远期疗效，并探索 MAEs 的独立危险因素，进而构建术后风险预测模型，以优化个体化治疗与随访策略。

方法：

本研究为回顾性队列分析，纳入 2013 年 1 月至 2019 年 6 月在西安交通大学第一附属医院接受 EVT 治疗的 TRAS 患者，共计 59 例，所有患者均接受至少 5 年随访。收集基线临床信息、术中数据及术后实验室指标、超声参数与不良事件发生情况。评估术后 5 年内血压、肾功能及超声指标的变化趋势，并依据是否发生 MAEs 进行分组比较。采用单因素及多因素 Cox 回归模型筛选术后 MAEs 的独立危险因素，并基于最终模型构建风险预测方程和 Nomogram 图。通过 ROC 曲线及 Brier 评分评价模型预测性能。

结果：

研究共纳入 59 例患者，男性占 66.1%，平均年龄为 35.4±10.5 岁。EVT 术后 5 年内患者平均动脉压、肌酐水平显著下降，肾小球滤过率（eGFR）显著上升（均 P < 0.001），提示长期疗效良好。术后初始技术成功率达 100%。MAEs 累计发生率为 25.4%（15 例），包括死亡、移植肾动脉再狭窄、夹层、造影剂肾病及肾丢失。多因素 Cox 回归分析显示：术后骨髓抑制（HR=6.37, P=0.008）、狭窄程度（HR=1.129, P=0.028）、单纯球囊扩张治疗（HR=4.548, P=0.005）为术后 MAEs 的独立危险因素。基于上述变量构建的预测模型 AUC 为 0.772（95%CI: 0.632–0.912），Brier 评分为 0.114，优于参考模型，显示良好的区分度与校准能力。进一步绘制 Nomogram 图，可用于临床个体化风险评估。

结论：

EVT 治疗可显著改善 TRAS 患者的血压与移植肾功能，并在术后 5 年内维持较好疗效。骨髓抑制、狭窄程度及治疗方式为 EVT 术后 MAEs 发生的关键影响因素。本研究首次建立了 EVT 术后 MAEs 的预测模型，具备良好的预测效能，可为高风险患者早期识别和精准干预提供参考依据。

股动脉穿刺术后严重并发症 - 感染性股动脉假性动脉瘤（IFPA）的处理和预防

陈世远 学组委员

蚌埠医科大学第一附属医院

【摘要 】 目的 感染性股动脉假性动脉瘤（IFPA）是医源性介入操作（如穿刺或切开置管）的严重并发症，常因感染控制困难导致治疗复杂化。本研究通过分析 3 例典型病例，探讨 IFPA 的临床特点、治疗策略及预防措施，旨在为降低并发症发生率及优化治疗方案提供参考。**方法** 回顾性分析蚌埠医科大学第一附属医院血管外科收治的 3 例 IFPA 患者资料：1. 病例 1：76 岁男性，颅内动脉瘤介入治疗后右股动脉假性动脉瘤伴感染，初期行破口缝合 + 清创，后因复发接受覆膜支架植入（失败），最终行髂总 - 股浅动脉解剖外旁路术。 2. 病例 2：73 岁男性，主动脉瓣修复术后假性动脉瘤感染，大隐静脉重建失败后改为解剖外旁路术。3. 病例 3：68 岁女性，ECMO 拔管后假性动脉瘤，经血凝酶注射无效后手术缝合破口并清创，术后切口感染经换药愈合。 治疗方法包括：破口缝合、感染组织清除、抗生素应用、覆膜支架植入（效果有限）及解剖外旁路术。预防措施强调规范穿刺后按压、加压包扎及高年资医师操作指导。**结果** 1. 治疗效果：解剖外旁路术（病例 1、2）和破口缝合 + 清创（病例 3）效果良好，但覆膜支架因感染易失效。病例 1 经历多次手术，耗时 6 个月，费用超 70 万元。 2. 并发症：感染导致动脉破口再破裂（病例 1、2）、皮肤坏死（病例 1）及深静脉血栓（病例 1）。3. 预防经验：穿刺前常规彩超评估入路血管，钙化严重，选择切开置管；选择股总动脉穿刺；穿刺鞘≤ 6F 时，有效按压 30 分钟 + 加压包扎；> 7F 时建议血管缝合器闭合。大鞘管（> 8F）推荐切开置管，安全性高。 **结论** 1. 治疗策略：IFPA 需个体化处理。轻度感染可尝试破口缝合 + 清创；严重感染或复发者首选解剖外旁路术，避免支架植入。2. 预防关键：严格规范穿刺后按压技术（着力点准确、时间≥ 20 分钟）、评估血管条件（如动脉硬化者慎穿刺），对大鞘管操作优先选择切开置管。3. 临床意义：早期干预和多学科协作可减少并发症。

Aortic Remodeling After Thoracic Endovascular Repair of Acute Type B Aortic Dissection Underwent Anti-Thrombotic Therapy

Zhan-Kui Du[1], Ya-Song Wang[2], Zhi-Qiang Zhang[2], Ruo- Gu[2], Quan-Min Jing[2], Xiao-ZengXueZuWeiYuanTongXunZuoZhe Wang[2]

1. the Second Hospital Affiliated to Xi'an Medical University

2. General Hospital of Northern Theater Command

Objective: To investigate the effect of anti-thrombotic (AT) drugs on aortic remodeling after thoracic endovascular aortic repair (TEVAR) for acute type B aortic dissection (TBAD).

Methods: This retrospective observational study included consecutive patients with acute TBAD who underwent TEVAR and had computed tomography angiography (CTA) in preoperative and follow-up from January 2012 to September 2023 in the general hospital of northern theater command. The patients were divided into AT group (aspirin, clopidogrel and/or warfarin/NOAC) and non-anti-thrombotic (NAT) group based on whether it was anticoagulant or not. AT group, patients were further divided into single anti-thrombotic (SAT) group (only aspirin, clopidogrel or warfarin/NOAC) and dual anti-thrombotic (DAT) group (aspirin combined with clopidogrel or warfarin/NOAC; clopidogrel combined with warfarin/NOAC).Preoperative and follow-up period images data were analyzed for the thrombosis status of false lumen (FL), the changes of the maximum diameter of true lumen (TL), FL, transaortic lumen (TAL) in the stented thoracic aorta (STA), unstented thoracic aorta(UTA), and abdominal aorta (AA).

Results: 175 patients of acute TBAD were included in this study. 175 consecutive acute TBAD patients with AT group (n =73) and NAT group (n=102) who underwent TEVAR in this study. The two groups had comparable baseline characteristics. For preoperative and 12 months follow-up images, there were no significant differences in the FL status (patent, partial thrombosis and complete thrombosis) and the changes of the maximum diameter of TL, FL, and TAL, respectively, at the STA, UTA, and AA segments between the AT and NAT groups (all P > 0.05). The FL status

of patent and complete thrombosis had significantly favourable in 12 months follow-up compared to preoperative image in all segments (all P < 0.001). The changes of maximum diameter of TL, FL and TAL at all segments were significant statistical differences in 12 months follow-up, respectively, in the AT and NAT groups (all P < 0.001). For the diameter variation, the expansion of TAL was 4.0%, 14.9% and 53.7%, respectively, at the STA, UTA and AA segments; the stabilization of TAL was 62.3%, 36.6% and 44.6%, respectively, at the STA, UTA and AA segments; the shrinkage of TAL was 33.7%, 48.6% and 1.7%, respectively, at the STA, UTA and AA segments. However, there were no significant statistical differences between the AT and NAT groups at aforementioned segments. For the FL status of patent, partial thrombosis, and complete thrombosis at the STA, UTA and AA segments, there were also no significant differences between the SAT and DAT groups in the 12 months follow-up (all P > 0.05). For the maximum diameters of the TL, FL, and TAL, there were also no significant differences between the SAT and DAT groups at the STA, UTA and AA segments in the 12 months follow-up (all P > 0.05).

Conclusions: The patients with AT drugs have comparable aortic remodeling prognosis than without AT drugs for acute TBAD underwent TEAVR in 12 months follow-up. The maximum diameter of the STA and UTA are stable, and the aneurysmal growth of the AA is mainly attributed to FL expansion.

Key word: acute type B aortic dissection, thoracic endovascular aortic repair, aortic remodeling, anti-thrombotic, computed tomography angiography

构建 A 型主动脉夹层患者 I 期心肺康复护理方案的临床应用评价

李娟

西安交通大学第一附属医院

目的 构建 A 型主动脉夹层患者 I 期心肺康复护理方案并临床应用评价其效果。方法 构建 A 型主动脉夹层患者 I 期心肺康复护理方案。采用类实验研究设计．根据目 的抽样法，选取西安某三级甲等医院 2021 年 1 月一 2024 年 9 月 223 例 A 型主动脉夹层手术患者作为研究对象。自愿选择 A 型主动脉夹层患者 I 期心肺康复护理方案的患者纳入试验 组，选择常规心肺康复方案的患者纳入对照组。比较两组 6 min 步行距离、Borg 主观劳累程度得分、术后首次下床时间、呼吸机待机时间、肺不张的发生率、低氧血症的发生率、低氧相关并发症发生率、康复护理相关不良事件发生率。结果 共纳入研究对象 223 例，23 例因手术并发症或中途退出．予以排除，最终 纳入 200 例，试验组 100 例，对照组 100 例。干预后，试验组的 6 min 步行距离、Borg 主观劳累程度得分、肺不张的发生率、低氧血症的发生率均低于对照组 (P<0．05)：两组患者术后首次下床时间、低氧相关并发症发生率、康复护理相关不良事件发生率比较，差异无统计学意义 (尸>0．05)。结论 构建的 A 型主动脉夹层患者 I 期心肺康复护理方案科学、可行，紧密结合临床，可提高患者的运动能力，降低其低氧血症发生率。

累及头颈部血管的急性 Stanford A 型主动脉夹层外科治疗的临床效果分析

韩帅贤 [1] 刘建平 [2]

1. 川北医学院

2. 遂宁市中心医院

目的：探讨急性 Stanford A 型主动脉夹层（acute Stanford type A aortic dissection, ATAAD）累及头颈部血管的外科治疗策略及其临床效果。ATAAD 是一种起病急骤、进展迅速、死亡率极高的心血管急症，若合并头颈部血管受累，将显著增加围术期神经系统并发症发生率与死亡风险。因此，明确该类复杂病变的外科干预策略、优化术中脑保护方案、评估术后神经功能恢复情况，对于提高患者生存率与生活质量具有重要意义。

方法：本研究为回顾性病例分析，纳入 2024 年 12 月至 2025 年 2 月期间在遂宁市中心医院心脏大血管外科接受手术治疗的 7 例急性 Stanford A 型主动脉夹层合并头颈部血管受累患者。其中男性 6 例，女性 1 例，年龄范围为 32 至 68 岁，平均年龄为（50.67±10.4）岁。所有患者术前均接受胸腹主动脉 CTA、头颈部 CTA 及冠状动脉 CTA 检查，明确夹层破口位置、头颈部血管受累程度（包括颈总动脉闭塞或重度狭窄）、Willis 环完整性及冠脉病变情况。术前由心脏大血管外科与脑血管外科联合开展多学科会诊，制定个体化手术方案，术中同期处理主动脉根部、弓部病变及颈动脉病变，确保一次性完成血运重建与神经保护。

术中操作方面：主动脉根部处理方面，5 例患者行升主动脉置换术，2 例患者因合并主动脉瓣病变行 Bentall 手术（主动脉根部替换 + 人工瓣膜置换 + 冠状动脉开口移植）。主动脉弓部病变均采用孙氏手术（全弓置换 + 支架象鼻植入）进行处理，共计 7 例。颈动脉处理方面，3 例患者行左侧颈总动脉人工血管置换，1 例患者行右侧颈总动脉置换，3 例患者因双侧颈总动脉受累行双侧颈总动脉置换。术中脑保护措施采用中低温（25-28℃）停循环联合顺行性脑灌注（antegrade cerebral perfusion, ACP）策略，其中 6 例患者采用单侧脑灌注（通过右腋动脉或左颈总动脉），1 例患者因术前头颈部 CTA 提示 Willis 环不完整，采用双侧脑灌注以确保脑组织充分灌注。所有患者术中均行脑氧饱和度监测与颈部血管造影，评估脑灌注效果及血管通畅情况。

结果：所有患者手术均顺利完成，无术中死亡。平均手术时间为（10.9±1.2）小时，体外循环时间为（5.2±1.9）小时，停循环时间为（21.6±9.3）分钟。术后 ICU 住院时间中位数为 2.4 天（四分位数间距 2.1~7.3 天）。术后 30 天内死亡 1 例，该患者术前合并双侧颈总动脉闭塞，术中行 Bentall+ 双侧颈动脉置换，术后出现持续性昏迷，头颅 CT 提示大面积低密度影，术后第 9 天，家属决定终止治疗，患者出院。术后新发神经系统并发症 2 例，其中 1 例表现为持续性昏迷（永久性神经功能障碍），另 1 例表现为短暂性意识不清（短暂性神经功能障碍），经对症治疗后恢复。围术期未观察到其他严重并发症，如急性肾损伤、严重出血或感染等。所有存活患者出院前复查主动脉 CTA 及头颈部 CTA，提示人工血管通畅，吻合口无狭窄，主动脉弓部及分支血管重建良好。

结论：急性 Stanford A 型主动脉夹层累及头颈部血管是一种复杂且高危的病变类型，传统单一处理主动脉病变而忽视颈部血管受累的策略已无法满足临床需求。本研究通过联合心外 - 脑血管外科团队，采用同期处理主动脉根部、弓部及颈部血管病变的综合手术策略，结合个体化脑保护措施（如单侧或双侧脑灌注），实现了良好的手术效果与神经功能保护。尽管术后仍存在一定神经系统并发症风险，但总体死亡率低，远期血管通畅率高，提示该策略在复杂 A 型主动脉夹层治疗中具有重要临床应用价值。未来仍需更大样本量、长期随访研究以进一步验证其安全性与有效性。

房颤患者急性下肢血栓形成的危险因素护理分析

徐阳 张喜维

北京安贞医院

摘要

目的： 探讨房颤患者发生急性下肢深静脉血栓形成的危险因素。

方法 ： 选取 2023 年 1 月 -2024 年 1 月入住三甲医院心内科及血管科； 年龄≥ 18 岁； 符合 ESC 房颤诊断标准的确诊房颤患者 100 名。无确诊急性下肢血栓形成的房颤患者为对照组和确诊急性下肢血栓形成的房颤患者为观察组。收集两组患者的临床资料，包括：人口学特征：年龄、性别； 基础疾病：高血压、糖尿病、冠心病、慢性肾功能不全等； 实验室检查指标 :D- 二聚体、低密度脂蛋白胆固醇、脂蛋白 (a)、C- 反应蛋白、白介素 -6 等； 心脏超声检查结果：左心房内径、左心室射血分数等; 抗凝治疗情况：是否接受抗凝治疗、抗凝药物种类及治疗时间。

结果 ： 在房颤患者中发生急性下肢血栓形成与未发生者，单因素分析结果显示，两组在年龄、高血压、糖尿病、冠心病、慢性肾功能不全、D- 二聚体水平、低密度脂蛋白胆固醇水平、脂蛋白 （a）水平、C- 反应蛋白水平、白介素 -6 水平、左心房内径、左心室射血分数、抗凝治疗等方面差异有统计学意义（P<0.05）。多因素回归分析显示，年龄≥ 75 岁，高血压 ,D- 二聚体水平≥ 500μg/L. 脂蛋白 (a) 水平 >30mg/dL, 左心房内径 >40mm 是房颤患者急性下肢血栓形成的独立危险因素。

结论 ： 房颤患者急性下肢血栓形成的危险因素较多，包括高龄、高血压、D- 二聚体水平升高、脂蛋白 （a）水平升高以及左心房扩大等。临床工作中应重视对这些危险因素的评估和管理，尤其是对于高危患者，需加强监测和积极的抗凝治疗，以降低急性下肢血栓形成的发生风险，改善患者的预后。

The gut metabolite phenylacetylglutamine inhibits the angiogenic potential of human umbilical vein endothelial cells via the β-adrenergic receptor-LDHA axis

Shuning Zhang

Fudan University Affiliated Zhongshan Hospital

Background & objective

Phenylacetylglutamine (PAGln), a gut microbiota-derived metabolite produced through the downstream metabolism of phenylacetic acid, has been demonstrated to enhance platelet responsiveness and thrombosis potential and significantly elevate the risk of major adverse cardiovascular events. Beyond arterial thrombosis, endothelial dysfunction is also recognized as an independent predictor of major adverse cardiovascular events. However, whether PAGln leads to endothelial cell dysregulation and affects the angiogenic ability is currently unclear. Mechanistic studies have revealed that PAGln interacts with G protein-coupled receptors. Specially, the β-adrenergic receptor is widely recognized to be associated with angiogenesis. The present study aims to elucidate whether PAGln regulates angiogenesis through β-adrenergic receptor-dependent mechanisms.

Methodologies

The mouse hind limb ischemia model was utilized as a preclinical surrogate for peripheral artery disease, with assessment of lower limb perfusion via laser Doppler imaging on days 0, 1, 7, and 14 post-operation. Gastrocnemius and adductor muscles from ischemic limbs were harvested at these time points for immunofluorescence staining, while angiogenesis was evaluated through both hindlimb blood flow recovery and CD31, α-SMA quantification. Human umbilical vein endothelial cells (HUVECs) were cultivated to assess proliferative (CCK-8 and EdU test), migratory (transwell assay), and endothelial tube formulation capabilities in vitro. Further RNA-Seq analysis and Gene set enrichment analysis (GSEA) were performed for biological process and pathway enrichment analyses. Glycolysis Rate Test Kit and extracellular lactate content detection were performed to qualitatively evaluate glycolysis, while western blotting, reverse transcription-real-time PCR were conducted to evaluate the expression of key glycolytic enzymes. Finally, Lentivirus transfection in cells and mice was performed to clarify the underlying mechanism.

Results

In the hindlimb ischemia model, a significant inverse correlation was observed between circulating PAGln concentrations and post-ischemic recovery of limb perfusion, as quantified by laser Doppler perfusion imaging (p<0.05): the higher the PAGln concentration, the worse the limb blood flow recovery, and the lower the percentage of CD31 and α-SMA

expression. Moreover, PAGln inhibited the proliferation, migration, and tubular formation ability of human umbilical vein endothelial cells in vitro. β-receptor blocker zenidolol was able to reverse the vascular inhibitory effects. Gene set enrichment analysis of RNA-seq data identified significant downregulation (FDR q<0.05) of the glycolytic pathway, with particular suppression of rate-limiting enzymes: hexokinase 2, pyruvate kinase M, phosphofructokinase muscle type, and lactate dehydrogenase A (LDHA). Furthermore, the glycolysis proton efflux rate decreased following PAGln intervention. Significant inhibition of LDHA expression was also observed and extracellular lactate content was significantly reduced. In contrast, The pivotal role of LDHA was established through rescue experiments: adenoviral-mediated LDHA overexpression completely reversed PAGln induced inhibition of endothelial proliferation, migration, and angiogenesis ability in vitro and significantly improved perfusion recovery in vivo.

Conclusion

In conclusion, our study demonstrates that the gut-derived metabolite PAGln significantly inhibits angiogenesis in human umbilical vein endothelial cells through β-adrenergic receptor-dependent mechanisms, with lactate dehydrogenase A serving as a key downstream effector mediating this angiogenic inhibitory effect. The finding not only elucidate a novel PAGln-β receptor-LDHA signaling axis that regulates endothelial function, but also open new therapeutic possibilities for targeting angiogenesis-related disorders through modulation of gut metabolite signaling.

异物参与的胺碘酮致急性闭塞性血栓性静脉炎 1 例

郭彩虹 张春然 蒋卢映

武汉亚洲心脏病医院

目的 探讨胺碘酮和体内异物致闭塞性血栓性静脉炎的作用机制和治疗方案，提高对闭塞性血栓性静脉炎的认识。

方法 结合 1 例存在体内异物的患者静脉使用胺碘酮过程中引起闭塞性血栓性静脉炎的临床资料和文献复习，详细分析该病的发病机制、治疗过程及预后。

结果 经联合应用局部药膏（消炎类药膏百多邦、肝素类药膏喜辽妥）、低分子肝素、溶栓药物及康复运动等综合治疗后，患者闭塞性血管完全再通。

结论 胺碘酮作为 III 类抗心律失常药物广泛用于各类心律失常的治疗，同时也常用于房颤消融术后窦性心律的维持。当高浓度高剂量胺碘酮通过外周浅表静脉输注时，容易引发各类静脉炎。经外周静脉输注低浓度低剂量胺碘酮引发静脉炎特别是闭塞性血管性静脉炎较为少见。除了胺碘酮本身容易刺激静脉血管壁和易沉淀性特点参与血栓形成机制外，该患者局部异物的存在可能对血栓的形成起了重要的作用。一方面，局部异物的物理压迫作用导致静脉管腔变窄，使得胺碘酮流经此处速度变缓容易淤滞。另一方面，异物诱发慢性炎症反应导致了凝血系统的激活。故我们考虑是胺碘酮和异物的共同作用导致了该患者急性闭塞性血栓性静脉炎的发生。输液时避开存在异物的肢体可显著降低血栓事件的发生率。除常规的局部用药及抗栓治疗外，康复运动在该患者治疗中起着重要的作用。

The Role and Mechanism of GRP94 in Hindlimb Ischemia of Murine

Qinyan Gong

The Second Affiliated Hospital Zhejiang University School of Medicine

Objectives

The present study was designed with the following objectives:

1. To characterize the temporal expression patterns of GRP94 at critical stages of hindlimb ischemia in order to lay the groundwork for understanding its involvement in specific biological processes related to ischemia.
2. To investigate the functional role of GRP94 in modulating angiogenic phenotypes under ischemic conditions.
3. To identify molecular targets and elucidate the mechanisms through which GRP94 regulates angiogenesis, with the goal of discovering novel therapeutic targets for vascular diseases.

To examine the association between GRP94 expression levels and clinical outcomes in patients with peripheral arterial disease (PAD), and to evaluate its potential as a diagnostic and therapeutic biomarker.

Methods and Results

Initial in vivo studies demonstrated that GRP94 expression was significantly upregulated following the induction of hindlimb ischemia in mice. Consistently, in vitro experiments revealed that GRP94 levels were markedly elevated in human umbilical vein endothelial cells (HUVECs) subjected to hypoxia-ischemia (HI) conditions. These concordant findings across models suggest that GRP94 may play a critical role in the biological response to ischemia.

To elucidate the functional significance of GRP94 in vivo, wild-type mice subjected to hindlimb ischemia were randomly assigned to either a control group or a group treated with PU-WS13, a specific GRP94 inhibitor. Various outcomes were systematically evaluated, including hindlimb blood perfusion assessed by laser Doppler imaging, the degree of limb necrosis, motor function recovery, histopathological alterations, and angiogenic capacity. The results demonstrated that pharmacological inhibition of GRP94 led to impaired angiogenesis and delayed restoration of blood flow in the ischemic limbs, underscoring the essential role of GRP94 in vascular repair processes.

In parallel, in vitro knockdown of GRP94 in HUVECs was achieved using small interfering RNA (siRNA), followed by exposure to hypoxic-ischemic conditions to simulate the ischemic microenvironment. Functional assays revealed that GRP94 depletion significantly attenuated endothelial cell proliferation, migration, and tube formation–processes that are fundamental to effective angiogenesis.

To further delineate the underlying molecular mechanisms, transcriptomic analysis was performed to identify potential downstream effectors of GRP94. This approach pinpointed integrin alpha 6 (ITGA6) as a key mediator of GRP94's pro-angiogenic effects. Functional validation using lentiviral constructs demonstrated that modulation of ITGA6 expression could recapitulate the angiogenic outcomes associated with GRP94 activity. Mechanistically, the data suggested that GRP94 exerts its regulatory influence on angiogenesis through ITGA6 and its downstream PI3K/AKT signaling pathway.

Conclusions

Collectively, these findings establish that GRP94 is a pivotal regulator of endothelial function and angiogenesis in the context of ischemic injury. Loss of GRP94 disrupts endothelial cell behavior, compromises vascular remodeling, and impairs perfusion recovery in murine hindlimb ischemia. The mechanistic link between GRP94, ITGA6, and the PI3K/AKT signaling cascade provides novel insights into the molecular basis of ischemia-induced angiogenesis.

Importantly, this study positions GRP94 as a potential therapeutic target for enhancing vascular repair in ischemic diseases such as PAD. By targeting GRP94 or its downstream integrin-mediated pathways, there may be opportunities to develop innovative strategies for improving vascular outcomes in patients suffering from ischemia-related vascular disorders. This research thus contributes to the broader understanding of endothelial biology and offers a promising direction for the diagnosis and treatment of cardiovascular and peripheral vascular diseases.

CCNY 缺失通过影响平滑肌细胞凋亡促进胸主动脉夹层的发生

杨眉 李千一 柴珂 张力

上海交通大学医学院附属新华医院

目的：胸主动脉夹层是高危致死性的疾病，目前尚缺乏有效的防治手段。血管平滑肌细胞是主动脉夹层发病过程的关键细胞之一，平滑肌细胞调亡一直被认为是主动脉夹层病理的重要标志。揭示胸主动脉夹层发生过程中调控平滑肌细胞凋亡的机制具有重要的意义。

方法：采用人和小鼠的主动脉夹层样本检测细胞周期蛋白 Y（CyclinY，CCNY）表达水平，构建 CCNY 敲除小鼠及平滑肌细胞特异性敲除 CCNY 小鼠，并通过 BAPN 诱导构建了胸主动脉夹层模型，记录小鼠死亡情况，并通过 EVG、HE 等染色方法评估病理改变。采用单细胞测序技术解析分子机制。

结果：首先，我们发现在主动脉夹层组织中 CCNY 表达升高。其次，与野生型（Wildtype， WT）小鼠相较，CCNY 敲除小鼠胸主动脉夹层的发生率增加，死亡率升高，主动脉弹力膜断裂程度增加，明确了 CCNY 敲除促进胸主动脉夹层的形成。通过对 CCNY 敲除小鼠和 WT 小鼠的主动脉夹层样本进行单细胞测序分析发现，CCNY 敲除后平滑肌细胞的凋亡增加。采用平滑肌细胞特异性敲除 CCNY 小鼠进行验证，结果显示，与 $CCNY^{fl/fl}$ 小鼠相较，平滑肌细胞特异性敲除 CCNY 小鼠主动脉夹层的发生率增加，死亡率升高，中膜平滑肌细胞凋亡增加，进一步明确 CCNY 敲除通过促进平滑肌细胞的凋亡促进主动脉夹层的发生。机制方面，通过对平滑肌细胞凋亡亚群的功能富集分析发现，CCNY 敲除后脂肪酸氧化增强，活性氧的解毒减弱，CCNY 可能通过调控脂肪酸氧化影响活性氧解毒进而细胞平滑肌细胞凋亡，最终影响主动脉夹层的发生。

结论：研究揭示了 CCNY 通过影响平滑肌细胞凋亡参与胸主动脉夹层中的作用和机制，为主动脉夹层的防治提供了新的靶点。

缩窄性心包炎引起的复杂斯坦福 A 型主动脉夹层伴硬膜下血肿的手术治疗 -- 病例报告

范伶林 [1,2] 何伟波 [1] 孙冬梅 [1] 匡锋 [1] 伍源 [1]

1. 粤北人民医院 (汕头大学医学院附属粤北人民医院)

2. 南昌大学江西医学院第二附属医院

目的：探讨复杂 A 型主动脉夹层合并缩窄性心包炎并且术后并发硬膜下血肿的危重病例的发病特点及围术期治疗体会。

方法：我们报道一例斯坦福 A 型主动脉夹层破裂并发缩窄性心包炎的患者，该患者心脏内血肿形成一个巨大的假性动脉瘤，严重压迫右心房及右心室，紧急情况下予以急诊手术，术后患者并发硬膜下血肿及反复抽搐，经过加强脑保护、甘露醇脱水、丙戊酸钠控制抽搐，以及腰椎穿刺降低颅内压等综合治疗，患者顺利出院并且预后良好的病例进行分析和讨论。

结果：A 型主动脉夹层合并缩窄性心包炎的患者病情危重，进展快，死亡率高，

急诊手术是此类患者最佳的选择。与体外循环的传统双腔插管技术相比，我们的研究结果表明，通过联合动脉灌注（右股动脉和无名动脉）和静脉引流（股静脉和上腔静脉 插管）建立体外循环，是治疗高风险主动脉夹层并发缩窄性心包炎的创新手术方法。此外，我们的围手术期方案 - 纳入了早期脑保护措施，包括甘露醇诱导脱水、丙戊酸钠控制癫痫发作、腰椎穿刺管理颅内压升高 - 为术后出现神经系统并发症的患者提供了全面的管理策略。

结论： 因此，早期急诊通过联合动脉灌注（右股动脉和无名动脉）和静脉引流（股静脉和上腔静脉 插管）进行体外循环手术及围手术期纳入早期脑保护措施，可为治疗这种复杂的高风险主动脉夹层合并慢性缩窄性心包炎的患者提供一种新的治疗策略。

康复护理路径在 Stanford A 型主动脉夹层患者中的应用价值

张远莹

西安交通大学医学院第一附属医院

目的 探讨康复护理路径在 Stanford A 型主动脉夹层患者中的应用价值研究。

方法 选取 2022 年 2 月–2023 年 1 月西安交通大学第一附属医院心血管外科收治的 100 例 Stanford A 型主动脉夹层患者，采用随机数字表法分为对照组和观察组，各 100 例。对照组实施基础护理，观察组实施康复护理路径干预。对比两组患者术后恢复时间、负性情绪水平、护理依赖性及不良反应发生情况。

结果 干预后，观察组机械通气时间、ICU 停留时间、胃肠蠕动恢复时间、引流时间、住院时间均短于对照组（P<0.05）；干预后，两组抑郁 - 焦虑 - 压力量表中文精简版（Chinese short version of depression anxiety and stress scale，DASS-C21）中焦虑、抑郁、压力评分均低于干预前，且观察组低于对照组（P<0.05）；干预后，观察组对护理依赖性低于对照组（P<0.05）。干预期间，观察组不良反应发生率低于对照组（P<0.05）。

结论 康复护理路径干预可提升 Stanford A 型主动脉夹层患者术后机体康复速度，降低不良情绪的影响及其对护理的依赖性，降低术后干预期间不良事件发生风险。

Jagged1 inhibits the osteogenic phenotypic transition of vascular smooth muscle cells by downregulating NFATc1 in exosomes derived from vascular endothelial cells

yi xuejiao, De-Hui Qian

Second Hospital Affiliated to the Army Medical University (Xinqiao Hospital)

Background and Aims: Vascular calcification, a significant pathological feature of cardiovascular diseases, is particularly prevalent in the elderly. It is of great significance to explore the specific mechanisms of the osteogenic phenotypic transition of VSMCs for understanding the process of vascular calcification in the elderly and identifying effective intervention strategies. The key mechanism underlying vascular calcification is the osteogenic phenotypic transition of vascular smooth muscle cells (VSMCs). This study aims to explore the molecular mechanism by which Jagged1 regulates the expression of NFATc1 in exosomes derived from vascular endothelial cells (ECs) to inhibit the osteogenic phenotypic transition of VSMCs and to investigate the role of BMP7 in this process.

Methods: Primary aortic ECs and VSMCs from young and aged mice were used for in vitro experiments. Lentivirus was employed to overexpress Jagged1 and BMP7 in aged ECs and to overexpress NFATc1 in VSMCs. Additionally, siRNA was used to knock down the expression of NFATc1 in aged ECs. The expression levels of NFATc1, Jagged1, BMP7, and osteogenic markers Runx2 and OPN were detected using Western blot, qPCR, and immunofluorescence. Alizarin red staining was performed to assess the calcification degree of VSMCs. We observed the exosomes secreted by primary aortic endothelial cells (ECs) from aged mice using transmission electron microscopy. The results showed that the exosomes had a typical cup-shaped structure with a diameter of approximately 100 nm, which is consistent with the morphological characteristics of exosomes.Similarly, we compared the expression of the exosome marker protein CD63 in the lysates of ECs and exosomes by Western blot. The expression of CD63 was increased in both exosome lysates, confirming that the substances separated by ultracentrifugation were exosomes . We further detected the expression levels of NFATc1 in exosomes derived from young and aged mice ECs using qPCR and Western blot. The results showed that the mRNA and protein expression levels of NFATc1 in exosomes derived from aged mice ECs were significantly higher than those from young mice .

Results: Jagged1 is an important ligand of the Notch signaling pathway and plays a significant role in vascular development and homeostasis. It was found that the expression of NFATc1 in exosomes derived from aged ECs was significantly higher than that from young ECs. Knocking down NFATc1 or overexpressing Jagged1 in aged ECs significantly inhibited the osteogenic phenotypic transition and calcification of VSMCs. In contrast, overexpression of NFATc1 in VSMCs could reverse the inhibitory effects of Jagged1 on the osteogenic phenotypic transition and calcification of VSMCs. Moreover, upregulation of BMP7 decreased the expression of Jagged1 in exosomes derived from aged ECs while increasing the expression of NFATc1, thereby promoting the calcification and osteogenic phenotypic transition of VSMCs.

Conclusion: Jagged1 inhibits the osteogenic phenotypic transition of VSMCs and alleviates vascular calcification by downregulating the expression of NFATc1 in exosomes derived from ECs. BMP7, by downregulating Jagged1 and upregulating NFATc1 in exosomes from aged ECs, is involved in this process. This result reveals the pro-calcific role of BMP7 in vascular calcification and further clarifies its relationship with Jagged1 and NFATc1. On the other hand, by combining clinical samples, the expression levels of Jagged1, NFATc1, and BMP7 in human vascular calcification should be studied to explore their potential as biomarkers or therapeutic targets.These findings provide new insights into the molecular mechanisms of vascular calcification and offer potential therapeutic targets.

Diagnostic value of platelets to high-density lipoprotein ratio in abdominal aortic aneurysm

Xiao Du[1], Jin Xu[2], Shilan Zhang[3], Ling Liu[2]

1. Department of Cardiology, Beijing Friendship Hospital, Capital Medical University, Beijing, China

2. Department of Cardiovascular Medicine, The Second Xiangya Hospital, Central South University, Hunan, China

3. epartment of Cardiology, Songjiang Hospital and Songjiang Research Institute School of Medicine, Shanghai Jiao Tong University, Shanghai, China.

Title: Diagnostic value of platelets to high-density lipoprotein ratio in abdominal aortic aneurysm.

Key words: abdominal aortic aneurysm; platelets to high-density lipoprotein ratio; diagnostic marker

Introduction Pan-vascular diseases are a series of vascular disorders that share atherosclerosis as their common pathological feature. Among them, abdominal aortic aneurysm (AAA) is a disease with a relatively high mortality risk. AAA refers to the localized and progressive dilation of the abdominal aorta. Once it ruptures, the fatality rate can reach as high as 80%. Early diagnosis of AAA is of vital importance for its treatment and the prevention of adverse events. However, the diagnosis of AAA still relies on imaging examinations, and there is a shortage of simple and rapid screening indicators. Previous studies have demonstrated that both high-density lipoprotein cholesterol (HDL-C) and platelets are closely associated with the occurrence of AAA. The platelet-to-HDL-C ratio (PHR) is a novel biomarker for evaluating the inflammatory state and hypercoagulability. It holds significant value in the diagnosis and prognosis assessment of cardiovascular diseases such as coronary artery disease, heart failure, and stroke. However, there are currently no relevant reports on the clinical application of PHR in AAA. This study aims to explore the clinical value of PHR in AAA, so as to provide a rapid and convenient laboratory screening indicator for the clinical diagnosis of AAA.

Methods In this study, we included 156 patients with AAA who were treated in the Emergency Department and the Department of Vascular Surgery at Xiangya Second Hospital, Central South University, from January 2018 to December 2018. Among them, 80 patients had concomitant thrombosis，while 113 healthy individuals were recruited to serve as the control group. Serum samples were collected from the patients upon their admission to the hospital and before they received any treatment. The calculation formula for the PHR is: PHR = [PLT (1000 cells/μL) / HDL-C (mmol/L)]. The optimal cut-off point of PHR was determined through receiver operating characteristic (ROC) curve analysis, and logistic regression analysis was used to identify the predictors of AAA.

Results In this study, the baseline PHR level of patients with AAA was significantly higher than that of the control group [127.00 (109.74, 163.42) vs. 192.35 (159.08, 231.66); $p < 0.0001$] (Figure A). Additionally, the PHR level was even higher in AAA patients with thrombosis [161.80 (135.54, 193.41) vs. 220.61 (186.49, 262.27); $p < 0.0001$] (Figure B). The ROC curve analysis revealed that PHR had a good predictive value for the diagnosis of AAA, with an area under the curve (AUC) of 0.805 and an optimal cut-off value of 170.7 (sensitivity: 84.96%, specificity: 66.03%) (Figure C). For the diagnosis of AAA with thrombosis, the AUC of PHR was 0.814, and the optimal cutoff value was 204.6 (sensitivity: 86.84%, specificity: 66.25%) (Figure D). Multivariate logistic regression analysis further demonstrated that the PHR level was an independent predictor of AAA (OR: 1.022, 95% CI: 1.012-1.031; p<0.001).

Conclusions PHR has good diagnostic value for AAA and can serve as a rapid screening indicator for its clinical diagnosis. Additionally, PHR can also be used to screen for thrombosis in patients with AAA.

Long-Term Outcomes of Different Surgical Modalities for Aneurysms in Patients with Rheumatic Immune Diseases: a Single-Center Cohort Study for 20-Year

Zi- Zhao, Ce Wang, Cheng-Jie Ma, Yue Sun, Ming Ni

The First Affiliated Hospital of Naval Medical University（Shanghai Changhai Hospital）

Background and Objectives

Rheumatic immune diseases, such as Takayasu's arteritis, systemic lupus erythematosus, and Behçet's disease, are systemic conditions characterized by chronic inflammation. Their pathological processes often involve damage to the vessel wall, leading to a significantly higher incidence of aneurysms compared to the general population. These inflammatory aneurysms are characterized by rapid progression, high risk of rupture, and numerous perioperative complications, posing a severe threat to patients' quality of life and long-term prognosis.

Surgical intervention is the cornerstone of preventing aneurysm rupture. The main options include traditional open surgical repair (OSR) and minimally invasive endovascular repair (EVR). However, the optimal surgical choice for this specific patient population remains highly controversial. While OSR allows for the complete resection of the diseased vessel, it is associated with significant surgical trauma and slower recovery, which are heightened risks in immunocompromised patients. EVR presents an attractive alternative due to its minimally invasive nature, but its long-term efficacy in a chronic inflammatory environment is questionable. Persistent vessel wall remodeling may lead to complications like endoleaks and stent-graft migration, while the use of immunosuppressants could potentially affect the process of graft endothelialization.

Currently, there is a scarcity of high-quality research directly comparing the long-term outcomes (e.g., reintervention rates, survival) of these two modalities. Furthermore, existing studies have seldom performed stratified analyses to explore the heterogeneous effects of different rheumatic disease subtypes or disease activity levels on surgical outcomes. This study, through a 20-year single-center retrospective cohort analysis, aims to systematically evaluate and directly compare the long-term prognoses of OSR versus EVR for aneurysms associated with rheumatic immune diseases. The core objective is to define the risk-benefit profile of each modality and investigate the influence of key covariates, such as disease activity, to provide evidence-based guidance for individualized clinical decision-making.

Methods

This study was conducted as a single-center, retrospective, longitudinal cohort study. Data were sourced from the electronic medical record (EMR) system and surgical follow-up databases of the First Affiliated Hospital of Naval Medical University. The study cohort included all patients with a confirmed diagnosis of a specific rheumatic immune disease, a co-existing aneurysm (affecting the aorta or peripheral arteries) confirmed by imaging, and who underwent their first OSR or EVR between January 1, 2003, and December 31, 2022. All included patients had at least two years of complete follow-up data.

A total of 218 patients were included in the final analysis and were divided into the OSR group (n=78) and the EVR group (n=140) based on their initial surgical procedure. The primary outcome was a composite endpoint including major postoperative complications within one year, any subsequent surgical or endovascular reintervention, and aneurysm-related death. The secondary outcome was all-cause mortality.

Detailed baseline data were collected as covariates, including demographics (age, sex), comorbidities (hypertension, diabetes, history of malignancy), characteristics of the rheumatic disease (type, duration, baseline inflammatory markers like ESR and CRP), and aneurysm features (location, type, size, rupture status).

Statistical analysis was performed using R software. Baseline characteristics were compared using the t-test, Mann-Whitney U test, or chi-square test. Kaplan-Meier curves were plotted to compare survival, with group differences assessed using the log-rank test. To control for confounding, a multivariable Cox proportional hazards regression model was constructed. Furthermore, to address selection bias, propensity score matching (PSM) was performed, with inverse probability of treatment weighting (IPTW) used as a sensitivity analysis to verify the robustness of the findings.

Results

The two groups were comparable across most baseline characteristics. However, the mean age of patients in the EVR group was significantly higher than in the OSR group (45.8 vs. 40.2 years, p=0.015). In terms of etiology, Takayasu's arteritis was predominant in the OSR group (64.1%), whereas the EVR group had a higher proportion of both Takayasu's arteritis (48.6%) and systemic lupus erythematosus (15.7%).

In the primary outcome analysis, after adjusting for age, sex, comorbidities, aneurysm characteristics, and disease activity in the multivariable Cox regression model, patients who underwent EVR had a significantly increased risk of the composite endpoint compared to those who underwent OSR (Hazard Ratio [HR] = 2.29, 95% Confidence Interval [CI]: 1.15-4.56, p=0.0184). Kaplan-Meier analysis also confirmed that the long-term survival rate was significantly lower in the EVR group (log-rank p = 0.014).

Subgroup analysis revealed a critical and counter-intuitive finding: the elevated risk associated with EVR was most pronounced in patient subgroups with seemingly well-controlled systemic inflammation preoperatively. For instance, among patients with a baseline Erythrocyte Sedimentation Rate (ESR) ≤28 mm/h, the HR for EVR versus OSR was 4.24. A similar trend was observed in patients with a C-reactive protein (CRP) level ≤ 20 mg/L (HR=4.26). This pattern also held for patients older than 43 years (HR=2.74) and those with a disease duration longer than one year (HR=3.02).

Conclusion and Implications

In this 20-year retrospective study, traditional open surgical repair (OSR) was associated with superior long-term outcomes compared to endovascular repair (EVR) for the treatment of aneurysms in patients with rheumatic immune diseases. Critically, the long-term risks of EVR were paradoxically higher in patients whose systemic inflammation appeared to be well-controlled.

This counter-intuitive finding challenges the conventional wisdom that "disease stability" automatically makes a patient a suitable candidate for minimally invasive therapy. It suggests a crucial clinical concept: systemic "clinical stability" (judged by serological markers) does not equate to "vessel wall stability" at the aneurysm site. In the context of rheumatic diseases, a subclinical level of inflammation or structural degeneration may persist in the vessel wall even when systemic inflammatory markers are normal. This "hidden vulnerability" could severely compromise the long-term anchoring, endothelialization, and integration of endografts, leading to a higher risk of late failure.

Therefore, clinicians must look beyond simple inflammatory markers when devising treatment strategies for this unique patient population. The choice of EVR should be approached with significant caution and not be adopted simply for its minimally invasive appeal. Treatment decisions must be based on a comprehensive assessment by a multidisciplinary team (including rheumatology, vascular surgery, and radiology), taking into full account the patient's vascular anatomy, life expectancy, and the potential long-term impact of chronic inflammation on the endograft. For select patients, particularly those with complex anatomy or a long life expectancy, OSR may remain the more durable and reliable long-term option, even if their rheumatic disease appears quiescent. Future prospective, multicenter studies are warranted to validate these findings and to further investigate the biological mechanisms governing the interaction between the inflammatory microenvironment and implanted endovascular devices.

主动脉缩窄（CoA）的诊断、病理机制与治疗进展

李昌

武汉大学中山医院

主动脉缩窄（CoA）是一种先天性心血管畸形，部分患者可长期无症状，导致漏诊风险增加。由于出生后肺部气体干扰可能影响超声对主动脉弓的观察，胎儿超声心动图在早期诊断中至关重要。

临床实践中，CoA 常与室间隔缺损（VSD）等心脏畸形共存。本例患者在出生后 50 天接受 VSD 修复术时漏诊 CoA，可能与手术视野受限或检查重点偏差有关。VSD 患者中 CoA 发病率较高，因此建议常规检查足背动脉搏动及上下肢血压以降低漏诊风险。故年轻高血压患者若出现上肢血压升高伴下肢脉搏减弱，需警惕 CoA，并通过血管造影或非侵入性成像明确诊断。

球囊扩张术和支架置入术是治疗青少年和成人主动脉缩窄的优选微创方法，能快速降低收缩压梯度（ > 20mmHg），显著改善症状并减少降压药物需求。然而，青少年患者因血管发育未成熟、弹性较强，面临更高的再狭窄、动脉瘤形成及支架断裂风险。为此，临床推荐采用渐进式扩张策略：首次扩张直径控制在横弓直径的 80-90%（如 14mm），后续根据随访结果逐步增加 1-2mm（如 15mm、16mm）。支架植入后提供的径向支撑可降低血管破裂风险，后续扩张可参考远端正常降主动脉直径的 90%-100%。

分期干预是该策略的核心，通过多次扩张（间隔≥ 6 个月）可减少血管壁急性损伤风险，适应患者生长发育需求，同时降低夹层或破裂概率。术中需实时监测压差变化（目标降至≤ 20mmHg），并通过血管造影评估血管完整性、动脉瘤迹象及球囊 " 腰征 " 改善情况。若出现夹层、动脉瘤、无法解释的低血压或剧烈胸背痛，需立即终止操作。对于复杂病例（长段或不规则狭窄），分期扩张能更精准地优化血流动力学，平衡治疗效果与安全性。

4D 血流 MRI 等新技术可量化血流动力学参数，预测术后再狭窄风险，优化手术方案。

未来研究方向包括提高产前诊断率、开发可吸收支架及利用人工智能预测再狭窄风险。综合影像学评估、遗传筛查及个体化治疗，有望进一步改善 CoA 患者的长期预后。

Association between complete blood cell derived inflammatory biomarkers and Short-Term Adverse Events in Patients with Acute uncomplicated Type B Aortic Intramural Hematoma

Yasong Wang, Tienan Zhou, Xiaozeng Wang

General Hospital of Northern Theater Command

Introduction

Aortic intramural hematoma (IMH) presents significant clinical challenges due to its potential for rapid progression to severe complications.

Inflammation is a hallmark of the initial development and progression of Type B Aortic IMH. Individual inflammatory markers may not fully capture systemic inflammation. This study aimed to investigate the value of preoperative inflammatory biomarkers in predicting aorta-related adverse events (ARAEs) in patients with acute uncomplicated Type B IMH.

Methods

We retrospectively analyzed 387 patients diagnosed with acute uncomplicated Type B IMH from April 2018 to April 2025. Patients were categorized into the stable group (N=255) and the exacerbation group (N=123) based on the occurrence of ARAEs within a 30-day follow-up period. ARAEs were defined as outcomes related to aortic disease, or the progression of IMH to aortic dissection or penetrating aortic ulcer. Preoperative inflammatory biomarkers were recorded, including neutrophil-to-lymphocyte ratio (NLR), monocyte-to-lymphocyte ratio (MLR), platelet-to-lymphocyte ratio (PLR), systemic immune inflammation index (SII), systemic coagulation inflammation index (SCI),and systemic inflammatory response index (SIRI). Patients were followed-up for the development of AAEs. Prediction accuracy of inflammatory biomarkers for AAEs were evaluated using the area under the receiver operating characteristic curves. A complete blood count was performed upon admission and immediately analyzed using an automated hematology analyzer. Logistic regression analyses were used to identify odds ratio with 95% confidence intervals . Variables with P<0.05 in the univariate analysis were included in the multivariate analysis, using the Enter method to determine independent risk factors associated with ARAEs.

Results

This study included 387 patients with acute uncomplicated Type B IMH, comprising 256 males (66.1%) and 121 females (33.9%), with a mean age of 64.4±8.4 years. Among these patients, 96developed PAU, 19 developed AD, and 10 cases resulted in death due to aortic disease or sudden death. Compared to the stable group, the exacerbation group exhibited a significant increase monocyte counts (P=0.001), but a lower lymphocyte count (P=0.048). The preoperative NLR, PLR, MLR, SII, SCI and SIRI were significantly different between the exacerbation and stable groups. The AUCs of NLR, PLR, MLR, SII, SCI and SIRI for AAEs were 0.609, 0.660 ,0.580, 0.424, 0.583, 0.645, respectively. The ROC analysis showed that SCI had the highest sensitivity of 92.3%, while MLR had the highest specificity of 63.8%. The risk of patients with NLR(>9.905), PLR(>250.462), MLR(>0.503), SII(>1794.016), SCI(>32.397) and SIRI ,SIRI(>5.048), of developing adverse events in comparison to patients with the below complete blood cell countderived inflammatory biomarkers. Multivariate logistic regression s identified SIRI(>5.048), anemia, diabetes, maximum diameter of aortic diameter, and ulcer like projection as independent predictors of ARAEs.

Conclusion

Our study underscores the critical role of inflammation in the pathogenesis of acute uncomplicated Type B IMH and highlights the potential of complete blood cell countderived inflammatory biomarkers as a valuable prognostic marker. The complete blood cell countderived inflammatory biomarkers offers a practical and effective means of predicting short-term outcomes in patients with acute uncomplicated Type B IMH. By enabling the early identification of high-risk patients, this study can guide clinical management and ultimately improve patient prognosis.

Keywords

Type B aortic intramural hematoma, Biomarkers, Prognosis.

Analysis of clinical characteristics and related factors of patients with post-implanta tion syndrome following prophylactic application of non-steroidal anti-inflammatory drugs after thoracic endovascular aortic repair

Tie-Nan Zhou, Xuan Wu, Ya-Song Wang, Xiao-Zeng Wang

General Hospital of Northern Theater Command

Analysis of clinical characteristics and related factors of patients with post-implanta

tion syndrome following prophylactic application of non-steroidal anti-inflammatory

drugs after thoracic endovascular aortic repair

Tienan Zhou，Wu Xuan，Yasong Wang，Xiaozeng Wang

1.Department of Cardiology, General Hospital of Northern Theater Command, Shenyang, Liaoning 110016, China

Abstract: AIM: Thoracic endovascular aortic repair (TEVAR) is an important therapeutic measure for thoracic aortic diseases such as Type B aortic dissection (TABD) and thoracic aortic penetrating ulcer. Compared with traditional surgery, TEVAR has the advantages of less trauma, quicker recovery, and relatively lower intensity of postoperative inflammatory response.The aim of this study is to investigate the clinical characteristics and related factors of post-implantation syndrome (PIS) following the prophylactic application of nonsteroidal anti-inflammatory drugs (NSAID) afte TEVAR.

Methods: A total of 510 adult patients who had received prophylactic NSAIDs after TEVAR at General Hospital of Northern Theater Command from September 2013 to April 2024 were consecutively included in the study. The patients were divided into two groups based on the occurrence of PIS postoperatively: the PIS group (34 patients, 6.67%) and the non-PIS group (476 patients, 93.33%).General information, past medical history and surgical features were compared between the two groups. Univariate and multivariate logistic regression analyses were used to identify predictors of PIS. The ROC curve is used to assess the overall diagnostic performance of the risk factors.

Results: The rate of gender as male, chest and back pain on adimission, limb ischaemia on admission, systolic blood pressure on admission, use of angiotensin converting enzyme inhibitor (ACEI)/angiotensin II receptor antagonist (ARB) drugs during hospitalisation, preoperative white blood cell count(WBC) and surgical approach involving an incision were higher than those in non-PIS group , and the age, preoperative eGFR level and use of statin drugs during hospitalisation were lower than those in non-PIS group, all differences were statistically significant. Postoperative C-reactive protein level, incidence of clinical adverse events during postoperative hospitalization, and length of postoperative hospitalization were increased in the PIS group compared with those in the non-PIS group.The presence of symptoms of thoracic and back pain in the patients in the PIS group at the 1-month postoperative review was The proportion was higher (P < 0.05). Univariate and multivariate logistic regression analyses identified patients'age < 60 years(OR=4.671, 95%CI 1.348-16.188, P=0.015), elevated preoperative WBClevels(OR=3.582, 95%CI 1.469-8.735, P=0.005) , and surgical approach involving an incision (OR=8.339, 95%CI 1.849-37.610, P=0.006)as independent predictors for PIS. The results of the ROC curve analysis showed that the area under the curve for patient age <60 years, increased preoperative WBC count, femoral arteriotomy access, and the three combined diagnoses predicting the occurrence of PIS after TEVAR were 0.653(95%CI: 0.573 ~ 0.733)、0.686(95%CI: 0.600 ~ 0.771)、0.699(95%CI: 0.627 ~ 0.770)、0.826(95%CI: 0.765 ~ 0.887).

Conclusions: The level of inflammatory response is associated with the pathogenesis and changes in aortic disease, and PIS can, to some extent, reflect the level of inflammatory response in patients after TEVAR surgery. Despite the prophylactic use of NSAIDs, some patients developed PIS after TEVAR. Patients'Age < 60 years, elevated preoperative WBC levels, and femoral artery incision approach are independent risk factors for PIS. Additionally, the incidence of PIS increased with the number of independent risk factors present.

Key words: thoracic endovascular aortic repair; nonsteroidal anti-inflammatory drug; post-implantation syndrome; independent predictors

Correlation Between Hypertension and Panvascular Disease: A Prospective Vascular Magnetic Resonance Imaging Study

Shiqi Ouyang, Hai-Bo Jia

心内科

Background: Panvascular disease (PVD) represents a spectrum of systemic vascular disorders unified by the common underlying pathological hallmark of atherosclerosis. This condition can extensively involve diverse vascular beds, including large conduit arteries , medium-sized vessels and the microvasculature. The systemic nature of PVD inevitably leads to multi-organ dysfunction and damage, critically endangering vital structures such as the heart (eg:manifesting as coronary artery disease, heart failure), brain (eg:causing stroke, vascular dementia), kidneys (eg:leading to chronic kidney disease, renovascular hypertension), extremities (eg:resulting in peripheral artery disease, critical limb ischemia), and the aorta itself (eg:aortic aneurysms, dissection). Globally, the burden attributable to panvascular disease is immense and constitutes the foremost cause of mortality among the general population. While substantial research efforts have historically concentrated on elucidating the impact of hypertension on single-organ vascular pathologies（eg: hypertensive nephropathy, hypertensive heart disease, or hypertensive cerebrovascular disease) there exists a significant knowledge gap concerning the comprehensive relationship between systemic hypertension and the development or progression of multi-territory, systemic panvascular disease. This prospective study specifically aims to investigate this complex correlation, utilizing advanced multi-vascular territory magnetic resonance imaging (MRI) as a primary assessment tool.

Methods: A prospective cohort study was conducted, enrolling a total of eighty-seven (87) consecutive patients who underwent clinically indicated coronary angiography between November 2023 and June 2024. Subsequent to coronary angiography, all participants underwent a dedicated, standardized multi-vessel magnetic resonance imaging (MRI) protocol. This protocol comprehensively evaluated vascular territories beyond the coronary circulation, specifically including: (1) Intracranial arterial vasculature (using MRA to assess circle of Willis and

major branches for stenosis, aneurysms, or other anomalies), (2) Carotid arteries (employing carotid MRA to evaluate common carotid, internal carotid, and external carotid arteries for plaque burden, stenosis, and morphology), (3) Renal arteries (utilizing renal MRA to identify renal artery stenosis, or accessory renal arteries). Based on the comprehensive findings from this multi-territory MRI assessment, the study population was stratified into two distinct groups: (1) Patients exhibiting evidence of panvascular disease (defined as atherosclerotic involvement in two or more distinct vascular territories assessed);(2) Patients without evidence of multi-territory involvement (disease confined to a single vascular bed or no significant disease). Detailed baseline demographic characteristics (age, sex), established cardiovascular risk factors (hypertension status, diabetes mellitus, dyslipidemia, smoking history, body mass index), relevant medical history, and laboratory parameters were systematically collected for all participants. Inter-group comparisons between the PVD group (Group 1) and the non-PVD group (Group 2) were rigorously performed for all baseline variables and the specific imaging findings. Statistical analyses employed appropriate methods: continuous variables were reported as mean ± standard deviation or median (interquartile range). Univariate and multivariate logistic regression analyses were conducted to identify factors independently associated with the presence of panvascular disease, with results presented as odds ratios (OR) along with their corresponding 95% confidence intervals (CI). P-value of less than 0.05 was considered statistically significant for all analyses.

Results: The prevalence of panvascular disease was significantly higher among patients diagnosed with hypertension compared to their normotensive counterparts. Multivariate logistic regression analysis confirmed that hypertension itself is a potent independent predictor for the presence of panvascular disease. Patients with hypertension exhibited an odds ratio (OR) of 2.72 (95% CI: 1.01 - 7.32; p < 0.05) for having panvascular disease compared to patients without hypertension. This elevated risk underscores the profound systemic impact of hypertension on the vasculature.

Conclusion: This prospective vascular MRI study provides compelling evidence of significant correlation between hypertension and the presence of panvascular disease. Crucially, the findings demonstrate that hypertension is not merely associated with PVD but functions as a independent risk factor for the development and progression of this systemic vascular condition. These results highlight the paramount importance of rigorous hypertension detection, diagnosis, and aggressive, sustained management as a fundamental cornerstone strategy for the primary and secondary prevention of panvascular disease and its devastating multi-organ complications. Effectively controlling blood pressure represents a critical, modifiable intervention to mitigate the pervasive global burden of systemic vascular morbidity and mortality.

盐皮质激素受体在主动脉夹层病变组织的表达及临床意义

朱晴 骆秦 李南方

新疆维吾尔自治区人民医院高血压中心

目的：明确盐皮质激素受体在主动脉夹层病变组织中的表达及临床意义。**方法：**收集 2021 年 1 月至 2022 年 6 月在新疆维吾尔自治区人民医院心脏外科住院诊断为主动脉夹层并行血管置换术患者的主动脉病变组织；同期收集非夹层（主动脉瓣膜病）行主动脉瓣修补或置换术患者的主动脉组织作为对照组；采用 RT-PCR 和免疫组化检测方法分别检测两组人群主动脉组织中盐皮质激素受体的基因和蛋白表达水平；并采用相关性分析探索其表达水平与血浆醛固酮浓度的关系。**结果：**本研究共纳入 50 例，其中 37 例 AD 患者和 13 例非夹层患者（主动脉瓣置换术），平均年龄为 53.78 岁，男性占 70.0%，血浆醛固酮浓度为 18.58 ng/dL。盐皮质激素受体在人的主动脉组织中有表达。主动脉夹层患者的主动脉病变组织中盐皮质激素受体蛋白表达水平高于非夹层患者的主动脉组织（120.48±14.28 vs 104.64±10.18，P =0.001）。主动脉夹层患者的盐皮质激素受体表达水平与血浆醛固酮浓度存在相关性（r = 0.394，P =0.011；调整后 r =0.402，P=0.028）。**结论：**主动脉夹层患者主动脉组织中盐皮质激素受体表达上调，其水平与血浆醛固酮浓度升高正相关，提示醛固酮可能通过上调主动脉组织中 MR 表达损害血管壁，从而引起 AD，具体详细的分子机制需进一步研究阐明。

Piezo1 介导 NETs 释放诱导巨噬细胞焦亡促腹主动脉瘤进展的机制研究

张鸿久 [1,2] 常润泽 [1,2] 樊可奕 [1,2] 鲁传龙 [1,2] 高思琦 [1,2] 张瑞婧 [1,2] 董红霖 [1,2]

1. 山西医科大学第二医院

2. 山西医科大学血管疾病研究中心

目的：本研究旨在探讨 Piezo1 介导的中性粒细胞胞外诱捕网（NETs）释放如何诱导巨噬细胞焦亡，从而促进腹主动脉瘤（AAA）的进展及其潜在机制。腹主动脉瘤是一种严重的血管疾病，其特征是腹主动脉管壁的局限性扩张，破裂风险极高，死亡率可达 80%。尽管已有研究表明炎症在 AAA 的形成和发展中起重要作用，但其具体机制仍未完全明确。本研究聚焦于 NETs 在 AAA 中的作用，特别是 NETs 如何通过激活巨噬细胞焦亡来加速 AAA 的进展。研究试图揭示机械应力通道 Piezo1 在这一过程中的角色，为 AAA 的治疗提供新的靶点。

方法：本研究分为三个主要部分进行。首先，在动物水平上，我们构建了 C57BL/6J 小鼠腹主动脉瘤模型，通过不同时间点的取材和检测，观察 NETs 与 AAA 发生发展的相关性。具体步骤包括：选择 8 周龄健康雄性 C57BL/6J 小鼠，随机分为对照组和 AAA 组，后者接受开腹手术并用弹性蛋白酶处理腹主动脉。随后，在不同时间点（1w、2w、3w、4w）取材，进行 HE、MASSON、EVG 染色等病理学检查，检测血清中的炎性指标和 NETs 特异性标志物（如 MPO-DNA 复合物）。第二部分，我们通过体内和体外实验验证 NETs 对巨噬细胞焦亡的调控作用。体内实验中，我们将小鼠分为不同处理组（如 AAA+Cl 脒抑制剂组、AAA+DNase Ⅰ组、PADI4$^{-/-}$ 小鼠 AAA 模型组），检测巨噬细胞中 Caspase-1 p20、GSDMD 等标志物的表达。体外实验则通过提取人外周血中性粒细胞并诱导 NETosis，收集 NETs 后与 THP-1 细胞共培养，检测细胞上清液中 Piezo1、Caspase-1 p20、GSDMD 等蛋白的表达。第三部分，我们构建了 Piezo1 抑制的小鼠模型，验证 Piezo1 在 NETs 诱导巨噬细胞焦亡中的作用。通过给予小鼠 GsMTx4（Piezo1 拮抗剂），检测血液和组织中的相关指标，进一步确认 Piezo1 与 NETs 表达的关系。

结果：研究结果显示，在小鼠腹主动脉瘤模型中，NETs 的生成与 AAA 的进展密切相关。通过 HE、MASSON、EVG 染色和电镜观察，我们发现随着 AAA 的发展，NETs 的数量显著增加，且与中性粒细胞浸润密切相关。体内实验表明，NETs 能够显著上调巨噬细胞中 Caspase-1 p20 和 GSDMD 的表达，提示 NETs 确实可以调控巨噬细胞的焦亡。此外，通过抑制 NETs（如使用 DNase Ⅰ或 Cl 脒抑制剂），我们观察到巨噬细胞焦亡减少，腹主动脉瘤的进展也有所延缓。体外实验进一步证实，NETs 可以直接诱导巨噬细胞焦亡，且这一过程依赖于 Piezo1 的激活。在 Piezo1 抑制模型中，我们发现抑制 Piezo1 可以显著降低 NETs 的生成，并减少巨噬细胞的焦亡，从而延缓 AAA 的进展。

结论：本研究首次系统地揭示了 Piezo1 通过激活 NETs 诱导巨噬细胞焦亡，进而促进腹主动脉瘤进展的机制。研究结果表明，NETs 不仅是 AAA 进展的重要参与者，而且其生成受到机械应力通道 Piezo1 的调控。通过抑制 Piezo1 或 NETosis，可以有效延缓 AAA 的发展，为临床防治 AAA 提供了新的策略。此外，本研究还为理解 AAA 的发病机制提出了新的假说，即“Piezo1-NETs- 焦亡”轴可能是 AAA 进展的因果驱动因素。未来的研究可以进一步探讨这一机制的具体细节，并开发针对性的治疗手段，以提高 AAA 患者的生存率和生活质量。

主动脉壁纤维结构的研究进展

戚

海南省人民医院

摘要 主动脉管壁分为内膜、中膜和外膜三层，其中，中膜层是组织结构最复杂、承载功能最多的部位，也是主动脉疾病的最主要病因和病变部位。主动脉中膜层主要结构成份是弹力纤维（EF）和胶原纤维（CF）组成的细胞外基质（ECM）。EF 和 CF 不仅参与主动脉壁局部微环境的构成，更重要的作用在于共同维持主动脉管壁的正常形态和力学特性，弹力纤维与管壁良好的顺应性有关，胶原纤维则与管壁的极限强度有关，两者交织在一起，使主动脉既有弹性又有韧性。本文从主动脉管壁纤维结构的组成，各成份合成、表达及功能等相关问题展开综述。

关键词 弹力纤维；胶原纤维；细胞外基质；主动脉平滑肌细胞；赖氨酰氧化酶

Abstract The aortic wall is divided into three layers, intima, media, and adventitia. Among them, the media is the most complex and load-bearing part of the tissue structure, and is also the main cause and lesion site of aortic diseases. The main structural components of the aortic media are the extracellular matrix (ECM) composed of elastic fibers (EF) and collagen fibers (CF). EF and CF not only participate in the formation of the local microenvironment of the aortic wall, but also play a more important role in jointly maintaining the normal morphology and mechanical properties of the aortic wall. Elastic fibers are related to the good compliance of the wall, while collagen fibers are related to the ultimate strength of the wall. The two fibers interweave with each other, making the aorta both elastic and resilient. The article reviews the composition of the fiber structure of the aortic wall, the synthesis, expression, and function of the fibers.

Key words Elastic Fiber; Collagen Fiber; Extracellular Matrix; Aortic Smooth Muscle Cell; Lysyloxidase

The Potential Role of Neutrophil-to-Red Cell Distribution Width Ratio in the Diagnosis of Aortic Dissection

Xinxin Tian[1], Yi-Ning Yang[2]

1. Heart Center, the First Affiliated Hospital of Xinjiang University, Urumqi, Xinjiang 830054, China

2. Department of Cardiology, People's Hospital of Xinjiang Uygur Autonomous Region, Urumqi, Xinjiang 830001, China

Abstract:

Objective: Inflammation plays an important role in the occurrence and development of aortic dissection (AD). New inflammatory indicators and their differences from whole blood cell count may be associated with an increased risk of AD. A retrospective study was conducted to investigate the level of Neutrophil-to-RDW Ratio (NRR) in AD patients, and further explore its potential diagnostic role in AD patients.

Methods: This retrospective study selected eligible patients with aortic dissection from the First Affiliated Hospital of Xinjiang Medical University. 1215 AD patients who visited the First Affiliated Hospital of Xinjiang Medical University from December 2012 to May 2023 were selected as the AD group. All patients were diagnosed with computed tomography angiography (CTA) of the aorta, and the diagnosis of AD was in accordance with the 2014 ESC guidelines for the diagnosis and treatment of aortic diseases.The exclusion criteria were as follows: 1) Patients with acute myocardial infarction or acute cerebrovascular disease; 2) Patients with

severe liver and kidney dysfunction, malignant tumors, hematological disorders, or autoimmune diseases; 3) Patients with hereditary connective tissue diseases such as Marfan's syndrome; 4) Has a history of malignant tumors; 5) Pregnant women; 6) Those who have not completed the inspection and have incomplete information; 7) Patients with renal or liver failure. A total of 1,215 patients diagnosed with AD were enrolled in this comprehensive study, while an additional 1,559 healthy individuals were included to form a robust healthy control group for comparative analysis. The research protocol conforms to the ethical guidelines of the Declaration of Helsinki, and was approved by the Ethics Committee of the First Affiliated Hospital of Xinjiang Medical University (KY2022072259). Various demographics, laboratory indexes, and potential risk factors were meticulously compared between the two groups to identify significant differences. A receiver operating characteristic (ROC) curve analysis was applied to assess the diagnostic performance and predictive capability of the NLR with an area under the curve (AUC); sensitivity and specificity, as well as likelihood ratios (LR) and predictive values (PV), were also calculated.

Results: The patients in the AD group had a higher NRR, white blood cells, systolic blood pressure, diastolic blood pressure, and hypertension compared to the healthy group.Compared with the healthy control group, the NRR level in AD group was significantly higher [0.47 (0.33,0.66) vs.0.28 (0.22, 0.35)]. The results of the multivariate logistic regression analysis verified that age，smoking，Hypertension, NRR,LDL-C and TG were the affecting factors of AD.After adjusting for age, smoking history, diabetes, hypertension, systolic blood pressure, diastolic blood pressure, heart rate, fasting blood glucose, and TG, the NRR remained a risk factor for AD. The area under receiver operating ROC curve for patients with AD versus control patients was 0.802 (0.785, 0.819) for NRR.

Conclusion: The expression of NRR in patients with aortic dissection is significantly higher than that in the control group, and is closely related to the inflammatory parameters and coagulation related parameters in AD.The level of NRR is closely related to AD, and is an independent risk factor for AD. It has implications for the diagnosis of AD. NRR may provide diagnostic information in patients with AD, whether may contribute to prognosis assessment should be further investigated.

Key words: Aortic Dissection; serum biomarker; diagnosis

Soluble ST2: A Novel Biomarker for Diagnosis and Prognosis of Cardiovascular Disease

Yin Feng, Li-Qun He

Wuhan NO1 hospital

[Abstract] The increasing incidence of cardiovascular disease (CVD) is a significant global health concern, Cardiovascular disease (CVD) is now the leading cause of death not only worldwide but also in China ，affecting millions of individuals each year. Despite advances in diagnosis, treatment and prognosis, there is an urgent need for new indicators to prevent and treat CVD effectively Accurate diagnosis of acute CVD poses a formidable challenge, as misdiagnosis can significantly decrease patient survival rates. Traditional biomarkers have played a vital role in the diagnosis and prognosis of CVDs, but they can be influenced by various factors, such as age, sex, and renal function. Soluble ST2 (sST2) is a novel biomarker that is closely associated with different CVDs. Its low reference change value makes it suitable for continuous measurement, unaffected by age, kidney function, and other confounding factors, facilitating risk stratification of CVDs. Furthermore, the combination of sST2 with other biomarkers can enhance diagnostic accuracy and prognostic value. This review aims to provide a comprehensive overview of sST2, focusing on its diagnostic and prognostic value as a myocardial marker for different types of CVDs and discussing the current limitations of sST2.

Keywords: soluble ST2; cardiovascular disease; combined biomarker; diagnosis and prognosis; limitations

单分支支架在主动脉弓部病变应用研究

马强

西安交通大学第一附属医院

目的：该研究通过回顾在西安交通大学第一附属医院周围血管科就诊的主动脉弓部病变患者应用单分支支架后至少半年随访的有效性和安全性。

方法：研究纳入 2018.1-2024.12 在西安交通大学第一附属医院就诊的主动脉病变患者共 392 例，病变位于 Z1 至 Z3 区，其中夹层 360 例，动脉瘤 22 例，主动脉溃疡 10 例。应用单分支支架结合烟囱或开窗支架进行处理，观察随访至少半年，主要随访指标为手术成功率，围手术期并发症率，术后生存率，二次干预率术后各类并发症率（包括内漏，逆撕，SINE，分支闭塞率，其他并发症率）。

结果：所有患者随访至少半年，其中手术成功率 392/392(100%)；术后生存率 390/392(99%)；围手术期并发症率 10/392(2%)，其中分支后移 3 例，分支再次处理 3 例，术后穿刺点并发症 3 例，术后即刻脑梗死 1 例；术后内漏 3/392(0.8%)；术后逆撕 1/392（0.27%）；术后 SINE3/392(0.8%)；术后分支闭塞率 3/392(0.8%)；其他并发症 2/392(0.54%)。总并发症率 22/392(5.6%)。

结论：单分支支架联合多种技术在主动弓病变中的应用短期安全有效，长期效果值得期待。

Association Between Serum Bilirubin and Prevalence of Abdominal Aortic Aneurysm: Results from a Chinese Screening Program and UK Biobank Study

Ting Zhou

Guangdong Provincial People's Hospital

Objective

This study aimed to investigate the association between serum total bilirubin (TBIL) levels and abdominal aortic aneurysm (AAA), and to evaluate the potential mediating role of lipid parameters in the TBIL-driven development of AAA. Additionally, these findings were further validated using the large-scale UK Biobank (UKB) cohort.

Methods

Data were obtained from 7,953 Chinese adults enrolled in a multicenter ultrasound screening cohort for AAA in China, and 360,292 British adults from the UKB. The relationship between serum TBIL levels and AAA was systematically examined using univariate and multivariate regression analyses. Subgroup analyses were performed to assess this relationship in different demographic and clinical strata. Restricted cubic spline (RCS) analysis was conducted to delineate the dose-response

association between TBIL levels and AAA risk. To further elucidate potential mechanisms, mediation analysis was applied to evaluate the role of various lipid parameters in the TBIL–AAA association. Finally, sensitivity analyses, including propensity score matching (PSM), were performed to verify the robustness of the findings.

Results

In the Chinese multicenter AAA ultrasound screening cohort, the prevalence of AAA was 2.6%. After adjusting for potential confounders, multivariate logistic regression analysis demonstrated that TBIL was significantly inversely associated with AAA, both as a continuous variable (OR: 0.968, 95% CI: 0.944–0.993, P=0.011) and as a three-category variable (TBIL II: OR = 0.592, 95% CI: 0.415–0.844, P = 0.004; TBIL III: OR = 0.695, 95% CI: 0.492–0.983, P = 0.040). Subgroup analyses revealed that this negative association was particularly pronounced in males, individuals aged ≥ 65 years, those with a BMI <25 kg/m², patients with hypertension, and those with coronary artery disease. The RCS curve indicated a nonlinear negative relationship between TBIL levels and AAA risk (P for overall = 0.001). Mediation analysis suggested that high-density lipoprotein cholesterol (HDL-C) mediated 17.62% of the total effect of TBIL on AAA. The PSM results were consistent with these primary findings.

In the UKB cohort, over a median follow-up of 13.66 years (interquartile range), 1,534 AAA cases were documented. After controlling for confounders, multivariate Cox regression analysis revealed that TBIL, whether analyzed as a continuous variable (HR: 0.986, 95% CI: 0.974–0.999, P = 0.031) or as a four-category variable (TBIL II: HR = 0.824, 95% CI: 0.706–0.961, P = 0.014; TBIL III: HR = 0.877, 95% CI: 0.755–1.018, P = 0.084; TBIL IV: HR = 0.846, 95% CI: 0.726–0.984, P = 0.030), was significantly inversely associated with AAA. Subgroup analyses further

demonstrated that this inverse relationship was significant among males, individuals aged <65 years, those with BMI <25 kg/m², smokers, and participants without hypertension, diabetes, or coronary artery disease—with sex emerging as a key confounding factor. Mediation analysis indicated that HDL-C accounted for 9.51% of the mediating effect between TBIL and AAA. These associations remained consistent after further exclusion of potential confounders.

Conclusion

The findings from the Chinese multicenter AAA ultrasound screening cohort indicate a significant negative association between TBIL levels and AAA, with HDL-C serving as a potential mediator in this relationship. These results were further corroborated in the UKB cohort. Consequently, TBIL may represent a promising novel biomarker for predicting the development and progression of AAA, thereby aiding in the early identification of high-risk individuals and providing robust evidence for timely screening and intervention in clinical practice.

KEYWORDS: Abdominal aortic aneurysm; Total bilirubin; UK Biobank; High-density lipoprotein cholesterol

下肢动脉股腘动脉支架内再狭窄减容联合药物球囊治疗的单中心回顾研究

马强

西安交通大学第一附属医院

目的：该研究通过回顾在西安交通大学第一附属医院周围血管科就诊的股腘动脉支架再狭窄患者应用新型减容方式联合药物球囊进行治疗，观察两种减容方式联合药物球囊治疗的有效性和安全性。

方法：该研究纳入 2016.5-2024.5 在西安交通大学第一附属医院就诊的股腘动脉支架再狭窄患者 125 例，其中 Tosaka I 型 1 例，II 型 10 例，III 型 114 例。所有患者均利用准分子激光或 Rotarex 减容联合药物球囊扩张进行治疗。随访术后 1 年，观察各种分型手术成功率，TLR 及术后再狭窄率，及两种减容方式在成功率及并发症方面的比较。

结果：所有患者手术成功率 124/125(99.2%)；术后随访一年 TLR Tosaka I 型 1/1(100%)，II 型 9/10(90%)，III 型 100/114(87.7%)；亚组分析后 TosakaIII 型开通时间长，远期效果不佳；两种减容方式在手术时间，手术后效果方面没有差异。其中激光减容引起远端栓塞并发症较少。

结论：减容结合药物球囊在支架内再狭窄中的治疗短期有效，两种减容方式短期内效果基本一致，长期效果需要进一步研究。但 TOSAKA III 型长段支架内再狭窄的治疗长期通畅性依旧是难题，需要进一步评估。

探究“医院 - 社区 - 家庭”三位一体延续性护理模式对主动脉夹层患者放射介入术后护理的应用效果分析

张燕 刘华芬 黄磊

武汉大学人民医院东院

目的

探究“医院 - 社区 - 家庭”三位一体延续性护理模式在主动脉夹层（AD）患者放射介入术后护理中的应用效果，分析其对患者术后并发症发生率、康复质量、自我管理能力的影响，为优化主动脉夹层患者放射介入术后护理路径提供循证依据。

方法

采用混合性研究方法，选取 2022 年 7 月至 2024 年 7 月在武汉大学人民医院接受主动脉夹层放射介入手术的患者 100 例，随机分为干预组（n=50）与对照组（n=50）。干预组实施“医院 - 社区 - 家庭”延续性护理模式：①院内阶段：组建放射介入医师、放射介入护士、康复治疗师组成的多学科团队，制定个性化出院计划；②转介阶段：通过区域医疗信息平台共享电子病历，建立社区护士与家庭医生联合随访机制，实现术后 72 小时内访视全覆盖；③居家阶段：利用智能穿戴设备（远程血压监测仪、移动心电监护）实时传输数据，配合每周线上专科护理门诊及每月社区集中康复训练。对照组接受常规出院指导。两组均随访 6 个月，比较术后并发症、Barthel 指数（BI）、主动脉夹层疾病知识问卷（ADKQ）得分、6 分钟步行距离（6MWD）及再入院率差异，并采用质性访谈法分析患者及家属的护理体验。

结果

干预组术后 6 个月核心指标显著优于对照组（p<0.05）：并发症发生率降至 8.99%（对照组 23.60%），再入院率降低至 6.74%（对照组 20.22%）；BI 评分提升至 78.32±9.15（对照组 65.41±10.28），ADKQ 得分达 82.47±6.33（对照组 68.55±8.71），6MWD 增加至 398.6±45.3 米（对照组 325.4±52.1 米）。质性访谈显示，85.2% 的干预组患者认为远程监护系统有效缓解了术后焦虑，91.1% 的家庭照顾者表示标准化症状管理手册提升了应急处理能力。

结论

医院 - 社区 - 家庭延续性护理模式通过整合多学科资源及强化信息监测，显著改善了主动脉夹层患者术后康复质量。其核心价值体现在：①通过早期预警降低迟发性并发症风险；②依托社区联动机制弥补家庭护理的专业性缺口；③以数据驱动的个性化干预提升患者疾病管理能力。建议将该模式纳入血管外科加速康复外科（ERAS）路径，并完善社区 - 家庭护理质量评价体系，以推动危急重症患者放射介入术后护理的连续性转型。

慢性肾脏病患者血浆 miR-423-5p 含量与高凝状态的相关性研究

冯雪莹

西安交通大学第一附属医院

一、目的：

慢性肾脏病（Chronic Kidney Disease，CKD）已经逐渐成为严重的全球公共卫生问题，机体高凝状态导致的心血管血栓并发症是 CKD 患者死亡率升高的主要原因。已有研究证明，D-D 升高是机体高凝状态的标志。而导致高凝状态的原因很复杂，血管内皮细胞、血小板、凝血级联反应和纤维蛋白溶解系统均受到肾功能不全期间累积的尿毒症毒素、炎症因子和代谢产物的影响。微小 RNA（microRNA，miRNA）是约 20 个碱基对的非编码 RNA，在转录后基因调控中发挥重要作用。既往研究提示，miR-423-5p 参与调控氧化应激及炎症相关通路，其血浆表达水平与 CKD 患者中颈动脉粥样硬化斑块的发生和严重程度有关。同时，它作为血小板中表达水平最高的 miRNA 之一，是血小板活化通路的重要调节因子，可能通过激活血小板促进凝血过程。然而，目前关于 miR-423-5p 与 CKD 患者高凝状态发生间关系的研究尚缺乏。为了深入了解慢性肾功能不全相关高凝状态发生所涉及的机制，进一步探索 CKD 患者血栓形成前状态的生物标志物和治疗靶点，本研究将主要探究 CKD 患者血浆 miR-423-5p 水平与凝血指标间的关系，同时对 miR-423-5p 下游潜在靶基因进行预测。

二、方法：

在西安交通大学第一附属医院肾内科以及心内科收集确诊为 CKD 及非 CKD 患者的清晨空腹血样，离心得到血浆后进行 qPCR 获得 miR-423-5p 的相对表达水平。使用 t 检验、卡方检验和 Kruskal-Wallis 检验等方法比较基线资料。通过 spearman 相关计算相关系数以确定 miR-423-5p 与各凝血指标之间的变量关系，而后采用线性回归分析在总人群及亚组人群中对该变量关系进一步分析评估。最后，利用终末期肾病（End-stage Renal Disease，ESRD）患者血浆转录组分析的数据集 GSE97709 进行差异表达分析和功能通路富集分析，并通过与 miRNA 数据库取交集进行 miR-423-5p 的下游靶基因预测。

三、结果：

1. 相对于非 CKD 患者，CKD 患者血浆中 miR-423-5p 相对表达水平显著升高（P<0.001）。

2. 总人群血浆中 miR-423-5p 水平与 eGFR 呈显著负相关关系（β= -0.070(-0.093--0.048)，P<0.001），即随着肾功能的下降血浆 miR-423-5p 的水平逐渐升高。

3. 在总人群中，血浆 miR-423-5p 水平与 PT、INR、FIB、D-D、FDP 值之间存在正相关关系，与 PA 值之间存在负相关关系，其中与 D-D 的相关性最强（r=0.270，P<0.001）。在调整协变量后，血浆 miR-423-5p 水平对 FIB（β=0.018(0.005-0.032)，P=0.007） 和 D-D（0.020(0.003-0.037)，P=0.024）影响显著。

4. 在 CKD 患者中，血浆 miR-423-5p 仅与 D-D 水平显著正相关（β=0.024(0.004-0.043)，P=0.020）。

5.ESRD 患者的血浆转录组数据分析显示差异表达基因显著富集在凝血调节、血小板活化等通路。

6. 筛选 ESRD 患者中显著表达下调的基因，采用 miRDB、TargetScan 和 miRTarBase 数据库预测 miR-423-5p 可能通过下游靶基因 MFGE8（log-2FC=-357.92，P=3.42E-07）参与对凝血功能的调节。

四、结论：

CKD 患者血浆 miR-423-5p 的水平显著升高，与高凝状态指标 D-D 显著正相关。对 miR-423-5p 进行干预，可能是减少 CKD 患者心血管血栓并发症的有效治疗手段。

肺栓塞 79 例临床诊治分析

钟伟

重庆荣昌区人民医院

【摘要】目的 增强对肺栓塞的认识，提高对肺栓塞的诊治水平，减少误诊率。**方法** 对 2006 年 1 月至 2009 年 l2 月收治入院的 79 例肺栓塞患者的临床资料进行回顾性分析。**结果** 79 例中首诊误诊 49 例(62.03%)，溶栓治疗 35 例(44.30%)，抗凝治疗 62 例（78.48%），死亡 11 例 (13.92%)。**结论** 肺栓塞临床症状和体征缺乏特异性；及时准确诊断肺栓塞，制定恰当的治疗策略对改善预后具有积极意义。

【关键词】肺栓塞；诊断； 误诊； 治疗

肺栓塞 (PE) 是各种栓子阻塞肺动脉系统的一组疾病或临床综合征的总称。目前，因其高发病率、高死亡率和低诊断率已成为全球的医疗保健问题 [1]，且发病率有明显升高趋势，是一种极易被误诊的急危重症疾病，可见于各临床科室。据研究在老年人群中，PE 的患病率和病死率均随年龄的增长而增加，在 65 ~ 69 岁的患者中年发病率为 1．8% ，85 ~ 89 岁的患者中年发病率为 3.1 %。美国每年新发病人数约 60 万，其中近 20%死亡，占死亡原因的第 3 位，仅次于肿瘤和心肌梗死。曾有 12 个尸检研究荟萃分析显示，严重 PE 漏诊率达 70%以上。我国临床上对此一度认识不足，误诊率和漏诊率高，治疗上亦不尽合理。为提高肺栓塞的临床诊治水平，降低误诊率，现将我院 2006 年 1 月 - 2009 年 l2 月收治的 79 例肺栓塞患者的临床资料作一回顾性分析。

Association Between Life's Essential 8 Score and the Risk of Abdominal Aortic Aneurysm: A Prospective Cohort Study from UK Biobank data

Chen Sixv, Hai-Feng Zhang, Yang-Xin Chen

Sun Yat-Sen Memorial Hospital, Sun Yat-Sen University

Background

Abdominal aortic aneurysm (AAA) represents a common life-threatening disease with high morbidity and mortality due to severe complications, such as aortic rupture. The healthy lifestyle factors have been closely associated with the risk of AAA. The American Heart Association (AHA) recently released a checklist of health factors known as Life's Essential 8 (LE8) to optimize cardiovascular health. The aim of this study was to test the hypothesis that greater adherence to the LE8 score was associated with a decreased risk of new-onset AAA.

Methods

This study included 279,251 UK Biobank participants without a history of AAA. LE8 score was calculated using 8 metrics according to the AHA's definition, including three health behaviours (sleep duration, smoking, and physical activities) and four health factors (blood pressure, HbA1c,

BMI, and non-HDL cholesterol). The primary outcome in this study was the incidence of new-onset AAA, which was identified by linking the cohort database with death register and hospital inpatient admissions base on ICD-10 codes (I71.3 or I71.4), or AAA-related surgical procedure (L18, or L19, L254, or L27, or L28, or L464). The study population was divided into four groups based on LE8 quartile. The Cox proportional hazard model was used to assess the association between LE8 score and risk of AAA. Restricted cubic spline (RCS) models with three knots (10th, 50th, and 90th percentiles) were conducted to estimate the dose-response association between LE8 and risk of AAA. The subgroup analyses were stratified by sex, age, and ethnicity. Several sensitivity analyses were used to verify the robustness of the results.

Results

During a median follow-up of 12.77 years (interquartile range: 12.08–13.04), 1042 cases of incident AAA were identified. Kaplan-Meier curves demonstrated that a higher LE8 score was associated with a lower risk of AAA during follow-up. After adjustment for potential confounders, the hazard ratio (95% confidence interval) of AAA was 0.52 (0.43, 0.64) for the Q2 group, 0.39 (0.32, 0.49) for the Q3 group, and 0.20 (0.12, 0.28) for the Q4 group, when compared with the Q1 group (the lowest LE8 score). When analyzed as a continuous variable, each 5-point increase in LE8 score was associated with a 20% lower risk of AAA (HR: 0.80, 95% CI: 0.73–0.85). A restricted cubic spline (RCS) revealed that the risk of AAA decreased continuously with increasing LE8 score across the range from 5.0 to 100.0, with the p for nOnlinear= 0.232. The results of the subgroup analysis stratified by age, sex, or ethnicity were consistent with the main analysis. In the sensitivity analyses, the results did not change when participants with outcome events within the first 2 years of follow-up were excluded. Moreover, consistent results were observed when analyses were repeated without performing multiple imputation of covariates. In addition, the association of LE8 and risk of AAA was assessed by Fine-Gray Model, and the results remained generally robust. Finally, after imputing these missing LE8 data, the results still consistent with the primary analysis.

Conclusion

In conclusion, this study showed that CVH as assessed by LE8 score was inversely associated with the risk of AAA in the general population. Our findings emphasize the importance of taking primordial approaches to maintain cardiovascular health and prevent the incidence of AAA.

Dietary Components of Curcuma longa Ameliorate Renal Artery Stenosis: Network Pharmacology and Experimental Validation

chunliang Zhang[1], De-Hui Qian[1]

1. Xinqiao Hospital, Army Medical University

2. Nanjing Normal University

Renal artery stenosis(RAS) is a common vascular disease, currently mainly treated with surgery, however its treatment methods are relatively limited.Curcuma longa (CUL) has been proven to have anti-inflammatory and antioxidant effects, and is a medicinal and edible plant with a long history and rich value.The objective of this study was to investigate the mechanism of Curcuma longa (CUL) on Renal artery stenosis(RAS), based on network pharmacology and molecular docking. We screen for common targets of CUL and RAS and verify the targets genes in cell experiments. The common targets of CUL and RAS were screened and obtained using different databases. These target genes were analyzed by GO and KEGG pathway enrichment analysis. PPI network analysis was performed and to analyze the key targets. A serizes of Wb models was constructed to confirm the relationship about the key targets and the core components of CUL.Then, we further use molecular dynamics simulations to simulate its binding interactions.The results demonstrated that GO functional enrichment analysis and KEGG pathway enriched top 10 pathways including Pathways in cancer,Diabetic cardiomyopathy,AGE − RAGE signaling pathway in diabetic complications,Renin secretion,Phospholipase D signaling pathway,Neuroactive ligand − receptor interaction involving inflammation and stress effects.The key genes were identifed in the Cytoscape3.10.1. The molecular docking analysis showed that each component bound strongly to the targets PPARG,IL6,HIF1A and ESR1. The cell experiments showed the core targets reduced by the core components of CULadministration. We identifed some common target genes of CUL and RAS and identifed these key genes. The anti-inflammatory efect of CUR was associated with the inhibition of upregulation of PPARG,IL6,HIF1A and ESR1 in vascular endothelial cell.Molecular docking and molecular dynamics simulations show that they have good binding effects.Taken together, this investigation highlights the potential of turmeric in anti-inflammatory and antioxidant functions,It regulates the physiological function of renal artery endothelial cells by downregulating the expression of proteins such as PPARG, HIF1A, ESR1, etc., laying the foundation for its development as a novel therapeutic drug for renal artery stenosis.

Our work leveraged network pharmacology to predict active ingredients and key targets for liver injury repair.Our study primarily focused on the beneficial effects of Curcuma longa. It is also important to acknowledge that some compounds may interact with unintended targets, potentially leading to adverse effects. Future studies should aim to investigate these off-target interactions to ensure the safety and efficacy of Curcuma longa.Network pharmacology revealed that stigmasterol and campesterol are the main active components in Curcuma longa, and PPARG, HIF1A, ESR1, and IL-6 genes may be potential targets for the core components of Curcuma longa to act on renal artery stenosis. The main pathways involved include the RASS hormone system, endothelial cell function regulation, and glucose metabolism pathways. Our cell experiments demonstrated that stigmasterol and campesterol downregulate the protein expression of these core targets and effectively reduce the inflammation level in inflammatory cell models. Further molecular docking and molecular dynamics studies showed that campesterol had the best binding effect with HIF1A and ESR1 targets, which are involved in the RAAS hormone system and corresponding glucose metabolism pathways.

GW501516 对低氧条件下肺动脉平滑肌细胞增殖的作用及其机制

陈昌贵 贺立群

武汉市第一医院

【摘要】目的：观察过氧化物酶体增殖物激活受体δ(PPA R δ) 激动剂 GW501516 对低氧原代大鼠肺动脉平滑肌

细胞 (PASMCs) 增殖的影响，并探讨其可能机制，为低氧肺血管重构的防治寻找新靶点。方法：对照组 PASMCs 采

用 21% 氧气培养，低氧组采用 3% 氧气诱导 PASMCs 增殖，通过不同浓度的 GW501516(10、30、100 nmol /L) 低氧条

件下孵育 PASMCs 12、24、48 h 筛选 GW501516 抑制低氧 PASMCs 增殖的最适浓度；选择 100 nmol /L GW501516 和

(或) 蛋白激酶 B(AKT) 激动剂 SC79 在低氧条件下孵育 PASMCs 24 h，探讨 GW501516 抑制 PASMCs 增殖可能机

制，通过 CCK-8 与 BrdU 试剂盒检测细胞增殖与 DNA 的合成，流式细胞仪分析细胞周期，实时定量 PC R (R T-PC R)

检测细胞周期蛋白 (Cyclin) D1，细胞周期蛋白激酶抑制蛋白 p27(p27) m R NA 的表达，Western blot 检测 PPA R δ、总

的和磷酸化蛋白激酶 B(AKT) 与糖原合酶激酶 3β(GSK3β) 的表达。结果：与低氧组相比，不同浓度的 GW501516

(10、30、100 nmol /L) 干预 12、24、48 h 后能够抑制低氧条件下 PASMCs 增殖与 DNA 的合成，且 100 nmol /L

GW501516 抑制作用最强 (P < 0. 05 或 P < 0. 01) ；与对照组相比，100 nmol /L GW501516 干预 PASMCs 24 h 能够显著

上调 PPA R δ 的表达，而低氧可显著下调 PPA R δ 的表达 (P < 0. 01) ；与低氧组相比，100 nmol /L GW501516 干预 24 h

后能够显著抑制 PASMCs 增殖与 DNA 的合成 (P < 0. 01) ，增加处于 G0 /G1 期的 PASMCs 比例，明显减少 S 期和 G2 /

M 期的 PASMCs 比例 (P < 0. 05 或 P < 0. 01) ，显著抑制 Cyclin D1 m R NA 的表达并促进 p27 m R NA 的表达 (P < 0. 01) ，

显著抑制 AKT 与 GSK3β 磷酸化 (P < 0. 01) ，而与 100 nmol /L GW501516 低氧组相比，AKT 激动剂 SC79 能够逆转

100 nmol /L GW501516 上述作用 (P < 0. 05 或 P < 0. 01) 。结论：GW501516 通过抑制 AKT/GSK3β 信号通路抑制低氧

条件下 PASMCs 增殖。

【关键词】低氧；肺动脉平滑肌细胞；GW501516; 过氧化物酶体增殖剂激活受体 δ; 增殖；蛋白激酶 B/ 糖原

合酶激酶 3β

健康促进与自我效能理论在急性 A 型主动脉夹层术后早期康复护理中的应用效果研究

何媛 张喜维

首都医科大学附属北京安贞医院

目的： 探讨基于健康促进模型（HPM）和自我效能理论（SET）的综合早期康复护理干预方案对改善急性 A 型主动脉夹层（TAAD）术后患者心理健康、生活质量及社会功能的效果。

方法： 采用前瞻性随机对照试验设计。纳入 80 例 TAAD 术后患者，随机分为实验组（n=40）和对照组（n=40）。对照组接受常规护理。实验组在常规护理基础上，接受为期 12 周的整合 HPM 和 SET 的综合干预，包括分阶段（术后早期、中期、晚期、远期）实施的心理教育、个体化咨询、同伴支持小组讨论及音乐治疗。在干预前（T0）、干预中期（T1，约 6 周）、干预结束（T2，12 周）及干预结束后 3 个月（T3）四个时间点，使用医院焦虑抑郁量表（HADS）、创伤后应激障碍自评量表（PCL-C）、世界卫生组织生活质量简表（WHOQOL-BREF）及社会功能缺陷筛查量表（SDSS）评估两组患者的焦虑抑郁水平、创伤后应激障碍风险、生活质量及社会功能。采用 SPSS 26.0 进行统计分析，计量资料组间比较采用独立样本 t 检验或重复测量方差分析，计数资料采用 χ^2 检验，以 P<0.05 为差异有

统计学意义。

结果： 实验组在 T1、T2 及 T3 时间点的 HADS 焦虑评分均显著低于对照组（实验组 5.8±2.1 vs 对照组 8.2±2.7, P<0.001）。实验组 PCL-C 评分在 T2、T3 显著低于对照组（实验组 28.5±7.4 vs 对照组 35.8±8.6, P<0.01）。实验组 WHOQOL-BREF 总分评分在 T2、T3 均显著高于对照组（实验组 78.3±9.5 vs 对照组 68.9±10.2, P<0.001）。实验组 SDSS 评分在 T3 显著低于对照组（实验组 1.2±0.8 vs 对照组 2.1±1.2, P<0.05）。方差分析显示实验组在 HADS、PCL-C、WHOQOL-BREF 及 SDSS 得分的时间主效应、组间主效应及交互效应均具有统计学意义（P<0.05）。

结论： 基于健康促进模型和自我效能理论的综合早期康复护理干预能有效降低 TAAD 术后患者的焦虑抑郁情绪和创伤后应激障碍风险，显著提升其生活质量和改善社会功能，且效果具有持续性和稳定性。该方案为优化 TAAD 术后康复护理实践提供了科学依据和有效路径。

借助单细胞转录组绘制胸主动脉瘤图谱

刘雪晗

山东大学齐鲁医院

目的：血管疾病领域单细胞测序（scRNA-seq）的研究开展较晚，目前尚无跨物种分部位的联合主动脉瘤单细胞微环境图谱绘制及数据库报道，本研究旨在提供全面、细胞量和测序深度高通量的多维度主动脉瘤单细胞图谱及数据库。

方法：通过 BAPN 喂水联合血管紧张素 2 泵注构建小鼠胸主动脉瘤模型，各组模型构建完成后按解剖结构剥离主动脉病变组织，同时进行消化解离制备单细胞悬液，通过台盼蓝染色和荧光细胞计数等方法判断单细胞悬液质量是否达到测序要求，即细胞活性大于 90%，细胞浓度在 700~1200 个 /uL。使用官方建库试剂盒 (10X Genomics Chromium Single-Cell 3’kit，V3) 进行细胞捕获后（捕获目标细胞 5000），进行 cDNA 扩增和文库构建。构建文库后采用 NovaSeq 6000 测序平台进行测序，单个样本测序深度 20,000 reads 以上。

结果：前期已完成小鼠正常主动脉、胸主动脉瘤单细胞测序建库及结果分析，对单细胞数据进行质控和细胞类型定义等，进行 GO 和 KEGG 差异基因富集分析，完成细胞轨迹分析，SCENIC 转录因子析，WGCNA 分析以及细胞互作分析，发现 GAS6-MERTK 互作对在胸主动脉瘤发生发展过程中起到重要作用。

结论：本研究首次揭露了胸主动脉瘤破裂在空间转录组水平的全景图谱，通过构建小鼠健康主动脉、胸主动脉瘤单细胞转录组数据库，探究在胸主动脉瘤发生过程中起到决定性作用的互作对。此外，联合临床胸主动脉瘤患者的血浆检测，筛选具有临床诊断和预测前景的生物学标志物，弥补了人胸主动脉瘤 / 夹层缺乏临床靶向药物治疗靶点与血清学诊断标志物的缺口。

Single-cell and spatial transcriptomics uncover age-associated smooth muscle de-differentiation and macrophage behavior in acute aortic dissection

Jing Tao[1,2], Jia-Hui Yong[1,2], Yi-Ning Yang[1,2]

1. People’s Hospital of Xinjiang Uygur Autonomous Region

2. Xinjiang Key Laboratory of Cardiovascular Homeostasis and Regeneration Research

Objectives

Type A acute aortic dissection (TAAAD) is a life-threatening cardiovascular emergency with a significantly earlier onset in the Chinese population (mean age 51.6 years) compared to Europeans (mean age 61.3 years). However, existing research has predominantly focused on elderly patients, leaving critical gaps in understanding age-specific pathogenic mechanisms, particularly in early-onset cases. This study aimed to investigate age-dependent molecular mechanisms underlying TAAAD using single-cell and spatial transcriptomics, identify key regulatory factors and pathways, and explore potential therapeutic targets for early-onset TAAAD, with a specific focus on unraveling the interplay between vascular smooth muscle cell (vSMC) phenotypic changes and immune cell behavior across different age groups.

Methods

A total of 23 TAAAD patients (stratified into early-onset [<40 years, n=6], mid-onset [40–55 years, n=10], and late-onset [>55 years, n=7]), 5 aortic aneurysm (AA) patients, and 3 healthy controls were included. Surgically resected aortic tissues from 53 anatomically annotated regions were collected. Single-cell RNA sequencing (scRNA-seq) and spatial transcriptomics were performed, generating transcriptomic data from 599,544 cells. Unsupervised clustering, principal component analysis (PCA), weighted gene co-expression network analysis (WGCNA), and trajectory analysis were used to characterize cellular heterogeneity and age-related molecular features. In vitro, human vascular smooth muscle cells (vSMCs) were subjected to hypoxic conditions, and ENO1 knockdown was used to verify its role in vSMC phenotypic switching. An AAD mouse model was established, and lentivirus-mediated Eno1 knockdown was performed to evaluate its impact on AAD progression and survival. Cell-cell communication analysis and co-culture experiments were conducted to explore the interaction between vSMCs and macrophages, focusing on the role of MIF and its receptors (CD74/CD44/CXCR4).

Results

Early-onset TAAAD patients exhibited higher white blood cell counts and a significantly increased male predominance (OR=8.57). Histologically, they showed more extensive medial destruction and inflammatory cell infiltration. scRNA-seq revealed elevated frequencies of NKT cells and proliferating macrophages in early-onset TAAAD, with myeloid cell enrichment as a characteristic immune phenotype. Twelve vSMC subtypes were identified, with the “Stressed SMC2/3” subtype specific to early-onset TAAAD. This subtype was associated with the transition from contractile to synthetic vSMCs, with its differentiation trajectory (Lineage 1) enriched in hypoxia response and glycolysis pathways, and negatively correlated with age (R=-0.3, p=0.033). WGCNA identified ENO1 as a hub transcription factor in Stressed SMC2/3. In vitro, ENO1 promoted vSMC phenotypic switching (downregulation of contractile marker α-SMA, upregulation of synthetic markers OPN/MMP9) and enhanced proliferation/migration, while ENO1 knockdown inhibited these processes under hypoxia. High ENO1 expression in Stressed SMC2/3 increased MIF secretion, which bound to macrophage receptors (CD74/CD44/CXCR4) to promote macrophage retention and pro-inflammatory (M1) polarization. In AAD mice, Eno1 knockdown reduced MIF expression and M1 polarization, significantly decreasing dissection incidence (from 80% to 30%) and improving survival (from 40% to 80%).

Conclusions

This study uncovers age-dependent molecular mechanisms in TAAAD using single-cell and spatial transcriptomics, identifying the ENO1-MIF axis as a pivotal driver of early-onset TAAAD pathogenesis. ENO1 promotes vSMC phenotypic switching and MIF-mediated macrophage pro-inflammatory polarization, while targeting ENO1 attenuates AAD progression in mouse models. These findings highlight the ENO1-MIF axis as a potential therapeutic target for early-onset TAAAD, advancing understanding of age-related differences in aortic dissection mechanisms.

Trem2/Tyrobp/Syk 信号通路通过抑制巨噬细胞促炎活化抑制主动脉夹层及破裂研究

张增辉 陈样新

中山大学孙逸仙纪念医院

目的：主动脉夹层（AD）的发生发展与炎症反应密切相关。Trem2/Tyrobp 信号通路作为免疫炎症的关键调控因子，在心血管疾病中具有重要作用，但其在 AD 中的具体功能尚未明确。本研究旨在于明确巨噬细胞 Trem2/Tyrobp 通路在 AD 中的作用及机制探索。

方法：为探究其功能机制，研究人员构建了 Tyrobp 全身性敲除（Tyrobp⁻/⁻）、髓系细胞特异性 Tyrobp 敲除（Tyrobp□□/□□ Lyz2cre）以及 Trem2 敲除（Trem2⁻/⁻）小鼠模型，通过饮水给予 β- 氨基丙腈（BAPN）诱导 AD。利用氯膦酸脂质体清除巨噬细胞以解析巨噬细胞在 Tyrobp 缺失介导 AD 进展中的作用。通过 Toll 样受体 4（TLR4）小分子抑制剂抑制巨噬细胞促炎活化及主动脉炎症反应。通过批量及单细胞 RNA 测序、免疫荧光染色和实时定量 PCR 等技术评估炎症反应及 Tyrobp 的作用机制。

结果：研究通过分析人类和小鼠 AD 主动脉组织的转录组数据，基于差异表达基因构建蛋白质互作网络，发现 Tyrobp 是 AD 的核心枢纽基因，且在人类和小鼠 AD 组织中表达显著升高。动物实验结果显示，Tyrobp 全身性或髓系细胞特异性缺失显著增加小鼠 AD 发生率，并加剧主动脉壁细胞外基质降解和巨噬细胞浸润。巨噬细胞清除可减轻 Tyrobp 缺失对 AD 进展的不利影响。机制研究表明，Tyrobp 缺失以及其下游 Syk 靶分子抑制剂均可增强 TLR4 炎症信号通路和巨噬细胞活化，而 TLR4 抑制剂可阻断上述效应。此外，Trem2 缺失显著加重小鼠 AD 发展，而 Trem2 激动剂治疗则对 AD 具有保护作用。

结论：本研究揭示了 Trem2/Tyrobp 信号通路在 AD 发展中的新作用，该通路通过抑制 TLR4 介导的巨噬细胞活化发挥保护效应。增强 Trem2/Tyrobp 信号通路可能成为预防和治疗 AD 的新策略，其在人类 AD 中的作用值得进一步研究。

超声评估受压段流速比与远心段呼吸相性变化对髂静脉压迫综合征的诊断效能分析

陈菁 谢培凯

珠海市人民医院

目的：探讨超声诊断下肢髂静脉压迫综合征（IVCS）与数字减影血管造影（DSA）检查结果的一致性，为临床诊断与筛查 IVCS 提供循证依据。

方法：选取 2024 年 1 月至 2025 年 4 月期间因下肢疼痛或静脉曲张住院的 78 例患者为研究对象。所有患者入院后均同时接受髂静脉彩色多普勒超声和 DSA 血管造影检查。依据 DSA 检查结果，将患者分为 IVCS 阳性组（n=15）和阴性组（n=63）。超声诊断 IVCS 的标准为: 1）受压处流速与扩张处流速比值 > 2.5; 2）受压远心段静脉血流呼吸相性变化减弱或消失。所有纳入患者资料完整，排除合并影响下肢静脉回流的其他疾病及无法完成相关检查者。

结果：以 DSA 结果作为 “金标准”，共检出 IVCS 阳性 15 例、阴性 63 例。超声检查诊断 IVCS 阳性 16 例，其中 12 例为 DSA 确诊的真阳性，4 例为假阳性；超声诊断阴性 62 例，其中 59 例与 DSA 一致为真阴性，3 例为假阴性。由此计算，超声诊断 IVCS 的敏感性为 80.0%，特异性为 93.7%，阴性预测值为 95.2%，阳性预测值为 75.0%，总体准确率为 91.0%。Kappa 一致性检验结果显示，超声与 DSA 在 IVCS 诊断上一致性较高，Kappa 值为 0.718，且 $p < 0.01$，表明两种方法的一致性具有统计学意义。

结论：本研究结果表明，超声检查在下肢髂静脉压迫综合征的诊断中，与 DSA

这一金标准检查结果具有较高的一致性。作为一种无创、操作简便、可重复性强的检查方式，超声对于 IVCS 的初步筛查、随访及疗效评价均具有重要临床应用价值。

白细胞计数与血红蛋白比值对心力衰竭患者院内死亡风险的预测价值

涂佩 刘海珍 涂焰明 宗文霞 李昌

湖北省中山医院 (湖北省第三人民医院)

目的：本研究旨在探讨白细胞计数与血红蛋白比值（WHR）对心力衰竭（HF）患者院内死亡的预测价值，并评估其作为预后标志物的临床应用潜力。

方法：本研究采用回顾性队列研究，连续纳入 2022 年 8 月至 2024 年 8 月期间在江汉大学附属湖北省第三人民医院心血管内科住院治疗的心力衰竭患者，根据住院期间转归将患者分为存活组（n=202）和死亡组（n=50）。收集患者的一般资料及实验室指标，通过统计学分析，分析 WHR 对心力衰竭患者院内死亡风险的预测价值。

结果: WHR 是 HF 患者院内死亡的独立危险因素（OR=1.95，95%CI: 1.075-1.329，P<0.001）。ROC 分析显示，WHR 对心衰患者院内死亡具有良好的预测价值（AUC 0.7357，95%CI：0.6581-0.8134），最佳截断点为 6.4495（灵敏度 68.0%，特异度 70.3%）。Cox 生存分析表明，高 WHR 患者死亡风险增加 2.684 倍（95%CI: 2.010-6.752）。

结论：WHR 是 HF 患者院内死亡的独立预测因子，具有较高的临床预测价值，可作为早期风险评估和预后评估的可靠生物学标志物。该指标简便易得，有助于临床医生识别高危患者并优化干预策略。

远端孤立性血栓的临床策略与治疗进展

胡会社 田红燕

西安交通大学医学院第一附属医院

目的

总结孤立性远端深静脉血栓（IDDVT）最新循证证据，建立以危险分层为核心的个体化诊疗路径，并比较新型口服抗凝药（NOAC）与传统方案的疗效与安全性。

方法

系统回顾 2020-2025 年发表的 6 项多中心研究（共纳入 >9 500 例 IDDVT 患者），提取 ACCP-10、ESC 及中国共识等指南意见；采用 Meta 分析比较 NOAC（利伐沙班 20 mg/d）与华法林（INR 2-3）在 6 个月内血栓蔓延、肺栓塞、大出血及全因死亡；同时汇总 RIDTS、CACTUS、LERIT 等研究对低危患者监测策略的随访数据。

结果

1. 抗凝疗效: NOAC 组血栓蔓延 / 肺栓塞发生率显著低于华法林（1.8 % vs 3.6 %，P = 0.002）；大出血风险亦降低（7.9 % vs 10.5 %，P = 0.013）。

2. 疗程与剂量：标准剂量利伐沙班 20 mg/d×3 个月较 6 周疗程可进一步降低 VTE 复发（HR 0.42，95 %CI 0.25-0.71），且不增加出血；低剂量（10-15 mg/d）疗效劣于标准剂量。

3. 风险分层：LERIT 评分≥ 3 分或超声显示血栓直径 > 7 mm、累及多支静脉者，抗凝 3 个月获益最大；低危患者 2 周内连续超声未见进展者，可安全采取“监测 - 不抗凝” 策略（VTE 复发率 < 1 %）。

4. 特殊人群：活动性肿瘤患者仍以低分子肝素为首选，但 NOAC 可作为肾功能正常者的替代；术后 / 高出血风险人群短程抗凝（4-6 周）联合机械预防可减少出血事件。

结论

IDDVT 治疗应首先完成危险分层：高危患者给予标准剂量 NOAC 3 个月为当前最佳方案；低危患者可考虑 2 周影像学监测，无进展则免抗凝。未来需验证生物标志物和新型评分系统以实现更精准个体化。

Precision Alignment in Minimalist Fenestrated TEVAR: A Novel Physician-Modified Technique Utilizing Self-Aligning Relay Non-Bare Stent-Grafts for Thoracic Aortic Endovascular Repair

Junzhou Pu, Wen-Hui Wu

Beijing Anzhen Hospital, Capital Medical University

Abstract

Objective:

To address the technical complexities of conventional fenestrated thoracic endovascular aortic repair (f-TEVAR) for aortic diseases involving the arch, we developed a streamlined approach utilizing a novel physician-modified Relay Non-bare stent-graft, eliminating the need for time-consuming marker suturing or guidewire-assisted fenestration alignment. This study evaluates the clinical application of this minimalist modification protocol.

Methods

This retrospective study analyzed 33 patients undergoing minimalist f-TEVAR using Relay Non-bare stent-grafts between January and December 2023. Preoperative ECG-gated CTA guided precise fenestration planning. The stent-graft's proprietary self-alignment mechanism enabled marker-free orientation via its pre-curved design and 12/6 o'clock markers. The Terumo Relay NBS stent-graft's proprietary self-alignment technology ensures precise arch conformation through a pre-curved inner catheter matching anatomical curvature, S-bar reinforcement along the greater curve, and a 12 o'clock alignment marker at the outer curvature. This integrated system automatically oriented the stent-graft's black midline marker to the aortic arch's superior aspect, enabling accurate fenestration positioning based on preoperative measurements.

Following angiographic confirmation of anatomical parameters, stent-graft customization proceeded in the Cath Lab. The proximal inner sheath was advanced beyond the outer primary sheath after shipping retainer removal, with first-stage stent deployment exposing modification zones. Preplanned window positions were marked using sterile surgical rulers and skin markers, followed by precise fenestration creation using low-temperature radiofrequency punch devices. The NBS system's inherent alignment accuracy eliminated the need for supplemental marker sutures.

The dual-sheath NBS delivery system (soft inner/rigid outer configuration) facilitated safe recapture through silk ligature-mediated stent compression during inner sheath retraction and continuous thread tension-guided outer sheath repositioning. Fluoroscopic confirmation of maintained 12/6 o'clock marker alignment ensured preserved spatial orientation post-resheathing.

All minimalist f-TEVARs employed local anesthesia with bilateral femoral access using ProGlide ™ preclosure (Abbott Laboratories, Chicago, IL). Mandatory 12 o'clock flush port alignment during introducer insertion ensured proper device orientation. Critical deployment steps included LAO projection-guided D-shaped marker alignment along the aortic greater curvature, continuous advancement of the deployment grip until proximal markers reached the planned landing zone, and reliance on the integrated self-orientation system to position fenestrations at predefined anatomical targets. The stent-graft was deployed in a single continuous motion, followed by retrograde (LSA) or antegrade (LCCA) fenestration cannulation.

Intraoperative modifications included partial deployment, low-temperature fenestration punching, and simplified re-sheathing with dual-layer delivery.The primary endpoints were technical success, stent-graft modification time, fluoroscopy time, procedure time, endoleak rate, procedure related complications, length of stay, 30-day, and late mortality.

Results

The cohort (mean age 63.2±10.6 years, 75.8% male) presented with different aortic diseases: penetrating ulcers (42.4%), type B dissections (27.3%), non-A non-B dissections (18.2%), and aneurysms (12.1%).The technique demonstrated our efficiency: graft modification time was 6.8±1.8 minutes, fluoroscopy exposure was 8.2±3.9 minutes and total procedure time was 57.9±13.1 minutes. All procedures achieved technical success (100%), with no instances of endoleak, retrograde dissection, or neurological complications. All patients survived after a mean follow-up of 12.6 ± 3.7 months. Supra-arch branches were all patent by the end of follow-up.

Conclusions

Our experience demonstrates that the Relay Non-bare stent-grafts self-aligning design characteristics enable safe and efficient fenestration while maintaining excellent sealing properties and branch vessel patency. This stent-graft selection strategy provides a reliable foundation for simplified arch repair, potentially expanding the accessibility of complex endovascular aortic interventions.

Basal Metabolic Rate and Risk of Aortic Aneurysm and Dissection: Results from Two Cohort Studies

Xiaosi Chen

Guangdong Provincial People's Hospital

Background

Aortic aneurysm and dissection(AAD) is a fatal and irreversible vascular disease. Previous studies have shown that a high basal metabolic rate (BMR) is associated with a high incidence of cardiovascular disease. This study aimed to comprehensively investigate the potential association between BMR and the risk of AAD, encompassing abdominal aortic aneurysm (AAA), thoracic aortic aneurysm (TAA), and aortic dissection (AD).

Methods

Utilizing prospective data from 360,292 participants enrolled in the UK Biobank (UKB) cohort, the study examined the relationship between BMR and AAD events. Univariable and multivariable Cox proportional hazards model was used to estimate the hazard ratios (HRs) and 95% confidence intervals (CIs) of outcomes associated with BMR quartiles, with the lowest quartile used as the reference group. Cumulative incidence curves were generated to visualize risk over time. Restricted cubic spline (RCS)

analyses assessed potential non-linear dose-response relationships.

To validate these findings, this study further analyzed data from a multicenter ultrasound screening cohort for AAA in China comprising 10,169 Chinese participants specifically recruited for AAA research, utilizing univariable and multivariable logistic regression models to calculate odds ratios (ORs).

Additionally, a mediation analysis was conducted using 44 pre-specified circulating metabolic biomarkers derived from the UKB's high-throughput nuclear magnetic resonance (NMR) metabolomics platform.

Results

Within the UKB cohort, during a median follow-up period of 13.65 years, 1620 new cases of AAA, 684 new cases of TAA and 180 new cases of AD were documented. After adjusting for potential confounders, multivariate Cox regression analysis revealed that individuals in the highest quartile of BMR exhibited a significantly elevated risk of incident AAA (HR = 1.70, 95% CI 1.27–2.27, P < 0.01) and TAA (HR = 2.01, 95% CI 1.29–3.13, P < 0.01) compared to those in the lowest quartile. However, no statistically significant association was observed for AD (HR = 2.04, 95% CI 0.86–4.83, P = 0.10). The RCS model confirmed a significant non-linear, J-shaped relationship between increasing BMR levels and the risk of AAA and TAA (P for non-linearity < 0.001).

The Chinese cohort study included 263 patients with AAA. After adjusting for common risk factors in Model 4, individuals in the third and fourth quartiles of BMR were found to have a significantly increased risk of AAA (OR = 1.61 , 95% CI 1.22–2.01, P = 0.02; OR = 1.78, 95% CI 1.33–2.23, P = 0.01, respectively).

Mediation analysis within the UKB NMR data identified three specific metabolic factors partially mediating the BMR-AAA/TAA association: leucine (mediation proportion: 15%), medium-sized high-density lipoprotein cholesterol (HDL-C) particles (18%), and small HDL-C particles (8%).

Conclusion

This large-scale study demonstrates a significant positive association between elevated BMR and increased AAA/TAA risk, consistently observed across European and Asian cohorts. While AD risk showed a non-significant trend, further investigation is needed. Partial mediation by specific HDL-C subfractions and leucine suggests metabolic pathways linking BMR to aortic vulnerability. These findings establish BMR as an emerging independent risk factor for AAA and TAA, offering a potential target for risk stratification and interventions to reduce morbidity.

Keywords: Basal metabolic rate; Abdominal aortic aneurysm; Thoracic aortic aneurysm; Aortic dissection; Mediation analysis

The causal association between body mass index and abdominal aortic aneurysm via obstructive sleep apnea, a two-step mendelian analysis

Xiao-lu Hu, Ting-Fang Zhu, Hao-Ran Chen, Lai-Hai Zhang, Ying-Mei Zhang

Fudan University Affiliated Zhongshan Hospital

The prevalence and disease burden of high body mass index are increasing globally. High BMI increases the risk of type 2 diabetes mellitus, hyperlipemia and hypertension. Over two-third of deaths attributable to high BMI are due to cardiovascular diseases (CVD). Furthermore, Obstructive sleep apnea (OSA), a condition characterized by repeated episodes of partial or complete obstruction of the respiratory passages during the sleep, is the most common type of obesity-relate sleep disorders. Chronic intermittent hypoxia (CIH) is one of the main features of OSA. CIH is considered to be the main pathological cause of OSA-related CVD, and CIH model has been widely in the biological researches. While evidence on BMI in relation to abdominal aortic aneurysm originates from observation studies, which are susceptible to confounding and reverse causation bias and thus cannot infer causality, uncertainties remain about the causal status of BMI for aortic abdominal aneurysm and the possible mediators. Hence, the present study applied the Mendelian randomization (MR) design to evaluate the association between BMI and AAA and examined whether BMI affect AAA through OSA by using two-step MR.

In this study, we conducted a mendelian randomization (MR) study to evaluate the association of body mass index (BMI) and abdominal aortic aneurysm (AAA). The potential mediating effect of obstructive sleep apnea (OSA) on BMI-AAA was analysis using two-step MR.

We extracted genetic variants associated with BMI from a meta-analysis of genome-wide association study. We used SNPs associated with BMI at the genome wide significance threshold ($P < 5x10^{-8}$) in a meta-analysis of genome-wide association studies, including 339 224 individuals. This study identified 97 BMI-associated loci, 56 of which are novel. The data of OSA were retrieved from the FinnGene Study. Cases of OSA were defined based on the international classification of disease codes (ICD-10: G47.3, ICD-9: 3472A). The summary-level data of AAA were retrieved from a recent genome-wide study association study (GWAS) published by Jiang's Lab, containing 556 AAA patients and 455,792 controls of European ancestry.

We performed two-sample MR analyses to explore the causal association of BMI with the risk of AAA. The two sample MR analysis in this study of each step was achieve mainly through the following operations: Firstly, extracted independent SNPs strongly correlated with exposure with filtration criteria of $P < 5*10^{-8}$ in 10000kb window around a leader SNP with low association with other SNPs in this region (LD, r2 < 0.001). Secondly, extract SNPs effects from outcome GWAS dataset with filtration criteria of MAF > 0.01. Next, obtained valid IVs after harmonizing exposure and outcome effects and removing SNPs with failure to harmonize, including containing incompatible alleles and being palindromic with intermediate allele frequencies. Then, the MR evaluation of valid IVs was carried out. The two-step MR analysis was used to evaluate the mediating effect of OSA from BMI to AAA. In the first step, BMI was taken as exposure, OSA was taken as outcome, respectively. In the second step, OSA was taken as exposure, AAA were taken as outcomes. Finally, we employed a Bayesian bootstrap procedure to calculate the confidence intervals of mediation effect.

We found that genetically predicted BMI was significantly positively associated with AAA. The odd ratio (OR) per genetically predicted $1kg/m^2$ increase of BMI ranged from 2.001 (95% CI: 1.554-2.449, P = 1.205E-09). The causal association between BMI and AAA was partly mediated by OSA, with a mediated proportion of 36% (95% CI:0.250-0.470). The results were robust and consistent in all sensitivity analyses.

Keywords: body mass index, aortic abdominal aneurysm, obstructive sleep apnea.

Take home message: This study reveals that there is a causal relationship between genetically predicted high body mass index and the risk of abdominal aortic aneurysm, and this relationship is partly mediated by obstructed sleep apnea.

Internal Migration of Calcification on Non-Contrast Computed Tomography: Is It Always Indicative of Acute Aortic Syndrome?

Wen-Ying Liu, Jie Zou, Jing-Yuan Zhong, Xing-Yue Li, Jia-Bing Huang, Liang-Geng Gong

The Second Affiliated Hospital, Jiangxi Medical College, Nanchang University,

Background: Displacement of calcification stands out as the most easily observable imaging feature on Non-Contrast Computed Tomography (NCCT). However, in clinical practice, the value of its presence on NCCT as a diagnostic indicator for AAS remains uncertain. Clinicians typically proceed with further aortic computed tomography angiography (CTA) due to its high sensitivity and specificity in diagnosing AAS. However, a substantial proportion of these patients are eventually confirmed to have non-AAS conditions. This study aimed to explore the feasibility of developing a combined diagnostic model for Acute aortic syndrome (AAS) by integrating inward migration of calcification and other NCCT-derived imaging features.

Methods: Patients who underwent chest or abdominal NCCT and CTA scans within 2 weeks at the Second Affiliated Hospital of Nanchang University between June 2017 and September 2024 were included. The data of 69 patients with 120 lesions of inward migration of calcification who underwent chest or abdominal NCCT due to unexplained chest or abdominal pain were analyzed retrospectively. The presence or absence of AAS and its subtypes were confirmed through CTA. The distance from the migrated calcification to the aortic adventitia, the CT attenuation values (Hounsfield, HU) on both the inner (defined as HU_I) and outer sides (defined as HU_O) of the endoluminal displacement of calcification, the thickness of the endoluminal displacement of intimal calcification (maximum value), the main body length of such displacement, and other imaging parameters were measured and recorded. The imaging and clinical differences between the AAS-positive and AAS-negative groups, as well as among different AAS subtypes, were analyzed using appropriate statistical methods, including t-test, Mann-Whitney U test, Chi-square test, Fisher's exact test, Kruskal-Wallis test, and one-way ANOVA. Diagnostic models were developed using logistic regression (Enter method) with clinical factors, imaging features, and combined variables. The receiver operating characteristic (ROC) curves analysis evaluated diagnostic efficacy, while the Youden Index determined optimal cutoff values for the distance.

Results: The median age of the AAS group (71 [57–85] years) was significantly lower than that of the non-AAS group (79 [65–93] years) (P= 0.010). Compared with the patients in the non-AAS group, the incidence of dyslipidemia in the AAS group was lower (3.9% vs 18.2%, P= 0.011), and the incidence of D-dimer ≥ 0.5 mg/L was higher (97.4% vs 84.1%, P=0.009). The median HU_I in the AAS group (40 [29–51] HU) was significantly lower than that in the non-AAS group (42.5 [33.5–51.5] HU) (P=0.031). However, the distance was significantly higher in the AAS group (8.2 [2.5 - 13.9] mm) than in the non-AAS group (5.65 [1.35 - 9.95] mm), (P<0.001). The incidences of linear high density (28.9% vs 4.5%, P= 0.001), high-density

hematomas (17.1% vs 0%, P<0.001) and pleural effusion (44.7% vs 11.4%, P<0.001) were significantly more frequent in the AAS group than in the non-AAS group. Among clinical, radiological, and combined diagnostic models, the combined model exhibited superior performance in detecting AAS (area under the curve=0.842, 95% CI: 0.773-0.911). The clinical model demonstrated an AUC of 0.772, whereas the radiological model showed an AUC of 0.797. Additionally, the distance ≥ 5.95 mm had a relatively high sensitivity for identifying AAS. After CTA examination, the final diagnostic results were 34 cases of AD, 17 cases of IMH, and 25 cases of PAU. Subtype analysis revealed that the distance was significantly greater in the AD group compared to the IMH group (Adjusted P Value=0.045). However, there was no statistically significant difference in the distance between the AD group and the PAU group (Adjusted P Value=0.089), as well as between the IMH group and the PAU group (Adjusted P Value=0.999).

Conclusions: NCCT emerges as a potential screening tool for AAS. The combined model based on the displacement of calcification on NCCT could minimize AAS misdiagnosis while curtailing excessive CTA testing.

D-Dimer and ADAMTS8 Based Multi-marker Score : Potential Biomarkers for Predicting Aortic Dissection

Ting Tian[1], xinxin Tian[1], Fen Liu[1], Xiao-Mei Li[1], Yi-Ning Yang[2]

1. 1Heart Center, the First Affiliated Hospital of Xinjiang University, Urumqi, Xinjiang 830054, China

2. Department of Cardiology, People's Hospital of Xinjiang Uygur Autonomous Region,

Abstract

Background:

Acute aortic dissection (AAD) is a rapidly fatal clinical emergency, with high rates of mortality. The aim of this study was to explore biomarkers that can help optimize the diagnosis of AAD.

Methods: AAD related genes were screened by spatial transcriptomics experiments in the previous study, and their encored proteins were validated in aortic tissues. We measured plasma concentrations of potential proteins in 302 participants, including 173 AAD cases and 129 controls, and developed diagnostic panels to differentiate AAD from healthy individuals.

Results:

In our previous studies, we have collected AAD tissues and conducted an initial exploration of AAD-related genes by spatial transcriptomics (ST). We identified PTMA, ADAMTS8 and CD36 as new genes related to AAD and evaluate cell types. To confirm the expression of the candidate proteins, we utilized aorta tissues from AAD patients for both IHC and WB detection. IHC and WB findings showed that PTMA, ADAMTS8 and CD36 were strongly expressed in the thickened walls of aortic arteries in patients from AAD compared with controls. To confirm the protein expression in blood circulation in larger clinical blood samples, we found that compare to the controls, patients with AAD showed higher expression of these encoded proteins in their aortic arteries and blood circulation. Our case-control analysis revealed that the AAD patients exhibited significantly higher levels of the independent risk factors including systolic blood pressure (SBP), smoking, hypertension, standing height and D-Dimer levels, along with high PTMA, ADAMTS8 and CD36 proteins in the blood circulation. Univariate logistic analysis identified that protein levels of ADAMTS8 and CD36, along with sex, height, SBP, smoking history, white blood cells, high-density lipoprotein cholesterol (HDL-C) and D-Dimer were the independent risk factors for AAD. The protein levels of ADAMTS8, CD36, D-Dimer and HDL-C were remained significant predictors for AAD after adjustment for sex, SBP, heart rate, smoking history, white blood cells, creatinine and triglyceride. Our case-control analysis revealed that elevated levels of PTMA, ADAMTS8 and CD36 along with D-Dimer, increased SBP, standing height and smoking history were risk factors for AAD. A PCA model based on ADAMTS8, D-Dimer and clinical cardiovascular risk factors demonstrated a partition of AAD patients and controls. The area under the curve values were 0.596, 0.765 and 0.881 for PTMA, ADAMTS8 and CD36, respectively. A multi-marker score based on D-Dimer, ADAMTS8, Height, SBP and Age was developed to distinguish AAD patients from controls, with an AUC of 0.962, and a sensitivity of 91.0%, a specificity of 92.3% respectively.The multi-marker score was significantly higher in AAD patients than in controls. Regression analysis with restricted cubic spline described the relationship between multi-marker score as a continuous variable and AAD events, suggesting that the likelihood of AAD events increased with the multi-marker score.

Conclusions: We identified PTMA, ADAMTS8 and CD36 as novel proteins associated with AAD. A 5-item biomarker-based risk score is developed to differentiate AAD from healthy individuals. This multi-marker score could serve as a sensitive tool, offering the potential for rapid and cost-effective diagnostic testing. It also potentially provides guidance for therapeutic strategies in AAD patients.

SIRT3 suppresses vascular endothelial senescence by inhibiting eNOS uncoupling

Yuan Zhao, Pei-Li Bu

State Key Laboratory for Innovation and Transformation of Luobing Theory; Key Laboratory of Cardiovascular Remodeling and Function Research of MOE, NHC, CAMS and Shandong Province; Department of Cardiology, Qilu Hospital of Shandong University, Jinan, China, 250012

Abstract

Aims

Vascular aging has become the prominent physiopathological basis of various organ systems aging and many chronic diseases in the elderly. Sirtuin 3 (SIRT3) is a deacetylase present in the mitochondrial matrix, and associated with several cardiovascular diseases, such as hypertension, ischemic heart disease, and heart failure. However, the mechanisms by which SIRT3 regulates vascular senescence remain to be investigated. Therefore, the present study verifies that SIRT3 protects vascular endothelial cells from aging via regulating endothelial nitric oxide synthase (eNOS) uncoupling, which would provide new insights into the clinical prevention and treatment of aging-related cardiovascular diseases.

Methods

1. To verify the beneficial role of SIRT3 on inhibiting vascular aging, wild type (WT) and Sirt3 knockout (Sirt3-KO) mice were purchased. D-galactose (D-gal) was injected intraperitoneally to construct vascular senescence models in mice. Mice were randomly grouped into WT group, WT+D-gal-induced aging group, Sirt3-KO group, Sirt3-KO+D-gal-induced aging group. Immunohistochemistry staining and western blot assay were used to evaluate the effects of SIRT3 on the vascular aging. And H&E, Masson's trichrome, Sirius Red and Verhoeff's Van Gieson staining were used to detect the function of SIRT3 on protecting aging aortas from pathological remodeling.

2. In vitro, mouse aortic endothelial cells (MAECs) were cultured with D-gal treatment. SIRT3 was knocked down by SIRT3 small interfering RNA (siRNA) in vitro. SIRT3 was overexpressed by plasmid in vitro. After that, β-galactosidase staining, transwell migration, wound healing and tube-formation experiments were used to detect the protective effects of SIRT3 on senescent endothelial cells in vitro. Western blot assay was used to measure the expression levels of aging-related proteins including p53, p21 and LaminB1.

3. In vitro, DCFH-DA and JC-1 probes were incubated with ECs to reveal SIRT3's function on regulating reactive oxygen species (ROS) production and mitochondrial membrane potential (MMP) disruption in senescent endothelial cells. Immunofluorescence staining and western blot assay were used to explore the mitochondrial redistribution and phosphorylation of eNOS in senescent endothelial cells with D-gal administration.

Results

1. Histochemical staining demonstrated that SIRT3 deficiency significantly aggravated aortic intima-media thickening, collagen deposition, elastic damage caused by vascular senescence in D-gal-induced aging aortas. And the expression levels of VCAM-1, p53 and p21 were upregulated in D-gal-induced aging aortas, while SIRT3 knockout aggravated the increasing role of those proteins. Immunohistochemistry showed that SIRT3 knockout upregulated the expressions of p53, MCP-1 and CXCL9 in D-gal-induced aging aortas.

2. SIRT3 knockdown upregulated the protein levels of p53 and p21, and downregulated the expression level of LaminB1. SIRT3 overexpression decreased the protein levels of p53 and p21 and upregulated LaminB1 protein level in senescent endothelial cells. Likewise, SIRT3 knockdown exacerbated the migration and tube-formation function of senescent endothelial cells And SIRT3 knockdown promoted MMP disruption and the production of ROS induced by senescence in endothelial cells, however, SIRT3 overexpression mitigated MMP disruption and oxidative stress in senescent endothelial cells.

3. It was found that the phosphorylation of eNOS-Thr495 and mitochondrial translocation of eNOS causing to eNOS uncoupling increased in senescent endothelial cells. After SIRT3 knockdown, the phosphorylation of eNOS at Thr495 and eNOS mitochondrial redistribution was upregulated. At the same time, SIRT3 overexpression by plasmid downregulated the phosphorylation of eNOS at Thr495 and eNOS mitochondrial translocation.

Conclusion

SIRT3 shows beneficial effects in preventing vascular endothelial aging through suppressing eNOS uncoupling, which provides new targets for treating cardiovascular diseases associated with vascular aging.

环丙沙星重塑肠道菌群提高吲哚乳酸水平并加重动脉瘤与夹层

蔡嘉庚（CSC 指南共识学组祖凌云）

北京大学第三医院

目的：以环丙沙星为代表的氟喹诺酮类抗生素增加动脉瘤与夹层（Aortic Aneurysm and Dissection，AAD）的破裂风险逐渐引起医学界的关注，本研究尝试探讨环丙沙星介导 AAD 加重的潜在病生理原因。

方法：我们以 β- 氨基丙腈（β-Aminopropionitrile，BAPN），一种常规的 AAD 模型构建药物，作为 C57 小鼠的基础诱导背景。宏基因组、血浆非靶与靶向代谢组、单细胞转录组、肠道菌群移植等手段用以观察小鼠肠道菌群构成与血浆代谢谱变化，评估 AAD 的发生发展，分析潜在的病生理原因。

结果：环丙沙星干预 BAPN 诱导下的 C57 小鼠后，AAD 的发生率与严重程度显著增加，表现为血管内径的显著提升以及血管弹力板的断裂。血浆非靶与靶向代谢组学提示，吲哚乳酸（Indolelactic Acid，ILA）水平在环丙沙星干预组中均呈现显著提高，是环丙沙星导致 AAD 加重的潜在代谢物。后续我们对 BAPN 诱导下的 C57 小鼠进行 ILA 灌胃，结果发现，ILA 同样可以介导 AAD 的加重。单细胞结果提示 ILA 减少血管平滑肌细胞的占比并促进平滑肌细胞表型转化。为了探究导致循环 ILA 增加的潜在原因，我们对上述小鼠肠道内容物分别进行了宏基因组与代谢组学检测。结果提示，环丙沙星可重塑肠道菌群构成，主要表现为 Duncaniella_Dubosii 与 Muribaculum_Intestinale 的增加；此外，肠道内容物中 ILA 水平也同水平增高，这与循环中的表现一致。为了探究环丙沙星是否是通过重塑肠道菌群而加重的 AAD，我们后续单独对环丙沙星干预下的肠道内容物进行小鼠的供受体移植，而不进行环丙沙星的灌胃。结果提示，单纯肠道环境的复制依然增加肠道及循环 ILA 的产生并加重 AAD 的发生。

结论：环丙沙星通过改变以 Duncaniella_Dubosii 与 Muribaculum_Intestinale 增加为特征的肠道菌群构成，增加肠道代谢产物 ILA 水平；增加的 ILA 进入循环并介导血管平滑肌细胞的流失与表型转化，削弱血管中层，进而加重 AAD 的发生。

LncSRLR is up-regulated in Thoracic Aortic Dissection and Regulated Phenotype Switch of Smooth Muscle Cells

Lianbo Shao, Ying-Long Ding, Ting-Yu Wang, Shan Liu, Zhen-Ya Shen

Department of Cardiovascular Surgery, The First Affiliated Hospital of Soochow University

Thoracic aortic dissection (TAD) is a vascular disease that presents acute onset, rapid progression and a high mortality rate. Currently, there are no effective medical therapeutic therapy for it. The pathological changes of aortic dissection mainly involve the tunica media degeneration induced by smooth muscle cells phenotypic transformation. Recent studies have shown that lncRNA can participate in numerous biological processes by regulating gene expression. At present, there are relatively few studies on the mechanism of lncRNA in the pathogenesis of aortic dissection. Studying the function and molecular mechanism of lncRNA in the pathogenesis of aortic dissection and screening out the hub lncRNA related to the onset of aortic dissection will provide new therapeutic targets for aortic dissection therapy.

Methods and Results: Aortic wall tissues from TAD patients and control were collected and perform RNA-seq. Bioinformatics analysis on the differentially expressed genes was confirmed, including GO analysis, KEGG analysis, and GSEA analysis, screened out LNCSRLR as one key pathogenic lncRNA. LNCSRLR overexpressed HASMCs were constructed, and the role of LNCSRLR in SMC phenotypic transformation was investigated in LNCSRLR overexpressed-HASMCs. The results showed overexpression of LNCSRLR can promote the phenotypic transformation of HASMC induced by angiotensin II (Ang II), specifically manifested as changed expression of OPN and CNN1 and the upregulation of inflammatory factors (IL6, CD68, CXCL2, NOS2), and the enhanced migration and proliferation of HASMCs.

The ceRNA regulatory network of LNCSRLR was constructed: miRNA sequencing found that there were 50 differentially expressed miRNAs in LNCSRLR overexpressed-HASMCs. RNA hybrid predicted potential target miRNA molecules of LNCSRLR, and integrated analysis of differentially expressed miRNAs. It was found that hsa-let-7c-5p might be the downstream target miRNA of LNCSRLR; KEGG enrichment analysis showed that the genes differentially expressed in the sequence were mainly involved in extracellular matrix-receptor interaction, cell adhesion molecules, and the PI3K-AKT signaling pathway; Further, the dual-luciferase reporter assay confirmed that ST6GAL2 was a candidate gene of hsa-let-7c-5p. Inhibiting the expression of ST6GAL2 with siRNA also inhibited the promotion of HASMCs phenotypic transformation by LNCSRLR. The experimental results also showed that the PI3K-AKT signaling pathway was included in the phenotypic transformation regulation of HASMCs by LNCSRLR; In vivo experiments showed that upregulating the expression of mmu-let-7c-5p or inhibiting the expression of ST6GAL2 could reduce the incidence rate of aortic dissection, the dilation of the aorta, and the fracture and degradation of elastic fibers, playing a protective role in alleviating the occurrence and development of aortic dissection.

Clinical correlation analysis: Clinical data of patients with thoracic aortic dissection and healthy subjects undergoing physical examinations were collected. Quantitative real-time polymerase chain reaction (RT-qPCR) was used to detect the expression level of LNCSRLR in plasma, and logistic regression was performed to analyze the predictive and diagnostic value of LNCSRLR in thoracic aortic dissection. The expression level of LNCSRLR in the peripheral plasma of patients with thoracic aortic dissection was significantly higher than that in healthy subjects undergoing physical examinations. Multivariate logistic regression analysis showed that the expression level of plasma LNCSRLR had a statistically significant impact on patients with aortic dissection (OR = 1.17, 95% CI (1.07~1.29), P

Conclusion: The expression of LNCSRLR is upregulated in thoracic aortic dissection tissues. LNCSRLR competitively binds to hsa-let-7c-5p, thereby upregulating the expression of ST6GAL2, regulating the expression of phenotypic markers of HASMCs, as well as the migration and proliferation abilities of VSMCs. This promotes the transformation of VSMCs into a synthetic phenotype, leading to the occurrence of thoracic aortic dissection. This study provides a theoretical basis for LNCSRLR to serve as an early diagnostic marker and a therapeutic target for thoracic aortic dissection.

Using the NoSAS Score to Stratify Long-Term Cerebrovascular Risk: A 5-Years Retrospective Analysis

Yuli Cai[1], Huan Li[1], Siyu He[1], Deyi Zhou[1], Zhongling Xiong[1], Rui Zhou[1], Boyang Xiao[1], Kunning Li[1], Tong Lu[1], Junfen Cheng[1], Yibin Wang[1], Jinhui Pan[1], Zixing Wu[1], Chengheng Tan[1], Guanhan Chen[1], Xing Li[1], Nanshan Lai[1], Sihan Lin[1], Huizhao Liao[2], Riken Chen[1]

1. The Second Affiliated Hospital of Guangdong Medical University

2. The First Affiliated Hospital of Guangzhou Medical University

Objective

Obstructive Sleep Apnea (OSA) is a well-established independent risk factor for cerebrovascular disease, largely due to the detrimental physiological consequences of recurrent nocturnal asphyxia. The associated intermittent hypoxemia and sleep fragmentation trigger a cascade of pathophysiological responses, including systemic inflammation, oxidative stress, and endothelial dysfunction, all of which promote vascular damage. Despite the serious risks, a vast number of individuals with OSA remain undiagnosed because the clinical gold standard, polysomnography (PSG), is both costly and has limited accessibility. This diagnostic challenge underscores an urgent need for simple, effective screening tools for use in frontline clinical settings. The NoSAS score, an easily calculated metric based on five clinical variables (Neck circumference, Obesity, Snoring, Age, and Sex), represents a promising, equipment-free tool for risk stratification. This study, therefore, aimed to evaluate the long-term predictive value of the NoSAS score for the five-year incidence of new-onset cerebrovascular disease in a clinical cohort.

Methods

This study retrospectively included patients who underwent sleep breathing monitoring at the Sleep Medicine Center of the First Affiliatedl Hospital of Guangzhou Medical University and the Sleep Research Institute of the Second Affiliated Hospital of Guangdong Medical University from September 1, 2016, to December 31, 2019. Patients with a pre-existing diagnosis of cerebrovascular disease at baseline or before admission were excluded. Based on their baseline NoSAS score, participants were stratified into a low-risk group (score < 8) and a high-risk group (score ≥ 8). The primary endpoint was the first documented incidence of a new-onset cerebrovascular event (ischemic stroke, hemorrhagic stroke, or transient ischemic attack) within a five-year follow-up period. Endpoint data were ascertained by systematically reviewing electronic health records and conducting standardized telephone follow-ups. A multivariate logistic regression model was constructed to assess the independent association between NoSAS risk category and the study endpoint, adjusting for key demographic and clinical confounders such as age, sex, body mass index, smoking status, hypertension, and diabetes. A planned stratified analysis was also performed using the Epworth Sleepiness Scale (ESS) to examine the score's utility in patients with and without significant daytime sleepiness (ESS ≤ 9).

Results

The final analysis included 1,348 participants, of whom 690 (51.2%) were categorized as high-risk. Over the five-year follow-up, the incidence of cerebrovascular disease in the high-risk group was 9.71%. After adjusting for all potential confounders in the multivariate model, a high NoSAS score was significantly associated with future cerebrovascular events. Compared to the low-risk group, individuals in the high-risk group had a 1.85-fold greater odds of experiencing an event (adjusted Odds Ratio [aOR]: 1.85, 95% Confidence Interval [CI]: 1.01–3.38; p=0.045). The stratified analysis provided a critical insight: the predictive association of the NoSAS score was particularly strong and statistically significant in the subgroup of patients who did not report excessive daytime sleepiness (ESS ≤ 9). This demonstrates the score's unique ability to identify at-risk individuals who lack the classic OSA symptom of sleepiness.

Conclusion

The high-risk group identified by the NoSAS score exhibited a higher incidence of cerebrovascular diseases and can serve as an independent predictor of the disease, particularly among high-risk OSA individuals without excessive daytime sleepiness.

冷休克蛋白 DbpA 乙酰化修饰调控线粒体功能障碍促主动脉夹层的机制研究

张凯玥 王洪杰 曾和松

华中科技大学同济医学院附属同济医院心血管内科

目的：主动脉夹层（Aortic dissection, AD）是一种致命性的心血管疾病。在我国随着人口老龄化和饮食结构的改变，主动脉夹层的发病率在迅速攀升。目前临床上对主动脉夹层主要采用外科手术进行血管置换或者通过介入手术行腔内隔绝治疗，但仍缺乏有效的药物干预手段。本研究旨在探究冷休克蛋白 DbpA 在主动脉夹层中的作用及作用机制，为主动脉夹层的防治提供新的理论依据。

方法：本研究首先通过分析人群和小鼠主动脉组织的转录组测序数据明确对照组与夹层组之间存在差异表达基因 Ybx3；采用免疫组织化学染色和免疫荧光染色进一步探究和验证 Ybx3 编码的蛋白 DbpA 在主动脉夹层中差异表达的具体部位。构建血管平滑肌细胞特异性 Ybx3（DbpA 编码基因）敲除小鼠，明确 DbpA 在体对 AD 发病率和死亡率的影响；在 MOVAS 细胞中通过敲低 / 过表达 DbpA 探究和明确其调控 AD 的具体作用机制。采用质谱分析联合蛋白质免疫印迹法，阐明 DbpA 在 AngII 刺激下线粒体转位的具体机制；进一步运用 Seahorse 检测、JC-1 染色、mitoSOX 染色明确 DbpA 对粒体功能的影响；通过检测 SM22α 和 calponin 和 α-SMA 水平，阐明 DbpA 通过诱导线粒体功能障碍促进平滑肌细胞表型转换的具体机制。最后，构建 DbpA K116R 突变体，探究靶向 DbpA 乙酰化在 AD 中的潜在治疗作用。

结果：DbpA 在 AD 患者和小鼠 AD 模型的主动脉血管平滑肌细胞中显著上调。血管平滑肌细胞特异性 Ybx3 敲除可降低小鼠 AD 发病率（从 63% 降至 25%）和死亡率（从 21% 降至 0%）（P<0.001）。机制上，AngII 刺激促进 DbpA 在赖氨酸 116（K116）位点发生乙酰化，从而导致其由细胞质转位至线粒体，增加线粒体活性氧（ROS）并损害呼吸功能。DbpA 诱导的线粒体功能障碍可以进一步诱导血管平滑肌发生表型转换和凋亡，最终促进主动脉夹层的发生和发展。此外，K116R 突变可阻断 DbpA 的线粒体转运并对 AD 起到保护作用。

结论：在主动脉平滑肌中，DbpA K116 位点的乙酰化修饰驱动其线粒体转运，从而诱导线粒体功能障碍和血管平滑肌细胞表型转换，参与主动脉夹层的发生。靶向 DbpA 的乙酰化修饰有望成为 AD 新的治疗策略。

颈动脉狭窄中血管周围脂肪 CD4+T 细胞 ICOS 的作用及机制研究

陈俊冶 朱展 舒克强 李康 刘暴

中国医学科学院北京协和医院

目的

颈动脉狭窄（Carotid artery stenosis, CAS）是导致卒中的主要病因，严重威胁人类健康。近年来，血管周围脂肪组织（Perivascular adipose tissue, PVAT）因其在动脉粥样硬化疾病进展过程中具有促进与保护的双重作用受到关注。我们利用单细胞转录组测序和生信分析初步发现 $CD4^+$T 细胞上的诱导性 T 细胞共刺激分子（Inducible T-cell co-stimulator, ICOS）基因在 CAS 患者与健康对照的颈动脉 PVAT 中存在差异性表达。既往研究提示 ICOS 可能具有抗动脉粥样硬化的作用，但 $CD4^+$T 细胞上的 ICOS 通过 PVAT 中在动脉粥样硬化中发挥的具体功能以及分子机制尚未明确。本研究旨在探究 ICOS 调节 $CD4^+$T 细胞分化，从而激发 PVAT 的动脉粥样硬化保护性作用的具体机制，为动脉粥样硬化治疗的精准医学研究奠定理论基础。

方法

本研究通过临床样本研究和小鼠模型实验，系统探讨 PVAT 中特定免疫细胞类型 $CD4^+$T 细胞及其关键分子 ICOS 对动脉粥样硬化的作用以及具体的分子机制。人体 PVAT 来源于在北京协和医院接受颈动脉内膜剥脱术（Carotid endarterectomy, CEA）的动脉粥样硬化源性 CAS 患者和作为有限对照的接受手术切除的良性颈动脉体瘤（Carotid body tumor, CBT）患者。人颈动脉粥样硬化斑块和外周血单个核细胞（Peripheral blood mononuclear cell, PBMC）来源于在北京协和医院接受 CEA 的 CAS 患者。高通量单细胞转录组测序和生信分析揭示了细胞亚群类型、数量以及 Marker 基因表达的谱系特征；免疫组化染色分析 ICOS 表达水平。对 6 周龄的 $Apoe^{-/-}$ 小鼠高脂饮食（High-fat diet, HFD）4 周和 18 周，构建早期和晚期的动脉粥样硬化小鼠模型。通过 CRISPR Cas9 联合 Cre-LoxP 重组酶系统，构建 $Apoe^{-/-}$ 背景的 $CD4^+$T 细胞条件性 Icos 敲除和过表达的小鼠模型。流式分析评估人颈动脉 PVAT 和小鼠主动脉 PVAT 中 ICOS 表达和 $CD4^+$T 细胞组分变化。主动脉瓣膜和全主动脉油红 O 染色评估脂质沉积程度。磁珠分选小鼠主动脉 PVAT 中和脾脏中的 $CD4^+$T 细胞后，进行全转录组测序（Bulk RNA sequencing, Bulk RNA-seq）并联合蛋白互作预测与分子对接挖掘机制。p<0.05 被认为有统计学意义。

结果

通过对 8 例 CAS 患者和 3 例有限对照的颈动脉 PVAT 样本进行单细胞转录组测序，共鉴定出 18 种细胞类型，其中 $CD4^+$T 细胞比例最高，并发现 ICOS 在 CAS 患者中显著上调。通过对 3 例 CAS 患者的颈动脉 PVAT、斑块和 PBMC 进行单细胞转录组测序并联合数据库资料分析，发现 ICOS 在 PVAT 中呈现组织特异性升高态势。基于早、晚期动脉粥样硬化小鼠模型，发现 PVAT 中 ICOS 表达水平的动态变化与辅助性 T 细胞 2（T helper 2 cell, Th2）比例密切相关。进一步构建 $CD4^+$T 细胞条件性 Icos 敲除和过表达的 $Apoe^{-/-}$ 小鼠模型，发现敲除 Icos 促进脂质沉积并特异性降低 PVAT 中 Th2 细胞分化，而过表达 Icos 则抑制脂质沉积并特异性增加 PVAT 中 Th2 分化。此外，全转录组测序和分子对接分析显示，ICOS 可能通过 FOXO1/CCR7 通路调控 Th2 细胞的分化和定位。

结论

本研究首次揭示 PVAT 中 ICOS 在颈动脉粥样硬化中的关键作用，为探索动脉粥样硬化的分子机制和潜在的预测以及治疗策略提供了新视角。

Creatinine-to-albumin ratio predicts mortality in patients with aortic aneurysms

Dong-Qin Cai, Jianfang Luo, Yuan Liu, Songyuan Luo

PersonalUse

Abstract

Background:

Aortic aneurysm is a severe and potentially life-threatening vascular disorder characterized by progressive dilation of the aorta. In its early stages, the condition is often asymptomatic, making timely diagnosis and intervention challenging. Most cases are identified incidentally through imaging studies, which limits opportunities for early treatment. Conventional biomarkers of inflammation and thrombosis, while widely used, exhibit limited specificity and are often influenced by systemic confounders, reducing their reliability in clinical practice. The serum creatinine-to-albumin ratio (CAR), a composite marker reflecting inflammation, metabolic stress, and nutritional status, has demonstrated prognostic significance in various cardiovascular conditions. However, its utility in the context of aortic aneurysm remains unexplored.

Methods:

To investigate the prognostic value of CAR in aortic aneurysm, we conducted a retrospective cohort study using data from the MIMIC-III and MIMIC-IV intensive care databases, which include detailed clinical information on critically ill patients. Baseline serum creatinine and albumin levels were used to calculate CAR, and an optimal cutoff value of 0.391 was determined using maximally selected rank statistics. Patients were stratified into high- and low-CAR groups based on this threshold. Survival probabilities at 28 days and one year were compared between the groups using Kaplan-Meier analysis. Multivariable Cox proportional hazards models were employed to quantify the association between CAR and mortality, adjusting for demographic factors and clinical covariates. Restricted cubic spline regression was used to assess potential nonlinear relationships between CAR and mortality risk. Sensitivity analyses at 90 and 180 days were conducted to confirm the temporal consistency of the findings. Subgroup analyses explored the impact of age, aneurysm rupture, and other key factors on the observed associations.

Results:

The study included 1,970 patients diagnosed with aortic aneurysm. A CAR value of ≥ 0.391 was strongly associated with worse survival outcomes. Kaplan-Meier analysis revealed significantly reduced survival rates in the high-CAR group at all time points (P < 0.001). Multivariable Cox regression analysis further confirmed the prognostic significance of CAR, with higher levels linked to increased mortality risk. Specifically, patients with elevated CAR demonstrated a hazard ratio (HR) of 1.53 (95% confidence interval (CI): 1.09–2.14) for 28-day mortality and an HR of 1.51 (95% CI: 1.24–1.85) for one-year mortality. Sensitivity analyses at 90 and 180 days consistently supported these findings (P < 0.001). Restricted cubic spline regression revealed a nonlinear relationship between CAR and mortality risk, with higher CAR values associated with progressively greater risk. Subgroup analyses identified older patients and those with ruptured aneurysms as particularly vulnerable, suggesting that CAR may be especially useful in risk stratification for these high-risk populations.

Conclusion:

The serum creatinine-to-albumin ratio represents a simple, cost-effective, and clinically valuable biomarker for prognostic assessment in patients with aortic aneurysm. A cutoff value of 0.391 reliably identifies individuals at elevated risk of both short-term and long-term mortality, making it a useful tool for early risk stratification and personalized management. By integrating CAR into routine clinical practice, healthcare providers may improve the identification of high-risk patients and optimize treatment strategies, potentially reducing mortality associated with this life-threatening condition. Further research is warranted to validate these findings in larger, prospective cohorts and to explore the underlying mechanisms linking CAR to adverse outcomes in aortic aneurysm.

通过肾动态显像结合肾动脉血流分数评价冠状动脉药物球囊治疗肾动脉纤维肌性结构不良 1 例

孙亚东 李迎 贺媛

中国人民解放军空军军医大学第一附属医院

本文题目为《通过肾动态显像结合肾动脉血流分数评价冠状动脉药物球囊治疗肾动脉纤维肌性结构不良 1 例》，作者包括空军军医大学第一附属医院医师孙亚东、李迎，空军军医大学第一附属医院心血管内科副主任医师贺媛（通讯作者）。本文报告了一例通过肾动态显像结合肾动脉血流分数来评价冠状动脉药物球囊治疗右肾动脉纤维肌性结构不良（fibromuscular dysplasia ，FMD）导致的继发性

高血压的安全性及有效性。目的：通过术前、术后肾动态显像结合肾动脉定量血流分数（Quantitative Flow Ratio，QFR）测量作为评价是否需要手术及手术成功的指标，验证冠状动脉药物球囊能否应用于肾动脉 FMD 的治疗。方法：用 1.5 mm×15mm 冠状动脉顺应性球囊扩张狭窄部位，序贯使用 2.5 mm×12mm、3.0 mm×12mm 冠状动脉非顺应性球囊缓慢扩张靶病变，造影提示扩张效果满意，残余狭窄 < 30%，靶病变处无夹层、穿孔，遂于靶病变处使用 4.0 mm×20mm 的冠状动脉药物球囊以 12 个大气压扩张 60 秒，多角度造影显示血管残余狭窄小于 30%，且无夹层、血管破裂、假性动脉瘤等并发症发生。球囊扩张前后患者肾动脉定量血流分数（QFR）结果分别为 0.20、0.92，表明球囊扩张显著改善了肾动脉狭窄及血流。结果：经冠状动脉药物球囊扩张狭窄的肾动脉后，血管残余狭窄 < 30%，术后患者血压逐步恢复正常。手术前后肾动态显像结果（治疗前总 GFR79.54，左 GFR48.52，右肾功能轻度受损 GFR31.02，治疗后 1 月总 GFR99.52，左 GFE55.05，右 GFR44.47）。结论：冠状动脉药物球囊用于 FMD 的治疗效果良好，且通过肾动态显像结合肾动脉 QFR 来评价手术的安全性及有效性具有可行性。冠状动脉药物球囊扩张系统为肾动脉 FMD 所致的肾动脉狭窄提供了一种新的安全、高效的器械选择。同时，结合 QFR 制定介入治疗策略，可有效评估球囊成形术效果，提高治疗成功率，降低手术风险。

Machine learning combined with omics-based approaches reveals T-lymphocyte cellular fate imbalance in abdominal aortic aneurysm

De-Min Li, Ge Zhang, Pei-yu Yuan, Jin-Ying Zhang, Jun-nan Tang

The First Affiliated Hospital of Zhengzhou University

Background:

Abdominal aortic aneurysm (AAA) represents a significant vascular pathology characterized by the progressive, often silent, dilation of the aorta. Its asymptomatic nature frequently leads to late diagnosis, with rupture carrying catastrophic mortality. While the etiology is multifactorial, dysregulated immune responses, particularly involving T lymphocytes, are recognized as central drivers of the inflammatory processes degrading the aortic wall. Despite this understanding, the precise molecular mechanisms orchestrating the fate imbalance within T-cell populations–critical for their pathogenic contribution to AAA progression–remain inadequately defined. A deeper elucidation of these mechanisms is paramount for advancing diagnostic precision and developing targeted therapeutic interventions to halt this life-threatening condition.

Methods:

To dissect the complex immune landscape of AAA, this study employed a robust integrative multi-omics approach. We systematically combined high-resolution single-cell RNA sequencing (scRNA-seq) data, enabling the dissection of cellular heterogeneity within AAA tissues, with bulk RNA sequencing data from larger patient cohorts to capture broader transcriptional trends. Leveraging this combined dataset, we constructed a comprehensive global regulatory network model. This sophisticated model facilitated the identification of: 1)Key T-cell infiltration regulatory features, pinpointing molecular signatures associated with aberrant T-cell recruitment and activation; 2)Critical transcription factors (TFs) driving the observed transcriptional programs; and 3)Dysregulated immune signaling pathways and their defining pathway markers. To rigorously extract the most significant biomarkers and therapeutic insights from this complex network, we utilized multiple advanced machine learning algorithms. These algorithms were applied for in-depth data mining, focusing on screening for pivotal diagnostic/prognostic biomarkers and computationally predicting potential therapeutic compounds capable of modulating the identified dysregulated pathways.

Results:

Our integrated analysis successfully illuminated the core molecular mechanisms underpinning T-lymphocyte fate imbalance within the AAA microenvironment. We generated a detailed and comprehensive regulatory map, encompassing:Specific molecular features governing pathological T-cell infiltration.

Critical transcription factors identified as master regulators of the dysregulated T-cell states. Notably,FOSB and JUNB emerged as central hubs within the regulatory network, exhibiting significant dysregulation. Key immune signaling pathways found to be aberrantly activated or suppressed, along with their associated molecular markers, providing a pathway-centric view of AAA immunopathogenesis. Applying machine learning algorithms to this rich dataset yielded highly significant translational findings:The transcription factors FOSB and JUNB were robustly identified as key diagnostic biomarkers for AAA.

Crucially, the diagnostic and biological significance of FOSB and JUNB underwent rigorous validation. Their dysregulation and biomarker potential were consistently confirmed across multiple independent AAA gene expression datasets sourced from public repositories. Furthermore, validation extended to clinical samples (e.g., blood or tissue samples from AAA patients versus controls), utilizing techniques such as qPCR, immunohistochemistry, or ELISA, which reinforced their feasibility and accuracy for clinical diagnostic application.

Conclusion:

This study provides asystematic and multi-faceted elucidation of the substantial contribution made by T lymphocytes to the pathogenesis and advancement of AAA. We successfully uncovered the intricate regulatory mechanisms responsible for the fate imbalance observed in these critical immune cells within the aneurysmal aorta. Beyond mechanistic insights, the research delivers significant translational value: We identified FOSB and JUNB as highly promising diagnostic biomarkers with demonstrable accuracy across diverse datasets and clinical samples, holding substantial potential for improving early AAA detection.

“精准护航”一例颈动脉狭窄 TCAR 手术患者的全程护理实践

吴岚 张喜维

首都医科大学附属北京安贞医院

目的：颈动脉狭窄是导致缺血性脑卒中的重要病因之一，不仅严重影响患者的生活质量，还可能引发如脑梗死、高灌注综合征等严重的并发症，甚至危及生命。经颈动脉血运重建技术及相关核心产品（Transcarotid Artery Revascularization, TCAR）于 2024 年引入中国，为中国患者带来新的治疗选择。与传统的颈动脉内膜剥脱术相比，具有创伤小、恢复快、术后并发症发生率低等优势，已成为治疗颈动脉狭窄的重要选择。然而，手术的成功与否不仅取决于医生的技术水平，还与患者围术期的护理质量密切相关。全程精准护理作为一种以患者为中心、注重细节和个体化的护理模式，能够有效提高手术成功率，减少并发症，并促进患者快速康复。因此，在 TCAR 手术患者的治疗过程中，实施全程精准护理具有重要的临床意义。本研究旨在通过对一例颈动脉狭窄患者接受经颈动脉血运重建术（TCAR）围术期的全程精准护理，探索提高手术成功率与患者康复质量的有效护理模式。旨在总结颈动脉狭窄最新手术方式–TCAR 手术患者的围术期护理经验，为临床护理实践提供参考。

方法：本次护理实践旨在探索一套精准、高效的全程护理模式，以应对 TCAR 手术患者在围术期护理中的特殊需求。在护理过程中，从患者入院即开始进行全面细致评估，为患者选择最优手术方式，依据评估结果制定个性化护理方案，涵盖术前、术中及术后各个阶段。其次，加强术中护士与医生之间的精准配合，确保手术过程顺利进行，减少手术时间和并发症的发生风险。术后密切监测病情，特别是针对常见并发症如低血压、高灌注综合征等的预防与处理，同时提供科学的康复指导，促进患者尽快恢复健康。通过多维度个性化围术期监测，有效预防了并发症发生。

结果：通过上述措施，实践结果显示，手术顺利完成，患者术后恢复良好，取得了良好的治疗效果。通过精准护理的实施，本例患者的术后并发症发生率显著降低，充分体现了精准护理在保障手术安全和促进患者康复中的重要作用。本研究期望能够显著提高 TCAR 手术的成功率，降低术后并发症的发生率，并为临床护理实践提供可借鉴的经验和参考依据，最终推动颈动脉狭窄患者护理质量的整体提升。

结论：通过对该例颈动脉狭窄 TCAR 手术患者的全程护理实践，我们深刻体会到精准全程护理的重要性，护士在护理过程中要密切观察患者病情变化，及时发现并处理问题，同时要给予患者心理支持和健康教育，促进患者早日康复。随着医疗技术的不断发展，护理工作也将不断面临新的挑战，我们应该综合运用一线指南、循证依据、多学科协作、个性化评估，多维度护理，早期发现问题，及时处理。精准护航，保证护理安全性、有效性对减少术后并发症发生，促进患者康复，提高手术成功率和患者生活质量至关重要。此次精准全程护理实践为颈动脉狭窄 TCAR 手术患者的临床护理提供了宝贵经验，同时也指出未来护理工作中需进一步精准化、个性化的发展方向，通过将精准护理模式应用于更多类似病例，有望进一步提升护理服务质量，为患者带来更好的治疗体验和预后效果。

12HETE is an endogenous modulator of BLT2 triggering vascular degeneration, dissection and rupture

yuyu Li[1]

1. The First Affiliated Hospital of Wenzhou Medical University

2. Beijing An Zhen Hospital: Capital Medical University Affiliated Anzhen Hospital

Background:

Thoracic aortic dissection (TAD) is a catastrophic vascular condition characterized by the separation of the aortic wall layers, leading to high morbidity and mortality if left untreated. Despite advances in surgical interventions, effective pharmacological strategies to prevent TAD progression and rupture remain limited. Emerging evidence suggests that inflammation and vascular homeostasis disruption play pivotal roles in TAD pathogenesis. Arachidonic acid (AA) metabolites, key mediators of inflammation and vascular function, have been implicated in various cardiovascular diseases. However, their specific contributions to TAD remain poorly understood. This study aimed to investigate the role of AA metabolites, particularly those derived from the 12/15-lipoxygenase (12/15-LOX) pathway, in TAD development and evaluate their potential as therapeutic targets.

Methods:

To characterize AA metabolic alterations in TAD, we performed plasma metabolomic profiling in both TAD patients and a β-aminopropionitrile monofumarate (BAPN)-induced TAD mouse model. We further examined 12/15-LOX expression in aortic tissues from these cohorts. To elucidate the functional role of 12/15-LOX, we utilized Alox15 knockout mice (Alox15-/-) and adeno-associated virus-mediated Alox15 suppression

in BAPN-treated mice. Additionally, we administered exogenous 12-hydroxyeicosatetraenoic acid (12-HETE), the 12/15-LOX inhibitor ML351, and the leukotriene B4 receptor 2 (BLT2) antagonist LY255283 to assess their effects on TAD progression. Molecular docking and immunoblotting were employed to investigate the interaction between 12-HETE and BLT2 on macrophages. Single-cell RNA sequencing (scRNA-seq) data from TAD patient aortas were reanalyzed to identify intercellular communication networks involving 12-HETE-producing and BLT2-expressing cells.

Results:

Metabolomic analysis revealed a significant elevation of 12-HETE in the plasma of TAD patients and BAPN-treated mice, accompanied by upregulated 12/15-LOX expression in aortic tissues. Genetic ablation or pharmacological inhibition of Alox15 markedly attenuated BAPN-induced TAD formation, rupture, and mortality, suggesting a critical role for 12/15-LOX in disease progression. Mechanistically, 12-HETE was found to bind BLT2 receptors on macrophages, triggering the activation of the NOX-1/ROS/NF-κB signaling cascade. This pathway promoted the release of pro-inflammatory cytokines (e.g., IL-6, TNF-α), which in turn recruited additional immune cells and exacerbated extracellular matrix (ECM) degradation. Furthermore, 12-HETE-driven inflammation induced pathological phenotype switching in vascular smooth muscle cells (VSMCs), shifting them from a contractile to a synthetic state, thereby weakening aortic wall integrity.

Single-cell transcriptomic analysis corroborated these findings, revealing enhanced crosstalk between 12-HETE-producing macrophages and BLT2-expressing cells in TAD tissues. Pharmacological interventions with ML351 (12/15-LOX inhibitor) or LY255283 (BLT2 antagonist) significantly reduced TAD incidence and severity in mice. Strikingly, combined treatment with both agents yielded synergistic protective effects, nearly abolishing aortic rupture in the BAPN model.

Conclusion:

Our study identifies 12-HETE as a key mediator of TAD pathogenesis, acting through macrophage BLT2 receptor activation to amplify inflammatory responses and disrupt VSMC homeostasis. The 12-HETE/BLT2 axis drives a vicious cycle of inflammation, ECM degradation, and VSMC dysfunction, ultimately predisposing the aorta to dissection. Targeting this pathway—either by reducing 12-HETE production (via 12/15-LOX inhibition) or blocking its downstream signaling (via BLT2 antagonism)—represents a promising therapeutic strategy for TAD. These findings not only deepen our understanding of TAD pathophysiology but also provide a rationale for developing novel pharmacotherapies to mitigate this life-threatening condition. Future studies should explore the translational potential of 12/15-LOX inhibitors and BLT2 antagonists in clinical settings, particularly in high-risk patients with predisposing conditions such as hypertension or genetic aortopathies.

Keywords: Thoracic aortic dissection, 12-HETE, 12/15-LOX, BLT2, inflammation, vascular smooth muscle cells, metabolomics, single-cell RNA sequencing.

Systematic evaluation of a predictive model for the risk of bloodstream infections associated with intravenous infusion port in oncology patients

Kun-Yan Peng

Zigong First People's Hospital

Introduction: Fully implantable IV port is an important mode of drug infusion, which is an infusion device implanted subcutaneously and left in the body for a long period of time, and is becoming more and more common in clinical use. It is mostly used in the infusion of antibiotics, blood products, chemotherapeutic drugs, nutritional fluids and repeated taking of venous blood in oncology patients. There are many practical studies in the academic world on the use of fully implantable intravenous infusion ports to confirm their utility value. However, due to its invasive characteristics, the fully implantable IV port is prone to a series of complications such as drug extravasation, catheter displacement, bloodstream infection, and intratubular embolism, among which bloodstream infection is more common, which directly affects the therapeutic effect of the patients and is not conducive to recovery. Therefore, this study systematically evaluates the risk prediction model of bloodstream infection associated with intravenous infusion ports in tumor patients to provide reference for clinical practice and related research. **Methods:** The systematic search of China Knowledge Network, Wanfang Database, China Biomedical Literature Service System (SinoMed), Wipo database, PubMed, Web of Science, The Cochrane Library and Embase database published literature related to the predictive model of the risk of bloodstream infections associated with intravenous infusion port in oncology patients, using a combination of subject terms and free words, as well as manually searching for published and retrieved through review studies and review articles The reference list identified other literature as complementary. The search time limit is from the establishment of the database to December 31, 2024 The languages were limited to Chinese and English. Literature was screened and data extracted independently by 2 researchers to analyze and compare the population characteristics, study types, predictors, model construction methods and model prediction results of the included studies. **Results:** A total of 14 papers were included in the literature, including 19 predictive models for the risk of bloodstream infections associated with intravenous port placement in oncology patients, with total sample sizes ranging from 116 to 983 cases, the number of outcome events ranging from 19 to 123, and the area under the operator characteristic curve of the subjects ranging from 0.715 to 0.969. Predictive factors appearing in the models at a high frequency were mainly malignant hematological disorders, neutropenia, prolonged steroid use, peri lack of antimicrobial use during surgery, port placement surgical incision infection, skin infection around the port placement site, parenteral nutrition, immediate post-implantation chemotherapy, and inexperienced surgeons. The results of the prediction model risk of bias assessment tool showed that the overall applicability of the included risk prediction models was good, but the risk of bias was high, which was related to the inappropriate source of data for the study samples, inappropriate methodological treatment of continuous variables, failure to handle missing data, insufficient assessment of the model's performance, and irregularities in the evaluation indicators. **Discussion:** There are some deficiencies in the predictive model for the risk of bloodstream infections associated with the port of infusion in oncology patients, and the study design and study report should be improved in the future, especially to be more standardized in the selection of predictors and evaluation of the model, and to externally validate the developed model.

A Preliminary Study on the Correlation between 18F-NaF Uptake and Aortic Calcification, Aneurysm Sac Expansion and Endoleak after Endovascular Repair of Abdominal Aortic Aneurysm

Xiao Bi, Long Cao, Jia-Jin Liu, Shi-Na Wu, Xiao-Jun Zhang, Zhi-Wei Guan, Wei Guo, Bai- Xu, Rui-Min Wang

The First Medical Center of the PLA General Hospital

Objective: 18F-fluoride (18F-NaF) can non-invasively detect vascular inflammation and active microcalcification. This study aimed to investigate the relationship between 18F-NaF uptake in the proximal, distal and aneurysmal sac of the endovascular aneurysm repair (EVAR) stent and aortic calcification and aneurysmal sac expansion, and to evaluate its predictive value for endoleak.

Methods: Seven patients with abdominal aortic aneurysms who underwent EVAR were included. All patients underwent CTA before the operation, and the maximum cross-sectional area of the abdominal aortic aneurysm was recorded. 18F-NaF PET/CT was performed within one week after the operation (two patients also underwent 18F-NaF PET/CT before the operation). The maximum standardized uptake value (SUVmax) at the proximal and distal ends of the stent, the aneurysm sac, ascending aorta, aortic arch, and descending aorta was measured, and the target-to-background ratio (TBR) was calculated using the muscle tissue in the left groin as the reference. The uWS MI software was used to quantify the calcium score of the aorta (including ascending aorta, aortic arch, descending aorta, 3 cm of the aorta above the proximal end of the stent, and 3 cm of the internal iliac artery below the distal end of the stent). CTA was performed 4-6 months after the operation to evaluate the changes in aneurysm size and the occurrence of endoleaks. Spearman correlation was used for data analysis.

Results: It showed that the 18F-NaF uptake at the distal end of the stent was positively correlated with the calcification score of the iliac internal artery 3 cm below the distal end of the stent ($\rho = 0.86$, $p = 0.014$) after EVAR for abdominal aortic aneurysm. The 18F-NaF uptake at the proximal end of the stent was not significantly correlated with the calcification score of the aortic area 3 cm above the proximal end of the stent, but was positively correlated with the 18F-NaF uptake of the ascending aorta ($\rho = 0.79$, $p = 0.036$). The 18F-NaF uptake at the aneurysm sac was positively correlated with the maximum cross-sectional change of the abdominal aortic aneurysm ($\rho = 0.82$, $p = 0.023$). The higher the TBR value at the aneurysm sac, the more obvious the expansion of the abdominal aortic aneurysm. In two patients who underwent 18F-NaF PET/CT before and after the operation, the TBR values at the proximal and distal ends of the stent increased after the operation, while the TBR of the aneurysm sac wall decreased. Among the 7 patients, the TBR value of the aneurysm sac wall in the patient with type II endoleak found during follow-up was significantly higher than that of the other cases (TBR = 2.69).

Conclusion: The 18F-NaF uptake at the distal end of the stent after EVAR for abdominal aortic aneurysm is associated with local calcification progression. An increase in the TBR of the aneurysm wall may indicate the risk of aneurysm expansion and endoleak. 18F-NaF PET/CT can dynamically assess postoperative vascular repair and metabolic changes in the aneurysm sac, providing potential imaging markers for early identification of endoleak and poor aneurysm sac remodeling. However, larger sample sizes and continuous follow-up are needed to further validate its predictive value.

低密度脂蛋白颗粒大小与主动脉瘤之间的因果关系：孟德尔随机化和中介分析的启示

可奕 郑霖 王恒 常润泽 张鸿久 李亚玲 张瑞婧 董红霖

山西医科大学第二医院

目的：大量证据表明，不同大小的低密度脂蛋白（LDL）在多种心血管疾病的发病机制中起着关键作用。然而，LDL 亚群与主动脉瘤（AA）之间的精确因果关系尚未完全明了，高血压是否与这一效应相关也尚不清楚。这项研究旨在探讨了 LDL 亚组大小和 AA 之间的潜在关联。此外，我们试图确定高血压是否介导了因果关系。

方法：我们进行了两项样本孟德尔随机化（MR）分析和中介分析。汇总统计数据来自 FinnGen（样本量 =209,366）、医学研究委员会综合流行病学单元（MRC-IEU）联盟（样本量 =462,933）和一个全基因组循环代谢物研究（样本量 =19,273）。我们使用一组单核苷酸多态性（SNPs）作为工具变量，这些变量符合低于全基因组统计显著性阈值（p <5e-8）和独立（r2 <0.001）的标准。进行了单变量和多变量 MR 分析。还进行了反向 MR 和 MR Steiger 测试。

结果：大（比值比（OR）= 1.20, 95% 置信区间（CI）：1.04-1.39, P = 0.0136）、中（OR = 1.25, 95% CI: 1.07-1.49, P = 0.0081） 和 小（OR = 1.27, 95% CI: 1.07-1.51, P = 0.0081）LDL 颗粒浓度的增加与 AA 风险升高有因果关系。高血压中介了中等大小 LDL 颗粒浓度与 AA 之间的关系，中介比例为 8.04%。

结论：本研究为大、中、小 LDL 颗粒水平与 AA 之间的因果关联提供了经验支持。我们揭示了较小的 LDL 颗粒在预测 AA 方面具有更强的效应，并强调了高血压的中介影响，为 AA 的发病机制提供了新的见解。这一发现为 AA 的靶向治疗提供了潜在策略。

1990-2021 年全球、区域和国家老年主动脉瘤全球负担的系统分析

樊可奕 王恒 李亚玲 姜建桦 张瑞婧 董红霖

山西医科大学第二医院

目的：主动脉瘤是发生在主动脉局部的节段性、进行性扩张的血管疾病，可累及胸部和 / 或腹部各部分。主动脉瘤的形成和发展具有隐蔽性，多数患者可无症状，然而一旦破裂，生存率不及 20%，年龄是其发病的独立危险因素。据统计，主动脉瘤疾病是 55 岁以上个体第 15 大最常见的死因。本研究旨在描述老年主动脉瘤患者的疾病负担及主动脉瘤的最新流行病学模式。

方法：根据最新全球疾病负担 (GBD) 数据库，计算全球 204 个国家，21 个地区以及 5 个社会人口指数 (SDI) 类别人群的年龄标准化死亡率 (ASDR)、年龄标准化残疾调整生命年率 (ASDALYR)。

结果: 2021 年 GBD 研究估计全球 55 岁及以上人群中有 138450 人死于主动脉瘤。全球年龄标化死亡率 (ASDR) 为 9.93/10 万 (8.69,10.84)，年龄标准化伤残调整寿命年率 (ASDALYs)。为 166.53(149.30,181.22)。按地区划分，高收入亚太地区、热带拉美地区和东欧地区负担最高，ASDR 分别为 23.71(19.61,26.32)、20.74(18.39,22.52) 和 18.97 (17.09,20.77)，ASDALYs 分 别 为 375.73(325.23,409.72)、395.97(358.27,427.61) 和 375.65(339.68,411.94)。按国家划分，亚美尼亚的 ASDR 最高，为 48.85(40.01,58.53)；其次是黑山，为 46.35(32.23,65.50) 和瑙鲁，为 32.25(14.32,58.44)。此外，大约 68.22% 的主动脉瘤死亡发生在高 SDI 和高 - 中 SDI 国家。

结论：全球范围内老年人群的动脉瘤负担较高，在不同国家、地区间存在差异。不同 SDI 类别的主动脉瘤负担存在显著差异，SDI 和 ASDR 之间呈正相关。了解特定地区的医疗系统和加强血管健康策略对于提供政策信息和改善主动脉瘤管理至关重要。

ENOX2 and the related mechanisms as potential genetic targets for varicose veins of lower extremities: an integrated bioinformatics and Mendelian analysis

Qiurui He, -Rong Yue Shi, -Ya Sheng Fu, -Da Hua Fu

The Third Hospital of Zhangzhou, Fujian, Chian

Objective: We employed an integrated bioinformatics screening approach along with Mendelian randomization (MR) analysis to explore potential genetic targets for varicose veins of lower extremities (VVs) and identify potential treatment options for VVs. **Methods:** Our study utilized publicly available genome-wide association study data from the IEU OpenGWAS Project (https://gwas.mrcieu.ac.uk/) to investigate the relationship between genetic susceptibility to EXON2 and the risk of VVs. Summary-level data for ENOX2 involved 3301 individuals with 10534735 SNPs, while the VVs data were extracted from a GWAS comprising 10044 cases and 452966 controls, with a total of 9851867 SNPs. Differential expression analysis was conducted using R software to identify differentially expressed genes (DEGs) of VVs from the Gene Expression Omnibus (GEO) database. Weighted gene co-expression network analysis (WGCNA) was performed to identify co-expression networks. Functional enrichment analyses were conducted for the identified genes. A protein-protein interaction (PPI) network was constructed to analyze the interactions among the identified genes. Additionally, genome-wide association studies (GWAS) data for VVs were downloaded for MR analysis. We conducted Two-sample MR analyses using R Studio to assess the causal relationship between genetic susceptibility to EXON2 and the risk of VVs. SNPs were selected as instrumental variables (IVs) based on the genome-wide significance threshold (P 10 as indicative of a sufficiently strong correlation between the IVs and the exposure, thus avoiding weak instrument bias. For univariable analysis, we employed the Inverse-variance weighted (IVW), MR-Egger, weighted median methods, and other approaches. The primary estimation method utilized was IVW, providing an asymptotic estimate of the standard error of the causal estimate from each variant. A two-sided P value **Results:** The DEGs identified from the VVs GEO dataset included 180 upregulated genes and 335 downregulated genes. Gene Ontology (GO) and Kyoto Encyclopedia of Genes and Genomes (KEGG) analysis revealed that the downregulated DEGs were significantly associated with nuclear protein-containing complexes and nucleic acid binding (P<0.05). WGCNA highlighted a highly significant “turquoise” module comprising 78 downregulated genes (P= 2e – 04). The PPI network analysis of the significant DEGs and the WGCNA “turquoise” module identified 224 nodes and 491 edges, uncovering several hub genes such as BRCA1, NCBP2, GTPBP4, HDAC2, KHDRBS1, and HNRNPR. Detailed functional enrichment analysis indicated involvement in tumor-like cellular proliferation and differentiation processes, including protein acetylation, RNA splicing, and metabolic processes. MR analysis revealed a causal association between the tumor-related gene ENOX2 and VVs, with genetically predicted ENOX2 increasing the risk of VVs (OR: 12.780; P = 0.012) according to IVW analysis. Sensitivity analysis confirmed the absence of heterogeneity and horizontal pleiotropy in the observed associations (P>0.05). “Leave-one-out” validation analysis did not indicate any changes. **Conclusions:** Our study initially employed transcriptomic data of varicose veins to compare gene expression profiles between veins with varicosities and non-varicose veins, identifying differentially expressed genes. Through enrichment functional analysis, we preliminarily determined the functions and molecular pathways associated with these differentially expressed genes. Our results revealed statistically significant enrichment in cellular functions and molecular pathways for upregulated and downregulated genes, with particular significance observed in the enrichment analysis of downregulated genes.Through screening, we found out a target, ENOX2, which is also a target related to tumor dilation oxidative stress. Our Mendelian analysis revealed a positive correlation between ENOX2 and venous varicosity gene SNPs, which can promote the incidence of venous varicosity. ENOX2 is a NADH oxidase that can regulate cell growth and division. Our study unveils the involvement of ENOX2 and the related mechanisms in the pathogenesis of VVs, suggesting their potential as genetic targets for treatment.

Keywords: varicose veins of lower extremities; ENOX2; bioinformatics; Mendelian.

Funding: The Natural Science Foundation of Zhangzhou City, China (No. ZZ2024J57) .

有氧运动降低脂质重塑改善肺动脉高压的分子机制研究

王友华 孙研 李素娟 张嘉敏 王亮 宋磊

陕西师范大学

研究目的

前期研究表明，有氧运动可以改善肺动脉高压导致的肺动脉血管重构，降低肺动脉高压，但其机制尚不明确。本研究将有氧运动作为主要干预手段，探讨有氧运动活化副交感神经以及抑制 ALCAT1 对低氧诱导的肺动脉高压小鼠肺血管重构以及右心肥大的改善作用，为肺动脉高压的预防和治疗提供实验参考。

研究方法

动物实验：雄性 9 周龄 C57BL/6 小鼠 40 只，随机分为 4 组：常氧对照组（C），低氧组（H），低氧 + 有氧运动组（HE），低氧 + 吡啶斯的明（PYR）组（HP）。雄性 9 周龄 ALCAT1 血管平滑肌特异性敲除小鼠 16 只，随机分为 2 组：ALCAT1 血管平滑肌特异性基因敲除组（AC），ALCAT1 血管平滑肌特异性基因敲除低氧组（AH）。采用动物低氧系统建立小鼠肺动脉高压模型，将 H 组，HE 组，HP 组和 AH 组放入 10% 氧气浓度的低氧箱中，24h/d 低氧，持续 5w。HE 组采用小动物跑台有氧运动干预，12m/min，1h/d，持续 5w，HP 组采用 PYR 灌胃干预，干预剂量为 3mg/kg/d，持续 5w，直至建模结束，C 组和 AC 组常氧环境饲养 5w。取材前，通过 Lab Chart 分析右心室收缩压（RVSP）验证小鼠肺动脉高压模型建模成功，心电图分析心率变异性（HRV），HE 染色，Masson 染色和血管造影观察小鼠肺组织形态学变化，脂质组学分析检测小鼠肺组织膜磷脂含量，评定小鼠肺组织膜磷脂的改变。小动物心动超声测右心室腔大小，小鼠心脏组织称重测定右心室肥厚指数，WGA 染色评定小鼠心肌细胞大小，Western blotting 检测小鼠肺组织和右心心肌组织低氧相关蛋白 HIF1α，内质网应激相关蛋白 CHOP，炎症和凋亡相关蛋白 IL-1β，BAK，血管重构相关蛋白 ET-1，PCNA，α-SMA 等指标。

研究结果

（1）肺动脉高压小鼠 RVSP 显著升高，有氧运动与 PYR 以及 ALCAT1 血管平滑肌敲除显著改善肺动脉高压小鼠血流动力学参数，降低肺动脉高压小鼠 RVSP。（2）肺动脉高压小鼠 HE 染色，Masson 染色和血管造影结果显示肺血管壁厚度显著增加，纤维化水平升高，有氧运动与 PYR 以及 ALCAT1 血管平滑肌敲除显著降低肺动脉高压小鼠肺血管壁厚度，降低纤维化水平，改善肺动脉高压小鼠肺血管重构。（3）肺动脉高压小鼠肺组织肺动脉内皮细胞蛋白 ET-1，肺动脉平滑肌增殖蛋白 PCNA，肺动脉平滑肌肌化蛋白 α-SMA 显著升高，有氧运动与 PYR 以及 ALCAT1 血管平滑肌敲除降低 ET-1，PCNA，α-SMA 表达，改善肺动脉高压小鼠肺血管重构。（4）肺动脉高压小鼠肺组织 ALCAT1，低氧相关蛋白 HIF1α，内质网应激相关蛋白 CHOP，炎症和凋亡相关蛋白 IL-1β，BAK 显著升高，有氧运动与 PYR 以及 ALCAT1 血管平滑肌敲除显著降低 ALCAT1，HIF1α，CHOP，IL-1β，BAK 表达，改善肺动脉高压小鼠肺血管重构。（5）肺动脉高压小鼠肺组织磷脂成分改变，有氧运动与 PYR 以及 ALCAT1 血管平滑肌敲除调控肺组织磷脂成分，改善肺动脉高压小鼠脂质组学紊乱。

研究结论

本研究通过胆碱酯酶抑制剂 PYR 以及 ALCAT1 血管平滑肌敲除平行实验，证实有氧运动可以激活副交感神经以及抑制 ALCAT1 降低小鼠体内炎症凋亡相关蛋白和内质网应激相关蛋白表达，改善肺动脉高压小鼠脂质组学紊乱，在改善低氧诱导的肺动脉高压小鼠肺血管重构以及右心肥大方面发挥作用，进而改善小鼠肺动脉高压。

Integrated analysis of bulk RNA-seq, Mendelian randomization, and eQTL reveals the Pathogenesis of Pan-Vascular Diseases

yuhang Zhang

The Second Hospital of Shanxi Medical University

Integrated analysis of bulk RNA-seq, Mendelian randomization, and eQTL reveals the Pathogenesis of Pan-Vascular Diseases

Yuhang Zhang[1], Chuanlong Lu[1], Keyi Fan[1], Heng Wang[1], Yaling Li[1],Ruijing Zhang[2]*, Honglin Dong[1]*

[1] Department of Vascular Surgery, The Second Hospital of Shanxi Medical University, Taiyuan, Shanxi, People's Republic of China

[2] Department of Nephrology, The Second Hospital of Shanxi Medical University, Taiyuan, Shanxi, People's Republic of China

*** Correspondence:**

Ruijing Zhang: 15035180085@163.com

Honglin Dong: honglindong@sxmu.edu.cn

Introduction

Pan-vascular diseases refer to systemic disorders affecting the human vascular system, a complex network comprising arteries, veins, and lymphatic vessels, with vascular lesions as their shared pathological feature, predominantly based on atherosclerosis (accounting for approximately 95%). Currently, the burden of pan-vascular diseases in China remains substantial, representing the leading cause of mortality among the Chinese population, with patient prognosis urgently requiring improvement. This study aims to investigate the potential associations and shared comorbid mechanisms between peripheral vascular diseases, particularly lesions of the aorta and lower extremity arteries, and carotid artery disease, thereby enhancing our understanding of the etiological factors and underlying molecular events in pan-vascular diseases.

Methods

The bulk-sequencing (bulk-seq) datasets for pan-vascular diseases were sourced from the Gene Expression Omnibus (GEO) database. We employed multiple methods to analyze and characterize the heterogeneity of pan-vascular diseases. Using Mendelian randomization (MR) and expression quantitative trait loci (eQTL) analyses, we screened for potential pathogenic genes implicated in pan-vascular diseases. Subsequently, we compared nine types of machine learning algorithms to select the optimal approach for identifying diagnostic features associated with pathogenicity, thereby constructing a nomogram model. Consensus clustering was utilized to stratify patients with pan-vascular diseases into distinct subgroups. Finally, we conducted immune cell infiltration and clinical correlation analyses on diagnostic features linked to comorbidity-related genes.

Results

By integrating eQTL data from genome-wide association studies (GWAS) of pan-vascular diseases with XGBoost (XGB) machine learning, we identified a total of four relevant diagnostic features (GNAI3, TCTN3, AVIL, and NCF1C). Consensus clustering analysis revealed that pan-vascular diseases could be classified into two distinct patterns (Cluster 1 and Cluster 2), with Cluster 2 exhibiting a higher pathogenic gene score than Cluster 1. These two clusters were involved in different biological pathways and displayed distinct immune cell infiltration profiles.There were no differences in age or gender between the two distinct patterns. Additionally, in patients with pan-vascular diseases, GNAI3 and AVIL showed a positive correlation with age. Among them, NCF1C encodes the neutrophil cytosolic factor 1 protein, which is expressed in neutrophils. The NCF1 protein serves as a component of the NADPH oxidase complex and participates in the oxidative burst process.It has been revealed that neutrophils play a significant role in the mechanisms underlying pan-vascular diseases.

Conclusion

Our study identified four shared pathogenic genes for pan-vascular diseases (including abdominal aortic aneurysm, aortic dissection, carotid artery stenosis, and peripheral arterial disease). The construction of a pathogenesis-related diagnostic model provides valuable resources for guiding immunotherapeutic strategies for pan-vascular diseases and lays a foundation for exploring the comorbidity mechanisms underlying these conditions.Among them, we have discovered that neutrophils play a crucial role in the onset and progression of pan-vascular diseases. Next, we will conduct in-depth research on the mechanisms by which neutrophils contribute to the development of these diseases.

1990-2021 年 55 岁及以上成人主动脉瘤的风险因素差异性分析

李亚玲 樊可奕 王恒 张瑞婧 董红霖

山西医科大学第二医院

目的

主动脉瘤（Aortic aneurysm，AA）是指主动脉局部节段性不可逆扩张，受高龄、高血脂、高血压、吸烟等多种因素影响。AA 是慢性进行性血管疾病，起病隐匿，通常没有临床症状，但由于破裂风险高，对人类生命构成重大威胁。AA 的危险因素很多，包括不良的生活习惯和其他慢性疾病，早期控制管理危险因素有助于降低 AA 发病风险。

方法

从 2021 年全球疾病负担 (Global burden of disease，GBD) 研究中提取 AA 负担数据，覆盖 5 个社会人口指数（Socio-demographic index，SDI）类别，按性别分层，通过分解分析法分析 AA 的归因危险因素，探索疾病负担的驱动因素。

结果

从 1990 年至 2021 年，全球 55 岁以上人群的 AA 死亡和伤残可归因于 7 个危险因素，包括：吸烟、蔬菜摄入少、水果摄入少、钠摄入多、高收缩压、高体质指数和环境铅暴露。我们依据性别分别讨论了不同 SDI 地区的危险因素。吸烟是男性 AA 的主要危险因素，在高 SDI 地区，吸烟的 ASDR 由 1990 年的 20.11(17.14,23.16) 降至 2021 年的 7.91(6.42,9.53)，在低中 SDI 地区，吸烟的 ASDR 从 1.84(1.04,3.39) 增加到 2.87(2.08,4.52)。收缩压高是女性 AA 的主要危险因素，高 SDI 地区归因危险因素总体呈下降趋势，ASDR 由 1990 年的 3.96(2.96,4.97) 降至 2021 年的 2.68(1.85,3.62)，在 SDI 低 - 中等地区，高收缩压导致的 ASDR 从 1990 年的 0.58(0.34,1.09) 增加至 2021 年的 0.87(0.59,1.26)。

结论

AA 仍然是一个重大的公共卫生问题。我们的研究结果强调 AA 的风险因素具有明显的性别差异和地区差异。迫切需要政府机构和非政府机构针对不同地区、不同人群制定预防工作和公共卫生规划，以减轻当前和未来的全球疾病负担。

中性粒细胞与主动脉瘤之间的因果关系：孟德尔随机化的启示

樊可奕 李亚玲 王恒 张瑞婧 董红霖

山西医科大学第二医院

目的

主动脉瘤是全球主要的心血管疾病之一，先前研究表明中性粒细胞被招募到动脉瘤壁并发挥一系列作用。活化的中性粒细胞通过多种机制损害血管内皮细胞的屏障功能，内皮细胞屏障功能障碍加重动脉瘤的发展。本研究旨在从遗传学角度确定中性粒细胞计数与动脉瘤之间的因果关系。

方法

双向两样本孟德尔随机化分析被用来识别动脉瘤与中性粒细胞计数之间是否存在因果关系。满足显著性阈值 (r2 <0.001 和 p <5e-8) 的单核苷酸变异（SNP）作为工具变量计算因果效应。计算 F 统计量和最小等位基因频率（MAF）来评估弱工具变量对偏倚的影响。此外，我们使用 PhenoScannerV2 去除与混杂因素 (如吸烟和高血压) 相关的工具变量。采用逆方差加权 (IVW)、加权中位数估计 (WME)、简单模态、加权模态和 MR-Egger 回归方法 (MR-ER) 进行分析，进行异质性检验、水平多效性检验和留一分析等敏感性分析以验证结果的稳健性。

结果

中性粒细胞计数增加与动脉瘤风险较高有因果关系（OR=1.431，95%CI：1.041-1.967，P = 0.027），而动脉瘤对中性粒细胞计数具有促进作用（OR=1.026，95%CI：1.007-1.045，P = 0.008）。在双向因果关系中均未检测到异质性或水平多效性。

结论

这项研究从基因水平证实了动脉瘤发生风险和中性粒细胞计数之间存在相互促进的因果关系，然而中性粒细胞在动脉瘤的发生发展过程中所起作用的具体机制还需进一步深入阐明。

单侧复发性缺血性脑卒中与同侧颈动脉 CTA 特征关系的定量分析研究

金晶

安徽医科大学第二附属医院

目的 基于 VascuCAP 软件对头颈 CTA 的颈动脉斑块图像进行分析，探讨单侧复发性缺血性脑卒中患者双侧颈动脉斑块特征的差异，以及颈动脉斑块与临床脑血管事件发生的相关性。

方法 回顾性分析 116 例单侧复发性急性前循环缺血性脑卒中患者颈动脉 CTA 图像，将颈动脉分为有症状侧和无症状侧两组，记录受试者血清学指标，计算血浆动脉粥样硬化指数（AIP），并记录两组颈动脉斑块特征，比较两组间的差异，分析颈动脉斑块特征与动脉狭窄程度的关系，以及颈动脉斑块特征与 AIP 的相关性。

结果 单侧复发性脑卒中患者双侧颈动脉粥样硬化斑块成分存在差异，有症状侧组颈动脉斑块内出血（IPH）体积（Z=7.862，P < 0.001）与百分比（Z=7.348，P < 0.001）、MATX 体积（Z=2.288，P=0.022）、最大重塑比例（Z=2.012，

P=0.044）大于无症状侧；两组间其他斑块成分的体积、百分比及动脉狭窄程度无明显差异。Spearman 相关性分析显示有症状侧颈动脉最大狭窄程度与钙化斑块（CALC）体积、富含脂质的坏死核心（LRNC）体积和百分比、总斑块体积呈正相关；无症状侧颈动脉最大狭窄程度与 IPH 体积和百分比、LRNC 体积和百分比、总斑块体积之间呈正相关性；AIP 与有症状侧血管壁大分子物质（MATX）呈负相关（r=-0.241，P=0.009）。

结论 利用半自动软件量测的 CTA 颈动脉斑块特征分析显示单侧复发性脑卒中患者有症状侧 IPH 体积和百分比明显大于对侧，颈动脉血管壁弹性结构减少与心血管事件风险增加相关。

肺循环与右心研究

Effectiveness of chest pain center accreditation on the in-hospital outcome of acute pulmonary embolism in China: Findings from the Chinese Cardiovascular Association Database

Beijian Zhang[1], Duo Lin[2], Jun-Bo Ge[1], Jing Yang[3]

1. Zhongshan Hospital, Fudan University, Shanghai Institute of Cardiovascular Diseases, China

2. China Heart House, Suzhou, 215124, China

3. Shanghai Xuhui Central Hospital, Zhongshan-Xuhui Hospital, Fudan University, Shanghai, 200237, China

Abstract

Background: Acute pulmonary embolism (APE) represents a critical, time-sensitive cardiovascular emergency with substantial in-hospital mortality. Optimizing care pathways is paramount to improving outcomes. While China's National Chest Pain Center Program (NCPCP) has proven effective in managing acute coronary syndromes, its specific impact on APE care and patient outcomes required comprehensive evaluation. This study aimed to determine whether Chest Pain Center (CPC) accreditation is associated with improved processes of care and clinical outcomes for patients hospitalized with APE.

Methods: Utilizing a nationwide registry, the Chinese Cardiovascular Association Database-Chest Pain Center (2016–2022), we conducted a self-controlled retrospective cohort study involving 43,428 APE patients admitted to 2,498 hospitals. Patients were stratified into pre-accreditation (n=14,258) and post-accreditation (n=29,270) groups based on their admission date relative to the individual hospital's CPC accreditation date. Primary outcomes were in-hospital mortality and misdiagnosis rate. Secondary outcomes included system delays (various time metrics in the care pathway) and diagnostic testing utilization. Generalized linear mixed models, adjusting for patient demographics (age, sex), clinical presentation (symptoms like dyspnea, syncope, persistent chest pain/tightness; vital signs including SBP <100 mmHg, heart rate ≥ 110 bpm; complications such as malignant arrhythmia, heart failure, bleeding; biomarkers NT-proBNP >600 ng/L, elevated troponin, D-dimer; risk stratification), arrival mode (walk-in, EMS, in-hospital onset), and hospital-level factors (geographic region, administrative hierarchy, tier), were employed to assess the independent association of CPC accreditation with outcomes. Extensive subgroup analyses were performed based on patient sex, age (<65 vs ≥ 65 years), arrival mode, geographic region (Eastern, Central, Western), hospital administrative hierarchy (Provincial Capital, Prefecture-level City, County), and hospital tier (Grade III A, Grade III B, Grade II).

Results: Following CPC accreditation, significant improvements were observed across multiple domains. Primary Outcomes: In-hospital mortality decreased significantly from 2.7% pre-accreditation to 2.0% post-accreditation (P<0.001). The misdiagnosis rate also declined substantially from 9.2% to 6.9% (P<0.001). Secondary Outcomes: System delays at all measured time points were significantly shorter post-accreditation (P<0.001 for all). Diagnostic testing rates increased significantly. Although total expenditure was higher, the median length of hospital stay decreased by 1 day in the post-accreditation group. Multivariable Analysis: After adjusting for confounders and hospital-level clustering, CPC accreditation was independently associated with an 18% reduction in the odds of in-hospital mortality (adjusted Odds Ratio [aOR] 0.822, 95% Confidence Interval [CI] 0.707–0.956) and a 10.2% reduction in the odds of misdiagnosis (aOR 0.898, 95% CI 0.819–0.985). Key independent predictors of mortality identified included systolic blood pressure <100 mmHg (aOR 3.385), malignant arrhythmia (aOR 3.285), heart rate ≥ 110 bpm (aOR 2.395), heart failure (aOR 1.681), and age ≥ 65 years (aOR 1.327). Major risk factors for misdiagnosis included persistent chest pain/tightness (aOR 1.206), malignant arrhythmias (aOR 2.283), and elevated troponin (aOR 1.122). Subgroup Analyses: The beneficial effects of CPC accreditation on mortality reduction were consistently observed but were significantly more pronounced in males, patients aged <65 years, EMS-transported patients, hospitals in the Central region, Provincial Capital hospitals, and Grade III A hospitals (P<0.05 for interaction). Similarly, the reduction in misdiagnosis was significantly greater in males, patients aged <65 years, walk-in patients, hospitals in the Eastern region, Provincial Capital hospitals, and Grade III A hospitals (P<0.05 for interaction). Sensitivity analyses confirmed the robustness of these findings.

Conclusion: CPC accreditation is independently associated with significantly improved quality of care and enhanced in-hospital outcomes for patients with acute pulmonary embolism across a large, diverse national cohort in China. Key benefits include reduced mortality, lower misdiagnosis rates, shorter system delays, increased diagnostic testing, and decreased length of stay. The magnitude of benefit varied meaningfully across patient subgroups and hospital types, with particularly strong effects observed in high-volume tertiary centers (Provincial Capital, Grade III A) and specific patient demographics. These findings provide robust evidence supporting the effectiveness of the NCPCP accreditation process in optimizing care pathways and improving survival for APE, a critical time-dependent condition, and advocate for its broader implementation and tailored enhancement across different healthcare settings.

S-nitrosylated Cys133 of Annexin A2 improves pulmonary arterial hypertension by inhibiting WNT/β-catenin pathway

Wande Yu, QIANQIAN Chen, HANG Zhang

nanjing first hospital

Abstract

Background

The excessive proliferation and migration of pulmonary artery smooth muscle cells (PASMCs) resulting in pulmonary vascular remodeling is the crucial pathological features of pulmonary arterial hypertension (PAH). Protein S-nitrosylation as a downstream of nitric oxide has been shown to be critically involved in PASMCs proliferation and PAH, but the underlying mechanism remains largely unknown.

Methods

Using a combination of membrane and nuclear localization, iodoTMT switch assay, molecular biology, in vitro and in vivo approaches, we investigated the effect of S-nitrosylated Cys133 of ANXA2 on the proliferation and migration of PASMCs in PAH.

Results

The protein expression of ANXA2 was increased in PASMCs from PAH rats. Interference with ANXA2 significantly inhibited the excessive of proliferation and migration PASMCs. Using inhibitor of ANXA2 or conditionally knockdown ANXA2 in PASMCs improved pulmonary vascular remodeling of experimental models of PAH. Moreover, we found the Cys133 of ANXA2 can be S-nitrosylated by the NO donor GSNO under hypoxic stimulation. S-nitrosylated Cys133 (SNO-Cys133) of ANXA2 inhibited hypoxia mediated PASMCs proliferation and migration by regulating the subcellular localization of ANXA2 in cells. Besides, SNO-Cys133 of ANXA2 regulates the WNT pathway by inhibiting Tyr24 phosphorylation of ANXA2. Lastly, SNO-Cys133 of ANXA2 improves pulmonary vascular remodeling and RV function in vivo.

Conclusions

SNO-Cys133 of ANXA2 suppresses relocation of ANXA2 activity and WNT pathway to improve pulmonary vascular remodeling in pulmonary hypertension.

Keywords: pulmonary arterial hypertension, ANXA2, S-nitrosylation, pulmonary artery smooth muscle cells

Introduction

Pulmonary arterial smooth muscle cells (PASMCs) play central roles in pathologic vascular remodeling because of their similar abilities to cancer cells for excessive proliferation and migration under hypoxia conditions[1]. Despite the combination therapy of multiple drugs, the long-term prognosis of pulmonary arterial hypertension (PAH) is still poor, which is related to the complex pathogenic mechanism leading to pulmonary small vessel remodeling[2,3]. The molecular mechanisms underlying PASMCs contribution to pulmonary vascular lesions associated with PAH have been a major focus of research, and it is currently unclear.

S-nitrosylation (SNO), a post-translational modification of cysteines by nitric oxide (NO), regulates protein activity, stability, and protein-protein interactions[4]. NO derived from endothelial cells diffuses into PASMC and directly modify G protein coupled receptors through S-nitrosylation, thereby inhibiting vasoconstriction[5]. Besides, a study indicated that sodium nitrite reversed chronic hypoxic pulmonary hypertension in juvenile rats by increasing lung S-nitrosylation[6]. However, the molecular mechanisms involved in protein S-nitrosylation in the pathological mechanism of PAH has not been fully elucidated, even though the NO signaling pathway is important for the pathological mechanism and drug development of PAH.

ANXA2, a calcium ion dependent phospholipid binding protein, is widely distributed in the cytoplasm and membrane. The C-terminus of ANXA2 consists of highly conserved four similar repetitive sequences, while the N-terminus contains multiple modification sites that regulate ANXA2 activity, including tyrosine 24 (Tyr24), serine 25 phosphorylation sites, Ser1 acetylation sites, S100A10 molecular binding sites, etc[7,8]. It should be noted that phosphorylation at the Tyr24 plays a role in membrane translocation and nucleus translocation of ANXA2, thereby participating in the regulation of various biological behaviors of cells[9,10]. A study showed that the cysteine 133 (cys133) site of ANXA2 is regulated by reversible glutathioneization, which downregulates the ability of ANXA2 to interact with phospholipid liposomes and F-actin[11]. However, the S-nitrosylation of ANXA2 has not been evaluated until today.

ANXA2 promotes cell proliferation, stabilizes the cytoskeleton, mediates endocytosis and exocytosis, and activates plasmin to dissolve the extra-

cellular matrix by transferring to the cell membrane or nucleus[12,13]. Bleomycin, as a cytotoxic drug with side effects leading to pulmonary arterial hypertension, direct binds with ANXA2 resulting in pulmonary fibrosis. Genetic depletion of ANXA2 in mice mitigates bleomycin-induced pulmonary fibrosis[14]. Besides, recent findings have established the essential role of high expression of ANXA2 in controlling the phenotypic modulation of PASMCs in pulmonary vascular remodelling associated with hepatopulmonary syndrome[15,16]. Moreover, hypoxia-induced mitogenic factor promotes the migration of PASMCs by stimulating S100A11 translocate to plasma membrane in PAH, and ANXA2 also synergistically undergoes membrane translocation[17]. These studies imply that ANXA2 is involved in regulating the development of PAH, but the specific mechanism has not been elucidated.

WNT signaling plays an important role in pulmonary vascular remodeling by enhancing the proliferation and migration of PASMCs[18,19]. Activated WNT signaling depends on the nuclear translocation of β-catenin as a downstream effector[20]. Many studies have revealed that ANXA2 regulates WNT signaling to promote cell proliferation and migration in tumor development[21-23]. This is related to ANXA2 promoting the translocation of β-catenin to nucleus, and further studies have shown that ANXA2 may directly regulate β-catenin to enhance the resistant phenotype tumor cells[24].

In this study, we show that the level of ANXA2 was increased in PASMCs from PAH patients, thereby participating in the regulation of the β-catenin mediated downstream signaling pathway. More importantly, we demonstrated that the Cys133 site of ANXA2 undergoes nitrosylation modification, improving the development of PAH by inhibiting its Tyr24 phosphorylation level.

靶向治疗联合 SGLT2-i 对肺高血压的疗效和安全性研究

荣春妍

吉大一院

目的：探索 PAH 和 CTEPH 患者应用靶向治疗联合达格列净治疗的疗效与安全性。

方法：1、本研究为一项前瞻性、探索性研究，前瞻组：纳入 2024 年 7 月至 2024 年 12 月于我院就诊的 PAH 和 CTEPH 患者，接受 DAPA 治疗联合靶向治疗。历史对照组：纳入 2022 年 1 月至 2024 年 6 月于我院就诊的 PAH 和 CTEPH 患者，仅接受靶向治疗。2、收集治疗前后两组患者的相关临床资料。3、主要终点事件定义为 6 分钟步行距离的改善情况，次要终点是 NT-proBNP、超声心动图、WHO-FC 分级、危险分层。不良事件。4、比较治疗前两组的基线特征，侧面分析目前 PH 患者的诊疗现状。5、治疗 3 个月后，比较两组治疗前后及组间各项指标的变化，并对靶向联合 DAPA 治疗的安全性进行分析。

结果：1、本研究最终纳入 73 例，其中 DAPA 组 28 例，对照组 45 例。所有 PH 患者中男性 20 例，女性 53 例，平均年龄 44.99±14.14 岁。2、治疗前，相关指标无统计学差异。3、DAPA 组 3 个月后随访，上述指标较治疗前下降，差异有统计学意义。危险分层、NT-proBNP、心脏超声相关指标较治疗前下降，但差异没有统计学意义。4、对照组 3 个月后随访，相关指标无统计学差异，心脏超声相关指标较治疗前下降，但差异没有统计学意义。5、治疗 3 个月后，两组之间进行比较，6MWD 组间差异没有统计学意义。与治疗前相比，治疗后，对照组血红蛋白明显下降，DAPA 组血红蛋白未见明显变化。6、DAPA 治疗期间患者病情及生命体征平稳，无肝肾损伤、尿路感染、严重的低血糖和低血压、离子紊乱等不良事件发生。

结论：1、应用靶向药物治疗，可明显改善 PAH 和 CTEPH 患者的右心功能和活动耐力。2、应用靶向药的基础之上，联合 DAPA 治疗，右心功能和活动耐力未见明显的进一步改善。3、DAPA 治疗可改善 PH 患者疾病原因或药物原因引起的血红蛋白下降，减轻靶向药物引起的副作用。

基于心肺运动试验的肺栓塞患者个体化阶梯式肺康复方案构建与效果评价

张璐

陆军军医大学第二附属医院新桥医院

目的：构建适用于急性肺栓塞患者的个体化阶梯式肺康复干预方案，并验证其对心肺功能、运动耐力及生活质量的改善效果。**方法：**采用单盲随机对照研究设计，纳入 2023 年 1 月至 2024 年 6 月收治的 92 例急性肺栓塞患者，通过心肺运动试验（CPET）评估个体心肺储备功能后，实验组（n=46）实施为期 12 周的阶梯式康复方案，包括呼吸模式重建、抗阻 - 有氧复合训练及健康教育三阶段，对照组（n=46）接受常规康复指导。分别于干预前后检测 VO2 峰值、VE/VCO2 斜率、6 分钟步行距离（6MWD），采用 SF-36 量表评估生活质量，并通过焦虑抑郁量表（HADS）进行心理状态评估。**结果：**干预后实验组 VO2 峰值较基线提升（23.5±3.1 vs 18.2±2.8 mL/kg/min，P<0.01），6MWD 增加（412±45 vs 338±52 m，P<0.01），VE/VCO2 斜率下降（28.3±4.2 vs 34.1±5.6，P<0.05），SF-36 生理职能维度评分显著高于对照组（75.6±8.3 vs 62.4±9.1，P<0.01），焦虑抑郁评分降低幅度达临床最小重要差异（MID）。**结论：**基于 CPET 制定的阶梯式肺康复方案能有效改善肺栓塞患者心肺适能，其分阶段、渐进式干预模式为精准康复提供了新路径，具有临床推广价值。

靶向药物治疗高原性肺动脉高压的疗效与安全性：一项聚焦藏族人群的 Meta 分析

车千秋

西藏自治区人民政府驻成都办事处医院 四川大学华西医院西藏成办分院

目的

系统评价靶向药物治疗高原性肺动脉高压（HAPH）的有效性及安全性，重点关注藏族世居人群的疗效差异，为高海拔地区临床用药提供循证依据。

方法

计算机检索 PubMed、Embase、Cochrane Library、CNKI 等 7 大数据库（建库至 2025 年 6 月），纳入比较靶向药物（PDE5 抑制剂、内皮素受体拮抗剂、sGC 激动剂、前列环素类）与对照组的随机对照试验（RCT）及前瞻性队列研究。研究对象为常住海拔≥ 2500m 的 HAPH 成人患者（mPAP ≥ 25 mmHg）。主要结局包括：①平均肺动脉压（mPAP）变化值；② 6 分钟步行距离（6MWD）；次要结局包括右心室功能指标（TAPSE、RVFAC）、NT-proBNP、生活质量及不良事件。采用 RevMan 5.4 进行数据合并，连续变量用加权均数差（WMD），二分类变量用风险比（RR），均报告 95% 置信区间（CI）。异质性用 I^2 检验，>50% 时采用随机效应模型。预设亚组分析：世居 vs 移居、单药 vs 联合治疗、药物类别。

结果

共纳入 12 项研究（7 项 RCT，5 项队列；总样本量 n=609，藏族占比 58.3%）：1）mPAP 改善效果：靶向药物组较对照组显著降低 mPAP（WMD= -9.6 mmHg, 95% CI: -12.3~-6.9, P<0.001, I^2=43%）；亚组分析：藏族患者降幅更大（WMD= -11.2 mmHg vs 移居者 -7.1 mmHg, P<0.01）。2）运动耐量：药物治疗后 6MWD 平均增加 64.3 米（95% CI: 48.7~79.9, P<0.001）；西地那非在藏族人群中效果最优（WMD=82 米，Zhao 2024）。3）右心功能：TAPSE 显著改善（WMD=1.8 mm, 95% CI: 1.2~2.4, P<0.001）；他达拉非对移居者 RVFAC 提升更显著（WMD=5.2% vs 波生坦 2.7%, Lu 2023）。4）联合治疗优势：安立生坦 + 西地那非降低 mPAP 效果优于单药（WMD= -4.3 mmHg, 95% CI: -6.8~-1.8, Chen 2021）。5）安全性：总体不良事件率与对照组无差异（RR=1.12, 95% CI: 0.97~1.30），但波生坦肝酶升高风险较高（RR=3.05, 95% CI: 1.2~7.8）。

结论

靶向药物（尤以 PDE5 抑制剂）可显著改善 HAPH 患者的血流动力学、运动耐量及右心功能，且对藏族世居人群疗效更优；联合治疗（内皮素拮抗剂 +PDE5 抑制剂）可能是重度 HAPH 的优选策略；临床用药需权衡疗效与安全性：移居者优先选择他达拉非，世居藏族推荐西地那非，需监测波生坦的肝毒性。

Arteridin 通过调控线粒体自噬在肺动脉高压的作用及机制研究

杨培丽

陆军军医大学大坪医院

目的：探讨长链非编码 RNA 编码蛋白 Arteridin 对大鼠低氧性肺动脉高压 (HPH) 及其肺血管结构重建的影响。

方法：采用低压低氧法建立大鼠 HPH 模型。选取 8-12 周龄大鼠用于实验，雌雄各半，分组为野生型 SD 大鼠作为对照组，Arteridin 过表达和 Arteridin 敲除大鼠为实验组；使用低压低氧舱（相当于海拔 5000m 高度）喂养大鼠 3 周构建肺动脉高压大鼠模型，对照组于常压常氧条件下正常喂养。喂养 3 周后采集肺动脉高压相关检测指标，如：肺动脉收缩压、右心室收缩压、超声心动图（右室游离壁厚度、三尖瓣环移动距离）等指标；并进行免疫荧光及 HE 染色，观察 Arteridin 对大鼠肺血管重构、肺微血管肌化指数、右心室重构的影响；以及 ki-67、TUNEL 染色，观察肺动脉平滑肌增殖、凋亡情况。为了进一步寻找受 Arteridin 调控的下游靶分子，我们使用野生型 (WT) 大鼠及 Arteridin-/- 大鼠原代肺血管平滑肌细胞，并使用 RNA-seq 检测敲除 Arteridin 细胞转录组的改变；

结果：模型组 mPAP、RVHI、肺小动脉管壁厚度与外径比值 (WT%)、管壁面积与管总面积比值 (WA%) 均明显高于对照组；且 Arteridin 敲除组上述指标明显高于模型组；转库组测序结果显示众多差异性表达的基因进行通路富集，我们发现线粒体自噬信号通路改变显著，且泛素依赖型线粒体自噬 PINK1-parkin 信号通路为主导。

结论：非编码 RNA 编码蛋白 Arteridin 对低氧所致的肺动脉高压、右心室肥厚及肺血管结构重建具有较好的预防和逆转作用。

Noninvasive PECS Model for Detection of Combined Post-Capillary Pulmonary Hypertension

Chenyu Wan[1], Yu-Xuan Liu[1], Rong Jiang[2,3]

1. Tongji University School of Medicine

2. Shanghai Jiao Tong University School of Medicine

3. Shanghai General Hospital

Abstract:

Background: Combined post-capillary pulmonary hypertension (Cpc-PH) is a severe and complex condition that occurs as a result of elevated pulmonary pressures due to left heart disease (LHD). It is associated with high morbidity and mortality, and its early detection is critical for improving patient outcomes. However, the current gold standard for diagnosing Cpc-PH–right heart catheterization (RHC)–is invasive, costly, and not always feasible, especially in patients who are frail or elderly. RHC also has associated risks and logistical limitations. This creates an urgent need for non-invasive diagnostic methods that are accurate, accessible, and cost-effective. This study aims to address this gap by developing and validating a novel non-invasive diagnostic model, the Predictive Echocardiography Cpc-PH Score (PECS), which utilizes echocardiographic parameters to facilitate the early and accurate detection of Cpc-PH in pa-

tients with suspected pulmonary hypertension due to left heart disease.

Methods: This study was a retrospective cohort analysis that included 198 patients who were admitted to the Shanghai Pulmonary Hospital between July 2010 and December 2023, with suspected pulmonary hypertension due to left heart disease (PH-LHD). All patients underwent both RHC and echocardiography. They were categorized into two groups: those with Cpc-PH and those without (non-Cpc-PH), based on the diagnostic criteria outlined in the 7th World Symposium on Pulmonary Hypertension (WSPH). A range of echocardiographic parameters were selected for the development of the PECS model, including valvular heart disease (VHD), left atrial systolic diameter (LAD), interventricular septal thickness (IVS), mitral valve E/Em ratio, left ventricular fractional shortening (LVFS), and tricuspid regurgitation velocity (TR Vmax). To identify the most relevant predictive indicators, we performed chi-square tests and L1-regularized backward elimination. The diagnostic performance of the PECS model was evaluated using receiver operating characteristic (ROC) curve analysis, and its stability and generalizability were further assessed using five-fold cross-validation.

Results: The PECS model, which incorporated the selected echocardiographic parameters, demonstrated good predictive performance for diagnosing Cpc-PH, with an area under the ROC curve (AUC) of 0.761 (95% CI: 0.692–0.823, P < 0.001). The model achieved a sensitivity of 66.7%, specificity of 72.0%, positive predictive value (PPV) of 72.9%, negative predictive value (NPV) of 65.7%, and an overall accuracy of 69.2%. In five-fold cross-validation, the model maintained consistent performance, with an AUC of 0.752 ± 0.070. This confirms that the PECS model is stable and reliable across different subsets of the patient population, further validating its potential as a robust diagnostic tool.

Conclusion: The PECS model provides a promising, non-invasive approach for diagnosing Cpc-PH. It allows for early detection of Cpc-PH using routinely collected echocardiographic data, which is widely accessible and non-invasive, making it an attractive alternative to RHC. By improving early diagnosis, the PECS model could reduce the need for invasive procedures and allow for more timely and effective management of Cpc-PH, especially in patients who are not suitable candidates for RHC. This model could also be beneficial for patient populations that are at higher risk, such as the elderly or those with multiple comorbidities, who may have difficulty undergoing invasive testing. The PECS model could serve as an important screening tool in clinical practice, potentially enhancing clinical decision-making and improving patient outcomes by identifying patients at risk for Cpc-PH earlier. Additionally, the model's simplicity and use of standard echocardiographic measurements make it feasible for widespread clinical implementation. Further validation through larger multicenter studies is needed to establish its generalizability, particularly in diverse patient populations and settings. Once validated, the PECS model has the potential to become an essential tool in the early diagnosis and management of Cpc-PH, thereby enhancing the care and prognosis of patients with this complex condition.

剪切力通过 Sema3C-NRP2 通路介导内皮 - 平滑肌对话加重肺动脉高压的机制研究

周文颖

南京市第一医院

肺动脉高压（Pulmonary Artery Hypertension, PAH）是一种以肺血管阻力进行性升高为主要特征的致命性疾病，其核心病理环节是肺血管重塑。近年来，生物力学因素尤其是剪切力（shear stress）在 PAH 发生发展中的作用日益受到关注。作为血管内皮细胞感知的主要力学刺激之一，高流量产生的高剪切力可直接损伤肺血管内皮并激活下游机械信号转导通路。然而，这种机械力如何转化为细胞内生化信号并驱动血管重塑的具体机制尚未明晰，成为当前 PH 研究领域的重要科学问题。本课题组前期研究发现，在 PH 模型中，高剪切力可显著上调肺动脉平滑肌细胞（PASMCs）中神经纤毛蛋白 2（Neuropilin-2, NRP2）的表达。通过构建平滑肌特异性 NRP2 敲低小鼠模型，我们首次证实平滑肌 NRP2（而非内皮 NRP2）是高剪切力诱导肺高压进展的关键介质。这一发现具有重要理论意义：它揭示了力学刺激的细胞特异性响应机制，提示血管不同层细胞对剪切力的感知和转导存在显著异质性。进一步机制研究表明，高剪切力可能通过促进肺动脉内皮细胞（PAECs）分泌 Semaphorin 3C（Sema3c），进而激活平滑肌细胞表面的 NRP2/PlexinD1 受体复合物。这一通路通过下调抑制性缺氧诱导因子调控因子 FIH1（Factor Inhibiting HIF-1α），导致 HIF-1α 蛋白稳定性增加，最终增强糖酵解通量。这一发现将力学刺激与代谢重编程联系起来，为理解 PH 中著名的 "Warburg 效应 " 提供了新视角。基于上述发现，本研究拟通过多层次研究体系深入解析该通路的分子机制：在细胞水平，采用微流控芯片模拟生理 / 病理剪切力，结合 CRISPR-Cas9 基因编辑技术，系统研究 Sema3C/NRP2 轴在内皮 - 平滑肌旁分泌对话中的时空动力学特征；在动物水平，利用平滑肌特异性 NRP2 条件性敲除小鼠和 Sema3c 功能获得 / 缺失小鼠模型，通过血流动力学测量、显微 CT 血管三维重建等技术，明确该通路在血管重塑中的贡献度；在临床转化层面，将检测 PH 患者肺组织及血清中 NRP2/Sema3C 的表达谱，分析其与疾病严重程度的相关性，同时评估小分子 NRP2 抑制剂在 PH 动物模型中的治疗潜力

红景天苷通过调控 BKCa 改善野百合碱诱导的肺动脉高压

许美扬 唐碧 孙红燕 陈庆 康品方

蚌埠医科大学第一附属医院

目的： 探讨红景天苷对大电导钙活化钾（BKCa）通道在慢性肺动脉高压（PAH）中的保护作用，旨在为 PAH 的治疗提供新思路与潜在机制。

方法： 选取健康的雄性 SD 大鼠，通过单次腹腔注射野百合碱（MCT）（60 mg/kg）建立 PAH 大鼠模型。将大鼠随机分为对照组、野百合碱（MCT）组及 MCT + Sal 组，每组各 8 只。MCT 组大鼠仅给予 MCT 处理，MCT + Sal 组给予红景天苷（100 mg/kg，i.g.），每日一次，持续 28 天。造模结束后，采用超声心动图和右心导管技术评估血流动力学，包括测量肺动脉收缩压、舒张压及平均压等指标，以量化评估肺动脉压力变化；利用离体血管环检测肺动脉血管收缩及舒张活性，观察血管对不同刺激的反应性；通过 HE 染色观察肺血管壁和心脏微观形态与变化，了解组织结构的病理改变；运用 Western blot 检测大鼠肺血管组织 BKCa α、PCNA、Cleaved - Caspase - 3、Bax、Bcl - 2 蛋白的表达，分析相关蛋白在细胞增殖、凋亡以及 BKCa 通道功能中的作用；采用免疫荧光染色检测 BKCa α、Ki67、Tunel 和 α - SMA 蛋白表达和定位，直观观察蛋白质在细胞内的分布及表达情况；同时利用全细胞膜片钳检测 BKCa 电流密度变化，从电生理角度探究 BKCa 通道的功能变化。

结果： 红景天苷可减轻肺血管及右心重构，提升肺血管收缩和舒张活性，增加肺动脉平滑肌的 BKCa 通道激活和蛋白的表达，增加 BKCa 电流密度，从而抑制肺动脉平滑肌的增殖，促进其凋亡。

结论： 红景天苷通过 BKCa 通道调控肺动脉增值与凋亡失衡，在改善 MCT 诱导的肺动脉高压方面具有显著效果，为红景天苷治疗肺动脉高压提供了新的潜在机制，为后续的深入研究和临床应用奠定了基础，有望为 PAH 患者带来新的治疗选择。

STING 信号通路调控 TASK-1 钾通道在低氧性肺动脉高压中的机制研究

孙红燕 许美扬 康品方 唐碧

蚌埠医科大学第一附属医院

目的： 探讨 STING 信号通路激活影响 TASK-1 钾通道表达在低氧性肺动脉高压（HPH）发生发展中的作用机制。

方法： 体内采用 SU5416 联合慢性低氧（10% O_2，4 周）（SuHx 模型）建立大鼠 HPH 模型，通过气管内滴注 STING 腺相关病毒血清型 9 载体，实现肺血管内 STING 表达的特异性敲低。通过右心导管术测量右心室收缩压（RVSP）和平均肺动脉压（mPAP），经胸超声心动图评估右心室肥厚（Fulton 指数）和右心功能。采用苏木精 - 伊红（H&E）和弹力纤维（EVG）染色对肺组织切片进行肺血管重塑的组织病理学分析。利用离体血管张力测定技术评估肺动脉收缩和舒张反应，采用全细胞膜片钳电生理技术测量离体 PASMCs 的 TASK-1 电流密度。体外培养原代大鼠 PASMCs，并置于常氧（21% O_2）或低氧（1% O_2，48 小时）条件下，利用 5- 乙炔基 -2´- 脱氧尿苷（EdU）探针法和 Ki67 免疫染色、划痕愈合实验和 Transwell 小室评估 PASMCs 增殖、迁移能力，采用 qRT-PCR、Western blotting 评估 STING 和 TASK-1 的 mRNA 及蛋白表达水平。

结果： 体内 SuHx 模型和体外培养的 PASMCs 中，低氧暴露均导致 STING 通路激活，表现为 STING、TBK1、p-TBK1、IRF3、p-IRF3 蛋白水平升高。同时，在低氧条件下，PASMCs 中观察到 TASK-1 mRNA 和蛋白表达显著下调，且 TASK-1 电流密度显著降低。靶向敲低 STING 可减轻慢性低氧对 SD 大鼠的肺循环损伤，降低右心室压力，减弱缺氧对酸敏感钾离子通道 TASK-1 电流的抑制作用，抑制了低氧诱导的 PASMCs 的异常增殖和迁移；同时，STING 抑制剂 C-178 降低了急性缺氧时肺血管张力，TASK-1 参与 C-178 介导肺动脉的舒张作用。

结论： 慢性低氧激活肺动脉中 STING 信号通路，敲低 STING 能够逆转低氧抑制肺动脉平滑肌细胞中 TASK-1 钾通道表达，STING 抑制剂有望成为治疗低氧性肺动脉高压的新型有效疗法。

The Post-Marketing Safety Profile of Sotatercept: A Disproportionality Analysis of Real-World Data from the FAERS Database

Hai-Long Li, Peng Liu, Qi-Wei Shen, Hong Chen, Hua-Long Liu, Jin-Zhu Hu

Department of Cardiovascular Medicine, The Second Affiliated Hospital of Nanchang University, China

Background

Pulmonary arterial hypertension (PAH) is a severe and progressive vasculopathy characterized by the proliferative remodeling of distal pulmonary arterioles, which leads to a sustained increase in pulmonary vascular resistance and, ultimately, right-ventricular failure. Despite advances in therapy, the five-year survival rate remains suboptimal at approximately 60%. Current guideline-recommended treatments, which target the endothelin, nitric-oxide, and prostacyclin pathways, primarily act as vasodilators. However, they do not fully reverse the underlying proliferative and inflammatory vascular pathology, leaving a significant therapeutic ceiling.

This has shifted research focus toward pathways governing vascular homeostasis. Sotatercept, a first-in-class activin signaling inhibitor, represents a paradigm shift. It is a fusion protein that acts as a ligand trap for members of the TGF-β superfamily, thereby rebalancing pro-proliferative and anti-proliferative signaling. Pivotal clinical trials, including PULSAR, STELLAR, and ZENITH, have demonstrated its efficacy in improving

exercise capacity, hemodynamics, and clinical outcomes in PAH patients. These trials identified common adverse events (AEs) such as increased hemoglobin, epistaxis, and telangiectasia. However, the safety profile of Sotatercept in a broader, more heterogeneous real-world population remains unclear. Spontaneous reporting systems like the FDA Adverse Event Reporting System (FAERS) are critical for post-marketing pharmacovigilance, enabling the detection of rare, delayed, or unexpected AEs not apparent in controlled clinical trials. This study aimed to conduct a comprehensive analysis of FAERS data to characterize the post-marketing safety profile of Sotatercept, validate known AEs, and identify novel safety signals.

Methods

A retrospective pharmacovigilance study was conducted using individual case safety reports (ICSRs) from the FAERS database, spanning from Q1 2004 to Q1 2025. All reports where Sotatercept was listed as the primary suspect drug were extracted. A rigorous de-duplication process was applied according to FDA guidelines to ensure each case was unique.

Adverse events were coded using the Medical Dictionary for Regulatory Activities (MedDRA v27.1) at the System Organ Class (SOC) and Preferred Term (PT) levels. The clinical severity of each report was classified based on FAERS seriousness criteria (e.g., death, life-threatening, hospitalization).

Data analysis was multifaceted. Descriptive statistics were used to summarize patient demographics, reporter type, and event seriousness. The time-to-onset (TTO) of AEs was analyzed using the Kaplan-Meier method to estimate cumulative incidence, while a Weibull model was fitted to determine the failure pattern via the shape parameter (β). A disproportionality analysis using a case/non-case methodology was the core of the study. To ensure robustness, this analysis employed four complementary algorithms: the frequentist methods of Reporting Odds Ratio (ROR) and Proportional Reporting Ratio (PRR), and the Bayesian methods of Information Component (IC) and Empirical Bayes Geometric Mean (EBGM). A significant signal was defined by meeting stringent, predefined criteria across these metrics (e.g., ROR 95% CI > 1, PRR ≥ 2, $\chi 2 \geq 4$, and case count ≥ 3). Further stratified analyses were performed by sex and age, and potential drug-drug interactions (DDIs) were investigated by calculating a shrinkage-adjusted odds ratio (Ω).

Results

An initial search yielded 2,745 reports, which were refined to 992 unique cases after de-duplication. The cohort was predominantly female (72.8%), with a median patient age of 56.0 years. Consumers (44.1%) and pharmacists (36.2%) were the most common reporters. Overall, 40.3% (400 cases) of the reports were classified as serious, with hospitalization being the most frequent serious outcome (29.8%).

The TTO analysis, limited by missing date information in 94.2% of reports, was feasible for only 58 cases. Among these, the median TTO for all AEs was 26.5 days, with over half of the events occurring within the first 30 days. The Weibull shape parameter of β=0.80 (95% CI: 0.64–1.00) suggested a random-failure pattern.

The disproportionality analysis successfully confirmed known AEs from clinical trials. Extremely strong signals were detected for expected events, including **haemoglobin increased** (ROR 456.85, 95% CI: 365.40–571.19), **telangiectasia** (ROR 292.64, 95% CI: 165.32–518.00), and **epistaxis** (ROR 27.14, 95% CI: 21.94–33.57).

Crucially, the analysis uncovered a novel and exceptionally strong signal for **pulmonary arteriovenous fistula** (ROR 2869.07, 95% CI: 1220.18–6746.19), an AE not prominently featured in trial publications or prescribing information. Other significant signals included **heart and lung transplant** (ROR 496.91) and **headache** (ROR 4.58).

Stratified analyses revealed distinct risk profiles. While increased hemoglobin was a strong signal in both sexes, **telangiectasia** was particularly prominent in females (ROR 242.7), whereas **right ventricular failure** showed a stronger signal in males (ROR 55.3). Age stratification highlighted **pulmonary arteriovenous fistula** (ROR 35,655) as the dominant signal in the 45-64 age group and **pericardial effusion** (ROR 80.5) in patients aged ≥ 65. The DDI analysis identified a significant interaction signal for "Laboratory test abnormal" when Sotatercept was co-administered with treprostinil (Ω 2.67, 95% CI 1.40–3.93).

Conclusion

This comprehensive pharmacovigilance study of the FAERS database provides the first real-world safety assessment of Sotatercept. The findings corroborate the known hematologic and vascular adverse event profile established in clinical trials, thereby validating the sensitivity of the analytical approach. More importantly, this study identified a novel, marked, and biologically plausible safety signal for pulmonary arteriovenous fistula. The mechanism may be related to Sotatercept's potent modulation of the TGF-β/BMP signaling pathway, which is integral to vascular integrity and is dysregulated in genetic conditions like Hereditary Hemorrhagic Telangiectasia that feature such malformations.

The median time-to-onset of approximately 27 days suggests that enhanced clinical vigilance is warranted, particularly during the first three months of therapy. These findings underscore the critical importance of continuous post-marketing surveillance to complement clinical trial data. While the results must be interpreted with caution due to the inherent limitations of spontaneous reporting systems—including under-reporting, missing data (notably for TTO and age), and the inability to establish causality or true incidence—the strength of the signal for pulmonary arteriovenous fistula demands attention. Further investigation through robust epidemiological studies is essential to confirm this association and quantify the risk. Despite this new safety consideration, the overall benefit-risk balance of Sotatercept for patients with PAH likely remains favorable, but these findings highlight the necessity of ongoing safety monitoring for this transformative therapy.

中性粒细胞通过释放基质金属蛋白酶 -8 促进 PH-LHD 小鼠心肌纤维化的机制研究

仇海花 李江

中南大学湘雅二医院心内科

目的：左心疾病相关肺高血压（PH-LHD）是最常见的肺高血压类型，其发病机制主要与左心功能障碍导致肺静脉压升高及进行性的肺血管和心肌重构密切相关。研究表明 PH-LHD 患者心肌纤维化程度与不良预后显著相关，具体机制尚未阐明。基质金属蛋白酶 -8（MMP-8）作为胶原酶重要成员之一，被发现可通过促进细胞外基质降解在心梗后心肌重塑过程中发挥重要作用。本研究旨在明确压力负荷合并代谢综合征诱导的 PH-LHD 小鼠中性粒细胞释放 MMP-8 水平显著升高，并阐明中性粒细胞来源的 MMP-8 促进心肌纤维化的深入机制。

方法：成年雄性昆明小鼠采用腹主动脉缩窄术联合代谢综合征构建 PH-LHD 模型，在第 10 周末对 PH-LHD 组小鼠进行左、右心功能以及肺血管相关指标鉴定评估造模情况，并对 PH-LHD 模型小鼠心肌组织行 RNA-seq 测序分析、流式细胞学及免疫荧光检测心脏中性粒细胞 MMP-8 表达情况。给予 MMP-8 抑制剂（GM6001）腹腔注射并评估三组小鼠左心功能、右心功能以及肺血管重构程度，比较中性粒细胞激活情况、心肌组织中性粒细胞浸润程度及其 MMP-8 表达水平、心肌重构情况。此外，分离 PH-LHD 和 GM6001 组小鼠骨髓中性粒细胞体外培养，检测上清液中 MMP-8 的水平；并将所提取的中性粒细胞分别与乳鼠心肌成纤维细胞共培养 48h 后，比较各组胶原蛋白及细胞外基质降解产物水平、纤维化相关指标及通路的 RNA 和蛋白水平。

结果：PH-LHD 模型小鼠左室肥厚、舒张功能减退、左室舒张末压以及右室压显著升高，且肺血管以及心室重构明显。PH-LHD 小鼠与对照小鼠心肌组织 RNA seq 测序分析发现 520 个差异基因，对差异基因行 GO 富集分析发现差异基因富集到了心肌细胞外基质（ECM），进一步 real time-PCR 和 western blot 验证筛选发现 MMP-8 在 PH-LHD 小鼠心肌组织中表达均显著升高。流式细胞学及免疫荧光染色显示 PH-LHD 小鼠心脏中性粒细胞比例较对照组小鼠升高，并且其 MMP-8 阳性水平也明显升高。采用 MMP-8 抑制剂，GM6001 可明显减轻 PH-LHD 小鼠心脏结构异常以及右室收缩压、改善血流动力学异常，减轻肺血管重构、改善心肌纤维化，并且 GM6001 干预后小鼠心肌组织 MMP-8 表达降低，心脏中性粒细胞中 MMP-8 阳性水平也明显下降。同时 ELASA 结果也显示 PH-LHD 小鼠骨髓中性粒细胞上清液中 MMP-8 水平较对照组显著升高，而 GM6001 干预组明显降低。分离提取 PH-LHD 小鼠骨髓中性粒细胞并检测 Histone H3 表达水平较对照组明显升高，中性粒细胞活化水平显著提高、GM6001 组则较 PH-LHD 组下降。将上述分离的中性粒细胞与乳鼠心脏成纤维细胞共培养 48h，结果显示与 PH-LHD 小鼠中性粒细胞共培养的心脏成纤维细胞胶原蛋白表达明显增多，TIMPs 表达减少，ECM 降解产物 ICTP 水平升高，而 GM6001 干预组则较 PH-LHD 组趋势相反。此外，与 PH-LHD 小鼠中性粒细胞共培养的心脏成纤维细胞纤维化程度也明显加重，免疫荧光染色显示其纤维结构紊乱，α-SMA 表达水平也明显增多，而 GM6001 干预组则可有效缓解心脏成纤维细胞肌化进程。

结论：腹主动脉缩窄术联合代谢综合征诱导的 PH-LHD 小鼠中性粒细胞产生 MMP-8 显著升高，加重心肌重构。而 GM6001 可通过抑制中性粒细胞中 MMP-8 的表达有效改善 PH-LHD 小鼠左、右心功能以及肺血管重构，纠正血流动力学紊乱。从机制上来说，中性粒细胞通过释放 MMP-8，促进心肌细胞外基质降解，促进心肌成纤维细胞肌化，加重纤维化。

PIEZO1 Regulates Smooth Muscle Cell Plasticity by Integrating Mechanical Stretch with Glycolytic Metabolism

Ya-Peng Cao[1], Li-Ran Xu[1], Min Zhang[1], Ai-Ling Su[1], Si-Yu Wang[1], Li[1], Si-Yu Liu[1], Zi-Yang Mao[1], Yu He[1], Ze-Hua Shao[1], Jia-Min Zhang[2], You-Hua Wang[2], Hui-Jing Tian[1], Yu-Zhuo Sun[1], Yong-Xin Li[1], Lu-Qin Yan[1], Guang-Jian Zhang[1], Na Mei[1], Fang-Yuan Chen[1], Guo-Zheng Liang[3], OFFERMANNS STEFAN[3], [1], Zu- Yuan[1], Sheng-Peng Wang[1]

1. the First Affiliated Hospital of Xi'an Jiaotong University

2. Shaanxi Normal University

3. Max Planck Institute for Heart and Lung Research

Background Pulmonary artery smooth muscle cells (PASMCs) are constantly exposed to mechanical strain and their ability to respond to mechanical forces is essential for the structure and function of the pulmonary vascular network. Mechanical stimuli and altered glycolytic metabolism are intrinsically intertwined in proliferative PASMCs undergoing a phenotypic switching. However, it remains unclear how biophysical forces and glycolysis are coupled in PASMCs during the remodeling of pulmonary artery in lung disease.

Methods We used the in vivo models of pulmonary hypertension (PH)

and fibrosis with vascular smooth muscle-specific knockout and lineage tracing mice (Myh11-CreER^{T2}; Piezo1$^{flox/flox}$; ROSA$^{mT/mG}$), Piezo1 reporter and lineage mice (Piezo1$^{P1\text{-}tdT}$ and Piezo1-CreER; ROSA$^{mT/mG}$) to investigate the role of Piezo1 in pulmonary artery remodeling. To analyze whether PIEZO1 is involved mechanosensation in PASMCs, we generated the inducible smooth muscle specific Piezo1-deficient mice (hereafter named Sm-Piezo1-KO) by crossing mice carrying floxed alleles of Piezo1 with the Myh11-CreER^{T2} mouse line. To test whether loss of PIEZO1 in PASMCs promotes pulmonary fibrosis by expansion of pre-existing SMCs, pulmonary SMC fate was traced with the Myh11-CreER^{T2}; mT/mG mice with or without floxed allele of Piezo1 during the process of bleomycin injury. To gain mechanistic insight into how PIEZO1 activation promotes glycolysis and proliferation, we performed RNA sequencing (R-seq) analysis in PASMCs treated with Yoda1 or mechanical stretch. Using a battery of in vitro assays, including uniaxial cell stretching, enhanced extracellular acidification rate (ECAR), patch clamp, $[Ca^{2+}]_i$ recording and immunohistochemistry, the mechano-regulation of glycolytic metabolism and proliferation in PASMCs were assessed. To further explore how PIEZO1-mediated mechano- and metabolic-signaling are altered in hypoxia, we used the fluorescent lipid tension sensor, FliptR to determine the membrane tension in PASMCs. To test whether loss of PIEZO1 in PASMCs promotes pulmonary fibrosis by expansion of pre-existing SMCs, pulmonary SMC fate was traced with the Myh11-CreER^{T2}; mT/mG mice with or without floxed allele of Piezo1 during the process of bleomycin injury. To gain mechanistic insight into how loss of PIEZO1 promotes expansion of SMCs and aggravates fibrosis in response to bleomycin injury, we performed RNA-seq analysis comparing SMCs from bleomycin treated Control or Sm-Piezo1-KO mT/mG mice. Human PAH and IPF samples were used to further confirmed the relevance of PIEZO1 in PASMC metabolism.

Results We report here that the mechanosensitive cation channel PIEZO1 plays a critical role in glycolysis and proliferation of PASMCs in vitro and in vivo by sensing plasma membrane tension. Hypoxia and bleomycin-injury differently rewire PIEZO1-mediated signaling into pro- and anti-glycolytic directions. Under hypoxic conditions, activation of PIEZO1 promotes glycolysis in PASMCs through activation of calcineurin/NFAT and upregulation of HIF1α and PFKFB3, resulting in profound lactate production and cell proliferation. In sever pulmonary injury condition induced by bleomycin, PIEZO1 is hyper-activated, which led to PPARγ activation, thereby antagonizing TGFβ signaling and restraining glycolysis and proliferation via FBP1. Loss of smooth muscle Piezo1 attenuates hypoxia-induced PH but aggravates bleomycin-induced pulmonary fibrosis in mice.

Conclusions Our study reveals that PIEZO1-mediated mechano-metabolic coupling contributes to PASMC plasticity. This discovery identified an intrinsic mechanism that integrates mechanical stretch with cellular glycolysis during pulmonary vascular remodeling.

房间隔缺损肺动脉高压患者克隆性造血相关基因的初步研究

李昇铃 卢祥婷 常开丽 张洁 杨红艳 晋珮云 鲁一兵 戴海龙

昆明医科大学附属延安医院

【目的】研究房间隔缺损（Atrial septal defect，ASD）肺动脉高压 (Pulmonary arterial hypertension, PAH) 患者中克隆性造血（Clonal hematopoiesis, CH）相关基因的突变情况。

【方法】纳入 2017 年 11 月至 2022 年 2 月我院诊治的 88 例房间隔缺损患者，其中单纯 ASD 组 37 例，ASD-PAH 组 51 例。所有入选患者均经心脏彩超、右心导管检查、心脏结构 CTA 等影像学检查证实为单纯 ASD 患者，不合并其他类型先天性心脏病（Congenital heart disease，CHD）。筛选入组后，收集所有患者的外周静脉血液标本，提取全基因组 DNA 序列，进行全外显子测序。利用 GATK、Samtools、Varscan 等数据处理软件与 refGene、rmsk 、gwasCatalog 、1000g、HGMD 等人类大型基因组数据库相对比，对目标区域的覆盖范围的质量进行评估，最终得出 CH 相关基因的突变情况。数据分析均使用 IBM SPSS statistic 27 软件完成， P<0.05 认为差异有统计学意义。

【结果】

ASD 组患者 37 例，其中女性 31 例（83.8%），年龄 38（26 ，52.50）岁；ASD-PAH 组 51 例，其中女性 38 例（74.5%），年龄 41（30 ，53）岁。两组间性别、年龄、房间隔缺损大小、六分钟步行距离、混合静脉血氧饱和度均无统计学差异（P 均 >0.05），但 ASD-PAH 组患者 NT-proBNP 高于 ASD 组（P<0.05）。在 37 例 ASD 患者中发现有 15（40.5%）例发生 CH 突变，在 51 例 ASD-PAH 中发现有 33（64.7%）人发生 CH 突变，两组间比较差异有统计学意义（P<0.05）。ASD 组中 CH 相关基因突变最多的是 SETD2 基因；ASD-PAH 组中 CH 突变最多的是 SETD2 和 TNFAIP3 基因，其次为 NOTCH1、SETBP1、KANSL1、 SH2B3 、ASXL1 、PTPRF 和 CBLB 基因。

【结论】

在房间隔缺损肺动脉高压患者中，存在克隆性造血患者比例较高。克隆性造血可能在房间隔缺损肺动脉高压患者发病过程中起一定作用。

TAPSE/SPAP 作为肺动脉高压预后指标的临床意义：一项单中心回顾性研究

陈文杰 李江

中南大学湘雅二医院

目的

本研究旨在探讨三尖瓣环收缩期位移与肺动脉收缩压之比（TAPSE/SPAP）在新诊断的肺动脉高压（PAH）患者中的预后价值。TAPSE/SPAP 是近年来被提出用于反映右心室 - 肺动脉耦合（RV-PA coupling）状态的无创指标，能够综合评估右心收缩功能和肺血管负荷之间的匹配情况。本研究通过系统分析 TAPSE/SPAP 比值与临床指标、右心功能参数及随访生存情况之间的关系，旨在评估其作为风险分层和预后预测工具的临床应用价值。

方法

本研究为回顾性研究，共纳入 125 例首次诊断的、尚未接受特异性药物治疗的 PAH 患者。所有患者均接受系统性临床评估，包括右心导管检查、超声心动图及相关生物标志物检测。根据 TAPSE/SPAP 比值的中位数（0.15 mm/mmHg），将患者分为低 TAPSE/SPAP 组和高 TAPSE/SPAP 组。比较两组间在右心室结构功能、血流动力学参数、治疗反应及生存率等方面的差异。采用 Kaplan-Meier 生存分析评估生存率差异，并通过 Cox 回归模型分析 TAPSE/SPAP 比值对死亡风险的影响。

结果

研究共纳入 125 例新诊断且尚未接受特异性药物治疗的 PAH 患者，年龄中位数为 34 岁，女性占比 72%。根据 TAPSE/SPAP 比值的中位数（0.15 mm/mmHg），将患者分为低 TAPSE/SPAP 组（<0.15 mm/mmHg）和高 TAPSE/SPAP 组（≥ 0.15 mm/mmHg）。低 TAPSE/SPAP 组在基线时表现出更严重的右心功能损害，包括 TAPSE 显著降低、右室面积扩大及心输出量下降。同时，该组肺动脉收缩压（SPAP）更高，肺血管阻力（PVR）显著升高，提示肺血管负荷更重。此外，该组患者的 6 分钟步行距离（6MWD）更短，WHO 功能分级更差，NT-proBNP 水平明显升高，显示出更差的运动耐量和更高的心衰风险。

超声心动图显示，低 TAPSE/SPAP 组右室 - 肺动脉耦合失调更明显，其右室室间隔运动异常更为显著，右心室 - 左心室尺寸比（RV/LV ratio）显著升高，提示右心压力负荷所致的构型变化更重。

Kaplan-Meier 生存分析显示，低 TAPSE/SPAP 组的累积生存率在 3 年和 5 年均明显低于高 TAPSE/SPAP 组（P = 0.028）。具体来看，低 TAPSE/SPAP 组 5 年生存率为 64.7%，而高 TAPSE/SPAP 组为 84.1%。单因素 Cox 回归分析中，TAPSE/SPAP < 0.15 mm/mmHg 显著关联于较高的全因死亡风险（HR = 2.575，95% CI: 1.067–6.214，P = 0.035），提示其具有良好的预后判别能力。然而在调整心功能分级和 NT-proBNP 的多因素模型中，TAPSE/SPAP 未能维持统计学显著性，表明其独立性有限，可能更多作为一个综合风险指标而非独立预测因子。

结论

TAPSE/SPAP 比值作为反映右心室 - 肺动脉耦合状态的指标，能够较好地识别新诊断 PAH 患者的高危人群。较低的 TAPSE/SPAP 值提示右心功能不全与肺血管负荷不匹配，预示患者生存率较差。尽管 TAPSE/SPAP 在单因素分析中表现出良好的预后能力，但其独立性需进一步通过前瞻性、多中心研究加以验证。总体而言，TAPSE/SPAP 是一项简便、非侵入性的临床评估工具，具有潜力用于 PAH 的风险评估和疾病监测。

重组人脑利钠肽治疗动脉型肺动脉高压所致右心衰竭的有效性及安全性研究

胡立星 赵青 赵智慧 罗勤 邓丽 蒋萍 柳志红

中国医学科学院阜外医院（国家心血管病中心）

目的：观察重组人脑利钠肽（rhBNP）治疗动脉型肺动脉高压所致右心衰竭的有效性及安全性。

方法：连续性纳入 2019 年 1 月至 2024 年 6 月期间中国医学科学院阜外医院呼吸与肺血管疾病诊治中心收治的动脉型肺动脉高压所致右心衰竭患者 421 例，均在包括规范化肺动脉高压靶向药物、传统利尿剂的常规治疗基础上加用 rhBNP，观察治疗期间患者尿量、摄入量、体重变化以及治疗前、后肝肾功能指标、电解质、血尿酸、红细胞分布宽度、心功能指标、血压、心率（治疗前、出院前 ）的变化，并记录治疗后患者临床症状、体征改善情况及治疗期间不良事件发生情况。

结果：rhBNP 治疗期间 24 h 尿量增多，体重减轻；与治疗前比较，治疗后丙氨酸氨基转移酶、总胆红素、直接胆红素、血尿酸、红细胞分布宽度、收缩压、心率、N 末端 B 型利钠肽原水平均明显下降（ P 均< 0.05），血肌酐、三尖瓣环收缩期位移 / 肺动脉收缩压比值的差异均无统计学意义（ P 均> 0.05）。经治疗后，患者的呼吸困难改善率为 75.2%（227/302），下肢水肿改善率为 66.9%（281/420）。治疗期间不良事件发生率为 1.19%（5/421），严重不良事件发生率为 0.48%（2/421）。

结论：对于动脉型肺动脉高压所致右心衰竭患者，在常规治疗基础上加用 rhBNP 可有效增加尿量，减轻体重，改善部分预后指标及临床症状和体征，且对肾功能无明显影响，但需严密监测血压。

克隆性造血与肺动脉高压因果关系的遗传学证据

邱家勇 [1,2] 黄伸伸 [2] 毛毅敏 [2] 荆志成 [1]

1. 广东省心血管病研究所，广东省医学科学院，南方医科大学附属广东省人民医院

2. 河南科技大学第一附属医院

背景： 肺动脉高压 （PAH） 是一种严重的进展性心肺血管疾病。虽然已经确定了克隆性造血 （CH） 与心血管疾病之间的潜在联系，但 CH 和 PAH 之间的因果关系仍不清楚。本研究旨在使用双样本孟德尔随机化 （MR） 方法探索 CH 对 PAH 风险的因果影响。

方法： 我们使用与 CH 相关的遗传变异作为工具变量，从两项大型全基因组关联

研究 （GWAS） 中确定，涉及发现队列中的 359,088 例参与者和验证队列中的 184,121 例参与者，均为欧洲血统。此外，我们获得了 PAH 的 GWAS 汇总统计数据。采用逆方差加权 （IVW） 方法作为主要分析，并辅以敏感性分析以评估我们研究结果的稳健性。我们还进行反向 MR 分析以分析 CH 和 PAH 之间的因果关系。

结果：结果表明在发现队列中，CH 对 PAH 风险存在因果效应，TET2 显示 IVW 比值比 （OR） 为 1.200 （95% CI：1.001-1.438，P = 0.049）。敏感性分析未显示显著的多效性或异质性。在验证队列中，我们发现 TET2 仍然是 PAH 的危险因素 （OR = 2.3E+08, 95% CI 17.007-3.1E+15，P = 0.022）。此外，未发现其他 CH 基因与 PAH 之间有因果关系，例如 DNMT3A 和 PAH（ P> 0.05）。反向 MR 分析 PAH 对 CH 不存在的因果影响的证据。

结论： 这些发现表明，由 TET2 突变引起的 CH 个体患 PAH 的风险可能更高，这提示 CH 患者可能需要接受 TET2 基因突变检测。

栀子苷通过调控 PFKFB3 改善肺血管重构降低肺动脉高压的研究

常瑞蕊

南京市第一医院

肺动脉高压（Pulmonary arterial hypertension，PAH）是一组以肺动脉压力进行性增高（安静状态下 mPAP（平均肺动脉压力）> 20mmHg、PAWP（肺动脉楔压）≦ 15mmHg 及 PVR（肺血管阻力）> 2WU），最终导致右心衰竭为特征的临床综合征。PAH 的发生主要是由肺动脉平滑肌细胞（PASMCs）的异常增殖引起的肺血管重构，然而目前临床中用于治疗 PAH 的药物主要是减轻血管舒张和收缩的临床症状，并不能改善肺血管重构，因此开发直接改善肺血管重构的药物迫在眉睫。栀子苷（Geniposide，GE）是从茜草科植物栀子的成熟干燥果实中提取的环烯醚萜苷类化合物，具有抗增殖和抗血管生成等多种功效，其有望通过减少 PASMCs 的异常增殖，改善肺血管重构，成为治疗 PAH 的潜在药物。

目的：从细胞及动物水平，明确 GE 通过肺血管重构影响 PAH，探究 GE 通过调控 PFKFB3 抑制糖酵解进而改善肺血管重构的机制。

方法：（1）利用 CCK8、划痕实验和 Edu 实验，检测 GE 对正常组、模型组和 GE 组 PASMCs 增殖和迁移的影响，明确 GE 抑制缺氧 PASMCs 的增殖迁移。（2）利用 PAH 大鼠肺组织切片染色评价肺血管重构和肺动脉肌化，同时在体检测 PAH 大鼠右心功能相关指标及肺动脉压力，验证 GE 通过改善肺血管重构影响 PAH 的作用。（3）使用 LC-MS/MS 检测不同时间 GE 及其有效代谢物京尼平在正常大鼠和 PAH 大鼠血浆中的浓度，并绘制血药浓度 - 时间曲线，对比 GE 在正常大鼠和 PAH 大鼠体内的药代动力学行为的差异，评价 GE 在 PAH 大鼠中药代动力学行为的优势。（4）利用缺氧 PASMCs 并结合转录组测序，筛选出 GE 干扰后具有显著性差异的基因。**（5）**利用 qRT-PCR 和 WB 实验，检测 GE 的干扰下，Pfkfb3 在缺氧 PASMCs 和 PAH 大鼠肺组织的蛋白和 mRNA 的表达，证实 Pfkfb3 是 GE 改善 PAH 的作用靶点。（6）从细胞和动物两方面，检测 GE 干扰后乳酸的水平，证实 GE 在 PAH 中可以抑制糖酵解。

结果：（1）CCK8 实验中，通过检测缺氧 PASMCs 干扰不同浓度（25、50 和 100μM）GE 后发现细胞活性与药物浓度成正比。Edu 实验结果 GE（50μM）可以改善缺氧引起 PASMCs 的增殖。划痕实验显示 GE（50μM）可以改善缺氧引起 PASMCs 的迁移。（2）GE 可以降低 PAH 大鼠的右心室收缩压，增加右心室射血分数，降低右心室肥厚，减少肺血管重构和肺血管肌化程度。（3）PAH 大鼠口服 GE 后，GE 及其代谢物京尼平在大鼠血浆中的暴露高于正常大鼠。（4）对 PASMCs 进行转录组测序并对结果数据分析，发现 GE 组 PFKFB3 的表达显著降低。（5）对两组样品进行 qRT-PCR 和 WB 检测，结果发现 GE 组的 PFKFB3 的 mRNA 水平和蛋白表达均降低。（6）PASMCs 和大鼠实验均显示，GE 可以降低由缺氧引起的乳酸升高。

结论：GE 通过下调 PFKFB3 抑制糖酵解，减少 PASMCs 的增殖迁移，改善肺血管重构，进而降低 PAH 的发生发展

慢性肺动脉狭窄解除后健侧肺的双相反效应

苏红玲

甘肃省人民医院

慢性肺动脉狭窄可引发双侧肺血管适应性改变：狭窄远端肺血管床因长期低灌注导致毛细血管萎缩、血管稀疏化及持续性低氧性血管收缩，致使微血管静水压低下；而健侧肺因代偿性高灌注诱发血管内皮损伤与微血管通透性增加，其淋巴回流不足以完全代偿高灌注相关的毛细血管渗漏，最终形成胸腔积液。

当狭窄解除后，健侧肺呈现特征性双相反效应：

1. 压力差显著改善时：狭窄侧肺血管阻力骤降引发血流 " 偷窃效应 "，导致健侧肺灌注锐减，触发 " 灌注突增 - 再灌注损伤 " 综合征。其机制包括：健侧肺因急性缺氧致血管内皮紧密连接破坏、通透性剧增；狭窄侧再灌注激活中性粒细胞及氧自由基，进一步损伤微血管屏障；淋巴泵功能因血流锐减退化，叠加微血管静水压短暂升高，最终导致高通透性肺水肿。

2. 压力差改善较小时：健侧肺血流仅轻度减少，避免急性缺氧损伤；同时全肺循环压力梯度下降使健侧毛细血管静水压降低，内皮通透性渐进性恢复。加之慢性狭窄中健侧肺已建立的淋巴代偿机制增强，促使原高灌注相关的胸腔积液消退。

临床意义：术前跨狭窄压力差是预测术后并发症的关键指标——

显著改善者需警惕肺水肿，建议采用肺保护性通气（低潮气量 + 呼气终末正压）、目标性抗炎（如糖皮质激素）及利尿治疗；

轻度改善者则有望出现胸腔积液自发减少。

Global Burden of pulmonary arterial hypertension from 1990 to 2021 and predictions to 2035: results from the GBD Study 2021

Ya-Fen Yang[1], Bin Liang[1], Hong-Xuan Fan[2], Jia-Hui Li[1], Zhuo-Lin Huang[1], Zhao-yu Ren[1]

1. The Second Hospital of Shanxi Medical University

2. Beijing Tsinghua Changgung Hospital, School of Clinical Medicine, Tsinghua University

Objective: Pulmonary Arterial Hypertension (PAH) is a rare, progressive, and fatal cardiopulmonary disorder characterized by pulmonary vascular remodeling, elevated pulmonary vascular resistance, and eventual right heart failure. Despite advancements in high-income countries, significant knowledge gaps persist regarding its global epidemiology, particularly trends across socio-demographic gradients and in low- and middle-income countries. This study provides the comprehensive analysis of PAH burden globally, regionally, and nationally from 1990 to 2021, incorporating forecasts to 2035.

Methods: Utilizing data from the Global Burden of Diseases, Injuries, and Risk Factors Study (GBD) 2021, we estimated PAH incidence, prevalence, deaths, and disability-adjusted life years (DALYs) across 204 countries and territories, stratified by age, sex, Socio-demographic Index (SDI), and 21 GBD regions. Age-standardized rates (ASRs) were calculated using a standard population. Temporal trends were quantified using Estimated Annual Percentage Change (EAPC) derived from linear regression models. The Bayesian Age-Period-Cohort (BAPC) model was employed to forecast burden metrics to 2035. Correlations between ASRs, SDI, and Human Development Index (HDI) were assessed using Pearson correlation coefficients.

Results: Globally in 2021, PAH affected 191,808 (95% UI: 155,356-235,787) individuals, with 43,251 (95% UI: 34,704-52,441) new cases, causing 22,020 (95% UI: 18,239-25,351) deaths and 642,104 (95% UI: 552,272-728,993) DALYs. Compared to 1990, incidence and prevalence counts increased by 85.6% and 81.8%, respectively. However, age-standardized death rate (ASDR) decreased by 23.0% (EAPC = -0.57, 95% CI: -0.72 to -0.42) and age-standardized DALYs rate (ASDAR) decreased by 37.7% (EAPC = -1.31, 95% CI: -1.43 to -1.19), indicating improved survival per capita. Females bore a higher burden overall (prevalence, incidence, deaths), but males experienced faster declines in ASDR and ASDAR. Burden peaked in older age groups, although the PP<0.001), but a positive correlation with ASPR (r= 0.62, P

Conclusions: This study reveals a persistent and substantial global burden of PAH, marked by significant inequalities across sex, age, geography, and SDI. While mortality rates per capita have improved, the absolute number of cases and deaths continues to rise. The disproportionate burden in females, older adults, children

1990 年至 2021 年全球、区域及国家层面的肺动脉高压负担：基于 2021 年全球疾病负担研究的年龄 - 时期 - 队列分析

沈季然 杜舟 喻荣辉

安徽医科大学第一附属医院

目的：本研究利用了全球疾病负担研究（Global Burden of Disease）的数据，对 1990 年至 2021 年期间肺动脉高压（PAH）的全球疾病负担进行了调查。它分析了不同人群以及在不同社会人口指数（SDI）水平下的患病率趋势、死亡率以及残疾调整生命年（DALYs），以评估肺动脉高压的全球影响和管理进展情况。

方法：采用年龄 - 时期 - 群体（APC）分析和 ARIMA 模型来评估肺动脉高压（PAH）的年龄标准化率（ASR）、死亡率和残疾调整生命年（DALY）的趋势，并根据社会发展指数（SDI）的水平进行分层分析。同时，利用预测模型来预测未来疾病负担。

结果：在 1990 年至 2021 年期间，全球肺动脉高压（PAH）的患病人数和死亡人数呈上升趋势，但是肺动脉高压的年龄标准化死亡率和残疾调整生命年数呈下降趋势，这可能反映了诊断和治疗水平的提高。在不同社会经济发展指数（SDI）地区，低 SDI 地区的年龄标准化发病率最高，而所有 SDI 类别的年龄标准化死亡率和残疾调整生命年数均有所下降。预计肺动脉高压的患病率将继续上升，但死亡率和残疾调整生命年数可能会继续下降，尤其是在低收入和中等收入国家。此外，老年人和女性患肺动脉高压的风险更高。

结论：尽管肺动脉高压的管理有了改善，但全球范围内仍存在显著的社会经济差异。未来的工作重点应放在加大对低收入和中等收入国家预防和治疗的投入，并优化诊断和治疗策略上。

GPNMB Drives Pulmonary Vascular Remodeling and Right Ventricular Fibrosis via ITGB2-STAT1-CXCL10 and TGF-β Pathways and Serves as a Biomarker in PAH

Lin Deng, Yuan Li, Bin Lengl, Jian Shi, Wen-Bin Wei, Gui-Fu Wuw

Department of Cardiology, The Eighth Affiliated Hospital of Sun Yat-sen University, Shenzhen, Guangdong, China

OBJECTIVES: Pulmonary arterial hypertension (PAH) is a progressive and life-threatening condition characterized by extensive pulmonary vascular remodeling, right ventricular (RV) fibrosis, and eventual heart failure.

Inflammation is widely recognized as a central trigger in the initiation and progression of this disease, contributing to the pathological changes observed in the pulmonary vasculature and the heart. Glycoprotein nonmetastatic melanoma protein B (GPNMB), a type I transmembrane protein featuring an integrin-binding RGD motif, is known to be secreted and plays a significant role in regulating inflammation, cell adhesion, fibroblast activation, and cardiac injury across various pathological contexts. Despite its established involvement in other diseases, the specific role of GPNMB in PAH, particularly in the context of pulmonary vascular remodeling, RV fibrosis, and its potential as a diagnostic or prognostic biomarker, remains largely unexplored and warrants detailed investigation.

METHODS: To address this knowledge gap, the expression of GPNMB was systematically evaluated in lung and RV tissues obtained from PAH patients as well as in rodent models of pulmonary hypertension, including the Sugen 5416/hypoxia (SuHx) model and the pulmonary artery banding (PAB) model. To further dissect the cellular and molecular contributions of GPNMB, macrophage-specific GPNMB knockout ($GPNMB^{LyZ}$-KO) mice and their littermate controls were employed to assess the progression of pulmonary hypertension (PH) and RV fibrosis in both SuHx and PAB models. Comprehensive molecular analyses were conducted using single-cell RNA sequencing (scRNA-Seq), bulk RNA-Seq, and a series of functional assays involving macrophages, pulmonary artery smooth muscle cells (PASMCs), pulmonary artery endothelial cells (PAECs), and cardiac fibroblasts to elucidate the underlying mechanisms. Additionally, the effects of recombinant human GPNMB (rhGPNMB) were examined to study its inflammatory impact, while plasma GPNMB levels in PAH patients were measured and analyzed to evaluate its potential as a biomarker for disease monitoring and prognosis.

RESULTS: The scRNA-Seq analysis of lung tissues from PAH patients and RV tissues from the monocrotaline (MCT) model revealed significantly elevated GPNMB expression across multiple cell types, including macrophages, PASMCs, PAECs, and cardiac fibroblasts. This upregulation was consistently observed in lung and RV tissues from rodent PH models, with expression levels showing a strong correlation with the severity of RV hypertrophy in PAB rats. In functional studies, $GPNMB^{LyZ}$-KO mice demonstrated attenuated pulmonary vascular remodeling and reduced RV hypertrophy in both SuHx and PAB models, highlighting GPNMB's pathological role. Mechanistically, GPNMB was found to bind integrin β2 (ITGB2) in macrophages, activating the STAT1-CXCL10 axis, which promotes macrophage infiltration into the vascular walls, with increased ITGB2 expression noted in PAH settings. In PASMCs and PAECs, GPNMB similarly upregulates the STAT1-CXCL10 axis, enhancing vascular inflammation and macrophage adhesion, effects that were further amplified following rhGPNMB treatment. In the RV, GPNMB derived from macrophages and fibroblasts induces cardiac fibroblast activation through TGF-β signaling, thereby promoting fibrosis. Functionally, knockdown of GPNMB significantly reduced PASMC and PAEC proliferation, migration, and fibroblast activation, underscoring its pro-fibrotic and pro-inflammatory effects. Clinically, elevated plasma GPNMB levels in PAH patients were found to correlate strongly with disease severity, supporting its potential as a reliable biomarker for assessing PAH progression and prognosis.

CONCLUSION: GPNMB synergistically interacts with ITGB2 to activate the STAT1-CXCL10 axis, driving pulmonary vascular inflammation and remodeling, while simultaneously promoting RV fibrosis through TGF-β signaling pathways. These findings position GPNMB as a critical mediator in PAH pathogenesis and suggest that targeting GPNMB could represent a promising therapeutic strategy for mitigating both pulmonary vascular and RV remodeling. Furthermore, the elevation of plasma GPNMB levels in PAH patients highlights its potential as a non-invasive biomarker for disease monitoring, prognosis assessment, and guiding personalized treatment approaches in clinical settings.

Riociguat Replacement Therapy in Eisenmenger Syndrome: A Prospective Real-World Study of Efficacy and Safety Following Transition from Phosphodiesterase-5 Inhibitors

Yingjie Tan, Jiang Li

Second Xiangya Hospital of Central South University

Background:

Eisenmenger syndrome (ES) represents a critical subtype of pulmonary arterial hypertension associated with congenital heart disease, characterized by progressively elevated pulmonary vascular resistance leading to right heart failure. ES patients frequently exhibit severe endothelial dysfunction, manifested by reduced production of vasodilatory substances such as nitric oxide. Although phosphodiesterase type 5 inhibitors (PDE5i) are widely used in pulmonary hypertension management, some patients develop tachyphylaxis or exhibit inadequate therapeutic responses. Notably, while both PDE5i and the soluble guanylate cyclase (sGC) stimulator riociguat target the NO-sGC-cGMP pathway, riociguat activates sGC independently of NO availability, conferring a theoretical advantage for ES patients with endothelial impairment who respond inadequately to PDE5i. International studies have demonstrated improved outcomes following transition from PDE5i to riociguat in pulmonary hypertension, yet evidence specific to the ES population remains scarce. This study aimed to prospectively evaluate the safety and efficacy of riociguat as replacement therapy in ES patients with suboptimal PDE5i responses.

Method:

This prospective, open-label, non-controlled interventional trial systematically evaluated the clinical transition fromPDE5i therapy to riociguat in patients diagnosed with ES, employing a standardized protocol whereby eligible adult participants meeting stringent inclusion criteria—specifically documented receipt of stable PDE5i treatment for a minimum duration of 3 months concurrent with World Health Organization Functional Class (WHO FC) II or III designation and baseline 6-minute walk distance (6MWD) measurements falling within the 165-440 meter range—underwent comprehensive screening assessments followed by a mandatory 1-3 day PDE5i washout period to preclude pharmacological interactions prior to initiating riociguat administration, which was subsequently carefully up-titrated according to a predefined schedule starting from 1.0 mg three times daily (TID) with biweekly 0.5 mg dose escalations contingent upon individual tolerability profiles until achieving either the target therapeutic maintenance dosage of 2.5 mg TID or the patient-specific maximally tolerated dose, with exploratory efficacy endpoints encompassing changes in 6MWD, WHO FC, peripheral oxygen saturation (SpO_2), and N-terminal pro-B-type natriuretic peptide (NT-proBNP) alongside rigorous safety monitoring through structured adverse event documentation, all clinical parameters being systematically collected during scheduled study visits to holistically assess both the safety profile and therapeutic effectiveness of this pharmacological transition strategy, with the trial protocol having been prospectively registered in the publicly accessible Chinese Clinical Trial Registry under the unique identifier ChiCTR2500096733 (www.chictr.org.cn).

Result:

Among the 36 enrolled Eisenmenger syndrome patients, 30 subjects (83.3%) successfully completed the 24-week study protocol, with 29 (96.7%) receiving concurrent endothelin receptor antagonist or selexipag therapy. At the 24-week endpoint, patients demonstrated significant clinical improvements including a mean NT-proBNP reduction of 216.68 ± 502.28 pg/mL, increased peripheral oxygen saturation (SpO_2) by 2.2% ± 3.2%, alongside enhanced 6-minute walk distance, improved WHO functional class, and ameliorated cardiac function parameters relative to baseline. Throughout the therapeutic transition period, drug-related adverse events were documented in 46% of participants; however, no treatment discontinuations occurred due to adverse drug reactions. Notably, two instances of clinical worsening were observed, both adjudicated as unrelated to the study medication and attributed to underlying disease progression.

Conclusion:

Transition from PDE5i to riociguat in ES patients is safe and feasible, significantly enhancingexercise tolerance, peripheral oxygen saturation, and cardiac function. Riociguat provides a viable therapeutic alternative for patients with suboptimal PDE5i responses.

基于血流动力学分层的阶梯式呼吸 - 运动耦联训练方案对中重度 PAH 患者心肺功能的影响

代芬

陆军军医大学第二附属医院新桥医院

摘要：目的：探讨阶梯式呼吸 - 运动耦联训练在中重度肺动脉高压（PAH）患者中的应用价值。

方法：将 62 例 WHO 功能 II - IV级 PAH 患者随机分为对照组（常规康复）与干预组（基于右房压、心指数及肺血管阻力的血流动力学分层训练），实施 12 周阶梯式干预。通过心肺运动试验（CPET）、6 分钟步行距离（6MWD）、N 末端脑钠肽前体（NT-proBNP）及 WHO 心功能分级评估干预效果。

结果：干预组峰值摄氧量（VO2 peak）较基线提升（18.7±3.2 vs 15.4±2.8 ml/kg/min，P<0.01），6MWD 增加（423±68 vs 358±59 m，P<0.05），且 NT-proBNP 水平显著下降（256±98 vs 542±156 pg/ml，P<0.01）。对照组各指标改善幅度均低于干预组（P<0.05）。分层分析显示肺血管阻力≤ 10 Wood 单位亚组 VO2 peak 提升更为显著（Δ+4.1 vs Δ+2.3 ml/kg/min，P=0.016）。

结论：基于血流动力学特征的阶梯式训练能有效改善中重度 PAH 患者运动耐量及右心功能，其效应与基线血流动力学状态密切相关。

关键词：阶梯式呼吸 - 运动耦联训练；肺动脉高压；心肺功能；运动耐量；右心功能

肺动脉高压（Pulmonary Arterial Hypertension, PAH）是一种以肺血管阻力进行性升高为特征，最终导致右心衰竭甚至死亡的严重心肺血管疾病。中重度 PAH 患者常伴有显著的运动耐量下降、呼吸困难及生活质量严重受损。运动康复作为心血管疾病管理的重要组成部分，其在 PAH 患者中的应用价值日益受到关注。然而，传统康复训练方案往往忽视患者个体间显著的右心功能和血流动力学差异，可能导致训练强度不当——强度不足则效果有限，强度过高则存在诱发右心功能失代偿的风险。因此，亟需探索一种能根据患者个体化血流动力学状态精准制定和调整训练强度的康复策略，以期在保障安全的前提下最大化运动康复的临床获

益。基于此，本研究旨在设计并验证一种基于血流动力学分层的阶梯式呼吸 - 运动耦联训练方案，并系统评价其对中重度 PAH 患者心肺功能及运动耐量的影响。

YBX1 Lactylation Modulates Endothelial-Mesenchymal Transition in Pulmonary Arterial Hypertension

Zhifu Guo[1], Jing-Yu Zhang[1], Qiang Xu[2], Yun-Pu Niu[1], Pan Li[1]

1. Changhai Hospital, Naval Medical University

2. Navy 905 Hospital, Naval Medical University

Abstract

Objective: Pulmonary arterial hypertension (PAH) is a progressive and fatal disease characterized by pulmonary vascular remodeling, endothelial dysfunction, and right heart failure, with a 5-year survival rate below 60% in severe cases. Despite advances in vasodilatory therapies, PAH remains incurable due to unresolved metabolic and epigenetic dysregulation. Recent studies highlight lactate accumulation and its derived lactylation modification (Kla) as critical drivers of vascular pathology, but the role of Y-box binding protein 1 (YBX1) lactylation in endothelial-mesenchymal transition (EndMT) and PAH progression remains unexplored. This study aims to: (1) establish the correlation between hypoxia-induced YBX1 lactylation and EndMT in PAH; (2) identify the downstream pathways regulated by lactylated YBX1; and (3) validate YBX1 as a novel diagnostic marker and therapeutic target for PAH.

Methods: A multi-dimensional approach was employed:Clinical and Preclinical Models: Analyzed plasma and lung tissues from PAH patients (GSE228644) and two hypoxic rodent models (SU5416/hypoxia mice and MCT-treated rats) for lactate levels and lactylation profiles. Performed single-cell RNA sequencing (scRNA-seq) to map YBX1 expression in endothelial cells.

Lactylation Profiling: Conducted pan-lactylation (Pan-Kla) sequencing in hypoxic pulmonary microvascular endothelial cells (PMVECs) and PAH tissues.

Validated YBX1 lactylation via co-immunoprecipitation (Co-IP) and immunofluorescence (co-localization with CD31/α-SMA).

Functional Validation: Modulated lactate levels in PMVECs using L-lactate supplementation or lactate dehydrogenase inhibitors (LDHi).

Assessed EndMT markers (CD31 ↓ , α-SMA ↑ , COL1A1 ↑) via qPCR, Western blot, and transwell assays. Generated YBX1-knockdown (siRNA) and site-directed mutagenesis models to dissect lactylation-dependent mechanisms.

In Vivo Studies: Developed endothelial-specific YBX1 knockout mice (Ybx1[flox/flox]; Cdh5-CreERT2) to evaluate PAH phenotypes (right ventricular hypertrophy, vascular remodeling).

Mechanistic and Therapeutic Exploration: Employed Cut&Tag to map YBX1-lactylation-bound genes and regulatory enzymes (e.g., p300/CBP). Screened potential inhibitors via molecular docking targeting YBX1-lactylation interactions

Results: Metabolic Dysregulation in PAH: PAH patients and hypoxic rodent models (SU5416/hypoxia mice and MCT-treated rats) exhibited elevated lactate and 3-hydroxybutyrate levels in plasma and lung tissues ($P < 0.01$), consistent with a Warburg-like metabolic shift toward aerobic glycolysis. Single-cell RNA sequencing (scRNA-seq, GSE228644) of PAH lung tissues revealed YBX1 upregulation specifically in endothelial cells, with a 1.8-fold increase compared to controls ($P < 0.05$). Immunofluorescence co-localization confirmed YBX1 enrichment in CD31+ endothelial cells of remodeled pulmonary arterioles.

YBX1 Lactylation Drives EndMT: Hypoxia (1% O_2) induced YBX1 lactylation in pulmonary microvascular endothelial cells (PMVECs), which correlated with EndMT activation:α-SMA expression increased 2.5-fold ($P < 0.001$), while CD31 decreased by 60% ($P < 0.01$). Exogenous L-lactate (25 mM) exacerbated these effects, further reducing endothelial markers (VE-cadherin ↓ 70%) and increasing mesenchymal markers (COL1A1 ↑ 3.2-fold). YBX1 silencing (siRNA) reversed hypoxia-induced EndMT, restoring CD31 expression and reducing collagen deposition by 45% ($P < 0.001$).

Mechanistic Insights: Cut&Tag analysis identified YBX1-lactylation binding sites enriched in promoters of fibrotic genes (COL1A1, S100A4) and inflammatory mediators (NF-κB, IL-6). p300/CBP was identified as the primary "writer" enzyme for YBX1 lactylation, with p300 inhibition reducing YBX1 lactylation by 80% ($P < 0.001$). EMSA assays confirmed lactylated YBX1 directly binds to the COL1A1 promoter, enhancing its transcription (luciferase activity ↑ 2.1-fold).

Therapeutic Potential: Ybx1-cKO mice showed attenuated PAH progression (RVSP ↓ 30%, Fulton index ↓ 25%). Molecular docking prioritized small molecules (e.g., resveratrol analogs) that disrupted YBX1-lactylation interactions.

Conclusion: This study pioneers the mechanistic link between YBX1 lactylation and PAH vascular remodeling via EndMT, establishing a novel metabolic-epigenetic axis in PAH pathogenesis. Hypoxia-induced lactate accumulation promotes YBX1 lactylation, which transcriptionally activates profibrotic (e.g., COL1A1, S100A4) and inflammatory (e.g., NF-κB) pathways, driving endothelial dysfunction and vascular stiffening. The integration of Cut&Tag technology and functional genomics revealed that lactylated YBX1 binds to promoters of genes enriched in vascular remodeling, extracellular matrix deposition, and hypoxia response, confirming its role as a master regulator of EndMT in PAH.

Key Innovations:

First evidence of YBX1 lactylation in endothelial dysfunction and PAH.

Multi-omics approach (scRNA-seq, Cut&Tag) to map lactylation-dependent gene networks.

Preclinical validation of YBX1-targeted therapy in PAH.

Significance:

This work not only elucidates a previously unrecognized mechanism of PAH progression but also provides a translational roadmap for targeting the lactate-YBX1 axis, potentially transforming PAH therapeutic strategies.

Keywords: Pulmonary arterial hypertension , YBX1, Lactylation, Endothelial-mesenchymal transition, Vascular remodeling

PAD4 通过 HIF1α–ENO1 信号轴介导 NETosis 促进肺动脉高压血管重塑的作用机制研究

郭煜[1,2,3] 高振强[1,2,3] 隆寰宇[4] 张牧之[1,2,3] 贾玉峰[1,2,3] 崔烨[1,2,3] 王蕾[5] 孙英[1,2,3] 刘杰[1,2,3] 王炜[1,2,3]

1. 首都医科大学基础医学院免疫学系

2. 首都医科大学呼吸病学系

3. 首都医科大学免疫异常与肺纤维化基础临床联合实验室

4. 北京大学第三医院呼吸与危重症医学科

5. 西安交通大学第二附属医院呼吸与危重症医学科

目的：

本研究旨在系统阐明 NETosis 在肺动脉高压（pulmonary hypertension, PH）发生发展中的作用机制，特别聚焦于低氧条件下低氧诱导因子 1α（hypoxia-inducible factor 1-alpha，HIF1α）- 烯醇酶 α（enolase-1，ENO1）代谢轴对肽基精氨酸脱亚氨酶 4 型（peptidyl arginine deiminase 4，PAD4）介导 NETosis 形成的调控机制，并验证 NETosis 在血管内皮功能障碍中的重要作用。

方法：

本研究利用 SU5416 联合低氧（SuHx）构建小鼠肺动脉高压模型，造模完成后获取肺组织样本进行单细胞转录组测序并系统性分析中性粒细胞中 PAD4 的表达特征及其在 PH 发生发展过程中发挥的潜在机制。采用 Western blot 检测肺组织中 PAD4、citH3、MPO、HIF1α 与 ENO1 的表达变化，并结合免疫荧光染色分析 NETosis 形成情况。利用 PAD4 基因敲除小鼠和 PAD4 特异性抑制剂 GSK484 干预模型，评价 PAD4 对肺血流动力学和肺血管重塑（小动脉中膜增厚、肌化程度）的影响。在体外，通过低氧刺激诱导中性粒细胞形成 NETosis，并通过干预 HIF1α 与 ENO1 表达（使用 HIF1α 激动剂 / 抑制剂、ENO1 siRNA）以明确二者在调节 NETosis 形成中的作用，并将中性粒细胞胞外捕获网（neutrophil extracellular traps，NETs）与人肺动脉内皮细（human pulmonary arterial endothelial cells，hPAECs）共培养，观察其对内皮细胞功能的影响。

结果：

单细胞数据分析显示，PAD4 在 SuHx-PH 小鼠肺组织中性粒细胞中显著上调，且高度富集于伴随低氧应答的糖酵解基因表达簇中。体内实验结果表明，SuHx 诱导肺组织中 PAD4、citH3、HIF1α 和 ENO1 表达均明显升高；PAD4 缺失或对其表达进行抑制可显著减少 NETosis 形成，同时，可改善血管重塑程度并逆转右心功能障碍。体外实验进一步证实，低氧刺激（1% O_2）人中性粒细胞后其 HIF1α 和 ENO1 蛋白表达显著升高，并伴随 NETosis 形成增加，而使用 HIF1α 抑制剂处理则显著降低 ENO1 和 PAD4 表达水平，NETosis 形成也明显减少。在常氧条件下应用 HIF1α 激动剂，可显著增强 ENO1 和 PAD4 的表达，并促进中性粒细胞形成 NETosis。进一步使用 ENO1 抑制剂处理后，即使在低氧条件下，PAD4 及其下游标志物 citH3 的表达也明显下降，NETosis 程度显著减弱，提示 ENO1 可能是 HIF1α 调控 PAD4 并驱动 NETosis 的关键中介分子。随后，将低氧和 PMA 条件下诱导形成的 NETs 收集并与 hPAECs 共培养，结果发现 NETs 可增强内皮细胞的黏附能力和血管生成能力，提示其可能通过调控内皮功能，参与肺动脉高压相关的血管重塑过程。

结论：

本研究发现低氧通过激活 HIF1α 上调其下游代谢酶 ENO1，增强糖酵解并促进 PAD4 参与的 NETosis，揭示了 HIF1α–ENO1–PAD4 轴调控 NETosis 的新机制。体外实验结果提示 NETs 可能通过调控内皮细胞功能参与肺血管重塑，而 PAD4 作为该通路的核心分子，有望成为肺动脉高压免疫代谢治疗的潜在靶点。

高强度间歇训练联合抗凝治疗对肺栓塞患者心肺功能及血栓再发风险的调控作用

金竹

陆军军医大学第二附属医院新桥医院

摘要：目的：探讨高强度间歇训练（HIIT）联合抗凝治疗对肺栓塞患者心肺功能及血栓再发风险的协同调控机制。

方法：采用随机对照试验设计，纳入 86 例急性肺栓塞康复期患者，分为联合治疗组（HIIT+ 利伐沙班）与常规抗凝组。通过心肺运动试验评估峰值摄氧量（VO2peak）、无氧阈及 6 分钟步行距离，运用超声心动图监测右心室功能，同时检测 D- 二聚体、凝血酶 - 抗凝血酶复合物（TAT）等血栓标志物。

结果：干预 12 周后，联合治疗组 VO2peak 提升幅度达 29.7±4.2%（vs 对照组 14.5±3.1%，P<0.01），右心室 Tei 指数改善 0.38±0.05（vs 对照组 0.21±0.04，P<0.05）。血栓再发率显著降低至 3.2%（对照组 13.9%，P<0.05），纤维蛋白降解产物（FDP）水平下降 58.3%±6.7%。

结论：HIIT 通过改善内皮功能及纤溶活性，与抗凝药物产生协同效应，既能显著提升运动耐量及心肺储备，又可降低高凝状态，为肺栓塞康复提供创新性综合治疗方案。

关键词：高强度间歇训练；运动康复；内皮功能；纤溶活性；血栓形成

肺栓塞（Pulmonary Embolism, PE）是一种由内源性或外源性栓子阻塞肺动脉或其分支引起的严重心肺血管疾病，具有高发病率、高致残率和高死亡率的特点。目前，抗凝治疗是肺栓塞患者的标准基础治疗，能有效预防血栓复发，但对于改善患者心肺功能、运动耐量及内皮功能障碍等方面作用有限。心肺功能下降及长期高凝状态是影响肺栓塞患者康复进程及预后的关键因素，亟需探索更优化的综合干预策略。近年来，运动康复在心血管疾病管理中的核心地位日益凸显，其中高强度间歇训练（HIIT）因其高效改善心肺适能的特性受到广泛关注。基础研究提示 HIIT 可能通过调节内皮功能、改善纤溶系统活性及降低炎症反应等多途径发挥抗血栓形成作用。然而，HIIT 与标准抗凝治疗联用对肺栓塞患者心肺功能恢复及血栓再发风险的协同调控效应尚缺乏系统研究，其潜在机制亦未明确。

肺栓塞后内皮功能障碍与运动耐量恢复的分子机制及康复干预靶点研究

翁容容

陆军军医大学第二附属医院新桥医院

摘要：目的：探讨肺栓塞患者急性期后内皮功能障碍与运动耐量恢复迟缓的分子关联机制，明确血管内皮生长因子（VEGF）-A/Notch 信号轴在肺微循环重建中的调控作用，揭示高强度间歇训练（HIIT）通过调控 SIRT1/PGC-1α 通路改善线粒体生物合成的分子机制。

方法：采用前瞻性队列研究，通过心肺运动试验（CPET）评估 56 例肺栓塞幸存者的峰值摄氧量（VO2peak），联合血管内皮功能检测（FMD%）、血浆内皮微粒（EMP）定量及单细胞转录组测序技术，建立内皮功能障碍生物标志物谱。构建大鼠肺栓塞模型，应用 Ad-Cre 介导的 VE-cadherin 条件性敲除技术，结合 RNA 干扰和腺相关病毒载体靶向调控关键分子表达。

结果：发现肺栓塞后 EMP 表面 CD144+/CD31+ 亚群比例与 VO2peak 呈显著负相关（r=-0.72，P<0.01），单细胞测序揭示内皮细胞中 HIF-1α/NF-κB 通路持续活化导致 eNOS 磷酸化异常。动物实验证实 HIIT 通过激活 SIRT1/PGC-1α 轴使线粒体 DNA 拷贝数提升 2.3 倍（P<0.001），同时抑制 NLRP3 炎症小体活化使 IL-1β 水平下降 58%（P<0.01）。

结论：内皮 - 线粒体耦联障碍是运动耐量恢复延迟的关键机制，靶向调控 SIRT1/PGC-1α-AMPK 信号网络可能成为新型康复干预策略。

关键词：肺栓塞；内皮微粒；线粒体生物合成；血管重构；代谢重编程

肺栓塞（Pulmonary Embolism, PE）作为血栓栓塞性疾病的重要类型，其急性期后遗症对患者长期预后构成严峻挑战。近年来，内皮功能障碍被确认为肺微循环障碍的核心病理基础，其通过影响血管通透性、炎症反应及氧化应激水平，直接加剧组织缺氧和运动耐量下降。流行病学数据显示，约 30-50% 的幸存者面临持续性运动耐量恢复延迟，这不仅降低生活质量，还增加心血管事件复发风险。尽管现有研究聚焦于血流动力学异常，但内皮 - 线粒体耦联机制在康复过程中的调控作用仍未被充分阐明。值得注意的是，VEGF-A/Notch 信号轴作为血管生成的关键通路，其失调可能导致微血管重塑失败，而 SIRT1/PGC-1α 通路的抑制则加剧线粒体功能障碍，阻碍能量代谢恢复。因此，深入探究这些分子网络的交互作用，不仅有助于解析康复迟缓的生物学本质，还为靶向干预提供理论依据。本研究通过整合临床队列与动物模型，系统评估 HIIT 等康复策略的分子效应，以期填补该领域的研究空白，推动个性化康复方案的优化。

营养 - 运动 - 心理 " 三位一体 " 干预方案对 PAH 患者生存质量影响的随机对照研究

田敏

陆军军医大学第二附属医院新桥医院

摘要：目的：探讨基于营养指导、运动康复及心理疏导构建的综合干预模式对肺动脉高压（PAH）患者生存质量指标的改善效果。

方法：采用随机对照试验设计，将确诊为 PAH 的 120 例患者按 1:1 比例随机分为干预组（常规治疗 + 三位一体干预）和对照组（仅常规治疗），通过 SF-36 生存质量量表和 6 分钟步行距离测试进行为期 6 个月的动态评估，采用重复测量方差分析比较两组患者生理功能、心理状态及运动耐量的组间差异。**结果：**干预组在干预 3 个月后 SF-36 量表总分较基线提高 18.7±3.2 分（P<0.01），对照组仅提高 5.4±2.1 分（P=0.032），组间差异具有统计学意义（F=22.43，P<0.001）。6 分钟步行距离（6MWD）数据显示，干预组 6 个月后步行距离达 412±45 米，显著高于对照组的 358±39 米（95%CI 32-67，P=0.004）。重复测量方差分析显示，干预组在生理职能（β=6.21，P=0.013）、情感职能（β=4.97，P=0.028）及社会功能维度（β=5.63，P=0.017）改善幅度均显著高于对照组。亚组分析表明，WHO 功能分级 II 级患者干预后 NT-proBNP 水平下降幅度达 43%（P=0.002），显著优于 III 级患者的 28%（P=0.047）。

结论：三位一体干预模式能有效改善 PAH 患者多维度生存质量指标，其中营养 - 运动联合干预对血流动力学改善效应（r=0.71，P<0.01）与心理干预对焦虑抑郁症状缓解效应（HADS-A 评分 Δ=-4.8，P=0.006）具有协同作用。

关键词：肺动脉高压；三位一体干预；生存质量；运动耐量；心理疏导

肺动脉高压（PAH）作为一种进展性的心血管疾病，严重影响患者的生活质量和预后。近年来，尽管医疗技术的进步和治疗手段的不断丰富，PAH 患者的生存率有所提高，但其生存质量的改善仍面临诸多挑战。本研究聚焦于探索一种更为全面、系统的干预方案，以期在常规治疗的基础上，进一步促进 PAH 患者的康复进程。营养、运动和心理状态是影响 PAH 患者生存质量的关键因素。营养不良不仅削弱患者的体力，还可能加剧其生理机能衰退；而缺乏适当的运动则可能导致肌肉废用性萎缩，进一步降低患者的运动耐量。此外，PAH 患者常常面临巨大的心理压力，焦虑、抑郁等情绪问题频发，这些心理问题反过来又会影响其治疗效果和康复进程。因此，我们提出 “营养 - 运动 - 心理” 三位一体的综合干预模式，旨在通过全面的营养指导、个性化的运动康复计划和专业的心理疏导，为患者提供全方位的支持和帮助。

The value of sST2 in risk stratification and short-term prognosis of acute pulmonary embolism: a pilot study focusing on intermediate-risk subgroups

Jian Wang, Zhen Liu, Yan Jiao, Jin-Long Li, Yan-Li Cheng

Binzhou Medical University Hospital

Background: Intermediate-risk acute pulmonary embolism (APE) represents a heterogeneous group that is temporarily hemodynamically stable and still has a high mortality. The aim of this study was to assess the predictive value of soluble growth stimulation expressed gene 2 (sST2) in risk stratification and short-term prognosis in this group.

Methods: This retrospective observational study included 128 patients with intermediate-risk APE between February 2020 to November 2023. Univariate or multivariate analysis were carried out for exploring the associations of sST2 with risk stratification and adverse event. Univariate logistic regression analysis and characteristic curve (ROC) were performed.

Results: Among 128 patients included in the study, the average age was 66.6±9.0 years, and 42.2% were male. More than half of patients (60.9% ,78/128, 95% CI 52.4% - 69.5%) were classified in the intermediate-high risk group. A total of 26 patients (20.3%,26/128, 95% CI 13.2% - 27.4%) developed adverse events (as defined in the methods), of which 22 occurred in the intermediate-high risk group and 4 in the intermediate-low risk group. sST2 levels were 16.0(10.1,32.1) ng/mL, and 27 patients (21.1%) had abnormally elevated (35ng/mL). Level of NT-proBNP was 1412.0 (825.0,3772.3) pg/mL. The percentage of occurrence of dyspnea was high (93.8%).Compared with the intermediate-low risk group, higher proportion of RVD (100.0% vs 32.0%, P<0.001), higher levels of sPESI (2.0, 1.0-3.0 vs 1.0, 1.0-2.0, P<0.001), NT-proBNP (1954.0,1313.0-4070.0pg/mL vs 810.0,368.8-1430.0pg/mL, P<0.001), sST2 (25.8,12.2-50.0ng/mL vs 11.5,8.0-16.0 ng/mL, P<0.001) and more adverse events (28.2% vs 8.0%, P=0.006) were observed in the intermediate-high risk group. Similarly, a higher proportion of RVD (92.3% vs 68.6%, P=0.015), higher levels of sPESI (2.0, 2.0-4.0 vs 2.0, 1.0-3.0, P=0.002), NT-proBNP (4559.0,2932.8-8482.0pg/mL vs 1234.0,638.0-3205.0pg/mL, P<0.001) and sST2 (44.9,24.1-72.8ng/mL vs 13.3,8.8-26.0, P<0.001) were observed in the adverse event group compared to the no adverse event group. In addition, higher levels of CTnI (0.21,0.12-0.44mmol/L vs 0.09,0.05-0.30, P=0.011) and lactate (1.3,1.0-1.5mmol/L vs 1.0,0.8-1.3, P=0.004) were also significantly higher in the adverse event group compared to the no adverse event group.Univariate logistic regression analysis showed that sST2 was associated with intermediate-high risk stratification (OR = 1.085, 95%CI 1.042~1.129, P<0.001). Age, gender, HR, CTnI, NT-proBNP, adverse event and sST2 were included to construct a multifactorial regression equation, and it was found that sST2 was still associated with intermediate-high risk stratification (OR = 1.071, 95%CI 1.018~1.127, P= 0.008).The ROC analysis showed that the area under the curve for sST2 identification of the intermediate-high risk stratification was 0.754 (95% CI: 0.671-0.837; P<0.001), and the optimal cut-off value was 16.20 ng/mL with a sensitivity of 66.70% and specificity of 84%.Univariate logistic regression analysis showed that sST2 was associated with adverse event (OR =1.049, 95%CI 1.027~1.072, P<0.001). After adjusting for confounding factors (age, gender, CTnI, NT-proBNP, intermediate-high risk stratification, RVD, DBP, Lac), sST2 was still associated with adverse event (OR

=1.038, 95%CI 1.007~1.070, P= 0.017). Other influencing factors were NT-proBNP (OR =1.001, 95%CI 1.000~1.001, P=0.002), DBP (OR =0.910, 95%CI 0.841~0.984, P= 0.018).Regarding sST2, the area under the ROC curve (AUC) for predicting adverse event was 0.832 (95% CI 0.751-0.913; P<0.001). The optimal cut-off value was 16.20ng/mL with a sensitivity of 92.30% and specificity of 64.47%. For NT-proBNP, the AUC was 0.830(95% CI: 0.735-0.924; P<0.001), and the optimal cut-off value was 3581.50pg/

mL with a sensitivity of 69.20% and specificity of 82.40%. When combining sST2 and NT-proBNP, the AUC was 0.860 (95% CI: 0.765–0.954; P <0.001). The optimal cut-off value was 0.173 with a diagnostic sensitivity of 84.60% and specificity 82.40%.

Conclusions: sST2 is associated with risk stratification and poor short-term prognosis for intermediate-risk APE, and it is a promising new biomarker that may contribute to further stratification for intermediate-risk subgroups and identification of individuals with a propensity to develop adverse events during hospitalization.

A Novel tRNA-Derived Small RNA, tRF-1:32-Glu-TTC-2-M2, Regulates RV Remodeling and Fibrosis by Targeting P4HA2 in Pulmonary Arterial Hypertension

Yusi Chen, Jiang Li

The Second Xiangya Hospital of Central South University

Background:

Right ventricular (RV) function is a critical determinant of exercise tolerance and long-term survival in patients suffering from pulmonary arterial hypertension (PAH). As the RV adapts to chronic pressure overload from elevated pulmonary vascular resistance, progressive structural and functional remodeling ensues, eventually leading to right heart failure—a primary cause of death in PAH. Despite its clinical relevance, the precise subcellular and molecular mechanisms driving maladaptive RV remodeling—particularly fibrosis—remain insufficiently defined. This persistent knowledge gap continues to hinder the development of targeted therapies and robust biomarkers for early detection, disease monitoring, or prognosis. Recently, tRNA-derived small RNAs (tsRNAs), a novel class of non-coding RNAs derived from mature or precursor tRNAs, have emerged as important post-transcriptional regulators in various biological processes, including stress response, metabolism, and cardiovascular disease. However, their functional relevance and mechanistic roles in PAH-induced RV dysfunction have not yet been systematically explored.

Methods:

To investigate the potential role of tsRNAs in RV remodeling, we employed high-throughput small RNA sequencing and microarray analysis to comprehensively profile tsRNA expression in the plasma of PAH patients and in RV tissues from monocrotaline (MCT)-induced rat models of pulmonary hypertension. Among differentially expressed candidates, we focused on **tRF-1:32-Glu-TTC-2-M2**, a tsRNA significantly downregulated in diseased RV tissues. Functional analyses were conducted using adeno-associated virus serotype 9 (AAV9) to overexpress this tsRNA in two well-established preclinical models of RV failure: the MCT model and a model combining chronic hypoxia with the VEGF receptor blocker Su5416. Comprehensive in vivo assessments were performed, including echocardiography, cardiac MRI, right heart catheterization, histopathological examination, and molecular analyses. In vitro, tRF-1:32-Glu-TTC-2-M2 mimic transfection was performed in primary rat cardiac fibroblasts under fibrotic and hypoxic stimuli. To identify interacting proteins and downstream targets, we employed chromatin isolation by RNA purification-mass spectrometry (ChIRP-MS), RNA pull-down, and RNA immunoprecipitation assays. Rescue experiments were conducted to validate the direct involvement of candidate proteins.

Results:

Our data revealed a profoundly altered tsRNA expression landscape in PAH, with **tRF-1:32-Glu-TTC-2-M2**consistently reduced in the RV (but not lungs) of both human patients and animal models. Its expression inversely correlated with the extent of RV fibrosis and dysfunction. AAV9-mediated overexpression of this tsRNA significantly improved RV systolic function, reduced myocardial fibrosis and capillary rarefaction, and prolonged survival, without significantly altering pulmonary vascular pathology. Mechanistically, tRF-1:32-Glu-TTC-2-M2 was found to bind directly to **prolyl 4-hydroxylase subunit alpha-2 (P4HA2)**, a key enzyme responsible for collagen stabilization. Overexpression of the tsRNA inhibited P4HA2 expression and enzymatic activity, thereby suppressing collagen synthesis and cardiac fibroblast activation in vitro. Restoration of P4HA2 reversed these protective effects, confirming its role as a direct functional target. Clinically, circulating plasma levels of tRF-1:32-Glu-TTC-2-M2 effectively discriminated PAH patients from healthy controls, correlated with RV function indices, and predicted long-term event-free survival in two independent PAH cohorts.

Conclusions:

This study uncovers a previously unrecognized **tRF-1:32-Glu-TTC-2-M2-P4HA2 axis** that regulates RV fibrosis in PAH. By suppressing P4HA2-mediated collagen biosynthesis, tRF-1:32-Glu-TTC-2-M2 exerts protective effects against maladaptive RV remodeling. These findings highlight a novel epigenetic mechanism and position this tsRNA as a promising **therapeutic target and prognostic biomarker**, paving the way for future RV-specific precision medicine strategies in PAH.

基于机器学习模型评估慢性肾衰竭患者发生肺动脉高压的风险

李玲玲

西安交通大学第一附属医院

目的：慢性肾衰竭 (CRF) 患者肺动脉高压 (PH) 的发病率升高，且此类患者的死亡风险较不伴 PH 的 CRF 患者明显增加。目前缺乏 CRF 患者发生 PH 的临床预测模型，本研究通过真实世界研究，探讨两种疾病之间临床特征的相关性，利用机器学习算法构建简便高效的 CRF 患者的 PH 风险预测模型，为 CRF 合并 PH 患者的早诊早治提供理论依据。

方法：回顾性筛选西安交大一附院 440 名 CKD3b-5 期患者（包括病例组 220 例 CKD 合并 PH 患者及对照组 220 例 CKD 无 PH 的患者），本研究采用 LASSO 回归分析方法，结合单因素及多因素 logistic 回归对预测变量进行筛选。基于筛选结果构建了预测 PH 风险的列线图模型。随后通过受试者工作特征曲线下面积（AUROC）评估 8 种机器学习模型的预测能力，并使用 Brier 评估准确性。其中 8 种模型分别为极端梯度提升（XGBoost）、逻辑回归（LR）、随机森林（RF）、自适应增强（AdaBoost）、高斯朴素贝叶斯（GNB）、多层感知器（MLP）、支持向量机（SVM）以及 k- 近邻（KNN）。模型通过计算验证队列中的表现进行外部验证，并评估它们的性能，最后使用决策曲线分析和临床影响曲线评估模型的临床实用性。

结果：共纳入 440 例患者（队列按 7：3 比例随机划分为建模队列 308 例和验证队列 132 例），8 种机器学习模型中 Logistic 回归分析及预测模型表现最佳，最终列线图包含五个特征：血红蛋白、γ- 谷氨酰转移酶、甘油三酯、冠心病病史和 NT-proBNP。模型 AUROC 为 0.772(95%CI:0.731-0.806)，外部验证证实了模型的良好性能，AUROC 为 0.782(95%CI：0.696-0.854)。

结论：我们开发了一个基于实验室检测结果的机器学习模型，用于评估 CRF 患者的 PH 风险。根据模型得出患者的 Hb 降低、GGT 升高、TG 降低、CHD 病史以及 NT-proBNP 升高是 CRF 发生 PH 的独立危险因素。该模型支持随访期间的风险评估，并有助于早期发现 PH。

关键词：肺动脉高压；慢性肾衰竭；机器学习；风险模型

Development of a lactate-related, gene signature-based predictive model in pulmonary arterial hypertension using transcriptome and single-cell sequencing

Dawei Lin[1], Li-Hua Guan[2]

1. Zhongshan hospital, Fudan university

2. The Pulmonary Circulation and Right-Heart Group of CSC

Background/Objective: Pulmonary arterial hypertension (PAH) is a progressive disease characterized by elevated pulmonary vascular resistance, leading to right heart failure and high mortality. Lactate metabolism and protein lactylation are thought to be involved in the pathological mechanisms of PAH. However, research specifically linking lactate-related mechanisms to PAH remains limited. This study aim to identify lactate-related key genes and pathways in PAH pathogenesis using bioinformatics and single-cell sequencing to guide therapeutic strategies.

Methods: Gene expression datasets (GSE117261, GSE113439, GSE185479) were obtained from the GEO database. Differential expression analysis (limma, |logFC|>1, P<0.05), weighted gene co-expression network analysis (WGCNA), and functional enrichment (GO/KEGG) were performed. A predictive model was constructed via LASSO regression and validated using ROC curves. Immune infiltration (CIBERSORT), gene set enrichment (GSEA/GSVA), and transcriptional regulation (RcisTarget, miRDB) were analyzed. Single-cell RNA-seq data were processed (Seurat, Harmony) for cell-type annotation and pathway activity assessment (AUCell).

Results:

This study provides novel insights into the molecular pathogenesis of pulmonary arterial hypertension (PAH) through an integrated multi-omics approach combining transcriptomic profiling, weighted gene co-expression network analysis (WGCNA), machine learning-based predictive modeling, and single-cell RNA sequencing. Our analysis of the GSE117261 dataset (25 healthy controls vs 58 PAH patients) identified 72 significantly differentially expressed genes (DEGs), comprising 39 upregulated and 33 downregulated genes, which formed the foundation for subsequent investigations into disease mechanisms. The WGCNA revealed 20 distinct co-expression modules, with the dark_gray module containing 2,938 genes demonstrating the strongest positive correlation with lactylation levels (Pearson r=0.79, p=8×10^{-19}), suggesting a crucial role of lactate metabolism in PAH pathophysiology. Intersection analysis between DEGs and the dark_gray module yielded 32 lactate-related genes that were functionally enriched in neutrophil chemotaxis and migration (GO analysis) as well as hematopoietic cell lineage and fluid shear stress pathways (KEGG analysis), indicating potential involvement of inflammatory processes and hemodynamic forces in disease progression. To develop clinically relevant biomarkers, we constructed a predictive model using LASSO regression that identified 19 signature genes with strong diagnostic potential. This model demonstrated exceptional discriminative capacity in both training (AUC=1.0) and validation datasets (AUC=0.824), highlighting its robustness for PAH detection. Protein-protein interaction network analysis of these candidate genes

revealed five central hub genes - CD163, POSTN, S100A12, IL1R2, and HMOX1 - that emerged as key molecular players in PAH pathogenesis. These hub genes exhibited significant associations with specific immune cell populations, with CD163, HMOX1, IL1R2 and S100A12 showing positive correlations with neutrophils and M0 macrophages but negative correlations with CD8+ T cells, while POSTN demonstrated an inverse relationship with neutrophils but positive association with resting CD4+ memory T cells. These findings suggest complex immunomodulatory roles of these genes in shaping the PAH microenvironment. Functional enrichment analyses revealed distinct pathway associations for each hub gene: CD163 was linked to steroid biosynthesis and fatty acid metabolism; HMOX1 to galactose metabolism and MTorC1 signaling; IL1R2 to amino acid biosynthesis and angiogenesis; POSTN to extracellular matrix-receptor interaction and KRAS signaling; and S100A12 to HIF-1 signaling and oxidative phosphorylation. These pathway associations provide mechanistic insights into how these genes may contribute to vascular remodeling, metabolic reprogramming, and oxidative stress responses characteristic of PAH. Single-cell RNA sequencing of 43,088 cells further delineated the cellular landscape of PAH, identifying 11 distinct cell populations including immune cells (macrophages, T cells, B cells) and structural cells (endothelial cells, smooth muscle cells, fibroblasts). Cell-type-specific analysis of lactate pathway activity revealed that S100A12 was particularly active in glial lactate shuttling pathways, while IL1R2, HMOX1 and CD163 were associated with circulating lactate dehydrogenase-related pathways, suggesting cell-specific metabolic adaptations in PAH. Transcriptional regulation analysis identified cisbp__M0494 as the most significantly enriched transcription factor motif (NES=7.86) regulating the hub genes, while miRNA network prediction revealed 157 potential mRNA-miRNA regulatory pairs involving POSTN, HMOX1, S100A12 and CD163. These regulatory networks provide additional layers of understanding about the molecular control of PAH-associated genes. Collectively, our findings highlight the central roles of lactate metabolism, immune dysregulation, and specific signaling pathways in PAH pathogenesis, while identifying potential diagnostic biomarkers and therapeutic targets. The integration of bulk and single-cell transcriptomics with network analysis approaches has yielded a comprehensive molecular framework for understanding PAH, offering new directions for both basic research and clinical translation in this devastating cardiopulmonary disorder.

Conclusion: This study highlights the roles of CD163, POSTN, S100A12, IL1R2, and HMOX1 as lactate-associated genes in PAH progression via immune modulation and metabolic reprogramming. The predictive model and single-cell insights offer potential biomarkers and therapeutic targets for PAH management.

Global, regional and national burden of disease analysis and projections for pulmonary hypertension, 1990 to 2023

Da-wei Lin[1], Li-Hua Guan[2]

1. Zhongshan hospital, Fudan university

2. Pulmonary Vascular and Right Heart Research Group of CSC

Background and Objectives: Pulmonary arterial hypertension (PAH) is a progressive and life-threatening pulmonary disorder that severely compromises patients' health while creating substantial clinical and economic challenges. A comprehensive assessment of its worldwide epidemiological impact and temporal trends remains insufficient.

Methods: This study evaluated the worldwide impact of PAH in 2023, examining differences across sex, age groups, Socio-Demographic Index (SDI) categories, and individual nations while comparing trends with historical data from 1990. Bayesian age-period-cohort (BAPC) analysis was applied to forecast future disease burden patterns.

Result: The global incidence and prevalence of PAH demonstrated consistent increases, with age-standardized rates (ASRs) showing an estimated annual percentage change (EAPC) of 0.06 for incidence and 0.01 for prevalence. By 2023, there were 45,321 new cases (ASR 0.52/100,000) and 197,669 prevalent cases (ASR 2.26/100,000) worldwide. While absolute deaths increased slightly (22,808 in 2023 vs 20,263 in 1990), ASRs for mortality and disability-adjusted life years (DALYs) showed substantial declines (EAPC -1.74 and -2.11 respectively), with 705,248 DALYs recorded in 2023 (ASR 8.8/100,000).

Gender disparities were prominent, with females consistently exhibiting higher incidence, prevalence, and, by 2023, higher mortality and DALY rates compared to males. Age-specific analysis revealed the highest incidence and prevalence rates among 75-79-year-olds, while the greatest mortality and DALY burdens shifted from children under five in 1990 to those aged 95+ by 2023. Socio-demographic index (SDI) analysis showed complex patterns: age-standardized incidence and DALYs decreased with higher SDI, while prevalence increased, particularly in high-SDI regions. Middle-SDI regions exhibited the lowest absolute case numbers across all metrics, whereas high-SDI regions bore the greatest burden.

Geographically, East Asia maintained the highest PAH burden throughout the study period, followed by South Asia, with both regions showing rising incidence and prevalence but divergent mortality trends (decreasing in East Asia, increasing in South Asia). Eastern Sub-Saharan Africa and Western Europe initially had the highest age-standardized incidence rates, though these declined significantly by 2023. Prevalence rates surged in Central Latin America, Western Europe, and Western Sub-Saharan Africa, while mortality and DALY rates decreased across all regions, with Central Asia and North Africa/Middle East emerging as hotspots by 2023.

SDI correlation analysis demonstrated that higher development levels generally corresponded with lower incidence and DALYs but higher prevalence. Zambia had the highest incidence rate, Georgia led in mortality and DALYs, and Switzerland recorded the highest prevalence. Projections to 2053 suggest a continued rise in incidence (peaking at 0.52/100,000 in 2052) followed by a decline, while prevalence is expected to decrease slightly (2.19/100,000). Encouragingly, mortality and DALYs are projected to drop by approximately 50%, indicating improved outcomes. However, the persistent growth in incident cases underscores the critical need for enhanced prevention strategies and equitable healthcare access to address this escalating global health challenge. These findings highlight both progress in PAH management and the ongoing requirement for targeted interventions across diverse populations and regions.

Conclusions: While PAH prevalence rises globally, falling mortality and DALYs reflect treatment advances. This paradox underscores the need for targeted interventions in high-risk groups—elderly women with hormonal/autoimmune drivers and pediatric cases in low-SDI regions with diagnostic delays. Prioritizing early detection and equitable access is key to reducing outcome gaps.

The protective effect and mechanism of SIRT3 in pulmonary hypertension

Da-wei Lin[1], Li-Hua Guan[2]

1. Zhongshan hospital, Fudan university

2. Pulmonary Vascular and Right Heart Research Group of CSC

Background and objective:Pulmonary artery hypertension (PAH) is a disease characterized by progressive stenosis of pulmonary arterioles and endothelial cell damage. The pathophysiology of PAH has not been fully elucidated. It is currently recognized that there are ion channel mechanisms, vasoactive substance imbalance mechanisms, immune inflammation mechanisms and genetic mechanisms. Inflammation plays a vital role in the progression of PAH. Various types of inflammatory cells and inflammatory factors are key factors in promoting pulmonary vascular remodeling. Sirtuins (SRIT) are a class of enzymes belonging to nicotinamide adenine dinucleotide (NAD+-)-dependent histone deacetylases. Many studies have found that SIRT3 has a protective effect in cardiovascular diseases, but its role in PAH, especially its effect on pulmonary artery smooth muscle cells (PASMCs), has not been clearly explained.This study aims to clarify the role and potential mechanism of SIRT3 in the pathophysiology of PAH development.

Method and Result: We collected and detected the concentrations of SIRT3 and various inflammatory factors (including IL-1β, IL-6, Tumor Necrosis Factor-α [Tumor Necrosis Factor-α, TNF-α], Monocyte Chemotactic Protein-1 (Monocyte Chemotactic Protein-1, MCP-1]) in the serum of PAH patients and healthy people. The results showed that the SIRT3 content in the serum of PAH patients was significantly decreased, while the levels of IL-1β, IL-6, TNF-α, and MCP-1 were significantly increased compared with the control group. In addition, the SIRT3 level in the patient's serum was correlated with the patient's pulmonary artery pressure, pulmonary vascular resistance, and right ventricular anterior wall thickness. The levels of serum SIRT3 and MCP-1 were positively correlated with the above indicators. Furthermore, we studied the diagnostic efficacy of serum SIRT3, and the results showed that serum SIRT3 level can be used as a specific diagnostic factor for PAH patients, with high specificity and sensitivity. We further analyzed the risk of all-cause mortality of PAH patients within 2 years and found that serum SIRT3 was an independent predictor of all-cause mortality in PAH patients. Therefore, we speculate that SIRT3 may affect the development of PAH through related mechanisms.

Next, at the animal level, we constructed a monocrotaline-induced PAH rat model to explore the role of SIRT3 in PAH. We performed tissue sequencing, immunohistochemistry, and Western Blot experiments. The results showed that compared with the control group, SIRT1, SIRT6, and SIRT3 in the SIRT family in the PAH group were key differences, among which SIRT3 had the largest difference, and the SIRT3 content in the lung tissue of PAH rats was significantly decreased. We used adenovirus to overexpress SIRT3 (AAV1.SIRT3) to intervene in PAH rats, and found that the pulmonary artery systolic pressure of this group of rats was reduced, and the pulmonary vascular and right ventricular remodeling was alleviated. Our sequencing also found that differential genes were enriched in inflammatory signaling pathways, and the intervention of AAV1.SIRT3 significantly reduced inflammatory factors.

Furthermore, we explored the potential mechanism of the protective effect of SIRT3 at the cellular level. We selected pulmonary artery smooth

muscle cells (PASMCs) for experiments. The results showed that SIRT3 overexpression can reduce the proliferation and migration of PASMCs induced by PDGF-bb, and SIRT3 is directly connected to the STAT3 promoter, inhibiting the activation of STAT3 to p-STAT3 and its function in the nucleus. p-STAT3 and CCNA2 co-localize in the nucleus to function. We performed a response experiment at the animal level to verify. Therefore, SIRT3 overexpression inhibits the proliferation and migration of PASMCs induced by TNF-α through the STAT3/CCNA2 signaling pathway.

Conclusion: In summary, we found that serum SIRT3 was significantly decreased in PAH patients and rat models, and SIRT3 overexpression could reduce pulmonary vascular remodeling, right heart remodeling and inflammatory factor levels. SIRT3 overexpression inhibited the proliferation and migration of PASCMs induced by TNF-α by inhibiting STAT3/CCNA2.

房间隔缺损介入封堵后右心重塑的变化

陈伟

中国人民解放军空军军医大学第一附属医院

目的 评估不同年龄段房间隔缺损患者经导管封堵后的右心重塑情况。**方法** 回顾性分析自 2019 年 1 月 1 日～ 2021 年 12 月 31 日在空军军医大学第一附属医院心血管内科诊断为房间隔缺损，并行导管封堵的 428 名患者右心重塑情况。根据年龄将患者分为 4 组，< 7 岁组，(8~18) 岁组，(19~60) 岁组，> 60 岁组。通过超声心动图分别在术前、术后 1 月、术后 6 月评估右心重塑情况。**结果** < 7 岁患儿右心房和右心室在术后 1 月明显缩小（均 P<0.01），与术后 1 月相比，术后 6 月右心房、右心室进一步缩小（均 P<0.01）。（8~18）岁 ASD 患者右心房和右心室在术后 1 月明显缩小（均 P<0.01），与术后 1 月相比，术后 6 月右心房、右心室缩小无统计学差异；（19~60）岁患者 ASD 闭合后，右心房、右心室在术后 1 月明显缩小（均 P<0.01），与术后 1 月相比，术后 6 月右心房、右心室缩小无统计学差异；> 60 岁患者，ASD 闭合后，右心室内径在术后 1 月明显缩小 (P<0.01)，右心房变化无统计学差异，与术后 1 月相比，术后 6 月右心房、右心室缩小无统计学差异。**结论** 60 岁以前的房间隔缺损患者在介入封堵后 1 月出现右心房、右心室明显缩小，年龄越小，重塑越明显；60 岁以后，房间隔缺损患者在介入封堵后 1 月出现右心室明显缩小，右心房缩小不明显。

外周血血小板活化特征揭示慢性血栓栓塞性肺动脉高压患者中 CD16 ⁺单核细胞功能障碍

金俊灏 [1] 曹云山 [2]

1. 兰州大学第一医院（兰州大学第一临床医学院）

2. 四川省医学科学院·四川省人民医院

题目： 外周血血小板活化评分揭示慢性血栓栓塞性肺动脉高压患者中 CD16 ⁺单核细胞功能障碍

作者： 金俊灏 [1]，曹云山 [2*]

单位: 1 兰州大学第一临床医学院，兰州，730000；2 四川省医学科学院·四川省人民医院，成都，610000

目的： 慢性血栓栓塞性肺动脉高压（chronic thromboembolic pulmonary hypertension，CTEPH）是一种少见但具有进展性的肺动脉高压，其发病机制尚未完全阐明。已有研究提示，血小板活化在 CTEPH 的病理过程中可能发挥关键作用，并可能通过调控 CD16⁺ 单核细胞的功能影响疾病进展。本研究旨在构建 CTEPH 相关的血小板活化评分（CTEPH-platelet activation score，CTEPH-PAS），并探讨其临床意义及其在外周血 CD16⁺ 单核细胞中的潜在免疫调控机制。

方法： 本研究收集健康被试及 CTEPH 的患者外周血，并开展血小板转录组测序分析。通过筛选 CTEPH 患者中显著上调的差异表达基因，并与基因本体论数据库中“血小板活化”基因集取交集，基于交集基因构建单样本基因集富集评分即 CTEPH-PAS，并评估其预后价值。进一步整合多个单细胞转录组数据外周血单核细胞数据及 CTEPH 患者肺动脉内膜切除组织数据，以探讨 CTEPH-PAS 在不同免疫细胞亚群中的表达分布及功能关联。

结果： CTEPH 患者（n=29）中血小板活化水平显著高于健康对照组 (n=102)。CTEPH-PAS 评分在 CTEPH 患者中明显升高，且高评分（>0.71）与较差的预后显著相关（风险比 =5.42，95% 置信区间：1.31-22.35）。单细胞分析显示，CTEPH-PAS 在 PBMC 中主要富集于 CD16⁺ 单核细胞，其高表达与炎症相关通路的下调及细胞通讯强度的减弱密切相关。拟时序分析进一步揭示，CD16 ⁺单核细胞在分化为组织巨噬细胞过程中，CTEPH-PAS 逐渐下降，而炎症信号则逐步增强。此外，在 CTEPH-PAS 较低状态下，血小板与 CD16⁺ 单核细胞之间的 MIF-CD74+CXCR4 信号显著增强，提示血小板可能通过该途径参与单核细胞的免疫调控。

结论： CTEPH-PAS 是一项基于外周血血小板转录组构建的活化评分，在 CTEPH 患者中显著升高，并具有一定的预后评估价值。该评分主要富集于 CD16⁺ 单核细胞，且与其炎症相关通路下调及细胞通讯能力减弱密切相关。研究结果提示，血小板活化可能通过影响 CD16⁺ 单核细胞的功能状态参与 CTEPH 的发病过程，为进一步探索其免疫调控机制提供了线索。

有氧运动通过抑制 NLRP3 上调 Treg 细胞活性在改善肺动脉高压血管重构中的作用及机制

王天宇 李江

中南大学湘雅二医院

目的：肺动脉高压是一种以肺血管阻力进行性升高为主要特征，进而导致患者右心衰竭，病死率及致残率均高的一种疾病。目前临床上主要有三大类靶向药物，其主要机制是扩张肺动脉血管，这些药物可在一定程度上延缓 PAH 的进展，改善患者右心功能，提高生活质量，延长生存时间，但患者远期预后仍不容乐观。PAH 患者仍需要多药联合以及多种治疗手段综合治疗，有氧运动作为一种非药物辅助治疗手段，定期进行有氧运动对病情稳定的患者的治疗产生积极作用。本研究旨在探讨有氧运动减少肺血管重构的具体机制是有氧运动下调 NLRP3 而上调 Treg 细胞数目及功能相关。

方法：本研究通过建立低氧 +Su5416 诱导的 PAH 小鼠模型，对 PAH 模型小鼠和未进行低氧 +Su5416 诱导的对照组小鼠均进行 0 周和 8 周的有氧运动干预，光镜下评估肺血管重构情况，检测肺组织和血清中炎症水平含量及血液中 Treg/Th17 比值，评估小鼠有氧运动干预后的炎症水平。

结果：结果表明，对肺动脉高压小鼠进行有氧运动干预可以改善肺血管重构，降低血液和肺组织中 NLRP3 炎症小体及其下游的 IL-1β、IL-6 及 IL-18 水平，并升高 Treg/Th17 的比值。

结论：有氧运动可以下调 NLRP3 水平，并有效地改善了 Treg 细胞数量和功能，减轻肺动脉高压的血管重塑，为更好地治疗 PAH 提供新思路，具有重要的研究价值和临床应用前景。

凝血状态对阻塞性睡眠呼吸暂停合并肺高血压患者疾病严重程度的影响

吴振华 [1] 曹云山 [2]

1. 甘肃中医药大学第一临床医学院

2. 四川省医学科学院 • 四川省人民医院

目的：探讨凝血功能异常在阻塞性睡眠呼吸暂停（OSA）合并肺高血压（PH）患者中的作用影响，明确其和疾病严重程度的关系，为早期干预提供理论依据。

方法： 本研究为病例对照研究。纳入 2019 年 1 月到 2021 年 12 月在甘肃省人民医院就诊且诊断为 OSA 的患者。根据心脏彩超估测的肺动脉收缩压将纳入的患者分为两组，OSA 不合并 PH 组（PASP ≥ 36mmHg）和 OSA 合并 PH 组（PASP < 36mmHg）。收集患者的临床资料，包括凝血功能相关数据及多导睡眠监测（PSG）数据等。结局变量为二分类（合并 PH=1/ 不合并 PH=0）变量。通过二元 Logistic 回归、倾向评分匹配等分析凝血功能与 OSA 合并 PH 的关系。

结果： 共纳入 1194 例诊断 OSA 的患者，其中 1013 例不合并 PH，患者年龄为 48（38，55）岁；181 例合并 PH，患者年龄为 50（40，57）岁。倾向评分匹配前的组间差异分析显示，两组间年龄、BMI、LVEF、FVC、FEV1、凝血酶原活动度、INR、凝血酶原比率、凝血酶原时间、纤维蛋白原降解产物、血小板计数、同型半胱氨酸、总睡眠时间、睡眠效率、平均血氧值、血氧低于 90% 在总睡眠时间中比值差异有统计学意义 (P<0.05)，单因素 Logistic 回归分析显示，同型半胱氨酸与结局呈正相关（OR=1.01，95% CI：1.01~1.02，P=0.016）、血氧低于 90% 在总睡眠时间中比值与结局呈正相关（OR=1.01，95% CI：1.01~1.02，P=0.002），而在多因素分析中，同型半胱氨酸（OR=1.04，95% CI：1.02~1.07，P=0.002）、血氧低于 90% 在总睡眠时间中比值（OR=1.02，95% CI：1.01~1.04，P=0.003）仍有统计学意义。经倾向评分匹配（1:2 最近邻匹配，卡钳值 =0.1）后，两组基线特征均衡。单因素 Logistic 回归分析显示，同型半胱氨酸与结局仍呈正相关（OR=1.02，95% CI：1.01~1.03，P=0.003）。

结论： OSA 合并 PH 患者存在凝血功能异常，有高凝状态倾向。同型半胱氨酸水平升高是 OSA 合并 PH 患者的独立危险因素。针对凝血功能异常，特别是高同型半胱氨酸血症的 OSA 患者，早期干预可能改善预后，需进一步研究验证。

NAFLD is associated with right heart function and prognosis in pulmonary hypertension

Jingyuan Chen, Jiang Li

Second Xiangya Hospital of Central South University

AIM: pulmonary hypertension (PH) is a disease of pulmonary vascular remodeling that can lead to right ventricular failure and death within a few years of diagnosis. Patients with PH exhibit systemic metabolic dysfunctional changes. Among these, abnormalities in glucose and lipid metabolism are independent risk factors for the prognosis of patients with both PH. Patients with PH and right heart failure develop multiple patterns of hepatic impairment due to hepatic stasis. When hepatic stasis occurs, the lack of blood flow leads to a decrease in oxygen and accumulation of toxic substances, resulting in cellular damage and death. It is also one of the triggers that can lead to the development of non-alcoholic fatty liver disease (NAFLD). Studies have shown that the prevalence of PH combined with NAFLD is increased approximately 2-fold compared to controls, but no study has ever examined whether the combination of NAFLD has an impact on the prognosis of patients with PH.

METHODS: A retrospective analysis was performed on 1,100 patients with pulmonary artery hypertension (PAH) and chronic thrombo embolic pulmonary hypertension (CTEPH) who were admitted to the Second Xiangya Hospital of Central South University from 2015 to 2025, and those with complete abdominal ultrasound or abdominal computed tomography (CT) were screened. Patients were analyzed for the diagnosis of NAFLD by ultrasound and abdominal CT, and differences in laboratory findings, cardiac ultrasound findings, right heart catheterization findings, and prognosis were compared between the two groups.

RESULTS: From 1100 patients with PAH and CTEPH, 269 patients who complete CT or ultrasound as well as right heart catheterization and cardiac ultrasound related findings were finally screened, and the number of PH patients with NAFLD was 44. Compared to PH patients

without NAFLD, PH patients with NAFLD had a higher body mass index (P<0.01), higher serum total bilirubin, higher fasting glucose (P<0.01), higher serum triglycerides (P<0.05), and lower High-density lipoprotein cholesterol (P<0.001). However, there were no significant differences between alanine aminotransferase, aspartate aminotransferase and other lipoproteins. There were no significant differences in the proportions of NYHA cardiac function classification and ESC risk stratification between the two groups. Furthermore, patients with NAFLD and PH showed slightly higher levels of NT-proBNP, but there was no significant statistical difference between the two groups. In terms of cardiac ultrasound parameters, the right atrium and right ventricle were somewhat larger in PH patients with NAFLD (P<0.05). However, there were no significant differences in the left atrium, left ventricle, or ejection fraction. In terms of hemodynamic parameters, there was no significant difference in the mean pulmonary artery pressure and pulmonary vascular resistance between the two groups, but the right atrial pressure was higher in PH patients with NAFLD (P<0.01). In terms of prognosis, mortality as well as event rates were higher in patients with NAFLD (P<0.05).

CONCLUSION: Compared with PH patients without NAFLD, PH patients with NAFLD had higher body mass index, more abnormal liver function, glucose, and lipid levels, larger right hearts, higher right atrial pressures. Patients with PH who have NAFLD have a poor prognosis.

ATGL 在肺动脉高压中的作用研究

孔雪 陈静远

中南大学湘雅二医院

目的：肺动脉高压 (PAH) 是一类以进行性肺动脉压力增高和肺小动脉重塑为特征的致死性肺血管病，伴随右心室超负荷，引起右心室肥厚、扩张甚至衰竭。 脂代谢紊乱是 PAH 的关键病理机制之一。脂肪甘油三酯脂肪酶 (ATGL) 作为脂解过程的关键限速酶，通过调控脂滴动态代谢参与细胞能量稳态调控，但其在 PAH 中的作用尚未明确。本研究旨在揭示 ATGL 通过调控脂滴代谢影响 PAH 进展的机制，为靶向脂代谢重编程治疗 PAH 提供新的理论依据。

方法：(1) 使用 PAH 患者和健康人的肺组织进行免疫荧光染色，检测 ATGL 的表达情况及定位。(2) 构建 Sugen- 缺氧 (SuHx) 诱导的大鼠 PAH 模型，并通过气管内滴注腺相关病毒 (AAV) 干扰肺血管 ATGL 的表达。将 SD 雄性大鼠随机分为四组：正常对照 (CON)+AAV-Con 组、CON+AAV-shAtgl 组，SuHx+AAV-Con 组和 SuHx+AAV-shAtgl 组，每组大鼠 8 只。右心导管测量右心室收缩压 (RVSP)，超声心动图测量右心室功能，病理切片评估肺动脉重构，Western blot 检测 ATGL 表达的变化。(3) 提取大鼠肺动脉平滑肌细胞 (PASMC)，转染 shRNA 质粒干扰 ATGL 的表达，将细胞置于低氧培养箱 (1% O_2，5%CO_2) 中给与缺氧环境，分为 Ctrl 组、Ctrl+shAtgl 组，低氧组 (Hyp 组)，Hyp+shAtgl 组。Western blot 检测 ATGL 和 PCNA 表达情况，细胞计数、CCK8 及 Edu 检测细胞增殖情况。(4) 提取大鼠 PASMC，转染过表达质粒 (flag-ATGL)，将细胞置于低氧培养箱 (1% O_2，5%CO_2) 中给与缺氧环境，分为 Ctrl 组、Ctrl+Atgl-flag 组，低氧组 (Hyp 组)，Hyp+Atgl-flag 组。Western blot 检测 ATGL 和 PCNA 表达情况，细胞计数、CCK8 及 Edu 检测细胞增殖情况。

结果: (1) 与健康人相比，PAH 患者的肺动脉平滑肌层 ATGL 表达升高 (P<0.0001)；(2) 与 CON-AAV-Con 组相比，SuHx+AAV-Con 组 RVSP 升高 (P < 0.01)，右心室功能下降 (P<0.05)，出现肺动脉重构 (P < 0.01)，管腔狭窄，肺动脉中膜层 ATGL 表达升高 (P<0.05)。与 SuHx+AAV-Con 组相比，SuHx+AAV-shAtgl 组 ATGL 的蛋白水平降低 (P<0.01)，RVSP 显著降低 (P < 0.05)，肺血管重构减轻 (P<0.01)；(3) 与 Ctrl 组比，Hyp 组的 ATGL 表达显著升高 (P<0.0001)，细胞计数、CCK8 和 Edu 检测显示细胞增殖水平增强 (P<0.0001)。与 Hyp 组相比，Hyp+shAtgl 组 ATGL 表达显著降低 (P<0.0001)，细胞计数、CCK8 和 Edu 检测显示细胞增殖水平下降 (P<0.0001)；(4) 与 Hyp 组相比，Atgl-flag 组 ATGL 表达显著升高 (P<0.0001)，细胞计数、CCK8 和 Edu 检测显示细胞增殖水平显著增强 (P<0.0001)；

结论：ATGL 在 PAH 患者及动物模型的肺动脉平滑肌中表达增高，敲低 ATGL 显著降低 PAH 动物模型肺动脉压力，改善其肺血管增殖重构，并且在细胞模型中证实其可以影响低氧肺动脉平滑肌增殖，有望成为 PAH 的治疗靶点。

Burden of Pulmonary Arterial Hypertension and Associated Heart Failure in Reproductive-Age and Postmenopausal Women: Global and Regional Trends from 1990 to 2021

Xin-Cheng Li

Shenzhen University

Burden of Pulmonary Arterial Hypertension and Associated Heart Failure in Reproductive-Age and Postmenopausal Women: Global and Regional Trends from 1990 to 2021

Xincheng Li[1]*, Jing Ma[2]*, Min Liu[3], Xiaofan Ji [4], Lu Sun [4], Han Tian [4], Hong Chen[2]†, Zhenguo Zhai [4]†, Deming Gou[1]†

(*These authors contributed equally to this work; †Corresponding authors)

Affiliations

1. College of Life Sciences and Oceanography, Shenzhen University, Shenzhen, Guangdong, China

2. Department of Respiratory and Critical Care Medicine, The Second Affiliated Hospital of Harbin Medical University, Harbin, China

3. Department of Pulmonary and Critical Care Medicine, Affiliated Hospital of Jianghan University, Wuhan, Hubei, China

4. National Center for Respiratory Medicine; State Key Laboratory of Respiratory Health and Multimorbidity; National Clinical Research Center for Respiratory Diseases; Institute of Respiratory Medicine, Chinese Academy of Medical Sciences; Department of Pulmonary and Critical Care Medicine, China-Japan Friendship Hospital, Beijing, China

Objectives

Pulmonary arterial hypertension (PAH) and PAH-associated heart failure (PAH-HF) represent severe cardiovascular conditions with a rising global burden. Women, especially those of reproductive age and postmenopausal status, may face increased susceptibility due to age-related hormonal changes and comorbidity profiles. However, comprehensive assessments of how these burdens differ by life stage and region remain limited. This study aimed to analyze the global, regional, and national trends in PAH and PAH-HF among reproductive-age (15–49 years) and postmenopausal (≥ 50 years) women from 1990 to 2021, and to project future trends through 2040.

Methods

Data on the incidence, prevalence, disability-adjusted life years (DALYs), and years lived with disability (YLDs) for PAH and PAH-HF were obtained from the Global Burden of Disease Study 2021 (GBD 2021). Age-standardized rates (ASRs) were calculated to facilitate cross-population and temporal comparisons. The estimated annual percentage change (AAPC) was used to assess trends from 1990 to 2021. To estimate future burden through 2040, we applied a Bayesian age-period-cohort (BAPC) model. Stratified analyses were conducted by age group (15–49 and ≥ 50 years), geographical region (21 GBD regions), and Socio-demographic Index (SDI) quintiles.

Results

Between 1990 and 2021, the global number of new PAH cases increased to 8,533 among reproductive-age women and 12,853 among postmenopausal women. Although the age-standardized incidence rates (ASIRs) slightly increased (AAPC: +0.16% in reproductive-age women; +0.09% in postmenopausal women), the age-standardized prevalence rate (ASPR) and DALY rate (ASDR) declined, especially in the younger group (ASPR AAPC: −0.05%; ASDR AAPC: −0.86%). Nonetheless, due to global population growth and aging, absolute DALYs rose to 11,520 and 20,991 person-years, respectively. Postmenopausal women consistently showed higher absolute burden across all metrics.

PAH-HF contributed significantly to disability, with global YLDs increasing from 9,788 in 1990 to 17,765 in 2021. Severe heart failure remained the primary contributor. Regionally, the burden was highest in middle- and low-middle SDI areas, particularly in South Asia, Sub-Saharan Africa, and East Asia. Western Europe and East Asia showed the highest age-standardized YLDs for PAH-HF, reflecting better detection and longer survival with chronic heart failure. Forecasts to 2040 indicated continued increases in absolute burden, particularly among postmenopausal women in developing regions.

Conclusions

Over the past three decades, the global burden of PAH and PAH-HF among women has increased, particularly in absolute terms. While age-standardized rates have declined modestly, the growing number of affected individuals, especially in older age groups and low- and middle-SDI regions, reflects a shifting demographic and healthcare challenge. Postmenopausal women are disproportionately affected, with higher incidence, disability, and mortality burden. These findings underscore the urgent need to strengthen early screening, age- and sex-specific management strategies, and resource allocation in underserved populations. Preventive efforts should prioritize timely diagnosis, guideline-based therapy, and multidisciplinary care models to reduce PAH-related heart failure and its societal burden globally.

The HIF- 1α/miR- 26a- 5p/PFKFB3/ULK1/2 axis regulates vascular remodeling in hypoxia-induced pulmonary hypertension by modulation of autophagy

Pan Li[1], Chao-Qun Ma[2], Qiang Xu[3], -Wen Song[1], Jing-Yu Zhang[1], Ming-Lei Sun[1], Bi-Li Zhang[1], Yuan Bai[1], Xian-Xian Zhao[1], Zhong-Kai Wang[1]

1. Changhai Hospital, Naval Medical University

2. General Hospital of Northern Theater Command

3. Navy 905 Hospital, Naval Medical University

Abstract

Objective:

Pulmonary arterial hypertension (PAH) is a progressive and life-threat-

ening disease characterized by pulmonary vascular remodeling, driven by excessive proliferation and autophagy of pulmonary arterial smooth muscle cells (PASMCs). Hypoxia-inducible factor-1α (HIF-1α) is a key regulator of cellular responses to hypoxia, but its interplay with microRNAs (miRNAs) in PAH pathogenesis remains unclear. MicroRNAs, particularly those responsive to hypoxia, have emerged as key modulators of cardiovascular diseases, including PAH. Among these, miR-26a-5p has been reported to play dual roles in tumor suppression and cardiovascular protection, but its specific function in PAH remains underexplored. Preliminary evidence suggests that miR-26a-5p is downregulated in PAH patients and hypoxia-exposed PASMCs, potentially due to HIF-1α-mediated transcriptional repression. This downregulation may disrupt critical pathways involving glycolysis (via PFKFB3) and autophagy initiation (via ULK1/2), thereby exacerbating PASMC dysfunction.This study aimed to investigate the role of miR-26a-5p, a hypoxia-responsive miRNA, in regulating PASMC autophagy and proliferation via the HIF-1α/miR-26a-5p/PFKFB3/ULK1/2 axis, and to explore its diagnostic and therapeutic potential in PAH .

Methods:

1. Clinical Samples: Plasma and lung tissues from PAH patients (n=14), non-PAH congenital heart disease (CHD) patients (n=15), and healthy controls (n=11) were analyzed for miR-26a-5p expression using qRT-PCR and fluorescence in situ hybridization (FISH) .

2. In Vitro Models: Human PASMCs were exposed to hypoxia (2% O_2) to induce autophagy. Autophagy markers (LC3B-II, p62) were assessed via Western blot, transmission electron microscopy (TEM), and tandem mRFP-GFP-LC3B fluorescence microscopy. HIF-1α's transcriptional regulation of miR-26a-5p was validated by chromatin immunoprecipitation (ChIP) and luciferase reporter assays .

3. Functional Studies: PASMCs were transfected with miR-26a-5p mimics/inhibitors or PFKFB3/ULK1/2-targeting siRNAs. Proliferation (CCK-8, EdU assays), migration (scratch wound, transwell assays), and autophagy flux were evaluated. Direct targeting of PFKFB3, ULK1, and ULK2 by miR-26a-5p was confirmed via dual-luciferase assays .

4. In Vivo Studies: Hypoxia-induced PAH rats received intratracheal adeno-associated virus (AAV) expressing miR-26a-5p. Hemodynamics (right ventricular systolic pressure, RVSP), pulmonary vascular remodeling (H&E staining), and autophagy markers were analyzed .

Results:

1. miR-26a-5p Downregulation in PAH: Circulating miR-26a-5p was significantly reduced in PAH patients ($p<0.05$) and negatively correlated with mean pulmonary arterial pressure (mPAP; $r = -0.322$). Hypoxia downregulated miR-26a-5p in PASMCs in a HIF-1α-dependent manner, as HIF-1α bound to the miR-26a promoter to suppress its transcription .

2. Autophagy and Proliferation Regulation:

o miR-26a-5p overexpression inhibited hypoxia-induced autophagy (reduced LC3B-II, increased p62) and suppressed PASMC proliferation/migration. Conversely, miR-26a-5p inhibition exacerbated these effects .

o PFKFB3, ULK1, and ULK2 were identified as direct targets of miR-26a-5p. PFKFB3 knockdown mimicked miR-26a-5p's anti-autophagic effects, while PFKFB3 overexpression rescued miR-26a-5p-mediated inhibition of ULK1 phosphorylation and autophagy .

3. In Vivo Therapeutic Effects: Intratracheal miR-26a-5p delivery attenuated pulmonary vascular remodeling (reduced arterial wall thickness by 40%, $p<0.05$) and right ventricular hypertrophy (RV/LV+S ratio decreased by 30%, $p<0.05$) in hypoxia-exposed rats. PFKFB3 and autophagy markers (LC3B-II, p62) were similarly modulated in lung tissues .

Conclusion:

This study elucidates a novel HIF-1α/miR-26a-5p/PFKFB3/ULK1/2 axis in PAH pathogenesis, where hypoxia-induced HIF-1α suppresses miR-26a-5p, leading to PFKFB3/ULK1/2 upregulation, enhanced PASMC autophagy, and vascular remodeling. miR-26a-5p emerges as a potential diagnostic biomarker and therapeutic target for PAH, with intratracheal delivery demonstrating efficacy in preclinical models. These findings highlight the interplay between hypoxia-responsive miRNAs and metabolic-autophagic pathways in PAH development

Key Words: Pulmonary hypertension, hypoxia, miR-26a-5p, PFKFB3, autophagy, vascular remodeling.

内皮特异性靶向 SIRT7 通过去乙酰化 KLF4 改善肺高压的机制研究

张瑾

西安交通大学第一附属医院

目的：肺高压是一类致死率高的肺血管疾病。作为肺动脉血管直接接触血液的细胞，肺动脉内皮细胞直接受到多种刺激因素的作用，包括血流剪应力和缺氧应激等。肺动脉内皮细胞功能异常往往引发血管重构进而影响肺高压的病理过程。本研究拟探索 NAD+ 依赖的去乙酰化酶 SIRT7 在肺高压疾病中对内皮细胞功能的重要调控作用。

方法：利用肺高压患者临床标本和肺高压动物模型检测 SIRT7 在肺内皮中的表达；利用基因编辑小鼠构建肺高压模型探索 SIRT7 缺失或获得对疾病的表型影响；在体外细胞实验中探索 SIRT7 对肺血管内皮功能的调控作用；使用生物信息学技术和分子生物学方法证实 SIRT7 对 KLF4 的翻译后修饰调控作用；利用基因治疗和现有药物对肺高压模型小鼠进行治疗，研究 SIRT7 作为肺高压治疗靶点的可行性。

结果：SIRT7 的表达水平在肺高压患者肺组织和肺动脉内皮细胞中显著减少，且在 Sugen5416 + hypoxia（SuHx）诱导的肺高压模型小鼠肺组织中同样显著降低。在 SuHx 小鼠模型中，内皮细胞特异性敲除 Sirt7 显著加剧小鼠的肺高压表型，增加小鼠右心室收缩压（right ventricularsystolic pressure，RVSP）和右心室肥厚情况。在细胞水平上，SIRT7 调控肺动脉内皮细胞的稳态，调节其增殖、迁移和血管形成能力。在分子水平上，我们发现 SIRT7 可以去乙酰化修饰内皮稳态维持的关键转录因子 Krüpple-like factor 4（KLF4）。SIRT7 对 KLF4 蛋白赖氨酸 K288 位点的去乙酰化修饰可显著抑制其泛素化降解，进而增加其蛋白稳定性。除此之外，在动物水平上，我们发现利用 adeno-associated virus type 1（AAV1）介导的内皮靶向性高表达 Sirt7，或者口服 nicotinamide riboside（NR）可显著改善小鼠肺高压表型。

结论：本研究证实了 SIRT7-KLF4 轴维持肺动脉内皮细胞稳态，内皮特异性靶向 SIRT7 显著抑制肺高压病理过程，可作为肺高压治疗的新靶点。

超声心动图联合定量 CT 剖析肺气肿表型与 COPD-PH 心肺功能关联的研究

谢思敏 华玮 方跃华 过依 周敏

上海交通大学医学院附属瑞金医院

目的：

肺高压（PH）是慢性阻塞性肺疾病（COPD）的常见的并发症，早期筛查及干预 COPD 相关 PH（COPD-PH）具有重要的临床意义。肺气肿是 COPD 的重要表型之一，其与心血管不良事件密切相关。本研究旨评估 COPD-PH 患者的心肺功能特征，探讨肺气肿表型与 COPD-PH 的关联，为早期筛查干预 COPD-PH 提供依据。

方法：

本研究纳入 2022 年 3 月至 2024 年 12 月间至上海交通大学医学院附属瑞金医院就诊的 COPD 患者。通过完成问卷调查、肺功能、定量 CT 和斑点追踪及三维超声心动图等检查，全面评估受试者的心肺功能。根据是否存在 PH 将患者分为 COPD-PH 组和 COPD 组。同时，根据低衰减区占肺野面积百分比（LAA%）是否 > 6%，将患者分为肺气肿表型组和非肺气肿表型组。分析各组间心肺功能特征的差异。用 Pearson 相关性分析探讨 LAA% 与肺动脉压力及心肺功能的关联，Logistic 回归分析 COPD-PH 风险因素，并构建风险预测模型。受试者操作特征（ROC）曲线用以评估该模型的预测效能。

结果：

共纳入 122 例 COPD 患者，COPD-PH 的患病率为 30.3%，肺气肿表型占比 59.8%。与单纯 COPD 患者相比，COPD-PH 患者年龄更大，呼吸困难评分更高，肺功能更差，肺气肿程度更严重，右心室 - 肺动脉耦联指标（TAPSE/sPAP、S′/sPAP、RVFAC/sPAP、RV FWLS /sPAP、RVEF/sPAP）均更差（P 均 <0.05），RV-FAC 和 RV-EF 显著降低（P <0.05），81.1% 的 COPD-PH 患者存在至少 1 项的左心室舒张功能异常；与非肺气肿表型患者相比，肺气肿表型 COPD 患者的肺功能下降，PH 比例升高（32.8% vs. 18.6%），具有更小的心腔结构，LVSV 及 RVSV 均显著减少（P <0.05），右心室 - 肺动脉耦联指标（TAPSE/sPAP、S′/sPAP、RVFAC/sPAP、RV FWLS /sPAP）均较非肺气肿组更差（P 均 <0.05）；LAA% 与三尖瓣反流速度（TRV）（r = 0.53，P <0.001）、肺动脉收缩压（sPAP）（r = 0.55，P <0.001）呈显著正相关；单因素 Logistic 回归显示年龄、HR、mMRC 评分（> 2）、FEV1%pred、FEV1/FVC、IC、DLCO%pred 及 LAA% 是 COPD-PH 的危险因素（P 均 <0.05），多因素 Logistic 回归进一步证实年龄、IC 和 LAA% 是 COPD-PH 的独立危险因素（P 均 <0.05）。LAA% 每增加 1 个标准差，COPD-PH 的风险增加 148.3%（OR = 2.483，95%CI 1.329-4.637）。ROC 曲线分析显示，基于年龄、IC 和 LAA% 构建的风险预测模型具有最佳效能（AUC = 0.850，95%CI 0.769-0.931），敏感性为 88.46%，特异性为 71.83%。

结论：

与单纯 COPD 患者相比，COPD-PH 患者的肺气肿严重程度更高，右心室收缩功能和左心室舒张功能更差，肺气肿严重程度与 COPD-PH 风险显著正相关。研究表明肺气肿表型的 COPD 患者更易发生 PH，应高度重视肺气肿表型 COPD 患者 PH 的早期筛查。基于定量 CT 的 LAA% 的测定有望成为 COPD-PH 风险的常规筛查和评估方法。

Integrated bioinformatics analysis reveals marker genes and immune infiltration for pulmonary arterial hypertension

Sheng-Xin Tang

重庆医科大学附属第三医院

Pulmonary arterial hypertension (PAH) is a chronic cardiopulmonary syndrome with high pulmonary

vascular load and eventually causing RV heart failure even death. However, the mechanism of

pulmonary hypertension remains unclear. The purpose of this research is to detect the underlying

key genes and potential mechanism of PAH using several bioinformatic methods. The microarrays

GSE22356, GSE131793 and GSE168905 were acquired from the GEO. Subsequently, a host of

bioinformatics techniques such as DAVID, STRING, R language and Cytoscape were utilized to

investigate DEGs between PAH and healthy controls and conduct GO annotation, KEGG enrichment

analysis and PPI network construction etc. Additionally, we predicted the transcription factors

regulating DEGs through iRegulon plugin of Cytoscape and CIBERSORT was used to conduct immune

infiltration analysis. One thousand two hundred and seventy-seven DEGs (403 up-regulated and 874

down-regulated) were identified from peripheral blood samples of 32 PAH patients and 29 controls,

among which SLC4A1, AHSP, ALAS2, CA1, HBD, SNCA, HBM, SELENBP1, SERPINE1 and ITGA2B were

detected as hub genes. The functional enrichment changes of DEGs were mainly enriched in protein

binding, extracellular exosome, extracellular space, extracellular region and integral component

of plasma membrane. The hub genes are chiefly enriched at extracellular exosome, hemoglobin

complex, blood microparticle, oxygen transporter activity. Among TF-DEGs network, 42 target DEGs

and 6 TFs were predicted with an NES> 4 (TEAD4, TGIF2LY, GATA5, GATA1, GATA2, FOS). Immune

infiltration analysis showed that monocytes occupied the largest proportion of immune cells. The

trend analysis results of infiltration immune cells illustrated that PAH patients had higher infiltration

of NK cell activation, monocyte, T cell CD4 memory activation, and mast cell than healthy controls

and lower infiltration of T cell CD4 naive. We detected SLC4A1, AHSP, ALAS2, CA1, HBD, SNCA, HBM,

SELENBP1, SERPINE1 and ITGA2B as the most significant markers of PAH. The PAH patients had

higher infiltration of NK cell activation, monocyte, T cell CD4 memory activation, and mast cell than

healthy controls and lower infiltration of T cell CD4 naive. These identified genes and these immune

cells probably have precise regulatory relationships in the development of PAH.

Results

Identification of DEGs in PAH. There are 580 DEGs screened from GSE22356 between PAH group with

healthy group which consists of 162 up-regulated and 418 down-regulated genes (Fig. 2A,D). Simultaneously,

heatmaps and volcano plots vividly showed that 156 up-regulated and 13 down-regulated DEGs were iden

tified from GSE131793, 102 up-regulated and 456 down-regulated DEGs were identified from GSE168905

(Fig. 2B,C,E,F) (p value<0.05 and |log2FC| ≥ 0.5). Then, we merged up-regulated and down-regulated DEGs

in the three datasets, which revealed a total of 403 up-regulated DEGs and 874 down-regulated DEGs in the

microarrays.

Discussion

PAH is a rare chronic refractory syndrome accompanied with pathological changes of distal pulmonary arteries

such as vasculature remodeling, lumen stenosis, laminar intimal proliferation and fibrosis, plexiform lesions

with excessive poorly formed capillaries14. The current clinical definition of PAH is that the average pulmonary

arterial pressure (m PAP) ≥ 25 mm Hg measured during right heart catheterization (1 mmHg = 0.133 kPa)15.

PAH is divided into many subgroups due to different etiologies worldwide. According to the latest Chinese PAH

Impact of Pretest HFpEF Probability on Clinical Outcomes in Patients with Chronic Thromboembolic Pulmonary Hypertension

Yijia Wang, Xin Li, Zhihua Huang, Anqi Duan, Qi Wang, Luyang Gao, Sicong Li, Qing Zhao, Zhihui Zhao, Qin Luo, Zhihong Liu

Fuwai Hospital

Impact of Pretest HFpEF Probability on Clinical Outcomes in Patients with Chronic Thromboembolic Pulmonary Hypertension

Yijia Wang[1†], Xin Li[1†], Zhihua Huang[1], Anqi Duan[1], Qi Wang[1], Luyao Gao[1], Sicong Li[1], Qing Zhao[1], Zhihui Zhao[1]*, Qin Luo[1]*, Zhihong Liu[1]*

[1] Department of Cardiology, Fuwai Hospital, Chinese Academy of Medical Sciences & Peking Union Medical College, Beijing, China.

† Yijia Wang and Xin Li have made equal contributions to this work.

*** Correspondences:**

Zhihong Liu, Department of Cardiology, Fuwai Hospital,100037, Beijing, China.

E-mail: zhihongliufuwai@163.com

Qin Luo, Department of Cardiology, Fuwai Hospital,100037, Beijing, China.

E-mail: luoqin2009@163.com

Zhihui Zhao, Department of Cardiology, Fuwai Hospital,100037, Beijing, China.

E-mail: zhaozhihui2008@126.com

Abstract

Background: Pulmonary hypertension (PH), characterized by a mean pulmonary artery pressure (mPAP) > 20 mmHg at rest, encompasses a range of pathophysiological conditions stemming from diverse etiological factors that induce pulmonary vascular remodeling and a gradual elevation in pulmonary vascular resistance (PVR), ultimately culminating in right heart failure or mortality. Contemporary classification systems stratify PH into five etiopathogenetically distinct groups with divergent therapeutic implications. **Chronic thromboembolic pulmonary hypertension (CTEPH), classified as Group 4 PH, arises from organized thrombi obstructing proximal pulmonary arteries and remodeling of distal vessels, severely impacting pulmonary circulation and patient health. CTEPH and left heart disease, particularly heart failure with preserved ejection fraction (HFpEF), show overlapping clinical features despite distinct pathophysiology.**

Objectives: The HFpEF-ABA algorithm (age, body mass index, atrial fibrillation) was used to characterize the pretest probability of HFpEF in patients with CTEPH. The main aims of our study are as follows: (1) to quantify the pretest probability of HFpEF in patients with CTEPH using the HFpEF-ABA algorithm, and (2) evaluate correlation between HFpEF-ABA score and prognostic outcomes.

Methods: In 466 patients with CTEPH stratified by HFpEF-ABA score (low < 25%, intermediate 25-74%, high ≥ 75%), we assessed associations between HFpEF-ABA scoreand clinical deterioration through Spearman's correlation analysis, Kaplan-Meier, Cox regression analysis, and restricted cubic splines. The endpoint was defined as clinical worsening, including all-cause mortality, lung transplantation initiation, unplanned hospitalization for PH progression.

Results: The final sample comprised of 466 patients, with median age 57 years (IQR 49-65years), and 49.4% were female. Among them, 52.4% (n = 244) and 9.0% (n = 42) of patients with CTEPH had intermediate and high HFpEF probabilities, respectively, and elevated HFpEF-ABA score was positively associated with left heart disease comorbidities and risk factors (obesity, hypertension, CHD, DM, OSA) (all P < 0.05). After adjusting for confounders, each standard deviation increase in the probability of HFpEF was associated with an approximately 65% increase in clinical deterioration (P < 0.001). Consistent results were found when HFpEF probability was used as a categorical variable (P < 0.05). No significant interactions were identified in subgroup analyses. Linking the HFpEF-ABA score in combination with the COMPERA 2.0 risk score significantly improved their prediction, reclassification and identification.

Conclusions: HFpEF probability stratification identifies high-risk CTEPH patients with subclinical left heart dysfunction, and improves prognostic precision when combined with existing risk models. These findings advocate for routine HFpEF probability evaluation in CTEPH management

and warrant investigation of phenotype-specific therapies.

Keywords Chronic thromboembolic pulmonary hypertension, Heart failure with preserved ejection fraction, HFpEF-ABA score; Clinical worsening

Mechanism study on the involvement of MIF in acute lung injury through regulation of the NLRP3 inflammasome-mediated pyroptosis pathway

An-Xia Deng

State Key Laboratory of Pathogenesis, Prevention and Treatment of High Incidence Diseases in Central Asian, Department of Cardiology. The First Affiliated Hospital and Clinical Medical Research Institute of Xinjiang Medical University

Objective: The present project was designed around two interlocking aims that together chart a clear path from mechanism to therapy in acute lung injury (ALI). The first aim was to dissect, at molecular and cellular resolution, how macrophage migration inhibitory factor (MIF) functions as a master upstream driver of deleterious inflammation in ALI. Using intact mice and cultured primary epithelial cells, we asked whether MIF initiates pyroptosis–the lytic, caspase-1-dependent form of programmed cell death–and whether it does so by licensing the NLRP3 inflammasome. If validated, this circuitry would place MIF at the apex of a positive-feedback loop in which dying epithelial cells release alarmins that further recruit and activate innate immune cells, amplifying tissue damage. The second aim was to translate these mechanistic insights into therapeutic proof of concept. We therefore tested whether genetic deletion of MIF or pharmacological blockade with the small-molecule inhibitor ISO-1 could interrupt the MIF–NLRP3–pyroptosis axis and, consequently, reduce lung edema, inflammation, and loss of pulmonary function in a clinically relevant murine model of LPS-induced ALI.

Methods: All animal work was approved by the institutional animal care committee and followed ARRIVE guidelines. Male C57BL/6J wild-type (WT) and global MIF-knockout (MIFKO) mice, 8–10 weeks old, received a single intratracheal instillation of Escherichia coli O55:B5 LPS (5 mg kg^{-1}) to generate sterile ALI. Sham controls received an equal volume of sterile saline. For longitudinal monitoring we used high-resolution lung ultrasound (LUS) to quantify B-line artifacts as a surrogate of extravascular lung water, and whole-body plethysmography (WBP) to record tidal volume, respiratory frequency, and enhanced pause (Penh) as indices of ventilatory efficiency. At 24 h post-challenge, mice were euthanized under deep anesthesia. Bronchoalveolar lavage fluid (BALF) and plasma were collected for multiplex cytokine arrays and differential cell counts. Lungs were harvested for wet-to-dry weight ratio (edema), histopathology (H&E, Masson), and immunostaining (CD45 for leukocyte infiltration, dihydroethidium for reactive oxygen species, and NLRP3/ASC immunofluorescence). Western blots quantified pyroptosis-relevant proteins (NLRP3, cleaved caspase-1, GSDMD-N, IL-1β). Microvascular leakage (MVL) was quantified with Evans blue extravasation, while ultrastructural features of pyroptosis were captured by transmission electron microscopy. In parallel, MLE-12 murine alveolar epithelial cells were transfected with MIF-targeting siRNA or scrambled control, then stimulated with LPS (1 μg ml^{-1}) plus Nigericin (10 μM) in the presence or absence of recombinant MIF (rMIF, 100 ng ml^{-1}) or the NLRP3 inhibitor MCC950 (10 μM). Propidium iodide uptake and lactate dehydrogenase release served as cell-permeability readouts, with pyroptosis proteins assessed by Western blot. Finally, a therapeutic arm tested ISO-1 (30 mg kg^{-1}, intraperitoneal, 1 h post-LPS) in WT mice, reproducing all in-vivo endpoints above.

Results: LPS instillation rapidly elevated MIF protein in lung homogenates, BALF, and plasma. Compared with WT littermates, MIFKO mice exhibited markedly fewer ultrasound B-lines, improved WBP indices, lower lung wet-to-dry ratios, and reduced histological injury scores. These advantages were accompanied by significant reductions in neutrophil influx, systemic and local cytokine storms, $CD45^{+}$ cell infiltration, and ROS production. NLRP3 inflammasome activation and downstream pyroptotic markers were attenuated, as was microvascular leakage. In MLE-12 cells, LPS + Nigericin increased membrane permeability and pyroptosis protein expression; MIF knockdown blunted these changes, whereas rMIF exacerbated them. MCC950 fully reversed the damage, confirming NLRP3 as the downstream executor. ISO-1 treatment phenocopied the protective effects observed in MIFKO mice: less edema, better respiratory mechanics, dampened inflammation, and suppressed pyroptosis.

Conclusion: This study highlights MIF's pivotal role in ALI, linking its upregulation to NLRP3 inflammasome activation and pyroptosis-related lung injury. MIF targeting, via genetic or pharmacological inhibition, curbs pyroptosis and lung damage. The research also unveils a synergistic interplay between MIF and NLRP3 inflammasome inhibition in ALI, supported by the therapeutic efficacy of the MIF inhibitor ISO-1. Furthermore, it introduces an innovative lung ultrasound technique for non-invasive edema monitoring in ALI mice, offering a new tool for precise lung injury assessment and underpinning novel MIF-focused ALI therapies.

Ac2-26 Reduced Lung Injury After Cardiopulmonary Bypass via the AKT1/GSK3b/eNOS Pathway

Lulu Zhang

the secend affiliated hospital of Harbin University

Introduction:Cardiopulmonary bypass (CPB) is an essential method for cardiac surgery. However, the application of CPB also leads to severe lung injury after CPB.1 Postoperative lung injury not only prolongs intensive care unit and hospital stays but also leads to death.2 It has been reported that the incidence of postoperative acute respiratory distress syndrome after CPB is approximately 0.4%-0.6%, but the mortality rate is high (15%-41.5%).3 Therefore, effective therapy for lung injury induced by CPB is important for patients undergoing cardiac surgery. The mechanism of lung injury after CPB is mainly attributed to endotoxemia and pulmonary inflammation secondary to systemic inflammation.4-6 Although many experimental and clinical studies have provided various treatments for lung injury induced by CPB, few effective therapies have been demonstrated.Annexin A1 is a glucocorticoid-regulated calcium- and phospholipid-binding protein that can inhibit phospholipase A2 activity, suppress the migration and activation of monocytes and modulate inflammation.7-9 Ac2-26 (an active terminal peptide of Annexin A1), which is a major active biological peptide of Annexin A1, has been shown to protect against lung injury10,11 and brain injury induced by reperfusion via the promotion of endothelial nitric oxide synthase (eNOS).12,13 Considering the pivotal role of inflammation in lung injury after CPB, we hypothesized that Ac2-26 could reduce lung injury after CPB through its anti-inflammatory and antiapoptotic effects. In this study, we generated a rat CPB model and investigated the effect of Ac2-26 on CPB induced lung injury. Previous studies have suggested that serine/threonine kinase 1 (AKT1) and glycogen synthase kinase (GSK)-3b play important roles in organ protection by regulating eNOS.14-16 In this study, we generated short hairpin RNA (shRNA) to interfere with the expression of AKT1 and administered a GSK3b inhibitor to investigate the possible mechanism by which Ac2-26 affects lung injury after CPB.

Methods: Forty rats were randomly divided into the sham, CPB, Ac, Ac/ serine/threonine kinase 1 (AKT1), and Ac/ glycogen synthase kinase (GSK)-3b groups. The rats in the sham group only received anesthesia, intubation, and cannulation. The rats in the other 4 groups received the standard CPB procedure. The rats in the CPB, Ac, Ac/AKT1, and Ac/GSK3b groups were immediately injected with saline, Ac2-26 (1 mg/kg), Ac2-26 combined with short hairpin RNA (AKT1), or Ac2-26 combined with a GSK3b inhibitor after CPB. At 12 h after the end of CPB, the PaO2/ fraction of inspired oxygen ratio, wet/dry weight ratio and protein content in the bronchoalveolar lavage fluid (BALF) were recorded. The numbers of macrophages and neutrophils in the BALF and blood were determined. Cytokine levels in

the blood and BALF were investigated. Lung tissue histology and apoptosis were estimated. The expression of nuclear factor kappa- B, AKT1, GSK3b, endothelial nitric oxide synthase and apoptosis-related proteins was analyzed. The survival of all the rats was recorded.

Results: Compared with the rats in the sham group, all the parameters examined worsened in the rats that received CPB. Compared with those in the CPB group, Ac2-26 significantly improved pulmonary capillary permeability, reduced cytokine levels, and decreased histological scores and apoptosis. The protective effect of Ac2-26 on lung injury was significantly reversed by AKT1 short hairpin RNA or a GSK3b inhibitor.

Conclusions: Ac2-26 significantly reduced lung injury and inflammation after CPB. The protective effect of Ac2-26 mainly depended on the AKT1/GSK3b/endothelial nitric oxide synthase pathway.

急性肺栓塞患者血清钙水平与急性肾损伤风险的相关性：一项回顾性队列研究

王云梦 王家琦 鲁静朝

河北医科大学第二医院

目的：急性肺栓塞（Acute Pulmonary Embolism, APE）是一种严重的静脉血栓栓塞性疾病，其 30 天全因死亡率高达 9.2%-17.4%。约 20%-30% 的 APE 患者会继发急性肾损伤（Acute Kidney Injury, AKI），且合并 AKI 者的住院死亡率显著增加。血清钙水平异常与多种疾病的发生发展及预后存在密切联系，但目前尚缺乏针对 APE 患者血清钙水平与 AKI 风险关联性的系统性研究。本研究旨在通过回顾性队列研究的方法，分析急性肺栓塞患者血清钙水平与急性肾损伤风险之间的相关性，为早期识别高危患者、优化 APE 患者的治疗策略以及改善其预后提供新的视角和循证医学依据。

方法：研究基于 MIMIC-IV 数据库，纳入了 1544 名 APE 患者，根据血清钙水平四分位数分组。通过 COX 回归分析，探讨血清钙水平与院内 AKI 风险的关联性；应用逻辑回归分析，评估血清钙水平与院内肾脏替代治疗（Renal Replacement Therapy, RRT）使用率的关联性。同时，绘制限制性立方样条图，分析血清钙与 AKI 风险的非线性关系，并进行亚组分析以评估血清钙在不同人群中的稳定性。

结果：血清钙水平与 AKI 风险呈 "U 型" 关联。COX 回归显示血清钙水平与 AKI 风险显著相关（HR 0.89, 95% CI 0.82-0.96，P=0.003）。血清钙在 8.1-9.8 mg/dL 范围内 AKI 风险较低，8.83 mg/dL 时风险最低。血清钙水平与 RRT 使用概率也显著相关（HR 0.60, 95% CI 0.46-0.78，P<0.001）。亚组分析显示在多数人群中关联稳定。

结论：血清钙水平与 APE 患者院内 AKI 风险及 RRT 使用概率显著关联，维持适

当血清钙水平可能降低 APE 患者 AKI 风险。本研究为 APE 患者的肾脏功能管理提供了新的视角，提示在临床实践中，关注 APE 患者的血清钙水平，尤其是在 8.1-9.8 mg/dL 范围内维持血清钙水平，可能有助于降低患者发生 AKI 的风险，从而改善患者的预后。

Application of Ultrasound in Assessment of Acute Lung Injury in Mice

An-Xia Deng

the First Affiliated Hospital of Xinjiang Medical University

Acute lung injury (ALI) is an acute hypoxic respiratory disorder of the lungs ALI can progress to acute respiratory distress syndrome (ARDS), which is characterized by increased alveolar capillary permeability with acute bilateral pulmonary edema and severe hypoxia. This study comprehensively evaluated the effectiveness of non-invasive ultrasound technology for monitoring pulmonary edema in a well-characterised murine model of ALI. The B-line, an lung ultrasound (LUS) sign, is a useful and simple imaging indices for assessing extravascular lung water. The aim of the study is to evaluate noninvasive ultrasound technique in precise detection of pulmonary edema in mice with ALI. Using LUS to detect and characterize changes of "B-lines" during the development of LPS-induced ALI, meanwhile, lung function, weight, histological changes and circulating levels of inflammatory mediators are also measured to validate the usefulness of LUS in assessment of the severity of pulmonary edema. Compared to micro-CT and X-ray, LUS has advantages in terms of cost and convenience. Eight-week-old male C57BL/6J mice received a single intratracheal instillation of lipopolysaccharide (LPS, 5 mg/kg) dissolved in 50 μL sterile saline, while sham controls received vehicle alone. Longitudinal imaging was performed using the high-resolution Vevo 3100 platform equipped with a 40 MHz linear transducer. Animals were lightly anaesthetised with isoflurane and scanned in the supine position; the thorax was divided into four quadrants, and still images as well as cine-loops were acquired from each quadrant to generate a cumulative lung ultrasound (LUS) score based on the number and confluence of B-lines. Temporal dynamics revealed a stereotypical pattern: non-converging B-lines appeared within the first 6 h, gradually increased in number and began to coalesce, peaking on day 3. Thereafter, B-line burden diminished progressively, becoming almost undetectable by day 11. This imaging trajectory was paralleled by whole-body plethysmography (WBP) data recorded via unrestrained chambers. Peak deterioration of tidal volume, respiratory rate, and enhanced pause (Penh) occurred between 6 and 24 h, with most ventilatory indices returning to baseline by day 3. Morphological outcomes corroborated the imaging findings. Lung wet weight and wet-to-tibial length ratio rose markedly by day 3, reflecting maximal vascular congestion and alveolar flooding, and normalised by day 11. Histopathological analysis of formalin-fixed, paraffin-embedded sections stained with haematoxylin–eosin confirmed severe inflammatory injury on days 3–5, characterised by pronounced neutrophilic infiltration, thickening of alveolar septa, perivascular cuffing, alveolar collapse, and hyaline membrane formation. These lesions regressed thereafter, paralleling the decline in B-line burden. Statistical correlation analyses strengthened the validity of LUS as a quantitative biomarker. The cumulative LUS score exhibited a strong positive relationship with the semiquantitative lung injury index ($r = 0.783$, $P < 0.001$) and with the lung weight-to-tibial length ratio ($r = 0.695$, $P < 0.001$), underscoring its sensitivity to the degree of pulmonary oedema. At 24 h post-LPS, LUS scores were also significantly correlated with key WBP parameters: positive correlations with Penh ($r = 0.672$, $P < 0.001$) and respiratory rate ($r = 0.618$, $P < 0.001$), and negative correlations with tidal volume ($r = -0.589$, $P < 0.001$) and minute ventilation ($r = -0.555$, $P < 0.01$). Taken together, the study demonstrates that LUS is an effective, reliable and non-invasive tool for real-time monitoring of pulmonary oedema in the mouse LPS-ALI model. The tight temporal alignment between ultrasonographic findings and functional, morphological and histopathological readouts validates LUS as a powerful surrogate marker for injury severity. These results encourage broader adoption of LUS in pre-clinical ALI research, offering the dual advantages of reduced animal use through longitudinal imaging and enhanced translational relevance for future therapeutic studies.

Keywords: Acute lung injury; pulmonary edema; lung ultrasound; B-lines; whole-body plethysmography

基于超声心动图的深度学习模型预测肺血管阻力的研究

黄陶然 费洪文

广东省人民医院

目的：以右心导管数据作为金标准，构建一个基于多切面超声心动图的深度学习模型，对肺血管阻力（Pulmonary vascular resistance, PVR）进行预测，识别肺血管阻力的异常。

方法：建模组纳入了自 2020 年 10 月至 2023 年 9 月就诊于广东省人民医院、中国医学科学院阜外医院（深圳医院）、广州医科大学附属第一医院的 410 例可疑肺高压患者，收集其右心导管数据及超声心动图动态图像，由超声医师进行超声图像感兴趣区域（Region of interest, ROI）的描记，以右心导管结果（PVR_{CATH}）作为金标准，进行深度学习模型的构建。另外，收集 PADN-CFDA 多中心临床试验的 64 例肺高压患者数据作为外部验证组。比较深度模型结果（PVR_{DL}）与传统多普勒法参数（TRV^2/VTI_{RVOT}）的预测效能，使用相关分析、Bland-Altman 一致性检验、Kappa 一致性检验、受试者工作特征曲线 (Receiver operating characteristic curve, ROC) 对模型进行评价。

结果：基于提取到的右室面积变化率、左室离心指数等特征，建立了一个深度学习模型，对 PVR 进行预测。在建模组中，PVR_{DL} 与 PVR_{CATH} 呈显著正相关（$r=0.931$, $P < 0.001$），相关系数高于 TRV^2/VTI_{RVOT}（$r=0.603$, $P < 0.001$）；PVR_{DL} 诊断肺血管阻力异常（$PVR_{CATH} > 2WU$）的曲线下面积（AUC）高于 TRV^2/VTI_{RVOT}（0.924 vs 0.894，P=0.150），PVR_{DL} 诊断肺血管阻力严重升高的（$PVR_{CATH} > 5WU$）的 AUC 显著高于 TRV^2/VTI_{RVOT}（0.953 vs 0.869，$P < 0.001$）；对于肺血管阻力分级，PVR_{DL} 与 PVR_{CATH} 一致性较强，Kappa 系数为 0.742（0.684-0.800，$P < 0.001$），TRV^2/VTI_{RVOT} 与 PVR_{CATH} 一致性中等，Kappa 系数为 0.572（0.498-0.647，$P < 0.001$）；在 Bland-Altman 分析中，深度学习模型预测阻力的 95% 一致性界限（95% LoA）为 -5.34WU 至 5.26WU，较传统多普勒法（95% LoA, -10.19WU 至 10.19WU）一致性明显提高。在外部验证中，深度学习模型也表现出良好的诊断效能，与 PVR_{CATH} 相关性较强（$r=0.76$, $P < 0.001$），其诊断 $PVR_{CATH} > 2WU$ 和 $PVR_{CATH} > 5WU$ 的 AUC 分别为 0.984（95%CI，0.952-1.000）、0.856（95%CI，0.761-0.951），Bland-Altman 分析的 95% LoA 为 -6.60WU 至 5.38WU。

结论：深度学习模型对于肺血管阻力异常的识别优于传统超声参数，对于阻力的分级与右心导管呈现出较高的一致性。作为一个无创的肺血管阻力评估方法，有望应用于肺高压的筛查和随访，为临床治疗提供有力支持。

关于急性致死性肺血栓栓塞症急救策略的一点商榷意见

王文利 [1,2] 李楚麒 [2]

1. 麻阳苗族自治县中医院

2. 怀化红雅医院

目的：众所周知：既往与肺栓塞相关的指南、共识均要求要获得确诊依据、至少有超声心动图证实右室负荷增加才能启动肺血栓栓塞症的再灌注（溶栓）治疗，而临床上，间常会遇到突发的极重症肺栓塞病例，发作后病情危重、进展迅猛，让医生和家属很难做下决断将病人推出病房去做 CTPA 检查，等待床旁超声检查所需的时长常伴随着病情的急剧加重，一定数量的病例甚至在此等待过程中心跳停搏，严重影响病人的最后转归。或许也是关注到了临床的这一困境，在今年 6 月 30 日发布的《中国肺血栓栓塞症诊治、预防和管理指南（2025 版）》里，加入了"对于临床高度怀疑急性高危 PTE 的患者，无法进行确诊检查，无其他原因可以解释，且没有溶栓禁忌，在充分权衡利弊后可考虑系统性溶栓治疗。"这样的推荐意见说明，这就打开了容许在未获得确诊依据也未获得超声依据情形下溶栓救治急性致死性 PTE 的规范窗口，然而，这又带出了新的问题：我们如何去尽量规范的判断哪些才是"临床高度怀疑急性高危 PTE 的患者"呢？单纯 Wells 或 Geneva 评分高度可能加上血流动力学不稳定显然是不够的；表 2 所列 PTE 的各项临床表现亦因没有特异性显然难以提供足够的支持力度；那就真的没办法规范了吗？

其实，结合肺栓塞发病机制病理生理我们并不难推断得出：需要医生在没有机会获取确诊依据做出溶栓决断的急性致死性肺栓塞，肯定还是会具备一些临床上能观察到也具备一定特征性的临床表现的：一、循环衰竭且补液和血管活性药物不能持续有效纠正，包括心脏骤停、梗阻性休克、持续性低血压状态，其中持续性低血压状态指体循环收缩压 <90 mmHg，或较基础值下降幅度≥ 40 mmHg，持续 5 min 以上。需除外新发生的心律失常、低血容量或脓毒症所致的血压下降。二、除外肺损伤、气道阻塞、血气胸的急发持续加重的气促、呼吸困难、氧饱和度降低，面罩给氧不能持续纠正，缺氧程度与血压下降程度大致平行（氧饱和度低于 85% 或较前下降 10% 以上有意义）。三、新发的右室负荷增加等符合肺栓塞表现的心电图改变且有动态变化。四、无神经、精神异常依据出现新发晕厥、淡漠、烦躁不安、惊恐或濒死感。五、新出现的颈静脉充盈、搏动或中心静脉压显著增高。六、肺动脉瓣区第二心音亢进（P2>A2）或分裂。七、无体温迅速上升和胸部皮下出血等指向脂肪栓塞征象。仔细分析病理生理，以上前六点征象，在急性致死性肺栓塞病例中，应该是都会出现的，第七点，主要是与跟 PTE 表现类似的脂肪栓塞做鉴别，这些应该是在病房都可以识别出来的。

方法：我们的方案：在疑诊急性致死性 PTE 病例，倘使具备上面前三项表现加上后四项中任意两项表现，则跟家属沟通启动溶栓再灌注治疗。

溶栓方案：阿替普酶 10mg，1-2 分钟推注，接 40mg 阿替普酶加生理盐水 200ml，按 50 滴 / 分静滴，期间仍尽快安排床旁超声，病人情况略趋于平稳后完善 CTPA 检查后转 ICU 病房。

结果：我们遇到的六例急性致死性 PTE 病例，采用上述方案，均获得成功救治，三月内死亡仅有一例，是急救成功（停跳的心搏恢复且神志恢复清醒）后 15 天，死于严重肺部感染，所有病例没有发生出血并发症。

结论：长期以来，江湖传言 PTE 临床表现不具备特异性，让很多医生对肺栓塞的认识陷入了不可知论的大坑，对致死性肺栓塞望而生畏，不去深究。而只要认真的思考了 PTE 的病理生理改变，是可以从它看似凌乱的临床表现中梳理出清晰的规律的，重视心变，电图反映出来的右室负荷增加表现及动态变化，结合 PTE 的特征性动态性的心肺功能改变，可以更迅捷的对致死性 PTE 作出诊断和再灌注治疗的决断，更有效的挽救此类重症患者。

Global Burden of Pulmonary Arterial Hypertension in Adults Aged 55 and Older: A Systematic Analysis of the Global Burden of Disease Study 2021

Ru-Yi Jia, Bing-Xiang Wu

Department of Cardiology, the Second Affiliated Hospital of Harbin Medical University, Harbin, Heilongjiang Province, China.

BACKGROUND: Pulmonary arterial hypertension (PAH) is a rare but progressive and life-threatening cardiopulmonary disorder characterized

by elevated pulmonary vascular resistance, right ventricular dysfunction, and eventual heart failure. While PAH has historically been associated with younger populations, increasing recognition of late-onset and secondary forms—such as those linked to connective tissue diseases, congenital heart disease, or chronic lung conditions—has highlighted its growing prevalence among aging individuals. Despite therapeutic advancements, including targeted vasodilators and combination therapies, prognosis remains poor, with high morbidity and mortality. Population-based epidemiological data on PAH's global burden, particularly in adults aged 55+, remain scarce due to diagnostic challenges, underreporting, and regional disparities in healthcare access. This study seeks to address this gap by quantifying PAH's prevalence, disability-adjusted life years (DALYs), and mortality across global, regional, and national levels in older adults, providing critical insights for resource allocation and aging-related healthcare strategies.

METHODS: Using data from the Global Burden of Disease (GBD) 2021 Study, we assessed the burden of PAH in adults aged ≥ 55 years across 204 countries and territories from 1990 to 2021. Age-standardized prevalence, DALYs, and mortality rates were reported per 100,000 population, stratified by age, sex, region, and sociodemographic index (SDI). Temporal trends were evaluated using estimated annual percentage change (EAPC) based on log-linear regression models.

RESULTS: Globally in 2021, the age-standardized prevalence, DALY, and mortality rates of PAH in individuals aged ≥ 55 years were 6.01 (95% CI: 4.45 to 7.96), 19.29 (95% CI: 15.14 to 22.62), and 1.11 (95% CI: 0.87 to 1.31) per 100,000 population, respectively. From 1990 to 2021, prevalence increased slightly (EAPC: 0.03, 95% CI: 0.01 to 0.05), DALYs declined (EAPC: -0.26, 95% CI: -0.42 to -0.09), and mortality rose modestly (EAPC: 0.23, 95% CI: 0.04 to 0.42). Prevalence peaked at ages 75-79, while DALY and mortality rates were highest in those aged ≥ 95 years. Females consistently exhibited higher burden across all metrics. High-SDI countries had the highest prevalence, whereas middle-SDI countries bore the greatest DALY and mortality burdens. Western Europe showed the highest prevalence regionally, East Asia the highest DALY and mortality, and country-level extremes were noted in Mongolia and Moldova. Temporal trends varied widely across countries.

CONCLUSIONS: PAH represents a growing health burden among older adults, with substantial heterogeneity across demographic and geographic subgroups. These findings underscore the need for targeted strategies that address the unique challenges of PAH in aging populations, particularly in light of rising mortality despite therapeutic advances.

CONDENSED ABSTRACT: Pulmonary arterial hypertension (PAH) is a progressive cardiopulmonary condition increasingly affecting older adults. Using Global Burden of Disease (GBD) 2021 data, we analyzed PAH burden in individuals aged ≥ 55 years across 204 countries from 1990 to 2021. In 2021, global age-standardized rates per 100,000 population were 6.01 for prevalence, 19.29 for DALYs, and 1.11 for mortality. While prevalence increased slightly, DALY rates declined and mortality rose modestly over time. Burden peaked at ages 75-79 (prevalence) and ≥ 95 (DALY and mortality), with consistently higher rates among females. High-SDI countries showed the highest prevalence, while middle-SDI countries experienced the highest mortality. Substantial geographic and temporal variations were observed. These findings highlight the growing and uneven burden of PAH in aging populations and underscore the need for targeted public health strategies.

内皮细胞中的 TXNIP 在肺动脉高压中的作用探究

高振强 [1,2,3] 郭煜 [1,2,3] 张牧之 [1,2,3] 隆寰宇 [4] 吕佳璐 [2,3] 贾玉峰 [1,2,3] 崔烨 [1,2,3] 王蕾 [5] 孙英 [1,2,3] 刘杰 [1,2,3] 王炜 [1,2,3]

1. 首都医科大学基础医学院免疫学系

2. 首都医科大学呼吸病学系

3. 首都医科大学免疫异常与肺纤维化基础临床联合实验室

4. 北京大学第三医院呼吸与危重症医学科

5. 西安交通大学第二附属医院呼吸与危重症医学科

目的：肺动脉高压（pulmonary hypertension, PH）是一种以肺动脉压力异常升高为主要特征的异质性临床疾病。在缺氧、炎症等因素的刺激下 PH 患者会出现血管内皮细胞受损及功能障碍。内皮功能障碍是大多数以血管重构为主要特征疾病的常见初始事件。与此同时，内皮细胞功能障碍会加重 PH 患者肺部活性氧积累、炎性细胞浸润以及其他血管结构细胞损伤。因此，内皮细胞功能障碍是肺血管重塑的重要原因。硫氧还蛋白相互作用蛋白（Thioredoxin-interacting protein，TXNIP）是一种炎症和氧化应激关键调控因子，其表达在低氧、氧化应激及促炎细胞因子等刺激下表达上调。本研究旨在探究 TXNIP 在 PH 发生发展中的具体功能及其潜在机制。

方法：收集慢阻肺病合并 PH 患者及对照组肺组织样本；采用低氧（10% O_2）-SU5416 联合应用构建 PH 小鼠模型，利用转录组测序和蛋白质组测序筛选共同的差异基因和差异蛋白；通过构建内皮细胞特异性敲减或过表达 TXNIP 的小鼠模型，以及腹腔注射 TXNIP 特异性抑制剂 SRI-37330 等体内干预手段，系统评估 TXNIP 在 PH 发生发展中的作用。在模型建立完成后，采用小动物超声对小鼠 PH 相关指标进行综合评估。体外实验中，分别利用 si-TXNIP、质粒过表达 TXNIP 或 SRI-37330 刺激人肺动脉内皮细胞（Human Pulmonary Arterial Endothelial Cells，hPAECs），通过细胞活性检测、细胞血管生成实验和细胞黏附实验分析 TXNIP 对内皮细胞功能的影响。同时，采用 Western blot 技术探究 TXNIP 参与内皮功能障碍的具体机制。

结果：（1）多组学联合分析发现，SuHx-PH 小鼠模型肺组织中，TXNIP 的转录水平和翻译水平在造模的第 1-4 周均升高；（2）免疫组织化学染色结果显示，TXNIP 在慢阻肺病合并 PH 患者以及 SuHx-PH 小鼠模型肺组织中升高，并且定位于血管内皮细胞。通过 MCT 诱导的肺动脉高压大鼠模型以及单纯低氧诱导的小鼠模型也同样验证这一结果；（3）采用内皮细胞特异性敲减 / 过表达 TXNIP 及 SRI-37330 进行体内干预小鼠模型均证实，靶向抑制 TXNIP 可缓解 SuHx 诱导的的肺血管重塑及肺动脉压力升高；（4）体外实验显示，hPAECs 过表达 TXNIP、低氧刺激后可导致内皮细胞功能障碍（血管生成能力和细胞黏附能力增强），采用 si-TXNIP 或 SRI-37330 干预后可改善上述功能障碍；（5）机制上，TXNIP 通过激活 NLRP3 信号通路，诱导炎症反应，从而促进内皮细胞功能障碍。

结论：在低氧等因素刺激作用下，TXNIP 通过介导内皮细胞功能障碍，促进肺血管重塑从而参与肺动脉高压的发生发展。

利拉鲁肽通过激活 AMPK/USP10 环路增强 ACE2 的表达：在肺动脉高压中的意义

陈子旋 [1] 龚开政 [1] John-shyy[2,3] 沈慧 [1]

1. 扬州市第一人民医院

2. 西安交通大学

3. UCSD 美国圣地亚哥分部

目的：研究肺血管内皮细胞中泛素羧基末端水解酶 10（USP10）是否可以通过对血管紧张素转换酶 2（ACE2）进行 K48 连接去泛素化从而稳定后者蛋白水平，最终在肺血管系统中发挥保护作用。并深入探究胰高血糖素样肽 -1（GLP-1）受体激动剂——利拉鲁肽治疗肺动脉高压的效果与机制。

方法：通过生物信息学分析和体外细胞实验，探究 USP10 在人类特发性肺动脉高压与啮齿类肺动脉高压模型中的作用，及其涉及肺内皮细胞中 AMPK/USP10 正反馈环的分子机制。采用内皮细胞特异性 USP10 转基因小鼠和利拉鲁肽给药小鼠，验证 AMPK/USP10 环路对啮齿类肺动脉高压的改善效应。单细胞测序研究利拉鲁肽对肺血管表型改善与分子机制影响。

结果：在人类特发性肺动脉高压及啮齿类肺动脉高压模型的肺内皮细胞中均发现 USP10 表达下调。AMPK/USP10 环路通过促进 ACE2 Ser-680 位点磷酸化和 Lys-788 位点去泛素化，维持 ACE2 稳态水平及肺血管通透性。利拉鲁肽给药小鼠呈现与内皮特异性 USP10 转基因小鼠相似的肺动脉高压缓解表型，部分归因于 AMPK/USP10 环路激活。单细胞测序证明利拉鲁肽治疗对肺血管内皮与平滑肌细胞生物学功能的改善，内皮细胞中分子水平的影响以及血管内皮 - 平滑肌细胞串扰的干预。

结论：通过基因干预（USP10 过表达）或药物手段（GLP-1 受体激动剂）激活 AMPK/USP10 环路可提升肺内皮 ACE2 水平。这种 ACE2 增强模式对人类肺动脉高压及啮齿类肺动脉高压均具有保护作用，为 GLP-1 受体激动剂治疗肺动脉高压提供了理论依据。

SPECT/CT 肺灌注 / 通气显像定量分析在 CTEPH 患者 BPA 术后疗效评估的应用

马荣政 杨森 王玲 韩萍萍 李环 富丽萍

中日友好医院

目的：探讨 SPECT/CT 肺灌注 / 通气显像定量分析方法在慢性血栓栓塞性肺高压 (CTEPH) 肺动脉球囊扩张成形术 (BPA) 术后疗效评估中的应用价值。

方法：前瞻性收集 2020.1 月至 -2024.2 月就诊于中日医院诊断为 CTEPH 并行 BPA 手术患者 50 例，手术共处理肺段 262 个，涉及 83 个肺叶，用 HERMES 工作站（HERMES Medical Solutions AB，瑞典）进行图像重建及分析，分别获得术前、术后灌注 / 通气显像各肺叶的功能体积（ml）。分别比较手术肺叶、非手术肺叶的灌注 / 通气显像功能体积。$P < 0.05$ 为差异有统计学意义。

结果：手术共处理 83 个肺叶，术前平均灌注功能体积为（762.99±334.80）ml，术后平均灌注功能体积为（903.99±356.92）ml，配对 t 检验结果有统计学意义（t=-2.813, P=0.037）。术前平均通气功能体积为（781.27±334.95）ml，术后平均通气功能体积为（885.63±365.72）ml，配对 t 检验结果没有统计学意义（t=-1603, P=0.170）。50 例患者手术未处理的共 167 个肺叶，术前平均灌注功能体积为（841.53±339.72）ml，术后平均灌注功能体积为（803.37±337.96）ml，配对 t 检验结果有统计学意义（t=3.410, P=0.009)ml。术前平均通气功能体积为（864.16±341.70）ml，术后平均通气功能体积为（852.14±352.12）ml，配对 t 检验结果没有统计学意义（t=0.263, P=0.799)。

结论：BPA 手术处理肺叶术后灌注功能体积较术前提升，而手术未处理肺叶，术后灌注功能体积较术前有所降低。BPA 手术处理肺叶、非手术肺叶通气功能体积术前、术后未见明显差异。SPECT/CT 肺灌注 / 通气显像定量分析能反应 CTEPH 患者 BPA 术后血流灌注的改善及肺内再分布情况。

Deciphering the Common Mechanisms of Pulmonary Hypertension Subtypes Using Multi-Omics and Machine Learning

Yajie Chen[2], Zhu Chen[2], Yuan Guo[1,2]

1. Zhuzhou Hospital Affiliated to Xiangya School of Medicine, Central South University

2. University of South China

Deciphering the Common Mechanisms of Pulmonary Hypertension Subtypes Using Multi-Omics and Machine Learning

Yajie Chen[2], Zhu Chen[2], Yuan Guo[1,2]

[1.] Department of Cardiovascular Medicine, Zhuzhou Hospital Affiliated to Xiangya School of Medicine, Central South University, Zhuzhou 412000, China.

[2.] University of South China, Hengyang 421001, China.

Aims:

Pulmonary hypertension (PH) is a heterogeneous disease characterized by elevated pulmonary artery pressure and right heart dysfunction, classified into five major subtypes based on different etiologies. Most current research focuses on individual subtypes, limiting the understanding of shared mechanisms and impeding the development of broadly effective diagnostic and therapeutic strategies. Single-cell RNA sequencing (scRNA-seq) enables high-resolution analysis of cellular heterogeneity, while machine learning offers powerful tools to integrate multi-omics and clinical data for pattern recognition and biomarker discovery. This study aims to combine multi-omics profiling with machine learning to identify common cellular-level mechanisms across PH subtypes, laying the groundwork for more comprehensive and universal treatment approaches.

Method:

This study systematically analyzed the common mechanisms of different PH subtypes by combining single-cell sequencing and machine learning techniques. The research collected human single-cell and Bulk RNA-seq data related to PH from the GEO database, which included samples from different tissues. After quality control and integration, the study identified dysfunctional cell subpopulations across PH subtypes at the single-cell level, screened differentially expressed genes (DEGs), and analyzed their differentiation trajectories. At the Bulk level, weighted gene co-expression network analysis (WGCNA), protein-protein interaction (PPI) analysis, and functional enrichment analysis were used to identify conserved gene modules and functional pathways of different types of PH. Six machine learning models, including random forest, support vector machine, and gradient boosting machine, were combined to screen core genes across PH subtypes. Subsequently, we constructed rat models of type I pulmonary hypertension induced by MCT, mouse models of type II pulmonary hypertension related to heart failure, mouse models of type III pulmonary hypertension induced by hypoxia, and mouse models of type IV pulmonary hypertension constructed by polyethylene microspheres combined with SU5416. We respectively explored the expression levels and functions of the identified core genes in different types of pulmonary hypertension. At the same time, peripheral blood was collected from patients with heart failure combined with pulmonary hypertension and patients with COPD combined with pulmonary hypertension, and the expression levels of core genes were detected.

Results:

Using “pulmonary hypertension” as the keyword to search the GEO database, with sample type restricted to Homo sapiens, we selected two scRNA-seq datasets and four bulk RNA-seq datasets for a systematic analysis of shared mechanisms across PH subtypes. Cell type proportion analysis on the two quality-controlled PH scRNA-seq datasets (PAH and CTEPH) revealed a significant increase in the proportion of endothelial cells (ECs) in PH samples compared to controls. This suggests abnormal enrichment of ECs within the PH pathological microenvironment. Subsequently, we employed CellChat to visualize potential cell-cell interactions among all cell types in the PAH and CTEPH groups. Overall cell communication was significantly enhanced during PH progression in both PAH and CTEPH. Crucially, EC communication strength was markedly augmented in both PH subtypes, indicating their pivotal role within the PH cellular communication network. Further investigation into altered communication patterns revealed that pathways exhibiting enhanced interactions in both PAH and CTEPH were significantly enriched in biological processes including angiogenesis, vasodilation and vasoconstriction, leukocyte-endothelial adhesion and transendothelial migration, inflammation, and immune responses. This further confirms the aberrant activation of vascular function regulation and immune-inflammatory pathways in PH. Focusing on ECs, we performed differential gene expression analysis (DEG)on ECs from both PH groups and further subcluster them. The dysfunctional EC subpopulation was identified based on high expression of vascular remodeling-related genes. Monocle2 was then used to reconstruct EC differentiation trajectories, revealing branch point characteristics associated with differentiation towards the dysfunctional subpopulation during disease progression. Intersecting the DEGs from both PH groups’ ECs with the differentially expressed genes at the branch point yielded 43 shared candidate genes across PH subtypes. To further identify cross-PH-subtype shared genes with broader relevance, Weighted Gene Co-expression Network Analysis (WGCNA) was performed on the four quality-controlled bulk RNA-seq datasets. This identified the gene module most significantly associated with PH. Intersecting this module with the 43 shared candidate genes derived from endothelial cell subpopulation analysis yielded 12 key genes. Finally, employing six machine learning algorithms with these 12 key genes as candidate inputs, we screened for top-ranked core molecules. Endothelial cell-selective adhesion molecule (ESAM) consistently performed excellently across all six algorithms, suggesting it as a potential shared core gene across PH subtypes. Furthermore, existing research indicates that elevated soluble ESAM (sESAM) levels significantly correlate with traditional cardiovascular risk factors (hypertension, diabetes, hyperlipidemia, obesity) and positively correlate with inflammatory markers.

Conclusions:

Breaking through the traditional research framework focusing on single subtypes, this study, for the first time, analyzes the common mechanisms of pulmonary hypertension from a cross-subtype perspective. By integrating multi-omics data analysis with machine learning techniques, it explores the shared mechanistic molecules across different subtypes of pulmonary hypertension, reveals the pivotal role of ESAM as a key gene in pulmonary hypertension, and validates its biological functions through animal experiments.

ALDH2 缺失通过调控铜死亡促进低氧性肺动脉高压诱导的右心室重塑

付程文 许美扬 孙红燕 唐碧 张晓红

蚌埠医学院第一附属医院

目的：本研究的目的是探讨 ALDH2 是否能通过调节细胞铜死亡影响 HPH 诱导的心肌重塑及其潜在机制。

方法：在体水平：将 ALDH2 敲除 (ALDH2 – / –) 小鼠和野生型 (WT) 小鼠暴露于氧浓度为 10±0.5% 的缺氧环境中 4 周，建立慢性缺氧 PAH (HPH) 诱导的右心室重构小鼠模型，通过超声心动图、右心导管技术、HE 染色、WGA、Masson、ELISA、蛋白质免疫印迹等方法评估 ALDH2 缺陷对 HPH 右心室功能及结构的影响体外水平：将 H9C2 心肌细胞置于缺氧环境中 48 小时，构建缺氧模型，通过 CCK-8、ELISA、JC-1、RT-qPCR 和蛋白免疫印迹等技术探讨 ALDH2 对缺氧心肌细胞的影响。

结果：ALDH2 – / –小鼠在缺氧暴露下表现出显著的肺血管壁增厚、右心室肥厚、肺动脉压力升高、心肌细胞肥大以及纤维化；进一步研究发现，ALDH2 缺失导致心肌组织中铜死亡相关蛋白 FDX1、LIAS、DLAT 及 HSP70 表达上调体外实验证实，抑制 ALDH2 表达加剧了缺氧诱导的心肌细胞损伤、铜离子水平升高、铜死亡相关蛋白表达上调，进而引起线粒体膜电位降低；而铜离子螯合剂 TTM 可降低缺氧条件心肌细胞中铜死亡相关蛋白的表达。

结论： ALDH2 缺失导致心肌组织中铜离子蓄积，激活铜死亡相关蛋白表达，进而引起心肌细胞损伤及右心室重塑，为改善 HPH 患者预后提供了新的治疗策略。

Balloon pulmonary angioplasty combined with riociguat for the treatment of inoperable chronic thromboembolic pulmonary hypertension (PRACTICE study)

null null

上海市肺科医院

Abstract

Background: In recent years, several prospective cohort studies conducted abroad have validated the efficacy of balloon pulmonary angioplasty (BPA) for inoperable chronic thromboembolic pulmonary hypertension (CTEPH). However, research on this treatment remains limited in China.

Method: This study is a single-center randomized controlled trial. Subjects with inoperable CTEPH are randomized into either a BPA combined with riociguat （R+B）or riociguat monotherapy group （R） (2:1) and observed for 12 months after initiation of treatment. The primary endpoint is the change in pulmonary vascular resistance from baseline to 12 months after initiation of treatment. The secondary endpoints include 6-min walk distance (6MWD), WHO-FC, N-terminal pro-B-type natriuretic peptide (NT-proBNP), and other hemodynamic parameters.

Results: Eighty-one patients with inoperable CTEPH were randomly assigned to the R+B group (n=54, age 63.6 ± 11.4 years, 43% male) and the R group (n=27, age 65.3 ± 11.1 years, 26% male). After 12 months of follow-up, the R+B group demonstrated a significant reduction in pulmonary artery systolic pressure (PASP) from 72.7 ± 24.1 mmHg to 44.5 ± 13.8 mmHg (P<0.001), while the R group experienced a decrease from 70.4 ± 19.7 mmHg to 57.8 ± 21.0 mmHg (P<0.001). Notably, pulmonary vascular resistance (PVR) in the R+B group significantly improved from 8.4 ± 3.7 to 3.3 ± 1.5 Wood units (WU, P=0.001), whereas the R group showed no significant change (8.7 ± 4.1 to 8.3 ± 6.4 WU, P=0.45). Mean pulmonary artery pressure (mPAP) in the R+B group decreased from 43.2 ± 8.9 mmHg

to 26.1 ± 6.9 mmHg, while the R group remained stable (41.6 ± 11.3 vs 41.3 ± 16.0 mmHg, P=0.26). Additionally, the 6MWD in the R+B group increased from 354.9 ± 130.9 meters to 442.7 ± 87.8 meters (P=0.002), in contrast to the R group's negligible change (344.6 ± 139.4 vs 384.6 ± 117.8 meters, P=0.35). The median level of NT-proBNP decreased significantly in the R+B group, from 535.6 pg/mL (IQR 119.8-1011.6) to 78.4 pg/mL (35.1-173.9, P<0.001), indicating a notable difference compared to the R group (NT-proBNP 236.0 to 235.4 pg/mL, P=0.15). The WHO FC in the R+B group showed significant improvement compared to the R group (P < 0.001 vs P = 0.166).

Conclusion: BPA combined with riociguat significantly improves hemodynamics and exercise tolerance in patients with inoperable CTEPH compared to riociguat alone.

Keywords: Balloon pulmonary Angioplasty, Riociguat, Chronic thromboembolic Pulmonary hypertension

Figure 1. Comparison of the trends of echocardiographic indicators between the two patient groups. In the R+B group, there were significant improvements in PASP, RAA, TAPSE, and PA compared to baseline. In the R group, both PASP and RAA showed improvements from baseline, while TAPSE and PA demonstrated less significant changes. RA, right room; PA, pulmonary artery; PASP, systolic pulmonary artery pressure; TAPSE, tricuspid value systolic displacement.

Figure 2. Comparison of hemodynamic parameters and exercise tolerance parameters between the two patient groups. In the R+B group, both mPAP and PVR showed significant improvement compared to baseline, along with notable enhancements in 6MWD and NT-proBNP. In contrast, the R group exhibited no significant improvements in these parameters compared to baseline. mPAP, mean pulmonary arterial pressure; NT-proBNP, N-terminal pro-brain natriuretic peptide; PVR, pulmonary vascular resistance; 6MWD, 6-minute walking distance.

m6A 修饰酶基因 METTL3 缺失对小鼠右室结构与功能障碍的影响及其作用机制探究

吴向起

南京医科大学附属南京医院

目的：研究证实右心室的结构与功能障碍在众多心血管疾病中扮演着至关重要的角色，然而，目前尚缺乏针对右心室结构与功能的表观调控机制的研究资料。因此，本研究旨在观察 m6A 甲基化基因 METTL3 在右心室结构和功能中的作用，并探讨其潜在机制。

方法：采用 Mef2c-Cre 在小鼠第二心场敲除 METTL3 基因。通过超声心动图、心电图、压力检测、Masson 染色和 TUNEL 检测，评估心脏功能、右室压力、心电情况、纤维化面积及细胞凋亡。利用 mRNA 测序、蛋白质印迹法、RT-PCR 和 RNA pull down 实验等方法，探究其潜在机制。

结果：与 $METTL3^{F/F}$ 小鼠相比，$METTL3^{F/F}$; Mef2c-Cre 小鼠在出生约 3 个月后，心超检查显示右心室收缩与舒张功能下降，左心室收缩与舒张功能亦降低；右室测压显示右室压力显著增高；Masson 染色显示右室明显扩大和室壁变薄，高倍镜下可见右室较多胶原聚集和少量心肌细胞类似脂肪变性；心电图显示肢导联长 QRS 间期及室性心律失常发生率显著增加；心肌细胞凋亡明显增多。与 $METTL3^{F/F}$ 小鼠相比，$METTL3^{F/F}$; Mef2c-Cre 小鼠右室心肌组织中筛选出 220 个差异表达的 mRNA（其中 42 个基因的 mRNA 表达显著上调，178 个基因的 mRNA 表达显著下调），并进行了 GO 及 KEGG pathway 分析。通过 RT-PCR 和 Western blot 验证，发现小鼠右室组织 PKP2 的 mRNA 和蛋白水平显著下降。RNA pull down 实验也提示 METTL3 蛋白可直接调控 PKP2 mRNA。

结论：在小鼠第二心场中，METTL3 基因的缺失可能通过影响 PKP2 mRNA 的 m6A 位点，导致其稳定性下降，进而显著降低 PKP2 mRNA 和蛋白的表达水平，最终引发右室结构与功能障碍的发生及发展。

The Role of USP7-Mediated Endothelial Cell Senescence in Vascular Remodeling Associated with Pulmonary Arterial Hypertension: Regulation of the p53 Pathway and Underlying Mechanisms

Ya-Nan Qi[1,2,3], Xiao-Wen Wu[1,2,3], Ping Luo[1,2], Jie Du[1,2], Jun Peng[3], Bin Liu[1,2,3]

1. Department of Pharmacy, Xiangya Hospital, Central South University

2. National Clinical Research Center for Geriatric Disorders, Xiangya Hospital, Central South University

3. Department of Pharmacology, Xiangya School of Pharmaceutical Sciences, Central South University

Pulmonary vascular remodeling is the fundamental characteristic of the pathological process associated with pulmonary arterial hypertension (PAH). This process involves multiple pathological mechanisms, including endothelial dysfunction, abnormal proliferation of pulmonary arterial smooth muscle cells, and dynamic remodeling of the extracellular matrix. Endothelial cell senescence represents a significant pathological phenotype of endothelial dysfunction and serves as a crucial driving factor in the progression of irreversible pulmonary vascular remodeling.

Ubiquitin-specific protease 7 (USP7) is a key component of the deubiquitinating enzyme family, playing a crucial role in the regulation of target protein stability through the specific recognition and hydrolysis of substrate proteins. This enzyme is pivotal in the process of cellular senescence. Previous investigations conducted by our research group revealed that USP7 expression is markedly upregulated in the lung tissues of patients with PAH, as well as in the lung tissue of rat models induced by hypoxia combined with Su5416 (SuHx) or monocrotaline (MCT). Notably, the expression of the senescence marker p21 was significantly elevated within the pulmonary vascular endothelial layer, indicating that USP7 may contribute to the irreversible remodeling of pulmonary vasculature by modulating the senescence phenotype of endothelial cells. This study aims to delineate the molecular mechanisms through which USP7 mediates endothelial cell senescence and fosters pulmonary vascular remodeling, thereby providing a novel theoretical framework and prospective intervention strategies for targeted treatment of PAH. By constructing PAH animal models induced by SuHx and MCT, we administered the USP7 inhibitor P22077. Our findings demonstrated that, in comparison to the control group, mice in the SuHx group and rats in the MCT group exhibited hallmark features of pulmonary vascular remodeling and compromised right heart function. Specifically, we observed a significant increase in the percentage and area ratio of pulmonary small artery vessel thickness, enhanced collagen deposition around the pulmonary vessels, decreased measurements of cardiac function such as the time velocity integral (VTI) and tricuspid valve ring systolic displacement (TAPSE), increased right ventricular wall thickness, and elevated expression levels of USP7 and p21 within the pulmonary vascular endothelial layer. Following intervention with P22077, the aforementioned pathological indicators showed marked improvement, suggesting that USP7 plays a role in promoting endothelial cell senescence and regulating pulmonary vascular remodeling. Additionally, the administration of P22077 and USP7 siRNA to a hypoxia-inducing human pulmonary artery endothelial cell (HPAEC) senescence model revealed that HPAECs subjected to hypoxia conditions (1% O_2) exhibited classic senescence characteristics. These included a significant increase in the proportion of β-galactosidase-positive cells and G1 phase cells, heightened fluorescence intensity of the DNA damage marker γ-H2AX, decreased expression of nuclear lamina protein Lamin B1, increased mRNA levels of senescence-related secretory phenotype factors such as IL-8 and MMP2, and an imbalance in mitochondrial oxidative stress. Molecular mechanism studies indicated a strengthened interaction between USP7 and the p53 protein in the hypoxia-induced HPAECs, concomitant with a marked reduction in both the total ubiquitination level and K48-specific ubiquitination of p53, as well as a significant upregulation of p21 expression. Treatment with 10 μM P22077 or USP7 siRNA transfection effectively reversed these alterations. In conclusion, our findings suggest that USP7 promotes endothelial cell senescence by regulating the deubiquitination of p53, thereby driving the process of pulmonary vascular remodeling associated with PAH. Moreover, the USP7 inhibitor P22077 demonstrates potential for alleviating endothelial cell senescence and the pulmonary vascular remodeling process in the context of PAH, with its mechanism linked to the inhibition of the USP7/p53 signaling pathway.

Key words: endothelial cell senescence; USP7; p53; deubiquitination; pulmonary arterial hypertension

Acute Pulmonary Hemodynamic Changes Following Pulmonary Artery Denervation in Pulmonary Hypertension Patients Undergoing Prior Transcatheter/Surgical Mitral Valve Repair

Xiang Chen[1], Ze-Ying Zhang[1], Huai-Bin Huang[1], Yan-Er Yao[1], Shao-Liang Chen[2], Yan Wang[1]

1. Xiamen Cardiovascular Hospital of Xiamen University

2. Nanjing First Hospital of Nanjing Medical University

Background: Elevated mean pulmonary artery pressure (mPAP) constitutes a key hemodynamic determinant of adverse outcomes in mitral regurgitation patients undergoing transcatheter mitral valve edge-to-edge repair (M-TEER) or surgical mitral valve replacement (SMVR). Despite procedural success in reducing regurgitant volume, persistent pulmonary hypertension (PH) mediated by residual valvular dysfunction continues to portend elevated mortality risk. Emerging evidence suggests pulmonary artery denervation (PADN) is beneficial in certain PH clinical groups, yet its therapeutic potential in post-M-TEER/SMVR PH remains uncharacterized.

Methods: All patients were >18 years of age. Patients with symptomatic World Health Organization-defined group II PH (mPAP > 20mmHg as measured by right heart catheterization) and prior M-TEER/SMVR for severe mitral regurgitation were evaluated for PADN as an alternative to mPAP reduction therapy. Included patients did not have cardiomyopathy, valvular stenosis, untreated congenital heart disease, systematic inflammation malignant cancer, severe renal dysfunction (evaluated GFR < 30 mL/min/1.73m2), severe hepatic dysfunction (Child-Pugh C), a blood platelet count of < 50 × 109/L, and an expected lifespan of < 12 months. Clinical data were collected from electronic medical records including demographics data, symptoms, medication, morbidities, laboratory examination, baseline echocardiographic measurements, baseline and post-PADN right heart catheterization measurements, PADN ablation parameters and hospital stay length. Data were tested for distribution using the Shapiro-Wilk test. Continuous variables were expressed as mean

± standard deviation (SD) if data were normally distributed or median (inter-quartile range, [IQR]) for continuous variables that did not conform to a normal distribution. Normally distributed data were compared using Student's t-test for paired samples. When the continuous variables were not normally distributed and the difference distribution was symmetrical, the Wilcoxon signed-rank test was used, otherwise the signed-rank test is used. Categorical data are presented as counts and percentages. Two-sided value of P < 0.05 in all statistical tests was considered to indicate statistical significance. All analyses were performed with SPSS version 26.0 (SPSS Institute Inc).

Results: Overall, 8 patients (M-TEER = 4, SMVR = 4) were included. Patient ages were from 59 to 79 years, with significant symptoms (NYHA functional class II - III) and various morbidities. 75.0% of patients had atrial fibrillation, and 12.5% of patients had hypertension. Diuretics, beta-blockers, and anticoagulants were the most commonly used medications. Echocardiography showed a mean value of left ventricular ejection fraction of 61.4 ± 10.2 % and of TAPSE of 16.9 ± 3.8 mm. The functional assessment showed that the median value of NT-pro BNP was 659.5 (IQR: 976.8) ng/L and the mean value of 6MWD was 342.3 ± 83.0 m. The mean right atrial pressure was 13.8 ± 8.0 mmHg, with a median value of mPAP of 35.0 (IQR: 8.8) mmHg. The mean duration of ablation at 3 sites during the PADN procedure was 91.3 ± 31.6 minutes. The ablation time in each site ranged from 7 seconds to 144 seconds. There were no morbidities or uncomfortablity complained by the patients during and after the procedure. As shown in Figure 1, The sign test indicated that the median mPAP after PADN (median = 31.5 mmHg) was significantly lower than before PADN (median = 35 mmHg, P = 0.008). Among 8 participants, 100% showed a decrease in mPAP after PADN. There were also significant reductions in sPAP (mean difference: -3.9 mmHg, P = 0.038, 95% CI: 0.3 to 7.5) and PVR (median difference: -0.51 wood, P = 0.012) while not in dPAP (P = 0.154) measured by right heart catheterization.

Conclusions: Based on the safety and short-term efficacy observed in this case series, we suggest that PADN may be an appropriate therapy for symptomatic PH patients underwent M-TEER/SMVR despite optimal medical therapy. These encouraging observational short-term results generate a need for mid-term and long-term studies looking at PADN as an alternative to current therapeutic strategies.

Integrated Single-Cell and Transcriptomic Profiling Reveals Lactylation-Driven Molecular Mechanisms in Pulmonary Arterial Hypertension

Zhifu Guo, Jing-Yu Zhang, Jin Luo, Ming Ni, Song-Qun Huang

海军军医大学附属第一医院长海医院

Objective

Pulmonary arterial hypertension (PAH) is a progressive and life-threatening disease characterized by elevated pulmonary vascular resistance, right ventricular failure, and poor prognosis. Despite advances in therapeutic strategies, the molecular mechanisms underlying PAH pathogenesis, particularly the role of metabolic dysregulation and lactic acidosis, remain poorly elucidated. Lactic acidosis, emerging as a critical metabolic hallmark, has been implicated in PAH progression through modulation of immune responses, fibrotic remodeling, and endothelial dysfunction. However, the precise molecular interplay between lactic acidosis and PAH pathobiology, especially at the single-cell level, remains undefined. This study aims to dissect the molecular mechanisms of lactic acidosis in PAH by integrating single-cell RNA sequencing (scRNA-seq) and bulk transcriptomics, with a focus on identifying key metabolic regulators, immune-metabolic interactions, and potential therapeutic targets.

Methods

This study employed a multi-omics approach combining scRNA-seq and bulk RNA-seq data from patients with PAH and healthy controls. The scRNA-seq dataset (GSE228644) included 3 PAH and 3 control samples, while the bulk RNA-seq dataset (GSE117261) comprised 58 PAH and 25 control samples. Data preprocessing involved quality control using Seurat v4.3.0, filtering cells based on gene counts (>200 genes/cell), mitochondrial gene ratios (

To identify lactate-associated gene signatures, lactate-related genes were curated from literature and intersected with differentially expressed genes (DEGs) in PAH-derived fibroblasts (AUCell scoring, p < 0.05). Machine learning algorithms (LASSO regression and random forest) were applied to prioritize hub genes, validated via ROC curve analysis. Immune infiltration landscapes were characterized using CIBERSORT, while ligand-receptor interactions were mapped using CellChat. Functional enrichment analysis (GSEA, GSVA) and pseudotime trajectory analysis (Monocle) were conducted to elucidate pathway activities and cellular differentiation dynamics. Transcriptional regulatory networks were inferred using SCENIC, and a nomogram model integrating clinical and molecular features was constructed for risk stratification.

Results

Single-Cell Profiling Reveals Fibroblast-Dominated Lactate Metabolism: scRNA-seq identified 9 distinct cell clusters, including fibroblasts, endothelial cells, and immune subsets. Fibroblasts exhibited significantly higher lactate scores compared to controls (p < 0.01), driven by upregulation of lactate transporters (e.g., SLC16A3) and glycolytic enzymes. Pseudotime analysis demonstrated a metabolic shift towards aerobic glycolysis in PAH fibroblasts, coinciding with reduced oxidative phosphorylation. **Key Gene Discovery and Validation**: Integrating DEGs in PAH fibroblasts with lactate-related genes yielded 149 candidate genes. LASSO regression and random forest algorithms prioritized five hub genes (ACAT2, FABP5, FUBP1, VIM, PAK2), which showed robust diagnostic performance (AUC > 0.85). ACAT2 correlated with monocyte/macrophage infiltration (r = 0.62), while VIM expression was linked to epithelial-mesenchymal transition (EMT) pathways. **Immune Microenvironment Dysregulation**: PAH samples exhibited increased M1 macrophages (23.5% vs. 12.1%), exhausted CD8+ T cells, and reduced regulatory T cells (p < 0.05). Key genes showed distinct immune correlations: FUBP1 correlated with B-cell memory and dendritic cell activation, whereas PAK2 inversely correlated with plasma cells and memory T cells. Cytokine-cytokine receptor interactions (e.g., CXCL12-CXCR4) were enriched in PAH, suggesting pro-inflammatory signaling. **Pathway Enrichment and Regulatory Networks**: GSEA revealed activation of hypoxia-related pathways (HIF-1α, VEGF) and metabolic reprogramming (glycolysis, fatty acid oxidation) in PAH. GSVA highlighted upregulation of oxidative phosphorylation (OXPHOS) and cholesterol biosynthesis in ACAT2-high fibroblasts. SCENIC identified KLF4, ETS1, and CEBPD as master transcription factors governing hub gene expression. **Prognostic Model Development**: A nomogram integrating ACAT2, FABP5, and clinical parameters (e.g., mean pulmonary artery pressure) achieved superior predictive accuracy (AUC = 0.92). Calibration plots confirmed alignment between predicted and observed risks, supporting clinical utility.

Conclusion

This integrative study elucidates the metabolic-immune axis in PAH, demonstrating that fibroblast-driven lactate production orchestrates immune dysregulation and fibrotic remodeling via HIF-1α and TGF-β signaling. The identified hub genes (ACAT2, FABP5, etc.) and their associated pathways (e.g., PPARγ, NF-κB) represent promising therapeutic targets. The nomogram model provides a practical tool for risk stratification, emphasizing the clinical relevance of metabolic profiling in PAH management. Future studies should validate these findings in longitudinal cohorts and explore lactate-modulating therapies to halt disease progression.

Keywords: Pulmonary arterial hypertension, Lactylation, Vascular remodeling, Post-translational modification, Nomogram model

Predictive Value of Right Atrial Strain Combined with Right Atrial Area for Clinical Deterioration in Patients with Pulmonary Hypertension

jinxin XU

Guangdong Provincial People's Hospital

Background:Pulmonary arterial hypertension (PAH) is a severe condition marked by elevated pulmonary arterial pressure, leading to increased pulmonary vascular resistance (PVR), right ventricular dysfunction, and high mortality. Although the prevalence in the general population is relatively low (15–50 cases per million), certain high-risk groups, such as those with congenital heart disease, exhibit significantly higher rates (5–10%). Untreated PAH carries a dismal median survival of 2.8 years, and even with targeted therapies, the 5-year survival remains below 60%. Elevated PVR (>5 Wood units) is a critical prognostic marker, often indicating severe disease and guiding treatment decisions across various PAH subtypes, including those associated with left heart disease, lung diseases, chronic thromboembolic pulmonary hypertension, and congenital heart disease. However, emerging evidence suggests that even patients with PVR <5 Wood units may experience adverse outcomes, underscoring the need for refined risk stratification tools to identify high-risk individuals early. Current risk assessment relies on parameters such as WHO functional class, exercise capacity, and biomarkers like BNP, but these may not fully capture the compensatory mechanisms of right heart function, particularly in early-stage or atypical PAH cases where right atrial adaptation plays a pivotal role.

Objective: This study aimed to evaluate the prognostic value of the right atrial area-to-atrial contraction strain ratio (RAA/RASct) in Pulmonary arterial hypertension (PAH)patients with pulmonary vascular resistance (PVR) ≤ 5 Wood units and to optimize the risk stratification model.

Methods: A prospective cohort of 359 suspected PAH patients was screened, with 97 meeting inclusion criteria after exclusions for inadequate hemodynamic or echocardiographic data. Echocardiographic parameters, including right atrial strain (reservoir, conduit, and contraction phases), were measured using speckle-tracking techniques, while right heart catheterization confirmed hemodynamic profiles. The primary endpoint was clinical worsening, encompassing mortality, PAH-related hospitalization, therapy escalation, or functional decline. Results demonstrated that RAA/RASct was a powerful independent predictor of adverse events (AUC=0.837, HR=1.063), outperforming traditional biomarkers like NT-proBNP. Even after adjusting for established risk factors, RAA/RASct

retained its prognostic significance, highlighting its utility in identifying high-risk patients who might otherwise be misclassified by conventional models.

Results:The integration of RAA/RASct into the 2022 ESC/ERS four-strata risk model significantly enhanced predictive accuracy, with the adjusted model showing a more pronounced risk gradient and superior discriminative performance (AUC=0.855 vs. 0.611). The net reclassification improvement (51.61%) and integrated discrimination improvement (29.38%) further validated its incremental value. Mechanistically, RAA/RASct reflects the imbalance between right atrial dilation and contractile dysfunction, suggesting that right atrial impairment may precede overt hemodynamic deterioration in low-PVR PAH. This finding underscores the importance of early echocardiographic monitoring to detect subclinical right atrial dysfunction and guide timely interventions. Limitations include the single-center design, modest sample size, and lack of external validation, necessitating further multicenter studies to confirm generalizability.

Conclusion: RAA/RASct is a robust prognostic marker in low-PVR PAH, offering superior risk stratification compared to current guidelines. Its incorporation into clinical practice could facilitate earlier identification of high-risk patients, enabling personalized therapeutic strategies and improving outcomes. Future research should focus on prospective validation in larger, diverse cohorts and explore the pathophysiological mechanisms linking right atrial dysfunction to disease progression in this distinct PAH subgroup.

芦丁通过与 PKCα 相互作用抑制铁死亡延缓肺动脉高压的发生发展

车海霞 李倩

哈尔滨医科大学

目的：肺动脉高压（PAH）是一种进行性的心血管疾病，发病率、死亡率高，且预后较差。芦丁是一种广泛存在于植物中的膳食类黄酮，因其卓越的抗氧化活性而受到广泛关注。铁死亡是一种由脂质过氧化引发的新型细胞死亡形式，已有研究表明其在 PAH 的发生发展中发挥重要作用。蛋白激酶 Cα（PKCα）是一种丝氨酸 / 苏氨酸激酶，参与包括铁死亡在内的多种细胞过程。然而，芦丁能否通过抑制铁死亡延缓 PAH 进程，以及 PKCα 在这一过程中所扮演的具体角色，仍需进一步探究。

方法：本研究首先构建了 PAH 动物和细胞模型，探讨了芦丁对 PAH 大鼠和缺氧处理的肺动脉平滑肌细胞（PASMCs）铁死亡的影响。随后，利用线粒体代谢组学、网络药理学和筛选芦丁调控铁丝亡的靶蛋白。最后，利用分子对接技术，以及固有荧光、同步荧光、表面等离子体共振、傅立叶变换红外光谱和圆二光谱等多光谱技术，探究了芦丁与靶蛋白的结合机制。

结果：结果显示，芦丁能够有效抑制 PAH 大鼠肺组织及缺氧 PASMCs 中铁死亡的发生。线粒体代谢组学和网络药理学结果显示 PKCα 是芦丁调控 PAH 相关线粒体代谢的关键靶点。分子对接和多光谱分析结果表明，芦丁可以通过氢键直接与 PKCα 相互作用，诱导 PKCα 静态淬灭，进而改变其二级结构。

结论：本研究首次揭示了芦丁可能通过改变 PKCα 结构、影响其活性，进而抑制铁死亡，最终发挥对 PAH 的保护作用。这项研究有助于从揭示小分子和生物大分子之间的相互作用的角度开发天然生物活性成分，并深入了解类黄酮在健康和疾病中的潜在应用。

Right atrial adaptation to impaired right ventricular function and increased afterload in precapillary pulmonary hypertension: a cardiac magnetic resonance feature-tracking study

Ning Wang

Chinese Academy of Medical Sciences and Peking Union Medical College

Right atrial adaptation to impaired right ventricular function and increased afterload in precapillary pulmonary hypertension: a cardiac magnetic resonance feature-tracking study

Yanyu Li1#, Yining Wang1*

1, Department of Radiology, State Key Laboratory of Complex Severe and Rare Diseases, Peking Union Medical College Hospital, Chinese Academy of Medical Sciences and Peking Union Medical College, Beijing, China

Abstract

Objectives Pulmonary hypertension (PH) is defined by mean pulmonary artery pressure (mPAP) > 20 mmHg at rest by invasive right heart catheterization (RHC). Pre-capillary PH encompasses most of the WHO classification groups (1, 3, 4, and 5). Current cardiac magnetic resonance (CMR) imaging in pre-capillary PH focuses more on measures of right ventricular (RV) function and RV-pulmonary artery (PA) coupling. This study aimed to evaluate RA function and the adaptation of RA to increased afterload in patients with pre-capillary PH using CMR FT technology.

Methods This retrospective study included 85 pre-capillary PH patients (59 female, mean 35 ± 18 years, median mPAP 48 [36, 57] mmHg) who underwent CMR and RHC within 7 days, as well as 37 healthy controls (HCs, 22 female, mean 42 ± 13 years) at peking union medical college hospital from January 2020 to December 2021. Pre-capillary PH was defined as mPAP > 20 mmHg associated with pulmonary artery wedge pressure (PAWP) < 15 mmHg and pulmonary vascular resistance (PVR) > 2 WU measured using RHC. RA and RV volumes were measured and compared. RA phasic strains and RV global strains were evaluated by using CMR FT. RA-RV coupling was calculated by volumes (RA minimal volume/RV end-diastolic volume), while RV-PA coupling was calculated using three different methods based on CMR-derived indices.

Results Patients with pre-capillary PH exhibited impaired RA ejection fraction (RAEF, 44.0±11.6 vs. 50.8±13.3, p=0.017) and RA phasic strains compared to HCs. In pre-capillary PH patients with preserved RVEF (≥ 45%, n = 41), RA reservoir strain (35.5 ± 16.0 vs. 47.2 ± 15.0, p = 0.002), passive strain (21.0 ± 12.5 vs. 30.9 ± 12.0, P < 0.001), and RV global strains [-19.5 ± 4.1 vs. -25.6 ± 2.5, p < .001; -13.5 ± 3.0 vs. -18.1 ± 2.0, P < .001; 21.2 ± 5.7 vs. 28.1 ± 5.6, p < .001, respectively for global longitudinal strain (GLS), global circumferential strain (GCS), and global radial strain (GRS)] remained impaired, while RA active strain (16.5 ± 8.7 vs. 19.0 ± 8.3, p = 0.102) and couplings (0.25 ± 0.11 vs. 0.25 ± 0.09, p = 0.694 for RA-RV coupling, and 0.8 ± 0.2 vs. 0.8 ± 0.2, P = 0.176 for RV-PA coupling) were preserved compared to HCs. RA reservoir and passive strains were associated with impaired RV myocardial function and increased RA-RV coupling and RV-PA coupling in patients with pre-capillary PH. RA active strain was the only parameter associated with invasive mean RA pressure (mRAP, r = -0.280, P = 0.010).

Conclusion

In patients with pre-capillary PH, CMR-determined RA reservoir and passive strain were impaired even when RVEF was preserved. RA phasic strains serve as surrogates of RA adaptation to increased afterload in pre-capillary PH patients.

Upregulation of CXCL10/CXCR3 axis induced by pulmonary hemodynamic stress promotes vascular remodeling in chronic thromboembolic pulmonary hypertension

Jianmin Lu, Cheng Hong

The First Affiliated Hospital of Guangzhou Medical University

Background:

Chronic thromboembolic pulmonary hypertension (CTEPH) is a serious and progressive form of pulmonary hypertension characterized by persistent obstruction of the pulmonary arteries due to organized thrombi and subsequent vascular remodeling. Among the numerous pathological factors contributing to CTEPH, hemodynamic stress plays a pivotal role in triggering inflammatory responses and subsequent structural changes in the pulmonary vasculature. A growing body of evidence suggests that perivascular inflammation, particularly mediated by macrophages and other immune cells, is a key driver in the progression of vascular remodeling in pulmonary hypertension.

Recent studies have highlighted the involvement of chemokines in the orchestration of immune cell infiltration into pulmonary arteries. Notably, CXCL10 (C-X-C motif chemokine ligand 10), also known as IP-10 (interferon gamma-induced protein 10), has emerged as a key inflammatory mediator in various cardiovascular and inflammatory diseases. CXCL10 exerts its biological effects primarily through binding to its receptor CXCR3, which is expressed on multiple cell types including T lymphocytes, macrophages, and vascular smooth muscle cells. Elevated circulating levels of CXCL10 have been reported in patients with CTEPH, and its expression has been shown to correlate with the severity of pulmonary hemodynamic abnormalities. However, the mechanistic role of the CXCL10/CXCR3 signaling axis in mediating vascular remodeling under conditions of chronic hemodynamic stress remains poorly understood.

In this study, we hypothesized that CXCL10, secreted by perivascular macrophages, may promote pulmonary arterial smooth muscle cell (PASMC) proliferation and contribute to vascular remodeling in CTEPH via activation of the CXCL10/CXCR3 axis. To test this hypothesis, we employed a combination of patient-derived tissue analysis and an experimental animal model of pulmonary hypertension that mimics the disturbed hemodynamic conditions of CTEPH.

Methods and Results:

To elucidate the cellular sources and localization of CXCL10 and its receptor CXCR3 in human CTEPH tissues, we performed immunohistochemical and immunofluorescence staining on pulmonary endarterectomy (PEA) specimens obtained from CTEPH patients. These analyses revealed that CXCL10 expression was prominently localized to CD68- and MRC1-positive M2-type macrophages within the remodeled pulmonary arteries, suggesting that alternatively activated macrophages are a major source of this chemokine. Furthermore, strong CXCR3 expression was observed throughout the PEA tissue, notably in the medial and intimal layers, indicating widespread involvement of CXCR3-expressing cells in CTEPH lesions.

To further investigate the functional relevance of CXCL10/CXCR3 signaling under hemodynamic stress, we employed a left pulmonary artery ligation (LPAL) rat model. This model induces increased blood flow and

pressure in the right lung, simulating the abnormal hemodynamic conditions observed in CTEPH. In the LPAL-induced pulmonary hypertension rats, we observed significant infiltration of CXCL10+ and CXCR3+ M2 macrophages in the pulmonary arteries of the right lung. These findings suggest that disturbed hemodynamics directly promote recruitment and activation of CXCL10-producing macrophages in vivo.

At the molecular level, both mRNA expression analysis and ELISA confirmed elevated levels of CXCL10 in the right lungs and systemic circulation of LPAL rats compared to sham-operated controls. Moreover, PASMCs isolated from the right pulmonary arteries of LPAL rats exhibited hyperproliferative phenotypes along with increased CXCR3 expression. In vitro experiments further demonstrated that stimulation with CXCL10 enhanced the proliferation of PASMCs, an effect that was significantly attenuated by the CXCR3 antagonist AMG487. These results indicate that CXCL10 directly promotes PASMC proliferation via activation of CXCR3.

To investigate the crosstalk between macrophages and PASMCs, we treated bone marrow-derived macrophages with CXCL10 and collected the conditioned media. When PASMCs were cultured with this conditioned media, a robust increase in cell proliferation was observed, supporting the hypothesis that macrophage-derived CXCL10 acts in a paracrine manner to influence PASMC behavior. Again, this effect was suppressed by the blockade of CXCR3, emphasizing the central role of the CXCL10/CXCR3 axis in mediating intercellular communication between macrophages and vascular smooth muscle cells.

Finally, to determine the therapeutic relevance of targeting CXCL10/CXCR3 signaling, LPAL rats were treated with AMG487 in vivo. Compared to vehicle-treated animals, rats receiving AMG487 showed significantly reduced pulmonary vascular remodeling, with decreased macrophage infiltration and suppression of PASMC proliferation. These findings demonstrate that pharmacological inhibition of CXCR3 can effectively ameliorate vascular changes induced by chronic hemodynamic stress.

Conclusions:

Taken together, our results reveal a novel mechanism in which CXCL10-secreting M2 macrophages accumulate in the pulmonary vasculature under chronic hemodynamic stress, activating the CXCL10/CXCR3 axis and promoting PASMC proliferation. This contributes to pathological vascular remodeling in the setting of CTEPH. These findings not only provide mechanistic insight into the inflammatory pathways driving pulmonary hypertension but also suggest that targeting CXCR3 may offer a promising therapeutic strategy for preventing or reversing vascular remodeling in CTEPH patients.

研究 BRCC3 和 Sotatercept 在重平衡 TGF-β 和 BMP 信号通路中的作用机制

正芹

扬州大学附属医院

摘要

目的：转化生长因子 -β（TGF-β）与骨形态发生蛋白（BMP）信号通路失衡是肺动脉高压（PAH）的关键驱动因素。已有研究表明 BRCC3 可在肺动脉平滑肌细胞中重平衡上述通路，但其在肺动脉内皮细胞（PAH 发病中的关键细胞）中的作用尚未明确。本研究旨在探究 BRCC3 在内皮细胞中重平衡 TGF-β/BMP 信号的作用及其在实验性 PAH 中的治疗潜力，并与已知药物 Sotatercept 进行比较。

方法：体外实验中，对人肺动脉内皮细胞（HPAECs）进行低氧处理以模拟 PAH，同时取特发性肺动脉高压（IPAH）患者的内皮细胞，分别给予 Sotatercept 处理或腺病毒介导的 BRCC3 过表达（Ad-BRCC3）。通过蛋白质印迹法检测 Smad 蛋白（TGF-β/BMP 通路的下游效应分子）的磷酸化水平。体内实验中，对 SuHx 诱导的 PH 小鼠以及 MCT 诱导的 PH 大鼠分别给予 Sotatercept 或 BRCC3 病毒鼻腔滴送治疗，评估血流动力学参数（RVSP、RV ±dP/dt、Fulton 指数）、血管重构（通过组织学和血管造影）及右心功能（超声心动图），并分析肺组织中 Smad 的磷酸化水平。

结果：在低氧 HPAECs 和 IPAH 患者内皮细胞中，Sotatercept 可抑制 TGF-β 通路下游 p-Smad2/3 及 BMP 通路下游 p-Smad1/5/9 的磷酸化；而 Ad-BRCC3 在抑制 p-Smad2/3 的同时激活 p-Smad1/5/9，实现了更优的通路重平衡效果。在 SuHx 诱导的 PH 小鼠和 MCT 诱导的 PH 小鼠中，Sotatercept 和 BRCC3 均降低了 RVSP、RV ±dP/dt 及 Fulton 指数，减轻了血管重构（通过组织学显示壁厚度减少等），改善了血管造影参数（分支长度及连接数恢复），并提高了超声心动图中 TAPSE 和 PAAT/PEET 值（提示右心功能改善）。与 Sotatercept 组相比，BRCC3 组小鼠的右心功能超声结果更优。肺组织分析显示，Sotatercept 组中 Smad3 和 Smad1/5 的磷酸化水平均降低，而 BRCC3 组中 Smad3 磷酸化水平降低、Smad1/5 磷酸化水平升高。

Balloon Pulmonary Angioplasty for Inoperable Chronic Thromboembolic Pulmonary Hypertension: A 9-Year, Multicenter Cohort Study

Yu-Ping Zhou[1], Lu-Hong Qiu[2], An-Yi Wang[2], Chao Liu[1], Fu-Hua Peng[3], Xi-Qi Xu[4], Xin Jiang[1], Zhi-Cheng Jing[1]

1. Department of cardiovascular medicine, Guangdong Provencal People's Hospital, Guangdong Academy of Medical Sciences, Southern Medical University

2. Department of cardiology, Peking Union Medical College Hospital, Chinese Academy of Medical Sciences and Peking Union Medical College

3. Department of cardiovascular medicine, Fuwai Hospital, National Center for Cardiovascular Diseases, Chinese Academy of Medical Sciences and Peking Union Medical College

4. Neuro Cardio Vascular Diseases Center, Xuanwu Hospital, Capital Medical University

BACKGROUND Balloon pulmonary angioplasty (BPA) has been reported to be a therapeutic option for patients with inoperable CTEPH. However, there is a relative scarcity of long-term survival results about BPA for inoperable CTEPH, and previous studies were single-arm, non-comparative studies, and confounders including medical therapies and baseline characteristics limited the interpretation of survival benefits of BPA for inoperable CTEPH.

OBJECTIVES This study aims to evaluate the long-term survival benefit of BPA, with a contemporary control group, in a multicenter cohort of consecutive patients with inoperable CTEPH.

METHODS In this multicenter, prospective cohort study, a total of 232 patients with inoperable CTEPH who received the BPA procedures (the BPA group) and 70 patients who refused the BPA procedure (the non-BPA group), from January 1st, 2016 to December 31st, 2024, were enrolled. Of the 232 patients in the BPA group, 129 patients who completed the BPA procedure were further divided into the Full-BPA group and other 103 patients were divided into the Partial-BPA group. The primary outcome was all-cause mortality. The safety outcomes included BPA procedure-related complications. The primary analysis was to assess the differences in the outcomes between the BPA group and the non-BPA group whereas the secondary analysis was to compare the Full-BPA group and the Partial-BPA group against the non-BPA group. The survival rates were estimated with the Kaplan-Meier method and compared by log-rank test. Furthermore, three Cox regression models were constructed to calculate the unadjusted and adjusted hazard ratio of all-cause death: Model 1 had group as the only study variable, Model 2 was the Model 1 plus age and gender, and Model 3 was the Model 2 plus comorbidities, pulmonary vascular resistance, World Health Organization functional class and Riociguat treatment.

RESULTS Baseline characteristics and medical therapies were comparative between the BPA group and the non-BPA group, except for more female patients (56.9% vs. 42.9%, p = 0.039) in the BPA group. During a median follow-up time of 6.0 (3.7-7.3) years, 17 patients in the BPA group and 26 patients in the non-BPA group died, contributing to the 9-year survival rate of 86.9% (95% CI, 80.5 to 93.9) in the BPA group and 48.6% (95% CI, 34.6 to 68.1) in the non-BPA group (Figure 1, p

CONCLUSIONS BPA tended to be associated with a reduced risk of all-cause mortality with acceptable safety profiles in inoperable CTEPH, even in those received partial BPA sessions.

FIGURE 1. Survival of Inoperable CTEPH Patients in the BPA Group and Non-BPA Group.

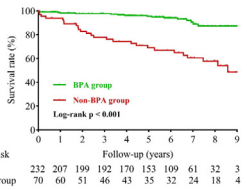

Patients at risk										
BPA group	232	207	199	192	170	153	109	61	32	3
Non-BPA group	70	60	51	46	43	35	32	24	18	4

Nine-year survival rates were 86.9% and 48.6% in the BPA group and the non-BPA group, respectively. The survival rate was significantly better in the BPA group compared with the non-BPA group. BPA = balloon pulmonary angioplasty; CTEPH = chronic thromboembolic pulmonary hypertension.

Figure 2. Survival of Inoperable CTEPH Patients in the Full-BPA Group, Partial-BPA Group, and Non-BPA Group.

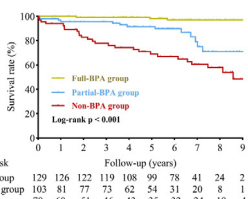

Patients at risk										
Full-BPA group	129	126	122	119	108	99	78	41	24	2
Partial-BPA group	103	81	77	73	62	54	31	20	8	1
Non-BPA group	70	60	51	46	43	35	32	24	18	4

Nine-year survival rates were 97.1% in the Full-BPA group, and 70.3% in the Partial-BPA group, both were better than 48.6% in the non-BPA group respectively. BPA = balloon pulmonary angioplasty; CTEPH = chronic thromboembolic pulmonary hypertension.

伴心血管合并症的特发性肺动脉高压患者临床特征分析

王齐 黄志华 罗勤 柳志红

中国医学科学院阜外医院

目的：了解伴心血管合并症的特发性肺动脉高压（IPAH）患者的临床特征。

方法：回顾性纳入 2014 年 10 月至 2024 年 6 月于中国医学科学院阜外医院住院的 150 例 IPAH 患者，分析伴心血管合并症的 IPAH 患者的临床指标、心脏结构及血液动力学特点。

结果：150 例 IPAH 患者的平均年龄为（35.9±12.5）岁，女性 110 例（73.3%），其中 88 例（58.7%）伴心血管合并症。伴心血管合并症的 IPAH 患者年龄明显大于不伴心血管合并症的 IPAH 患者 [（38.9±12.3）岁 vs.（31.7±11.9）岁]，血清 N 末端 B 型利钠肽原水平 [1 469.0（656.8，2 615.8）pg/ml vs. 923.5（304.4，1 958.8）pg/ml] 和右心房平均压升高 [6.0（3.3，9.0）mmHg vs. 4.0（3.0，6.3）mmHg（1 mmHg=0.133 kPa）], 混合静脉血氧饱和度 [（67.0±7.0）% vs.（70.3±6.9）%] 和心脏指数 [2.4（1.9，2.9）L/（min·m^2）vs. 2.8（2.3，3.8）L/（min·m^2）] 则显著降低（P 均 <0.05）。伴≥ 2 种心血管合并症的 IPAH 患者年龄明显大于伴 1 种心血管合并症的 IPAH 患者 [51.0（40.0，63.3）岁 vs. 35.0（29.3，43.8）岁]，左心房前后径 [（35.6±4.8）mm vs.（30.4±4.4）mm] 和左心室舒张末期前后径 [（40.8±7.5）mm vs.（35.8±5.5）mm] 均显著增加（P 均 <0.05）。在伴心血管合并症的 IPAH 患者中，高血压是最常见的合并症（48.9%）。

结论：伴心血管合并症的 IPAH 患者呈现出年龄增大的趋势，以高血压为首的一系列心血管合并症对 IPAH 患者的临床特征、心功能指标及血液动力学状态有重要影响，临床医师需重视对 IPAH 患者的合并症评估和管理。

Total Flavonoids of Epimedium Improve Pulmonary Vascular Remodeling in Pulmonary Hypertension: A Study Combining Network Pharmacology and Experimental Verification

Huan Li[1], Huizhao Liao[2], Weifeng Liao[1], Zijie Huang[1], Junyan Lin[2], Zhenzhen Zheng[1], Weimin Yao[1], Wenliang Chen[1], Riken Chen[1]

1. The Second Affiliated Hospital of Guangdong Medical University

2. The First Affiliated Hospital of Guangzhou Medical University

Objective

Pulmonary hypertension (PH) is a severe pathophysiological condition defined by elevated pulmonary artery pressure, which leads to right heart failure and has a historically low survival rate. The underlying pathology involves excessive pulmonary vascular remodeling, driven by the abnormal proliferation and migration of pulmonary artery smooth muscle cells (PASMCs). While current targeted drug therapies provide symptomatic relief, they do not fundamentally reverse the underlying vascular dysfunction. Total Flavonoids of Epimedium (TFE), a multi-component extract from a traditional medicinal herb, has demonstrated broad cardiovascular effects, including phosphodiesterase type 5 (PDE5) inhibition. However, the complex, multi-target pharmacological mechanism by which TFE may treat PH has not been systematically elucidated. This study aimed to investigate the molecular mechanisms of TFE against PH using an integrated approach of network pharmacology, molecular docking, and rigorous experimental verification in both in vivo and in vitro models.

Methods

A network pharmacology approach was first employed to identify the active components of TFE and their potential therapeutic targets. Component and target information was retrieved from the TCMSP, PubChem, and SwissTargetPrediction databases, while PH-related targets were sourced from the GeneCards database. A protein-protein interaction (PPI) network was constructed using Cytoscape software to identify core targets, followed by Gene Ontology (GO) and Kyoto Encyclopedia of Genes and Genomes (KEGG) pathway enrichment analysis using R language.

For experimental validation, an in vivo PH model was established in male Sprague-Dawley rats via a single intraperitoneal injection of monocrotaline (MCT). The rats were then treated daily for four weeks with either low-dose (60 mg/kg) or high-dose (180 mg/kg) TFE. Therapeutic efficacy was evaluated through hemodynamic measurements of Right Ventricular Systolic Pressure (RVSP) and histological assessment of pulmonary artery remodeling. In vitro, rat PASMCs were stimulated with PDGF-BB to induce proliferation and migration. The effects of TFE, with and without specific inhibitors of the p53/p21 pathway, were assessed using EDU, scratch, and TUNEL assays. Finally, molecular docking technology was used to analyze the binding affinity between key TFE compounds and the primary identified target, p53.

Results

The network pharmacology analysis identified 13 primary monomer components in TFE, which shared 140 common targets with PH. PPI network analysis highlighted several core targets, including TP53, TNF, and AKT1. In the in vivo experiments, high-dose TFE (180 mg/kg) significantly attenuated the MCT-induced increases in RVSP and reduced pulmonary vascular wall thickness, while the low-dose TFE treatment showed no statistically significant improvement. High-dose TFE also reversed the MCT-induced downregulation of p53 mRNA in lung tissue. In the in vitro studies, TFE effectively inhibited PDGF-BB-induced PASMC proliferation and migration while promoting apoptosis. These beneficial effects were significantly reversed by the addition of p53 and p21 inhibitors, confirming the critical role of this signaling pathway in TFE's mechanism of action. Furthermore, molecular docking simulations revealed strong binding affinities between the primary active compounds in TFE and the p53 protein, with binding energies all less than -5 kcal/mol.

Conclusion

This study successfully integrated network pharmacology with experimental validation to demonstrate that TFE ameliorates pulmonary hypertension. The underlying mechanism involves the inhibition of pulmonary artery smooth muscle cell proliferation and migration and the promotion of apoptosis, effects which are mediated through the activation of the p53/p21 signaling pathway. The dose-dependent efficacy observed in the animal model suggests that high-dose TFE holds significant potential as a therapeutic agent for improving pulmonary vascular remodeling and hemodynamics in PH. These findings provide a robust scientific basis for the therapeutic effects of TFE and support further development of its components for the treatment of pulmonary hypertension.

Hemodynamic effects of dobutamine versus dopamine in preterm infants: a meta-analysis

li jiang

Jiangsu Province Hospital, the First Affiliated Hospital of Nanjing Medical University

Objective: For the past few years there has been a steady increase in the incidence of preterm birth, and now the number of preterm infants accounts for 9.6% of births worldwide, a total of approximately 13 million births annually. Preterm birth is associated with a range of adverse hemodynamic problem, which may be attributed to altered development of cardiovascular and central nervous systems following preterm birth. Dobutamine and dopamine are the commonly used drugs in preterm infants, but the majority of what is known about these drugs is the result of adults studies. Guidelines published by National Association of Neonatal Nurses support the administration of vasopressors to hypotensive infants with clinical signs of low systemic blood flow. Therefore, it is important to focus the review on the response of not only hypotension but also low blood flow and organ perfusion by using dobutamine and dopamine. To compare the effects and safety of dobutamine versus dopamine in preterm infants with abnormal hemodynamic status.

Method: Study sources were from PubMed, EMBASE, the Cochrane Library, ISI Web of Knowledge and Google Scholar up to 2017 for RCTs in which dobutamine and dopamine treatment was adopted. Included studies were conducted on preterm infants

with abnormal hemodynamic status that reported mortality < 28 days, treatment failure and organ effects.

Results: 72 citations were identified, and 7 articles were included with a total 286 patients. 4 studies only focused on the change of blood pressure after treatment in cardiac aspects. Studies of Roze1993 stated the relationship between blood pressure (BP), left ventricular output (LVO) and SVR, in which dobutamine significantly reduced SVR (1035 ± 188 to 1171 ± 237 dynes/sec/cm5/m2 with dobutamine vs. 1124 ± 186 to 1952 ± 300 dynes/sec/cm5/m2 with dopamine) and enhanced LVO (+21 ± 7% with dobutamine vs. -14 ± 8% with dopamine) while dopamine increase the mean arterial BP (25.6 ± 1.2 to 37.7 ± 1.5 mmHg with dopamine vs. 24.4 ± 1.0 to 32.0 ± 1.4 mmHg with dobutamine) mainly. Hentscel1995 stated the relationship between BP and partial blood flow and vascular resistance. In this study, both dobutamine and dopamine significantly enhanced mean artery pressure (31.0 ± 6.8 to 37.7 ± 9.8 mmHg with dobutamine vs. 27.7 ± 3.6 to 36.0 ± 9.3 mmHg with dopamine) and reduced vascular resistance of superior mesenteric artery (SMA) (0.81 ± 0.07 to 0.74 ± 0.11 with dobutamine vs. 0.89 ± 0.06 to 0.79 ± 0.07 with dopamine), meanwhile only dobutamine managed to increase partial blood flow velocity (25.8 ± 13.5 to 31.5 ± 16.5 cm/s with dobutamine vs. 16.3 ± 5.0 to 19.0 ± 6.0 cm/s with dopamine). Osborn2002 focused on low blood flow rather than hypotension. Authors revealed that dobutamine resulted in a more significant increase in superior vena cava (SVC) flow (30.8 ± 7.2 to 85.6 ± 24.7 mL/kg/min with dobutamine vs. 33.8 ± 5.4 to 68.0 ± 30.2 mL/kg/min with dopamine) and only at 24h it had a preponderant effect of right ventricular output (RVO) (130.2 ±

42.3 to 294.5 ± 81.3 mL/kg/min with dobutamine vs. 126.7 ± 49.7 to 169.2 ± 51.9 mL/kg/min with dopamine), in the meantime dopamine resulted in a greater increase in BP (29.9 ± 4.8 to 39.8 ± 4.9 mmHg with dobutamine vs. 26.0 ±7.1 to 35.4 ± 4.9 mmHg with dopamine). 5 studies reported mortality (180 patients), 4 studies reported P/IVL (145 patients), 4 studies reported P/IVH (160 patients), 2 studies reported severe P/IVH (105 patients), 3 studies reported NEC (140 patients), 2 studies reported BPD (55 patients), and 6 studies reported treatment failure (266 patients). Meta-analysis showed an increased probability in treatment failure using

dobutamine treatment (RR, 1.67; 95% CI, 1.14-2.45; P = 0.008), whereas there was no significant difference in mortality < 28 days (RR, 1.16; 95% CI, 0.70– 1.91; P = 0.57), P/IVL (RR, 2.90; 95% CI, 0.93-9.11; P = 0.07), P/IVH (RR, 1.23; 95% CI, 0.73-2.08; P = 0.44), severe P/IVH (RR, 0.58; 95% CI, 0.21-1.62; P = 0.30), NEC (RR, 2.21; 95% CI, 0.60-8.09; P = 0.23) and BPD (RR, 1.04; 95% CI, 0.38-2.82; P = 0.94) between two groups.

Conclusion: Dopamine showed more effective in treatment success in treatment of preterm infants with abnormal systemic hemodynamic status. No evidence of difference was found existed in mortality < 28 days and the incidence of adverse organ effects including P/IVL, P/IVH, NEC and BPD between dobutamine and dopamine. However, more RCTs need to be performed to firm the safety and benefit of the two drugs to make a clear choice to solve systemic hemodynamic problem of preterm infants and their effects on the interaction of systemic BP, cardiac output and SVR.

儿童期起病肺动脉高压合并 FLNA 基因突变 1 例

谭瑞

武汉亚洲心脏病医院

目的：肺动脉高压是指由各种原因导致的肺血管阻力和肺动脉压力升高的病理综合征，继而发展为右心衰竭甚至死亡。本文报道儿童起病肺动脉高压合并 FLNA 基因突变一例，总结其诊疗经过并分析发病原因。

诊疗经过：7 岁男性患儿，因“发现三尖瓣反流半年”于 2025.01.14 就诊。入院查体示 P2 增强，完善心脏彩超提示右心稍大（右房 3.6cm, 右室 3.6cm），三尖瓣轻度反流，肺动脉高压轻度（估测 46mmHg），进一步行右心导管：PAP55/20/32mmHg，PCWP 17/7/10mmHg，PP/PS 0.38，PVR 3.7WOOD。肺动脉高压诊断明确，进一步排查病因，完善肺血管 + 腹部 + 心脏 CTA 提示主肺动脉增宽、右心稍大；肺功能提示轻度阻塞性通气功能障碍、弥散功能正常；风湿免疫抗体无异常，全外显子基因检测提示 FLNA:NM_001456.4:exon44:c.7160G>C:p.R2387P 变异。

讨论：儿童肺动脉高压病因复杂，起病隐匿，心脏彩超可为潜在患儿的筛查提供重要意义，右心导管检测可明确诊断。染色体的异常改变与遗传相关因素在儿童肺动脉高压的发病中有着重要意义，目前研究证实 BMPR2、ACVRL1、CAV1、TBX4 等基因突变与肺动脉高压相关。FLNA 基因心编码的 Filamin A 蛋白是细胞骨架的核心组件，负责调控细胞形态、迁移和信号转导，尤其在神经元发育、血管形成中起关键作用，其错义突变目前尚未明确为肺动脉高压致病基因，但研究发现与心血管发育不良、Melnick-Needles 综合征密切相关，同时 Melnick-Needles 综合征的重要表现之一为肺动脉高压，FLNA 错义突变可能为肺动脉高压潜在致病基因之一。

经皮机械血栓清除术治疗中、高危急性肺栓塞： 初步疗效与安全性研究

潘泓 王皓辰 蒋鑫 荆志成

广东省医学科学院 广东省人民医院

目的：评估应用国产新型机械取栓装置（Tendvia，上海腾复）行经皮机械血栓清除术（PMT）治疗中、高危急性肺栓塞（APE）患者的初步疗效和安全性。

方法：本研究为前瞻性设计，纳入 2024 年 11 月至 2025 年 6 月期间就诊于广东省人民医院且使用 Tendvia 机械取栓装置行 PMT 治疗的中、高危 APE 患者。主要疗效指标为基线至术后 48 小时右心室 / 左心室比值（RV/LV）的下降值（CT 肺动脉造影评价）。次要疗效指标包括术后即刻患者肺动脉平均压（mPAP）变化，术后 48 小时 N 端脑钠肽前体（NT-proBNP）、肌钙蛋白 T（TnT）及 D- 二聚体变化。安全性指标包括术中及住院期间 PMT 相关并发症及不良事件发生情况。

结果：本研究共纳入 18 例接受 PMT 治疗的 APE 患者，平均年龄 56.0±15.7 岁，66.7% 患者为女性，其中高危 3 例，中危 15 例。所有患者 PMT 术中均使用 Tendvia 抽吸导管抽吸血栓，14 例患者同时使用网篮血栓清除装置，术中取栓成功率为 100%。除 1 例患者在成功行 PMT 治疗后因考虑存在微血管栓塞而在局部应用导管内尿激酶溶栓，余患者术中及术后均未使用溶栓药物治疗。相比术前，术后 48 小时 RV/LV 比值显著降低（1.39±0.35 vs.1.01±0.18, P<0.001）。此外，相比术前，术后即刻 mPAP 显著降低（27.0±9.0mmHg vs. 20.0±7.0mmHg，P<0.001）；术后 48 小时 NT-proBNP [1079.0（277.0, 2633.5）pg/mL vs. 322.2（74.4, 1450.0）pg/mL, P=0.003）]、TnT [53.6（22.5, 190.3）pg/mL vs. 26.5（15.0, 93.6）pg/mL，P=0.033] 和 D- 二聚体 [7580.0（4565.0, 18655.0）ng/mL vs. 2325.0（1690.0, 5030.0）ng/mL，P<0.001] 均有显著降低。1 例高危 APE 患者在顺利取栓后发生心脏骤停，余患者术中及住院期间内未发生严重不良事件。

结论：初步研究显示，对于中、高危急性肺栓塞患者，应用国产 Tendvia 机械取栓装置可快速清除双肺动脉血栓，大幅降低血栓负荷，同时迅速降低肺动脉压力，改善右心功能和心肌损伤指标，且安全性良好，为中、高危 APE 患者提供一种新的治疗选择。

“Treat-and-Repair” 策略在成人房间隔缺损合并重度肺动脉高压患者中的疗效与安全性分析——基于单中心回顾性研究

张家兴 刘梦宜 蒋鑫 荆志成

广东省医学科学院、南方医科大学附属广东省人民医院

目的 探讨 “Treat-and-Repair” 策略在成人房间隔缺损合并重度肺动脉高压（ASD-PAH）患者中的疗效及安全性。

方法 回顾性纳入 2011 年 2 月 –2024 年 11 月广东省人民医院收治的 36 例重度 ASD-PAH 患者（女 27 例；年龄 29.3±7.2 岁；缺损直径 21.8±7.8 mm）。首次右心导管确诊 PAH 且无手术指征者，接受靶向药物治疗（内皮素受体拮抗剂 / 磷酸二酯酶 -5 抑制剂 / 前列环素类似物）。治疗中位 183 天后行二次右心导管评估，经多学科团队确认手术指征后行缺损介入 / 外科闭合术。术后中位随访 574 天，34 例接受超声心动图检查，7 例复查右心导管。主要评价指标为平均肺动脉压（mPAP）、肺血管阻力（PVR）及超声估测的肺动脉收缩压（PASP），采用配对 t 检验比较各阶段指标的差异。

结果 靶向药物治疗后，36 例患者中 mPAP 由基线 56.0±8.7 mmHg 降至 44.2±11.4 mmHg，平均下降 11.75 mmHg（95% CI 7.93–15.57，p<0.001）；PVR 由 8.0±3.1 WU 显著减少至 4.2±1.8 WU（p<0.001），经多学科讨论后全部患者进行缺口闭合手术。术后随访结果提示，34 例超声心动图随访显示 PASP 由术前 75.6±17.6 mmHg 进一步降至 35.7±13.2 mmHg，平均下降 39.9 mmHg（95% CI 32.4–47.4，p<0.001）；7 例患者行右心导管评估，mPAP 由 44.2±11.4 mmHg 降至 25.4±8.8 mmHg，平均下降 18.8 mmHg（95% CI 11.6–25.9，p= p<0.001），术后 PVR 维持在 4.0±1.5 WU。全程未见严重不良事件。

结论 “Treat-and-Repair” 策略通过靶向药物显著改善重度 ASD-PAH 患者血流动力学指标，使传统禁忌患者成功接受缺损闭合术，术后血流动力学持续优化。PVR 维持在低水平提示肺血管重构改善，但需扩大样本验证长期获益。

早期强化靶向治疗在房间隔缺损合并重度肺动脉高压患者中的应用探索一项前瞻性病例系列报告

张家兴 刘梦宜 蒋鑫 荆志成

广东省医学科学院、南方医科大学附属广东省人民医院

目的 探讨在经右心导管确诊重度 PAH 且暂不具备手术指征的 ASD 患者中，立即启动曲前列尼尔联合口服靶向治疗对改善血流动力学并桥接缺口闭合手术的临床价值。

方法 本前瞻性病例系列自 2024 年 1 月至 2024 年 12 月纳入 3 例经右心导管确诊重度 PAH 且暂不具备手术指征的 ASD 患者，早期启动皮下曲前列尼尔持续泵入（根据耐受性及血流动力学目标逐步调整至 35-40 ng/kg·min），并联合口服至少两种靶向药物（马昔腾坦、他达拉非或利奥西胍等）。所有患者在治疗期间定期行右心导管和超声心动图评估，并于治疗 20±4 周后在多学科团队评估下实施 ASD 缺口闭合手术；术后三个月通过超声心动图随访疗效。

结果 3 例女性患者（平均年龄 32.7 ± 4.1 岁），经早期曲前列尼尔联合口服靶向治疗 20 ± 4 周后，肺血流动力学显著改善：mPAP 由 55.7 ± 9.3 降至 44.7 ± 6.4 mmHg，PVR 由 10.5 ± 5.5 降至 3.8 ± 2.2 WU，Qp/Qs 由 1.40 ± 0.27 升至 2.09 ± 0.2。多学科评估后 3 例顺利行 ASD 修补术，无严重并发症；术后 3 个月超声复查显示左心腔明显扩张（左室舒张末期内径由 35.3 ± 3.1 增至 41.0 ± 4.4 mm；收缩末期内径由 21.7 ± 0.6 增至 25.7 ± 4.0 mm）而右心腔显著缩小（右房上下径由 53.3 ± 2.9 降至 44.0 ± 3.5 mm；右室上下径由 70.3 ± 2.1 降至 62.0 ± 4.4 m），三尖瓣返流明显减轻，进一步证明该治疗策略在改善肺血流动力学和重构心腔方面的有效性。

结论 在重度 ASDPAH 患者中，自首次诊断起即启动早期曲前列尼尔皮下注射联合口服靶向治疗，可有效降低 PVR 并改善血流动力学参数，为外科修补或内科封堵创造可行的“桥接”条件，且术后继续发挥优化肺动脉压力与右心功能的作用。该前瞻性小样本观察提示该策略具有良好的临床潜力，需进一步在更大样本与多中心研究中加以验证。

复杂高危冠脉介入有关研究

A Retrospective Cohort Study on Long-Term Outcomes of Ticagrelor versus Clopidogrel After Retrograde Percutaneous Coronary Intervention for Chronic Total Occlusion

Fei-Huang Han

Guangdong Provincial People's Hospital

Background

Chronic total occlusion (CTO) is a common and clinically significant lesion subtype encountered in 15% to 25% of patients undergoing coronary angiography. Successful percutaneous coronary intervention (PCI) for CTO can alleviate myocardial ischemia, relieve angina symptoms, and significantly improve quality of life. However, CTO-PCI—particularly when performed via the retrograde approach—is technically complex and associated with higher rates of complications. The increased risk of acute and long-term stent thrombosis, restenosis, and procedural failure is often attributed to features such as longer lesion length, severe calcification, and extensive stent deployment.

Dual antiplatelet therapy (DAPT), typically combining aspirin with a P2Y12 receptor inhibitor, remains a cornerstone of post-PCI pharmacotherapy to prevent thrombotic complications. While clopidogrel has long been the standard P2Y12 inhibitor for patients with chronic coronary syndrome (CCS), newer and more potent agents like ticagrelor have shown superior efficacy in acute coronary syndrome (ACS) settings. Nonetheless, their role in CTO-PCI—especially in CCS patients undergoing retrograde interventions—remains inadequately defined. Conflicting data from previous observational studies and trials underscore the need for focused investigations in this subset. This study aims to evaluate the long-term clinical outcomes of ticagrelor-based DAPT compared to clopidogrel-based therapy in patients undergoing elective retrograde CTO-PCI.

Methods

We conducted a retrospective cohort study involving 836 consecutive patients who underwent elective retrograde CTO-PCI at a single tertiary center from January 2011 to April 2023. Patients were stratified based on their post-procedural DAPT regimen: ticagrelor or clopidogrel in addition to aspirin. Baseline demographic data, lesion characteristics, procedural details, and post-procedural outcomes were systematically recorded. The primary endpoint was the incidence of major adverse cardiovascular events (MACE), including all-cause mortality, cardiac death, myocardial infarction, and target vessel revascularization, during follow-up. Secondary outcomes included safety endpoints and individual components of the composite endpoint.

Results

Of the 836 patients, 767 (91.2%) completed clinical follow-up, with a median duration of 1,041 days (interquartile range: 531–1,511 days). The baseline characteristics were well balanced between both treatment groups. The retrograde technical success was high and similar between two treatment group (92.5% vs. 88.0%, p = 0.42), as well as CC tracking success (95.7% vs. 92.9%, p = 0.23) and recanalization success (94.1% vs. 89.4%, p = 0.075). The incidence of cardiac tamponade, pericardiocentesis, emergency surgery, and in-hospital death was similar between the groups (all p > 0.05). No significant bleeding events were observed in any of the treatment groups. Patients treated with ticagrelor demonstrated a significantly lower rate of MACE compared to those treated with clopidogrel (8.8% vs. 18.5%, p = 0.005). The difference was primarily driven by reduced all-cause mortality (1.9% vs. 8.1%, p = 0.009) and cardiac death (0.6% vs. 5.8%, p = 0.012).

Conclusion

Our findings indicate that ticagrelor-based DAPT may offer superior long-term cardiovascular protection in CCS patients undergoing retrograde CTO-PCI. The significant reduction in MACE, all-cause mortality, and cardiac death without a concomitant rise in bleeding events highlights the potential role of potent P2Y12 inhibition in this high-risk population. These results provide supportive evidence for considering ticagrelor as a favorable DAPT option in selected CTO-PCI patients, though prospective randomized controlled trials are warranted to confirm these observations and to refine antiplatelet strategies tailored to CTO complexity and patient-specific risk profiles.

Prediction of percutaneous coronary intervention success in moderate-to-severe coronary artery calcification patients using machine learning based on coronary angiography

ZIXIANG YE, KEFEI DOU

Chinese Academy of Medical Sciences & Peking Union Medical College Fuwai Hospital

Background: Given the challenges faced during percutaneous coronary intervention (PCI) for heavily calcified lesions, accurately predicting PCI success is crucial for enhancing patient outcomes and optimizing procedural strategies.

Objective: This study aimed to utilize machine learning to identify coronary angiographic vascular characteristics and PCI procedures associated with the immediate procedural success rates of PCI in patients exhibiting moderate-to-severe coronary artery calcification (MSCAC).

Methods: This study included patients who underwent PCI between January 2017 and December 2018 in a cardiovascular hospital, comprising 3,271 patients with MSCAC and 17,998 with no or mild coronary artery calcification. Six machine learning models—K-nearest neighbors, Gradient Boosting Decision Tree, Extreme Gradient Boosting (XGBoost), logistic regression, random forest, and support vector machine —were developed and validated, with SMOTE used to address imbalance data. Model performance was compared using multiple parameters, and the optimal algorithm was selected. Model interpretability was facilitated by SHapley Additive exPlanations (SHAP), identifying the top six coronary angiographic features with the highest SHAP values for inclusion in the optimal predictive model. The importance of different PCI procedures was also elucidated via SHAP values. Testing validation was performed in a separate cohort of 1,437 MSCAC patients in 2013. Sensitivity analyses were conducted in patients with acute coronary syndrome (ACS) and chronic coronary syndrome (CCS).The definition of immediate PCI procedure success was a restoration of grade 2 or 3 Thrombolysis in myocardial infarction (TIMI) flow with residual stenosis of less than 50% as well as without significant operational complications, such as intraoperative stent thrombosis, coronary artery dissection, perforation of the coronary artery and in-hospital MACE.

Results: In the development cohort, 7.6% of MSCAC patients experienced PCI failure, compared to 4.5% of patients with no or mild CAC. The XGBoost model demonstrated superior performance, achieving the highest area under the receiver operator characteristic curve (AUC) of 0.984, average precision (AP) of 0.986, F1 score of 0.970, and G-mean of 0.970 among the six models. Calibration curves indicated reliable predictive accuracy. The key predictive factors identified included lesion length, minimum lumen diameter, TIMI flow grade, chronic total occlusion, reference vessel diameter, and diffuse lesion (SHAP value 1.65, 1.40, 0.92, 0.60, 0.54, and 0.47, respectively). The lesion length, MLD, and RVD were found to have a nonlinear relationship with the probability of PCI failure with the cut-off value is 30mm, 0.3mm, and 3.0mm. The use of modified balloons for calcified lesion preparation had a positive effect on PCI success in MSCAC patients (SHAP value 0.16). The five most important PCI procedures predicting success included stent implantation, use of the tandem stenting technique, number of stents implanted, post-dilation, and the use of balloon pre-dilation. Sensitivity analyses showed consistent model performance across ACS and CCS subgroups, with similar top five coronary angiographic variables (lesion length, MLD, TIMI flow, RVD, and CTO). The optimized XGBoost model maintained robust predictive performance in the testing cohort, with an AUC of 0.972, AP of 0.962, F1 score of 0.940, and G-mean of 0.930.

Conclusions: The interpretable XGBoost models with the best performance in predicting PCI immediate procedure success for MSCAC patients were established and validated. Six important CAG predictors, including lesion length, MLD, TIMI, CTO, RVD, diffuse lesion, and a PCI treatment (modified balloon) were explored. Machine learning models can precisely predict the success rate of PCI in patients with MSCAC. This capability assists clinicians in identifying challenging cases, enabling cardiologists to allocate their efforts more effectively toward delivering safer and more efficient treatments.

Effect of paclitaxel-coated balloon angioplasty on side branch lesion and cardiovascular outcomes in patients with de novo true coronary bifurcation lesions undergoing percutaneous coronary intervention Qi Mao Department of Cardiology, Institute of Cardi

Mao Qi

Xinqiao Hospital

Effect of paclitaxel-coated balloon angioplasty on side branch lesion and cardiovascular outcomes in patients with de novo true coronary bifurcation lesions undergoing percutaneous coronary intervention

Qi Mao

Department of Cardiology, Institute of Cardiovascular Research, Xinqiao Hospital, Army Medical University, Chongqing 400037, China

Abstract

Purpose To compare the effects of paclitaxal-coated balloon (PCB) versus conventional balloon (CB) on side branch (SB) lesion and cardiovascular outcomes in patients with de novo true bifurcation lesions.

Methods In total, 219 patients with de novo true bifurcation lesions were enrolled and divided into PCB group (102 cases) and CB group (117 cases) according to angioplasty strategy in SB. Drug-eluting stent (DES) was implanted in main vessel (MV) for each subject. All subjects underwent

a 12-month follow-up for late lumen loss (LLL), restenosis and major adverse cardiovascular events (MACE) after percutaneous coronary intervention (PCI). MACEs included cardiac death, nonfatal myocardial infarction and unstable angina requiring admission.

Results There were no differences in diameter, minimum lumen diameter (MLD) and stenosis for bifurcation lesions between the two groups before and immediately after PCI (P>0.05). After 12-month follow-up, no differences occurred in MV-MLD and MV-LLL between the two groups (P>0.05); SB-MLD in PCB group was higher than that in CB group (1.97±0.36 mm vs. 1.80±0.43 mm, P=0.007); SB-LLL in PCB group was lower than that in CB group (0.11±0.18 mm vs. 0.19±0.25 mm, P=0.024). Multivariate COX analyses indicated that PCB group had lower MACE risk than CB group (HR=0.480, 95%CI 0.244-0.941, P=0.033).

Conclusion PCB could decrease SB-LLL and MACE risk in patients with de novo true coronary bifurcation lesion 12 months after single-DES intervention.

Key words paclitaxal-coated balloon, percutaneous coronary intervention, bifurcation lesion, late lumen loss, cardiovascular events

Effect of paclitaxel-coated balloon angioplasty on side branch lesion and cardiovascular outcomes in patients with de novo true coronary bifurcation lesions undergoing percutaneous coronary intervention

Qi Mao

Department of Cardiology, Institute of Cardiovascular Research, Xinqiao Hospital, Army Medical University, Chongqing 400037, China

Abstract

Purpose To compare the effects of paclitaxal-coated balloon (PCB) versus conventional balloon (CB) on side branch (SB) lesion and cardiovascular outcomes in patients with de novo true bifurcation lesions.

Methods In total, 219 patients with de novo true bifurcation lesions were enrolled and divided into PCB group (102 cases) and CB group (117 cases) according to angioplasty strategy in SB. Drug-eluting stent (DES) was implanted in main vessel (MV) for each subject. All subjects underwent a 12-month follow-up for late lumen loss (LLL), restenosis and major adverse cardiovascular events (MACE) after percutaneous coronary intervention (PCI). MACEs included cardiac death, nonfatal myocardial infarction and unstable angina requiring admission.

Results There were no differences in diameter, minimum lumen diameter (MLD) and stenosis for bifurcation lesions between the two groups before and immediately after PCI (P>0.05). After 12-month follow-up, no differences occurred in MV-MLD and MV-LLL between the two groups (P>0.05); SB-MLD in PCB group was higher than that in CB group (1.97±0.36 mm vs. 1.80±0.43 mm, P=0.007); SB-LLL in PCB group was lower than that in CB group (0.11±0.18 mm vs. 0.19±0.25 mm, P=0.024). Multivariate COX analyses indicated that PCB group had lower MACE risk than CB group (HR=0.480, 95%CI 0.244-0.941, P=0.033).

Conclusion PCB could decrease SB-LLL and MACE risk in patients with de novo true coronary bifurcation lesion 12 months after single-DES intervention.

Key words paclitaxal-coated balloon, percutaneous coronary intervention, bifurcation lesion, late lumen loss, cardiovascular events

Effect of paclitaxel-coated balloon angioplasty on side branch lesion and cardiovascular outcomes in patients with de novo true coronary bifurcation lesions undergoing percutaneous coronary intervention

Qi Mao

Department of Cardiology, Institute of Cardiovascular Research, Xinqiao Hospital, Army Medical University, Chongqing 400037, China

Abstract

Purpose To compare the effects of paclitaxal-coated balloon (PCB) versus conventional balloon (CB) on side branch (SB) lesion and cardiovascular outcomes in patients with de novo true bifurcation lesions.

Methods In total, 219 patients with de novo true bifurcation lesions were enrolled and divided into PCB group (102 cases) and CB group (117 cases) according to angioplasty strategy in SB. Drug-eluting stent (DES) was implanted in main vessel (MV) for each subject. All subjects underwent a 12-month follow-up for late lumen loss (LLL), restenosis and major adverse cardiovascular events (MACE) after percutaneous coronary intervention (PCI). MACEs included cardiac death, nonfatal myocardial infarction and unstable angina requiring admission.

Results There were no differences in diameter, minimum lumen diameter (MLD) and stenosis for bifurcation lesions between the two groups before and immediately after PCI (P>0.05). After 12-month follow-up, no differences occurred in MV-MLD and MV-LLL between the two groups (P>0.05); SB-MLD in PCB group was higher than that in CB group (1.97±0.36 mm vs. 1.80±0.43 mm, P=0.007); SB-LLL in PCB group was lower than that in CB group (0.11±0.18 mm vs. 0.19±0.25 mm, P=0.024). Multivariate COX analyses indicated that PCB group had lower MACE risk than CB group (HR=0.480, 95%CI 0.244-0.941, P=0.033).

Conclusion PCB could decrease SB-LLL and MACE risk in patients with de novo true coronary bifurcation lesion 12 months after single-DES intervention.

Key words paclitaxal-coated balloon, percutaneous coronary intervention, bifurcation lesion, late lumen loss, cardiovascular events

步步为营，险中求生 -IVUS 应用急性心肌梗死合并左主干、前三叉分叉病变救治一例

俊

马鞍山市人民医院

本文记录一例 NSTEMI、OMI、PCI 术后患者，既往 1 年前下壁心梗植入支架，此次 1 月前因心绞痛入院行冠脉造影术示左主干合并前三叉分叉病变，当时患者及家属拒绝介入治疗，出院后再次入院，诊断 NSTEMI，患者及家属同意手术，术中根据 IVUS 指南及患者病情变化情况最终选择了 T 术式，最终安全下台，患者血运重建后心脏功能改善、康复出院，现随访一般情况良好。

病例亮点

1. 缺血性心肌病，有条件的建议完全血运重建，改善患者远期预后。

2. 对于 CHIP 冠心病患者（存在无保护左主干病变、严重三支病变、多支闭塞病变、慢性完全闭塞病变、严重前三叉病变、冠脉桥血管病变、严重血栓负荷病变等）这类高危患者，术前需充分评估制定好策略及应急预案，术中需严密监测患者生命体征，术后需防范相关并发症出现，另有条件的可使用机械循环辅助装置（ECMO/IABP/Impella）保驾。

3. 对于左主干病变，术前 7F 鞘管及指引导管，术中去甲肾上腺应用，注意造影配比，球囊支架快起快放；对于分叉病变，熟练掌握几种术式的流程，同时需根据术中患者情况，及时灵活调整治疗方案。

4. 对于高危介入患者，术前需要与患者及家属的充分知情沟通，同时术中患者的安全永远是第一位。

探究 ETcath200 系统在经皮冠状动脉介入治疗（PCI）复杂病变中的安全性与有效性

翟光耀 杨婧 房宇琦 闫奕竹

首都医科大学附属北京潞河医院

目的：本研究旨在评估中国自主研发的冠状动脉介入手术控制系统 ETcath200 在经皮冠状动脉介入治疗（PCI）复杂病变中的安全性与有效性。

方法：本研究采用前瞻性、单中心、单组目标值临床试验设计。研究纳入标准为（1）年龄 >18 岁，性别不限；（2）B2/C 型病变（根据 1988 年 ACC/AHA 冠状动脉病灶分类）；（3）自愿参加并签署知情同意书。本研究对所有受试者采用介入手术控制系统 ETcath200 辅助完成 PCI，该系统由导丝执行机构、导管执行机构、控制盒、控制机柜、触摸屏及液晶显示器六部分组成，支持操作员对导丝、球囊 / 支架及导引导管进行精准操控。主要研究终点包括：①临床成功，定义为术后目测残余狭窄 <30%、TIMI 血流 3 级，且术后 48 小时内或出院前（以先到者为准）无主要不良心血管事件（MACE）发生；②技术成功，定义为达到临床成功标准，且介入过程中导管、导丝、球囊扩张导管及支架系统的推送、回撤、旋转均由介入手术控制系统完成，无中转人工操作。

结果：研究共纳入 20 例受试者（80% 为男性，20% 为女性），共 24 个靶病变，其中 B2 型病变 4 个（16.67%），C 型病变 20 个（83.33%），临床成功率 100%，无 MACE 事件发生；技术成功率为 80%，4 例受试者（20%）中转人工操作，机器人手术平均时间 68.50 分钟（IQR：41.75-74.25 分钟），术者平均辐射剂量为 0.0900uSv（IQR：0.0325-0.1000uSv），15 例患者放置直径为 2.75mm（IQR：2.50- 3.00mm）且长度为 22mm（IQR：16-30mm）的药物洗脱支架，机器人器械性能评价、阻力显示功能评价、操作模式评价均优秀率 100%。

结论：本研究为 ETcath200 介入机器人应用于 PCI 全流程的首次临床验证，初步证实 ETcath200 系统用于冠状动脉复杂病变介入治疗具有良好的可行性、安全性和有效性。

准分子激光冠状动脉成形术在慢性完全闭塞性病变中的应用

关韶峰 陈阳 曲新凯

复旦大学附属华东医院

目的：观察准分子激光冠状动脉成形术 (ELCA) 在冠状动脉慢性完全性闭塞 (CTO) 病变中应用的安全性和有效性。

方法：：总结自 2021 年 1 月至 2025 年 3 月在华东医院应用 ELCA 治疗的 CTO 病变患者，共 30 例，其中 LAD 病变占 40%，造影提示合并钙化占 60%。所有患者导引钢丝在对侧冠状动脉造影指引下成功通过闭塞段病变，应用 1.0mm 或 1.25mm 直径球囊均无法通过病变，其中 7 例患者应用延长导管支持球囊亦无法通过，ELCA 治疗后球囊均顺利通过病变，使用的脉冲频率 35~60Hz, 能量密度 30~60mJ/mm，激光消融导管直径均为 0.9mm，13 例（43%）患者消融时用对比剂冲管以增加消融强度，激光消融次数在 5 次以内后消融导管顺利通过病变的为 15 例（50%），其中 2 例消融后再行旋磨治疗，最终均进行药物洗脱支架置入。观察手术成功率及并发症，并随访主要心脏不良事件发生情况。

结果：30 例患者 ELCA 器械操作全部成功、介入治疗全部成功 . 术中无 1 例发生

血管夹层、穿孔、慢血流及血栓形成，随访期间无 1 例发生心绞痛、心肌梗死、靶病变再次血运重建及死亡。

结论：准分子激光冠状动脉成形术应用于球囊无法通过的慢性闭塞病变是安全有效的。

Retrograde Protected Antegrade Puncture Reentry: A Novel Strategy to Improve Procedural Efficiency in Retrograde CTO PCI

Qi-Heng Wan, Ze-Han Huang, Song Wen, Dun-Liang Ma, Fei-Huang Han, Yu-Qing Huang, Shao-Yu Wu, Feng Wang, Bin Zhang

Department of Cardiology, Guangdong Cardiovascular Institute, Guangdong Provincial People's Hospital, Guangdong Academy of Medical Sciences,

Background: Reverse CART is the predominant strategy for retrograde chronic total occlusion (CTO) percutaneous coronary intervention (PCI), but it is technically demanding, requiring successful retrograde microcatheter tracking through collateral channels (CCs) and precise spatial alignment between the collateral exit and the distal CTO cap. These limitations hinder procedural efficiency and success, especially in anatomically challenging cases. To overcome these challenges, we developed a novel technique called retrograde protected antegrade puncture reentry (RPR), which enables controlled antegrade reentry under retrograde wire guidance while minimizing reliance on retrograde microcatheter CCs crossing.

Purpose: To evaluate the procedural efficiency, success rate, and safety of the RPR technique compared to conventional Reverse-CART in patients undergoing retrograde CTO PCI.

Methods: We retrospectively analyzed 320 consecutive patients who underwent retrograde CTO PCI by high-volume operators at Guangdong Provincial People's Hospital between July 2022 and May 2025. Patients were divided into the RPR group and the Reverse-CART group. Lesion complexity was assessed using the J-CTO score. Procedural efficiency was defined as the time from retrograde wire crossing of the CCs and arrival at the distal CTO cap to the externalization of the antegrade wire. Procedural success, microcatheter cross CCs rate, and periprocedural complications were evaluated. The RPR technique involves advancing a retrograde guidewire through the CCs to the distal CTO, advancing to the proximal cap as closely as possible. Under retrograde guidewire guidance, a high-penetration, non-hydrophilic guidewire (mainly CP12 or CP12ST) is used for antegrade puncture, with directional adjustment from at least two orthogonal angles. The Stick and Drive technique is applied to facilitate true lumen reentry. If antegrade reentry fails, the procedure is converted to Reverse CART.

Results: Of 320 patients, 79 underwent RPR and 241 underwent Reverse CART. The RPR group was younger (56.8 ± 10.3 vs. 60.2 ± 10.3, P < 0.01)) and had higher lesion complexity (J-CTO 3.5 ± 1.0 vs. 3.0 ± 1.0, P < 0.01)), more blunt occlusions (91% vs. 65 %), and less calcification (37% vs. 57 %, P < 0.01)). The RPR group demonstrated significantly shorter occlusion crossing time (18.1 ± 20.2 vs. 33.2 ± 30.3 minutes, P < 0.01)) and required fewer cases of microcatheter collateral tracking (68% vs. 100%, P < 0.01). Among the 79 RPR patients, 55 achieved successful RPR, 20 cases required conversion to Reverse-CART, and 4 had retrograde guidewires directly crossing the occlusion (overall RPR success rate 73 percent).

Subgroup analysis showed that successful RPR cases had more reattempted lesions, shorter occlusion length, and less calcification compared to bailout RPR cases. Multivariate analysis identified occlusion length as the only independent predictor of RPR failure (OR 0.096, 95%CI:0.005 to 0.558, P = 0.032). Among patients with J-CTO scores of 3 or higher (RPR n = 66, non-RPR n = 172), RPR was associated with significantly shorter occlusion crossing times. Importantly, conversion from primary to bailout RPR did not prolong the total procedure time. No major complications such as tamponade, vessel perforation, or death occurred in the RPR group.

Conclusion: The RPR technique offers a safe and efficient strategy when used prior to Reverse CART in retrograde CTO PCI. It improves procedural efficiency without increasing the risk of complications, and may serve as a preferred first-line approach in appropriately selected cases.

复杂冠脉病变与结构性心脏病介入治疗的疗效分析及个体化方案探索

段天凤 田丹 刘华芬

武汉大学人民医院

背景：随着人口老龄化及心血管疾病发病率攀升，介入心脏病学作为微创治疗的核心技术，在冠心病、结构性心脏病等领域的应用日益广泛。然而，复杂病变的手术安全性、新型器械的长期疗效及个体化治疗策略的优化仍为当前研究热点与难点，亟需通过临床与基础研究探索解决方案。

目的：本研究旨在（1）分析复杂冠状动脉病变（如慢性完全闭塞病变、分叉病变）介入治疗的近期及远期预后，评估新型支架（如生物可吸收支架、药物涂层球囊）的疗效与安全性；（2）探讨结构性心脏病（如主动脉瓣狭窄、先天性心脏病）介入治疗的技术创新与临床转归；（3）构建基于影像组学、生物标志物的介入治疗风险预测模型，为个体化治疗决策提供依据。

方法：纳入 2019 年 1 月至 2024 年 6 月在本院接受介入治疗的心血管疾病患者共 1200 例，根据病变类型及治疗方案分为不同亚组。收集患者临床基线资料、手术相关数据（如手术时长、造影剂用量、并发症）及随访数据（6 个月、1 年、2年主要不良心血管事件发生率）。采用多因素回归分析影响预后的独立危险因素，通过 ROC 曲线评估预测模型的效能，并结合 Meta 分析系统评价新型介入器械的临床价值。

结果：初步结果显示，复杂冠状动脉病变患者采用药物涂层球囊联合支架治疗的 1 年靶病变血运重建率显著低于传统支架组（5.2% vs. 9.8%，P<0.05）；经导管主动脉瓣置换术（TAVR）在高龄高危患者中 30 天死亡率为 2.1%，显著低于外科手术组（4.8%，P<0.01）。基于影像组学构建的风险预测模型对术后大出血的预测 AUC 值达 0.83，具有较高临床应用价值。

结论：新型介入器械与技术可有效改善复杂心血管疾病患者的预后，个体化风险评估模型有助于优化治疗决策。本研究为介入心脏病学的临床实践提供了循证依据，对提升治疗安全性与有效性具有重要意义。

透视下确定左主干分叉最佳投照角度

王斌

中国人民解放军北部战区总医院（原沈阳军区总医院）

针对左主干分叉病变，经常由于前降支和回旋支近段重叠或缩短，导致左主干分叉病变在透视下不能良好暴露，使该部位尤其是开口病变不能获得精准治疗。本文拟对这一问题进行研究。目的：探讨仅利用透视确定左主干分叉最佳投照角度的可能性。方法：共入选 30 个拟行左冠状动脉介入治疗的患者。其在治疗前或治疗后已行冠状动脉计算机断层扫描（Computed tomography, CT）检查。利用透视和冠状动脉 CT 分别找出左主干分叉最佳投照角度。比较两种方法获得的最佳投照角度差异。结果：对比两种方法获得的左主干分叉最佳投照角度，一致性分析显示，组内相关系数在左右投照，即左前斜或右前斜为 0.713[95% 可信区间 (CL)，0.292-0.874]；在上下投照，即头位或足位为 0.711[95% 可信区间 (CL)，0.214-0.879]。通过透视获得的左主干分叉最佳投照角度为左 8.83° ±38.21° / 足 60.13° ±11.46°，通过 CT 获得左主干分叉最佳投照角度为右 10.56° ±30.86° / 足 52.63° ±12.50°。两种方法获得的左主干最佳投照角度差值为 17.57° ±10.60°。结论：利用透视确定左主干分叉最佳投照角度是可能的。90% 的患者两种方法获得的左主干最佳投照角度差异较小。

Rota-Tripsy or step-up-approach rotational atherectomy for severe coronary artery calcification treatment: a comparative effectiveness study

Feng-Wen Cui, Ya-Liang Tong, Bei-Bei Du, Xiang-Dong Li, Yu-Quan He

吉林大学中日联谊医院

Background: Severe coronary artery calcification (CAC) presents significant challenges for percutaneous coronary intervention (PCI), impacting stent expansion and clinical outcomes. While step-up-approach rotational atherectomy (RA) is established, rota-tripsy (combining initial small-burr RA with intravascular lithotripsy [IVL]) has emerged as a novel alternative. Comparative data on their efficacy and safety are limited.

Objective: To evaluate and compare the immediate efficacy and safety of rota-tripsy versus step-up-approach RA for treating severe CAC under intravascular imaging guidance.

Methods: This retrospective, comparative effectiveness cohort study analyzed data from 3652 patients undergoing PCI with intracoronary imaging (IVUS/OCT) at a single center between February 2021 and February 2024. Patients with severe CAC (OCT calcium score=4 or IVUS calcium score=2-4) requiring plaque modification beyond initial small-burr RA and non-compliant balloon (NCB) failure (16 atm) were included. 37 patients (38 lesions) were enrolled: 18 in the rota-tripsy group (Group A) and 19 in the step-up-approach RA group (Group B). All received drug-eluting stents (DES) post-modification. Calcification severity was assessed using standardized IVUS or OCT scoring systems post-initial burr. The primary efficacy endpoint was procedural success (stent expansion >70% by IVUS/OCT + no in-hospital major adverse cardiac events [MACEs]). The primary safety endpoint was absence of serious angiographic complications (slow/no flow, perforation, Type C-F dissection, abrupt closure, acute thrombosis). Secondary safety endpoints included absence of in-hospital and 30-day MACEs (cardiac death, MI, TVR). Procedural efficiency (fluoroscopy time, dose-area product [DAP], interval time) was also compared.

Results:

Patient/Lesion Characteristics: Baseline characteristics (age, sex, comorbidities, LVEF, ACS presentation) and lesion characteristics (target vessel, calcification score, calcium arc/length, reference diameter, lesion length) showed no significant differences between groups.

Efficacy Endpoints: Both groups achieved 100% procedural success (stent expansion >70% and no in-hospital MACEs). The overall mean stent expansion was 83% in both groups (P=0.954). Rates of stent expansion categories (≥ 90%, 80-90%, 70-80%) were also similar (P=0.696).

Safety Endpoints: Group A (rota-tripsy) had a significantly lower incidence of serious angiographic complications (0% vs 31.6% in Group B, P=0.02). All complications in Group B were slow/no flow events. No perforations, dissections, abrupt closures, or acute thromboses occurred in either group. Freedom from in-hospital and 30-day MACEs was 100% in

both groups.

Procedural Efficiency: Group A demonstrated significantly better efficiency metrics compared to Group B:

Shorter Fluoroscopy Time: Median 46 min (IQR 40.75-61.25) vs 70 min (IQR 60-75); difference -20 min (95% CI -28, -8); P<0.01.

Lower Radiation Dose (DAP): Median 450.8 Gy·cm² (IQR 373.75-514.03) vs 532.6 Gy·cm² (IQR 479.4-650.3); difference -104.1 Gy·cm² (95% CI -196.3, -26); P<0.01.

Shorter Interval Time: Median 8 min (IQR 7-9) vs 15 min (IQR 13-19); difference -7 min (95% CI -10, -5); P<0.01.

Other Outcomes: Minimal lumen area (MLA) gains post-modification (MLA1 to MLA2) and post-stenting (MLA1 to MSA), stent length, and number of stents per vessel showed no significant differences. Length of stay trended shorter in Group A but was not statistically significant (P=0.061).

Conclusions: Both rota-tripsy and step-up-approach RA demonstrated high procedural success rates (100%) and excellent short-term safety (no in-hospital or 30-day MACEs) for the treatment of severe CAC under intravascular imaging guidance. However, rota-tripsy offered significant advantages in procedural safety, with a complete absence of angiographic complications (notably slow/no flow) compared to step-up RA. Additionally, rota-tripsy was significantly more efficient, requiring less radiation exposure (DAP), shorter fluoroscopy time, and shorter specific modification interval time. These findings suggest rota-tripsy is a highly effective, safer, and more efficient plaque modification strategy for severe CAC compared to the step-up-approach RA. Further multi-center studies with larger samples and longer-term follow-up are warranted to confirm these results.

Keywords: Coronary artery calcification, Rotational atherectomy, Intravascular lithotripsy, Rota-tripsy, Step-up approach, Percutaneous coronary intervention, Intravascular ultrasound, Optical coherence tomography.

Safety and Outcomes of Retrograde Percutaneous Coronary Intervention for Chronic Total Occlusions in Patients with Reduced Left Ventricular Ejection Fraction: A Single-Center Retrospective Cohort Study

Song Wen, Qi-heng Wan, Ze-Han Huang, Dun-Liang Ma, Fei-Huang Han, Ji-Quan Xiao, Feng Wang, Yu-Qing Huang, Bin Zhang

Department of Cardiology, Guangdong Cardiovascular Institute, Guangdong Provincial People's Hospital, Guangdong Academy of Medical Sciences, Southern Medical University, Guangzhou, 510080, Guangdong, China.

Background

Approximately 15-20% of angiograms diagnostic of coronary artery disease (CAD) are found to have a concomitant coronary chronic total occlusion (CTO). The success rate of the percutaneous coronary intervention (PCI) for CTO was 65-70% when using only the antegrade approach, so it was difficult to expect a high success rate. However, the introduction of the retrograde approach has significantly increased the success rate of the procedure. In the early days of the retrograde approach, the complexity and variability of the procedure and the possibility of complications caused practitioners to hesitate to use this method. Several studies suggested that retrograde CTO PCI has been associated with lower technical and procedural success rates and higher in-hospital and long-term major adverse cardiac event (MACE) rates compared with antegrade approach. Therefore, the retrograde approach was used in critically ill patients with particular caution.

Left ventricular ejection fraction (LVEF) is a well-established independent prognostic factor in patients with CAD. Recent studies have indicated that in patients with ischemic heart failure, the presence of CTO was associated with worse long-term outcomes. Previous studies have suggested that PCI was a safe and effective revascularization strategy, yielding good midterm outcomes and LVEF improvement in CTO patients with low LVEF. However, the majority of patients in these studies were employed an antegrade approach, with only a small proportion utilizing the retrograde approach, potentially introducing selection bias. There is a dearth of data regarding the procedural success and clinical outcomes of retrograde CTO PCI in real-world practice, particularly in patients with reduced LVEF (≤ 40%). Therefore, we aimed to assess the procedural results and long-term outcome of retrograde CTO PCI in individuals with reduced LVEF.

Methods

836 patients undergoing retrograde CTO PCI in the 2nd division of Cardiovascular Department, Guangdong Province People's Hospital from January 2011 to April 2023 were selected retrospectively. Based on echocardiographic assessment, cases were divided into two groups: LVEF ≤ 40% and LVEF>40% LVEF. Baseline clinical data, angiography data and follow-up information were collected and compared between the two groups. The primary clinical endpoint was defined as all-cause death. The secondary endpoint was MACE, defined as a composite of all-cause death, cardiac death, nonfatal myocardial infarction (MI), stroke, and target vessel revascularization (TVR) during follow-up. The prognostic effect of successful CTO PCI on CTO patients with decreased LVEF was evaluated by Kaplan-Meier survival analysis and Cox regression analysis.

Results

1. Retrograde CTO PCI was attempted in a total of 836 patients, with 764 males (91.4%), averaging 59.5±10.6 years old. According to baseline LVEF, the study population was divided as follows: group 1 (LVEF ≤ 40%) with 156 (18.7%) patients and group 2 (LVEF > 40%) with 680 (81.3%) patients. The mean LVEF of group 1 and group 2 were 33.4±5.5 and 58.6±7.8 respectively (PPcholesterol (TC), low-density lipoprotein cholesterol (LDL-C), blood urea nitrogen (BUN), N-terminal pro B-type natriuretic peptide (NT-proBNP), Troponin T (TNT), and fasting blood glucose (FBG) were significantly elevated, whereas estimated glomerular filtration rate (eGFR) and albumin (ALB) were significantly reduced (all P < 0.05). Moreover, compared with group 2, the patients in group 1 had larger left ventricular end-systolic dimension (LVESD) and left ventricular end-diastolic dimension (LVEDD).

2. The right coronary artery was the most common CTO territory, followed by the left anterior descending artery and the left circumflex artery. The number of CTO lesions was significantly higher in patients in group 1 (41.0% vs. 25.1%, Pollateral channel tracking success was high (overall 93.5%) and similar among the 2 groups (94.2% vs. 93.4%, P=0.835), as well as retrograde technical success (89.9% vs. 87.8%, P=0.548) and recanalization success (91.5% vs. 87.8%, P=0.281). A total of 148 in-hospital procedural complications were reported, including 112 cases (13.4%) of coronary injury, 29 cases (3.5%) of cardiac tamponade, 19 cases (2.3%) requiring pericardiocentesis, 2 cases (0.2%) of emergency surgery, and 5 cases (0.6%) of in-hospital death. Moreover, the incidence of coronary injury, cardiac tamponade, pericardiocentesis, emergency surgery, and death in hospital was no significant differences between the groups (all P > 0.05).

3. Clinical follow-up was available in 767 (91.2%) patients with a medium follow-up duration of 1041 (531-1511) days. A total of 126 (16.4%) patients experienced MACE, comprising 52 patients (6.8%) with all-cause mortality, 36 patients (4.7%) with cardiac death, 6 patients (0.8%) with nonfatal MI, 11 patients (1.4%) with stroke, and 62 patients (8.1%) with TVR. Among patients with reduced LVEF, the risk of MACE was significantly higher (23.2% vs. 14.9%, P=0.021), primarily driven by all-cause mortality (15.4% vs. 4.1%, P < 0.001) and cardiac death (12.2% vs. 2.5%, P < 0.001).

4. Successful CTO recanalization was independently associated with reduced the risk of MACE, all-cause mortality, cardiac death, and TVR regardless of left ventricular systolic function. Age (hazard ratio [HR]: 1.03, 95% confidence interval [CI]: 1.01-1.04, P=0.008), LVEF ≤ 40% (HR: 1.21, 95%CI: 1.01-1.45, P=0.039), and revascularization success (HR: 0.38, 95% CI: 0.22-0.66, P

Conclusion

1. Retrograde PCI may represent a safe and efficient management strategy in CTO patients with reduced LVEF.

2. CTO patients with reduced LVEF had a significantly increased risk of long-term mortality and MACE, and early initiation of standard anti-heart failure therapy may be necessary.

3. Successful CTO recanalization is associated with significant survival benefits, regardless of left ventricular systolic function.

KEYWORDS: Chronic total occlusion; Percutaneous coronary intervention; Left ventricular ejection fraction; Retrograde; Recanalization

右冠慢性完全闭塞病变逆向介入治疗中假腔旋磨的分期处理策略：1 例高龄复杂病例报告

张海山 史础宁

中国医科大学附属第一医院

目的：冠状动脉慢性完全闭塞（CTO）病变经皮冠状动脉介入治疗（PCI）中，导丝误入内膜下假腔是常见挑战，发生率高达 15%-30%。传统观念认为在假腔内进行器械操作（尤其是旋磨术）具有极高风险，可能导致血管穿孔、夹层扩展等严重并发症，因此被视为禁区。本病例旨在探讨并报告一种基于最新证据的策略：在严格的血流动力学稳定条件下，于假腔内实施旋磨术，用于开通传统方法难以处理的严重钙化性 CTO 病变，并评估其安全性与可行性。

方法：报告一例典型病例：70 岁男性患者，因劳力性心绞痛入院。冠状动脉造影确诊右冠状动脉（RCA）近中段 CTO，伴严重钙化。首次尝试正向 PCI 未能成功开通。遂行逆向介入治疗 **。术中克服侧枝通道后成功逆向送入导丝通过 CTO 段，但前向送入血管内超声（IVUS）导管因严重钙化无法通过病变。为克服钙化障碍，在 IVUS 及造影引导下确认导丝位于假腔后，谨慎地在假腔内实施了旋磨术（使用较小尺寸旋磨头）。旋磨术后造影显示远端血流受限。

结果：1. 术中即刻结果：旋磨术后即时 IVUS 检查，明确证实导丝及旋磨头全程操作均位于血管假腔（内膜下）内，血管壁结构相对完整，未见明显穿孔征象或

夹层灾难性扩展。

2. 一期处理：基于对假腔状态相对稳定可控的判断，一期手术在远端确认的真腔内精准植入一枚药物洗脱支架（DES）。该操作旨在：a) 确保远端血管床的有效血流灌注；b) 为后续操作建立稳固的远端着陆区。

3. 二期计划：手术策略设定为分期处理。一期结束于远端真腔支架植入。二期手术计划在 IVUS 精确引导下，从近端支架边缘重新穿刺内膜，将导丝再次引入近端真腔，最终实现全程真腔内的支架优化植入，完成功能性及解剖学上的完全再通。

结论：本病例实践表明，对于伴有严重钙化的复杂 CTO 病变，在血流动力学稳定、操作精细可控的前提下，假腔内旋磨术并非绝对禁忌，具有一定的可控性和安全性。其成功实施的关键要素包括：严格的患者选择与血流动力学监测、精细的旋磨操作（避免过度扩展）、旋磨后即时影像学（IVUS）对假腔范围及血管壁完整性的精准评估、以及一期远端真腔支架植入为二期真腔重穿提供的安全保障和目标引导。这标志着在处理特定复杂钙化 CTO 时，可以更加灵活和积极地应用内膜下技术，最终实现血管的安全有效开通。

AI 驱动的冠状动脉旋磨术旋转速度预测及其临床意义研究

马士新 陈昱 马智会

上海市第六人民医院（上海交通大学附属第六人民医院）

目的：本研究旨在通过集成机器学习方法预测在不同冠脉钙化严重程度病变中的旋磨速度，并探讨旋磨转速不低于 18 万转 / 分在临床操作中的优势。

方法：我们回顾性分析了 2020 年至 2024 年间我院接受旋磨治疗的患者数据。数据经预处理后分为连续和离散变量，并通过 One-Hot 编码处理离散变量。分类模型包括随机森林、逻辑回归、决策树、梯度提升、KNN、AdaBoost、极端随机树、MLP 和高斯朴素贝叶斯等，通过 train_test_split(·) 将数据集划分为训练集和测试集，并使用 VotingClassifier 实现集成学习。模型评估采用准确率、精度、召回率、F1 分数等多项指标，选择 F1 分数最高的组合作为最优模型。进一步使用 SHAP 进行特征重要性分析，通过 SHAP 值评估每个特征对预测结果的贡献，绘制特征重要性图。为应对数据不平衡问题，采用了随机欠采样方法平衡样本比例，以提高模型的预测性能。最终，模型的评估结果通过 ROC 曲线、精度 - 召回率曲线和混淆矩阵等方式进行了可视化。

结果：在分析冠状动脉旋磨术 (coronary rotational atherectomy) 时，使用多变量 AI 集成模型可以帮助识别与旋转速度相关的临床因素，并通过 SHAP 包提供的可解释性结果来理解这些因素的生物学意义。研究发现，肌酐水平、丙氨酸氨基转移酶、血红蛋白水平、初始旋磨头大小、体质指数、低密度脂蛋白、高血压持续时间、旋磨时间以及术中心动过缓发生与否等因素与最终通过病变的旋转速度相关。特别是，当旋磨转速达到 18 万转 / 分以上时，可以更有效地处理钙化病变，提高手术的成功率和安全性。这一转速范围能够更好地适应不同患者的血管条件，减少手术并发症，改善患者的临床预后。

结论：通过集成机器学习方法成功预测了冠状动脉旋磨术中的旋转速度，并揭示了旋磨转速不低于 18 万 / 分转在临床操作中的显著优势。这一发现为临床医生提供了重要的参考依据，有助于优化手术策略，提高冠状动脉旋磨术的疗效和安全性。

关键词：冠状动脉旋磨术；旋转速度；集成机器学习；SHAP 特征分析

基于危险因素评分模型指导高速旋磨策略在严重钙化病变中的应用研究

马士新 陈昱 马智会

上海市第六人民医院（上海交通大学附属第六人民医院）

目的：本研究旨在探讨高速旋磨技术在处理严重钙化病变中的有效性与安全性，重点解决何时应直接采用不低于 180 000 rpm 的高速旋磨而非传统低速递增策略并比较主动与被动旋磨的优劣。

方法：通过回顾性分析 2020–2024 年间共 197 例严重钙化病变患者的旋磨数据，我们系统评估了病变成角 >70°、尿毒症、糖尿病病程 >10 年、超高龄（≥ 80 岁）、女性合并低 BMI(<22 kg/m²)、钙化长度 >15 mm 以及前降支病变等危险因素对旋磨策略的影响。

结果：多因素 logistic 回归显示上述因素均与直接选择高速旋磨显著相关，据此构建的积分模型在验证队列中 AUC 达 0.87。与低速递增策略相比，直接高速组总旋磨时间显著缩短（p<0.05），慢血流发生率降低至 3.6%，穿孔风险仅 0.9%。在手术技术层面，主动旋磨较被动旋磨成功率更高；起始转速每提升 30 000 rpm，总旋磨时间可再缩短约 18%。此外，主动旋磨虽能进一步缩短操作时间，但在成角 >70°或长钙化病变中需谨慎使用，临床仍以被动旋磨为主（占比 82%）。

结论：通过危险因素积分识别高风险病变并直接采用高速旋磨，同时优选主动旋磨，合理匹配旋磨头尺寸与转速，可显著提高钙化病变旋磨的成功率并减少并发症，为临床实践提供循证依据。

关键词：高速旋磨；钙化病变；风险因素分析；主动旋磨与被动旋磨；旋磨技术优化

冠状动脉慢性完全闭塞患者 术后 MACE 风险预测模型研究

张博晖 [1] 禹天同 [3] 赵帅 [1] 韩鹏 [1] 王车 [2] 张玺 [1] 廉坤 [1]

1. 空军军医大学附属西京医院

2. 陕西中医药大学

3. 西安市红会医院

目的

构建机器学习模型以识别冠状动脉慢性完全闭塞（CTO）经皮冠状动脉介入治疗（PCI）术后主要不良心血管事件（MACE）的危险因素，优化临床决策，提升患者生存质量。

方法

数据收集与预处理

纳入 2018-2021 年西京医院接受 CTO-PCI 的 1069 例患者，数据涵盖基本信息、病史、术前检查、干预细节及住院期间 MACE 事件。对患者进行为期一年的随访，记录 MACE 发生情况。数据经标准化处理，按 8:2 比例划分为训练集和验证集。

模型构建

采用三种方法构建模型：

① 逻辑回归模型：通过单因素分析筛选显著变量，纳入二元逻辑回归。

② 机器学习模型：结合人工与机器学习筛选变量，通过主成分分析（PCA）和随机森林（RF）降维，采用朴素贝叶斯构建模型。

③ 自动机器学习：使用 TPOT 和 H2O AutoML 框架，分别在未采样、SMOTE 过采样和欠采样数据上构建模型。

模型评价

采用 ROC 曲线、决策分析曲线（DCA）、准确率、召回率和 F1 分数评估模型性能。

模型解释

逻辑回归模型基于 sigmoid 函数解释。机器学习模型通过 SHAP、随机森林特征重要性评分和 LIME 进行解释。

结果

逻辑回归模型

基于 7 个显著变量（年龄、住院并发症、他汀类药物、利尿剂、闭塞近端 3mm 有分支、主要支架数量、手术成功）构建模型，最佳截断值 0.1663，敏感性 0.5762，假阳率 0.1839，AUC 0.7345。

机器学习模型

① 人工与机器学习结合的变量筛选优于单一方法。

② 朴素贝叶斯模型在测试集上表现为：准确率 0.7746，精确率 0.7500，召回率 0.7800，F1 分数 0.7647，AUC 0.8281，DCA 显示较高净收益，表明模型具有临床实用性。

③ 关键预测因子包括心脏功能（射血分数、收缩末期容积、分数缩短率）、心肌损伤（肌酸激酶、肌酸激酶 -MB、心肌肌钙蛋白）、代谢健康（丙氨酸氨基转移酶、甘油三酯、总胆固醇）及术前 D- 二聚体和 NT-proBNP（呈非线性预测模式）。肝 - 代谢 - 心血管轴交互效应显著，手术复杂性（如 J-CTO 评分）及高风险干预（如 IABP+ECMO）增加 MACE 风险。

自动机器学习

① TPOT 在原始数据集上表现最佳，准确率 86.45%，多数类（类 0）精确率 0.87、召回率 0.98、F1 分数 0.92，但少数类（类 1）召回率仅 0.24（精确率 0.73，F1 分数 0.36）。

② H2O AutoML 最佳模型（GBM）准确率 87.61%，多数类表现优异（召回率 0.99，F1 分数 0.93），但少数类召回率低（0.26，F1 分数 0.39）。

结论

逻辑回归模型预测能力中等，敏感性低，假阳性率高，难以捕捉复杂非线性关系。

朴素贝叶斯模型有效识别 CTO-PCI 术后一年 MACE 高危患者，支持临床决策。

人工与机器学习结合的特征选择方法性能优异，人工筛选确保统计相关性与解释性，机器学习挖掘非线性关系，提升模型稳定性与临床价值。

多因素非线性交互（如炎症、代谢健康、病变复杂性）对 MACE 预测至关重要，SHAP 和 LIME 分析揭示亚群异质性，为精准治疗提供方向。

自动机器学习框架潜力大，但对不平衡数据集处理能力有限，需优化数据预处理以提升临床应用价值。

关键词：冠状动脉慢性完全闭塞病变；机器学习；MACE；朴素贝叶斯；临床决策。

清醒 VA-ECMO 支持下复杂钙化病变多支血管 PCI 术及术后心脏康复 1 例

贾凌梅 贾敏 陈亚丽

河北医科大学第二医院

目的：冠状动脉复杂病变（尤其是慢性完全闭塞病变及弥漫性钙化病变）的血运重建始终是介入心脏病学的重大挑战。对于高龄、多支血管病变且合并血流动力学高危因素的患者，经皮机械循环支持（pMCS）已成为保障手术安全的核心技术。传统静 - 动脉体外膜肺氧合（VA-ECMO）虽可提供充分循环支持，但全身麻醉与镇静带来的呼吸抑制、神经功能监测缺失及撤机延迟等问题，显著增加了并发症风险。

方法：近年来，清醒 ECMO 策略的兴起正重塑高危经皮冠状动脉介入治疗（PCI）的支持范式，通过保留患者自主呼吸与意识状态，实现实时症状反馈，如心绞痛

发作的早期识别，并能够显著降低呼吸机相关损伤，加速患者术后康复。然而，该技术在高龄钙化病变患者中的应用仍缺乏系统报道，其适应证筛选、抗凝管理及撤机时机亟待规范。

结果：本文报道一例 71 岁右冠慢性完全闭塞（CTO）合并前降支重度钙化病变患者，在清醒 ECMO 支持下成功完成多支 PCI 术，并重点探讨清醒 ECMO 的建立与术中管理、术后即刻撤机的可行性标准以及术后心脏康复策略。本案例为高危 PCI 的循环支持策略提供了新证据，并为相关共识的更新贡献临床经验。

结论：清醒 ECMO 支持下 PCI 联合术后心脏康复代表了危重症支持从“生命支持”向“精准介入康复”的理念跃迁，其成功实施依赖于严格的生理学筛选标准、创新的血管管理技术及多学科团队的实时响应能力，术中管理的复杂性要求团队不仅掌握先进设备操作，更需具备应对生理 - 心理综合挑战的系统化策略。

基于目标血管差异的冠状动脉旋磨术治疗慢性完全闭塞病变的疗效与短期预后研究

张斌 张晓娇 栾波

辽宁省人民医院

目的 比较 RA 用于不同靶血管（左前降支、左回旋支和右冠状动脉）CTO 病变中的术中特点、治疗效果及短期预后差异，探讨 RA 操作的解剖适配性与临床获益关系。

方法 回顾性收集 2019 年 1 月至 2024 年 12 月于辽宁省人民医院接受 RA 辅助 CTO-PCI 治疗的 119 例单支 CTO 患者，按靶血管分为 LAD 组（n=55）、LCX 组（n=14）和 RCA 组（n=50）。比较三组患者的基线特征、实验室指标、手术过程及半年主要不良心脑血管事件（MACCE）发生情况。采用 Kaplan-Meier 法绘制生存曲线，COX 回归分析影响短期预后的独立预测因子。

结果 RCA-CTO 组患者年龄更大（71.52±12.21 岁），三支病变比例更高（78.0%），但半年 MACCE 发生率最低（10.0%，对比 LAD 组 23.6%，LCX 组 28.6%，P=0.116），RCA 组与非 RCA 组比较差异有统计学意义（P=0.042）。RA 操作中三组患者在磨头直径、转速、腔内影像学指导率等方面差异不显著，但 RCA 组支架总长度和造影剂使用量显著增加。COX 回归分析提示腔内影像应用、HDL 水平、三支病变状态为 MACCE 发生的趋势性因素，但未达到统计学显著性。

结论 在高度钙化、非顺应性 CTO 病变中，RA 辅助治疗总体安全可行，具有相对较好的安全性与可操作性。RA 治疗不同靶血管 CTO 病变在结果存在差异，可能与 RCA 解剖适配性更高，从而可能具有更高的临床获益和更佳的短期预后。腔内影像学技术在 RA 操作中具有重要的指导意义，在提升 RA 精度、避免并发症中发挥关键作用。

老年冠状动脉原位大血管严重钙化弥漫病变旋磨术后不同处理策略临床结局对比

郭权 聂铭 李牧蔚

阜外华中心血管病医院 河南省人民医院心脏中心

目的：探索在老年冠状动脉严重钙化弥漫病变旋磨术（RA）后不同处理策略的临床结局。

方法：回顾性连续收集在阜外华中心血管病医院 2018 年 1 月 -2022 年 5 月期间 PCI 中因严重钙化使用 RA 术的 60 岁及以上且靶病变长度 > 40mm 患者，根据不同治疗策略分为 DES 组（n=326）：指整支血管病变均由 DES 处理；DCB 组（n=183）指整支血管病变均由 DCB 处理；DES+DCB 组（n=67）：整支血管病变由 DES 与 DCB 串联处理。主要终点事件为主要心脑血管不良事件（MACCE）发生率，包含心血管死亡，非致死性心梗，靶血管血运重建（TLR），脑卒中。次要终点事件为 MACCE 的组成成份以及出血学术研究联合会（BARC）定义的 2、3 或 5 型出血事件，并分析影响患者预后的危险因素。

结果：（1）在基线资料中，DCB 组年龄较 DES+DCB 组大 [71(66.00, 76.00) vs. 69(64.00, 74.00) 岁，P<0.05]，肾功能不全患者较 DES 组及 DES+DCB 组多 (9.29% vs. 2.76%vs.1.49%, P<0.05)；DES+DCB 组男性占比其余两组更多 (74.63% vs. 53.07% vs. 53.38%, P<0.05)，吸烟占比较 DES 组及 DCB 组更高 (47.76% vs. 33.13% vs. 31.15%, P<0.05)，其余临床基线资料无明显差异。（2）手术资料中，DES+DCB 组及 DCB 组使用腔内影像学（指血管内超声或光学相干断层扫描）均较 DES 组更多 (74.63% vs. 67.76% vs. 51.84%, P<0.05)。DES+DCB 组较多病变涉及左主干，DCB 组较 DES 组及 DES+DCB 组最少 (3.83% vs. 15.95% vs. 25.37%, P<0.05)。DCB 组较 DES 组使用了更大的旋磨头 (1.59±0.22 vs. 1.52±0.17mm, P<0.05)。DES 组置入物总长度较 DCB 组及 DES+DCB 组最短 [60.00(52.00,67.00) vs. 60.00(55.00,70.00) vs. 65.00(61.00,70.00)mm, P<0.05]。（3）三组患者在不良事件中的对比：所有患者至少有 1 年的随访记录，中位随访时间为 812 天。DCB 组 MACCE 发生率高于 DES 组（22.4% vs. 16.56%, P<0.05）和 DES+DCB 组（22.4% vs. 11.94%, P<0.05），后两者之间差异无统计学意义。DCB 组非致死性心梗率高于 DES 组和 DES+DCB 组（4.37% vs. 0.92% vs 0, P<0.05）。DCB 组靶血管血运重建率高于 DES 组（14.75% vs. 5.83%, P<0.05）和 DES+DCB 组（14.75% vs. 5.97%, P<0.05），后两者之间差异无统计学意义。三组患者在心血管死亡、脑卒中、出血学术研究联合会 2/3/5 型出血发生率上无统计学差异。COX 回归显示，在排除混杂因素后，与 DES 组相比，DCB 组增加了 MACCE 的风险 (HR=2.054, 95% CI：1.315-3.208, P<0.05)；

结论：在冠状动脉严重钙化弥漫病变 RA 术后，单纯使用 DCB 导致主要心脑血管不良事件发生率增加，而 DES+DCB 策略与使用 DES 组无明显差异。提示在老年冠脉严重钙化弥漫病变中，DES 联合 DCB 治疗方案是安全可行的，可在一定程度上减少永久性支架的置入。

不同旋磨策略对冠脉钙化病变斑块修饰及支架膨胀的影响： 一项单中心 IVUS 研究

刘玉婷 潘亮 邱竞 王玺 彭猛 单迎光 邱春光

郑州大学第一附属医院

目的：严重冠脉钙化是当前冠脉介入领域的关键挑战之一，常导致支架膨胀不良，是支架内血栓与再狭窄的核心预测因素。旋磨术是有效的斑块修饰手段，但关于采用小磨头（磨头 / 血管直径比 <0.6）的保守策略与采用大磨头（≥ 0.6）的积极减容策略的优劣尚存争议。本研究旨在通过血管内超声（IVUS）全程指导，对比两种策略对中重度钙化病变斑块修饰、支架膨胀及一年期临床预后的影响。

方法：本研究为单中心回顾性队列研究，连续入选 2023 年 6 月至 2024 年 5 月因中重度冠脉钙化（IVUS 证实钙化弧度 >180°或造影提示）接受旋磨 PCI 的患者。患者据策略分为：积极减容组（大磨头 + 特殊球囊预处理）与保守策略组（小磨头 + 非 / 半顺应性球囊预扩张）。所有操作均在 IVUS 全程指导下完成。主要终点为 IVUS 测量的术后支架膨胀率。次要终点包括术后最小支架面积（MSA）及 1 年 MACE（心源性死亡、靶血管心肌梗死、临床驱动的靶病变血运重建的复合终点）。

结果：共纳入 83 例患者（89 处病变），分为保守策略组（n=46）和积极减容组（n=37）。两组基线特征具有可比性（P 均 >0.05）。积极减容组使用了更大的磨头（1.85±0.22 vs. 1.44±0.15mm, P<0.001）和更高比例的特殊球囊（95.0% vs. 44.9%, P<0.001）。围术期并发症发生率无差异。主要终点方面，积极减容组的支架膨胀率显著更优（89.8±3.3% vs. 82.0±7.0%, P<0.001）。同时，积极减容组获得了更大的 MSA（7.65±1.57 vs. 6.29±1.36mm², P<0.001）及更优的支架对称性。1 年随访中，两组 MACE 率无统计学差异（积极减容组 10.8% vs. 保守策略组 19.6%, P=0.136），但积极减容组的临床驱动的靶病变血运重建（CD-TLR）呈降低趋势（5.4% vs. 10.9%, P=0.052）。

结论：对于中重度冠脉钙化病变，采用大磨头的积极减容策略能实现更有效的斑块修饰，获得更优的即刻支架膨胀和更大的术后管腔。尽管 1 年 MACE 率差异未达统计学意义，但优异的即刻血管成形结果是长期获益的基石，其临床价值有待更大规模研究证实。

复杂高危冠心病患者择期 PCI 术中清醒 ECMO 支持：单中心经验

贾敏 贾凌梅 陈亚丽

河北医科大学第二医院

目的：随着人口老龄化，有多种合并症及不能耐受心外科手术的高危冠心病患者数量逐渐增加，这些患者往往存在严重多支血管病变、左心室功能显著低下（如左心室射血分数 <35%）、无保护的左主干病变、严重合并症（如慢性肾脏病、慢性阻塞性肺疾病）等特征，要么选择保守治疗，要么冒险行 PCI，术中极易因短暂性心肌缺血、再灌注损伤、心律失常或血流动力学崩溃而出现循环衰竭，导致手术失败甚至死亡，面临着巨大的挑战和风险。但是目前关于预防性植入静 - 动脉体外膜肺氧合 (VA-ECMO) 对复杂高危经皮冠状动脉介入治疗 (PCI) 的影响的证据有限。本文对本中心的 6 例患者评估清醒 ECMO 支持下复杂 PCI 患者住院期间和干预后 30 天的结果。

方法：本研究为一项观察性回顾性研究，包括我科室 2025 年 4 月 -2025 年 6 月所有接受高风险 PCI 并接受 VA-ECMO 心肺支持的患者。主要终点是住院期间和出院 30 天主要不良心脑血管事件 (MACCE) 发生率。次要终点是血管并发症、出血和手术成功。

结果：共纳入 6 例患者。所有患者均被外院心内科认定为不能手术，且所有患者均拒绝进行冠脉搭桥手术。采用复杂 PCI 技术 :5 例患者行慢性闭塞病变（CTO）开通，3 例患者行冠状动脉旋磨术，所有患者均行多支冠脉支架植入术，PCI 在所有靶区和附加病灶血运重建的患者中均取得成功。6 例患者中有 5 例术后存活至少 30 天。并发症发生率方面，肢体缺血 2 例行顺行灌注，股动脉假性动脉瘤 1 例行介入封堵，局部血肿 2 例，血红蛋白明显下降大于 20g/l 的患者 3 例，输血 2 例。

结论：清醒 VA-ECMO 是高危 PCI 血运重建术的有效支持策略，对于因风险高被认为不能手术且预期有明显临床获益的患者具有良好预后。

The Impact of Intracoronary Imaging Guidance on Long-term Outcomes for Patients Undergoing Coronary Rotational Atherectomy

Xiao-Chen Liu[1], Ya- Chen[1], Yue-Kun Zhang[1], Guo[1], Ying-Ying Guo[2], Fei-Yu Zhang[1], Wen Hao[1], Xiao Wang[1], Shao-Ping Nie[1]

1. Beijing AnZhen Hospital, Capital Medical University

2. Chinese Academy of Medical Sciences & Peking Union Medical College Fuwai Hospital

Objectives: This study sought to investigate the impact between angiography-guided RA and intravascular guided RA on clinical outcomes and final angiographic results.

Methods: This study included 980 patients undergoing RA at 19 sites between July 2018 and December 2020 from the Rota China Registry (NCT03806621), a prospective and multicenter registry study. All patients had a follow-up office visit or telephone contact at 30 days and up to 1 year after procedure. The primary outcome was major adverse cardiac event (MACE), the composite of cardiac death, MI, or ischemia-driven target lesion revascularization.

Results: A total of 980 patients were included in the final analysis, with 660 underwent angiography-guided RA and 330 underwent intravascular imaging (IVUS or OCT) guided RA. The final angiographic findings were analyzed. The average lumen diameter was significantly higher in intravascular-guided RA group (2.85±0.33 vs 2.77±0.32, P<0.001). The incidence of 30-days MACE (5.5% vs 3.7%, log-rank P=0.24) and 1-year MACE (8.6% vs 7.2%, log-rank P=0.41) was similar between angiogra-

phy-guided and intravascular image-guided group.

Conclusion: RA guided by intravascular image or angiography showed a similar clinical outcome. Intravascular imaging demonstrated a larger post-procedure lumen diameter, underscoring its value in optimizing procedural outcomes.

心房颤动有关研究

导管消融术后房颤复发预测模型的建立

黄源[1] 利龙昌[2]

1. 广西壮族自治区江滨医院

2. 广西壮族自治区人民医院

目的：本研究旨在确定导管消融术后房颤复发的独立危险因素，并建立一个评估复发可能性的预测模型。

方法：本研究纳入了 2020 年 1 月至 2021 年 9 月接受首次导管消融治疗的 303 例房颤患者。收集临床资料、治疗细节和超声检查结果。进行统计学分析，以确定预后因素，包括套索和多变量逻辑回归。建立了一个预测模型，并利用校准曲线对该预测模型进行了评价。

结果：最终，21.8% 的患者发生了房颤复发。通过 LASSO 回归和多变量 logistic 回归，确定了列线图模型的 5 个预后因素：三尖瓣反流程度、CHA2DS2-VASc 评分、左心室射血分数、房颤类型和左心房内径。AF 复发的 AUC 为 0.862（95%CI 为 0.809~0.916），该模型的 c 指数为 0.86。进行了引导抽样验证，结果校正后的 c 指数为 0.841。该模型采用留一交叉验证方法进行评估，结果校正后的 c 指数为 0.861，校准曲线斜率为 1.0。这些结果显示了良好的鉴别能力和校准性能。

结论：本研究确定了导管消融术后房颤复发的独立危险因素，并建立了一个评估复发可能性的预测模型。该模型可以帮助对个别患者进行个性化的管理和治疗决策。需要进行外部验证来进一步证实其临床效用。

A Novel Predictive Model for Identifying Left Atrial Low-Voltage Area in Patients with Paroxysmal Atrial Fibrillation

Baowei Zhang

Shanghai East Hospital

Purpose: Atrial fibrillation (AF) is the most common sustained cardiac arrhythmia encountered in clinical practice, with the prevalence of 4.48% in the general population. Left atrial low-voltage area (LVA), indicative of structural remodeling of the left atrium, is an important factor in the initiation and maintenance of AF. It also serves as a major predictor of recurrence following AF radiofrequency ablation. Although LVA is more commonly observed in patients with persistent AF, it can also be present in some individuals with paroxysmal AF. However, the high-risk factors associated with the presence of LVA in patients with paroxysmal AF remain unclear. This study aims to investigate the risk factors and effective predictors for the presence of LVA in patients with paroxysmal AF.

Methods: This study enrolled patients with paroxysmal AF who underwent their first radiofrequency ablation procedure in the Department of Cardiology at Shanghai East Hospital between January 2020 and August 2023. Left atrial endocardial voltage mapping was performed with the PentaRay catheter guided by a 3D electro-anatomical mapping system. LVA was defined as regions with a bipolar voltage of less than 0.5 mV, and patients with LVAs exceeding 5% of the total left atrial surface area were classified into the LVA group. Demographic characteristics, comorbidities, electrocardiographic findings, and echocardiographic parameters were collected and used to develop a predictive model for left atrial LVA in patients with paroxysmal AF using logistic regression analysis. To validate the predictive performance of this model, a prospective cohort of patients with paroxysmal atrial fibrillation undergoing first-time radiofrequency ablation at the Department of Cardiology, Shanghai East Hospital, between September 2023 and April 2025 was enrolled.

Results: A total of 383 patients with paroxysmal AF were ultimately included in this study, among whom 104 patients (27.2%) were found to have left atrial LVA. Compared with patients with normal left atrial substrate, those with LVA had a significantly higher proportion of females and a higher incidence of prior stroke. Patients with LVAs also had older age, larger left atrial diameter, prolonged PR interval, lower hemoglobin levels, and elevated levels of troponin I and BNP. Multivariate logistic regression analysis revealed that female sex, history of stroke, left atrial diameter, PR interval, hemoglobin level, and serum creatinine level were independently associated with the presence of LVAs. Based on these six independent risk factors, we developed the HALF-PC model to predict the presence of LVA in patients with paroxysmal AF. Receiver operating characteristic (ROC) curve showed that the HALF-PC model effectively predicted the presence of left atrial LVA in patients with paroxysmal AF (AUC= 0.81, 95% CI 0.76-0.86). Furthermore, the HALF-PC model was more accurate than the ZAQ score in predicting the presence of left atrial LVA in patients with paroxysmal AF (AUC: 0.81 vs 0.77, p=0.04). By decision curve analysis, the clinical benefit of the HALF-PC model was also superior to ZAQ score. Subgroup analysis showed that the predictive value of the HALF-PC model was not influenced by age, sex, diabetes, hypertension, history of stroke, or left atrial diameter. In the validation cohort, we prospectively enrolled 173 patients with paroxysmal atrial fibrillation, among whom 60 (34.7%) were found to have left atrial LVA. ROC analysis demonstrated that the HALF-PC model maintained stable performance in predicting left atrial LVA in the validation cohort, with an AUC of 0.83 (95% CI: 0.76–0.90).

Conclusions: In this study, we identified several independent risk factors for the presence of left atrial LVA in patients with paroxysmal AF, including female sex, history of stroke, left atrial diameter, PR interval, hemoglobin level, and serum creatinine level. Based on these variables, the HALF-PC model was developed and demonstrated good predictive performance for identifying left atrial LVA in this patient population.

Prognostic Value of Red Cell Distribution Width-to-Serum Calcium Ratio for All-Cause Mortality in Critically Ill Atrial Fibrillation Patients

Qi-Qiang Jie[1], Gang Li[2], Jian-Ping Wang[1], Ming-Zhu He[1], Hai-Bo Jia[1], Feng-Fu Zhang[1], -Chun Qian[1]

1. Nanjing First Hospital

2. the First Affiliated Hospital of Zhengzhou University

Background: In the intensive care unit (ICU), atrial fibrillation (AF) is a common arrhythmia associated with significant morbidity and mortality. Accurate risk stratification is paramount for optimizing clinical management in this high-risk population. The red cell distribution width (RDW), a measure of erythrocyte size variability, and serum calcium levels are routine laboratory parameters that reflect underlying systemic inflammation, oxidative stress, and electrolyte homeostasis—all critical in cardiovascular pathophysiology. The red cell distribution width-to-serum calcium ratio (RCR) has recently emerged as a novel, integrated biomarker potentially reflecting a composite of these pathological states. It has been linked to poor outcomes in various cardiovascular disorders. Nevertheless, the prognostic significance of this easily calculated factor in the specific, complex setting of critically ill patients with AF remains insufficiently explored. This study aims to bridge this knowledge gap by assessing the predictive value of the RCR concerning both short-term (30-day) and long-term (365-day) all-cause mortality in this vulnerable patient population.

Methods: A large-scale, retrospective cohort study was performed utilizing data from 6,323 critically ill adult patients with a diagnosis of AF, sourced from the comprehensive Medical Information Mart for Intensive Care IV (MIMIC-IV) database. We calculated the RCR for each patient based on their initial laboratory values upon ICU admission. The cohort was subsequently stratified into tertiles based on these RCR levels to facilitate comparative analysis. The primary outcomes of interest were all-cause mortality, evaluated at two distinct clinical time points: 30 days and 365 days post-ICU admission. The analytical approach was multifaceted, employing Kaplan-Meier survival curves to visually represent mortality differences between the RCR tertiles, multivariable Cox proportional-hazards regression models to identify RCR as an independent predictor while adjusting for a wide range of potential clinical and laboratory confounders, and restricted cubic spline (RCS) regression to flexibly investigate and characterize potential non-linear relationships between RCR and mortality risk.

Results: The analysis revealed a robust and significant association between elevated RCR values and an increased risk of all-cause mortality at both follow-up intervals. The Kaplan-Meier curves showed a clear separation, with the highest RCR tertile experiencing significantly worse survival. After adjusting for confounders, the Cox regression models confirmed RCR as an independent predictor. A key finding from the RCS analyses was the identification of J-shaped associations between RCR and mortality, which suggests a more complex relationship than a simple linear trend. These analyses identified critical thresholds at an RCR of approximately 2.25, with minor variations depending on the duration of follow-up. Notably, mortality risk markedly escalated for RCR values above this threshold. For patients in the highest RCR tertile, a particularly notable hazard ratio (HR) of 7.42 (95% CI, 5.78–9.53) was observed for 365-day mortality, indicating a more than seven-fold increased risk of death within a year compared to the reference group.

Conclusion: An elevated red cell distribution width-to-serum calcium ratio (RCR) at the time of ICU admission is a significant and independent predictor of both short- and long-term mortality in critically ill patients with atrial fibrillation. The identification of a J-shaped relationship and a distinct risk threshold provides nuanced insight into this association. These findings highlight the potential clinical utility of RCR, a biomarker derived from two inexpensive and universally available laboratory tests, for enhancing bedside risk stratification. This could allow for the early identification of high-risk patients and the development of tailored, more aggressive management strategies to potentially improve outcomes.

Keywords: Atrial fibrillation; Red cell distribution width; Serum calcium; Prognosis; Mortality; MIMIC-IV

Association of Glycopyrrolate With New-Onset Atrial Fibrillation in Critically Ill Patients: A Retrospective Cohort Study

Qi-Qiang Jie[1], Gang Li[2], Jian-Ping Wang[1], Ming-Zhu He[1], Hai-Bo Jia[1], Feng-Fu Zhang[1], -Chun Qian[1], Shao-Liang Chen[1]

1. Nanjing First Hospital

2. the First Affiliated Hospital of Zhengzhou University

Background: Glycopyrrolate is a frequently administered anticholinergic agent in the intensive care unit (ICU), valued for its ability to reduce secretions and reverse neuromuscular blockade without significant central nervous system effects. Its primary mechanism involves blocking muscarinic receptors, including the M2 receptors in the heart. The blockade of these M2 receptors attenuates vagal input, leading to an increased heart rate. This physiological effect raises theoretical concerns about its potential to be proarrhythmic, specifically by creating an electrical environment conducive to the development of new-onset atrial fibrillation (NOAF). Given that NOAF is already a common and serious complication in the critically ill, associated with increased morbidity, mortality, and length of stay, clarifying any iatrogenic risk factors is of paramount clinical importance. However, despite these well-founded theoretical concerns, large-scale, robust evidence regarding this association in a general, heterogeneous ICU population has been notably limited. This study therefore sought to investigate whether the systemic administration of glycopyrrolate is independently associated with an increased risk of developing NOAF in critically ill patients.

Methods: To address this question, we conducted a large-scale retrospective cohort study, leveraging the extensive, real-world data contained within two major critical care databases: the Medical Information Mart for Intensive Care IV (MIMIC-IV), which served as our primary cohort, and MIMIC-III, used as a validation cohort to ensure the reproducibility of our findings. The study included adult critically ill patients who were free of atrial fibrillation at the time of ICU admission. Exposure was strictly defined as the administration of at least one dose of systemic glycopyrrolate within the first 48 hours of their ICU stay. The primary outcome was the incidence of NOAF within the first 7 days of ICU admission. To mitigate selection bias and confounding inherent in observational data, we performed rigorous propensity score matching (PSM) in the primary cohort, creating well-balanced groups of patients who did and did not receive glycopyrrolate. In both cohorts, multivariable logistic regression analyses were employed to further adjust for a comprehensive set of potential confounders.

Results: Our analysis revealed a consistent and statistically significant association between glycopyrrolate administration and an increased risk of developing NOAF. After propensity score matching in the MIMIC-IV cohort, glycopyrrolate use was associated with a 20% increase in the odds of NOAF (Odds Ratio [OR], 1.20; 95% Confidence Interval [CI], 1.06–1.37). This finding was corroborated and even more pronounced in the MIMIC-III validation cohort, where multivariable logistic regression showed a 60% increase in the odds of NOAF (adjusted OR, 1.60; 95% CI, 1.27–2.00). In a secondary analysis of mortality in the MIMIC-IV cohort, glycopyrrolate was associated with a surprising reduction in in-hospital mortality (PSM OR, 0.67; 95% CI, 0.52–0.86). However, this potential protective effect was not replicated in the MIMIC-III cohort (P = .088), indicating that this finding may be inconsistent. Furthermore, no significant association was observed between glycopyrrolate use and ICU mortality in either cohort.

Conclusions: Systemic glycopyrrolate administration was consistently and independently associated with a significantly increased risk of new-onset atrial fibrillation in a large, diverse population of critically ill patients, a finding robust across two separate large databases. This suggests that the proarrhythmic potential of glycopyrrolate is a tangible clinical risk. Conversely, the findings regarding a potential benefit on in-hospital mortality were inconsistent across the cohorts and should be interpreted with caution. No association with ICU mortality was observed. Clinicians should therefore remain vigilant and weigh the known benefits of glycopyrrolate against this quantified risk of NOAF when prescribing it to critically ill patients.

Keywords: Glycopyrrolate, New-Onset Atrial Fibrillation, Critical Illness, Intensive Care Unit, Cohort Study

心房颤动患者治疗方式选择的影响因素分析

黄燕

陆军军医大学第一附属医院心血管内科

目的：通过了解心房颤动患者的一般情况、疾病状况和治疗决策，分析各要素之间的关系，判断显著影响治疗意愿和选择的因素，总结原因，为未来房颤治疗技术发展提供方向。

方法：本研究为回顾性研究，收集病历系统中住院接受治疗的房颤患者资料，根据治疗方式分为药物治疗组和射频消融手术治疗组，共收集病历数据 3759 份。将患者一般人口学资料（年龄、性别、受教育程度、医保类型、婚姻状况）、临床相关指标（CHA_2DS_2-VASc-60 评分、HAS-BLED 出血评分、症状 EHRA 评分、BMI）等纳入研究。将符合正态分布的定量资料采用 t 检验；定性资料采用 $\chi 2$ 检验进行单因素分析，以 P<0.05 为差异有统计学意义。之后以房颤患者治疗方式作为因变量，以单因素分析中差异有统计学意义的变量作为自变量进行 Logistic 回归分析。

结果：本研究最终统计得出药物治疗患者 2039 例，占比 57%，比例较高。单因素分析中年龄、CHA_2DS_2-VASc-60 评分、HAS-BLED 出血评分、症状 EHRA 评分、医保付费方式、受教育程度、婚姻状况具有统计学意义（P < 0.05）。将上述变量进行多因素 Logistic 回归分析显示年龄、受教育程度、BMI、CHA_2DS_2-VASc 评分的差异具有统计学意义。

结论：年龄、受教育程度、BMI 和 CHA_2DS_2-VASc 评分是显著影响治疗方式的因素。年龄越大、卒中评分越高，患者越倾向于选择药物治疗；而 BMI 指数和受教育程度越高，患者越偏向手术治疗。年龄大、卒中评分高，患者对于手术的耐受程度及术后恢复能力减弱；体重指数越大，手术治疗的效果优于保守治疗；受教育程度越高，对于先进技术的接受程度越高，顾虑少。因此，应根据患者实际情况以获得最好的预后、减少复发及死亡为原则选择合适的抗凝措施，推荐最有效的一线治疗方式，在现有基础上根据影响因素作用大小发掘更安全、更有效的新思路。

不同类型心房颤动患者心脏结构与功能的差异性分析：一项观察性研究

宋诗飞 谢伟

新疆生产建设兵团医院

目的 探讨不同类型心房颤动（房颤）患者心脏结构和功能之间是否存在相互关联。**方法** 采用查询电子病历及存档病历的方式，对 2014 年 01 月 ~ 2024 年 12 月期间在我院住院患者病历进行筛选，筛选出出院诊断为房颤的病例。**结果** 共纳入 505 例房颤患者，根据房颤持续时间分为阵发性房颤组（简称“阵发组”，n=237）、持久性房颤组（简称“持久组”，n=268）。不同类型房颤患者的左心房结构和功能存在差异，主要心脏结构指标：LA（Left Atrium）、RA（Right Atrium）、IVSd (Interventricular Septal thickness at end-diastole)、LVPW（Left Ventricular Posterior Wall Thickness）及功能指标：LVEF(Left Ventricular Ejection Fractions) 差异有统计学意义（分别为：Z=14.80，P=0.00、Z=9.70，P=0.00、Z=6.66，P=0.01、Z=5.50，P=0.02、Z=8.02，P=0.01）。持久组结构指标与阵发组相比有增大趋势，心力衰竭发生率更高。**结论** 不同类型心房颤动之间心脏结构和功能存在着密切的相互关系，可以为临床诊治及病情预后评估提供有力的依据。

基于机器学习的阵发性房颤导管消融术后复发风险预测模型研究

孙颖

吉大一院

目的：基于机器学习算法构建多参数融合的预测体系，评估不同算法对阵发性房颤（Paroxysmal atrial fibrillation ,PAF）患者导管消融术（Catheter Ablation,CA）术后复发的预测效能，筛选最优预测模型，通过可解释性分析量化关键生物标志物的预测贡献度，最终为临床决策提供依据，优化个体化风险评估和术后随访策略。

方法：回顾性纳入 2019 年 6 月 1 日至 2023 年 6 月 1 日在吉林大学第一医院首次接受 CA 的 PAF 患者 . 随访截至 2024 年 12 月 31 日，最终纳入 501 例患者。收集并预处理患者的多维度临床特征，采用多阶段特征筛选策略确定预测变量，并基于这些变量分别构建逻辑回归、支持向量机、K 邻近算法、随机森林、极端梯度提升机和轻量梯度提升机学习模型。使用分层随机抽样法按 7:3 比例将数据划分为训练集

结果：1. 共纳入 501 例首次行 CA 的 PAF 患者，复发率为 13.8%（95%CI:10.7-16.9%）。2. 经特多阶段征筛选，房颤负荷、二尖瓣反流程度、身体质量指数、B 型钠尿肽、左房内径、左室舒张末期内径、P 波时限、校正 QT 间期、病程时长、房间传导阻滞 11 项变量纳入最终模型。3.LightGBM 为最优模型，校准曲线与理想校准重合度较高，决策曲线分析显示其在广泛阈值区间都有较高的净收益。4.SHAP 分析贡献度，对复发的贡献度相对较小。

结论：1、阵发性房颤患者导管消融术后有一定的复发率，提示临床需重视术后复发风险的早期识别与管理，以改善患者长期预后并降低医疗负担。2、通过多阶段特征筛选与 SHAP 可解释性分析，研究证实房颤负荷、P 波时限、二尖瓣反流程度、LAD 及 QTc 与复发相关，其中房颤负荷与 P 波时限的贡献度最为显著，揭示了电生理重构与结构重塑的协同作用机制。3. 本研究构建的基于 LightGBM 算法的多维临床参数机器学习预测模型，有助于优化术后随访策略及个体化干预方案的制定。

The Predictive Value of Real-world Cardiologist Performance (RWCP) Score in Atrial Fibrillation Recurrence Risk After Radiofrequency Ablation

Yang-Yang Wang[1], Jing-Chao He[1], Yang Shao[2], Tong Liu[3], Ao-Lin Ding[4], Guo-Hua Xue[1], Yu-Bing Guo[1], Peng-Yu Wu[1], Yun-Fei Gu[1], Hao Wang[1]

1. Luoyang Central Hospital Affiliated to Zhengzhou University

2. Sahlgrenska University Hospital

3. The Second Hospital of Tianjin Medical University

4. Biosense Webster Medical Technology

Abstract

Objective To explore the predictive value of Real-world Cardiologist Performance (RWCP) score for atrial fibrillation (AF) recurrence risk after radiofrequency catheter ablation (RFCA).

Methods Patients with non-valvular AF who underwent first-time RFCA at Luoyang Central Hospital affiliated to Zhengzhou University between October 2021 and June 2023 were included in this study. All enrolled participants provided written informed consent, who voluntarily agreed to participate in the study. Detailed ablation data were exported from CARTO®3 system (Biosense Webster, USA), based on which, four parameters, including discharge time proportion, Catheter Contact Force Stability (C3-FOT proportion), Ablation Index Consistency (SURPOINT/TOP-

4 proportion) and fragmented points proportion, were calculated. Then, the RWCP score was calculated from these parameters for each patient. Predictive value of the RWCP score for AF recurrence risk were assessed using Cox regression and Kaplan-Meier analyses.Statistical analyses were performed using SPSS 23.0 for Windows (Chicago, IL, USA), with statistical significance set at p < 0.05 (two-sided).

Results A total of 148 AF patients were enrolled, including 68 males and 80 females. During follow-up, 30 patients (20.3%) experienced AF recurrence. Patients in the recurrence group were found to be relatively older (P=0.048) and had a significantly lower. Catheter Contact Force Stability (C3-FOT proportion) of right ring (P=0.01). Although the fragmented points proportion of right ring in the recurrence group showed a lower trend, the difference did not reach statistical significance. The RWCP score was calculated using Cox regression coefficients, due to the regression coefficient being too small, they were amplified by 10 times to derive the RWCP score formula. The final RWCP score was as follows: RWCP score = (left ring discharge time ratio×2.853)-(left C3-FOT proportion×0.91)+(left SURPOINT/TOP4×2.943)+(left fragmented point proportion×0.423)-(right ring discharge time ratio×4.039)-(right C3-FOT proportion×6.159)-(right SURPOINT/TOP4×1.312)-(right fragmented proportion×4.425). Univariate Cox regression analysis did not identify any clinical indicators with statistically significant predictive value for AF recurrence risk. Based on well-established AF recurrence risk factors reported in previous researches, variables such as sex, age, AF onset type, and left atrial diameter (LAD) were included in a multivariable Cox regression for adjustment. The results across all three levels of adjustment, including unadjusted model, minimally adjusted model (adjusting only for sociodemographic factors such as sex and age), and fully adjusted model (adjusting AF onset type and LAD, besides sex and age) were summarized. All three adjustment models suggested that RWCP score was an independent predictor of AF recurrence risk. In the fully adjusted model, each one-point increase in RWCP score was associated with an approximately 10% increase in AF recurrence risk (P=0.0009). To facilitate clinical application, patients were further classified into three groups (high, medium and low RWCP score) based on tertiles, as well as two groups (high and low RWCP score) according to median. Kaplan-Meier survival analysis demonstrated a clear trend in survival curves across the three groups (high, medium, and low RWCP score). In the two-group comparison, patients in the high RWCP score group showed significantly higher recurrence risk than those in the low score group. To further improve clinical utility, an online RWCP score calculator was developed and released (https://doctorwanghao.shinyapps.io/RWCP_English/).

Conclusion The RWCP score shows promise as a tool for evaluating ablation completeness, assessing cardiologist performance and predicting AF recurrence risk after ablation.

Keywords: atrial fibrillation; radiofrequency catheter ablation; recurrence; prediction

Research Progress on Insulin Resistance Indicators and Recurrence after Radiofrequency Ablation of Atrial Fibrillation

Shi Yongfeng, Guang-Zhi Yongfeng

The Second Hospital of Jilin University

Objective

The primary objective of this review is to summarize the current research progress on the association between various surrogate markers of insulin resistance (IR), including the estimated glucose disposal rate (eGDR), triglyceride-glucose (TyG) index, metabolic score of insulin resistance (METS-IR), and uric acid to high-density lipoprotein cholesterol (HDL-C) ratio (UHR), and the recurrence of atrial fibrillation (AF) after radiofrequency catheter ablation (RFCA). We aim to identify a suitable predictor that can be used in clinical practice to improve the prediction of AF recurrence after RFCA.

Methods

To achieve this objective, we conducted a comprehensive literature search on PubMed to identify studies that have investigated the relationship between IR indicators and AF recurrence after RFCA. The search terms included "insulin resistance," "AF recurrence," "radiofrequency ablation," "estimated glucose disposal rate," "triglyceride-glucose index," "metabolic score of insulin resistance," and "uric acid to HDL cholesterol ratio." The retrieved articles were reviewed and analyzed to extract relevant data and findings. The results were then summarized and generalized to provide an overview of the current research progress in this field.

Results

In a study involving 899 patients with AF who underwent RFCA, the median follow-up period was 11.63 months. During this period, 296 patients experienced AF recurrence. The cumulative recurrence rate of AF was significantly higher in the lowest eGDR group compared to the highest eGDR group (log-rank p < 0.01). Specifically, subjects with an eGDR ≥ 8 mg/kg/min had a significantly higher rate of AF recurrence compared to those with an eGDR < 4 mg/kg/min. The hazard ratio (HR) for AF recurrence was 0.28 [95% confidence interval (CI) 0.18, 0.42] for subjects with lower eGDR values, indicating a lower risk of recurrence.

In another study that included 575 patients with AF, the risk of AF recurrence was found to increase with higher cumulative TyG index values. After adjusting for potential confounders, the risk of AF recurrence was significantly higher in patients with moderate (HR = 4.949, 95% CI: 1.778–13.778, p = 0.002) and high (HR = 8.716, 95% CI: 3.371–22.536, p < 0.001) cumulative TyG index values compared to those with low cumulative TyG index values.

A third study included 2,242 AF patients who underwent RFCA. At the 1-year follow-up, 31.7% of patients experienced AF recurrence. Multivariate analysis revealed that the TyG index, METS-IR, and TyG-BMI index were independent risk factors for AF recurrence. Restricted cubic spline analysis further demonstrated a significant association between METS-IR, TyG-BMI index, and AF recurrence (P < 0.001).

In a smaller study involving 163 patients who underwent RFCA for AF, 39 (23.93%) experienced AF recurrence. The mean age of the participants was 57.49 ± 11.22 years, and 59.51% were male. The study found that a UHR value greater than 15.1 was an independent predictor of AF recurrence.

Conclusion

The findings from the reviewed studies collectively suggest that decreased eGDR is associated with an increased risk of AF recurrence after RFCA. The TyG index, METS-IR, and TyG-BMI index are independently associated with AF recurrence after ablation. Additionally, the UHR has emerged as an independent biomarker for predicting AF recurrence. These surrogate markers of IR offer potential clinical utility for predicting AF recurrence after RFCA. Further prospective studies with larger cohorts are warranted to validate these findings and to determine the optimal cutoff values for these markers in clinical practice.

Impact of Sodium-Glucose Cotransporter 2 Inhibitor on Recurrence After Catheter Ablation for Atrial Fibrillation in Patients With or Without Metabolic Syndrome

Yang Xu[1], Zi-Xu Zhao[1], Hui Xu[1], Chao Jiang[1], Xiao Wang[2], Ze-Jun Yang[1], Wen-Yu Shao[1], Hang Guo[1], Liu He[1], Qi Guo[1], Cai-Hua Sang[1], De-Yong Long[1], Xin Du[1,3], Jian-Zeng Dong[1], Chang-Sheng Ma[1]

1. Beijing Anzhen Hospital

2. Beijing Fuwai Hospital

3. Heart Health Research Cente

Impact of Sodium-Glucose Cotransporter 2 Inhibitor on Recurrence After Catheter Ablation for Atrial Fibrillation in Patients With or Without Metabolic Syndrome

Yang Xu*, MS1, Zixu Zhao*, MD1, Hui Xu*, MS1, Chao Jiang, MD1†, Xiao Wang, MD2†, Zejun Yang, MS1, Wenyu Shao, MS1, Hang Guo, MS1, Liu He, PhD1, Qi Guo, MD1, Caihua Sang, MD1, Deyong Long, MD1, Xin Du, MD1,3, Jianzeng Dong, MD1, Changsheng Ma, MD1†

*The authors contributed equally to the study.

1 Department of Cardiology, Beijing Anzhen Hospital, Capital Medical University, National Clinical Research Center for Cardiovascular Diseases, Beijing, China

2 Cardiometabolic Medicine Center, Fuwai Hospital, National Center for Cardiovascular Diseases, Chinese Academy of Medical Sciences and Peking Union Medical College, Beijing, China

3 Heart Health Research Center, Beijing, China

ACKNOWLEDGEMENTS

This study is supported by Beijing Municipal Health Commission, Capital Health Development Research Project (2024-4-20610) and Beijing Physician Scientist Training Project (BJPSTP-2024-21).

DISCLOSURE

None reported.

Address for correspondence: Chao Jiang, E-mail: superj@zju.edu.cn; Changsheng Ma, E-mail: chshma@vip.sina.com. Department of Cardiology, Beijing Anzhen Hospital, Capital Medical University, No.2, Anzhen Road, Chaoyang District, 100029 Beijing, China. Xiao Wang, E-mail: spaceeye123@126.com; Fuwai Hospital, National Center for Cardiovascular Diseases, Chinese Academy of Medical Sciences and Peking Union Medical College, 167A Beilishi Road, Xicheng District, Beijing 100037, China

ABSTRACT

Aims: The impact of sodium-glucose cotransporter-2 inhibitors on atrial fibrillation recurrence after catheter ablation is still inconclusive. Besides, their efficacy on atrial fibrillation recurrence stratified by metabolic syndrome status remains unknown.

Methods: Patients with atrial fibrillation undergoing initial catheter ablation between January 2017 and December 2023 from the China-AF Registry were included. Patients were 1:1 propensity score-matched by sodium-glucose cotransporter-2 inhibitors use at discharge and stratified by baseline metabolic syndrome status. The main outcome was the atrial fibrillation recurrence after a 3-month blanking period. Kaplan-Meier curves and the log-rank test were used to compare outcomes, and hazard ratios with 95% confidence intervals were derived from univariate Cox proportional hazards models. Nonlinear associations between baseline body mass index and atrial fibrillation recurrence were assessed using restricted cubic splines with interaction testing for sodium-glucose cotransporter-2 inhibitors use.

Results: After propensity score matching, 573 patients in the sodium-glucose cotransporter-2 inhibitors group and 573 in the non-sodium-glucose cotransporter-2 inhibitors group were included in the study. During the 20.5 ± 13.7 months follow-ups, atrial fibrillation recurrence occurred in 100 patients (17.5%) in the sodium-glucose cotransporter-2 inhibitors group and 168 patients (29.3%) in the non-sodium-glucose cotransporter-2 inhibitors group. Sodium-glucose cotransporter-2 inhibitors was associated with lower atrial fibrillation recurrence (17.5% vs. 29.3%; HR 0.59, 95% CI 0.46–0.75, P<0.001), with consistent benefits in metabolic syndrome (HR 0.61, 95% CI 0.39–0.75, P=0.03) and non-metabolic syndrome subgroups (HR 0.58, 95% CI 0.43–0.78, P<0.001, Pinteraction=0.841). The effect of sodium-glucose cotransporter-2 inhibitors on the atrial fibrillation recurrence also remained consistent across the body mass index spectrum (Pinteraction=0.740).

Conclusion: Sodium-glucose cotransporter-2 inhibitors was associated with a lower risk of AF recurrence after catheter ablation. The effect of SGLT2 inhibitors on the recurrence of AF was consistent across the MetS status and a wide range of BMI spectrum.

Keywords: Atrial fibrillation, Catheter ablation, Sodium-glucose cotransporter-2 inhibitors, Metabolic syndrome, Body mass index.

Impact of Sodium-glucose Cotransporter 2 Inhibitor on Recurrence and Cardiovascular Outcomes after Catheter Ablation for Atrial Fibrillation in Patients with Chronic Kidney Disease

Hui Xu[1], Zi-Xu Zhao[1], Yang Xu[1], Chao Jiang[1], Xiao Wang[3], Ze-Jun Yang[1], Hang-Yu Yan[1], Ting Shen[1], Hang Guo[1], Liu He[1], Qi Guo[1], Chen-Xi Jiang[1], Ri-Bo Tang[1], Cai-Hua Sang[1], De-Yong Long[1], Xin Du[1,2], Jian-Zeng Dong[1], Chang-Sheng Ma[1]

1. Department of Cardiology, Beijing Anzhen Hospital, Capital Medical University, National Clinical Research Center for Cardiovascular Diseases

2. Heart Health Research Center

3. Cardiometabolic Medicine Center, Fuwai Hospital, National Center for Cardiovascular Diseases, Chinese Academy of Medical Sciences and Peking Union Medical College

Impact of Sodium-glucose Cotransporter 2 Inhibitor on Recurrence and Cardiovascular Outcomes after Catheter Ablation for Atrial Fibrillation in Patients with Chronic Kidney Disease

Hui Xu*, MS1, Zixu Zhao*, MD1, Yang Xu*, MS1, Chao Jiang, MD1†, Xiao Wang, MD3†, Zejun Yang, MS1, Hangyu Yan, MS1, Ting Shen, MS1, Hang Guo, MS1, Liu He, PhD1, Qi Guo, MD1, Chenxi Jiang, MD1, Ribo Tang, MD1, Caihua Sang, MD1, Deyong Long, MD1, Xin Du, MD1,2, Jianzeng Dong, MD1, Changsheng Ma, MD1†

*The authors contributed equally to the study.

Affiliations

1 Department of Cardiology, Beijing Anzhen Hospital, Capital Medical University, National Clinical Research Center for Cardiovascular Diseases, Beijing, China

2 Heart Health Research Center, Beijing, China

3 Cardiometabolic Medicine Center, Fuwai Hospital, National Center for Cardiovascular Diseases, Chinese Academy of Medical Sciences and Peking Union Medical College, Beijing, China

Address for correspondence

Changsheng Ma

Department of Cardiology, Beijing Anzhen Hospital, Capital Medical University, No.2, Anzhen Road, Chaoyang District, Beijing 100029, China. E-mail: chshma@vip.sina.com

Chao Jiang

Department of Cardiology, Beijing Anzhen Hospital, Capital Medical University, No.2, Anzhen Road, Chaoyang District, Beijing 100029, China. E-mail: superj@zju.edu.cn

Xiao Wang

Cardiometabolic Medicine Center, Fuwai Hospital, National Center for Cardiovascular Diseases, Chinese Academy of Medical Sciences and Peking Union Medical College, Beijing, 167A Beilishi Road, Xicheng District, Beijing 100037, China. E-mail: spaceeye123@126.com

Abstract

Objective: Emerging evidence suggests that sodium-glucose cotransporter 2 inhibitor (SGLT2i) exerts antiarrhythmic effects and is associated with a reduced risk of atrial fibrillation (AF) recurrence after catheter ablation in patients with diabetes or heart failure. This study aimed to evaluate the effect of SGLT2i on AF recurrence and cardiovascular outcomes after catheter ablation in patients with chronic kidney disease (CKD).

Methods: From the multicenter, prospective Chinese-AF Registry, we identified 628 AF patients with CKD who underwent initial catheter ablation for AF from January 2019 to December 2023. Based on discharge prescriptions, patients were stratified into the SGLT2i group (n=119) and the non-SGLT2i group (n=509). Propensity score-derived overlap weighting was employed to balance baseline characteristics, with standardized mean differences <0.1 confirming adequate covariate balance. Cox proportional hazards models were employed to assess the association between SGLT2i treatment and clinical outcomes. The primary outcome was AF recurrence after the three-month blanking period from the ablation.

Results: With a mean follow-up duration of 13.1 ± 5.3 months, patients in the SGLT2i group had a lower rate of AF recurrence compared to the non-SGLT2i group after overlap weighting adjustment (21.8% [26/119] vs 31.2% [159/509]; adjusted HR 0.56, 95% CI 0.32–0.98, P = 0.044). Additionally, the SGLT2i group demonstrated a significantly lower rate of the composite cardiovascular outcome (cardiovascular mortality, cardiovascular hospitalization, or thrombotic events; adjusted HR 0.38, 95% CI 0.20–0.73, P = 0.004), with the most substantial reduction observed for cardiovascular hospitalization (adjusted HR 0.33, 95% CI 0.16–0.68, P = 0.002). Subgroup analyses demonstrated consistent treatment effects across major baseline characteristics. No significant differences were observed in all-cause mortality, cardiovascular mortality, and thrombotic events between the SGLT2i and non-SGLT2i groups.

Conclusion: SGLT2i treatment was associated with reduced risks of AF recurrence and the composite cardiovascular outcome (cardiovascular mortality, cardiovascular hospitalization, or thrombotic events) in CKD patients receiving catheter ablation for AF.

MBNL2 在房颤发生发展中的作用机制及治疗潜力：最新研究进展与展望

嘉豪

哈尔滨医科大学附属第一医院

目的：

房颤（Atrial Fibrillation, AF）是最常见的心律失常之一，其发病机制涉及电重构、结构重构和自主神经调节异常。近年来，RNA 结合蛋白 MBNL2（Muscleblind-like 2）被发现在心脏发育和疾病中发挥关键作用，但其在房颤中的具体机制尚不明确。本文旨在 MBNL2 与房颤的关联性，探讨其通过调控选择性剪接、离子通道表达及纤维化通路影响房颤的分子机制，并评估其作为治疗靶点的潜在价值。

方法：

通过系统检索 PubMed、Web of Science 及 bioRxiv 等数据库，筛选近 5 年关于 MBNL2 与房颤的临床研究、动物模型实验及分子机制研究。结合单细胞测序、基因编辑（如 CRISPR-Cas9）和蛋白质组学等

结果：

1、房颤患者心房组织及动物模型中 MBNL2 表达显著下调，其低表达与心房电重构 KCNQ1、SCN5A 剪接异常和纤维化 TGF-β/Smad 通路激活密切相关。

2、MBNL2 通过结合 pre-mRNA 调控钙处理蛋白 RyR2、SERCA2a 和钠通道 SCN5A 的剪接变体，影响动作电位时程和传导速度。

3、MBNL2 缺失导致促纤维化 miRNA（如 miR-21）上调，促进胶原沉积。

4、在房颤小鼠模型中，AAV 介导的 MBNL2 过表达可减轻电重构和纤维化，而反义寡核苷酸（ASO）靶向恢复 MBNL2 功能可减少房颤诱发率。

结论：

MBNL2 作为 RNA 代谢的核心调控因子，通过多途径参与房颤的发生发展，其表达恢复或功能增强可能成为新型治疗策略。MBNL2 对房颤的调控具有时空特异性，其在心房肌细胞与成纤维细胞中的作用可能不同。未来需进一步明确其组织特异性调控网络，并开发临床可用的靶向递送系统。结合人工智能预测剪接靶点及基因编辑技术，MBNL2 相关研究有望推动房颤的精准治疗。

关键词：MBNL2；房颤；RNA 剪接；电重构；纤维化；靶向治疗

Integrated Single-Cell and Bulk Transcriptome Analysis Reveals a Lactate Metabolism-Related Signature and T-Cell Alterations in Atrial Fibrillation

Xianglin Long, Zhi-Hui Zhang

The Third Xiangya Hospital of Central South University

Objective: Atrial fibrillation (AF) is characterized by significant T-cell immune dysregulation. While lactate metabolism is a critical regulator of T-cell function, its role in the immunopathology of AF remains poorly defined. This study aimed to identify a lactate metabolism-related gene signature and elucidate associated T-cell alterations in AF through an integrated transcriptomic approach.

Methods: We performed an integrated analysis of bulk and single-nucleus RNA-sequencing (snRNA-seq) data from human atrial tissue of patients with AF and sinus rhythm. Lactate metabolism-related genes were curated from the Molecular Signatures Database (MSigDB). Key genes were identified using Weighted Gene Co-expression Network Analysis (WGCNA) and differential expression analysis. A machine learning-based diagnostic signature was constructed and validated in external cohorts. Findings were validated by quantitative real-time PCR (qRT-PCR) in a murine AF model. T-cell subpopulations and intercellular communication networks were characterized using Seurat and CellChat, respectively.

Results: We identified a six-gene lactate metabolism-related signature strongly associated with AF status and correlated with CD4+/CD8+ T-cell abundance. A diagnostic model built from this signature demonstrated excellent performance in external validation datasets (Area Under the Curve [AUC] = 0.909). SnRNA-seq analysis revealed a distinct, metabolism-related T-cell subcluster (CLM-T) that was significantly depleted in AF tissues. Furthermore, we observed enhanced CD45 and thrombospondin-1 (THBS1) signaling from CLM-T cells to other T-cell subsets in AF. The upregulation of the signature genes was successfully validated in atrial tissue from a murine AF model.

Conclusion: By integrating bulk and single-cell transcriptomics, this study identifies a novel lactate metabolism-related gene signature as a robust diagnostic biomarker for AF. Our findings reveal a distinct T-cell subpopulation remodeling in AF, directly linking altered cellular metabolism to immune dysregulation in the atrial microenvironment. These insights advance our understanding of AF immunopathology and highlight lactate metabolism as a potential therapeutic and diagnostic target.

Keywords: Atrial fibrillation; Lactate metabolism; T cell; Single-cell RNA sequencing; Transcriptomics; Biomarker.

Objective: Atrial fibrillation (AF) is characterized by significant T-cell immune dysregulation. While lactate metabolism is a critical regulator of T-cell function, its role in the immunopathology of AF remains poorly defined. This study aimed to identify a lactate metabolism-related gene signature and elucidate associated T-cell alterations in AF through an integrated transcriptomic approach.

Methods: We performed an integrated analysis of bulk and single-nucleus RNA-sequencing (snRNA-seq) data from human atrial tissue of patients with AF and sinus rhythm. Lactate metabolism-related genes were curated from the Molecular Signatures Database (MSigDB). Key genes were identified using Weighted Gene Co-expression Network Analysis (WGCNA) and differential expression analysis. A machine learning-based diagnostic signature was constructed and validated in external cohorts. Findings were validated by quantitative real-time PCR (qRT-PCR) in a murine AF model. T-cell subpopulations and intercellular communication networks were characterized using Seurat and CellChat, respectively.

Results: We identified a six-gene lactate metabolism-related signature strongly associated with AF status and correlated with CD4+/CD8+ T-cell abundance. A diagnostic model built from this signature demonstrated excellent performance in external validation datasets (Area Under the Curve [AUC] = 0.909). SnRNA-seq analysis revealed a distinct, metabolism-related T-cell subcluster (CLM-T) that was significantly depleted in AF tissues. Furthermore, we observed enhanced CD45 and thrombospondin-1 (THBS1) signaling from CLM-T cells to other T-cell subsets in AF. The upregulation of the signature genes was successfully validated in atrial tissue from a murine AF model.

Conclusion: By integrating bulk and single-cell transcriptomics, this study identifies a novel lactate metabolism-related gene signature as a robust diagnostic biomarker for AF. Our findings reveal a distinct T-cell subpopulation remodeling in AF, directly linking altered cellular metabolism to immune dysregulation in the atrial microenvironment. These insights advance our understanding of AF immunopathology and highlight lactate metabolism as a potential therapeutic and diagnostic target.

Keywords: Atrial fibrillation; Lactate metabolism; T cell; Single-cell RNA sequencing; Transcriptomics; Biomarker.

Bleeding Risk of Rivaroxaban and Edoxaban with and without Amiodarone in Atrial Fibrillation Patients: A Prospective Cohort Study

Zi Wang[1], Fan Yang[2], Qi-Ming Wang[2], Hong-Yi Wu[1], Qian-Zhou Lv[1]

1. Zhongshan hospital, Fudan University

2. Shanghai Geriatric Medical Center

Background

Rivaroxaban and edoxaban are commonly used for stroke prevention in patients with atrial fibrillation (AF). However, the differential impact of these anticoagulants combined with amiodarone on bleeding risk remains unclear.

Objective

The aim of this study was to compare the bleeding risk between rivaroxaban and edoxaban in patients with atrial fibrillation, both with and without the combination of amiodarone.

Methods

We conducted a prospective cohort study involving patients with AF. Participants were divided into four groups based on the type of direct oral anticoagulant they received: rivaroxaban monotherapy, edoxaban monotherapy, rivaroxaban combined with amiodarone, and edoxaban combined with amiodarone. A 3-month follow-up was performed to record bleeding events. Propensity score matching (PSM) and inverse probability of treatment weighting (IPTW) methods were used to control for confounding factors. The primary endpoint was the time to the first occurrence of a composite of major bleeding, clinically relevant non-major bleeding (CRNM), and minor bleeding, as defined by the International Society on Thrombosis and Haemostasis (ISTH). Secondary endpoints included stroke, recurrence of AF, and discontinuation of anticoagulant therapy or amiodarone due to adverse drug reactions.

Results

A total of 910 patients with AF were included in the study. Of these, 298 received rivaroxaban alone, 151 received edoxaban alone, 321 received rivaroxaban with amiodarone, and 140 received edoxaban with amiodarone. After propensity score matching, no significant differences in baseline characteristics were found between the monotherapy and combination treatment groups. During follow-up, the bleeding risk was similar between the rivaroxaban (9.01%) and edoxaban (13.51%) monotherapy groups (P = 0.403). However, the bleeding risk in the rivaroxaban-amiodarone group was significantly higher than in the edoxaban-amiodarone group, both in the PSM analysis (HR = 2.015, 95% CI = 1.026–3.958, P = 0.042) and the IPTW analysis (HR = 2.278, 95% CI = 1.232–4.211, P = 0.009). Stroke incidence was low across all groups, with no significant differences observed between rivaroxaban and edoxaban, whether used alone or with amiodarone. Atrial fibrillation recurrence was higher with rivaroxaban monotherapy than edoxaban (0.78% vs. 5.47%, P = 0.022), but this difference disappeared when combined with amiodarone. Discontinuation due to adverse events showed no significant differences among the groups. Further analysis revealed that patients receiving standard-dose rivaroxaban with amiodarone had a significantly higher bleeding risk than those receiving edoxaban with amiodarone (HR = 2.678, 95% CI = 1.017–7.045, P = 0.046). Additionally, rivaroxaban with amiodarone was associated with a significantly higher bleeding risk compared to edoxaban with amiodarone in patients with renal dysfunction (HR = 2.186, 95% CI = 1.016–4.702, P = 0.045).

Conclusion

In this prospective cohort study, we found that when used as monotherapy, the bleeding risks associated with rivaroxaban and edoxaban were similar. However, when combined with amiodarone, rivaroxaban was associated with a higher bleeding risk compared to edoxaban. Additionally, our results indicate that drug dosage and renal function can influence the bleeding risk associated with these drug combinations. These findings highlight the importance of considering individual patient characteristics, such as renal function and medication dose, when selecting anticoagulant therapy, particularly in combination with amiodarone, to minimize bleeding risks. Further research is needed to confirm these results and refine treatment strategies for patients with atrial fibrillation.

持续性房颤射频消融术中应用尼非卡兰复律前冠状窦 A-A 间期在识别高危复发人群的意义

蔡萧旭

南昌大学第二附属医院

研究目的：本研究旨在探讨持续性房颤射频消融术中，行尼非卡兰复律前冠状窦 A-A 间期在识别术后高危复发人群中的预测价值，以期为临床优化消融策略及术后管理提供一个便捷的心电生理参数。

研究方法：本研究回顾性纳入了 2021 年 1 月至 2024 年 1 月期间在南昌大学第二附属医院接受导管射频消融术的持续性房颤患者。完成递进式射频消融术式未能成功复律后使用尼非卡兰药物复律的患者共 294 例被最终纳入分析。所有患者均在使用尼非卡兰复律前段测量了冠状窦 A-A 间期。根据 A-A 间期是否可测得，划分为 2 组：不可测出组与可测出组。在可测出组中，根据 A-A 间期的长度，划分为 3 组：T1 组（A-A 间期＜ 160ms）、T2 组（A-A 间期≥ 160ms，＜ 180ms）和 T3 组（A-A 间期≥ 180ms）。术后随访 1 年，记录房颤复发情况。采用多因

素 Cox 回归分析评估 A-A 间期与术后复发风险的关系。

研究结果：术后 1 年总体复发率为 28.9%。其中，不可测出组复发率为 51.3%，高于可测出组的 25.6%。不同 A-A 间期组的复发率也具有显著差异（P < 0.001），T1 组（A-A 间期< 160ms）为 31.5%，T2 组（A-A 间期≥ 160ms，< 180ms）为 28.3%，T3 组（A-A 间期≥ 180ms）为 16.6%。多因素 Cox 回归分析显示，A-A 间期可测出组的患者术后复发风险显著降低（HR=0.36,95%CI:0.21-0.61,p < 0.001），且 A-A 间期与术后复发风险呈负相关（HR=0.98,95%CI:0.97-0.99,p=0.003）。A-A 间期≥ 180ms 的患者复发风险显著低于 A-A 间期< 180ms 的患者（HR=0.39, 95%CI:0.21-0.74,p=0.003）。

研究结论：持续性房颤射频消融术中，行尼非卡兰复律前冠状窦 A-A 间期与术后远期复发呈负相关，提示 A-A 间期可作为术中识别高复发风险患者的有效工具，对于优化消融策略以及制定个体化随访管理方案具有一定的临床意义。

脉冲场消融用于不同类型心肌组织治疗心房颤动：犬实验研究

李云浩 [1,2] 宣风琦 [3] 梁明 [2] 王祖禄 [2]

1. 中国医科大学北部战区总医院培养基地

2. 北部战区总医院

3. 天津市胸科医院

目的：本研究旨在评估脉冲场消融（PFA）在消融不同类型心肌组织时的疗效和安全性。

方法：8 只犬被随机分配到 48 小时或 4 周观察组。在不同心脏结构上应用了不同剂量的脉冲场消融。通过电生理标测以及大体和组织学观察来评估消融的有效性。通过监测食管温度、膈肌收缩以及周围器官的潜在损伤来评估消融的安全性。

结果：所有 8 只犬均成功通过脉冲场消融（PFA）进行了消融，每个消融部位均实现了 100% 的急性电隔离。用于上腔静脉（SVC）、右心房（RAA）和左心房（LAA）以及肺静脉消融的能量设置分别为 1000 伏、16 次脉冲；1000 伏、24 次脉冲；以及 1200 伏、36 次脉冲。所有消融部位的急性电隔离率均为 100%。实验动物在消融过程中表现出轻微的骨骼肌震颤，连续心电图监测未发现缺血性变化，未发生恶性心律失常，导管表面未出现血栓形成和烧焦现象。术后大体解剖显示形成了连续的、环形的、透壁的损伤。未出现心包填塞、血肿形成或对邻近组织（如食管或膈神经）的损伤等并发症。使用不同剂量的脉冲场能量对不同心脏部位进行消融没有观察到明显的食管温度上升，膈肌受损或其他周围器官的损伤。

结论：使用不同剂量的脉冲场能量对不同心脏部位进行消融被证明是安全且有效的。

脉冲电场应用于小血管相关心律失常消融——一种新的导管和方法

李云浩 [1,2] 宣风琦 [3] 梁明 [2] 王祖禄 [2]

1. 中国医科大学北部战区总医院培养基地

2. 北部战区总医院

3. 天津市胸科医院

目的: 设计一款 3F 中空脉冲电场标测与消融导管用于治疗小血管相关心律失常，并通过犬实验验证了该导管的有效性和安全性。

方法：一共 8 只实验犬（体重 35-40kg，年龄 2.90±0.56 岁）在实施消融后随机分入短期观察组（48 小时）和长期观察组（30 天）中。利用中空的 3F 12 极导管在心大静脉、左室侧静脉、前室间静脉以及心大静脉系统细小分支内消融，通过大体和镜下观察消融灶损伤特征。

结果：所有的手术过程成功实施，脉冲电场能够能量能够透过血管壁及脂肪组织传递到心肌组织上。30 天组的消融深度（2.37±0.53 mm）比 48 小时组的消融深度（3.92±0.62 mm）变浅了 39%（P<0.001）。除此之外，在 48 小时组中发现消融灶内存在组织过渡带。术中及术后未出现不良事件，毗邻小动脉中未发现明显损伤，术中 1 只犬出现一过性冠状动脉痉挛。

结论：本研究中使用的 3F 导管具有较好的操作性和灵活性，被设计成中空，便于 PCI 导丝通过做靶血管超选后的指引。该导管在心大静脉系统中能够同步多极标测，一旦标测到理想电位，可以立即在靶点附近电极之间发放脉冲能量，提高消融的准确性。用于发放脉冲能量的电极可以灵活选择，不但可以用于 Marshall 静脉的全长消融，也能够用于局部电极间的靶点消融。除了能够被用于心律失常领域消融之外，还有望被用应用在冠状动脉穿间隔支中以治疗肥厚性梗阻性心肌病。

脉冲电场消融关键参数对消融灶特征的影响：马铃薯实验

李云浩 [1,2] 宣风琦 [3] 梁明 [2] 王祖禄 [2]

1. 中国医科大学北部战区总医院培养基地

2. 北部战区总医院

3. 天津市胸科医院

目的: 本研究旨在通过土豆模型研究脉冲场消融（PFA）的关键参数（包括电压 V、脉冲宽度 PW、脉冲数量 P 和消融次数 N）对损伤深度的影响。

方法： 该研究利用马铃薯显示不可逆电穿孔的区域。将新鲜马铃薯切成大约 3 厘米厚的块，并在每个组织块的中心仔细挖掘一个最大横向直径约为 4 厘米的楔形结构，旨在模拟肺静脉口的解剖特征，利用 9 极环形导管模拟肺静脉消融时的贴靠（图 1A-1B）。

结果：900V×5μs 组和 1420V×2μs 组的平均消融深度分别为 4.43±0.16mm 和 4.11±0.09mm（p<0.01），表明脉宽对消融深度的影响大于电压。1000V×100 个组和 1300V×60 个组的平均消融深度分别为 4.47±0.27mm 和 4.88±0.32mm（p<0.01），表明电压对消融深度的影响大于一次放电脉冲数。2μs×500 个组和 5μs×200 个组的平均消融深度分别为 4.02±0.18mm 和 4.28±0.11mm（p<0.01），表明脉宽对消融深度的影响大于一次放电脉冲数。300 个 ×12 次组和 60 个 ×60 次组的平均消融深度分别为 4.25±0.19mm 和 5.06±0.30mm（p<0.01），表明消融次数对消融深度的影响大于一次放电脉冲数。综上所述，各脉冲场参数对消融深度的影响程度应为 PW>V>P；N>P。

在其他参数保持不变的情况下，将电压分别设置为 200V、400V、600V、800V、1000V、1200V、1400V、1600V，相应的消融深度分别为 0mm、1.04±0.17mm、2.06±0.18mm、3.44±0.19mm、4.14±0.16mm、4.60±0.22mm、5.12±0.27mm、5.53±0.23mm（p<0.01）。随着电压的增加，消融深度逐渐增加（图 2），而当电压低于 400V 时，未观察到明显的消融损伤。当电压增加到 1600V 时，体外可见明显的气泡。在一次放电脉冲数保持不变的情况下，通过将总脉冲数增加到 2400 个（400×6）、4800 个（480×10）、7200 个（400×18）、9600 个（480×20）、12000 个（400×30），消融深度分别为 4.28±0.18mm、4.54±0.19mm、4.77±0.19mm、5.25±0.30mm、5.11±0.21mm。在消融次数保持不变的情况下，通过将总脉冲数增加到 2400 个（400×6）、4800 个（800×6）、7200 个（1200×6）、9600 个（1600×6）、12000 个（2000×6），消融深度分别为 4.23±0.16mm、4.49±0.18mm、4.73±0.20mm、4.98±0.19mm 和 5.03±0.16mm（图 2）。随着总脉冲数的增加，消融深度逐渐增加，两组均表明当总脉冲数超过 9600 个时，消融深度未显著增加，即消融深度达到饱和点。

结论：在脉冲电场消融关键参数中，PW 对消融深度的影响最大，其次是 V 和 P。有趣的是，N 对消融深度的影响大于 P。消融深度与 V 和总脉冲数呈同向变化，但当总脉冲数达到一定值时，损伤深度会饱和。电压和总脉冲数是在临床应用中经常调整的消融参数。了解它们对消融灶的影响可以方便在临床中更好地调整消融参数。虽然体外实验虽然允许在直视下直接操作导管，确保一致的接触力，并减少设备和技术专长的要求，但是马铃薯实验只能提供关于关键参数影响 PFA 损伤深度趋势的有限信息。

一种体外评估脉冲电场消融灶的方法

李云浩 [1,2] 张洁 [2] 梁明 [2] 王祖禄 [2]

1. 中国医科大学北部战区总医院培养基地

2. 北部战区总医院

目的： 利用 4% 单质碘 - 无水乙醇溶液对离体脉冲电场消融组织染色，评估染色方法有效性并验证其可靠性。

方法： 比格犬离体心肌脉冲电场消融后经固定、梯度脱水，利用 4% 单质碘 - 无水乙醇溶液染色，并测量消融深度、宽度，计算消融灶横截面积。

结果： 使用 4% 碘单质 - 无水乙醇溶液染色后，消融区域清晰可见，消融损伤呈深棕色，未消融组织呈现浅棕色的非特异性染色，两者之间界限分明（见图 1A）。通过测量消融深度和宽度，可以计算出消融损伤面积。在电压组中，1200 伏、1500 伏和 1800 伏的消融深度分别为 3.22±0.50 毫米、3.59±0.29 毫米和 4.37±0.43 毫米（P<0.001），对应的面积分别为 4.90±1.31 平方毫米、6.49±0.87 平方毫米和 7.44±0.76 平方毫米（P<0.001）。电压增加与消融深度的逐渐加深和面积的扩大相对应。在消融时间组中，6 次、12 次、15 次、21 次和 27 次脉冲应用的消融深度分别为 2.96±0.55 毫米、3.22±0.50 毫米、3.88±0.41 毫米、5.13±0.39 毫米和 5.21±0.58 毫米（P<0.001），对应的面积分别为 3.65±0.64 平方毫米、4.90±1.31 平方毫米、4.94±0.61 平方毫米、8.02±0.70 平方毫米和 8.27±0.65 平方毫米（P<0.001）。消融时间的增加导致消融深度更深和面积更大。在接触力组中，接触力为 0 克、0-10 克、10-20 克、20-30 克和 30-40 克时的消融深度分别为 1.61±0.71 毫米、3.22±0.50 毫米、3.79±0.57 毫米、4.27±0.59 毫米和 4.87±0.34 毫米（P<0.001），对应的面积分别为 1.81±1.18 平方毫米、4.90±1.31 平方毫米、7.70±1.21 平方毫米、8.74±1.52 平方毫米和 8.70±1.69 平方毫米（P<0.001）。接触力的增加导致消融深度更深和面积更大。

结论： 4% 单质碘溶液对离体脉冲电场消融染色有效、可靠。随着电压、消融次数和贴靠压力的增加，消融深度和消融灶面积都随之增加，存在并能够达到饱和水平。

Pulsed field ablation on different types of myocardial tissues for the treatment of atrial fibrillation: canine experiments

Yun-Hao Li[1,2], Feng- Xuan[3], Ming Liang[2], Zu-Lu Wang[2]

1. General Hospital of Northern Theatre Command of China Medical University

2. General Hospital of Northern Theater Command

3. Tianjin Chest Hospital

Objectives

Pulsed field ablation (PFA), a novel therapeutic technology based on electroporation, disrupts cell membrane integrity through high-frequency pulsed electric fields to achieve selective tissue injury. This non-thermal mechanism theoretically minimizes risks of adjacent tissue damage compared to conventional thermal (radiofrequency) or cryoablation. However, varying electrophysiological properties and fibrous architectures among cardiac structures (e.g., atrial myocardium, pulmonary vein antrum, auricular tissues) may necessitate different energy requirements and yield distinct tissue responses. This study aimed to determine optimal energy parameters for PFA targeting specific cardiac structures–superior vena cava (SVC), right/left atrial appendages (RAA/LAA), and

pulmonary veins–and systematically evaluate its efficacy and safety through electrophysiological mapping, histopathological analysis, and safety monitoring.

Methods

Eight healthy mongrel dogs were randomized into 48-hour acute observation (n=4) and 4-week chronic observation (n=4) groups. Under general anesthesia, ablation catheters were implanted via jugular and femoral veins to target SVC, RAA/LAA, and pulmonary veins. Energy parameters were tailored to tissue thickness and fibrous density: SVC (1000 V, 16 pulses), RAA/LAA (1000 V, 24 pulses), and pulmonary veins (1200 V, 36 pulses), with all pulses delivered at 200μs duration. Efficacy assessments included: ① Electrophysiological mapping to measure local potential amplitude changes and acute electrical isolation rates; ② Gross anatomical examination to evaluate lesion continuity, transmurality, and adjacent tissue adhesion immediately post-ablation and at 4 weeks; ③ Histological analysis via HE staining (cell necrosis) and Masson trichrome staining (fibrosis quantification). Safety monitoring included esophageal temperature control (≤ 42 ℃), diaphragmatic electromyography (to exclude phrenic nerve stimulation), continuous ECG (malignant arrhythmia detection), and 30-day post-op complication tracking (pericardial effusion, thrombus formation, esophageal injury).

Results

All eight dogs underwent successful PFA with 100% acute electrical isolation across all target sites. Energy responses varied by anatomical location: pulmonary veins, characterized by thicker myocardium and dense fibrous alignment, required higher energy (1200 V, 36 pulses) to achieve transmural lesions, while thinner-walled SVCs achieved effective isolation with lower energy (1000 V, 16 pulses). Transient skeletal muscle tremors occurred during ablation–likely due to neuromuscular stimulation from pulsed fields–without persistent diaphragmatic contraction or abnormal esophageal heating (average temperature increase: 1.2±0.3 ℃). Continuous ECG monitoring revealed no ST-segment changes, ventricular fibrillation, or atrioventricular block. Gross anatomy demonstrated uniform, circumferential, and transmural lesions: 3-4mm diameter in SVC/auricles, 5-6mm in pulmonary vein antrum, with no charring on catheter surfaces or thrombus formation. Histologically, acute lesions showed edematous myocytes with pyknosis and clear boundaries, while chronic lesions exhibited fibrous scarring without inflammatory infiltration or abnormal myocyte proliferation. Safety evaluations identified no major complications (pericardial tamponade, hematoma, esophageal ulcer, or phrenic nerve palsy), except mild reactive pericardial effusion in one dog, which resolved within 4 weeks.

Conclusions

This study confirms that tailored PFA energy parameters, adjusted for anatomical and electrophysiological characteristics of different cardiac structures, safely and effectively achieve transmural electrical isolation. The differentiated protocols for SVC, auricles, and pulmonary veins provide experimental evidence for clinical precision ablation. PFA's non-thermal mechanism demonstrates significant advantages in reducing thrombus risk and avoiding adjacent organ damage. While intraoperative neuromuscular stimulation warrants careful neuroprotection, results support PFA's application potential in anatomically complex regions (e.g., left atrial appendage, pulmonary vein antrum). Future research should explore long-term efficacy and tissue remodeling mechanisms to optimize individualized treatment strategies for cardiac arrhythmias.

1 例房颤脉冲场消融围手术期护理经验

陈慕洁

清华大学附属北京清华长庚医院

摘要 目的 总结 1 例房颤患者行脉冲场消融（PFA）的围手术期护理要点及效果。**方法** 对 2024 年 5 月 8 日在北京清华长庚医院首例应用国产锦江电子 PFA 系统行房颤消融的患者实施结构化护理。核心措施包括：1. 术前评估与心理干预：充分评估基础状态及血管条件，重点针对患者作为新技术首例接受者的焦虑，进行针对性宣教及沟通，解释 PFA 优势（如安全、快速、微痛），建立信任。2. 术中关键护理配合：保障舒适体位与沟通；严密动态监测生命体征（心电、血压、血氧），特别关注 PFA 发放时的心律变化；实时评估神经系统功能（如膈神经活动、语言能力）。备齐急救设备药品。3. 术后严密监测与康复：重点防治穿刺点并发症（加压包扎、卧床管理、观察末梢循环）；系统筛查心包填塞（生命体征、症状）、肺静脉狭窄（呼吸音）等主要并发症；指导早期非负重活动与渐进性离床；得益于 PFA 特性，术后疼痛管理简单。4. 出院教育：强化抗凝及抗心律失常药物管理、症状识别、生活方式指导及随访安排。**结果** 患者手术顺利，全程清醒配合，体验良好。手术时间短（约 90 分钟）。术中及术后均未发生任何并发症。患者术后无显著疼痛，心理负担轻，康复进程顺利，术后第 4 日出院。与房颤射频消融相比，PFA 护理流程显著简化（如无需热效应管理、疼痛护理减少）。**结论** PFA 基于非热能机制，具备选择性消融特点，可有效避免食管、膈神经等邻近组织损伤，安全性提升，手术耗时明显缩短。本例护理实践表明，其配套的围手术期护理流程相对简化，尤其体现在术中监测压力减轻、术后疼痛护理需求低及患者舒适度高。精心、结构化的围术期护理是保障 PFA 成功应用的重要环节，有助于提升手术安全性与患者康复质量。PFA 前景广阔，但其护理模式的优化仍需更多病例积累与深入研究。

关键词 脉冲场消融；心房颤动；围手术期护理；安全；护理管理

Effects of Key Parameters on Pulsed Field Ablation of Atrial Fibrillation: Potato Experiments

Yun-Hao Li[1,2], Feng- Xuan[3], Ming Liang[2], Zu-Lu Wang[2]

1. General Hospital of Northern Theatre Command of China Medical University

2. General Hospital of Northern Theatre Command

3. Tianjin Chest Hospital

AIMS: The study aims to investigate the impact of key parameters of pulsed field ablation (PFA) on lesion depth, including voltage (V), pulse width (PW), number of pulses (P), and ablation number (N), using potato models.

METHODS: Potatoes are utilized as a display of the irreversible electroporation lesion. The key ablation parameters were varied systematically to explore its influences on lesion depths.

RESULTS: All the ablations were successfully conducted on potatoes. The mean ablation depths of the 900 V × 5 μs group and the 1420 V × 2 μs group were 4.43 ± 0.16 mm and 4.11 ± 0.09 mm, respectively ($p < 0.01$), indicating that the PW had a greater influence on the ablation depths than the V (Table 1). The mean ablation depths of the 1000 V × 100 pieces and 1300 V × 60 pieces groups were 4.47±0.27 mm and 4.88±0.32 mm, respectively ($p<0.01$), suggesting that the V had a greater influence than the P on the ablation depths (Table 1). The mean ablation depths in the 2 μs×500 pieces and 5 μs×200 pieces groups were 4.02±0.18 mm and 4.28±0.11 mm, respectively ($p<0.01$), suggesting that the PW had a greater influence than the P on the ablation depths. The mean ablation depths in the 300 pieces × 12 times and 60 pieces × 60 times groups were 4.25±0.19 mm and 5.06±0.30 mm ($p < 0.01$), respectively ($p<0.01$), suggesting that the N had a greater influence than the P on the ablation depths. In summary, the degree of influence of each pulsed field parameter on ablation depth should be PW > V > P; N > P.

With other parameters kept constant and V was set to 200V, 400V, 600V, 800V, 1000V, 1200V, 1400V, 1600V, the corresponding ablation depths were 0mm, 1.04±0.17mm, 2.06±0.18mm, 3.44±0.19mm, 4.14±0.16mm,4.60±0.22mm, 5.12±0.27mm, 5.53±0.23mm($p < 0.01$)(Table 2, Figure 3). The ablation depths increased with increased V (Figure 2), while there was no obvious ablation injury when the voltage was <400V. And when the voltage was increased to 1600 V, obvious bubble was visible in vitro. With P controlled the same, by increasing the total numbers of pulses to 2400 (400×6), 4800 (480×10), 7200 (400×18), 9600 (480×20), 12000 (400×30), the ablation depths were 4.28 ± 0.18mm, 4.54 ± 0.19mm, 4.77 ± 0.19mm, 5.25 ± 0.30mm, 5.11 ± 0.21mm. With N controlled unchanged, by increasing the total number of pulses to 2400 (400×6), 4800 (800×6), 7200 (1200×6), 9600 (1600×6), 12000 (2000×6), the ablation depths were 4.23±0.16mm, 4.49±0.18mm, 4.73±0.20mm, 4.98±0.19mm and 5.03±0.16 mm, respectively (Table 2, Figure 3). The ablation depths gradually increased as the total number of pulses increased, and both groups suggested that the ablation depths did not significantly increase when the total number of pulses was more than 9600, i.e. when the ablation depth reached the saturation point.

CONCLUSION: The key ablation parameters have varying degrees of influence on lesion depths, following the order of PW > V; V > P; PW > P; N > P. Lesion depths increased with higher values of V and P. However, when the total number of pulses reached 9600, there was no significant increase in injury depth.

A Novel Method for Assessing the Lesion Size of in Vitro Pulsed Field Ablation

Yun-Hao Li[1,2], Jie Zhang[2], Ming Liang[2], Zu-Lu Wang[2]

1. General Hospital of Northern Theatre Command of China Medical University

2. General Hospital of Northern Theatre Command

Objective: Pulsed field energy can induce irreversible cell membrane electroporation, leading to apoptosis, and has demonstrated significant potential in the interventional treatment of arrhythmias. It has been applied in various diseases, including atrial fibrillation ablation, premature ventricular contraction ablation, and dual-pathway arrhythmia ablation. The ablation lesions created by pulsed field ablation (PFA) are subject to multiple influencing factors, such as voltage, pulse widths, ablation times, and the configuration of the catheter. Precise evaluation of lesion size is essential for the optimization of ablation parameters. However, current methods for assessing PFA lesion size are limited and exhibit low precision.

This study aims to assess the efficacy of staining ex vivo pulsed electric field ablation tissues using a 4% elemental iodine-anhydrous ethanol solution and to confirm its reliability.

Methods: Ex vivo myocardial tissues from canines were treated with pulsed field ablation. After fixation and graded dehydration, the tissues

were stained using a 4% elemental iodine-anhydrous ethanol solution. The depth and width of the ablation lesion were measured to determine the cross-sectional area of the ablation lesion.

Results: Following staining with a 4% elemental iodine-anhydrous ethanol solution, the ablation region was distinctly visible, with the ablation lesion exhibiting a deep brown color and the non-ablated tissue showing a light brown, non-specific staining, demarcating a precise boundary (Figure 1A). Measurements of the ablation depths and widths allowed calculating the ablation lesion areas. In the voltage group, depths at 1200 V, 1500 V, and 1800 V were 3.22±0.50 mm, 3.59±0.29 mm, and 4.37±0.43 mm (P<0.001), respectively, with corresponding areas of 4.90±1.31 mm^2, 6.49±0.87 mm^2, and 7.44±0.76 mm^2 (P<0.001), respectively. Increased voltage corresponded to a progressive deepening of the ablation depth and an area enlargement. In the ablation times group, depths for 6, 12, 15, 21, and 27 applications were 2.96±0.55 mm, 3.22±0.50 mm, 3.88±0.41 mm, 5.13±0.39 mm, and 5.21±0.58 mm (P<0.001), respectively, with areas of 3.65±0.64 mm^2, 4.90±1.31 mm^2, 4.94±0.61 mm^2, 8.02±0.70 mm^2, and 8.27±0.65 mm^2 (P<0.001), respectively. Increased ablation times resulted in a deeper ablation depth and a larger area. In the contact force group, depths at 0 g, 0-10 g, 10-20 g, 20-30 g, and 30-40 g were 1.61±0.71 mm, 3.22±0.50 mm, 3.79±0.57 mm, 4.27±0.59 mm, and 4.87±0.34 mm (P<0.001), respectively, with areas of 1.81±1.18 mm^2, 4.90±1.31 mm^2, 7.70±1.21 mm^2, 8.74±1.52 mm^2, and 8.70±1.69 mm^2 (P<0.001). Increasing contact force led to a deeper ablation depth and a larger area.

Conclusion: The 4% elemental iodine solution demonstrates efficacy and reliability in staining ex vivo pulsed field ablation lesions. With the escalation of voltage, ablation times, and contact force, there is a corresponding increase in the depth and area of the ablation lesions, which can reach and maintain a plateau level. Overall, the application of 4% elemental iodine staining for evaluating lesions in ex vivo PFA experiments presents several benefits: 1) It facilitates the assessment and execution of PFA ex vivo experiments, thereby circumventing errors introduced by confounding factors in vivo settings; 2) In contrast to TTC staining and NTZ, this method is independent of tissue oxidative reactions, minimizing errors associated with the tissue incubation process; 3) It can concurrently highlight regions of thermal damage, which is advantageous for refining catheter parameter configurations.

Beverage consumption and mortality among adults with atrial fibrillation: a prospective study from UK biobank

Zhaowei Zhu, Wen Gong, Sheng-Hua Zhou

Department of Cardiovascular Medicine, The Second Xiangya Hospital, Central South University

Abstract

Background: Atrial fibrillation (AF) represents a significant global health burden as the most prevalent clinically significant cardiac arrhythmia. It is strongly associated with heightened risks of stroke, heart failure, and all-cause mortality. While established risk factors such as age, hypertension, and structural heart disease are well-recognized, there is growing evidence that modifiable lifestyle factors, including dietary patterns, play a crucial role in the development, progression, and clinical outcomes of AF. However, despite the central role beverages play in daily caloric intake and nutrient supply, a substantial gap persists in robust epidemiological evidence comprehensively evaluating the longitudinal relationships between distinct beverage categories and critical hard endpoints—mortality and cardiovascular events—in diagnosed AF populations. Clarifying the impact of specific beverages, ranging from commonly consumed sugary drinks and artificially sweetened alternatives to potentially protective options like coffee or fruit juices, is paramount for developing targeted dietary guidance aimed at improving prognosis in this vulnerable patient group.

Methods: This prospective cohort, from the UK biobank included 3,904 AF patients who completed at least one 24-hour dietary recall questionnaire, and were free of heart failure and stroke. The beverage categories included artificially sweetened beverages (ASBs), sugar-sweetened beverages (SSBs), natural fruit juices (NJs), coffee, tea, milk, and water. The Cox proportional hazards regression model was used to assess the associations between beverage consumption and the risk of outcomes in AF patients.

Results: During the median follow-up period of 11.62 years, 575 all-cause deaths, 211 cardiovascular deaths, 781 heart failure, and 344 stroke cases were recorded. Higher ASBs consumption (>1 drink per day) was associated with an increased risk of all-cause mortality (HR: 1.14, 95% CI: 1.02–1.28), cardiovascular mortality (HR: 1.81, 95% CI: 1.21–2.71), and stroke (HR: 2.32, 95% CI: 1.41–3.80). Compared with the categories of lowest consumption of beverages, NJs (>1 drink per day) (HR: 0.67, 95% CI: 0.47–0.95), coffee consumption (1-2 drink per day) (HR: 0.77, 95% CI: 0.61–0.97), and tea (>4 drink per day) (HR: 0.71, 95% CI: 0.52–0.97) were associated with a lower risk of all-cause mortality. Substitution analyses suggested that replacing ASBs with NJs, coffee, or tea significantly reduced all-cause mortality risk.

Conclusions: This large, long-term prospective cohort study provides compelling evidence that beverage choice significantly impacts clinical outcomes in patients with established Atrial Fibrillation. Specifically, higher consumption of Artificially Sweetened Beverages (ASBs) is robustly linked to an elevated risk of death from any cause, death from cardiovascular disease, and incident stroke. Conversely, consumption of Natural Fruit Juices, Coffee, and Tea is associated with a lower risk of overall mortality, suggesting these beverages may confer protective effects. The substitution analyses further indicate that replacing ASBs with NJs, coffee, or tea represents a potentially beneficial dietary strategy for reducing mortality risk in AF patients. These findings underscore the profound impact of modifiable dietary factors, particularly beverage selection, on long-term prognosis in individuals living with AF. Public health initiatives and clinical dietary counseling for AF patients should prioritize strategies to reduce ASB intake and promote healthier alternatives such as natural juices, coffee, or tea, potentially serving as an adjunctive approach alongside standard medical therapy to improve survival and reduce cardiovascular complications.

Keywords: Atrial fibrillation, Beverage consumption, Mortality, Cardiovascular events, Cohort study, UK biobank.

房颤消融术后左心结构与功能的变化与预后的影响

张奇 梁明

中国人民解放军北部战区总医院

目的：观察心房颤动患者经冷冻或射频导管消融术后左心结构功能的变化以及与术后复发的影响因素分析。

方法：选取 2023 年 7 月至 2023 年 12 月我院行冷冻或射频消融术治疗的阵发或持续性心房颤动患者共 94 例。术后随访 6 个月，收集患者术前术后左心结构及功能的变化，分析复发的危险因素。

结果：分析阵发性及持续性房颤患者术前术后左心房前后径（LAD）、左心室舒张末期前后径（LVEDD）、左室射血分数（LVEF）的变化。阵发组与持续组对比，阵发性房颤患者术前术后 LAD、LVEDD、LVEF 均较持续性房颤患者术前术后各项指标显著改善（P < 0. 01）。阵发组中 LAD 术前术后有显著改善（P=0.05），余指标比较差异无统计学意义。持续性房颤患者术后均较术前明显改善（P < 0.05）。阵发性房颤患者术后 6 个月复发与未复发相关各指标均无统计学差异，持续性房颤患者术后 6 个月未复发组 LAD、LVEF 较复发组明显改善（P < 0.05）。对术前 LAD 与房颤复发进行 ROC 分析并绘制曲线，曲线下面积为 0.698，P=0.008，差异有统计学意义。当术前 LAD 大小等于 43.5 mm 时 ROC 曲线取到最佳界点，此时敏感度 0.579，特异度 0.792。

结论：导管消融治疗房颤可改善左心结构和功能，尤其是持续性房颤患者改善尤为明显；若术前 LAD 超过 43.5 mm 为房颤患者消融术后复发的危险因素，对于持续性房颤患者若 LAD < 43.5 mm 应考虑更积极的导管消融治疗。

下壁导联 F 波参数与房颤病程对持续性房颤射频消融术后复发联合预测价值的双中心研究

王月刚 陈圆圆

南方医科大学南方医院

目的：预测持续性心房颤动（房颤）患者射频消融术后复发仍具有挑战性。本研究旨在探讨下壁导联心电图 f 波振幅（FWA）、f 波宽度（FWD）及房颤病程对持续性房颤患者射频消融术后复发的预测价值。

方法： 采用双中心回顾性观察性研究设计，纳入 2017 年 1 月–2022 年 11 月在南方医科大学南方医院、江苏省人民医院首次接受射频消融术的 763 例持续性房颤患者。使用 MATLAB 软件测量术前 12 导联心电图的 FWA 和 FWD。收集临床数据并完成了 12 个月的随访。通过二元 Logistic 回归分析确定独立危险因素，采用梯度提升机（GBM）构建预测模型。通过接收者操作特征（ROC）曲线、校准曲线和决策曲线分析（DCA）评估模型性能，同时进行了内部验证（随机分组法）和外部验证（中心间验证）。

结果： 在 12 个月的随访期间，有 198 名患者（26%）出现房颤复发。复发组的下壁导联 FWA（0.108 [0.076 - 0.157] mV 比 0.126 [0.087 -0.173] mV，P = 0.003）、下壁导联 FWD（54.96 [40.26 - 71.31] ms 比 61.46 [42.7 -76] ms，P = 0.038）显著低于非复发组，房颤病程显著长于非复发组（13.8 [4 -38] 个月比 6.5 [3 -21] 个月，P <0.001）。多因素分析确定下壁导联 FWA（OR = 0.788，95%CI 0.662 -0.937，P = 0.007）和房颤病程（OR = 1.014，95%CI 1.007 -1.021，P <0.001）是复发的独立预测因素。结合房颤病程和下壁导联 FWA 的模型 AUC 为 0.692（95%CI 0.648 -0.737），在纳入下壁导联 FWD 后提升至 0.746（95%CI 0.701 -0.787）。该模型在内部验证（AUC = 0.722，95%CI 0.680 -0.762）和外部验证（AUC = 0.703，95%CI 0.659 -0.747）中均显示出良好的鉴别能力。

结论：下壁导联 FWA 和房颤病程是持续性房颤患者射频消融术后复发的独立预测因素。结合这些参数和 FWD 的预测模型具有良好的鉴别能力和临床实用性。

睡眠呼吸障碍与房颤导管消融术后复发的相关性研究

范凌华 潘雁楠 贺鹏康 陈尔冬 黄波 李康 周菁 蒋捷 马靖

北京大学第一医院

目的

已有研究表明睡眠呼吸暂停是房颤的危险因素。本研究的目的是进一步探究

睡眠呼吸障碍与房颤患者导管消融术后房颤复发的相关性。

方法

本研究为单中心双向性队列研究，纳入了 2018 至 2024 年在北京大学第一医院心内科行房颤导管消融手术且术前行多导睡眠图或便携式呼吸睡眠监测的成年人群。导管消融术后患者常规于房颤门诊随访，定期行 12 导联心电图及动态心电图检查，失访人群则被排除。研究终点为消融术后 1 年是否出现房颤复发，术后 3 个月作为空白期，期间的房颤发作不纳入研究终点。

结果

研究共纳入 382 例患者，其中复发组 116 例（30.4%），无复发组 266 例（69.6%）。基线与超声心动图参数方面，复发组女性占比更高（40.5% vs 29.0%，p=0.03），房颤病程更长（12.0 vs 6.0 月，p=0.01），左房容积指数（49.56 vs 44.04 ml/m^2，p=0.01）及右房容积指数（30.77 vs 28.01 ml/m2，p=0.04）更高，基线超敏 C 反应蛋白水平更高（1.38 vs 1.08 μg/L，p=0.03），射频消融占比更高（91.4% vs 82.7%，p=0.02），出院带药包含 I 类或 III 类抗心律失常药的比例更低（85.3% vs 92.1%，p=0.04）。睡眠呼吸参数方面，复发组与无复发组人群的呼吸暂停低通气指数（AHI）（14.10 vs 12.65 次 / 时，p=0.64）、睡眠时 SpO2 的平均值（94.26% vs 94.17%，p=0.35）与最低值（84.02% vs 84.54%，p=0.46）均无明显差异，复发组的睡眠平均心率高于无复发组（67.68 vs 65.13 次 / 分，p=0.04）。经过多因素校正后，AHI ≥ 15 与 AHI<15 患者相比，消融术后房颤复发的风险并不增加（HR 1.43，95% CI 0.82-2.49，p=0.21），Kaplan-Meier 曲线未发现不同 AHI 组别间的差异（p=0.577）。亚组分析表明，对于阵发性房颤人群，女性亚组及左房扩大亚组中 AHI ≥ 15 显著增加消融术后房颤复发风险。

结论

本研究表明，房颤消融术后复发组较无复发组的睡眠平均心率更高，但两组间 AHI 及睡眠时 SpO2 无明显差异。女性及左房扩大的阵发性房颤患者中，中重度睡眠呼吸障碍（AHI ≥ 15）会增加消融术后房颤复发风险。

肿瘤合并心房颤动患者射频导管消融的疗效与安全性评估

王璇 孙鸣宇 王祖禄 梁明 金志清 丁建

中国人民解放军北部战区总医院

背景 在恶性肿瘤幸存者中，心房颤动是一种常见的心律失常，对患者的生活质量和预期寿命造成严重影响。对于恶性肿瘤患者接受导管消融术的疗效和安全性，仍存在争议。**目的** 本研究旨在评估合并恶性肿瘤病史的房颤患者导管消融的疗效和安全性。**方法** 本研究采用回顾性研究方法，收集在 2019 年 1 月 -2022 年 12 月接受导管消融术的房颤患者的临床资料。数据来源于中国人民解放军北部战区总医院病历系统。收集的数据包括患者的一般情况、肿瘤类型及病程、心房颤动类型、导管消融方式及术后随访情况等。将其中有恶性肿瘤病史的非瓣膜性房颤患者作为肿瘤组，以无恶性肿瘤病史的非瓣膜性房颤患者为对照组。比较了两组患者接受导管消融治疗的疗效及安全性，相关结果包括房颤复发、围手术期及随访期并发症等。**结果** 研究的 140 名患者中，70 名伴有恶性肿瘤病史，倾向性配对评分匹配 70 名无恶性肿瘤史患者为对照组。两组基线资料对比均无统计学差异（P 均 > 0.05）。术中结果与术后抗心律失常药物及抗凝药物使用，肿瘤组与对照组相比均无统计学差异（P 均 > 0.05）。肿瘤组平均随访 318.79±101.77 天，对照组平均随访 339.79±77.35 天，两组房颤复发率无统计学差异（18.57% VS 20.00%,P=0.830）。围术期及随访期并发症的发生率无统计学差异。Kaplan-Meier 生存分析结果显示，随访期间内房颤复发在恶性肿瘤患者和非恶性肿瘤患者之间差异无统计学意义（Log-Rank 检验 P=0.937）。多因素 Cox 回归分析，经过校正其他混杂因素后，房颤复发率差异无统计学意义（P=0.800），风险指数（hazard ratio, HR）为 0.863（95% CI：0.397-1.877）。**结论** 与对照组患者相比，合并恶性肿瘤的房颤患者导管消融术后手术成功率、房颤复发率、围术期及随访期并发症发生率无统计学差异。导管消融术能有效治疗心房颤动，改善患者的生活质量，对合并恶性肿瘤史房颤患者是一种安全有效的治疗方法。

Effect of ablation index-guided baseline impedance on tissue damage

jinhong guo, Ying-Jie Wang, Mei-Xue Jia, Shuai Chen

Fuyang People's Hospital

Effect of ablation index-guided baseline impedance on tissue damage

Jinhong Guo1, Yingjie Wang1, Meixue Jia1, Shuai Chen1，and Bin Ning1 □

1 Department of Cardiology， the Affiliated Fuyang People's Hospital of Anhui Medical University, Fuyang,236300, Anhui province, China

Aims: The extent of tissue damage under the control of radiofrequency ablation power modes is influenced by several factors, including applied pressure, tissue impedance, and perfusate. The purpose of this study was to investigate the effect of baseline impedance and its variation on the extent of tissue damage under conditions of similar ablation index (Ablation Index AI) and fixed power.

Methods: In the ex vivo porcine heart experiments, the AI was set to 500, the fixed output power was 40 W, and a contact force (CF) of 10-15 g was applied to simulate clinical ablation conditions. Baseline Impedance (BI) was artificially controlled by adjusting the impedance value of the varistor in the circuit, which was divided into three groups: the low impedance group (100-135 Ω), the medium impedance group (135-170 Ω), and the high impedance group (170-214 Ω). The focus of the study was to analyze the correlation between the baseline impedance level and impedance drop and the myocardial tissue damage caused by radiofrequency ablation, including lesion width, depth, and Volume. The experiment aimed to investigate the effect of impedance parameters on ablation efficacy and to provide an experimental basis for optimizing the ablation strategy.

Results: At similar AI and fixed power, the degree of impedance decrease in the medium impedance group was not statistically different from that of the low impedance group (P=0.145) and statistically different from that of the high impedance group (P=0.011), and there was a negative correlation between baseline impedance and the degree of impedance decrease, with a correlation coefficient of R=-0.591 (P<0.0001). The width of the injury was 8.23±0.39, 7.19±0.73, and 6.07±0.39 mm (P<0.0001), the depth was 5.55±0.36, 4.72±0.25, and 3.86±0.59 mm (P<0.0001), and the volume was 111.06±15.08, and 72.80±15.82 and 42.71±11.21 mm3 (P<0.0001), respectively, for the low impedance group, the medium impedance group and the high impedance group. There was a significant negative linear correlation between baseline impedance and the size of tissue damage. The correlation coefficients of baseline impedance with the width, depth, and volume of injury were R=-0.879, R=-0.932, and R=-0.917, respectively (P<0.0001). A positive correlation was found between the degree of impedance change and the magnitude of tissue damage. The correlation coefficients between the decrease in impedance and the width, depth, and volume of injury were R=0.653, R=0.556, and R=0.639, respectively (P<0.0001). Steam bursts occurred 3 times in all experimental modes (2/15 cases in the low impedance group; 0/15 cases in the medium impedance group; 1/20 cases in the high impedance group). However, the difference was not statistically significant, P=0.467.

Conclusion: In the power control mode, radiofrequency ablation guided by AI will lead to significant differences in the size of damage due to the difference in baseline impedance. It is shown that ablation at lower impedance will lead to enhanced tissue heating and form larger damage, and the size of damage has a significant negative linear correlation with the initial impedance.

Keywords: Radiofrequency ablation, Ablation index, Baseline impedance, Lesion size

Association between rivaroxaban and the prognosis of patients with acute myocardial infarction and new-onset atrial fibrillation

Yi Zheng[1], Ying Liu[1], Xin-Yu Zheng[1], Gary Tse[1,2], Gregory Lip[1,3,4], Kang-Yin Chen[1], Tong Liu[1]

1. Second Hospital of Tianjin Medical University

2. Hong Kong Metropolitan University

3. Liverpool Heart & Chest Hospital

4. Aalborg University

Objective: New-onset atrial fibrillation (AF) in the setting of acute myocardial infarction (AMI) is associated with higher risks of stroke and mortality. However, current guidelines lack specific antithrombotic recommendations for this population. This study aimed to explore the association between rivaroxaban and the prognosis of patients with AMI and new-onset AF.

Methods: This retrospective cohort study included patients with AMI and new-onset AF receiving dual antiplatelet therapy between August 2016 and June 2023 in China. New-onset AF, including transient and non-transient AF, was defined as the first diagnosis of AF in the setting of AMI. Transient AF was defined as those with new-onset AF and without a non-transient AF episode after a 2-week "blanking period", and the non-transient AF group was defined as those with new-onset AF and additional medical documentation of AF after a 2-week "blanking period". The primary outcome was stroke. The secondary outcomes included ischemic stroke, hemorrhagic stroke, all-cause mortality, cardiovascular mortality, bleeding, and major bleeding. Proportional Cox regression models were used to evaluate associations between rivaroxaban use and the outcomes of interest. Hazard ratios (HRs) with corresponding 95% confidence intervals (CIs) were reported. Propensity score matching (PSM) was performed with a 1:3 ratio for rivaroxaban users versus non-users in the transient and non-transient AF group, respectively. Kaplan-Maier survival curves were plotted to illustrate survival curves between patients with and without rivaroxaban. Sensitivity analysis was conducted using multivariable competing risk analysis to assess the robustness of the results.

Results: A total of 2,477 patients with AMI and new-onset were identified, including 141 rivaroxaban users and 2,336 non-users. After a median follow-up time of 922 days, 627 (25.3%) patients experienced stroke. Rivaroxaban users had an approximate 5.7% lower risk of stroke compared to non-users, although this was not statistically significant (19.9% vs. 25.6%; P=0.152). Despite the suggestion of a protective trend, multivariable Cox regression showed that rivaroxaban use was not associated with a lower risk of stroke (HR 0.77, 95% CI 0.52-1.13, P=0.187). Regarding secondary outcomes, no significant associations between rivaroxaban use and risks of ischemic stroke, hemorrhagic stroke, all-cause mortality, bleeding, and major bleeding were observed. However, rivaroxaban use was associated with a significantly lower risk of cardiovascular

mortality (HR 0.29, 95%CI 0.09-0.90, P=0.033) among patients with AMI and new-onset AF. Among 1,451 patients with AMI and transient AF, 46 (3.2%) were discharged on rivaroxaban, while 1,405 (96.8%) were not discharged on rivaroxaban. Despite the point estimate of HR suggesting a protective trend, the association remained non-significant between rivaroxaban use and the risk of stroke (HR 0.66, 95%CI 0.29-1.49, P=0.314). There were also no statistically significant associations between rivaroxaban use and risks of secondary outcomes. PSM was sequentially performed with a 1:3 ratio, leading to 42 patients in the rivaroxaban group and 113 in the non-rivaroxaban group. Kaplan-Meier survival curves showed no significant difference in risks of stroke, ischemic stroke, hemorrhagic stroke, all-cause mortality, cardiovascular mortality, bleeding, and major bleeding between rivaroxaban users and non-users. Sensitivity analyses using multivariable competing risk models also revealed no significant association between rivaroxaban use and risks of outcomes. Among 1,026 patients with AMI and non-transient AF, 95 (9.3%) were discharged on rivaroxaban, while 931 (90.7%) were not discharged on rivaroxaban. Although the point estimate of the HR indicated a potential protective trend, multivariable Cox regression showed that the association between rivaroxaban and the risk of stroke remained statistically non-significant (HR 0.81, 95%CI 0.52-1.27, P=0.362). Regarding secondary outcomes, no statistically significant association was observed between rivaroxaban use and risks of ischemic stroke, hemorrhagic stroke, all-cause mortality, cardiovascular mortality, and major bleeding. However, rivaroxaban use was associated with a significantly higher risk of bleeding (HR 3.33, 95%CI 1.18-9.44, P=0.024) among patients with non-transient AF. PSM was sequentially performed with a 1:3 ratio, leading to 85 patients in the rivaroxaban group and 210 in the non-rivaroxaban group. Kaplan-Meier survival curves showed no significant difference in the risks of outcomes between rivaroxaban users and non-users. Sensitivity analyses using multivariable competing risk models also revealed no significant association between rivaroxaban use and risks of study outcomes.

Conclusions: Among patients with AMI and new-onset AF receiving dual antiplatelet therapy, no significant association was observed between rivaroxaban use and the risks of stroke, ischemic stroke, hemorrhagic stroke, all-cause mortality, cardiovascular mortality, bleeding, or major bleeding. Future prospective large-scale studies and randomized controlled trials are needed to further examine the role of rivaroxaban in this special population.

Adherence to Dabigatran versus Warfarin and Associated Factors in Patients with Non-Valvular Atrial Fibrillation after Percutaneous Coronary Intervention

Yulai Yan, Ming Liang, Zu-Lu Wang

General Hospital of Northern Theater Command

Objective: The optimal antithrombotic strategy for patients with non-valvular atrial fibrillation (NVAF) after percutaneous coronary intervention (PCI) remains controversial. Optimizing antithrombotic therapy can reduce thromboembolic events while minimizing bleeding risks, and adherence to medication is critical for ensuring treatment efficacy. This study aimed to compare adherence to dabigatran versus warfarin in NVAF patients post-PCI, analyze the relationship between adherence and bleeding events, and identify factors influencing adherence.

Methods: This multicenter, prospective, randomized controlled trial enrolled 540 NVAF patients undergoing PCI between April 2018 and January 2022. All patients received dual antiplatelet therapy (DAPT: clopidogrel 75 mg daily + aspirin 100 mg daily) preoperatively. Post-PCI, patients were randomized to dabigatran or warfarin groups with open-label administration: Dabigatran group: Dabigatran (110 mg twice daily) + DAPT. Warfarin group: Warfarin (target INR 2.0–3.0) + DAPT. Aspirin was discontinued at 1 month post-PCI in both groups, and dabigatran/warfarin + clopidogrel continued until 6 months. Follow-up data were collected via telephone and outpatient visits at 1, 3, and 6 months. Adherence differences, bleeding event correlations, and influencing factors were analyzed using logistic regression.

Results: A total of 451 patients were included in the final analysis (dabigatran group: 249; warfarin group: 202). Baseline preoperative and intraoperative characteristics showed no significant differences between the two groups (P > 0.05). 1. Medication Regularity and Adherence: At 1, 3, and 6 months post-PCI, the proportion of patients with regular medication use was significantly higher in the dabigatran group compared to the warfarin group: 1 month: 91.20% vs. 79.70% (P = 0.04). 3 months: 90.80% vs. 78.70% (P < 0.001). 6 months: 90.76% vs. 78.71% (P < 0.001). Similarly, adherence rates were consistently higher in the dabigatran group at all follow-up intervals: 1 month: 92.7% vs. 81.3% (P < 0.001). 3 months: 93.0% vs. 80.3% (P < 0.001). 6 months: 93.0% vs. 80.3% (P < 0.001). 2. Nuisance Bleeding (NB) Incidence: At 1 month, there was no significant difference in NB incidence between the two groups (P = 0.295). However, at 3 and 6 months, the warfarin group had significantly higher NB rates: 3 months: 14.1% vs. 4.1% (P < 0.001). 6 months: 21.8% vs. 8.8% (P < 0.001). Subgroup Analysis by Adherence: arfarin group: Patients with poor adherence had higher NB rates at all follow-ups: 1 month: 18.9% vs. 4.3% (P = 0.002). 3 months: 28.2% vs. 10.7% (P < 0.001). 6 months: 30.8% vs. 19.5% (P = 0.021). Dabigatran group: NB incidence correlated with adherence only at 1 month (16.7% vs. 3.0%, P = 0.029); no significant association was observed at 3 or 6 months (P > 0.05). 3. Medication Behavior in Patients with NB: Patients experiencing NB exhibited significantly higher rates of non-adherence compared to those without NB. Warfarin group: 2–3 months post-PCI: Among 14 patients with NB, 6 (42.9%) showed poor adherence. Retrospective analysis of their 1-month and 6-month follow-ups revealed only 1 case (7.1%) of non-adherence. 4–6 months post-PCI: Among 15 patients with NB, 11 (73.3%) were non-adherent. Retrospective review of their 3-month and 1-month follow-ups showed 3 (20%) and 1 (6.7%) cases of non-adherence, respectively. Dabigatran group: 2–3 months post-PCI: Among 14 patients with NB, 6 (42.9%) had irregular medication use. Retrospective analysis of their 1-month and 6-month follow-ups showed only 1 case (7.1%) of non-adherence. 4–6 months post-PCI: Among 7 patients with NB, 3 (42.9%) discontinued medication. Notably, all 7 patients had adhered to treatment during prior follow-ups when no NB occurred. 4. Multivariate Logistic Regression Analysis: Independent protective factor: Dabigatran use significantly improved adherence compared to warfarin (P < 0.001; OR = 3.50). Independent risk factors: ≥ 3 vessels with >50% stenosis (P = 0.027; OR = 0.46) Occurrence of bleeding events (P < 0.001; OR = 0.28).

Conclusion: 1. Dabigatran demonstrated superior adherence and regularity compared to warfarin. 2. Dabigatran reduced nuisance bleeding events, which were a primary driver of non-adherence. 3. Dabigatran use, multivessel disease (≥ 3 vessels with >50% stenosis), and bleeding events independently influenced adherence.

Key Words: Warfarin; Dabigatran; Non-valvular atrial fibrillation; Post-PCI; Medication adherence

Body Roundness Index, Visceral Adiposity Index, and Metabolic Score for Visceral Fat in Predicting New-Onset Atrial Fibrillation: A UK Biobank Cohort Study

Yi Zheng[1], Lei Liu[2], Xin-Yu Zheng[1], Tong Liu[1], Xiao-Ping Li[3]

1. Second Hospital of Tianjin Medical University

2. Suining central hospital

3. Sichuan Provincial People's Hospital, School of Medicine

Objective: Obesity represents an established modifiable risk factor for atrial fibrillation (AF). Novel adiposity indices, including body roundness index (BRI), visceral adiposity index (VAI), and metabolic score for visceral fat (METS-VF), have been developed to better reflect fat distribution. However, the predictive utility of these indices in predicting new-onset AF remains understudied. This study aims to investigate the longitudinal associations of BRI, VAI, and METS-VF with the risk of new-onset AF.

Methods: This study included participants from the UK Biobank who were free of AF or pregnancy at baseline and completed the first and second assessments of BRI, VAI, and METS-VF. The changes in BRI, VAI, and METS-VF were classified using K-means clustering analyses, and the cumulative adiposity indices were also calculated. The primary outcome was new-onset AF. Three Cox regression models were employed to investigate the longitudinal associations of the BRI, VAI, and METS-VF changes with the risk of incident new-onset AF. The results were presented as hazard ratios (HRs) and the corresponding 95% confidence intervals (CIs). Restricted cubic spline analyses were performed to explore potential non-linear associations between baseline or cumulative adiposity indices and the risk of new-onset AF. C-index analyses were conducted to evaluate the predictive value of BRI, VAI, and METS-VF for new-onset AF. Subgroup analyses were performed according to age, sex, race, smoking status, alcohol consumption, and physical activity. Polygenic risk scores were applied to account for genetic susceptibility and investigate potential interactions between adiposity indices and genetic risk. Univariate linear regression analyses were performed to evaluate the relationships of cumulative adiposity indices and magnetic resonance imaging and dual X-ray absorptiometry parameters, including visceral adipose tissue (VAT) volume, VAT mass, trunk fat volume, and trunk fat mass. We further applied the eXtreme Gradient Boosting (XGBoost) algorithm, with the feature importance being measured to evaluate the predictive value of each adiposity index for imaging parameters. Mendelian randomization analysis was further conducted to investigate the potential causal relationship between trunk fat mass and AF.

Results: A total of 12,776 participants were included. Over a median follow-up of 9.60 years, 761 (5.96%) new-onset AF events were recorded. Participants were divided into four classes based on the changes in adiposity indices. In the fully adjusted model, compared to participants in Class 1 of BRI, those in Class 3 (HR, 1.30, 95%CI 1.04-1.63, P=0.023) and Class 4 (HR, 2.17, 95%CI 1.61-2.93, P<0.001) were associated with significantly higher risks of new-onset AF. Regarding METS-VF, participants in Class 4 of METS-VF also demonstrated a significantly higher risk of new-onset AF compared to those in Class 1 (HR, 1.66, 95%CI 1.15-2.39, P=0.007). However, no significant association was observed between different classes of VAI and the risk of new-onset AF. For every 1 standard deviation increase in cumulative BRI, VAI, and METS-VF, the fully adjusted HRs of new-onset AF were 1.23 (95%CI 1.13-1.35), 1.02 (95%CI

0.94-1.10), and 1.23 (95%CI 1.12-1.35), respectively. Cumulative adiposity indices (BRI, VAI, and METS-VF) were divided into quartiles. Using the first quartile as reference, participants in the highest quartiles of BRI (HR, 1.40, 95%CI 1.10-1.79, P=0.007) and METS-VF (HR, 1.44, 95%CI 1.13-1.83, P=0.003) both exerted a significantly higher risk of new-onset AF. Regarding VAI, no significant association was observed (HR, 1.00, 95%CI 0.81-1.23, P=0.988). Restricted cubic spline analyses revealed non-linear relationships between cumulative BRI, baseline/cumulative VAI, and baseline/cumulative METS-VF with new-onset AF risk (all P-overall <0.05, P-non-linear <0.05). In the C-index analysis, BRI demonstrated the highest predictive performance for new-onset AF, followed by METS-VF and VAI. Subgroup analysis indicated a stronger association between METS-VF and the risk of new-onset AF amongst participants younger than 60 years (P interaction =0.008). Polygenic risk score analysis stratified by genetic risk demonstrated a synergistic effect between BRI and genetic risk with new-onset AF, with the overall risk of new-onset AF increasing as both BRI and genetic risk increased. Linear regression analysis revealed a positive correlation between cumulative BRI with VAT volume, VAT mass, trunk fat volume, and trunk fat mass. The feature importance plot derived from the XGBoost algorithm indicated that cumulative BRI had the greatest predictive value on VAT volume, VAT mass, trunk fat volume, and trunk fat mass. Mendelian randomization analysis confirmed a significant causal relationship between trunk fat mass and AF.

Conclusions: There were significant non-linear associations between BRI, METS-VF, and VAI with new-onset AF. Higher BRI and METS-VF were significantly associated with a higher risk of new-onset AF, whereas no significant association was observed for the VAI. BRI exhibited a positive correlation with VAT and trunk fat, and demonstrated superior performance in predicting new-onset AF compared to VAI and METS-VF. Monitoring and managing BRI may be important in the early detection and intervention of AF.

评价微创冷冻消融系统用于治疗心房颤动的有效性和安全性：一项前瞻、单组、多中心临床试验

张萍 梁明 王祖禄

中国人民解放军北部战区总医院

目的：评价微创冷冻消融系统治疗阵发性房颤的安全性和有效性。

方法：本研究为一项前瞻性、多中心、目标值法、单臂性的临床研究。共纳入来自中国 8 家医院的 159 例非瓣膜性阵发性房颤患者，均接受上海微创公司冷冻消融系统治疗。分析即刻消融成功率、标测成功率及围术期安全性，并进行术后 1、3、6、12 个月的随访，记录器械相关不良事件发生率及术后 3-12 个月的治疗成功率。

结果：研究共纳入 159 例患者，其中男性 81 例（50.94%），平均年龄为 61.89±8.69 岁。去除 8 家中心第一例入组（roll-in）患者，151 例受试者手术即刻隔离成功率为 100%；术后 3-12 月随访成功率为 82.78%，95%CI 为（75.80%-88.43 %）。试验期间，共发生 2 例受试者危及生命或死亡的严重不良事件：其中 1 例因术中心脏压塞而接受了外科手术，另 1 例则在术后 1 个月因主动脉瘤破裂不幸死亡，整个试验过程中未发现器械缺陷。与试验用医疗器械相关的不良事件共有 3 例（3 例次），而严重不良事件则达到了 19 例，共发生了 25 例次，其中与器械直接相关的严重不良事件为 1 例（1 次）。

结论：根据临床试验，使用微创冷冻消融系统进行的冷冻球囊消融术治疗阵发性房颤被证实是安全且有效的。

甲状腺激素敏感性受损与甲状腺功能正常人群的心房颤动风险的联系

尹晓盟 公涵

大连医科大学附属第一医院

目的：心房颤动是一种以规则有序的心房电活动被快速无序的颤动波所取代为特征的慢性进行性疾病，是临床最常见的心律失常之一。除了疾病本身带来的不适症状，AF 还会诱发患者卒中、心力衰竭、认知功能障碍甚至死亡等诸多风险，显著提高患者的致残率和致死率，降低了患者的生活质量，然而，甲状腺激素敏感性与心房颤动进展的关系尚不清楚，本研究旨在阐明甲状腺功能正常人群中甲状腺激素敏感性受损与房颤进展的关系。

方法: 共纳入 1190 名房颤患者，分为阵发性房颤（n=623）和持续性房颤（n=567）两组，收集心脏超声和血清生化指标。使用 parametric thyroid feedback quantile-based index（PTFQI）、thyrotropin thyroxine resistance index（TT4RI）以及外周性指标 FT3/FT4 ratio 计算甲状腺激素敏感性指数。采用 Logistic 回归分析探讨甲状腺激素敏感性指数与房颤分型的关系。

结果：相较于阵发性房颤组，持续性房颤组的患者 PTFQI、TT4RI 较高，FT3/FT4 ratio 较低（P < 0.001），多因素 logistic 回归分析显示，TT4RI、PTFQI 升高及 FT3/FT4 ratio 降低均与持续性房颤显著正相关（P 均 < 0.05）。在完全调整混杂因素的模型中，TT4RI、PTFQI 和 FT3/FT4 比值的 OR 值分别为 1.038 (95%CI: 1.010-1.067)、3.952 (1.470-10.626) 和 0.008 (0-0.130)。四分位数分析进一步证实了 PTFQI 在每个分位数上都显著促进持续性房颤的发生发展 (P 均 < 0.01)。FT3/FT4 ratio 在第三分位数显著促进持续性房颤的发生 (P < 0.05)，而 TT4RI 的四分位数分组差异无统计学意义。

结论：甲状腺激素敏感性受损可能在甲状腺功能正常患者中促进阵发性房颤向持续性房颤的进展，其临床预测价值有待大样本研究进一步证实。

The Causal Role of Atrial Fibrillation in Anxiety and Depression:A Bidirectional Mendelian Randomization Study

null null

The First People's Hospital of Changde City

Background: Atrial fibrillation (AF), the most prevalent cardiac arrhythmia, exhibits complex clinical associations with anxiety disorders and depression. Observational studies suggest bidirectional relationships, yet confounding factors and reverse causation impede definitive causal inference. This study employed bidirectional Mendelian randomization (MR) to investigate genetic evidence for causal pathways between AF, anxiety, and depression—addressing critical gaps in understanding their etiological interplay.

Methods: Utilizing summary statistics from large-scale, population-based genome-wide association studies (GWAS), we conducted bidirectional two-sample MR analyses. Exposure and outcome datasets included:AF: FinnGen study (ID: finn-b-I9_AF; 22,068 cases/116,926 controls; European ancestry).Anxiety Disorders: UK Biobank (ID: ukb-b-6519; 255,812 self-reported cases/194,953 controls).Depression: UK Biobank (ID: ukb-b-6848; 80,611 self-reported cases/69,288 controls).Instrument Selection: Single-nucleotide polymorphisms (SNPs) associated with exposures ($P < 5\times10^{-8}$) were selected as instrumental variables (IVs). Rigorous quality control included: linkage disequilibrium clumping ($r^2 < 0.001$, 10,000 kb window), exclusion of palindromic/ambiguous SNPs and those with minor allele frequency < 0.01, PhenoScanner screening for confounding traits (e.g., BMI, blood pressure), and F-statistic calculation (F > 10 retained to mitigate weak instrument bias).Analytical Approach:Forward MR: Estimated causal effects of genetically predicted AF on anxiety and depression.Reverse MR: Estimated causal effects of genetically predicted anxiety/depression on AF.Primary analysis used inverse-variance weighted (IVW) regression (random-effects). Sensitivity analyses included MR-Egger, weighted median, weighted mode, and simple mode methods. Robustness was assessed via:Cochran's Q test (heterogeneity), MR-Egger intercept test (horizontal pleiotropy), Leave-one-out analysis (influential SNP detection), Directionality testing (MR Steiger), Visualization (scatter, funnel, forest plots)

Results: Forward MR (AF → Anxiety/Depression):Anxiety Disorders: Genetically predicted AF significantly increased anxiety risk (IVW OR = 1.006; 95% CI: 1.002–1.009; p = 0.002). Weighted median analysis corroborated this (OR = 1.006; 95% CI: 1.001–1.011; p = 0.025). Sensitivity analyses confirmed robustness: no heterogeneity (Cochran's Q p = 0.159), no horizontal pleiotropy (MR-Egger intercept p = 0.931), and consistent effects in leave-one-out analysis.Depression: No causal association was observed (IVW OR = 0.998; 95% CI: 0.991–1.006; p = 0.685).Reverse MR (Anxiety/Depression → AF):Anxiety → AF: Null effect (IVW OR = 0.644; 95% CI: 0.338–1.224; p = 0.179).Depression → AF: Null effect (IVW OR = 0.977; 95% CI: 0.303–3.157; p = 0.970), though limited by few IVs (n = 6 SNPs).Visualization (scatter/funnel plots) and supplementary methods (MR-Egger, weighted mode) consistently supported primary findings.

Discussion: This study provides novel genetic evidence for a unidirectional causal pathway: AF is a risk factor for anxiety disorders, but not depression. The AF-anxiety link (OR = 1.006) aligns with proposed biological mechanisms:Autonomic Dysregulation: AF-induced sympathetic hyperactivity promotes anxiety neurocircuitry activation.Neuroendocrine Effects: HPA-axis dysregulation and elevated cortisol from AF-related stress may exacerbate anxiety.

Indirect Pathways: AF impairs quality of life, sleep, and physical activity—established anxiety triggers.The null findings for depression and reverse causation challenge some observational literature but highlight the specificity of AF's psychological impact. Comparatively, a recent MR study reported depression → AF effects (OR = 1.073), underscuring methodological differences (e.g., GWAS sources, IV selection) that may explain discrepancies.

Strengths and Limitations:Strengths:MR design minimizes residual confounding and reverse causation.Large GWAS samples enhance statistical power.Rigorous IV selection ($P < 5\times10^{-8}$, F > 10, confounder screening). Comprehensive sensitivity analyses validate robustness.Limitations:European ancestry restriction limits generalizability.Anxiety/depression based on self-report (UK Biobank), not clinical diagnoses.Limited power in reverse MR (depression → AF: n = 6 SNPs).Residual pleiotropy possible despite PhenoScanner screening.Clinical and Research Implications:-Clinical Practice: Routinely screen AF patients for anxiety using validated tools (e.g., GAD-7). Integrate evidence-based interventions:

Cognitive Behavioral Therapy (CBT) for symptom management.Mindfulness and autonomic regulation training.Lifestyle optimization (sleep hygiene, exercise, caffeine reduction).Research Directions:Validate findings in diverse ancestries and clinically diagnosed cohorts.Elucidate molecular mechanisms (e.g., inflammation, autonomic biomarkers).Develop integrated "psycho-cardiology" care models for AF.

Conclusion: This bidirectional MR study establishes AF as a causal risk factor for anxiety disorders but not depression. It refutes reverse causation (anxiety/depression → AF), highlighting the need for proactive

anxiety management in AF care. Future work should prioritize multi-ethnic validation and mechanistic studies to translate these findings into targeted therapies.

Rituximab prevents atrial fibrillation by depressing B cell function and regulating CCR2+ T lymphocyte infiltration and differentiation

Miao Jiang

The First Affiliated Hospital of Dalian Medical University

Background: Atrial fibrillation (AF) is a common cardiac arrhythmia characterized by a multifactorial pathogenesis involving electrophysiological disturbances, structural remodeling, and inflammatory responses. Recent studies emphasize the central role of inflammation and immune cell activation in AF initiation and maintenance. As key adaptive immune cells, B and T lymphocytes play pivotal roles in cardiovascular diseases, but their exact mechanisms in AF remain unclear. CD20, a transmembrane protein predominantly expressed on the surface of B lymphocytes, is involved in calcium channel regulation and B lymphocyte activation. B lymphocytes contribute to immune modulation through the secretion of pro-inflammatory cytokines, while T lymphocytes mediate inflammatory responses and tissue damage via differentiation into subsets such as Th1 and Th17. In AF, chronic inflammation may lead to aberrant immune cell activation and infiltration, exacerbating atrial structural remodeling and electrophysiological dysfunction. Nevertheless, the mechanisms by which B and T lymphocytes participate in AF pathogenesis through interactions involving chemokines and cytokines require further elucidation.

This study aims to investigate the mechanisms underlying the infiltration and differentiation of B and T lymphocytes in atrial tissue, elucidating their roles in AF pathogenesis through the modulation of inflammatory responses and the immune microenvironment. A particular focus is placed on $CD20^+$ B lymphocytes and their mediated CCL2/7 signaling pathway, as well as the evaluation of the therapeutic potential of the CD20 monoclonal antibody Rituximab (RTX) in attenuating AF by inhibiting CD20 activation, reducing immune cell infiltration, and mitigating atrial inflammation and remodeling. By integrating clinical samples and animal models, this research seeks to provide a theoretical foundation and potential therapeutic targets for immunomodulatory strategies in AF, while establishing a basis for the application of RTX in precision medicine for AF treatment.

Objectives: AF is not merely a prevalent cardiac arrhythmia but also a significant public health concern with extensive detrimental implications. This study aims to investigate the mechanisms underlying the infiltration and differentiation of B and T lymphocytes within atrial tissue, elucidating their roles in AF pathogenesis through the modulation of inflammatory responses and the immune microenvironment. Specifically, the research focuses on $CD20^+$ B cells and their mediated CCL2/7 signaling pathway, while evaluating the therapeutic potential of Rituximab in attenuating atrial inflammation and remodeling via the suppression of CD20 activation and the reduction of B and T cell infiltration.

Methods: This study utilized male C57BL/6 wild-type mice to establish an AF model through continuous infusion of angiotensin II (Ang II; 2000 ng/kg/min) for three weeks, with the objective of investigating the role of $CD20^+$ B cells in AF pathogenesis. A subset of mice was administered the CD20 monoclonal antibody Rituximab during the model induction phase. Throughout the experimental period, blood pressure was monitored using the tail-cuff method, while cardiac ultrasound was employed to evaluate atrial structure and function. Histological analyses, including Masson's trichrome staining, were conducted to assess atrial fibrosis and inflammatory infiltration. To further dissect the underlying inflammatory and immune mechanisms, Western blotting was utilized to detect the expression of CD20, the IKK/IκBα/NF-κB signaling pathway, and the chemokines CCL2/7. Flow cytometry was performed to quantify the proportions of $CD20^+$ B cells and $CCR2^+$ T cells. Quantitative reverse transcription polymerase chain reaction (qRT-PCR) was employed to measure mRNA levels of CCL2/7, IFN-γ, and IL-17, while enzyme-linked immunosorbent assay (ELISA) was used to determine the protein concentrations of relevant cytokines in serum and atrial tissues. By integrating multiple analytical techniques, this study aims to comprehensively elucidate the contributions of B cells and T cells to the pathogenesis of AF and to evaluate the potential therapeutic efficacy of Rituximab in attenuating atrial inflammation and remodeling through the suppression of $CD20^+$ B cell activation and $CCR2^+$ T cell infiltration. These findings provide a theoretical foundation and experimental evidence to support immunomodulatory strategies for AF treatment.

Results: The results revealed a time-dependent increase in CD20 expression at the mRNA and protein levels in the atria of Ang II-infused mice. Besides, $CD20^+$ B-cell and T-cell counts were elevated in both AF patients and mice, accompanied by atrial inflammation, fibrosis, and ion channel abnormalities, which collectively contributed to the maintenance of AF. Additionally, the levels of CCL2/7 chemokines secreted by B cells, the expression of CCR2 receptors on T cells, and the secretion of pro-inflammatory cytokines IFN-γ and IL-17 by $CCR2^+$ T cells were also elevated. Administration of the Rituximab in AF model mice reduced AF inducibility and duration, likely due to decreased atrial inflammation and structural remodeling. Mechanistically, these effects were attributed to suppressed $CD20^+$ B lymphocyte activation and hyperactivation of the IKK/IκBα/NF-κB pathway, which decreased CCL2/7 chemokine secretion. Finally, the decrease in CCL2/7 secretion was accompanied by reduced recruitment of $CCR2^+$ T cells to the atria and decreased secretion of the inflammatory cytokines IFN-γ and IL-17.

Conclusions: This study elucidates the pivotal role of B cells and T cells in the pathogenesis of AF through their regulation of the inflammatory and immune microenvironment. The activation of the CCL2/7 signaling pathway, mediated by $CD20^+$ B cells, promotes the infiltration of $CCR2^+$ T cells and the secretion of pro-inflammatory factors (e.g., IFN-γ, IL-17), thereby exacerbating atrial inflammation and remodeling. Rituximab, by inhibiting the activation of $CD20^+$ B cells and the IKK/IκBα/NF-κB signaling pathway, reduces the secretion of CCL2/7, diminishes the recruitment of $CCR2^+$ T cells, and attenuates inflammatory responses, ultimately mitigating the occurrence of AF. These findings substantiate the therapeutic potential of targeting $CD20^+$ B cells as a novel strategy for AF treatment.

Key Words: B lymphocyte differentiation antigen CD20; Chemokines CCL2 and CCL7; T lymphocyte differentiation; Atrial remodeling; Atrial fibrillation

乳腺癌细胞来源 CXCL11 激活 CXCR3+Th17 细胞促进心肌细胞焦亡在房颤发生中的作用及机制研究

曹宇开

哈尔滨医科大学第一附属医院

目的：乳腺癌患者排除抗肿瘤治疗等因素后心房颤动（房颤）发病率仍显著增加。肿瘤细胞可通过调控辅助 T 细胞功能介导炎症反应，但在肿瘤相关心脏病中的作用尚不明确。本研究探索 $CXCR3^+Th17$ 细胞在乳腺癌相关房颤中的作用，解析肿瘤相关心脏病的免疫调控机制，为临床提供新的治疗靶点。

方法：构建 E0771 乳腺癌荷瘤小鼠模型，对其心房组织行质谱流式检测（CytoF）挖掘目标细胞亚群，行蛋白质组学及转录组学测序挖掘下游作用机制，行流式细胞术分析循环目标亚群比例变化，Western Blot 及免疫组化检测相关通路蛋白表达；构建 $CXCR3^{fl/fl,CD4\text{-}Cre}$E0771 乳腺癌荷瘤小鼠检测房颤诱发率；人类乳腺癌及外周血液样本检测目标免疫细胞亚群相关蛋白表达。

结果：

① CytoF 及流式细胞术结果表明，乳腺癌荷瘤小鼠循环及心房组织 $CXCR3^+Th17$ 细胞比例显著增加；人类乳腺癌细胞、乳腺癌癌旁组织及外周血高表达 CXCR3 配体 CXCL11（P<0.05）。

②敲除辅助 T 细胞中 CXCR3（$CXCR3^{fl/fl,CD4\text{-}Cre}$）可有效减少乳腺癌荷瘤导致的房颤易感性增加（P<0.0001），房颤持续时间显著缩短（P=0.0021）。

③测序结果显示，乳腺癌荷瘤小鼠心房组织差异基因富集于 IL17 信号通路、焦亡相关 NF-κB 通路。实验证实荷瘤小鼠心房 CXCR3（P=0.0004）及 IL17（P=0.0411）表达显著上调，焦亡相关蛋白 NLRP3、GSDMD 及 IL-18 表达（P<0.05）显著升高。

结论：乳腺癌细胞来源 CXCL11 激活 $CXCR3^+Th17$ 细胞释放 IL17，引起心肌细胞焦亡，促进房颤。

左心室舒张功能对非瓣膜性心房颤动患者左心耳功能的影响

焦晓芳 周微微

中国人民解放军北部战区总医院

目的 探讨非瓣膜性心房颤动患者左心室舒张功能不全对左心耳功能的影响

方法 选取本医院收治的 96 例心房颤动患者，根据经食道超声结果分为无自发显影组（A 组）及自发显影或血栓形成组（B 组）。经食道超声测量两组患者左心耳 (LAA) 血流排空流速 (LAA-PEV) 及 45°和 135°左心耳入口内径 (LAAD); 常规经胸超声心动图测量两组患者的左室舒张末期内径 (LVEDD)、左心房收缩末期内径 (LAD), 左心室射血分数 (LVEF); 频谱多普勒测量二尖瓣口血流频谱舒张早期峰值流速 (E) 及舒张早期 E 峰减速时间 (DT), 同时选取四腔心切面应用组织多普勒 (DTI) 测量二尖瓣瓣环室间隔位的组织多普勒速度 e，并计算 E/e'。比较两组各超声技术检测参数间的差异，并进行相关性分析。

结果 两组患者 LVEDD、LVEF、E 及 LAAD 比较，差异无统计学意义 (P > 0.05); 两组患者间隔 E/e'、LAD、E 峰减速时间 (DT)、LAA-PEV 比较，差异有统计学意义 (P<0.05), 心房颤动患者的左心耳 LAA-PEV 与间隔 E/e'升高相关。

结论 左心室舒张功能不全影响非瓣膜性房颤患者左心耳功能，增加左心耳血栓形成风险，可能是左心耳血栓形成的独立危险因素之一。

心房颤动患者合并出血性卒中的抗凝治疗现状

张凯 彭建军

首都医科大学附属北京世纪坛医院

心房颤动（atrial fibrillation, AF）是临床中最常见的持续性心律失常之一，

是缺血性卒中的重要原因。相关数据表明，抗凝治疗能降低 AF 患者近 2/3 的系统栓塞率 [1]。然而，抗凝治疗在降低血栓栓塞事件的同时也增加了颅内出血（intracerebral hemorrhage, ICH）的风险。本文旨在总结 AF 患者合并 ICH 后的抗凝治疗相关研究及策略，探讨重启或开始抗凝治疗的安全性和有效性。最近的研究表明，AF 相关的住院率急剧上升，给患者和全球医疗系统带来了沉重的负担 [2]，1990 至 2021 的 30 年间，AF 的患病率翻了 1 倍，全球大约有 5970 万的 AF 患者。此外，随着人口老龄化，AF 的患病率将不断激增 [3]。AF 患者的血栓栓塞风险显著增加，尤其是导致缺血性卒中的发生，严重威胁人类健康。口服抗凝药（oral anticoagulants, OACs）包括直接口服抗凝药（direct oral anticoagulants, DOACs）和维生素 K 拮抗剂（vitamin K antagonists, VKAs），已被广泛用于预防血栓栓塞事件。然而，对于合并 ICH 的患者，抗凝治疗成为了一个复杂的问题。ICH 占所有卒中的 15%-25%，具有较高的致残率和死亡率，是抗栓治疗中最令人恐惧的并发症，因此对于 ICH 后存活的 AF 患者，尽管其 AF 相关的缺血性卒中风险很高，大多数医生仍不愿意重启 / 开始 OACs，只有少数患者在 ICH 后数月才恢复治疗，因而近期合并 ICH 病史的患者被 RCT 中排除 [4]。针对合并 ICH 的 AF 患者的抗凝治疗策略需要谨慎权衡利弊。

Intracardiac echocardiography improves lesion quality and ablation efficiency of pulmonary vein isolation in atrial fibrillation patients: A propensity score-matched analysis

Ye Deng[1], Li Deng[1], Qing Qing Gu[1], Qian Wen Chen[1], Yang Zhang[3], Jun Wei[3], Xu Liu[4], Yuan Ji[1], Qing Jie Wang[1], Ling Sun[2]

1. The Third Affiliated Hospital of Nanjing Medical University

2. The Affiliated Wuxi People's Hospital of Nanjing Medical University

3. The Affiliated Hospital of Xuzhou Medical University,

4. Johnson & Johnson (Shanghai) Medical Equipment Co

Background: Pulmonary vein isolation (PVI) is a cornerstone of catheter ablation for atrial fibrillation (AF). Intracardiac echocardiography (ICE) offers real-time imaging that may enhance procedural outcomes compared to traditional X-ray guidance. This study evaluates the impact of ICE on PVI lesion quality and efficiency using a novel Ablation Index Functional Validation (AIFV) system.

Methods: This single-center, retrospective, matched cohort study included AF patients undergoing catheter ablation between June 2022 and June 2023 at The Third Affiliated Hospital of Nanjing Medical University. Patients were grouped based on ICE use (ICE vs. No-ICE), with intraoperative data recorded via the VisiTag system and analyzed by AIFV. Propensity score matching (1:1) was applied to compare procedural efficiency and lesion quality (primary endpoints) and AF recurrence (secondary endpoint) between groups.

Results: Of 126 patients enrolled (61 ICE, 65 No-ICE), 46 matched pairs were analyzed. PVI was achieved in all cases without severe complications. The ICE group demonstrated significantly shorter total PVI time [2819 s (2565 s, 2953 s) vs. 3153 s (2696 s, 3831 s), p = 0.006], higher radiofrequency (RF) time ratio (59.1 ± 13.9% vs. 48.2 ± 11.6%, p<0.001), and higher effective ablation-index (AI) ratio (96.1 ± 4.5% vs. 91.2 ± 3.9%, p<0.001) compared to the No-ICE group. Left and right PVI times were also reduced (p=0.034 and p=0.029, respectively). At 12-month follow-up, AF recurrence rates were significantly lower in the ICE group (7.7% vs. 30.8%, p = 0.038) in persistent AF patients.

Conclusion: ICE enhances the quality of lesions and the ablation efficiency of PVI in AF patients, as shown by the AIFV system.

Atrial fibrillation and 28-day mortality risk in sepsis: an observational and Mendelian randomization study

Xiaoping Peng

The First Affiliated Hospital, Jiangxi Medical College

Observational studies have long indicated that the association between atrial fibrillation (AF) and 28-day mortality in sepsis remains controversial, with conflicting findings across different clinical cohorts—some reporting a 30% higher mortality risk in AF patients, others showing no significant correlation. These discrepancies may arise from variations in patient selection criteria, such as differing proportions of community-acquired versus hospital-acquired sepsis, or inconsistencies in adjusting for confounders like renal function and mechanical ventilation use. However, the critical question of whether a causal relationship exists between atrial fibrillation and 28-day mortality in sepsis has remained unresolved, creating uncertainty for clinicians in risk assessment and treatment decisions, thus highlighting the need for integrated real-world and genetic epidemiological investigations.

To address this knowledge gap, we designed a multi-faceted study combining observational analysis and Mendelian randomization (MR) approaches. First, we conducted a real-world observational analysis using the MIMIC-IV database, a large-scale critical care dataset encompassing over 60,000 intensive care unit admissions with detailed clinical, laboratory, and outcome data—including daily vital signs and medication records—to explore the relationship between AF and 28-day mortality in septic patients. We applied Kaplan-Meier survival curves to visualize survival differences, with stratification by AF onset (pre-existing vs. new-onset in sepsis), and Cox proportional-hazards models to quantify the association, adjusting for potential confounding variables such as age, sex, comorbidities, and disease severity—including parameters like SOFA scores and lactate levels that reflect sepsis acuity.

Subsequently, to investigate potential causal relationships, we accessed genome-wide association study (GWAS) data for AF (exposure) and sepsis-related 28-day mortality (outcome) from the MRC-IEU consortium, which aggregates high-quality genetic datasets with sample sizes exceeding 1 million individuals, ensuring sufficient statistical power. We employed bidirectional MR to assess both forward (AF to sepsis mortality) and reverse (sepsis mortality to AF) causal directions, as well as multivariable MR to account for confounding by other cardiovascular and inflammatory traits like coronary artery disease and C-reactive protein levels. Additionally, a two-step mediated MR analysis was conducted to identify potential indirect factors (e.g., inflammatory markers, cardiac function indices) that might mediate the relationship. To elucidate underlying genetic mechanisms, we performed expression quantitative trait locus (eQTL) MR, which links genetic variants to gene expression, and integrated this with gene expression data from the GEO database—specifically focusing on datasets profiling immune cell and cardiac tissue transcriptomes in sepsis—to identify functionally relevant genes.

In the real-world analysis, AF was not associated with 28-day all-cause mortality in the overall cohort of septic patients (HR=0.98, 95% CI=0.89-1.07, P=0.65). However, age-stratified analyses revealed inconsistent results: in patients over 65 years, AF was associated with poorer 28-day mortality (HR=1.12, 95% CI=1.01-1.24, P=0.03), suggesting age may modify this relationship, possibly due to age-related declines in cardiac reserve and immune function.

In the genetic epidemiological component, univariable MR analysis demonstrated a causal effect of genetically predicted AF on sepsis-related 28-day mortality (OR=1.14, 95% CI=1.05-1.24, P=0.001). This association remained significant in multivariable MR, which adjusted for potential confounders like hypertension and diabetes, confirming that AF independently increases the risk of 28-day death in sepsis (OR=1.09, 95% CI=1.02-1.16, P=0.008). Reverse MR analysis found no evidence that sepsis-related 28-day mortality causally increases AF risk (OR=1.01, 95% CI=0.99-1.03, P=0.310).

Finally, eQTL MR and GEO data integration identified four co-expressed genes—NDRG3, SIGLEC5, RORA, and CNRIP1—that may play roles in the genetic mechanism linking AF to sepsis mortality, potentially through regulation of inflammatory responses (e.g., cytokine production in macrophages during infection) or cardiac electrical stability (e.g., ion channel regulation in atrial myocytes).

Marshall 静脉周围心外膜脂肪组织与心房颤动的相关性研究

张飞龙 胡宇豪 喻荣辉

安徽医科大学第一附属医院

目的: 评估Marshall静脉(VOM)周围心外膜脂肪组织(EAT)容积与心房颤动(AF)类型及术后复发的相关性。

方法：本研究为回顾性研究，纳入了 2022 年 8 月至 2024 年 8 月于安徽医科大学第一附属医院接受射频消融术治疗、具备术前胸部 CT（层厚 1.25 mm）影像数据且术后随访时间 ≥ 6 月的房颤患者，根据疾病诊断将患者分为阵发性房颤组与持续性房颤组。使用 3D Slicer 定量测量 VOM-EAT 容积，使用多因素 Logistic 回归分析其与房颤类型的相关性，并绘制受试者工作特征（ROC）曲线评估其区分能力。使用多因素 Cox 比例风险回归分析评估其在不同房颤类型中与射频消融术后复发的相关性。

结果：共纳入 765 名房颤患者，年龄（63.1 ± 11.3）岁，男性 324 名（42.4%），持续性房颤患者 408 例（53.3%），持续性房颤患者 VOM-EAT 容积较高（1.0 ± 0.6 vs. 0.8 ± 0.4，P <0.001）。Logistic 回归分析提示 VOM-EAT 与持续性房颤类型密切相关（OR=1.66，95% CI 1.33~2.06，P <0.001），ROC 曲线表明其区分持续性房颤能力较强（AUC=0.645）。中位随访时间 15 月，阵发性房颤术后复发 90 例（25.2%），持续性房颤术后复发 141 例（34.6%），多因素 Cox 回归分析结果提示 VOM-EAT 在阵发性房颤患者（HR=2.10，95% CI 1.58~2.78，P <0.001）及持续性房颤患者（HR=1.75，95% CI 1.46~2.10，P <0.001）中均为术后复发的独立危险因素。

结论：VOM-EAT 容积与房颤的类型及术后复发密切相关，可能提示附加 Marshall 静脉酒精消融的指征，为未来研究提供了新的方向，有助于实现房颤的个体化治疗。

Oral Anticoagulant Treatment in Dialysis-Dependent Atrial Fibrillation: A Network Meta-analysis of 137574 Patients

Yao Du[1], Yu-Wen Zeng[1], Si-Xin Xu[1], Qi-Wei Shen[1], Jin-Zhu Hu[1], Gregory Lip[2,3,4]

1. Department of Cardiovascular Medicine, the Second Affiliated Hospital, Jiangxi Medical College, Nanchang University, Nanchang, Jiangxi, People's Republic of China.

2. Liverpool Centre for Cardiovascular Science at University of Liverpool, Liverpool John Moores University and Liverpool Heart & Chest Hospital, Liverpool, United Kingdom.

3. Department of Clinical Medicine, Aalborg University, Aalborg, Denmark.

4. Medical University of Bialystok, 15-089 Bialystok, Poland.

Abstract

Background: Patients with atrial fibrillation and end-stage renal disease (ESRD) requiring chronic dialysis therapy exhibit a substantially elevated dual risk profile: heightened susceptibility to thromboembolic stroke and increased vulnerability to major bleeding complications. Despite this critical clinical dilemma, consensus regarding optimal oral anticoagulation (OAC) strategies in this high-risk population remains elusive, with current guidelines reflecting persistent controversy. Given the limited number of prior studies, it becomes imperative to anticipate the most effective treatment strategy for patients with AF on long-term dialysis, as more research accumulates. To address this evidence gap, our study employs comparative effectiveness methodology to quantitatively evaluate net clinical benefits across OAC regimens, thereby identifying the optimal therapeutic approach for atrial fibrillation patients receiving long-term dialysis.

Methods: A comprehensive systematic literature search adhering to PRISMA guidelines and MOOSE guidelines was executed across three core biomedical databases (PubMed, EMBASE, and Web of Science). The search encompassed all available records from each database's inception through October 9, 2024, to identify studies evaluating OAC strategies in atrial fibrillation patients receiving maintenance dialysis. Primary efficacy outcomes were ischemic stroke and/or systemic thromboembolism; secondary efficacy outcomes included all-cause mortality. Major bleeding events served as the prespecified safety endpoint, per protocol. Given the distinct hemorrhagic profiles associated with hemodialysis (HD) versus peritoneal dialysis (PD), we subsequently performed sensitivity analyses by excluding studies involving exclusively PD patients to mitigate potential confounding heterogeneity on our conclusions. The network meta-analysis was conducted using MetaXL 5.3 (Epigear International Pty Ltd., Sydney, Australia). The pooled HR with 95% CI were estimated for the dichotomous outcomes (ischemic stroke and/or systemic thromboembolism, major bleeding, and all-cause mortality). If data on the HR was not reported, the risk ratio was calculated (two RCT applied this calculation) by reporting the number of events and participants, and then combined with the HR of other observational studies. Heterogeneity among studies was quantified using the Cochran's Q the I^2 statistics, which described the percentage of total variation across studies attributable to heterogeneity rather than probability.

Results: This comprehensive evidence synthesis integrated data from 31 observational studies and two randomized controlled trials, collectively comprising an aggregate population of 137,574 atrial fibrillation patients receiving long-term maintenance dialysis therapy. In comparative analyses against no anticoagulant therapy, none of the evaluated oral anticoagulants demonstrated statistically significant reductions in ischemic stroke or systemic thromboembolism risk: warfarin (HR, 0.963; 95% CI, 0.841-1.104), rivaroxaban (HR, 0.523; 95% CI, 0.163-1.677), apixaban 5mg (HR,0.744; 95%CI, 0.540-1.025) and apixaban 2.5mg (HR,0.954; 95%CI, 0.745-1.220). All confidence intervals crossed the null threshold (HR=1.0), indicating no statistically significant protective effects at α=0.05 significance level. Only apixaban 5 mg twice daily was associated with a lower risk of all-cause mortality compared to non-OAC use (HR, 0.671; 95% CI, 0.490-0.919). Dabigatran (HR, 2.140; 95% CI, 1.734-2.642) and Phenprocoumon (HR, 2.419; 95% CI, 1.241-4.713) were associated with significantly higher risk of major bleeding than non-OAC use. Results from sensitivity analyses undertaken after the exclusion of studies comprising exclusively long-term peritoneal dialysis patients showed a high degree of concordance with the main analysis findings.

Conclusions: All OACs were not associated with a reduced risk of ischemic stroke and/or systemic thromboembolism in patients with atrial fibrillation on long-term dialysis. Dabigatran and Phenprocoumon were associated with significantly higher major bleeding risk. Only apixaban 5 mg twice daily was associated with a decrease in all-cause mortality when compared with non-OAC use.

Key words: atrial fibrillation; dialysis; anticoagulant; all-cause mortality; network meta-analysis

Plasma corin levels provide minimal prognostic utility in left atrial reverse remodeling after catheter ablation of atrial fibrillation

Qian-Qian Wang, Fei-Fei Chen

The First Affiliated Hospital of Dalian Medical University

Plasma corin levels provide minimal prognostic utility in left atrial reverse remodeling after catheter ablation of atrial fibrillation

Qianqian Wang, Yang Li, Keyi Song, Chunkai Li, Feifei Chen

Department of Cardiology, The First Affiliated Hospital of Dalian Medical University, Dalian, China

Abstract

Aims To assess the impact of pre- and post-procedural plasma corin levels on the left atrial reverse remodeling (LARR) in patients atrial fibrillation (AF) after catheter ablation (CA).

Methods This prospective, single-center, observational study included 335 patients undergoing their first CA of AF. All patients underwent at least 2 echocardiographic examinations with the interval more than 3 months. Corin was measured before and one day after CA. LARR was defined as a reduction ≥ 20% in the left atrial volume (LAV) , inversely as non-LARR group.

Results After a median 29.53 months follow-up, 94 patients (28.06%) exhibited LARR. Patients in the LARR group had lower rates of paroxysmal AF (PaAF), hypertension and type 2 diabetes mellitus (T2DM), higher frequency of heart failure (HF), longer PR interval and corrected QT interval than without LARR. The plasma corin concentrations drawn pre- and post-procedure in the LARR group were 442.85 [241.25, 631.68] and 516.83 [362.4,697.84] pg/mL, respectively, and those were significantly higher than those in the non-LARR group (393.82 [207.09, 558.11] and 473.77 [320.88, 665.75] pg/mL; P=0.036 and P=0.047, respectively), with a sensitivity of 40.4%, a specificity of 73.4%, and an area under the curve (AUC) of 0.574 pre-ablation and a sensitivity of 90.4%, a specificity of 21.6%, and an AUC of 0.570 post-ablation (P=0.036, P=0.047, respectively) . The ROC curve analysis of plasma corin drawn pre- and post-ablation identified threshold values of >535.22 pg/mL and >307.69 pg/mL, respectively, as having the best predictive value for LARR in AF patients after CA. Kaplan-Meier survival curve showed that high corin concentrations measured before the procedure indicated a significantly higher rate of LARR than low corin concentrations in the total group, persistent AF group, male group and female group (P=0.014, 0.036, 0.018, and 0.046, respectively) other than PaAF group (P=0.069). However, post-ablation corin concentrations were not associated with LARR, whether in the total group, different types of AF, or different sex. Besides, Cox regression found that plasma corin levels before or after the procedure, whether in total group, PaAF or persistent AF, male or female, were not associated with LARR in AF patients after CA without or with adjusting for confounding factors. Absence of hypertension (P=0.001, OR=0.33, 95%CI: 0.168–0.649) and T2DM (P=0.007, OR=0.269, 95%CI: 0.104–0.701), were associated with a greater likelihood of LARR in AF patients after CA.

Conclusions Although plasma corin concentrations drawn pre- and post-ablation in the LARR group are higher than those in the non-LARR group, the difference is weakened after adjusting for confounding factors. It indicates that plasma corin levels provide minimal prognostic utility in LARR after CA of AF. Absence of hypertension and T2DM are associated with greater likelihood of LARR.

Keywords Atrial fibrillation; Corin; Catheter ablation; Left atrial reverse remodeling; Left atrial volume index

阵发性房颤左心房心肌传导速度重构特点的探索

孙源君 戴世煜 马成鸣 肖宪杰 王忠振 王楠 张荣峰 于晓红 高连君 尹晓盟 尹晓盟

大连医科大学附属第一医院

目的：心肌传导速度是重要的电生理参数，速度减缓、异质性增加是心律失常折返发生的重要条件。本研究拟在三维标测系统高密度激动标测指导下，探索阵发性房颤的患者心房传导速度重构特点（多部分变化及差异性）。

方法：入选接受左房操作的射频消融治疗的患者 40 例，包括阵发性房颤 20 例（房颤组），阵发性室上性心动过速 20 例（非房颤组），阵发性室上性心动过速患者不合并心血管危险因素，阵发性房颤患者除房颤外，不合并其他心血管危险因素。术中窦性心律下行左房高密度激动标测，计算不同区域传导速度，局部传导速度的计算方法如下：传导速度 =Δ 距离 /Δ 时间（单位：mm/ms）（**Δ 距离**是根据系统激动时间颜色变化及洋流图判断的激动方向上，取标测的两点（距离约 10mm），测量两点实际距离；**Δ 时间**是两个点的激动时间差值）。并计算离散度（最大速度减最小速度）和相邻部位差异（差值取绝对值）。

结果：两组患者左房各部位电压无统计学差异，房颤组患者左房平均传导速度显著低于非房颤（0.85±0.12 mm/ms vs.1.02±0.11 mm/ms, P<0.01），左房底部、顶部、前壁、二尖瓣峡部的传导速度均较非房颤患者下降，房颤组的左房传导速度速离散度明显增加（0.43±0.14 mm/ms vs. 0.26±0.13 mm/ms, P<0.01），左房后壁与底部之间（0.28±0.19 mm/ms vs. 0.11±0.08 mm/ms, P<0.01）、顶部与后壁之间的差异（0.22±0.2 mm/ms vs. 0.13±0.09 mm/ms, P=0.04）更为显著。

结论：房颤的左房传导速度重构发生在电压重构前，在阵发性房颤阶段，已出现包括左房传导速度均值减低、离散度增加以及部分区域速度异质性增加的重构特点。

The impact of sacubitril/valsartan on catheter ablation for atrial fibrillation complicated with hypertension: A comprehensive retrospective analysis

Manli Yu

Changhai Hospital

The impact of sacubitril/valsartan on catheter ablation for atrial fibrillation complicated with hypertension: A comprehensive retrospective analysis

Rongbing Peng*, Ke Li*, Jianhan Yao, Chao Liu, Feifei Dong, Zhifu Guo, Manli Yu

Department of Cardiovascular Medicine, Changhai Hospital, Naval Medical University, Shanghai, China

*Both authors equally contributed to the study.

Correspondence to:

Manli Yu, MD,

Department of Cardiovascular Medicine,

Changhai Hospital, Naval Medical University,

168 Changhai Road, Shanghai, 200433, China,

phone: +86 21 311 612 63,

e-mail: yumanli2006@163.com

INTRODUCTION

Atrial fibrillation (AF) is one of the most common type of arrhythmias, which is an important cause of ischemic stroke and heart failure. catheter ablation (CA) is considered as a first-line treatment for symptomatic AF, but there is still a certain recurrence rate, due to atrial structural and/or electrical remodeling and autonomic nervous system dysfunction [1]. This implies the reverse of atrial structural remodeling may be a promising therapeutic strategy in reducing the AF recurrence after CA [2].

Sacubitril/valsartan (Sac/Val) is a combined inhibitor of angiotensin receptor and enkephalin receptor, commonly used for patients with heart failure. In addition to the function of valsartan, Sac/Val inhibits the degradation of biologically active natriuretic peptides, which in turn stimulate natriuresis, diuresis and vasodilation. It is showed Sac/Val can reverse ventricular remodeling and reduce readmission rate and mortality

[3]. Up to now, most researches of Sac/Val focused on the patients with heart failure (HF) and hypertension. Our study aims to examine the impact of Sac/Val for AF patients with hypertension who have undergone CA, in order to provide a new idea for the comprehensive treatment of AF.

METHODS

202 patients (≥ 18 years) with AF and hypertension, who had undergone CA between January 2021 to April 2023, were enrolled in this study. All eligible patients were divided into Sac/Val group (n = 124) and angiotensin-converting enzyme inhibitor/angiotensin II receptor blocker (ACEI/ARB) group (n = 98). The anteroposterior diameter of left atrium measured by echocardiography was no more than 50mm.All individuals enrolled had left ventricular ejection fraction (LVEF) ≥ 35%. The detailed descriptions about inclusion/exclusion criteria and follow-up schedule are seen in the Supplementary material.

This study was reviewed and approved by the ethics committee at Changhai Hospital, Naval Medical University, and was conducted in accordance with the Declaration of Helsinki and its amendments. The patients/families provided their written informed consent to participate in this study prior to the procedures.

Mapping and ablation were performed under the guidance of CARTO (Biosense Webster, Diamond Bar, CA, US) or EnSite (St. Jude Medical, St Paul, MN, US) mapping systems in addition to standard fluoroscopy. For patients with paroxysmal AF (Par-AF), standard pulmonary vein isolation was performed, while for those with persistent AF (Per-AF), additional linear and/or complex fragmented atrial electrogram ablations were carried out according to the physician's discretion. Sinus rhythm was restored by either ablation or electric cardioversion. Class III drugs (amiodarone) were recommended for Per-AF patients with structural cardiomyopathy and class I C (propafenone) otherwise. Antiarrhythmic drugs were only used during the 3-month blanking period. No pharmacotherapy was taken after CA for Par-AF.

Statistical analysis

Statistical analysis was performed using SPSS 26. The quantitative data were represented as mean (standard deviation) or median (interquartile range), whereas the categorical data were displayed as frequencies in percentages. The study utilized independent sample t-tests or Wilcoxon rank-sum tests to compare quantitative data, while $\chi 2$ analysis was applied to compare categorical data. P <0.05 was considered statistically significant. Kaplan-Meier estimate analyzed the freedom of atrial arrhythmia with P-value achieved by the log-rank test. Multivariable logistics regression analysis was applied to determine the risk factors of the recurrence of atrial arrhythmias, the items which P <0.2 were chosen to build the multivariable model. Besides, we have ever seen that the AF recurrence after CA maybe of gender-related. Other variables such as the left atrium dimension (LAD) and stroke history are strongly related to the treatment effect of atrial fibrillation, so were built in the multivariable model.

RESULTS AND DISCUSSION

A total of 202 patients were enrolled in the study, 124 received Sac/Val and 98 received ACEI/ARB treatment (Supplementary material, Figure S1). Clinical baseline characteristics between the two groups were showed in Supplementary material, Table S1.

In patients with Per-AF, LVEF increased and N-terminal pro-B-type natriuretic peptide and LAD decreased 1 year after CA compared toACEI/ARB group, which were not found in Par-AF (Supplementary material, Table S2). Sac-Val group has the reduction of AF recurrence 1 year after CA in Per-AF (47.22% vs. 17.65%; P = 0.005) (Supplementary material, Table S3).

Univariate logistic regression analysis showed LAD and Sac/Val were related to the recurrence of AF (Supplementary material, Table S4). The Kaplan–Meier curve analysis (Figure 1) showed taking Sac/Val after CA in Per-AF can improve the AF-free survival probability (persistent: log rank P = 0.011).

This study has shown compared with ACEI/ARB, Sac-Val can reduce the AF recurrence rate, improve cardiac remodeling, reduce the LAD and N-terminal pro-B-

type natriuretic peptide and increase LVEF after CA for Per-AF, which demonstrates the additional clinical efficacy of dual-acting ARB and neprilysin inhibitor in AF treatment. However, the above findings were not observed in Par-AF.

Atrial remodeling is characterized by atrial enlargement and interstitial fibrosis, which is considered to be the main cause and an independent risk factor of AF [4]. The purpose of upstream therapy of AF is to reverse or stop the negative pathophysiological process leading to atrial remodeling, so as to reduce the occurrence and recurrence of AF [5].

The left atrial function of patients with AF who received Sac/Val treatment was better than that of valsartan, reflected by the LA peak systolic strain increase, left atrial appendage emptying speed and ejection fraction [6]. In our study, on the basis of maintaining sinus rhythm after CA, the changes of cardiac structure and LAD in Per-AF have been observed. Growing evidences indicate that anti- atrial fibrosis may be a potential therapeutic target for AF. PARABLE trial showed Sac/Val can increase LA volume index in the setting of reduced markers of filling pressure in patients with HF. Natriuretic peptide modulating therapy delivered improved vascular compliance and reduced cardiac chamber stiffness [7], which maybe indicate atrial structure improvements are the main benefits in Per-AF, then function improvement are followed behind. It has also been reported Sac-Val can improve atrial matrix and electrical remodeling and reduce the susceptibility to AF by inhibiting atrial fibrosis [8]. An experiment on the susceptibility to atrial arrhythmias in rats showed Sac-Val can reverse LAremodeling, reduce collagen deposition, inhibit the progression of atrial fibrosis and reduce the susceptibility to atrial arrhythmias by inhibiting p-Smad2/3, p-p38 MAPK and p-JNK pathways [9]. No AF recurrence difference was found in Par-AF, which may be due to healthy atrial substrate.

Our study demonstrated compared with ACEI/ARB, Sac-Val treatment after ablation of Per-AF can enhance AF-free survival time and improve cardiac remodeling. However, it was just a retrospective study and patients enrolled in our study had both AF and hypertension, whether Sac/Val can achieve the same effect in patients with normal blood pressure remains to be further studied.

心脏计算机断层扫描增强成像对房颤患者左心耳不同部位血栓的诊断价值

杨龙 [1,2] 欧巧巧 [1] 蒋智 [1] 何炯红 [1] 刘启方 [1] 田野 [1] 田龙海 [1]

1. 贵州省人民医院

2. CSC 第 12 届心房颤动学组

目的：以经食道超声心动图（TEE）检查为心房颤动（AF）患者左心耳（LAA）血栓诊断金标准，评价心脏计算机断层扫描增强成像（CCTA）对不同部位 LAA 血栓诊断的准确性。

方法：连续纳入 2016 年 6 月至 2023 年 12 月就诊于贵州省人民医院确诊 AF 拟行导管消融术治疗，并同期行 CCTA 及 TEE 检查的患者。收集患者临床资料（临床特征及辅助检查结果），以 TEE 检查结果为参考标准，根据 LAA 血栓位置分为 LAA 开口处血栓组及 LAA 内血栓组，计算 CCTA 对 LAA 不同部位血栓的敏感度、特异度、阴性预测值、阳性预测值，评估 CCTA 对检测 LAA 不同部位血栓的准确性。

结果：共 710 位患者，男性 60.3%，平均年龄 (61±11) 岁。TEE 检出 LAA 血栓患者 71 例（10.0%），其中 36 例（50.7%）位于 LAA 开口处，35 例（49.3%）位于 LAA 内。CCTA 检出 LAA 血栓患者 52 例（7.3%），其中 LAA 开口处血栓 17 例（32.7%），LAA 内血栓 29 例（55.8%），其余 6 例（11.5%）TEE 检查未见 LAA 血栓。CCTA 对 LAA 血栓的总体敏感性为 64.8%，特异性为 99.1%，阴性预测值为 96.2%，阳性预测值为 88.5%。CCTA 对 LAA 开口处血栓的敏感性低于 LAA 内血栓（47.2% vs 82.9%，P=0.002）。Logistic 多因素回归分析显示，LAA 开口处血栓 (OR=0.185, CI: 0.037-0.936, P=0.041) 及 LAA 血栓最大直径 (OR=1.323, CI: 1.077-1.625, P=0.008) 是 CCTA 检出 LAA 血栓敏感性低于 TEE

的独立预测因素。

结论：对于 AF 拟行导管消融患者，CTTA 检测 LAA 血栓的敏感性低于 TEE，尤其是对于 LAA 开口处、最大直径更小的血栓准确性较低。

Dapagliflozin attenuates atrial fibrosis by inhibiting ferroptosis and Warburg effect via activating the SIRT1/FOXO3a signaling pathway

Hengjing Hu

First Affiliated Hospital of University of South China

Background: Atrial fibrillation (AF) is the most common cardiac arrhythmia globally, with a rising prevalence in Chinese adults now at 1.6%. This increase poses a significant economic burden on society and individuals. Atrial fibrosis, a hallmark of AF's structural remodeling, is crucial for its persistence, highlighting the importance of targeting atrial fibrosis to curb AF progression. Despite this, the mechanisms driving atrial fibrosis remain incompletely elucidated.

Myocardial fibrosis can be categorized into reactive and reparative forms. In reparative fibrosis, cardiomyocyte death leads to fibroblast-mediated tissue replacement, maintaining the myofibril structure. Emerging evidence suggests that ferroptosis, an iron-dependent cell death characterized by lipid peroxidation accumulation, plays a role in atrial fibrosis in mice. Inhibition of ferroptosis has been shown to mitigate Ang II-induced cardiac remodeling and fibrosis . As ferroptosis can induce fibrosis through cardiomyocyte death, it has emerged as a pivotal factor in the pathogenesis of cardiovascular diseases. This insight implies that ferroptosis may be a critical pathway in atrial fibrosis, and thus, its inhibition in cardiac cells could offer a therapeutic strategy for managing atrial fibrosis.

Glucose serves as the primary source of cellular energy and plays a critical role in glucose metabolism. In normal organisms, the vast majority of adenosine triphosphate (ATP)—approximately 90%—is derived from the mitochondrial oxidative phosphorylation pathway, with only a small fraction (approximately 10%) generated via the glycolytic pathway. Yet cells prefer glycolysis for ATP and lactate production even under aerobic conditions, a process called the Warburg effect (aerobic glycolysis). Local lactate accumulation—a Warburg effect hallmark—induces an acidic environment linked to cardiovascular diseases and myocardial fibrosis. Inhibiting this effect significantly improves AF-induced myocardial fibrotic remodeling. Aerobic glycolysis also drives succinate production to stabilize hypoxia-inducible factor 1 (HIF-1), promoting transforming growth factor-β (TGF-β)-induced fibroblast-to-myofibroblast differentiation. Thus, the Warburg effect contributes to myocardial fibrosis development.

SIRT1, a key enzyme within the SIRT family, is predominantly found in the cytoplasm and nucleus of cardiomyocytes, where it plays a critical role in sensing cellular energy changes and maintaining metabolic health. Recognized as a significant regulator of programmed cell death, SIRT1 influences cellular iron metabolism, which is vital for cell function and survival, as iron imbalance can trigger oxidative stress and cell death. SIRT1's regulatory influence is particularly evident in its modulation of FOXO3a, a crucial downstream target. By deacetylating FOXO3a, SIRT1 controls the transcriptional activity of this factor, thereby affecting genes related to cell survival, stress resistance, and apoptosis. The interplay between SIRT1 and FOXO3a is central to the regulation of programmed cell death. Moreover, increased SIRT1 expression leads to the deacetylation of FOXO3a, reducing oxidative stress and apoptosis, highlighting the importance of the SIRT1-FOXO3a axis in preserving cellular integrity and preventing premature cell death. Additionally, SIRT1 supports gluconeogenesis, suppresses glycolysis, enhances fatty acid utilization, and regulates the homeostasis of both fatty acid and glucose metabolism. This regulatory mechanism is pivotal for the heart's stress response and has broader implications for cellular metabolism and iron homeostasis, underscoring SIRT1's multifaceted role in cellular biology.

Dapagliflozin (DAPA), an SGLT2 inhibitor, reduces renal glucose reabsorption, promoting urinary excretion and lowering blood sugar. It significantly decreases cardiovascular events and heart failure hospitalizations in type 2 diabetes mellitus （T2DM）patients. DAPA mitigates cardiac strain and blood volume, potentially preventing atrial fibrillation. Studies suggest DAPA's role in heart remodeling involves the TGF-β1/Smad pathway, independent of glycemic control. Additionally, DAPA activates SIRT1, attenuating endothelial-mesenchymal transition in non-diabetic heart failure, and counteracts Ang II-induced SIRT1 suppression in cardiomyocytes. The interaction between DAPA, SIRT1, and FOXO3a in atrial fibrosis prevention remains under investigation, highlighting a potential role in atrial fibrillation susceptibility and myocardial remodeling.

Consequently, our hypothesis suggests that DAPA could be a gamechanger in atrial fibrosis therapy by neutralizing ferroptosis and metabolic dysregulation, and activating the SIRT1/FOXO3a pathway. In this study, AngII is used to establish in vivo and in vitro atrial fibrosis models to investigate the protective role of DAPA and associated cellular phenotype changes. SIRT1-specific knockout rats (Ad-SIRT1-shRNA) are employed to validate the molecular target, providing a potential therapeutic strategy for atrial fibrillation and atrial fibrosis.

Dapagliflozin (DAPA), a novel SGLT2 inhibitor, has shown promise in reducing atrial fibrosis, but its mechanism remains elusive. Our study delves into DAPA's role in ferroptosis—a form of regulated cell death linked to fibrosis—and glucose metabolism dysfunction (Warburg effect).

Methods: We employed both in vivo and in vitro models using angiotensin II (AngII) to induce atrial fibrosis and measured fibrosis, ferroptosis and Warburg effect markers.

Results: Our findings reveal that DAPA significantly suppresses ferroptosis and Warburg effect, thereby reducing fibrosis markers in both models. Intriguingly, bioinformatics pointed to the Silent Information Regulator 1 (SIRT1) / Forkhead Box O (FOXO) pathway's potential involvement in myocardial fibrosis. DAPA was found to boost SIRT1 and reduce FOXO3a, a key regulator in this pathway. The benefits of DAPA were negated by SIRT1 inhibition or silencing, underscoring its crucial role.

Conclusion: This research suggests that DAPA's cardioprotective effects against atrial fibrosis are mediated through the modulation of the SIRT1/FOXO3 axis, offering a new therapeutic strategy for heart disease management.

SIRT3 sulfhydrylation by hydrogen sulphide: A novel approach to prevent ferroptosis and atrial fibrosis

Hengjing Hu

First Affiliated Hospital of University of South China

Background: Atrial fibrillation (AF) is the most common and severe arrhythmia, with an incidence exceeding 6 % in individuals over 60 years old . AF is often associated with serious cardiovascular events, including stroke and heart failure. The death of atrial myocytes plays a cru cial role in atrial structural remodeling, leading to atrial enlargement and fibrosis—key factors in AF progression. In AF patients, the rate of myocyte death is significantly elevated, which is closely linked to an giotensin II (Ang-II) release. Ang-II activation of the renin angiotensin-aldosterone system promotes myocyte death and cardiac fi broblast proliferation, resulting in atrial fibrosis and persistent AF. However, the specific form of cell death in atrial myocytes remains un clear.

Ferroptosis, an iron-dependent form of cell death, is increasingly recognized as a key player in cardiomyocyte injury, contributing to the electrical remodeling seen in AF. Several ferroptosis markers, in cluding glutathione peroxidase 4 (GPX4), Solute Carrier Family 7 Member 11 (SLC7A11), and prostaglandin-endoperoxide synthase 2 (PTGS2), are increasingly recognized as key regulators of ferroptosis in cardiac tissues. GPX4 and SLC7A11, essential for the antioxidant defense against lipid peroxidation, have been shown to influence myocardial fibrosis and atrial remodeling, both of which contribute to AF progression. Moreover, PTGS2 involved in lipid metabolism, is also a critical marker in ferroptosis regulation. Alterations in the ex pression levels of these markers could reflect the severity and progres sion of AF, making them potential biomarkers for predicting disease onset, development, and prognosis. Monitoring these markers may of fer valuable insights into AF pathophysiology and provide new av enues for targeted therapeutic strategies.

SIRT3, a mitochondrial deacetylase, plays a crucial role in regulat ing cellular metabolism, mitochondrial function, and oxidative stress. When SIRT3 activity is reduced, mitochondrial dysfunction, increased reactive oxygen species (ROS), and iron accumulation occur, leading to decreased levels of GPX4, a key regulator of ferroptosis . This cas cade promotes ferroptosis and contributes to cardiac fibrosis, a hall mark of AF. Conversely, SIRT3 activation or overexpression has been shown to protect against ferroptosis and alleviate fibrosis, sug gesting its potential as a therapeutic target for AF. One key mecha nism by which SIRT3 exerts its protective effects is S-sulfhydration, a post-translational modification by hydrogen sulfide (H2S). S sulfhydrated SIRT3 enhances mitochondrial function and mitigates cel lular stress, thus preventing ferroptosis and reducing fibrosis. Fur thermore, SIRT3 is thought to regulate myocardial fibrosis through modulation of the Wnt/β-catenin pathway, a signaling cascade in volved in cellular processes like proliferation and differentiation. While it is known that SIRT3 can inhibit the Wnt/β-catenin pathway in some contexts, whether S-sulfhydrated SIRT3 specifically impacts this pathway to influence ferroptosis and the progression of fibrosis in AF remains unclear. Based on the above, we hypothesize that S-sulfhydrated SIRT3 in hibits ferroptosis in atrial myocytes by antagonizing the Wnt/β-catenin pathway, thereby reducing atrial fibrosis and improving susceptibility to AF. This study aims to explore the potential of S-sulfhydrated SIRT3 as a novel therapeutic target for AF, providing new insights into the molecular mechanisms underlying atrial fibrosis and ferroptosis. By tar geting this pathway, the study offers a promising direction for the pre vention and treatment of AF.

Hydrogen sulfide (H2S) has been shown to counteract ferroptosis and atrial fibrosis, yet the underly ing mechanisms remain incompletely understood. This study aims to investigate how H2S regulates ferroptosis to alleviate atrial fibrosis.

Methods: In vivo and in vitro models of atrial fibrosis were established using Angiotensin II (Ang-II) to modu late the expression of SIRT3, β-cat-

enin, and ferroptosis markers. Western blotting was employed to analyze changes in proteins related to ferroptosis and fibrosis. Histological evaluations, including Hematoxylin and Eosin (HE), and Masson's staining were performed to assess atrial fibrosis. Cardiac ultrasound was used to as sess left atrial function in vivo. In vitro, reactive oxygen species (ROS) levels and iron staining were used to monitor ferroptosis and oxidative stress.

Results: In atrial tissue from patients with AF, significant increases in ferroptosis markers and atrial fibrosis were observed. In both animal and cell models of atrial fibrosis, reduced sulfhydrylated SIRT3 and elevated β catenin expression were associated with increased ferroptosis and fibrosis markers. Treatment with NaHS, a donor of H2S, reversed these changes, reducing both ferroptosis and fibrosis. Importantly, inhibition of sulfhydrylated SIRT3 further upregulated β-catenin, exacerbating ferroptosis and fibrosis. However, blocking β-catenin effectively alleviated Ang-II-induced ferroptosis and fibrosis in the atrial fibrosis model.

Conclusion: H2S alleviates atrial fibrosis and inhibits ferroptosis by upregulating SIRT3 sulfhydrylation and an tagonizing the Wnt/β-catenin signaling pathway. These findings suggest that targeting the H2S-SIRT3-β-catenin signaling axis may offer a promising therapeutic strategy for atrial fibrosis and associated arrhythmias

巯基化修饰 SIRT3 抑制 NLRP3 炎性小体和 Warburg 效应改善心房纤维化

胡恒境

南华大学附属第一医院

目的：旨在探讨 H_2S 改善心房纤维化的机制及 SIRT3 在其中的作用。

方法 :1. 将 HL- 1 细胞随机分为 Control 组、血管紧张素 II 组（AngII），分别予以不同时间处理后，使用 Western Blot 检测纤维化相关指标、NLRP3 炎性小体组成成分、 Warburg 效应关键酶和 SIRT3 蛋白表达水平。

2. 将 HL- 1 细胞随机分为 Control 组、血管紧张素 II 组（AngII）、AngII+MCC950 组（MCC950，NLRP3 炎性小体选择性抑制剂）、AngII+DCA 组 （DCA，Warburg 效应特异性抑制剂）共四组，分别予以不同时间处理后，使用 Western Blot 检测纤维化相关指标和 SIRT3 的蛋白表达水平。

3. 将 HL- 1 细胞随机分为 Control 组、AngII 组、3-TYP 组 (3-TYP,SIRT3 特异性抑制剂）、AngII+3-TYP 组共四组，分别予以不同时间处理后，使用 Western Blot 检测纤维化相关指标、NLRP3 炎性小体组成成分、Warburg 效应关键酶和 SIRT3 蛋白表达水平，通过 MDA 、T-SOD 检测试剂盒检测相应指标，检测线粒体活性氧水平。

4. 将 HL- 1 细胞随机分为 Control 组，AngII 组，AngII+NaHS 组， NaHS 组 (H2S 外源性供体), AngII+DTT 组，DTT（巯基化抑制剂）组，共六组，分别予以不同时间处理后，使用 Western Blot 检测纤维化相关指标、NLRP3 炎性小体组成成分、Warburg 效应关键酶、 SIRT3 和 S- SIRT3 蛋白表达水平，通过 MDA 、T-SOD、葡萄糖、乳酸检测试剂盒检测相应指标，Elisa 试剂盒检测炎症因子 IL-1β 和 IL-18，检测线粒体活性氧水平。

5. 将 HL- 1 细胞随机分为 Control 组，AngII 组，AngII+NaHS 组、AngII+ NaHS+si-NC 组、AngII+NaHS+si-SIRT3 组，共五组，分别予以不同时间处理后，使用 Western Blot 检测纤维化相关指标、NLRP3 炎性小体组成成分、 Warburg 效应关键酶和 SIRT3 蛋白表达水平。

结果 :1. AngII 诱导后，HL-1 细胞中 SIRT3 表达显著下调，伴随心肌纤维化增加，NLRP3 炎性小体活化增强，以及 Warburg 效应激活增加。

2. MCC950 或 DCA 处理显著改善 AngII 诱导的 HL-1 细胞中 SIRT3 蛋白表达的下调。同时，MCC950 和 DCA 能够逆转 AngII 导致的心肌纤维化、NLRP3 炎性小体活化以及 Warburg 效应的激活。

3. 予以 3-TYP 抑制 SIRT3 进一步增强 AngII 诱导的 NLRP3 炎性小体表达以及 Warburg 效应激活。此外，3-TYP 加剧 AngII 介导的心肌纤维化，同时促进线粒体 ROS 的过量产生，并导致 MDA 和 T-SOD 水平显著升高。

4. DTT 处理增强 AngII 诱导的 NLRP3 活化，也进一步促进 Warburg 效应的激活，并加剧了 AngII 所介导的纤维化。此外，DTT 导致线粒体 ROS 产生增加，并伴随着 MDA、T-SOD 水平升高。通过 NaHS 巯基化修饰 SIRT3，可以有效减轻 NLRP3 炎性小体活化及 Warburg 效应激活介导的心肌纤维化的程度，同时降低线粒体 ROS、MDA、T-SOD 蓄积。

5.SIRT3 敲低后，NaHS 无法改善 AngII 诱导的 NLRP3 炎性小体活化、Warburg 效应的增强以及纤维化的加重。

结论：巯基化修饰 SIRT3 抑制 NLRP3 炎性小体和 Warburg 效应改善心房纤维化。

Systemic Immune-Inflammation Index and Blood Pressure Control Are Independent and Interactive Predictors of Atrial Fibrillation Recurrence After Ablation

Yu-Hang Wei, Gang-Qiong Liu, Chen-Xi Cao, Yun-Zhe Wang, Wen-Jing Zhang, Xi-Jia Wang, JiaHong ShangGuan

The First Affiliated Hospital of Zhengzhou University

Abstract

Background:

Atrial fibrillation (AF) recurrence remains a significant challenge following radiofrequency catheter ablation (RFCA), particularly in patients with comorbid hypertension (HTN), affecting over 70% of AF patients. Hypertension contributes to AF pathogenesis and recurrence through structural, electrical, and inflammatory remodeling. The systemic immune-inflammation index (SII), a composite marker derived from peripheral neutrophil, platelet, and lymphocyte counts (SII = Platelets × Neutrophils/Lymphocytes), has emerged as a robust indicator of systemic inflammatory dysregulation and has shown associations with cardiovascular diseases, including AF. While inflammation is a recognized contributor to AF recurrence, the specific prognostic value of pre-ablation SII in hypertensive AF patients undergoing RFCA, and crucially, the potential modifying effect of blood pressure (BP) control status on this association, remain inadequately explored. Prior studies have seldom integrated inflammatory markers like SII with hemodynamic factors such as BP control in risk stratification for post-ablation recurrence.

Objective:

This study aimed to: (1) Evaluate the independent predictive value of pre-ablation SII for AF recurrence after RFCA specifically in a cohort of patients with hypertension; (2) Investigate whether BP control status modifies the association between SII and recurrence risk; and (3) Assess the incremental predictive value of SII over established clinical predictors.

Methods:

A single-center, retrospective observational cohort study was conducted. Consecutive patients with AF and comorbid hypertension undergoing first-time RFCA at the First Affiliated Hospital of Zhengzhou University between January 2020 and December 2022 were screened (n=630). Exclusion criteria included prior left atrial ablation/cardiac surgery, significant structural heart disease, secondary AF, active infection/malignancy/severe hepatic/renal dysfunction, and incomplete data/loss to follow-up, resulting in 568 eligible patients for final analysis. Baseline demographic, clinical, laboratory (including complete blood counts for SII calculation), and echocardiographic data were collected. Hypertension was defined as systolic BP ≥ 140 mmHg, diastolic BP ≥ 90 mmHg, or current antihypertensive medication use. Poor BP control was defined as requiring ≥ 3 antihypertensive agents with persistently elevated BP on ambulatory or home monitoring. All patients received antiarrhythmic drugs for ≥ 3 months post-ablation. Recurrence was defined as any documented atrial tachyarrhythmia lasting ≥ 30 seconds on ECG or 24-hour Holter monitoring occurring after a 3-month blanking period. Patients were followed for a mean of 39.5 months. Statistical analyses employed R (v4.3.1) and SPSS (v29.0). Patients were stratified by SII quartiles (Q1-Q4) and BP control status (good/poor). Group comparisons used appropriate parametric/non-parametric tests. The predictive performance of SII for recurrence was assessed using receiver operating characteristic (ROC) curve analysis (AUC comparison via DeLong test). Kaplan-Meier curves with log-rank tests evaluated recurrence-free survival. Multivariable Cox proportional hazards models were constructed to assess associations, adjusting sequentially for demographics (Model 2: age, sex) and key clinical confounders (Model 3: BMI, AF type, AF duration, left atrial diameter (LAD), left atrial volume (LAVOL), CHA_2DS_2-VASc score). Restricted cubic splines (RCS) modeled the dose-response relationship. Net Reclassification Improvement (NRI) and Integrated Discrimination Improvement (IDI) quantified the incremental value of SII added to a baseline clinical risk model. Subgroup analyses assessed consistency across clinical characteristics.

Results:

1. Baseline & Outcomes: Among 568 patients (mean age 62.5±9.3 years, 41.0% female), 98 (17.3%) experienced AF recurrence during follow-up. Recurrence patients had significantly longer AF history, higher CHA_2DS_2-VASc scores, larger left atrial volumes, elevated platelet counts, neutrophil counts, SII values, and a higher prevalence of poor BP control (all P<0.05) compared to non-recurrence patients. The poor BP control group (n=238) itself had a higher recurrence rate (26.1% vs 10.9%, P<0.001), longer AF history, higher prevalence of CAD and DM, higher CHA_2DS_2-VASc scores, and lower eGFR than the good control group (n=330).

2. SII Predictive Performance: ROC analysis demonstrated SII had superior predictive ability for recurrence (AUC = 0.739, 95% CI: 0.689-0.789, P<0.001) compared to AF duration (AUC=0.602, P<0.001) and left atrial volume (AUC=0.570, P<0.001). The optimal SII cut-off was 554.63 (sensitivity 78.6%, specificity 72.1%).

3. SII Quartiles & Survival: Patients in higher SII quartiles (Q3, Q4) had significantly higher recurrence rates (Q1: 4.9%, Q2: 5.6%, Q3: 20.4%, Q4: 38.0%, P<0.001). Kaplan-Meier analysis confirmed a stepwise decline in recurrence-free survival across increasing SII quartiles (log-rank P<0.001).

4. Multivariable Cox Regression: After full adjustment (Model 3), elevated SII remained a significant independent predictor of recurrence (HR per unit increase = 1.01, 95% CI: 1.01-1.01, P<0.001). Poor BP control was also independently associated with increased recurrence risk (HR = 2.40, 95%

CI: 1.58-3.64, P<0.001).

5. Interaction Effect: A significant synergistic interaction was observed. Patients with both high SII (Q4: >682.49) and poor BP control had a markedly elevated risk of recurrence (Adjusted HR = 4.02, 95% CI: 2.60-6.21, P<0.001) compared to the reference group. RCS analysis confirmed a significant non-linear relationship between baseline SII and recurrence risk (P for non-linearity=0.005). Cumulative incidence curves visually demonstrated the highest recurrence burden in the "Poor BP Control + High SII" group.

6. Incremental Value: Adding SII to the baseline clinical risk model (age, sex, AF type, BMI, CHA_2DS_2-VASc, AF duration, LAD, LAVOL) significantly improved predictive performance: C-statistic increased from 0.645 (95% CI: 0.586-0.704) to 0.755 (95% CI: 0.711-0.800, P<0.001), IDI=0.033 (95% CI: 0.011-0.065, P<0.001), and NRI=0.395 (95% CI: 0.164-0.511, P<0.001).

7. Subgroup Analysis: The positive association between SII and recurrence risk was consistent across all subgroups stratified by sex, age, BMI, AF type, smoking, alcohol use, CAD, DM, TIA, and BP control status (all interaction P>0.05).

Conclusion:

This study provides robust evidence that pre-ablation systemic immune-inflammation index (SII) is a potent, independent, and superior predictor of atrial fibrillation recurrence following catheter ablation in patients with hypertension, outperforming traditional markers like AF duration and left atrial volume. Crucially, it identifies blood pressure control status as a significant effect modifier of the SII-recurrence association. A profound synergistic interaction exists, whereby patients exhibiting both elevated SII (indicating systemic inflammatory dysregulation) and poorly controlled hypertension face a more than fourfold increased risk of recurrence (HR=4.02). The integration of SII into established clinical prediction models significantly enhances their discriminative capacity for identifying high-risk individuals. These findings underscore the intertwined pathophysiological roles of inflammation and hemodynamic stress in AF recurrence post-ablation. Joint assessment of SII and BP control status offers a promising, readily accessible approach for improved risk stratification and could guide personalized post-procedural management strategies, potentially targeting intensive anti-inflammatory interventions and rigorous blood pressure control in high-risk subgroups to mitigate recurrence. Future prospective studies should investigate the impact of combined anti-inflammatory and intensive BP lowering therapies on long-term outcomes in this population.

窦性心律下左心房超声重构参数对阵发性房颤的预测价值

李晶洁

李晶洁

哈医大一院

背景及目的：

心房颤动是常见心律失常，与卒中、心衰等相关，约 1/3 阵发性房颤（PAF）患者无症状导致检出率低，故需探索新识别方法。左心房重构与房颤关联密切，左心房机械离散度（LAMD）及应变已证实对 PAF 识别有效，左心房僵硬度指数（LASI）在 PAF 识别中尚无研究，或有应用潜力。结合窦性心律下左心房重构参数与机器学习，可能提升 PAF 识别效果。本研究旨在评估窦性心律下 PAF 患者左心房改变，探究 LASI 对 PAF 的预测价值，结合机器学习构建模型，为 PAF 识别提供新思路。

方法：

选取 2022 年 4 月至 12 月哈尔滨医科大学附属第一医院心血管内科住院的 58 名 PAF 患者（PAF 组）和 51 名无心律失常患者（对照组），年龄性别匹配。采集临床基线资料，进行超声心动图检查，用二维斑点追踪超声心动图测得左心房相关应变、LASI、LAMD 等参数。采用 R 语言统计分析，行组间对比、单因素及多因素 Logistic 回归分析，筛选独立危险因素，绘制 ROC 曲线评价诊断性能，基于机器学习算法结合相关资料构建 PAF 诊断模型。

结果：

1. 两组在年龄、性别、BMI 等基线资料无显著差异（P > 0.05）。

2.PAF 组 LAD 高于对照组（P < 0.05）。

3.PAF 组 LASr 显著减小，LAScd、LASct、LAMD、LASI 均显著高于对照组（P < 0.001）。

4. 多因素 Logistic 回归分析显示，LASr、LAMD、LASI 与 PAF 独立相关，其 ROC 曲线 AUC 分别为 0.866、0.899、0.868。

5. 按 LAD 将 PAF 组分为三组，三组间 LASr、LAMD 及 LASI 无显著差异（P > 0.05）。

6. 纳入 26 个特征构建 5 个机器学习预测模型，除 K 最邻近算法外其他模型表现良好，支持向量机模型效果最佳，准确率及 F1-score 均达 0.97，AUC 最大。

结论：

1. 窦性心律下 PAF 患者的左心房储存功能、管道功能及辅泵功能均受损。

2. 运用左心房重构参数可以识别 PAF。LAMD、LASI、LASr 是 PAF 的独立影响因素，且优于临床危险因素及常规超声心动图参数，其在早期识别 PAF 方面可提供重要价值。

3. 将临床基线指标、常规超声指标、左心房应变及 LASI、LAMD 纳入数据集，构建的支持向量机模型能够更加准确识别 PAF，具有较高临床价值及推广价值。

老年长程持续性房颤患者射频消融对比冷冻球囊消融疗效及安全性分析

金震 孙鸣宇 王祖禄

中国人民解放军北部战区总医院

目的 探讨射频消融和冷冻球囊消融治疗老年长程持续性房颤患者的疗效及安全性。

方法 回顾性研究 2021 年 1 月至 2023 年 6 月于北部战区总医院心内科行导管消融的 60 岁以上老年长程持续性房颤患者，分为射频消融组及冷冻消融组。两组患者基线资料包括：性别、年龄、体重指数、临床合并症、烟酒史、实验室相关检查、心脏超声、CHA2DS2-VASC 评分及 HAS-BLED 评分。比较两组患者围手术期并发症发生率及手术复发率。

结果 本研究共纳入 237 例老年长程持续性房颤患者，与冷冻消融组（93 例）相比，射频消融组（144 例）患者房颤病程长 [（51.05±57.02）个月 vs（30.66±33.90）个月，P=0.001]，且射频组合并其他心律失常比例明显增高（11.81%vs4.3%，P=0.047）。两组患者在性别、年龄、体重指数、临床合并症、烟酒史、实验室相关检查、心脏超声、CHA2DS2-VASC 评分及 HAS-BLED 评分等指标无统计学差异（均 P>0.05）。两组肺静脉隔离即刻成功率均为 100%，手术时间无统计学差异，射频组射线曝光时间显著低于冷冻组 [（14.31±6.60）min vs（26.93±10.16）min，P<0.001]。射频消融组及冷冻消融组分别随访（24.55±8.48）个月和（25.27±8.27）个月，两组复发率无统计学差异（25% VS 27.96%，P=0.613）。

结论 射频组患者房颤病程长，合并其它心律失常比例更高；射频组术中曝光时间更短，线性消融比例更高；射频消融和冷冻球囊消融治疗老年长程持续性房颤患者的疗效及安全性无统计学差异。

替格瑞洛与氯吡格雷对急性心肌梗死合并心房颤动患者预后的影响

邱久纯

天津医科大学第二医院

目的 比较替格瑞洛与氯吡格雷对急性心肌梗死（acute myocardial infarction, AMI）合并心房颤动（atrial fibrillation, AF）患者预后的影响。

方法 纳入 2010 年 1 月至 2023 年 6 月天津市 72 家二、三级医院 AMI 合并 AF 且接受双联抗血小板治疗的患者进行回顾性分析，根据患者出院带药分为替格瑞洛联合阿司匹林组和氯吡格雷联合阿司匹林组。主要结局指标是卒中与全因死亡。结局指标包括缺血性卒中、出次要血性卒中、心血管死亡和大出血事件。采用倾向性评分匹配（propensity score matching, PSM）、多变量 Cox 回归和 Kaplan-Maier 生存曲线等方法比较替格瑞洛及氯吡格雷对 AMI 合并 AF 患者预后的影响。

结果 纳入使用双联抗血小板治疗的 AMI 合并 AF 患者共 5084 例，其中替格瑞洛联合阿司匹林组 670 例，氯吡格雷联合阿司匹林组 4414 例。替格瑞洛联合阿司匹林组患者卒中（21.0% vs 34.1%）、全因死亡（8.4% vs 29.3%）、缺血性卒中（20.4% vs 33.0%）、出血性卒中（1.0% vs 2.8%）、心血管死亡（6.9% vs 23.6%）和大出血事件（1.3% vs 3.9%）发生率显著低于氯吡格雷联合阿司匹林组。经过 1:1 倾向性评分匹配后，替格瑞洛联合阿司匹林组患者卒中 [风险比（hazard ratio, HR）=0.69，95% 置信区间（95%confidence interval, 95%CI）：0.54 ~ 0.88] 、全因死亡（HR=0.49，95%CI：0.36 ~ 0.68）、缺血性卒中（HR = 0.71，95%CI：0.55 ~ 0.91）、心血管死亡（HR=0.51，95%CI：0.36 ~ 0.73）的发生风险显著低于氯吡格雷联合阿司匹林组，而两组患者出血性卒中（HR=0.51，95%CI：0.20 ~ 1.30）和大出血事件（HR=0.58，95%CI：0.25 ~ 1.35）的发生风险无统计学差异。死亡竞争风险模型分析结果与多变量 Cox 回归结果一致。亚组分析表明，替格瑞洛在既往房颤患者中对卒中及全因死亡的保护作用更为显著。

结论 在 AMI 合并 AF 人群中，替格瑞洛与氯吡格雷相比卒中、全因死亡、缺血性卒中和心血管死亡事件发生风险较低，而出血性卒中和大出血风险无明显增加。

Eicosanoid Metabolomics as a Novel Biomarker for Predicting Atrial Fibrillation Recurrence After Cryoballoon Ablation

Jiuchun Qiu

The Second Hospital of Tianjin Medical University

Objective: Atrial fibrillation (AF), the most prevalent sustained cardiac arrhythmia, poses significant clinical challenges. Cryoballoon ablation (CBA) has emerged as an innovative and effective catheter-based intervention for achieving pulmonary vein isolation in AF patients. Concurrently, dysregulation within the eicosanoid metabolic pathway - a complex network of bioactive lipid mediators derived from polyunsaturated fatty acids, critically involved in inflammation, vascular tone, and fibrosis - plays a pivotal role in the pathogenesis, perpetuation, and clinical prognosis of AF. Given the profound impact of CBA on cardiac tissue and the known significance of eicosanoids in AF, this study specifically aimed to evaluate the influence of a successful CBA procedure on the systemic metabolism of eicosanoids. Furthermore, leveraging these metabolic insights, the study sought to construct a predictive model for AF recurrence based on identifiable changes in eicosanoid metabolites.

Methods: A prospective cohort study was conducted involving fifty-two AF patients who underwent successful CBA at the Second Hospital of Tianjin Medical University between September 2022 and December 2023. Peripheral blood samples were collected under standardized conditions immediately prior to the ablation procedure and again at 24 hours post-CBA. These samples were processed for comprehensive eicosanoid metabolomics profiling. The primary study endpoint was clinical recurrence of atrial tachyarrhythmia following the ablation procedure. Recurrence was rigorously defined as any documented episode of atrial fibrillation, atrial flutter, or atrial tachycardia lasting ≥ 30 seconds, detected either on a standard 12-lead electrocardiogram (ECG) or during 24-hour ambulatory ECG monitoring, occurring beyond the 3-month post-procedural blanking period. Ultra high-performance liquid chromatography tandem mass spectrometry (UPLC-MS/MS)-based metabolomics was employed to meticulously investigate and quantify differences in the profile of eighty eicosanoid metabolites between the pre-ablation and 24-hour post-ablation time points. To explore potential biological links, Pearson correlation analysis was performed to reveal statistical associations between the identified differential metabolites and relevant clinical characteristics. Finally, the predictive value of significant metabolite changes for AF recurrence was assessed using receiver operating characteristic (ROC) curve analysis.

Results: Comparative metabolomic analysis revealed significant alterations in eight out of the eighty measured eicosanoid metabolites following cryoablation compared to pre-procedural baseline levels. These metabolites were: 12,13-dihydroxy-9Z-octadecenoic acid (12,13-diHOME), 9,10-dihydroxy-12Z-octadecenoic acid (9,10-diHOME), Prostaglandin E2 (PGE2), Thromboxane B2 (TXB2), Prostaglandin D2 (PGD2), Eicosapentaenoic acid (EPA), 12-Hydroxyeicosatetraenoic acid (12-HETE), and Prostaglandin F2α (PGF2α). Pearson correlation analysis identified specific associations: EPA levels showed a significant correlation with left atrial diameter, while PGF2α levels correlated significantly with NT-proBNP concentration. ROC analysis demonstrated that the magnitude of change (difference) between preoperative and postoperative plasma levels of specific eicosanoids possessed predictive capacity for AF recurrence. Individually, the change in 9,10-diHOME concentration exhibited an area under the curve (AUC) of 0.729 (95% CI, 0.574-0.884). Importantly, a model based on the combined detection of multiple differential metabolites significantly enhanced predictive performance for atrial fibrillation recurrence, achieving an AUC of 0.803 (95% CI, 0.667-0.938; P <0.05).

Conclusion: This study demonstrates that the systemic eicosanoid metabolism profile undergoes significant alteration within 24 hours following successful cryoballoon ablation in patients with atrial fibrillation. The identified changes in specific eicosanoid metabolites, particularly when evaluated in combination, exhibit a statistically significant capacity to predict the likelihood of AF recurrence after the procedure. Consequently, these findings position the post-ablation eicosanoid metabolomic signature as a promising novel class of biomarkers for stratifying recurrence risk following catheter ablation for AF.

Catheter ablation combined with left atrial appendage closure for non-valvular atrial fibrillation: A Single-Center Retrospective Study

Manli Yu

Changhai Hospital

1.Introduction

According to the epidemiological study of atrial fibrillation (AF) conducted by Hu Daichi et al. in 13 provinces and cities in China, the age-adjusted prevalence rate of AF was 0.65%, and as high as 7.5% in people older than 80 years[1-2]. AF could reduce cardiac function, exercise tolerance, and increase the incidence of ischemic stroke as well as systemic thromboembolic events. Catheter ablation (CA) is the first-line treatment for symptomatic AF in selected patients. Guidelines suggest for AF patients at high risk of stroke, anticoagulation therapy should be maintained even after successful postoperative conversion and sinus rhythm maintenance[3]. However, patients exposed to a high risk of stroke often had a relatively high bleeding risk score, and long-term oral anticoagulants increased the risk of bleeding. As an alternative treatment to oral anticoagulant drugs, left atrial appendage closure (LAAC) could safely and effectively prevent thromboembolic events[3].

AF can cause structural and functional changes in the heart, especially for left atrial enlargement. CA can reverse left atrial remodeling and reduce the increased left atrial diameter. In recent years, the safety of CA combined with LAAC (referred to as combined procedure) has been proven[4-8]. However, LAAC can increase the left atrial volume of patients in some studies[9-11]. Problems thus appear that how the diameter of the left atrium will change when CA and LAAC are combined, and whether this change will affect the success rate of AF ablation. To this end, the statistical method of propensity score matching (PSM) was used to investigate the effect of combined procedure on the ablation effect of AF in patients with a high risk for stroke. At the same time, the influence of combined procedure on left atrial remodeling was also discussed.

2.Methods

2.1 Studied Population

In this study, non-valvular AF patients aged > 18 years and ≤ 90 years with a high risk of stroke (CHA2DS2-VASc score ≥ 2 in men and ≥ 3 in women) who received the combined procedure of CA and LAAC in Shanghai Changhai Hospital from October 2020 to December 2021 were retrospectively included as the combined group (n=150), including persistent AF (n=64) and paroxysmal AF (n=86). All participants were included based on the following indications for unsuitable long-term anticoagulant therapy: a clear history and/or tendency to bleed; allergy to anticoagulants; poor compliance with long-term oral anticoagulants; or increased blood risk (HAS-BLED score ≥ 3).

During the same period of time, CA procedures were performed on 480 patients, including persistent AF (n=226) and paroxysmal AF (n=254) respectively. PSM was used to select controls to minimize potential confounding bias. Patients of the combined group were matched 1:1 to those who underwent CA alone (CA-only group). A total of 300 patients in both groups were included in the final analysis (Tab.1). This retrospectively study was approved by the Ethics Committee of Changhai Hospital and complied with the Declaration of Helsinki.

2.2 Pre-procedural assessment

All the procedures were performed by experienced operators having passed the learning curves of either CA or LAAC. Left atrial appendage (LAA) thrombus exclusion and size measurement were carried out by transesophageal echocardiography (TEE) before procedures on 30% (90/300) of patients. A cardiac computed tomography (CT) scan and 3-dimensional reconstruction of the left atrium were performed in advance to assist CA and/or LAAC for all patients.

2.3 Ablation procedure

Under conscious sedation, a decapolar catheter was positioned in the coronary sinus, and two transseptal accesses were obtained through the right femoral vein. Mapping and ablation were performed under the guidance of CARTO (Biosense Webster, Diamond Bar, CA, USA) or EnSite (St. Jude Medical, St Paul, MN, USA) 3- dimensional electroanatomic mapping systems in addition to standard fluoroscopy. For patients with paroxysmal AF, standard pulmonary vein isolation (PVI) was performed, while for those with persistent AF, additional linear and/or complex fragmented atrial electrogram (CFAE) ablations were carried out according to the physician's discretion. Sinus rhythm was restored by either ablation or electric cardioversion.

2.4 LAAC procedure

All patients underwent successful LAA closure with the guidance of WATCHMAN. 14F guide wire and pigtail catheters were advanced into the LAA following AF ablation. The size, depth, and shape of LAA was observed and recorded by angiogram under fluoroscopy guidance and TEE or ICE. The device was released after confirmation of an adequate position [no or minimal peridevice leakage (PDL)≤3 mm by TEE/ICE] and a tug test.

2.5 Follow-Up

All patients routinely received anticoagulation therapy for at least 3 months after the combined procedure. The anticoagulation regimen was usually either warfarin or novel OACs depending on the individual patient, Cardiac computed tomography angiography (CCTA) was performed 3-6 months after the combined procedure to assess device stability, LAA sealing and device-related thrombus (DRT). If the CCTA suggested PDL < 3mm or no DRT during follow-up, the patient was subsequently treated with dual antiplatelet therapy to the 6th months after procedure, then oral aspirin or clopidogrel for long-term.. Holter and echocardiography was routinely obtained at the 3,6,and12months outpatient clinic appointment for all patients. Freedom of AF, cardiac function, left ventricular ejection fraction (LVEF) and left atrial diameter (LAD) were compared between the combined group and CA-only group. Incidence of perioperative complications and thromboembolic events such as stroke, transient ischemic attack (TIA), and systemic embolism were observed during follow-up between the two groups.

2.6 Statistical Analysis

Continuous variables were described as mean ± standard deviation (SD). Categorical variables were described as percentage (%). Kaplan-Meier estimate analyzed the freedom of atrial arrhythmia with p value achieved by the log-rank test. Multivariate logistics regression analysis was applied to determine the risk factors of the recurrence of atrial arrhythmias and residual leakage after left atrial appendage closure. All data were analyzed by SPSS 26.0, and P < 0.05 was considered statistically significant.

基于临床检验检查指标建立老年非瓣膜性房颤患者诊断判别模型

石世林 [1] 许严锴 [2] 刘克坚 [2]

1. 第八师石河子市人民医院

2. 石河子大学第一附属医院

目的 基本研究旨在基于患者基线资料、实验室检验指标及心脏超声检查指标，构建适用于新疆南疆地区老年非瓣膜性心房颤动（NVAF）患者的诊断判别模型，以解决该地区医疗资源分布不均、房颤知晓率低且患病率高的问题，为临床早期识别高风险人群和制定区域性防治策略提供依据。

方法 回顾性收集 2014 年 1 月至 2023 年 12 月南疆地区 5 家医院住院的 2118 例老年患者（≥ 60 岁）资料，包括 1059 例 NVAF 患者和 1059 例非 NVAF 对照。通过单因素 Logistic 回归初步筛选变量，采用 LASSO 回归（十折交叉验证）从 28 个候选变量中提取显著预测因子。基于筛选变量构建 4 种模型：多因素 Logistic 回归模型、支持向量机（SVM）模型、极度梯度提升树（XGBoost）模型、随机森林模型。数据集按 7:3 划分为训练集（1482 例）和测试集（636 例）。模型性能通过受试者工作特征曲线下面积（AUC）、准确率、精确率、召回率、F1 评分、灵敏度及特异度综合评价。

结果 1. 变量筛选：LASSO 模型自身 AUC 达 0.85。LASSO 回归确定 13 个核心预测变量。危险因素：糖尿病（DM）、高血压（HTN）、收缩压（SBP）、中性粒细胞 / 淋巴细胞比值（NLR）、总胆红素（TBIL）、间接胆红素（IBIL）、左房内径（LAD）、左室舒张末期内径（LVDd）。保护因素：钙离子（Ca^{2+}）、高密度脂蛋白胆固醇（HDL-C）、低密度脂蛋白胆固醇（LDL-C）、左室射血分数（EF）、左室收缩末期内径（LVDs）。2. 模型性能比较：XGBoost 模型表现最优，其中训练集：AUC=0.931（95%CI: 0.919-0.943），准确率 85.2%，灵敏度 81.4%，特异度 89.1%。测试集：AUC=0.856（95%CI: 0.827-0.888），准确率 78.5%，灵敏度 73.4%，特异度 83.4%。其余模型测试集 AUC：Logistic 回归（0.847）、SVM（0.834）、随机森林（0.836）。3. 临床因素分析：南疆地区 NVAF 独立危险因素包括：高血压（患病率 70.10% vs 全国 66.8%）、糖尿病（58.07% vs 对照组 22.95%）、高 NLR（OR=1.07）及左心房扩大（LAD: 41.68±7.35 mm vs 对照组 35.94±6.75 mm）。LDL-C 的保护作用可能与当地高肉类 / 乳制品饮食相关（NVAF 组 LDL-C: 2.27±0.77 mmol/L vs 对照组 2.57±0.83 mmol/L）。

结论 基于 DM、HTN、SBP、NLR、HDL-C、LDL-C、TBIL、IBIL、Ca^{2+}、LAD、LVDs、LVDd、EF 构建的 XGBoost 模型，对南疆老年 NVAF 具有显著判别价值（测试集 AUC=0.856）。该模型整合了反映炎症（NLR）、代谢（血脂）、心脏重构（LAD/LVDd）及地域特性（高胆红素）的多维指标，可为基层医疗提供高效诊断工具，助力区域性房颤早期干预。

Marshall 静脉乙醇灌注在有二尖瓣置换术史的持续性心房颤动患者导管消融治疗中的应用

汤日波 程小航 刘筱莹 王伟 赵欣 李昌义 喻荣辉 刘念 李松南 刘晓霞 郭雪原 左嵩 李梦梦 刘佟 黄丽洪 吕文鹤 李玉昆 王学思 李佳霖 杜卓航 李心茹 蒋晨曦 桑才华 龙德勇 董建增 马长生

首都医科大学附属北京安贞医院

目的： Marshall 静脉乙醇灌注在非瓣膜性持续性心房颤动患者中的疗效已得到证实。然而，在既往接受过二尖瓣置换术的持续性心房颤动患者的导管消融治疗中，Marshall 静脉乙醇灌注是否能取得相同的效果仍有待讨论。本研究主要探讨 Marshall 静脉乙醇灌注在既往接受二尖瓣置换术的持续性心房颤动患者导管消融治疗中的有效性与安全性。

方法：研究采用回顾性病例对照研究设计方法，纳入首次接受导管消融治疗的既往接受过二尖瓣置换术的持续性心房颤动患者。根据是否接受 Marshall 静脉乙醇灌注，患者被分为酒精消融组（27 例）和常规消融组（33 例）。两组患者均接受双侧肺静脉隔离及线性消融。在酒精消融组的手术方案中增加 Marshall 静脉乙醇灌注。通过比较两组患者的二尖瓣峡部阻滞成功率、手术相关并发症及窦性心律维持率评价 Marshall 静脉乙醇灌注在既往接受二尖瓣置换术的持续性心房颤动患者导管消融治疗中的有效性与安全性。

结果：两组患者的基线特征无显著差异。在酒精消融组的 27 例患者中，有 22 例患者成功接受 Marshall 静脉乙醇灌注。酒精消融组的二尖瓣峡部阻滞成功率显著高于常规消融组（77.8% vs. 51.5%，P 值 =0.036）。经过 15.4±9.4 个月的随访，酒精消融组的窦性心律维持率显著高于常规消融组（62.9% vs. 36.4%，P 值 =0.032）。多变量 Cox 回归分析显示，Marshall 静脉乙醇灌注与更高的窦性心律维持率有关（风险比 0.35，95% 置信区间 0.16 ~ 0.78，P 值 =0.009）。酒精消融组中 1 例患者术后出现心包积液，经观察后自行缓解。

结论：在既往接受过二尖瓣置换术的持续性房颤患者的导管消融治疗中，Marshall 静脉乙醇灌注与更高的二尖瓣峡部线性阻滞成功率及窦性心律维持率有关，且并未显著增加手术相关并发症。

房颤射频消融术对心脏搭桥合并心脏瓣膜手术患者心功能、心肌损伤及预后的影响

刘馨羽

中国医科大学附属盛京医院南湖院区

目的：探究房颤射频消融术 (RA) 对心脏搭桥合并心脏瓣膜手术患者心功能、心肌损伤及预后的影响。

方法：选取我院 2023 年 2 月至 2024 年 3 月接受心脏搭桥合并心脏瓣膜手术患者 50 例，随机数字表法将其分为观察组 25 例 (房颤 RA 治疗) 与对照组 25 例 (保守药物治疗)。对比两组手术相关指标、不同时间点心肌损伤 [肌酸激酶同工酶 (CK-MB)、肌钙蛋白 I(cTnI)、N 末端脑钠肽前体 (NT-proBNP)] 及心功能 [左心室射血分数 (LVEF)、左心室舒张末期内径 (LVEDD)、左心室收缩末期内径 (LVESD)] 指标，术后随访 3 个月，统计患者窦性心律转复及心脑血管不良事件 (MACCE) 发生率。

结果：观察组体外循环时间比对照组长，总住院时间比对照组短，差异均有统计学意义 (P < 0. 05)。两组术后血清 CK-MB、cTnI、NT-proBNP 水平均呈现先上升、后下降趋势 (P < 0. 05); 观察组术后 2 h 血清 CK-MB、cTnI、 NT-proBNP 水平均显著高于对照组 (P < 0. 05), 但两组间术后 48 h 上述指标差异均无统计学意义 (P > 0. 05)。术后 3 个月，观察组比对照组 LVEF[(49. 78 ± 2. 35)% vs. (45. 03 ± 2. 17)%] 显著上升 ,LVEDD[(54. 93 ± 4. 30) mm vs. (57. 38 ± 4. 16)mm]、LVESD[(39. 62 ± 4. 37)mm vs. (46. 15 ± 5. 23)mm] 显著下降 (P < 0. 05)。观察组术后第 1 天、出院时及术后 3 个月窦性心律转复率均显著高于对照组 (P < 0. 05), 术后 3 个月内 MACCE 两组对比差异无统计学意义 (P > 0. 05)。

结论：房颤 RA 能有效改善心脏搭桥合并心脏瓣膜手术患者心功能，提高窦性心律转复率，短期预后好，但可能引发一过 性心肌酶上升。

心源性猝死风险分层对肥厚型心肌病合并心房颤动患者导管消融结局预测价值的研究

汤日波 杜卓航 王伟 赵欣 李昌义 喻荣辉 刘念 李松南 刘晓霞 郭雪原 左嵩 李梦梦 刘佟 戴雯莉 黄丽洪 郭琦 高明阳 吕文鹤 李玉昆 王学思 李佳霖 刘筱莹 李心茹 蒋晨曦 桑才华 龙德勇 董建增 马长生

首都医科大学附属北京安贞医院

目的： 肥厚型心肌病的心源性猝死风险预测模型包含多项影响心房颤动（房颤）导管消融结局的因素。本研究探讨不同猝死风险的肥厚型心肌病合并房颤患者行导管消融的疗效和安全性。

方法： 连续纳入 2015 年 1 月至 2023 年 12 月于北京安贞医院行首次房颤导管消融术的肥厚型心肌病患者共 339 例。根据肥厚型心肌病心源性猝死风险预测模型，研究对象被分为低风险组（n=292）和中高风险组（n=47）。比较两组患者导管消融术后的心律失常复发率以及远期预后。

结果： 经过中位随访时间 43.0 [12.0-69.0] 个月后，中高风险组首次消融后的复发率显著高于低风险组（70.2% vs. 41.8%，P < 0.001）。无论是在阵发性房颤亚组还是持续性房颤亚组，中高风险组的复发率均显著高于低风险组（64.3% vs. 42.2%，P=0.014；78.9% vs.41.3%，P=0.008）。最后一次消融后，中高风险组的复发率也高于低风险组（57.4% vs. 32.2%，P < 0.001）。多因素 COX 回归分析显示，中高猝死风险是房颤导管消融术后复发的独立危险因素（HR=1.77，95%CI=1.14 ~ 2.74; P=0.010）。随访期间，低风险组和中高风险组在心源性死亡发生率（6.5% vs. 2.4%，P=0.283）、心力衰竭加重而住院发生率（8.1% vs. 5.5%，P=0.648）和卒中发生率（10.6% vs. 3.8%，P = 0.071）方面无显著差异。

结论： 肥厚型心肌病猝死中高风险与房颤导管消融术后复发率升高相关。

Association between antithrombotic therapy adherence and adverse events after “one-stop” procedures of combined catheter ablation and left atrial appendage closure for atrial fibrillation

null null, Ming-Yu Sun

the General Hospital of Northern Theater Command of the Chinese People’s Liberation Army

Revised Abstract

Objective: The “one-stop” procedure, combining catheter ablation (CA) for atrial fibrillation (AF) with left atrial appendage closure (LAAC), has emerged as a viable therapeutic strategy for non-valvular AF patients at high thromboembolic risk who are unsuitable for long-term oral anticoagulation (OAC). However, robust evidence regarding the correlation between adherence to post-procedural antithrombotic therapy (ATT) and adverse events (AEs) remains limited. This study aimed to comprehensively evaluate the association between ATT adherence and the incidence of adverse events following the “one-stop” procedure.

Methods: A retrospective analysis was conducted on 472 consecutive non-valvular AF patients who underwent a “one-stop” procedure (CA combined with Watchman device implantation) at the General Hospital of Northern Theater Command, Chinese People’s Liberation Army, between January 2019 and June 2023. Comprehensive baseline, perioperative, and clinical follow-up data were systematically collected. Post-operative ATT usage patterns and specific reasons for non-adherence were meticulously recorded. Based on adherence to the prescribed discharge ATT regimen, patients were stratified into two groups: Non-Adherence Group (n=178, 37.7%) and Adherence Group (n=294, 62.3%). ATT adherence status at the time of any AE occurrence was documented, and the correlation between AEs and ATT adherence was rigorously assessed.

Results: The Non-Adherence Group exhibited significantly younger age (Median 64.0 [IQR 57.0-69.0] vs. 66.0 [61.0-70.0] years, P=0.005) and lower CHA2DS2-VASc scores (3.34±1.64 vs. 3.72±1.59, P=0.013) compared to the Adherence Group. However, they demonstrated significantly higher rates of redo ablation (5.62% vs. 1.36%, P=0.008) and BARC ≤ 2 bleeding events, specifically gingival bleeding (25.84% vs. 10.54%, P<0.001), conjunctival bleeding (4.49% vs. 1.02%, P=0.015), and cutaneous bleeding (7.30% vs. 0.34%, P<0.001). Multivariate logistic regression analysis identified redo ablation (OR=0.212, 95% CI=0.064-0.705, P=0.011), gingival bleeding (OR=0.336, 95% CI=0.199-0.569, P<0.001), and cutaneous

bleeding (OR=0.035, 95% CI=0.004-0.278, P=0.001) as significant independent negative predictors of ATT adherence.

Phase-stratified analysis revealed dynamic temporal patterns in AE risk. Overall, patients in the non-adherence phase experienced a 2.3-fold increased risk of serious adverse events (SAEs: stroke, thromboembolism, cardiac tamponade, severe bleeding, all-cause death) compared to those in the adherence phase (OR=0.428, 95% CI=0.199-0.921, P=0.030). Thromboembolic risk (ischemic stroke/systemic embolism) was significantly elevated by 3.7-fold during non-adherence phases (OR=0.362, 95% CI=0.158-0.830, P=0.016). During Phase 1 (0-3 months post-op; OAC), non-adherence was strongly associated with higher bleeding risk (23.81% vs. 3.32%; OR=0.110, 95% CI=0.036-0.339, P<0.001). Paradoxically, during Phase 3 (>6 months post-op; SAPT), adherence was associated with a significantly increased bleeding risk compared to non-adherence (16.42% vs. 7.97%; OR=2.268, 95% CI=1.148-4.479, P=0.018).

Analysis of non-adherence reasons identified patient cognitive factors (misunderstanding, behavioral habits) as the predominant driver across all phases (67%, 73%, 58% in Phases 1, 2, 3 respectively). Non-adherence due to other medical conditions increased notably in Phase 3.

Conclusion: Adherence to ATT following the "one-stop" procedure is associated with a reduced overall risk of SAEs, particularly thromboembolism. However, long-term adherence (specifically in Phase 3 SAPT) is paradoxically associated with an elevated risk of late-phase bleeding events. Factors significantly impairing ATT adherence include younger age, lower CHA2DS2-VASc scores, occurrence of BARC ≤ 2 bleeding events (gingival, cutaneous), undergoing redo ablation procedures, and crucially, patient-related cognitive/behavioral factors. These findings underscore the critical need for implementing individualized ATT regimens tailored to patient-specific risk profiles, incorporating phase-specific monitoring protocols, and instituting early interventions for bleeding events to optimize long-term clinical outcomes after combined CA and LAAC therapy.

Keywords: Adherence; Antithrombotic Therapy; Left Atrial Appendage Closure; "One-Stop" Procedure; Catheter Ablation; Atrial Fibrillation; Serious Adverse Events; Bleeding; Thromboembolism.

The Impact of Sacubitril/Valsartan on Catheter Ablation Therapy Outcomes for Atrial Fibrillation Complicated With Hypertension: A Comprehensive Retrospective Analysis

Zhifu Guo, Rong-Bing Peng, Chao Liu, Jian- Yao, - Dong, Man-Li Yu

Changhai Hospital of Second Military Medical University

The Impact of Sacubitril/Valsartan on Catheter Ablation Therapy Outcomes for Atrial Fibrillation Complicated With Hypertension: A Comprehensive Retrospective Analysis

Zhifu Guo†, Rongbing Peng†, Ke Li†, Jianhan Yao, Chao Liu, Feifei Dong, Manli Yu

Department of Cardiovascular Medicine, Changhai Hospital, Naval Medical University, No. 168, Changhai Road, Yangpu District, Shanghai 200433, China

†These authors share first authorship

Zhifu Guo: Email address: guozhifu@126.com

Rongbing Peng: pengrb1995@126.com

Chao Liu: liuchao19960416@163.com

Jianhan Yao: 398231564@qq.com

Feifei Dong: feifdong@outlook.com

Manli Yu: yumanli2006@163.com

*Correspondence authors

Zhifu Guo

Department of Cardiology, Changhai Hospital, Naval Medical University

168 Changhai Road, Shanghai, China, 200433, China

Email address: guozhifu@126.com

and

Manli Yu

Department of Cardiology, Changhai Hospital, Naval Medical University

168 Changhai Road, Shanghai, China, 200433, China

Email address: yumanli2006@163.com

[Abstract]**Background:** Atrial fibrillation (AF) is one of the most common type of arrhythmias, which is an important cause of ischemic stroke and heart failure. CA is considered as a first-line treatment for symptomatic atrial fibrillation, but there is still a certain recurrence rate, because of atrial structural and/or electrical remodeling and autonomic nervous system dysfunction. Studies have shown that atrial remodeling after activation of renin-angiotensin-aldosterone system (RAAS) is one of the main causes of AF occurrence. Angiotensin II (Ang II) is the main mediator in RAAS which can contribute to atrial fibrosis, and patients with higher level of Ang II in peripheral blood usually have a higher incidence of AF. Previous studies have shown that Sacubitril/Valsartan(Sac-Val) may reverse atrial remodeling in patients with atrial fibrillation(AF) complicated with hypertension. The purpose of this study is to detect the efficacy of Sac-Val and angiotensin converting enzyme inhibitor(ACEI)/angiotensin receptor blocker(ARB) in the treatment of AF by catheter ablation(CA), in order to evaluate the impact of Sac-Val on sinus rhythm maintenance and recurrence after CA. **Methods and Results:** This study has retrospectively enrolled 202 patients with AF and hypertension, who had undergone CA between January 2021 to April 2023. All eligible patients were divided into Sac-Val group (n = 104) and ACEI/ARB group (n = 98) according to whether they received Sac-Val after ablation. In patients with persistent AF (Per-AF), there were significant differences in the AF recurrence with Sac-Val (47.22% vs 17.65%, P=0.005), N-terminal pro-brain natriuretic peptide (NT-proBNP) (223.46±94.94 vs 121.31±105.96, P < 0.001), left atrial diameter (LAD) (4.08±0.42 vs 3.75±0.36, P=0.002), and left ventricle ejection fraction (LVEF) (58.91±3.64 vs 63.04±4.36, P < 0.001). Compared with ACEI/ARB, patients treated with Sac-Val had higher AF-free survival probability. Logistic regression analysis showed that Sac-Val was a risk factor for reducing the recurrence of Per-AF after CA. In patients with paroxysmal AF (Par-AF), there was no significant difference in LAD, LVEF, NT-proBNP, recurrence of AF whether Sac-Val used or not. **Conclusion:** Sac-Val can improve the cardiac structure and function of patients with AF, reduce the recurrence rate after CA in Per-AF. Sac-Val is a risk factor for reducing recurrence of Per-AF after CA.

Keywords Sacubitril/Valsartan; Atrial Fibrillation; Catheter Ablation; Hypertension

What Is New?

1. Sac-Val can improve left atrial (LA) structure in patients with Per-AF after CA.

2. Sac-Val can reduce the recurrence in patients with Per-AF who undergone with CA.

3. The above results were not observed in Par-AF.

导管消融对心房颤动合并功能性瓣膜反流预后的危险因素分析

郭志福 彭荣兵 刘超 姚建晗 倪铭

第二军医大学附属长海医院

研究目的：

探究功能性瓣膜反流的相关危险因素以及 AF 合并 FVR 导管消融术后复发的危险因素，探讨导管消融对 AF 合并 FVR 预后的影响。

研究方法：

本研究连续回顾性纳入从 2022 年 8 月至 2023 年 12 月期间于我院心血管内科首次接受导管消融术的心房颤动患者。系统收集患者的基线临床资料，术后于 3 月、6 月、12 月于我院门诊随诊，完善并记录随访超声心动图、心电图、动态心电图及 NT-ProBNP 结果。分析患者基线资料差异，采用 Logistic 回归分析探讨 FMR/FTR 的危险因素。根据是否复发将患者分为复发组和窦性心律组，采用多因素 COX 比例风险回归模型，分析 AF 合并 FMR/FTR 患者消融术后复发的独立危险因素。通过 Kaplan-Meier 生存曲线评估 FMR/FTR 严重程度对 AF 患者消融术后复发时间的影响。

结果：

本研究共纳入我院行 AF 射频消融的患者 572 例，平均随访时间 10.44±3.83 月。共纳入无或轻度功能性瓣膜反流（None to Mild Functional Valvular Regurgitation, NM-FVR）组患者 390 例，FMR/FTR 患者 182 例，与 NM-FVR 组相比，AF 合并 FMR/FTR 的患者中持续性 AF 的比例明显增高（71.43% vs 28.72%，P<0.001）。在消融方式选择上，FMR/FTR 组患者接受射频消融的比例显著高于冷冻消融（P=0.005）。相较于 NM-FVR 组患者，FMR/FTR 组患者的 NT-ProBNP 水平明显更高（637.20±576.92ng/L vs. 298.78±429.63ng/L）、LVEF 水平显著降低（59.00±7.72% vs. 62.15±5.38%）、左心房容积（Left Atrial Volume, LAV）、左心房前后径（Left Atrial Diameter, LAD）明显增大，均为 P<0.05。Logistic 回归分析显示年龄、持续性 AF、LAV 是 FMR/FTR 的独立相关因素。

结论：

AF 合并 FMR/FTR 组患者导管消融术后 AF 复发率较 NM-FVR 组明显升高，其术后无房颤生存时间较 NM-FVR 明显缩短。LAV、持续性是 AF 合并 FMR/FTR 患者术后复发的独立预测因子。

A simplified multislice computed tomography image integration-guided procedure in catheter ablation of atrial fibrillation

Zhuo Wang, Song-Yun Wang, Hui Chen, Hui-Hui Hu

Renmin hospital of Wuhan University

This study investigated the feasibility and safety of a simplified multislice computed tomography (MSCT) image integration-guided procedure for catheter ablation of atrial fibrillation (AF).MSCT imaging of the left atrium (LA) and pulmonary veins (PVs) in the post-absorptive state within 7 days before RF ablation. The mean distance between image and the electroanatomic map was only 2 mm, accurately depicting the anatomy of the left atrium and the pulmonary veins and allowing accurate visualization of the catheter position on real surface anatomy during the ablation procedure. Also, complications can be avoided to some extent by integrating preprocedural acquired MSCT images and the 3D mapping images. 472 consecutive patients with paroxysmal or persistent AF were included. The atrial model constructed from MSCT images was then integrated to the PV models to guide ablation. A circular mapping catheter was placed in pulmonary veins (PV) to generate the PV electroanatomic models using the Carto® 3 mapping system. After the models of four PVs (left superior, left inferior, right superior and right inferior PVs) were all created, the atrial model generated from the MSCT images acquired before procedure were displayed next to the PV models. The atrial MSCT model was then manually moved and rotated in several directions to make it fit well with all the four PV models. The accuracy of the integrated LA model was further confirmed by examining the contact force on the edges of this model using the ablation catheter (THERMOCOOL SMARTTOUCH Navigation Catheter, Biosense Webster (Israel) Ltd., Yokneam, Israel) and moving the catheter through the atrium and assessing its relationship to well-recognized landmarks (e.g., PVs and left atrium appendage). These processes took only a few minutes and could accurately fit the atrial MSCT model to the real 3-D location, which was critical to the precise ablation later. Procedural outcomes were recorded, and complications were assessed. PV antrum isolation (PVI) was performed in all patients. PVI was achieved by ablation around the large circumference of left or right PV antrum, which encircled all PV ostia on the left or right side. The procedural end point of electrical PVI was LA-PV entrance block as proved by complete elimination of all PV potentials on the electrophysiological recording system. And the complete electrical isolation was then reconfirmed by mapping of residual potentials around the entire circumference of the PV antrum. If sinus rhythm was not restored after complete PVI, additional linear ablations (e.g. a left atrial roof line, a mitral isthmus line, etc.) were further performed. If AF termination was not achieved, sinus rhythm was then restored by electrical cardioversion.

A total of 266 patients (202 paroxysmal and 64 persistent) were followed 24 months after ablation. Electrophysiological end points were achieved in all patients. The whole procedure time was 80±22 min with an ablation time of 34±5 min. The fluoroscopy time was 10.7±1.9 min and the radiation dose per procedure was 719±200 mGy. In conventional operation PVI alone was reported to have a procedure time of 167~187 min and an ablation time of around 82 min. The total procedure time (80±22 min) and ablation time (34±5 min) were both evidently shortened compared with conventional operation. After a follow-up of 24 months, 163 patients from paroxysmal AF (80.7%) and 23 patients from persistent AF (35.9%) were free from atrial tachyarrhythmias.

The simplified MSCT image integration procedure for catheter ablation of AF needed only the electroanatomic mapping of PVs. The integration of PV models with MSCT images was easy to maneuver and could provide a clear view of the inner face of the atrium, which was critical for precise ablation. This procedure was highly effective, time-saving and safe, which might be worthy of more extensive application. This simplified MSCT image integration-guided ablation is an effective, time-saving and safe procedure for catheter ablation of paroxysmal AF.

BRD4 通过 P53/PAI-1 途径诱导衰老心房 纤维化促心房颤动发生的机制研究

易宏 薛玉梅 饶芳 刘慧意

广东省心血管病研究所

目的：心房结构重塑和电重塑是心房颤动（简称“房颤”，Atrial fibrillation，AF）发生发展的病理生理机制。心房结构重塑包括心房纤维化和心房扩大，而心房

纤维化是心房结构重塑的重要特征和 AF 维持的基质，衰老与心房纤维化密切相关。BRD4 是 BET 家族的一员，在表观遗传调控、转录控制和染色质结构维护中有多方面的作用。BRD4 可能通过调控 p53 参与细胞衰老，可能通过 TGF-β 诱导纤维化，但具体机制尚不明确。本研究旨在探讨 BRD4 诱导心房纤维化及促 AF 发生的机制。

方法：

1. 人心房组织获取：本研究经过广东省人民医院伦理委员会批准(No.GDREC20160128H)。心耳组织取自广东省人民医院心脏外科进行体外循环手术或胸腔镜手术的患者。将心耳进行原代细胞培养，培养至第 3 代及（P3）第 11 代 (P11)，建立衰老细胞模型，用于后续实验。

2. 动物实验：C57/BL6 小鼠在无病原体条件下饲养，饲养在温度和湿度受控的环境中，光照 / 黑暗周期为 12 小时，自由进食和饮水，直至 18-20 月龄，建立

小鼠衰老模型。将 32 只小鼠随机分为 4 组。其中 3 组（每组 8 只小鼠）从 17 月龄至 18 月龄接受 JQ1 溶液尾静脉注射，50 或 100 mg/kg BID，或等量生理盐水作为安慰剂。8 只 5 月龄小鼠作为青年组，亦注射等量生理盐水。使用 iWorx 数摘 要据采集和分析系统记录和分析小鼠的体表 ECG 和心内电图。

3. 小鼠细胞实验：从 C57BL/6 小鼠（3 周龄）的心耳中分离原代小鼠心房成纤维细胞。传代至 P3 及 P11 用于细胞实验。对 P3 细胞过表达 BRD4、P53 及

PAI-1，对 P11 细胞敲低 BRD4 及 PAI-1，或使用 JQ1 抑制 BRD4。

4. 人心房成纤维细胞实验：将获得的人心房成纤维细胞，对 P3 细胞过表达 BRD4、P53 及 PAI-1，P11 敲低 BRD4 及 PAI-1 或使用 JQ1 抑制 BRD4。用人 BRD4 和 PAI-1 特异性的 shRNA 质粒转染人心房成纤维细胞，敲低基因表达。

5. 对处理后细胞进行 β- 半乳糖苷酶染色及免疫荧光检查，对小鼠组织进行 Masson 三色染色。

6. 蛋白质免疫印迹分析及 CO-IP：在 RIPA 裂解缓冲液中均质化心房成纤维细胞或心房组织，进行蛋白质免疫印迹分析。

结果：

（1）对比人 P3 心房成纤维细胞，P11 人心房成纤维细胞的 BRD4/p53/PAI-1 及细胞相关纤维化蛋白的表达升高。BRD4 与 p53 共定位，提示二者存在相互作

用；（2）RNAi 技术敲低以及用 JQ1 抑制人及小鼠（P11）心房成纤维细胞的 BRD4 表达降低，p53/PAI-/p21 及细胞相关纤维化蛋白的表达下调，细胞衰老程

度减轻；（3）过表达人及小鼠 P3 的心房成纤维细胞 BRD4 表达，p53/PAI-1/p21 及细胞相关纤维化蛋白表达量升高，细胞衰老程度加重；同时过表达 p53，PAI-1/p21 及细胞相关纤维化蛋白表达增加；（4）敲低人及小鼠 P11 细胞 PAI-1 可以使细胞相关纤维化蛋白及 TGF-β 的表达量降低；过表达人及小鼠 P3 细胞 PAI-1 可以使细胞相关纤维化蛋白升高，但 TGF-β 表达量仍降低；（5）年老小鼠相较于年轻小鼠的心房组织 BRD4/p53/PAI-1 及细胞相关纤维化蛋白的表达量更高；（6）年老小鼠 AF 诱发率高于年轻小鼠（71.4%VS12.5%，P<0.01），且持续时间明显延长，应用 JQ 1 抑制 BRD4 表达后年老小鼠的 AF 诱发率下降为 28.7%。

结论：

BRD4 可诱导衰老相关的心房纤维化，AF 易感性增加；BRD4 可能通过 p53/PAI-1 信号途径促进 AF 发生。

Neutrophil-to-lymphocyte ratio and blood pressure control status stratify atrial fibrillation recurrence risk in hypertensive patients after ablation

Zixi Zhang, Yi-Chao Xiao, Tao Tu, Qi-Ming Liu

The Second Xiangya Hospital of Central South University

Background

Atrial fibrillation (AF) is the most common arrhythmia encountered in clinical practice and is associated with an increased risk of thromboembolic events, particularly stroke. Catheter ablation has emerged as a standard therapy for rhythm control in patients with symptomatic AF, particularly in those with hypertension. However, despite the benefits of catheter ablation, the recurrence of AF remains a significant challenge, especially in hypertensive patients. Hypertension is known to increase the risk of AF recurrence due to the impact it has on atrial remodeling, but reliable predictors of recurrence following catheter ablation are still lacking. The identification of early and effective biomarkers to predict AF recurrence is essential to improving patient outcomes, guiding therapeutic interventions, and refining post-ablation management. One such potential marker that has garnered attention in recent years is the neutrophil-to-lymphocyte ratio (NLR), a simple, cost-effective marker of systemic inflammation. This study aims to investigate the predictive value of NLR for AF recurrence, particularly in patients with hypertension.

Objective

This study sought to assess the role of NLR as a predictor of AF recurrence following catheter ablation in hypertensive patients. Specifically, the study aimed to evaluate whether NLR could predict recurrence, determine an optimal threshold for prediction, and assess the impact of hypertension control on this relationship.

Methods

This was a retrospective cohort study that included patients who underwent catheter ablation for AF and had a history of hypertension. The primary outcome was the recurrence of AF after ablation, defined as a documented episode of AF lasting more than 30 seconds, detected via ECG or Holter monitoring. Baseline NLR was calculated using pre-ablation blood samples, and patients were followed for a median duration of 12 months.

Cox regression models were utilized to examine the association between NLR and the risk of AF recurrence, adjusting for potential confounders

including age, sex, body mass index (BMI), and hypertension control status. Restricted cubic splines (RCS) were used to explore the non-linear relationship between NLR and AF recurrence, allowing for the identification of an optimal threshold. Receiver operating characteristic (ROC) curves were generated to evaluate the predictive accuracy of NLR for AF recurrence, and interaction and joint analyses were performed to assess the effect of blood pressure control on the relationship between NLR and recurrence. Mediation analysis was conducted to explore the potential role of inflammation in mediating the association between hypertension and AF recurrence.

Results

Of the 350 patients included in the analysis, AF recurrence occurred in 17.94% (n=63) of patients during the follow-up period. The baseline NLR was significantly higher in patients with recurrence compared to those without. The univariate Cox regression analysis demonstrated that higher NLR was associated with an increased risk of AF recurrence. Specifically, for each unit increase in NLR, the hazard ratio (HR) for AF recurrence was 1.30 (95% CI: 1.12–1.50, P <0.001), indicating that a higher NLR was an independent predictor of recurrence.

RCS analysis revealed a non-linear relationship between NLR and the risk of AF recurrence, with a threshold value of 2.37. Above this threshold, the risk of recurrence significantly increased. Patients with an NLR ≥ 2.37 had a 1.5-fold higher risk of recurrence compared to those with an NLR

Furthermore, no significant interaction effect was found between NLR and blood pressure control status. However, a subgroup analysis revealed that patients with both high NLR (≥ 2.37) and uncontrolled hypertension had the highest risk of AF recurrence, with an HR of 3.92 (95% CI: 1.82–8.42, P

Conclusions

The NLR is a reliable and easily measurable predictor of AF recurrence in hypertensive patients following catheter ablation. An NLR ≥ 2.37 is associated with a significantly increased risk of recurrence, particularly when combined with uncontrolled hypertension. These findings underscore the importance of integrating anti-inflammatory strategies alongside optimal blood pressure control in managing AF patients at high risk for recurrence. Future prospective studies are needed to further validate these findings and evaluate the efficacy of targeted anti-inflammatory therapies in preventing AF recurrence. The role of NLR as a simple, cost-effective biomarker may enhance clinical decision-making, allowing for personalized risk stratification and better management of AF recurrence in hypertensive patients.

Cryoballoon ablation for patients with atrial fibrillation and heart failure with preserved ejection fraction: A systematic review and meta-analysis

Zixi Zhang, Yi-Chao Xiao, Jia-Yi Zhu, Tao Tu, Qi-Ming Liu

The Second Xiangya Hospital of Central South University

Background

Atrial fibrillation (AF) and heart failure with preserved ejection fraction (HFpEF) represent two of the most significant challenges in contemporary cardiovascular medicine. Both conditions are becoming increasingly prevalent, particularly in the aging population, and are often coexisting in patients. AF is the most common arrhythmia, significantly contributing to stroke, mortality, and morbidity, while HFpEF, which is characterized by the preservation of left ventricular ejection fraction despite symptoms of heart failure, continues to present a diagnostic and therapeutic challenge. Despite advancements in pharmacological treatment, both AF and HFpEF are associated with poor long-term outcomes, including hospitalizations, decreased quality of life, and increased risk of mortality. Traditional pharmacological therapies, including rate and rhythm control strategies, have been shown to have limited efficacy, with considerable side effects. These limitations have prompted the exploration of non-pharmacological approaches, such as catheter ablation (CA), to manage these conditions more effectively. Among the various ablation techniques, cryoballoon ablation (CBA) has emerged as a promising method for rhythm control, particularly in patients with paroxysmal AF. However, its role in patients with concomitant HFpEF has been less thoroughly investigated. Therefore, this meta-analysis aims to assess the safety and efficacy of CBA in patients with AF and HFpEF.

Methods

This meta-analysis evaluates studies that assessed the outcomes of CBA in patients diagnosed with both AF and HFpEF. The literature search was conducted up until April 2024, focusing on human studies that reported essential baseline clinical data, including AF recurrence rates, levels of N-terminal pro-B-type natriuretic peptide (NT-pro BNP), left atrial diameter (LAD), and left ventricular ejection fraction (LVEF). The primary objective was to assess the short-term effects of CBA on AF burden, while secondary outcomes included changes in NT-pro BNP levels, LAD, LVEF, and the incidence of procedure-related complications. Studies included in the analysis were required to report on both clinical outcomes and safety parameters, such as phrenic nerve palsy, which is the most common complication associated with CBA.

Results

Seven studies were included in the analysis, with a total of 948 patients. These studies predominantly involved patients with paroxysmal AF and indications for anticoagulation therapy. Interestingly, only 59.2% of patients received anticoagulation treatment, indicating that a significant portion of the cohort was not optimally managed in terms of stroke prevention. The results from the meta-analysis showed that CBA effectively reduced the burden of AF in the short term, as evidenced by decreased AF recurrence rates. Additionally, NT-pro BNP levels, a marker for heart failure severity, were significantly reduced post-procedure, suggesting that CBA may alleviate the strain on the heart in patients with HFpEF. However, no significant improvements were observed in left atrial diameter (LAD) or left ventricular ejection fraction (LVEF) after CBA, indicating that while the procedure may be beneficial for controlling rhythm, it does not result in substantial structural or functional improvements in the heart. The incidence of complications related to CBA was relatively low, with phrenic nerve palsy being the most common adverse event. Other complications, such as esophageal injury and pericardial effusion, were rarely reported.

Conclusion

Cryoballoon ablation (CBA) is a safe and effective procedure for patients with AF and HFpEF, providing short-term benefits in terms of reducing AF recurrence and alleviating heart failure symptoms as evidenced by decreased NT-pro BNP levels. However, it does not appear to improve the structural remodeling of the left atrium or left ventricular function, as indicated by unchanged LAD and LVEF. While the complication rate remains low, phrenic nerve palsy remains a notable concern. Given the mixed results regarding the long-term benefits, further large-scale, well-designed randomized controlled trials are needed to validate the efficacy and safety of CBA in patients with AF and HFpEF. Future studies should also investigate whether combining CBA with other therapies could further improve outcomes in this high-risk population.

Explore potential targets and mechanisms of Diabetes mellitus with Atrial fibrillation by bioinformatics analysis

zhang yujie

Department of Cardiology, General Hospital of Northern Theatre Command

Objective: As the population ages and the survival period for chronic diseases extends, the burden of diabetes (DM) and atrial fibrillation (AF) is escalating rapidly. While DM is acknowledged as a risk factor for AF, the underlying mechanisms by which DM induces AF remain poorly understood. In recent years, bioinformatics analysis has emerged as a powerful tool for investigating genetic alterations and identifying novel biomarkers across various diseases. Furthermore, the advancement of numerous public databases, such as the Gene Expression Omnibus (GEO), has significantly facilitated transcriptomics and genomics research. Utilizing these public platforms, we employ bioinformatics analysis to investigate the comorbidity genes associated with DM and AF, thereby enhancing our understanding and providing new insights for the prevention and treatment of DM and AF.

Method: We retrieved datasets pertaining to DM and AF from the GEO database. Limma, a differential expression screening technique using a generalized linear model, was employed via the R package limma (version 3.40.6) to identify DEGs in each dataset. For DM , DEGs were screened with criteria of |log2FC| ≥ 1.5 and P<0.05, while for AF, the criteria were |log2FC| ≥ 2.0 and P<0.05. RStudio was used to create volcano plots and heatmaps. Venny 2.1.0 identified overlapping DEGs between DM and AF for further functional enrichment analysis. GO and KEGG were utilized to annotate genes and explore biological functions and pathways. Metascape analyzed GO enrichment and KEGG pathways for these overlapping genes, focusing on key molecular processes and signaling pathways. To enhance the visualization of the relationships among these overlapping genes, limit the maximum number of interactors to 10. Subsequently, import the resulting PPI network data into Cytoscape software version 3.7.2 for visualization purposes. Key genes, typically identified as those with the highest degree of interaction, are likely to play a pivotal role in the pathogenesis of these diseases.

Result: In our study, 101 DEGs were identified by analyzing and integrating the expression profiles of two genes, GSE23561 and GSE14975. The functional enrichment analysis suggested that ribosome biogenesis may play a role in the comorbidity of DM and AF. The construction of the PPI network indicated that the comorbidity of DM and AF is potentially associated with a hub gene, RPS9. Previous research indicates that RPS9 is crucial in various diseases, with its expression linked to disease progression. In non-small cell lung cancer, high RPS9 levels correlate with poor prognosis, promoting cancer via STAT3 and ERK pathways. In acute myeloid leukemia, RPS9 interacts with LAPTM4B to stabilize itself, activating

STAT3 and advancing leukemia. RPS9 is also upregulated in osteosarcoma, enhancing tumor growth through the MAPK pathway. These findings suggest RPS9's role in cancers might involve a shared signaling pathway, hinting at its potential involvement in cardiovascular and cerebrovascular diseases by influencing cell proliferation, apoptosis, and signaling. While research on the specific mechanisms of RPS9 in cardiovascular and cerebrovascular diseases remains limited, findings from studies on other diseases offer valuable insights.

Conclusion: Ribosome-related genes have been implicated in the pathogenesis of diabetes with atrial fibrillation, and RPS9, as a pivotal gene, may underlie the comorbidity of these conditions. Future investigations should aim to elucidate the precise role of RPS9 in the context of diabetes with atrial fibrillation, thereby potentially identifying novel targets and strategies for the diagnosis and treatment of these diseases.

A Comparative Analysis of the Prognostic Value of Multiple Atrial Fibrillation Prognostic Scoring Systems for Recurrence in Patients with Non-Paroxysmal Atrial Fibrillation Undergoing Pulmonary Vein Isolation Alone

Lin-Xin Guan, Fei-Long Zhang

Department of Cardiology, Fujian Medical University Union Hospital

OBJECTIVES Pulmonary vein isolation (PVI) serves as the cornerstone of catheter ablation for treating atrial fibrillation (AF), aiming to eliminate abnormal electrical triggers originating from the pulmonary veins. Nevertheless, a substantial proportion of patients experience AF recurrence post-ablation, with this issue being particularly pronounced in the non-paroxysmal atrial fibrillation (non-PAF) population—characterized by more persistent arrhythmias and often more complex underlying cardiac conditions, which contribute to higher recurrence risks. To date, over a dozen prognostic models have been developed to predict post-ablation recurrence, each incorporating different combinations of clinical, electrocardiographic, or imaging parameters. Against this backdrop, the present study seeks to compare the prognostic performance of these multiple scoring systems specifically in non-PAF patients who underwent PVI alone, with the goal of identifying the most reliable tool for guiding clinical decision-making.

METHODS A single-center retrospective study was conducted, enrolling 166 patients with non-paroxysmal atrial fibrillation (non-PAF) who underwent their first pulmonary vein isolation (PVI) alone, with a female proportion of 22.3% and a mean age of 60 ± 9 years. All participants met the diagnostic criteria for non-PAF and had no history of previous atrial fibrillation ablation. Clinical data collected included baseline information (such as medical history, medication use, and laboratory test results), as well as imaging data: transthoracic echocardiography (TTE) was used to assess parameters like left atrial diameter and left ventricular ejection fraction, while either cardiac computed tomography (CT) or transesophageal echocardiography (TEE) was performed to evaluate pulmonary vein anatomy and rule out left atrial thrombus. Based on these collected data, 11 commonly used prognostic risk scores were calculated for each patient, including APPLE, BASE-AF_2, C2HEST, CAAP-AF, CHA_2DS_2-VASc, $CHADS_2$, DR-FLASH, HATCH, MB-LATER, PAT_2C_2H, and SCALE-CryoAF—all of which are widely applied in clinical practice to predict recurrence after atrial fibrillation ablation, integrating multiple dimensions such as age, gender, comorbidities (e.g., hypertension, diabetes), and cardiac structural indicators.

RESULTS Atrial fibrillation recurrence after a 90-day blanking period was observed in 41 patients (24.7%), 24 (51.8%) in the cryo-balloon ablation (CBA) subgroup, and 17 (48.2%) in the radiofrequency ablation (RFCA) subgroup. BASE-AF_2 (AUC=0.666, 95%CI 0.572- 0.759, P=0.001), MB-LATER (AUC = 0.734, 95%CI 0.646-0.821, P<0.001) and SCALE-CryoAF (AUC=0.702, 95%CI 0.600-0.804, P<0.001) had better prognostic value for atrial fibrillation recurrence. By propensity score matching, MB-LATER (AUC=0.734, 95%CI 0.570-0.899, P=0.019) was found to have a better prognostic value for recurrence in the cryo-balloon ablation subgroup than other prognostic scoring systems. BASE-AF_2 (AUC=0.758, 95%CI 0.578-0.937, P=0.013) had a better prognostic value for recurrence in the radiofrequency ablation subgroup than other prognostic scoring systems.

CONCLUSIONS Among the multiple prognostic scoring systems evaluated, the BASE-AF_2, MB-LATER, and SCALE-CryoAF scoring systems consistently demonstrated superior prognostic value in predicting recurrence risk in non-paroxysmal atrial fibrillation (non-PAF) patients who underwent pulmonary vein isolation (PVI) alone, showing better discriminative ability and clinical applicability in this patient cohort. Further subgroup analysis based on ablation modality revealed that in non-PAF patients who underwent PVI alone via cryo-balloon ablation—characterized by its unique tissue interaction and lesion formation mechanism—the MB-LATER scoring system emerged as the preferred tool for prognostic assessment of recurrence risk, likely due to its incorporation of parameters more closely aligned with the physiological and procedural features of cryo-ablation. In contrast, for non-PAF patients who underwent PVI alone via radiofrequency ablation, which relies on thermal energy for lesion creation, the BASE-AF_2 scoring system was identified as the optimal choice for predicting recurrence risk, potentially attributable to its inclusion of factors that better reflect the biological and procedural nuances of radiofrequency-based ablation. These findings may provide actionable guidance for clinicians in selecting the most appropriate prognostic tool based on the specific ablation modality used, thereby enhancing personalized risk stratification and management of non-PAF patients post-PVI.

Remimazolam-Flumazenil versus Propofol for procedural sedation in patients undergoing electrical cardioversion: A prospective randomized controlled trial.

Zhifu Guo, Xin-Miao Huang, Chao Liu

长海医院

Abstract

Background

Direct current cardioversion (DCC) is a well-established and effective procedure for restoring sinus rhythm in patients with atrial fibrillation, offering advantages over antiarrhythmic drugs such as higher success rates, rapid onset, and lower proarrhythmic risk. However, DCC is associated with significant pain, necessitating procedural sedation that balances three critical requirements: adequate depth of sedation to ensure patient comfort, rapid recovery of consciousness to minimize post-procedural monitoring time, and preservation of cardiovascular and respiratory stability. Currently used sedatives, such as propofol, while effective in inducing sedation, are often limited by adverse effects including hypotension, respiratory depression, and variable recovery times. Remimazolam, a novel ultra-short-acting benzodiazepine, exerts its sedative effects through GABA-A receptor modulation and has demonstrated promise in procedural sedation due to its favorable pharmacokinetic profile—including minimal injection pain, reduced cardiovascular and respiratory depression, and rapid reversibility with flumazenil. Despite its increasing use in endoscopy and dental procedures, data on remimazolam's efficacy and safety in DCC remain limited, highlighting the need for comparative studies with established agents like propofol.

Aims

This prospective randomized controlled trial aimed to compare the efficacy and safety of remimazolam (reversed with flumazenil) versus propofol for procedural sedation in patients undergoing DCC. The primary objective was to evaluate differences in sedation recovery time (SRT), with secondary assessments including sedation induction time (SIT), hemodynamic stability (heart rate [HR], mean arterial pressure [MAP], and oxygen saturation [SpO_2]), and the incidence of adverse events.

Methods

The study enrolled 82 patients with atrial fibrillation requiring DCC after catheter or cryoballoon ablation, conducted at Changhai Hospital between June 2024 and October 2024. Patients were randomized to either the remimazolam-flumazenil group (R-F group, n=41) or the propofol group (P group, n=39), with two patients excluded from the P group due to refractory hypotension and multiple cardioversions. Inclusion criteria included age ≥ 18 years, planned DCC, and signed informed consent; exclusions included ASA class IV status, history of epilepsy or myasthenia gravis, severe hepatic/renal dysfunction (eGFR <30 ml/min·1.73m²), and BMI ≥ 32 kg/m². The study was approved by the institutional ethics committee and conducted in accordance with the Helsinki Declaration.

All patients fasted for 8 hours pre-procedure, with continuous monitoring of ECG, HR, MAP, and SpO_2, and received 3L/min nasal oxygen. Sedation protocols were as follows:

R-F group: Remimazolam (diluted to 1mg/ml) was administered at an initial dose of 0.1mg/kg over 30 seconds, with additional 2.5mg doses every minute (maximum 5 doses) until a Ramsay score ≥ 5 was achieved. Immediately after successful DCC, flumazenil (0.5mg initially, with 0.2mg increments as needed, maximum 1.0mg) was given to reverse sedation to a Ramsay score of 2.

P group: Propofol (10mg/ml) was administered at an initial dose of 0.8mg/kg over 30 seconds, with 20mg increments every 2 minutes until a Ramsay score ≥ 5 was reached.

Primary endpoints included SRT (time from sedative administration to recovery of consciousness, defined as Ramsay score=2). Secondary endpoints included SIT (time from sedative administration to loss of consciousness, defined as Ramsay score ≥ 5). Safety endpoints included changes in HR, MAP, and SpO_2 at predefined time points (T0: baseline; T1-T20: 1 to 20 minutes post-induction) and adverse events (bradycardia, hypotension, respiratory depression, involuntary movements, delirium).

Results

Baseline characteristics were comparable between groups, with no significant differences in age, gender, CHA_2DS_2-VASc scores, comorbidities (hypertension, diabetes, stroke), or baseline hemodynamics (all P>0.05).

Hemodynamic changes showed an overall decrease in MAP from T0 to T20 in both groups, but the P group exhibited significantly lower MAP at T5 (97.95±15.69 vs. 105.95±15.70 mmHg, P<0.05). SpO_2 declined from T0 to T1 in both groups but remained significantly lower in the P group at T3, T5, and T9 (all P<0.05). HR decreased slightly from baseline in both groups, with no significant between-group differences at any time point (P>0.05).

Efficacy outcomes revealed no significant difference in SIT between groups (P group: 63.71±43.44s vs. R-F group: 52.52±24.36s, P=0.157). However, SRT was significantly shorter in the R-F group (162.62±71.73s vs. P group: 349.32±149.02s, P<0.001).

Adverse events were significantly more common in the P group (17/39 vs. R-F group: 6/41, P=0.004). Specifically, respiratory depression (8/39 vs. 2/41, P=0.035) and hypotension (9/39 vs. 3/41, P=0.048) were more frequent in the P group, while involuntary movements and delirium showed no significant differences.

Conclusion

Remimazolam, when reversed with flumazenil, provides effective and safe procedural sedation for DCC, offering significant advantages over propofol. Key benefits include shorter sedation recovery time, reduced cardiovascular and respiratory depression, and a lower incidence of adverse events. These findings support remimazolam-flumazenil as an ideal sedation strategy for DCC, balancing efficacy, safety, and rapid recovery to enhance patient outcomes and procedural efficiency.

Keywords: Direct current cardioversion; procedural sedation; propofol; remimazolam; flumazenil; hemodynamic stability.

在 CHA2DS2-VASc 评分基础上构建列线图预测心房颤动患者消融术后的复发

蒋林倩 张飞龙

福建医科大学附属协和医院心内科

目的：通过对心房颤动（Atrial Fibrillation，AF）消融术后复发危险因素进行单因素和多因素分析筛选相关的预测因子，在 CHA_2DS_2-VASc 评分基础上开发列线图模型以预测 AF 消融术后的复发情况，并验证模型预测能力和临床适用性，个体化评估房颤术后复发的风险。

方法：纳入 2019 年 6 月至 2021 年 6 月期间就诊于我院并首次行经导管消融术的症状性心房颤动患者共 398 例。收集纳入患者的临床基线资料和检验、检查数据，手术记录及患者术后随访 12 个月的复发情况。根据患者的复发情况分为复发组和非复发组，采用单因素分析和 COX 多因素回归分析选取与 AF 消融术后复发显著相关的预测因子。在 CHA_2DS_2-VASc 评分基础上联合 COX 多因素回归分析结果得出的预测因子构建列线图预测模型，评估列线图的预测能力和适用性。同时对不同房颤类型及不同术式的亚组进行该列线图模型的预测价值检验。

结果：共有 398 例患者完成随访。其中，阵发性房颤 260 例，持续性房颤 138 例。复发组 81 例，非复发组 317 例。

1、 两组单因素分析结果提示复发组的房颤病程、空白期复发、中性粒细胞计数（NE）、中性粒细胞 / 淋巴细胞比值（NLR）、红细胞分布宽度（RDW）、左房前后径（LAD）显著高于非复发组（$p < 0.05$）。

2、 两组 COX 多因素回归分析提示房颤病程、空白期复发、NE、NLR、LAD 是预测 AF 消融术后复发相关的独立预测因子。

3、 进行 Kaplan-Meier 分析：房颤病程、NE、NLR、LAD 不同分层对患者复发的影响 p 值均小于 0.05，具有统计学差异。房颤病程越长，AF 发生消融术后复发的风险越高；当 NE > $3.54*10^9$ /L、NLR > 1.24、LAD > 36.75 mm 时，AF 发生消融术后复发的风险较高。

4、 根据上一步结果，基于 CHA_2DS_2-VASc 评分、房颤病程、NLR、LAD 构建 AF 患者导管消融术后复发的列线图预测模型。列线图提示随着房颤病程的延长、NLR 及 LAD 增大、CHA_2DS_2-VASc 评分≥ 2 分，总得分逐渐增大，可预测 AF 消融术后复发概率越高。其中 NLR 得分为 100 分，LAD 得分为 40 分，房颤病程得分为 20 分，CHA_2DS_2-VASc 评分得分为 15 分，总分范围为 0-180 分。校准曲线得出该列线图在实际观察结果和预测之间有着较佳的一致性。列线图模型的一致性指数（C-index）为 0.707（95%CI=0.566-0.847），明显高于 CHA_2DS_2-VASc 评分（C-index=0.499；95%CI=0.359-0.640）。根据 DCA 决策曲线图可得出：列线图预测模型与 CHA_2DS_2-VASc 评分相比，该列线图的临床适用性较高。对于亚组间进行 ROC 曲线统计结果提示：该列线图模型对于亚组间均适用。

结论：

1、 房颤病程、空白期复发、中性粒细胞计数（NE）、中性粒细胞 / 淋巴细胞比值（NLR）、左房前后径（LAD）是预测心房颤动经导管消融术后复发的独立危险因素。

2、基于 CHA_2DS_2-VASc 评分，联合房颤病程、NLR、LAD 构建列线图预测模型，该预测模型中：NLR 分值最大，对 AF 术后复发的预测价值最大，其次为 LAD，再者为房颤病程，最后为 CHA_2DS_2-VASc 评分。随着房颤病程时间的增加、NLR 及 LAD 的增大、CHA_2DS_2-VASc 评分≥ 2 分，该列线图预测模型的总得分增加，AF 消融术后发生复发的概率越高。

3、 列线图预测模型对于不同房颤类型（持续性心房颤动、阵发性心房颤动）及不同消融术式（射频消融、冷冻消融、射频消融肺静脉电隔离、射频消融肺静脉电隔离 + 基质改良术）的复发有临床预测价值。

Research on exploring the common characteristics and clinical significance of atrial fibrillation and chronic kidney disease based on machine learning

Chenxi Cao, Yunzhe Wang, Gangqiong Liu

The First Affiliated Hospital of Zhengzhou University

Background: Atrial fibrillation (AF) is the most common type of arrhythmia in the heart. It disrupts the contraction of the atria, leading to strokes and heart failure. Chronic kidney disease (CKD) is one of the most significant cardiovascular risk factors, playing a crucial role in various cardiovascular diseases, including AF. This study aims to explore the common features of AF and CKD through bioinformatics analysis and multiple machine learning techniques, and to identify biomarkers associated with patients with CKD and AF.

Methods: Gene expression data for AF and CKD cohorts were selected from the GEO database (https://www.ncbi.nlm.nih.gov/geo/). The limma package in R software was used to screen for differentially expressed genes (DEGs) in AF and CKD respectively. Subsequently, the expression patterns of DEGs were visualized in the form of volcano plots and heatmaps with the "ggplot2" package and "pheatmap" package in R software. The intersecting genes, which may represent common pathogenic genes for both diseases, were identified. GO and KEGG functional enrichment analyses were performed on the differential genes of the two diseases to explore the relationships between the pathways of these genes and to investigate the pathophysiology of the two diseases. Machine learning was applied to the intersecting genes to further identify hub genes in both diseases. Finally, single-cell data analysis of AF was conducted using data from the GEO database to analyze the expression distribution of hub genes at the cellular level and intercellular communication.

Results: The strategy of bioinformatics analysis is performed as shown in Fig. 1. Two raw datasets of AF atrial and CKD-PBMC samples were collected from the GEO database, including 26 (12 control and 14 AF) samples in the AF group and 115 (40 control and 75 CKD) samples in the CKD group. Detailed descriptive information of datasets was shown in Table 1. Through differential expression analysis of the AF dataset (GSE79768), 1397 upregulated genes and 1338 downregulated genes were identified. Similarly, for the CKD dataset (GSE37171), 5032 upregulated genes and 7755 downregulated genes were identified. Taking the intersection of these genes resulted in 684 upregulated genes and 420 downregulated genes. Further enrichment analysis revealed that these genes were primarily enriched in metabolic and protein synthesis regulation. Six candidate hub genes (IDH3A, LBH, LINC00527, RAB8A, RPS11, SETED5) were identified through various machine learning algorithms including LASSO regression (a logistic regression method for fltering variables to enhance the predictive performance) and random forest (RF) algorithm (integrating multiple trees through the idea of ensemble learning to gain better accuracy), and five of these (IDH3A, LBH, RAB8A, RPS11, SETED5) were selected as candidate biomarkers. The distribution and variation trajectory in cells were explored in the single-cell dataset (GSE224959) of atrial fibrillation.

Conclusion: Our study has untangled common biomarkers for CKD and AF, providing insights into the abnormalities of metabolic and protein synthesis regulation in patients with comorbid CKD and AF. This offers new perspectives for future serum-based diagnosis and therapeutic interventions for comorbid CKD and AF, and aids in the development of combined cardio-renal protection.

Keywords: Chronic kidney disease, Atrial fibrillation, Metabolic abnormalities, Protein synthesis

心房颤动并射血分数保留型心力衰竭患者冷冻消融术后复发的预测参数探索

宋文华 王乔 上官文锋 赵志强 刘恩照 许纲 李广平 刘彤

天津市心血管病离子与分子机能重点实验室，天津医科大学第二医院心脏科，天津心脏病学研究所，天津，300211

目的 探讨冷冻球囊消融术治疗心房颤动 (房颤 , AF) 合并射血分数保留型心力衰竭 (HFpEF) 患者的有效性 , 并分析冷冻球囊消融术后 AF 复发相关影响因素。方法 前瞻性收集截至 2023 年 12 月于天津医科大学第二医院心脏内科行 AF 冷冻消融术的患者。采用倾向得分匹配 , 最终确定 207 名患者 , 分为非心力衰竭组 (n=138) 和 HFpEF 组 (n=69)。术前收集受试者基线资料 , 随访 292(135,574) 天 , 根据随访期间是否出现 AF 复发分为复发组 (n=40) 和非复发组 (n=167), 对比 2 组临床资料 , 采用 Cox 回归模型分析影响预后的因素。结果 共计纳入 207 名患者 , 女性 106(51.21%) 例，平均年龄 68.16±9.46 岁。与非复发组相比，复发组患者早发房性心律失常发生率更高，左心耳最大排空速度更低，差异具有统计学意义 ($p<0.05$**)。单因素 COX 分析显示，HFpEF (HR=0.845, 95%CI:0.429~1.662,** $P=0.625$**) 不是冷冻球囊消融术后 AF 复发的预测因素 , 多因素 Cox 回归分析显示，早发房性心律失常 (HR=3.586, 95%CI:1.680~7.651,** $P=0.001$**) 和游离三碘甲腺原氨酸 (HR=0.661, 95%CI:0.479~0.911,** $P=0.011$**) 是冷冻球囊消融术后 AF 复发的独立预测因素。结论 冷冻球囊消融术可作为 HFpEF 患者有效的治疗方案。**

【关键词】心房颤动；心力衰竭；冷冻球囊消融术；复发；预测

The impact of early cryoballoon ablation on clinical outcomes in pa-

tients with non-paroxysmal atrial fibrillation

Wenhua Song[1], Runze Gao[1], Wenfeng Shangguan[1], Enzhao Liu[1], Zhiqiang Zhao[1], Gang Xu[1], Qiao Wang[1], Gary Tse[1,2], Tong Liu[1]

1. Tianjin Key Laboratory of Ionic-Molecular Function of Cardiovascular Disease, Department of Cardiology, Tianjin Institute of Cardiology, the Second Hospital of Tianjin Medical University, Tianjin 300211, China

2. School of Nursing and Health Sciences, Hong Kong Metropolitan University, Hong Kong, China

Background and aims: Atrial fibrillation (AF) is the most common arrhythmia in clinical settings and exhibits a mortality rate that is twice as high as that of sinus arrhythmias. Cryoballoon ablation is a safe and efficient rhythm control strategy in patients suffering from AF. Diagnosis-to- ablation time (DAT) has been defined as a predictor of ablation outcomes, early intervention strategies should be encouraged after the diagnosis of atrial fibrillation. Although the feasibility and effectiveness of cryoballoon ablation for patients with paroxysmal AF were demonstrated previously, the impact of early ablation among non-paroxysmal AF patients is unclear. The aim of this study was to examine the impact of early cryoballoon ablation on AF recurrence in a prospective single-center cohort of non-paroxysmal AF patients.

Methods: Patients with non-paroxysmal AF defined as continuous AF of at least 7 days' duration admitted to the Second Hospital of Tianjin Medical University until July 2024 and underwent first-time cryoballoon ablation were enrolled. The patients were divided into two groups to evaluate differences in AF recurrence risk associated with early-ablation (n=78), defined as within 6 months of first AF diagnosis, and delayed-ablation (n=70), defined as > 6 months after first AF diagnosis. The primary outcome was AF recurrence, defined as any atrial arrhythmias lasting more than 30s by electrocardiogram (ECG) or Holter. Within 3 months after ablation, the blank period, recurrence was defined as early recurrence of atrial fibrillation (ERAF). Patients were followed from every 3 months post ablation at the outpatient clinic. At each follow-up visit, patients underwent surface 12-lead ECG or Holter monitoring examinations to check for recurrence. All participants were followed up until October 31, 2024, or until they were diagnosed with AF recurrence or passed away. The follow up was until October 31, 2024. Cox regression models were used to identify predictors of recurrence.

Results: A total of 148 subjects were included and followed up for a mean of 293 (119-398) days. The cohort included 78(52.70%) in the early-ablation group and 70 (47.30%) in the delayed-ablation group. The mean age was 65.82±9.75 years and 56(37.84%) were female. AF recurrence was found in 45 subjects (30.41%)**.** Compared to participants without recurrence, those with AF recurrence had larger right atrium diameter (RAD) (55.02±5.37mm vs 52.34±6.68mm,P=0.027) and higher prevalence of ERAF (53.33% vs 20.39%, P<0.001), but lower likelihood of undergoing early-ablation (31.11% vs 62.14%, P=0.001) and lower level of platelet count (188[168,226] *10^9/L vs 204[183,261] *10^9/L, P=0.003). Multivariate Cox regression analysis showed that early-ablation (HR=0.496, 95%CI:0.248-0.991, P=0.047), low-density lipoprotein/high-density lipoprotein ratio (HR=0.589, 95%CI:0.377-0.920, P=0.020) and early recurrence (HR=2.750, 95%CI:1.418-5.333, P=0.003) were independent predictors of AF recurrence after cryoballoon ablation. The cumulative incidence of AF recurrence was higher with longer DAT, lower LDL/HDL ratio and early recurrence.Subgroup analysis identified that the risk of AF recurrence was significantly lower in early-ablation group for the male(female:HR:0.370, 95%CI:0.126-1.093; male: HR: 0.355, 95% CI: 0.162-0.778; P for interactions: 0.045), the eldly (age≥65 years: HR: 0.311, 95% CI: 0.129-0.749; age<65 years:HR:0.411,95%CI:0.164-1.033; P for interactions: 0.009), the overweight patients (BMI ≥ 24kg/m^2: HR: 0.281, 95% CI: 0.130-0.618; BMI<24kg/m^2: HR:0.568, 95%CI:0.178-1.818; P for interactions: 0.015) or those with heart failure (heart failure: HR: 0.206, 95% CI: 0.063-0.676; non-heart failure: HR:0.493, 95%CI:0.233-1.042; P for interactions: 0.008). LDL/HDL ratio was associated with lower risk of AF recurrence among the eldly (age ≥ 65 years: HR:0.532, 95%CI:0.285-0.991; age<65 years: HR:0.726, 95%CI: 0.432-1.220; P for interactions 0.006).For the male(female:HR:1.055, 95%CI:0.358-3.107; male:HR:5.642, 95%CI:2.664-11.951; P value for interaction<0.001) and the overweight patients (BMI ≥ 24kg/m^2:HR: 3.311, 95% CI: 1.624-6.748; BMI<24kg/m^2:HR:3.091,95%CI:0.994-9.612; P for interactions=0.001), compared with the non-ERAF group, the risk of AF recurrence in patients with ERAF was significantly increased.

Conclusion: Early cryoablation reduced the risk of recurrence in patients with non-paroxysmal atrial fibrillation. It was supported that early cryoballoon ablation might improve the outcomes in non-paroxysmal AF patients requiring ablation for rhythm control.

Key word: Cryoballoon ablation; Early-ablation; Non-paroxysmal atrial fibrillation; Recurrence; Predictors.

沙库巴曲缬沙坦对持续性房颤患者心脏结构及功能的影响

张骏 高玉英 李巧 代容 郭盛 陈杰

重庆荣昌区人民医院

目的：观察沙库巴曲缬沙坦钠片对持续性心房颤动（简称房颤）患者心脏结构及功能的影响。

方法：选取持续性房颤患者 120 例（房颤发作时间 > 12 月）为研究对象，随机分为对照组和观察组，每组 60 例。对照组服用盐酸胺碘酮片复律和维持治疗，观察组在对照组用药基础上加用沙库巴曲缬沙坦钠片（根据患者肾功、血压、电解质等情况逐渐滴定至靶剂量）。治疗后 1、6 和 12 个月进行随访，观察患者房颤复发率、血流动力学、左心房、左心室结构及功能指标的变化。

结果：与对照组比较，观察组治疗后 1、6 和 12 个月心率、左心房内径 (LAD)、左心房容积 (LAV)、左心房容积指数 (LAVI)、舒张末期内径 (LVEDD)、收缩末期内径 (LVESD)、氨基末端脑钠肽前体 (NT-proBNP) 明显降低 (P<0.05), 左心房存储应变 (LASr)、左室射血分数 (LVEF) 明显升高 (P<0.05), 平均动脉压、血氧饱和度无明显差异 (P>0.05); 观察组治疗后 12 个月 LAD、LAVmax、房颤复发率明显降低，而左心房射血分数 (LAEF) 明显升高 (P<0.05)。

结论：沙库巴曲缬沙坦有助于改善持续性房颤患者心脏结构及功能，减少房颤复发率。

内蒙古某医院心房颤动患者临床治疗现状及预后影响因素分析

武强 沙禹

内蒙古医科大学附属医院

摘要：目的：调查内蒙古某医院心房颤动患者的临床治疗现状，分析影响心房颤动患者预后的相关因素，为内蒙古自治区心房颤动的临床防治及管理提供建议，为改善患者生活质量、降低复发风险提供参考。

方法：研究者通过查阅国内外相关文献，结合心房颤动临床诊疗特点及现有评估量表，修改完善形成《心房颤动患者临床特征及预后影响因素调查问卷》，包括《患者一般资料调查表》和《心房颤动预后评估量表》，该问卷条目为 35 个。问卷经对 60 名心房颤动患者进行预调查，且经多次咨询心血管领域专家并反复修订后，测得信度为 Cronbach's α=0.930，效度为 0.780，均满足量表信效度要求。采用问卷调查结合临床病例回顾的方法，对内蒙古某医院心内科 150 例心房颤动患者进行调查，最终分析符合有效标准的 145 例患者的临床资料及预后影响因素。

结果：维度标准化得分最高的三个依次是：治疗依从性、合并高血压情况、日常活动能力。年龄维度（≥65 岁 vs < 65 岁）和病程维度（≥5 年 vs < 5 年）比较，差异具有统计学意义（P < 0.05）。此外，规律服用抗凝药物患者的血栓事件发生率显著低于未规律服药者（P < 0.01）。

结论：治疗依从性及合并疾病对心房颤动患者的预后影响显著，临床中应针对性加强患者健康教育，优化合并症管理，提高治疗规范性，为改善心房颤动患者预后、降低不良事件发生率发挥积极作用。

Clinical Comparison of Cryoballoon Ablation and Radiofrequency Ablation in the Treatment of Persistent Atrial Fibrillation

Xinyu Zhang[2], Jiaxin Luan[1], Jianqing She[1], Hongbing Li[1]

1. The First Affiliated Hospital of Xi'an Jiaotong University

2. Xi'an Jiaotong University

Aims Persistent atrial fibrillation (PerAF) accounts for an increasing proportion of the global AF burden, yet optimal catheter ablation strategies remain debated. Although radiofrequency ablation (RFA) is the established standard, second-generation cryoballoon ablation (CBA) has proven non-inferior for paroxysmal AF, while evidence in PerAF is scarce. We therefore undertook a real-world comparison to determine whether CBA achieves comparable 1-year freedom from arrhythmia and perioperative safety relative to RFA when used as first-line therapy in patients with drug-refractory PerAF.

Methods We retrospectively screened all AF ablation cases performed at our tertiary center from January 2019 to June 2021 and enrolled 116 consecutive patients (mean age 61.7 ± 10.6 years, 64.7 % male) with documented PerAF undergoing first-time catheter ablation. Inclusion required age ≥ 18 years, left atrial diameter ≤ 60 mm, failure of ≥ one antiarrhythmic drug (excluding beta-blockers), and absence of prior left-atrial ablation, severe valvular disease, or contraindications to anticoagulation. Patients were assigned to CBA (n = 56) or RFA (n = 60) according to operator preference and anatomical suitability. In the CBA arm, a 28 mm second-generation cryoballoon was used to achieve pulmonary vein isolation (PVI); additional linear ablation (roof or mitral isthmus lines) was performed in 21.4 % of cases. The RFA arm employed contact-force sensing catheters with 3-D mapping systems; after circumferential PVI, substrate modification (low-voltage area ablation and linear lesions) was added in 80 % of patients. All procedures were performed under conscious sedation with uninterrupted anticoagulation bridging. The primary endpoint was freedom from documented or symptomatic atrial tachyarrhythmia ≥ 30 s between 3 and 12 months post-ablation; secondary endpoints included perioperative complications and need for repeat ablation. Propensity score matching (PSM) was performed on twelve baseline variables (age, sex, BMI, comorbidities, CHA_2DS_2-VASc score,

AF duration) to mitigate confounding.

Results After PSM, 37 well-matched pairs were analyzed. Baseline characteristics were balanced (P > 0.05 for all variables). Procedural success—defined as acute PVI—was achieved in 100 % of patients. One-year arrhythmia-free survival did not differ between CBA and RFA (83.9 % vs 76.7 %; hazard ratio [HR] 0.75, 95 % CI 0.32–1.74; P = 0.360) and remained similar after PSM (89.2 % vs 73.0 %; P = 0.084). Subgroup analyses revealed no influence of additional linear ablation on recurrence rates within either modality (P = 0.056–1.000). Perioperative complications occurred in 25.0 % of CBA and 35.0 % of RFA patients (P = 0.312). Specific adverse events included transient phrenic nerve palsy in two CBA patients (3.6 %), pericardial tamponade requiring drainage or surgical repair in three RFA patients (5.0 %), and minor hemorrhage or vascular complications without long-term sequelae. Post-ablation creatine kinase and CK-MB levels were higher after CBA (P < 0.001), reflecting greater acute myocardial injury, but these elevations did not correlate with late arrhythmia recurrence.

Conclusions In this single-center real-world cohort, cryoballoon ablation achieved equivalent 1-year efficacy and non-inferior safety compared with radiofrequency ablation for initial treatment of persistent atrial fibrillation. The absence of incremental benefit from extensive substrate modification suggests that durable PVI remains the cornerstone of PerAF ablation, regardless of energy source. These data support CBA as a safe and effective alternative to RFA in the PerAF population, particularly when procedural simplicity and reduced fluoroscopy time are desired. Prospective multicenter randomized trials with longer follow-up are warranted to confirm long-term durability and broader applicability of these findings.

U-shaped association between HDL-c and late recurrence after atrial fibrillation ablation

JINGMING Wang, FEILONG Zhang

Fujian Medical University Union Hospital

Title: U-shaped association between HDL-c and late recurrence after atrial fibrillation ablation

Background: Atrial fibrillation (AF), as a common type of clinical arrhythmia, the issue of postoperative recurrence has long been a focus of attention in the field of cardiovascular medicine. High-density lipoprotein cholesterol (HDL-c), as a lipid index closely related to cardiovascular health, is generally recognized to have protective effects such as anti-atherosclerosis, anti-inflammation, and anti-oxidation. However, the association between high-density lipoprotein cholesterol (HDL-c) and the postoperative recurrence rate of atrial fibrillation remains unclear at present. This study aims to investigate the relationship between the preoperative serum concentration of high-density lipoprotein cholesterol and late postoperative recurrence in patients with non-valvular atrial fibrillation..

Methods: A total of 376 non-valvular atrial fibrillation patients attending the Department of Cardiology of Fujian Medical University Union Hospital for treatment from 2018 to 2022 were selected. Grouped according to preoperative HDL-c level (tertile method) into high level HDL-c group (Q3), low level HDL-c group (Q1), and intermediate level HDL-c group (Q2). Radiofrequency ablation or cryoablation of AF was performed in each group of patients. According to the follow-up results were classified as late recurrence and non-late recurrence, risk factors related to late recurrence of AF were analyzed.Meanwhile, the Kaplan-Meier method was used to plot survival curves to compare the recurrence-free survival rates among patients in different HDL-c level groups, and the Log-rank test was applied to compare the differences between groups.

Results: Postoperative follow-up of 376 patients. There were 60 cases (14.5%) with late recurrence of atrial fibrillation, among which 20 cases (16.5%) were in the high-level HDL-c group (Q3), 28 cases (21.7%) in the low-level HDL-c group (Q1), and 12 cases (9.5%) in the intermediate-level HDL-c group (Q2). There was a significant difference in the late recurrence rate among the three groups (P=0.028). The results of multivariate Cox proportional hazards regression analysis showed that after adjusting for confounding factors, the serum concentration of HDL-c in the intermediate range was an independent protective factor against late recurrence after atrial fibrillation surgery (P=0.012, HR=0.4, 95% CI: 0.2-0.8), meaning that patients with preoperative HDL-c at the intermediate level had a significantly lower risk of late postoperative recurrence than those in other level groups.The results of the Kaplan-Meier survival curve indicated that the recurrence-free survival time of patients in the intermediate-level HDL-c group was significantly longer than that in the high-level group and the low-level group. Further analysis revealed that there might be a special U-shaped relationship between the late recurrence rate after non-valvular atrial fibrillation ablation and the serum concentration of HDL-c, that is, when the HDL-c level is too low or too high, the late postoperative recurrence rate of patients is relatively high, while when it is at the intermediate level, the recurrence rate is the lowest.

Conclusion: The results of this study indicate that HDL-c serum concentrations in the intermediate range are an independent protective factor against late recurrence after AF.The relationship between HDL-c levels and the risk of postoperative recurrence of atrial fibrillation is not a simple linear one, but rather a complex U-shaped association.

心房颤动患者左心房低电压区预测模型的建立

杜文娟 张欣宁 林小涵 解晓龙

哈尔滨医科大学附属第二医院

目的：心房颤动（Atrial Fibrillation， AF）是常见的心律失常之一。环肺静脉隔离导管消融（Pulmonary Vein Isolation， PVI）已成为全球范围内治疗 AF 最广泛应用的节律控制策略之一。尽管 PVI 在多数患者中具有良好的短期疗效，但其长期成功率却存在显著差异。而许多患者在术后仍会出现律失常的复发，这一问题为 AF 的治疗来了重大挑战。近年来的研究表明，左心房低电压区的存在是影响导管消融术后 AF 复发率的重要因素，目前术前有效预测左心房低电压区的手段仍不够成熟因此，进一步探索无创、精准且简便的左心房低电压区评估方法，已成为优化 AF 治疗的重要研究方向。本研究旨在分析 AF 患者左心房低电压区的独立危险因素，并建立预测模型，提供更为简便的 AF 术前左心房低电压区评估的方法。

方法：纳入从 2020 年 1 月到 2024 年 6 月在我院首次接受经导管射频消融手术的 405 例患者进行回顾性分析，在 Carto3 三维标测系统下完成 PVI，通过使用面积测量工具（以 cm^2 为单位）来确定，如果在覆盖 $1cm^2$ 的区域中至少有三个相邻点的双极电压 <0.5mV，则确定为低电压区。根据标测结果将患者分为无低电压区组和有低电压区组，收集患者临床资料，使用 R4.2.2 版本软件进行分析左心房低电压区独立危险因素并建立预测模型，评估模型效能。

结果：共纳入 405 例符合要求的患者，无低电压区组共 118 人，有低电压区组共 287 人，先进行两组间比较，其中年龄、AF 类型、卒中评分，出血评分，CAD，LVEF，LAD，左室舒张末期内径，左室收缩末期内径，是否服用胺碘酮，直接胆红素，尿酸，凝血酶时间测定，血浆 D- 二聚体，BNP 的 P 值小于 0.05，具有统计学意义，将两组间比较有意义（P < 0.05）的变量纳入单因素 logistic 归分析，单因素分析结果显示年龄、AF 类型、CAD，LVEF，LAD、左室舒张末期内径、左室收缩末期内径、胺碘酮、尿酸、BNP 具有统计学差异。使用逐步回归法筛选变量，筛选得到五个自变量最终纳入多因素 logistic 回归模型，分别是：年龄、AF 类型、CAD，LAD 和 BNP。基于以上危险因素绘制列线图。自变量结果的解释分别为：年龄每增长一岁，发生低电压区的风险就增加 2.1%（95%CI：0.996-1.048，P= 0.102）；持续性 AF 组发生低电压区的风险是阵发性 AF 组的 1.777 倍（95%CI：1.011-3.119，P=0.044）；冠心病组发生低电压区的风险是非冠心病组的 2.028 倍（95%CI：0.988-4.420，P=0.062）；左房内径每增加一个单位，发生低电压区的风险就增加 18.6%（95%CI：1.112-1.271，P<0.001）；BNP 每增加一个单位，发生低电压区的风险就增加 0.1%（95%CI：1.001-1.002，P=0.002）。本模型的 AUC 值为 0.843（95%CI：0.804-0.8817），该模型判断效果较好。

结论：年龄、AF 类型、CAD，LAD 和 BNP 是预测心房颤动患者左心房低电压区的独立危险因素，基于以上危险因素得到的预测模型具有良好的预测效能，对于 AF 导管消融术前低电压区的评估具有一定参考价值，可以成为导管消融术前的无创便捷评估手段。

尿酸和血脂对非瓣膜性房颤患者卒中事件的综合预测价值

唐雨琦 杨晓蕾 夏云龙

大连医科大学附属第一医院

目的：血清尿酸 (Serum uric acid, SUA) 和血脂代谢紊乱与心房颤动 (Atrial fibrillation, AF) 及其预后密切相关。在非瓣膜性房颤 (Non-valvular atrial fibrillation, NAF) 患者中，我们评估了血清尿酸、甘油三酯 (Triglycerides, TG) 和低密度脂蛋白 (Low-density lipoprotein cholesterol, LDL-C) 对缺血性卒中的综合预测价值，以提高缺血性卒中风险的预测和管理。

方法：我们纳入了 2020 年 1 月至 2023 年 12 月在大连医科大学附属第一医院就诊的 3,176 名 NAF 住院患者。分析了包括 SUA 和血脂在内的生物标志物及相关临床数据，以评估它们对 NAF 患者发生缺血性卒中 (Ischemic stroke, IS) 的影响。

结果：由于卒中与非卒中患者中，TG 和 SUA 水平的性别差异 ((男性为 1.39 mmol/L vs. 1.28 mmol/L，P=0.031；女性为 1.5 mmol/L vs. 1.28 mmol/L，P=0.001) 和 (男性为 424 μmol/L vs. 397 μmol/L，P=0.008；女性为 361 μmol/L vs. 328 μmol/L，P=0.004))。我们通过限制性立方样条曲线确定了预测 NAF 患者卒中事件的 SUA(男性 400 μmol/L，女性 330 μmol/L) 和 TG(男性 1.28 mmol/L，女性 1.29 mmol/L) 的临界值。Kaplan-Meier 累积风险分析表明，基于性别的 SUA 和 TG 综合评估能增强 NAF 患者的 IS 风险分层。与 SUA 和 TG 水平较低的患者相比，具有高水平 SUA 和 TG 的患者 IS 风险更高 (HR 1.98)。在多变量 Cox 回归分析中 (矫正混杂因素后)，升高的 SUA 和 LDL-C 生物标志物与增加的卒中风险显著相关。综上所述，我们构建了 CHA2DS2-VASc+SUA+TG+LDL-C 卒中风险预测模型。其临床预测价值通过 C 指数、综合判别改善指数和净重新分类指数进行评估。

结论：SUA、TG 和 LDL-C 与非瓣膜性房颤患者 IS 风险密切相关。SUA、TG 和 LDL-C 的结合有效提升了 CHA2DS2-VASc 评分对 IS 的预测价值。

心房颤动患者射频消融术后晚期复发风险预测模型的建立和验证

杜文娟 林小涵 张欣宁 谢晓龙

哈尔滨医科大学附属第二医院

目的：心房颤动是最常见的心律失常之一，射频消融术是治疗手段之一，其术后

复发风险评估对于优化消融策略和改善患者预后具有重要意义。尽管已有多种评分体系用于预测其术后复发风险，但准确性和适用性尚有提升空间以及大部分都缺少对模型的验证。为此，本研究旨在建立并验证一个预测首次行 AF 射频消融术后复发风险的列线图模型，整合多种临床指标，提供个性化的复发概率预测，更好的识别术后复发高风险患者，优化医疗资源的使用。

方法：本研究纳入哈尔滨医科大学附属第二医院首次行 AF 射频消融术的 377 例患者。通过回顾性分析患者术前相关实验室检查及心脏彩超、术中左房的低电压面积、术后随访等相关临床数据，按照 7:3 的比例分为训练集与验证集，训练集用于模型构建，验证集用于模型验证，筛选术后复发的潜在危险因素，采用逐步回归法构建多因素 logistic 回归模型，并以列线图形式实现风险可视化。通过 ROC 曲线、校准曲线及决策曲线验证模型的区分能力、校准能力及临床应用价值。

结果：多因素回归分析显示，LVZ%（95%CI：1.0001~1.028，p=0.048）；血浆纤维蛋白原(95%CI: 1.163~3.638, p=0.013)；BNP(95%CI: 1.00006~1.0007, p=0.016）；早期复发（95%CI：8.796~39.008，p<0.001）是术后复发的独立危险因素。所构建的模型在训练集和验证集的 ROC 曲线下面积（AUC）分别为 0.857（95%CI：0.807-0.908）和 0.780（95%CI：0.665-0.895），具有良好的预测能力与泛化性能。校准曲线与理想线高度吻合，决策曲线分析显示该模型在实际决策中具有显著的净收益。

结论：该研究发现 LVZ%、血浆纤维蛋白原、BNP 水平、早期复发是房颤术后复发的独立危险因素，并根据多因素回归结果建立并验证了一个房颤射频消融术后复发风险的预测模型，本研究模型具有良好的区分能力、校准性能和泛化能力，该模型能够有效评估术后复发风险，为房颤患者个体化诊疗和术后随访管理提供重要依据。未来可通过增加样本量、整合更多临床数据及生物标志物，进一步优化模型性能及预测能力。

回顾性分析甘油三酯葡萄糖指数对非瓣膜性心房颤动患者导管消融术后晚期复发的影响

马薇 张飞龙

福建医科大学附属协和医院

目的：探讨甘油三酯葡萄糖指数（TyG）与非瓣膜性心房颤动（NVAF）患者消融术后晚期复发的相关性及其预测价值。

方法：回顾性收集 2018.05-2022.10 于我院首次行导管消融术的 401 例 NVAF 患者的资料，术后随访 2 年。Cox 回归分析探索房颤复发的危险因素，TyG 计算公式为：ln [空腹甘油三酯 [mg/dL]× 空腹葡萄糖 [mg/dL]/2]，由结果建立风险模型，通过绘制受试者工作曲线（ROC）并计算曲线下面积（AUC）、计算 C 指数、构建列线图模型、绘制校准曲线、决策曲线分析，从预测性能、临床收益、预测准确性等多维度评价模型性能；Kaplan-Meier 法对比生存曲线，比较术后 2 年内无房颤晚期复发生存率；Spearman 相关性分析及限制性立方样条（RCS）探索 TyG 与与其他研究变量及术后房颤复发风险的相关性；在糖尿病及非糖尿病组开展亚组分析。

结果：研究纳入 401 名 NVAF 患者，平均年龄 60.7±10.0 岁，女性占 41.4%；糖尿病患者占 12.7%；持续性房颤占 37.7%；晚期复发率为 16.2%，早期复发率为 8.0%。无晚期复发组（n=336）与晚期复发组（n=65）的基线对比显示，晚期复发组的 TyG、左心房前后径（LAD）、女性比例、持续性房颤占比、早期复发率更高（P<0.05）。Cox 回归分析提示：TyG、女性、持续性房颤、LAD 是房颤术后晚期复发的独立危险因素（P<0.05）。中介效应分析提示：早期复发是 TyG 与晚期复发的中介变量。对风险模型评分、TyG、LAD 分别划分的高 / 低分组，有 / 无早期复发组、阵发性与持续性房颤组、男性与女性绘制组间 K-M 曲线，各组间的无房颤晚期复发生存率存在显著差异（P<0.05）。Spearman 相关性分析发现：TyG 与房颤术后早期复发、晚期复发 (P<0.05) 存在显著正相关。RCS 分析发现：在调整混杂因素前后，TyG 与房颤术后晚期复发风险均存在线性关系，TyG 升高对应着较高的房颤复发风险。对糖尿病及非糖尿病组开展的亚组分析显示：两组中 TyG 指数均是房颤术后晚期复发的独立危险因素（P<0.05）。

结论：TyG、女性、持续性房颤、LAD 是 NVAF 患者消融术后晚期复发的独立危险因素。早期复发是 TyG 与晚期复发的中介变量和关联的关键环节。TyG 对糖尿病及非糖尿病人群房颤消融术后的复发均有一定预测价值。

Elevated resting heart rate in hospitalized patients with atrial fibrillation is associated with increased cardiovascular risk

Kangning Han, De-Yong Long

Beijing Anzhen Hospital, Capital Medical University

Background

The management of atrial fibrillation (AF) has evolved beyond the simple dichotomy of rate versus rhythm control, with most patients now receiving a tailored combination of both strategies. This has created uncertainty regarding the optimal heart rate target, particularly for patients hospitalized with AF who face an elevated risk of adverse outcomes such as stroke, heart failure (HF) exacerbation, and hemodynamic instability. While rate control remains a cornerstone of therapy, the evidence guiding resting heart rate (RHR) targets for this specific, high-risk inpatient population is limited. This study aimed to determine the dose-response relationship between RHR at admission and in-hospital adverse outcomes using a large-sample database from the Improving Care for Cardiovascular Disease in China-AF (CCC-AF) project.

Methods

This study utilized data from the CCC-AF project, a nationwide, multicenter quality improvement initiative involving 236 hospitals across China.[1] From January 2015 to December 2019, clinical data were collected from 61,136 inpatients with AF.[2] For this analysis, the population was refined to include only patients whose primary discharge diagnosis was AF and whose admission 12-lead electrocardiogram (ECG) confirmed AF, resulting in a final sample of 12,775 patients. The RHR was recorded from the first ECG performed after a five-minute rest period upon hospital admission and prior to the initiation of in-hospital treatment.

The primary outcome was a composite of new-onset acute heart failure (AHF) and all-cause mortality during hospitalization. Secondary outcomes included in-hospital stroke/transient ischemic attack (TIA) and bleeding events. A comprehensive set of variables was collected, including patient demographics, AF type (e.g., paroxysmal, persistent), comorbidities (hypertension, diabetes, coronary artery disease, HF), clinical measurements (LVEF, eGFR), and both pre-hospital and in-hospital treatments.

Statistical analysis involved comparing patients with an RHR <80 bpm versus those with an RHR ≥ 80 bpm. Multivariable logistic regression models were employed to assess the association between RHR and outcomes, adjusting for a wide range of potential confounders. Model 1 was unadjusted; Model 2 adjusted for demographics and clinical comorbidities; Model 3 further adjusted for pre-hospital and in-hospital treatments. To explore the continuous relationship, restricted cubic splines (RCS) were used within the fully adjusted model. The floating risk method was also used to compare risk across nine distinct RHR categories without relying on a fixed baseline group.

Results

The final cohort consisted of 12,775 patients with a median hospital stay of 8 days. Patients with an admission RHR <80 bpm were generally older, more likely to be male, and had a higher prevalence of hypertension and cerebrovascular disease, but a lower incidence of pre-existing HF.

A significantly higher risk for the primary composite outcome was observed in patients with an RHR ≥ 80 bpm. In the fully adjusted model (Model 3), an RHR ≥ 80 bpm was associated with an odds ratio (OR) of 1.79 (95% Confidence Interval [CI]: 1.44-2.22, P <0.001) for the primary outcome. This corresponded to an absolute risk increase of 2.11% (95% CI: 1.40%-2.83%). This association was predominantly driven by the risk of AHF. For AHF alone, an RHR ≥80 bpm was associated with an OR of 1.77 (95% CI: 1.42-2.20, P <0.001) in the fully adjusted model, translating to an absolute risk increase of 2.03%.

The RCS analysis revealed a general U-shaped relationship between RHR and the primary outcome. The risk began to increase significantly at an RHR above 72 bpm, continuing to rise with higher heart rates. Further analysis showed that patients with more advanced forms of AF (e.g., long-standing persistent/permanent AF) experienced a higher risk of the primary outcome across the entire RHR spectrum. Conversely, the use of catheter ablation during hospitalization was associated with a lower risk of the primary outcome across all RHR values.

Discussion

To our knowledge, this is the first large-scale, nationwide study to specifically investigate the association between admission RHR and in-hospital outcomes in patients whose primary reason for hospitalization is AF. The findings reveal a significant and robust association, where an RHR exceeding 80 bpm is linked to a substantially increased risk of in-hospital new-onset AHF and all-cause mortality.

These results provide important context to the current guidelines, which have increasingly favored a lenient rate control strategy (target RHR <110 bpm), largely based on the RACE II trial. However, the authors note that the RACE II trial had several limitations, including a small difference in achieved heart rates between the strict (75 bpm) and lenient (85 bpm) control groups and low statistical power to detect benefits of stricter control. This study, with its large sample size, suggests that the optimal RHR target in the acute setting may be lower than currently recommended. The observed inflection point at 72 bpm, above which risk begins to rise, aligns with other studies suggesting that elevated heart rates are a risk factor for adverse cardiovascular events.

The study also highlights that the risk associated with a high RHR is magnified in patients with more persistent forms of AF. Furthermore, the finding that catheter ablation, but not antiarrhythmic drug therapy, was associated with a reduced risk of the primary outcome is consistent with recent clinical trials demonstrating the superiority of ablation for improving outcomes in select AF populations, particularly those with concurrent HF.

Limitations

The authors acknowledge several limitations. As an observational study, it can only establish association, not causation; it remains unknown if actively lowering RHR to a specific target would improve outcomes. The study lacked data on HF-specific biomarkers like NT-proBNP.[3] Additionally, since only admission RHR was available, the direct effect of catheter ablation on RHR could not be assessed, and data on medication dosag-

es were not available.

Conclusion

In a large, nationwide cohort of patients hospitalized for AF, an admission RHR of ≥ 80 bpm was independently associated with a significantly increased risk of in-hospital new-onset acute heart failure and all-cause mortality. The risk appeared to increase progressively for RHR values above 72 bpm. These findings challenge the sufficiency of a lenient rate control strategy in the acute hospital setting and suggest that a stricter RHR target (<80 bpm) may be more appropriate for mitigating adverse events in this high-risk population. Further randomized controlled trials are warranted to confirm whether a strategy targeting a lower RHR can prospectively improve clinical outcomes.

循证式督导护理在持续性心房颤动导管消融术后管理中的效果评价

闫石芳 张喜维

北京安贞医院

【摘要】目的：探究循证式督导护理在持续性心房颤动（persistent Atrial Fibrillation, psAF）患者在经皮心脏导管消融（Catheter Ablation）术后管理中的应用效果。

方法：纳入 2022 年 1 月至 2023 年 6 月在某三级甲等医院心内科接受射频消融手术的 psAF 患者 148 例，将其随机分为试验组（78 例）与观察组（70 例），并同期接受导管消融治疗。出院时观察组接受常规健康指导，试验组则在标准组的护理和健康教育的前提下，经由拥有 3 年及以上专业经验的循证督导护理小组进行 12 个月及以上的督导随访。主要终点为患者出院 12 个月期间的服药依从性及生活质量得分，次要终点为心血管事件再住院率。

结果：两组患者基线临床特征无统计学差异（P > 0.05）。出院 12 个月后，试验组病人的药物依从性评分 (7.55±0.75 vs.5.24±2.55，P <0.001) 较对照组更高，房颤生活质量量表（Atrial Fibrillation Effect on Quality-of-Life, AFEQT）得分（86.27±10.55 vs.72.48±10.80, P=0.013）及中文版生活质量评估表总得分 [578.2 (IQR 470-610) vs.449.5 (IQR 358-599), P < 0.001] 均较对照组更优。多因素 Cox 回归模型显示，试验组病人的心血管事件较对照组降低 9% (HR = 0.91，95% CI = 0.72 - 0.99, P = 0.031)。

结论：对持续性心房颤动患者导管消融术后实施至少 12 个月以上的循证督导护理可以有效地改善病人的术后自我管理能力，提升术后生活质量，同时可降低心血管病再住院率，对改善持续性心房颤动患者的长期预后具有重要临床价值。

Non-optimal Temperature is Associated with Higher Atrial Fibrillation Hospitalizations in China: A Nationwide Case-crossover Study

Shi-hao Wang[1], Xiao-Lei Yang[1], Shao-Bo Shi[2], Cong-Xin Huang[2], He Huang[2], Yun-Long Xia[1]

1. The First Affiliated Hospital of Dalian Medical University

2. The Renmin Hospital of Wuhan University.

Title: Non-optimal Temperature is Associated with Higher Atrial Fibrillation Hospitalizations in China: A Nationwide Case-crossover Study

Authors' names: Shihao Wang MD, PHD [a†], Xiaolei Yang MD, PHD [a†], Shaobo Shi MD, PHD [b], Congxin Huang MD, PHD [b], He Huang MD, PHD [b*], Yunlong Xia MD, PHD [a*]

Abstract

Background and Objectives

Atrial fibrillation (AF) is the most common sustained cardiac arrhythmia worldwide, affecting approximately 59.7 million individuals and causing substantial healthcare burden through increased risks of stroke, heart failure, and mortality. While previous studies have examined temperature impacts on cardiovascular mortality, limited evidence exists regarding temperature-AF hospitalization associations across diverse geographical contexts. Given that AF typically presents as recurrent episodes requiring hospitalization rather than immediate mortality, and considering projected increases in extreme weather events due to climate change, understanding these relationships is crucial for developing targeted prevention strategies. This study aimed to comprehensively quantify the association between ambient non-optimal temperatures and AF-related hospitalizations across China, identify vulnerable populations, and estimate the attributable disease burden.

Methods

We conducted a nationwide two-stage time-stratified case-crossover study using the Chinese Atrial Fibrillation Real-World Study (RWS-CAF) database. The analysis included 1,665,014 patients with primary AF discharge diagnoses from 802 centers across 251 cities between June 2014 and June 2023. Daily meteorological data were obtained from China's Meteorological Data Sharing Service System, and air pollution data from the National Urban Air Quality Real-time Publishing Platform. In stage one, conditional quasi-Poisson generalized linear models combined with distributed lag non-linear models characterized city-specific temperature-AF relationships over 0-14 day lag periods. The exposure-response relationship was modeled using quadratic B-splines with knots at the 10th, 50th, and 90th percentiles of city-specific temperature distributions. The time-stratified design, matching on city, year, month, and day-of-week, controlled for individual-level confounders and temporal trends. In stage two, random-effects meta-analysis pooled city-specific estimates. We identified the minimum hospitalization temperature (MHT) as the temperature with lowest AF hospitalization risk. Relative risks were calculated for extreme cold (1st percentile) and heat (99th percentile) versus MHT. Stratified analyses examined effect modification by demographics, comorbidities, and regions. Population-attributable fractions were calculated with bootstrap-derived confidence intervals.

Results

The study population averaged 72±12 years old, with 57% males and high cardiovascular comorbidity prevalence. The exposure-response relationship showed an inverse J-shaped curve with national MHT at 24.3 ° C (74th percentile). Extreme cold exposure demonstrated significantly stronger associations than extreme heat. The cumulative relative risk for extreme cold (-6.4° C) was 1.32 (95% CI: 1.24-1.42), while extreme heat (31.5° C) showed no significant association (RR: 1.03, 95% CI: 0.99-1.07). Cold effects displayed delayed onset, with initial protective associations at lag 0-1 days before adverse effects peaked at lag 2-4 days and persisted throughout the observation period. Significant geographical heterogeneity emerged, with northern China experiencing higher cold-related risks (RR: 1.53, 95% CI: 1.35-1.73) compared to southern China (RR: 1.27, 95% CI: 1.16-1.39; Pinteraction=0.019). Overall, 14.3% (95% empirical CI: 12.2-14.8%) of AF hospitalizations were attributable to non-optimal temperatures, with cold effects accounting for 91.4%. Moderate cold temperatures contributed most substantially (12.0%), while extreme temperatures had smaller contributions. Regional variations were pronounced, with northern China experiencing 18.4% attributable fraction versus southern China's 12.4%. Subgroup analyses revealed no significant effect modifications by age or sex, though patients with hypertension and vascular disease showed higher attributable fractions.

Conclusions

In conclusion, exposure to non-optimal ambient temperatures is associated with increased risks of hospitalization related to AF in China. Excess risk was evident in northern China, where cold temperatures dominate. The study also found that patients with a history of hypertension, diabetes, stroke/transient ischemic attack, and vascular disease have a higher population-attributable fraction. The potential impact of these findings could be substantial, as they provide crucial insights into the management and prevention of AF.

Keywords: Atrial fibrillation; Ambient temperature; Cardiac arrhythmia; Case-crossover study; China; Environmental epidemiology

† Shihao Wang,Xiaolei Yang, and Shaobo Shi contributed equally as primary authors.

* Corresponding author.

Extracellular vesicles from LAA facilitate atrial fibrillation

Jing Wang

the First Affiliated Hospital of Kunming Medical University,

Objective

This study aimed to investigate the role of extracellular vesicles (EVs) derived from the Left Atrial Appendage (LAA) in the pathogenesis of Atrial Fibrillation (AF). Atrial fibrillation is a common arrhythmia characterized by atrial fibrosis, inflammatory responses, and thrombus formation. Although the LAA plays a significant role in the occurrence and thrombogenesis of AF, the specific mechanisms of LAA-derived EVs in AF pathophysiology remain unclear. This study explored, at the molecular level, the mechanisms by which LAA-derived EVs may promote inflammation, fibrosis, and thrombosis to drive the initiation and progression of AF, providing research direction and a theoretical basis for identifying novel therapeutic targets for AF.

Methods

One hundred patients were enrolled from the Department of Cardiology and Inpatient Wards of the First Affiliated Hospital of Kunming Medical University between May 2021 and May 2022. This included 48 AF patients and 52 non-AF arrhythmia patients. AF classification followed the 2021 Chinese Society of Cardiology (CSC) AF guideline criteria. LAA blood and peripheral blood were collected from AF patients, and LAA blood was collected from non-AF patients for EV extraction and identification.

Immunofluorescence was used to verify cellular uptake of LAA-EVs.

Transwell assays assessed cardiomyocyte migration ability. Flow cytometry detected apoptosis, mitochondrial membrane potential, and Ca^{2+} influx. ELISA measured CRP, IL-6, IL-8, and adiponectin levels.

Apoptosis and reactive oxygen species (ROS) were detected in HUVECs and HAECs. A tube formation assay assessed angiogenesis capability.

Western Blot analysis measured the expression levels of CD106, CD54, PAI-1, Vascular Endothelial Growth Factor (VEGF), Growth Hormone, Serpin C1, and tPA.

LAA-EVs were injected into the ventricular wall of SD rats to evaluate their effects on cardiac tissue inflammation and fibrosis.

LAA blood samples from 3 non-AF arrhythmia patients and 3 AF patients were collected for miRNA sequencing.

The effects of LAA-EVs on the expression of ESRRA, FKBP4, and HS3ST1 were analyzed.

Results

Immunofluorescence showed that atrial-like cardiomyocytes could take up LAA-EVs. LAA-EVs from AF patients most effectively reduced cardiomyocyte migration ability. LAA-EVs from AF patients significantly increased apoptosis and Ca^{2+} influx. These EVs decreased mitochondrial membrane potential and increased intracellular ROS levels. Furthermore, LAA-EVs from AF patients elevated CRP, IL-6, and IL-8 levels while decreasing adiponectin levels.

LAA-EVs from AF patients significantly enhanced ROS generation and increased the apoptosis rate in endothelial cells. Additionally, they significantly reduced angiogenesis capability.

Western Blot results showed that the AF patient LAA-EV intervention group (EV-1) and the AF patient peripheral blood EV intervention group (EV-2) promoted the expression of CD106, CD54, and PAI-1 in HUVECs, while inhibiting the expression of VEGF, Growth Hormone, Serpin C1, and tPA. The effects on HAECs were consistent with those observed in HUVECs.

Myocardial injection of EVs in SD rats. LAA-EVs from AF patients induced the most significant inflammatory response and disorganization of myocardial tissue arrangement.

MiRNA sequencing identified three target genes (ESRRA, FKBP4, and HS3ST1) associated with miRNAs.

In cardiomyocytes, EV-1 significantly downregulated the expression of ESRRA, FKBP4, and HS3ST1, while EV-2 also downregulated ESRRA and FKBP4 expression, but the effect of non-AF patient LAA-EVs (EVs) on these markers was not significant. In HAECs, EVs (non-AF LAA-EVs) increased the expression of these three proteins. In HUVECs, HCFBs (Human Cardiac Fibroblasts), and atrial tissue, EVs (AF LAA-EVs) significantly reduced the expression of ESRRA, FKBP4, and HS3ST1. (Note: Interpretation of point 6 requires careful reading of the original context regarding which EVs were used in which cell type. This translation reflects the described results but clarifies the likely EV groups based on the patterns.)

Conclusion

This study reveals the significant role of LAA-derived EVs in atrial fibrillation. These EVs promote inflammation, fibrosis, and thrombosis through multiple mechanisms, thereby driving the initiation and progression of AF. The findings not only provide new perspectives for understanding the pathophysiological mechanisms of AF but also offer a theoretical basis for developing novel diagnostic biomarkers and therapeutic targets for AF and its complications.

Comparative Efficacy of Catheter Ablation Versus Antiarrhythmic Drug Therapy in Asymptomatic and Symptomatic Atrial Fibrillation: Insights from the CABANA Trial

Shi Yongfeng

the Second Hospital of Jilin University

Abstract

Background: The optimal rhythm control strategy for patients with asymptomatic atrial fibrillation (AF) remains uncertain. This study aimed to assess the comparative efficacy of catheter ablation versus antiarrhythmic drug (AAD) therapy in asymptomatic versus symptomatic AF patients using data from the CABANA trial. Building upon the CABANA trial dataset, this study aims to systematically compare the treatment outcomes of catheter ablation and antiarrhythmic drug therapy in patients with asymptomatic versus symptomatic AF. While the CABANA trial has demonstrated that catheter ablation effectively reduces AF recurrence and cardiovascular hospitalization rates, its impact on clinical endpoints in asymptomatic patients remains unclear. Given the increasing recognition of asymptomatic AF as a significant predictor of stroke and cardiovascular morbidity, understanding whether early intervention with ablation confers a clinical advantage over pharmacologic therapy is critical. This research is expected to refine treatment algorithms by providing robust evidence on the risk-benefit profile of catheter ablation in asymptomatic AF patients, potentially advocating for earlier rhythm control strategies in this population. Additionally, the findings may contribute to the ongoing discourse on AF screening, risk stratification, and precision-based management.

Methods and results: This was a secondary analysis of the multicenter, randomized CABANA trial, including 2,204 AF patients randomized to catheter ablation or AAD therapy. The original CABANA trial enrolled patients with AF who were randomized to receive either catheter ablation or medical therapy, with long-term follow-up to assess major cardiovascular outcomes. Ethical approval for the CABANA trial was obtained from institutional review boards at each participating center, and all patients provided written informed consent. Patients were classified as asymptomatic (CCS-SAF class 0–2, n=1,265) or symptomatic (CCS-SAF class 3–4, n=926). The primary endpoint was a composite of all-cause mortality, disabling stroke, serious bleeding, or cardiac arrest. Secondary endpoints included cardiovascular hospitalization, AF recurrence, and health-related quality of life (HRQoL), measured by EQ-5D-3L scores. Over a median follow-up of 48.5 months, the primary composite endpoint showed no significant difference between ablation and drug therapy groups in asymptomatic (6.28% vs. 7.92%; hazard ratio [HR] 0.79, 95% CI 0.52–1.20, P=0.238) or symptomatic patients (10.02% vs. 10.51%; HR 0.94, 95% CI 0.62–1.41, P=0.844). However, catheter ablation significantly reduced AF recurrence in both asymptomatic (HR 0.56, 95% CI 0.49–0.64, P<0.001) and symptomatic patients (HR 0.65, 95% CI 0.56–0.75, P<0.001). Ablation was also associated with reduced cardiovascular hospitalization or death in asymptomatic (HR 0.85, 95% CI 0.73–1.00, P=0.044) and symptomatic (HR 0.79, 95% CI 0.67–0.94, P=0.013) patients. Improvement in HRQoL was significantly greater in asymptomatic compared with symptomatic patients (adjusted mean difference 3.06 vs. 1.93; both P<0.0001).

Conclusion:

Catheter ablation significantly reduces AF recurrence and cardiovascular morbidity in both asymptomatic and symptomatic patients. While no survival advantage was observed, ablation led to substantial HRQoL improvements, particularly in asymptomatic patients. These findings support ablation as an effective rhythm control strategy beyond symptom management and suggest that risk-stratified approaches should be considered to identify asymptomatic patients who may benefit from early intervention. Future studies are needed to evaluate long-term outcomes, stroke prevention, and the role of anticoagulation discontinuation following ablation in asymptomatic AF patients.

心房颤动的发作频率是独立于心房颤动类型的死亡危险因素：一项来自全国范围注册研究

王一萌 杨艳敏

中国医学科学院阜外医院

目的：

心房颤动（房颤）负荷被视为患者不良预后的危险因素。然而，既往研究多集中于探索房颤的持续时间对于预后的影响，忽视了房颤的发作频率在其中的作用。因此，本研究拟探索房颤发作频率对于患者不良预后的影响。

方法：

本研究是基于一项全国范围、多中心注册研究。主要研究终点为自入组 1 年内患者的全因死亡；次要研究终点为自患者入组 1 年内卒中 / 体循环栓塞以及大出血事件。

结果：

本研究共计纳入 1544 名受试者。平均年龄为 69±13 岁，其中 54.5% 的受试者为女性。399 名受试者被视为随访期间房颤低发作频率，1145 名受试者被视为随访期间房颤高发作频率组。在随访期间共计 241（15.6%）名受试者发生了死亡。多因素 Cox 回归分析表明房颤高发作频率独立于房颤类型作为受试者死亡事件的危险因素 (HR: 2.542, 95%CI: 1.670-3.871, P<0.001)。然而房颤发作频率对于卒中 / 体循环栓塞事件（HR: 0.773, 95%CI: 0.497-1.202，P=0.253）及大出血事件 (HR: 0.904, 95%CI: 0.322-2.537, P = 0.849) 无统计学意义。亚组分析表明，在高龄患者人群中房颤发作频率与受试者 1 年内全因死亡相关（HR: 2.565， 95%CI：1.640-4.014，P<0.001），在年轻患者人群（HR：3.226，95%CI：0.947-10.992，p=0.061）中不具有统计学意义。

结论：

房颤发作频率是独立于房颤类型作用于患者 1 年全因死亡的危险因素。在老年人群患者中房颤发作频率与 1 年全因死亡事件相关。

Long-term effects of SGLT2 inhibitors on arrhythmias: a systematic review and meta-analysis

Beibei Du, Pei-Pei Li, Ping Yang, Yu-Quan He

China-Japan Union Hospital of Jilin University

Background: Sodium-glucose co-transporter 2 (SGLT2) inhibitors are established cardioprotective agents in heart failure guidelines, but their specific impact on various arrhythmia types, particularly beyond atrial fibrillation/flutter (AF/AFL), remains incompletely understood. While some studies suggest potential antiarrhythmic benefits, findings have been inconsistent. This systematic review and meta-analysis aimed to comprehensively evaluate the long-term effects of SGLT2 inhibitors on the risk of AF/AFL, ventricular tachycardia (VT), ventricular fibrillation (VF),

and sinus bradycardia.

Methods: This study adhered to PRISMA guidelines and was registered with PROSPERO (CRD42022371089). A systematic search of PubMed, Embase, Web of Science, and ClinicalTrials.gov was conducted from database inception until June 30, 2024, to identify randomized controlled trials (RCTs) with a minimum follow-up duration of 52 weeks. Inclusion criteria required adult participants (≥ 18 years), comparison of SGLT2 inhibitors (dapagliflozin, empagliflozin, canagliflozin, ertugliflozin, tofogliflozin, luseogliflozin, ipragliflozin, remogliflozin, sergliflozin) or SGLT1/2 inhibitors (sotagliflozin, licogliflozin) against placebo, and reporting of specific arrhythmia events (AF, AFL, VT, VF, sinus bradycardia). Non-randomized trials, animal studies, reviews, and non-English literature were excluded. Two reviewers independently performed study selection, data extraction, and risk of bias assessment using the Cochrane tool. The primary outcome was the incidence of AF/AFL; secondary outcomes were VT, VF, and sinus bradycardia. Pooled risk ratios (RRs) with 95% confidence intervals (CIs) were calculated using fixed-effects (I^2<50%, Q-test P>0.1) or random-effects models. Sensitivity analyses (leave-one-out method) and publication bias assessment (funnel plots) were performed.

Results: Thirty-nine RCTs, encompassing 107,770 participants, were included. Trials assessed dapagliflozin (n=12), empagliflozin (n=7), canagliflozin (n=6), sotagliflozin (n=9), ertugliflozin (n=4), and licogliflozin (n=1). Populations included diabetes mellitus (DM, n=31 trials), heart failure (HF, n=5 trials), and chronic kidney disease (CKD, n=8 trials). Risk of bias was generally low.

AF/AFL: Meta-analysis of all 39 trials demonstrated a statistically significant 14% reduction in the risk of AF/AFL with SGLT2 inhibitors compared to placebo (RR 0.86; 95% CI, 0.77–0.95; I^2 = 0%; P = 0.003). Subgroup analysis showed significant risk reduction in DM patients (RR 0.84; 95% CI, 0.73–0.96; P=0.01) and CKD patients (RR 0.72; 95% CI, 0.55–0.94; P=0.02), but not in HF patients (RR 0.90; 95% CI, 0.64–1.27; I^2=69%; P=0.56).

Dose Effect (AF/AFL): Analysis of 19 trials comparing high-dose vs. low-dose SGLT2 inhibitors showed a non-significant trend towards reduced AF/AFL risk with higher doses (RR 0.78; 95% CI, 0.60–1.02; I^2 = 0%; P = 0.07). Sensitivity analysis excluding one trial (NCT01986881) yielded a statistically significant result (RR 0.68; 95% CI, 0.48–0.96; P=0.03), but this requires cautious interpretation.

VT: Analysis of 16 trials found no significant difference in VT risk between SGLT2 inhibitors and placebo (RR 0.99; 95% CI, 0.81–1.22; I^2 = 0%; P = 0.96).

VF: Analysis of 14 trials found no significant difference in VF risk (RR 1.06; 95% CI, 0.73–1.54; I^2 = 0%; P = 0.75).

Sinus Bradycardia: Analysis of 8 trials found no significant difference in sinus bradycardia risk (RR 1.12; 95% CI, 0.57–2.18; I^2 = 0%; P = 0.74).

Sensitivity analyses confirmed the robustness of the primary results for all arrhythmia types. Funnel plots indicated low publication bias probability.

Conclusion: This large systematic review and meta-analysis demonstrates that SGLT2 inhibitors significantly reduce the long-term risk of atrial fibrillation and atrial flutter (AF/AFL) by 14% compared to placebo. This beneficial effect was observed in patients with diabetes and chronic kidney disease, but not significantly in heart failure patients within this analysis. Importantly, SGLT2 inhibitors showed no significant effect on the risk of ventricular tachycardia (VT), ventricular fibrillation (VF), or sinus bradycardia. Furthermore, different doses of SGLT2 inhibitors did not demonstrate a statistically significant differential effect on AF/AFL incidence. These findings support the potential antiarrhythmic benefit of SGLT2 inhibitors specifically for atrial arrhythmias in certain high-risk populations and reinforce their cardiovascular safety profile regarding ventricular arrhythmias and bradycardia. Future large-scale RCTs specifically designed to assess arrhythmia outcomes are warranted to confirm these effects, particularly exploring dose relationships and effects in heart failure subgroups.

Systematic Review Registration: PROSPERO (CRD42022371089)

Keywords: Sodium-glucose co-transporter 2 inhibitors, SGLT2i, arrhythmia, atrial fibrillation, atrial flutter, ventricular tachycardia, ventricular fibrillation, sinus bradycardia, meta-analysis.

住院心房颤动患者睡眠质量及其影响因素分析

王永涛 杨毅宁 彭辉

新疆维吾尔自治区人民医院

目的 旨在了解住院心房颤动患者睡眠质量，并分析其影响因素。**方法** 以 2024 年 9 月至 2025 年 1 月在新疆维吾尔自治区人民医院心内科住院的 150 例心房颤动患者为研究对象，患者入院时均采用匹兹堡睡眠质量指数量表 (PSQI) 测评睡眠质量。以 PSQI 总分 > 7 分定义为睡眠障碍，依据 PSQI 评分将患者分为睡眠障碍组和无睡眠障碍组，调取病历内容收集一般临床资料、临床诊断、生化指标、心脏超声、心电图等资料，采用单因素及多因素 Logistic 回归分析影响心房颤动患者睡眠质量的危险因素。以 P < 0.05 为差异具有统计学意义。 **结果** 本研究共入选 150 例心房颤动患者为研究对象，平均年龄 59.43±12.15 岁，其中男性 112 例（74.67%），经统计共有 49 例心房颤动患者发生睡眠障碍（32.67%），单因素分析显示，年龄、女性、焦虑、合并心衰是心房颤动患者发生睡眠障碍的危险因素，多因素分析显示年龄（OR=1.113,95%CI 1.097-3.254，P= 0.023）、合并心衰（OR=1.354,95%CI 1.134-4.023，P= 0.015）是心房颤动患者发生睡眠障碍的独立危险因素。**结论** 住院心房颤动患者睡眠障碍发生率较高，与年龄、合并心衰密切相关。

Circulating transthyretin with atrial fibrillation risk, and the modifying role of BMI

Nan Zhang[1], Zi-Heng Jia[1], Jin-Hua Zhao[1], Gary Tse[1], Jian-Dong Zhou[2], Kang-Yin Chen[1], GREGORY Y.H. Lip[3], Tong Liu[1]

1. Tianjin Key Laboratory of Ionic-Molecular Function of Cardiovascular Disease, Department of Cardiology, Tianjin Institute of Cardiology, Second Hospital of Tianjin Medical University, Tianjin 300211, China

2. Department of Family Medicine and Primary Care, School of Clinical Medicine, Li Ka Shing Faculty of Medicine, The University of Hong Kong, Hong Kong, China

3. Liverpool Centre for Cardiovascular Science at University of Liverpool, Liverpool John Moores University and Liverpool Heart & Chest Hospital, Liverpool, UK

Background: Low circulating transthyretin (TTR) concentration has been suggested as a biomarker of transthyretin tetramer instability, a prerequisite for the development of transthyretin cardiac amyloidosis (ATTR). Important clinical manifestations of ATTR include cardiac arrhythmias such as atrial fibrillation (AF). Whether low circulating TTR concentration confers increased risk of incident arrhythmias in the general population is unknown. This study aimed evaluate the associations between circulating TTR levels with incident AF and other cardiac arrhythmias in the general population.

Methods: This study used data form the UK Biobank. Participants with available TTR data and without prior arrhythmias were included. The primary outcome was new-onset AF. The secondary outcomes were new-onset supraventricular arrhythmias (SVA), bradyarrhythmias, cardiac block, and ventricular arrhythmias (VA). Multivariable Cox model was applied to evaluate the associations between circulating TTR levels with outcomes, adjusting for demographic characteristics, laboratory measurements, comorbidities, and medication history.

Results: A total of 40,725 participants (mean age 56.7 ± 8.2 years; 55% women) were included. During a median follow-up of 14.6 years, new-onset AF, SVA, bradyarrhythmias, cardiac block, and VA developed in 2930 (7.2%), 3098 (7.6%), 2016 (4.9%), 1590 (3.8%), and 701 (1.7%) participants, respectively. After adjusting for potential confounders, one standard deviation (SD) decrease in TTR levels was associated with an increased risk of incident AF in the general population [HR 1.06, P = 0.005] (**Figure 1**). Furthermore, significant associations between low TTR with atrial structural remodeling were observed, manifesting as increased LA volume index [LAVi β=0.51, p=0.017] and RA volume index [RAVi β=0.87, p<0.001]. In the general population, there was a significant association between lower TTR levels with higher incident SVA risk, but not for bradyarrhythmias, cardiac block, or VA. Notably, a consistently significant interaction effect was identified between TTR levels and BMI for the risk of AF, SVA, bradyarrhythmias and cardiac block (all $P_{interaction}$ <0.05), with lower TTR levels being significantly associated with a higher risk of AF [HR 1.15, p<0.001], SVA [HR 1.15, p<0.001], bradyarrhythmias [HR 1.17, p=0.003], and cardiac block [HR 1.15, p=0.023] among individuals with a BMI < 25 kg/m² (**Figure 2**). In addition, the associations between lower TTR and increased AF risk were greater among individuals with an older age, as well as those with lower polygenic risk score for AF ($P_{interaction}$ <0.05).

Conclusions: Our study suggests a potential mechanistic association between low circulating TTR concentration as a marker of tetramer instability and incident AF in the general population. Exposure to low TTR and low BMI may be associated with a higher risk of AF, SVA, bradyarrhythmias and cardiac block.

SGLT2 抑制剂对房颤合并心衰患者导管消融术后房颤复发及心脏功能的影响

陈可心 耿璐 史晨晨 鲁静朝

河北医科大学第二医院

目的 探讨 SGLT2 抑制剂（SGLT2i）对房颤合并心衰患者导管消融术后房颤复发及心脏功能的影响。

方法 回顾性纳入首次行导管消融术的房颤合并心衰患者 168 例，根据是否应用 SGLT2i 分为 SGLT2i 组及非 SGLT2i 组 2 组，收集患者导管一般临床资料、实验室指标、手术相关指标、术后口服药物、术前及术后 1、3、6、12 个月心脏超声参数及术后房颤复发情况等指标。比较两组术后房颤复发率及心脏功能结构变化。

结果 两组基线资料比较无统计学差异（P >0.05）。SGLT2i 组的房颤复发率

明显低于非 SGLT2i 组（13.25% vs 25.88%，P <0.05）。左房高度纤维化和应用 SGLT2i 是房颤合并心衰患者导管消融术后房颤复发的独立影响因素（P <0.05）。SGLT2i 对不同亚组人群房颤复发的影响基本一致（P >0.05）。两组患者术前及术后 1、3、6 个月各项心脏超声参数比较无统计学差异（P >0.05）。术后 12 个月，SGLT2i 组的左房内径、舒张早期二尖瓣峰值速度 / 二尖瓣环峰值速度低于非 SGLT2i 组，左室射血分数高于非 SGLT2i 组（P <0.05），左室内径、E 峰与 A 峰比值较非 SGLT2i 组无统计学差异（P >0.05）。

结论 房颤合并心衰患者应用 SGLT2i 可降低导管消融术后房颤复发风险，且对心脏功能和结构有改善作用。

SGLT2 抑制剂对房颤合并 2 型糖尿病患者导管消融术后复发及心脏功能的影响

史晨晨 裴玮娜 鲁静朝

河北医科大学第二医院

目的：本研究探讨 SGLT2 抑制剂对房颤合并 2 型糖尿病患者导管消融术后房颤复发及心脏结构功能的影响。

方法：本研究采用回顾性研究方法，收集 2022 年 1 月至 2023 年 6 月期间于河北医科大学第二医院接受导管射频消融术的房颤合并 2 型糖尿病患者，根据是否应用 SGLT2i 分为 SGLT2i 组和非 SGLT2i 组。研究随访 18 个月，收集患者基线临床特征、生化指标、手术相关参数、各时间心脏超声指标，以及术后房颤复发情况等资料。比较 SGLT2i 组和非 SGLT2i 组患者术后房颤复发情况及心脏结构功能的变化情况。

结果：两组患者基线资料比较无统计学差异（P>0.05）。SGLT2i 组消融术后 18 个月房颤复发率低于非 SGLT2i 组（11.25% vs 24.10%，P=0.032），差异有统计学意义。多因素 Cox 回归分析显示未应用 SGLT2i（HR 0.44，95%CI 0.20~0.97，P=0.043）和心房高度纤维化（HR 4.28，95%CI 1.85~9.87，P<0.001）是房颤术后复发的独立预测因子。两组患者术后 1、3 个月心脏超声各项指标比较，差异均无统计学意义（P>0.05）。术后 6、12 个月比较，SGLT2i 组 LAD 指标明显低于非 SGLT2i 组（6 个月 37.87 ± 4.56mm vs 36.20 ± 4.08mm，12 个月 37.48 ± 4.80 mm vs 35.35 ± 4.66mm），差异有统计学意义（P<0.05）。

结论：房颤合并 2 型糖尿病患者应用 SGLT2 抑制剂可降低导管射频消融术后房颤复发的风险，并且改善左心房结构重构。

Exploring T-Cell Exhaustion-Associated Genes in Atrial Fibrillation: A New Diagnostic Perspective and Pathogenic Mechanism Analysis

Jiao Wang[1], Yu-Chun Yang[1], Mei-Juan Zheng[1], Muhuyati Wulasihan[2]

1. First Affiliated Hospital of Xinjiang Medical

2. Xinjiang Medical University

Abstract

Background: T cell exhaustion (TEX) plays an important role in infection immunity and auto immune. New study finds link between T cell-mediated inflammation and atrial fibrillation (AF) disease progression, but mechanism not yet elucidated. Therefore, the present study aimed to investigate TEX-related genes (TEX-RGs) and their regulatory mechanisms in AF.

Methods: Transcriptomic and single-cell RNA sequencing (scRNA-seq) data for AF, as well as information on TEX-RGs, were sourced from the public databases. Key genes for this study were selected based on differential expression analysis, protein-protein interaction (PPI) network, expression validation, and diagnostic performance evaluation. Following that, the molecular mechanisms of key genes in AF were further explored through enrichment and immune infiltration analyses. Lastly, cell clusters in AF were further refined through scRNA-seq analysis, allowing for an in-depth exploration of molecular regulatory mechanisms at the cellular level. The expression of the key genes was verified using reverse transcription quantitative polymerase chain reaction (RT-qPCR).

Results: Transcriptomic and single-cell RNA sequencing (scRNA-seq) data for AF, as well as information on TEX-RGs, were sourced from the public databases. This study identified three key genes: IGFBP2, LTBP2, and RCAN1. These genes demonstrated excellent diagnostic capabilities, with area under curve (AUC) exceeding 0.7 within GSE2240 and GSE115574. The nomogram model was constructed by IGFBP2, LTBP2 and RCAN1. Subsequently, the AUC values of the nomogram model was 0.955, as the ROC curve showed. Meanwhile, the DCA curves showed a high net clinical benefit for both the key genes and the nomogram model. The GSEA results revealed that all 3 key genes demonstrated concurrent enrichment in the pathways of "ECM receptor interaction". Moreover, IGFBP2 and RCAN1 were all enriched in "focal adhesion", these analyses revealed the importance of these pathways in the pathogenesis of AF. Those three key genes were significantly positively correlated with CD56dim natural killer cell and Natural killer T cell with correlation coefficients greater than 0.3 (P<0.05), while three key genes were significantly negatively correlated with Natural killer cell with correlation coefficients less than -0.5 (P<0.01). Additionally, the DSigDB database was utilized to predict targeting agents for key genes and to identify small molecule compounds with potential therapeutic effects in AF patient. 48 drugs such as alvespimycin, anisomycin, and astemizole, etc. were interrelated with the RCAN1; camptothecin and GW-8510 were interrelated with the IGFBP2. In single cell dataset, 6 cell types were annotated and Macrophage and Smooth muscle cells were defined as key cells. Notably, the expression trends of the three key genes differed during Macrophage and Smooth muscle cell differentiation. Among them, both IGFBP2 and LTBP2 showed a downward trend in the later stages of macrophage differentiation, whereas they were stable throughout smooth muscle cell differentiation. The expression levels of LTBP2 and IGFBP2 were significantly upregulated in AF samples compared to controls, consistent with its expression in GSE2240 and GSE115574. Whereas RCANA expression was up-regulated in AF, but not significantly, and these may be attributed to the limitation of small sample size.

Conclusion: IGFBP2, LTBP2, and RCAN1 were recognized as TEX-related key genes in AF. These findings shed new light on diagnostic methods, preventive measures, and elucidation of the pathogenic mechanisms underlying AF.

Personalized risk prediction of late recurrence outcome of atrial fibrillation after radiofrequency catheter ablation based on 4S-AF scheme

Nai-Yuan Cui, De-Yong Long

Beijing Anzhen Hospital, Capital Medical University

Background Atrial fibrillation (AF) is the most common cardiac arrhythmia and recurrence after catheter ablation remains a significant challenge. 4S-AF scheme was a structured pathophysiology-based characterization scheme that encompasses four domains: stroke risk (St), symptom (Sy), severity of AF burden (Sb), and substrate (Su). The 4S-AF scheme provides personalized prognostic information for AF adverse outcomes but has limited application in predicting AF recurrence following catheter ablation.

Methods A prospective cohort study was conducted with 426 patients undergoing radiofrequency catheter ablation (RFCA) for AF. Baseline clinical data, echocardiographic parameters, and biomarkers [including red blood cell distribution width (RDW) and high-sensitivity C-reactive protein (hs-CRP)] were measured and collected. The 4S-AF scheme comprised of four domains was used to characterize all participants by two independent researchers. The total score was the sum of each domain with a maximum score of 10 (St =1, Sy =2, Sb=2, and Su=5). St domain score was characterized as if at non-low stroke risk and had indication for oral anticoagulant therapy based on CHA_2DS_2-VASc score. Sy domain was based on symptom severity ranging from none to disabling accessed by European Heart Rhythm Association symptom score, and Sb domain score was categorized based on the AF classification. Su domain score was the sum of three subdomain scores: comorbidity/ cardiovascular risk factors score, left atrial enlargement score, and elder age score. The primary endpoint of this study was late AF recurrence, defined as any documented episode of AF, atrial flutter, or atrial tachycardia lasting >30 seconds occurring more than 3 months after RFCA, as confirmed by 12-lead ECG or Holter monitoring during follow-up. A multivariate Cox regression model was applied to identify independent predictors of AF recurrence, and a nomogram was developed for prediction. The performance of the model was assessed using receiver operating characteristic (ROC) curves, calibration curves, and decision curve analysis (DCA).

Results A total of 426 enrolled patients were included in our analysis and randomly divided into training cohort (n=298) and internal validation cohort (n=128) with a ratio of 7:3. Over a median follow-up of 29 months, 35.9% of participants experienced AF recurrence. Univariable Cox regression analysis showed that 4S-AF scheme score, hs-CRP>1.2 mg/L, RDW, and total AF history duration were independent predictors for AF recurrence in the training cohort. Finally, variables were selected as predictors in the multivariate Cox model to establish a prediction model, including 4S-AF scheme score (HR 1.361, 95% CI: 1.194-1.550, P<0.001), hs-CRP>1.2 mg/L (HR 1.532, 95% CI: 1.043-2.251, P=0.030), and RDW (HR 1.074, 95% CI: 1.005-1.146, P=0.034). ROC analysis demonstrated that the predictive performance of the nomogram (AUC 0.711, 95% CI: 0.652–0.771) is superior to BASE-AF2 (AUC 0.683, 95% CI: 0.622–0.744) and APPLE scores (AUC 0.628, 95% CI: 0.566–0.691) in the training set. The nomogram incorporating these predictors demonstrated favorable performance, with C-index values of 0.654 and 0.725 in the training and validation cohorts. Calibration plots showed mean absolute error in the training and validation cohorts was respectively 0.046 and 0.016, indicating adequate agreement between prediction and observation in the training and validation cohorts of the nomogram model. DCA indicated that the nomogram provided net benefits across a range of threshold probabilities for predicting AF recurrence.

Conclusions This study demonstrates that integrating the 4S-AF scheme with systemic biomarkers such as hs-CRP and RDW enhances the prediction of late AF recurrence following RFCA. The developed nomogram provides a personalized risk stratification tool that may guide post-ablation management and improve patient outcomes. Further validation in larger, diverse populations is needed to confirm its clinical utility.

Keywords Atrial fibrillation; Radiofrequency catheter ablation; Recurrence; 4S-AF scheme; Nomogram; Risk stratification

日间患者局麻深度镇静下房颤脉冲电场消融手术患者围术期的护理实践经验

沈建平 马燕 吴黎莉

浙江大学医学院附属邵逸夫医院

日间患者局麻深度镇静下房颤脉冲电场消融手术患者围术期的护理实践经验

沈建平 马燕 吴黎莉

浙江大学医学院附属邵逸夫医院

310000

13738100702

Sjp520@189.cn

【摘要】房颤是指心房无序的电活动导致心房机械活动不协调，心房失去有效的收缩与舒张，心功能受损，还可能引发其他严重并发症作为一种常见的心律失常疾病，严重影响患者的心脏功能与生活质量。在 2022 年开展的一项全国范围的横断面流行病学研究中，发现我国房颤的患病率达到了 1.6%，[1] 研究指出，与传统的治疗方法相比，经导管房颤射频消融治疗能够显著提高患者的生活质量，因此，该治疗方式在临床指南中的推荐等级逐步上升。脉冲电场消融手术以其独特优势，如精准的组织选择性消融、对周围组织损伤小等，逐渐成为多列房颤治疗的重要手段。手术成功不仅依赖于先进的技术和精湛的医术，围手术期间护理同样发挥着关键作用，它贯穿手术全程，从患者从进入医院至病房到入手术室和手术结束直到出院后，每一个护理细节都关乎患者的安全与手术效果以及复发率。本文将通过总结 18 例日间局麻深度镇静下房颤脉冲电场消融手术患者围术期的护理实践经验。通过构建“精准评估 - 智能防控 - 分层管理 - 数字延伸”整合式医护技多团队合作模式使患者康复痊愈出院。其护理要点如下：1. 提前系统化精细化术前评估，缩短住院时间，提高手术效率，优化手术策略；2. 严格防控感染并优化空间布局，缩短手术时间，提高紧急抢救的成功率；3. 阶梯性使用镇静镇痛药物达到深度镇静使患者舒适化的护理技术；4. 团队合作早期识别致命性并发症的预防及处理；5. 并发症分层管理，减少穿刺血肿，心包填塞，肺静脉狭窄发生率和食道损伤；6. 术后交班和延续性护理以及智能远程监测和随访，通过构建多学科协作机制与精准化，人性化的护理技术融合为房颤脉冲电场消融手术提供围术期个体化护理方案及优质护理，助力 18 例房颤患者得到的有效治疗并康复痊愈出院。

Association of red blood cell distribution width with long-term recurrence outcome of atrial fibrillation after radiofrequency catheter ablation

Nai-Yuan Cui, De-Yong Long

Beijing Anzhen Hospital, Capital Medical University

Background: Red cell distribution width (RDW) has recently been recognized as a potential marker of potential marker of red cell dysfunction, inflammation and oxidative stress. Elevated RDW has been associated with various cardiovascular adverse outcomes. Systemic inflammation may contribute to the atrial fibrosis and remodeling process. However, the association of RDW with AF recurrence after radiofrequency catheter ablation (RFCA) is controversial. This study aims to investigate the association between RDW and the long-term recurrence outcome of AF after RFCA.

Methods: This single-centre, prospective observational cohort study included 647 consecutive AF patients aged ≥ 18 years who underwent initial RFCA at Beijing Anzhen Hospital between January 2019 and December 2019. Patients were regularly followed for 3, 6, 12 months, or longer after RFCA. Baseline characteristics, laboratory data, and echocardiographic parameters were collected. Red blood cell distribution width-standard deviation (RDW-SD) levels and red blood cell distribution width-coefficient of variation (RDW-CV) were assessed. The primary outcome assessed was AF recurrence after RFCA, defined as any documented atrial tachyarrhythmia episode lasting at least 30 seconds. Univariate and multivariate Cox regression analyses were performed to determine risk factors for AF recurrence, and the hazard ratio (HR) and 95% confidence intervals (CI) were calculated. The baseline model was adjusted by age, sex, persistent AF, AF duration, coronary artery disease, hypertension, heart failure, diabetes, stroke/ transient ischemic attack, left atrial diameter and estimated glomerular filtration rate. The predictive capability of biomarkers and predictive models for AF recurrence was tested using receiver-operating characteristic (ROC) curves and area under the curve (AUC) analysis.

Results: A total of 426 patients were included in the final analysis [age 62 (IQR: 53-68) years, 34.5% female, 70.7% paroxysmal AF]. The median total duration of AF was 12 (4-48) months. RDW-SD [43.10 (41.60-45.65) vs. 42.30 (40.90-43.95), P<0.001] of the AF recurrence group were significantly greater than those of the non-recurrence group. During a follow-up period of 29 (IQR: 13-36) months, 153 patients (35.9%) experienced AF recurrence. Multivariate Cox regression analysis revealed that AF history (HR, 1.005, 95% CI, 1.002-1.009, P=0.002), persistent AF (HR, 1.633, 95% CI, 1.148-2.322, P=0.006), RDW-SD (HR, 1.069, 95% CI, 1.012-1.129, P=0.016), hs-CRP (HR, 1.048, 95% CI, 1.011-1.086, P=0.01) and LAD (HR, 1.066, 95% CI, 1.025-1.108, P=0.001) were independent predictors for AF recurrence. When a cut-off value of 43.85 fL was set, elevated RDW-SD was significantly associated with increased AF recurrence (HR: 1.676, 95% CI: 1.216-2.309, P=0.002). Subgroup analyses demonstrate that male sex, age < 65 years, no CAD, no DM, and LAD ≥ 40 mm combined with high RDW-SD level could better predict AF recurrence after RFCA. Combining with the conventional clinical model, RDW-SD (AUC 73.95%, 95% CI: 69.04-78.85) and RDW-CV (AUC 72.97%, 95% CI: 67.98-77.95) demonstrated comparable predictive performance to well-established biomarkers such as hs-CRP (AUC 73.25%, 95% CI: 68.23-78.26) and BNP (AUC 72.91%, 95% CI: 67.92-77.89).

Conclusions: Elevated RDW-SD is significantly associated with AF recurrence following RFCA. These findings suggest that RDW may be a valuable prognostic marker for identifying patients at high risk of AF recurrence.

Keywords: Atrial fibrillation; Radiofrequency catheter ablation; Red cell distribution Width; Recurrence; Biomarker; Inflammation

Predictive Value of Left Atrial Global Longitudinal Strain (LAGLS) for Recurrence After Catheter Ablation in Hypertensive Patients with Atrial Fibrillation

Xiyang Li[1], Tingting Zheng[1], Suining Xu[1], Kamili Kamila[1], Danni Wang[1], Pengjie Gao[1], Yan Zhuo[1], Yiran Yan[1], Gang Tian[1], Xin Jin[2]

1. The First Affiliated Hospital of Xi'an Jiaotong University

2. Xi'an International Medical Center Hospital

Background: Atrial fibrillation (AF) is one of the most common sustained cardiac arrhythmias and imposes a substantial burden of stroke, heart failure and all-cause mortality worldwide. Catheter ablation, which electrically isolates arrhythmogenic foci and remodels atrial substrate via radio-frequency or cryothermal energy, has become a first-line rhythm-control strategy for symptomatic Atrial fibrillation refractory to, or intolerant of, anti-arrhythmic drugs. Nevertheless, long-term efficacy remains limited; reported rates of late AF recurrence range from 20 % to 45 %, and are particularly high among patients with concomitant hypertension. Chronic blood-pressure overload promotes atrial pressure elevation, structural fibrosis and electrical heterogeneity, thereby increasing the likelihood of post-procedural arrhythmia recurrence. Identifying reliable pre-procedural markers that capture hypertension-related atrial remodelling and accurately predict recurrence is therefore crucial for optimising patient selection and personalising follow-up.Speckle Tracking Echocardiography (STE) provides angle-independent, high-resolution myocardial deformation analysis and is well established for ventricular assessment. Its application to the left atrium (LA)—especially derivation of Left Atrial Global Longitudinal Strain (LAGLS)—offers a quantitative, non-invasive measure of LA reservoir function that reflects myocardial compliance and interstitial fibrosis. Although STE has gained traction, evidence for the incremental prognostic value of LAGLS in hypertensive patients undergoing AF ablation remains scarce.

Methods: We prospectively enrolled 168 consecutive patients who underwent first-time catheter ablation for AF at our centre between March 2022 and January 2023. Baseline demographics, cardiovascular risk factors and comprehensive echocardiographic parameters, including LAGLS measured offline by STE, were recorded. Post-ablation, patients were followed in a structured programme with 12-lead electrocardiograms or 24-h Holter monitoring at each visit. AF recurrence was defined as any atrial tachyarrhythmia lasting > 30 s occurring beyond a 3-month blanking period. Participants were stratified into recurrence and non-recurrence groups, and predictors were explored using single-factor logistic regression (SFLR) followed by multivariate analysis.

Results: Of the 168 patients (mean age 62 ± 8 years; 37 % female), 28 (16.67 %) experienced late AF recurrence during a median follow-up of 11 months. Baseline age, sex, body-mass index, blood pressure, lipid profile and fasting glucose were comparable between groups (all P value > 0.05). SFLR identified LA anteroposterior diameter (OR = 1.507, 95 % CI 1.007–1.110), LA end-diastolic volume (OR = 1.015, 95 % CI 1.002–1.029), LA end-systolic volume (OR = 1.024, 95 % CI 1.009–1.040), LA volume index (OR = 1.028, 95 % CI 1.005–1.052) and LAGLS (OR = 0.880, 95 % CI 0.808–0.958) as significant factors. After adjustment for confounders, LAGLS remained the sole independent predictor of recurrence (OR = 0.981, 95 % CI 0.805–0.987; P < 0.05). Receiver-operating-characteristic analysis yielded an area under the curve of 0.687 (95 % CI 0.593–0.780); the optimal cut-off value of 5.85 % produced 60.4 % sensitivity and 71.4 % specificity.

Conclusions: In hypertensive patients with AF undergoing first-time catheter ablation, impaired LAGLS is an independent predictor of late arrhythmia recurrence. As a simple, non-invasive STE-derived parameter, LAGLS may complement conventional echocardiographic indices to refine risk stratification and guide personalised follow-up in this high-risk population.

Keywords: atrial fibrillation; hypertension; left atrial strain; speckle tracking echocardiography; catheter ablation; recurrence.

多共病对房颤导管消融术后疗效影响的观察研究

阳文青 [1,2] 梁明 [2] 王祖禄 [2]

1. 大连医科大学北部战区总医院培养基地

2. 中国人民解放军北部战区总医院

目的：通过观察消融 3 月后复发率和 1 年后复发率等疗效指标，分析多共病对房颤导管消融术后疗效的影响。

方法：本研究为回顾性研究，纳入从 2023 年 1 月到 2023 年 12 月在中国人民解放军北部战区总医院心内科确诊房颤且并接受了导管消融术治疗的患者病例。纳入标准：年龄 18-80 岁；术前通过心电图或动态心电图确诊为房颤；术前 24h 行食道超声排除左心房血栓；患者及家属签署知情同意书；配合术后随访。排除标准：严重心脏瓣膜病；抗凝禁忌；不配合术后随访的患者；全身情况差，预期寿命小于 1 年的患者。收集患者基本信息（年龄、性别、房颤类型、临床症状、心脏超声等）、共病情况（高血压、心功能不全、2 型糖尿病、肥胖和超重、阻塞性睡眠呼吸暂停、运动情况、过量饮酒）以及手术资料（手术方式、手术时间、额外线性消融数量、术后并发症等）。通过 logistic 回归分析，探究多共病与房颤术后复发的关联。

结果：BMI 下降（P 值 0.048，OR 0.12）、心功能恶化（P 值 < 0.001，OR 11.72）及术后血压控制不佳（P 值 0.036，OR 6.99）显著增加房颤术后复发风险。术后糖尿病改善（P 值 0.475，OR 1.49）、术后 OSA 改善（P 值 0.705，OR 0.76）、术后戒酒（P 值 0.773，OR 0.89）、术后运动改善（P 值 0.890，OR 1.18）对房颤术后复发无显著影响。

结论：积极推动患者减重、改善心功能、调控血压有助于降低房颤术后复发可能性，提醒临床医生优化管理策略。糖尿病及 OSA 管理、术后戒酒、适当运动等因素受限于样本量较小，虽暂未明确其与复发的关联，但是，从患者整体健康出发，术后仍应倡导健康生活方式（如戒酒、适度运动等），助力康复，我们也会持续探索多共病对房颤术后的长期影响。

Periprocedural Intravascular Hemolysis and Renal Function in Persistent Atrial Fibrillation Patients Undergoing Pulmonary Vein Isolation with Pulsed-Field Ablation

Daile Jia, LiLian Bao, Xueting Han, ChunFeng Dai, ZhenNing Nie

Department of Cardiology, Zhongshan Hospital, Fudan University

Periprocedural Intravascular Hemolysis and Renal Function in Persistent Atrial Fibrillation Patients Undergoing Pulmonary Vein Isolation with Pulsed-Field Ablation

Daile Jia1,2, Lilian Bao1,2, Xueting Han1,2, Chunfeng Dai1,2, Zhenning Nie1,2

1Department of Cardiology, Zhongshan Hospital, Fudan University, Shanghai Institute of Cardiovascular Diseases, Shanghai, China

2State Key Laboratory of Cardiology, Zhongshan Hospital, Fudan University, Shanghai, China

Abstract

Background:

Pulmonary vein isolation (PVI) is a cornerstone of catheter ablation therapy for atrial fibrillation (AF), with radiofrequency and cryothermal energy being the conventional modalities. Recently, pulsed-field ablation (PFA) has emerged as a novel, non-thermal technique based on electroporation, offering tissue selectivity and favorable procedural safety. While early studies have demonstrated excellent efficacy of PFA for paroxysmal AF, increasing clinical experience has revealed that hemolysis may occur during ablation, potentially leading to transient renal dysfunction. This concern is particularly relevant in patients undergoing more extensive ablation for persistent AF, who often require additional substrate modification beyond pulmonary vein isolation—such as ablation of the left atrial roof, posterior wall, or mitral isthmus—thereby increasing energy exposure. Although large registries have reported rare cases of PFA-induced hemolysis-related acute kidney injury, data specific to the biochemical and clinical consequences of hemolysis in persistent AF populations remain scarce. Understanding the incidence and extent of periprocedural hemolysis in this context is crucial for improving patient safety and guiding intraprocedural fluid management strategies.

Objectives:

This study aimed to evaluate the degree of intravascular hemolysis and its short-term impact on renal function in patients with persistent AF undergoing PFA-based catheter ablation. Specifically, the investigation focused on changes in established hemolytic biomarkers and serum creatinine levels in the periprocedural period, providing insight into the safety profile of contemporary PFA protocols during complex left atrial substrate modification. The study also sought to determine whether the extent of hemolysis observed translates into clinically meaningful renal impairment, especially in procedures involving a moderate number of pulsed field applications.

Methods:

Patients with persistent AF underwent isolation of pulmonary vein, left atrial roof, posterior wall and superior vena cava using PFA with FarapulseTM (Boston Scientific, USA) catheter. If AF still persisted or was converted to atrial flutter, mitral and/or cavotricuspital isthmus was ablated accordingly. At least 2 liters of normal saline were intravenously infused during and after the procedure. Blood samples were collected at baseline and the following morning post-procedure. Markers of hemolysis—including lactate dehydrogenase (LDH), haptoglobin, indirect and direct bilirubin—and serum creatinine were measured at both time points.

Results:

A total of thirty-eight patients (mean age: 63.2 ± 10.5 years; 33% female) were enrolled. A mean of 58.29 ± 9.7 pulsed field applications were delivered without evidence of clinically significant hemolysis. Compared with baseline, haptoglobin levels significantly decreased post-PFA (0.76 ± 0.35 vs. 0.20 ± 0.24 g/L, P < 0.0001), while LDH increased markedly (187.1 ± 37.2 vs. 313.7 ± 52.1 U/L, P < 0.0001). Direct and indirect bilirubin levels also rose significantly (direct: 2.08 ± 1.85 vs. 8.78 ± 3.81 μmol/L; indirect: 11.38 ± 7.52 vs. 27.18 ± 15.10 μmol/L; both P < 0.0001). In contrast, serum creatinine remained stable (78.8 ± 18.6 vs. 82.6 ± 21.2 μmol/L, P = 0.60001), indicating no short-term renal impairment.

Conclusions:

In patients with persistent AF, PFA is associated with significant periprocedural hemolysis, but not with clinically relevant renal dysfunction. Further studies are warranted to assess thresholds of PFA applications and long-term renal safety.

Efficacy and Safety of a Novel Method Stimulating Superior Vena Cava Approach via Femoral Vein to Facilitate Ethanol Infusion of the Vein of Marshall in Atrial Fibrillation

qinchao wu, Yun-Long Wang

Beijing Anzhen Hospital affiliated to Capital Medical University

Abstract:

Aims: Ethanol infusion of the vein of marshall (EI-VOM) has been widely used to facilitate atrial fibrillation (AF) ablation and block of mitral isthmus. However, some sophisticated cases can't be finished limited by anatomical constraints. This study aimed to introduce and evaluate a novel method of EI-VOM stimulating superior vena cava approach using steerable sheath.

Methods: From July 2024 to July 2025, consecutive AF or atrial flutter (AFL) patients scheduled for radiofrequency catheter ablation and EI-VOM at Beijing Anzhen Hospital were enrolled. When the VOM venography was successfully performed, the conventional method of EI-VOM was attempted firstly and if it failed or took more than 20 minutes, the novel method stimulating superior vena cava approach was applied. Procedural process for the novel method included: 1) The VOM is identified by CS venography; 2) the wire is advanced to the distal coronary sinus to ensure adequate support; 3) the steerable sheath is shaped into a 90° - 180 ° curve to form an inverted U-configuration with the wire providing support; 4) the JR4 guiding is withdrew and rotated to align the guiding catheter's tip with the VOM 7ostium; 5) the wire and balloon is advanced into the VOM; 6) the balloon is inflated at 6-8 atm; 7) the VOM is stained after ethanol injection. We analyzed the efficacy and safety of EI-VOM by new method in detail. Meanwhile, the anatomical structure of VOM and isthmus of tricuspid valve were analyzed by X-ray. The length of CTI and the angle between VOM and the branch of distal CS was measured in the right anterior oblique (RAO) view. The distance from the VOM ostium to the CS ostium in the left anterior oblique (LAO) and RAO views was recorded.

Results: Of the 200 patients enrolled in this study, the novel method was applied in 39 patients and led to a 97.4% successful rate of EI-VOM (38/39). Patients had a mean age of 60.18±8.8 years old, and 71.8% were male. In the overall population, paroxysmal AF was present in 7.7%, persistent AF in 82.1%, and AFL in 10.2%. The mean LA dimension and LA volume were 44.72±4.7 mm and 144.15±27.5 ml, respectively. Of the 39 patients, eighteen (46.2%) had long a cavo tricuspid isthmus, fifteen (38.5%) had a VOM ostium close to the coronary sinus ostium, nine (23.1%) had a prominent Eustachian ridge, and six (15.4%) had abnormal VOM ostium. The mean distance from the VOM ostium to the CS ostium in the RAO and LAO view was 8.82±4.50 and 24.06±10.97mm, respectively. The mean distance of CTI was 39.27±7.23 mm in the RAO view. The mean angle between the VOM and the main branch of CS was 35.59± 25.05. The total mean procedure time of EI-VOM using novel method was 29.82±4.3 min, radiated with exposure of X-ray at a dose of 735.46±529.4 mGy. No serious complications occurred in the patients using novel method.

Conclusions: For patients with specific anatomical structures, we developed a novel method stimulating superior vena cava approach using steerable sheath with high successful rate of EI-VOM and favorable safety.

Mechanism of hydrogen sulfide alleviating atrial fibrillation induced by acute obstructive sleep apnea based on proteomic differential protein glutaredoxin-1

Hui-Ning Huang[1], Ya-Qing Zhao[2], Yi Sun[3], Ying-Long Hou[3], Mei Gao[3,4]

1. The First People's Hospital of Pinghu

2. The People's Hospital of Jiaxiang

3. The First Affiliated Hospital of Shandong First Medical University & Shandong Provincial Qianfoshan Hospital

4. member of the lipid management committee

Mechanism of hydrogen sulfide alleviating atrial fibrillation induced by acute obstructive sleep apnea based on proteomic differential protein glutaredoxin-1

Huining Huang[1], Yaqing Zhao[2], Yi Sun[3], Yinglong Hou, Mei Gao[3,4#]

1 Department of Cardiology, The First People's Hospital of Pinghu, Jiaxing, Zhejiang, 314000, China.

2 Department of Cardiology, The People's Hospital of Jiaxiang, Jining, Shandong, 272000, China.

3 Department of Cardiology, The First Affiliated Hospital of Shandong First Medical University & Shandong Provincial Qianfoshan Hospital, Shandong Medicine and Health Key Laboratory of Cardiac Electrophysiology and Arrhythmia, Jinan, Shandong, 250012, China.

4 member of the lipid management committee

Correspondence: gaomei0217@163.com

Abstract

Objective: This study aims to quantify the differentially expressed proteins in the left atrial appendage (LAA) between the acute obstructive sleep apnea (OSA)-induced atrial fibrillation (AF) group and the control group using TMT-based quantitative proteomics. Additionally, the study explores the mechanism through which hydrogen sulfide (H2S) mitigates acute OSA-induced AF by focusing on the differentially expressed protein glutaredoxin-1.

Methods: Twelve adult New Zealand white rabbits were randomly assigned to either the control group or the OSA-induced AF group (n = 6). TMT-based proteomics was employed to quantify the differentially expressed proteins in the LAA, followed by bioinformatics analysis. The upregulated protein ACTB and the downregulated protein GLRX were selected for validation through Western blotting. Sodium hydrosulfide (NaHS), an exogenous H2S donor, was administered. Twenty-four adult male SD rats were randomly divided into four groups: control group, OSA-induced AF group (OSA group), NaHS + OSA group (NaHS group), and cadmium chloride + NaHS + OSA group (CdCl2 group) (n = 6). An OSA-induced AF model was established as per previous studies. After the experiment, the rats were euthanized, and LAA tissues were collected. Immunofluorescence and ELISA were used to measure the expression of glutaredoxin-1 in the LAA. Western blotting assessed the expression of gap junction protein connexin-43 (Cx43), while the thiobarbituric acid reactive substances (TBARS) assay was used to determine malondialdehyde (MDA) levels.

Results: A total of 3,596 proteins were identified, with 54 showing statistically significant differential expression (fold change > 1.2 for upregulated proteins or < 0.83 for downregulated proteins, P < 0.05). Of these, 24 proteins were upregulated, and 30 were downregulated. Western blotting confirmed that the expression patterns of ACTB and GLRX were consistent with the proteomic data. Bioinformatics analysis indicated that the differentially expressed proteins were primarily involved in binding, structural molecular activity, catalytic activity, molecular function regulation, and transcription regulation. These proteins were implicated in key biological processes, including cellular processes, biological regulation, stimulus responses, and metabolic pathways. Significant alterations were observed in important pathways such as hypertrophic cardiomyopathy, dilated cardiomyopathy, and adherens junctions. Compared to the OSA group, the NaHS group exhibited reduced frequency and duration of atrial fibrillation (P < 0.05). Additionally, compared to the control group, the OSA group showed decreased glutaredoxin-1 expression, elevated MDA levels, and reduced Cx43 expression. In contrast, the NaHS group demonstrated increased glutaredoxin-1 expression, decreased MDA levels (P < 0.01), and upregulated Cx43 expression. Following the application of the glutaredoxin-1 inhibitor CdCl2 in the NaHS group, MDA levels increased (P < 0.01), Cx43 expression was downregulated, and the protective effect of H2S on OSA-induced AF was abolished.

Conclusion: Exogenous H2S mitigates acute OSA-induced AF by modulating oxidative stress through glutaredoxin-1, thereby regulating Cx43 expression in the LAA.

心房颤动经皮射频消融护理质量评价指标体系的构建及应用

童可欣 刘华芬

武汉大学人民医院

目的：房颤是最常见的心律失常，经皮射频消融作为一线治疗手段，其成功率与围手术期护理质量密切相关，构建心房颤动患者经皮射频消融护理质量评价指标体系并验证其应用效果，从而提高心房颤动患者射频消融护理质量，本研究基于护理质量管理理论构建专科化评价体系，为临床护理质量改进提供依据。方法：运用三维质量模型，通过文献资料分析、访谈、专家函询法及层次分析法，从结构（资源配置）、过程（护理行为）、结果（健康结局）三个维度构建指标体系，确立心房颤动经皮射频消融护理质量评价标准，并在临床验证其效果。结果：研究构建了包含 3 个一级指标、10 个二级指标、32 个三级指标的心房颤动经皮射频消融护理质量评价体系。临床应用后干预组术中与术后中重度疼痛发生率、感染发生率、24 小时日常生活需他人照护数低于对照组（P < 0.5），平均住院费用低于对照组，差异无统计学意义（P > 0.5）。指标体系的特点：专科特异性、过程导向性、量化可操作（如“术后 2h 内完成首次心电图复查率达 100%），局限性：未纳入经济指标，需多中心验证远期效果。结论：研究构建的心房颤动经皮射频消融护理质量评价指标体系有较好的科学性和实用性，有利于改善患者结局，促进护理质量的提升，应用后可显著改善患者预后，建议后续开发智能化评价系统以实现动态检测。

AI 智能管理平台对房颤患者射频消融术后心脏康复干预效果分析

刘平 刘华芬

武汉大学人民医院

目的：探讨 AI 智能管理平台对房颤患者射频消融术后心脏康复干预效果分析。方法：选取武汉大学人民医院心律失常科 2024 年 1 月至 2024 年 12 月收治的行射频消融术后的房颤患者 100 例，采用投掷法将患者随机分为对照组和观察组，每组 50 例。对照组患者接受常规居家运动康复指导及随访管理，观察组患者患者需佩戴可监测心率及血压的移动智能设备，由 AI 智能平台对患者移动数据及综合信息进行实时动态分析督导下进行为期 6 个月的运动、心理、用药、风险预警等综合干预的远程家庭指导，制定个性化的康复运动计划，并根据患者生命体征及自诉症状进行动态评估调整。两组患者干预 6 个月后对患者康复运动行为，生活质量及满意度等情况进行比较分析。结果：干预后有 3 例对照组和 1 例观察组患者失访，其余 96 例患者完成全部资料的收集。干预前两组在性别、年龄、文化程度、既往病史等一般资料比较，无统计学差异（P > 0.05）。干预 6 个月后观察组在心率控制、康复运动行为、满意度情况均高于对照组，差异均有统计学意义 (P<0.05). 结论：通过 AI 智能管理平台管理有助于提高房颤患者射频消融术后心脏康复运动的依从性及满意度，改善患者的生活质量，为提高房颤患者安全风险管控提供临床参考。

风险评分系统在预测胸腔镜下心房颤动消融术后复发中的价值

刘文杰 [1,2] 杨沐 [1,2] 郦明芳 [1]

1. 江苏省人民医院 / 南京医科大学第一附属医院

2. 南京医科大学附属泰州人民医院

目的：评估 CHA_2DS_2-VASc、APPLE、CAAP-AF 三种风险评分系统对心房颤动（简称房颤）患者接受胸腔镜下房颤消融术后房颤复发的预测价值。

方法：本研究为基于 5A 队列（胸腔镜下房颤消融 + 左心耳切除队列）的二次数据分析。原始队列为前瞻性队列研究，纳入在 2013 年 5 月至 2021 年 5 月期间在本中心接受胸腔镜下房颤消融联合左心耳切除术的房颤合并血栓栓塞患者共 173 例。本研究筛选出可计算 CHA2DS2-VASc、APPLE 及 CAAP-AF 评分的患者作为研究对象。使用受试者工作曲线（Receiver Operating characteristic Curves, ROC）和 logistic 回归分析评估不同评分系统对消融后 3-12 个月房颤复发的预测价值。

结果：本研究最终纳入 158 例患者进行分析，平均年龄为 62 ± 8 岁， 男性 112 例（70.9%），阵发性房颤 86 例（54.4%）。患者的平均 CHA_2DS_2-VASc 积分为 4 ± 1 分，HAS-BLED 评分平均为 2 ± 1 分。消融后 3-12 个月复发 60 例 (38.0%)，未复发 98 例 (62.0%)。logistic 回归分析显示 APPLE 评分 (OR:1.54，95% CI: 1.08 - 2.20 , p=0.018） 和 CAAP-AF 评 分（OR：1.34，95% CI: 1.10 - 1.62 , p=0.004）是消融后 3-12 月内复发的预测因子，而 CHA_2DS_2-VASc 积分与术后房颤复发之间的关联无显著性（OR：0.89，95% CI: 0.67 - 1.19 , p=0.437）。ROC 曲线显示， APPLE 评分曲线下面积为 0.614，CAAP-AF 评分为 0.641，两者之间差异无统计学意义（p=0.37）。

结论：本研究提示对于接受胸腔镜下房颤消融联合左心耳切除的患者，APPLE 和 CAAP-AF 评分系统对术后 1 年内房颤复发具有一定的预测价值。APPLE 和 CAAP-AF 评分系统可作为筛选更适合接受该术式患者的参考工具。

瓣膜病房颤和非瓣膜病房颤的区别和抗凝策略的差异

向珍贤

重庆医科大学附属第一医院

心房颤动（房颤）是临床最常见的心律失常之一，可分为瓣膜病房颤和非瓣膜病房颤，但临床医生常将其混淆。根据目前的指南，瓣膜病房颤是指机械瓣置换术后或二尖瓣中 - 重度狭窄合并的房颤，其他的均为非瓣膜病房颤。区别瓣膜病和非瓣膜病房颤是由于其血栓形成的机制和栓塞风险及抗凝策略不同，目前瓣膜病房颤只能使用维生素 K 拮抗剂（华法林）抗凝，而非瓣膜病房颤可选择华法林或新型口服抗凝药（NOACs），首选 NOACs。现就瓣膜病和非瓣膜病房颤定义的演变和药物治疗的循证作一综述，旨在让临床医生对瓣膜病和非瓣膜病房颤的诊治有更好的理解。心房颤动（房颤）是临床最常见的心律失常之一，可分为瓣膜病房颤和非瓣膜病房颤，但临床医生常将其混淆。根据目前的指南，瓣膜病房颤是指机械瓣置换术后或二尖瓣中 - 重度狭窄合并的房颤，其他的均为非瓣膜病房颤。区别瓣膜病和非瓣膜病房颤是由于其血栓形成的机制和栓塞风险及抗凝策略不同，目前瓣膜病房颤只能使用维生素 K 拮抗剂（华法林）抗凝，而非瓣膜病房颤可选择华法林或新型口服抗凝药（NOACs），首选 NOACs。现就瓣膜病和非瓣膜病房颤定义的演变和药物治疗的循证作一综述，旨在让临床医生对瓣膜病和非瓣膜病房颤的诊治有更好的理解。

Catheter Ablation versus Non-ablation in Atrial Fibrillation Patients Aged ≥ 80 years: Results from the China Atrial Fibrillation Registry

Mei-qi Zhao[1], Si-Tong Li[1], Cong Yuan[2], Liu He[1], Ning Zhou[1], Cai-Hua Sang[1], De-Yong Long[1], Xin Du[1], Jian-Zeng Dong[1,3], Chang-Sheng Ma[1]

1. Department of Cardiology, Beijing Anzhen Hospital, Capital Medical University, National Clinical Research Center for Cardiovascular Diseases, Beijing, China

2. The Affiliated Changsha Hospital of Xiangya School of Medicine, Central South University, Changsha, Hunan, China

3. First Affiliated Hospital of Zhengzhou University: Zhengzhou, Henan Province

Aims: Atrial fibrillation (AF) is increasingly prevalent among the elderly due to rapid population aging. Although catheter ablation has been shown to provide greater benefit than antiarrhythmic drugs (AADs) in reducing atrial arrhythmia recurrence and healthcare utilization in AF patients, the evidence in patients aged ≥ 80 years are limited. Our study aimed to evaluate the effect of catheter ablation in these population.

Methods: This study utilized data from the China Atrial Fibrillation Registry (China-AF), a prospective, multi-centered cohort enrolling patients with documented AF from 31 hospitals in Beijing between August 2011 and December 2022. Patients with age ≥ 80 years, documented type of AF, echocardiographic assessment and a follow-up ≥ 6 months were included in this study, with regular follow-up of every 6 months. Patients were divided into ablation and non-ablation groups based on baseline ablation status. The primary outcome was the composite of cardiovascular hospital and all-cause death. Secondary outcomes included cardiovascular hospitalization, cardiovascular death, thromboembolism, major bleeding and AF recurrence. Multivariate Cox proportional hazards models and overlap weighting Cox model were performed to evaluate the association between ablation and outcomes, respectively. Subgroup analyses were also conducted using multivariable Cox proportional hazards regression model, stratified by gender, body mass index, type of AF, left ventricular ejection fraction, left atrial diameter, history of thromboembolism, major bleeding, diabetes mellitus, vascular disease, heart failure, hypertension, chronic kidney disease and OAC use at 6 months. All statistical analyses were performed using R version 4.4.2. A P value of <0.05 on the two-sided test was considered statistically significant.

Results: A total of 1,331 patients were included (mean age 83.6 ± 3.0 years, 49.3% female, 19.9% underwent ablation). In non-ablation group, 177 (16.6%) used AADs,

712 (66.8%) used rate control drugs and the remaining 314 (29.5%) used neither of the drugs. Patients who underwent catheter ablation were younger, had a shorter duration of AF, a lower proportion of persistent AF, heart failure and left atrial enlargement. Compared with non-ablation patients, patients underwent ablation had a significantly lower incidence rate of the composite outcome (12.5 vs. 21.3 per 100 person-years). After multivariable adjustment, catheter ablation was associated with a reduced risk of the composite outcome (HR 0.73, 95% CI: 0.59–0.91, P = 0.005), and this association remained significant after overlap weighting (HR 0.74, 95% CI: 0.58–0.95, P = 0.018). Catheter ablation was also associated with a markedly lower risk of cardiovascular death (adjusted HR 0.32, 95% CI: 0.18–0.57; overlap weighted HR 0.28, 95% CI: 0.14–0.57; both P < 0.001) and AF recurrence (adjusted HR 0.31, 95% CI: 0.26–0.38; overlap weighted HR 0.29, 95% CI: 0.24–0.36; both P < 0.001). No significant differences were observed in cardiovascular hospitalization, thromboembolism, or major bleeding between groups after adjustment or weighting (P all > 0.05). No significant interaction effects were found in most subgroups for the primary outcome and AF recurrence, except for hypertension status subgroup. Among patients with hypertension, catheter ablation showed a stronger association with reduced risk of the composite outcome than non-hypertension group (P for interaction < 0.05).

Conclusion: In patients aged ≥ 80 years, catheter ablation was associated with significantly lower risks of the composite outcome of cardiovascular hospitalization or death, cardiovascular death, and AF recurrence, without increasing risks of thromboembolism or major bleeding. These findings indicate possible effectiveness of catheter ablation in AF patients aged ≥ 80 years. Further randomized controlled trial are needed to provide more robust evidence.

LOXL2 as a Predictive Biomarker for Breakthrough Stroke Risk in Paroxysmal Atrial Fibrillation Patients

Fang Liu, De-Yong Long

首都医科大学附属北京安贞医院

Background:

Breakthrough stroke, defined as an ischemic stroke that occurs despite adequate oral anticoagulation, remains a significant clinical concern in patients with paroxysmal atrial fibrillation (PAF). These events are associated with substantial morbidity and mortality and pose diagnostic and prognostic challenges. Although the CHA2DS2-VASc score remains the standard tool for assessing stroke risk in atrial fibrillation (AF), it often fails to identify high-risk individuals who may still develop stroke while on anticoagulation. Emerging evidence suggests that atrial remodeling, particularly atrial fibrosis, plays a critical role in the pathophysiology of cardioembolic events. Lysyl oxidase-like 2 (LOXL2), an enzyme involved in collagen cross-linking and fibrotic remodeling, has been implicated in the development of atrial fibrosis and arrhythmogenesis. However, its clinical relevance in predicting stroke events in anticoagulated AF patients remains largely unexplored and uncertain.

Objective:

This study aimed to investigate the predictive value of serum LOXL2 levels for breakthrough stroke in anticoagulated patients with PAF and to evaluate whether incorporating LOXL2 improves upon existing clinical risk stratification tools, particularly the CHA2DS2-VASc score.

Methods:

We conducted a prospective cohort study involving 197 patients with non-valvular PAF who were receiving oral anticoagulant therapy. Serum LOXL2 levels were measured using enzyme-linked immunosorbent assay (ELISA). Patients were dichotomized into LOXL2+ and LOXL2 – groups based on the median serum LOXL2 level (275.9 pg/mL). The primary outcome was the incidence of ischemic stroke during follow-up, defined as new neurologic deficits confirmed by neuroimaging. Patients were followed for a median duration of 3.88 years. Kaplan-Meier and Nelson-Aalen analyses were used to assess time-to-event differences between groups. Multivariate Cox regression was used to identify independent predictors of stroke. The added predictive value of LOXL2 was evaluated using ROC analysis, net reclassification improvement (NRI), and decision curve analysis (DCA).

Results:

During follow-up, 24 patients (12.2%) experienced a breakthrough stroke. Those with stroke were significantly older and had higher baseline serum LOXL2 levels (419.8 ± 229.4 vs. 278.8 ± 81.4 pg/mL, P = 0.006). Multivariate Cox regression identified LOXL2 (HR = 1.01, P < 0.001), age (HR = 1.13, P = 0.012), and antiplatelet use (HR = 3.21, P = 0.037) as independent predictors of stroke. Kaplan-Meier survival analysis showed significantly lower stroke-free survival in the LOXL2+ group (P = 0.030). ROC curve analysis revealed that a model incorporating LOXL2 and age (Model C) had the highest predictive value (AUC = 0.842), outperforming both the CHA2DS2-VASc score and other combinations. Model C also showed greater clinical utility in DCA and yielded a significant NRI of 15.0% over CHA2DS2-VASc alone (P < 0.001).

Conclusion:

Serum LOXL2 is an independent predictor of breakthrough stroke in patients with PAF receiving anticoagulation therapy. Elevated LOXL2 levels reflect underlying atrial fibrosis and may serve as a valuable biomarker for identifying patients at residual risk of thromboembolism despite guideline-directed therapy. Incorporating LOXL2 into conventional risk models significantly enhances predictive performance, offering a novel and more precise strategy for individualized stroke risk assessment. These findings highlight the potential of LOXL2 to improve secondary stroke prevention and support its further evaluation in larger, multicenter prospective trials worldwide.

CEP68/FLRT2: The potential druggable genes for Atrial Fibrillation identified by Systematic druggable genome-wide Mendelian randomization

Jing-Han Zhou[1], -Yu Dong[1], Fei Liu[1], Jin-Pu Zhang[1], - Peng[1], Yu-Hang Wen[1], Yu Gao[1], Tesfaldet Hidru[1], Jia-Yue Yang[2], Yun-Long Xia[1], Xiao-Lei Yang[1]

1. First Affiliated Hospital of Dalian Medical University

2. Liverpool School of Tropical Medicine

Background

Atrial fibrillation (AF), a globally prevalent arrhythmia with escalating incidence, still lacks effective treatments focusing on its substrate. Antiarrhythmic agents like amiodarone, which focus on rhythm control, are associated with more hospitalizations and adverse effects, such as bradycardia and extracardiac toxicities. Despite catheter ablation has been applied to maintain sinus rhythm, it is an invasive procedure associated with complications ranging from cardiac tamponade to stroke. Contemporary management strategies predominantly focus on symptomatic relief rather than addressing the underlying substrate of AF. Furthermore, preventative measures aimed at averting the onset of AF are inadequately defined within current paradigms, and upstream treatment strategies for AF are not well understood. Mendelian Randomization (MR) has been widely used to discover potential druggable targets. Leveraging the genetic predisposition to AF, this study employed systematic druggable genome-wide MR to identify novel therapeutic targets.

Method

We performed traditional two-sample MR and Summary-data-based Mendelian Randomization (SMR) analyses to assess causal relationships between druggable genes and AF risk. A comprehensive list of 5,883 druggable genes sourced from the Drug-Gene Interaction Database and a review conducted by Finan was compiled from the Drug-Gene Interaction Database and a published review. We integrated cardiac (atrial/ventricular) expression quantitative trait loci (eQTLs) from GTEx, blood eQTLs from eQTLGen, and blood protein QTLs (pQTLs) from the deCODE study with AF genome-wide association study (GWAS) data (60,620 cases; 970,216 controls). Colocalization analysis and heterogeneity in dependent instruments (HEIDI) tests distinguished shared causal variants. Phenome-wide association studies (PheWAS) evaluated potential side effects using phenotype statistics of the UK Biobank cohort. Sensitivity analyses included MR-PRESSO for pleiotropy and F-statistics for instrument strength. Statistical power was calculated by using the mRnd method.

Result

Our integrated analysis identified 21 potential druggable genes significantly associated with AF risk (ALB, BAZ2A, CASQ2, CEP68, F10, FLRT2, GYPC, HABP4, JAM2, KCNJ5, KDM1B, PMVK, PRKD3, PROZ, PSMC5, PXN, SF3B1, THRB, TNNT3, TPMT, WDR1). Crucially, two genes (CEP68, FLRT2) demonstrated significance in both cardiac and blood tissues.

CEP68 showed a positive association with AF in MR analyses for atrial (OR: 1.13, 95% CI: 1.04-1.22) and ventricular tissue (OR: 1.15, 95% CI: 1.05-1.25), with SMR analyses confirming this relationship. PheWAS further validated its specific link to AF/atrial flutter phenotypes. Similarly, FLRT2 exhibited significant protective effects in MR for atrial tissue (OR: 0.86, 95% CI: 0.80-0.93) and blood (OR: 0.93, 95% CI: 0.90-0.97), supported by SMR evidence including blood pQTL data (pSMR<0.001). Colocalization (ppH4 > 0.75) and HEIDI tests (p > 0.05) confirmed shared causal variants for both genes. In contrast, MR analysis of genes targeted by conventional antiarrhythmic drugs (e.g., Amiodarone) yielded no significant associations after multiple-testing correction.

Conclusion

This study identified 21 potential drug target genes for AF using MR and SMR analyses. Among these, two genes, CEP68 and FLRT2, exhibited significant associations in both cardiac tissue and blood. Our findings provide genetic evidence supporting these targets. Although the roles of CEP68 and FLRT2 in AF are not yet fully understood, this study paves the way for future investigations into the pathophysiology of AF and the development of novel therapies. Further clinical studies evaluating the safety and efficacy of drugs targeting these genes are essential for confirming their potential therapeutic benefits.

经皮左心耳封堵术后中期口服抗凝治疗与抗血小板治疗的疗效的比较

李松南 李昌义 周篪 李梦梦 龙德勇

首都医科大学附属北京安贞医院

背景与研究目的

在临床实践中，左心耳封堵术中期阶段的抗栓治疗策略尚缺乏明确证据。通常，单独进行左心耳封堵术术后的“早期阶段”定义为术后 45 天，而联合射频消融治疗时则定义为术后 3 个月。因此，我们将术后早期阶段结束至术后 6 个月的时间段定义为“中期阶段”。在此阶段，抗凝治疗与抗血小板治疗之间的疗效与安全性差异仍未明确。为填补这一证据空白，本研究旨在评估现实世界中在左心耳封堵术术后中期阶段使用 WATCHMAN 装置植入的患者中，不同抗栓治疗策略的安全性和有效性。

方法

本研究为前瞻性、单中心、队列研究，共纳入 374 例连续接受经皮左心耳封堵术的患者，所用装置为 WATCHMAN 封堵器。患者根据术后抗栓策略分为两组：口服抗凝治疗组和抗血小板治疗组。主要复合终点为术后 6 个月内发生的心源性死亡、缺血性卒中 / 短暂性脑缺血发作（TIA）/ 全身性栓塞事件及主要出血事件。次要终点包括心血管死亡、装置相关血栓栓塞事件以及主要终点中各单项事件的发生率。

结果

多变量 Cox 回归分析结果显示，抗血小板组与抗凝治疗组在主要复合终点的风险上无统计学差异（调整后风险比 HR=0.76，95% 置信区间 CI：0.40-1.49，P=0.447）。在次要终点方面，两组间包括心源性死亡、心血管死亡、缺血性卒中 / 全身栓塞、主要出血事件以及器械相关血栓栓塞事件的发生率也均无显著差异。

结论

本研究结果提示，在 WATCHMAN 封堵装置植入术后的中期阶段，口服抗凝治疗与双联抗血小板治疗在安全性与疗效方面可能具有相似的表现。这为临床在术后中期阶段的抗栓策略选择提供了现实世界证据支持。

关键词：房颤；左心耳封堵术；抗凝治疗；抗血小板治疗

心腔内超声结合全三维技术实施零射线个体化房间隔穿刺

魏博 李志勇 王历 苟文 苏婷 张海涛 赖溱 喻荣辉 刘念

重庆市第二人民医院

目的：评估经我们整合及改进后的心腔内超声（intracardiac echocardiography,ICE）结合全三维（total 3-dimensional,T3D）技术实施零射线个体化房间隔穿刺的可行性和安全性。

方法：入选 2021 年 4 月至 2024 年 3 月于重医附属永川医院行房颤射频消融术的房颤患者 112 例。根据所采用房间隔穿刺方法按 1:1 比例随机分为 ICE+T3D 组（n=56 例）和 ICE 组（n=56 例）。记录两组患者基线资料，统计两组患者的心房重建时间、冠状窦电极到位时间、房间隔穿刺过程中超声扇面调整次数、房间隔穿刺时间、消融前预处理时间、并发症发生率、X 线曝光时间及暴露剂量等参数。

结果：两组患者基线资料差异无统计学意义。ICE+T3D 组的房间隔穿刺过程中超声扇面调整次数、房间隔穿刺时间小于 ICE 组 [(1.70±0.63) 次 VS.(5.34±1.71) 次 ,P < 0.001]、[(3.66±1.09)min VS.(4.90±1.92)min,P < 0.001]。 但 ICE+T3D 组的心房重建时间、消融前预处理时间长于 ICE 组 [(22.44±3.13)min VS.(12.34±2.12)min,P < 0.001]、[(49.41±3.52)min VS.(37.65±4.04)min,P < 0.001]。ICE+T3D 组有 43（76.8%）例患者在消融前预处理阶段实现零射线，有 13 例患者因推送导管困难而使用 X 射线 , 但这些患者的 X 射线暴露时间及剂量均小于 ICE 组 [(1.68±0.72)min VS.(3.14±1.95)min,P=0.010]、[(6.28±2.78) mGy VS.(23.85±21.32) mGy,P=0.004]。在房间隔穿刺阶段中，ICE+T3D 组全部实现零射线，而 ICE 组有 11(19.6%) 例使用 X 射线。并发症方面，两组均无心包填塞、误穿主动脉、栓塞等致命性并发症，均有 1(1.8%) 例血管并发症。

结论：经我们整合及改进后的心腔内超声结合全三维技术可以安全可靠地实施零射线个体化房间隔穿刺。

房颤发生率在胸腔镜肺段切除与肺叶切除肺癌患者中的差异性研究

张玉琨

中国人民解放军空军军医大学第二附属医院

一、研究目的

比较肺癌患者接受不同胸腔镜手术方式后房颤的发生率，探索术后房颤发生的相关影响因素，为临床治疗策略优化提供参考。

二、研究方法

回顾性分析 2022 年 12 月 1 日至 2024 年 12 月 1 日期间，我院胸腔外科同一手术组实施胸腔镜手术的肺癌患者临床资料。根据手术方式分为肺叶切除组与肺段切除组，统计两组术后房颤发生率，并分析可能影响房颤发生的相关因素。

三、研究结果

基线数据与术后房颤发生率

共纳入符合标准的患者 325 例，其中肺叶切除组 212 例，肺段切除组 113 例。术后共有 21 例患者出现房颤，总发生率为 6.46%。

肺叶切除组：18 例发生房颤，发生率为 8.49%；

肺段切除组：3 例发生房颤，发生率为 2.65%。

单因素分析结果

对比房颤患者与无房颤患者的临床指标，发现以下因素差异具有统计学意义（P<0.05）：

平均年龄（P=0.034）；

术前一秒率（第一秒用力呼气容积占用力肺活量比值，FEV_1/FVC，P=0.001）；

淋巴结清扫方式（P=0.036）；

手术时间（P=0.043）。

多因素 Logistic 回归分析结果

进一步分析显示，以下因素为术后房颤发生的独立影响因素（P<0.05）：

手术方式（肺叶切除相较于肺段切除，风险更高）；

术前 $FEV_1/FVC \leq 70\%$；

手术时间延长。

四、结论

手术方式对肺癌患者术后房颤发生率有显著影响，与肺叶切除术相比，肺段切除术可显著降低术后房颤发生风险（2.65% vs 8.49%）。

患者术前肺功能（$FEV_1/FVC \leq 70\%$）及手术时间是术后房颤发生的重要影响因素，临床中应针对性优化术前评估与手术流程，以减少术后房颤的发生。

Ablation Lesion Characteristics with ODOT MICRO Catheter Modes Versus Conventional Power Control: A Comparative Analysis

Mei-Xue Jia, Bin Ning

Fuyang People’s Hospital

Background: With the advent of novel radiofrequency ablation (RFA) modalities including temperature/flow-controlled (TFC) QDOT MICRO ™

catheters and very high-power short-duration (vHPSD) approaches, this study systematically quantifies biomechanical lesion characteristics under ablation index (AI) guidance, comparing differential effects of TFC/vHPSD versus conventional power-controlled (PC) modes across critical procedural parameters.

Methods and Results: An ex vivo perfused porcine heart model (37 ° C saline perfusion at 300 mL/min flow rate simulating intracardiac blood flow) was employed to evaluate lesions under three experimental dimensions:Mode comparison: Fixed contact force (CF=10g) conditions assessing TFC (AI targets: 400/500), vHPSD (50W power with 5-10s duration), and PC (AI400/500).Graded CF effects: Controlled pressures of 5g, 15g (TFC/PC), and additional 25g (vHPSD).Sequential ablation: Consecutive applications (1-3) at identical sites.Morphometric analysis included surface width (SW), maximum depth (Dmax), lesion volume (Vol), and impedance drop (ΔImp), quantified after triphenyltetrazolium chloride (TTC) staining with strict viability thresholds (pale lesion area <10% total ablation zone). Statistical validation used one-way ANOVA with Tukey's post-hoc testing (significance: α=0.05).

Key Findings: Mode-specific differentials:TFC vs PC: At AI400, TFC produced 26.4% shallower lesions versus PC (Dmax: 2.64±0.36mm vs 3.58±0.41mm; P<0.001) with no SW difference (P=0.12). Conversely, at AI500, TFC expanded SW by 18.9% (6.78±0.43mm vs PC's 5.70±0.52mm; P=0.003) while maintaining equivalent Dmax (5.21±0.39mm vs 5.18±0.41mm; P=0.87). PC consistently exhibited higher baseline impedance (mean Δ13.7Ω; P<0.01).vHPSD vs TFC: vHPSD generated 34.2% smaller Vol than TFC-AI500 (15.21±2.8mm^3 vs 23.12±3.4mm^3; P<0.0001), accompanied by reduced ΔImp at AI400 (Δ16.1Ω vs TFC's Δ22.4Ω; P=0.008), indicating distinct energy-delivery efficiency.CF-driven depth modulation:Increasing CF to 15g significantly enhanced Dmax-:TFC-AI400: 27.7% depth increase (3.37±0.56mm vs 2.64±0.36mm at 5g; P=0.013);TFC-AI500: 31.6% depth augmentation (6.78±0.43mm vs 5.15±0.82mm; P<0.0001);vHPSD exhibited CF hyper-sensitivity: At 25g, Dmax surged 103.1% relative to 5g (5.81±0.38mm vs 2.86±0.41mm; P<0.0001), whereas SW remained pressure-insensitive across all modes (CV<8%).Sequential ablation amplification:Repeat applications fundamentally altered lesion geometry:vHPSD achieved maximal Dmax at second application (21.4% increase: 4.19±0.52mm vs 3.45±0.44mm; P<0.0001);TFC400 expanded SW by 23.1% post-second ablation (5.91±0.73mm vs 4.80±0.65mm; P=0.002);TFC500 demonstrated dramatic 109.2% Vol inflation after two ablations (P<0.001), suggesting cumulative thermal effects.Transmural continuity optimization:When deploying 6-mm spacing:TFC500 achieved 100% continuous transmural lines (0 gaps), significantly surpassing vHPSD (75% gap incidence, max gap=0.95mm) and TFC400 (87.5% gaps, max=0.7mm) (P<0.05).Gap formation correlated with Vol reduction in vHPSD (R^2=0.73) and low-AI TFC (R^2=0.68), revealing volumetric thresholds for continuity.

Conclusion: AI settings, CF magnitude, and ablation sequence collectively govern lesion architecture through three mechanistic axes: (1) AI dictates depth-width equilibrium shifts (high-AI favors width, low-AI favors depth), (2) CF selectively potentiates tissue penetration without altering surface dimensions, and (3) repeat applications exponentially expand damage geometry. Crucially, TFC500 uniquely enables >6-mm continuous ablation lines – a critical threshold for pulmonary vein isolation efficacy.

Innovation and Significance: This work provides four transformative advances:First biomechanical validation of CF-dependent depth ceilings for vHPSD (>25g required for deep lesions)Quantification of "Ablation Sequence Multipliers" : Demonstrated 2.09× Vol inflation in TFC500 repeat ablations.Clinical-engineering bridge: TFC500's continuity at wide spacing (6-mm vs. current 4-5mm clinical standards) may reduce procedural time by ≥ 40%.Safety implications: vHPSD's impedance stability (ΔImp<17Ω) correlates with reduced steam pop risk (R^2=0.82 in supplementary data)This framework redefines RFA parameter optimization, offering actionable insights for designing efficient, durable, and complication-minimized ablation protocols.

Trends and Appropriateness of OACs Use in Atrial Fibrillation: A Decade of Real-World Evidence from the China-AF Registry (2011–2022)

Yuexin Jiang, De-Yong Long, Liu He, Shengma Chang

Beijing AnZhen Hospital, Capital Medical University, Beijing, China

Background:

Atrial fibrillation (AF) is a major risk factor for thromboembolic complications, especially ischemic stroke. Oral anticoagulants (OACs), including vitamin K antagonists (VKAs) and direct oral anticoagulants (DOACs), are the cornerstone of stroke prevention in AF. In recent years, DOACs have become increasingly favored over warfarin due to their improved safety and convenience. However, inappropriate dosing of DOACs remains a major clinical concern. This study aimed to assess the trends, dosing appropriateness, and predictors of DOAC use in patients with non-valvular AF (NVAF) based on a decade of nationwide registry data from China.

Methods:

The China-AF Registry is an ongoing, prospective, multicenter observational study involving 31 hospitals in Beijing (18 of which perform AF ablation). The study was approved by the Human Research Ethics Committee of Beijing Anzhen Hospital and the ethics committees of all participating institutions. Between February 2011 and November 2022, a total of 33,488 patients with AF were enrolled. After excluding those with rheumatic valvular disease, those not prescribed OACs at discharge, or those with missing OAC prescription data, 25,292 patients with NVAF receiving OACs were included in the final analysis. Among them, 10,205 patients were prescribed warfarin and 15,087 were prescribed DOACs (either dabigatran or rivaroxaban). Dosing appropriateness was evaluated according to Chinese product labeling, which considers age and creatinine clearance (CrCl). Dabigatran was recommended at 150 mg or 110 mg twice daily, with dose reduction to 110 mg for patients aged ≥ 80 or with CrCl 30–49 mL/min. Rivaroxaban was given at 20 mg daily, with reduction to 15 mg for CrCl 15–49 mL/min. DOAC use below or above these recommendations was defined as inappropriate. Statistical analyses included descriptive summaries, Wilcoxon tests, chi-square tests, and multivariable logistic regression using R.

Results:

The mean age of the overall cohort was 64 ± 15.7 years, with 62.5% being male. Compared to patients receiving warfarin, DOAC users were younger (63.7 vs. 64.3 years), had better renal function (mean CrCl 63.3 vs. 54.0 mL/min), and had lower prevalence of hypertension (46.5% vs. 57.4%), diabetes (15% vs. 18.4%), stroke/TIA history (10.9% vs. 15.5%), and previous bleeding (2.8% vs. 3.8%). DOAC users were more likely to undergo in-hospital catheter ablation (66.1% vs. 53.5%) and less likely to receive antiplatelet co-therapy at discharge (3.9% vs. 19.8%). Among OAC prescriptions, dabigatran accounted for 29.5% and rivaroxaban 22.8%. Inappropriate dosing occurred in 16.8% of DOAC users, with underdosing accounting for 86.5% of cases and overdosing for 13.5%. Dabigatran had a significantly higher rate of appropriate dosing (93.9%) than rivaroxaban (51.1%). Rivaroxaban was underdosed in nearly half (48.4%) of its users, whereas dabigatran had a higher rate of overdosing (5.3%). Stratified analysis showed that inappropriate dosing increased with higher CHA_2DS_2-VASc and HAS-BLED scores. Specifically, the inappropriate dosing rate rose from 24.4% at CHA_2DS_2-VASc = 0 to 44.5% at >6, and from 21% at HAS-BLED = 0 to 62.5% at ≥ 5. By age, inappropriate DOAC use increased substantially among patients aged 80–84 (up to 84%) but slightly declined beyond age 85 (53.4%). Renal function also influenced dosing: among patients with CrCl ≥ 50 mL/min, 23% received inappropriate doses, rising to 63.2% with CrCl 30–49 and 54.5% with CrCl

Conclusion:

In this large, real-world registry spanning over a decade, DOAC use among Chinese NVAF patients increased significantly and gradually replaced warfarin. While the overall appropriateness of DOAC dosing improved over time, especially in elderly and renally impaired populations. Age is the dominant risk factor for inappropriate dosing. These findings underscore the need for improved clinician awareness and adherence to guideline-recommended DOAC dosing, particularly in high-risk subgroups.

Left Atrial Epicardial Adipose Tissue Dispersion Predicts Low Voltage Areas in Hypertensive Atrial Fibrillation Patients

Yu-Hang Yang, Tong-Shuai Chen, Pei-Li Bu

Qilu Hospital of Shandong University

Left Atrial Epicardial Adipose Tissue Dispersion Predicts Low Voltage Areas in Hypertensive Atrial Fibrillation Patients

Yuhang Yang[1], Tongshuai Chen[1], Peili Bu[1]

Affiliations

1 State Key Laboratory for Innovation and Transformation of Luobing Theory; Key Laboratory of Cardiovascular Remodeling and Function Research of MOE, NHC, CAMS and Shandong Province; Department of Cardiology, Qilu Hospital of Shandong University, Jinan, China, 250012

Objective: Atrial fibrillation (AF) is the most common tachyarrhythmia encountered in clinical practice, significantly increasing the risk of various diseases including heart failure, myocardial infarction, cardioembolic stroke, and vascular dementia. The risk of atrial fibrillation is markedly higher in hypertensive patients, where left atrial epicardial adipose tissue (LA-EAT) may play an important role. Numerous studies have identified a bidirectional relationship between hypertension and EAT, with hypertensive patients often exhibiting thicker epicardial fat and lower radiodensity. However, the accuracy of EAT measurement remains controversial due to multiple influencing factors. This study aims to evaluate differences in two novel imaging characteristic including LA-EAT enhancement fraction and LA-EAT dispersion between hypertensive and non-hypertensive atrial fibrillation patients, and explore their correlations with left atrial low voltage areas (LVAs) which is considered as the substrate of atrial fibrillation.

Methods: From June 2022 to December 2024, atrial fibrillation patients who underwent coronary computed tomography angiography and catheter ablation were included and assigned into hypertensive or non-hypertensive group according to the clinical practice guidelines for the management of hypertension in China. The differences in imaging data and electrophysiological data between the two groups were analyzed. Additionally, univariate and multivariate logistic regression analyses were performed to identify risk factors predictive of LVAs.

Results: 106 (54.64%) of 194 patients (median age, 65.00 [55.00, 70.00] years; 119 men) included suffered from hypertension. Compared to non-hypertensive patients, the patients with hypertension exhibited higher CHA_2DS_2-VASc scores, creatinine levels, troponin I levels, ascending aortic diameter, interventricular septal thickness, and left ventricular posterior wall thickness. However, there were no significant differences in other general characteristics such as gender, age, type of atrial fibrillation, and duration of atrial fibrillation. In terms of total EAT, the hypertension group had a lower total EAT attenuation (P = 0.018), while there was no significant difference in volume. However, patients in hypertension group (vs. non-hypertensive group) had lower LA-EAT attenuation (median [IQR], -85.78 [-95.21, -80.80] HU vs. -81.47 [-89.47, -74.97] HU, P <0.001), higher LA-EAT volume (33.25 [26.65, 39.54] ml vs. 29.83 [23.82, 36.21] ml, P = 0.008), higher dispersion (54.89 [47.40, 62.41] HU vs. 49.29 [42.46, 56.64] HU, P <0.001), and higher enhancement fraction (38.53 [33.20, 43.84] % vs. 33.69 [30.06, 39.05] %, P <0.001). The hypertension group also had larger LVAs compared to non-hypertensive group (18.89 [16.05, 20.37] cm^2 vs. 15.61 [12.98, 18.05] cm^2). Left atrial EAT attenuation was negatively correlated with left atrial LVA area (r = -0.207, P = 0.004), while left atrial EAT volume (r = 0.338, P <0.001), enhancement fraction (r = 0.387, P <0.001), and dispersion (r = 0.401, P . Univariate and multivariate logistic regression analysis revealed that LA-EAT dispersion (OR=1.11; 95%CI=1.02-1.21, P = 0.016) was an independent risk factor for the presence of LVAs.

Conclusion: In atrial fibrillation patients with hypertension, lower LA-EAT density, higher enhancement fraction, and higher diffusivity are common, which may reflect inflammatory and myocardial infiltration of LA-EAT. It is associated with LVAs formation and may contribute to the atrial fibrosis in hypertensive atrial fibrillation patients.

The Predictive Role of Tumor Necrosis Factor Superfamily 14 in Atrial Fibrillation Recurrence Following Catheter Ablation: A Prospective Cohort Study

Dong-Tao Zhou, De-Yong Long

Beijing Anzhen Hospital, Capital Medical University

Title: The Predictive Role of Tumor Necrosis Factor Superfamily 14 in Atrial Fibrillation Recurrence Following Catheter Ablation: A Prospective Cohort Study

Authors: Dongtao Zhou, MD; Deyong Long

From the Department of Cardiology, Beijing Anzhen Hospital, Capital Medical University, National Clinical Research for Cardiovascular Diseases, Beijing, China.

Abstract

Objective:

Atrial fibrillation (AF) is a common arrhythmia with high recurrence rates following catheter ablation (CA), largely due to structural and inflammatory remodeling of the atria. Tumor Necrosis Factor Superfamily 14 (TNFSF14), a pro-inflammatory cytokine also known as LIGHT, has been implicated in cardiovascular inflammation and fibrosis. However, its value in predicting AF recurrence post-ablation remains unexplored. This study aimed to assess whether serum TNFSF14 levels are independently associated with AF recurrence and whether it can improve current risk prediction models.

Methods:

In this prospective cohort study, 263 patients undergoing CA for AF at Beijing Anzhen Hospital between October 2022 and September 2023 were enrolled. Blood samples were collected prior to ablation, and serum TNFSF14 levels were measured using a standardized enzyme-linked immunosorbent assay (ELISA). Patients were followed for AF recurrence, defined as any atrial tachyarrhythmia lasting more than 30 seconds after a 3-month blanking period, with routine electrocardiogram or 24-hour Holter monitoring over an average follow-up of 362.83 ± 143.81 days. Clinical data including baseline characteristics, echocardiographic measurements, biomarker levels, and ATLAS scores were collected. Cox proportional hazards models were used to evaluate the association between TNFSF14 and recurrence. Predictive performance was assessed by receiver operating characteristic (ROC) analysis, time-dependent area under the curve (AUC), decision curve analysis (DCA), net reclassification improvement (NRI), and integrated discrimination improvement (IDI). A new model was constructed by integrating TNFSF14 and B-type natriuretic peptide (BNP) into the ATLAS score.

Results:

Among 263 patients (mean age: 62.6 ± 11.0 years; 61.6% male), 81 (30.8%) experienced AF recurrence. Baseline TNFSF14 levels were significantly higher in the recurrence group than in the non-recurrence group (1.21 ± 0.24 vs. 1.02 ± 0.29 ng/ml, P < 0.001). In multivariate Cox regression, TNFSF14 was independently associated with AF recurrence (adjusted hazard ratio: 3.65; 95% CI: 2.19–6.09; P < 0.001), along with BNP, left atrial volume index (LAVI), and the ATLAS score. ROC analysis showed that TNFSF14 had a superior predictive performance (AUC: 0.70) compared to BNP (AUC: 0.66) and the ATLAS score (AUC: 0.65). Kaplan–Meier analysis revealed that elevated TNFSF14 levels were significantly associated with shorter recurrence-free survival (P < 0.001). Incorporating TNFSF14 and BNP into the ATLAS score significantly improved model performance, with time-dependent AUC increasing over time. The new model yielded an NRI of 0.44 (95% CI: 0.25–0.57, P < 0.001) and an IDI of 0.12 (95% CI: 0.06–0.19, P < 0.001), and also demonstrated greater net clinical benefit on decision curve analysis.

Conclusion:

This is the first study to demonstrate that baseline TNFSF14 is an independent and robust predictor of AF recurrence after CA. TNFSF14 outperforms traditional risk scores and biomarkers and shows increasing predictive strength over time. Furthermore, combining TNFSF14 and BNP with the ATLAS score substantially improves recurrence prediction, suggesting its potential utility in personalized AF management. Future studies are needed to validate these findings and to explore the mechanistic role of TNFSF14 in atrial remodeling and fibrosis.

From Single Cells to Causality: Decoding Atrial Fibrillation Mechanisms via Transcriptomics and Mendelian Randomization

Zhifu Guo, Jing-Yu Zhang, -Pu Niu, Cheng Jiang, Song-Qun Huang

Changhai Hospital, Naval Medical University

Objective

Atrial fibrillation (AF), affecting 2–3% of the global adult population, is a leading cause of stroke, heart failure, and mortality. Its pathogenesis involves complex interplays between genetic susceptibility, structural remodeling, and immune dysregulation. Current treatments, including anticoagulation, ablation, and rate/rhythm control, remain suboptimal due to high recurrence rates and off-target effects. This study aims to dissect the molecular underpinnings of AF by integrating scRNA-seq and MR analyses to: Characterize atrial cellular heterogeneity and identify disease-specific cell subpopulations. Construct co-expression networks to pinpoint AF-associated pathways. Validate causal relationships between gene expression and AF using MR. Elucidate immune and metabolic mechanisms contributing to AF pathogenesis.

Methods

Data Acquisition and Preprocessing: ScRNA-seq data (GSE238242, 7 atrial samples) and bulk RNA-seq data (GSE79768, 26 samples) were downloaded from the GEO database. Samples were partitioned into control (n=16) and AF (n=17) groups. Quality control involved filtering cells with 7000 genes, >10% mitochondrial reads, or extreme gene expression variability. Normalization and batch correction were performed using Seurat's LogNormalize and Harmony algorithms. Cell clusters were annotated using CellMarker and SingleR, revealing 12 cell types, including cardiomyocytes, fibroblasts, and immune subsets. Subclustering and Differential Analysis: Cardiomyocytes were subjected to secondary clustering, identifying two AF-specific subpopulations (C3, C7). Differential gene expression analysis compared AF vs. control samples, with genes exhibiting $|log2FC| > 1$ and adjusted $P < 0.05$ deemed significant. Co-expression Network Construction: hdWGCNA was applied to construct gene co-expression networks. Modules were identified using dynamic tree cutting, and module-trait correlations were calculated to link modules to AF. Pathway enrichment analysis (Metascape) prioritized pathways, including AMPK signaling and ECM remodeling. Mendelian Randomization: Cis-eQTLs from eQTLGen ($P < 1e-5$) served as instrumental variables. AF GWAS summary statistics (EBI: ebi-a-GCST006414) were used as outcomes. Causal effects were estimated using IVW, MR-Egger, and weighted median methods. Heterogeneity (Q statistic) and pleiotropy (MR-Egger intercept) tests ensured validity. Functional and Immune Analyses: Gene set enrichment (KEGG, GO) and ssGSEA quantified immune cell infiltration. Transcription factor regulatory networks were inferred using RcisTarget. Metabolic pathway activity was assessed via GSVA.

Results

Single-Cell Profiling Reveals Disease-Specific Cardiomyocyte Subpopulations: ScRNA-seq identified 12 cell clusters in atrial tissues. Cardiomyocytes dominated AF samples (62 ± 8%), with subclusters C3 and C7 exhibiting unique gene signatures. C3 cells showed upregulation of fibrosis-related genes (e.g., COL1A1, FN1), while C7 cells exhibited enrichment in oxidative phosphorylation and calcium-handling pathways. hdWGCNA Identifies AF-Associated Pathways: The brown module (1,247 genes) correlated strongly with AF (correlation = 0.75, P = 4e – 12).

Enrichment analysis revealed overrepresentation of AMPK signaling, ECM-receptor interaction, and sphingolipid signaling pathways. Key hub genes included CABLES1, COL24A1, and ITGB1. Mendelian Randomization Validates Causal Genes: MR identified two causal genes: CABLES1 (OR = 1.20, P = 0.003): Enriched in sphingosine-1-phosphate signaling and metabolic pathways. rs11746922 (IVW β = 0.18, P = 3e – 4) mediated its effect. COL24A1 (OR = 1.14, P = 0.035): Linked to antigen processing (HLA-DQA1/DRB1) and interferon responses. rs7278467 (IVW β = 0.13, P = 0.01) was the top IV. Functional and Immune Correlates: CABLES1 correlated negatively with T follicular helper cells (ρ = – 0.42, P = 0.009) and positively with cytochrome P450 activity (GSVA score = 0.35 ± 0.12 vs. 0.18 ± 0.07 in controls). COL24A1 correlated with type I/II interferon responses (ρ = 0.51, P = 0.002) and mast cell infiltration (ρ = 0.38, P = 0.02). Immune profiling showed elevated neutrophils (P = 0.004) and reduced MHC class I expression (P = 0.03) in AF tissues

Conclusion

This study integrates multi-omics approaches to identify CABLES1 and COL24A1 as causal drivers of AF. CABLES1 modulates cardiomyocyte metabolism and calcium homeostasis, while COL24A1 exacerbates fibrosis and immune dysregulation. MR validation confirms their causal roles, offering actionable targets for precision therapies. Future directions include CRISPR-based gene silencing and immune-modulatory interventions to disrupt AF progression.

Keywords: Atrial fibrillation, Mendelian randomization, AMPK signaling, Immune infiltration, Precision medicine

合并心力衰竭与心房血栓的心房颤动患者的临床特征及预后

杨沭 [1,2] 刘文杰 [1,2] 郦明芳 [2] 陈明龙 [1,2]

1. 泰州市人民医院

2. 江苏省人民医院（南京医科大学第一附属医院）

目的 旨在探讨合并心力衰竭（心衰）与心房血栓的非瓣膜性心房颤动（NVAF）患者的临床特征，并通过随访分析心房血栓的消退情况及患者的临床预后。

方法 本研究为单中心回顾性观察性研究。选取 2012 年 1 月至 2024 年 4 月在南京医科大学第一附属医院心内科心律失常病区住院的拟行导管消融的 NVAF 患者，其中明确诊断心衰与心房血栓并完成影像学复查的 NVAF 患者被纳入最终分析。本研究首先描述了合并心衰与心房血栓的 NVAF 患者的临床特征，并进一步探究了心房血栓的消退情况及随访期间心血管不良事件的发生情况。

结果 共有 40 例明确诊断心衰与心房血栓并完成影像学复查的 NVAF 患者被纳入最终分析。所有患者的平均年龄为（59.4±11.5）岁，男性 23 例（57.5%，23/40），非阵发性房颤 36 例（90.0%，36/40）。其中，5 例为射血分数降低的心衰（HFrEF），8 例为射血分数轻度降低的心衰（HFmrEF），27 例为射血分数保留的心衰（HFpEF）。诊断心房血栓后，34 例（85.0%，34/40）患者调整了抗凝方案，中位复查时间 3 个月（IQR：3 ~ 6 个月）期间，20 例（50.0%，20/40）患者的心房血栓取得了消退，其中以 HFpEF 组的消退率最低（37.0%，10/27）。共 28 例（70.0%，28/40）患者的心衰得到了改善。心衰改善组的血栓消退率显著高于未改善组（64.3% 比 16.7%，P=0.006）。随访期间，共发生 2 例缺血性脑卒中事件，均在抗凝治疗中断后发生。

结论 合并心衰，尤其是合并 HFpEF 的 NVAF 患者，心房血栓的发生不容忽视。随访期间心衰状态的变化对于这部分患者的临床管理具有重要意义。

J 形弯导丝房间隔穿刺术随机对照研究

刘元伟

清华大学附属北京清华长庚医院

目的：本研究将进一步探索 ICE 引导的 Vizigo 可调弯鞘 J 形导丝行房间隔穿刺术在导管消融手术中的有效性与安全性。

方法：本研究为随机、单盲对照研究，根据房间隔穿刺方式分为 J 形弯导丝穿刺组（实验组）和传统房间隔穿刺组（对照组）。入选拟行房间隔穿刺术的年龄 18-80 岁的导管消融手术患者 100 例为研究对象，随机分配到 J 形弯导丝穿刺组（实验组）和传统房间隔穿刺组（对照组），随机化方法采用区组随机化的方法。随访期为 3 个月。随访信息通过 ESR 从医院电子病历系统、研究对象居住地医疗机构信息系统的信息中获得。受试者的随访数据包括：安全性终点事件（主动脉穿孔、新发或进展的心包积液、症状性卒中或系统性栓塞、医源性心房分流以及死亡）发生情况，超声心动图数据（心包积液、心房分流数据等）、头颅 CT/核磁结果等。本研究通过门诊随访、电子病历系统随访 2 种方式进行随访，随访间期为 3 个月。术后 48h：（1）如果术后患者出现神经系统缺失症状或无症状患者同意进行检查，术后 48 小时内安排两组入选患者均进行头颅 MRI 检查以排查脑梗。（2）复查 12 导联心电图、24 小时动态心电图、超声心动图，确定房间隔缺损面积，除外心包积液、其他心电事件。术后 3 个月：（1）随访安排超声心动图检查，查看心包积液，并评估医源性房间隔缺损是否已闭合。

结果：入选 34 例房间隔穿刺患者，导丝穿刺组的射线曝光量、费用、穿刺时间小于常规穿刺组（分别为 15mGy vs 24mGy, 4712 vs 6928 元，2.3 vs 3.4 分钟），而尝试次数及并发症明显差别。

结论：使用 J 形弯钢丝穿刺房间隔安全性不劣于传统 BRK 针穿法，但是手术时间、费用、X 射线曝光量更低。

心电图 f 波振幅预测老年持续性心房颤动患者射频消融术后 1 年复发的价值

颜清 [1] 王林林 [2] 陈红武 [3] 陈明龙 [3]

1. 南京医科大学附属明基医院

2. 苏州大学附属第四医院

3. 南京医科大学第一附属医院

目的 探索心电图 f 波振幅在预测老年持续性心房颤动并行射频消融术的患者术后 1 年复发方面的价值。

方法 纳入 2014 年 09 月至 2022 年 05 月在南京医科大学第一附属医院明确诊断为持续性心房颤动并接受射频消融术的 60 岁及以上患者。根据患者术后 1 年是否复发分为未复发组与复发组，分析两组患者临床特征，将具有明显差异的指标纳入 logistic 回归分析。

结果 共纳入 369 人，其中未复发组 281（76.15%）人，复发组 88（23.85%）人。两组在年龄、体重指数、合并症、左心室舒张末期内径、左心室射血分数、肺动脉压力、脑钠肽前体、尿酸、低密度脂蛋白胆固醇、抗心律失常药物使用上无明显差异（P 均 > 0.05）。与未复发组比较，复发组的女性比例高（39.77% vs. 26.69%，P=0.019），病程长【17.00（6.00，60.00）月 vs.8.00（3.00，24.00）月，P < 0.001】，III 导联【0.07（0.06，0.08）mv vs. 0.09（0.08，0.11）mv，P < 0.001】、avF 导联【0.06（0.05，0.07）mv vs. 0.08（0.07，0.10）mv，P < 0.001】、V2 导联【0.07（0.06，0.09）mv vs. 0.10（0.08，0.12）mv，P < 0.001】f 波振幅低，左心房内径【44.00（41.00，47.00）mm vs.42.00（40.00，45.00）mm，P=0.039】、右心房内径【42.00（40.00，44.00）mm vs.40.00（39.00，43.00）mm，P=0.038】更大。Logistic 回归分析显示心房颤动病程长是老年持续性心房颤动患者射频消融术后 1 年复发的危险因素，而 avF 导联、V2 导联 f 波振幅高则是其保护因素。

结论 心电图 f 波振幅及病程可预测老年持续性心房颤动患者射频消融手术效果。

犬尿酸升高通过抑制心脏神经节丛 γ- 氨基丁酸信号传导介导“房颤诱发房颤”

韩欣睿 [1,2,3,4,5,6] 周丽平 [1,2,3,4,5,6] 周晓亚 [1,2,3,4,5,6] 江洪 [1,2,3,4,5,6] 余锂镭 [1,2,3,4,5,6]

1. 武汉大学人民医院心血管医院

2. 武汉大学复杂生命体代谢与调控全国重点实验室

3. 自主神经调控湖北省重点实验室

4. 武汉大学心脏自主神经研究中心

5. 武汉大学泰康生命医学中心

6. 武汉大学人民医院分子医学研究院

目的：代谢紊乱在房颤（atrial fibrillation，AF）发生发展中有重要作用。组学技术已经鉴定了与 AF 进展相关的多种代谢变化，以及代谢重构与自主重构在 AF 中的相互作用。然而，在房颤进展和治疗中的代谢物筛选、机制探索和临床转化之间仍存在差距。

方法：我们通过非靶向代谢组学确定了对照患者和 AF 患者之间的血清代谢差异，以及房颤患者治疗前后的差异。在 AF 患者血清和快速心房起搏诱导的犬 AF 模型血清中测量所选代谢产物水平进行验证。我们进一步在犬 AF 模型中探索了所选代谢物的生物学功能。我们首先测量了心脏神经节丛（ganglionated plexuses，GPs）中选定代谢物的局部浓度。并将选定的代谢产物和相关酶抑制剂微量注射到四个主要 GP 中，以探索其对 GP 功能、心房电生理和 AF 易感性的影响。

结果：非靶向代谢组学分析显示，一共有 13 种代谢物和 8 种途径在对照患者和 AF 患者之间以及 AF 患者治疗前后存在差异。我们选择色氨酸 - 犬尿氨酸途径中的代谢物进行验证。AF 患者和犬 AF 模型的血清犬尿酸（kynurenic acid，Kyna）水平升高。有趣的是，在犬 AF 模型的 GPs 中也检测到 Kyna 升高和犬尿氨酸转氨酶 2（kynurenine aminotransferase 2，KAT2）上调，这与房颤相关炎症以及雪旺细胞的异常激活有关。Kyna 进一步加剧了 AF 易感性、心房电生理紊乱和 GP 过度激活。KAT2 抑制剂改善了这些变化。从机制上讲，Kyna 抑制了 GPs 中 γ- 氨基丁酸（gama-aminobutyric acid，GABA）信号的突触前和突触后传递。

结论：我们的研究结果表明，Kyna 升高是“房颤引发房颤”的中介因素，主要抑制心脏 GPs 中的 GABA 信号传导。

Nrf2 Overexpression Attenuates Erastin-Induced Ferroptosis in Cardiac Fibroblasts

meixue jia, Bin Ning

Fuyang People’s Hospital

Purpose

To systematically investigate the cytoprotective role of nuclear factor erythroid 2-related factor 2 (Nrf2) in counteracting Erastin-induced ferroptosis within cardiac fibroblasts, and to elucidate the therapeutic efficacy of ginsenoside RG1 in mitigating atrial fibrillation (AF)-associated myocardial fibrosis through Nrf2-mediated molecular pathways. The study addresses a critical gap in understanding how redox regulation intersects with iron-dependent cell death in fibrotic heart disease patho-

genesis.

Methods

In vitro investigations: Primary murine cardiac fibroblasts were cultured in DMEM/F12 supplemented with 10% FBS. Ferroptosis was induced by 24-hour exposure to 10 μM Erastin (MedChemExpress, USA). Mitochondrial integrity was assessed using JC-1 staining (λex 485 nm/λem 530 nm for monomers; λex 535 nm/λem 590 nm for aggregates) with quantification via fluorescence microscopy (Nikon Eclipse Ti). Intracellular ROS generation was measured using DCFH-DA probe (Sigma-Aldrich; λex 488 nm/λem 525 nm). Nrf2 overexpression was achieved through lentiviral transduction (HANBIO, Shanghai) at MOI 50, validated by qPCR and immunofluorescence. Protein expression profiles (Nrf2, SLC7A11, GPX4, collagen I/III) were analyzed by Western blot using β-actin normalization (primary antibodies: Abcam). Iron metabolism was evaluated colorimetrically (Fe^{2+} detection kit, Biovision; MDA assay, Jiancheng Bioengineering). SOD activity was determined via nitroblue tetrazolium reduction assay. Inflammatory cytokines (IL-1β, IL-6, TNF-α) were quantified using high-sensitivity ELISA kits (R&D Systems). Nrf2 knockdown utilized siRNA transfection (Santa Cruz Biotechnology), and viability was assessed via CCK-8 absorbance (450 nm).

In vivo modeling: Adult C57BL/6 mice (male, 8-weeks-old) were subjected to AF induction via continuous 7-day acetylcholine-$CaCl_2$ infusion (Ach 66 μg/kg/min + $CaCl_2$ 10 mg/kg/min). Treatment groups (n=10/group) received: 1) saline, 2) Rg1 (20 mg/kg/day i.p., Chengdu Herbpurify), or 3) ferrostatin-1 (5 mg/kg/day i.p., Selleckchem) for 28 days. Transthoracic echocardiography (VisualSonics Vevo 2100) quantified cardiac function. Post-sacrifice, myocardial sections underwent H&E and Masson's trichrome staining for fibrosis quantification (ImageJ). Serum cytokines were analyzed via Luminex multiplex assay (Millipore).

Results

Ferroptosis induction dynamics: Erastin triggered mitochondrial depolarization (ΔΨm reduction: 62.3 ± 5.1% vs control, ***p<0.001**) and ROS overproduction (2.7-fold increase, **p<0.01**). Molecular profiling revealed Nrf2 suppression (0.4 ± 0.06-fold), accompanied by GPX4 downregulation (0.5 ± 0.08-fold) and collagen I/III overexpression (2.1 ± 0.3-fold and 1.8 ± 0.2-fold, respectively; **p<0.01**).

Nrf2 rescue mechanisms: Overexpression restored ΔΨm to 89.2 ± 6.3% control levels (**p<0.01**) and attenuated ROS by 58.4 ± 4.7% (**p<0.05**). Immunoblotting demonstrated Nrf2 upregulation (3.1 ± 0.4-fold vs Erastin group) leading to complete GPX4/SLC7A11 recovery and collagen I/III suppression (68.2 ± 6.1% and 61.3 ± 5.4% reduction, respectively; ***p<0.001**).

Multi-parameter cytoprotection: Erastin elevated Fe^{2+} (3.2 ± 0.5-fold) and MDA (2.9±0.4-fold) while diminishing SOD activity (45.7 ± 4.2% residual activity, ***p<0.001**). Nrf2 transduction reduced Fe^{2+} accumulation by 51.3±3.8% (**p<0.01**), decreased lipid peroxidation (MDA reduction: 48.2 ± 5.3%, **p<0.05**), and restored SOD activity to 92.8 ± 7.6% baseline. Inflammatory cascades (IL-1β: 4.3-fold, IL-6: 3.6-fold, TNF-α: 3.1-fold increase; ***p<0.001**) were fully abrogated by Nrf2 overexpression.

Ginsenoside RG1-driven therapeutic modulation:Viability rescue: Nrf2 knockdown reduced survival to 43.2±3.9%, while ginsenoside Rg1 restored viability to 78.5±6.2% (***p<0.001** vs. knockdown group).Fibrosis attenuation:ginsenoside Rg1 decreased collagen deposition by 64.3±5.7% (***p<0.001**) in AF mice, equaling ferrostatin-1 efficacy (67.1±4.9% reduction). Serum IL-1β and IL-6 decreased by 57.2 ± 3.4% and 61.8±4.1% (***p<0.001**).Integrated molecular regulation: ginsenoside Rg1 upregulated Nrf2 nuclear translocation (2.8±0.3-fold), enhancing SLC7A11 (3.1±0.5-fold) and GPX4 (2.5±0.4-fold) while suppressing collagen I/III synthesis (72.1±5.3% and 68.9±6.7% inhibition, respectively; ***p<0.001**). Fe^{2+} accumulation diminished by 53.4 ± 4.1% (**p<0.01**).

Conclusion

This study establishes Nrf2 as a master regulatory nexus coordinating three-tiered cardioprotection: 1) ferroptosis inhibition via SLC7A11/GPX4 axis stabilization, 2) oxidative stress resolution through SOD reactivation and lipid peroxidation blockade, and 3) fibrotic remodeling suppression via collagen transcriptional downregulation. Ginsenoside RG1 emerges as a multifunctional therapeutic agent that pharmacologically amplifies endogenous Nrf2 signaling, demonstrating superior efficacy over selective ferroptosis inhibitors by simultaneously targeting iron dyshomeostasis, inflammation, and extracellular matrix deposition. These findings validate Nrf2 potentiation as a promising paradigm for treating ferroptosis-exacerbated cardiac pathologies including AF-related fibrosis.

国内外心房颤动与心房重构的研究热点与趋势的比较——基于 WOS 和 CNKI 文献的可视化分析

刘琴[1] 郑美娟[1] 王若楠[1] 木胡牙提·乌拉斯汉[2]

1. 新疆医科大学第一附属医院

2. 新疆医科大学

目的 通过可视化分析方法，比较国内外近二十年心房颤动（AF）与心房重构领域的研究现状、热点及发展趋势，揭示该领域的国际差异与互补潜力，为未来研究提供参考。**方法** 检索 2005–2024 年 Web of Science（WOS）核心数据库与中国知网（CNKI）中关于 AF 与心房重构的文献，筛选后纳入 WOS 文献 587 篇、CNKI 文献 622 篇。采用 Excel、VOSviewer 和 CiteSpace 对文献进行计量学分析，绘制科学知识图谱，对比国内外发文量、研究机构合作网络、作者合作模式及关键词分布特征。**结果** 国内外研究热点存在显著差异：WOS 研究集中于诊断技术（如导管消融、超声心动图）、病理机制（如纤维化、炎症）及基因编辑等前沿领域；CNKI 研究则聚焦致病因素、药物干预（如胺碘酮、缬沙坦）及中医药应用。炎症反应是国内外共同关注的核心主题。国际合作网络显示，中国、美国、德国等国家合作紧密，而国内以天津医科大学第二医院为核心形成区域性团队，跨机构合作较少。关键词突现分析表明，氧化应激和心外膜脂肪组织（EAT）是近年新兴热点，可能成为未来研究方向。**结论** 国内外研究在技术应用与本土化问题上各具特色，国际研究更注重技术创新，国内研究则侧重临床实践与中医药探索。未来需加强跨学科、跨机构及国际合作，重点关注 EAT 与代谢 - 炎症 - 电重构的关联机制，推动 AF 治疗的精准化与个体化发展。本研究通过文献计量学方法，为优化科研资源配置和制定国际合作策略提供了实证依据。

Management for stroke secondary prevention in patients refusing anticoagulation therapy after atrial fibrillation catheter ablation without recurrence: A Prospective Cohort Study

Qi-Bin Chen, Fang-Yi Xiao

The First Affiliated Hospital of Wenzhou Medical University

Background:

Non-valvular atrial fibrillation (NVAF) significantly increases the risk of ischemic stroke, especially in patients with prior cerebrovascular events such as ischemic stroke or transient ischemic attack (TIA). Catheter ablation has become a cornerstone treatment to maintain sinus rhythm and reduce AF burden. However, despite successful ablation and absence of documented AF recurrence, current clinical guidelines recommend long-term oral anticoagulation (OAC) for secondary stroke prevention. Many patients, however, refuse or discontinue OAC due to bleeding concerns, drug intolerance, or personal preference, creating a clinical challenge due to the lack of alternative effective stroke prevention strategies in this population. Hence, integrated approaches that combine anatomical thrombus prevention with rhythm control and minimize anticoagulation are urgently needed.

Objective:

To evaluate the safety and efficacy of combining percutaneous left atrial appendage closure (LAAC) with intra-procedural pulmonary vein (PV) reconnection assessment and repeat isolation specifically in NVAF patients with prior stroke or TIA who maintain sinus rhythm after catheter ablation but refuse long-term oral anticoagulation. This study aims to clarify whether this combined strategy offers effective secondary stroke prevention without compromising rhythm control in this high-risk, anticoagulation-intolerant population.

Methods:

This prospective study enrolled 38 NVAF patients with prior ischemic stroke or TIA who had undergone prior successful radiofrequency catheter ablation and demonstrated no AF recurrence confirmed by serial 12-lead electrocardiograms, 24-hour Holter monitoring, and symptom review during outpatient follow-up. The median time from last ablation to enrollment was 156 days (interquartile range 132–185 days). All patients had formally declined long-term anticoagulation following informed discussion with their treating physicians.During the percutaneous LAAC procedure, transesophageal echocardiography (TEE) and fluoroscopic guidance were used to deploy the occlusion device. Simultaneously, intracardiac electroanatomic mapping with a circular mapping catheter was performed to assess for pulmonary vein reconnection. In cases where electrical reconnection was identified, immediate radiofrequency re-isolation was carried out. Devices used for left atrial appendage occlusion included the Watchman device (Boston Scientific) in 88.9% of cases and the LACbes device in 11.1%.

Results:

LAAC was successfully performed in 36 out of 38 patients, corresponding to a procedural success rate of 94.7%. Pulmonary vein reconnection was detected in 11 patients (28.9%), all of whom underwent successful repeat isolation. Over a median follow-up duration of 775 days (range 582–934 days), one patient (3.7%) suffered an ischemic stroke. Two patients (5.6%) developed device-related thrombosis (DRT), which resolved after a short course of anticoagulation therapy. Minor bleeding events occurred in two patients (5.3%) without the need for hospitalization. Only two patients (5.3%) experienced late AF recurrence, resulting in a sinus rhythm maintenance rate of 94.7%.

Conclusion:

In NVAF patients with prior ischemic stroke or TIA who maintain sinus rhythm following catheter ablation but refuse long-term oral anticoagulation, a combined approach of LAAC and intra-procedural pulmonary vein reconnection assessment with repeat isolation is a feasible, safe,

and effective strategy for secondary stroke prevention. This hybrid procedural approach addresses both the anatomical substrate of thrombus formation and the electrophysiological triggers of AF recurrence, offering a comprehensive treatment alternative for this challenging patient population. Larger randomized controlled trials are warranted to confirm these findings and further define the clinical applicability of this strategy.

Keywords:Non-valvular atrial fibrillation; Left atrial appendage closure; Pulmonary vein isolation; Secondary stroke prevention; Oral anticoagulation intolerance

Long-term clinical efficacy of vein of Marshall ethanol infusion combined with catheter ablation for persistent atrial fibrillation

ge weili

Taizhou hospital of Zhejiang province

Background: Atrial arrhythmia recurrence following radiofrequency catheter ablation (RFCA) remains a relatively common and clinically challenging problem in the management of persistent atrial fibrillation (AF). Despite procedural refinements, the long-term success rates for persistent AF ablation with conventional RFCA strategies alone are suboptimal, highlighting a significant unmet need for more effective therapeutic approaches. The complex and sustained nature of persistent AF often involves triggers and substrates beyond the pulmonary veins, including those associated with the ligament of Marshall and its vasculature. Consequently, the development and integration of reformative, upgraded ablation strategies targeting these additional pathways are critically required to improve patient outcomes. Recently, ethanol infusion of the vein of Marshall (EI-VOM) has emerged as a promising adjunctive therapy, potentially enhancing the efficacy of standard RFCA procedures for persistent AF. Ethanol infusion induces controlled chemical ablation within the VOM region, targeting autonomic ganglia and arrhythmogenic substrates that are difficult to eliminate with RF energy alone. While initial and mid-term studies suggest potential benefits of combining EI-VOM with RFCA, comprehensive data evaluating the sustained, long-term clinical efficacy of this combined approach compared to conventional RFCA alone remains notably lacking in the current literature. Filling this evidence gap is essential for guiding optimal treatment selection.

Objective: This study aimed to conduct a direct, comparative assessment of the long-term arrhythmia-free survival outcomes between patients with persistent AF undergoing combined EI-VOM and RFCA therapy versus those receiving RFCA alone. A secondary objective was to identify and analyze potential clinical, procedural, or anatomical factors influencing the long-term maintenance of sinus rhythm in this patient population.

Methods: A cohort of patients diagnosed with persistent atrial fibrillation (AF) undergoing de novo ablation procedures was prospectively enrolled and systematically grouped based on treatment strategy: (1) the EI-VOM + RFCA group received combined therapy, and (2) the RFCA group received standard ablation alone. The foundational RFCA strategy was consistent across both groups and included extensive electrophysiological mapping followed by wide-area, circumferential bilateral pulmonary vein isolation (PVI) to achieve electrical isolation, confirmed by entrance and exit block. Additionally, linear ablation lesions were routinely performed, typically including a roof line connecting the superior aspects of the left and right pulmonary vein isolation circles and a mitral isthmus line extending from the left inferior pulmonary vein to the mitral valve annulus, with confirmation of bidirectional conduction block. The defining procedural difference lay in the EI-VOM group: prior to initiating any RFCA, ethanol (99% dehydrated alcohol) was selectively infused under fluoroscopic and/or intracardiac echocardiography (ICE) guidance into the vein of Marshall via an angioplasty balloon catheter positioned within the coronary sinus. Only after successful EI-VOM completion did the standard RFCA protocol (PVI + linear ablation) proceed. All patients underwent rigorous clinical follow-up, including scheduled outpatient visits, 12-lead ECGs, 24-hour Holter monitoring at 3, 6, and 12 months, and subsequently at least annually, supplemented by event recorders for symptomatic episodes.

Results: A total of 112 consecutive patients meeting the criteria for persistent AF were included in the final analysis (mean age: 62.3 ± 9.1 years; 71 patients in the EI-VOM + RFCA group, 41 patients in the RFCA alone group). In the EI-VOM + RFCA group, ethanol infusion into the VOM was successfully performed first in all cases, followed by comprehensive bilateral PVI and linear ablation using RF energy. The RFCA alone group underwent the identical PVI and linear ablation protocol using only RF energy. Over a mean follow-up period of 38.2 ± 6.5 months, freedom from any documented atrial arrhythmia recurrence (AF, atrial flutter, or atrial tachycardia lasting >30 seconds, off antiarrhythmic drugs after a 3-month blanking period) was significantly higher in the combined therapy group at all assessed time points. Specifically, Kaplan-Meier estimated freedom from recurrence was 87.32% at 12 months, 80.25% at 24 months, and 77.46% at 36 months post-procedure in the EI-VOM + RFCA group. In contrast, the RFCA alone group demonstrated significantly lower success rates: 78.05% at 12 months, 65.85% at 24 months, and 58.54% at 36 months (Log-rank p < 0.05 for overall comparison). Multivariable Cox proportional hazards regression analysis identified two independent predictors significantly associated with long-term maintenance of sinus rhythm: 1) Adjunctive EI-VOM therapy (Hazard Ratio [HR] for recurrence: 0.42, 95% CI: 0.23-0.78, p=0.006), and 2) Smaller left atrial diameter (HR: 1.08 per mm increase, 95% CI: 1.02-1.14, p=0.008).

Conclusion: This comparative study provides robust evidence that adjunctive Ethanol Infusion of the Vein of Marshall (EI-VOM) significantly enhances the long-term efficacy of radiofrequency catheter ablation for persistent atrial fibrillation. The combined EI-VOM + RFCA strategy resulted in substantially higher rates of freedom from atrial arrhythmia recurrence at 12, 24, and 36 months compared to conventional RFCA alone. EI-VOM was identified as a strong independent predictor of successful rhythm maintenance, alongside left atrial diameter. These findings strongly suggest that EI-VOM effectively modifies key arrhythmogenic substrates, leading to a durable reduction in recurrence rates. The present research offers compelling, long-term outcome data supporting the integration of EI-VOM as a valuable adjunctive therapy to standard ablation in the management of persistent AF, addressing a critical evidence gap.

Impact of Catheter Ablation on Left Ventricular Diastolic Function and Remodeling in Atrial Fibrillation Patients Stratified by Left Ventricular Diastolic Dysfunction Severity

Ying Cao, Rui Zeng

West China Hospital, Sichuan University West China School of Medicine

Aims:

This study aimed to investigate the effects of catheter ablation (CA) on left ventricular (LV) diastolic function, cardiac remodeling, and clinical outcomes in atrial fibrillation (AF) patients with varying grades of left ventricular diastolic dysfunction (LVDD), and to identify early predictors of sustained LVDD improvement.

Methods:

This retrospective study analyzed 182 predominantly paroxysmal AF patients undergoing CA between January 2018 and February 2023. Patients were stratified into four groups based on preoperative echocardiography: Group A (No LVDD, n=97), Group B (LVDD Grade 1, n=43), Group C (LVDD Grade 2, n=32), and Group D (LVDD Grade 3, n=10). Transthoracic echocardiography was performed preoperatively and at 1, 3, 6 and 12 months post-ablation to assess LV diastolic parameters and cardiac structure. Major statistical analyses included generalized estimating equations, Kaplan-Meier analysis and Cox regression.

Results:

LV Diastolic Function: LVDD Grade (LVDDG): Group B showed transient improvement at 3 months (1.00 vs. 0.75, p=0.045). Groups C and D demonstrated significant and sustained LVDDG improvement at all follow-up intervals (all p<0.001): C group (Δ -0.35 [95% CI -0.01 to -0.70] at 1m; Δ -0.88 [95% CI -0.55 to -1.21] at 3m; Δ -0.84 [95% CI -0.46 to -1.22] at 6m; Δ -0.53 [95% CI -0.21 to -0.86] at 12m); D group (Δ -1.23 [95% CI -0.83 to -1.63] at 1m; Δ -1.78 [95% CI -1.05 to -2.51] at 3m; Δ -1.06 [95% CI -0.12 to -1.99] at 6m; Δ -1.91 [95% CI -1.35 to -2.48] at 12m). Group A had statistically significant (all p<0.001) but clinically insignificant shifts, as 95% CI upper bounds remained below the LVDDG 1 threshold. Filling Pressure (E/e'): Group C showed significant E/e' reduction at 3 months (15.63 vs. 18.83, p=0.006) and 12 months (15.28 vs. 18.83, p=0.008). Group D demonstrated sustained improvements at 1, 6, and 12 months (14.91/12.28/14.64 vs. 19.00, all p<0.05). E/e' remained unchanged in Group B but transiently increased in Group A at 6 months (11.30 vs. 10.26, p=0.010).

Reverse Cardiac Remodeling: Left Atrium: Significant LAD reductions occurred at specific intervals: Group B at 3m (38.83 vs. 37.25 mm, p=0.045) and 12m (38.83 vs. 37.36 mm, p=0.036); Group C at 6m (40.07 vs. 37.58 mm, p=0.005); Group D at 12m (41.08 vs. 38.24 mm, p=0.020). Group A showed no significant change. LV Concentric Remodelings: Group D exhibited a significant time-dependent reduction in concentric remodeling prevalence (p<0.001), declining from 40% pre-op to 12% at 12 months (p=0.041 vs. baseline). Group C showed non-significant downward trends (3/6/12m: 16%/19%/21% vs. pre-op 29%, all p>0.05).

Early Improvement as Predictor: Early LVDD improvement (≥ 1-grade reduction) at 1 month strongly predicted sustained diastolic recovery throughout follow-up (adjusted OR 4.51, 95% CI 1.81-11.25; p=0.001). Patients with 1-month improvement had significantly higher probabilities of maintained recovery at subsequent assessments (3m: 79% vs. 46%; 6m: 75% vs. 39%; 12m: 87% vs. 61%; all p<0.01), with an absolute probability difference of 32% (81% vs. 49%) for composite 12-month improvement.

Clinical Outcomes: No significant difference was observed in AF recurrence rates among groups (log-rank p=0.22). Major Adverse Cardiovascular Events (MACE) included myocardial infarction (n=1, Group A, 1.03%) and heart failure hospitalizations (n=3: Group A n=1, 1.03%; Group B n=2,

4.65%).

Association of LVDD Improvement with Rhythm Status: In Groups B-D, patients maintaining sinus rhythm (SR, n=58) and those with AF recurrence (AF, n=27) had comparable trajectories of diastolic improvement. GEE models adjusted for age, BMI, and LVDDG showed no significant association between rhythm status and diastolic improvement (adjusted OR 1.27, 95% CI 0.58-2.82; p=0.552).

Conclusion:

Catheter ablation induces significant and sustained improvement in LV diastolic function in AF patients with moderate-to-severe LVDD (Grades 2-3). Patients with severe LVDD (Grade 3) additionally demonstrate significant left atrial reverse remodeling and reversal of LV concentric remodeling. Early diastolic improvement (≥ 1-grade reduction) at 1 month post-ablation is a strong predictor of sustained long-term functional recovery. Notably, these functional and structural benefits were not directly associated with strict maintenance of sinus rhythm, suggesting potential benefits of ablation beyond rhythm control. This study provides robust evidence supporting the role of CA in ameliorating LV diastolic impairment in AF patients with LVDD.

Clinical effect of vein of Marshall ethanol infusion on mitral isthmus ablation Running title: Marshall ethanol infusion

ge weili

Taizhou hospital of Zhejiang province

Purpose: This study aimed to rigorously investigate the specific electrophysiological effect of adjunctive ethanol infusion into the vein of Marshall (VOM-Et) on the achievement of bidirectional conduction block across the mitral isthmus (MI) during catheter ablation for persistent atrial fibrillation (AF). The primary objective was to compare the immediate procedural success rate of achieving durable MI block between patients receiving combined VOM-Et and radiofrequency (RF) ablation versus those undergoing conventional RF ablation alone. Secondary objectives included conducting a stratified analysis to identify patient characteristics associated with the benefit of VOM-Et for facilitating MI block.

Methods: A cohort of consecutive patients diagnosed with persistent AF undergoing first-time catheter ablation at Taizhou Hospital of Zhejiang Province between January 2018 and December 2021 was prospectively enrolled. Patients were systematically allocated into two treatment groups based on the ablation strategy: 1) The VOM-Et-RF group received combined therapy involving ethanol infusion into the VOM followed by extensive RF ablation; 2) The RF group underwent standard catheter ablation using RF energy exclusively. The standard RF ablation protocol for both groups encompassed wide-area circumferential pulmonary vein isolation (PVI) confirmed by entrance and exit block, followed by deliberate linear ablation targeting the mitral isthmus (MI line). In the VOM-Et-RF group, selective cannulation and ethanol infusion (using dehydrated alcohol) into the VOM were performed via the coronary sinus under fluoroscopic and/or intracardiac echocardiography (ICE) guidance prior to initiating any RF ablation. MI ablation in the RF group relied solely on endocardial and/or epicardial (within the coronary sinus) RF applications. The primary outcome measure was the acute procedural success rate defined as the achievement of confirmed bidirectional conduction block across the mitral isthmus immediately following the completion of the ablation procedure, assessed using established electrophysiological criteria (differential pacing and demonstration of widely separated double potentials along the line during coronary sinus pacing). Stratified subgroup analyses were performed to evaluate the influence of specific baseline factors (sex, age, left atrial diameter, AF duration) on the primary outcome.

Results: A total of 118 consecutive patients meeting the inclusion criteria were included in the final analysis (72 patients in the VOM-Et-RF group, 46 patients in the RF group). Acute bidirectional perimitral block was successfully achieved in 96% (69 out of 72) of patients in the VOM-Et-RF group. In contrast, significantly lower success was observed in the RF group, with block achieved in 76% (35 out of 46) of patients (P < 0.01, Chi-square test). Subgroup analysis revealed that the significant benefit of VOM-Et in achieving higher MI block rates was particularly pronounced in patients with the following characteristics: Male sex, Age older than 60 years, Left atrial diameter < 55 mm, and AF duration < 3 years. These subgroups derived the greatest advantage from the adjunctive VOM-Et strategy compared to RF ablation alone.

Conclusion: Ethanol infusion into the vein of Marshall (VOM-Et) used adjunctively with conventional radiofrequency catheter ablation significantly improves the acute procedural success rate in achieving bidirectional conduction block across the mitral isthmus (MI) in patients with persistent atrial fibrillation. This enhancement in creating a complete, durable MI line is a critical determinant of long-term ablation success in preventing perimitral flutter. Furthermore, specific patient demographics and disease profiles appear to influence the magnitude of benefit derived from VOM-Et. The findings strongly suggest that male patients, those older than 60 years, individuals with a smaller left atrial diameter (<55 mm), and patients having a shorter duration of AF (<3 years) are most likely to experience significant improvements in MI block rates with the VOM-Et approach. These results support the targeted use of VOM-Et as a valuable adjunct to improve the efficacy and potentially the long-term outcomes of catheter ablation for persistent AF, particularly in the identified beneficiary subgroups.

结缔组织生长因子与房颤及心房纤维化的相关性研究

陈丽雯 白瑾 孙丽杰 崔鸣

北京大学第三医院

目的：心房颤动（Atrial Fibrillation，AF）是一种常见的心律失常，严重影响患者的心脏功能和生活质量，并导致高昂的医疗费用。本研究旨在探讨结缔组织生长因子（Connective Tissue Growth Factor，CTGF）在心房颤动患者中的表达水平及其与心房纤维化和射频消融术后复发的相关性。

方法：本研究纳入 2020 年 7 月至 2021 年月 7 月于北京大学第三医院心血管内科住院首次行射频消融术 89 例房颤患者，选择同期住院的无房颤病史的 45 例窦性心律患者为对照组。收集入组患者的临床资料，包括病史、实验室指标、超声心动图指标、肺静脉相关指标，采用酶联免疫吸附法检测血浆 CTGF 水平。房颤组患者在射频消融术中标测左房低电压区面积，并随访术后 24 月，评估预后情况。

结果: 与对照组相比较，阵发性房颤组和持续性房颤组血浆 CTGF 浓度均明显升高，且持续性房颤组明显高于阵发性房颤组（13.4 ± 4.2 ng/ml vs 11.4 ±3.0ng/ml vs 10.0±3.1ng/ml，P < 0.05）。相关分析表明，CTGF 水平分别与左房低电压区面积 (r=0.316, P=0.012)、左房面积 (r=0.245, P=0.005) 呈正相关。多因素分析中 CTGF 是房颤发生发展的独立危险因素（HR=1.4, p =0.008）。

结论：CTGF 与心房纤维化相关，与房颤发生发展相关，推测 CTGF 可能通过促进心房纤维化参与房颤发生发展的过程。

缩窄性心包炎合并心房颤动及心房扑动行射频消融术的疗效和安全性分析

金书琪 刘念

首都医科大学附属北京安贞医院

摘要：心房颤动（AF）与心房扑动（AFL）均为心房电生理活动异常及心室节律不规则，导致血流动力学稳定性受损的心律失常。缩窄性心包炎（CP）是一种心包慢性炎症性疾病，其特征为心包纤维化、粘连及钙化。在临床实践中，部分 CP 患者合并 AF/AFL，然而，针对此类患者是否适宜进行射频消融术（RFA）、术后疗效及预后情况，现有临床数据尚显不足。

研究方法与结果：本研究回顾性分析了首都医科大学附属北京安贞医院自 2019 年 2 月至 2025 年 2 月期间接受经导管 RFA 治疗的 34 例合并 CP 的 AF/AFL 患者。其中，11 例患者未曾接受心包剥脱术，而 23 例患者已有心包剥脱术史。在未接受心包剥脱术的 11 例患者中，5 例为持续性 AF，3 例为阵发性 AF，3 例为持续性 AFL；所有患者均成功完成消融，消融成功率为 100%；9 例患者术后未出现复发，2 例患者术后复发，且均有 2 次及以上 RFA 术史，复发率为 18.2%。在已接受心包剥脱术的 23 例患者中，14 例为持续性 AF，4 例为阵发性 AF，5 例为持续性 AFL；22 例患者消融成功，1 例消融失败，消融成功率为 95.7%；14 例患者术后未复发，8 例患者术后复发，且均有 2 次及以上 RFA 术史，复发率为 36.4%。综合分析显示，总体消融成功率为 97.1%，总体复发率为 29.4%。

结论：对于合并 CP 且已行心包剥脱术的 AF/AFL 患者，RFA 治疗仍具有较高的成功率，但同时较高的远期复发率亦应引起重视。此外，未行心包剥脱术的患者在 RFA 后心功能改善不显著，而已行心包剥脱术的患者在 RFA 后心室舒张功能可得到部分改善。

术前高敏 C 反应蛋白水平与非瓣膜性房颤射频消融术后长期预后的关系：一项中位 7 年随访的前瞻性队列研究

毕雨欣 彭晓东 李玉昆 逯峰源 孟凡超 金书琪

首都医科大学附属北京安贞医院

背景 房颤射频消融术（RFCA）是治疗非瓣膜性房颤（NVAF）的重要方法，但术后长期预后仍存在不确定性，部分患者面临死亡、卒中及大出血等严重不良事件的风险。高敏 C 反应蛋白（hs-CRP）作为炎症标志物，与心房结构重塑及房颤进展密切相关，可能影响术后预后。然而，hs-CRP 对术后长期硬终点及软终点事件的预测价值尚不明确。

方法 本研究基于中国房颤注册（CAFR）队列，纳入 2011 年至 2022 年在北京安贞医院接受首次 RFCA 治疗的 NVAF 患者，中位随访 7 年。术前采集血清 hs-CRP 水平，结合临床及影像学资料，分别分析 hs-CRP 与两个复合硬终点（全因死亡 + 卒中 +ISTH 大出血；心血管死亡 + 卒中 +ISTH 大出血）及两个软终点（房颤复发、主要出血）的关联。采用多变量 Cox 比例风险模型及限制性立方样条（RCS）分析剂量 - 反应关系，调整潜在混杂因素，并开展亚组及敏感性分析。

结果 患者按 hs-CRP 三分位数分组，高组患者具有更高心血管风险负担及更多持续性房颤。多变量调整后，hs-CRP 水平升高显著增加两个复合硬终点的风险（完全调整 HR 约 1.12，P<0.05），呈线性剂量 - 反应趋势。亚组分析显示，该关联在 < 65 岁患者中更为显著（HR=1.30，P<0.001），而年龄≥65 岁组无明显相关性。hs-CRP 升高亦与术后房颤复发和主要出血风险增加相关，但对复发预测的统计学意义较边缘。

结论 术前 hs-CRP 水平是 NVAF 患者接受射频消融术后长期硬终点风险的独立预测因子，尤其在年轻患者中具有更高的预后价值。该炎症标志物可能参与房颤的电结构重塑及相关并发症的发生，提示术前炎症评估对患者风险分层和个体化管理具有重要意义。未来应进一步探讨抗炎策略在术后长期管理中的潜在作用。

Clinical Outcomes in Asymptomatic and Symptomatic Atrial Fibrillation Patients With or Without Rhythm Control Therapy: A Prospective Multicenter Registry Study

Xiao-Dong Peng, Liu He, Xiao-Xia Liu, Chang-Sheng Ma

Beijing AnZhen Hospital, Capital Medical University

Background

Current guidelines recommend rhythm control for atrial fibrillation (AF) based primarily on symptom management, though accumulating evidence indicates potential prognostic benefits beyond symptom relief. This study aimed to assess the association between rhythm control and clinical outcomes according to symptomatic status.

Methods Of the 15,603 patients enrolled in the China-AF registry, symptom status was classified as asymptomatic or symptomatic according to the European Heart Rhythm Association (EHRA) score. Cox proportional hazards models were applied to assess the associations between symptom status, rhythm control, and composite outcomes (cardiovascular death and stroke). The interaction effect of symptom status and rhythm control on outcomes was also examined. Results Among the patients, 1,345 (8.6%) were asymptomatic, with a higher proportion of males, non-paroxysmal AF, a prolonged AF course, and eccentric hypertrophy. Rhythm control treatment was applied in 48.9% of asymptomatic patients and 62.9% of symptomatic patients. Over a median follow-up of five years, the incidence of composite outcomes was similar between asymptomatic and symptomatic patients (1.99% person-year vs. 2.12% person-year, adjusted hazard ratio [aHR]: 0.96; 95% confidence interval [CI], 0.81–1.14). For asymptomatic patients, rhythm control was associated with a reduced risk of composite outcomes (aHR: 0.37; 95% CI, 0.23–0.60), comparable to that observed in symptomatic patients (aHR: 0.52; 95% CI, 0.49–0.62) (P for interaction=0.111). Conclusions This observational study suggests that asymptomatic patients exhibited a similar risk of adverse outcomes compared to symptomatic patients, with no significant difference in the benefit of rhythm control between the groups. These results highlight the value of rhythm control strategies in meeting the unaddressed clinical needs of asymptomatic AF patients, who are frequently under-treated due to the symptom-driven management. This observation supports a potential paradigm shift in AF care, and may inform future updates to management guidelines.

导管消融对心房颤动合并颅内出血病史患者的远期预后影响

李景业 赖一炜 赵一泽 何柳 郭雪原 桑才华 马长生

首都医科大学附属北京安贞医院

目的 心房颤动（房颤）合并颅内出血史的患者同时面临血栓栓塞与再发出血的双重风险，临床决策极具挑战。导管消融治疗在此类特殊高危人群中的临床获益尚不明确。本研究旨在评估导管消融与单纯药物治疗相比对房颤合并颅内出血史患者的远期心血管预后影响，为个体化治疗提供依据。

方法 本研究基于中国房颤注册研究（China-AF），纳入 2011 年 8 月至 2022 年 6 月间入组时明确存在颅内出血病史的房颤患者，根据治疗策略不同将其分为消融组和非消融组。研究的主要终点为心血管死亡、血栓栓塞（缺血性卒中 / 短暂性脑缺血发作 / 系统性栓塞）及危及生命大出血事件构成的复合终点。

结果 本研究纳入共计 310 例符合入排标准的房颤患者，其中消融组 126 例（40.6%）。与非消融组相比，消融组更年轻（平均年龄 64.0±9.6 岁 vs. 70.1±9.9 岁，p<0.001），持续房颤的比例较低（36.5% vs. 57.6%, p<0.001）且房颤病史的时程更短（中位病程 1.4 年 vs. 2.8 年，p=0.004）。中位随访 60.2 个月，消融组的累积终点事件发生率显著低于非消融组（7.9% vs. 30.4%，Log-rank p<0.001）。校正潜在混杂因素后，与药物治疗相比，导管消融与主要复合终点事件风险降低相（HR: 0.40, 95% CI: 0.19-0.87, p=0.025），主要由血栓栓塞风险下降驱动（HR 0.23，95%CI 0.07–0.78；p=0.024），而心血管死亡（HR, 0.46; 95% CI, 0.15-1.40; p=0.182）和危及生命的大出血事件（HR, 1.11; 95% CI, 0.33-3.67; p=0.872）无统计学差异。

结论 对于房颤合并颅内出血史这一特殊高危人群，导管消融治疗与远期血栓栓塞及复合心血管事件风险降低相关，且与危及生命的大出血事件风险无关。

基于集成于智能手表的单导联心电图：人工智能增强校正 PPG 评估的心房颤动负荷的前瞻性验证研究

左嵩 李法东 马长生

首都医科大学附属北京安贞医院

背景： 采用光电容积描记术（PPG）的智能手表在评估心房颤动（AF）负荷方面展现出应用前景，但其无法准确识别心律的局限性导致测量效果欠佳。本研究旨在通过结合智能手表的单导联心电图（ECG），利用人工智能（AI）增强校正技术，提高基于智能手表 PPG 的房颤负荷评估准确性。

方法： 本前瞻性验证研究于 2024 年 1 月至 6 月在北京安贞医院的房颤患者中开展。患者佩戴具备 PPG 算法和单导联心电图记录功能的智能手表及心电图贴片，进行 24 小时监测。监测期间，患者需主动使用智能手表记录单导联心电图，作为校正参考片段，以贴片心电图（P-ECG）结果作为评估金标准。采用卷积神经网络与长短期记忆网络相结合的 AI 算法对数据进行分割、分类和校正。

结果： 共纳入 1054 名参与者（中位年龄 64 岁；男性占 66.5%），每日佩戴智能手表的中位时长为 16.3 小时，每位参与者平均记录 3.7 次单导联心电图，共完成 3847 次 AI 校正。AI 校正算法诊断性能优异，在房颤负荷检测中的敏感性达 98.60%（95% 置信区间：98.57%–98.63%），特异性达 99.27%（95% 置信区间：99.25%–99.29%），曲线下面积（AUC）为 98.94%。值得注意的是，平均绝对百分比误差（MAPE）降低 23.4%（从 1.11% 降至 0.85%），皮尔逊相关系数达 0.9988，表明一致性极高。该算法在高依从性组中表现尤为突出：在单导联心电图触发次数超过 8 次的患者中，房颤负荷估计误差降低 70.6%。此外，假阳性和假阴性检测分别减少 30.37% 和 13.19%，进一步验证了该算法在真实世界监测中的可靠性。

解读： 集成于智能手表中的 AI 增强校正算法显著提高了房颤负荷评估的准确性，大幅减少了因 PPG 算法在心律识别方面的局限性所致的假阳性和假阴性结果。本研究的 AI 校正模型有效解决了 PPG 技术的固有缺陷，尤其在单导联心电图触发频繁的患者中效果显著。该研究提出了一种具有临床可行性、可扩展性且前景广阔的方法，可为个性化房颤管理策略提供支持，并促进真实世界环境下的大规模房颤监测。（NCT06552468）

单导联长程心电监测对中国东部某农村地区 75 岁及以上老年人房颤筛查的有效性：一项社区人群研究

赵一泽 周乐 王珏 李法东 何柳 左嵩 马长生

首都医科大学附属北京安贞医院

目的 评估单导联长程（7 日）心电监测与常规 12 导联心电图相比，对提高中国农村地区 75 岁及以上老年人群心房颤动（房颤）检出率的影响，并描述房颤负荷的分布特征。

方法 纳入 2024 年 8 月至 12 月期间居住于浙江省衢州市衢江区自愿参加房颤筛查且既往无房颤病史的 75 岁及以上居民，所有受试者均佩戴单导联心电贴片连续 7 天监测，并同时接受标准 12 导联心电图检查。

结果 研究共纳入 3424 人，中位年龄 79（Q1-Q3: 76-83）岁，男性 1595 人（46.6%）。长程心电监测共检出房颤患者 268 例（7.8%），其中持续性房颤 155 例（4.5%），均经 12 导联心电图检出；检出阵发性房颤 113 例（3.3%），仅 11 例（0.3%）被 12 导联心电图检出（3.3% vs. 0.3%, P < 0.001）。房颤患者中位房颤负荷为 97.3% (Q1-Q3：14.0%-99.8%)，阵发性房颤患者中位负荷为 10.5%（Q1-Q3：5.4%-36.7%），阵发性房颤最长持续时间的中位数为 24.5 分钟（Q1-Q3：8.0–58.0），其中 86 例（76.1%）< 60 分钟，8 例（7.1%）> 200 分钟。在阵发性房颤患者中，房颤负荷与单次最长持续时间呈正相关，差异具有统计学意义（r=0.155, P < 0.001）。

结论 在≥ 75 岁老年人群中，与标准 12 导联心电图相比，长程心电监测可显著提高房颤检出率，尤其是阵发性房颤的检出。此外，长程心电监测能更全面地评估房颤负荷，可能对老年人群基于房颤负荷行个体化抗凝治疗具有指导意义。

Validation of Photoplethysmography-Based Smartwatch for Continuous Evaluation of Atrial Fibrillation Burden

SONG ZUO, Le Zhou, Jue Wang, Yi-Ze Zhao, Fa-Dong Li, Liu He, Chang-Sheng Ma

Beijing AnZhen Hospital, Capital Medical University

Objective:

To verify the effectiveness of a smartwatch equipped with the PPG algorithm in continuously monitoring AF burden.

Methods:

This prospective study included patients diagnosed with AF at Beijing Anzhen Hospital between January and December 2024. Each participant continuously wore a smartwatch equipped with the PPG algorithm and a patch-based electrocardiograph (P-ECG) as the reference to validate algorithm performance for estimation of AF burden. The watch-based PPG (W-PPG) data will be segmented into 30-second intervals and verified with the data from P-ECG to analyze its accuracy, sensitivity, and specificity.

Results:

The study recruited 728 participants, with a mean age of 62.0 ± 10.5 years, of whom 412 (56.6%) had paroxysmal AF. The average monitoring time for each participant was 20.4 ± 4.5 hours. The overall effective recording rate for P-ECG was 96.2%, while the effective recording rate for W-PPG was 62.5%. After segmentation, a total of 1,440,826 PPG records were generated. At the interval level, sensitivity was 98.6% (95% CI: 98.5%–98.7%), specificity was 99.5% (95% CI: 99.4%–99.6%), with an AUC of was 99.1%. At the patient level, W-PPG demonstrated a sensitivity of 92.0% (95% CI: 89.3%–94.6%) and specificity of 96.4% (95% CI: 94.3%–98.4%), and the area under the curve (AUC) was 94.2%. The Bland-Altman analysis showed excellent agreement between the AF burden estimates from PPG and ECG, with a mean difference of -1.34% and 95% limits of agreement ranging from -6.45% to 3.77%. A strong correlation (r = 0.999) was observed between PPG-based and ECG-measured AF burden (NCT 05333380). Conclusions: Smartwatches with PPG algorithm offer a practical and non-invasive approach for continuous AF burden monitoring. The results suggest that PPG can be an effective approach for long-term AF management, providing an accessible alternative to traditional ECG monitoring.

Continuous Evaluation of Atrial Fibrillation Burden

Yi-Ze Zhao, Le Zhou, Jue Wang, Fa-Dong Li, Liu He, Song Zuo, Chang-Sheng Ma

Beijing AnZhen Hospital, Capital Medical University

Objective:

This trial aims to evaluate the effectiveness of an AI-driven seven-day single-lead ECG patch in improving the detection of newly diagnosed AF and reducing the risk of cardiovascular events in the elderly population in rural China.

Methods:

The cluster-randomized controlled trial will randomly assign 128 village clinics in a 1:1 ratio to either the long-term screening group (seven-day ECG patch and 12-lead ECG) or the routine screening group (only 12-lead ECG in Qujiang District, Zhejiang Province. Each village will enroll at least 100 elderly participants aged 60 years or older. Both screening approaches will be performed in their group annually, and for three consecutive years. All participants will be followed up to three years.

Results:

The primary outcome is the detection rate of newly diagnosed AF in the first year for the first phase, and a composite endpoint of all-cause mortality, stroke, and hospitalization for heart failure for the second phase.

房颤导管消融术后口服抗凝治疗与血栓栓塞风险降低无关：一项纵向队列研究

任岚 马长生

首都医科大学附属北京安贞医院

背景

心房颤动（AF）患者行导管消融（CA）术后口服抗凝（OAC）治疗的最佳策略尚未明确。本研究旨在探讨接受与未接受 CA 治疗的 AF 患者 OAC 治疗与血栓栓塞及出血事件风险的关系，并评估消融术后停用 OAC 的潜在可行性。

方法

这项前瞻性队列研究连续纳入 2011 年 8 月至 2022 年 6 月期间中国房颤注册研究（China-AF）中年龄≥ 18 岁的 AF 患者，中位随访 4.7 年。血栓栓塞事件定义为缺血性卒中、体循环栓塞或短暂性脑缺血发作，大出血事件采用国际血栓与止血学会（ISTH）标准判定。

结果

共纳入 24,587 例患者，基线时分为 CA 组与非 CA 组，并根据 6 个月时的 OAC 治疗状态分为 4 组：CA 组持续 OAC（n=2,637）、CA 组停用 OAC（n=11,032）、非 CA 组持续 OAC（n=3,410）及非 CA 组停用 OAC（n=7,508）。CA 组总体血栓栓塞发生率显著低于非 CA 组（0.81% 人年 vs. 1.77% 人年；校正后 P<0.001）。在 CHA2DS2-VA 评分≥ 3 且未抗凝的患者中，CA 组与非 CA 组的血栓栓塞发生率分别为 1.47% 人年和 2.75% 人年。6 个月界标分析显示，CA 组中 OAC 治疗在所有 CHA2DS2-VA 评分分层均未进一步降低血栓栓塞风险（CHA2DS2-VA ≤ 1：校正风险比 [aHR] 1.11，95% CI 0.70-1.77；CHA2DS2-VA 评分 =2：aHR 0.64，95% CI 0.36-1.16；CHA2DS2-VA 评分 ≥ 3：aHR 1.05，95% CI 0.74-1.48），且无分层交互作用（交互作用 P=0.930）。对于 CHA2DS2-VA 评分≥ 3 的消融术后患者，OAC 治疗显著增加大出血风险（aHR 2.32，95% CI 1.19-4.50）。

结论

与未接受 CA 治疗者相比，消融术后 AF 患者的血栓栓塞风险降低。在消融术后患者中，OAC 治疗未减少血栓栓塞风险，反而增加大出血风险（尤其 CHA2DS2-VA 评分≥ 3 的患者）。研究结果提示，未来亟需开展高质量随机对照试验来指导 CA 术后抗凝策略的制定。

左心室几何重构与房颤合并射血分数保留型心衰患者的预后及疗效的关系

任岚 马长生

首都医科大学附属北京安贞医院

左心室几何重构与房颤合并射血分数保留型心衰患者预后及疗效的关系

任岚，彭晓东，李明宵，何柳，郭雪原，董建增，马长生

背景与目的：

左心室几何重构是射血分数保留型心衰（HFpEF）的关键病理生理特征，但对合房颤（AF）合并 HFpEF 患者的预后影响尚不明确。本研究旨在探讨左心室几何重构与 AF 合并 HFpEF 患者临床结局的关联性，并分析不同左室几何重构亚型对治疗反应的差异。

方法：

本研究为基于中国房颤注册登记研究（China-AF）的前瞻性多中心队列研究，通过超声心动图评估左心室质量指数（LVMI）和相对室壁厚度（RWT），将基线左室几何构型分为四类：正常构型、偏心性肥厚、向心性重构和向心性肥厚。主要终点为包括心血管死亡、血栓栓塞和大出血的复合终点。次要终点包括全因死亡及复合终点的各单项事件。采用多变量 Cox 回归模型分析关联性及治疗的交互作用。

结果：

共纳入 1,691 例 AF 合并 HFpEF 患者，中位随访 4.8 年。50.9% 的患者存在 LV 几何构型异常。向心性重构（校正风险比 [aHR]：1.53；95% CI：1.17–2.01）和向心性肥厚（aHR：1.48；95% CI：1.10–1.99）与主要终点风险升高独立相关。向心性几何构型与心血管死亡和血栓栓塞事件增加显著相关。导管消融术与向心性重构患者的主要终点事件风险的降低显著相关（aHR：0.29；95% CI：0.12–0.74），但各构型间与治疗方式无显著交互作用（交互作用 P 值 =0.15）。RAAS 抑制剂和 β 受体阻滞剂在不同几何亚型中的获益均不一致。

结论：

左室几何重构对 AF 合并 HFpEF 患者具有重要的预后分层价值，其中向心性重构和向心性肥厚患者不良结局风险更高。尽管导管消融在向心性重构患者中显示出风险降低趋势，但由于缺乏统计学显著的交互作用，该结果需谨慎解读。未来需进一步研究验证针对不同左室几何重构患者的个体化治疗策略。

心血管互联网与人工智能有关研究

TabPFN 在心 - 肾 - 代谢综合征冠脉狭窄诊断模型构建中的探索性应用

朱时典 [1,2] 刘福明 [1]

1. 南京中医药大学附属医院，江苏省中医院

2. 南京中医药大学第一临床医学院

目的: 探索表格先验数据拟合网络（TabPFN）在医学诊断模型开发中的应用价值; 基于心 - 肾 - 代谢综合征（CKM）研究框架，构建并验证 CKM 患者冠脉重度狭窄的中西医诊断模型，为临床提供辅助决策支持。

方法：回顾性纳入江苏省中医院本部（2024 年 1 月 -2024 年 8 月）及紫东院区（2024 年 9 月 -2024 年 12 月）住院患者共 535 例。将本部数据按 4:1 随机分层分为训练集（n=376）和内部验证集（n=95），紫东数据作为外部验证集（n=64）。综合文献综述、专家访谈和 LASSO 回归筛选变量。利用 TabPFN 构建诊断模型，并与 9 种传统机器学习算法（决策树、随机森林、极限梯度提升、弹性网络、支持向量机、浅层神经网络、逻辑回归、轻量级梯度提升机、K 近邻）从区分度、校准度及临床实用性等方面进行多维度评估。最后，实际应用于冠脉 CTA 临界病变患者。

结果：LASSO 回归筛选出 9 个独立危险因素：中医病性证素（滞、痰、瘀、虚）、性别、高血压病程、动脉硬化指数（ASI）、糖化血红蛋白（HbA1c）及尿酸 / 高密度脂蛋白胆固醇（UHR）。综合性能比较表明，TabPFN 模型表现最优，AUC 在训练集、内部和外部验证集中分别为 0.963 (95% CI: 0.947~0.979)、0.862 (95% CI: 0.790~0.933) 和 0.900 (95% CI: 0.814~0.986); 外部验证集中，校准曲线预测概率一致性良好，决策曲线全程均具临床净获益，置换特征重要性排序为：滞、瘀、虚、UHR、性别、HbA1c、高血压病程、ASI、痰。在冠脉 CTA“临界病变”患者中，识别重度狭窄 AUC 达 0.853 (95% CI: 0.741~0.966)，可使 60% 实际重度狭窄患者获益。

结论：TabPFN 在小样本医学数据中，综合效能优于传统机器学习模型，应用前景良好；本研究构建的诊断模型可为 CKM 患者临床诊疗提供决策依据。

基于人工智能的心血管疾病信息化护理管理系统的构建与应用研究

徐心雨

中国人民解放军陆军特色医学中心

目的

心血管疾病（CVD）患者的管理需要长期、动态的护理干预，传统护理模式存在数据碎片化、预警滞后等问题。本研究旨在构建一种基于人工智能（AI）的心血管信息化护理管理系统，实现患者数据的智能整合、风险评估及个性化护理决策支持，以提高护理效率及患者预后。

方法

1. 系统架构：

数据层：整合电子健康档案（EHR）、可穿戴设备（如智能手环）实时生命体征（心率、血压、血氧）、患者自报告症状及用药记录。

AI 模型层：

采用随机森林（RF）和长短期记忆网络（LSTM）构建动态风险评估模型，预测急性事件（如心衰加重、心律失常）。

自然语言处理（NLP）技术分析护理记录文本，自动识别高危患者（如依从性差、症状恶化）。

应用层：开发护士端移动终端，提供实时预警、护理路径推荐及患者教育内容推送。

2. 验证设计：

前瞻性纳入 200 例 CVD 患者（心衰、冠心病各半），随机分为 AI 护理组（n=100）和常规护理组（n=100），比较 6 个月内再入院率、护理响应时间及患者满意度。

结果

1. 模型性能：AI 系统对心衰恶化的预测准确率达 89.3%（F1-score=0.87），预警时间较传统方法平均提前 48 小时。

2. 临床效果：

AI 护理组再入院率显著低于常规组（12% vs. 28%，p<0.01），护理响应时间缩短 65%（p<0.001）。

患者满意度评分提高（4.6±0.3 vs. 3.9±0.4，p<0.05）。

3. 护理效率：NLP 自动识别高危患者的敏感度为 92.1%，减少护士手工筛查时间 70%。

结论

本研究构建的 AI 驱动心血管护理管理系统，通过多源数据融合与智能分析，显著提升护理精准度和时效性，为慢性心血管疾病患者的长期管理提供了一种高效、可推广的信息化解决方案。未来可扩展至社区护理及居家监护场景。

心血管信息化与 AI 融合提升诊疗效能的探索

张蕾

西安交通大学第一附属医院

目的：

目的： 探讨心血管信息化系统与 AI 技术对提升疾病诊疗效率、准确性、可及性及个体化管理的潜力。

方法：1. 构建集成信息系统：整合电子健康记录（EHR）、诊疗方案及医疗影像，实现全流程数字化。

2. 开发 AI 辅助工具：

影像分析：基于深度学习算法，实现超声心动图标准切面自动识别（>90% 准确率）、左心室全自动分割及射血分数（LVEF）实时计算。

无创监测：利用光纤传感床采集心冲击图（BCG）信号，结合降噪算法；通过脉搏波（PW）特征提取与机器学习筛查慢性肾病患者的冠脉钙化风险。

风险预测：运用自监督学习处理 EHR 数据构建患者关系图谱（心衰预测 AUROC=0.9137），筛选跨疾病标志物如 S100A12。

结果：

1. 效率提升：AI 辅助冠脉 CTA 后处理使日检查量增加 15 倍，报告 24 小时内完成；AI 超声床旁分析缩至 5 分钟。

2. 准确性增强：LVEF 计算与二尖瓣环位移（MAPSE）测量误差 <5%；PW 模型筛查冠脉钙化平衡准确率达 83%（AUC 0.89）；BCG 与 ECG 心率检测相关性 R=0.98。

3. 新知识发现：揭示 MAPSE<8mm 提示心肌能量效率不足与休克风险；鉴定 S100A12 为 COVID-19 血栓并发症标志物；无创 BCG/PW 技术支持连续监测。

4. 赋能基层：AI 数字化专家经验辅助基层诊断，缓解资源短缺。

结论 ： 心血管信息化与 AI 融合显著优化诊疗流程，通过自动化分析、精准无创监测及高效风险预测，提升效率与客观性，赋能早期预警和个体化管理。未来需扩大数据集、推动多学科合作与标准化应用，深化基层及预防场景，实现心血管医疗的普惠可及。

数字 AI 预测护理系统联合护士主导模式降低冠心病再入院率的阶梯楔形随机试验研究

张玲玲

中国人民解放军陆军特色医学中心

目的 探讨护士主导的数字 AI 预测护理系统对降低冠心病患者再入院率、改善生活质量及提升自我管理能力的效果。

方法 开展多中心阶梯楔形随机试验，纳入多家三级医院心内科病房，随机分为对照组（常规护理）与干预组（数字 AI 预测护理系统 + 护士主导干预）。AI 系统整合患者基础信息（年龄、性别、合并症）、临床数据（心电图、心肌标志物、冠脉造影结果）、用药情况及动态监测数据（血压、心率、血氧饱和度），通过机器学习算法实时预测再入院风险。护士依据 AI 风险预警，对高风险患者实施强化干预：包括每周 2 次电话随访、个性化用药指导（如他汀类药物依从性管理、抗血小板药物出血风险监控）、远程心电监测异常结果的即时处理，以及基于患者认知水平的心血管疾病防治教育。主要观察指标为出院后 30 天、90 天、180 天的再入院率，同时采用西雅图心绞痛量表（SAQ）评估生活质量，冠心病自我管理行为量表（CSMS）评估自我管理能力，分别在基线、干预 3 个月、6 个月、12 个月进行测量。

结果：共纳入 1500 例冠心病患者（对照组 750 例，干预组 750 例）。出院 30 天，干预组再入院率为 6.8%，显著低于对照组的 11.2%（P<0.001）；90 天再入院率分别为 13.5% vs 19.8%（P<0.001）；180 天再入院率为 18.3% vs 26.7%（P<0.001）。干预组 SAQ 总分在 3 个月后显著提升（82.5±7.3 vs 75.2±8.1，P<0.001），CSMS 评分从基线的 62.4±6.5 提升至 12 个月的 78.6±5.8（P<0.001），均优于对照组。

结论：护士主导的数字 AI 预测护理系统可显著降低冠心病患者再入院率，有效改善患者生活质量及自我管理能力，为冠心病长期管理提供了高效、精准的数字化解决方案，具备临床推广价值。

人工智能在心脏重症中血流动力学监测的应用进展

吴诗文

北京清华长庚医院

目的：心脏重症患者常因严重心功能不全、循环衰竭或复杂心脏术后状态而面临显著的血流动力学不稳定情况，危及生命。传统监测手段如脉波指示剂连续心排血量监测（PiCCO）和肺动脉漂浮导管（PAC）虽能提供心输出量、肺动脉压等重要数据，但其临床应用受到有创操作相关风险、技术要求高、费用昂贵以及难以实现动态监测的局限制约。当前，经胸心脏超声（TTE）和经食管心脏超声（TEE）凭借其微创、可重复性高、能实时评价心脏结构与功能的独特优势，已成为心脏重症血流动力学监测的重要工具，研究证实其能为疾病诊断、疗效评估、重复血流动力学监测及解剖结构观察提供关键信息。然而 TTE 和 TEE 在应用中仍然存在短板，其操作高度依赖医师的专业技术水平和经验，存在操作者差异；无法提供连续、实时的血流动力学数据流，限制了其在危重症场景的应用。

方法：查阅国内外前沿文献与资料，进行综述

结果：人工智能（AI）技术的崛起为突破 TEE 上述瓶颈提供了革命性的解决方案。AI 的核心优势在于其强大的模式识别与深度学习能力、精准的自动化控制潜力、实现了持续动态检测的可能性，以及对图像中细微且复杂变化的高度敏感捕捉能力。国外前沿研究显示，将经食管心脏超声（TEE）与人工智能技术（如 autoMAPSE）结合应用时，AI 测量较手动测量展现出更优的趋势预测能力、更

低偏差及更高精准度与一致性，且大幅度减少了对操作者经验的依赖。

结论：本文综述人工智能技术在心脏重症护理血流动力学监测中的应用进展，旨在为临床工作者提供优化心脏重症患者监测策略的循证新思路、高效工具选择依据及未来研发方向参考，以期最终提高监测效率、诊疗精准度及患者预后。

基于生成式人工智能技术赋能的心内科复杂急救情境虚拟仿真训练体系在护理人员培训中的应用与效果研究

zhang

中国人民解放军陆军特色医学中心

目的： 鉴于心内科复杂急救场景对护理人员的高要求及传统培训方式的局限性，本研究旨在构建基于生成式人工智能（Gen AI）的心内科复杂急救场景虚拟仿真训练体系，并评估其在护理人员培训中的应用效果。

方法： 融合 Gen AI 技术与虚拟仿真平台，设计涵盖心源性休克、急性心律失常、急性冠脉综合征、肺栓塞、主动脉夹层等复杂急救场景的多模块交互系统，包含病情快速识别、精准急救处理、高效团队协作及延续性护理指导四大核心模块，共 15 项交互任务，其中 6 项任务嵌入 Gen AI 生成的多路径急救决策与动态反馈机制。于 2024 年 3 月至 12 月，选取 80 名心内科护理人员随机分为试验组（n=40）与对照组（n=40）。试验组采用 Gen AI 辅助的虚拟仿真系统培训，系统依据操作实时生成个性化急救案例与反馈；对照组接受传统人工设计案例培训。对比两组急救方案制定时长、急救操作考核成绩、培训满意度及案例专业质量的专家评分（由 5 名心内科专家盲评，从急救流程创新性、动态应变能力、操作规范性、医学逻辑严谨性四个维度进行）。

结果： 试验组急救方案制定平均用时（38.2±7.5）分钟，显著短于对照组（72.3±12.1）分钟（P<0.01）；急救操作考核得分试验组（90.1±5.8）分，明显高于对照组（79.6±8.3）分（P<0.05）。试验组培训满意度达 95%（38/40），显著高于对照组 80%（32/40）（P<0.05）。专家评审显示，试验组在急救流程创新性（4.7/5）与动态应变能力（4.6/5）评分优于对照组，但操作规范性（4.3/5 vs. 4.6/5）与医学逻辑严谨性（4.4/5 vs. 4.7/5）评分低于对照组（P<0.05）。

结论： Gen AI 赋能的心内科复杂急救场景虚拟仿真训练体系可有效提升护理人员急救培训效率与实践操作能力，培训满意度高。然而，该体系在急救流程规范性和医学逻辑严谨性方面仍需通过人工审核与专业校准进一步完善。未来可探索将该体系与其他培训方式结合，推广至更多科室，为心内科护理人员急救能力培养提供智能化、高效化的新路径。

Machine Learning Identifies ECG Biomarkers for 28-Day Mortality Risk Stratification in ICU Patients

null null

Beijing Tsinghua Changgung Hospital

Background: Risk stratification in intensive care units (ICUs) remains one of the most complex tasks in critical care medicine due to the dynamic and heterogeneous nature of critically ill patients. Traditional clinical scoring systems such as SOFA, APACHE II, and SAPS II are widely used for outcome prediction; however, they often fail to capture subtle but clinically relevant physiological changes that may precede adverse events. Electrocardiogram (ECG) recordings, which are routinely collected in ICU settings, contain rich temporal and morphological information that may reflect underlying cardiac dysfunction, autonomic imbalance, and systemic stress. Despite their potential value, ECG-derived features have not been systematically evaluated across large, unselected ICU populations for mortality risk prediction. This study aimed to address this gap by identifying and validating interpretable ECG biomarkers for predicting 28-day all-cause mortality using machine learning techniques.

Methods: The data for this retrospective cohort study were obtained from the Medical Information Mart for Intensive Care IV (MIMIC-IV), a publicly available database containing de-identified health records of over 40,000 ICU admissions. From this dataset, we selected 29,326 adult ICU patients who had at least one high-quality 12-lead ECG recording during their stay. A total of 283 ECG-derived features were extracted using automated signal processing algorithms. These included time-domain parameters (e.g., QRS duration, QT interval), amplitude-based measures (e.g., ST deviation, R-wave amplitude), frequency-domain metrics (e.g., power spectral density), heart rate variability (HRV) indices (e.g., SDNN, RMSSD), and vectorcardiographic (VCG) features derived from Frank lead transformation. To ensure robustness and generalizability, we applied a multi-stage feature selection pipeline: first removing highly correlated features (Pearson's r > 0.8), then eliminating multicollinear variables using variance inflation factor (VIF > 10), and finally applying bootstrap-enhanced LASSO-Cox regression over 1000 iterations to retain only those features selected in ≥ 95% of the samples.

Results: Two survival-based machine learning models—Random Survival Forest (RSF) and XGBoost—were trained to predict the probability of 28-day all-cause mortality. Model performance was evaluated using the concordance index (C-index), time-dependent receiver operating characteristic (timeROC) curves, and precision-recall analysis. The RSF model achieved a C-index of 0.740 and a 28-day timeROC AUC of 0.766 (95% CI: 0.751–0.780), indicating good discriminative ability. The XGBoost model demonstrated superior performance, with a C-index of 0.761 and a 28-day timeROC AUC of 0.781 (95% CI: 0.767–0.795). Both models were further assessed for interpretability using SHAP (SHapley Additive exPlanations) values and built-in feature importance scores, which helped identify the most influential predictors and provided insight into the biological mechanisms underlying the predictions.

Following the feature selection process, 21 ECG-derived biomarkers were identified as independently associated with 28-day mortality. Among these, several showed particularly strong predictive power. The maximum QRS velocity (speed_qrs_max), reflecting the speed of ventricular depolarization, was the most important predictor in the XGBoost model (gain = 0.126), suggesting that impaired conduction velocity may be a marker of severe myocardial dysfunction or systemic illness. Other significant features included RMSSD_all, a measure of short-term heart rate variability reflecting parasympathetic activity (gain = 0.072), and avL_qrst_area, a metric derived from the aVL lead that quantifies repolarization heterogeneity (gain = 0.068). These findings indicate that abnormalities in cardiac conduction, autonomic regulation, and electrical recovery patterns are closely linked to mortality risk in ICU patients. SHAP value analysis further confirmed that slower depolarization, increased repolarization dispersion, and reduced HRV were consistently associated with higher mortality probabilities.

Conclusion: In conclusion, this large-scale retrospective analysis of ICU patients from the MIMIC-IV database demonstrates that specific ECG-derived features—particularly those related to ventricular depolarization speed and repolarization heterogeneity—are independent and robust predictors of 28-day mortality. When integrated into survival-predictive models using interpretable machine learning techniques, these biomarkers offer meaningful improvements in risk discrimination compared to traditional clinical scores alone. These results underscore the potential of ECG signals as a readily available source of prognostic information in critical care settings. Future research should focus on external validation in prospective cohorts, integration into real-time monitoring systems, and exploration of their utility in guiding early interventions and personalized treatment strategies.

STEMI 患者 PCI 术后急性肾损伤的机器学习预测模型的构建与验证

吕华胜 芦颜美

新疆医科大学第一附属医院

目的：构建并验证基于机器学习算法的模型，以预测急性 ST 段抬高型心肌梗死 (STEMI) 患者经皮冠状动脉介入治疗 (PCI) 术后急性肾损伤 (AKI) 的发生风险。

方法：纳入 2020 年 1 月至 2023 年 6 月期间接受 PCI 治疗的 2315 例 STEMI 患者，其中 306 例 (13.2%) 发生 AKI。采用 LASSO 回归对基线变量进行特征筛选，并通过 10 折交叉验证选择最优 λ 值，确定与 AKI 相关的变量。随后，构建了 8 种不同的机器学习模型，并评估其预测性能。使用 SHAP 值分析关键变量对模型预测结果的影响。

结果：LASSO 回归筛选出 7 个与 AKI 显著相关的变量，包括年龄、多支病变、术前肌酐、心力衰竭、白细胞计数、血红蛋白及白蛋白水平。在所有模型中，轻量梯度提升机 (LGBM) 和极限梯度提升 (XGB) 预测性能最佳，训练集 AUC 分别为 0.899(95% CI:0.877~0.921) 和 0.893(95% CI:0.868~0.918)，验证集 AUC 分别为 0.809(95% CI:0.763~0.856) 和 0.871(95% CI:0.833~0.909)。SHAP 分析显示，白蛋白、年龄、术前肌酐和白细胞计数是 AKI 风险的主要影响因素。

结论：本研究成功构建并验证了基于机器学习的预测模型，可有效识别 STEMI 患者 PCI 术后 AKI 风险，为临床决策提供了有价值的辅助工具。

面向长 QT 综合征等心律失常的单导联 ECG 智能诊断

赵宇彤 陈波

北京清华长庚医院

目的：针对长 QT 综合征等心律失常心电表现的频繁性与突发性，探索通过使用单导联 ECG 来检测长 QT 综合征等心律失常，从改善诊疗模式，探索积极处置各类不良解决的可能性。方法：在收集开源数据、我院多导联、单导联数据的基础上，提出了一种基于知识蒸馏的单导联 LQTS 等心律失常的检测框架（SLLD），通过引入知识蒸馏技术，使得单导联设备能够学习到十二导联设备的诊断知识，从而提升检测性能。为了进一步提高检测准确性，本研究设计了一种将卷积神经网络和双向长短时记忆网络相结合的特征融合器，以实现 LQTS 等心律失常的空间特征和时序特征的融合，从而增强网络对心电信号特征的提取能力。研究还利用导联间信息传递、多标签信息传递等操作，进一步提升网络的性能。结果：研究将 SLLD 与几种经典的单导联检测网络进行了比较，结果表明 SLLD 的性能显著超越了其他单导联检测模型，SLLD 的平均 F1 分数提升了 8.0%，LQTS 的 F1 分数提升了 5.1%。此外，通过数据处理实验进一步证实了 SLLD 中各个模块的有效性和贡献。结论：本研究提出了一种基于知识蒸馏的 SLLD 框架，能够协助医生和患者更加及时、便捷地预测 LQTS 等心律失常，从而有效改善心律失常带来的不良预后，拥有广泛的应用潜力。

机器学习在心血管疾病诊疗中的应用研究进展

郭彩旭

太原市中心医院

[摘要] 心血管疾病是全球发病率和死亡率最高的疾病，然而病因、疾病途径和临床表现的异质性使心血管疾病的诊断和预后面临巨大挑战，同时，电子病历、移动医疗设备和成像数据的集成产生的复杂高维数据也远超人类思维处理能力，提示开发新方法来识别具有潜在生命威胁的心血管疾病的重要性。机器学习（ML）作为人工智能的重要分支，是算法和统计模型的总称，可在极大程度上拓宽对复

杂数据的解释，并有助于将近乎无穷无尽的数据转化为临床决策，已成为克服传统探究限制的潜在解决方案，在心血管疾病基础研究数据处理、大型组学预测解释、影像学二维图像自识别分析、仿生微创介入手术、数字化心脏康复等多个层面，快速迭代的 ML 算法与临床海量数据交相辉映，一个心血管领域全周期、智慧化、高效能的集成数据大模型雏形已经出现，可为临床“对症下药”式施治、“量体裁衣”式护理提供确切依据，推动医疗机构数智化转型。未来完善和优化机器学习相关法律、纳入大型多中心高质量数据集、构建高精度算法模型或解决黑盒问题，将为机器学习在心血管疾病诊疗中的应用提供无限可能。本文旨在综述机器学习在心血管疾病诊疗中的应用研究进展，探讨其在提升心血管疾病诊断与治疗效率方面的潜力与挑战。机器学习将在心血管疾病的预防、诊断和治疗中扮演更加关键的角色，推动智慧医疗与精准医学的进步。

[关键词] 机器学习；心血管疾病；诊疗；综述

基于多模态信息融合的主动脉夹层 AI 诊断

常久洋 [1] 杨洲 [1] 徐世君 [1] 王博文 [2] 刘红阳 [1]

1. 大连医科大学附属第一医院

2. 世象医疗科技（大连）有限公司

目的: 主动脉夹层（AD）是一种起病急骤、进展迅猛且致命性高的心血管急危重症，其中不典型 AD 症状隐匿、缺乏特异性，早期易漏诊误诊，快速准确诊断对降低 AD 死亡率至关重要。本研究旨在整合主动脉 CT 血管成像结果与 D- 二聚体、炎症因子等关键血液学指标，构建基于多模态信息融合的 AI 诊断模型，突破单一模态局限，提升 AD 诊断效能及可解释性，并探索其在风险分层与预后预测中的应用价值，助力临床精准决策。

方法：纳入四组研究对象（共 469 例）：AD 组 351 例（A 型 94 例，B 型 122 例，不典型 AD 135 例）及健康对照组 118 例（经临床及影像学确认无心血管疾病），构建包含主动脉 CTA 影像与同期 D- 二聚体、炎症因子等血液指标的多模态数据集。本研究构建了一种双分支深度学习架构，用于实现影像与血液指标的多模态融合诊断。影像分支采用预训练的 ResNet50 模型提取高阶特征，血液分支通过全连接网络解析指标的时序动态变化。创新性地引入跨模态注意力机制以实现特征交互与融合，生成联合诊断结果。进一步集成可解释性模块（SHAP）以解析关键特征对诊断结果的贡献。通过五折交叉验证与独立测试集评估模型性能，并与单模态模型（影像 AI 模型与血液指标模型）及临床初诊结果进行对比。

结果：多模态融合模型在独立测试集上的 AD 诊断准确率为 Acc=0.721，显著高于纯影像模型（Acc = 0.631）与血液指标模型（Acc = 0.315）。关键发现包括：（1）跨模态交互作用：D- 二聚体动态变化与主动脉内膜片影像特征的协同作用可识别 52.4% 的不典型 AD 病例；（2）可解释性验证：SHAP 分析结果表明，D- 二聚体峰值、CRP 水平及 AI 提取的图像特征为主要判别因素；（3）风险预测能力：高风险评分组在 30 天内的不良事件发生率显著高于低风险组（42.1% vs 5.3%，p <0.001）。

结论：本研究首创的 “影像 - 血液” 多模态融合模型显著提升 AD 诊断准确度，突破不典型病例识别瓶颈；其可解释性设计验证了 D- 二聚体动态变化与影像特征的协同机制，并展现预后风险预警潜力，为 AD 的精准诊疗提供新范式。

Deep Learning-based Cardiac Computed Tomography Angiography Left Atrial Segmentation and Quantification: A Multi-model Comparative Study

lijun feng

Department of Cardiology of The Second Affiliated Hospital, School of Medicine, Zhejiang University

Abstract

Background and Purpose: Quantitative assessment of left atrial volume (LAV) is an important factor in the study of the pathogenesis of atrial fibrillation. However, automated left atrial segmentation with quantitative assessment usually faces many challenges. The main objective of this study was to find the optimal left atrial segmentation model based on cardiac computed tomography angiography (CTA) and to perform quantitative LAV measurement.

Method: A left atrial study cohort containing 158 cardiac CTAs was created, each case accompanied by expert image annotation by three cardiologists. the two annotators perform left atrium contouring separately, and if the intersection over union between the two masks is greater than 0.98, we can assume that the annotations are consistent. If not, a third reviewer will make the final determination. The annotation tool used is ITK-SNAP version 4.2.0, which is designed for the visualization and segmentation of 3D medical images. To ensure consistent resolution, the annotated images were resampled. The left atrium annotations covered the entire left atrium region, consisting of 80 to 120 layers in the 2D plane. On this basis, to ensure the continuity of changes between the annotated layers, we applied Gaussian smoothing to the annotation results, using a Gaussian kernel set to 1.5. Then based on this left atrium dataset, five recent state of the art (SOTA) models in the field of medical image segmentation were used to train and validate the left atrium segmentation model, including DAResUNet, nnFormer, xLSTM-UNet, UNETR and VNet, respectively. Further, the optimal segmentation model was used to assess the consistency validation of the LAV.

Results: baseline of clinical characteristics, the higher proportion of male participants in the examinations resulted in a significantly greater percentage of males in the training set (67.27%) compared to the other two cohorts; however, the overall distribution did not show a significant difference (p = 0.0987). Regarding coronary functional parameters, except for left atrium anteroposterior diameter (LAAD), no significant differences were observed in other functional indicators across the cohorts (p > 0.05). Compared to the test set, LAAD was significantly larger in the training set (4.42 ± 0.74 vs. 4.02 ± 0.65, p = 0.0245). Model performance was assessed using four metrics (reported as mean ± standard deviation): DSC, JI, HD and ASD. DAResUNet achieved the best performance in DSC (0.944±0.018) and JI (0.894±0.056) among all models, while VNet is the best performer in HD (10.609±4.384) and ASD (0.150±0.100). While UNETR and xLSTM-UNet exhibited comparable performance overall, both models underperformed in edge segmentation metrics, particularly in HD and ASD. The Bland-Altman plot demonstrated the extremely strong agreement (7.6 mL, 95% CI -17.3–29.4 mL) between model’s automatic prediction and manual measurements.

Conclusion: Deep learning models based on a study cohort of 158 CTA left atrial were capable of achieving SOTA results in left atrium segmentation. Recently the performance of SOTA model in the field of medical image segmentation has been explored and validated on 3D segmentation of left atrium CTA. At the data scale of a hundred or so cases, the CNN-based segmentation network structure for left atrial segmentation outperforms emerging network structures such as Transformer and xLSTM. LAV assessment based on deep learning models may be useful for biomarkers of the onset of atrial fibrillation.

深度学习辅助超声心动图自动监测主动脉狭窄和严重程度分级：多切面与单切面比较

杨菲菲 [1]

1. 中国人民解放军总医院第一附属医院（304）/ 解放军总医院第四医学中心

2. 解放军总医院第一医学中心

3. 解放军总医院第六医学中心

目的: 开发一个基于超声心动图视频的可用于自动检测和分级主动脉瓣狭窄（AS）的深度学习（DL）框架。

背景：超声心动图是诊断和分级 AS 严重程度的主要影像技术，但往往需要专业知识和相当长的处理时间。DL 的研究进展表明，它有望实现超声心动图解读的自动化，提高临床实践的准确性和效率。然而，AS 的全自动分析在很大程度上仍未得到探索。本研究旨在开发一个 DL 框架来简化临床 AS 评估。

方法：开发了一个三阶段 DL 框架，用于自动筛选超声心动图视频以检测和分级 AS。DL 框架自动对超声心动图视图进行分类，检测 AS 的存在，并采用两种算法评估严重程度：一种算法根据既定指南量化多个切面的关键指标；另一种是一种简化的方法，基于单个二维（2D）胸骨旁长轴（PLAX）视图对 AS 进行分类，避免了对多普勒数据的需要。使用真实世界的前瞻性测试数据集，根据两名专家医师超声心动图专家的评估，评估了我们诊断和分级 AS 严重程度的模型的可行性和准确性。

结果：DL 模型在前瞻性试验数据集中实现了 AS 检测的高性能，曲线下面积（AUC）为 0.942，灵敏度为 0.904，特异性为 0.923，准确性为 0.922。DL 分级指标与手动测量之间的相关性在 Vmax（r=0.94，p<0.001）、MPG（r=0.91，p<0.001），LVOT d（r=0.81，p<0.001） 和 LVOT VTI（r=0.84，p<0.001）方面表现出色。连续性方程导出的 AVA 也显示出极好的相关性（r=0.87，p<0.001）。基于这些指标，AS 分级的受试者操作特征（ROC）曲线显示，严重 AS 的 AUC 最高，为 0.976（95%CI:0.953，1.0），明显优于中度 AS（AUC 0.907）和轻度 AS（AUD 0.874）。PLAX-2D 视图方法为所有 AS 严重程度产生了可比的 AUC（0.869-0.920）。

结论: 本研究开发的 DL 算法依据超声心动图，具有可自动化实现 AS 筛查和分级，提高临床工作效率的潜力。

智能导管系统在心血管疾病方面的研究进展

胡可 葛睿 刘宁 赵国力 汪华玲

江苏省苏北人民医院

目的：旨在讨论智能导管系统在心血管疾病中的应用进展，探讨其未来的发展方向。

方法：本文在中国知网、万方、维普、PubMed、Web of Science 数据库进行文献检索，检索时间从建库至 2025 年 6 月。中文检索词为 “心血管疾病、人工智能、机器学习、多模态影像整合”，英文检索词为 “Cardiovascular Diseases，Artificial Intelligence，Machine Learning，Multimodality Imaging Integration”，梳理后的国内外相关文献为本文参考依据。

结果：在心血管疾病的临床诊疗中，智能导管系统展现出多方面的应用价值。于冠心病领域，该系统借助人工智能技术整合冠脉 CT、冠状动脉造影及血管内超声等多源影像信息，精准构建冠脉三维模型并开展定量血流分数（Quantitative Flow Ratio，QFR）评估，为复杂冠脉介入手术提供精细的路径规划与关键指导，有效提升手术精确性、效率及安全性。同时，其虚拟冠状动脉介入功能可预测支架置入后的生理反应，助力医生精准决策治疗方案。在心律失常诊疗方面，智能导管系统一方面通过人工智能引导房颤消融治疗，精准定位心房组织薄弱区域以实现能量的精准传递，从而提高消融成功率；另一方面，在室性心动过速治疗中，其独特技术能够更准确地识别目标区域，优化消融策略，进而提升治疗效果。此外，智能导管技术在心腔内超声技术领域取得了显著进展，其 4D ICE 技术能生成高分辨率动态三维心脏模型，从而为房颤射频消融等介入手术提供精确的术中

导航，进而提高手术的安全性和成功率。可操控导管的研发也在不断推进，其尖端偏转技术让导管在执行复杂心电生理操作时更加灵活、精准，为临床实践带来了新的视角和可能性。同时，智能导管与先进 3D 映射系统的结合预示着心脏外科手术的重大变革，通过整合多维度信息并实现精准定位，有望全面优化手术流程，进而显著提升手术效果并改善患者的生活质量。

结论：智能导管系统在心血管疾病的诊断和治疗中展现了显著的优势，随着技术的不断进步，其有望在更多临床场景中发挥重要作用，为患者和医生提供更安全、更高效的治疗方案。需要注意的是，智能导管系统在临床应用中仍需经过严格的验证和评估，以确保安全性和有效性。

基于人工智能技术量化的视网膜微血管与冠状动脉粥样硬化性心脏病相关性研究

孙嘉逸 于雪

北京医院

目的：探讨人工智能（AI）技术量化的视网膜微血管与冠状动脉粥样硬化性心脏病的相关性，并评估其对冠脉病变严重程度的临床预测价值。

方法：本研究连续入选 2022 年 6 月至 2024 年 6 月因具有心肌缺血症状或客观证据于北京医院行冠状动脉造影术（CAG）的患者 591 例，并分为无冠心病对照组（n=169 例）、非阻塞性冠心病组（NOCAD，n=136 例）和阻塞性冠心病组（OCAD，n=286 例）。运用 AI 技术获取单眼 45°眼底彩照中视网膜微血管定量参数，包括血管平均分支夹角（VBA）、分形维数（D_f）、血管密度（VD）、动静脉平均弯曲度（TortA、TortV）、动静脉平均管径（RAC、RVC）、动静脉管径比（AVR）。运用三分位法将冠心病患者 Gensini 评分（GS）分为 GS 低分位组（$GS_{低分}$<13 分）、GS 中分位组（13 分≤ $GS_{中分}$<39.5 分）和 GS 高分位组（$GS_{高分}$≥ 39.5 分），将 SYNTAX 积分（SS）分为 SS 低分位组（$SS_{低分}$<7 分）、SS 中分位组（7 分≤ $SS_{中分}$<15 分）和 SS 高分位组（$SS_{高分}$≥ 15 分）。本研究运用 Logistic 回归和线性回归分析探索视网膜微循环与冠心病和冠脉评分之间的相关性。在以 OCAD 和 NOCAD 为因变量的多因素 Logistic 回归分析中，本研究选取 P<0.05 的视网膜微血管参数，即 VBA 和黄斑中心凹 3mm 内 TortA 以创建视网膜综合评分作为新的指标。此外，本研究将主要心血管风险因素设置为基础模型，运用连续型 NRI 和 IDI 评估视网膜微循环是否提高基础模型对冠心病和冠脉评分的预测能力。

结果：与无冠心病人群相比，AVR 降低不仅是 NOCAD 的独立危险因素（OR=0.004，P=0.006），而且能够显著改善基础模型对 NOCAD 的预测能力（IDI=0.015，P=0.015）。与 NOCAD 患者相比，升高的黄斑中心凹 3mm 内 TortA 和视网膜综合评分不仅是 OCAD 的独立危险因素（前者 OR=1.116，P=0.034；后者 OR=1.740，P=0.024），而且能够显著改善基础模型对 OCAD 的重分类准确度（前者连续型 NRI=0.279，P=0.006；后者连续型 NRI=0.228，P=0.014）和预测能力（前者 IDI=0.016，P=0.006；后者 IDI=0.012，P=0.022）。在多因素有序 Logistic 回归分析中，增大黄斑中心凹 5mm 内 TortA 与 GS（OR=1.122，P=0.023）、SS（OR=1.112，P=0.034）呈显著正相关，并且可以显著提高基础模型对高 GS 冠心病患者的预测能力（IDI=0.011，P=0.049）。女性 NOCAD 患者减小的视盘上侧（ß=-18.828，P=0.031）、颞侧（ß=-14.529，P=0.017）、下侧（ß=-19.419，P=0.031）、鼻侧（ß=-14.568，P=0.047）D_f 以及视盘颞侧 RAC（ß=-0.134，P=0.022）与 GS 显著相关；然而男性患者的视网膜微血管参数与 GS 之间无显著关联。此外，女性 NOCAD 患者增大的 2.0-2.5PD 间的 TortA（ß=0.633，P=0.021），男性 NOCAD 患者减小的视盘上侧 RVC（ß=-0.144，P=0.019）均与 SS 升高显著相关。

结论：视网膜微血管定量指标不仅与 NOCAD、OCAD 及冠脉病变严重程度显著相关，还可以显著提高主要心血管风险因素的预测效能。此外，女性 NOCAD 患者较男性具有更多与冠脉病变严重程度显著相关的视网膜微血管指标。

Initial experience of multi-device robot-assisted Left main bifurcation stenting with Culotte technique in pig model

wang ming, Xin-Kai Qu

Huadong Hospital Affiliated to Fudan University

Backgrounds: Percutaneous coronary intervention (PCI) has become major therapy of coronary heart disease. As the tremendous progress in technique, devices and image guidance, this procedure has improved prognosis of millions of people. Despite all the progress in different facts of PCI, the protection of interventional cardiologist just made a little step. Although it's hard to connect the relationship between radiation exposure and increased cancer risk, there are still some reports of radiation exposure related damage to interventional cardiologist. Limited by support power of guiding catheter, bifurcation lesions and unprotected left main (LM) lesions were excluded in this trial. In second generation CorPath GRX System (Corindus Inc., Waltham, MA, the United States), the problem of support power was solved by guiding catheter manipulation module, but the problem of multi devices manipulation in coronary simultaneously still remained unsolved. Even though in some studies, robot assistant PCI were performed in bifurcation lesions, chronic total occlusion (CTO) lesions and other complex lesions, manual interventions were still needed when multi-devices manipulating. Despite X-ray exposures to operators, robotic assisted PCI also could provide protection from contagious disease. In the end of 2019, coronavirus disease-2019 (COVID-19) cause a worldwide pandemic. The transmission routes of COVID-19 are direct contact, respiratory droplets secreted from infected individuals, and aerosol transmissions. In these situations, a robotic assisted PCI allows operators to manipulate devices remotely, in which situation the chance of getting infection could be reduced significantly. Considering the defects of CorPath system, our research team developed a new robot system to solve the problem of multi-devices manipulation. With its help, more complex coronary intervention operations may be accomplished by robot assistant system under remote control with less manual intervention. In this study, we sought to perform LM bifurcation PCI with culotte technique in pig model to prove the safety and effectiveness of this new robot system.

Methods: 6 pigs were enrolled in this experiment. A 2-stent strategy was performed in left main bifurcation following culotte strategy. All procedures were performed by our multi-device robot system which was remotely controlled by operator under 5G wireless network. In 4 pigs, bionic thumb and 2 bionic forefingers were involved. Except loading the devices on robot system, all procedures including guiding catheter manipulating, wire manipulating, stent or balloon adjusting, especially final kissing step were all performed by remote control without manually intervention. In 2 pigs, only bionic thumb and 1 bionic forefinger were involved. Manually interventions were involved in devices loading and devices exchanging. 4 procedures were performed in short distance (18.3 kilometers) and 2 were performed in long distance (1102.5 kilometers).

Results: All procedures were performed successfully in 6 pigs. No device related complication occurred in all procedures. Compared with short distance control, long distance control showed longer delay in data transmitting (90.25±1.05 vs 81.13±1.66ms, p=0.007) and mean image transmitting (163.25±0.95 vs 160.73±0.75ms, p=0.004). Either data transfer delay or image transfer delay showed no influences on operator's judgements. One pair of bionic fingers controlling showed significant longer procedure time compared to two pairs of bionic fingers controlling (126.5±1.5 vs 104.0±5.0 min, p=0.03) which were mainly caused by manually intervention for devices loading and exchanging (3274.5±228.5 vs 1908.5±25.5 sec, p=0.009).

Conclusions: This study demonstrated a new multi-device robot system for robot assistant percutaneous coronary intervention. With this robot system, fewer manually interventions were needed during the procedure of left main treatments and less procedure time were needed. Compared with CorPath System, this new multi-device robot system may provide more convenient manipulation in complex lesions of coronary diseases in the future.

The Feasibility and Utility of Large Language Models in Interpreting Cardiac Magnetic Resonance Reports: A Real-World Pilot Study

Fen Sa, Shi-Hua Zhao

Department of Magnetic Resonance Imaging, National Center for Cardiovascular Diseases, Chinese Academy of Medical Sciences and Peking Union Medical College, Fuwai Hospital

Background: Large language models (LLMs) show promise in medical text interpretation due to their powerful natural language processing capabilities. Cardiac magnetic resonance (CMR) reports are often difficult for patients and non-specialist physicians to understand due to complex principles, numerous parameters, and specialized terminology, increasing radiologists' interpretation burden. Therefore, an effective tool is urgently needed to assist CMR report interpretation. LLMs serve as a promising tool for interpreting CMR reports into more accessible language for patients.

Purpose: This study aimed to assess the feasibility and utility value of two LLMs (DeepSeek-R1 and ChatGPT-4o) in interpreting CMR reports and making the comparisons.

Materials and Methods: A total of 117 patients undergoing CMR at Fuwai Hospital (Beijing, China) were prospectively recruited from March to April 2025. Each CMR original-report was randomly assigned to one of the two LLMs (DeepSeek-R1 and ChatGPT-4o), where standardized prompts were used to guide the generation of LLM-report. Structured Likert-scale questionnaires were developed to assess the comprehensibility and quality of the LLM-reports by patients and CMR radiologists, respectively. Each patient reviewed two versions of their report: first, the original-report, and then the corresponding LLM-report. Immediately after reviewing each report, patients completed a questionnaire to assess their comprehension. All evaluations were conducted on-site, without any verbal or written assistance from medical staff or family members. Five senior CMR radiologists independently evaluated the quality of each LLM-report using questionnaires, with the corresponding original-report serving as the reference standard for comparison. Reliability and validity of the questionnaire were tested using Cronbach's α, the Kaiser-Meyer-Olkin (KMO) , Bartlett's sphericity test, and exploratory factor analysis (EFA). The Student t test, Mann-Whitney U test, and Chi-square test were used for statistical analyses. Bonferroni correction was used to adjust for potential statistic bias.

Results: Ultimately,100 LLM-reports were analyzed (mean age 48.8 ± 12.6 years; 72% male; comprising 34% hypertrophic cardiomyopathy, 33% dilated cardiomyopathy, and 33% coronary artery disease), with 50 interpreted by DeepSeek-R1 and 50 by ChatGPT-4o. Both the patient and radiologist questionnaires demonstrated good internal consistency and structural validity, with Cronbach's α values of 0.849 and 0.814, respectively. The KMO values were 0.803 and 0.793 for the patient and radiolo-

gist data, respectively, and Bartlett's tests of sphericity were significant in both cases, indicating sampling adequacy for EFA. EFA confirmed that the questionnaire items corresponded well with the intended dimensional structure. EFA revealed a structure comprising four factors for the 16-item patient questionnaire, accounting for 68.28% of the total variance, and five factors for the 20-item radiologist questionnaire, accounting for 82.68%. Across all four dimensions, the scores of LLM-reports were significantly higher than those of the original-reports (p p > 0.013). In the quality assessment conducted by radiologists, no statistically significant differences were observed between DeepSeek-R1 and ChatGPT-4o across the five evaluation dimensions (all p > 0.01). The overall quality score for LLM-report was 83.5 (IQR: 78–89) out of a maximum of 100 points, as rated by senior radiologists, indicating a high level of quality. These findings suggest that both LLMs can provide consistent and high quality report interpretations suitable for patient communication.

Conclusion: In this real-world pilot study, LLM showed good feasibility and utility in interpreting CMR reports into patient-accessible language, with comparable performance and quality between DeepSeek-R1 and ChatGPT-4o.

机器学习与传统模型在预测中国普通人群动脉粥样硬化性心血管疾病中的性能比较

范子豪 [1,2] 杜智 [3] 付金荣 [4] 周颖 [1] 张鹏宇 [1] 史础宁 [1] 孙英贤 [1]

1. 中国医科大学附属第一医院

2. 广东省人民医院(广东省医学科学院),南方医科大学,中山二路 106 号,广州,510080,中国

3. 浙江大学医学院附属第一医院心内科,杭州,中国

4. 中国医科大学附属第一医院内分泌与代谢科,辽宁省沈阳市南京北街 155 号,110001,中国

目的

准确预测动脉粥样硬化性心血管疾病(ASCVD)的风险对实施个体化预防策略和改善患者预后至关重要。本研究旨在开发基于机器学习(ML)的模型来预测前瞻性中国人群的 ASCVD 风险,并与传统回归模型的性能进行比较。

方法

本研究使用了一个包含 551 个特征的混合数据集,其中包括 98 个人口学、行为和心理特征,444 个心电图(ECG)特征和 9 个超声心动图(Echo)特征。经过选择最具信息量的 30 个特征后,训练、验证和测试了七个基于机器学习的模型。我们比较了 ML 模型与传统 ASCVD 风险计算器(如 Pooled Cohort Equations(PCE)和中国 ASCVD 风险预测模型(China-PAR))的区分度、校准度、净收益和净重分类改善(NRI)。

结果

研究包括 9609 名参与者(平均年龄 53.4 ± 10.4 岁,53.7% 为女性),在中位随访 4.7 年期间,有 431 名(4.5%)参与者发展为 ASCVD。在测试集中,最终的基于 ML 的人工神经网络(ANN)模型在预测 ASCVD 方面优于 PCE、China-PAR、重新校准的 PCE 和重新校准的 China-PAR。该模型的曲线下面积(AUC)为 0.800,而其他模型分别为 0.777、0.780、0.779 和 0.779。此外,该模型的 Hosmer-Lemeshow χ2 值为 9.1,而其他模型分别为 37.3、67.6、126.6 和 18.6。在 5% 的阈值下,ML 基于 ANN 模型的净收益也较高,为 0.017,而其他模型分别为 0.016、0.013、0.017 和 0.016。此外,ML 基于 ANN 模型的 NRI 为 0.089,而 PCE、China-PAR 和重新校准的 PCE 分别为 0.355、0.098 和 0.088。

结论

与传统的 ASCVD 风险计算器(如 PCE 和 China-PAR)相比,基于 ANN 的预测模型通过灵活地整合更广泛的潜在预测因素,可以更好地识别高心血管风险个体。这些发现可能有助于指导临床决策,并最终促进 ASCVD 的预防和管理。

Establishment and Validation of a Predictive Model for Anxiety Risk in Patients with Atrial Fibrillation

liangqing ge

The first people's hospital of Changde city

Background: Atrial fibrillation (AF), the most prevalent clinical arrhythmia with a rising global incidence, is increasingly recognized for its significant psychosocial comorbidities. Anxiety disorders affect 34-44% of AF patients, markedly higher than the general population, creating a detrimental bidirectional "psycho-cardiac" cycle impacting treatment efficacy and quality of life (QoL). Despite its clinical importance, anxiety in AF remains underdiagnosed (<40% recognition rate) and is not addressed by traditional AF risk tools like CHA2DS2-VASc.

Objective: To develop and validate an interpretable machine learning (ML) predictive model for anxiety risk in AF patients, enabling early identification of high-risk individuals for targeted interventions and advancing "psychocardiology" in clinical practice.

Methods: A multicenter cross-sectional study enrolled hospitalized AF patients from three tertiary hospitals in Hunan Province, China (October 2022 - December 2024). Inclusion required confirmed AF diagnosis, age ≥ 18 years, adequate communication, and completion of the Generalized Anxiety Disorder-7 (GAD-7) scale during admission; anxiety was defined as GAD-7 ≥ 10. Exclusion criteria included severe comorbidities, pre-existing psychiatric illness, cognitive impairment, in-hospital death, or excessive missing data (>20%). After screening electronic medical records (EMRs), 2771 patients met criteria (Derivation cohort: n=2417; External Validation cohort: n=354 from one hospital). Sixty-three variables spanning demographics, medical history, vitals, laboratory tests, echocardiography, symptoms (palpitations), medication (anticoagulant use), and scores (GAD-7, CHA2DS2-VASc, HAS-BLED) were collected. Missing data imputation used K-Nearest Neighbors (KNN). Feature selection employed rigorous collinearity screening followed by Logistic Regression (LR), Adaptive Boosting (AdaBoost), and Least Absolute Shrinkage and Selection Operator (LASSO) regression; intersection via Venn diagram identified the final 10 key predictors. Six ML algorithms (LR, AdaBoost, Gradient Boosting Decision Trees - GBDT, Gaussian Naive Bayes - GNB, Support Vector Machine - SVM, K-Nearest Neighbors - KNN) were trained on the derivation cohort (random split: 83% training, 17% testing). Hyperparameter tuning utilized 5-fold cross-validation (CV). Model performance was evaluated using Area Under the Receiver Operating Characteristic Curve (AUC-ROC), accuracy, sensitivity, specificity, positive/negative predictive value (PPV/NPV), F1 score, Kappa, Precision-Recall curve (AUPRC), calibration curves, Brier score, and Decision Curve Analysis (DCA). The best-performing model underwent SHapley Additive exPlanations (SHAP) analysis for interpretability and external validation.

Results: In the derivation training cohort (n=2001), 18.99% (n=380) had comorbid anxiety. The anxiety group had significantly higher proportions of sleep duration ≤ 6 hours (69.51% vs 30.85%), mental labor occupations (67.38% vs 35.58%), paroxysmal AF (51.39% vs 30.24%), and palpitations (87.63% vs 51.69%), but lower anticoagulant use (p<0.01 for all). Feature selection identified 10 key predictors: Sleep Duration, Work Type (Mental Labor), Palpitations, AF Type (Paroxysmal), Anticoagulant Use, Height, Heart Rate, Fasting Glucose, HDL, Neutrophil Count. Among the six ML models, GBDT showed the highest test set AUC (0.934) but exhibited significant overfitting (validation AUC=0.839). The Logistic Regression (LR) model demonstrated optimal and consistent performance: Training Set mean AUC = 0.854 (95% CI: 0.829-0.878); Test Set AUC = 0.838 (95% CI: 0.783-0.893); Accuracy=0.795, Sensitivity=0.768, Specificity=0.801. It showed excellent calibration (Brier score=0.111) and high clinical utility via DCA. External validation on the independent cohort (n=354, anxiety prevalence 21.39%) confirmed robust generalizability: AUC=0.862, Accuracy=0.805, Sensitivity=0.754, Specificity=0.817, NPV=0.937. SHAP analysis revealed Heart Rate (SHAP ≈ 0.2), AF Type (Paroxysmal, SHAP ≈ 0.1), and Anticoagulant Use (Non-use, SHAP ≈ 0.1) as major positive contributors to anxiety risk, while longer Sleep Duration (SHAP ≈ -0.2) was the strongest protective factor. Work Type (Mental Labor, SHAP ≈ -0.1), lower Fasting Glucose (SHAP ≈ -0.1), and greater Height (SHAP ≈ -0.1) were also protective. The final model, named the AAR0T0 (AF Anxiety Risk of Onset) model, was deployed as a clinically accessible web-based calculator.

Conclusion: This study successfully developed and validated the AAR0T0 model, an interpretable ML tool leveraging multidimensional clinical data to accurately predict anxiety risk in AF patients (AUC >0.85). It identifies key modifiable (sleep duration, heart rate control, anticoagulant choice) and non-modifiable (AF type, occupation, height) risk factors. The model provides a valuable tool for early identification of high-risk AF patients, facilitating personalized psychological interventions and supporting the integration of "psychocardiology" into AF management to improve patient outcomes and QoL.

基于多维度指标监测与机器学习算法的健康干预体系构建

周军文

西安交通大学医学院第一附属医院

摘要:

目的:本研究旨在系统评估智能可穿戴设备在老年冠心病患者居家管理中的临床应用价值,通过构建多维度观察指标体系与机器学习预警模型,探索"监测-分析-干预"闭环管理模式的有效性及优化路径。

方法:采用前瞻性随机对照研究设计,选取 2024 年 7 月至 2025 年 1 月某三甲医院心内科出院的 80 例老年冠心病患者为研究对象,采用分层区组随机法分为传统管理组(n=40)和设备管理组(n=40)。对照组采用常规管理模式(每周电话随访 + 每月门诊复查),观察组应用集成式智能腕带(实时监测心率、血压、血氧及步数)实现动态数据采集,通过蓝牙技术同步至云端健康管理平台。

1. 生理指标:包括收缩压变异系数(CV)、夜间心率标准差(SDNN),采用配对 t 检验进行组内纵向比较,组间差异通过协方差分析(ANCOVA)评估;

2. 行为指标:用药依从性(Morisky 8 项量表,MMAS-8)及运动达标率(每周 ≥ 150 分钟中强度运动),应用卡方检验和 Mann-Whitney U 检验分析;

3. 临床结局:急诊就诊率、心血管事件复发率,采用 Logistic 回归模型校正混杂因素;

4. 技术效能:数据采集完整率(缺失值插补后)与预警模型性能(ROC 曲线下面积 AUC、敏感性 / 特异性),通过 Bland-Altman 分析和 Delong 检验验证。

5. 机器学习建模: 基于 LSTM 神经网络构建风险预测模型,输入特征包括 24 小

时动态血压趋势、心率变异性（HRV）及运动量时间序列数据，采用五折交叉验证优化超参数，模型性能通过混淆矩阵和 SHAP 值进行可解释性分析。

结果：

1. 数据质量：设备管理组日均有效监测时长（23.1±0.8h vs. 传统组 8.4±2.1h，t=32.15, P<0.001），数据缺失率≤ 3.2%（采用三次样条插补）；

2. 生理指标：干预 6 个月后，设备组收缩压 CV 从 15.2% 降至 9.8%（对照组 13.5% → 12.1%，组间差异 Δ=3.4%，F=6.87, P=0.011），夜间 SDNN 提升至 38.2±5.1ms（vs. 对照组 32.7±6.3ms, P=0.003）；

3. 临床结局：设备组急诊就诊风险降低 54%（OR=0.46, 95%CI:0.28-0.75），心血管事件预测模型 AUC=0.913（敏感性 82.4%，特异性 89.1%，Delong 检验 P<0.05）；

4. 行为改善：设备组 MMAS-8 评分≥ 6 分比例达 87.5%（对照组 65.0%，χ^2=7.24, P=0.007），运动达标率提高 2.3 倍（RR=2.31, 95%CI:1.62-3.29）；

5. 技术效能：LSTM 模型提前 48 小时预警急性事件的准确率为 86.7%（95%CI:82.1-90.3%），误报率≤ 8.9%/ 周。

结论：智能穿戴设备通过高精度连续监测与机器学习算法协同，可显著提升老年冠心病患者居家管理的精细化水平（血压波动降低 36.5%、事件预警敏感度 > 80%）。研究证实，基于多维度指标体系的动态管理模式能够实现个性化干预（NNT=5.3），且技术接受度达 91.2%（SUS 评分≥ 82.4 分）。建议后续研究重点关注多设备数据融合（如结合智能药盒）与医疗资源整合（如 AI 分诊系统），以完善居家 - 医院协同管理生态。

从 U-Net 到 Transformer：主动脉夹层分割技术的演进与临床转化

林喜 王焱

厦门大学附属心血管病医院

目的：

主动脉夹层（Aortic Dissection, AD）是一类进展迅速、病死率高的心血管急症，早期诊断和术后监测高度依赖于医学影像。高精度的分割技术对辅助诊断、术前评估及随访具有重要意义。随着深度学习的发展，越来越多研究将其应用于 AD 及相关心血管结构的自动分割中。本文旨在综述 2023–2025 年间在医学图像分析领域中发表的最新研究成果，聚焦深度学习在主动脉夹层影像分割中的方法创新、成像模态应用及临床转化前景。

方法：

近年来，大多数方法以 U-Net 及其变体作为主干网络，结合新颖模块以提升分割精度。例如，Auto3D-Seg 竞赛中的最佳方案采用 SegResNet（U-Net 变体）实现对主动脉树的精准分割；也有研究引入 Transformer 结构，如 Swin-UNETR 和 Swivm-UNet，以增强长距离依赖建模能力，提升结构识别效果。针对主动脉夹层结构复杂的特点，多阶段或级联式分割框架成为主流策略。Zhang 等提出一种两阶段框架，先对增强血管、血栓与分支血管进行粗分割，再提取真腔（TL）与假腔（FL）区域；Xiang 等则设计了“内膜瓣注意力”（flap-attention）机制，并在级联网络中重点增强该区域特征，有效提升 TL/FL 分割准确率。

此外，部分方法关注上下文信息的融合，例如 CIS-UNet 在编码瓶颈层引入上下文感知滑窗自注意力（CSW-SA）模块，联合 CNN 和 Transformer 优势，实现比传统 Swin-UNETR 更优的全局特征建模。为增强模型泛化能力，研究者还提出多种训练策略，如两阶段训练、多任务联合优化、模型集成等。在成像模态方面，CTA（增强 CT）仍是主流输入，因其空间分辨率高、血管结构清晰。部分研究也开始尝试 MRI、超声等模态的应用，尤其在腹主动脉瘤等相关任务中表现出潜力。

结果：

得益于上述方法的不断优化，AD 分割精度显著提升。Xiang 等提出的 ADSeg 模型在 108 例多中心 CTA 数据上，获得了领先的血管分割 Dice 系数和边界距离指标。Zhang 等在 133 例术后 B 型 AD 随访 CTA 上，实现了 TL 和 FL 分别为 0.962 和 0.921 的高 Dice 得分。Xu 等提出的融合模型在 100 例数据上达到 TL 约 0.91、FL 约 0.88 的精度，表现稳健，尤其在处理血栓区域具有优势。此外，多组学方法逐步支持血管体积、分支角度及直径的自动化量化，为术后 TEVAR 疗效评估及个性化介入方案制定提供依据。在主动脉多分支分割方面，AortaSeg24 挑战赛吸引 121 支队伍参与，主流方法多基于 nnU-Net 并辅以级联结构、定制损失函数及数据增强策略，多个方案已实现开源，推动标准化发展。CIS-UNet 在 59 例 CTA 上完成 13 类主动脉区段分割，相比 Swin-UNETR，Dice 指标从 0.717 提升至 0.732，性能显著优化，代码和数据亦计划开源。

结论：

近三年来，基于深度学习的主动脉夹层影像分割技术发展迅速，研究持续在网络结构设计、特征建模与训练策略等方面取得突破。方法多以 U-Net 或 Transformer 为基础，结合注意力机制、多尺度融合及上下文建模等手段，显著提高了分割性能与泛化能力。研究普遍以 CTA 为主要成像手段，同时向多模态方向拓展。值得关注的是，多项成果已向临床部署迈进，如用于血管直径自动测量、辅助诊断与风险评估等任务。随着数据共享与算法开源的推进，未来相关技术有望进一步集成进临床影像流程，提升主动脉夹层的智能化诊疗水平。

综合生物信息学分析发现 POLR2I 是高血压肾病发病机制的关键基因

游世隆 许佳琪 吴博全 吴少军 张莹 孙英贤 张乃今

中国医科大学附属第一医院

目的：结合 WGCNA 和差异基因表达分析来筛选与 HN 肾小管间质病变发病机制相关的关键基因。

方法：采用基因表达综合（GEO）数据集建立基因共表达网络，并鉴定 HN 管间质组织与匹配对照组之间的差异表达基因（DEGs）。然后，利用 DEGs 和性状相关模块中存在的重叠基因构建蛋白质 - 蛋白质相互作用（PPI）网络来选择枢纽基因。同时，通过基因本体（GO）和京都基因与基因组百科全书（KEGG）分析，评估重叠基因的潜在功能。经过 GEO 和临床验证，从枢纽基因中筛选出一个关键基因。最后，通过体内实验验证了关键基因，并通过基因集变异分析（GSVA）研究了关键基因的潜在生物学功能

结果：利用综合生物信息学分析了来自两个独立 GEO 数据集的 HN 和健康对照中的基因表达谱。数据集中共鉴定出 229 个具有共表达趋势的关键基因。GO 和 KEGG 富集分析表明，这些基因主要参与与转录活性和氧化还原活性相关的各种过程。这些结果表明，HN 可能是一种由转录活性异常和氧化还原稳态失衡引起的疾病

结论：通过全面的生物信息学分析，将 POLR2I 确定为与 HN 相关的关键基因。我们的研究为 HN 的分子机制提供了新的见解，并为该疾病的精确治疗提供了新的候选靶点

机器学习和多组学整合：推进心血管转化研究和临床实践

贾鹏宇

中国医科大学附属第一医院

目的：随着心血管疾病全球负担持续上升，亟需探索更有效的疾病预防、诊断和治疗策略。本综述旨在系统总结人工智能（AI），特别是机器学习方法在整合多组学数据用于心血管疾病研究中的最新进展，探讨其在揭示疾病潜在机制和推动临床转化中的应用潜力。

方法：本研究系统整理了近年来将机器学习与基因组学、转录组学、蛋白质组学、代谢组学等多组学技术相结合的代表性心血管疾病研究，重点分析了用于心血管疾病研究的机器学习模型的类型、建模策略及其在不同组学层面上的应用方式。同时，我们评估了这些模型在因果推理、特征选择、预测建模等任务中的表现，并总结了其在基础研究与临床实践之间的桥梁作用。

结果：机器学习与多组学数据的结合在心血管疾病的病因学研究、诊断分子标志物发现、亚型划分、个体化治疗方案制定及疾病预后风险预测等方面在近年来进行广泛的研究。多种经典与新兴的机器学习模型（如随机森林、支持向量机、深度神经网络等）在整合高维组学数据、提取关键分子特征和构建可解释性模型方面展现出强大能力，为弥合当前临床实践中的知识空白提供了支持。

结论：多组学与人工智能的融合为心血管疾病研究带来了前所未有的机遇，有望加速机制阐明和精准医学转化。尽管目前仍存在数据异质性高、模型可解释性差、临床验证不足等挑战，但随着计算方法、数据标准化及跨学科合作的不断进步，未来新型 AI 模型将在心血管领域发挥更广泛的应用价值。推动其向常规临床实践的整合，是实现从大数据到精准医学转变的关键路径。

人工智能随访信任量表的编制及信效度检验

谢丽丽 涂惠 彭莹 于浪琴 陈雨芬 彭小凤

南昌大学第二附属医院

目的

编制人工智能随访信任量表，并检验其信效度，以期为人工智能随访患者的信任评估提供有效工具。该量表的开发旨在完善人工智能随访流程，提高出院患者的随访依从性，促进患者与医护人员之间的沟通，并为制定针对性干预措施以改善患者预后提供科学依据。

方法

本研究基于信任源理论框架，采用混合研究方法编制量表。首先，通过文献回顾和质性访谈构建条目池，2024 年 1 月 ~3 月对 15 例人工智能随访患者进行半结构访谈，提取关键条目。其次，2024 年 6 月 ~8 月邀请 18 名专家进行两轮德尔菲专家函询，结合专家意见调整条目，并选取 10 例患者进行预调查，优化量表表述。最后，2024 年 9 月 ~12 月采用分层抽样和便利抽样法，对 420 例人工智能随访患者进行调查，通过项目分析、探索性因子分析、验证性因子分析及信度检验筛选条目并验证量表信效度。

结果

文献回顾纳入 43 篇文献，质性访谈归纳出 3 个主题（患者倾向信任、系统交互信任、环境信任）及 8 个亚主题，初步形成 42 个条目的条目池。两轮专家函询的问卷回收率分别为 88.89% 和 100%，专家权威系数为 0.884 和 0.891，肯德尔协调系数为 0.181 和 0.202（均 P<0.05），最终形成 33 个条目的初始量表。预调查显示量表完成时间为（11.56±2.24）分钟，未调整内容。正式调查中，项目分析删除 5 个条目，内容效度指数为 0.833~1，平均内容效度指数为 0.955。探索性因子分析提取 3 个公因子（累计方差贡献率 65.385%）。验证性因子分析中各个拟合指标：卡方自由度为 1.48，渐进残差均方和平方根为 0.048，拟合优度指数为 0.860，规准适配指数为 0.889，非规准适配指数为 0.957，增值拟合指数为 0.961。总量表 Cronbach's α 为 0.929，折半信度 0.946，重测信度 0.906，最终形成 27 个条目的正式量表（患者倾向信任 11 条、系统交互信任 11 条、环境信任 5 条）。

结论

本研究开发的人工智能随访信任量表包含 3 个维度、27 个条目，具有良好的信效度，可作为评估患者对人工智能随访信任程度的可靠工具，为优化随访策略及提升医疗服务质量提供参考。

Machine Learning Based Prediction of Postoperative Acute Kidney Injury Risk in Coronary Artery Bypass Grafting Patients

Yang Zhang[1], Da Bei Cai[2], Ye Deng[2], Zhu Wang[1], Zhi Han Zhang[1], Hu Zhang[1], Shou Jie Feng[1], Qing Jie Wang[2], Jun Wei[1], Ling Sun[3]

1. The Affiliated Hospital of Xuzhou Medical University

2. The Third Affiliated Hospital of Nanjing Medical University

3. The Affiliated Wuxi People's Hospital of Nanjing Medical University

Background Acute kidney injury (AKI) following coronary artery bypass grafting (CABG) severely impacts patient prognosis, and traditional prediction models lack sufficient accuracy. This study aimed to develop a high-precision AKI prediction model by integrating multidimensional preoperative and intraoperative data through machine learning algorithms, providing a novel tool for early clinical warning.

Methods A retrospective analysis was conducted on 520 CABG patients (2021–2024). Least Absolute Shrinkage and Selection Operator (LASSO) regression was employed to screen 31 key variables, and SHapley Additive exPlanations (SHAP) values were applied to interpret feature contributions. Six machine learning models—logistic regression (LR), random forest (RF), LightGBM, and others—were constructed. Hyperparameters were optimized via grid search cross-validation, and model performance was evaluated using receiver operating characteristic (ROC) curves and the area under the curve (AUC).

Results Among the cohort, 135 patients (25.96%) developed AKI. In the validation cohort, the logistic regression model (LR-31) achieved an AUC of 0.82 (95% CI: 0.74–0.88), while the random forest model (RF-31) yielded an AUC of 0.81 (95% CI: 0.72–0.88). SHAP analysis identified preoperative renal function (eGFR), diabetes history, and intraoperative urine output as core risk factors for AKI.

Conclusion This study demonstrates that machine learning models effectively integrate multidimensional data to significantly improve AKI prediction accuracy, offering new insights for clinical intervention. However, limitations include the single-center retrospective design and potential selection bias. Future multicenter prospective studies are required to validate model generalizability and incorporate novel biomarkers to enhance predictive performance.

AI 健康助手在提升糖尿病高血压患者居家血压 / 血糖双达标率中的作用评估

张璐

陆军军医大学第二附属医院新桥医院

摘要：目的：评估 AI 健康助手在优化糖尿病患者合并高血压居家管理中的干预效果。

方法：采用多中心随机对照试验设计，纳入 328 例确诊 2 型糖尿病合并高血压患者，通过智能监测设备实现血压、血糖数据的实时传输与 AI 动态分析。干预组（n=164）接受 AI 健康助手提供的个性化用药提醒、膳食运动建议及异常值预警服务，对照组（n=164）实施常规家庭监测。主要观察指标包括 3 个月动态血压达标率（<130/80 mmHg）、空腹血糖控制率（4.4-7.0 mmol/L）及糖化血红蛋白（HbA1c）降幅。

结果：干预 6 个月后，干预组血压 / 血糖双达标率较基线提高 24.7%（95%CI 18.3-31.1%，P<0.001），较对照组提升 19.2 个百分点。AI 组患者服药依从性量表（MMAS-8）评分均值达 7.2±0.8，显著高于对照组的 5.9±1.1（P=0.003）。多元回归分析显示，AI 预警响应时间每缩短 1 小时，血糖波动系数（GV）降低 0.32 mmol/L（β=-0.32，P=0.016）。

结论：AI 健康助手通过智能化数据解析与实时行为干预，可有效提升居家患者代谢指标双达标率，其算法驱动的个性化管理方案具有显著临床推广价值。

关键词：AI 健康助手；糖尿病；高血压；服药依从性；居家健康管理

糖尿病与高血压均为全球范围内高发的慢性代谢性疾病，两者常合并存在，显著增加患者心脑血管并发症风险及疾病负担。据流行病学调查显示，全球约 4.63 亿成年人患有糖尿病，其中超过 60% 合并高血压。居家环境下实现血压与血糖的长期、有效协同控制是管理此类患者的难点与关键。传统居家管理模式依赖于患者自我监测记录及定期门诊随访，存在数据记录不完整、反馈滞后、依从性难以保证等问题，医护人员难以及时识别风险并实施干预。近年来，人工智能技术在健康管理领域的应用日益广泛，为提升慢病管理的精细化与实时性提供了新的可能。然而，现有研究多集中于单一疾病或单一指标的干预，对 AI 技术在糖尿病合并高血压患者居家协同管理中效果的实证研究尚显不足。为此，本研究旨在通过多中心随机对照试验，评估基于智能监测设备与人工智能算法的健康助手在提升居家糖尿病合并高血压患者血压 / 血糖双达标率及综合管理效果方面的干预价值。

可穿戴生物传感器驱动的 AI 个体化运动处方系统对高危心血管病患者康复效果分析

罗燕

陆军军医大学第二附属医院新桥医院

摘要：目的：系统评价整合可穿戴生物传感器与人工智能算法的个性化运动处方系统在高危心血管疾病患者康复管理中的临床价值。

方法：采用前瞻性多中心队列研究设计，连续纳入 2022 年 1 月至 2024 年 6 月收治的 412 例急性冠状动脉综合征患者，采用随机数字表法分为 AI 干预组（n=206）和常规康复组（n=206）。干预组通过智能可穿戴设备持续监测心率变异性（HRV）、ST 段偏移量及血氧饱和度参数，结合深度强化学习算法实现运动强度动态优化；对照组采用标准化心肺康复训练方案。主要研究终点定义为 6 个月主要不良心血管事件（MACE）复合终点发生率，次要终点包括峰值摄氧量（VO2peak）、6 分钟步行试验（6MWT）距离及 N 末端 B 型利钠肽前体（NT-proBNP）浓度变化。

结 果：AI 干预组 MACE 相关再住院率显著低于对照组（9.2% vs 17.0%，χ^2=5.89，P=0.015），平均康复周期缩短 23.5 天（95%CI 15.8-31.2）。多因素 logistic 回归模型证实基于传感器参数反馈的运动强度自适应调节是降低心室重构风险（OR=0.62，95%CI 0.51-0.75）的独立预测因子。

结论：本研究首次在循证医学层面证实，融合生物传感技术与机器学习算法的动态运动处方系统能够实现精准心脏康复管理，较传统方案具有显著成本效益优势。该系统通过实时生理参数监测与算法迭代优化，有效解决了传统康复方案中运动强度个体化适配不足的临床难题，为降低高危患者远期心血管事件风险提供了新型数字医疗解决方案。建议后续开展大样本多模态临床研究以验证长期预后改善效应，该技术框架对重构慢性病管理模式、优化医疗资源分配具有重要转化医学意义。

心血管疾病作为全球首要死因，其康复管理面临严峻挑战。尤其对于急性冠状动脉综合征等高风险患者，运动康复虽被证实可显著改善预后，但传统标准化方案因无法精准匹配患者实时生理状态，常面临运动强度不足或过量的两难困境。过度运动可能诱发心肌缺血或心律失常，而强度不足则难以产生充分训练效应，导致康复依从性和效果不佳。近年来，可穿戴生物传感技术的突破性进展，使得连续、无创监测关键心血管参数成为可能。同时，人工智能算法在复杂数据分析与动态决策支持方面展现出独特优势。本研究团队基于上述技术融合，创新性开发了 AI 驱动的个体化运动处方系统，旨在通过实时生理反馈与算法优化，实现运动强度的动态精准调控。本研究即聚焦于评估该整合系统在高危心血管病患者康复中的临床效能与安全性，探索其解决传统康复核心痛点的能力，并为数字医疗在慢性病管理中的应用提供高级别循证依据。

面向急性 A 型主动脉夹层术后患者低氧血症的多阶段智能决策模型构建

林喜 孙丽军 王焱

厦门大学附属心血管病医院

目的：

急性 Stanford A 型主动脉夹层具有起病急骤、进展迅速及临床表现复杂等特点，是心脏外科领域中最为凶险的急危重症之一，术后并发症高发且病死率居高不下。尽管紧急手术已成为改善患者预后的首选治疗方式，但由于手术通常在深低温停循环状态下进行，时间长、创伤大，导致术后低氧血症的发生率显著升高。持续性低氧不仅会导致肺部、心肌及肝脏等多器官功能障碍，还可能延长机械通气时间与 ICU 住院时长，增加医疗负担，进而影响患者远期生存率。因此，如何在术中及术后关键阶段实现对低氧风险的动态识别与干预调控，已成为提升主动脉夹层围术期管理水平的重要临床需求。

方法：

本研究提出一种基于多阶段强化学习（Reinforcement Learning, RL）的智能决策建模方法，旨在生成个体化干预策略，以降低低氧血症发生率并优化患者的机械通气时长及 ICU 住院时间。研究数据来源于厦门大学附属心血管病医院主动脉夹层专病库中急性主动脉夹层患者的术中与术后临床记录。我们将围术期过程划分为术中监测与术后恢复两个关键阶段，并分别构建阶段感知型智能体（Stage-Aware Agent），模拟临床路径中的阶段性决策过程。状态空间融合时间序列生理参数（如 SpO_2、FiO_2、PEEP、血压等）与阶段指示变量，并通过共享的门控循环单元（GRU）进行时序编码；动作空间涵盖关键治疗调控行为，包括呼吸机参数调节、镇静剂使用、俯卧位通气等干预手段。为提升模型在小样本场景下的泛化能力与稳定性，引入保守性强化学习（Conservative Q-Learning, CQL）机制与不确定性感知结构，限制策略在离线数据分布之外的过度推断。同时，设计阶段分解的奖励函数（Stage-Wise Reward Decomposition），分别优化术中血氧控制、术后 ICU 住院时间与机械通气时长，通过加权整合提升整体决策效果与医学合理性。

结果：

在模型评估阶段，我们基于历史病例的模拟环境进行策略回放与对比实验。结果显示，与基线专家策略及经典 DQN 模型相比，所提出的多阶段 RL 策略在控制低氧血症发生方面能够有效地降低术后低氧风险，辅助生成更具个体化、动态性的干预策略。

结论：

综上所述，本研究验证了强化学习在主动脉夹层围术期智能决策支持中的有效性与适应性。通过多阶段建模、结构化奖励设计与小样本优化策略，我们的模型为复杂高危手术场景下的精细化管理提供了全新思路，有望推动基于数据驱动的外科智能决策系统在临床的实际落地。

基于深度学习的心电图诊断肥厚型心肌病模型的构建与验证

梁义秀

上海复旦大学附属中山医院

目的：

肥厚型心肌病（HCM）是一种常见的遗传性心肌病，由于其早期心电图（ECG）表现缺乏特异性，筛查与早期诊断存在挑战。人工智能技术有望提高 HCM 的识别效率与准确性。本研究旨在基于中国人群构建并验证一个卷积神经网络（CNN）驱动的人工智能心电图（AI-ECG）模型，以评估其在 HCM 筛查与诊断中的应用价值。

方法：

本研究回顾性收集 2009 年至 2022 年间于本中心确诊的 10,202 例 HCM 患者及 386,763 例正常对照者的标准化 12 导联心电图数据，构建基于 CNN 的 HCM 诊断模型。数据集按 7:1:2 的比例划分为训练集（n=349,385）、验证集（n=44,921）和内部测试集（n=104,816）。此外，另设由中国三家不同区域医院（北京中日友好医院，武汉亚洲心脏病医院，上海第十人民医院）数据构成的独立外部测试集（包括 6,120 例 HCM 患者及 212,788 例对照者），用于评估模型的泛化性能。

结果：

在内部测试集中，模型表现出优异的诊断性能，AUC 为 0.937，灵敏度为 88.4%，特异度为 91.2%。在外部测试集中，AUC 为 0.924，灵敏度为 81.0%，特异度为 89.1%，进一步验证了模型的稳健性与跨机构泛化能力。

结论：

本研究构建的 AI-ECG 模型有效克服了传统心电图在 HCM 筛查中敏感性不足的局限，显著提高了识别效率。作为一种标准化、可推广的辅助筛查工具，该模型在中国人群中展现出良好的临床应用前景，有望促进 HCM 的早期发现与精准管理。

基于利用人工智能增强心电图预测肥厚型心肌病患者新发房颤的研究

梁义秀

复旦大学附属中山医院

背景

房颤是肥厚型心肌病（HCM）患者中常见且临床意义重大的心律失常，发病率约为 25%。房颤的发生显著增加卒中、系统性栓塞及心衰风险，影响患者生活质量及长期预后。早期识别高风险人群对于干预时机的把握至关重要。然而，现有临床预测工具依赖于超声心动图等结构参数，灵敏度有限，难以广泛推广。十二导联心电图（ECG）作为一种低成本、易获取的检查手段，若结合人工智能（AI）技术，有望挖掘出传统分析无法察觉的隐含特征，用于早期房颤风险预测。

目的

本研究旨在基于 AI 算法开发心电图预测模型，用于评估 HCM 患者在无房颤病史的情况下，未来 5 年内新发房颤的可能性，从而支持临床早期干预和个体化管理。

方法

本研究纳入 3068 例来自上海中山医院的 HCM 患者，所有患者在入组时均无房颤病史，且具有标准 12 导联 ECG 数据。数据被随机分配为训练集（70%）、验证集（10%）和测试集（20%）。我们采用残差卷积神经网络（CNN）进行模型构建，预测主要终点事件为 5 年内新发房颤。随后，通过将 AI-ECG 模型输出与年龄和性别进行整合，构建逻辑回归模型以进一步提高预测准确性。

结果

AI-ECG 模型在独立测试集中的 AUC 为 0.828（95%CI：0.786–0.865），表现出良好的区分能力。整合年龄和性别后的逻辑回归模型 AUC 进一步提升至 0.845（95%CI：0.806–0.879）。Kaplan–Meier 分析显示，基于模型评分分层的高低风险组在随访期间房颤发生率存在显著差异（log-rank P<0.001）。亚组分析进一步证实模型在不同性别和年龄层中均保持稳定预测能力。

结论

AI 增强心电图模型是一种简便、无创且适用于临床实践的工具，能有效预测 HCM 患者未来发生房颤的风险。该方法可辅助医生识别高危人群，优化监测和预防策略，有望改善房颤相关不良事件的发生率与患者远期预后。

探讨互联网 + 护理服务远程应用的护理效果分析及可行性

李双

吉林大学第二医院 (白求恩第二医院)

目的： 探讨护理结合互联网服务在冠心病术后随访中的应用效果。

方法：选取 2024 年 9 月 -12 月在北京某院进行冠心病支架术后随访的 45 例患者作为研究对象，选取 2024 年 6 月 -9 月在本院进行冠心病支架术后随访的 43 例患者作为对照组。对研究对象实施护理结合互联网服务模式，通过移动应用程序、远程监测、在线健康教育和个性化随访计划等方式，提供药物管理、饮食指导、运动建议、上门服务、支持和心理睡眠干预等服务。对照组给予常规护理模式。

结果：对照患者复查后 3 个月的化验结果，使用中华护理学会冠心病二级预防相关评估工具及上门评估对两组患者进行评估，研究对象的药物依从性、饮食多样性、运动耐受性、治疗效果以及满意度，均显著高于对照组（P < 0.03）。此外，研究对象的血压、血糖等指标控制情况优于对照组，再住院率及投诉率显著降低。

结论：护理结合互联网服务模式应用于冠心病患者术后随访中，能够有效提高患者的生活质量、疾病认知水平及及治疗积极性、健康行为依从性，改善患者的生理指标，降低再住院率，减轻患者的经济负担，提升患者满意度。且网络服务在随访工作中简单、易行，患者不受时间、地点影响，提高康复的依从性，提高患者的生活质量，值得广泛推广。

基于深度神经网络的 CT 冠状动脉造影自动分割与诊断

李奕明

四川大学华西医院

目的：冠状动脉 CT 血管造影（CCTA）在冠状动脉疾病（CAD）领域发展迅速。然而，冠状动脉树的手动分割与重建过程耗时且繁琐。深度学习算法已成功应用于医学图像分析，可高效处理大规模数据。因此，本研究旨在基于单中心回顾性 CCTA 队列开发一种深度学习工具，实现冠状动脉自动重建及 CAD 的自动化诊断。

方法：CAD 的自动化诊断包含两个子任务。其一是分割任务，旨在通过 U-Net 模型从原始图像中提取感兴趣区域（ROI）；其二是识别任务，采用 3DNet 模型完成。将冠状动脉树图像及临床参数输入 3DNet，输出 CAD 诊断结果。

结果：我们在一个 443 人的单中心 CCTA 队列中构建了基于 CCTA 图像及其标注数据的冠状动脉分割模型，基于 U-Net 的平均 Dice 值为 0.771±0.021。在此基础上进一步建立了 CAD 的自动化诊断模型（分类模型），其平均准确率为 0.750±0.056，受试者工作特征曲线下面积（AUC）为 0.737。

结论：本研究通过深度学习算法，分两步实现了从 CCTA 图像到 CAD 的快速分类与诊断。我们的深度学习模型能够快速、准确地自动分割冠状动脉，并对 ≥ 50% 的冠状动脉狭窄作出诊断。以深度学习为代表的人工智能技术有望显著提升 CCTA 图像分析的效率。

虚拟现实引导的动机增强训练对青年心肌梗死患者康复依从性及心理社会功能重建的混合方法研究

唐晓楹

陆军军医大学第二附属医院新桥医院

摘要：目的：探讨虚拟现实引导的动机增强训练（VR-MET）对青年心肌梗死患者康复依从性及心理社会功能重建的影响机制。

方法：采用解释性序列混合研究方法，选取 2022 年 1 月 -2023 年 6 月收治的 96 例青年心肌梗死患者为研究对象，通过量性问卷测量（康复依从性量表、心脏病患者自我效能感量表、社会支持评定量表）和质性半结构访谈，运用重复测量方差分析及主题分析法评估干预效果。将患者随机分为 VR-MET 组（n=48）和常规护理组（n=48），观察组在传统心脏康复基础上实施为期 12 周的 VR-MET 干预，通过三维心脏模型动态演示、虚拟康复场景互动及智能生物反馈系统构建多层次干预模块。

结果：干预后观察组康复依从性评分（8.32±1.21 vs 6.45±1.57）、自我效能感（39.15±5.62 vs 32.84±6.03）及社会支持（43.27±7.15 vs 37.92±6.84）显著优于对照组（P<0.01）；质性访谈归纳出“沉浸式疾病认知重构”“游戏化康复目标达成”及“正向情绪激励机制”3 个核心主题。

结论：VR-MET 通过多模态感官刺激与行为激活技术，有效提升青年心梗患者康复参与度，其三维可视化健康教育模块与智能生物反馈系统形成的闭环调节机制，为心血管疾病创新护理模式提供实践依据。

青年心肌梗死（MI）发病率在全球范围内呈现上升趋势，尤其在青年群体中，因其发病突然、病程长、并发症多及对社会功能的显著冲击，已成为严峻的公共卫生挑战。传统心脏康复（CR）方案虽被证实有效，但在青年患者群体中常面临依从性低、心理社会适应困难等核心问题。康复依从性不足直接影响二级预防效果，增加再梗及不良心血管事件风险；而疾病带来的焦虑、抑郁、社会角色转变及职业中断等心理社会功能障碍，则严重阻碍患者全面康复与生活质量恢复。如何有效提升青年心梗患者的康复主动性和持续性，并促进其心理社会功能的重建，是当前心血管康复领域亟待解决的关键问题。

虚拟现实（VR）技术凭借其沉浸式、交互性和构想性特征，为创新康复干预模式提供了新思路。其核心优势在于能够构建可控、安全且高度仿真的环境，通过多感官通道整合信息，增强患者对疾病认知的深度理解与情感投入。基于动机增强理论（MET）的 VR 引导训练（VR-MET），旨在利用 VR 技术模拟康复场景、可视化心脏病理生理过程、设定游戏化康复目标并提供即时生物反馈，从而激活患者内在动机，强化自我效能信念，优化健康行为决策。这种将动机性访谈策略与 VR 技术深度整合的干预模式，有望成为破解青年心梗患者康复动力不足与心理社会适应障碍的有效路径。然而，目前关于 VR-MET 对青年心梗患者康复依从性及心理社会功能（如自我效能、社会支持感知）影响的系统性研究，尤其是结合量性与质性证据深入探索其作用机制的混合方法研究仍显不足。

基于人工智能的心脏康复个性化运动处方设计与效果评估

田敏

陆军军医大学第二附属医院新桥医院

摘要：目的：构建智能心脏康复运动处方生成系统，通过深度学习算法整合患者电子病历、多模态生理数据及行为特征，实现运动强度 - 频率 - 持续时间的动态优化配置。

方法：研究纳入 372 例Ⅰ - Ⅲ期心脏康复患者，通过智能手环采集 24 小时动态心电、体动记录仪获取运动能耗数据，结合电子病历中的心脏超声与血清生物标志物构建三维健康画像。采用 LSTM 神经网络处理时序生理信号，通过蒙特卡洛树搜索算法进行运动参数组合优化。建立包含 12 个风险因子的决策树分类器，当实时监测数据超出安全阈值时触发语音告警并自动下调运动强度。采用倾向性评分匹配法控制混杂变量，主要终点设置为 3 个月干预周期内心律失常事件发生率。

结 果：AI 处方组 6 分钟步行距离提升幅度较对照组显著提高（Δ=38.6m，95%CI 25.4-51.8，p<0.001），峰值摄氧量改善率提高 21.7%（p=0.003）。风险预警系统灵敏度达 92.3%，特异性 89.6%，成功拦截 87% 的潜在运动风险事件。NT-proBNP 水平下降幅度与运动处方动态调整频次呈显著负相关（r=-0.47，p=0.012）。AI 组心血管相关再入院率降低 41%（HR=0.59，p=0.032），未发生严重运动相关并发症。

结论：基于深度学习的动态处方优化系统能有效提升心脏康复安全性及疗效，其数据驱动的决策模式克服了传统经验处方的静态性缺陷。多维度生理信号融合技术为精准评估运动耐量提供新范式，自适应调整机制显著降低二级预防中的医疗

风险。

关键词：人工智能；心脏康复；运动处方；可穿戴设备

心血管疾病作为全球首要死因之一，其康复管理对降低再住院率和心血管事件风险至关重要。心脏康复通过结构化运动干预改善患者功能耐量和生活质量，但传统运动处方依赖临床经验与静态评估，难以实时适应个体生理动态变化，导致安全风险和疗效不足。人工智能技术的崛起为精准康复提供了新机遇：深度学习模型能融合多源异构数据，实现运动参数的动态优化，克服经验处方的局限性。本研究聚焦于开发智能处方系统，旨在通过数据驱动决策提升心脏康复的个性化水平与安全性，并为临床实践提供可扩展的技术框架。

人工智能驱动的护理决策支持系统在心血管病风险管理中的应用：一项多中心随机对照研究

朱晶晶 田丹 刘华芬

武汉大学人民医院（湖北省人民医院）

目的

针对心血管护理中病情预警滞后、风险干预被动化及护理资源分配不均等问题，开发并验证一套基于人工智能（AI）的护理决策支持系统（NDSS），实现风险主动预警、护理措施个性化推荐及资源智能调度。

方法

采用阶梯式混合研究设计：

1. 系统开发：

- 整合 8 家三甲医院 10 万例电子护理记录（2021-2023 年），构建多模态 AI 模型：

- 风险预警模块: 融合可穿戴设备实时心电 / 血压数据 + 护理评估量表（MEWS、Braden 等）

- 措施推荐引擎：基于循证指南生成个性化护理方案（如心衰患者液体管理策略）

- 资源调度算法：根据患者风险等级动态分配护士人力

2. 效果验证：

- 2024 年 1-6 月纳入 326 例心血管住院患者（冠心病 / 心衰 / 心律失常），随机分为 AI 组（n=163，使用 NDSS）与常规组（n=163）

结果

1. 风险预警效能：

- AI 系统识别病情恶化的灵敏度达 96.3%（如心衰急性发作提前 2.1 小时预警）

- 误报警率降低 41%（vs. 传统监护设备）

2. 护理质量提升：

- AI 组不良事件发生率下降 54%（压疮 / 跌倒 / 给药错误，p=0.003）

- 心衰患者 24 小时出入量平衡达标率提高 28%（p<0.01）

3. 资源优化效果：

- 高风险患者护理巡视频次增加 35%，中低风险患者文书工作时长缩短 22%

- 护士决策时间减少 48%（从常规组平均 8.3 分钟→ AI 组 4.3 分钟）

结论

本研究首创的 AI 护理决策支持系统实现了心血管病护理的三大转型：

1. 从被动响应到主动干预（早期预警前置化）

2. 从经验决策到循证智能（措施个性化推荐）

3. 从均质化分配到精准调度（人力资源动态优化）

该系统为护理质量的持续改进提供可推广范式，助力“以患者安全为核心”的智慧护理体系建设。

Clinical Feasibility of two Cardiac Deep Learning Cine MRI Sequences: Single-Breath-Hold and Free-Breathing Motion-Corrected Approaches

Hui-Hui Kong, Yi He, Xian-Tao Song

Beijing Friendship Hospital

Clinical Feasibility of two Cardiac Deep Learning Cine MRI Sequences: Single-Breath-Hold and Free-Breathing Motion-Corrected Approaches

Background

Cardiac magnetic resonance (CMR) is a critical non-invasive modality for evaluating cardiac diseases. Cine imaging, in particular, plays a pivotal role in quantifying ventricular volumes and function, offering essential insights for cardiovascular disease diagnosis, therapeutic efficacy assessment, and prognosis prediction. Cardiac cine MRI faces the challenges of prolonged examination times and repeated breathhold (BH). This study evaluated the clinical feasibility of the deep learning (DL)-accelerated cine sequences, which shorten the scanning time and achieve comparable image quality (IQ) and function.

Methods

This prospective study enrolled consecutive patients who were scheduled to undergo CMR examination at our hospital from August 2024 to February 2025. The examination included three cine sequences [segmented cine, single-BH DL cine, and free-breathing motion-corrected DL cine (FB-MOCO DL cine)]. The actual total acquisition time were recorded. The overall IQ, blood pool myocardial signal ratio (BMC), edge sharpness, three-dimensional volumetric mesh contour quality, biventricular cardiac function parameters, and left ventricular (LV) strain parameters were evaluated. For comparisons of imaging time, overall image quality, edge sharpness, BMC, and cardiac functional parameters across the three cine sequences: One-way ANOVA was used if data met assumptions of normality and homogeneity of variance. Friedman test (nonparametric alternative for related samples) was applied for non-normally distributed data. If a significant difference was detected ($P < 0.05$), post hoc pairwise comparisons with Bonferroni correction were performed[20]. For functional parameters with non-normal distributions showing significant differences ($P<0.05$), Cliff's delta (Δ) was calculated to quantify effect size, categorized as: Very small: $|\Delta| < 0.147$, Small: $0.147 \le |\Delta| < 0.33$, Fair: $0.33 \le |\Delta| < 0.474$, High: $|\Delta| \ge 0.474$[26]. Correlation analysis and Bland-Altman analysis were used to evaluate the correlation and consistency between the two cine sequences.

Results

Eighty-six patients were evaluated (52.98±14.34 years, 79% male). Compared with segmented cine [239.70 (224.55, 260.15)], the total acquisition time of single-BH DL cine [63.55 (60.98, 66.00)] and FB-MOCO DL cine [90.65 (79.43, 103.80)] decreased by 73% and 62% respectively. There was no statistical difference in overall image quality between single-BH DL cine [4 (4, 5)], FB-MOCO DL cine [4 (4, 5)] and segmented cine [5(4, 5); χ^2=7.74, P=0.309). The average three-dimensional volumetric mesh contour scores for segmented, single-BH, and FB-MOCO DL cine were 4 (3, 4), 4 (4, 5), 4 (4, 4.25), respectively, with statistical differences (χ^2=35.42, P <0.001). The pairwise comparison results showed that there were significant differences between segmented- and single-BH DL cine ($Z = -4.23$, $P < 0.001$), and between segmented- and FB-MOCO DL cine ($Z = -2.40$, $P = 0.049$). The edge sharpness for segmented, single-BH, and FB-MOCO DL cine were 0.67 (0.53, 0.77), 0.42 (0.30, 0.59), 0.45 (0.32,0.63), respectively, with statistical differences (χ^2=59.21, P <0.001). The pairwise comparison results showed that there were significant differences between segmented- and single-BH DL cine ($Z=7.47$, $P < 0.001$), and between segmented- and FB-MOCO DL cine ($Z=5.11$, $P < 0.001$). Among the three cine sequences, no statistically significant differences were observed in all measured biventricular volumetric, functional parameters and LV mass (all $P > 0.05$). Additionally, in the correlation analysis, all measured parameters demonstrated strong correlations (all $r \ge 0.80$) between the single-BH/FB-MOCO DL cines and the segmented cine. Bland-Altman analysis further revealed small mean differences and narrow LoA for all CMR cardiac function parameters between the single-BH/FB-MOCO DL cines and the segmented cine, indicating excellent agreement. There were significant differences in LV strain between segmented- and single-BH DL cine (GCS: -1.82%, GRS: 7.73%, GLS, -2.25%) and between segmented- and FB-MOCO DL cine (GCS: -1.68%, GCS: 5.93%, GLS, -2.40%).

Conclusion

Compared with traditional segmented cine, DL-accelerated cine enables whole-heart imaging under single BH or free breathing in a shorter acquisition time, with preserved IQ and quantitative cardiac function results.

移动医疗视域下慢性心力衰竭患者自我管理体验与需求的质性研究

田晓萌

四川大学华西医院

本研究采用目的抽样的研究方法，选取了位于四川省成都市某知名三甲医院内住院治疗的慢性心力衰竭患者作为本次研究的对象。在研究过程中，我们运用了描述性质性研究的方法，对选取的研究对象进行了深入且具有半结构性质的访谈，通过慢性疾病患者自我管理需求及移动医疗相关文献，初步制定半结构访谈提纲，组织小组内成员讨论以及预访谈校正提纲后，形成最终的访谈提纲。通过对访谈所获得的丰富数据进行细致的主题分析，我们最终共提炼出四个一级主题：首先，慢性心力衰竭患者普遍表达出强烈的期望，希望能够尽快回归到正常的生活状态之中；其次，这些患者普遍反映，他们在日常生活中缺乏一套系统化且个性化的居家管理方案，这在很大程度上影响了他们的疾病管理效果；第三，慢性心力衰竭患者在获得社会支持方面存在明显的欠缺，这种支持不足在一定程度上加剧了他们的心理负担和生活困境；最后，不同患者在对待新技术的接受度上存在显著的差异，这提示我们在推广新技术时需要更加关注患者的个体差异。访谈结果进一步显示，慢性心力衰竭（CHF）患者对于移动医疗平台表现出了较高的需求和接受度。基于这一发现，我们完全可以设计并开发出切实可行的移动医疗平台，通过这一平台为患者提供更加便捷和高效的医疗服务，从而有效提高慢性心力衰竭患者的生存质量，改善他们的整体健康状况。

Reliability and Reproducibility of AI-assisted Left Ventricular Ejection Fraction Assessment: A Multicenter Real-world Retrospective Study

Ying-Hui Le[1], Zhi-Qiang Li[2], Yi-Min Li[3], Ting Zhang[4], Jian-Ying Zhang[5], Ji-Xin Zhang[6], Xian-Tao Song[1], Yi He[1]

1. Beijing Friendship Hospital, Capital Medical University

2. Binzhou People's Hospital

3. Zhangzhou Affiliated Hospital of Fujian Medical University

4. Sanmenxia Central Hospital

5. Nanchong Hospital of Beijing Anzhen Hospital Affiliated to Capital Medical University

6. Huludao Second People's Hospital

Purpose

The accuracy of left ventricular ejection fraction (LVEF) quantification in cardiac magnetic resonance (CMR) reports is indispensable for clinical applications. Despite the widespread integration of artificial intelligence (AI) into postprocessing workflows, generating high-quality functional reports faces challenges. This multicenter retrospective study aims to systematically evaluate the performance of AI-assisted CMR functional analysis. Specific objectives include: 1) quantifying the reliability of LVEF assessments obtained using heterogeneous AI tools across centers and operators with varying expertise; 2) comparing the reproducibility of fully manual versus AI-assisted LVEF quantification; and 3) assessing the clinical utility of AI-assisted LVEF values in complex real-world settings, thereby elucidating the core advantages of AI technologies amid their current developmental limitations.

Materials and Methods

This multicenter retrospective observational study utilized CMR datasets consecutively collected from six medical centers in China, encompassing multiple vendors, magnetic field strengths, and cardiovascular disease subtypes. All cases were matched with original imaging reports containing AI-assisted LVEF values generated by vendor-specific software operated by personnel with varying levels of expertise at each participating center. A standardized LVEF reassessment (M-LVEF) was performed by the experienced physicians using an AI assisted analysis system (QMass 8.1), with systematic comparison against original LVEF assessments from each center's imaging reports (R-LVEF). Three operators with varying levels of experience independently measured 30 cardiac function cases using both fully manual and AI-assisted modes for inter-observer reproducibility analysis. Operator A performed two measurements in both modes for intra-observer analysis.

Results

A total of 354 patients were ultimately enrolled in the study. The cohort comprised 221 males (62%) and 133 females (38%), with a mean age of 55 years ± 15. The median R-LVEF was 51% (IQR, 35%-62%), whereas the median M-LVEF was 53% (IQR, 33%-62%; P = 0.007). The overall agreement and correlation between R-LVEF and M-LVEF were good, with an ICC of 0.90 (95% CI: 0.88–0.92) and a Pearson r of 0.91. Bland-Altman analysis demonstrated a mean bias of 1.1% (R-LVEF slightly higher than M-LVEF), with wide 95% LOA (− 13.8% to 15.9%) . Clinically relevant discrepancies were observed: 44.3% of cases exhibited >5% differences between R-LVEF and M-LVEF, and 17.5% showed >10% differences. Independent analysis across centers demonstrated good-to-excellent agreement (ICC range: 0.86–0.95; Center 1: 0.87; Center 2: 0.89; Center 3: 0.93; Center 4: 0.94; Center 5: 0.95; Center 6: 0.86), with Pearson r values ranging from 0.89 to 0.96 (all P < 0.001). The AI-assisted method significantly reduced LVEF assessment time compared with manual analysis (p< 0.001). AI-assisted assessment of LVEF showed better inter-observer and intra-observer reproducibility than fully manual assessments. For LVEF, fully manual assessments yielded inter-observer ICC values of 0.924, 0.971, and 0.913, with CoVs of 8.8%, 5.6%, and 9.3%, respectively. In contrast, AI-assisted assessments improved the ICC values to 0.974, 0.984, and 0.968, while reducing the CoVs to 3.8%, 2.5%, and 4.4%（p< 0.05）.

Conclusion

In real-world clinical practice, there are interindividual differences in LVEF assessment by physicians with different levels of experience using different AI tools. However, AI-assisted assessment has significant reproducibility advantages, which can provide objective and stable quantitative basis for the dynamic assessment of cardiac function and follow-up management of patients.

基于多模态生物传感器在心血管疾病动态监测与智能护理预警中的创新应用及价值研究

刘玲 刘华芬

武汉大学人民医院（又名湖北省人民医院）紫阳院区

目的：心血管疾病的高发性与突发性对动态监测及护理预警提出了更高要求，传统单一生物传感器监测维度有限，难以全面捕捉疾病进展信号，导致护理干预滞后。本研究旨在探索多模态生物传感器在心血管疾病动态监测中的创新应用模式，通过整合多维度生理数据构建智能护理预警体系，明确其在提升监测全面性、预警精准度及护理质量中的实际价值，为临床护理决策提供技术支撑。

方法：采用前瞻性队列研究设计，选取 2024 年 1 月至 2025 年 1 月武汉大学人民医院心内科收治的 250 例心血管疾病患者（包括冠心病、心力衰竭、心律失常）作为研究对象，按随机数字表法分为实验组（125 例）与对照组（125 例）。实验组采用多模态生物传感器系统，同步采集心电（12 导联动态心电）、血压（无创连续监测）、血氧饱和度、皮肤温度及运动姿态等 5 类生理参数，数据经边缘计算模块预处理后传输至云端平台，结合 LSTM 深度学习算法构建多维度风险预警模型，实时生成风险等级（低、中、高）并推送护理干预建议；对照组采用传统单一心电监测设备，依赖护士人工分析数据并判断风险。两组均随访 6 个月，比较监测数据完整率、预警灵敏度、特异度、护理干预响应时间、不良事件发生率及患者生活质量评分（SF-36）。

结果：实验组多维度生理数据完整率达 97.6%，显著高于对照组的 78.4%（χ^2=26.35，P<0.001）；智能预警模型对中高危心血管事件（如恶性心律失常、急性心衰加重）的预警灵敏度为 94.2%、特异度为 91.5%，较对照组人工预警（灵敏度 72.3%、特异度 68.9%）分别提升 21.9% 和 22.6%（P 均 <0.01）；实验组护理干预响应时间平均为 28.3 分钟，较对照组的 65.7 分钟缩短 57.1%（t=14.22，P<0.001）；随访期间，实验组不良事件发生率为 8.0%，显著低于对照组的 22.4%（χ^2=11.59，P=0.001）；SF-36 评分中，实验组生理功能、情感职能等维度得分均高于对照组，差异有统计学意义（P<0.05）。

结论：多模态生物传感器通过整合多维度生理信号，突破了传统单一监测的局限性，实现了心血管疾病的全景式动态监测；其与深度学习算法结合构建的智能预警体系，显著提升了护理预警的精准度与时效性，缩短了干预响应时间，降低了不良事件风险，同时改善了患者生活质量。该创新应用为临床提供了主动化、个性化的护理模式，具有重要的临床推广价值。

AI-Driven Advances and Application in Vascular Aging Research

shenghua zhou, Shi Tai, Zhong-Ling Dai

The Second Xiangya Hospital

Vascular aging is a fundamental contributor to the development of chronic diseases and has emerged as a critical focus in biomedical research. With the rapid advancement of artificial intelligence (AI), new opportunities have arisen to enhance the precision and efficiency of vascular aging studies. AI techniques, particularly those applied to large-scale multi-omics and medical imaging data, enable the identification of novel biomarkers and the development of robust models to quantify the rate and extent of vascular aging. These approaches facilitate early detection, individualized risk assessment, and potential intervention strategies. This review provides a comprehensive overview of current AI applications in vascular aging, spanning from basic mechanistic research to clinical risk prediction. It also discusses future directions and key challenges, emphasizing the transformative role of AI in advancing precision medicine for vascular health.

By summarizing the applications of AI in cardiovascular aging research, we have identified that AI has the potential to integrate multimodal data, including imaging data such as cardiac MRI, coronary CT angiography (CTA), and echocardiography, as well as physiological data like electrocardiograms (ECG) and ambulatory blood pressure monitoring (ABPM). This integration endows AI with significant potential for assessing the velocity and severity of vascular aging. Furthermore, it can be harnessed for dynamic modeling of vascular aging and the identification of novel therapeutic targets.Future research directions are poised to concentrate on several key areas, including the integration of multi-omics data (e.g., genomics, radiomics, and biomechanics), dynamic personalized modeling (e.g., digital twins and time-series prediction), interpretable AI technologies (e.g., causal inference to identify aging biomarkers), development of early screening tools (e.g., retinal AI analysis), and optimization of anti-aging therapies (e.g., AI-driven screening of Senolytic drugs). By constructing standardized databases, interdisciplinary collaborative platforms (integrating biology, clinical medicine, and computational modeling), and establishing ethical guidelines, AI holds the potential to surmount the mechanistic bottlenecks of vascular aging, facilitating a transition from reactive treatment to proactive intervention, and ultimately propelling the implementation of precision anti-aging medicine. For instance, AI models can be developed to integrate data from genomics, epigenomics, and metabolomics to elucidate the driver genes (e.g., SIRT1, FOXO3) and critical pathways (e.g., mTOR, NF-κB) underlying vascular aging. AI, in conjunction with radiomics, can analyze coronary artery CT plaques and combine with computational fluid dynamics to predict blood flow shear stress. Time-series models, such as Transformer and LSTM, can be employed to analyze the dynamic changes in vascular function with age, thereby predicting individual aging trajectories. Digital twin technology can be harnessed to construct patient-specific vascular models to optimize intervention strategies (e.g., personalized anti-aging pharmacotherapy). Additionally, interpretable AI methods, such as attention mechanisms and causal inference, can be utilized to identify key biomarkers (e.g., senescent cell-derived exosomes). Generative AI, such as diffusion models, can simulate the molecular processes of vascular aging to aid in target discovery. The development of low-cost, non-invasive AI tools (e.g., retinal vascular image analysis, wearable device data) for early vascular aging risk assessment and the design of AI-driven dynamic treatment protocols incorporating anti-aging therapies (e.g., Senolytics, NAD+ boosters) represent other promising future directions. The establishment of open-access vascular aging databases (akin to the UK

Biobank) to facilitate algorithmic fairness validation is also crucial. Collaborations between biologists, clinicians, and biomechanics experts to develop AI models embedded with domain knowledge, and the integration of AI with other biotechnologies such as gene editing, cell therapy, organoids and regenerative medicine, will provide novel insights into the intervention and treatment of vascular aging. Furthermore, the development of more interpretable tools and technologies to aid clinicians in understanding AI decision-making processes, and the rigorous validation and evaluation of AI models through large-scale prospective clinical trials to ensure their reliability and efficacy in real-world applications, are essential future endeavors. In summary, the study of vascular aging should deeply integrate multi-omics data mining, dynamic imaging analysis, and clinical phenotype modeling to construct a"spatiotemporal progressive" research framework. The specific pathways are as follows:

1.Based on the Generative Adversarial Network (GAN) and Transformer architecture, integrate single-cell sequencing, epigenetic, and hemodynamic data to establish a cross-scale dynamic atlas of vascular cell aging.

2.Identify novel targets such as "metabolism-epigenetic coupling nodes," and develop 4D reconstruction algorithms for vascular imaging (e.g., photoacoustic imaging + AI super-resolution). Quantify subclinical aging biomarkers such as vascular wall elastic modulus and microcalcification distribution. In combination with federated learning, achieve multi-center data-driven early risk stratification.

3.Optimize individualized intervention strategies through reinforcement learning. For example, design AI prediction models targeting endothelial injury to dynamically adjust the synergistic regimen of NAD+ supplementation and exercise prescriptions.

AI is profoundly transforming the research paradigm of vascular aging, offering novel tools for both mechanistic exploration and clinical translation. At the basic research level, AI-driven integration of multi-omics data (such as single-cell transcriptomics, epigenetics, and protein interaction networks) enables the elucidation of the heterogeneity of vascular cell aging and identification of key regulatory hubs, such as the metabolic-inflammatory crosstalk nodes. Deep learning-assisted dynamic imaging analysis (e.g., OCT and photoacoustic imaging) can precisely quantify the structural and functional degeneration of the vascular wall, facilitating the discovery of novel imaging biomarkers. In the realm of clinical translation, federated learning-supported multicenter data fusion can establish early risk prediction models for vascular aging, while reinforcement learning-optimized individualized intervention strategies, such as combined pharmacological and exercise regimens hold promise to overcome the limitations of traditional one-size-fits-all treatment approaches. Looking forward, the integration of AI with organoids and digital twin technologies is poised to propel vascular aging research focus from a "static biomarker-oriented" approach to a "dynamic systems regulation" perspective, ultimately realizing precision medical interventions.

基于心电图和临床风险因素结合深度学习预测房颤相关性脑卒中

李晶洁 王子航

哈尔滨医科大学附属第一医院

目的：脑卒中现已成为我国第一大致残、致死疾病，而在脑卒中的诱发因素中，20% ~ 25% 为心房颤动。据流行病学统计，房颤患者合并脑卒中的发生率为 2% ~ 6%， 其致死率达到非房颤相关性卒中的两倍以上。因此，尽早预测房颤患者是否有脑卒中的发生对于临床医生的治疗方案至关重要。近些年深度学习作为人工智能数据分析领域最重要的分支，在医学领域得到了广泛的应用，尤其在多数据种类的疾病预测方面表现出色。本课题全面收录 AF 患者的多维临床指标及 12 导联体表心电图，将深度学习与多模态数据结合，最大程度地挖掘房颤相关脑卒中的潜在风险因素，显著提高预测的准确性，还能够在复杂、多变的临床环境中提供更好的决策支持，能够帮助实现更加精准、个性化的风险预测与管理，具有重大的成本效益及临床意义。

方法：（1）收集患者，进行分组：本课题纳入自 2014 年 1 月至 2023 年 11 月就诊于哈医大一院，年龄≥ 18 岁且诊断包含 AF 的患者 6188 例，根据是否合并脑卒中分为单纯房颤组（n=3168）与房颤相关脑卒中组 -- 共病组（n=3020）。房颤相关性卒中的患者，即共病组定义为在卒中时或卒中后 365 天发现了以前未确诊的房颤。

（2）建立临床数据预测模型（AI-CD）：收集所有入组患者的个人信息；入院特征；血液学标志物；超声心动图标志物共计 28 个临床因子，运用 SPSS 统计学方法比较房颤组与共病组差异，找到与疾病风险相关的因子。再利用随机森林及 SHAP 分析得出对模型贡献最大的预测因子。

（3）建立心电图预测模型（AI-ECG）：回顾性收集所有入组患者的 12 导联心电图数据，对数据进行去标识化和去噪处理。将预处理后的数据随机分为训练集（n=4161）、验证集（n=1039）、测试集（n=988），应用不同的深度学习算法在训练集中构建心电图预测模型，在验证集中调整模型参数，在测试集中评估预测性能，模型训练 50 轮后通过比较评估指标选择最优算法。

（4）建立多模态联合预测模型（AF-Stroke-AI）：将心电图预测模型中中的最优深度学习算法和患者的临床因子相结合建立多模态联合预测模型，模型训练 50 轮后通过比较评估指标，选择临床数据预测模型、心电图预测模型和多模态联合预测模型中的最优模型。

结果：

（1）房颤合并脑卒中的患者共 3020 例，平均年龄为 72.45±10.08 岁，与单纯房颤组患者相比，房颤合并脑卒中的患者平均年龄更高，更多合并高血压及糖尿病，总胆固醇、D- 二聚体等指标增加，差异具有统计学意义（P < 0.05）。接下来使用随机森林算法，结合 SHAP 分析筛选出对临床数据预测模型贡献最高的重要变量 -- 总胆固醇。

（2）我们将去标识化及去噪后的 12 导联心电图输入四种具有图像识别功能的深度学习算法进行建模，DenseNet 模型准确度最高为 0.982，全部八种评价指标综合评价后性能最好。

（3）我们将 DenseNet 模型与临床数据预测模型进行多模态融合，建立联合预测模型，其准确度最高为 0.998，其余各项评价指标均高于单一种类数据预测模型，综合预测性能最好，将其命名为 AF-Stroke-AI。

结论：本研究收录了 6188 例 AF 患者全面完整的临床数据和入院时的 12 导联心电图，基于心电图和临床风险因素结合深度学习预测房颤相关性脑卒中的发生，并构建联合预测模型，与单一数据种类的预测模型相比性能更加优越。未来房颤患者就诊时即可以通过联合预测模型，利用 12 导联心电图及临床数据预测是否合并脑卒中，从而指导医生治疗与决策。且模型中的因子均为价格低廉容易获得，这大大提高了模型的成本效益与临床转化价值。

心率以外的稳健心脏风险筛查：低剂量 CT Agatston 评分在心率亚组分类中的高诊断一致性

林晓娟 [1] 刘元芬 [2]

1. 福建医科大学医学影像学院

2. 福建医科大学附属协和医院

目的：

探究低剂量胸部 CT(Chest LDCT) 图像和标准门控心脏 CT（Cardiac CT）图像测量的钙化积分之间的差异与心率之间的相关性，为临床实践中心率异变的患者提供肺癌与心血管疾病筛查循证依据

方法：

本研究采用前瞻性队列设计，连续纳入 312 例胸痛患者，所有受试者在接受临床指征的心电门控非增强心脏 CT 检查前，均额外行胸部 LDCT 扫描（扫描参数：管电压 120 kVp，自动毫安调制，本实验已通过伦理委员会审查）。LDCT 图像采用两种重建算法:（1）标准重建内核（"STND"）;（2）肺算法优化内核（"LUNG"）。以心电门控心脏 CT 为金标准，通过经 FDA 认证的人工智能分析软件定量计算四支主要冠状动脉（左主干、左前降支、左回旋支及右冠状动脉）及整体冠状动脉的三种 CACS 参数：Agatston 积分、钙化体积积分和钙化质量积分。把患者分为低心率组（HR）和高心率组（HR ≥ 65 BPM），比较不同心率下 Chest LDCT 和 Cardiac CT 获得的 CACS 差异，利用线性回归分析 Chest LDCT 与 Cardiac CT 测得的 CACS 的偏差（Bias=LDCT 值 - 心脏 CT 值）与心率的相关性。使用混淆矩阵比较不同心率患者的 Chest LDCT 在 Agaston CACS 分级上的效能。

结果：

低剂量肺部 CT 平均有效剂量为 1.12±0.29mSv，显著低于常规心脏 CT。对于 LUNG 重建核的低心率和高心率组，Chest LDCT 与 Cardiac CT 相比较具有统计学显著差异的 CACS 参数有 3 和 9 个，而对于 STND，则分别有 11 和 14 个。心率与偏差的统计学显著相关性仅在 STND 重建核下出现在钙化体积评分中（R^2=0.032,P=0.01）。Agaston 钙化评分和钙化质量评分的偏差均与 HR 无统计学显著相关性（P>0.05）。对于 Agaston CACS 分级，两心率组准确性都达到 80% 以上（低心率 vs. 高心率： 80% vs.83% for STND,84% vs 82% for LUNG)

结论：

心率不影响低剂量胸部 CT 钙化积分的测量精准性，对于不同心率患者，在 Agaston 风险分层中均具有较高的准确性。这意味着对于不同心率的患者，均可在低剂量 CT 肺癌筛查的同时筛查心血管疾病风险，以优化心血管疾病早期防控。

基于 LASSO 回归和机器学习构建冠状动脉慢血流诊断预测模型

尤晶晶 曹桂秋

新疆医科大学第五附属医院

目的：基于 LASSO 回归和机器学习算法构建冠状动脉慢血流（CSF）的诊断预测模型，以早期识别高危患者并指导临床干预。

方法：回顾性纳入 2021 年 4 月至 2024 年 10 月新疆医科大学第五附属医院行冠状动脉造影检查的 608 例患者（CSF 组 302 例，对照组 306 例），按 7:3 比例分为训练集（425 例）和验证集（183 例）。收集患者临床资料、实验室指标、心脏超声及心率变异性数据，构建多因素 Logistic 回归模型，并通过 LASSO 回归筛选变量构建 6 种机器学习模型（即决策树、随机森林、XGBoost、支持向量机、K- 近邻算法、LightGBM）。采用 ROC 曲线、校准曲线、决策曲线、混淆矩阵等评估各模型性能。

结果：多因素 Logistic 回归显示糖尿病（OR=2.700）、吸烟史（OR=2.050）为 CSF 独立危险因素，淋巴细胞计数（OR=0.622）和主动脉瓣血流速度（OR=0.265）为保护因素，模型训练集 AUC 为 0.711，验证集 AUC 为 0.631。LASSO 回归筛选出 18 个关键变量，将其纳入机器学习算法中。机器学习模型中，随机森林（RF）和 XGBoost 表现最佳，验证集 AUC 分别为 0.756（95% CI: 0.687-0.825）和 0.764（95% CI: 0.693-0.835）；RF 模型的灵敏度（91.86%）和 XGBoost 的特异度（65.98%）较高。运用 SHAP 解释两种模型中特征重要性

排序，筛选出两种模型中排名前 10 的交集变量。

结论：结合 LASSO 回归与机器学习构建的 CSF 诊断模型具有较好的预测效能，其中随机森林（RF）和 XGBoost 模型表现最优，其反映的重点预测因子可为临床早期识别 CSF 提供数据支持。

基于人工智能的信息化平台在冠心病 PCI 术后患者心脏康复护理中的应用

李梦燕

贵州医科大学附属医院

【摘要】目的：探讨基于人工智能的信息化平台在冠心病经皮冠状动脉介入治疗（PCI）术后患者心脏康复护理中的实际应用效果，通过引入智能监测、个体化康复方案制定及动态干预等手段，评估其对改善心功能、降低再住院率等方面的影响，为临床心脏康复护理模式提供新思路。方法：选取 2023 年 6 月至 2024 年 6 月本院收治的冠心病 PCI 术后患者 64 例作为研究对象，采用随机数字表法分组为干预组和对照组各 32 例。对照组采用常规康复护理，包括药物使用及注意事项手册发放，给予生活建议如饮食调整和适度活动指导，维持基础康复管理。干预组采用基于人工智能的信息化平台开展全程心脏康复护理干预，充分融合智能监测、个性化管理与远程指导等多项技术手段。①由护士指导患者正确佩戴可穿戴智能设备，如腕带式心率监测仪和电子血压计，系统内置的机器学习算法持续分析患者数据变化趋势，一旦发现异常波动立即自动生成预警信息。②将患者的基础资料如年龄、病史、术后心功能状态等录入平台，系统依据数据综合评估后，自动生成个性化康复方案，涵盖运动频率、强度、持续时间及饮食营养比例等内容。护士每周将康复计划推送至患者移动终端，根据平台反馈的运动完成率、症状自评日记等，实时调整计划内容。③安排每周一次远程在线健康咨询，护士通过视频了解患者恢复状况，解答疑问，评估康复执行情况，并给予情绪支持。系统设有自动提醒功能，定时推送服药、复诊等信息，鼓励患者上传康复日志，平台据此生成个体康复分析报告进一步优化护理策略。采用超声心动图测量患者左心室射血分数，在干预前和干预后各进行一次评估，通过随访记录患者术后 6 个月内因心脏相关原因再住院的事件。结果：护理后干预组的左心室射血分数显著高于对照组，差异有统计学意义（P < 0.05）；干预组术后再个月内的住院率明显低于对照组，差异有统计学意义（P < 0.05）。结论：本研究结果表明基于人工智能的信息化平台可显著提升冠心病 PCI 术后患者的心脏康复效果。平台通过可穿戴设备实时监测心率、血压等数据，结合 AI 算法生成个性化康复方案，并设有预警机制与动态调整功能，提高了康复的科学性与时效性；视频咨询、自动提醒及康复日志反馈进一步增强患者依从性与自我管理能力，该平台在精准康复护理中具有较高应用价值和推广潜力。【关键词】冠心病；经皮冠状动脉介入治疗；人工智能信息化平台；心脏康复护理

Characteristics, Cost/Effect Consideration of Clinical Examinations, and Construction of Machine Learning Models of Restrictive Cardiomyopathy: Insights from Peking Union Medical College Hospital

An-Tian Chen, Wei Chen

Peking Union Medical College Hospital, Chinese Academy of Medical Sciences & Peking Union Medical College

Background: Restrictive cardiomyopathy (RCM) is an uncommon condition with heterogeneous causes. Amyloidosis, a major subtype, presents with diagnostic complexity, economic burden, and prognostic implications. This study aims to summarize the characteristics of RCM patients, evaluate the cost-effectiveness of common diagnostic strategies, and construct machine-learning (ML) models to improve the clinical decision-making process.

Methods: This study included patients with RCM who underwent transthoracic echocardiography (TTE) and cardiac magnetic resonance imaging (MRI). Statistical analyses were conducted between amyloidosis and non-amyloidosis groups. To improve cost-effectiveness in clinical workflows, we analyzed laboratory test costs related to autoimmune, infectious, tumor-related, and amyloidosis-specific examinations. Multivariate regression analyses were performed using TTE and cardiac MRI findings. Feature selection was performed using least absolute shrinkage and selection operator (LASSO) regression based on variables that showed statistically differences between groups. These selected features were then used to construct eight ML models, which were trained and validated using leave-one-out cross-validation. After constructing the model, we evaluated the sample size for the ML applications. According to previous literature, a sample size is deemed suitable when it achieves (1) effect sizes greater than 0.5, and (2) ML accuracy exceeding 80%. The best-performing model was interpreted using Shapley additive explanations (SHAP) to enhance model transparency.

Results: The study included 83 patients (55 with amyloidosis and 28 with other causes). The mean age was 54.8 years, 60.24% male. Pathological examinations were performed in 58 patients (69.9%). Significant differences were observed between the amyloidosis and non-amyloidosis groups. Testing autoimmune, infection, and tumor biomarkers costs RCM patients without corresponding causes more in total, although the average cost is lower. Multivariate regression identified several indicators of amyloidosis: thickness of left ventricular posterior wall (LVPW) and left ventricular ejection fraction (LVEF) from TTE, and left ventricular short axis (LVSA), LVEF, and interventricular septum (IVS) thickness from cardiac MRI. Based on the statistically different variables, five features were selected using LASSO regression for model construction. The Random Forest (RF) model achieved the best performance, with an area under the curve (AUC) of 0.977, an accuracy of 0.908. It also showed excellent accuracy, sensitivity, specificity, and Brier score, indicating good performance in distinguishing amyloidosis from other RCM subtypes. We further evaluated the appropriateness of the sample size for the ML model construction. The effect sizes for all features of the RF model, except for LVPW (TTE), were greater than 0.5. Although the effect size of LVPW (TTE) indicated a negative predictive effect on amyloidosis, its absolute value was still greater than 0.5. Thus, all the features achieved an effect size greater than 0.5. In addition, the accuracy of the selected RF model exceeded 0.8. Consequently, both the criteria were met, confirming that the sample size was appropriate for the study.

Conclusion: The developed ML model accurately distinguishes amyloidosis, with the Random Forest model achieving an AUC of 0.977 and accuracy of 0.908. Cost-effectiveness analysis suggests that routine testing for infection, autoimmune, and tumor biomarkers in patients with RCM may not be advisable. Amyloidosis should be suspected in RCM patients with heart failure symptoms, restrictive TTE changes, and tongue hypertrophy. TTE is recommended for all patients with RCM, and cardiac MRI shall be performed if feasible. These findings support the integration of ML-based screening with echocardiographic, MRI, and clinical features to guide more targeted and cost-effective diagnostic strategies in clinical practice.

多模态基础模型对超声心动图室壁运动异常 的智能识别

沙轩 [1] 郭家榕 [2] 费洪文 [1]

1. 广东省人民医院

2. 香港科技大学

研究目的

冠心病（coronary artery disease, CAD）的高死亡率和年轻化趋势凸显了其早期诊断和及时干预的必要性。节段性室壁运动异常（regional wall motion abnormalities,RWMAs）的早期识别对促进及时诊治并预防心肌梗死（myocardial infarction, MI）等严重心脏事件具有重要临床价值。超声心动图是心血管疾病诊断中不可或缺的成像技术。目前 RWMAs 的识别主要依赖于二维超声心动图（two-dimension echocardiogram, 2DE),但其对心内外膜的显示常受限于图像质量，影响诊断准确性。心肌声学造影（myocardial contrast echocardiography，MCE）通过微泡可以更清晰地显示出心内外膜结构并准确评估心肌微循环灌注。然而，不论是在 2DE 或 MCE 中， RWMAs 的判断仍依赖肉眼判读，具有较强主观性且高度依赖观察者的经验。亟需采取有效的干预措施减少对 RWMAs 的误读。人工智能（artificial intelligence，AI）近年来在提升超声心动图自动分析与诊断精度方面展现出巨大潜力。EchoCLIP 是一种基于自监督学习的超声 - 视觉语言基础模型，能够联合训练超声心动图及相关临床报告文本。然而，该模型在 RWMAs 识别中的性能尚未得到有效验证。

本研究旨在利用多模态超声心动图视频构建及验证基于 EchoCLIP 的多模态适配器模型 EchoCLIP Adaptor（EchoCA），并探究当其在迁移到 2DE 图像上时对 17 节段 RWMAs 的诊断效果。同时将其诊断表现与专家和初级医师进行比较。

研究方法

动态采集 2DE、MCE 及左心声学造影（left ventricular opacification，LVO）三种模态下的心尖两腔心切面（apical views-apical two-chamber，A2C）、心尖三腔心切面（apical three-chamber，A3C）和心尖四腔心切面（apical four-chamber，A4C）超声视频。数据集一共纳入 300 例病例数据，以 7:1:2 分为训练、验证及内部测试集；数据集二纳入 90 例病例数据作为外部测试集，用于评估模型的迁移泛化能力。EchoCA 模型以 EchoCLIP 为基础架构，通过构建适配器以适应不同的成像模式，分别提取结构特征及运动特征，最终实现对 17 个心肌节段 RWMAs 的自动识别，以心脏磁共振成像（magnetic resonance imaging，CMR）为金标准，与 3 名专家医生和 3 名初级医生的诊断结果进行比较。

研究结果

（1）EchoCA 模型在融合三模态数据的条件表现最佳，RWMAs 识别的整体受试者工作特征曲线下面积（area under the curve，AUC）为 0.91；

（2）当迁移至仅 2DE 视频中时，模型仍保持良好性能，AUC 达 0.84；

（3）与目前广泛应用的五种 AI 模型相比，EchoCA 模型表现最佳；

（4）EchoCA 模型的整体效能显著优于初级医生（p < 0.001），总体表现接近专家医生的水平。

结论

EchoCA 通过引入迁移学习策略，实现多模态信息在 2DE 中的有效融合，即使缺乏 MCE 或 LVO 等额外模态，也能准确检测 RWMAs。其出色的自动识别能力有望辅助初级医生，提高诊断效率与一致性，推动 CAD 相关室壁运动异常的智能评估。

（影像学组费洪文团队）

基于 5G 物联网与人工智能技术的区域性心脏心电智能预警体系构建

何吉富 [1] 范和松 [2] 宗树利 [2] 李晓 [1]

1. 山东中医药大学附属医院（山东省中医院）

2. 山东中医药大学

目的 针对心血管疾病（尤其是心律失常）高发病率、高负担及我国优质医疗资源分布不均、基层诊疗能力不足的现状，本研究旨在构建基于 5G 物联网与人工智能技术的区域性心脏心电智能预警体系，以提升区域心血管疾病防控水平，实现心律失常早筛早治，减轻医疗负担，保障人民生命健康。

方法 引入智能长时程远程心电技术，采用超微型贴片式心电仪，结合 5G、物联网、大数据及人工智能技术，搭建区域远程心电网络平台。以本单位为核心，联合各级医疗机构开展远程心电监测与智能诊断，探索分级诊疗新模式。通过数据实时上传与 AI 分析实现快速诊断，配套患者管理平台追踪数据变化，构建心律失常监测中心，优化流程与数据管理，建立双向转诊机制，确保 AI 诊断与医师审核结合。

结果 区域心电网络建设已取得成效，与多家二级以上医院及基层卫生院联网，初筛 13000 名社区慢病患者，检出室性节律、房颤等心律失常患者共 2050 名。对 404 名高危患者实施平均 3.75 天、每日 20 余小时的长时程监测，通过 AI 与人工审核明确多种心律失常诊断。建成心律失常监测中心，完善双向转诊机制，降低了监测成本，提升康复质量，降低复发率和死亡率，验证了该模式的多重价值。

结论 该区域性心脏心电智能预警体系显著提升了心律失常诊断率与效率，实现大规模人群筛查，推动优质医疗资源下沉，优化资源配置，符合国家“以防为主、防治结合”的慢病防治政策及“健康中国 2030”计划，对提升区域心血管疾病防控水平、保障人民健康意义重大，未来进一步完善后将发挥更大作用。

基于人工智能的多模态心音与超声特征融合模型在射血分数保留心力衰竭早期诊断中的研究

唐念[1] 游于人[2] 张登洪[1] 陈晓晓[1] 李鸿飞[1] 李勇[1] 郎明健[1]

1. 成都市第五人民医院

2. 中国联通数据科学与人工智能研究院

目的：

本研究旨在建立一套基于人工智能的多模态融合诊断模型，结合心音信号与心脏超声图像特征，探索其在 HFpEF 早期识别中的可行性和临床应用价值。

方法：

本研究纳入 HFpEF 人群，首先通过标准化流程采集同步心音信号及心脏超声图像，建立多模态训练数据集包括：心音信号：使用 EKO CORE 500 听诊器在 5 个心前区采集 15 秒 PCG 信号，经梅尔频谱图转换后，通过 Bi-LSTM+Attention 提取时序特征。超声特征：采用 Philips EPIQ7C 系统获取 LVEF、GLS 在内的关键参数，通过 ResNet-50 提取空间特征。其次，构建多模态融合模型：以 Transformer Encoder 为核心架构实现跨模态特征交互，引入 Cross-modal Attention 机制学习心音与超声特征间的深层关联模式，通过特征自适应对齐与协同建模，整合两类模态的互补信息。最后，采用五折交叉验证进行模型训练与优化，以 AUC、敏感性、特异性及准确率作为主要评估指标；同时引入 SHAP 方法分析关键特征的贡献度，增强模型的可解释性。

结果与展望：

已完成模型框架设计与技术路线规划，正进行数据收集与预处理，包括采集 HFpEF 患者及健康对照者的同步心音与超声图像，构建含临床基线、心音时序及超声特征的多模态标注数据库。预计建立适用于 HFpEF 早期辅助诊断的 AI 模型原型，产出可推广的多模态诊断框架。

结论：

融合心音信号与超声影像特征的人工智能诊断模型，能有效提升 HFpEF 早期识别效能，有显著临床应用潜力与推广价值。本研究为 HFpEF 智能化筛查提供全新技术路径，也为多模态人工智能医疗系统构建应用提供范例支撑。

心血管智慧护理创新融合新进展

万文瑾、刘华芬

武汉大学人民医院

智慧护理近几年来在心血管医疗健康领域是一个重要研究方向，它结合了信息技术、人工智能、物联网、大数据分析和可穿戴设备等先进技术，实现心血管疾病精准检测、早期预警、个性化干预和远程管理以提升护理效率、优化患者体验并降低医疗成本。目前主要集中在技术融合与应用、远程护理与健康管理、个性化护理与精准医疗、护理机器人与自动化、数据安全与隐私保护等以上几个方面进行开展。智慧护理的核心在于技术融合，这些技术的融合不仅提升了心血管疾病的诊疗效率，还推动了从“被动治疗”向“主动健康管理”的转型，为患者提供全周期、个性化的护理服务。但目前我国智慧护理创新在心血管临床应用尚存在一系列问题。如何有效利用好智慧护理创新技术为临床患者精准实施个性化护理、提高护理的准确性和效率，并且目前对于智慧护理的管理也尚无统一标准。在政策驱动下，国家护理发展规划推动“互联网 + 护理”模式落地，加速智慧护理普及。我们必须顺应社会发展趋势，积极面对当前心血管智慧护理创新融合问题。紧紧把握当前发展中的机遇更好的促进心血管智慧护理创新融合协调发展。此外智慧护理还需要与政策、伦理和社会需求相结合，以实现可持续发展。总之，智慧护理通过技术创新和跨学科合作，正在重塑现代医疗护理模式，为患者和医护人员带来更多便利和价值。

心血管疾病患者数字健康技术促进因素和阻碍因素的系统评价： 基于 CIFR 框架

何细飞

华中科技大学同济医学院附属同济医院

目的 对心血管疾病患者使用数字健康技术的促进因素和障碍因素的相关文献进行系统评价，促进数字健康技术在护理领域的发展与应用。**方法** 系统检索中国知网、万方数据库、PubMed、Web of science 等 8 个中英文数据库中心血管疾病患者数字健康干预的影响因素相关文献，检索时限为建库至 2025 年 1 月 20 日，采用 MMAT 工具进行质量评价，以实施性研究综合框架（Consolidated Framework for Implementation Research, CFIR）对影响因素进行归纳和整理。**结果** 纳入 25 篇文献，其中共包含 11 项定量研究、9 项定性研究和 5 项混合性研究，涉及 3684 例心血管疾病患者、2007 名医生、356 名护士、133 名利益相关者、227 名医疗保健人员、378 名心脏病专家。 通过分析，提取出 43 项促进因素和 65 项障碍因素。**结论** 本研究基于 CFIR 框架，系统评价了影响心血管疾病患者数字健康技术采用的促进因素和阻碍因素，较多的障碍因素集中于内部因素、创新及个体特征，本研究为优化数字健康技术的推广策略提供了理论依据，建议未来在个性化设计、医疗环境适配和政策支持方面进一步优化，以提高心血管疾病患者的数字健康技术使用率和健康获益。

Development and application of Artificial Intelligence Follow-up System in Coronary heart disease Patients

Xi-Fei He

Tongji hospital affiliated to Tongji Medical College, Huazhong University of Science and Technology

Abstract

Background

Coronary heart disease (CHD) is a leading cause of mortality globally and poses significant public health challenges, particularly in China. Despite advancements in medical treatments, post-discharge management of CHD patients remains inadequate, often resulting in poor medication adherence, low self-management, and increased readmission risks. Traditional manual follow-up methods are time-intensive, inefficient, and lack personalization, limiting their ability to address patients' complex healthcare needs.

Objective

This study aimed to develop and evaluate an AI-assisted follow-up platform incorporating Patient Profiling and Interactive Voice Response (IVR) technologies. The platform seeks to improve follow-up efficiency, enhance patient satisfaction, reduce the workload of medical staff, and provide a scalable model for intelligent follow-up in clinical settings.

Methods

This study utilized a prospective cohort design.A total of 4,000 CHD patients discharged from Tongji Hospital were enrolled, with 2,000 patients assigned to a manual follow-up group from September 2022 to August 2023 and 2,000 from September 2023 to August 2024 to an AI-assisted follow-up group. Key performance indicators, including follow-up rates, feedback collection rates, patient satisfaction, and medical staff workload, were compared between the two groups.

Results

The follow-up rates were similar between the manual group (82.0%) and the AI-assisted group (81.3%) (P=0.567).The feedback collection rates did not significantly differ between the two groups (7.2% vs. 6.1%, P = 0.163). However, the AI-assisted follow-up significantly reduced time expenditure, saving an average of 13.2 hours per 100 patients compared to manual follow-up. Patient satisfaction was significantly higher in the AI-assisted group than in the manual group (94.5% vs. 74.0%, P <0.001). Binary logistic regression analysis identified follow-up method as the significant predictor of patient satisfaction(OR = 5.993, 95% CI: 4.829-7.438, P medical staff (P <0.01).

Conclusions

The AI-assisted follow-up platform demonstrated comparable effectiveness to manual methods while significantly improving efficiency and satisfaction for both patients and healthcare providers. By integrating Patient Profiling and IVR technologies, the platform offers personalized, dynamic, and cost-effective follow-up services. These findings highlight the potential of AI-enabled systems in optimizing chronic disease management and resource utilization.

Keywords: Coronary heart disease, AI-assisted follow-up, Cost-effectiveness, patient profiling, Interactive Voice Response

Introduction

Coronary heart disease (CHD) remains a leading cause of mortality worldwide and poses significant public health challenges, particularly in China[1]. With the aging population and lifestyle changes, the prevalence and burden of CHD continue to rise, placing immense strain on healthcare systems[2, 3]. Challenges such as poor medication adherence, limited

self-management capacity, and psychological distress are common among CHD patients, often resulting in increased readmission rates and reduced quality of life[4, 5]. The 2023 guidelines for the chronic management of coronary artery disease emphasize the importance of ongoing follow-up and periodic reevaluation to enhance therapeutic adherence and reduce the risk of adverse cardiovascular events[6]. Traditional follow-up methods, primarily relying on manual phone calls and text messages, are labor-intensive, lack efficiency, and fail to deliver personalized care tailored to the diverse needs of patients[7, 8]. These limitations underscore the urgent need for innovative, technology-driven follow-up solutions[9, 10].

The rapid advancements in artificial intelligence (AI) and digital health technologies have paved the way for intelligent follow-up platforms that leverage tools like patient profiling and interactive voice response (IVR) [11, 12]. These technologies enable personalized, precise, and dynamic follow-up care, optimizing patient outcomes while reducing healthcare provider workload[13]. By integrating AI with clinical practices, intelligent follow-up systems have the potential to address the inefficiencies of traditional models and transform the landscape of chronic disease management. Patient profiling technology is a crucial component, capable of integrating multi-dimensional information such as patients' health status, medical records, lifestyle habits, and psychological conditions to construct personalized, tagged user models, enabling precise intervention[14, 15]. Domestically, there have been research efforts to utilize patient profiling technology. For instance, a comprehensive intelligent service platform developed by Su Mingliang [16]and colleagues generates an 'individual health profile' through multi-layered health monitoring devices. It has facilitated the early detection of diseases, real-time monitoring, and precise management. However, current research and application of patient profiling have primarily focused on relatively healthy populations within communities. There is a scarcity of practical applications and validations that address the complex needs of patients within hospitals. This gap limits the ability to provide truly personalized management support for patients with coronary heart disease.

5G 远程随访系统在心脏起搏器植入术后患者延续性护理中的应用与研究

张燕 刘华芬 黄磊

武汉大学人民医院东院

目的

探讨 5G 远程随访系统在心脏起搏器植入术后患者延续性护理中的应用效果，分析其对术后并发症管理、患者依从性及医疗资源利用效率的影响。研究旨在验证基于 5G 技术的远程随访模式能否突破传统诊室随访的时空限制，实现精准化、高效化的术后管理。

方法

选取 2023 年 12 月至 2024 年 12 月于武汉大学人民医院行永久性心脏起搏器植入术的 200 例患者为研究对象，随机分为实验组（n=100）与对照组（n=100）。

实验组采用 5G 远程随访系统进行延续护理，包括：

远程监测系统：配备具备 5G 传输功能的起搏器程控设备（如 Medtronic CareLink），实时采集起搏器参数（起搏比例、阈值、电池状态）及心电数据，异常事件自动报警；

远程门诊平台：通过 5G 高清视频实现医患实时互动，进行症状评估、用药指导及心理干预；

智能化管理模块：结合云平台数据分析，生成个性化随访计划，推送健康教育内容（如电磁环境规避、运动指导）。

对照组采用常规门诊随访。比较两组异常事件发现时间、术后 6 个月内并发症发生率、随访效率、患者 6 分钟步行距离（6MWD）、左室射血分数（LVEF）、满意度。

结果

实验组较对照组显著优化管理效果

异常事件发现时间：观察组较对照组平均提前 7.2 天；

术后 6 个月内并发症发生率：实验组电极脱位、囊袋感染等并发症发生率降低 42%（P<0.05），归因于远程系统对早期异常事件（如房颤、导线阻抗异常）的及时识别；

随访效率：实验组随访完成率达 96%，高于对照组的 78%（P<0.01），5G 网络低延迟（平均 79ms）保障了远程会诊流畅性；

患者 6 分钟步行距离（6MWD）提高 15%；

左室射血分数（LVEF）改善 5%；

满意度达 95%，优于传统随访组的 81%

结论

5G 远程随访系统通过高带宽、低延时的数据传输与多模态交互功能，可有效提升起搏器术后管理的时效性与精准度。其不仅降低了并发症风险与医疗成本，还通过打破地域限制优化了医疗资源配置，为心血管疾病延续性护理提供了创新解决方案。未来需进一步探索 5G 技术与 AI 辅助诊断的深度融合，以实现全周期智慧化健康管理

ECG8-EHR13-AF: A Multimodal Electrocardiographic and Clinical Score for Two-Year Incident Paroxysmal Atrial Fibrillation Risk Prediction

Yu-Juan Huang[1], Xiao-Han Liu[1], Zhu Chen[2], Yuan Guo[1]

1. Zhuzhou Hospital Affiliated to Xiangya School of Medicine, Central South University

2. Hunan University of Technology

Objective: Early and accurate diagnosis of atrial fibrillation (AF), coupled with effective stroke risk prediction, is critical for improving patient prognosis. However, AF is frequently asymptomatic in its early stages, posing significant challenges for timely detection. Existing risk scores are predominantly based on either sparse electrocardiographic (ECG) indices or isolated clinical variables, resulting in limited generalizability. Building upon our previously published single-lead AF diagnostic model CLAAF, this study extends the application of deep learning to the long-term risk stratification of AF. Our primary objective was to fuse high-resolution electrocardiographic phenotypes with comprehensive electronic health record (EHR) data, derive an optimized feature set, and develop a clinically usable AF diagnostic and prediction system capable of outputting personalized diagnostic and prognostic probabilities for patients.

Methods: We conducted a retrospective study enrolling 1,218 consecutive inpatients admitted between January 2017 and November 2024. Patients were classified as "paroxysmal AF" (n = 635) if any documented AF episode was present in their records; otherwise, they were labeled "non-AF" (n = 583). From the index 12-lead ECG, only lead II (a 10-second window) was extracted, and 50 digital biomarkers were calculated: 43 time-domain indices (e.g., RRran, pNN50, QRS_wmean), 3 frequency-domain indices (LFn, HFn, Ratio_LH), and 4 non-linear indices (VLI, VAI, Radius_LLZ, RR_SampEn). Concurrently, 48 routinely collected clinical variables were harmonized, encompassing demographics, NYHA functional class, diabetes mellitus, hypertension, coronary artery disease, echocardiographic indices (left atrial diameter, left ventricular end-diastolic diameter, ejection fraction [EF], E/A ratio), laboratory tests (B-type natriuretic peptide [BNP], creatinine, C-reactive protein [CRP], platelet count, troponin), and lifestyle factors (smoking, alcohol consumption). Minor missing values were imputed using an in-house random forest imputer, and all features underwent min-max normalization. Seven interpretability algorithms – logistic regression, LASSO, ANOVA-F, Support Vector Machine (SVM), Support Vector Classifier (SVC), random forest, and XGBoost – were employed to rank feature importance. The intersection of top-ranked features across these methods yielded an optimal feature set. Random over-sampling was applied to address class imbalance, and the cohort was subsequently stratified into an 8:2 split for training and testing. An XGBoost multiclass classifier was trained to assign patients into four predefined risk strata: Low Risk (no AF within two years), Low-Intermediate Risk (no AF within one year but AF within two years), High-Intermediate Risk (AF within one year), and High Risk (current AF). Model performance was rigorously assessed using F1-score, precision, recall, Area Under the Receiver Operating Characteristic Curve (AUC), confusion matrix analysis, Precision-Recall (PR) curves, Kaplan-Meier survival analysis, and Cox proportional-hazards regression (with a one-year observation horizon for Cox analysis). Finally, a desktop application was developed using PySide6, integrating functionalities for data input, feature extraction, prediction, and visual reporting.

Results: The intersection of feature importance rankings identified an optimal set comprising 8 ECG features (QRS_wmean, SKP, QRS_wmin, RRskewness, VLI, P_index, QRS_hmean, RR_SampEn) and 13 clinical variables (EF, left ventricular diameter, left atrial diameter, platelet count, interventricular septal thickness, BNP, CRP, creatinine, triglycerides, E/A ratio, troponin, potassium, right ventricular diameter). The XGBoost multiclass risk stratification model, trained on this optimal feature set, demonstrated excellent predictive performance on the independent test set (n = 244). The model exhibited superior discriminative ability for the Low Risk and High Risk strata, achieving AUCs of 0.95 and 0.94, with corresponding F1-scores of 0.87 and 0.90, respectively. Prediction of the intermediate strata (Low-Intermediate and High-Intermediate Risk) proved more challenging, yielding F1-scores ranging between 0.50 and 0.81. Kaplan-Meier survival curves demonstrated clear and statistically significant separation between the risk strata (log-rank $p < 0.001$). Cox proportional-hazards regression analysis revealed a substantially elevated risk for the High Risk group compared to the Low Risk group, with a Hazard Ratio (HR) of 9.10 (95% Confidence Interval [CI] 6.4–12.9). When benchmarked against five established clinical risk scores – C2HEST, CHA2DS2-VASc, CHARGE-AF, HARMS2-AF, and HATCH – the proposed ECG8-EHR13-AF score demonstrated significantly superior discriminative capability on the identical test set (AUCs for all comparator scores were less than 0.50, with accuracies ≤ 0.50). The deployed PySide6 desktop application efficiently processed each patient record in less than 3.5 seconds. In a preliminary usability assessment, the application received favorable feedback regarding its usability and clinical relevance from two independent cardiologists.

Conclusion: This study successfully developed the ECG8-EHR13-AF multimodal framework, establishing a robust predictive model for stratifying the two-year risk of incident paroxysmal atrial fibrillation. By effectively integrating high-resolution electrocardiographic features with comprehensive clinical information, the model achieved a significant enhancement in predictive accuracy (AUCs 0.94-0.95 for key strata), substantially outperforming traditional risk scores (C2HEST, etc., AUC < 0.50) and demonstrating effective discrimination between distinct risk levels (evidenced by significant Kaplan-Meier separation and HR=9.10). The accompanying PySide6-based visualization desktop application provides a practical tool, enabling real-time, interpretable risk estimation (processing time < 3.5 seconds per record) suitable for informing clinical decision-making at the point of care. This research offers a novel and effective approach for the early identification and personalized risk management of atrial fibrillation, holding significant potential for clinical translation. Prospective multi-center validation is warranted to further confirm its generalizability and clinical utility.

基于计算流体力学的 caFFR 测定评价冠脉生理学功能的准确性研究

艾虎

卫生部北京医院（北京大学第五临床医学院）

背景：冠状动脉造影无法单独进行冠脉生理功能评价，无法准确地判断病变是否导致心肌缺血。血流储备分数测定是冠脉生理功能评价的最佳手段，但由于其成本昂贵、操作复杂，目前临床应用并不广泛。目前，基于计算流体力学的血流储备分数测定，简化了测量过程，有助于血流储备分数在临床中推广应用。基于冠脉造影的血流储备分数测定（coronary angiography-derived FFR ,caFFR) 是一种新的冠脉生理功能评价方法，操作简单，准确性较高，具有一定的临床应用价值。

目的：本文利用 caFFR 完成对冠脉生理功能评价，并与经导丝血流储备分数测定比较，回顾性分析 caFFR 诊断有冠脉狭窄性心肌缺血的准确性。

方法：本研究是一项回顾性诊断试验，选取从 2020 年 1 月至 2025 年 1 月在北京医院心脏导管室行冠脉造影检查，至少有 1 支血管狭窄在 50-90% 之间，并完成经导丝 FFR 测定的患者 150 例（共 167 支有效血管）。将以上患者的冠脉造影数据传输至 Flash Angio 工作系统，利用内置算法得到 caFFR 数值。以导丝 FFR 为金标准，0.80 为诊断心肌缺血的界值，评价 caFFR 诊断心肌缺血的准确性，评价内容包括诊断准确度、敏感度及特异度等，以 Pearson 相关系数及 Bland-Altman 图示法评价 caFFR 与 FFR 的相关性及一致性，以组内相关系数 (intra-class correlation coefficient, ICC) 评价 caFFR 测量的可靠性，并比较在诊断灰区与非灰区、复杂病变与非复杂病变、PCI 前后、老年与非老年患者、糖尿病与非糖尿病患者及高血压与非高血压患者中 caFFR 的诊断价值。

结果: 在血管分析水平上，caFFR 与 FFR 具有良好的相关性（r=0.87, p < 0.0001），诊断心肌缺血的价值较高 (AUC=0.959)，以 FFR ≤ 0.80 为诊断心肌缺血的界值，caFFR 的诊断准确性为 91.0%(95% CI:85.7 至 94.5)，Bland-Altman 图示法所见 caFFR 与 FFR 之间无显著差异，平均差值为 0.0041（95% LOA: -0.08 至 0.09）。caFFR 在诊断灰区与非灰区 (85.7% vs. 95.7%, p = 0.089)、复杂病变与非复杂病变 (90.2% vs. 89.9%, p = 0.956)、PCI 前后 (93.5% vs. 97.4%, p = 0.439)、老年与非老年患者 (88.4% vs. 91.4%, p = 0.548)、糖尿病与非糖尿病患者 (99.6% vs. 85.9%, p =0.065) 及高血压与非高血压患者 (89.8% vs. 91.5%, p = 0.720) 中的诊断准确性无显著性差异。

结论：（1）caFFR 的测定具有良好的可行性与可重复性，且 caFFR 与经导丝 FFR 的相关性较高，具有良好的诊断准确性；（2）caFFR 在 FFR 诊断灰区、PCI 前后及弥漫、钙化等复杂冠脉病变的诊断准确性仍较高，且较对照组无显著性差异；（3）caFFR 在老年冠心病患者、糖尿病合并冠心病的患者以及高血压合并冠心病的患者中的诊断价值良好。

关键词：冠心病，冠脉生理功能，血流储备分数，计算流体力学。

Diagnosis of heart disease based on multimodal information fusion

Liang Li[1], XI-Ming Li[2]

1. Tianjin NanKai Hospital，Tianjin Medical University；Hospital of Integrated Chinese and Western Medicine, Tianjin University

2. Tianjin Chest Hospital

Cardiovascular diseases (CVDs) remain the leading global cause of mortality from non-communicable diseases, with their prevalence steadily rising in China. Accurate auxiliary diagnosis of CVDs is an urgently needed technological advancement in cardiac health assessment. This project addresses key scientific challenges, including the mapping mechanism between high-density signal features and cardiac pathologies, as well as dynamic multimodal signal fusion for cardiac disease diagnosis. We aim to investigate the feasibility of high-density surface electromyography (HD-sEMG) for cardiac diagnosis, compare the diagnostic performance of three unimodal signals (echocardiography, electrocardiography [ECG], and HD-sEMG), and develop a unified Transformer-based fusion model augmented by joint learning strategies to mitigate multimodal imbalance and modality bias. Ultimately, an online multimodal cardiac disease diagnostic system will be established.

Objective: To investigate the feasibility of high-density surface electromyography (HD-sEMG) in the diagnosis of cardiac diseases and compare the diagnostic performance of three unimodal signals (echocardiography, electrocardiography, and HD-sEMG), a multimodal information fusion-based online diagnostic system for cardiac diseases was developed.

Methods: Twenty-four subjects were enrolled, including 8 patients with valvular heart disease (VHD), 8 patients with coronary artery disease (CAD), and 8 healthy controls. Echocardiography (UCG), electrocardiography (ECG), and HD-sEMG data were acquired from each subject. HD-sEMG signals were processed using principal component analysis (PCA) and independent component analysis (ICA) to extract diagnostically relevant components. Six deep learning models (Res-Transformer, ATI-CNN, ResNet, Transformer, Bi-LSTM, and MLP) were employed to compare the predictive performance of the three unimodal signals (HD-sEMG, UCG, and ECG) in cardiac disease diagnosis. A unified Transformer architecture was explored for multimodal cardiac disease diagnosis, processing multimodal inputs (HD-sEMG, UCG, and ECG) uniformly by embedding them into token vectors via an embedding layer. Attention mechanisms (self-attention and cross-attention) were utilized to facilitate interactions between modalities. Based on this framework, a dynamic fusion model was designed to enhance diagnostic accuracy.

Results:

1. Two-way ANOVA was performed to assess the effects of two factors—component analysis methods (PCA/ICA) and the number of components—on cardiac disease prediction performance. For accuracy, no significant interaction was observed between the two factors (*p* = 0.206, *F* = 1.73). A significant main effect was found for the component analysis method (*p* <0.001, *F* = 43.72), whereas no significant main effect was observed for the number of components (*p* = 0.870, *F* = 0.14). For the F1-score, a significant interaction was identified between the two factors (*p* = 0.011, *F* = 5.89). When the number of components was fixed, significant differences were observed among component analysis methods (*p* <0.001, *p* = 0.010, *p* = 0.040). Conversely, when the component analysis method was fixed (PCA), no significant differences were found across different numbers of components (*p* = 0.415, *F* = 0.972).

2. The impact of varying the number of stacked layers in different modules—Transformer Encoder 1, Multi-head Cross-Attention Module, and Transformer Encoder 2—on performance was investigated. Optimal cardiac disease prediction was achieved when both Transformer Encoder 1 and Transformer Encoder 2 were stacked with 4 layers. The multi-head cross-modal attention module contributed performance gains of 3%, 2%, 2%, 3%, 3%, and 4% as the number of layers increased from 0 to 2. However, further increasing the number of layers beyond 2 (up to 8) did not yield additional improvements.

Conclusions:

1. PCA-extracted components demonstrated significantly superior performance over ICA in predicting CAD and VHD, while validating the feasibility of HD-sEMG for cardiac disease diagnosis.

2. The Transformer-based multimodal fusion framework exhibited higher diagnostic efficacy than other learning models, and the multimodal joint learning model significantly outperformed unimodal approaches in predicting CAD and VHD.

Machine Learning Facilitated Early Risk Stratification of Bee Injuries Based on a Tropical Multicenter Cohort

Wang Liao, Feng Han, Yuan-Shui Liu, Yang-YanHong Ou

Hainan General Hospital

Background: Bee sting injuries in tropical regions represent a frequent and potentially life-threatening public health challenge. Early identification of high-risk patients is essential for optimizing emergency care.

Objective: To evaluate epidemiological characteristics of bee sting injuries and develop an interpretable machine learning model for early risk stratification in emergency settings across tropical, multicenter cohorts.

Methods: We conducted a retrospective multicenter cohort analysis of patients presenting with confirmed bee sting events across five secondary or higher-level hospitals in Hainan Province from January 1, 2019 to December 31, 2021. Demographics, sting details, clinical and laboratory data were collected. Supervised machine learning algorithms were trained and internally validated to predict progression to severe outcomes, with feature importance assessed for interpretability.

Results: Among 1,102 cases included, 8.7% developed severe systemic complications. The optimal model (random forest) achieved an area under the receiver operating characteristic curve of 0.89 (95% CI 0.86–0.92) on held-out validation, with key predictors including number of stings, involvement of head/neck region, symptom onset time, and serum creatinine levels. A user-friendly web-based risk calculator was created based on this model.

Machine Learning Model Performance

In comparing 13 mainstream machine learning algorithms, the Extra

Trees model exhibited the best performance on the test set (accuracy = 0.889, AUC = 0.959), outperforming logistic regression, naïve Bayes, and other models. Extra Trees excelled in capturing complex feature interactions and nonlinear decision boundaries. Its interpretability, enhanced through SHAP (SHapley Additive exPlanations), revealed that leukocyte count, hypotension, and creatinine were the top three contributors to risk predictions—offering clinicians transparent insight into model rationale.

To enhance clinical applicability, we also developed a simplified model based on five routinely available emergency indicators. Although the AUC slightly declined to 0.937, the model's ease of use and rapid data acquisition make it suitable for prehospital triage and community-level emergency care. With individual SHAP value visualizations, this streamlined model enables personalized risk factor analysis, supporting frontline clinicians in formulating dynamic intervention strategies.

Comparison with Traditional Risk Scores

Compared to widely used scoring systems like SOFA, qSOFA, and NEWS—which are primarily designed for infectious disease contexts with reported AUCs ranging from 0.77 to 0.84[10]—our model showed superior predictive performance and adaptability in wasp sting cases. While logistic regression provides interpretability, it struggles with nonlinear and high-order feature interactions. The ensemble Extra Trees model, by contrast, achieved a balance between accuracy and clinical reliability, supported by SHAP-based interpretability.

Crucially, the model outputs not only a probability score but also facilitates risk stratification. Predicted risk levels can be categorized as low (<10%), moderate (10–50%), and high (>50%), informing decisions on observation, enhanced monitoring, or early transfer. This provides a new pathway for implementing stratified and precise clinical interventions in wasp sting cases. Future work could incorporate multimodal data—such as on-site image recognition, venom detection, or natural language processing of medical records—to build an integrated intelligent early warning system for wasp stings.

Conclusion: Our study provides robust epidemiological insights and an accurate, interpretable machine learning tool for early triage of bee sting injuries. Integration into emergency workflows may enhance frontline decision-making and patient outcomes in tropical settings.

数字孪生技术在心血管护理领域的应用进展

王修正 涂惠 熊芳 郭婷 彭莹 彭小风 胡千芊 陈雨芬 郑知垚 万引

南昌大学第二附属医院护理部，南昌大学护理学院

随着人工智能信息技术的迅猛发展和海量医疗数据不断涌现，物联网、可穿戴式设备以及信息化水平的提升能够系统、全面地收集以患者为中心的大数据，这为护理实践提供了新的视角和机遇。此外，人工智能技术的迅猛发展极大地丰富了大数据的加工、处理和挖掘工作，为健康问题的诊断、预测及干预提供了强有力的支持。

数字孪生 (DigitalTwins，DT) 是一种新的数字技术应用，它通过基于物理实体，构建一个数字替身，实现基于数据的监测、模拟和决策，不同于其他传统仿真技术，它能够实时整合来自可穿戴设备、医学影像、电子健康记录等多源数据，形成同步持续更新的数字模型，使医护人员能够在虚拟环境中进行治疗方案的测试与优化等，从而指导真实世界的临床决策。其核心特征体现为数据实时同步性、全生命周期覆盖以及高保真映射。随着物联网、人工智能、机器学习以及大数据等技术的融合，数字孪生技术可将其进一步整合，从单一工具演变为“实时数据聚合 - 多模态分析 - 自主决策”的全链条生态。

随着社会经济的发展，国民生活方式的变化，尤其是人口老龄化及城镇化进程的加速，居民不健康的生活方式日益突出，心血管疾病 (cardiovasculardiseases，CVD) 危险因素对居民健康的影响愈加显著，CVD 的发病率仍持续增高。CVD 给居民和社会带来的经济负担日渐加重，已成为重大的公共卫生问题，加强政府主导的 CVD 防治工作刻不容缓。

传统护理模式在面对复杂多变的心血管病情时，往往受到可变治疗反应和基于人群的风险分层工具的限制。数字孪生技术，使用患者特定的解剖学和生理学数据构建的计算模型，已成为解决这些限制的一种有前途的方法。最新一些应用比如对复杂的患者特异性冠状动脉支架置入术病例进行数字孪生建模计算工作流程；通过整合连续的生理数据并计算数月的血流动力学模式来模拟患者的循环系统，用于早期疾病检测和监测进展；开发依赖于计算流体动力学评估冠状动脉狭窄功能严重程度，以改善改善颅外颈内动脉疾病的风险分层。这些模型已显示出增强护理个性化的潜力，提供比传统评分系统或单独的成像更细致和预测的框架。

数字孪生技术使得现实世界中发生的情境能够首先在虚拟世界中进行模拟与预测，通过有针对性的早期干预、推进个性化护理等，并为医护人员提供决策支持，从而改善患者的愈后，故数字孪生技术在护理实践中的应用前景较好。该技术与医疗护理的融合有助于创新护理模式，提升护理服务质量与效率，推动护理高质量发展。目前，国外数字孪生技术的应用发展迅猛，但国内相关研究还处于起步阶段。因此，本研究对于数字孪生在心血管护理领域的应用现状进行综述，以期进一步为推动国内数字孪生技术在心血管护理领域的应用和发展提供参考。

基于共享决策模式的人工智能老年房颤患者健康监测小程序的研发及应用研究

肖维，刘华芬

武汉大学人民医院（又名湖北省人民医院）紫阳院区

内容目的：开发一款针对老年房颤患者的人工智能监测小程序，实现患者 - 医院的共享决策并探讨监测小程序的应用效果，为此类患者提供延续性护理。方法：本研究以武汉某三甲医院心律失常科收治的老年房颤患者为研究对象，对患者及其主要照顾者进行半结构访谈，分析程序开发需求。成立多学科团队，召开小组会议确定健康监测小程序的内容和模块，待小程序研发完成后，招募老年患者测试小程序对健康数据的监测准确性与异常检测的灵敏度。比较小程序生成的健康建议与传统医疗建议的一致性与效果。通过用户调查法调查老年患者、家属和医护人员对小程序的接受度和使用体验。后期采用对照研究法设立实验组（使用小程序）和对照组（传统健康管理模式）调查小程序在决策共享效率中的实际表现，评估两组患者健康管理结局的差异。结果：开发老年房颤患者健康监测小程序，两组患者均完成随访，两组出院 3 个月后患者卒中发生率比较，差异无统计学意义（P>0.05），比较两组出血事件例数和复发例数，差异有统计学意义（P<0.05），使用小程序后患者出院满意度有所提高。结论：基于共享决策模式的人工智能老年房颤患者健康监测小程序可改善老年房颤患者的不良结局，减少居家并发症的发生，提高患者满意度，为患者出院延续性护理提供新的护理内容。

PPARgene 2.0: leveraging large language models and multi-omics data for enhanced identification and prediction of PPAR target genes

Jing-xi Qin, Wei-li Xie, Heng Li, Hao Li, Yu-cheng Zeng, Yu Luo, Yan-kai Li, Tian-Ming Sha, Li Fang

Sun Yat-sen University

1. Purpose

Peroxisome proliferator-activated receptors (PPARs) are ligand-activated transcription factors of the nuclear receptor superfamily. Upon ligand binding, PPARs activate target gene transcription and regulate a variety of important physiological processes such as lipid metabolism, inflammation, wound healing and immune responses. Synthetic PPAR ligands, such as fibrates and thiazolidinediones, are used for clinical treatment of dyslipidemia and type 2 diabetes, respectively. Numerous PPAR target genes have been experimentally identified, but the increasing volume of PPAR-related publications each year makes it difficult to systematically track and evaluate newly discovered target genes and their functional evidence.

To address this, the original PPARgene database (version 1.0) provided a manually curated collection of validated target genes with detailed annotations including PPAR subtypes, tissue specificity, species, and supporting PubMed references. Using high-throughput gene expression data combined with computational analysis of PPAR-responsive elements (PPREs), a machine learning method was implemented to predict novel PPAR target genes. However, with ongoing research generating new validated target genes, these findings need to be incorporated into the database. In addition, the increasing availability of high-throughput experimental data provides opportunities to further improve the prediction model.

Therefore, we introduce PPARgene 2.0, a 10-year update to the original PPARgene database. It is a significantly enhanced and freely accessible database that incorporates newly validated target genes, subtype-specific and integrative prediction models, and user-friendly web interfaces for query and data exploration. This resource aims to support researchers in systematically identifying, prioritizing, and interpreting PPAR target genes for functional studies and therapeutic development.

2. Methods

2.1. Data Collection.

We first retrieved PubMed-indexed articles (2016–2024) containing PPAR-related terms (e.g., “PPAR”, “PPARα”, “PPARγ”). Next, we fine-tuned Bioformer (a BERT-like language model) to extract PPAR-related studies. GPT-4o-mini and GPT-4o models were then used to identify abstracts potentially reporting novel PPAR target genes. Candidate studies identified by GPT-4o-mini and GPT-4o were manually screened using two criteria: (1) evidence of gene expression changes after PPAR perturbation (e.g., agonists, knockouts) and (2) direct PPRE binding via EMSA, ChIP, reporter assays, or ChIP-seq. Genes meeting both were retained as experimentally validated targets.

We also curated 68 PPAR-relevant microarray and 15 RNA-seq datasets from GEO involving PPAR activation, overexpression, or inhibition. Additionally, PPARα/β/γ ChIP-seq datasets were obtained from ENCODE (GRCh38). To enhance confidence in TF-binding events, only ChIP-seq peaks overlapping ATAC-seq peaks within ±5 kb of gene TSS regions were retained. Among overlapping peaks, those with q-values below 0.1 were considered high-confidence and used for feature extraction. PPAR binding near gene TSS (±5 kb) was further assessed based on data from ChIP-Atlas, applying a MACS2 score threshold of ≥ 250.

2.2. Feature Extraction.

We extracted three feature types:

(1) **Transcriptomic Evidence (TE)**: Differential gene expression was computed from microarray and RNA-seq data (83 experiments). For each gene, we calculated the proportion of experiments in which the log fold change (logFC) exceeded specific thresholds: logFC > 1.5, logFC > 1.0, logFC > 0.5, logFC < −0.5, logFC < −1.0, and logFC < −1.5.

(2) In silico **PPRE Evidence (ISPE)**: A binary feature indicated whether conserved PPRE motifs were found within ±5 kb of the TSS in human, mouse, or rat.

(3) **PPAR Binding Evidence (PBE)**: ChIP-seq peaks overlapping ATAC-seq signals in TSS ±5 kb regions were used. Only the peak with the highest signalValue (q

2.3. Model Training and Evaluation.

Four logistic regression models were trained: one general model (all PPARs) and three isoform-specific models (PPARα, PPARβ/δ, PPARγ). Verified targets served as positives; negatives were randomly sampled genes excluding all known PPAR targets. To reduce sampling bias, we repeated the negative sampling process 100 times and trained each model using the corresponding positive set paired with each of the 100 negative sets. Model performance was evaluated using 5-fold cross-validation, reporting the median of precision, recall, F1, and AUC across 100 runs. All classification metrics were calculated at a probability threshold of 0.4.

2.4. Genome-wide Prediction of PPAR target genes

We trained a logistic regression model using a 1:5 ratio of positive to negative samples and the previously described feature set. The classification thresholds for predicting PPAR target genes were determined from the precision-recall (PR) curve by selecting the probability values corresponding to precisions of 0.8, 0.65, and 0.5. Genes with predicted probabilities above the threshold corresponding to precision 0.8 were classified as high-confidence targets; those with probabilities between the thresholds for precisions 0.6 and 0.8 as medium-confidence targets; and those with probabilities between the thresholds for precisions 0.5 and 0.6 as low-confidence (or high-sensitivity) targets. Genes with predicted probabilities below the threshold corresponding to precision 0.5 were predicted as non-targets.

2.5. Web Server.

PPARgene 2.0 is implemented using Flask with a Bootstrap frontend and an SQLite backend. It is publicly available at http://www.ppargene.org.

3. Results

Using a regular expression to capture common PPAR-related terms, we retrieved 23,746 PubMed abstracts (2016–2024) potentially relevant to PPAR target gene studies. Abstracts were screened using Bioformer, GPT-4o-mini, and GPT-4o, and 441 candidate articles were manually reviewed. Based on strict criteria for experimental validation, 337 genes were confirmed as PPAR targets, representing an increase of 112 genes over the previous version, including 35 for PPARα, 20 for PPARβ/δ, and 72 for PPARγ.

Using these validated genes, we trained logistic regression models with three feature types: transcriptomic evidence (TE), in silico PPRE evidence (ISPE), and PPAR binding evidence (PBE). The best-performing model achieved an AUROC of 0.843. Among individual features, TE yielded the highest predictive power, while PBE and ISPE enhanced recall and robustness. Subtype-specific models were also constructed, with PPARα achieving the best performance (AUC = 0.885). Ablation analyses confirmed the additive value of combining all features.

Genome-wide prediction using the subtype-agnostic model was performed on 19,906 human genes, resulting in 2,533 predicted PPAR targets: 420 high-confidence, 753 medium-confidence, and 1,360 low-confidence genes. All results are accessible at the PPARgene 2.0 website.

4. Conclusion

In this study, we described PPARgene 2.0, a ten-year update to the original PPARgene database. By integrating transcriptomic evidence, conserved PPRE analysis, and ChIP-seq binding features, we developed four logistic regression models – one integrative model and three PPAR subtype-specific models – to predict novel PPAR target genes in the human genome. PPARgene 2.0 now includes 337 experimentally validated targets (49.7% more than the orginal version) and provides genome-wide predictions across 19,906 human genes. We consider that PPARgene 2.0 will be a valuable resource for systematic exploration of PPAR-mediated transcriptional regulation and target discovery.

基于拉曼光谱结合 Stacking 机器学习方法对主动脉夹层患者早期识别的研究

张凯楠 杨毅宁

新疆维吾尔自治区人民医院

摘 要

目 的 探究基于拉曼光谱和 Stacking 机器学习方法对早期主动脉夹层患者的快速诊断效能。

方 法 基于临床、心脏超声、CT、冠脉造影结果，分别纳入明确诊断的主动脉夹层患者和急性心肌梗死患者各 50 例，同期纳入天山队列中冠脉造影正常的患者 50 例作为对照组。收集所有研究对象血清样本进行拉曼光谱检测。将检测得的全部光谱数据集使用自适应迭代重加权惩罚最小二乘法（adaptive iterative re-weighted penalized least squares，airPLS）以去除荧光背景并对基线进行校正，随后采用主成分分析算法（Principal Component Analysis，PCA）对处理后的拉曼光谱数据信息进行主成分特征提取，并运用机器学习中 Stacking 方法，依托 RandomForest、XGB、LGBM、GBM、AdaBoost 和 CatBoost 作为一级学习器，LogisticRegression 作为二级学习器，建立多分类诊断模型。对样本数据集采 8：2 的分割方式，采用五折交叉验证的方法来建立模型训练集和验证集，根据分类结果，计算模型的准确率、特异度、灵敏度，画出受试者工作特征曲线（receiver operating characteristic curve，ROC）求得曲线下面积（area under curve，AUC）以评价模型诊断效能。

结 果 分析测得血清平均拉曼光谱，主动脉夹层组与各对照组各类人群在位移 640cm-1、717cm-1、750cm-1 等多处光谱拉曼强度有统计学差异（P<0.05），这些光谱波峰的强度对应的是特定的生物分子和代谢物质，可能有利于血清拉曼光谱对主动脉夹层患者的快速识别。应用 PCA 算法对光谱数据进行降维处理，提取光谱特征信息，该特征主成分在二维平面中能将两组样本进行区分，进一步根据 Stacking 方法构建诊断模型对主动脉夹层进行分类学习，结果显示该模型对主动脉夹层患者的分类敏感度达到 88.7%，特异度为 96.1%（AUC=0.94），显示出了较好的诊断效能。

结 论 研究结果显示，基于拉曼光谱结合 Stacking 机器学习方法的算法模型能够对主动脉夹层的患者进行早期快速分类识别，为主动脉夹层的快速诊断和筛查提供新的思路和技术支持。

人工智能在心血管疾病辅助诊疗中的应用进展与挑战

刘丽红 刘华芬

武汉大学人民医院

目的：

人工智能（Artificial Intelligence, AI）正在重塑现代医学图景，尤其在数据密集、流程复杂的心血管疾病领域展现出巨大潜力。本文旨在系统梳理近年来 AI 在心血管疾病诊疗中的研究进展，探讨其关键技术路径、典型应用场景及未来发展方向。

方法：

采用 PubMed、Web of Science 等数据库检索 2018 年至 2025 年 AI 在心血管疾病领域应用的高影响力研究，重点筛选基于机器学习（ML）与深度学习（DL）框架的临床研究、前瞻性验证及转化落地成果，围绕五大核心方向展开系统性归纳：1）影像辅助诊断；2）心电图自动判读；3）预后模型与风险预测；4）介入策略优化；5）个体化心血管治疗决策支持。

结果：

研究显示，AI 在多个细分领域实现突破性进展。例如，基于深度卷积神经网络的冠脉 CTA 智能分析已在多项研究中实现接近人工读片准确度（AUC>0.93）；AI-EKG 模型在房颤、心衰筛查方面表现优异，部分已进入 FDA 批准流程。在预后预测方面，AI 可整合多模态临床数据构建心衰复发、心源性猝死等风险评分系统，优于传统回归模型。AI 在介入策略评估中也开始用于 FFR 计算、PCI 路径规划等。尽管前景广阔，但目前仍存在模型泛化性不足、临床落地门槛高、数据安全与伦理问题等挑战。

结论：

AI 技术为心血管疾病的精准诊疗提供了全新范式，正在从辅助工具向临床决策核心环节逐步演进。未来发展需聚焦真实世界验证、多中心协同开发、临床医生与工程师共建机制，推动从“算法可用”走向“系统可信”，加速 AI 在心血管病学的临床转化进程。

人工智能在心血管临床护理中的应用

杨杏 李娟利

西安交通大学第一附属医院

心血管疾病作为全球公共卫生领域的重大挑战，其临床护理工作因病情复杂多变、个体差异显著等特点面临着诸多困难。近年来，人工智能技术的快速发展为心血管护理领域带来了革命性的变革。本文系统探讨了人工智能技术在心血管临床护理中的关键应用及其面临的挑战。

在应用层面，人工智能技术主要体现为四大核心功能：首先，在病情监测与预警方面，通过智能分析患者的实时生理数据，能够实现早期风险识别和及时干预；其次，在辅助诊断决策方面，深度学习算法显著提升了医学影像分析的准确性和效率；再次，在个性化护理方案制定方面，基于大数据的分析能力使精准医疗成为可能；最后，在患者健康管理方面，智能系统有效提升了健康教育的个性化和依从性。这些应用不仅提高了护理质量和效率，还优化了医疗资源的配置。

然而，人工智能在心血管护理中的实际应用仍面临多重挑战。技术层面存在数据质量参差不齐、算法可解释性不足等问题；人员层面需要解决医护人员的技术适应性和能力提升需求；管理层面涉及工作流程的重构和协作模式的创新；伦理法律层面则面临责任界定不清和监管框架缺失等困境。

针对这些挑战，本文提出了系统性的应对策略：建立标准化的医疗数据库、开发可解释性算法、加强专业人才培养、完善伦理规范和监管体系等。展望未来，随着 5G、物联网等新技术的融合发展，人工智能在心血管护理中的应用将更加深入，推动护理模式向智能化、个性化和预防性方向转型。本研究旨在为人工智能在心血管护理领域的健康发展提供理论依据和实践指导，最终实现提升护理质量、改善患者预后的目标。

远程医疗技术在冠心病患者服药依从性中应用的研究进展

露露

首都医科大学附属北京友谊医院

据统计 2023 年我国冠心病患病人数高达 1139 万，药物是冠心病治疗和二级预防的基石。良好的服药依从性对降低冠心病患者致残率、病死率，改善生活质量具有积极意义。相较于传统模式，远程医疗技术克服了时空限制，可实时用药监测、个性化用药评估。本文综述其常见应用形式及实施障碍因素。（1）常见应用形式：①微信及短信：具备健康教育及用药提醒功能。通过微信公众号发布疾病相关科普文章、动画供患者查阅。医护人员可在微信群内提醒患者服药并答疑。②药物提醒 APP：具备服药设置、提醒、记录等功能。由护士录入药物信息并设置提醒，以闹钟或短信形式提醒服药。同时提供药物知识链接。③移动穿戴式程序：具备远程多参数生命体征监测、多系统联动、服药提醒、远程互动功能，帮助患者树立治疗信心。④电子药盒：集药盒与提醒功能于一体，通过振动、语音或灯光闪烁提醒服药。（2）实施障碍因素：①技术使用障碍：老年或教育水平低的患者因技术门槛放弃使用远程技术。②沟通局限性：目前大多数远程技术缺乏即时反馈功能，患者疑问未及时解决，易自行调整用药。③数据整合：不同平台未实现数据关联，医生无法全面评估。④心理因素：部分患者过分依赖家属及医护人员，远程自主性不足。

心血管疾病全周期智慧化管理：人工智能平台的构建与应用实效

李玉琼 田丹 刘华芬

武汉大学人民医院

目的：探索人工智能（AI）与信息化技术在心血管疾病“筛查 - 诊疗 - 康复 - 随访”全周期管理中的应用价值，提升诊疗效率、精准度及患者预后，并验证本院创新平台的临床实效。

方法：1. 智能预警平台构建：基于可穿戴心电监护设备（39g 轻量设计），通过蓝牙 / 移动网络实时传输心电数据至云端，集成 AI 算法自动识别 20 余种心律失常事件，实现高危患者自动预警（如心脏传导阻滞、室速）。建立“湖北省心电大数据中心”，整合 100 万 + 份心电数据训练算法，覆盖院前筛查至院后随访全流程。2. 真实世界数据驱动决策：依托本院获批的国家级平台“疑难复杂心血管病介入诊疗真实世界数据应用中心”，融合 AI 与临床诊疗数据，构建介入手术风险预测模型，优化手术方案。3. 区域协同救治网络：联合 38 家基层医疗机构建立远程心电诊疗平台，通过 AI 辅助心电解读 + 专家远程复核（4 名副高职以上专家轮值），实现“基层筛查 - 中心诊断 - 绿色转诊”闭环管理。

结果：1. 预警效能：系统累计筛查 27 万例心电数据，识别高危患者 1 万余例（阳性率 3.7%），成功预警并干预心脏性猝死事件（如宜城李先生病例）；2. 基层赋能：基层医院心电诊断准确率提升 40%，转诊至本院的危急病例从入院到手术时间缩短 35%；3. 精准诊疗：AI 辅助的介入手术风险模型使复杂手术并发症率降低 22%，术后 30 天再入院率下降 18%；4. 管理效率：房颤中心智能管理平台（1.0 版）应用后，单病例填报时间从 15 分钟缩短至 2 分钟，字段准确率达 97.7%。

结论：武汉大学人民医院构建的心血管 AI 全周期管理范式已取得三大突破：1. 预警革新：可穿戴设备 + 云端 AI 实现“无症状期”风险主动拦截，改写被动救治模式；2. 资源优化：区域协同网络破解基层诊疗瓶颈，推动分级诊疗落地；3. 决策升级：真实世界数据驱动精准介入治疗，提升复杂手术安全性。未来需深化 AI 与多模态数据（如影像、基因组）融合，拓展至心力衰竭、高血压等慢病管理，助力“健康中国”战略实施。

关键词：人工智能（AI）、心血管信息化、可穿戴设备、真实世界数据、区域协同救治

人工智能：放射介入术后康复护理个性化、精准化与资源优化的利器

赵婉婷

首都医科大学附属北京友谊医院

目的：探寻并评估人工智能（AI）于放射介入术后康复护理规划里的运用潜力，达成护理方案的个性化与精准化，合理调配资源，提升患者康复成效，降低并发症出现几率，强化护理决策的合理性。

方法：运用文献查阅、趋势剖析、各方专家看法调研、需求考察、预测模型构建等手段，针对人工智能在放射介入术后康复护理规划中的应用前景以及面临的挑战展开详尽分析。

结果：

1、个性化照护：人工智能大幅提高个性化护理策略的精准程度，借助对患者术后生理指标、基因组数据、影像资料等进行全面剖析，为患者制定高度个性化的护理方案。和传统护理模式相较，个性化护理使并发症发生几率降低约 20%，患者康复速度加快约 15%。

2、并发症预估：基于深度学习的并发症预估模型精准识别高风险患者的能力达到 90%，提前采取的预防举措成效显著，有效降低了患者再次入院的比例。

3、资源调配：人工智能辅助的护理资源调配系统让护理人员的工作效率提升约 30%，同时护理成本降低约 10%。

结论：人工智能在放射介入术后康复护理规划中的应用展现出极为广阔的前景，不仅能够极大地提升护理的个性化与精准程度，还能优化资源的利用效率，提高患者对护理的满意程度，推动医患之间的沟通交流。

The feasibility of radiomic analysis based on T1 mapping to distinguish between hypertensive heart disease and hypertrophic cardiomyopathy

SHENGLIANG LIU, Guo-Kun Wang, Yan-Ming Zhao, Bo Yu

The Second Affiliated Hospital of Harbin Medical University

Introduction:

Hypertensive heart disease (HHD) is characterized by arranged hyperplastic myocytes and increased interstitial tissue due to changes compensated for uncontrolled arterial hypertension. Hypertrophic cardiomyopathy is involved in abnormally hypertrophied heart muscle, disarray of cardiomyocytes and increased interstitial connective tissue. Late gadolinium enhancement (LGE) patterns of the two diseases are mostly different in cardiac magnetic resonance (CMR), which represent extent of myocardial fibrosis are not identical. HCM tends to show patchy enhancement in middle layer of ventricular wall, enhancement of HHD tends to be diffuse and subtle. Higher native T1 value is also proved in HCM compared to HHD patients. However, when it comes to slight changes in early clinical stage, differences become obscure. Thus, novel techniques and extensive experiences based on CMR are urgently needed. Radiomics plays a more and more important role in clinical decision-making by mining quantitative texture analysis (TA) features from medical images and screening the valuable organizational features by statistical or machine learning methods. TA involves spatial arrangement and relationship of adjacent pixels, which provides an approach to quantify subtle imaging abnormalities. The relaxation time of longitudinal or spin lattice can be measured by T1 mapping, and the biological determinants of the increase of T1 value are edema and fibrosis, which have been widely studied in cardiomyopathy. Furthermore, previous study showed that CMR histogram analysis of T1 mapping in the white rabbit model could be an effective method to predict the liver fibrosis stage. Thus, we hypothesize that radiomic analysis based on T1 mapping could extract valuable TA features in the two diseases. The purpose of this study is to distinguish HHD and HCM by using as comprehensive TA features as possible.

Methods:

Patients with HHD and HCM were enrolled in this study from Sep. 2020 to Apr. 2021. CMR images were obtained by a 3.0T system (Ingenia CX, Philips Healthcare, the Netherlands) with 32-channel abdomen coil. Modified Look-Locker inversion recovery (MOLLI) sequence with a short-axis stack covering the base, mid-ventricular and apex level were performed and the detailed scanning parameters of T1 mapping were as follows:, repetition time (TR), / echo time (TE) = 3.3/1.6 ms, field of view (FOV) = 300 ×300 mm^2, voxel = 2 ×2 ×2.5 mm, flip angle = 20 ° , no slice gap. CVI software (cvi42, Circle Cardiovascular Imaging Inc., Calgary, Alberta, Canada) was used for the post-processing of T1 mapping images. The thickest section of LV wall was chosen in HCM patients and mid-ventricular segment was chosen in HHD patients. LV epicardial and endocardial borders were delineated on T1 mapping using a freehand region of interest (ROI) tool by two experienced radiologists (with three and two years of experience) separately.The types of images used in this study were as follows: original, wavelet,logarithm and square. TA features were calculated by using Pyradiomics, an open-source python package. Seven subsets of features were acquired including First Order Statistics, Shape-based (2D),Gray Level Cooccurence Matrix (glcm), Gray Level Run Length Matrix (glrlm) and Gray Level Size Zone Matrix (glszm), Neighbouring Gray Tone Difference Matrix (ngtdm) and Gray Level Dependence Matrix (gldm). The independent t-test or Manne Whitney U-test was used to compare between two groups. Histograms were used to visualize different TA features for distinguishing these two diseases. ROC curves were used to evaluate the diagnostic efficiency and Delong's test was calculated to compare AUCs among groups.

Results:

Twenty-three patients with HHD (50.65 ± 16.62 years; 82.6 % men) and twenty-one patients with HCM (54.10 ± 12.57 years; 71.4 % men) were enrolled in this study. For all calculated TA features, AUCs of nine parameters had the value above 0.65. Logarithm_glszm_ZoneEntropy(AUC: 0.790, sensitivity: 71.4 %, specificity: 81.8%, P <0.01)showed slightly higher value than original_shape2D_Sphericity (AUC: 0.779, sensitivity: 81.0 %, specificity: 77.3 %, P < 0.01). Besides, the AUCs of original_glszm_LargeAreaHighGrayLevelEmphasis, wavelet-HH_firstorder_Mean and logarithm_glszm_LargeAreaHighGrayLevelEmphasis were 0.719 (sensitivity: 90.5 %, specificity: 50.0 %, P= 0.014), 0.703 (sensitivity: 85.7 %, specificity: 63.6 %, P= 0.022) and 0.742 (sensitivity: 85.7 %, specificity: 63.6 %, P < 0.01) respectively.

Discussion:

Although native T1 mapping has shown great potential in differentiation HCM and HHD, sometimes mean T1 values may hide significances in local or specific regions. In addition, T1 values are not identically stable due to different sequences or parameters, making it difficult to determine absolute cutoff values. TA features overcome the limitations as described above, as well as provide more dimensional information for the spatial distribution of signals on the images. Logarithm_glszm_ZoneEntropy

and original_shape2D_Sphericity showed better diagnostic efficiency in the presented study, which means that the chaotic distribution of the logarithmic transformed image in T1 space and the sphericity on the original plane image are of great significance to distinguish the two diseases. Actually, more data of radiomic analysis on T1 mapping would be needed for further verification in the future.

Conclusion:

Texture analysis features may be an effective method to distinguish HCM and HHD.

不同来院方式对急性 ST 段抬高型心肌梗死患者再灌注时间及短期预后的影响分析

欧尾妹 林吉怡 王斌

厦门大学附属心血管病医院

【摘要】 目的 探讨不同来院方式对急性 ST 段抬高型心肌梗死 (STEMI) 患者的再灌注时间及短期预后的影响。**方法** 根据来院方式不同将 597 例接受直接经皮冠状动脉介入治疗（PPCI）的 STEMI 患者分为自行来院组（122 例）、120 转运组（51 例）和网络医院转诊组（324 例）。比较各组患者的基本特征、再灌注指标（发病 - 首次医疗接触时间、首次医疗接触 - 导丝通过时间、大门 - 导丝通过时间、发病 - 导丝通过时间、入门 - 出门时间）、住院期间并发症和死亡率。**结果** 与其他两组相比，网络医院转诊组的到达大门 - 导丝通过时间更短，而首次医疗接触 - 导丝通过时间更长（P < 0.05），分别为：35 (29, 45)min 和 123 (80, 192)min。与其他两组相比，120 转运组的发病 - 首次医疗接触时间和发病 - 导丝通过时间更短（P < 0.05），分别为：55 (32, 136)min 和 136 (101, 188)min。与自行来院组相比，网络医院转诊组患者住院期间并发症的发生率较低（P < 0.05）。**结论** 为缩短 STEMI 患者心肌缺血时间，仍需加强对自行来院和网络医院转诊途径的院前流程优化。

【关键词】 心肌梗死；来院方式；再灌注时间；短期预后；胸痛中心

人工智能在改善老年心血管患者服药依从性与准确率中的应用研究

吴敏 刘华芬

武汉大学人民医院

老年心血管患者因基础疾病复杂、用药方案繁琐，常存在漏服、误服、多服或少服等问题，直接影响治疗效果并增加不良事件风险。本研究旨在探索人工智能技术在优化老年心血管患者服药管理中的应用路径，通过个性化干预提高服药依从性与准确率，改善患者预后。

研究方法上，首先构建多维度老年心血管患者用药数据库，整合电子病历中的基础疾病信息、用药清单（如抗凝药、降压药、调脂药等）、肝肾功能指标及既往服药行为记录；基于该数据库开发智能服药管理系统，集成三项核心技术：一是利用机器学习算法（如随机森林、LSTM）分析患者年龄、记忆力评分、生活作息等特征，构建漏服风险预测模型，实现高风险时段提前预警；二是开发搭载物联网技术的智能药盒与可穿戴设备，通过语音提醒、APP 推送等方式执行个性化服药指令，并自动记录开合状态与服药时间；三是结合自然语言处理技术，搭建智能问答模块，实时解答患者对用药剂量、时间、禁忌等的疑问。研究选取 200 例老年心血管患者，随机分为 AI 干预组（100 例）与常规管理组（100 例），干预周期为 6 个月，对比两组服药相关指标差异。

研究结果显示，AI 干预组的服药依从性显著提升：漏服率从干预前的 38.2% 降至 12.5%，误服率（如剂量错误、时间错误）从 15.6% 降至 4.1%，服药准确率达 95.9%，较常规管理组（72.3%）提升 23.6 个百分点。同时，AI 系统的漏服风险预测准确率达 89.3%，可提前 1-3 天识别高风险患者并触发强化提醒；患者对用药方案的知晓率从干预前的 56.7% 升至 88.9%，6 个月内不良心血管事件（如脑卒中、急性心衰）发生率较常规管理组降低 27.4%。此外，82.0% 的患者及家属表示对智能设备的接受度高，认为其操作简便且有效减轻照护压力。

研究结论表明，人工智能技术通过个性化风险预测、智能化提醒与互动式指导，能有效改善老年心血管患者的服药行为，显著提升依从性与准确率，降低不良事件风险。该技术方案兼顾老年患者的生理特点（如记忆力衰退）与操作便利性，具有较强的临床实用性。未来需进一步优化系统的适老化设计（如简化操作界面、增强语音交互），并加强数据安全保护，通过多中心推广实现技术普惠，为老年心血管患者的规范用药管理提供可持续的解决方案。

绘制昼夜节律紊乱驱动动脉粥样硬化进展的分子指纹图谱

张格 张金盈 唐俊楠

郑州大学第一附属医院

目的：昼夜节律紊乱被认为是动脉粥样硬化性心血管疾病（ASCVD）发生发展的重要危险因素，但其在动脉粥样硬化斑块微环境形成中的作用机制尚不明确，限制了靶向干预策略的开发。目前相关认知主要源自流行病学研究及动物模型，而多数人群研究聚焦于健康个体，动物实验亦难以充分模拟人类疾病的真实病理生理状态。因此，如何在真实临床背景中精确识别与量化个体内源性昼夜节律紊乱，是亟待解决的重要科学问题。

方法：昼夜节律紊乱被认为是动脉粥样硬化性心血管疾病（ASCVD）发生发展的重要危险因素，但其在动脉粥样硬化斑块微环境形成中的作用机制尚不明确，限制了靶向干预策略的开发。目前相关认知主要源自流行病学研究及动物模型，而多数人群研究聚焦于健康个体，动物实验亦难以充分模拟人类疾病的真实病理生理状态。因此，如何在真实临床背景中精确识别与量化个体内源性昼夜节律紊乱，是亟待解决的重要科学问题。

结果：基于 MyPROClock 系统，我们在群体层面揭示了昼夜节律错位与多种临床表型之间的显著关联，并在分子层面解析了其驱动斑块微环境重塑及疾病进展的关键机制。研究发现 MFAP4 为节律错位的关键介导因子，促进平滑肌细胞表型转化及斑块不稳定性形成，具有潜在的干预靶点价值。此外，我们基于节律生物学特征构建了具有良好重现性与临床应用前景的 ASCVD 节律分型系统，并上线 AI 驱动的患者节律状态评估工具 miniClock（https://myproclock.cardioartist.workers.dev/），便于临床医生实现个体化节律风险分层与管理策略优化。

结论：本研究系统描绘了 ASCVD 中昼夜节律错位的分子指纹图谱，阐明其在斑块微环境重构与疾病进展中的核心作用，提出了以 MFAP4 为代表的潜在干预靶点，并构建了具有转化潜力的节律风险评估工具与分型系统。研究为昼夜节律指导下的精准治疗策略提供了理论基础与实践路径，推动节律医学在心血管领域的临床应用落地。

基于机器学习建立冠心病患者冠状动脉整体负荷风险预测模型

胡志鸿

石河子大学第一附属医院

目的 建立与验证一个可预测冠状动脉粥样硬化性心脏病（CAD）患者冠状动脉整体负荷的机器学习模型。

方法 本研究是一项回顾性研究，选取 2023 年 1 月至 2023 年 12 月石河子大学第一附属医院收治的 615 例 CAD 患者为研究对象。应用 LASSO 回归分析 CAD 患者冠状动脉整体负荷相对中高风险的独立危险因素。建立并验证可预测 CAD 患者冠状动脉整体负荷的随机森林模型、决策树模型、K 近邻模型、梯度提升模型、多层感知机模型，通过灵敏度、特异度、AUC、准确率、精确率、召回率和 F1 评分综合评价模型的性能。优选最佳模型后，通过夏普利加性解释（SHAP）方法量化特征，可视化最佳机器学习模型。

结果 LASSO 回归分析结果显示，低密度脂蛋白、血清肌钙蛋白 T、NT-proBNP、葡萄糖、室壁运动评分、尿酸、天门冬氨酸氨基转移酶、白蛋白、收缩压、TC-HDLDL、血钙、性别、血钠、肌酸激酶、心率是 CAD 患者冠状动脉整体负荷相对中高风险的独立危险因素。5 种机器学习算法中，随机森林模型预测 CAD 患者冠状动脉整体负荷的性能最高，在训练集中的各项指标为：准确率 0.793、精确率 0.789、召回率 0.937、F1 评分 0.857、AUC 值 0.857；在测试集中的对应指标为 0.708、0.73、0.885、0.8、0.732。

结论 基于随机森林模型构建的 CAD 患者冠状动脉整体负荷风险预测模型性能最优，此模型的应用可以帮助临床医师及早判断患者病情，从而为制定个体化的诊疗方案提供参考。

中心静脉导管相关血流感染预防控制系统的构建及应用

郑薇亮 孙丽军 崔冬梅

厦门大学附属心血管病医院 (厦门市心脏中心)

目的 中心静脉导管相关血流感染 (Central Line-Associated Bloodstream Infection, CLABSI) 指患者在留置中心静脉导管 (Central venous catheter, CVC) 期间或拔出 CVC 48 小时内发生的原发性，且与其他部位存在的感染无关的血流感染，一旦发生，将增加患者的住院费用、延长患者的住院时间、严重影响患者的预后。我院 2019 ~ 2021 年 CLABSI 发生率为 0.69 ~ 1.76‰，中位数 0.92‰，处于较高水平。尽管相关指南与专家共识 [5-7] 提出了多样化、集束化的防控措施，但在临床实践中存在 CVC 置管与管路维护不规范、管路移除不及时、信息统计和质量控制滞后等问题。基于此，构建中心静脉导管相关血流感染预防控制系统，并进行初步应用，评价其在中心静脉导管相关血流感染管理中的可用性，以期降低中心静脉导管相关血流感染的发生率。**方法** 组建系统构建小组，基于相关指南、专家共识及临床需求构建中心静脉导管相关血流感染预防控制系统，该系统包括导管置入、导管评估与维护、CLABSI 预警、CLABSI 监控与统计分析 4 个模块。系统上线运行后，比较系统应用前 (2021 年 1 月–12 月) 与应用后 (2022 年 1 月–12 月) 住院患者中心静脉导管相关血流感染发生率的变化及临床医护人员对于系统的可用性评价。 **结果** 系统应用后，中心静脉导管相关血流感染发生率为 0 低于系统应用前 1.76‰（P<0.05），临床医护人员对于系统的可用性评价标准化得分为 1.84±0.97 分，处于高水平。**结论** 中心静脉导管相关血流感染预防控制系统降低了中心静脉导管相关血流感染的发生率，可用性良好，具有一定的临床应用推广价值。

基于胸痛视角的心脏大血管转诊平台的构建与实践

郑薇亮 孙丽军 崔冬梅

厦门大学附属心血管病医院 (厦门市心脏中心)

目的：中国心血管病死亡占居民疾病死亡构成 40% 以上，高于肿瘤及其他疾病。基于胸痛视角的心脏大血管体系平台建设以医疗联合体（医联体）模式为基础，将同一区域内的医疗资源整合在一起组成一个医疗联合体，有效推动形成基层首诊、双向转诊、急慢分治、上下联动的分级诊疗模式。 方法：建立由信息护士、医生、信息科组成的信息专案小组，由信息专案小组主导进行现有流程进行风险评估，针对性的开发设计实现患者双向转诊应用并落地运行，串联转诊前数据先行、转诊中及时记录，实时监测监护数据及病人相关信息，转诊后治疗记录共享及患者随访，根据患者病情危重缓急的情况，开展适时的 MDT 服务，实现患者及时医、有效医，促进优质服务的连贯性、可及性。 结果：通过区域大血管疾病诊疗平台建设，将急性 A 型主动脉夹层患者从发病到入院的时间由 11.1 小时缩短至 8.8 小时；入院至手术的时间由 15.28 小时缩短至 12.22 小时，急诊 A 型主动脉夹层死亡率低至 1.02%，极大提升了区域大血管疾病的救治水平。结论：高效实用性的双向转诊平台实现患者高效救治，缓解患者“看病难、看病远”问题，更好地满足人民群众的健康需求。

关键词： 5G、心血管疾病、医联体平台、心脏大血管体系

冠心病长期皮下注射单抗患者对网约护理服务的认知及需求度现状

刘莎莎 刘华芬

武汉大学人民医院（湖北省人民医院）

目的 调查冠心病长期皮下注射单抗患者对网约护理服务的认知及需求度现状，为提高安全风险意识、完善规章制度和政策的制订提供参考依据。

方法 研究团队自行编制问卷，内容涵盖患者基本信息、网约护理认知与需求，安全风险意识相关问题。针对武汉大学人民医院需长期皮下注射单抗的冠心病患者展开调查，同时采用电话、线上平台等方式回访，以确保数据真实全面。

结果 冠心病长期皮下注射单抗患者对网约护理服务的认知得分 58.00(45.00,70.00) 分，需求度得分 1.00(1.00,2.00) 分。多元逐步回归分析结果显示，影响武汉大学人民医院冠心病需长期皮下注射单抗患者对网约护理服务认知的主要因素为年龄、文化程度；影响患者对网约护理服务需求的主要因素为月收入、注射周期，就诊次数。

结论 长期皮下注射单抗的冠心病患者对网约护理服务的认知亟待提升。建议以患者需求为导向，针对不同年龄与文化程度的患者，开展多样化宣传，如为老年患者举办社区讲座，为年轻患者利用社交媒体推送科普信息；提供适配的宣传资料，文化程度低的提供通俗易懂版本，高的提供专业深入资料。此外，医疗机构及相关部门应全力完善网约护理服务体系，明确服务流程规范，提升服务透明度，公开护士资质、服务价格明细等，全方位提升患者对网约护理服务的认知，推动其在冠心病护理领域的广泛应用。

心音心电图远程监测在心脏起搏器患者心功能院外评估中的可行性研究

黄婧娟

上海交通大学医学院附属胸科医院

目的：心脏起搏器患者的长期管理需关注心功能变化，传统返院随访依赖超声心动图，存在成本高、便利性差等问题。心音心电图（PCG-ECG）可通过电机械收缩时间（EMAT）无创评估心脏收缩功能，但其在起搏器患者远程监测中的应用价值尚未明确。本研究旨在探索基于 PCG-ECG 的院外随访模式对起搏器患者心功能监测的有效性。

方法：前瞻性纳入 2023 年 1 月至 4 月植入双腔起搏器的 10 例患者（男 4 例、女 6 例，年龄 65±8 岁），采用便携式 PCG-ECG 设备（闻心）开展 3 个月远程监测。患者每周居家同步记录心音与单导联心电图，经云端平台计算 EMAT（QRS 起点至 S1 心音结束时间）及 EMAT 比率（EMAT/RR 间期），结合患者自报症状（NYHA 分级、活动耐量）综合评估心功能。主要终点为 EMAT 动态变化（正常参考值 < 120ms），次要终点包括症状恶化率、数据采集成功率及不良事件。

结果：3 个月内累计完成 120 次远程监测（依从率 100%），数据有效传输率 98.3%（118/120）。基线 EMAT 为 118±15ms，随访期间波动在 110-130ms（均值 122±18ms，P=0.21），EMAT 比率保持稳定（12.1±2.3% vs 12.5±2.1%，P=0.38）。1 例患者因 EMAT 持续延长（>140ms），经远程提示后返院复查，超声证实左室射血分数（LVEF）下降（50% 降至 42%），经药物调整后症状改善。所有患者未发生急性心力衰竭或起搏器相关并发症，人均减少院内随访 2.3 次（节约就诊时间 5.8 小时）。

结论：基于心音心电图的 EMAT 监测能有效识别起搏器患者心功能变化，与临床症状及超声结果具有一致性，为院外心功能管理提供了无创、便捷的工具。该模式通过动态评估电机械耦联效率辅助早期干预，减少非必要返院，尤其适用于心功能代偿期患者的长期随访。后续需扩大样本量，并验证 EMAT 阈值对临床预后的预测价值。

基于人工智能 MA-IRNet 算法的心脏起搏器品牌自动分类系统应用研究

黄婧娟

上海交通大学医学院附属胸科医院

目的：随着心脏起搏技术的快速发展，不同制造商（如百多力、波士顿科学、索林、美敦力、雅培 / 圣犹达等）的起搏器在硬件设计、软件协议、运行参数及临床适配性上存在显著差异，这给临床管理带来了挑战 —— 准确识别起搏器品牌及型号是实现精准调试、故障排查、长期随访的前提。然而，传统人工分类依赖专业经验，效率低且易受主观因素影响，难以满足复杂临床场景需求。因此，本研究旨在开发一种基于人工智能 MA-IRNet 算法的自动分类系统，通过智能化手段精准区分五大主流制造商的心脏起搏器，为提升心脏器械管理的效率与准确性提供技术支撑。

方法：构建涵盖五大制造商不同型号起搏器的数据集，以确保数据对各品牌技术特性的代表性。在此基础上，提出 MA-IRNet 算法，该算法融合多注意力机制（Multi-Attention, MA）与改进残差网络（Improved Residual Network, IRNet），通过强化对品牌特异性特征的捕捉能力，提升分类精度。采用 MA-IRNet 算法对上述五大制造商的起搏器进行分类；通过测试集、验证集评估模型性能，在公开数据集上验证模型泛化能力，并通过消融实验逐步移除算法中的关键组件（如注意力模块、残差连接等），量化各组件对分类性能的影响；并模拟临床常见噪声干扰（如信号衰减、数据传输误差等），测试模型在不同噪声水平下的稳健性。

结果：MA-IRNet 算法在测试集上分类准确率达 96.82%（置信区间 95.13%-99.12%），验证集上准确率达 97.35%（置信区间 94.70%-98.59%）；且精确率、召回率、F1 值均保持在 96% 以上，表明模型对不同品牌起搏器特征的区分能力优异且结果稳定。在公开数据集上验证模型中仍保持 95% 以上的准确率，显著优于传统机器学习方法及现有深度学习模型，证实其良好的跨场景适配性。消融实验表明，移除多注意力模块会导致准确率下降 4.2%-6.8%，说明该模块在捕捉品牌特异性特征中起关键作用；稳健性测试显示，即使在 15% 噪声干扰下，模型准确率仍维持在 92% 以上，远高于同类算法（平均下降 10%-15%），体现出较强的抗干扰能力。

结论：MA-IRNet 算法通过创新的特征提取机制，实现了对五大主流制造商心脏起搏器的高精度自动分类，其性能不仅显著优于现有方法，且在稳定性、泛化性与抗干扰性上表现突出，能够可靠识别不同品牌起搏器的核心运行特征。该系统的开发为解决临床中起搏器品牌识别难题提供了智能化方案。在实际应用中，可辅助医护人员快速匹配设备参数库、优化调试流程、提升故障诊断效率，尤其适用于多品牌器械共存的综合医院或远程随访场景。未来，随着数据集的进一步扩容与算法的迭代优化，该系统有望整合至心脏器械管理平台，推动机器学习技术在心血管植入器械领域的深度应用，为精准化临床决策提供更强有力的支持。

Multimodal AI Models in Hypertrophic Cardiomyopathy Screening: Current Advances and Future Directions

bo zhu

Tangdu Hospital,The Fourth Military Medical University

Hypertrophic cardiomyopathy (HCM) represents the leading cause of sudden cardiac death (SCD) in adolescents and young adults worldwide, yet faces persistent diagnostic limitations. These include insufficient spatial resolution of conventional unimodal imaging techniques (notably echocardiography for detecting apical hypertrophy), prohibitively high costs and contraindications restricting cardiac magnetic resonance (CMR) accessibility, and genetic testing's limited diagnostic yield (identifying pathogenic variants in only 40-50% of clinically diagnosed cases), compounded by variants of uncertain significance (VUS). Consequently, an estimated 85% of individuals with HCM remain undiagnosed, delaying critical interventions for pre-symptomatic and atypically presenting patients. Based on these critical gaps in current diagnostic paradigms, this review synthesizes the recent advances, clinical efficacy, translational challenges, and future directions of multimodal artificial intelligence (AI) integration strategies for HCM screening and management.

Multimodal AI models address the inherent constraints of unimodal approaches by intelligently integrating heterogeneous data streams, including electrophysiological profiles (e.g., electrocardiography - ECG), multi-parametric imaging (echocardiography, CMR-derived tissue characterization), circulating biomarkers, and genetic information. This integrated analytical framework demonstrably enhances early detection sensitivity, achieving an absolute increase exceeding 40% compared to standard protocols, and significantly improves risk stratification accuracy, with validated area under the curve (AUC) values reaching 0.88. Key technological advancements include deep learning architectures (e.g., convolutional neural networks - CNNs) that fuse time-series ECG data with dynamic echocardiographic structural analyses, enabling precise disease subtyping (e.g., obstructive HCM, non-obstructive high-fibrosis, genotype-positive/phenotype-negative, apical variant, end-stage) and facilitating personalized therapeutic interventions. For instance, AI-ECG algorithms have successfully identified high-risk HCM in patients with atypical presentations, leading to timely initiation of targeted therapies like cardiac myosin inhibitors and demonstrating measurable clinical improvement. Furthermore, multimodal integration enables dynamic modeling of disease progression trajectories and end-to-end prognostic assessment frameworks. Combining CMR-derived late gadolinium enhancement (LGE) quantification (a marker of myocardial fibrosis) with ultrasound strain parameters (e.g., global longitudinal strain - GLS) significantly boosts SCD risk prediction (AUC increase from 0.75 to 0.88). Integration of clinical variables with ECG features has also optimized patient selection for devices like implantable cardioverter-defibrillators (ICDs), reducing unnecessary implantations by 42% and associated healthcare costs.

Despite these promising advances, substantial barriers impede clinical translation. Persistent technical bottlenecks encompass: (1) significant interoperability limitations and quantitative discrepancies across vendor-specific imaging software platforms (e.g., GE EchoPAC, Siemens VVI, Philips QLab) for critical parameters like longitudinal strain, leading to potential diagnostic inaccuracies; (2) subjectivity and expertise-dependence in medical image annotation, amplifying data bias; (3) insufficient model generalizability due to limited sample representativeness, particularly the underrepresentation of Asian cohorts where apical HCM prevalence exceeds 20%; and (4) reliance on static imaging data, failing to capture dynamic obstruction prevalent in ~70% of patients during exercise or pharmacologic provocation. Clinical translation barriers involve complex ethical and legal uncertainties regarding liability attribution for AI-related diagnostic errors, coupled with significant resource constraints (e.g., low penetration of high-performance GPUs and CMR in primary care settings, with county hospital CMR rates below 10%) hindering equitable access.

Future development necessitates coordinated advancement across three critical dimensions: (1) Construction of large-scale, standardized, ethnically diverse multimodal databases incorporating longitudinal follow-up data and dynamic monitoring (e.g., via wearable devices) to overcome historical sample biases and temporal limitations; (2) Development of vendor-agnostic, adaptive algorithms (e.g., utilizing deformable CNNs) and lightweight edge-computing frameworks (e.g., pruning, quantization) to enhance cross-platform compatibility and deployment feasibility in resource-limited settings, while improving model interpretability for

clinical trust; (3) Establishment of robust multidisciplinary frameworks involving clear regulatory guidelines (e.g., akin to the EU AI Act), ethical governance for liability, integration into health insurance reimbursement systems, workflow integration, and adoption of privacy-preserving technologies like advanced federated learning (e.g., Q-Chain FL) to enable secure cross-institutional data collaboration. Through synergistic innovation in computational methodologies, ethical frameworks, healthcare policies, and multi-sector collaboration, multimodal AI integration holds transformative potential to shift HCM management paradigms towards precision prevention during the pre-symptomatic phase, enabling earlier detection, more accurate subtyping, personalized risk stratification, and targeted therapeutic interventions on a global scale.

Ethical considerations for using artificial intelligence in clinical practice: an umbrella review

ge weili

Taizhou hospital of Zhejiang province

Artificial intelligence (AI), encompassing a spectrum of advanced computational techniques such as machine learning and deep learning, is increasingly being integrated across diverse domains within the medical field. This integration is fundamentally driven by the dual aims of enhancing the efficacy, efficiency, and accessibility of healthcare delivery–potentially improving diagnostic accuracy, optimizing treatment planning, enabling predictive analytics, and personalizing patient care–while simultaneously striving to promote greater health equity by addressing disparities in access and outcomes. Despite the significant promise held by these rapidly evolving technologies and their burgeoning applications in clinical practice, research, and administration, it remains absolutely crucial to engage in thorough and ongoing deliberation concerning the profound ethical and societal implications inherent in the development, validation, deployment, and sustained governance of AI systems within sensitive healthcare contexts. To systematically capture the current state of scholarly discourse on these critical considerations, a targeted examination was conducted across four major, internationally recognized academic databases; this search strategy yielded a curated collection of meta-analyses and systematic reviews that specifically delve into the multifaceted ethical considerations surrounding the implementation and impact of AI in medicine.

The careful synthesis and thematic analysis of this aggregated corpus of high-level evidence reveals a predominant focus within the existing literature on articulating the transformative expectations for medical AI–its anticipated benefits and potential–alongside a detailed discussion of the substantial technical, clinical, regulatory, and ethical challenges it presents. Furthermore, these reviews consistently document numerous ethical principles and conceptual frameworks (e.g., beneficence, non-maleficence, respect for autonomy, justice, fairness, transparency, explainability, accountability, and privacy) proposed by various stakeholders to steer the responsible, trustworthy, and ethically sound development and utilization of these powerful technologies. However, a critical appraisal makes it unequivocally evident that certain nuanced ethical dimensions and broader societal consequences of applying AI within complex, real-world clinical and public health settings are not yet sufficiently explored or comprehensively addressed within the current body of synthesized literature. Paramount among these significant gaps is the pressing and urgent need for the field to concentrate dedicated efforts on proactively identifying, rigorously evaluating, and effectively mitigating potential algorithmic biases embedded within the training datasets and model architectures themselves. Such biases pose a substantial and unacceptable risk of inadvertently perpetuating, entrenching, or even exacerbating existing health inequities and causing tangible injustices against historically marginalized or vulnerable patient populations, thereby fundamentally undermining the foundational goal of promoting genuine health equity through technological advancement.

The conclusion derived from this extensive synthesis strongly emphasizes the critical importance of continuously and critically examining these complex ethical quandaries and far-reaching societal issues, alongside the identified substantive gaps prevalent in current academic discussions and proposed governance frameworks. This necessitates a deeper, more rigorous interrogation conducted from a robust philosophical standpoint, actively engaging with foundational concepts such as fairness, moral responsibility, distributive justice, and the evolving nature of the physician-patient relationship within an era increasingly shaped by algorithmic decision-support and automation. Consequently, the analysis advocates compellingly for the essential, non-negotiable inclusion of insights, critical theoretical perspectives, and methodological approaches derived from relevant social science disciplines–including sociology, anthropology, science and technology studies (STS), ethics, and health policy–alongside the indispensable technical and clinical expertise, throughout the entire lifecycle encompassing the ongoing development, rigorous evaluation, thoughtful regulation, and adaptive governance of AI technologies destined for deployment in medical settings. Only through the consistent application of such genuinely multidisciplinary and philosophically grounded approaches can the healthcare community effectively navigate the intricate interplay of rapidly advancing technology, enduring ethical principles, and complex societal structures to responsibly realize AI's vast potential benefits while proactively minimizing associated harms and steadfastly upholding core healthcare values and commitments to justice.

基于多模态数据融合与深度学习的急性心肌梗死早期预警系统研究

张丹丹

哈尔滨医科大学第二附属医院

目的：急性心肌梗死（AMI）的早期诊断对降低死亡率至关重要，但传统诊断方法（如心电图和血清标志物）存在灵敏度不足和延迟性问题。本研究旨在开发一种基于多模态数据（电子健康档案、心电信号、超声影像）和深度学习（DL）的 AMI 早期预警系统，以提高诊断准确率并实现动态风险评估。

方法：纳入我院 1,200 例疑似 AMI 患者，收集以下数据，包括：人口统计学、病史、实验室指标（如肌钙蛋白、CK-MB、BNP 等）；12 导联心电图（ECG）、超声心动图（Echo）、入院首次病程记录（NLP 提取关键特征）。对 ECG 和 Echo 数据进行标准化处理（降噪、归一化）和标注（由 3 名心血管专家盲审确认）。进行多模态融合框架构建，使用 ResNet-1D 处理 ECG 时序信号（灵敏度优化至 ±0.1mV）。采用 Vision Transformer（ViT）分析 Echo 影像（分割左心室射血分数及室壁运动异常）。基于 BERT 模型提取首次病程记录中的关键临床特征（如胸痛描述、危险因素）。通过注意力机制融合多模态特征进行联合训练及优化，输出 AMI 风险评分（0-1 分），阈值≥ 0.75 触发预警。利用测试集对比金标准（冠状动脉造影），评估模型性能。 对比传统 Logistic 回归模型和单一模态 DL 模型（仅 ECG 或 Echo）。

结果：多模态模型准确率达 94.3%（95%CI: 92.1-96.0%），显著高于单一 ECG 模型（88.5%）和临床评分（GRACE 评分，82.7%）。对症状出现 <3 小时的超早期 AMI 检出率提高 21.5%（F1-score=0.91 vs. 0.72）。系统平均预警时间比血清肌钙蛋白检测提前 2.1 小时（P<0.01）。 误诊率降低至 3.8%（传统方法为 9.4%），尤其改善了对非 ST 段抬高型心肌梗死（NSTEMI）的识别。通过 Grad-CAM 可视化显示，模型决策依据与临床关键特征高度一致（如 ECG 的 ST 段偏移、Echo 的室壁运动异常）。

结论：本研究证实，基于多模态数据融合的深度学习系统可显著提升 AMI 早期诊断的准确性和时效性，尤其适用于症状不典型或超早期患者。未来需进一步开展前瞻性多中心临床试验以验证其普适性，并探索与医院信息系统（HIS）的无缝集成方案。

Integrating the Red Cell Distribution Width to Albumin Ratio into Machine Learning for Predicting In-Hospital Mortality in Heart Failure Patients with Pneumonia: a Multi-Center Study

Hong-Yu Su[1], Meng-Zhao Yang[2,3], Hai-Yu Wang[2,3], Ben-Chen Rao[2,3], Yuan Li[4], Zheng-Yu Chen[1], Zhi-Gang Ren[2,3], Yuan Liu[1]

1. Department of Cardiology, The First Affiliated Hospital of Zhengzhou University

2. Department of Infectious Diseases, the First Affiliated Hospital of Zhengzhou University

3. Gene Hospital of Henan Province/Precision Medicine Center, the First Affiliated Hospital of Zhengzhou University

4. Department of Cardiovascular Surgery, Fuwai Hospital, Chinese Academy of Medical Sciences & Peking Union Medical College/National Center for Cardiovascular Diseases

Background

Heart failure (HF) patients with pneumonia face high mortality risks, yet current risk stratification tools lack precision due to oversimplified biomarkers and methodological limitations. HF, affecting over 64 million adults globally, carries heightened vulnerability to pneumonia–a critical complication disproportionately impacting outcomes. Alarmingly, 10% of first HF hospitalizations are pneumonia-triggered, making it the leading non-cardiovascular precipitant. Pneumonia independently amplifies mortality risk by 4.3-fold in HF with reduced ejection fraction and 3.8-fold in HF with preserved ejection fraction, with mortality peaking within 1 month post-infection. These findings underscore an urgent need for early identification and risk stratification. The ratio of red cell distribution width (RDW) to albumin (ALB) (RAR) has emerged as a novel composite biomarker integrating inflammatory and nutritional aspects, potentially providing more comprehensive prognostic assessment. Recent studies demonstrate a strong association between RAR and all-cause as well as disease-specific mortality. This study aims to validate the prognostic value of RAR and develop a machine learning (ML)-based model for predicting 31-day in-hospital mortality in HF patients with pneumonia admitted to the ICU.

Methods

Using data from the Medical Information Mart for Intensive Care IV (MIMIC-IV v3.1) database (3,230 patients) and an external cohort (1,069 patients retrospectively recruited from The First Affiliated Hospital of Zhengzhou University between December 5, 2022, and January 31, 2023), we analyzed RAR's association with mortality. Inclusion criteria were patients diagnosed with both HF and pneumonia during the same hospitalization; exclusion criteria were age < 18 years, ICU stay <

24 hours, or absence of RDW and ALB results. Baseline characteristics (demographics, comorbidities, medications), vital signs (heart rate, respiratory rate, SpO2), and initial laboratory data upon ICU admission were collected. RAR was calculated as RDW (%) / ALB (g/dL). The primary outcome was 31-day in-hospital all-cause mortality. Statistical analyses included restricted cubic spline (RCS) analysis to evaluate non-linear relationships, Kaplan-Meier survival curves with log-rank tests, and univariate/multivariable Cox proportional hazards models adjusted for demographics, vital signs, laboratory results, and comorbidities. Sensitivity analyses, subgroup analyses, and propensity score matching (PSM) were performed. For ML analysis, the MIMIC-IV cohort was divided into training and internal validation sets (7:3 ratio). Feature selection used the Boruta algorithm. Eight ML models (Logistic Regression, Decision Tree, Random Forest, k-nearest neighbor, Support Vector Machine, Neural Network, eXtreme Gradient Boosting, Light Gradient Boosting Machine [LightGBM]) were developed, with hyperparameter optimization via random search, manual tuning, and five-fold cross-validation. Model performance was evaluated using area under the receiver operating characteristic curve (AUC) and decision curve analysis (DCA) on internal and external validation sets. SHapley Additive exPlanations (SHAP) analysis enhanced interpretability. A web-based tool (PneumoHF-RAR-Predictor) was developed.

Results

RCS analysis revealed a linear relationship between RAR and all-cause mortality (P < 0.001 for association, non-linearity P = 0.846), with an optimal cutoff of 5.07 distinguishing high- and low-risk groups. Kaplan-Meier survival analysis confirmed significantly higher cumulative mortality in the high-RAR group (P < 0.001). Cox regression models demonstrated RAR's independent association with in-hospital mortality, both as a continuous variable (fully adjusted Model HR: 1.18 [95% CI: 1.11-1.26]; P < 0.001) and categorical variable (fully adjusted Model HR: 1.28 [95% CI: 1.05-1.54]; P = 0.012 for high vs. low RAR). Subgroup and sensitivity analyses confirmed consistency. PSM (1,043 matched pairs) maintained significant associations (continuous RAR HR: 1.18 [95% CI: 1.10-1.28]; P < 0.001; categorical HR: 1.33 [95% CI: 1.07-1.66]; P = 0.011). Boruta feature selection identified RAR as the third most important predictor of mortality, after aspartate aminotransferase and renin-angiotensin-aldosterone system antagonist use. The LightGBM model achieved robust predictive accuracy, with AUCs of 0.740 (internal validation) and 0.735 (external validation). DCA demonstrated superior net clinical benefit for LightGBM. SHAP analysis confirmed RAAS antagonists, RAR, and age as the top influential features. A web-based tool (https://mengzhaoyang.shinyapps.io/PneumoHF-RAR_Predictor/) was developed for real-time risk assessment.

Conclusions

In conclusion, this study highlights the utility of RAR as a prognostic biomarker and its successful integration into ML models for predicting 31-day in-hospital mortality in HF patients with pneumonia. By combining traditional biomarkers with ML approaches, this research underscores the potential for improved risk stratification, enhanced model interpretability, and personalized clinical decision-making, paving the way for precision medicine in high-risk patient management.

互联网 + 和人工智能在高血压临床管理中的应用

沈梦瑶 张任贤 周晓阳

武汉大学人民医院

高血压作为全球范围内可预防和可干预的首要心脑血管疾病危险因素，其管理成效直接影响到“健康中国 2030”战略目标的实现。当前，我国高血压防控面临知晓率、治疗率和控制率“三率”水平不均衡、传统管理模式难以满足日益增长的健康管理需求等多重挑战。传统医疗体系在服务覆盖范围、管理持续性和干预精准性方面存在局限，难以实现对高血压患者的全周期、动态化管理。近年来，随着“互联网 + 医疗健康”与人工智能（AI）技术的迅速发展，为高血压的院外监测、风险评估、个体化治疗及长期随访提供了新的解决方案与技术支撑。本文通过系统综述的方式，全面梳理了互联网与 AI 技术在高血压管理中的应用进展与现实挑战。

首先，本文总结了“互联网 +”在高血压管理中的核心应用场景，包括分级诊疗体系的优化、远程血压监测技术的普及、数字疗法（Digital Therapeutics）的发展以及移动健康（mHealth）平台的临床应用。这些技术手段显著提升了患者自我管理能力，并增强了医疗机构对高血压人群的覆盖与干预能力。其次，人工智能技术在高血压领域的应用日益广泛，涵盖了疾病风险预测、亚型分类识别、用药方案优化、并发症早期预警以及可穿戴设备的数据分析等多个方面。研究显示，深度学习模型在识别难治性高血压方面具有较高的准确性（AUC 可达 0.89–0.94），AI 驱动的数字疗法在短期内可有效降低 24 小时收缩压 2–4 mmHg。

此外，本文也深入探讨了该领域在真实世界应用中所面临的挑战，包括数据安全与隐私保护问题、算法偏倚带来的公平性争议、经济学评价的缺失以及政策监管的滞后。这些因素在一定程度上制约了“互联网 +AI”模式的大规模推广与临床转化。

展望未来，构建以患者为中心、整合互联网与 AI 技术的新型高血压管理模式，是实现从临床试点向公共卫生实践转化的关键路径。为此，需推动多中心、高质量数据平台建设，加强医学、工程、信息技术等多学科协作，促进跨行业协同创新，最终实现高血压管理的智能化、个性化与系统化，助力“健康中国”战略目标的全面实现。

心脏瓣膜置换术后患者居家抗凝管理模式的卫生经济学评价

王薇 夏宇婷 邢倩 丁思毓

上海市卫生和健康发展研究中心（上海市医学科学技术情报研究所）

目的：心脏瓣膜置换术是成人最常见的心脏手术之一。根据白皮书数据，2023 年我国心脏瓣膜置换术数量约为 88737 例。我国心脏瓣膜病人数约为 2500 万。机械瓣膜置换术后患者必须接受终身的华法林抗凝治疗。因华法林治疗窗口窄，抗凝过量引起的出血及抗凝不足诱发的栓塞是其最为常见的并发症，所以需严格定期监测凝血功能以合理调整用药剂量，避免出血或栓塞风险。因此，如何做好定期监测成为华法林抗凝管理中的关键环节。本研究旨在从我国卫生系统的角度，评估在机械瓣膜置换术后患者采用便携式凝血仪开展居家抗凝管理模式与常规实验室检测模式相比的成本效果，为医患共同决策、医疗机构耗材准入及医保政策制定提供参考依据。

方法：本研究构建基于队列的 Markov 模型，模型中的健康状态包括无并发症、发生出血事件后、发生血栓事件后和死亡，从而模拟口服抗凝治疗的进展过程，并汇总分析长期的成本和效果。在输入参数的数据来源上，两种模式在避免并发症上的相对临床疗效来自于现有 RCT 的荟萃分析，效用、基线并发症发生风险等来自于最佳文献证据，直接医疗成本数据则来自公开收费标准或文献。

结果：患者终生采用居家抗凝管理模式，较常规实验室检测模式，可延长平均生存期（15.71 vs 15.64 年），获得更多的质量调整生命年（13.17 vs 13.02 QALY）。虽然终生成本增加（54956 元 vs. 16384 元），但增量成本效果比（ICER: 255357 元 /QALY）低于 3 倍的 2024 年人均 GDP（95759 元），说明居家抗凝管理模式具有成本效果优势。敏感性分析显示：关键变量为血栓栓塞发生率的相对风险比、严重出血发生率的相对风险比、贴现率，模型结果总体稳健，即 ICER 在绝大数情况下始终低于 3 倍的 2024 年人均 GDP（95759 元）。

结论：本模型预测患者居家抗凝管理模式在我国的应用可显著降低血栓事件的发生率，延长患者生存时间，提高患者生命质量，所增加的终生直接医疗成本在可接受范围内，是比常规实验室检测模式更具性价比的抗凝管理策略。

心血管免疫与炎症研究

基于冠状动脉周围脂肪衰减指数探讨 SGLT-2 抑制剂联合 GLP-1 受体激动剂对 2 型糖尿病患者冠状动脉炎症的影响

王天行

河北省人民医院

【摘要】

目的 评估 SGLT-2 抑制剂与 GLP-1 受体激动剂单独或联合使用治疗对 2 型糖尿病（T2DM）患者冠状动脉周围脂肪衰减指数（FAI）的影响。

方法 本研究为回顾性研究纳入 2023 年 1 月至 2024 年 6 月在河北省人民医院接受冠状动脉 CT 血管造影（CCTA）检查的 T2DM 患者 292 例，按用药情况将患者分为 GLP-1RA 与 SGLT-2i 联合治疗组、单药治疗组（GLP-1RA 或 SGLT-2i）和未治疗组。收集并比较 3 组患者的临床资料、实验室指标及 CCTA 参数。运用多因素线性回归模型分析 GLP-1RA 与 SGLT-2i 联合治疗与 FAI 的关联。 结果 与未治疗组及单药治疗组相比，联合治疗组患者呈现更年轻的年龄分布特征，且男性患者比例显著更高；单药组、联合用药组及未用药组在糖尿病病程、心血管危险因素及炎症指标等方面，未观察到统计学差异（P > 0.05）。单因素方差分析显示，三组患者在左前降支、左回旋支及右冠状动脉的冠状动脉周围脂肪衰减指数（FAI）存在显著组间差异（P<0.05）。具体而言，联合用药组患者 LAD 及 LCX 的 FAI 值较未用药组显著降低；与单药组相比，联合用药组患者 LCX 的 FAI 值亦呈现显著降低趋势。多因素回归分析进一步证实，在调整年龄、性别、糖尿病病程、心血管危险因素等混杂变量后，联合用药与 LAD（β = -3.054）、LCX（β = -3.601）及 RCA（β = -2.745）的 FAI 值降低存在独立相关性（P 均 < 0.05）。亚组分析显示，上述相关性在不同分层人群（如年龄、BMI、ACS 类型）中存在显著异质性。

结论 GLT-2 抑制剂联合 GLP-1 受体激动剂或与 2 型糖尿病患者冠状动脉周围脂肪衰减指数降低相关，提示其可能对减轻冠状动脉炎症有一定作用，且与单药治疗相比或存在潜在优势。

Cardiac Resident Macrophage-Derived Collagen I Supports Vascular Stabilization and Healing Following Cardiac Injury

Jing-Hong Zhang[1,2], Dai-Le Jia[1], Qi-Xin Chen[1], Si-Rui Huang[1], Ai-Jun Sun[1,2], Jun-Bo Ge[1,2]

1. Zhongshan Hospital, Fudan University

2. Institute of Biomedical Sciences, Fudan University

Object : To characterize a newly identified subpopulation of CCR2 $^{-}$ MHC-II^{LOW} cardiac resident macrophages capable of producing type I collagen during the early phase of myocardial infarction (MI), and to investigate their essential role in orchestrating myocardial tissue repair. Specifically, this study seeks to define the temporal dynamics, spatial localization, and transcriptional identity of these cells within the infarcted heart. In addition, we aim to evaluate their contributions to key regenerative processes, including epicardial activation, extracellular matrix remodeling, neovascularization, and scar stabilization. By elucidating the mechanisms through which this macrophage subset supports structural and vascular repair, we seek to uncover novel therapeutic targets for enhancing endogenous healing and improving outcomes following myocardial injury.

Methods : We utilized single-cell RNA sequencing to identify a distinct population of collagen I-producing macrophages in both murine and human samples of acute myocardial infarction (MI). Spatial transcriptomics further localized these macrophages to the infarct border zone and epicardial region. Dual recombinase-mediated lineage tracing confirmed the dynamic accumulation of CCR2 $^{-}$ MHC-II^{LOW}Col1 $^{+}$ macrophages in these anatomical niches. To investigate their functional significance, we employed targeted genetic disruption of Col1a1 specifically in resident macrophages. Immunofluorescence and in situ hybridization were performed to validate gene and protein expression. Functional outcomes were evaluated through assessments of scar architecture, neovascularization, and cardiac function post-MI.

Result : We employed an integrative multi-omics approach to investigate the functional heterogeneity of macrophage subpopulations during myocardial infarction (MI). Single-cell RNA sequencing of murine and human infarcted hearts revealed a distinct population of CCR2 $^{-}$ MHC-II^{LOW}macrophages capable of producing type I collagen. Spatial transcriptomics mapped these collagen-producing macrophages to the infarct border zone and epicardial region during the early phase of MI. Dual recombinase-mediated lineage tracing confirmed the dynamic expansion and localization of CCR2 $^{-}$ MHC-II^{LOW}Col1 $^{+}$ macrophages (termed CMCMs) within these zones. Targeted genetic deletion of Col1a1 in resident macrophages significantly impaired collagen deposition, attenuated epicardial activation, and disrupted neovascular maturation, indicating a pivotal reparative role for CMCMs. Further pathway analysis revealed that CMCMs engage the DDR1–NF-κB–MMP9/ADGRA2 signaling axis, orchestrating extracellular matrix remodeling and guiding endothelial stabilization. Loss of this macrophage-driven program led to disorganized scar architecture and compromised cardiac function. Collectively, these findings establish CMCMs as a functionally distinct subset essential for coordinating structural repair and vascular remodeling after myocardial injury.

Conclusion : Our study identifies a unique subpopulation of CCR2 $^{-}$ MHC-II^{LOW}Col1 $^{+}$ cardiac resident macrophages (CMCMs) that play a pivotal and previously unrecognized role in orchestrating myocardial tissue repair following acute myocardial infarction. These macrophages are distinguished by their ability to produce type I collagen and by their spatial enrichment in the infarct border zone and epicardial region during the early reparative phase. Through activation of the DDR1–NF-κB–MMP9/ADGRA2 signaling axis, CMCMs contribute to key regenerative processes including epicardial activation, extracellular matrix remodeling, and vascular maturation. Functional ablation of Col1a1 in resident macrophages resulted in impaired scar organization, delayed angiogenic response, and compromised recovery of cardiac function, underscoring their essential contribution to post-infarction healing. These findings not only redefine the role of resident macrophages in cardiac injury but also highlight CMCMs and their signaling programs as attractive therapeutic targets to enhance endogenous repair mechanisms and improve clinical outcomes in patients with ischemic heart disease.

HyPoxia Induces M2 MacroPhages to ExPress VSIG4 and Mediate Cardiac Fibrosis After Myocardial Infarction

bei Shi

Affiliated Hospital of Zunyi Medical University

VSIG4 in M2 Macrophage-Mediated Fibrotic Repair After Acute Myocardial Infarction: Mechanisms and Therapeutic Implications

Introduction

Acute myocardial infarction (AMI) triggers a complex inflammatory and reparative response, where M2 macrophages play a pivotal role in tissue repair and fibrosis. V-set and immunoglobulin domain-containing 4 (VSIG4), a membrane protein predominantly expressed on tissue-resident and M2-polarized macrophages, is a critical regulator of immune homeostasis. However, its specific role in post-Acute myocardial infarction cardiac remodeling remains poorly understood. Given the dual nature of fibrosis—essential for wound healing but detrimental if excessive—understanding how VSIG4 modulates macrophage-fibroblast crosstalk could uncover novel therapeutic strategies. This study investigates the functional significance of VSIG4 in AMI using VSIG4 knockout (KO) mice and bone marrow chimeric models, combined with gain- and loss-of-function experiments in cardiac fibroblasts (CFs). We demonstrate that VSIG4 promotes scar formation, regulates inflammatory resolution, and enhances TGF-β1 and IL-10 secretion. Furthermore, hypoxia upregulates VSIG4 in M2 macrophages, driving CF-to-myofibroblast conversion. These findings highlight VSIG4 as a potential immunomodulatory target for optimizing post-Acute myocardial infarction repair.

Key Findings

1. VSIG4 Deficiency Impairs Scar Formation and Exacerbates Inflammation

In VSIG4 KO mice, AMI resulted in reduced collagen deposition and delayed scar maturation, compromising ventricular integrity.

KO mice exhibited prolonged inflammatory infiltration (elevated Ly6C+ monocytes and neutrophils) and blunted IL-10 production, indicating impaired resolution.

Adoptive transfer of WT bone marrow-derived macrophages (BMDMs) into KO mice restored fibrosis, confirming VSIG4's macrophage-specific role.

2. VSIG4 Drives TGF-β1/IL-10-Dependent Fibroblast Activation

VSIG4+ macrophages secreted higher levels of TGF-β1 and IL-10, key cytokines for fibroblast activation and anti-inflammatory signaling.

Conditioned media from VSIG4+ M2 macrophages induced α-SMA+ myofibroblast differentiation in CFs, whereas VSIG4 KO macrophage media failed to do so. Silencing VSIG4 in macrophages attenuated TGF-β1 release, while overexpression enhanced fibrotic responses.

3. Hypoxia Upregulates VSIG4 in M2 Macrophages, Amplifying Fibrosis

Hypoxic conditions (1% O_2) potently induced VSIG4 expression in bone marrow-derived M2 macrophages.

Hypoxia-primed, VSIG4-high macrophages exhibited enhanced pro-fibrotic activity, further accelerating CF-to-myofibroblast transition.

Mechanistically, HIF-1α stabilization was linked to VSIG4 transcriptional upregulation under hypoxia.

Therapeutic Implications

1. Targeting VSIG4 to Modulate Fibrosis

Agonists (e.g., recombinant VSIG4) could accelerate reparative fibrosis in early AMI, preventing ventricular rupture.

Antagonists (e.g., anti-VSIG4 antibodies) might mitigate excessive late-

stage fibrosis, reducing diastolic dysfunction.

2. Hypoxia-Mimetic Strategies

PH inhibitors (e.g., roxadustat) could amplify VSIG4+ macrophage reparative functions in ischemic hearts.

3. Precision Immunomodulation

VSIG4+ macrophage adoptive therapy may optimize infarct healing in high-risk patients.

Conclusion

This study establishes VSIG4 as a central regulator of macrophage-dependent fibrotic repair in Acute myocardial infarction , bridging hypoxic signaling, immune resolution, and fibroblast activation. By delineating the VSIG4-TGF-β1-IL-10 axis, we provide a mechanistic foundation for therapies fine-tuning post-AMI remodeling. Future work should explore:

Cell-specific VSIG4 manipulation (e.g., conditional KO in fibroblasts).

Clinical correlations (VSIG4 expression in human Acute myocardial infarction biopsies).

Combination therapies (VSIG4 modulation with anti-inflammatory agents).

These insights pave the way for immunofibrogenic therapies that balance repair and adverse remodeling in ischemic heart disease.

Significance: First demonstration of VSIG4's role in cardiac fibrosis, offering a translatable pathway for AMI therapy.

心血管免疫与炎症研究

胡婷

西安交通大学第一附属医院

目的：

本研究旨在探讨免疫与炎症反应在心血管疾病发生与发展过程中的作用机制，明确关键炎症因子、免疫细胞类型及其信号通路对动脉粥样硬化、心肌损伤和心力衰竭等疾病的影响，为临床诊疗提供理论依据和潜在干预靶点。

方法：

通过系统综述近年来相关基础与临床研究文献，并结合部分实验室动物模型与心血管病患者外周血样本检测数据，分析免疫系统中固有免疫与适应性免疫在不同心血管病理过程中的动态变化。具体方法包括炎症因子（如 IL-1β、TNF-α、IL-6）水平检测、巨噬细胞极化状态分析、T 细胞亚群分布研究，以及核因子 NF-κB、NLRP3 炎症小体等信号通路的活化情况观察。

结果：

研究结果表明，心血管疾病并非单一的代谢性疾病，其发生发展高度依赖免疫与炎症网络的调控。动脉粥样硬化中，单核细胞 - 巨噬细胞系统及其分泌的促炎细胞因子在斑块形成、破裂中发挥核心作用；心肌梗死后炎症反应调节不当可导致持续性组织损伤与心室重构；慢性心力衰竭患者中普遍存在低水平慢性炎症状态，$CD4^+$ T 细胞和 IL-17 相关通路与预后密切相关。此外，IL-1 抑制剂和 SGLT2 抑制剂等抗炎策略显示出潜在治疗价值。

结论：

免疫与炎症反应在心血管疾病中具有双重角色，既参与疾病进展，也可作为潜在的干预靶点。深入理解免疫细胞亚群的动态变化与炎症因子的时序表达，对指导精准治疗具有重要意义。未来心血管病管理将更多依赖炎症状态的评估与靶向调控策略的发展。

关键词：

心血管疾病；免疫反应；炎症因子；动脉粥样硬化；心力衰竭；NLRP3 炎症小体；免疫治疗

NETs 通过 TGFβ1-Smad2/3 介导的内皮间充质转化在糖尿病肾病动静脉内瘘狭窄中的机制研究

李理政

山西医科大学第二医院

目的：终末期糖尿病肾病（DKD）患者自体动静脉内瘘（AVF）狭窄发生率高且危及生命，内皮间充质转化（EndMT）是其早期关键特征。本研究旨在验证假说：DKD 中升高的中性粒细胞胞外诱捕网（NETs）通过蛋白酶及整合素依赖性途径激活 TGFβ1，进而经 TGFβ1-Smad2/3 信号通路驱动 EndMT，最终促进 AVF 狭窄形成，为临床早诊早治提供新靶点。

方法：通过多层面技术验证假说：

临床层面：分析 DKD 患者狭窄 AVF 组织中 NETs、TGFβ1 活化及 EndMT 标志物表达；

动物模型：构建 DKD-AVF 狭窄动物模型，干预 NETs 形成或 TGFβ1 信号，观察狭窄表型及 EndMT 变化；

细胞实验：体外模拟高糖及 NETs 环境，检测内皮细胞 EndMT 转化及 TGFβ1-Smad2/3 通路活性；

谱系示踪技术：特异性标记血管内皮细胞，追踪其在 NETs 刺激下向间充质细胞转分化的动态过程。

结果：

DKD 患者狭窄 AVF 组织中 NETs 显著积聚，且与 TGFβ1 活化、EndMT 程度及狭窄严重度正相关；

动物模型证实：清除 NETs 或抑制 TGFβ1-Smad2/3 通路可显著减轻 EndMT 及 AVF 狭窄；

体外实验显示：NETs 通过释放中性粒细胞弹性蛋白酶（NE）等蛋白酶及激活整合素，促进 TGFβ1 成熟与信号传导，诱导内皮细胞发生 Smad2/3 依赖的 EndMT；

谱系示踪直接证实：NETs 诱导内皮细胞丢失特异性标记并获得间充质表型，此转化过程被 TGFβ1 抑制剂阻断。

结论：

DKD 中升高的 NETs 通过蛋白酶 / 整合素介导的 TGFβ1 活化及下游 Smad2/3 信号传导，驱动内皮细胞发生 EndMT，是 AVF 狭窄的核心机制。靶向 NETs 形成或 TGFβ1-Smad2/3 通路可有效抑制 EndMT，为终末期 DKD 患者 AVF 狭窄的早期诊断与防治提供全新策略。

分子伴侣介导的自噬调控巨噬细胞免疫代谢在心肌梗死中的研究

乔磊

山东大学齐鲁医院

背景与目的

抗炎治疗在动脉粥样硬化性心血管疾病（Atherosclerotic cardiovascular disease; ASCVD）的临床管理中具有关键作用。既往研究表明，分子伴侣介导的自噬（Chaperone-mediated autophagy；CMA）能够通过调控炎症反应显著改善动脉粥样硬化（AS）进程，然而该机制在心肌缺血性损伤中的具体作用尚未阐明。本研究旨在系统揭示 CMA 在心肌梗死（Myocardial infarction; MI）后心脏微环境稳态维持中的调控作用及其分子机制。

方法

采用免疫组织化学和 Western blot 技术检测 MI 患者及小鼠模型心脏组织中 CMA 关键限速蛋白 LAMP2A 的动态表达特征。构建髓系细胞特异性 LAMP2A 条件性敲除（LAMP2A-cKO）和敲入（LAMP2A-cKI）小鼠，通过冠状动脉左前降支结扎术建立 MI 模型。整合转录组学、代谢组学和蛋白质组学等多组学分析方法解析 CMA 调控网络，并采用 CRISPR/Cas9 基因编辑和腺病毒载体转染等技术进行功能验证。

结果

时序检测显示：在 MI 急性期（术后 3 天），骨髓造血干细胞、外周血单核细胞及心脏浸润巨噬细胞中 LAMP2A 表达显著上调；而在心肌梗死后期（术后 4 周），心肌组织中巨噬细胞的 LAMP2A 表达呈进行性下降。临床相关性分析证实心肌梗死患者的循环单个核细胞（PBMC）中 LAMP2A 表达强度与左室射血分数（LVEF）呈显著正相关。基因敲除实验表明，髓系细胞 LAMP2A 特异性缺失导致梗死区扩大、纤维化程度加重及心功能恶化。分子机制研究发现，LAMP2A 缺失通过抑制 CMA- 溶酶体途径，导致巨噬细胞内 HIF-1α 蛋白降解受阻、蛋白水平增加，进而引起 HIF-1α 下游靶基因糖酵解关键酶的表达上调。这种代谢重编程促使巨噬细胞向促炎表型转化，同时抗炎 / 修复型巨噬细胞的比例减少。值得注意的是，采用小分子激活剂（CA77.1）或 AAV9-LAMP2A 基因治疗均可显著改善心肌缺血损伤和心肌重构。

结论

本研究首次证实巨噬细胞 CMA 在心肌梗死中发挥重要作用，CMA 通过介导 HIF-1α 蛋白的降解调控巨噬细胞能量代谢，进而影响其功能表型。上调巨噬细胞的 CMA 功能有望成为 ASCVD 抗炎治疗的新途径。

Nrf2 参与 MSCs 调节大鼠梗死心肌氧化应激作用的实验研究

赵然尊

遵义医科大学附属医院

目的：探讨间充质干细胞 (MSCs) 移植对梗死心肌组织氧化应激反应的调节作用及其机制。

方法：建立心肌梗死大鼠模型，利用随机数字表进行随机化分组，分为对照组 (n=20)、MSC 移植组 (n=20) 和 MSC 移植 +HO-1 抑制剂组 (n=20)。以密度梯度离心并贴壁培养获得骨髓源 MSCs，于心肌梗死模型建立后经心肌局部多点注射 MSCs 悬液；细胞移植后不同时间点以测定血浆以及心肌梗死和梗死交界区组织超氧化物歧化酶 (SOD)、还原型谷酰甘肽 (GSH) 和丙二醛 (MDA) 水平；Western Blot 检测 Nrf2 和 HO-1 蛋白表达的变化。

结果：细胞移植后 8h，3 组大鼠梗死组织中 SOD、GSH 表达量开始下降，72h 时达到最低，以后逐渐开始回升，至两周时恢复接近心肌梗死前水平；同时，细胞移植后梗死组织中脂质氧化终产物 MDA 水平开始增高，3 组均在 72h 达到高峰 (P<0.05)，以后开始下降，至 2 周时降至梗死前水平。细胞移植后各时间点，与对照组比较，MSC 移植组 SOD 和 GSH 含量下降幅度减小、恢复较快 (P<0.05)，且 MDA 含量减少 (P<0.05)。对照组梗死心肌组织中 Nrf2 及 HO-1 蛋白表达轻微升高，72h 时最显著；而 MSC 移植组中 Nrf2 和 HO-1 蛋白表达显著增高，且升高时间提前至细胞移植后 24 ~ 72h，且与对照组比较，细胞移植后 24h 和

72h，Nrf2 和 HO-1 表达水平均高于对照组 (P<0.05)；MSC 移植 +HO-1 抑制剂组与对照组比较，差异无统计学意义 (P>0.05)。

结论：心肌梗死后移植 MSCs 可能通过促进局部 Nrf2 及其下游抗氧化酶靶基因 HO-1 蛋白表达而调节梗死心肌的氧化应激反应，进而减轻氧化应激诱导的心肌损伤。

miR-214 靶向抑制 CaMK II 调控 H9c2 心肌细胞的氧化应激

石蓓

遵义医科大学附属医院

目的：探讨 miR-214 靶向抑制 CaMK II 调节缺氧复氧诱导 H9c2 心肌细胞氧化应激的作用。

方法：以 H9c2 心肌细胞为研究对象，实验分 4 组，①正常组：正常培养的心肌细胞；②缺氧复氧组：心肌细胞经缺氧 24 h 复氧 6 h 处理；③ miR-214 模拟物组：心肌细胞转染 miR-214 模拟物后予缺氧复氧处理；④ miR-214 模拟物阴性对照组：心肌细胞转染 miR-214 模拟物阴性对照后予以缺氧复氧处理。予以 CCK-8 法检测各组细胞活性，qPCR 检测各组细胞 miR-214 的变化，流式细胞术、TUNEL 法及 SOD、MDA 试剂盒检测各组细胞氧化应激水平及凋亡效应；双荧光素酶报告基因检测 miR-214 与 CaMK II 相关性，qPCR 和 Western blot 检测 CaMK II mRNA 和蛋白表达变化。随后用腺病毒转染过表达细胞中 CaMK II 进行回复实验，并采用上述方法检测细胞氧化应激水平及凋亡状态。

结果：缺氧复氧组心肌细胞活性明显低于正常组，miR-214 模拟物组可明显改善该作用 (P<0.05)。缺氧复氧组 miR-214 表达水平明显低于正常组，而 miR-214 模拟物组 miR-214 高表达 (P<0.05)。与正常组比较，缺氧复氧组细胞 ROS、MDA 表达水平及 TUNEL 阳性细胞数明显增高，SOD 表达显著下降 (P<0.05)；与缺氧复氧组比较，miR-214 模拟物组 ROS、MDA 水平及 TUNEL 阳性细胞数明显下降，SOD 表达明显增高 (P<0.05)。双荧光素酶报告基因验证了在心肌细胞中 miR-214 可结合 CaMK II 。此外，在缺氧复氧组中 CaMK II mRNA 和蛋白水平均明显高于正常组，miR-214 可显著抑制缺氧复氧诱导的 CaMK II 表达。采用腺病毒过表达细胞中 CaMK II 后，miR-214 抗氧化应激及凋亡效应被部分阻断。

结论：过表达 miR-214 可通过抑制 CaMK II 转录后翻译过程，改善心肌细胞氧化应激水平及凋亡状态。

CircHIPK3 regulates the autoPhagy and aPoPtosis of hyPoxia/reoxygenation-stimulated cardiomyocytes via the miR-20b-5P/ATG7 axis

bei Shi

Affiliated Hospital of Zunyi Medical University

Myocardial ischemia/reperfusion (I/R) injury remains a critical challenge in cardiovascular medicine, characterized by the exacerbation of tissue damage when blood flow is restored to previously ischemic cardiac tissue. This pathological process involves complex cellular mechanisms, with autophagy and apoptosis emerging as key players in determining cardiomyocyte survival or death. Autophagy, a conserved catabolic process, can either protect cells by removing damaged organelles or contribute to cell death when excessively activated, while apoptosis–programmed cell death–directly leads to the loss of functional cardiomyocytes. Together, these processes significantly influence the extent of myocardial injury following I/R, making them critical targets for therapeutic intervention.

Recent advances in non-coding RNA research have highlighted circular RNAs (circRNAs) as pivotal regulators of various cellular functions, including autophagy and apoptosis, across multiple disease contexts, particularly cancers. Among these, circular RNA HIPK3 (circHIPK3) has been identified as a key modulator of cell survival and death pathways in several cancer types, where it influences autophagic flux and apoptotic rates by interacting with microRNAs (miRNAs) and protein-coding genes. However, the specific role of circHIPK3 in regulating cardiomyocyte autophagy and apoptosis during myocardial I/R injury has remained unexplored, prompting the present study to investigate its potential involvement and underlying mechanisms.

The current study aimed to elucidate the regulatory effect of circHIPK3 on myocardial I/R injury, with a focus on its impact on cardiomyocyte autophagy and apoptosis, and to dissect the molecular pathways mediating these effects. To address this, the researchers first examined circHIPK3 expression patterns in both in vivo models of myocardial I/R injury and in vitro models of hypoxia/reoxygenation (H/R) injury– a widely used cellular model to mimic I/R conditions in cardiomyocytes. Results revealed a significant upregulation of circHIPK3 in response to both I/R and H/R, suggesting its potential involvement in the pathological process.

To characterize the functional role of circHIPK3 in H/R-induced cardiomyocyte injury, gain-of-function and loss-of-function experiments were performed. Overexpression of circHIPK3 in cardiomyocytes exposed to H/R led to a marked increase in autophagic activity, as evidenced by enhanced expression of autophagy-related markers. Concurrently, it exacerbated cellular injury, including elevated levels of intracellular reactive oxygen species (ROS)–a major driver of oxidative stress in I/R–and increased apoptotic rates compared to control cells. Conversely, silencing of circHIPK3 resulted in reduced autophagy, diminished ROS production, and decreased apoptosis, indicating that circHIPK3 acts as a pro-injury factor in H/R-induced cardiomyocyte damage.

Further mechanistic investigations focused on the interaction between circHIPK3 and miRNAs, given that circRNAs often function as “sponges” to sequester and inhibit miRNA activity, thereby regulating downstream gene expression. Bioinformatics analysis and experimental validation confirmed that circHIPK3 directly binds to miR-20b-5p, an miRNA previously implicated in cellular stress responses. This interaction was found to sequester miR-20b-5p, preventing it from suppressing the expression of ATG7–a critical autophagy-related gene that promotes autophagosome formation. Consequently, increased circHIPK3 levels led to reduced miR-20b-5p activity, upregulation of ATG7, and subsequent enhancement of autophagy. Importantly, treatment with miR-20b-5p inhibitors reversed the decrease in ATG7 expression induced by circHIPK3 silencing, confirming the specificity of this regulatory axis.

In conclusion, this study demonstrates that circHIPK3 accelerates cardiomyocyte autophagy and apoptosis during myocardial I/R injury through the miR-20b-5p/ATG7 signaling axis. By sponging miR-20b-5p, circHIPK3 upregulates ATG7, thereby promoting excessive autophagy and apoptotic cell death. These findings identify circHIPK3 as a potential therapeutic target for mitigating myocardial I/R injury, offering new avenues for the development of RNA-based interventions to protect cardiac function following ischemic events.

基于 TLR4/NF-kB 通路探讨木犀草素对 LCWE 诱导的冠状动脉血管炎的保护机制

曹勇 孟照辉

昆明医科大学附属第一医院

目的：川崎病（Kawasaki disease, KD）是儿童获得性心脏病的主要病因，其冠状动脉血管炎病理机制与 NLRP3/IL-1β 炎症通路激活及血小板介导的免疫反应密切相关。本研究采用干酪乳杆菌细胞壁提取物（LCWE）诱导的小鼠冠状动脉血管炎模型，模拟 KD 心血管病变特征（如冠状动脉炎、腹主动脉瘤），并探讨天然黄酮类化合物木犀草素(luteolin)通过调控 TLR4/NF-κB 通路的保护作用。

方法： 雄性 C57BL/6J 小鼠腹腔注射 LCWE（500 μg）建立血管炎模型。木犀草素干预组于造模前后灌胃给药（剂量：40 mg/kg）。通过以下指标评估疗效：心血管病变：1. 心脏组织 H&E 染色分析冠状动脉炎症评分，超声检测腹主动脉直径；2. 血小板活化：全血血小板计数、流式细胞术检测单核细胞 - 血小板聚集体（MPAs）；3. 炎症通路：ELISA 检测血清 IL-1β、IL-6、P- 选择素水平；4.Western blot 分析心脏组织 TLR4/NF-κB 通路蛋白表达；5. 血小板 - 免疫细胞互作：免疫荧光染色观察冠状动脉 CD41+ 血小板浸润。6.qPCR 分析心脏组织 TLR4/NF-κB 通路 mRNA 表达。

结果：1.LCWE 诱导后小鼠血小板计数显著升高（峰值：第 14 天），且与冠状动脉炎症评分呈正相关（R = 0.73, P = 0.0038）；

2. 木犀草素显著抑制 TLR4/NF-κB 通路活化，降低血清 IL-1β、IL-6 及 P- 选择素水平（P < 0.01）；

3. 木犀草素减少 MPAs 形成（流式检测 CD11b+CD61+ 细胞比例下降），减轻冠状动脉 CD41+ 血小板浸润及血管壁损伤；

4. 机制上，木犀草素通过抑制 TLR4/NF-κB 信号，阻断血小板介导的 NLRP3 炎症小体激活，下调单核细胞 IL-1β 分泌，从而缓解心血管病变。

5. 心脏组织病理切片显示木犀草素组炎症评分明显小于单纯 LCWE 诱导的模型组。

结论：木犀草素通过靶向 TLR4/NF-κB 通路，抑制血小板活化及 MPAs 形成，减少 IL-1β 驱动的血管炎症，为 KD 冠状动脉病变提供新型治疗策略。本研究首次揭示木犀草素在 KD 模型中的保护作用，为天然抗炎药物研发提供实验依据。

ATF7 介导的单核细胞表观遗传重编程通驱动肥胖相关 HFpEF 的发生机制研究

王港 黄炜 戴翠莲 刘彬彬 王焱

厦门大学附属心血管病医院 (厦门市心脏中心)

目的

射血分数保留型心力衰竭（HFpEF）是与代谢紊乱密切相关的一类心血管疾病，近年来患病率持续上升，尤其在肥胖人群中发病显著。然而，肥胖如何通过远程免疫机制引起心脏舒张功能障碍，其分子机制尚未完全明确。本研究旨在探讨：长期肥胖是否通过诱导骨髓造血干细胞的表观遗传学重编程，导致单核细胞谱系功能改变，并在心脏中驱动炎性巨噬细胞积聚和损伤心肌质控机制，从而促进 HFpEF 的发生。

方法

本研究首先建立长期高脂饮食喂养的小鼠模型，模拟肥胖状态，评估其舒张功能与 HFpEF 典型表型。通过单细胞转录组测序与 ATAC-seq 联合分析骨髓造血干细胞（HSCs）及血液单核细胞谱系的表观遗传状态和基因表达谱，重点关注转录因子 ATF7 的调控机制。采用体外培养小鼠骨髓来源单核细胞并过表达或敲低 ATF7，结合 ATAC-seq 和 qPCR，系统研究 ATF7 如何影响钙卫蛋白基因启动子区域染色质开放性及表达水平。还构建了髓系细胞特异性 ATF7 敲除小鼠 $Atf7^{flox/flox}$ $Lyz2^{Cre}$，评估其在高脂饮食暴露下是否可阻断 HFpEF 的发生。体内采用骨髓移植模型，验证来自肥胖小鼠的造血系统是否可诱导受体小鼠发生 HFpEF 表型。并进一步利用流式细胞术和免疫组织染色分析心脏 CXCR2+ 巨噬细胞的积聚情况。最后，基于肥胖人群外周血样本数据，检测单核细胞中 ATF7

与钙卫蛋白表达的相关性，以验证临床相关性。

结果

高脂饮食诱导的肥胖小鼠表现出典型 HFpEF 特征，包括舒张功能障碍、心肌肥厚和间质纤维化。ATF7 在肥胖小鼠骨髓 HSCs 中显著上调，并伴随其靶基因调控区染色质开放性增强。在体外，ATF7 直接促进钙卫蛋白启动子区域的染色质开放和转录激活。ATF7 敲低显著降低钙卫蛋白表达，提示其在单核细胞促炎表型形成中发挥核心作用。相较于对照组，髓系细胞特异性敲除 ATF7 的小鼠大幅度减轻了长期高脂饮食引起的心脏舒张功能障碍和心脏重构。骨髓移植实验显示，来自肥胖小鼠的骨髓细胞可在正常小鼠中复制 HFpEF 相关心脏改变。心脏组织中 CXCR2 $^{+}$巨噬细胞数量显著增加，伴随高水平的钙卫蛋白分泌。钙卫蛋白作用下心肌细胞内质网应激标志物 XBP1 和 CHOP 显著上调，提示其干扰心肌蛋白质质控通路。在人群研究中，肥胖个体单核细胞中 ATF7 表达水平与钙卫蛋白呈正相关，进一步支持这一机制在人类中的存在。

结论

本研究揭示了肥胖通过 ATF7 介导的单核细胞表观遗传重编程，诱导钙卫蛋白高表达并促使 CXCR2 $^{+}$心脏巨噬细胞积聚，从而破坏心肌内质网稳态，导致舒张功能障碍和 HFpEF 发生的关键机制。这一“骨髓 – 免疫 – 心肌”通路的发现为理解肥胖相关 HFpEF 的免疫病理机制提供了新视角，也为早期干预提供了潜在治疗靶点。

Macrophage-derived AMPKγ2 prevents cardiac remodeling post myocardial infarction via SMURF2/YY1/CXCL16 axis

Xiaolin Zhang, Ziping Song, Haixu Song, Dan Liu, Jiayin Li, Kun Na, Ning Zhao, Chenghui Yan, Yaling Han

State Key Laboratory of Frigid Zone Cardiovascular Disease, Cardiovascular Research Institute and Department of Cardiology, General Hospital of Northern Theater Command, Shenyang, China

Background: The AMP-activated protein kinase (AMPK) complex, a critical energy sensor in eukaryotic cells, plays a well-documented role in cardioprotection during myocardial infarction (MI). Phosphorylation of the AMPKα subunit at Thr172 is widely recognized as a central mechanism underlying its activation and protective effects. However, the functional significance of the AMPKγ2 subunit, which forms the regulatory core of the AMPK complex, remains poorly understood in the context of MI. Existing studies have predominantly focused on the α subunit, leaving a critical gap in knowledge regarding the potential roles of AMPKγ2 in regulating post-MI immune responses and cardiac remodeling. This study aims to elucidate the specific role of AMPKγ2 in macrophage-mediated inflammation and CD8+ T cell infiltration during MI progression, providing novel insights into therapeutic targets for mitigating cardiac dysfunction.

Methods: To investigate AMPKγ2 dynamics in MI, we employed a multifaceted approach combining clinical and experimental models. First, plasma AMPKγ2 levels were measured via enzyme-linked immunosorbent assay (ELISA) in patients with acute MI and compared with healthy controls. For in vivo studies, a left anterior descending (LAD) coronary artery ligation model was established in C57BL/6 mice to simulate MI. Genetically modified mouse lines, including Lyz2-cre AMPKγ2 knockout (KO) mice and adeno-associated virus (AAV)-F4/80-AMPKγ2 overexpression mice, were utilized to modulate AMPKγ2 specifically in macrophages. Macrophage migration and inflammatory responses were assessed using Transwell assays and scratch wound healing assays. Additionally, the chemotactic activity of CD8+ T cells toward macrophage supernatants was evaluated in vitro. Western blotting, quantitative PCR (qPCR), and Western blots (WB) were performed to explore molecular mechanisms, including CXCL16/CXCR6 signaling, NF-κB pathway activation, and ubiquitination processes.

Results: AMPKγ2 was highly expressed in macrophages. AMPKγ2 levels were decreased in monocytes of myocardial infarction patients. Lyz2-cre AMPKγ2 mice developed worse cardiac dysfunction post MI by boosting macrophage and CD8^{+} T cell infiltration. AAV-F4/80-AMPKγ2 mice developed improved cardiac dysfunction post MI by decrease macrophage and CD8+ T cell infiltration. In vitro , AMPKγ2 levels were downregulated by inflammatory stimuli of IFN-γ in RAW264.7 cells. In the myocardial infarction microenvironment, knockdown of AMPKγ2 increased the migration and inflammation levels of macrophages. Overexpression of AMPKγ2 reduces macrophage migration and inflammation levels. The CXCL16 was a key contributor to CD8+ T cell infiltration, macrophage migration and inflammation, which was alleviated by AMPKγ2 administration via transcriptional regulation. Moreover, the CXCL16/CXCR6 and NF-κB-MCP1/IL-6 pathways jointly formed a positive feedback loop. AMPKγ2 repressed the CXCL16/CXCR6 axis by restraining YY1 expression to rescue CD8+ T cell infiltration, macrophage migration and inflammation dependent on AMPKα1 subunit-mediated AMPK activity. A769662, but not the classic AMPK agonist metformin can rescue deficiency of AMPKγ2 induced-the myocardial dysfunction. AMPKγ2 phosphorylated smurf2 to promote YY1 degradation via the ubiquitin proteasome pathway. Finally, IFN-γ downregulated HOXA5 to repress AMPKγ2 transcriptional activity and protein expression in vitro and in vivo.

Conclusion: AMPKγ2 inhibits the YY1-CXCL16-CXCR6 pathway, which plays an important role in cardiac dysfunction following MI, and may be a potential therapeutic target for myocardial remodeling after MI.

This study reveals a previously unrecognized role for AMPKγ2 in restraining post-MI inflammation through suppression of the YY1-CXCL16-CXCR6 axis. By modulating macrophage migration, CD8+ T cell infiltration, and inflammatory cytokine production, AMPKγ2 emerges as a critical regulator of cardiac remodeling after MI. The identification of HOXA5-AMPKγ2-YY1-CXCL16 signaling provides novel mechanistic insights and supports AMPKγ2 as a promising therapeutic target for mitigating myocardial injury. Future studies should explore pharmacological strategies to enhance AMPKγ2 activity while avoiding off-target effects associated with broad AMPK activation.

Molecular Mechanisms of Nanoplastic-Induced Impairment in Early Endothelial Tube Formation Derived from Human iPSCs

rui Zhang[1], Bo-da Zhou[1], Jie Na[2]

1. Beijing Tsinghua Changgung Hospital

2. Tsinghua University

Background: Microplastics (MPs) and nanoplastics (NPs) represent pervasive global environmental contaminants, with documented human bioaccumulation in multiple organs including the vascular system. Critically, NPs have been identified within human atherosclerotic plaques and correlated with increased plaque inflammation, vulnerability, and adverse cardiovascular outcomes. While this establishes NPs as an emerging cardiovascular risk factor, the precise cellular and molecular mechanisms driving their vascular toxicity remain poorly understood.

Endothelial cells (ECs) are central targets, forming the vascular barrier and actively regulating inflammation and hemodynamics. Crucially, their capacity for neovascularization – specifically migration and tube formation (tubulogenesis) – is fundamental for post-ischemic tissue repair and collateral vessel development in cardiovascular diseases. This angiogenic function, however, is not uniform across the endothelial spectrum.

Of paramount importance are early-stage endothelial cells. These cells exhibit unique phenotypic properties critical for initiating vascular repair: enhanced plasticity, high proliferative and migratory capacity, and robust tubulogenic potential. Unlike quiescent mature endothelium, early ECs are metabolically active and inherently more responsive to pro-angiogenic cues, making them essential responders to ischemic injury. Consequently, early ECs may possess heightened vulnerability to environmental stressors like NPs that could disrupt these critical repair mechanisms before mature vascular networks form.

Despite the identification of NPs in plaque and epidemiological links to CVD, the specific impact of NPs on the distinctive function of early endothelial progenitors remains a critical knowledge gap. Exposure could impair their unique tubulogenic capacity, directly sabotaging vascular repair pathways vital for recovery from myocardial infarction, peripheral artery disease, and stroke. Understanding NP toxicity specifically within this sensitive and therapeutically relevant cell population is therefore essential to elucidating a key mechanism of environmental cardiovascular damage.

Therefore, investigating the mechanistic effects of NPs on the specialized tubulogenic function of early human endothelial cells is imperative for defining their cardiovascular hazard profile and identifying potential therapeutic targets to preserve vascular repair capacity.

Methods: To investigate the mechanistic impact of nanoplastics (NPs) on early human endothelial cell (EC) function, we employed a well-defined in vitro model system. Human induced pluripotent stem cells (hiPSCs) derived from healthy volunteers were directed to differentiate into early-stage endothelial cells (D5-D6 post-differentiation) using established protocols. Differentiation efficiency was rigorously quantified by flow cytometry, confirming a highly pure population (97% CD31+ cells), ensuring the relevance of our model to authentic vascular endothelium.

We utilized carboxylate-modified fluorescent polystyrene nanoparticles as model NPs, characterized by two distinct average diameters: 40 nm (NPs 40nm) and 100 nm (NPs 100nm). To establish a non-cytotoxic exposure regime for functional assessment, early hiPSC-ECs were exposed to a concentration gradient (0, 5, 10, 20, 40, 80 μg/ml) of each NP size for 24 hours. Cell viability was meticulously assessed using flow cytometry-based live/dead staining. Concurrently, NP internalization dynamics were evaluated using a combination of flow cytometry (exploiting NP fluorescence) and high-resolution immunofluorescence microscopy to distinguish surface-bound versus internalized particles.

Based on the viability results, a sub-cytotoxic concentration (10 μg/ml) was selected for both NP sizes to specifically investigate functional impairment independent of overt cell death. Following 24-hour exposure to NPs 40nm or NPs 100nm at 10 μg/ml, the critical angiogenic function of tube formation (tubulogenesis) was assessed using a standardized in vitro Matrigel assay. Tubulogenesis capacity was quantified by measuring key parameters: number of branch points (nodes) and total tube length per field. To elucidate the molecular underpinnings of observed

functional deficits, bulk RNA sequencing (RNA-seq) was performed on hiPSC-ECs exposed to NPs 40nm or NPs 100nm (10 μg/ml, 24h) and compared to untreated controls. Bioinformatic analysis focused on identifying significantly dysregulated genes and enriched pathways related to angiogenesis, endothelial function, and stress responses.

Results: Our hiPSC differentiation protocol robustly generated early endothelial cells, as evidenced by high CD31 expression (97% purity via flow cytometry), confirming a suitable model for studying NP effects on vascular biology. Critical screening experiments revealed distinct NP size-dependent interactions and cytotoxic profiles: Exposure to NPs 40nm, even at the highest concentration tested (80 μg/ml), exhibited no significant cytotoxicity compared to untreated controls. Strikingly, immunofluorescence imaging combined with flow cytometry unequivocally demonstrated that NPs 40nm were efficiently internalized by the early hiPSC-ECs. In contrast, exposure to NPs 100nm resulted in a significant, concentration-dependent decrease in cell viability at concentrations ≥ 20 μg/ml. Furthermore, NPs 100nm were not internalized by the cells; imaging revealed particles predominantly associated with the cell surface or remaining in suspension.

Consequently, the sub-cytotoxic concentration of 10 μg/ml was selected for both NP sizes to isolate functional effects from overt toxicity. Assessment of tubulogenesis, a fundamental angiogenic process crucial for vascular repair, yielded significant findings. Compared to untreated control ECs (CTL-EC), both NPs 40nm-exposed ECs (NPs 40nm-EC) and NPs 100nm-exposed ECs (NPs 100nm-EC) exhibited profound impairment in tube-forming capacity. Quantitative analysis demonstrated a substantial and statistically significant reduction in both key metrics: the number of nodes (branch points) decreased by 67%, and the total tube length decreased by 74% in NP-exposed groups relative to controls. Notably, despite the stark difference in their cellular interaction (internalization vs. surface adherence), NPs 40nm and NPs 100nm induced remarkably similar and severe deficits in tubulogenic function at 10 μg/ml, with no statistically significant difference observed between the two NP-exposed groups.

To probe the mechanistic basis for this pronounced impairment in angiogenic capacity, we conducted bulk RNA-seq analysis. Transcriptomic profiling identified significant dysregulation of numerous genes in NP-exposed early hiPSC-ECs compared to controls. Pathway enrichment analysis pinpointed specific disruption in biological pathways intimately linked to endothelial cell migration, vascular development, and tube formation. These findings strongly suggest that sub-cytotoxic NP exposure, irrespective of internalization capability (40nm) or surface interaction (100nm), disrupts core molecular programs essential for early endothelial cell function, directly contributing to the observed vascular network formation failure.

Conclusion: Our findings demonstrate that exposure to carboxylated nanoplastics (40nm and 100nm) at sub-cytotoxic concentrations profoundly impairs the tubulogenic capacity of early human endothelial cells (hiPSC-ECs), a critical function for vascular repair. Strikingly, despite divergent cellular interactions—efficient internalization of 40nm NPs versus surface association without uptake of 100nm NPs—both particle sizes induced remarkably similar and severe deficits in endothelial network formation (67% reduction in nodes, 74% reduction in tube length). Transcriptomic analysis revealed significant dysregulation of pathways integral to angiogenesis, vascular development, and cell migration. This work provides novel mechanistic evidence that nanoplastics disrupt fundamental endothelial repair programs independently of direct cytotoxicity or the mode of cellular interaction, establishing a crucial link between nanoplastic exposure and compromised vascular regenerative capacity, a key factor in cardiovascular disease pathogenesis.

Adenylyl cyclase 7 of cardiac macrophages protects myocardial ischemia/reperfusion injury by suppressing inflammation

Guofang Xia, Cong-Feng Xu

Shanghai Jiaotong University School of Medicine Affiliated Sixth People's Hospital

Background

Myocardial ischemia/reperfusion (I/R) injury substantially diminishes the therapeutic efficacy of percutaneous coronary intervention (PCI) for myocardial infarction, contributing to 25-40% of the final infarct area despite reperfusion therapy, with no effective clinical interventions currently available. This injury involves microvascular damage, cardiomyocyte injury (Ca^{2+} overload, oxidative stress), and DAMP-triggered sterile inflammation. Cardiac macrophages, particularly recruited monocyte-derived $CCR2^{+}$ subsets, are pivotal orchestrators of this inflammatory response. While essential for initial debris clearance, excessive $CCR2^{+}$ macrophage activation exacerbates tissue damage and adverse remodeling. Adenylate cyclases (ACs) generate cyclic AMP (cAMP), a known modulator of inflammation, but their specific role, particularly ADCY7, in cardiac macrophages during I/R injury remained unexplored.

Methods

Spatial transcriptomics analysis of murine I/R hearts identified potential inflammatory regulators. Expression dynamics of ADCY7 were validated in murine I/R models (temporary coronary artery ligation) via qPCR, immunoblotting, immunofluorescence (co-staining with CD68), and multi-parameter flow cytometry (using MHC-II and CCR2 markers) of cardiac macrophages and bone marrow-derived macrophages (BMDMs). ADCY7 expression was also assessed in peripheral blood monocytes from ST-elevation myocardial infarction (STEMI) patients versus healthy controls. A macrophage depletion/reconstitution (D/R) model was established using clodronate followed by intravenous infusion of genetically modified BMDMs (CRISPR/Cas9-generated Adcy7 knockout (KO) or lentivirus-mediated Adcy7 overexpressing (OE) BMDMs; engraftment was confirmed by flow cytometry. Myocardial I/R injury was assessed by echocardiography (LV ejection fraction), infarct size measurement (EB/TTC staining), and apoptosis (TUNEL assay). Inflammation was evaluated via flow cytometry of cardiac leukocyte infiltration ($CD45^{+}$, $CCR2^{+}$ macrophages), immunofluorescence ($CD68^{+}$), and qPCR for pro-inflammatory cytokines (Il1, Tnfa, Cxcl1, Nos2). Transcriptomic (RNA-seq) and unbiased phospho-proteomic analyses were performed on Adcy7-KO BMDMs. Mechanisms of NF-κB regulation (P65 nuclear translocation) were investigated using subcellular fractionation, immunofluorescence, and pharmacological modulation (PKA agonist 6-Bnz-cAMP and antagonist H-89). An optogenetic therapeutic strategy was developed using lentiviral overexpression of the photoactivatable adenylyl cyclase *b*PAC in BMDMs, combined with intravital optical clearing of the thoracic wall and in vivo blue light illumination post-I/R.

Results

Spatial transcriptomics identified Adcy7 as a key regulator enriched in the infarct/border zones. ADCY7 protein and mRNA expression significantly increased in murine hearts from day 3 to day 7 post-I/R, specifically within recruited $MHC\text{-}II^{-}$ $CCR2^{+}$ macrophages. ADCY7 was the predominant AC isoform in BMDMs. In STEMI patients, ADCY7 was markedly elevated in peripheral blood monocytes, correlating positively with NT-proBNP and inversely with LVEF. Reconstitution of macrophage-depleted I/R mice with Adcy7-KO BMDMs exacerbated injury: impaired LVEF, increased infarct-to-AAR ratio, elevated apoptosis, enhanced infiltration of $CD45^{+}$ leukocytes and $CCR2^{+}$ macrophages (but not $CCR2^{-}$ macrophages or neutrophils), and upregulated pro-inflammatory genes (Il1, Tnfa, Cxcl1, Nos2). Conversely, reconstitution with Adcy7-OE BMDMs conferred protection: improved LVEF, reduced infarct size/apoptosis, decreased leukocyte/$CCR2^{+}$ macrophage infiltration, and suppressed pro-inflammatory gene expression. RNA-seq on Adcy7-KO BMDMs revealed 950 upregulated genes enriched in pro-inflammatory pathways (chemokine signaling, leukocyte chemotaxis, IL-1 response), with NF-κB identified as the master regulator. Adcy7 deficiency significantly increased nuclear translocation of NF-κB P65, while Adcy7 overexpression suppressed it. Phospho-proteomics linked ADCY7 to PKA Cα activation. Mechanistically, ADCY7-generated cAMP activates PKA, which inhibits P65 nuclear translocation: 6-Bnz-cAMP (PKA agonist) rescued the translocation defect in Adcy7-KO BMDMs, while H-89 (PKA antagonist) abolished the suppression in Adcy7-OE BMDMs. Optogenetic activation of *b*PAC in reconstituted BMDMs via blue light significantly reduced $CD45^{+}$/$CCR2^{+}$ macrophage infiltration and pro-inflammatory genes, improved LV systolic function, and diminished infarct size and apoptosis in I/R hearts.

Discussion

This study establishes ADCY7 within recruited $CCR2^{+}$ cardiac macrophages as a critical regulator of inflammation and injury following myocardial I/R. Its upregulation coincides with the early reparative phase in both murine and human settings. Functional studies using a macrophage-specific D/R model definitively demonstrate that macrophage ADCY7 deficiency exacerbates inflammation and injury, while its overexpression or targeted optogenetic activation is potently protective. The mechanism involves ADCY7/cAMP/PKA signaling inhibiting NF-κB P65 nuclear translocation, thereby restraining transcription of key pro-inflammatory mediators (cytokines, chemokines). Although other AC isoforms (e.g., ADCY6) influence inflammation differently, ADCY7 emerges as the dominant and functionally essential isoform in macrophages for mitigating I/R injury. The successful application of an optogenetic strategy (*b*PAC + blue light) to activate ADCY7/cAMP signaling spatiotemporally in macrophages demonstrates significant therapeutic efficacy, reducing inflammation and tissue damage in vivo. This highlights the translational potential of targeting macrophage ADCY7. While other candidates (e.g., Arrb2) exist and ADCY7 expression may occur in other cell types, the D/R model specifically implicates macrophage ADCY7 as the key effector. Future research should explore ADCY7's subcellular localization and potential isoform-specific interactors. Overall, macrophage ADCY7 is a promising therapeutic target for developing novel anti-inflammatory strategies to ameliorate myocardial I/R injury and improve outcomes post-reperfusion therapy.

ATF4 regulates PI3K/AKT signaling axis to promote angiogenesis after myocardial infarction

Yan Wang

Affiliated Hospital of Zunyi Medical University

The persistent ischemic-hypoxic response of tissues after acute MI leads to ventricular remodeling and heart failure . Effective tissue repair after MI relies on robust neovascularization in the infarct border zone . Therefore, finding effective ways to promote neovascularization after MI is a major challenge in cardiovascular research.

Activating transcription factor 4 is a key factor in the unfolded protein response and the integrated stress response, and is involved in the regulation of gene transcription in the endoplasmic reticulum stress response, antioxidant response, autophagy, and angiogenic response and senescence . Recent studies have shown that a subpopulation of ATF4-positive endothelial cells exists in skeletal muscle, which can promote cell proliferation and neovascularization by increasing amino acid metabolism after exercise, while a subpopulation of endothelial cells with low expression of ATF4 does not have such a function, which suggests that ATF4 is a key regulator of the endothelial cell's ability to proliferate, migrate, and become a member of the vasculature. Studies in the heart have shown that ATF4 can regulate the mitochondrial stress response in cardiomyocytes through the mitotic scaffold 1, promoting cell division during proliferation of cardiomyocytes after MI in mice with a single allele of mitochondrial ribosomal protein S5 (MRPS5), thus promoting the regenerative response of cardiomyocytes . Interestingly, overexpression of ATF4 in neonatal rat ventricular myocytes can contribute to cellular NADPH production via the pentose phosphate pathway and the mitochondrial serine/glycine/folate metabolic signaling pathway pathway; thus, in vivo cardiomyocyte-specific deletion of ATF4 may partially lead to a decrease in NADPH production thereby exacerbating cardiomyopathy and accelerating the progression of heart failure in the presence of aortic constriction .However, whether ATF4 is involved in neovascularization after MI and related mechanisms has not been reported.

Here, we found that ATF4 is a promoter gene of angiogenesis in endothelial cells in vitro and after MI in vivo in mice under hypoxic conditions by gain-of-function or lack-of-function and that this may act by regulating PI3K/AKT signaling through in endothelial cells.

Neovascularization is the process by which vascular endothelial cells proliferate, migrate, and form new blood vessels in existing vessels under pathophysiological conditions such as repair of tissue damage, and ischemic regeneration . Vascular regeneration holds promise for therapy and enhancing perfusion in ischemic tissues, playing a pivotal role in tissue repair and cardiac function improvement post-myocardial infarction. Transcription factor regulation represents a crucial dimension of gene expression network control . With ATF4 playing a pivotal role in promoting cardiomyocyte proliferation and ameliorating oxidative damage in cardiac regeneration and heart failure. However, its involvement and underlying mechanisms in mediating neovascularization in the hypoxic tissue environment post-myocardial infarction remain to be elucidated .

Effective neovascularization is critical for tissue repair and the enhancement of cardiac function following myocardial infarction (MI). However, the hypoxic microenvironment post-MI significantly impedes neovascular formation. Although ATF4 has been implicated in heart failure and myocardial cell regeneration and repair, its role in angiogenesis remains unclear. This study utilized both in vitro and in vivo models to investigate the role of ATF4 in neovascularization after MI.In hypoxia-cultured murine endothelial cells (ECs), hypoxia was observed to inhibit EC proliferation, migration, and tube formation. In contrast, overexpression of ATF4 ameliorated these hypoxia-induced impairments. Conversely, inhibition of ATF4 further exacerbated the reduction in EC proliferation, migration, and tube formation induced by hypoxia. Notably, the beneficial effects of ATF4 were reversed by the PI3K/AKT inhibitor LY294002. Under hypoxic conditions, ATF4 overexpression significantly upregulated phosphorylated (p)-PI3K, p-AKT (T308), and p-AKT (S473) in ECs. LY294002, however, markedly reduced the expression of p-PI3K, p-AKT (T308), and p-AKT (S473) in hypoxic ECs overexpressing ATF4.In a murine MI model, ATF4 overexpression partially mitigated cardiac dysfunction and promoted neovascularization, effects that were significantly attenuated by LY294002. These findings suggest that ATF4 plays a crucial role in endothelial cell-mediated neovascularization under post-MI hypoxia by modulating the PI3K/AKT signaling pathway.

心脏归巢肽功能化修饰的脂质体纳米材料负载秋水仙碱的制备及其改善心肌梗死后炎症和神经重构的作用

丁欢欢 周贤惠

新疆医科大学第一附属医院

目的：构建心脏归巢肽 (Cardiac Homing Peptide，CHP）修饰的载有秋水仙碱（Colchicine，COL）的脂质体纳米颗粒（Liposomal Nanomaterials，LP），研究其对心肌梗死后（Myocardial Infarction，MI）后心脏炎症反应与神经重构的作用。**方法：**确定 COL 的作用靶点 β- 微管蛋白（β-tubulin，TUBB），使用孟德尔随机化（Mendelian Randomization，MR）分析，研究遗传预测的 TUBB 水平与 MI 发生风险之间的因果关系。制备心脏归巢肽功能化修饰的脂质体纳米颗粒负载秋水仙碱（Cardiac-Homing Peptide-Functionalized Liposomal Nanomaterials loaded with Colchicine，CCP）。采用透射电子显微镜（TEM）、动态光散射（DLS）等技术测定 CCP 和秋水仙碱脂质体纳米颗粒（Liposomal Nanoparticles loaded with Colchicine，CP）和形貌、粒径及电位。与大鼠心肌细胞（H9C2）共培养验证 CCP 与心肌细胞共定位情况；透析法考察 CCP 包封率及载药量；细胞增殖 - 毒性检测法（CCK8）检测各组干预后细胞增殖活力；激光共聚焦显微镜观察 各组与 H9C2 细胞的共定位情况。SD 大鼠按随机数字表法等分为六组：对照组、假手术组（Sham 组）、CCP 组、CP 组，LP 组以及 COL 组，尾静脉注射各组脂质体纳米颗粒，通过小动物活体成像系统（IVIS）验证各干预组的靶向作用。MI 大鼠干预 3 天后，取左室心脏组织转录组学初步探究 CCP 在 MI 模型的分子机制。MI 大鼠干预 14 天后，在体评价脂质体纳米颗粒的生物安全性。心脏组织进行 Masson 染色和天狼星红染色，取血检测炎症因子指标，探究脂质体纳米颗粒对 MI 后纤维化和炎症作用。心脏组织免疫荧光（IF）染色检测神经重构指标，ELISA 测定神经肽 Y（NP-Y）表达水平，探究脂质体纳米颗粒对于 MI 后神经重构的作用。测量并记录各组第 28 天后 MI 大鼠超声心动图指标。**结果：**遗传预测的 TUBB 水平与 MI 呈正相关，COL 作为 TUBB 的靶向抑制剂，可能对 MI 的发生具有抑制作用。制得的 CCP 和 CP 表面规整，呈圆形，CCP 粒径为 213.2±2.7nm，PDI 为 0.36±0.03。CP 粒径为 203.9±3.2nm，PDI 为 0.43±0.02。体外结果显示，CCP 组与 CP 组 14μg/mL 浓度时，细胞存活率均大于 80%，H9C2 细胞对 CCP 的荧光摄取表达显著高于 COL 和 CP（P < 0.001），共定位荧光定量结果显示 CCP 能有效靶向到 H9C2 细胞中。IVIS 实验显示 CCP 组的荧光显著增强，8 小时后能有效靶向到缺血心脏（P < 0.001）。 各组大鼠的肝肾功能指标检测结果显示均维持在正 常生理范围内。与 MI 组相比，CCP 组 H&E 染色显示心肌纤维细胞数量减少，大多数心肌细胞排列有序，中性粒细胞浸润减少。Masson 染色和 天狼星红染色结果显示 CCP 组、CP 组 Masson 染色纤维化面积较 MI 组（42%）明显减轻（P < 0.001）。ELISA 结果表明 CCP 组和 CP 组 炎症因子较 MI 组表达减少。 CCP 组和 CP 组较 MI 组 LVEF 和 LVFS 显著升高。IF 染色 CP 组和 CCP 组较 MI 组 GAP43、TH、NGF 表达明显减弱（P < 0.001）。**结论：**CCP 能准确靶向到缺氧的心肌，并能有效减轻 MI 所致心肌纤维化以保护心脏 功能，明显改善 MI 后炎症细胞浸润以及炎症因子的表达，减轻 MI 后心脏的神经重 构，为治疗 MI 提供新思路。

系统免疫炎症指数在心血管疾病中临床应用的研究进展

田亚楠

中国医科大学附属盛京医院南湖院区

关键词：系统免疫炎症指数；心血管病；预后； Systemic Immune Inflammatory Index ; Cardiovasculardisease ; prognosis

摘要：

1. 目的：系统免疫炎症指数（ systemic immunoinflammatory index , SII ）是一种基于中性粒细胞、血小板和淋巴细胞计数的新型炎症标志物，其可有效且全面的反映出机体炎症状态及免疫系统状况。近年来，有许多的研究表明， SII 与多种心血管疾病（ cardiovascular disease , CVD ）的病理生理及预后具有相关性。本文就目前 SII 在 CVD 中的临床研究进展进行综述。

2. 方法：心血管疾病（ cardiovascular disease , CVD ）是全球最常见的非传染性疾病，估计在 2017 年造成 1770 万人死亡。当前，随着我国人口老龄化及城镇化进程加快，居民不良生活方式的影响，心血管病危险因素对健康的影响越加显著，其发病率仍持续增高。2020 年， CVD 是我国城乡居民的首要死亡原因，农村为 48.00%，城市为 45.86%。为我国居民及社会带来的经济负担日渐加重，已成为重大的公共卫生问题。 CVD 的防控、心血管急重症患者社会医疗资源的投入、降低 CVD 存活患者复发、再住院和失能的风险，成为了我国医疗服务迫切需要解决的问题。疾病的诊治重点从疾病本身向疾病预防和健康促进转变。由于目前血清学标志物受当地医院实验室水平及辅助检查医院等级的限制，基层居民 CVD 就诊更多是因为严重的心脑血管并发症。因此，尽早识别 CVD 发生的相关因素显得极为重要。大量证据表明，慢性低度炎症在动脉粥样硬化和心血管疾病的发病机制中起着关键作用，血管内皮损伤、氧化应激、血栓形成可能是潜在的潜在机制，全血细胞计数成分可作为冠心病风险预测因子，淋巴细胞也参与了动脉粥样硬化的适应性免疫。 BoHu 等人在 2014 年开发出系统免疫炎症指数（ SII ）= 为血小板数 x 中性粒细胞数 / 淋巴细胞计数的比值，最初被证明是预测肝癌的预后，是一种结合淋巴细胞计数、中性粒细胞及血小板的新型炎症指数，其可有效且全面的反映出机体炎症状态及免疫系统状况。后被临床广泛研究并证明为呼吸系统肿瘤、消化系统肿瘤、妇科肿瘤及炎症性疾病的预后标志物。

3. 结果: 随后 SII 被应用于 CVD 的预后研究中，M . Xu 等人进行了一项队列研究，纳入了 13,929 名平均年龄为 62.56 岁（范围 35~91 岁）且没有心血管疾病和癌症的中老年人进行分析。在中位 8.28 年（最长 8.98 年）的随访中，共发现了 3386 例心血管疾病病例，包括 801 例中风病例和 2585 例冠心病病例。经过多变量 Cox 回归分析后发现，高 SII 与 CVD 事件（包括中风和冠心病）显著相关。SII 可作为中老年人群心脑血管疾病发展中的作用的有用标志物。本文通过检索近年来 SII 与 CVD 相关及预后的文献，对其研究进展进行综述。

4. 结论：目前，随着居民物质条件进步和人均预期寿命提高， CVD 仍是阻碍生活质量的首要病因。 CVD 包含多种疾病，且临床表现多以其他系统的症状。但早期诊断十分困难，很容易被临床医生误诊，延误治疗。 SII 可以预测 CVD 的不良预后及疾病严重程度,在常规检查中发现高 SII 患者,可以采取个体化干预措施,建议改善不良生活方式，加强锻炼，并增加相关实验室及辅助医疗检查，让更多的高危患者从二级预防中获益。但 SII 与 CVD 发生发展的具体机制尚不明确，未来需要更多前瞻性研究深入验证，最终服务临床，使患者受益。

Clinical features and prognosis of idiopathic inflammatory myopathy complicated by heart failure with preserved ejection fraction

Lei Zhou

The First Affiliated Hospital With Nanjing Medical University

Background Idiopathic inflammatory myopathy (IIM) is increasingly recognized as a systemic disorder with subclinical myocardial involvement. Although skeletal muscle is the primary target, IIM frequently involves multiple organ systems, with cardiac involvement being particularly concerning due to its substantial contribution to morbidity and mortality.

However, the co-occurrence of IIM and heart failure with preserved ejection fraction (HFpEF) has not been systematically explored. Emerging evidence suggests that autoimmune-driven myocardial injury and interstitial fibrosis may underlie this overlap, warranting a structured approach to risk stratification.

Objective A total of 134 patients with IIM from August 2016 to February 2025 were retrospectively analyzed and divided into a low-risk group (low risk of HFpEF), a medium-risk group (suspected HFpEF), and a high-risk group (confirmed HFpEF) according to the HFA-PEFF score. To characterize the clinical, serological, and imaging profiles of IIM patients with HFpEF, and to evaluate the prognostic utility of the HFA-PEFF score in this specific context.

Methods A cohort study was conducted, analyzing 134 patients with IIM and stratifying them into low-risk, medium-risk, and high-risk groups according to the HFA-PEFF score. A comparative analysis was performed on the clinical characteristics and prognosis of these three risk groups.

Results Among 134 IIM patients, 22 (16.4%) were classified as high-risk (HFA-PEFF ≥ 5), exhibiting significantly older age, lower free triiodothyronine (FT3) levels, and elevated C-reactive protein (CRP) and cardiac troponin T levels (P <0.05]. Notably, positive rates of antinuclear antibodies (ANA), anti-SSA, anti-Jo-1, and anti-Ro52 antibodies were significantly enriched in the high-risk group (P <0.05), suggesting a potential link between autoimmunity and myocardial remodeling. By May 09, 2025, a total of 26 deaths were recorded among the 134 enrolled IIM patients, corresponding to an overall survival rate of 80.6% during a mean follow-up period of 52.6±28.9 months. Survival analysis demonstrated a significantly reduced 5-year survival in high-risk patients (50%) compared to low- and medium-risk groups (90% and 84.7%, respectively; P

Conclusion This study is the first to propose a quantitative risk stratification framework for HFpEF in IIM using the HFA-PEFF score. The findings highlight the prognostic relevance of specific antibody profiles and cardiac fibrosis, offering novel insights into the immune-cardiac axis in IIM. Stratified management based on HFA-PEFF score may inform early intervention strategies and personalized monitoring in this high-risk population.

NLRP3 介导的中性粒细胞焦亡在川崎病冠脉瘤的作用及机制研究

易岂建 李梦玲

重庆医科大学附属儿童医院

目的：研究中性粒细胞的 NOD 样受体热蛋白结构域相关蛋白 3（NOD-like receptor thermal protein domain associated protein 3,NLRP3）炎症小体在川崎病冠脉瘤中的作用和机制研究。

方法: 利用 RNAseq 检测川崎病巨大冠脉瘤患儿外周血的中性粒细胞转录组水平，扫描电镜及 WB 进一步验证中性粒细胞的焦亡。通过腹腔注射 CAWS 建立 KD 小鼠模型，将动物分为溶剂组（control 组，n=6）、模型组（CAWS 组，n=6）和 MCC950 组（NLRP3 抑制剂组，n=6）取小鼠心脏组织、骨髓中性粒细胞以及全身大动脉血管进行后续实验。通过 HE、Masson 染色和免疫荧光技术检测心脏结构的改变，利用免疫荧光染色检测中性粒细胞在冠脉周围的情况、RT-qPCR、Western Blot 技术检测焦亡相关蛋白的表达。通过 HL-60 和 HASMC 共培养方法模拟中性粒细胞体外炎症模型，利用流式细胞技术检测细胞凋亡、划痕实验检测细胞迁移、PI/Hoechest 共染法检测细胞死亡。

结果： 中性粒细胞 RNAseq 转录组水平显示有 208 个基因上调，1124 个基因下调。KEGG 通路富集分析结果显示，这些基因主要涉及 NOD 样受体信号通路。巨大冠脉瘤患儿全血提取的中性粒细胞扫描电镜以及 WB 证实中性粒细胞发生焦亡。动物实验 HE 染色观察 4W 冠脉周围炎症明显；Masson 染色观察冠脉损伤后胶原纤维及肌成纤维细胞增殖明显，血管组织的 RT-qPCR 以及骨髓的中性粒细胞 WB 结果也显示焦亡通路 NLRP3 相关分析基因及蛋白表达明显上调。免疫荧光检测 CAWS 4W 小鼠冠脉周围中性粒细胞聚集。NLRP3 抑制剂 MCC950 抑制剂能挽救 CAWS 导致的血管炎症。将 LPS 刺激后的 dHL-60 细胞和 HASMA 细胞共培养，划痕实验、流式检测凋亡、PI/Hoechest 共染色提示炎症环境下影响平滑肌细胞的的增殖、凋亡和衰老。

结论：中性粒细胞焦亡在 KD 冠脉瘤中发挥重要作用，该研究为进一步阐明 KD 的病理生理过程提供了新的证据。

基于单细胞测序技术对动脉粥样硬化斑块中干细胞样 CD8+T 细胞的探讨

罗仁飞 周恩格 沈天舟 刘世兴 欧阳鑫 江龙

南昌大学第二附属医院 心血管内科

目的：

动脉粥样硬化（Atherosclerosis,AS）是心血管疾病的主要病理基础，涉及脂质沉积、慢性炎症和免疫细胞活化。CD8+T 细胞在 AS 中具有促进和拮抗的双重作用，但其亚群异质性及功能调控机制尚不明确。干细胞样 CD8+T（$Tcf7^{hi}$CD8+T）细胞在肿瘤、慢性感染中作用显著，但在 AS 中未见报道。本研究旨在应用单细胞 RNA 测序（Single-cell RNA sequencing,ScRNA-seq）鉴定分析 AS 斑块中的 $Tcf7^{hi}$CD8+T 细胞亚群，探究其功能、来源及与脂质代谢的关联。

方法：

1. 亚群鉴定：对普通和高脂饮食（High-Fat Diet,HFD）喂养 24 周的 $LDLR^{-/-}$ 及野生型小鼠主动脉进行 ScRNA-seq，鉴定分析 $Tcf7^{hi}$CD8+T 细胞。分析公共 $LDLR^{-/-}$ 小鼠及人斑块数据集。

2. 功能验证：对 $LDLR^{-/-}$ 小鼠主动脉进行免疫荧光共染和流式细胞术，检测 Tcf7+CD8+T 细胞比例及功能状态（IFN-γ, MKI67, PD-L1），外周血同步检测。

3. 来源探讨：分析健康人主动脉及冠脉周围脂肪组织公共数据。流式检测 $LDLR^{-/-}$ 小鼠脂肪组织及脾脏 Tcf7+CD8+T 细胞比例。收集家族性高胆固醇血症（Familial hypercholesterolemia，FH）患者和健康人外周血，流式检测 Tcf7+CD8+T 细胞比例，分析其与血脂（LDL-C, TC）相关性。

结果：

1.$LDLR^{-/-}$ 小鼠 ScRNA-seq 显示主动脉中存在具备干性特征的 $Tcf7^{hi}$CD8+T 细胞及终末毒性表型的 $Tcf7^{lo}$CD8+T 细胞。HFD 促进 $Tcf7^{hi}$CD8+T 细胞增殖、促炎能力增强，并向 $Tcf7^{lo}$ 细胞分化。小鼠和人主动脉公共数据集的结果一致。

2. 流式证实小鼠主动脉存在 Tcf7+CD8+T 细胞，HFD 组比例显著下降（63.36% vs. 32.38%, p<0.01）。免疫荧光支持此结果。HFD 组该细胞促炎（IFN-γ+: 18.96% vs. 33.52%, p<0.01）、增殖（MKI67+: 5.40% vs. 11.92%, p<0.01）增强，和耗竭（PD-L1+: 7.03% vs. 16.35%, p<0.01）水平升高。外周血趋势相同。

3. 无病变人主动脉及冠动脉周围脂肪组织的公共 ScRNA-seq 数据显示 Tcf7 表达低。流式细胞术结果表明 $LDLR^{-/-}$ 小鼠脂肪组织中 Tcf7+CD8+T 比例普遍较低，主要存在于特定脂肪（胸主动脉周围脂肪、腹股沟白色脂肪和附睾白色脂肪）。在 HFD 组中，胸主动脉周围脂肪组织（19.97% vs. 8.15%，p < 0.05）、腹股沟白色脂肪（16.28% vs. 4.79%，p < 0.05）和附睾白色脂肪（18.52% vs. 2.10%，p < 0.0001）中 Tcf7+CD8+T 细胞比例均更低。脾脏和外周血中存在大量 Tcf7+CD8+T 细胞，提示其可能是主动脉该细胞的来源。

4. 未治疗 FH 患者外周血 Tcf7+CD8T 细胞比例低于健康人（92.39% vs. 85.57%, p<0.05），且与 LDL-C（r=-0.539, p<0.001）和 TC（r=-0.539, p<0.001）水平呈显著负相关。

结论：本研究首次揭示 AS 斑块中存在干细胞样 CD8+T 细胞，其在高脂环境下可分化为促炎和“耗竭”表型细胞。循环中该细胞比例与 LDL-C 和 TC 水平负相关，显示其在 AS 进展中的重要角色，未来需更多研究证实。

单细胞测序联合代谢组学揭示免疫相关心肌炎中的代谢重编程与免疫互作机制

谢子嫣 李怡 王怡宁

中国医学科学院北京协和医院

目的

免疫相关心肌炎是一类由免疫系统异常激活引发的严重心脏并发症，尤其在免疫检查点抑制剂（ICI）治疗的肿瘤患者中，尽管其发病率仅为 0.3%-1.7%，但死亡率高达 67%，对患者预后造成严重威胁。目前尚缺乏特异性诊断指标和有效治疗手段，临床治疗主要依赖糖皮质激素，面临免疫抑制副作用大、疗效不稳定等限制。**深入阐明其发病机制、识别可干预的特异性代谢通路，对于提高肿瘤免疫治疗的安全性和改善患者结局具有重要意义。**近年来，代谢与免疫互作机制成为研究热点。**代谢不仅决定细胞能量供需，还通过代谢物、代谢酶和通路调控免疫细胞的功能与效应状态，**特别在自身免疫病和肿瘤免疫中密切相关。然而，免疫相关心肌炎的代谢图谱尚未被系统揭示，代谢重编程如何调控心脏局部免疫反应仍属空白。**本研究联合单细胞转录组、代谢组和脂质组数据，系统解析免疫相关心肌炎的代谢异常特征，识别代谢 - 免疫互作的关键节点，并结合功能实验验证其致病机制。**

方法

本研究构建免疫相关心肌炎小鼠模型，采集心脏组织样本，开展单细胞转录组测序、代谢组学和定量脂质组学联合分析。基于 KEGG 和 Reactome 数据库的代谢通路基因集，采用 AUCell 算法对每个细胞通路活性进行评分，评估其在不同细胞类型中的活跃程度，并识别细胞类型特异性差异代谢基因。结合代谢组和脂质组检测到的差异代谢物和脂类成分，开展通路富集及拓扑分析，并整合构建代谢 - 基因联合变化网络。通过免疫组化、流式细胞术及体外功能实验，进一步验证关键代谢通路对免疫效应的调控作用。

结果

单细胞测序分析共鉴定出 14 种心脏细胞类型。随后对 83 条代谢通路进行评分，筛选出包括**产热作用、糖尿病性心肌病、氧化磷酸化、嘌呤代谢、癌症中心碳代谢等 10 条活跃通路，提示心脏代谢重塑与氧化应激和免疫信号密切相关。**进一步筛选出 1734 个差异代谢基因，其中成纤维细胞、心肌细胞和内皮细胞代谢表达重塑最为显著。代谢组学分析发现，心肌炎小鼠心脏中 L- 脯氨酸、L- 甲硫氨酸、丝氨酸等氨基酸显著升高；乳酸和乙酰辅酶 A 水平下降，提示糖酵解效率降低；腺苷、脱氧腺苷、黄素腺嘌呤二核苷酸（FAD）显著下降，反映核苷酸代谢紊乱。**KEGG 通路富集结果显示，差异代谢物主要富集在氨基酸代谢、嘌呤代谢、丙酮酸代谢、中心碳代谢和糖酵解等通路。**脂质组学分析显示，心肌炎组中性脂质如三酰甘油和二酰甘油显著减少，**提示心肌细胞储能能力下降。**

整合单细胞通路评分与代谢组学分析，**识别出在基因表达与代谢物层面共同改变的核心代谢通路，包括嘌呤代谢、嘧啶代谢、脂肪酸合成与分解通路。**其中，嘌呤代谢通路中关键代谢物腺苷水平下降，其合成酶 CD73 在间皮细胞中显著下调。体外功能实验显示，外源性腺苷可剂量依赖性抑制 $CD8^+$ T 细胞杀伤分子 GZMB 表达，提示**腺苷作为代谢性免疫抑制信号可调控 T 细胞效应功能。**脂肪酸合成关键酶 FASN 和 ACC 在成纤维细胞中显著下调，提示脂质合成能力下降。已有研

究表明，中性脂质水平下降可减少 T 细胞内脂质储存，促进其转向脂肪酸氧化供能，进而增强其效应活性。本研究结果提示，**这种脂质代谢重编程可能加剧 T 细胞介导的心肌炎症损伤。**

结论

本研究首次整合单细胞转录组、代谢组和脂质组，系统描绘了免疫相关心肌炎中心脏局部的代谢重编程图谱，**明确嘌呤代谢紊乱与中性脂质减少是免疫异常激活的重要代谢背景。**腺苷和脂质等免疫抑制代谢信号的显著减少，可能解除 T 细胞代谢限制，增强其活化与效应功能。研究**揭示了代谢 - 免疫互作在免疫相关心肌炎发病机制中的核心作用，为靶向腺苷合成或脂质代谢通路干预免疫相关心脏毒性提供潜在思路，**并为提升肿瘤免疫治疗的安全性和有效性提供理论基础与实践依据。

Dual Epigenetic Control by p16INK4a via ISGylation and m ⁶ A/m ⁷ G Epitranscriptomic Reprogramming Governs Macrophage Efferocytic Dysfunction in Cardiac I/R Injury

Hao-Yu Meng[1], Xiao-Yan Wang[2], Xin Gu[2,3]

1. Department of Cardiology, The First Affiliated Hospital with Nanjing Medical University, Nanjing, Jiangsu, 210029, China

2. Department of Cardiology, The Affiliated Hospital of Jiangnan University, Wuxi, Jiangsu, 214062, China

3. Department of Cardiology/Angiology I, University Heart Center Freiburg-Bad Krozingen, Germany Medical University

Background: Myocardial ischemia/reperfusion (I/R) injury remains a major clinical challenge, characterized by excessive inflammation, oxidative stress, and impaired ventricular remodeling. Macrophage-mediated efferocytosis is essential for post-infarction tissue repair, yet its efficiency declines significantly with age and contributes to poor cardiac recovery. Although p16^Ink4a is a classical marker of cellular senescence, its role in regulating macrophage dysfunction during I/R injury remains poorly understood. ISGylation—the covalent conjugation of interferon-stimulated gene 15 (ISG15) to target proteins—has gained increasing attention beyond its classical antiviral role. Recent studies suggest that ISGylation is involved in broader physiological processes, including inflammation, oxidative stress, and immune regulation, all of which are tightly linked to cardiovascular health. In this study, utilizing clinical samples from patients with ischemia/reperfusion (I/R) injury, alongside macrophage-specific p16 knockout mice ($p16^{fl/fl}Lyz2^{Cre}$), whole-body p16 knockout mice ($p16^{-/-}$), and bone marrow transplantation models, we elucidated the protective role of p16 deficiency in macrophages following I/R injury. Through bulk RNA sequencing, m ⁶ A-seq, and m ⁷ G-seq analyses on macrophages, we discovered that p16 deletion leads to a profound epitranscriptomic remodeling of the macrophage transcriptome, mediated by alterations in mRNA methylation patterns.Further mechanistic investigations using co-immunoprecipitation coupled with mass spectrometry (Co-IP/MS) revealed a novel regulatory axis wherein the senescence-associated marker p16 promotes ISGylation of IGF2BP1—a key m ⁶ A/m ⁷ G reader protein—thereby reshaping the epitranscriptomic landscape and enhancing the efferocytic capacity of macrophages, ultimately alleviating myocardial I/R injury. Notably, this modification was dependent on ISGylation, a ubiquitin-like post-translational process, suggesting that p16 stabilizes IGF2BP1 by inhibiting its ubiquitin-mediated degradation via ISGylation. To explore the translational potential of targeting this pathway, we performed molecular dynamics simulations and virtual screening, identifying a first in class small molecule, HIT211526174, that disrupts the p16–IGF2BP1 interaction. In both in vitro and in vivo models, this compound improved m ⁷ G modifications, enhanced the cytosolic function of macrophages, and ameliorated cardiac function after I/R injury. Together, our findings establish a critical link between RNA epigenetic modifications, cellular senescence signaling, and innate immune function. This work provides novel insights into the regulation of macrophage-mediated clearance and identifies potential therapeutic avenues for the treatment of ischemic heart disease.

Methods and Results: Using clinical samples from I/R patients, macrophage-specific p16 knockout mice ($p16^{fl/fl}Lyz2^{Cre}$), whole-body $p16^{-/-}$ mice, and bone marrow transplantation models, we demonstrate that p16 deficiency enhances macrophage efferocytic capacity and protects against myocardial I/R injury. Multi-omics analysis including bulk RNA-seq, m ⁶ A-seq, and m ⁷ G-seq revealed that p16 deletion reshapes the macrophage transcriptome through altered RNA methylation, suggesting an epitranscriptomic mechanism of functional restoration. Mechanistically, we identified that p16 promotes ISGylation of IGF2BP1—a key reader of m ⁶ A/m ⁷ G modifications—stabilizing its expression by inhibiting ubiquitin-mediated degradation. This ISGylation-dependent interaction modifies the RNA methylation landscape and facilitates macrophage-mediated clearance of apoptotic cells.

Furthermore, molecular dynamics simulations and in silico drug screening identified a small molecule, HIT211526174, capable of disrupting the p16–IGF2BP1 interaction. Treatment with HIT211526174 in vitro and in vivo restored m ⁷ G modification, enhanced macrophage function, and significantly improved cardiac performance following I/R injury.

Conclusions: This study uncovers a previously unrecognized regulatory axis linking p16-driven ISGylation to RNA methylation and macrophage function. Our findings establish a mechanistic connection between cellular senescence, epitranscriptomic remodeling, and immune clearance, offering a promising therapeutic strategy for myocardial I/R injury.

Anti-Atherosclerotic Effects and Mechanisms of Narciclasine via Histone Lactylation-Mediated Inhibition of Endothelial Inflammation

Zi-Qian Wang, Zheng-Bin Zhang, Ming-Rui Ma, Ying-Qian Zhang, Yun-Dai Chen

中国人民解放军总医院

Background: Cardiovascular diseases (CVDs) are a leading cause of death worldwide, with atherosclerosis (AS) being a critical pathological process contributing to adverse CVD events. AS is a chronic inflammatory disease characterized by lipid deposition beneath the intima, with major complications like myocardial infarction and stroke posing significant health threats. While statins effectively reduce LDL-C levels and AS-related events, 10%-20% residual cardiovascular risk persists, largely attributed to persistent vascular inflammation. Although IL-1β receptor antagonists and colchicine show promise, long-term monoclonal antibody treatments face clinical challenges and infection risks. Thus, identifying novel anti-inflammatory small-molecule compounds is urgent. Endothelial cell inflammation triggers AS progression, where ox-LDL, hyperglycemia, or hemodynamic changes activate pro-inflammatory pathways, recruiting monocytes that differentiate into macrophages, exacerbating plaque formation. Despite endothelial inflammation's central role, clinical therapies directly targeting it remain scarce. Systems biology advances, particularly transcriptomics and proteomics integration, enable deciphering endothelial inflammation's complex networks. The Connectivity Map (Cmap) database offers a crucial platform for drug repurposing, potentially identifying endothelial-specific anti-inflammatory compounds. This study identified narciclasine, a DNA topoisomerase inhibitor with anti-tumor properties, as a potential endothelial anti-inflammatory agent. Emerging evidence suggests narciclasine treats inflammatory diseases, though its AS mechanism remains unclear. Transcriptomics indicates narciclasine may regulate glycolysis, a key endothelial energy pathway whose overactivation drives dysfunction and inflammation. Lactate, a glycolysis byproduct, regulates gene expression via histone lactylation, particularly H3K18la, which activates NF-κB signaling. We hypothesize narciclasine inhibits endothelial inflammation and plaque formation by modulating H3K18la-mediated NF-κB activation.

Methods: (1) An in vitro shear stress model using HUVECs was established. Proteomics analyzed gene expression changes post-oscillatory shear stress (OSS). Public transcriptomics data from OSS/TNF-α-treated HUVECs identified differentially expressed genes input into Cmap for anti-inflammatory compound screening. Narciclasine cytotoxicity was assessed via cell viability assays. VCAM1, ICAM1, SELE, and CCL2 protein/mRNA levels were measured post-treatment. PKH26-labeled THP-1 monocyte adhesion to HUVECs and RAW264.7 migration were evaluated, alongside oxidative stress levels. In ApoE-/- mice with carotid ligation, narciclasine's dose-dependent effects on plaque formation were assessed. Immunofluorescence detected plaque VCAM1 and macrophage infiltration. Mouse TC, TG, LDL-C, and HDL-C levels were measured. (2) Public narciclasine-treated cell transcriptomics data underwent bioinformatics analysis. WB/qPCR measured GLUT1/PFKFB3 expression post-treatment. Glucose uptake/glycolysis changes were assessed. Sodium pyruvate restored glycolysis, measuring VCAM1/ICAM1 changes and monocyte adhesion. In ApoE-/- mice, immunofluorescence detected carotid GLUT1 changes. AMPK pathway activation, mitochondrial membrane potential, and oxidative phosphorylation were measured. (3) Cellular lactate production and Pan Kla levels were measured post-narciclasine. WB/immunofluorescence detected H3K18la inhibition. In ApoE-/- mice, carotid H3K18la changes were assessed. H3K18la was inhibited using 2-DG, sodium oxalate, or P300 inhibitors (A-485/C646), measuring adhesion molecule expression. Sodium lactate or EX-527 restored H3K18la, assessing VCAM1/ICAM1 changes, monocyte adhesion/migration, and NF-κB activity. CUT&Tag sequencing with transcriptomics identified H3K18la regulatory sites on NF-κB molecules.

Results: (1) GEO database analysis showed OSS/TNF-α altered HUVEC gene expression, enriching endothelial inflammation/AS pathways. Cmap screening identified seven compounds, including anti-inflammatory/antioxidant narciclasine. Cellular experiments showed narciclasine inhibited ox-LDL-induced VCAM1, ICAM1, SELE, and CCL2 expression, reducing monocyte migration/adhesion and oxidative stress. In vivo, 0.02 mg/kg narciclasine every other day inhibited plaque formation, reduced plaque VCAM1 and macrophage infiltration, without affecting mouse plasma lipids. (2) Transcriptomics revealed narciclasine regulated glycolytic genes. Cellular experiments showed it inhibited ox-LDL-induced GLUT1/PFKFB3 expression, reducing glucose uptake/glycolysis. Sodium pyruvate reversed narciclasine's suppression of adhesion molecules and monocyte adhesion. In mice, narciclasine inhibited plaque GLUT1 without affecting AMPK, mitochondrial potential, or oxidative phosphorylation. (3) Narciclasine inhibited ox-LDL-induced lactate/Pan Kla levels, particularly H3K18la (not H3K9la/14la). In mice, it reduced carotid H3K18la. H3K18la inhibition via 2-DG, sodium oxalate, or P300 inhibitors reduced

ox-LDL-induced adhesion molecules. Narciclasine upregulated SIRT1; sodium lactate/EX-527 restored adhesion molecule expression, monocyte adhesion/migration, and NF-κB activation. CUT&Tag/transcriptomics showed narciclasine-regulated genes enriched in NF-κB pathways, with TRAF6, cIAP1/2, RIP1, and IKKB promoters showing lactate-dependent H3K18la regulation.

Conclusions: Integrating multi-omics and bioinformatics, we identified narciclasine as an effective anti-inflammatory compound inhibiting AS plaque formation. Narciclasine reduces endothelial glycolysis and lactate accumulation, modulating H3K18la-mediated NF-κB activation to suppress inflammation and plaque progression. This study elucidates narciclasine's anti-inflammatory mechanism in AS, providing novel molecular insights and therapeutic strategies for inflammation-targeted AS treatment.

免疫检查点抑制剂相关心血管不良事件影响因素的 Meta 分析

李婷婷 汪正艳 史铁英

大连医科大学附属第一医院

目的 系统分析免疫检查点抑制剂患者发生心血管不良事件的危险因素，为临床护理实践提供参考。方法 在 Pubmed、Embase、Cochrane Library、Web of Science、中国知网、万方数据、维普数据库、中国生物医学文献数据库中搜集相关文献，检索时限为建库至 2024 年 10 月 31 日，由 2 名研究者对文献进行筛选、资料提取和质量评价后，采用 RevMan 5.4 软件进行分析。结果 本研究共纳入的 21 篇文献，其中 14 篇为队列研究，6 篇为病例对照研究，2 篇为横断面研究。研究中的 21 篇文献共提取了 16 个危险因素。分析结果显示，Khorana 评分≥ 2、高血压、血栓栓塞史、心衰史、冠心病史、心脏病史、存在疾病（肝、脑）转移、存在免疫相关不良事件史、接受抗凝治疗、免疫联合治疗、联合其他治疗和中性粒细胞 / 淋巴细胞比值是免疫检查点抑制剂患者发生心血管不良事件的危险因素（均 P < 0.05），男性是免疫检查点抑制剂患者发生心血管不良事件的保护因素（均 P < 0.05）。结论 免疫检查点抑制剂患者发生心血管不良事件受较多因素影响，医护人员应针对心血管不良事件危险因素，进行早期筛查、及早干预。临床医护人员可参考本研究相关分析结果，根据提出的危险因素及保护因素进行评估，对患者给予针对性预防措施，提供精准化干预，降低免疫检查点抑制剂患者的心血管不良事件发生率，进而改善患者的预后。

Associations of Metabolic Vulnerability Index with microvascular complications and all-cause mortality intype 2 diabetes mellitus patients: a prospective cohort study of UK Biobank

Gaoyu Yu, Yilin ChenChen, Yao Xie

The Second Affiliated Hospital, Zhejiang University School of Medicine

Background:

Diabetic microvascular complications (MCD) significantly impact long-term prognosis in type 2 diabetes mellitus (T2DM) patients. The Metabolic Vulnerability Index (MVX), a novel biomarker integrating systemic inflammation and metabolic malnutrition, is associated with mortality in patients with cardiovascular diseases. However, the association between MVX and the risk of microvascular diseases and mortality in patients with T2DM is unknown. This study aims to evaluate the utility of the MVX score in assessing the risk of microvascular complications in T2DM patients, with the goal of providing new insights for long-term complication risk stratification and intervention.

Methods:

The UK Biobank is a prospective cohort study that enrolled approximately half a million participants from the UK between 2006 and 2010, aged 40 to 69 years. At baseline, data on self-reported health conditions, physical measurements, and biological samples were collected through touchscreen questionnaires, verbal interviews, and assessment centers nationwide. This prospective analysis included 11,207 T2DM participants without baseline microvascular complications from the UK Biobank. The MVX score was derived from nuclear magnetic resonance (NMR)-measured metabolites (GlycA, small HDL, branched-chain amino acids, citrate concentration). Outcomes included incident nephropathy, neuropathy, retinopathy, and all-cause mortality. Kaplan-Meier curve, Cox proportional hazards models and restricted cubic spline (RCS) were performed to evaluate the associations between MVX score and the risk of microvascular complications and all-cause mortality. The impact of MVX on model improvement was additionally accessed.

Results:

Over 13.15 years (median follow-up), 22.6% developed microvascular complications. Adjusted hazard ratios (HRs) for the highest MVX quartile (vs. lowest) were 1.32 (95% confidence interval: 1.15–1.51) for composite microvascular complications, 1.41 (95% confidence interval: 1.18–1.69) for diabetic nephropathy, 1.62 (95% confidence interval: 1.18–2.22) for diabetic neuropathy, and 1.36 (95% confidence interval: 1.17–1.58) for all-cause mortality. No significant association was observed for diabetic retinopathy (HR=0.97, 95% confidence interval: 0.79–1.20). RCS analyses indicated linear association of the MVX score with microvascular complications and all-cause mortality (all P values for nonlinearity>0.05). In stratified analyses, no statistically significant interactions were identified between MVX and other stratified variables, including age, sex, ethnicity, baseline diabetes duration, hypertension, or dyslipidemia. Sensitivity analyses largely confirmed the robustness of the findings. Excluding patients with undefined diabetes, those with events occurring within two years, or those with baseline cardiovascular disease (CVD), and adjusting for the age of onset of Type 1 diabetes (T1D), produced consistent results. Similarly, restricting the analysis to cases with complete data or applying the Fine-Gray competing risk model yielded comparable associations between the MVX score and all outcomes. Finally, model improvement was assessed by comparing the parameters of the fully adjusted model before and after incorporating the MVX score. The Harrell's C-statistic, NRI, and IDI demonstrated the modest incremental value of MVX in improving the model after adjusting for established traditional risk factors.

Conclusions:

Higher MVX scores were associated with an increased risk of developing microvascular complications, especially diabetic nephropathy, diabetic neuropathy, and all-cause mortality. The interaction of systemic inflammation and metabolic dysregulation may play a crucial role in the development of microvascular complication and all-cause mortality. This study represents one of the few large-scale prospective investigations of T2DM microvascular complications. To our knowledge, this is the first to evaluate the risk stratification capability of composite biomarkers for T2DM microvascular complications and all-cause mortality.

Threshold Effect of Systemic Immune-Response Index on In-Stent Neoatherosclerosis Among Patients With Drug-Eluting Stent Restenosis

Shuang-Ya Yang, Ning Gu, Chan-Cui Deng, Yong-Chao Zhao, Zhi-Jiang Liu, Ran-Zun Zhao, Bei Shi

The Affiliated Hospital of Zunyi Medical University

Background:

In-stent neoatherosclerosis (ISNA) has become an important pathological mechanism underlying in-stent restenosis (ISR) following drug-eluting stent (DES) implantation. Although DES significantly reduces the incidence of early restenosis by inhibiting neointimal hyperplasia, the proportion of late and very late stent failures has gradually increased, with ISNA playing a key role. The characteristics of neoatherosclerosis include the accumulation of lipid-laden foam cells and the presence of thin fibrous caps within the neointima, with a pathological process similar to native coronary atherosclerosis. Studies have shown that inflammation plays a predominant role in the occurrence and development of ISNA; however, reliable biomarkers for accurately predicting ISNA risk are still very limited. The systemic immune-response index (SIRI), which is calculated from routine blood cell counts (neutrophil count × monocyte count / lymphocyte count), has been found in recent years to be associated with adverse cardiovascular outcomes. However, its role in the process of ISNA development in DES-ISR patients has not been fully explored.

Methods:

This was a retrospective analysis involving 212 patients with DES-ISR. All patients underwent coronary angiography and optical coherence tomography (OCT) at least 12 months after the initial stent implantation. ISR was confirmed based on coronary angiography results, and researchers used OCT to perform detailed assessments of the presence and features of in-stent neoatherosclerosis and thin-cap fibroatheroma (TCFA). All patients were divided into three groups according to SIRI tertiles, with SIRI data obtained from routine blood tests prior to the procedure. To comprehensively evaluate the association between SIRI and ISNA risk, multivariate logistic regression was used to adjust for multiple confounding factors, including age, sex, common cardiovascular risk factors, and medication use. In addition, smooth curve fitting and threshold effect analyses were performed to explore the nonlinear relationship between the two, and subgroup analyses were conducted to validate this relationship in different populations.

Results:

The analysis showed that the incidence of ISNA and TCFA was significantly higher in patients with high SIRI compared with those with low SIRI (both P < 0.05), suggesting that elevated systemic inflammation is closely associated with in-stent neoatherosclerotic changes. In multivariate regression analysis, SIRI, as a continuous variable, remained an independent risk factor for ISNA (OR per unit increase = 1.23, 95% CI: 1.04–1.47, P = 0.018). Further statistical analysis revealed a significant nonlinear relationship between SIRI and ISNA risk, with an inflection point at a SIRI value of 3.95: below this threshold, ISNA risk increased sharply as SIRI rose; above this threshold, the risk plateaued. Additionally, subgroup analysis showed that the association between SIRI and ISNA risk was generally consistent across most populations, with a significant interaction observed only in patients younger than 60 years (OR = 1.94, 95% CI: 1.23–3.05, P for interaction = 0.010).

Conclusion:

This study suggests that in patients with DES-ISR, SIRI is independently and nonlinearly associated with the risk of in-stent neoatherosclerosis, with a key inflection point at a SIRI value of 3.95. Notably, even mild elevations in SIRI below 3.95 are significantly associated with increased ISNA risk. Clinically, dynamic assessment of SIRI may serve as a simple tool to identify high-risk patients for restenosis and neoatherosclerosis after DES implantation, providing support for individualized secondary prevention strategies. However, large-scale prospective studies are still needed to further validate these findings and explore the underlying mechanisms.

AMPK-CLYBL 乙酰化正反馈环路通过代谢重编程与炎症反应加剧心脏重塑

张乃今

中国医科大学附属第一医院

目的：巨噬细胞代谢重编程是炎症反应的核心驱动因素，但其调控机制尚未完全阐明。本研究旨在揭示 AMPK-CLYBL 乙酰化正反馈环路在连接代谢重编程与炎症反应中的作用，并探究其对高血压相关心脏重塑的病理影响。

方法：通过定量乙酰化组学分析鉴定 CLYBL 为 SIRT2 的作用底物及关键乙酰化位点（K154）。采用免疫共沉淀技术验证 CLYBL 与乙酰转移酶 CBP、去乙酰化酶 SIRT2 的相互作用。在 RAW264.7 巨噬细胞模型中，使用脂多糖（LPS）模拟炎症刺激，联合 AMPK 激动剂（AICAR）处理，通过 Western blot 检测 AMPK 磷酸化、SIRT2 表达及 CLYBL 乙酰化水平。构建 CLYBL-K154R（不可乙酰化突变体）评估其对 NLRP3 炎性体活化和巨噬细胞极化（流式细胞术检测 CD86，免疫荧光分析 iNOS）的影响。建立血管紧张素 II（Ang II，1.4 mg/kg/d，4 周）诱导的高血压心脏重塑模型，利用 SIRT2 基因敲除（SIRT2-KO）和 SIRT2-Flag 转基因（SIRT2-Flag-TG）小鼠分别模拟 CLYBL 高乙酰化和低乙酰化状态，通过超声心动图（检测射血分数和短轴缩短率）、Masson 三色染色（评估胶原沉积）、CD68 免疫荧光（分析巨噬细胞浸润）及炎性因子 mRNA 检测评估心脏结构与功能变化。

结果：乙酰化组学证实 CLYBL-K154 是 SIRT2/CBP 调控的关键位点。LPS 刺激通过抑制 AMPK 磷酸化降低 SIRT2 活性，显著增强 CLYBL-K154 乙酰化，形成 AMPK 低磷酸化 -CLYBL 高乙酰化正反馈环路。CLYBL-K154R 突变有效抑制 LPS 诱导的 NLRP3 炎性体活化、促炎因子释放及巨噬细胞向 M1 型极化。在心脏重塑模型中，CLYBL 高乙酰化状态加剧 Ang II 诱导的心肌损伤：表现为胶原沉积增加、心功能下降、单核 / 巨噬细胞浸润及心脏局部炎性因子表达升高；而 CLYBL 低乙酰化状态则显著改善上述病理改变。

结论：TLR 激活通过 AMPK 低磷酸化 -SIRT2 下调 -CLYBL-K154 高乙酰化轴形成正反馈环路，驱动巨噬细胞代谢重编程与炎症反应。CLYBL 乙酰化通过促进单核细胞心脏浸润和炎性因子释放，直接加剧高血压性心脏重塑进程。靶向抑制 CLYBL-K154 乙酰化可阻断该病理机制，为炎症相关心血管疾病提供新干预策略。

泛血管疾病的视角下的胞葬作用

赵永超 李滢

遵义医科大学附属医院

目的：本综述旨在深入探讨胞葬在泛血管疾病中的重要性，尤其在动脉粥样硬化形成和进展中的作用机制，并总结最新的研究成果。通过对胞葬的生物学机制及其对泛血管健康影响的分析，本文希望为未来的研究方向和临床应用提供新的视角。

方法：总结最新的研究成果。

结果：胞葬（Efferocytosis）是巨噬细胞、树突状细胞等通过识别凋亡细胞表面磷脂酰丝氨酸，经 MerTK、Axl 等受体及 PI3K/Akt、NF-κB 等信号通路清除凋亡细胞的过程，能维持组织稳态、调节炎症反应，与多种疾病相关。泛血管疾病作为全球范围内的主要健康威胁，其各种病理机制复杂，胞葬在其中起到一定作用，能够通过清除凋亡细胞来维持组织的稳态，减轻炎症反应，并促进修复过程。动脉粥样硬化中，其效率影响泡沫细胞形成，能力下降会促进泡沫细胞生成，加速病变；抑制巨噬细胞胞葬会加剧斑块不稳定性。心脏缺血再灌注损伤时，胞葬通过清除受损细胞、调节炎症与细胞信号，影响心脏修复再生。糖尿病相关心血管疾病中，高血糖抑制巨噬细胞胞葬功能，引发慢性炎症，加速动脉粥样硬化，延缓相关伤口愈合。治疗上，调控胞葬为潜在策略，如靶向 Legumain 可增强巨噬细胞胞葬能力，改善心功能。

结论：研究显示胞葬对动脉粥样硬化有双重影响，虽作为治疗靶点前景广阔，但机制理解需深化，未来需探究其在疾病不同阶段的作用，开发特异性药物，推动基础与临床研究结合以促进转化应用。

MicroRNA-27a-5p Protects Against Diabetic Vascular Injury by Suppressing NOX4-Driven Autophagy via MAPK Signaling

Yi-wen Wang, Feng Zhang, Jia-Tian Cao

Zhongshan Hospital, Fudan University

Background: Diabetes mellitus (DM) is recognised as a worldwide epidemic that drives macro- and micro-vascular complications responsible for the majority of diabetes-related disability and mortality. Endothelial dysfunction, impaired post-ischaemic angiogenesis, and deregulated autophagy/apoptosis represent core pathophysiological processes linking chronic hyperglycaemia to tissue ischaemia, non-healing ulcers and major adverse cardiovascular events. MicroRNAs (miRNAs) have emerged as pivotal post-transcriptional regulators of endothelial homeostasis; nonetheless, the precise roles and downstream targets of individual miRNAs in diabetic vascular injury remain incompletely defined. MiR-27a-5p is highly enriched in vascular endothelium, yet its contribution to diabetic vasculopathy has not been systematically investigated.

Objective: We set out to elucidate (i) whether miR-27a-5p is mechanistically involved in hyperglycaemia-driven endothelial injury and angiogenic failure, (ii) how it modulates autophagy and apoptosis under diabetic conditions, and (iii) which downstream effector(s) mediate its vascular actions in vitro and in vivo.

Methods: Human umbilical vein endothelial cells (HUVECs) were exposed to advanced glycation end-products (AGE-BSA, 100 μg ml $^{-1}$) to emulate the diabetic milieu. Gain- and loss-of-function approaches included transfection with miR-27a-5p mimics/inhibitor, NOX4 siRNA, or NOX4 over-expression plasmid. Autophagy flux was quantified by LC3B-II/p62 immunoblotting, mCherry-GFP-LC3 dual fluorescence and transmission electron microscopy. Apoptosis was assessed by Annexin-V/PI cytometry and cleaved caspase-3/BAX expression. Functional readouts encompassed proliferation (CCK-8), migration (scratch assay), tube formation, and intracellular ROS profiling (DCFH-DA, Amplex-Red, DHE). Whole-transcriptome RNA-seq followed by KEGG/GO enrichment, miRWalk/TargetScan prediction and dual-luciferase validation identified direct miRNA targets. For translational corroboration, type-2 diabetic (db/db) and age-matched C57BL/6 mice underwent femoral artery ligation to induce hind-limb ischaemia (HLI). A recombinant adenovirus expressing the miR-27a precursor (Ad-miR-27a-5p) or control vector was injected intramuscularly on days 1 and 7 post-HLI. Perfusion recovery was serially quantified by laser Doppler imaging; gastrocnemius tissue was subjected to immunoblotting, CD31 immunohistochemistry, and CD31-co-localised TUNEL/LC3B immunofluorescence.

Results:

1.AGE exposure triggered a dose- and time-dependent suppression of endogenous miR-27a-5p, accompanied by excessive LC3B-II accumulation, p62 build-up, ROS generation, apoptotic signalling and profound impairment of endothelial proliferation, migration and tubulogenesis (all $p < 0.01$ versus BSA). NAC abrogated ROS, normalised autophagy markers and restored endothelial function, supporting a ROS-dependent mechanism.

2.Ectopic miR-27a-5p expression reinstated autophagic flux (reduced LC3B-II/p62, fewer autolysosomes), curtailed apoptosis (↓ cleaved caspase-3/BAX, ↓ Annexin-V $^{+}$ cells), and rescued proliferation, migration and tube formation under AGE stress ($p < 0.001$ versus AGE + miR-NC). Conversely, miR-27a-5p inhibition aggravated all deleterious AGE effects.

3.Transcriptomics highlighted the AGE-RAGE axis and reactive-oxygen species pathways; NOX4 emerged as the most up-regulated mRNA repressed by miR-27a-5p. Bioinformatics revealed a conserved 8-mer seed match within the NOX4 3□-UTR. MiR-27a-5p markedly reduced NOX4 mRNA/protein and dampened NOX4-derived H_2O_2 (but not superoxide). A wild-type NOX4 3□-UTR luciferase construct was suppressed by miR-27a-5p mimics (-55 %, $p < 0.0001$), whereas the mutant reporter was unresponsive, confirming direct targeting.

4.NOX4 over-expression re-induced LC3B-II/p62 accumulation and autophagic flux blockade despite miR-27a-5p presence, whereas NOX4 knock-down phenocopied miR-27a-5p over-expression, normalising autophagy and diminishing apoptosis. Mechanistically, NOX4 drove phosphorylation of MAPK family members (ERK1/2, JNK, p38); silencing NOX4 or scavenging ROS attenuated MAPK activation, positioning NOX4-derived H_2O_2 upstream of MAPK-dependent autophagy.

5.In vivo, diabetic mice displayed blunted perfusion recovery (14-day perfusion ratio 0.46 ± 0.05) versus non-diabetic controls (0.81 ± 0.04, $p < 0.001$), associated with elevated NOX4, autophagy and apoptosis markers and reduced CD31 $^{+}$ capillary density. Ad-miR-27a-5p delivery (confirmed 12-fold miR-27a-5p up-regulation) accelerated perfusion recovery to 0.74 ± 0.06 ($p < 0.01$ versus Ad-NC), increased CD31 $^{+}$ microvessel density by 1.8-fold, and decreased endothelial TUNEL and LC3B puncta, concomitant with lowered NOX4 and MAPK phosphorylation.

Conclusions: MiR-27a-5p is down-regulated by AGEs and serves as an endogenous brake on NOX4-mediated oxidative stress, MAPK hyper-activation, and maladaptive autophagy/apoptosis in endothelial cells. Restoring miR-27a-5p expression re-equilibrates autophagic flux, protects endothelial viability and function, and markedly improves post-ischaemic neovascularisation in diabetic limbs. The miR-27a-5p/NOX4/MAPK axis therefore represents a compelling therapeutic target and biomarker nexus for mitigating diabetic vascular complications.

Significance: This work provides the first integrated mechanistic and translational proof that miR-27a-5p supplementation can reverse diabetes-induced vascular damage through precise modulation of redox-autophagy crosstalk. Given the current lack of clinically effective strategies to enhance angiogenesis in diabetic patients, miR-27a-5p-based interventions—or pharmacological mimetics that inhibit NOX4—hold promise for novel RNA-therapeutic and drug-discovery programmes aimed at limb salvage, myocardial repair and broader vasculo-protective indica-

tions in diabetes.

SGLT-2 Inhibition Mitigates Neutrophil-Driven Endothelial Injury in Diabetic Coronary Artery Disease by Suppressing GREM1 and Restoring TGF-β/Smad Signalling

wenyuan zheng, Jia-Tian Cao,

Zhongshan Hospital, Fudan University

Background:Type 2 diabetes mellitus (T2DM) accelerates atherosclerosis and nearly doubles the incidence of adverse events in coronary artery disease (CAD). Mounting clinical and experimental evidence implicates excessive neutrophil activation—including over-production of reactive oxygen species (ROS), release of neutrophil elastase and pro-inflammatory cytokines, and formation of neutrophil-extracellular traps (NETs)—as a pivotal driver of endothelial dysfunction and plaque instability in this setting. Sodium-glucose cotransporter-2 inhibitors (SGLT-2i) have emerged as first-line glucose-lowering agents that consistently reduce cardiovascular events, yet the immunomodulatory mechanisms behind their vascular benefits remain incompletely understood. Gremlin-1 (GREM1), an antagonist of bone morphogenetic protein (BMP) family ligands, has recently been linked to acute coronary syndromes in diabetes; by binding BMPs, GREM1 attenuates canonical TGF-β/Smad signalling, a pathway known to restrain neutrophil cytotoxicity. We therefore postulated that SGLT-2 inhibition protects the diabetic coronary vasculature by down-regulating neutrophil GREM1, thereby restoring TGF-β/Smad activity and curbing neutrophil-mediated endothelial injury.

Methods:We adopted a multi-tiered translational strategy encompassing (i) human peripheral blood studies, (ii) in-vitro cell-interaction assays, and (iii) an in-vivo murine model of diabetic cardiomyopathy. Peripheral neutrophils were isolated from three well-matched groups: healthy controls (n = 15), patients with CAD + T2DM (n = 15), and CAD + T2DM patients treated with SGLT-2i for ≥ 12 weeks (empagliflozin or dapagliflozin; n = 15). Bulk RNA-sequencing identified differentially expressed genes (DEGs) and enriched pathways; key hits were validated by qPCR, immunoblotting, and flow cytometry. Systemic neutrophil activation was quantified by serum cell-free double-stranded DNA (dsDNA) and elastase-2 ELISAs. Functional cytotoxicity was gauged by co-culturing patient-derived neutrophils with luciferase-labelled human aortic endothelial cells (HAEC-Luc) at graded effector-to-target ratios (2.5–20:1). Endothelial viability (luciferase activity), supernatant H_2O_2, TNF-α, and nitric oxide (NO) were measured ± SGLT-2i (10 μmol/L) or an anti-GREM1 neutralising antibody. For in-vivo corroboration, streptozotocin/high-fat diet–induced diabetic C57BL/6J mice were randomised to vehicle or empagliflozin (10 mg kg^{-1} d^{-1}) for 6 weeks; sham-fed non-diabetic littermates served as controls. End-points included fasting glucose, serum creatine kinase (CK), CK-MB, peripheral neutrophil counts ($CD11b^+Ly6G^+$), cardiac MPO staining, myocardial collagen deposition (Masson), and expression of Grem1 and Smad1/5/9 phosphorylation.

Results:1. Transcriptomic profilingrevealed 186 DEGs between untreated and SGLT-2i–treated neutrophils, with GREM1 ranking among the top down-regulated genes . KEGG enrichment highlighted the TGF-β pathway as the most significantly restored signalling cascade following SGLT-2 inhibition.

2. Compared with healthy controls, CAD + T2DM patients exhibited a 1.6-fold rise in circulating neutrophil percentage, 2.3-fold higher dsDNA, 1.9-fold higher elastase-2, and a 3.4-fold increase in neutrophil GREM1 protein, accompanied by a 47 % reduction in phospho-Smad1/5/9 (all $p < 0.01$). SGLT-2i therapy normalised these metrics toward control values without altering total leukocyte counts or ejection fraction.

3. Patient-derived neutrophils induced proportional HAEC-Luc death, elevated H_2O_2 and TNF-α, and depleted NO in a ratio-dependent manner. Addition of SGLT-2i or anti-GREM1 antibody reduced endothelial death by >45 %, cut H_2O_2 and TNF-α by 40–50 %, restored NO by 35 %, suppressed neutrophil elastase and CitH3, and re-phosphorylated Smad1/5/9 (all $p < 0.01$ vs. untreated neutrophils).

4. In diabetic mice, empagliflozin lowered fasting glucose, CK , CK-MB , and peripheral $CD11b^+Ly6G^+$ neutrophils Serum dsDNA, elastase-2, and cardiac Grem1 expression decreased by 48 %, 53 %, and 60 %, respectively, while myocardial p-Smad1/5/9 rose 2.1-fold. Histology confirmed marked reductions in MPO-positive infiltrates and interstitial fibrosis (collagen area 11 % vs. 22 % in vehicle, $p < 0.001$).

Conclusion:Our integrated human, cellular, and animal data identify neutrophil GREM1–mediated blockade of TGF-β/Smad signalling as a previously unrecognised mechanism linking metabolic stress to endothelial injury in diabetic CAD. SGLT-2 inhibition dismantles this pathological axis—down-regulating GREM1, re-activating Smad phosphorylation, dampening neutrophil cytotoxicity, and ultimately preserving vascular and myocardial integrity. Beyond illuminating how SGLT-2i confer cardiovascular benefit independent of glycaemia, the study positions the neutrophil GREM1/TGF-β pathway as a promising therapeutic target for cardio-metabolic disease. Prospective trials integrating GREM1 or NET biomarkers could refine patient selection and serve as pharmacodynamic readouts for next-generation vascular immunotherapies.

Liensinine Attenuates Coxsackievirus B3-Induced Viral Myocarditis by Inhibiting NLRP3-Mediated Pyroptosis via Improved Mitochondrial Function

梁 馨月 , Chao Ma, Hai-Tao Yuan

Shandong Provincial Hospital Affiliated to Shandong First Medical University

Abstract: Viral myocarditis (VMC), predominantly caused by Coxsackievirus B3 (CVB3), is a severe inflammatory cardiac disorder critically involving cardiomyocyte pyroptosis and mitochondrial dysfunction. Liensinine (Lien), a natural alkaloid, exhibits diverse pharmacological properties including antioxidant, anti-arrhythmic, and anti-fibrotic effects. Prior evidence indicates Lien ameliorates mitochondrial dysfunction in doxorubicin cardiomyopathy by inhibiting dynamin-related protein 1 (Drp1) phosphorylation at Serine 616 (Ser616), thereby reducing apoptosis. This study systematically investigated the therapeutic efficacy of Lien in a CVB3-induced VMC model and elucidated its underlying molecular mechanisms, particularly its role in regulating NLRP3 inflammasome-mediated pyroptosis. In vivo, 48 male BALB/c mice were randomly allocated into four groups: Control (Con), Lien alone (Lien), CVB3-infected VMC model (VMC), and CVB3-infected + Liensinine treated (VMC+Lien). Cardiac systolic function was assessed via echocardiography on day 7 post-infection. Histopathological evaluation of myocardial inflammation and fibrosis was performed using Hematoxylin & Eosin (H&E) and Masson's trichrome staining. Serum levels of cardiac injury markers (cardiac Troponin I, cTnI; Creatine Kinase-MB, CK-MB) and inflammatory cytokines (Tumor Necrosis Factor-alpha, TNF-α; Interleukin-6, IL-6; Interleukin-1 beta, IL-1β; Interleukin-18, IL-18) were measured by enzyme-linked immunosorbent assay (ELISA). Expression of key pyroptosis-related proteins (NLRP3, cleaved caspase-1, N-terminal Gasdermin D [N-GSDMD]) was analyzed using Western blotting. In vitro, an H9c2 cardiomyoblast model of CVB3 infection was established. Pyroptosis-related protein expression was quantified using Western blotting and confirmed by cellular immunofluorescence. Mitochondrial function was comprehensively assessed: mitochondrial membrane potential (ΔΨm) was measured using the fluorescent probe JC-1; intracellular reactive oxygen species (ROS) levels were determined fluorometrically using 2′,7′-dichlorofluorescin diacetate (DCFH-DA); and cellular adenosine triphosphate (ATP) levels were quantified colorimetrically. **Key findings:** (1) **Liensinine ameliorates CVB3-induced myocardial injury and cardiac dysfunction** in vivo**:** Administration of Lien significantly improved the survival rate of VMC mice and markedly enhanced left ventricular systolic function assessed by echocardiography. Lien treatment effectively attenuated myocardial inflammatory cell infiltration and suppressed collagen deposition/fibrosis as observed histologically. Concordantly, serum levels of cardiac injury markers (cTnI, CK-MB) and pro-inflammatory cytokines (TNF-α, IL-6, IL-1β, IL-18) were significantly reduced in the VMC+Lien group compared to the untreated VMC group. (2) **Liensinine suppresses CVB3-induced pyroptosis in myocardium and H9c2 cells:** CVB3 infection significantly upregulated the expression of key pyroptosis markers (NLRP3, cleaved caspase-1, N-GSDMD) in both mouse myocardial tissue and infected H9c2 cells. Critically, Liensinine treatment potently inhibited the activation of the NLRP3 inflammasome and effectively suppressed downstream pyroptotic events, evidenced by reduced expression of these crucial proteins in both experimental models. (3) **Liensinine enhances mitochondrial function and reduces oxidative stress:** Assessment of mitochondrial parameters revealed that Liensinine significantly restored the CVB3-induced loss of mitochondrial membrane potential (ΔΨm) in H9c2 cells, indicated by JC-1 staining. Furthermore, Lien treatment significantly increased cellular ATP levels, demonstrating improved energy metabolism. Crucially, Lien effectively curtailed the excessive generation of intracellular ROS triggered by CVB3 infection, as detected by DCFH-DA fluorescence. **Conclusion:** This study demonstrates that Liensinine confers substantial cardioprotection against CVB3-induced VMC. Its therapeutic efficacy is mechanistically linked to the amelioration of mitochondrial dysfunction (restoring ΔΨm, enhancing ATP production, mitigating oxidative stress), which subsequently leads to the suppression of NLRP3 inflammasome activation and the downstream pyroptotic cell death pathway. These concerted actions culminate in reduced myocardial injury, diminished inflammation and fibrosis, improved cardiac systolic function, and enhanced survival. Liensinine represents a promising therapeutic candidate targeting mitochondrial integrity and the NLRP3-mediated pyroptotic cascade for the treatment of viral myocarditis.

Integrative Analysis of Lactylation-Associated Features in Abdominal Aortic Aneurysm and Its Immune Microenvironment Utilizing scRNA-seq and Bulk RNA Sequencing

Jiexin Li, Yang-Xin Chen

Sun Yat-sen Memorial Hospital

Background

Abdominal aortic aneurysm (AAA) is a life-threatening vascular disorder characterized by abdominal aortic dilation exceeding 30 millimeters

in diameter, with rupture mortality rates surpassing 80 percent and an age-standardized global death rate of 2.19 per 100,000 individuals. Current clinical management relies exclusively on surgical intervention and endovascular repair due to the absence of effective pharmacological therapies. Immune dysregulation plays a pivotal role in AAA pathogenesis, where infiltrating immune cells promote apoptosis of aortic wall cells, facilitate phenotypic transition of vascular smooth muscle cells, and drive extracellular matrix degradation through protease secretion. Although lactate metabolism and its derivative post-translational modification lactylation have been implicated in immune regulation across various diseases–including the transformation of proinflammatory M1 macrophages to anti-inflammatory M2 macrophages via lactylation–their specific contributions to AAA pathogenesis remain uncharacterized.

Methods

This study integrated single-cell RNA sequencing (scRNA-seq) data from the GSE166676 dataset (4 AAA samples, 2 control samples) and bulk RNA sequencing data from five independent cohorts (GSE269845, GSE183464, GSE57691, GSE47472, GSE7084; total 80 AAA samples, 37 controls). Single-cell data underwent stringent quality control: genes expressed in fewer than 3 cells were excluded; cells with fewer than 200 or more than 2,500 detected genes were removed; and cells with mitochondrial gene content exceeding 25 percent were eliminated, retaining 8,350 high-quality cells and 19,823 genes. Unsupervised clustering identified 20 cell clusters subsequently annotated into eight major types (B cells, T cells, natural killer cells, smooth muscle cells, fibroblasts, stem cells, macrophages, endothelial cells) via marker genes and the ACT database. Lactylation activity was quantified using ten computational methods (AUCell, singscore, ssGSEA, UCell, JASMINE, viper, AddModuleScore, scSE, zscore, GSVA), with cells stratified into high- and low-lactylation groups by median scores. Differential expression analysis identified 389 upregulated genes in high-lactylation groups, while correlation analysis detected 595 lactylation-associated genes; their intersection defined 65 lactylation-related genes (LRGs). ConsensusClusterPlus stratified 49 AAA patients into lactylation-based subtypes (Cluster 1: n=23; Cluster 2: n=26). Machine learning evaluated 113 algorithm combinations through 10-fold cross-validation, selecting an integrated glmboost and Naive-Bayes model (mean AUC=0.903) to identify hub genes. Validation included immune deconvolution (CIBERSORTx) and quantitative PCR in an angiotensin II-induced AAA mouse model (1,000 nanograms per kilogram per minute for 4 weeks in Apoe – / – mice versus saline controls).

Results

Western blot analysis confirmed significantly elevated global lactylation levels in AAA tissues compared to controls. Single-cell resolution revealed pronounced heterogeneity: smooth muscle cells, natural killer cells, and B cells exhibited substantially higher lactylation activity than endothelial cells, stem cells, T cells, macrophages, and fibroblasts. Immune cells within high-lactylation groups demonstrated markedly increased immune response scores, showing strong positive correlation with lactylation levels. Gene set variation analysis linked high lactylation to activated Kras signaling, Hedgehog signaling, MYC targets, and G2M checkpoint pathways. Cell-cell communication analysis indicated enhanced outgoing and incoming signaling interactions in high-lactylation immune cells. Functional annotation of the 65 LRGs highlighted enrichment in primary immunodeficiency, B cell receptor signaling, and systemic lupus erythematosus pathways, with Gene Ontology terms implicating immune system processes and cell surface localization. Lactylation-based subtyping showed Cluster 2 (high lactylation) had significantly elevated lactylation scores and immune infiltration compared to Cluster 1 (low lactylation), characterized by increased M1 macrophages, memory B cells, and plasma cells. Machine learning identified eight diagnostic hub genes (TNFSF8, HIST1H2AG, CD79B, CD69, BANK1, RPL17, RPL36A, RPS29), all achieving area under the curve values exceeding 0.7 across five validation cohorts. Animal experiments confirmed significant upregulation of Tnfsf8, Hist1h2ag, Cd79b, Cd69, and Bank1 alongside downregulation of Rpl36a and Rps29 in AAA tissues.

Conclusions

This study establishes lactylation as a critical regulator of immune dysregulation in abdominal aortic aneurysm, demonstrating cell-type-specific activity patterns with highest intensity in B cells and natural killer cells. The identification of 65 lactylation-related genes enables stratification of AAA patients into distinct immunological subtypes, while eight machine learning-derived hub genes–experimentally validated in vivo–correlate with specific immune infiltration profiles and demonstrate diagnostic potential. These findings provide mechanistic insights into lactylation-mediated pathways in AAA pathogenesis.

Neutrophil Methylmalonic Acid Promotes Microthrombis Formation and Adverse Cardiac Remodeling Post-Myocardial Infarction Through Activating IL-6 Signaling Pathway-mediated NETosis

Yige Liu, Jiaxin Wang

Second Affiliated Hospital of Harbin Medical University

Background:

Despite advances in reperfusion therapies that have reduced acute infarct size in acute myocardial infarction (MI), adverse ventricular remodeling remains a major cause of heart failure and death worldwide. Beta receptor blockers and RAS inhibitors, targeting the excessive activation of the neuroendocrine system, have been proven to improve cardiac remodeling after MI and reduce the risk of adverse cardiovascular events. Neutrophils, as early responders after MI, have emerged as central mediators of maladaptive cardiac remodeling, yet the upstream immunometabolic mechanisms remain insufficiently understood. Our previous work identified methylmalonic acid (MMA) as a novel prognostic biomarker in cardiovascular disease, with recent evidence implicating MMA in neutrophil activation in congenital methylmalonic acidemia. However, whether neutrophil-derived MMA actively drives NETosis and subsequent adverse cardiac remodeling after MI has not been elucidated.

Methods:

We measured serum and neutrophil MMA levels in both human MI patients and animal models of MI. To establish causality, we generated neutrophil-specific Mmut knockout (Mmut CKO) mice, in which MMA accumulates exclusively in neutrophils. These mice and controls were subjected to MI and treated with either GSK484 (a PAD4 inhibitor targeting NETosis) or DNase I (a NET-degrading agent) to evaluate the contribution of MMA-induced NET formation to post-infarction thrombosis and ventricular remodeling. We further performed high-throughput RNA sequencing on isolated neutrophils to clarify the molecular mechanisms linking MMA accumulation to NETosis.

Results:

Serum and neutrophil MMA levels were significantly higher in AMI patients than in angina controls, with especially pronounced elevation in neutrophils. Notably, elevated NET biomarkers were found in coronary thrombus tissue from patients with higher neutrophil MMA. In the animal model, neutrophil-specific MMA accumulation in Mmut CKO mice led to greater NET formation, increased microthrombus burden, and more severe cardiac dysfunction and remodeling after MI, compared to S100a-8Cre controls. Pharmacologic inhibition of NETosis with GSK484 or DNase I dramatically reduced microthrombus formation and improved cardiac structure and function, particularly in Mmut CKO mice. Transcriptomic and pathway analyses revealed that MMA accumulation in neutrophils drove NETosis through marked activation of the IL-6/JAK1/STAT3 signaling cascade. Administration of IL-6 neutralizing antibody to Mmut CKO mice post-MI significantly suppressed NET formation, reduced cardiac inflammation and microthrombosis, and alleviated ventricular dysfunction and fibrosis. Additionally, colchicine treatment robustly inhibited neutrophilic IL-6 expression, NETosis, and microthrombus formation, resulting in preserved cardiac function and reduced fibrosis post-MI in both wild-type and Mmut CKO mice.

Conclusions:

Our study demonstrates for the first time that neutrophil-intrinsic MMA accumulation is a crucial immunometabolic trigger that promotes IL-6-mediated NETosis and microvascular thrombosis, leading to adverse ventricular remodeling after MI. These findings reveal a novel pathophysiological axis linking neutrophil mitochondrial metabolism, sterile inflammation, and cardiac injury. Targeting the IL-6 signaling pathway, IL-6 neutralizing effectively mitigates MMA-induced NET formation and subsequent maladaptive remodeling, providing a promising and translatable therapeutic strategy to prevent post-MI heart failure–particularly in patients with elevated neutrophil MMA. Overall, our results underscore the clinical relevance of metabolic-immune crosstalk in neutrophils and identify MMA as both a biomarker and driver of post-infarction inflammation and thrombosis, thereby opening new avenues for precision therapy in cardiovascular disease.

Key words: AMI, MMA, Neutrophils, NETosis, thrombosis

α- 酮戊二酸激活心肌细胞 FTO 影响中性粒细胞募集改善脓毒性心肌的机制研究

梁陈陈 杨爽

哈尔滨医科大学附属第二医院

目的：探究 α- 酮戊二酸激活心肌细胞 FTO 通过 m6A 去甲基化转录后调控影响中性粒细胞募集改善脓毒性心肌的具体分子机制。

方法：采用脂多糖腹腔注射构建脓毒性心肌病模型，外源性补充 α- 酮戊二酸，微板法检测各组小鼠心肌细胞 α- 酮戊二酸变化，观察小鼠生存状态，评价心脏功能及心肌组织病理，同时比较各组小鼠血清及心肌组织炎症因子、心肌损伤标志物及凋亡指标变化，使用免疫荧光观察白细胞等免疫细胞分布情况，荧光激活细胞分选分析心脏组织及骨髓中性粒细胞积聚情况，流式细胞术观察中性粒细胞活化及凋亡，随后分析小鼠心脏组织中性粒细胞趋化因子谱。使用腺病毒转染后敲除心肌细胞 FTO，斑点印记法检测 CXCL8 m6A 甲基化水平，WB 和 qPCR 检测 FTO 蛋白及 mRNA 表达情况。使用单因素方差分析用于多组之间的比较，T 检验用于两组之间的统计学分析。

结果：α- 酮戊二酸与脓毒性心肌损伤负相关，且心肌细胞变化最显著。α- 酮戊二酸补充后改善脓毒性心脏功能和小鼠存活率，且 α- 酮戊二酸促进中性粒细胞

在脓毒性心肌中积聚，并增加趋化因子 CXCL8 mRNA 稳定性及蛋白水平，减少 CXCL8 mRNA 的 m6A 修饰。心肌细胞特异性敲减 FTO 会抵消 α- 酮戊二酸对脓毒性心脏的保护作用。

结论：脓毒性心肌病外源性给予 α- 酮戊二酸可以激活心肌细胞 FTO 从而使趋化因子 CXCL8 去甲基化，增加其 mRNA 稳定性及蛋白水平，进而吸引中性粒细胞在心脏中快速有效募集发挥抗菌防御作用。

Systemic inflammation indices affect the association between pericoronary fat attenuation index and adverse prognosis in patients with coronary artery disease

Huang-Tao Ruan, Xiao-Zhao Lu, Jin Liu, Hao-Zhang Huang, Shang-Yi Tang, Zi-Yao Yuan, Zu-Xian Huang, Ji-Yan Chen, Yong Liu, Ning Tan

Guangdong Provincial People's Hospital

Background:

By the time of 2023, there had been still approximately 315 million people with coronary artery disease (CAD) worldwide, which has imposed a huge economic and health burden on society. Inflammation is associated with adverse prognosis of patients with CAD. Hematological indices such as monocyte count, neutrophil count, lymphocyte count and their composite indices, can reflect the state of systemic inflammation (SI). In recent years, the coronary computed tomographic angiography (CCTA)-based imaging index pericoronary fat attenuation index (pFAI) has been proposed, providing a quantitative indicator of coronary artery local inflammation. The above indices have wide applications in evaluating severity and predicting poor prognosis of CAD. However, the joint association of SI indices and pFAI remains unclear. This study aims to investigate whether the pFAI-associated adverse prognosis is affected by SI indices in CAD patients.

Methods:

This study included patients who underwent CCTA and diagnosed with CAD by coronary angiography within 6 months from the Cardiorenal ImprovemeNt-II. Patients who had undergone coronary artery bypass grafting, coronary artery revascularization or cardiac valve surgery were excluded from the study. All the enrolled patients were aged over 18 years and had complete follow-up information. SI indices included systemic immune-inflammation index (SII), systemic inflammation response index (SIRI), monocyte-to-lymphocyte ratio (MLR) and neutrophil-to-lymphocyte ratio (NLR), were extracted from electronic clinical management systems. pFAI represented coronary arteries local inflammation and was quantitatively measured around the 10 mm to 50 mm length segment proximal to the right coronary artery (RCA) from CCTA images. High SI state was defined as SI index level exceeding the median value. High RCA-pFAI values were determined from the median levels of RCA-pFAI (≥ -80.27 Hounsfield units). The primary outcome was major adverse cardiovascular and cerebrovascular event (MACCE), including cardiovascular mortality, acute myocardial infarction and stroke. Cox proportional hazards models were used to calculate the association among SI indices, pFAI and MACCE. Interaction test was used to estimate the interaction between pFAI and SI indices relative to MACCE.

Results:

560 participants with CAD (mean age: 67.7±10.7 years; 29.1% female) were enrolled. After a follow-up of median 5.5 years, a total of 90 (16.1%) MACCEs occurred. After fully adjusted, the Cox regression analysis showed that a high RCA-pFAI level was associated with higher risk of MACCE (adjusted Hazard Ratio [aHR]: 2.16, 95% confidence interval [CI]: 1.30–3.58, P=0.003). Interaction test indicated that the interaction among SIRI, MLR and RCA-pFAI was significant (P for Interaction=0.037 for SIRI and RCA-pFAI; P for Interaction=0.042 for MLR and RCA-pFAI). Elevated level of SIRI, MLR or pFAI alone was not associated with an increased risk of MACCE, while the combined increasing in both SIRI or MLR and RCA-pFAI was associated with higher MACCE risk (aHR: 3.14, 95% CI: 1.55–6.33, P=0.001 in $pFAI_{high}/SIRI_{high}$ group; aHR: 2.82, 95% CI: 1.39–5.73, P=0.004 in $pFAI_{high}/MLR_{high}$ group).

Conclusion:

RCA-pFAI was a risk factor for poor prognosis of CAD patients and can enhance the risk stratification value for adverse prognosis when combined with the systemic inflammation indices. Individuals with high coronary artery local inflammation and high SI state require more aggressive monitoring and risk intervention.

Association between Aggregate Inflammatory Score Index and Hypertension Patients with Coronary Heart Disease: A Cross-Sectional Study Based on NHANES (2005–2016)

Ruiyuan Li, Guang-Yao Zhai

Beijing Luhe Hospital

Abstract

Objective: Atherosclerosis is the underlying cause of coronary heart disease (CHD). Chronic inflammation plays a critical role throughout the entire process of atherosclerotic development and is closely related to the immune mechanisms underlying hypertension (HT). Traditional inflammatory markers, such as C-reactive protein (CRP), procalcitonin, and IL-6, have been shown to be associated with atherosclerosis, acute coronary syndromes, and adverse clinical outcomes. In recent years, as inflammatory markers have been further explored in cardiovascular disease research. Consequently, novel inflammatory biomarkers (AISI) derived from neutrophil, lymphocyte, monocyte, and platelet counts have emerged, reflecting an immune-inflammatory equilibrium. Compared to traditional inflammatory markers, this new indice offer the advantages of being cost-effective and readily accessible, without necessitating active patient involvement. This characteristic renders it particularly valuable for evaluating patients with limited mobility or cognitive impairment.This study aims to investigate novel inflammatory marker (aggregate inflammatory score index, AISI), and its relationship with coronary heart disease (CHD) in patients with hypertension (HT) using data from the National Health and Nutrition Examination Survey (NHANES).

Methods: We conducted a cross-sectional study using complete data from the 2005–2016 NHANES survey. A total of 9,242 hypertensive participants aged 18 years or older were included in the study(2,055 with CHD; 7,187 without CHD). Univariate analysis, multivariate logistic regression analysis, and independent nomogram models were used to explore the relationship between CHD risk and AISI.Participants were divided into HT group and HT combined with CHD group. AISI was calculated as MC × PC × NC/LC. Additionally, demographic, lifestyle factors and health-related information was gathered. Logistic regression models were utilized to pinpoint AISI associated with HT combined with CHD, and constructed three nomogram models to forecast HT combined with CHD risk.

Results: In our cohort of 9,242 patients, 2,055 (30.77%) had CHD.Univariate logistic regression analysis identified gender, age, race, family poverty-to-income ratio (PIR), education level, marital status, smoking status, log2-AISI as significant risk factors (all P < 0.05). Higher levels of log2-AISI (OR 1.13, 95%CI: 1.07 - 1.19, P<0.001) was associated with an increased likelihood of CHD in hypertensive patients. Elevated log2-AISI, along with male gender, older age, non-Mexican American ethnicity, family poverty income ratio (PIR) < 1.5, and smoking, were identified as risk factors for CHD in hypertensive populations. Optimized model using backward stepwise regression also showed log2-AISI (OR 1.13, 95%CI: 1.07 - 1.19, P<0.001) was significant risk factors (Figures 3). The model likelihood ratio chi-square value of the optimized model was 1039.952 (log2-AISI model) (all P < 0.001), and the model was successful. Calibration curve was constructed to assess the deviation between predicted and actual values, with 1,000 bootstrap iterations showing good consistency between predictions and observed outcomes. AUC value of the model was 0.726 (95% CI: 0.714–0.737), respectively. The model had good discrimination power. Decision curve analysis indicated that the nomogram model is effective in clinical practice.

Conclusion: This novel immune-inflammatory marker (AISI) offer a simple, non-invasive, and cost-effective screening tool with promising clinical application for predicting CHD risk in HT population. It have the potential to guide personalized treatment, aligning with the goals of precision medicine.

复方丹参滴丸、乙酰唑胺和红景天苷在急性高原缺氧诱导早期肺损伤中对 HIF1α/CXCR4 通路的调控

张依曼 [1,3] 王飞 [2,3] 刘兵 [1,3] 刘佳 [3] 来宝长 [3] 贾璞 [2] 张军波 [1] 马强 [1] 孟燕 [1] 赵晔 [2] 乌仁塔娜 [5] 郑晓晖 [1,2] 殷倩 [1,3,4] 田红燕 [1]

1. 西安交通大学医学院第一附属医院

2. 西北大学生命科学学院

3. 西安交通大学基础医学院心血管研究中心

4. 陕西省分子心脏病学重点实验室

5. 青海大学医学院高原医学研究中心，青海大学高原医学应用重点实验室

目的：肺血管内皮细胞的炎症反应是低压低氧诱发急性肺损伤的关键病理机制，阐明其潜在作用机制及治疗靶点具有重要意义。复方丹参滴丸、乙酰唑胺和红景天苷是目前治疗急性高原反应的常用药物，本研究拟探讨这些药物防治急性高原缺氧诱导早期肺炎症反应的机制。

方法：采用模拟海拔 6000 米的低压低氧大舱，将小鼠暴露 8、24 和 72 小时构建急性肺损伤模型。通过苏木精 - 伊红染色、组织病理学分析和免疫组化评估炎症程度。采用 Western blotting 检测内皮型一氧化氮合酶（eNOS）磷酸化水平评估内皮损伤。通过高通量 RNA 测序筛选早期炎症调控因子。利用 Western blotting 检测缺氧诱导因子 -1α（HIF1α）、CXC 趋化因子受体 4（CXCR4）等蛋白表达，采用实时荧光定量 PCR 测定 CXCR4 及相关炎症因子的 mRNA 水平。

结果：小鼠肺组织在低压低氧暴露 8 小时后即出现显著炎症浸润，24 小时达到高峰。HIF1α 表达在 8 小时显著上调，随后逐渐降低；CXCR4 作为 HIF1α 的靶基因呈现出相同的变化趋势。预防性地复方丹参滴丸、乙酰唑胺和红景天苷干预可显著抑制低压低氧 8 小时后肺组织中 HIF1α、CXCR4 及相关炎症因子的表达

水平。此外，这些药物干预 72h 对血管内皮功能障碍及炎症反应具有协同保护效应。

结论：本研究表明，内皮细胞 HIF1α/CXCR4 信号轴在低压低氧所致急性肺损伤早期阶段起关键调控作用。复方丹参滴丸、乙酰唑胺和红景天苷对该通路的抑制作用，为急性高原缺氧性肺损伤的临床防治提供了潜在治疗策略。

Prevalence and Risk Factors of Subclinical Atherosclerosis in Chinese Patients with Systemic Lupus Erythematosus

Jiabo Wu, Shuyuan Zhang, Zhuang Tian

Peking Union Medical College Hospital, Chinese Academy of Medical Sciences

Objective: Systemic lupus erythematosus (SLE) is a chronic autoimmune disease associated with markedly increased cardiovascular risk, particularly due to accelerated atherosclerosis. This risk is frequently underrecognized when relying solely on traditional lipid parameters such as low-density lipoprotein cholesterol (LDL-C). To more accurately identify early vascular damage, we aimed to determine the prevalence of subclinical atherosclerosis among Chinese SLE patients using carotid intima-media thickness (CIMT) and to elucidate key clinical, immunological, and therapeutic factors associated with atherosclerotic risk, with particular attention to residual cholesterol (RC), immunosuppressive regimens, and glucocorticoid exposure.

Methods: This prospective observational study included 819 SLE patients from the Chinese CSTAR registry, all of whom were consecutively followed at Peking Union Medical College Hospital between 2022 and 2024. Subclinical atherosclerosis was defined as CIMT > 0.9 mm, measured using standardized carotid ultrasound protocols. Clinical and laboratory characteristics were compared between patients with and without subclinical atherosclerosis. Multivariable logistic regression was used to identify independent risk factors. In addition, restricted cubic spline (RCS) analysis was applied to explore potential non-linear relationships between continuous predictors (age, disease duration, and residual cholesterol) and atherosclerosis risk.

Results: Of the 819 patients (94.5% female; median age 35.0 years), 90 individuals (11.0%) met the criteria for subclinical atherosclerosis. Compared to non-atherosclerotic patients, these individuals were significantly older (median 46.5 vs. 34.0 years, P<0.001), had longer disease duration (96.3 vs. 74.8 months, P=0.004), and demonstrated a higher frequency of hypertension (24.4% vs. 10.4%, P<0.001) and cumulative organ damage as assessed by the SLICC/ACR Damage Index (P=0.007). Interestingly, traditional lipid markers, including LDL-C and total cholesterol, were not significantly different between the two groups (LDL-C: P=0.392; TC: P=0.13), highlighting the limitations of conventional risk stratification in SLE. In contrast, both residual cholesterol (RC) and non-HDL-C levels were significantly elevated in patients with subclinical atherosclerosis (RC: P<0.001; non-HDL-C: P=0.005). Among lipid ratios, Castelli I and the non-HDL/HDL ratio were also higher in the atherosclerotic group. Multivariate logistic regression confirmed that RC was a robust independent predictor of subclinical atherosclerosis (OR=3.31, 95% CI: 1.90–5.81, P<0.001), independent of age, hypertension, and organ damage. The RCS models revealed a non-linear, dose-dependent association between RC levels and the risk of atherosclerosis, with a sharp increase in risk at higher concentrations. Similarly, age and SLE disease duration displayed non-linear trajectories, with risk rising exponentially after certain thresholds (age > 50 years and disease duration > 120 months). In terms of immunosuppressive therapy, no significant associations were found for most conventional agents in univariate comparisons. However, subgroup analysis based on drug combinations revealed trends worthy of further exploration. Patients on HCQ+GC+CYC regimens exhibited the highest odds of subclinical atherosclerosis (OR=1.20), and this regimen was significantly more common among affected patients (P=0.008). In contrast, regimens such as HCQ+MMF and HCQ+GC+MTX appeared to confer a lower risk (OR=0.23 and 0.32, respectively), although the wide confidence intervals preclude definitive conclusions. Glucocorticoid exposure—quantified by cumulative use, frequency of dose adjustments, and maximum dose—did not show significant differences in mean values across groups. Nonetheless, patients with subclinical atherosclerosis had numerically higher maximum GC doses (119.5 vs. 91.9 mg) and shorter GC interval durations, suggesting possible fluctuation and cumulative vascular burden. Additionally, antiphospholipid antibody positivity, particularly anti-cardiolipin antibodies (ACL), was more common among patients with atherosclerosis (26.7% vs. 14.4%, P=0.006), aligning with the prothrombotic component of lupus-related vascular damage.

Conclusion: In this large Chinese SLE cohort, 11% of patients had subclinical atherosclerosis. Residual cholesterol, rather than traditional lipid measures, emerged as a robust early indicator with a non-linear risk trajectory. Additionally, treatment regimens may influence atherosclerosis risk, suggesting potential cardioprotective or aggravating effects. These findings underscore the importance of incorporating RC and treatment stratification into cardiovascular risk assessment for SLE patients..

Complement component C4B prioritization through drug□target Mendelian randomization reveals a novel therapeutic target for calcific aortic valve stenosis

Weijie Li, Jianfang Luo, Yuan Liu, Songyuan Luo

Guangdong Provincial People's Hospital

Background:

Calcific aortic valve stenosis (CAVS) is a progressive cardiovascular disease characterized by the thickening and calcification of the aortic valve, ultimately leading to impaired blood flow and heart failure. Despite its significant morbidity and mortality, no pharmacological therapies currently exist to effectively halt or reverse its progression. Given the limitations of surgical and transcatheter interventions, there is an urgent need to identify novel drug targets for CAVS. Mendelian randomization (MR) analysis, a genetic epidemiological approach that leverages naturally occurring genetic variants as instrumental variables, provides a powerful tool to infer causal relationships between potential drug targets and disease outcomes. In this study, we integrated druggable genome data with cis-expression quantitative trait loci (eQTLs) to systematically identify and validate potential therapeutic targets for CAVS.

Method:

We employed a multi-step analytical framework to identify and validate druggable genes associated with CAVS. First, we integrated the druggable genome—a curated list of genes encoding proteins that are known or predicted to be modulated by drugs—with cis-eQTL data from the eQTLGen Consortium to pinpoint genes with available genetic regulatory variants. We then conducted MR analyses using two independent genome-wide association study (GWAS) datasets for CAVS: the Finngen dataset (discovery cohort) and a genome-wide meta-analysis (replication cohort). Genes demonstrating significant associations in both cohorts underwent further validation, including Bayesian colocalization to assess shared causal variants, as well as Gene Ontology (GO) and Kyoto Encyclopedia of Genes and Genomes (KEGG) enrichment analyses to explore biological pathways. To evaluate potential off-target effects, we performed a phenome-wide association study (PheWAS) to assess horizontal pleiotropy. Additionally, reverse causality MR analysis was conducted to confirm the directionality of the causal relationship. Finally, immunohistochemical (IHC) staining was performed on human aortic valve tissues to validate the expression of the identified target gene at the protein level.

Results:

Among 2,525 MR analyses, seven druggable genes exhibited significant associations with CAVS in both GWAS cohorts. Bayesian colocalization analysis revealed strong evidence of shared causal variants between CAVS and two complement system genes, C4A and C4B, with posterior probabilities (PP.H4) exceeding 75% (C4A: 81.44%; C4B: 81.23%). However, only C4B was consistently identified as a risk factor for CAVS, with an odds ratio (OR) of 1.05 (95% CI: 1.03–1.07, *p* = 6.97E-08) in the discovery phase. Reverse causality MR confirmed the unidirectional effect of C4B on CAVS risk, with no evidence of reverse causation. PheWAS analysis further supported the specificity of C4B, as no significant associations were found with other phenotypes, minimizing concerns about pleiotropic effects. IHC analysis demonstrated significantly stronger C4B immunostaining in calcified aortic valves compared to non-calcified controls. The IHC scores for C4B were markedly higher in CAVS tissues (median: 4 [IQR: 3, 4]) than in controls (median: 3 [IQR: 2, 3], *p* = 0.014). Quantitative assessment of staining intensity revealed that the integrated density values of C4B-positive regions were nearly fourfold higher in calcified valves (1916.95 ± 1118.89) compared to controls (502.34 ± 474.27, *p* = 0.025), further corroborating its role in CAVS pathogenesis.

Conclusion:

Our study identifies C4B, a key component of the immune-complement system, as a novel and genetically supported therapeutic target for CAVS. The robust convergence of MR, colocalization, and protein-level validation highlights the potential of complement inhibition as a pharmacological strategy to mitigate CAVS progression. Future studies should explore the mechanistic role of C4B in valvular calcification and assess the efficacy of complement-modulating therapies in preclinical and clinical settings. These findings open new avenues for the development of targeted therapies to address the unmet clinical need in CAVS management.

载 BNN6/RAPA 纳米粒调控巨噬细胞极化抑制心脏移植急性排斥反应

崔楠

华中科技大学同济医学院附属医院协和医院

目的：

本研究旨在构建并评估一种可调控巨噬细胞极化的新型载药纳米系统，以期用于抑制心脏移植急性排斥反应。在心脏移植排斥反应中，单一免疫抑制剂难以实现“系统 - 局部 - 时空”三重调控。本研究中，我们将雷帕霉素与 NO 供体 BNN6 协同封装于 PLGA 纳米粒内，意在实现多层次、协同机制的免疫干预。雷帕霉素作为系统性基础免疫抑制药物，可广泛降低 T 细胞和 M1 型巨噬细胞活性，起到

“扫清免疫高反应”的作用； BNN6 作为精准免疫调控因子，在超声触发下局部释放 NO，调节巨噬细胞极化状态，诱导 M2 型表型形成，从而在移植局部微环境中发挥“再平衡、再塑型”功能；二者联用形成“系统免疫压制 + 局部炎症调控”的多通路干预模式，有效增强抗排斥治疗的选择性、安全性与靶向性。

方法：

通过双乳液溶剂挥发法制备同时包载 RAPA 和 BNN6 的 PLGA 纳米粒（PLGA-BNN6/RAPA），并采用透射电子显微镜（TEM）、动态光散射（DLS）等手段对其粒径、形貌及稳定性进行表征。通过体外透析实验评估药物释放行为，并在超声刺激下检测 NO 响应对协同释放的调控作用。以大鼠肺泡巨噬细胞 NR8383 为模型，利用流式细胞术及 ELISA 检测其对巨噬细胞 M1 型向 M2 型极化的调控效果，同时采用划痕实验、Transwell 实验和 CCK-8 检测分析材料对细胞活力与迁移能力的影响。在动物实验中，建立大鼠异位心脏移植模型，进一步验证该载药系统对移植物炎症微环境的免疫调控效果。

结果：

PLGA-BNN6/RAPA 纳米粒呈球形，粒径约为 200–270 nm，表面电位稳定，具备良好的分散性和生物相容性。在超声刺激下，BNN6 快速释放 NO 并协同促进 RAPA 的释放。体外实验显示，该载药系统能有效抑制 M1 型标志物（CD86、TNF-α、IL-6、IFN-γ）的表达，同时显著上调 M2 型标志物（CD163、IL-10、TGF-β）的水平。体内实验进一步证实，PLGA-BNN6/RAPA 组在超声作用下可显著诱导心移植物中 M1 型巨噬细胞向 M2 型转化，减少 T 细胞浸润，降低炎症因子水平，减轻急性排斥反应，心移植物存活时间延长。

结论：

本研究成功构建了一个基于 PLGA 纳米载体的双药协同释放系统，通过“系统免疫抑制 + 局部炎症调控”策略，实现对心脏移植排斥反应的多通路干预。雷帕霉素通过 mTOR 通路广泛抑制免疫激活，BNN6 在超声刺激下局部释放 NO，有效诱导 M2 型极化，两者协同作用显著改善巨噬细胞极化状态与免疫微环境。该纳米系统为器官移植后免疫调控提供了新的技术路径与策略支持，具有良好的应用前景。

孟德尔随机化探究心脏淀粉样变危险因素

袁耀

山东大学齐鲁医院

背景 心脏淀粉样变（cardiac amyloidosis, CA）是由于异常折叠蛋白分子构成的不可溶性纤维沉积物在心肌聚集而导致的以心力衰竭、心律失常和心肌缺血为主要表现的临床综合征，是限制性心肌病最常见的病因。近年来，孟德尔随机化（Mendelian Randomization, MR)方法被广泛应用于探索潜在因果风险因素，克服传统观察性研究的混杂偏倚。

方法 本研究利用大规模全基因组关联研究（GWAS）汇总数据，通过两样本孟德尔随机化分析，系统评估了血脂、炎症标志物、心脏代谢特征及多种心血管疾病等与 CA 的因果关系。

结果 遗传预测的低密度脂蛋白胆固醇（LDL-C）升高和脂蛋白 (a) [Lp(a)] 水平增加与 CA 风险显著正相关，而高密度脂蛋白胆固醇（HDL-C）呈保护性关联。此外，系统性炎症标志物（如 IL-6）和收缩压的遗传倾向也与 CA 风险相关。同时，研究也发现门静脉血栓形成的风险也与 CA 患病也成正相关。但糖尿病及冠心病未显示显著因果效应。敏感性分析支持结果的稳健性，且未发现水平多效性。

结论 本研究首次通过 MR 证实了血脂异常和炎症通路在 CA 发生中的潜在因果作用，为早期干预靶点提供了遗传学证据，并提示降脂及抗炎治疗可能对 CA 预防具有临床价值。

关键词: 心肌淀粉样变性，孟德尔随机化，脂蛋白 (a)，低密度脂蛋白胆固醇，炎症，门静脉血栓

Prenatal and Postnatal Ambient Air Pollution and Kawasaki Disease: A Systematic Review and Meta-Analysis

Penghui Yang[1], Jing Zhang[2]

1. West China Second University Hospital, Sichuan University

2. Sichuan Provincial People’s Hospital

Background: Kawasaki disease (KD) is a systemic vasculitis that affects mainly children and has been reported across all ethnicities spanning all continents, with the highest rates in East Asia. Despite the availability of effective treatments, KD still poses a great risk for coronary artery and myocardial inflammatory injury because of either delayed treatment or aggressiveness of the disease. KD is the most common cause of acquired heart disease in children in high-income regions and is associated with a higher risk for cardiovascular events in adulthood, leading to public health concerns. The causes of KD are not completely understood, most likely resulting from the interplay between genetic susceptibility and environmental triggers, involving mechanisms related to immune cell activation, exaggerated inflammatory response, and increased oxidative stress. Air pollution has become a major contributor to the global disease burden, leading to 8.1 million deaths in 2021, including 709,000 deaths in children under 5 years of age. Emerging studies have indicated that exposure to high levels of ambient air pollutants is associated with immune-mediated inflammatory diseases and cardiovascular diseases by triggering innate and adaptive immune responses, inducing inflammation, stimulating oxidative stress, and mediating genetic and epigenetic mechanisms. The geographical clustering and seasonal variation of KD incidence and the multiple overlapping mechanisms of KD and air pollutants link KD with environmental factors, including ambient air pollution. Accumulating evidence indicates associations between ambient air pollution and KD, but the results remain inconsistent. This systematic review and meta-analysis aimed to comprehensively summarize the current evidence on the effects of ambient air pollutants on KD.

Methods: Four electronic databases (PubMed, Web of Science, Embase, and Scopus) were searched from inception to 11 May 2024 (initial search) and 18 January 2025 (final search) for relevant studies investigating the risk of KD after exposure to ambient air pollution. No limitations were placed on publication year or language. A fixed- or random-effects model was used to calculate pooled ORs with 95% CIs for an increase in ambient air pollutant concentration of 10 $\mu g/m^3$. The risk of bias was assessed using the Risk of Bias In Nonrandomized Studies of Exposures tool, and the quality of evidence was assessed by the Grading of Recommendations, Assessment, Development, and Evaluations framework. The protocol was registered with PROSPERO (CRD42024545321).

Results: Thirteen studies with 124,857 participants were included. Seven studies were at high risk of bias. The meta-analysis revealed an increased risk of KD after short-term postnatal exposure to $PM_{2.5}$ (OR: 1.011; 95% CI: 1.003-1.019; I^2 = 0%; high-quality evidence) and PM_{10} (OR: 1.004; 95% CI: 1.000-1.008; I^2 = 38%; high-quality evidence), as well as long-term postnatal exposure to $PM_{2.5}$ (OR: 1.415; 95% CI: 1.179-1.697; I^2 = 41%; high-quality evidence). Prenatal exposure to carbon monoxide, nitric oxide, nitrogen oxides, and sulfur dioxide; short-term postnatal exposure to nitric oxide; and long-term postnatal exposure to carbon monoxide and nitrogen oxides were also associated with KD occurrence.

Conclusions: The present systematic review and meta-analysis revealed that prenatal and postnatal exposure to several ambient pollutants are associated with a higher incidence of KD. Appropriate policies and actions are suggested to ameliorate this global public health concern.

PKM2/PPARγ 代谢重编程调控 CXCR4+ 中性粒细胞促进 NETs 介导的心肌细胞焦亡，是脓毒症心肌病的关键因素

尹哲辉

浙江大学医学院第二附属医院

目的：

脓毒症是由感染引起的全身性炎症反应，其可导致严重心脏损伤，显著增加患者死亡率。$CXCR4^+$ 中性粒细胞已被证实可在相关疾病中促进炎症和组织损伤。然而，$CXCR4^+$ 中性粒细胞影响脓毒症心肌病的具体作用机制尚未可知。最近的研究表明，糖脂代谢重编程对细胞功能改变发挥关键作用。我们假设，PKM2/PPARγ 介导的糖脂代谢重编程调节 $CXCR4^+$ 中性粒细胞 NETs 释放，从而促进脓毒症心肌病中心肌细胞焦亡。本研究旨在阐明代谢重编程与炎症之间的复杂相互作用，为阐明脓毒症心肌病发病机制提供新见解，并识别潜在的治疗靶点。

方法：

在本研究中，我们采用体外和体内方法来研究脓毒症心肌病病理形成中 $CXCR4^+$ 中性粒细胞的具体作用机制，探索 PKM2/PPARγ 介导的糖脂代谢重编程在 $CXCR4^+$ 中性粒细胞 NETs 释放中的作用及其对心肌细胞焦亡的影响。

体内，构建 CXCR4 髓系特异性敲除小鼠，并建立脂多糖（LPS）和盲肠结扎穿刺（CLP）脓毒症模型，以模拟脓毒症心脏损伤。我们评估了各组心脏组织损伤和炎症水平。并采用免疫染色和蛋白印迹检测 NETs 成分及焦亡相关的蛋白质。

体外，从小鼠骨髓中分离出中性粒细胞并刺激。评估各处理方式后糖脂代谢指标，并量化 NETs 释放。进一步使用药物抑制剂和 siRNA 靶向 PKM2 和 PPARγ 以研究其调节作用。

结果：

我们研究发现，在脓毒症心肌病小鼠模型的心肌组织中，$CXCR4^+$ 中性粒细胞数量显著增加，这表明它们参与了脓毒性心肌病的病理过程。为了探讨这一现象，我们培育了髓系特异性敲除 CXCR4 基因小鼠，并诱导其发生脓毒症心肌病。我们发现，中性粒细胞特异性敲除 CXCR4 可通过 Caspase-1/GSDMD/NLRP3 经典通路调控心肌细胞焦亡，以显著改善脓毒症后心脏功能障碍。并通过中性粒细胞心肌内注射实验，我们证实了 $CXCR4^+$ 中性粒细胞在脓毒症心肌病进展中起着关键作用。

为了进一步研究 CXCR4 敲除后中性粒细胞的功能变化，我们观察到 CXCR4 敲除后中性粒细胞 NETs 释放显著减少。随即利用 NETs 消除剂 Dnase I 发现消除小鼠体内 NETs 可显著降低心肌细胞焦亡发生，并在 CXCR4 敲除鼠中也观察到此现象。此外，通过单细胞测序我们发现在病理心脏组织中低表达 CXCR4 可增强中性粒细胞脂质水解代谢功能，并利用 qPCR 及相关糖酵解速率和脂滴含量检测，发现敲除 CXCR4 后中性粒细胞糖酵解能力下降，脂质分解代谢能力升高。进一步探究糖脂代谢重编程中的具体分子机制，我们发现，在中性粒细胞中敲除 CXCR4 会导致 PKM2 核转位减少，但上调 PPARγ 表达，从而促进过氧化物酶体的增殖，最终减少 NETs 的释放。最后，我们利用 PKM2 调节剂 DASA-58 抑制中性粒细胞 PKM2 核转位，发现其上调 PPARγ 表达并减少 NETs 释放。

结论：

我们的研究表明，PKM2/PPARγ 介导的糖脂代谢重编程调节 $CXCR4^+$ 中性粒细胞中的 NETs 释放，而 NETs 促进心肌细胞焦亡，从而促进由脓毒症心肌病的进展。

Group 2 Innate lymphoid cell derived IL-9 activates regulatory T cells to

Facilitate post myocardial infarction repair

Yuxiao Feng

Shanghai Chest hospital

Objective: Myocardial fibrosis is a pivotal pathological driver of post-infarction ventricular remodeling and heart failure progression. While cardiac immune responses play indispensable roles in post-MI tissue repair, the regulatory mechanisms by which type 2 innate lymphoid cells (ILC2s) – a key cardiac-resident immune subset – modulate fibrotic remodeling and cross-talk with other immune cells in the cardiac inflammatory microenvironment remain poorly defined. This study aims to elucidate the ILC2-centric molecular circuitry governing myocardial fibrosis and adverse remodeling following MI. Specifically, we seek to (1) delineate the spatiotemporal dynamics of ILC2-mediated cytokine signaling (IL-4/IL-13/IL-9) during fibrotic progression, (2) characterize the immunoregulatory interplay between ILC2s and cardiac T cell subsets, and (3) evaluate the therapeutic potential of targeting the ILC2-immune microenvironment axis. Our findings may establish a novel paradigm for innate immunity-guided myocardial repair strategies and identify actionable targets to mitigate maladaptive remodeling in ischemic heart disease.

Methods: Male C57BL/6 mice (8–12 weeks old) were randomized into five groups: a sham-operated group and myocardial infarction (MI) groups (postoperative Day 1, 3, 5, and 7), with MI induced by ligating the left anterior descending coronary artery. Cardiac immune cells were analyzed via flow cytometry to quantify the proportion of type 2 innate lymphoid cells (ILC2s) within $CD45^+$ leukocytes and their intracellular cytokines (IL-4, IL-13, and IL-9). ILC2s were depleted by intraperitoneal anti-CD90.2 antibody injection, with depletion efficiency and IL-9 reduction validated by flow cytometry and Western blotting. Recombinant IL-9 was administered to assess therapeutic effects: cardiac function was evaluated through echocardiography (LVEF and FS), while fibrosis (Masson's trichrome/Sirius red), apoptosis (Cleaved-Caspase 3/TUNEL), tissue morphology (HE staining), and myocardial inflammation biomarkers（TNF-α、IL-1β、IL-6、IL-10、IFN-γ、IL-17a via ELISA) were analyzed histologically. Post-IL-9 treatment, cardiac T cell subsets ($CD4^+$/$CD8^+$) and activation markers (CD107a/CD25) were profiled by flow cytometry.

Results: Our study demonstrates that ILC2s and their derived IL-9 exhibit time-dependent expansion during the first week post-myocardial infarction (MI), with IL-9 serving as a cardioprotective effector. Exogenous IL-9 supplementation significantly improved cardiac functional recovery, as evidenced by echocardiography showing elevated left ventricular ejection fraction and fractional shortening. Histopathological analysis (Masson's trichrome; Sirius red) revealed attenuated fibrosis, reduced myocardial injury (HE staining), and diminished apoptosis (TUNEL+ cells; Cleaved-Caspase 3+ area). Mechanistically, single-cell RNA sequencing identified IL-9 receptor (IL-9R) enrichment in both ILC2s and regulatory T cells (Tregs). Flow cytometry confirmed that exogenous IL-9 administration did not alter ILC2 quantity or activation status, but markedly expanded the Treg population and upregulated TGF-β secretion. Conversely, $CD8^+$ T cell infiltration decreased, accompanied by reduced IFN-γ level. Immunofluorescence co-localization analysis excluded direct IL-9R signaling in $CD8^+$ T cell, while demonstrating robust IL-9R/$CD4^+$ co-expression. These findings collectively establish that ILC2-derived IL-9 mediates cardio-protection post-MI by engaging Treg-expressed IL-9R to amplify immunosuppressive TGF-β signaling, rather than through autocrine or $CD8^+$ T cell-dependent pathways.

Conclusion: This research confronts the critically important challenge of pathological cardiac fibrosis and adverse ventricular remodeling following myocardial infarction (MI) by introducing a novel mechanistic framework. We demonstrate that an immunosuppressive signaling pathway, specifically the IL-9/T regulatory cell (Treg) axis originating from type 2 innate lymphoid cells (ILC2s), functions as a central and indispensable regulator governing the progression of fibrotic tissue deposition. Within this axis, IL-9 acts as the key orchestrator, directing the activation and function of Tregs, which subsequently act to suppress detrimental maladaptive remodeling processes. These significant findings do more than just advance our understanding; they fundamentally redefine the intricate immune-metabolic cross-communication that underpins the heart's repair mechanisms after MI. Furthermore, the study establishes a completely new therapeutic avenue focused on targeting the dynamic interactions between the innate and adaptive immune systems. This breakthrough insight holds considerable transformative potential for the future development of precision immunotherapeutic strategies aimed at treating ischemic heart disease.

系统性红斑狼疮合并急性心肌炎 12 例临床分析

宁夏

延安大学附属医院

摘要：目的 了解系统性红斑狼疮 (SLE) 合并急性心肌炎患者的临床特点和转归。

方法 收集 2020 年 1 月 -2023 年 7 月在延安大学附属医院住院的急性心肌炎合并 SLE 患者的一般临床资料，实验室等生化检查以及超声心动图等辅助检查，并且对诊断和治疗过程进行分析。 结果 12 例患者中男 2 例，女 10 例；年龄 19 ~ 42 岁，平均 27.8±3.6 岁；病程 2 个月 ~ 9 年。其中 2 例心肌炎为首发症状之一，3 例为 SLE 病情反复时出现。除心肌炎之外，还有狼疮肾炎、狼疮肺炎、以及脑病和血液系统受累等多系统受累的表现。根据评分表进行评分，将所有的患者进行评估后，其 SLE 病情活动指数评分平均为 17 分 (12 ~ 21 分)。超声心动图中 12 例患者存在左室收缩功能损害，其中 4 例严重存在左室功能不全 (左室射血分数 23% ~ 32%)。7 例患者应用甲基泼尼松龙和环磷酰胺冲击治疗，3 例口服足量泼尼松和环磷酰胺冲击治疗。2 例患儿应用 IVIG。治疗后 12 例患者心脏功能均有不同程度改善。结论 SLE 患者合并急性心肌炎多在病情活动时出现，不仅症状隐匿，而且可以出现心功能不全以及全身多系统症状。采取不同的治疗方案针对性的患者进行治疗，不仅可以积极控制原发病，而且可以延缓患者病情的发展，通过及时应用免疫抑制剂，可取得满意疗效。

关键字：系统性红斑狼疮 急性心肌炎 临床

Mitochondrial One-Carbon Metabolism Drives CD34 Lineage Cells to Differentiate into Tfh Cells to Form Tertiary Lymphoid Organ in Transplant Arteriosclerosis

Junru Wu[1], Xuejing Sun[1], Hong Yuan[1], Qing-Bo Xu[2], Jingjing Cai[1]

1. Department of Cardiology, The Third Xiangya Hospital, Central South University, Changsha, Hunan, China

2. Department of Cardiology, the First Affiliated Hospital, School of Medicine, Zhejiang University, Zhejiang, China

Background

Organ transplantation is a critical life-saving procedure for end-stage organ failure. However, its long-term success is frequently compromised by transplant arteriosclerosis, a form of chronic rejection characterized by diffuse vascular lumen narrowing that is a significant contributor to graft failure. For example, cardiac allograft vasculopathy (CAV) affects nearly half of heart transplant recipients by 10 years post-transplantation. A key pathological feature of this condition is the formation of tertiary lymphoid organs (TLOs)—ectopic, organized immune cell aggregates—within the adventitia of the grafted artery. In allograft arteriosclerosis, these TLOs are considered detrimental, fostering proinflammatory responses and autoantibody production. The development of functional TLOs hinges on the establishment of germinal centers (GCs), a process orchestrated by follicular helper T (Tfh) cells. Tfh cells, a specialized subset of CD4+ T cells, provide essential signals for B cell maturation, affinity selection, and the generation of long-lived plasma and memory B cells. Therefore, controlling Tfh cell differentiation represents a critical checkpoint for preventing pathological B cell activation and mitigating chronic inflammatory diseases. Despite their importance, the precise origin of the Tfh cells that drive TLO formation in transplanted vessels and the molecular mechanisms governing their differentiation remain poorly understood. This study sought to comprehensively trace the developmental source of pathogenic Tfh cells in a model of allograft arteriosclerosis and to identify the specific metabolic pathways that regulate their function, with the ultimate aim of uncovering novel therapeutic targets to prevent chronic rejection and improve long-term transplant outcomes.

Methods

We employed a multi-faceted approach to investigate Tfh cell origins and regulation. A Cd34-CreERT2;Rosa26-tdTomato mouse model was used for lineage tracing of CD34+ cells in an aortic allograft model. The cellular composition of remodeled arteries was analyzed at 2 and 4 weeks post-transplantation using single-cell RNA sequencing (scRNA-seq), flow cytometry, and immunofluorescence. The origin of graft-infiltrating T cells was interrogated through thymectomy experiments and bone marrow transplantation models. The role of lymphatic transport was assessed using a VEGFR-3 inhibitor and lymph node dissection. Metabolic signatures were identified via untargeted and targeted ultra-performance liquid chromatography/high-resolution mass spectrometry (UHPLC-HRMS) metabolomics and computational flux analysis on ex vivo differentiated Tfh cells. The functional role of mitochondrial one-carbon metabolism was validated using deuterium-labeled serine tracing, pharmacological inhibition of the key enzyme MTHFD2, and a CD4+ T cell-specific Mthfd2 knockout (CD4+ T-Mthfd2-KO) mouse model.

Results

Lineage tracing revealed that CD34+ lineage cells are the predominant source of T cells infiltrating the allograft, accounting for over 80% of the T cell population at 4 weeks post-transplantation. These CD34+ lineage T cells were found to originate primarily from the thymus, not bone marrow, and were transported to the graft via lymphatic vessels. Depletion of CD34+ lineage cells or disruption of lymphatic transport significantly reduced TLO formation and intimal hyperplasia. ScRNA-seq analysis identified that CD34+ lineage CD4+ T cells differentiate into various effector subsets, with Tfh cells being a key population that interacts with B cells to form GCs. Metabolomic profiling demonstrated a distinct upregulation of one-carbon metabolism during the differentiation of CD4+ T cells into Tfh cells. Isotope tracing with D3-serine confirmed that this process relies predominantly on the mitochondrial, rather than cytosolic, one-carbon pathway. Critically, both pharmacological inhibition of the mitochondrial enzyme MTHFD2 with DS18561882 and conditional knockout of Mthfd2 in CD4+ T cells markedly suppressed Tfh cell differentiation, abolished TLO

formation, and ameliorated transplant-associated vascular remodeling in vivo.

Conclusions

This study provides definitive evidence that Tfh cells driving TLO formation and vascular pathology in allograft arteriosclerosis originate from a distinct population of thymic-derived CD34+ lineage cells. We demonstrate that these cells are transported to the graft via the lymphatic network and that their subsequent differentiation into a pathogenic Tfh phenotype is critically dependent on metabolic reprogramming toward MTHFD2-mediated mitochondrial one-carbon metabolism. These findings unveil a comprehensive pathway from cellular origin to metabolic regulation and alloimmune pathology. The central role of MTHFD2 as a metabolic checkpoint in Tfh cell differentiation highlights it as a highly specific and promising therapeutic target for inhibiting chronic allograft rejection and improving the long-term survival of transplanted organs.

Regulatory Dendritic Cells enhance the survival and cardioprotective effect of mesenchymal stromal cells via improving immune microenvironment

Wen-Qi Tian, Ji-Long Liu, Xiao-Juan Zhao, Xiu-Hong Dou, Fan-Di Niu, Meng-Meng Wang, Jin-Yang Xu, Wen-Qiang Gao, Yun-Chu Li, Cong-Ye Li, Yun-Long Xia, Xiao-Ming Xu, Yong-Zhen Guo, Feng-Yue Ding, Ling Tao, Wen-Jun Yan, Hui-Shou Zhao

The First Affiliated Hospital of Air Force Medical University (Xijing Hospital)

Wenqi Tian[1,#], Jilong Liu[1,#], Xiaojuan Zhao[1], Xiuhong Dou[1], Fandi Niu[1], Mengmeng Wang[1], Jinyang Xu[1], Wenqiang Gao[1], Yunchu Li[1], Congye Li[1], Yunlong Xia[1], Xiaoming Xu[1], Yongzhen Guo[1], Fengyue Ding[1], Ling Tao[1], Wenjun Yan[1*], Huishou Zhao[1*],

[1]Department of Cardiology, Xijing Hospital, Fourth Military Medical University, Xi'an 710032, China.

#These authors contributed equally to this work.

*Correspondence authors:

Huishou Zhao, M.D., Ph.D. Department of Cardiology, Xijing Hospital, Fourth Military Medical University, E-mail: 13934838479@163.com;

Wenjun Yan, M.D., Ph.D. Associate Professor, Department of Cardiology, Xijing Hospital, The Fourth Military Medical University, E-mail: yanyan517032@163.com

Background: Ischemic heart disease (IHD) is a leading cause of death. Mesenchymal stromal cells (MSCs) therapy holds promise for treating IHD. However, the adverse immune microenvironment in the infarcted myocardium leads to rapid loss of transplanted MSCs. Regulatory dendritic cells (DCregs) are a specialized subset of dendritic cells that play a key role in inducing immune tolerance in organ transplantation. The current study aimed to explore the cardioprotective effect of co-transplantation of DCregs with MSCs following myocardial infarction (MI), and to investigate the immune regulatory function of DCregs as well as the underlying molecular mechanisms.

Methods: Mouse bone marrow mononuclear cells were cultured in the presence of GM-CSF, IL-4, 1,25-dihydroxyvitamin D3, and dexamethasone for 1 week to generate DCregs. Flow cytometry was used to detect the levels of CD40, CD80, CD86, and MHC-II in DCregs. MSCs specific-antigen loaded DCregs were induced via exposure of DCreg to MSCs debris. After murine MI model was established, fluorescently labeled MSCs specific-antigen loaded DCregs were injected subcutaneously, and their distribution was tracked in vivo by organ imaging. Fluorescently labeled adipose-derived mesenchymal stromal cells (ADSCs) were directly injected into the infarcted myocardium either alone or in combination with subcutaneous injection of DCregs. Cardiac function was assessed by consecutive echocardiographic measurements. The survival of ADSCs was evaluated using immunofluorescence staining and heart imaging. Cardiac remodeling including cardiomyocyte apoptosis, angiogenesis, and fibrosis were detected using TUNEL staining, CD31 staining, and Masson-trichrome staining. The distribution of DCregs in organs and their impact on the immune microenvironment of the heart, liver and spleen were examined using immunofluorescence staining.

Results: We successfully generated DCregs with stable immune-tolerant phenotypes from bone marrow mononuclear cells, as evidenced by increased expression and secretion of IL-10 and TGF-β, decreased expression of inflammatory cytokines (IL-1β, IL-6, and TNF-α), co-stimulatory molecules (CD40, CD80, CD86), and antigen-presenting molecule MHC-II. In addition, DCregs successfully intaked MSCs-derived cell debris. After subcutaneous injection of DCregs into the left abdominal region, DCregs migrated to the left inguinal lymph nodes, mediastinal lymph nodes, and major organs such as the spleen and liver. DCregs promoted the polarization of macrophages towards the M2 phenotype in the liver and spleen. MSCs specific-antigen loaded DCregs significantly improved the immune microenvironment of ischemic heart as indicated by increased M2 macrophages, regulatory T cells (Tregs), and reduced M1 macrophages, $CD8^+$ T cells surrounding MSCs, and pro-inflammatory cytokines. In addition, MSCs specific-antigen loaded DCregs significantly increased retention of ADSCs 3 days and 1 week post-MI. Finally, DCregs enhanced the cardioprotective effect of the intramyocardially injected ADSCs, as indicated by increased cardiac function and angiogenesis and reduced apoptotic cardiomyocytes and fibrosis. Neutralizing IL-10 with its antibody reduced the cardiac retention of ADSCs in 3 days post-MI.

Conclusion: Subcutaneous injection of MSCs specific-antigen loaded DCregs enhances the survival and cardioprotective effect of the intramyocardially injected ADSCs by improving the immune microenvironment in the ischemic heart. This study provides a new strategy to optimize MSCs-based therapy for IHD.

Key Words: Myocardial infarction, Mesenchymal stromal Cells, Regulatory dendritic cells, Immune tolerance

Funding: This work was supported by the Program for National Science Funds of China (Grant Nos. 82370252, 82022004), the Key R&D Program of Shaanxi Province (Grant No. 2024SF-GJHX-44).

Single-cell RNA sequencing atlas of peripheral blood mononuclear cells from subjects with Premature ST-segment elevation myocardial infarction

Fan Han

中国人民解放军总医院第一医学中心

Fan Han[1,2], Ran Zhang[1,2]

[1] Department of Cardiovascular Medicine, Chinese PLA General Hospital, Beijing 100853, China

[2] Graduate School of Chinese PLA Medical School, Beijing 100853, China

Background:

Cardiovascular diseases (CVD), and, in particular, coronary artery disease (CAD) continue to represent one of the most important causes of morbidity and mortality all around the world.Thus, coronary heart disease continues to be a major health problem, and while there are a lot of studies available for adults, there is a scarcity of data on myocardial infarction in the "young". This may cause an underestimation of the importance of CAD in young patients, in whom both the short-and long-term consequences can be devastating.Premature ST-segment elevation myocardial infarction (STEMI) is increasingly prevalent in younger populations, with these cases exhibiting unique immunoregulatory characteristics. Monocytes play a crucial role in the destabilization of atherosclerotic plaques and the pathogenesis of myocardial ischemia-reperfusion injury, primarily through their modulation of inflammatory responses and oxidative stress. Despite their central role, the immunological profiles and underlying mechanisms contributing to premature STEMI remain poorly defined. This knowledge gap highlights the need for a deeper understanding of the distinct immunopathological features of STEMI in younger individuals.

Objective:

This study aims to perform whole transcriptome sequencing of peripheral blood mononuclear cells (PBMCs) from patients with premature STEMI to identify age-specific immunological profiles. The findings will provide valuable insights into the pathogenesis of premature STEMI and identify potential biomarkers specific to younger populations.

Methods:

Single-cell RNA sequencing (scRNA-seq) was conducted on PBMCs from three premature STEMI patients (n=3) and three age- and gender-matched controls (n=3). Subsequent analyses involved cellular and gene-level approaches, including clustering, enrichment analysis, Cell-cell communication networks analysis, cellular trajectory analysis, and weighted co-expression network analysis, to comprehensively characterize monocyte subsets.

Results:

A total of 27 distinct cell populations were identified from 62,658 cells, including monocytes, T cells, B cells, NK cells, neutrophils, and platelets. Significant differences in monocyte abundance were observed between the STEMI and control groups. Monocytes were further classified into clusters 3, 4, 12, 13, and 17, with enrichment analysis showing that monocytes were significantly enriched in the inflammatory response, oxidative phosphorylation, and IL-6/JAK-STAT3 signaling pathways. Cluster 3 exhibited significant enrichment in reactive oxygen species and hypoxia response pathways, while Cluster 4 was notably enriched in the oxidative phosphorylation pathway. Cluster 12 was significantly enriched in both the inflammatory response and IL-6/JAK-STAT3 signaling pathways. Cluster 13 was predominantly enriched in angiogenesis pathways, and Cluster 17 was significantly enriched in coagulation and NOTCH signaling pathways. Differential gene expression analysis revealed that six key genes—AC020656.1, PIM3, PIM1, PRDX2, AC007952.4,

and FAM118A–were expressed across all five monocyte subsets in both groups. Among these, AC020656.1, PIM3, PIM1, and PRDX2 were significantly upregulated in the STEMI group, while AC007952.4 and FAM118A were significantly downregulated.

Conclusion:

In this study, significant monocyte characteristics in the premature STEMI population were elucidated through single-cell sequencing analysis. Five monocyte subsets with functional heterogeneity were enriched in the hypoxia/reactive oxygen species response, oxidative phosphorylation, inflammation/IL-6-JAK-STAT3 signaling, angiogenesis, and coagulation/NOTCH pathways. Six core genes were identified, including four upregulated genes (AC020656.1, PIM3, PIM1, and PRDX2) and two downregulated genes (AC007952.4 and FAM118A). Notably, among these core genes, AC020656.1, PIM3, and AC007952.4 exhibited significant expression specificity in monocytes. These findings collectively highlight the central role of monocytes in the inflammatory pathology of the premature STEMI population and provide potential molecular targets for targeted therapy.

Keywords:

Premature STEMI; Monocytes; Single-cell RNA sequencing; Differentially expressed genes; Weighted co-expression network analysis

Prognostic Value of Serum Total Bilirubin in Patients with In-Stent Restenosis: A Stratified Analysis Based on Inflammatory Status

Miao Yu

Fuwai Hospital, Beijing, China

Abstract

Background: In-stent restenosis (ISR) remains a persistent and challenging complication following percutaneous coronary intervention (PCI), even with the widespread use of second-generation drug-eluting stents (DES). Although inflammation is recognized as a key driver of ISR pathophysiology and recurrence, current prognostic tools such as high-sensitivity C-reactive protein (hsCRP) are limited by their sensitivity to acute changes and external influences. Total bilirubin (TBIL), an endogenous antioxidant and anti-inflammatory molecule, has recently emerged as a potential biomarker reflecting chronic inflammation and vascular health. This study aimed to assess the predictive value of serum TBIL, alone and in combination with hsCRP, for long-term major adverse cardiovascular events (MACEs) in ISR patients undergoing repeat PCI.

Methods: A total of 2,055 ISR patients who underwent revascularization at Fuwai Hospital between January 2017 and December 2018 were consecutively enrolled in this single-center observational cohort study. They were routinely followed-up via office visit or telephone contact until January 31, 2021. Patients were stratified into four groups based on serum TBIL (cutoff: 12.385 μmol/L) and hsCRP (cutoff: 2 mg/L) levels: TBIL-High/hsCRP-Low, TBIL-Low/hsCRP-Low, TBIL-High/hsCRP-High, and TBIL-Low/hsCRP-High. The primary endpoint was the occurrence of MACEs, defined as a composite of all-cause mortality, myocardial infarction (MI), stroke, repeat revascularization, and stent thrombosis. Multivariable Cox proportional hazards models were used to identify independent predictors of outcomes, and subgroup analyses explored interactions by clinical characteristics.

Results: Over a median follow-up of 36 months, 457 patients (22.3%) experienced MACEs. Patients with low TBIL levels were significantly more likely to suffer adverse events, regardless of hsCRP levels. Compared to the reference group (TBIL-High/hsCRP-Low), patients in the TBIL-Low/hsCRP-High group had the highest risk of MACEs (adjusted hazard ratio [HR] = 2.208; 95% confidence interval [CI]: 1.395–2.426; P < 0.001), followed by the TBIL-High/hsCRP-High group (HR = 1.512; 95% CI: 1.131–2.020; P = 0.005) and the TBIL-Low/hsCRP-Low group (HR = 1.322; 95% CI: 1.021–1.712; P = 0.034). Kaplan-Meier survival analysis further confirmed that patients with both low TBIL and elevated hsCRP had the poorest long-term prognosis (P < 0.001).

Subgroup analysis showed that this prognostic pattern remained consistent across age, sex, hypertension status, and clinical presentation (acute or chronic coronary syndrome). Notably, the prognostic value of TBIL was significantly more pronounced in diabetic patients (P for interaction = 0.001), suggesting a potential role for TBIL in refining risk stratification in this high-risk population.

Conclusion: Serum TBIL is an independent and stable predictor of long-term adverse cardiovascular outcomes in ISR patients undergoing PCI. When used in combination with hsCRP, TBIL enhances risk stratification by capturing both chronic and acute inflammatory states. This dual-biomarker approach is especially valuable in diabetic patients, who are at elevated risk of ISR recurrence and poor outcomes. Given its affordability, accessibility, and biological relevance, TBIL may serve as a practical tool for guiding individualized management strategies in ISR care. Further prospective and multicenter studies are warranted to confirm its utility.

Limitations:

This single-center retrospective study may involve selection bias, single-time biomarker measurement, and limited generalizability due to population-specific factors. Unmeasured confounders may exist, and findings require validation through larger, multi-center, prospective cohort studies.

Keywords

In-stent restenosis; Total bilirubin; High-sensitivity C-reaction protein; Percutaneous coronary intervention; Inflammation

泛素连接酶 RNF216 调控心脏内皮细胞炎症性衰老在心脏衰老中的作用机制

朱思濛 许从峰

上海市第六人民医院

目的：近数十年来我国老龄化人口逐年增加，导致老龄相关疾病，尤其是心血管疾病的发病率急剧增加。作为衰老的重要机制，炎症性衰老对心血管系统的影响也得到了越来越多的关注。目前已有的研究大多聚集于免疫细胞对心脏衰老的调控。内皮细胞的衰老已被证实参与多种心血管疾病的发生，但其衰老机制目前仍缺乏充分研究。因此，本研究拟探讨炎症导致内皮细胞衰老的发生机制及其对心脏衰老的作用。

方法：通过从衰老小鼠心脏中分选内皮细胞进行 SMART-RNA seq 筛选参与其衰老的关键分子，构建关键分子泛素连接酶 Rnf216 稳定过表达与敲减的细胞株，并通过多种细胞生物学试验明确其细胞生物学行为变化，以及通过 qPCR 检测 SASP 表达。继续通过细胞核 - 质蛋白分离以明确 RNF216 定位，免疫荧光进行确认。进一步通过免疫共沉淀联合质谱分析探究 RNF216 的互作蛋白，并构建 RNF216 不同位点突变体研究相互作用结构域和作用模式。

结果：泛素连接酶 RNF216 在衰老小鼠心脏内皮细胞表达升高，在诱导衰老的人脐静脉内皮细胞系（Human Umbilical Vein Endothelial Cells, HUVEC）中也发生明显的特异性表达升高。过表达 RNF216 的 HUVEC 细胞在多种细胞生物学行为如细胞侵袭、细胞迁移及血管形成能力均有明显的增强，而衰老相关分泌表型（Senescence-associated secretory phenotype, SASP），如白介素 1b、金属蛋白酶 MMP-9 等则在 Rnf216 敲减后表达显著增加，提示 RNF216 对内皮细胞的生物学行为具有重要的调控作用。亚细胞定位提示，RNF216 在衰老内皮细胞中发生向细胞核内的转移，而敲减 GTP 结合蛋白 RAN 后 RNF216 在核内的表达明显减少，表明衰老内皮细胞中 RNF216 在 RAN 的协助下转移至细胞核发挥作用。免疫共沉淀联合质谱分析提示 RNF216 与 RNA 结合蛋白 HNRNP A2B1 存在相互作用，并通过蛋白酶体途径调控其降解，从而调控多种炎症因子的表达与转录，抑制 SASP 的分泌，参与维持内皮细胞的正常功能。

结论：衰老心脏内皮细胞中 RNF216 在 RAN 的协助下转移至细胞核内促进 HNRNP A2B1 的泛素化降解从而抑制 SASP 的产生，参与维持衰老心脏的免疫稳态与正常功能。

Integrative Immune–Echo Profiling Reveals B Cell–Cardiac Function Association: A Retrospective Analysis

Miao Tian[1], Bo-Kai Yang[2], Shuo Feng[2], Xiao-Quan Rao[1]

1. Department of Cardiology, Tongji Hospital, Tongji Medical College, Huazhong University of Science and Technology

2. School of Public Health, Huazhong University of Science and Technology

Background: Immune cell activity is now recognized as an important part of cardiovascular homeostasis. Changes in peripheral immune cell subsets often occur during myocardial stress, fibrosis, and ventricular remodeling. However, routine cardiac evaluation rarely includes quantitative immune phenotyping. Most human studies on immune cells and echocardiographic parameters are limited by small sample sizes or focus on specific diseases.

Understanding how peripheral immune cell profiles relate to common cardiac measures-such as left ventricular ejection fraction (LVEF), diastolic filling pressure (E/E ′), and structural parameters of the cardiac wall, may help improve risk assessment and guide immunomodulatory treatment.

Among immune cells, B lymphocytes are of particular interest due to their roles in antibody production and cytokine secretion. However, their overall impact on cardiac function in general clinical populations remains unclear.

Methods: This study retrospectively analyzed a total of 2,457 inpatient records from Tongji Hospital, Wuhan, between January 2016 and March 2025. Each record included transthoracic echocardiographic examinations and flow cytometric immune profiling performed during the same hospitalization. Relevant data were extracted from the hospital's electronic medical record system and laboratory information management system. Inclusion criteria required that patients had both qualified echocardiographic and immune profiling results. Additional variables including demographic characteristics (such as age, sex), clinical diagnoses, medication use (such as immunosuppressants, antihypertensives, and biologic agents), and selected laboratory parameters were collected as covariates for adjustment.

Based on echocardiographic reports, patients were categorized into two groups: those with normal findings (n = 1,074) and those with abnormal

findings (n = 1,383). Spearman correlation analysis was performed to assess monotonic relationships between immune cell subsets and echocardiographic parameters, including left ventricular ejection fraction (LVEF), E/E ′ ratio, and relative wall thickness (RWT). Multivariable linear regression models were further used to control for confounding factors such as age, sex, clinical diagnosis, and medication exposure.

Additionally, 50 patients who received B cell-depleting monoclonal antibodies (rituximab or belimumab) were identified for paired echocardiographic comparison before (≤ 60 days pre-treatment) and after therapy (3-12 months post-treatment). EF changes before and after treatment were assessed using a paired Wilcoxon signed rank test.The selection of the non-parametric test was based on the non-normal distribution of EF values and the small sample size of the treatment group.

Results: Across both normal and abnormal echocardiogram cohorts, B cells were most consistently correlated with multiple echocardiogram parameters. Higher B cell levels, whether calculated as absolute count (cells/μL), percentage of total lymphocytes, or percentage of white blood cells (WBC), were associated with lower LVEF (r = -0.11, all p < 0.001), higher E/E ′ ratio (surrogate of filling pressure, r = 0.08 to 0.10, all p < 0.01), and markers of geometric remodeling (increased septal thickness, posterior wall thickness, and relative wall thickness). Correlation magnitude was comparable across the two cohorts (|Δr| < 0.03). In pooled multivariable linear regression analysis, the inverse association between B cell (%WBC) and LVEF remained significant (β = -0.158; p = 0.022) after adjustment. Among patients receiving B cell-targeted antibody therapy, median LVEF increased from 65% (IQR 63–68 %) before treatment to 68% (IQR 65–72 %) post treatment, with a median improvement of 3 % (IQR 1–6 %; p = 0.0003).

Conclusion: This study identified a consistent inverse association between peripheral Bcell burden and EF in a large realworld inpatient cohort, observed across both normal and abnormal echocardiographic subgroups. These associations remained robust after adjusting for demographic and clinical confounders. Additionally, exploratory analysis of patients who had received B-cell-targeted monoclonal antibody therapy showed modest but significant improvements in EF over time. These findings suggest that peripheral B-cell metrics may serve as potential biomarkers of cardiac function and support further investigation into their clinical relevance.

Explainable Machine Learning Diagnostic Model for Coronary Heart Disease Using Inflammatory Factors Combined with Traditional Risk Factors: A Retrospective Single-Center Study

KEXIN YANG, SHENG LIU, MING ZHANG

北京安贞医院

Objective:

Coronary artery disease (CAD) is a leading cause of mortality worldwide, and early accurate diagnosis is crucial for improving patient outcomes. Although coronary angiography (CAG) remains the gold standard for diagnosis, its invasiveness and high cost limit widespread application. Atherosclerosis, the underlying pathology of CAD, is fundamentally a chronic inflammatory process, with inflammatory markers playing critical roles in disease initiation and progression. However, most existing diagnostic models primarily rely on traditional risk factors, neglecting the predictive value of these inflammation-related biomarkers. Machine learning (ML) has shown great potential in assisting CAD diagnosis, yet many studies have not fully integrated inflammatory markers, limiting the models' ability to detect early disease and to provide biological interpretability. This study aims to develop and interpret an explainable ML model combining inflammatory and traditional risk factors to enhance auxiliary diagnosis of CAD and evaluate its clinical utility.

Methods:

A retrospective single-center study was conducted, including 4,656 patients who underwent coronary angiography (CAG) for suspected CHD at Beijing Anzhen Hospital between August 8, 2021, and November 10, 2023. CHD was defined as at least one coronary artery stenosis ≥ 50%, excluding patients with acute myocardial infarction. Demographic characteristics, clinical data, biochemical indicators, and 12 serum inflammatory markers measured by multiplex flow cytometry were collected.

After data preprocessing (missing value imputation and standardization), the dataset was randomly stratified into training and independent testing sets at a ratio of 7:3. Feature selection was performed using L1-regularized LASSO regression combined with the Synthetic Minority Oversampling Technique (SMOTE). Ten machine learning algorithms, including logistic regression, random forest, support vector machine, and XGBoost, were developed and optimized using the R package caret. All models were tuned via repeated 5-fold cross-validation with grid search on the training set and evaluated on the testing set by accuracy, sensitivity, specificity, F1 score, and area under the receiver operating characteristic curve (AUC). The interpretability analysis of the model was conducted using SHapley Additive exPlanations (SHAP) to comprehensively evaluate the contribution of key variables, thereby achieving transparent interpretation of the model's diagnostic mechanisms.

Results:

A total of 4,656 patients were included, of whom 3,180 were diagnosed with CHD. The CHD group showed significantly higher proportions of males, hypertension, diabetes, hyperlipidemia, and smoking history compared to the non-CHD group (all P <0.001), as well as significantly higher prevalence of hypertension (62.9% vs. 21.5%), diabetes (38.1% vs. 14.6%), hyperlipidemia (78.5% vs. 44.7%), and smoking history (46.6% vs. 28.7%) (all P

Regarding inflammatory markers, IL-6, IL-8, IL-2, and IFN-alpha showed significant differences between groups, indicating a close association between inflammation and CAD. Using LASSO regression, 21 key variables were selected, covering traditional risk factors such as age, sex, hypertension, diabetes, smoking, lipid indicators, as well as multiple inflammatory markers (IL-6, IL-8, IFN-alpha, etc.) and hematological and biochemical indicators.

The performance of ten machine learning models varied on the independent test set. XGBoost and C5.0 models showed outstanding results in accuracy, sensitivity, and F1 score, with accuracies of 0.924 and 0.917 and AUCs of 0.832 and 0.847, respectively. However, considering the balance between model complexity and interpretability, the generalized linear model (GLM) was ultimately selected as the optimal model, demonstrating good overall balance with an accuracy of 0.810, sensitivity of 0.820, specificity of 0.711, F1 score of 0.887, and an AUC of 0.815.

Further SHAP analysis revealed that hypertension, hyperlipidemia, male sex, triglycerides, smoking, and diabetes were the most important positive predictors for CAD diagnosis. IL-6 and lipoprotein(a) also contributed significantly. Other factors such as age, albumin, uric acid, potassium, GGT, LDH, and platelet distribution width-related indices were also confirmed to influence the model's diagnostic results to varying degrees, reflecting the multidimensional biological associations of the disease.

Conclusion:

Combining inflammatory markers with traditional risk factors effectively improves the diagnostic performance for CHD. The explainable machine learning model developed in this study achieves accurate prediction while enabling feature contribution visualization and clinical decision support, showing promising clinical utility, especially for individualized risk assessment and precision intervention in CHD.

心血管信息化与大数据有关研究

“互联网 + 智慧医院背景下” 医 - 护 - 患三维联动模式的创新与实效 ——在缩短老年急性心肌梗死患者平均住院日的应用研究

张素云

西安交通大学医学院第一附属医院

目的 探究“互联网 + 智慧医院背景下” 医 - 护 - 患三维联动模式对缩短老年急性心肌梗死患者平均住院日的影响探究。方法 选取 2024 年 2 月–2024 年 11 月陕西某三甲医院急诊入院的 120 例急性心肌梗死的老年患者作为研究对象，随机分为对照组和观察组各 60 例。对照组采用常规护理模式，观察组在常规护理的基础上予以“互联网 + 智慧型医院背景下” 医 - 护 - 患三维联动模式线上线下相结合的干预模式。结果 观察组的总有效率高于对照组（98.15% > 80.00%），死亡率低于对照组（1.82% < 12.31%），P<0.05。观察组的平均住院日和平均住院费均低于对照组（P<0.05）。观察组的床位周转率、病床使用率和患者满意度均高于对照组（P<0.05）。结论 “互联网 + 智慧医院背景下” 应用“医 - 护 - 患三维联动” 模式，为老年急性心肌梗死患者的救治争取大量宝贵时间，提高临床抢救效率，为患者的健康提供良好保障的同时，大大降低了患者的死亡率，从而为改善患者预后质量，缩短平均住院时间，提高患者满意度提供了另一种选择。同时此模式，丰富了临床医疗服务模式，建立了医 - 护 - 患平等合作关系，和谐了医疗服务氛围，为临床医疗的稳步发展开辟了新的赛道。

基于可解释机器学习的房颤消融围术期心脏压塞风险预测模型的开发与验证

鲍志鹏 周丽华 孙国珍

江苏省人民医院（南京医科大学第一附属医院）

背景： 急性心脏压塞是房颤经导管消融术中最严重的并发症之一。有效防治心脏压塞对保障手术安全至关重要。机器学习（ML）为分析围手术期并发症的危险因素提供了有力工具。

目的： 开发一种可解释的机器学习模型，用于预测房颤消融术中心脏压塞的风险，以优化围术期管理。

方法： 本研究采用回顾性队列研究，纳入 2015 至 2024 年期间接受经导管消融的全部心脏压塞患者（n=91），并通过系统随机抽样选取同期未发生心脏压塞的患者（n=1390）共 1481 例房颤患者，通过系统文献回顾与多学科专家共识初筛 37 个临床及手术相关变量。采用多重插补法处理缺失值，并通过合成少数类过采样技术（SMOTE）解决数据不平衡问题。基于 LASSO 回归筛选出 12 个关键预测变量（包括 D- 二聚体、华法林使用、HAS_BLED 评分等），并构建八种分类模型（Logistic 回归、随机森林、k 近邻、神经网络、XGBoost、支持向量机、朴素贝叶斯、LASSO 回归）。采用 5 折交叉验证进行内部验证，以 ROC 曲线下面积（AUC）、精确率 - 召回率曲线（PRAUC）、敏感性和特异性评估模型性能，并通过决策分析曲线（DCA）和 SHAP 值分析临床实用性与特征重要性。

结果： 1481 例患者中心脏压塞患者 91 例。XGBoost 模型在内部验证中表现最佳（AUC=0.908，PRAUC=0.805，F1 Score=0.714，特异性 =0.973）。SHAP 分析显示，前五大预测因素为术者介入年限、D- 二聚体、肝素总剂量、房颤类型、左房大小。DCA 表明 XGBoost 在临床决策中具有较高的净收益。

结论： 本研究为个性化术前风险评估和围术期患者管理提供了有价值的管理工具，将机器学习模型集成到围术期管理系统中可以促进实时风险评估。

基于人工智能心电图构建改善型心力衰竭的预测模型

刘璐 郭俊含

大连大学附属中山医院

目的：基于标准 12 导联心电图，利用深度卷积神经网络构建改善型心力衰竭的预测模型。

方法：在这项回顾性研究中，纳入了 2018 年 3 月至 2023 年 8 月在大连大学附属中山医院和大连市第三人民医院住院的 415 例 LVEF ≤ 40% 患者的 12 导联静息心电图，将患者分为改善组（HFimpEF）和未改善组（Non-HFimpEF）。HFimpEF 组心电图共 194 张，Non-HFimpEF 组心电图有 221 张。我们利用卷积神经网络来分析和处理心电数据，构建了四种不同的改善型心力衰竭预测模型，并将搜集的 ECG 数据按照 8：2 比例随机分配给训练集和测试集。通过计算准确率、精确率、召回率、特异性、F1 评分和 AUC 值来评估模型性能。同时收集了患者的临床资料包括一般资料、实验室指标、合并症、用药情况，进一步分析两组患者基线特征是否存在显著差异，并根据临床基线资料，利用 logistic 回归分析构建预测模型，用以与利用卷积神经网络构建的模型比较模型性能。

结果：与未改善型心力衰竭患者相比，改善型心力衰竭患者的 D- 二聚体、左室舒末内径、室间隔厚度、左房内径、左房上下径较低（P < 0.05），心绞痛患病率更低，β 受体阻滞剂使用率较高。利用患者基线资料构建的预测模型 AUC 值为 0.646。利用人工智能心电图构建预测模型方面，在测试数据集上，四种不同卷积神经网络模型都表现出较高的准确性和特异性，其中以 InceptionV3 的准确性最佳，而 Densenet161 和 MobilenetV2 的特异度最高。通过绘制了各模型的 ROC 曲线，以评估和比较四种模型在预测 HFimpEF 任务的性能。四种模型的 AUC 值分别为 0.60、0.68、0.66 和 0.74，其中以 InceptionV3 模型的 AUC 值最高。

结论：基于深度卷积神经网络心电图构建的改善型心力衰竭的预测模型可以很好的预测改善型心力衰竭，从而有利于判断患者预后和帮助疾病管理。

基于机器学习的急性冠脉综合征智能风险评估系统构建与护理实践

曾琳

重庆医科大学附属璧山医院

目的 针对急性冠脉综合征（ACS）患者传统风险评估滞后问题，开发基于机器学习的智能预警系统，实现不良事件早期预警，提升护理安全管理水平。

方法 依托医院信息平台，整合 2021-2023 年 5 家三甲医院 CCU 的 ACS 患者数据（n=4,263）。构建分层预警模型： ①数据整合：实时采集心电、血压（每 5 分钟）、实验室指标（cTnT、BNP）、护理评估（胸痛程度、Killip 分级）等多维度特征； ②算法开发：XGBoost 模型预测恶性心律失常（输入特征：ST 段变异度、QTc 离散度）； LightGBM 模型识别心源性休克（关键特征：乳酸 >4mmol/L+CI<1.8 L/(min·m²)）；SHAP 可解释模块可视化风险贡献度（如“收缩压波动率 >15%” 贡献风险值 38%）； ③系统部署：开发移动护理终端，实时推送风险等级及干预清单（如“高危：准备除颤仪 + 呼叫医生”）。

结果 ①模型效能：心律失常预测 AUC 0.91（敏感度 87.3%，特异度 93.1%），心源性休克预测 AUC 0.85； ②临床效果：高风险患者识别时间从（45.6±11.8）分钟缩短至（7.2±2.4）分钟（P<0.01）； 不良事件发生率下降 36.7%（对照组 16.2% vs. 干预组 10.2%，P=0.001）； 护士临床决策时间减少 64%（从 12.3 分钟至 4.4 分钟，P<0.01）。 ③典型案例：62 岁 NSTEMI 患者术后 4 小时，系统预警室颤风险（SHAP 提示：频发室早 +ST 段抬高 0.3mV），护士提前备好除颤仪，3 分钟后成功抢救室颤发作。

结论 基于机器学习的智能风险评估系统显著提升 ACS 患者不良事件预警效率，实现从被动处置到主动防控的护理模式转型。建议：①深化多模态数据融合（如影像学特征）；②建立护理预警响应标准化流程；③拓展模型在社区 - 医院联动的应用。

家庭支持系统对青年冠心病患者二级预防行为依从性的影响研究

曾琳

重庆医科大学附属璧山医院

目的

青年冠心病患者（≤ 45 岁）二级预防行为依从性普遍较低，而家庭作为核心支持源尚未被充分干预。本研究旨在量化分析家庭支持强度与患者用药、生活方式改良及随访依从性的相关性，为构建以家庭为纽带的护理干预模式提供依据。

方法

1. 研究对象：纳入 2023 年 1 月 -2025 年 1 月我院收治的青年冠心病患者 102 例（年龄 28-45 岁，平均 37.2±4.8 岁）；排除独居、认知障碍或合并严重并发症者。

2. 评估工具: 家庭支持评定量表(APGAR): 评估情感支持、决策参与等 5 个维度(总分 0-10 分)；二级预防行为依从性量表: 含用药规范(MMAS-8 量表)、戒烟限酒、运动执行（IPAQ）、复诊准时率 4 项核心指标；出院后 3 个月进行随访评估。

3. 数据分析：SPSS 25.0 进行 Pearson 相关性分析及多元线性回归。

结果

1. 关键数据：高支持组规范服药率，戒烟成功率均高于对照组（P<0.01）。

2. 相关性分析：APGAR 总分与用药依从性呈强相关（r=0.72, P<0.01）； 家庭决策参与度是生活方式改善的最大预测因子（β=0.61, P=0.003）；情感支持不足导致 3 个月内再入院风险增加 2.3 倍（95%CI 1.2-4.4）。

结论与护理对策

1. 核心结论：家庭支持强度直接决定青年患者二级预防行为质量，尤以用药和运动依从性最为显著；家属参与医疗决策是改善生活方式的关键杠杆点。

2. 护理实践建议：建立“家庭 - 护士” 共管模式：将家属纳入出院计划制定，签署行为监督承诺书；开发家庭支持数字化工具：用药提醒共享 APP、家庭运动打卡小程序；开设家属教育课程：聚焦药物管理技能（如他汀类药物漏服处理）、应急症状识别；设立家庭支持积分制：将患者行为达标率与家属健康管理奖励挂钩。

基于心电图及多模态临床特征的机器学习模型预测危重症患者死亡风险

王秋雨 王一斐 陈波 王斌 张萍

北京清华长庚医院，清华大学临床医学院

目的： 重症监护病房（ICU）患者多存在严重基础疾病及复杂并发症，具有较高的短期死亡风险。针对该类患者短期死亡风险的准确预测，依然是目前临床实践中的重大挑战。本研究旨在构建一种融合心电图衍生风险评分与多模态临床指标的机器学习模型，有效预测 ICU 患者的 28 天死亡率。

方法： 本研究为回顾性队列研究，数据来源于 MIMIC-IV v2.2 数据库。主要结局为 28 天全因死亡。通过深度残差卷积神经网络对 ICU 患者入院后首次心电图数据进行分析，生成心电风险评分。特征筛选结合 XGBoost 特征重要性排序、SHapley 加性解释（SHAP）及临床意义综合判定，最终构建了包含五个变量的简约模型，并与四种主流机器学习算法进行了比较。模型性能从区分度（AUC）、校准性及临床应用价值等方面进行评估。

结果： 共纳入 18,256 例 ICU 患者（中位年龄 68 岁，女性占 41.1%），其中 2,412 例于 28 天内死亡。死亡患者的心电风险评分显著高于存活患者（中位数 [IQR]：34.1[20.7–50.3] vs. 13.7[6.7–25.4]，p < 0.001）。全变量 XGBoost 模型 AUC 为 0.880（95% CI: 0.865–0.895）。SHAP 分析结果显示，心电评分、急性肾损伤分期、去甲肾上腺素应用、年龄及 APS-III 评分为最具预测价值的五项变量，进而据此构建了 EANAS 评分。基于 EANAS 的逻辑回归模型表现出良好的区分能力（AUC: 0.845；95% CI: 0.829–0.862）。单纯心电评分的 AUC 为 0.787（95% CI: 0.769–0.805）。决策曲线分析显示，EANAS 模型在相关风险阈值范

围（0-78%）内具有更高的净临床获益。

结论：本研究将心电信息与多模态临床变量深度融合，建立了兼具准确性与稳健性的 ICU 患者 28 天死亡风险预测模型。其中，心电信息在提升模型预后判断准确性方面发挥了关键作用，为危重症患者的早期风险识别与精准管理提供了新的技术手段和理论依据。该模型有望为危重症患者的个体化风险评估和早期干预策略制定提供有力支持。

人工智能赋能心血管信息化：我国心血管病防治进展与科研成果整合分析

盛思琪 董增祥

哈尔滨医科大学附属第一医院

人工智能赋能心血管信息化：

我国心血管病防治进展与科研成果整合分析

盛思琪 董增祥 *

哈尔滨医科大学附属第一医院

目的：

随着心血管疾病（CVD）负担持续加重，我国亟需整合信息化与人工智能（AI）技术以优化防治体系。本研究旨在总结近五年我国心血管病防治领域的关键进展，评估 AI 技术在风险预测、影像诊断、远程监护及个性化治疗中的应用效果，并提出未来科研与临床转化的方向。

方法：

通过系统检索 2019–2024 年中国知网（CNKI）、PubMed 及 IEEE 数据库中我国心血管 AI 相关研究，纳入临床研究、队列分析及技术创新类文献 127 篇。采用文献计量学方法分析研究热点，结合多中心临床试验数据（如国家心血管病中心发起的“智慧心链”项目），评估 AI 模型在以下场景中的效能：（1）风险预测：基于电子健康记录（EHR）的深度学习模型（如 XGBoost、Transformer）对 10 年 ASCVD 风险的预测准确性；（2）影像诊断：AI 辅助 CT-FFR、超声心动图自动分析的应用现状；（3）远程管理：可穿戴设备结合 AI 算法对心力衰竭患者的再入院率影响；（4）治疗优化：强化学习在个体化抗凝方案制定中的探索。

结果：

（1）风险预测：AI 模型在社区筛查中显著提升高风险人群识别率（AUC 0.92 vs. 传统模型 0.81），但跨区域泛化能力仍需改进；（2）影像诊断：AI 辅助冠状动脉 CTA 分析缩短诊断时间 40%，敏感度达 94%，但小样本研究显示基层医院应用存在硬件限制；（3）远程监护：基于 PPG 信号的可穿戴设备预警系统使心衰急性发作检出率提升 35%，但误报率（12%）仍是瓶颈；（4）治疗决策：AI 推荐抗凝方案与专家共识符合率 88%，但缺乏前瞻性 RCT 证据支持。此外，我国已建立 12 个省级心血管 AI 示范平台，但数据标准化与伦理框架建设滞后于技术发展。

结论：

我国心血管 AI 研究在技术创新层面与国际同步，尤其在影像诊断和风险分层领域成果显著，但临床转化仍面临数据孤岛、算法透明度及医疗资源不均等挑战。未来需推动以下方向：建立国家级心血管多模态数据库；开展 AI 工具的前瞻性多中心验证；制定 AI 辅助决策的伦理指南。本研究为心血管信息化建设的政策规划与科研布局提供了实证依据。

Development and validation of an interpretable machine learning model for predicting Coronary Artery Aneurysms in Children with Kawasaki Disease: A Multicenter Study from Southwest China

Jing Fengchuan[1], Dong Liu[2], Bin Li[3], Yan-Xia Xu[4], Zhong-You Tan[5], Yan-Feng Yang[6], Wen-Liang Jiang[7], Tao Wang[7], Qi-Jian Yi[1]

1. Children’s Hospital of Chongqing Medical University

2. The Affiliated Hospital of Southwest Medical University

3. Kunming Children’s Hospital

4. Guiyang Maternal and Child Health Care Hospital

5. Chongqing University Three Gorges Hospital

6. Chengdu Women’s and Children’s Central Hospital

7. Dazu Hospital of Chongqing Medical University

Development and validation of an interpretable machine learning model for predicting Coronary Artery Aneurysms in Children with Kawasaki Disease: A Multicenter Study from Southwest China

Fengchuan Jing[1,2,3], Dong Liu[4], Bin Li[5], Yanxia Xu[6], Zhongyou Tan[7], Ouyang Chen[7], Yanfeng Yang[8], Feifei Si[8], Wenliang Jiang[9], Tao Wang[10], Qijian Yi[1,2,3]

Affiliation

1.Department of Cardiovascular Medicine, Children’s Hospital of Chongqing Medical University, National Clinical Research Center for Child Health and Disorders, Ministry of Education Key Laboratory of Child Development and Disorders, Chongqing, People’s Republic of China.

2.Chongqing Key Laboratory of Structural Birth Defect and Reconstruction, Chongqing, People’s Republic of China.

3.National Clinical Key Cardiovascular Specialty, Key Laboratory of Children’s Important Organ Development and Diseases of Chongqing Municipal Health Commission, Chongqing, People’s Republic of China.

4. Department of Pediatrics, The Affiliated Hospital of Southwest Medical University, Sichuan Clinical Research Center for Birth Defects, Luzhou, People’s Republic of China.

5.Department of Cardiovascular Medicine, Kunming Children’s Hospital, Yunnan, People’s Republic of China.

6.Department of Pediatric Cardiovascular Medicine, Guiyang Maternal and Child Health Care Hospital, Guiyang Children’s Hospital, Guizhou, People’s Republic of China.

7.Department of Pediatric Cardiovascular Medicine, Chongqing University Three Gorges Hospital, Chongqing, People’s Republic of China.

8.Department of Pediatric Cardiovascular Medicine, Chengdu Women’s and Children’s Central Hospital, School of Medicine, University of Electronic Science and Technology of China, Sichuan, People’s Republic of China.

9. Department of Pediatric Cardiovascular Medicine, Dazu Hospital of Chongqing Medical University, Chongqing, People’s Republic of China.

10. Internal Medicine-Cardiovascular Department, Dazu Hospital of Chongqing Medical University, Chongqing, People’s Republic of China.

Corresponding Author: Qijian Yi, E-mail: qjyi2003@aliyun.com.

Author Fengchuan Jing and author Dong Liu contributed equally to this work.

Background: Coronary artery aneurysm (CAA) is a severe complication of Kawasaki disease (KD), associated with long-term disability and significant cardiovascular morbidity. This imposes substantial emotional, financial, and healthcare burdens on patients, families, and medical systems. Early risk prediction prior to symptom onset is critical to initiate targeted interventions, optimize resource allocation, and mitigate adverse outcomes. Despite clinical scoring systems, accurate pre-symptomatic CAA risk stratification remains challenging. This multicenter study aimed to develop and rigorously validate an interpretable machine learning (ML) model to predict CAA risk in children with KD across Southwest China.

Methods: We conducted a retrospective cohort analysis using clinical data from 11,671 KD patients admitted to six tertiary pediatric hospitals in Southwest China between January 1, 2015, and May 31, 2021. After stringent data preprocessing to handle missing values and outliers, 6,018 patients (2,406 with CAA, 3,612 without CAA) met inclusion criteria. The cohort was randomly allocated into training (60%, n=3,611), internal validation (20%, n=1,204), and external test (20%, n=1,203) sets. Feature engineering involved collating 26 clinically plausible variables encompassing demographics, laboratory indices, and echocardiographic markers. Sequential dimensionality reduction was performed using univariate logistic regression ($p<0.05$), Boruta-based recursive feature elimination (RFE), and embedded algorithm importance rankings. Eight ML algorithms, including Random Forest (RF), eXtreme Gradient Boosting(XGBoost), Category Boosting (CatBoost), Light Gradient Boosting (LightGBM), Lasso regression, K-nearest neighbors (KNN), Support Vector Machine (SVM) and Multilayer Perceptron (MLP) were trained and optimized using 10-fold cross-validation. Performance was evaluated using AUC, precision-recall curves, F1-score, calibration metrics, and decision curve analysis (DCA) to quantify net clinical benefit. Model generalizability was externally validated, and the best-performing algorithm was deployed into a web-based interface for real-time risk calculation.

Results: Feature selection refined the initial 26 variables to 8 key predictors incorporated into the final model. The CatBoost classifier demonstrated superior discrimination: training set AUC=0.768 (95% CI: 0.752–0.783), internal validation AUC=0.723 (95% CI: 0.694–0.752), and external test AUC=0.731 (95% CI: 0.702–0.760). Performance remained robust across all centers (external test center AUCs=0.652–0.728). Calibration curves showed optimal agreement between predicted and observed risks. DCA confirmed significant clinical net benefit across threshold probabilities. SHAP analysis identified the following drivers of CAA risk: age, monocyte-to-lymphocyte ratio (MLR), hemoglobin-to-red blood cell distribution width ratio (HRR), fever duration, gamma-glutamyl transpeptidase (GGT), mean corpuscular hemoglobin concentration (MCHC), albumin (ALB), and globulin (GLB). A user-friendly web-based interface was developed to facilitate clinical application.

Conclusion: We developed and validated an interpretable ML model for predicting CAA risk in pediatric KD patients. The model provides individualized risk stratification with high generalizability across diverse settings, achieving robust performance in unseen multicenter external data. SHAP analysis enhanced model transparency, enabling clinicians to identify key risk factors, implement proactive interventions, and optimize patient outcomes.

Keywords: Machine learning, Coronary artery aneurysm, Kawasaki dis-

ease, Prediction modeling, SHAP values

基于人工智能的儿童先天性心脏病院后随访体系构建与管理模式探索

邢文露 刘馨允 江继承

阜外华中心血管病医院；河南省人民医院心脏中心；郑州大学华中阜外医院；河南省心血管疾病防治大数据中心

目的：基于人工智能技术，构建标准化、结构化的儿童 CHD 院后智能随访体系，探索覆盖效率与临床干预有效性兼顾的智能化随访新模式。

方法：围绕儿童 CHD 人群，设计涵盖六项核心指标的标准化 AI 语音随访话术，包括：身体不适（如胸闷、发热、头晕）、饮食与活动情况、服药依从性、心脏超声与心电图复查情况。系统集成语义识别与逻辑分类模型，自动识别阳性事件信号，辅以“语音 + 文本双检”人工质控机制，构建问题台账并持续优化模型算法与话术表达。引入院级 - 科级随访联动机制，实现阳性事件定向反馈与随访闭环管理。

结果：截至 2025 年 6 月，系统共完成儿童 CHD 出院患者院后智能随访 11259 人次。2024 年出院患者随访接通率达 76%，完成率达 67%，接通率、完成率持续提升。在质控样本中，语义识别准确率超过 95%，结构化随访数据准确率接近 100%。常见识别事件包括：活动后耐力下降、反复发热、饮食不良、术后未复查心脏功能等。临床科室反馈表明该随访体系显著提升随访效率与门诊复诊依从性。

结论：本研究建立了一套适用于儿童 CHD 人群的人工智能院后随访体系，在多项环节实现标准化与自动化突破。未来将进一步拓展病种适配与大模型语义理解能力，支撑儿童 CHD 的高质量慢病管理与队列研究。

ComPrehensive Bioinformatics Analysis Reveals the Role of Shared CuProPtosis- and FerroPtosis-Related DEG DLD in Abdominal Aortic Aneurysm

bei Shi

Affiliated Hospital of Zunyi Medical University

Abdominal aortic aneurysm (AAA), a life-threatening vascular disorder characterized by progressive dilation and weakening of the abdominal aortic wall, poses a significant clinical challenge due to its asymptomatic progression and high risk of rupture. The pathogenesis of AAA involves complex interactions between vascular inflammation, extracellular matrix degradation, and vascular smooth muscle cell (SMC) dysfunction, with regulated cell death pathways emerging as critical drivers of disease progression. Among these, ferroptosis—a form of iron-dependent lipid peroxidation-mediated cell death—has been increasingly recognized for its role in promoting SMC loss and aortic wall destabilization in AAA. More recently, cuproptosis, a copper-dependent regulatory cell death mechanism characterized by mitochondrial dysfunction and protein lipoylation, has gained attention for its overlapping molecular features with ferroptosis, including involvement in oxidative stress and metabolic perturbations. However, the interplay between these two cell death pathways and their shared regulatory genes in AAA remains largely unexplored, highlighting the need to identify key molecules that bridge ferroptosis and cuproptosis in this pathology.

To address this gap, the present study aimed to investigate the role of shared differentially expressed genes (DEGs) associated with both cuproptosis and ferroptosis in AAA progression, with the goal of identifying potential biomarkers and therapeutic targets. The research employed a multi-step approach combining transcriptomic analysis and experimental validation. Initially, RNA sequencing was performed on human AAA tissues and matched normal aortic samples to profile global gene expression patterns. This was followed by comprehensive bioinformatics analyses, including functional enrichment and pathway analysis, to identify DEGs linked to cuproptosis (CRDEGs) and ferroptosis (FRDEGs). Among the overlapping DEGs, dihydrolipoamide dehydrogenase (DLD)—a mitochondrial enzyme involved in energy metabolism and redox regulation—emerged as a key candidate, given its established role in both cuproptosis (via modulation of lipoylated protein homeostasis) and ferroptosis (through regulation of reactive oxygen species generation).

To validate the differential expression of DLD in AAA, quantitative real-time polymerase chain reaction (qRT-PCR) and immunohistochemical (IHC) assays were conducted. These experiments confirmed that DLD mRNA and protein levels were significantly elevated in human AAA tissues compared to control samples, consistent with the transcriptomic data. Further validation using murine AAA models replicated these findings, demonstrating conserved upregulation of DLD across species and reinforcing its potential relevance to AAA pathogenesis.

To explore the functional role of DLD in AAA-related processes, experimental studies were performed using SMCs, the primary cell type responsible for maintaining vascular wall integrity. In vitro assays revealed that DLD overexpression promoted multiple pathological processes in SMCs, including necrosis, apoptosis, and mitophagy. Necrosis and apoptosis contribute directly to SMC loss, weakening the aortic wall, while mitophagy—selective autophagy of damaged mitochondria—may disrupt energy metabolism and enhance oxidative stress, further exacerbating SMC dysfunction. Conversely, DLD knockdown attenuated these effects, supporting a causal role for DLD in driving SMC-mediated aortic wall damage.

The molecular mechanisms underlying DLD’s actions likely involve its dual involvement in cuproptosis and ferroptosis pathways. As a component of mitochondrial enzyme complexes, DLD regulates the balance of lipoylated proteins—a key feature of cuproptosis—and modulates redox status, influencing iron-dependent lipid peroxidation in ferroptosis. By promoting both pathways, DLD may amplify SMC death and mitochondrial dysfunction, creating a feedforward loop that accelerates AAA progression.

In summary, this study identifies DLD as a conserved differentially expressed gene in AAA, linking cuproptosis and ferroptosis through its regulation of SMC necrosis, apoptosis, and mitophagy. The consistent upregulation of DLD in human and murine AAA samples, combined with its functional role in promoting SMC dysfunction, positions it as a promising biomarker for AAA diagnosis and a potential therapeutic target. Targeting DLD could offer a novel strategy to inhibit both cuproptosis and ferroptosis, preserving SMC integrity and slowing AAA progression. Further research is warranted to explore the clinical applicability of DLD, including its utility as a diagnostic marker and the development of DLD-targeted therapies for AAA management.

Machine Learning-Derived Strategy for Predicting Long-Term Ischemic Stroke Among Type 2 Diabetes Mellitus Patients with Non-ST-Elevation Acute Coronary Syndrome: A Nationwide Multicenter Cohort Study

Xiaomeng Yang[1], Jun Wang[2]

1. Shenzhen Hospital of Southern Medical University, Shenzhen, Guangdong, China

2. The First Affiliated Hospital of Bengbu Medical University, Bengbu, Anhui, China

Abstract

Background: Acute coronary syndrome (ACS) and stroke remain leading contributors to global morbidity and mortality, collectively accounting for approximately one-third of worldwide deaths annually. The complex interplay among metabolic disturbances, inflammation and their combined impact on stroke incidence in type 2 diabetes mellitus (T2DM) patients with non-ST-elevation acute coronary syndrome (NSTE-ACS) remains unclear. Importantly, ACS and stroke share a spectrum of risk factors, with T2DM being a potent mediator driving pathological alterations across both cardiac and cerebral vascular networks.

Methods: This multicenter cohort study enrolled 2,432 T2DM patients with NSTE-ACS from seven hospitals in China between January 2019 and February 2021, with patient allocation to specific cohorts based on geographical distribution to ensure external validity. In this study, we implemented a novel multi-algorithmic feature selection framework incorporating three complementary computational approaches: Random Forest, Least Absolute Shrinkage and Selection Operator (LASSO) regression, and the Boruta algorithm. Subsequently, a prognostic model was developed based on multivariate COX regression analysis. The nomogram’s predictive performance underwent rigorous validation through a multi-faceted approach across three independent cohorts. Discriminative performance was assessed using time-dependent receiver operating characteristic (ROC) analysis with corresponding area under the curve (AUC) values calculated at 30-, 40-, and 50-month intervals with 95% confidence intervals. Model calibration was assessed through calibration plots comparing observed event rates against predicted probabilities, with Hosmer-Lemeshow tests confirming goodness-of-fit across risk deciles. To evaluate clinical relevance beyond conventional statistical metrics, decision curve analysis (DCA) was performed to quantify net benefit across clinically relevant decision thresholds.

Results: Patients were divided into a training cohort (n=624), an external validation cohort (n=594), and a test cohort (n=725) based on their province of origin. Over a median follow-up period of 50 months, ischemic stroke occurred in 5.86% of patients (n=142). The incidence of ischemic stroke was similar among the training (n=42, 6.73%), validation (n=77, 6.56%), and test (n=32, 6.10%) cohorts (p=0.187). four clinically significant biomarkers emerged as independent prognostic indicators for ischemic stroke: NLR (hazard ratio [HR]= 1.104, 95% confidence interval [CI]: 1.056-1.153, p<0.001), triglyceride (HR=1.170, 95% CI: 1.042-1.314, p=0.008), TyG-BMI (HR=1.008, 95% CI: 1.002-1.013, p= 0.005), and lipoprotein(a) (HR=1.002, 95% CI: 1.001-1.003, p<0.001). We established a nomogram that identified the neutrophil-to-lymphocyte ratio, triglyceride levels, triglyceride-glucose index, body mass index, and lipoprotein(a) as key predictive factors. The nomogram model achieved area under the curve (AUC) values of 0.712 (95% CI: 0.653-0.771), 0.702 (95% CI: 0.610-0.794), and 0.718 (95% CI: 0.618-0.818) in the training, external validation, and test cohorts, respectively. Calibration curves revealed strong concordance between predicted and observed outcomes, while decision curve analysis showed a net clinical utility across multiple risk thresholds. Finally, we developed the CASCADE platform, a web-based platform that computationally implements the nomogram model. This user-friendly interface enables clinicians to input four specific patient features into

designated fields

Conclusion: In this comprehensive nationwide multicenter cohort study, several significant advances in stroke risk prediction were achieved for patients with T2DM experiencing NSTE-ACS. Through rigorous multi-algorithmic feature selection combining Random Forest, LASSO regression, and Boruta algorithms, we identified a parsimonious set of four independent predictors that collectively constitute a novel multifactorial signature of cerebrovascular vulnerability: NLR representing systemic inflammation, triglyceride reflecting dyslipidemia, TyG-BMI capturing insulin resistance, and lipoprotein(a) indicating genetic predisposition to vascular disease. This constellation of biomarkers transcends traditional risk factors, integrating complementary pathophysiological pathways implicated in the brain-heart axis. By leveraging readily available clinical biomarkers to capture these diverse pathophysiological domains, our model offers a clinically accessible and mechanistically comprehensive evaluation of stroke risk, thereby facilitating more precise and targeted interventions for high-risk individuals.

Keywords: Machine Learning; Non-ST-Elevation Acute Coronary Syndrome; Type 2 Diabetes Mellitus; Metabolic-Inflammatory Biomarkers; Ischemic Stroke.

智能化技术在心血管护理管理中的应用与创新

彭娜

西安交通大学第一附属医院

摘要：目的 探究智能化信息技术在心血管护理管理中的应用情况。

方法：择取 2024 年 3 月 -2024 年 12 月来我院就医的心血管患者作为此次研究对象（100 例），实行动态化随机分组原则，对照组予以常规护理，观察组予以智能化技术护理管理，分析不良情绪评分、生存质量评分、心血管不良事件发生率等。

结果 显示：在不良情绪评分中，观察组数据（焦虑：32.36±3.99 分、抑郁：31.06±3.88 分）低于对照组（P<0.05），在生存质量评分中，观察组生存质量评分（情绪功能：75.36±3.98 分、躯体功能：77.85±5.49 分、认知功能：78.45±5.57 分、角色功能：77.98±4.16 分、整体功能：79.65±3.48 分）高于对照组，差异性显著（P<0.05），观察组心血管不良事件发生率低于对照组，P<0.05，数据之间存在差异性。

结论： 智能化技术在心血管护理管理中具有明显显著的应用价值，也属于临床医学护理中的创新之举，新颖且实际运用于临床工作中。使用智能化管理技术，能够显著改善患者病情及愈后，缓解患者负性情绪，进而提升生存质量，还可有效避免心血管不良事件的发生率，值得临床采纳使用。

A Bibliometric Study and Visualization Analysis of Chronotherapy

Ya-Jun Xue

北京清华长庚医院

Objective: This study aimed to review the research status and to demonstrate the hotspots and frontiers of chronotherapy.

Method: Literatures regarding chronotherapy from inception to 2024 were retrieved from the Web of Science Core Collection database. CiteSpace 5.6.R3 was used to generate network maps about the distributions of authors, countries, institutions, references, journals and reveal hot spots and frontiers of chronotherapy.

Results: A total of 1059 studies related to chronotherapy were included. The number of literatures regarding chronotherapy was generally increased with some fluctuations. The field of vascular calcification research involves many disciplines, such as pharmacology pharmacy, biology, and physiology. High-yielding countries include the United States and European countries, with China also having a place. Major research institutes include the Hôpital Paul Brousse, Universidade de Vigo, and so on. High-yielding and most cited authors include Levi FA and Hermida RC. Chronobiol Int published the most of research regarding chronotherapy. The first co-cited reference reported the MAPEC trial which analyzed the effect of circadian rhythm time of hypertension treatment on cardiovascular risk. Hot topics focused on the circadian rhythm, hypertension, sleep deprivation, cancer and rheumatoid arthritis. It can be predicted that future correlative studies of chronotherapy will revolve around hypertension, cancers, immune system disorders, and psychiatric disorders.

Conclusions: This study suggested the prosperous research trends and close cooperation. Major ongoing research trends include the timing of antihypertensive medication dosing, sleep deprivation, cancer and rheumatoid arthritis.

: Interpretable Prediction of Hospitalization Costs for Patients with Ischemic Heart Disease Using Artificial intelligence

Ya-Jun Xue, Ping Zhang

北京清华长庚医院

Background: Ischemic heart disease (IHD) is a major contributor to global mortality and disability, resulting in a significant social and economic burden on both individuals and healthcare systems.To optimize medical resource management and ultimately benefit a larger population, accurately predicting healthcare costs is essential.

Objective: This study proposes an interpretable feature extraction approach based on network analytics to enhance IHD hospitalization cost prediction. A diagnosis-procedure concurrence network is constructed, and a graph kernel-based method is employed to capture and represent information on diseases and treatments.

Results: This study presents a hospitalization cost prediction model that leverages a diagnosis-procedure concurrence network to extract features that balance predictability and interpretability. Due to the unique nature of our research focus and the specific dataset used, comparing our results with other studies can be challenging. Considering that the average cost for all patients in the HQMS dataset is around 20,000 CNY and the average cost for our IHD patient dataset is 37,853 CNY, our model demonstrates superior performance. This indicates the effectiveness of our approach in predicting hospitalization costs for a specific patient population with complex treatment options like IHD.

Conclusions:The results of our analysis demonstrate that the proposed model balances predictive accuracy and interpretability, highlighting its potential to support intelligent IHD management.

《心血管信息平台与人工智能协同：从精准诊断到风险防控的体系化研究》

王宏研

哈尔滨医科大学附属第一医院

目的：心血管疾病作为全球主要致死病因，给社会和家庭带来沉重负担。传统心血管疾病诊疗面临诸多困境，如诊断效率低下、漏诊误诊率较高、患者管理缺乏精准性与连续性。本研究旨在深度融合心血管信息化与人工智能技术，打造智能化、精准化的心血管疾病诊疗与管理新范式，提升疾病早期诊断的准确性、优化临床治疗决策、强化患者长期管理效果，为心血管疾病防治开辟新路径，助力“健康中国”战略目标的实现。

方法：本研究运用多学科协同的研究策略。数据层面，汇聚电子病历、影像数据、动态监测数据等多源异构心血管信息，借助大数据清洗、标准化处理等技术，搭建高质量心血管数据库，为后续分析奠定基础。人工智能技术应用方面，基于深度学习算法，构建心血管疾病影像识别模型，如针对冠脉造影图像的斑块精准分析模型、心脏超声图像的结构智能识别模型；同时，结合患者全面信息，开发临床决策支持模型，为医生提供个性化、精准化治疗方案建议。此外，运用自然语言处理技术，对医疗文本数据进行深度挖掘，提取关键诊断信息。研究过程中，通过回顾性分析历史数据与前瞻性开展临床试验，对构建的各类模型进行严格验证与持续优化。

结果：从目前研究结果来看，在疾病诊断环节，影像识别模型对心血管疾病的识别准确率较传统方法提升显著。如基于深度学习的冠脉斑块识别模型准确率达到 92% ，相比传统人工识别，大大降低了人为误差 ；心脏瓣膜病变检测敏感度提高至 88%，能够更早发现潜在病变。临床决策支持模型在模拟测试与实际应用中，成效斐然。以急性冠状动脉综合征为例，该模型能有效辅助医生制定治疗方案，减少决策时间约 30%，降低不合理用药与治疗方案的发生率。在患者管理方面，基于人工智能的随访系统可自动分析患者健康数据，及时预警病情变化。以高血压患者管理为例，患者复诊依从性提高 25%，心血管事件复发风险降低 18%。

结论：心血管信息化与人工智能的深度融合为心血管疾病诊疗与管理带来了新的突破。通过整合多源数据与先进人工智能技术，能够显著提升疾病诊断的准确性与效率，优化临床决策过程，强化患者长期管理效果。然而，研究也发现，模型在复杂病例诊断中的泛化能力仍需进一步提升，医疗数据的隐私安全与伦理规范问题也亟待完善。未来，需持续深化技术创新，加强跨机构数据共享与协作，完善相关法律法规，推动心血管信息化与人工智能技术在临床实践中的广泛应用与可持续发展，为心血管疾病防治事业注入新动能。

基于多模态深度学习的心血管疾病智能诊断框架

涂永波 郭应坤 文凌仪

重庆大学附属人民医院

目的：该研究旨在利用人工智能深度学习技术，整合临床资料、生化检测数据、冠脉 CTA 影像组学特征及心电图时间序列特征等多模态数据，以提高对冠状动脉粥样硬化、冠心病、心衰、心肌损伤和心肌缺血等心血管疾病的分类准确性，为临床诊断和个性化治疗提供更精准的依据，推动心血管疾病诊疗技术的发展。

材料与方法：收集 2022 年至 2024 年在两家医院放射科进行冠状动脉 CTA 检查的连续性患者的临床、实验室、心电图及冠脉 CTA 图像资料。剔除资料不全、重复检查、影像质量差的患者，利用卷积神经网络进行特征提取，并采用加权融合策略建立多模态预测模型。以 7:1.5:1.5 的比例建立内部验证评价体系。使用独立的数据集进行外部测试。采用受试者工作特征曲线下面积（AUC-ROC）评估模型与病变的相关性。

结果：最后在内部验证集中有 460 名患者收集齐四种模态数据，外部验证集中有 217 名患者收集齐四种模态资料。多模态模型在内部测试集的曲线下面积（area under The curve， AUC）为 0.86，外部测试的 AUC 为 0.83。这一性能显著优于单峰模型 0.79 和 0.77（p <0.001）。在 50% 临床数据缺失的情况下，注意机制的 AUC 仍为 0.76，注意机制的可视化与临床决策的关键特征具有高度的一致性。

结论：多模态融合模型通过跨域特征互补显著提高了心血管疾病的诊断性能，对

缺失的临床数据具有良好的适应性，有助于心血管疾病的智能辅助诊断建立。需要进一步的多中心验证和预后预测研究。

用于心血管疾病分类的多模态机器学习：一项基于临床、生化、影像学和心电图数据的综合研究

涂永波 郭应坤 文凌仪

重庆大学附属人民医院

目的：整合临床数据、生化指标、心电图和冠状动脉 ct 血管成像（CCTA）图像等多模态数据，构建高效能的心血管疾病机器学习分类模型。

方法：采用多中心回顾性研究方法，收集行 CCTA 检查的连续性患者资料。使用 Pyradiomics 从 CCTA 图像中提取影像组学特征，使用 Tsfresh 从 ECG 时间序列中提取特征。结合临床和生化指标，建立了 7 个机器学习模型（logistic regression (LR)、random forest(RF)、support vector machine (SVM)、decision tree(DT)、KNN、xgboost、LightGBM）。使用内部和外部验证集评估这些模型的性能。

结果：从重庆人民医院获得内部验证数据集 965 例用于模型开发，包括训练数据集中的 675 例（70%）和测试数据集中的 290 例（30%）。外部验证数据集来自重庆医科大学附属永川医院 342 例患者。7 个模型中，XGBoost 模型表现最佳，AUC 为 0.94，灵敏度为 0.73，特异度为 0.95。整合临床、生化、影像和心电图数据的多模态融合模型显著优于单模态模型，AUC 提高了 11%。包括心肌缺血和冠心病在内的 10 种循环系统疾病的 AUC 范围为 0.95 ~ 0.98。在模型中确定的关键特征包括高敏肌钙蛋白水平、影像组学纹理分析和 ECG 的 r 波峰。外部验证进一步证实了模型的稳健性，AUC 为 0.91。

结论：多模态数据融合可显著提高心血管疾病（CVD）的分类准确率，为高危人群的筛查和个体化干预提供了新思路。未来需要增加样本量，整合超声数据进行进一步优化研究。

基于 AI 的心血管患者智能护理管理系统构建及应用效果研究

喻帅

重庆荣昌区人民医院

目的

心血管疾病（CVD）患者需长期、动态的护理干预，传统护理模式依赖人工记录与经验判断，存在护理流程碎片化、风险预警滞后、患者随访效率低等问题。本研究基于心血管信息化与人工智能（AI）技术，构建“智能护理管理系统”，旨在优化护理流程、提升风险预警准确性及患者照护质量，为心血管专科护理的智能化转型提供实践依据。

方法

需求分析与系统设计：通过半结构化访谈（35 名心血管专科护士、50 例 CVD 患者及家属）明确核心需求：①护理数据自动采集与整合；②患者风险（如心衰急性发作、压疮、跌倒）实时预警；③个性化健康宣教方案生成。系统采用“数据层 - 算法层 - 应用层”架构：数据层整合医院电子护理记录（2020-2024 年）、床旁生命体征监测数据（心率、血压、血氧）及患者问卷（用药依从性、症状自评）；算法层通过自然语言处理（NLP）提取护理文本中的“高风险事件关键词”（如“呼吸困难加重”“下肢水肿 ++”），结合 XGBoost 模型训练“护理风险预测模块”；应用层开发“智能排班”“患者随访”“宣教推送”三大功能模块。

临床验证：选取心血管内科 2 个病区（A 区为实验组，B 区为对照组），纳入 2024 年 6-12 月住院的 300 例 CVD 患者（实验组 150 例，对照组 150 例）。实验组护士使用智能系统完成护理记录、风险评估及随访；对照组采用传统人工模式。观察指标：①护理操作时间；②风险预警准确率；③患者满意度。

结果

系统功能表现：智能护理管理系统实现了护理数据的自动采集与整合（与医院 HIS 系统对接，数据录入时间缩短 78%）；风险预测模块对心衰急性发作、压疮的预警准确率分别为 89%、85%（传统人工评估分别为 62%、58%）；个性化宣教方案生成时间从人工整理的 30 分钟 / 例缩短至 2 分钟 / 例。

临床应用效果：实验组单例患者护理记录耗时（8.2±1.5 分钟）显著低于对照组（21.3±3.8 分钟）（P<0.01）；风险事件漏报率（2.7%）较对照组（11.3%）降低 8.6 个百分点；患者满意度评分（92.5±3.1 分）高于对照组（81.2±4.5 分）（P<0.01）；护士工作负荷量表（NWI）得分（28.6±4.2）低于对照组（41.7±5.6）（P<0.01），提示系统有效减轻了护理人力负担。

结论

基于 AI 的心血管智能护理管理系统通过数据整合、风险预测及功能模块开发，显著优化了护理流程，提升了风险预警准确性与患者照护质量，同时减轻了护士工作负荷。本研究为心血管护理的智能化转型提供了可行路径，未来可进一步扩大多中心验证，并结合可穿戴设备（如智能手环）实现院外患者的连续监测与护理干预，推动“医院 - 社区 - 家庭”全周期护理模式的落地。

信息化在心血管临床护理创新中的应用研究

王媛媛

武汉大学人民医院（湖北省人民医院）

信息化在心血管临床护理创新中的应用研究

王媛媛 刘华芬

摘要

目的：探讨信息化在心血管临床护理创新中的应用效果，旨在优化护理流程，提高护理质量，改善患者的整体就医体验。

方法：研究将以 2023 年 10 月至 2024 年 10 月我院心血管内科诊收治的 80 例心血管疾病患者作为案例，本次分组将会结合随机数字法的形式，将患者分为对照组和实验组，每组的患者确保各 40 例。其中，对照组中男性患者有 23 例，女性患者有 17 例，平均年龄 54.16±2.13 岁，平均病程 8.13±3.61 年；实验组中男性患者有 24 例，女性患者有 16 例，平均年龄 55.21±2.54 岁，平均病程 8.63±3.42 年。在本次研究中，对照组患者会应用常规性的护理管理操作，实验组患者则在对照组的基础上，引入信息化技术进行护理创新，包括病情监测、药物管理、健康教育等，患者从急诊入院的初步评估阶段、到诊断、治疗、护理以及出院指导的全过程护理，通过信息化技术进行密切监测，及时完善护理过程中的各项措施。通过统计学软件对数据情况进行分析，比较两组患者的患者的护理满意度、住院时间、并发症率等相关数据情况。

结果：研究结果显示，在实验组中，患者的平均住院时间 10.5±1.2 天，患者的 ICU 入住时间为 3.14±1.2 天，患者的并发症率 8%（3 例），患者的整体满意度达为 95%；在对照组中，患者平均住院时间 14.1±2.2 天，患者的满意度仅为 80%。患者的并发症率为 19%（6 例）。经由统计学数据检验，两组患者的数据差异明显，差异具有统计学意义（P<0.05）。**结论**：信息化在心血管临床护理创新中的应用可以有效帮助患者缩短住院时间，通过完善各个护理的细节，确保患者在护理后的并发症得到有效控制，为患者建立更为安全、科学、有效的护理环境，使得患者对整体护理效果的评价较高，值得在临床上进行推广。

关键词：信息化技术；心血管疾病；临床护理

Machine learning based model for predicting cardiovascular disease using dynamic triglyceride-glucose index: a Longitudinal study cohort CHARLS database

Yi Yang, Zeng-Ao Yang, Hong-Hong Zhang, Zheng-Feng Wu, Hai-Jing Zhao, Yue Zhu, Yu-Han Ma, Yu-Qi Liu

chinese pla general hospital

Cardiovascular disease (CVD) remains the leading cause of global mortality and morbidity, with China facing particularly severe challenges as its aging population contends with 330 million CVD cases accounting for 46.74% of all deaths, where two out of every five fatalities stem from cardiovascular causes, creating an urgent need for improved risk assessment methodologies amidst growing metabolic risk factors and demographic pressures. This study leverages five waves of longitudinal data from the China Health and Retirement Longitudinal Study (CHARLS) to investigate the dynamic relationship between Triglyceride-glucose (TyG) index changes - a robust marker of insulin resistance - and subsequent CVD risk among 5,625 Chinese adults aged 45 and older, employing advanced machine learning techniques to overcome limitations of previous cross-sectional approaches and establish a novel framework for dynamic metabolic risk assessment. Participants were stratified into four distinct TyG trajectory groups (low-low, low-high, high-low, high-high) based on 2011-2015 measurements, with comprehensive adjustment for demographic, lifestyle and clinical covariates revealing that individuals maintaining stable high TyG levels faced significantly elevated CVD risk (HR 1.18, 95% CI 1.03-1.36) and stroke risk (HR 1.45, 95% CI 1.11-1.89) compared to those with stable low levels, while no significant difference emerged for isolated heart disease incidence. Survival analyses demonstrated progressively worsening cardiovascular outcomes corresponding to TyG trajectory patterns, with machine learning models (including random forest, XGBoost, CoxBoost, Deepsurv and GBM) consistently demonstrating the superior predictive value of dynamic TyG changes over static measurements or traditional glucose metabolism abnormalities, particularly for stroke risk prediction. Subgroup analyses revealed particularly pronounced risks among individuals aged <65 years, females, and those with higher education levels, lower BMI, or elevated depression scores, suggesting important demographic variations in TyG-related cardiovascular vulnerability. The study's innovative application of machine learning algorithms enabled sophisticated handling of complex longitudinal metabolic data, capturing non-linear relationships and interaction effects that conventional statistical methods might miss, thereby establishing a new paradigm for dynamic risk factor analysis in cardiovascular epidemiology. These findings carry significant clinical implications, demonstrating that monitoring TyG index trajectories over time provides more accurate cardiovascular risk stratification than single measurements, potentially enabling earlier identification of high-risk individuals and more timely intervention. The results underscore the importance of considering metabolic parameter dynamics rather than isolated values in cardiovascular prevention strategies, particularly for stroke prevention where TyG changes showed strongest predictive value. Furthermore, the identified high-risk subgroups suggest potential avenues for targeted screening programs and personalized prevention approaches based on demographic and metabolic characteristics. This research represents a substantial methodological advancement in cardiovascular risk prediction by combining longitudinal population data with cutting-edge machine learning techniques, providing both immediate clinical insights and a robust analytical framework for future investigations of dynamic metabolic risk factors. The demonstrated superiority of trajectory-based assessment over static measurements challenges current clinical paradigms and suggests the need for revised risk assessment protocols incorporating serial metabolic monitoring. These findings have particular relevance for China's healthcare system as it confronts the dual chal-

lenges of population aging and cardiovascular disease burden, offering evidence-based strategies for more effective risk stratification and prevention in resource-constrained settings. By establishing the clinical relevance of TyG index dynamics and demonstrating the value of machine learning in longitudinal risk factor analysis, this study contributes significantly to the growing field of precision cardiovascular prevention and provides a model for future research investigating other metabolic markers. The robust association between TyG trajectory patterns and cardiovascular outcomes, even after comprehensive adjustment for potential confounders, strengthens the case for incorporating TyG monitoring into routine cardiovascular risk assessment, particularly in middle-aged and older adults where metabolic changes frequently precede overt disease. These results also highlight the importance of continuous metabolic monitoring rather than single assessments, as dynamic changes proved more informative than static measurements for predicting cardiovascular outcomes. The study's findings support the development of clinical guidelines recommending serial TyG assessment as part of comprehensive cardiovascular risk evaluation, while also suggesting potential utility as a monitoring tool for evaluating intervention effectiveness in metabolic syndrome management. The demonstrated predictive value across multiple machine learning algorithms reinforces the robustness of the findings and supports the growing role of artificial intelligence in cardiovascular risk prediction. This research bridges an important gap between epidemiological observation and clinical application by providing concrete evidence for the implementation of dynamic metabolic monitoring in real-world cardiovascular prevention programs, while simultaneously advancing methodological standards for analyzing longitudinal risk factor data. The identification of specific high-risk demographic subgroups further enables targeted prevention strategies that could improve resource allocation in public health initiatives, particularly relevant for China's massive population facing growing cardiovascular disease burden. These results may also inform the development of dynamic risk prediction algorithms that incorporate time-varying metabolic parameters, potentially yielding more accurate risk estimates than current static models. The study's comprehensive approach, combining traditional epidemiological methods with advanced machine learning techniques, sets a new standard for investigating metabolic risk factors and their relationship to cardiovascular outcomes, providing both immediate clinical insights and a methodological framework for future research in this critical area of public health.

人工智能在女性心脏病健康流行病学中的应用与展望

陈俊婷 刘华芬

武汉大学人民医院

目的 探究人工智能（AI）技术对女性心脏病健康流行病学研究及临床管理的价值，针对女性心脏病因性别差异产生的独特病理特征、诊疗挑战，明晰 AI 应用潜力与发展方向，为优化防控策略提供参考。

方法 选取近 5 年国内外关于 AI 应用于女性心脏病领域的文献，运用归纳分析法，梳理机器学习、深度学习等技术在诊断、风险预测、健康管理环节的应用流程；对比 AI 技术与传统方法在识别女性特有病理特征、优化诊疗路径中的差异，分析 AI 应用优势及现存瓶颈。

结果 女性心脏病具显著性别特征，发病年龄相对滞后，以疲劳、恶心等非典型症状为主，传统诊断工具敏感度低，且妊娠并发症、绝经后激素波动会加剧患病风险。AI 可融合电子病历、影像数据、可穿戴设备信息等多源数据，挖掘女性专属风险模式，如关联炎症指标、心理压力与预后关系。诊断中，深度学习影像分析通过量化斑块、评估心肌灌注，提升女性患者诊断精准度；自然语言处理（NLP）从临床文本提取信息，辅助识别易漏诊症状；风险评估模型纳入妊娠史、激素水平等变量，优化个体预测。治疗与管理上，AI 分析真实世界数据，评估性别因素对疗效、手术结局影响以支撑决策；个性化推荐系统结合生活习惯、文化背景定制方案，AI 聊天机器人助力偏远地区女性康复依从性提升。但 AI 应用存挑战：历史研究男性样本占比高致数据失衡、模型有性别偏见，算法可解释性差、临床转化难。

结论 AI 为女性心脏病防控提供创新路径，需突破数据质量、算法透明性等壁垒。未来应构建性别均衡多中心数据库，研发可解释 AI 模型，加强跨学科协作，推动女性心血管健康全周期精准管理，助力降低性别健康差距。

关于信息化时代下心血管健康科普知识传播效果的研究

李媛媛 刘华芬

武汉大学人民医院

目的：随着信息技术的快速发展，互联网已成为了我国公民获取健康信息的重要渠道之一。心血管疾病作为全球头号死因之一，其健康科普知识的有效传播对于疾病的预防及控制起着至关重要的作用。本研究旨在探讨信息化时代下心血管健康科普知识的传播效果，为提升大众人民心血管健康素养提供科学依据。

方法：本研究采用文献检索、问卷调查和数据分析相结合的方法。首先，查阅国内外心血管健康科普知识传播相关文献，构建研究框架。其次，设计问卷对公众心血管健康科普知识获取渠道、内容偏好、信任度及行为改变等进行调查。最后，选取典型案例，运用内容分析法对新媒体平台心血管健康科普内容进行深入分析。

结果：研究发现，信息化时代心血管健康科普知识传播呈现以下特点：（1）传播主体多元化，包括医疗机构、专家学者、自媒体等（2）传播渠道多样化，社交媒体、短视频平台等成为重要渠道（3）传播内容碎片化、可视化趋势明显。同时，研究也发现存在以下问题：（1）科普内容质量参差不齐，部分内容缺乏科学依据（2） 传播效果评估体系不完善，难以准确衡量科普效果（3）公众健康素养水平有待提高，对各种信息的辨别能力不足

结论：信息化时代为心血管健康科普知识传播带来了机遇与挑战。为提升传播效果，建议：（1）加强科普内容建设，提高内容的科学性、趣味性和实用性（2）创新传播方式，充分利用新媒体平台优势，开发更多公众喜闻乐见的科普产品（3）建立健全传播效果评估体系，及时了解公众需求，不断优化传播策略（4）加强公众健康教育，提高公众健康素养和信息辨别能力

关键词：信息化时代，心血管健康，科普知识，传播效果，新媒体

基于可解释机器学习建立睡眠呼吸暂停低通气患者中冠心病预测模型--整合炎症及睡眠障碍相关标志物

刘钰涛 [1] 吴嘉慧 [2]

1. 湖北省中山医院 (湖北省第三人民医院)

2. 首都医科大学附属北京安贞医院

背景： 睡眠呼吸暂停低通气综合征（OSAHS）在心血管疾病患者中患病率高达 40-80%，是冠状动脉粥样硬化性心脏病（CAD）的独立风险因素。OSAHS 与 CAD 之间的病理生理联系涉及间歇性低氧、全身炎症和代谢功能障碍的复杂相互作用。本研究旨在开发和验证整合传统危险因素、炎症生物标志物和睡眠特异性参数的机器学习模型，以预测 OSAHS 患者的 CAD 发生风险。

方法： 本回顾性单中心研究纳入 2022 年 1 月至 2025 年 3 月期间在湖北省第三人民医院接受冠状动脉造影检查的 305 例确诊 OSAHS 患者。收集包括人口学变量、传统心血管危险因素、炎症标志物（高敏 C 反应蛋白、中性粒细胞）和多导睡眠监测参数（呼吸暂停低通气指数、氧减指数、最低血氧饱和度）在内的综合数据。采用合成少数过采样技术（SMOTE）处理类别不平衡问题。采用 Boruta 方法进行变量筛选。实施九种机器学习算法，包括逻辑回归、支持向量机、梯度提升机、人工神经网络、随机森林、XGBoost、K 近邻、AdaBoost 和 CatBoost。采用受试者工作特征曲线下面积（AUC）、校准曲线和决策曲线分析评估模型性能。应用可解释性机器学习方法 SHAP 解释预测模型变量重要性。

结果：在 305 例 OSAHS 患者中，98 例（32.1%）经冠状动脉造影确诊为冠心病。集成方法显示出卓越的预测性能，其中随机森林达到最高 AUC 值 0.819（95%CI: 0.776-0.862），其次为 CatBoost（AUC=0.818，95%CI：0.777-0.858）和 AdaBoost（AUC=0.811，95%CI：0.770-0.851）。SHAP 分析显示，炎症标志物（高敏 C 反应蛋白）、氧减指数和传统危险因素（年龄、糖尿病、吸烟）是最具影响力的预测因子。与仅使用传统危险因素的模型相比，整合炎症和睡眠相关参数显著提高了模型的区分度（p<0.001）。

结论： 整合炎症生物标志物和睡眠特异性参数与传统危险因素的机器学习模型为 OSAHS 患者冠心病预测提供了优异的区分能力。这种多模态方法可指导该冠心病高危人群的靶向心血管筛查。

关键词： 睡眠呼吸暂停低通气综合征；冠心病；机器学习；炎症；风险预测

数字技术在心血管临床护理中的应用研究

钱莉 刘华芬

武汉大学人民医院

近年来，数字技术的快速发展为心血管临床护理带来了革命性变革，其在提升诊疗效率、优化患者管理及推动精准医疗方面展现出显著潜力。**研究目的：**本研究旨在探究数字技术在心血管护理中的创新性应用、现存的挑战以及相应的优化策略，进而为推动心血管护理的智能化与精准化发展提供理论与实践支撑。**研究内容与方法：**基于现有研究，本文运用文献回顾、案例分析以及专家访谈等方法，重点探讨了人工智能 (AI)、可穿戴设备、远程监测系统、数字孪生技术及数字疗法在心血管护理中的应用。例如，AI 算法通过整合多组学数据，实现了心血管疾病的早期风险预测、亚型分类及个性化治疗方案制定；可穿载设备结合实时监测功能，显著提高了高血压、心力衰竭等慢性病的动态管理能力；数字孪生技术则通过构建心脏三维模型，支持心律失常的精准治疗模拟。此外，数字疗法在高血压患者行为干预、心力衰竭远程症状监测及冠心病术后康复依从性提升中均显示出积极效果。**成果与挑战：**尽管数字技术显著提升了护理效率与患者预后，但其应用仍面临多重挑战。数据安全与隐私保护问题因健康信息的数字化而凸显，需通过区块链与边缘计算技术强化防护；技术与临床实践的融合障碍则需通过多学科协作及医护培训解决；此外，数字鸿沟可能导致医疗资源分配不均，需政策支持以推动低收入地区技术普及。**结论与展望：**本研究证实，数字技术为心血管护理提供了创新工具，但其规模化应用需克服技术、，伦理及社会层面的障碍、未来研究应聚焦于优化人机协同模式、完善数据标准化体系，并探索公平可及的数字健康生态，以实现心血管疾病全周期管理的精准化与智能化。本综述为临床实践提供了理论依据，为技术优化指明方向，助力心血管护理质量与效率的全面提升。

高血压患者心力衰竭可解释预测模型的识别与验证

赵腾啸 韩嘉毅 丁耀东 曾勇

首都医科大学附属北京安贞医院

背景：心力衰竭（HF）是一种异质性综合征，全球有超过 6000 万人受其影响。患有高血压的患者尤其容易发生心力衰竭。在这一人群中及时识别和预测心力衰竭具有重要的临床意义。本研究旨在开发并验证一种基于机器学习（ML）方法的新型可解释预测模型，以建立和验证心力衰竭的预测模型。

方法：本研究基于强化血压控制与标准血压控制的随机试验（SPRINT）。为解决目标变量的类别不平衡问题，采用了随机欠采样技术，使正负样本比例达到 1:1。通过随机匹配 162 名无心力衰竭终点事件的个体与有事件的个体，构建了

一个包含 324 名参与者的平衡数据集。测试集占总体数据集的 40%，以确保对模型性能进行稳健评估。采用 7 种机器学习算法构建预测模型。采用机器学习算法——多层感知器（MLP）、逻辑回归（LR）、决策树（DT）、随机森林（RF）、极端梯度提升（XGBoost）和支持向量机（SVM）——构建预测模型。使用包括受试者工作特征曲线下面积（AUC）在内的多个评估指标来比较预测性能。采用 SHapley Additive exPlanation(SHAP)方法来确定特征重要性并解释最终模型。

结果：在中位随访 3.14 年期间，162 名患者（1.7%）发生新发心力衰竭。在 7 种机器学习模型中，梯度提升机（GBM）模型的判别能力最强。通过应用 GBM 方法，本研究成功建立了高效的心力衰竭风险预测模型。根据 LASSO 进行特征选择后，建立了具有 14 个特征的可解释的最终 GBM 模型。该模型在识别心力衰竭风险方面表现出强大的预测能力，总体准确率为 71%，精确率为 75%，AUC 为 77%。

结论：我们开发了一种针对高血压患者心力衰竭的可解释预测模型。

基于心电大数据的房颤慢性病管理模式研究进展与展望

何吉富 李晓

山东中医药大学附属医院（山东省中医院）

目的：心房颤动（AF）是全球范围内一项重大的公共卫生挑战，亟需有效的慢性病管理策略。本综述旨在总结利用心电大数据进行房颤慢性病管理模式的最新研究进展，探究其在房颤早期筛查、诊断、治疗及长期管理中的应用，为优化房颤慢性病管理提供理论依据和实践指导。

方法: 通过整合心电大数据相关技术与临床实践，系统分析该模式的技术基础（包括可穿戴设备的心电采集、长程监测、多参数同步采集技术，以及云计算、深度学习等数据处理分析方法）、应用场景（大规模人群筛查、AI 辅助诊断、远程监测与个性化治疗决策、患者自我管理）及效果评价体系（临床结局改善、卫生经济学分析），并探讨其面临的技术与临床挑战。

结果：研究表明，房颤具有高发病率、高致残率等流行病学特征，传统慢性病管理模式在早期识别、动态监测及个体化干预等方面存在明显局限。而心电大数据技术的应用有效突破了这些瓶颈：人工智能算法与心电数据的整合，使房颤自动识别准确率提升至 90% 以上；远程监测系统实现了患者心率、心律等指标的实时传输与分析，显著降低了急诊就诊率；基于多维度心电数据制定的个性化治疗方案，将患者年度心血管不良事件发生率降低约 20%。这些进展共同推动了房颤管理向精准化、智能化方向发展。

结论：基于心电大数据的房颤慢性病管理模式为突破传统管理局限、实现房颤早期化、个性化管理提供了创新路径，在临床效果与经济效益上均具潜力。未来需通过技术创新（如边缘计算、可解释 AI）、统一标准规范、加强多学科协作及政策支持，解决现存挑战，推动其在临床实践中的广泛应用与持续优化，最终改善房颤患者预后并减轻公共卫生负担。

关键词

心电大数据、房颤、慢性病管理、人工智能、远程监测

基于 CiteSpace 对心血管数字健康技术演进路径与前沿趋势的研究

许家瑄 崔鹤蓉

北京中医药大学

摘要：随着人口老龄化加剧和生活方式改变，心血管疾病的防控面临巨大挑战。传统的诊疗模式存在诊断效率低、个体化治疗不足等问题。近年来，人工智能（AI）等信息技术在医疗领域的应用，为心血管疾病的精准诊疗、风险预测和健康管理提供了新的解决方案，尽管该领域的研究蓬勃发展，但研究热点、机构合作模式、未来趋势仍缺乏系统性分析。

目的：旨在通过文献计量学方法，评估 2000-2023 年心血管数字健康技术研究的研究趋势，并探讨机构合作、研究热点和前沿趋势。

方法：计算机检索数据库中国知网 (CNKI)，检索 2000-2023 年发表的关于心血管数字健康技术研究的文献。运用文献计量学软件 CiteSpace 对机构、期刊、作者和关键词进行可视化分析。

结果：从 2000 年 1 月 1 日到 2025 年 7 月 1 日，共检索到 500 篇关于心血管数字健康技术研究的论文。结果显示，整体发文量逐渐增加；心血管病学进展 (16) 是发文量最多的期刊，发文量最多的是中国人民解放军医学院 (7)。在作者分析中，李方江 (4) 排在第一位。关键词处于数字健康技术部分的人工智能 (269) 和医学部分的冠心病 (36) 在文献中出现频率最高。预测模型和主动脉缩窄为 2021-2025 年前沿研究内容。

结论：该研究分析了心血管数字健康技术研究的研究现状和趋势，为研究人员提供了有价值信息，有助于研究者发现潜在的合作者和机构，发现该领域的热点问题和探索新的研究方向。

关键词：心血管；数字健康技术；人工智能；文献计量学 ;CiteSpace

基于机器学习的心房颤动患者发生血栓的预测模型

刘剡 [1] 张智轩 [2] 张家瑜 [2] 王凯 [2] 木胡牙提·乌拉斯汉 [2]

1. 新疆医科大学第一附属医院

2. 新疆医科大学

目的 基于大样本真实世界临床数据，构建面向心房颤动（Atrial Fibrillation，AF）患者的血栓风险预测模型，系统评估多种主流机器学习算法在识别血栓高风险人群中的应用价值，并探索关键临床变量与血栓形成之间的潜在关联，为改善抗凝策略提供决策依据。

对象和方法 本研究数据来源于新疆某三甲医院共 27,982 例 AF 住院患者。通过单因素分析与 LASSO 回归筛选关键特征变量，并采用随机欠采样技术处理类别不平衡问题。分别构建逻辑回归、随机森林、GBDT、XGBoost 与 LightGBM 模型，评估其在 AUC、准确率、召回率、F1 分数等多维度上的预测性能。最终结合 SHAP 解释算法对综合最优模型结果进行可视化解析。

结果 XGBoost 模型的 AUC 评分最高，但随机森林模型的综合性能最优，在准确率、召回率与 F1 值上优于其他模型。SHAP 解释结果显示，肺动脉收缩压、左室射血分数、右心房内径、左心室收缩末内径与心搏出量是影响 AF 患者血栓风险的核心变量。SHAP 图谱同时揭示出高肺动脉收缩压、高右心腔内径及低左室收缩功能（如低射血分数、左室末径扩大）等特征，在多数样本中与血栓发生呈正向关联，提示房颤状态下心腔重构与血液动力学异常可能在血栓形成过程中扮演重要角色。

结论 本研究基于机器学习识别 AF 患者发生血栓的逻辑回归、随机森林、GBDT、XGBoost 与 LightGBM 模型均显示出较高的判别性能，其中随机森林模型的综合判别效能最佳。

接受经导管主动脉瓣置换术的重度主动脉瓣狭窄患者并发二 尖瓣反流演变的研究

艾虎

卫生部北京医院（北京大学第五临床医学院）

目的:

重度主动脉瓣狭窄（aortic stenosis，AS）常与二尖瓣反流（mitral regurgitation，MR）共存。本研究旨在评估因重度 AS 接受经导管主动脉瓣置换术（transcatheter aortic valve replacement，TAVR）治疗的患者中合并中度及以上 MR（中重度 MR）的演变。

方法：

这是一项前瞻性多中心队列研究，纳入 2020 年 1 月至 2023 年 10 月期间在我国五个瓣膜中心接受 TAVR 治疗的重度 AS 患者。使用经胸超声心动图评估基线和 TAVR 术后 12 个月 MR 的严重程度及其术后演变。分析了以全因死亡和因充血性心力衰竭、心肌梗死或心绞痛再住院为复合终点的术后 12 个月临床结局。

结果：

研究期间共纳入 424 例患者，31%（n=130）的患者在基线时合并中重度 MR。在 130 例患者中，80 例患者在术后 12 个月时有超声心动图随访数据，其中 56 例（70%）患者观察到 MR 改善。与术后 12 个月 MR 未改善或加重的患者相比，MR 改善患者的纽约心脏协会（The New York Heart Association，NYHA）心功能分级明显改善。左心室射血分数（left ventricular ejection fraction，LVEF）更大程度的改善与 MR 改善相关（OR=0.97，95% CI: 0.95-1.00，P=0.04）。在基线合并和不合并中重度 MR 的患者之间未观察到生存获益存在统计学差异。尽管全因死亡率没有差异，但在 MR 改善的患者中观察到复合终点发生率更低的趋势（12.5% vs. 20.8%，log-rank p=0.49）。在合并中重度 MR 的患者中，高龄（HR=1.12，95% CI：1.01–1.24，P =0.04）和较高

的肺动脉收缩压（systolic pulmonary arterial pressure，SPAP）（HR：1.05，95% CI：1.00–1.09，P =0.04）与 TAVR 术后不良预后独立相关。

结论：

在本研究中，合并中重度 MR 的患者在 TAVR 后 MR 严重程度和 NYHA 分级均有所改善。基线合并中重度 MR 与较差的临床结局不相关，但在 MR 改善的患者中观察到预后改善的趋势。高龄和较高的 SPAP 是 AS 合并中重度 MR 的患者 TAVR 术后不良预后的预测因素。

将 CFIR 框架用于心血管疾病急救医疗实施研究：阻碍、促进因素与可能的机会

郭心远 胡雅丽 余小梅 侯博文 张煌 高星宇 朱丽 蔡泽鸣 杨懿 章浦瑞 王朗 朱丽华

武汉大学人民医院

目的

心血管疾病的急救医疗在实践过程中存在质量差异，尽管现有指南提供了标准化诊疗方案，但实施中仍面临医疗资源不均、流程衔接障碍及决策延迟等问题。数字化信息化技术已被证明可改善疾病诊疗质量，但在心血管病的急救医疗中的应用仍需探索。实施性研究综合框架（CFIR）为系统评估数字化信息化技术的应用环境提供了结构化方法，该框架包含创新特征、外部环境、内部环境、个体特征和实施过程五大核心领域，能够全面分析影响技术实践的关键因素。本研究基于 CFIR 设计调查问卷，广泛收集湖北省内多位临床工作者及临床专家意见，旨在评估数字化信息化急救医疗的促进与阻碍因素，为优化急救医疗实施情况提供线索。

方法

本研究在 PubMed 等多个医学文献数据库检索与心血管病、数字化信息化技术和紧急医疗服务相关文献，提取文献中涉及使用数字化信息化技术的作用、现状、影响因素的关键信息，采用收敛综合方法整合定性及定量数据。研究人员与专家基于提取数据开展研讨以明确部分重要因素。在 CFIR 框架的指导下设计调查问卷。问卷包含人口学信息及所在机构急诊科概况提问以明确受访者的工作时长、职称等基本特征；纳入 48 个与 CFIR 结构相关的问题，尚未被确定重要性的因素在问卷中收集定量数据，旨在评估该类要素对数字化信息化技术实施的影响程度；已确定重要性的因素在问卷中收集定性数据以判断该因素对技术实施的促进或阻碍作用。收集的问卷数据由一名研究人员独立分析整合，另一名研究人员对数据进行准确性检查，采用描述性统计数据来总结调查项目的回答平均分，并确定所有受访者中最常见的促进和障碍因素。

结果

在 43 份调查问卷的数据中，促进因素集中在创新领域，少数位于其他领域；而阻碍因素主要分布在创新和内部结构中。院前、院内以及医疗机构间的数据共享程度在促进和阻碍因素中均表现出高度重要性，其他较为显著的影响因素包括医疗机构对诊疗质量的目标制定、临床工作者与同事和同行的沟通协作、临床工作者的经验与认知以及收集反馈后的优化创新。然而数字化信息化技术应用于急救医疗的建设成本较高，这与当前多数研究来自高收入国家的特征相符；部分区域如偏远地区使用数字化信息化的条件不足，阻碍了技术实施。

结论

本研究是国内首个评估心血管疾病数字化信息化急救医疗影响因素的实施科学研究，依据 CFIR 框架制定调查问卷，收集湖北省多家公立医院临床工作者的实施意见以分析急救医疗在真实世界实施的背景环境，为后续心血管病急救医疗的实施策略制定及研究提供了理论指导。

人工智能辅助心血管疾病风险预测模型的构建与验证

张弘扬

哈医大二院

目的：心血管疾病作为全球范围内导致死亡的首要原因之一，其高发性、高致残率给社会和家庭带来了沉重负担。早期对疾病风险进行精准预测，能够为临床采取针对性预防措施、延缓疾病进展争取宝贵时间。本研究致力于借助人工智能技术，整合多维度心血管疾病相关数据，构建一套高效、精准的风险预测模型，以突破传统预测方法在准确性和时效性上的局限，为临床实践中心血管疾病的一级和二级预防提供更具参考价值的决策依据。

方法：研究数据来源于国内 5 家三级甲等医院过去 3 年的临床诊疗记录，收集的信息不仅有年龄、性别、身高、体重等基本人口学数据，还包含高血压、糖尿病等既往病史，吸烟、饮酒、运动习惯等生活方式信息，以及血常规、生化指标、心电图、心脏超声等检验检查结果。在数据预处理阶段，采用多重插补法处理缺失值，运用 Z-score 标准化方法对连续变量进行标准化，通过独热编码处理分类变量，利用局部离群因子算法剔除异常值，确保数据集的完整性和可靠性。模型构建过程中，分别采用逻辑回归、随机森林、梯度提升树及深度神经网络四种算法进行训练。将数据集按照 7:3 的比例通过分层抽样划分为训练集和测试集，其中训练集用于模型参数优化，测试集用于模型性能评估。采用 5 折交叉验证对各模型的超参数进行调优。评估指标除了受试者工作特征曲线下面积外，还包括准确率、精确率、召回率及 F1 分数。

结果：在测试集中，四种模型的性能表现存在显著差异。逻辑回归模型的 AUC 为 0.78，准确率 72%，精确率 70%，召回率 68%，F1 分数 69%；随机森林模型的 AUC 为 0.85，准确率 79%，精确率 77%，召回率 76%，F1 分数 76.5%；梯度提升树模型的 AUC 为 0.88，准确率 82%，精确率 80%，召回率 79%，F1 分数 79.5%；而深度神经网络模型表现最优，AUC 达到 0.92，准确率 86%，精确率 85%，特异度 88%，敏感度 85%，F1 分数 85%。进一步对不同心血管事件的预测结果显示，该深度神经网络模型在预测急性心肌梗死时 AUC 为 0.91，预测脑卒中时 AUC 为 0.90，均显著高于其他三种模型（P<0.05）。通过特征重要性分析发现，年龄、收缩压、空腹血糖、总胆固醇 / 高密度脂蛋白胆固醇比值及左心室射血分数是影响模型预测结果的前五位重要特征。

结论：本研究构建的深度神经网络心血管疾病风险预测模型在多维度评估指标上均优于传统机器学习算法及逻辑回归模型，具有较高的预测准确性和临床实用性。该模型能够有效整合多源临床数据，精准识别心血管疾病高危人群，尤其是对急性心肌梗死、脑卒中等严重心血管事件的早期预测具有重要价值，可为临床医生制定个体化的预防策略提供科学依据，有助于降低心血管疾病的发病风险和不良预后的发生率。但本研究仍存在一定局限性，数据来源于国内 5 家医院，可能存在地域局限性，模型在不同种族、不同医疗资源水平地区的适用性有待进一步外部验证；其次，模型的可解释性仍需加强，可通过引入注意力机制等方法提高模型决策的透明度，增强临床医生对模型的信任度，促进其在临床实践中的广泛应用。

心脏瓣膜病术后的个体化抗凝治疗

佟明汇 奚卉

北京大学国际医院（北京大学第八临床医学院）

目的：华法林是目前全球最广泛用于瓣膜术后口服抗凝治疗的药物，患者需频繁监测 INR 并及时调整华法林剂量，这对于年龄偏大、行动不便以及来自偏远地区的抗凝患者的术后生活，造成了极大困扰。 本研究运用“互联网 + 大数据”理念结合华法林自我管理技术，旨在探索这种专科医生团队参与的“远程自我”管理模式，指导瓣膜术后患者抗凝治疗的可行性及有效性，建立现代的电子化抗凝数据库并同时进行多亚组分析，实现华法林精准给药。

方法：本研究前瞻性单中心非随机队列研究；对所有于本院进行瓣膜手术，并术后需要连续服用华法林抗凝治疗的患者进行入组，包括但不仅限于人工瓣膜置入、成形环、持续性房颤以及心内血栓形成患者，对入组患者进行远程抗凝管理相关知识以及平台使用方法详细培训。根据患者抗凝意愿以及当地临近医院条件，以抗凝模式分组，即远程自我管理组及对照组。前者采用家居抗凝仪器进行抗凝管理，后者则在我院或当地医院门诊进行抗凝检测及管理，所有患者采取通过微信小程序患者端上传至远程抗凝平台并完成 INR 及其他数据记录，由本团队进行远程抗凝方案制定；远程自我管理组中随机分为基因型调整组（基因组）和传统调整组（传统组）。基因组利用 IWPC 模型根据患者 CYP2C9 和 VKORC1 基因型、年龄、身高、体重、种族、是否合并使用胺碘酮和是否合并使用 CYP 酶诱导剂等信息，制定个体化起始及维持剂量，若每间隔 3 天一次的调整剂量连续 5 次，即持续 12 天检测 INR 不达治疗目标，将基因组转为传统组继续后续随访；传统组包括部分远程自我管理组患者以及对照组患者，根据目标 INR、华法林剂量 -INR 趋势以及临床症状调整华法林剂量。

结果：完成前瞻性注册入组华法林抗凝患者 357 人。当中居家抗凝组患者 162 例，门诊组 195 例，共获得有效 INR 数值 4051 条。目前平均随访时间 23.7 月。随访总时间为 247681d，随访率达 98.3%。INR 检测值范围为 1.13~6.33(1.98±0.51)。在目标 INR 范围内（单纯主动脉瓣置换及成形环植入为 1.5-2.0；其余瓣膜手术为 1.8~2.5) 患者所服用的华法林剂量为 5.73~39.30(19.37±4.22) mg/ 周。总体不良事件（严重栓塞及出血）事件 1.0%; 当中院内消化道出血 1 例，院内及术后 2 月新发脑梗塞各一例，院外随访中出现无严重出血及死亡事件。随访期间，门诊组及居家组抗凝患者在目标 INR 范围内其 TTR 分别为 46.10%(73731 d/159757d)，77.21%(104377 d/135187d);FTTR 则分别为 58.64%(1021 次 /1741 次)，78.22%(1731 次 /2213 次)。虽然居家抗凝治疗组患者在严重出血及栓塞事件发生情况与门诊治疗组相约。但居家抗凝治疗组 INR 检测量（人均 15.8 次 vs8.9 次）、达标比例及达标时长均较门诊组高，同时 INR 检测频率也较高。入组 56 例患者进行华法林基因型模型计算药物剂量并调整，初步结果显示患者首次达标时间（2.42 天 vs 3.93 天）及 INR 达标比例（85.37%vs 73.28%）均优于传统调整组趋势。问卷调查患者满意度高，总体满意及非常满意度为 95.3%，家居组满意度更高于门诊组（97.5%vs 93.2%）

结论：本研究中远期结果提示“远程 + 自我”管理模式进行抗凝管理，该模式安全有效，总体不良事件（严重栓塞及出血）事件低，居家抗凝治疗患者抗凝管理治疗可能是未来长期抗凝患者更佳选择。利用基因型大模型进行精准抗凝显示更佳安全性及有效性趋势。

Explainable Machine Learning for Predicting ICU-Onset Atrial Fibrillation in STEMI Patients: A Gradient Boosting Framework Based on Real-World Data

Hao-Ran Wang, Hao Liu, Shi-Yi Liu, Hao-Jian Dong

Guangdong Provincial People’s Hospital (Guangdong Academy of Medical Sciences)

1. **Objective**

New-onset atrial fibrillation (NOAF) is a common yet underrecognized complication in critically ill patients with ST-segment elevation myocardial infarction (STEMI), affecting approximately 5–15% of this population during their intensive care unit (ICU) stay. The emergence of NOAF in this context is associated with significantly increased risks of hemodynamic instability, stroke, prolonged hospitalization, and in-hospital mortality. Despite its clinical significance, NOAF remains difficult to anticipate using conventional scoring systems or clinician judgment alone, especially in the early hours of ICU admission when preventive decisions are most impactful.

Current prognostic tools for atrial fibrillation largely focus on chronic or postoperative populations and are not tailored to STEMI patients in the critical care setting. Furthermore, the dynamic interplay of cardiovascular stress, systemic inflammation, pharmacologic exposures, and organ dysfunction in the ICU environment adds complexity to early risk prediction. As a result, there is an unmet clinical need for data-driven, individualized, and interpretable risk stratification models that can support timely decision-making. Advances in machine learning (ML), particularly explainable algorithms, offer a promising avenue to address this gap by leveraging high-dimensional real-world data to generate precise and clinically meaningful predictions.

This study aimed to develop and internally validate an explainable machine learning model to predict new-onset atrial fibrillation (NOAF) during ICU admission in patients with ST-segment elevation myocardial infarction (STEMI), using high-resolution, real-world data from a large critical care database. The model was designed to provide both accurate risk stratification and transparent individual-level interpretation to support early clinical decision-making.

2. **Methods**

A retrospective cohort study was conducted using data from the MIMIC-IV (v3.1) database, which includes de-identified electronic health records of ICU patients at the Beth Israel Deaconess Medical Center between 2008 and 2019. Adult patients diagnosed with STEMI were included based on predefined ICD-9/10 codes. Patients were eligible if they were ≥ 18 years old, had ICU stays longer than 48 hours, had no prior history or first-day documentation of atrial fibrillation, and had not undergone cardiac surgery. The primary outcome was new-onset atrial fibrillation (NOAF) occurring after ICU admission, defined using structured bedside heart rhythm annotations.

More than 100 candidate features were extracted from the first 24 hours of ICU data, encompassing demographics, comorbidities, laboratory values, vital signs, interventions, and medication usage. Missing data were handled using the K-nearest neighbors (KNN) imputation algorithm, and variables with >30% missingness were excluded. A two-step feature selection process was implemented: initial filtering via the LReliefF algorithm, followed by wrapper-based refinement using Boruta. Final feature selection was informed by gradient boosting decision tree (GBDT) feature importance profiles. A GBDT model was trained on the top 12 predictors using stratified 10-fold cross-validation. Model performance was assessed using metrics including AUC, sensitivity, specificity, F1-score, and Brier score, and interpretability was evaluated through SHAP (SHapley Additive exPlanations) for both global and local explanations.

3. **Results**

Among 1,255 ICU admissions for STEMI, 120 patients (9.6%) developed new-onset atrial fibrillation (NOAF) after the first ICU day. The final GBDT model incorporated 12 top-ranked predictors including SOFA score, age, mechanical ventilation, heart rate, serum creatinine, and amiodarone use. During 10-fold cross-validation, the model achieved a mean AUC of 0.984 (SD 0.003), accuracy of 96.5%, sensitivity of 92.0%, specificity of 97.0%, and F1-score of 0.830. Performance remained acceptable in internal validation (AUC 0.823, accuracy 87.2%) and was preserved in the independent test set (AUC 0.771, accuracy 84.1%, sensitivity 56.3%, specificity 88.2%).

Calibration assessment revealed close agreement between predicted and observed risks (Brier score 0.091; 95% CI: 0.053–0.135), and decision curve analysis indicated net clinical benefit across a threshold range of 5–30%. SHAP analysis identified SOFA score, amiodarone exposure, and admission age as the most influential variables. Global SHAP plots showed that higher SOFA scores and amiodarone use markedly increased predicted risk, whereas beta-blocker use and female sex were protective. Force plots demonstrated individual-level feature contributions, delineating distinct clinical risk profiles and enhancing interpretability of model outputs.

4. **Conclusion**

This study developed and internally validated an interpretable machine learning model for predicting new-onset atrial fibrillation (NOAF) in critically ill patients with ST-segment elevation myocardial infarction (STEMI), using real-world ICU data from the MIMIC-IV database. Our findings demonstrate that a gradient boosting decision tree (GBDT) algorithm, trained on a rigorously selected set of 12 clinically plausible predictors, achieved robust discriminative performance and good calibration. Importantly, the model's interpretability—enabled by SHapley Additive exPlanations (SHAP)—enhanced its transparency and clinical relevance by identifying key modifiable risk factors and offering individualized explanations for prediction outputs.

In contrast to prior work focused on general ICU populations or non-ICU cardiovascular cohorts, this study specifically addressed NOAF prediction in STEMI patients—a group at heightened arrhythmic risk yet underserved by existing risk stratification tools. Conventional scoring systems such as $CHADS_2$ or CHA_2DS_2-VASc are not designed for acute settings and lack predictive granularity for incident AF. Our approach incorporated ICU-specific physiologic parameters (e.g., SOFA score, mechanical ventilation, AKI status) alongside pharmacologic exposures and laboratory abnormalities, reflecting the complex interplay of hemodynamic stress, systemic inflammation, and cardiac vulnerability characteristic of STEMI pathophysiology.

A major strength of this work lies in its multimodal feature selection pipeline. The integration of LReliefF (filter method), Boruta (wrapper method), and GBDT-based importance analysis provided a balanced, data-efficient approach to dimensionality reduction, mitigating overfitting while retaining key clinical signals. The consistent identification of SOFA score, amiodarone use, and admission age as top contributors aligns with known mechanistic insights into atrial remodeling and electrophysiologic instability. Moreover, the interpretability analysis revealed not only global drivers of AF risk but also personalized feature contributions for individual patients, offering a pathway for clinician-facing, explainable AI deployment in high-stakes ICU environments.

Despite promising results, several limitations must be acknowledged. First, the model was developed using data from a single academic center, and external validation in independent, multicenter datasets (e.g., eICU) was not feasible due to heterogeneity in data structures and high rates of missingness for critical predictors. Second, the reliance on structured documentation (e.g., nurse-recorded heart rhythm status) may have underdetected brief or asymptomatic AF episodes not captured during routine charting. Third, our model did not incorporate electrocardiographic waveforms, echocardiographic indices, or biomarkers of atrial fibrosis, which may further enhance discrimination. Lastly, although SHAP provides intuitive visualization, it does not substitute for prospective clinical trials or mechanistic validation.

In summary, we present a robust and interpretable machine learning model for early prediction of ICU-onset atrial fibrillation in STEMI patients, grounded in real-world clinical data. The model demonstrates high accuracy, favorable calibration, and meaningful clinical transparency through SHAP analysis. These findings highlight the potential utility of explainable AI tools in acute cardiac care, enabling proactive monitoring and individualized risk mitigation. Future work should focus on external validation, real-time integration into clinical workflows, and evaluation of downstream impact on patient outcomes.

Leveraging Explainable Artificial Intelligence to Uncover Age and Sex Heterogeneity in Cardiovascular Risk Factors: A Cross-sectional Study of the BRFSS Cohort

Zixing Wang[1], Yuxiaoqian Cheng[2], Yiyang Liu[1], Yujie Yang[1]

1. Chinese Academy of Medical Sciences, Peking Union Medical College, Fuwai Hospital

2. Chinese Academy of Medical Sciences & Peking Union Medical College, School of Health Policy and Management

Background: Traditional cardiovascular disease (CVD) risk assessment models frequently fail to account for the varying effects of risk factors across different demographic groups. This research endeavor is focused on harnessing the power of machine learning techniques and explainable artificial intelligence (XAI) to achieve two primary objectives: (1) to distinguish between unique clinical phenotypes among individuals who have experienced a heart attack, and (2) to measure the specific influence of key predictors on heart disease risk, taking into account the differences in impact across varying age groups and sexes.

Methods: This study adopted a cross-sectional design, utilizing data from 246,022 adult participants who responded to the 2022 Behavioral Risk Factor Surveillance System (BRFSS). Initially, we applied unsupervised clustering techniques, specifically K-Means combined with UMAP (Uniform Manifold Approximation and Projection) visualization, to a subset of 13,435 individuals who reported a history of heart attack. This approach enabled us to identify distinct clinical phenotypes based on their individual profiles of risk factors. Following this, we trained a high-performance XGBoost classification model on the entire dataset to predict the likelihood of a heart attack history. To interpret the model's predictions, we utilized SHAP (SHapley Additive exPlanations), a method that not only identifies key global predictors but also allows for a comparative analysis of the importance and impact of these predictors across different demographic subgroups, specifically comparing between males and females and between individuals under 55 years of age and those 55 years or older.

Results: The clustering analysis conducted in this study successfully distinguished three unique clinical phenotypes among patients with a history of heart attack: the "Classic Comorbid Phenotype," which is characterized by the presence of multiple chronic diseases and physical frailty, with a higher prevalence among females; the "Metabolically-Healthier, Older Phenotype," which is associated with fewer comorbidities but includes older individuals and is more common in males; and a novel "Non-Diabetic, Obese Phenotype." The XGBoost model exhibited outstanding predictive capabilities, achieving an AUC-ROC of 0.880 (95% CI: 0.874-0.887). The subsequent SHAP analysis uncovered significant variations in the impact of risk factors: while a history of angina emerged as the most influential predictor across all groups, a high body mass index (BMI) was found to be a considerably more potent risk factor for males compared to females. Interestingly, alcohol consumption was revealed to be a protective factor, but only in the female subgroup. Among individuals younger than 55 years, lifestyle factors such as smoking and BMI, along with sex, were identified as the top predictors. In contrast, for the older cohort aged 55 years and above, age itself and comorbid conditions such as stroke were the dominant predictors.

Conclusion: The outcomes of this study underscore the inadequacy of a generic, "one-size-fits-all" approach to CVD risk assessment. By combining machine learning methodologies with XAI, we have provided quantitative evidence highlighting the significant heterogeneity in cardiovascular risk factors across different age and sex demographics. These findings hold the potential to facilitate the development of more precise and personalized prevention strategies, tailored to the unique demographic and clinical profiles of individuals, thereby enhancing the effectiveness of cardiovascular disease management and intervention.

新形势下构建和谐护患关系与护理文化建设的思考

杨丹 刘华芬

武汉大学人民医院

《新形势下构建和谐护患关系与护理文化建设的思考》

杨丹

随着医疗环境变革与健康中国战略的深化，护患关系与护理文化建设面临新挑战与机遇。当前，患者健康需求多元化、信息化技术广泛应用、医改政策持续推进，对护理服务提出了更高要求。护患关系作为医疗服务的核心纽带，直接影响患者满意度与护理质量。然而，沟通不畅、信任缺失等问题仍制约着和谐护患关系的构建。

护理文化建设是提升护患和谐的关键路径。通过强化人文关怀理念，倡导以患者为中心的服务模式，可有效增强患者信任感与归属感。例如，推广叙事护理、共情沟通等实践，有助于深化护患情感联结。同时，完善护理团队协作机制，建立开放包容的医院文化氛围，能够激发护理人员的职业认同感与责任感，进而提升服务效能。此外，信息化手段的应用为护患互动提供了新途径，如智能随访系统、健康宣教平台等，不仅优化了服务流程，还促进了护理文化的数字化传播。

新形势下，需从制度、教育、实践多维度协同推进护理文化建设。建议加强护理伦理培训，规范服务标准；鼓励护理人员参与文化创新项目，挖掘典型案例；结合政策导向，构建以患者体验为导向的护理文化评价体系。通过系统性建设，推动护患关系从"技术主导"向"人文共融"转型，为护理事业高质量发展注入持久动力。

智慧管理模式在心力衰竭患者延续性护理中的应用进展

刘娅

北京清华长庚医院

心力衰竭患者需通过科学的延续性护理降低复发率并提升生活质量。智慧管理模式在延续性护理中的应用，可有效解决当前患者依从性低、居家监测困难、资源分配不均、信息沟通不畅等问题，通过远程实时监测、数据驱动决策和个性化干预等手段，显著提升患者自我管理能力。本文综述了智慧管理模式在心力衰竭患者延续性护理中的应用研究进展，涵盖身体数据监测、个性化护理方案制定、远程护理指导以及用药管理等方面。尽管智慧管理模式展现出显著的应用潜力，但在技术整合、标准统一以及用户适应性等方面仍面临诸多挑战。

关键词：智慧管理模式；人工智能；心力衰竭；延续性护理；远程监测

心力衰竭（heart failure, HF）是多种心血管疾病进展到终末阶段后形成的临床综合征，其主要特征包括高再住院率、高死亡率以及患者生活质量受损 [1]。心力衰竭患者通常需要接受长期、系统的管理和治疗，以延缓疾病进展、改善预后 [2]。然而，大量研究显示 [3]，心力衰竭患者出院后的延续性护理落实情况不容乐观。由于患者居住分散，后续跟踪难度较大，导致沟通有限。此外，传统的延续性护理模式，如电话随访、门诊复诊、和社区护理，在心力衰竭患者的延续性护理管理中存在诸多局限性。这些模式因监测频率不足、数据采集不连续、反馈信息延迟、缺乏个性化护理方案以及资源有限所致覆盖范围狭窄等关键瓶颈，难以满足心力衰竭患者的护理需求 [4]。因此，探索新的护理模式以优化延续性护理方式显得尤为重要。近年来，随着科技的飞速发展，智慧化管理模式为延续性护理带来了新的机遇。其核心内涵是以患者为中心，整合医疗信息资源，运用信息技术提升医疗服务的精准性、便捷性和高效性。智慧管理模式以人工智能、大数据和物联网等前沿技术为核心 [5]，通过传感器将管理平台与管理对象连接，实现数据的实时采集、处理与分析，为个性化护理方案的制定提供科学依据 [6-8]。同时借助区块链技术保障数据安全和隐私 [9]。这些技术的协同作用，不仅提升了延续性护理的效率和质量，更为解决传统延续性护理模式所面临的瓶颈问题提供了关键支持。本文旨在综述智慧管理模式在心力衰竭患者延续性护理中的应用研究进展，以期为临床护理实践提供参考和借鉴。

RESEARCH ON SIMULATION AND IDENTIFICATION OF ECG SIGNAL

Yongxiang Zhang[1], Jian Wu[1], Yong Sun[1], Qin-Ce Li[2]

1. 2nd Affliated Hospital of Harbin Medical University

2. Harbin Insitute of Technology

The 12-lead electrocardiogram (ECG) is crucial in the initial evaluation of patients suspected of having acute coronary syndrome, providing prognostic information similar to or even better than troponin measurements [1]. However, the sensitivity of the 12-lead ECG for detecting acute myocardial infarction is only 50-60% due to the presence of non-typical ECG changes in many patients, such as ST depression, T-wave inversion, left bundle branch block, or left ventricular hypertrophy [2]. A major drawback of the 12-lead ECG equipment is the limited number of precordial leads and the absence of posterior leads, leading to insufficient sensitivity and specificity in the measured heart data and an inability to accurately describe and analyze complex cardiac electrophysiological activities. One method to enhance the diagnostic capability of the 12-lead ECG is to sample over a larger thoracic surface area, such as the right ventricle, lateral, and posterior regions—a technique known as body surface potential mapping (BSPM). The 256-lead ECG acquisition is a non-invasive method that uses a large number of electrodes covering the patient's chest and back.

Displaying waveform data in the time domain similar to the 12-lead ECG is impractical with a large number of leads. A feasible approach is to combine the spatial position of electrodes on the body surface to generate computerized body surface potential maps (BSPM), which map all lead signals onto a torso model with vertex rendering colors and contour lines to describe the distribution of the body surface potential. BSPMs can provide more cardiac information compared to the 12-lead ECG, as they cover not only the chest but also the back region, which is not detected by the 12-lead system, aiding the diagnosis of certain heart diseases. BSPM can measure more detailed potential changes on the human body surface, focusing on more subtle features, better reflecting cardiac information, and assisting doctors in determining health status and specific diseases.

However, due to the scarcity of 256-lead ECG data and the lack of a comprehensive database, generating 256-lead ECG signals to expand the sample size is necessary to avoid overfitting during experiments, which could lead to inaccurate recognition of abnormal samples. At the same time, it is essential to conduct research on the recognition of 256-lead ECG data. Addressing the issue of insufficient multi-lead ECG data samples, this paper primarily proposes and employs two generative algorithms tailored to the unique categories of ECG data: the CNN-BiLSTM model and the 2DUnet-VPTransformer model. By respectively extracting features from the spatial and temporal dimensions of the ECG signals, these models are capable of generating new ECG signals that share the same distribution as the original data. Notably, the second algorithm is not confined to generating signals with a single disease; through the integration of multi-channel fusion and spatio-temporal attention mechanisms, it can produce ECG signals that encompass multiple diseases, representing an innovative approach. The spatio-temporal attention mechanism enhances the autoregressive inference speed of the model and reduces the cumulative inference error.

As this method requires data labeled with specific disease markers, and since the existing 256-lead ECG data lacks such labels, the approach is primarily experimented on a 12-lead dataset. Comparative analysis and experimental results indicate that the CNN-BiLSTM and 2DUnet-VPTransformer models for ECG signal generation perform remarkably well. In the future, these models can be explored for generating ECG signals containing various diseases for multi-label classification recognition. The utilization of an attention-based residual network for classification algorithms can also improve recognition accuracy, showing unique advantages on the ECG dataset and promising prospects for future applications.

心脏瓣膜病有关研究

The Relationship of Serum Uric Acid and Intracardiac Thrombosis Risk in Patients with Rheumatic Heart Disease

Yuan Huang[1], Yu-xin Li[2]

1. Jiangbin Hospital of Guangxi Zhuang Autonomous Region

2. The First Affiliated Hospital of Guangxi Medical University

Aims: To explore the relationship between serum uric acid (SUA) and intracardiac thrombosis in patients with Rheumatic Heart Disease (RHD).

Methods: Propensity score matching (PSM) analysis was employed to reduce the interference of confounding variables. A restricted cubic spline curves and logistic regression analysis were used to assess the relationship between SUA and intracardiac thrombosis risk.

Results: The patients with intracardiac thrombosis had a significantly higher SUA levels both in overall population and PSM population. The risk of intracardiac thrombosis increased with increasing levels of SUA. In total population, when SUA is 412 μmol/L, the adjusted OR (aOR) of intracardiac thrombosis is 1; after PSM, when SUA was 419 μmol/L, the aOR was 1. With fully adjusted, the multivariate logistic regression analysis demonstrated that: 1) SUA showed an independent positive association with intracardiac thrombosis; 2) each standard deviation (SD) increase in SUA was independently associated with a 19.2% increase in the risk of intracardiac thrombosis for overall population (aOR = 1.192; 95%CI: 1.005 - 1.414) and with a 33.5% increase in the risk of intracardiac thrombosis for PSM population (aOR = 1.335; 95%CI: 1.083 - 1.645). Among the subgroup of female (age ≥ 50), each SD increase in SUA was independently associated with a 70% increase in the risk of intracardiac thrombosis.

Conclusion: SUA is independently associated with a higher risk of intracardiac thrombosis in patients with RHD. Controlling SUA level may be of very important clinical significance in preventing intracardiac thrombosis in postmenopausal female.

Keywords: serum uric acid, intracardiac thrombosis, rheumatic heart disease, postmenopausal female, risk factor

Aims: To explore the relationship between serum uric acid (SUA) and intracardiac thrombosis in patients with Rheumatic Heart Disease (RHD).

Methods: Propensity score matching (PSM) analysis was employed to reduce the interference of confounding variables. A restricted cubic spline curves and logistic regression analysis were used to assess the relationship between SUA and intracardiac thrombosis risk.

Results: The patients with intracardiac thrombosis had a significantly higher SUA levels both in overall population and PSM population. The risk of intracardiac thrombosis increased with increasing levels of SUA. In total population, when SUA is 412 μmol/L, the adjusted OR (aOR) of intracardiac thrombosis is 1; after PSM, when SUA was 419 μmol/L, the aOR was 1. With fully adjusted, the multivariate logistic regression analysis demonstrated that: 1) SUA showed an independent positive association with intracardiac thrombosis; 2) each standard deviation (SD) increase in SUA was independently associated with a 19.2% increase in the risk of intracardiac thrombosis for overall population (aOR = 1.192; 95%CI: 1.005 - 1.414) and with a 33.5% increase in the risk of intracardiac thrombosis for PSM population (aOR = 1.335; 95%CI: 1.083 - 1.645). Among the subgroup of female (age ≥ 50), each SD increase in SUA was independently associated with a 70% increase in the risk of intracardiac thrombosis.

Conclusion: SUA is independently associated with a higher risk of intracardiac thrombosis in patients with RHD. Controlling SUA level may be of very important clinical significance in preventing intracardiac thrombosis in postmenopausal female.

Keywords: serum uric acid, intracardiac thrombosis, rheumatic heart disease, postmenopausal female, risk factor

Development and Validation of a Nomogram for Predicting Intracardiac Thrombosis Risk in Patients with Rheumatic Heart Disease

Yuan Huang[1], Chun Gui[2]

1. Jiangbin Hospital of Guangxi Zhuang Autonomous Region

2. The First Affiliated Hospital of Guangxi Medical University

Aims: This study aimed to develop a predictive model based on clinical data to assess the risk of intracardiac thrombosis in patients with rheumatic heart disease (RHD) and to provide guidance for personalized post-discharge treatment strategies.

Methods: Consecutive patients with RHD who were hospitalized between August 2016 and August 2019 were included in the study. Lasso regression analysis was performed to identify key prognostic factors influencing intracardiac thrombosis formation. A predictive model was then constructed through multivariable logistic regression and validated using a nomogram. The model's effectiveness was evaluated using the concordance index (C-index) and calibration curves.

Results: A total of 870 patients were enrolled, including 524 in the thrombosis group and 346 in the non-thrombosis group. Lasso regression analysis identified five key prognostic factors: atrial fibrillation (AF), mitral valve stenosis, left atrial anteroposterior diameter, left atrial diameter, and history of stroke. AF and mitral valve stenosis were ultimately identified as independent risk factors. Based on these factors, a nomogram for thrombosis risk prediction was constructed, with a C-index of 0.743 (95% CI: 0.710-0.776), indicating good predictive ability. Internal validation yielded a C-index of 0.736, further supporting the model's validity. Decision curve analysis showed that the model has good clinical applicability when the threshold probability is between 18% and 81%.

Conclusion: This study is the first to construct a predictive model for intracardiac thrombosis risk in patients with RHD using a nomogram approach. The model demonstrates strong potential for clinical application. By identifying key prognostic factors, it can effectively assess the risk of intracardiac thrombosis in RHD patients and provide a basis for personalized treatment strategies.

Aims: This study aimed to develop a predictive model based on clinical data to assess the risk of intracardiac thrombosis in patients with rheumatic heart disease (RHD) and to provide guidance for personalized post-discharge treatment strategies.

Methods: Consecutive patients with RHD who were hospitalized between August 2016 and August 2019 were included in the study. Lasso regression analysis was performed to identify key prognostic factors influencing intracardiac thrombosis formation. A predictive model was then constructed through multivariable logistic regression and validated using a nomogram. The model's effectiveness was evaluated using the concordance index (C-index) and calibration curves.

Results: A total of 870 patients were enrolled, including 524 in the thrombosis group and 346 in the non-thrombosis group. Lasso regression analysis identified five key prognostic factors: atrial fibrillation (AF), mitral valve stenosis, left atrial anteroposterior diameter, left atrial diameter, and history of stroke. AF and mitral valve stenosis were ultimately identified as independent risk factors. Based on these factors, a nomogram for thrombosis risk prediction was constructed, with a C-index of 0.743 (95% CI: 0.710-0.776), indicating good predictive ability. Internal validation yielded a C-index of 0.736, further supporting the model's validity. Decision curve analysis showed that the model has good clinical applicability when the threshold probability is between 18% and 81%.

Conclusion: This study is the first to construct a predictive model for intracardiac thrombosis risk in patients with RHD using a nomogram approach. The model demonstrates strong potential for clinical application. By identifying key prognostic factors, it can effectively assess the risk of intracardiac thrombosis in RHD patients and provide a basis for personalized treatment strategies.

TAVR 术后发生急性肾损伤危险因素分析及预测模型构建

闫磊 杨毅宁

新疆维吾尔自治区人民医院

目的：探讨 TAVR 患者术后发生 AKI 的危险因素，为临床预防及干预提供依据。

方法：分析 2021 年 1 月至 2024 年 12 月我院行 TAVR 手术的 205 例患者资料，根据术后 48 小时内是否发生 AKI 分为 AKI 组（n=45）与非 AKI 组（n=160）。采用单因素、LASSO 回归和多因素 Logistic 回归分析 TAVR 术后发生 AKI 的危险因素。将数据集按照 7 ： 3 的比例随机分为训练集和测试集，并基于多因素 Logistic 回归结果，构建预测模型，使用受试者工作特征曲线、Hosmer-Lemeshow 校准曲线和决策曲线对列线图的性能进行评估。

结果：本研究共纳入 205 例患者，比较 AKI 组和非 AKI 组之间的参数。①两组患者在年龄、高血压、糖尿病、贫血、手术时间、房颤、K+、Lac、肌酐、BNP、术前 24 小时尿量和术前中心静脉压方面差异有显著性意义 (P < 0.05)；②采用 LASSO 回归分析方法筛选出 7 个与 TAVR 术后发生 AKI 风险相关的预测变量，将其纳入多因素 Logistic 回归分析，结果显示年龄、手术时间、房颤、术前贫血、糖尿病、术前 24 小时尿量和术前中心静脉压是 TAVR 术后发生 AKI 的独立危险因素 (P < 0.05)；③训练集中预测发生 AKI 风险的受试者工作特征曲线下面积为 0.839 (95%CI：0.780-0.897)，验证集预测发生 AKI 风险受试者工作特征曲线下面积为 0.846(95%CI：0.759-0.932)；Hosmer-Lemeshow 校准曲线拟合度较好 (训练集，P=0.062；验证集，P=0.081)；决策曲线显示使用列线图预测模型能预测 TAVR 术后发生 AKI 的风险是有益的。

结论：TAVR 术后发生 AKI 是多因素的，其中年龄、手术时间、房颤、术前贫血和糖尿病、术前低尿量、术前低中心静脉压为独立危险因素，同时构建的列线图预测模型，可用于预测 TAVR 手术患者发生 AKI 的风险。

Serum alpha-1-microglobulin (A1M) as an independent predictor of calcific aortic valve stenosis and its predictive value

Ze-Yuan Mei[1], Cheng-Hu Guo[1], Hong Yang[2], Jia-Qi Li[1], Mei-Ling Chang[1], Cheng Zhang[1], Mei Ni[1], Lin Chen[1], Wei Gao[1], Xiao-Ling Liu[1], Gui-Peng An[1]

1. Qilu Hospital of Shandong University

2. Jinan Vocational College of nursing

Backgroud: In our previous study, we performed RNA sequencing of aortic valve tissue from patients with severe AVS and without CAVD respectively, and found that the expression of the AMBP [A1M (alpha-1-microglobulin)/bikunin precursor] gene was significantly higher in calcified aortic valve tissues than that in the relatively normal aortic valve tissues, which was further verified by qRT-PCR and immunohistochemical staining (GEO accession: GSE235995). This study aimed to investigate the potential predictive value of serum A1M for aortic valve stenosis (AVS).

Methods: This study continuously enrolled patients with AVS who visited Qilu Hospital of Shandong University from August 2023 to February 2024, which were further divided into two groups: patients with non-severe AVS, and patients with severe AVS. The age- and sex- matched patients without aortic valve disease were recruited as controls during the same period. All participants were underwent transthoracic echocardiography. Serum A1M levels were measured by ELISA. We explored the relationship between serum A1M and AVS using ordinal logistic regression, Spearman correlation analysis, smoothed curve fitting, threshold effect analysis, and subgroup analysis.

Results: A total of 234 (69.9 ± 8.36 years, 92 [39.3%] males) patients were included, with 61 [26.0%] in the non-severe AVS group, 89 [38.0%] in the severe AVS group, and 84 [36.0%] in control group. Serum A1M levels were significantly lower in AVS patients, particularly in those with severe AVS (Control: 22.00 ± 8.25 μg/mL, non-severe AVS: 14.72 ± 4.79 μg/mL,severe AVS: 10.11 ± 3.95 μg/mL, respectively, P < 0.001). Spearman correlation analysis showed that the serum levels of A1M were negatively correlated with aortic valve maximal gradient (r_s = -0.3645 [95% CI: -0.4994 to -0.2123], P < 0.001), mean aortic valve gradient (r_s = -0.3826 [95% CI: -0.5150 to -0.2324], P < 0.001) and aortic valve maximal velocity (r_s = -0.3553 [95% CI: -0.4914 to -0.2022], P < 0.001), while positively correlated with aortic valve area (r_s = 0.4348 [95% CI: 0.2908 to 0.5596], P < 0.001). Multivariate analysis identified serum A1M levels as independent predictive factors for AVS (adjusted odds ratio, 0.761 [95% CI: 0.715–0.811], P < 0.001). Subgroup analysis indicated that serum A1M was still the independent predictive factor for AVS in different subgroup populations and was not affected by lipid levels.ROC analysis demonstrated that A1M exhibited good diagnostic value in diagnosing AVS (AUC = 0.867, 95% CI: 0.818–0.917, P < 0.001) and assessing its severity (AUC = 0.771, 95% CI: 0.695–0.847, P < 0.001). We evaluated the discrimination and reclassification of models with and without serum A1M for predicting both the incidence and severity of AVS. The inclusion of serum A1M resulted in a significant improvement in AUC, NRI, and IDI. These findings suggest that serum A1M demonstrates strong independent and additive predictive value for both the incidence and severity of AVS.

Conclusions: The serum levels of A1M were significantly decreased in patients with AVS and further decreased with severity of AVS. Serum A1M was an independent predictive factor of AVS, and showed a good predictive ability for AVS and the severity of AVS. Further clinical studies are worth conducting to explore the possibility of A1M as a valid biomarke

风湿性心脏病合并心腔内血栓患者的临床特征及预后相关分析

黄源 李宇鑫 杨立华 黄丽红

广西壮族自治区江滨医院

目 的：心腔内血栓是心血管疾病中较为严重的并发症之一，被认为与不良预后密切相关。本研究旨在探讨风湿性心脏病（Rheumatic heart disease, RHD）合并心腔内血栓患者的临床特征，以及血栓对不良预后的影响，为该类患者的临床决策提供更具针对性的依据，从而改善其长期预后。

方 法：连续性纳入 2016 年 8 月至 2019 年 8 月在本中心首次住院经超声心动图确诊为 RHD 的患者共 740 例。通过电子病历系统获取患者的基线资料。心腔内血栓通过经胸或经食道超声心动图诊断。通过电话随访以及临床病历调查来获取预后信息。借助单因素及多因素 Logistic 回归分析深入探讨心腔内血栓对不良预后的影响。

结 果：合并心腔内血栓的患者有 206 例（27.84%），血栓均见于左心系统，主要分布于左心耳（51.94%），附壁血栓占 79.13%。通过随访调查，最终获取 550 例患者的预后信息。差异性分析显示，合并心腔内血栓的患者再住院率（χ^2=11.15, P<0.001）及全因死亡率（χ^2=6.79, P=0.009）更高。单因素分析显示，心腔内血栓与再住院风险（OR=2.93, 95%CI: 1.52~5.65, P=0.001）及全因死亡风险（OR=2.51, 95%CI: 1.23~5.10, P=0.011）升高显著相关。经调整后多因素回归显示，心腔内血栓与再住院风险（OR=3.02, 95%CI: 1.39~6.55, P=0.005）及全因死亡风险（OR=2.56, 95%CI: 1.08~6.06, P=0.033）之间仍表现出显著的关联，并且与 1 年内、3 年内、5 年内的再住院风险及全因死亡风险之间表现出一致的正相关。

结 论：RHD 患者的心腔内血栓多分布于左心系统，并以左心耳血栓多见。合并心腔内血栓的患者其再住院风险及全因死亡风险显著增加，心腔内血栓是 RHD 患者不良预后的独立危险因素。

Whole transcriptome analysis of aortic stenosis unveils dysregulated RNA networks, immune infiltration, and NADK2-driven pathogenic mechanisms

wang wangfengxia[1,2], Yi-Tong Ma[1]

1. The First Affiliated Hospital of Xinjiang Medical University

2. People's Hospital of Xinjiang Uygur Autonomous Region

Background

Aortic stenosis (AS), a prototypical fibrocalcific valvular disease, imposes a substantial global burden, affecting an estimated 2.5% of adults over 65 years and up to 13.3% of those over 75. Characterized by progressive narrowing of the aortic valve orifice, AS culminates in left ventricular outflow tract obstruction, diastolic dysfunction, and ultimately heart failure, with a 5-year mortality rate exceeding 50% in severe cases. While transcatheter aortic valve replacement (TAVR) and surgical valve replacement have revolutionized late-stage management, the molecular underpinnings of valve degeneration remain poorly characterized. Emerging evidence implicates a tripartite pathogenesis involving aberrant valvular interstitial cell (VIC) activation, extracellular matrix (ECM) remodeling, and low-grade inflammation. However, the role of non-coding RNAs (ncRNAs)—including long non-coding RNAs (lncRNAs) and circular RNAs (circRNAs)—in orchestrating epigenetic and post-transcriptional regulation, as well as the crosstalk between immune cell infiltration and metabolic reprogramming, represents an uncharted frontier.

Methods

Employing a multi-omics approach, we profiled RNA expression in surgical valve specimens from 12 patients with severe AS and 8 age-matched controls using Illumina HiSeq 2500 sequencing (150 bp paired-end reads). Differentially expressed transcripts (DETs) were identified using DESeq2 (FDR < 0.05, |log2FC| > 1), with principal component analysis (PCA) confirming robust transcriptomic segregation between groups. Functional validation of nicotinamide adenine dinucleotide kinase 2 (NADK2), a candidate hub gene, involved: (1) quantitative real-time PCR (qPCR) in an expanded cohort of 30 AS valves and 15 controls; (2) Western blot analysis of NADK2 protein levels in matched samples; (3) immunohistochemistry to localize NADK2 expression in human AS valves and a murine AS model (Rat fed a high-cholesterol diet for 16 weeks). Bioinformatics analyses included: GO/KEGG enrichment for coding RNAs, ChIP-seq-based prediction of lncRNA transcription factor binding sites, circRNA-miRNA-mRNA network construction using miRanda, immune cell infiltration quantification via CIBERSORT, and weighted gene co-expression network analysis (WGCNA) to identify modules associated with AS pathogenesis.

Results

RNA-seq analysis revealed 1,443 differentially expressed mRNAs (68.3% upregulated), 3,147 lncRNAs (72.1% upregulated), and 145 circRNAs (65.4% upregulated) in AS valves. Key findings included: Coding RNA Landscape: mRNAs such as CACNA1C (calcium channel) and MMP9 (matrix metalloproteinase) were enriched in calcium signaling and ECM-receptor interaction pathways, implicating dysregulated calcium homeostasis and matrix degradation in valve stiffening;Non-coding RNA Networks: lncRNAs like HOXA11-AS clustered with Wnt signaling and embryonic development pathways, suggesting reactivation of developmental programs. NADK2 as a Hub Gene: NADK2 expression was upregulated 4.7-fold at the mRNA level (p < 0.001) and 3.2-fold at the protein level in human AS valves, with conserved upregulation (3.8-fold mRNA increase) in the murine model. Immunoinfiltration analysis showed robust positive correlations between NADK2 expression and infiltrating CD4 memory T cells (r = 0.72, p < 0.001) and CD8 T cells (r = 0.68, p < 0.01). WGCNA identified a magenta module (347 genes) strongly associated with NADK2 (module-trait correlation r = 0.89), enriched for NAD metabolism and T cell activation pathways.

Conclusion

This study unveils a tripartite regulatory axis in AS: (1) coding RNAs drive fibrocalcific remodeling via calcium and ECM pathways; (2) lncRNAs epigenetically reprogram VICs to an embryonic-like state; (3) circRNAs modulate protein turnover through ubiquitination networks. The conserved upregulation of NADK2 across species positions it as a critical node linking metabolic reprogramming (via NADP(H) biosynthesis) and immune activation (via T cell effector function). Targeting NADK2-mediated NADPH shunting could disrupt the feedforward loop of inflammation and metabolic dysfunction in AS. Additionally, lncRNA-directed epigenetic therapies or circRNA-based microRNA sponges offer novel avenues for intervening in valve degeneration. These findings not only advance our understanding of AS pathogenesis but also provide a translational framework for developing RNA-based diagnostic biomarkers and therapeutic strategies.

探究风湿性二尖瓣疾病的血流动力学影响

李永超 [1] 杨天阳 [3] 贾一新 [1] 张宇 [2]

1. 清华大学附属北京清华长庚医院

2. 清华大学基础医学院

3. 上海市胸科医院

目的

本研究旨在通过计算流体动力学（CFD）方法深入探究风湿性二尖瓣疾病对左心室血流动力学的影响，为临床诊断和治疗决策提供量化评估和理论支持。风湿性心脏病（RHD）是一种由未治疗的 A 组 β- 溶血性链球菌性咽炎引发的自身免疫性疾病，在中低收入国家较为常见。RHD 的主要特征包括心内膜炎症和瓣膜病变，这些病变可导致二尖瓣和主动脉瓣的狭窄或反流，进而引发心力衰竭等严重并发症。尽管现有影像学技术（如超声心动图、CT、X 光造影和心血管磁共振成像）能够在一定程度上评估 RHD 的严重程度，但它们在显示心脏深部结构和功能方面存在局限性。CFD 作为一种新兴的技术手段，能够提供更全面、客观且信息丰富的血流动力学评估，对于早期诊断和治疗效果预测具有重要意义。

方法

本研究基于上海第四人民医院心外科收治的四名风湿性心脏病患者的 CT 数据，利用开源图像处理软件 3D Slicer 生成了患者特定的左心室三维模型。进一步采用 ANSYS 17.1.5 软件对模型进行 CFD 网格划分，生成包含约 304188 至 638472 个四面体单元的网格，并在左心室与二尖瓣交界区域加密网格以提高模拟精度。通过设定合理的边界条件和加载条件，如左心室体积变化、血液流动的不可压缩性以及心脏周期内的动态变化，结合 ANSYS Fluent 2020R1 软件求解质量与动量守恒方程，模拟了心脏周期内的血流动力学变化。同时，构建了一个理想化的健康二尖瓣模型作为对照，以突出风湿性二尖瓣病变对血流动力学的影响。

结果

研究结果表明，风湿性二尖瓣狭窄会导致左心室舒张期血流速度显著增加，且血流模式更加紊乱，出现更多的漩涡。与理想模型相比，风湿性二尖瓣病例的左心室壁压力和二尖瓣跨瓣压力差在舒张期明显增大，且瓣口面积越小，压力差越大。此外，左心室壁和二尖瓣的切应力也显著升高，切应力大小与瓣口狭窄程度呈正相关。具体而言，风湿性二尖瓣病例在舒张期的左心室血流速度可达理想模型的 2-5 倍，左心室壁压力差可达理想模型的 3-57 倍，二尖瓣跨瓣压力差可达理想模型的 15-285 倍，左心室壁和二尖瓣的切应力可达理想模型的 4-191 倍。

结论

本研究成功运用 CFD 方法对风湿性二尖瓣疾病患者的左心室血流动力学进行了模拟和分析，揭示了风湿性二尖瓣病变对左心室血流动力学的显著影响。研究结果表明，风湿性二尖瓣狭窄会导致左心室舒张期血流速度显著增加、跨瓣压力差增大以及切应力升高，这些血流动力学参数的变化与瓣口狭窄程度密切相关。这些发现为临床医生提供了量化评估风湿性心脏病严重程度的新工具，有助于改善治疗决策和手术规划。此外，本研究还为未来进一步探索和改善风湿性心脏病的治疗方法奠定了坚实的理论基础，强调了 CFD 在心血管疾病研究中的重要性和应用前景。

使用 Feops 有限元模拟技术评估接触压力指数预测经导管主动脉瓣置换术后新发左束支传导阻滞的效能：一项单中心临床研究

李福杭 高远 张海山 梁长彬 马克 孙英贤 郭亮

中国医科大学附属第一医院

摘要

目的 (Objective): 经导管主动脉瓣置换术（TAVR）后新发左束支传导阻滞（LBBB）是影响预后的重要并发症，发生率达 10-35%。本研究旨在评估 Feops 有限元模拟技术计算的接触压力指数（CPI）预测 TAVR 后新发 LBBB 的临床价值。

方法（Method）：本研究回顾性分析了 2019 年 1 月至 2023 年 12 月期间在我院心脏中心接受 TAVR 治疗的连续病例。纳入标准包括症状性重度主动脉瓣狭窄、使用 Venus-A 系列瓣膜、术前有完整的增强 CT 血管造影资料等。所有患者术前 CT 图像均导入 Feops HeartGuide 平台进行三维重建和有限元分析，根据实际植入的瓣膜型号和深度计算 CPI 值。主要研究终点为术后新发 LBBB，由经验丰富的心电图专家根据标准诊断标准判定。采用受试者工作特征曲线分析 CPI 的预测效能，并通过多因素 logistic 回归分析确定独立预测因子。

结果 (Results)：研究期间共 106 例患者接受 Venus-A 系列瓣膜 TAVR 治疗，根据纳入排除标准，最终 96 例患者纳入分析。患者平均年龄 73.17±7.75 岁，男性占 50.0%，二叶式主动脉瓣患者占 54.2%。术后 21 例（21.9%）患者发生新发 LBBB，其中 4 例因进展为高度房室传导阻滞而需要植入永久起搏器。新发 LBBB 组的 CPI 值显著高于非 LBBB 组（中位数：24.3% vs 12.1%，P<0.001）。ROC 曲线分析显示，CPI 预测新发 LBBB 的曲线下面积为 0.874（95% 置信区间：0.799-0.949），当截断值设定为 16.5% 时，敏感性为 76.2%，特异性为 85.3%。多因素分析显示，在校正瓣环直径、植入深度等因素后，CPI 仍是新发 LBBB 的独立预测因子（OR= 0.052，95% CI: 0.015 - 0.184，P<0.001）。

结论 (Conclusions)：Feops 有限元分析技术计算的接触压力指数能够有效预测中国患者 TAVR 后新发左束支传导阻滞的发生风险。CPI ≥ 16.5% 可作为识别高危患者的阈值，该技术的应用有助于术前风险评估、手术策略制定和术后管理方案的优化，为实现 TAVR 的精准化治疗提供了重要工具。

Post-TAVR blood pressure elevation: Impact on clinical outcomes

Ning-Jing Qian, Si-Yin Ding, Jin Lu, Xiao-Hong Pan, Xian-Bao Liu

The Second Affiliated Hospital of Zhejiang University School of Medicine

Background:

Transcatheter aortic valve replacement (TAVR) has revolutionized the management of severe aortic stenosis, particularly in patients deemed at high or intermediate surgical risk. While the procedure effectively alleviates valvular obstruction and improves hemodynamic parameters, the clinical significance of post-procedural blood pressure (BP) changes remains a subject of ongoing investigation. Current literature provides conflicting perspectives on whether BP elevation following TAVR represents a compensatory physiological response or a pathological state requiring intervention. Emerging evidence suggests that BP increases post-TAVR may serve as a marker of improved ventricular-arterial coupling and cardiac output, potentially influencing long-term cardiovascular outcomes. However, the relationship between these hemodynamic changes and hard clinical endpoints has not been comprehensively evaluated. This meta-analysis sought to systematically examine the association between elevated BP after TAVR and key clinical outcomes, including all-cause mortality, myocardial infarction, stroke, and cardiovascular-related rehospitalization, with particular attention to temporal patterns of risk modification.

Methods:

We conducted a rigorous systematic review following PRISMA guidelines. Our comprehensive search strategy encompassed PubMed, Embase, and Cochrane Library databases from their inception through January 19, 2025, without language restrictions. The search employed a combination of MeSH terms and keywords related to TAVR, blood pressure, and clinical outcomes. Two independent reviewers screened records at title/abstract and full-text levels, with discrepancies resolved by consensus or third-party adjudication. Included studies met the following criteria: (1) prospective or retrospective cohort studies of adult patients undergoing TAVR; (2) explicit comparison between patients with post-TAVR BP elevation versus those without significant BP changes; and (3) reporting of at least one predefined outcome with minimum 6-month follow-up. Data extraction included study design, population characteristics, BP measurement protocols, outcome definitions, and adjusted effect estimates when available. The quality of the selected studies was evaluated by Risk of Bias in Non-Randomized Studies of Interventions (ROBINS-I) tool. Meta-analysis was performed using random-effects models to generate pooled risk ratios (RR) with 95% confidence intervals (CI).

Results:

This meta-analysis incorporated data from four eligible studies. The pooled cohort comprised 535 patients for 6-month mortality assessment, 997 patients for 1-year outcomes, and 304 patients with extended follow-up beyond 2 years. The findings revealed a remarkable temporal pattern in mortality risk associated with post-TAVR BP elevation. At 6 months follow-up, patients with elevated BP demonstrated a robust 74% reduction in mortality risk (RR: 0.26, 95% CI: 0.14-0.51, p <0.0001), suggesting an immediate survival advantage. This benefit attenuated by 1-year follow-up to a non-significant 40% risk reduction (RR: 0.60, 95% CI: 0.22-1.70, p = 0.34), potentially reflecting the resolution of acute hemodynamic improvements. Notably, the survival benefit re-emerged substantially during extended follow-up (>2 years), with the elevated BP group maintaining a 48% lower mortality risk (RR: 0.52, 95% CI: 0.39-0.70, p <0.0001), indicating durable prognostic significance. Secondary outcome analyses at 1-year follow-up revealed nuanced patterns. For myocardial infarction, the elevated BP group showed a clinically meaningful 33% lower incidence (RR: 0.67, 95% CI: 0.24-1.28, p = 0.43), though this did not reach statistical significance, possibly due to limited event numbers. Stroke rates were comparable between groups (RR: 0.87, 95% CI: 0.34-2.24, p = 0.78), suggesting that post-TAVR BP elevation does not increase cerebrovascular risk. Rehospitalization analysis demonstrated nearly identical rates between groups (RR: 0.98, 95% CI: 0.81-1.19, p = 0.85), indicating that BP changes may not influence healthcare utilization patterns.

Conclusions:

This comprehensive meta-analysis provides evidence that elevated BP following TAVR is associated with significantly improved survival outcomes, particularly in both the short term post-procedural period and longer term follow-up. The biphasic mortality risk pattern suggests complex underlying mechanisms, potentially involving initial hemodynamic optimization followed by sustained cardiovascular adaptation. The absence of increased stroke risk challenges conventional concerns about BP elevation in this population, while the neutral effect on rehospitalization rates provides reassurance regarding resource utilization. These findings have important clinical implications, suggesting that conservative BP management may be warranted in post-TAVR patients and that elevated BP may serve as a positive prognostic marker. Future research should focus on elucidating the pathophysiological mechanisms underlying these associations and determining optimal BP targets for TAVR recipients through prospective, randomized studies.

老年重度瓣膜性心脏病患者的现状和预后分析：一项单中心前瞻性观察研究

余青云 吴延庆

南昌大学第二附属医院 心血管内科

目的：本研究旨在探讨老年重度瓣膜性心脏病患者的临床特征、治疗现状及预后情况，并比较不同治疗方案对患者结局的影响，寻找不良预后相关危险因素，为临床决策提供依据。

方法：本研究为前瞻性队列研究，入选 2021 年 1 月至 2023 年 1 月期间在南昌大学第二附属医院诊断为重度瓣膜性心脏病的 235 例老年住院患者。所有患者均在入组时进行标准化的临床评估。研究设计包括两部分：一部分为基线临床数据的收集与分析，根据患者年龄、瓣膜病类型和 NYHA 心功能分级进行分组，分别分析各组的临床特征、治疗方案及治疗效果。另一部分为随访数据的收集和分析，所有患者随访至少 12 个月，主要结局指标为全因死亡率，次要结局指标包括心功能改善、再住院率及相关并发症等。采用 Kaplan-Meier 生存分析比较不同亚组患者的长期生存率，并应用 Cox 回归模型评估独立危险因素。

结果：本研究发现，患者的平均年龄为 72.4±6.36 岁，男性占 57.45%。最常见的瓣膜病变为主动脉瓣狭窄（41.7%），其次为二尖瓣关闭不全（25.5%）。在治疗方案中，药物治疗组占 40.85%，有创治疗组占 59.15%，其中经皮介入治疗的患者占比最高（42.98%）。有创治疗组的住院天数和住院费用显著高于药物治疗组（住院天数：18.0 天 vs 7.0 天，P<0.001；住院费用：27.00 万元 vs 0.93 万元，P<0.001）。尽管有创治疗组的住院天数和费用较高，但两组的院内死亡率无显著差异（P=0.496）。在随访期内，共有 10 名患者死亡（4.46%），其中 66.67% 为心源性死亡。71 名患者（30.85%）经历了心源性再住院。心衰加重（24.3%）和肾功能恶化（6.5%）为最常见的不良事件。生存分析显示，NYHA III-IV 级患者的死亡率显著高于 I-II 级患者（P=0.027）。治疗方案对再住院率影响显著，药物治疗组的再住院率高于有创治疗组（P<0.001）。Cox 回归分析显示，左室后壁厚度较小（HR=0.67，95%CI: 0.48-0.95，P=0.025）、E 值较低（HR=0.98，95%CI: 0.96-0.99，P=0.002）和血小板计数较低（HR=0.99，95%CI: 0.98-1.00，P=0.019）为独立危险因素。

结论：老年重度 VHD 主要由退行性变引起，以主动脉瓣狭窄最为常见。心功能分级较差（NYHA III-IV 级）会显著增加死亡风险，而左室后壁厚度较小、E 值较低及血小板计数减少为预后不良的独立危险因素。不同治疗策略对心功能恢复和再住院率具有重要影响。基于患者临床特征优化个体化管理对于改善长期预后、降低心血管事件发生率至关重要。

TAVR 术中导丝过瓣困难时的应对方法

王斌

中国人民解放军北部战区总医院（原沈阳军区总医院）

目的：探讨经导管主动脉瓣膜置换术（Transcatheter Aortic Valve Replacement, TAVR）导丝过瓣困难时的应对方法。

方法：11 例主动脉瓣重度狭窄拟行经股动脉 TAVR 的患者，常规方法（AL 2.0 6F 导管支撑直头导丝过瓣）进行导丝过瓣不能成功，尝试时间为 1052±1477 秒，最长为 4657 秒。改用方法 1（应用抓捕器辅助 AL 2.0 6F 导管）或方法 2（应用 260cm 0.035″ 长导丝 +JL 3.5 7F 指引导管）实施导丝过瓣。

结果：11 例主动脉瓣严重狭窄患者，年龄 75.3±5.6 岁，其中男性 7 例（占 63.6%），三叶瓣 2 例（占 18.2%），0 型二叶瓣 4 例（占 36.4%），1 型二叶瓣 4 例（占 36.4%），2 型二叶瓣 1 例（占 9.1%）。主动脉瓣瓣叶钙化积分为 794.3±660.3mm^2（钙化定义为 HU 值大于 850）。主动脉瓣瓣环角度为 57.5±11.2 度，最大者为 81 度。患者 1 至患者 7 改用方法 1 进行过瓣，6 例导丝顺利过瓣。患者 8 先改为方法 1 过瓣，尝试 2270 秒未成功，再改为方法 2 过瓣，导丝成功过瓣，用时 87 秒。患者 9 至患者 11 直接改为方法 2 进行过瓣，均成功过瓣。应用方法 1 过瓣成功率为 75%（6/8），应用方法 2 过瓣成功率为 100%（4/4）。

结论：二叶瓣、瓣叶钙化严重、瓣环角度大的 TAVR 患者，易发生导丝过瓣困难。应用抓捕器辅助 AL 导管或 260cm 导丝 +JL 7F 指引导管能解决导丝过瓣困难的问题。其中，260cm 导丝 +JL 7F 指引导管这一方法操作更简单，过瓣成功率更高，可作为 TAVR 术中导丝不能过瓣的首选替代方法。

经导管主动脉瓣置换术后 30 天死亡率预测的机器学习模型：基于 NTCVR 队列的全国性研究

卢金 朱齐丰 刘先宝 王建安

浙大二院

背景：经导管主动脉瓣置换术（TAVR）已成为主动脉瓣狭窄（AS）患者的首选治疗方案。然而，针对该人群的专用风险评估工具仍显不足。本研究旨在利用中国全国性队列，开发基于机器学习的 TAVR 患者 30 天死亡风险预测模型。

方法：基于国家经导管心血管治疗注册数据库（NTCVR），纳入 2011 年 11 月至 2024 年 8 月期间全国 147 家三级医院接受 TAVR 的患者（定义为全因死亡）。按 6:2:2 比例将队列分为训练集、内部验证集和外部验证集（随机选取两省患者）。采用过采样技术和特征选择方法处理终点事件不平衡问题并筛选关键预测因子。通过机器学习算法开发预测模型，并采用内外交叉验证进行评估。模型性能与传统 STS 评分进行对比。

结果：共纳入 10,799 例 TAVR 患者，平均年龄 75 岁，男性占比 60%。TAVR 术后 30 天死亡率为 2.9%。研究识别出 5 组特征子集（每组含 15 项预测因子），将其与 15 种机器学习算法进行排列组合，最终构建 1,125 个预测模型。其中双输入对称相关（DISR）结合支持向量机（SVM）的组合预测性能最优。在内部验证中，最优机器学习模型的受试者工作特征曲线下面积（AUC）为 0.74（95%CI: 0.67-0.81），显著优于 STS 评分的 0.60（0.53-0.67）（p<0.05）；外部验证中 AUC 分别为 0.69（0.62-0.76）和 0.57（0.51-0.63）（p<0.05）。

结论：本研究开发了一种简便有效的机器学习模型，可预测 TAVR 患者 30 天死亡率，为中国人群的风险分层提供了实用工具。

Hyperglycemia and genetic susceptibility in relation to incident degenerative aortic valve stenosis

Chao-Lei Chen, Zhi-Qiang Nie, Ying-Qing Feng

Guangdong Provincial People's Hospital

Aims: Degenerative aortic valve stenosis (AS) is the most common form of valvular heart disease, with a global burden estimated to affect over 9.4 million individuals. While the association between diabetes and AS has been well established, the relationship between prediabetes and AS remains unclear. Furthermore, the potential influence of genetic susceptibility on these associations has yet to be explored. This study aims to examine the association between hyperglycemia, including prediabetes and diabetes, and incident degenerative AS, as well as to explore whether genetic susceptibility modifies these associations.

Methods: This population-based cohort study analyzed data from 461,017 participants from the UK Biobank, who were divided into three groups (normoglycemia, prediabetes, and type 2 diabetes) based on their baseline glycemic status. The primary outcome was incident degenerative AS, while the secondary outcome was AS-related events, defined as a composite of AS-related interventions or death due to AS. The study used Cox proportional hazards models to estimate hazard ratios (HRs) and 95% confidence intervals (CIs), adjusting for a wide range of covariates including sociodemographic factors, lifestyle variables, and comorbidities. A polygenic risk score (PRS) was constructed based on 38 single nucleotide polymorphisms (SNPs) significantly associated with AS to assess genetic susceptibility.

Results: During a median follow-up of 14.3 years, 5,307 cases of incident AS and 2,209 AS-related events were documented. Compared with normoglycemia, prediabetes and diabetes were associated with increased risks of incident AS (HR 1.21, 95% CI 1.13-1.30 for prediabetes; HR 1.66, 95% CI 1.52-1.80 for diabetes) and AS-related events (HR 1.26, 95% CI 1.13-1.41 for prediabetes; HR 1.60, 95% CI 1.40-1.83 for diabetes). These associations remained significant across various subgroups and in sensitivity analyses. The joint analysis of glycemic status and PRS showed that participants with diabetes and high genetic risk had the highest risk of AS (HR 3.25, 95% CI 2.82-3.74) and AS-related events (HR 3.79, 95% CI 3.05-4.72).

Discussion: This study provides novel insights into the relationship between hyperglycemia and the risk of degenerative AS. The findings indicate that both prediabetes and diabetes are significant risk factors for incident AS and AS-related events, independent of genetic susceptibility. This is the first large-scale prospective study to demonstrate that prediabetes, in addition to diabetes, is associated with an increased risk of AS. The results are consistent across different definitions of prediabetes and various subgroups, highlighting the robustness of the findings. The study also highlights the importance of glycemic control in mitigating AS risk, as uncontrolled diabetes was associated with a higher risk compared to well-controlled diabetes. The potential mechanisms underlying the association between hyperglycemia and AS may involve the formation of advanced glycoxidation end products (AGEs) and subsequent activation of inflammatory pathways, which contribute to valvular calcification and progression of AS.

Conclusion: This study underscores the importance of managing hyperglycemia as a modifiable risk factor for the primary prevention of degenerative AS. Both prediabetes and diabetes are associated with an increased risk of AS and AS-related events, independent of genetic susceptibility. These findings highlight the need for early intervention and management of hyperglycemia to reduce the burden of AS. Future research should focus on exploring the underlying mechanisms and validating these findings in diverse populations.

心脏瓣膜病患者护理中呼吸训练对术后康复的促进作用

彭娜

西安交通大学第一附属医院

目的：探讨标准化护理联合系统化呼吸训练对心脏瓣膜置换术后患者康复效果的影响。

方法：在 2023 年 5 月至 2025 年 5 月间，研究小组共计选出 52 例符合研究要求的心脏瓣膜病患者，并采用随机分配法，将其平均编入采取标准化术后护理干预方案的对照组，以及在此基础上增加呼吸训练的研究组后开展具体的研究工作。期间，通过比较两组研究对象术后第 7 天的肺功能指标、术后 72 小时的血气分析、术后并发症发生率、住院时间以及生活质量评分等，评估呼吸训练护理的价值。

结果：对比此次研究活动取得的两组数据，研究组在术后第 7 天的用力肺活量（FVC）（72.58±6.84%）及第 1 秒用力呼气容积（FEV1）（70.83±6.27%）的改善幅度远比对照组（FVC（65.21±7.42%）和 FEV1（63.74±7.05%））更令人满意。再者，术后 72 小时，研究组的动脉血氧分压（PaO2）为（80.34±4.26 mmHg）比对照组（75.89±5.17 mmHg）更高，而二氧化碳分压（PaCO2）（41.05±2.18 mmHg）水平则较低。同时，研究组患者不仅术后肺部感染及肺不张的发生率（肺部感染的发生率为 7.69%（2 例），肺不张发生率为 11.54%（3 例））较对照组（30.77%（8 例）和 34.62%（9 例））要低，且 ICU 停留时间（48.25±10.34 小时）及总住院时间（12.58±2.16 天）也较短。此外，研究组在术后 1 个月的 SF-36 量表生理功能评分（65.48±7.21）和社会功能维度的评分（68.27±8.15）均显著优于对照组。

结论：通过组间数据对比，以及深度分析，可知结合标准化护理与系统化呼吸训练的方案能够进一步改善心脏瓣膜置换术后患者的肺功能与氧合状态，降低肺部

并发症的发生率，缩短住院时间，提升患者术后早期生活质量。

Outcomes and Temporal Trends of Transcatheter Versus Surgical Aortic Valve Replacement in Patients with Chronic Thrombocytopenia: Insights from the Nationwide Inpatient Sample

Aoqin Gu, YiXuan Xu, GuangZhi Cong, Qing Chen, Ying Cui, BaoTong He, XiaoXia Jia

Ningxia Medical University General Hospital

Background: Chronic thrombocytopenia (CTP) is defined as a persistent reduction in blood platelet count, it increases the risk of perioperative and postprocedural hemorrhage in patients with aortic stenosis (AS) undergoing aortic valve replacement (AVR). CTP posing a clinical challenge in selecting the optimal intervention–transcatheter aortic valve replacement (TAVR) or surgical aortic valve replacement (SAVR). While TAVR, a minimally invasive surgery, has demonstrated superior safety in high-risk populations, there remains a deficiency of data comparing its outcomes and temporal trends with SAVR specifically in patients with CTP. Given the elevated hemorrhage risk in this cohort, determining the safer intervention is crucial for optimizing patient outcomes.

Methods: We performed a retrospective cohort analysis using the US National Inpatient Sample (NIS) database from 2016 to 2022. Patients with AS and concomitant CTP who underwent isolated AVR were identified using ICD-10 codes and stratified into TAVR and SAVR cohorts. The primary outcome was postprocedural hemorrhage, Secondary outcomes were in-hospital mortality, blood transfusion, cardiogenic shock, cardiac arrest, cardiac tamponade, paravalvular leak, and Cerebrovascular infarction. Given the differences in baseline characteristics, we employed propensity score matching (PSM) to match hospitalizations with AS undergoing TAVR to those undergoing SAVR at 1:1 ratio. Nearest neighbor technique was adopted to match each case to a control which is closest in terms of calculated propensity score, with a caliper width of 0.2, and 22 variables were adjusted, including age, sex and comorbidities. Multivariable logistic regression models adjusting for demographics, hospital characteristics, and procedural complications, were used to compare differences in in-hospital outcomes between the two cohorts.

Results: Among 112,725 hospitalizations for AS, 16.19% (n=18,254) complicated by CTP. Patients with missing data on demographic data, in-hospital death, length of stay, or concomitant coronary artery bypass grafting and mitral, tricuspid, pulmonary valve procedures were excluded to minimize confounding, with 5,545 undergoing TAVR and 10,912 undergoing SAVR. After PSM, 4,468 matched pairs were analyzed. The key findings of this study include: the rate of postprocedural hemorrhage of TAVR group was significantly lower than that of SAVR group, and the postprocedural hemorrhage risk in the TAVR group was even lower (2.2% vs. 3.8%; aOR: 0.54, 95% CI: 0.41-0.71; P < 0.001). TAVR was associated with lower risks of in-hospital mortality (aOR: 0.57, P < 0.001), blood transfusion (aOR: 0.29, P < 0.001), cardiogenic shock (aOR: 0.13, P < 0.001), and cardiac arrest (aOR: 0.42, P = 0.014). No significant differences were observed in cardiac tamponade, paravalvular leak, or Cerebrovascular infarction between the two groups. Compared with the SAVR group, the median length of stay (9.7 vs. 5.3 days; P < 0.001) and hospitalization costs ($261,328.8 vs. $253210.8; P =0.026) were reduced in the TAVR group. The proportion of TAVR procedures in CTP patients rise from 37.84% to 60.94% in 2016 - 2022 (P-trend < 0.001), and the rate of postprocedural hemorrhage of patients undergoing TAVR treatment showed a downward trend (4.12% - 2.66%, P-trend = 0.016).

Conclusions: This nationwide observational analysis indicates that TAVR is independently associated with lower risks of postprocedural hemorrhage and multiple adverse hospitalization outcomes compared to SAVR in AS patients with CTP. Its overall safety supports its consideration as the preferred intervention in this high-bleeding-risk population. These findings emphasize the importance of individualized decision-making, particularly in AS patients with thrombocytopenia, where minimizing postprocedural adverse outcomes is crucial. Further prospective studies are warranted to verification these observations and refine patient selection standard.

Keywords: aortic stenosis; chronic thrombocytopenia; transcatheter aortic valve replacement; surgical aortic valve replacement

The Comparative Effectiveness of Single versus Double Perclose ProGlideTM Devices in Achieving Transfemoral AortIc Valve Replacement Access Site Closure: A Prospective, Multicenter, Randomized Controlled Trial (Single-Closure)

Yu-Chao Guo, Ju-Bo Jiang, Po Hu, Xian-Bao Liu, Jian-An Wang

Second Affiliated Hospital Zhejiang University

Transfemoral transcatheter aortic valve replacement (TF-TAVR) is a well-established treatment for patients with severe aortic stenosis across all surgical risk categories. Access site closure is a critical component of procedural success and patient safety. The Perclose ProGlide ™ suture-mediated closure system is widely used to achieve hemostasis following large-bore vascular access. While the use of two ProGlide devices (“double closure”) has been adopted as the standard approach, recent clinical observations suggest that a single ProGlide device (“single closure”) may achieve comparable outcomes with potential benefits, including reduced cost, shorter procedure time, and fewer complications. Previous studies comparing these strategies have been limited to observational and nonrandomized designs, with inconsistent findings and risk of bias. Therefore, a well-designed randomized controlled trial is needed to provide definitive evidence on the comparative effectiveness and safety of single versus double Perclose closure.

Methods

This is an investigator-initiated, open-label, multicenter, randomized controlled trial conducted across multiple centers in China. Eligible patients are aged ≥ 65 years with symptomatic severe aortic stenosis and an indication for transfemoral TAVR. Participants are randomized 1:1 to receive either single or double Perclose ProGlide closure following TAVR. Randomization is stratified by site using a block size of four, and is managed through an interactive web response system (IWRS). The primary endpoint is the rate of access site- or access-related major and minor vascular complications, as defined by the Valve Academic Research Consortium-3 (VARC-3) criteria. Secondary endpoints include device failure, bleeding complications, vascular interventions, transfusion requirements, time to hemostasis, hospital stay, and mortality at discharge and 30 days. The study uses Modified Intention-to-Treat (mITT) and Per Protocol analyses. A total of 876 patients (438 per arm) will be enrolled to provide 80% power to detect superiority (δ = 0), assuming complication rates of 9.1% (double closure) and 7.1% (single closure), accounting for a 1% dropout rate. Statistical analyses will be conducted using SAS® 9.4.

Results

As of July 7th, 2025, the trial has been initiated at 20 participating centers and has enrolled 476 patients. Study enrollment and follow-up are ongoing. Baseline demographic and procedural data, as well as interim safety assessments, will be reviewed by an independent Data and Safety Monitoring Board. Final analysis will evaluate non-inferiority of the single closure strategy compared to double closure.

Discussion

Despite improvements in device profile and procedural techniques, vascular complications remain a significant concern in TF-TAVR. While the double Perclose strategy is common practice, emerging observational evidence suggests that a single Perclose device may suffice in many cases, with potential benefits in cost, efficiency, and procedural simplicity. However, these prior studies lack randomization and may be influenced by confounding factors. This trial is designed to provide high-quality evidence to determine whether the single Perclose closure is non-inferior to the standard double closure in terms of vascular safety and procedural efficacy.

Conclusion

The SINGLE-CLOSURE trial is the first prospective, multicenter randomized study designed to evaluate whether a single Perclose ProGlide device is non-inferior to the conventional double-device strategy in closing large-bore vascular access after TF-TAVR. The results of this trial will offer valuable evidence to inform clinical decision-making and optimize vascular access management in TAVR procedures.

冠状动脉疾病对经导管主动脉瓣置换术患者预后的影响

方毅 徐凯

中国人民解放军北部战区总医院寒地心血管病全国重点实验室

摘要

目的：评估冠状动脉疾病（CAD）对接受经导管主动脉瓣植入术（TAVR）患者预后的影响。

方法：回顾性分析北部战区总医院 2016–2022 年接受 TAVR 患者的临床资料，根据冠脉 CTA 或冠状动脉造影及经皮冠状动脉介入治疗（PCI）病史明确是否合并 CAD 分为合并 CAD 组和不合并 CAD 组。主要终点是超过 1 年的全因死亡和主要不良心脑血管事件（MACCE，包括心原性死亡、心梗、血运重建、心衰再入院、卒中的复合终点）。采用生存分析评估 CAD 对事件发生时间结局的影响。

结果：共纳入 262 例患者，TAVR 合并 CAD 组 128 例 (48.9%)，TAVR 不合并 CAD 组 134 例 (51.1%)，CAD 发病率 48.9%，平均随访 2.5±1.2 年。在随访时间内，合并 CAD 组中长期全因死亡率较不合并 CAD 组明显增高，差异有显著统计学意义（7.8% vs. 2.2%, HR 3.30, 95%CI 1.13~ 4.67, P=0.007）；同时，合并 CAD 组 MACCE 发生率较不合并 CAD 组增高，两组间有显著差异 (24.0% vs.9.7%, HR 3.02, 95%CI 1.71 ~ 5.31, P<0.001).

结论：接受 TAVR 治疗的患者中，合并 CAD 患者无论是在全因死亡还是在心原性死亡、心梗、血运重建、心衰再入院、卒中的复合终点较无 CAD 患者发生率均显著增高，提示合并 CAD 的 TAVR 患者未来预后更差。

关键词：经导管主动脉瓣植入术，冠状动脉疾病，经皮冠状动脉介入治疗

可穿戴心音图技术在主动脉瓣二叶畸形相关升主动脉扩张早期预警中的应用价值研究

张文俐 张瑞岩 朱政斌

上海交通大学医学院附属瑞金医院

目的

主动脉瓣二叶畸形（Bicuspid Aortic Valve, BAV）作为最常见的先天性心脏畸形，其患者常在较年轻时并发升主动脉扩张，增加了主动脉事件的风险。当前临床实践中，缺乏能够早期、无创且连续监测主动脉扩张进展的生物标志物，导致影像学检查频率和干预时机决策困难。本研究旨在利用可穿戴设备采集心音信号，探索 BAV 患者的心音图（Acoustic Cardiogram, ACG）特征，并重点评估其作为升主动脉扩张早期预警新型指标的临床应用潜力。

方法

本研究回顾性纳入了于瑞金医院就诊的 200 例心脏瓣膜病患者，其中包括 74 例经超声心动图确诊的 BAV 患者及 126 例非 BAV 患者作为对照。所有受试者均于同一天接受了标准的经胸超声心动图检查，并使用可穿戴设备在二尖瓣区（M）、主动脉瓣第二听诊区（E）及主动脉瓣区（A）同步采集了 1 分钟的心电图与心音图信号。我们对心音信号的形态学特征进行分析，并提取了一系列心音参数，包括电机械激活时间比值（EMAT%）、左室射血时间（LVET）、射血前期比值（PEP%）、PEP/LVET 比值，以及第一、第二心音（S1、S2）的最大能量点（S1Emax、S2Emax）、最大振幅（S1Amax、S2Amax）和能量峰频率（S1EmaxFreq、S2EmaxFreq）。依据升主动脉内径是否≥ 45mm 进行分组，对上述参数进行比较分析。

结果

基线资料显示，与非 BAV 组相比，BAV 组患者年龄显著更轻（41.5 岁 vs. 74.0 岁，P<0.001），但其升主动脉内径更大（39.00mm vs. 36.00mm，P=0.01），且升主动脉扩张（≥ 45mm）的发生率更高（21.62% vs. 7.14%，P=0.003）。在心音形态上，BAV 患者中观察到一种独特的“S1 额外能量峰”现象，其发生率显著高于非 BAV 组（45.95% vs. 1.59%，P<0.001）。关键发现是，升主动脉扩张（≥ 45mm）组患者的 S2 能量峰频率（S2EmaxFreq）显著高于非扩张组（46.00hz vs. 38.00hz，P<0.001）。ROC 曲线分析表明，S2EmaxFreq 对升主动脉扩张具有中等程度的预测效能（曲线下面积 [AUC]=0.783，敏感性 76.0%，特异性 74.3%，P<0.001）。尤为重要的是，在 BAV 患者亚组中，S2EmaxFreq 的预测准确性显著提升（AUC=0.862，敏感性 93.7%，特异性 79.3%，P<0.001）。

结论

本研究首次揭示，在升主动脉扩张患者中，S2EmaxFreq 显著升高。该参数表现出强大的敏感度，尤其是在主动脉瓣二叶畸形（BAV）这一高危队列中，提示 S2EmaxFreq 具潜力成为一种评估升主动脉扩张的新型、无创性声学标志物。此项基于可穿戴设备的监测策略，有望通过动态风险分层来优化超声心动图、CTA 或 MRI 等影像学检查的随访间隔，从而为心血管风险较高的年轻 BAV 患者群体，提供一种连续、便捷的主动脉重塑进展监测新途径，具有重要的临床转化价值。

基于人工智能的影像学分析方法自动检出并定级 TAVR 术后低密度瓣叶增厚的研究

王墨扬 吴永健

北京阜外心血管病医院

目的：

经导管主动脉瓣置换术（TAVR）后，患者可能发生低密度瓣叶增厚（HALT），这一变化可能影响血流动力学和瓣膜耐久性，并潜在地导致不良预后。尽管通过术后 CT 影像可以进行 HALT 的诊断与分级，但人工评估不仅要求丰富的经验，还需要消耗大量时间。本研究旨在开发并验证一种基于 TAVR 术后 CT 影像的人工智能（AI）全自动 HALT 检出与分级方法。

方法：

本研究为一项多中心回顾性研究，我们收集了 852 例接受 TAVR 手术患者的术后 CT 影像，并完成了结构分割标注和 HALT 分级标注。所有患者随机分配为训练集（602 例）和验证集（250 例）。基于这些数据，我们设计、训练并验证了 HALT 检出与分级模型（图 1 展示了本研究的基本流程）。在验证集中，我们采用准确度、灵敏度、特异度、阳性预测值（PPV）、阴性预测值（NPV）、F1 分数以及 Kappa 系数等指标评估模型在 HALT 检出任务中的性能。此外，使用多分类混淆矩阵、准确率、加权 F1 分数、加权 Kappa 系数以及平均绝对误差（MAE）等指标评估模型在 HALT 分级（0 至 4 级）任务中的表现。

结果：

在 250 例患者组成的验证集中，本研究开发的人工智能算法在 HALT 检出任务中表现优异，准确度为 98.8%，灵敏度 95.4%，特异度 100%，阳性预测值（PPV）为 100%，阴性预测值（NPV）为 98.4%，F1 分数为 0.976，Cohen’s Kappa 系数为 0.968。在进一步的 HALT 分级（0 至 4 级）任务中，算法同样显示出良好的性能，多分类混淆矩阵见图 4，总体准确率达到 96.8%，加权 F1 分数为 0.966，加权二次 Kappa 系数为 0.977，平均绝对误差（MAE）仅为 0.040 级，表明模型预测的 HALT 分级与专家人工评估结果具有高度一致性。

结论：

本研究开发的人工智能算法能够基于 TAVR 术后 CT 影像实现 HALT 的准确自动检出与精确分级，其表现与专家评估高度一致，有望作为临床实践中 HALT 评估的一种高效可靠工具。

单纯食管超声心动图引导经导管二尖瓣缘对缘修复术后中期疗效分析

韩宇

阜外华中心血管病医院

目的：随着超声在介入治疗过程中的广泛应用，超声已成为优化经导管介入治疗的重要工具，单纯超声引导可以避免使用 X 线透视，从而避免辐射损伤。探讨单纯食管超声心动图引导下经导管二尖瓣缘对缘修复术（transcatheter edge-to-edge repair of the mitral valve,MV-TEER）的有效性、安全性及中期预后。

方法：回顾性选取 2023 年 1 月至 2024 年 1 月于阜外华中心血管病医院接受单纯食管超声心动图引导下行 MV-TEER 的二尖瓣反流（mitral regurgitation,MR）患者 46 例，手术方法：本中心经验，CDS 外露的距离在 5ml 注射器 2-3 之间（“5ml 注射器修正骑跨法”），可实现骑跨（straddle）。入选患者在术后 1、3、6 及 12 月应用心脏超声评估左心结构及 MR 分级，研究终点定义为手术成功（MR 分级降低≥ 1 级）、患者因心力衰竭入院、二尖瓣再次干预（包括二尖瓣手术和再次 MV-TEER）以及全因死亡。

结果：共纳入 46 例患者，年龄 67.50（59.00 73.00）岁，男性 29 例（63.04%），所有患者顺利完成手术，即刻效果满意，术中无并发症发生。所有患者术前 MR 分级均处于中重度反流（3+）及以上，左心室收缩末期内径为 39.71±7.44mm，左心室收缩末期容积为 87.02±20.63ml，左心室射血分数为 44.98±11.78%。末次随访时，二尖瓣反流程度处于 3+ 患者为 5 例，其余患者均在 3+ 以下，左心室收缩末期内径为 39.71±7.44mm，左心室收缩末期容积为 72.18±17.30ml，左心室射血分数为 51.84±10.03%，NT-proBNP 从术前 3245（1751 3839）ng/L 降至 968（729 1433）ng/L。NYHA 心功能分级及 6 分钟步行试验均得到了显著改善。

结论：单纯食管超声引导下 MV-TEER 是安全有效的，并且避免了辐射损伤，且中期预后良好。

Case Report of snare-assisted coaxiality optimized technique during valve deployment in patient with pure aortic regurgitation

Ji-Wei Yu, Zheng-Bin Zhu, Rui-Yan Zhang

Rui Jin Hospital, Shanghai Jiao Tong University School of Medicine

Abstract

An 84-year-old male was diagnosed with severe PNAR with anatomical challenges, including a large sinus of valsalva and horizontal aorta. We attempted TAVR procedure with an innovative technique we named “snare-assisted coaxiality optimized technique” (SACOT) during valve deployment.

KEYWORDS

aortic valve regurgitation, snare catheter, snare-assisted coaxiality optimized technique, transcatheter valve replacement (TAVR)

INTRODUCTION

Utilizing TAVR in high-risk patients with pure native aortic regurgitation (PNAR) is still regarded as an off-label intervention. Given the variations in the anatomical structure of the aortic root and the technical difficulties tailored specifically for PNAR, transcatheter TAVR via the transfemoral approach (TF-TAVR) still requires ongoing experience accumulation and technological advancements. In this context, we successfully and safely executed a snaring-assisted TF-TAVR procedure for a PNAR patient presenting with a notably large aortic angulation with an innovative technique we named“snare-assisted coaxiality optimized technique”(SACOT) during valve deployment. This technique was crucial in optimizing valve positioning, resulting in improved coaxiality and a more ideal implantation depth in PNAR. Post-procedure assessments showed stability and no PVR.

CASE DESCRIPTION

This 84-year-old male presents with intermittent chest tightness and shortness of breath, with a significant exacerbation of symptoms over the past two weeks. He has a history of diabetes mellitus and chronic lung disease, and underwent surgery for pulmonary abscess in the past. Additionally, he has a long-standing history of heavy smoking. Blood pressure was 174/47 mmHg, heart rate was 74 bpm, and oxygen saturation was 92% in room air. Physical examination revealed normal respiratory sounds, diastolic murmur, and mild pedal edema. Screening of the pre-operative laboratory values revealed elevated levels of N-terminal pro-brain natriuretic peptide (1065pg/mL, normal range 5-738pg/mL) and elevated creatinine (1.41mg/dL, normal range 0.7-1.29mg/dL) level; thus, a heart disease wan suspected. A transthoracic echocardiography (TTE) was performed, reveling severe aortic regurgitation with volume 64ml/beat accompanied with mild mitral and tricuspid regurgitation. The left ventricular ejection fraction was 62%, the left ventricular end-diastolic diameter (LVEDd) was 62mm and the end-systolic diameter was 41mm. Electrocardiography revealed sinus rhythm and left ventricular high voltage (Fig 1).

Following a comprehensive heart team discussion, we decided to perform a TAVR using a 27mm VitaFlow Liberty valve (MicroPort, Shanghai). This decision was influenced by the patient’s Society of Thoracic Surgeons score, which was assessed at 7.78%.

A computed tomography (CT) angiography unveiled a substantial sinus

of Valsalva, with an average diameter of 43.4mm, and a sinotubular junction (STJ) with an average diameter of 39.2mm. There was no calcification observed in the annulus or leaflets, with the aortic annulus area measuring 489.7 mm^2 and the perimeter measuring 79.6mm. The left ventricular outflow tract (LVOT) perimeter was 85mm, and the maximal ascending aorta diameter was 44.9mm. Assessment of the coronary arteries and the arterial iliofemoral system anatomy indicated suitability for the TAVR procedure. Notably, the aortic angulation was 62 ° , which increase the surgical complexity for a patient with PNAR .

PROCEDURAL DETAILS

The procedure was conducted under general anesthesia with guidance from a transthoracic echocardiogram. One pigtail catheter was placed in the Sinus of Valsalva to serve as annular landmark. The transcatheter heart valve (THV) was carefully advanced until reaching the aortic annulus and was deployed under rapid ventricular pacing at 180 beats/min. Despite our attempts to position the valve as high as feasible, after the initial try, the lack of coaxial alignment resulted in an excessively deep implantation of the valve in the left coronary sinus .

Therefore, we decided to pre-place a snare. In the second deployment, we employed an unconventional approach by continuously pulling the THV during deployment to improve the coaxiality. This resulted in a more ideal implantation depth below the left coronary sinus . After TTE assessment, no apparent perivalvular leak was observed, and the anterior leaflet motion of the mitral valve was unaffected. We released the valve completely under rapid pacing at 120 beats/min, facilitating the stability of the valve. Upon a follow-up TTE before discharge, it was noted that the LVEDd had decreased to 56mm, and no residual AR was observed. The CT showed a will-positioned and normo-function THV .

CONCLUSION

This case presents typical challenges of PNAR, including a horizontal aorta and the absence of anchoring regions. Therefore, coaxiality during valve deployment becomes particularly crucial. Conventional self-expanding valve deployment in such cases frequently leads to paravalvular leaks or excessive implantation depth. We have detailed an innovative snare-assisted technique which helped coaxial adjustment during TAVR procedure.

中国西北地区大型三甲医院瓣膜性心脏病患者的病因及分布研究

徐锐 赖红梅

新疆维吾尔自治区人民医院

背景：关于中国西北地区瓣膜性心脏病（VHD）临床特征的现代数据相对有限，因此亟需系统性探讨该地区 VHD 的流行病学特征。本研究旨在调查新疆地区一家大型三级甲等医院中 VHD 的最新临床表现及其特点，通过对大规模患者数据的分析，为该地区 BVD 的早期筛查、诊断和管理提供科学依据。近年来，随着人口老龄化程度不断加深和相关疾病的高发率，VHD 的疾病负担逐步增加，了解其发生特点、危险因素以及性别差异对于疾病的早期预警和预防策略的制定具有重要意义。

方法：本研究以 2010 年 1 月至 2021 年 10 月期间在新疆维吾尔自治区人民医院接受超声心动图检查的所有成年人（年龄范围 18-80 岁）为研究对象，共计 260,159 例。利用医院内部数据库检索系统，识别出首次被诊断为 VHD 的患者案例，同时对患者的基础信息、临床表现和超声检查结果进行详细整理。通过对患者年龄进行分层，分析不同年龄段 VHD 的发生率和变化趋势。研究重点关注各种瓣膜疾病的具体类型，包括二尖瓣返流（MR）、主动脉瓣返流（AR）、二尖瓣狭窄（MS）以及其他类型，同时评估其性别差异和不同病因。采用 Logistic 回归模型，分析年龄、性别、吸烟、血压、糖尿病、慢性肾脏疾病等因素与 VHD 发生之间的关系，以明确独立风险因素。

结果：研究发现，任何 VHD 的总体患病率为 3.06%，其中以 MR（0.75%）、AR（0.58%）和 MS（0.35%）最为常见，它们共同占据了绝大部分的 VHD 病例。随年龄增长，VHD 的发生率显著提高，且存在明显的性别差异：男性在 AR 和主动脉瓣狭窄（AS）中的比例明显高于女性（P<0.05），而 MS 则更常见于女性患者。根据病因分析，功能性（36%）为主要类型，其次是风湿性（27%）和退行性（17%）病变。多变量 Logistic 回归显示，男性、年龄逐渐增长、吸烟史、高血压、糖尿病和慢性肾脏疾病均为 VHD 发生的重要独立危险因素。这些因素与患者的疾病发展密切相关，提示生活方式和基础疾病管理对于 VHD 的预防具有潜在价值。

结论：本研究显示，功能性病变已成为新疆地区 VHD 的主要病因，提示心血管疾病管理的重点已逐渐从外围疾病向瓣膜病变转变。性别方面，AR、AS 在男性中更为常见，MS 则在女性中更占优势。年龄增长和多种基础疾病（如高血压、糖尿病、慢性肾脏疾病）是 VHD 发生的独立危险因素。这些发现有助于临床识别高危人群，指导早期筛查和预防策略，以减轻 VHD 带来的疾病负担，同时也提示公共卫生需加强相关健康教育，控制危险因素，降低 VHD 的发生率和进展速度。

基于 SF-36 量表的生物瓣与机械瓣置换术后中老年患者健康相关生命质量的动态差异比较研究

何萌 张喜维

首都医科大学附属北京安贞医院

[摘要]

背景：随着心脏瓣膜病治疗技术的进步，生物瓣与机械瓣的选择成为关注焦点。本研究基于 SF-36 量表，比较生物瓣与机械瓣置换术后中老年患者健康相关生命质量的差异，旨在为临床决策提供科学依据。

方法：我们对北京安贞医院心脏外科中心接受单纯主动脉瓣置换术（AVR）的 60 - 65 岁患者进行了回顾性研究。通过电话随访采用 36 项简短健康调查问卷（SF-36）评估术后生活质量。

研究结果：本次调查共收集到 628 份有效问卷，其中机械瓣膜患者 353 例，生物瓣膜患者 275 例。患者平均年龄为 62.5±1.7 岁，男性占比 57.8%（363 例）。平均随访时间为 7.3±3.9 年。机械瓣膜与生物瓣膜患者在生活质量各维度评分及 SF-36 总分上均无显著差异。经校正手术年龄、性别、射血分数、人工瓣膜类型及有效开口面积指数等因素后，体质指数（β=-0.109，p=0.014）和术后时间（β=-0.251，p<0.001）被证实为影响生活质量的独立预测因子。两组患者每年的卒中发生率与心血管再介入率相似。然而，在主动脉瓣置换术后 12 年的随访中，机械瓣膜组表现出更优的临床效果。

结论：在 60 至 65 岁接受单纯主动脉瓣置换术的患者中，机械瓣与生物瓣术后生活质量无显著差异，但机械瓣在远期表现上可能更具优势。

[关键词]：主动脉瓣置换术；生物瓣膜；机械瓣膜；生活质量；SF-36 量表

Optimal Oversizing Degree of Self-Expanding Transcatheter Valve in Patients with Bicuspid versus Tricuspid Aortic Stenosis

Wenjing Sheng

The Second Affiliated Hospital Zhejiang University School of Medicine

Optimal Oversizing Degree of Self-Expanding Transcatheter Valve in Patients with Bicuspid versus Tricuspid Aortic Stenosis

Wenjing Sheng, MD[a,b†], Jiaqi Fan, MD[a,b†], Jun Chen, MD[a,b], Dao Zhou, MD[a,b], Hanyi Dai, MD[a,b], Qiong Liu, PhD[a], Jian'an Wang, MD, PhD[a,b,c,d*], Xianbao Liu, MD, PhD[a,b,c*]

[a]Department of Cardiology, The Second Affiliated Hospital, School of Medicine, Zhejiang University, Hangzhou 310009, China

[b]State Key Laboratory of Transvascular Implantation Devices, Hangzhou 31009, China.

[c]Heart Regeneration and Repair Key Laboratory of Zhejiang province, Hangzhou 31009, China

[d]Transvascular Implant Instrument Research Institute, The Second Affiliated Hospital Zhejiang University School of Medicine，Binjiang District，Hang Zhou 310053，China

Disclosure:

All authors have reported that they have no relationships relevant to the contents of this paper to disclose.

Correspondence author*:

Jian'an Wang, MD, PhD

Tel +86-571-87783992; fax +86-571-87037885

E-mail: wangjianan111@zju.edu.cn

Address: Department of Cardiology, Second Affiliated Hospital Zhejiang University School of Medicine, Hangzhou 310009, China

Xianbao Liu, MD, PhD

Tel +86-571-87783992; fax +86-571-87037885

E-mail: liuxb@zju.edu.cn

Address: Department of Cardiology, Second Affiliated Hospital Zhejiang University School of Medicine, Hangzhou 310009, China

†These authors contributed equally to this work.

Abstract

Background : The impact of annular oversizing on paravalvular regurgitation (PVR) and new-onset conduction disturbances (NOCD) in bicuspid (BAV) and tricuspid aortic valve (TAV) patients undergoing transcatheter aortic valve replacement (TAVR) with self-expanding valves (SEV) remains unclear.

Aims: To identify the optimal perimeter-based annular oversizing strategy in BAV and TAV patients to reduce PVR and NOCD.

Methods: We included 580 consecutive severe aortic stenosis (AS) patients who underwent TAVR with SEV from March 2013 to December 2020. The perimeter-based oversizing ratio (OSr) was determined by annular dimensions assessed via computed tomography. PVR was evaluated by 30-day transthoracic echocardiography, and NOCD was assessed using a 12-lead electrocardiogram. The predictors associated with increased PVR and NOCD was determined using logistic regression analysis. Receiver operating characteristic curves analyses were used to determine the sensitivity and specificity of the thresholds of OSr to predict PVR and NOCD

in BAV and TAV patients.

Results: In this study, BAV patients comprised 67.1% (389/580) and the median of systolic annular perimeter-based OSr was 8.1% (IQR：3.0%-12.4%). Among 580 patients, 54.2% experienced ≥ mild PVR, and 15.2% developed new-onset atrioventricular block (AVB). A higher OSr correlated with decreased ≥ mild PVR ($p < 0.001$) but increased new-onset AVB ($p = 0.021$). There was an interaction between BAV and OSr ($p_{interaction}=0.007$). In BAV patients, a 5% increase in OSr was associated with a 27% reduction in ≥ mild PVR (adjusted OR 0.732, 95% CI: 0.617-0.869; $p < 0.001$) and a 45% increase in new-onset AVB (adjusted OR 1.451, 95% CI: 1.145-1.838; $p = 0.002$). The optimal OSr for predicting ≥ mild PVR was 7.37 % (AUC 0.621, 95% CI: 0.575-0.667; $p < 0.001$), with an optimal value of 7.09% in BAV patients (AUC 0.647, 95% CI: 0.591-0.703; $p < 0.001$). For predicting new-onset AVB, the optimal OSr was 5.30% in overall patients (AUC 0.595, 95% CI: 0.503-0.627; $p = 0.0053$), and BAV patients (AUC 0.595, 95% CI: 0.522-0.669; $p = 0.0001$). No optimal OSr was identified for TAV patients.

Conclusion: Greater perimeter-based oversizing was associated with decreased PVR but increased new-onset AVB, especially in BAV patients. In BAV patients, an OSr of 7.09% optimally predicted ≥mild PVR, and 5.3% optimally predicted new-onset AVB. No optimal OSr was identified for TAV patients.

Outcomes of Transcatheter Aortic Valve Implantation for Bicuspid Versus Tricuspid Mixed Aortic Valve Disease

Bo-Ren Tan, Xian-Bao Liu

The Second Affiliated Hospital of Zhejiang University, School of Medicine

Purpose: Prior studies rarely distinguished bicuspid valve morphology in mixed aortic valve disease (MAVD) populations, and no study has evaluated long-term transcatheter aortic valve implantation (TAVI) outcomes between bicuspid aortic valve (BAV) and tricuspid aortic valve (TAV) in this setting. This study aimed to compare procedural and longitudinal outcomes of TAVI in BAV versus TAV patients with MAVD.

Methods: This study used data from the TORCH registry (NCT02803294), an ongoing, real-world TAVI registry at the Second Affiliated Hospital of Zhejiang University. Between March 2013 and December 2024, a total of 615 patients with severe mixed aortic valve disease defined as severe aortic stenosis with concomitant ≥ moderate aortic regurgitation were enrolled, after excluding patients with quadricuspid valves, pure regurgitation, or valve-in-valve procedures. Patients were stratified into BAV and TAV groups based on multidetector computed tomography (MDCT). All patients underwent comprehensive pre-TAVI and post-TAVI echocardiography. Clinical follow-up was performed at 30 days and annually thereafter. The primary outcome was all-cause mortality at long-term follow-up. Outcomes were adjudicated per VARC-3 criteria. Baseline and follow-up data were compared between groups according to variable type and distribution. Kaplan–Meier and Cox proportional hazards models were used to compare outcomes between groups. Statistical analyses were conducted using SPSS (version 27.0) and R (version 4.3.0).

Results: A total of 615 patients with mixed aortic valve disease were included in the final analysis, comprising 221 (35.4%) patients with BAV and 394 (64.6%) with TAV. The median age was 75 (IQR: 70-79) years in the BAV group and 73 (IQR: 68-77) years in the TAV group (pp=0.066). Patients with TAV had a higher STS score compared to the BAV group (4.15 [IQR: 2.38-7.77]% vs. 3.45 [IQR: 1.69-6.10]%, p<0.001), and higher proportion of hypertension (58.1% vs. 47.5%, p=0.011), peripheral vascular disease (12.7% vs. 6.8%, p=0.022). Preprocedural echocardiographic evaluation revealed that patients with BAV exhibited higher aortic stenosis severity compared to those with TAV, as evidenced by greater peak aortic jet velocity (4.85 [IQR: 4.35-5.45] m/s vs. 4.60 [IQR: 4.17-5.13] m/s, p<0.001), higher mean transvalvular gradient (55 [IQR: 44-71] mmHg vs. 49 [IQR: 40-61] mmHg, p<0.001), and smaller aortic valve area (0.63 [IQR: 0.48-0.81] cm^2 vs. 0.70 [IQR: 0.55-0.86] cm^2, pp=0.237). During a median follow-up of 750 (IQR: 365-1465) days, the overall all-cause mortality was 29 (13.1%) in the BAV group and 92 (23.4%) in the TAV group. Time-to-event Kaplan-Meier survival analysis for all-cause mortality demonstrated better survival in patients with BAV compared to TAV (log-rank p=0.023). The unadjusted hazard ratio (HR) for all-cause mortality in the BAV group versus the TAV group was 0.34 (95% confidence interval [CI], 0.15-0.77; p=0.009). Cardiovascular mortality rates were 3.2% in BAV vs. 9.6% in TAV during the follow-up. Multivariable Cox regression of all-cause mortality adjusted for baseline confounders confirmed no significant independent association between valve morphology and mortality (adjusted HR 0.77, 95% CI 0.50-1.18, p=0.224). These findings suggest that long-term survival after TAVI in patients with mixed aortic valve disease is comparable regardless of valve anatomy. Follow-up echocardiographic evaluations at 30 days, 1 year, and 2 years post-TAVI revealed stable hemodynamic performance in both BAV and TAV groups. Mean transvalvular gradients, peak aortic jet velocity and LVEF remained comparable throughout follow-up, all with no statistically significant differences between groups (p>0.05 for all). However, moderate or greater paravalvular leak (PVL) was consistently more prevalent in the BAV group across all time points, occurring in 14.4% vs. 8.5% at 30 days (p=0.026), 17.0% vs. 9.9% at 1 year (p=0.030), and 19.4% vs. 8.9% at 2 years (p=0.014). This higher PVL burden in BAV patients underscores the persistent challenge of achieving optimal valve sealing in anatomically complex bicuspid valves and may necessitate tailored procedural strategies or closer post-procedural monitoring.

Conclusion: In patients with mixed aortic valve disease undergoing TAVI, bicuspid valve anatomy is characterized by more severe aortic stenosis and presents unique procedural challenges. Despite these challenges, the adjusted risk of long-term all-cause and cardiovascular mortality were similar between BAV and TAV groups. Echocardiographic follow-up demonstrated durable valve function and stable left ventricular performance over long-term in both groups; however, the persistently higher paravalvular leak burden in BAV patients highlights the need for tailored procedural strategies and vigilant post-procedural monitoring. These findings affirm the feasibility and safety of TAVI in patients with bicuspid valves and underscore the importance of optimizing device selection and implantation techniques to improve clinical outcomes.

二叶式和三叶式主动脉瓣重度狭窄行 TAVR 术前术后对比分析研究

张婷婷 周微微

中国人民解放军北部战区总医院

目的 比较二叶式主动脉瓣（BAV）狭窄和三叶式主动脉瓣（TAV）狭窄行经导管主动脉瓣置换术（TAVR）术前、术后对比分析。

方法 本研究为回顾性研究。入选 2023 年 1 月至 2023 年 12 月于北部战区总医院因主动脉瓣重度狭窄接受 TAVR 的患者。根据术前主动脉增强 CT 将患者分为 BAV 组和 TAV 组。收集患者术前、术后即刻及术后 1、6、12 个月超声心动图检查结果。主要指标包括主动脉瓣最大速度（AVmax）、主动脉瓣峰值压差（AVPGmax）、主动脉瓣平均压差（AVPGmean）、主动脉瓣口面积（AVA）、左室射血分数（LVEF）、升主动脉内径（AAO）等。对比分析两组术前和术后心超数据，并对每组术前及术后不同时间点的心超数据进行分析。

结果 共入选 52 例患者，其中 BAV 组 22 例，TAV 组 30 例。术前 BAV 组 AVPGmean 大于 TAV 组（$P < 0.05$）；BAV 组术后 1 个月、6 个月和 12 个月的 AVVmax、AVPGmax、AVPGmean 大于 TAV 组（$P < 0.05$）；BAV 组 AAO 在术前和术后各时间点均大于 TAV 组（$P < 0.05$）；BAV 组术后 12 个月的 AVA 小于 TAV 组（$P < 0.05$）；BAV 组 IVST 在术前和术后各时间点大于 TAV 组（$P < 0.05$）；两组术后 AVmax、AVPGmax、AVPGmean 均较术前明显减小（$P < 0.05$）；两组术后 1 个月、6 个月和 12 个月的 AVVmax、AVPGmax、AVPGmean 均较术后即刻增加（$P < 0.05$）；两组 AVA 在术后均较术前显著增大（$P < 0.05$）；TAV 组术后各时间点的 LVEDD 与术前比较显著减小（$P < 0.05$）；两组术后各时间点的 LVEF 均较术前升高（$P < 0.05$）。

结论 BAV 狭窄患者和 TAV 狭窄患者在行 TAVR 术后主动脉瓣血流动力学明显改善，左室发生部分逆向重构，且随着术后随访时间延长各项指标趋于稳定。

经导管主动脉瓣置换术中球扩瓣与自展瓣的瓣周漏与患者预后的 Meta 分析

高远 李福杭 张海山 梁长彬 郭亮

中国医大一院

目的：经导管主动脉瓣置换术（TAVR）是治疗主动脉瓣狭窄的重要手段，瓣周漏（PVL）作为术后常见并发症，对患者预后影响显著。临床中自膨胀瓣膜与球囊扩张瓣膜的 PVL 发生率存在差异，本研究旨在通过 Meta 分析，系统比较 TAVR 中球扩瓣与自展瓣的 PVL 发生率及对患者预后的影响，为临床治疗决策提供循证依据。

方法：检索 PubMed、Embase、Cochrane 图书馆、Web of Science、收集建库至 2025 年 3 月关于 TAVR 中球扩瓣与自展瓣 PVL 及患者预后的研究。由两名研究者独立筛选文献、提取数据并评价质量，采用 RevMan 5.4 软件进行 Meta 分析，计数资料以风险比（RR）及 95% 置信区间（CI）表示，通过 I^2 统计量评估异质性，选择合适模型分析，P<0.05 为差异有统计学意义。

结果：最终纳入 28 项研究，共 8567 例患者，其中球扩瓣组 4235 例，自展瓣组 4332 例。Meta 分析显示，自展瓣组 PVL 发生率（32.0%）显著高于球扩瓣组（24.2%）（RR=1.32，95% CI：1.18-1.48，P<0.001），研究间存在中度异质性（I^2=48%）。预后方面，球扩瓣组与自展瓣组全因死亡率（10.8% vs 11.6%，RR=1.05，95% CI：0.92-1.20，P=0.47）、心血管死亡率（7.0% vs 7.7%，RR=1.08，95% CI：0.92-1.26，P=0.35）、心力衰竭再住院率（9.1% vs 10.2%，RR=1.10，95% CI：0.94-1.28，P=0.23）、脑血管事件发生率（4.9% vs 5.3%，RR=1.08，95% CI：0.89-1.31，P=0.43）差异均无统计学意义，研究间存在中高度异质性（I^2=55%-78%）。亚组分析显示不同随访时间亚组中，两组预后指标差异均无统计学意义。

结论： TAVR 中自展瓣的 PVL 发生率高于球扩瓣，但在全因死亡率、心血管死亡率等主要预后指标上，两种瓣膜类型无显著差异。临床医生应结合患者个体情况选择瓣膜类型，以降低 PVL 风险，改善预后。

老年中 - 重度主动脉瓣狭窄人群不同治疗方式远期预后及危险因素研究

刘靓靓 [1,2] 孙泽瑜 [2] 张颖倩 [2] 王晶 [2] 蒋博 [2] 陈韵岱 [1,2] 刘长福 [2]

1. 中国人民解放军总医院 / 解放军医学院

2. 中国人民解放军总医院第六医学中心

目的：探究接受非手术治疗的老年中重度主动脉瓣狭窄（aortic stenosis，AS）

患者全因死亡的危险因素。方法：选取 2021 年 1 月 1 日 ~2022 年 12 月 31 日就诊于解放军总医院第一医学中心的老年中重度 AS 患者 238 例。收集患者基线时的临床资料、超声心动图数据和治疗方式，应用多因素 Cox 回归模型探索全因死亡的危险因素。结果：多因素 Cox 回归分析显示，Log N 末端 B 型利钠肽前体（N terminal pro B type natriuretic peptide，NT-proBNP）（HR：3.48；95% 置信区间：1.41-9.19）是接受非手术治疗的中重度 AS 患者 2 年全因死亡发生的独立预测因素。在接受非手术治疗的中重度 AS 患者中，相较于左心室收缩末期内径（left ventricular end systolic diameter，LVESD）≤ 27.50mm 组，LVESD > 27.50mm 的患者的全因死亡率明显升高（Z=-3.56，P < 0.010）。合并左心室射血分数（left ventricular ejection fraction，LVEF）< 60%（37.93% vs. 8.06%；HR：0.19；95% 置信区间：0.07-0.54）或 NT-proBNP > 450 pg/ml（27.50% vs. 10.34%；HR：0.31；95% 置信区间：0.11-0.89）的中度 AS 患者全因死亡率明显增高。结论：接受主动脉瓣置换术治疗的重度 AS 患者全因死亡率明显降低，而接受非手术治疗的中重度 AS 合并左室收缩末内径增大的患者全因死亡率明显升高。中度 AS 合并 LVEF 下降或 NT-proBNP 升高的患者，生存率进一步下降，应给予密切关注、及时评估以改善患者预后。

March2 缺失促进 ALDH3B2 介导的氧化应激加重钙化性主动脉瓣疾病

陈浩然 朱婷芳 张来海 胡晓璐 张英梅

上海复旦大学附属中山医院

背景：钙化性主动脉瓣膜疾病（CAVD）是以主动脉瓣硬化和纤维化为特征的退行性疾病，目前缺乏有效的药物治疗。蛋白质泛素化在心血管疾病中发挥着关键作用。然而，E3 泛素连接酶 March2（膜相关 RING 指蛋白 2）在 CAVD 发病中的潜在作用仍未阐明。

方法：通过高通量转录组测序联合公共数据库分析，我们确定了在钙化性主动脉瓣疾病中存在表达差异的 E3 泛素连接酶。构建 March2/ApoE 双基因全身敲除小鼠，使用高胆固醇饮食喂养 24 周诱导主动脉瓣钙化小鼠模型以检测 March2 在主动脉瓣钙化（AVC）中的作用。体外实验中，通过促钙化培养基诱导体外细胞钙化模型，利用功能获得和丧失实验以确定 March2 在诱导人类瓣膜间质细胞（hVICs）的成骨分化中的作用。

结果：在钙化性主动脉瓣膜疾病患者的主动脉瓣和高胆固醇饮食诱导的 AVC 小鼠中，March2 的表达水平均上调，体外实验也得到了相同的结果。高胆固醇饮食诱导的 AVC 在 March2/ApoE 基因全身敲除小鼠中显著加重。此外，我们通过酵母双杂交实验发现 March2 可以与 ALDH3B2 相互作用，并促进其 K48 连接的多泛素化。March2 的缺失减少了 ALDH3B2 的降解，明显加重了瓣膜间质细胞氧化应激水平，从而促进瓣膜间质细胞成骨分化。

结论：我们发现 March2 的缺失可以促进 ALDH3B2 介导的氧化应激加重瓣膜间质细胞成骨分化，提示 March2 可能成为 CAVD 的潜在治疗靶点。

江苏地区二叶式主动脉瓣畸形患者的临床特征及超声心动图在随访管理中的价值：一项单中心回顾性研究

吴婷婷 潘昊天 赵锟 袁伟 周蕾 周滨 孙伟 孔祥清

江苏省人民医院（南京医科大学第一附属医院）

目的：探讨江苏地区人群中的二叶式主动脉瓣畸形（Bicuspid aortic valve，BAV）患者的临床特征，以及超声心动图在其随访管理中的应用价值，为该类患者的早期识别、风险评估及随访策略提供依据。

方法：回顾性分析 2013 年 1 月 1 日至 2019 年 12 月 31 日期间在江苏省人民医院（南京医科大学第一附属医院）接受超声心动图检查并确诊为 BAV 的患者临床资料，包括其构成比、男女比例、是否合并其他先心病、瓣膜形态及功能、主动脉内径等。进一步筛选具有心超随访数据的患者，评估和比较患者初诊和末次心超（尚未手术者，手术者在主动脉瓣手术或升主动脉手术之前）时的瓣膜功能和升主动脉内径等心超指标的变化情况。采用 Excel 整理数据并使用 SPSS 25.0 软件进行统计分析。

结果：1、汇总 7 年间接受超声心动图检查共 271185 人次，诊断为 BAV 者 1608 人次（占比 0.59%）。过滤掉复查患者后，共 1154 位 BAV，其中男性 768 人（66.55%，48.85±17.52 岁），女性 386 人（33.45%，50.34±16.55 岁），男女比例约 2：1；合并先心病者 74 人（6.40 %）；发生主动脉瓣狭窄 646 人（55.98%），关闭不全者 829 人（71.84%），主动脉窦部增宽 294 人（25.48%，41.26±4.27mm），升主动脉增宽 743 人（64.38%，43.89±5.13mm）；发生感染性心内膜炎 30 人（2.60%），主动脉夹层 9 人（0.78%）。2、按初诊时年龄分组，发现不同性别在各年龄组中的构成比无明显差异；但瓣膜狭窄的发生率及病变程度随年龄增加呈升高和加重趋势，而瓣膜关闭不全在各年龄组中的发生并无明显差异；升主动脉内径随年龄增长呈逐渐增宽趋势。3、按性别分组发现：男性更易出现瓣膜关闭不全和升主动脉扩张，女性则以瓣膜狭窄为主。4、BAV 患者中仅 21.06%（243 人）完成两次及以上心超随访。多因素 Cox 回归分析显示，年龄 >36 岁是 BAV 患者发生主动脉瓣或升主动脉手术事件的独立危险因素（HR=5.119，P < 0.001）。

结论：本研究中 BAV 构成比 0.59%，具有显著的年龄和性别相关的临床差异。超声心动图在 BAV 的初始诊断、病情评估和长期随访中具有关键价值。应加强对 BAV 患者的标准化超声随访管理，特别是高龄患者和存在瓣膜功能异常及主动脉扩张者，以降低手术风险并改善长期预后。

Impact of Concomitant Pulmonary Hypertension on Outcomes after Transcatheter Edge-to Edge Repair for Mitral Regurgitation

Yi-Xuan Xu, Ao-Qin Gu, Guang-Zhi Cong, Qing Chen, Ying Cui, Xiao-Xia Jia, Bao-Tong He

宁夏医科大学总医院

Background: Transcatheter mitral valve edge-to-edge repair (M-TEER) has emerged as a safe and effective treatment option for patients with mitral regurgitation (MR). MR causes elevated left atrial pressure, which passively transmits backward into the pulmonary veins and arteries, leading to pulmonary hypertension (PH). Current data on the association between PH and postprocedural outcomes after TEER are limited to small case reports and case series. There is still a lack of relevant real-world research on M-TEER in related patients.

Objective: To evaluate clinical application trends of MTEER and to investigate the impact of PH on outcomes after M-TEER.

Methods: The National Inpatient Sample (NIS) database is the largest publicly available all-payer inpatient care database in the United States (US). We queried the NIS from 2012 to 2022 and identified hospitalizations for adult patients (age ≥ 18 years) who underwent M-TEER. We identify all cases by using the International Classification of Diseases, 10th Revision, Procedure Coding System (ICD-10-PCS) claims code. To identify PH patients, we used ICD-10 codes of I27. Cohorts were stratified based on the etiology of PH. Baseline patient characteristics included the demographic variables (age, sex, race and region) and baseline comorbid medical conditions such as hypertension, type 2 diabetes mellitus (T2DM), atrial fibrillation, hyperlipidemia, obesity, liver and renal impairment. Primary endpoints comprised all-cause death and clip related complications. Secondary endpoints included postoperative cardiogenic shock, acute postoperative bleeding, pericardial tamponade, endocarditis, blood transfusion and acute ischemic stroke. This study is a large, retrospective study. We used propensity score overlap weighting analysis to compare outcomes between PH and non-PH patients, accounting for measured confounders.

Results: A total of 64345 weighted cases of M-TEER were identified. Of the included patients, 46665 patients had the PH diagnosis. The average age of the PH group was 76.6 ± 10.5（P < 0.01）vs 76.7 ± 11.1（P < 0.01）for the non-PH group. Both groups have a higher morbidity of Caucasian (P < 0.001). However, there were no significant statistical differences between the two groups in terms of postoperative cardiogenic shock (aOR 1.46; 95% CI 0.96–2.20; p = 0.07), acute postoperative bleeding (aOR 1.03; 95% CI 0.89–1.21; p = 0.67), pericardial tamponade (aOR 1.47; 95% CI 0.87–2.48; p = 0.15), endocarditis (aOR 1.09; 95% CI 0.58–2.03; p = 0.79), blood transfusion (aOR 1.15; 95% CI 0.95–1.40; p = 0.15), and acute ischemic stroke (aOR 0.67; 95% CI 0.37–1.19; p = 0.17). Combined with stratified analysis, we found that patients with PH who also exhibited abnormal lipid metabolism or renal impairment were more susceptible to occur death (P

Conclusion: Over the past decade, the clinical application of M-TEER in PH patients in US had accelerated significantly. Although PH does not increase the incidence of common postoperative complications, it constitutes an independent risk factor for in-hospital mortality and device-related complications. Whether TEER can be performed on patients with PH remains to be discussed. More prospective and long-term data regarding quality of life and functional status improvement after the TEER is needed to assess its feasibility and safety.

基于转录组学和生物信息学分析的主动脉瓣钙化关键通路及核心基因研究

赵鹏辉 蔡嘉庚 陈露 祖凌云

北京大学第三医院

背景

钙化性主动脉瓣膜疾病（Calcified Aortic Valve Disease, CAVD）是继冠心病和高血压之后的第三大心血管疾病。长期以来，CAVD 被认为是一种退行性病变，但最新研究表明，其进展是一个主动的、可调节的过程。然而，CAVD 发生发展的分子机制仍不明确。转录组学和生物信息学分析为研究 CAVD 的分子机制提供了强有力的工具，能够从海量数据中筛选出差异表达基因、关键信号通路以及潜在的治疗靶点，从而为揭示 CAVD 的病理机制和寻找新的治疗策略奠定基础。

方法

本研究收集了外科瓣膜置换术后的主动脉瓣样本，根据病理结果分为钙化组和对照组，并进行转录组学测序。通过 R 语言对数据进行生物信息学分析，挖掘钙化相关的关键机制。此外，从基因表达综合数据库（GEO）下载公开数据集（GSE235995 和 GSE267949），对挖掘的靶点进行验证。最后，基于 CMap 数据库预测与相关靶点负相关的潜在治疗分子。

结果

测序结果显示，与对照组相比，钙化组存在 216 个上调基因和 260 个下调基因。通过 KEGG 信号通路富集分析，细胞外基质 - 受体相互作用信号通路和硒化合物代谢信号通路被筛选为可能参与主动脉瓣钙化的关键通路，通路上的关键基因包括 **IBSP**、**SPP1**、**LAMA3**、**LAMC3**、**KYAT1**、**TXNRD3** 和 **CTH**。进一步验证显示，在人和动物的主动脉瓣钙化数据集中，**IBSP** 在钙化组中呈显著上调，而 **ADRB1** 和 **HSPA2** 在钙化组中显著下调，提示这些基因可能是 CAVD 的关键调控因子。此外，将共有差异基因上传至 CMap 数据库后发现，**茴香霉素**、**3,5- 二甲基苯甲酸托品酯** 和 **吐根酚碱** 是与主动脉瓣钙化负相关排名前 3 的分子。

结论

本研究表明，细胞外基质 - 受体相互作用信号通路及硒化合物代谢信号通路可能是 CAVD 的关键调控通路；**IBSP**、**SPP1**、**LAMA3**、**LAMC3**、**KYAT1**、**TXN-**

RD3、**CTH**、**ADRB1** 和 **HSPA2** 可作为 CAVD 的潜在关键基因；**茴香霉素**、**3,5-二甲基苯甲酸托品酯** 和 **吐根酚碱** 是潜在的治疗分子，为 CAVD 的干预提供了新的研究方向。

Left Atrial Function Index-Tricuspid Regurgitation Interplay Predicts Midterm Prognosis Following Transcatheter Aortic Valve Replacement: A Hemodynamic Remodeling Perspective

GuangWei Zhou, Ben He

Shanghai Dongfang Hospital

Abstract

Background: Severe aortic stenosis (AS) induces chronic pressure overload, leading to left ventricular (LV) hypertrophy, elevated filling pressures, and maladaptive left atrial (LA) remodeling ("atrial cardiomyopathy"). The left atrial function index (LAFI), a rhythm-independent composite metric integrating LA reservoir function (LA emptying fraction, LAEF), indexed LA volume (LAESVi), and stroke volume (LV outflow tract velocity-time integral, LVOT-VTI), provides a robust assessment of LA-LV coupling. Concomitant tricuspid regurgitation (TR) is prevalent (~40%) in transcatheter aortic valve replacement (TAVR) candidates and independently predicts adverse outcomes. The interplay between post-TAVR LA functional recovery (via LAFI) and TR evolution, and their collective prognostic impact, remains unexplored.

Objectives: This study aimed to: (1) Characterize midterm LAFI trajectories after TAVR and their determinants; (2) Elucidate the bidirectional relationship between LAFI dynamics and TR evolution; (3) Evaluate the prognostic value of LAFI for mortality and cardiovascular events.

Methods: This retrospective single-center study analyzed 59 patients with severe symptomatic AS undergoing transfemoral TAVR (Nov 2019 - Oct 2023). Baseline characteristics included mean age 75.7 ± 5.2 years, 56% male, STS score 6.29 ± 5.69. Patients with adequate echocardiograms for standardized LAFI calculation (LAFI = [LAEF × LVOT-VTI] / LAESVi) were included; 6 patients had atrial fibrillation. A subgroup of 48 patients had serial echocardiography for LAFI assessment pre-TAVR and at midterm (3-6 months, median 3 months [IQR 3-6]) and/or long-term (12 months) follow-up. TR severity was graded (0-4) per ESC/ASE guidelines using jet area, vena contracta width, and PISA. LA strain analysis was performed using speckle tracking (EchoPAC). ΔLAFI was defined as change from baseline; patients were categorized as Improvers (ΔLAFI ≥ +3%), Decliners (ΔLAFI ≤ -3%), or Stable (|ΔLAFI| <3%). The primary endpoint was 1-year all-cause mortality. Secondary endpoints included cardiovascular events (stroke/TIA, MI, pacemaker, bleeding) at 30 days (VARC-3 criteria). Multivariable logistic regression identified predictors of 1-year mortality and residual TR. Generalized Estimating Equations (GEE) modeled associations between LAFI dynamics and TR progression, adjusting for age, sex, BSA, NYHA class, STS score, sPAP, and BNP.

Results:

1.Baseline Stratification & Outcomes: Using LAFI ≤ 13.5 (based on Youden Index) for stratification, 40.6% (n=24) had low LAFI. This group had higher female prevalence (62% vs 31%, p=0.018), BNP (1242.98±1699.78 vs 443.45±503.06 pg/mL, p<0.001), atrial fibrillation (25% vs 0%, p=0.003), smaller AVA (0.46±0.17 vs 0.6±0.19 cm^2, p=0.04), worse LV GLS (-12.08±4.6% vs -15.24±3.01%, p=0.002), and higher sPAP (31.29±15.58 vs 24.8±8.93 mmHg, p13.5 group. No significant difference in 1-year mortality (8% vs 2.8%, p=0.35) or secondary endpoints was observed between groups. However, multivariable analysis identified higher baseline BNP (HR 1.001, 95% CI 1.001-1.002, p=0.046) and lower post-TAVR LAFI (HR 0.03, 95% CI 0.001-0.994, p=0.05) as independent predictors of 1-year mortality.

2.LAFI Trajectories: Overall midterm LAFI change was non-significant (25.61±4.43 vs 29.75±3.23, p=0.356). However, dynamic patterns emerged: 55.6% of the baseline LAFI ≤ 13.5 group and 44.3% of the LAFI>13.5 group were Improvers. Improvers had significantly lower baseline TR grade (p<0.001), lower sPAP (p<0.001), better LV GLS (p=0.02), and no chronic dialysis (p=0.019) compared to non-improvers. Decliners constituted 31.3% of the baseline LAFI ≤ 13.5 group and 46.7% of the LAFI>13.5 group, associated with higher STS scores and renal dysfunction.

3.LAFI-TR Interplay: Post-TAVR TR severity diverged:

1.LAFI ≤ 13.5 Group: Moderate-severe TR increased (20.8% vs 8.3% baseline).

2.LAFI>13.5 Group: Moderate-severe TR decreased (5.7% vs 11.4% baseline), with only 2 severe TR cases.

Multivariable analysis identified baseline AF (OR 0.498, 95% CI 0.783-2.882, p=0.001), lower post-TAVR LAFI (OR -0.462, 95% CI -2.008 - 0.444, p=0.003), and negative ΔLAFI (OR -0.28, 95% CI -0.693 - 0.049, p=0.025) as independent predictors of residual TR. GEE modeling confirmed an inverse relationship: Each unit increase in LAFI reduced the odds of TR deterioration by 4.7% (adjusted OR 0.953, 95% CI 0.914-0.994, p=0.024). Baseline TR severity inversely correlated with likelihood of LAFI improvement.

Discussion: This is the first study to investigate the LAFI-TR relationship post-TAVR. Key findings are:

1.Prognostic Markers: Lower post-TAVR LAFI and elevated baseline BNP synergistically predict 1-year mortality, indicating persistent ventricular strain and irreversible atrial remodeling despite afterload reduction.

2.Bidirectional LAFI-TR Relationship: Baseline TR severity impedes LAFI improvement post-TAVR. Conversely, higher post-TAVR LAFI and positive ΔLAFI independently protect against TR progression. Mechanistically, LA dysfunction (low LAFI) exacerbates pulmonary hypertension, perpetuating RV overload and TR - a cycle potentially modifiable by TAVR in suitable patients. Residual TR may hinder LA reverse remodeling.

3.Heterogeneous LAFI Response: Midterm LAFI improvement (47% overall) was significant in patients with favorable profiles (milder baseline TR, lower sPAP, better LV GLS, no dialysis). Decliners had higher comorbidity burdens, suggesting irreversible LA damage limits hemodynamic benefit. ΔLAFI itself emerged as a mortality predictor.

4.Clinical Implications: LAFI provides a rhythm-independent measure of LA-LV coupling and post-TAVR adaptation. Integrating LAFI, BNP, and TR grade may optimize risk stratification. Patients with low baseline LAFI, significant TR, AF, and renal dysfunction represent a high-risk phenotype potentially benefiting from intensified GDMT, pulmonary vasodilators, LA appendage closure, or consideration of staged tricuspid intervention guided by serial LAFI/TR assessment and ΔLAFI.

Limitations: The primary limitation is the relatively small sample size (n=59 overall, n=48 with serial imaging), reducing power to detect subtle effects and subgroup differences and potentially limiting multivariable model robustness. The single-center, retrospective design and median 3-month follow-up for LAFI trajectories warrant validation in larger, prospective, multicenter studies with longer follow-up. Phenotyping using advanced analytics (e.g., machine learning) or pooled multi-institutional data could further elucidate heterogeneity.

Conclusion: LAFI is a valuable prognostic marker reflecting atrial-ventricular interdependence in AS patients undergoing TAVR. A bidirectional relationship exists between LAFI and TR: Baseline TR severity impedes LAFI improvement, while higher post-TAVR LAFI and positive ΔLAFI mitigate TR progression. Serial assessment of LAFI and TR dynamics post-TAVR, particularly ΔLAFI, offers insights into hemodynamic adaptation and identifies high-risk patients who may benefit from adjunctive therapies or tricuspid valve intervention.

Keywords: Aortic stenosis; Transcatheter aortic valve replacement (TAVR); Left atrial function index (LAFI); Tricuspid regurgitation (TR); Prognosis; Atrial cardiomyopathy; Hemodynamic adaptation.

Effects of transcatheter aortic valve replacement on hemodynamics and left atrial reverse remodelling for aortic stenosis with progressive to severe mitral stenosis

null null, Ben He

Dongfang Hospital

Abstract

Background: Transcatheter aortic valve replacement (TAVR) is established for severe symptomatic aortic stenosis (AS), yet 7-18% of candidates present with significant concomitant mitral stenosis (MS). The hemodynamic impact of isolated TAVR in AS-MS patients remains poorly characterized, particularly regarding left atrial (LA) remodeling and mitral valve dynamics. Existing evidence on outcomes is conflicting, and MS etiology (rheumatic vs. calcific) may differentially influence results.

Objectives: This study aimed to: (1) Evaluate acute hemodynamic changes and LA reverse remodeling after isolated TAVR in severe AS with MS; (2) Characterize mitral valve parameter (MVA, MPG) trajectories; (3) Assess early safety and functional outcomes.

Methods: This single-center retrospective study analyzed 8 patients with severe AS (AVA ≤ 1.0 cm^2) and MS (MVA ≤ 2.0 cm^2) undergoing TAVR (Jan 2018–Jan 2024). Exclusion criteria included prior mitral valve surgery. Etiology: rheumatic MS (n=6, 75%; 1 with prior PBMV) and annular calcification (n=2, 25%). Baseline characteristics: age 72.6±5.1 years, 75% male, 63% with LVEF<50%, high comorbidity burden (37% moderate-severe AR, 88% MR, 75% TR). Transthoracic echocardiography (GE Vivid E95) assessed LA volume (LAV), mitral valve area (MVA), mean pressure gradient (MPG), and LVEF pre-TAVR and at 1-month follow-up. Adverse events (cardiovascular mortality, HF hospitalization, bleeding) and NYHA class were tracked.

Results:

Hemodynamics & LA Remodeling: Significant LAV reduction occurred post-TAVR (121.8±50.5 mL vs. 87.0±44.8 mL; p=0.028). No significant changes in MPG (9.3±5.0 vs. 7.8±2.5 mmHg; p=0.614) or MVA (1.8±0.5 vs.

2.1±0.8 cm²; p=0.196) were observed.

LV Function & Symptoms: Patients with baseline LVEF<50% (n=5) showed greater LVEF improvement (Δ LVEF +21.2±8.7%) than those with LVEF ≥ 50% (n=3; Δ LVEF +2.8±5.3%; p=0.01). NYHA class improved significantly in all patients by 1 month.

Safety: All procedures succeeded via femoral access (Peijia: 38%, Venus: 50%, Microport: 12%). No intraprocedural deaths. Adverse events: 1 patient (rheumatic MS) died 6 months post-TAVR (non-cardiac: gastric malignancy); 1 required hospitalization for warfarin-related bleeding (resolved); 1 continued hemodialysis for pre-existing renal failure.

Etiology-Specific Trends: The single patient with prior failed PBMV (rheumatic MS) exhibited post-TAVR MVA improvement despite calcific MS patients showing no significant change.

Discussion: Isolated TAVR in AS-MS patients demonstrated:

Significant LA Reverse Remodeling: Rapid LAV reduction suggests immediate LA pressure unloading, corroborating AS hemodynamic studies.

Heterogeneous Mitral Valve Response: Stable MPG/MVA contrasts with reports of improvement, potentially reflecting etiology (rheumatic vs. calcific) and baseline severity. Calcific MS may resist change due to annular rigidity, while rheumatic MS showed variable responses (1 improved post-TAVR despite failed PBMV).

LV Functional Recovery: Pronounced Δ LVEF in systolic dysfunction patients highlights TAVR's afterload reduction benefit in this high-risk subgroup.

Symptomatic Benefit: Uniform NYHA improvement supports symptom palliation despite unchanged mitral metrics in some.

Safety Profile: Feasibility was demonstrated, though comorbidities (renal failure, anticoagulation needs) contributed to non-cardiac events.

Limitations: Small sample size (n=8), single-center retrospective design, mixed MS etiologies, heterogeneous regurgitation (AR/MR/TR), and concomitant medications limit generalizability. Short-term follow-up precludes assessment of MS progression. Lack of surgical comparator (SAVR) and advanced hemodynamic imaging.

Conclusion: Isolated TAVR is feasible and improves symptoms and LA remodeling in severe AS with concomitant MS. While mitral valve parameters (MVA/MPG) remained stable acutely, significant LVEF recovery occurred in patients with baseline systolic dysfunction. Etiology may influence mitral hemodynamic response, warranting larger studies to define long-term MS progression and guide patient selection for concomitant interventions. TAVR represents a viable initial strategy for high-risk AS-MS patients, particularly those with impaired LV function.

Keywords: Transcatheter aortic valve replacement (TAVR); Aortic stenosis; Mitral stenosis; Left atrial remodeling; Hemodynamics; Rheumatic heart disease; Mitral annular calcification.

Feasibility and Outcomes of Intra-aortic Balloon Pump Support in Patients with Severe Aortic Valve Stenosis and Acute Decompensated Heart Failure

Kaimin WU, Bin Wang, Hui-Yuan Kang, Xiang Chen, Yan Wang

厦门大学附属心血管病医院 (厦门市心脏中心)

Objective

Transcatheter aortic valve replacement (TAVR) has emerged as a transformative therapeutic modality for patients with severe aortic valve stenosis (AS) who are at high or prohibitive risk for surgical aortic valve replacement, markedly enhancing both survival rates and functional status. Nevertheless, a considerable proportion of patients with severe AS presenting with acute decompensated heart failure (AHF) or cardiogenic shock (CS) continue to pose significant clinical challenges. Their profound hemodynamic instability often renders immediate definitive interventions unfeasible, creating a critical need for effective bridging strategies. The ability to achieve even temporary stabilization in these critically ill individuals is of paramount importance, as it affords clinicians the opportunity to conduct a comprehensive review of clinical data, thoroughly evaluate procedural feasibility, and engage in informed shared decision-making with patients and their families. The present retrospective study was designed to assess the feasibility, safety profile, and clinical outcomes associated with intra-aortic balloon pump (IABP) support as a bridging intervention in patients with severe AS and AHF, with a specific focus on those presenting with concurrent CS.

Methods and Results

This retrospective observational study was conducted at Xiamen Cardiovascular Hospital, Xiamen University, and included a consecutive cohort of patients with severe AS and AHF who underwent IABP support as a bridging strategy between January 2018 and January 2025. The inclusion criteria were strictly defined as follows: (1) confirmation of severe AS via echocardiography, characterized by an aortic valve area following AHA guidelines; and (3) implementation of IABP implantation as a bridging measure to definitive therapy. A total of 29 patients were enrolled in the study, with a mean age of 74.3±9. 3years, and 15 (51.7%) were male. Among the study population, 15 patients (51.7%) presented with CS, 9 (31.0%) had a concurrent acute myocardial infarction, and 6 (20.7%) required endotracheal intubation and mechanical ventilation at baseline. Echocardiographic and hemodynamic assessments confirmed the severity of AS, with the following key parameters: peak aortic valve gradient (91.3±32.8 mmHg), mean gradient (55.5±21.1 mmHg), peak flow velocity (4.7±0.8 m/s), aortic valve area (0.53±0.21 cm²), and left ventricular ejection fraction (42.2%±10.2%). IABP implantation was technically successful in all 29 patients, with a mean support duration of 49.1±46.5 hours. Hemodynamic stabilization was achieved in 25 patients (82.8%), as evidenced by a significant improvement in mean arterial pressure and a notable reduction in inotropic requirements. Unfortunately, 4 patients (13.8%) succumbed to refractory shock even with IABP support. Among the stabilized patients, 23 proceeded to undergo TAVR, while 2 patients underwent percutaneous balloon aortic valvuloplasty (PBAV) as the definitive intervention. No peri-procedural deaths or major IABP-related complications, such as limb ischemia, aortic dissection, or major bleeding, were observed. Following the definitive interventions, 3 patients died after TAVR: 1 due to gastrointestinal bleeding, and 2 due to malignant arrhythmias leading to cardiac arrest. The overall in-hospital and 30-day mortality rates were 27.6% (8/29).

Conclusions

Intra-aortic balloon pump support demonstrates favorable safety and efficacy as a bridging strategy in patients with severe AS and AHF, including those with concurrent CS, enabling the majority of patients to proceed to subsequent definitive interventions such as TAVR. These findings underscore the value of IABP in stabilizing hemodynamically unstable patients with severe AS, thereby facilitating access to life-saving valve replacement therapies. Further prospective, larger-scale studies are warranted to validate these observations and refine the selection criteria for optimal patient outcomes.

Key Words

Aortic valve stenosis; Acute decompensated heart failure; Cardiogenic shock; Transcatheter aortic valve replacement; Intra-aortic balloon pump

合并冠心病的 TAVR 患者同期行 PCI 的安全性和有效性研究

刘荣 黄琼 袁义强 邓秋琼

河南省胸科医院

目的：探讨在经导管主动脉瓣置换术（TAVR）合并冠心病（CAD）患者中，同期行冠脉介入治疗（PCI）对比单纯药物治疗的临床疗效。

方法：本研究为回顾性研究，纳入 2019 年 12 月至 2023 年 9 月在河南省胸科医院接受 TAVR 治疗且存在严重冠脉狭窄的患者。根据不同治疗方法分为 TAVR+PCI 组和单纯 TAVR 组，分别纳入 48 例和 57 例患者。收集患者的基线资料、冠脉病变情况及随访数据，主要终点为全因死亡，次要终点包括

急性心肌梗死（MI）、中风、手术成功率、出血并发症、入路并发症、脑血管事件、急性肾损伤等。数据采用 SPSS 25.0 软件进行统计分析。

结果: 两组患者在年龄、性别、BMI 等多项基线特征上差异无统计学意义(P>0.05)，但高血压病史在 TAVR+PCI 组更为常见（75% vs 31.58%，P<0.05）。在冠脉病变情况方面，两组在单支、双支、三支病变比例上差异无统计学意义（P 值分别为 0.622、0.092、0.263）。随访结果显示，TAVR+PCI 组发生主要不良心血管事件（MACE）的患者有 3 例（6.25%），单纯 TAVR 组有 1 例（1.75%），两组间差异无统计学意义（P=0.492）；但在总事件数上，TAVR+PCI 组（17 例）显著多于单纯 TAVR 组（7 例），P=0.005。

结论：在 TAVR 患者中同期行 PCI 治疗并未显著增加主要不良心血管事件的风险，但次要终点事件总发生数较多，提示在选择联合 PCI 治疗时需谨慎权衡手术风险和潜在获益。

单把血管缝合器对比双把在闭合 TAVR 患者股动脉入路的安全性及有效性研究

马玲 王婧雅 王钊 余小林 杨毅宁

新疆维吾尔自治区人民医院

目 的：探讨 TAVR 术前预埋单把缝合器对比双把对股动脉止血的安全性与有效性。**方 法：**连续纳入 2021 年 3 月至 2024 年 12 月就诊新疆维吾尔自治区人民医院并行经股 TAVR 的患者，根据 TAVR 术前预埋缝合器数量分为单把缝合器组和双把缝合器组两组，统计分析两组在止血成功率、鞘管型号、术中并发症及随访 MACE 事件等方面的差异。**结 果：**根据纳入排除标准筛选后，本研究最终共纳入 190 例经股行 TAVR 的重度主动脉瓣狭窄患者，其中男性 100 名，女性 90 名，根据 TAVR 术前预埋缝合器数量分为单把组（n=98）和双把组（n=92）两组。统计分析两组患者在鞘管型号及住院天数上存在显著差异（P < 0.05），但在使用同一鞘管型号时两组主入路血管并发症无统计学差异（P > 0.05），但单把组并发症发生率小于双把组（5.1% vs 7.6%）；且在闭合大于 18F 的鞘管器械通路时单把缝合器缝合止血有效且并发症发生率低于双把（3.1% vs 6.8%），但两组并发症无统计学差异（P > 0.05）；两组患者在术中并发症及随访 MACE 事件方面无统计学差异（P > 0.05）。**结 论：**单把缝合器对比双把缝合器在 TAVR 术中对股动脉的止血效果相似，且均未显著增加术后并发症的风险，单把缝合器

对行 TF-TAVR 的患者止血效果不劣于双把缝合器。

经导管主动脉瓣置换术治疗重度主动瓣狭窄合并射血分数降低型心衰经验总结

李福杭 张海山 高远 梁长彬 邹麓 孙璐璠 (血脂异常学组委员) 郭亮

中国医科大学附属第一医院

目的：重度主动脉瓣狭窄合并射血分数降低型心衰心衰患者往往已经进入了失代偿阶段，尤其进展至低 EF- 低流量 - 低压差型主动脉瓣狭窄的患者，传统外科手术存在术中风险高，恢复时间长等问题，TAVR 是这部分患者的可选治疗方案，为重度主动脉瓣狭窄合并射血分数降低型心衰心衰患者带来了生存希望。

方法：回顾性分析 2020 年 1 月至 2025 年 1 月于中国医科大学附属第一医院因主动脉瓣重度狭窄行 TAVR 治疗的 201 例患者，其中主动脉瓣重度狭窄合并射血分数降低型心衰的患者有 20 例。从医院的电子病历系统提取患者的基线信息、心电图、术前及术后心血管超声、主动脉根部 CTA 进行分析；记录患者的基线信息包括：年龄、性别、体重指数（BMI）、体表面积、心功能分级（NYHA 分级）、既往病史（心绞痛、心肌梗死、冠脉内介入治疗、冠脉搭桥术后）。由经验丰富的的心血管超声医生明确患者的主动脉瓣重度狭窄的诊断及 EF 值的测量。

结果：共纳入 20 例主动脉瓣重度狭窄合并射血分数降低型心衰患者，其中男性 18 例（90.0%），平均年龄 68.05 岁，术前平均 NT-pro BNP 为 15692.75pg/ml，术前心源性休克患者 3 例（15.0%），术前急性心衰患者 2 例（10.0%）。超声提示左室射血分数平均为 30.5%，左室舒末内径平均为 61.6mm， 低 EF- 低流量 - 低压差患者 5 例（25.0%），主动脉瓣二叶畸形 16 例 (80.0%)，外科瓣膜术后衰败患者 1 例（5.0%），合并主动脉瓣中度以上关闭不全 4 例 (20.0%)，合并二尖瓣中度以上关闭不全患者 5 例（25.0%），合并肺动脉高压患者 8 例（40.0%）；19 例（95.0%）患者于全麻下行 TAVR，1 例（5.0%）患者于镇静监护下行手术。19 例患者以股动脉为主入路 ,1 例患者以腋动脉为主入路。16 例使用自膨式主动脉瓣，4 例使用球扩式瓣膜。3 例患者同台行 PCI 治疗；2 例围术期 V-A ECMO 支持，术后均成功撤机；3 例患者植入瓣中瓣；无中度以上瓣周漏；患者术后心功能均得到改善，术后 1 周内复查 EF 值平均值为 33.5%，左室舒末内径平均值为 59.65mm，平均跨瓣压差的平均值为 10.38mmHg，峰值跨瓣血流速度的平均值为 2.22m/s。所有患者均在规律随访，1 名患者术后 2 年非心源性死亡。

结论：射血分数降低型心衰患者应早期行 TAVR 治疗；围术期心源性休克患者及恶性心律失常患者均难以按照预定日期进行 TAVR 治疗，且在血流动力学不稳定早期使用生命支持设备可以提高这类患者的生存率。本研究中共 2 例患者行 V-A ECMO 支持，1 例于手术室外行 V-A ECMO，1 例于手术室内术前行 V-A ECMO 支持；2 例患者均于术后成功撤机。

孤独感与退行性心脏瓣膜疾病风险的关联：一项大规模前瞻性队列研究

朱兆伟 周胜华 龚文

中南大学湘雅二医院心内科

目的

心脏瓣膜疾病是全球范围内的重要公共卫生问题，随着人口老龄化进程加速，其发病率呈现显著上升趋势。退行性心脏瓣膜病（如主动脉瓣狭窄和二尖瓣反流）在老年人群中的发病率逐渐升高，严重影响患者生活质量并导致较高的医疗负担。孤独感作为一种普遍存在的社会心理现象，在现代社会中呈现出日益严峻的公共卫生挑战。随着城市化进程加速和社会结构变迁，越来越多的人群正经历着不同程度的孤独体验，尽管已有孤独感与心血管疾病的研究， 但尚无针对心脏退行性瓣膜性疾病的研究。本研究旨在研究孤独感与退行性心脏瓣膜疾病风险之间的关联及其潜在机制。

方法

研究人群平均年龄 58 岁，女性占 55%，白人占 95%。根据孤独感指数将参与者分为三组：无孤独感组 (331,946 人)、轻度孤独感组 (108,822 人) 和重度孤独感组 (22,149 人)。采用多变量 Cox 比例风险模型分析孤独感与退行性心脏瓣膜疾病风险的关联。

结果

本研究通过对英国生物样本库 462,917 名参与者的长期追踪，揭示了孤独感与退行性心脏瓣膜疾病风险之间存在的显著关联。在调整了年龄、性别、种族、社会经济地位、生活方式因素及基础疾病等多重变量后，数据分析显示孤独感程度与退行性心脏瓣膜疾病发病率呈现明确的剂量反应关系。具体而言，与无孤独感个体相比，具有重度孤独感的参与者发生退行性心脏瓣膜病的风险增加了 19%（HR=1.19，95%CI 1.09-1.28），主动脉瓣狭窄风险增加 21%（HR=1.21，1.06-1.37），而二尖瓣反流风险也显著升高 23%（HR=1.23，1.09-1.39）。

结论

本研究首次在大规模人群队列中证实了孤独感与退行性心脏瓣膜疾病风险之间存在显著的独立关联，并揭示了这种关联呈现出明确的剂量反应关系。研究结果表明，孤独感不仅是传统心血管危险因素之外的重要预测指标，更可能通过影响生活方式行为和代谢状态对心脏瓣膜健康产生实质性损害。

经导管主动脉瓣置换术后失败的处理策略：瓣膜取出与二次 TAVR 疗效比较的系统综述与荟萃分析

白明 郎泽昆 董康 赵彦航

兰州大学第一医院（兰州大学第一临床医学院）

目的：随着经导管主动脉瓣置换术（TAVR）在主动脉瓣病变治疗中的应用日益广泛，失败的发生率也随之上升。因此，TAVR 失败的处理已成为关键临床问题。针对 TAVR 失败的治疗策略需要采取个体化、多学科协作的诊疗模式。本系统综述与荟萃分析旨在综合现有证据，比较瓣膜取出与二次 TAVR 在 TAVR 术后失败患者中的临床结局差异。

方法：通过系统检索主要数据库，筛选出直接比较外科 TAVR 瓣膜取出术与二次 TAVR 治疗 TAVR 失败的临床研究。本研究严格遵循 PRISMA 指南，并在 PROSPERO 数据库注册（注册号：CRD420251046720）。统计学分析中，二分类变量采用相对危险度（RR）表示，连续变量采用均数差（MD）表示。使用 Review Manager（RevMan）5.4 版和 Stata SE 16.0 软件进行荟萃分析。

结果：共纳入 4 项研究，合计 905 例患者。汇总分析显示：二次 TAVR 组与瓣膜取出术组在总住院时间方面无显著差异（MD：-0.25；95%CI：-0.55 至 0.04）。但瓣膜取出术组的重症监护病房（ICU）停留时间显著延长（MD：-0.37；95%CI：-0.44 至 -0.30）。二次 TAVR 组短期死亡率显著降低（RR：0.36；95%CI：0.22 至 0.59），而两组长期死亡率相当（RR：0.78；95%CI：0.46 至 1.33）。在永久起搏器植入率及大出血发生率方面，两组无显著差异。但瓣膜取出术组急性肾功能衰竭发生率显著增高（RR：0.50；95%CI：0.33 至 0.77）。

结论：本荟萃分析表明，与瓣膜取出术相比，二次 TAVR 可能具有更优的短期临床结局，包括缩短 ICU 停留时间、降低短期死亡率及减少肾脏并发症风险。两种治疗策略在长期死亡率及出血、起搏器植入等不良事件方面效果相当。这些研究结果支持根据患者风险特征和手术可行性采取个体化治疗策略。

Sex-Specific Differences in the Incidence of New-Onset Left Bundle Branch Block and Need for Pacemaker Implantation Following Transcatheter Aortic Valve Replacement

Cong-Yan Ye[1], Guang-Zhi Cong[2], Jin-Wei Tian[1]

1. The Second Affiliated Hospital of Harbin Medical University, Harbin

2. Hospital of Ningxia Medical University, Yinchuan

Background: Left bundle branch block (LBBB) is one of the most frequent conduction disturbances following transcatheter aortic valve replacement (TAVR) and may precipitate significant adverse events, including the need for permanent pacemaker implantation (PPI). While previous studies have described the overall burden of LBBB and PPI in TAVR populations, sex-specific differences in the prevalence, clinical correlates, and prognostic implications of these complications remain poorly defined. A better understanding of gender-based disparities is essential for the development of targeted preventive and therapeutic strategies in this increasingly prevalent patient population. To address this knowledge gap, we utilized data from the National Inpatient Sample (NIS), a large, representative hospital administrative database, to assess clinical characteristics, the frequency of LBBB after TAVR, and sex-associated differences in the risk for PPI among men and women treated with TAVR in the United States.

Methods: This retrospective cohort study included patients who underwent TAVR between 2016 and 2021, identified within the NIS database by International Classification of Diseases, 10th Revision, Clinical Modification (ICD-10-CM) codes. Both principal and secondary diagnoses and procedures were screened to capture all relevant cases. Patient demographics, comorbidities, and hospitalization characteristics were abstracted, with adjustments made for age, race/ethnicity, socioeconomic status, and comorbidities measured by the Elixhauser Comorbidity Index. Weighted logistic regression modeling was implemented to examine associations between sex and outcomes, with stratification for key variables. The primary endpoint was the incidence of new-onset LBBB within the postprocedural period. Secondary endpoints included the frequency of PPI in those who developed new-onset LBBB. Additionally, temporal trends in the prevalence of LBBB and PPI over the study period were explored.

Results: We identified a total of 315,330 hospitalizations for TAVR between 2016 and 2021, with 54.78% male (n=172,725) and 45.22% female (n=142,605), and a mean age notably higher among females (79.33 versus 78.00 years; P < 0.001). Female patients also presented with a higher burden of comorbidities. Among the cohort, 15.96% developed new-onset LBBB post-TAVR, with females showing a significantly elevated risk compared to males (17.28% vs. 14.84%; adjusted OR, 1.20; 95% CI, 1.15–1.26; P < 0.001). Subgroup analysis indicated particularly increased odds in patients with fluid and electrolyte disorders (aOR 1.49; 95% CI, 1.31–1.69; p-interaction = 0.001) and those with depression (aOR 1.40; 95% CI, 1.19–1.63; p-interaction = 0.013). Among patients who developed LBBB, females had a significantly lower rate of PPI compared to males (aOR 0.61; 95% CI, 0.50–0.75; P < 0.001). Notably, annual PPI rates in males with new-onset LBBB consistently exceeded those in females, although both declined over the observation period.

Conclusions: Our findings suggest that women undergoing TAVR are at increased risk of developing new-onset LBBB, especially those with fluid and electrolyte imbalances or depression, yet are less likely to require PPI once LBBB develops compared to their male counterparts. These results highlight the necessity for implementing sex-specific management strategies for conduction disturbances in TAVR recipients and point to the need for further prospective studies to elucidate mechanisms underlying these observed disparities.

Key Words: transcatheter aortic valve replacement, left bundle branch block, sex, permanent pacemaker implantation, gender differences, con-

duction disorders.

Effect and Mechanism of Calcium Binding Protein S100A8/A9 on Calcific Aortic Valve Disease

zai-qiang liu, Yu-Xiu Yang, Qiu-Xuan Li, Yang Zheng, Jing-Yao Yang, Xiao-Teng Ma, Zhi-Jian Wang

Beijing Anzhen Hospital, Capital Medica University

Research Background

Calcific Aortic Valve Disease (CAVD) is the most prevalent condition affecting cardiac valves, characterized by the thickening, fibrosis, and mineralization of aortic valve leaflets. The pathogenesis of CAVD is influenced by multiple factors, among which immune-inflammatory mechanisms play a significant role. S100A8/A9, a calcium-binding protein, is constitutively expressed in neutrophils and monocytes/macrophages, serving as a Ca^{2+} sensor. During inflammatory processes, S100A8/A9 is actively secreted by monocytes/macrophages and plays a pivotal role in regulating inflammatory responses. Studies have demonstrated that S100A8/A9 promotes the progression of various cardiovascular diseases; however, its role in CAVD remains poorly understood.

Objectives

1. Investigate the expression and distribution of S100A8/A9 protein in valvular tissues of CAVD patients and in a CAVD mouse model.

2. Utilize an in vitro valvular interstitial cell calcification model to explore the impact of S100A8/A9 protein on valvular calcification.

3. Elucidate the specific mechanisms by which S100A8/A9 protein promotes calcification of valvular interstitial cells in vitro.

Methods

Aortic valve tissues from CAVD patients were collected for transcriptomic sequencing analysis to determine the expression of S100A8/A9 in calcified valvular tissues. A CAVD mouse model was established by feeding APOE $^{-/-}$ C57BL/6J mice a high-fat diet. Valvular tissue sections were prepared and subjected to hematoxylin and eosin (HE) staining to assess valve thickness, alizarin red staining to detect calcified nodule deposition, and immunofluorescence staining to analyze the expression and distribution of the osteogenic differentiation marker RUNX2 and S100A8/A9 protein. Using an in vitro valvular interstitial cell calcification model, recombinant S100A8/A9 protein was added under osteogenic induction culture conditions. The expression of osteogenic differentiation-related markers RUNX2 and BMP2 was detected by Western blot and qRT-PCR, and alizarin red staining was performed to assess calcium nodule deposition in valvular interstitial cells. Subsequently, the mRNA and protein expression of molecules associated with the TLR4/MyD88/NF-κB signaling pathway were examined to investigate the signaling pathway activated by S100A8/A9 in valvular interstitial cells.

Results

Through the analysis of calcified valve tissues from patients with calcific aortic valve disease (CAVD) and bulk RNA-Seq results of calcified valve tissues from the GEO database, it was found that the expression of S100A8 and S100A9 genes was significantly higher than that in normal valve tissues. Histological staining of valve tissues from CAVD model mice revealed that the expression of S100A8/A9 proteins in calcified valve tissues was significantly greater than that in the control group. Using an in vitro calcification model of valve interstitial cells, after adding recombinant S100A8/A9 proteins, Western Blot analysis showed an increased expression of osteogenic differentiation markers RUNX2 and BMP2, indicating that the osteoblastic differentiation of valve interstitial cells was aggravated, as evidenced by increased deposition of calcified nodules indicated by Alizarin Red staining. Furthermore, the study assessed the expression levels of S100A8/A9 protein receptors and downstream inflammatory molecules such as MyD88, NFκB, ICAM-1, and IL-6, revealing an exacerbation of the inflammatory response in valve interstitial cells.

Conclusion

In this study, through the construction of a CAVD mouse model and an in vitro model of osteogenic-like differentiation of valvular interstitial cells, we demonstrated that S100A8/A9 protein promotes osteogenic-like differentiation of valvular interstitial cells by activating the TLR4/MyD88/NF-κB signaling pathway. Blocking the function of S100A8/A9 protein within the valve may serve as a potential therapeutic target to mitigate valvular calcification.

一例经心尖主动脉瓣置换术后全身皮下气肿的护理体会

何君子

新疆维吾尔自治区人民医院

目的：经导管主动脉瓣置换术（Transcatheter aortic valvreplacement,TAVR）是指将组装好的主动脉瓣经导管置入到主动脉根部，替代原有主动脉瓣，是一种微创心脏手术，经心尖主动脉瓣置换是其中的一种手术入路方式，适用于高危主动脉瓣狭窄患者，尽管其创伤较小，但术后并发症如皮下气肿（Subcutaneous Emphysema, SE）仍可能发生。皮下气肿表现为气体在皮下组织异常积聚，可导致高碳酸血症、循环波动等问题，护理工作的关键在于早期识别与及时干预，密切监测患者的生命体征，特别是呼吸频率和血氧饱和度，是预防并发症恶化的基础。一旦发现患者出现皮下气肿症状，应立即通知医疗团队，并启动紧急护理流程。此外，针对 TAVR 术后患者可能出现的其他并发症，如出血、感染等，也需制定详细的预防和应对措施。通过加强团队协作，优化护理流程，确保患者在术后能够得到全面、细致的护理。

方法：从呼吸道管理、感染防控、心输出量优化护理、多管路安全管理、并发症预防性护理、广泛性皮下气肿护理、高碳酸血症的多因素干预以及疼痛管理、营养支持、心理干预、早期活动促进、家属教育与参与、持续病情监测与评估、以及适时调整治疗方案等多方面进行综合护理。

结果：患者呼吸功能得到显著改善，动脉血气分析指标恢复正常，氧合指数稳定在正常范围。患者未出现其他严重并发症，病情好转后顺利转出 ICU，最终康复出院

结论：本研究通过回顾性分析 1 例经心尖经导管主动脉瓣置换术（TAVR）后发生全身皮下气肿患者的临床资料及护理过程，不仅总结了护理要点与难点，还为未来 TAVR 术后并发症的护理提供了宝贵的临床参考。我们期待通过不断优化护理措施，提升护理质量，为患者带来更好的预后和生活质量。

Predicting new-onset persistent conduction disturbance following transcatheter aortic valve replacement: the usefulness of FEOPS finite element analysis

Shi-Yong Yu, Mao-De Wang

Xinqiao Hospital, Army Medical University

Background: Despite the frequency of persistent new-onset conduction disturbances after transcatheter aortic valve replacement (TAVR), few preoperative methods of prediction exist.

Methods: Patients who underwent TAVR in the Department of Cardiology of the Second Affiliated Hospital of the Army Medical University from December 2020 to September 2021 and postoperative aortic root modeling via the FEOPS finite element analysis were included in this single-center case-control study, divided into persistent conduction disturbances (PCD) and non-PCD groups according to their pre- and postoperative electrocardiograms in the first month. Risk factors affecting PCD were identified by comparing the baseline data of these two groups, including echocardiograms, computed tomography angiography of the aortic root, surgical decision-making, and FEOPS data. Independent risk factors were screened using logistic regression modeling, and the receiver operating characteristic (ROC) curve was used to test the predictive ability.

Results:

1.Comparison of baseline data and preoperative echocardiograms

A total of 56 patients were included in this study, comprising 37 patients with bicuspid aortic valve (BAV) (22 Type 0, 14 Type 1, and 1 Type 2) and 19 patients with trileaflet aortic valve (TAV). Postoperative PCD was observed in 17 (30.4%) patients, of whom 14 (25.0%) exhibited persistent complete left bundle branch block and three demonstrated third-degree atrioventricular block. Among these 17 patients, five received a PPM prior to discharge. A total of 39 (69.6%) patients did not experience postoperative PCD, or exhibited postoperative conduction disturbance but recovered to normal before discharge or during follow-up. No statistically significant differences were identified in the comparison of patients' baseline data ($P>0.05$). The prevalence of diabetes mellitus was found to be statistically different between the two groups of patients with TAV ($P<0.05$), but not among patients with BAV or all patients. A comparison of the preoperative echocardiograms revealed a statistically significant difference in the prevalence of preoperative severe aortic regurgitation among patients with TAV ($P=0.05$). However, no statistically significant difference was observed among the overall patient cohort or patients within the BAV group ($P>0.05$). Furthermore, no statistically significant difference was identified in the remaining indicators ($P>0.05$).

2.Comparison of preoperative CTA data, surgical selection, and FEOPS data

A statistically significant difference was observed in the LVOT area between patients with TAV ($P<0.05$), but no difference was observed in the overall patient cohort or those patients with BAV. The remaining CTA indicators were not found to be statistically different ($P>0.05$). However, the valve oversize ratio and ΔMSID were observed to be statistically different within the overall patient cohort ($P<0.05$), although no differences were identified in the bicuspid and trileaflet valve subgroups. The valve implantation depth was found to be statistically different within the overall patient cohort and the subgroup of patients with BAV ($P<0.05$). However, no statistically significant differences were observed in the TAV group. Furthermore, the CPI was found to be statistically different ($P<0.05$) both within the overall population and in the subgroups of bicuspid and trileaflet valves.

3.Logistic multifactor regression analysis

The univariate analysis revealed statistically significant differences in the

effects of CPI, valve implantation depth, ΔMSID, LVOT area, and diabetes mellitus on PCD. However, given that the differences in LVOT area and diabetes mellitus were only observed in the trileaflet subgroup, the absence of differences in the overall subgroup or the diaphragm subgroup, and the relatively small and inadequately represented sample size of the trileaflet subgroup, these two factors were not included in the multifactorial analysis. A binary logistic regression analysis utilising the input method was conducted, and the analysis yielded no statistically significant differences (P>0.05), with the exception of the CPI (P<0.05).

4.ROC curve analysis

The predictive value of the factors was analyzed using ROC curves. The results demonstrated that the CPI (AUC=0.806, 95% CI: 0.684–0.928, P=0.001), valve implantation depth (AUC=0.677, 95% CI: 0.521–0.833, P=0.46), valve oversize ratio (AUC=0.681, 95% CI: 0.523–0.839, P=0.043), and ΔMSID (AUC=0.669, 95% CI: 0.502–0.835, P=0.058) were also identified as factors with predictive value.

5.FEOPS predictive model accuracy analysis

Previous research has demonstrated that a CPI threshold of ≥14% can predict conduction disturbance following TAVR [10]. However, our results indicated that only 26 patients had accurate predictions. Consequently, we recalculated the prediction bounds. The CPI was calculated by conducting a ROC curve analysis to identify the optimal Jordon index (sensitivity=81.25%, specificity=66.67%) when the CPI was set at 32. This analysis also informed the accuracy grouping, whereby a CPI value of ≥32 was designated as PCD following TAVR, while a CPI value of<32 was excluded. A statistically significant difference was observed in the right ventricular transverse diameter between the two groups (P≤0.05). Additionally, a notable difference was noted in the right atrial transverse diameter and moderate or more AR, although this did not reach statistical significance (P>0.05).

Conclusions: The CPI of FEOPS has better predictive value for new-onset conduction disturbance after TAVR compared to other known predictors.

High High-Density Lipoprotein Cholesterol Is Associated with Elevated Bleeding Risk in Patients With Aortic Stenosis Undergoing Transcatheter Aortic Valve Replacement

Bang-Yuan Yang, Song-Yuan Luo, Yuan Liu, Jian-Fang Luo

Department of Cardiovascular, Guangdong Provincial People's Hospital (Guangdong Academy of Medical Sciences), Southern Medical University

Background:

High-density lipoprotein cholesterol (HDL-C) has long been regarded as a cardioprotective lipid fraction, primarily through its established role in reverse cholesterol transport and its associated anti-inflammatory and antioxidant properties within the vascular system. However, a growing body of contemporary epidemiological and clinical research challenges this uniformly beneficial perspective, revealing a more complex association with cardiovascular outcomes. Notably, recent investigations have identified a U-shaped or J-shaped relationship curve between HDL-C levels and cardiovascular events, suggesting that both very low and potentially very high concentrations may be linked to an increased risk of adverse events, contrary to the linear inverse relationship traditionally assumed. Further complicating the understanding of HDL-C's physiological role, emerging data specifically examining bleeding complications – a critical aspect of patient safety – has begun to surface. For instance, studies focusing on patients undergoing percutaneous coronary intervention (PCI) have reported a nonlinear pattern between HDL-C concentrations and the incidence of bleeding events, indicating that lower HDL-C levels might paradoxically correspond to a reduced hemorrhagic risk in that specific procedural cohort. Within the field of structural heart interventions, transcatheter aortic valve replacement (TAVR) has become the standard therapy for patients with severe, symptomatic aortic stenosis (AS) deemed at high or prohibitive surgical risk. Despite significant procedural advances enhancing safety profiles, bleeding complications remain a frequently encountered and clinically significant adverse event following TAVR, with these bleeding episodes consistently demonstrating a strong association with heightened in-hospital and long-term all-cause mortality rates. Despite the recognized importance of HDL-C in vascular biology and the established prognostic significance of post-TAVR bleeding, a substantial gap exists in current clinical knowledge regarding the potential interplay between circulating HDL-C levels and the subsequent risk of developing significant bleeding complications specifically in the population of severe AS patients undergoing TAVR procedures. This knowledge gap forms the critical context and rationale for our current investigation.

Methods:

To address this clinical question, we conducted a single-center, observational, retrospective cohort study designed to evaluate the association between pre-procedural HDL-C concentrations and bleeding outcomes after TAVR. The study population encompassed 547 consecutive adult patients diagnosed with severe, hemodynamically significant AS who subsequently underwent successful TAVR procedures at our institution between April 2016 and March 2023. Patient identification, data extraction, and detailed characterization were performed by systematic review of comprehensive electronic health records and dedicated procedural databases. The primary exposure variable of interest was the baseline serum level of HDL-C, measured prior to the TAVR intervention. Patients were systematically stratified into two distinct comparison groups based on a pre-specified HDL-C threshold level of 1.12 mmol/L (equivalent to 43.3 mg/dL), forming a low HDL-C group (<1.12 mmol/L) and a high HDL-C group (≥ 1.12 mmol/L). The primary outcome measure for evaluating bleeding risk was the incidence of clinically significant bleeding events, rigorously defined as Bleeding Academic Research Consortium (BARC) type ≥ 2 bleeding, captured from the index procedure through 30 days post-procedural follow-up. Secondary outcome measures included all-cause mortality and non-cardiovascular death occurring during the identical post-procedure follow-up window. To elucidate the independent association between elevated HDL-C status (≥ 1.12 mmol/L) and the primary bleeding outcome, multivariate logistic regression analysis was employed. This statistical model incorporated key covariates, including age, sex, baseline hemoglobin levels, platelet count, chronic kidney disease status, use of concomitant antithrombotic therapy (antiplatelet agents and/or anticoagulants), and key procedural variables, to account for potential confounding influences of established bleeding risk factors.

Results:

Analysis of the cohort stratified by HDL-C levels demonstrated a significant disparity in clinically relevant bleeding events between the comparison groups. Patients categorized into the high HDL-C group (≥ 1.12 mmol/L) exhibited a substantially higher incidence of BARC type ≥ 2 bleeding within 30 days post-TAVR compared to patients in the low HDL-C group (<1.12 mmol/L) (11.6% vs. 6.6%; hazard ratio analysis confirmed this difference achieved statistical significance, p=0.041). Furthermore, the analysis of secondary mortality endpoints revealed a significant difference in the occurrence of non-cardiovascular deaths during the 30-day post-procedural period: non-cardiovascular deaths occurred in 1.5% of patients within the high HDL-C group, whereas no non-cardiovascular deaths (0%) were observed in the low HDL-C group (p=0.050). There was no statistically significant difference observed between the groups regarding the endpoint of all-cause mortality during the study's follow-up timeframe. Crucially, the multivariate logistic regression analysis, after comprehensive adjustment for the collected demographic, clinical, laboratory, and pharmacological confounding variables, robustly confirmed high HDL-C level (≥ 1.12 mmol/L) as an independent predictor significantly associated with an increased risk of experiencing significant post-TAVR bleeding. The adjusted hazard ratio was calculated to be 2.66 (95% confidence interval: 1.159–6.108), yielding a p-value of 0.021, indicating strong statistical independence from other known bleeding risk factors included within the model.

Conclusion:

This retrospective cohort study provides novel evidence that elevated pre-procedural levels of high-density lipoprotein cholesterol (≥ 1.12 mmol/L) are significantly and independently associated with an increased risk of clinically relevant bleeding complications (BARC ≥ 2) during the critical 30-day period following transcatheter aortic valve replacement in patients suffering from severe, symptomatic aortic stenosis. This association remains statistically significant even after meticulous multivariable adjustment encompassing an extensive range of variables known to influence hemorrhagic risk, including baseline anemia, thrombocytopenia, renal dysfunction, and exposure to antiplatelet or anticoagulant medications. The finding of a heightened bleeding risk linked to higher HDL-C levels in the TAVR population directly challenges the long-standing concept of HDL-C functioning exclusively as a protective cardiovascular biomarker. It necessitates a paradigm shift towards recognizing a potential dual nature of HDL-C physiology related to thrombosis and hemostasis. These results strongly warrant further dedicated research, ideally incorporating larger, prospective, multi-center study designs, to substantiate this critical association, explore the underlying pathobiological mechanisms – which may involve platelet reactivity, coagulation cascade interactions, vascular integrity functions, or HDL particle subfraction heterogeneity – and elucidate the potential clinical implications for risk stratification models or personalized management strategies in patients undergoing contemporary transcatheter aortic valve therapies. The study underscores the complexity of HDL biology beyond simple cholesterol transport in the setting of complex interventional cardiovascular procedures.

心肺康复调控心脏瓣膜术后患者心肺耦合机制的系统评价：基于血流动力学参数与自主神经功能的 Meta 回归

马姣 李娟利 石媛媛

交大一附院

背景（Background）

心脏瓣膜术后患者普遍存在心肺功能失调，表现为运动耐量下降与自主神经失衡。

尽管心肺康复（CR）被广泛推荐，其通过调控心肺耦合机制（Cardiopulmonary Coupling, CPC）改善血流动力学效率与自主神经功能的潜在通路尚未系统阐明。

目的（Objective）

通过系统评价与 Meta 回归分析，综合评估 CR 对瓣膜术后患者 CPC 的影响，并探索血流动力学参数（如心输出量、肺动脉压）与自主神经功能指标（如心率变异性、压力反射敏感性）的调控关联。

方法（Methods）

1. 文献检索：检索 7 大数据库（PubMed/Embase/Cochrane 等），时限从建库至 2023 年，纳入比较 CR 与非 CR 的 RCTs/ 队列研究（PROSPERO 注册号：XXXXXX）。2. 结局指标：核心结局为 CPC 相关参数（通气效率斜率 VE/VCO2、氧脉搏）、血流动力学指标、自主神经功能标志物。

3. 数据分析：采用随机效应模型计算标准化均数差（SMD），通过 Meta 回归分析 CR 剂量（频率 / 周期 / 强度）与血流动力学 - 自主神经交互效应的量化关系。

结果（Results）

纳入 12 项研究（n=876），CR 显著降低 VE/VCO2（SMD=-0.82, 95%CI: -1.15 至 -0.49, p<0.001），提升氧脉搏（SMD=0.67, CI: 0.41-0.93）。血流动力学改善与迷走神经活性增强呈显著正相关（Meta 回归 β=0.43, p=0.02），高强度间歇训练（HIIT）对肺动脉压的调控效应优于持续训练（亚组 p=0.03）。

结论（Conclusion）

CR 通过优化心肺耦联效率与自主神经再平衡促进瓣膜术后功能恢复，其中 HIIT 可能通过降低肺血管后负荷增强迷走神经调控。未来研究需标准化 CPC 评估以指导精准康复。

经导管主动脉瓣置换术相关脑卒中的危险因素探究

李云峰 [1] 李飞 [2]

1. 中国人民解放军联勤保障部队第 940 医院

2. 空军军医大学西京医院

目的：

探究中国人群经股动脉经导管主动脉瓣置换术（transcatheter aortic valve replacement, TAVR）术后隐匿性脑卒中（silent cerebral infarction, SCI）的发生率；识别中国人群经股动脉 TAVR 相关脑卒中的潜在危险因素。

方法：

TAVR 相关脑卒中危险因素分析。连续纳入 2023 年 6 月 1 日至 2024 年 12 月 31 日在西京医院心血管内科接受经股动脉入路 TAVR 治疗并完成术前及术后头颅 DW-MRI 检查的患者。通过头颅 DW-MRI 和患者临床症状，明确中国人群 TAVR 术后 SCI 的发生率。基于影像学特征，包括总病灶数（total lesion number, TLN）（中位数）、总病灶体积（total lesion volume, TLV）（中位数）或最大单个病灶体积（individual lesion volume, ILV）（中位数），将脑卒中进一步分为轻度脑损伤和重度脑损伤。采用单因素及多因素 Logistic 回归分析，探讨 TAVR 相关重度脑损伤的危险因素。

结果：

研究共纳入 137 例患者，107 例（78.10%）在术后头颅 DW-MRI 检查中发现了新发脑卒中病灶，其中显性脑卒中患者 5 例（3.65%），SCI 患者 102 例（74.45%）。病灶累及双侧大脑半球的概率为 59.81%，以累及左侧额叶频率最高（40.30%）。影像学分析显示，TLN 中位数为 4 个 ［四分位数间距（interquartile range, IQR）：2.00-7.50 个］、TLV 中位数为 0.24 cm^3（IQR: 0.08-0.52 cm^3）、最大 ILV 中位数为 0.11 cm^3（IQR: 0.05-0.18 cm^3）。根据 TLN ≥ 4 个、TLV > 0.24 cm^3 或 ILV > 0.11 cm^3 的标准，将脑卒中进一步分轻度脑损伤和重度脑损伤。单因素和多因素 Logistic 回归分析结果表明，较长的手术持续时间［比值比（odds ratio, OR）:1.03, 95% 置信区间（confidence interval, CI）：1.01-1.04, P=0.001）］和较低的术中激活凝血时间（activated clotting time, ACT）水平（OR=0.99, 95%CI: 0.98-0.99, P < 0.001）是 TAVR 相关重度脑损伤独立危险因素。糖尿病、房扑 / 房颤、主动脉根部钙化体积、球囊后扩张、基础心功能较差和单纯主动脉瓣返流等因素也与脑卒中病灶的体积或数量密切相关。

结论：

本研究人群发现，经股动脉 TAVR 术后脑卒中的总体发生率达 78.10%，其中 SCI 发生率为 74.45%。较长手术持续时间和较低术中 ACT 水平是发生严重脑损伤的独立危险因素。此外，糖尿病、房扑 / 房颤、主动脉根部钙化体积、球囊后扩张、基础心功能较差和单纯主动脉瓣返流等因素也与脑卒中病灶的体积或数量密切相关。

关键词：经导管主动脉瓣置换术；脑卒中；危险因素

Transcatheter aortic valve replacement for pure native aortic valve regurgitation: a real-world, prospective, multi-center Study (TRUST TAVR REGISTRY)

Ru-Tao Wang[1], Ai-Yuan Cheng[1], Rong-Zhen Zhang[1], Jian Yang[1], Lian-Pin Wu[2], Xin-Lei Wu[2], Jun-Jie Wen[3], Xiao-Ping Peng[4], Ling Tao[1]

1. The First Affiliated Hospital of the Air Force Medical University of the Chinese People's Liberation Army

2. The Second Affiliated Hospital of Wenzhou Medical University

3. Guang'an People's Hospital

4. The Second Affiliated Hospital of Nanchang University

Background

Transcatheter aortic valve replacement (TAVR) has achieved a primary role as a first-choice treatment for elderly patients with aortic stenosis regardless of surgical risk. Beyond aortic stenosis, the role of TAVR has also expanded in patients with aortic regurgitation. The latest European guidelines state that TAVR may be considered in experienced centers for selected patients with pure severe native aortic valve regurgitation (NAVR) who are ineligible for SAVR. Due to the unique anatomical characteristics among patients with NAVR, TAVR for NAVR is challenging and remains an "off-label" indication. The safety and efficacy of TAVR or NAVR in a real-world setting ave not been fully investigated.

Aims

The safety and efficacy of TAVR for native aortic valve regurgitation (NAVR) with "off-label" self-expanding valves in a real-world setting have not been fully investigated. We aimed to explore the procedural safety and clinical outcomes of TAVR with "off-label" self-expanding valves for NAVR.

Methods and results

The TRUST TAVR trial (NCT 06381271) is a multicenter, prospective, observational registry intended to collect data on patients with severe NAVR treated with self-expanding devices from 2018 to 2024. Baseline clinical characteristics, TAVR procedural details, and follow-up data were collected. The study was approved by Ethics Committee of all participating sites and was complied with the Declaration of Helsinki. All patients provided written informed consent.

The primary outcome was a composite consisting of all-cause death, any stroke, and heart failure rehospitalization at 1 year. Secondary outcomes were composed of all-cause death, any stroke, life-threatening or fatal bleeding, major vascular complications, access-related or cardiac structural complication, acute kidney injury stage 3 or 4, surgery or intervention related to the device, moderate or severe paravalvular regurgitation, new permanent pacemaker due to procedure-related conduction abnormalities, conduction block and arrhythmia, surgery or intervention related to the device, heart failure rehospitalization, myocardial infarction, technical success, and device success at 30-day according to the Valve Academic Research Consortium-3 definition.

A total of 221 patients were included. The mean age was 68.5 ± 8.0 years, 132 (59.7%) of the patients were men. The mean Society of Thoracic Surgeons score was 2.8% ± 2.1%. The mean annulus perimeter was 79.5 (75.7-84.5) mm. Device size was ≥ 29 mm in 87.3% of patients. The "off-label" self-expanding valves included VitaFlow/VitaFlow Liberty valves (65.2%, 144/221), Venus A-valve/Venus A-Plus valves (26.2%, 58/221), and Tarnusone/TaurusElite valves (7.2%, 16/221). A second valve implantation was needed in 14.9% of patients. Technical and device success rates were 82.8% and 81.0%, respectively. At 30-day follow-up, all-cause death, any stroke, heart failure rehospitalization, life-threatening or fatal bleeding, major vascular complications, acute kidney injury stage 3 or 4, surgery or intervention related to the device, moderate or severe paravalvular regurgitation, new permanent pacemaker were 4.5%, 2.0%, 3.7%, 6.8%, 3.6%, 2.7%, 3.6%, 1.4%, and 12.8%, respectively. At 1-year follow-up, the primary outcome, a composite of all-cause death, any stroke and heart failure rehospitalization was 17.7% (all-cause death: 6.0%, any stroke: 2.8%. and heart failure rehospitalization: 10.6%).

Conclusions

In this multi-center, real-world Chinese cohort of patients with NAVR, TAVR with "off-label" self-expanding valves showed acceptable safety and efficacy outcomes, suggesting TAVR with self-expanding valves may be an alternative strategy in selected NAVR patients who are at low surgical risk.

经导管主动脉瓣置换术对单纯主动脉瓣反流患者心功能及心室重构的影响

王汝涛 张茸祯 程爱媛 李昀初 陶凌

中国人民解放军空军军医大学第一附属医院（西京医院）

目的：观察经导管主动脉瓣置换术（Transcatheter aortic valve replacement，TAVR）对单纯主动脉瓣反流（Aortic regurgitation，AR）患者心功能及心室重构的影响。

方法：连续入选 2018 年 10 月至 2023 年 7 月在西京医院行 TAVR 治疗的单纯 AR 患者。收集术前、术后 7 天内和 12 个月超声心动图检查结果，观察 TAVR 治疗后单纯 AR 患者心功能变化及心脏结构改变。

结果：本研究共纳入 62 例因 AR 行 TAVR 治疗的患者，其中男 35 例、女 27 例，平均年龄 67.66±7.16 岁。与术前心脏超声结果进行比较，术后 7 天的左室射血分数（Left ventricular ejection fraction，LVEF）与术前相比呈下降趋势（45.81±10.40 vs 48.10±9.86，P=0.066），但未达统计学差异；术后

12 个月时 LVEF 与术前比较显著增加（52.60%±7.93% vs 48.10%±9.86%，P=0.001）；术后 12 个月时左心室收缩末期内径（37.82±8.87 vs 46.35±9.50，P<0.001）、左心室舒张末期内径（51.56±8.30 vs 60.66±8.36，P<0.001）、左心室收缩末期容积（55.46±39.25 vs 91.72±44.06，P<0.001）和左心室舒张末期容积（112.53±50.87 vs 172.64±60.32，P<0.001）与术前相比较显著减少。

结论：TAVR 可改善 AR 患者术后 12 个月的心功能并逆转左心室重构。

分析重度主动脉瓣狭窄对左室各壁心肌收缩功能 损伤的差异及对心肌收缩同步性的影响

杨捷

北京大学第三医院

目的 对左室射血分数（LVEF）≥ 50%的重度主动脉瓣狭窄（AS）患者进行左室长轴心肌应变（LS）及心肌运动同步性收缩分析，评价重度 AS 对左室各壁心肌损伤的差异及对左室各壁心肌收缩同步性的影响。

方法 纳入 2024 年 1 月 ~2024 年 12 月北京大学第三医院 LVEF ≥ 50%的 32 例重度 AS 患者和超声心动图结果正常的 37 例志愿者。2 组患者均完成常规超声心动图检查，同时采用自动功能成像技术（AFI）测定左室心肌长轴应变值及心肌收缩达峰时间离散度（PSD）。并搜集两组心电图结果。

结果 两组年龄、性别、伴随疾病、LVEF 均无统计学差异。重度 AS 组左房大小、室壁厚度、左室心肌重量均明显大于对照组（均 P < 0.01））。重度 AS 组 LS 明显大于对照组：4CH-G (-14.1±5.2 % vs. -19.7±2.7 %，P < 0.01)、2CH-G (-14.8±4.2 % vs. -20.5±2.6 %，P < 0.01)、Apx-G (-15.4±4.9 % vs. -21.3±3.4 %，P < 0.01)、Avg-G (-14.8±4.4 % vs. -20.5±2.4 %，P < 0.01)。分析重度 AS 对主动脉瓣周围心肌收缩力影响的差异，比较重度 AS 组与对照组左室基底段不同室壁间长轴应变的差值：前壁△ LS 4.82%，前间隔△ LS 9.08%，室间隔△ LS5.58%、下壁△ LS3.86%，后壁△ LS8.61%，侧壁△ LS8.77%。分析重度 AS 对左室各壁心肌收缩同步性的影响：重度 AS 患者 PSD 明显高于对照组 [68.0（56.6，79.2）vs.44.0（38.2，50.6），P < 0.01]，心电图 QRS 波群宽度明显大于对照 [94.0 ms（85.5，113.5）vs. 86.5ms（82.0，95.5），P < 0.05]。

结论 LVEF 正常的重度 AS 患者心肌收缩功能已受到明显损伤，主动脉瓣周围心肌前间隔、后壁、侧壁基底段心肌损伤可能更大，同时重度 AS 已影响左室收缩同步性，虽然心电图 QRS 波群时间仍在正常范围，但已明显大于对照组，且 PSD 明显大于对照组，提示重度 AS 患者左室心肌收缩同步性亦受损。

合并肺动脉高压对 TEER 手术术后结局的影响

徐艺轩 顾奥琴 丛广志 贾小霞 陈青 崔莹 贺宝童

宁夏医科大学总医院

目的：评估全国范围内 MTEER 的临床使用趋势，并比较有无 PH 的患者在围手术期的安全性及临床终点上的差异。

方法：本研究使用 NIS 数据库进行，采用 ICD10 代码提取涉及 M-TEER 的成人数据样本。以是否患有肺动脉高压来进行分层。主要结局为全因死亡和夹合器相关并发症。使用多元回归和倾向性评分匹配进行分析。

结果：2012-2022 年共查询到 13271 例 TEER 病例。在纳入的患者中，3536 例患者诊断为 PH。PH-TEER 组的平均年龄为 76.6 ± 10.5（P < 0.01），而非 teer 组的平均年龄为 76.7 ± 11.1（P < 0.01）。两组人群均以白种人（P < 0.01）和男性（P < 0.01）患者为主。研究发现，合并 PH 的患者术后有更高的死亡率，较无 PH 的患者可升高 172%（P < 0.01）。其次合并 PH 的患者更易发生夹合器相关并发症，其发生率可达 4.96%，较无 PH 的患者提升 156%（P < 0.01）。同时，合并 PH 的患者术后有更高的急性出血风险和输血需求（P < 0.01）。然而，对于两组人群来说，术后出现心源性休克、心包填塞、心内膜炎及急性缺血性中风无明显的统计学差异（P > 0.01）。经过分层分析，合并脂代谢异常或肾功能损害的 PH 患者更容易发生死亡结局（P < 0.01）。合并慢性阻塞性肺疾病（COPD）或肝损害或既往发生过心肌梗死的患者更易出现夹合器相关并发症（P < 0.01）。

结论：在 2012-2022 的十年中，M-TEER 在 PH 患者中的使用在美国的临床实践中显著增加。虽然 PH 不会增加不良心脏事件（如心源性休克、心包填塞等）的发生率，但它是院内死亡率和夹合器相关并发症的独立危险因素。

慢性血小板减少症患者经导管与外科主动脉瓣置换术的结果和时间趋势的比较：来自全国住院患者样本的见解

顾奥琴 徐艺轩 丛广志 陈青 崔莹 贺宝童 贾晓霞

宁夏医科大学总医院

背景：慢性血小板减少症（CTP）增加了主动脉瓣狭窄 （AS） 患者接受主动脉瓣置换术（AVR）术后出血的风险。CTP 在经导管主动脉瓣置换术（TAVR）或外科主动脉瓣置换术（SAVR）选择最佳干预措施方面构成了临床挑战。TAVR 是一种微创手术，在高危人群中显示出卓越的安全性，但目前仍然缺乏将其结果和时间趋势与 SAVR 进行比较的数据，特别是在 CTP 的患者中。鉴于该队列的出血风险升高，确定更安全的干预措施对于优化患者预后至关重要。

方法： 我们使用 2016 年至 2022 年的美国国家住院样本（NIS）数据库进行了回顾性队列分析。使用 ICD-10 代码确定接受孤立 AVR 的 AS 合并 CTP 患者，并将其分为 TAVR 和 SAVR 队列。主要结局是术后出血，次要结局是院内死亡、输血、心源性休克、心脏骤停、心包压塞、瓣周漏和脑血管梗死。鉴于基线特征的差异，我们采用倾向评分匹配 （PSM），调整了 22 个变量，包括年龄、性别和合并症。使用多变量 logistic 回归模型调整人口统计学、医院特征和手术并发症，以比较两个队列之间院内结局的差异。

结果： 在 112,725 例 AS 住院患者中，16.19%（n=18,254）合并了 CTP，排除了基线数据缺失的患者，其中 5,545 例接受 TAVR，10,912 例接受 SAVR。PSM 后，分析了 4,468 个匹配队列，TAVR 组术后出血率显著低于 SAVR 组，并且 TAVR 组术后出血风险更低（2.2% vs. 3.8%；aOR：0.54，95% CI：0.41-0.71，P < 0.001）。TAVR 与较低的院内死亡风险（aOR：0.57，P < 0.001）、输血（aOR：0.29，P < 0.001）、心源性休克（aOR：0.13，P < 0.001）和心脏骤停（aOR：0.42，P = 0.014）相关。两组心包压塞、瓣周漏或脑血管梗死差异无统计学意义。与 SAVR 组相比，TAVR 组中位住院时间更短（9.7 vs.5.3 days；P < 0.001），住院费用更低（$261,328.8 vs.$253210.8；P = 0.026）。2016-2022 年合并 CTP 的患者行 TAVR 手术比例从 37.84% 上升到 60.94%（P-trend < 0.001），接受 TAVR 治疗的患者术后出血率呈下降趋势（4.12% - 2.66%，P-trend = 0.016）。

结论： 这项全国性的观察性分析表明，TAVR 与 AS 合并 CTP 患者术后出血和多种不良住院结局的风险降低独立相关。其整体安全性支持将其视为这一高出血风险人群的首选干预措施。这些发现强调了个体化决策的重要性，尤其是在合并血小板减少症的 AS 患者，尽量减少术后不良结局至关重要。需要进一步的前瞻性研究来验证这些观察结果并完善患者选择标准。

关键词：主动脉瓣狭窄；慢性血小板减少症；经导管主动脉瓣置换术；外科主动脉瓣置换术

基于免持超声多普勒技术经颈无创连续评估主动脉瓣功能的研究

魏思萌 陈韵岱 王晶

中国人民解放军总医院第六医学中心

目的

本研究旨在基于免持超声多普勒技术探索颈动脉血流参数与主动脉瓣功能的关联性，评估其在无创连续评估主动脉瓣膜病变及经导管主动脉瓣置换术（TAVR）围术期动态演变中的临床应用价值。

方法

采用前瞻性单中心观察性研究设计，纳入 133 例受试者（主动脉瓣疾病组 30 例，非瓣膜病组 103 例）。使用 CADFlow® 免持超声贴片监测双侧颈动脉血流参数（ccFT、dv.MAX、Vmax 等），结合心脏超声评估主动脉瓣功能指标（跨瓣压差、瓣口面积）。研究分为两部分：第一部分对比瓣膜病组与对照组的颈动脉血流特征；第二部分对 30 例中 - 重度主动脉瓣疾病患者行 TAVR 围术期纵向监测，分析术前至术后 72 小时颈动脉血流动态变化与瓣膜功能的相关性，并通过多元线性回归模型验证颈动脉参数对主动脉瓣功能变化的预测能力。

结果

1. 瓣膜病组颈动脉血流参数特征显著异常：双侧 ccFT 延长（368.74±31.9 ms vs. 327.44±30.45 ms，P<0.001）、dv.MAX 降低（9.64±2.85 m/s^2 vs. 12.16±2.87 m/s^2，P=0.001），多普勒频谱呈现“延迟钝化”（狭窄）与“双峰分离”（反流）特征。

2. 颈动脉参数与主动脉瓣功能显著相关：Vmax、dv.MAX 与跨瓣压差负相关（r=-0.765，P<0.001），ccFT 与跨瓣压差正相关（r=0.520，P<0.001）。

3. TAVR 术后颈动脉参数即时改善：术后 2 小时 dv.MAX 提升 23.5%，ccFT 缩短 10.2%，与瓣膜功能改善显著相关（P<0.001）。

4. 多元回归模型显示，cVTI 和 Vmax 是预测主动脉瓣峰值流速（AV-Vmax）和平均跨瓣压差（PGmean）的核心指标，模型调整 R^2 分别为 0.650 和 0.671。

结论

免持超声技术通过连续监测颈动脉血流动力学特征，可敏感反映主动脉瓣功能异常及 TAVR 术后动态变化。颈动脉参数 ccFT、dv.MAX 及频谱形态特征为无创评估主动脉瓣病变及术后疗效监测提供了新思路，具有临床转化潜力，尤其适用于基层医疗场景与围术期连续监测需求。

Study on cardiac function and ventricular wall motion after transcatheter aortic valve replacement (TAVR)

LiTing He

The First Affiliated Hospital of Kunming Medical University

Aortic stenosis (AS) constitutes the predominant acquired left-sided valvulopathy encountered in the geriatric demographic, predominantly emanating from progressive, age-mediated calcific degenerative remodeling of the aortic leaflets and, secondarily, from congenital bicuspid aortic valve malformations that predispose to premature fibro-calcific alterations. In the setting of severe AS, the abrupt and sustained augmentation in left-ventricular (LV) afterload initiates a cascade of compensatory concentric hypertrophy driven by sarcomeric hypertrophic signaling pathways; however, prolonged pressure overload precipitates maladaptive myocardial remodeling characterized by interstitial fibrosis, capillary rarefaction, and impaired calcium-handling proteins, ultimately culminating in symptomatic heart failure with preserved or reduced ejection fraction. At present, surgical aortic valve replacement (SAVR) and transcatheter aortic valve replacement (TAVR) remain the only evidence-based, guideline-endorsed definitive therapies for symptomatic moderate-to-severe AS, with selection contingent upon anatomical, frailty, and risk-stratification indices. Given the substantial economic expenditure, resource intensity, and intricate multidisciplinary orchestration inherent to TAVR programs, its post-procedural survival trajectory

and durability metrics have attracted intensive scientific scrutiny. Patients referred for TAVR frequently manifest advanced New York Heart Association (NYHA) functional class III–IV symptomatology, accompanied by overt congestion-related clinical signs, profound exercise intolerance, and markedly diminished health-related quality-of-life indices as quantified by validated instruments such as the Kansas City Cardiomyopathy Questionnaire (KCCQ). Following successful transcatheter valve implantation, immediate mechanical relief of valvular obstruction normalizes transvalvular pressure gradients and expands effective orifice area, thereby initiating reverse LV remodeling characterized by regression of LV mass index, reduction in end-diastolic and end-systolic volumes, and improvement in global longitudinal strain and diastolic strain rate. Nevertheless, a substantial proportion of recipients exhibit significant preoperative comorbid cardiovascular burden—including coronary artery disease, atrial fibrillation, renal insufficiency, and pulmonary hypertension—along with varying degrees of baseline myocardial dysfunction, thereby engendering heterogeneous post-interventional phenotypes and discordant trajectories of functional recovery. Accordingly, rigorous serial multimodality assessment of post-TAVR cardiac performance and segmental ventricular wall-motion dynamics—integrating transthoracic echocardiography, cardiac magnetic resonance imaging, and biomarker profiling—is indispensable for accurate prognostication and for tailoring individualized postoperative surveillance paradigms. Objective: To systematically delineate pre-, intra-, and post-procedural determinants governing cardiac functional recuperation and segmental wall-motion normalization following TAVR; to refine evidence-based, precision-driven patient-selection algorithms that optimize procedural candidacy and risk-benefit stratification; and to devise targeted, multidisciplinary discharge interventions—including guideline-directed pharmacotherapy, structured cardiac rehabilitation, and remote hemodynamic monitoring—that mitigate outcome-limiting factors, thereby enhancing long-term survival, improving patient-reported health status, and reducing 30-day and mid-term heart-failure-related readmission rates.

Method: A comprehensive longitudinal data acquisition protocol was implemented, prospectively collating serial transthoracic echocardiographic parameters and biochemical profiles—including, but not limited to, B-type natriuretic peptide (BNP), comprehensive metabolic panel (hepatic and renal indices), total protein, and full lipidogram—from consecutive TAVR recipients at three predefined time-points: pre-procedure, immediate pre-discharge, and 1- to 6-month post-intervention. Anthropometric variables (body-mass index, BMI) and additional clinical covariates were integrated into an initial univariate analytical framework to screen for potential predictors of cardiac functional recovery.

Results:

1. Following TAVR, there were statistically significant improvements in peak aortic jet velocity, aortic root dimension, ascending aorta diameter, interventricular septal excursion amplitude, left-ventricular ejection fraction (LVEF), fractional shortening (LVFS), stroke volume (SV), BNP, and left-atrial anteroposterior diameter. Notably, the magnitude of improvement was more pronounced during the immediate postoperative phase than at mid-term follow-up.

2. Indices of systolic performance (LVEF and LVFS) exhibited significant enhancement after valve implantation, whereas SV failed to achieve a comparable statistically significant increment.

3. Serial echocardiographic surveillance disclosed segmental wall-motion abnormalities in a subset of patients during the follow-up interval.

Conclusion:

1. Relative to baseline, TAVR elicits rapid and efficacious amelioration of cardiac chamber geometry, global contractile function, and ventricular wall kinetics.

2. From discharge to mid-term assessment, these echocardiographic and biochemical indices continue to improve, albeit at a decelerated rate.

Key words: TAVR; cardiac function; ventricular wall motion

Potential Inhibition of Aortic Valve Calcification by Eicosapentaenoic Acid: Implications for Non-Invasive Treatment of Aortic Stenosis

Xin-Yue Yang, Li-Xin Fang, Yuan-Wei Chen, Jian-Fang Luo, Jiao-Hua Chen

Guangdong Provincial People's Hospital

Introduction

Aortic stenosis (AS) is a progressive, degenerative condition, and is characterized by pathological calcification of the aortic valve. Given the lack of pharmacologic treatments for AS, novel therapies that target the calcification process could offer significant clinical benefits.

Eicosapentaenoic acid (EPA), an omega-3 fatty acid, has demonstrated a cardiovascular risk reduction in ASCVD patients, beyond simple lipid lowering, as evidenced by the REDUCE-IT trial. Given the lipid-driven nature of both ASCVD and AS, we hypothesized that EPA could exert similar benefits in AS by attenuating valve calcification.

Methods

Primary Human valvular interstitial cells (VICs) were purchased from Fenghui Company (Fenghbio, China) and cultured at 37 ° C in 5% CO2 with 90% humidity. human VICs were exposed to a calcifying medium with and without EPA intervention. Calcium deposition was assessed with Alizarin Red staining, and the expression of osteogenic markers (ALPL, RUNX2) and extracellular matrix-related gene COL1A1 was analyzed via qPCR.

Results

EPA Reduces Calcification in VICs

VICs cultured in osteogenic media (OM) exhibited substantial calcium deposition, as visualized by Alizarin Red staining. In contrast, EPA treatment markedly reduced calcification in VICs compared to the OM group ($p < 0.001$) (Figure 1).

Effect of EPA on Osteogenic Marker Expression

Quantitative real-time PCR analysis revealed ALPL and RUNX2 mRNA levels were significantly elevated in VICs treated with OM relative to cells in CM (ALPL $p < 0.05$, RUNX2 $p < 0.01$). EPA intervention, however, significantly suppressed the expression of ALPL and RUNX2, indicating reduced osteogenic differentiation ($p < 0.05$) (Figure 2, A-B).

COL1A1 Expression and Extracellular Matrix Modulation

The extracellular matrix component COL1A1, implicated in vascular mineralization, also showed increased expression in VICs under calcifying conditions ($p < 0.01$). EPA treatment notably inhibited the OM-induced elevation of COL1A1 mRNA expression, suggesting a protective effect on the extracellular matrix against calcification-related alterations ($p < 0.05$) (Figure 2C).

Discussion

Our study provides initial evidence that EPA may represent a novel, non-surgical treatment avenue for AS. By inhibiting osteogenic differentiation and reducing extracellular matrix mineralization in VICs, EPA could potentially slow AS progression.

The observed downregulation of osteogenic markers (ALPL and RUNX2) and COL1A1, an extracellular matrix component associated with vascular calcification, further supports EPA's potential role in modulating the calcification process. These findings align with recent evidence suggesting that EPA's cardiovascular benefits in ASCVD patients may be independent of LDL-cholesterol levels, underscoring its multifaceted mechanisms of action.

Our results provide a strong foundation for future studies investigating EPA's impact on AS progression. This line of inquiry could ultimately lead to a paradigm shift in AS management, introducing a pharmacologic option to complement current invasive approaches.

Conclusion

Our findings demonstrate that EPA may inhibit VIC calcification and osteogenic differentiation, positioning it as a potential therapeutic agent for AS. While further in vivo studies are essential to confirm these effects, our study opens the door to new pharmacologic strategies for managing AS.

Figure 1. EPA Reduces Calcification in VICs.

A, Representative Alizarin red staining of primary human VICs cultured in different medium with or without EPA incubation (50 μM) for 21 days. Scale bars, 500 um. B, Quantification of Alizarin red staining results. *$p < 0.05$, **$p < 0.01$, ***$p < 0.001$, by one-way ANOVA. Data are presented as mean ± SD.

Figure 2, Effect of EPA on osteogenic marker expression and extracellular matrix modulation.

A-B, RT-qPCR analysis of osteogenic marker ALPL and RUNX2 in VICs after osteogenic and EPA incubation. C, RT-qPCR analysis of COL1A1 in VICs after osteogenic and EPA incubation. *$p < 0.05$, **$p < 0.01$, by one-way ANOVA. Data are presented as mean ± SD.

经导管经间隔途径二尖瓣置入术治疗二尖瓣生物瓣衰败的疗效观察

谭洪文

贵州省人民医院

背景：症状性重度二尖瓣反流预后差，传统的治疗方法为经胸瓣膜置换术，但部分患者高龄或伴有多种合并症，外科手术死亡率及并发症发生率高。再次开胸瓣膜置换术较首次手术死亡率增加。二尖瓣瓣中瓣手术是二尖瓣生物瓣毁损后高手术风险患者的替代治疗方法。

目的：本研究旨在评估经导管经间隔途径二尖瓣瓣中瓣置入术（TMViV）治疗二尖瓣生物瓣衰败的高危手术患者的有效性和安全性。

方法：回顾性纳入了 2023 年 7 月至 2025 年 3 月期间在本院接受 TMViV 手术的高手术风险患者。采用 Edwards SAPIEN-3 瓣膜经间隔入路行 TMVR 手术。

结果：5 例患者，中位年龄 74 岁，中位 STS 评分 8.5，术前 5 例患者纽约心功能分级均为Ⅳ级。5 例（100%）患者技术成功；1 例患者合并冠心病，术前先行冠脉支架植入术治疗；1 例患者术前评估新左室流出道面积 104mm^2，术中行二尖瓣前叶电切割术处理，随访 3 月至 2 年，5 例患者心功能均为Ⅰ～Ⅱ级。在整个随访过程中，5 例患者均存在小于 5mm 的房间隔缺损，左向右分流，无二尖瓣反流、二尖瓣明显狭窄、瓣周漏、瓣膜移位，没有患者出现死亡。

结论：TMVR 是治疗二尖瓣生物瓣衰败一种安全有效的手术方法。但需要大样本研究及更长时间的随访。

Temporal and Spatial Evolution Dynamics and Sociodemographic Gradient Effects of Disease Burden (Prevalence, DALYs, and Mortality) of Valvular Heart Diseases (RHD/CAVD/DMVD) Under a Cross-National Spatial Spectrum from 1990 to 2021: An Epidemiological Mod

Yuanxin Liu, Xinmeng Xie

Fujian Medical University Union Hospital

Objective:

This study aims to systematically analyze the disease burden of valvular heart disease (VHD) at the global, regional, and national levels from 1990 to 2021. Specifically, it focuses on examining the epidemiological trends and changes in disability-adjusted life years (DALYs) of three major types of VHD: rheumatic heart disease (RHD), non-rheumatic calcific aortic valve disease (CAVD), and non-rheumatic degenerative mitral valve disease (DMVD). Additionally, the research intends to explore the regional disparities, associations with sociodemographic characteristics, and temporal dynamics of these diseases. The ultimate goal is to provide a scientific basis for formulating targeted prevention and control strategies to alleviate the global burden of VHD.

Methods:

The study is based on data from the 2021 Global Burden of Disease (GBD) database, from which relevant information on VHD was extracted, covering the period from 1990 to 2021 and encompassing 204 countries and regions worldwide. Key indicators analyzed include prevalence, DALYs, and other related metrics. To assess the temporal trends of the diseases, the estimated annual percentage change (EAPC) was employed. Stratified analyses were conducted according to the sociodemographic index (SDI), geographical region, gender, and age group to evaluate the distribution characteristics of different types of VHD and their associated factors. This multi-dimensional analytical approach ensures a comprehensive understanding of the epidemiological patterns of VHD across various populations and regions.

Results:

In 2021, the global number of cases of RHD, CAVD, and DMVD was 54.8 million, 13.3 million, and 15.5 million, respectively. Age-standardized prevalence rates revealed distinct patterns across different SDI levels: RHD was most prevalent in low-SDI regions, with a rate of 1184.2 per 100,000 population, while CAVD had the highest prevalence in high-SDI regions, reaching 349.8 per 100,000 population. Among the population aged 70 years and above, the age-standardized prevalence rates of CAVD and DMVD were particularly high, at 1803.6 per 100,000 and 2148.9 per 100,000, respectively, highlighting the significant burden of these degenerative diseases in elderly populations.

Regional disparities were striking: sub-Saharan Africa bore the heaviest burden of RHD, whereas high-income regions faced a more prominent burden of CAVD and DMVD. Over the period from 1990 to 2021, the age-standardized prevalence rates of CAVD and DMVD showed the most significant increases in middle-SDI and low-middle-SDI regions, with respective growth rates of 60.6% and 44.4%. Gender differences were also evident: the prevalence of RHD was higher in women, at 754.8 per 100,000 population, while men had higher prevalence rates of CAVD and DMVD, at 193.2 per 100,000 and 257.9 per 100,000 population, respectively. Notably, despite the overall increase in the prevalence of all three types of VHD, the age-standardized DALYs for each showed a downward trend, indicating improvements in the impact of these diseases on healthy life expectancy.

Conclusion:

The global burden of valvular heart disease exhibits significant sociodemographic and regional disparities. In low-SDI regions, RHD remains a major public health challenge, reflecting the continued impact of socioeconomic factors and limited access to healthcare resources. In contrast, high-SDI regions, due to population aging, are facing an increasingly prominent burden of CAVD and DMVD, which are closely associated with age-related degenerative processes.

To effectively reduce the global burden of VHD, it is crucial to formulate targeted prevention and control strategies based on the specific disease types and risk characteristics of different regions. For low-SDI regions, efforts should be focused on strengthening the prevention and treatment of RHD, including improving access to healthcare, promoting primary prevention measures, and enhancing early diagnosis and intervention. For high-SDI regions, greater attention should be paid to the management of degenerative valvular diseases in the elderly population, such as implementing regular screening programs, optimizing treatment protocols, and addressing comorbidities associated with aging.

By acknowledging and addressing these disparities, public health authorities and healthcare systems can develop more effective interventions, ultimately mitigating the impact of valvular heart diseases on global health and well-being. This study underscores the importance of a tailored, region-specific approach to tackling VHD, considering the diverse epidemiological landscapes shaped by sociodemographic factors and aging populations.

Valve-in-Valve Transcatheter Aortic Valve Replacement Versus Redo Surgical Aortic Valve Replacement for Structural Valve Degeneration: An d Meta-Analysis

Lu Yan, Wei Wang

Department of Geriatrics, Southwest Hospital, Third Military Medical University (Army Medical University), Chongqing, China. Cardiovascular Center, Southwest Hospital, Third Military Medical University (Army Medical University), Chongqing, China.

Abstract

OBJECTIVE Valve-in-valve TAVR (ViV-TAVR) and redo surgical aortic valve replacement (Redo-SAVR) are the main treatment modalities for structural valve degeneration (SVD) after the first surgical aortic valve replacement (SAVR) procedure. There is still controversy surrounding the short- and long-term complications and risk-benefit situation. In order to perform a more up-to-date and comprehensive comparison of the short and midterm outcomes of ViV-TAVR versus Redo-SAVR for SVD, we conducted this systematic review and meta-analysis.

DATA SOURCES PUBMED/MEDLINE, Embase, the Cochrane Controlled Trials Register, and ClinicalTrials.gov were searched as of July 20th, 2024, for studies comparing clinical outcomes of ViV-TAVR and Redo-SAVR.

STUDY SELECTION Studies comparing ViV-TAVR and Redo-SAVR were identified through a systematic retrieval of published articles. We followed the protocols recommended by the Meta-analysis Of Observational Studies in Epidemiology (MOOSE) group, using a strategy of population, intervention, comparison, outcome, and study design.

DATA EXTRACTION AND SYNTHESIS Data were extracted in accordance with Preferred Reporting Items for Systematic Reviews and Meta-Analyses guidelines. Two authors extracted and assessed the risk of bias independently. When disagreements arose, the third author examined the data and made the final decision. Data were compared in two groups: ViV-TAVR and Redo-SAVR. Pooled prevalence was calculated using a random-effects or fixed-effects meta-analysis model.

MAIN OUTCOMES AND MEASURES 30-day mortality, 1-year mortality, stroke, major bleeding (MB), permanent pacemaker implantation (PPI), severe patient-prosthesis mismatch (SPPM), moderate to severe paravalvular leakage (PVL), myocardial infarction (MI), acute kidney injury requiring dialysis, major vascular complications, length of stay (LOS), readmission.

RESULTS A total of 20 studies published between 2015 and 2024 were included in our study, including 17,891 patients (ViV-TAVR, n = 8,857; Redo-SAVR, n = 9,034). In the pooled analysis, ViV-TAVR was associated with lower overall 30-day mortality (OR: 0.52; 95% CI: 0.37 to 0.73; p < 0.001) and lower stroke rates (OR: 0.62; 95% CI. 0.44 to 0.88; p = 0.007), rate of major bleeding (OR 0.45; 95% CI: 0.33 to 0.60; p < 0.001), permanent pacemaker implantation (OR: 0.65; 95% CI: 0.44 to 0.96; p = 0.032), and a shorter hospital stay (OR: -0.67; 95% CI: -0.92 to -0.43; p < 0.001). One-year mortality (OR: 0.83; 95% CI: 0.62 to 1.12; p = 0.22), severe patient-prosthesis mismatch (OR: 1.64; 95% CI: 0.31 to 8.83; p = 0.562), myocardial infarction (OR: 1.05; 95% CI: 0.58 to 1.90; p = 0.864), acute kidney injury requiring dialysis (OR: 0.66; 95% CI: 0.37 to 1.18; p = 0.161), and major vascular complications (OR: 1.09; 95% CI: 0.7 to 1.69; p = 0.70) did not differ between the ViV-TAVR and Redo-SAVR groups, although ViV-TAVR was associated with a higher moderate to severe paravalvular leakage (OR: 7.1; 95% CI: 2.14 to 23.57; p = 0.001) and a higher readmission (OR: 1.16; 95% CI: 1.03 to 1.30; p = 0.014).

CONCLUSIONS AND RELEVANCE ViV-TAVR is a valuable option in the treatment of patients with SVD as of its lower incidence of postoperative complications and better early survival compared with Redo-SAVR.

Keywords: structural valve degeneration (SVD), transcatheter aortic valve replacement (TAVR), surgical aortic valve replacement (SAVR), valve-in-valve (ViV)

胸痛与急性心梗有关研究

Kinetics and Prognosis Value of Heparin Binding Protein at the Acute ST-Segment-Elevation Myocardial Infarction

Yue-ying Wang, Tian-Qi Zhu, Wen-Li Zhang, Hong-Yang Xie, Xue-Zheng Qu, E-REMU BUAYIXIMU K, Zheng-Bin Zhu, Jing-Wei Ni, Run Du, Jin-Zhou Zhu, Xiao-Qun Wang, Feng-Hua Ding, Xiao-Xiang Yan, Ping Li, Zhi-Hong Xu, Rui-Yan Zhang, Wei-wei Quan

Department of Cardiovascular Medicine, Ruijin Hospital, Shanghai Jiao Tong University School of Medicine, Shanghai 200025, PR China.

Background: heparin-binding protein (HBP) is released from reperfused coronary circulation, alongside coronary neutrophil adhesion and myocardial injury, suggesting its potential role in ischemia-reperfusion processes. However, the association between HBP and clinical outcomes in patients with ST-segment elevation myocardial infarction (STEMI) has not yet to be well investigated. This study aimed to investigate the role of HBP, a neutrophil-derived inflammatory marker, as a prognostic biomarker in patients with STEMI undergoing primary percutaneous coronary intervention (pPCI).

Methods: The study population was derived from the Ruijin Acute ST-Segment Elevation Myocardial Infarction (RJH-STEMI, NCT05450757) cohort, a prospective registry conducted at Ruijin Hospital, Shanghai Jiao Tong University School of Medicine. From July 2022 to June 2023, we prospectively enrolled 251 consecutive STEMI patients who underwent pPCI. HBP were tested at 4 time points sequent: at admission (HBP_{0h}) during the coronary angiography (CAG) and then at 24 hours (HBP_{24h}), 48 hours (HBP_{48h}), and 72 hours (HBP_{72h}) after admission. The primary endpoint was major adverse cardiac events (MACE), defined as a composite of all-cause mortality, hospitalization for heart failure (HF), relapse MI, or stroke. Over a median follow-up period of 1.5 (interquartile range, 0.9–1.9) years, MACEs were recorded.

Results: In contrast to hs-CRP, HBP levels peaked early in STEMI and progressively declined between 24-72 hours post-pPCI. Global plasma HBP increased from 43.43 (28.60, 71.96) ng/mL at admission and decreased gradually to 21.24 (11.10, 45.21) ng/mL at 24 hours, 21.86 (13.49, 45.84) ng/mL at 48 hours, and 19.54 (12.34, 32.28) ng/mL at 72 hours after pPCI. This kinetic pattern paralleled myocardial injury markers like CK, CK-MB and hs-cTnI. Later HBP measurements (HBP_{48h}: β = -0.257, P = 0.015; HBP_{72h}: β = -0.364, P $_{0h}$ and HBP_{24h} levels showed no predictive value (all P > 0.05). These findings were corroborated by multivariate analysis, where HBP_{72h} (β = -0.291, P = 0.005) remained independently associated with reduced LVEF after adjustment for clinical confounders.

Forty-six patients (21.4%) experienced MACE during a mean follow-up of 1.5 years (IQR 0.9-1.9). Patients with MACE had higher plasma levels of HBP_{48h} and HBP_{72h} compared with those without MACE (P P = 0.017). The highest HBP_{72h} quartile remained independently associated with a 5 times increased risk of MACE during the follow-up (HR 5.156, 95%CI 1.380 – 19.271, P = 0.0148) compared to the lowest group, after adjusted for established clinical variables. Landmark analysis at 180 days revealed significant survival divergence during the initial 180-day period (P = 0.017), while no statistically significant difference was observed beyond this timepoint (post-landmark P = 0.495). However, no significant associations between MACE and HBP_{0h}, HBP_{24h}, HBP_{48h} quartiles.

Receiver-operating characteristic curve analysis demonstrated that an HBP_{72h} cut-off level of 29.12 ng/mL predicted MACE had 61.9% sensitivity and 78.0% specificity with AUC 0.730. Moreover, adding HBP_{72h} to hs-cTnI improved MACE prediction better than hs-cTnI (NRI 0.578, P <0.001), NT-proBNP (NRI 0.483, P = 0.003), hs-CRP (NRI 0.448, P = 0.006) alone.

Conclusions: Our study establishes HBP as a clinically useful biomarker that complements existing tools for risk stratification in STEMI patients. The 72-hour window appears optimal for measurement, with potential to guide personalized therapeutic decisions. These findings underscore the importance of neutrophil-mediated inflammation in STEMI outcomes and pave the way for investigating targeted anti-inflammatory strategies in high-risk patients identified by HBP elevation. This is the first study by our knowledge to systematically characterize HBP temporal dynamics and establish its independent prognostic value in STEMI patients undergoing pPCI.

Impact of the first-wave COVID-19 pandemic on emergency acute coronary syndrome: a multicenter retrospective study from a non-epicenter region

Mao Qi

Xinqiao Hospital

Impact of the first-wave COVID-19 pandemic on emergency acute coronary syndrome: a multicenter retrospective study from a non-epicenter region

Qi Mao[1]

1. Department of Cardiology, Institute of Cardiovascular Research, Xinqiao Hospital, Army Medical University, Chongqing 400037, China

Abstract

Background: The COVID-19 pandemic presented severe challenges to emergency practice of acute coronary syndrome (ACS). However, poor evidence was shown on ACS in a non-hot-spot region.

Purpose: We sought to clarify the influence of the first-wave COVID-19 pandemic on emergency ACS from a non-epicenter region.

Methods: This retrospective multicenter study was conducted in emergency ACS patients during the pandemic (from 2020-01-23 to 2020-03-29) and the ones during the same period in 2019. Clinical characteristics, timeline parameters and treatment strategies were compared between different groups. Association of the pandemic with non-invasive therapy was further assessed.

Results: Compared with 2019, ACS had a drop in admission (267 cases vs. 475 cases) and invasive therapy (140 cases vs. 318 cases). Also, process delays were detected including the period from symptom onset to first medical contact (S-to-FMC, 5h vs. 2.5h), the period from FMC to electrocardiogram (ECG) completed (8min vs. 4min) and the period from FMC to dual antiplatelet therapy (FMC-to-DAPT, 25min vs. 19min). Primary percutaneous coronary intervention (PPCI) decreased by 54.9% in STEMI and early invasive therapy decreased by 59.2% in NSTE-ACS. The proportion of invasive therapy in NSTE-ACS decreased more than in STEMI (16.9% vs. 10.1%) with longer process delay. The pandemic was associated with increased non-PPCI in STEMI (OR=1.707, 95%CI 1.082-2.692, P=0.021) and elevated medication in NSTE-ACS (OR=2.029, 95%CI 1.268-3.247, P=0.003), respectively.

Conclusion: Even in a non-epicenter region, the first-wave COVID-19 pandemic caused a significant reduction of invasive therapy and evident process delays in emergency ACS.

Keywords: COVID-19, Acute coronary syndrome, Invasive therapy, Emergency care, Non-epicenter region

Impact of the first-wave COVID-19 pandemic on emergency acute coronary syndrome: a multicenter retrospective study from a non-epicenter region

Qi Mao[1]

1. Department of Cardiology, Institute of Cardiovascular Research, Xinqiao Hospital, Army Medical University, Chongqing 400037, China

Abstract

Background: The COVID-19 pandemic presented severe challenges to emergency practice of acute coronary syndrome (ACS). However, poor evidence was shown on ACS in a non-hot-spot region.

Purpose: We sought to clarify the influence of the first-wave COVID-19 pandemic on emergency ACS from a non-epicenter region.

Methods: This retrospective multicenter study was conducted in emergency ACS patients during the pandemic (from 2020-01-23 to 2020-03-29) and the ones during the same period in 2019. Clinical characteristics, timeline parameters and treatment strategies were compared between different groups. Association of the pandemic with non-invasive therapy was further assessed.

Results: Compared with 2019, ACS had a drop in admission (267 cases vs. 475 cases) and invasive therapy (140 cases vs. 318 cases). Also, process delays were detected including the period from symptom onset to first medical contact (S-to-FMC, 5h vs. 2.5h), the period from FMC to electrocardiogram (ECG) completed (8min vs. 4min) and the period from FMC to dual antiplatelet therapy (FMC-to-DAPT, 25min vs. 19min). Primary percutaneous coronary intervention (PPCI) decreased by 54.9% in STEMI and early invasive therapy decreased by 59.2% in NSTE-ACS. The proportion of invasive therapy in NSTE-ACS decreased more than in STEMI (16.9% vs. 10.1%) with longer process delay. The pandemic was associated with increased non-PPCI in STEMI (OR=1.707, 95%CI 1.082-2.692, P=0.021) and elevated medication in NSTE-ACS (OR=2.029, 95%CI 1.268-3.247, P=0.003), respectively.

Conclusion: Even in a non-epicenter region, the first-wave COVID-19 pandemic caused a significant reduction of invasive therapy and evident process delays in emergency ACS.

Keywords: COVID-19, Acute coronary syndrome, Invasive therapy, Emergency care, Non-epicenter region

Influence of COVID-19 pandemic on mechanical reperfusion in ST-segment-elevation myocardial infarction undergoing primary percutaneous coronary intervention: a multicenter retrospective study from a non-epicenter region

Mao Qi

Xinqiao Hospital

Influence of COVID-19 pandemic on mechanical reperfusion in ST-segment-elevation myocardial infarction undergoing primary percutaneous coronary intervention: a multicenter retrospective study from a non-epicenter region

Qi Mao

Department of Cardiology, Institute of Cardiovascular Research, Xinqiao Hospital, Army Medical University, Chongqing 400037, China

Abstract

Objective: The COVID-19 pandemic placed heavy burdens on emergency care and posed severe challenges to ST-segment-elevation myocardial infarction (STEMI) treatment. This study aimed to investigate the impact of COVID-19 pandemic on mechanical reperfusion characteristics in STEMI undergoing primary percutaneous coronary intervention (PPCI) in a non-epicenter region.

Methods: STEMI cases undergoing PPCI from January 23 to March 29 between 2019 and 2020 were retrospectively compared. PPCI parameters mainly included total ischemic time (TIT), the period from symptom onset to first medical contact (S-to-FMC), the period from FMC to wire (FMC-to-W) and the period from door to wire (D-to-W). Furthermore, the association of COVID-19 pandemic with delayed PPCI risk was further analyzed.

Results: A total of 14 PPCI centers were included, with 100 and 220 STEMI cases undergoing PPCI in 2020 and 2019, respectively. As compared to 2019, significant prolongations occurred in reperfusion procedures (P<0.001) including TIT (420 min vs. 264 min), S-to-FMC (5h vs. 3h), FMC-to-W (113 min vs. 95 min) and D-to-W (83 min vs. 65 min). Consistently, delayed reperfusion surged including TIT ≥ 12h (22.0% vs.3.6%), FMC-to-W ≥ 120 min (34.0% vs. 6.8%) and D-to-W ≥ 90 min (19.0% vs. 4.1%). During the pandemic**,** the patients with FMC-to-W ≥ 120 min had longer durations in FMC to ECG completed (6 min vs. 5min, P=0.007), FMC to DAPT (24 min vs. 21 min, P=0.001), catheter arrival to wire (54 min vs. 43 min, P<0.001) and D-to-W (91 min vs. 78min, P<0.001). The pandemic was significantly associated with high risk of delayed PPCI (OR=7.040, 95%CI 3.610-13.729, P<0.001).

Conclusions: Even in a non-epicenter region, the risk of delayed STEMI reperfusion significantly increased due to cumulative impact of multiple procedures prolongation.

Keywords: COVID-19, ST-segment-elevation myocardial infarction, primary percutaneous coronary intervention, mechanical reperfusion, non-epicenter region

Influence of COVID-19 pandemic on mechanical reperfusion in ST-segment-elevation myocardial infarction undergoing primary percutaneous coronary intervention: a multicenter retrospective study from a non-epicenter region

Qi Mao

Department of Cardiology, Institute of Cardiovascular Research, Xinqiao Hospital, Army Medical University, Chongqing 400037, China

Abstract

Objective: The COVID-19 pandemic placed heavy burdens on emergency care and posed severe challenges to ST-segment-elevation myocardial infarction (STEMI) treatment. This study aimed to investigate the impact of COVID-19 pandemic on mechanical reperfusion characteristics in STEMI undergoing primary percutaneous coronary intervention (PPCI) in a non-epicenter region.

Methods: STEMI cases undergoing PPCI from January 23 to March 29 between 2019 and 2020 were retrospectively compared. PPCI parameters mainly included total ischemic time (TIT), the period from symptom onset to first medical contact (S-to-FMC), the period from FMC to wire (FMC-to-W) and the period from door to wire (D-to-W). Furthermore, the association of COVID-19 pandemic with delayed PPCI risk was further analyzed.

Results: A total of 14 PPCI centers were included, with 100 and 220 STEMI cases undergoing PPCI in 2020 and 2019, respectively. As compared to 2019, significant prolongations occurred in reperfusion procedures (P<0.001) including TIT (420 min vs. 264 min), S-to-FMC (5h vs. 3h), FMC-to-W (113 min vs. 95 min) and D-to-W (83 min vs. 65 min). Consistently, delayed reperfusion surged including TIT ≥ 12h (22.0% vs.3.6%), FMC-to-W ≥ 120 min (34.0% vs. 6.8%) and D-to-W ≥ 90 min (19.0% vs. 4.1%). During the pandemic**,** the patients with FMC-to-W ≥ 120 min had longer durations in FMC to ECG completed (6 min vs. 5min, P=0.007), FMC to DAPT (24 min vs. 21 min, P=0.001), catheter arrival to wire (54 min vs. 43 min, P<0.001) and D-to-W (91 min vs. 78min, P<0.001). The pandemic was significantly associated with high risk of delayed PPCI (OR=7.040, 95%CI 3.610-13.729, P<0.001).

Conclusions: Even in a non-epicenter region, the risk of delayed STEMI reperfusion significantly increased due to cumulative impact of multiple procedures prolongation.

Keywords: COVID-19, ST-segment-elevation myocardial infarction, primary percutaneous coronary intervention, mechanical reperfusion, non-epicenter region

Iodixanol-associated acute kidney injury and prognosis in patients undergoing elective percutaneous coronary intervention: a prospective, multicenter study

Mao Qi

Xinqiao Hospital

Iodixanol-associated acute kidney injury and prognosis in patients undergoing elective percutaneous coronary intervention: a prospective, multicenter study

Qi Mao

Department of Cardiology, Institute of Cardiovascular Research, Xinqiao Hospital of Army Medical University, Chongqing 400037, China

Abstract

Objective: To evaluate iodixanol-associated acute kidney injury (AKI) and prognosis in patients undergoing elective percutaneous coronary intervention (PCI).

Methods: Patients undergoing elective PCI and iodixanol administration were prospectively enrolled in 8 centers between May 2020 and November 2021. The primary endpoint was AKI, defined as an increase in SCr of ≥ 0.3 mg/dL (26.4 μmol/L) or relative elevation ≥ 50% from baseline in the 48–72 h after PCI. Prognosis evaluations included the major adverse renal and cardiovascular events (MARCE): all-cause mortality, new-onset renal replacement therapy (NRRT), non-fatal myocardial infarction, and non-fatal stroke. AKI predictors were identified using multivariable logistic regression and associations between AKI and outcomes were examined using Cox regression.

Results: A total of 3630 patients were included in the final analysis and 2.9% of patients (107/3,630) suffered AKI. Among them, 95.3% (102/107) of AKI were stage 1, and 4.6% (5/107) of stage 2. The multivariable analysis indicated that age over 75-year-old, diabetes, NT-pro-BNP > 300 pg/mL, hemoglobin < 110 g/L, eGFR < 60 mL/min/1.73m2, and diuretics were independently associated with AKI (p < 0.05). After a median follow-up of 13 months, MARCE occurred in 3.6% (131/3630) of the study population, and their incidence was higher in AKI (9.4%, 10/107) vs. non-AKI

patients (3.4%, 121/3,523). However, after multivariable adjustment, there was no statistically significant association between AKI and MARCE (p = 0.382).

Conclusions: In patients undergoing elective PCI, cases of iodixanol-associated AKI were mostly mild and, after multivariable adjustment, held no statistically significant association with MARCE on mid-term follow-up.

Keywords Acute kidney injury · Contrast media · Percutaneous coronary intervention · Prognosis

Iodixanol-associated acute kidney injury and prognosis in patients undergoing elective percutaneous coronary intervention: a prospective, multicenter study

Qi Mao

Department of Cardiology, Institute of Cardiovascular Research, Xinqiao Hospital of Army Medical University, Chongqing 400037, China

Abstract

Objective: To evaluate iodixanol-associated acute kidney injury (AKI) and prognosis in patients undergoing elective percutaneous coronary intervention (PCI).

Methods: Patients undergoing elective PCI and iodixanol administration were prospectively enrolled in 8 centers between May 2020 and November 2021. The primary endpoint was AKI, defined as an increase in SCr of ≥ 0.3 mg/dL (26.4 μmol/L) or relative elevation ≥ 50% from baseline in the 48–72 h after PCI. Prognosis evaluations included the major adverse renal and cardiovascular events (MARCE): all-cause mortality, new-onset renal replacement therapy (NRRT), non-fatal myocardial infarction, and non-fatal stroke. AKI predictors were identified using multivariable logistic regression and associations between AKI and outcomes were examined using Cox regression.

Results: A total of 3630 patients were included in the final analysis and 2.9% of patients (107/3,630) suffered AKI. Among them, 95.3% (102/107) of AKI were stage 1, and 4.6% (5/107) of stage 2. The multivariable analysis indicated that age over 75-year-old, diabetes, NT-pro-BNP > 300 pg/mL, hemoglobin < 110 g/L, eGFR < 60 mL/min/1.73m2, and diuretics were independently associated with AKI (p < 0.05). After a median fol-

low-up of 13 months, MARCE occurred in 3.6% (131/3630) of the study population, and their incidence was higher in AKI (9.4%, 10/107) vs. non-AKI

patients (3.4%, 121/3,523). However, after multivariable adjustment, there was no statistically significant association between AKI and MARCE (p = 0.382).

Conclusions: In patients undergoing elective PCI, cases of iodixanol-associated AKI were mostly mild and, after multivariable adjustment, held no statistically significant association with MARCE on mid-term follow-up.

Keywords Acute kidney injury · Contrast media · Percutaneous coronary intervention · Prognosis

Risk of post-contrast acute kidney injury in patients with heart failure undergoing elective percutaneous coronary intervention: a prospective, multi-center study based on iodixanol administration

Mao Qi

Xinqiao Hospital

Risk of post-contrast acute kidney injury in patients with heart failure undergoing elective percutaneous coronary intervention: a prospective, multi-center study based on iodixanol administration

Qi Mao

Department of Cardiology, Institute of Cardiovascular Research, Xinqiao Hospital, Army Medical University, Chongqing 400037, China

Background: Prevalence, risk factors, and prognostic significance of post-contrast acute kidney injury (PC-AKI) have not been well described in patients with heart failure (HF) undergoing percutaneous coronary intervention (PCI).

Methods: Patients with HF undergoing elective PCI with iodixanol administration were prospectively enrolled in eight medical centers between May 2020 and November 2021. The primary endpoint was PC-AKI, as defined by the European Society of Urogenital Radiology (ESUR). Post-hoc analysis included new-onset renal replacement therapy (NRRT) and major adverse cardiovascular events (MACE). Logistic and Cox regression analyses were performed to identify risk factors for PC-AKI and MACE. Restricted cubic spline analysis was conducted to explore the dose-response relationship between estimated glomerular filtration rate (eGFR) and PC-AKI.

Results: In total, 1048 patients were included in the final analysis. The incidence of PC-AKI was 6.1% in the updated ESUR definition and 8.7% in the old definition. Diabetes, eGFR<60 ml/min´1.73 m^2 and diuretics were independent risk factors for PC-AKI. The median change in serum creatinine was only 1μmol/L for the overall population and just 6.8μmol/L for high-risk patients. The correlation of eGFR with PC-AKI presented a nonlinear dose-response mode, the risk of PC-AKI increased significantly when eGFR<77.6 ml/min´1.73 m^2 upon updated definition. After follow-up, no patient developed NRRT; the incidence of MACE was only 6.1%, and no association was found between PC-AKI and MACE.

Conclusions: The incidence of PC-AKI was low and mainly ascribed to mild renal impairment in HF patients undergoing elective PCI with iodixanol use.

Keywords: post-contrast acute kidney injury, heart failure, percutaneous coronary intervention, iodixanol, dose-response, prognosis

Risk of post-contrast acute kidney injury in patients with heart failure undergoing elective percutaneous coronary intervention: a prospective, multi-center study based on iodixanol administration

Qi Mao

Department of Cardiology, Institute of Cardiovascular Research, Xinqiao Hospital, Army Medical University, Chongqing 400037, China

Background: Prevalence, risk factors, and prognostic significance of post-contrast acute kidney injury (PC-AKI) have not been well described in patients with heart failure (HF) undergoing percutaneous coronary intervention (PCI).

Methods: Patients with HF undergoing elective PCI with iodixanol administration were prospectively enrolled in eight medical centers between May 2020 and November 2021. The primary endpoint was PC-AKI, as defined by the European Society of Urogenital Radiology (ESUR). Post-hoc analysis included new-onset renal replacement therapy (NRRT) and major adverse cardiovascular events (MACE). Logistic and Cox regression analyses were performed to identify risk factors for PC-AKI and MACE. Restricted cubic spline analysis was conducted to explore the dose-response relationship between estimated glomerular filtration rate (eGFR) and PC-AKI.

Results: In total, 1048 patients were included in the final analysis. The incidence of PC-AKI was 6.1% in the updated ESUR definition and 8.7% in the old definition. Diabetes, eGFR<60 ml/min´1.73 m^2 and diuretics were independent risk factors for PC-AKI. The median change in serum creatinine was only 1μmol/L for the overall population and just 6.8μmol/L for high-risk patients. The correlation of eGFR with PC-AKI presented a nonlinear dose-response mode, the risk of PC-AKI increased significantly when eGFR<77.6 ml/min´1.73 m^2 upon updated definition. After follow-up, no patient developed NRRT; the incidence of MACE was only 6.1%, and no association was found between PC-AKI and MACE.

Conclusions: The incidence of PC-AKI was low and mainly ascribed to mild renal impairment in HF patients undergoing elective PCI with iodixanol use.

Keywords: post-contrast acute kidney injury, heart failure, percutaneous coronary intervention, iodixanol, dose-response, prognosis

Non-anticoagulant heparin alleviates myocardial ischemia-reperfusion injury through inhibiting GSDMD-mediated cardiomyocyte pyroptosis via the HMGB1/RAGE pathway

xuewen wang, Gang Pan

Yueyang Central Hospital

Background: Heparin reduces myocardial ischemia-reperfusion (I/R) injury, which is associated with pyroptosis. As a derivative of heparin, non-anticoagulant heparin (NAH) is rarely researched in this field. This study aims to explore the mechanisms of NAH in myocardial I/R injury and pyroptosis. **Methods:** Cardiomyocytes (H9C2) were exposed to hypoxia/reoxygenation (H/R) to simulate myocardial I/R injury in vitro. Cells were successively treated with NAH, ov-gasdermin D (GSDMD), ov-caspase 11, H_2O_2, N-acetyl-L-cysteine, and rHMGB1. The binding of NAH to HMGB1 was detected by molecular docking and DARTS. In vivo, mice underwent myocardial I/R surgery and were treated with NAH and rHMGB1. Myocardial infarction, injury, and fibrosis were detected. **Results:** NAH inhibited H/R-induced pyroptosis of H9C2 cells as evidenced by a reduction in caspase 11 and GSDMD activation, a decrease in IL-18 and LDH release, and an increase in ATP yields. Moreover, overexpression of caspase 11 or GSDMD-N attenuated the therapeutic effect of NAH. Similar to N-acetyl-L-cysteine, NAH inhibited H/R and H_2O_2-induced oxidative stress. Moreover, NAH reversed the promoting effects of rHMGB1 on cell pyroptosis and oxidative stress. Studies revealed that NAH bound to HMGB1 and that HMGB1 interacted with RAGE. At the animal level, NAH effectively alleviated myocardial infarction, injury, and fibrosis in mouse models and reduced pyroptosis and myocardial oxidative stress. However, rHMGB1 reversed these therapeutic effects of NAH. **Conclusions:** NAH inhibited GSDMD-mediated pyroptosis through the HMGB1/RAGE pathway, thereby alleviating myocardial I/R injury. NAH may serve as a potential drug for treating myocardial I/R injury.

Keywords:Non-anticoagulant heparin; myocardial ischemia-reperfusion injury; GSDMD; pyroptosis; HMGB1/RAGE pathway

Background: Heparin reduces myocardial ischemia-reperfusion (I/R) injury, which is associated with pyroptosis. As a derivative of heparin, non-anticoagulant heparin (NAH) is rarely researched in this field. This study aims to explore the mechanisms of NAH in myocardial I/R injury and pyroptosis. **Methods:** Cardiomyocytes (H9C2) were exposed to hypoxia/reoxygenation (H/R) to simulate myocardial I/R injury in vitro. Cells were successively treated with NAH, ov-gasdermin D (GSDMD), ov-caspase 11, H_2O_2, N-acetyl-L-cysteine, and rHMGB1. The binding of NAH to HMGB1 was detected by molecular docking and DARTS. In vivo, mice underwent myocardial I/R surgery and were treated with NAH and rHMGB1. Myocardial infarction, injury, and fibrosis were detected. **Results:** NAH inhibited H/R-induced pyroptosis of H9C2 cells as evidenced by a reduction in caspase 11 and GSDMD activation, a decrease in IL-18 and LDH release, and an increase in ATP yields. Moreover, overexpression of caspase 11 or GSDMD-N attenuated the therapeutic effect of NAH. Similar to N-acetyl-L-cysteine, NAH inhibited H/R and H_2O_2-induced oxidative stress. Moreover, NAH reversed the promoting effects of rHMGB1 on cell pyroptosis and oxidative stress. Studies revealed that NAH bound to HMGB1 and that HMGB1 interacted with RAGE. At the animal level, NAH effectively alleviated myocardial infarction, injury, and fibrosis in mouse models and reduced pyroptosis and myocardial oxidative stress. However, rHMGB1 reversed these therapeutic effects of NAH. **Conclusions:** NAH inhibited GSDMD-mediated pyroptosis through the HMGB1/RAGE pathway, thereby alleviating myocardial I/R injury. NAH may serve as a potential drug for treating myocardial I/R injury.

Keywords:Non-anticoagulant heparin; myocardial ischemia-reperfusion injury; GSDMD; pyroptosis; HMGB1/RAGE pathway

老年急性 ST 段抬高型心肌梗死患者膜联蛋白 A1 与 eGFR 水平、冠脉病变程度及不良心血管事件的相关性

赵亮 谢伟

新疆生产建设兵团医院

摘要：目的：探讨血清膜联蛋白 A1（AnxA1）与肾小球滤过率（eGFR）水平及

老年急性 ST 段抬高型心肌梗死（STEMI）患者冠脉病变程度以及对近期预后的观察。**方法：** 选择纳入 2021 年 7 月至 2023 年 1 月我院收治后出院的老年急性 ST 段抬高型心肌梗死患者 130 例，所有患者均接受规范的抗血小板等治疗，收集患者临床资料，采用 Gensini 评分评定冠脉病变程度，采用 ELISA 法检测患者入院时血清 AnxA1 水平。根据 180 天内是否发生主要心血管不良事件（major adverse cardiovascular events，MACE），分为 MACE 组和非 MACE 组，对比两组患者临床资料、利尿效果、肾功能指标；**结果**：截止随访结束共发生 36 例 MACE，发生率为 29.75%。MACE 组使用利尿剂总剂量、血清 AnxA1 含量、LDL-C 含量高于非 MACE 组，基准 eGRF 水平低于非 MACE 组，差异具有统计学意义（P<0.05）；入组患者冠脉多支病变 Gensini 评分最高，明显高于双支、单支患者。多支患者不良心血管事件发生率最高，显著高于双支、单支（P<0.05）。血清 AnxA1、eGRF 水平与冠脉病变程度呈正相关（P<0.05）。**结论**：老年急性 ST 段抬高型心肌梗死（STEMI）患者血清 AnxA1 与 eGFR 水平、冠脉病变程度及预后存在相关性。

中国高原地区急性 ST 段抬高型心肌梗死的特点和转归：基于胸痛中心数据的回归性分析

陈垦

陆军军医大学大坪医院

急性冠脉综合征（ACS）是严重危害生命健康的疾病。高原特殊环境低温、低氧、低压等可能是导致或加重 ACS 的重要危险因素。但高原地区 ACS 患者的特点与转归是否与平原地区存在差异，目前尚不清楚。本研究基于苏州工业园区东方华夏心血管健康研究院 - 胸痛中心数据库（Chinese Cardiovascular Association (CCA) Database-Chest Pain Center），获取 2015 年 1 月至 2021 年 9 月中国中西部高原地区的急性冠脉综合征人群数据，包括分布在 11 个省、自治区的 505 个胸痛中心，分别是西藏、青海、甘肃、宁夏、陕西、山西、内蒙古、云南、贵州和四川，位于青藏高原、黄土高原、内蒙古高原和云贵高原。每个胸痛中心的海拔信息来自于谷歌地球，不同胸痛中心的海拔自 60 米至 3836 米，按海拔数据研究将 ACS 人群分为 4 个组，即 <500 米，500-1000 米，1000-1500 米和 >1500 米。研究共计纳入 ACS 患者 320743 人，其中 SETMI 患者 128510 人 (40.1%)，NSTEMI 患者 65731 人 (20.4%)，UA 患者 126502 人 (39.5%)。海拔 1500 米以上胸痛中心有更多的急性心梗患者，其心肌损伤标志物较较低海拔升高。针对 STEMI 研究，研究发现，1500 米海拔以上的 SETMI 患者高脂血症发生率较其他海拔高，但更少的人合并糖尿病或吸烟。在治疗上，高海拔的 STEMI 患者更倾向于进行转运 PCI。总的来说，最高海拔（>1500m）STEMI 患者新发急性心衰的发生率更低，同时最高海拔（>1500m）STEMI 患者的心血管死亡率和全因死亡率并不是最高。综上所述，本研究发现，尽管在高海拔地区胸痛中心会收治更多的急性心梗患者，但高海拔并不会增加 STEMI 患者的终点事件发生。

Development and Validation of a LASSO-Enhanced GRACE Model for Predicting Major Adverse Cardiac Events After PCI in AMI Patients

Xiaofei Gao, Jing-Yu Zhao, Jun-Jie Zhang, Shao-Liang Chen

Department of Cardiology, Nanjing First Hospital, Nanjing Medical University, Nanjing, China

Development and Validation of a LASSO-Enhanced GRACE Model for Predicting Major Adverse Cardiac Events After PCI in AMI Patients

Xiao-Fei Gao, MD[a], Jing-Yu Zhao, MSc[a], Jun-Jie Zhang, MD, PhD[a], Shao-Liang Chen, MD, PhD[a]

[a]Department of Cardiology, Nanjing First Hospital, Nanjing Medical University, Nanjing, China

Abstract: Objective: To develop and validate an enhanced clinical prediction model based on the GRACE score, aiming to improve individualized risk stratification and predictive performance for major adverse cardiovascular events (MACE) at 1-year follow-up after percutaneous coronary intervention (PCI) in patients with acute myocardial infarction (AMI).

Methods: We retrospectively analyzed 1,719 consecutive patients with AMI who underwent PCI between January and December 2023 across four medical centers. After applying exclusion criteria, 1,502 patients were included. The study cohort was randomly divided into a training set (70%) and a validation set (30%). In the training cohort, LASSO regression was applied to identify additional predictors beyond those included in the GRACE score. These variables were then combined with GRACE components and incorporated into a multivariable Cox proportional hazards model to build an enhanced prediction model. A nomogram was constructed based on the final Cox model to provide individualized risk estimation.

Result: Compared to the GRACE score, the new model showed better fit (lower Akaike's Information Criterion and Bayesian Information Criterion), superior discrimination (training net reclassification improvement (NRI) : 0.101; validation NRI: 0.200; training integrated discrimination improvement (IDI): 0.047; validation IDI: 0.095; all P < 0.05), and higher C-index (training: 0.831 (95% CI: 0.787-0.872) vs. 0.787 (95% CI: 0.739-0.831), P = 0.001; validation: 0.801(95% CI: 0.720-0.871) vs. 0.735 (95% CI: 0.642-0.824), P < 0.001, with all based on 1,000 bootstrap resamples for 95% CI estimation). Calibration was assessed using 1,000 bootstrap resamples, yielding calibration slopes of 1.000 (95% CI: 0.843–1.157) in the training set and 1.000 (95% CI: 0.765–1.235) in the validation set, with corresponding integrated Brier scores (IBS) of 0.045 and 0.050, respectively. The decision curve analysis (DCA) and clinical impact curve (CIC) confirmed improved net clinical benefit and applicability.

Conclusion: The enhanced prediction model significantly outperforms the traditional GRACE scoring system in discrimination, calibration, and clinical utility, providing a more accurate and clinically valuable tool for risk stratification in the studied population. This model may better guide individualized patient management and improve clinical decision-making.

Key Words: acute myocardial infarction, percutaneous coronary intervention, GRACE score, Clinic predict model, nomogram

USP13 Ameliorates Myocardial Infarction Injury by Inhibiting Ferroptosis via Stabilizing ALDOA

Peng-cheng Li, De-Long Chen, Chen-yun Zhang, Qin-yan Gong, Jia-Cheng Fang, Yidilisi Abuduwufuer , Jun-Yan Jin, Yu-Xuan Zhang, Ji-Niu Huang, Jun Jiang

The Second Affiliated Hospital, School of Medicine, Zhejiang University

Introduction: Myocardial infarction(MI) is a serious clinical condition triggered by coronary artery thrombotic occlusion, characterized by the transformation of cardiac tissue into fibrotic scar tissue and a reduction in cardiac output or an increase in intracardiac pressure. Even with reperfusion therapy and other related therapies, patients with MI usually continue to suffer from continued cell death and adverse remodeling of the heart, which in turn leads to heart failure. Therefore, an in-depth study of the pathogenesis of MI as well as the identification of new therapeutic targets is extremely important for the development of effective prevention and treatment strategies.

Ubiquitination is a reversible post-translational modification associated with a variety of cellular processes such as protein degradation, DNA damage repair, cell cycle, signal transduction, cell division and immune response. Ubiquitination can be inversely regulated by deubiquitinases (DUBs), which plays an important role in a variety of diseases by precisely controlling protein function and degradation. To date, more than 100 DUBs have been identified in humans and some DUBs such as USP25, UCHL1, and OTUD5 have been reported to play key roles in cardiovascular diseases. USP13 belongs to the family of USPs and is widely involved in a variety of cellular processes. A number of studies conducted in recent years have demonstrated the significant role of USP13 in various diseases, including lung cancer, ovarian cancer and breast cancer. Previous study suggests that USP13 regulates ferroptosis in chicken follicle granulosa cells by deubiquitinating ATG7, while USP13 also reduces septic mediated cardiomyocyte oxidative stress and inflammation by inducing Nrf2. Notably, ferroptosis has emerged as a key mediator of ischemic tissue damage. During ischemia, oxidative stress plays an important role, which leads to overproduction of reactive oxygen species, mitochondrial dysfunction, increased inflammatory response, apoptosis and necrosis. However, the role of USP13 in myocardial infarction and its potential involvement in ferroptosis and oxidative stress within myocardial cells warrant further exploration.

Objectives: Our study aims to elucidate how a DUB, ubiquitin-specific protease 13(USP13) improves MI, and preliminarily discuss its mechanism.

Methods: The role of USP13 in myocardial infarction was evaluated in murine cardiomyocytes in response to oxygen-glucose deprivation and myocardial infarction stimulation and in myocardium tissues of myocardial infarction patients. Liquid chromotography with mass spectrometry/mass spectrometry analysis combined with Co-IP was used to identify ALDOA (fructose-bisphosphate aldolase A), as an interacting protein of USP13. To clarify the molecular mechanism of USP13 in the regulation of ALDOA, we constructed a series of mutant plasmids of USP13. In addition, we overexpressed USP13 and ALDOA in the heart with adeno-associated virus serotype 9 vectors to validate the biological function of USP13 and ALDOA interaction.

Results: This study delineates a previously unrecognized cardioprotective mechanism orchestrated by USP13 in ischemic cardiomyopathy. USP13 expression is downregulated in the infarct border zone of mouse heart post-MI. Subsequent investigation revealed that USP13 gene knockdown exacerbates cardiac ferroptosis induced by MI. Through integrated mass spectrometry analysis and functional validation, we identified ALDOA as the principal substrate through which USP13 executes its protective effects via site-specific (K13) deubiquitination that stabilizes K48-linked ubiquitination patterns. Crucially, USP13-mediated preservation of ALDOA was shown to disrupt hypoxia-driven lipid peroxidation cascades in cardiomyocytes. Finally, the study demonstrated that cardiac-specific overexpression of USP13 prevents MI-induced cardiac injury. Collectively, these findings offer novel insights into the complex interplay between protein deubiquitination and ferroptosis in cardiomyocytes and propose new potential targets for therapeutic strategies in MI.

Conclusion: We confirmed that USP13 inhibited MI-induced cardiac injury by deubiquitinating and stabilizing ALDOA. These findings suggest that USP13 may serve as a promising therapeutic target for myocardial infarction, providing a foundation for developing novel treatment strate-

gies focused on ferroptosis.

Keywords: USP13; myocardial infarct; ubiquitination; cardiac injury

Albumin-to-Globulin ratio as an independent risk factor for predicting prognostic risk in patients with acute coronary syndrome undergoing percutaneous coronary intervention.

linlin wang, Shuang Xie, Ao-Xue Mei, Ying Fu, -Chen Wang, Ge Song, -Xian Sun, Ying Zhang

The Affiliated Hospital of Chengde Medical University

Authors:

[1]Linlin Wang, MM

[1]Shuang Xie, MM

[1]Aoxue Mei, MM

[1]Ying Fu, MM

[1]Xinchen Wang, MM

[1]Ge Song, MM

[1,2,3]Lixian Sun, MD

[1,2,3]Ying Zhang, MD

1 Department of Cardiology, The Affiliated Hospital of Chengde Medical University, Chengde, 067000, China

2 Hebei Key Laboratory of Panvascular Diseases, Chengde, 067000, China

3 The Cardiovascular Research Institute of Chengde, Chengde, 067000, China

Correspondence: Ying Zhang

Hebei Key Laboratory of Panvascular Diseases, Department of Cardiology, The Affiliated Hospital of Chengde Medical University, Chengde, Hebei, 067000, China

Email: cyfyzy@126.com

Abstract:

Purpose: Acute coronary syndromes (ACS) is a leading cause of death worldwide. Albumin and globulin are the main components of serum proteins. The albumin-to-globulin ratio (AGR) is often used to assess nutritional status. However, the clinical significance of the AGR in predicting the prognosis of patients with ACS remains unclear.We aimed to further delineate the prognostic role of the AGR in predicting the risk of MACEs in patients with ACS undergoing PCI.

Patients and methods: A total of 1408 patients with ACS who underwent percutaneous coronary intervention (PCI) were consecutively enrolled between January 2016 and December 2018 at The Affiliated Hospital of Chengde Medical University. The follow-up endpoints were defined as cardiac death or recurrent acute myocardial infarction.

The Kolmogorov-Smirnov test was employed to assess the normality of continuous variables, with normally distributed and non-normally distributed variables reported as mean ± standard deviation and median with interquartile range, respectively. Differences in non-normally distributed continuous variables between the MACEs and non-MACE groups were analyzed using the Mann-Whitney U-test. Categorical variables were expressed as counts (%) and compared using the χ^2 test. The Kaplan-Meier method was used to evaluate the incidence of adverse cardiovascular events across groups, while the log-rank test was used to assess differences between the two groups. Receiver operating characteristic (ROC) curves were used to determine the diagnostic value of AGR, with Youden's index (sensitivity + specificity - 1) employed to identify the optimal cutoff point. Additionally, time-dependent ROC curves were used to examine temporal correlations. The dose-response relationship between the AGR and MACEs in patients with ACS undergoing PCI was illustrated using restricted cubic spline (RCS) curves. Univariate and multivariate Cox proportional hazards models were used to evaluate predictive capacity of AGR for prognostic risk.

All statistical analyses were performed using SPSS (version 26, SPSS Inc., Chicago, IL, USA), GraphPad Prism 8.0 (GraphPad Software Inc., La Jolla, CA, USA), and R version 4.3.3. Statistical significance was set at $P < 0.05$.

Results: A total of 1363 patients responded in the follow-up period, of whom 49 had MACEs. AGR was significantly different between the MACEs and non-MACE groups. The area under the curve for the AGR was 0.619 (P =0.004, 95% confidence interval [CI]: 0.542–0.697). The optimal cut-off value for the AGR was determined to be 1.350 using Youden's index. The cumulative survival rate of the low AGR group was significantly lower than that of the high AGR group, according to the Kaplan-Meier curve (log-rank P =0.008). Multivariate Cox proportional hazards model showed age ≥ 60 years, HR:2.689 (95%CI:1.288-5.615, P =0.008), left ventricular ejection fraction (LVEF) <40%, HR: 3.527, (95%CI: 1.357–9.164, P =0.010), and AGR<1.350, HR: 2.180, (95%CI: 1.078–4.407, P =0.030) were all independent risk factors. A restricted cubic spline showed that a decreasing AGR was correlated with increasing risk of MACEs.

Conclusion:

The AGR was independently associated with a higher risk of cardiac death and recurrent acute myocardial infarction in patients with ACS who underwent PCI. This indicator combines inflammation, infection, and nutritional factors, and is easy to obtain, convenient, and effective. It may serve as a useful biomarker for identifying patients with ACS at an increased risk of MACEs.

Prognostic Nutritional Index as an Independent Risk Factor for Predicting Outcomes in Acute Coronary Syndrome Patients Undergoing Percutaneous Coronary Intervention.

linlin wang, Ao-Xue Mei, Shuang Xie, Ying Fu, Ge Song, -Xian Sun, Ying Zhang

The Affiliated Hospital of Chengde Medical University

Authors:

[1]Linlin Wang, MM

[1]Aoxue Mei, MM

[1]Shuang Xie, MM

[1]Ge Song, MM

[1]Ying Fu, MM

[1,2,3]Lixian Sun, MD

[1,2,3]Ying Zhang, MD

1 Department of Cardiology, The Affiliated Hospital of Chengde Medical University, Chengde, 067000, China

2 Hebei Key Laboratory of Panvascular Diseases, Chengde, 067000, China

3 The Cardiovascular Research Institute of Chengde, Chengde, 067000, China

Correspondence: Ying Zhang

Hebei Key Laboratory of Panvascular Diseases, Department of Cardiology, The Affiliated Hospital of Chengde Medical University, Chengde, Hebei, 067000, China

Email: cyfyzy@126.com

Abstract:

Purpose: Acute coronary syndrome (ACS) remains a leading cause of global mortality, with ischemic heart disease accounting for nearly half of all cardiovascular deaths. Emerging evidence highlights the connections between malnutrition, systemic inflammation, and cardiovascular outcomes, fueling interest in potential biomarkers. The Prognostic Nutritional Index (PNI), derived from serum albumin and lymphocyte counts, has garnered significant attention. However, its specific impact on cardiovascular prognosis remains uncertain.

The relationship between nutritional status and ACS outcomes requires further investigation, particularly in patients undergoing percutaneous coronary intervention (PCI). Although inflammation and malnutrition are linked to unstable plaques and post-PCI complications, the exact mechanisms driving the prognostic significance of the PNI in ACS—beyond its correlation with mortality—remain unclear .

Patients and methods: From January 2016 to December 2018, 1,408 ACS patients undergoing percutaneous coronary intervention (PCI) were recruited at the Affiliated Hospital of Chengde Medical University. The primary endpoint was major adverse cardiac events (MACEs), defined as cardiac death or recurrent acute myocardial infarction (AMI).

The Kolmogorov-Smirnov test was applied to evaluate the normality of continuous variables. Normally distributed variables were expressed as mean ± standard deviation, whereas non-normally distributed variables were reported as median (interquartile range). Differences in non-normally distributed continuous variables between the MACE and non-MACE groups were assessed using the Mann-Whitney U-test. Categorical variables were presented as counts (%) and compared via the χ^2 test. The Kaplan-Meier method was employed to estimate the incidence of adverse cardiovascular events across groups, with the log-rank test used to examine intergroup differences. Receiver operating characteristic (ROC) curves were generated to evaluate the diagnostic performance of PNI, and Youden's index (sensitivity + specificity - 1) was utilized to determine the optimal cutoff point. Time-dependent ROC curves were also constructed to analyze temporal correlations. Restricted cubic spline (RCS) curves were used to illustrate the dose-response relationship between

PNI and MACEs in ACS patients undergoing PCI. Lastly, univariate and multivariate Cox proportional hazards models were applied to evaluate the predictive value of AGR for prognostic risk.

All statistical analyses were conducted using SPSS (version 26, SPSS Inc., Chicago, IL, USA), GraphPad Prism 8.0 (GraphPad Software Inc., La Jolla, CA, USA), and R (version 4.3.3). Statistical significance was set at $p < 0.05$.

Results: Among the 1,369 patients followed, 52 experienced MACEs. PNI significantly differed between the MACE and non-MACE groups. The area under the curve (AUC) for PNI was 0.714 ($p < 0.001$, 95% CI: 0.642–0.785). Based on Youden's index, the optimal PNI cut-off was 46.905. Kaplan-Meier analysis revealed lower cumulative survival in the low PNI group (log-rank $p < 0.001$). Multivariate Cox regression identified Cr ≥ 110 μmol/L (HR: 4.353, 95% CI: 1.632–11.611, $p = 0.003$), LVEF <40% (HR: 5.646, 95% CI: 2.126–14.992, $p = 0.001$), and PNI <46.905 (HR: 2.822, 95% CI: 1.429–5.575, $p = 0.003$) as independent risk factors. A restricted cubic spline demonstrated that lower PNI is associated with a higher MACE risk.

Conclusion:

The PNI was independently associated with a higher risk of cardiac death and recurrent acute myocardial infarction in ACS patients undergoing PCI. This composite indicator incorporates inflammation, infection, and nutritional status, distinguished by its simplicity, convenience, and effectiveness. It may, therefore, serve as a valuable biomarker for identifying ACS patients at elevated risk.

急性心肌梗死“肥胖悖论”的机制阐释与临床启示：一项系统性观点综述

韩冬雨 董增祥

哈尔滨医科大学第一附属医院

目的：系统性梳理当前关于急性心肌梗死（AMI）患者中存在“肥胖悖论”（即超重 / 轻度肥胖患者短期至中期生存率高于正常或低体重患者）的循证证据，深入探讨其潜在生物学机制，并基于现有研究提出对临床实践的启示及未来研究方向。

方法：

1. 文献检索策略：在 PubMed、EMBASE 等数据库中系统检索截至 2025 年 6 月的相关文献。

2. 纳入标准：

①观察性研究（队列研究、注册研究）、荟萃分析及大型临床试验的亚组分析报告。

②研究对象为成人 AMI 患者（STEMI/NSTEMI）。

③主要探讨 BMI 与短期（住院 /30 天）或中期（1-3 年）死亡率、主要心血管不良事件（MACE）的关系。

④涉及潜在机制探讨（如炎症、代谢、神经内分泌、治疗差异等）的研究。

3. 数据整合与评价：对纳入研究的主要结论、研究方法学质量、潜在偏倚及机制假说进行定性综合与批判性评述，重点关注一致性发现、争议点及证据强度等级。

结果：

1.“悖论” 存在的广泛证据：

①绝大多数大型观察性研究及荟萃分析证实，在 AMI（尤其是接受 PCI）患者中，超重（BMI 25-25.9 kg/m²）及轻度肥胖（BMI 30-34.9kg/m²）患者的住院死亡率、30 天死亡率及 1-3 年全因死亡率显著低于正常体重（BMI 18.5-24.9 kg/m²）患者，呈现典型的“U 型” 或 “J 型” 曲线关系。

②低体重（BMI <18.5 kg/m²）患者被一致认为是预后最差的群体。

③该现象在校正年龄、性别、合并症、病变程度（如 SYNTAX 评分）、心功能（Killip 分级）及治疗方式后仍然存在。

2. 核心潜在机制阐释：

①代谢储备与营养状态优势： 超重 / 肥胖患者通常具有更高的瘦体重、能量储备（如肌糖原、肝糖原）及循环中脂联素水平，在急性应激状态下可能提供更好的代谢缓冲能力。

②神经内分泌激活差异：部分研究提示肥胖患者基础交感神经张力较高，可能在 AMI 后相对 “耐受” 儿茶酚胺风暴；其肾素 - 血管紧张素 - 醛固酮系统（RAAS）激活程度与瘦素 / 脂联素轴的相互作用也可能影响心肌修复。

③治疗时机与强度的 “肥胖优势”：临床观察显示，超重 / 肥胖患者因症状更易被识别或就医意愿更强，可能获得更及时的 PCI；部分研究提示其在急性期接受指南推荐药物（如 β 受体阻滞剂、ACEI）的耐受性更好，停药率较低。

3. 争议与局限性：

① BMI 的局限性：BMI 无法区分脂肪与肌肉含量，亦不能反映脂肪分布（如中心性肥胖）。腰围、腰臀比或身体成分分析可能提供更精确的风险评估。

②长期预后反转：多数研究显示 “悖论” 在 3-5 年后减弱甚至反转，长期随访中重度肥胖（BMI ≥ 35 kg/m²）患者的心血管风险显著增加。

结论：

1. 现象确认：现有高质量证据强烈支持在 AMI（尤其急性期）患者中存在 “肥胖悖论”，超重及轻度肥胖与短期至中期生存优势相关，而低体重是明确的高危标志。

2. 机制核心：肥胖患者的代谢 - 营养储备优势及可能获得的更积极治疗是解释该悖论的主要路径，神经内分泌适应及脂肪组织的潜在保护作用仍需深入研究。

3. 临床启示：

①避免急性期盲目减重：AMI 急性期管理的首要目标是优化血流动力学、血运重建和药物治疗，而非降低体重。

②重视低体重患者：需对低体重 AMI 患者进行营养风险评估与强化干预（如蛋白质补充、康复训练）。

③个体化长期管理：在稳定期（>6 个月），应依据个体情况（如脂肪分布、合并症）制定包括体重管理在内的二级预防策略，平衡短期悖论与长期风险。

4. 未来方向：需开展前瞻性研究探索更精准的体成分指标（如肌肉质量指数）的预后价值，并通过代谢组学技术阐明能量代谢储备的分子基础，为精准干预提供靶点。

关键词：急性心肌梗死、肥胖、肥胖悖论

Short-Term Exposure to Ozone and $PM_{2.5}$ and Their Components Increases the Risk of In-Hospital Mortality in Patients with Acute Myocardial Infarction: A Time-Stratified Case-Crossover Study

Yuan-Song Zhuang, Ya-Kun Zhao, Zhong-Jie Fan

Peking Union Medical College Hospital, Peking Union Medical College and Chinese Academy of Medical Sciences

Background: Air pollution is a significant environmental risk factor for mortality in patients with acute myocardial infarction (AMI). Despite existing research indicating adverse cardiovascular effects of ozone (O_3) and fine particulate matter ($PM_{2.5}$), the impact of short-term exposure to O_3, $PM_{2.5}$, and their chemical components on in-hospital mortality in AMI patients remains unclear. Notably, there is limited evidence regarding potential synergistic effects between O_3 and $PM_{2.5}$ components.

Methods: This time-stratified case-crossover study included 10,869 AMI patients hospitalized in Beijing from 2013 to 2019 who experienced in-hospital mortality. Conditional logistic regression models were used to analyze the relationship between short-term exposure to O_3, $PM_{2.5}$, and their five chemical components (sulfate, nitrate, ammonium, organics, and black carbon) before onset and the risk of in-hospital mortality. The analysis evaluated effects at different lag times (single-day lag0–7, moving average MA1–7), explored multiplicative and additive interactions between O_3 and $PM_{2.5}$ components, and estimated the population attributable risk percentage (PAF).

Results: A threshold effect for O_3 was observed at a concentration of 90 μg/m³. When exposure exceeded this threshold, for every 10 μg/m³ increase in concentration, the risk of in-hospital mortality in AMI patients increased by 6.2% (OR = 1.062, 95%CI: 1.037–1.087) at an average lag of 4 days. The exposure effects of $PM_{2.5}$ and its five chemical components showed a linear positive correlation. At an average lag of 1 day, for every 10 μg/m³ increase in $PM_{2.5}$ concentration, the risk of death increased by 1.4% (OR = 1.014, 95%CI: 1.009–1.019), with sulfate (OR = 1.078) and organics (OR = 1.058) showing the strongest health effects. Significant multiplicative interactions were found between O_3 and all $PM_{2.5}$ components ($P < 0.05$), particularly with organics (interaction OR = 1.054). On an additive scale, the additive interaction between O_3 and organics had an estimated relative excess risk (RERI) of 0.155 (95%CI: 0.053–0.258), and between O_3 and black carbon, the RERI was 0.137 (95%CI: 0.033–0.240), suggesting a synergistic effect. Subgroup analyses revealed that women, patients aged ≥ 65 years, and those with diabetes or chronic kidney disease were more sensitive to air pollution, with higher mortality risks associated with exposure. Additionally, the effect of O_3 on mortality risk was more pronounced in summer, while the effects of $PM_{2.5}$ and its components were more prominent in winter. Population attributable risk analysis showed that the PAF for exposure to O_3 alone was 1.83% (95%CI: 1.47–2.18) and for $PM_{2.5}$ alone was 6.97% (95%CI: 4.48–9.45). When exposed to both pollutants, the PAF increased to 8.67% (95%CI: 7.43–9.90), indicating that the combined effects of pollutants contribute more to the mortality burden.

Conclusion: Short-term exposure to high concentrations of O_3 (≥ 90 μg/m³) and $PM_{2.5}$ components significantly increases the risk of in-hospital mortality in hospitalized AMI patients. There is a synergistic effect between O_3 and organics, as well as between O_3 and black carbon, suggesting that exposure to multiple pollutants may pose higher risks. Research on pollutant interactions should be prioritized, and pollution control strategies should focus on high-risk groups and seasonal differences to reduce the mortality burden associated with AMI.

HMGB-1 联合 MSCs 移植对急性心肌梗死大鼠心脏功能影响的实验研究

石蓓

遵义医科大学附属医院

目的：研究高迁移率组蛋白 -1(HMGB-1) 联合骨髓间充质干细胞 (MSCs) 移植对于大鼠发生急性心肌梗死后心功能的影响及其相关作用机制。

方法：将 144 只雄性 SD 大鼠分为健康对照组、模型对照组、MSCs 移植组、HMGB-1 注射组、HMGB-1 注射 +MSCs 移植组及 HMGB-1BoxA 注射 +MSCs 移植组等 6 组，术后第 28 天对大鼠的心脏功能、心肌的病理切片、心肌梗死的面积及梗死区新生血管的密度进行检测。并在心肌梗死术后第 3、7、28 天测定血清中相关细胞因子的水平。

结果：在术后第 28 天，HMGB-1 注射 +MSCs 移植组较其余 5 组的左心室舒张末期内径和左心室收缩期内径明显缩小，左心室短轴缩短率和射血分数明显增加 (P<0.05)；HMGB-1 注射 +MSCs 移植组梗死面积与其余模型组相比明显缩小 (P<0.05)，梗死区的新生血管数目显著增加 (P<0.05)。在术后第 3 天和第 7 天，HMGB-1 注射 +MSCs 移植组的大鼠血清 TLR4、VEGF 水平最高 (P<0.05)；术后第 7 天及第 28 天，HMGB-1 注射 +MSCs 移植组大鼠的血清中白细胞介素 6、核因子 KaPPa 及肿瘤坏死因子 α 的水平最低 (P<0.05)。

结论：通过使用 HMGB-1 注射联合 MSCs 移植的治疗方法可以有效改善心肌梗死预后。

HMGB1 预处理骨髓间充质干细胞移植治疗心肌梗死大鼠的实验研究

刘志江 石蓓

遵义医科大学附属医院

目的：研究高迁移率族蛋白 -1(1HMGB1) 预处理的骨髓间充质干细胞 (BMSCs) 移植治疗大鼠心肌梗死的有效性及其机制。

方法：建立急性心肌梗死 (AMI) 大鼠模型，体外传代培养大鼠 BMSCs，以 25.0μg/L HMGB1 预处理细胞后 48h 移植到大鼠心脏梗死区域。实验分为假手术组、模型对照组、BMSCs 组、HMGB1+BMSCs 组。心电图检测确定心肌梗死模型的建立。细胞移植 28d 后进行以下检测：HE、Masson 染色检测梗死心脏形态学变化；TTC 染色测定心肌梗死面积；超声心动图测定心脏功能；免疫组织化学染色检测心肌梗死交界区血小板内皮细胞黏附分子 -1(CD31) 的表达；Western-blot 检测梗死心肌组织血管内皮生长因子 (VEGF) 的表达。

结果：心电图结果表明大鼠心肌梗死模型成功建立。与模型对照组相比，细胞移植组能有效减轻大鼠心肌纤维化程度及梗死面积，以 HMGB1+BMSCs 组更为明显 (P<0.05)。单纯 BMSCs 以及 HMGB1 预处理 BMSCs 移植均能增加心肌梗死区 CD31、VEGF 的表达，有效改善梗死心脏功能，HMGB1 预处理作用更显著 (P<0.05)。

结论：HMGB1 预处理 BMSCs 较单纯的 BMSCs 移植更能有效减轻心肌梗死程度，改善心脏功能，并且该效应可能与 HMGB1 促进 BMSCs 的旁分泌有关。

干扰 Nrf2 基因后骨髓间充质干细胞移植对大鼠心肌梗死后心肌凋亡的影响

赵然尊

遵义医科大学附属医院

目的：观察干扰核因子相关因子 2(Nrf2) 的骨髓间充质干细胞 (MSCs) 注射大鼠心肌梗死局部后细胞凋亡情况及对心功能的影响。

方法：建立心肌梗死大鼠模型，随机分为三组：干扰 Nrf2 基因的 MSCs 移植 (Nrf2 干扰组) 组；空载慢病毒修饰的 MSCs 移植 (Nrf2 正常组)；生理盐水注射对照组 (对照组，n=12)。心肌梗死细胞移植后 7 d，细胞免疫荧光法检测心肌局部 casPase3 蛋白的表达；移植后 28 d HE 染色评价梗死后心肌组织病理变化，TTC 染色评估梗死面积；采用蛋白印迹法 (Western blot) 检测心肌梗死区 Nrf2 和凋亡蛋白 Bcl2、Bax 的蛋白表达水平。

结果：心梗细胞移植后 7d，心肌梗死区域有 EGFP 标记的 MSCs，部分 EGFP 表达位置检测到 CasPase3 表达阳性，Nrf2 干扰组凋亡蛋白 CasPase3 的荧光强度强，Nrf2 正常组 CasPase3 的荧光强度弱，对照组无 EGFP 表达；细胞移植后 28 d，HE 染色结果显示，与 Nrf2 正常组比较，Nrf2 干扰组心肌组织肌纤维排列紊乱，炎性细胞浸润明显，而 Nrf2 正常组细胞排列整齐，炎性细胞浸润减少；心肌 TTC 染色结果显示，Nrf2 干扰组的心肌梗死面积较 Nrf2 正常组明显增加 (P<0.05)，与对照组比较无差异 (P>0.05)；Western blot 结果显示，与 Nrf2 正常组比较，Nrf2 干扰组心肌中 Nrf2 蛋白和抗凋亡蛋白 Bcl-2 表达下降，而促凋亡蛋白 Bax 表达增加 (P<0.05)，Nrf2 干扰组与对照组比较，各蛋白表达无差异性 (P>0.05)；心功能改善方面，Nrf2 干扰组 EF 较 Nrf2 正常组降低 (P<0.05)，而心室容积较 [(LVDd，LVDs] 较 Nrf2 正常组增加。

结论：移植干扰 Nrf2 的 MSCs 后，心肌梗死区凋亡相关蛋白表达增加，降低了外源性 MSCs 对梗死心脏的修复能力。

沉默 Nrf2 基因的骨髓间充质干细胞移植对大鼠心肌梗死后心室重构和纤维化的影响

龙仙萍 石蓓 赵然尊

遵义医科大学附属医院

目的：探讨以 si RNA 为载体沉默骨髓间充质干细胞 (MSC) 中核因子 E2 相关因子 2(Nrf2) 基因后细胞移植对大鼠心肌梗死后心肌纤维化和心室重构的影响及可能机制。

方法：建立心肌梗死大鼠模型，随机分为沉默 Nrf2 基因的 MSC 移植组 (MSCNrf2-/- 组)、过表达 Nrf2 基因的 MSC 移植组 (MSCNrf2+/+ 组) 和生理盐水转染 MSC 移植组 (对照组)，每组 12 只。细胞移植后 28 天，采用 Masson 染色检测心肌梗死边缘区胶原沉积含量和纤维化程度，Western blot 检测梗死心肌 Nrf2 和血红素氧合酶 1(HO-1) 蛋白表达水平，超声心动图评价梗死后心功能。

结果：siRNA-Nrf2 转染 MSC 后，Nrf2 蛋白表达明显减少。移植后第 28 d，MSCNrf2-/- 组心肌组织纤维化程度较对照组加重，MSCNrf2+/+ 组心肌组织纤维化程度较对照组减轻 (P<0.05)；MSCNrf2-/- 组梗死心肌中 Nrf2、HO-1 蛋白表达较对照组下降 (P<0.05)，而 MSCNrf2+/+ 组梗死心肌中 Nrf2、HO-1 蛋白表达较对照组增加 (P<0.05)；超声心动图结果显示，与对照组比较，MSCNrf2-/- 组左心室舒张期末内经 (LVEDD) 和左心室收缩期末内经 (LVESD) 增大，左心室射血分数 (LVEF) 下降 (P<0.05)，MSCNrf2+/+ 组 LVEDD 和 LVESD 均减小，LVEF 无下降 (P<0.05)。

结论 siRNA-Nrf2 可有效干扰 MSC 中 Nrf2 蛋白的表达，降低外源性 MSC 对梗死心脏的修复能力，增加心肌梗死区胶原沉积，进而促进心室重构，降低心功能。由此推测 Nrf2 信号通路在干细胞移植治疗心肌梗死后心肌重构和纤维化中起了关键作用。

钙素基因相关肽调节间充质干细胞存活对大鼠颈动脉损伤后血管修复的作用

赵然尊

遵义医科大学附属医院

目的：探讨降钙素基因相关肽 (CGRP) 调节间充质干细胞 (MSC) 存活和对大鼠颈动脉损伤后血管修复的作用及其可能机制。

方法：分离培养获得大鼠 MSC，分为 CGRP 组和对照组，均给予过氧化氢 (H2O2) 处理，前者再同时加入 CGRP 处理，以流式细胞仪检测 MSC 的存活和凋亡情况，并采用 Western 印迹法检测磷酸化糖原合成酶激酶 -3β(PGSK3β) 和 β- 链蛋白 (β-catenin) 的表达情况。构建大鼠颈动脉球囊损伤模型，分为 MSC-CGRP 组、MSC 组和对照组，前两组分别给予 MSC-CGRP 和 MSC 移植治疗，采用 Western 印迹法检测血管局部 CGRP、PGSK3β 和 β-catenin 的表达情况，免疫荧光染色检测损伤血管 CD31 的表达，苏木精 - 伊红 (H-E) 染色检测损伤血管新生内膜、中膜面积。

结果：H2O2 处理 8、24h 时，CGRP 组 MSC 的早期凋亡率、晚期凋亡 / 死亡细胞比例均显著低于对照组同时间点 (P 值均 <0.05)，细胞存活率均显著高于对照组同时间点 (P 值均 <0.05)。H2O2 处理后 8h，CGRP 组的 PGSK3β 和 β-catenin 蛋白表达水平均显著高于对照组 (P 值均 <0.05)；应用 CGRP 阻断剂 CGRP8-37 后 (CGRP+CGRP8-37 组) 均显著低于 CGRP 组 (P 值均 <0.05)，而与对照组的差异无统计学意义 (P 值均 >0.05)。大鼠颈动脉损伤模型中，细胞移植后 28d，对照组、MSC 组的新生内膜与中膜面积比均显著高于 MSC-CGRP 组 (P 值均 <0.05)。细胞移植后 3d，MSC 组血管局部 PGSK3β、β-catenin 表达水平均显著高于对照组 (P 值均 <0.05)；MSC-CGRP 组均显著低于 MSC 组 (P 值均 <0.05)。

结论：CGRP 可能通过激活 GSK3β/β-catenin 信号通路，促进移植的 MSC 存活，并增强 MSC 对损伤血管的修复作用。

TLR4 基因修饰 BMSCs 移植对大鼠急性心肌梗死后心功能的影响

陈文明 石蓓

遵义医科大学附属医院

目的：探讨 Toll 样受体 -4(TLR4) 修饰的骨髓间充质干细胞 (BMSCs) 对心肌梗死后心脏心功能的影响。

方法：将携带目的基因重组慢病毒载体 (Lv-EGFP-TLR4) 及空病毒载体 (Lv-EGFP) 分别转染至 BMSCs；用 ELISA 检测细胞上清液 TLR4 的表达。选用成年 SD 大鼠建立急性心肌梗死模型，随机分为 3 组 (n=18)：对照组、Lv-EGFP 组、Lv-EGFP-TLR4 组。分别将 Lv-EGFP 和 Lv-EGFP-TLR4 转染的 BMSCs 多点注射到大鼠心肌梗死区周边，对照组注射等量 PBS；细胞移植第 7 d，用荧光显微镜追踪 EGFP 阳性细胞表达，Western blot 检测梗死区周边 TLR4 的蛋白表达；细胞移植第 28 d，用超声心动图检测大鼠心功能，HE 和 MASSON 染色观察心肌胶原纤维化程度，用 ELISA 检测血清 I 型前胶原羧基端肽 (P Ⅰ CP) 和III型前胶原氨基端肽 (P III NT) 表达水平。

结果：TLR4 转染至 BMSCs 后，细胞上清液中 TLR4 的表达明显增多。细胞移植第 7 d，心肌梗死区域有 EGFP 标记的 BMSCs，Lv-EGFP-TLR4 组的绿色荧光强度明显优于 Lv-EGFP 组，对照组无 EGFP 表达，TLR4 蛋白表达也明显高于 Lv-EGFP 组 (P<0.01)。细胞移植第 28 d，Lv-EGFP-TLR4 组左室射血分数 [LVEF] 和短轴缩短率 [LVFS] 较 Lv-EGFP 组均明显增加 (P<0.01)，左心室收缩末径 [LVDs] 和左心室舒张末径值较 Lv-EGFP-BMSCs 组均明显缩小 (P<0.01)；血清中 Lv-EGFP-TLR4 组 P Ⅰ CP 和 P III NP 蛋白浓度较 Lv-EGFP 组均明显减少 (P<0.05)；Lv-EGFP-TLR4 组心肌纤维化程度也明显低于 Lv-EGFP 组。

结论：TLR4 基因修饰 BMSCs 移植治疗心肌梗死，进一步减轻心肌纤维化程度，从而改善心肌梗死大鼠的心功能。

CircERBB2IP Promotes Post-infarction revascularization via the miR-145a-5P/Smad5 axis

Xian-Ping Long, Bei Shi, Ran-Zun Zhao

Affiliated Hospital of Zunyi Medical University

Myocardial infarction is one of the leading diseases causing death and disability worldwide， and the revascularization of damaged tissues is essential for myocardial-injury rePair. Circular RNAs (circRNAs) are widely

involved in Physiological and Pathological Processes in various systems throughout the body, and the role of circRNAs in cardiovascular disease is gaining attention. In this study, we determined that circERBB2IP is highly exPressed in the hearts of newborn mice. Silencing or overexPression of circERBB2IP inhibited and Promoted angiogenesis in vivo and in vitro, resPectively. Mechanistically, the transcriPtion factor GATA4 Promotes the Production of circERBB2IP. Furthermore, circERBB2IP functioned as an endogenous miR-145a-5P sPonge and was able to sequester and rePress miR-145a-5P activity, which led to an increased exPression level of Smad5. In summary, circERBB2IP can Promote angiogenesis after myocardial infarction through the miR-145a-5P/Smad5 axis. These data suggest that circERBB2IP may be a Potential theraPeutic target for the treatment of myocardial infarction.

ANNEXIN A2 FACILITATES NEOVASCULARIZATION TO PROTECT AGAINST MYOCARDIAL INFARCTION INJURY VIA INTERACTING WITH MACROPHAGE YAP AND ENDOTHELIAL INTEGRIN B3

bei Shi

Affiliated Hospital of Zunyi Medical University

Myocardial infarction (MI) remains a leading cause of cardiovascular mortality worldwide, characterized by irreversible cardiomyocyte death and subsequent ventricular remodeling, which often progresses to heart failure. A growing body of evidence highlights the critical role of immune cells, particularly macrophages, in orchestrating the post-infarction repair process. Macrophages exhibit remarkable phenotypic plasticity, with distinct polarization states—pro-inflammatory (M1) and reparative (M2)—exerting opposing effects on tissue healing: M1 macrophages initiate the inflammatory response to clear debris, while M2 macrophages promote angiogenesis, collagen deposition, and tissue regeneration. However, the molecular mechanisms regulating macrophage polarization and their interplay with vascular cells during post-MI remodeling remain incompletely understood.

Annexin A2 (ANXA2), a calcium-dependent phospholipid-binding protein, has emerged as a key player in various physiological and pathological processes, including inflammation, cell migration, and angiogenesis. Previous studies have suggested that ANXA2 modulates macrophage function, driving polarization toward a reparative phenotype, and enhances neovascularization—two processes critical for mitigating MI-induced damage. Despite these insights, the specific role of ANXA2 in post-MI cardiac remodeling, as well as the underlying cellular and molecular mechanisms, has remained elusive, limiting its potential as a therapeutic target.

To address this knowledge gap, our study systematically investigated the dynamic expression and functional significance of ANXA2 in a murine model of MI. We first analyzed ANXA2 expression patterns in the infarcted heart and observed a striking temporal regulation: ANXA2 levels increased rapidly following MI, peaking on the second day post-injury, suggesting a potential role in the early reparative phase. To directly assess its functional impact, we employed adeno-associated virus (AAV) vectors to selectively overexpress or silence ANXA2 in the heart. Remarkably, ANXA2 overexpression in the infarcted myocardium led to significant improvements in cardiac function, as evidenced by enhanced ejection fraction and reduced left ventricular dilation. Concomitantly, we observed a marked reduction in cardiac fibrosis—characterized by decreased collagen deposition in the infarct border zone—and a robust increase in peri-infarct angiogenesis, as indicated by higher density of CD31-positive microvessels, compared to control animals. Conversely, cardiac-specific silencing of ANXA2 exacerbated post-MI injury, resulting in impaired cardiac function, increased fibrosis, and diminished neovascularization, confirming ANXA2's protective role.

To dissect the cellular mechanisms underlying these observations, we established in vitro coculture systems to study the crosstalk between macrophages and cardiac microvascular endothelial cells (CMECs), the primary cell type responsible for new blood vessel formation. Our results demonstrated that ANXA2-engineered macrophages—genetically modified to overexpress ANXA2—significantly enhanced CMEC proliferation, migration, and tubule formation, key hallmarks of angiogenesis. Mechanistic investigations revealed a dual mode of action for ANXA2: in macrophages, ANXA2 physically interacted with yes-associated protein (YAP), a transcriptional coactivator known to regulate macrophage polarization. This interaction inhibited YAP activity, shifting macrophage polarization toward a pro-angiogenic, reparative phenotype. In parallel, ANXA2 directly bound to integrin β3 on CMECs, activating downstream signaling pathways that promoted endothelial cell growth, migration, and tubule formation—a critical step in neovascularization.

Taken together, our findings uncover a novel protective role for ANXA2 in MI-induced cardiac injury. By promoting neovascularization in the infarcted area through two distinct mechanisms—YAP inhibition in macrophages to enhance reparative polarization and integrin β3 activation in endothelial cells to stimulate angiogenesis—ANXA2 effectively mitigates ventricular remodeling and preserves cardiac function. These results not only shed light on the complex molecular networks governing post-MI repair but also identify ANXA2 as a promising therapeutic target. Strategies aimed at enhancing ANXA2 expression or activity could potentially improve clinical outcomes in MI patients by accelerating vascular repair and limiting adverse cardiac remodeling, offering new hope for the treatment of this devastating disease.

Serum liPidomics reveals PhosPhatidylethanolamine and PhosPhatidylcholine disorders in Patients with myocardial infarction and Post-myocardial infarction-heart failure

bei Shi

Affiliated Hospital of Zunyi Medical University

Myocardial infarction (MI) and post-MI heart failure (PMIHF) represent critical global health burdens, accounting for a substantial proportion of mortality and morbidity worldwide. Despite advances in clinical management, the transition from acute MI to PMIHF remains poorly understood, with limited biomarkers available to predict this progression. This knowledge gap underscores the urgent need to identify early molecular indicators that can facilitate timely intervention and improve patient outcomes. In response, the present study aimed to characterize lipid metabolites as potential early biomarkers for the development of PMIHF, leveraging lipidomic profiling to explore differential lipid expression between patients with MI and those with established PMIHF.

To achieve this, serum samples were collected from 18 patients diagnosed with MI and 24 patients with PMIHF at the Affiliated Hospital of Zunyi Medical University. Lipidomic analysis was performed using Ultra High Performance Liquid Chromatography (UHPLC) coupled with a Q-Exactive High Resolution Mass Spectrometer, a state-of-the-art approach that enables high sensitivity and specificity in identifying and quantifying lipid species. Multivariate statistical analysis, specifically orthogonal Partial Least Squares Discriminant Analysis (OPLS-DA), was applied to distinguish metabolomic profiles between the two groups. Further, receiver operating characteristic (ROC) curves were used to evaluate the diagnostic potential of candidate biomarkers, while correlation analyses explored relationships between these lipids and clinical parameters, including B-type natriuretic peptide (BNP), total cholesterol (TC), and blood urea nitrogen (BUN).

Baseline characteristics revealed notable differences between the cohorts: the average age of MI patients was 57.83 ± 9.28 years, compared to 64.38 ± 10.89 years in the PMIHF group. Clinically relevant markers also diverged, with BNP levels (a key indicator of heart failure severity) being significantly higher in PMIHF patients (3535.96 ± 3025 pg/mL) than in MI patients (328.5 ± 299.842 pg/mL). Additionally, PMIHF patients exhibited lower TC (4.69 ± 1.13 mmol/L vs. 5.59 ± 1.51 mmol/L) and higher BUN (7.20 ± 3.49 mmol/L vs. 5.24 ± 2.15 mmol/L), reflecting potential metabolic and renal dysfunction in the PMIHF state.

Lipidomic profiling identified 88 differentially expressed lipids between the two groups, with 76 (86.36%) showing downregulation in PMIHF. Among these, two lipids emerged as promising biomarkers: phosphatidylethanolamine (PE) (12:1e_22:0) and phosphatidylcholine (PC) (22:4_14:1). ROC analysis demonstrated that PE (12:1e_22:0) had an area under the curve (AUC) of 0.9306, indicating excellent discriminative ability, while PC (22:4_14:1) showed good performance with an AUC of 0.8380. Correlation analyses further supported their clinical relevance: PE (12:1e_22:0) was inversely correlated with BNP and BUN but positively correlated with TC, whereas PC (22:4_14:1) displayed the opposite trend—positive associations with BNP and BUN and a negative correlation with TC. These relationships suggest that these lipids may reflect underlying pathophysiological processes, such as cardiac stress, lipid metabolism dysregulation, and renal impairment, in the transition to PMIHF.

In conclusion, this study highlights the potential of lipidomics in identifying early biomarkers for PMIHF. PE (12:1e_22:0) and PC (22:4_14:1) emerge as robust candidates, capable of distinguishing MI from PMIHF and correlating with key clinical parameters. These findings contribute to a deeper understanding of the metabolic shifts driving PMIHF and lay the groundwork for future studies to validate these biomarkers in larger cohorts, ultimately aiming to improve risk stratification and therapeutic targeting for post-MI patients.

Clinical Feature-Based Machine Learning Model for 1-Year Mortality Risk Prediction of ST-Segment Elevation Myocardial Infarction in Patients with HyPeruricemia: A RetrosPective Study

bei Shi

Affiliated Hospital of Zunyi Medical University

Accurate risk assessment of high-risk Patients is essential in clinical Practice. However, there is no Practical method to Predict or monitor the Prognosis of Patients with ST-segment elevation myocardial infarction (STEMI) comPlicated by hyPeruricemia. We aimed to evaluate the Performance of different machine learning models for the Prediction of 1-year mortality in STEMI Patients with hyPeruricemia. We comPared five machine learning models (logistic regression, k-nearest neighbor, CatBoost, random forest, and XGBoost) with the traditional global (GRACE) risk score for acute coronary event registrations. We registered

Patients aged >18 years diagnosed with STEMI and hyPeruricemia at the Affiliated HosPital of Zunyi Medical University between January 2016 and January 2020. Overall， 656 Patients were enrolled (average age，62.5 ± 13.6 years； 83.6%， male). All Patients underwent emergency Percutaneous coronary intervention. We evaluated the Performance of five machine learning classifiers and the GRACE risk model in Predicting 1-year mortality. The area under the curve (AUC) of the six models， including the GRACE risk model， ranged from 0.75 to 0.88. Among all the models，CatBoost had the highest Predictive accuracy (0.89)，AUC (0.87)，Precision (0.84)， and F1 value (0.44). After hybrid samPling technique oPtimization， CatBoost had the highest accuracy (0.96)， AUC (0.99)，Precision (0.95)， and F1 value (0.97). Machine learning algorithms，esPecially the CatBoost model，can accurately Predict the mortality associated with STEMI comPlicated by hyPeruricemia after a 1-year follow-uP.

钠 - 葡萄糖协同转运蛋白 2 抑制剂在急性冠状动脉综合征患者中的疗效

宋佳蔚 张澄

山东大学齐鲁医院心内科

目的

钠 - 葡萄糖协同转运蛋白 2 抑制剂 (Sodium-Glucose Cotransporter 2 Inhibitors, SGLT2i) 在治疗 2 型糖尿病或慢性心力衰竭方面的证据充足，但在急性冠状动脉综合征 (ACS) 患者中的疗效尚不明确。因此，本研究针对 SGLT2i 对 ACS 患者心血管结局的影响进行荟萃分析。

方法

本研究严格按照 PRISMA guidelines 和 the Cochrane Handbook version 6.4, 2023 进行。全面检索英文数据库 (PubMed、Web of Science、Cochrane Library) 和中文数据库 (中国知网、万方数据库、维普数据库和中国生物医学文献数据库) 自建库以来至 2023 年 12 月 25 日前有关 SGLT2i 在 ACS 患者中疗效的中英文研究。由两名研究人员独立筛选文献并提取数据后，利用 Cochrane 偏倚风险评价工具以及 Newcastle-Ottawa Scale 分别对纳入的随机对照试验以及观察性研究进行质量评估。结果包括全因死亡、主要心血管不良事件、心脏重构 (包括左室舒张末期内径 (LVEDD) 和左室收缩末期内径 (LVESD))、心功能 (包括左室射血分数 (LVEF) 和 NT-proBNP)，以及血糖。使用 Review Manager 5.3 软件对所纳入的研究进行结果数据分析，并进行异质性检验和亚组分析、偏倚分析和敏感性分析。

结果

最终纳入 24 项研究，包括 15 项随机对照临床试验和 9 项观察性研究。共纳入 12413 名患者，SGLT2i 治疗组 6175 人，非 SGLT2i 治疗组 6238 人。在心血管结局方面，与未使用 SGLT2i 治疗的组相比，SGLT2i 在减少全因死亡 (OR 0.72, 95% CI [0.61, 0.85])、主要心血管不良事件 (OR 0.44, 95% CI [0.30, 0.64])、心血管死亡 (OR 0.66, 95% CI [0.54, 0.81])、心力衰竭 (OR 0.52, 95% CI [0.44, 0.62])、心肌梗死 (OR 0.68, 95% CI [0.56, 0.83])、心绞痛 (OR 0.37, 95% CI [0.17, 0.78]) 和脑卒中 (OR 0.48, 95% CI [0.24, 0.96]) 方面显示出优势。在心脏重构方面，与未使用 SGLT2i 治疗的组相比，SGLT2i 在降低 LVEDD (MD -2.03, 95% CI [-3.29, -0.77]) 中显示出优势。在心功能方面，与未使用 SGLT2i 治疗的组相比，SGLT2i 有效提高 LVEF (MD 3.22, 95% CI [1.71, 4.72])，降低 NT-proBNP (MD -171.53, 95% CI [-260.98,-82.08])。

结论

SGLT2i 治疗可减少 ACS 患者的全因死亡和主要心血管不良事件风险，并改善心脏重构和心功能。

18 至 45 岁急性冠脉综合征患者中代谢表型与心血管事件的关联

徐榕笛 [1,2] 王乐 [2] 丛洪良 [2]

1. 天津医科大学研究生院

2. 天津市胸科医院

目的： 肥胖和代谢综合征与心血管事件相关。然而，在 18-45 岁急性冠脉综合征（acute coronary syndrome, ACS）患者中，不同代谢表型与肥胖对心血管事件的关联性仍不明确。本研究旨在根据代谢表型评估该年龄段 ACS 患者的预后。

方法：本研究纳入了 1787 名年龄≤ 45 岁的 ACS 患者，均接受冠状动脉造影检查。根据代谢表型将患者分为四组：代谢健康型非肥胖（metabolically healthy non-obesity，MHN）、代谢健康型肥胖（metabolically healthy obesity，MHO）、代谢不健康型非肥胖（metabolically unhealthy non-obesity，MUN）和代谢不健康型肥胖（metabolically unhealthy obesity，MUO）。主要终点为复合主要不良心血管事件（major adverse cardiovascular events, MACE），包括全因死亡、心肌梗死、卒中或非计划性血运重建。

结果：在 1787 名 ACS 患者中，中位年龄为 41.6 岁，1675 人（93.7%）为男性，1111 人（62.2%）患有肥胖，659 人（36.9%）被归类为 MHO。在中位 65 个月的随访期间，共发生 404 例 MACE 事件。多因素 Cox 分析显示，与 MHN 相比，MHO 与 MACE 风险降低相关，而 MUN 显著增加风险（MHO：风险比 [HR] 0.69，95% 置信区间 [CI] 0.52-0.92，P=0.011；MUN：HR 1.47，95% CI 1.07-2.02，P=0.012）。此外，限制性立方样条分析表明，体重指数（body mass index, BMI）与 MACE 发生率呈线性关系（非线性 P=0.304，总体 P<0.001）。

结论：在 18-45 岁的 ACS 患者中，MHO 与 MACE 风险降低相关，而 MUN 较 MHN 显著增加风险。此外，BMI 与 MACE 发生率呈线性关系。

Superlubricity DAPA-PDMAMPC-PCM Nanoparticles Boost Dapagliflozin's Therapeutic Effects in Diabetic Myocardial Infarction: Mitochondrial Repair and Targeted Delivery Synergy

Yan-Ru Yang[1], Zhen-Hong Fu[1], Chu-Nan Zhao[2], Ji-Hang Wang[1]

1. Chinese PLA General Hospital

2. Beijing Institute of Radiation Medicine

Purpose/Objective(s):

We hypothesized that dapagliflozin (DAPA) attenuates diabetic myocardial infarction (MI) injury by activating AMPK to restore mitochondrial fusion dynamics,and that myocardial-targeted DAPA-PDMAMPC-PCM nanoparticles with superlubricity properties would enhance this therapeutic effect.This study aimed to:(1) define the AMPK-mitochondrial pathway underlying DAPA's cardioprotection in diabetic MI,and (2) engineer and validate a nanoparticle-based delivery system to optimize drug targeting and efficacy.

Materials/Methods:

Diabetic MI was induced in C57BL/6J mice (high-fat diet + streptozotocin, 50 mg/kg/day) via permanent Left Anterior Descending (coronary artery) ligation. Five groups (n=6-8/group) included:DM+Sham,DM+AMI,DM+AMI+Dapa (1.5 mg/kg/day),DM+AMI+AMPK agonist (A769662) and DM+AMI+Dapa+AMPK inhibitor (Compound C). Cardiac function (LVEF/LVFS), remodeling (HE staining), and apoptosis (TUNEL) were assessed at 3/7 days post-MI. In vitro, H9c2 cells under high-glucose hypoxia were treated with Dapa ± AMPK modulators to evaluate mitochondrial fusion (WB for MFN1/2, OPA1; TEM), ROS (DCFH-DA), and apoptosis (Annexin V/PI).

The copolymer P(DMA-co-MPC) was synthesized according to a previously established protocol and employed to encapsulate dapagliflozin (DAPA) within its hydrophobic core. Concurrently, DSPE-PEG2000-PCM was synthesized via thiol-maleimide click chemistry and subsequently integrated into pre-formed nanoassemblies through hydrophobic insertion. The chemical structure of P(DMA-co-MPC) and DSPE-PEG2000-PCM was evaluated by 1H NMR spectrum and Gel Permeation Chromatography.While their physicochemical properties were evaluated using transmission electron microscopy (TEM) and dynamic light scattering (DLS).The tribological experiment is performed to investigate the lubrication performance of DAPA-PDMAMPC-PCM nanoparticles in aqueous suspension.In vivo imaging detection of small animals is performed to verify the targeting properties of different nanoparticles.Cytocompatibility was assessed via CCK-8 staining.After intravenous injection of nanoparticles into mice, the therapeutic effects on cardiac structure and function were systematically evaluated and compared with free dapagliflozin (DAPA) treatment.

Results:

In diabetic MI mice,Dapagliflozin (DAPA) significantly improved cardiac function,increasing LVEF by 23.01±1.88% (vs. DM+MI, p<0.01) at 7-day post-MI .The DAPA-treated group showed the most substantial preservation of cardiac architecture. This was characterized by: (1) a minimal increase in cardiomyocyte cross-sectional area (29.56% vs 102.32% in DM+MI controls, p<0.01), and (2) a significant 21.65±4.95% reduction in myocardial apoptosis rate (p<0.01 versus DM+MI group) .All these cardioprotective effects were completely abrogated by AMPK inhibition (p<0.01) .

In hypoxic cardiomyocytes,DAPA upregulated MFN1 and OPA1 expression (2.1-fold, p<0.01), reduced ROS by 50% (p<0.05), and decreased apoptosis (2.3-fold, p<0.01).Additionally, DAPA restored mitochondrial membrane potential, as evidenced by a 1.7-fold increase in the JC-1 ratio (p<0.01). Transmission electron microscopy (TEM) further confirmed the restoration of mitochondrial ultrastructure.

Optimized 5% PCM-modified nanoparticles exhibited the highest zeta potential and a uniform size (~1 μm, confirmed by DLS/TEM). The formulation showed no cytotoxicity and enhanced myocardial retention (2.09-fold vs. non-targeted, p<0.001), leading to superior therapeutic effects: 30.77% less fibrosis, 3.59% greater apoptosis suppression vs. free DAPA (p<0.05), and 17.36% reduced cardiomyocyte hypertrophy (p<0.05)

Conclusion:

1. Dapagliflozin improves cardiac function after myocardial infarction and reduces cardiac remodeling in diabetic mice.

2. Dapagliflozin up-regulates the expression of mitochondrial fusion protein by activating AMPK pathway, and promotes mitochondrial fusion in high glucose and high lipid hypoxia cardiomyocytes.

3. Dapagliflozin can reduce intracellular ROS production, improve mitochondrial energy metabolism of cardiomyocytes and reduce myocardial cell apoptosis by promoting mitochondrial fusion of cardiomyocytes with high glucose and fat.

4. DAPA-PDMAMPC-PCM nanoparticles can target the infarct site and play a more efficient myocardial protection effect.

BMI Differences on Anticoagulation with Bivalirudin vs. Heparin During Primary PCI: a BRIGHT-4 subanalysis

Da-li Zhang[1], Yi Li[1], Miao-han Qiu[1], Zhen-Yang Liang[1], Kai Xu[1], Yang Li[1], Guan-Shan Zhang[2], Wen Xie[3], He-Song Zeng[4], Yu-Cai Cheng[5], Ji-Dong Liu[6], Qiu-Tang Zeng[7], Xiang Cheng[7], Ke Zhu[8], Jun-Xing Hu[9], Kang Cheng[10], Jing-Ping Wang[11], Ren-Li Cheng[12], Yin-Pin Zhou[13], Ben-Yun Wang[14], Gui-Qiu Cao[15], Ya-Ling Han[1], Gregg W Stone[16]

1. State Key Laboratory of Frigid Zone Cardiovascular Diseases, Department of Cardiology, General Hospital of Northern Theater Command, Cardiovascular Research Institute, Shenyang, China

2. Hengshui Cardiovascular Hospital, Hengshui, China

3. Hospital of Chengdu University of TCM, Chengdu, China

4. Tongji Hospital, Tongji Medical College of Hust, Wuhan, China

5. Zaozhuang Central Hospital of Shandong Healthcare Group, Zaozhuang, China

6. Shandong Second Provincial General Hospital, Jinan, China

7. Union Hospital, Tongji Medical College of Hust, Wuhan, China

8. Xuzhou Central Hospital, Xuzhou, China

9. The First People's Hospital of Ruzhou, Pingdingshan, China

10. The Affiliated Hospital of Northwest University, Xi'An No.3 Hospital, Xi'An, China

11. Shanxi Cardiovascular Hospital, Taiyuan, China

12. Suzhou Municipal Hospital of Anhui Province, Suzhou, China

13. Chongqing University Fuling Hospital, Chongqing, China

14. Heze Mudan People's Hospital, Heze, China

15. The Fifth Affiliated Hospital of Xinjiang Medical University, Urumqi, China

16. Icahn School of Medicine at Mount Sinai, New York, NY, USA

Background Body mass index (BMI) is associated with ischemic and bleeding events in patients with ST-segment elevation myocardial infarction (STEMI) undergoing primary percutaneous coronary intervention (PCI). Procedural anticoagulation with bivalirudin followed by a prolonged high-dose post-PCI infusion was shown in the BRIGHT-4 trial to reduce mortality and major bleeding compared with heparin monotherapy. We aimed to assess the outcomes of bivalirudin compared with heparin in relation to BMI in STEMI patients undergoing primary PCI.

Methods This prespecified subgroup analysis from the BRIGHT-4 trial evaluated the treatment effects of bivalirudin with a high-dose infusion for 2-4 hours after primary PCI compared with heparin monotherapy in 6,016 randomized STEMI patients undergoing primary PCI predominantly via radial artery access stratified according to baseline BMI. A total of 3284 (54.6%) patients had a BMI <25 kg/m^2, the pre-specified stratification threshold.

Results The primary endpoint of all-cause death or Bleeding Academic Research Consortium (BARC) types 3-5 bleeding events at 30 days in all enrolled patients occurred less often in patients with BMI ≥ 25 kg/m^2 compared with those with BMI <25 kg/m^2 [2.9% vs. 4.4%; unadjusted hazard ratio (HR) 0.66, 95% confidence interval (CI) 0.50-0.87; P=0.003], which was no longer significant after adjusting for confounders (adjusted HR 0.99, 95% CI 0.74-1.31; P=0.92). Bivalirudin reduced the rate of the primary endpoint compared with heparin in patients with BMI <25 kg/m^2 (3.2% vs. 5.7%; adjusted HR 0.56, 95% CI 0.40-0.79) but not in those with BMI ≥ 25 kg/m^2 (2.9% vs. 2.9%; adjusted HR 0.97, 95% CI 0.62-1.52; $P_{interaction}$=0.04). A similar pattern was observed for the individual components of the primary endpoint, as well as for the composite of all-cause death or BARC types 2-5 bleeding. As shown in the exploratory analysis based on further stratification of BMI into underweight (BMI <18.5 kg/m2), normal (18.5 kg/m2 ≤ BMI <25 kg/m2), overweight (25 kg/m2 ≤ BMI <30 kg/m2) and obese (BMI ≥ 30.0 kg/m2) groups, those with lower BMI had higher incidence of primary endpoint compared with patients with higher weight, which peaked in those underweight patients (12.4% vs. 3.9%; unadjusted HR 3.32, 95% CI 2.16-5.11; P < 0.0001). The benefit of bivalirudin compared with heparin for the primary endpoint was seen in underweight (7.1% vs. 19.1%; unadjusted HR 0.35, 95% CI 0.15-0.82; P=0.02) and normal-weight patients (2.9% vs. 4.9%; unadjusted HR 0.59, 95% CI 0.41-0.86; P=0.005), but not overweight (3.2% vs. 3.3%; unadjusted HR 0.97, 95% CI 0.62-1.54; P=0.91) or obese patients (1.4% vs. 1.2%; unadjusted HR 1.13, 95% CI 0.23-5.61; P=0.88). The benefit of bivalirudin vs. heparin tended to increase with decreased BMI. Further analysis evaluating the association of BMI and anticoagulation strategy in high-risk subgroup with cardiogenic shock and/or cardiac arrest showed that the benefit of bivalirudin vs. heparin for the primary endpoint was not observed in either BMI group among those high-risk patients.

Conclusions Among patients with STEMI undergoing primary PCI in the BRIGHT-4 trial, greater rates of adverse ischemic and bleeding events were observed in patients of lower BMI, although this "obesity paradox" was eliminated after adjustment for measured confounders. Procedural anticoagulation with bivalirudin plus a 2-4-hour high-dose post-PCI infusion decreased the 30-day rate of all-cause death or BARC types 3-5 bleeding in patients with lower BMI (<25 kg/m2) but not those with higher BMI (≥ 25 kg/m2).

Trial registration The BRIGHT-4 trial is registered with ClinicalTrials.gov (NCT03822975).

Keywords Bivalirudin, heparin, ST-segment elevation myocardial infarction, primary percutaneous coronary intervention, body mass index, obesity paradox

司美格鲁肽对非糖尿病大鼠急性心肌梗死后心肌细胞凋亡的影响及机制研究

李艳红

河北省人民医院

目的：探究司美格鲁肽对非糖尿病大鼠急性心肌梗死后心脏结构、功能及心肌细胞凋亡的影响，并阐明其潜在分子机制。

方法：36 只雄性 SD 大鼠随机分为假手术组（Sham）、模型组（Model）和司美格鲁肽组（SEMA）。Model 组和 SEMA 组左前降支结扎法建立急性心肌梗死大鼠模型；术后第 1 天起，SEMA 组每日皮下注射 0.12 mg/kg 司美格鲁肽，Sham 组与 Model 组注射等量生理盐水，持续干预 4 周。采用 ELISA 检测血清 NT-proBNP 水平，超声心动图评估心脏结构与功能；心肌组织切片 HE 染色观察心肌细胞排列及形态，Masson 染色分析梗死面积及间质纤维化程度，TUNEL 法检测心肌细胞凋亡。基于 4D-label-free 蛋白质组学技术定量分析心肌组织蛋白表达谱，筛选差异表达蛋白，并应用生物信息学方法进行功能富集分析。采用 Western Blot 验证凋亡相关蛋白（Bcl-2/Bax、Cleaved Caspase-3）及 cGMP/PKG 通路关键分子（p-PKG、p-CREB）表达水平。

结果：与 Model 组相比，SEMA 组血清 NT-proBNP 水平显著降低（P < 0.05），LVEDD 与 LVES 减小，左室短轴缩短率（left ventricular fractional shortening, LVFS）和 LVEF 显著改善（P < 0.05）；组织病理学显示，与 Model 组相比，SEMA 组梗死面积降低无统计学意义，但心肌细胞排列紊乱程度明显减轻，胶原体积分数显著下降（P < 0.05）；TUNEL 染色提示 SEMA 组非梗死区细胞凋亡指数较 Model 组显著下降（P < 0.05）；蛋白质组学筛选出 108 个 SEMA/Model 组间差异表达蛋白，功能富集分析表明 cGMP/PKG 信号通路显著激活； Western Blot 证实，与 Model 组相比，SEMA 组 Bcl-2 与 Bax 比值升高，Cleaved Caspase-3 表达下调，同时 PKG 和 p-CREB 显著增加（P < 0.05）。

结论：司美格鲁肽可能通过影响 cGMP/PKG/CREB 通路抑制非梗死区心肌细胞凋亡，发挥心脏保护作用。

穿戴心音心电同步设备对急性心肌梗死 PCI 术后左室收缩功能障碍及预后的预测价值

彭庆龄

南昌大学第二附属医院 心血管内科

目的：可穿戴心音心电同步设备是一项全新的技术，在心血管疾病的快速诊断及预后方面具有很大的优势。本研究旨在探讨可穿戴心音心电设备同步分析在急性心肌梗死（AMI）患者经皮冠状动脉介入治疗（PCI）后左室收缩功能障碍及预后预测中的临床价值。

方法：本研究纳入了 202 例急性心肌梗死患者入组研究，所有患者均入院行皮冠状动脉介入治疗，中位随访时间为 150 天。入院用超声心动图测定左室射血功能（LVEF），并在 PCI 术前用可穿戴心音心电设备同步记录心音图和心电图信号。分析心音图和心电图信号，以确定电机械激动时间（EMAT）、经时间校正的电机械激动时间（EMATc）、射血前期时间（PEP）、左室射血时间（LVET）、左室收缩时间（LVST）。主要终点定义为急性心肌梗死 PCI 术后主要心血管不良事件（MACE）的发生率，次要终点定义为急性心肌梗死 PCI 术后左室收缩功能障碍的发生率。

结果：左室收缩功能障碍组的 EMAT 、EMATc 高于非左室收缩功能障碍组（p <0.05），LVET 和 LVST 低于非左室收缩功能障碍组（p <0.05）。EMAT 和 EMATc 是 AMI 患者 PCI 后左室收缩功能障碍的独立风险因素 [EMAT（OR：1.71，95%CI(1.12, 2.62)，P=0.0135）、EMATc（OR：2.07，95%CI(1.31, 3.26)，P=0.0017）]。在 cox 比例风险回归模型中，EMAT Z-score 及 EMATc Z-score 每增加一个单位，急性心肌梗死患者的主要心血管不良事件发生率升高 29%（95%CI 1.07, 1.56）、37%（95%CI 1.12, 1.67）。

结论：本研究表明 EMAT 及 EMATc 能预测 AMI 患者左室收缩功能障碍及主要心血管不良事件。可穿戴心音心电同步设备可作为一种无创、快速、有效、简便的预测急性心肌梗死患者 PCI 术后预后的方法。

注射用心肌肽干预急性 ST 段抬高型心肌梗死直接 PCI 术后改善心肌梗死面积的多中心临床研究

钱赓[1] 马翔[1] 张颖[1] 郭自同[4] 尹秋林[3] 陈韵岱[1] 孙志军[1]

1. 中国人民解放军总医院

2. 新疆医科大学附属第一医院

3. 江西省人民医院

4. 新疆自治区人民医院

目的：心肌肽是一种从乳猪心脏提取的多肽类活性物质，具有清除活性氧及其他自由基的能力，从而保护心肌免受多种因素导致的损伤。尽管直接经皮冠状动脉介入治疗（PCI）能够恢复急性 ST 段抬高型心肌梗死（STEMI）患者的血流，但再灌注损伤仍可能进一步加重心肌损害。本研究旨在评估静脉注射心肌肽对 PCI 直接术后患者心梗面积的改善效果。

方法：本研究采用前瞻性、多中心、随机、单盲、平行对照的设计。计划纳入拟行直接 PCI 的急性 ST 段抬高型心肌梗死患者，将其随机分为两组。干预组是在常规治疗基础上，于导管室前缓慢静脉滴注注射用心肌肽 3mg/kg 直至手术结束，术后 3 天每日继续静脉滴注注射用心肌肽 3mg/kg；对照组在围术期采用常规的心肌梗死治疗手段。两组患者在直接 PCI 术后 5-7 天，进行心脏磁共振检查，定量评估心肌梗死面积、心脏挽救指数及微循环阻塞（MVO）等。

结果：研究共筛选 322 名急性 ST 段抬高型心肌梗死患者，最终入组 172 例，其中心肌肽干预组 85 例，对照组 87 例。135 例患者完成心肌核磁检查并纳入分析，包括干预组 67 例，对照组 68 例。两组患者在年龄、性别、基础疾病（高血压、高血脂、糖尿病）、吸烟史、血压、心率、血常规、血肌酐、罪犯血管分布及术前肌钙蛋白水平等基线资料方面无显著差异（P 值均 > 0.05）。干预组的心肌梗死面积显著低于对照组（20.8±9.2% vs 25.1±10.4%，P=0.013）；心脏挽救指数显著提高（45.8±12.2% vs 39.4±12.9%，P=0.004）；而 MVO 发生率（35.8% vs 41.2%，P=0.523）及 MVO 质量（1.15±2.31g vs 1.69±3.59g，P=0.303）无显著差异。

结论： 在直接 PCI 围术期应用注射心肌肽能够显著缩小心肌梗死面积并提升心肌挽救指数，表明心肌肽有望成为急性 ST 段抬高型心肌梗死患者再灌注治疗的辅助治疗策略。

miR-21 联合冠脉狭窄程度对急性心肌梗死患者介入术后 MACE 的预测价值

麦尔江克力木

新疆喀什地区喀什第二人民医院

【摘要】 目的：建立基于急性心肌梗死（Acute Myocardial Infarction，AMI）患者经皮冠状动脉介入术 (Percutaneous Coronary Intervention，PCI) 后主要心血管不良事件 (Major adverse Cardiovascular Events，MACE) 预测模型并进行内部验证。**方法：**选取 **20**21 年 01 月 01 至 2022 年 06 月 30 日于新疆喀什地区第二人民医院心血管内科住院并接受 PCI 治疗的 AMI 的患者 149 例，为建立和验证预测模型，将研究对象分为两部分，2021 年 01 月至 2021 年 06 月的数据作为训练组（105 例），2021 年 06 月至 2021 年 07 月的数据作为验证组（44 例）。收集患者的基本特征、实验室检查、辅助检查情况，通过单因素和多因素 Cox 回归分析建立预测模型，并绘制列线图。采用受试者工作特征（ROC）曲线、校准曲线和 Hosmer-Lemeshow 拟合优度检验验证和评价预测模型的区分度和校准度；决策曲线分析（DCA）评估预测模型的临床有效性。**结果：**基于能独立预测主要心血管不良事件 (MACE) 的 miR-21 分界值 1.460，将所有 AMI 患者分为低 miR-21 组和高 miR-21 组。基于单因分析显示 CK（HR=1.000, P=0.008），AST(HR=1.004,P = **0.021**），CHOL(HR=1.606,P =**0.037**），Gensini 评分（HR=1.019,P =0.001）和高 miR-21 状态（HR=5.540,P < 0.001）与 MACE 事件发生显著相关；多因素分析证实 Gensini 评分 (HR=1.014,P =0.003) 和高 miR-21 状态 (HR=4.390,P=0.022) 为独立预测因子。制定了列线图来预测 MACE 事件的发生，C- 指数和 ROC 曲线下的面积证实了列线图的预测准确性有所提高。校准曲线表明，观测到的概率与列线图预测的概率在训练，验证和整个队列中具有很高的一致性。DCA 证实，在训练组中列线图提供更大的净获益。最后，Kaplan-Meier 分析显示，高风险组患者发生 MACE 事件的概率最高，预后最差（P<0.0001）。 **结论：**入院时高 miR-21 水平及高 Gensini 评分与 AMI 患者 PCI 术后发生 MACE 事件存在相关性，对临床诊断的确立和预测预后提供帮助。

miR-126 联合纤维蛋白原与白蛋白比值对急性心肌梗死患者介入术后 MACE 的预测价值

麦尔江克力木

新疆喀什地区喀什第二人民医院

【摘要】 目的：建立基于急性心肌梗死（Acute Myocardial Infarction，AMI）患者经皮冠状动脉介入术 (Percutaneous Coronary Intervention，PCI) 后主要心血管不良事件 (Major adverse Cardiovascular Events，MACE) 预测模型并进行内部验证。**方法：**选取 **20**21 年 01 月 01 至 2022 年 06 月 30 日于新疆喀什地区第二人民医院心血管内科住院并接受 PCI 治疗的 AMI 的患者 149 例，为建立和验证预测模型，将研究对象分为两部分，2021 年 01 月至 2021 年 06 月的数据作为训练组（105 例），2021 年 06 月至 2021 年 07 月的数据作为验证组（44 例）。收集患者的基本特征、实验室检查、辅助检查情况，通过单因素和多因素 Cox 回归分析建立预测模型，并绘制列线图。采用受试者工作特征（ROC）曲线、校准曲线和 Hosmer-Lemeshow 拟合优度检验验证和评价预测模型的区分度和校准度；决策曲线分析（DCA）评估预测模型的临床有效性。**结果：**基于能独立预测主要心血管不良事件 (MACE) 的 miR-21 分界值 1.460，将所有 AMI 患者分为低 miR-21 组和高 miR-21 组。基于单因分析显示 CK（HR=1.000, P=0.008），AST(HR=1.004,P = **0.021**），CHOL(HR=1.606,P =**0.037**），Gensini 评分（HR=1.019,P =0.001）和高 miR-21 状态（HR=5.540,P < 0.001）与 MACE 事件发生显著相关；多因素分析证实 Gensini 评分 (HR=1.014,P =0.003) 和高 miR-21 状态 (HR=4.390,P=0.022) 为独立预测因子。制定了列线图来预测 MACE 事件的发生，C- 指数和 ROC 曲线下的面积证实了列线图的预测准确性有所提高。校准曲线表明，观测到的概率与列线图预测的概率在训练，验证和整个队列中具有很高的一致性。DCA 证实，在训练组中列线图提供更大的净获益。最后，Kaplan-Meier 分析显示，高风险组患者发生 MACE 事件的概率最高，预后最差（P<0.0001）。 **结论：**入院时高 miR-21 水平及高 Gensini 评分与 AMI 患者 PCI 术后发生 MACE 事件存在相关性，对临床诊断的确立和预测预后提供帮助。

SBAR 标准化沟通模式：在急性心肌梗死患者转交接护理中的应用研究

闫茂芳

太原市中心医院

目的: 探讨 SBAR(现状 - 背景 - 评估 - 建议)标准化沟通模式在急性心肌梗死 (AMI) 患者转交接护理中的应用效果，以提高信息传递的准确性、缩短交接时间并降低不良事件发生率。

方法：采用对照研究设计，选取某三甲医院 2023 年 1 月至 2024 年 6 月收治的 AMI 患者 200 例，随机分为对照组（常规交接）和干预组（SBAR 标准化交接），每组 100 例。比较两组交接时间、信息完整率、护理差错发生率及医护人员满意度。

结果：干预组平均交接时间显著缩短（15.2±2.8 min vs. 28.5±4.6 min，P<0.05）；信息完整率由常规组的 78.3% 提升至 96.5%（P<0.05）；护理差错发生率从 12.0% 降至 3.0%（P<0.05）；医护人员满意度由 72.4% 提高至 94.6%（P<0.05）。

结论：SBAR 沟通模式能够帮助护理人员接受更有效的患者信息，最大程度上确保护理实施的安全性。采用 SBAR 沟通模式进行交接，护理人员对患者的病情变化、治疗、检查等相关情况做到心中有数，并且在患者跨院区间转运护理操作的过程中，其护理思路清晰，可以做到有条不紊有预见性地实施护理干预措施；同时实施 SBAR 沟通模式进行转交接能够避免交接遗漏，及时发现护理工作中所存在的问题。SBAR 模式可优化 AMI 患者的转交接流程，提高护理连续性和安全性，值得临床推广。

基于单细胞技术研究 LEF1 调控 IL6ST 转录抑制 CD56dimCD16+NK 细胞凋亡在心 肌梗死中的机制研究

永 [1]

1. 自治区人民医院

2. 新疆心脏血管稳态与再生医学研究重点实验室

[摘要] 目的：通过探究 LEF1 和 IL6ST 对 CD56 dimCD16+NK 细胞凋亡的影响，

基于单细胞层面揭示 LEF1 对 IL6ST 转录的调控作用，在 NK 细胞中对 MI 的分子

机制，为 MI 的诊治提供理论依据。方法：收集我院 MI 患者（实验组）与健康人

（对照组）各 5 例血液 PBMC 样本。单细胞测序检测 CD56 dimCD16+NK 细胞比

例及 LEF1 和 IL6ST 在 CD56 dimCD16+NK 细胞中的表达，并利用流式细胞分选

技术对 CD56 dimCD16+NK 细胞在 MI 中的比例变化进行验证，利用 RT-qPCR、

Western Blot（WB）技术，检测实验组和对照组 PBMC 中 LEF1 和 IL6ST 的整体表

达水平，根据检测实验组和对照组中 LEF1 和 IL6ST 的表达，对它们的表达量进行

相关性分析。结果：（1）与对照组相比，MI 组中 CD8+T 细胞、CD14+ 单核细

胞细胞比例明显增加，CD4+T 细胞、CD16+ 单核细胞和 NK 细胞比例明显降低；

（2）MI 中的 NK 细胞亚群，可分为 CD56 dimCD16+ NK 细胞和

CD56 brightCD16- NK 细胞，CD56 dimCD16+ NK 细胞的占比最大，且 MI 组中

CD56 dimCD16+ NK 细胞比例明显降低，对其中的差异表达基因分析，发现

CD56 dimCD16+ NK 细胞发生下调表达的基因最多；（3）SCENIC 分析 LEF1 所

调控的靶基因，发现 LEF1 调控的基因富集到细胞凋亡的负调控信号通路中，

在该通路中 IL6ST 基因与 MI 的发展紧密相关，且 LEF1 和 IL6ST 在 MI 中都低表达

。结论：LEF1 可能通过调控 IL6ST 的转录并上调其表达，抑制

CD56 dimCD16+NK 细胞凋亡，最终抑制 MI 的进展。

Axl 受体通过保护内皮屏障与减轻钙超载在心肌缺血再灌注损伤中发挥保护作用

李悠然 钱菊英 陈章炜

上海复旦大学附属中山医院

目的

Axl 是 TAM 家族的一员，该家族包含三种受体酪氨酸激酶，即 Tyro3、Axl 和 MerTK。已有研究证明 Axl 与多种疾病相关，然而 Axl 影响心血管疾病的具体机制仍不清楚。本研究旨在探究 Axl 在心肌缺血再灌注损伤过程中对心脏微血管功

能的保护作用。

方法

采用雄性 C57BL/6 小鼠，通过结扎左前降支冠状动脉（LAD）1 小时后松开结扎线，使缺血组织再灌注，以此建立心脏缺血再灌注（I/R）损伤模型。利用蛋白质印迹法（Western blotting）和免疫荧光法（Immunofluorescence）检测 I/R 损伤后不同时间点（12 小时、1 天、3 天、7 天、28 天）对照组织与缺血组织中 Axl 的水平。此外，我们使用人源心脏微血管内皮细胞（HCMEC）在体外分析了 Axl 表达的调控。

通过蛋白质印迹法和免疫荧光法检测缺血组织以及经历氧糖剥夺 / 复氧（OGD/R）损伤的 HCMEC 中 Axl 的表达。进一步利用靶向 Axl 的 shRNA 进行基于细胞的实验，以明确其在 OGD/R 损伤中扮演的角色。

将动物随机分为两组，腹腔注射溶剂（DMSO）或选择性 Axl 拮抗剂 R428（50mg/kg），连续 5 天。然后，通过在体内施用 R428 抑制 Axl 受体，评估 Axl 对 I/R 损伤的影响。

结果

Axl 在缺血组织中的表达上调（图 1A, C），但在 I/R 损伤的内皮细胞簇以及遭受 OGD/R 损伤的 HCMEC 中表达下调（图 1B, E, F）。Axl 与 CD31 在缺血组织中共表达，且与正常组织相比，缺血组织展现出显著更高的 Axl 表达（图 1D）。选择性 Axl 拮抗剂 R428 处理导致心肌梗死面积显著扩大（图 2A）。在 OGD/R 损伤后，Axl 敲低的 HCMEC 细胞活力急剧下降（图 2B）。Axl 敲低导致 HCMEC 中血管内皮钙粘蛋白（VE-Cadherin）和 SERCA2 的蛋白表达下调，表明 Axl 在增强内皮屏障功能和维持心脏钙稳态中发挥作用（图 2C）。Axl 敲低导致线粒体活性氧（ROS）产生增加并加剧钙超载（图 2D, E）。

结论

Axl 受体酪氨酸激酶可能通过保护内皮细胞屏障、减轻钙超载和氧化应激，在心血管损伤中发挥保护作用。目前，关于 Axl 改善心血管疾病的研究尚不完整。本研究结果可能为心肌微血管保护的机制研究提供新思路。发现潜在的靶向激动剂或能为心肌微血管再灌注损伤的预防和治疗提供新的选择。

血浆致动脉粥样硬化指数与急性心肌梗死患者预后的相关性研究

王凯阳

新疆维吾尔自治区人民医院

目的：探讨基线血浆致动脉粥样硬化指数 (AIP) 对急性心肌梗死 (AMI) 患者长期预后的影响。

方法：连续纳入 2018 年 1 月至 2019 年 12 月期间新疆维吾尔自治区人民医院收治的 712 名 AMI 患者作为研究对象，依据 AIP 三分位数将研究对象分为低值组(AIP≤0.280, n=237)，中值组(AIP 0.280-0.852, n=238)和高值组(AIP>0.852, n=237)。终点事件定义为主要心血管不良事件 (MACEs) 的发生。采用多因素 Cox 回归分析 MACEs 发生的独立影响因素；采用限制性立方样条图分析 AIP 与 MACEs 发生风险之间的非线性关系; 采用 Kaplan-Meier 曲线分析组间生存差异; 亚组分析评估 AIP 对 MACEs 预测价值的一致性。

结果：随着 AIP 三分位数分组递增，患者血脂异常和 MACEs 发生比例升高，白细胞计数、空腹血糖、甘油三酯、总胆固醇、低密度脂蛋白、AIP 升高，高密度脂蛋白降低，差异具有统计学意义 (P＜0.05)。多因素 Cox 回归分析结果显示：AIP 是 MACEs 发生的独立危险因素 (HR=2.024, 95%CI: 1.211-3.381, P=0.007)。限制性立方样条图分析结果显示：AIP 与 MACEs 发生风险之间呈“L”形非线性效应关系 (P-NOnlinear=0.008)，当 AIP>0.613 时，AMI 患者 MACEs 风险随 AIP 升高而升高。Kaplan-Meier 生存曲线分析结果显示：随着 AIP 升高 AMI 患者 MACEs 累积发生率显著增加 (Log-rank test, P=0.032)，与低值组相比，高值组患者 MACEs 发生风险增加 131%(HR=2.311, 95%CI: 1.261-4.234, P=0.007)。亚组分析结果显示，各亚组内交互作用 P 值均不显著，AIP 对 MACEs 预测能力适用于所有亚组人群。

结论：基线 AIP 升高是 AMI 患者远期不良预后的独立预测因子。

血清 sTREM2 与老年急性冠脉综合征的相关性研究

段馨悦

石河子大学第一附属医院

目的：探讨血清可溶性髓样细胞触发受体 2（soluble triggering receptor expressed on myeloid cells 2，sTREM2）对老年急性冠脉综合征（acute coronary syndromes，ACS）的诊断价值和血清 sTREM2 与老年 ACS 患者冠状动脉病变程度的相关性。

方法：选取 2024 年 3 月至 2024 年 8 月于石河子大学第一附属医院住院疑诊为 ACS 并行冠状动脉造影的老年患者（年龄≥ 60 岁）165 例。收集患者的一般资料及检验结果，记录患者的冠状动脉造影结果并计算 Gensini 评分以评估其冠状动脉病变程度，通过 ELISA 法检测患者的血清 sTREM2 水平。统计分析血清 sTREM2 对老年 ACS 的诊断价值及与老年 ACS 患者冠状动脉病变程度的相关性。

结果：1.ACS 组的糖尿病病史比例、WBC、FIB、sTREM2 水平升高，HDL-C、ALB 水平降低，差异具有统计学意义（P < 0.05）；血清 sTREM2 水平在非冠心病组、不稳定性心绞痛组、急性心肌梗死组依次升高，各组间差异有统计学意义（P < 0.05）。2. 吸烟患者的血清 sTREM2 水平明显高于未吸烟患者（P < 0.001）；血清 sTREM2 水平与 TG（r = -0.281，P < 0.001）、LDL-C（r = -0.196，P = 0.012）、HDL-C（r = -0.333，P < 0.001）、ALB（r = -0.358，P < 0.001）水平呈负相关，血清 sTREM2 水平与 WBC（r = 0.240，P = 0.002）、FIB（r = 0.232，P = 0.003）水平呈正相关。3. 糖尿病病史（OR = 3.681，95% CI：1.183-11.451，P = 0.024）、血清 sTREM2 水平升高（OR = 1.260，95% CI：1.102-1.441，P = 0.001）是 ACS 的独立危险因素，HDL-C 水平升高是 ACS 的独立保护因素（OR = 0.145，95% CI: 0.027-0.798，P = 0.026）。4.ROC 曲线分析显示，血清 sTREM2 对老年 ACS 有一定的诊断价值，以 14.77 为截断值，AUC 为 0.771（95 % CI = 0.694-0.847，P < 0.001），敏感性为 66.90 %，特异性为 78.00 %。5. 血清 sTREM2 水平与 Gensini 评分呈正相关（r=0.311，P < 0.001）。6. 多元线性回归分析显示，血清 sTREM2 水平升高是 Gensini 评分的独立危险因素（B = 1.971，P < 0.001）。

结论：1. 血清 sTREM2 水平升高是老年 ACS 的危险因素，血清 sTREM2 对老年 ACS 有一定的诊断价值。2. 血清 sTREM2 水平升高是老年 ACS 患者 Gensini 评分的独立危险因素，对提示冠状动脉病变程度有潜在价值。

A youth acute myocardial infarction patient during high-altitude de-acclimatization: A case report and literature review

Zhiling He[1,3], Lu-Xun Tang[3], Jing-Tang Hu[3], Jia-Jie Liao[2], Peng Wang[3], Shuang Li[3]

1. Department of Clinical Medicine, North Sichuan Medical College

2. Chengdu Medical College

3. Department of Cardiology, The General Hospital of Western Theater Command

Background: High-altitude exposure (>2,500 m) imposes profound multisystem physiological strain, with the cardiovascular system exhibiting exceptional vulnerability due to hypoxia-inducible factor (HIF)-mediated maladaptations. The synergistic triad of chronic hypobaric hypoxia, reduced atmospheric pressure (≈ 60% sea-level at 4,000m), and thermal extremes triggers a pathological cascade: endothelial dysfunction via nitric oxide synthase suppression, sympathetic overactivation elevating resting heart rate by 15-20 bpm, and metabolic dysregulation characterized by insulin resistance and leptin dysregulation. Consequently, residents aged 30-50 years in high-altitude regions demonstrate significantly elevated cardiometabolic disorders: 1) Atherogenic dyslipidemia: 2.1-fold higher LDL and lipoprotein(a), 2) Hypertension prevalence: 34.2% vs. 24.8% in lowlands, 3) Diabetes incidence: adjusted OR 1.83 (95% CI: 1.4-2.4).This risk profile drives disproportionate acute myocardial infarction (AMI) burdens: 2.3-fold higher incidence (95% CI: 1.7-3.1), multivessel disease prevalence (68.4% vs 47.1%), and 19.7% 12-month recurrence versus 8.9% in low-altitude counterparts. Mechanistically, chronic hypoxia induces secondary polycythemia (hematocrit >52%), enhanced platelet aggregability, and HIF-1α-mediated vascular inflammation - creating a thrombogenic milieu. Alarmingly, while these altitude-acclimatized risks are documented, the de-acclimatization phase remains critically understudied. During this transition, rapid hemodilution, autonomic instability, and rebound oxidative stress create vulnerability windows for plaque rupture. Less than 5% of current altitude-cardiology literature addresses this vulnerable phase characterized by hemodynamic instability and rebound oxidative stress, creating dangerous knowledge gaps in preventive strategies.

Methods: Through an integrated analysis of a young adult AMI case during high-altitude de-acclimatization, we synthesized a systematic literature review with retrospective assessment of pathogenic mechanisms. This methodology elucidated critical disease progression patterns, enabling formulation of evidence-based clinical management recommendations. These tailored protocols provide actionable guidance for diagnostic and therapeutic decision-making in this vulnerable physiological transition period.

Case presentation: A previously healthy 34-year-old male presented with 9 hours of crushing substernal chest pain. Electrocardiogram (ECG) demonstrated anteroseptal ST-segment elevation in leads V1-V3 with reciprocal changes in inferior leads. Emergency coronary angiography (CAG) revealed thrombus-containing total occlusion of the proximal left anterior descending (LAD) artery (TIMI 0 flow), accompanied by diffuse non-culprit coronary plaques (30-40% stenosis). Primary percutaneous coronary intervention (PCI) with drug-eluting stent implantation restored TIMI 3 flow, confirming acute ST-elevation myocardial infarction secondary to plaque rupture. The event occurred 36 hours post-descent from 4,200m altitude after intensive exercise, highlighting de-acclimatization-associated cardiovascular vulnerability in young high-altitude workers.

Conclusions: Acute myocardial infarction (AMI) risk during high-altitude de-acclimatization involves multifactorial pathophysiology, prominently featuring dyslipidemia-induced endothelial dysfunction and exercise-triggered hemodynamic stress. Our analysis confirms hyperlipidemia (LDL >4.1 mmol/L) amplifies plaque vulnerability through hypoxia-enhanced oxidation of LDL particles, while intense physical activity during this transitional phase provokes catecholamine surges that destabilize coronary lesions. Critically, the convergence of altitude-acclimatized cardiovascular adaptations with rapid re-exposure to normobaric conditions creates a distinct risk window. For young high-altitude workers and military personnel, we advocate: 1) Mediterranean-diet adoption to optimize lipid profiles pre-descent, 2) graded aerobic exercise protocols (<60% VO_2 max) during initial 7-day reacclimatization, and 3) abstinence from vigorous activity until hematocrit stabilizes (<48%).

These evidence-based countermeasures address the unique pathophysiological triad of hemoconcentration, autonomic dysregulation, and oxidative stress rebound characterizing de-acclimatization–a previously underappreciated period of cardiovascular vulnerability requiring protocolized management.

急性心肌梗死新发房颤预后模型的开发与验证：一项多中心回顾性研究

魏毅东

上海市第十人民医院

目的：

开发并验证用于预测急性心肌梗死（AMI）合并新发心房颤动（NOAF）患者 5 年内发生主要不良心脏事件（MACE）风险的预测模型。

方法：

回顾性多中心队列研究。纳入 2014 年 1 月至 2022 年 1 月三家三甲医院连续收治的 663 例心梗后 NOAF 患者。采用逐步多变量 Cox 回归分析确定独立危险因素，建立预测 5 年 MACE 风险的模型。通过时间依赖性受试者工作特征曲线下面积（AUC）、C 指数、校准曲线和决策曲线分析（DCA）在建模与外部验证队列中评估模型性能。

结果：

中位随访 4.6 年（IQR：3.0-6.3）的建模队列和 3.4 年（IQR：2.1-5.7）的验证队列中，分别有 195 例和 68 例心梗后 NOAF 患者发生 MACE。逐步回归分析确定预测模型（NOAFCAMI 评分）包含 7 个变量：年龄、心衰病史、Killip 分级、经皮冠状动脉介入治疗、NT-proBNP 峰值、房颤负荷及症状性房颤。建模队列 5 年 AUC 为 0.83（95%CI：0.77-0.88），内部验证的乐观校正 C 指数为 0.72（95%CI：0.68-0.76）；外部验证 5 年 AUC 达 0.79（95%CI：0.69-0.89）。校准分析显示建模队列（Brier 评分：0.17[95%CI：0.15-0.19]）与验证队列（Brier 评分：0.19[95%CI：0.16-0.22]）的预测一致性良好。DCA 证实该模型在广泛风险阈值内较全球急性冠脉事件注册评分具有更优的临床净获益。模型在线计算器已公开（https://noafcamiscore.shinyapps.io/dynnomapp/

）。

结论：

NOAFCAMI 评分是首个经外部验证、可个体化评估心梗后 NOAF 患者 MACE 风险的预测工具，为精准管理和二级预防提供重要依据。

心肌梗死后睡眠对心脏左室射血分数的短期影响

丁欢欢 周贤惠

新疆医科大学第一附属医院

目的：通过匹兹堡睡眠质量指数量表 (Pittsburgh Sleep Quality Index PSQI) 探索初次诊断心肌梗死 (myocardial infarction MI) 患者的睡眠改变及各个睡眠周期对 MI 后心脏左室射血分数 (the left ventricular ejection fraction LVEF) 的短期影响，从而为 MI 的治疗方案提供新的临床思路，达到改善患者临床预后的目的 **方法：**选取 2023 年 5 月 ~2024 年 7 月就诊于新疆医科大学第一附属医院的患者，根据纳入标准及排除标准，筛选出原始病例组（初次诊断 MI 患者）原始对照组（非 MI 患者），入院 5~7 天后均对其进行 PSQI 调查及睡眠监测，通过倾向性评分匹配调整混杂因素，最终得到病例组 (n=109)，对照组 (n=109)；对收集的 PSQI 评分及睡眠监测报告进行对比分析，明确 MI 后患者睡眠改变的情况及睡眠对心脏 LVEF 的影响 **结果：**①本研究发现病例组睡眠质量总评分 7(6,9.5)，对照组睡眠质量总评分 5(3,6),P <0.001；②睡眠持续性（小时）：病例组 6.5(5.5,7)，对照组 7(7,7.5)，P<0.001；习惯性睡眠效率 (%)：病例组 80.0(73.7,87.5)，对照组 87.5(83.3,88.9),P<0.001；③病例组睡眠质量总评分：病例组 7(6,9.5)，随访病例组 8(7,10)，P<0.001；病例组习惯性睡眠效率 (%)：病例组 80.0(73.7,87.5)，随访病例组 75(68.3,79.3)，P<0.05；④非 MI 组睡眠片段均值 150.6 分钟，MI 组 55.12 分钟 P<0.05，存在统计学差异；⑤非 MI 组 N1+N2 睡眠片段均值 213.9 分钟，MI 组 60.65 分钟 P<0.05，存在统计学差异；⑥非 MI 组与觉醒次数≤ 10 组的 N1+N2 睡眠片段均值差为 123.2 分钟 P<0.05，非 MI 组与觉醒次数 >10 组的睡眠片段均值差为 183.3 分钟，P<0.0001，以上均具有统计学差异；⑦ MI 患者的总睡眠片段均值 N1+N2 睡眠片段均值均分别随着总觉醒次数 N1+N2 觉醒次数的增加呈下降趋势，P<0.001；⑧ MI 患者的 LVEF 随着总睡眠时长的增加呈下降趋势，P<0.05；⑨ MI 患者的 LVEF 随着总觉醒次数 N1+N2 的觉醒次数的增加呈下降趋势，P<0.05；⑩ MI 患者的 LVEF 随着睡眠片段均值 N1+N2 睡眠片段均值的延长呈上升趋势，P<0.05 结论：1. 患者发生 MI 后睡眠发生改变，可表现为睡眠质量的下降及睡眠效率的降低；2. 与非 MI 患者相比，MI 患者的睡眠片段均值缩短，与此同时 N1+N2 期睡眠片段均值显著缩短，且随着觉醒次数的增加差距愈发显著，睡眠呈现碎片化；3. 患者发生 MI 后心脏 LVEF 与总睡眠时长呈负相关；4. 患者发生 MI 后心脏 LVEF 与总睡眠片段均值、N1+N2 期睡眠片段均值呈正相关；

Multi-Omics Mendelian Randomization Identifies Genes for High Platelet Reactivity in Myocardial Infarction

Yi-An Yao, Yu Tang, Ke-Ke Ding, Zi Ye, Cui-Mei Zhao, Yan Lai, Wen-Wen Yan, Xue-Bo Liu

上海市同济医院（同济大学附属同济医院）

Background and Aims: Myocardial infarction (MI) is a leading cause of mortality worldwide, with high platelet reactivity (HPR) recognized as a potential risk factor. However, the genetic causal association between HPR and MI remains unclear. To identify potential pathogenic genes for Myocardial infarction(MI) by exploring the association between HPR-related genetic variants and MI risk using a multi-omics Mendelian randomization(SMR) approach.

Methods: We utilized summary data from genome-wide association studies(GWAS) for MI and blood-based methylation quantitative trait loci(mQTLs), expression QTL(eQTLs),and protein QTL(pQTLs). Tissue-specific eQTL data from GTEx v8 was also included. SMR analysis and the HEIDI test were employed for pleiotropy. Colocalization analysis identified shared genetic variants.

Results The SMR analysis identified 52 methylation sites (corresponding to 36 genes) associated with MI (P-SMR < 0.05, P-SMR multi < 0.05 and P-HEIDI > 0.05). For instance, the methylation site cg20216752 located in ALOX12 shows a positive association with MI risk (OR = 1.10, 95% CI:1.02-1.19). Conversely, another methylation site cg14375499 within the same gene, ALOX12, exhibits a negative association with the risk (OR = 0.91, 95% CI:0.83-0.99).

The SMR analysis identified 9 genes related to HPR that are associated with MI risk (P-SMR < 0.05, P-SMR multi < 0.05 and P-HEIDI > 0.05). Among them, the expression levels of 3 genes (MAPK7, VAMP8, SCARB1) were negatively associated with MI risk, while the expression levels of the other 6 genes were positively associated.

Colocalization analysis showed that 3 of these genes have strong colocalization evidence in the colocalization window (PPH4 > 0.5). GPX1, PIK3CB, and VAMP8 were validated in the GCST011364 MI cohort (P-SMR < 0.05, P-SMR multi < 0.05 and P-HEIDI > 0.05), and VAMP8 (ENSG00000118640, OR = 0.997, 95% CI: 0.996-0.999, P =1.11×10^{-4}, P-multi = 1.21×10^{-3} and P-HEIDI = 0.596) was validated in the UKB MI cohort (P-SMR < 0.05, P-SMR multi < 0.05 and P-HEIDI > 0.05)

The SMR analysis identified four proteins related to HPR–PCSK9, PECAM1, SHH, and SOD1–as being associated with MI risk (P-SMR < 0.05, P-SMR multi < 0.05 and P-HEIDI > 0.05). SHH and SOD1 protein abundance were all negatively associated with MI risk, and PCSK9 and PECAM1 protein abundance were positively associated with MI risk.

Colocalization analysis revealed that 13 of these sites (corresponding to 12 genes) have strong colocalization evidence in the SNP colocalization window (PPH4 > 0.5). AGT (cg19125606); CFTR (cg11606570); GPX1 (cg24011261); ITGB3 (cg06568783); NOS3 (cg19475224); PECAM1 (cg02459519); TRAF3 (cg18185554); VAMP8 (cg23752985) were validated in the GCST011364 MI cohort (P-SMR < 0.05, P-SMR multi < 0.05 and P-HEIDI > 0.05). ABO (cg07241568); CFTR (cg11606570); ITGB3 (cg06568783); SCARB1 (cg15282973); VAMP8 (cg23752985) were validated in the UKB MI cohort (P-SMR < 0.05, P-SMR multi < 0.05 and P-HEIDI > 0.05).

Colocalization analysis revealed that both PCSK9 and PECAM1 proteins had strong colocalization evidence in the colocalization window (PPH4 > 0.5). The PECAM1 (OR = 2.13, 95% CI: 1.27-3.59, P = 4.29×10^{-3}, P-multi = 4.29×10^{-3} and P-HEIDI = 0.891) protein was validated in the GCST011364 MI cohort (P-SMR < 0.05, P-SMR multi < 0.05 and P-HEIDI > 0.05). The PECAM1 (OR = 1.023, 95% CI: 1.005-1.041, P = 0.0131, P-multi = 0.0131 and P-HEIDI = 0.253) protein was also validated in the UKB MI cohort (P-SMR < 0.05, P-SMR multi < 0.05 and P-HEIDI > 0.05).

Both CSK (cg20552236, OR = 0.25, 95% CI: 0.17-0.37, P = 3.77×10^{-12}, P-multi = 3.77×10^{-12} and P-HEIDI = 0.501) and GPX1 (cg24011261, OR = 1.57, 95% CI: 1.35-1.82, P = 1.94×10^{-9}, P-multi = 1.94×10^{-9} and P-HEIDI = 0.115) were significantly validated in these results (P-SMR < 0.05, P-SMR multi < 0.05 and P-HEIDI > 0.05)

Conclusions: This study identified potential causal associations between HPR and MI. Specifically, CSK and GPX1 emerged as key genes with potential pathogenic roles in MI.

Keywords: Myocardial Infarction, Platelet Reactivity, Multi-Omics, Mendelian Randomization, Colocalization

MIF 在心肌缺血 / 再灌注后的微血管损伤中的作用及机制

赵帮豪 高晓明

新疆医科大学第一附属医院心脏中心，新疆医科大学临床医学研究院，新疆医学动物模型研究重点实验室

目 的：（1）动物模型中，研究不同心肌缺血及再灌注（ischemia/reperfusion，I/R）时间对微血管损伤（microvascular obstruction，MVD）的影响。（2）在细胞和动物模型中，研究巨噬细胞移动抑制因子（macrophage migration inhibitory factor，MIF）在 I/R 所致的 MVD 中的作用及机制。

方 法：对 10-14 周龄雄性野生型（wild type，WT）C57BL/6J 小鼠进行不同心肌缺血时间或不同再灌注时间的 I/R 手术，随后采用①硫黄素 S 和 Evans 蓝双重染色法测定各组术后心肌微血管阻塞（microvascular obstruction，MVO）程度；②Evans 蓝尾静脉注射后左心室切片图像分析微血管渗漏（microvascular leakage，MVL）程度；③三氯乙酸（trichloroacetic acid，TCA）化学法提取心肌的 Evans 蓝定量检测 MVL 程度；④以 C57BL/6J 小鼠为背景，建立 MIF 基因敲除小鼠（MIFKO），与 WT 小鼠同时进行 I/R（1 h/24 h）造模手术。检测两组小鼠的心脏毛细血管管腔开放数量，MVL 组织学测量和定量检测，连接蛋白

的表达水平，检测细胞凋亡蛋白的表达水平，超声分析 WT 和 MIFKO 小鼠在 I/R（1 h/24 h）后的心功能变化；⑤通过基因干预方法，给内皮细胞用 siRNA 敲低 MIF 基因，用质粒过表达 MIF 基因和使用 SP600125 抑制 JNK 磷酸化，在缺氧 / 复氧（hypoxia/reoxygenation，H/R）刺激后检测内皮细胞的增殖情况、迁移能力、NO 分泌水平、通透性、连接蛋白和细胞凋亡蛋白的表达水平。

结 果：（1）MVO 和 MVL 的严重程度依赖于缺血时间和再灌注时间，但再灌注 3 天后渗漏程度明显减轻。（2）1 h-I/24 h-R 后，WT 小鼠循环和心肌 MIF 表达水平均增高，MIF 通过激活 JNK 通路增加凋亡相关蛋白的表达水平，下调连接蛋白的表达水平，造成 MVO 和 MVL，而 MIF 基因的缺失可减轻 I/R 导致的微血管损伤。超声结果提示敲除 MIF 基因可以改善 I/R 后的左心室收缩功能。在内皮细胞模型中，H/R 会导致内皮细胞增殖水平、NO 分泌水平、迁移能力下降，通透性增加，连接蛋白表达水平下降，细胞凋亡蛋白表达增加。敲低 MIF 可减轻 H/R 对细胞的损伤程度，改善这一效应，过表达 MIF 则会加重 H/R 对细胞的损伤程度，但在使用 JNK 抑制剂 SP600125 后得到逆转和改善。

结 论：I/R 对微血管损伤的严重程度依赖于缺血及再灌注时间，且 MVL 在再灌注 3 天后开始消退。缺血或缺氧后，受损的心脏微血管内皮细胞释放 MIF，激活 JNK 通路，诱导血管内皮细胞凋亡和血管内皮间连接蛋白减少，内皮屏障功能障碍，通透性增加，加重微血管渗漏，最终导致不可逆的心功能障碍。

支架置入策略对前降支真性分叉病变患者术后一年主要不良心血管事件的影响

赖红梅

新疆维吾尔自治区人民医院

目的：冠状动脉分叉病变（CBL）作为临床常见且复杂的冠心病病变类型，一直是心血管介入治疗中的研究热点。尽管经皮冠状动脉介入治疗（PCI）在改善患者预后方面已取得显著成效，但对于分叉病变的支架策略选择仍存在较大争议。本研究旨在系统探讨在冠状动脉前降支（LAD）真性分叉病变中，单支架与双支架策略在术后 1 年内发生主要不良心血管事件（MACE）的差异，为临床医师在治疗策略的选择提供科学依据和临床经验支持。

方法：本研究纳入新疆维吾尔自治区人民医院心内科接受经皮冠状动脉介入治疗的 482 例前降支真性分叉病变患者。这些患者均通过冠状动脉造影确诊分叉病变，其中依据手术策略的不同，将患者分为即刻单支架策略组（295 例）和双支架策略组（187 例）。研究对比了两组患者的基本临床特征（如年龄、性别、血脂水平、糖尿病、高血压等），并详细记录了 PCI 术中涉及的病变血管情况，包括分叉血管的血管直径、病变长度和血管狭窄程度。同时，患者在手术后定期随访，通过电话和门诊复查，收集其术后的 1 年内主要心血管事件，包括心肌梗死、血管再狭窄、再次血运重建和死亡等，评估两组的临床预后。

结果：随访期间，观察到双支架组患者的 1 年 MACE 发生率高于单支架组，统计分析显示差异具有统计学意义（P < 0.05），提示双支架策略可能增加不良事件的风险。具体而言，双支架组的血管再狭窄和血运重建需求显著高于单支架组，但在血管内再狭窄的发生率方面，两组之间未表现出明显差异（P > 0.05），提示两者在再狭窄发生方面不存明显差异。生存分析进一步支持上述结论，显示采用双支架策略的患者在随访期间发生 MACE 的总体风险明显较高（P < 0.05），说明双支架策略在此类患者中可能存在潜在的风险。

结论：对于冠状动脉前降支真性分叉病变患者，通过本研究可以看出，采用双支架策略的患者在随访一年内，其发生主要不良心血管事件的风险显著高于采用即刻单支架策略的患者。未来还需更多大样本、多中心的前瞻性研究，以优化分叉病变的支架策略，提升患者的长期预后质量，为临床实践提供更具科学性和指导性的治疗方案。

Sex-related differences in clinical outcomes of octogenarians with STEMI in China

Shao-Feng Guan, Jia- Cai, Xin-Kai Qu

Huashan Hospital Fudan University

Backgrounds and aims: Women have a worse prognosis after ST-segment elevation myocardial infarction (STEMI) than men. However, it is unclear if these differences persist among octogenarians.

Methods and Results: This is a country-wide population-based cohort study performed on octogenarians with STEMI between January 2014 and December 2021 across 2812 different chest centers in China. The analysis included 24,402 male patients (mean age 83.8 ±3.4 years), 22,155 female patients (mean age 84.3 ±3.7 years), and a total of 20,924 (49.0%) patients underwent primary PCI strategy. Men exhibited a shorter time for Onset- FMC and STD compared to women in the overall study population or primary PCI population. men and women differed significantly in baseline characteristics, except for persistent chest pain, pattern of patient arrival, CVD family history, AF, valvular disease and the treatment of dual antiplatelet, anticoagulation drug, and beta-blocker. Additionally, men were more likely to undergo primary PCI compared to women. Men had a lower prevalence of calcification and a higher rate of stent implantation and PCI success, and there were no sex differences in proportion of bifurcation lesion, chronic total occlusion (CTO), acute thrombosis, and multivessel disease. Women exhibited a higher risk of in-hospital mortality (odds ratio [OR], 1.13; 95% confidence interval [CI], 1.05- 1.21) and the composite outcome (OR, 1.22; 95% CI, 1.16- 1.27) compared to men after multivariable adjustment, regardless of whether they received a primary percutaneous coronary intervention (PCI) strategy or not. Meanwhile, primary PCI strategy was associated with a reduced risk of in-hospital mortality (OR, 0.61; 95% CI, 0.55- 0.68) and the composite outcome (OR, 0.79; 95% CI, 0.74- 0.84) among female octogenarians, whereas, thrombolytic therapy conferred no significant short-term benefit in both survival (OR, 1.10; 95% CI, 0.91- 1.32) and the composite outcome (OR, 1.16; 95% CI, 1.02- 1.33). These associations persisted after adjusting for baseline clinical covariates by PSM and IPTW analysis, and subgroup analysis demonstrated the robustness of these findings across nearly all subgroups. During a median follow-up of 6.6 months after hospital admission, 31.6% of patients had died, and female sex remained associated with an increased incidence of all-cause mortality (hazard ratio [HR], 1.11, 95% CI: 1.07–1.15) among octogenarians with STEMI. Subgroup analysis revealed that in both overall study population and primary PCI population, women was consistently associated with an elevated risk of in-hospital mortality and the composite outcome in nearly all subgroups (P < 0.05), even after adjusting for confounders. Meanwhile, primary PCI was associated with significantly lower risks of both in-hospital mortality and the composite outcome in nearly all subgroups in women (P < 0.05), whereas, thrombolytic therapy only showed significant associations with the composite outcome in subgroups of patients with age > 85 years, no current smoking, no AF, and no CKD.

Conclusions: Among octogenarians with STEMI in China, female sex was significantly associated an increased risk of in-hospital mortality and the adverse composite outcome. Additionally, primary PCI strategy could mitigate these risks, whereas thrombolytic therapy did not confer a short-term benefit among female octogenarians with STEMI.

Keywords: ST-segment elevation myocardial infarction; octogenarian; mortality; primary percutaneous coronary intervention.

基于急性心肌梗死患者血浆的核酸适配体筛选及其临床诊断价值研究

廖仙莹 解玉泉 卜军

上海交通大学医学院附属仁济医院

目的：急性心肌梗死（acute myocardial infarction, AMI）是心血管疾病致死的主要原因之一，早期快速诊断对改善患者预后至关重要。目前临床依赖的心肌损伤标志物如肌钙蛋白（cTn）等检测存在时间窗口延迟、灵敏度不足等问题，亟需开发新型生物标志物及快速诊断工具。核酸适配体（Aptamer）是一类通过体外筛选技术（如 SELEX）获得的单链 DNA 或 RNA 分子，能够通过特定的三维空间构象，以高亲和力和高特异性结合靶标分子（如蛋白质、小分子等）。核酸适配体具有优异的化学稳定性、灵活的功能修饰、低成本生产、多靶标同步检测等优点，在临床不同类型的疾病标志物检测中展现出独特优势。本研究的核心目标在于通过构建 AMI 特异性核酸适配体检测体系，显著提升 AMI 超急性期（<4 小时）的诊断效能，突破现有生物标志物时间窗的限制，为临床实施早期再灌注治疗提供关键时间窗口，从而有效降低心肌不可逆损伤风险，改善患者预后转归，同时为探索 AMI 发病机制中新型分子靶标提供研究思路。

方法：1.SELEX 技术筛选并验证：利用 SELEX 技术筛选针对 AMI 血浆的特异性核酸适配体，利用筛选得到的核酸适配体进行体内实验与体外实验验证。

2. 靶蛋白及亲和力测定：利用质谱检测核酸适配体富集到的蛋白，表面等离子共振技术（SPR） 验证核酸适配体与靶标的结合动力学（KD 值）及特异性，明确核酸适配体的靶蛋白。

3. 核酸适配体功能验证：通过分子对接预测核酸适配体与靶蛋白的结合区域，评估核酸适配体与靶蛋白的结合强度，指导适配体进行合理优化，与靶蛋白更好地结合。

4. 临床诊断价值评估：通过 ROC 曲线分析核酸适配体单独或联合 cTnI 的诊断效能，并追踪 STEMI 患者预后（如 30d 再梗死率、左心室射血分数），分析靶目标核酸适配体水平与预后的相关性。

结果：本研究项目利用 AMI 患者与冠状动脉无狭窄患者的血浆样本，采用 SELEX 技术，针对血浆中潜在的 AMI 相关生物标志物进行特异性核酸适配体筛选，得到 2 条针对 AMI 的特异性核酸适配体，并在体内小动物活体成像和体外实验免疫荧光、ELISA 等实验中进行验证，并且 AMI 组与对照组的靶蛋白 SerpinD1 和 MDH2 水平差异具有显著性，并且与 cTnI 水平具有相关性，诊断效果良好。

结论：本研究基于 AMI 患者血浆的核酸适配体筛选，我们首次鉴定并获得了分别靶向 SerpinD1 和 MDH2 的高亲和力、高特异性的核酸适配体。这些成功筛选得到的核酸适配体，为开发针对 SerpinD1 和 MDH2 的新型 AMI 诊断试剂（如快速检测试纸条、生物传感器）及功能研究工具奠定了坚实基础，有望推动 AMI 的液体活检和精准诊疗发展。利用核酸适配体分子识别技术的 AMI 血浆标志物检测新方法，突破传统免疫检测技术受限于抗体开发周期长、稳定性不足的技术瓶颈，为临床提供具有高灵敏度、高特异性且可实现多重检测的分子诊断工具。

王不留行黄酮苷改善心肌梗死后心肌细胞焦亡的研究

曹阳

哈尔滨医科大学第一附属医院

目的

急性心肌梗死（AMI）是全世界死亡的主要原因之一，其病理特征为心肌细胞死亡。细胞焦亡是心肌细胞死亡的重要方式之一，但目前针对心肌梗死后细胞焦亡的治疗方法较少且效果有限。本研究旨在探讨王不留行黄酮苷（Vaccarin, VAC）对心肌梗死后心肌细胞焦亡的影响，以期为心肌梗死治疗提供新的药物选择。

方法

动物实验

实验分组：将 40 只 C57BL/6 小鼠随机分为假手术（Sham）组、心肌梗死（MI）组、

MI+VAC 组和 MI+MCC950 组（MCC950 为 NLRP3 特异性抑制剂），每组 10 只。

心肌梗死模型建立：通过结扎小鼠左前降支建立心肌梗死模型。

药物处理：MI+VAC 组小鼠心梗建模后腹腔注射 VAC(30mg/kg/d)，连续 4 周；MI+MCC950 组小鼠腹腔注射 MCC950（10mg/kg），每周两次，连续 4 周；Sham 组和 MI 组小鼠注射等量生理盐水。

心脏功能评估：使用多普勒超声心动图测定小鼠心脏功能。

氧化应激和细胞焦亡检测：通过 ELISA 检测心肌组织氧化应激指标（MDA、SOD），通过 IHC 染色、WB 和 qPCR 评估心肌细胞焦亡相关蛋白（NLRP3、Caspase-1、GSDMD-N、IL-1β）表达水平。

细胞实验

细胞分组与处理：将原代心肌细胞随机分为对照组、缺氧组、缺氧 +VAC 组和缺氧 +MCC950 组。

细胞活力与损伤检测：通过 CCK-8 检测细胞活力，通过 LDH 释放实验评估细胞损伤。

氧化应激和细胞焦亡检测：通过 ELISA 检测细胞氧化应激指标（MDA、SOD），通过 WB、qPCR 和 caspase-1 活性测定评估细胞焦亡相关蛋白表达水平。

结果

动物实验

心脏功能改善：与 MI 组相比，MI+VAC 组和 MI+MCC950 组小鼠的 LVEF 和 LVFS 显著升高，LVEds 和 LVEdd 显著降低。

氧化应激抑制：VAC 显著降低了心肌组织 MDA 水平，提高了 SOD 水平。

细胞焦亡减轻：VAC 显著降低了心肌组织 NLRP3、Caspase-1、GSDMD-N 和 IL-1β 的表达水平。

细胞实验

细胞活力提高：与缺氧组相比，缺氧 +VAC 组和缺氧 +MCC950 组细胞活力显著提高。

细胞损伤减轻：缺氧 +VAC 组 LDH 释放水平显著降低。

氧化应激抑制和细胞焦亡减轻：VAC 显著降低了原代心肌细胞 MDA 水平，提高了 SOD 水平，并降低了 NLRP3、Caspase-1、GSDMD 和 IL-1β 的表达水平。

结论

VAC 可以显著改善心肌梗死小鼠的心脏功能，抑制心肌组织氧化应激和细胞焦亡。在细胞实验中，VAC 同样表现出对缺氧诱导的原代心肌细胞氧化应激和细胞焦亡的抑制作用。因此，VAC 可能为心肌梗死治疗提供一种新的有效药物

王不留行黄酮苷（Vaccarin）改善小鼠心肌梗死后 心室重构

曹阳

哈尔滨医科大学第一附属医院

目的

本研究旨在探讨王不留行黄酮苷（Vaccarin, VAC）对小鼠心肌梗死后心室重构的影响，评估其改善心脏功能及心肌纤维化的效果，为心肌梗死后心室重构的防治提供新的治疗策略。

方法

动物实验

· **分组与模型构建**：将 C57BL/6 小鼠随机分为四组：假手术组（Sham 组）、心肌梗死组（MI 组）、MI+VAC 组、MI+MCC950 组。通过结扎左前降支（LAD）构建心肌梗死模型。

· **药物处理**：MI+VAC 组小鼠心梗建模后腹腔注射 VAC(30mg/kg/d)，连续 4 周；MI+MCC950 组注射 MCC950（NLRP3 特异性抑制剂，10mg/kg，每周两次，累计剂量 80mg/kg）。

· **评估指标**: 多普勒超声心动图评估心脏功能，ELISA 检测血清脑钠肽（BNP）水平，HE 染色、Masson 染色、免疫组化（IHC）染色及 Western Blotting 评估心肌纤维化。

细胞实验

· **细胞分组与处理**：永生化小鼠心肌成纤维细胞分为四组：对照组、TNF-α 组、TNF-α+VAC 组、TNF-α+MCC950 组。通过 CCK-8 筛选 VAC 的治疗浓度（10μM），TNF-α 处理浓度为 15μg/L。

· **评估指标**: CCK-8 检测细胞增殖，细胞划痕实验和 Transwell 实验评估细胞迁移，Western Blotting、RT-qPCR 和免疫荧光评估纤维化相关基因及蛋白表达。

结果

动物实验

· **心脏功能改善**：VAC 显著提高 MI 小鼠的左心室射血分数（LVEF）和左心室短轴缩短率（LVFS），降低左心室收缩末期内径（LVESD）和左心室舒张末期内径（LVEDD），并显著降低血清 BNP 水平。

· **心肌纤维化改善**：VAC 显著减少 MI 小鼠心肌胶原纤维沉积，降低纤维化相关蛋白 α-SMA、Fibronectin、Collagen I、Collagen III、TGF-β1 的表达。

细胞实验

· **细胞增殖与迁移抑制**：VAC 显著抑制 TNF-α 诱导的心肌成纤维细胞增殖和迁移。

· **纤维化改善**：VAC 显著降低 TNF-α 诱导的心肌成纤维细胞纤维化相关蛋白和基因的表达。

结论

VAC 通过改善心脏功能、抑制心肌纤维化和心肌成纤维细胞增殖迁移，有效减轻小鼠心肌梗死后的心室重构。本研究为心肌梗死后心室重构的防治提供了新的候选药物和治疗策略。

血清转酮醇酶（Tkt）水平对急性冠脉综合征患者临床预后的预测价值

金玮 李晴川

上海交通大学医学院附属瑞金医院

目的：

探讨急性冠脉综合征患者中血清转酮醇酶（Tkt）水平是否升高，并评估其对诊断及临床预后的相关性

方法：

进行了一项前瞻性研究，纳入了 230 名急性冠脉综合征患者和 230 名对照受试者，使用酶联免疫吸附试验（Elisa）测定血清 Tkt 浓度。主要终点是中位随访时间 3 年内（四分位数间距 780 天 -1452 天）再发心梗、因新发心衰入院及心血管事件死亡的时间；

结果：

ACS 患者的血清 Tkt 水平显著高于对照受试者（275.75±26.55 vs. 217.53±82.53ng/mL，P<0.001），且 Tkt 水平与冠脉堵塞程度（Gensini 评分）相关。在一组 ACS 患者（n=88）中，经急性期 PCI 及长期抗心室重构治疗后，患者血清 Tkt 水平显著降低，且与 NT-proBNP 水平下降、LVEF 恢复及左室重构（LVEDV、LVESV）相关；在调整多个心血管危险因素后，高 Tkt 水平使主要终点的风险增加了 1.3 倍；Tkt 在临床预测因子和 N 端前脑钠肽（NT-proBNP）之外，提供了额外的预后价值（P<0.05）

结论：

Tkt 水平升高与 ACS 患者的主要终点和因新发心衰入院相关。Tkt 是 ACS 患者中新发心衰诊断和预后的潜在生物标志物。

All-trans retinoid acid pre-treatment reduced myocardial ischemia/reperfusion-induced cell death in vitro

null null, Jin-Zhou Zhu, Zheng-Bin Zhu, Rui-Yan Zhang

Rui Jin Hospital, Shanghai Jiao Tong University School of Medicine

Background: Myocardial ischemia/reperfusion (I/R) injury represents a significant clinical challenge, paradoxically undermining the critical therapeutic goal of restoring blood flow (reperfusion) to ischemic heart tissue. While timely reperfusion is essential to salvage myocardium at risk, the sudden reintroduction of oxygen triggers a cascade of detrimental events, including a profound burst of reactive oxygen species (ROS) and the activation of inflammatory pathways. This reperfusion phase can inflict additional damage, contributing to overall myocardial cell death and limiting the recovery of cardiac function. Oxidative stress, a hallmark of I/R injury characterized by an imbalance between ROS production and cellular antioxidant defenses, has been robustly demonstrated to play a central role in initiating and propagating cardiomyocyte apoptosis - a programmed form of cell death. Consequently, strategies aimed at mitigating oxidative stress and its downstream apoptotic consequences are of substantial therapeutic interest.

All-trans retinoic acid (ATRA), the principal biologically active metabolite of vitamin A (retinol), is a well-characterized molecule with pleiotropic effects. Beyond its critical role in embryonic development and cellular differentiation, a growing body of preclinical evidence highlights ATRA's potent anti-oxidative properties and anti-apoptotic activities in various pathological contexts. It has been shown to modulate the expression and activity of key antioxidant enzymes and directly scavenge free radicals. Furthermore, ATRA can influence apoptotic pathways by regulating the expression of Bcl-2 family proteins and caspases. Despite these promising attributes documented in other cell types and disease models, the specific efficacy of ATRA in ameliorating myocardial I/R injury and its precise mechanisms of action within cardiac cells remain incompletely defined and warrant direct investigation.

Methods: To elucidate the potential cardioprotective effects of ATRA and delineate its underlying mechanisms, we employed an established in vitro model of I/R injury using the rat embryonic cardiomyocyte-derived H9c2 cell line. Cells were systematically pretreated with increasing concentrations of ATRA (ranging from 1 μM to 10 μM) for a duration of 24 hours prior to inducing injury. The simulated I/R injury protocol consisted

of subjecting the cells to 6 hours of hypoxia (achieved using a specialized gas mixture in a hypoxia chamber) followed by 1 hour of re-oxygenation under normal atmospheric conditions. Cell viability, a primary indicator of overall cellular health and survival, was quantitatively assessed using the WST-1 colorimetric assay, which measures mitochondrial metabolic activity.

To specifically evaluate apoptosis, two complementary and highly specific techniques were utilized: Annexin V-FITC/propidium iodide staining analyzed by flow cytometry, which detects phosphatidylserine externalization (an early apoptotic marker) and loss of membrane integrity, and the Terminal deoxynucleotidyl transferase dUTP nick end labeling (TUNEL) assay, which directly visualizes and quantifies DNA fragmentation, a late-stage apoptotic event. Intracellular ROS generation during the re-oxygenation phase was measured using the fluorescent probe 2',7'-dichlorofluorescin diacetate (DCFH-DA), with quantification performed via both fluorescence microscopy imaging and flow cytometric analysis. To investigate the molecular signaling pathways implicated in ATRA's effects, particularly the stress-responsive Mitogen-Activated Protein Kinases (MAPKs) known to be activated by ROS and involved in apoptosis regulation (p38, JNK, ERK1/2), we conducted Western blot analysis. This assessed both the total levels and, crucially, the phosphorylation status (activation state) of these kinases. Additionally, key apoptosis regulatory proteins, specifically the anti-apoptotic protein Bcl-2 and the executioner caspase-3 (both its pro-form and cleaved, activated form), were also analyzed by Western blot.

Results: Pretreatment with ATRA conferred significant protection against hypoxia/reoxygenation (H/R) injury in H9c2 cardiomyocytes. The WST-1 assay demonstrated a statistically significant, concentration-dependent enhancement in cell viability in ATRA-pretreated groups compared to the H/R injury control group ($p < 0.05$). Corroborating this finding, both flow cytometric analysis of Annexin V/PI staining and TUNEL assay revealed a marked, concentration-dependent reduction in the proportion of apoptotic cells following H/R injury in cells pre-exposed to ATRA ($p < 0.05$). These results strongly indicate that ATRA possesses potent anti-apoptotic properties in this model of cardiac I/R injury.

At the molecular level, Western blot analysis provided mechanistic insights. ATRA pretreatment significantly upregulated the expression of the anti-apoptotic protein Bcl-2 ($p < 0.05$) and concurrently reduced the levels of activated (cleaved) caspase-3 ($p < 0.05$) compared to control cells subjected to H/R without ATRA. Furthermore, ATRA demonstrated a significant anti-oxidative capacity, evidenced by a partial but statistically significant attenuation of intracellular ROS production during re-oxygenation as measured by DCFH-DA fluorescence ($p < 0.05$). Crucially, analysis of the MAPK signaling pathway revealed that the protective effects of ATRA were associated with a significant reduction in the phosphorylation (and thus activation) of the stress kinases p38, JNK, and ERK1/2 ($p < 0.05$ for all) following H/R injury.

Conclusion: Our comprehensive in vitro investigation demonstrates that ATRA pretreatment effectively protects H9c2 cardiomyocytes against simulated ischemia/reperfusion injury. The primary mode of protection manifests as a significant reduction in apoptotic cell death and a concomitant increase in overall cell viability. The observed anti-apoptotic effect is mechanistically linked, at least in part, to ATRA's inherent anti-oxidative capacity, which attenuates the damaging ROS burst associated with reperfusion. Furthermore, the cardioprotection afforded by ATRA is strongly associated with the modulation of key pro-apoptotic signaling cascades, specifically the down-regulation of the activated states of p38, JNK, and ERK1/2 MAP kinases. These findings collectively suggest that ATRA holds potential as a therapeutic agent for mitigating myocardial I/R injury, primarily through its anti-oxidative and anti-apoptotic actions mediated via suppression of detrimental MAPK signaling pathways. Further in vivo studies are warranted to validate these promising effects in a more physiologically relevant context.

Keywords: All-trans retinoid acid, Ischemia and reperfusion, Hypoxia and re-oxygenation, Apoptosis, Mitogen-activated protein kinases

All-trans Retinoic Acid prevent reperfusion injury post-myocardial infartion in diabetic mice by incresing RAGE cut.

Ji-Wei Yu, Zheng-Bin Zhu, Rui-Yan Zhang

Rui Jin Hospital, Shanghai Jiao Tong University School of Medicine

Background

Previous scientific investigations have established that All-trans-retinoic acid (ATRA), the principal biologically active metabolite of vitamin A, exhibits significant anti-apoptotic properties across a diverse range of cell types. This protective effect is primarily mediated through its ability to modulate key signaling pathways, leading to the down-regulation of pro-apoptotic signals and promotion of cell survival. Despite this well-documented cytoprotective capacity in various contexts, the specific utility and efficacy of ATRA in mitigating the complex damage caused by ischemia-reperfusion (I/R) injury, particularly within cardiac tissue and especially under diabetic conditions, remain incompletely understood and warrant further investigation. Diabetic states significantly exacerbate the severity of myocardial I/R injury, partly due to altered metabolic and signaling environments. A critical mediator implicated in the pathogenesis of I/R injury, particularly in diabetes, is the Receptor for Advanced Glycation End Products (RAGE). RAGE activation upon binding its ligands (including AGEs, HMGB1, S100 proteins) triggers pro-inflammatory, pro-oxidant, and pro-apoptotic signaling cascades, significantly contributing to cellular damage during ischemia and, more potently, upon reperfusion. Elevated RAGE expression and signaling are hallmarks of diabetic complications and are strongly associated with worse outcomes following cardiac I/R. Given ATRA's known anti-apoptotic effects and RAGE's established detrimental role, this study was specifically designed to investigate two interconnected aspects: first, the potential protective effect of ATRA against myocardial I/R injury in a diabetic mouse model; and second, whether this protection correlates with or involves modulation of the RAGE signaling pathway. The aim was to elucidate if ATRA could be a viable therapeutic strategy for diabetic patients at high risk of I/R injury following events like myocardial infarction.

Methods

To address these objectives, a diabetic mouse model was utilized. Diabetes was experimentally induced in 6-week-old mice via intraperitoneal injection of streptozotocin (STZ), a compound toxic to pancreatic beta-cells, following standard protocols to establish hyperglycemia. Diabetic mice confirming hyperglycemia were then randomly allocated into two experimental groups. One group received All-trans-retinoic acid (ATRA) dissolved in corn oil, administered daily via esophageal gavage (oral gavage) at a dosage of 0.75 mg per day. The control group received an equivalent volume of the blank corn oil vehicle alone, administered via the same route. This pretreatment regimen continued for a period of ten days. Each group comprised ten mice (n=10 per group). Following the pretreatment phase, all mice underwent a standardized surgical procedure to induce myocardial I/R injury. This involved transient occlusion of the left anterior descending (LAD) coronary artery for precisely 30 minutes to induce regional myocardial ischemia, followed by carefully controlled reperfusion for 48 hours to allow the manifestation of reperfusion injury. At the conclusion of the 48-hour reperfusion period, the extent of cardiac damage was comprehensively assessed using multiple established techniques. The size of the myocardial infarct (the area of irreversible tissue death) was quantitatively measured using the triphenyltetrazolium chloride (TTC) staining method, which distinguishes metabolically active (viable, red) tissue from infarcted (non-viable, pale) tissue. Cardiac function was evaluated non-invasively using echocardiography (echo) to assess parameters such as left ventricular ejection fraction and fractional shortening, providing a measure of the heart's pumping capacity post-injury. Blood samples or cardiac tissue homogenates were analyzed to determine the levels of well-established biochemical markers released upon cardiomyocyte injury, specifically lactate dehydrogenase (LDH) and creatine kinase (CK), whose elevated levels in circulation correlate with the degree of myocardial damage. Furthermore, to investigate the molecular mechanisms underlying apoptosis and the potential role of RAGE, myocardial tissue samples were analyzed to determine the activation status (phosphorylation levels) of key pro-apoptotic signaling molecules, namely phospho-c-Jun N-terminal kinase (p-JNK) and phospho-p38 mitogen-activated protein kinase (p-p38MAPK). Additionally, the study specifically measured the expression level of α-disintegrin and metalloprotease 10 (ADAM 10), a protease known to cleave membrane-bound receptors, and assessed its downstream effect on RAGE levels and the production of soluble RAGE (sRAGE).

Results

Analysis of myocardial infarct size using the TTC staining method provided clear evidence of ATRA's protective effect. Diabetic mice pretreated with ATRA exhibited a significantly smaller infarct area (20.2% of the area at risk) compared to diabetic mice pretreated only with the corn oil vehicle (31.1% of the area at risk), with this difference being statistically significant ($P<0.05$). This reduction in tissue damage was corroborated by functional assessment. Echocardiographic data demonstrated that ATRA pretreatment significantly improved cardiac function recovery following I/R injury in diabetic mice compared to the vehicle-treated diabetic controls ($P<0.05$). Consistent with these morphological and functional improvements, the biochemical markers of cardiomyocyte injury, LDH and CK, were significantly lower in the blood or tissue of ATRA-pretreated diabetic mice compared to vehicle-pretreated diabetic mice ($P<0.05$), indicating reduced cellular necrosis and membrane damage.

Conclusion

The data obtained from this study demonstrate that pretreatment with ATRA is effective in reducing myocardial ischemia/reperfusion (I/R) injury in a streptozotocin-induced diabetic mouse model. This protection is evidenced by a significant reduction in infarct size, improved recovery of cardiac function, decreased levels of cardiomyocyte injury markers (LDH, CK), and attenuation of pro-apoptotic signaling (reduced p-JNK and p-p38MAPK). Crucially, the results elucidate a specific molecular mechanism underlying ATRA's cardioprotective effect in this diabetic context. The key role, at least partially if not entirely, involves the up-regulation

of ADAM 10 expression by ATRA. This increased ADAM 10 level facilitates the proteolytic cleavage of the membrane-bound Receptor for Advanced Glycation End Products (RAGE), generating soluble RAGE (sRAGE) and consequently down-regulating the levels and presumably the detrimental signaling activity of membrane-bound RAGE. This modulation of the RAGE pathway represents a significant mechanism by which ATRA confers protection against I/R injury in the diabetic heart. Therefore, the outcome of this study supports the potential therapeutic application of ATRA supplementation as an adjunctive strategy to help prevent or mitigate I/R injury following myocardial infarction, specifically targeting the high-risk population of diabetic patients where RAGE signaling is pathologically heightened.

CREG1 protects myocardium from hypoxic injury by regulating autophagy through Lysosomal Stress Response

Cheng-Hui Yan, Jia-Xin Xu, Ya-Ling Han

State Key Laboratory of Frigid Zone Cardiovascular Disease, Cardiovascular Research Institute and Department of Cardiology, General Hospital of Northern Theater Command

AIMS

Myocardial Infarction (MI) is one of the most serious forms of cardiovascular disease. MI occurs when coronary artery occlusion leads to ischemia and hypoxia of local cardiomyocytes, resulting in irreversible damage or death. Apoptosis is the most important Programmed Cell Death mode of cardiomyocyte hypoxic injury. The Cellular repressor of E1A-stimulated genes (CREG1) is a lysosomal associated protein that plays an important role in the regulation of differentiated tissues and cell homeostasis. It is very low expressed in embryonic tissues, but widely expressed in mature tissues and cells. Previous studies have shown that CREG1 deficiency can lead to cardiac fibrosis, suggesting that CREG1 has a potential protective effect on myocardial cell damage. However, the detailed regulatory mechanism has not been elucidated. This study attempted to use an in vitro model of primary cardiomyocytes. To investigate the hypoxia-induced cardiomyocyte death mode and protective mechanism, and elucidate the protective mechanism of lysosomal protein CREG1 against cardiomyocyte hypoxic injury.

Methods

The hypoxia injury model of primary cardiomyocytes cultured in vitro was established by the intervention of different concentrations of $CoCl_2$. Different cell death markers were used to detect cell death. The main death modes of hypoxic-induced cardiomyocyte death were detected by different cell death inhibitors. Western blot and RT-PCR were used to detect the expression of CREG1. Primary cardiomyocytes with CREG1 overexpression and low expression were prepared by adenovirus infection and siRNA transfection, and the regulatory effect of CREG1 on cell death was detected. Lysosome correlation assay was used to detect the changes of cellular lysosome and determine whether the regulation of cardiomyocyte death by CREG1 is related to lysosome function.

Results

The hypoxia injury model of primary cardiomyocytes cultured in vitro was established by the intervention of different concentrations of cobalt chloride ($CoCl_2$). $CoCl_2$ induced the death of primary cultured cardiomyocytes in a dose-dependent manner. Selected $CoCl_2$ (1000uM, 24 hours) as the effective intervention concentration and time. Inhibition of HIF-1α activation by Oltipraz treatment suggests that CREG1 protein expression is rapidly reduced during hypoxia-induced apoptosis of CoCl2 cells. Different cell death markers were used to detect cell death. Application of different cell death inhibitors testing oxygen induced myocardial cell death of the main manner of death, found that apoptosis inhibitor Z-VAD-FMK could significantly inhibit $CoCl_2$-induced cell death in both in vitro and in vivo studies, suggesting that apoptosis is the main mode of cardiomyocyte death caused by hypoxia. Meanwhile, administration of lysosomal inhibitor chloroquine (CQ) and lysosomal enzyme CA-079 also significantly inhibited $CoCl_2$-induced cell death. Given early autophagy inhibitor 3-MA $CoCl_2$ induced cell death are increased significantly. On the contrary, intervention with the Autophagy agonists Resveratrol could inhibit cardiac cell death. The results suggest that $CoCl_2$-induced cell death is mainly apoptosis. The occurrence of apoptosis may be related to the lysosome excessive activation and spillover damage on the lysosomal enzyme, and activate cell autophagy suppresses early myocardial cell death occurred.L-Leucyl-L-Leucine methyl ester (LLOMe) hydrochloridecan induce lysosomal pathway stress to inhibit myocardial cell death. Western blot and RT-PCR detection confirmed that the protein expression of CREG1 decreased rapidly during $CoCl_2$-induced apoptosis, while the RNA level did not change significantly. Primary cardiomyocytes with CREG1 overexpression and low expression were prepared by adenovirus infection and siRNA transfection, and the regulatory effect of CREG1 on cell death was detected. Overexpression of CREG1 can significantly inhibit $CoCl_2$-induced apoptosis, while Silence CREG1 can aggravate $CoCl_2$-induced apoptosis. Lysosome correlation assay was used to detect the changes of cellular lysosome and determine whether the regulation of cardiomyocyte death by CREG1 is related to lysosome function. CREG1 deficiency can affect lysosome maturation and inhibit early autophagy activation of cardiomyocytes. Overexpression of CREG1 increased LC3B and Beclin-1, indicating a significant increase in autophagosomes. Conversely, silencing CREG1 blocked autophagy. Further studies suggest that CREG1 regulates autophagy and apoptosis of cardiomyocytes through STAT3 signaling pathway.

Conclusion Apoptosis was the main cell death induced by hypoxia. CREG1 is involved in the regulation of autophagolysosomal function, reducing apoptosis and alleviating myocardial cell damage.

基于淋巴细胞的炎症指数对急性心梗合并心源性休克预测价值研究

席荣 李瑞康 樊星星 员峰莉 刘慧 牛晓琳

中国人民解放军空军军医大学第二附属医院

目的：急性心肌梗死 (acute myocardial infarction, AMI) 与炎症机制有关，这可能会导致诸如心源性休克 (cardiogenic shock, CS) 等严重并发症。基于淋巴细胞的炎症指标 (lymphocyte-based inflammation indices, LBIIs) 作为固有免疫细胞和适应性免疫细胞的综合衡量指标，能够为生理和病理条件下的炎症状态提供定量的见解。我们旨在阐明 LBIIs 在预测急性心肌梗死合并心源性休克（acute myocardial infarction complicated with cardiogenic shock，AMICS）中的价值。

方法：回顾性纳入了被诊断为 AMICS 和急性心肌梗死非合并心源性休克（AMI non CS，AMInCS）的患者。通过 logistic 回归分析、受试者工作特征曲线 (receiver operating characteristic curve, ROC) 和限制性立方样条 (restricted cubic spline, RCS) 评估 LBIIs 对 AMICS 患者的影响。

结果：本研究纳入了 718 名 AMI 患者，其中 234 名患者出现了 AMICS。通过单因素 logistic 分析发现，除血小板与淋巴细胞比率（Platelet-lymphocyte ratio，PLR）外，中性粒细胞与淋巴细胞比率（Neutrophil-lymphocyte ratio，NLR）、单核细胞与淋巴细胞比率（Monocyte-lymphocyte ratio，MLR）、系统性炎症反应指数（Systemic inflammatory response index，SIRI）和系统性免疫炎症指数（Systemic immune-inflammation index，SII）四个 LBIIs 指标均为 AMI 患者合并 CS 的危险因素。ROC 分析结果显示，SIRI 对 AMICS 的预测性能最佳（AUC:0.72）。在调整血糖、尿酸和尿素氮等混杂因素后，logistic 分析表明 SIRI 与 AMICS 独立相关（OR:2.83，95%CI：1.41-5.68，p<0.001）。此外，通过 RCS 分析显示表明 SIRI 与 AMICS 之间呈非线性关联。最后根据分层分析，发现相较于男性患者，SIRI ≥ 4.58 的女性 AMICS 患者面临更高的风险。

结论：多项 LBIIs 与 AMICS 显示出显著的相关性。SIRI 表现出最佳性能，并且可能作为早期识别 AMI 患者心源性休克的新预测指标。

Protective effect of ALG-2 interacting protein X on hypoxic injury of cardiomyocytes

Cheng-Hui Yan, Jia-Xin Xu

State Key Laboratory of Frigid Zone Cardiovascular Disease, Cardiovascular Research Institute and Department of Cardiology, General Hospital of Northern Theater Command

Objective

Myocardial Infarction (MI) is one of the most serious forms of cardiovascular disease. MI occurs when coronary artery occlusion leads to ischemia and hypoxia of local cardiomyocytes, resulting in irreversible damage or death.The formation of autophagosomes is coordinated by a wide range of cellular factors and culminates in the closure of the cup-shaped double membrane or phagophore. The endosomal sorting complex required for transport (ESCRT) machinery has been proposed to mediate the sealing of the autophagic membranes. We recently described the role of ALIX (ALG-2 interacting protein-X) in autophagosome maturation during salt stress in Arabidopsis. To investigate the protective effect of ALG-2-interacting protein X (ALIX) on hypoxia-induced injury in cardiomyocytes.

Methods

A hypoxia-induced injury model was established in H9C2 cardiomyocytes by stimulating them with cobalt chloride (CoCl2) for 24 hours. Changes in ALIX expression in the hypoxia-induced injury model were detected using Western Blot and cellular immunofluorescence. GFP-ALIX fusion plasmids and ALIX RNA knockdown constructs were generated in vitro. After using cell transfection techniques to achieve endogenous overexpression or knockdown of ALIX in H9C2 cells, the cells were stimulated with CoCl2. Subsequently, real-time fluorescent quantitative polymerase chain reaction (PCR) and Western Blot were used to detect ALIX mRNA and protein levels, as well as the expression of apoptosis-related proteins. The TdT-mediated dUTP nick end labeling (TUNEL) assay was employed to assess cell apoptosis. At the time points of 3 days, 7 days and 28 days after myocardial infarction, paraffin sections were performed on the hearts of C57 mice and mice injected with overexpressing ALIX adeno-associated viruses. HE and Masson staining were then carried out to observe myocardial fibrosis.

Results

ALIX expression was increased in cardiomyocytes stimulated with

CoCl2. In the ALIX overexpression group stimulated with CoCl2, the expression levels of Bax/Bcl-2 and Cleaved-caspase 3 were lower than those in the hypoxia-induced injury group. In contrast, the expression levels of these proteins were higher in the ALIX knockdown group stimulated with CoCl2 compared to the hypoxia-induced injury group, with statistical significance observed in all differences (P < 0.05). TUNEL assay results showed that overexpression of ALIX reduced cell apoptosis in the group stimulated with CoCl2, while knockdown of ALIX increased the apoptosis rate in the corresponding group, with statistical significance observed in both differences (P < 0.05). The results of HE staining and Masson staining showed that the degree of myocardial fibrosis in mice overexpressing ALIX was lower than that in the control group, indicating that ALIX can protect myocardial cells.

Conclusion ALG-2-interacting protein X exhibits a protective effect on cobalt chloride-induced hypoxia injury in cardiomyocytes.

[Keywords] ALG-2-interacting protein X; myocardial infarction; hypoxia; apoptosis

急性心肌梗死并发心脏破裂的危险因素分析及预测模型建立

谷新顺 仝帅

河北医科大学第二医院

目的：分析急性心肌梗死（acute myocardial infarction，AMI）患者并发心脏破裂（cardiac rupture，CR）的危险因素，并建立预测模型。

方法：收录 2016 年 1 月 -2025 年 1 月就诊于医院的 AMI 患者 2893 例，其中 AMI 并发 CR 的患者 40 例，包括游离壁破裂（free wall rupture，FWR）患者 10 例，室间隔穿孔（ventricular septal rupture，VSR）患者 27 例，乳头肌断裂（papillary muscle rupture，PMR）患者 3 例。选取 699 例未并发 CR 的 AMI 患者为非 CR 组。

1．收集患者资料，包括（1）人口学资料：包括年龄、性别、入院血压、入院心率、既往病史（高血压、糖尿病）。（2）临床特征：缺血预适应、梗死部位、Killip 分级。（3）实验室资料：N 末端脑钠肽前体、高敏肌钙蛋白 I、肌红蛋白、肌酸激酶、肌酸激酶同工酶 MB、白细胞计数、血红蛋白、血小板计数、中性粒细胞百分率、超敏 C 反应蛋白、肌酐、血清钾、高密度脂蛋白胆固醇、低密度脂蛋白胆固醇、葡萄糖、D- 二聚体。

2．通过对比 CR 组和非 CR 组的观察资料，分析得出 CR 的独立危险因素，并由此建立预测模型。

结果：

1．两组间年龄、女性、心率、白细胞计数、肌酸激酶同工酶 MB 差异具有统计学意义，P < 0.001。两组间无缺血预适应、Killip 分级III ~ IV级、前壁心肌梗死差异具有统计学意义，P < 0.05。

2．多因素 Logistic 回归分析：女性（OR=1.465，95%CI：1.369~1.568，P < 0.001），年龄≥ 60 岁（OR=0.906，95%CI：0.903~0.909，P < 0.001），心率≥ 96 次 / 分（OR=0.946，95%CI：0.944~0.948，P < 0.001），白细胞计数≥ $14.95\times10^{9}\cdot L^{-1}$（OR=0.819，95%CI：0.811~0.826，P < 0.001），肌酸激酶同工酶 MB ≥ $248U\cdot L^{-1}$（OR=0.999，95%CI：0.999~0.999，P < 0.001）；前壁心肌梗死（OR=0.282，95%CI：0.251~0.317，P < 0.001）是 AMI 并发 CR 的独立危险因素。

3．由上述独立危险因素建立预测模型，各独立危险因素均赋值 1 分，评分≤ 2 分为低风险，评分≥ 3 分为高风险，预测模型具有较好的区分度和校准度。

结论：本研究发现女性、年龄≥ 60 岁、入院心率≥ 96 次 / 分、前壁心肌梗死、WBC ≥ $14.95\times10^{9}\cdot L^{-1}$、CKMB ≥ $248U\cdot L^{-1}$ 是 AMI 并发 CR 的独立危险因素。由以上独立危险因素建立的预测模型具有良好的区分能力和校准度，对于预测 AMI 并发 CR 有指导意义。

急性前壁 ST 段抬高型心肌梗死患者发生左心室血栓的危险因素

谷新顺

河北医科大学第二医院

目的：探究急性前壁 ST 段抬高型心肌梗死（ST elevation myocardial infarction，STEMI）患者发生左心室血栓（Left Ventricular Thrombus，LVT）的危险因素。

方法：本研究为单中心、回顾性研究。收集整理 2022 年 5 月 1 日至 2024 年 12 月 1 日就诊于河北医科大学第二医院心内科诊断为“急性前壁 STEMI”的 31 例患者的临床资料，均根据经胸超声心动图（Transthoracic echocardiography，TTE）检查证明存在 LVT 为观察组；同时随机纳入同时期诊断为急性前壁 STEMI 且 TTE 未探及血栓的患者 90 例为对照组。记录分析两组患者的临床资料，统计整理两组患者的 TTE 相关指标，对比两组有无统计学差异；通过单因素分析及多因素 Logistic 回归分析探究急性前壁 STEMI 患者发生 LVT 的危险因素。所有数据通过 SPSS26.0 统计软件进行分析，P<0.05 **认为其差异具有统计学意义。**

结果：

1. 两组患者的年龄、性别、吸烟史、高血压病史、糖尿病病史、体重指数（Body mass Index，BMI）、白细胞（White blood cell，WBC）、血红蛋白（Hemoglobin，HGB）、肌酐（Creatinine，Cr）、低密度脂蛋白（Low density lipoprotein，LDL）、应用阿司匹林、替格瑞洛、吲哚布芬、氯吡格雷、肝素类抗凝药物、β 受体阻滞剂、肾素 - 血管紧张素 - 醛固酮受体拮抗剂（Renin-Angiotensin-Aldosterone System Inhibitor，RAASi）、钠葡萄糖同向转运蛋白 2 抑制剂（Sodium-glucose isotransporter 2 inhibitors，SGLT2i）等方面均无统计学意义（P>0.05）；而 Killip 分级、延迟再灌注、超敏 C 反应蛋白（hypersensitive C-reactive proteinhs，hsCRP）具有统计学差异（P<0.05）。

2. 两组患者的 TTE 相关指标，包括左室射血分数（Left ventricular ejection fraction，LVEF）、室壁运动积分（Wall Motion Score Index，WMSI）、左室室壁瘤（Left Ventricular aneurysm，LVA）具有的统计学差异（P<0.05），而左室舒张末期内径（Left ventricular end-diastolic dimension，LVEDd）无统计学差异。

3. 通过单因素 Logistic 回归分析发现，延迟再灌注、hsCRP、LVEF、WMSI、LVA 为 LVT 发生的危险因素。

4. 以 LVT 为因变量，以上述单因素回归分析得到的危险因素为自变量，进行多因素 Logistic 回归分析，结果示：LVEF<42.6%（OR=0.13,95%CI：0.02-0.77，p=0.02）、WMSI>1.4 分（OR=8.61，95%CI：2.42-30.64，P<0.01）、延迟再灌注（OR=11.98，95%CI：3.16-45.43，P<0.01）、存在 LVA（OR=14.58，95%CI：2.89-73.42，P<0.01）是发生 LVT 的独立危险因素。

结论：

对于急性前壁 STEMI 患者，并发 LVT 的独立危险因素包括延迟再灌注、存在 LVA、WMSI>1.4 分、LVEF<42.6%。

关键词：左心室血栓、前壁 ST 段抬高型心肌梗死，危险因素，室壁运动积分

急性心肌梗死多支病变合并糖尿病不同血运重建的预后比较

门冰欣 胡娜娜 张亚苹 张军兰 师晓雷 张锦

兰州大学第一医院

急性心肌梗死多支病变合并糖尿病不同血运重建的预后比较

门冰欣[1]，胡娜娜[1]，张亚苹[1]，张军兰[1]，师晓雷[1]，张锦[1, 2*]

(1. 兰州大学第一临床医学院，甘肃 兰州 730000；2. 兰州大学第一医院心内科，甘肃 兰州 730000)

第一作者：门冰欣，E-mail：mbx2935719940@163.com，Tel：15934842157

通讯作者：张锦，E-mail：chzhangjin@163.com，Tel：18919808653

目的：探讨不同血运重建方式对急性心肌梗死（AMI）冠脉多支病变合并糖尿病患者产生的预后差异。

方法：回顾性纳入 2022 年 1 月 -2024 年 6 月兰州大学第一医院心内科收治的 AMI 冠脉多支病变合并糖尿病患者。根据血运重建方式分为不完全血运重建组（NCR）、分期完全血运重建组（SCR）和即刻完全血运重建组（ICR）。记录并比较各组患者的基线临床特征、冠状动脉造影资料和术后用药情况。随访终点事件为不良心脑血管事件（MACCE），MACCE 包括全因死亡、心原性死亡、非致死性心肌梗死、计划外的再次血运重建及脑卒中。采用 Log-rank 检验分析三组 MACCE 累计发生率差异的显著性。运用 Cox 回归探讨患者预后不良的影响因素。

结果：本研究回顾性纳入 2022 年 1 月 -2024 年 6 月兰州大学第一医院心内科收治的 AMI 冠状动脉多支病变合并糖尿病患者 645 例。经纳入排除标准筛选后剔除不符合病例 113 例，因未按计划 PCI 排除 55 例，失访 39 例，最终纳入 438 例。NCR 组 166 例，SCR 组 152 例，ICR 组 120 例。通过中位随访 21（11，25）个月，发现 NCR 组 59 例（35.5%），SCR 组 26 例（17.1%），ICR 组 30 例（25%）发生 MACCE 事件。三组间 MACCE 累计发生率的差异具有统计学意义（P < 0.001），两两比较发现，NCR 组与 SCR 组（log-rank P < 0.001）、ICR 组（log-rank P=0.011）差异均有统计学意义，SCR 组与 ICR 组差异无统计学意义（P=0.228）。多因素 Cox 回归分析表明，既往高血压病史是 AMI 冠状动脉多支病变合并糖尿病患者发生 MACCE 的独立危险因素 (HR=1.71，95%CI：(1.10 ~ 2.64)，P < 0.05），SCR 与 NCR 间 MACCE 累计发生率的差异具有统计学意义（HR=0.45，95%CI：(0.28 ~ 0.73)，P=0.001）。

结论: 推荐 SCR 作为 AMI 冠脉多支血管病变合并糖尿病患者优先的血运重建方式，并且对合并高血压的患者，应加强血压管理降低 MACCE 的发生风险。

关键词：急性心肌梗死；冠状动脉多支病变 ;2 型糖尿病；冠状动脉支架植入术

中性粒细胞与血小板比值（NPR）对行经皮冠脉介入治疗的急性冠脉综合征患者预后的预测价值

孙兆青

中国医科大学附属盛京医院

目的：本研究探讨了中性粒细胞与血小板比值（Neutrophil to platelet ratio, NPR）与接受经皮冠状动脉介入治疗（Percutaneous coronary intervention, PCI） 的急性冠脉综合征（Acute coronary syndrome, ACS）患者全因死亡风险之间的关 系。NPR 是一项反映机体炎症状态的血液学指标，在多种疾病的预后评估中具 有潜在价值。然而，目前关于 NPR 在接受 PCI 治疗的 ACS 患者人群中的临床意 义尚缺乏系统研究。因此，本研究旨在评估 NPR 水平与该类患者短期及长期全 因死亡率的关联，以期为临床风险分层和预后评估提供新的生物标志物依据，并 为优化 ACS 患者的个体化治疗策略提供参考。

方法：本研究为单中心回顾性研究，连续入选 2010 年 1 月至 2016 年 12 月 期

间在中国医科大学附属盛京医院住院并接受 PCI 治疗的 4,993 例 ACS 患者，所有患者均在入院后 24 小时内采集空腹静脉血样本并计算 NPR 值，同时收集所 有患者的一般资料、实验室检查结果、冠状动脉造影及介入治疗相关指标、住院 期间用药情况。2023 年 10 月进行回顾性随访，随访方式包括电话随访或查阅患 者的门诊及急诊住院病历。主要研究终点为全因死亡，同时记录 30 天的全因死 亡率作为短期结局。根据 NPR 中位数，将患者分为低 NPR 组（n=2496）及高 NPR 组（n=2497），对两组患者的基线资料进行对比。NPR 同时作为连续变量及 分类变量进行分析，采用 Kaplan-Meier 法评估高低 NPR 组患者生存率并采用 Log-rank 检验进行比较。采用 Cox 回归模型进行单因素、多因素回归分析，以 探讨 NPR 与接受 PCI 治疗的 ACS 患者全因死亡率之间的关联。此外我们进行了 亚组分析，亚组根据年龄、性别、高血压及糖尿病病史进行分组，结果以森林图 的形式展示。

结果：本研究共纳入 4993 例 ACS 患者，平均年龄为 62.0±11.4 岁，其中女 性占 30.8%。在中位随访时间 8.7 年内，共记录 815 例（16.3%）全因死亡事件，43 例（0.9%）30 天内全因死亡事件。多因素 COX 回归分析显示，NPR 升高与 全因死亡风险显著相关（HR 1.065，95% CI 1.023-1.109，p=0.002）。当 NPR 作 为分类变量分析时，高 NPR 组患者的全因死亡发生风险显著高于低 NPR 组（HR 1.213，95% CI 1.053-1.398，p=0.007）。对于 30 天全因死亡，NPR 每增加 0.01， 30 天内全因死亡风险增加 41.2%（HR 1.412，95% CI 1.268-1.573，p<0.001）。且高 NPR 组全因死亡风险显著增加（HR 3.290，95% CI 1.558-6.947，p=0.002）。 亚组分析结果表明，NPR 在按年龄、高血压、2 型糖尿病分层后，仍与全因死亡 风险的增加显著相关。然而，NPR 与全因死亡之间的相关性在性别亚组中有差 异（交互作用 P=0.008）。在女性中，NPR 对全因死亡风险的预测性能更佳。

结论：NPR 与行 PCI 治疗的 ACS 患者长期及短期全因死亡风险显著相关。 NPR 可作为接受 PCI 治疗的 ACS 患者全因死亡率的潜在预测指标。NPR 对女性 群体全因死亡风险的预测性能更佳。NPR 可能有助于临床医生识别高风险 ACS 患者。

空腹应激性高血糖比率对经皮冠状动脉介入治疗的急 性冠脉综合征患者预后的影响

孙兆青

中国医科大学附属盛京医院

目的: 近年来，研究表明，空腹应激性高血糖比率（Stress Hyperglycemia Ratio，SHR）能够反映急性心肌梗死（AMI）患者真实的急性高血糖状态，并与 AMI 患者的短期不良预后相关，但其与长期预后的关系尚不明确，且对于急性冠脉综合征（Acute Coronary Syndrome，ACS）的患者探究较少。因此，本文探究空腹 SHR 与接受经皮冠状动脉介入治疗（Percutaneous Coronary Intervention，PCI）术后的 ACS 患者预后的相关性；并在不同亚组分析空腹 SHR 与预后的关系。

研究方法：本研究采用回顾性队列研究方法，共纳入中国医科大学附属盛京医院 2010 年 1 月至 2016 年 12 月期间诊断为 ACS 并接受 PCI 治疗的 4729 例患者。对纳入人群进行一般基线资料的收集，中位随访时间 8.7 年，主要临床终点事件定义为全因死亡。次要临床终点事件定义为 30 天内全因死亡。依据空腹 SHR 的四分位数分为 4 组（Q1-Q4），将 Q1-Q3 定义为低 SHR 组（3547 例），Q4 定义为高 SHR 组（1182 例）。依据糖尿病史将所有纳入患者分为糖尿病组（1615 例）和非糖尿病组（3114 例）。我们建立了 Cox 比例风险回归模型进行单因素、多因素回归分析，以探究空腹 SHR 对于 ACS 患者全因死亡率的预测价值。并绘制 2 种分组患者全因死亡的 Kaplan-Meier 曲线，以分析两组死亡率差异。在亚组分析中，绘制森林图探究年龄、性别、高血压史、糖尿病史、射血分数、是否为 AMI 人群中是否存在交互作用。

结果：本研究共纳入 4729 例患者。低 SHR 组和高 SHR 组在糖尿病史、既往 PCI、慢性肾脏病史、入院心率、FPG、HbA1c、D 二聚体、HDL-C、LDL-C、LVEF、Grace 风险评分、诊断类型以及全因死亡风险之间存在显著差异（P<0.05）。糖尿病组和非糖尿病组在性别、高血压、吸烟史、既往 PCI、入院心率、收缩压、诊断类型、左主干或三支病变、慢性完全闭塞以及全因死亡风险之间差异显著（P<0.05）。针对 ACS 人群，多因素 Cox 回归显示可得出年龄、吸烟史、既往 PCI、既往 CABG、血红蛋白、LVEF、诊断类型、左主干或三支病变和空腹 SHR 与全因死亡风险显著相关（P<0.05），其中空腹 SHR 每增加 1，全因死亡风 险 增 加 63.9%（HR=1.639，95%CI：1.232-2.179，P<0.001），高 SHR 组的全因死亡风险是低 SHR 组的 1.336 倍（HR=1.336，95%CI：1.146-1.556，P<0.001）。与 30 天内全因死亡风险显著相关的有年龄、LVEF 和 SHR（P<0.05），其 中 空 腹 SHR 与 死 亡 风 险 显 著 相 关（HR=5.803，95%CI：2.804-12.007，P<0.001），高 SHR 组的全因死亡风险更高（HR=2.738，95%CI：1.482-5.060，P=0.001）。并且无论在糖尿病人群中还是非糖尿病人群中，均可得出类似结论。Kaplan-Meier 生存曲线显示，无论是在总人群、糖尿病患者还是非糖尿病患者中，高 SHR 组的全因死亡率均显著高于低 SHR 组（Log-rank P<0.05）。亚组分析显示，空腹 SHR 与年龄、性别、高血压、糖尿病、射血分数和是否急性心肌梗死人群未见明显交互作用（p>0.05）。

结论：本研究表明，在经 PCI 术后的 ACS 患者中，无论是否合并糖尿病，空腹 SHR 与长期和 30 天内全因死亡风险密切相关，空腹 SHR 可能是危险分层的标志物。

CONUT 评分对经皮冠状动脉介入治疗的急性心肌梗死患者 预后的预测价值

孙兆青

中国医科大学附属盛京医院

目的：控制营养状况（Controlling Nutritional Status，CONUT）评分是一种反 映营养不良的新指标，已被广泛证实能够预测多种疾病中的全因死亡率和主要不 良心血管事件（major adverse cardiovascular events，MACE）。本研究旨在评估急 性心肌梗死（acute myocardial infarction，AMI）患者在接受经皮冠状动脉介入治 疗（percutaneous coronary intervention，PCI）后，营养不良对其临床预后的影响。

研究方法：本研究采用回顾性队列研究方法，连续纳入了 2010 年至 2016 年 期间在中国医科大学附属盛京医院住院并接受 PCI 治疗且确诊 AMI 的 3294 名患 者。对纳入人群进行一般基线资料的收集，中位随访时间 8.6 年。主要临床终点 事件定义为全因死亡。次要临床终点事件定义为入院后 30 天内全因死亡。所有患 者根据 CONUT 评分分为营养正常组（1687 例）、轻度营养不良组（1437 例）和 中重度营养不良组（170 例）比较两组参数之间的差异。我们建立了 Cox 回归模型 进行单因素、多因素回归分析，以探究 CONUT 评分与经 PCI 术后的 AMI 患者中 全因死亡率之间的预测价值。使用 Kaplan-Meier 法绘制三组患者全因死亡的生存 曲线，用 Log-rank 检验进行比较。并且绘制了 CONUT 联合全球急性冠脉事件登 记（Global Registry of Acute Coronary Events，GRACE）风险评分以及 GRACE 模 型对全因死亡预测的受试者工作特征（ROC）曲线，计算曲线下面积（AUC）， 同时通过绝对综合判别改善（Absolute Integrated Discrimination Improvement， IDI）指数和无类别净重新分类改善（Category-free Net Reclassification Improvement，NRI）指数比较新旧模型的预测能力。

结果：根据 CONUT 评分，43.6% 的患者为轻度营养不良，5.2% 的患者为中度 和重度营养不良。在中位随访 8.6 年期间，共记录了 622 例（18.8%）全因死亡事 件。主要终点事件的发生率随着营养不良严重程度的增加而逐渐升高。多变量调 整后，与正常营养组相比，中度和重度营养不良组的主要终点事件的比值比为 1.38（95% 置信区间 1.01 至 1.90，P=0.008）。绘制三组患者 PCI 术后全因死亡的 Kaplan-Meier 生存曲线，结果示中重度营养不良组患者术后发生全因死亡的风险显 著高于 营养正 常组（Log-rank P < 0.001）。此外，CONUT 评分 显著提 高 了 GRACE 风险评分对全因死亡的预测能力（IDI=0.008，P < 0.001；NRI=0.144， P=0.001）。

结论：在经 PCI 术后的 AMI 患者中，CONUT 评分与全因死亡风险增加独立相关。未来需要更多的前瞻性临床试验来评估营养干预对 AMI 患者 PCI 术后结局 的影响。

STEMI 合并应激性高血糖对患者临床预后及血小板功能的影响

朱倩倩 陈飞

上海同济大学附属同济医院

目的：本研究旨在通过对接受经皮冠状动脉介入术（PCI）的 STEMI 患者进行血糖状态评估及血小板功能、血栓负荷分析，进而探究应激性高血糖对患者临床预后及血小板功能的影响。

方法：连续入选 2020 年 1 月至 2022 年 12 月于上海市同济医院诊断为 STEMI 并接受 PCI 治疗的患者 680 例。根据既往研究结果，将非糖尿病患者入院血糖≥ 7.8mmol/L，糖尿病患者入院血糖≥ 12.8mmol/L 诊断为应激性高血糖，以此分为应激性高血糖组（SH）和非应激性高血糖组（Non-SH）。同时对前瞻性入组的患者进行动态血糖监测，PCI 术后采用辅理善瞬感扫描式葡萄糖监测系统对患者的血糖予以动态监测。血小板功能主要通过测定血栓弹力图两侧曲线的最宽距离（MA），MA 值在一定程度上可以反映血小板的功能。

结果： 1. 无论是在 DM 组还是 Non-DM 组中，住院期间 SH 组 MACE 事件发生率显著高于 Non-SH 组，具有统计学差异（DM：22.1% vs 12.6%，P=0.025；Non-DM：21.7% vs 13.6%，P=0.048）；且两组在高血栓负荷方面具有统计学差异（P < 0.05）。

2．Kaplan-Meier 曲线分析显示，在 DM 组中，SH 组相较于 Non-SH 组具有更高的 6 个月内 MACE 事件发生风险（25.5% vs 15.7%，HR=1.797，95%CI:1.072-3.012；Log-rank P=0.0071）。多因素 COX 回归分析显示，SH(HR=1.661，95%CI：1.083-2.804，P=0.04) 是 STEMI 患者临床预后的独立危险因素。同样在 Non-DM 组中，SH 组相较于 Non-SH 组具有更高的 6 个月内 MACE 事件发生风险（19.7% vs 10.0%，HR=1.971，95%CI：1.110-3.499;Log-rank P=0.016）。多因素 COX 回归分析显示，SH(HR=1.506，95%CI 1.084-2.677，P=0.01) 是 STEMI 患者临床预后的独立危险因素。

3. 单因素回归分析显示，在 DM 组中，平均血糖漂移幅度（HR=1.218，95%CI：1.099-1.484，P=0.04）、血糖变异系数 (HR=1.146，95%CI：1.058-1.241，P=0.01) 及低血糖事件均 (HR=1.115，95%CI：1.033-1.205，P=0.005) 均与 STEMI 患者临床预后相关。在 Non-DM 组中，平均血糖漂移幅度（HR=1.432，95%CI: 1.037-2.449，P=0.01）和血糖变异系数 (HR=1.107，95%CI: 1.016-1.206，P=0.02) 与 STEMI 患者临床预后相关，但低血糖事件（HR=1.068，95%CI：0.974-1.171，P=0.163）与 STEMI 患者临床预后无显著相关性。

4. 在 DM 组中，SH 组患者血栓弹力图中 MA 平均值明显高于 Non-SH 组（75.91±5.65 vs 65.00±6.20，P < 0.001）。在 Non-DM 组中，SH 组 MA 平均值也显著大于 Non-SH 组（68.14±6.69 vs 59.08±5.76，P < 0.001）。相关性分析结果显示，无论是在糖尿病患者还是非糖尿病患者中，SH 组和 Non-SH 组中血栓弹力图 MA 值与患者入院血糖成正相关。

结论：应激性高血糖与 STEMI 患者的临床预后独立相关。STEMI 患者住院期间血糖波动也与患者的临床预后相关。应激性高血糖会使血小板功能增加，血小板功能增加与梗死相关血管高血栓负荷形成存在一定的相关性，两者共同增加了 STEMI 患者 6 个月内主要不良心血管事件的发生。

Machine learning prediction model and nomogram to predict risk of cardiovascular events in patients with acute coronary syndrome

Juan Wang, Kui-Bao Li, Wei-Ming Li

Beijing Chaoyang Hospital Affiliated to Capital Medical University

Background: There is no generally accepted biomarker-based risk model appliable for acute coronary syndrome (ACS) cohorts. We sought to develop a machine learning (ML) model, utilizing multiple variables predict

the long-term cardiovascular events for ACS patients.

Methods: In a prospective, randomized trial cohort of 3687 patients with ACS, we analyzed several candidate variables for median follow-up of 8.1 years from the Observation of Cardiovascular Events of ACS patients (OCEA) study. The OCEA group is the main prospective observational study data source for machine learning derivation, including 3687 ACS patients from PLA general hospital, 55.0% experienced unstable angina, 26% had ST elevated myocardial infarction (STEMI), 19% of which had non-ST elevated myocardial infarction (NSTEMI). The MCRH group is the prospective observational study data source for the ML model validation, including 542 ACS patients from Chao-Yang hospital with a median follow-up duration of 1.3 years (IQR 1.1–1.4). External validation was performed in 542 patients with ACS for median follow-up of 1.3 years from the management of cardiovascular risk and health (MCRH). The OCEC group is the main prospective observational study data source for machine learning derivation, including 3687 CAD patients from PLA general hospital, 25.62% of which had stable angina, 74.38% of which had other CAD subtypes such as unstable angina, STEMI, and NSTEMI and the percentage of which are 62.41%, 8.25%, and 3.29%, respectively. ML involved an automated process encompassing feature selection through information gain ranking, model construction utilizing a boosted ensemble algorithm, and 5-fold stratified cross-validation for the entire process. For ML, a boosted ensemble algorithm was used with data split into a training set (80%) on which 5-fold cross-validation was done and a test set (20%). In order to thoroughly compare the prognostication of cardiovascular events, the boosting tree-based ML model including clinical factors (C), organ dysfunction (O), biomarkers of plasma (B)-ML-COB was evaluated against a nomogram model. Furthermore, for the construction of a clinical prediction model, the COB candidate variables mentioned above were at our disposal. A complete-case analysis was undertaken, and no imputation measures were employed. We initially fitted an extensive Cox regression model that encompassed all candidate variables. In cases where biomarkers levels fell below the limit of detection biomarker levels below the limit of detection, they were set to half of that limit.

Results: We developed a novel biomarker-based risk model for predicting cardiovascular events and all-cause death in a large clinical trial cohorts of patients with ACS during a median follow-up of 8.1-year. We utilized ML as an advanced analytic approach, optimized to construct an accurate predictive model containing clinical risk factors (C), organ functional parameters (O) and biomarkers of plasma (B). The ML-COB model demonstrated strong predictive capabilities for cardiovascular events and also performed well compared with ML-C model containing traditional risk factors only or ML-OB model containing biomarkers only for the predication of all clinical events. ML-COB model had a good calibration and produced better performance compared with nomogram model for 9-year follow up. The predictive value of ML-COB model was confirmed to be superior to the clinical risk model in both the derivation [area under the curve (AUC) 0.847 vs. 0.69; P (<0.001)] and the validation cohort [AUC 0.755 vs. 0.66; P (<0.001)].

Conclusion: ML-COB model was found to accurately predict long term cardiovascular events in ACS patients. The utilization of ML-COB may improve risk stratification and help guide future clinical treatment management.

身体活动、久坐行为与生物年龄对心肌梗死后死亡风险的联合影响及中介作用

王玥莹 权薇薇 张瑞岩

上海交通大学医学院附属瑞金医院

背景

急性心肌梗死（AMI）后的身体活动（PA）与预后的关系已有较多研究，但多数聚焦于初级预防，且缺乏对不同强度 PA（如中强度 PA [MPA] 和高强度 PA [VPA]）的比较。此外，PA 降低死亡风险的机制是否通过代谢表型或生物年龄介导尚不明确。本研究基于美国国家健康与营养调查（NHANES，2007-2018 年）数据，探讨 PA 与 AMI 幸存者死亡率的关系，并分析生物年龄（以表型年龄 PhenoAge 为指标）的中介作用。

方法

研究纳入 40 岁以上的 AMI 幸存者，通过问卷评估 PA（MPA 和 VPA）及每日久坐时间（DST）。PA 按代谢当量（MET）分级，MPA 和 VPA 分别分为三类（0-149、150-300、>300 min/ 周和 0-74、75-150、>150 min/ 周）。生物年龄通过 PhenoAge 计算，基于 9 项生物标志物和实际年龄。主要结局为全因死亡和心血管死亡。采用 Cox 比例风险模型分析 PA、DST 与死亡率的关系，并通过因果中介分析评估生物年龄的中介效应。敏感性分析包括 3 年 landmark 分析。

结果

PA 与死亡率：增加 PA（尤其是 MPA）与全因死亡风险降低显著相关。每周 MPA 超过 300 分钟仍可进一步降低风险，而 VPA 仅在 MPA ≥ 300 分钟且每周 75-150 分钟时表现出额外益处。久坐时间过长（≥ 8 小时 / 天）与死亡风险增加相关（HR=1.35）。

生物年龄与死亡率：PhenoAge 每增加 1 岁，全因死亡和心血管死亡风险分别增加 9% 和 7%。久坐时间过长与生物年龄加速显著相关。

中介分析：总 PA 通过降低生物年龄间接减少全因死亡风险，中介比例为 31.6%；久坐时间通过生物年龄介导死亡风险的比例为 18.0%。但 MPA 和 VPA 单独分析时，生物年龄的中介作用不显著（中介比例 <6%）。

结论

AMI 后增加 PA（特别是 MPA）可显著降低死亡风险，且超出 WHO 推荐量仍有益处。VPA 的益处需建立在足够 MPA 基础上。久坐时间过长直接增加死亡风险，部分通过加速生物衰老介导。生物年龄（PhenoAge）是 AMI 预后的独立预测因子，也是 PA 与死亡率关联的重要中介。研究支持将减少久坐和个性化 PA（以 MPA 为主）纳入 AMI 二级预防策略，并提示生物年龄可作为干预效果的评价指标。

Multiomics reveals gut dysbiosis links to fatty acid dysmetabolism in early phase of acute myocardial infarction

cui hanbin, Jia-Jun Ying

The First Affiliated Hospital of Ningbo University

Abstract

Background: Acute myocardial infarction (AMI) remains a major cause of death, with limited understanding of its early risk stratification. The exact underlying mechanism responsible for the progression of coronary artery disease and occurrence of adverse event remains unclear. While gut microbiome disturbances have been associated with late-stage AMI, the connection to early-stage AMI (eAMI) is less explored.

Methods: Using metabolomics and metagenomics, we analyzed 56 samples, comprising 30 eAMI patients (within 12 hours of onset) and 26 age- and gender-matched healthy controls, to discern the influence of gut microbes and their metabolites.We discovered the potential mechanism of long-chain fatty acids (LCFAS) dominated by gut microbiota in the occurrence of early phase of AMI through in silico molecular docking and in vitro thrombogenic assay.

Results: We found the eAMI plasma is dominated by increased LCFAs, 14 of which provide differentiating power of eAMI patients from HCs. Multiomics analysis reveals up to 70% of the variance in LCFAs of eAMI patients can be explained by altered gut microbiome. We found that eAMI and HC samples were significantly different in the beta-diversity of structural variations composition (PWilcoxon = 1.4e-05) and composition of bacterial genetics in eAMI individuals has less heterogeneity than that of HC subjects. Higher-resolution profiling of gut bacterial species demonstrated that bacterial structural variations are mechanistically linked to LCFAs dysregulation. By in silico molecular docking and in vitro thrombogenic assay in isolated human platelets, we highlighted that eAMI-associated LCFAs contribute to platelet aggregation, a driving factor for AMI initiation.

Conclusions: LCFAs hold significant potential as early biomarkers of AMI and gut microbiome contributes to altered LCFAs in eAMI. Further studies are imperative to expand upon these observations to better leverage LCFAs as a potential biomarker for eAMI and as a therapeutic target for inhibition of platelet aggregation in eAMI.

Relationship Between the Atherogenic Index of Plasma and New-Onset Atrial Fibrillation in Acute Myocardial Infarction

Yan-Ni Ji, Yun-Jie Yin, Yan-Chun Chen

Yixing People's Hospital

Objective Atherogenic index of plasma(AIP), a novel biomarker reflecting lipid metabolism and systemic inflammation, has been found to exhibit a significant correlation with cardiovascular disease. Clinical studies suggest that Blood lipid levels are closely related to the occurrence of atrial fibrillation, and different components of blood lipids are also closely associated with the release of atrial fibrillation. AIP is the logarithmic value of the ratio of triglycerides to high-density lipoprotein, which is a novel lipid indicator used to evaluate the occurrence and prognosis of cardiovascular diseases. To our knowledge, no prior studies have investigated the correlation between AIP and NOAF following myocardial infarction. This study aims to evaluate the relationship between AIP and new-onset atrial fibrillation (NOAF) in acute myocardial infarction (AMI). **Methods** This study is a retrospective case-control study. A total of 598 AMI patients admitted to the Department of Cardiology at Yixing People's Hospital from January 2016 to January 2023 were enrolled. According to whether the patient experienced atrial fibrillation during hospitalization, they were divided into AMI group and AMI combined with NOAF group, with 542 patients in the AMI group and 56 patients in the AMI combined with NOAF group. Clinical data, including blood biochemistry, blood glucose, and glycated hemoglobin, were collected. At the same time, all patients underwent echocardiography to evaluate the left atrial diameter. Restricted cubic spline (RCS) analysis was used to examine the nonlinear relationship between AIP and NOAF. Logistic regression was employed to identify risk factors for NOAF, and receiver operating characteristic (ROC) curve analysis was performed to evaluate the predictive performance of relevant indicators. **Results** Notably, patients who developed NOAF exhibited significantly lower baseline AIP levels compared to those without NOAF(-0.035±0.289 vs 0.191±0.291, P<0.05). RCS regression analysis demonstrated no significant nonlinear association between AIP and NOAF incidence (P=0.106 for nonlinearity). The dose-response curve

exhibited a near-linear inverse trend, where increasing AIP values correlated with a progressive decline in NOAF risk until reaching a plateau at approximately AIP=0.2, beyond which the relationship stabilized . In univariate logistic regression, AIP emerged as a statistically significant protective factor against NOAF (OR=0.065, P<0.05) , suggesting that each 0.1 unit increase in AIP was associated with a 9.35% reduction in NOAF risk. This association persisted after multivariate adjustment for clinically relevant confounders, including sex, age, smoking status, hypertension, and diabetes mellitus (OR=0.099, P<0.05) . The ROC analysis results showed that the area under the AIP ROC curve was 0.728 (95% CI 0.653-0.804, p<0.001); By calculating the Youden Index, the optimal cutoff of AIP was found to be -0.008, with corresponding sensitivity and specificity of 64.3% and 77.0%, respectively. **Conclusion** This study initially investigated the relationship between AIP and NOAF in AMI. Lower AIP levels appear to confer a protective effect for NOAF, potentially mediated by reduced oxidative stress, improved endothelial function, and attenuated pro-inflammatory pathways. These findings highlight the potential utility of AIP as both a prognostic tool and a therapeutic target in AMI patients at high risk for atrial fibrillation. Further research is warranted to elucidate the mechanistic links between AIP and NOAF in AMI.

Keywords Atherogenic index of plasma; Acute myocardial infarction; New-onset atrial fibrillation

加权基因共表达网络分析和单细胞测序分析揭示了心肌缺血再灌注损伤中巨噬细胞坏死性凋亡的核心基因

晋群

中国人民解放军联勤保障部队第九六〇医院

目的：通过生物信息学分析和动物实验验证，确定 MIRI 中巨噬细胞坏死性凋亡的核心基因，并探索其免疫调控机制。

方法：本研究采用加权基因共表达网络分析 （WGCNA） 算法建立加权基因共表达网络，使用最小绝对收缩、选择运算符 （LASSO） 回归和支持向量机 （SVM） 特征选择算法确定 MIRI 中巨噬细胞坏死性凋亡的关键基因，并通过 MIRI 动物模型验证核心基因的表达。

结果：1. 生物信息学分析发现 Casp1 、 Hpse 、 Myd88 、 Ripk1 和 Tpm3 作为坏死性凋亡的生物标志物；2. 单细胞测序分析表明，坏死性凋亡的核心基因集中在巨噬细胞上，巨噬细胞主要通过 TNF/TNFRSF1A 相互作用介导单核细胞、成纤维细胞、造血干细胞和心肌细胞的功能变化；3. 巨噬细胞的极化和功能激活受其他细胞的 MIF 信号网络 （MIF CD74/CXCR4 和 MIF CD74/CD44） 的影响；4. 免疫浸润试验结果显示，参与坏死性凋亡的 5 个基因与 M2 巨噬细胞的浸润和功能活性显著增加相关；5. 预计 TWS-119 是一种靶向关键 MIRI 基因的分子药物；6. 通过建立小鼠模型确认可这 5 个核心基因的表达，缺血再灌注损伤 （IRI） 后心室重塑随时间增加。

结 论：在心肌缺血再灌注损伤过程中，Casp1、Hpse、Myd88、Ripk1 和 Tpm3 可能是调节巨噬细胞坏死性凋亡和极化并引起心室重塑的核心基因。

Serpina7 介导中性粒细胞胞外诱捕网产生加重心肌梗死损伤的研究

郭彦 范国勇 王思梦 黎炫 郑梦姣 余凯 蒋世翠 张驰 *

瑞安市人民医院

目的：

心肌梗死（Myocardial Infarction，MI）是发病率和死亡率均极高的世界性疾病。心肌梗死会引发心脏多种病理性变化，包括剧烈的炎症反应，心肌细胞凋亡，心肌纤维化，左心室收缩功能抑制，氧化应激等。本课题组利用蛋白质组学检测血清结果发现当发生心肌梗死时有 80 个上调蛋白，其中 Serpina7 蛋白水平上调更加显著，这暗示 Serpina7 作为心肌梗死的新基因治疗靶点的潜力。本文旨在探索 Serpina7 与心肌梗死诱导的心肌损伤的关系，解析 Serpina7 在心肌梗死导致的心肌损伤中的具体作用机制。

方法：

1. 构建雄性 Serpina7-KO 小鼠后，将之与其同窝对照 WT 小鼠随机分为 WT-sham、KO-sham、WT-MI、KO-MI 四组。在分别进行假手术和左冠状动脉前降支结扎后十四天，收集心脏组织样本及血液检测纤维化、凋亡、炎症、氧化应激等心肌损伤相关指标；同时构建过表达 Serpina7（AAV-serpina7）小鼠，分 AAV-EGFP-sham、AAV-Serpina7-sham、AAV-EGFP-MI、AAV-Serpina7-MI 四组进行上述相同实验操作。从两个不同角度出发探索 Serpina7 在心肌梗死导致的心肌损伤中的作用。

2. 构建 AAV-serpina7 小鼠，分 AAV-EGFP-sham、AAV-EGFP-MI、AAV-Serpina7-MI、AAV-Serpina7-MI-DNase1 四组进行上述相同实验操作。在 serpina7 基因高表达以及额外添加中性粒细胞胞外诱捕网（NETs）抑制剂 DNase1 的环境下检测小鼠心梗后心肌损伤的变化情况。

3. 构 建 Serpina7-KO 小 鼠， 分 WT-sham、WT-MI、KO-MI、WT-MI-DNase1、KO-MI-DNase1 五组进行上述相同实验操作，在 serpiana7 基因缺失以及 DNase1 干预的环境下检测小鼠心梗后心肌损伤的变化情况。

结果：

1. 功能缺失性研究表明 Serpina7 缺失可缓解心肌梗死诱导的心肌损伤，表现在改善心脏功能、缓解心肌纤维化、抑制心肌细胞凋亡、减轻炎症反应、抑制氧化应激。同时功能获得性研究表明 Serpina7 过表达可加重心肌梗死诱导的心肌损伤。

2. 蛋白组学分析发现，WT-MI 组与 (Serpina7-)KO-MI 组差异表达蛋白在 NETs 形成相关通路中显著富集（p-value = 0.0215，FDR = 0.0384）。因此，引入 NETs 抑制剂（DNase1）进行体内研究，结果表明与 AAV-Serpina7-MI 组相比，AAV-Serpina7-MI-DNase1 组能够改善心肌梗死诱导的心肌损伤。

3. 实验结果表明，与 WT-MI-DNase1 组相比，KO-MI-DNase1 组在心肌梗死后的心肌组织并没有进一步的保护作用。

结论：

Serpina7 是通过介导中性粒细胞胞外诱捕网产生，来加重心肌梗死后的心肌损伤。

血清乙酰肝素酶水平对急性心肌梗死患者 MACE 事件的预测价值

晋群

中国人民解放军联勤保障部队第九六〇医院

目的：探讨血清乙酰肝素酶（Heparanase, HPSE）在急性心肌梗死（Acute Myocardial Infarction, AMI）患者中的表达水平及其与主要心血管不良事件（major adverse cardiovascular events，MACE）发生的相关性，评估其作为新型生物标志物对 MACE 的预测价值，为风险分层和早期干预提供依据。

方法：选取 2023 年 9 月至 2024 年 9 月于中国人民解放军联勤保障部队第九六〇医院心血管内科住院的 217 例 AMI 患者为研究对象，收集患者的基线资料及采用酶联免疫吸附试验（enzyme linked immunosorbent assay, ELISA）法测定患者血清 HPSE 水平。患者出院后进行为期 6 个月的随访，随访终点事件为出现 MACE 事件。随访结束后依据是否发生 MACE 事件将患者分为 MACE 组（n=51）和非 MACE 组（n=166）。采用单因素和多因素 Cox 比例风险回归模型分析探讨患者发生 MACE 事件的影响因素。绘制受试者工作特征（ROC）曲线评估血清 HPSE 水平预测患者发生 MACE 事件的价值并计算 ROC 曲线下面积（AUC）。绘制 Kaplan-Meier 生存曲线比较患者随访过程中累积生存率的差异，组间比较采用 Log-rank 检验。

结果：MACE 组和非 MACE 组资料比较结果显示，MACE 组肌钙蛋白 I(cTnI)、低密度脂蛋白 (LDL-C)、肌酐 (Cr)、血清 HPSE 水平高于非 MACE 组，左心室射血分数（LVEF）低于非 MACE 组（P<0.05）。多因素 Cox 比例风险回归分析结果显示，LVEF 降低：HR=1.042(95%CI: 1.032~1.404, P=0.018)、Cr 升高 (HR=1.015，95%CI=1.007~1.023，P<0.021)、血清 HPSE 水平升高 (HR=1.103，95%CI=1.029~1.175，P<0.001) 为患者发生 MACEs 的危险因素。ROC 曲线结果显示血清 HPSE 水平预测 AMI 患者发生 MACE 事件的 AUC 为 0.802 (95%CI=0.745~0.859, P<0.001)，最佳截断值为 5.24 ng/ml。将所有受试者以 ROC 曲线计算所取得的最佳截断值为界，分为高 HPSE 组和低 HPSE 组，绘制的 Kaplan-Meier 生存曲线结果显示，低 HPSE 组累积生存率高于高 HPSE 组（P=0.01）。

结论：HPSE 是 AMI 患者发生 MACE 事件的独立预测因子，其血清水平的高低可作为 AMI 风险分层和早期干预的新型生物标志。HPSE 联合 LVEF 与 Cr 等指标，能够进一步优化对 MACE 事件的预测效能，为改善患者预后管理和制定个体化治疗策略提供重要依据。

分析预见性护理干预措施对急性心肌梗塞患者的影响

田冰心

新疆维吾尔自治区人民医院

摘要：目的：分析急性心肌梗塞的临床干预中，实施预见性护理干预措施的临床应用价值。**方法：**研究样本限定为本院接诊的急性心肌梗塞患者共计 64 例，研究时间为 2019 年 5 月到 2020 年 8 月，采用随机数字分组法分为对照、干预两组，分析组间并发症发生率、健康认知评分差异。**结果：**干预组并发症发生率 3.13%，对照组并发症发生率 25.00%，数据分析存在意义（P < 0.05）；干预组病理认知、生理认知、并发症预防、预后认知等各项评分数据相较于对照组数据差异存在差异（P < 0.05）。**讨论：**急性心肌梗塞疾病的护理干预中，预见性护理措施的临床实施有效的促进患者并发症降低，提升患者健康认知程度，应用价值显著。

关键词：预见性护理干预措施；急性心肌梗塞；影响

研究数据分析得知：干预组并发症发生率 3.13%，对照组并发症发生率 25.00%，数据分析存在意义（P < 0.05）；干预组病理认知、生理认知、并发症预防、预后认知等各项评分数据相较于对照组数据差异存在差异（P < 0.05），有效促进患者生理状态改善，提升病理认知及相关认知内容，应用价值显著。

综上所述，基于急性心肌梗塞患者病情表现，实施预见性护理措施能够有效改善患者生理状态，促进其生存质量的有效提升。

基于多组学与孟德尔随机化解析代谢综合征与心肌梗死的遗传因果网络

卢杨芳 刘华芬

武汉大学人民医院

目的 代谢综合征（MetS）是心肌梗死（MI）的重要危险因素，但其通过遗传调控影响 MI 发生的分子机制尚未完全明确。本研究旨在整合多组学数据（基因组、转录组、代谢组），结合孟德尔随机化（MR）因果推断方法，构建 MetS 与 MI 的遗传因果网络，揭示二者关联的核心遗传调控通路及关键分子节点，为疾病预防和靶向治疗提供理论基础。

方法 基于公共数据库及临床队列数据，筛选 MetS 相关遗传变异（SNP）、差异表达基因及特征性代谢物；通过 MR 分析验证 MetS 及其组分（如肥胖、高血糖、血脂异常）与 MI 的遗传因果关系；利用多组学整合分析（如表达数量性状位点分析、代谢物 - 基因关联分析）挖掘介导因果关系的中间分子（基因 / 代谢物）；最终通过网络分析构建“遗传变异 - 分子表型 -MetS-MI”的多层级遗传因果网络，

并通过独立队列验证核心节点的有效性。

结果 共筛选出 28 个与 MetS 和 MI 均相关的核心 SNP，MR 分析证实 MetS 对 MI 存在显著遗传因果效应（OR=1.62，95%CI：1.45~1.81，P<1e-8）。多组学整合显示，SNP 调控的脂代谢基因（如 LPL、APOB）及炎症相关代谢物（如甘油三酯、C 反应蛋白）是介导因果关系的关键中间节点，形成 “遗传变异 - 脂代谢紊乱 - 慢性炎症 -MetS-MI” 的核心调控网络。独立队列验证显示该网络对 MI 发病风险的预测效能良好（AUC=0.82）。

结论 本研究通过多组学与孟德尔随机化的结合，首次系统构建了 MetS 与 MI 的遗传因果网络，明确了脂代谢基因及炎症代谢物在二者关联中的核心介导作用，为解析疾病遗传机制及开发精准防治策略提供了全新视角。

麝香保心丸对 STEMI 患者长期预后的影响

于云

鄂尔多斯市中心医院（内蒙古自治区超声影像研究所）

目的：研究麝香保心丸 (SBP) 对接受直接经皮冠状动脉介入治疗 (PPCI) 的首次 ST 段抬高型心肌梗死 (STEMI) 患者长期预后的影响。

方法：回顾性分析 2016-09-01 至 2019-03-31 于鄂尔多斯市中心医院心内科行 PPCI 的首发 STEMI 患者 110 名。根据是否接受 SBP 治疗，分为对照组 (PPCI 组)：55 例，其中 2 例有陈旧性心肌梗死病史，1 例有严重心力衰竭 (kilipIII 级)，共计 3 例患者被排除，最终 52 例；麝香保心丸组 (PPCI+SBP 组)：55 例，其中 1 例有陈旧性心肌梗死病史，1 例有严重心力衰竭 (kilipII 级)，1 例有严重心力衰竭 (kilip IV 级),1 例有急性炎症，共计 4 例患者被排除，最终 51 例。两组均予指南推荐的标准药物及 PPCI。PPCI+SBP 组入院即刻含服 SBP 45mg，继以 45mg tid 口服 1 个月。记录并比较所有患者一般资料，包括是否服用麝香保心丸、性别、年龄、吸烟史、危险因素（高血压、糖尿病、脑梗死病史），用药情况（阿司匹林、ACEI、ARB、β 受体阻滞剂、ARNI、他汀类、螺内酯、糖尿病药物、叶酸片、维生素 D），检测患者心率、收缩压、舒张压、血常规、生化、空腹血糖、糖化血红蛋白、血脂、维生素 D、BNP、同型半胱氨酸；颈动脉超声测量患者颈动脉斑块 Crouse 积分，用心脏超声测定患者心功能：左室舒张末期内径、左室收缩末期内径、左房内径、左室射血分数、三尖瓣返流峰值速度及肺动脉压收缩压、左心室质量指数、左心室整体纵向收缩应变等指标。主要随访终点为主要心脑血管不良事件 (MACCE)：心源性死亡、非致死性再梗死、新发心力衰竭、新发脑梗死、短暂性脑缺血发作。

结果：临床中位随访时间为 87 个月，随访中死亡 11 例（10.7%），发生 MACCE 事件 27 例（26.2%）。Kaplan-Meier 分析显示，PPCI+SBP 组患者 MACCE 事件的发生率较低（P<0.05）。

结论：麝香保心丸能够改善 ST 段抬高型心肌梗死患者的长期预后，提高患者生存率，降低 STEMI 患者主要心血管不良事件。

急性心肌梗死并发肾功能不全的危险因素分析及预测模型构建

冯龙 信满坤 潘奕霖 王睿 贺晓楠

首都医科大学附属北京安贞医院

目的: 研究急性心肌梗死(AMI)患者并发肾功能不全(RI)的临床特征及危险因素，并构建风险预测模型。

方法：回顾选取 2020 年 1 月至 2024 年 12 月在首都医科大学附属北京安贞医院住院治疗的 173 例 AMI 并发 RI 患者为病例组，以同院同期诊断为单纯 AMI 的 1672 例住院患者为对照组。比较两组一般资料及实验室指标，筛选 AMI 患者并发 RI 的独立危险因素，通过绘制受试者工作特征曲线（ROC）评估模型的预测效能。

结果：与对照组患者比较，病例组患者男性较多、年龄较大，既往合并高血压、糖尿病、心力衰竭、房颤、脑卒中病史比例以及入院时 BMI、TC、LDL-C、WBC、HB、PLT 水平的差异有统计学意义（P<0.05）。多因素 Logistic 回归分析显示，既往合并心力衰竭及入院时 LDL-C、HB、PLT 是 AMI 患者并发 RI 的独立危险因素（P<0.05）。基于以上四项指标建立预测模型，预测模型 ROC 曲线下面积（AUC）为 0.817（95%CI：0.781~0.852，P<0.001），提示已构建的模型具有较好的预测效能。

结论：既往合并心力衰竭及入院时 LDL-C、HB、PLT 是 AMI 患者并发 RI 的独立危险因素，基于以上四项指标构建的预测模型，对早期识别 AMI 患者并发 RI 的效能较好。

Development and Validation of a Nomogram for Predicting Atrial Fibrillation in Patients with Acute Myocardial Infarction: A Retrospective Cohort Study

Long Feng, Yi-Lin Pan, Man-Kun Xin, Wen-Wen Duan, De-Cheng Chen, Shi-Jie Yang, Xiao-Nan He

Beijing Anzhen Hospital,Capital Medical University

Objective: Analyze the risk factors of Atrial Fibrillation (AF) in patients with Acute Myocardial Infarction (AMI), and build a corresponding risk prediction model to provide reference for clinical personalized prediction of AF risk in AMI patients.

Methods: A total of 126 AMI patients complicated with AF who were hospitalized in Beijing Anzhen Hospital Affiliated to Capital Medical University from January 2020 to December 2024 were selected as the case group, and 1719 inpatients diagnosed with simple AMI in the same hospital during the same period were selected as the control group. The clinical characteristics and laboratory test results of the two groups of patients were compared, and independent risk factors for AF in AMI patients were screened. The predictive performance of the model was evaluated by drawing each independent predictor and the Area Under the Curve (AUC) for joint diagnosis R software was used to draw nomograms, calibration charts and Decision Curve Analysis (DCA) based on the multi-factor Logistic regression model to evaluate the clinical efficacy of the Nomogram model.

Results: Multivariate Logistic regression analysis showed that older age (OR=1.067, 95% CI: 1.044~0.092, P<0.001), longer hospitalization days (OR=1.039, 95% CI: 1.013~1.066, P<0.005), Previous history of coronary heart disease (OR=1.602, 95% CI: 1.042~2.462, P<0.05), Heart rate is fast (OR=1.021, 95% CI: 1.007~1.035, P<0.005), high INR levels (OR=2.047, 95% CI: 1.111~3.773, P<0.05), low Hemoglobin level (OR=1.018, 95% CI: 1.007~1.028, P<0.005), and large mean platelet volume (OR=1.227, 95% CI: 1.009~1.493, P<0.05) were independent risk factors for AF in AMI patients. The AUC of age, hospitalization days, history of coronary heart disease, heart rate, INR, Hemoglobin, and mean platelet volume were 0.721, 0.663, 0.577, 0.614, 0.688, 0.438, and 0.607. The AUC of Nomogram model for predicting AF in AMI patients was 0.833 (95% CI: 0.796~0.870, P<0.001), the best cutoff value was 0.543, the sensitivity was 0.817, and the specificity was 0.726. Nomogram model predicts that the risk threshold of AF in AMI patients is greater than 0.06.

Conclusion: A joint prediction model based on age, hospital stay, coronary heart disease history, heart rate, INR, hemoglobin, and average platelet volume has good prediction effect. The variables in this Nomogram model are easily obtained in clinical practice and can provide reference for individualized prediction of AF in AMI patients.

Objective: Analyze the risk factors of Atrial Fibrillation (AF) in patients with Acute Myocardial Infarction (AMI), and build a corresponding risk prediction model to provide reference for clinical personalized prediction of AF risk in AMI patients.

Methods: A total of 126 AMI patients complicated with AF who were hospitalized in Beijing Anzhen Hospital Affiliated to Capital Medical University from January 2020 to December 2024 were selected as the case group, and 1719 inpatients diagnosed with simple AMI in the same hospital during the same period were selected as the control group. The clinical characteristics and laboratory test results of the two groups of patients were compared, and independent risk factors for AF in AMI patients were screened. The predictive performance of the model was evaluated by drawing each independent predictor and the Area Under the Curve (AUC) for joint diagnosis R software was used to draw nomograms, calibration charts and Decision Curve Analysis (DCA) based on the multi-factor Logistic regression model to evaluate the clinical efficacy of the Nomogram model.

Results: Multivariate Logistic regression analysis showed that older age (OR=1.067, 95% CI: 1.044~0.092, P<0.001), longer hospitalization days (OR=1.039, 95% CI: 1.013~1.066, P<0.005), Previous history of coronary heart disease (OR=1.602, 95% CI: 1.042~2.462, P<0.05), Heart rate is fast (OR=1.021, 95% CI: 1.007~1.035, P<0.005), high INR levels (OR=2.047, 95% CI: 1.111~3.773, P<0.05), low Hemoglobin level (OR=1.018, 95% CI: 1.007~1.028, P<0.005), and large mean platelet volume (OR=1.227, 95% CI: 1.009~1.493, P<0.05) were independent risk factors for AF in AMI patients. The AUC of age, hospitalization days, history of coronary heart disease, heart rate, INR, Hemoglobin, and mean platelet volume were 0.721, 0.663, 0.577, 0.614, 0.688, 0.438, and 0.607. The AUC of Nomogram model for predicting AF in AMI patients was 0.833 (95% CI: 0.796~0.870, P<0.001), the best cutoff value was 0.543, the sensitivity was 0.817, and the specificity was 0.726. Nomogram model predicts that the risk threshold of AF in AMI patients is greater than 0.06.

Conclusion: A joint prediction model based on age, hospital stay, coronary heart disease history, heart rate, INR, hemoglobin, and average platelet volume has good prediction effect. The variables in this Nomogram model are easily obtained in clinical practice and can provide reference for individualized prediction of AF in AMI patients.

新冠感染后急性冠脉综合征患者血浆淋巴细胞亚群及炎性因子特点的临床研究

刘冉 翟光耀

首都医科大学附属北京潞河医院（首都医科大学附属潞河临床医学院）

目的：研究急性冠脉综合征患者在新冠感染后及感染不同阶段淋巴细胞亚群及炎性因子的变化。

方法：本课题为病例对照研究，入组从 2023 年 1 月 1 日至 2023 年 5 月 31 日在北京潞河医院诊断急性冠脉综合征患者 234 例，其中急性 ST 段抬高型心肌梗死（STEMI）患者 109 例，非 ST 段抬高型急性冠脉综合征（NSTE-ACS）125 例，同期感染新冠且不符合排除标准的健康患者 78 例作为对照，采集患者血液样本，采用流式细胞术检测淋巴细胞亚群，采用化学发光法检测 IL6、IL8、TNF-α 水平。比较上述指标在新冠感染后及各阶段的差别。

结果：1）新冠感染后 STEMI、NSTE-ACS 组 CD4+T 淋巴细胞均下降，STEMI 组 IL-6、TNF-α 升高，与对照组比较差别显著（P<0.05）；2）进一步比较感染不同阶段的数据，结果显示：①新冠感染 3 月内 STEMI 组 CD4+、CD8+T 淋巴细胞均下降，CD4+/CD8+、IL-6、TNF-α 则升高，NSTE-ACS 组仅 CD4+ 下降，

与对照组比较差别显著（P<0.05）；②新冠感染 3 月内 STEMI 组 CD8+T 淋巴细胞下降，CD4+/CD8+T 淋巴细胞升高，与 NSTE-ACS 组比较差别显著（P<0.05）③新冠感染 3 月至 6 月，与对照组比较，STEMI 组仅 IL-6、TNF-α 仍显著升高（P<0.05），但 CD4+、CD8+、CD4+/CD8+T 淋巴细胞及 IL-8 则差别不显著（P>0.05）；与对照组比较，NSTE-ACS 组淋巴细胞亚群及各项炎性指标均无显著差别（P>0.05）

结论： 新冠感染后 NSTE-ACS 组淋巴细胞亚群的变化主要发生在感染 3 月内，主要表现为 CD4+T 淋巴细胞的显著下降，提示新冠感染对 NSTEMI 患者的影响可能主要集中在感染的 3 月内；新冠感染后 STEMI 患者 CD4+T 淋巴细胞亚群持续减少，早期同时有 CD8+T 淋巴细胞的显著减少，提示新冠感染对 STEMI 患者的影响可能更显著且持久；新冠感染后 STEMI 患者表现持续 IL-6、TNF-α 的升高，提示新冠感染后 STEMI 患者存在持续的炎性反应。

酮替芬治疗 STEMI 直接 PCI 患者有效性和安全性的临床研究

谢鹏昕 崔鸣

北京大学第三医院

目的：

部分急性 ST 段抬高型心肌梗死（ST-segment elevation myocardial infarction，STEMI）患者开通罪犯血管后出现缺血再灌注损伤和心室不良重构，其发生机制与过度炎症反应密切相关。肥大细胞（mast cells，MCs）作为一种重要的炎症细胞，在心肌梗死中发挥重要的作用。MCs 在心肌梗死早期迅速活化，释放多种效应因子，放大炎症级联反应。其中，类胰蛋白酶是 MCs 释放的特异性蛋白酶，是评估活化程度的金标准。本课题组既往研究表明，类胰蛋白酶在 STEMI 急性期显著升高，且与远期预后相关。动物实验提示，通过稳定 MCs 或拮抗其释放产物可减轻缺血再灌注损伤，缩小心肌梗死面积，但相关临床证据仍较为匮乏。酮替芬是经典的肥大细胞稳定剂，被广泛应用于治疗过敏性疾病，但其在心肌梗死患者中是否具有保护作用值得深入探讨，因此拟进一步探讨肥大细胞稳定剂酮替芬治疗 STEMI 患者的有效性和安全性。

方法：

本研究拟开展一项随机对照试验，纳入 2022 年 9 月到 2023 年 9 月就诊于北京大学第三医院心内科的 STEMI 直接 PCI 患者，按照 1:1 比例区组随机方式分组：① 对照组：给予 STEMI 标准治疗；② 酮替芬组：标准治疗方案基础上给予酮替芬 3 个月（每日 2 次，每次 1 mg）。于心肌梗死后 3 个月行心脏磁共振扫描评估心肌梗死面积，作为主要观察终点。

结果：

在本研究中，酮替芬组和对照组各纳入了 56 例患者。酮替芬组患者的心肌梗死面积小于对照组（12.86 ± 5.63 g VS.15.87 ± 4.87 g，P <0.01），在不同年龄、CKMB 峰值和心肌梗死部位的亚组中，均观察到酮替芬对心肌梗死面积的影响。次要终点方面，酮替芬组患者的细胞外体积分数低于对照组（27.27 ± 5.65% VS.30.14 ± 5.14%，P <0.01），左室整体纵向应变改善值高于对照组（3.24 ± 0.50% VS. 2.45 ± 0.73%，P <0.001）。随访期间，共 5 例患者出现轻度精神萎靡等不良反应，均发生在酮替芬组，症状轻微且持续约 1 周后逐渐缓解，未影响治疗的依从性。

结论：

肥大细胞稳定剂酮替芬可以减少 STEMI 直接 PCI 患者的心肌梗死面积和纤维化程度，改善心肌应变，且安全性良好，提示酮替芬具有潜在的临床应用价值，为急性心肌梗死抗炎治疗提供新思路。

Usefulness of Albumin-to-D-dimer ratio in predicting the long-term outcome after hospital discharge in patients with ST-elevation myocardial infarction: a retrospective cohort study

Pei-Ren Shan, Guang-Ze Xiang

温州医科大学附属第一医院

Abstract

Objective: The Albumin-to-D-dimer ratio (ADR), a novel systemic inflammatory marker, has been linked to adverse outcomes in patients with cardiovascular disease. However, limited research has explored its prognostic value in ST-elevation myocardial infarction (STEMI) survivors following hospital discharge. This study aimed to evaluate the prognostic significance of ADR in hospital-discharged STEMI patients.

Methods: In this retrospective study, we analyzed data from 2675 STEMI patients admitted to our hospital between January 2014 and December 2021. Patients were stratified into two groups based on their natural logarithmic ADR (Ln ADR): a high Ln ADR group (≥ 3.998) and a low Ln ADR group (<3.998). Univariate and multivariate Cox regression analyses were performed to assess the association between Ln ADR levels and clinical outcomes, including all-cause mortality and new-onset stroke.

Results: Over a mean follow-up period of 1013 days (interquartile range: 466–1449 days), the incidence of major adverse cardiovascular events (MACE) was significantly higher in the low Ln ADR group compared to the high Ln ADR group (20.87% vs. 12.33%, P < 0.001). This disparity was particularly evident in all-cause mortality (6.58% vs. 1.00%, P < 0.001) and new-onset stroke (4.19% vs. 0.90%, P < 0.001). Multivariate analysis revealed that low Ln ADR was an independent predictor of all-cause mortality (HR = 2.46, 95% CI: 1.25–4.81, P = 0.009) and new-onset stroke (HR = 2.93, 95% CI: 1.35–6.35, P = 0.006).

Conclusions: Reduced ADR levels were independently associated with increased long-term all-cause mortality and new-onset stroke in STEMI patients following hospital discharge. These findings suggest that ADR may serve as a valuable prognostic marker for risk stratification in this population.

Keywords: Albumin, D-dimer, Albumin-to-D-dimer ratio, ST-elevation myocardial infarction, All-cause Mortality, New-onset Stroke

Introduction

Coronary artery disease (CAD) remains the predominant cause of global morbidity and mortality [1][2]. Although significant progress has been made in the management of ST-elevation myocardial infarction (STEMI)–including timely reperfusion via percutaneous coronary intervention (PCI), advancements in acute cardiovascular care, and the adoption of more effective pharmacotherapies [3][4]–the mortality and complication rates among post-discharge patients persist at concerning levels, especially in high-risk populations [5]. Consequently, there is an urgent need to identify more reliable indicators for early recognition of high-risk patients and to optimize post-discharge management strategies.

Previous studies have established that both albumin [6][7][8] and D-dimer [9][10][11] are valuable predictors of long-term outcomes in patients with CAD. In recent years, the albumin-to-D-dimer ratio (ADR), an emerging biomarker, has gained recognition as a significant prognostic indicator, particularly in the context of cardiovascular diseases [12][13]. For instance, Li et al. [14] demonstrated in a study of 3707 patients with heart failure and multivessel disease undergoing elective PCI that a higher D-dimer-to-albumin ratio was independently associated with major adverse cardiovascular events (MACE) and all-cause mortality in diabetic patients with ischemic heart failure. This finding underscores the potential of ADR as a reliable prognostic tool for this high-risk population. Additionally, Yuan et al. [15] highlighted a significant relationship between serum albumin and D-dimer levels in patients with non-valvular atrial fibrillation (NVAF), revealing an inverse correlation between D-dimer and albumin levels. Despite these advancements, no studies to date have specifically explored the prognostic utility of ADR in patients with STEMI.

Therefore, this study aims to investigate the prognostic role of the ADR in predicting long-term outcomes in patients with STEMI and to compare its predictive efficacy with that of albumin and D-dimer individually.

急性心肌梗死患者应激性高血糖比率、白蛋白与院内预后的关联：一项队列研究

杨毓秀 [1,2] 严妍 [1,2] 王志坚 [1,2] 周玉杰 [1,2]

1. 首都医科大学附属北京安贞医院

2. 国家心血管病临床研究中心

目的：应激性高血糖比率（Stress Hyperglycemia Ratio, SHR）升高被认为是急性心肌梗死（AMI）的潜在风险指标。然而，SHR、白蛋白与后续心血管不良结局之间的关系尚不明确。

方法：本研究连续纳入 2022 年 1 月至 2023 年 10 月来自多中心前瞻性注册研究（NCT05337319）的患者，分析其基线 SHR 和白蛋白水平。采用最佳截断值定义低 SHR 组与高 SHR 组。主要终点为院内主要不良心血管事件（MACEs），包括全因死亡、心源性休克、急性充血性心力衰竭（ACHF）、再梗死和脑卒中。通过多变量逻辑回归模型评估白蛋白分层下 SHR 与结局的关联。

结果：本研究共纳入 5,269 例 AMI 患者，其中 27.7% 存在高 SHR，19.5% 合并低白蛋白血症。分析显示，低 SHR 且白蛋白正常患者的院内主要不良心血管事件（MACEs）发生率最低（1.4%）；与之相比，高 SHR 合并低白蛋白血症患者的 MACEs 风险显著升高（校正后 OR=6.800，95% CI: 3.883–11.907，P<0.001）。此外，低 SHR 但合并低白蛋白血症组（校正后 OR=3.033，95% CI: 1.775–5.182，P<0.001）以及高 SHR 而白蛋白正常组（校正后 OR=2.375，95% CI: 1.335–4.226，P=0.003）的 MACEs 风险亦显著增加。关键发现表明，无论基线白蛋白水平如何，高 SHR 均独立增加 MACEs 风险：白蛋白正常组校正后 OR=2.325（95% CI: 1.307–4.136，P=0.004），低白蛋白血症组校正后 OR=2.213（95% CI: 1.343–3.647，P=0.002），且交互作用检验无显著性（P=0.866）。这一关联模式在心源性休克和急性充血性心力衰竭（ACHF）的次级终点分析中同样成立。

结论: SHR 升高在 AMI 患者中普遍存在，尤以合并低白蛋白血症的群体更为显著；无论患者基线白蛋白水平如何，较高的 SHR 均一致提示更差的院内预后，白蛋白状态不削弱 SHR 对不良结局的独立预测效力。

TSTEMI 影响因素分析及列线图的构建与验证

郑一歌 [1,3] 董浩铖 [1,3] 李晓萌 [1,3] 赵雨静 [1,3] 关世杰 [1,2] 郝潇 [3] 李树仁 [3]

1. 河北医科大学研究生院

2. 河北北方学院研究生院

3. 河北省人民医院

目的 初始表现为心电图 ST 段抬高，但在再灌注治疗前出现 ST 段恢复超过 50% 和症状缓解的急性冠脉综合征患者，被称为短暂性 ST 段抬高型心肌梗死（STEMI），指南建议这类患者早期介入治疗，而目前诊断方法仅有反复观察急性心梗患者心电图变化来确定，部分人群因未及时完善心电图或入院时 ST 段已经回落而不能得到辨认。本文旨在探讨 TSTEMI 发生的影响因素并建立列线图预测模型，构建

更简单的预测评分，有助于临床诊断并及时进行有效的处理措施。

方法 回顾性分析 2016 年 9 月至 2024 年 9 月于河北省人民医院心血管内科就诊的急性心梗患者，最终纳入 TSTEMI 组 71 人、NSTEMI 组 88 人。采用单因素及多因素 Logistic 回归法分析与 TSTEMI 发生相关的影响因素，基于影响因素分析结果构建和验证预测 TSTEMI 发生的列线图模型，并通过 ROC 曲线以及临床决策模型检验列线图的效能。

结果 多因素 Logistic 回归分析显示，TSTEMI 发生的独立预测因素包括：术前双抗使用阿司匹林 + 替格瑞洛（OR=0.23）、院前 3 个月心绞痛发作史（OR=0.13）、入院呼吸频率(OR=1.41)、入院收缩压(OR=0.98)、合并多支血管病变(OR=0.18)。预测模型的 AUC 为 0.93，临床决策曲线显示预测模型净获益较高。

结论 TSTEMI 发生的影响因素主要包括术前双抗使用阿司匹林 + 氯吡格雷（而非替格瑞洛）、院前 3 个月心绞痛发作史、入院呼吸频率、入院收缩压、合并多支血管病变。预测模型可以为临床快速辨别 TSTEMI 患者提供更快速、精准的评分指标，便于临床医生决策。

重复远隔缺血适应对急性心肌梗死患者血清胰岛素样生长因子水平的影响

何立芸 艾丽玛·艾尔肯 王贵松

北京大学第三医院

目的：观察重复远隔缺血适应（remote ischemia conditioning,RIC）对急性心肌梗死（AMI）患者急诊 PCI 术后血清胰岛素样生长因子（IGFs）水平的影响；分析血清 IGFs 水平变化与反映心肌损伤和心功能状态的临床参数间的相关性，以初步确定 IGFs 做为 RIC 保护性体液因子的可能性。

方法：本研究纳入 2020 年 9 月至 2021 年 1 月于北京大学第三医院行急诊 PCI 治疗的 80 例 AMI 患者，随机分为重复 RIC 组 (40 例) 和对照组（40 例）。重复 RIC 组患者在急诊 PCI 术后 24 小时内启动肢体 RIC 处理，每日一次，连续进行 1 周，同时给予常规药物治疗；对照组于急诊 PCI 术后仅给予常规药物治疗。比较两组患者血清心肌酶和 cTnT 峰值以及急诊 PCI 术后 24 小时至术后 1 周血浆 NT - proBNP 水平的变化；比较两组间超声心动图测得的心功能参数变化；采用 ELISA 方法测定两组患者急诊 PCI 术前及术后 1 周血清 IGF-1，IGF-2 及其受体 IGF-1R 水平并比较两组间的变化；对血清 IGF s 水平与反映心肌损伤和心功能状态的临床参数进行相关性分析。

结果：重复 RIC 组患者急诊 PCI 术后 1 周血浆 NT-proBNP 水平显著低于对照组 [290.50（122.25 ~ 1073.50）VS 888.00（399.00 ~ 2144.00），P=0.01], 且术后 1 周内血浆 NT-ProBNP 降低幅度 RIC 组显著高于对照组 [233.50（20.00 ~ 976.50）VS 376.50.50（213.75 ~ 1510.50），P < 0.05]。两组患者入院 48 小时内及术后 1 周超声心动图参数间差异无统计学意义（P > 0.05）。重复 RIC 组术后 1 周血清 IGF-1、IGF-2 水平显著高于对照组（P < 0.05），血清 IGF-1R 水平较对照组有升高趋势，但差异无统计学意义（P > 0.05）。重复 RIC 组术后 1 周血清 IGF-1、IGF-2、IGF-1R 水平较术前显著升高（P < 0.05），而对照组术后 1 周的血清 IGF-2 水平较术前显著下降（P=0.02），血清 IGF-1 及 IGF-1R 水平亦较术前有下降趋势（P > 0.05）。重复 RIC 组术后 1 周血浆 NT-proBNP 水平与血清 IGF-1 水平呈显著负相关（r=-0.323，P=0.04）。

结论：重复 RIC 可使接受急诊 PCI 治疗的 AMI 患者血清 IGFs 水平升高，同时降低血浆 NT-proBNP 水平，改善心功能。血清 IGF-1 水平升高与 NT-proBNP 水平下降具有相关性，提示 IGFs 可能是重复肢体 RIC 心脏保护作用的体液因子。

急性心肌梗死早期应用 PCSK9 抑制剂对患者心功能的影响

刘梦茜 邵春丽 王贵松

北京大学第三医院

目的：PCSK9 抑制剂作为一种新兴降脂药物已被广泛应用于冠心病患者的二级预防，可有效降低 LDL-C 水平和主要不良心血管事件。本研究旨在探究急性心肌梗死（AMI）早期应用 PCSK9 抑制剂在降脂治疗的同时对患者心功能的影响。

方法：本研究为一项单中心前瞻性、开放标签、随机对照的探索性研究。对于符合入排标准的 84 名 AMI 患者以 1:1 随机分为治疗组和对照组。治疗组在急诊 PCI 术后 24 小时内给予首次依洛尤单抗 140 mg 皮下注射，第 2 周、第 4 周再分别注射一次，之后是否继续应用 PCSK9 抑制剂由门诊随访医师酌定；对照组患者急诊 PCI 术后接受常规药物治疗，术后 4 周内降脂治疗主要采用他汀类药物或合用胆固醇吸收抑制剂。患者出院后随访 6 个月，主要终点为患者住院期间与急诊 PCI 术后 1 个月超声心动图测得 LVEF 值的变化，次要终点为患者基线与应用 PCSK9 抑制剂后 3 天及 PCI 术后 1 个月血清 NT-proBNP 水平的变化。

结果：治疗组患者血浆 LDL-C 水平显著下降，且降幅显著优于对照组（Δ=-0.76；95% CI：-1.30 至 0.26；P=0.003）。治疗组与对照组患者的血浆 PCSK9 浓度在用药后 3 天均显著升高，而治疗组升高幅度显著高于对照组（Δ=449.68；95% CI：273.66 至 625.70；P<0.001）。治疗组 AMI 患者急诊 PCI 术后 1 个月 LVEF 值平均增加 5.51±8.55%（P<0.001），对照组急诊 PCI 术后 1 月后 LVEF 值无明显改善（P=0.190），治疗组相较于对照组能够显著改善急诊 PCI 术后 1 月 LVEF 水平（Δ=4.36；95% CI：1.125 至 7.57，P=0.008）。亚组分析显示，前壁心肌梗死患者 LVEF 水平的改善程度差异具有统计学意义（Δ=6.52；95% CI：1.93 至 11.13；P=0.007），而非前壁心肌梗死患者改善程度无统计学差异（P=0.310）。治疗组患者应用 PCSK9 抑制剂后 3 天及急诊 PCI 术后 1 个月血清 NT-proBNP 浓度分别平均下降 408.50 pg/ml（P<0.001）和 561.00 pg/ml（P<0.001），对照组 3 天及 1 月 NT-proBNP 浓度分别平均下降 389.50 pg/ml 和 428.00 pg/ml，但其下降幅度两组间差异无统计学无意义。

结论：AMI 患者早期应用 PCSK9 抑制剂可显著降低 LDL-C 水平、改善左心室功能 LVEF，提示 PCSK9 抑制剂的早期应用可能对 AMI 患者的心功能具有保护作用。

改善“生命八要素”可以降低急性心肌梗死的风险，延迟发病时间，并预防近六成的病例：一项来自英国生物银行的证据

程文珂 赵懿 康品方 （血脂学组委员） 唐碧 （肺动脉高压委员）

蚌埠医科大学第一附属医院

背景

2022 年，美国心脏协会（AHA）提出了更新版的心血管健康评估工具——“生命八要素”（Life's Essential 8, LE8），在原有的“生命七要素”基础上新增了睡眠维度，全面涵盖了饮食、体力活动、烟草暴露、睡眠健康、体重指数、血脂、血糖和血压八个方面，旨在更科学评估个体心血管健康（CVH）水平。已有研究表明，较高的 CVH 评分可显著降低心血管疾病（CVD）整体风险，但其与急性心肌梗死（AMI）及其不同亚型（ST 段抬高型 STEMI 和非 ST 段抬高型 NSTEMI）之间的具体关系仍缺乏系统性研究。此外，当前尚不清楚改善 CVH 能否延缓 AMI 发病时间，以及改善 CVH 能否显著降低 AMI 发病负担。本研究旨在评估 LE8 评分与 AMI 风险、发病时间的关联，并探讨炎症和代谢生物标志物在其中的中介作用。

方法

本研究纳入英国生物样本库中 122,914 名 40–69 岁、基线无心血管病的参与者。根据 LE8 得分将 CVH 划分为低（<50）、中（50–79）和高（≥ 80）三类。通过多变量 Cox 比例风险模型评估 CVH 与 AMI 及其亚型的关联，采用加速失效时间模型（AFT）分析 CVH 与 AMI 发病时间的关系，限制性立方样条（RCS）用于评估剂量 – 反应关系。采用中介分析评估炎症与代谢生物标志物（hs-CRP、白细胞、血小板、甘油三酯、尿酸）的中介效应，并计算人群归因风险（PAF）和可预防事件数（IER），以估算改善 CVH 对 AMI 预防的潜在影响。

结果

在中位随访 163.2（IQR: 124.5-194.1）个月中，共记录 2,892 例 AMI 事件，其中 844 例为 STEMI，1,490 例为 NSTEMI。每升高 1 分 CVH 评分，AMI 风险降低 3%（HR=0.970，95%CI: 0.967–0.973）。与低 CVH 组相比，中、高 CVH 组 AMI 风险分别下降 41.2%（HR=0.588，95%CI: 0.534–0.648）和 75.0%（HR=0.250，95%CI: 0.205–0.306），该趋势在 STEMI 与 NSTEMI 中均一致。高 CVH 组 AMI 发病时间较低 CVH 组延迟约 33.6 个月。中介分析显示，炎症与代谢标志物在 CVH 与 AMI 之间解释的效应占比为 1.57%–8.62%。人群归因分析表明，若低 CVH 人群提升至中或高水平，约 58.65%（95%CI: 45.16%–72.14%）的 AMI 事件可被预防。

结论

较高的 CVH 水平与 AMI 风险降低和发病延迟显著相关，该关系部分由炎症与代谢通路介导。提升 CVH 可在群体层面预防约六成 AMI 事件，凸显“生命八要素”在心血管一级预防中的临床和公共卫生价值。未来干预策略应聚焦于提升 CVH 各维度，尤其是饮食、血脂及血压控制，以实现更有效的 AMI 预防。

YY1 在心肌梗死后心脏损伤和重塑中的保护作用

杨德忠

陆军军医大学大坪医院

目的： 潜在的治疗靶点对心肌梗死（MI）和 MI 后心力衰竭具有重要意义。转录因子 YY1）是凋亡和血管生成的重要调节因子，但其在心肌梗死中的作用尚不清楚。

方法：检测心肌梗死后 C57BL/6J 小鼠心脏中 YY1 的表达。通过注射腺相关病毒 9 实现了 YY1 在小鼠心脏中的过表达或沉默。评估存活率、心脏功能和瘢痕大小，以及凋亡、血管生成、心脏纤维化、T 辅助 2 淋巴细胞细胞因子产生和巨噬细胞极化。还研究了 YY1 对 Akt 磷酸化和血管内皮生长因子产生的影响。

结果：心肌梗死显著刺激了 YY1 在心脏中的表达。YY1 过表达提高了小鼠的存活率、心功能、瘢痕大小和左心室容积，但 YY1 沉默使其恶化。YY1 减轻了心肌梗死后心脏的凋亡和纤维化，促进了血管生成、T 辅助 2 细胞因子的产生和 M2 巨噬细胞的极化，还增强了内皮细胞的成管和迁移能力。在 YY1 过表达的情况下，观察到 Akt 磷酸化增强，血管内皮生长因子水平升高。

结论：YY1 通过抑制心肌细胞凋亡和促进血管生成来改善心肌梗死后的心脏损伤和重塑，这可能归因于 Akt 磷酸化的增强和随后血管内皮生长因子的上调。增加 T 辅助 2 细胞因子的产生和 M2 巨噬细胞极化也可能参与 YY1 的心脏保护作用。这些发现支持 YY1 作为心肌梗死治疗研究的潜在靶点。

新型 Wnt 通路抑制剂对心肌梗死后心脏再生的治疗作用

杨德忠

陆军特色医学中心（陆军军医大学大坪医院）

目的：心肌梗死（MI）后，由于心肌细胞大量丢失和心脏再生不足，心脏难以修复。传统的药物主要针对病理性重塑，但对于刺激心脏再生的新型候选药物却鲜有报道。

方法：在本研究中，我们确定了新型 wnt 抑制剂 CGX1321 是否以及如何影响 MI 和心脏再生。在小鼠中进行左前降支 (LAD) 冠状动脉的永久结扎以诱导 MI 损伤。通过超声心动图测量心脏功能，通过 TTC 染色检查梗塞大小。用 masson 三色染色和 vimentin 染色评估纤维化。

结果：CGX1321 给药阻断了 Wnt 蛋白的分泌，并抑制了经典和非经典 Wnt 信号通路。 CGX1321 改善了心脏功能，减少了心肌梗死面积和 MI 后心脏的纤维化。 CGX1321 显着增加了 MI 后心脏梗死边界区新形成的心肌细胞，EdU+ 心肌细胞的增加证明了这一点。同时，CGX1321 增加培养中的 Ki67+ 和磷酸组蛋白 H3 (PH3+) 心肌细胞，表明增强的心肌细胞增殖。 mRNA 微阵列显示 CGX1321 上调细胞周期调节基因，如 Ccnb1 和 Ccne1 CGX1321 不会改变心肌细胞中 YAP 蛋白的磷酸化和核易位。

结论：wnt 抑制剂 CGX1321 通过限制纤维化和促进再生来减少 MI 损伤。它通过不依赖 Hippo/YAP 的途径刺激细胞周期调节基因来促进心肌细胞增殖。

Predictive Value of Triiodothyronine in Long-term Outcomes of Left main and/or three-vessel Disease in Patients with Acute Myocardial Infarction

Yan Chen, Lei Song, Jin-Qing Yuan

Fuwai hospital

Background: Low Triiodothyronine (T3) syndrome, characterized by reduced serum T3 levels without primary thyroid dysfunction, is frequently observed in acute myocardial infarction (AMI) patients and correlates with adverse cardiovascular outcomes in general coronary artery disease populations. However, its specific prognostic utility in the high-risk cohort of AMI patients presenting with left main coronary artery disease (LMD) and/or three-vessel disease (3VD) remains inadequately defined. This study aimed to comprehensively evaluate the association between admission serum T3 levels and long-term clinical outcomes, particularly mortality, in this complex and vulnerable patient group undergoing percutaneous coronary intervention (PCI).

Methods: We consecutively enrolled 800 AMI patients with angiographically confirmed LMD/3VD (left main stenosis >50% or three-vessel stenosis >50%) undergoing percutaneous coronary intervention (PCI) at Fuwai Hospital (2013). Serum T3 was measured at admission. Receiver operating characteristic (ROC) analysis identified 0.84 ng/ml as the optimal T3 cutoff for predicting 2-year mortality, stratifying patients into low-T3 (<0.84 ng/ml, n=196) and high-T3 (≥ 0.84 ng/ml, n=604) groups. Primary and secondary endpoints were 2-year all-cause death and major adverse cardiovascular/cerebrovascular events (MACCE: death, MI, stroke, unplanned TVR, or stent thrombosis). Multivariable Cox regression adjusted for significant confounders.

Results: Baseline characteristics revealed substantial differences. Low-T3 patients were older (63.6±10.4 vs. 56.1±10.7 years; p<0.001), more frequently female (28.1% vs. 13.4%; p<0.001), and had higher hypertension prevalence (71.9% vs. 60.3%; p=0.003), prior PCI (35.7% vs. 19.5%; p<0.001), and Killip class ≥ II (12.2% vs. 5.5%; p=0.001). They exhibited lower left ventricular ejection fraction (LVEF: 58.0% vs. 60.0%; p=0.001), higher hs-CRP (8.6±5.4 vs. 5.2±4.7 mg/dL; p<0.001), and greater angiographic complexity (SYNTAX score: 18.1±9.6 vs. 15.8±8.3; p=0.001). Procedural characteristics showed higher primary PCI rates (40.3% vs. 16.2%; p<0.001) and intra-aortic balloon pump use (10.2% vs. 2.3%; p<0.001) in low-T3 patients. In-hospital management were generally comparable between groups, though pre-discharge medical therapy data, showed similar rates of guideline-recommended secondary prevention medications (Dual antiplatelet therapy: 98.5% vs. 99.1%; Beta-blockers: 89.2% vs. 90.1%; ACEI/ARB: 85.6% vs. 87.2%; High-intensity statins: 86.7% vs. 89.0%; p>0.05 for all).

At 2-year follow-up, outcomes demonstrated a stark divergence based on T3 status. Low-T3 patients experienced significantly higher all-cause mortality (5.6% [11/196] vs. 0.7% [4/604]; p<0.001), cardiac death (4.1% vs. 0.7%; p=0.002), definite/probable stent thrombosis (2.6% vs. 0.5%; p=0.024), stroke (3.1% vs. 0.7%; p=0.017), and MACCE (25.5% [50/196] vs. 15.6% [94/604]; p=0.011). Kaplan-Meier analysis confirmed significantly reduced survival in low-T3 patients. Rates of recurrent non-fatal MI (3.6% vs. 2.8%; p=0.558) and unplanned TVR (14.3% vs. 10.6%; p=0.129) showed numerical but not statistically significant differences.

In the Multivariable analysis, low serum T3 levels (<0.84 ng/ml) at admission remained an independent predictor of 2-year all-cause mortality. In the most fully adjusted model, which included age, sex, comorbidities (hypertension, diabetes, dyslipidemia, smoking), prior PCI, Killip class ≥ II, peak cTnI, LVEF, hs-CRP, BNP, and SYNTAX Score, the Low-T3 Group retained a strong association with increased mortality risk (Adjusted HR = 5.09, 95% CI: 1.22–21.30; p=0.026). In contrast, while univariable analysis suggested an association with MACCE, low T3 status was not independently predictive of the composite MACCE endpoint after comprehensive multivariable adjustment (Adjusted HR = 0.87, 95% CI: 0.58–1.33; p=0.525). ROC analysis validated T3's predictive capacity in mortality, A T3 cut-off value of 0.84 ng/ml had an AUC of 0.763 (95% CI 0.617-0.910), with a sensitivity of 76.4% and a specificity of 73.3% for the prediction of 2-year all-cause death.

Conclusions: Admission T3 level <0.84 ng/ml independently predicts 2-year all-cause mortality in AMI patients with LMD/3VD, beyond established risk factors. T3 assessment provides valuable prognostic information for risk stratification in this high-risk population.

SCFAs Block Macrophage Osteoclastogenesis via FFAR2-RANKL Signaling to Promote Post-MI Cardiac Repair

Caixia Guo, Qun Zhang

Capital Medical University Affiliated Tongren Hospital

Abstract

Background: Myocardial infarction triggers a cascade of pathophysiological processes that thereby facilitate post-infarction cardiac repair. The pathophysiological mechanisms by which short-chain fatty acids (SCFAs) facilitate early post-myocardial infarction cardiac repair via Free fatty acid receptor 2(FFAR2) remain poorly defined. Osteoclast-like macrophage-driven inflammation critically contributes to post-MI cardiac injury and repair, yet intrinsic mechanisms constraining these immune responses—essential for homeostasis and effective infarct healing—are incompletely understood. This study determines whether SCFAs suppress osteoclast differentiation signaling through myeloid FFAR2 receptors, consequently reducing post-infarction osteoclast-like macrophage infiltration and attenuating cardiac macrophage inflammation.

Methods: From April to December 2023, we recruited 50 percutaneous coronary intervention (PCI)-treated STEMI patients alongside 50 concurrent matched controls at Beijing Tongren Hospital, Capital Medical University to investigate the correlation between plasma SCFAs concentrations and short-term prognosis as well as coronary lesion complexity in patients with MI, while documenting major cardiovascular events. Peripheral blood samples were collected immediately prior to PCI, with subsequent targeted plasma SCFAs metabolomic profiling conducted on the obtained specimens. Subsequent follow-up recorded major adverse cardiovascular events including recurrent MI, heart failure (HF) rehospitalization, stroke, and cardiovascular death, with concurrent quantitative assessment of STEMI coronary lesion complexity using validated angiographic scoring systems. The median duration of follow-up was 3 months. Additionally, FFAR2 receptor mRNA expression was quantified in peripheral blood leukocytes from both cohorts. In murine models investigating SCFAs-mediated cardioprotection post-MI, myocardial infarction was surgically induced in global (FFAR2-KO) and myeloid-specific ($FFAR2^{\Delta myeloid}$) FFAR2-deficient mice following three-month pre-MI oral SCFA supplementation (100mM), with subsequent functional and histopathological evaluation. To delineate mechanisms of myeloid FFAR2-dependent early cardiac repair (MI-D3), RNA sequencing (RNA-seq) combined with single-nucleus/single-cell RNA sequencing (snRNA-seq/scRNA-seq) assessed SCFAs-attenuated osteoclast-like macrophage infiltration and repair-associated cellular dynamics. Flow cytometry further confirmed that SCFAs attenuated the infiltration of osteoclast-like macrophages at day 3 post-MI through myeloid-restricted FFAR2 signaling. For in vitro validation that SCFAs promote fibroblast-to-myofibroblast transition by acting on macrophage FFAR2 receptors, neonatal mouse macrophage-fibroblast co-cultures examined myeloid FFAR2-dependent pro-fibrotic responses. Finally, to elucidate the mechanism whereby SCFAs attenuate early post-MI cardiac rupture through FFAR2 receptor-mediated suppression of osteoclast-like macrophage activation, we employed neonatal mouse macrophages subjected to in vitro SCFA/RANKL stimulation to assess FFAR2-dependent inhibition of RANKL-RANK pathway activation.

Results: Based on validation within our case-control cohort, reduced plasma SCFAs levels were associated with poorer short-term prognosis in patients with MI. Plasma SCFA concentrations were inversely correlated with coronary lesion complexity. Furthermore, FFAR2 receptor expression levels in peripheral blood leukocytes were significantly lower in STEMI patients compared to the matched control group. Genetic ablation of FFAR2—whether global or myeloid-specific—exacerbated cardiomyocyte necrosis/apoptosis in the early post-MI phase, increased infarct size, attenuated infarct fibrotic deposition, and elevated the incidence of cardiac rupture. Conversely, supplementation with SCFAs (100 mM) for three months prior to MI reduced cardiomyocyte death and infarct size while enhancing fibrotic deposition and decreasing rupture rates in both WT and $FFAR2^{flox/flox}$ mice. Integrated RNA-seq and snRNA-seq/scRNA-seq analyses revealed that, compared to myeloid-specific knockout, $FFAR2^{flox/flox}$ mice exhibited expansion of fibroblast/cardiomyocyte populations, reduced infiltration of osteoclast-like macrophages, and enhanced macrophage-cardiomyocyte-fibroblast crosstalk. Concurrently, flow cytometry confirmed that SCFAs attenuated early post-MI infiltration of osteoclast-like macrophages via myeloid FFAR2 (MI-D3), thereby reducing collagen degradation, promoting early fibrotic repair, and ultimately decreasing the incidence of post-MI cardiac rupture. Macrophage-fibroblast co-culture experiments demonstrated that the SCFA-induced pro-fibrotic response requires macrophage FFAR2. Mechanistically, SCFAs attenuated post-MI infiltration of osteoclast-like macrophages through FFAR2 and suppressed RANKL-RANK activation via FFAR2-dependent G_i signaling.

Conclusion:

We identified an inverse association between plasma SCFA concentrations and major adverse cardiovascular event risk in STEMI patients undergoing PCI; SCFAs enhanced early post-MI fibrotic repair by attenuating osteoclast-like macrophage infiltration through myeloid FFAR2-mediated suppression of RANKL-RANK signaling. Targeting the SCFAs-FFAR2-RANKL-RANK signaling axis represents a promising novel therapeutic strategy for MI patients.

急诊 PCI 冠脉血流相关因素及 其与预后的关系

杨丽霞

中国人民解放军联勤保障部队第九二〇医院

【目 的】基于我院胸痛中心的数据构建预测模型以探究 ST 段抬高型心肌梗死患者急诊行冠状动脉介入手术术后出现慢血流 / 无复流的影响因素，为改善患者的预后提供依据。

【方 法】回顾性研究自 2023 年 1 月至 2024 年 6 月本胸痛中心急诊行 PCI 术并符合入选标准的 STEMI 患者 520 例，根据校正的 TIMI 帧数分为正常血流组（n=361）、慢血流 / 无复流组（n=159）。记录患者临床资料、实验室检验指标、术后 48 小时内心脏彩超指标、围手术期相关数据等，并通过患者门诊复查、电话回访等方式进行随访并记录，统计患者随访期间 MACCE 的发生情况、心脏彩超数据。采用多因素 Logistic 回归分析 STIEMI 患者行 PCI 术后发生慢血流 / 无复流的影响因素，建立预测模型后进行内外部验证，最后分析 STEMI 患者术后半年的预后情况。

【结 果】本研究最终纳入了 520 例行急诊 PCI 术的 STEMI 患者，其中发生慢血流 / 无复流的 159 例，正常血流的患者 361 例。慢血流 / 无复流组与正常血流组相比吸烟史暴露时间更长（中位数 28 vs. 20，P=0.020）、糖尿病患病率更高（40.9% vs. 26.9%，P=0.001）、肌钙蛋白峰值更高（87.29 vs. 65.08，P=0.001）、肌酸激酶（CK）峰值更高（2669 vs. 1790，P<0.001）、肌酸激酶同工酶（CK-MB）峰值更高（218 vs. 138，P<0.001）、BNP 更高（291.2 vs. 194.1，P=0.002）、低密度脂蛋白胆固醇（LDL-C）更高（3.48 vs. 3.08，P<0.001）、术前 Killip III 级（13.8%）和 IV 级（24.5%）的比例更高（P<0.001）、FMC-B 时间更长（186 vs. 133，P<0.001）、2 支严重病变血管（34.0%）和 3 支严重病变血管（40.3%）的比例更高（P<0.001），病变位置位于近段病变的比例较高（79.2% vs. 67.3%，P=0.008）、3 枚支架数量比例较高（13.2% vs. 3.9%，P<0.001）、支架最大直径较大（3.5 vs. 3.25，P=0.001）、球囊扩张次数较多（3 vs. 2，P<0.001）；其中病变位置（OR=2.14，95% CI：1.43-3.32，P<0.001）、支架数量（OR=2.14，95% CI：1.45-3.32，P<0.001）、支架最大直径（OR=1.93，95% CI：1.21-3.32，P=0.007）及球囊扩张次数（OR=2.05，95% CI: 1.72-2.46，P<0.001）是发生慢血流 / 无复流的独立危险因素。短期预后：半年后随访心脏彩超提示：慢血流 / 无复流组的左室射血分数显著低于正常血流组（50 vs. 56，P<0.001），左房内径（34 vs. 33，P=0.007）及左室舒张末期内径（51 vs. 50，P<0.001）显著大于正常血流组；半年内慢血流 / 无复流组的 MACCE 事件发生率显著高于正常血流组（16.4% vs. 8.8%，P=0.018）。

【结 论】1. 单因素及多因素 logistic 回归分析显示，病变位置、支架数量、支架最大直径、球囊扩张次数是慢血流 / 无复流发生的独立危险因素；2. 发生慢血流 / 无复流的患者与正常血流的患者相比心功能预后较差，其中发生慢血流 / 无复流的患者左室射血分数较低、左室舒张末期内径较大；3. 发生慢血流 / 无复流的患者 MACCE 发生率高于正常血流的患者

The redistribution of cadmium after acute myocardial infarction in mice

Hung-Chen Lin

Tongji Hospital of Tongji Univeristy

Objective

Cadmium, a heavy metal which has a lot of effects on cardiovascular system, have been proved to be a stable conjunction to metallothioneins in human body. However, some research showed that under several circumstances, cadmium can release from the stable conjunction and have further damage to tissue or organ function[1-3]. Our team have previously proof that acute myocardial infarction patients with higher urine cadmium will have high 30-days mortality rate, therefore, whether cadmium will distribution after acute myocardial and have further damage to organs' function is needed to be proven.

Methods

Sixty 8-weeks old wild type mice was included in our study. Mice were randomly divided into two groups: cadmium exposure mice (chronic cadmium exposure group) and cadmium exposure with AMI mice (chronic cadmium exposure with acute myocardial infarction group). Both groups were fed with 100mg/L $CdCl_2$ water for 12 weeks. At the end of 12 weeks, experiment group were induced acute myocardial infarction by left descending coronary artery ligation, the effectiveness of the induction is confirmed by electrocardiogram and echocardiogram. After 24 hours of the induction, both control and experiment group were sacrifice. Serum sample between this 24 hour gap were collect. Heart, aorta, kidney, liver, intestine, spinal bone and thigh bone were collected. ICP-MS were used to measure cadmium, lead, magnesium, zinc and other heavy metals in the organ samples. H&E dye, silver stain, and trichrome stain were used to access the pathological change of the organs.

Result

Different cadmium concentration in different organs showed in figure 1 and table 1. In the small intestine, mice in the chronic cadmium exposure acute myocardial infarction group showed a decrease in cadmium concentration compared to mice in the chronic cadmium exposure group, with no statistically significant changes in other metals. In the kidneys, mice in the acute myocardial infarction group had lower concentrations of cadmium, zinc, iron, and magnesium compared to mice in the non-acute myocardial infarction group, while calcium concentration was higher. In the liver, mice in the chronic cadmium exposure acute myocardial infarction group had lower concentrations of cadmium, zinc, and magnesium compared to mice in the chronic cadmium exposure non-acute myocardial infarction group, while iron and calcium concentrations were higher. In the heart tissues of mice in the chronic cadmium exposure acute myocardial infarction group, calcium, iron, and copper concentrations were higher than in mice in the non-acute myocardial infarction group, while cadmium, zinc, and magnesium concentrations were lower. In the femurs and vertebral bones, concentrations of calcium, iron, zinc, and cadmium were higher in mice in the chronic cadmium exposure acute myocardial infarction group compared to mice not subjected to acute myocardial infarction treatment.

Misra et al.[1] confirmed that nitric oxide can replace cadmium in stable binding with metallothionein, resulting in the liberation of cadmium into a free state. Satarug et al.[2] found a 27.8% decrease in renal cadmium content in rats injected with LPS following cadmium loading; LPS can significantly increase the concentration of nitric oxide in the body[4], which also supports the theory that nitric oxide-induced changes in cadmium concentration could lead to its redistribution. During acute myocardial infarction, the NOS system is activated to produce large amounts of nitric oxide[5], and based on our experimental results, it is reasonable to infer that the massive production of nitric oxide stimulated by acute myocardial infarction causes the release and redistribution of accumulated cadmium in the body. Our experiments also revealed that, except for the femur and vertebral bones, cadmium concentrations decreased in all organs after acute myocardial infarction. This phenomenon might be due to the extensive activation of the NOS system after acute myocardial infarction, which stimulates osteoblastic activity in bones, promoting calcium transfer into bones and thus increasing bone mass [6]; cadmium may enter bones through calcium channels and get deposited [7], but this requires further investigation. We also observed consistent changes in zinc and copper concentrations with cadmium changes in the liver and kidneys, the primary organs of cadmium-metallothionein complex accumulation. Indeed, in the human body, zinc and copper also bind with metallothionein [8, 9], and an increase in nitric oxide concentration could lead to changes in zinc and copper levels[10], potentially displacing them from metallothionein, similar to cadmium. This study is the first to confirm that acute myocardial infarction can lead to redistribution of cadmium across various organs in the body; the redistribution of cadmium, initially deposited in the body caused by the rise in nitric oxide following acute myocardial infarction, poses a potential risk of secondary harm. It also raises the question of whether chelators should be used concurrently during acute myocardial infarction to bind the liberated cadmium and potentially reduce further damage to the human body, which requires further research validation. Moreover, due to the stable nature of cadmium in the body, chelation therapy for cadmium has been ineffective. Based on the characteristics of nitric oxide in liberating cadmium, a new approach to cadmium chelation therapy might be proposed.

Conclusion

Acute myocardial infarction will cause cadmium redistribution between organs, and might cause further damage to body function.

[1] MISRA R R, HOCHADEL J F, SMITH G T, et al. Evidence That Nitric Oxide Enhances Cadmium Toxicity by Displacing the Metal from Metallothionein [J]. Chemical Research in Toxicology, 1996, 9(1): 326-32.

[2] SATARUG S, BAKER J R, REILLY P E B, et al. Evidence for a Synergistic Interaction between Cadmium and Endotoxin Toxicity and for Nitric Oxide and Cadmium Displacement of Metals in the Kidney [J]. Nitric Oxide, 2000, 4(4): 431-40.

[3] ERDEM O, YAZIHAN N, KOCAK M K, et al. Influence of chronic cadmium exposure on the tissue distribution of copper and zinc and oxidative stress parameters in rats [J]. Toxicol Ind Health, 2016, 32(8): 1505-14.

[4] SERRELI G, MELIS M P, CORONA G, et al. Modulation of LPS-induced nitric oxide production in intestinal cells by hydroxytyrosol and tyrosol metabolites: Insight into the mechanism of action [J]. Food and Chemical Toxicology, 2019, 125(520-7.

[5] WILMES V, SCHEIPER S, ROEHR W, et al. Increased inducible nitric oxide synthase (iNOS) expression in human myocardial infarction [J]. Int J Legal Med, 2020, 134(2): 575-81.

[6] VAN'T HOF R J, RALSTON S H. Nitric oxide and bone [J]. Immunology, 2001, 103(3): 255-61.

[7] SADDALA M S, KANDIMALLA R, ADI P J, et al. Novel 1, 4-dihydropyridines for L-type calcium channel as antagonists for cadmium toxicity [J]. Scientific Reports, 2017, 7(1): 45211.

[8] ANZELLOTTI A I, FARRELL N P. Zinc metalloproteins as medicinal targets [J]. Chem Soc Rev, 2008, 37(8): 1629-51.

[9] LIU J, CHAKRABORTY S, HOSSEINZADEH P, et al. Metalloproteins containing cytochrome, iron-sulfur, or copper redox centers [J]. Chem Rev, 2014, 114(8): 4366-469.

[10] SATARUG S, BAKER J R, REILLY P E, et al. Evidence for a synergistic interaction between cadmium and endotoxin toxicity and for nitric oxide and cadmium displacement of metals in the kidney [J]. Nitric Oxide, 2000, 4(4): 431-40.

运动预适应通过 IL-13 调控中性粒细胞抑制胞外诱捕网形成在心肌梗死后的作用研究

张颖男 杨爽

哈尔滨医科大学附属第二医院

目的：心血管疾病是影响全球人类身体健康的主要原因。诱发心血管疾病的因素丰富多样，仍需继续开发治疗方法。心肌梗死是心血管疾病中引起死亡的最重要原因，每年全球内有高达 700 多万人受其影响。运动是有效的心血管疾病治疗手段，对免疫有着别样的影响。IL-13 近来被证明是由运动诱导的耐力调节因子，它本身也参与了心梗后的系列反应。中性粒细胞胞外诱捕网是中性粒细胞的杀菌手段之一，但它在无菌性炎症中其实会加重组织损伤。目前运动对免疫细胞的调控机制研究方兴未艾，对于其中的效应因子和作用通路还不够明确。因此，深入研究运动对 NETs 的可能调控机制将有助于扩大运动的益处。

方法：（1）构建中等强度有氧运动小鼠心梗模型，通过心脏超声检测心功能，TTC 检测心肌损伤程度，HE、Masson 染色检测纤维化水平，进一步通过 WB 及 ELISA 检测 NETs 关键酶 PAD4 和标志物 H3Cit 的表达水平；（2）通过 ELISA 检测小鼠运动后 IL-13 的水平；（3）应用 IL-13 基因敲除小鼠构建心梗模型，检测心功能及纤维化水平；（4）使用重组 IL-13 蛋白体外刺激小鼠骨髓原代中性粒细胞，检测 NETs 水平；（5）进一步构建中等强度有氧运动 IL-13-/- 小鼠心梗模型，检测心功能及 NETs 水平；（6）体外补充 IL-13 检测 IL-13-/- 小鼠中性粒细胞的 NETs 生成水平；（7）检测不同预处理的小鼠的线粒体耗氧率；（8）体外 IL-13 刺激 IL-13-/- 小鼠中性粒细胞并检测各组线粒体耗氧率。

结果：运动预适应的小鼠心梗后第一天的心肌组织损伤程度较低，远期的左室射血分数和缩短分数较静坐组更高，纤维化程度更轻，并且运动组心梗小鼠 PAD4 和 H3Cit 的水平较低。运动后小鼠血浆和心肌组织中的 IL-13 的水平升高。体外重组 IL-13 蛋白刺激后，中性粒细胞 NETs 生成减少。敲除 IL-13 导致小鼠的左室射血分数和缩短分数较野生型低，纤维化程度更重。运动未完全挽回 IL-13-/- 心梗小鼠的左室射血分数和缩短分数的降低，运动的 IL-13-/- 心梗小鼠心脏纤维化程度同样较重。运动预适应的 IL-13-/- 心梗小鼠 PAD4 和 H3Cit 的水平偏高。心梗小鼠的中性粒细胞线粒体功能显著活跃，运动及体外补充 IL-13 增强了线粒体呼吸功能。

结论：（1）运动改善心肌梗死后心功能及心脏重塑；（2）运动减少了心肌梗死后 NETs 的生成；（3）运动通过 IL-13 发挥其对心肌梗死的有益效应；（4）运动通过 IL-13 调控心肌梗死后 NETs 的生成；（5）运动通过 IL-13 调控中性粒细胞线粒体功能。

血管内成像引导的稳定性冠心病日间经皮冠状动脉介入治疗：临床结局与安全性的回顾性队列研究

朱友琦 白明 苏昱润 胡威

兰州大学第一医院（兰州大学第一临床医学院）

目的：日间经皮冠状动脉介入治疗（PCI）方案旨在降低住院负担，但关于其联合血管内成像（IVUS/OCT）用于稳定性冠心病（SCAD）的真实世界证据仍然有限。本回顾性队列研究旨在评估血管内成像引导的日间 PCI 与传统住院 PCI 的临床结局差异。

方法：通过单中心电子健康记录数据库（2022-2023 年），将 520 例接受择期 PCI 的 SCAD 患者分为两组：日间 PCI+IVUS/OCT 组（暴露队列，n=760）：术后 8 小时内出院并实施标准化远程监测；住院 PCI+ 血管造影组（非暴露队列，n=760）：常规住院行血管造影引导 PCI。采用倾向评分匹配（1:1，卡钳值 =0.1）平衡 32 项基线变量（包括 SYNTAX 评分、肾功能等）。主要结局指标包括 24 小时非计划再住院率和 30 天主要不良心血管事件（MACE：心血管死亡、心肌梗死、血运重建）。安全性终点涵盖 BARC ≥ 2 级出血、穿刺部位血肿（超声确诊）及患者满意度（采用经过验证的 5 项量表进行回顾性调查）。

结果：IVUS/OCT 引导的日间组尽管住院观察时间更短（中位数 6.2 小时 vs. 22.5 小时），但 24 小时再住院率更低（校正后 OR 0.42，95% CI 0.28-0.63）。30 天 MACE 风险降低（HR 0.91，95% CI 0.73-0.98）与成像优化的支架参数相关（最小管腔面积 >6.0 mm^2 达成率 89% vs. 血管造影引导组 64%，P<0.001）。安全性相当：大出血发生率 1.2% vs. 1.5%（绝对差异 -0.3%，95% CI -1.1-0.5）；血肿发生率 2.4% vs. 3.1%（绝对差异 -0.7%，95% CI -1.9-0.5）。患者满意度方面，日间 PCI 在便利性（4.3/5 vs. 3.1/5，P<0.01）和心理压力减轻（视觉模拟评分 8.1 vs. 5.9，P<0.001）方面评分更高。

结论：本回顾性分析表明，血管内成像引导的日间 PCI 在不影响安全性的前提下，可改善早期临床结局并提高患者满意度。这些真实世界数据证实了精准支架优化联合当日出院方案的可行性，为 SCAD 治疗中更广泛的应用提供了依据。

定量血流分数联合腔内影像学指导的精准 PCI 在冠心病日间手术中的应用：一项回顾性队列研究

朱友琦 白明 苏昱润 胡威

兰州大学第一医院（兰州大学第一临床医学院）

摘要

目的：评估定量血流分数（QFR）联合血管内影像学（IVUS/OCT）指导的精准经皮冠状动脉介入治疗（PCI）在冠心病日间手术模式中的可行性与安全性。

方法：回顾性分析 2024 年 1 月至 2024 年 12 月在兰州大学第一医院心脏中心接受 PCI 治疗的冠心病患者临床资料。根据手术策略将患者分为日间手术组（QFR+ 血管内影像学指导，n=386）和常规住院组（传统造影指导，n=382）。主要终点为 24 小时内安全出院率，次要终点包括手术成功率、支架植入率、手术时间、造影剂用量、30 天主要不良心血管事件（MACE）及再入院率。

结果：共纳入 768 例患者，其中男性 542 例，女性 226 例，平均年龄（62.4±12.9）岁。日间手术组 386 例，常规手术组 382 例。两组人口学基线特征比较差异无统计学意义（P>0.05）。日间手术组 24 小时内出院率达 94.3%（364/386），显著高于常规组的 35.6%（136/382）（P<0.001）。两组手术成功率均为 100%。日间手术组在手术时间（43.8±16.2 min vs 54.3±18.6 min）、造影剂用量（85±25 mL vs 130±35 mL）及支架使用数量（1.1±0.3 vs 1.5±0.5）方面均显著优于常规组（均 P<0.05）。30 天随访显示，两组 MACE 发生率（1.2% vs 2.8%，P=0.45）和再入院率（2.4% vs 3.5%，P=0.62）差异均无统计学意义。

结论：QFR 联合血管内影像学指导的精准 PCI 可安全有效地应用于冠心病日间手术模式，显著缩短住院时间、优化医疗资源配置，且不增加短期不良事件风险，具有显著的临床价值和广阔的推广前景。

Dapagliflozin in acute myocardial infarction with left ventricular systolic dysfunction

Ge Gao[1,2], Wei-Ying Hui[1,2], Yan-Jie Yang[1,2], Jing-Jin Li[1,2], Tong-Shuai Guo[1,2], Tao Chen[1,2]

1. Department of Cardiology, First Affiliated Hospital of Xi'an Jiaotong University, Xi'an, China; Xi'an, Shaanxi 710061, China.

2. Key Laboratory of Environment and Genes Related to Diseases, Ministry of Education, Xi'an Jiaotong University, Xi'an, Shaanxi 710061, China.

Background and aims: Acute myocardial infarction (AMI) is a severe ischemic event in atherosclerotic cardiovascular disease, with high morbidity and mortality. Left ventricular systolic dysfunction is a strong predictor of poor outcomes in AMI, affecting approximately 40% of AMI patients. For those patients, more treatment strategies besides guideline-directed medical therapies are still needed to reduce residual cardiovascular risk. Dapagliflozin, a sodium glucose co-transporter 2 inhibitor, has been verified its efficacy in heart failure. In this study, we aimed to explore whether AMI patients with left ventricular systolic dysfunction could benefit from dapagliflozin treatment.

Methods: This retrospective cohort analysis included a total of 1310 AMI patients with newly reduced left ventricular ejection fraction (LVEF) to <50% enrolled from December 2019 to December 2022, among whom 356 received dapagliflozin plus conventional treatment (dapagliflozin group) and the remaining 954 received conventional treatment only (control group). All patients had successfully undergone percutaneous coronary intervention. Demographic information, clinical characteristics, medical treatment, and laboratory test results at baseline and follow-up were collected. The primary outcome was a composite of all-cause death, recurrent myocardial infarction, hospitalization for recurrent angina, hospitalization for heart failure, and stroke. The secondary outcomes are independent events of primary outcome. A propensity score matching analysis was conducted based on age, sex, LVEF, past medical histories, and laboratory test results at a 1:1 ratio using a 0.05 caliper.

Results: Compared with control group, dapagliflozin group had more patients with three-vessel disease (58.7% vs. 49.5%, P=0.003), history of diabetes (70.5% vs. 14.7%), P<0.001), and hypertension (53.4% vs. 46.3%, P=0.023), had less patients with ST-segment elevation myocardial infarction (73.3% vs. 81.3%, P=0.001), Killip Ⅰ / Ⅱ (87.1% vs. 92.7%, P=0.002), and history of smoke (57.3% vs. 63.5%, P=0.039), had a higher level of NT-proBNP (2,105 [1,120, 4,289] vs. 1,815 [941, 3,333] pg/mL, P=0.005), had a lower level of myocardial injury biomarkers (peak CKMB level: 139 [32, 378] vs. 232 [70, 455] U/L, P<0.001), had a poorer LVEF (43.5% [40.0%, 46.0%]vs. 45.0% [41.0%, 47.0%], P<0.001). A total of 263 patients experienced primary composite outcome events during follow-up, including 64 patients (18.0%) in dapagliflozin group and 199 (20.9%) in control group, with no significant difference between groups (P=0.247). After propensity score matching, 466 patients (233 in each group) were included in further analysis, and the above covariates were well balanced between groups (P<0.05 for all comparisons). During a median follow-up of 28 months, the incidence of primary outcome events in dapagliflozin group was significantly lower than control group (15.5% vs. 26.6%, P=0.003). Kaplan-Meier survival analysis showed that patients in dapagliflozin group had a significantly decreased risk of primary outcome events (HR=0.64, 95%CI: 0.43-0.96, P=0.032), which was mainly reflected in the risk of hospitalization for heart failure (HR=0.51, 95%CI: 0.31-0.83, P=0.007). In multivariate analysis, the independent predictors of primary outcome events were: dapagliflozin treatment (HR=0.558, 95%CI: 0.365-0.851, P=0.007), age (HR=1.023, 95%CI: 1.001-1.045, P=0.038), three-vessel disease (HR=2.001, 95%CI: 1.238-3.236, P=0.026), LVEF (HR=0.949, 95%CI: 0.901-0.999, P=0.048), and systolic blood pressure (HR=0.984, 95%CI: 0.971-0.998, P=0.024). A further subgroup analysis showed that patients with these characteristics can benefit more from dapagliflozin treatment in comparison with control group: men (HR=0.543, 95%CI: 0.322-0.917, P=0.022), Killip Ⅰ / Ⅱ (HR=0.623, 95%CI: 0.39-0.993, P=0.047), three-vessel disease(HR=0.531, 95%CI: 0.321-0.877, P=0.013) , angiotensin receptor-neprilysin Inhibitor treatment (HR=0.384, 95%CI: 0.192-0.77, P=0.007), beta-blockers treatment (HR=0.565, 95%CI: 0.359-0.89, P=0.014).

Conclusion: Dapagliflozin can significantly reduce the risk of composite cardiovascular events in AMI patients with left ventricular systolic dysfunction, especially the risk of hospitalization for heart failure.

Keywords: Dapagliflozin; Left ventricular systolic dysfunction; Acute myocardial infarction

中性粒细胞 Irgm1 促进胞葬作用在心肌梗死后心脏修复中作用及相关机制研究

房绍红 [1,2] 汪增 [1,2] 魏来 [1,2] 王明洋 [1,2] 于波 [1,2]

1. 哈尔滨医科大学附属第二医院，心内科

2. 心肌缺血教育部重点实验室

目的：探讨免疫相关 GTP 酶 Irgm1 影响中性粒细胞清除和胞葬作用在心肌梗死后心脏修复中的作用及机制研究。

方法：临床获得对照组和心梗患者外周血中性粒细胞，qPCR 和 WB 检测 MI 患者中性粒细胞 IRGM 的表达及其与预后指标的相关性。利用野生型小鼠和中性粒细胞 Irgm1 特异性敲除（Irgm1-cKO）小鼠构建心梗模型，通过超声检测心功能；TTC 染色检测心肌梗死面积；TUNEL 染色检测心肌细胞凋亡；Masson 染色评价瘢痕纤维化面积；HE 染色检测心梗后炎症细胞浸润；流式细胞术检测心梗后中性粒细胞的浸润情况检测 Irgm1 对心梗预后影响；利用质谱、RNA 测序、免疫沉淀、免疫共沉淀和邻近连接测定（PLA）相互结合蛋白验证机制。

结果：MI 患者外周血中性粒细胞中 IRGM 表达增加与预后改善显著正相关。小鼠中性粒细胞特异性 Irgm1 敲除会导致心功恶化，心肌梗死面积扩大，心脏纤维化加剧，加重不良心脏修复。Irgm1 缺失导致心脏浸润中性粒细胞清除延迟，抑制中性粒细胞凋亡和胞葬作用。体外研究发现中性粒细胞 Irgm1 缺失通过抑制 Caspase3 途径抑制 Ptdser 暴露，进而抑制巨噬细胞对中性粒细胞的胞葬作用和巨噬细胞修复表型转化。通过质谱分析、分子对接、COIP 和 WB 等生物学技术研究发现 Irgm1 与 PDIA3 相互作用，通过自噬降解途径介导促进 PDIA3 降解。

结论：中性粒细胞 Irgm1-PDIA3 轴通过促进胞葬作用加快心梗后中性粒细胞清除，在 MI 后心脏修复中发挥保护作用。

Prognostic Value of Interleukin-6 in Predicting Heart Failure with Reduced Ejection Fraction and In-Hospital Mortality in Patients with Acute Myocardial Infarction

Jian-Quan Liao, Zhen Dong, Run-Da Wu, Ju-Ying Qian, Kang Yao, Jun-Bo Ge

Zhongshan Hospital Fudan University

Background: Acute myocardial infarction (AMI) remains a major contributor to global cardiovascular morbidity and mortality. Inflammation plays a pivotal role in the pathogenesis and progression of AMI, with interleukin-6 (IL-6) recognized as a key mediator in myocardial injury and post-infarction remodeling. Although IL-6 has been associated with adverse cardiovascular outcomes in chronic heart failure and acute coronary syndromes, its prognostic utility for predicting short-term complications such as heart failure with reduced ejection fraction (HFrEF) and in-hospital mortality following AMI remains insufficiently characterized.

Methods: This retrospective cohort study included 650 patients diagnosed with AMI (414 with ST-elevation myocardial infarction [STEMI] and 236 with non-ST-elevation myocardial infarction [NSTEMI]) who were admitted to Zhongshan Hospital, Fudan University, between January 2020 and September 2023. Serum IL-6 levels were measured within 24 hours of admission using chemiluminescent immunoassay technology. Transthoracic echocardiography was used to assess left ventricular ejection fraction (LVEF), with HFrEF defined as LVEF <40%. Clinical endpoints included the development of HFrEF during hospitalization and all-cause in-hospital mortality. Multivariate logistic regression analyses were conducted to evaluate the association between IL-6 quartiles and outcomes, adjusting for age, sex, hypertension, diabetes mellitus, and smoking. Receiver operating characteristic (ROC) curves were used to determine the discriminative performance of IL-6.

Results: Among the 650 patients analyzed, the incidence of HFrEF was 5.54%, and the in-hospital mortality rate was 4.46%. IL-6 levels were significantly elevated in patients who developed HFrEF (median 33.1 pg/mL [IQR: 16.13–76.65]) compared to those who did not (13.75 pg/mL [IQR: 8.18–27.00], p<0.001). Similarly, IL-6 concentrations were markedly higher in non-survivors than survivors (51.60 [29.55–107.00] vs. 13.60 [8.20–25.70] pg/mL, p<0.001). Patients in the highest IL-6 quartile (Q4) demonstrated a 6.17-fold increased risk of HFrEF (adjusted OR 6.17, 95% CI: 1.75–21.79) and an 8.50-fold higher risk of in-hospital mortality (adjusted OR 8.50, 95% CI: 1.91–37.94) compared to the lowest quartile (Q1). ROC analysis revealed good discriminative ability of IL-6 for predicting HFrEF (AUC 0.721, 95% CI: 0.635–0.806, p<0.001) and in-hospital mortality (AUC 0.832, 95% CI: 0.747–0.918, p<0.001). The optimal IL-6 cutoff was 16.05 pg/mL for HFrEF (sensitivity 77.8%, specificity 57.3%) and 25.5 pg/mL for mortality prediction (sensitivity 86.2%, specificity 74.7%).

Conclusion: Elevated serum IL-6 levels at the time of admission are independently associated with increased risk of HFrEF development and in-hospital mortality in patients with AMI. These findings support the use of IL-6 as a dual-purpose prognostic biomarker and provide further rationale for targeting IL-6–mediated inflammation in the management of acute coronary syndromes. Incorporating IL-6 into early risk stratification protocols may facilitate timely identification of high-risk patients and guide more personalized treatment strategies aimed at improving short-term outcomes following AMI.

Keywords: Interleukin-6; acute myocardial infarction; heart failure with reduced ejection fraction; in-hospital mortality; inflammation; biomarker; prognosis.

中国胸痛救治单元项目对急性冠状动脉综合征转诊患者救治效率的影响研究

刘胜聪 [1] 王宗斌 [2] 张龙 [1] 李建平 [1,3] 周书铎 [2]

1. 北京大学第一医院心内科

2. 北京大学第一医院临床流行病学研究室

3. 北京大学第一医院心内科研究所

目的：2020 年初，中国胸痛中心联盟实施了面向基层医疗机构的胸痛救治单元（Chest Pain Unit，CPU）项目，以加速对首诊在这些医疗机构的急性冠状动脉综合征（Acute Coronary Syndrome，ACS）患者的快速诊断，并将其转诊到附近的胸痛中心。本文研究了该项目对此类需要转诊的 ACS 患者的救治效率的影响。

方法：本研究为回顾性队列研究，数据来源于 2020 年 1 月 1 日至 2022 年 12 月 31 日中国心血管协会 - 胸痛中心和胸痛救治单元的胸痛患者登记数据。参与者包括被诊断为 ACS，并从其他医疗机构转诊到胸痛中心的患者。符合条件的患者被分为 CPU 转诊组和非 CPU 转诊组。CPU 转诊组首诊在 CPU，接受标准化的诊断、治疗和转诊程序; 非 CPU 转诊组首诊在其他基层医疗设施，接受既往的诊断、治疗和转诊流程。所有患者最终转诊到胸痛中心接受标准化管理，直到出院或死亡。主要结局是院内死亡率、在转诊医院的进门出门时间以及从发病到到达胸痛中心的时间。次要结局是从发病到首次医疗接触的时间、到达时他汀类药物和抗凝药的应用、从胸痛中心到 PCI 导丝通过的时间、出院带他汀类药物和抗血小板药物、院内心衰率、住院时间和住院费用等。使用倾向性评分匹配和广义线性混合模型来估计效应，并对医院聚类进行了调整。

结果：倾向性评分匹配后，9980 人纳入研究队列。CPU 转诊组在院内死亡率（比值比 [OR] = 0.68, 95% CI：0.53 ~ 0.87）、进门出门时间 （β = -0.29, 95% CI：-0.35 ~ -0.22）、从发病到到达胸痛中心门的时间 （β = -0.13, 95% CI：-0.20 ~ -0.06）均显著优于非 CPU 转诊组。CPU 转诊组也更有可能在出院时带他汀类药物（OR = 1.33，95% CI：1.14 ~ 1.57）和抗血小板药物（OR = 1.37，95% CI：1.16 ~ 1.63），并且住院支出也较低（β = -0.07，95% CI：-0.10 ~ -0.04）。

结论：胸痛单元项目能够缩短 ACS 转诊患者的院前延误，降低院内死亡率，提高服务质量，并有助于降低住院成本。

非高密度脂蛋白与载脂蛋白 B 的比值与急性心肌梗死患者 PCI 术后预后的关系的摘要

崔恰 杨爽

哈尔滨医科大学附属第二医院

研究目的：非高密度脂蛋白胆固醇与载脂蛋白 B 的比值可作为预测普通人群长期死亡率的潜在生物标志物，独立于传统的危险因素。但是其是否可用来预测急性心肌梗死患者 PCI 术后发生心血管不良事件尚未可知。

研究方法：本研究基于哈尔滨医科大学附属第二医院随访中心的数据，回顾性分析非高密度脂蛋白胆固醇与急性心肌梗死患者 PCI 术后发生心血管不良事件的关系。收集患者入院时的血脂、年龄、性别、合并症及实验室指标。采用卡方检验和 T 检验来进行单因素分析，然后用逻辑回归分析血脂等与 PCI 术后发生心血管不良事件的关系。此外，进行亚组分析用于验证结果的稳健性。

研究结果：本研究共纳入 12721 例满一年随访的急性心肌梗死 PCI 术后的患者，单因素分析结果显示非高密度脂蛋白胆固醇与载脂蛋白 B 的比值小于 1.4 的组发生心血管不良事件的概率远高于非高密度脂蛋白胆固醇与载脂蛋白 B 的比值大于 1.4 的组；但是多因素分析显示非高密度脂蛋白与载脂蛋白 B 的比值与急性心肌梗死患者 PCI 术后心血管事件的发生无显著关系。当前可以看出非高密度脂蛋白胆固醇与载脂蛋白 B 的比值不能用来预测急性心梗死 PCI 术后短期心血管不良事件的发生，但是能否用来预测急性心梗死 PCI 术后长期心血管不良事件的发生还不得而知。

研究结论：非高密度脂蛋白胆固醇与载脂蛋白 B 的比值不能用来预测急性心梗死 PCI 术后短期心血管不良事件的发生，但是能否用来预测急性心梗死 PCI 术后长期心血管不良事件的发生还不得而知。

血管特征与心肌损伤标志物的交互作用对 AMI 患者远期预后的影响

李妍宁 杨爽

哈尔滨医科大学第二附属医院

研究目的：临床对于急性心肌梗死（AMI）患者远期预后的传统评估多单独依据血管病变特征或心肌损伤标志物，忽略了二者间的复杂交互作用。本研究旨在明确不同罪犯血管特征（包括位置、病变性质）与心肌损伤标志物（CK-MB、cTnI、proBNP）动态变化间的交互作用，及其对 AMI 患者远期预后的具体影响，并评估主要不良心血管事件（MACE）如心源性死亡、再梗死及心衰住院的发生情况。

研究方法：本研究基于哈尔滨医科大学附属第二医院心内科 PCI 术后患者随访中心数据库，采用回顾性分析方法，纳入确诊 STEMI 或 NSTEMI 并行冠脉造影、且至少完成 3 次连续心肌标志物检测的患者。主要变量包括血管解剖特征（罪犯血管位置、病变性质、多支病变）、功能特征（如 TIMI 血流分级、慢血流 / 无复流现象）及心肌损伤标志物的动态变化。统计分析采用乘法模型，在 Cox 回归分析中加入血管特征与心肌损伤标志物（CK-MB、cTnI、proBNP）变化率的乘积项，以揭示两者交互作用。

研究结果：“双高危型”患者需强化治疗措施（LAD 病变合并 cTnI 快速上升）需

强化治疗措施；“标志物主导型”患者（非 LAD 病变但 proBNP 持续升高）应重点关注心衰预防；“血管主导型”患者（左主干病变）无论心肌损伤标志物水平如何，均应优先进行血运重建。

研究结论：本研究揭示血管特征与心肌损伤标志物交互作用显著影响 AMI 患者预后。提出“血管 - 损伤 - 预后”评估框架，指导分型治疗：“双高危型”强化心衰管理，“标志物主导型”优化心律失常预防，“血管主导型”优先血运重建。

Early Diagnosis of Acute Myocardial Infarction via Hub Genes Identified by Integrated Weighted Gene Co-expression Network Analysis

Kun Huang, Yi-hong Chen, Chun Liang

Second Affiliated Hospital of Naval Medical University

Abstract

Background: Acute myocardial infarction (AMI) is a leading cause of morbidity and mortality worldwide. Circulating endothelial cells (CECs) have been reported to be involved with the early stages of AMI. The specific objective of our study was to discover early diagnostic markers of CECs in circulation using bioinformatics analysis.

Methods: Raw microarray data of the GSE66360 dataset were acquired from the Gene Expression Omnibus (GEO) database. The R software was used to filtrate differentially expressed genes (DEGs) from the discovery cohort of GSE66360 (n=43). A weighted gene co-expression network analysis (WGCNA) was performed to explore the key modules connected with AMI. Next, main roles of the pathological states in AMI were analyzed using GO and KEGG and PPI networks. Diagnostic biomarkers were selected and identified using three machine learning algorithms. Additionally, the expression and diagnostic efficiency of seven hub genes were verified in the validation cohort (n=56).

Results: 366 DEGs were identified (20 upregulated and 306 downregulated). A total of 276 intersecting genes were markedly associated with AMI in the pink and turquoise modules. Based on multiple machine learning algorithms, seven genes were identified as hub genes and showed satisfactory diagnostic efficiency in the discovery cohort. Among these, LILRA1, CCL20, IL1R2, TYROBP, CXCL16 and NFKBIA were valuable for predicting AMI in the validation cohort.

Conclusion: Our data provides evidence supporting a list of seven hub genes to be trapped in the pathophysiology of AMI and proposes six of these as candidate biomarkers for the early diagnosis of AMI.

Keywords: WGCNA, machine learning, acute myocardial infarction, circulating endothelial cells, hub genes

静脉注射硫酸镁与急性心肌梗死危重患者 1 年病死率的相关性：一项队列研究

苏昱润 赵晶 白明

兰州大学第一医院（兰州大学第一临床医学院）

背景：急性心肌梗死（AMI）是全球心血管死亡的主要原因。尽管再灌注治疗技术已取得进展，但硫酸镁（MgSO4）静脉给药在重症监护期间对死亡率的影响仍不明确。为填补这一知识空白，本研究旨在探讨重症监护病房（ICU）内 MgSO4 给药与全因死亡率之间的关联。

方法：本研究纳入医疗信息市场重症监护 IV 数据库（Medical Information Market for Intensive Care IV database）中的 AMI 患者。主要结局指标为 365 天全因死亡率，次要结局指标包括 ICU 死亡率、30 天及 90 天死亡率、28 天无机械通气时长及无血管加压药时长。采用倾向评分匹配（PSM）以确保研究结果的可靠性。

结果：2008 至 2022 年间共纳入 3,745 例 ICU 住院 AMI 患者（MgSO4 使用组 3,092 例，非使用组 653 例）。总体 1 年死亡率在 MgSO4 使用组和非使用组分别为 30.8%（953/3,092）和 38.7%（253/653）。校正潜在混杂因素后，ICU 期间 MgSO4 给药与 365 天死亡率降低 17% 相关（校正风险比 [aHR]=0.83；95% 置信区间 [CI]：0.72–0.97；P=0.016）。在匹配队列（n=1,234）中，使用组的 365 天、30 天及 90 天死亡率均低于非使用组（aHR=0.71–0.79）。所有亚组分析在 PSM 前后结果一致。采用倾向评分、标准化死亡率加权（SMRW）和重叠加权（OW）的敏感性分析均验证了上述发现。

结论：AMI 危重患者入住 ICU 期间静脉给予 MgSO4 可能降低长期死亡率，该结论仍需进一步研究验证。

CAMI-DM: Development and Validation of a Multi-Algorithm Model for In-Hospital Mortality Risk Prediction in Diabetic Patients With Acute Myocardial Infarction – The China Acute Myocardial Infarction Registry

Zuoxiang Wang, Xiao-Jin Gao, Yong-Jian Wu, Yue-Jin Yang

Fuwai Hospital, National Center for Cardiovascular Diseases, Chinese Academy of Medical Sciences and Peking Union Medical College

Objective

Patients with diabetes constitute a substantial proportion of those with acute myocardial infarction (AMI) and exhibit distinct pathophysiological characteristics. However, existing guideline-recommended traditional and generic risk prediction models show limited performance in this specific population. This study aimed to develop a dedicated in-hospital mortality risk prediction tool tailored to diabetic patients with AMI, based on representative real-world data from a multicenter registry in China, by leveraging machine learning (ML) and deep learning algorithms (DL) integrated with diabetes-related metabolic indicators.

Methods

Based on the China Acute Myocardial Infarction (CAMI) registry, a total of 6,091 diabetic patients meeting strict inclusion and exclusion criteria were enrolled and randomly divided into training and testing sets in an 8:2 ratio. A comprehensive set of 62 multidimensional candidate features was extracted, including demographic characteristics, physical examination, medical history, laboratory data, composite metabolic indicators—such as the stress hyperglycemia ratio (SHR) and triglyceride-glucose index— and treatment strategies. Under the premise of significant univariate associations, three feature selection strategies—Elastic Net (EN), Recursive Feature Elimination, and Consensus Feature Selection—were applied to develop 12 mainstream ML and deep learning models. These models spanned six algorithm categories: (1) tree-based models: CatBoost, XGBoost, LightGBM, GBM, Random Forest, and Decision Tree; (2) linear models: Generalized Linear Model (GLM); (3) probabilistic models: Naive Bayes; (4) distance-based models: K-Nearest Neighbors Classifier; (5) kernel-based models: Support Vector Machine; and (6) deep learning models: Deep Neural Networks (DNN) and TabNet. All models underwent hyperparameter tuning via five-fold cross-validation in the training set, with the optimal combination selected based on area under the curve (AUC). The optimized models were then evaluated in the independent test set. Following the development of individual models, two post-hoc ensemble strategies—stacking and probability averaging—were employed to explore various combinations of top-performing models from different algorithm categories, aiming to construct the final ensemble model, thereby improving overall predictive performance and stability. Finally, the predictive performance and clinical utility of the CAMI-DM models versus the GRACE score was compared in the independent testing set using multiple evaluation metrics, including confusion matrix indicators, receiver operating characteristic curves, DeLong test, calibration plots, the Hosmer–Lemeshow (HL) goodness-of-fit test, integrated discrimination improvement, net reclassification improvement, and decision curve analysis.

Results

Predictive models across algorithm categories, developed using 11 features selected by EN (age, sex, ejection fraction, serum creatinine, hemoglobin, SHR, heart rate, systolic blood pressure, Killip class, malignant arrhythmia, and emergency PCI) demonstrated optimal performance. After evaluating various fusion strategies, the ensembled GLM+TabNet model was ultimately selected as CAMI-DM 2.0, achieving an AUC of 0.875 (95% CI: 0.856-0.893) in the independent test set. To balance predictive performance and model simplicity, CAMI-DM 1.0 adopted a linear framework and was developed using five features from Strategy 3 (age, ejection fraction, serum creatinine, plasma glucose, and HR). Based on regression coefficients and intercepts, simplified categorical thresholds were defined for each variable, and a point-based scoring system was constructed accordingly, which attained an AUC of 0.821 (95% CI: 0.799-0.842) in testing set. The total score of CAMI-DM 1.0 ranged from 0 to 20. According to score-based tertiles, patients were stratified into three risk groups: low risk (0–3 points, predicted risk 0.38%–1.53%), intermediate risk (4–5 points, 2.41%–3.78%), and high risk (≥ 6 points, 5.89%–91.25%). Comparative analyses revealed that CAMI-DM 2.0 outperformed CAMI-DM 1.0 in terms of discrimination, accuracy, calibration, and clinical net benefit. Furthermore, CAMI-DM 1.0, with its simplified structure, still outperformed the GRACE score in overall predictive ability and generalizability.

Conclusion

This study focused on the specific population of diabetic patients with AMI, and for the first time developed two dedicated models to predict in-hospital mortality risk. CAMI-DM 1.0, a simplified point-based model, requires only five key features to facilitate rapid risk assessment. CAMI-DM 2.0, by contrast, is a fusion model based on 11 features and implemented via an ensemble of GLM and TabNet, delivering superior predictive performance alongside improved clinical interpretability enabled by SHAP. Both models outperformed the traditional GRACE score in terms of predictive accuracy. The tailored application of these models in different clinical settings allows for more precise identification of high-risk diabetic AMI patients and facilitates personalized treatment strategies, thereby optimizing clinical management.

Pan-immune inflammation value is associated with poor outcomes among patients with acute coronary syndrome undergoing percutaneous coronary intervention

Zai-Qiang Liu[1], Yu-Xiu Yang[1], Qiu-Xuan Li[1], Yang Zheng[1], Jing-Yao Yang[1], wei Li[2], Zhi-Jian Wang[1]

1. Beijing Anzhen Hospital, Capital Medica University

2. The Second Affiliated Hospital of Inner Mongolia Medical University

Background

Inflammation has been recognized as a key factor contributing to adverse outcomes in coronary artery disease (CAD) patients undergoing percutaneous coronary intervention (PCI). Post-PCI patients require dual antiplatelet therapy to prevent stent thrombosis and represent a high-risk subgroup for adverse cardiovascular outcomes. Current evidence indicates that systemic inflammation significantly impacts prognosis in PCI-treated populations. Landmark randomized controlled trials (COLCOT and CANTOS) have demonstrated the therapeutic benefits of targeted anti-inflammatory interventions in post-myocardial infarction, significantly reducing recurrent cardiovascular events. The Pan-Immune-Inflammation Value (PIV), a novel biomarker derived from blood cell counts, has been proposed to reflect systemic inflammatory status. However, it remains unclear whether PIV is associated with poor prognosis in acute coronary syndrome (ACS) patients receiving PCI.

Methods

This retrospective cohort analysis utilized data from the Coronary Artery Disease-Specific Database (CAD-SD) project, a multicenter, prospective, dynamic registry (ClinicalTrials.gov ID: NCT05337319) led by Beijing An Zhen Hospital, Capital Medical University, and coordinated by the National Clinical Research Center for Cardiovascular Diseases. A total of 10598 ACS patients undergoing PCI were retrospectively analyzed. PIV was calculated based on (neutrophil count [×10 ^{9} /L] × platelet count [×10 ^{9} /L] × monocyte count [×10 ^{9} /L])/lymphocyte count [×10 ^{9} /L], PIV was grouped according to the median. The primary endpoint was major adverse cardiovascular events, including death, nonfatal myocardial infarction, and nonfatal stroke.

Results

During the median 465-day follow-up period, 188 MACEs were documented, comprising 69 deaths, 50 non-fatal myocardial infarctions, and 69 non-fatal strokes. Comparative analysis revealed significantly higher event rates in the high-PIV group versus the low-PIV group for mortality, non-fatal MI, non-fatal stroke, and composite MACEs (2.19% vs. 1.36%; p=0.0012). The high-PIV group demonstrated 116 MACEs occurrences compared with 72 in the low-PIV group, corresponding to an odds ratio of 1.62 (95% CI: 1.24-2.09). We found that compared with the low PIV group, the high PIV group had higher rates of death (0.51% vs. 0.79%, p=0.0321), nonfatal myocardial infarction (0.36% vs. 0.59%, p=0.0486), nonfatal stroke (0.49% vs. 0.81%, p =0.0486), and higher rates of death (0.51% vs. 0.79%, p=0.0321). p=0.0087) and MACE (1.36% vs. 2.19%, p=0.0012). After adjustment for age, sex, BMI, hypertension, diabetes mellitus, LDL-C, creatinine, homocysteine, hsCRP, and BNP, the association between continuous PIV and MACEs remained significant (HR = 1.006 per 10-unit, 95% CI 1.002–1.011; p =0.004), with persistent risks for non-fatal myocardial infarction (HR = 1.009, 95% CI 1.002–1.016; p=0.008). However, the mortality association attenuated to marginal significance (HR = 1.007, 95% CI 1.000–1.013; p=0.054), and no significant link was observed for non-fatal stroke (HR = 1.002, 95% CI 0.992–1.013; P = 0.671). In categorical analyses, high PIV independently predicted non-fatal stroke (HR = 1.952, 95% CI 1.074–3.545; p=0.028) and MACEs (HR = 1.718, 95% CI 1.196–2.468; p=0.003), whereas associations with mortality (HR = 1.507, p=0.19) and non-fatal myocardial infarction (HR = 1.698, p=0.132) were no longer statistically significant. Restricted cubic spline curve showed a linear relationship between PIV and MACE (overall p=0.001, non-linear p=0.11). Subgroup analysis showed that PIV had an interaction effect on MACE in gender and age subgroups (p for interaction=0.032; p for interaction=0.043).

Conclusion

In conclusion, we identified a linear association between PIV and adverse cardiovascular events in ACS patients undergoing PCI. The risk of MACE is significantly increased in patients with high PIV, and the predictive value of PIV is more obvious in women and people younger than 65 years old. Risk stratification of patients by PIV, which may facilitate early identification of high-risk patients and prompt treatment strategies.

高血栓负荷急性心肌梗死不同时期血运重建对其预后的影响

姚义安 席鹏 严文文 叶梓 汤宇 来晏

上海市同济医院（同济大学附属同济医院）

研究目的：观察高血栓负荷急性心肌梗死患者不同时期血运重建对该类患者预后的影响

研究方法：回顾性分析 2017.01-2023.12 在我院诊断急性 ST 段抬高型心肌梗死并行冠脉造影的患者 1023 例，其中血栓负荷五级以上患者 124 例；在血栓负荷五级以上的患者中，根据造影所见血栓长度与罪犯血管靶病变直径的关系，将患者分为四组，一组血栓长度为罪犯血管直径的 2 倍（38 例），二组为 3 倍（30 例），三组为 4 倍（35 例），四组为 5 倍及以上（21 例）；

研究结果：血栓负荷五级以上患者与血栓负荷五级以下的患者，发病到手术时间（38±29 小时 VS. 12±7 小时，P<0.05）有统计学差异；而在血栓负荷五级以上的患者中，四组间发病到手术时间无显著差异（24±15 VS. 22±17 VS. 25±18 VS. 21±16 小时，P>0.05）；造影结果发现，与血栓负荷五级以下的患者相比，血栓负荷五级以上的患者中，右冠高血栓负荷最多见，前降支次之，回旋支最少；而且后者瘤样扩张的比例较高（5.7 % VS. 12.3%，P<0.05）；即刻血管开通率，血栓负荷五级以下的患者为 97.6%，五级以上者 86.5%，两者具有统计学差异（P<0.05）；两者之间，即刻支架植入的患者，远端栓塞的比例（4.2% VS. 9.6%，P<0.05），无复流比例（3.5% VS. 8.4%，P<0.05），均具有统计学意义；同时发现，血栓长度越长，即刻血管开通率越低（一、二、三、四组开通比率为 94.3% VS. 91.2% VS. 87.4% VS. 83.2%）；而对比分析血栓长度 4 倍于血管直径以上的患者，即刻支架植入组（36 例）与择期组（1 周后）延迟支架植入（20 例），急性血栓事件（21.4% VS. 10%，P<0.05），死亡率（10.7% VS. 10.1%，P>0.05）。

研究结论：高血栓负荷患者，就诊到发病时间较长，提示血栓负荷与发病时间长短密切相关；高血栓负荷已发生于右冠和瘤样扩张的患者，相对而言，高血栓负荷血运重建术中易发生远端栓塞及无复流，而对血栓长度大于 4 倍血管直径的患者，延迟支架植入是安全的，而且效果优于即刻支架植入。

关键词：急性心肌梗死 血栓 冠脉造影 支架植入

Correlation between early arterial lactate levels, arterial bicarbonate ion levels, and the lactate/albumin ratio and in-hospital mortality in patients with acute myocardial infarction complicated with cardiac shock

Jiao Wang[1], Mei-Juan Zheng[1], Yu-Chun Yang[1], Kai-Li Wang[1], Muhuyati Wu-LaSiHan[1]

1. First Affiliated Hospital of Xinjiang Medical

2. Xinjiang Medical University

Abstract

Background: To investigate the predictive value of early arterial lactate levels, arterial bicarbonate ion levels and the lactate/albumin ratio (L/A) for in-hospital mortality in patients with acute myocardial infarction complicated with cardiac shock (AMICS).

Methods: Three hundred ninety-five adult patients with AMICS who were hospitalized at the First Affiliated Hospital of Xinjiang Medical University between January 2018 and August 2024 were included in this study. All-cause mortality during hospitalization was taken as the study endpoint. The patients' general data, test and examination results, surgical data and prognoses were recorded. The patients' clinical features, coronary lesion characteristics, and laboratory and imaging findings were retrospectively analyzed. A receiver operating characteristic (ROC) curve was drawn to analyze the predictive value of early arterial lactate levels, arterial bicarbonate ion levels and the L/A for in-hospital mortality in patients with AMICS. Subgroup analysis was performed according to the optimal cutoff value, and a Kaplan–Meier survival curve was drawn to analyze the median survival time of each group. A Cox fitted proportional risk model was used to verify the association between arterial bicarbonate ion levels, arterial lactate levels, and the L/A and all-cause mortality during hospitalization.

Results: Three hundred ninety-five patients were included in this study, 171 of whom died in the hospital and 224 were discharged because their conditions had improved, and the mortality rate was 43.29%. Univariate analysis revealed that the arterial lactate level was higher in the death group than in the survival group (2.90 vs. 2.00, P < 0.001), the arterial bicarbonate ion level was lower in the death group than in the survival group (16.20 vs. 19.50, P < 0.001), and the L/A was greater in the death group than in the survival group (0.08 vs. 0.06, P < 0.001). ROC curve analysis revealed that the areas under the curve for arterial bicarbonate ion level, arterial lactate level and L/A were 0.707, 0.679 and 0.670, respectively, indicating that these parameters have certain value for predicting in-hospital mortality in patients with AMICS; however, arterial bicarbonate ion level had the highest predictive value. The Kaplan–Meier survival curve revealed that the median survival time of the low bicarbonate ion group was shorter than that of the high bicarbonate ion group (log–rank test: χ2=40.460, P < 0.001), and the median survival time of the low lactic acid group was longer than that of the high lactic acid group (log–rank test: χ2=65.810, P < 0.001). The median survival time of the low L/A group was longer than that of the high L/A group (log–rank test: χ2=63.690, P < 0.001). The Cox proportional risk model indicated that higher arterial bicarbonate ion levels were a protective factor for in-hospital death in AMICS patients and that higher arterial lactate levels and a higher L/A were independent risk factors for in-hospital death in AMICS patients.

Conclusion: Early arterial bicarbonate ion levels, arterial lactate levels and the L/A were predictive of all-cause death in AMICS patients. Higher arterial bicarbonate ion levels were protective factors for in-hospital death in AMICS patients, whereas higher arterial lactate levels and the L/A were independent risk factors for in-hospital death in AMICS patients.

早发 AMI 患者一年内心源性死亡及卒中风险因素与风险预测模型构建： 基于前瞻性队列研究

刘家彤 张金玲 侯欣宇 孙勇

哈尔滨医科大学第二附属医院

目的

探讨≤ 55 岁早发急性心肌梗死 (Premature Acute Myocardial Infarction，PAMI) 患者一年内发生心源性死亡及卒中复合事件的风险因素，构建预后风险预测模型以及风险评分表，辅助制定个体治疗决策，进而改善 PAMI 患者预后。

方法

基于“十三五”国家重点研发计划项目“急性心肌梗死全程心肌保护体系构建及关键技术研究”，从 2017 年 1 月至 2022 年 8 月入组于哈尔滨医科大学附属第二医院并确诊为 AMI 的 11752 名患者中，根据纳排标准筛选出 3630 例 PAMI 患者，并纳入最终研究队列。收集研究对象临床资料（包括临床及影像学共 49 个特征）以及一年随访信息，记录其一年内心源性死亡及卒中发生情况。按照 7:3 的比例，将研究对象随机分为训练队列和验证队列。牵头单位同期构建的随访中心数据库患者作为外部验证队列（n=800）。利用训练队列数据，应用 Cox 风险回归分析进行预测因子筛选，进一步为简化模型结构，对最终应用于建模的连续变量进行数据分箱，分箱界值结合 RCS 曲线切点值及 cutoff 值确定，通过多因素 Cox 比例风险回归，计算各预测因子 β 系数并转化为评分量表。量表中不同预测因子分值确定方法如下：以最终模型系数中绝对值最小的 β 值作为参考值，指定其参考分值为 1 分，对其他系数进行标准化，确保评分尺度成比例且一致。

结果

早发队列共纳入 3630 名患者，其中训练队列 2541 人，验证队列 1089 人，二者基线特征分布均衡。在本研究所构建的模型中 ，发病时气温、纤维蛋白原、促甲状腺激素、血红蛋白、红细胞、是否多支病变为 PAMI 患者重要预后特征。分类转换后模型训练队列及验证队列 AUC 为 0.777（95%CI：0.710-0.844），优于初始模型 0.798（95%CI：0.715-0.881）及 Grace 评分 0.612（95%CI：0.551-0.672）。评分表如下：（1）发病时气温 0.99-7.98℃ 分数为 1，<0.99℃为 5，> 7.98℃ 为 0；（2）纤维蛋白原≥ 3.33g/ml 分数为 7，<3.33g/ml 为 0；（3）促甲状腺激素 0.74-9.87mIU/L 分数为 -1，>0.87mIU/L 为 5，< 0.74mIU/L 为 0；（4）血红蛋白 >154g/L 分数为 4，<133g/L 为 12，133-154 为 0；（5）红细胞 <8.7*10^12/L 分数为 3，>13.7*10^12/L 为 5，8.7-13.7*10^12/L 为 0；（6）存在多支病变评分为 3，未存在多支病变为 0。最终总评分 < 17 为低风险，17-29 为中风险，> 29 为高风险，三个风险组事件发生率存在显著差异（P<0.001）。

结论

本研究开发了一种新颖便捷的评分量表，可良好预测 PAMI 患者一年内心源性死亡及卒中的风险。该评分量表不仅能够有效评估 PAMI 患者的预后风险，还进一步实现了风险分层，以辅助临床决策过程。

院内无明显出血情况下血红蛋白下降与急性心肌梗死患者经皮冠状动脉介入治疗 1 年预后的相关性

周鹤

中国人民解放军北部战区总医院

目的

目前，在因急性心肌梗死（AMI）住院期间接受经皮冠状动脉介入治疗（PCI）的患者中，院内存在无明显出血情况下，但血红蛋白较基线下降，且与 1 年临床预后之间的关系尚不明确。

方法

共纳入 5036 例接受 PCI 治疗的 AMI 患者，这些患者均出现院内无明显出血的血红蛋白下降。根据血红蛋白下降程度的三分位数，将患者分为 3 组：血红蛋白下降 < 8 g/L 组（1652 例）、血红蛋白下降 8~<14.9 g/L 组（1652 例）和血红蛋白下降≥ 15 g/L 组（1733 例）。

结果

随着血红蛋白下降程度从 < 8 g/L 增至≥ 15 g/L，1 年缺血事件和全因死亡率呈显著升高趋势（分别从 1.88% 升至 3.46%、从 1.15% 升至 2.37%）。血红蛋白每下降 1 g/L，校正后的缺血事件风险和全因死亡风险分别增加 2% 和 3%。血红蛋白下降 < 8 g/L 组患者的 1 年心肌梗死（MI）发生率显著低于其他两组患者。随着血红蛋白下降程度的增加，卒中发生率和出血发生率（包括 BARC 2、3、5 型及 BARC 3、5 型）无显著差异。

结论

在调整众多患者特征后，即使无明显出血，血红蛋白下降与 1 年不良事件（包括缺血事件和全因死亡）之间仍存在强烈的独立相关性。

急性心肌梗死患者 PCI 术后支架内再狭窄的影响因素

王涵桐

吉林大学中日联谊医院

目的：探讨急性心肌梗死患者 PCI 术后支架内再狭窄的影响因素。

方法：纳入 2021 年 4 月至 2023 年 4 月于吉林大学中日联谊医院因急性心肌梗死首次接受药物洗脱支架（DES）治疗的患者，并在术后 6-12 个月返院复查或再发心绞痛来院进行二次造影、资料完整，根据复查造影结果分为支架内再狭窄（ISR） 组及非 ISR 组，使用单因素和多因素二元 Logistic 回归模型，分析比较两组患者的一般临床资料、手术资料、生化资料、TyG 指数（甘油三酯 - 葡萄糖指数）、AIP 指数（血浆动脉粥样硬化指数）、NHHR（非高密度脂蛋白胆固醇 / 高密度脂蛋白胆固醇）、Gensini 评分等在两组间是否存在统计学差异。

结果：本研究共纳入 288 例患者，其中 ISR 患者 71 例（24.65%）。单因素分析显示，Gensini 评分（P=0.004）、支架个数（P=0.025）、支架总长度（P=0.012）、甘油三酯（P<0.001）、总胆固醇（P=0.002）、低密度脂蛋白胆固醇（P=0.019）、高密度脂蛋白胆固醇（P < 0.001）、非高密度脂蛋白胆固醇（P < 0.001）、载脂蛋白 B（P=0.007）、淋巴细胞计数（P=0.008）、血红蛋白（P=0.006）、凝血酶原活动度（P=0.011）、白蛋白（P<0.001）、TyG 指数（P=0.002）、AIP 指数（P<0.001）、NHHR（P<0.001）是 ISR 的影响因素。多因素分析中的协变量为单因素分析中 P<0.1 的变量，并剔除 VIF>10 的共线性变量。二元 Logistic 回归分析显示，血红蛋白（OR=0.027，95%CI：1.006-1.049，P=0.012）、凝血酶原活动度（OR=1.031，95%CI：1.005-1.056，P=0.017） 、白蛋白（OR=0.813，95%CI：0.719-0.919，P<0.001）、TyG 指数（OR=1.625，95%CI：1.110-2.378，P=0.012）、AIP 指 数（OR=7.202，95%CI：2.478-20.930，P<0.001）、NHHR（OR=2.915，95%CI：1.810-4.692，P<0.001）、Gensini 评 分（OR=1.017，95%CI：1.005-1.029，P=0.007） 是 ISR 的独立影响因素。

结论：急性心肌梗死患者 PCI 术后支架内再狭窄的独立影响因素有血红蛋白、凝血酶原活动度、白蛋白、TyG 指数、AIP 指数、NHHR，这些影响因素对于支架内再狭窄的早期预防具有重要意义，识别这些因素有助于优化治疗策略，改善预后。

急性左主干完全闭塞所致急性心肌梗死患者的预后影响因素

周航 王晶 陈韬

解放军总医院第六医学中心

急性左主干完全闭塞所致的急性心肌梗死可到达医院进行诊治的患者很罕见，对此类患者的危险因素了解甚少。目的：本研究分析急性左主干完全闭塞所致急性梗死患者的临床特点，及探讨其院内死亡的预后影响因素。方法 ：回顾性分析自 5 家医院心内科接受治疗的急性左主干（LM）完全闭塞所致急性心肌梗死（AMI）患者 53 例。根据患者是否发生院内死亡，分为院内存活组与院内死亡组。比较分析两组患者的预后影响因素。结果：本研究最终纳入急性 LM 完全闭塞致 AMI 的患者总共 53 例，患者整体平均年龄为 60.0 岁 , 男性有 43 例。其中院内存活组 26 例，院内死亡组 27 例。77% 的入院患者心电图表现为 STEMI，且有 51% 的所有患者有 LAH。院内死亡组心电图有 RBBB 伴 LAH 的患者明显多于院内存活组（37% vs. 4%，p=0.003）。所有患者冠脉均为右优势型。49% 的患者存在侧枝循环，其中院内存活组患者存在侧枝循环的百分比明显高于院内死亡组（77% vs. 22%, p<0.001）。死亡患者住院时间中位数为 7 小时，最长住院时间为 1440 小时。单因素 COX 回归分析结果显示，入院心功能 Killip III~IV 级、存在侧枝循环和 RBBB+LAH 与患者院内死亡相关；多因素 COX 回归分析结果显示，入院心功能 Killip III~IV 级（HR 7.91, 95% 置信区间 1.81-34.62; p=0.006）为院内死亡的独立危险因素，而存在侧枝循环（HR 0.31, 95% 置信区间 0.12-0.79; p=0.014）为院内死亡的独立保护因素。结论：入院心功能 Killip III~IV 级为院内死亡的独立危险因素，而存在侧枝循环为院内死亡的独立保护因素。

双膦酸盐类药物的使用与心肌梗死的风险的荟萃分析和系统性回顾

丁茹 梁春

上海长征医院

【摘要】

目的：双膦酸盐类药物和心血管事件之间的关系引起了极大的关注。然而，心肌梗死（MI）的风险与使用双膦酸盐类药物的心脏病死亡率的数据是矛盾的。所以我们系统评价双膦酸盐类药物使用相关的心肌梗死和心源性死亡的风险。

方法：通过检索 PubMed、EMBASE、Cochrane 对照试验登记，Cochrane 数据库，和临床试验注册数据库的随机对照试验（RCT）以及观察性研究等数据库，从 1966 年到 2015 年 4 月报告的关于双膦酸盐治疗心肌梗死和心脏病死亡率的结果的论文进行荟萃分析和系统性回顾。

结果：对 6 个随机对照试验和 12 个观察性研究进行分析。在共享的随机对照试验采用随机效应荟萃分析，双磷酸盐类药物的使用与心源性死亡（RR 0.92，95% CI 0.68-1.26，P = 0.62）和心肌梗死（RR 1.02，95% CI 0.61-1.69，P = 0.95）的风险是不相关的。观察性研究的数据具有不汇集高异质性，然后进行系统性回顾。与基线的风险因素调整后分析，研究显示双膦酸盐对心脏死亡率的没有影响。五项研究报告显示双膦酸盐类药物对心肌梗死没有影响，三项研究表明，双膦酸盐类药物的使用与降低心肌梗死，冠状动脉疾病或急性冠状动脉综合征的风险相关。但也有三项研究报道了在双磷酸盐类药物的使用者中，出现增加心肌梗死的风险：第一项研究显示只在以前有心血管事件和服用药物超过 1 年的患者具有较大的风险；第二项研究显示双磷酸盐和心肌梗死发生之间的反剂量反应关系；最后一个队列研究主要是在男性受试者之间进行。

结论：根据我们的荟萃分析，双膦酸盐类药物的使用是与心脏病死亡率或风险增加相关。至少在女性患者依从性高，既往无心血管疾病，双膦酸盐的使用并不增加心肌梗死的发生，应进一步分析，应该从更大的前瞻性，随机和安慰剂对照研究数据进一步分析和证实。

【关键词】双膦酸盐；心肌梗死；心脏性猝死；动脉粥样硬化

Incremental prognostic value of hemodynamic forces misalignment by cardiac magnetic resonance for major adverse cardiac events after ST-segment elevation myocardial infarction

Yu-Meng Sun

Capital Medical University Affiliated Anzhen Hospital

Background:

The prognostic value of left ventricular (LV) hemodynamic forces (HDFs)

derived from cardiac magnetic resonance (CMR) cine imaging in patients with ST-segment elevation myocardial infarction (STEMI) remains an important yet incompletely understood area of cardiovascular research. While CMR has become an indispensable tool for assessing cardiac structure and function post-STEMI, the specific role of LV HDFs—which reflect the dynamic forces generated during myocardial contraction—in predicting long-term clinical outcomes requires further investigation. Current risk stratification models primarily rely on conventional parameters such as LV ejection fraction (LVEF) and infarct size (IS), but these may not fully capture the complex hemodynamic alterations that occur following STEMI. This study sought to address this knowledge gap by systematically evaluating the prognostic significance of CMR-derived LV HDFs, with particular emphasis on identifying which specific HDF parameter—whether apex-base (A-B) forces, latero-septal (L-S) forces, or their angular relationship (angle ϕ)—holds the strongest predictive value for major adverse cardiac events (MACEs), defined as the composite of all-cause mortality, reinfarction, or new-onset congestive heart failure.

Methods:

In this retrospective cohort study, we analyzed consecutive STEMI patients who underwent primary percutaneous coronary intervention (PCI) at our institution between January 2019 and June 2024, followed by a comprehensive CMR examination within 1 to 10 days post-revascularization. CMR cine images were acquired using standardized protocols and subsequently analyzed using advanced feature-tracking software to quantify LV HDFs in both the A-B and L-S directions throughout the entire cardiac cycle. The angle ϕ, representing the directional orientation of the resultant HDF vector, was also calculated to assess potential alterations in force distribution patterns. Clinical follow-up data were meticulously collected through hospital records and telephone interviews, with MACEs serving as the primary endpoint. Multivariable Cox proportional hazards models were constructed to evaluate the independent prognostic value of HDF parameters after adjusting for established clinical predictors including infarct location (anterior vs. non-anterior STEMI), Killip classification, global longitudinal strain (GLS), LVEF, IS, and the presence of microvascular obstruction (MVO). Receiver operating characteristic (ROC) curve analysis was performed to assess the incremental predictive value of HDF parameters beyond traditional risk markers.

Results:

The study population comprised 280 STEMI patients with a median age of 58 years (interquartile range: 51-65 years), of whom 85% were male—a demographic profile consistent with typical STEMI populations. During a mean follow-up duration of 26 ± 18 months (range: 6-60 months), 72 patients (25.7%) experienced at least one MACE event. Comprehensive multivariable analysis revealed that the L-S/A-B HDFs ratio maintained a robust, independent association with MACEs (hazard ratio: 1.06 per unit increase, 95% confidence interval: 1.04-1.09, P < 0.001) even after rigorous adjustment for anterior STEMI location, Killip class, impaired GLS, reduced LVEF, larger IS, significant MVO, and baseline A-B HDFs magnitude. Notably, the L-S/A-B HDFs ratio demonstrated significant incremental prognostic value when added to conventional risk models: its incorporation improved the C-statistic for MACE prediction from 0.675 (LVEF alone) to 0.749 (P = 0.022), and from 0.732 (IS alone) to 0.802 (P = 0.012).

Conclusion:

The findings of this study highlight the prognostic relevance of CMR-derived LV HDFs in STEMI patients. Specifically, the L-S/A-B HDFs ratio emerged as an independent predictor of MACEs, offering incremental prognostic value beyond conventional parameters such as LVEF and IS. These results suggest that incorporating HDF analysis into routine CMR assessments may improve risk stratification and guide therapeutic decision-making in STEMI patients. Future prospective studies are warranted to validate these findings and explore the potential role of HDFs in personalized post-STEMI management.

Non-Linear Associations of Shock Index and Modified Shock Index with New-Onset Atrial Fibrillation in Patients with Acute Myocardial Infarction

Ping Jin[1], Peng Wu[2], Juan Ma[2], Xueping Ma[2], Shaobin Jia[2], Qiangsun Zheng[1]

1. Second Affiliated Hospital Of Xi'an Jiaotong University

2. General Hospital of Ningxia Medical University

Background: New-onset atrial fibrillation (NOAF) occurs in 4-12% among patients with acute myocardial infarction (AMI) and is associated with increased mortality, prolonged hospitalization, and higher risk of stroke and heart failure. Understanding factors associated with NOAF occurrence is crucial for optimal patient management and resource allocation. Shock index (SI) and modified shock index (MSI) are simple hemodynamic parameters calculated from routine vital signs that reflect cardiac output, peripheral resistance, and sympathetic activation. While these indices have demonstrated associations with adverse outcomes in various cardiovascular conditions, their relationship with NOAF occurrence in AMI patients remains unexplored. This study aimed to investigate the associations between SI and MSI with in-hospital NOAF occurrence in patients with AMI, with particular focus on potential non-linear relationships and their relative association strength.

Methods: This retrospective cohort study analyzed consecutive AMI patients admitted to a tertiary cardiac center from January 2016 to December 2019. Patients with pre-existing atrial fibrillation, admission atrial fibrillation, or incomplete hemodynamic data were excluded. SI was calculated as heart rate divided by systolic blood pressure (SBP), and MSI as heart rate divided by mean arterial pressure (MAP), using vital signs obtained within 24 hours of admission. The primary outcome was in-hospital NOAF occurrence documented by continuous cardiac monitoring or 12-lead electrocardiography. Multivariable logistic regression models were constructed adjusting for age, sex, hypertension, diabetes, smoking status, Killip class, laboratory parameters (including creatinine, hemoglobin, and white blood cell count), and AMI characteristics. Generalized additive models (GAM) were employed to explore non-linear relationships between SI/MSI and NOAF occurrence. Threshold effect analysis was performed to identify specific turning points where the association patterns changed. Comprehensive subgroup analyses were conducted across different demographic and clinical characteristics, including age groups and hypertension status. Mediation analyses were performed to examine whether white blood cell (WBC) count mediated the observed associations between hemodynamic indices and NOAF occurrence.

Results: Among 3,343 consecutive AMI patients, 287 (8.6%) developed in-hospital NOAF. Patients with NOAF were significantly older, had higher prevalence of hypertension and cardiac dysfunction, with elevated SI (0.738 vs. 0.672, P<0.001) and MSI (0.970 vs. 0.893, P<0.001). Both indices demonstrated dose-response relationships with NOAF incidence progressively increasing across tertiles. In multivariate analysis, both indices showed strong independent associations with NOAF occurrence, with SI demonstrating superior association strength (OR 4.10, 95% CI 2.15-7.83) compared to MSI (OR 2.80, 95% CI 1.67-4.71), both P<0.001. Generalized additive model analysis revealed distinct non-linear associations with threshold effects. Threshold effect analysis identified specific turning points at SI = 0.586 and MSI = 0.785, below which neither index showed significant associations with NOAF occurrence, but above which both demonstrated strong positive associations (SI: OR 6.168, 95% CI 2.916-13.046; MSI: OR 3.896, 95% CI 2.133-7.117, both P<0.0001). Subgroup analyses demonstrated robust associations across most clinical characteristics, with significant interaction effects for age and hypertension status, showing stronger associations in patients ≥ 65 years and those with hypertension. Mediation analysis demonstrated that WBC count significantly mediated the associations, accounting for 9.81% of the SI-NOAF association and 11.88% of the MSI-NOAF association (both P<0.05).

Conclusions: This study demonstrates that SI and MSI are independently associated with in-hospital NOAF occurrence in AMI patients through distinct non-linear threshold effects. SI showed superior association strength compared to MSI, with clinically meaningful cut-points identified at SI > 0.586 and MSI > 0.785. The associations were robust across most clinical subgroups but stronger in elderly patients (≥ 65 years) and those with hypertension. WBC count partially mediated these associations, suggesting inflammatory pathways may contribute to the observed relationships. These simple, readily available hemodynamic indices calculated from routine vital signs offer practical tools for real-time risk assessment and may inform enhanced monitoring strategies in clinical practice, particularly for vulnerable population.

HA-Hypoxia Dual-Engineered Exosomes from ADSCs Target Myocardial Infarction by Modulating miR-331-5P Pathways

Jia-Bin Zang[1], Jia-Jie Pan[2], Yi-Ying Yang[2]

1. Department of Cardiology, Shanghai Sixth People's Hospital Affiliated to Shanghai Jiao Tong University School of Medicine

2. Department of Cardiology, The Eighth Affiliated Hospital of Sun Yat-sen University

Objective: Myocardial infarction (MI) triggers detrimental inflammatory and oxidative cascades, hindering repair. This study aimed to develop a novel dual-engineered exosome delivery system (HA@Hypo-ADSCs-exo) to enrich within the MI zone, ameliorate the inflammatory and oxidative microenvironment, and enhance cardiac repair, providing a new therapeutic strategy for post-MI functional recovery.

Methods:

1.Exosome Isolation and Characterization: Exosomes were isolated from adipose-derived mesenchymal stem cells (ADSCs) under normoxia (ADSC-exo) or hypoxia (1% O2, Hypo-ADSC-exo) via differential and ultracentrifugation. Characterization involved Transmission Electron Microscopy (TEM), Nanoparticle Tracking Analysis (NTA), and Western blot (WB) for morphology, size, surface markers (CD81, ALIX, TSG101, CD63 positive; calnexin negative), and zeta potential.

2.In Vitro Functional Assessment: Hypo-ADSC-exo and ADSC-exo were co-cultured with H/R-injured cardiomyocytes. Anti-inflammatory and antioxidant effects were evaluated via: WB (VCAM-1, ICAM-1, p-p65,

NRF2, HO-1); CCK-8 assay (viability); LDH release (cytotoxicity); DCFH-DA fluorescence (ROS levels). miRNA sequencing identified differentially expressed miRNAs in Hypo-ADSC-exo. Key miRNA (miR-331-5p) function was validated using inhibitors/mimics and assessing downstream genes (VCAM-1, ICAM-1, NRF2, HO-1, CYBB, AGTR1).

3.Targeting Modification and Validation: Hypo-ADSC-exo was surface-modified with Hyaluronic Acid (HA) via chemical conjugation (HA@Hypo-ADSCs-exo). Targeting to CD44 receptors on cardiomyocytes was confirmed using DiR-labeled exosomes via confocal microscopy (cellular uptake efficiency over 48h) and in vivo imaging system (IVIS) tracking in MI mice.

4.In Vivo Therapeutic Efficacy: MI was induced in mice (LAD ligation). Groups received: PBS (Control), Hypo-ADSCs-exo, or HA@Hypo-ADSCs-exo via tail vein injection. Assessments included:

(1)Function: Echocardiography (LVEF%, LVFS%, wall thickness) at days 7, 14, 28 post-MI.

(2)Inflammation/Oxidative Stress: Serum ELISA (TNF-α, IL-6, VCAM-1, MDA, SOD); Heart tissue WB (p-p65, NRF2, HO-1); HE staining (inflammatory infiltration); DHE staining (ROS); Immunofluorescence.

(3)Tissue Remodeling: Masson's Trichrome (fibrosis area); WGA (cardiomyocyte size); TUNEL (apoptosis).

(4)Safety: Serum AST/ALT; Histopathology of major organs.

Results:

1.TEM/NTA/WB confirmed successful isolation and characterization of ADSC-exo and Hypo-ADSC-exo (50-200nm, cup-shaped, exosome markers positive).

2.Hypo-ADSC-exo demonstrated superior efficacy vs. ADSC-exo in vitro: significantly higher cardiomyocyte viability (CCK-8), lower LDH release, reduced ROS (DCFH-DA), decreased pro-inflammatory markers (VCAM-1, ICAM-1, p-p65), and increased antioxidant markers (NRF2, HO-1).

3.miRNA sequencing identified miR-331-5p as the most significantly upregulated miRNA in Hypo-ADSC-exo (~4-fold vs. ADSC-exo). Inhibiting miR-331-5p in Hypo-ADSCs abolished the protective effects of their exosomes on H/R cardiomyocytes. Conversely, miR-331-5p mimic downregulated VCAM-1, ICAM-1, CYBB, AGTR1 and upregulated NRF2/HO-1 in injured cells. Bioinformatic prediction and luciferase reporter assays confirmed KEAP1 and TRAF6 as direct targets of miR-331-5p.

4.HA conjugation was confirmed (FTIR). HA@Hypo-ADSCs-exo showed significantly enhanced CD44-mediated cellular uptake (confocal) and targeted accumulation within the MI region (IVIS) compared to unmodified Hypo-ADSCs-exo.

5.In vivo, HA@Hypo-ADSCs-exo treatment yielded the most significant benefits:

(1) Improved Cardiac Function: Significantly higher LVEF% and LVFS% vs. Control and Hypo-ADSCs-exo groups at days 14 and 28.

(2) Reduced Inflammation/Oxidative Stress: Markedly lower serum TNF-α, IL-6, VCAM-1, MDA; higher SOD; reduced myocardial ROS (DHE), inflammatory infiltration (HE), p-p65; increased NRF2/HO-1.

(3) Attenuated Remodeling: Smaller infarct size, reduced fibrosis (Masson's), less cardiomyocyte apoptosis (TUNEL), decreased cardiomyocyte hypertrophy (WGA).

(4) Safety: No significant changes in AST/ALT or histopathology in major organs.

Conclusion: We successfully constructed a dual-engineered exosome system (HA@Hypo-ADSCs-exo). This system efficiently targets the MI heart via HA-CD44 interaction. It exerts potent anti-inflammatory and antioxidant effects, significantly improving cardiac function and attenuating remodeling in MI mice. The cardioprotective mechanism is primarily mediated by the hypoxia-induced enrichment of miR-331-5p within the exosomes, which suppresses inflammation and oxidative stress by targeting KEAP1 and TRAF6. HA@Hypo-ADSCs-exo represents a highly promising and safe targeted nanotherapeutic strategy for myocardial repair after infarction.

Keywords: Exosomes, Adipose-derived mesenchymal stem cells (ADSCs), Hypoxia preconditioning, Hyaluronic Acid (HA), Myocardial Infarction, Inflammation, Oxidative Stress.

冠心病急性心梗不同病变血管缺血时间与 SII 的相关性研究

黄日红 刘珈宁

大连医科大学附属第一医院

目的：本研究旨在探讨急性心肌梗死（AMI）患者不同罪犯血管病变分组中，心肌缺血时间与全身免疫炎症指数（Systemic Immune-Inflammation Index, SII）的相关性。通过分析前降支（LAD）、右冠状动脉（RCA）和回旋支（LCX）病变患者的缺血时间与 SII 值的关联性，评估 SII 作为反映心肌损伤后机体炎症反应强度的潜在生物标志物的临床价值，为 AMI 病情评估和预后判断提供理论依据。

方法：纳入共 5335 例确诊 AMI 患者，根据冠脉造影结果分为前降支病变组（n=2685）、右冠状动脉病变组（n=2548）和回旋支病变组（n=102）。记录所有患者心肌缺血时间（从症状发作至血运重建时间）及入院时的 SII 值（基于中性粒细胞、淋巴细胞及血小板计数的复合指标）。采用 Pearson 相关系数分析各组缺血时间与 SII 值的线性相关性，并计算统计显著性（p 值），以评估二者关联强度与临床意义。

结果：前降支病变组（n=2685）：缺血时间与 SII 值呈显著正相关（r = 0.0523, p = 0.0081）；右冠病变组(n=2548)：缺血时间与 SII 值呈显著正相关(r = 0.0660, p = 0.0020)；回旋支病变组(n=102)：缺血时间与 SII 值无显著相关性(r = 0.0630, p = 0.5551）。提示在前降支与右冠状动脉病变患者中，心肌缺血时间越长，机体炎症反应强度（SII 值）越高；而在回旋支病变患者中，当前数据未显示二者显著关联。

结论：本研究发现，对于前降支及右冠状动脉病变导致的 AMI 患者，心肌缺血时间与 SII 值呈显著正相关，提示更长的缺血时间可能激活更强烈的全身性炎症反应，SII 值可作为评估此类患者炎症状态和病情严重程度的潜在参考指标。然而，回旋支病变组未见显著关联，可能与样本量有限（n=102）及解剖区域生理特点相关，需未来扩大样本进一步验证。该研究为基于罪犯血管分层的 AMI 炎症反应评估提供了新证据，支持 SII 在 LAD/RCA 相关心梗临床管理中的应用价值，强调缺血时间对炎症级联反应的调控作用，为个体化抗炎治疗时机选择提供了理论支持。

Stress Hyperglycemia Ratio Predicts Short- and Long-Term Mortality in Acute Myocardial Infarction Patients Undergoing Intra-Aortic Balloon Pump Support

Caixia Guo, Xue-Qian Shen, haosheng Wu, Pan-Pan Yu, Xue Jiang

Beijing Tongren Hospital Affiliated to Capital Medical University

Objective

Stress-induced dysglycemia is common after acute myocardial infarction (AMI) and may be amplified in critically ill patients requiring intra-aortic balloon pump (IABP) support. We aimed to determine whether the stress hyperglycemia ratio (SHR)—the admission glucose normalized to chronic glycemic status—independently predicts both short-term (28-day) and long-term (1-year) mortality in AMI patients treated with IABP.

Methods

We performed a retrospective cohort study using the MIMIC-IV critical-care database (2008-2019). Adults whose first intensive-care admission included IABP placement for AMI were identified by ICD-9/10 codes, leaving 337 unique patients after excluding non-AMI indications and missing key laboratory values. SHR was calculated as admission plasma glucose (mmol L^{-1}) divided by (1.59 × HbA1c [%] − 2.59). Patients were stratified into SHR quartiles, and survival was analyzed with Kaplan–Meier curves, log-rank tests, and Cox proportional-hazard models. Three increasingly adjusted multivariable models incorporated demographic factors, comorbidities (e.g., diabetes, heart failure, chronic kidney disease), critical illness variables (cardiac arrest, septic shock, extracorporeal membrane oxygenation), and laboratory indices. Restricted cubic splines (RCS) explored non-linear SHR–mortality relationships, and predefined subgroup analyses assessed effect modification. Missing covariates (<20 %) were multiply imputed. Statistical significance was set at $P < 0.05$.

Results

The cohort was predominantly older (median age ≈ 70 years), male, and overweight; hypertension, hyperlipidemia, and heart failure were frequent. Overall 28-day and 1-year mortality were 21 % and 31 %, respectively. Mortality rose stepwise across SHR quartiles: Kaplan–Meier curves showed the highest risk in Q4 (median SHR ≈ 2.0) and the lowest in Q2 (median SHR ≈ 1.1; log-rank $P < 0.001$). In unadjusted Cox analysis, each one-unit increase in SHR doubled 28-day mortality (HR = 2.07, 95 % CI 1.73-2.49) and similarly elevated 1-year mortality (HR = 2.17, 95 % CI 1.80-2.62). After full adjustment (Model 3), SHR remained an independent predictor: HR = 2.24 (95 % CI 1.76-2.87) for 28-day and HR = 2.01 (95 % CI 1.57-2.56) for 1-year mortality per unit increase. Compared with Q2, the highest quartile carried a fourfold (28-day) and four- to five-fold (1-year) excess risk.

RCS modelling revealed a significant U-shaped association ($P_{non\text{-}linear} = 0.004$) with a nadir at SHR ≈ 1.146. For SHR > 1.146, mortality climbed steeply (e.g., HR = 2.52 for 28-day); below this threshold, the slope reversed and risk plateaued without statistical significance.

Subgroup analyses were largely consistent, but a significant interaction emerged with septic shock: SHR strongly predicted mortality among patients without septic shock, whereas its effect was attenuated in those with septic shock (interaction $P < 0.05$). No meaningful interactions were observed for age, diabetes, chronic kidney disease, or heart failure.

Conclusion

In AMI patients receiving IABP support, the stress hyperglycemia ratio is

an marker of both early and late mortality. The U-shaped relationship indicates that relative hypoglycemia and pronounced hyperglycemia are harmful, with an optimal SHR near 1.1. Incorporating SHR into bedside risk stratification may help clinicians identify high-risk individuals, tailor glycemic management, and improve prognostication beyond traditional comorbidities and laboratory indices. Prospective studies are warranted to test whether interventions targeting aberrant SHR can translate into better clinical outcomes.

Unraveling the Therapeutic Potential of Sophora flavescens Aiton in Myocardial Infarction: An Integrative Approach Combining Bioinformatics, Network Pharmacology, and Experimental Validation

Zhong-Bai Zhang

海军军医大学第二附属医院 / 上海长征医院

Abstract

Aims: To elucidate the relationship between potential MI targets and SFA's mechanism of action, providing a theoretical basis for clinical development of new drugs.

Background: Myocardial infarction (MI) has been identified as one of major cardiovascular diseases with adverse consequences. Sophora flavescens Aiton (SFA) is indicated for the therapeutic treatment of MI. However, there is no systematic research on the new therapeutic targets for MI and the exact action mechanism of SFA.

Objective: This study explores the potential mechanisms of SFA in treating MI by integrating bioinformatics, network pharmacology analyses and experimental verification.

Methods: New MI targets were predicted using bioinformatics techniques. Network pharmacology and molecular docking jointly served for predicting the key targets and underlying mechanism of SFA. A machine learning model was developed to identify the core MI targets. Subsequently, H9c2 cardiomyocytes hypoxia model was established for experimental verification.

Results: 140 active components were ascertained in SFA and 59 differentially expressed genes (DEGs) were screened for MI. 87 shared genes were achieved by WGCAN. 80 proteins and 413 interactions were identified by PPI network. After building the machine model, three core targets were identified (STAT1, TNFRSF1A and MCL1). According to in vitro experiments, SFA exerts protective effect relying on three core targets and biological processes including cell viability, the inflammatory response, and antiapoptotic effects, etc.

Conclusions: This study finds new core targets for MI and the therapeutic activity of SFA against MI, of which the experimental verification provides valuable insights into the molecular mechanisms underlying SFA's efficacy in MI treatment and paving the way for targeted drug development strategies.

Keywords: bioinformatics; network pharmacology; machine learning model; core targets; myocardial infarction

Abstract

Aims: To elucidate the relationship between potential MI targets and SFA's mechanism of action, providing a theoretical basis for clinical development of new drugs.

Background: Myocardial infarction (MI) has been identified as one of major cardiovascular diseases with adverse consequences. Sophora flavescens Aiton (SFA) is indicated for the therapeutic treatment of MI. However, there is no systematic research on the new therapeutic targets for MI and the exact action mechanism of SFA.

Objective: This study explores the potential mechanisms of SFA in treating MI by integrating bioinformatics, network pharmacology analyses and experimental verification.

Methods: New MI targets were predicted using bioinformatics techniques. Network pharmacology and molecular docking jointly served for predicting the key targets and underlying mechanism of SFA. A machine learning model was developed to identify the core MI targets. Subsequently, H9c2 cardiomyocytes hypoxia model was established for experimental verification.

Results: 140 active components were ascertained in SFA and 59 differentially expressed genes (DEGs) were screened for MI. 87 shared genes were achieved by WGCAN. 80 proteins and 413 interactions were identified by PPI network. After building the machine model, three core targets were identified (STAT1, TNFRSF1A and MCL1). According to in vitro experiments, SFA exerts protective effect relying on three core targets and biological processes including cell viability, the inflammatory response, and antiapoptotic effects, etc.

Conclusions: This study finds new core targets for MI and the therapeutic activity of SFA against MI, of which the experimental verification provides valuable insights into the molecular mechanisms underlying SFA's efficacy in MI treatment and paving the way for targeted drug development strategies.

Keywords: bioinformatics; network pharmacology; machine learning model; core targets; myocardial infarction

基于目诊仪探究心肌梗死患者的中医证候：一项前瞻性，观察性研究

高占群[2] 张迪瑞[1,3] 胡思宁[1,3] 郝伟[1,3] 赵晨[1,3] 高语博[1,3] 贾海波[1,3] 房超[1,3] 张智[4,5] 于波[1,3]

1. 哈尔滨医科大学第二附属医院

2. 湖南医药学院 总医院

3. 中国教育部心肌缺血重点实验室

4. 国家工程研究中心北京生物芯片技术

5. 北京博奥生物有限公司

摘要：

目的：本研究旨在利用目诊仪技术分析心肌梗死患者的眼像特征，探讨其与中医证候分型的相关性，为心肌梗死的中西医结合诊断提供客观化依据。

方法：采用前瞻性观察性研究设计，分两个阶段（2019 年 11 月 18 日 -2020 年 1 月 24 日及 2021 年 11 月 15 日 -2022 年 2 月 25 日）纳入 1086 例疑似或确诊心肌梗死并行冠脉造影检查的患者。通过目诊仪采集眼像数据后，首先排除图像质量不达标者，再依据冠脉造影结果（至少 1 支血管狭窄 > 70%）及临床标准（典型症状、心肌损伤标志物异常、心电图缺血性改变）确诊心肌梗死的患者。采用中医证候量表评估患者证型，分析其与眼像特征的关联性。

结果：105 例心肌梗死患者中，男性占比 87.62%（92 例），平均年龄 57.3±9.5 岁，BMI 25.5±3.5 kg/m²，提示超重人群比例较高。临床分型显示非 ST 段抬高型心肌梗死（NSTEMI）占 54.3%，冠脉病变复杂程度（Syntax 评分）为 16.0±7.7。中医证候分析发现，湿热证占比最高（44.8%），其次为血瘀证（28.6%）和气虚证（19.0%）。眼像特征显示，湿热证患者在心眼区即眼睛内眦，出现特有的中医表现，如雾漫或者异常血管等。

结论：本研究首次通过目诊仪技术证实，冠脉造影确诊的心肌梗死患者中，湿热证为其核心中医证型，眼像特征可为中医辨证提供可视化依据。未来需扩大样本量以验证目诊仪在中医证候客观化诊断中的价值。

关键词：目诊仪，心肌梗死，中医证候，湿热证，冠脉造影

不同海拔地区患者冠脉支架植入术后再狭窄发率情况比较

李燕

西藏自治区人民政府驻成都办事处医院 四川大学华西医院西藏成办分院

目的：系统比较不同海拔地区患者冠脉支架植入术后再狭窄发生率与海拔高度的影响关系、差异以及危险因素。

方法 ： 采用单中心回顾性队列研究设计，分析 2023 年 1-2023 年 12 月西藏驻成都办事处医院收治的 217 例不同海拔高度的冠心病患者，按居住地海拔分为高海拔组（>3000m，n=126）和低海拔组（<1000m，n=91）。术后 30 天检测血脂、hs-CRP，1 年后复查冠脉造影，比较两组血脂和血清 CRP-hs 水平、比较一年后冠脉支架术后再狭窄发生率、比较一年后冠脉造影多支血管病变分布情况。

结果 ： 高海拔组 LDL-C 达标率（<1.8mmol/L）显著低于低海拔组（19% vs 12.1%, P=0.04），支架内再狭窄（19% vs 12.1%, P=0.04）、多支血管病变（42.9% vs 20.9%, P=0.02）及闭塞血管比例（19% vs 12.1%, P=0.04）均较高，高海拔地区患者的术后血管病变再发生率显著高于低海拔地区。

结论： 不同海拔地区患者冠脉支架植入术后恢复情况有显著差异，高海拔地区患者术后恢复较差，高海拔环境通过低氧诱导的炎症反应、血脂代谢紊乱及血液流变学改变，显著增加冠脉支架术后再狭窄及多支血管病变风险。未来需结合多组学技术（如转录组学）深入解析分子机制，并为高海拔地区患者制定 "降脂 - 抗炎 - 氧疗 - 随访" 四位一体的个体化精准管理策略，对高海拔地区冠脉支架植入术后康复和预防具有一定临床价值。

残余 R 波对急性 ST 段抬高型心肌梗死血管再通的预测价值

李颖

重庆市第二人民医院

【摘要】目的 探讨残余 R 波（Residual R wave, RR）对急性 ST 段抬高型心肌梗死（ST-segment elevation myocardial infarction,STEMI）血管再通的预测价值。方法 选取 2019 年 1 月 1 日至 2020 年 12 月 31 日我院因急性 STEMI 接受冠状动脉介入治疗患者，根据术中罪犯血管 TIMI 血流分级（thrombolysis in myocardial infarction,TIMI）分为非再通组（TIMI 血流 0 级、1 级）和再通组（TIMI 血流 2 级、3 级），收集患者临床资料，分析残余 R 波与血管再通的相关性及血管再通影响因素。结果 共收集 2019 年 1 月 1 日至 2020 年 12 月 31 日因急性 STEMI 于我院接受冠状动脉介入治疗患者 451 例，根据纳排标准，最终纳入 375 例，包括接受 PPCI 的 305 例及择期 PCI 的 70 例。分为非再通组（n=202）和再通组（n=173）。采用单因素分析比较两组患者一般临床资料，年龄、性别、高血压、糖尿病、房颤、胸痛时间、药物使用（替格瑞洛、肝素、比伐泸定），Q 振幅、残余 R/Q 振幅比值、罪犯血管、射血分数（Ejection Fraction,EF）、总胆固醇（Total cholesterol,TC）、低密度脂蛋白（low density lipoprotein,LDL）、C 反应蛋白（C-ractive protein,CRP）、肌红蛋白（myoglobin,MB）在两组间无统计学差异，残余 R 波、R 波振幅、ST 段抬高振幅（ST-elevation,STE）、

脑钠肽（brain natriuretic peptide,BNP）、氯吡格雷、溶栓、急诊在两组间差异显著（p<0.05），对上诉自变量采用二元 logistic 回归分析，证实残余 R 波是血管再通的独立危险因素（OR=2.974,95%CI=1.151-7.683,p=0.024），存在残余 R 波提示更高的 TIMI 血流分级，无残余 R 波提示更低水平的 TIMI 血流。采用逐步回归法进行分析，得出残余 R 波、STE、溶栓、急诊是血管再通的相关危险因素。结论 残余 R 波的存在与罪犯血管再通有相关性，存在残余 R 波可预测 STEMI 罪犯血管再通，对临床再灌注决策有指导意义。

关键词：急性心肌梗死；残余 R 波；血管再通。

冠状动脉痉挛诱发急性心肌梗死 1 例

朱其中 任洁

山西白求恩医院（山西医学科学院）

目的：探讨冠状动脉痉挛导致急性心肌梗死的临床特点、诊断方法及治疗策略。

方法：采用病例回顾性研究方法，对 1 例典型冠状动脉痉挛诱发急性心肌梗死的患者资料进行分析。

结果：患者男性，42 岁，因 " 突发胸痛 2 小时 " 急诊入院。既往有吸烟史（20 支 / 日 ×20 年），否认高血压、糖尿病病史。入院查体：血压 150/90mmHg，心率 98 次 / 分，心肺听诊未及明显异常。心电图示 II、III、aVF 导联 ST 段抬高 0.3-0.4mV，肌钙蛋白 I 5.6ng/ml（正常 <0.04ng/ml），初步诊断为急性下壁心肌梗死。急诊行冠状动脉造影显示右冠状动脉中段 99% 局限性狭窄（TIMI 血流 2 级），但未发现明显粥样硬化斑块。经冠状动脉内注射硝酸甘油 200μg 后复查造影，原狭窄病变完全消失（TIMI 血流 3 级），确诊为冠状动脉痉挛导致的急性心肌梗死。术后给予地尔硫卓缓释片 90mg q12h、单硝酸异山梨酯 60mg qd 抗痉挛治疗，联合阿司匹林、氯吡格雷双抗血小板治疗。住院期间行心脏 MRI 检查显示下壁心内膜下延迟强化，符合心肌梗死改变，但左心室射血分数保持正常（58%）。患者出院后严格戒烟，规律服用钙拮抗剂，随访 6 个月期间未再发胸痛，运动负荷试验阴性，24 小时动态心电图未发现缺血性 ST 段改变。本病例具有以下临床教学价值：（1）冠状动脉痉挛好发于中年吸烟男性，可表现为典型 ST 段抬高型心肌梗死，约占急性心梗病因的 2%-3%；（2）诊断需依靠冠脉造影动态观察，硝酸甘油试验是鉴别痉挛与固定性狭窄的关键；（3）治疗应着重于解除血管痉挛（钙拮抗剂为首选）和危险因素控制（特别是戒烟）；（4）若无合并明显冠脉狭窄，应避免不必要的支架植入。

结论：1. 冠状动脉痉挛是导致急性心肌梗死的非动脉粥样硬化性重要原因；2. 冠脉造影联合药物试验是确诊的关键方法；3. 长期钙拮抗剂治疗可有效预防复发；4. 临床医师需提高对血管痉挛性心梗的认识，避免过度支架植入。

急性 STEMI 患者心肌结构与功能的影像学综合评估：基于分形分析法与 CMR 特征追踪技术

张沁 文丹 余洪

遵义医科大学附属医院

目的：微血管阻塞（microvascular obstruction，MVO）是急性 ST 段抬高型心肌梗死（ST-elevation myocardial infarction，STEMI）患者预后不良的重要决定因素。心脏磁共振特征追踪（cardiac magnetic resonance feature tracking，CMR-FT）可量化左心室应变功能，分形分析法则可评估心肌小梁结构的复杂性。本研究旨在通过分析 STEMI 患者经皮冠状动脉介入治疗（（percutaneous coronary intervention， PCI）后的心脏磁共振（cardiac magnetic resonance，CMR）数据，定量评估心肌结构重构，并探索其与 MVO 之间的关系。

方法：本研究共纳入 91 例 PCI 术后 STEMI 患者及 56 名健康对照。依据钆对比剂延迟强化（late gadolinium enhancement，LGE）成像结果，将患者分为 MVO 组（n=50）与 nMVO 组（n=41）。所有受试者于 PCI 术后 2–10 天接受 CMR 检查，采集左室三向应变参数：整体径向应变（global radial strain，GRS）、整体环向应变（global circumferential strain，GCS）和整体纵向应变（global longitudinal strain，GLS），及其峰值收缩 / 舒张速率；应用分形分析法提取分形维数（fractal dimension，FD），包括平均整体 FD 值（mean global FD）、最大基底部 FD（max basal FD）和最大心尖部 FD（max apical FD）。组间比较采用单因素方差分析及 LSD 法进行多重比较。

结果：MVO 组与 nMVO 组的 mean global FD 均显著高于正常组（p<0.05），提示 STEMI 患者心肌小梁结构复杂性普遍增加；且 nMVO 组 mean global FD 值高于 MVO 组。STEMI 患者的左室射血分数（left ventricular ejection fraction，LVEF）及左室每搏输出量（left ventricular stroke volume，LVSV）均低于正常组，左室质量（left ventricular mass，LVM）、左室质量指数（left ventricular mass index）、左室舒张末期容积（left ventricular end-diastolic volume，LVEDV）和左室收缩末期容积（left ventricular end-systolic volume，LVESV）均显著升高（p<0.05）。左室三向应变参数在三组间依次递减（正常组 > nMVO 组 > MVO 组），组间差异均具有统计学意义（p<0.05）。

结论：分形分析法联合 CMR-FT 应变参数可全面、定量评估 STEMI 患者左室结构与功能损害，尤其在识别 MVO 方面表现出良好敏感性。mean global FD 有望成为早期识别 MVO 的新型影像生物标志物。

1,3-Butanediol Enhances Autophagy via PI3K/Akt/FOXO3 Pathway to Ameliorate Cardiac Remodeling Post-Myocardial Infarction

Hailin Zhang, Dajun Chai

The First Affiliated Hospital of Fujian Medical University

Background: Myocardial infarction (MI) is the leading cause of cardiovascular death and a serious threat to global health. In recent years, ketone bodies have been found not only to act as a 'super fuel' for the heart, but also to inhibit adverse cardiac remodeling by improving vascular endothelial function, reducing oxidative stress and regulating inflammation, providing a novel target for the treatment of cardiovascular disease. Autophagy is an important means of self-repair after injury, and levels of autophagy in cardiomyocytes are reduced after infarction. It is not clear whether ketone bodies can increase the level of autophagy in cardiomyocytes and thus improve the structure and function of the heart in MI rats.

Methods: 1,3-butanediol (1,3-BD) is a precursor for ketone body metabolism that can be converted to β-hydroxybutyric acid (β-HD) in the liver. β-HD is not only an energetic substrate but also an important molecule for cellular signaling. In this study, the MI rat model was established by continuous ligation of the left anterior descending coronary artery in standard SD rats for 5 weeks, and non-infarcted rats were excluded by cardiac ultrasound at week 1 after surgery and randomly divided into control (Ctr), MI and MI+1,3-BD intervention groups. In the MI+1,3-BD group, 1,3-BD was administered by gavage (10 mg/100 g) daily from the 1st postoperative week to the 5th postoperative week, and the effects of 1,3-BD on the structural function of the heart and pathological damage to the myocardium were clarified at various levels, such as cardiac ultrasound, hemodynamics, hematology and histopathology, in MI rats. Transmission electron microscopy and laser confocal microscopy were used to observe the changes in myocardial mitochondrial ultrastructure and autophagy levels in the infarct border zone, and possible regulatory mechanisms were explored in conjunction with transcriptomic and metabolomic analyses and verified by immunoblotting.

Results: 1,3-BD treatment for 4 weeks significantly increased serum β-Hb levels in rats. After 5 weeks of continuous ligation of the left anterior descending coronary artery, cardiac ultrasound and invasive hemodynamic monitoring showed that the left ventricular chambers of rats in the MI group were significantly enlarged and the systolic and diastolic functions were significantly reduced, and 1,3-BD intervention significantly improved the cardiac structure and function of rats and reduced serum B-type natriuretic peptide (BNP) levels (left ventricular end-diastolic diameter: 7.70±0.25 cm vs 8.45±0.71 cm, left ventricular ejection fraction: 71.92±6.08 % vs 50.39±5.94 %, maximum rise rate of left ventricular pressure: 3871.07±272.35 mmHg vs 2899.65±554.38 mmHg, maximum drop rate of left ventricular pressure: -3431.68±363.66 mmHg vs -2726.04±552.97 mmHg, BNP: 61.95±9.62 pg/ml vs 91.20±14.10 pg/ml, all $P < 0.05$). Compared with rats in the MI group, HE staining of rats in the MI+1,3-BD group showed a reduction in the size of the left ventricular chamber, a reduction in the extent of necrotic thinning of the ventricular wall, a reduction in the infiltration of inflammatory cells, and a reduction in the deposition of collagen fibres in myocardial tissue as shown by Masson's staining. Mitochondrial transmission electron microscopy confirmed that MI+1,3-BD significantly improved the structure and number of myocardial mitochondria in the marginal zone, and autophagic vesicles were significantly increased. LC3 immunofluorescence in situ staining of myocardial tissue and observation by laser confocal microscopy showed that LC3 expression in myocardium in the marginal zone of the MI+1,3-BD group was significantly enhanced compared with that of the MI group, suggesting that the level of myocardial autophagy was increased. Transcriptomic and metabolomic analyses of myocardial tissue from the infarct border zone further revealed that exogenous supplementation of 1,3-BD not only enhanced the metabolic pathways for energy supply to the myocardium, but also autophagy, glycerophospholipid metabolism, phosphatidylinositol metabolism and the PI3K-Akt-FOXO3 signaling pathway were significantly enriched. The protein levels of Atg7, Atg13, Beclin1, SQSTM1/p62, ULK1 and LC3II/LC3 I were significantly decreased in the MI group compared to the Ctr group, and the expression of autophagy-related proteins was significantly upregulated by 1,3-BD intervention. Meanwhile, the MI group activated the PI3K-Akt pathway, upregulated HDAC1 expression and inhibited FOXO3 expression compared with the Ctr group, and 1,3-BD intervention significantly inhibited the PI3K-Akt pathway, downregulated HDAC1 and increased FOXO3 expression. It is suggested that 1,3-BD may inhibit the deacetylation of HDAC1 and increase the autophagy level of injured cardiomyocytes by regulating the PI3K/Akt/FOXO3 pathway.

Conclusion: 1,3-BD significantly improved cardiac structural function, attenuated myocardial pathological injury and mitochondrial destruction in MI rats, and could upregulate the autophagy level of marginal zone cardiomyocytes by modulating the biological functions of the PI3K/Akt/FOXO3 pathway and HDAC1. Exogenous supplementation of 1,3-BD not only provides richer energy support to the ischemic heart, but also improves the poor prognosis of MI by enhancing autophagy in injured cardiomyocytes via ketone body β-Hb. Appropriate ketone body supplementation could be a potentially effective means of preventing ischemic cardiomyopathy.

Keywords: Myocardial infarction, 1,3-butanediol, β-hydroxybutyrate, autophagy, PI3K/Akt/FOXO3 signaling pathway

RXRα Mediates the Effect of Atorvastatin on the Function of Foxp3+

Regulatory T-cells in Patients with Acute Coronary Syndrome

Hailin Zhang, Wangjin Zhang, Dajun Chai

The First Affiliated Hospital of Fujian Medical University

Background: Acute coronary syndrome (ACS) is characterized by increased effector cells and decreased regulatory T cells (Tregs). Tregs expressing the transcription factor forkhead box P3 (Foxp3) play an essential role in maintaining immune homeostasis and preventing peripheral self-tolerance. Sustained expression of Foxp3 in Tregs is essential for their phenotypic stability, metabolic fitness and regulatory function. Statins have been shown to be clinically beneficial in ACS patients via the induction of Tregs, but the mechanism remains unknown. The aim of this study was to investigate the effect of atorvastatin on the induction of Foxp3+ Tregs in ACS patients and to elucidate the role of RXRα in this process.

Methods: Clinically suspected and previously untreated ACS patients were enrolled. Patients were divided into ACS and control groups. CD4+ T cells were collected from the patients' peripheral blood, purified and stimulated with ImmunoCult™ Human CD3/CD28 T Cell Activator. Immunoblotting and flow cytometry were used to determine the expression of Foxp3 and the percentage of Foxp3+ Tregs in CD4+ T cells, respectively. CD4+ T cells were pre-stimulated with CD3 (5 μg/ml) / CD28 (2 μg/ml) antibodies and then treated under different conditions with or without TGF-β1 (5ng/ml) and (or), atorvastatin (10-7 mol/L), Smad2 inhibitor (10-6 mol/L), RXRα agonist 9-cis-RA (10-8 mol/L) and RXRα inhibitor UVI3003 (10-7 mol/L). The expression of Foxp3 and the percentage frequency of Foxp3+ Tregs in CD4+ T cells were determined by flow cytometry. Foxp3 expression, the variation of Foxp3 expression and the proportion of Foxp3+ Tregs in CD4+ T cells were observed by the above methods, also the phosphorylated of Smad2 (P-Smad2), total Smad2 (t-Smad2) and RXRα were detected by immunoblotting, the serum levels of IL-10 expression were quantified by ELISA and, and the levels of IL-10 mRNA were detected by real-time PCR.

Results: Compared with the control group, the proportion of Foxp3+ Tregs and the levels of Foxp3, P-Smad2 and RXRα expression in CD4+ T cells were significantly reduced in the ACS group. Under the combined stimulation of atorvastatin and TGF-β1, the proportion of Foxp3+ Tregs and the levels of Foxp3, P-Smad2 and RXRα in CD4+ T cells from ACS patients were significantly increased, while there was no significant difference in the levels of t-Smad2. After pretreatment with Smad2 inhibitor in CD4+ T cells, the co-stimulatory function of TGF-β1 and atorvastatin was significantly suppressed. The stimulatory effects of atorvastatin and TGF-β1 on Foxp3+ Tregs were promoted by the RXRα agonist 9-cis-RA and inhibited by the RXRα antagonist UVI3003 separately. Both combined intervention of TGF-β1 and atorvastatin or TGF-β1 and 9-cis-RA could significantly promote the secretion of IL-10 by Foxp3+ Tregs, and the secretion of IL-10 was prominently suppressed by RXRα inhibitor UVI3003.

Conclusions: Atorvastatin promotes Foxp3 expression and increases the distribution ratio of the induction and immunomodulatory effects of Foxp3+ Tregs in the peripheral blood of ACS patients by activating the TGF-β1/Smad2 pathway. The nuclear receptor RXRα plays an important mediating role in anti-inflammation, mediating the effect of atorvastatin on the TGF-β1/Smad2 pathway and IL-10 production.

Keywords: Acute coronary syndrome; Regulatory T cells; Statin; TGF-β1/Smad2 pathway; Retinol X receptor

探究 STEMI 患者血清 Omentin-1 水平与斑块易损性、微循环灌注及临床预后的相关性

肖居正 刘芳

哈尔滨医科大学附属第二医院

目的 探讨急性 ST 段抬高型心肌梗死（STEMI）患者血清网膜素 -1（Omentin-1）水平与冠状动脉斑块易损性、心肌微循环灌注及临床预后的相关性，为 STEMI 风险分层及预后评估提供潜在生物学标志物。

方法 选取 2024 年 1 月至 2025 年 6 月在本院确诊为 STEMI 并接受急诊经皮冠状动脉介入治疗（PCI）的患者 256 例，根据血清 Omentin-1 水平三分位数分为低水平组（<300 ng/mL）和高水平组（>300ng/mL）。检测所有患者入院时血清 Omentin-1 水平，通过光学相干断层扫描（OCT）评估斑块易损性指标（包括脂质核心占比、纤维帽厚度、斑块破裂及微血栓），采用心肌 blush 分级（MBG）和 TIMI 心肌灌注分级（TMPG）评价微循环灌注情况，并记录术后 1 年主要不良心血管事件（MACE，包括心源性死亡、再发心肌梗死、靶血管血运重建及心力衰竭住院）的发生情况。

结果 低 Omentin-1 组患者脂质核心占比显著高于高水平组（P<0.05），纤维帽厚度显著降低（P<0.05），斑块破裂及微血栓发生率更高（P<0.05）；MBG 0~1 级及 TMPG 0~1 级比例显著高于高水平组（P<0.05）。Spearman 相关分析显示，血清 Omentin-1 水平与脂质核心占比呈负相关（r=-0.426，P<0.001），与纤维帽厚度呈正相关（r=0.382，P<0.001），与 MBG 及 TMPG 分级呈正相关（r=0.357、0.341，均 P<0.001）。多因素 Logistic 回归分析显示，低血清 Omentin-1 水平是 STEMI 患者 PCI 术后 1 年 MACE 发生的独立危险因素（OR=2.847，95%CI：1.362~5.951，P=0.005）。

结论 STEMI 患者血清 Omentin-1 水平降低与斑块易损性增加、微循环灌注不良及临床预后不佳密切相关，可作为评估 STEMI 患者病情严重程度及预后的潜在生物学标志物。

Analysis of the effectiveness and regression of intra-aortic balloon er pulsation in the treatment of AMI

yanqiu LI

The Third Affiliated Hospital of Chongqing Medical University

Abstract: Objective To investigate the therapeutic effect and regression analysis of intra-aortic balloon counter pulsation (IABP) combined with percutaneous coronary intervention (PCI) in patients. Methods: 83 patients with AMI who underwent emergency PCI with IABP support were selected as the IABP group. 48 patients with AMI with cardiogenic shock who underwent emergency PCI without IABP support were set as the control group. The peak post-PCI Tn I levels were compared between the two groups, and the left ventricular ejection fraction at 2 weeks and 3 months post-PCI was compared with the mortality rate at 3 months post-PCI. Results: There was no significant difference between the CRP levels of the two groups on admission, while the CRP levels on day 3 and 7 were significantly lower in the IABP group than in the control group [(80 · 3±42 · 8): (98 · 9±31 · 6) mg/L (70 · 6±34 · 3): (85 · 8±25 · 8) mg/L; all P<0 · 05]; the postoperative TNI peak was significantly lower in the IABP group than in the control group [(21 · 6): (85 · 8±25 · 8) mg/L]. The left ventricular ejection fraction at 2 weeks and 3 months after surgery was significantly better than in the control group [(44 · 7±7 · 3) %: (40 · 5±6 · 2) % (45 · 1±6 · 6) %: (40 · 7±4 · 4) %; both P<0 · 05]; and the rate of death at 3 months after surgery was significantly lower in the IABP group (P<0 · 05). The mortality rate was significantly lower in the IABP group (P < 0 · 05). Conclusion: Emergency PCI with IABP in patients with AMI complicated by cardiogenic shock significantly reduced postoperative CRP levels, and was effective in improving left ventricular function and reducing the mortality rate at 3 months after the procedure.

Abstract: Objective To investigate the therapeutic effect and regression analysis of intra-aortic balloon counter pulsation (IABP) combined with percutaneous coronary intervention (PCI) in patients. Methods: 83 patients with AMI who underwent emergency PCI with IABP support were selected as the IABP group. 48 patients with AMI with cardiogenic shock who underwent emergency PCI without IABP support were set as the control group. The peak post-PCI Tn I levels were compared between the two groups, and the left ventricular ejection fraction at 2 weeks and 3 months post-PCI was compared with the mortality rate at 3 months post-PCI. Results: There was no significant difference between the CRP levels of the two groups on admission, while the CRP levels on day 3 and 7 were significantly lower in the IABP group than in the control group [(80 · 3±42 · 8): (98 · 9±31 · 6) mg/L (70 · 6±34 · 3): (85 · 8±25 · 8) mg/L; all P<0 · 05]; the postoperative TNI peak was significantly lower in the IABP group than in the control group [(21 · 6): (85 · 8±25 · 8) mg/L]. The left ventricular ejection fraction at 2 weeks and 3 months after surgery was significantly better than in the control group [(44 · 7±7 · 3) %: (40 · 5±6 · 2) % (45 · 1±6 · 6) %: (40 · 7±4 · 4) %; both P<0 · 05]; and the rate of death at 3 months after surgery was significantly lower in the IABP group (P<0 · 05). The mortality rate was significantly lower in the IABP group (P < 0 · 05). Conclusion: Emergency PCI with IABP in patients with AMI complicated by cardiogenic shock significantly reduced postoperative CRP levels, and was effective in improving left ventricular function and reducing the mortality rate at 3 months after the procedure.

高敏肌钙蛋白与急性心肌梗死患者不良预后的研究进展

陈宇

重庆医科大学附属第三医院（方大医院）

随着人民生活水平的提高，心血管疾病（Cardiovascular disease，CVD）目前已成为我国人民死亡的主要原因之一，占我国死亡总人数的 40%[1]。冠状动脉粥样硬化性心脏病（Coronary atherosclerotic heart disease，CHD）是一种缺血性心脏病，简称冠心病，是由于冠状动脉发生粥样硬化改变造成血管腔狭窄并形成血栓，导致心肌缺血缺氧甚至坏死 [2]。目前我国的冠状动脉粥样硬化性心脏病的负担正在迅速逐渐增加，在 20 世纪 80 年代和 90 年代初，我国冠心病发病率和死亡率都很低，但是在 2016 年，冠心病在我国造成了至少 170 万人死亡，在过去 20 年里，冠心病的疾病负担正在迅速增加，其中，急性心肌梗死（Acute myocardial infarction，AMI）因为其高致死率及致残率，目前已经是我国人民在医疗卫生领域所面临的重要挑战 [3]。经皮冠脉介入治疗（Percutaneous coronary intervention，PCI）是治疗冠心病的一种安全且有效的方法，相较于外科冠脉搭桥术，其更简便、创伤更小、更经济等特点为患者提供了更多的选择。尽管我国 PCI 技术目前已经相对完善，冠脉介入死亡率已经控制在了极低的水平 [4]，但是术后短期内患者发生不良心血管事件 (Major adverse cardiovascular events，MACEs) 的概率仍较高。高敏肌钙蛋白（High-sensitivity cardiac troponin，hs-cTn）是心肌损伤的特异性标志物，已被指南推荐用作诊断急性心肌梗死的标准生物标志物 [5]。高敏肌钙蛋白不仅可以应用于急性心肌梗死的诊断，同样在危险分层、治疗决策和疗效评估等方面有着重要的地位。目前，关于高敏肌钙蛋白与急性心肌梗死患者不良预后的研究越来越丰富，因此本篇综述就高敏肌钙蛋白的临床意义，急性心肌梗死的概念、治疗以及不良预后的危险因素等方面进行阐述，为改善急性心肌梗死患者预后提供一定的参考依据。

.BCL10 通过调节炎症和细胞凋亡促进心肌缺血 / 再灌注损伤

杨智勇

中国医科大学附属盛京医院南湖院区

1. **目的：**探讨 BCL10 通过 NF-κB 信号通路调控细胞凋亡及炎症反应参与心肌缺血 / 再灌注损伤（MIRI）进展的分子机制

2. **方法：**

动物实验：8-10 周龄 C57BL/6 小鼠随机分为四组（sham 组、IR 组、IR+LV-shNC 组、IR+LV-shBCL10 组），尾静脉注射 BCL10 沉默慢病毒后建立 IR 模型，随后进行以下检测：①超声心动图检测小鼠心脏功能（LVESD、LVEDD、EF、FS）；② ELISA 检测血清中 CK-MB、cTnI、TNF-α、IL-1β、IL-6 水平；③ Western blot 检测心肌梗死半影区 BCL10、cleaved caspase-3、cleaved caspase-9、p-p65 NF-κB（Ser536）、核 p65 NF-κB 蛋白的表达；④ Real-time PCR 检测心肌梗死半影区 TNF-α、IL-1β、IL-6 mRNA 水平；⑤ TTC 染色检测心肌梗死面积；⑥ HE 染色检测心肌梗死半暗带区病理变化；⑦试剂盒检测心肌组织髓过氧化物酶（MPO）的活性、免疫组化检测 MPO 的表达；⑧ TUNEL 染色检测心肌梗死半影区细胞凋亡。

细胞实验：沉默 HL-1 细胞中 BCL10，随后建立 OGD/R 模型（Control 组、OGD/R 组、OGD/R+LV-shNC 组、OGD/R+LV-shBCL10 组），进行以下检测：① Western blot 检测细胞中 BCL10、cleaved caspase-3、cleaved caspase-9、p-p65 NF-κB（Ser536）、核 p65 NF-κB 蛋白表达；② ELISA 检测细胞培养上清中 TNF-α、IL-1β、IL-6 含量；③ Real-time PCR 检测细胞中 TNF-α、IL-1β、IL-6 mRNA 水平；④ TUNEL 染色检测细胞凋亡；⑤免疫荧光检测细胞中 p65 NF-κB 表达和分布。

3. **结果：**

动物实验：与 sham 组相比，IR 小鼠① LVESD 和 LVEDD 显著升高、EF 和 FS 显著降低；②小鼠血清中 CK-MB、cTnI、TNF-α、IL-1β、IL-6 水平显著升高；③心肌梗死半影区 BCL10、cleaved caspase-3、cleaved caspase-9、p-NF-κB（p65）（Ser536）、核 NF-κB（p65）、TNF-α、IL-1β、IL-6 的表达显著上调；④心肌梗死面积显著增多；⑤心肌梗死半暗带区出现明显损伤；⑥ MPO 活性及表达显著上调；⑦心肌梗死半影区细胞凋亡数量明显增加。在 IR 模型中沉默 BCL10 后，以上指标趋势均被逆转。

细胞实验：与对照组相比，OGD/R 细胞① BCL10、cleaved caspase-3、cleaved caspase-9、p-p65 NF-κB（Ser536）、核 p65 NF-κB、TNF-α、IL-1β、IL-6 的表达显著上调；②细胞培养上清中 TNF-α、IL-1β、IL-6 水平显著升高；③细胞凋亡数量明显增加；④ p65 NF-κB 的表达及入核均明显增加。在 OGD/R 模型中沉默 BCL10 后，以上指标趋势均被逆转。

4. **结论：**BCL10 通过促进心肌损伤、炎症、细胞凋亡和激活 NF-κB 信号通路参与 MIRI 发病。

敲低 SFPI1 通过调控 BCL10 转录减轻心肌缺血 / 再灌注损伤

杨智勇

中国医科大学附属盛京医院南湖院区

1. **目的：**探究 SFPI1 通过影响细胞凋亡、炎症反应、氧化应激参与 MIRI 进展的分子机制

2. **方法：**

动物实验：8-10 周龄 C57BL/6 小鼠随机分为四组（sham 组、IR 组、IR+LV-shNC 组、IR+LV-shSFPI1 组），尾静脉注射 SFPI1 沉默慢病毒后建立 IR 模型，随后进行以下检测：①超声心动图检测小鼠心脏功能（LVESD、LVEDD、EF、FS）；② Western blot 检测心肌梗死半影区 SFPI1、cleaved caspase-3、cleaved PARP 蛋白表达；③ Real-time PCR 检测心肌缺血半影区 IL-6、iNOS、BCL10 表达水平；④ TTC 染色检测心肌梗死面积；⑤ TUNEL 染色检测心肌缺血半影区细胞凋亡；⑥试剂盒检测血清中 MDA 含量和 SOD 活性、心肌缺血半影区的 ROS 含量。

细胞实验：沉默 HL-1 细胞中 SFPI1，随后建立 OGD/R 模型（Control 组、OGD/R 组、OGD/R+LV-shNC 组、OGD/R+LV-shSFPI1 组），进行以下检测：① Western blot 检测细胞中 SFPI1、cleaved caspase-3、cleaved PARP 蛋白表达；② CCK-8 检测细胞活性；③ TUNEL 检测细胞凋亡；④ Real-time PCR 检测细胞中 IL-6、iNOS、BCL10 表达水平；⑤试剂盒检测细胞中 MDA 含量、SOD 活性；⑥流式检测细胞中 ROS 含量。随后在 HL-1 细胞中过表达 SFPI1：① Western blot 验证细胞中 SFPI1 表达；② Real-time PCR 和 Western blot 检测细胞中 BCL10 表达；③双荧光素酶检测 SFPI1 与 BCL10 启动子序列的结合情况。

3. **结果：**

动物实验：与 sham 组相比，IR 小鼠① LVESD 和 LVEDD 显著升高、EF 和 FS 显著降低；②心肌梗死半影区 SFPI1、cleaved caspase-3、cleaved PARP、IL-6、iNOS、BCL10 表达显著上调；③心肌梗死面积明显增加；④细胞凋亡数量明显上调；⑤血清中 MDA 含量显著增加，SOD 活性显著下降，心肌缺血半影区 ROS 含量明显增加。在 IR 模型中沉默 SFPI1 后，以上指标趋势均被逆转。

细胞实验：与对照组相比，OGD/R 细胞① SFPI1、cleaved caspase-3、cleaved PARP、IL-6、iNOS、BCL10 表达显著上调；②细胞活性显著降低；③细胞凋亡数量明显增加；④细胞中 MDA 含量显著增加，SOD 活性显著下降，细胞中 ROS 含量显著增加。在 OGD/R 模型中沉默 SFPI1 后，以上指标趋势均被逆转。细胞中过表达 SFPI1 后，BCL10 表达水平显著增加；SFPI1 与 BCL10 启动子序列存在结合。

4. **结论：**SFPI1 促进 BCL10 表达，诱导心肌细胞凋亡、炎症反应和氧化应激，加速 MIRI 的疾病进展。

PTBP1 通过诱导炎症和细胞凋亡促进心肌缺血 / 再灌注损伤

杨智勇

中国医科大学附属盛京医院南湖院区

1. **目的：**探讨 PTBP1 参与 MIRI 进展的分子机制

2. **方法：**8-10 周龄 C57BL/6 小鼠随机分为四组（sham 组、IR 组、IR+LV-shNC 组、IR+LV-shPTBP1 组），尾静脉注射 PTBP1 沉默慢病毒后建立 IR 模型，随后进行以下检测：① Western blot 检测小鼠心肌组织中凋亡相关蛋白和 MAPK 通路相关蛋白（PTBP1、Bax、Bcl-2、Mcl-1、p-JNK、JNK、p-ERK、ERK、p-p38、p38）的表达；② Real-time PCR 检测小鼠心肌组织中 PTBP1、IL-6、IL-8、IL-1α、Mcl-1 mRNA 表达水平；③免疫荧光检测小鼠心肌组织中 PTBP1 和 Mcl-1 的蛋白表达；④ ELISA 检测小鼠血清中 cTnI、CK-MB、IL-8、IL-1α、IL-6、LDH 含量；⑤试剂盒检测小鼠心肌组织中 MPO 活性；⑥ TTC 染色检测小鼠心肌梗死面积；⑦ HE 染色检测小鼠心肌组织的病理变化；⑧ TUNEL 染色检测小鼠心肌细胞凋亡情况。

3. **结果：**与 Sham 组相比，I/R 组①小鼠心肌组织中 PTBP1、IL-6、IL-8、IL-1α、Bax、p-JNK、p-ERK、p-p38 表达水平明显上调，Bcl-2 和 Mcl-1 表达水平明显下调；②小鼠血清中 cTnI、CK-MB、LDH、IL-6、IL-8 和 IL-1α 水平显著增加；③小鼠心肌梗死面积显著增加；④小鼠心肌组织中可见心肌细胞核形态不规则，出现水肿和出血，炎性细胞浸润增多；⑤小鼠心肌组织中 MPO 活性显著增加；⑥小鼠心肌细胞凋亡数目显著增加。在 IR 模型中沉默 PTBP1 后，IR 引起的小鼠心肌组织细胞凋亡和炎症损伤得到明显改善。

4. **结论：**PTBP1 通过激活 MAPK 信号通路，诱导心肌细胞凋亡和炎症反应，加速 MIRI 进展。

Clinical Characteristics and Predictors of Acute Myocardial Infarction Complicating Out-of-Hospital Cardiac Arrest

Ya-Lin Zhu, Xiao-Jin Gao, Yue-Jin Yang

Fuwai Hospital, Chinese Academy of Medical Sciences and Peking Union Medical College, State Key Laboratory of Cardiovascular Disease, National Center for Cardiovascular Diseases

Background and objective: Out-of-hospital cardiac arrest (OHCA) is a severe complication of acute myocardial infarction (AMI). However, the characteristics of AMI patients complicated with OHCA have not been well studied. We aim to identify the characteristics at higher risk for OHCA.

Methods: This multicenter retrospective study analyzed data from 24,223 AMI patients enrolled in the CAMI (China Acute Myocardial Infarction) registry between January 2013 and September 2014. Multivariate logistic regression identified independent risk factors for OHCA. Subsequently, a matched sub-cohort (599 OHCA cases versus 2,995 controls; 1:5 ratio matched by age, sex, and ST-segment elevation status) was constructed to develop the Internal Environment Disorder (IED) score, designed to quantify the cumulative impact of metabolic derangements on OHCA risk. The IED score incorporated four admission metabolic parameters: hypokalemia (serum potassium

Results: Multivariate analysis confirmed that beyond well-established conventional risk factors (including male sex, absence of diabetes mellitus, short prehospital delay, STEMI presentation, and culprit lesion in the left main coronary artery), disturbances in the internal metabolic milieu demonstrated significant independent associations with OHCA risk. The newly developed IED score exhibited a remarkably strong and graded relationship with the likelihood of OHCA. Using the group with a 0-point IED score (no metabolic derangements) as the reference, the adjusted odds ratios (ORs) exhibited a strong graded relationship with OHCA:1-point score: OR 1.62 (95% CI 1.11-2.36); 2-point score: OR 3.02 (95% CI 2.10-4.34); 3-point score: OR 7.60 (95% CI 5.20-11.10); 4-point score: OR 9.57 (95% CI 5.55-16.48). Crucially, the time-sensitive analysis in IHCA patients reinforced this finding. Analysis of metabolic parameters measured prior to the arrest event in 883 IHCA patients revealed a virtually identical pattern: escalating IED scores were associated with progressively higher risk of IHCA, mirroring the relationship observed with OHCA. This temporal validation further supports the IED score's association with cardiac arrest risk independent of arrest-induced physiological changes. Regarding outcomes, experiencing OHCA was independently associated with a significantly increased risk of in-hospital mortality (adjusted Hazard Ratio [HR] 1.84, 95% CI 1.52-2.24). However, for patients who survived to discharge, a history of OHCA during the index AMI admission was not significantly associated with increased post-discharge mortality risk (adjusted HR 1.33, 95% CI 0.98-1.80).

Conclusion: The IED score assists in identifying AMI patients at high OHCA risk based on four modifiable metabolic parameters (hypokalemia, hyperglycemia, hyperleukocytosis, low eGFR). The IED score provides clinicians with a pragmatic tool to stratify OHCA risk during initial evaluation and prioritize timely correction of physiological homeostasis disturbances. Future prospective studies should validate the IED score's predictive performance and investigate whether targeted correction of these derangements based on the score translates into improved clinical outcomes, particularly a reduction in OHCA incidence.

血浆外泌体 miRNA 与 CKD 加速的动脉粥样硬化（AS）病程进展的关系及其早期预测价值

王建东 周娟

西安交通大学医学院第一附属医院

背景：

慢性肾脏病（Chronic Kidney Disease, CKD）作为全球公共卫生难题，其患病率较高，而心血管并发症是导致 CKD 患者死亡的首要原因，其中动脉粥样硬化（Atherosclerosis, AS）的发生率较普通人群明显增高。CKD 患者 AS 呈现进展迅速、病变弥漫的特点，传统危险因素（高血压、高血脂、糖尿病等）难以完全解释其病理机制，近年研究发现炎症反应、氧化应激、内皮功能障碍及代谢紊乱等非传统因素在 CKD 加速 AS 进程中起关键作用。外泌体作为细胞间通讯的重要介质，可通过传递蛋白质、mRNA 及微小 RNA（miRNA）调控靶细胞功能。已有研究证实，CKD 患者血浆外泌体中存在特异性 miRNA 表达谱改变，这些 miRNA 通过调控血管内皮细胞凋亡、平滑肌细胞表型转换及巨噬细胞极化等途径参与 AS 的发生发展。但目前关于 CKD 患者外泌体 miRNA 与 AS 病程进展的系统性研究仍较缺乏，特别是缺乏早期预测生物标志物的探索。本研究旨在系统解析 CKD 患者血浆外泌体 miRNA 的表达特征，揭示其与 AS 病理进程的关联，为开发基于外泌体 miRNA 的早期预测模型提供理论依据，同时为靶向血管微环境的新型治疗策略奠定基础。目的：探讨血浆外泌体 miRNA 与慢性肾脏病（Chronic Kidney Disease，CKD）加速的动脉粥样硬化（Atherosclerosis，AS）病程进展的关系及其早期预测价值。方法：

选取 2020 至 2021 年于西安交通大学第一附属医院住院治疗的 190 例冠状动脉粥样硬化性心脏病（Cornary artery disease，CAD）患者，其中合并 CKD 患者（CKD 组）90 例，未合并 CKD 患者（对照组）100 例，并采用 ROC 曲线分析 miR-148b-3p 对 CKD 和非 CKD 患者颈动脉粥样硬化的预测。结果：

1. CKD 组男性 66 例（73.33%），女性 24 例（26.67%）；年龄 71（60,78）岁；高血压 78 例（86.67%）、糖尿病 24 例（26.67%）、卒中 25 例（27.78%）、PCI 29 例（32.22%）、ARB 治疗 39 例（43.33%）、eGFR65.55（47.75,84.52）ml/min per1.73m2。以上资料与对照组患者对比差异有统计学意义（P < 0.05）。CKD 组患者颈动脉斑块 74 例（82.22%），斑块厚度 2.60（1.50,4.63）mm，均大于对照组（P < 0.05）。2. CKD 组患者血浆 miR-148b-3p 水平（9.63±1.45），高于对照组（P < 0.05）。Spearman 相关性分析显示，eGFR 与血浆 miR-148b-3p 水平呈负相关性（r=-0.310，P < 0.001）。且限制性立方样条曲线分析显示 eGFR 与血浆 miR-148b-3p 水平之间存在非线性关联。

3. miR-148b-3p 低、中、高表达组（此处内容省略）。

结论：1. 相较于非 CKD 患者，CKD 患者更易出现 AS，提示 CKD 与 AS 存在关联。2. 相较于非 CKD 患者，CKD 患者血浆 miR-148b-3p 水平明显升高，且 eGFR 与血浆 miR-148b-3p 水平呈负相关，说明随着血浆 miR-148b-3p 水平升高肾功能下降。3. 血浆 miR-148b-3p 水平与颈动脉粥样硬化斑块的危险因素、严重程度相关，表明其影响 AS 进程。4. 血浆 miR-148b-3p 水平对非 CKD 患者颈动脉粥样硬化的预测效能较低，但对 CKD 患者颈动脉粥样硬化的预测效能较高，其可作为潜在的生物标志物，为早期识别 CKD 患者发生 AS 的风险提供参考，有助于临床早期干预和病情监测。

Comparison of In-Hospital Net Clinical Outcomes of Ticagrelor and Clopidogrel in Acute Coronary Syndrome Patients Stratified by CRUSADE Score: Findings from the CCC-ACS Registry

Zuo-Yi Zhou[1], Hao-Tai Xie[1], Fang-Fang Fan[1], Fan Yang[1], Jie Jiang[1], Bo Zheng[1], Yan Zhang[1], Yong-Chen Hao[2], Jing Liu[2], Yan-Jun Gong[1], Dong Zhao[2], Sidney C. Smith[3], Yong Huo[1]

1. Peking University First Hospital

2. Beijing Anzhen Hospital

3. University of North Carolina, Chapel Hill

Objective: The selection of optimal P2Y12 inhibitors for acute coronary syndrome (ACS) patients remains a critical clinical decision, particularly in East Asian populations where the balance between ischemic protection and bleeding risk presents unique challenges. Current guidelines recommend potent P2Y12 inhibitors like ticagrelor, but the "East Asian Paradox" suggests these patients may experience disproportionate bleeding complications compared to Western populations. This study aimed to comprehensively compare the in-hospital outcomes between ticagrelor and clopidogrel in a large, real-world Chinese ACS population, while evaluating whether the CRUSADE bleeding risk score could serve as a practical tool to guide personalized antiplatelet therapy selection. By examining both efficacy and safety endpoints across different risk strata, we sought to provide evidence-based recommendations for optimizing treatment strategies in this specific patient population.

Methods: We conducted a nationwide cohort study using data from the CCC-ACS registry, which finally included 70,319 ACS patients treated with dual antiplatelet therapy (DAPT) within 24 hours of presentation between November 2014 and December 2019. We performed 1:1 propensity score matching to balance baseline characteristics between the ticagrelor and clopidogrel groups, resulting in 17,767 well-matched pairs. The primary endpoint was net adverse clinical events (NACE), defined as a composite of all-cause mortality, major ischemic events (including recurrent myocardial infarction, stent thrombosis, and ischemic stroke), and major bleeding (BARC types 3b, 3c, and 5). Secondary endpoints included individual components of the primary endpoint, major adverse cardiovascular events (MACE), and specific bleeding subtypes such as intracranial and gastrointestinal bleeding. We conducted detailed subgroup analyses stratified by CRUSADE score categories to evaluate treatment effect modification by bleeding risk.

Results: First, there was no significant difference in the primary endpoint of NACE between ticagrelor and clopidogrel (1.6% vs 1.6%, OR 0.97, 95% CI 0.82-1.16), nor in all-cause mortality (0.7% vs 0.7%, OR 0.92, 95% CI 0.71-1.20). However, ticagrelor demonstrated superior efficacy in preventing ischemic events, with a 20% reduction in MACE (1.0% vs 1.2%, OR 0.80, 95% CI 0.65-0.99) and a 30% reduction in major ischemic events (0.4% vs 0.5%, OR 0.70, 95% CI 0.51-0.96). This benefit was offset by significantly higher bleeding risks, including a 50% increase in major bleeding (1.6% vs 1.1%, OR 1.50, 95% CI 1.24-1.81), a 2.24-fold higher risk of intracranial hemorrhage (0.3% vs 0.1%), and a 74% increase in gastrointestinal bleeding (0.9% vs 0.5%, OR 1.74, 95% CI 1.33-2.28). The CRUSADE score effectively stratified treatment responses, with ticagrelor showing particular benefit in low-risk patients (CRUSADE <30) but increased harm in high-risk patients (CRUSADE >40), particularly for bleeding outcomes.

Conclusion: This large-scale, real-world study provides important insights into the risk-benefit balance of ticagrelor versus clopidogrel in Chinese ACS patients. While ticagrelor offers superior ischemic protection compared to clopidogrel, this comes at the cost of significantly increased bleeding risks, particularly intracranial hemorrhage. The CRUSADE score emerged as a valuable tool for personalizing treatment decisions, with low-risk patients deriving greater benefit from ticagrelor's anti-ischemic effects and high-risk patients potentially being better served by clopidogrel to avoid excessive bleeding complications. These findings support the incorporation of bleeding risk assessment into clinical decision-making for ACS management in East Asian populations and suggest that a one-size-fits-all approach to P2Y12 inhibitor selection may not be optimal. Future studies should prospectively validate this risk-score guided approach to further refine personalized antiplatelet therapy strategies.

Omentin-1 Mitigates Myocardial Ischemia-Reperfusion Injury by Regulating Fatty Acid β-Oxidation via the AMPK-PPARβδ-CPT1A Pathway

wei hao, Li Yin, Fang Liu

the 2nd Affiliated Hospital of Harbin Medical University

Omentin-1 Mitigates Myocardial Ischemia-Reperfusion Injury by Regulating Fatty Acid β-Oxidation via the AMPK-PPARβ/δ-CPT1A Pathway

Wei Hao, Li Yin ,Fang Liu, Department of Cardiology，the 2nd Affiliated Hospital of Harbin Medical University，Harbin 150001，China.

Objective:

Significant advances over recent decades have substantially reduced morbidity and mortality following ST-segment elevation myocardial infarction (STEMI). However, despite prompt revascularization—which ultimately limits infarct size—reperfusion itself activates injurious processes affecting both cardiomyocytes and the coronary microvasculature. Upon blood flow restoration, microvascular integrity becomes compromised, leading to edema, intramyocardial hemorrhage, and exacerbation of infarct size. Given the critical need to mitigate microvascular dysfunction, this study investigates the effect of Omentin-1 on coronary microvascular integrity during myocardial ischemia-reperfusion (I/R), elucidates its role and molecular mechanisms in reducing infarct size and improving cardiac function, and identifies novel therapeutic targets for alleviating I/R injury.

Methods:

Clinical Cohort: A total of 300 ST-segment elevation myocardial infarction (STEMI) patients undergoing emergency percutaneous coronary intervention (PCI) were enrolled. Serum Omentin-1 levels were measured preoperatively and at 6h, 24h, and 72h postoperatively. Myocardial reperfusion was assessed using cardiac magnetic resonance (CMR). Major adverse cardiovascular events (MACE) were recorded during a 2-year follow-up period, and the relationship between Omentin-1 levels and prognosis was analyzed.

Animal Experiments: Myocardial I/R models were established in male C57BL/6 mice. Mice were divided into four groups: sham-operated, Omentin-1-overexpressing sham, I/R, and Omentin-1-overexpressing I/R. Infarct size was measured using Evans Blue and triphenyltetrazolium chloride (TTC) staining; myocardial edema was assessed via Evans Blue leakage assay; immunofluorescence staining was used to detect endothelial junction proteins (e.g., VE-cadherin, ZO-1) and pericytes (NG2); cardiac function was evaluated by echocardiography at 1 day and 4 weeks. A transgenic mouse model with cardiac endothelial-specific CPT1A knockout was generated to validate the central role of CPT1A. The therapeutic potential of recombinant human Omentin-1 was evaluated by in vivo administration.

In Vitro Experiments: Human coronary microvascular endothelial cells (CMECs) and cardiomyocytes (CMs) were subjected to oxygen-glucose deprivation/reoxygenation (OGD/R). Cell viability was assessed by MTT

assay; reactive oxygen species (ROS) production was measured using a fluorescent probe; endothelial barrier function was evaluated by FITC-dextran permeability assay. The interaction between CMECs and CMs was explored using a co-culture system. Furthermore, the effects of AMPK, PPARβ/δ, and CPT1A inhibitors on cell junction integrity, fatty acid β-oxidation rate, and related signaling molecule expression were examined.

Results:

In the clinical cohort, serum Omentin-1 levels in STEMI patients showed a compensatory increase within 72 hours post-PCI. Higher Omentin-1 levels were negatively correlated with the severity of microcirculatory injury and associated with a lower incidence of MACE over 2 years.

Animal experiments demonstrated that Omentin-1 overexpression enhanced microvascular barrier function, reduced myocardial edema and infarct size, and improved cardiac function. This protective effect was significantly attenuated following endothelial-specific CPT1A knockout.

In vitro experiments confirmed that Omentin-1 alleviated CMEC injury, reduced ROS generation and vascular permeability, and improved cell survival in the CMEC-CM co-culture system. It also decreased levels of inflammatory factors (TNF-α) and injury markers. Mechanistically, Omentin-1 activated the AMPK-PPARβ/δ pathway, promoting CPT1A-mediated fatty acid β-oxidation. These effects were reversed by specific inhibitors.

Conclusion: Omentin-1 enhances microvascular barrier function and reduces myocardial I/R injury by activating the AMPK-PPARβ/δ-CPT1A signaling pathway. It holds promise as both a biomarker for STEMI diagnosis and prognosis evaluation and a potential therapeutic target.

肥大细胞 MRGPRX2 受体介导神经免疫互作诱发急性心肌梗死后室性心律失常

王长毅 [1,2,3,4,5,6] 周晓亚 [1,2,3,4,5,6] 余锂镭 [1,2,3,4,5,6] 江洪 [1,2,3,4,5,6]

1. 武汉大学人民医院心血管医院

2. 武汉大学复杂生命体代谢与调控全国重点实验室

3. 自主神经调控湖北省重点实验室

4. 武汉大学心脏自主神经研究中心

5. 武汉大学泰康生命医学中心

6. 武汉大学人民医院分子医学研究院

目的：急性心肌梗死（AMI）后室性心律失常（VAs）是心源性猝死的主要原因，我们前期研究表明肥大细胞（MCs）与心脏交感神经–星状神经节（LSG）的交互在其中发挥重要作用。然而，发挥关键作用的 MCs 受体仍然未知。

方法：建立大动物心肌梗死模型，收集心脏交感神经节组织（LSG、4 个心脏神经节丛，GPs）和外周血以初步检测多个 MCs 受体的表达。同时纳入于我院行急诊 PCI 术的 AMI 患者，以冠脉造影阴性患者为对照组，收集血清样本进一步验证指标变化。敲低 LSG 中 MRGPRX2 受体表达，探索其对 LSG 的影响及在 AMI 后 VAs 的作用；取 LSG 组织进行 RNA 测序，揭示下游的关键因子及潜在机制并进一步体内验证。

结果：AMI 模型 LSG 中 MRGPRX2 表达显著升高，而其他 2 个 MCs 受体（FcεRI 和 NK1R）无差异，同时伴随交感神经共递质 NPY 表达增加，免疫荧光共定位提示 NPY 与 MRGPRX2 结合；临床数据进一步证实，AMI 组血清 MRGPRX2 和 NPY 水平高于对照组，且两者水平呈正相关。敲低 LSG 中 MRGPRX2 可抑制 AMI 后 LSG 功能、活性和全身交感神经活性，改善心室电生理稳定性，表现为 ERP 和 APD90 延长、室颤阈值升高等，减少 AMI 后 VAs 发生率；此外，LSG 交感神经重构减轻，NPY 释放减少。RNA 测序提示 IL18 及其上下游因子显著改变；体外细胞培养提示 NPY 可通过 MRGPRX2 激活 MCs 释放 IL18，免疫荧光显示 LSG 中 IL18、IL18R1 与交感神经标记物 TH 共定位。最后，局部调控 LSG 中 IL18 表达，证实 IL18 通过 NFKB 相关信号通路激活交感神经元，促进 AMI 后 VAs，而 IL18 天然抑制剂可逆转这一效应。临床数据提示，AMI 患者血清 IL18 水平显著升高，高 IL18 水平与高敏 C 反应蛋白、心肌损伤标志物、左室射血分数相关。

结论：肥大细胞 MRGPRX2 受体是介导 LSG 中神经免疫紊乱的关键“放大器”，通过 NPY/MRGPRX2/IL18 轴促进 AMI 后交感神经过度激活诱发 VAs。靶向干预 MRGPRX2 或 IL18 可显著降低 VAs 风险，为 AMI 后 VAs 的临床防治提供了新的干预策略。

冠状动脉内自体骨髓细胞移植治疗急性心肌梗死的长期临床研究

史张伟 张富龙 于进

中国人民解放军空军军医大学第一附属医院（西京医院）心血管内科

目的：通过长达 20 年的长期临床研究，深入探究骨髓单核细胞（BMC）移植治疗对急性 ST 段抬高型心肌梗死患者（STEMI）左心室功能及生活质量的长期影响。方法：纳入既往在空军军医大学第一附属医院心血管内科就诊的 86 例急性 ST 段抬高型心肌梗死（STEMI）患者，开展骨髓单核细胞移植试验。在这项试验中，86 名成功接受了经皮冠状动脉介入治疗（PCI）的 STEMI 患者被随机分组，其中 41 例接受冠状动脉内注射骨髓单核细胞（BMC）治疗，而另外 45 例则接受生理盐水作为对照组。本次研究对此 86 例患者进行长达 20 年的临床随访，主要终点是生存分析、左心室射血分数（LVEF）、生存质量评分。次要终点是术后再次血运重建率、术后心律失常发生率、术后心衰发生率、术后肿瘤发生率。结果：本研究发现，在骨髓单核细胞移植治疗急性 ST 段抬高型心肌梗死患者的二十年研究中，两组生存分析结果显示无统计学差异（P > 0.05），但左室射血分数显著改善（49.5% ± 5.1% vs 44.5 ± 4.0%，P < 0.01），并且可以显著改善患者生存质量（0.62 ± 0.1 vs 0.52 ± 0.1，P < 0.01），两组间术后再次血运重建率、心律失常发生率、术后心力衰竭发生率、肿瘤发生率无统计学差异（P > 0.05）。结论：本研究深入探索了冠状动脉内自体骨髓单核细胞移植在急性 ST 段抬高型心肌梗死治疗中的长期效果。研究结果表明，这种治疗方法不仅能够持续改善患者的心功能，表现为左室射血分数的显著提高和心脏功能的优化，还能够显著提升患者的生存质量。此外，经过长期观察和研究，我们确认这种治疗方法是安全可行的，没有增加不良事件的发生率或降低患者的生存率。

急性心肌梗死血清中神经调节蛋白 4 的水平变化及临床意义

李颜超 候静波

哈尔滨医科大学附属第二医院

目的：神经调节蛋白 4（Nrg4）是一种新型脂肪因子，在能量及糖脂代谢中起重要作用，且与代谢综合征的指标呈负相关。然而，目前尚无急性心肌梗死（AMI）患者血清 Nrg4 的水平变化及意义研究，本研究旨通过探讨 AMI 患者血清 Nrg4 水平变化，分析其与 AMI 相关性，旨在为临床诊治 AMI 提供依据。

方法：选取 2024 年 9 月至 2025 年 5 月于我院心内科住院的急性 ST 段抬高型心肌梗死（STEMI）患者 106 例，稳定性冠心病（CHD）患者 104 例，平均年龄（62.49±11.45），记录受试者一般资料，测定 hs-CRP、NT-proBNP、CK-MB 及 cTnI 等急性指标，测定肝肾功能、血脂等相关生化代谢指标，利用心脏超声测定患者心功能，记录冠脉造影结果，采用酶联免疫吸附法检测患者入院即刻血清循环 Nrg4 水平。

结 果：在住院人群中，STEMI 患者即刻血清 Nrg4 水平升高 34.72[24.72，34.68]，高于 CHD 患者 23.92[16.58，27.06](p < 0.0001)。进一步校正性别、年龄、血压、BMI、吸烟史、饮酒史、糖尿病病程、血糖后，STEMI 患者血清 Nrg4 水平仍升高。皮尔逊相关分析表明，调整 BMI 后，Nrg4 水平与左室射血分数，左室缩短率呈负相关，与 NT-proBNP、cTnI、CRP 呈正相关（p < 0.05）。造影结果显示，Nrg4 的水平与多支血管病变呈负相关。多元线性回归分析表明，收缩压和 Nrg4 在内的几种变异是 cTnI 升高的独立危险因素（p < 0.01）。

结论：STEMI 患者入院即刻血清 Nrg4 水平升高，提示血清 Nrg4 水平作为应激因子，可能影响 AMI 的发生发展。

基于四道防线对冠心病家族史患者经皮冠状动脉介入（PCI）治疗后再发心梗的预防策略研究

董甜甜

首都医科大学附属北京友谊医院

目的 通过对有冠心病家族史经皮冠状动脉介入（PCI）治疗后患者实施健康宣教，问卷调查，电话回访等方式守护心梗的四道防线，降低了患者再发心梗。方法 选择 2022 年 1 月至 2024 年 11 月于我院住院的有冠心病家族史经皮冠状动脉介入（PCI）治疗后患者 107 例，按方便采样法分为观察组和对照组，观察组每组 53 人，对照组每组 54 人，对照组采用常规护理措施。观察组在此基础上应用健康宣教，守护第一道防线：管好 6 匹马：健康宣教、坚持运动、控制体重、远离烟酒、不要熬夜、好的心态。第二道防线：驾好 3 辆车：即高血压、糖尿病、高脂血症。第三道防线：正规控制斑块，遵医嘱定时服药。第四道防线：学会识别心梗在敲门：心绞痛是心梗最后一道防线，若出现心前区疼痛、胸痛、肩膀痛、牙痛等，及时就诊。应用问卷调查，每个月通过发布问卷调查填写 BMI 指数，血脂指数，每周运动情况，健康饮食情况，戒烟戒酒情况，每日睡眠情况。应用电话回访指导监督患者守护心梗四道防线完成情况。对比两组患者满意度、EORTC 生命质量测定量表、生活质量、心血管不良事件发生率，再发心梗发生率。结果 观察组应用健康宣教，问卷调查，电话回访等方式守护心梗的四道防线，出院后患者满意度、EORTC 生命质量测定量表、生活质量、心血管不良事件发生率，再发心梗发生率均高于对照组提高（P < 0.05），统计学有意义。结论 四道防线对冠心病家族史经皮冠状动脉介入（PCI）治疗后降低了患者再发心梗，能有效增加患者满意度、自我价值实践，生活质量提高、能有效的提高护患关系和护理质量。

Omentin-1 通过 AMPK-PPARβδ-CPT1A 通路调控脂肪酸 β 氧化改善心脏缺血再灌注损伤

郝伟 尹力 刘芳

哈尔滨医科大学附属第二医院

Omentin-1 通过 AMPK-PPARβ/δ-CPT1A 通路调控脂肪酸 β 氧化改善心脏缺血再灌注损伤

郝伟，尹力，刘芳，哈尔滨医科大学附属第二医院，心内科

目的:

缺血再灌注 (I/R) 损伤通过氧化应激加速心肌细胞 (CMs) 死亡，从而恶化心功能，这严重限制了 STEMI 患者冠状动脉血运重建后的临床获益。在本研究中，我们探讨了 Omentin-1 对心脏缺血再灌注中冠状动脉微血管完整性的影响，探讨其在减少心肌梗死面积、改善心功能中的作用及分子机制，为减轻心肌梗死后缺血再灌注损伤提供新治疗靶点和策略。

方法：

(1) 临床队列：纳入 300 例接受急诊 PCI 的 STEMI 患者，检测术前及术后 6h、24h、72h 外周血 Omentin-1 水平，结合心脏磁共振评估心肌再灌注，随访 2 年记录主要不良心血管事件，分析其与预后的关系。

(2) 动物实验：采用 C57BL/6 雄性小鼠构建心肌缺血再灌注模型，分为假手术组、过表达 Omentin-1 假手术组、缺血再灌注组、过表达 Omentin-1 缺血再灌注组。通过 Evansblue 与 TTC 染色测梗死面积，Evansblue 渗漏实验评估心脏水肿，免疫荧光染色检测内皮连接蛋白（VE-cad、ZO-1 等）及周细胞（NG2），超声心动图检测评估心脏功能（1 天和 4 周）。构建心脏内皮特异性敲除 CPT1A 转基因小鼠模型，验证 CPT1A 的核心作用；在体回输重组人 Omentin-1 评估其对心肌梗死的挽救能力。

(3) 体外实验：采用缺氧复氧（OGD）模型处理人冠状动脉微血管内皮细胞（CMECs）和心肌细胞（CMs），通过 MTT 法检测细胞存活率，ROS 荧光探针检测活性氧生成，FITC- 葡聚糖通透性实验评估血管内皮屏障功能；通过 CMECs 与 CMs 共培养体系，探究两者间的相互作用。进一步给予 AMPK 抑制剂、PPARβ/δ 抑制剂及 CPT1A 抑制剂处理，检测细胞连接功能变化、脂肪酸 β 氧化速率及相关信号分子的表达水平。

结果：

(1) 临床队列中，STEMI 患者血清 Omentin-1 在 72h 内代偿性升高，水平与微循环损伤程度呈负相关，高水平者 2 年不良事件发生率更低。

(2) 动物实验显示，Omentin-1 过表达可增强微血管屏障功能，减少水肿和梗死面积，改善心功能；内皮特异性敲除 CPT1A 后，其保护作用显著削弱。

(3) 体外实验证实，Omentin-1 减轻 CMECs 损伤，减少 ROS 生成及血管通透性，通过 CMECs 与心肌细胞相互作用提高细胞存活，降低炎症因子（TNF-α）及损伤标志物。机制上，其通过激活 AMPK-PPARβ/δ 通路促进 CPT1A 介导的脂肪酸 β 氧化，抑制剂可逆转该效应。

结论：

Omentin-1 通过激活 AMPK-PPARβ/δ-CPT1A 通路增强微血管屏障功能，减少心肌损伤，有望成为 STEMI 诊断、预后评估的生物标志物及治疗靶点。

基于 SOP 模型理论的急性心肌梗死患者早期心理康复干预研究

朱明辉

首都医科大学附属北京友谊医院

目的：探讨刺激 - 组织 - 处理（Stimulus-Organism-Process, SOP）模型理论在急性心肌梗死（AMI）患者早期心理康复中的应用价值。方法：选取 2022 年 1 月至 2023 年 12 月收治的 120 例 AMI 患者，采用分层随机法分为对照组与干预组各 60 例。对照组实施常规护理，干预组基于 SOP 模型理论开展早期心理康复干预，通过刺激评估、个性化干预策略制定以及效果追踪，引导患者调整心态，干预周期为 4 周。比较两组干预前后心理状态（HADS 评分）、疾病认知水平（AMI 知识问卷）及康复依从性（Morisky 量表）。结果：干预后，干预组焦虑评分、抑郁评分显著低于对照组（P<0.05）；疾病认知优良率、康复依从性均优于对照组（P<0.05）。结论：SOP 模型理论指导下的早期心理康复干预，能够显著改善患者的心理状态，增强患者对康复知识的认知，提升康复依从性，对促进患者的身心康复具有积极的临床意义，建议在临床实践中建立“医院 - 社区 - 家庭”三级联动机制，将 SOP 模型纳入 AMI 标准化治疗路径，为患者提供全周期、立体化的心理支持。未来研究可进一步探索该模型与心脏康复运动方案的整合效果，以及在老年、糖尿病合并 AMI 等特殊人群中的适用性。

改良应激性高血糖比值是急性心肌梗死患者不良预后的独立危险因素

张浥[1] 端家豪[1] 黄帆[1] 黄凯[1] 王茹婷[1] 刘伟[1] 杨晓宇[1] 朱滨[2] 杨春[3] 杨玲[1]

1. 苏州大学附属第三医院心血管内科

2. 苏州大学附属第三医院重症医学科

3. 南京医科大学第一附属医院麻醉与围术期医学科

目的：探讨改良应激性高血糖比值（mSHR）对急性心肌梗死（AMI）患者不良预后的预测价值及其临床意义。

方法：本研究为多中心观察性研究。将美国重症监护医学信息数据库 -IV 中符合纳入标准的 AMI 患者作为发现队列，将苏州大学附属第三医院心血管内科冠心病监护病房收治的符合纳入标准的 AMI 患者作为验证队列，提取临床资料并进行回顾性和前瞻性分析。mSHR 计算公式：mSHR= 入监护病房 24 h 最高血糖（mmol/L）/［1.59× 糖化血红蛋白（HbA1c）（%）-2.59］。主要结局为住院期间发生的早期心血管并发症（ECC），定义为心血管死亡、心脏骤停复苏、危及生命的缓慢性或快速性心律失常、机械并发症、急性心力衰竭、心原性休克或左心室血栓形成的复合结局。次要结局为第 6、12 个月随访时的全因死亡。采用 Logistic 回归、受试者工作特征曲线（ROC）、机器学习、修正 Poisson 回归、敏感性分析、亚组分析及逆概率处理加权法（IPTW）评估及验证 mSHR 与不良预后的关系。

结果：发现队列共纳入 1349 例患者，其中 322 例（23.9%）发生 ECC。多因素 Logistic 回归分析显示，mSHR 与 ECC 的发生独立相关（校正后 OR=1.164，95% CI 1.124~1.206，P<0.001）。ROC 分析显示，mSHR 曲线下面积为 0.714（95% CI 0.680~0.748），高于其他糖代谢相关参数，包括应激性高血糖比值、入监护病房随机血糖及 HbA1c，差异具有统计学意义（P 均 <0.001），mSHR 最佳截断值为 1.216。机器学习分析确定 mSHR 为识别 ECC 最重要的特征。验证队列共纳入 303 例患者，根据 mSHR 三分位数分为 3 组（T1 组为 mSHR ≤ 0.984，共 101 例；T2 组为 0.984<mSHR ≤ 1.202，共 101 例；T3 组为 mSHR>1.202，共 101 例）。修正 Poisson 回归分析显示，T3 组 ECC 发生风险显著高于 T2 组（校正后 RR=2.271，95% CI 1.307~3.946，P=0.004）。敏感性分析显示，合并 T1 组和 T2 组后，T3 组仍具有更高的 ECC 发生风险（校正后 RR=2.337，95% CI 1.479~3.693，P<0.001）。亚组分析显示，mSHR>1.202 对 ECC 发生的影响在各亚组间一致（交互作用 P 均 >0.05）。IPTW 分析后，修正 Poisson 回归结果较前相仿。发现队列共 1307 例患者参与出院后随访，多因素 Cox 回归分析显示，mSHR ≥ 1.216 是第 6 个月（校正后 HR=2.198，95% CI 1.101~4.386，P=0.025）及第 12 个月（校正后 HR=1.819，95% CI 1.029~3.215，P=0.039）全因死亡的独立危险因素。

结论：mSHR 对 AMI 患者 ECC 及短期全因死亡具有较好的预测价值，可作为 AMI 风险分层工具，或为临床决策提供指导。

冠脉内低温联合 KATP 通道开放剂干预对 STEMI 患者 PPCI 术后慢血流 / 无复流及心功能的影响

汪永生

合肥市第一人民医院

目的 观察冠脉内低温联合 ATP 敏感性钾离子 (K_{ATP}) 通道开放剂对急性 ST 段抬高型心肌梗死（STEMI）患者行直接经皮冠状动脉介入（PPCI）慢血流 / 无复流及心功能的影响。

方法 连续入组 2021 年 06 月到 2023 年 6 月在合肥市第一人民医院行 PPCI 术的 STEMI 患者 130 例，通过随机数字表平均分为干预组和对照组。两组均接受常规 PPCI 术，干预组术中通过抽吸导管向梗死相关动脉灌注 K_{ATP} 通道开放剂（0.06mg/kg）后行冠脉内低温处理，术后 24h 持续静脉应用尼可地尔（2mg/h），对照组仅行冠脉内低温处理。比较两组入门至导丝通过的时间、慢血流 / 无复流、电除颤 / 电复律、心肌损伤标志物和心功能指标，观察术后 1 年不良心血管事件发生情况。

结果 干预组中 PPCI 术后慢血流 / 无复流的发生率低于对照组，差异有统计学意义（P<0.05），联合干预提高了术后心电图 ST 段回落 >70% 的比率、减少室性期前收缩的数量和降低术后心肌损伤标志物的水平，差异有统计学意义（P<0.05）。术后 3 个月干预组中左室射血分数高于对照组，差异有统计学意义（P<0.05），术后 1 年随访显示不良心血管事件发生率在两组间无统计学差异（P>0.05）。

结论 STEMI 患者 PPCI 术中冠脉内低温联合应用 K_{ATP} 通道开放剂可减少慢血流 / 无复流发生，改善冠脉微循环障碍、ST 段回落和左室射血分数，有助于左心功能的恢复。

青年英语演讲交流

Stress Hyperglycemia Ratio Index Predicts All-Cause Mortality in Aortic Diseases: A Retrospective Analysis of the MIMIC-IV Database

wang wangfengxia[1,2], Yi-Tong Ma[1]

1. The First Affiliated Hospital of Xinjiang Medical University

2. People's Hospital of Xinjiang Uygur Autonomous Region

Background

Stress hyperglycemia, a transient elevation in blood glucose levels during severe stress states such as trauma or infection, is underpinned by neuroendocrine dysregulation and activation of inflammatory responses. The Stress Hyperglycemia Ratio Index (SRHI), a composite metric for quantifying the severity of stress hyperglycemia, has been consistently linked to poor outcomes in conditions like sepsis and acute coronary syndrome. However, its association with all-cause mortality in aortic diseases—including aortic dissection and aortic aneurysm—remains undefined. Aortic diseases are characterized by acute onset and high mortality, making early and precise prognostic assessment critical for clinical decision-making. Leveraging the large-scale publicly available MIMIC-IV database, this study aims to fill this research gap and provide novel biomarkers for identifying high-risk patients.

Methods

This retrospective cohort study screened 3,145 patients with aortic diseases from the MIMIC-IV database (encompassing over 700,000 hospitalized patients). Data collection included demographic characteristics (age, sex), comorbidities (hypertension, diabetes), laboratory parameters (blood glucose, creatinine, inflammatory markers), and clinical outcomes (all-cause mortality). SRHI was calculated as: (maximum blood glucose / baseline blood glucose) × 100, where baseline glucose was defined as the average level in the 3 months prior to admission or the first emergency department measurement.

Patients were stratified into three groups based on SRHI levels: low SRHI (<120), medium SRHI (120–150), and high SRHI (>150). Baseline characteristics were compared across groups using chi-squared tests and analysis of variance. The independent association between SRHI and all-cause mortality was evaluated via Cox proportional hazards modeling, with adjustment for confounders including age, sex, comorbidities, and Acute Physiology and Chronic Health Evaluation II (APACHE II) score. Survival analysis was performed using Kaplan-Meier methods, with intergroup comparisons via log-rank tests.

Results

In the study cohort, patients in the high SRHI group had a mean age of 68.2±9.5 years, significantly higher than the low SRHI group (59.8±8.3 years). The prevalence of diabetes was 42% in the high SRHI group, surpassing that in the medium (28%) and low (19%) SRHI groups. The median APACHE II score of 22 in the high SRHI group indicated more critical illness. Multivariate Cox regression analysis revealed that after adjusting for all confounders, each standard deviation increase in SRHI was associated with a 39% higher risk of all-cause mortality (HR=1.39, 95% CI: 1.11–2.23, P<0.001). Kaplan-Meier survival curves showed a 1-year survival rate of 58.7% in the high SRHI group, significantly lower than the medium (72.4%) and low (81.5%) SRHI groups (Log-rank P<0.001). Subgroup analysis highlighted a stronger association in patients with diabetes (HR=1.62, 95% CI: 1.23–2.14).

Conclusion

This study, based on large-scale real-world data, is the first to confirm that SRHI is an independent risk factor for all-cause mortality in aortic diseases. The underlying mechanisms may involve interactions between excessive inflammatory responses, endothelial dysfunction, and glycemic derangements during stress. Clinically, monitoring SRHI can aid in identifying high-risk patients with poor prognoses, particularly those with diabetes, who require intensified glycemic control and multi-organ protection. Future research may explore optimal SRHI thresholds for personalized therapy or combine SRHI with other biomarkers (e.g., D-dimer, NT-proBNP) to develop more precise prognostic models. This finding offers a new perspective on risk stratification for aortic diseases, with significant clinical translation potential.

Epidemiology of ischemic heart disease in Chinese population from 1990 to 2023: Findings from the Global Burden of Disease Study 2023

Zheng Long

Xuanwu Hospital Capital Medical University

Abstract

Objective: Against the backdrop of rapid socioeconomic transformation and evolving cardiovascular risk profiles in China, this study aims to comprehensively characterize the burden of ischemic heart disease and quantify its temporal dynamics from 1990 to 2023 using a multi-dimensional framework. By integrating six key epidemiological metrics—mortality, prevalence, incidence, disability-adjusted life years, years lived with disability, and years of life lost—the analysis seeks to: 1) dissect age- and sex-specific disparities in disease manifestation and progression; 2) evaluate trends in age-standardized rates to isolate population-level changes independent of demographic shifts, such as aging and urbanization; and 3) identify critical periods of burden escalation across the lifespan. This granular assessment of temporal and subgroup variations aims to inform evidence-based policy formulation and resource allocation for IHD prevention and control, particularly amid China's ongoing transition toward an aging society with rising non-communicable disease burdens.

Methods: Using data from the Global Burden of Disease 2023 (GBD 2023) study, we analysed six key indicators: the mortality, prevalence, incidence, disability-adjusted life years, years lived with disability, and years of life lost. Age-standardized rates were analysed using the global age structure as a reference. Joinpoint regression was used to assess the annual percentage change and average annual percentage change.

Results: In 2023, 66,695,396 prevalent cases, with 1,906,927 incidence cases and 1,982,120 deaths due to ischemic heart disease, were reported from China. The number crude rates of the mortality, prevalence, incidence, disability-adjusted life years, years lived with disability, and years of life lost significantly increased in 2023 compared with 1990. The age-standardized rates per 100,000 were 3019.97 for prevalence (+6.83% from 1990), 89.53 for incidence (-3.15%), 92.67 for mortality (-21.29%), 1688.14 for disability-adjusted life years (-35.19%), 126.44 for years lived with disability (+8.91 %), and 1561.70 for years of life lost (-38.76%). The burden of ischemic heart disease was higher in males than in females during 1990-2023. With age increasing, the rate of mortality, prevalence, incidence, disability-adjusted life years, years lived with disability, and years of life lost all rose. In 2023, lead exposure (34.47%), particulate matter pollution (30.35%), smoking (24.00%), high sodium diet (14.26%), and low whole grain diet (11.20%) were the leading risk factors contributing to disability-adjusted life years.

Conclusion: From 1990 to 2023, China experienced a substantial increase in the absolute burden of IHD, reflected by rising counts of prevalent cases, incident cases, and deaths. While age-standardized mortality, incidence, disability-adjusted life years, and years of life lost demonstrated significant declines, indicating potential improvements in risk factor management and clinical care, the simultaneous rise in absolute disease burden and age-standardized prevalence/years lived with disability highlights the growing impact of population aging and secular trends in risk factors. The persistent male-female disparity and age-dependent escalation in all burden indicators underscore the need for gender-tailored prevention strategies and enhanced healthcare services for aging populations. These findings emphasize the continuing public health imperative to address ischemic heart disease through integrated approaches targeting primary prevention, early intervention, and systemic improvements in cardiovascular care, particularly amid demographic transitions and evolving lifestyle risks.

Keywords: ischemic heart disease, burden of disease, trend

Dynamic Cardiac Toxicity Monitoring Based on Time Threshold and Chemotherapy Stratification in Hematologic Malignancies

Ming-Xuan Zhang

Sir Run Run Shaw Hospital, Zhejiang University College of Medicine

Background

Early warning of cardiac dysfunction related to cancer therapy urgently requires quantification of time effects and regimen specificity. This study enrolled 43 patients with hematologic malignancies (lymphoma 58.1%, myeloma 27.9%, leukemia 14.0%) receiving chemotherapy. It systematically analyzed the evolution patterns of subclinical cardiac dysfunction.

Methods

A pre-post treatment paired design was employed. Comprehensive cardiac monitoring utilized advanced echocardiographic techniques, with core parameters including: Global Longitudinal Strain (GLS), a highly sensitive marker of left ventricular systolic function; right ventricular free wall strain; left atrial reservoir strain; conventional left ventricular ejection fraction (EF); the diastolic function parameter average E/E' (ratio of early mitral inflow velocity to mitral annular early diastolic velocity); and the novel myocardial work index, which incorporates afterload. Statistical analyses utilized the Wilcoxon paired test to assess changes in cardiac function (effect size Cliff's delta) and Spearman correlation to examine time interval effects. Subgroup analyses were performed based on diagnostic groups. All p-values underwent Holm-Bonferroni multiple correction.

Results

The overall cohort analysis revealed significant subclinical cardiac injury despite stable conventional measures. Absolute GLS worsened signifi-

cantly (median decrease: 0.5%, p=0.028, δ = -0.32), indicating impaired left ventricular systolic function. Right ventricular strain also deteriorated substantially (median decrease: 1.3%, p=0.009, δ = -0.38). Concurrently, a significant compensatory enhancement in left atrial reservoir strain was observed (median increase: 0.7%, p=0.038, δ = +0.29), suggesting an adaptive mechanism. Crucially, neither EF nor average E/E' showed significant changes, underscoring the limitations of relying solely on these traditional parameters for early detection.

Time effect analysis identified critical temporal patterns. Patients with intervals exceeding 2 months between treatment cycles exhibited a markedly higher GLS worsening rate (73.7%) compared to those with intervals ≤ 2 months (41.7%). This translated to a 2.92-fold increased risk of GLS deterioration (Odds Ratio [OR] = 3.92, 95% Confidence Interval [CI]: 1.24-12.41). Furthermore, a linear relationship was established: each additional month of cumulative treatment duration accelerated GLS worsening by an average of 0.16% (ρ = -0.41, p=0.003). Right ventricular damage also progressed significantly with longer treatment time (ρ = -0.44, p=0.001).

Diagnostic subgroup analysis revealed disease-specific compensatory responses:

Lymphoma: Had the highest incidence of GLS worsening (68.0%) but effectively maintained stable EF through compensatory mechanisms.

Myeloma: Uniquely activated significant compensatory enhancement in left atrial strain (p=0.019), potentially mitigating ventricular dysfunction.

Leukemia: Exhibited a significant decline in myocardial work efficiency (p=0.047), indicating reduced cardiac performance per unit of energy expended.

Conclusion

This study identified establishes **2 months as a critical time threshold** for the development of subclinical cardiac injury during chemotherapy. GLS and right ventricular strain are most significant in monitoring changes in cardiac function in chemotherapy patients, while left atrial strain often shows compensatory increase. Lymphoma patients require prioritized tracking of GLS changes, while myeloma patients warrant focused assessment of left atrial compensatory mechanisms

Clinical Significance

This study discovered the linear pattern of 0.16% GLS worsening per additional month of treatment, and reveals the protective mechanism of left atrial compensation in myeloma. The revelation of a **protective left atrial compensatory mechanism specifically in myeloma patients** offers new insights into differential cardiac adaptation. These findings drive the precision revolution in cardiac function monitoring strategies during cancer therapy. Implementing these insights can fundamentally alter the paradigm from reactive heart failure management to proactive prevention.

Human-Machine Collaborative Enhancement in Perioperative Care for Atrial Fibrillation Catheter Ablation: Optimization and Application of Key Nursing Technologies

zhipeng bao

the first affiliated hospital with Nanjing medical university

[background]

Atrial fibrillation (AF) is a common supraventricular arrhythmia linked to stroke, heart failure, and high morbidity and mortality. China bears the highest AF burden globally, with over 20 million cases and rising incidence. Catheter ablation is the first-line therapy, yet systematic, standardized perioperative rehabilitation remains insufficient. Traditional care models are constrained by time, geography, limited workforce, and lack of personalized, data-driven approaches. These gaps hinder patient recovery and long-term disease management. Therefore, there is a pressing need to develop innovative, technology-enabled care pathways that enhance outcomes, support continuous follow-up, and reduce healthcare resource consumption and economic burden.

[Objective]

This interdisciplinary research project focuses on optimizing perioperative care for patients undergoing catheter ablation for atrial fibrillation (AF) by integrating human-machine collaborative technologies. The overarching goal is to enhance the precision, efficiency, patient-centeredness, and cost-effectiveness of clinical care through the innovative application of generative artificial intelligence (AI), brain-computer interface (BCI) systems, Internet of Things (IoT), and big data analytics. The project aims to bridge the gap between advanced technological capabilities and real-world clinical needs, creating a new paradigm of intelligent, personalized, and proactive perioperative nursing care in cardiovascular interventions.

[Methods]

The project implemented five key technological and methodological innovations:

Generative AI tools were developed and deployed to assist with preoperative patient triage, screening, and education. AI-powered conversational agents (chatbots) provided tailored health information, addressed patient concerns, and guided shared decision-making.

BCI-guided intraoperative mindfulness interventions were introduced to reduce anxiety and pain during the procedure. In a randomized controlled trial involving 84 patients, BCI devices captured real-time neural feedback and facilitated dynamic mindfulness prompts.

A **machine learning-based heparin anticoagulation prediction model** was constructed to support intraoperative anticoagulation management, aiming to prevent complications such as cardiac tamponade.

IoT-enabled remote rehabilitation systems utilizing wearable sensors were used to monitor patient activity and support personalized exercise programs during the postoperative recovery period.

A **comprehensive health economic evaluation** was conducted using Markov decision models to assess the cost-effectiveness of the integrated human-machine intervention framework.

[Results]

The BCI-guided mindfulness protocol significantly alleviated intraoperative pain, as measured by the Numeric Rating Scale (NRS), and led to reduced intraoperative opioid consumption (mean 3.96 vs. 4.85 mcg/kg, P=0.003), indicating improved procedural comfort and reduced reliance on sedative medications. The machine learning-driven anticoagulation management system demonstrated improved safety outcomes by optimizing real-time heparin dosing. Patients in the IoT rehabilitation group showed significantly higher compliance with exercise prescriptions, with improvements in cardiorespiratory endurance (VO_2 max, P<0.05). The health economic analysis revealed that the integrated intervention resulted in an incremental cost-effectiveness ratio (ICER) of ¥33,572 per quality-adjusted life year (QALY) gained, which is well below the cost-effectiveness threshold based on China's per capita GDP (¥85,698), thereby confirming the economic feasibility of the system.

[Conclusions]

This study demonstrates that human-machine collaborative technologies can significantly enhance the quality, safety, and efficiency of perioperative care in AF catheter ablation procedures. By synergizing AI, BCI, IoT, and health economics, the framework offers both clinical efficacy and economic value. The results suggest that this integrative, intelligent approach can serve as a scalable and adaptable model for future cardiovascular care, with potential applicability to other interventional procedures and chronic disease management scenarios.

Downregulation of Alox5 inhibits ferroptosis to improve doxorubicin-induced cardiotoxicity via the P53/SLC7A11 pathway

wenxi Fang

Renmin Hospital of Wuhan University

Abstract

Objective: Doxorubicin (DOX) is an anthracycline chemotherapy drug used for tumor treatment. Due to DOX-induced cardiotoxicity (DIC), its clinical application is widely limited. The pathogenesis of DIC includes cell death, inhibition of DNA/RNA/protein synthesis, increased reactive oxygen species (ROS) production, impaired energy metabolism, mitochondrial dysfunction, interstitial fibrosis, autophagy disorders, and intracellular calcium homeostasis disorders.Although there are many unknown factors associated with the pathogenesis of DIC, ferroptosis is a form of cell death, which includes the fenton reaction, lipid peroxidation, and ROS accumulation. Lipoxygenase, as one of the three key enzymes involved in lipid peroxidation, Alox5 is involved in the production of ROS. Alox5 is known to participate in various physiological and pathological processes. Alox5 has been studied in hepatitis, pancreatic cancer, asthma, Alzheimer's disease and other diseases. More importantly, there have been relevant studies on pulmonary hypertension, atherosclerosis, ischaemic heart disease, septic heart disease, and pressure overload-induced heart failure. However, the pathogenic role of Alox5 in DIC is still unclear. Therefore, our aim was to understand whether Alox5 is involved in DIC and the extent to which it causes myocardial damage and cardiac dysfunction after DOX stimulation.

Method: A mouse cardiomyopathy model and a primary rat cardiomyocytes model were constructed using doxorubicin. Alox5 was overexpressed in vivo and in vitro using adenovirus and adenovirus, respectively. Subsequently, in vivo and in vitro experiments were conducted using the ferroptosis inhibitor dexrazoxane to knock down Alox5 in mice and small interfering RNA in primary rat cardiomyocytes. Regularly monitor mouse echocardiography, hemodynamics, morphological staining, and

myocardial injury markers. After the completion of modeling, further molecular biology experiments and morphological staining were used to detect ferroptosis related indicators in both in vivo and in vitro experiments. And further validate its phenotype and mechanism through transcriptome sequencing, and finally use molecular biology experiments and morphological staining to further verify its mechanism in both forward and reverse directions. Ultimately, Alox5 was suppressed from Pharmacological inhibition in DIC in vivo and in vitro.

Results: In vivo and vitro experiments showed that Alox5 expression was significantly upregulated in DIC. Overexpression of Alox5 was found to exacerbate DIC in cardiac function, hemodynamics, morphological staining, myocardial injury markers, and survival analysis curves. Knocking down Alox5 was found to improve DIC in cardiac function, hemodynamics, morphological staining, myocardial injury markers, and survival analysis curves. Next, transcriptome sequencing revealed that knocking down Alox5 improved ferroptosis and inflammation in DIC, which was further confirmed by morphological staining and molecular biology experiments. Next, it was found that the ferroptosis inhibitor dexrazoxane can improve DIC exacerbated by overexpression of Alox5 in cardiac function, hemodynamics, morphological staining, myocardial injury markers, and survival analysis curves. The final prediction of Alox5 through transcriptomics suggests that it may improve DIC by inhibiting ferroptosis through the P53/SLC7A11 pathway, which has been further confirmed through morphological staining and molecular biology experiments. Finally, pharmacological inhibition of Alox5 could prevent DIC in vitro and in vivo in cardiac function, hemodynamics, morphological staining, myocardial injury markers, and survival analysis curves. Importantly, our study contributed to the understanding of the role of Alox5 in cardiomyocytes and demonstrated its potential as a therapeutic target for treating DIC.

Conclusion: Alox5 inhibits ferroptosis and improves DIC through the P53/SLC7A11 pathway.

IL4I1+ Macrophages maintain the contractile phenotype of vascular smooth muscle cells via I3P/AhR axis in atherosclerosis

Yunchang Liu

Daping Hospital of Army Medical University

IL4I1+ Macrophages maintain the contractile phenotype of vascular smooth muscle cells via I3P/AhR axis in atherosclerosis

Background

Cardiovascular diseases (CVDs) remain the leading cause of global mortality, accounting for over 18 million deaths annually according to WHO estimates. In China, rapid urbanization and demographic aging have precipitated an alarming rise in atherosclerotic cardiovascular disease (ASCVD), creating an unprecedented healthcare burden. Despite aggressive management of traditional risk factors through lipid-lowering therapies (e.g., statins, PCSK9 inhibitors) and antithrombotic agents, approximately 40% of ASCVD patients experience recurrent cardiovascular events due to residual inflammatory risk. This therapeutic gap underscores the critical need to identify novel pathophysiological mechanisms driving plaque progression. Beyond hyperlipidemia and thrombosis, chronic low-grade inflammation has emerged as a central mediator of atherosclerotic plaque destabilization. Within this inflammatory milieu, macrophages exhibit extraordinary functional plasticity, dynamically shifting between pro-inflammatory and reparative states throughout disease progression. The advent of single-cell RNA sequencing (scRNA-seq) has revolutionized our understanding of macrophage heterogeneity, revealing specialized subsets with spatiotemporally restricted functions. Our previous work identified IL4I1 $^{+}$ macrophages (IL4I1 $^{+}$ Macs)—an immunoregulatory subset expressing the enzyme interleukin-4-induced-1—within advanced human atheromas. This subset exhibits distinct immunosuppressive properties, though its metabolic crosstalk with vascular cells remains unexplored.

Method

To characterize IL4I1 $^{+}$ Macs, we integrated scRNA-seq data from human atherosclerotic lesions with a comprehensive myeloid reference atlas spanning tumor and chronic inflammatory diseases. Subtype specificity was validated using spatial transcriptomics and immunofluorescence co-staining of LYZ/IL4I1 in human and murine specimens. We generated Il4i1-overexpressing bone marrow-derived macrophages (BMDMs) via AAV9 transduction, profiling transcriptomes through bulk RNA-seq. For in vivo validation, we employed two complementary models: 1) Myeloid-specific Il4i1-knockout mice (Lyz2-Cre; Il4i1fl/fl) underwent PCSK9-AAV8 transduction and 2) ApoE $^{-}$ / $^{-}$ recipients of Il4i1-overexpressing bone marrow transplantation (IL4i1-BMT). Both cohorts administrated Western diet feeding to induce advanced atherosclerosis. Plaque burden was quantified by en face Oil Red O staining. Single-cell transcriptomics delineated microenvironmental changes in IL4i1-BMT mice, while targeted metabolomics measured tryptophan pathway intermediates. To investigate VSMC phenotypic modulation, we established Transwell co-cultures between IL4I1 $^{+}$ Macs and PDGF-BB-stimulated pulmonary artery smooth muscle cells (PASMCs), assessing contractile markers (ACTA2/CNN1/TAGLN), proliferation (BrdU), and migration (scratch assay). The functional contribution of the enzymatic product indole-3-pyruvate (I3P) was tested using pharmacological AhR inhibitors. Therapeutic efficacy was evaluated via adoptive transfer of Il4i1-modified myeloid cells into mice with established plaques.

Result

IL4I1+ Macs localized preferentially in advanced plaque cores, validated by LYZ/IL4I1 co-staining. Il4i1-overexpressing BMDMs recapitulated immunosuppressive signatures. Myeloid-specific IL4I1 knockout increased lesion area, while IL4i1-BMT reduced lesions. Metabolomics confirmed indole-derived metabolite elevation in IL4i1-BMT mice while decrease. Co-culture with IL4I1+ Macs and I3P preserved VSMC contractile phenotype (↑ ACTA2/CNN1/TAGLN; ↓ proliferation/migration) via AhR activation. Adoptive transfer attenuated plaque progression.

Conclusion

This study elucidates a previously unrecognized immunometabolic axis in atherosclerosis: IL4I1 $^{+}$ macrophages catabolize tryptophan to generate I3P, which activates AhR signaling in VSMCs to preserve their contractile phenotype and inhibit synthetic-state transition. Beyond their established immunosuppressive functions, IL4I1 $^{+}$ Macs thus serve as metabolic sentinels maintaining vascular homeostasis. The I3P/AhR axis represents a promising therapeutic target against plaque destabilization—particularly for statin-resistant patients with residual inflammatory risk. Future studies should explore I3P analogs or macrophage-directed gene therapies to harness this endogenous protective mechanism.

Magnesium sulfate in cardiogenic shock patients: a retrospective propensity score-matched cohort study

Xie Linfeng

The First Affiliated Hospital of Chongqing Medical University

Purpose: Cardiogenic shock (CS) is a low-cardiac-output state resulting in life-threatening end-organ hypoperfusion and hypoxia. Although treatment measures continue to advance recently, the mortality rate of CS remains high, reaching 27% -51%. Moreover evidence-based therapeutic interventions known to clearly improve patient outcomes are limited. Magnesium ions are essential inorganic ions in the body, playing a crucial role in normal physiological functions. Previous studies have shown that supplementing magnesium sulfate can provide survival advantages for critically ill patients. Our study aimed to explore whether intravenous magnesium sulfate could provide a survival advantage in patients with cardiogenic shock (CS).

Methods: This is a retrospective cohort study based on the Medical Information Mart in Intensive Care (MIMIC) IV database. The study participants were CS patients. The study endpoints were 30-day, 90-day, and 360-day all-cause mortality. Propensity score matching, Kaplan-Meier analyses, Cox proportional hazards analyses, and subgroup analysis was conducted. The external validation was performed in eICU 2.0 database.

Results: Totally, 2547 eligible CS patients were included in this study, among which 2119 patients received magnesium sulfate and 428 patients did not receive magnesium sulfate during ICU stay. The mean (SD) age of this cohort was 69.98 (14.33) years, 1535 (60.27%) were male. Before PSM, patients administrated intravenous magnesium sulfate had lower 30-day (34.9% vs. 50.7%, p<0.001), 90-day (42.7% vs. 59.6%, p<0.001), and 360-day (49.7% vs. 70.3%, p<0.001) all-cause mortality compared with those without intravenous magnesium sulfate. Similarly, in the PSM cohorts, patients administrated intravenous magnesium sulfate had lower 30-day (36.6% vs. 50.6%, p<0.001), 90-day (45.3% vs. 59.8%, p<0.001), and 360-day (54.2% vs. 70.4%, p<0.001) all-cause mortality compared with those without intravenous magnesium sulfate. The Kaplan-Meier survival analyses showed that the survival probability was significantly higher in patients administrated intravenous magnesium sulfate compared with those without intravenous magnesium sulfate (all log-rank p<0.001). In the overall patient cohort, multivariable Cox regression showed that magnesium supplementation was associated with a reduced risk of 30-day (HR=0.635 95%CI: 0.539, 0.749, p<0.001), 90-day (HR=0.687 95%CI: 0.591, 0.749, p<0.001), and 360-day all-cause mortality (HR=0.681 95%CI: 0.593, 0.782, p<0.001). This association remained consistent after PSM in 30-day (HR=0.624; 95% CI, 0.506, 0.768; p<0.001), 90-day (HR=0.640; 95% CI, 0.530, 0.774; p<0.001), and 360-day all-cause mortality (HR=0.629; 95% CI, 0.529, 0.749; p<0.001). Subgroup analysis found that the effect of magnesium supplement was consistent in different subgroup patients including in patients with hypomagnesemia versus non-hypomagnesemia (all p-interaction>0.05). What's more, the 30-day, 90-day, and 360-day all-cause mortality of patients with lower dosage and long duration of magnesium reduced more significantly. In 1867 CS patients from eICU 2.0 for external validation, after PSM, intravenous magnesium sulfate use was associated with lower in-hospital (HR=0.742; 95% CI, 0.578, 0.952; p=0.019) and in-ICU all-cause mortality (HR=0.729; 95% CI, 0.555, 0.958; p=0.023).

Conclusion: Our study revealed that magnesium supplementation can

be considered a routine therapeutic adjunct for patients with CS to reduce 30-day, 90-day, and 360-day all-cause mortality, and the benefits from magnesium supplementation were consistent in patients with higher or lower serum magnesium. More importantly, our research revealed that the 30-day, 90-day, and 360-day all-cause mortality of patients with lower dosage and long duration of magnesium reduced more significantly, is essential for evaluating the dose-response relationship and optimizing treatment protocols. However, prospective studies, especially rigorously designed randomized controlled trials, are needed to confirm this finding.

Proteome Profiling by High-Resolution Mass Spectrometry Discriminates HFimpEF from HFrEF

Chen-Die Yang, Rui-Yan Zhang, Xiao-Qun Wang

Ruijin Hospital, Shanghai Jiao-Tong University School of Medicine, Shanghai, P. R. China

Background: Heart failure (HF) with improved ejection fraction (HFimpEF) has emerged as a distinct HF subtype, characterized by left ventricular reverse modeling and myocardial recovery. However, the underlying pathophysiological mechanisms remain unclear, and specific diagnostic and predictive biomarkers are still lacking.

Objectives: This study characterized the serum proteome profiles of HFimpEF patients compared to those with reduced ejection fraction (HFrEF), aiming to identify novel protein biomarkers that could both inform pathogenic mechanisms specific to HFimpEF and enhance diagnostic accuracy.

Methods: This study performed untargeted serum proteome profiling using data-independent acquisition-based label-free quantitative liquid chromatography–tandem mass spectrometry on 55 HFimpEF patients, as compared with 33 HFrEF patients. Significant changes in protein intensities were determined with nonpaired Student's t-tests and were further classified by the Boruta algorithm. The proteins' diagnostic performance was evaluated by area under the curve (AUC) and validated using the 10-fold cross-validation. Gene Ontology (GO) enrichment analysis and pathway enrichment analysis were performed to identify significantly enriched biological functions and pathways associated with the differentially expressed proteins.

Results: Quantitative proteomic analysis identified 2,461 serum proteins across 88 patients with HFimpEF or HFrEF. Of these, 1,712 proteins showed high detection consistency (≥ 60% prevalence) and were retained for comparative analysis, which revealed 35 differentially expressed proteins. Specifically, HFimpEF patients exhibited 33 up-regulated and 2 down-regulated proteins compared to HFrEF. The Boruta machine learning algorithm prioritized 9 signature proteins as key discriminators between the two phenotypes. The combination of immunoglobulin superfamily member 1, immunoglobulin heavy constant gamma 1, pentraxin-related protein PTX3, and 55 kDa erythrocyte membrane protein had the best diagnostic precision (AUC: 0.90; 95% CI: 0.83-0.97) to distinguish patients with HFimpEF from HFrEF. Salient biologic themes related to thrombosis, immune regulation, cellular motility and membrane integrity were predominant in HFimpEF.

Conclusions: These newly identified proteins warrant further evaluation to establish their role in the pathogenesis of HFimpEF and potential use as predictive or diagnostic biomarker, as well as therapeutic targets.

Background: Heart failure (HF) with improved ejection fraction (HFimpEF) has emerged as a distinct HF subtype, characterized by left ventricular reverse modeling and myocardial recovery. However, the underlying pathophysiological mechanisms remain unclear, and specific diagnostic and predictive biomarkers are still lacking.**Objectives:** This study characterized the serum proteome profiles of HFimpEF patients compared to those with reduced ejection fraction (HFrEF), aiming to identify novel protein biomarkers that could both inform pathogenic mechanisms specific to HFimpEF and enhance diagnostic accuracy.**Methods:** This study performed untargeted serum proteome profiling using data-independent acquisition-based label-free quantitative liquid chromatography-tandem mass spectrometry on 55 HFimpEF patients, as compared with 33 HFrEF patients. Significant changes in protein intensities were determined with nonpaired Student's t-tests and were further classified by the Boruta algorithm. The proteins' diagnostic performance was evaluated by area under the curve (AUC) and validated using the 10-fold cross-validation. Gene Ontology (GO) enrichment analysis and pathway enrichment analysis were performed to identify significantly enriched biological functions and pathways associated with the differentially expressed proteins.**Results:** Quantitative proteomic analysis identified 2,461 serum proteins across 88 patients with HFimpEF or HFrEF. Of these, 1,712 proteins showed high detection consistency (≥ 60% prevalence) and were retained for comparative analysis, which revealed 35 differentially expressed proteins. Specifically, HFimpEF patients exhibited 33 up-regulated and 2 down-regulated proteins compared to HFrEF. The Boruta machine learning algorithm prioritized 9 signature proteins as key discriminators between the two phenotypes. The combination of immunoglobulin superfamily member 1, immunoglobulin heavy constant gamma 1, pentraxin-related protein PTX3, and 55 kDa erythrocyte membrane protein had the best diagnostic precision (AUC: 0.90; 95% CI: 0.83-0.97) to distinguish patients with HFimpEF from HFrEF. Salient biologic themes related to thrombosis, immune regulation, cellular motility and membrane integrity were predominant in HFimpEF.**Conclusions:** These newly identified proteins warrant further evaluation to establish their role in the pathogenesis of HFimpEF and potential use as predictive or diagnostic biomarker, as well as therapeutic targets.

Mediating effect of systemic inflammation on sleep duration and all-cause/CVD mortality

Lihua Hu

Peking university first hospital

Objective: No studies have examined the mediating role of these novel inflammatory indicators in the relationship between sleep duration and all-cause and cause-specific mortality. Therefore, this study aimed to investigate the mediating role of systemic inflammation, measured by four distinct biomarkers (neutrophil-to-lymphocyte ratio [NLR], red cell distribution width to platelet ratio [RPR], systemic immune-inflammation index [SII] and platelet-to-lymphocyte ratio [PLR]), in the relationship between sleep duration and all-cause and CVD mortality.

Methods: This prospective cohort study included 22,939 adults from the NHANES (2007-2018), linked to the National Death Index through December 31, 2019. Sleep duration was self-reported. Multivariable-adjusted Cox proportional hazards models assessed mortality risks. Mediation analysis evaluated the proportion of the total effect of sleep duration on mortality explained by each inflammatory index.

Results: Over a median follow-up period of 7.83 years (interquartile range: 5.33-10.25 years), 1,802 deaths from all causes, including 435 deaths attributed to CVD were recorded. Our results revealed a U-shaped relationship between sleep duration and mortality, independent of other factors. Threshold effect analysis suggested that a sleep duration of 7 hours may be considered optimal for minimizing mortality risk. when sleep duration was less than 7 h (insufficient sleep duration), it was inversely associated with a reduced risk of all-cause mortality (HR = 0.91; 95% CI, 0.85-0.96; P = 0.001). In contrast, when sleep duration exceeded 7 hours (prolonged sleep duration), it was positively linked to an increased risk of all-cause mortality (HR = 1.16; 95% CI, 1.09-1.23; P < 0.001). The results also showed an positive association between sleep duration and CVD mortality only for sleep duration > 7 h (HR = 1.19; 95% CI, 1.07-1.33; P = 0.002). Among participants with prolonged sleep duration (> 7 h), every hour increase of sleep duration was associated with the increases of 2.2% and 0.06% in NLR and RPR, respectively, further resulting in a 16% higher risk of all-cause mortality. Moreover, for per unit increment in NLR and lgSII, the risk of all-cause mortality increased by 6% (HR = 1.06; 95% CI, 1.04-1.09) and 46% (HR = 1.46; 95% CI, 1.19-1.79), respectively. Every 10-unit increase in RPR was associated with 52% increased risk of all-cause mortality (HR = 1.52; 95% CI, 1.37-1.68). The similar results were observed for inflammation biomarkers and CVD mortality. Of the four systemic inflammation indices examined, NLR mediated a substantial proportion of the association between prolonged sleep duration and increased risk of both all-cause mortality (mediation proportion: 2.40%; P = 0.025) and CVD mortality (mediation proportion: 2.42%; P = 0.042). Conversely, none of the four inflammatory biomarkers significantly mediated the association between insufficient sleep duration (<7 hours) and mortality.

Conclusion: Notably, only NLR demonstrated a significant mediating effect in the association between prolonged sleep duration and increased mortality risk. NLR may serve as a key biomarker identifying individuals with prolonged sleep at heightened risk due to inflammatory dysregulation. By understanding how sleep affects inflammation and how this process contributes to the risk of mortality, researchers can better identify potential interventions aimed at improving sleep and reducing inflammation to prevent premature death.

Evaluating the Role of Traditional Chinese Medicine as an Adjunctive Therapy in Chronic Heart Failure: A Retrospective Study

xuanxuan li

Shijiazhuang Great Wall Hospital of Integrated Traditional Chinese and Western Medicine

Abstract

Objective: This retrospective study aimed to evaluate the effectiveness and safety of the Xinjihuoli Formula (XJHLF), a traditional Chinese medicine, as an adjunctive therapy for patients with CHF, focusing on its impact on cardiac function and inflammatory markers.

Methods: A total of 114 patients with CHF were included in this retrospective study. Participants were assigned to either a treatment group or a control group based on the therapies they received. The treatment group (n=57) received XJHLF in addition to standard care, while the control group (n=57) received standard care alone. All outcomes were assessed at baseline and after three months of treatment. **Results**: The

primary outcomes assessed were cardiac function and inflammatory markers, which were evaluated using left ventricular end-diastolic diameter (LVEDD), left ventricular end-systolic volume (LVESV), left ventricular ejection fraction (LVEF), effective cardiac output (ECO), plasma N-terminal B-type natriuretic peptide (NT-proBNP), interleukin-6 (IL-6), and C-reactive protein (CRP). Adverse events (AEs) were also recorded. Compared to the control group, the treatment group showed significant improvements in cardiac function, with better LVEF , LVEDD , LVESV , ECO , and NT-proBNP levels. Additionally, inflammatory markers IL-6 ($P < 0.05$) and CRP ($P < 0.05$) were significantly lower in the treatment group. There were no significant differences in adverse events between the two groups.

Results

A total of 114 patients were initially enrolled in this retrospective study. Baseline characteristics were comparable between the treatment and control groups, with no significant differences observed prior to the intervention . Outcome measures are shown in Figures 1-3. Patients in the treatment group exhibited statistically significant improvements compared to the control group in several key outcomes, including LVEDD, LVESV, LVEF, and ECO, as well as biomarkers such as NT-proBNP, IL-6, and CRP ($P < 0.05$). Improvements in cardiac function (LVEF and echocardiographic outcomes) and biomarkers (NT-proBNP, IL-6, and CRP) observed at the three-month assessment were largely maintained at the one-year follow-up. This suggests that the adjunctive use of XJHLF may provide lasting benefits in the management of CHF. Additionally, significant enhancements were observed in functional assessments, including the 6MWT and the MLHFQ scores. A 10% improvement in 6MWT was associated with enhanced survival rates in CHF patients. No AEs or treatment-related deaths were reported during the study period.

Conclusion: XJHLF may improve cardiac and motor function while effectively reducing inflammation in patients with CHF.

The therapeutic approach combines methods to strengthen vitality, remove blood stasis, promote fluid metabolism, warm the body, and detoxify. These principles are the foundation for the "Myocardial Vitality Drink," a prescription aimed at detoxifying the heart, invigorating qi, and enhancing blood circulation[5]. The formula includes the following traditional Chinese medicines: Astragali Radix and Radix Codonopsis as primary herbs to tonify qi; Salvia miltiorrhiza, Panax notoginseng powder, and Peony bark to clear heat, cool the blood, and promote circulation, supporting the primary herbs' effects on improving blood flow; Forsythia, Coptis chinensis, and Sophora flavescens to clear heat, dry dampness, detoxify, and purify the heart; Schisandra to strengthen the kidneys, calm the heart, and provide astringency; Wheat and Rehmannia to nourish yin, moisten the lungs, and soothe the heart; and Licorice to harmonize the formula, facilitate the circulation of qi and blood, ensure detoxification without harm, and reinforces qi without residual pathogens. Additionally, this formula helps mitigate the side effects of Western diuretics, such as dry mouth and irritability caused by fluid depletion.

However, this study has certain limitations. The observed efficacy may be attributed to the combined effect of XJHLF with routine treatment, rather than XJHLF alone, despite the baseline medications being similar between the two groups. The generalizability of the results may be limited due to potential variations in efficacy across different populations, differences in background treatments, the acceptability of the intervention in other clinical settings, and varying levels of compliance among the treatment groups.

Deep learning fusion of CTA and clinical features to predict small abdominal aortic aneurysm prognosis

Jiaxin Cheng[1,2], Ya-Song Wang[2], Zhi-Qiang Zhang[2], Xiao-ZengXueZuWei-Yuan Wang[2]

1. Northeastern University College of Medicine and Biological Information Engineering

2. National Key Laboratory of Frigid Zone Cardiovascular Disease, Cardiovascular Research Institute and Department of Cardiology, General Hospital of Northern Theater Command

Abstract

Background: Abdominal aortic aneurysm (AAA) rupture is a catastrophic event with high mortality. While larger AAAs warrant intervention, managing small AAAs (SAAAs) relies heavily on surveillance based primarily on maximum diameter to gauge rupture risk and time interventions. However, diameter alone is an imperfect prognostic indicator, as a significant proportion of SAAAs rupture before reaching the established intervention threshold. This limitation underscores an unmet clinical need for more precise, individualized risk stratification tools for SAAA patients. Enhanced prediction of abdominal aortic-related adverse events (AARAEs), including rupture, emergency intervention, and aortic-related death, over the critical medium-term (e.g., 5-year) horizon is essential to optimize personalized surveillance intensity and timely, potentially life-saving interventions. Current approaches often fail to fully integrate the complex interplay between aneurysm morphology, captured through imaging like computed tomography angiography (CTA), and relevant clinical biomarkers. Therefore, there is a compelling rationale to develop advanced predictive models that leverage both radiomic features from medical imaging and comprehensive clinical data to uncover hidden risk factors and significantly improve prognostic accuracy beyond diameter measurements for SAAA patients.

Objective: Current prognostic assessment of the patients with SAAA relies primarily on aneurysm diameter, yet its predictive utility remains limited, as some SAAAs still rupture. This study aimed to develop a deep learning-driven multimodal framework integrating CTA images and clinical data to enhance 5-year AARAE prediction in patients with SAAA.

Methods: A single-center retrospective study screened patients with SAAA treated at our center, stratified into AARAE and non-AARAE groups based on follow-up records. Clinical data such as demographics, medical history, laboratory indices, and CTA images were analyzed. SHapley Additive exPlanations (SHAP) analyses identified critical predictors. A multimodal model fused a residual neural network extracted imaging features dependent on multi-head attention with clinical data. The multimodal fusion architecture integrated: Firstly, ResNet-18 (ImageNet-pretrained) extracted features from localized CTA slices, processed by a transformer encoder and mean pooling. Then, a multilayer perceptron (MLP) processed the six SHAP-selected features. Finally, a multi-head self-attention block explicitly modeled interactions between image and clinical embeddings (512D).The fused output fed a classifier for AARAE prediction. The model was trained using AdamW optimization, 5-fold cross-validation with class-balancing weights, rigorous data augmentation (rotation, flipping, intensity shifts), gradient clipping, and early stopping. Statistical analyses employed appropriate tests (t-test, Mann-Whitney U, chi-square/Fisher's) with significance at $p<0.05$.

Results: Over 34.5 months median follow-up, of the 206 participants enrolled with 85.4% males, and the median age of 72 years. 30.1% experienced AARAE (48 requiring emergency intervention), with 18.9% all-cause and 2.4% aortic-related mortality. SHAP highlighted fibrinogen, estimated glomerular filtration rate, age, simple renal cyst, low-density lipoprotein cholesterol, and maximum aneurysm diameter as key predictors. The model achieved an area under the receiver operating characteristic curve of> 0.999, 95.5% accuracy, and 94.2% F1-score for AARAE prediction.

Conclusions: This model significantly improves 5-year risk precision in patients with SAAA by revealing morphology-clinical biomarker interactions, supporting personalized surveillance and timely intervention. Its integration of radiomics and clinical data advances vascular disease management.

Keywords: multihead attention mechanism; multimodal model; SHapley Additive exPlanations analysis; residual neural network; abdominal aortic-related adverse events.

Clinical AI Diagnosis and Reasoning for Cardiovascular Diseases Based on Large Language Models and Knowledge Graphs

Jiu-Yang Chang[1], Bo-Wen Wang[2], Hong-Yang Liu[1]

1. The First Affiliated Hospital of Dalian Medical University

2. Worldview Medical Technology Company

Objective: Cardiovascular diseases (CVDs) are the leading cause of death and a major threat to global health. Early risk assessment, timely diagnosis, and prognosis determination are critical for CVD management. While an increasing number of artificial intelligence (AI) technologies and tools are being introduced into clinical practice, they often face challenges related to lack of interpretability and trustworthiness. Large language models (LLMs), deep learning models trained on massive text corpora, have seen limited application in the medical field, particularly in cardiovascular diseases.

Methods: We created the Diagnostic Reasoning for Cardiovascular Tasks (DiReCT) dataset, containing clinical records of 521 patients with common cardiovascular diseases, to evaluate the diagnostic reasoning capabilities and interpretability of LLMs compared to human cardiovascular physicians. Utilizing the MIMIC critical care database, board-certified cardiologists extracted patient data including chief complaints, present and past medical history, and examination results (blood tests, imaging, pathology, secretions, physical exams). Medical data were meticulously annotated based on internationally recognized AHA/ESC guidelines to reflect diagnostic logic. Crucially, we provided a CVD diagnostic knowledge graph, essential for logical reasoning, which is absent in current LLM training data.

Results: Testing on several high-performance LLMs revealed that even the current top-performing model, GPT-4-Turbo, achieved only a classification accuracy of 0.572 (for 16 disease categories) and a reasoning consistency score of 0.199 compared to human physicians. Analysis of outputs demonstrated that while GPT-4 excels at identifying potential symptom descriptions within text, it struggles to explain and correlate findings to reach a diagnosis. Providing GPT-4 with the knowledge graph yielded improvements of 0.042 in classification accuracy and 0.058 in

reasoning consistency. This indicates that current LLMs lack robust diagnostic reasoning capabilities, but knowledge graphs can partially mitigate this deficiency. Overall, our evaluation reveals a significant performance gap between leading LLMs and human experts, highlighting the urgent need to develop interpretable AI diagnostic models for clinical settings.

Conclusion: We propose the DiReCT dataset as a benchmark for evaluating the diagnostic reasoning capabilities of interpretable LLMs for cardiovascular diseases. We will continue to expand this dataset. The significance of this work lies in its potential to: First, deliver diagnostic results comparable to or exceeding the accuracy of cardiovascular specialists. Second, establish diagnosis logic and evidence based on international guidelines, providing clear explanations for diagnostic decisions. Third, automatically extract key disease-related information from patient data for initial screening. The future application of such models in the healthcare industry holds profound implications, promising significant reductions in human resource demands, expansion of medical resource coverage, and enhanced CVD diagnosis and treatment support in primary care hospitals.

Limitations: DiReCT encompasses only a subset of disease categories and considers only one PDD, omitting the inter-diagnostic relationships due to their complexity–a significant challenge even for human doctors. Additionally, our baseline may not use optimal prompts or address issues related to hallucinations in task responses. Our dataset is solely intended for model evaluation but not for use in clinical environments. The use of the diagnostic knowledge graph is also limited to serving merely as a part of the input and once a knowledge graph is provided, the focus shifts to whether the LLM follows the graph's rules well. Future work will focus on constructing a more comprehensive disease dataset and developing an extensive diagnostic knowledge graph.

Serial Myocardial Fibrosis Assessments Predict Outcomes in Patients with Hypertrophic Cardiomyopathy

YUN TANG, Shihua Zhao

Fuwai Hospital, Chinese Academy of Medical Sciences & Peking Union Medical College/National Center for Cardiovascular Diseases

Title: Serial Myocardial Fibrosis Assessments Predict Outcomes in Patients with Hypertrophic Cardiomyopathy

Running Title: Prognostic value of LGE progression in HCM

STRUCTURED ABSTRACT

BACKGROUND

The prognostic value of serial myocardial fibrosis assessments in patients with hypertrophic cardiomyopathy (HCM) remains to be elucidated.

OBJECTIVES

To investigate the progression of late gadolinium enhancement (LGE), as assessed by follow-up cardiac magnetic resonance (CMR) imaging, in patients with HCM, as well as its associated prognostic value.

METHODS

Patients with HCM who underwent two CMR examinations between 2010 and 2019 were retrospectively evaluated. The LGE mass progression (ΔLGE%) was defined as the number of increased grams of enhanced myocardium added divided by the number of years between the two scans. Primary endpoint was the combination of cardiac death, heart transplantation, aborted sudden cardiac death (SCD), appropriate implantable cardioverter defibrillator discharge, hospitalization for heart failure and stroke. Secondary endpoint was the combination of cardiac death, aborted SCD and heart transplantation. A maximally selected rank statistical analysis was conducted to identify the optimal cut-off for ΔLGE% for prognostic stratification.

RESULTS

A total of 313 patients with HCM (median scan interval: 4.2 years) were evaluated. LGE mass progressed from a median of 2.9 (Q1-Q3: 0.0 to 8.1) g at CMR-1 to 8.3 (Q1-Q3: 3.6 to 16.3) g at CMR-2. During a median follow-up of 7.7 (Q1-Q3: 6.0-9.8) years from initial CMR, the primary endpoint occurred in 66 patients, of whom 22.7% reached the secondary endpoint (n=15). For primary endpoint and secondary endpoint, the optimal cut-off for ΔLGE% were >1.50 and 3.75g/year, respectively. In the multivariable model, New York Heart Association class III/IV at baseline (HR 5.39, 95% CI: 2.92-9.94, P<0.0001), left ventricular ejection fraction <50% at CMR-1 (HR 2.65, 95% CI: 1.27-5.52, P=0.0096), and ΔLGE% >1.50g/year (HR 5.86, 95% CI: 3.41-10.08, P<0.0001) were associated with the primary endpoint.

CONCLUSIONS

In HCM patients, myocardial fibrosis increased over time. Serial assessments of myocardial fibrosis on CMR may improve risk stratification and clinical decision-making in HCM patients.

Key words:

myocardial fibrosis, hypertrophic cardiomyopathy, cardiac magnetic resonance, late gadolinium enhancement, sudden cardiac death, heart failure

Condensed Abstract:

Patients with hypertrophic cardiomyopathy (HCM) had varying degrees of late gadolinium enhancement (LGE) progression. Rapid LGE progression (>1.50g/year) conferred a 5-fold increase in event risk for patients with HCM. Rigorous and serial evaluations of LGE facilitate more informed clinical decision-making.

Addressing disparities in hypertension care cascades to reduce cardiovascular disease burden: a residence- and sex- stratified analysis in China

Xue Cao

Fuwai Hospital, Chinese Academy of Medical Sciences

Background

Although hypertension remains the leading modifiable contributor to CVD-related deaths and disability, improving hypertension management performance in China has uncertain implications across different socioeconomic and demographic groups. In this study, we developed a microsimulation model to estimate how scale-up in hypertension care cascade performance could prevent CVD cases and advance health equity in the Chinese adult population.

Methods

Using 86,071 individual-level data from nationally and provincially representative survey in China, we simulated two scenarios for the hypertension care cascades (diagnosis scenario and treatment scenario) based on a microsimulation model. Diagnosis (diagnosis scenario) and treatment (treatment scenario) levels for all urban and rural areas to match the best-performing province's urban or rural rates. We then estimated the effects of intervention scenarios on CVD risk and prevented occurrences of CVD cases per 1,000 people with hypertension, stratified by demographic and regional subgroups. Key outcomes were computed as the difference between CVD risk levels in the baseline and intervention scenarios (diagnosis or treatment). We also calculated the percentage point gap in CVD risk between urban and rural populations within each province and scenario to examine the intervention's effect on urban-rural disparities in CVD risk. Results were further disaggregated by human development index (HDI) categories and seven geographic regions. All analyses were conducted independently by urban-rural residence and sex.

Results

The total number of individual respondents included in the simulated population was 86,071 adults aged 20-85 years with hypertension. The median age was 56.3 years (IQR 45.4-68.1), with 46.3% (39,817) of female. HDI regions exhibited non-linear disparities in hypertension care cascade performance. Transitioning from baseline to diagnosis and treatment scenarios substantially reduced mean 10-year CVD risk across all provinces, with rural populations and males experiencing the most pronounced improvements. Most provinces saw narrowed urban-rural CVD risk gaps and national inequalities in CVD burden would be reduced, particularly under treatment scenarios. Nationally, the number of CVD occurrences prevented during the 10-year period for diagnosis and treatment scenarios were 1.75 million and 2.41 million, respectively. Under treatment scenarios, rural areas in Northwest China demonstrated the highest CVD case averted (11.3 per 1,000 individuals with hypertension), followed by urban Northeast China (9.6 per 1,000) and rural Northeast China (9.5 per 1,000). For different HDI regions, rural areas in upper-middle HDI regions averted the most CVD cases (9.7 per 1,000 individuals with hypertension) under treatment scenario, surpassing urban counterparts (6.9 per 1,000), while lower-middle HDI regions showed narrower urban-rural differences (7.3 vs. 7.0 per 1,000) under treatment scenarios. Provincial-level analyses highlighted rural Shaanxi as the top performer in CVD cases prevention under treatment scenario (15.3 per 1,000), followed by rural areas in Shandong (12.2 per 1,000) in the treatment scenario and rural areas in Shaanxi in the diagnosis scenario (12.0 per 1,000). Sex-specific analyses revealed consistent male-favoring disparities, with upper-middle HDI regions achieving the highest male-specific CVD reduction (11.1 per 1,000). Males in Shaanxi, Shandong, and Liaoning showed the largest improvements in CVD cases preventions in the treatment scenarios. The health gains of hypertension management strategies varied significantly depending on the target definition in the simulated intervention scenarios.

Conclusions

Strengthening hypertension care cascade performance across China could substantially prevent CVD burden, particularly among rural pop-

ulation and among males in upper-middle HDI regions. Prioritizing targeted enhancements in hypertension diagnosis and treatment adherence would not only reduce preventable CVD outcomes but also address persistent residence- and sex-based disparities in healthcare equity.

Complement C3a and C5a receptors-mediated activation of FoxP3+ Tregs promotes adipocyte browning and attenuates diet-induced obesity

ling-ran kong, Xin-Kai Qu

Huadong Hospital Affiliated to Fudan University

Aims: Complement activation closely related to the regulation of obesity-related metabolic disorders. Complement C3a or C5a receptor (C3aR or C5aR) blockade is thought to reduce proinflammatory adipokines in adipose tissue and improve insulin sensitivity in obesity. Previous studies have showed that C3a/C3aR and C5a/C5aR signaling downregulates Foxp3 expression in Tregs and inhibits their immune-suppressive capacity. The present study aimed to elucidate whether the loss of C3aR and C5aR is involved in the regulation of adipocyte browning and diet-induced obesity .

Methods: Balb/c (WT) mice, C3aR and C5aR double knockout (DKO) mice were randomly assigned to room temperature (RT, 25 ℃) or cold (4 ℃) group for 7days. For high-fat diet (HFD)-induced obesity, male WT and DKO mice had free access to the HFD (45% fat;) or NCD (10% fat) for 12 weeks.The expressional of browning-related genes were detected by quantitative real time PCR. Flow cytometric analysis was used to assess serum and adipose tissue CD4+Foxp3+ Tregs. Oxygen consumption, respirometry and physical activity were measured for male mice after cold exposure using Promethion Metabolic Cage System in cold or after 12-weeks HFD. Heat production and RER were calculated as described previously. In order to determine whether the regulation of C3aR and C5aR in adipose browning is Foxp3+ Tregs dependent, WT mice were subcutaneous injection in fat situ and intravenously injected via the tail vein one time with 4*105 WT or 4*105 DKO CD4+CD25+ Tregs, followed by exposure at RT or 4 C for 7 days. Adenosine was detected by liquid chromatography coupled with mass spectrometry.We also generated adenosine 2a receptor (A2aR), C3aR, and C5aR triple-knockout (TKO) mice, which were subjected to cold exposure at 4℃ for 7 days or introduction of high-fat diet (HFD) for 12 weeks.

Results: DKO mice had a higher proportion of multilocular, brown-like adipocytes and an increase of UCP1 staining in sWAT after cold exposure. QPCR analyses showed increased expressions of most browning-related genes (UCP1, peroxisome proliferatoractivated receptor [PPARg], peroxisome proliferator-activated receptor gamma coactivator 1a [PGC1a], PRDM16, cell deathinducing DNA fragmentation factor alpha-like effector a [Cidea], and ELOVL fatty acid elongase 3 [ELOVL3]) and Leptin in sWAT of DKO mice after cold exposure. Flow cytometric analysis showed that the percentage of CD4+Foxp3+ Tregs was significantly increased in sWAT of DKO mice after cold exposure compared with WT mice. Adoptive transfer of Tregs demonstrated that Treg accumulation was more pronounced in DKO Treg-donor mice compared with WT Treg-donor after cold exposure. Moreover, the increased Tregs percentage was accompanied by sWAT browning. C3aR/C5aR DKO displayed more beneficial sWAT phenotypes with smaller adipocytes, along with increased UCP1 staining and browning-related gene expression than WT mice after intake of HFD. Principal-component analysis showed significantly distinctive expression of different substances between WT and DKO Tregs, including adenosine. Unexpectedly, no significant difference in adenosine level was found in sWAT of DKO compared with WT mice. Inosine, an endogenous purine nucleoside,was significantly increased in sWAT and serum of DKO mice compared with WT mice. Adenosine and inosine mediate a wide range of physiological and pathological functions through interacting with A2aR. HE and IHC analysis showed that the higher proportion of brown-like adipocytes and increased UCP1 staining induced by C3aR/C5aR DKO were abolished in TKO mice in sWAT and iBAT after cold exposure.C3aR/C5aR deficiency attenuated HFDinduced weight gain compared with WT mice, whereas this beneficial effect of DKO on HFD-induced obesity was abolished in TKO mice.

Conclusions: We identify C3aR and C5aR as critical switches to control adipocyte browning and energy balance in male mice. Loss of C3aR and C5aR in combination, more than individually, increases cold-induced adipocyte browning and attenuates diet-induced obesity in male mice. Mechanistically, loss of C3aR and C5aR increases regulatory T cell (Treg) accumulation in the subcutaneous white adipose tissue during cold exposure or high-fat diet. Activated Tregs produce adenosine, which is converted to inosine by adipocyte-derived adenosine deaminases. Inosine promotes adipocyte browning in a manner dependent on activating adenosine A2a receptor. These data reveal a regulatory mechanism of complement in controlling adaptive thermogenesis and suggest that targeting the C3aR/C5aR pathways may represent a therapeutic strategy in treating obesity-related metabolic diseases.

Study on the role and mechanism of frailty in left atrial remodelling and dysfunction after myocardial infarction in aging mice by activating AIM2 and NLR Inflammasome-Mediated Cardiomyocyte Pyroptosis

Di Zhao

The First Affiliated Hospital of Nanjing Medical University

Background and Objectives

Myocardial infarction (MI) tended to result in left atrial dysfunction and myocardial remodeling, which could significantly increase the risk of cardiovascular events such as heart failure and stroke. It could be indicated by previous clinical studies that frailty exhibited a negative connection with left atrial function in elderly MI patients after percutaneous coronary intervention, which could indicate that frailty might exacerbate the decline in left atrial function. Based on this clinical observation, this study aimed to further explore the impact of frailty on left atrial myocardial remodeling after myocardial infarction in aged mice, alongside the investigation of its potential molecular mechanisms. Based on this research, it was expected to provide new theoretical evidence for early diagnosis and intervention of cardiovascular diseases connected with the frailty.

Methods

24-month-old Interleukin 10 knockout (IL10-KO) mice were utilized in this study to construct a frailty model, alongside the construction of a MI model by ligating the left anterior descending coronary artery. Additionally, the function and morphology of the left ventricle and left atrium were assessed by techniques such as echocardiography, hematoxylin and eosin (H&E) staining, and Masson's trichrome staining. Besides, the differential gene expression profiles in the left atrial tissue of aged mice from the control and frailty groups post-MI were analyzed by transcriptome sequencing (RNA-sequencing), alongside the analysis based on bioinformatics tools such as DESeq2 and Clusterprofile. Furthermore, the mRNA and protein expression levels of relevant genes were detected by the techniques including reverse transcription quantitative PCR (RT-qPCR), Western blot (WB), and immunofluorescence staining (IF). Finally, the effects of NLRP3/AIM2-in-3, an inflammasome-dependent pyroptotic inhibitor of NLRP3 and AIM2, on the morphology and function of the left atrium after MI in frailty-induced aged mice were explored.

Results

The successful construction of a frailty syndrome model in aged mice was validated by the Frailty Index (FI) score in this study, and it was found that frailty exhibited no significant effects on the function and morphology of the left atrium under the physiological conditions. Subsequently, a MI model was constructed, and it was found that the left atrial diameter and area were significantly enlarged in the frailty group (MI+Frailty) according to a series of functional and morphological tests 28 days post-MI, alongside a marked increase in myocardial fibrosis and inflammatory infiltration. Moreover, the survival of aged mice in the frailty group (MI+Frailty) appeared to be significantly worse than that of the control group (MI+WT). It could be indicated by the RNA-seq sequencing analysis that the differentially expressed genes between the two groups of aged mice (MI+WT vs MI+Frailty) were mainly enriched in pathways related to pyroptosis, immune-inflammatory response and cytokine release. Additionally, it was revealed by further experiments that the levels of pyroptosis and inflammation in left atrial cardiomyocytes exhibited a significant increasing trend in the frailty group (MI+Frailty). According to the Gene Set Enrichment analysis (GSEA) and experiments, it was found that the NOD-like receptor signaling pathway (NLR signaling) and absent in melanoma 2 (AIM2) were significantly activated in the left atrial tissue of aged mice in the frailty group (MI+Frailty). Further studies have shown that the application of the inhibitor NLRP3/AIM2-IN-3 could significantly alleviate the pathological remodeling of the left atrium after MI in frailty-induced aged mice, alongside the significant improvement of left atrial function.

Conclusions

It could be demonstrated by this study that the frailty could exacerbate the pathological remodeling and dysfunction of the left atrium in aged mice post-MI, alongside the significant promotion of cardiomyocyte pyroptosis. Mechanistically, frailty contributes to post-MI left atrial dysfunction in aging mice by activating AIM2 and NLR signaling pathways, which mediate inflammation and cardiomyocyte pyroptosis. Additionally, it was revealed by further research that the inhibitor NLRP3/AIM2-IN-3 could effectively alleviate the pathological remodeling of the left atrium in frailty-induced aged mice post-MI, alongside the reduction of cardiomyocyte pyroptosis, thereby contributing to the improvement of the atrial function. Based on the above findings, NLRP3/AIM2-IN-3 exhibited its potential application prospects as a therapeutic agent in the treatment of left atrial lesions post-MI in the elderly. Overall, the therapeutic effects of NLRP3/AIM2-IN-3 and its action mechanisms required to be further verified by future research, which could provide novel strategies for the clinical treatment of cardiovascular diseases related to frailty.

Keywords

Frailty; Myocardial infarction; NLR signaling pathway; AIM2; Inflammation; Pyroptosis; NLRP3/AIM2-IN-3

Yangxinshi tablet protects against myocardial injury and increases skeletal muscle exercise capacity by regulating mitochondrial bioener-

getics

宋海旭 Song, Chun-Ying Liu, -Ming Yang, Ya-Ling Han

State Key Laboratory of Frigid Zone Cardiovascular Disease, Cardiovascular Research Institute and Department of Cardiology, General Hospital of Northern Theater Command

Background: Heart failure is a systemic disease in which impairment in skeletal muscle structure and function contributes to cachexia and skeletal muscle atrophy, and reduced exercise tolerance.Reduced exercise tolerance is not only due to deterioration of cardiac function, but also because of the body's metabolic disorder, myocyte apoptosis and skeletal muscle atrophy. In particular, the imbalance of energy metabolism, mitochondrial structural abnormalities and dysfunction, the conversion of slow fibers to fast fibers, and muscle atrophy in skeletal muscle, are key factors leading to the decline in exercise capacity in patients with heart failure.Traditional Chinese medicine (TCM) has been studied extensively and offers unique scientific theories and practical applications. TCM has the potential to serve as a novel therapeutic approach for treating heart failure due to its multi-component and multi-target advantages Yangxinshi tablet (YXST), as the traditional Chinese medicine, could significantly improve cardiac function and exercise tolerance in patients with coronary heart disease.In the current study, the potential effect and underlying molecular mechanisms of YXST in heart failure and skeletal muscle injury were investigated However, molecular mechanisms of YXST protecting against myocardial injury and promoting skeletal muscle exercise capacity is still unclear.

Purpose: This study aimed to clarify the efficacy and potential mechanisms of YXST in myocardial injury and skeletal muscle exercise capacity.

Methods: Mice were randomly divided into 6 groups (n=10-20 every group) and administrated for 6 weeks: control group, myocardial ischemia□reperfusion group (I/R group), YXST group (I/R mice treated with YXST, respectively 250,500 and 1000 mg/kg/day) and I/R treated with trimetazidine (TMZ) group (20 mg/kg/day). Meanwhile, the mice were divided into 4 groups (n=8-9 every group), which were control group, YXST group (250, 500 and 1000 mg/kg/day for 6 weeks). Cardiac function, exercise tolerance, grip strength, skeletal muscle structure and myoblasts proliferationwere detected. RNA-sequence assays and mass spectrometry analysis of C2C12 myotubes were performed and analyzed. UHPLC was employed to detect YXST's characterize and its principal components. The target protein of YXST were assessed by molecular docking methods. Mitochondria oxygen consumption rate was detected by Seahorse.

Results: YXST improved cardiac function and exercise tolerance, enhanced the slow type I fibers expression, ameliorated mitochondrial biogenesis, and attenuated inflammation level under I/R condition in vivo. YSXT could directly promote exercise capacity and satellite cells proliferation of skeletal muscle under normal condition in vivo. We also found that YXST promoted C2C12 myoblasts differentiation and myotubes formation by regulating mitochondrial biogenesis, mitophagy, and oxidative phosphorylation in vitro. Molecular docking analysis demonstrated that the top 9 compounds identified in blood may bind with BTB and CNC homology 1 protein (BACH1). CETSA assay revealed that YXST had a significantly effect on increasing the thermal stability of BACH1 protein. Interestingly, YXST stimulated the secretion of cardioprotective myokines.

Conclusion: This study revealed that YXST improved cardiac function and exercise tolerance in I/R mice, particularly we found that YXST could directly enhance the exercise capacity of mice under normal condition. Mechanismly, YXST significantly regulated mitochondrial biogenesis, oxidative phosphorylation and myokine production in vivo and in vitro. Our findings provide novel mechanistic insights and pharmacological basis for the application of YXST against coronary heart disease and skeletal muscle injury.

Rescue of Cardiac Dysfunction in Mice with Dilated Cardiomyopathy by Administration of Induced Pluripotent Stem Cell-Derived Exosomes in Utero

Gu Li[1,2], Jie Tian[1], Xiao-Li Liu[2]

1. Department of Cardiology, Children's Hospital of Chongqing Medical University

2. Department of Pediatrics, Brigham and Women's Hospital, Harvard medical university

Background / Aims

Dilated cardiomyopathy (DCM), primarily driven by genetic factors, is an early-onset disease with high mortality and no curative therapies. It accounts for about 50% of pediatric cardiomyopathies, with 40% mortality within two years post-diagnosis. Our prior studies identified that deficiency in **striated preferentially expressed gene** (**SPEG**), a serine/threonine kinase regulating cardiac structure and function, causes embryonic mitochondrial abnormalities and downregulation of **peroxisome proliferator-activated receptor γ coactivator-1α (PGC-1α)**—a master regulator of mitochondrial biogenesis. SPEG deficiency impairs ATP production and mitochondrial cristae formation in developing cardiomyocytes, contributing to heart failure and early death. We hypothesize that **induced pluripotent stem cell-derived cardiomyocyte exosomes (iPSC-CMs-EVs)** enriched with PGC-1α and its phosphorylated forms can rescue mitochondrial dysfunction in SPEG-deficient DCM via in utero delivery. This project aims to: 1) Validate SPEG deletion-induced PGC-1α suppression and mitochondrial defects. 2) Elucidate SPEG-PGC-1α interaction mechanisms. 3) Assess iPSC-CMs-EVs transplantation in rescuing cardiac phenotypes in utero.

Materials and Methods

This study employed SPEGf/f;NKX2.5-Cre mice to establish a cardiac-specific SPEG-deficient DCM animal model. Primary cardiomyocytes transfected with AAV-shSPEG served as the in vitro counterpart. Human iPSCs were differentiated into cardiomyocytes (iPSC-CMs) for 15 days followed by exosome isolation via ultracentrifugation (100,000g, 75 min, 4° C). EVs were characterized for size distribution (nanoparticle tracking), bilayer membrane structure (electron microscopy), surface markers (CD9/CD81$^+$, histone$^-$ measured by immunoblotting), and cardiomyocyte uptake capacity (PKH26 labeling visualized through immunofluorescence). Molecular assessments were performed, including proteomics and KEGG pathway analysis of phosphorylated proteins. To investigate SPEG-PGC-1α interactions, co-immunoprecipitation (Co-IP) was conducted and immunofluorescence colocalization was assessed. Chromatin immunoprecipitation (ChIP) was employed to examine transcriptional regulation. Additionally, PGC-1α pathway components (NRFs, ERRs, PPARs, TFAM) and mtDNA/nDNA ratios were quantified using quantitative PCR and immunoblotting. Functional evaluations encompassed mitochondrial cristae integrity (NAO staining), ATP production (Seahorse XF Analyzer), reactive oxygen species (MitoSOX), and membrane potential (TMRM). Cardiac structure and function was monitored via echocardiography (ejection fraction), survival tracking, and histology (H&E staining of ventricular dimensions). For in utero intervention, ultrasound-guided microinjection (Vevo 2100 + embryo injection system) delivered PBS or EVs directly into E13.5 fetal hearts.

Results

Cardiac-specific SPEG knockout (SPEGf/f;NKX2.5-Cre) mice exhibited severe dilated cardiomyopathy phenotypes, including ventricular dilation (H&E staining), significantly reduced ejection fraction (20% vs. 60% in controls at 3 weeks, $p<0.05$), and high mortality (40% survival vs. 100% in controls by day 21, pIn vitro, EVs co-culture restored cristae integrity and normalized ATP synthesis in shSPEG cardiomyocytes ($p<0.05$ vs. untreated). In utero delivery (E13.5 ultrasound-guided injection) reversed DCM progression, improving EF to 60% ($p<0.05$ vs. SPEG-cKO+PBS) and survival to 80% at 3 weeks ($p<0.05$), while restoring mitochondrial metrics for ≥ 3 weeks. Inhibiting PGC-1α by SR-18292 abolished these benefits, confirming pathway specificity.

Conclusions

SPEG deficiency disrupts mitochondrial structure and function by suppressing PGC-1α expression and phosphorylation, leading to DCM and early death. iPSC-CMs-EVs deliver functional PGC-1α/p-PGC-1α to cardiomyocytes, rescuing mitochondrial defects and heart failure in SPEG-deficient mice via in utero transplantation. Mechanistically, SPEG directly interacts with PGC-1α to regulate its activity. This work identifies a novel SPEG-PGC-1α-mitochondria axis in DCM pathogenesis and provides proof-of-concept for EVs-based prenatal therapy as a translational strategy for incurable pediatric cardiomyopathies.

Suboptimal Control of Small Dense Low-Density Lipoprotein Cholesterol is Associated with Coronary Plaque Progression: An Intravascular Ultrasound Study

You Ran Li, Abulikemu Amuti, Rui Yan Zhang, Chen Die Yang, Xiao Qun Wang

Ruijin Hospital, Shanghai Jiaotong University School of Medicine

BACKGROUND : Plaque progression (PP), a critical step between subclinical atherosclerosis and plaque rupture, is one of the major pathological processes driving the onset of acute coronary events. A number of conventional risk factors, such as diabetes, hypertension, and dyslipidemia, are related to PP. As a subfraction of low-density lipoprotein particles, small dense low-density lipoprotein cholesterol (sdLDL-C) is considered as the most atherogenic lipoprotein. It is characterized by a higher density of 1.044 g/mL to 1.063 g/mL and a smaller particle size with a diameter <25.5 nm, compared with other LDL subclasses. However, the relationship between sdLDL-C and PP is still unclear. In this study, we performed repeat intravascular ultrasound (IVUS) examinations on untreated marginal coronary lesions in patients with coronary artery disease (CAD) and analyzed the relationship between time-averaged sdLDL-C levels and PP determined by changes in atheroma volume.

METHODS : We retrospectively analyzed 86 patients with stable CAD and untreated lesions who underwent IVUS examinations at baseline and during follow-up after ~12 months in Ruijin Hospital, Shanghai Jiao-Tong

University School of Medicine, between January 2020 and May 2023. The cohort comprised both patients with marginal lesions without percutaneous coronary intervention, as well as those with multivessel disease and untreated marginal lesions after percutaneous coronary intervention. PP was determined by increases in percent atheroma volume (PAV), defined as the atheroma volume in proportion to the volume occupied by the entire vascular wall, ≥ 5% during follow-up. Time-averaged values were calculated for all cardiometabolic parameters including sdLDL-C. Multivariate logistic regression analysis was performed to interrogate the association between the time-averaged sdLDL-C and PP.

RESULTS : During a median follow-up of 12.6 months, the mean changes in atheroma volumes were 4.1%±10.2% of PAV and 4.3±11.8 mm^3 of total atheroma volume (TAV). PP was detected in 65 lesions (44.5%), with 12 lesions (18.5%) in 9 patients (18.8%) progressing to require stenting during follow-up. Time-averaged sdLDL-C was significantly correlated to changes in TAV (Pearson r=0.29, P=0.006). Furthermore, subgroup analysis showed that this correlation was significant in diabetic (Pearson r=0.58, P<0.001) but not in nondiabetic (P=0.393) patients. Univariate analysis demonstrated that PP was associated with lower baseline plaque burden, represented by TAV (odds ratio [OR], 0.982 [95% CI, 0.969–0.994]), normalized TAV (OR, 0.971 [95% CI, 0.951–0.990]) and PAV (OR, 0.946 [95% CI, 0.919– 0.972]), and higher time-averaged levels of apoB (OR, 11.357 [95% CI, 1.406–102.908]) and sdLDL-C (OR, 1.191 [95% CI, 1.048–1.367]). Per-lesion multivariate analysis showed that time-averaged sdLDL-C level was associated with PP after adjusting for age and sex. After further adjustments for conventional risk factors, lesion characteristics, and other significant predictors from the univariate analysis, every 0.1-mmol/L increase in time-averaged sdLDL-C conferred a 1.2-fold increased risk of PP. This association remained to be significant after additional adjustment for time-averaged level of LDL-C, but no longer existed after controlling for time-averaged level of apoB. Per-patient analysis exhibited similar findings. In addition, subgroup analysis showed that this association was not affected by diabetic conditions (P for interaction=0.448).

CONCLUSIONS : Our findings suggest that elevated sdLDL-C is independently associated with PP in patients with CAD. Intensive control of sdLDL-C along with other risk factors by lifestyle intervention and optimized medication therapies may maximally inhibit PP, thereby leading to a reduction in cardiovascular events.

Key Words : coronary artery disease ■ intravascular ultrasound ■ plaque progression ■ small dense low-density lipoprotein

Discriminatory and Prognostic Value of MRI-Derived Myocardial Work Efficiency in Heart Failure with Preserved Ejection Fraction: Beyond Left Ventricular Global Longitudinal Strain

Leyi Zhu, Min-Jie Lu

Chinese Academy of Medical Sciences & Peking Union Medical College Fuwai Hospital

Background: Left ventricular global longitudinal strain is an established diagnostic and prognostic marker in heart failure with preserved ejection fraction; however, it is sensitive to left ventricular afterload. Pressure-volume loop analysis accounts for left ventricular loading conditions and may provide additional insights beyond global longitudinal strain into myocardial energetics and work efficiency. Compared with echocardiography, MRI-derived pressure-volume loop analysis offers superior geometric accuracy and direct volumetric measurements; nevertheless, evidence supporting its clinical value in heart failure with preserved ejection fraction remains limited.

Purpose: The purpose of this study is to determine the discriminatory and prognostic value of myocardial work efficiency derived from cardiac MRI in patients with heart failure with preserved ejection fraction.

Methods and Materials: This retrospective study included 158 participants, comprising 124 patients with heart failure with preserved ejection fraction (age 53.8±13.7 years; 77% male) and 34 sex- and age-matched healthy controls (age 56.4±7.2 years; 65% male). All participants were scanned on 3.0-T systems. Left ventricular global longitudinal strain was measured using the feature-tracking technique. Pressure-volume loop analysis was performed by integrating left ventricular myocardial strain analysis with brachial systolic and diastolic blood pressure data, and work efficiency was subsequently calculated. Analysis of covariance was used to compare work efficiency across healthy controls and patient subgroups with adjustment for global longitudinal strain. Logistic regression analysis was conducted to evaluate the ability of work efficiency to discriminate between healthy controls and patients with heart failure with preserved ejection fraction. The primary endpoint was a composite of all-cause death and heart failure hospitalization. Cox regression analysis was performed to examine the associations between work efficiency and clinical outcomes.

Results: In all participants, work efficiency showed moderate correlations with left ventricular ejection fraction (r = 0.62; P < .001) and global longitudinal strain (r = -0.58; P < .001). Participants were divided into three groups: healthy controls, heart failure with preserved ejection fraction patients with global longitudinal strain ≤ median, and those with global longitudinal strain > median. Work efficiency demonstrated a stepwise decline across these three groups (P for trend < .001; all Bonferroni-corrected P < .001), and this trend in work efficiency remained significant after adjustment for global longitudinal strain (P for trend < .001). In multivariable logistic regression analysis, lower work efficiency was significantly associated with higher odds of heart failure with preserved ejection fraction (adjusted odds ratio per 1% decrease, 1.33 [95% CI: 1.03, 1.82; P = .044]), even after adjusting for global longitudinal strain. During a median follow-up of 5.4 years, 49 patients with heart failure with preserved ejection fraction reached the primary endpoint. Multivariable Cox regression analysis revealed that lower work efficiency (<71.15%) was an independent predictor of the primary endpoint (adjusted hazard ratio, 1.92 [95% CI: 1.03, 3.57; P = .040]) even after adjustment for age, sex, late gadolinium enhancement, and extracellular volume fraction, whereas global longitudinal strain was not.

Conclusion: Left ventricular work efficiency derived from cardiac MRI provided independent discriminatory and prognostic value in patients with heart failure with preserved ejection fraction, even after adjustment for global longitudinal strain.

Clinical Relevance/Application: Cardiac MRI-derived myocardial work efficiency is impaired in patients with heart failure with preserved ejection fraction, and it may serve as a promising non-invasive marker for both diagnosis and risk stratification in this condition, providing a new dimension beyond global longitudinal strain.

Keywords: Heart failure with preserved ejection fraction, cardiac magnetic resonance, strain, pressure-volume loop analysis, work efficiency

Nuclear AGO2 exacerbated high-fat diet-induced heart failure by activating transcription of HMGCS2 to promote ketogenesis in the heart

Kunying Jin, Hua-Ping Li, Chen Chen

Department of Cardiology, Tongji Hospital, Tongji Medical College, Huazhong University of Science and Technology

Background and Aims: Heart failure (HF) is a clinical syndrome that results from structural or functional cardiac abnormalities and is characterized by high morbidity and mortality, reduced ability, and poor quality of life. Clinically, despite the fact that general anti-HF therapies are proposed for treating established cardiac dysfunction, including β-blockers, ACE inhibitors, aldosterone antagonism, and SGLT2 inhibitors, the morbidity and mortality of patients with HF remain high. It is reported that unhealthy lifestyles, prolonged survival of patients with various cardiovascular diseases, and aged populations all contribute to the increased overall prevalence of HF. Especially, hyperglycemia is associated with the development of HF. Meanwhile, hyperlipidemia is also associated with HF risk. Therefore, metabolism-related targets may bring therapeutic effects against HF. Recent studies suggested that microRNAs (miRNAs) located in different subcellular organelles could regulate lipid metabolism and cardiac function. However, the functional property of subcellular AGO2, the core member of miRNA machinery, remained elusive in hyperlipidemia-related HF.

Methods: The causal role of nuclear AGO2 in inducing cardiac dysfunction was revealed with a recombinant adeno-associated virus (serotype 9) vector. All animal experiments followed ARRIVE guidelines and were performed in compliance with the Institutional Animal Care and Use Committee guidelines at Tongji Medical College, Huazhong University of Science and Technology (Wuhan, China, ethics permit number: 199-20220714). Male C57BL/6J mice (22-25 g, seven-week-old) were purchased from GemPharmatech (Nanjing, China). Mice were housed at 22 ° C with a 12 h light, 12 h dark cycle and were given free access to food and water. All mice were allowed to acclimatize to the animal facility environment for 1 week before being used for experimentation, and they were subjected to either a standard chow diet (Cat #12031, containing 10% fat, 70% carbohydrate, 20% protein, Medicience Diets, Jiangsu, China) or high-fat diet (Cat #12033, containing 60% fat, 20% carbohydrate, 20% protein, Medicience Diets Jiangsu, China) feeding. After feeding for 16 weeks, mice were randomly allocated into experimental groups and received the recombinant adeno-associated virus serotype 9 (rAAV9) (ViGene Biosciences, Shandong, China) containing 5 x 10^{11} AAV9 vector genomes. Eight weeks after the rAAV injection, echocardiography (Vevo1100, VisualSonics, Toronto, Canada) and Millar catheter system (Millar Instruments, Houston, Texas, USA) were used to assess left ventricle systolic and diastolic function. Then, mice were anesthetized and sacrificed, their organs and plasma were isolated, followed by storage at -80 ° C, and portions of the heart were fixed in 4% phosphate-buffered paraformaldehyde for histopathological examination. The underlying mechanisms were explored with echocardiography, catheter manometer system, proteomics analyses, chromatin immunoprecipitation assays, luciferase assays, Western blotting, immunofluorescence, seahorse assays, β-hydroxybutyrate and ATP measurements.

Results: Knockdown of AGO2 attenuated high-fat diet (HFD)-induced cardiac dysfunction. Mechanistically, AGO2 could activate the transcrip-

tion of HMGCS2. Knockdown of either cardiac AGO2 or HMGCS2 protected against cardiac dysfunction in HFD-induced HF. Subsequent high-through profiling further identified ATP5F1E and UQCR10 as the key downstream targets for AGO2/HMGCS2 mediated β-hydroxybutyrate over-production, and a feed forward loop involving lipo-toxicity and ketone-toxicity was discovered. Furthermore, a PKCα-ERK-EGR1-AGO2-HMGCS2 axis in the initiation of fatty acids-induced cardiomyocyte dysfunction was revealed. Importantly, overexpressing of nuclear AGO2 rather than cytosolic AGO2 exacerbated the cardiac dysfunction in HFD-induced HF mice.

Conclusions: In this study, we found that cardiac AGO2 was significantly upregulated in the HFD-induced HF mice and translocated into the nucleus to directly enhance HMGCS2 transcription, leading to enhanced ketogenesis and mitochondrial dysfunction. We demonstrated that AGO2 or HMGCS2 shRNA delivered by recombinant adeno-associated virus (rAAV) was able to rescue inappropriate ketone body accumulation and cardiac dysfunction in HFD-induced HF mice, suggesting a potential therapy for hyperlipidemia-associated cardiac dysfunction.

The impact of short-term exposure to nitrogen dioxide on endothelial function in Chinese elders: A cross-sectional study

Qi-Xia Jiang[1], Lin-Shan Zhong[2], Kai Zhang[2]

1. Shanghai General Hospital, Shanghai Jiao Tong University School of Medicine

2. Tong Ren Hospital, Shanghai Jiao Tong University School of Medicine

Abstract

Background and Objectives

Nitrogen dioxide (NO_2), a critical component of ambient air pollution generated primarily through combustion processes, has been consistently associated with adverse cardiovascular outcomes in epidemiological studies. While existing research has established links between NO_2 exposure and increased cardiovascular disease (CVD) mortality (demonstrating 13% elevation per 10 μg/m³ annual increase according to meta-analyses), the specific pathophysiological mechanisms mediating these effects, particularly regarding vascular endothelial function in vulnerable elderly populations, remain incompletely characterized. This study aimed to comprehensively investigate the temporal dynamics, concentration-response relationships, and population susceptibility patterns of short-term NO_2 exposure effects on vascular endothelial function, as measured by flow-mediated dilation (FMD), among community-dwelling elderly individuals in Shanghai, China. The utilization of FMD, a well-validated non-invasive measure of endothelial function, provides unique insights into the early vascular effects of air pollution exposure preceding clinical cardiovascular events.

Materials and Methods

We conducted a rigorous cross-sectional analysis of 812 elderly participants (aged ≥ 65 years, mean age 70.6±5.4 years, 61% female) who underwent standardized FMD assessment at Tongren Hospital, Shanghai Jiao Tong University School of Medicine between January 2020 and December 2022. All participants completed comprehensive questionnaires documenting demographic characteristics, lifestyle factors (including smoking and alcohol consumption), and medical history (encompassing hypertension, diabetes mellitus, dyslipidemia, coronary artery disease [CAD], and CVD). Individualized NO_2 exposure assessment was achieved through the Tracking Air Pollution in China (TAP) platform, which utilizes an advanced two-stage machine learning algorithm incorporating: a first-stage random forest model integrating multi-source data (satellite observations, ground monitoring measurements, population density, and land use statistics), and a second-stage gradient boosting model that enhances prediction accuracy (cross-validated R^2=0.91). Residential address-specific daily NO_2 concentrations were obtained at 10×10 km spatial resolution.

Vascular endothelial function was quantified via brachial artery FMD using high-resolution ultrasound (UNEXEF18VG, Unex Co. Ltd., Japan) following established protocols. After obtaining baseline arterial diameter measurements, transient ischemia was induced via blood pressure cuff inflation to 200 mmHg for 5 minutes, with subsequent FMD calculated as the maximal percentage increase in post-deflation diameter relative to baseline. Vascular endothelial dysfunction (VED) was defined as FMD <6.0%. All examinations were performed by a single certified technician to ensure consistency (intraclass correlation coefficient=0.93).

Statistical analyses employed distributed lag nonlinear models (DLNM) coupled with generalized additive models (GAM) to characterize both immediate and delayed exposure-response relationships. Three progressively adjusted models were implemented: Model 1 (unadjusted), Model 2 (demographic and meteorological adjustments), and Model 3 (full adjustment including comorbidities). Effect estimates were expressed as percentage change in FMD or odds ratios for VED per interquartile range (IQR) increase in NO_2 concentration.

Results

Our analysis of 812 elderly participants (mean age 70.6±5.4 years) revealed significant associations between short-term NO_2 exposure and vascular endothelial dysfunction. The distributed lag nonlinear models demonstrated that NO_2 exposure induced time-dependent endothelial impairment, with flow-mediated dilation (FMD) showing statistically significant reductions at lag days 1 (-26.87%, 95%CI: -44.34% to -9.40%), 5 (-19.64%, 95%CI: -36.48% to -2.81%), and 6 (-15.93%, 95%CI: -33.49% to 1.63%), while the risk of vascular endothelial dysfunction (VED, FMD<6.0%) increased significantly only at lag day 5 (OR=1.27, 95%CI:1.05-1.53). Cumulative effect analysis established a clear concentration-response relationship, with NO_2 levels between 35-85 μg/m³ showing progressive FMD decline (p<0.05), as visualized through three-dimensional response surface models that mapped the combined effects of concentration and exposure timing. Notably, subgroup analyses identified enhanced susceptibility in participants without coronary artery disease (CAD) or hyperlipidemia history, who exhibited 23% greater FMD reduction (p<0.05) and prolonged effect duration (7 days vs 5-6 days in the overall population), with significant interaction terms for both CAD status (p-interaction=0.007) and hyperlipidemia (p-interaction=0.018). These findings collectively demonstrate that NO_2 exposure impairs endothelial function through distinct temporal patterns and concentration-dependent mechanisms, with particular vulnerability observed in ostensibly healthier elderly subgroups lacking traditional cardiovascular risk factors.

Discussion and Conclusions

This study provides robust epidemiological evidence that short-term NO_2 exposure at concentrations within current regulatory limits (China's secondary standard of 80 μg/m³ for 24-hour exposure) induces measurable endothelial dysfunction in elderly individuals through time-dependent mechanisms. The characteristic lag pattern (peaking at 5 days post-exposure) implicates biological processes such as oxidative stress-mediated reduction in nitric oxide bioavailability and subsequent vascular inflammation. The paradoxical vulnerability of ostensibly healthier subgroups may reflect the absence of compensatory vascular adaptations present in patients with established cardiometabolic diseases.

From a public health perspective, these findings suggest that current air quality standards may inadequately protect elderly populations from NO_2-mediated vascular injury. The demonstration of significant effects at concentrations below regulatory thresholds highlights the need for: revised air quality guidelines specifically considering endothelial health endpoints, targeted protective measures for susceptible subgroups, and incorporation of vascular function monitoring in environmental health risk assessment.

Methodologically, this study advances the field through its application of distributed lag modeling to characterize temporal effect patterns, residential-level exposure assessment, and standardized FMD protocols. The identification of specific susceptibility patterns provides important insights for both clinical practice and environmental policy development. Future research should investigate the potential benefits of pharmacological and behavioral interventions to mitigate NO_2-induced endothelial dysfunction in high-risk populations.

Association Between Serum Cartilage Oligomeric Matrix Protein (COMP) Levels and Calcification Burden in Aortic Valve Calcification Disease, and Its Predictive Value for Prognosis After Transcatheter Aortic Valve Replacement

zheng Zheng[1,2], Fen Liu[1], qian Zhao[1], Jun-Yi Luo[1], Ning Song[1], Xiao-Mei Li[1], Yi-Ning Yang[2]

1. The First Department of Coronary Heart Disease, Heart Center of the First Affiliated Hospital

2. Department of Cardiology, People's Hospital of Xinjiang Uygur Autonomous Region

Objective: To investigate the association between serum COMP levels and aortic valve calcification volume in patients with calcific aortic valve disease (CAVD) and to evaluate its predictive value for major adverse cardiovascular and cerebrovascular events (MACCE) in patients undergoing transcatheter aortic valve replacement (TAVR).

Methods: This retrospective cohort study consecutively enrolled patients with severe aortic stenosis who underwent TAVR at the First Affiliated Hospital of Xinjiang Medical University and the People's Hospital of Xinjiang Uygur Autonomous Region between January 2016 and December 2023. Baseline serum COMP concentrations were measured using enzyme-linked immunosorbent assay (ELISA), and aortic valve calcification volume was quantitatively assessed via imaging techniques. The relationship between COMP levels and calcification volume was analyzed using linear regression, while the predictive efficacy of COMP for MACCE was evaluated using Cox proportional hazards models.

Results: A total of 223 patients (mean age 71.3±8.3 years, 59.6% male) were included. Serum COMP levels were normally distributed (62.71±26.98 ng/mL), and the median aortic valve calcification volume was 517.9 mm³ (interquartile range: 238.8–743.1). Linear regression

revealed a significant inverse correlation between COMP levels and calcification volume (β = -6.5, R^2 = 0.22, p < 0.0001). When stratified by calcification volume (cutoff: 500 mm^3), the severe calcification group exhibited significantly lower COMP levels than the mild calcification group (52.96±3.52 vs. 69.53±2.69 ng/mL, p < 0.0001). Logistic regression indicated that every 10 ng/mL increase in COMP reduced the risk of severe calcification by 8% (OR = 0.92, 95% CI: 0.87–0.97). During a median follow-up of 31.3 months, the incidence of MACCE was 21.84%. Survival analysis demonstrated significantly higher all-cause mortality in the low COMP group (≤ 45 ng/mL) compared to the high COMP group (24.1% vs. 4.9%, HR = 0.15, 95% CI: 0.04–0.55), which remained significant after adjusting for age and sex (adjusted HR = 0.07, 95% CI: 0.01–0.54). The area under the ROC curve for COMP in predicting all-cause mortality was 0.71 (sensitivity 63.6%, specificity 77.8%).

Conclusion: Serum COMP levels serve as a novel biomarker inversely associated with calcification burden in CAVD. Low COMP levels (≤ 45 ng/mL) are an independent predictor of all-cause mortality post-TAVR, highlighting its potential clinical value for prognostic assessment.

Objective: To investigate the association between serum COMP levels and aortic valve calcification volume in patients with calcific aortic valve disease (CAVD) and to evaluate its predictive value for major adverse cardiovascular and cerebrovascular events (MACCE) in patients undergoing transcatheter aortic valve replacement (TAVR).

Methods: This retrospective cohort study consecutively enrolled patients with severe aortic stenosis who underwent TAVR at the First Affiliated Hospital of Xinjiang Medical University and the People's Hospital of Xinjiang Uygur Autonomous Region between January 2016 and December 2023. Baseline serum COMP concentrations were measured using enzyme-linked immunosorbent assay (ELISA), and aortic valve calcification volume was quantitatively assessed via imaging techniques. The relationship between COMP levels and calcification volume was analyzed using linear regression, while the predictive efficacy of COMP for MACCE was evaluated using Cox proportional hazards models.

Results: A total of 223 patients (mean age 71.3±8.3 years, 59.6% male) were included. Serum COMP levels were normally distributed (62.71±26.98 ng/mL), and the median aortic valve calcification volume was 517.9 mm^3 (interquartile range: 238.8–743.1). Linear regression revealed a significant inverse correlation between COMP levels and calcification volume (β = -6.5, R^2 = 0.22, p < 0.0001). When stratified by calcification volume (cutoff: 500 mm^3), the severe calcification group exhibited significantly lower COMP levels than the mild calcification group (52.96±3.52 vs. 69.53±2.69 ng/mL, p < 0.0001). Logistic regression indicated that every 10 ng/mL increase in COMP reduced the risk of severe calcification by 8% (OR = 0.92, 95% CI: 0.87–0.97). During a median follow-up of 31.3 months, the incidence of MACCE was 21.84%. Survival analysis demonstrated significantly higher all-cause mortality in the low COMP group (≤ 45 ng/mL) compared to the high COMP group (24.1% vs. 4.9%, HR = 0.15, 95% CI: 0.04–0.55), which remained significant after adjusting for age and sex (adjusted HR = 0.07, 95% CI: 0.01–0.54). The area under the ROC curve for COMP in predicting all-cause mortality was 0.71 (sensitivity 63.6%, specificity 77.8%).

Conclusion: Serum COMP levels serve as a novel biomarker inversely associated with calcification burden in CAVD. Low COMP levels (≤ 45 ng/mL) are an independent predictor of all-cause mortality post-TAVR, highlighting its potential clinical value for prognostic assessment.

Liraglutide Attenuates High-Glucose-Induced Hypoxia/Reoxygenation Injury in Cardiomyocytes by Regulating Fatty Acid Metabolism and Inhibiting Apoptosis via the GLP-1R/AMPK Pathway

Bin-Bin Fang[1,2], Fen Liu[1,2], Jun-Yi Luo[2], Ning Song[2], Hong-Li Wang[1], Wei Ji[2], qian Xie[2], Yi-Ning Yang[3], Xiao-Mei Li[2]

1. State Key Laboratory of Pathogenesis, Prevention and Treatment of High Incidence Diseases in Central Asia, Clinical Medical Research Institute, the First Affiliated Hospital of Xinjiang Medical University

2. Department of Coronary Heart Disease, Heart Center of the First Affiliated Hospital

3. Department of Cardiology, People's Hospital of Xinjiang Uygur Autonomous Region

Objective To investigate whether liraglutide alleviates hypoxia/reoxygenation (H/R) injury in cardiomyocytes under high-glucose conditions by activating the AMPK signaling pathway to regulate fatty acid metabolism and to elucidate the underlying mechanisms involved.

Methods Rat H9C2(2-1) cardiomyocytes were divided into six groups: the control group (Con), high-glucose group (HG), high-glucose hypoxia/reoxygenation group (HG+H/R), liraglutide intervention group (HG+H/R+Lir), AMPK inhibition group (HG+H/R+Lir+CC), and GLP-1R inhibition group (HG+H/R+Lir+GLP-1R). A high-glucose model was established by culturing cardiomyocytes in high-glucose DMEM (25 mM glucose), and an H/R model was constructed using a hypoxia chamber. Each group was treated with liraglutide (200 nM), the AMPK inhibitor Compound C (0.5 μM), or a GLP-1R inhibitor (0.163 μM). Western blotting was used to detect the expression of AMPK, GLP-1R, PPARα, CPT1a, ACC, and the apoptosis-related proteins BCL2 and BAX. Flow cytometry was used to elucidate early apoptosis rates, and immunofluorescence was used to assess the expression of the liraglutide receptor GLP-1R.

Results Compared with the Con group, the HG and HG+H/R groups presented reduced GLP-1R expression and p-AMPK/AMPK ratios (P < 0.05), whereas the HG+H/R+Lir group presented significantly increased GLP-1R expression and increased AMPK phosphorylation, indicating that liraglutide increases GLP-1R expression and activates the AMPK signaling pathway in cardiomyocytes under high-glucose conditions. Additionally, liraglutide significantly increased the expression of the fatty acid metabolism-related proteins PPARα and CPT1a, as well as ACC phosphorylation levels (P < 0.05). Moreover, the HG+H/R group presented increased early apoptosis rates and a decreased Bcl2/Bax ratio, whereas liraglutide intervention reduced early apoptosis rates and increased the Bcl2/Bax ratio. The immunofluorescence results revealed decreased GLP-1R expression in the HG group, which was significantly increased by liraglutide (P < 0.05). However, Compound C or the GLP-1R inhibitor partially counteracted these protective effects.

Conclusion Liraglutide activates the AMPK signaling pathway in a GLP-1R-dependent manner, promoting fatty acid metabolism and inhibiting apoptosis, thereby alleviating H/R injury in cardiomyocytes under high-glucose conditions. This study provides new theoretical insights and potential therapeutic targets for the treatment of patients with diabetes complicated by coronary heart disease.

Objective To investigate whether liraglutide alleviates hypoxia/reoxygenation (H/R) injury in cardiomyocytes under high-glucose conditions by activating the AMPK signaling pathway to regulate fatty acid metabolism and to elucidate the underlying mechanisms involved.

Methods Rat H9C2(2-1) cardiomyocytes were divided into six groups: the control group (Con), high-glucose group (HG), high-glucose hypoxia/reoxygenation group (HG+H/R), liraglutide intervention group (HG+H/R+Lir), AMPK inhibition group (HG+H/R+Lir+CC), and GLP-1R inhibition group (HG+H/R+Lir+GLP-1R). A high-glucose model was established by culturing cardiomyocytes in high-glucose DMEM (25 mM glucose), and an H/R model was constructed using a hypoxia chamber. Each group was treated with liraglutide (200 nM), the AMPK inhibitor Compound C (0.5 μM), or a GLP-1R inhibitor (0.163 μM). Western blotting was used to detect the expression of AMPK, GLP-1R, PPARα, CPT1a, ACC, and the apoptosis-related proteins BCL2 and BAX. Flow cytometry was used to elucidate early apoptosis rates, and immunofluorescence was used to assess the expression of the liraglutide receptor GLP-1R.

Results Compared with the Con group, the HG and HG+H/R groups presented reduced GLP-1R expression and p-AMPK/AMPK ratios (P < 0.05), whereas the HG+H/R+Lir group presented significantly increased GLP-1R expression and increased AMPK phosphorylation, indicating that liraglutide increases GLP-1R expression and activates the AMPK signaling pathway in cardiomyocytes under high-glucose conditions. Additionally, liraglutide significantly increased the expression of the fatty acid metabolism-related proteins PPARα and CPT1a, as well as ACC phosphorylation levels (P < 0.05). Moreover, the HG+H/R group presented increased early apoptosis rates and a decreased Bcl2/Bax ratio, whereas liraglutide intervention reduced early apoptosis rates and increased the Bcl2/Bax ratio. The immunofluorescence results revealed decreased GLP-1R expression in the HG group, which was significantly increased by liraglutide (P < 0.05). However, Compound C or the GLP-1R inhibitor partially counteracted these protective effects.

Conclusion Liraglutide activates the AMPK signaling pathway in a GLP-1R-dependent manner, promoting fatty acid metabolism and inhibiting apoptosis, thereby alleviating H/R injury in cardiomyocytes under high-glucose conditions. This study provides new theoretical insights and potential therapeutic targets for the treatment of patients with diabetes complicated by coronary heart disease.

Epicardial Adipose Tissue Volume and Density are Associated with Heart Failure with Improved Ejection Fraction

Chendie Yang, Rui-Yan Zhang, Xiao-Qun Wang

Ruijin Hospital, Shanghai Jiao-Tong University School of Medicine, Shanghai, P. R. China

Background: Heart failure (HF) with improved ejection fraction (EF, HFimpEF) gains increasing attention as a distinct HF subtype, characterized by left ventricular reverse modeling and myocardial functional recovery. Multiple cardiometabolic factors are implicated in this process. Epicardial adipose tissue (EAT), emerging as an endocrine and paracrine organ, contributes to the onset and progression of HF. However, the relation between EAT and the incidence of HFimpEF is still unclear.

Methods: A total of 203 hospitalized HF patients with reduced EF (HFrEF, EF ≤ 40%) who underwent coronary CT angiography (CCTA) during index hospitalization were consecutively enrolled between November 2011 and December 2022. Routine follow-up and repeat echocardiograms

were performed. The incidence of HFimpEF was defined as (1) an absolute EF improvement ≥ 10% and (2) a second EF > 40% (at least 3 months apart). EAT volume and density were semiautomatically quantified on non-enhanced series of CCTA scans.

Results: During a median follow-up of 8.6 (4.9~13.3) months, 104 (51.2%) patients developed HFimpEF. Compared with HFrEF patients, HFimpEF patients had lower EAT volume (115.36 (87.08~154.78) mL vs 169.67 (137.22~218.89) mL , P< 0.001) and higher EAT density (-74.92 ± 6.84 HU vs -78.76 ± 6.28 HU, P< 0.001) both in HF patients with and without an ischemic etiology. Meanwhile, EAT density was inversely correlated with EAT volume (r=-0.33, P<0.001). Multivariate analysis showed lower EAT volume (OR: 0.885 [95%CI 0.822~0.947]) and higher density (OR: 1.845 [95%CI 1.023~3.437]) were both independently associated with the incidence of HFimpEF, after adjustment for conventional risk factors, pharmacological therapies and baseline anthropometric parameters including body mass index. Subgroup analysis revealed that the association between EAT properties and HFimpEF was not modified by HF etiology.

Conclusions: This study reveals that lower EAT volume and higher EAT density are associated with development of HFimpEF. Therapies targeted at reducing EAT quantity and improving its quality might provide favorable effects on myocardial recovery in HF patients.

Background: Heart failure (HF) with improved ejection fraction (EF, HFimpEF) gains increasing attention as a distinct HF subtype, characterized by left ventricular reverse modeling and myocardial functional recovery. Multiple cardiometabolic factors are implicated in this process. Epicardial adipose tissue (EAT), emerging as an endocrine and paracrine organ, contributes to the onset and progression of HF. However, the relation between EAT and the incidence of HFimpEF is still unclear. **Methods:** A total of 203 hospitalized HF patients with reduced EF (HFrEF, EF ≤ 40%) who underwent coronary CT angiography (CCTA) during index hospitalization were consecutively enrolled between November 2011 and December 2022. Routine follow-up and repeat echocardiograms were performed. The incidence of HFimpEF was defined as (1) an absolute EF improvement ≥ 10% and (2) a second EF > 40% (at least 3 months apart). EAT volume and density were semiautomatically quantified on non-enhanced series of CCTA scans. **Results:** During a median follow-up of 8.6 (4.9~13.3) months, 104 (51.2%) patients developed HFimpEF. Compared with HFrEF patients, HFimpEF patients had lower EAT volume (115.36 (87.08~154.78) mL vs 169.67 (137.22~218.89) mL , ^{P}< 0.001) and higher EAT density (-74.92 ± 6.84 HU vs -78.76 ± 6.28 HU, ^{P}< 0.001) both in HF patients with and without an ischemic etiology. Meanwhile, EAT density was inversely correlated with EAT volume (r=-0.33, ^{P}<0.001). Multivariate analysis showed lower EAT volume (OR: 0.885 [95%CI 0.822~0.947]) and higher density (OR: 1.845 [95%CI 1.023~3.437]) were both independently associated with the incidence of HFimpEF, after adjustment for conventional risk factors, pharmacological therapies and baseline anthropometric parameters including body mass index. Subgroup analysis revealed that the association between EAT properties and HFimpEF was not modified by HF etiology. **Conclusions**: This study reveals that lower EAT volume and higher EAT density are associated with development of HFimpEF. Therapies targeted at reducing EAT quantity and improving its quality might provide favorable effects on myocardial recovery in HF patients.

Visit-to-Visit Glycemic Variability is Associated with the Incidence of Heart Failure with Improved Ejection Fraction

Chendie Yang, Rui-Yan Zhang, Xiao-Qun Wang

Ruijin Hospital, Shanghai Jiao-Tong University School of Medicine, Shanghai, P. R. China

Aims: With advanced guideline-directed therapies, a substantial portion of heart failure (HF) patients have experienced improvement of ejection fraction (EF), termed HFimpEF. We sought to investigate the association between visit-to-visit glycemic variability (GV) and the incidence of HFimpEF.

Methods: From January 2013 to December 2020, 951 hospitalized HF patients with reduced EF (HFrEF, EF ≤ 40%) were consecutively enrolled and followed up for around 12 months. The incidence of HFimpEF, defined as (1) an absolute EF improvement ≥ 10% and (2) a second EF > 40% and its relationship with visit-to-visit fasting plasma glucose (FPG) variability were analyzed.

Results:

A total of 519 HFrEF patients were finally enrolled. During a mean follow-up of 12.2 ± 0.6 months, 218 (42.0%) patients developed HFimpEF. Multivariate analysis showed visit-to-visit FPG variability was independently associated with incidence of HFimpEF after adjustment for baseline HBA1c, mean FPG during follow-up and other traditional risk factors (odds ratio [OR] for highest vs. lowest quartile of CV of FPG: 0.487 [95% CI 0.257~0.910]). Assessing FPG variability by alternative measures yielded similar results. Subgroup analysis revealed the relationship between GV and HFimpEF was only observed in HF of ischemic etiology and the association persisted significant irrespective of glycemic levels and diabetic conditions.

Conclusions: This study reveals that greater visit-to-visit FPG variability is associated with compromised development of HFimpEF independent of mean glycemic levels and diabetic conditions. Therapies targeted at improving GV might provide favorable effects on myocardial recovery in HF patients even without diabetes.

Aims: With advanced guideline-directed therapies, a substantial portion of heart failure (HF) patients have experienced improvement of ejection fraction (EF), termed HFimpEF. We sought to investigate the association between visit-to-visit glycemic variability (GV) and the incidence of HFimpEF. **Methods:** From January 2013 to December 2020, 951 hospitalized HF patients with reduced EF (HFrEF, EF ≤ 40%) were consecutively enrolled and followed up for around 12 months. The incidence of HFimpEF, defined as (1) an absolute EF improvement ≥ 10% and (2) a second EF > 40% and its relationship with visit-to-visit fasting plasma glucose (FPG) variability were analyzed.**Results:** A total of 519 HFrEF patients were finally enrolled. During a mean follow-up of 12.2 ± 0.6 months, 218 (42.0%) patients developed HFimpEF. Multivariate analysis showed visit-to-visit FPG variability was independently associated with incidence of HFimpEF after adjustment for baseline HBA1c, mean FPG during follow-up and other traditional risk factors (odds ratio [OR] for highest vs. lowest quartile of CV of FPG: 0.487 [95% CI 0.257~0.910]). Assessing FPG variability by alternative measures yielded similar results. Subgroup analysis revealed the relationship between GV and HFimpEF was only observed in HF of ischemic etiology and the association persisted significant irrespective of glycemic levels and diabetic conditions. **Conclusions**: This study reveals that greater visit-to-visit FPG variability is associated with compromised development of HFimpEF independent of mean glycemic levels and diabetic conditions. Therapies targeted at improving GV might provide favorable effects on myocardial recovery in HF patients even without diabetes. **Aims:** With advanced guideline-directed therapies, a substantial portion of heart failure (HF) patients have experienced improvement of ejection fraction (EF), termed HFimpEF. We sought to investigate the association between visit-to-visit glycemic variability (GV) and the incidence of HFimpEF. **Methods:** From January 2013 to December 2020, 951 hospitalized HF patients with reduced EF (HFrEF, EF ≤ 40%) were consecutively enrolled and followed up for around 12 months. The incidence of HFimpEF, defined as (1) an absolute EF improvement ≥ 10% and (2) a second EF > 40% and its relationship with visit-to-visit fasting plasma glucose (FPG) variability were analyzed.

Visit-to-Visit Fasting Plasma Glucose Variability is Associated with Left Ventricular Adverse Remodeling in Diabetic Patients with STEMI

Chendie Yang, Rui-Yan Zhang, Xiao-Qun Wang

Ruijin Hospital, Shanghai Jiao-Tong University School of Medicine, Shanghai, P. R. China

Background:

Patients with type 2 diabetes mellitus (T2DM) are predisposed to poor cardiovascular outcomes after ST-segment elevation myocardial infarction (STEMI). Left ventricular adverse remodeling (LVAR) triggered upon myocardial infarction is recognized as the predominant pathological process in the development of heart failure. In the present study, we sought to investigate whether visit-to-visit fasting plasma glucose (FPG) variability is a potential predictor of LVAR in T2DM patients after STEMI.

Methods:

From January 2014 to December 2018 in Ruijin Hospital, T2DM patients with STEMI who underwent primary percutaneous coronary intervention were consecutively enrolled and followed up for ~12 months. The changes in left ventricular geometric and functional parameters between baseline and 12-month follow-up were assessed by echocardiography. The incidence of LVAR, defined as 20% increase in indexed left ventricular end-diastolic volume (LVEDV), and its relationship with visit-to-visit FPG variability were analyzed. Multivariate regression models were constructed to test the predictive value of FPG variability for post-infarction LVAR.

Results:

A total of 437 patients with type 2 diabetes and STEMI were included in the final analysis. During a mean follow-up of 12.4±1.1 months, the incidence of LVAR was 20.6% and mean enlargement of indexed LVEDV was 3.31±14.4 mL/m^2, which was significantly increased in patients with higher coefficient variance (CV) of FPG (P=0.002) irrespective of baseline glycemic levels. In multivariate analysis, FPG variability was independently associated with incidence of post-infarction LVAR after adjustment for traditional risk factors, baseline HbA1c as well as mean FPG during follow-up (OR: 3.021 [95% CI:1.081~8.764] for highest vs. lowest tertile of CV of FPG). Assessing FPG variability by two measures, including standard deviation (SD) and variability independent of the mean (VIM), yielded similar findings.

Conclusions:

This study suggests that visit-to-visit FPG variability is an independent predictor of incidence of LVAR in T2DM patients with STEMI.

Background: Patients with type 2 diabetes mellitus (T2DM) are predisposed to poor cardiovascular outcomes after ST-segment elevation myocardial infarction (STEMI). Left ventricular adverse remodeling (LVAR) triggered upon myocardial infarction is recognized as the predominant pathological process in the development of heart failure. In the present study, we sought to investigate whether visit-to-visit fasting plasma glucose (FPG) variability is a potential predictor of LVAR in T2DM patients after STEMI. **Methods:** From January 2014 to December 2018 in Ruijin Hospital, T2DM patients with STEMI who underwent primary percutaneous coronary intervention were consecutively enrolled and followed up for ~12 months.

The changes in left ventricular geometric and functional parameters between baseline and 12-month follow-up were assessed by echocardiography. The incidence of LVAR, defined as 20% increase in indexed left ventricular end-diastolic volume (LVEDV), and its relationship with visit-to-visit FPG variability were analyzed. Multivariate regression models were constructed to test the predictive value of FPG variability for post-infarction LVAR. **Results:** A total of 437 patients with type 2 diabetes and STEMI were included in the final analysis. During a mean follow-up of 12.4±1.1 months, the incidence of LVAR was 20.6% and mean enlargement of indexed LVEDV was 3.31±14.4 mL/m2, which was significantly increased in patients with higher coefficient variance (CV) of FPG ($_p$=0.002) irrespective of baseline glycemic levels. In multivariate analysis, FPG variability was independently associated with incidence of post-infarction LVAR after adjustment for traditional risk factors, baseline HbA1c as well as mean FPG during follow-up (OR: 3.021 [95% CI:1.081~8.764] for highest vs. lowest tertile of CV of FPG). Assessing FPG variability by two measures, including standard deviation (SD) and variability independent of the mean (VIM), yielded similar findings. **Conclusions:** This study suggests that visit-to-visit FPG variability is an independent predictor of incidence of LVAR in T2DM patients with STEMI.

Insulin Resistance is Associated with Heart Failure with Recovered Ejection Fraction in Non-diabetic Patients

Chendie Yang, Rui-Yan Zhang, Xiao-Qun Wang

Ruijin Hospital, Shanghai Jiao-Tong University School of Medicine, Shanghai, P. R. China

Background:

Due to advances in medical treatments, a substantial proportion of heart failure (HF) patients have experienced recovery of ejection fraction (EF), termed HF with recovered EF (HFrecEF). Insulin resistance (IR) is prevalent in HF and tightly related with prognosis. This study investigates the relationship between IR and the incidence of HFrecEF in non-diabetic patients.

Methods and Results:

A total of 262 non-diabetic HF patients with reduced EF (HFrEF) were consecutively enrolled. Patients were classified into HFrecEF (follow-up EF > 40% and ≥ 10% absolute increase) or otherwise persistent HFrEF based on repeat echocardiograms after 12 months. IR was estimated by an updated homeostasis model assessment (HOMA2-IR). The median HOMA2-IR level was 1.05 (IQR 0.67~1.63) in our cohort of non-diabetic HF patients. During follow-up, 121 (46.2% [95% CI 40.2%~52.2%]) patients developed HFrecEF. Compared with HFrEF patients, HFrecEF patients had significantly lower HOMA2-IR levels (0.92 [IQR 0.61 ~ 1.37] vs. 1.14 [IQR 0.75 ~ 1.78], P=0.007), especially in HF of nonischemic etiology. Log_2-transformed HOMA2-IR was inversely correlated to improvements in EF (Pearson's r = -0.25, P<0.001). After multivariable adjustment, a doubling of HOMA2-IR was associated with a 42.8% decreased likelihood of HFrecEF (OR 0.572 [95% CI 0.385~0.827]).

Conclusions:

This study reveals that IR is independently associated with compromised development of HFrecEF in non-diabetic patients.

Background: Due to advances in medical treatments, a substantial proportion of heart failure (HF) patients have experienced recovery of ejection fraction (EF), termed HF with recovered EF (HFrecEF). Insulin resistance (IR) is prevalent in HF and tightly related with prognosis. This study investigates the relationship between IR and the incidence of HFrecEF in non-diabetic patients. **Methods and Results:** A total of 262 non-diabetic HF patients with reduced EF (HFrEF) were consecutively enrolled. Patients were classified into HFrecEF (follow-up EF > 40% and ≥ 10% absolute increase) or otherwise persistent HFrEF based on repeat echocardiograms after 12 months. IR was estimated by an updated homeostasis model assessment (HOMA2-IR). The median HOMA2-IR level was 1.05 (IQR 0.67~1.63) in our cohort of non-diabetic HF patients. During follow-up, 121 (46.2% [95% CI 40.2%~52.2%]) patients developed HFrecEF. Compared with HFrEF patients, HFrecEF patients had significantly lower HOMA2-IR levels (0.92 [IQR 0.61 ~ 1.37] vs. 1.14 [IQR 0.75 ~ 1.78], P=0.007), especially in HF of nonischemic etiology. Log2-transformed HOMA2-IR was inversely correlated to improvements in EF (Pearson's r = -0.25, P<0.001). After multivariable adjustment, a doubling of HOMA2-IR was associated with a 42.8% decreased likelihood of HFrecEF (OR 0.572 [95% CI 0.385~0.827]). **Conclusions**: This study reveals that IR is independently associated with compromised development of HFrecEF in non-diabetic patients.**Background:** Due to advances in medical treatments, a substantial proportion of heart failure (HF) patients have experienced recovery of ejection fraction (EF), termed HF with recovered EF (HFrecEF). Insulin resistance (IR) is prevalent in HF and tightly related with prognosis. This study investigates the relationship between IR and the incidence of HFrecEF in non-diabetic patients. **Methods and Results:** A total of 262 non-diabetic HF patients with reduced EF (HFrEF) were consecutively enrolled. Patients were classified into HFrecEF (follow-up EF > 40% and ≥ 10% absolute increase) or otherwise persistent HFrEF based on repeat echocardiograms after 12 months. IR was estimated by an updated homeostasis model assessment (HOMA2-IR). The median HOMA2-IR level was 1.05 (IQR 0.67~1.63) in our cohort of non-diabetic HF patients. During follow-up, 121 (46.2% [95% CI 40.2%~52.2%]) patients developed HFrecEF. Compared with HFrEF patients, HFrecEF patients had significantly lower HOMA2-IR levels (0.92 [IQR 0.61 ~ 1.37] vs. 1.14 [IQR 0.75 ~ 1.78], P=0.007), especially in HF of nonischemic etiology. Log2-transformed HOMA2-IR was inversely correlated to improvements in EF (Pearson's r = -0.25, P<0.001). After multivariable adjustment, a doubling of HOMA2-IR was associated with a 42.8% decreased likelihood of HFrecEF (OR 0.572 [95% CI 0.385~0.827]).

Effect of gender on the association between high density lipoprotein cholesterol level and prognosis of patients with coronary heart disease undergoing percutaneous coronary intervention

徐颖 Xu, -Han , Zi- Qi, Jing Li, Yi Li, Ya-Ling Han

State Key Laboratory of Frigid Zone Cardiovascular Diseases，Cardiovascular Research institute and Department of Cardiology, General Hospital of Northern Theater Command, No.83, Wenhua Road, Shenhe District,Shenyang, 110016, China

Objective: Recent studies found that the use of drugs to raise high density lipoprotein cholesterol (HDL-C) levels did not reduce the risk of cardiovascular disease (CVD) in some people, and research also suggested that elevated levels of HDL-C may be related to an increased risk of CVD. However, it is not clear whether this is the case in patients with coronary artery disease (CAD) undergoing percutaneous coronary intervention (PCI), and whether this association is affected by gender.

Methods:The OPT-CAD (Optimal antiPlatelet Therapy for Chinese patients with Coronary Artery Disease) was a large registration study, with a total of 14032 CHD patients enrolled. In this study, 7747 patients with CAD undergoing PCI who completed 5-year follow-up in the OPT-CAD study were included and divided into quartile groups according to HDL-C, including 5861 men and 1886 women. The primary outcomes were ischemic events including the composite of cardiac death, myocardial infarction (MI), and/or ischemic stroke at 5 years. The secondary outcomes were independent components of ischemic events and all-cause death, bleeding events as defined by Bleeding Academic Research Consortium (BARC), including BARC 2-5 and BARC 3-5 bleeding at 5 years. The restricted cubic splines (RCS) were used to test the nonlinear relationship between continuous HDL-C levels and outcomes.

Results: Male patients were divided into Q1: < 0.80mmol/L, Q2:0.80-0.97mmol/L, Q3:0.98-1.18mmol/L, Q4: ≥ 1.19mmol/L. And female patients were divided into Q1: < 0.90mmol/L, Q2:0.80-1.07mmol/L, Q3:1.08-1.30mmol/L, Q4: ≥ 1.31mmol/L. With the increase of HDL-C level, the body mass index (BMI), combined diabetes mellitus (DM), hypertension, hyperlipidemia, the proportion of previous MI, previous PCI and anemia, as well as the levels of estimated glomerular filtration rate (eGFR) and left ventricular ejection fraction (LVEF) decreased, while the proportion of smoking and ST-segment elevation myocardial infarction (STEMI), total cholesterol (TC) and low-density lipoprotein cholesterol (LDL-C) levels increased in male patients. And the BMI, combined DM, hyperlipidemia, the proportion of smoking, previous MI and previous PCI, as well as the levels of eGFR and LVEF decreased, but the proportion of NSTEMI and STEMI, TC and LDL-C levels elevated in female patients. Compared with low HDL-C levels, the positions of target vessels, the proportion of chronic complete occlusion and bifurcation lesions, the number of stents, the average stent diameter and the total stent length in male patients were lower in the higher group (P < 0.05). The medication rates of β-blockers and Angiotensin converting enzyme inhibitor/Angiotensin receptor blocker decreased, with statistically significant differences (P < 0.05). Among female patients, the number of stents and the total length of stents were lower in high group (P < 0.05). There was no statistically significant difference in the medication use after discharge. The usage rates of aspirin and clopidogrel for both male and female patients were above 97%. Ischemic events and MI were statistically different between groups in male patients, with HDL-C in the range of 0.98mmol/L -1.18 mmol/L having the lowest incidence (P < 0.05). All bleeding events decreased considerably with increasing HDL-C levels (P < 0.001). There was no statistical difference in the ischemic and bleeding events for women. The ischemic events were connected with HDL-C in a U-shaped relationship in CAD patients undergoing PCI, and in male patients, ischemic events and all-cause death were U-shaped with HDL-C, outcomes risk increased at both high and low levels of HDL-C ($P_{nonlinearity}$ =0.007). However the nonlinear relationship did not shown in females.

Conclusions: This study revealed a U-shaped association between ischemic events, all-cause death and HDL-C in male patients with CAD who underwent PCI, but no nonlinearity was observed in females.

Lipoprotein(a) molar concentrations rather than genetic variants better predict coronary artery disease risk and severity in Han Chinese population

Jie Li, Hu Ding, Yan Wang

Department of Cardiovascular Medicine, Tongji Hospital, Tongji Medical College, Huazhong University of Science and Technology

Background It is well established that increased lipoprotein(a) [Lp(a)] is a significant risk factor for coronary artery disease (CAD). Plasma Lp(a) levels are genetically determined and vary widely between different races, regions and individuals. However, most studies on Lp(a) associated genetic variants have focused on the Caucasian population currently. Our study aimed to test the associations among LPA genetic variants, Lp(a) concentrations, and CAD in a Han Chinese cohort.

Methods The study is a cross-sectional study. A total of 3779 Han Chinese patients who underwent coronary angiography were recruited from Tongji Hospital. Clinical information was recorded from a large scientific research data center in the hospital. Lp(a) molar concentrations were measured in nanomoles per liter (nmol/L) using latex enhanced immunoturbidimetry in the central laboratory of the hospital. LPA Kringle IV type 2 (KIV-2) copies were detected using TaqMan probe real-time

quantitative polymerase chain reaction (qPCR) analysis and fifteen single nucleotide polymorphisms (SNPs) within the LPA gene were detected using TaqMan probe genotyping analysis. LPA genetic risk score (GRS) was computed based on seven SNPs associated with Lp(a). Associations of LPA genetic variants with Lp(a) were evaluated using linear regression analyses and associations of LPA genetic variants and Lp(a) with CAD risk and severity were evaluated using Logistic regression analyses. Restricted cubic splines were used to assess the associations between Lp(a), as a continuous variable, and CAD, multivessel CAD, or high Gensini scores. In all multivariable-adjusted analyses, age, sex, smoking status, hypertension, diabetes, total cholesterol (TC), low-density lipoprotein cholesterol (LDL-C) and high-density lipoprotein cholesterol (HDL-C) were adjusted.

Results When Lp(a) was treated as a continuous variable, the odds ratios (ORs) for CAD, multivessel CAD and high Gensini (Gensini > median) increased with elevated concentrations of Lp(a) after adjustment for traditional cardiovascular risk factors and conventional lipids. Compared with the first quartile of Lp(a), the fourth quartile exhibited a significant association with CAD [OR: 2.08, 95% conffdence interval (CI): 1.67–2.59, p < 0.001], multivessel CAD [OR: 2.54, 95% CI: 2.06–3.12, p < 0.001], and high Gensini scores [OR: 2.17, 95% CI: 1.77–2.66, p < 0.001] after multivariable adjustment. Elevated Lp(a) quartiles were significantly associated with a stepwise increased in the incidence of CAD, multivessel CAD and high Gensini scores (all p for trend < 0.001). Seven SNPs were significantly associated with inverse normal-transformed Lp(a) levels and the LPA GRS was defined according to the above seven SNPs. Both LPA GRS and KIV-2 quartiles were associated with Lp(a) concentrations (both p for trend < 0.001). However, after false discovery rate (FDR) correction, there were no significant associations of LPA SNPs with CAD, multivessel CAD or high Gensini scores (corrected p > 0.05). Meanwhile, no significant associations were observed between LPA GRS, KIV-2 copies, and CAD, multivessel CAD or high Gensini scores.

Conclusions Our findings indicate LPA genetic variants can affect Lp(a) levels, but compared with LPA genetic variants, Lp(a) molar concentrations are better at predicting CAD incidence and severity, highlighting the importance of Lp(a) detection and management.

Keywords LPA gene, Kringle IV type 2 copies, Single nucleotide polymorphism, Genetic risk score, Genetics, Epidemiology

Analysis of the correlation between helper T-lymphocyte subsets and atrial fibrillation: An observational and Mendelian randomization study

Jia-Hui Li, Bin Liang, Ya-Fen Yang, Hong-Xuan Fan

the second hospital of Shanxi medical university

Objective:

The objective of this research was to examine the distribution of absolute numbers of helper T-lymphocyte subpopulations in peripheral blood in patients with atrial fibrillation and the association between atrial fibrillation risk and helper T-lymphocyte subpopulations.

Methods:

1. The case-control method was used in this observational study. Our study retrospectively included 302 patients diagnosed with atrial fibrillation (AF) attending the Department of Cardiovascular Medicine of the Second Hospital of Shanxi Medical University from 2020.06.01 to 2023.11.30 as the AF group, and 183 healthy people attending the Department of Health Checkup of the Second Hospital of Shanxi Medical University for perfecting T-lymphocyte subset testing as the healthy control group. The relevant electronic medical record system was consulted to obtain the relevant clinical laboratory and examination information of the study subjects. The covariates between the two groups were balanced by 1:1 propensity score matching analysis (PSM). Potential independent predictors of AF were investigated by multivariate logistic regression analysis. Patients with AF were subsequently divided into paroxysmal AF group and persistent AF group, and multivariate logistic regression analyses were used to investigate the potential relationship between the absolute counts of lymphocyte subpopulations and different types of AF.

2. The causal effect of 731 immune cells on the risk of developing AF was determined using Mendelian Randomization (MR). The GWAS dataset of 731 immune cells includes T cells, T cells at all stages of maturation, B cells, NK cells, DC cells, monocytes, myeloid cells, and Treg cell subsets. The GWAS dataset for AF was derived from a large meta-analysis of six study cohorts (Health of North Trendelagh Study (HUNT), deCODE, Michigan Genomics Initiative (MGI), DiscovEHR, the UK Biobank and the AFGen Consortium), which consisted of 1,030,836 European-origin subjects who were categorized into 60,620 AF cases and 970,216 controls. The primary MR analysis method employed was inverse variance weighted (IVW), but three additional MR analysis methods—weighted median (WM), simple mode, and weighted mode—based on various model assumptions were also used to assess the results' consistency. To evaluate heterogeneity and multiplicity in MR causal estimation, Cochran's Q test, MR-PRESSO analysis, Leave-one-out sensitivity (LOO) analysis, and MR-Egger regression intercept term test were employed.

3. Drug-targeted MR approach was used to explore the causal relationship between multiple immunomodulatory drugs and AF. Using data from immunomodulatory drug-targeted protein genes, drug-targeted protein gene expression quantitative trait Loci (eQTL), a large AF GWAS dataset, and a C-reactive protein GWAS dataset, we explored the causal relationship between multiple immunomodulatory drugs and AF using drug-targeted MR analysis and summary-data-based MR (SMR) method to explore the causal relationship between multiple immunomodulatory drugs and AF and to provide new ideas for the use of immunomodulatory drugs to prevent and control AF.

Results:

1. The AF patients' absolute value counts of Th1 cells, Th17 cells, B-lymphocytes and Th cells and the ratio of Th1/Th2, Th17/Treg were all considerably greater than those of the healthy control group (P < 0.05). Multivariate logistic analysis showed that the absolute value counts of Th1 cells (OR=1.01, 95% CI: 1.01~1.02, P<0.001), absolute value counts of Th17 cells (OR=1.22, 95%CI: 1.12~1.32, P<0.001), Th1/Th2 (OR=1.04, 95%CI: 1.01~1.08, P=0.011), Th17/Treg*0.1 (OR=1.63, 95%CI: 1.3~2.05, P<0.001) [Each 0.1 unit increase in Th17/Treg was associated with a 63% increased risk of developing atrial fibrillation], absolute value counts of B-lymphocyte (OR=1.01, 95%CI: 1.0~1.01, P=0.022) and absolute value counts of Th cell (OR=1.0, 95%CI: 1.0~1.0, P=0.004) were independent risk factors for AF.

2. There was no statistically significant difference found in the absolute value counts of any helper T-lymphocyte subpopulation between the paroxysmal AF group and the persistent AF group (P > 0.05). Multivariate logistic analysis showed that the absolute value counts of various types of helper T lymphocyte subsets were not associated with progression between different types of AF. It is suggested that the disorganization of lymphocyte subsets and T-lymphocyte subsets in patients with AF occurs at the early stage of AF formation and may promote the development of AF.

3. Among the 731 types of immune cells, 2 types of immune cells were significantly associated with the risk of developing AF. IVW analysis showed a strong causal relationship between increased absolute CD4+CD8dim T-cell counts and increased risk of developing AF (OR=1.03, 95% CI: 1.01-1.05, P=0.002); increased absolute IgD-CD38dim B-cell counts were also strongly and causally associated with an increased risk of developing AF (OR=1.06, 95% CI: 1.03-1.10, P=0.0003).

4. Drug-targeted MR analysis method showed that IL-6R-mediated CRP elevation was significantly associated with increased risk of AF in IVW-MR analysis (OR=1.33, 95% CI: 1.19-1.49, P=0.000000518). SMR analysis showed that there was a causal relationship between increased IL-6R gene expression in the blood and a high risk of AF (OR=1.29, 95%CI: 1.115-1.493, P=0.00063), suggesting that IL-6R inhibitors may reduce the risk of AF. Expression of the IL-18 gene in the blood was causally associated with a reduction in the occurrence of AF, (OR=0.95, 95%CI: 0.905-0.997, P=0.036), suggesting that the use of IL-18 inhibitors may increase the risk of AF occurrence.

Conclusion:

1. Immune dysfunction, especially disorders of T-lymphocyte subsets, is a risk factor for the development of AF. Elevated absolute value counts of Th1 cell, Th17 cell, B lymphocyte, Th cell and the elevated ratio of Th1/Th2, Th17/Treg are risk factors for the development of AF.

2. Absolute value counts of various helper T-lymphocyte subpopulations were not associated with progression between different types of AF. It is suggested that the disorganization of lymphocyte subsets and T-lymphocyte subsets in patients with AF occurs at the early stage of AF formation and may promote the development of AF.

3. Mendelian randomization study showed a strong causal relationship between increased absolute CD4+CD8dim T-cell counts, increased absolute IgD-CD38dim B-cell counts, and increased risk of AF development.

4. Drug-targeted MR analysis revealed IL-6R inhibitors as potential agents to reduce the risk of AF development, whereas IL-18 inhibitor use may increase the risk of AF development.

Temporal Shifts in Ischemic Heart Disease Burden Among Premenopausal and Postmenopausal Women Worldwide: Insights from the Global Burden of Disease Study 2021 and Projections

Ya-Fen Yang[1], Bin Liang[1], Jia-Hui Li[1], Zhuo-Lin Huang[1], Hong-Xuan Fan[2], Zhao-Yu Ren[1], Li-Qiang Zheng[3]

1. The Second Hospital of Shanxi Medical University

2. Beijing Tsinghua Changgung Hospital, School of Clinical Medicine, Tsinghua University

3. School of Public Health, Shanghai Jiao Tong University School of Medicine

Objective: To comprehensively assess the global burden of ischemic heart disease (IHD) in premenopausal (15-49 years) and postmenopausal (≥ 50 years) women from 1990 to 2021, identify key temporal trends and disparities, evaluate the contribution of modifiable risk factors, and project the burden to 2040.

Methods: Utilizing data from the Global Burden of Disease (GBD) Study 2021, we analyzed IHD incidence, prevalence, deaths, disability-adjusted life years (DALYs), and corresponding age-standardized rates (ASRs: ASIR, ASPR, ASMR, ASDR) across 204 countries and territories, stratified by menopausal status. Temporal trends from 1990 to 2021 were quantified using estimated annual percentage changes (EAPCs) with 95% confidence intervals (CIs). The Socio-demographic Index (SDI) was used to stratify analyses by regional development level. Pearson correlation assessed associations between ASRs, EAPCs, SDI, and the Human Development Index (HDI). Hierarchical clustering analyzed regional trend patterns. Bayesian age-period-cohort (BAPC) modeling projected IHD burden metrics through 2040. The attributable burden of IHD deaths and DALYs to metabolic, behavioral, and environmental/occupational risk factors, as defined by GBD 2021, was assessed.

Results: In 2021, the global IHD burden was substantially higher in postmenopausal compared to premenopausal women: ASIR (1160.4 vs. 66.2 per 100,000), ASMR (315.8 vs. 8.5 per 100,000), ASPR (9590.1 vs. 425.0 per 100,000), and ASDR (5904.2 vs. 431.4 per 100,000). From 1990 to 2021, significant global declines were observed in ASMR (Postmenopausal EAPC = -1.54 [95% CI: -1.59 to -1.49]; Premenopausal EAPC = -1.00 [-1.05 to -0.95]) and ASDR (Postmenopausal EAPC = -1.48 [-1.53 to -1.43]; Premenopausal EAPC = -0.98 [-1.03 to -0.93]) for both groups. However, ASIR (EAPC = 0.43 [0.40 to 0.46]) and ASPR (EAPC = 0.31 [0.28 to 0.33]) significantly increased among premenopausal women, while postmenopausal ASIR showed a slight decline (EAPC = -0.48 [-0.53 to -0.43]) and ASPR remained stable (EAPC = 0.05 [0.01 to 0.09]). The highest age-standardized burden occurred consistently in low-middle SDI regions. Notably, middle SDI regions experienced significant increases in postmenopausal ASIR (EAPC = 0.11 [0.05 to 0.16]) and ASPR (EAPC = 0.34 [0.31 to 0.36]). Geographically, North Africa and the Middle East had the highest postmenopausal ASIR/ASPR, while Central Asia had the highest ASMR/ASDR. Metabolic risks were the primary driver of attributable deaths and DALYs globally (led by high systolic blood pressure), followed by behavioral risks (led by dietary risks). Environmental/occupational risks, particularly air pollution, were the third-leading contributor in low-SDI regions. Attributable burden patterns varied by age and SDI; for example, high BMI impacted younger premenopausal women in high-SDI regions, while air pollution disproportionately affected low-SDI regions. Projections to 2040 indicate rising ASIR (66.1 to 66.8 per 100,000) and ASPR (424.9 to 472.6 per 100,000) for premenopausal women, and substantial increases in ASIR (1160.3 to 1398.9 per 100,000) and ASPR (9590.1 to 12918.1 per 100,000) for postmenopausal women, despite projected continued declines in ASMR and ASDR, leading to a widening absolute burden gap favoring postmenopausal women.

Conclusion: This first global assessment of IHD burden stratified by menopausal status reveals persistently marked disparities, with postmenopausal women bearing a significantly higher burden. While mortality rates are declining globally, the rising incidence and prevalence among premenopausal women and the persistently high absolute burden in postmenopausal women represent major public health challenges. Profound geographic and socioeconomic inequalities exist, with the highest age-standardized burden concentrated in low-middle SDI regions. Metabolic, behavioral (dietary), and environmental (air pollution) risks are the dominant drivers, exhibiting distinct patterns by SDI, region, and age. The projected increase in IHD cases, particularly among postmenopausal women, underscores the urgent need for targeted, context-specific interventions focusing on early prevention in premenopausal women, optimized management of metabolic risks (especially hypertension), dietary improvements, air pollution mitigation, and enhanced healthcare access in high-burden regions to mitigate the growing IHD burden by 2040.

Novel Transthoracic Pulmonary Valve Implantation Using Self-expanding Salus ™ Valve: A Prospective Study of Safety and Mid-term Outcomes

Zi-Qin Zhou, Shu-Sheng Wen, Ji-Mei Chen

Guangdong Provincial People's Hospital

Background: Transcatheter pulmonary valve replacement (TPVR) has become a standard treatment for severe pulmonary regurgitation (PR) in patients with right ventricular outflow tract (RVOT) dysfunction. Traditional transcatheter valves, such as the Melody and Sapien valves, are primarily designed for use in allografts or valved conduits, which significantly limits their applicability in patients with enlarged native RVOT. The Salus ™ valve, a novel self-expanding valve stent, addresses this limitation by offering a wider diameter range (16-34 mm) and a transthoracic approach, which allows for direct access and immediate intervention if needed. This study aims to evaluate the mid-term safety and efficacy of the Salus ™ valve in patients with severe PR.

Methods: This prospective cohort study enrolled 38 patients who underwent transthoracic pulmonary valve stenting at Guangdong Provincial People's Hospital from September 2021 to September 2024. Inclusion criteria included moderate-to-severe PR following RVOT reconstruction, age ≥ 14 years, and specific clinical/imaging parameters. Primary endpoints were pulmonary regurgitation fraction <20%, freedom from reintervention at 12 months, and major adverse events (MAE), defined as death, reintervention, recurrent severe PR, worsening heart failure, cardiac arrest, new severe ventricular arrhythmias, and third-degree AV block. Preoperative assessments included comprehensive imaging evaluations using CT angiography and echocardiography to determine the optimal valve size and deployment position.

Results: All 38 patients (mean age 24.08±8.12 years) successfully underwent the procedure, although intraoperative valve displacement occurred in three cases, which were promptly corrected using cardiopulmonary bypass. During a median follow-up of 24 months, significant improvements were observed in right ventricular volumes: Right Ventricular End-Diastolic Volume Index (RVEDVI) decreased from 141.45 to 109.98 mL/m² and Right Ventricular End-Systolic Volume Index (RVESVI) decreased from 74.27 to 56.62 mL/m² (both p<0.01). No mortality or need for reintervention was observed during the follow-up period. The estimated freedom from MAE at 36 months was 87.2%. At 12 months, CMR examination showed a significant reduction in RVEDVI and RVESVI, and echocardiography demonstrated a decrease in right atrial and ventricular dimensions and PR grades. At 2 to 3 years post-implantation, echocardiography showed that 14 patients exhibited no or mild PR, while moderate PR was observed in 5 patients. Notably, 1 patient experienced a recurrence of severe PR.

Conclusion: The Salus ™ valve demonstrated safety and efficacy in treating severe PR through its transthoracic approach, which offers unique advantages in terms of direct access and immediate complication management. The study highlights the potential of the Salus ™ valve to address the needs of patients with enlarged native RVOT who are not suitable candidates for traditional transcatheter valves. Longer follow-up is needed to assess long-term durability. Future studies with larger sample sizes and longer follow-up periods are necessary to further validate these findings and confirm the long-term outcomes of this novel approach. Additionally, the transthoracic approach provides a viable alternative for patients with small or occluded femoral veins, expanding the applicability of TPVR in a broader patient population. The results of this study suggest that the Salus ™ valve could become a valuable addition to the armamentarium of treatments for severe PR, particularly in patients with complex anatomies.

Relationship between hs-CRP and MACCEs risk in patients with drug-eluting stents undergoing statin therapy: A comparison of diabetic and non-diabetic patients—A prospective registry-based study

Xin-Yue Chen, Hao-Yu Wang, Dong Yin, Ke-Fei Dou

Fuwai Hospital, Chinese Academy of Medical Sciences and Peking Union Medical College

Abstract

Purpose:

Inflammation is a critical driver in the pathogenesis of both type 2 diabetes mellitus (T2DM) and coronary heart disease (CHD). While statin therapy effectively reduces low-density lipoprotein cholesterol (LDL-C) and provides anti-inflammatory benefits, a significant residual inflammatory risk (RIR) persists in many patients, predisposing them to major adverse cardiovascular and cerebrovascular events (MACCEs). This RIR, often measured by the simple and economical biomarker high-sensitivity C-reactive protein (hs-CRP), is distinct from residual cholesterol risk. Patients with T2DM exist in a state of chronic low-grade inflammation, which complicates risk assessment. However, it remains unclear whether the prognostic value of hs-CRP for predicting MACCEs is altered by the presence of T2DM in patients with CHD receiving modern treatment. This large-scale prospective study aimed to evaluate how T2DM status modifies the relationship between baseline hs-CRP levels and long-term clinical outcomes in a contemporary cohort of CHD patients treated with statins and drug-eluting stent (DES) implantation

Patients and methods:

This prospective registry-based study enrolled 8,628 consecutive patients with CHD who underwent percutaneous coronary intervention (PCI) with DES implantation and were receiving statin therapy at Fuwai Hospital. Participants were first stratified by their T2DM status, defined as a prior diagnosis or a baseline hemoglobin A1c (HbA1c) level of ≥ 6.5%. Within each group, patients were further categorized based on baseline hs-CRP levels into three tiers: low (<1 mg/L), moderate (≥ 1 to <2 mg/L), and high (≥ 2 mg/L). The primary endpoint was the incidence of MACCEs, a composite of all-cause mortality, myocardial infarction, stroke, and target vessel revascularization. Statistical analysis involved Kaplan-Meier survival curves and multivariate Cox proportional hazards regression models to calculate hazard ratios (HR) and 95% confidence intervals (CI).

Results:

Over a median follow-up of 2.4 years, 999 MACCEs were recorded. The final cohort consisted of 3,729 patients with T2DM and 4,899 without. At baseline, patients with T2DM exhibited a more adverse risk profile, including significantly higher hs-CRP levels and a greater burden of severe coronary artery disease compared to their non-diabetic counterparts. Kaplan-Meier analysis revealed that increasing hs-CRP levels were significantly associated with a higher incidence of MACCEs in the Non-T2DM group (Log-rank p = 0.011), but this association was absent in the T2DM group (Log-rank p = 0.310). After comprehensive adjustment for potential confounders in the final multivariate Cox model, an hs-CRP level ≥ 2 mg/L remained a strong and independent predictor of MACCEs in patients without T2DM (HR = 1.39, 95% CI: 1.14-1.85, p = 0.002) when compared to those with hs-CRP <1 mg/L. Conversely, in the T2DM group, no significant association was found between hs-CRP levels and MACCEs risk (HR = 1.02, 95% CI: 0.73-1.23, p = 0.453). A formal interaction analysis confirmed that the prognostic impact of hs-CRP on MACCEs was significantly modified by diabetic status (p for interaction = 0.040). These findings were robust across multiple sensitivity and subgroup analyses.

Conclusion:

Among CHD patients receiving contemporary statin therapy following DES implantation, higher hs-CRP levels appeared to be associated with future MACCEs in those without T2DM, though not in T2DM patients. Hs-CRP, an important diagnostic marker of inflammation, shows different value depending on diabetes status, revealing how diabetes and inflammation jointly influence cardiovascular outcomes and providing clinical insights for optimizing the application of inflammatory biomarkers in personalized cardiovascular risk stratification.

Keywords:

High-sensitivity C-reactive protein, Risk of residual inflammation, Coronary heart disease, Statin therapy, Diabetes mellitus, Major adverse cardiovascular and cerebrovascular events

Association between healthy lifestyle and the risk of multiple cardiometabolic diseases: a prospective cohort study based on the UK Biobank

Xin-Yue Chen, Hao-Yu Wang, Dong Yin, Ke-Fei Dou

Fuwai Hospital, Chinese Academy of Medical Sciences and Peking Union Medical College

Aim: Primary prevention of cardiometabolic diseases (CMDs), a leading cause of global morbidity and mortality, requires robust risk stratification tools. This study aimed to systematically evaluate the association between a comprehensive set of lifestyle factors and the risk of a wide range of CMDs using data from the UK Biobank. The research also sought to determine if incorporating these lifestyle factors could improve the performance of traditional disease risk prediction models.

Methods: We analyzed data from 148,155 participants in the UK Biobank without baseline CMDs. Cox proportional hazards models were used to assess the impact of healthy lifestyle factors (non-smoking, alcohol consumption, physical activity, healthy diet, and healthy sleep) on 11 types of CMDs (coronary heart disease, type 2 diabetes, atrial fibrillation, hypertension, stroke, heart failure, Alzheimer's disease, non-alcoholic fatty liver disease, valvular heart disease, cardiomyopathy, and pulmonary hypertension). Based on the β coefficients from a Cox proportional hazards model, a weighted healthy lifestyle score was developed. Improvements in predictive models after incorporating lifestyle factors were evaluated.

Results: Through Cox model analysis, this study quantified the contribution weights of five lifestyle factors to health. The results showed that healthy sleep contributed the most (weighted β coefficient: 0.342), followed by non-excessive alcohol consumption (0.288), non-smoking (0.239), regular physical activity (0.082), and healthy diet (0.049). A nomogram developed from the model visually confirmed the relative importance of each factor, showing that unhealthy sleep contributed the most points to the total risk score, followed by smoking and drinking. Adhering to a healthier lifestyle demonstrated a significant and dose-response association with a reduced risk of composite CMDs. After multivariable adjustment, compared with the "Very Unhealthy" group, the hazard ratios (HRs) for the composite outcome were 0.87 (95% CI: 0.83-0.91) for the "Unhealthy" group, 0.77 (95% CI: 0.73-0.80) for the "Healthy" group, and 0.70 (95% CI: 0.67-0.74) for the "Very Healthy" group. This protective association was observed across most individual CMDs, with the most pronounced effect seen in pulmonary arterial hypertension (HR: 0.34, 95% CI: 0.24-0.50). Kaplan-Meier analysis confirmed that healthier lifestyle groups had significantly longer disease-free survival (p < 0.0001). Furthermore, adding the lifestyle score to established risk models (Framingham, FINDRISC, CHARGE-AF, QStroke) significantly improved risk prediction across all metrics, including the area under the curve (AUC), continuous Net Reclassification Improvement (NRI), and Integrated Discrimination Improvement (IDI) (all P < 0.001). The protective association of a healthy lifestyle was largely consistent across subgroups based on sex, ethnicity, BMI, and sedentary time, although the magnitude of the effect showed a statistically significant interaction by age and Townsend deprivation index. Furthermore, the findings remained robust in several sensitivity analyses, including using an unweighted lifestyle score, excluding events within the first two years of follow-up to account for reverse causation, and using a separate data partition to derive the score weights, which confirmed the stability of the results.

Conclusion: This study systematically reveals that a healthy lifestyle is associated with a significant reduction in the risk of a wide range of CMDs, and it enhances the accuracy of existing risk prediction models. This underscores its critical role in the primary prevention of cardiovascular and metabolic diseases.

Superior Predictive Value of TyG-ABSI for Cardiovascular Disease and Mortality in Individuals with Metabolic Syndrome: Evidence from the US NHANES

Xin Zheng[1,2], Wen-Jing Zhang[2], Lei-Gang Yuan[2], Bin Liang[2]

1. Yangquan First People's Hospital

2. Shanxi Medical University

Abstract:

Background:

Metabolic syndrome (MetS) is a metabolic disorder characterized primarily by central obesity and insulin resistance (IR), significantly increasing the risk of cardiovascular disease (CVD), type 2 diabetes mellitus, and premature mortality. In recent years, the triglyceride-glucose (TyG) index has been widely used as a surrogate marker for IR. To improve predictive performance, composite indices such as TyG-BMI, TyG-WC, and TyG-WHtR have been developed by integrating TyG with anthropometric parameters. However, these traditional indices have limitations in accurately capturing visceral adiposity and the actual metabolic burden, especially in high-risk MetS populations. Meanwhile, A Body Shape Index (ABSI), which adjusts waist circumference for height and weight, more effectively reflects central obesity and has been shown to outperform conventional anthropometric measures. The combination of TyG and ABSI—termed TyG-ABSI—offers a novel composite index that may better reflect the underlying pathophysiology of MetS. Nevertheless, its prognostic value in individuals with MetS remains unclear.

Methods:

This study utilized data from nine continuous cycles of the US National Health and Nutrition Examination Survey (NHANES), spanning 2001 to 2018, including 10,059 adults who met the NCEP ATP III criteria for MetS. TyG, TyG-ABSI, and other TyG-derived indices (TyG-BMI, TyG-WC, TyG-WHtR) were calculated and categorized into tertiles. Associations between these indices and major outcomes—CVD, cardiovascular mortality, and all-cause mortality—were assessed using multivariable logistic regression and Cox proportional hazards models. Covariates included demographic, socioeconomic, lifestyle, clinical, and biochemical factors. Predictive performance was evaluated using receiver operating characteristic (ROC) curves, Kaplan-Meier survival analysis, and restricted cubic spline (RCS) modeling. Subgroup analyses were also conducted to examine consistency across population strata.

Results:

The findings showed that while traditional TyG and its composite indices demonstrated certain predictive capabilities, TyG-ABSI consistently exhibited superior predictive power across all evaluated outcomes. After full adjustment, each one-unit increase in TyG-ABSI was associated with significantly higher risks of CVD (OR = 1.32; 95% CI: 1.19–1.47), cardiovascular mortality (HR = 1.29; 95% CI: 1.11–1.51), and all-cause mortality (HR = 1.28; 95% CI: 1.18–1.40), all with p-values < 0.001. Compared to the lowest tertile, individuals in the highest tertile of TyG-ABSI had a 38% higher risk of CVD, a 45% higher risk of cardiovascular mortality, and a 32% higher risk of all-cause mortality. ROC analysis demonstrated the highest area under the curve (AUC) values for TyG-ABSI across all outcomes, with 95% confidence intervals that did not overlap with those of the other indices, indicating statistically significant superiority. Kaplan-Meier survival curves showed distinct stratification by TyG-ABSI tertiles, and RCS modeling revealed a nearly linear, dose-response relationship between TyG-ABSI and adverse outcomes. As shown in the subgroup analyses, TyG-ABSI remained significantly associated with all outcomes in most subgroups, with no significant interactions observed (p for interaction > 0.05), suggesting robust and consistent predictive performance across diverse population strata.

Conclusion:

Although traditional TyG and its composite indices are useful for assessing metabolic risk, they may inadequately capture the synergistic effects of central obesity and IR. TyG-ABSI, by integrating both components, provides a more comprehensive reflection of metabolic dysfunction. It not only overcomes the limitations of single-parameter models but also demonstrates superior predictive accuracy and robustness across various

outcomes and analytical approaches. Given its simplicity, accessibility, and strong prognostic value, TyG-ABSI holds promise as an effective clinical tool for early risk stratification and personalized prevention strategies in individuals with MetS.

Inflammatory and Bleeding Risks on Clinical Outcomes in Acute Coronary Syndrome Patients Undergoing Percutaneous Coronary Intervention

Yi- Duan[1,2], -Han [1], Na[1], Dao-Shen Liu[1,2], Shang- Zhou[1,2], Ying Xu[1], Zi- Qi[1], Hai-Wei Liu[1], Kai Xu[1], Xiao-Zeng Wang[1], Jing Li[1], Yi Li[1], Ya-Ling Han[1]

1. State Key Laboratory of Frigid Zone Cardiovascular Diseases，Cardiovascular Research institute and Department of Cardiology, General Hospital of Northern Theater Command, No.83, Wenhua Road, Shenhe District,Shenyang, 110016, China

2. The Department of Cardiology, Xijing Hospital, Air Force Medical University, Xi'an, Shaanxi, 710000, China

Objective Even after undergoing a series of evidence-based therapeutic regimens, acute coronary syndrome (ACS) patients who received percutaneous coronary intervention (PCI) still carry significant residual risks of cardiovascular and thrombotic complications.Nevertheless, it remains unclear whether there is a synergistic effect of bleeding and inflammation risks on both ischemic and bleeding events among patients treated with DAPT. Hence, we analyzed a large-sample, real-world PCI cohort to evaluate the potential influence of long-term outcomes according to the existence of bleeding and inflammation risk conditions in ACS patients who are receiving DAPT after PCI.This study aimed to evaluate the impact of systemic inflammation burden using high-sensitivity C-reactive protein (hsCRP) and long-term prognosis in ACS patients undergoing PCI stratified by bleeding risk status.

Methods Consecutive patients admitted for ACS and who received PCI between March 2016 and March 2022 were enrolled in the analysis. Elevated systemic inflammation was defined as hsCRP >2mg/L, and high bleeding risk (HBR) was defined the Academic Research Consortium (ARC)-HBR criteria. UpSet plots were performed to illustrate the most frequent combinations of HBR major and minor criteria. The subgroup analyses were further stratified by the components of the HBR conditions to evaluate the impact of hsCRP. Sensitivity analyses included repeat analysis by using the PRECISE-DAPT score to evaluate bleeding risk, and competing- risk analysis through Fine-Gray model accounting for the competitive risk of death and employing alternative hsCRP thresholds (1 and 3 mg/L). The primary outcome was ischemic events at 12 months, composed of cardiac death, myocardial infarction, and/or stroke. The main secondary outcomes included all-cause death, and Bleeding Academic Research Consortium (BARC) types 2, 3, and 5 bleeding and types 3 and 5 bleeding. To address potential confounding factors, the following variables were selected for multivariate regression: age, sex, hypertension, diabetes, previous MI, previous stroke, previous PCI, peripheral artery disease, smoking status, presentation, estimated glomerular filtration rate (eGFR), anemia, and medical treatment at discharge.

Results Of 15,013 patients, 4,606 (30.7%) were qualified as HBR and 8,395 (55.9%) had hsCRP>2mg/L. In both the non-HBR and HBR groups, patients with elevated hsCRP levels were more likely to be tobacco smokers, have acute MI at presentation, and less likely to have a history ofMI and PCI. These patients also had lower ejection fraction, estimated glomerular filtration rate, and hemoglobin levels. The procedural

information between the two groups was similar, with only numerical differences in the characteristics of

stent implantations. Moderate or severe anemia, taking oral anticoagulant agents, and prior moderate or severe cerebrovascular accident (CVA) were the first three major ARC-HBR criteria. Elevated hsCRP was consistently associated with higher risk of ischemic events in both HBR (adjusted hazard ratio [aHR]: 1.20; 95% confidence interval [CI]: 0.91–1.58) and non-HBR (aHR: 1.34; 95% CI: 1.01–1.78) subgroups (P interaction=0.755). Although the incidence of bleeding events was higher in HBR patients, an elevated hsCRP level was not associated with bleeding events regardless of HBR status. Sensitivity analyses using alternative cut-off values for hsCRP (1 and 3 mg/L) yielded results consistent with the primary analysis. Restricted cubic spline regression represented an inverse J-shaped relation between hsCRP and non-HBR for ischemic events (P nonlinearity <0.001) and all-cause death (P nOnlinearity=0.003). Forest plots showed a significant difference in the major criteria of taking oral anticoagulant (OAC) agents and outcomes (ischemic events: OAC: HR 2.94, 95% CI 1.63–5.31; No OAC: HR 1.35, 95% CI 1.01–1.81, $P_{interaction}$ = 0.02; all-cause death: OAC: HR 5.99, 95% CI 2.73–13.18; No OAC: HR 1.62, 95% CI 1.18–2.23, $P_{interaction}$<0.01), which demonstrated an interaction between high bleeding status and high inflammatory burden for ischemic events and all-cause death.

Conclusion Irrespective of HBR status, elevated levels of hsCRP were associated with an augmented risk of ischemic events, and all-cause mortality, but not for bleeding events in ACS patients receiving DAPT

following PCI. Thus, anti-inflammatory therapies could have potential benefits, offering the reduction of thrombotic events without appreciable effect on bleeding in these patients.

Effect of CYP2C19 Genotype on Outcomes of Treatment with Ticagrelor versus Clopidogrel in Acute Coronary Syndrome Patients with Diabetes Mellitus: A Analysis in a Large-Scale, Real-World Study

Hao-Fu Tian[1,2], -Han [1], Na[1], Zi- Qi[1], Kai Xu[1], Hai-Wei Liu[1], Xiao-Zeng Wang[1], Jing Li[1], Yi Li[1], Ya-Ling Han[1]

1. State Key Laboratory of Frigid Zone Cardiovascular Diseases，Cardiovascular Research institute and Department of Cardiology, General Hospital of Northern Theater Command, No.83, Wenhua Road, Shenhe District,Shenyang, 110016, China

2. The Department of Cardiology, Postgraduate Training Base of General Hospital of Northern Theater Command, Jinzhou Medical University, Jinzhou, Liaoning, 121001, China.

Background: Dual antiplatelet therapy (DAPT) is a cornerstone treatment strategy for preventing ischemic events in patients with acute coronary syndrome (ACS) undergoing percutaneous coronary intervention (PCI). Diabetes mellitus (DM), a common comorbidity in ACS, elevates thrombosis and mortality risks. CYP2C19 genetic polymorphisms influence antiplatelet pharmacodynamics and prognosis. But evidence linking CYP2C19 genotypes to antithrombotic efficacy in ACS patients with DM is limited.

Purpose: This study analyzed a large-sample real-world dataset to evaluate the potential influence of ticagrelor versus clopidogrel-based antiplatelet strategies in ACS patients with DM based on different CYP2C19 alleles.

Methods: This was a post-hoc analysis of a prospective real-world PCI registry (March 2016–March 2023) in China, including 10,376 ACS patients with DM who received ticagrelor (n=2,931) or clopidogrel (n=7,445) after PCI and underwent CYP2C19 genotyping. Patients were categorized into CYP2C19 LOF allele non-carriers (n=4,326) and carriers (n=6,050). The primary outcome was a composite of fatal or irreversible ischemic and bleeding events at 12 months, which was defined as a composite of cardiac death, myocardial infarction (MI), ischemic stroke and Bleeding Academic Research Consortium (BARC) types 3, 5 bleeding at 12 months after discharge. The secondary endpoints were all-cause mortality, ischemic events (a composite of cardiac death, MI, ischemic stroke), BARC types 2-5 bleeding, and BARC types 3 or 5 bleeding within 12 months. Propensity score matching (PSM) was used to adjust for bias due to confounders across treatment regimens, and Cox proportional hazards models were applied for outcome analysis.

Results: Among 4326 CYP2C19 LOF allele non-carriers, 3304 (76.38 %) were treated with clopidogrel and 1022 (23.62 %) were treated with ticagrelor. Among 6050 CYP2C19 LOF allele carriers, 4141 (68.45 %) were treated with clopidogrel and 1909 (31.55 %) were treated with ticagrelor. In the CYP2C19 LOF allele non-carriers, ticagrelor use was not associated with a significant difference in the primary outcome of fatal or irreversible ischemic and bleeding events compared to clopidogrel (4.67 % vs. 4.87%; hazard ratio [HR], 1.04; 95%CI: 0.70-1.55; p=0.853). However, ticagrelor was associated with a significantly higher incidence of BARC types 2-5 bleeding events (5.07% vs. 7.95%; HR=1.59, 95% CI: 1.12-2.26; p=0.009), primarily driven by an increase in BARC type 2 bleeding (3.38% vs. 5.77%; HR=1.72, 95% CI: 1.13-2.63; p=0.012). There were no significant differences in BARC types 3 and 5 bleeding (1.69% vs.2.19%; HR=1.29, 95%CI: 0.69-2.44; p=0.424). Among patients carried CYP2C19 loss-of-function (LOF) alleles, those treated with ticagrelor were associated with a lower risk of fatal or irreversible ischemic and bleeding events (4.82% vs. 3.36%; HR=0.69, 95% CI: 0.50-0.95; p=0.025), Ticagrelor also significantly reduced the risk of ischemic events (3.31% vs. 1.79%; HR=0.54, 95% CI: 0.35-0.82; p=0.004) and all-cause mortality (2.06% vs. 1.19%; HR=0.58, 95% CI: 0.34-0.97; p=0.040). Albeit with a higher incidence of BARC type 2 bleeding (HR=1.86; 95% CI, 1.38-2.51; p=0.0001). No significant differences in BARC types 3/5 bleeding were observed between groups.

Conclusions: The CYP2C19 genotype could be used to identify potential patients who would derive benefit from the ticagrelor-based antiplatelet strategy. In ACS patients with DM carrying (LOF) alleles, ticagrelor provides greater benefits by reducing ischemic events and all-cause mortality, despite an increased risk of minor bleeding. For non-carriers, clopidogrel remains a reasonable option due to similar efficacy and a lower bleeding risk. These findings support CYP2C19 genotyping to guide personalized DAPT in this high-risk population. Further research is needed to trade off the bleeding complications from potent P2Y12 inhibitors.

Key words: acute coronary syndrome; CYP2C19 genotype; diabetes mellitus; dual antiplatelet therapy.

PTPN14 aggravates neointimal hyperplasia via boosting PDGFRβ signaling in smooth muscle cells

Qiannan Ma

Tianjin Medical University

Abstract

Background: Vascular smooth muscle cells (VSMCs) are the predominant constituents of arteries and play a fundamental role in maintaining the normal physiological functions of blood vessels. In response to pathological stimuli or vascular injury, VSMCs migrate to the subintima and undergo pathological proliferation, inducing stenosis in the vascular lumen and then causing vascular restenosis, thereby contributing to the development of atherosclerosis and restenosis. PDGF/PDGFRβ signaling is prominently responsible for phenotypic modulation of VSMCs and occlusive cardiovascular diseases. During neointima formation, PDGF is locally produced and initiates a multitude of biological effects through the activation of its receptor PDGFRβ and subsequent intracellular signaling that contribute to VSMC proliferation, migration, and dedifferentiation. Although numerous studies have demonstrated the central role of PDGFRβ and elucidated the downstream signaling of PDGFRβ, the precise regulatory mechanisms governing PDGFRβ signaling, both in terms of its promotion and inhibition, remain largely unknow.

PTP non-receptor type 14 (PTPN14) belongs to the classical phosphotyrosine-specific phosphatase family, which is involved in the balance of protein tyrosine phosphorylation by interaction with tyrosine kinases (PTPs). Previous studies have reported that PTPN14 is involved in the occurrence and development of various cancers by regulating cell migration, metastasis, adhesion, and turnover. Moreover, we have recently reported that PTPN14 inhibited the disturbed flow-induced athero-prone phenotype of endothelial cells (ECs). Despite these findings, the role of PTPN14 in VSMCs and neointimal hyperplasia remains unclear.

Methods: In this study, PTPN14 level was systematically evaluated in carotid arteries across three distinct mouse models of neointimal formation, as well as in human coronary arteries with restenosis lesions. Multiple gain- and loss-of-function genetic approaches were conducted to investigate the potential role of PTPN14 in wire-injured-induced neointimal hyperplasia. RNA-seq and mass spectrometry were employed to elucidate PTPN14-mediated signaling in SMCs. Integrated multi-omics analyses including RNA-seq and mass spectrometry were employed to elucidate PTPN14-interacting proteins and phosphorylation-dependent signaling networks.

Results: Our study observes a marked upregulation of PTPN14 in SMCs across multiple murine vascular injury models, including atherosclerotic, complete ligation, and wire-injured carotid arteries. This finding was corroborated in human coronary arteries, where PTPN14 expression was significantly elevated in hyperplastic coronary arteries compared to non-hyperplastic vessels and positively correlated with the degree of stenosis. PTPN14 overexpression promoted PDGF-BB-induced proliferation, migration, and dedifferentiation of SMCs, and aggravated wire-injured-induced neointimal hyperplasia in mice in a phosphatase activity-dependent manner, while SMC-specific deficiency of PTPN14 attenuated neointimal hyperplasia in mice. Besides, RNA-seq indicated that PTPN14 deficiency inhibited PDGF-BB/PDGFRβ signaling-induced SMC phenotypic modulation. Moreover, we found that PTPN14 interacted with intracellular region of PDGFRβ and mediated its dephosphorylation on Tyr692 site. Using gain- and loss-of-function experiments, we demonstrated that phosphorylation of PDGFRβ^{Y692} negatively regulated PDGFRβ signaling activation. Overexpression of phosphomimetic mutant of PDGFRβ recapitulated, while the phospho-null mutant of PDGFRβ counteracted, the protective effects of SMC-specific deficiency of PTPN14 on wire-injured-induced neointimal hyperplasia in mice. Finally, we found that the phosphorylation level of PDGFRβ^{Y692} was negative correlated with the degree of stenosis in human coronary arteries.

Conclusions: Our study establishes PTPN14 as a PDGF-BB-inducible novel modulator of vascular smooth muscle cell phenotype and neointimal hyperplasia pathogenesis. We demonstrate that PDGF-BB stimulation upregulates PTPN14 expression in SMCs, creating a positive feedback loop that amplifies PDGFRβ signaling through selective dephosphorylation of the self-inhibitory Tyr692 site on PDGFRβ. PDGFRβ^{Y692} serves as a self-inhibitory site to control PDGFRβ activation and targeting PTPN14/PDGFRβ^{Y692} might offer a potential therapeutic strategy for neointimal hyperplasia related diseases.

Keywords:

PTPN14, PDGFRβ, vascular smooth muscle cells, dephosphorylation, neointimal hyperplasia

Impact of Renal Function on Prognostic Value of Post-PCI High-Sensitivity Troponin T in Acute Coronary Syndrome: A Retrospective Cohort Study

kun Na, Yi Li, Jing Li, Ya-Ling Han

State Key Laboratory of Frigid Zone Cardiovascular Diseases，Cardiovascular Research institute and Department of Cardiology, General Hospital of Northern Theater Command, No.83, Wenhua Road, Shenhe District,Shenyang, 110016, China

Background: High-sensitivity troponin T (hsTnT) serves as the gold standard biomarker for myocardial injury detection and risk stratification in acute coronary syndrome (ACS), with Class I recommendation in clinical guidelines. However, interpreting hsTnT levels presents significant challenges in patients with renal impairment, as renal function substantially influences circulating troponin concentrations through altered clearance mechanisms and complex pathophysiological interactions. Patients with chronic kidney disease frequently demonstrate elevated troponin levels without acute coronary events, creating clinical uncertainty in distinguishing between chronic elevation due to impaired clearance and acute elevation signifying new myocardial injury. Current risk assessment models inadequately account for the potential interaction between renal function and troponin levels, potentially leading to misclassification of cardiovascular risk. The relationship between hsTnT levels and clinical outcomes may follow non-linear patterns across the spectrum of renal function that existing prognostic models fail to capture, necessitating more sophisticated risk stratification approaches for this complex patient population.

Methods: This retrospective analysis utilized data from a single-center, prospective, real-world percutaneous coronary intervention (PCI) registry conducted at the General Hospital of Northern Theater Command. From March 2016 to March 2019, we enrolled 14,208 consecutive ACS patients aged 18 years or older who underwent PCI with at least one stent implanted. Patients were stratified by renal function using estimated glomerular filtration rate (eGFR) calculated with the Modification of Diet in Renal Disease equation: impaired renal function (eGFR < 60 mL/min/1.73m²) versus preserved renal function (eGFR ≥ 60 mL/min/1.73m²). Peak hsTnT levels measured 6-12 hours post-PCI were categorized as < 5 versus ≥ 5 times the 99th percentile upper reference limit (URL). The primary endpoint was one-year all-cause mortality, with secondary endpoints including ischemic events defined as a composite of cardiac death, myocardial infarction, or stroke. Statistical analysis employed Kaplan-Meier survival analysis, multivariable Cox regression models adjusted for clinical and procedural characteristics, and restricted cubic spline regression to evaluate non-linear relationships between hsTnT concentrations and clinical outcomes.

Results: Among 14,208 patients, 1,206 (8.5%) had impaired renal function and 13,002 (91.5%) had preserved renal function. Patients with impaired renal function were significantly older (68.12 ± 9.98 vs. 60.36 ± 10.15 years, P < 0.001) with higher cardiovascular risk burden and elevated peak hsTnT levels [0.12 (0.03-0.74) vs. 0.04 (0.02-0.23) ng/L, P < 0.001]. Elevated hsTnT (≥ 5 URL) was more prevalent in impaired renal function patients (30.3% vs. 17.8%). In patients with impaired renal function, elevated hsTnT was associated with dramatically increased one-year all-cause mortality (12.84% vs. 4.29%, adjusted hazard ratio [aHR] 3.63, 95% confidence interval [CI] 2.04-6.49, P < 0.0001) and ischemic events (10.66% vs. 4.88%, aHR 2.72, 95% CI 1.51-4.88, P = 0.0008). Conversely, in patients with preserved renal function, the mortality association was markedly attenuated (1.42% vs. 0.98%, aHR 1.40, 95% CI 0.85-2.29, P = 0.1864), though ischemic events remained significantly elevated. Restricted cubic spline analysis revealed a significant non-linear relationship between hsTnT levels and all-cause mortality specifically in the impaired renal function cohort (P for non-linearity = 0.0004), while patients with normal renal function exhibited a predominantly linear relationship (P for non-linearity = 0.2647). A statistically significant interaction was observed between renal function status and hsTnT for mortality prediction (P interaction = 0.0089).

Conclusions: These findings demonstrate that renal function fundamentally transforms the prognostic significance of elevated troponin T in ACS patients undergoing PCI. This critical interaction—where elevated troponin carries three-fold greater mortality risk in renal impairment but minimal impact with normal function—establishes the necessity for integrated risk assessment incorporating both parameters to identify patients requiring intensified surveillance and intervention.

Prolonged Dual Antiplatelet Therapy Strategy in Acute Coronary Syndrome Patients Post-Standard Therapy and Adverse Event-Free: An Analysis Based on OPT-CAD Risk Score Stratification

Xiao-Lin Su[1,2], miao-Han qiu[1], Hai-Wei Liu[1], Kai Xu[1], Xiao-Zeng Wang[1], Jing Li[1], Yi Li[1], Ya-Ling Han[1]

1. State Key Laboratory of Frigid Zone Cardiovascular Diseases，Cardiovascular Research institute and Department of Cardiology, General Hospital of Northern Theater Command, No.83, Wenhua Road, Shenhe District,Shenyang, 110016, China

2. Department of Traditional Chinese Medicine, Shengjing Hospital of China Medical University, Shenyang, China

Background: The optimal antiplatelet strategy for patients with acute coronary syndrome (ACS) after the standard 12-month dual antiplatelet therapy (DAPT) is still a matter of concern. We aimed to apply the OPT-CAD (Optimal antiPlatelet Therapy for Chinese patients with Coronary Artery Disease) score for risk stratification and to identify those who would derive benefit from prolonged DAPT beyond 12 months.

Methods: In this post hoc analysis of OPT-CAD study, a large-scale, multicentre, prospective, real-world observational registry conducted at 109 centres in 31 provinces in China, 7,154 patients with ACS, who completed 12-month DAPT without any adverse events, were divided into low-risk (n=4,171) and medium-to-high-risk (n=2,983) groups based on the OPT-CAD risk score, which consists of 10 variables, including age, heart rate, hypertension, prior myocardial infarction (MI), prior stroke, renal insufficiency, anaemia, low ejection fraction, positive cardiac troponin and ST-segment deviation. The primary endpoint was ischemic events, defined as the composite of cardiac death, MI or stroke occurring between 12 and 24 months. The secondary endpoints included all-cause death and Bleeding Academic Research Consortium (BARC) types 3 or 5 bleeding. Propensity score matching (PSM) was performed in the low-risk and medium-to-119 high-risk groups at a 1:1 ratio to minimize potential confounding factors.

Results: Based on the OPT-CAD risk score, 4,171 patients (58.30%) were at low risk and 2,983 (41.70%) were at medium-to-high risk. The patients at medium-to-high risk had a significantly higher incidence of ischemic events (hazard ratio [HR] 3.01, 95% confidence intervals [CI] 2.13-4.26, P< 0.0001) and all-cause death (HR 3.14, 95%CI 1.98-4.99, P< 0.0001) than those at low risk. In the low-risk cohort, patients treated with prolonged DAPT exhibited a higher proportion of males, lower LVEF, and a reduced prevalence of prior MI and PCI. At discharge, patients in the prolonged DAPT group were more commonly prescribed clopidogrel but less frequently administered PPIs. After PSM, among 1,287 propensity-matched pairs, ischemic events, all-cause death, and BARC type 3 or 5 bleeding were comparable between prolonged DAPT and single antiplatelet therapy (SAPT) regimens. Among the medium-to-high-risk patients, prolonged DAPT, as compared to SAPT, was more prevalent among younger patients with hyperlipidaemia and lower BMI, and with a lower proportion of previous MI and PCI. At discharge, patients treated with prolonged DAPT were more inclined to be prescribed clopidogrel and ACEI/ARB. After propensity score matching, a total of 950 propensity-matched pairs, prolonged DAPT was associated with a reduction in ischemic events (2.21% vs. 4.53%, HR 0.48, 95%CI 0.29-0.81, P=0.0062) and all-cause death (1.16% vs. 2.63%, HR 0.44, 95%CI 0.21-0.89, P=0.0220) without apparently increasing the risk of BARC type 3 or 5 bleeding (0.32% vs. 0.32%, HR 1.49, 95%CI 0.25-8.92, P=0.6622).

Conclusions: The OPT-CAD risk score demonstrated a moderately effective capability to predict long- term ischemic events and all-cause death in ACS patients who completed standard 12- month DAPT and were free from any adverse events. Patients classified as medium-to- high risk according to the OPT-CAD risk score might benefit from the prolonged DAPT beyond 12 months, as it was associated with a reduction in ischemic events and all-cause death without increasing the risk of bleeding complications between 12 and 24 months. Additional trials are warranted to assess the value of the OPT-CAD risk score in guiding DAPT duration.Additional trials are warranted to assess the value of the OPT-CAD risk score in guiding DAPT duration.

Prognostic Value of Persistent Microvascular Obstruction in Post-myocardial Infarction Patients After Reperfusion: A Cardiac Magnetic Resonance Study

Peng-Yu Zhou, Xiu-Yu Chen, Shi-Hua Zhao

Fuwai Hospital, Chinese Academy of Medical Sciences and Peking Union Medical College

Background: Multiple randomized clinical trials have failed to demonstrate improved long-term outcomes after coronary revascularization. One remarkable potential explanation for these results is the negative impact of coronary microvascular dysfunction. Microvascular obstruction (MVO), a common phenomenon in obstructive coronary artery disease following percutaneous coronary intervention (PCI), serves as an important prognostic biomarker of microvascular injury that can be accurately quantified by cardiac magnetic resonance (CMR) imaging. While acute-phase MVO is a well-established predictor of adverse outcomes, the clinical significance of persistent-MVO on follow-up CMR remains poorly understood. Persistent microvascular injury likely reflects unresolved tissue damage and has been strongly associated with adverse left ventricular remodeling (ALVR), a key structural alteration linked to subsequent heart failure (HF) development. However, the prognostic value of persistent-MVO for HF-related adverse outcomes, particularly its incremental value beyond established clinical and imaging markers, remains unclear. To bridge these gaps, this study reviewed a cohort of post-MI patients with the previous PCI following objectives: 1) to quantify the prevalence of persistent-MVO and describe its associated clinical characteristics, and 2) assess the prognostic value of persistent-MVO and determine its incremental predictive value for HF-related adverse outcomes over established clinical and imaging markers.

Methods: In this single-center retrospective study, 798 post-MI patients with previous PCI who underwent CMR were consecutively included between June 2017 and February 2022. Persistent-MVO was defined as the presence of MVO on late gadolinium enhancement (LGE) imaging performed at least 60 days after PCI. The endpoint was a composite event of heart failure (HF) comprising HF-related death, heart transplantation, left ventricular assist device implantation, and HF hospitalization. Sudden cardiac death (SCD), aborted SCD, and non-cardiovascular death were also recorded to address the competing influence. Competing risk analysis was performed using Fine-Gray subdistribution hazard modeling. The incremental value of each variable was assessed using Harrell's C-statistic (with bootstrap-based 95% confidence intervals (CI) and 1,000 replicates for pairwise comparisons) and the likelihood ratio test.

Results: In the 504 eligible patients (mean age 56.2 years, 89.1% male), 44 (8.7%) patients had persistent-MVO. The median interval time of the PCI and CMR was 87 (69-290) days. Patients with persistent-MVO were less likely to use statin medicine (70.5% vs. 92.2%, p<0.001), lower left ventricular ejection fraction (LVEF) (32.2 ± 10.9% vs. 37.3 ± 14.4%, p=0.04), larger end-diastolic volume index (EDVi) (142.4 ± 40.3 vs. 122.8 ± 48.4, p=0.001) and end-systolic volume index (ESVi) (101.3 ± 38.1 vs. 87.7 ± 47.8, p=0.02), as well as larger LGE extent (29.2 ± 10.9% vs. 21.4 ± 11.8%, p<0.001), compared to those without persistent-MVO. During a median follow-up of 64.5 (IQR, 45.0 to 79.4) months, 91 patients (18.1%) experienced the endpoint. Persistent-MVO was independently associated with HF-related events (sHR=2.26, 95% CI: 1.25–4.08, p < 0.01), after adjusting for New York Heart Association functional classification (NYHA) class (sHR = 1.89, 95%CI, 1.17-3.05, p < 0.01), LVEF (sHR = 0.96, 95%CI, 0.94-0.99, p = 0.02), EDVi (sHR = 1.01, 95%CI, 1.00-1.01, p = 0.03), and LGE extent (sHR = 1.02, 95%CI, 1.01-1.04, p = 0.04). Persistent-MVO significantly improved the model discrimination and the model fit (C-index: increased from 0.76 to 0.78, p=0.01; -2 Likelihood ratio: decreased from 498.4 to 492.4, p<0.001) compared with the model including NYHA class, LVEF, and LGE extent for the HF-related events.

Conclusion: Persistent-MVO was observed in 8.7% of post-MI patients more than 60 days after reperfusion. It emerged as a significant predictor of HF-related events and demonstrated incremental prognostic value beyond conventional markers. These findings highlight the role of persistent microvascular injury in post-infarction risk and support future research into microvascular repair strategies.

Nonischemic Late Gadolinium Enhancement Associated with Adverse Remodeling is an Underrecognized Predictor of Heart Failure Outcomes Post-Myocardial Infarction

Peng-Yu Zhou, Xiu-Yu Chen, Shi-Hua Zhao

Fuwai Hospital, Chinese Academy of Medical Sciences and Peking Union Medical College

Background and Aims:

Advances in acute myocardial infarction (MI) management—such as timely revascularization, evidence-based pharmacotherapy, and secondary prevention—have substantially improved short-term survival over recent decades. However, many patients still experience adverse left ventricular remodeling (ALVR) and eventually develop heart failure (HF), which significantly contributes to long-term morbidity and mortality. Early identification of patients at high risk of post-MI HF remains a clinical challenge. Conventional markers such as infarct size and left ventricular ejection fraction (LVEF) offer only modest predictive power. Indeed, adverse remodeling can occur even in patients with relatively small infarcts or preserved LVEF, suggesting that additional pathophysiologic mechanisms—such as diffuse fibrosis or inflammation—may be involved. Cardiac magnetic resonance (CMR) imaging is the gold standard for assessing cardiac function and myocardial tissue characteristics. Late gadolinium enhancement (LGE) imaging enables visualization of replacement fibrosis with high spatial resolution. While ischemic-pattern LGE has been extensively validated as a predictor of mortality, arrhythmia, and HF, increasing attention has turned to nonischemic LGE (NI-LGE) patterns—including mid-wall, subepicardial, and insertion point enhancement—that have been identified in patients with ischemic heart disease. These patterns are typically associated with nonischemic cardiomyopathies or myocarditis but may also occur in the setting of ischemic injury, possibly reflecting secondary remodeling or regional inflammation. The clinical significance and prognostic impact of NI-LGE in post-MI patients, however, remain poorly characterized. Recent studies have hinted that NI-LGE may be associated with increased risk of adverse outcomes, including HF progression, but large-scale, event-specific analyses are lacking. Furthermore, whether NI-LGE provides incremental prognostic value beyond established clinical (e.g., NYHA class) and imaging markers (e.g., LVEF, infarct size) has not been definitively addressed. Finally, it is unclear whether the prognostic impact of NI-LGE varies based on specific patterns (e.g., mid-wall vs. subepicardial) or locations (e.g., septal vs. free wall). To bridge these knowledge gaps, the present study aimed to (1) quantify the prevalence of NI-LGE and characterize its clinical and imaging associations in a large cohort of post-MI patients; (2) evaluate the independent prognostic value of NI-LGE for HF-related and sudden cardiac death (SCD)-related outcomes; and (3) determine whether NI-LGE confers incremental predictive utility beyond traditional clinical and CMR-based markers.

Methods:

A total of 956 post-MI patients (mean age: 56.2±10.9 years, 88.4% male)

confirmed by cardiac MR were retrospectively included. NI-LGE was defined as mid-wall, subepicardial, or insertion point enhancement. Patients concomitant with nonischemic cardiomyopathies or myocarditis were excluded. HF- and sudden cardiac death- (SCD) related events were recorded. Competing risk analysis was used to address the competing influence. The incremental value of each variable was assessed using Harrell's C-statistic (with bootstrap-based 95% confidence intervals (CI) and 1,000 replicates for pairwise comparisons) and the likelihood ratio test. Model fit was evaluated using the Akaike Information Criterion (AIC), with a lower value indicating a better fit.

Results:

Among the 86 patients (9.0%) with NI-LGE, the most prevalent pattern and location were the mid-wall enhancement (71 patients) and the septum involvement (74 patients). NI-LGE patients had lower left ventricular ejection fraction (LVEF, 28.3% vs. 36.9%, p<0.001) and larger EDVi (160.7 vs. 122.6, p<0.001), with EDVi independently associated with NI-LGE (OR=1.01, p<0.001). During a median follow-up of 69.6 months, 101 (10.6%) and 65 (6.8%) experienced the HF- and SCD-related events, respectively. NI-LGE was independently associated with the HF-related events (sHR = 5.75, 95%CI, 3.71-8.92, p<0.001) after adjusting for the NYHA class (sHR = 1.95, 95%CI, 1.27-3.00, p < 0.001), LVEF (sHR = 0.94, 95%CI, 0.90-0.97, p < 0.001), and LGE extent (sHR = 1.04, 95%CI, 1.02-1.06, p < 0.001). NI-LGE improved the model discrimination and fit performance (C-index: increased from 0.84 to 0.87; Likelihood ratio: decreased from 1168.0 to 1106.1; AIC: decreased from 1174.0 to 1114.1, all p < 0.001) compared with the model including NYHA class, LVEF, and LGE extent for the HF-related events. However, NI-LGE was not associated with the SCD-related events (p=0.65). In location analysis, dual-involvement patients had a higher HF-related events risk than isolated-involvement patients (sHR = 2.30, 95% CI: 1.18–4.47, p = 0.02). No significant differences in the risk of the HF-related endpoint were observed between isolated- and dual-pattern (p = 0.19) or between mid-wall and subepicardial LGE (p = 0.89).

Conclusion:

In this large retrospective CMR study, NI-LGE occurs in 9% of post-MI patients and is associated with ALVR, which is most commonly observed as mid-wall enhancement of the septum. NI-LGE serves as a promising predictor of HF-related events rather than SCD-related events, and provides incremental prognostic value beyond conventional markers. Identifying NI-LGE may help risk stratification and facilitate more accurate and HF-specific management in this population in the future.

Mediation of the Relationship Between Myocardial Replacement Fibrosis and Sudden Cardiac Death by Left Ventricular Ejection Fraction Post-Myocardial Infarction

Peng-Yu Zhou, Xiu-Yu Chen, Shi-Hua Zhao

Fuwai Hospital, Chinese Academy of Medical Sciences and Peking Union Medical College

Background and Aims

Sudden cardiac death (SCD) remains a leading cause of mortality in patients with ischemic heart disease (IHD), accounting for a substantial proportion of cardiovascular deaths worldwide. Patients who have experienced a myocardial infarction (MI) are particularly vulnerable due to their increased risk of life-threatening ventricular arrhythmias. Current clinical guidelines recommend implantable cardioverter-defibrillator (ICD) therapy primarily for patients with left ventricular ejection fraction (LVEF) ≤ 35%, as these patients are considered at highest risk of SCD. However, this selection criterion has important limitations: a significant number of SCD cases occur in patients with preserved or mildly reduced LVEF (>35%), and many patients with severely reduced LVEF never receive appropriate ICD therapy. Thus, LVEF alone is insufficient to fully capture SCD risk, and improved risk stratification tools are urgently needed. Cardiac magnetic resonance (CMR) imaging with late gadolinium enhancement (LGE) enables noninvasive identification of myocardial replacement fibrosis, a key arrhythmogenic substrate implicated in SCD. LGE not only directly contributes to electrical instability but also promotes adverse ventricular remodeling, which in turn leads to LVEF decline. Therefore, fibrosis could increase SCD risk via two complementary pathways: a direct pro-arrhythmic effect and an indirect effect mediated by impaired ventricular function. Despite these insights, the extent to which LVEF mediates the association between LGE and SCD remains incompletely understood, particularly across different LVEF strata relevant to ICD implantation. To address this knowledge gap, we aimed to investigate the mediation effect of LVEF on the relationship between LGE and SCD in a large cohort of post-MI patients. We also sought to evaluate whether this mediation differs in subgroups of patients with LVEF ≤ 35% and >35%, thus providing insight into the utility of LGE for SCD risk stratification beyond current guidelines.

Methods

We retrospectively analyzed 917 patients with prior myocardial infarction (mean age 56.3 ± 11.0 years; 88.8% male) who underwent CMR imaging at a median of 2.3 ± 3.2 years following their last MI event. The composite endpoint comprised sudden cardiac death, aborted SCD, and appropriate ICD discharges. Causal mediation analysis was performed using an accelerated failure time (AFT) model with 1,000 quasi-Bayesian simulations to estimate 95% confidence intervals (CIs). Effect estimates (aβ) represent log time ratios, with negative values reported as absolute values (-aβ) for intuitive interpretation, so that larger values indicate stronger effects. All models were adjusted for age and sex to account for their potential confounding effects. Subgroup analyses stratified patients into those with LVEF ≤ 35% and those with LVEF >35%, reflecting current ICD implantation criteria.

Results

During a median follow-up of 63.3 months (IQR 43.6 to 76.6 months), 65 patients (7.1%) experienced SCD-related events. Patients with SCD showed significantly greater LGE extent (30.1% vs. 19.7%, p<0.001), lower LVEF (30.7% vs. 36.6%, p=0.001), and worse New York Heart Association (NYHA) functional classification compared to patients without SCD. LGE extent was independently associated with lower LVEF (β = -0.35, p<0.001) and higher risk of SCD (subdistribution hazard ratio [sHR] = 1.06, p<0.001). LVEF was also independently associated with SCD risk (sHR = 0.95, p=0.03). Mediation analysis revealed a significant direct effect of LGE on SCD (-aβ = 23.2, 95% CI: 5.4 to 61.7, p<0.001), while LVEF partially mediated this association (-aβ = 5.5, 95% CI: 0.6 to 17.2, p<0.001), accounting for 19.7% of the total effect. In the LVEF >35% subgroup (n=436), the mediation effect was more pronounced, with LVEF explaining 40.4% of the LGE–SCD relationship (-aβ for indirect effect = 104.6, p=0.02). Conversely, in the LVEF ≤ 35% subgroup (n=481), no significant mediation was detected as LGE was not independently associated with LVEF (p=0.08). Inter- and intra-observer reproducibility for LGE extent and LVEF measurement were excellent, with intraclass correlation coefficients exceeding 0.95.

Conclusion

In patients with prior MI, LVEF partially mediates the effect of LGE on SCD risk, explaining less than one-fifth of the total association overall. Notably, the mediation effect is stronger in patients with preserved or mildly reduced LVEF (>35%), highlighting the potential added value of LGE for SCD risk stratification beyond conventional LVEF-based criteria. These findings support the incorporation of LGE assessment into clinical decision-making for ICD implantation, pending confirmation by large-scale prospective trials.

The U-shaped Relationship of Stress Hyperglycemia Ratio with Ventricular Arrhythmias and Sudden Cardiac Death in Acute Myocardial Infarction

Li Deng[1], Jun Wei[2], Ye Deng[3], Jing Yi Wang[3], Jian Ya Huang[3], Qian wen Chen[3], Qing Qing Gu[3], Xiao Jing Bao[1], Hua Yan You[1], Lu Pan[1], Yuan Ji[3], Qing Jie Wang[3], Ru Xing Wang[1], Ling Sun[1]

1. The Affiliated Wuxi People's Hospital of Nanjing Medical University

2. The Affiliated Hospital of Xuzhou Medical University

3. The Third Affiliated Hospital of Nanjing Medical University,

Background: Ventricular arrhythmias (VA) and sudden cardiac death (SCD) are life-threatening complications in acute myocardial infarction (AMI) patients. Although the stress hyperglycemia ratio (SHR) is recognized as a potential AMI prognostic factor, its association with VA and SCD development remains unclear.

Objective: This study aimed to explore the relationship between SHR and the risk of VA/SCD in patients with AMI.

Methods: A prospective cohort study enrolled 3,320 AMI patients, stratified by the occurrence of VA/SCD. The restricted cubic spline (RCS) method explored the non - linear relationship between SHR and the incidence of VA/SCD during hospitalization, with logistic regression analysis adjusting for confounders to validate the association.

Results: Among 3,320 participants (mean age 64.68 years, 74.2% male), 165 (5.0%) experienced VA/SCD during hospitalization. RCS analysis showed a U - shaped association between SHR and VA/SCD with an inflection point of 0.96. When SHR > 0.96, each standard deviation (SD) increases raised VA/SCD risk by 25% (odds ratio [OR]: 1.25, 95% confidence interval [CI]: 1.02 – 1.54); when SHR < 0.96, a SD increase reduced the risk by 25% (OR: 0.75, 95% CI: 0.63 – 0.89, P = 0.001), consistent with logistic regression results.

Conclusion: This study established a U-shaped association between SHR and VA/SCD risks in hospitalized AMI patients, highlighting its potential as a biomarker for precise severity assessment and personalized treatment. Further prospective validation are needed before clinical application.

C-reactive Protein-Albumin-Lymphocyte (CALLY) Index as an Independent Risk Factor for Postoperative Atrial Fibrillation Recurrence

Ye Deng[1], Jian Ya Huang[1], Li Deng[1], Yu Xuan Zhou[2], Lu Pan[3], JIng Yi Wang[1], Qian Wen Chen[1], Qing Qing Gu[1], Yang Zhang[4], Jun Wei[4], Yuan Ji[1], Qing Jie Wang[1], Ling Sun[3]

1. the Third Affiliated Hospital of Nanjing Medical University

2. Fudan University Affiliated Shanghai Fifth People's Hospital

3. The Affiliated Wuxi People's Hospital of Nanjing Medical University

4. The Affiliated Hospital of Xuzhou Medical University,

Background Atrial fibrillation (AF) recurrence following catheter ablation remains a significant clinical challenge despite reported procedural efficacy. Emerging evidence suggests inflammatory biomarkers may predict arrhythmia recurrence. This study evaluates the novel CALLY index, a composite inflammatory marker, as a prognostic tool for AF recurrence post-ablation.

Methods I n a prospective cohort study, 556 consecutive patients with AF undergoing catheter ablation between June 2018 and June 2023 were enrolled. Patients were categorized into recurrence and sinus rhythm (SR) maintenance groups. The CALLY index was calculated pre-ablation. Cox proportional hazards regression and Kaplan-Meier survival analyses assessed the association between CALLY index levels and AF recurrence risk. Predictive accuracy was evaluated using receiver operating characteristic (ROC) curves and area under the curve (AUC).

Results During a median follow-up of 12 months, 102 patients (18.3%) experienced AF recurrence. The SR maintenance group exhibited significantly higher CALLY index values compared to the recurrence group (3.24 ± 1.68 vs. 1.89 ± 0.57; P < 0.001). Univariate Cox regression analysis revealed an inverse association between the CALLY index and recurrence risk (hazard ratio [HR]: 0.439, 95% confidence interval [CI]: 0.292–0.659; P < 0.001), which persisted after multivariable adjustment (HR: 0.887, 95% CI: 0.789–0.956; P = 0.031). Patients in the highest CALLY index tertile had a 29% lower recurrence risk compared to the lowest tertile (HR: 0.71, 95% CI: 0.68–0.76; P = 0.017). ROC analysis identified a CALLY index threshold of ≥ 1.433, yielding an AUC of 0.790 (sensitivity: 76.4%, specificity: 74.8%; P < 0.001).

Conclusion The CALLY index is an independent predictor of AF recurrence following catheter ablation, demonstrating robust discriminatory power. Its integration into clinical practice may enhance risk stratification and optimize post-ablation management strategies.

Risk Reclassification and Cost-Effectiveness of Echocardiography for Cardiovascular Primary Prevention in Hypertension in China

Anping Cai

广东省人民医院

Objective: Subclinical cardiac changes are common among individuals with hypertension and are associated with increased cardiovascular risk, yet current hypertension guidelines do not routinely recommend echocardiography for risk assessment due to concerns about cost-effectiveness and limited risk reclassification data. This study aimed to evaluate the incremental value of echocardiography in cardiovascular risk reclassification and assess its cost-effectiveness among Chinese hypertensive adults without pre-existing cardiovascular disease (CVD).

Methods: We analyzed data from 3,243 hypertensive participants free of baseline CVD enrolled in the China PEACE Million Persons Project in Guangdong Province between 2016 and 2020. All participants underwent standardized clinical evaluation, including measurements of blood pressure, anthropometrics, fasting glucose, lipid profile, and lifestyle risk factors. Echocardiographic examinations were performed by trained personnel using a standardized protocol and included assessment of left atrial (LA) size, left ventricular diastolic dysfunction (LVDD), and global longitudinal strain (GLS). Echocardiographic abnormalities were defined as enlarged LA, presence of LVDD (by septal/lateral e' or LA enlargement), and reduced GLS (<18%). The primary outcome was major adverse cardiovascular events (MACE), a composite of coronary heart disease, myocardial infarction, stroke, heart failure (HF), or cardiovascular death. Cox proportional hazards models were used to estimate the association between predictors and MACE. Risk prediction models were constructed using conventional clinical variables (age, sex, smoking, obesity, diabetes, and dyslipidemia), and then updated by incorporating echocardiographic measures. Discrimination was assessed using the C-statistic. Based on the observed incidence rates of MACE, participants were categorized into low-, intermediate-, or high-risk groups. Number needed to test (NNT) and associated costs were calculated to assess the utility and cost-effectiveness of echocardiographic screening.

Results: Over a median follow-up of 4.5 years, 368 participants (11.3%) experienced MACE. Echocardiographic abnormalities were prevalent and significantly associated with outcomes. Multivariable analysis showed that enlarged LA, LVDD, and reduced GLS were independently associated with increased MACE risk, with hazard ratios ranging from 1.30 to 1.57. The addition of these echocardiographic markers to the clinical model significantly improved predictive performance, increasing the C-statistic from 0.615 to 0.643 (P = 0.003). Reclassification analyses revealed that 22% of patients originally classified as low-risk were reclassified to higher risk categories, with 18% to intermediate-risk and 4% to high-risk based on the presence of echocardiographic abnormalities. The 1-year MACE incidence in the reclassified high-risk group was 12.3%, while the 3-year incidence in the intermediate-risk group was 12.0%, both exceeding thresholds used to define high 10-year CVD risk. At 1-year follow-up, the NNT to identify one intermediate- and one high-risk individual was 77 and 11, respectively, with corresponding costs of approximately USD 3,080 and USD 440. These improved to 20 and 6 (USD 800 and USD 240) by year three. These values fall well below China's cost-effectiveness threshold of USD 14,952 per quality-adjusted life year. Furthermore, echocardiographic abnormalities were more strongly associated with incident HF than with atherosclerotic cardiovascular disease (ASCVD) (e.g., LVDD HR for HF: 5.72 vs. 1.80 for ASCVD, P = 0.005).

Conclusion: This study demonstrates that echocardiographic assessment meaningfully improves cardiovascular risk stratification and is cost-effective for primary prevention in hypertensive individuals in China. Importantly, the identified subclinical cardiac changes were more strongly linked to HF risk than to ASCVD, emphasizing the value of early detection and intervention to prevent HF development. These findings support the integration of echocardiography into routine hypertension management, particularly in resource-appropriate settings, and warrant future research evaluating echocardiography-guided treatment strategies.

Single-cell multi-omics identifies a specialized cytotoxic and migratory CD8+ effector T cells in acute myocarditis

zhonghua tong, Xiang-Yu yan, Tao Chen, Wei-Jun Song, Di Su, Mao-Mao Zhang, Bo Yu

The Second Affiliated Hospital of Harbin Medical University

BACKGROUND: Acute myocarditis (AM), particularly fulminant myocarditis (FM), is an infrequent yet life-threatening cardiac inflammation, with limited effective precision-targeted treatments currently available. This urgent clinical challenge has prompted further investigations into the mechanisms underlying this pathology to develop novel therapeutic approaches.

METHODS: We enrolled 40 patients diagnosed with AM (24 mild, 16 fulminant) between December 2022 and November 2023. Using a multi-omics approach, we analyzed their peripheral blood mononuclear cells (PBMCs) and plasma integrated single-cell RNA sequencing (scRNA-seq), single-cell T cell receptor sequencing (scTCR-seq), cytometry by time of flight (CyTOF), and Olink proteomics to identify specific pathogenic immune subsets and molecular alterations. In-vitro experiments validated the function and inducing signals of identified pathogenic subsets. In coxsackievirus B3 induced FM mice, CyTOF analysis was performed on PBMCs and cardiac infiltrating immune cells. Pharmacological blockade of key molecular was tested to assess potential therapeutic efficacy.

RESULTS: Single-cell transcriptomics and proteomics analyses revealed that circulating $CD8^+$ T cells displayed the most prominent changes in both cellular density and transcriptional profiles following the onset of AM, exhibiting increased immune activation and recruitment likely contributing to tissue damage and inflammation. Futher sub-clustering identified a specialized type of $CD8^+$ effector T cells, $CD57^+CD8^+$ T cells with high cytotoxicity and migration potential, significantly enriched and exhibited large clonal expansion in AM. However, resembling $CD57^+CD8^+$ effector T cells were not identified in the peripheral blood of patients with other inflammatory diseases (COVID-19, influenza, and systemic lupus erythematosus) nor in the cardiac tissue of patients with heart failure or myocardial infarction, with the exception of those with immune checkpoint inhibitor (ICI)-induced myocarditis. These findings indicate that the effector phenotype of $CD57^+$ $CD8^+$ T cells in myocarditis reflects a disease-specific transcriptional program.

Trajectory analysis delineated a continuum from $CD57^-$ naïve T cells toward mild-associated $CD57^+$ effectors, and subsequently to fulminant-associated $CD57^+$ subsets. The sustained up-regulation of cytotoxic and migratory genes throughout this process, suggesting escalating immune activation and recruitment with increasing disease severity. Differential expression analysis further revealed up-regulation of natural killer (NK)-like receptor genes in $CD57^+CD8^+$ effector T cells from FM compared to mild cases, which positively associated with enhanced cytotoxicity and migration potential.

In-vitro experiments confirmed the existence of circulating $CD57^+CD8^+$ effector T cells and their high cytotoxic degranulation and migration function, where they were shown to induce cardiomyocyte apoptosis. Consistent with this, both cardiac biopsy samples and single-nucleus RNA sequencing of heart tissue detected the presence of resembling $CD57^+CD8^+$ effector T cells, suggesting that these pathogenic cells may migrate from the circulation to cardiac tissue and contribute directly to immune-mediated myocardial injury.

Proteomic profiling using Olink further revealed a heightened inflam-

matory protein signature in FM, supporting the precence of cytokine storms. Among these, IL18 was significantly increased and showed a strong correlation with the frequency of $CD57^+CD8^+$ T cells, implicating IL-18 as a potential upstream regulator. In vitro stimulation with IL-18, as well as serum from AM patients, significantly increased the proportion of $CD57^+CD8^+$ effector T cells and promotes the expression of genes associated with cytotoxicity and chemotaxis. This differentiation process was effectively attenuated by IL-18 antagonism, underscoring a functional role for IL-18 in promoting effector T cell pathogenicity.

Further analysis identified a distinct subset of $CXCL8^+$ $CD14^+$ pro-inflammatory monocytes that was significantly expanded in FM and likely contributed to the observed cytokine storms, including elevated IL-18 production. Ligand–receptor interaction analysis revealed that $CXCL8^+CD14^+$ monocytes may promote the differentiation and activation of $CD57^+$ $CD8^+$ effector T cells via IL18-IL18R1 and HLA-E-KLRC2 signaling pathways, suggesting that the pathogenic role of $CD57^+CD8^+$ effector T cells was further amplified by $CXCL8^+CD14^+$ monocytes in FM

To validate these observations, immune profiling was conducted in an A/J mouse model of coxsackievirus B3 induced FM. Comparable expansions of $CD57^+CD8^+$ effector T cells and $CXCL2^+LY6C^+$ inflammatory monocytes were observed in both peripheral blood and cardiac tissue, accompanied by elevated plasma IL-18 levels. Importantly, disruption of the pathological axis involving pro-inflammatory monocytes, IL-18 signaling, $CD57^+CD8^+$ effector T cell activation, and CCR5-mediated recruitment significantly ameliorated disease severity in the murine model, providing multifaceted strategies to mitigate immune-mediated cardiac injury in FM.

CONCLUSIONS: The identification of clonally expanded $CD57^+CD8^+$ effector T cells—marked by high cytotoxicity and migratory potentia—together with their upstream inflammatory regulators, underscores a pathogenic axis that may serve as a promising therapeutic target to alleviate immune-mediated cardiac injury. These findings offer critical mechanistic insights and valuable resources for advancing early diagnostic strategies and developing targeted interventions for AM, especially in its fulminant form.

Optimizing Long-term Cardiovascular Risk Stratification: Integrating Biomarkers into the Very High-Risk ASCVD Definition in Asian Patients

Hao-Yu Wang, Dong Yin, Ke-Fei Dou

Fuwai hospital

Background: The 2018 American Heart Association/American College of Cardiology (AHA/ACC) cholesterol guideline defines very high-risk (VHR) atherosclerotic cardiovascular disease (ASCVD) patients to guide intensive lipid-lowering therapy.

Objectives: This study sought to evaluate VHR's effectiveness in assessing cardiovascular (CV) risk in an Asian population and examine the predictive value of additional biomarkers for improving risk stratification.

Methods: 26,752 ASCVD patients were prospectively enrolled at Fuwai Hospital (2017–2018). Patients were classified as very high risk (VHR) based on the 2018 AHA/ACC cholesterol guideline, which defines VHR as having multiple major ASCVD events or one major event accompanied by multiple high-risk conditions. The primary outcome was a composite of 3-year CV events, including cardiovascular mortality, myocardial infarction, stroke, and coronary revascularization.

Results: A total of 26,752 patients with clinical ASCVD were included (mean age 59.7 years, 23% female). Recent ACS occurred in 45.6%, 24.5% had a prior MI unrelated to recent ACS, 12.4% had a history of stroke, and 6.2% had symptomatic peripheral artery disease. 14,475 (54.1%) patients were classified as VHR, with higher 3-year event rates than non-VHR (9.6% vs. 7.3%). In age- and sex-adjusted Cox regression, VHR classification was a significant predictor of 3-year CV events (HR: 1.25 [95% CI 1.12–1.40]). Notably, a history of multiple ASCVD events was a stronger predictor of future events (HR: 1.36 [95%CI 1.20–1.55]) compared to a history of one event with multiple risk factors (HR: 1.17 [95%CI 1.03–1.32]).

Hemoglobin (Hb), high-sensitivity C-reactive protein (hs-CRP), lipoprotein(a) (Lp(a)), and high-density lipoprotein cholesterol (HDL-C) were significant CV risk influencers in VHR patients (hazard ratios [95% CI]: 0.93 [0.90–0.96], 1.13 [1.06–1.21], 1.07 [1.04–1.11], 0.73 [0.61–0.89], respectively) , but not in non-VHR patients. Within the VHR category, patients with ≥ 2 abnormal biomarkers (Hb <12 g/dL for men, <11 g/dL for women; hs-CRP >3 mg/L; Lp(a) ≥ 50 mg/dL; HDL-C <1 mmol/L) were categorized as Very Very High Risk (VVHR), showing significantly higher event rates than those with fewer abnormal biomarkers (11.7% vs. 8.9%, P < 0.001).

Incorporating each biomarker into the VHR definition significantly improved predictive metrics, including Harrell's C-index, NRI, IDI, and AUC. A model combining all four biomarkers achieved a C-index of 0.632, compared to 0.589 for the VHR definition alone, with an NRI of 0.343 (95%CI 0.275–0.389) and an IDI of 0.039 (95%CI 0.035–0.044), demonstrating substantial added predictive value. Four biomarker-based high-risk conditions were identified: anemia (Hb <12 g/dL for men, <11 g/dL for women), inflammation (hs-CRP >3 mg/L), high Lp(a) (≥ 50 mg/dL), and low HDL-C (<1 mmol/L). Incorporating additional high-risk conditions into the original VHR definition resulted in a refined VHR classification, which remained a significant predictor of 3-year cardiovascular events (HR: 1.23 [95% CI 1.14–1.36]).

Conclusions: The VHR definition identifies high-risk Asian ASCVD patients but can be refined by incorporating biomarker-based high-risk conditions. Anemia, inflammation, elevated Lp(a), and low HDL-C can be incorporated into the original VHR criteria as additional high-risk conditions to refine risk stratification by addressing biomarker-related risks. The proposed VVHR category (VHR with ≥ 2 abnormal biomarkers) enhances risk stratification, identifying those who may benefit most from targeted intensive lipid-lowering therapy.

Stress Hyperglycemia Ratio, Albumin, and In-hospital Outcomes in Patients with Acute Myocardial Infarction: A Cohort Study

Yuxiu Yang[1,2], Yan Yan[1,2], ZhiJian Wang[1,2], YuJie Zhou[1,2]

1. Beijing Anzhen Hospital

2. National Clinical Research Center for Cardiovascular Disease

Background: Stress hyperglycemia ratio (SHR), calculated as acute-to-chronic glycemic markers, has emerged as a robust predictor reflecting true acute hyperglycemic stress beyond chronic hyperglycemia burden in critically ill patients. While elevated SHR is increasingly recognized as a putative risk indicator for adverse outcomes in acute myocardial infarction (AMI), the complex interplay between SHR and albumin—a biomarker integrating nutrition, inflammation, and frailty—remains inadequately characterized. Specifically, whether albumin status modifies the prognostic value of SHR for in-hospital cardiovascular events lacks large-scale evidence. This multi-center cohort study aims to delineate the albumin-stratified associations between SHR and composite major adverse cardiovascular events (MACEs) in a contemporary AMI cohort.

Methods: From January 2022 to October 2023, we consecutively enrolled AMI patients within 24 hours of symptom onset from the prospective Cardiovascular Biomarker Registry (NCT05337319). Baseline SHR was computed as fasting glucose (mmol/L) divided by estimated average glucose derived from admission glycated albumin (GA%) using the formula: [GA(%) × 0.31 + 1.9]. Hypoalbuminemia was defined as serum albumin <35 g/L. Optimal SHR cutoffs (high vs. low) were determined via maximally selected rank statistics for MACEs prediction. The primary endpoint was in-hospital MACEs, a rigorously adjudicated composite of all-cause mortality, cardiac shock, acute congestive heart failure (ACHF), reinfarction, and ischemic stroke. Multivariable logistic regression models adjusted for age, sex, systolic blood pressure, creatinine, troponin peak, Killip class, and revascularization strategy estimated odds ratios (ORs) with 95% confidence intervals (CIs) for MACEs across SHR-albumin subgroups and tested multiplicative interaction effects.

Results: A total of 5,269 consecutive patients presenting with acute myocardial infarction (AMI) were prospectively enrolled from the multi-center registry (NCT05337319) between January 2022 and October 2023. The cohort had a mean age of 60 years (range 51–68 years), and was predominantly male (79.0%). Elevated stress hyperglycemia ratio (SHR ≥ 0.92, defined by maximally selected rank statistics) was identified in 27.7% (n=1,462) of the population, while hypoalbuminemia (serum albumin <35 g/L) affected 19.5% (n=1,027). The primary endpoint of in-hospital MACEs occurred in 4.7% (n=252) of the overall cohort. Risk stratification based on SHR-albumin status demonstrated substantial prognostic divergence. Patients with low SHR and normal albumin manifested the lowest MACE incidence (1.4%, reference group). Conversely, those with high SHR and concomitant hypoalbuminemia experienced the most pronounced risk elevation, exhibiting a 6.800-fold increase in MACEs risk (adjusted OR=6.800; 95% CI: 3.883–11.907; P<0.001) after multivariable adjustment. Intermediate risk tiers were observed in low-SHR hypoalbuminemia (adjusted OR=3.033; 95% CI: 1.775–5.182; P<0.001) and high-SHR normalbuminemia subgroups (adjusted OR=2.375; 95% CI: 1.335–4.226; P=0.003), confirming the independent contribution of both metabolic derangements. Critically, high SHR consistently portended increased cardiovascular risk across albumin strata. In the normal albumin subgroup, high SHR independently predicted higher MACEs risk (adjusted OR=2.325; 95% CI: 1.307–4.136; P=0.004). Similarly, among hypoalbuminemic patients, high SHR remained significantly associated with adverse outcomes (adjusted OR=2.213; 95% CI: 1.343–3.647; P=0.002). Formal testing for multiplicative interaction between SHR and albumin yielded a non-significant P value of 0.866, indicating that albumin status did not modify the prognostic impact of SHR. This consistent risk pattern extended to secondary endpoints, including cardiac shock and ACHF (interaction P>0.05 for both).

Conclusions: In a large-scale comprehensive registry of AMI patients in China, stress hyperglycemia is prevalent, especially among those with hypoalbuminemia. Higher SHR is associated with in-hospital cardiovascular risk independently and regardless of serum albumin level. Screening for SHR and albumin status is recommended in AMI patients to aid risk stratification and effective secondary prevention strategies.

Effect of PCSK9 Inhibitors on the Quality of Life in Patients with Acute Coronary Syndromes

An-Ran Jing[1], Jing-Xian Wang[1], Meng-Long Zhang[1], Yan Liang[2], Jing-Yu Liu[2], Nan Zhang[2], Ji-Xiang Wang[2], Xiao-Wei Li[2], Chang-Ping Li[3], Zhuang Cui[3], Yin Liu[2], Jing Gao[2]

1. Thoracic Clinical College, Tianjin Medical University

2. Tianjin Chest Hospital

3. School of Public Health, Tianjin Medical University

Background PCSK9 Inhibitors (PCSK9i) can reduce LDL-C levels and the risk of long-term major adverse cardiovascular events (MACE) of patients with acute coronary syndromes (ACS). The application of PCSK9i has been recognized by current clinical guidelines[1]. With the development of modern medicine, patients' quality of life (QOL) has become a focal point. The Patient-Reported Outcome Measurement Information System (PROMIS) can effectively assess the overall health of patients. To date, no study has used PROMIS to explore QOL of ACS patients treated with PCSK9i.

Purpose To assess PCSK9i's impact on ACS patients' QOL, compare PCSK9i plus statin vs statin-only therapy using PROMIS 10, and analyze the association between PROMIS scores and MACE.

Methods The EMSIACS trial is a prospective, randomized, open-label, parallel-group, multicenter study registered at ClinicalTrials.gov (NCT04100434)[2]. This study presents exploratory outcomes from this trial. From September 2020 to March 2022, a total of 500 ACS patients were enrolled. Patients were randomly assigned in a 1:1 ratio to receive Evolocumab plus statin therapy or statin-only therapy. QOL was assessed using PROMIS 10 at baseline, week 12, and week 48. PROMIS 10 includes two summary scores: Global Physical Health (GPH, including physical health, physical function, fatigue and pain intensity) and Global Mental Health (GMH, including overall quality of life, mental health, satisfaction with social activities, and emotional problems). At week 48, MACE were evaluated in the Evolocumab group.

Results At week 12, GPH and GMH scores in Evolocumab group were significant compared with baseline (P<0.05) and the changes in scores were significant compared with Statin group (P<0.05), and the improvement of pain intensity, mental health, and satisfaction with social activities of Evolocumab group were significant compared with Statin group(P<0.05). Meanwhile, Evolocumab group showed significant differences in physical health and pain intensity compared to baseline (P<0.05). No significant difference was observed for physical function and fatigue(P>0.05). GMH items were significant compared with baseline (P< 0.05). At week 48, GPH, GMH and all items of Evolocumab group significantly improvement compared with baseline (P<0.05), but there was no significant difference between Evolocumab group and Statin group (P>0.05). At week 48, emotional problems in patients with MACE in the Evolocumab group deteriorated, and the score difference was significant compared with non-MACE (P<0.05).

Conclusions In the short term, PCSK9i significantly improved QOL of ACS patients in both global physical health and global mental health, and the efficacy was better than that of statins, especially in pain intensity, mental health and satisfaction with social activities. In the long term, PCSK9i sustained global physical health, global mental health and improvements for ACS patients. The occurrence of MACE in ACS patients treated with PCSK9i may be correlated with emotional problems.

Funding: Key Discipline Project of Tianjin Municipal Health Commission (TJWJ2022XK032)

References

[1] Visseren, Frank L J et al. "2021 ESC Guidelines on cardiovascular disease prevention in clinical practice." European heart journal vol. 42,34 (2021): 3227-3337. doi:10.1093/eurheartj/ehab484

[2] Gao, Jing et al. "Effects of Evolocumab Added to Moderate-Intensity Statin Therapy in Chinese Patients With Acute Coronary Syndrome: The EMSIACS Trial Study Protocol." Frontiers in physiology vol. 12 750872. 23 Nov. 2021, doi:10.3389/fphys.2021.750872

Cultural Adaptation and Psychometric Evaluation of the Preference for Intuition and Deliberation in Eating Decision-making Scale among Chinese People with Cardiovascular Disease

Hui-Xia Huang

The second affiliated hospital of Harbin medical university

Background The way individuals make dietary decisions plays a crucial role in shaping their eating behaviors, which in turn influences the prevention and management of cardiovascular disease (CVD). The Preference for Intuition and Deliberation in Eating Decision-making Scale (E-PID) is an instrument originally developed to assess individuals' tendencies to rely on intuitive versus deliberative processes in making dietary choices. However, to date, there has been no culturally adapted version validated for Chinese populations with CVD. Given the unique dietary patterns, health beliefs, and decision-making contexts in China, it is imperative to culturally adapt and psychometrically evaluate the E-PID for this population.

Objectives: This study aimed to (1) translate and culturally adapt the E-PID into Chinese, (2) test the psychometric properties including construct validity, reliability, and measurement invariance among Chinese individuals with CVD.

Methods The E-PID was translated into Chinese following established guidelines for cross-cultural adaptation, including forward translation, synthesis, back-translation, expert committee review, and pretesting in a small patient sample to ensure cultural relevance and clarity. Content validity was evaluated by a panel of six cardiovascular nursing, nutrition, and behavioral psychology experts using a content validity index (CVI). The psychometric evaluation was conducted on a sample of 1463 patients with cardiovascular disease (CVD) recruited from a tertiary hospital in northeastern China between July 2024 and December 2024. The Chinese version of the E-PID was assessed through a series of analyses, including item analysis, measurement invariance, composite reliability, and criterion-related validity. To explore the underlying dimensionality and network structure of the scale, Exploratory Graph Analysis (EGA) was employed, followed by Confirmatory Factor Analysis (CFA) to test the factor structure. Internal consistency reliability was evaluated using Cronbach's α and McDonald's ω coefficients, and test-retest reliability was assessed in a subsample of 32 participants over a six-week interval. Convergent validity was further examined by correlating the E-PID with measures of dietary behavior adherence and decision-making style. Additionally, discriminative validity was analyzed to confirm the scale's ability to differentiate among relevant groups.

Results Item analyses indicated that deleting any single item resulted in a decrease in the Cronbach's αcoefficient of the total scale and its respective dimension, indicating that all items had good internal consistency. Furthermore, patients were divided into high-score and low-score groups based on the mean scores of the two dimensions. Independent sample t-tests showed that the item scores between the two groups were significantly different ($p < 0.001$), further supporting the discriminant validity of the items. Results from the exploratory factor analysis (EFA, n = 704) and the exploratory graph analysis (EGA, n = 704) were consistent, both supporting the two-factor structure of the 7-item original scale, namely intuitive preference (3 items) and deliberative preference (4 items). The EFA extracted two common factors, explaining 39.84% and 27.70% of the variance respectively, with a cumulative variance contribution rate of 67.54%. Confirmatory factor analysis (CFA)indicated that the scale demonstrated a satisfactory model fit with CFI = 0.99, GFI = 0.99, TLI = 0.98, RMSEA = 0.059 (90% CI [0.041, 0.077]), and SRMR = 0.026.The findings further indicated that the Chinese version of the E-PID possessed adequate criterion validity, internal consistency, and test-retest reliability. The Cronbach'sα coefficients for each dimension were 0.83 (95% CI [0.80, 0.86]) and 0.75 (95% CI [0.73, 0.77]); McDonald's ω values were 0.81 (95% CI [0.78, 0.84]), 0.87 (95% CI [0.85, 0.90]), and 0.73 (95% CI [0.70, 0.77]); and the test-retest reliability coefficients were 0.86 (95% CI [0.72, 0.93]) and 0.79 (95% CI [0.61, 0.89]). In addition, multi-group confirmatory factor analysis (n = 1463) indicated that the scale exhibited good measurement invariance across gender (Δ CFI ≤ 0.01, Δ RMSEA ≤ 0.015), supporting its suitability for testing gender differences.

Conclusion The E-PID showed sufficient psychometric properties in a Chinese sample, making it a valid instrument for assessing dietary decision-making preferences among people with cardiovascular disease in China and can serve as an effective tool for both clinical practice and research.

Left ventricular remodeling index to predict ventricular tachyarrhythmia in dilated cardiomyopathy with ejection fraction

Xi Jia, Shihua Zhao

Fuwai Hospital, National Center for Cardiovascular Diseases of China, Chinese Academy of Medical Sciences and Peking Union Medical College

Objectives

Myocardial fibrosis assessed by cardiac magnetic resonance (CMR) with late gadolinium enhancement (LGE) imaging has emerged as a powerful predictor for sudden cardiac death (SCD) in dilated cardiomyopathy (DCM). However, in the cohort of DCM patients with left ventricular ejection fraction (LVEF) <35%, isolated LGE may not exhibit significant difference between those with and without adverse outcomes. In such circumstances, morphological parameters may provide additional prognostic value for DCM patients with LVEF <35%. The predictive value of LV remodeling index (LVRI), a novel geometry parameter derived from CMR, for ventricular tachyarrhythmia (VTA) in this population remains unclear. Therefore, this study aimed to assess LVRI for predicting VTA in patients with DCM with left ventricular ejection fraction LVEF <35%.

Methods

In this retrospective single-center study, consecutive DCM patients with LVEF <35% (n=271) who underwent CMR imaging were followed up. The study endpoint was VTA, including sudden cardiac death and major ventricular arrhythmias. The newly derived LVRI was defined as the cubic root of the LV end-diastolic volume (LVEDV) divided by the maximal LV wall thickness (LVWT) (LVRI = [□ LVEDV]/LVWT). Competing risk regression analysis and Kaplan-Meier analysis were used to evaluate the association of LVRI with VTA. The incremental values of incorporating LVRI into Cox models were evaluated by calculating the improvement of Chi-square values and C index. Reclassification of patients by adding LVRI to the baseline model was further evaluated by integrated discrimination improvement (IDI).

Results

During a median follow-up of 71 months (interquartile range: 17–134 months), 35 (12.9%, mean age 46.7 years, 27 males) participants reached VTA events. The presence (62.9% vs. 60.2%, p = 0.761) and extent (6.9±6.6 vs. 6.5±8.3, p = 0.747) of LGE and LVEF (23.3±6 vs. 21.9±10.3, p = 0.197) were not significantly different between the patients with and without endpoint. Kaplan-Meier curve analysis showed that participants with LVRI ≥ 7.5 were more likely to experience VTA (p < 0.0001). In the univariable competing risk regression analyses, LVRI showed significant associations with VTA events both as a dichotomized variable (≥ 7.5: HR 2.82, 95% CI 1.37–5.79, p = 0.005) and as a continuous variable (per 1-unit increase: HR 1.21, 95% CI 1.02–1.43, p = 0.026). In contrast, the presence, extent and pattern of LGE were not associated with VTA events (all p > 0.05). In the multivariable competing risk regression model 1, when heart transplantation and heart failure-related death were counted as competing risks, LVRI ≥ 7.5 (adjusted HR 2.496 [95% CI 1.213–5.138], p = 0.013) was an independent predictor of VTA events. However, when LVRI was included as a continuous variable in model 2, the results showed that LVMI was the only independent predictor of VTA events (adjusted HR 0.983 [95% CI 0.968–0.998], p = 0.031), after adjusting for age, sex and left bundle branch block. The chi-square values for Model 1 (LVEF), Model 2 (LVEF + LGE presence), and Model 3 (LVEF + LGE presence + LVRI) were 0.0004, 2.1 (p = 0.149 vs Model 1), and 27.1 (p < 0.001 vs Model 2), respectively. The incorporation of LVRI provided significant incremental predictive discrimination (C-index: 0.75 [0.67-0.84]) with clinically meaningful reclassification (IDI = 0.144, p < 0.001).

Conclusions

For nonischemic DCM patients with LVEF <35%, LVRI ≥ 7.5 was associated with lethal VTA events and provided incremental value over conventional CMR parameters, including LVEF and the presence of LGE.

Subendocardium-Involved Late Gadolinium Enhancement Predicts Sudden Cardiac Death in Nonischemic Dilated Cardiomyopathy

Xi Jia, Shihua Zhao

Fuwai Hospital, National Center for Cardiovascular Diseases of China, Chinese Academy of Medical Sciences and Peking Union Medical College

Objective

Late gadolinium enhancement (LGE) is an established predictor of sudden cardiac death (SCD) in nonischemic dilated cardiomyopathy (DCM). However, the prognostic value of LGE phenotypes-particularly those involving the subendocardium - remain incompletely demonstrated. Therefore, this study aimed to evaluate the association between subendocardium - involved LGE and SCD events in a large cohort of patients with nonischemic DCM. We also sought to explore whether LGE phenotypes combining the pattern and location could improve SCD risk stratification in this population.

Materials and Methods

In this retrospective single-center study, adults with nonischemic DCM who underwent cardiac magnetic resonance (CMR) with LGE imaging between July 2015 and December 2018 were consecutively enrolled. Subendocardium-involved LGE pattern in nonischemic DCM was characterized by subendocardial or transmural LGE with noncoronary distribution. Patients with significant coronary disease that would lead to subendocardium-involved LGE were excluded. SCD-related events included SCD, appropriate implantable cardioverter-defibrillator shock, and resuscitation after cardiac arrest. Cox regression analysis and Kaplan-Meier analysis were performed to identify the association of LGE phenotypes with outcomes.

Results

Among 902 patients (mean age 46 years±14, 78.7% men), subendocardium-involved LGE and midwall LGE were observed in 14.3% and 29.1%, predominantly involving the lateral wall (65.1%) and interventricular septum (97.7%), respectively. During a median follow-up of 77 months (IQR 40-92 months), 51 (5.7%) patients experienced SCD events. In multivariable analysis, septal midwall LGE (adjusted HR 3.84; 95% CI 2.06-7.17; P < .001) and lateral subendocardium-involved LGE (HR 3.53; 95% CI 1.76-7.08; P < .001) were independent predictors of SCD-related events. Patients were stratified into three risk categories based on the presence or absence of septal midwall LGE and lateral subendocardium-involved LGE phenotypes: the high-risk group (n = 49 [5.4%]), defined as patients with both LGE phenotypes; the moderate-risk group (n = 243 [27%]), defined as patients with either LGE phenotype alone; and the low-risk group (n = 610 [67.6%]), defined as patients without either LGE phenotype. High-risk patients had the highest annual event rate of 0.58%, while low-risk patients had the lowest rate of 0.03%. Multivariable regression analysis confirmed significantly increased SCD risk in the moderate-risk group (HR 4.8, 95% CI 2.5-9.23, P < 0.001) and high-risk group (HR 12.8; 95% CI 5.35-30.51, P < 0.001) versus the low-risk group. Adding this novel risk stratification category to LVEF incrementally improved the discrimination (C-statistic 0.75 vs 0.56, AUC 0.71 vs 0.55); both P < 0.001) and reclassification (NRI 0.31, IDI 0.06; both P < 0.001) for SCD risk prediction. Compared with the 35% LVEF cutoff, the new category allowed reclassifying the SCD risk of 53.5% of patients in the entire cohort: 480 patients (low-risk group) were reclassified from high to low risk; 1 patient (moderate-risk group) were reclassified from low to moderate risk; and 2 patients (high-risk group) were reclassified from low to high risk.

Conclusion

In nonischemic DCM, both lateral subendocardial LGE and septal midwall LGE emerged as independent predictors of SCD. The novel SCD risk model integrating these LGE phenotypes demonstrated superior prognostic performance compared to conventional prognosticator, potentially enabling more precise implantable cardioverter-defibrillator candidate selection.

Multimodality Cardiac Magnetic Resonance Imaging for Discriminating Danon Disease from Hypertrophic Cardiomyopathy

Xi Jia, Shihua Zhao

Fuwai Hospital, National Center for Cardiovascular Diseases of China, Chinese Academy of Medical Sciences and Peking Union Medical College

Objectives

Danon disease (DD) presenting with an hypertrophic cardiomyopathy (HCM) phenotype often closely resembles HCM. Traditional diagnostic tools like echocardiography fail to distinguish DD from classical HCM due to overlapping morphological features. Cardiac magnetic resonance (CMR) offers unique advantages in tissue characterization through multiparametric assessment. However, systematic characterization of CMR features in DD and their discriminative value against HCM remain unexplored, posing significant diagnostic challenges. Therefore, this study aimed to evaluate multiparametric CMR features of DD with an HCM phenotype and investigate their discriminative value against classical HCM.

Materials and methods

From May 2015 to August 2023, 17 patients with genetically confirmed DD with HCM phenotype were retrospectively recruited. The comprehensive CMR-based comparison was performed between 17 DD, 17 HCM patients and 17 healthy controls matched on age and sex. Multiparameter CMR imaging included cardiac morphology, function, late gadolinium enhancement (LGE), native T1 mapping, extracellular volume (ECV), T2 mapping, biventricular and left atrial strains. Diagnostic performance of CMR parameters in discriminating DD from HCM was evaluated by analysis of binary logistic regression and receiver operating characteristic (ROC) curves.

Results

A total of 17 DD patients (mean age 22 years±12, 47.1% men), 17 HCM patients (mean age 21 years±12, 47.1% men) and 17 healthy controls (mean age 23 years±14, 47.1% men) were enrolled in this study. Compared with HCM patients, DD patients with an HCM phenotype exhibited greater lateral wall thickness (10.3±4.9 vs 6.7±2.9, p = 0.01), reduced left ventricular ejection fraction (LVEF) (44±19.4% vs 60.8±10.4%, p = 0.011), more extensive LGE (52.9% vs 5.9%, p = 0.006) (predominantly with midbasal septal sparing [52.9% vs 0%, p = 0.001] and free wall involvement [94.1% vs 35.3%, p < 0.001]), higher prevalence of free wall (94.1% vs 35.3%, p < 0.001) and apex LGE (70.6% vs 17.6%, p = 0004), elevated global native T1 (1334±84 vs 1287±51, p = 0.043), and more impaired left ventricular global circumstance strain (LVGCS) (-7.9±3.9% vs -13.9±3.4, p < 0.001) and left ventricular global radial strain (LVGRS) (11±6.5% vs 21.9±8.5%, p < 0.001). Global ECV values, T2 values, right ventricular and left atrial strains did not show significant differences between the two groups (all p > 0.05). Among these, binary logistic regression and analysis of ROC curves demonstrated that LVGCS (cutoff: -11.3%; AUC: 0.877; sensitivity: 81.3%; specificity: 86.7%) and LVGRS (cutoff: 16.9%; AUC: 0.863; sensitivity: 87.5%; specificity: 80%) had the best performance in screening for DD in patients with an HCM phenotype. During a median follow-up of 2 years, 11 (64.7%) patients experienced major adverse cardiovascular events, including all cause of death (n = 2), heart transplantation(n = 3), heart failure re-hospitalization (n = 5), stroke (n = 2), and malignant arrhythmia (n = 1).

Conclusion

DD should be strongly suspected in patients with an HCM phenotype presenting with extensive LGE (especially midbasal septum sparing pattern, free wall involvement LGE and apex LGE, globally elevated native T1 values, and more severely impaired LV strains. LVGCS is the best parameter for differentiating DD from classical HCM in Chinese populations, providing an effective method for rapid screening of DD in clinic, which may help identify patients for early treatment of DD.

Prognostic Impact of Early Cardiorenal Involvement in Fabry Disease: Rethinking When to Start Enzyme Replacement Therapy

Yanjia Chen, Yan OuYang, ZePing Qiu, Nan Chen, Wei Jin

Ruijin Hospital, Shanghai Jiao Tong University School of Medicine,

Background:

Anderson-Fabry disease (AFD) is a progressive, X-linked lysosomal storage disorder caused by mutations in the GLAgene, leading to deficient or absent α-galactosidase A (α-Gal A) enzyme activity. The enzymatic defect results in the accumulation of glycosphingolipids—primarily globotriaosylceramide (Gb3) and lyso-Gb3—within various cell types, particularly cardiomyocytes, renal tubular epithelial cells, and vascular endothelial cells. Cardiac and renal involvement are the leading causes of morbidity and mortality in AFD, and their interplay often accelerates disease progression. Enzyme replacement therapy (ERT) is the cornerstone of treatment and has been shown to stabilize or reverse organ damage when administered early. However, current clinical guidelines generally recommend initiating ERT only after overt organ damage—such as left ventricular hypertrophy or renal dysfunction—is observed. This approach may overlook a critical therapeutic window, during which subclinical organ involvement is already present but potentially reversible.

Objectives:

To evaluate the prognostic impact of early cardiac and renal involvement in a genetically confirmed Chinese cohort of AFD patients, and to validate the Cardiac Raw Score (CRS)—a structured, composite scoring system integrating structural, electrical, and functional cardiac parameters—as a practical and dynamic tool for risk stratification and early therapeutic decision-making.

Methods:

This multicenter, retrospective analysis included 105 AFD patients confirmed by genetic testing and enzyme activity assays, enrolled from three tertiary hospitals in China between 2011 and 2024. CRS was calculated at baseline and follow-up, capturing echocardiographic dimensions, electrocardiographic findings, and NYHA functional class on a 0–4 Likert scale per parameter. Renal dysfunction was staged using eGFR (calculated by the CKD-EPI formula) and albuminuria, with stage 1 representing preserved function and stage 2 indicating moderate impairment. The primary composite outcome included cardiovascular death, nonfatal myocardial infarction, nonfatal stroke, or heart failure hospitalization. Cox proportional hazards models were used to identify predictors of adverse outcomes, and Kaplan-Meier survival curves assessed differences in event-free survival.

Results:

Over a median follow-up of 41 months (IQR 22–107), 20 patients (19.0%) experienced a cardiovascular event. Univariable and multivariable Cox regression identified both baseline CRS and the slope of CRS progression (ΔCRS per month) as independent predictors of cardiovascular risk. A 1-point increase in baseline CRS was associated with a 29.4% increase in event risk (adjusted HR = 1.294, 95% CI: 1.125–1.488, P <0.001), while each 1-unit/month improvement in CRS slope reduced event risk by over 70% (HR = 0.257, 95% CI: 0.069–0.960, P = 0.043). Kaplan-Meier analysis showed that patients with CRS ≥ 1 had significantly lower event-free survival than those with CRS = 0 (P <0.0001).

Renal staging also demonstrated strong prognostic value. Patients with stage 2 renal dysfunction had a nearly threefold increased risk of cardiovascular events compared to those with stage 1 (28.9% vs. 9.8%, P = 0.03). Stratified analysis revealed that CRS ≥ 1 was prognostically significant even in stage 1 patients, whereas in stage 2 patients, a CRS threshold ≥ 3 identified those at highest risk.

Conclusions:

This study demonstrates that subclinical cardiac and renal abnormalities are powerful, independent predictors of adverse cardiovascular outcomes in AFD. The CRS offers a dynamic, quantitative, and accessible framework for cardiac assessment and longitudinal monitoring. When combined with early renal staging, CRS enables more refined risk stratification and can guide the timely initiation of ERT—well before irreversible organ damage develops. These findings support a paradigm shift from reactive to anticipatory management in AFD and highlight the potential for early intervention to meaningfully alter disease trajectory, especially in patients with preserved renal function and mild or asymptomatic cardiac involvement.

Efficacy Analysis of Cardiac Rehabilitation in a Patient with Heart Failure Due to Dilated Cardiomyopathy: A Case Report

Yu-jie Hu[1], Juan Wang[2], Ping Xie[1,2], Wei-Jie Lu[3], Kang Yang[3], Meng-Yang Liu[3], Yao-Ting Deng[3]

1. THE FIRST SCHOOL OF CLINICAL MEDICINE OF LANZHOU UNIVERSITY

2. GANSU PROVICIAL HOSPITAL

3. Gansu University of Chinese Medicine

Study Purpose:

This case report aimed to detail the implementation and outcomes of a structured, individualized cardiac rehabilitation (CR) program for a 42-year-old male patient with heart failure (HF) due to dilated cardiomyopathy (DCM). It specifically sought to demonstrate the efficacy of an early-initiated, comprehensive, and dynamically adjusted CR protocol integrating multiple modalities beyond standard pharmacotherapy. Furthermore, it intended to provide clinical insights for managing this specific patient population (younger DCM-HF patients) by evaluating improvements across cardiopulmonary function, physical fitness, and quality of life.

Methods:

Patient: A 42-year-old male diagnosed with DCM, severe HF (NYHA class IV, LVEF 30%), and pulmonary hypertension.

Rehabilitation Program: A 25-week, supervised program involving 95 sessions (3-4 sessions/week).

Core Approach: Dynamic adjustment of training intensity based on periodic multi-domain assessments conducted pre-rehabilitation, at 3 months, and at 6 months. Assessments included:

Cardiopulmonary Function (CPET: Peak VO_2, VO_2 at AT, Peak VE/VCO_2, Peak O_2/HR, Peak Qtc; Echocardiography: LVEF)

Exercise Tolerance (6-Minute Walk Test - 6MWT)

Physical Fitness Parameters (Grip strength, single-leg standing time, waist/hip circumference, waist-to-hip ratio)

Laboratory Biomarkers (NT-proBNP)

Quality of Life (SF-12, PSQI, GAD-7, PHQ-9)

Interventions: The comprehensive CR program combined:

Pharmacotherapy: Guideline-directed "quadruple therapy" (bisoprolol, sacubitril/valsartan, spironolactone, dapagliflozin) augmented with vericiguat.

Multimodal Exercise Training:

Enhanced External Counterpulsation (EECP)

Respiratory Muscle Training

Upper Limb Strength Training (wall push-ups progressing to dumbbells)

Lower Limb Strength Training (heel raises)

Traditional Chinese Exercises

Aerobic Training (cycle ergometry, walking - intensity progressed based on assessment)

Patient Education: Provided throughout all phases.

Key Results:

Following 6 months of CR, the patient demonstrated significant and clinically meaningful improvements across all measured domains:

Cardiopulmonary Function:

LVEF increased from 30% to 55%.

NT-proBNP decreased dramatically from 20,000 pg/mL to 23.27 pg/mL.

CPET showed substantial gains: Peak VO_2 (16.3 to 21.5 ml/min/kg), VO_2 at AT (9.3 to 10.1 ml/min/kg), Peak O_2/HR (12.4 to 14.4), Peak Qtc (8.4 to 11.2 L/min). Peak VE/VCO_2 also improved (23.16 to 26.01).

Exercise Tolerance:

6MWT distance increased from 402m to 654.7m.

Physical Fitness:

Grip Strength improved (Left: 30.7 to 37.2 Kg; Right: 32 to 38.5 Kg).

Single-Leg Standing Time increased (Left: 12 to 30 sec; Right: 8 to 27 sec).

Waist circumference decreased (101cm to 97cm), waist-to-hip ratio improved (1.06 to 1.02).

Respiratory pattern normalized (resolved shoulder shrugging).

Quality of Life & Psychological State:

SF-12 score significantly improved (35.63 to 89.38).

Sleep quality (PSQI) improved (14 to 5).

Anxiety (GAD-7) reduced (9 to 1).

Depression (PHQ-9) reduced (5 to 1).

Symptoms: Symptoms of chest tightness and shortness of breath were essentially resolved.

Conclusion:

This case report demonstrates that a systematic, early-initiated, personalized, and comprehensive cardiac rehabilitation program, incorporating multiple modalities (EECP, respiratory training, strength training, traditional exercises, aerobic training) alongside optimized pharmacotherapy and dynamically adjusted based on regular multi-domain assessments, can lead to remarkable improvements in cardiopulmonary function (LVEF, CPET parameters), exercise capacity (6MWT), physical fitness (strength, balance, body composition), symptoms, and quality of life/psychological well-being in a young patient with HF due to DCM.

Given the common limitations of traditional pharmacotherapy-focused approaches in this population (e.g., recurrent cardiac decompensation, hypotension restricting drug titration), this successful case provides compelling evidence for a paradigm shift. It strongly advocates that early cardiac rehabilitation should be considered an essential and equally important component of HF management, effectively complementing pharmacotherapy. Integrating such a structured, multifaceted CR program early in the care pathway offers significant potential to optimize outcomes for younger DCM-HF patients.

Extravascular Lung Water Index versus Central Venous Pressure: A Comparative Study on Predicting Global End-Diastolic Volume Index in Cardiogenic Shock

Jieyun You

Shanghai East Hospital

Background: Cardiogenic shock, a life-threatening condition leading to high mortality and poor prognosis, necessitates precise volume management to optimize cardiac output and prevent further complications. Extravascular lung water index (EVLWI) is a reliable indicator for assessing the severity of pulmonary edema. This study aims to compare the effectiveness of EVLWI and central venous pressure (CVP) in predicting the global end-diastolic volume index (GEDVI), a parameter of cardiac preload, in patients with cardiogenic shock.

Methods: In this prospective cohort study, 200 patients diagnosed with cardiogenic shock were enrolled. EVLWI and CVP were measured simultaneously by the pulse index continuous cardiac output (PiCCO) system. Spearman correlation analysis was used to assess the relationships between EVLWI (or CVP) and GEDVI. Receiver operating characteristic (ROC) curve analysis was performed to evaluate the predictive value of EVLWI and CVP for elevated GEDVI. Sensitivity, specificity, positive predictive value (PPV), negative predictive value (NPV), positive likelihood ratio (+LR), and negative likelihood ratio (-LR) of EVLWI and CVP were calculated, with GEDVI as the reference standard. The area under the curve (AUC) was also calculated to determine the accuracy of baseline EVLWI or CVP for predicting 30-day all-cause mortality.

Results: A total of 971 datasets from 166 patients with cardiogenic shock were included in the final analysis. The median age of the cohort was 73.46 ± 12.28 years, with 74.67% of the patients being male. The baseline mean GEDVI in the study population was 755.59 ± 164.47 mL/m^2, the mean EVLWI was 9.89 ± 3.40 mL/kg, and the mean CVP was 15.24 ± 6.25 mmHg. EVLWI demonstrated a significant correlation with GEDVI ($r = 0.47$, $p < 0.01$), whereas CVP showed no correlation ($r = 0.03$, $p = 0.38$). The optimal EVLWI cutoff value for predicting GEDVI > 800mL/m^2 was 10.35mL/kg, with area under the curve (AUC) of 0.76 (95 % CI: 0.73–0.79, $p < 0.01$). In contrast, CVP had a poor predictive performance (AUC = 0.53, 95% CI: 0.49–0.57, $p = 0.14$). The diagnostic accuracy of EVLWI was higher than CVP (53.35% vs. 47.27%; difference: 6.08%, $p < 0.01$). EVLWI also showed superior sensitivity in predicting elevated GEDVI compared to CVP (94.22% vs. 67.17%; difference: 27.05%, $p < 0.01$). Both EVLWI and CVP had relatively low specificity in predicting GEDVI > 800 mL/m^2 (32.40% vs. 37.07%; difference: 4.67%, $p > 0.05$). PPV, NPV, +LR, and -LR were 41.67%, 91.63%, 1.39, and 0.18 for EVLWI, respectively, and 35.36%, 68.79%, 1.07, and 0.89 for CVP, respectively. Furthermore, baseline EVLWI predicted 30-day all-cause mortality with an AUC of 0.78 (95% CI: 0.74–0.83, $p < 0.01$), while CVP lacked prognostic value (AUC = 0.52, 95% CI: 0.45–0.59, $p = 0.56$).

Conclusions: EVLWI outperforms CVP in predicting elevated GEDVI and short-term mortality in patients with cardiogenic shock. These findings support the use of EVLWI, rather than CVP, as a preferred parameter for volume management in this high-risk population. The study support a shift toward more advanced hemodynamic monitoring systems like PiCCO, which includes EVLWI, to improve the therapeutic strategies in cardiogenic shock.

KEYWORDS: cardiogenic shock, extravascular lung water index, central venous pressure, global end-diastolic volume index, hemodynamic monitoring.

Association between Transcatheter Heart Valve Deformation and Hypoattenuating Leaflet Thickening in Patients after Transcatheter Aortic Valve Replacement

Xiang-Ming Hu[1], Yun-Qing Ye[2], Hao-Wen Ma[2], Guan-Nan Niu[2], Jie Zhao[2], De-Jing Feng[2], Can Wang[2], Zhe Li[2], Yang Chen[2,3], Zhen-Yan Zhao[2], Zheng Zhou[2], Hong-Liang Zhang[2], Mo-Yang Wang[2], Yong-Jian Wu[2]

1. Guangdong Provincial People's Hospital (Guangdong Academy of Medical Sciences)

2. Fuwai Hospital, National Center for Cardiovascular Diseases, Chinese Academy of Medical Sciences and Peking Union Medical College

3. Peking University People's Hospital

Background: Transcatheter aortic valve replacement (TAVR), as a mature treatment option for severe aortic stenosis, has performed well across various surgical risk classifications and is increasingly being used in younger patients. In TAVR for native aortic stenosis, concerns arise regarding the risk for reduced transcatheter heart valve (THV) expansion and increased eccentricity, especially for those with bicuspid aortic valve. Hypoattenuating leaflet thickening (HALT) is relatively common after TAVR and may increase the risk of cerebral thromboembolism. However, the association between THV deformation and HALT remains unclear.

Methods: In this prospective study, 238 patients with severe aortic stenosis who underwent TAVR and had paired pre- and post-procedural computed tomography (CT) were included. Based on the presence of HALT, patients were classified into two groups. The analysis and evaluation of CT imaging was measured by the core laboratories of Fuwai Hospital. An artificial intelligence-based CT post-processing analysis platform can perform precise segmentation of THV scan images at a 1-mm resolution and automatically draw closed curves. We identified the THV core functional portion (CFP), which extends from the lowest edge of the artificial leaflets to the hinge points of the artificial leaflets. The evaluation of THV underexpansion and eccentricity was based on the THV CFP. THV underexpansion was defined as an expansion rate of CFP <90%, and THV eccentricity as an eccentricity index of CFP >50%. HALT was defined as >25% leaflet involvement along the curvilinear contour at least one leaflet according to the Valve Academic Research Consortium 3 criteria. All patients were followed up at 1 month, 3 months, 6 months, 1 year and each subsequent year after discharge via telephone interviews or outpatient visits. A Cox regression model was employed to evaluate the association between THV deformation and the occurrence of HALT. Variables with clinical and statistical effects were included as adjustment factors in the multivariate model.

Results: The average age was 73.20 ± 7.29 years, and 140 (58.82%) were male. The proportion of bicuspid aortic valve was 49.5% (n=118). The majority (n=204, 85.7%) of patients received a self-expanding valve, while the remaining received a balloon-expandable valve. Isolated THV underexpansion or eccentricity occurred in 43.7% of patients, while 19.75% had both. There were 64 patients (n=64, 26.9%) experienced HALT during a median follow-up of 1 year after TAVR. Univariate analysis indicated that THV underexpansion and eccentricity were associated with an increased risk of HALT (hazard ratio [HR]: 2.12, 95% CI [confidence interval]: 1.09–4.07; $p = 0.026$). Similar results were found in multivariate analysis (HR: 2.12, 95% CI: 1.09–4.19; $p = 0.032$), after adjusting for age, sex, anticoagulation regimen, and THV type. When the criteria of >50% leaflet involvement along the curvilinear contour at least one leaflet was adopted for HALT, the THV underexpansion and eccentricity still increased the risk of HALT (HR: 2.74, 95% CI: 1.13–6.61; $p = 0.025$) after adjusting for the above variate.

Conclusion: THV underexpansion and eccentricity were independently associated with HALT. Attention are needed to pay to the deformation of the THV formation after TAVR procedure. Further studies with larger sample sizes are warranted to validate this finding.

CircSMAD3 represses VSMC phenotype switching and neointima formation via promoting hnRNPA1 ubiquitination degradation

Shuai Mei, Hu Ding, Jiang-Tao Yan

华中科技大学同济医学院附属同济医院

Backgrounds: Vascular smooth muscle cells (VSMCs) are the prominent cells in the blood vessel wall that can transition from a contractile state to a synthetic state in a process known as 'phenotype switching', which is a typical characteristic for various of vascular diseases. Circular RNAs

(circRNAs), a novel regulatory RNAs with high evolutionary conservation and stability, significantly affect the progression, diagnosis, and treatment of human diseases, making them attractive therapeutic agents for various vascular diseases. The SMAD family, as mediators of the canonical transforming growth factor-beta (TGF-β) signalling pathway, reportedly plays a critical role in vascular homeostasis. However, the role of circRNAs derived from the SMAD family members in vascular physiology remains unclear.

Methods: CircRNA database and circRNA microarray were integrated to identify the critical circRNAs in vascular homeostasis. Real-time PCR, Western blot and immunofluorescence were used to detect the expression of target genes. Fluorescence in situ hybridization (FISH) was used to detect the distribution and level of circSMAD3 in vascular smooth muscle cell (VSMC). In vitro, Transwell, wound healing, cell-counting kit 8 assay (CCK-8), 5-Ethynyl-2′-deoxyuridine (EDU) to investigate the ability of circSMAD3 to affect VSMC proliferation. Cell contraction assay and phalloidin staining assay were performed to detect the contractility of VSMC. Flow cytometry was used to detect VSMC apoptosis. In vivo, the right carotid artery was wire-injured to construct the neointima formation model and the specific expression of circSMAD3 in artery was modulated by overexpression or knockdown adeno-associated virus type 9 with a transgelin promoter. RNA sequencing technology was conducted to comprehensively describe transcriptomic changes in circSMAD3 silencing HASMC by gene set enrichment analysis (GSEA). To explore the mechanisms of circSMAD3 in VSMC phenotype switching and neointima formation, RNA pulldown and mass spectrum were performed to identify the potential proteins interacting with circSMAD3. RNA immunoprecipitation assay was used to study the enrichment level of circSMAD3 by its binding proteins. ChIP-PCR assay was conducted to verify the binding of p53 with pro-apoptosis genes promotors. Co-immunoprecipitation assay was applied to conformed the interaction of hnRNPA1 with WDR76. Ubiquitination assay was used to detect the degradation process of protein ubiquitination.

.Results: By integrating the circBase database and circRNA microarray data from mouse aortic tissue, we identified a circRNA originated from SMAD3 gene, named circSMAD3, which was upregulated in response to the stimulation of TGF-β1 or serum deprivation and downregulated in response to platelet-derived growth factor subunit B (PDGF-BB) in primary aortic smooth muscle cells, and downregulated in vascular injury and atherosclerosis. Characterization analysis showed that circSMAD3 is a bona fide circRNA in VSMCs. In vitro, we explored that overexpression of circSMAD3 repressed VSMC proliferation and phenotype switching, promoted VSMC contraction capacity and apoptosis, and evidenced by multiple morphological assays. The silencing of circSMAD3 in VSMC promoted the proliferation and migration of VSMC, inhibited contraction and apoptosis. In vivo, circSMAD3 overexpression ameliorated arterial injury-induced neointima formation. While, the knockdown of circSMAD3 is in the opposite way. By RNA sequencing, we found the differential genes affected by circSMAD3 overexpression were enriched in p53 signalling pathway, which is critical for cell cycle progression and apoptosis. Mechanistically, circSMAD3 interacted with heterogeneous nuclear ribonucleoprotein A1 (hnRNPA1) within the nucleus, enhanced its interaction with E3 ligase WD repeat domain 76 (WDR76), which promoted hnRNPA1 ubiquitination degradation, facilitated p53 pre-RNA splicing, activated p53γ signalling pathway, and finally suppressed VSMC proliferation and phenotype switching and neointima formation.

Conclusions: Our study identifies circSMAD3 as a novel epigenetic regulator that suppresses VSMC proliferation and phenotype switching, thereby attenuating vascular remodelling and providing a new circRNA-based therapeutic strategy for cardiovascular diseases.

Circulating ketone bodies, genetic susceptibility, with left atrial structure, function and atrial fibrillation

Nan Zhang[1], Daiqi Liu[1], Jin-Hua Zhao[1], TSE Gary[1], Jian-Dong Zhou[2], Qing-Peng Zhang[4], GREGORY Y.H. Lip[3], Tong Liu[1]

1. Tianjin Key Laboratory of Ionic-Molecular Function of Cardiovascular Disease, Department of Cardiology, Tianjin Institute of Cardiology, Second Hospital of Tianjin Medical University, Tianjin 300211, China

2. Department of Family Medicine and Primary Care, School of Clinical Medicine, Li Ka Shing Faculty of Medicine, The University of Hong Kong, Hong Kong, China

3. Liverpool Centre for Cardiovascular Science at University of Liverpool, Liverpool John Moores University and Liverpool Heart & Chest Hospital, Liverpool, UK

4. School of Data Science, City University of Hong Kong, Hong Kong, China.

Background

Ketone bodies (KB) are important cardiac metabolic energy source. Metabolic remodeling has been recently pointed to play an important role in the pathological process of atrial fibrillation (AF). However, no prior study has investigated the associations between circulating KB levels with the risk of new-onset AF. We evaluated the association between circulating KB levels with incident AF risk in the general population.

Methods

We studied 237,163 participants (mean age, 56.5 years; 55% women) from the UK Biobank who were free of AF at baseline and had data about circulating levels of β-hydroxybutyrate (β-OHB), acetoacetate, and acetone at the time of enrollment. Restricted cubic spline analyses were used to explore the dose-response relationship between KB with AF and left atrial (LA) measurements. The associations between KB with AF were evaluated by multivariable Cox regression in the general population and across three genetic risk groups [low, moderate, and high polygenic risk score (PRS) of AF].

Results

After a follow-up of 3,309,367 person-years, 16,638 (7.0%) participants developed AF. There was a U-shaped association between total KB and β-OHB with incident AF, with nadirs at 60.6 and 40.8 μmol/L, respectively (P non-linear <0.05), whereas a positive association between acetoacetate and acetone with incident AF was observed (P overall <0.001, P non-linear >0.05). After adjusting for potential confounders, compared to those in tertile 2 of total KB level, participants in tertile 1 (HR, 1.04, 95%CI 1.00-1.08) and tertile 3 (HR, 1.07; 95%CI 1.04-1.11) had significant higher risks of new-onset AF. Compared to individuals in tertile 2 of β-OHB, those in tertile 3 (HR, 1.06; 95%CI 1.02-1.10) also demonstrated a significant increased risk of AF. Due to the linear associations, tertile 1 was used as reference group for acetoacetate and acetone, presenting with significant associations between higher acetoacetate (HR, 1.06; 95%CI 1.02-1.11) and acetone (HR, 1.11; 95%CI 1.07-1.15) with increased risk of AF. Consistently, a U-shaped association was also observed between total KB and β-OHB with LA volume parameters, including LA maximum volume (LAVmax), LA minimum volume (LAVmin), and their body surface area-indexed counterparts, and an inverted U-shaped association was observed for LA ejection fraction (all P non-linear <0.05). Significant interactions were observed between KB and genetic risk on incident AF ($P_{interaction}$ <0.05). The association between KB with AF was greater among individuals with low genetic risk, while the highest AF risk was for those at high genetic risk with high KB levels (**Figure**). Significant mediation effects of inflammatory markers on the associations between KB and AF were identified. Specifically, C-reactive protein contributed 9.6%, 12.8%, 7.5%, and 0.8% respectively to the total effect of circulating total KB, β-OHB, acetoacetate, and acetone on new-onset AF (all P <0.001).

Conclusions

There is a U-shaped association between circulating total KB and β-OHB with incident AF, LA structure and function measurements, as well as a positive association between acetoacetate and acetone level with AF risk in the general population. The associations are greater among individuals with low genetic risk for AF, while the highest is for those at high genetic risk with high KB levels. Our findings may facilitate risk stratification and prevention strategies for AF, and provide novel infights for future mechanistic studies.

Left Atrium Myocardial Remodeling and Prognostic Marker Derived from Cardiac MRI Feature Tracking in Pediatric Hypertrophic Cardiomyopathy

Xingrui Chen[1], Shi-Hua Zhao[2]

Fuwai Hospital, Chinese Academy of Medical Sciences and Peking Union Medical College

Background

Hypertrophic cardiomyopathy (HCM) is the most prevalent inherited myocardial disorder and a major contributor to sudden cardiac death (SCD) in young populations. While diastolic dysfunction is recognized as a hallmark feature in adult HCM, left atrial (LA) morphology and function serve as sensitive indicators of diastolic impairment, offering potential early prognostic insights. Cardiac magnetic resonance (CMR) is a robust imaging modality for assessing HCM, with LA longitudinal strain–encompassing reservoir, conduit, and booster pump functions–demonstrating prognostic relevance in prior CMR-based HCM studies. Nevertheless, the prognostic significance of LA strain in pediatric HCM remains poorly characterized. This study investigates the prognostic utility of CMR-derived LA strain parameters in children with HCM.

Methods

This retrospective study consecutively involved 249 HCM patients aged ≤ 21 years with contrast-enhanced CMR and 49 age- and sex-matched healthy controls. Strain parameters were assessed by feature-tracking analysis. Clinical and CMR features were analyzed using Cox proportional hazards models about the composite outcomes included SCD or equivalent events and heart failure-related events.

Results

Pediatric HCM patients were found to have thicker LV wall, higher LV

mass index and smaller LV diameter and LVEDVi than healthy control (all P<0.05). In terms of LA volumetric and functional indices, the decreased LA reservoir and conduit strain (LA reservoir strain 30.8 ± 11.3% vs. 41.2 ± 10.0%, P<0.001; LA conduit strain 16.6 ± 8.4% vs. 27.5 ± 7.9%, P<0.001), increased all phasic LA volume, reduced LAEF and deteriorated LA strain rate were shown significantly in HCM patients than in the normal controls (all P<0.05).

During a median follow-up of 62 months (IQR: 39-85), 26 (11.3%) patients reached composite outcomes. Patients were divided into two groups based on the median LA reservoir strain of 29.3%. The group with lower LA reservoir strain had thicker maximum wall thickness, lower LVEF, greater LGE extent, lower LA conduit strain and lower LA reservoir and conduit strain rate (all P < 0.05). Kaplan-Meier analysis showed a significantly increased risk of composite outcomes in the groups with LA reservoir strain (log-rank P < 0.001) and LA conduit strain (log-rank P = 0.001) lower than the median, respectively. In the univariable Cox regression analysis, LVEF (HR: 0.95, 95%CI: 0.92-0.98, P = 0.003), LV mass index(HR: 1.01, 95%CI: 1.00-1.01, P = 0.005), LGE presence(HR: 10.88, 95%CI: 1.46-80.97, P = 0.020) and extent(HR: 1.16, 95%CI: 1.10-1.22, P < 0.001), LA reservoir strain (HR: 0.94, 95%CI: 0.90-0.98, P = 0.002) and conduit strain (HR: 0.90, 95%CI: 0.85-0.96, P = 0.001), LA total EF(HR: 0.97, 95%CI: 0.94-0.99, P = 0.034) and LA maximum volume index(HR: 1.01, 95%CI: 1.00-1.02, P = 0.040) were identified as significant predictors for the occurrence of composite outcomes, whereas LA booster strain had no statistical significance (P = 0.295).Risk for composite outcomes increased with per percentage reduction in LA reservoir and conduit strains with statistical significance but not for LA booster strain in splined-adjusted analysis. After stepwise selection on predefined variables and significant clinical parameters (age and sex), age (HR: 0.88-0.89, 95% CI: 0.79-0.98, all P<0.05), LGE extent (HR: 1.16, 95% CI: 1.09-1.23, P < 0.001), LA reservoir strain (HR: 0.95, 95% CI: 0.91-0.99, P = 0.007) and conduit strain (HR: 0.92, 95% CI: 0.87-0.98, P = 0.005) remained significant predictors of composite outcomes.

Conclusion

In pediatric HCM, patients with worse LA reservoir strain and conduit strain showed poorer cardiac function and clinical outcomes. LA reservoir strain and conduit strain are associated with cardiovascular risk events. Cardiac MR examination, especially its feature-tracking technology, provides the possibility to prognosticate childhood HCM at an early stage.

Impact of Nanoplastics on Human Pluripotent Stem Cell-Derived Early Endothelial Cells

rui Zhang

Beijing Tsinghua Chunggung Hospital

Background: Microplastics (MPs) and nanoplastics (NPs) represent pervasive global environmental contaminants, with documented human bioaccumulation in multiple organs including the vascular system. Critically, NPs have been identified within human atherosclerotic plaques and correlated with increased plaque inflammation, vulnerability, and adverse cardiovascular outcomes. While this establishes NPs as an emerging cardiovascular risk factor, the precise cellular and molecular mechanisms driving their vascular toxicity remain poorly understood.

Endothelial cells (ECs) are central targets, forming the vascular barrier and actively regulating inflammation and hemodynamics. Crucially, their capacity for neovascularization – specifically migration and tube formation (tubulogenesis) – is fundamental for post-ischemic tissue repair and collateral vessel development in cardiovascular diseases. This angiogenic function, however, is not uniform across the endothelial spectrum.

Of paramount importance are early-stage endothelial cells. These cells exhibit unique phenotypic properties critical for initiating vascular repair: enhanced plasticity, high proliferative and migratory capacity, and robust tubulogenic potential. Unlike quiescent mature endothelium, early ECs are metabolically active and inherently more responsive to pro-angiogenic cues, making them essential responders to ischemic injury. Consequently, early ECs may possess heightened vulnerability to environmental stressors like NPs that could disrupt these critical repair mechanisms before mature vascular networks form.

Despite the identification of NPs in plaque and epidemiological links to CVD, the specific impact of NPs on the distinctive function of early endothelial progenitors remains a critical knowledge gap. Exposure could impair their unique tubulogenic capacity, directly sabotaging vascular repair pathways vital for recovery from myocardial infarction, peripheral artery disease, and stroke. Understanding NP toxicity specifically within this sensitive and therapeutically relevant cell population is therefore essential to elucidating a key mechanism of environmental cardiovascular damage.

Therefore, investigating the mechanistic effects of NPs on the specialized tubulogenic function of early human endothelial cells is imperative for defining their cardiovascular hazard profile and identifying potential therapeutic targets to preserve vascular repair capacity.

Methods: To investigate the mechanistic impact of nanoplastics (NPs) on early human endothelial cell (EC) function, we employed a well-defined in vitro model system. Human induced pluripotent stem cells (hiPSCs) derived from healthy volunteers were directed to differentiate into early-stage endothelial cells (D5-D6 post-differentiation) using established protocols. Differentiation efficiency was rigorously quantified by flow cytometry, confirming a highly pure population (97% CD31+ cells), ensuring the relevance of our model to authentic vascular endothelium.

We utilized carboxylate-modified fluorescent polystyrene nanoparticles as model NPs, characterized by two distinct average diameters: 40 nm (NPs 40nm) and 100 nm (NPs 100nm). To establish a non-cytotoxic exposure regime for functional assessment, early hiPSC-ECs were exposed to a concentration gradient (0, 5, 10, 20, 40, 80 μg/ml) of each NP size for 24 hours. Cell viability was meticulously assessed using flow cytometry-based live/dead staining. Concurrently, NP internalization dynamics were evaluated using a combination of flow cytometry (exploiting NP fluorescence) and high-resolution immunofluorescence microscopy to distinguish surface-bound versus internalized particles.

Based on the viability results, a sub-cytotoxic concentration (10 μg/ml) was selected for both NP sizes to specifically investigate functional impairment independent of overt cell death. Following 24-hour exposure to NPs 40nm or NPs 100nm at 10 μg/ml, the critical angiogenic function of tube formation (tubulogenesis) was assessed using a standardized in vitro Matrigel assay. Tubulogenesis capacity was quantified by measuring key parameters: number of branch points (nodes) and total tube length per field. To elucidate the molecular underpinnings of observed functional deficits, bulk RNA sequencing (RNA-seq) was performed on hiPSC-ECs exposed to NPs 40nm or NPs 100nm (10 μg/ml, 24h) and compared to untreated controls. Bioinformatic analysis focused on identifying significantly dysregulated genes and enriched pathways related to angiogenesis, endothelial function, and stress responses.

Results: Our hiPSC differentiation protocol robustly generated early endothelial cells, as evidenced by high CD31 expression (97% purity via flow cytometry), confirming a suitable model for studying NP effects on vascular biology. Critical screening experiments revealed distinct NP size-dependent interactions and cytotoxic profiles: Exposure to NPs 40nm, even at the highest concentration tested (80 μg/ml), exhibited no significant cytotoxicity compared to untreated controls. Strikingly, immunofluorescence imaging combined with flow cytometry unequivocally demonstrated that NPs 40nm were efficiently internalized by the early hiPSC-ECs. In contrast, exposure to NPs 100nm resulted in a significant, concentration-dependent decrease in cell viability at concentrations ≥ 20 μg/ml. Furthermore, NPs 100nm were not internalized by the cells; imaging revealed particles predominantly associated with the cell surface or remaining in suspension.

Consequently, the sub-cytotoxic concentration of 10 μg/ml was selected for both NP sizes to isolate functional effects from overt toxicity. Assessment of tubulogenesis, a fundamental angiogenic process crucial for vascular repair, yielded significant findings. Compared to untreated control ECs (CTL-EC), both NPs 40nm-exposed ECs (NPs 40nm-EC) and NPs 100nm-exposed ECs (NPs 100nm-EC) exhibited profound impairment in tube-forming capacity. Quantitative analysis demonstrated a substantial and statistically significant reduction in both key metrics: the number of nodes (branch points) decreased by 67%, and the total tube length decreased by 74% in NP-exposed groups relative to controls. Notably, despite the stark difference in their cellular interaction (internalization vs. surface adherence), NPs 40nm and NPs 100nm induced remarkably similar and severe deficits in tubulogenic function at 10 μg/ml, with no statistically significant difference observed between the two NP-exposed groups.

To probe the mechanistic basis for this pronounced impairment in angiogenic capacity, we conducted bulk RNA-seq analysis. Transcriptomic profiling identified significant dysregulation of numerous genes in NP-exposed early hiPSC-ECs compared to controls. Pathway enrichment analysis pinpointed specific disruption in biological pathways intimately linked to endothelial cell migration, vascular development, and tube formation. These findings strongly suggest that sub-cytotoxic NP exposure, irrespective of internalization capability (40nm) or surface interaction (100nm), disrupts core molecular programs essential for early endothelial cell function, directly contributing to the observed vascular network formation failure.

Conclusion: Our findings demonstrate that exposure to carboxylated nanoplastics (40nm and 100nm) at sub-cytotoxic concentrations profoundly impairs the tubulogenic capacity of early human endothelial cells (hiPSC-ECs), a critical function for vascular repair. Strikingly, despite divergent cellular interactions—efficient internalization of 40nm NPs versus surface association without uptake of 100nm NPs—both particle sizes induced remarkably similar and severe deficits in endothelial network formation (67% reduction in nodes, 74% reduction in tube length). Transcriptomic analysis revealed significant dysregulation of pathways integral to angiogenesis, vascular development, and cell migration. This work provides novel mechanistic evidence that nanoplastics disrupt fundamental endothelial repair programs independently of direct cytotoxic-

ity or the mode of cellular interaction, establishing a crucial link between nanoplastic exposure and compromised vascular regenerative capacity, a key factor in cardiovascular disease pathogenesis.

Targeting Notch2-Mediated Macrophage Mechanotransduction Alleviates Cardiac Fibrosis

Jin Wang, Xi Wang

Capital Medical University

Abstract

Background: Fibrosis, characterized by abnormal extracellular matrix (ECM) deposition and mechanical stiffening, is widely recognized as a common pathophysiologic process in most heart diseases. Macrophage-driven inflammation is closely linked to ECM stiffening. In our previous work, we demonstrated that ECM stiffening in the cardiovascular system promotes macrophage infiltration into the vessel wall and induces the expression of fibrotic genes. This highlights the importance of mechanical response of immune cells in fibrotic remodeling. However, the mechanisms by which macrophages sense and respond to biomechanical cues remain largely unknown.

Objective: This study aimed to identify key mechanotransduction mechanisms in macrophages contributing to cardiac fibrosis, and to explore targeted therapeutic strategies based on disruption of stiffness-induced signaling cascades

Methods: 1. We performed a meta-analysis of single-cell RNA sequencing datasets by using integrative clustering to identify mechanoresponsive macrophage subsets enriched in the fibrotic cardiac tissue. 2. Key gene expressions were validated in monocytes from heart failure patients using immunoblotting and flow cytometry. 3. Macrophage responses to matrix stiffness were assessed in vitro using polyacrylamide hydrogels with tunable elastic moduli simulating physiological and fibrotic conditions, and in vivo using a murine transverse aortic constriction (TAC) model to mimic pressure overload-induced cardiac remodeling, a well-established model for studying myocardial fibrosis. 4. Candidate compounds targeting mechanotransduction pathways were screened using the Connectivity Map (CMap) and validated by molecular docking, with computational scoring to assess predicted binding affinity.

Results: We identified the Notch2 as a macrophage-enriched mechanosensor: 1. Analysis of scRNA-seq data revealed a distinct Notch2^{high} macrophage subset enriched in fibrotic hearts, characterized by elevated expression of pro-inflammatory cytokines (CCL2, IL1β, and NFκB), suggesting activation of inflammatory signaling pathways. 2. Elevated Notch2 protein was confirmed in peripheral blood monocytes from heart failure patients. 3. In vitro, macrophages on stiffer polyacrylamide substrates showed increased Notch2 expression and nuclear translocation; Inhibition of Notch2 signaling attenuated the nuclear localization of YAP, a hallmark of mechanotransduction, suggesting that Notch2 modulates macrophage mechanical responsiveness. In the murine TAC models, Notch2 expression was elevated in cardiac macrophages within fibrotic regions, correlating with increased collagen deposition and inflammatory infiltration, as assessed by immunohistochemistry and gene expression profiling. 4. Connectivity Map (CMap) identified Cp6, a glucoside, as a Notch2 inhibitor. Cp6 inhibited Notch2-mediated mechanotransduction and suppressed inflammatory gene expression in vitro when macrophages were cultured on substrates with different stiffness. In TAC mice, Cp6 reduced Notch2 expression in cardiac macrophages, attenuated myocardial inflammation and fibrosis (histology), and improved cardiac function (echocardiography) as evidenced by increased left ventricular ejection fraction (EF) and fractional shortening (FS).

Conclusions: Notch2^{high} macrophages are a novel mechanosensitive subset that sustains a positive feedback loop between inflammation and fibrosis in the heart. Matrix stiffening promotes Notch2/YAP-mediated inflammatory and fibrotic genes expression, amplifying maladaptive remodeling, thereby contributing to tissue dysfunction and structural disorganization. Notch2 inhibition effectively dampens macrophage-driven inflammation, limits fibrotic progression, and preserves cardiac function. These results highlight Notch2-mediated mechanosensing as a potential therapeutic target in cardiac fibrosis.

Key words: Cardiac Fibrosis; Extracellular Matrix Stiffness; Notch2; Mechanotransduction; Single-Cell Transcriptomics.

CREG1 Enhances Postinfarction Cardiac Repair by Regulating HOXA5-Mediated miR-125a Cluster to Suppress Macrophage Inflammation

Jing-Jin Hou, Cheng-Hui Yan

State Key Laboratory of Frigid Zone Cardiovascular Disease, Cardiovascular Research Institute and Department of Cardiology, General Hospital of Northern Theater Command

Background

Acute myocardial infarction (AMI) remains one of the most significant contributors to cardiovascular morbidity and mortality globally. Despite advances in early revascularization strategies such as percutaneous coronary intervention (PCI), a considerable proportion of AMI survivors develop heart failure (HF), underscoring a critical need to identify novel molecular targets for post-infarction cardiac repair. Increasing evidence suggests that macrophage-mediated inflammation plays a pivotal role in post-MI remodeling; however, the molecular mechanisms that regulate macrophage phenotype and function in this context remain incompletely understood. This study investigates the role of Cellular Repressor of E1A-Stimulated Genes 1 (CREG1) and its downstream signaling axis in modulating macrophage-mediated inflammation and cardiac remodeling following AMI.

Methods

We generated macrophage-specific CREG1 knockout (Creg1 flox/flox Lyz2-cre) and CREG1-overexpressing transgenic (Creg1 Tg) mice. AMI was induced by permanent ligation of the left anterior descending (LAD) coronary artery. Cardiac function was assessed by echocardiography. Histopathological evaluation was performed using H&E and Masson's trichrome staining. Immune cell profiling was conducted via flow cytometry and immunofluorescence. In vitro studies employed bone marrow-derived macrophages (BMDMs) with genetic manipulation of CREG1 expression to assess changes in cytokine production, migration capacity, and miRNA expression. Luciferase reporter assays identified transcriptional regulators of target miRNAs. The clinical relevance of the CREG1–HOXA5–miR-125a/99b/let-7e axis was further evaluated in monocytes isolated from AMI patients.

Results

Macrophage-specific deletion of CREG1 resulted in exacerbated cardiac dysfunction following MI, as evidenced by significantly lower ejection fraction (EF%) and fractional shortening (FS%) compared with littermate controls. Histological analyses revealed increased infarct size, myocardial hypertrophy, and interstitial fibrosis in Creg1-deficient mice. Flow cytometry and immunostaining demonstrated elevated infiltration of Ly6C^hi^ pro-inflammatory macrophages and upregulated expression of inflammatory mediators including TNF-α, IL-6, and CCL2. Conversely, CREG1 overexpression attenuated these pathological changes, improved cardiac function, and promoted an anti-inflammatory macrophage phenotype.Microarray and qPCR analyses identified a CREG1-dependent microRNA cluster (miR-125a-5p, miR-99b-5p, and let-7e-5p) that was downregulated in CREG1-deficient macrophages. Functional studies revealed that these miRNAs suppressed pro-inflammatory cytokine expression and macrophage migration, with miR-125a-5p showing the most potent anti-inflammatory effects and let-7e-5p having the greatest impact on migration. Transfection with miRNA mimics reversed the pro-inflammatory phenotype induced by CREG1 knockdown, while miRNA inhibitors counteracted the anti-inflammatory effects of CREG1 overexpression.Further mechanistic analysis demonstrated that CREG1 upregulates the transcription factor HOXA5, which directly binds to and activates the shared promoter region of the miR-125a/99b/let-7e cluster. Dual-luciferase reporter assays confirmed HOXA5's regulatory role, and loss-of-function mutations within its binding sites abolished promoter activity. In vivo, administration of miR-125a-5p mimics in CREG1-deficient mice improved cardiac function and reduced myocardial inflammation and macrophage infiltration after MI.In human subjects, expression levels of CREG1, HOXA5, and miR-125a-5p were significantly reduced in circulating monocytes from AMI patients compared to non-infarct CAD controls. Moreover, expression levels of CREG1 positively correlated with HOXA5 and miR-125a-5p, and higher levels were associated with preserved cardiac function.

Conclusion

Our findings identify the CREG1–HOXA5–miR-125a/99b/let-7e axis as a critical immunoregulatory pathway in macrophage-mediated cardiac remodeling post-AMI. CREG1 enhances HOXA5 expression, which transcriptionally activates anti-inflammatory miRNAs that restrain NF-κB-driven macrophage activation and migration. This axis represents a promising therapeutic target for mitigating inflammation-induced cardiac injury and preventing the progression to heart failure following AMI.

Managing Sustained SVT in Pregnancy Without Structural Heart Disease: Is Catheter Ablation a Safer and more effective Alternative?

Liu Fang, De-Yong Long

Beijing Anzhen Hospital

BACKGROUND:

Supraventricular tachycardia (SVT) during pregnancy is associated with increased maternal and fetal morbidity, including higher risks of cesarean delivery, preterm birth, and, in rare cases, maternal cardiomyopathy. Although catheter ablation is a definitive and curative treatment for SVT (Class I, Level B), current guidelines recommend its use during pregnancy only for patients with drug-refractory or poorly tolerated SVT (Class IIa, Level C), primarily due to concerns over fetal exposure to ionizing radiation. However, recent advances in three-dimensional electroana-

tomical mapping and intracardiac echocardiography have enabled zero-fluoroscopy catheter ablation, making it a viable option for selected pregnant women when performed in experienced centers. Despite these technological advances, the optimal management strategy for sustained SVT during pregnancy—particularly in women without structural heart disease—remains inadequately defined.

OBJECTIVES:

To evaluate the safety and efficacy of catheter ablation compared with medical therapy for the treatment of sustained SVT during pregnancy in women without structural heart disease, and to assess their respective impacts on arrhythmia recurrence, obstetric outcomes, and fetal development.

METHODS:

This retrospective case-control study included 560 patients screened from all pregnancy-related hospital admissions between December 2010 and February 2025 at a tertiary referral center. Women aged 18–50 years were eligible for inclusion. The study group comprised 112 pregnant women diagnosed with sustained SVT in the absence of structural or significant cardiac disease, confirmed by comprehensive chart review and echocardiographic evaluation. Patients were stratified by treatment strategy into catheter ablation (n=49) and medical therapy (n=63) groups. A control group of 448 pregnant women without SVT or cardiac disease was randomly selected from the same period at a 4:1 ratio, matched by age and delivery date to minimize temporal and selection bias. Baseline characteristics, arrhythmia burden, obstetric outcomes, and fetal development were analyzed. Multivariable regression models adjusted for maternal age and parity were used to assess associations between treatment strategy and clinical outcomes.

RESULTS:

Among 188,957 pregnancy-related hospitalizations, 112 women were diagnosed with sustained SVT and structurally normal hearts. Compared to those receiving medical therapy, patients undergoing catheter ablation had significantly lower SVT recurrence rates (2.0% vs. 52.4%; OR: 0.03; 95% CI: 0.004–0.24; $P < 0.001$), reduced rates of emergency cesarean delivery (9.1% vs. 25.4%; OR: 0.29; 95% CI: 0.09–0.90; $P = 0.032$), shorter hospital stays (2.73 ± 1.72 vs. 4.43 ± 2.72 days; $P < 0.001$), and higher neonatal birth weights (3394.5 ± 388.2 g vs. 3216.4 ± 461.6 g; $P = 0.040$). Ablation was performed using a zero-fluoroscopy approach in 91.8% of cases, with no procedure-related maternal complications or fetal malformations observed. In contrast, medical therapy was associated with a higher incidence of intrapartum SVT episodes and several fetal anomalies. After adjusting for relevant covariates, catheter ablation remained independently associated with improved obstetric outcomes and significantly reduced arrhythmia recurrence.

CONCLUSIONS:

SVT during pregnancy, even in the absence of structural heart disease, is associated with increased maternal risk and adverse obstetric outcomes. The unpredictable recurrence of arrhythmia and the limited efficacy of antiarrhythmic medications complicate clinical management during both pregnancy and labor. Our findings demonstrate that catheter ablation is a safe, feasible, and highly effective treatment for sustained SVT during pregnancy in selected patients. Compared to medical therapy, catheter ablation significantly reduced arrhythmia recurrence, lowered the rate of emergency cesarean sections, shortened hospitalizations, and improved neonatal birth weights. These results support early consideration of catheter ablation, especially in patients with drug-refractory or poorly tolerated SVT, and highlight the potential role of zero-fluoroscopy techniques in ensuring fetal safety.

Plasma proteomic profiling reveals distinct molecular signatures associated with coronary collateral circulation in CTO patients

Jun-Yi Luo[1], Peng Ran[2], Fen Liu[1,3], Xiao-Mei Li[1], Ding[2], Yi-Ning Yang[4]

1. Department of Cardiology, the First Affiliated Hospital of Xinjiang Medical University, Urumqi, Xinjiang, 830054, China

2. Center for Cell and Gene Therapy, Fudan University Clinical Research Center for Cell-based Immunotherapy, Shanghai Pudong Hospital, Human Phenome Institute, State Key Laboratory of Genetic Engineering, School of Life Sciences, Fudan University, Shanghai 200433, China.

3. State Key Laboratory of Pathogenesis, Prevention and Treatment of High Incidence Diseases in Central Asia, Clinical Medical Research Institute, the First Affiliated Hospital of Xinjiang Medical University, Urumqi, Xinjiang, 830054, China.

4. Department of Cardiology, Xinjiang Key Laboratory of Cardiovascular Homeostasis and Regeneration Research, People's Hospital of Xinjiang Uygur Autonomous Region, Urumqi, Xinjiang, 830000, China

Abstract

Background: Coronary collateral circulation (CCC) provides a critical cardioprotective role in mitigating myocardial ischemia through its dynamic compensatory capacity. Clinical evidence demonstrated that good CCC development preserves relatively cardiac functional stability even in the context of complete native coronary artery occlusion. However, the molecular mechanisms underlying CCC formation remain poorly understood, and there is a lack of clinically actionable noninvasive biomarkers to classify CCC status in chronic total occlusion (CTO) patients. Precise characterization of CCC functional status holds significant clinical value for risk stratification and management of coronary CTO patients.

Methods: Using the data-independent acquisition (DIA) quantitative proteomic approach, we comprehensively analyzed 235 plasma samples from two independent CTO cohorts (discovery cohort: n=124; validation cohort: n=111). The grades of collateral filling from the contralateral vessel were categorized into four levels based on the Rentrop classification criteria: Grade 0: No collateral filling; Grade 1: Filling of side branches of the artery to be dilated via collateral channels without visualization of the epicardial segment; Grade 2: Partial filling of the epicardial segment via collateral channels; Grade 3: Complete filling of the epicardial segment of the artery being dilated via collateral channels. According to collateral flow, patients were classified into a good CCC group (Rentrop grades 2-3) or a bad CCC group (Rentrop grades 0-1). Participants were followed up every 3-6 months for endpoint events through telephone or clinic visits. The study endpoint was the occurrence of composite MACCEs during follow-up, including all-cause death, cardiac death, non-fatal myocardial infarction, non-fatal stroke, malignant arrhythmia, revascularization, severe heart failure (NYHA class III or IV), target vessel revascularization.

Results: Our findings revealed the significant clinical features (basophil counts, prothrombin time activity, medical history duration, serum chloride concentrations, high density lipoprotein- cholesterol levels, and red blood cell distribution width) associated with CCC status. However, the clinical feature-based model faces challenges in precisely classifying patients' CCC status. Proteome profiling revealed that protein degradation and ion transport pathways were enriched in good-CCC CTO patients, whereas immune responses and vascular remodeling pathways were predominant in bad-CCC patients. Using candidate plasma protein biomarkers (SOD1, UFD1, DDX5, MIA3, TOM1, and LMAN2) in conjunction with clinical data, we developed CCC classifiers that demonstrated high predictive accuracy, achieving an area under the curve of 0.91 in the discovery cohort. The model's robustness and generalizability were further confirmed in an independent validation cohort, with an AUC of 0.82. To validate the robustness and reproducibility of our findings, we performed additional confirmations in both the discovery cohort and an external validation cohort. We confirmed the plasma protein biomarkers identified in our discovery cohort by using ELISA. The ELISA results showed strong concordance with our proteomic data, with SOD1, MIA3, and LMAN2 being significantly elevated in the good CCC group, while UFD1, DDX5, and TOM1 were higher in the bad CCC group. Notably, the expression patterns for all six candidate biomarkers were consistent across both proteomic analysis and ELISA validation, with statistically significant differences observed for each biomarker. Additionally, we constructed a risk prediction model for MACCEs based on a panel of nine plasma proteins, providing a potential tool for the early identification of high-risk CTO patients. In conclusion, our findings provided new insights into the molecular characteristics of the CCC ecosystem, enhancing the understanding of CTO patients with distinct CCC statuses.

Conclusion: The identification of a circulating biomarker panel presented the potential for improving the clinical diagnosis and optimizing the clinical management strategies for CTO patients.

PCSK9 Inhibitor Improves Ventricular Remodeling via Regulating the Overexpression of TACE and Its Downstream Factors in Alcoholic Cardiomyopathy

Yi-Zhan Fan, H-AHADAT HOSSAIN S, Ying-Hao Yang, Hai-Long Cui, Yue-Heng Feng, E-BREMICHAEL MEKONNEN HAILEMICHAEL G, Jian-Qiang Li

The First Affiliated Hospital of Harbin Medical University

Background and purpose

Alcoholic cardiomyopathy (ACM) is a special type of cardiomyopathy caused by long-term heavy alcohol intake. Ventricular remodeling is considered to be an important part of the occurrence and development of ACM, and metalloproteinase family is an important factor affecting ventricular remodeling of ACM. Tumor necrosis factor-α converting enzyme (TACE) belongs to the metalloproteinase family. It can hydrolyze membrane-bound Tumor necrosis factor-α (TNF-α) precursors and release soluble TNF-α. The overexpression of TNF-α is closely related to extracellular matrix (ECM) degradation, cell apoptosis, cardiac hypertrophy and cardiac chamber enlargement, and is involved in the occurrence and development of a variety of cardiovascular diseases. Proprotein convertase subtilisin/kexin type 9 (PCSK9) exerts a pro-inflammatory effect by stimulating the expression of inflammatory factors such as soluble TNF-α and interleukin (IL). The aim of this study was to determine the expression of TACE and its substrates in ACM and their relationship with ventricular remodeling, and to observe the effect of PCSK9 inhibitor

on ventricular remodeling of ACM mediated by TACE and its downstream factors.

Methods

Three groups were formed by randomly dividing 40 8-week-old C57 mice: control group (Ctrl, n=10), ACM group (EtOH, n=15) and intervention group (EtOH+Drug, n=15). Mice in the EtOH and EtOH+Drug groups were fed with Lieber DeCarli alcohol diet for 12 weeks to establish an ACM model, while mice in the Ctrl group were given a normal diet. Mice in the EtOH+Drug group were subcutaneously injected with evolocumab (10mg/kg) every 10 days, while mice in the Ctrl and EtOH groups received saline at the same frequency. At the end of the experiment, the cardiac structure and function of each group were evaluated by echocardiography. After euthanizing the mice, blood samples and cardiac tissue were collected. HE staining, Masson staining, and Tunel staining were performed for histopathological analysis. Western blot was used to detect the protein expression of PCSK9, TACE, and TNF-α. Circulating TNF-α levels were measured with enzyme-linked immunosorbent assay (ELISA). Statistical analysis was conducted using GraphPad Prism 8.0 software, and analysis of variance was used to compare the data of each group.

Results

The ACM model was successfully established in C57 mice fed with Lieber-DeCarli liquid alcohol diet for 12 weeks. Compared with the Ctrl group, left ventricular ejection fraction (LVEF) was significantly reduced (P<0.01) in the EtOH group, while left ventricular end diastolic diameter (LVEDD) was significantly increased (P<0.05). Evolocumab markedly improved the cardiac structure and function in the EtOH+Drug group. Pathological examination revealed that myocardial and nuclear arrangement was dramatically disordered and apoptosis was obviously increased in the EtOH group (P<0.01), while the above pathological changes were markedly enhanced in the EtOH+Drug group (P<0.01). Compared with the Ctrl group, the protein expression of TACE, PCSK9 and TNF-α was significantly upregulated in the EtOH group (P<0.01 for TACE and PCSK9, and P<0.01 for TNF-α). Compared with the EtOH group, the protein expression of TACE, PCSK9 and TNF-α was significantly downregulated in the EtOH+Drug group (P<0.05 for TACE, P<0.01 for PCSK9 and P<0.01 for TNF-α). Compared with the Ctrl group, the levels of TACE and TNF-α were much higher in the EtOH group (P<0.01 for TACE and P<0.01 for TNF-α), while evolocumab considerably reduced the levels of PCSK9, TACE and TNF-α in the EtOH+Drug group (P<0.01 for TACE, P<0.01 for PCSK9 and P<0.01 for TNF-α).

Conclusions

Evolocumab could inhibit the expression of TACE and its downstream factors by inhibiting PCSK9, thus reversing the ventricular remodeling in ACM. Therefore, PCSK9 and TACE may be potential targets for the treatment of ACM.

Identifying Patients for Cardiac Resynchronization Therapy Beyond Current Guidelines: Insights from Cardiac Magnetic Resonance Imaging

di zhou, Min-Jie Lu

Fuwai Hospital, CAMS & PUMC

Objectives: Cardiac resynchronization therapy (CRT) is recommended for chronic heart failure (HF) patients with reduced left ventricular ejection fraction (LVEF) and prolonged QRS duration. Despite the extensive use of CRT guided by QRS duration and morphology, it is widely acknowledged that 30%-40% of patients do not benefit from its implantation. The reasons for this lack of effectiveness are multifaceted.

Recent clinical studies have highlighted the importance of assessing LV dyssynchrony and myocardial viability to enhance patient selection for CRT. Cardiac magnetic resonance (CMR) emerges as a pivotal tool for evaluating these aspects. According to current guidelines, CMR offers a noninvasive characterization of the myocardium, enabling precise assessment of cardiac structure and function with remarkable reproducibility. Myocardial strain has been utilized to evaluate dyssynchronous and predict outcomes in patients following CRT, such as circumferential uniformity ratio estimate and systolic dyssynchrony index derived from CMR, as well as myocardial work and septal flash derived from echocardiography. In addition, late gadolinium enhancement (LGE)-CMR imaging is considered the standard non-invasive method for identifying myocardial fibrosis, a critical factor in the risk assessment for severe arrhythmias. In a prospective multicentre study of 200 participants, J.M. Malen et al found that the absence of septal LGE enhances the accuracy of identifying CRT responders. Taylors et al demonstrated that mid-wall LGE in patients with systolic dysfunction leads to dyssynchronous circumferential myocardial strain and reduced response to CRT, resulting in poor outcomes. Although the results from these imaging studies are promising, few studies have conclusively shown that incorporating imaging indicators can reduce total mortality or hospitalizations through comparison between patients receiving and not receiving CRT. And no large cohort study has demonstrated improved survival or response rates through the use of imaging indicators. Hence, current guidelines do not recommend the use of any imaging tool for patient assessment in CRT.

In this study, we aimed to identify CMR risk factors for survival in patients with reduced ejection fraction and prolonged QRS and to improve the selection of CRT candidates by incorporating CMR factors beyond the current guideline criteria.

Methods: We retrospectively enrolled 711 patients with reduced ejection fraction and prolonged QRS who underwent CMR imaging. The primary endpoint was a composite of cardiac-related death, heart transplantation, and left ventricular (LV) assist device implantation. Outcomes were compared in CRT-eligible patients with and without CRT.

Results: Over a median follow-up of 4.8 years, LGE and LV strains emerged as independent risk factors for survival in 547 patients without CRT. Stratified by COR I, late gadolinium enhancement (LGE)-negative, LGE of 0 - 8.0%, global longitudinal strain (GLS) ≥ - 5.9%, global circumferential strain (GCS) ≥ -6.3%, or global radial strain (GRS) ≤ 8.0%, patients without CRT experienced significantly shorter event-free survival for the primary endpoint compared to CRT recipients. Among COR I patients with LGE ≥ 8.0%, GLS < -5.9%, GCS < -6.3%, or GRS > 8.0%, survival outcomes were comparable regardless of undergoing CRT or not. In COR IIa subgroup, GLS ≥ -5.9% (HR [95% CI]: 3.204 [1.339-7.670]), GCS ≥ -6.3% (HR [95% CI]: 3.050 [1.194-7.788]), and GRS ≤ 8.0% (HR [95% CI]: 2.743 [1.070-7.029]) independently correlated with worse outcomes in patients without CRT compared to those with CRT.

Conclusions: Our study highlights the potential of CMR as a valuable tool in enhancing risk stratification and refining indications for CRT over an extended period of long-term follow-up. The key findings offer several valuable insights. First, we established that the extent of LGE and LV strains independently correlated with total mortality and hospitalizations in patients with reduced LVEF and prolonged QRS who did not undergo CRT implantation. Second, LGE and LV strains reinforce a tailored approach in the choice of patients for CRT implantation. In patients with LGE ≥ 8.0%, GLS < -5.9%, GCS < -6.3%, or GRS > 8.0%, the implantation of CRT did not lead to improved clinical outcomes, regardless of whether they were in the COR I cohort or LBBB cohort. Among the COR I subgroup, we observed a significant 9.924-fold increased risk of the primary endpoint in LGE-negative patients who did not receive CRT implantation. Lastly, our findings suggest that CMR measures offer incremental prognostic value beyond the existing guideline criteria. Among patients with GLS ≥ - 5.9%, GCS ≥ -6.3%, or GRS ≤ 8.0%, CRT implantation was a predictor of a better outcome in patients who fulfilled COR IIa.

Risk Stratification of Sudden Cardiac Death in Non-Ischemic Cardiomyopathy

di zhou, Min-Jie Lu

Fuwai Hospital, CAMS & PUMC

Objective: MRI-derived arrhythmogenic substrate, including late gadolinium enhancement (LGE) and extracellular volume fraction (ECV), is indicative of sudden cardiac death (SCD) risk in non-ischemic dilated cardiomyopathy (DCM). The relative prognostic value of LGE and ECV remains unclear. In this study, we aimed to evaluate the clinical performance of LGE and T1 mapping in predicting SCD in DCM patients and to explore practical clinical implementation.

Methods: This study enrolled 1105 patients with DCM who underwent cardiac MRI at four centers. The data were analyzed in a development cohort (n=837, single-center) and an external validation cohort (n=268, three centers). The primary endpoint comprised SCD, appropriate implantable cardioverter-defibrillator shock, and resuscitated cardiac arrest. The secondary endpoint comprised heart failure death, heart transplantation, and LV assist device implantation. Risk algorithms and a clinically applicable workflow for SCD risk assessment were developed based on validated MRI predictors.

Results: Over a median follow-up of 58.3 months, in the development cohort 78 patients reached the primary endpoint, and 120 patients the secondary endpoint. In the adjusted analysis, LGE ≥ 7.2% (HR, 4.748 [95% CI: 2.911-7.744], P<.001), ECV ≥ 31.8% (HR, 2.913 [95% CI: 1.625-5.221], P=.001), and native T1 z-score ≥ 2.1 (HR, 1.686 [1.039-2.738], P = .035) were associated with SCD-related events. Patients with ECV ≥ 31.8% and no LGE were at higher risk of SCD events compared to those with ECV<31.8% and LGE between 0-7.2% or mid-wall/focal LGE. Patients with LVEF>35%, LGE<7.2%, and ECV<31.8% exhibited a low risk of SCD with an annual event rate of 0.2%. Patients with LGE ≥ 7.2% exhibited a high risk of SCD-related events with an annual event rate of 4.65%.

Conclusion: In this study, we sought to advance our understanding of arrhythmogenic substrate assessment in non-ischemic DCM and improve risk stratification strategies for predicting SCD. Our findings highlight several key points that address limitations of current methodologies and propose actionable improvements. Firstly, the reliance on qualitative analysis of LGE has constrained its effectiveness in predicting SCD. Our research demonstrates that a quantitative approach, specifically using a cutoff value of LGE ≥ 7.2%, offers a more robust assessment of SCD risk, with an annual event rate of 4.65%. Secondly, we observed that ECV aids in differentiating genuinely low-to-moderate risk populations when LGE

is less than 7.2% or focal or mid-wall LGE is present. By providing cutoff values for LGE and ECV, our research introduces a nuanced approach that enhances the predictive capability across clinical scenarios. For patients unable to undergo contrast-enhanced imaging, native T1 may provide an alternative value for predicting SCD-related events to some extent. This approach expands the utility of imaging in diverse clinical settings, where contrast agents are contraindicated or unavailable. Lastly, in response to current guidelines advocating for enhanced risk assessment tools, we developed a comprehensive workflow for cardiac MRI-based evaluation of SCD risk in DCM patients. This workflow aims to assist clinicians in implementing personalized prognostic strategies, thereby improving individualized patient care and management. Overall, our study proposes practical solutions for refining SCD risk stratification in DCM, ultimately contributing to better clinical outcomes in this high-risk population.

Multi-omics and biological validations identify TARS2 as a mediator of mitochondrial oxidative stress in dilated cardiomyopathy

Chen Liming, Xuan Li, Xiao-Lei Sun, Xiao-Lin Wang, Jian Wu, Shi-Jun Wang, Lei-Lei Ma, Yun-Zeng Zou

Zhongshan Hospital, Fudan University

Multi-omics and biological validations identify TARS2 as a mediator of mitochondrial oxidative stress in dilated cardiomyopathy

Liming Chen[1], Xuan Li[1], Xiaolei Sun[1], Xiaolin Wang[1], Jian Wu[1], Shijun Wang[1], Leilei Ma[1], Yunzeng Zou[1]

[1]Zhongshan Hospital, Fudan University, Shanghai 200032, China

Background

Dilated cardiomyopathy (DCM) is a leading etiology of heart failure, affecting over 6 million people worldwide and accounting for the majority of heart transplant referrals. It is pathologically defined by progressive left ventricular dilatation, impaired systolic function, and cardiomyocyte loss. Although ~30% of DCM cases are attributed to monogenic mutations in sarcomeric or cytoskeletal proteins, the molecular underpinnings of the remaining sporadic forms remain poorly characterized. Over the past decade, mitochondrial dysfunction—particularly excessive mitochondrial reactive oxygen species (mtROS) production—has emerged as a central driver of metabolic stress and cell death in DCM. Yet, a fundamental question persists: does mtROS dysregulation initiate myocardial remodeling, or is it merely a downstream consequence of structural damage? Addressing this knowledge gap is critical for identifying early biomarkers and druggable targets.

Objective

To systematically identify and functionally validate key mitochondrial oxidative stress (MitOS)-associated genes that causally regulate cardiomyocyte fate in DCM, and to translate these discoveries into a clinically actionable diagnostic and therapeutic framework.

Methods

We integrated bulk RNA-seq from 38 human DCM and 14 non-failing hearts with machine-learning pipelines (LASSO, Random Forest, SVM-RFE) to prioritize MitOS genes. Diagnostic accuracy was quantified by ROC AUC and nomogram modeling, validated in an independent cohort. A doxorubicin-induced mouse DCM model was established; cardiac function was tracked by echocardiography and speckle-tracking strain analysis. Single-cell and spatial transcriptomics mapped cell-type-specific gene expression in human left ventricular tissue, complemented by immunohistochemistry and CellChat to quantify cardiomyocyte-macrophage crosstalk. Mitochondrial phenotypes were assessed in freshly isolated adult mouse cardiomyocytes (JC-1, MitoTracker, MitoSOX) and by transmission electron microscopy. Knockdown of TARS2 were performed in human AC16 cardiomyocytes and mice exposed to doxorubicin. Mendelian randomization (MR) leveraged GTEx left-ventricular eQTLs and two large GWAS (n = 355,381 Europeans) to test causality. In-silico drug screening (DSigDB) and molecular dynamics simulations identified and optimized small-molecule TARS2 inhibitors.

Results

Three MitOS genes—TARS2, SNCA, and NOX4—were reproducibly selected by all algorithms and displayed superior diagnostic performance (combined AUC = 0.929, 95% CI: 0.859–0.998; external validation AUC = 0.928). Spatial and single-cell data localized TARS2 specifically to left-ventricular cardiomyocytes, where high expression coincided with mtROS accumulation and upregulation of apoptotic (CASP3/9) and efferocytic (CX3CL1, GAS6) signals. Overexpression of Tars2 induced mitochondria-dependent apoptosis in cultured HL-1 cells and promoted pro-efferocytic signaling. The conditioned medium derived from HL-1 cells transfected with a TARS2-overexpressing plasmid enhanced the adhesion molecule expression of bone marrow-derived macrophages (BMDMs), including Cd36, Tsp-1, and Mertk. DCM mice recapitulated transcriptomic signatures, showing 2.3-fold TARS2 up-regulation, fragmented mitochondria, and 38% reduction in ejection fraction. TARS2 knockdown in DCM mice and cultured human cardiomyocytes restored mitochondrial membrane potential, decreased mtROS, and reduced cardiomyocyte apoptosis. MR analyses confirmed a causal effect of genetically predicted TARS2 level on DCM risk (OR = 1.52, 95% CI: 1.11–2.10, P = 0.0098) and adverse remodeling traits including lower LVEF and wall thickness. Virtual screening nominated theophylline, raloxifene, and bisacodyl as TARS2 ligands; 100-ns molecular dynamics simulations revealed theophylline exhibited the lowest RMSD (1.9 Å) and tightest binding energy (– 8.5 kcal mol^{-1}), predicting favorable therapeutic potetial.

Conclusions

by integrating multi-scale transcriptomic datasets, machine learning algorithms, MR, and in silico drug screening, we propose a generalized, data-driven framework for discovering and prioritizing novel targets in cardiovascular disease. This study establishes a novel diagnostic model for DCM based on mitochondrial oxidative stress-associated genes, highlighting TARS2 as a promising therapeutic target. The identification of small-molecule drugs for TARS2 protein suggests potential avenues for targeted therapeutic interventions during DCM progression.

Burden of Ischemic heart disease in Postmenopausal Women and Its Attributable Risk Factors in 204 Countries and Territories, 1990-2021: Results from the Global Burden of Disease Study 2021.

pan wu

Lanzhou university

BACKGROUND

Globally, the burden of disease in women's health, particularly in the postmenopausal population, is significantly underestimated. Traditional biomedical models have long reduced sex differences to morphological differences in the reproductive system, ignoring sex-specific gene regulatory mechanisms and failing to adequately consider the impact of hormonal dynamics on disease susceptibility during pregnancy, menopause, and other physiological stages; in addition, the prevalence of gender imbalance in the allocation of healthcare resources in clinical practice has impeded the analysis of sex-specific disease mechanisms and the development of precise intervention strategies. The postmenopausal risk of ischemic heart disease (IHD), the leading cause of death globally, surges mainly due to endothelial dysfunction and metabolic feedback imbalance mediated by estrogen withdrawal. In view of this, the aim of this study was to characterize the epidemiological transition of IHD incidence, prevalence, and disability-adjusted life years (DALYs) in postmenopausal women globally from 1990 to 2021.

METHODS

In this study, based on the Global Burden of Disease Study (GBD) 2021, mortality, disability-adjusted life years (DALYs), years of life lost (YLLs), prevalence, and incidence of IHD in postmenopausal females and men of the same age in 204 countries and territories from 1990 to 2021 were included and estimated and compared. Age standardized rates (ASRs) were calculated with reference to global age standards and their temporal trends were analyzed by estimating annual percentage change (EAPC). The effects of gender, age, region and socio-demographic index (SDI) were also considered in this study. Based on relative risk, exposure and theoretical minimum exposure level inputs, the estimates were attributable to provide a basis for precise, gender-differentiated prevention and treatment strategies.

RESULTS

In 2021, an estimated 254 million people with IHD will be reported globally, including 109 million women (936,000 postmenopausal women).3.71 million postmenopausal women will die from IHD, and 4.29 million men of the same age will die from IHD.The global age-standardized prevalence of IHD in postmenopausal women with a (per 100,000) global age-standardized prevalence rate, death, and DALY rate of 11,900 (95% of the uncertainty interval 10188.1,14050.1), 472 (414.4,511.4), and 7701.5 (6970.1,8279.9).The prevalence of IHD in 2021 is 6.9% (2.3%-12.5%) higher in postmenopausal women compared with 1990 compared with men of the same age (2.2%-6.6%); the age-standardized prevalence of IHD in the 1990- IHD age-standardized mortality rates and DALYs generally trended downward between 1990 and 2021.In 2021, the highest age-standardized incidence rates of IHD (per 100,000) were found in postmenopausal females in Eastern Europe (23227.5) and North Africa and Middle East (23197.2), and in high income Asia Pacific (188.1) and Southern Latin America (259.4) showed the lowest IHD (per 100 000) age-standardized mortality rates, while High-income Asia Pacific (2218.7), Western Europe (3704.9) and Southern Latin America (3747.2) had the lowest IHD (per 100 000) age-standardized DALY. Among females, global DALY rates for IHD peaked in the 70-74 age group and then declined with age, notably, a small rebound in DALY rates was observed in the upper age group of 80-84 years, after which the overall declining trend was maintained; whereas, among males, global DALY rates for IHD peaked in the 65-69 age group and then declined with age. Regionally, there was an overall inverted V-shaped association between the sociodemographic index (SDI) and age-standardized DALY rates for IHD.

The major risk factors contributing to the global DALY rate of IHD in postmenopausal women include hypertension (55.2%), high LDL cholesterol (30%), atmospheric particulate pollution (18.6%), and kidney damage (15.9%).

CONCLUSION

Global IHD age-standardized mortality rates and DALYs are declining, but prevalence is increasing, with postmenopausal women's risk approaching that of men or even being higher, and the burden on low and intermediate SDI countries is high, requiring intensified prevention and control to reduce the burden.

Efficacy of Early Initiation of Vericiguat in Acute Heart Failure: A Prospective Study

Junlong Chen[1], Dong-Ying Zhang[2]

1. The First Affiliated Hospital of Chongqing Medical University

2. Chongqing University Central Hospital

Background: For heart failure (HF) patients, quadruple guideline-directed medical therapy (GDMT) can reduce rehospitalization and mortality[1]. Pillar GDMT consists of beta-blocker, angiotensin receptor-neprilysin inhibitor (ARNI)/ angiotensin converting enzyme inhibitor (ACEI)/ angiotensin receptor blocker (ARB), mineralocorticoid receptor antagonist (MRA), and sodium-glucose cotransporter 2 inhibitor (SGLT2i).Unfortunately, high-risk HF patients are less likely to receive full standard therapy due to the presence of multiple contraindications or drug side effects[2,3]. There is an urgent need for better treatment strategies for new-onset acute heart failure patients or HF patients with GDMT intolerance. Vericiguat, as the first and only soluble guanylate cyclase stimulator approved for the treatment of heart failure with reduced ejection fraction (HFrEF), is recommended in addition to pillar GDMT. However, the efficacy of vericiguat in patients with GDMT intolerance or new-onset heart failure is unknown.

Methods: This study was a real-world, prospective cohort study, which enrolled patients diagnosed with acute heart failure with left ventricular ejection fraction less than or equal to 45%. Patients attempted to initiate vericiguat in hospital and were classified into vericiguat group and non-vericiguat group according to whether or not vericiguat was initiated at discharge. The primary endpoint was the time to first worsening HF events within 180 days.

Results: Patient characteristics before and after PS-matching were presented in Table 1. In the original cohort, patients with vericiguat treatment exhibited higher percentage of ischemic HF patients (27.1% vs. 14.7%; p=0.022), higher percentage of AF history (25.2% vs. 43.1%; p=0.005), higher eGFR (70.9 ml/min/1.73m^2 vs 763.5 ml/min/1.73m^2; p=0.041) and lower levels of creatinine (90 ug/L vs 99 ug/L; p=0.047). After PS matching, the cohort comprised 80 matched patient pairs with vericiguat treatment (Median age 70 years; 67.5% men) or without vericiguat treatment (Median age 70 years; 66.3% men). There were no significant differences between the groups regarding baseline information, laboratory metrics, NYHA functional class, left ventricular function and diameters, proportions of GDMT intolerant patients, or other clinical history. In both pre- and post- propensity score matching cohorts, early initiation of vericiguat therapy was associated with a reduced risk of worsening heart failure (hazard ratio (HR) 0.479; 0.501, 95% confidence interval (95%CI) 0.299-0.768; 0.283-0.888, p=0.003; 0.020, respectively). More patients with vericiguat achieved NYHA cardiac class I (54.2% vs 22.4%), but there was no statistically significant difference between the two groups in terms of improvement in echocardiography at endpoint. In the subgroup analysis, Vericiguat has been shown to reduce worsening HF event in patients with a previous history of chronic heart failure (HR[95%CI]= 0.451[0.224-0.907]) and in patients with new-onset heart failure (HR[95%CI]=0.265[0.074-0.949]), as well as in patients combined with quadruple GDMT therapy (HR[95%CI]=0.501[0.283-0.888]) and those intolerant of GDMT therapy (HR[95%CI]= 0.583[0.292-1.163]) (all p-interaction > 0.2). Notably, whether in patients who could or could not tolerate quadruple GDMT, early initiation of vericiguat therapy was associated with fewer heart failure worsening events compared to no vericiguat therapy.

Conclusions: Vericiguat should be initiated as early as possible throughout the development of heart failure, as long as there are no contraindications, regardless of whether the patient can tolerate full quadruple GDMT. This may suggest a new strategy for the management of HFrEF patients, particularly for patients who are intolerant to GDMT.

Hs-CRP, Diabetic Status, and Adverse Events Among Patients Receiving Statin Therapy Following PCI—A Prospective Registry-Based Study

王浩宇 窦克非 谌昕悦

中国医学科学院阜外医院（国家心血管病中心）

Purpose: This study aims to evaluate the impact of T2DM on the relationship between residual inflammatory risk, as assessed by a simple, economical, and easily measurable biomarker—hs-CRP—and clinical outcomes in statin-treated coronary heart disease (CHD) patients with drug-eluting stent (DES) implantation.

Methods: 8,628 individuals with CHD treated with statins and DES implantation at Fuwai Hospital were included. Participants were first stratified according to T2DM status, and then baseline hs-CRP levels were further divided into three groups using 1 mg/L and 2 mg/L as the cut-off points. The primary endpoint was MACCEs, defined as the composite of all-cause mortality, myocardial infarction, stroke, and target vessel revascularization.

Results: After 2.4 years of median follow-up duration, 999 patients were defined as MACCEs, whose hs-CRP levels were significantly higher compared to the non-MACCEs group (p= 0.007). The cohort was stratified into T2DM (n = 3,729) and Non-T2DM (n = 4,899) groups. In full adjusted model: for the Non-T2DM group, hs-CRP ≥ 2 mg/L remained significantly associated with MACCEs [HR = 1.39, 95% CI (1.14– 1.85), p = 0.002]. In the T2DM group, no significant association was observed [HR = 1.02, 95% CI (0.73– 1.23), p = 0.453] (p for interaction= 0.040).

Conclusion: Hs-CRP, an important diagnostic marker of inflammation, shows different value depending on diabetes status, revealing how diabetes and inflammation jointly influence cardiovascular outcomes and providing clinical insights for optimizing the application of inflammatory biomarkers in personalized cardiovascular risk stratification.

Residual Atherosclerotic Risk in Older Patients with Atherosclerotic Cardiovascular Disease: Where Inflammation Meets Lipoprotein(a)

Haoyu Wang, Xiao-Hui Bian, Ke-Fei Dou

Fuwai hospital

Background: Inflammation and hyperlipidaemia contribute with similar magnitude to the risk of future atherothrombotic events. However, the relative importance of high-sensitivity CRP (hsCRP) and lipoprotein(a) [Lp(a)] as determinants of risk for major adverse cardiovascular events are not well defined among patients aged 75 year or older with established ASCVD.

Methods: The present study prospectively enrolled 2,333 patients aged 75 years or older diagnosed with ASCVD with measurement of hsCRP and Lp(a) at Fuwai hospital. The primary endpoint was major adverse cardiovascular event (MACE), defined as a composite of all-cause death, myocardial infarction (MI), stroke, or ischemia-driven coronary revascularization.

Results: The median follow-up time was 3.0 years (IQR: 2.5-3.2 years) and 293 first MACE accrued. Both hsCRP and Lp(a) showed skewed distribution, with a median of 1.8 mg/L (IQR: 0.9-4.4 mg/L) for hsCRP and 19.3 mg/dL (IQR: 8.6-44.2 mg/dL) for Lp(a) (Figure 1). RCS analysis indicated a positive and linear association between hsCRP and MACE risk (P for overall association = 0.004, P for non-linearity = 0.393). However, there was no significant association between Lp(a) and MACE risk (P for overall association = 0.756).

hsCRP was significantly associated with an increased risk of MACE (adjusted HR [aHR]: 1.05, 95% CI: 1.03-1.08 per 1 mg/L increment, P<0.001; highest versus lowest quartile: aHR: 1.70 [1.22-2.38]), whereas there was no significant association between Lp(a) and MACE risk (aHR: 1.02 [0.98-1.06] per 10 mg/dL increment, P = 0.341; highest versus lowest quartile: aHR: 1.06 [0.77-1.47]). When modeled as a continuous variable, each 1 mg/L increase in hsCRP was associated with a 5% increased risk of MACE (adjusted HR: 1.05, 95% CI: 1.02-1.08, P<0.001). However, each 10 mg/dL increase in Lp(a) was not associated with MACE (adjusted HR: 1.02, 95% CI: 0.98-1.06, P = 0.341). Risks of MACE were significantly higher in participants with hsCRP ≥ 2 mg/L than in those with hsCRP <2 mg/L, irrespective of Lp(a) strata (adjusted HR: 1.41 [1.12-1.79]; P=0.004). Conversely, no significant association between Lp(a) and MACE risk was observed in the Lp(a) categorical threshold of 30 mg/dL (Lp[a] ≥ 30 mg/dL vs. <30mg/dL, adjusted HR: 1.10, 95% CI: 0.86-1.40, P = 0.439).

In the total population, hsCRP was significantly associated with MACE assessed by either per 1 mg/L increase (adjusted HR: 1.05; 95% CI: 1.03-1.08; P<0.001), or categorical threshold of 2 mg/L (adjusted HR: 1.41; 95% CI: 1.12-1.79; P=0.004). No significant interaction was observed between hsCRP and Lp(a) (P for interaction = 0.903 when Lp(a) was tested as continuous variable, and 0.635 when Lp(a) was tested by 30 mg/dL threshold). Higher hsCRP was significantly associated with increased risk regardless of baseline Lp(a) for MACE.

Using 2 mg/L as the cutoff of hsCRP and 30 mg/dL as the cutoff of Lp(a), all participants were divided into four groups, in which the group with hsCRP <2 mg/L and Lp(a) <30 mg/dL was defined as reference. Compared with the reference group, individuals with both elevated hsCRP (≥2 mg/L) and Lp(a) (≥ 30 mg/dL) resulted in the highest overall absolute risk, with a 1.54-fold increased risk of MACE (adjusted HR, 1.54; 95% CI, 1.13-2.12; P = 0.007).

Conclusions: Inflammation assessed by hsCRP predicted risk for future cardiovascular events more strongly than Lp(a) in patients aged 75 year

or older with established ASCVD. These results provided real-world evidence on older patients potentially benefit by targeted anti-inflammatory strategies for secondary ASCVD prevention.

Validation and comparison of five chronic total occlusion scores to predict difficulty of percutaneous coronary intervention

Yahang Tan

Capital Medical University Affiliated Beijing Chaoyang Hospital

Objective:

Successful percutaneous coronary intervention (PCI) for chronic total occlusion (CTO) has been shown to relieve symptoms, improve left ventricular ejection fraction and enhance survival. However, uncertainty regarding procedural duration, success rates, and potential complications remains a significant barrier to CTO PCI. Several preprocedural assessment tools based on invasive coronary angiography (ICA) and coronary computed tomography angiography (CCTA) have been

developed to evaluate CTO lesion characteristics and gradeprocedural complexity.These scoring models provide quantitative measures of procedural difficulty and the likelihood of successful recanalization, enabling more informed case selection based on operator experience. However,the performance of these CTO scoring models has not been validated in an independent population. Therefore, we aimed to validate and compare the predictive performance of five CTO scoring systems in multicenter cohort in China.

Materials and methods:

A total of 220 patients with 220 CTO lesions who underwent CCTA prior to invasive coronary angiography (ICA) with CTO Percutaneous coronary intervention (PCI) in three centers were retrospectively enrolled. Procedural difficulty was classified using five scoring systems: the CT Registry of CTO Revascularization (CT-RECTOR), Korean Multicenter CTO CT Registry (KCCT), Multicenter CTO Registry of Japan (J-CTO), Prospective Global Registry for the Study of Chronic Total Occlusion Intervention (PROGRESS), the clinical and lesion-related score (CL-score). The primary endpoint was successful GW crossing within 30 minutes. Receiver operating characteristic (ROC) curves and net reclassification improvement (NRI) were used to compare the predictive performance of the scores.To examine the contribution to the NRI of the subgroups with and without successful GW crossing within 30 min, reclassification tables were constructed for patients with and without successful GW crossing within 30 min.

Results :

The baseline characteristics of the 220 consecutive patients (70% male) referred for CCTA and ICA are listed in Table 1.GW crossing within 30 minutes and final success were achieved in 55% and 81% of cases, respectively.The clinical characteristics were similar between the successful and failed GW crossing groups, except for frequency of previous coronary artery bypass grafting, previous attempt of PCI at CTO and occlusion duration 12 months or unknown.The chart illustrated the success rates of GW crossing within 30 minutes for different difficult levels according to five CTO scores. It showed that for each scoring system, the probability of GW crossing CTO lesion within 30 minutes decreased from easy to difficult. For the final CTO-PCI, the probability showed the same trend except PROGRESS system.The area under the ROC curve for predicting successful GW crossing within 30 minutes was 0.609 for PROGRESS,0.783 for KCCT,0.731 for CL-score,0.853 for CT-RECTOR and 0.774 for J-CTO. The NRI for CT-RECTOR was significantly higher than for the other models (vs. PROGRESS: 0.70, $p < 0.001$; vs. J-CTO: 0.32, $p < 0.001$; vs. CL-score: 0.52, $p < 0.001$; vs. KCCT: 0.35, $p < 0.001$).

Conclusions:

Compared to other scoring systems, our findings highlight the superior performance of the CT-RECTOR in accurately stratifying CTO patients based on the likelihood of procedural success.This enhanced predictive capability may facilitate more personalized and effective clinical decision-making in the planning and execution of CTO interventions.

最新研究进展专场

慢性心力衰竭患者血清 KLK1、KLF2 表达及其对室性心律失常的预测价值

樊亚宁 任洁

西安交通大学医学院第一附属医院

【摘要】目的：探讨慢性心力衰竭（CHF）患者血清组织激肽释放酶 1（KLK1）、Kruppel 样因子 2（KLF2）表达及其对室性心律失常（VA）的预测价值。**方法：**选取 133 例在本院 2023 年 1 月 -2023 年 12 月收治的 CHF 患者归为研究组，根据患者入院后是否发生 VA 分为 VA 组（n=45）、N-VA 组（n=88），另选取 110 例同期在本院进行体检的健康者为对照组。应用 ELISA 法检测血清 KLK1、KLF2 水平；分析影响 CHF 患者 VA 的相关因素；相对危险度分析不同水平 KLK1、KLF2 对 CHF 患者 VA 的影响；ROC 曲线分析血清 KLK1、KLF2 对 CHF 患者 VA 的预测价值。**结果：**与对照组比，研究组血清 KLK1、KLF2 水平较低（P < 0.05）。VA 组心功能分级 III 级 /IV 级占比明显高于 N-VA 组，LVEF、血清 KLK1、KLF2 明显低于 N-VA 组（P < 0.05）。血清 KLK1、KLF2、心功能分级、LVEF 为影响 CHF 患者 VA 的相关因素（P < 0.05）。血清 KLK1 低水平的 CHF 患者发生 VA 的风险是高水平患者的 1.511 倍，血清 KLF2 低水平的 CHF 患者发生 VA 的风险分别是高水平患者的 1.758 倍。血清 KLK1、KLF2 及联合预测 CHF 患者 VA 的曲线下面积（AUC）分别为 0.800、0.752、0.881，联合高于各自单独预测（$Z_{联合-KLK1}$=2.471、$Z_{联合-KLF2}$=2.563，P=0.014、P=0.010），其敏感度与特异度分别为 95.56%、72.73%。**结论：**CHF 患者血清 KLK1、KLF2 水平降低，与 CHF 患者 VA 的发生有密切联系，联合检测对 CHF 患者预测 VA 具有更佳的效能。

基于生物电阻抗法测量的骨骼肌含量和射血分数减低的慢性心力衰竭患者预后的相关性

陆凯 叶兴伟 邹璇 陈佳

重庆医科大学附属第一医院

目的 本研究旨在探讨射血分数下降的慢性心力衰竭（HFrEF）患者骨骼肌含量下降与预后之间的潜在相关性。

方法 本研究为队列研究，研究对象为 2020 年 8 月至 2022 年 5 月期间于我院心内科收治的 276 名 HFrEF 患者。所有研究对象入组后均接受了人体学测量（包括身高、体重）、血液学检测（包括肝肾功、肌钙蛋白、脑钠肽）和营养评估（包括血红蛋白、肱三头肌皮褶厚度和 NRS2002 营养风险筛查）。研究对象的四肢骨骼肌含量由韩国 Inbody S10 体成分分析仪通过生物电阻抗法（BIA）测量。本研究采用四肢骨骼肌含量指数（aSMI，即四肢骨骼肌含量 / 身高 2，kg/m2）来校正体型对于骨骼肌含量的影响，其中男性 aSMI <7.0 kg/m2 或女性 <5.4 kg/m2 被定义为四肢骨骼肌含量下降。所有研究对象随访一年，终点事件定义为随访期间内的全因死亡。采用多变量 COX 比例风险模型来分析 aSMI 与 HFrEF 患者 1 年内全因死亡之间的相关性。

结果 本研究中，随访结束时共发生全因死亡 84 例。在 NYHA 心功能为 II 到 IV 级的患者中，aSMI 下降的发生率分别为 30.0%, 34.5% 和 46,2%。和 aSMI 没有下降的患者相比，aSMI 下降的 HFrEF 患者在 1 年内的全因死亡的风险增加了 2.13 倍 (HR：2.21，95% CI：1.47-2.78，P<0.05)。进一步调整年龄、性别、BMI、Hb、NRS2002 评分和肱三头肌皮褶厚度等混杂因素后，全因死亡风险仍然增加了 2.36 倍 (HR: 2.36, 95% CI: 1.65-3.21, P<0.05)。K-M 曲线显示 aSMI 下降和未下降的 HFrEF 患者 1 年内全因死亡率具有显著差异（P<0.05）

结论 四肢骨骼肌含量下降的 HFrEF 患者 1 年内全因死亡的风险显著增加。四肢骨骼肌含量下降很可能是导致 HFrEF 患者预后不良的独立危险因素。

心磁图对静息心电图正常患者心肌缺血的诊断价值研究及评分模型的建立

蒋雨枫 周亚峰

苏州大学附属第四医院

目的

开发并验证基于心磁图（MCG）的列线图模型，提升静息心电图（ECG）正常患者的冠状动脉疾病（CAD）早期诊断能力。

方法

前瞻性纳入 421 例于苏州大学附属第四医院接受冠状动脉造影的患者，所有患者静息 ECG 结果正常。收集人口统计学、生命体征、实验室 / 影像学指标、合并症及超声心动图数据。使用 Cardiomox MCG-9 系统在电磁屏蔽环境下采集 MCG 数据。通过 LASSO 正则化逻辑回归筛选预测因子，整合关键 MCG 参数与传统生物标志物构建列线图模型。采用曲线下面积（AUC）、校准曲线（Brier 评分）及决策曲线分析（DCA）评估模型性能（R v4.2.2 和 MSTATA v3.1 软件，显著性阈值 p<0.05）。

结果

列线图在训练队列中 AUC 为 0.777（95% CI: 0.723-0.831），验证队列中 AUC 为 0.643（95% CI: 0.543-0.743）。MCG 参数（如 TT_mean_F_30, OR=1.01, p=0.035）可识别 ECG 无法检测的复极化异常亚临床改变。校准分析显示模型具中度准确性（Brier 评分 =0.191）。决策曲线证实模型对静息 ECG 正常患者的临床决策具有指导价值。

结论

本研究首次将 MCG 技术整合于 CAD 筛查流程，克服了静息 ECG 的敏感性局限。MCG 列线图为早期心肌缺血诊断（尤其资源有限地区）提供可推广工具，可作为现有筛查策略的补充。

急性下壁心肌梗死并发高度至三度房室传导阻滞患者急诊 PCI 术前植入临时起搏器的必要性及安全性

陈静

重庆医科大学附属第一医院

目的：房室传导阻滞（AVB）是急性下壁心肌梗死（AIMI）常见的并发症，但关于此类患者急诊冠脉介入治疗（PCI）术前植入临期起搏器（TP）的必要性和安全性目前尚无明确的结论。本研究旨在评估 AIMI 并发高度至三度 AVB 患者急诊 PCI 术前植入 TP 对 PCI 疗效和安全性的影响。

方法：回顾性纳入我院 2015 年 1 月至 2025 年 4 月诊断为 AIMI 并发高度至三度 AVB 的患者，分为 PCI 前植入 TP 组和未植入 TP 组。主要终点事件为两组患者门 - 球时间、房室传导阻滞恢复时间、PCI 术中血管活性药物的使用及血压、心率变化、术中发生恶性心律失常（心脏停搏、室速、室颤）。次要终点为两组患者的主要不良心血管事件（MACE），包括住院期间死亡、非致死性再梗、非致死性卒中、恶性心律失常、休克、心衰。安全性终点为临时起搏器感知 / 起搏不良、心肌穿孔、发热及穿刺部位血肿形成。

结果：2015 年 1 月至 2025 年 4 月间共计 1,901 例 AIMI 患者，其中 80 例并发高度至三度 AVB 患者行急诊 PCI 术，31 例（38.75%）患者植入 TP，49 例（61.25%）未植入 TP。与未植入 TP 组患者相比，植入 TP 组患者入院时血压更低（98.71±28.87 vs. 112.29±26.99 mmHg, p=0.036），并发右心室梗死的比例更高（58.6% vs. 26.5%, p=0.005），白细胞计数更高（15.72±5.92 vs. 13.32±4.59 *10^9/L），其余基线资料两组无显著差异（p>0.05）。植入 TP 组 PCI 手术时间更长（ 60.93±22.00 vs. 49.51±21.23 min, p=0.029），其罪犯血管多为左回旋支（67.7% vs. 20.4%，p < 0.001），而未植入 TP 患者的罪犯血管多为右冠状动脉（32.3% vs. 75.5%, p < 0.001），植入 TP 组患者术后 TIMI ≤ 2 级占比更大（16.1% vs. 2.0%，p=0.020），入院 24 小时以内使用抗血小板药物的比例更高（64.5% vs. 34.7%, p=0.009）。在终点事件上，两组患者门 - 球时间、术中血管活性药物的使用、术后血流动力学变化和 AVB 的恢复时间两组均无显著差异（p>0.05）。与未植入 TP 组相比，植入 TP 组术中、术后恶性心律失常、心源性休克和心衰的发生率更高（p < 0.05），但住院期间的全因死亡、再梗死、非致死性卒中和支架内血栓两组患者相当（p > 0.05）。在安全性终点事件上，仅有 1 例 TP 患者发生术后心包积液。

结论：AIMI 并发高度至三度 AVB 患者急诊 PCI 术前植入 TP 是安全的，对患者门 - 球时间和 MACE 事件无明显影响，但植入 TP 可能会降低患者术中因心率慢继发的心脏骤停的风险，对于术中发生恶性心律失常高危风险的患者，应考虑急诊 PCI 术前植入 TP。

Optimizing Long-term Cardiovascular Risk Stratification: Integrating Biomarkers into the Very High-Risk ASCVD Definition in Asian Patients

王浩宇 程佳曦 尹栋

中国医学科学院阜外医院（国家心血管病中心）

Background: This study sought to evaluate very high-risk (VHR) ASCVD criteria in assessing cardiovascular (CV) risk in an Asian population and examine the predictive value of additional biomarkers for improving risk stratification.

Methods: 26,752 ASCVD patients were prospectively enrolled at Fuwai Hospital (2017–2018). VHR was defined according to 2018 ACC/AHA Blood Cholesterol Guideline. The primary outcome was a composite of 3-year CV events, including cardiovascular mortality, myocardial infarction, stroke, and coronary revascularization.

Results: 14,475 (54.1%) patients were classified as VHR, with higher 3-year event rates than non-VHR (9.6% vs. 7.3%). In age- and sex-adjusted Cox regression, VHR classification was a significant predictor of 3-year CV events (HR: 1.25 [95% CI 1.12–1.40]). Hemoglobin (Hb), hs-CRP, lipoprotein(a) (Lp(a)), and HDL-C were significant CV risk influencers in VHR patients (HR [95% CI]: 0.93 [0.90–0.96], 1.13 [1.06–1.21], 1.07 [1.04–1.11], 0.73 [0.61–0.89], respectively) , but not in non-VHR patients. Within the VHR category, patients with ≥ 2 abnormal biomarkers (Hb 3 mg/L; Lp(a) ≥ 50 mg/dL; HDL-C <0.001).

Conclusions: The VHR definition identifies high-risk Asian ASCVD patients but can be refined by incorporating biomarker-based high-risk conditions. The proposed VVHR category (VHR with ≥ 2 abnormal biomarkers) enhances risk stratification, identifying those who may benefit most from targeted intensive lipid-lowering therapy.

静息 HFQRS 对急性心肌梗死 PCI 术后临床转归的评估价值

孔祥勇

中国科学技术大学附属第一医院南区

目的：探讨静息高频 QRS（HFQRS）对急性心肌梗死（AMI）急诊 PCI 术后临床转归的评估价值。

方法：纳入 2022 年 7 月 -2024 年 10 月中国科学技术大学附属第一医院南区冠心病监护病房（CCU）收治的 AMI 急诊 PCI 患者 121 例，术后 24 小时内采集静息 HFQRS，以≥ 3 个导联缺血为阳性组（n=67），≤ 2 个导联缺血为阴性组（n=54）。随访至 2025 年 1 月，比较两组基线资料、实验室指标及主要不良心血管事件（MACEs）发生率。

结果：阳性组年龄、左房 / 左室内径、NT-proBNP 水平及多支病变比例显著更高（均 P<0.05），而糖尿病患病率、LDL-C 及血红蛋白水平更低（均

P<0.05）。阳性组 MACEs 发生率显著高于阴性组（55.2% vs. 35.2%，P=0.028），其中再发心绞痛差异尤为显著（32.8% vs. 11.1%，P=0.005）。Cox 分析显示，HFQRS 缺血导联数是 MACEs 的独立危险因素（HR=1.105，95% CI:1.006-1.214，P=0.037）。

结论：静息 HFQRS 阳性是 AMI 患者 PCI 术后 MACEs 的独立预测因子，可作为无创评估预后的重要手段。

脂蛋白 a 和同型半胱氨酸的协同效应对早发心肌梗死患者预后的影响：一项前瞻性队列研究

王宇航[1] 刘婧宇[2] 李晓卫[2] 李平[1] 赛迪妮萨·如则麦麦提[1] 李长平[3] 刘寅[2] 高静[2]

1. 天津医科大学胸科临床学院

2. 天津市胸科医院

3. 天津医科大学公共卫生学院

目的：本研究旨在探究脂蛋白 a[Lp(a)] 和同型半胱氨酸（HCY）及其联合效应对早发心肌梗死（PMI）患者主要不良心血管事件（MACE）的影响。

方法：本前瞻性队列研究从天津市胸科医院连续纳入 1741 例 PMI 患者（年龄≤55 岁）。基于限制性立方样条（RCS）分析 Lp(a) 和 HCY 与 MACE 的非线性关系，根据临床参考阈值确定最佳截断值。将 Lp(a) 和 HCY 分别转化为二分类变量（高 / 低水平组），通过变量组合将患者分为 4 个亚组（低 Lp(a)+ 低 HCY、低 Lp(a)+ 高 HCY、高 Lp(a)+ 低 HCY、高 Lp(a)+ 高 HCY）。采用多变量 Cox 比例风险回归模型，系统评估 Lp(a) 与 HCY 的联合效应对 PMI 患者 MACE 的影响。研究通过分层分析策略，分别在总体及合并高血压或糖尿病患者中，评估不同临床背景下 Lp(a) 和 HCY 联合作用对 MACE 的影响。

结果：在平均随访 25.6 个月中，共 224 例（12.9%）发生 MACE。RCS 显示，Lp(a) 在总体（P=0.002）及合并糖尿病（P=0.049）时，与 MACE 存在非线性关系，而在合并高血压组的非线性关系不成立（P=0.163）。HCY 在总体（P=0.402）及合并高血压（P=0.092）或糖尿病（P=0.189）患者中与 MACE 均不存在非线性关系。总人群 Lp(a) > 50mg/dL（HR 2.383, 95% CI 1.778-3.193, P < 0.001）或 HCY > 15μmol/L（HR 1.964, 95% CI 1.486-2.596, P < 0.001）时 MACE 的风险比显著增加。与低 Lp(a)+ 低 HCY 组相比，PMI 患者高 Lp(a)+ 高 HCY 组在整体及合并高血压或糖尿病中的 MACE 风险最高，分别增加 4.162 倍（95% CI 2.851-6.077, P < 0.001）、4.140 倍（95% CI 2.487-6.892, P < 0.001）、4.277 倍（95% CI 2.112-8.658, P < 0.001）。Lp(a) 和 HCY 只在总体（P=0.003）及合并高血压（P=0.046）交互作用显著。

结论：高水平 Lp(a) 和 HCY 是 PMI 患者 MACE 的独立危险因素，且 Lp (a) 和 HCY 的联合升高放大了 PMI 人群发生 MACE 的风险。联合检测和管控高血压和糖尿病人群的 Lp (a) 和 HCY，为 PMI 患者的精准二级预防提供双重干预靶点。

基于 Murray 定律的 PCI 术后定量血流分数（μQFR）对长期不良心血管事件的预测价值

张锐 管常东 宋雷

中国医学科学院阜外医院

目的：验证基于 Murray 定律的 PCI 术后定量血流分数（μQFR）对长期不良心血管事件的预测价值。

方法：本回顾性研究纳入了 FAVOR III China 试验中的 3825 例患者。选取所有血管直径≥ 2.5mm 且直径狭窄率为 50%-90% 的血管，进行 PCI 术后离线 μQFR 分析。根据 μQFR 三分位数，将血管分为高危组、中危组和低危组。主要终点为 3 年血管导向复合终点（VoCE），定义为靶血管相关心血管死亡、靶血管相关自发性心肌梗死或缺血驱动的靶血管血运重建的复合事件。

结果：成功对 3293 例患者的 4196 条血管进行了离线分析。PCI 术后 μQFR 的平均值为 0.93±0.06。具体而言，1397 条血管（PCI 术后 μQFR ≤ 0.92）被归为高危组，1431 条血管（PCI 术后 μQFR 0.93-0.96）为中危组，1368 条血管（PCI 术后 μQFR>0.96）为低危组。经过 3 年随访，225 条血管（5.4%）发生了 VoCE。随着 μQFR 升高，3 年 VoCE 发生率显著降低（高危组：6.9%，中危组：5.4%，低危组：3.8%；Log-rank P=0.002），主要归因于缺血驱动的靶血管血运重建减少（4.7% vs. 3.7% vs. 2.2%，Log-rank P=0.002）。糖尿病、分叉病变、串联病变和中重度钙化被确定为 PCI 术后 μQFR 降低的独立预测因素。

结论：PCI 术后 μQFR 可有效预测长期不良心血管事件的风险。PCI 术后 μQFR 值越低，3 年 VoCE 发生率越高。

低剂量利伐沙班与阿司匹林分别联合氯吡格雷在合并胃肠疾病冠心病患者 PCI 术后的疗效与安全性：一项前瞻性、非劣性、随机对照研究

周铁楠（学组委员） 李悦 王亚松 王效增（学组委员）

中国人民解放军北部战区总医院

背景：本研究旨在探讨低剂量利伐沙班（10mg/d）与阿司匹林分别联合氯吡格雷对于合并胃肠疾病（GID）的冠状动脉粥样硬化性心脏病（CHD）患者经皮冠状动脉介入治疗（PCI）术后的疗效和安全性。

方法：本研究是一项前瞻性、单中心、非劣性、随机对照临床研究。患者在入院接受 PCI 治疗后分为两组：DPI 组：给予 12 个月的氯吡格雷（75mg 口服 1/ 日）联合利伐沙班（10mg 口服 1/ 日）治疗；DAPT 组：给予 12 个月的氯吡格雷（75mg 口服 1/ 日）联合阿司匹林（100mg 口服 1/ 日）治疗。主要安全终点是术后 6 个月内的美国出血学术研究联合会（BARC）定义的 2-5 型出血事件发生率。次要疗效终点是术后 6 个月内的主要不良心脑血管事件（MACCE）发生率。其他次要终点包括：①术后 6 个月内的 BARC 3-5 型出血事件、MACCE 各组成部分事件发生率；②术后 12 个月内的 BARC 2-5 型出血、BARC 3-5 型出血事件、MACCE 及各组成部分事件发生率。胃肠道不良事件包括胃肠道不适症状（腹痛、腹胀、反酸、嗳气）及胃肠道出血（呕血、黑便）。预设亚组根据糖尿病状态将患者分为糖尿病组和非糖尿病组。

结果：纳入 2021 年 4 月至 2023 年 5 月接受 PCI 治疗的合并 GID 的 CHD 患者 1042 例（DPI 组 522 例，DAPT 组 520 例）。术后 6 个月 BARC 2-5 型出血事件发生率在两组之间无显著差异（1.5% VS 1.2%，P=0.595），率差 95% 置信区间的下限大于所设非劣界值（-1.10% > -4.7%），表明 PCI 术后应用低剂量利伐沙班联合氯吡格雷术后 6 个月 BARC 2-5 型出血事件发生率不劣于阿司匹林联合氯吡格雷。DPI 组术后 6 个月（4.8% VS 9.6%，P=0.009）、12 个月（6.7% VS 11.9%，P=0.010）腹痛发生率显著低于 DAPT 组。基于年龄、性别、活动性吸烟、临床表现、糖尿病、高血压、心肌梗死史、PCI 史、多支血管病变和肾功能的亚组分析结果显示，术后 12 个月 BARC 2-5 型出血事件和 MACCE 发生率在两组之间均无显著差异（P 均 >0.05）。预设糖尿病亚组分析结果显示，术后 6 个月 BARC 2-5 型事件、BARC 3-5 型出血事件和 MACCE 及各组成部分发生率在糖尿病和非糖尿病患者之间均无显著差异（P 均 > 0.05）。术后 12 个月糖尿病患者脑卒中（P=0.012）和 BARC 3-5 型出血事件（P=0.037）发生率显著高于非糖尿病患者，非糖尿病患者缺血驱动靶血管血运重建（P=0.045）发生率显著高于糖尿病患者。

结论：对于接受 PCI 的 GID 合并 CHD 患者，在安全性方面，术后应用低剂量利伐沙班联合氯吡格雷不劣于阿司匹林联合氯吡格雷；在疗效方面，在术后 6 个月后，低剂量利伐沙班联合氯吡格雷可能进一步改善 MACCE 的预后；低剂量利伐沙班联合氯吡格雷在不增加胃肠道出血事件发生率的同时可显著降低腹痛发生率。

接受 TAVR 患者术后全生命周期管理模式的评估与优化

刘然

首都医科大学附属北京安贞医院

目的：经导管主动脉瓣置换术（TAVR）已成为主动脉瓣狭窄（AS）患者的标准治疗选择。然而，在长期随访中，术后并发症仍然是死亡和再住院率的重要因素。如何在出院后建立规范的术后管理制度是目前 TAVR 患者治疗领域的空白。

方法：共有 408 例成功接受 TAVR 的 AS 患者纳入本回顾性研究，依据术后管理模式分为两组：常规护理（UC）组 (n=186；2021 年 6 月 1 日至 2022 年 10 月 31 日) 和心脏多参数监测（HMM）组 (n=208 例，2022 年 11 月 1 日至 2023 年 8 月 31 日)。HMM 组接受了个性化的生命周期管理计划，包括基于互联网的智能医疗保健平台和远程可穿戴设备指导的心脏康复。所有患者在 TAVR 术后完成 1、6 和 12 个月随访评估。终点设定为净不良临床事件（NACE）和生活质量（QoL）评估。统计分析包括 Kaplan-Meier 分析和对数秩检验用于组间事件发生率比较，Cox 比例风险回归校正潜在混杂因素，卡方检验和 t 检验用于其他组间比较。

结果：与 UC 组相比，HMM 显著降低了复合不良 NACE 的发生率（94.5% 比 81.2%,P <0.001）。HMM 队列中复合 NACE 的降低主要是由于心脏死亡率（98.2% vs 93.6%）、致残性卒中（99.6% vs 98.0%）和心肌梗死（98.7% vs 96.0%）的改善。多因素分析进一步显示，复合不良事件的相对风险降低了 74.9%（HR 0.251, 95% CI 0.119-0.526,P <0.001），强调了 HMM 方法在传统危险因素之外具备独立的保护作用。与 UC 组相比，HMM 组的生活质量指标显著改善，达到 NYHA I 级的比例显著增加（12 个月时为 25.4% 比 2.2%），KCCQ 评分显著提高，分别为 81.67 [IQR: 74.30-86.67] 和 80.00 [IQR: 73.19-83.43]（P <0.01）。

结论：该研究结果表明，通过 HMM 系统优化生命周期管理可显著改善 TAVR 后的临床结果。建立这种普及性和教育性的模式可以作为当代临床实践的关键组成部分。

高敏 C 反应蛋白在经皮冠状动脉介入治疗后急性冠脉综合征合并肾功能不全患者中的长期预测价值

党丹 裘淼涵 李晶 李毅 韩雅玲

中国人民解放军北部战区总医院

目的: 本研究旨在评估高敏 C 反应蛋白（hsCRP）在行经皮冠状动脉介入治疗（PCI）的急性冠脉综合征（ACS）合并肾功能不全患者中的远期预测能力，并观察此类患者的临床预后。**方法：**本研究选取 2016 年 3 月至 2019 年 3 月在北部战区总医院心血管内科接受 PCI 治疗的 ACS 患者为研究对象，选取估算的肾小球滤过率 <90 ml/min/1.73m^2（Estimated Glomerular Filtration Rate，eGFR）患者并将该类患者依据 hsCRP 水平进行分组，以比较不同分组患者的临床结果。主要研究终点为患者出院后 12 个月随访期间发生的全因死亡及主要不良心血管事件（Major Adverse Cardiovascular Event，MACE）事件，包括心原性死亡、心肌梗死、缺血性卒中和 / 或任何原因导致的血运重建组成的复合终点。

结果：hsCRP 水平的中位数位 3.2mg/L。在纳入的 3450 例 eGFR<90 ml/min/1.73m^2 的肾功能不全患者中，根据美国疾病控制与预防中心和美国心脏协会的标准，所分为 hsCRP>3.0mg/L（1757 例，50.9%）和 hsCRP ≤ 3.0mg/L（1693 例，49.1%）两组。在平均 390 天的随访期间，一共有 496 例 MACE 事件和 145 例死亡事件，其中 hsCRP ≤ 3.0mg/L 组中分别为 236（47.6%）例 MACE 和 48（33.1%）例全因死亡，而 hsCRP>3.0mg/L 组则分别为 260（52.4%）例 MACE 和 97 例（66.9%）全因死亡。hsCRP>3.0mg/L 组的全因死亡以及 MACE 事件的发生率均高于前者（全因死亡 66.9% vs 33.1%， P<0.001；MACE 52.4% vs 47.6%，P=0.47）；在调整混杂因素（年龄、性别、体重指数、吸烟、高血压、糖尿病、卒中史、外周血管病史、既往经皮冠脉介入治疗史及陈旧性心梗病史）多变量 Cox 分析中，hsCRP 与全因死亡率之间仍然存在显著关联（P=0.01），风险比为 1.59（95%Cl：1.12-2.27）。然而 hsCRP 对 MACE 事件的预测作用未达到统计学意义。

结论：hsCRP 并对行 PCI 治疗的 ACS 合并肾功能不全患者的全因死亡的长期预

后有很好的预测价值；对于 hsCRP 升高的入院患者，建议出院后加强定期随访，并考虑采取针对性的抗炎治疗措施。

基于 GRACE 风险评分比较高缺血和高出血风险的急性冠脉综合征患者中氯吡格雷单药治疗与延长双联抗血小板治疗的疗效：OPT-BIRISK 随机临床试验的亚组分析

张诗宇 [1] 李晶 [1] 裘淼涵 [1] 李毅 [1] 王志方 [2] 苏淑红 [2] 张瑶俊 [3] 刘爱军 [4] 韩雅玲 [1]

1. 中国人民解放军北部战区总医院

2. 新乡市中心医院

3. 徐州市肿瘤医院

4. 本溪市中心医院

研究目的 本研究旨在探讨对于经皮冠状动脉介入治疗（PCI）后已完成 9-12 个月双联抗血小板治疗（DAPT） 且符合高出血和高缺血风险的患者，根据急性冠状动脉事件全球登记（GRACE）风险评分分层，氯吡格雷单药治疗是否优于延长双联抗血小板治疗。

研究方法 在 OPT-BIRISK 研究中，7758 名在植入药物洗脱支架（DES）治疗 ACS 后完成至少 9 个月但不超过 12 个月 DAPT 的患者被随机分配到阿司匹林加氯吡格雷组和安慰剂加氯吡格雷组。这项研究是 OPT-BIRISK 研究的一项预定义亚组分析，根据 GRACE 风险评分将纳入 OPT-BIRISK 研究的患者分为中高风险组（GRACE >88）和低风险组（GRACE ≤ 88）。研究的主要终点是 BARC 2、3 或 5 型出血。关键次要终点是随机分组后 9 个月的主要心脑不良事件 (MACCE) 发生率，定义为全因死亡、心肌梗死、卒中或临床驱动的血运重建的复合终点。

研究结果 根据 GRACE 评分对患者进行缺血风险分层，49% 的患者属于低风险组（3738 人），51% 的患者属于中高风险组（3884 人）。在 GRACE 评分为低风险的患者中，49 名接受氯吡格雷单药治疗的患者（2.7%）和 69 名接受延长 DAPT 的患者（3.6%）发生了 BARC 2、3 或 5 型出血（[HR] 0.73；95% CI 0.50-1.05；P=0.0883）。45 名接受氯吡格雷单药治疗的患者（2.4%）和 55 名接受延长 DAPT 的患者（2.9%）发生了 MACCE（[HR] 0.84; 95% CI 0.57-1.25; P=0.3947）。两组患者的主要终点和次要终点发生率没有统计学差异。在中高风险患者中，45 名接受氯吡格雷单药治疗的患者（2.3%）和 57 名接受延长 DAPT 的患者（3.0%）发生了主要终点（[HR] 0.77；95% CI 0.52-1.14；P=0.8377）。与延长 DAPT 组相比，氯吡格雷单药治疗组的 MACCE 率明显降低（2.9% vs 4.1%；HR 0.69，95% CI 0.49-0.97；P=0.033）。在整个试验人群中，GRACE 评分和治疗组之间在主要终点或关键次要终点上没有显著的交互作用。

研究结论： 与延长 DAPT 相比，无论 GRACE 评分如何，氯吡格雷单药治疗可显著降低高缺血性和高出血风险的 ACS 患者的出血事件发生率。此外，在中高危风险组中，氯吡格雷单药治疗在降低 MACCE 事件发生率方面优于延长 DAPT。

基于 CRUSADE 评分分层的比伐芦定与肝素在 ST 段抬高型心肌梗死患者中的疗效与安全性比较：BRIGHT-4 研究亚组分析

段一璇 裘淼涵 李晶 李毅 韩雅玲

中国人民解放军北部战区总医院

【背景】在接受急诊经皮冠状动脉介入治疗(PCI)的ST段抬高型心肌梗死(STEMI)患者中，比伐芦定与肝素抗凝治疗的临床结局存在争议，部分原因可能与患者出血风险差异有关。本研究基于 CRUSADE 评分分层，旨在比较术后高剂量持续输注比伐芦定与单用肝素在 STEMI 患者中的疗效与安全性。

【方法】本研究为 BRIGHT-4 试验的预设亚组分析，纳入行初始 PCI 治疗的 STEMI 患者，随机分配接受术后持续 2-4 小时高剂量输注的比伐芦定或单用肝素。根据 CRUSADE 评分≥ 30 定义为高出血风险。主要结局为 30 天全因死亡或出血学术研究联盟（BARC）3-5 型出血的复合终点。

【结果】共纳入 6016 例患者，其中 1435 例（23.9%）CRUSADE 评分≥ 30 分，4581 例（76.1%）评分 <30 分。CRUSADE 评分≥ 30 的患者在主要终点、全因死亡及 BARC3-5 型出血风险均显著高于 CRUSADE<30 分的患者（P<0.05）。CRUSADE 评分 <30 患者中，应用比伐芦定的患者主要终点事件风险显著降低（调整后风险比 [aHR]：0.53；95% 置信区间 [CI]：0.35-0.82；P=0.0041），全因死亡风险亦降低（aHR：0.59；95% CI：0.38-0.93；P = 0.0224）；BARC 3-5 型出血风险显著降低（aHR：0.12；95% CI：0.02-0.57；P = 0.0076）。而在评分≥30患者中,比伐芦定组患者在BARC 3-5型出血风险显著低于肝素组(aHR: 0.22；95% CI：0.06-0.88；P = 0.0316），两组在主要终点及其组成部分间未见显著差异。

【结论】在 CRUSADE 评分 <30 的 STEMI 患者中，术后给予高剂量持续输注的比伐芦定较肝素显著降低了 30 天全因死亡及 BARC 3-5 型出血复合终点的发生率。然而，在 CRUSADE 评分≥ 30 的高出血风险患者中，应用比伐芦定在减少出血事件的获益程度较小。

3 “A” 优化策略管理对预防性 VA-ECMO 植入的左主干急性冠脉综合征患者经皮冠状动脉介入治疗的影响：多中心回顾性队列研究

赵晓辉 解力

陆军军医大学第二附属医院新桥医院

目的：针对左主干急性冠脉综合征（ACS）的经皮冠状动脉介入治疗 (PCI) 存在显著的血流动力学不稳定风险。尽管预防性静脉 - 动脉体外膜肺氧合 (VA-ECMO) 的应用日益普及，但在这类高危人群中，其安全性和治疗效果仍缺乏充分研究。本实验旨在讨论 3 “A” 优化策略管理对预防性 VA-ECMO 植入的左主干急性冠脉综合征患者经皮冠状动脉介入治疗的影响。

方法：我们回顾性纳入了 2021 年 4 月至 2024 年 4 月期间在四家医疗中心接受预防性静脉 - 动脉体外膜肺氧合（VA-ECMO）支持下左主干经皮冠状动脉介入治疗（LM PCI）的急性冠脉综合征（ACS）患者。VA-ECMO 的管理采用以下 3 “A” 方案：1. 血管通路评估：在超声、透视和血管造影多模态影像引导下经皮股动脉穿刺，优化插管定位（使用 15-17Fr 动脉插管）；2. 人工循环：预防性 VA-ECMO 初始流量设为 1.5 升 / 分钟，通过实时血流动力学监测（平均动脉压≥ 65mmHg）指导 PCI 术后立即撤机；3. 自体输血：在撤管过程中以 50 毫升 / 分钟的速度回输 400-500 毫升管路残余血液。主要终点包括院内主要不良心脑血管事件（MACCEs，含心源性死亡、卒中、非致死性心肌梗死、血运重建）、手术并发症及失血量，中位随访 10 个月进行评估。

结果：从 24861 例经皮冠状动脉介入治疗 (PCI) 病例中筛选出 51 例接受预防性静脉 - 动脉体外膜肺氧合 (VA-ECMO) 支持的患者。所有患者均成功实现血运重建 (TIMI 3 级血流)，平均欧洲心脏手术风险评估系统 (Euroscore) 评分为中位 8 分 (6-13 分)。中位随访 10 个月期间，主要不良心脑血管事件 (MACCE) 发生率为 5.9%(3/51)：包括 1 例心源性死亡 (2.0%)、1 例急性肾损伤 (2.0%) 和 1 例支架内再狭窄 (2.0%)。所有患者均在局部麻醉下，采用 15-17Fr 插管经股总动脉行经皮 VA-ECMO 植入。PCI 术中 ECMO 中位持续转机时间为 165 分钟 (四分位距 84-335 分钟) 撤除 VA-ECMO，手术并发症包括 1 例穿刺部位血肿 (2.0%)。自体输血组 (n=16) 较对照组 (n=32) 显著降低血红蛋白下降幅度 (18.1±8.0 vs. 26.7±12.6 g/L，p=0.019) 和异体输血需求 (6.3% vs. 15.6%，p=0.04)。超声检查与压力监测显示自体输血期间未出现容量负荷或后负荷增加。

结论：预防性 VA-ECMO 支持下对急性冠脉综合征患者实施左主干经皮冠状动脉介入治疗成功率较高，主要不良心脑血管事件发生率较低。3 “A” 优化管理有望成为未来手术管理的前瞻性策略。

PrizvalvePro ™经导管主动脉瓣膜系统治疗中国高风险重度主动脉瓣狭窄患者的前瞻性多中心单组目标值研究

齐斌 徐凯 韩雅玲

中国人民解放军北部战区总医院

目的：本研究旨在评估 PrizvalveProTM 经导管主动脉瓣膜系统，在治疗中国人群传统手术高风险 , 或不适合行常规外科手术的重度主动脉瓣狭窄患者的安全性和有效性。

方法：本研究为前瞻性、多中心、单组目标值临床研究，纳入 2023 年 7 月 5 日至 2024 年 5 月 11 日在中国人民解放军北部战区总医院和四川大学华西医院收治的诊断重度主动脉瓣反流并行 TAVR 治疗的 44 例患者。研究采用 Prizvalve-Pro ™球囊扩张式瓣膜 (上海纽脉) 完成 TAVR 手术，收集并分析患者的基线信息、CT 测量和围术期情况和术后 30 天随访指标。

结果：术后 30 天复合终点事件发生率为 9.1%（95% 置信区间: 3.51%-22.43%）。器械成功率为 100%（44/44），手术成功率为 95.5%（42/44）。术后即刻超声心动图检查显示所有患者瓣膜功能良好，主动脉瓣平均压差（10.14±4.53）mmHg，主动脉瓣峰值血流速度（2.15±0.45）m/s，无中量及以上瓣周反流。术后 30 天随访结果显示，与基线相比，患者术后 30 天左心室射血分数逐渐增高；左心室舒张末期内径持续缩小；N 末端 B 型利钠肽原水平显著降低；NYHA 心功能分级改善；生活质量评分明显提高。

结论：PrizvalvePro ™球扩式经导管主动脉瓣膜系统在治疗重度主动脉瓣狭窄患者中有良好的安全性和有效性。

Background P2Y12 monotherapy in ACS patients after PCI has gradually become important, and a number of large-scale clinical studies have shown that it can reduce the incidence of adverse clinical outcomes. Implantation of different types of stents is crit

齐斌

中国人民解放军北部战区总医院

Aims

The purpose of this study was to evaluate the impact of clopidogrel monotherapy on birisk patients who underwent PCI and completed 9-12 months of DAPT, stratified by types of drug-eluting stents (DES).

Methods

This is a subgroup analysis of the OPT-BIRISK trial, which categorized patients into three groups based on DES types: those with biodegradable polymer-coated or polymer-free DES (BP-DES/PF-DES), those with durable polymer-coated DES (DP-DES), and those with more than two stent types. The OPT-BIRISK trial is an investigator-initiated, multicenter, double-blind, placebo-controlled study where patients are randomly assigned, with ischemia and bleeding outcomes assessed one year post-randomization.

Results

Of 7,515 total patients, 4,011 (53.4%) received BP-DES/PF-DES, 2,893 (38.5%) had DP-DES, and 611 (8.1%) used over two stent types. For single-stent-type patients, clopidogrel monotherapy showed lower BARC 2/3/5 bleeding risk vs DAPT: BP-DES/PF-DES (2.6% vs 3.6%; HR=0.71, 95%CI=0.50-1.02, P=0.062); DP-DES (2.1% vs 2.8%; HR=0.74, 95%CI=0.46-1.19, P=0.212). It also reduced major adverse cardiac and cerebral events (MACCE): BP-DES/PF-DES (2.9% vs 3.9%; HR=0.75, 95%CI=0.53-1.05, P=0.093); DP-DES (2.1% vs 3.3%; HR=0.65, 95%CI=0.41-1.02, P=0.062). For patients with ≥ 2 stent types, BARC 2/3/5 bleeding (3.8% vs 3.8%; HR=0.99, 95%CI=0.44-2.25, P=0.986) and MACCE (3.1% vs 3.4%; HR=1.08, 95%CI=0.45-2.60, P=0.861) showed no significant differences.

Conclusions

In birisk patients who completed 9-12 months of DAPT, clopidogrel monotherapy reduces bleeding and ischemic events compared to continued DAPT, irrespective of the DES type used.

非高密度脂蛋白胆固醇与高密度脂蛋白胆固醇比率和动脉僵硬度的 L 型关联：一项基于人群的研究

魏涛涛 余静

兰州大学第二医院

目的：虽然已知血脂比率和水平与心血管疾病有关，但美国人群中非 HDL/HDL 比率（NHHR）与动脉僵硬度之间的关系仍未探索。这将通过在美国人群中使用电子脉搏波速度（ePWV）评估动脉僵硬度来实现。

方法: 这项基于人群的研究利用了 2007-2016 年国家健康与营养调查（NHANES）的横断面数据。阐明 NHHR 与动脉僵硬度风险之间的关系。我们采用了多变量线性回归分析，阈值效应，平滑曲线拟合和亚组分析方法。

结果：本研究共纳入 23456 名成年美国人，平均年龄 49.56±17.58 岁，平均 NHHR 值为 2.97±1.48。经过充分调整，我们的分析显示 NHHR 与 ePWV 水平呈负相关（β=-0.01，95%CI：-0.02，-0.00）。此外，NHHR 最高四分位数内的个体的平均 ePWV 得分比最低四分位数低 0.06 个单位（β=-0.06，95%CI：-0.09，-0.02；趋势 P=0.0068）。平滑曲线拟合表明 NHHR 和 ePWV 评分之间存在 L 形关系，截止值为 2.13（高血压亚组为 1.93）。

结论：这项研究的结果表明，NHHR 与美国人群动脉僵硬风险之间存在 L 型关系。控制 NHHR 对于降低 AS 风险具有临床意义。然而，需要进一步的大规模前瞻性临床试验来验证管理动脉僵硬度的最佳 NHHR 范围。

院间转运对 ST 段抬高型心肌梗死患者接受直接经皮冠状动脉介入治疗后临床结局的影响：一项基于 BRIGHT-4 试验的二次分析

苏晓琳 [1,2] 裘淼涵 [1] 顾成圻 [3] 杨秀慧 [4] 刘斌 [5] 孟繁波 [6] 宁彬 [7] 李伟 [8] 钟志雄 [9] 王正忠 [10] 石蓓 [11] 商卓 [12] 梁振洋 [1] 李毅 [1] 韩雅玲 [1] Gregg W. Stone[13]

1. 中国人民解放军北部战区总医院

2. 中国医科大学附属盛京医院

3. 大同市第三人民医院

4. 漯河市中心医院

5. 吉林大学第二医院

6. 吉林大学中日联谊医院

7. 阜阳市人民医院

8. 贵州医科大学附属医院

9. 梅州市人民医院

10. 青岛市市立医院

11. 遵义医科大学附属医院

12. 蚌埠市第二人民医院

13. 西奈山伊坎医学院，美国纽约

背景：既往关于院间转运对接受直接经皮冠状动脉介入治疗（PCI）的 ST 段抬高型心肌梗死（STEMI）患者死亡率影响的研究结果并不一致。BRIGHT-4 试验显示，在 STEMI 患者中，与单纯使用肝素相比，PCI 术后高剂量比伐芦定输注（1.75mg/kg/h）能够降低 30 天内全因死亡或出血学术研究联盟（BARC）定义的 3-5 型出血的发生率。本研究旨在进一步评估院间转运对接受 PCI 治疗的 STEMI 患者临床结局的影响，并探讨在这一人群中比伐芦定相较于肝素在疗效上的差异。

方法与结果：在 BRIGHT-4 试验中，共有 2121 例（35.7%）患者被转运至三级医院接受直接 PCI，3817 例（64.3%）患者则直接就诊于具备介入治疗能力的医疗机构。研究的主要终点是 30 天内全因死亡或 BARC 3-5 型出血构成的复合事件。次要终点包括支架内血栓形成。研究对基线协变量及随机分组治疗药物进行了校正分析。结果显示，转运患者从症状发作到导丝通过梗死相关动脉的中位时间明显更长（6.00 h vs. 3.93 h，P<0.0001）。在 30 天时，转运组与直接入院组之间主要终点的发生率没有显著差异（4.2% vs. 3.4%，校正 HR 0.99，95%CI 0.73-1.33，P=0.94）。与单纯使用肝素相比，比伐芦定在 PCI 术后以高剂量持续输注的治疗方案，在转运患者（3.5% vs. 4.8%，校正 HR 0.66，95% CI 0.42-1.05）和直接入院患者（2.8% vs. 4.1%，校正 HR 0.62，95% CI 0.43-0.89）中均显示出降低主要终点事件趋势，且两组间的治疗效果无显著交互作用（交互 P=0.78）。在支架内血栓形成这一次要终点上，也观察到了一致的结果。

结论：在这项事后分析中，接受院间转运后接受 PCI 治疗的 STEMI 患者 30 天内的临床结局并不显著差于直接入院接受 PCI 治疗的患者。在 PCI 术后高剂量输注比伐芦定 2-4 小时，可有效降低 30 天全因死亡率、主要出血以及支架内血栓形成的发生率，且这一疗效在转运患者和直接入院患者中表现一致。

急性心肌梗死新发房颤负荷和左室射血分数的预后意义

魏毅东

上海市第十人民医院

目的：左心室射血分数（LVEF）在急性心肌梗死（AMI）后因危险因素差异导致预后截然不同。新发心房颤动（NOAF）负荷对 AMI 患者（尤其是不同 LVEF 亚组）的风险分层价值尚不明确。本研究旨在探讨 NOAF 负荷对不同 LVEF 分型 AMI 患者的预后影响。

方法：连续纳入 2014 至 2022 年期间 5 家医院首次发生院内 AF 且无 AF 病史的 AMI 患者。根据 LVEF 将心梗后 NOAF 患者分为 AMIrEF 组（LVEF < 40%）和 AMIpEF 组（LVEF ≥ 40%），并以 10.87% 的 AF 负荷临界值进一步分层。主要终点为包含心血管死亡和心衰住院的主要不良心血管事件（MACE）。此研究为 NOAFCAMI-China 注册研究：NCT05511649。

结果：812 例患者中 644 例（79.3%）具有基线 LVEF 数据，其中 AMIrEF 组 178 例（27.6%），AMIpEF 组 466 例（72.4%）。248 例（38.5%）患者住院期间呈现高 AF 负荷（ > 10.87%）。中位随访 4.2 年期间，低 / 高负荷 AMIrEF 组的 MACE 发生率分别为 18.9 和 23.0 例 /100 人年，AMIpEF 组分别为 7.2 和 17.5 例 /100 人年。校正混杂因素后，高负荷 NOAF 与 AMIpEF 组 MACE 风险显著相关 [风险比（HR）：2.63，95% 置信区间（CI）：1.82-3.78]，而 AMIrEF 组无此关联 [HR：0.78，95%CI：0.48-1.26]。倾向评分匹配分析结果一致 [AMIrEF 组 1.08（0.66-1.77），AMIpEF 组 2.45（1.75-3.45）]。

结论：高 NOAF 负荷是 AMIpEF 患者长期心血管不良结局的独立预测因子，该高危人群需优化临床管理策略。

微循环阻力指数对 MINOCA 患者微循环障碍的评估

徐良潇

哈医大二院

中文摘要

背景及目的：在全球范围内，针对非梗阻性心肌梗死（MINOCA）的研究日益增多。MINOCA 的病因机制极为复杂，其中微循环障碍（CMD）是重要因素之一，这些因素对患者的长期预后有着深远影响。尽管现有的少量研究已提供了部分见解，但该领域仍存在诸多知识空白。深入探究 MINOCA 的微循环障碍，有助于增进对这一病症的理解，进而推动更有效的临床治疗方案的开发。本研究旨在运用微循环阻力指数(AMR)评估 MINOCA 患者中微循环障碍的分布情况和发生率，同时探究微循环障碍对 MINOCA 患者预后，尤其是对心血管不良事件的影响。

方法：本研究前瞻性共纳入 246 例于哈尔滨医科大学附属第二医院心血管内科诊断为没有显著冠状动脉狭窄（狭窄程度 <50%）的 MINOCA 患者。通过定量的无创血管造影技术，计算患者的 AMR 值。定义 AMR 大于 250 mmHg*s/m 为微循环障碍。根据 AMR 的指数结果把患者分为微循环障碍组（n=132）和对照组（n=114）。研究终点定义为随访一年后的主要心血管不良事件（MACE），包括心源性死亡，全因死亡，靶血管血运重建事件。次要终点包括 MACE 事件中的单个事件。

结果：本研究纳入的 MINOCA 患者中微循环障碍患者占比高达 53.66%，其中微循环障碍组 AMR 指数远大于对照组（288 [264.25-318.5] vs 217 [199-234]； P < 0.001）。两组在血管造影方面，微循环障碍组的罪犯血管狭窄程度更小（34%vs36%； P=0.024），血管 QFR 更大（0.94 [0.9-0.97] vs0.89 [0.84-0.92]； P < 0.001），说明可能在大血管方面微循环组病变程度相对较轻；且 AMR 与狭窄程度呈负相关（r=-0.194; P=0.002）。在预后方面，在排除了 51 名随访丢失的患者后，微循环障碍组占比 52.82%，两组 MACE 事件发生率无明显差异（13.59%vs15.22%； P=0.747）；两组在次要终点发生率上也无明显差异。

结论：本研究纳入的 MINOCA 患者中微循环障碍高达 53.66%，这部分患者罪犯血管狭窄程度更小，提示相对于大血管，可能存在更为严重的小血管病变；由于人数数目较少的影响看不到临床不良结局的差异，但 AMR 在诊断 MINOCA 潜在病因方面可能具有重要价值，以后可进一步研究商讨。

急性冠状动脉综合征患者早期依洛尤单抗治疗抑制 IL-1β/IL-17A 并改善早期左心室功能：一项随机临床对照试验

张萌龙 [1] 刘靖宇 [2] 王静娴 [1] 靖安然 [1] 张峻峰 [3] 李长平 [3] 崔壮 [3] 刘寅 [2] 高静 [2]

1. 天津大学胸科医院

2. 天津市胸科医院

3. 天津医科大学公共卫生学院

目的：虽然前蛋白转化酶 Subtilisin/kexin 9 型抑制剂（PCSK 9 i）有效降低低密度脂蛋白胆固醇（LDL-C）水平并降低急性冠状动脉综合征（ACS）患者主要不良心血管事件（MACE）的发生率，但其抗炎作用和对早期心脏重塑的影响仍不清楚。这项研究探究了早期给予依洛尤单抗是否可以调节 ACS 患者体内炎症性细胞因子并改善早期左心室（LV）功能。

方法：在这项前瞻性、单中心、开放标签的随机对照试验中，302 名 ACS 患者被分配接受他汀类单药治疗或他汀类加依洛尤单抗治疗。在基线、1 周和 4 周时通过酶联免疫吸附试验（ELISA）测量外周血清白细胞因子（IL）-17A、IL-18、IL-1β 和 CC 趋化因子受体 2（CCR2）水平。在基线、第 4 周和第 12 周时通过超声心动图评估 LV 功能 [左室射血分数（LVEF）、左心室舒张末期内径（LVDd）和左心房内径（LAD）]。主要终点包括炎症标志物和 LV 功能参数的变化。

结果：从基线到 4 周时，依洛尤单抗组 IL-17A 的百分比变化为 -31.26% ± 14.57%（从平均值 5.75 mmol/L 降至 3.91 mmol/L），他汀组为 -25.46% ± 16.08%（从平均值 5.76 mmol/L 降至 4.22 mmol/L），组间平均差异为 -5.80%（95% 置信区间 [CI]：-9.59% 至 -2.02%；P= 0.003）；依洛尤单抗组 IL-1β 的百分比变化为 -29.46% ± 11.59%（从平均值 16.91 mmol/L 降至 11.93 mmol/L），而他汀类药物组为 -25.08%±10.93%（从平均值 16.77 mmol/L 降至 12.55 mmol/L），组间平均差异为 -4.37%（95% 置信区间 [CI]：-1.51% 至 -7.23%；P= 0.003）。12 周时，与他汀类药物单药治疗相比，依洛尤单抗改善了 LVEF（平均数变化：7.0% vs 4.0%，P=0.047）并提高了 ΔEF ≥ 0.05 的发

生率（73.3% vs 54.6%，P<0.001）。治疗 4 周时 IL-17A 和 IL-1β 的显著降低分别增加了 57%(OR 1.57, 95% CI 1.15-2.13)和 53%(OR 1.53, 95% CI 1.18-1.99) LV 功能在 12 周时发生改善的概率。中介效应分析证实，依洛尤单抗对于 LV 功能改善的影响 8.74%/9.60% 归因于其对 IL-1β/IL-17A 的抑制 (bootstrap 检验 P<0.05)。

结论：ACS 患者早期依洛尤单抗治疗可迅速减轻炎症 (IL-1β/IL-17A) 并促进 LV 功能恢复，这些作用部分由细胞因子调节介导。这些多效性作用支持了在 ACS 患者中，应用依洛尤单抗作为一种辅助治疗不仅是因为其降脂作用。这些发现支持早期开始使用 PCSK 9 抑制剂作为缓解 ACS 中由炎症驱动的心功能障碍的潜在策略。

基于冠脉造影微循环阻力指数的 STEMI 术后心肌内出血预测模型构建与验证

周亚峰 段洋

苏州大学附属第四人民医院

目的：

心肌内出血（intramyocardial hemorrhage，IMH）是急性 ST 段抬高型心肌梗死（STEMI）经初始经皮冠状动脉介入治疗（PCI）后常见的微循环损伤表现，显著增加主要不良心血管事件（MACE）和心力衰竭的风险。心脏磁共振（CMR）虽为评估 IMH 的“金标准”，但在急性期受限明显。冠脉造影衍生的微循环阻力指数（caIMR）可在术中实时获取，为构建术后即刻 IMH 预测模型提供新方向。本研究旨在结合 caIMR 与临床参数构建术后早期 IMH 预测列线图模型，并验证其对 IMH 及预后事件的预测效能。

方法：

本研究为回顾性单中心研究，纳入 2022 年 1 月至 2023 年 1 月于我院接受成功初始 PCI 并于术后 1 周内完成 CMR 检查的 STEMI 患者 309 例，按 4:1 比例随机分为训练队列（n=247）与验证队列（n=62）。计算术后 caIMR，并结合 CMR 评估是否存在 IMH。通过多因素 Logistic 回归筛选 IMH 的独立预测因子，构建列线图模型。采用受试者工作特征曲线（ROC）、校准曲线与决策曲线（DCA）评价模型的预测能力、校准度与临床获益，同时与单纯 CMR 评估的 IMH 进行比较。进一步分析列线图预测评分与住院心力衰竭、1 年 MACE 的关系。

结果：

最终列线图纳入两个独立预测因子：caIMR > 40 U（OR=17.27，P<0.001）和左室射血分数（LVEF）（OR=0.93，P<0.001）。模型在训练队列中 AUC 为 0.844（95%CI：0.793–0.896），验证队列中 AUC 为 0.834（95%CI：0.724–0.944），显示良好的区分度。Hosmer–Lemeshow 检验和校准曲线提示预测概率与实际概率一致性良好。DCA 分析表明，在训练与验证队列中，预测 IMH 的决策阈值范围分别为 10–88% 和 10–74%，具有较高的净收益。进一步分析发现：列线图评分优于 CMR 确认的 IMH 本身对住院心衰（AUC：0.748 vs. 0.633）和 MACE（AUC：0.726 vs. 0.584）的预测能力（P 均 <0.001）。

结论：

本研究首次构建并验证了结合 caIMR 和 LVEF 的 IMH 术后预测列线图模型，具有良好的准确性与实用性。该模型可在术后即时完成风险评估，辅助早期识别高危患者并指导预后管理。相比依赖 CMR 检查的传统策略，该模型更具可及性和实时性，尤其适用于急性 STEMI 的临床路径优化。未来仍需在多中心前瞻性队列中进一步验证模型的推广应用价值。

心脏电子植入装置治疗扩张性心肌病的临床疗效分析

阿卜杜如苏力·喀迪尔

新疆维吾尔族自治区人民医院

目的：本研究旨在深入探讨针对扩张性心肌病患者，采用心脏电子植入装置进行手术治疗与传统的药物保守治疗在疗效上的差异。**方法：**研究选取了 100 例确诊为扩张性心肌病的患者作为研究对象，依据其接受的治疗方式不同，将其分为对照组（n=60 例）和手术组（n=40 例）。对照组患者接受常规的药物保守治疗，而手术组患者则接受心脏电子植入装置的手术治疗。通过对两组患者在治疗前后心功能各项指标的变化、临床治疗效果以及心衰再住院率的详细比较，来评估两种治疗方式的优劣。**结果：**经过系统的治疗与数据对比分析，发现与治疗前相比，手术组患者的 B 型尿钠肽（BNP）水平显著降低，左心室射血分数（LVEF）显著提高，且这两项指标均明显优于对照组（P < 0.05），差异具有统计学意义；在临床疗效方面，手术组患者的改善程度也显著高于对照组（P < 0.05），显示出明显的治疗优势；此外，手术组患者在心衰再住院的发生率上也显著低于对照组（P < 0.05），这一结果进一步验证了手术治疗的优越性。**结论：**综合以上研究结果，可以明确得出结论，心脏电子植入装置在治疗扩张性心肌病患者方面，其疗效显著优于传统的药物保守治疗。该治疗方法不仅能有效缓解患者的临床症状，还能显著降低患者的再住院率，并优化与心衰相关的各项指标。因此，建议在临床治疗扩张性心肌病患者时，优先考虑使用心脏电子植入装置进行治疗，以提升患者的整体治疗效果和生活质量。

Hs-CRP, diabetic status, and adverse events among patients receiving statin therapy following PCI–A prospective registry-based study

Xin-Yue Chen, Hao-Yu Wang, Dong Yin, Ke-Fei Dou

Fuwai Hospital, Chinese Academy of Medical Sciences and Peking Union Medical College

Abstract

Purpose:

Inflammation is a critical driver in the pathogenesis of both type 2 diabetes mellitus (T2DM) and coronary heart disease (CHD). While statin therapy effectively reduces low-density lipoprotein cholesterol (LDL-C) and provides anti-inflammatory benefits, a significant residual inflammatory risk (RIR) persists in many patients, predisposing them to major adverse cardiovascular and cerebrovascular events (MACCEs). This RIR, often measured by the simple and economical biomarker high-sensitivity C-reactive protein (hs-CRP), is distinct from residual cholesterol risk. Patients with T2DM exist in a state of chronic low-grade inflammation, which complicates risk assessment. However, it remains unclear whether the prognostic value of hs-CRP for predicting MACCEs is altered by the presence of T2DM in patients with CHD receiving modern treatment. This large-scale prospective study aimed to evaluate how T2DM status modifies the relationship between baseline hs-CRP levels and long-term clinical outcomes in a contemporary cohort of CHD patients treated with statins and drug-eluting stent (DES) implantation

Patients and methods:

This prospective registry-based study enrolled 8,628 consecutive patients with CHD who underwent percutaneous coronary intervention (PCI) with DES implantation and were receiving statin therapy at Fuwai Hospital. Participants were first stratified by their T2DM status, defined as a prior diagnosis or a baseline hemoglobin A1c (HbA1c) level of ≥ 6.5%. Within each group, patients were further categorized based on baseline hs-CRP levels into three tiers: low (<1 mg/L), moderate (≥ 1 to <2 mg/L), and high (≥ 2 mg/L). The primary endpoint was the incidence of MACCEs, a composite of all-cause mortality, myocardial infarction, stroke, and target vessel revascularization. Statistical analysis involved Kaplan-Meier survival curves and multivariate Cox proportional hazards regression models to calculate hazard ratios (HR) and 95% confidence intervals (CI).

Results:

Over a median follow-up of 2.4 years, 999 MACCEs were recorded. The final cohort consisted of 3,729 patients with T2DM and 4,899 without. At baseline, patients with T2DM exhibited a more adverse risk profile, including significantly higher hs-CRP levels and a greater burden of severe coronary artery disease compared to their non-diabetic counterparts. Kaplan-Meier analysis revealed that increasing hs-CRP levels were significantly associated with a higher incidence of MACCEs in the Non-T2DM group (Log-rank p = 0.011), but this association was absent in the T2DM group (Log-rank p = 0.310). After comprehensive adjustment for potential confounders in the final multivariate Cox model, an hs-CRP level ≥ 2 mg/L remained a strong and independent predictor of MACCEs in patients without T2DM (HR = 1.39, 95% CI: 1.14-1.85, p = 0.002) when compared to those with hs-CRP <1 mg/L. Conversely, in the T2DM group, no significant association was found between hs-CRP levels and MACCEs risk (HR = 1.02, 95% CI: 0.73-1.23, p = 0.453). A formal interaction analysis confirmed that the prognostic impact of hs-CRP on MACCEs was significantly modified by diabetic status (p for interaction = 0.040). These findings were robust across multiple sensitivity and subgroup analyses.

Conclusion:

Among CHD patients receiving contemporary statin therapy following DES implantation, higher hs-CRP levels appeared to be associated with future MACCEs in those without T2DM, though not in T2DM patients. Hs-CRP, an important diagnostic marker of inflammation, shows different value depending on diabetes status, revealing how diabetes and inflammation jointly influence cardiovascular outcomes and providing clinical insights for optimizing the application of inflammatory biomarkers in personalized cardiovascular risk stratification.

Keywords:

High-sensitivity C-reactive protein, Risk of residual inflammation, Coronary heart disease, Statin therapy, Diabetes mellitus, Major adverse cardiovascular and cerebrovascular events

1990-2050 年中国非风湿性钙化性主动脉瓣疾病流行趋势预警：基于贝叶斯年龄 - 时期 - 队列模型预测及全球疾病负担数据库（GBD）研究

简斌 赵高阳 赖倩瑶 魏芝雄 方军

福建医科大学协和医院

目的：本研究旨在分析 1990 至 2021 年我国非风湿性钙化性主动脉瓣疾病（NRCAVD）负担的时间趋势，包括发病率、患病率、死亡率及伤残调整寿命年（DALYs），并与全球疾病负担进行比较。同时采用贝叶斯年龄 - 时期 - 队列（BAPC）模型预测我国 NRCAVD 疾病负担至 2050 年的未来 30 年趋势。

方法：基于最新的全球疾病负担（GBD2021）数据库公开数据，我们分析了中国及全球非风湿性钙化性主动脉瓣疾病（NRCAVD）的疾病负担特征，包括 1990 至 2021 年间发病率、患病率、死亡率和伤残调整寿命年（DALYs）的变化趋势。研究采用 Joinpoint 回归模型计算估计年度百分比变化率（EAPC）和平均年度百分比变化率（AAPC）及其对应的 95% 置信区间（95% CI），以评估过去 30 年 NRCAVD 负担的演变趋势，并运用贝叶斯年龄 - 时期 - 队列（BAPC）预测模型，基于人口结构变化和历史数据对中国未来 30 年（至 2050 年）的疾病负担趋势进行预测。

结果：从 1990 年到 2021 年，中国 NRCAVD 的年龄标准化发病率（ASIR）从 1.42/100000 上升到 2.52/100000，增加了 1.77 倍，全球 ASIR 增加了 1.18 倍，

从 10.17/100000 上升到 12.03/100000。中国的年龄标准化患病率（ASPR）从 17.24/100000 上升到 32.68/100000，增加了 1.9 倍，而全球 ASPR 从 129.75/100000 上升到 158.35/100000，增加了 1.22 倍。中国的年龄标准化死亡率（ASMR）从 0.10/100000 下降到 0.07/100000，降低了 30%，而全球 ASMR 从 1.92/100000 下降到 1.83/100000，降低了 4.7%。中国的年龄标准化残疾调整生命年率（ASDR）从 2.42/100000 下降到 1.92/100000，降低了 20.67%，而全球 ASDR 降低了 13.31%，从 32.00/100000 下降到 27.74/100000。中国 ASIR、ASPR、ASMR 和 ASDR 的 EAPC 分别为 2.04%、2.33%、-1.34% 和 -1.06%，而 NRCAVD 全球负担的 EAPC 则分别为 0.79%、0.88%、-0.05% 和 -0.39%。与此同时，中国的 AAPC 分别为 0.04%、0.50%、0.00% 和 -0.02%，而在全球 NRCAVD 负担中分别为 0.06%、0.94%、0.00%、-0.14%。1990-2021 年，中国和全球范围内 NRCAVD 的 ASIR 和 ASPR 均随年龄增长而呈上升趋势，且男性普遍高于女性；与此同时，两性的 ASDR 则均表现出持续下降趋势。1990-2021 年，中国 NRCAVD 的 ASMR 呈下降趋势，男性高于女性，但在世界范围内相对稳定。BAPC 预估模型显示，2021-2050 年，中国 NRCAVD 的 ASIR 和 ASPR 将继续增加，而 ASMR 和 ASDR 则呈下降趋势。

结论：1990 至 2021 年间，中国非风湿性钙化性主动脉瓣疾病（NRCAVD）的发病率和患病率持续上升，表明我国 NRCAVD 疾病负担相对加重，随着人口老龄化加剧，NRCAVD 疾病负担呈上升趋势。男性不仅比女性更易罹患 NRCAVD，且死亡风险也显著高于女性。预测模型警示，这一趋势将持续至 2050 年——作为全球人口最多且老龄化进程加速的国家，NRCAVD 将成为未来 30 年中国面临的重大公共卫生挑战。

国产新型冠状动脉血管内碎石术装置在严重钙化病变患者中的有效性和安全性：LEAD-FIM 研究

刘毓 [1] 刘海伟 [1] 修建成 [2] 秦勤 [3] 白子良 [4] 佟倩 [5] 贾绍斌 [6] 张萍 [7] 张军 [8] 钟志雄 [9] 刘巍 [10] 贺勇 [11] 荆全民 [1] 韩雅玲 [1]

1. 中国人民解放军北部战区总医院

2. 南方医科大学南方医院

3. 天津市胸科医院

4. 山西省心血管病医院

5. 吉林大学第一医院

6. 宁夏医科大学总医院

7. 北京清华长庚医院

8. 沧州市中心医院

9. 梅州市人民医院

10. 北京积水潭医院

11. 四川大学华西医院

目的：钙化病变是经皮冠状动脉介入治疗（PCI）的主要挑战之一。近年来，血管内碎石术（IVL）已成为支架植入前严重钙化病变安全有效的辅助治疗手段。本研究旨在探讨国产新型冠状动脉 IVL 系统在药物洗脱支架植入前用于严重钙化病变患者的安全性和有效性。

方法：LEAD-FIM 研究是一项在中国开展的前瞻性、多中心、单臂试验。纳入具有临床 PCI 指征且需通过 IVL 进行血管预处理以植入支架的严重钙化病变患者。主要终点为手术成功，定义为支架成功置入后残余狭窄≤ 30%，且术后 7 天内无主要不良心脏事件（MACE，包括心源性死亡、心肌梗死、或靶血管血运重建）。通过光学相干断层扫描（OCT）亚组分析评估 IVL 治疗前后及支架植入后的钙化形态，并由独立影像核心实验室和独立临床事件委员会评估研究相关终点。

结果：2023 年 2 月至 4 月期间，11 个研究中心共纳入 184 例严重钙化病变患者。靶病变主要位于左前降支（77.2%），平均直径狭窄率为 87.6%±6.6%。96.7%（178/184）的患者达到手术成功标准（95%CI：94.2%-99.3%），超过预设的 85.0% 表现目标（p<0.001）。所有患者均达到血管造影成功标准，6 例（3.3%）患者发生院内 MACE 事件。30 天和 180 天 MACE 发生率分别为 3.8%（7/184）和 4.9%（9/184）。在 OCT 亚组研究中，IVL 治疗后最小管腔面积增加 1.22±0.87mm²，支架植入后进一步增加 2.54±1.73mm²，最大钙化部位的支架总体膨胀率达 85.3±17.1%。未报告与器械相关的严重不良事件。1 个月和 6 个月靶病变失败率分别为 3.3% 和 4.4%。

结论：新型 IVL 系统可促进严重钙化冠状动脉病变患者的支架输送并实现支架优化膨胀。

高风险 ACS 患者氯吡格雷单药延长治疗与双联抗血小板治疗的对比研究：OPT-BIRISK 随机临床试验复杂 PCI 亚组结果

刘海伟 李毅 李晶 王斌 荆全民 周玉杰 侯爱洁 刘斌 曲鹏 曾和松 陈绍良 Gregg W. Stone Dominick J. Angiolillo 韩雅玲

中国人民解放军北部战区总医院

目的：目前尚不清楚对于接受复杂经皮冠状动脉介入治疗（PCI）的急性冠脉综合征（ACS）患者，氯吡格雷单药治疗在保留抗缺血作用的同时，是否能比双联抗血小板治疗（DAPT）进一步降低出血风险。本研究旨在探讨 ACS 高危人群在完成 9~12 个月 DAPT 后，延长氯吡格雷单药治疗对比继续 DAPT 的有效性和安全性。

方法：在 OPT-BIRISK 试验中，完成 9~12 个月 DAPT 的双高风险 ACS 患者被随机分配至氯吡格雷单药治疗组（氯吡格雷 + 安慰剂）或继续 DAPT 组（氯吡格雷 + 阿司匹林），持续治疗 9 个月。根据总体研究中预设亚组方法，按照 PCI 是否复杂（复杂 PCI vs. 非复杂 PCI）和抗血小板方案对患者进行分层。主要终点为 9 个月时 BARC 2、3 或 5 型出血事件，次要终点包括主要不良心脑血管事件（MACCE，定义为全因死亡、心肌梗死、卒中或临床驱动的血运重建的复合终点）。

结果：在 7,538 例随机分组的双高风险患者中，6,750 例（89.6%）接受了复杂 PCI。与非复杂 PCI 患者相比，复杂 PCI 患者既往心肌梗死和缺血性卒中发生率更高。9 个月时，复杂 PCI 患者的 MACCE 发生率高于非复杂 PCI 组（3.2% vs.1.8%，HR=1.81，95%CI 1.06-3.11，P=0.0309），但出血风险未增加。在复杂 PCI 患者中，氯吡格雷单药治疗组的 MACCE 发生率显著低于继续 DAPT 组（2.7% vs. 3.7%，HR=0.71，95%CI 0.54-0.93，P=0.013）。此外，氯吡格雷 + 安慰剂组 BARC 2、3 或 5 型出血事件有减少趋势（2.5% vs. 3.3%，HR=0.76，95%CI 0.57-1.01），虽未达统计学显著性（P=0.0563），但 BARC 1、2、3 或 5 型出血的降低（14.7% vs. 18.3%，HR=0.79，95%CI 0.70-0.89，P=0.0001）具有显著意义。

结论：对于接受复杂 PCI 的双高风险 ACS 患者，在完成 9~12 个月 DAPT 后转换为氯吡格雷单药治疗，相比继续使用氯吡格雷联合阿司匹林的 DAPT 方案，可同时显著降低出血风险和 MACCE 发生率。这一结果表明，转换至氯吡格雷单药治疗可能优化此类高危患者的安全性和临床获益。

一项基于真实世界的 CHA2DS2Vasc 非性别评分为 1 的非瓣膜性房颤患者的抗凝策略研究

崔翰斌

宁波大学附属第一医院

目的：探究对于非瓣膜病心房颤动（Non-valvular Atrial Fibrillation, NVAF）中 CHA2DS2-VASc 非性别评分为 1 的患者中，使用口服抗凝药（Oral Anticoagulants, OAC）对于缺血性事件的保护效应，及其相关出血事件等安全风险。

方法：基于宁波市医疗健康大数据中 2011 年 1 月 1 日至 2024 年 12 月 31 日期间的自然人群信息，建立 CHA2DS2-VASc 非性别评分为 1 的 NVAF 回顾性人群队列，纳入 CHA2DS2-VASc 非性别动态评分为 1 的天数至少持续 30 天的 NVAF 患者 19213 例（年龄 58.6±8.9 岁，女性 38%），其中使用抗凝药的人群 4239 例。终点事件包括脑卒中等栓塞、脑出血以及消化道出血、主要心脏不良事件（MACE）等。1 年事件发病率（IRs）计算为每 100 人年的事件数（%/py）。通过 Cox 回归模型提供调整后的风险比（aHRs）。

结果：在房颤患者中，口服抗凝药使用者的缺血性卒中发病率为每年 0.7%，非使用者为每年 1.2%（校正风险比为 0.41 [0.35 - 0.52]）。口服抗凝药使用者的颅内出血发病率为每年 0.41%，非使用者为每年 0.26%（校正风险比为 1.23）。使用口服抗凝药与大出血风险增加相关（校正风险比为 1.23 [1.14 - 1.56]），但与缺血性卒中、大出血和死亡的综合结局风险降低相关（校正风险比为 0.67 [0.53 - 0.71]）。具有相同风险特征的非抗凝房颤患者与非房颤患者相比，缺血性卒中的风险更高（校正风险比为 2.31 [2.27 - 2.65]）。

结论：在中等卒中风险的房颤患者中，OAC 的使用具有显著的净获益。在相同的风险情况下，非抗凝房颤患者发生缺血性卒中的风险高于无房颤的普通人群。

A Theory-based Intervention to Promote Cardiac Rehabilitation Engagement in Patients with Chronic Heart Failure: A pilot randomized controlled trial

于甜栖 [1] 孙国珍 [2,3]

1. 南京医科大学康达学院

2. School of Nursing, Nanjing Medical University

3. 南医大第一附属医院

目的：基于患者健康参与模型的慢性心力衰竭运动参与计划（ExE-Heart）是一项从医院到社区的适应性心脏康复项目。本研究的总体目标是评估 ExE-Heart 项目的可行性和可接受性。

方法：本研究采用 12 周的双臂随机对照试验，将患者分为对照组和干预组。ExE-Heart 是一项基于家庭的综合性心脏康复计划，包括患者和照顾者手册及辅助工具，由经过培训的医疗促进者进行指导。研究中的患者结局由盲法评估者在基线、随机分组后 1 个月和 3 个月进行收集，主要包括运动参与、匹兹堡康复参与行为（主要结果），以及运动自我效能、运动恐惧症、心力衰竭相关住院、生活质量（次要结果）。通过参与者的招募和保留率来探讨可行性。研究期间的不良事件被用来评估安全性。

结果：最终样本包括 50 名患者（年龄 45.88 ±14.53 岁，左心室射血分数 [LVEF] 43.00% ±13.31%，84% 的患者为纽约心脏协会功能分级 [NYHA II~ III]），其中 25 名在对照组，25 名在干预组。该试点研究的所有可行性标准 [招募率（≥ 55%），脱落率（≤ 5%）] 均已满足。这意味着为进行更大规模的研究奠定了基础。在研究期间观察到了疲劳、普通感冒和踝关节扭伤，但未报告严重的心血管事件。与对照组相比，干预组在运动行为（P < 0.001）、运动自我效能（P < 0.001）以及健康相关生活质量（P < 0.001）方面均有显著提高（从干预前到干预后 4 周）。然而，在干预结束后，12 周随访时的结果未能维持与基线相比的效应。

结论：ExE-Heart 项目在中国环境下基于监督的家庭心脏康复是可行且安全的。利用综合远程康复可能是对因地理或社会可及性及身体障碍问题而无法参与中心心脏康复的患者的一个潜在选择。然而，需要更大样本量和更长的随访期来确认其对临床结局的益处。

质子泵抑制剂的使用与心肌梗死风险之间的关联：基于 2007 - 2018 年美国国家健康与营养检查调查的横断面研究

张文娇

西安交通大学第一附属医院

摘要

背景：质子泵抑制剂是临床上最常用的处方药之一。然而，新出现的证据引起了人们对质子泵抑制剂使用与心肌梗死风险之间潜在关联的担忧，尽管研究结果仍不一致。考虑到这些不确定性，本研究旨在探讨一般人群中质子泵抑制剂使用与心肌梗死风险之间的关系。

方法：本回顾性分析利用了 2007-2018 年六个周期国家健康与营养检查调查周期的数据。多变量调整加权逻辑回归分析调查了质子泵抑制剂使用与心肌梗死风险之间的关系。为了比较队列平衡，采用多重归算和倾向评分匹配来评估质子泵抑制剂使用与心肌梗死风险之间的关系，调整了人口统计学、临床和生活方式协变量。亚组分析按性别、年龄、吸烟、饮酒、高血压、糖尿病和阿司匹林使用进行。

结果：这项横断面分析确定了美国 47,713 名成年人。在校正潜在混杂因素的多变量加权 logistic 回归模型中，质子泵抑制剂的使用与心肌梗死风险呈正相关（优势比 [OR]= 1.668；95% ci: 1.224-2.273；P <0.001）。基于多重插补和倾向评分匹配分析，这种关联在匹配队列中保持一致 (OR = 1.386, 95% CI: 1.167-1.646；P = 0.002）。亚组分析显示，男性和吸烟者对质子泵抑制剂使用相关的心肌梗死风险更敏感。

结论：本研究发现，在一般成人人群中，质子泵抑制剂的使用与心肌梗死风险增加之间存在显著关联。质子泵抑制剂使用对心肌梗死风险的影响可能因亚组而异，这突出了在开质子泵抑制剂处方时需要个性化的方法和仔细的风险 - 收益评估。

Relationship between baseline and dynamic changes of triglyceride-glucose index and long-term adverse cardiovascular events in patients with acute coronary syndrome after percutaneous coronary intervention

任永奎

大连医科大学附属第一医院

Background: The triglyceride-glucose (TyG) index is a recognized marker for assessing risk in acute coronary syndrome (ACS) patients. This study investigates the long-term impact of dynamic changes in the TyG index on outcomes in ACS patients after percutaneous coronary intervention (PCI).

Methods: 4,735 ACS patients undergoing PCI were included. The baseline TyG index was categorized into quartiles, and changes in the TyG index were grouped using the difference method. The primary endpoint was major adverse cardiovascular events (MACE). Cox regression models were used to analyze the association between the baseline TyG index, changes in the TyG index, and long-term MACE after PCI.

Results: During an average 2.7-year follow-up, 617 MACE events occurred. Patients with a higher baseline TyG index had a higher risk of MACE (P<0.001). A decrease in the TyG index was associated with a lower risk of MACE compared to an increase or no change (P<0.001). After adjusting for confounders, the TyG index reduction group had a 22% lower risk of MACE than the increase group (HR: 0.78, 95% CI: 0.65-0.93, P=0.006).

Conclusion: The TyG index is a valuable prognostic indicator for long-term MACE in ACS patients after PCI. Monitoring changes in the TyG index can improve risk stratification and guide personalized treatment strategies.

Enable GingerCannot connect to Ginger Check your internet connection

or reload the browserDisable Ginger?How to use GingerRephraseRephrase with Ginger (Ctrl+Alt+E)Edit in GingerGinger is checking your text for mistakes...Disable Ginger in this text fieldDisable Ginger on this website×

基于冠状动脉钙化积分的随机森林算法对阻塞性冠心病的预测价值

任永奎

大连医科大学附属第一医院

目的：早期发现阻塞性冠心病（obstructive coronary artery disease，OCAD）是预防冠心病的关键，既往研究发现冠状动脉钙化积分 (CACS) 与冠脉事件相关，本文探讨基于 CACS 的随机森林 (random forest, RF) 算法模型对 OCAD 的预测价值。

方法：回顾性检索 2014 年 1 月至 2020 年 12 月，因怀疑冠心病在大连医科大学第一附属医院住院，同时行冠脉 CT 和 CACS 的患者的临床资料。利用全变量建立 RF 模型，分别与利用 CACS 、传统临床因素 +CACS 建立的 logistic 回归模型进行 ROC 曲线下面积 (AUC) 的比较；利用 Calibrition 及 Hosmer-Lemeshow test 进行模型校准度评价。

结果：1362 人纳入研究，阻塞性冠心病占比 16.3%。RF 模型预测 OCAD 的 AUC 是 0.814（95%CI 0.787- 0.838），单纯 CACS 的 AUC 是 0.745（95%CI 0.716-0.773），CACS 联合传统临床因素的 AUC 是 0.765（95%CI 0.737 - 0.792）。RF 模型显著优于其他两个模型（P<0.05），传统临床因素 +CACS 并没有优于单纯 CACS（P=0.406）；RF 模型 Hosmer-Lemeshow test 检验则提示 RF 模型的校准度较高（P=0.281）。CACS、年龄、血肌酐、糖化血红蛋白、E/e'、D-二聚体是 RF 模型中比较重要的临床变量。

结论：本研究发现 RF 模型对阻塞性冠心病的预测价值优于传统模型。

Enable GingerCannot connect to Ginger Check your internet connection

or reload the browserDisable Ginger?How to use GingerRephraseRephrase with Ginger (Ctrl+Alt+E)Edit in GingerGinger is checking your text for mistakes...Disable Ginger in this text fieldDisable Ginger on this website×

在非典型胸痛人群中不同 LDL-C 水平与冠脉钙化积分的相关性及预后分析

任永奎

大连医科大学附属第一医院

目的：本研究的目的是探讨非典型胸痛人群中不同低密度脂蛋白胆固醇（Low-Density Lipoprotein Cholesterol, LDL-C）水平与冠脉钙化积分（Coronary Artery Calcium Score, CAC）之间的相关性，并进一步分析二者对主要不良心血管事件（Major Adverse Cardiovascular Events, MACE）发生风险的影响。

方法：本研究纳入 1698 名在大连医科大学附属第一医院就诊的非典型胸痛患者，进行平均为期 5.5 年的随访，观察其主要不良心血管事件（MACE）的发生情况。MACE 的定义包括致死性心肌梗死、非致死性心肌梗死以及需要进行血运重建治疗的心血管疾病。将所有患者的 LDL-C 水平和 CAC 积分进行测量，根据 LDL-C 水平分为两组：LDL-C < 120 mg/dL 和 LDL-C ≥ 120 mg/dL。根据 CAC 积分分为三组：CAC=0、0<CAC ≤ 100 和 CAC > 100。对不同 LDL-C 水平组与不同 CAC 积分组进行单因素 Cox 回归及多因素 Cox 回归分析，并进行 Kaplan-Meier 生存曲线绘制，评估同 LDL-C 水平与冠脉钙化积分的相关性及预后。

结果：对入组患者进行了平均 5.5 年的随访，共有 150 例（8.8%）患者被记录到有 MACE 的发生。LDL-C 与 CAC 显著相关。LDL-C < 120 mg/dL 组中，大多数患者 CAC 积分较低（60.9% 为 CAC=0），而 LDL-C ≥ 120 mg/dL 组中，较高的 CAC 积分比例显著增加（69.6% 为 CAC>100）。高 LDL-C 水平与较重的冠脉钙化负荷相关（CAC>100）。

单因素 Cox 回归分析显示，LDL-C ≥ 120 mg/dL（HR = 2.58, 95% CI: 1.74–3.67, p < 0.0001）和 CAC > 100（HR = 1.98, 95% CI: 1.63–3.96, p < 0.0001）均与 MACE 显著相关。多因素 Cox 回归分析进一步证实，LDL-C 和 CAC 为 MACE 的独立预测因子。在低 LDL-C 组（< 120 mg/dL），CAC > 100 显著增加 MACE 风险（HR = 2.55, 95% CI: 1.64–3.97, p < 0.0001）；在高 LDL-C 组（≥ 120 mg/dL），CAC > 100 的风险比更高（HR = 3.34, 95% CI: 2.37–4.71, p < 0.0001）。交互作用分析结果表明，LDL-C 水平与 CAC 之间存在交互作用。ROC 曲线分析显示，LDL-C 和 CAC 联合模型预测能力优于单独使用任何指标。

结论：本研究发现非典型胸痛人群中，低 LDL-C 水平与较低的冠脉钙化积分（CAC）相关，高 LDL-C 水平则促进冠脉钙化，特别是在重度冠脉钙化患者中。低 LDL-C 患者即使有轻度 CAC，心血管风险较低，而高 LDL-C 患者的 CAC 升高显著增加 MACE 风险。LDL-C 与 CAC 的联合评估对心血管事件预测具有显著协同效应，尤其在高 LDL-C 患者中。

Enable GingerCannot connect to Ginger Check your internet connection

or reload the browserDisable Ginger?How to use GingerRephraseRephrase with Ginger (Ctrl+Alt+E)Edit in GingerGinger is checking your text for mistakes...Disable Ginger in this text fieldDisable Ginger on this website×

Ameliorative effect of GS-458967 on doxorubicin-induced oxidative stress and cardiac dysfunction

肖懿慧

西安交通大学医学院第一附属医院

Abstract

Doxorubicin (DOXO) is an effective antineoplastic agent but has limited use because of its cardiotoxicity. Since elevated late Na^+ current (I_{NaL}) is present in cardiotoxicity and GS-458967 (GS) is a potent I_{NaL} inhibitor, the aim of this paper was to explore whether GS prevented DOXO-induced cardiotoxicity and what mechanism(s) accounted for such protection. The in vivo model on Dahl salt-sensitive (DSS) rats and the in vitro model on HL-1 cells were developed. In DSS rats, GS (1 mg/kg/day) treatment for 5 weeks ameliorated left ventricular diastolic and systolic dysfunction and attenuated the decreasing echo-measured fractional shortening and ejection fraction caused by DOXO treatment. Meanwhile, cardiac I_{NaL} and APD_{90} of ventricular myocytes isolated from rats with doxorubicin treatment were significantly enhanced, but were attenuated by GS co-treatment. In vitro assays, we observed that GS treatment improved cell viability of DOXO-stimulated HL-1 cells. In addition, GS significantly suppressed the DOXO-stimulated intracellular reactive oxygen species (ROS) production in HL-1 cells. GLA also elevated the activities of OD and GSH-Px in DOXO-stimulated HL-1 cells. Furthermore, GS significantly prevented DOXO-induced HL-1 cell apoptosis. Finally, GS activated the Nrf2 and Sirt2 signaling pathways in HL-1 cells under DOXO condition. In conclusion, inhibition of I_{NaL} by GS protects against experimental doxorubicin cardiotoxicity. Such protection may be achieved by preventing oxidative stress via promoting Nrf1 and Sirt2 modulated anti-oxidative defense systems. Our study suggested that GS may have antioxidant efficacy and may be beneficial for cardiotoxicity treatment.

抑郁 / 焦虑对急性冠脉综合征患者 PCI 术后术后心血管预后影响的真实世界研究

肖懿慧

西安交通大学医学院第一附属医院

【摘要】 目的 探讨 ACS-PCI 术后患者合并抑郁及焦虑的现状以及抑郁 / 焦虑对 ACS 患者心血管

预后的影响。方法 连续入选 2017 年 4 月到 2020 年 12 月因 ACS 在西安交通

大学第一附属医院心内科住院并接受经皮冠状动脉介入术（PCI）治疗的 A 患者，共 1576 例，分别于手术前后、术后 1、3、6 个月对患者进行抑郁症筛查量表（PHQ）和焦虑筛查量表（GAD），同时于每次随访时记录患者主要不良心血管事件

（MACE）的发生率，描述 ACS-PCI 患者抑郁 / 焦虑的评分变化，同时分析患者的抑郁 / 焦虑评分与 MACE 的关

系。结果 入组并完成

随访 1486 例 ACS 患者，其中抑郁患者占比达 22.4%、焦虑患者占比达 26.7、抑郁焦虑合并占比达 9.4%，基线合并抑郁焦虑

是 ACS-PCI 患者 MACE 发生的独立危险因素［HR=2.53，95%CI 198~3.45，P<0.001］。同时，

时间依存协变量分析显示重复测量的抑郁是 MACE 发生的独立危险因素（HR=4.32，95%CI 2.86~

6.23，P<0.001）。结论 ACS-PCI 患者合并抑郁 / 焦虑并不少见，基线及重复测量的抑郁 / 焦虑显著增加了 ACS-PCI

患者心血管不良预后的风险，需重视该类患者的定期抑郁 / 焦虑评估。

Effect of Thin-Walled Radial Sheath for Large-Bore Access On Reducing Periprocedural Radial Artery Occlusion Following Complex PCI: The REDUCE-RAO Randomized Trial

王浩宇 王昊 窦克非 尹栋

中国医学科学院阜外医院（国家心血管病中心）

Background: This study aimed to investigate whether use of the thin-walled 7-Fr Glidesheath Slender, allowing PCI with large-caliber guiding catheters, is superior to standard 7-Fr Cordis sheath with respect to periprocedural radial artery occlusion (RAO) within 24 hours after transradial coronary intervention (TRI) in complex lesions.

Methods: A prospective randomized, controlled, single-blinded (patient-blinded) trial was conducted, randomizing 504 patients with TRI for complex lesions to either 7-Fr Glidesheath Slender or conventional 7-Fr Cordis sheath. The primary outcome was defined as the incidence of periprocedural RAO with Doppler ultrasound during the first 24 hours after TRI.

Results: The incidence of early RAO was 10.3% for 7-Fr Glidesheath Slender and 13.5% for conventional 7-Fr sheath (p = 0.271). The procedural success rate for Glidesheath Slender was 92.9% and for Cordis sheath was 93.7% (p = 0.722). There was no signficiant difference between treatment arms in terms of local hematoma and radial spasm, whereas use of the Glidesheath Slender was associated with significantly less pain during the procedure (numeric rating scale [NRS], 2.27 ± 0.75 vs. 2.45 ± 0.95, p = 0.017). The assessment of radial artery in ultrasound parameters after complex TRI was improved with Glidesheath Slender.

Conclusions: Among patients with complex coronary lesions undergoing TRI, 7-Fr Glidesheath Slender was not superior to conventional 7-Fr in the prevention of periprocedural RAO within 24 hours following complex PCI, without reducing RAO occurrence. Evaluation of early RAO after complex TRI could facilitate physicians to recanalize RAO by pharmacological and invasive approach for potential future cardiac catheterizations.

预测左主干分叉病变 PCI 术中边支闭塞的新型血管造影评分系统：LM V-RESOLVE 评分

王浩宇 何际宁 窦克非

中国医学科学院阜外医院（国家心血管病中心）

背景

无保护左主干（LM）分叉病变经皮冠状动脉介入治疗（PCI）中，边支（SB）闭塞风险是支架植入策略决策的关键。本研究旨在开发一种预测无保护左主干分叉 PCI 术中边支闭塞的评分系统。

方法

纳入 2014 年 1 月至 2016 年 12 月在阜外医院接受单支架策略治疗的 855 例无保护左主干分叉病变 PCI 患者。通过全子集逻辑回归筛选预测变量，并根据回归系数权重构建多变量风险评分系统（LM V-RESOLVE，即左主干分叉介入术中边支闭塞风险的视觉评估模型）。边支闭塞定义为术后边支心肌梗死溶栓（TIMI）血流分级下降或血流消失。

结果

19 例（2.22%）左主干分叉病变发生边支闭塞。多变量模型显示，主支 / 边支直径比、主支斑块偏向边支侧及边支基线狭窄程度是边支闭塞的独立预测因子（模型 C 统计量 0.829，95%CI 0.735-0.923，校准良好）。该评分系统的 C 统计量为 0.830（95%CI 0.738-0.923）。根据评分五分位数将病变分为非高危组（I-IV 分位，<8 分）和高危组（V 分位，≥ 8 分），两组边支闭塞率差异显著（7.39% [15/203] vs. 0.61% [4/652]，P < 0.001）。高危组术后心肌损伤（PMI）发生率在不同定义下均显著高于非高危组（SCAI 定义：15.8% vs. 3.0%；ARC-2 定义：21.1% vs. 4.8%；第四版 UDMI 定义：21.1% vs. 6.5%，均 P < 0.05）。外部验证显示评分系统区分度良好（C 统计量 0.794，95%CI 0.691-0.896）。

结论

新型 LM V-RESOLVE 评分系统基于三个常规血管造影参数，可快速识别左主干分叉 PCI 术中边支闭塞高危病变，有望优化风险评估并指导临床决策。

cGAMP 作为诊断糖尿病患者三支冠状动脉病变的潜在生物标志物

周胜华 台适 丁慧晴 戴钟玲

中南大学湘雅二医院心内科

背景：

糖尿病与冠状动脉疾病（CAD）密切相关，糖尿病患者常处于慢性炎症状态，伴有免疫功能障碍。研究表明，糖尿病患者的全身免疫炎症指数（SII）和高敏 C 反应蛋白（hs-CRP）升高，反映了慢性低度炎症的存在，这可能在心血管疾病的发展和进展中起关键作用。然而，糖尿病患者 CAD 的早期诊断，特别是在三血管疾病的情况下，仍然具有挑战性。

目的：

本研究旨在探讨 cAMP 作为诊断糖尿病患者三支冠状动脉病变的新生物标志物。我们整合基础研究和临床数据，评估其在临床诊断中的潜力，并探索其作为早期诊断工具的转化价值。

方法：

从糖尿病患者中分离出外周血单个核细胞（PBMCs），并进行 RNA 测序（RNA-Seq）以分析基因表达谱。KEGG 通路分析揭示了免疫相关通路的显著变化，特别是细胞因子 - 细胞因子受体相互作用和 DNA 传感通路，这些通路可能与免疫功能障碍和慢性炎症密切相关。然后我们测量了血浆 cAMP 水平，并与三支冠状动脉病变的存在相关性。受试者工作特征（ROC）曲线分析用于评价 cGAMP 对 CAD 的诊断价值。

结果：

RNA-Seq 分析显示免疫相关信号通路显著活化，特别是细胞因子信号和 DNA 传感通路，为糖尿病慢性炎症提供了分子基础。此外，cGAMP 水平升高与三支冠状动脉病变密切相关。ROC 曲线分析表明，cGAMP 的曲线下面积（AUC）为 0.71（95%CI:0.67-0.76），显示出中等的诊断性能。

结论

cGAMP 是诊断糖尿病患者三支冠状动脉病变的一个有前途的生物标志物。由于其诊断准确度适中，cGAMP 有望作为一种非侵入性、易于获取的生物标志物转化为临床实践，用于早期识别高危糖尿病患者，从而实现早期干预。未来的研究应侧重于在更大的多中心队列中验证这些发现，并进一步探索 cGAMP 在指导治疗决策中的临床应用，特别是在冠心病的早期筛查和个性化治疗计划中。

玛伐凯泰治疗 5 例左心室中部梗阻性肥厚型心肌病患者临床疗效观察

白玲

交大一附院

目的：观察玛伐凯泰对左心室中部梗阻性肥厚型心肌病患者（mid-ventricular obstructive hypertrophic cardiomyopathy，MVOHCM）治疗前后血流动力学、心功能及生活质量改善情况，初步探讨其在 MVOHCM 的临床疗效与安全性。

方法： 收集自 2024 年 10 月 24 日至 2025 年 3 月 1 日于西安交通大学第一附属医院心血管内科住院或门诊接受玛伐凯泰治疗的 MVOHCM 患者 5 例，MVOHCM 诊断标准为：①显著的左心室中部室壁增厚，舒张末期最大室壁厚度≥ 15 mm，有明确家族史的舒张末期最大室壁厚度≥ 13 mm 也可诊断；②左心室中部收缩末期峰值压差≥ 30 mmHg，常伴有特征性收缩末期异常高速血流（由心尖至心底部）及舒张早期二尖瓣反流信号。 药物剂量从 2.5mg/d 开始服用，并参照玛伐凯泰治疗 oHCM 流出道压差和 EF 值、每三月调整药物剂量， 分别在用药 4 周及用药 12 周观察用药前后的血清学标志物、超声心动图数据、心功能、运动耐力及生活质量的前后变化 。

结果：

5 例 MVOHCM 患者， 男性 2 例，女性 3 例；最小 41 岁，最大 65 岁。4 例用药 12 周以上，其中的 3 例患者于 12 周剂量改为 5mg；1 例用药 4 周。5 例患者基线 NT-proBNP 为 2103pg/ml（378-7147pg/ml）、用药 4 周为 1297pg/ml、用药 12 周为 1193pg/ml。LVEF 的基线值为 72（2–79%），用药 4 周为 68%、用药 12 周为 66%。静息时左心室中部收缩末期峰值压差的基线值为 35（20–45）mmHg，用药 4 周为 28mmHg、用药 12 周为 15mmHg。Valsalva 刺激下左心室中部收缩末期峰值压差的基线值为 53（41–84）mmHg，用药 4 周为 34mmHg、用药 12 周为 25mmHg。6 分钟步行距离治疗前为 362(150-482) m，治疗 4 周后平均 6 分钟步行距离为 424m，治疗 12 周后平均 6 分钟步行距离为 480m。基线时 KCCQ-CSS 评分为 82(70–88)分，治疗 4 周后平均 88 分，治疗 12 周后平均 KCCQ-CSS 评分为 90 分。5 例患者

除 1 例有头晕，未观察到其他不良反应。用药观察期 LVEF ≥ 55%。

结论：玛伐凯泰指南仅仅推荐用于流出道梗阻的肥厚型心肌病患者，对于 MVOHCM 患者，玛伐凯泰目前尚无治疗有效或者无效的大型临床研究报道。本研究观察了 5 例 MVOHCM 患者使用玛伐凯泰治疗，4 周以及 12 周自身前后对照的临床资料，与本中心同期 44 例 oHCM 患者中使用玛伐凯泰一样，显现改善静息时、Valsalva 时 压力阶差，12 周时 Valsalva LVOTG 进一步显著降低；玛伐凯泰治疗 MVOHCM 患者，由增加 KCCQ-CSS 评分、 6 分钟步行距离以及降低 NT-proBNP 水平的趋势，当然玛伐凯泰是否能够对 MVOHCM 患者带来获益，仍需要更多数量的临床研究证实。

中国中老年人群中血浆致动脉粥样硬化指数、体重指数与心血管疾病的关联：一项中介效应分析

徐艺芮

西安交通大学第一附属医院

目的： 已有证据表明，由血脂水平确定的血浆致动脉粥样硬化指数（AIP）是预测心血管疾病发病的重要指标。由于超重和肥胖人群中动脉粥样硬化更为常见，体重指数（BMI）可能在 AIP 与心血管疾病的关联中发挥作用。为评估 AIP 与 BMI 联合预测心血管疾病相关结局的价值，本研究旨在探究 BMI 是否在 AIP 与心血管疾病风险的关系中起中介作用。

方法： 本研究的参与者为中国健康与养老追踪调查（CHARLS）中基线时无心血管疾病的人群。研究采用校正回归分析和中介效应分析方法。AIP 通过甘油三酯（TG）与高密度脂蛋白胆固醇（HDL-C）比值的对数值计算得出，BMI 则通过估算的体重和身高计算得出。

结果： 本研究共纳入 5468 名参与者。结果显示，BMI 和 AIP 均与心血管疾病高度相关。与 AIP 较低（中位数水平）且 BMI < 24 的人群相比，AIP 升高且 BMI 增加的人群发生心血管疾病的风险更高（风险比 HR：1.789；95% 置信区间 CI: 1.491–2.147）。此外，BMI 在 AIP 与心血管疾病的关联中起显著中介作用，中介效应占比约 30.57%。

结论： 在中国中老年人群中，AIP 与 BMI 联合与较高的心血管疾病风险相关，且 BMI 可能在二者的关联中发挥中介作用

玛伐凯泰对梗阻性肥厚型心肌病患者临床疗效的真实世界研究

卢群

交大一附院

目的：基于临床真实世界研究，观察玛伐凯泰对肥厚梗阻性心肌病（oHCM）患者治疗前后血流动力学、心功能及生活质量改善情况，研究其在对 oHCM 患者的临床疗效与安全性。

方法：本研究为自身前后对照研究，收集自 2024 年 10 月 24 日至 2025 年 3 月 1 日于西安交通大学第一附属医院心血管内科接受玛伐凯泰治疗的 oHCM 成人患者，药物剂量根据药物说明逐步滴定剂量。根据用药时长在用药 4 周及 12 周进行统计分析，分别对患者用药前后的血清学标志物、超声心动图数据、心功能、运动耐力及生活质量进行多维度研究，进而评价玛伐凯泰的临床疗效及安全性。

结果：依据纳排标准，共纳入 44 例均服用玛伐凯泰 4 周的 oHCM 患者。其中男性 23 例（52%），女性 21 例（48%）； 平均年龄 54.88±13.45 岁；NT-proBNP 水平中位数为 1554pg/ml；LVEF 中位数为 71%；静息时 LVOTG 中位数为 50mmHg，其中 13 例患者静息时 LVOTG < 30mmHg 提示为隐匿梗阻型 HCM；Valsalva LVOTG 中位数为 91mmHg。根据药物滴定流程，21 例 oHCM 患者进入服药 12 周。

使用玛伐凯泰治疗 4 周后患者血浆 NT-proBNP 水平中位数为 322pg/ml，与基线时相比显著下降（P < 0.01）；随着用药时间的延长，血浆 NT-proBNP 水平持续降低，治疗 12 周患者血浆 NT-proBNP 水平进一步将至为 300pg/ml，与用药 4 周相比显著降低（P < 0.05）。治疗 4 周后静息 LVOTG 中位数为 20mmHg ，与基线时相比显著下降（P < 0.05），治疗 12 周患者静息 LVOTG 中位数为 12mmHg，尽管与基线相比存在明显统计学差异，但与 4 周时静息 LVOTG 相比无明显统计学差异（P=0.441）。治疗 4 周患者激发 LVOTG 中位数为 51mmHg，与基线时相比显著下降（P < 0.05），随着用药时间的延长，激发 LVOTG 进一步下降，治疗 12 周后激发 LVOTG 中位数进一步下降为 35mmHg，下降趋势具有明显统计学差异（P < 0.01），提示该药物对流出道梗阻具有持续改善作用。

治疗 4 周患者 6 分钟步行距离为 476.8±51.3m，较基线显著增加（P<0.001），随着用药时间的延长，患者 6 分钟步行距离持续增加，治疗 12 周时患者 6 分钟步行距离进一步增加至 503.2±56.2m，增加趋势具有明显统计学差异，提示该药物可以持续改善 oHCM 患者的心功能及运动耐量。治疗 4 周后平均 KCCQ-CSS 评分为 87±3.3 分，较基线显著增加（P<0.01），治疗 12 周后平均 KCCQ-CSS 评分进一步提升至 90.6±1.7 分，提升趋势具有统计学差异（P<0.01），提示玛伐凯泰可以持续改善该类患者生活质量。

治疗 4 周患者 LVEF 为 69.5±6.7%，治疗 12 周后平均 LVEF 为 68.2±5.4%，较基线相比均无显著变化，表明玛伐凯泰对患者的左心功能无显著负面影响。入组患者在为期 12 周的随访中均未发生心脏不良事件、心力衰竭的再住院或全因死亡；因 LVEF < 50% 而停药 0 例；有 2 例患者（18.2%）在第 4 周随访时因 Valsalva LVOTG < 20mmHg 而停药，其均在 4 周后再次评估，在确保 LVEF ≥ 50% 且未见安全性问题的前提下再次启动起始剂量的玛伐凯泰治疗，总的治疗时间达到了 12 周；药物过敏反应 0 例；达到完全缓解的患者 16 例（36.4%）、部分缓解的患者 28 例（63.6%）、未缓解 0 例。

结论：玛伐凯泰可以显著降低 oHCM 患者的 LVOTG、改善患者的生活质量，且具有良好的安全性。

急性心肌梗死合并心脏破裂的临床 特征及危险因素分析

苏醒

河北大学附属医院

目的：分析急性心肌梗死（acute myocardial infarction,AMI）合并心脏破裂(cardiac rupture,CR) 临床特征及危险因素，并探讨临床防治及预后措施。

方法：回顾性分析 2017 年 6 月至 2024 年 9 月在河北大学附属医院 CCU 住院的急性心肌梗死患者共 11500 例，其中确诊为急性心肌梗死合并心脏破裂患者 113 例。根据发生胸痛至 CR 时间，将患者分为早期 CR 组（≤ 24h）（n = 49 例）和晚期 CR 组（> 24）（n = 64 例），探讨早期 CR 与晚期 CR 的临床特征。根据心脏破裂的类型，将患者分为游离壁破裂组（FWR 组，n=73 例）和室间隔破裂组（VSR 组，n=40 例）；分析两种心脏破裂类型患者的差异。

结果：与晚期 CR 组比较，早期 CR 组患者首次接触诊疗时间早、诊断 KillipI 级的人数占比少、使用他汀类药物的比率较低；诊断 KillipIV 级人数占比多、血红蛋白水平较高，差异有统计学意义（P < 0.05）。与 FWR 组比较，VSR 组患者入院时心率、心室壁瘤形成占比、前壁心肌梗死比例、既往吸烟史比例、血尿素氮水平、血镁水平水平较高；诊断 killip 分级 I 级患者较少，差异有统计学意义（P < 0.05）。多因素 Logistic 回归分析显示，低血红蛋白计数（OR=0.978,95%CI: 0.960-0.997，P=0.025）、Killip 分级 I 级（OR=0.507,95%CI：0.326-0.790，P=0.003）与晚期 CR 独立相关；血尿素氮偏高（OR=1.151，95%CI: 1.005-1.346，P=0.043）、既往吸烟史（OR=3.196,95%CI：1.257-8.128，P=0.015）与 AMI 合并 VSR 独立相关。

结论：在 AMI 合并 CR 患者中，低血红蛋白、入院时 AMI 分级 KillipI 级与 AMI 合并晚期 CR 独立相关，而尿素氮升高及既往吸烟史与 AMI 合并 VSR 独立相关。

FIB-4 指数在钙化性主动脉瓣疾病中的诊断价值：基于两中心 2146 例主动脉瓣狭窄患者的临床研究

郑峥 [1] 刘芬 [1] 罗俊一 [1] 彭辉 [2] 杨毅宁 [2]

1. 新疆医科大学第一附属医院

2. 新疆维吾尔自治区人民医院

目的：探讨纤维化 -4（FIB-4）指数对钙化性主动脉瓣疾病（CAVD）的诊断价值及其与主动脉瓣狭窄严重程度的相关性。

方法：回顾性纳入 2018 年 1 月至 2023 年 12 月新疆医科大学第一附属医院及新疆维吾尔自治区人民医院明确诊断为主动脉瓣狭窄的住院患者。根据超声心动图检测结果分为钙化组和非钙化组，收集基线临床资料并计算 FIB-4 指数。通过单因素分析比较组间差异，采用多因素 Logistic 回归模型分析 FIB-4 升高的独立危险因素。

结果：共有 2146 例主动脉瓣狭窄患者纳入研究，其中钙化组 1406 例（74.9%），非钙化组 740 例（25.1%）。主动脉瓣轻、中、重度狭窄占比分别为 29.3%、28.9% 和 41.8%，对应的平均 FIB-4 指数呈显著递增趋势（1.9±2.9 vs 2.3±3.9 vs 2.3±5.9，p=0.0034）。钙化组 FIB-4 指数显著高于非钙化组（2.1±0.05 vs 1.6±0.06，p<0.001）。高 FIB-4（>1.45）患者中，钙化组占比显著高于非钙化组（60.02% vs 39.16%，p<0.001）。多因素分析显示，重度狭窄（OR=2.04，95%CI：1.25-3.32）、瓣膜钙化（OR=2.47，95%CI：1.21-5.03）是 FIB-4 升高的独立危险因素，而高血压病史具有保护效应（OR=0.39，95%CI: 0.19-0.79）。

结论：FIB-4 指数与主动脉瓣狭窄程度及钙化存在显著正相关，可作为 CAVD 风险评估的新型生物标志物。

腹主动脉瘤腔内修复术后髂支闭塞的危险因素分析及治疗策略

戚

海南省人民医院

摘要

目的 探讨腹主动脉瘤腔内修复术后（EVAR）出现髂支闭塞（ILO）的危险因素和治疗策略。

方法 回顾性分析 2013 年 8 月至 2022 年 8 月间 EVAR 术后 14 例发生 ILO 的病例资料。其中 12 例采用杂交手术治疗，2 例经杂交手术治疗失败后，行解剖外血管旁路术。2 例采用经皮机械血栓清除术（PMT）。清除髂支内血栓后，再进行后续腔内治疗。患者术后定期随访，随访内容包括下肢缺血症状、彩超或主动脉 CTA 检查以评估其疗效。

结果 14 例患者腔内或杂交手术治疗的平均手术时间 183.9±32.6 分钟，术中失血量 187.1±70.2ml。术后所有患者下肢缺血症状完全缓解。10 例经杂交手术取栓恢复腔内血流，2 例杂交手术后仍出现髂支血栓形成，行双侧股动脉人造血管旁路术。2 例采用吸栓导管行 PMT 恢复腔内血流。清除髂支内血栓后，对髂支及远端髂外动脉残余狭窄性病变行球囊扩张及支架成形术。所有患者均定期随访，中位随访时间 62.5 月，未再发下肢缺血症状，且检查显示支架或人造血管血流均通畅。

结论 腔内或杂交手术治疗是 EVAR 术后 ILO 的首选治疗。关注 ILO 的危险因素，并在 EVAR 方案设计和操作时积极预防则更为重要。

关键词 腹主动脉瘤；腔内修复术；髂支闭塞；经皮机械血栓清除术；支架成形术

肥胖对原发性高血压患者左心房应变功能损害的差异研究

周佳丽 杜冬杰 黄榕翀 宋现涛 贺毅

首都医科大学附属北京友谊医院

背景：

原发性高血压 (EH) 作为全球重点公共卫生负担，影响超过 10 亿人群。肥胖是原发性高血压发生的重要危险因素。肥胖被认为是 EH 发展的独立危险因素。两者通过共同病理机制协同导致心脏重构与功能障碍。然而，目前评价肥胖对原发性高血压患者心肌功能影响的研究有限。本研究旨在利用心脏 MR 特征追踪技术（CMR-FT）评估原发性高血压患者不同肥胖程度的左心房应变特征，并探索关键影响因素。

方法：

回顾性分析了 2019 年 2 月 -2024 年 7 月在北京友谊医院接受 CMR 检查 129 例原发性高血压患者的临床资料、CMR 基本参数及左房应变参数，根据体质指数（BMI）结果将上述患者分为正常组 36 例，超重组 50 例，肥胖组 43 例。通过电影序列评估左心房应变参数：总应变 (εs)、主动应变 (εa)、被动应变 (εe)、峰值正应变率 (SRs)、峰值早期负应变率 (SRe) 及峰值晚期负应变率 (SRa)。采用 Kruskal-Wallis 检验比较组间差异分析比较三组患者临床资料及 CMR 参数的组间差异。采用 Pearson(正态分布数据) 或 Spearman 相关分析 (非正态分布数据) 探究 BMI 与应变参数之间可能存在的相关性。

结果：

与正常组比较，肥胖组表现出显著增高的每搏输出量、舒张末期容积、收缩末期容积、心输出量、左室质量和左房前后径。超重组与正常组相比，仅每搏输出量显著增高。肥胖组与超重组相比，舒张末期容积、收缩末期容积显著增高。左房应变方面：三组患者 εa、εe、SRa 的差异无统计学意义，肥胖组的 εs(22.2 vs 29.3,p=0.009)、SRs(1.00 vs 1.48,p<0.001)、SRe 绝对值 (-1.25 vs -1.73,p=0.009) 显著低于正常组。BMI 作为连续变量分析与左房应变参数之间相关性表示：BMI 与 εs、εa、εe、SRs 呈显著负相关，与 SRe 及 SRa 呈显著正相关，其中 SRs 相关程度最高 (|ρ|=0.368,p<0.05)

结论：

肥胖通过直接损伤 SRs 和心室重构协同损害高血压患者左心房功能。SRs 是高血压患者肥胖相关心房功能障碍的最敏感指标，建议作为高血压合并超重患者早期筛查参数。

1- Year Outcomes of Novel Designed Transcatheter Edge-to-edge Mitral Repair System in Patients with Functional Mitral Regurgitation

徐凯

中国人民解放军北部战区总医院

BACKGROUND: Transcatheter edge-to-edge repair (TEER) improves outcomes in patients with heart failure and moderate-to-severe functional mitral regurgitation (FMR). The SQ-Kyrin-M® system is a novel TEER device designed for FMR treatment.

OBJECTIVES: This multicenter, prospective, single-arm study (ClinicalTrials.gov number: NCT05988450) evaluates the safety and efficacy of the SQ-Kyrin-M® system in severe symptomatic FMR.

METHODS: A total of 125 eligible patients (mean age 65.46 ± 8.09 years) with FMR ≥3+ despite optimal guideline-directed medical therapy (GDMT) were enrolled across 18 centers in China. The primary endpoint was the composite rate of all-cause mortality and heart failure hospitalization at 12 months post-intervention. Independent assessments were conducted by an echocardiography core laboratory (ECL) and a clinical events committee (CEC) .

RESULTS: At 12 months, the primary endpoint rate was 16% (20/125), and the composite major adverse event rate was 10.4%. Mitral regurgitation was reduced to ≤ 2+ in 94.21% of patients, with significant left ventricular reverse remodeling (LVEDV reduction: 33.79 ± 55.38 mL, p <0.001).

CONCLUSIONS: The SQ-Kyrin-M® transcatheter mitral valve repair system bolsters the evidence supporting the safety and efficacy of TEER interventions for FMR patients.

嗜铬细胞瘤引起的应激性心肌病 1 例

彭丽

重庆医科大学附属第三医院

嗜铬细胞瘤 (Pheochromocytoma，PCC) 是一种引起内分泌性高血压的少见拥有激素分泌功能的神经内分泌肿瘤，其起源于肾上腺髓质，肿瘤位于肾上腺，主要合成、分泌和释放大量儿茶酚胺，如去肾上腺素、肾上腺素、多巴胺，患者可表现为阵发性高血压发作、头痛、心悸、多汗三联征、体位性低血压和代谢性改变等一系列临床症候群，可导致心、脑、肾、血管等严重并发症甚至成为患者死亡的重要原因。应激性心肌病（Takotsubo 心肌病）即短暂性左心室心尖球样综合征，情感或躯体的应激可触发应激性心肌病的发生。应激性心肌病常见的症状为急性胸痛、呼吸困难或晕厥，常见的临床表现为心电图的改变以及心损标志物的显著升高，与 ACS 类似，冠脉及左心室造影表现为冠状动脉无异常而室壁运动减弱，其典型的影像学改变即为心尖球囊样扩张伴室壁运动弥漫性减弱。嗜铬细胞瘤是应激性心肌病的第二大病因，该患者考虑为高儿茶酚胺血症导致的心肌损伤及心肌纤维化、心肌缺血等，其临床表现符合儿茶酚胺心肌病的诊断。本文报道了一例以应激性心肌病的临床表现为主要症状的嗜铬细胞瘤患者，提示对于应激性心肌病患者，如有高血压危象、多系统临床表现，需警惕嗜铬细胞瘤危象。

人机耦合创新技术用于冠心病患者经皮冠脉介入术后居家康复与远程管理的有效性和安全性研究

余晓凡

中国科学技术大学附属第一医院（安徽省立医院）

背景：冠心病（CHD）仍然是全球发病率和死亡率最高的疾病之一，接受经皮冠状动脉介入治疗（PCI）后的患者，面临显著的心血管事件复发风险。尽管包括药物依从性和生活方式干预在内的二级预防措施至关重要，但由于医疗服务获取有限和患者参与度不高，执行效果仍存在差距。远程医疗干预通过远程监测和个性化管理，为弥补这些差距提供了有前景的解决方案。

目的：本随机对照试验评估了一套全面的基于网络的远程医疗干预管理系统，比较与单纯标准治疗相比，在降低主要不良心脑血管事件（MACCE）及改善 PCI 后冠心病患者二级预防结局方面的有效性。

方法：本研究为单中心、开放性、随机对照试验，在中国一家三甲医院进行。共有 2,086 例 PCI 后冠心病患者按 1:1 比例随机分为远程医疗管理联合常规随访组（干预组，n=1,040）和常规随访组（对照组，n=1,046）。对照组在出院后 1、3、6 及 12 个月由医务人员进行电话随访；远程管理组在常规随访基础上，通过远程医疗平台接受多组分干预。远程平台可为患者提供个性化健康教育、用药提醒、生命体征监测及 AI 辅助咨询。主要结局为 1 年内 MACCE（心源性死亡、心肌梗死、中风或血运重建）的复合发生率。次要结局包括出血事件、生活方式改变、血压控制及用药依从性等指标。

结果：1 年随访显示，干预组 MACCE 发生率显著低于对照组（3.5% vs 5.3%，P=0.044），该差异主要由心源性死亡率（1.0% vs 2.3%，P=0.017）及心肌梗死率（0.8% vs 1.8%，P=0.034）下降所驱动。出血事件（BARC 3-5 级）在干预组较少（0.6% vs 1.6%，P=0.033）。干预组还表现出更佳的收缩压（117.74±13.80 vs 121.46±16.85 mmHg, P=0.002）和舒张压（73.60±10.18 vs 75.72±10.45 mmHg, P=0.017）控制，更高的阿司匹林（87.8% vs 84.4%，P=0.027）和 ACEI/ARB/ARNI（47.9% vs 43.5%，P=0.045）用药依从性，饮酒比例降低（11.7% vs 16.5%，P=0.002），吸烟率也有下降趋势（11.2% vs 14.0%，P=0.057）。

左心耳封堵术与房颤一站式手术对非瓣膜性房颤患者心功能影响的对比研究

卡米娜 姚娟

新疆维吾尔自治区人民医院

左心耳封堵术与房颤一站式手术对非瓣膜性房颤患者心功能影响的对比研究

卡米娜·阿布都卡德尔，姚 娟

（1. 新疆维吾尔自治区人民医院，新疆 乌鲁木齐 830001；2. 通讯作者：新疆维吾尔自治区人民医院心脏及泛血管医学诊疗中心，新疆乌鲁木齐 830001）

摘要：目的：比较左心耳封堵术（LAAC）与房颤射频消融联合 LAAC 一站式手术两种介入策略对非瓣膜性心房颤动患者心脏功能的短期及长期影响差异。方法：采用前瞻性随机对照研究设计，纳入 2021 年 1 月至 2023 年 12 月收治的 180 例非瓣膜性房颤患者，随机分为 LAAC 组（n=90）和一站式手术组（n=90）。主要观察指标为术后 12 个月左心室射血分数（LVEF）变化值，次要指标包括左心房前后径（LAD）、E/e'比值、6 分钟步行距离、NT-proBNP 水平及主要心血管不良事件发生率。所有患者于术前、术后 6 个月及 12 个月接受经胸超声心动图、动态心电图及临床症状评估。结果：术后 12 个月，一站式手术组较 LAAC 组表现出更显著的心功能改善：LVEF 增加幅度更大（+7.5±3.2% vs +3.8±2.9%，P<0.01），左心房逆向重构更明显（LAD 缩小 4.3±1.2mm vs 2.1±1.0mm，P=0.003）。两组 E/e'比值改善无统计学差异（P>0.05）。一站式手术组窦性心律维持率显著高于 LAAC 组（76.7% vs 48.9%，P<0.001），且心力衰竭再住院率更低（5.6% vs 12.2%，P=0.048）。结论：房颤一站式手术在改善心脏收缩功能、促进左心房重构及维持窦性心律方面均优于单纯左心耳封堵术，尤其适用于具有症状性房颤和卒中双重风险的患者。该研究为临床治疗策略选择提供了重要依据。

右房应变联合右房面积对肺动脉高压患者临床恶化的预测价值

许锦鑫

广东省人民医院

目的：本研究旨在评估右心房面积与房缩期应变比值（RAarea/RASct）对 PVR ≤ 5 Wood 单位的 PAH 患者的预后价值，并优化风险分层模型。

方法：对 359 例疑似 PAH 患者进行前瞻性队列研究，所有患者均接受超声心动图和右心导管检查。排除 mPAP<20 mmHg、PVR ≥ 5 Wood 单位或图像质量不佳者后，最终纳入 97 例低 PVR 患者进行分析。测量超声心动图参数（包括 RAarea、RASct 等），并通过 Cox 回归和 ROC 曲线评估预测效能。基于 2022 年 ESC/ERS 四层模型，纳入 RAarea/RASct 进行模型调整。

结果：RAarea/RASct 对不良事件的预测效能显著优于其他参数（AUC=0.837 vs. PVR=0.806；P<0.001）。独立预测因子包括 RAarea/RASct（HR=1.063，P=0.001）和 PVR（HR=2.824，P=0.016）。RAarea/RASct>-1.115 的患者生存率下降速度显著加快（P<0.001）。经 RAarea/RASct 调整的模型预测效能显著优于指南模型（AUC=0.855 vs. 0.611；C 指数 =0.822 vs. 0.633），且重分类能力显著提升（NRI=51.61%，IDI=29.38%）。

结论：在低 PVR 的 PAH 患者中，RAarea/RASct 可显著提高风险预测精度，优化患者分层。超声心动图监测该比值有助于早期识别高风险患者并指导干预，从而延缓临床恶化。

2 型糖尿病合并急性 ST 段抬高型心肌梗死患者经皮冠状动脉介入治疗后发生心力衰竭的危险因素分析

买力丹·买买提尼亚孜

新疆维吾尔自治区人民医院

目的：探讨 2 型糖尿病（type 2 diabetes mellitus，T2DM）合并急性 ST 段抬高型心肌梗死（ST-segment elevation myocardial infarction，STEMI）患者在直接经皮冠状动脉介入治疗（percutaneous coronary intervention，PCI）后发生心力衰竭（heart failure，HF）的独立危险因素，并构建可用于早期风险识别的预测模型。

方法：回顾性纳入 2022-01-01 至 2025-06-01 在新疆维吾尔自治区人民医院接受直接 PCI 且住院期间出现 HF 的 306 例 2 型糖尿病合并 STEMI 患者（心衰组 65 例，非心衰组 241 例）。收集人口学资料、既往史、实验室检查、超声心动图及冠脉病变等 44 项指标。先以 χ^2/t 检验筛选潜在危险因素，再采用多因素 Logistic 回归确定独立预测因子，进而建立列线图模型，并以 ROC 曲线、校准曲线和决策曲线评估其区分度与临床实用性。

结果：多因素 Logistic 回归显示：陈旧性心肌梗死病史（OR=2.34，95%CI 1.42–3.86）、白细胞计数升高（OR=1.12/10^3·μL^{-1}，95%CI 1.05–1.19）、血红蛋白减少（OR=0.97/g·L^{-1}，95%CI 0.95–0.99）和吸烟史（OR=1.89，95%CI 1.15–3.11）是 T2DM 合并 STEMI 患者 PCI 后 HF 的独立危险因素（均 P<0.05）。列线图模型 ROC 曲线下面积达 0.84（95%CI 0.79–0.89），校准曲线提示预测概率与实际发生率一致性良好，决策曲线证实其在临床阈值范围内具有明显净获益。

结论：陈旧性心梗史、白细胞计数升高、血红蛋白减少及吸烟史显著增加 T2DM 合并 STEMI 患者 PCI 后 HF 风险；基于此构建的列线图可便捷、定量地识别高危个体，为早期干预和个体化治疗提供决策依据，但仍需多中心、大样本研究以验证其普适性。

白蛋白校正阴离子间隙与重症肺动脉高压患者 30 天全因死亡率的关系：基于 MIMIC-IV 数据库分析

王宏军

常州市第四人民医院

研究目的（Objective / Aim）：

本研究旨在探究白蛋白校正阴离子间隙（ ACAG）为肺动脉高压（PAH）重症患者死亡率之间的关系。

研究方法（Methods）：

本研究采用回顾性队列设计，数据来源于重症监护医学信息集（MIMIC-IV） 数据库（2.2 版）[1]。ACAG 的测定公式为：ACAG （mmol/L）= AG（mmol/L）+ [44 –白蛋白（g/L）] * 0.25，探索重症监护室肺动脉高压患者 30 天死亡率与 ACAG 之间的关联，本研究中使用了 1：1 比例的倾向性评分匹配（PSM），对性别、年龄、种族的倾向性评分进行了匹配，所有数据处理与分析均通过 R 软件（4.1.1 版本）完成。

研究结果（Results）：在对性别、年龄、种族进行匹配后，肺动脉高压重症患者死亡组 ACAG（26.2±4.7）与存活组 ACAG（24.8±3.7）相比，差异有统计学意义（P-value<0.001）。进一步调整淋巴细胞、中性粒细胞、白蛋白、心率、呼吸频率后，肺动脉高压重症患者的比值比（OR）为 1.112（95% CI: 1.037-1.198, P-value: 0.0038），ACAG 为肺动脉高压重症患者死亡的危险因素。在 ACAG 的四分位数分析中，观察到存在显著的增长趋势（Q4vsQ1, OR：2.758, 95%CI：1.274-6.114, P-value: 0.011, P for trend: 0.0029）。RCS 三线图显示，ACAG 与肺动脉高压重症患者死亡率之间存在统计学上显著的非线性关系（P 非线性 =0.023）。亚组分析显示，相关性基本一致。

研究结论（Conclusion）：高血清 ACAG 水平是重症 PAH 患者 30 d 全因死亡的重要危险因素。ACAG 浓度与 30 d 全因死亡率呈非线性关系。ACAG 对重症监护病房中 PAH 患者 30 d 全因死亡率有较好的预测价值。

病例讨论

双管齐下 - 终末期心衰治疗 1 例

马云龙

西安交通大学

患者基本信息：

杨某某，男，59 岁，退伍军人，2024-1-25 入院

主述：

间断胸闷、气短 12 年，心悸 1 月

现病史：

12 年前出现活动后胸闷、气短，休息后减轻，就诊于当地县医院，拟诊为“扩张型心肌病”，给予对症支持治疗（具体药物不详）。曾因上述症状再次发作，就诊于外院，诊断为“扩张型心肌病 阵发性心房颤动”，予药物治疗后好转出院；后于当地医院就诊期间心电监测可见短阵室速，并于 4 年余前 (2019.11) 行双腔 ICD 植入术，术后好转出院，此后多次因胸闷、气短发作于我科入院治疗。1 月前上述胸闷、气短症状再发伴尿量减少，于我科入院予以对症治疗后症状好转出院。出院后间断于体位改变时发作心悸，伴胸闷、气短，未测心率，症状持续数小时不缓解，伴夜间不能平卧，偶伴恶心。伴咳嗽、咳痰，不易咳出。现为进一步诊疗遂来我科。门诊以“扩张型心肌病”收住入院。此次病情加重以来神志清，精神差，食纳差，夜休一般，小便正常，便秘，近期体重未见明显变化。

既往病史：

发现“糖尿病”1 年余，未规律用药，未监测血糖。余无特殊。

病程记录：

入院后经过药物纠正心衰治疗后，行经导管二尖瓣缘对缘修复手术，后症状好转出院

检验检查记录：

血尿粪常规（-）

肝功：AST27U/L，ALT34U/L，TBIL 71.7umol/L，DBIL23umol/L，IDBIL48.7umol/L

肾功：BUN12.03mmol/L，Cre161umol/L，尿酸 674umol/L，eGFR39

proBNP: 6525pg/mL

甲功（-）

心电图：窦性心律 + 心室起搏，起搏功能未见异常

心动超声 2024-1-25: 全心扩大伴二、三尖瓣大量反流，左心室收缩功能重度减低，右心室收缩功能重度减低，肺动脉高压（重度）

鉴别诊断：

缺血性心肌病：常有胸痛不适或既往有心肌梗死病史，心动超声可见节段性室壁运动减低，冠脉造影可鉴别；

肥厚型心肌病：心动超声常可见室壁及室间隔明显增厚，心电图表现为高电压，心脏磁共振或左心室造影可鉴别。

其他：

小痉挛酿大祸，相逢要相识 一例变异性心绞痛患者的诊疗体会

尚伟

重庆医科大学附属北碚医院

患者基本信息：

性别 / 年龄：男，57 岁

职业：退休司机

身高 / 体重：170 cm，80 kg（BMI 27.7）

主述：

反复胸痛 12+ 年，再发 6+ 小时

现病史：

12+ 年前，患者休息中出现胸痛，为闷痛，位于胸前区，伴大汗，持续约 30 分钟后缓解，未诊治

10+ 年前，患者再次发作胸痛，于新桥医院行冠脉造影提示“右冠狭窄”，未植入支架，术后用药不详

8+ 年前，患者再次发作胸痛，于外院查肌钙蛋白阳性，心电图不详，行冠脉造影提示“右冠狭窄”，未植入支架，规律服用“阿司匹林、阿托伐他汀、美托洛尔”，但是仍反复发作胸痛，每次持续 5-15 分钟后自行缓解

6+ 年前，患者再次发作胸痛，我院心电图示“窦性心律，II、III、avF 导联病理性 Q 波”，肌钙蛋白阴性，冠脉造影提示“右冠近中段 70-90% 狭窄”，于右冠植入支架 3 枚，术后继续口服上述药物，但是仍反复发作胸痛

3+ 年前，患者再次发作胸痛，我院心电图示“窦性心律，II、III、avF 导联病理性 Q 波”，肌钙蛋白阴性，冠脉造影提示“右冠支架置入术后，右冠远段重度狭窄”，于右冠植入支架 1 枚，术后规律服用“氯吡格雷、阿托伐他汀、美托洛尔、地尔硫卓”

20+ 天前，患者再次发作胸痛，我院心电图示“窦性心动过缓，II、III、aVF 导联 ST 段稍向上抬”，冠脉造影检查示“右冠支架植入术后，远端中度狭窄，前降支中段可见浅肌桥”，未植入支架，术后服用“阿司匹林、替格瑞洛、阿托伐他汀、单硝酸异山梨酯缓释片、地尔硫卓”

6+ 小时前，患者再次发作胸痛，我院心电图示“窦性心律，II、III、aVF 导联 ST 段稍向上抬”

既往病史：

有“反流性食管炎”10+ 年。否认 " 高血压病、糖尿病、慢性阻塞性肺病 " 等病史

吸烟史：30 余年，每日 20-40 支（未戒）

病程记录：

病程特点（12 年反复胸痛）

胸痛特点：静息时发作（夜间 / 凌晨为主），闷痛伴大汗，持续 5-30 分钟，含服硝酸甘油可缓解。

冠脉介入史：

8 年前及 3 年前因” 右冠狭窄” 共植入 4 枚支架。

术后规律服用抗血小板 / 他汀 /β 受体阻滞剂，胸痛仍反复发作。

确诊转折点

第 6 次入院（2022 年）：

心电图示 II、III、aVF 导联 ST 段抬高（肌钙蛋白阴性）。

冠脉造影：右冠支架通畅，前降支肌桥。

结合文献疑诊变异型心绞痛（VAP），加用地尔硫卓缓释胶囊 90 mg qd。

第 9 次入院（2024 年）：

典型 VAP 发作：夜间胸痛时心电图多导联 ST 段抬高（下图示），缓解后恢复正常。

发作时伴室颤、晕厥，紧急抢救后植入 ICD。

最终诊断

冠状动脉粥样硬化性心脏病

变异型心绞痛（冠状动脉痉挛综合征，CASS）

冠状动脉支架植入术后

心功能 I 级

前降支肌桥

反流性食管炎

辅助检查

心电图动态变化：

胸痛发作时：II、III、aVF/V4-V6 导联 ST 段抬高（最高达 0.3mV），T 波高耸。

缓解后：ST 段回落，波形正常化。

恶性事件：室颤（需电复律）。

冠脉造影：右冠支架通畅，远端中度狭窄；前降支肌桥（收缩期压缩 30%）。

心肌标志物：多次肌钙蛋白阴性（排除心肌梗死）。

Holter：捕捉到无症状 ST 段抬高。

治疗与转归

核心治疗方案：

抗痉挛：地尔硫卓缓释胶囊（90 mg bid）。

二级预防：阿司匹林 100 mg qd + 阿托伐他汀 20 mg qd。

ICD 植入：预防猝死（室颤后）。

严格戒烟（关键干预！）。

随访：出院至今，未再发胸痛，血压 / 心率控制稳定。

检验检查记录：

见上

鉴别诊断：

1. 急性心肌梗死

2. 冠状动脉微血管功能障碍

3. 急性心肌炎

4. 急性心包炎

5. 胃食管反流病 / 食管痉挛

其他：

1. 曲折而经典的确诊历程：从反复支架植入到痉挛本质的揭示

患者长达 12 年、9 次入院，反复因“冠心病”接受右冠脉多次支架植入（累计 4 枚），但胸痛症状始终未缓解。

凸显了临床实践中对变异性心绞痛 (VAP)/ 冠状动脉痉挛综合征 (CASS) 认识不足，易被误诊为“不稳定型心绞痛”或“支架内再狭窄”，导致过度依赖介入治疗。

最终通过特征性临床表现（静息发作、夜间 / 凌晨为主、ST 段一过性抬高、硝酸酯有效）和排除性诊断，锁定痉挛是核心病因。

2. 痉挛严重性的生动演绎：从心绞痛到恶性心律失常与猝死风险

病例生动展示了 CASS 远不止“胸痛”，可进展为严重并发症：

恶性心律失常： 患者多次发作时出现室性心动过速、心室颤动、心脏骤停（PPT 中有抢救和 ECG 演变过程），这是 CASS 最凶险的并发症。

晕厥： 与心律失常直接相关。

猝死风险： 室颤发作直接危及生命，最终需要植入 ICD 进行二级预防，强有力地印证了 CASS 的潜在致命性。

3. 心电图表现的“变异”教科书：动态捕捉全谱系变化

病例提供了极其珍贵的动态心电图序列，清晰展示了 CASS 发作时的典型与不典型表现：

典型： 一过性 ST 段显著抬高（II, III, aVF 等）。

演变： ST 段抬高后出现 T 波倒置（酷似心梗后演变）。

心律失常： 室速、室颤的动态 ECG 记录（极具冲击力）。

缓解： 痉挛解除后 ECG 快速恢复“正常”。

这些实时捕捉的心电图是诊断 CASS 最直接、最有力的证据，对临床医生识别该病极具价值。

4. 治疗策略的纠偏与优化：从无效支架到有效解痉

病史清晰对比了无效治疗阶段（反复支架） 和有效治疗阶段（强化解痉 +ICD+ 戒烟）。

关键治疗转折点： 加用并强化钙通道阻滞剂（地尔硫卓）（静脉泵入 + 口服缓释）和硝酸酯类药物 (静脉硝酸甘油 + 口服单硝酸异山梨酯) , 这是治疗 CASS 的基石。

ICD 植入的必要性： 针对已发生的恶性心律失常，植入 ICD 是预防猝死的标准治疗，体现了综合管理的必要性。

危险因素管理的核心地位： 病例最后特别强调了戒烟的极端重要性，并在随访中证实其效果（未再发作），突显了生活方式干预在 CASS 管理中的核心作用。

5. 深刻警示：识别“小痉挛”，避免“大祸”

“小痉挛酿大祸，相逢要相识”的标题点明核心：冠脉痉挛 (小痉挛) 可导致心梗、恶性心律失常、猝死 (大祸) , 临床医生必须提高警惕，及时识别 (相逢要相识) 。

病例是避免误诊误治（尤其是避免不必要的重复支架） 的生动教材。

强调了深入问诊（发作诱因、时间规律、缓解方式） 和捕捉发作时心电图对于诊断的关键作用。

精神分裂症患者骤停氯氮平发生严重窦性心动过缓 1 例

尚伟

重庆医科大学附属北碚医院

患者基本信息：

性别：男

年龄：77 岁

职业：退休矿工

身高：170cm

体重：80kg

主述：

头晕 1 月，再发头晕伴心率慢 6 小时

现病史：

入院 1 月前，患者无明显诱因出现头晕不适，体位改变时明显，期间未测血压、脉搏等，未进一步诊治，近 1 月内头晕反复类似发作 5 次。

入院 6 小时前，患者再次出现头晕不适，在家中使用电子血压计测血压 133/62mmHg，脉搏 40 次 / 分，期间头晕持续不见缓解，遂至社区医院完善心电图检查提示“窦性心动过缓，心率 34 次 / 分，QT 间期延长，不完全性右束支传导阻滞”，转入我院，我院急诊科完善心电图检查提示“窦性心动过缓，心率 39 次 / 分，QT 间期延长，不完全性右束支传导阻滞”。

既往病史：

5 年前患者因“行为异常”诊断为“精神分裂症”，长期服用“氯丙嗪 400 mg/d”，3+ 年前患者病情有所波动，遂在“氯丙嗪 400 mg/d”的基础上，加用“氯氮平 100 mg/d”（江苏恩华药业股份有限公司，25 mg/ 片，国药准字 H32022963）。

有“慢性阻塞性肺疾病”病史 10+ 年。

病程记录：

图 1 我院急诊科心电图 心率 39bpm，QT/QTc 560/451ms，QRS 112ms

图 2 3+ 年前初始使用氯氮平随访心电图，心率 92bpm，QT/QTc 376/465ms，QRS 84ms

体格检查：体温 36.7 ℃，脉搏 45 次 / 分，呼吸 18 次，血压 137/79mmHg，血氧饱和度 SPO2 100%，身高 170cm，体重 70kg，BMI 24.22kg/m^2。体型中等，意识清楚，精神差，定向正常，接触尚可，对答切题，注意力集中，记忆及智力尚可，思维逻辑稍有障碍。全身皮肤无紫纹，颈静脉无怒张，口唇发绀，双肺呼吸音粗，下肺闻及湿性啰音，未闻及哮鸣音。心界无扩大，心率 45 次 / 分，各瓣膜听诊区未闻及病理性杂音。腹平软，全腹无压痛，无反跳痛及肌紧张，肠鸣音约 4 次 / 分。双下肢无水肿，神经系统查体无异常。

辅助检查：（1）实验室检查。血气分析提示 PH 值 7.40，氧分压 101.00mmHg，二氧化碳分压 34.20 mmHg，乳酸 2.56 mmol/L。肝功提示总蛋白 62.4 g/L，白蛋白 32.9 g/L。B 型钠尿肽前体 1331.00pg/mL。超敏 C 反应蛋白 54.15 mg/L。尿微量白蛋白 111.83 mg/L 。心肌酶谱、肌钙蛋白、肾功能、血脂、电解质、甲功、糖化血红蛋白、血栓弹力图、粪便常规 + 隐血试验均未见明显异常。

（2）影像学检查。入院第一天心电图（予以盐酸异丙肾上腺素注射液提升心率后）提示窦性心律（心率 60 次 / 分）、频发房性早搏、不完全性右束支阻滞、左心室高电压、右室及后壁未见异常；入院第二天心电图提示交界性心律（心率 57 次 / 分）、不完全性右束支阻滞、T 波改变及 Q-T 间期延长（QT 间期 562 毫秒）、右胸壁无特殊、正后壁 T 波改变；入院第四天心电图提示显著窦性心动过缓（心率 49 次 / 分）、房性早搏、T 波改变、完全性右束支阻滞（见图 3）。心脏彩超提示 LVEF 63%，主动脉窦部及升主动脉增粗，二尖瓣、三尖瓣、主动脉瓣轻度返流，左室舒张顺应性下降，主动脉瓣瓣口流速增快。甲状腺彩超、腹部（肝胆胰脾）彩超未见异常。血管超声提示双侧颈动脉粥样硬化伴斑块形成，双侧椎动脉阻力指数增高；胸、腹主动脉粥样硬化伴斑块形成；双下肢动脉粥样硬化伴斑块形成。泌尿系超声提示左肾囊肿，前列腺增大伴钙化灶。胸部 (平扫 + 冠状面成像) 提示双肺间质性肺炎，右主支气管粘液；肺气肿征；主动脉、冠脉钙化；纵隔淋巴结增大；双侧胸膜增厚，双侧胸腔积液。

图 3 患者入院后第一天、第二天、第四天心电图

A．入院后第一天心电图 心率 60bpm，QT/QTc 439/439ms，QRS 120ms；B. 入院后二天心电图 心率 57bpm，QT/QTc 562/547ms，QRS 118ms；C. 入院后第四天心电图 心率 49bpm，QT/QTc 456/412ms，QRS 122ms。

诊断：窦性心动过缓（氯氮平撤药反应）、精神分裂症、慢性阻塞性肺病、间质性肺炎、胸腔积液、低蛋白血症、外周动脉粥样硬化、单纯性肾囊肿。诊断依据：患者老年男性，病程长，无明显电解质紊乱、严重心肌缺血、严重缺氧、甲状腺功能减低等危险因素，入院 1 月前反复出现头晕与体位改变相关，入院前 6 小时再次发作头晕与体位改变无关，当地医院完善心电图提示窦性心动过缓、心率 34 次 / 分、QT 间期延长，入院后多次完善心电图均提示窦性心动过缓。结合患者既往病史及用药史，患者长期服用氯丙嗪、氯氮平，且于入院 3 天前，患者自行停用氯氮平，故诊断为窦性心动过缓（氯氮平撤药反应）。窦性心动过缓应与其他缓慢性心律失常导致的心率减慢相鉴别，根据心电图中的 I 、II 和 aVL 导联上直立 P 波且 aVR 导联上负向 P 波提示心动过缓起源于窦房结，可行鉴别；同时，还应明确引起窦性心动过缓的原因，该患者缺少心肌梗死、心肌炎、甲状腺功能低下、高钾血症、高钙血症、服用 β 受体阻滞剂 / 非二氢吡啶类钙拮抗剂 / 洋地黄类药物 / 抗心律失常药物等证据，故考虑该患者为氯氮平撤药反应引起窦性心动过缓。

治疗：入我院后立即予以盐酸异丙肾上腺素注射液 0.5mg+5% 葡萄糖注射液 200ml 缓慢静滴以提升心率，使用 1 天后心电监护提示窦性心律过缓，心率波动于 50-60 次 / 分，故停用盐酸异丙肾上腺素注射液，并请心身医学科会诊后，调整抗精神分裂症治疗方案为氯丙嗪 400 mg（1 次 / 日）+ 氯氮平 100 mg（1 次 / 日），加用沙美特罗替卡松吸入剂 1 吸（2 次 / 日）抗炎、扩张支气管等治疗；随访心电图，监测心率、血压变化，入院第 5 天后，患者心率波动于 60 次 / 分左右，期间血压波动于 110-135/60-80mmHg；入院第七天随访心电图提示窦性心动过缓（心率 59 次 / 分）、完全性右束支阻滞、电轴轻度右偏、T 波改变及 Q-T 间期延长（QT 间期 479 毫秒）（见图 4）；并完善动态心电图显示 I. 窦性心律，窦性心动过缓伴不齐（平均心率 :58 bpm；最快心率 :85 bpm；最慢心率 :40 bpm）；II. 房性早搏 110 次，单发房早 86 次，成对房早 4 次，房速 1 阵；III. 偶发室性早搏 1 次，单发室早 1 次；IV. 心率变异性分析：正常（见图 5）。

图 4 入院第七天心电图 心率 59bpm，QT/QTc 479/474ms，QRS 122ms

图 5 动态心电图

治疗结果、 随访及转归：出院后 1 月随访。（1）心电图：出院后 1 月随访心电

图提示：窦性心动过缓（心率 53 次 / 分）、电轴轻度右偏、不完全右束支阻滞（见图 6）。（2）患者现诉长期坚持规律服药，未再出现头晕等不适，在家自测脉搏在 60 次 / 分左右。

图 6 出院 1 月随访心电图 心率 53bpm，QT/QTc 466/437ms，QRS 110ms

检验检查记录：

见上

鉴别诊断：

1. 急性冠脉综合征

2. 电解质紊乱

3. 甲状腺功能减退症

4. 药物中毒

其他：

无

过敏性休克掩盖下的 STEMI：一例造影剂诱发 II 型 Kounis 综合征的救治启示

尚伟

重庆医科大学附属北碚医院

患者基本信息：

性别：男

年龄：50 岁

职业：个体户

身高：166cm

体重：80kg

主述：

反复胸痛 1+ 周

现病史：

入院 1+ 周前，患者反复出现胸骨后闷痛，发作与活动无关，休息下亦可出现，可忍受，每次持续半小时左右后自行缓解，每天发作 1-2 次，偶伴喉部、口腔牵扯性疼痛，偶伴心悸、出汗不适。

既往病史：

有“2 型糖尿病”病史 10 年，未规范治疗和随访。有“河虾”过敏史。

病程记录：

初步处理

入院后首次心电图（17：07）示窦性心律。入院后初步考虑诊断“非 ST 段抬高性急性冠脉综合症”，进行了危险分层评分。按照 GRACE 评分，当时为 90 分（尚未计算血肌酐水平），提示低危；按照 TIMI 评分，当时为 2 分（尚未计算心脏标志物检查），为低危。入院时，患者无胸闷、胸痛、血流动力学不稳定、心力衰竭等情况，与患者沟通后，同意暂时先行冠脉 CTA 检查。期间询问，患者否认近期使用“二甲双胍”，否认既往使用“造影剂”。

急救过程

17：15 患者至放射科，静脉注射对比剂碘普罗胺注射液 50ml（优维显 370；拜耳公司，德国），顺利行冠脉 CTA 检查。17：40 检查结束，返回病房。17：50 患者出现面部、颈部、胸部、上肢的皮肤潮红、肿胀，伴意识模糊，伴胸痛。当时测血压 80/50mmHg，心率 130 次 / 分，SPO2 90%，无喉头水肿，心肺听诊未见异常。17：55 考虑患者发生过敏反应，立即给予肾上腺素 0.5mg 肌肉注射、地塞米松 10mg 静脉注射、多巴胺泵入、大量补液、吸氧等处理。18：05 患者血压升高至 130/80mmHg 左右，心率波动于 100 次 / 分，SPO2 波动于 97-98%；患者皮肤红肿逐渐消退、意识状态好转，但胸痛未缓解。期间心电监护提示 II 导联的 ST 段较前明显改变，表现为弓背向上型抬高，且持续存在。复查心电图：窦性心律，ST 段在 II、III、aVF、V4-V6 导联呈弓背向上型抬高 2-3mm，ST 段在 V1-V3 导联呈水平型及下垂型压低 1-2 mm。18: 20 因怀疑“变异性心绞痛”，前后给予“硝酸甘油片”2 片含服，ST 段未见变化，胸痛未见缓解。18：30 静脉滴入“硝酸甘油”，加用“地尔硫卓 90mg”口服，ST 段未见变化，胸痛未见缓解。期间完善床旁肌钙蛋白 I：2.01 ng/ml（参考范围 < 0.3 ng/ml）。考虑患者为“急性下壁、前侧壁 ST 段抬高性心肌梗死”。结合患者存在造影剂严重过敏反应，故行 PCI 存在禁忌，与家属沟通后，行急诊溶栓治疗。于 18:46 开始行溶栓治疗，溶栓方案如下：阿替普酶 50mg/ 支，用生理盐水稀释后，静脉注射 15mg 负荷剂量，后续 30min 内以 0.75mg/kg 静脉滴注（该患者使用 50mg），随后 60min 内以 0.5mg/kg 静脉滴注 (该患者使用 35mg)；溶栓治疗结束时间 19:47。19:40，患者胸痛明显缓解，全身皮疹逐渐消退，心电监护可见室性心律失常、一过性窦性心动过缓、窦房传导阻滞，提示出现再灌注性心律失常。20:54，心电监护提示抬高的 ST 段较前回落，偶见室性早搏，提示溶栓治疗积极有效。期间患者血压波动于 134-148/78-89mmHg，心率波动于 102-110 次 / 分，SPO2 波动于 98-99%。期间冠脉 CTA 检查回示：前降支近段狭窄 25%，回旋支远段狭窄 50%，右冠中段狭窄 20%。复查心电图（当日 21：12），提示窦性心律，ST 段在 II、III、aVF、V4-V6 导联呈弓背向上型抬高 1mm，较前回落，ST 段在 V1-V3 导联无明显压低。复查肌钙蛋白 33.66 ng/ml（参考范围 < 0.3 ng/ml）。

后续治疗

继续复查心电图（次日 01：02）提示：窦性心律，ST 段在 II、III、aVF、V4-V6 导联无抬高，ST 段在余导联无明显改变（与入院时第 1 份心电图比较相似）。1 周时复查心电图，提示窦性心律，ST 段在 II、III、aVF、V4-V6 导联无抬高，ST 段在余导联无明显改变。继续复查肌钙蛋白 > 50 ng/ml(参考范围 < 0.3 ng/ml），1 周时复查肌钙蛋白 3.43 ng/ml（参考范围 < 0.3 ng/ml）。期间查血脂：总胆固醇 4.27mmol/L、低密度脂蛋白 1.92 mmol/L、甘油三酯 5.43 mmol/L；D 二聚体、BNP、肝功能、肾功能、电解质、心脏彩超等未见明显异常；Holter 提示全程基础心律为窦性心律，平均心率 70 次 / 分，室性早搏 560 次，未见缺血型 ST-T 改变。

溶栓后给予患者“阿司匹林 100mg qn、替格瑞洛 90mg bid、瑞舒伐他汀 10mg qn、地尔硫卓 90mg qd、培哚普利 4mg qd、低分子肝素 5000iu bid”的治疗方案。之后患者未再出现胸闷、胸痛等不适，生命体征平稳，于 1 周时出院。1 月后患者再次来院，一般情况可，日常活动不受限，未出现胸痛、心悸等不适，测血压 122/78mmHg，测心率 63 次 / 分，心肺查体无异常。长期用药如下：阿司匹林 100mg qn，替格瑞洛 90mg bid，瑞舒伐他汀 10mg qn，地尔硫卓 90mg qd，培哚普利 4mg qd 等。

检验检查记录：

见上

鉴别诊断：

1. 肺栓塞

2. 主动脉夹层

3. 心肌炎

其他：

本病例展示了一例由造影剂诱发、过敏性休克完美掩盖的急性下壁前侧壁 STEMI，最终确诊为 II 型 Kounis 综合征。在抗休克治疗改善过敏症状后，持续性胸痛及特征性 ST 段弓背向上型抬高的心电图动态演变，成为识破心肌梗死伪装的关键线索。面对 PCI 禁忌的困境，团队果断选择并成功实施静脉溶栓，挽救了心肌。该病例深刻诠释了 Kounis 综合征的凶险性、诊断的挑战性（尤其在休克状态下识别心肌缺血信号），以及在特殊禁忌下个体化治疗策略（溶栓）的关键价值，为临床处理此类‘双危象’重叠患者提供了宝贵经验。

甜蜜的瘫痪 一例低钾型周期性瘫痪患者的诊疗体会

尚伟

重庆医科大学附属北碚医院

患者基本信息：

性别：男

年龄：23 岁

职业：电子厂工人

身高：173 cm

体重：80 kg (BMI ≈ 26.7 kg/m²，超重)

吸烟史：10 年，约 10 支 / 天

饮酒史：偶有少量饮酒

家族史：无类似疾病家族史

主述：

反复双下肢乏力 1+ 年，再发 4+ 天，加重 1+ 天。

现病史：

入院 1+ 年前，患者突然出现双下肢乏力，无法站立，双侧对称，双上肢等活动自如，未处理后，双下肢乏力持续约 10 小时后逐渐缓解，近 1+ 年反复发作约 5 次，每次发作情况类似。

入院 4+ 天前，患者再次出现双下肢乏力，基本可站立，但活动欠

灵活，双上肢等活动自如，未处理后，约 10 小时后逐渐缓解，2 天

前再次类似发作 1 次。

入院 1+ 天前，患者再次出现双下肢乏力，程度较前加重，无法站立，无法将腿抬离床面，双上肢活动时稍感乏力，未处理后，上述不适持续未见缓解。遂前来我院急诊科就诊，查心电图提示“窦性心律，T 波低平，U 波形成”，血气分析提示“血钾 2.1 mmol/L”。

既往病史：

无“高血压病、糖尿病、甲亢、消化道疾病”等病史

病程记录：

体格检查 (入院时)：

生命体征：T 36.5℃， P 82 次 / 分， R 18 次 / 分， BP 136/70mmHg， SPO2

100%。

神经系统：

四肢肌张力不高。

双侧上肢肌力 5 级。

双侧下肢肌力 1 级 (关键阳性体征)。

双侧病理征 (-)。

其他：体型中等，颈静脉无充盈，心肺听诊未及明显异常，双下肢无水肿。

辅助检查 (部分关键结果)：

急诊：

血气分析：血钾 2.1 mmol/L。

心电图：窦性心律，T 波低平，U 波形成。

入院后：

血钾动态监测：

入院时：2.1 mmol/L

治疗后：2.35 mmol/L (具体时间点未详述)

治疗后：4.43 mmol/L (具体时间点未详述)

其他检查 (用于鉴别诊断，均未见明显异常)：

血常规、肝功能、肾功能、甲状腺功能、BNP、血糖、糖化血红蛋白。

肾素、醛固酮、皮质醇水平及节律。

24 小时尿钾。

Holter：窦性心律，平均 75 次 / 分，室性早搏 170 次，无缺血型 ST-T 改变。

头颅 MRI + 腰椎 MRI。

心脏彩超、下肢血管彩超。

下肢肌电图 (NCV)：双下肢胫神经、腓神经运动及感觉传导速度未见明显异常。

诊疗经过：

入院诊断： 低钾血症 (病因待查)。

治疗： 积极补钾（口服 + 静脉）。

病因明确： 结合病史及诱因追问，明确为可乐性低钾。

关键干预： 严格指导患者避免摄入可乐等饮料。

转归： 治疗后患者双下肢肌力逐渐恢复。

出院情况： 入院第 3 天，患者拒绝复查血气分析、血钾及心电图，要求出院。出院时下肢功能已恢复。

出院诊断：

低钾型周期性瘫痪

可乐性低钾

出院医嘱：

保证日常钾摄入（橙子、豆类、坚果、菠菜、海产品等）。

严格避免高糖饮料（尤其可乐、冰红茶、果汁、奶茶等，包括无糖可乐）及高盐、高碳水化合物食物。

规律作息，避免劳累、熬夜、情绪波动。

剧烈运动或大量出汗后及时饮水。

随访： 出院后 2 周、4 周电话随访，患者诉未再出现下肢乏力不适。

检验检查记录：

见上

鉴别诊断：

1. 缺钾性低钾血症

2. 稀释性低钾血症

其他：

1."可乐性低钾"的生动实例：清晰地展示了一个由长期大量饮用可乐 (每次 1-2L) 诱发严重低钾血症 (血钾 2.1 mmol/L)，进而导致低钾型周期性瘫痪的典型病例。这是该病的特殊诱因，贴近生活，警示性强。

2. 隐匿诱因的挖掘过程： 强调了诊断的关键在于细致追问病史。在排除了常见病因（摄入不足、丢失过多、内分泌疾病、药物因素等）后，通过反复询问才最终发现 "大量饮用可乐" 这一关键诱因，体现了临床思维的重要性。

3. 典型临床表现与快速恢复： 病例呈现了低钾型周期性瘫痪的经典特征：

青年男性（23 岁）。

反复发作、对称性、近端重于远端的双下肢驰缓性瘫痪（下肢肌力 1 级）。

发作间期正常。

心电图特征性改变（U 波形成、T 波低平）。

补钾后症状迅速缓解（结合避免可乐后未再复发）。

4. 明确的"可乐 - 低钾 - 瘫痪"因果链验证： 通过治疗干预 (补钾 + 停饮可乐) 和随访（出院后 2 周、4 周未再发作），有效验证了可乐是导致低钾和瘫痪发作的直接诱因，为诊断提供了有力支持。

从绝望到希望：左主干心梗患者的重生之路

蒋雨枫

苏州大学

患者基本信息：

性别：男

年龄：24 岁

就诊日期：2023 年 4 月 21 日

主述：

突发胸痛 1 小时

现病史：

患者 1 小时前工作中突发心前区疼痛，程度剧烈，伴大汗淋漓，濒死感，持续不缓解，同伴立即拨打 120 送至我院急诊，血气分析：PH7.34， PCO2 37.8 mmHg，PO2 84.2mmHg，Lac4.1mmol/L，Glu17.8mmol/L，K3.7mmol/L，急查心电图示 aVR、I、aVL ST 段抬高，II、III、aVF、V1-V6 ST 段压低，请我科会诊后考虑左主干心肌梗死可能，立即予无创通气、双抗负荷，同时与家属电话沟通病情后拟急诊行 CAG 备 PCI。

既往病史：

基础疾病：否认冠心病、高血压、心肌病、糖尿病史。

手术史：无 PCI 或心血管手术史。

个人史：无吸烟饮酒史，饮食规律。

过敏史：无药物 / 食物过敏。

家族史：否认高血压、糖尿病、卒中家族史。

病程记录：

1. 急诊介入治疗（2023.04.21）

冠脉造影（CAG）：左主干（LM）闭塞，右冠脉（RCA）正常；血栓抽吸 + 替罗非班冠脉内注射，植入主动脉内球囊反搏（IABP），血流恢复 TIMI 3 级。

手术策略：参与 OPTIMAL 研究（延迟支架植入组），未直接植入支架。

2. 术后诊断与治疗

主要诊断：

急性 ST 段抬高型广泛前壁心肌梗死（Killip IV 级）

2 型糖尿病（随机血糖 17.8 mmol/L，OGTT 及抗体检测确诊）

抗磷脂综合征（APS）待确诊（抗心磷脂抗体 IgG ↑、IgM ↑）

高脂血症（TG 4.09 ↑，LDL-C 4.55 ↑）

药物治疗：

抗栓：华法林（INR 2-3）+ 双抗（阿司匹林 + 氯吡格雷）

降脂：瑞舒伐他汀 + 依洛尤单抗（PCSK9 抑制剂）

心衰管理：沙库巴曲缬沙坦 + 美托洛尔 + 螺内酯

降糖：恩格列净 + 二甲双胍

免疫调节：羟氯喹（0.2g bid）

3. 病情演变

心肌损伤标志物：肌钙蛋白 T 峰值 8456 pg/mL（显著升高→大面积心梗）。

心功能：EF 42%（↓），左室壁节段性运动异常。

并发症：急性心衰（ProBNP 1535 pg/mL）、乳酸酸中毒。

检验检查记录：

关键辅助检查

项目	结果	意义
心电图（急诊）	aVR/I/aVL ST ↑，下壁及胸前导联 ST ↓	左主干 / 前降支病变
冠脉造影（CAG）	LM 闭塞，血栓抽吸后血流恢复 TIMI 3 级	心梗直接证据
肌钙蛋白 T（峰值）	8456 pg/mL（↑↑）	大面积心肌坏死
心超（术后）	EF 42%，左室壁节段性运动异常	心功能受损
抗磷脂抗体	抗心磷脂 IgG/IgM ↑，β2-GP1 IgM 31.71 RU/mL（↑）	APS 可能
糖尿病相关	随机血糖 17.8 mmol/L，OGTT 异常，GADA 阴性	新发 2 型糖尿病
血脂	TG 4.09 ↑，LDL-C 4.55 ↑	高脂血症
Holter	偶发室早 / 房早	低心律失常风险

其他重要结果

凝血功能：APTT 延长（147.6 秒），需监测抗凝出血风险。

感染指标：WBC 19.44×10 ^{9} /L（↑），但 CRP 正常，无感染证据。

免疫检查：ANA 阴性，补体正常，排除 SLE 等结缔组织病。

鉴别诊断：

急性冠脉综合征（ACS）：

支持点：典型胸痛、ST 段改变、肌钙蛋白升高、CAG 证实 LM 闭塞。

特殊点：年轻男性无传统危险因素→需排查继发性病因。

抗磷脂综合征（APS）：

证据：抗心磷脂抗体（IgG 77.58 ↑、IgM 46.25 ↑）、β2-GP1 抗体阳性；

意义：APS 可导致冠脉血栓形成，需 12 周后复查抗体确诊。

其他病因：

心肌炎（年轻患者，但无感染史，心电图不符）；

冠脉痉挛（冠脉造影未见痉挛，血栓明确）。

其他：

核心问题：24 岁男性突发左主干心梗，病因可能与抗磷脂综合征相关，合并新发 2 型糖尿病及高脂血症。

治疗重点：抗凝（华法林）+ 免疫调节（羟氯喹）预防再梗，强化心衰及血糖管理。

随访计划：

12 周后复查抗磷脂抗体（确诊 APS）；

1 年后复查冠脉造影及心功能评估。

辗转三甲医院，多次消融术后复发的室上速到底有多硬核

蒋春英

上海市第十人民医院

患者基本信息：

患者 **，男性，66 岁

主述：

反复心悸 8 年，再发伴出汗 1 天

现病史：

患者 8 年前无明显诱因下开始出现心悸不适，为阵发性发作，每次持续数分钟至数小时不等，发作时血压低下，多次医院急诊就诊，严重影响生活。2018 年及 2020 年接受射频消融术，具体不详。2024 年 9 月发作频繁，意识丧失，查心电图示宽 QRS 波心动过速，某三甲医院行三尖瓣环典型房扑及双径路射频消融术（未见手术记录），术后再次发作，后一直服用抗心律失常药物治疗。一天来再次发作伴有出汗。

既往病史：

Ø2024 年 2 月行冠脉造影，前降支植入支架 1 枚，8 年前右颈内动脉支架植入术。有高血压病史。

病程记录：

1 反复发作，消融不成功。原因是什么？手术记录未见，电生理诊断错误，典型房扑消融？

2 冠心病，支架植入病史。发作伴有出汗，血压低下等表现。冠状动脉是否存在问题？

遂决定，先完善冠脉造影检查。

冠脉造影检查结果提示：未见明显问题。故继续完善动态心电图检查。

动态心电图提示另一种心动过速：窄 QRS 波心动过速。两种形态的心动过速，是同源还是来自不同部位？拟第四次手术，完善电生理检查。考虑快慢型房室结双径路，室上性心动过速。多次尝试，最终房室结位置消融成功。

消融方法：慢快型双径路室上性心动过速，解剖结合电位消融法。

准确的靶点，降低并发症发生风险。

分析原因：电生理检查诊断似乎不是很难，但靶点位于非常规慢径位置。前面数次消融失败。甚至第 3 次怀疑房扑，消融了三尖瓣峡部。

快径高位位置分析：① 没想到；② 想到，但消融导致高度房室传导阻滞风险较大

讨论：左侧间隔对面消融是否有效？

检验检查记录：

见 PPT

鉴别诊断：

见 PPT

其他：

见 PPT

迟发性 HIT 治疗后再发心梗 1 例

陈鸿武

中国科学技术大学附属第一医院（安徽省立医院）

患者基本信息：

男，87 岁，58Kg

主述：

2 月内晕厥 3 次住院

现病史：

• “半小时前胸闷伴晕厥一次”，于 2024 年 6 月 21 日急诊入院。无明显胸痛及咳嗽咳血发热等，无明显气喘。急诊心电图提示：下壁导联 ST 段弓背向上抬高，III° AVB。诊断：急性下壁 ST 段抬高型心肌梗死，III° AVB。急诊 CAG 提示右冠近段完全闭塞伴血栓，LAD 近中段 90% 狭窄。术中临时起搏保护，肝素 6000u，右冠顺利植入 1 枚进口 PP 支架（4.0/28mm），术后血流 TIMI3 级。术后恢复窦性心律，拔出临时起搏，EF50%，术后第六天（6.26）康复出院，口服氯吡格雷阿司匹林（多立维）抗血小板治疗。住院期间合并右侧小腿肌间静脉血栓，予以联合低分子肝素 3000u Qd 共 3 天。入院急诊血常规提示：血小板 165×109/L，术后第二天血小板 168×109/L，出院前血小板 146×109/L。

• “半天内晕厥一次伴黑便”，于 2024 年 7 月 6 日再次入急诊科，无明显胸闷胸痛，心电图提示窦性心律，无 ST 抬高。但血常规提示血小板 8×109/L。初步诊断：血小板减少，上消化道出血，心肌梗死亚急性期，PCI 术后，收住血液内科。入院后予以停用氯吡格雷阿司匹林，同时予以地塞米松、丙球、重组人血小板生成素、口服海曲泊帕乙胺醇片等治疗，并积极完善检查，血小板抗体（+）。但患者入院后血小板仍持续下降（由 8-5-5-4-2-7-16-41-70），最低下降至 2×109/L，因上述治疗效果不佳，间断输血小板 3 次。患者住院 18 天，未出现颅内出血等严重并发症，血小板恢复至 50×109/L 以上时口服氯吡格雷 50mg Qd（停药半月），7 月 24 日出院，血小板 70 ×109/L ，继续口服海曲泊帕乙胺醇片 5mg Qd。嘱患者出院 1 周复查血常规。

• “胸痛 8 小时伴晕厥一次”，于 2024 年 8 月 11 日下午入院。仍有胸闷胸痛，急诊心电图提示：下壁导联 ST 段弓背向上抬高，III° AVB。诊断：急性下壁 ST 段抬高型心肌梗死，III° AVB。比伐芦定抗凝下再次急诊 CAG 提示右冠近段完全闭塞伴血栓，LAD 近中段 90% 狭窄。术中临时起搏保护，使用比伐芦定抗凝，右冠中段顺利串联植入 1 枚国产 PP 支架（4.0/29mm），术后血流 TIMI3 级。予以氯吡格雷阿司匹林抗血小板，术后恢复窦性心律，第三天拔出临时起搏，EF47%。入院时血小板明显升高（ 457×109/L ），予以停用海曲泊帕乙胺醇片。动态监测血小板变化（由 400-411-423-441-398-332-324-296-287-263）。住院期间大便 OB 仍（+），复查上消化道备餐提示“幽门管粘膜脱垂”。术后第 8 天，比伐芦定抗凝下行前降支 PCI 术，术中前降支及右冠支架行 OCT 检查，提示支架贴壁及膨胀均满意。术后一过性轻度消化道出血，予以单用替格瑞洛 90mg Bid 抗血小板。 二次术后第 7 天（8.25）康复出院。

既往病史：

• 既往高血压，口服缬沙坦氨氯地平，有 COPD 及肾功能不全，否认糖尿病及脑梗塞。

病程记录：

•2024.6.21 12:20 “胸闷伴晕厥 1 小时” 急诊入院，急诊血小板 165×109

12:50 急诊心电图提示：III° AVB，下壁导联 ST 段弓背向上抬高；

13:55 急诊右冠近段植入 1 枚支架，术中肝素 6000u，植入临时起搏器；

15:10 术后低分子肝素 3000u。

•2024.6.22 血小板 168×109，窦性心律 + 起搏心律，阿司匹林 + 氯吡格雷，CYP2C19 中间代谢

•2024.6.23 血小板 151×109，阿司匹林 + 氯吡格雷，拔除临时起搏器

•2024.6.24 下肢肌间静脉血栓，低分子肝素 3000u，阿司匹林 + 氯吡格雷

•2024.6.25 血小板 146×109，低分子肝素 3000u，阿司匹林 + 氯吡格雷

•2024.6.26 低分子肝素 3000u, 阿司匹林 + 氯吡格雷，EF50%，出院。

•2024.7.5 黑便伴晕厥一次，急诊血小板 8×109，严密观察会诊。

•2024.7.6 急诊血小板 7×109，合并皮下出血点，收住血液内科，急诊予以输注丙球 2.5g，备血小板

•2024.7.7 急诊血小板 5×109，输血小板，皮下注射 TPO（重组人血小板生成素），口服海曲泊帕乙胺醇片 5mg Qd

•2024.7.8 口服海曲泊帕乙胺醇片 7.5mg Qd， TPO，地塞米松 20mg

•2024.7.9 急诊血小板 5×109，输血小板， TPO，建议骨穿（拒绝）。口服海曲泊帕乙胺醇片，地塞米松 20mg

•2024.7.10 急诊血小板 4×109， TPO，口服海曲泊帕乙胺醇片，地塞米松 20mg

•2024.7.13 急诊血小板 2×109， TPO，血小板抗体 +，双下肢出血点

•2024.7.14 输注配型血小板 2u， TPO

•2024.7.15 急诊血小板 7×109，输注丙球 2.5g， TPO

•2024.7.16 输注配型血小板 1u， TPO

•2024.7.20 急诊血小板 16×109， TPO，输注配型血小板 1u

•2024.7.22 急诊血小板 41×109， TPO，开始氯吡格雷 50mg Qd（停药 17 天）

•2024.7.24 急诊血小板 70×109，TPO，海曲泊帕乙胺醇片 5mg Qd，出院

•2024.8.11 13:00 “胸痛伴晕厥一次” 急诊入院，急诊血小板 457×109

14:23 急诊心电图提示：III° AVB，下壁导联 ST 段弓背向上抬高；

14:55 急诊右冠中段植入 1 枚支架，术中比伐芦定抗凝，植入临时起搏器；

•2024.8.12 血小板 400×109，窦性心律 + 起搏心律，阿司匹林 + 氯吡格雷，大便 OB+

•2024.8.13 血小板 411×109，拔除临时起搏器，阿司匹林 + 氯吡格雷

•2024.8.14 血小板 423×109， CYP2C19 中间代谢，替格瑞洛 + 吲哚布芬，TEG

•2024.8.15 血小板 441×109，

•2024.8.17 血小板 398×109，

•2024.8.18 上消化道钡餐：幽门管粘膜脱垂

•2024.8.19 前降支 PCI（术中使用比伐芦定），术前血小板 332×109，血红蛋白均为 114g/L，术后一过性上消化道出血，禁食水，术后血小板 324×109，血红蛋白均为 114g/L

•2024.8.20 血小板 296×109 血红蛋白 113g/L

•2024.8.21 试饮水

•2024.8.22 血小板 287×109，温凉流质

•2024.8.23 大便 OB+，软食

•2024.8.24 血小板 263×109，血红蛋白 124g/L

•2024.8.25 出院

检验检查记录：

•2024.6.21 急诊血小板 165×109；急诊心电图提示：III° AVB，下壁导联 ST 段弓背向上抬高；

•2024.6.22 血小板 168×109，窦性心律 + 起搏心律，CYP2C19 中间代谢

•2024.6.23 血小板 151×109 窦性心律

•2024.6.24 下肢肌间静脉血栓

•2024.6.25 血小板 146×109

•2024.6.26 EF50%，阿司匹林 + 氯吡格雷，带药出院。

•2024.7.5 黑便伴晕厥一次，急诊血小板 8×109。

急诊头颅 CT：右侧额颞部硬膜下积液，脑缺血改变，透明隔间隙增宽，脑萎缩。双下肢静脉血流通畅；

•2024.7.6 急诊血小板 7×109，合并皮下出血点，收住血液内科

•2024.7.7 急诊血小板 5×109，免疫球蛋白（IgG 升高，其余正常）

•2024.7.9 急诊血小板 5×109，抗核抗体阴性，抗磷脂抗体阴性

•2024.7.10 急诊血小板 4×109，TORCH 系列阴性。Coom’s 弱阳性

•2024.7.13 急诊血小板 2×109，血小板抗体 +，双下肢出血点

•2024.7.15 急诊血小板 7×109

•2024.7.20 急诊血小板 16×109

•2024.7.22 急诊血小板 41×109 开始氯吡格雷 50mg Qd（停药 17 天）

•2024.7.24 急诊血小板 70×109，出院

•2024.8.11 “胸痛伴晕厥一次” 急诊入院，急诊血小板 457×109，急诊心电图提示：III° AVB，下壁导联 ST 段弓背向上抬高；术后 EF47%。

•2024.8.12 急诊术后第二天血小板 400×109，窦性心律 + 起搏心律，阿司匹林 + 氯吡格雷，大便 OB+；双肺渗出性改变，两侧胸腔少许积液。

•2024.8.13 血小板 411×109，拔除临时起搏器

•2024.8.14 血小板 423×109， CYP2C19 中间代谢，替格瑞洛 + 吲哚布芬，TEG（血小板增多，血凝块力学强度增加）

•2024.8.15 血小板 441×109

•2024.8.17 血小板 398×109

•2024.8.18 上消化道钡餐：幽门管粘膜脱垂；男性肿瘤全套（CA125 轻度升高，其余正常）

•2024.8.19 前降支 PCI（术中使用比伐芦定），术前血小板 332×109，血红蛋白均为 114g/L，术后一过性上消化道出血，禁食水，术后血小板 324×109，血红蛋白均为 114g/L

•2024.8.20 血小板 296×109 血红蛋白 113g/L

•2024.8.22 血小板 287×109

•2024.8.23 大便 OB+

•2024.8.24 血小板 263×109，血红蛋白 124g/L

•2024.8.25 出院

鉴别诊断：

•I 型夹层导致下壁心肌梗死（心脏彩超及 CT 排除）

• 脑出血导致晕厥（头颅 CT 排除）

• 原发性血小板减少（病史否认）

• 继发性血小板减少

GIT（术中未用）

病毒感染导致血小板减少（检验否认）

风湿免疫疾病（检验否认）

肿瘤相关性（检验否认）

其他：

• 第一次住院（胸痛伴晕厥）STEMI 住院行急诊 PCI（2024.6.21-6.26）

• 第二次住院（黑便伴晕厥）迟发型 HIT 升血小板 （2024.7.6-7.24）

• 第三次住院（胸闷伴晕厥）升血小板过高再发 STEMI 行急诊 PCI （2024.8.11-8.25）

•2024.8.25 出院后至今未再有不适，一直口服替格瑞洛 90mg Bid、立普妥 20mg、泮托拉唑、螺内酯、达格列净、诺欣妥 50+50mg。

•2025.1.24 心电图：窦性心律，66bpm，下壁 Q 波；心脏彩超：EF50%，二尖瓣及主动脉瓣轻中度反流

血常规：WBC5.11×109/L，血小板 184×109/L ，血红蛋白 119g/L；肌酐 97umol/L，LDL-C2.19，空腹血糖 5.31，ALT9.2IU/L；大便 OB+；

•2025.4.1 心电图：窦性心律，67bpm，下壁 Q 波，房早；心脏彩超：EF51%，二尖瓣反流（中度偏少），主动脉瓣轻中度反流

血常规：WBC4.83×109/L，血小板 168×109/L ，血红蛋白 113g/L；肌酐 97umol/L，LDL-C1.59，空腹血糖 5.24，ALT9.2IU/L；大便 OB+，停替格瑞洛改波立维 75mg Qd（术后 7 月）；

•2025.6.10 心电图：窦性心律，49bpm，下壁 Q 波 . 心脏彩超：EF49%，二尖瓣反流（轻中度），主动脉瓣轻度反流

• 波立维 75mg、立普妥 20mg、泮托拉唑、螺内酯、达格列净、诺欣妥 50+50mg

IVUS 指导 ELCA 治疗静脉桥血管闭塞一例

王威

中国人民解放军总医院第六医学中心

患者基本信息：

67 岁男性

主述：

间断胸痛 7 年，再发 3 月

现病史：

患者自 2016 年初间断出现胸痛症状，疼痛位于胸骨后，呈闷胀痛，常在提重物等活动后出现，持续数分钟，休息后可缓解，偶有头痛，就诊于当地医院，诊断为“冠心病”，行冠状动脉搭桥手术（左乳内动脉桥至前降支，升主动脉至回旋支、后降支大隐静脉桥），术后胸痛症状缓解。2023 年 1 月，患者再次出现胸痛症状，疼痛位于胸骨后，呈闷胀痛，可在夜间休息时出现，持续十几分钟，休息后可缓解，无咳嗽、咳痰、咯血，无恶心、呕吐、呕血，无腹泻、腹痛、便血，无头晕。就诊于当地医院，行冠状动脉造影提示动脉桥通畅，静脉桥重度狭窄（具体不详）。未行介入治疗。

既往病史：

否认高血压、糖尿病病史，高脂血症病史 7 年，未规律治疗。吸烟 30 年，平均每天 20 支，已戒烟 7 年。

病程记录：

患者入院后予阿司匹林 100mg 口服每日一次，替格瑞洛 90mg 口服每日两次，瑞舒伐他汀 10mg 口服 1/ 日，依折麦布 10mg 口服 1/ 日治疗。后行冠状动脉造影示：左主干末端不规则，前降支自开口完全闭塞，回旋支近段弥漫性狭窄 90%，右冠近端节段性狭窄 90% 伴瘤样扩张、自中段起闭塞；动脉桥血管通畅，升主动脉至回旋支静脉桥血管段闭塞，回旋支至后降支静脉桥血管段通畅。术中静脉桥自开口闭塞，正向寻找困难，采用逆向导丝指引正向开通升主动脉至回旋支静脉桥血管段，血管内超声示静脉桥内斑块负荷较重，应用准分子激光消融后串联植入 4 枚药物支架，术中未发生慢血流、无复流。术后予阿司匹林 100mg 口服每日一次，替格瑞洛 90mg 口服每日两次，瑞舒伐他汀 10mg 口服 1/ 日，依折麦布 10mg 口服 1/ 日，美托洛尔缓释片 47.5mg 口服每日一次治疗。

检验检查记录：

心电图提示 II、III、aVF 导联，V3-V6 导联 T 波倒置。心脏超声示主动脉窦增宽，室间隔 12mm，主动脉瓣、三尖瓣、肺动脉瓣轻度反流，射血分数 61%。

鉴别诊断：

患者三支病变，已行搭桥手术治疗，外院冠脉造影证实动脉桥通畅、静脉桥狭窄。

主要与急性肺栓塞、主动脉夹层、心包积液等鉴别，行心脏超声、查血 D 二聚体等化验检查以资鉴别。

其他：

生死时速：一例暴发性心肌炎合并心源性休克与电风暴的救治

游洁芸

上海市东方医院（同济大学附属东方医院）

患者基本信息：

1. 中青年女性，发病前有发热

2. 胸闷伴消化道症状

3. 既往体健，无心脏病及慢性病史

4. 心肌损伤标志物明显升高

5. 心电图提示传导系统损害、广泛心肌损害，无明确定位

主述：

发热 3 天，胸闷 1 天

现病史：

患者 3 天前发热，最高体温 39.1℃，予头孢呋辛抗感染及对症治疗 3 天，体温恢复正常。入院前 1 天突发胸闷，伴呕吐一次，无胸痛、黑矇、晕厥，心悸、气促、腹痛、腹泻等症状。

既往病史：

1. 既往史：既往体健，否认慢性病史，否认手术史，否认过敏史。

2. 个人史、婚育史、月经史、家族史：未婚未育，平素月经正常，无家族遗传病。

病程记录：

1. 入院查体: T 36.8℃, BP 111/68mmHg。神清, 呼吸平稳, 皮肤无明显色素沉着。颈软, 颈静脉无充盈。双肺呼吸音粗, 未闻及明显干湿啰音, 心率 65 次 / 分, 律齐, 无杂音, 腹平软, 无压痛及反跳痛, 肝脾肋下未及, 双下肢无浮肿。四肢肌力 V 级, 肌张力正常，病理征阴性。

2. 综合救治过程：

机械循环支持：早期及时植入 VA-ECMO，联合 IABP、机械通气等高级生命支持。

药物干预：病因治疗（免疫调节、抗病毒）、补钾补镁、充分镇静、抗心律失常（利多卡因、β 受体阻滞剂、胺碘酮）、维持血流动力学稳定。

动态监测：血流动力学、心功能、凝血功能及感染指标等。

并发症管理：1）左心室扩张：IABP、降低前负荷（控制入量，加强利尿）、正性肌力药物增加心肌收缩力（小剂量肾上腺素）、降低后负荷（扩血管药物、优化 VA-ECMO 流量）。2）凝血功能异常：输血（红细胞悬液、血浆、冷沉淀、单采血小板）、止血（缩宫素、优思明）、根据凝血功能指标及时调整肝素剂量。3）多重耐药菌感染：根据药敏试验积极抗感染。

心脏康复。

3. 转归：经积极抢救治疗，患者心源性休克、室性心律失常电风暴、左心室扩张、凝血功能异常、多重耐药菌感染等均得到有效控制，第 16 天撤除 ECMO，第 19 天撤除 IABP，第 20 天拔除气管插管，第 39 天顺利出院，2 月后心超及心电图均恢复正常。

检验检查记录：

入院辅助检查结果：

1. 心肌损伤标志物：cTnT 0.807 ng/mL，CK-MB 23.68 ng/mL，MYO 115.7 ng/mL；

2. 生化：ALT、Scr、AMY、GLU 均正常，K 3.5 mmol/L；

3. D 二聚体：1.66 mg/L；

4. 血气分析（鼻导管吸氧 2L/min）：PH 7.519，PCO2 25.6 mmHg，PO2 116.5 mmHg，SpO2 99.6 %，BE -2.1 mmol/L，Lac 1.4 mmol/L；

5. 血常规及炎症指标：

入院前 3 天：WBC 3.39×109/L，N 76.3 %，L 14.5 %，CRP 7.24 mg/L；

入院当天：WBC 3.22×109/L，N 53.8 %，L 35.4%，CRP 3.17 mg/L，SAA 11.25 mg/L；

6. 病原学检查（入院前 3 天）：甲乙流、新冠均阴性。

7. 心超：左室节段性运动异常（下壁基底段及下侧壁基底段运动减低），二尖瓣及三尖瓣少量反流，LVEF 57%。

8. 心电图：窦性心律，T 波改变（I、aVL、V4、V5、V7 低平，II、III、aVF 倒置）。

9. 胸部 CT：未见明显异常。

10. 冠脉造影：未见明显异常。

鉴别诊断：

1. 急性心肌梗死

2. 急性肺动脉栓塞

3. 主动脉夹层

4. 急性心包炎

5. 原发性心肌病急性加重

6. 气胸

7. 急腹症

8. 其他引起胸闷的疾病

其他：

通过介绍一例暴发性心肌炎合并心源性休克与电风暴的救治过程，强调多学科协作下以 ECMO 为核心的生命支持体系的关键作用，同时介绍了 ECMO 运行过程中遇到的困境（包括左心室扩张、凝血功能异常、感染等）及解决措施。

暴发性心肌炎合并心源性休克与电风暴需早期识别、快速启动 ECMO 等高级生命支持，联合多学科协作，实现全生命周期管理。

生长激素促进心脏移植患者心脏再发育康复出院一例

蔡欢

新疆维吾尔自治区人民医院

患者基本信息：

52 岁中年男性，公务员，

主述：

反复胸闷气短 5 月，加重 3 天

现病史：

患者自诉于 5 月前受凉后出现胸闷、气短不适，伴有夜间不能平卧，咳嗽，咳白色黏痰，活动耐量明显下降，无发热、胸痛、黑朦、咯血等不适，就诊于我院，完善相关检查后，诊断“1. 心源性休克 缺血性心肌病 2. 左肺下叶肺动脉栓塞 3. 短阵室速 频发室早 4. 慢性心力衰竭（急性加重）5. 重症肺炎 6. 双侧胸腔积液 7. 冠心病 PCI 术后 陈旧性心梗”，经患者及家属同意，行胸腔穿刺引流术及强化抗血小板聚集，降脂、稳定斑块，减慢心率，降低心肌耗氧量，抑制心室重构等对症治疗，病情基本平稳后，于 2022-4-29 日行“心脏除颤器置入术 (S-ICD)+ 胸廓成形术 + 置入可充电的心脏收缩力调节 [CCM] 装置，全系统 + 右心导管置入 + 静脉穿刺术”，术后强化抗血小板聚集，调脂、稳斑，抑制心室重塑，改善心衰，抗感染，多次胸腔引流等综合治疗，病情未见好转，请多次院内疑难病例讨论及远程会诊，调整治疗方案，患者病情有所好转后报出院，此后因胸腔积液反复入住我院，并给予胸腔穿刺等对症治疗，好转后出院。此次次于 3 天前无诱因再次出现胸闷、气短不适，无发热、胸痛、黑朦、咯血等不适，伴有夜间不能平卧，咳嗽，咳白色黏痰，不易咳出，活动耐量明显下降。为进一步诊治来我院就诊，急诊以“心源性休克”收住。

既往病史：

2022 年 1 月份因胸痛不适，就诊于黄河路中医院，完善心电图及心肌酶，诊断为“急性心肌梗死”，择期完善冠脉造影提示血管狭窄 85% 以上，予以行冠状动脉支架植入，规律口服“阿司匹林 氯吡格雷 阿托伐他丁”治疗。

平素健康状况体健， 2013 年 5 月冠脉造影（血管狭窄 85% 以上）+PTCA 术，外伤：10 岁时右足粉碎性骨折及左小腿外侧划伤（具体不详）。

病程记录：

患者中年男性，2013 年明确诊断为冠心病，并行“冠脉造影 +PTCA 术”，此后先后置入多个冠脉支架，并因病情反复多次住院治疗，规律口服“阿司匹林 氯吡格雷 阿托伐他丁”治疗；2022-04-29 在我院因病情行“心脏除颤器置入术 (S-ICD)+ 胸廓成形术 + 置入可充电的心脏收缩力调节 [CCM] 装置，全系统 + 右心导管置入”，术后强化抗血小板聚集，调脂、稳斑，抑制心室重塑，改善心衰，抗感染，多次胸腔引流等综合治疗，病情未见好转，多次院内疑难病例讨论及远程会诊，病情未见好转，此次入院前 3 天再次出现病情加重，2022-09-05 以“反复胸闷、气短 5 月，加重 3 天”为主诉心内科 CCU 病区治疗，明确诊断为难治性心力衰竭 慢性心功能不全急性加重 心功能Ⅳ级，09-12 经过疑难病例讨论后行 IABP 植入术，强心、利尿降肺动脉压力、纠正凝血功能及内环境紊乱，并完善心脏移植前准备，等待心脏移植，于 2022-09-13 在全麻行“心脏移植术 + 体外膜肺氧合［ECMO］安装术 + 暂时性经静脉起搏器系统的置入 + 心包切开引流术 + 胸腔闭式引流术 + 延迟关胸术 + 漂浮导管检查 [Swan-Ganz 导管插入]”，因病情危重，术后转入重症医学科监护抢救治疗，予以报病危、心电监护、ECMO 及 IABP 辅助循环、BIS 监测、肺动脉压力持续测定等，治疗上稳定循环、改善心功能、输血改善贫血、输血浆改善凝血功能、输注血小板预防出血、抗凝、呼吸机辅助通气、抗感染、免疫抑制、补充白蛋白、营养支持、脏器功能维护等综合治疗；术后第 1 天（2022-09-14），完善双下肢血管彩超提示：右下肢动脉血栓形成，紧急请血管外科会诊后急诊行切开取栓术；术后第 2 天（2022-09-14），患者右侧小腿肿胀，完善心肌酶谱、肾功能等均有明显升高，提示脏器功能不全，经过讨论后由血管外科在床旁行“右下肢筋膜间隙切开减压术”，并行 CRRT 治疗，加强抗凝治疗；术后第 3 天（2022-09-15），患者下肢肌肉颜色暗红，弹性差，存在右侧小腿肌肉坏死表现，有导致多脏器功能不全进一步加重可能，经过疑难病例讨论行“右下肢截断术 + 筋膜皮瓣移植术”，去除病灶改善全身症状；经过以上积极调整治疗，患者循环逐渐稳定，下调 ECMO 参数后循环稳定，经过疑难病历讨论后，术后第 8 天（2022-09-21）在全麻行行“开胸探查术 + 体外膜肺氧合［ECMO］撤离术”，术后安返我科继续监护抢救治疗，治疗上根据每日疑难讨论后调整调整，完善 SBT 实验后，2022-09-22 拔除气管插管，治疗上予以高流量吸氧持续湿化气道、俯卧位、震动排痰等呼吸道管理治疗，但患者自主咳痰能力差，出现呼吸衰竭表现，2022-09-25 行气管插管辅助通气，完善支气管镜下见气道内大量粘痰堵塞气道，予以灌洗治疗后呼吸道情况有所改善，但因咳痰能力差，痰液引流不畅，每日行支气管镜下吸痰改善呼吸，并加强呼吸道管理；因患者神志未恢复，咳痰无力等原因，为加强呼吸道管理、利于痰液引流、改善感染等诸多原因，再次经过疑难病历讨论，于 2022-09-29 在局麻下行“气管切开术”，其后根据痰量、胸片炎症渗出等因素间断行气管镜肺泡灌洗吸痰治疗，治疗上继续抗感染、强心、改善心衰、稳定循环、严格容量控制、CRRT 改善肾功能、免疫抑制、呼吸道管理、营养支持、补充白蛋白、适当镇静镇痛、改善焦虑、辅助睡眠、术区换药保持切口清洁干燥、红外线治疗促进切口愈合、床旁康复、心理疏导等综合治疗；2022-10-04 患者出现体温波动，最高体温 38.5℃，并出现循环波动，结合病情经过疑难病例讨论后考虑感染反复，存在脓毒症、感染性休克，经过讨论后调整抗感染方案、稳定循环、免疫抑制方案调整、脏器功能维护等积极治疗，病情再次逐渐好转，进入平台期，治疗上根据病情微调治疗；2022-10-27 凌晨患者病情再次出现波动，表现为高热、循环波动，经过讨论后再次考虑为感染反复，患者一直存在感染与免疫之间的平衡问题，反复出现感染性休克，并多次调整抗感染方案，多次留取培养等查找致病菌，每日行全院疑难病例讨论调整治疗方案，积极控制感染并调整心脏功能，并血滤置管进行血滤治疗，密切监测患者全身情况，经积极治疗后患者感染得意控制，肾功能不全情况治疗效果满意，撤除血滤后尿量逐日增多，治疗效果显著。患者病情总体平稳后出院。

检验检查记录：

鉴别诊断：

（1）急性肺动脉栓塞：可发生胸痛、咯血、呼吸困难和休克。但有右心负荷急剧增加的表现如发绀、肺动脉瓣区第二心音亢进、颈静脉充盈，肝大、下肢水肿等。心电图示 I 导联 S 波加深，III导联 Q 波显著 T 波倒置，胸导联过度区左移，右胸导联 T 波倒置等改变可鉴别。（2）主动脉夹层：胸痛一开始即达高峰，常放射到背肋腹腰和下肢，两上肢的血压和脉搏可有明显差别，可有下肢暂时性瘫痪、偏瘫和主动脉关闭不全的表现，但无血清心肌坏死标记物升高等可资鉴别。二维超声心电图检查、X 线或磁共振体层显像有助于诊断。

其他：

-

猝死原因为何：一例肥厚型心肌病家系的遗传学调查

毛琦

陆军军医大学附属新桥医院心内科

患者基本信息：

樊某，女，43 岁，因“反复心悸、气促 4 年，头晕 1 年”入院。

主述：

反复心悸、气促 4 年，头晕 1 年

现病史：

4 年前无明显诱因出现心悸、气促，不伴胸闷，无黑矇、晕厥，遂就诊市内三甲医院，诊断为“肥厚型心肌病”（室间隔 17.7mm），予以药物治疗，但未规范服用。1 年前逐渐出现头晕不适，自测血压偏低，波动于“90-100/50-60mmHg”，无视物旋转，无黑矇、晕厥，活动较前明显受限，运动耐量降低。就诊时头晕、气促较前加重，曾自服“中药”治疗，但未见明显改善，无胸痛、黑矇、晕厥，无咯血、浮肿，遂于 2019 年 1 月 23 日入院

既往病史：

否认“高血压、糖尿病、冠心病”等病史，2014 年于当地医院行“剖宫产术”，余无特殊

病程记录：

生命体征： T 36.4℃ P 92 次 / 分 R 20 次 / 分 BP 93/52mmHg

神志清楚，精神正常，查体合作，言语清晰，对答切题。皮肤无黄染，全身浅表淋巴结无肿大，皮温正常，口唇无发绀，颈软，双肺呼吸音清晰，未闻及干湿啰音，心前区无隆起，心尖搏动正常，无抬举样搏动及震颤，心界不大，心率 92 次 / 分，心律规则，心音正常，各瓣膜区未闻及明显杂音。腹部平软，无压痛、反跳痛及肌紧张，双下肢无水肿。

随机血糖：5.7mmol/L；动脉血气：PH 7.43，氧合正常

血、尿及大便常规正常，肝肾功及甲功正常，凝血常规无异常

冠脉 CT 血管造影：冠脉未见明显异常

检验检查记录：

我们报道了一个高猝死风险的 HCM 家系并发现了一处位于 MYBPC3 基因的新发剪切位点突变 c.2737+1（IVS26）G>T

MYBPC3 c.2737+1（IVS26）G>T 突变导致转录本 26 号外显子跳跃缺失，造成 cMyBP-C 中 C7 结构域的结构崩塌和功能破坏，使 cMyBP-C 分子不能正确锚定在肌节 A 带中，导致心肌结构和功能障碍

对高 SCD 风险的肥厚型心肌病患者，建议植入 ICD，并给予 β- 受体阻滞剂以减少猝死风险

鉴别诊断：

心肌病

其他：

青年男性，反复心梗为哪般？

王方超

重庆大学附属人民医院

患者基本信息：

患者周某，男，33 岁

主述：

咽喉部紧缩感 2+ 月，胸闷 2 小时

现病史：

入院前 2+ 月，无明显诱因出现咽喉部紧缩感，未诊治。2 小时前无明显诱因出现持续胸闷，伴全身冷汗，未诉胸背部痛、咳嗽咳痰、呼吸困难、咯血等表现，

安静休息无好转，外院心电图提示“急性前间壁 ST 段抬高型心肌梗死”，为进一步诊治急诊入我院。

既往病史：

无特殊

病程记录：

33 岁男性，首次因 STEMI 急诊入院，冠脉造影提示前降支开口闭塞，前降支 - 左主干植入 1 枚支架，规律药物治疗，1+ 年后再次急性心梗入院，急诊造影提示左主干闭塞，血栓抽吸 + 球囊扩张后 2 小时再次出现左主干闭塞，再次上台，术中反复出现主干闭塞，术后强化抗凝治疗，调整抗板方案，后续出现两次消化道出血，完善相关检查，病因不明。后续复查再次出现支架内狭窄，再次植入 2

枚支架，最后于风湿免疫科诊断为白塞氏病。规律激素、免疫及生物制剂治疗后，复查冠脉造影，支架未再出现再狭窄。

检验检查记录：

见 PPT

鉴别诊断：

动脉粥样硬化、易栓症、血管炎等

其他：

病例亮点：

1. 青年男性急性心肌梗死，符合目前心肌梗死年轻化趋势

2. 中青年心肌梗死，不应只关注心肌梗死治疗，需注重病因筛查

3. 文献资料显示，白塞氏病累及冠脉导致狭窄、急性心肌梗死罕见

4. 该患者既往有白塞氏病相关临床表现，但被临床医师忽略，造成诊断延迟，如及时多学科 MDT 协作，有利于早期诊断明确，及时基础疾病治疗也有利于避免反复支架内再狭窄

“摇摇欲坠”的心脏 一例老年急性重症心肌炎的诊治

王方超

重庆大学附属人民医院

患者基本信息：

张某某，男，82 岁

主述：

发热 3 天，发现心电图异常 5 小时

现病史：

入院前 3 天，患者受凉后出现咳嗽咳痰，痰为白色粘痰，伴发热，体温最高 39.5℃，外院考虑肺部感染，予以头孢唑肟抗炎治疗，病程中未诉明显胸闷胸痛、

心累气短等不适。5 小时前当地医院心电图提示“窦性心律，I、II、AVL、V5、V6 导联 ST 段弓背抬高 0.1-0.5mv”，考虑急性侧壁 ST 段抬高型心肌梗死，

为进一步诊治入我院

既往病史：

既往体健，2021.01 于我院胸外科行“胸腔镜左肺下叶切除 + 纵膈淋巴结清扫 + 左喉返神经探查 + 胸腔黏连松解术”，术后病检：浸润性腺癌，术后未放化疗，

规律随访。余病史无特殊

病程记录：

82 岁老年男性，发热 3 天，外院住院期间心电图提示“STEMI”样表现，患者无不适，急诊行冠脉造影排除急性心肌梗死，临床诊断为急性心肌炎，住院期间心功能逐渐恶化，心衰加重，心律失常，心电图呈现典型心肌炎表现（低电压、束支阻滞、AVB、频发室早、室速），经积极纠正心衰、激素和免疫球蛋白冲击、代谢治疗后病情逐渐趋于稳定，心功能好转出院

检验检查记录：

见 PPT

鉴别诊断：

急性心肌梗死

其他：

病例亮点：

1. 急性心肌炎中青年常见，高龄老年相对少见

2. 该患者入院无任何症状，住院期间呈现为典型心肌炎发展过程（症状发展、血生化指标变化、心脏结构功能变化、传导系统演变），可作为典型病例展示

3. 老年患者急性心肌炎治疗方案是否区别于中青年人群，如何更好的改善这类人群预后，值得探讨

弥漫性大 B 细胞淋巴瘤心脏转移一例

王方超

重庆大学附属人民医院

患者基本信息：

患者曹某某，女，62 岁

主述：

短暂性意识丧失 1 次

现病史：

入院前 1+ 月，患者站立时无明显诱因突发意识丧失，跌倒在地，持续数十秒后意识恢复，发作前否认头昏头痛、心悸胸闷等不适，发作时无肢体抽搐、口吐白沫、大小便失禁等。醒后诉心累气短不适，伴头部外伤，未进一步诊治，病程中曾感一过性“精神恍惚”。入院前 9 天于当地医院就诊，心脏彩超提示“右房增大、右房异常回声、心包积液”，为进一步诊治入我院。

既往病史：

无特殊

病程记录：

62 岁女性，无基础心肺病史，因短暂性意识丧失入院，心电图提示交界性逸博心律，心脏彩超提示右心房占位、大量心包积液，胸部 CT 提示多发结节，结合心脏增强 MRI、心包穿刺、PET-CT、腋窝淋巴结活检，最终诊断为弥漫性大 B 细胞淋巴瘤伴多发转移。经规律抗肿瘤治疗后，患者心脏占位及心包积液完全消失，随访 2 年多，患者目前一般情况可

检验检查记录：

见 PPT

鉴别诊断：

1. 晕厥鉴别诊断

2. 心脏占位鉴别诊断

其他：

病例亮点：

1. 以“晕厥”为首发表现的继发性心脏肿瘤病例

2. 晕厥原因值得探讨：大量心包积液？交界性逸博心律？肺栓塞？

3. 右心房占位鉴别诊断：血栓？肿瘤？（原发 / 继发）

4. 患者右心房占位大，4.3cm*3.5cm，经抗肿瘤治疗后完全消失，随访 2 年多患者一般情况可，治疗方案值得探讨

顽固心律失常是何原因?

周佳

吉林大学第二医院

患者基本信息：

患者女，56 岁，

主述：

主因“间断心悸 38 年，加重 5 天”入院

现病史：

患者于 38 年前无明显诱因出现间断心悸，每次持续约 10 分钟至 1 小时不等，曾多次于当地医院就诊诊断为预激综合征，并行心电生理检查及射频消融术。5 天前上述症状再次出现，伴上腹痛、恶心、呕吐，症状持续不缓解。既往史：既往体健。入院检查：体温：36.5℃，脉搏 88 次 / 分，呼吸 18 次 / 分，血压 115/80mmHg。神志清，自主体位，双肺呼吸音清，未闻及干湿啰音，无胸膜摩擦音，心前区无隆起，心尖搏动点位于左侧第 5 肋间锁骨中线 0.5cm，未见异常搏动，未触及震颤，未触及心包摩擦感。心电图提示：窦性心律，一度房室传导阻滞，V2-V6 导联 ST 段压低 0.05-0.1mV。

既往病史：

体健

病程记录：

遂急检肌红蛋白、肌钙蛋白、NT-proBNP，心肌酶，完善心脏彩超等相关检查，肌红蛋白结果 47.77ng/ml（参考范围 0-70）、肌钙蛋白结果 0.055ng/ml（参考范围 0-0.08）、NT-proBNP 结果 741.6pg/ml（参考范围 0-900）均未见明显异常，心脏彩超提示：右心增大，右房（左右径 * 上下径）45*85mm，左房室内径正常，室间隔、左室后壁厚度正常。房室间隔回声连续。室壁各节段收缩活动未见异常。升主动脉 30mm，不增宽，主动脉瓣（左冠瓣、无冠瓣）增厚，回声增强，开放不受限，彩色多普勒探及主动脉瓣反流，反流面积 2.2 平方厘米，主动脉瓣前向最大流速 159cm/s，Pg10mmHg. 二尖瓣不增厚，开放不受限，二尖瓣环未见钙化，彩色多普勒谈及二尖瓣反流，反流面积 3.5 平方厘米，三尖瓣后叶和隔叶附着点向心尖部移位，三尖瓣隔叶与二尖瓣前叶距离为 47mm，致部分右室房化，二尖瓣前叶冗长，彩色多普勒探及三尖瓣反流，反流面积 9.5 平方厘米，最大反流速度 235cm/s，Pg22mmHg。估测肺动脉压力 Pg34mmHg，下腔静脉 14mm，塌陷率 < 50%，肺动脉不增宽，肺动脉瓣不增厚，彩色多普勒示肺动脉瓣微量反流，肺动脉瓣前向最大流速 77cm/s，Pg2mmHg。组织多普勒测定：二尖瓣环室间隔侧 E’/e’= 9.4. 超声印象诊断：先天性心脏病，三尖瓣下移畸形，右心增大，左心功能低限值，三尖瓣重度反流，主动脉瓣、二尖瓣轻度反流。主动脉瓣钙化（左冠瓣、无冠瓣）。患者入院第二日后再次发作心悸症状，性质同前，复查心电图提示：宽 QRS 心动过速伴多发室性期前收缩。

检验检查记录：

完善经食管超声心动图：各心腔及大血管内径同经胸超声，左房及左心耳内未探及血栓样回声，各瓣口血流未见异常。该患基础疾病为三尖瓣下移畸形，为明确

患者心动过速诊断及进一步治疗，建议患者行心电生理检查明确诊断，必要时行射频消融术，术中见：室房逆传，CS9-10A 波最早，行心室拖带心动过速终止时呈 VAVA 顺序排除房速考虑慢旁道，不除外不典型 AVNRT，应用 ST 消融导管行三尖瓣环激动标测，显示三尖瓣环 5 点处逆传 A 波最早，结合患者既往曾行 B 型预激消融，考虑右侧旁路逆传仍在。选择 ST 消融导管于三尖瓣环约 5 点钟处，标测到小 A 大 V 波，心室刺激，VA 融合，以此为消融靶点，55 度 35W 放电 5 秒钟出现 VA 分离，旁路逆传中断，继续巩固放电累计至 120s。此后患者出现宽 QRS 波心动过速，心率约 130 次 / 分，电生理检查示室房分离，考虑为室性心动过速，应用消融导管在三维下行激动标测显示后间隔三尖瓣瓣下 V 波激动最早，较体表心电图提前约 25ms，在此处放电约 20s 后室速终止，继续巩固放电至 180s，反复进行心房、心室 S1S2 和 S1S1 刺激，证明旁道无逆传，无心动过速发作。术后多次复查心电图未见异常心动过速发作。术中明确诊断：先天性心脏畸形、三尖瓣下移、预激综合征、阵发性室性心动过速、阵发性室上性心动过速、心功能 II 级。

鉴别诊断：

需与其余如完全性大动脉转位、动脉导管未闭等鉴别

其他：

心脏 T 细胞淋巴瘤继发暴发性心肌炎及多脏器损害一例

王一斐

北京清华长庚医院

患者基本信息：

73 岁男性

主述：

发作性意识丧失 1 周

现病史：

入院 1 周前患者由蹲位站立后出现黑朦，后立即出现意识丧失、摔倒，摔伤头部，数秒后意识恢复，有大汗、恶心、头晕等不适，否认大小便失禁、肌肉强直、抽搐、舌咬伤、胸痛等不适，未测血压。就诊我院急诊，测血压 131/78mmHg，心电图“窦性心律，电轴轻度左偏，室内传导阻滞”。后转诊至心内科，以“晕厥原因待查”收入院。

自发病来精神差，睡眠可，食欲下降 2 月，大小便无明显异常，近 2 月体重下降 3kg。

既往病史：

诊断胃溃疡 2 年，不规律口服奥美拉唑。2 周余前因间断右上腹痛、纳差持续不缓解，肝胆外科住院，腹部 CT 提示胆总管下段小结石可能，MRCP 提示肝外胆管轻度扩张，胃镜提示十二指肠息肉，病理提示慢性炎症，后患者调整为半流食口服，未予进一步干预。否认明确食物药物过敏史。

病程记录：

予冠心病二级预防治疗，后患者出现暴发性心肌炎，与甲泼尼龙 +IVIG，联合 IABP 及 ECMO 维持循环

检验检查记录：

心肌室间隔基底段活检：可观察到弥漫增生的非典型淋巴细胞，细胞大小不一，核轮廓不规则，伴少量嗜酸性细胞及组织细胞浸润

心肌活检 TCR：可见单克隆重排

心肌活检免疫组化：CD3(+), CD20(-), CD4 (+), CD5 (+), CD8 (+), Gran B (+), Ki67 (>85%)

考虑心脏 T 细胞淋巴瘤

鉴别诊断：

1、冠状动脉粥样硬化性心脏病

2、病毒性心肌炎

其他：

MitraClip 联合 PTSBME 治疗合并重度二尖瓣反流的肥厚型梗阻型心肌病 1 例

汪学文

岳阳市中心医院

患者基本信息：

患者男，51 岁。因“反复胸闷气促 2 年，加重半年”于 2024 年 04 月 29 日入院

主述：

反复胸闷气促 2 年，加重半年

现病史：

患者 2 年前始出现活动后胸闷气促，多于爬楼爬坡时出现，严重时伴乏力、头晕，休息后可缓解，近半年胸闷气促加重，一般活动明显受限，无胸痛、晕厥、心慌、大汗、夜间阵发性呼吸困难，于外院完善心脏彩超：左室壁增厚，左室流出道梗阻；二尖瓣返流（中 - 重度）；三尖瓣返流（中度）。予以中药治疗效果不佳，遂于我院门诊就诊，完善相关检查，拟“肥厚型心肌病”收入我科。

既往病史：

有冠心病病史，长期口服阿司匹林、他汀治疗；否认肝炎、结核等传染病史。否认药物、食物过敏史。否认手术史。否认输血史。否认肥厚型心肌病家族史。

病程记录：

予地尔硫卓、曲美他嗪等药物治疗，症状未见缓解。经结构性心脏病团队评估后行一站式室间隔支微球栓塞 + 经皮二尖瓣钳夹术。患者全身麻醉、气管插管后插入食道超声备用，首先使用微球颗粒进行室间隔支栓塞。冠脉造影显示相对粗大室间隔支。SIONblue 导丝成功送至粗大室间隔支远段，沿导丝送入微导管至室间隔支中段，在经食道超声指导下，经微导管行选择性超声造影显影，证实拟栓塞室间隔支有效（图 2）。静滴异丙肾使心率达到 100 次 / 分上做激发试验：血压明显下降至 60/40mmHg，LVOT 峰值压差 110mmHg。微导管送入 SIONblue 导丝交换 2.5*20mmOTW 球囊至室间隔支开口 - 近段。OTW 球囊 4atm 扩张后，从 OTW 球囊注入微球颗粒液约 2ml 栓塞。栓塞后食道超声再次测量流出道流速明显降低，提示栓塞有效。食道超声提示二尖瓣仍有明显反流，SAM 征未消失（图 3），经结构性心脏病团队讨论后决定进一步行二尖瓣钳夹。在经食道超声指导下穿刺房间隔，采用 MitraClip XTR 成形夹输送系统进行二尖瓣钳夹，在超声引导下调节 MitraClip XTR 成形夹输送系统指向二尖瓣口返流最明显处并能垂直活动，打开 MitraClip 成形夹的双臂至 120°，在经食道超声指导下调整 MitraClip XTR 成形夹使之位于二尖瓣前后瓣叶的中间，实时 3 维超声外科视野切面下进一步调整 MitraClip XTR 成形夹至二尖瓣瓣环外交界，并使两臂位于 12 点半和 6 点半，于心脏舒张期送入心室腔，缓慢回撤 MitraClip XTR 成形夹，并使 2 个瓣叶均落在 MitraClip 成形夹 的两个臂上，操作 MitraClip XTR 成形夹，使之夹住 2 瓣尖，经食道超声反复确认二尖瓣返流微量，再次激发试验证实有效心率达到 100 次 / 分上，血压 80/60mmHg 左右，跨瓣压差较前降低，最终释放 MitraClip XTR 成形夹。再次冠脉造影示：前降支及右冠无明显异常，床旁心电图证实无明显传导阻滞及前壁、下壁急性心肌梗死。

检验检查记录：

BNP、肌钙蛋白、三大常规、肝肾功能、电解质、凝血功能、甲状腺功能无明显异常。经食道心脏超声：符合非对称性梗阻性肥厚型心肌病声像图改变（室间隔不均匀增厚，基底段明显，最厚处约 18mm，凸向左室流出道，致左室流出道狭窄，V max：3.82m/s，平均跨瓣压差 29mmHg；心尖段各壁厚约 10 - 11mm，室间隔中间段厚约 12mm，余中间段各壁厚约 11 - 12mm）升主动脉内径增宽，左房增大（左房左右径约 55mm，上下径约 64mm）二尖瓣中度反流、三尖瓣及主动脉瓣轻度返流 房间隔膨胀瘤，卵圆孔未闭 肺动脉增宽。左心室造影 + 测压检查：收缩期左心室心尖部及基底节部明显受压，左室心尖、左室流出道与主动脉瓣上压差 80-90mmHg；符合肥厚型梗阻性心肌病改变。冠脉造影：前降支近段局限性狭窄 40-50%，左主干、回旋支、右冠无明显狭窄。六分钟步行实验 240m。

鉴别诊断：

1）高血压性心脏病：长期高血压可导致左心室对称性肥厚，而 HCM 多为非对称性室间隔肥厚。高血压患者通常有明确血压升高史，且心肌肥厚程度与血压控制相关。超声心动图显示室壁增厚均匀，无左室流出道梗阻表现；

2）主动脉瓣狭窄：主动脉瓣狭窄可引起左心室肥厚和胸痛、晕厥等症状，易与 HCM 混淆。超声心动图可明确瓣膜狭窄程度及瓣叶形态（如二叶式主动脉瓣），而 HCM 的主动脉瓣结构通常正常，梗阻位于左室流出道或心尖部。

其他：

一个月随访患者胸闷气促症状较前好转，心功能较前改善，活动耐量较前增加，六分钟步行实验由术前的 240m 增加到 480m。复查心脏彩超示室间隔基底部肥厚明显，约 14mm，LVOT 峰值压差 14mmHg，心脏 MRI 证实室间隔肥厚减轻，超声示二尖瓣反流较前减少，EF66%。

一年后复查心脏 MRI、心脏彩超示室间隔肥厚明显减轻，LVOT 峰值压差基本正常。无二尖瓣反流。

声尺量心路，术数判盈枯—— IVUS+FFR 指导无造影剂冠状动脉介入一例

王威

中国人民解放军第六医学中心

患者基本信息：

男性，67 岁

主述：

间断胸痛 9 年，加重 2 周。

现病史：

2016 年起，间断出现胸痛症状，呈针刺样，症状在步行上 3 楼等活动后出现，持续数分钟，休息后可好转。未行诊疗。

2025 年 3 月 18 日起，再次出现上述症状，疼痛在平路步行时也可出现，无恶心、呕吐、呕血，无咳嗽、咳痰、咯血，无腹痛、腹泻、便血，无头晕、头痛，就诊于中国人民解放军第一医学中心，行冠脉 CT 示：前降支中段重度狭窄，CT 检查时出现颜面部、双眼睑发红伴明显水肿，持续 2 天后逐渐消退。

既往病史：

高血压病 10 年，血压最高达 180/110mmHg，平时应用氨氯地平 5mg 口服每

日一次，血压波动在 150/80mmHg 上下。高脂血症病史 9 年，应用他汀类、依折麦布等效果欠佳。

病程记录：

入院后予阿司匹林 100mg 口服每日一次，氯吡格雷 75mg 口服每日一次，瑞舒伐他汀 10mg 口服每日一次，依洛尤单抗注射液 140mg 皮下注射每两周一次，美托洛尔 12.5mg 口服每日两次，氨氯地平 5mg 口服每日一次。术前 6 小时予甲泼尼龙琥珀酸钠 0.5g 静滴后行冠状动脉介入治疗，在已有冠状动脉 CT 指引下，在前降支、对角支分别置入导丝，沿前降支导丝行血管内超声示左主干最小管腔面积 7.92mm^2，斑块负荷 50%。前降支最小管腔面积 2.08mm^2，远段参考管腔直径 3.5mm，病变长度 27.9mm。行血流储备分数示前降支病变远端 0.74，左主干病变前后未发生压力跳跃。沿对角支导丝行血管内超声示对角支开口面积 6.46mm^2。在对角支行导丝拘禁，在前降支中段植入一枚 3.5×28mm 药物支架。术后沿前降支导丝行血管内超声示最小支架内面积 5.01mm^2，行血流储备分数示前降支支架远端 0.85。沿对角支导丝行血管内超声示对角支开口面积 6.31mm^2，行血流储备分数示对角支开口以远 0.89。术后患者症状缓解。出院带药：阿司匹林 100mg 口服每日一次，氯吡格雷 75mg 口服每日一次，瑞舒伐他汀 10mg 口服每日一次，依洛尤单抗注射液 140mg 皮下注射每两周一次，美托洛尔 12.5mg 口服每日两次，氨氯地平 5mg 口服每日一次。

检验检查记录：

心脏超声示：左房扩大（左右径 39mm），三尖瓣轻度反流，EF：66%。心电图示：窦性心动过缓，心率 57 次 / 分

鉴别诊断：

患者行冠状动脉 CT 后出现颜面部水肿，需与肾功能不全、心功能不全鉴别。行心脏超声、血肌酐等检查以资鉴别。

其他：

ICE 指导下 Ebstein 畸形合并 B 型预激综合征导管消融一例

孙胜楠

辽宁省人民医院

患者基本信息：

35 岁

女性

主述：

发作性心悸 1 年

现病史：

近 1 年来反复出现心悸，持续 1-2 分钟可自行缓解，近半年频繁发作

既往病史：

房间隔缺损，于 2014 年介入封堵房间隔

病程记录：

未予药物治疗，排除禁忌后择期心脏电生理检查、射频消融术

检验检查记录：

心电图

超声心动图

鉴别诊断：

其他：

冲击波球囊，钙化困局中的破壁者--钙化病变旋磨后支架膨胀不全补救一例

王威

中国人民解放军总医院第六医学中心

患者基本信息：

男性，66 岁

主述：

间断胸闷 1 个月

现病史：

2025 年 1 月起患者间断出现胸闷，位于左侧胸部，为闷胀不适感，夜间休息时也可出现，持续数分钟，可自行好转。偶有咳嗽，干咳少痰，无咯血，无恶心、呕吐、呕血，无腹痛、腹泻、便血，无头晕、头痛，就诊于北京仁和医院，诊断为“冠心病”，行冠状动脉造影示：前降支中段狭窄 90%，回旋支中段狭窄 80%。术中在回旋支植入 1 枚支架。前降支未行介入治疗。术后胸闷症状无明显好转。为求进一步治疗来我院就诊。

既往病史：

高血压病史 10 年，血压最高 160/90mmHg，高脂血症病史 10 年，应用他汀类药物效果欠佳，吸烟 30 年，每日 20 支，未戒烟。

病程记录：

患者入院后予阿司匹林 100mg 口服每日一次，替格瑞洛 90mg 口服每日两次，阿托伐他汀 20mg 口服每日一次，依折麦布 10mg 口服每日一次，美托洛尔 25mg 口服每日 2 次治疗。行冠状动脉造影示：前降支近中段节段性狭窄 90% 伴重度钙化，回旋支支架通畅，右冠细小。行光学相干断层成像提示：大于 270°的钙化病变长度大于 3mm，存在 360°的钙化，最小管腔面积 1.33mm^2，远端参考管腔直径 2.65mm。送入 1.5mm 旋磨头，以 16 万转至 18 万转行旋磨，旋磨后植入 2.75×28mm 支架，非顺应性球囊无法完全膨胀，行 OCT 示前降支最小支架内面积 3.22mm^2，支架膨胀率 57%。反复后扩张无效。在支架内应用 2.5×12mm 冲击波球囊，释放 20 次冲击波后，非顺应性球囊可以完全膨胀。复查 OCT 示：前降支最小支架内面积 4.79mm^2，支架膨胀率 77%。治疗后患者症状好转。出院带药阿司匹林 100mg 口服每日一次，替格瑞洛 90mg 口服每日两次，阿托伐他汀 20mg 口服每日一次，依折麦布 10mg 口服每日一次，美托洛尔 25mg 口服每日 2 次

检验检查记录：

心脏超声：二、三尖瓣轻度反流，射血分数 57% 。心电图示：窦性心律，完全性右束支传导阻滞。

鉴别诊断：

本例患者不稳定型心绞痛需要与慢性冠脉综合征、肺炎、肺动脉栓塞、主动脉夹层鉴别，需行心脏超声、血常规、血 D 二聚体，并根据患者症状、体征鉴别诊断。

其他：

1 例猝死青少年的起死回生：挑战与总结

杨靖

北京清华长庚医院

患者基本信息：

25 岁男性，慢性病程

主述：

反复晕厥 9 年余

现病史：

18 年前因“胃痛”就诊于北京儿童医院时查心电图发现 Brugada 波，考虑 Brugada 综合征可能，否认心悸、胸闷、胸痛，无黑矇、晕厥等，未予特殊诊治。

9 年余前看电脑时，情绪激动后出现晕厥，摔倒在地，晕厥前无心悸、胸闷等症状，摔倒在地，伴有口唇咬伤、小便失禁、大声吼叫、四肢抽搐，20min 后清醒，清醒后觉乏力，大连 120 急救到现场，送至外院，心电图示：室上性心动过速（未见报告资料，由患者陈述），测血压 90/60mmHg，血钾 3.02mmol/L，予以补钾治疗后，镇静后予以电复律治疗后好转。

转至我院就诊

既往病史：

既往史：否认高血压、糖尿病、冠心病、高脂血症、其他心律失常史、其他系统疾病史、传染病史、手术外伤史、输血史。酒精过敏。

个人史：否认吸烟饮酒史，否认疫区接触史、地方性疾病史、冶游史、毒品和放射线接触史。

家族史：父母及外公外婆、爷爷奶奶无晕厥及猝死病史，无兄弟姐妹，未婚，无子女，无早发心血管疾病史及猝死家族史，无家族性遗传病情况。

病程记录：

入院 5 分钟前患者外出时在车上意识丧失， 呼之不应、 肢体强直， 小便失禁，家属立即自驾至我院急诊， 血压、心率测不出，除颤仪监护界面提示心室颤动，予非同步双向 120J 直流电除颤 2 次，并立即予心肺复苏 、气管插管有创呼吸机辅助通气，及肾上腺素强心 、碳酸氢钠纠正酸中毒、补钾等治疗

检验检查记录：

入院时，紧急 ECG 显示室颤。迅速采取了包括外部电除颤、心肺复苏和肾上腺素注射在内的急救措施。复苏后的 ECG 显示心房心动过速和单形宽 QRS 心动过速，伴有右束支传导阻滞（RBBB）模式。值得注意的是，V2 导联的 J 波幅度显著增加，J 点在 V2-V3 导联中清晰可见。鉴于患者血流动力学不稳定，进行了同步电复律。随后的 ECG 显示，患者出现窦性心动过速，QRS 波形与之前的心动过速相似（。当心率降至每分钟 95 次时，血压升至 85/60mmHg，RBBB 异常现象消失。

鉴别诊断：

该患者表现为宽 QRS 波心动过速，需与以下诊断鉴别：

①室性心动过速

②房性心动过速伴不等比例下传

③窦性心动过速

其他：

房性心动过速的存在使得 BrS 患者中区分真正的 RBBB 和室性心动过速变得复杂。速率依赖性的 RBBB 模式可能代表一种短暂的传导异常。此外，J 波幅度的增加

突显了 BrS 的心律失常风险。密切监测并及时干预以管理 BrS 患者的危及生命的心律失常至关重要。

地高辛中毒救治一例

苏伟江

广东省人民医院 粤西医院

患者基本信息：

患者女性，80 岁。

主述：

头晕一天

现病史：

病人因为长期重度二尖瓣返流 心房颤动 诱发心衰，间断在本院住院。此次药物治疗好转后于 2024 年 11 月 22 号出院，但由于老人家在家里误服地高辛 5 片，自觉头晕明显，家属立刻送病人到广东省人民医院 粤西医院急诊科，洗胃后收治到心血管一区病房。

既往病史：

既往诊断 慢性心力衰竭 重度二尖瓣返流 心房颤动。

病程记录：

当时查地高辛浓度 4.0（正常范围 0.9 –2.0），心率 30-40 次 / 分，科室在严密的心电血压监护下，立刻联系'血液透析'治疗，并密切监测血中地高辛浓度，经过两天的密切观察，病人的地高辛浓度从 4.0 降低到 2.9，0.9，病人的心率也从 30 恢复到 60 次 / 分， 12 月 3 日顺利出院。

检验检查记录：

病人的地高辛浓度从 4.0 降低到 2.9。心电图 显示 3 度房室传导阻滞。

鉴别诊断：

病态窦房结综合征：以头晕为常见症状，多有高血压，糖尿病病史，心电图可以明确。

其他：

血液透析是有效的治疗方法。

如何打破反复住院的恶性循环？ 一例高龄心衰患者的“逆袭”之路

尚伟

重庆市第九人民医院

患者基本信息：

患者基本信息

性别：男

年龄：90 岁

职业：退休矿工

身高：165 cm

体重：55 kg

主述：

反复心悸、气促 1+ 年，加重 2+ 天。

现病史：

患者 1+ 年前开始反复于活动后出现心悸、气促，休息后可缓解，伴间断双下肢水肿。曾于外院诊断为“扩张型心肌病”，建议植入 CRT-D，但患者拒绝。长期服用沙库巴曲缬沙坦、达格列净、比索洛尔、螺内酯、呋塞米等药物，症状曾一度好转，但仍反复发作，多次因心衰加重住院。心脏彩超提示射血分数（EF）30-40%，心电图示窦性心律、完全性左束支传导阻滞（QRS 156-158 ms），BNP 多次 > 1000 pg/mL。2+ 天前受凉后症状加重，稍活动即感心悸、气促，伴咳嗽、夜间阵发性呼吸困难、双下肢水肿及尿量减少。

既往病史：

高血压病史 3+ 年，未规范治疗及随访。

吸烟史 40+ 年，偶有少量饮酒。

病程记录：

药物治疗：优化抗心衰方案（沙库巴曲缬沙坦、达格列净、比索洛尔、螺内酯、呋塞米），抗感染及营养支持。

器械治疗：行心脏再同步化治疗（CRT），术后 EF 提升至 40%+，QRS 波缩窄，症状显著改善。

随访：术后 2 周，6 分钟步行距离由 100 m 增至 305 m，NT-proBNP 降至 815.0 pg/mL，无心衰症状复发。

检验检查记录：

心脏彩超提示 EF 32%

心电图：窦性心律，完左，QRS 156-158 ms

[Marker] cTnT 0.06 ng/ml，NT-pro BNP 4660 pg/mL

[CBC] HG 111 g/l，PLT 125x109 /L，WBC 8.1x109 /L

[Bioch] TB/CB 24.3/12.2 umol/L，A/G 49/34 g/L，Urea 8.80 mmol/L，Cr 126.10 umol/L，GFR 50.91mL/min，K+ 4.4 mmol/L

[D-dimer] 0.17 mg/L

[Thyroid Function] FT3 2.99 pg/mL, FT4 1.07 ng/dL, TSH 4.1 uIU/mL

[HbA1c] 6.3%

[BGA] PH 7.43, PaCO2 35mmHg, PaO2 80mmHg，SpO2 96%，lactic acid 0.9 mmol/L

Holter：全程基础心律为窦性心律，平均心率 70 次 / 分，室性早搏 781 次，房性早搏 420 次

胸腔彩超：双侧胸腔积液

腹部彩超：胆囊息肉样病变

泌尿系统彩超：右肾囊肿

颈部血管彩超：颈动脉粥样硬化

胸、腹主动脉彩超：动脉粥样硬化

鉴别诊断：

左束支阻滞性心肌病

其他：

通过药物优化联合 CRT-D 治疗，该高龄患者成功打破心力衰竭反复住院的恶性循环，证实了年龄并非 CRT 治疗的绝对禁忌，综合干预与个体化随访是改善预后的关键。

迷雾中的血栓风暴

刘瑞闪

河南省胸科医院

患者基本信息：

患者 45 岁男性，货车司机，既往有肺栓塞病史，本次以低蛋白血症、大量蛋白尿、高血压、高血脂及下腔静脉血栓形成为主要表现。

主述：

间断活动后气短半年，再发 20 天，加重 2 天

现病史：

半年前因突发咳嗽，伴胸闷、胸痛并活动后气短，于鹤壁市第二人民医院急诊住院治疗，行冠脉造影提示右冠脉轻度粥样斑块浸润，肺动脉 CTA 提示肺动脉栓塞，予以抗凝等治疗后好转后转至我院继续治疗，期间查 D-D 明显升高，心电图示 III、aVF 导联异常 Q 波，心脏超声示左室下壁基底段运动幅度稍减低、左室收缩功能正常，胸部 CT 平扫示右下肺外基底段实变及磨玻璃影、肺梗死待鉴别，继续予以抗凝、利尿补钾等治疗，除外禁忌后于 2024-12-09 行肺动脉造影示左中、下肺动脉近段可见血栓影、前向血流通畅，术后继续上述治疗，病情好转后出院，院外继续服用利伐沙班 20mg qd 抗凝，病程中间断有踝部肿胀。1 月前复查肺动脉 CTA（2025-05-04）示未见明显栓塞征象、右肺下叶前基底段少许炎性改变，半月余前停药。20 天前，患者开车行至甘肃省再发活动后气短，伴头晕、心悸，于当地医院就诊考虑“高原反应”，予以吸氧等治疗后好转半月前，患者开车行至陕西省时出现发热，伴胸闷、胸痛，于当地医院就诊，查尿常规提示“尿蛋白阳性”、胸部 CT 提示“肺炎”可能，予以抗感染、补充白蛋白等治疗后好转出院 10 余天前，患者返回林州后至当地医院住院治疗，复查胸部 CT 提示“轻度肺水肿”可能，对症治疗后好转出院 2 天前，患者仍感活动后气短，再次于林州红旗渠医院住院治疗，期间查腹部超声扫及下腔静脉近右房口 50mm 处血栓形成可能、下肢静脉超声提示血流瘀滞，心脏超声无明显异常，予以抗凝等治疗后好转，今为进一步诊治急诊至我院，急诊以“下腔静脉血栓形成”收入我科。

4 年余前体检发现血压升高，最高血压 170+/100+mmHg，现服用“替米沙坦 40-80mg qd”降压，未规律监测血压，平素无明显头晕、头痛等。

半年前，患者于我院查空腹血糖升高，未监测血糖，近期因血糖偏高予以“二甲双胍缓释片 0.5g bid”降糖，血糖控制不详。

自发病来，神志清，精神可，睡眠及饮食可，近半年小便泡沫多，尿量可，近期体重无明显变化

既往病史：

既往有吸烟史，约 20 年，平均 40 支 / 日，已戒烟半年，余无特殊

病程记录：

本入院予以调脂、抗凝、利尿、降压、降糖、补充白蛋白、减轻尿蛋白、抑酸及改善循环等治疗，近 2 日进一步于河南省人民医院肾内科门诊查抗磷脂酶 A2 受

体抗体示 32.21RU/ml（0-20），目前考虑膜性肾病可能，后于肾内科专科进一步诊治。

检验检查记录：

既往我院 2024-12-07 尿常规示隐血 1+, 尿蛋白 2+。肝功能示白蛋白 35.0 g/L。血脂示甘油三酯 2.29 mmol/L。肾功能及泌尿系超声无异常。2025-05-04 我院门诊血脂示甘油三酯 2.66 mmol/L, 总胆固醇 5.31 mmol/L, 低密度脂蛋白 -C 2.78 mmol/L。**近期外院 2025-05-04 生化示葡萄糖 7.64 mmol/L, 白蛋白 33.4 g/L。血脂示总胆固醇 5.37mmol/L，低密度脂蛋白 3.35mmol/L，甘油三酯 1.85mmol/L。**本次入院查 2025-06-02 心肌损伤标志物示 N- 末端脑钠肽前体测定 843.7 pg/ml。肝功能示白蛋白 24.7 g/L。尿常规示尿蛋白 2+, 隐血 +-。随机尿微量白蛋白 1085.180 mg/24h, 尿微量白蛋白 / 尿肌酐 1054.41 mg/g。2025-06-05 尿微量白蛋白 25227.81 mg/24h。24h 尿蛋白定量 15864.2 mg/24h。凝血功能示 D- 二聚体 5.95 ug/mL。血便常规、肝功、肾功、电解质、糖化血红蛋白、甲功、输血前检查无明显异常。心电图示窦性心动过缓，III、aVF 导联异常 Q 波。静脉超声示下腔静脉低回声（考虑血栓形成），双下肢静脉血流通畅。泌尿系超声示双肾动脉未见明显异常，右肾囊肿，前列腺体积增大伴钙化灶。肺动脉 CTA 示与我院 2025.05.04 日检查相比：右下肺动脉栓塞，较前新见；双肺结节、索条，大部分较前新见；双侧胸腔积液，较前新见。

鉴别诊断：

见上述。

其他：

检查文件见 PPT 中。

1 例风心病双瓣置换术后合并心源性肝硬化行 TTVR 的围术期生死竞速

刘瑞闪

河南省胸科医院

患者基本信息：

患者女，55 岁，风心病双瓣置换术后合并心源性肝硬化行 TTVR 围术期管理及诊疗相关。

主述：

活动后喘累 15 年，间断乏力、纳差 7 年，加重半月

现病史：

15 年前（37 岁）因活动后喘累于当地医院就诊，诊断为“风湿性心脏瓣膜病”，除外手术禁忌后行“二尖瓣及主动脉瓣置换术、三尖瓣成形术”，术后长期抗凝、强心、利尿等治疗。7 年前（45 岁）开始间断出现纳差，伴头晕、乏力，活动后稍喘累，无夜间阵发性呼吸困难，偶有腹胀，间断有下肢水肿，无黑矇、晕厥，无胸闷、胸痛，无慢性咳嗽、咳痰，无腹痛、黑便等，未进一步诊治。4 年前（48 岁）因上述症状加重于当地医院就诊，查血常规提示贫血，心电图示“阵发性心房颤动”，心脏超声示主动脉瓣及二尖瓣置换术后、双房大、主动脉瓣中度关闭不全、三尖瓣重度关闭不全、肺动脉高压、LVEF 56%，腹部超声示淤血肝、腹腔积液，考虑“风心病换瓣术后右心衰”，予以利尿、纠正贫血、腹腔穿刺抽液等治疗后稍缓解。病程中上述症状反复发作，间断于当地医院及我院对症处理，症状仍反复。半月前，患者再发上述症状，逐渐加重，于当地卫生院查常规生化提示“低蛋白血症、贫血、低钾血症”，予以补充白蛋白、利尿等处理后症状缓解不明显，为进一步诊治至我院，门诊以“风心病换瓣术后 心力衰竭”收入院。自发病来，神志清，精神一般，纳差，睡眠欠佳，大便可，小便偏少，近半月体重增加 3kg

既往病史：

曾于 30 余年前发现“心脏病”，具体不详，因经济原因未诊治，否认“高血压病、脑梗塞、糖尿病、肝炎、结核”等病史，因“贫血”有反复输血史，否认食物或药物过敏史。育有 2 女，个人史及家族史无特殊。

病程记录：

入院后查 2023-08-26 血常规示血红蛋白 94 g/L。国际标准化比值 2.55。生化示白蛋白 33.8 g/L, 肌酐 142.0 umol/L。心电图示不纯性心房扑动，下壁 Q 波形成，部分导联 T 波异常。腹部超声示符合肝淤血声像图改变，胆囊壁毛糙、增厚，脾大，右肾囊肿，双肾动脉未见明显异常，腹腔积液；下肢静脉超声示双侧小腿肌间静脉局部增宽。心脏超声示 AVR+MVR+ 三尖瓣成形术后，三尖瓣返流（极重度），主动脉瓣、二尖瓣位机械瓣功能正常，左室收缩功能正常，右室功能正常，心包微量积液。胸部 CT 平扫示心影增大，二尖瓣、主动脉瓣置换术后状态，心包包裹积液，较前变化不大；右侧胸腔积液，较前新见；肝脾增大，腹水，较前变化不大；双下肺少许条片，较前稍加重；纵隔肿大淋巴结，较前部分稍增大。心脏 CTA 示心脏增大，二尖瓣、主动脉瓣术后改变；右心房右旁包裹积液或囊肿可能；双肺间质性改变伴感染可能；双肺透过度不均并多处小的节段不张可能；肝脾肿大伴腹水。入院予以强心、抗凝、利尿补钾、纠正低蛋白血症、补充造血原料、输血、护肾、抑酸等治疗后症状好转，经充分评估后拟择期行经导管三尖瓣置换术，但患者出现进食哽噎感伴呕血，经消化科会诊并完善钡餐、急诊胃镜（食管可见大量血凝块及新鲜血迹，内镜下圈套器取出大量血凝块及坏死物质后见食管黏膜坏死、撕裂并广泛渗血，距门齿约 30cm 后壁为重，经止血钳止血后见渗血明显减轻，同时应用肾上腺素及血凝酶喷洒止血）后考虑患者系心脏增大导致机械性压迫食道，进一步引起食道多发慢性缺血坏死伴出血，不除外胃肠道淤血、抗凝药物引起局部血肿形成后出血等，2023-09-01 经急诊内镜下止血等处理后症状缓解，2023-09-15 复查胃镜示 1. 食管出血，治疗后（食管距门齿 26-32cm，见条、片状粘膜缺损，对比 2023.9.1 未见出血、血凝块，余黏膜未见异常，蠕动可）；2. 慢性浅表性胃炎。除外手术禁忌后于 2023-09-23 全麻下行胃镜检查示慢性浅表性胃炎，食管原黏膜出血剥离部位已完全愈合，随后继续行二维及三维食道超声引导下右侧胸小切口微创三尖瓣置换术，术毕 TEE 提示三尖瓣位生物瓣固定好，瓣膜形态可，生物瓣正向流速约 0.7m/s，最大压差 2mmHg，平均压差 1mmHg，瓣周见少量返流信号，面积约 2.2C m²。术毕转至 EICU 给予呼吸机辅助呼吸及对症支持治疗后顺利拔除气管插管，随访血红蛋白进行性下降、血小板减低，胸部 CT 提示右侧胸腔积气并多发包裹性积液积血可能，双肺多发节段不张。除外手术禁忌后于 2023-9-25 急诊全麻下行开胸探查术，探查见右侧胸腔大量血凝块，彻底清除凝血块，胸壁、心房未见明显出血点。术毕转至 GICU 进一步治疗，术中及术毕患者出现大量鼻出血，不除外合并气道出血，经鼻出血止血术并支气管镜下抽吸止血、输注血液制品等治疗后症状较前明显好转，顺利拔除气管插管并拔出胸引管后自 GICU 转回普通病房，术后继续予以抗感染、化痰、强心、利尿补钾、纠正贫血、升血小板、补充白蛋白等治疗，现患者较前好转，出院前复查 2023-10-27 N- 末端脑钠肽前体测定 2841.4 pg/ml。血常规示白细胞计数 5.15*10^9/L, 中性粒细胞百分比 83.4 %, 红细胞计数 3.02*10^12/L, 血红蛋白 83 g/L, 血小板计数 77*10^9/L,C 反应蛋白 34.81 mg/L。INR 1.56。生化示谷草转氨酶 44.8 U/L, 白蛋白 34.4 g/L, 尿素 14.4 mmol/L, 肌酐 163.6 umol/L, 尿酸 679 umol/L。2023-10-26 复查心脏超声示 TTVR+AVR+MVR 术后，三尖瓣位生物瓣功能正常并瓣周返流，主动脉瓣、二尖瓣位机械瓣功能正常，右心、左房增大，左室收缩功能正常 右室功能减低（FAC25%），中度肺动脉高压可能。泌尿系超声示右肾囊肿，双肾动脉阻力指数增高。胸部 CT 平扫示与本院 2023-10-10 日胸部 CT 片：心脏增大，心脏瓣膜术后改变，心包右侧机化包裹形成，较前变化不大；右侧胸腔积液并多发包裹积液积血可能，较前积液增多，积血减少，原积气吸收；双肺多发节段不张，较前增多，加重；双肺广泛间质改变伴磨玻璃影，考虑间质性肺水肿并肺泡性肺水肿可能，较前新增；左肺多发磨玻璃斑片，较前增多，合并感染待排；纵隔见增大淋巴结；扫及肝硬化，脾大，腹水表现，较前腹水量增多；扫及甲状腺左侧叶低密度灶。2023-10-27 腹部超声示肝实质弥漫性改变并肝静脉、下腔静脉增宽，胆囊壁增厚、毛糙，脾大，腹腔积液。现要求今日出院，予以办理今日出院，嘱按时服药，定期复查，不适随诊。

检验检查记录：

见诊疗经过。

鉴别诊断：

见上述。

其他：

检查文件见 PPT。

心房颤动射频消融术后心房食管瘘 1 例

张建奇

吉林大学第二医院

患者基本信息：

患者男性，64 岁，主因“突发晕厥伴发热 1 天”于 2023 年 9 月 9 日入院。

主述：

突发晕厥伴发热 1 天

现病史：

患者 1 天前无明显诱因出现晕厥、意识障碍，事后不能回忆，伴发热、咳嗽、纳差，体温最高不详。遂就诊于我院急诊，完善检查：血常规：白细胞总数 19.8×10^9/L，中性粒细胞百分比 86.9%，中性粒细胞计数 17.17×10^9/L，血红蛋白含量 131g/l，血小板计数 137×10^9/L；降钙素原检测：3.371ng/ml；胰腺功能：淀粉酶 18U/L，脂肪酶 19U/L。心脏超声示心包积液；肺部 CT 示两肺下叶局部不张，两侧胸腔积液、心包积液；冠脉 CTA、主动脉 CTA、肺动脉 CTA 示冠状动脉粥样硬化，主动脉粥样硬化，肺动脉 CTA 未见异常；头部 MR 平扫 + 弥散示多发腔隙性脑梗死，部分形成软化灶；DWI 脑桥内不明低信号影，待除外微出血灶（图 1）；头部血管 MRA 示右侧大脑中动脉 M1 段局部管腔轻度狭窄。

既往病史：

既往高血压病史 3 年；5 天前因“阵发性心房颤动”于我院行房颤射频消融术。

病程记录：

入院后查体：体温 36.5 ℃，脉搏 74 次 / 分，呼吸 22 次 / 分，血压 83/62mmHg。双肺呼吸音粗，可闻及少许湿罗音。心率 76 次 / 分，心律齐，心音减弱。意识清，四肢肌力正常。完善检查：血常规：白细胞总数 18.7×10^9/L，中性粒细胞百分比 90.3%，中性粒细胞计数 16.86×10^9/L，血红蛋白含量 136g/l，血小板计数 138×10^9/L；降钙素原检测：3.763ng/ml；C 反应蛋白：328mg/l；血沉：67mmm；凝血常规：凝血酶原时间 16.6s，凝血酶原国际正常比值 1.52，部分凝血活酶时间 31s，凝血酶时间 13.1s，D- 二聚体 1.21mg/L。心电图示窦性心律，I II V_2-V_6 导联 ST 段弓背向下抬高，aVR 导联 ST 段压低，不除外心包炎；立即给予床旁心包穿刺，引流出 410ml 黄色液体，送检结果示心包积液常规检查：外观 黄色，李凡他试验 弱阳性，白细胞总数 45689×10^6/L，红细胞总数 10000×10^6/L；心包积液生化：总蛋白 58.7g/L，乳酸脱氢酶 1918U/L，葡萄糖 3.58mmol/L，氯 101.3mmol/L，腺苷脱氨酶 24.6U/L。拟诊：晕厥待查、急性心包炎、肺部感染、心脏射频消融术后、腔隙性脑梗死，予以禁食水、抗感染、抗凝、抑酸、抗心律失常、静脉营养及对症治疗。

次日复查肺部 CT 示与前片比较，两肺下叶肺不张范围增大，胸腔积液增多，心包出现气体影，吞服碘海醇后可见食管内造影剂向心包纵隔内扩散（图 2）。结合患者射频消融手术史，考虑存在心包食管瘘 / 心房食管瘘可能，遂急请胸外科急诊行开胸探查及修补术，术中直视下可见胸腔淡黄色渗出液，心包黄色积液夹杂气体溢出，纵膈胸膜脓性液体溢出，食管中下段肿胀增粗，与心房界限不清，可见食管存在一 0.3cm 瘘口，与食管瘘口临近之心房壁质地硬脆，存在少量渗血，

压迫 15 分钟后渗血趋势增大；术中于 ECMO 辅助下行食管修补术及心房修补术，手术过程顺利，术后以“心房食管瘘、纵隔感染”转入 ICU 继续治疗。术后患者出现发热症状，体温最高 38.8℃，复查血常规：白细胞总数 25×10^9/L，中性粒细胞百分比 92.6%，中性粒细胞计数 23.1×10^9/L，血红蛋白含量 120g/l，血小板计数 49×10^9/L；C 反应蛋白：185mg/l；白介素 -6：352.42pg/ml；凝血常规：凝血酶原时间 18.3s，凝血酶原国际正常比值 1.68，部分凝血活酶时间 42.4s，凝血酶时间 24.5s，D- 二聚体 8.32mg/L；血培养：缓症链球菌。患者病情持续恶化并出现脓毒血症，经积极抗感染、有创呼吸机辅助通气、连续肾脏替代治疗等生命支持治疗措施后，最终进展为感染性休克、多器官功能衰竭，生命体征难以维持，家属签署离院告知书返回当地后患者死亡。

检验检查记录：

血常规：白细胞总数 18.7×10^9/L，中性粒细胞百分比 90.3%，中性粒细胞计数 16.86×10^9/L，血红蛋白含量 136g/l，血小板计数 138×10^9/L；降钙素原检测：3.763ng/ml；C 反应蛋白：328mg/l；血沉：67mmm；凝血常规：凝血酶原时间 16.6s，凝血酶原国际正常比值 1.52，部分凝血活酶时间 31s，凝血酶时间 13.1s，D- 二聚体 1.21mg/L。心电图示窦性心律，Ⅰ Ⅱ V_2-V_6 导联 ST 段弓背向下抬高，aVR 导联 ST 段压低，不除外心包炎；立即给予床旁心包穿刺，引流出 410ml 黄色液体，送检结果示心包积液常规检查：外观 黄色，李凡他试验 弱阳性，白细胞总数 45689×10^6/L，红细胞总数 10000×10^6/L；心包积液生化：总蛋白 58.7g/L，乳酸脱氢酶 1918U/L，葡萄糖 3.58mmol/L，氯 101.3mmol/L，腺苷脱氨酶 24.6U/L。次日复查肺部 CT 示与前片比较，两肺下叶肺不张范围增大，胸腔积液增多，心包出现气体影，吞服碘海醇后可见食管内造影剂向心包纵隔内扩散。急请胸外科急诊行开胸探查及修补术，术中直视下可见胸腔淡黄色渗出液，心包黄色积液夹杂气体溢出，纵膈胸膜脓性液体溢出，食管中下段肿胀增粗，与心房界限不清，可见食管存在一 0.3cm 瘘口，与食管瘘口临近之心房壁质地硬脆，存在少量渗血，压迫 15 分钟后渗血趋势增大；术中于 ECMO 辅助下行食管修补术及心房修补术。

鉴别诊断：

无

其他：

Clinical diagnosis and treatment of a case of hypocalcemia due to hypoparathyroidism

刘郑一

吉林大学第二医院

患者基本信息：

The patient was a middle-aged female with an acute course. History of present illness: The cause of the disease began to have chest tightness, shortness of breath without obvious cause 1 month ago, no precordial pain, no obvious radiating pain, no palpitations, no dizziness and headache, no nausea and vomiting, no syncope, consciousness and limb movement disorders, each attack lasted for a few minutes, and could be relieved after rest, because it did not affect daily work and life, it has not been systematically diagnosed and treated. One week ago, the patient had no obvious cause for the aggravation of the above symptoms, and was awakened by night questioning, so he was admitted to the outpatient clinic of our hospital, and the outpatient clinic was admitted to the hospital with “heart failure”. During the course of the disease, the patient has paroxysmal tetany. Anamnesis: the patient had thyroidectomy 15 years ago (the exact extent and procedure of resection are unknown). He has a history of hypertension for 3 years, blood pressure is up to 160/90mmHg, and he has irregular oral antihypertensive drugs (specific medication is unknown). One month ago, during a physical examination at a local hospital, the patient was not concerned about the low blood calcium, and then there were paroxysmal tetans, which the patient did not care about because it did not affect daily life. Denial of history of diabetes, denial of coronary heart disease, no history of blood transfusion, no history of drug and food allergies, unknown history of vaccination, no history of surgical trauma. Specialist examination: no bulge in the precordial area, apical pulse point located 0.5cm outside the midclavicular line of the 5th intercostal space on the left side, no abnormal pulsation, no palpable tremor, no palpable pericardial friction, heart rate 110 beats/min, uniform heart rhythm, normal heart sounds, P2=A2, no murmur, no pericardial friction rub.

主述：

Chest tightness and shortness of breath lasted for a month and worsened within a week

现病史：

The patient was a middle-aged female with an acute course. History of present illness: The cause of the disease began to have chest tightness, shortness of breath without obvious cause 1 month ago, no precordial pain, no obvious radiating pain, no palpitations, no dizziness and headache, no nausea and vomiting, no syncope, consciousness and limb movement disorders, each attack lasted for a few minutes, and could be relieved after rest, because it did not affect daily work and life, it has not been systematically diagnosed and treated. One week ago, the patient had no obvious cause for the aggravation of the above symptoms, and was awakened by night questioning, so he was admitted to the outpatient clinic of our hospital, and the outpatient clinic was admitted to the hospital with “heart failure”. During the course of the disease, the patient has paroxysmal tetany.

既往病史：

Anamnesis: the patient had thyroidectomy 15 years ago (the exact extent and procedure of resection are unknown). He has a history of hypertension for 3 years, blood pressure is up to 160/90mmHg, and he has irregular oral antihypertensive drugs (specific medication is unknown). One month ago, during a physical examination at a local hospital, the patient was not concerned about the low blood calcium, and then there were paroxysmal tetans, which the patient did not care about because it did not affect daily life. Denial of history of diabetes, denial of coronary heart disease, no history of blood transfusion, no history of drug and food allergies, unknown history of vaccination, no history of surgical trauma.

病程记录：

Patients were given continuous pumping of neoactivin (rate 4 ml/h, no loading dose), oxygen inhalation, blood pressure control, thyroxine supplementation, anti-RAAS system, and symptomatic supportive therapy.

检验检查记录：

Thyroid function triathlon: free T3 (FT3) 3.83 pmol/L (3.1- 6.8); Free T4(FT4) 22.00 pmol/L (12-22); Thyroid-stimulating hormone (TSH) 1.3500 mlu/L 0.70 to 15.2 for newborns/child (6 days to 3 months) 0.72 to 11.0 for children (April to December) 0.73 to 8.35 for children (1 to 6 years) 0.70 to 5.97 for children (7 to 11 years) for children (7 to 11 years of age) 0.60 to 4.84 for adolescents (12 to 20 years of age) 0.51 to 4.30 for adolescents (12 to 20 years of age) and 0.27 to 4.20 for adults (> 20 years of age)；NT-proBNP：552.33pg/ml；Uric acid: 406 umol/L (89-375 umol/L); Creatinine: 104umol/L (41-73umol/L);potassium 4.46 mmol/L (3.5-5.3 mmol/L); sodium 145.0 mmol/L (137-147 mmol/L); chlorine 110.0 mmol/L (99-110 mmol/L); calcium 1.36 mmol/L (2.11-2.52 mmol/L); phosphorus 2.45 mmol/L (0.85-1.51 mmol/L); magnesium 0.78 mmol/L (0.75-1.02 mmol/L); eGFR51.9ml/min（>90）；ECG: abnormal ECG, QT interval: 404 ms, QTc: 521 ms.Cardiac ultrasound: diffuse reduction of wall motion, LV: 55mm, LA: 41mm, LVEF: 38% (indicating that the patient’s left heart is enlarged and left heart function is reduced).

鉴别诊断：

Differential diagnosis of heart failure involves distinguishing it from other conditions that may present with similar symptoms. Here are some key conditions to consider:

1. Chronic Obstructive Pulmonary Disease (COPD): Clinical Features: Patients with COPD often have a history of long-term smoking or exposure to pollutants. Symptoms include chronic cough, sputum production, and dyspnea that may worsen with activity. On physical examination, there may be signs of hyperinflation of the lungs, such as a barrel-shaped chest and decreased breath sounds.Distinguishing Features: Unlike heart failure, COPD is primarily a disease of the airways and alveoli. Pulmonary function tests typically show obstructive ventilatory defects in COPD, whereas heart failure is more likely to be associated with restrictive patterns or normal spirometry but with elevated BNP (B-type natriuretic peptide) levels.2. Pulmonary Embolism: Clinical Features: Sudden onset of dyspnea, pleuritic chest pain, and hemoptysis are classic symptoms. Patients may also have signs of deep vein thrombosis, such as unilateral leg swelling. Distinguishing Features: The presence of sudden onset of severe symptoms and risk factors for thromboembolism (e.g., recent surgery, prolonged immobility) helps differentiate it from heart failure. Imaging studies like CT pulmonary angiography can confirm the presence of pulmonary emboli, whereas heart failure is usually associated with chronic symptoms and signs of fluid overload.3.Coronary Artery Disease (CAD):Clinical Features: Patients may have angina (chest pain) on exertion or at rest, especially if there is significant ischemia. ECG changes such as ST-segment depression or T-wave inversion may be seen during episodes of ischemia.Distinguishing Features: While heart failure can be a complication of CAD, the primary presentation of CAD is usually related to myocardial ischemia. Stress testing, coronary angiography, or cardiac biomarkers (e.g., troponin) can help identify CAD as the primary issue.4. Valvular Heart Disease:Clinical Features: Symptoms depend on the specific valve involved. For example, aortic stenosis may present with exertional dyspnea, angina, and syncope. Mitral regurgitation can cause symptoms similar to heart failure, such as dyspnea and fatigue.Distinguishing Features: Physical examination findings such as heart murmurs (e.g., a harsh systolic murmur in aortic stenosis or a holosystolic murmur in mitral regurgitation) are crucial. Echocardiography is the gold standard for diagnosing and quantifying valvular abnormalities.5. Anemia:Clinical Features: Patients may present with fatigue, weakness, and dyspnea on exertion. Physical examination may reveal pallor, tachycardia, and a systolic flow murmur.Distinguishing Features: Laboratory tests showing low hemoglobin and hematocrit levels help differentiate anemia from heart failure. Anemia can cause symptoms of heart failure due to increased cardiac output to compensate for reduced oxygen-carrying capacity, but the underlying cause is different.6. Thyroid Disease:Clinical Features: Hyperthyroidism can present with symptoms

such as palpitations, weight loss, heat intolerance, and tremors. Hypothyroidism may cause fatigue, weight gain, and cold intolerance.Distinguishing Features: Thyroid function tests (TSH, free T4) can confirm the diagnosis. Both hyperthyroidism and hypothyroidism can affect cardiac function, but the clinical context and laboratory findings are distinct from heart failure.

其他：

宽松容量管理在慢性心力衰竭急性加重期应用病例分享

任泽鹏

鄂尔多斯市中心医院

患者基本信息：

患者，元某，男，汉族，60 岁；体重 100kg，身高 174cm；专业技术人员，已退休；2025-02-22 急诊入院

主述：

反复喘息、气短 24 年，加重 1 月

现病史：

患者于 24 年（前 2001 年）于饮酒后首次出现呼吸困难，之后反复出现活动后气短；于鄂尔多斯市中心医院就诊，行 CAG 提示前降支近段狭窄约 70%；经后阜外医院诊断为扩张型心肌病、冠状动脉粥样硬化性心脏病；开始接受规律的二级预防治疗以及金三角的药物治疗；并多次于长期在银川市第一人民医院及石嘴山第一人民医院住院以及门诊随诊；2023 年 5 月因患甲流诱发肺感染、心衰，转诊北京途中，发生急性心肌梗死，急诊就诊于北京世纪坛医院医院，行急诊 CAG+ LAD PCI 术治疗，以及抗感染、纠正心功能不全等治疗后出院；院外遵医嘱用药，日常活动无明显不适。2024 年淋水后受凉再次诱发心衰加重在我院住院诊疗，予以对症纠正心功能不全治疗后症状缓解出院；之后反复因气短加重在我院诊疗；均考虑诊断：1. 扩张性心肌病 [充血性心肌病]，1.1 全心衰竭；1.2 心功能 IV 级（NYHA 分级），2. 冠状动脉粥样硬化性心脏病，2.1 陈旧性心肌梗死；3.2 型糖尿病；4. 痛风；院外接受新四联 + 维立西呱联合治疗。近 1 月来患者再次出现气短加重，自行增加利尿剂效果不理想，症状进行性加重，夜间不能平卧，需要无创呼吸机辅助通气；为求进一步系统诊疗经我院急诊科以“急性左心衰竭”收住我科；病程中，患者无发热，偶有咳嗽、咳痰，精神差，饮食那差，腹部胀满，睡眠差，大小便未见明显异常，双下肢水肿且进行性加重。未监测体重 。

既往病史：

既往史：2 型糖尿病病史 2 年，目前口服达格列净 10mg/ 日，血糖控制尚可；否认高血压、脑血管疾病病史，否认肝炎、结核病史，患有传染性疾病：否，无外科手术史，无重大外伤史，无输血史，否认食物、药物过敏史，预防接种史随当地进行。

个人史 : 生于原籍，无外地长期居住史，无疫区长期居住史，吸烟 30 年，每日 5 支；戒酒 20 年。无工业毒物、粉尘、放射性物质接触史，无冶游史，无重大精神创伤史。

婚育史：适龄，育有 1 子 1 女；

病程记录：

1. 入院后予以基于生理需要的静脉扩容以及能量补充；同时予以重组人脑利钠肽 + 利尿纠正心功能治疗；

2. 维持院外新四联 + 维立西呱改善预后治疗；

2. 予以抑酸、促胃动力、促消化等对症治疗；

4. 患者于次日起进食改善，在患者进食显著改善后，逐步减少静脉液体的输入，允许患者根据自身感觉自由进食。

5. 患者在第 4 日起可自由行走，无明显气短不适。

检验检查记录：

入院后急诊检验：2025-2-22

生化：尿酸 660umol/L，尿素 8.70mmol/L，肌酐 103umol/L，K+ 4.52mmol/L；**总胆红素（TBIL）38**.9μmol/L，直接胆红素（DBIL） 15.6μmol/L；间接胆红素（IBIL）23.3μmol/L

NT-ProBNP 19261pg/ml；

D-dimer 0.59mg/L FEU；FDP 0.80ug/ml

危险因素筛查：GLU5.54 mmol/L，TC 1.85mmol/L，TG 0.75mmol/L，HDL-C 0.57mmol/L，LDL-C 0.88 mmol/L，HbA1c 6.9%

治疗后：

2025-2-27 NT-ProBNP 11494pg/ml; 尿素 9.10mmol/L, 肌酐 93.0 umol/L，尿酸 538umol/L；K+ 5.16mmol/L

2025-03-02 NT-ProBNP 1952/ml； 尿素 9.10mmol/L, 肌酐 71.0 umol/L，尿酸 458umol/L；K+ 3.86mmol/L

鉴别诊断：

患者既往有多次的诊疗资料，结合患者发病后症状，以及查体肺部湿罗音，双下肢水肿等；主要诊断明确。

1. 慢性阻塞性肺病急性加重

依据：患者无明确的 COPD 病史，且患者临床表现为以呼吸困难为主；

2. 支气管哮喘

依据：患者无过敏史，无哮喘病史，发病时肺部以湿罗音为主，无喘鸣音；不支持哮喘。

3. 胃食管反流

依据：患者平素无反酸、嗳气，但是考虑到患者晚间显著，不能排除，拟经验性予以 PPI 进一步观察。

4. 焦虑状态

依据：患者慢性病多年，且反复有加重住院诊疗，会对心理造成影响。拟行焦虑、抑郁量表评估，或经验性予以抗焦虑治疗。

其他：

遗漏的真凶及处理

钍戈

浙江大学医学院附属邵逸夫医院

患者基本信息：

患者，男，55 岁。自由职业。

主述：

发作性胸骨后闷痛 1 小时。

现病史：

患者于 1 小时前无诱因出现胸骨后疼痛，呈闷痛，向后背部放散，伴大汗，持续不缓解。自行至当地医院就诊，诊断为 “急性下壁心肌梗死” 并给予阿司匹林 300mg、氯吡格雷 300mg 嚼服。遂转送至我院急诊科，行心电图示 “II、III、aVF 导联 ST 段抬高”，TNI0.083ng/ml（0.000-0.160），诊断为 “急性下壁心肌梗死” 并至急诊导管室行介入治疗。

既往病史：

既往高血压病史 4 年，血压最高达 150/104mmHg，平素未系统用药。

病程记录：

2025-4-22 行急诊介入治疗：患者造影示冠状动脉扩张（CAE），初步导丝尝试开通右冠远端，发现非罪犯血管。后行造影示回旋支巨大冠状动脉瘤（CAA），给与 PTCA、抽吸导管血栓抽吸、冠脉内无复流药物注入、延长导管血栓抽吸，仍未恢复血流。期间患者出现抽搐、意识丧失，心电监护示室颤，给予胸外按压及电除颤 1 次，患者恢复窦性心律。

后收入 ICU 治疗，术后患者症状缓解，心电图 ST 段逐渐回落，完善血管炎性指标及抗核抗体谱，未见异常。给与秋水仙碱、利伐沙班、阿司匹林、阿托伐他丁、依洛尤单抗、螺内酯、呋塞米等药物口服治疗后病情稳定，后于 2025-4-29 再次行经皮冠状动脉造影术：提示冠状动脉扩张（CAE）血流通畅，遂出院继续口服药物治疗。

检验检查记录：

完善心电图、心脏彩超、心肌酶谱、血管炎相关抗体、并复查冠脉造影。

鉴别诊断：

冠状动脉瘤样扩张 (coronary artery aneurysms，CAAs)：冠状动脉扩张节段的直径是其正常相邻节段血管直径的 1.5 倍以上

巨大冠状动脉瘤 (coronary artery aneurysm, CAA)：冠状动脉扩张节段血管直径是正常相邻参考血管直径的 4 倍以上或扩张节段直径大于 20 mm；对于儿童，当冠状动脉扩张的血管直径大于 8 mm。

冠状动脉扩张 (coronary artery ectasia, CAE)：更长、更弥漫的动脉扩张，扩张血管长度超过所在血管总长度的三分之一。

其他：

药物治疗：受益 ----CCB/ 抗血小板（阿司匹林）/ 抗凝

争议 ----β 受体阻滞剂 / 硝酸酯类

手术治疗：急性伴血栓负荷 ---- 抽吸 /GPI；

1) 不累及主要侧支的囊状动脉瘤和小假性动脉瘤可采用覆膜支架；

2) 累及主要侧支的囊状或梭状动脉瘤可采用球囊或支架辅助线圈栓塞，或手术治疗；

3) 累及左主冠状动脉的 CAAs、多发或巨大（>20 mm，或 >4 倍参考血管直径）手术切除被认为是一线治疗；

4) 对于巨大或快速扩张的大隐静脉桥血管瘤或引起症状性外压迫的患者，使用 Amplatzer 封堵器或线圈栓塞进行经皮封堵，无论是否对移植血管进行 PCI，都是手术的可行替代方案。

中年女性心室肥厚的曲折诊治之旅

谢林峰

重庆医科大学附属第一医院心血管内科

患者基本信息：

患者是一名 58 岁女性

主述：

因“间断头晕 5 年，气短、胸闷 3 年”多次入院。

现病史：

一、诊断曲折之旅：

第一次住院（2017 年，54 岁）：患者无明显诱因出现间断发作头晕、黑朦，不伴晕厥，症状持续数秒可自行缓解，于当地县医院神经内科住院治疗，考虑“脑血管病”，予以口服药物治疗（具体不详），效果欠佳；既往史：否认高血压、糖尿病、冠心病病史。入院 1 年前，诊断“慢性胃炎”及“反流性食管炎”。家族史：父亲 47 岁死于“心脏病”（具体不详），母亲走失；2 个弟弟，其中一弟弟患“胃癌”。（遗憾未行心脏相关检查）。

第二次住院（2019 年，56 岁）：于重庆某三甲医院就诊，心脏彩超提示“左室肥厚”（室间隔 15mm，左室后壁 14mm），查肌钙蛋白：0.05ng/ml，动态心电图提示：窦性心律伴显著窦缓，窦性停搏及短暂性全心停搏（最长 RR 间期 4.7 秒），考虑“病窦综合征”，行双腔起搏器植入术，术后患者头晕、黑朦症状缓解，但逐渐出现劳力性胸闷、呼吸困难。（可惜为筛查心脏肥厚病因）。

第三次住院（2021 年，58 岁）：患者因劳力性呼吸困难症状加重，伴腹胀、双下肢水肿于当地医院就诊，考虑诊断“ 肥厚型心肌病 心力衰竭 心功能III级”，予以“比索洛尔、呋塞米、螺内酯、培哚普利、恩格列净”等药物口服，查肌钙蛋白：0.84ng/mL(升高 72 倍)，期间因服药后血压低调整比索洛尔及培哚普利剂量，因不耐受而停用，患者胸闷、气短症状无明显缓解。（错失细节，遗憾漏诊心室肥厚病因）。

第四次住院（2022 年，59 岁）：患者因呼吸困难、下肢水肿加重于 2022.7.19 于阜外医院就诊，以“肥厚型心肌病”收住院。针对患者心肌肥厚进行详细检查，最终完善 PYP 显像及基因检测诊断为遗传型转甲状腺素心脏淀粉样变。（盖棺定论，病因诊断明确）。

二、治疗曲折之旅：

初步治疗：诊断明确后患者于我院门诊规律随访，予以氯苯唑酸治疗，病情稳定，症状逐渐好转。同时完善家系筛查，哥哥和女儿基因筛查阴性。

看似一切向好，实则困难重重

第一次病情加重（2023 年 03 月）：下肢水肿及晨起眼睑水肿伴夜间阵发性呼吸困难。入院后查 NT-proBNP：4640pg/ml，心脏彩超 LVEF38%，胸水 B 超示右侧大量胸腔积液，入院后予以胸腔置管引流，新活素泵入，利尿等治疗后好转，出院方案：氯苯唑酸 61mg qd、维立西呱 2.5mg qd

第二次病情加重（2023 年 03 月）：患者出院当天再次出院病情加重，喘累明显，伴恶心、呕吐、上腹胀痛。入院后查 NT-proBNP：14050Pg/ml, 加强利尿、纠正心衰、对症治疗后好转出院。

第三次病情加重（2023 年 12 月）：患者受凉后呼吸困难加重，轻微活动即感呼吸困难，伴夜间阵发性呼吸困难、纳差、恶心呕吐。入院后查 NT-proBNP：24000Pg/ml, LVEF：31%，动态心电图示阵发性房颤，房扑。治疗：新活素，左西孟旦，达格列净，利尿，抗凝。出院方案：氯苯唑酸 61mg qd，达格列净 10mg qd，呋塞米 20mg qd，螺内酯 20mg qd，艾多沙班 15mg qd。

三、曲折病情总稳定

2023.12 至今，于我院规律输注左西孟旦，患者现心功能 II 级，近一年未再次因慢性心力衰竭急性失代偿住院。

病情稳定体现在：①心衰标志物（NTproBNP）稳定；②患者活动耐量变好（六分钟步行试验；③心脏结构及功能稳定（心脏彩超）；④自我感受。

既往病史：

否认高血压、糖尿病、冠心病病史。入院 1 年前，诊断“慢性胃炎”及“反流性食管炎”

病程记录：

一、诊断曲折之旅：

第一次住院（2017 年，54 岁）：患者无明显诱因出现间断发作头晕、黑朦，不伴晕厥，症状持续数秒可自行缓解，于当地县医院神经内科住院治疗，考虑“脑血管病”，予以口服药物治疗（具体不详），效果欠佳；既往史：否认高血压、糖尿病、冠心病病史。入院 1 年前，诊断“慢性胃炎”及“反流性食管炎”。家族史：父亲 47 岁死于“心脏病”（具体不详），母亲走失；2 个弟弟，其中一弟弟患“胃癌”。（遗憾未行心脏相关检查）。

第二次住院（2019 年，56 岁）：于重庆某三甲医院就诊，心脏彩超提示“左室肥厚”（室间隔 15mm，左室后壁 14mm），查肌钙蛋白：0.05ng/ml，动态心电图提示：窦性心律伴显著窦缓，窦性停搏及短暂性全心停搏（最长 RR 间期 4.7 秒），考虑“病窦综合征”，行双腔起搏器植入术，术后患者头晕、黑朦症状缓解，但逐渐出现劳力性胸闷、呼吸困难。（可惜为筛查心脏肥厚病因）。

第三次住院（2021 年，58 岁）：患者因劳力性呼吸困难症状加重，伴腹胀、双下肢水肿于当地医院就诊，考虑诊断“ 肥厚型心肌病 心力衰竭 心功能III级”，予以“比索洛尔、呋塞米、螺内酯、培哚普利、恩格列净”等药物口服，查肌钙蛋白：0.84ng/mL(升高 72 倍)，期间因服药后血压低调整比索洛尔及培哚普利剂量，因不耐受而停用，患者胸闷、气短症状无明显缓解。（错失细节，遗憾漏诊心室肥厚病因）。

第四次住院（2022 年，59 岁）：患者因呼吸困难、下肢水肿加重于 2022.7.19 于阜外医院就诊，以“肥厚型心肌病”收住院。针对患者心肌肥厚进行详细检查，最终完善 PYP 显像及基因检测诊断为遗传型转甲状腺素心脏淀粉样变。（盖棺定论，病因诊断明确）。

二、治疗曲折之旅：

初步治疗：诊断明确后患者于我院门诊规律随访，予以氯苯唑酸治疗，病情稳定，症状逐渐好转。同时完善家系筛查，哥哥和女儿基因筛查阴性。

看似一切向好，实则困难重重

第一次病情加重（2023 年 03 月）：下肢水肿及晨起眼睑水肿伴夜间阵发性呼吸困难。入院后查 NT-proBNP：4640pg/ml，心脏彩超 LVEF38%，胸水 B 超示右侧大量胸腔积液，入院后予以胸腔置管引流，新活素泵入，利尿等治疗后好转，出院方案：氯苯唑酸 61mg qd、维立西呱 2.5mg qd

第二次病情加重（2023 年 03 月）：患者出院当天再次出院病情加重，喘累明显，伴恶心、呕吐、上腹胀痛。入院后查 NT-proBNP：14050Pg/ml, 加强利尿、纠正心衰、对症治疗后好转出院。

第三次病情加重（2023 年 12 月）：患者受凉后呼吸困难加重，轻微活动即感呼吸困难，伴夜间阵发性呼吸困难、纳差、恶心呕吐。入院后查 NT-proBNP：24000Pg/ml, LVEF：31%，动态心电图示阵发性房颤，房扑。治疗：新活素，左西孟旦，达格列净，利尿，抗凝。出院方案：氯苯唑酸 61mg qd，达格列净 10mg qd，呋塞米 20mg qd，螺内酯 20mg qd，艾多沙班 15mg qd。

三、曲折病情总稳定

2023.12 至今，于我院规律输注左西孟旦，患者现心功能 II 级，近一年未再次因慢性心力衰竭急性失代偿住院。

病情稳定体现在：①心衰标志物（NTproBNP）稳定；②患者活动耐量变好（六分钟步行试验；③心脏结构及功能稳定（心脏彩超）；④自我感受。

检验检查记录：

略

鉴别诊断：

略

其他：

略

零射线内外膜联合消融治疗 Marshall 相关心房颤动一例

施尚淞

苏州大学附属第一医院

患者基本信息：

患者女，74 岁，

主述：

反复心悸 8 月

现病史：

反复劳累后心悸 8 月，位于心前区，伴胸闷，气短，持续数分钟，无胸痛，无出汗，无黑朦，休息可缓解。门诊动态心电图提示阵发性房颤，拟入院行射频消融。

既往病史：

否认高血压、糖尿病、肾病病史，否认传染病史。无输血史。否认药物、食物过敏史。

查体：T 36.5℃ P 68 次 / 分 R 16 次 / 分 BP 128/86mmHg，神志清，精神可。双肺呼吸音清，心律齐，心音可，各瓣膜区未闻及异常。

病程记录：

入院后行零射线内外膜联合房颤消融，具体如下：

心腔内超声构建左房模型，明确左心耳内无血栓。腔内超声指导下穿刺房间隔。行环肺静脉电隔离。术中自发房颤，电复律转为窦性，但无法维持，电复律两次结果一致，仍为房扑房颤交替，消融 Marshall 对应内膜面时可终止，但 CS9,10 房早仍可触发房颤房扑及房速，Marshall 内膜面电位最早，考虑 Marshall 相关触发房颤。在左肺静脉前庭 Marshall 对应内膜面局部线性巩固消融，继续消融二峡线，消融二峡线过程中房颤终止，并维持窦律。但验证并未阻断。继续至冠状窦内 Marshall 内膜面巩固消融，局部片状巩固消融后验证二峡线性阻断。异丙肾静脉推注后反复刺激未见明显房性心律失常。ICE 未见明显心包积液。手术顺利，术后复查心电图为窦性心律。

检验检查记录：

血细胞分析 +CRP 组套（急）：白细胞计数 * 4.16×10^9/L，红细胞计数 * 4.05×10^12/L，血红蛋白量 * 125g/L，血小板计数 * 84×10^9/L；

NT-pro BNP 288pg/L，肌钙蛋白阴性；

甲功、血凝、输血全套，肝肾功能均正常。

入院心电图：1. 窦性心律 2. 窦性心动过缓；

24 小时动态心电图示：1. 房性早搏 偶发短阵房速 阵发性房颤、房扑 2. 偶发室性早搏 3. 交界性逸搏心律。

心脏超声：左房左室增大，主动脉瓣中度反流，二尖瓣轻度反流。

冠脉 CTA：LAD 中段心肌桥；右肺中叶纤维灶及钙化灶。

鉴别诊断：

诊断明确

其他：

无

增强 CT 检出早期心脏破裂一例

谢颖

北京清华长庚医院

患者基本信息：

患者女性，72 岁，主因“突发胸痛 5 小时”于 2025 年 4 月入院。

主述：

突发胸痛 5 小时

现病史：

入院 5 小时前睡眠中突发胸痛伴后背及双上肢胀痛，自觉有撕裂感，伴胸闷恶心，无呕吐头晕头痛、腹痛腹胀，自测血压 170/90mmHg，先后口服布洛芬 1 片、速效救心丸 15 粒疗效欠佳，持续疼痛 1 小时后 120 至我院急诊，当时测血压 194/95mmHg，脉搏 91 次 / 分，心电图示 V3-V6 ST 段抬高，心肌酶示 TnT-hs 0.0411 ng/mL，考虑急性前侧壁心肌梗死，为进一步诊治入院。患者近期精神、饮食、睡眠、二便、体重较前无明显变化。

既往病史：

高血压病史 15 年，2 型糖尿病 10 年，高胆固醇血症 5 年。否认烟酒史，否认毒物暴露史，否认冠心病家族史。

病程记录：

14:10 患者突发意识丧失，呼之不应，心电图：房速伴快心室率。间隔 2min 复查心电图：窦律，ST 改变。约 3min 后，患者大动脉搏动无法触及，持续呼之不应，血压无法测出，考虑心脏骤停，予胸外按压，肾上腺素 1mg 每 3min 静脉推注，联合多巴胺及去甲肾上腺素升压治疗。超声心动图显示心包积液；予心包穿刺即刻引流出约 200mL 血性心包积液，置入 IABP、气管插管机械通气，后患者恢复脉搏，心电图提示房颤律，予电复律转复窦律。心包穿刺引流，在最初 24 小时引流出 1025 毫升血性液体，此后每日引流量 10-80 毫升。10 天后经胸超声心动图显示真性心尖部室壁瘤形成。随后的数周内，心包引流量逐渐减少，一个月后成功拔除引流导管。

检验检查记录：

血 常 规：CRP(B) 1.20 mg/L, WBC 10.10 10^9/L, HGB 121 g/L, PLT 197 10^9/L

心肌损伤标志物：MYO 68.6 ng/mL, NT-ProBNP 419 pg/ml, TnT-hs 0.0411 ng/mL

肝肾功能：ALT 13.9 U/L, TBIL 8.4 umol/L, ALB 43.9 g/L, Cre 67 umol/L, K 3.23 mmol/L, Na 139.4 mmol/L

动脉血气：pH(Blood Gas) 7.41, PCO2 40 mmHg, PO2 69 mmHg, Na(Blood Gas) 136 mmol/L, K(Blood Gas) 3.3 mmol/L, Lac(blood gas) 1.0 mmol/L

血脂及尿酸：UA 370 umol/L, HDL-C 1.03 mmol/L, LDL-C 2 mmol/L

糖化血红蛋白：Hb-A1c 6.7 %

鉴别诊断：

冠状动脉穿孔

其他：

无

一例心脏破裂患者的系列心电图改变

付丽

北京清华长庚医院

患者基本信息：

74 岁，男性。

主述：

突发胸痛 4 小时。

现病史：

患者 4 小时前无诱因突发胸痛，伴大汗，持续不缓解，自行开车就诊我院急诊，测血压 120/74mmHg，心率 58 次 / 分，心电图：窦性心律， I、AVL、 V 1 -V 5 ST 段 弓背抬高，T 波高尖，提示急性广泛前壁心肌梗死，急诊进行了冠脉造影，明确左前降支近中 100% 闭塞病变（图 15 A），前降支植入支架 1 枚后前降支血流恢复后收入 CCU 病房。收入 CCU 后给予规范的药物治疗。

既往病史：

患者既往高血压病史 40 年，血压控制在 130-140/70mmHg 左右。近 30 多年，晕厥 4 次，每次均有疼痛诱因（进食烫红薯、肌肉注射药物、腿抽筋、摔倒疼痛），曾就诊神经科考虑血管迷走性晕厥，2 天前就在搬冰箱过程中被撞倒后出现意识丧失，持续 3-5 分钟自行苏醒，就诊我院急诊，头颅 CT 未见明显异常，患者此次就诊时完善了心电图检查，给我们留下了心梗发生前的心电图记录（图 1）：窦性心律， 电轴左偏，非特异的 ST-T 改变。高尿酸病史 2 年。

病程记录：

复查心电图：窦性心律，V 1 -V 4 QS 型，急性广泛前壁、高侧壁心梗演变过程（图 3）。患者于心梗后第 3 天复查心电图：窦性心律，I、AVL、V2-V6 ST 段较前抬高及 QT 间期的延长（图 4）。患者于心梗后第 4 天午饭后，卧床休息状态下，心电监护首先监测到患者心率下降，窦性心律，心率 42 次 / 分，立即床旁查看患者，患者呼之不应，血压测不出，无自主呼吸，急性床旁超声检查提示大量心包积液，部分积液回声高，考虑心脏破裂，心包积血，血凝块，急予心包穿刺，积血难以抽出，最终可抽出血性液体约 100ml。给予患者一系列的抢救，最终患者死亡。患者患者病情变化时带有动态心电图检查，记录下患者心脏破裂前一系列的心电图变化：先出现了室早、房早、加速性室性自主节律，随后患者前壁的 ST 段显著抬高，在后出现交界性逸博及交界性逸博心律，室性逸博及室性逸博心律，可见完全性房室分离，室内阻滞，到最终心脏停搏的过程。

检验检查记录：

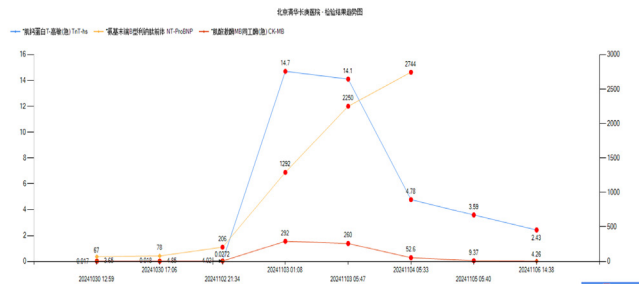

鉴别诊断：

肺栓塞

主动脉夹层

其他：

无

糖尿病酮症引发的复发型应激性心肌病

何榕

清华大学附属北京清华长庚医院

患者基本信息：

患者女性，64 岁

主述：

间断胸痛 4 年，再发 13 小时

现病史：

- 患者 4 年前无明显诱因出现恶心、呕吐，伴心前区针扎样疼痛，放射至后背部，程度可忍受，伴有喘憋、双下肢水肿，症状持续不缓解，就诊于安贞医院、急查心电图提示窦性心律、胸前导联 T 波倒置，心脏损伤标志物 cTnI 1.22ng/ml，随机血糖 21-22mmol/L，尿酮体 2+，诊断为“急性非 ST 段抬高型心肌梗死、糖尿病酮症酸中毒”，急诊冠状动脉造影提示“LCX 50% 狭窄”，超声心动图示左室各壁下 1/2 运动减低，给予药物治疗后患者

症状迅速缓解，出院后 1 月复查超声心动图示左室壁活动未见异常。院外规律口服阿司匹林、氯比格雷（1 年后自行停用）、阿托伐他汀（自行停用）治疗

- 患者自述期间未再发作胸闷、胸痛等不适，运动耐量正常。

•13 小时前患者安静休息时无明显诱因突发恶心、呕吐胃内容物，伴心前区针扎样疼痛及灼烧感，范围约手掌大小，放射至后背部，持续不缓解，否认呼吸困难、大汗、濒死感；

•8 小时前（2020-11-10 16:00）就诊我院急诊，测得血压 139/93mmHg，心电图示：窦性心律，胸前导联 R 波递增不良，心脏损伤标志物： TnT-hs 0.033->0.255 ng/mL，尿常规示尿糖 4+，酮体 2+，血气分析 pH 7.43。考虑急性非 ST 段抬高型心肌梗死、糖尿病酮症，给予心电监护、吸氧、口服替格瑞洛 180mg，补液纠酮治疗。为求进一步诊治，收入院

既往病史：

• 高血压 40 年，最高血压 220/90mmHg，口服厄贝沙坦氢氯噻嗪 1#qd、硝苯地平控释片 30mgqd 控制血压，血压控制在 120-140/60-70mmHg；

•2 型糖尿病病史 12 年，口服二甲双胍 500mgtid、阿卡波糖 50mgtid、胰岛素皮下注射治疗，2 月前自行停用胰岛素皮下注射，血糖控制差；

• 高脂血症 4 年，未规律口服他汀类药物调脂治疗；

•2 周前患者左侧膝关节摔伤，近期活动受限；

• 子宫切除术后 10 年，乳腺结节切除术后；

• 反复询问，近期无情绪波动；

“庆大霉素”药物过敏史，否认其它药物及食物过敏史。

病程记录：

入院后急诊冠脉造影未见明显有意义狭窄，UCG 左室心尖部球囊样膨出，左室射血分数减低 (LVEF=46%)，检查糖尿病酮症诊断明确，积极纠正糖尿病酮症。监测心肌损伤标志物 TnT-hs 最高 0.255ng/ml，

NT-ProBNP 88.81 pg/ml，阿司匹林 100mgqd、氯吡咯雷 75mgqd、瑞舒伐他汀 20mgqn、厄贝沙坦 150mgqd；静脉补钾补镁治疗；患者症状缓解，复查超声心动图完全恢复，心内结构及血流未见明显异常，左室射血分数正常范围 (LVEF=60%)，心电图 T 波改变恢复。

检验检查记录：

急诊冠脉造影：LM 见异常；LAD 开口 - 中段 30%~50% 弥漫性狭窄，LAD 远段可见长约 20mm 冠状动脉肌桥，收缩期缩窄 70%，前向血流 TIMI-3 级；LCX 中段不规则，远段 50% 局限性狭窄，前向血流 TIMI-3 级；RCA 近段不规则，远段不规则病变，前向血流 TIMI-3 级；未见侧支循环。暂不行进一步介入治疗。

UCG：左房增大，左室心尖部球囊样膨出，二尖瓣少量反流，左室射血分数减低 (LVEF=46%)

CTPA 未见明显异常

复查超声心动图完全恢复，心内结构及血流未见明显异常，左室射血分数正常范围 (LVEF=60%)

CMR：未见明显延迟强化，ECV 28%

鉴别诊断：

急性心肌梗死：中老年女性，危险因素多，胸痛伴心肌标志物升高，应考虑急性心肌梗死可能，但患者心电图仅表现为 T 波改变和 R 波递增不良，冠脉造影未见有意义狭窄，UCG 左室心尖部球囊样膨出，酮症纠正后心电图改变恢复，超声心动完全正常，不符合急性心肌梗死典型表现。

应激性心肌病：中老年女性，4 年前胸痛伴心肌标志物升高，冠脉造影未见明显狭窄，糖尿病酮症纠正后心电图改变完全恢复。本次发病再发糖尿病酮症，胸痛伴心肌标志物升高，但患者心电图仅表现为 T 波改变和 R 波递增不良，冠脉造影未见有意义狭窄，UCG 左室心尖部球囊样膨出，酮症纠正后心电图改变恢复，超声心动完全正常，符合应激性心肌病表现，两次症状及心电图改变发作均在糖尿病酮症发生时，患者无其他情绪应激的原因，考虑糖尿病酮症发作诱发复发型应激性心肌病可能性大。

其他：

主动脉内球囊反搏致多脏器血管栓塞 1 例

巫凯敏

厦门大学附属心血管病医院

患者基本信息：

患者王 XX，男，54 岁

主述：

间断胸痛 10 余天，加重 6 天

现病史：

患者 10 余天前无明显诱因出现胸骨后闷痛，范围约一手掌，无放射痛，无恶心、呕吐，无咳嗽、咳痰，无发热，无黑矇、晕厥，持续数分钟后自行缓解，未予诊治。6 天前上述症状加重，持续不缓解，伴出汗，伴气促，就诊于当地医院诊断“急性广泛前壁心肌梗死”，行急诊冠脉造影提示 LAD 及 LCX 闭塞（未见影像），术中出现心源性休克，遂在主动脉内球囊反搏（IABP）支持下行 LAD 支架植入术，术后继续给予升压、抗凝、抗血小板等药物对症治疗，效果不佳，仍有反复胸闷、气促，现为求进一步诊治由 120 转诊就诊急诊，急诊以“急性心肌梗死”收入院。病程中饮食、睡眠欠佳，二便如常，近期体重未监测体重。

既往病史：

既往高血压病史，血压控制不佳。

吸烟、饮酒史。

病程记录：

入院后予抗凝、抗血小板、利尿、抗感染等治疗，病情逐渐平稳。入院第 2 天凌晨突发中上腹痛，查体可及中上腹压痛，无肌紧张及反跳痛，完善血气分析未见代谢性酸中毒，化验提示 D 二聚体升高，予抑酸护胃、解痉止痛等药物治疗效果不佳，进一步完善胸腹主动脉 CT 血管成像提示：肝右动脉、脾动脉远段、肠系膜上动脉远段、双肾动脉远段分支多发动脉栓塞，请血管外科、胃肠外科、肝胆外科等多学科会诊，考虑：1.IABP 导致多血管栓塞可能性大，主动脉附壁血栓可能是栓子来源；2. 血栓位于血管远端，暂予保守治疗，若病情进展，必要时行急诊手术。综合讨论后，予立即拔除 IABP，并足剂量低分子肝素抗凝（100IU/kg），予禁食水、抑酸补液、解痉止痛、抗感染等治疗，腹痛逐渐缓解。后复查 D 二聚体、血清肌酐逐渐升高后稳定，未见肌红蛋白升高。

检验检查记录：

2024-10-17 凝血筛查：D- 二聚体 1.39 ↑ mg/L 活化部分凝血活酶时间 22.60 ↓ s 纤维蛋白原 8.27 ↑ g/L；

2024-10-17 糖化血红蛋白 5.60 %；

2024-10-17 N 端 - B 型钠尿肽测定 4125 ↑ ng/L 高敏肌钙蛋白 T 5524 ↑ ng/L 肌红蛋白测定 27.4 ↓ ng/mL 降钙素原检测 0.120 ↑ ng/mL；

2024-10-17 血气分析：pH 值 7.493 ↑ 氧分压 118 ↑ mmHg 动脉血氧饱和度 99.1 ↑ % 二氧化碳分压 29.2 ↓ mmHg 二氧化碳总量 19.4 ↓ mmol/L 氧合血红蛋白 98.3 ↑ % 还原血红蛋白 0.9 ↓ % 钙 (血气分析游离钙) 1.1 ↓ mmol/L 乳酸 0.8 ↓ mmol/L

2024-10-17 生化全套：白蛋白 36.50 ↓ g/L 丙氨酸氨基转移酶 60.5 ↑ U/L 天门冬氨酸氨基转移酶 63.1 ↑ U/L γ- 谷氨酰基转移酶 143.3 ↑ U/L 碱性磷酸酶 128.1 ↑ U/L 直接胆红素 6.2 ↑ umol/L 甘油三酯 1.67 mmol/L 总胆固醇 3.50 mmol/L 高密度脂蛋白胆固醇 1.07 mmol/L 低密度脂蛋白胆固醇 2.07 mmol/L 载脂蛋白 -A1 0.94 ↓ g/L 乳酸脱氢酶 908.6 ↑ U/L 尿素 8.80 ↑ mmol/L 肌酐 88.4 umol/L 碳酸氢盐 21.7 mmol/L 钾 3.81 mmol/L 钠 137.90 mmol/L 超敏 C 反应蛋白测定 149.87 ↑ mg/L 内生肌酐清除率 77 ↓ mL/(min*1.73m^2) 肾小球滤过率 84.95 mL/(min*1.73m2)；

2024-10-17 血常规检查：白细胞计数 11.14 ↑ 10^9/L 中性粒细胞计数 7.81 ↑ 10^9/L 单核细胞计数 1.35 ↑ 10^9/L 淋巴细胞比值 12.9 ↓ % 单核细胞比值 12.2 ↑ % 血红蛋白 145 g/L 血小板计数 185 10^9/L。

2024-10-19，CT 血管成像 (胸腹主动脉): 肝右动脉、脾动脉远段、肠系膜上动脉远段、双肾动脉远段分支多发动脉栓塞，左肾楔形低灌注区，建议复查。 肝左动脉局部显影浅淡。主动脉及其分支动脉粥样硬化，散在附壁血栓及溃疡灶。肠系膜下动脉远段显影浅淡。 肺气肿；左心增大；冠状动脉支架植入术后改变。

2024-10-17，心脏彩超 :1、左心扩大；室间隔基底段增厚。2、左室壁节段性运动异常。3、中度二尖瓣反流。4、左室整体收缩功能减低，舒张功能减退。

鉴别诊断：

1. 心房颤动；2. 左心室血栓（室壁瘤）；3. 主动脉夹层；4. 糖尿病酮症酸中毒；5. 消化性溃疡

其他：

目前 IABP 广泛应用于急性心肌梗死合并心源性休克的病人，临床上多见局部出血、下肢缺血、血小板减少等并发症，而出现多发脏器血管栓塞较为罕见，值得引起广大临床医师的注意。

且将新“履”试新“途”，“幽远”趁“通达”

顾崇怀

安庆市立医院

患者基本信息：

59 岁男性，以“反复痛 3 年余，再发 1 月”为主诉于 2025.2.17 入院，1 月前曾就诊于外院行 LCX-PCI，并尝试 RCA-CTO 失败此后仍然反复发作胸痛胸闷，此次入院为行 RCA-CTO

主述：

反复痛 3 年余，再发 1 月

现病史：

以“反复痛 3 年余，再发 1 月”为主诉于 2025.2.17 入院，1 月前曾就诊于外院行 LCX-PCI，并尝试 RCA-CTO 失败此后仍然反复发作胸痛胸闷，此次入院为行 RCA-CTO

既往病史：

DM

病程记录：

RCA-CTO

检验检查记录：

--

鉴别诊断：

--

其他：

由于幻灯过大，上传数次均失败现上传 pdf 版本

右房占位性病变 - 肝癌心脏转移 1 例

陈玲玲

北京清华长庚该医院

患者基本信息：

患者男，43 岁，因腹胀就诊当地医院诊断原发性肝癌，无遗传病或肿瘤家族史

主述：

发现肝细胞癌 10 个月

现病史：

2024 年因腹胀就诊当地医院完善检查提示肝癌，于佑安医院行介入治疗，效果欠佳，现为行进一步治疗就诊于我院

既往病史：

既往乙肝病史，无冠心病、高血压、糖尿病等病史。否认丙肝病史，否认结核及传染病史。

病程记录：

患者入院后完善超声心动图检查，提示右心房及下腔静脉占位，由于心脏风险较高，随时有猝死风险，建议心脏外科手术治疗，患者拒绝手术治疗，进行放射治疗

检验检查记录：

超声心动图检查示右心房内可见一异常回声影，大小约 58mm×30mm，回声不均匀，形状不规则，活动度较大，舒张期部分经三尖瓣口进入右室，收缩期返回右房，与三尖瓣相接触，无粘连，右心房异常回声物延伸至下腔静脉，部分充填腔管。

腹部增强 CT：肝右叶 23mm×17mm 类圆形低密度灶，下腔静脉及肝右静脉内见低密度影伴结节状高密度灶，提示癌栓形成。

腹部超声：肝右叶低回声区，符合肝癌表现。

PET-CT：肝右叶、肝右静脉及下腔静脉多发低密度灶伴高密度结节，放射性摄取增高；病变侵犯右心房及房室交界区，可见不规则软组织占位伴放射性摄取增高

鉴别诊断：

右心房占位需鉴别原发性肿瘤（如黏液瘤）与继发病变（如血栓）：

黏液瘤多有蒂，附着于卵圆窝，活动度大、形态可变；

血栓多继发于房颤或瓣膜疾病，基底宽、无活动性；

转移性癌栓特征为与下腔静脉病变连续，活动与心动周期不同步

其他：

诊断：

综合临床病史及影像学结果，诊断为原发性肝癌伴下腔静脉、右心房癌栓形成，右心房占位性病变，心脏转移性肿瘤

讨论：

肝细胞癌是一种高度恶性的肿瘤，肿瘤细胞常易侵犯邻近的血管系统，如肝静脉、门静脉、下腔静脉等造成肝内和肝外转移。肝外转移中以肺部最为常见，其次为骨、肾上腺等部位，而心脏转移少见，原发性肝癌合并右心房癌栓发生率很低。原发性肝癌心脏转移的临床表现缺乏特异性，大多数是无症状的，部分患者可引起胸闷、劳力性呼吸困难、心律失常及下肢浮肿、腹水等下腔静脉回流受阻的表现

本例癌栓通过下腔静脉直接延伸至右心房，形成连续性瘤栓。若转移肿瘤发生在房室瓣口或心室流出道，则可出现相应部位梗阻的症状和体征，严重者可发生猝死。需警惕肺栓塞这一常见致死并发症，超声可表现为右心扩大、室间隔左移等征象

结论：

结合文献，我们认为若患者有原发性肝癌病史，且在心腔内发生实质性占位，需注意观察下腔静脉切面，进一步结合腹部超声和 CT 检查，一旦发现下腔静脉及肝静脉官腔内出现癌栓回声，则可视为原发性肝癌心脏转移的支持诊断

双孔型房间隔缺损封堵术后封堵器脱落一例

曲朔晗

吉林大学第二医院

患者基本信息：

患者，男，66 岁，已婚，主因“阵发性头晕 1 年，加重 1 周”于 2024-10-08 8：48 入院。

主述：

阵发性头晕 1 年，加重 1 周

现病史：

该患者源于 1 年前明显诱因出现头晕症状，病程中无恶心，呕吐，无大汗，无呼吸困难，与体位，进食无明显关系，休息后可缓解，因未影响正常生活，未系统诊治。此后上诉症状有时发作，性质同前。1 周前无明显诱因上诉症状再次发作，行心脏彩超检查，诊断为”房间隔缺损”未治疗，近期发作频繁，今为求进一步系统诊治，遂来我院。

既往病史：

既往有高血压病史 15 年，血压最高可达 160/88mmHg，平素口服诺欣妥控制血压，血压控制不佳。

病程记录：

心脏彩超显示：右心增大，右房（左右径 * 上下径）44mm*50mm，余心腔内径正常范围。房间隔回声连续中断，房水平可探及两束左向右分流，大动脉短轴切面，一处断端约 9mm，另一处断端越 7mm，距主动脉侧无断端，距房顶 8mm，四腔心切面，断端约 12mm，距十字交叉 8mm，距房顶 10.6mm，剑下双房切面，可探及两处断端，一处断端约 10mm，另一处断端约 9mm，断端间距约 14.7mm，距腔上静脉 6mm，距下腔静脉 12mm。EF：56%，三尖瓣轻度反流，左心室舒张功能减退（见图 1），诊断为 “心功能 III 级，双孔型 ASD，房间隔缺损”（见图 1），综合以上病情，多学科团队综合评估患者基本情况，解剖结构等，确认患者适合行 ASDC 手术。遂给予阿司匹林每次 100mg，每日 1 次睡前口服，氯吡格雷每次 75mg，每日 1 次，晚餐后口服。

检验检查记录：

心脏彩超显示：右心增大，右房（左右径 * 上下径）44mm*50mm，余心腔内径正常范围。房间隔回声连续中断，房水平可探及两束左向右分流，大动脉短轴切面，一处断端约 9mm，另一处断端越 7mm，距主动脉侧无断端，距房顶 8mm，四腔心切面，断端约 12mm，距十字交叉 8mm，距房顶 10.6mm，剑下双房切面，可探及两处断端，一处断端约 10mm，另一处断端约 9mm，断端间距约 14.7mm，距腔上静脉 6mm，距下腔静脉 12mm。EF：56%，三尖瓣轻度反流，左心室舒张功能减退（见图 1），诊断为 “心功能 III 级，双孔型 ASD，房间隔缺损”（见图 1），综合以上病情，多学科团队综合评估患者基本情况，解剖结构等，确认患者适合行 ASDC 手术。遂给予阿司匹林每次 100mg，每日 1 次睡前口服，氯吡格雷每次 75mg，每日 1 次，晚餐后口服。

鉴别诊断：

二尖瓣狭窄、主动脉瓣狭窄

其他：

【手术过程】2024-10-10 行局麻下经皮介入房间隔缺损封堵术，拟分别选择 14mm 12mm 封堵伞对两个房间隔缺损进行同期封堵，治疗后患者症状好转。2024-10-10 复查心脏彩超后提示封堵伞脱落，并向家属交代病情，再次行经皮介入房缺封堵术。于 2024-10-11 行局麻下经皮房间隔缺损封堵术，透视下证实原 14mmASD 封堵器脱落至升主动脉弓部（见图 2 ），经右侧股动脉预埋 proglide 后置入 14F 鞘管，选择圈套器抓捕脱落 14mm 封堵器后取出。穿刺右侧股静脉，置入 6F 鞘管，沿右侧股静脉鞘管，加硬导丝通过房间隔缺损口到左房并放置于左肺上静脉，经过彩超证实通过房间隔缺损，置入 10F 封堵器可调弯输送鞘，置入 16mmASD 封堵器于缺损部位，反复牵拉封堵器无活动，并行心脏彩超见残余分流消失。

诊断为 “心功能 III 级，双孔型 ASD，房间隔缺损” （见图 1），综合以上病情，多学科团队综合评估患者基本情况，解剖结构等，确认患者适合行 ASDC 手术。遂给予阿司匹林每次 100mg，每日 1 次睡前口服，氯吡格雷每次 75mg，每日 1 次，晚餐后口服。

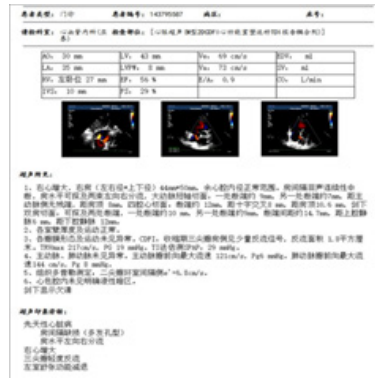

【手术过程】2024-10-10 行局麻下经皮介入房间隔缺损封堵术，拟分别选择 14mm 12mm 封堵伞对两个房间隔缺损进行同期封堵，治疗后患者症状好转。2024-10-10 复查心脏彩超后提示封堵伞脱落，并向家属交代病情，再次行经皮介入房缺封堵术。于 2024-10-11 行局麻下经皮房间隔缺损封堵术，透视下证实原 14mmASD 封堵器脱落至升主动脉弓部（见图 2 ），经右侧股动脉预埋 proglide 后置入 14F 鞘管，选择圈套器抓捕脱落 14mm 封堵器后取出。穿刺右侧股静脉，置入 6F 鞘管，沿右侧股静脉鞘管，加硬导丝通过房间隔缺损口到左房并放置于左肺上静脉，经过彩超证实通过房间隔缺损，置入 10F 封堵器可调弯输送鞘，置入 16mmASD 封堵器于缺损部位，反复牵拉封堵器无活动，并行心脏彩超见残余分流消失。

图 2　二次 ASDC 透视

【讨论】经皮介入房间隔缺损封堵术是治疗房间隔缺损的微创治疗手术方式，优势在于因其可在局麻下进行操作，手术创伤小，避免了传统手术开胸及体外循环等损伤，手术简便，疗效较佳，并且可以缩短患者术后的痛苦及住院周期时常。但是需要术前精确的心脏彩超来评估应选择的封堵器尺寸：1. 房间隔缺损的大小，位置，边缘支撑力；2. 综合评估肺动脉高压程度。本病例发生封堵器脱落，根据脱落后的心脏彩超检查分析，其原因：1. 封堵器尺寸偏小；2. 两孔间距较远。该患者出现封堵器脱落是发生在患者术后当天，不排除因患者剧烈运动导致的封堵器脱落。本例通过第二次 ASDC 术中透视证实 14mm 封堵器脱落至升主动脉根部，为下一步治疗提供了明确的方案。心脏彩超不仅对房间隔缺损是一个必不可少的参考指标，对其他所有的先天性心脏病都是重要的参考数据，如术前诊断，术中监测，术后疗效观测均有重要的应用价值，从房间隔缺损的大小，位置，封堵器尺寸的选择到术中确认封堵器是否牢固稳定预防术后脱落都起着至关重要的作用。

误诊为癫痫的 2 型长 QT 综合征家系报告

李锟

清华大学附属北京清华长庚医院

患者基本信息：

患者，女性， 21 岁

主述：

间断意识丧失 14 年

现病史：

患者 14 年前跑步上 2 楼后突发心悸、黑矇后意识丧失，伴双眼上吊、身体僵直，持续 1 min 后意识自行恢复，清醒后伴大汗，无恶心、呕吐、大小便失禁，未诊治。 2 个月后上课过程中无明显诱因再发意识丧失，性质同前，就诊当地医院，完善脑电图、头颅核磁，未见异常，诊断为“癫痫”， 予奥卡西平 300 mg 3 次 /d。此后上述症状仍间断发作，每年 5 ~ 10 次，多于紧张、晨起将醒、接电话、噪音、饥饿、情绪低落情况下诱发，每次发作前均有心悸、黑矇，发作过程中均有抽搐、双眼上吊、牙关紧闭,发作后均有出汗,偶有恶心、呕吐、大小便失禁。11 年开始外院诊断为“复杂性癫痫”，予丙戊酸镁缓释片 250 mg 2 次 /d、左乙拉西坦 500mg 2 次 /d，效果不佳。 20 d 前于外院拟行“额叶切除术”，术中心电图提示 QTc 480 ms， T 波双峰，终止手术，就诊我院。母亲、大姨、妹妹反复意识丧失病史。

既往病史：

否认特殊病史。

病程记录：

患者治疗包括 3 个方面： 1. 生活方式改善，避免发病诱因，避免应用延长 QTc 药物； 2. 药物治疗：起始予患者 β 受体阻滞剂 10mg 3 次 /d， Holter 记录到患者出现心动过缓并仍有室速反复发作，调整为普萘洛尔 5 mg 3 次 /d，加用美西律 150mg 3 次 /d、补钾； 3.ICD 植入。

检验检查记录：

心电图：窦性心律，左室高电压， T 波改变， QT 间期延长（图 1A）。 24 h 动态心电图：窦性心律（总心搏数 88490 次，平均心率 61 次 /min，最慢心率 38 次 /min，最快心率 121 次 /min）；短阵房性心动过速（7 次 / 阵，仅 1 阵）；短阵室性心动过速（3 ~ 6 次 / 阵，共 5 阵，频率 46 ~ 319 次 / min）； TdP（39 ~ 367 次 / 阵，共 2 阵）（图 1B）； QT 间期延长（最长 712ms，对应 QTc 602ms）； ST-T 改变。

超声心动图：左室心尖部致密化不全；左室射血分数正常范围。经过对全基因组外显子的分析（图 2），发现了患者存在 KCNH2 基因突变 (c.818 C>T, p.T273M; NM_001204798)。Sanger 法验证证实先证者及其母亲和妹妹均携带该变异。

鉴别诊断：

根据 2015 年 ESC 室性心律失常与猝死指南，患者的临床表现、家族史、心电图特征及基因检测结果均支持 2 型先天性长 QT 综合征诊断。鉴别诊断：1. 不同亚型的 LQTS 共同特征是 QT 间期延长，且致病机制及治疗策略不同，因此本病了主要需要鉴别不同亚型 LQTS；2. 需要鉴别电解质紊乱、心肌病等继发因素导致的获得性 LQTS。

其他：

左心交感神经节切除术治疗 Jervell-Lange Nielsen 综合征 1 例

李锟

清华大学附属北京清华长庚医院

患者基本信息：

患儿，女性， 12 岁

主述：

耳聋 11 年，反复意识丧失 10 年

现病史：

患儿 11 年前发现对声音无刺激，外院行脑干诱发电位发现先天性耳聋。 10 年前开始出现反复意识丧失,多于情绪紧激动、玩闹或受惊吓时发生,发作时伴胸闷、抽搐，外院多次脑电图检查未见异常，平均每年发作 5~6 次，每次持续 2~10 min 左右。2 年前开始较前频繁,严重时每月 2~3 次,外院心电图示 QT 间期延长，考虑“LQTS”， 予倍他乐克 12.5 mg 1 次 /d，症状发作无明显减少。家族史：父母体健，弟弟耳聋、反复意识丧失病史 。

既往病史：

否认特殊病史。

病程记录：

先证者及其弟弟行 LCSD 治疗，术后改善生活方式，避免情绪激动、剧烈运动等发病诱因，避免服用延长 QT 间期的药物；口服普萘洛尔 30 mg 3 次 /d 。

检验检查记录：

心电图: 窦性心律，QT=502 ms，QTc=492 ms（图 1B）；动态心电图: 窦性心律，偶发房性早搏，可见 QT 间期延长，最长 534 ms；超声心动图：心脏结果未见异常。经过对全基因组外显子的分析，发现了患者存在 KCNQ1 基因的剪接位点突变 c.224-2A>G，和错义突变 c.815G>A（p.G272D）。 Sanger 法验证证实先证者及其弟弟均携带该复合杂合子变异，两个变异分别来自父亲和母亲。

鉴别诊断：

心电图提示 QTc > 480ms，临床表现为反复意识丧失发作伴先天性耳聋，基因检测确定患者存在 KCNQ1 复合杂合子变异，故诊断 JLNS。

其他：

血小板增多症诱发年轻的急性心肌梗死一例

肖美明

广东省人民医院 粤西医院 （电白区人民医院）

患者基本信息：

患者 男，24 岁，急性起病

主述：

胸痛一小时入院

现病史：

患者于 2025 年 5 月 11 日 19：10 出现持续性胸痛，以胸骨后为主，呈压榨性，无他处放射痛，伴出汗，无伴心悸，无伴气促，无畏寒、发热，无濒死感，无黑矇，无晕厥，无咳嗽、咳痰，无咯血，无腹痛、腹胀，无恶心、呕吐。于 19：50 到达电白区人民医院急诊，于 19：54 完成心电图提示“窦性心律不齐，下壁导联 T 波异常，前壁导联 ST 段呈上斜型 J 点抬高 0.10-0.40mV 伴 T 波高尖。”，于 20:16 完成抽血，于 20:20 我科会诊，于 20:25TnI 提示 0.020mg/L,20:26 考虑诊断“急性前壁心肌梗死”，予替格瑞洛片 180 mg、阿司匹林肠溶片（合资）300 mg、阿托伐他汀钙片 40mg 口服，考虑患者发病在 12 小时内，有急诊介入指征，于 20：27 与患者及患者同事沟通病情后，告知介入手术风险，于 20：28 启动介入室，20：55 签署心导管诊疗知情同意书后，21：02 拟“胸痛查因”收入我科，于 21：03 送入介入室接诊，予介入治疗。

既往病史：

既往有血小板增高，未予治疗，同时发现糖尿病 2 年，间断给与胰岛素治疗。

病程记录：

冠脉造影显示：前降支闭塞，开通后，植入一枚支架。后续给与

1 阿司匹林肠溶片 100mg qd

2. 替格瑞洛 90mg bid

3. 阿托伐他汀钙片 20mg qn

4. 依折麦布 10mg qd

5. 酒石酸美托洛尔片 50mg bid

6. 泮托拉唑片 40mg qd

7. 德谷胰岛素利拉鲁肽注射液 14u ih qd

检验检查记录：

心电图 ST 段抬高，肌钙蛋白升高

鉴别诊断：

主动脉夹层：夹层患者往往有高血压病史，心电图没有 ST 改变，D 二聚体高，该病人都不符合。

其他：

冠脉造影显示 前降支闭塞

OCT 联合 FFR 精准指导钙化病变 PCI 一例

耿雨

清华大学附属北京清华长庚医院

患者基本信息：

患者信息：男性，55 岁，体重 67kg。

主述：

间断胸痛 10 月，再发 2 周。

现病史：

10 月前活动后出现胸痛，伴烧灼感，范围咽喉部至剑突下，持续时间约 5 分钟，休息后可缓解，未予重视。2 周前再次出现活动后胸痛，范围同前，程度较前加重，持续约 5-10 分钟，休息后缓解，无其他不适。

既往病史：

有高血压病、高脂血症、陈旧性脑梗死病史，有长期大量吸烟史。

病程记录：

一、冠状动脉造影结果

1. 左冠状动脉：前降支（LAD）近段严重钙化，狭窄 50%-80%，中段严重钙化，狭窄 50%-90%；回旋支（LCX）远段 70%-90% 狭窄伴重度钙化，OM 狭窄 50%-80% 狭窄。

2. 右冠状动脉（RCA）：中段严重钙化，狭窄 50%-70%，长度约 20mm，后侧支严重钙化，狭窄程度 50%-90%。

二、治疗策略

首先处理 LCX 远段病变，然后处理 LAD 近中段病变，采用 FFR 评估 LAD 近中段病变血流储备分数 (FFR)，后 OCT 评估 LAD 钙化情况，应用 IVL 处理严重钙化、狭窄的原发冠状动脉病变进行碎石和低压球囊扩张。

三、器械准备

1. 桡动脉入路，6F EBU 3.5 指引导管、Runthrough 导丝、Guidezilla 延长导管。

2. IVL 系统（Shockwave C2 冠状动脉 IVL 系统）、OCT 导管、FFR 压力微导管。

3. 半顺应性球囊、非顺应性球囊（NC 球囊）、切割球囊、药物涂层球囊（DCB）、支架

手术过程

四、左冠状动脉 LCX 病变治疗

1. 介入治疗：LCX 远段植入 2.25x30mm DES，OM 使用 2.0x16mm DCB 扩张，复查冠脉造影见支架贴壁良好，未见夹层。

行左冠状动脉 LAD 病变治疗

1.FFR 测定：对 LAD 近中段进行功能学评估，EQ 数值为 2，VERFIY 数值为 2，整体数据没有漂移，FFR 数值为 0.66。

2.OCT 评估 LAD 病变：术前 OCT 观察下 LAD 中段纤维增生伴钙化、狭窄严重，MLA 0.78mm²，钙化最厚 13.2mm。

3. IVL 治疗： 根据 OCT 观察到管腔直径 2.2mm 选择 2.5x12mm IVL 球囊对病变进行 40 次脉冲治疗，后扩张球囊能够完全充盈。

4. IVL 治疗后 OCT 评估：MLA 处面积从 0.78mm² 增加到 2.28mm²，钙化最厚处显著的裂痕。

5. 支架植入：植入 DES 支架，中段病变植入 2.5x18mm DES，近段病变植入 3.0x30mm DES 植入、3.0 x18mm NC 后扩。

6. 术后复查 OCT：术后 OCT 示支架贴壁良好。

7. 术后左冠脉多体位造影

检验检查记录：

心电图：窦性心律，未见明显 ST-T 改变；

超声心动：结构及功能未见明显异常。

鉴别诊断：

入院诊断：

1. 冠状动脉粥样硬化性心脏病（不稳定性心绞痛，心功能 I 级）

2. 高血压 3 级（很高危）

3. 高脂血症

4. 陈旧性脑梗死

鉴别诊断：

1. 急性心肌梗死

2. 肺栓塞

3. 急性主动脉夹层

4. 返流性食管炎

其他：

1. 功能学与形态学评估的协同作用

FFR（血流储备分数）：术前对 LAD 近中段进行功能学评估，FFR 值为 0.66（显著缺血阈值以下），明确了该病变对血流动力学的显著影响，为治疗必要性提供了客观依据。

OCT（光学相干断层扫描）：术前 OCT 清晰显示 LAD 中段严重钙化（钙化最厚 13mm）、最小管腔面积仅 0.78mm²，精准定位病变性质与范围；术后 OCT 验证 IVL 治疗后钙化斑块裂痕及管腔扩大（MLA 增至 2.28mm²），并确认支架贴壁良好，避免了支架膨胀不全或贴壁不良的风险。

2.IVL（冲击波球囊）在钙化病变中的应用优势

高效钙化修饰：针对 LAD 中段严重钙化，采用 2.5×12mm IVL 球囊进行 40 次脉冲冲击波治疗，成功破碎深层钙化环，显著改善血管顺应性，为后续支架植入创造理想条件。

安全性保障：IVL 治疗后 OCT 显示钙化斑块裂痕但无夹层或穿孔，结合低压球囊扩张，降低了血管损伤风险。

3. 综合治疗策略的制定与实施

分步处理: 优先处理 LCX 远段病变(植入 DES 联合 DCB 扩张),再聚焦 LAD 近中段，体现了“分阶段、精准化”的治疗理念。

器械协同：IVL 预处理后植入 DES 支架（2.5×18mm 及 3.0×30mm），结合非顺应性球囊（NC）后扩，确保支架充分膨胀；药物涂层球囊（DCB）用于分支血管（OM2）扩张，减少支架植入需求。

IOCA 相关的 CMVD 一例 ——左前降支 CFR 异常的预警价值

闫航语

首都医科大学附属北京安贞医院

患者基本信息：

女性，70 岁

第一次就诊于门诊：

主因“间断胸痛 10 年，二次支架术后加重 1 月”于 2023-4-19 就诊于我科门诊

既往史：糖尿病史 10 年，高脂血症病史 10 年

手术史 :2009 年右踝关节手术，2013 年于当地医院冠脉造影并于前降支植入支架 1 枚，2023 年 3 月 (1 月前) 于我院于前降支植入支架 2 枚

体检 :BP 130/80mmHg，HR70 次 / 分钟，未发现其他异常

实验室检查 :LDL-C:1.86mmo/L，HDL-C:0,87mmol/L，Hcy:15.9umolL，LPa:84.2nmol/L，糖化血红蛋白 (HbA1C):7.7%，B 型钠酸肽 (BNP) 检测 :35.0pg/ml，高敏肌钙蛋白 I(hsTnI):0.0pg/ml(参考值 0-11.6pg/ml)，甲功五项 :4.990mlu/L，血常规、便常规、凝血五项见明显异常

ECG: 窦性心律 (83 次 / 分)

UCG:LVEF:68%，LAD:31mm，LVDd:41mm，LVDs:26mm，IVS:9mm，TAPSE:23mm，二尖瓣反流 (轻度)，左室舒张功能减低

第二次就诊：

主因“间断胸痛 10 余年，加重 15 天于 2024-7-16 再次就诊于我科门诊

主述：

主因“间断胸痛 10 年，二次支架术后加重 1 月”于 2023-4-19 就诊于我科门诊

现病史：

2023-4-19 第一次就诊于我科门诊：

患者 10 年前出现活动后胸痛，2013 年就诊于当地医院，于**前降支置入支架 1 枚**，2023 年 3 月因症状加重，于我院行冠脉造影提示 "LAD **近段支架内再狭窄，最重狭窄 100%，TMI 血流 0 级**，LAD **中段，最重狭窄 100%**，**TMI 血流 0 级**，侧支循环：钝缘支 - 间隔支，钝缘支最重狭窄 95%，TIMI 血流 3 级"，于 LAD 近段至 LAD 中段，**行药物球囊扩张，植入 2 枚支架**。术后规律药物治疗，此次因胸痛症状间断发作就诊于我院门诊

2024-7-16 第二次就诊于我科门诊：

主因 "间断胸痛 10 余年，加重 15 天 " 于 2024-7-16 再次就诊于我院，完善冠状动脉造影提示 "LAD **近段支架内再狭窄，最重狭窄 100%**，**TIMI 血流 0 级**，LAD **中段支架内再狭窄，最重狭窄 100%，TIMI 血流 0 级**"，于 LAD 原支架内行**药物球囊扩张成形术**。

既往病史：

糖尿病史 10 年，高脂血症病史 10 年

病程记录：

该患者为门诊患者，通过电话及门诊随访收集病历资料，无入院后治疗记录

检验检查记录：

检查记录：

2023 年 3 月冠脉造影及介入治疗：行冠脉造影左前降支近段病变性质：支架内再狭窄，Mehran 分型：IV 型 支架断裂类型：支架未断裂，TIMI 血流：0 级，最重狭窄程度：100%，侧支循环：纯缘支（OM）一间隔支（Sept）：左前降支中段 TIMI 血流：0 级，最重狭窄程度：100%，侧支循环：钝缘支（OM）一间隔支（Sept）；钝缘支 b TIMI 血流：III 级，最重狭窄程度 :95%。左前降支近段 - 左前降支中段，行药物球囊扩张，置入支架 2 个。

2023 年 4 月 ECG: 窦性心律 (83 次 / 分)

2023 年 4 月 UCG:LVEF:68%，LAD:31mm，LVDd:41mm，LVDs:26mm，IVS:9mm，TAPSE:23mm，二尖瓣反流 (轻度)，左室舒张功能减低

2023 年 4 月静息 + 药物负荷心肌断层显像：药物负荷试验心电图阴性。左心室前壁中段（LAD 供血区）轻度心肌缺血改变，约占左心室面积 6%。左心室整体收缩功能正常。　LAD、LCX 及 RCA 支配区域及左心室整体冠状动脉血流灌注储备指数减低。LAD：1.55，LCX：1.58，RCA：1.75，TOT：1.61（正常参考值 ≥ 2.1）。

2024 年 4 月静息 + 药物负荷心肌断层显像：左心室部分心尖段、前壁心尖段及中段、部分前间隔中段及基底段（LAD 供血区）心肌缺血改变，约占左心室面积 15%。左心室整体收缩功能正常。LAD 支配区冠状动脉血流灌注储备指数减低；LCX、RCA 支配区域及左心室整体冠状动脉血流灌注储备指数正常。LAD：1.48，LCX：2.77，RCA：2.90，TOT：2.15（正常参考值≥ 2.1）。

2024 年 7 月冠脉造影及介入治疗：LAD 近段支架内再狭窄，最重狭窄 100%，中远段弥漫支架内再狭窄，自侧桥侧枝显影。于 LAD 原支架内行药物球囊扩张成形术，应用两枚药物球囊，并应用 OCT 进行影像学评估。

检验记录：

实验室检查 :LDL-C:1.86mmo/L，HDL-C:0,87mmol/L，Hcy:15.9umolL，LPa:84.2nmol/L，糖化血红蛋白 (HbA1C):7.7%，B 型钠酸肽 (BNP) 检测 :35.0pg/ml，高敏肌钙蛋白 l(hsTnl):0.0pg/ml(参考值 0-11.6pg/ml)，甲功五项 :4.990mlu/L，血常规、便常规、凝血五项见明显异常

鉴别诊断：

1. **X 综合征：**X 综合征多见于女性，心电图负荷试验常阳性，但冠状动脉造影则阴性且无冠状动脉痉挛。该患者上述症状及检查不符合，必要时行相关检查以明确。

2. **肋间神经痛及肋软骨炎：**本病常累及 1-2 个肋间，但并不一定局限在胸前，为刺痛或灼痛，多为特征性而非发作性，咳嗽、用力呼吸和身体转动可使疼痛加剧，肋软骨处或沿神经走行处有压痛，手臂上举活动时局部有牵拉疼痛，该患者上述症状及检查与之不同。

3. **心脏神经症：**本病患者常诉胸痛，但为短暂的刺痛或持久的隐痛，常喜欢吸一大口气或叹息性呼吸。胸痛部位多为左胸心尖部附近，或经常变动。症状多在疲劳后出现，而不在疲劳的当时，作轻度体力活动反觉舒适，有时可耐受较重的体力活动而不发生胸痛或胸闷。含服硝酸甘油无效或在 10 多分钟后才 "见效"，常伴有心悸、疲乏及其他神经衰弱的症状。该患者上述症状及检查不符合。

其他：

事件时间链：2013.3 诊断为不稳定型心绞痛于 LAD 型支架植入→ 2023.3 诊断为不稳定型心绞痛于 LAD 支架内再狭窄开通→ 2023.4（术后 1 月）第一次就诊于我科门诊，复查 CFR 提示 CFRLAD 及 CFRLCX/RCA/TOT ↓→ 2024.4（术后 1 年）第二次就诊于我科门诊，复查 CFR 提示 CFRLAD 持续↓，CFRLCX/RCA 改善→ 2024.7（术后 15 月）以不稳定型心绞痛入院，于 LAD 支架内再狭窄开通

本例患者为 70 岁女性，曾于 2013 年及 2023 年行经皮冠状动脉介入治疗。2023 年 3 月冠脉造影显示 LAD 近段及中段支架内再狭窄 100%，钝缘支狭窄 95%（TIMI 血流 3 级），并于 LAD 近段及中段成功植入 2 枚支架。核素心肌灌注显像提示左心室前壁中段放射性分布稀疏区较负荷像" 填充"，LAD、LCX 及 RCA 支配区域及左心室整体 CFR 减低，直接证实了微循环功能障碍的存在，并结合《冠状动脉微血管疾病诊断和治疗中国专家共识（2023 版）》中相关分类标准，考虑诊断为 IOCA 相关 CMVD。按照《共识》指示，强化生活方式干预、抗血小板治疗、冠心病二级预防治疗。2024 年 4 月复查显示，LCX 和 RCA 的 CFR 分别改善为 2.77 和 2.90，总 CFR 恢复至正常范围，但 LAD 区域 CFR 仍低，为 1.48。

IOCA 相关 CMVD 的诊疗困境，在本例中体现为 "解剖成功" 与 "功能失败" 的鲜明矛盾。患者于 2023 年 3 月行 LAD 药物球囊扩张及支架植入术，术后 LAD 血流恢复（TIMI 3 级），但 2024 年 4 月 CFR 复查显示 LAD 区域持续低下（1.48），而 LCX/RCA 区域显著改善（2.77/2.90）。这一结果曾引发困惑：为何 LAD 解剖开通后微循环仍无法复苏？ 直至 2024 年 7 月造影证实 LAD 近中段再狭窄，真相方浮出水面——CFR 的异常实为解剖狭窄复发的早期预警信号。

OCT 指导 IVL 处理复杂左主干真分叉钙化病变

耿雨

清华大学附属北京清华长庚医院

患者基本信息：

男性，82 岁，体重 62kg

主述：

间断胸痛 12 年，再发加重 5 天。

现病史：

患者 12 年前无明显诱因出现剑突下疼痛，疼痛性质为闷痛，伴紧迫感，范围约拳头大小，持续数分钟不缓解，伴胸闷、出汗，行冠脉造影检查并于右冠植入支架（具体不详），术后规律口服冠心病二级预防药物治疗，无胸闷、胸痛等不适。患者 5 天前大便用力时出现剑突下疼痛，性质为闷痛，伴紧迫感，无放射痛，持续时间 30 分钟不缓解。

既往病史：

有高血压、糖尿病、高脂血症病史多年，有长期大量吸烟史，未戒烟。

病程记录：

冠状动脉造影结果

造影结果

1. 左冠状动脉：左主干（LM）体尾部 50%-70% 狭窄伴钙化，前降支（LAD）近段至远段严重钙化，狭窄 70%-90%，第一对角支（D1）开口至近段 50%-70% 狭窄；回旋支（LCX）开口至近段 50%-80% 狭窄伴钙化，LM/LAD/LCX Medine 分型：1.1.1。

2. 右冠状动脉（RCA）：开口至近中段可见支架影，支架内血流通畅。

治疗策略

患者造影提示严重钙化病变，根据指南和共识，IVL 适用于严重钙化、狭窄的原发冠状动脉病变进行碎石和低压球囊扩张，拟采用 IVL 技术进行钙化病变预处理。

患者 LM 分叉病变，Medine 分型：1.1.1，拟使用 DK-CRUSH 双支架技术。

器械准备

1. 桡动脉入路，7F EBU 3.5 指引导管、Runthrough 导丝、6F Telescope 延长导管。

2.IVL 系统（Shockwave C2 冠状动脉 IVL 系统）、OCT 导管。

3. 半顺应性球囊、非顺应性球囊（NC 球囊）、切割球囊、支架（DES）。

手术过程

左冠状动脉 LAD 病变治疗

1. OCT 评估 LAD-LM：OCT 显示 LAD 到 LM 均为钙化病变，钙化积分 4 分，长度 20.9mm，最小管腔面积 1.52mm²，钙化最厚 1.90mm 。

2. IVL 预处理 LAD-LM：LCX 保护，预扩张球囊 2.5x 15mm 12atm 进行扩张后，3.5mm shockwave 无法通过，使用 IVL-Shockwave 3.0x 12mm 进行扩张 LM 及 LAD，50 个脉冲后，使用 3.5x 12mm shockwave 对 LM 进行扩张，复查造影可见钙化斑块体积减少。

3. IVL 后 OCT 评估 LAD-LM：OCT 显示钙化斑块破裂，管腔面积显著扩大。

左冠状动脉 LCX 病变治疗

1. IVL 预处理 LCX-LM：对 LCX 进行预扩张，并进行 3.0x30mm shockwave 球囊 IVL 治疗 LM-LCX，30 个脉冲。（图 8）

2. IVL 治疗后 OCT 评估 LCX-LM：OCT 显示钙化斑块破裂，管腔面积显著扩大。

3. 支架植入：6F Telescope 支撑下进行 DK-CRUSH 技术完成 LAD 3.0x18mm DES 拘禁保护，LCX 植入 3.0x18mm DES，造影观察；LAD 3.0x18mm DES 后造影观察，LM 植入 3.5x15mm DES 10atm 扩张；球囊对吻扩张并 POT。

术后评价

1. 冠脉造影：左冠状动脉 LM、LAD 和 LCX：支架通畅，贴壁良好，无残余狭窄。

2. 术后腔内影像：支架膨胀良好，无夹层。

检验检查记录：

体格检查：体温：36.4℃，脉搏：76 次 / 分钟，呼吸：19 次 / 分钟，血压：152/69mmHg。心肺腹查体（-）。

实验室检查：CK 78 U/L, CK-MB 12.4 ng/mL, NT-ProBNP 10811 pg/ml, TnT-hs 0.270 ng/mL。

心电图：窦性心律，前壁导联 ST 段压低。

鉴别诊断：

入院诊断

1. 冠状动脉粥样硬化性心脏病

急性非 ST 段抬高型心肌梗死

陈旧性心肌梗死

窦性心律

心界不大

心功能 I 级 (KILLIP 分级)

冠状动脉支架植入术后状态

2. 高血压病 3 级（很高危）

3.2 型糖尿病

4. 高脂血症

鉴别诊断：

1. 急性主动脉夹层

2. 急性肺栓塞

3. 不稳定性心绞痛

4. 返流性食管炎

其他：

拨开迷雾见真章

李璇璇

石家庄长城中西医结合医院

患者基本信息：

患　者：男，27 岁，身高 170cm，体重 68k

既往史：否认先天性心脏病、冠心病、心肌炎、高血压等病史。

家族史：否认家族遗传病史，否认类似疾病史。

主述：

间断胸闷、气短半年，加重 10 天

现病史：

半年前患者无明显诱因出现胸闷、气短、乏力，活动后为著，就诊于当地医院，查肺 CT 不除外肺炎。给予抗感染治疗，症状未见明显好转。逐渐出现心悸、纳差、腹胀、夜间不能平卧，查心脏超声：LA 51mm LV72mm EF24% 全心增大 左室弥漫性运动减弱 心包积液 右侧胸腔积液。诊断为“扩张型心肌病 心力衰竭”，给予对症治疗后病情好转出院。

10 天前患者病情较前加重，遂就诊。

既往病史：

体健

病程记录：

本例为一青年男性，反复出现心力衰竭，我们接诊时首先考虑的是，是否依然延续他院外的诊断扩张型心肌病？众所周知，扩张型心肌病是个除外性的诊断，那么这个患者，是否已经除外了包括高血压性心脏病、缺血性心肌病、炎性心肌病、淀粉样变性等疾病？

检验检查记录：

心电图：窦性心律，电轴左偏，肢体导联低电压，胸导 R 波递增不良，T 波倒置。

动态心电图：窦性心律，平均心率 83 次 / 分，室性早博共 6755 次，包括 6040 次单发室早，715 次成对室早和 2 次室速。

心脏超声：左心增大 左室部分心肌致密化不全 室间隔与左室壁运动幅度弥漫性减低 二尖瓣中度反流 少量心包积液。

心脏核磁增强：左室间隔室壁心肌中层线样延迟强化。

冠脉造影：未见异常。

B 型钠尿肽前体：12919.8pg/ml（参考值：0-450pg/ml）

心肌酶：肌酸激酶 CK 263（参考值：0-190U/L）；肌酸激酶同工酶 CK-MB 38（参考值：0-24U/L）

腹部彩超：肝淤血

胸部 CT：两肺散在纤维条索；心脏增大，全心为著

血、尿、便常规，凝血常规未见异常

血气分析、肌钙蛋白、肝功能、肾功能（院外肌酐曾一过性增高）、电解质、血脂、甲功未见明显异常

三角肌活检：肌源性损伤，神经纤维，考虑线粒体肌病。

HE 染色：肌纤维变性、坏死；SDH 染色见 SSV 现象；改良三色提示髓鞘缺失；ATP 酶染色提示神经纤维受损

考虑患者病理结果提示线粒体疾病，我们建议患者及其亲属行基因检测，患者表示院外已查基因，并带来了结果。

院外基因检测结果：院外行全外显子检测 +sanger 测序，变异基因：TTN MYBPC3，考虑肥厚性心肌病？

鉴别诊断：

本例为一青年男性，反复出现心力衰竭，我们接诊时首先考虑的是，是否依然延续他院外的诊断扩张型心肌病？众所周知，扩张型心肌病是个除外性的诊断，那么这个患者，是否已经除外了包括高血压性心脏病、缺血性心肌病、炎性心肌病、淀粉样变性等疾病？

其他：

现在我们面对病理和基因完全不同的结果，在患者临床特征不典型的情况下，我们的诊断是应该依据哪个？

后又再次行基因检测：我们收集了先证者及其父母的尿液样本，进行了 DNA 提取行全基因组检测，并利用 Sanger 测序法检测，结果患者携带线粒体 DNA 变异 m.3243A>G，原本应该是鸟嘌呤被置换成了腺嘌呤，变异来源于母亲。

病例启示

1. 对于合并多系统症状的心肌病患者、MCM 的高危人群 应尽早进行线粒体相关生物化学、基因检测及心脏相关筛查。

2. 临床在进行线粒体变异检测时采样的优先顺序应为：肌肉活检 > 口腔拭子 > 尿液 > 血液。

经股 TAVR 治疗单纯主瓣反流伴主动脉夹层 1 例

刘尚典

深圳市宝安区人民医院

患者基本信息：

man, 82-year-old

主述：

tachypnea for 2 years

现病史：

An 82-year-old man who had been hospitalized for repeated tachypnea for 2 years, recently experienced increased dyspnea with renal insufficiency. He has a history of hypertension and uncomplicated TBAD. TEE before surgery showed severe AR (Figure 1), regurgitation area was about 8.3 cm^2, aortic sinus diameter was about 46 mm. Tricuspid and mitral valve regurgitation was mild, and left ventricular diameter was about 56 mm.

Computed tomography angiography (CTA) measurements showed significant dilation of the descending thoracic aorta to approximately 38 mm.

既往病史：

hypertension 20 years;Stanford type B aortic dissection 2 years

病程记录：

TAVR was successfully performed under the guidance of transesophageal echocardiography (TEE). Postoperatively, the prosthesis worked well and there was no para-valvular regurgitation.

检验检查记录：

TEE before surgery showed severe AR , regurgitation area was about 8.3 cm2, Ascending aorta diameter was 33 mm. Tricuspid and mitral valve regurgitation was mild, and left ventricular diameter was about 60 mm.

Computed tomography angiography (CTA) measurements showed significant dilation of the descending thoracic aorta to approximately 38 mm. The dissection began at the distal end of the left subclavian artery (LSA) and extended through the descending aorta to the left common iliac artery (LCIA).

鉴别诊断：

Aortic regurgitation

Stanford type B aortic dissection

Stage 3 hypertension (high-risk category)

其他：

--

从两例 Kommerell 憩室的腔内修复治疗病例浅谈 Kommerell 憩室

刘尚典

深圳宝安区人民医院

患者基本信息：

王 XX，男性，42 岁

主述：

胸痛 2 小时

现病史：

患者 2 小时前左右吃饭时突然出现胸痛，为胸前区持续性剧痛，有后背部放射痛，伴大汗淋漓，无心悸，无呼吸困难，无晕厥，无意识障碍，无恶心、呕吐，无发热等不适，患者未予特殊处理，自行至当地医院就诊，行全主动脉 CTA 提示：主动脉夹层（DeBakey III 型），夹层累及肠系膜上动脉起始部、右侧髂总动脉。D 二聚体 7.74mg/L，NT-proBNP635.6pg/ml, 心肌酶、肌钙蛋白正常，予芬太尼镇痛、乌拉地尔降压治疗。考虑患者病情危重，予 120 救护车转我院，现拟“主动脉夹层” 收住我科。起病以来，患者精神、食欲、睡眠尚可，大小便正常，近期体重无明显改变。

既往病史：

既往 “高血压” 病史 10 余年，长期口服降压药物，具体不详，平时未监测血压，近 2 日未服药

病程记录：

应用 Castor 支架合并原位开窗技术全腔内治疗

检验检查记录：

术前全主动脉（CTA）显示: 1、主动脉夹层（DeBakey III 型），破口位于主动脉弓，累及双侧锁骨下动脉，远侧累及降主动脉、双侧髂总动脉、髂内动脉及右侧髂外动脉，考虑右侧髂外动脉假腔内附壁血栓形成；腹腔干起始部及右肾动脉近段受累，管腔狭窄；2、Kommerll 憩室，迷走右锁骨下动脉，左颈总动脉与右颈总动脉共干；3、主动脉硬化；4、双背侧胸膜下肺内炎症

鉴别诊断：

--

其他：

--

阻塞性睡眠呼吸暂停综合征合并扩张型心肌病患者诊治 1 例

邹济

南昌大学

患者基本信息：

性别：男

年龄：35 岁

身高 / 体重：1.74m / 101.5kg

BMI：33.5 kg/m²（肥胖）

就诊时间：2024 年 3 月 10 日

就诊科室：南昌大学第二附属医院心血管内科

主述：

胸闷 5 天余

现病史：

患者于 5 天前夜间 11 点无明显诱因出现持续性胸闷气喘，心慌，伴有呼吸困难，平卧时胸闷加重，无胸痛，无恶心呕吐，无晕厥黑朦，日间症状好转，仍感胸闷气促，2 天前于当地县医院就诊，心脏彩超示：1. 全心扩大，2. 左室壁运动弥漫性减低。3. 左心功能明显低下。予以美托洛尔，沙库巴曲缬沙坦，达格列净，螺内酯等药物治疗，患者胸闷较前明显缓解，后转入我院继续治疗。

既往病史：

既往体健，否认高血压、糖尿病、冠心病等病史，有外伤史，2008 年曾有过车祸史。否认吸烟、饮酒史，否认心脏病家族史。患者生活作息长期熬夜，体型肥胖。

病程记录：

入院予以 - 持续气道正压通气（continuous positive airway pressure,CPAP）

- 抗心衰四联：沙库巴曲缬沙坦 50mg bid、螺内酯 20mg qd、达格列净 10mg qd、呋塞米 20mg qod

- 调脂：阿托伐他汀 20mg qn

- 降尿酸：非布司他 40mg bid + 秋水仙碱 0.5mg qn + 碳酸氢钠 1g tid 暂缓起搏器植入（考虑患者年轻、代偿能力可及 OSAHS 可逆性）

出院后 规律服药 + CPAP 治疗

3 个月随访 动态心电图：窦性心律，偶发房早（房室传导阻滞消失）

6 个月随访 心脏超声：LVEF 63%（↑ 39%），体重降至 30.7 kg/m²；心力衰竭症状显著缓解

检验检查记录：

实验室检查

BNP：235 pg/ml（↑）；

肝功能：ALT 143.70 U/L（↑），AST 42.60 U/L（↑）；

肾功能：肌酐 118.30 μmol/L（↑），尿酸 587.30 μmol/L（↑）；

尿常规：葡萄糖 4+，蛋白质 +；

乙肝：HBsAg 阳性（19.112 IU/ml）。余检验无异常。

影像学与功能检查

检查项目 结果

心脏超声 左房前后径 47mm，左室舒张末径 65mm，LVEF 24%; 左房、左室扩大，整体收缩活动减弱

动态心电图 全天平均心率快、高度房室传导阻滞、交界性 / 室性逸搏心律、ST-T 改变

心脏磁共振 左心房扩大伴左室功能明显减低（符合 DCM 表型），心包少量积液

睡眠呼吸监测 (PSG) AHI 66.6 次 / 小时，最低血氧 64%（重度 OSAHS+ 重度低氧血症）

冠脉造影 前降支、回旋支、右冠散在斑块（狭窄 < 50%，TIMI 3 级）

腹部 CT 肝内钙化灶、双肾结石、左肾囊肿

关节超声 左侧膝关节痛风性关节炎并痛风石

鉴别诊断：

1. 高血压性心脏病：有高血压病史，出现左室对称甚至非对称性肥厚表现，一般不伴有左室流出道梗阻，有学者认为高血压左室肥厚与肥厚型心肌病可靠地鉴别点在于有无肥厚型心肌病的家族史，本例患者无高血压病史，不存在左室流出道梗阻，无左室不对称性肥厚，有肥厚型心肌病家族史均不支持高血压性心脏病诊断：

2. 冠心病：心绞痛、心电图 ST-T 改变为二者共有，但冠心病一般有年龄、女性绝经后、高血压、糖尿病、高血脂、吸烟、饮酒等危险因素，无特征性杂音，主动脉多增宽或有钙化，心脏彩超室间隔不增厚，但可能有节段性室壁运动异常。本例患者中年男性，无冠心病危险因素不支持，冠脉造影有助于明确诊断。

3. 室间隔缺损：收缩期杂音部位相似，但多为全收缩期粗糙喷射样杂音，心尖部多无杂音，本例患者未闻及杂音不支持，心脏彩超已明确排外。

4. 主动脉瓣狭窄：症状和杂音部位相似，但杂音部位较高，并常有主动脉瓣区收缩期喷射音，第二心音减弱，还可能合并舒张早期杂音。生理动作和药物左右对杂音影响不大，左心导管检查显示收缩期压力差在于主动脉瓣前后，心脏彩超已明确排外。

5. 风湿性二尖瓣关闭不全：杂音相似，但多为全收缩期，血管收缩药或下蹲杂音增强，Valsalva 动作杂音减弱，心脏彩超已明确排外。

其他：

治疗特殊性：未植入起搏器（突破点）：青年患者、扩张型心肌病可逆、CPAP+ 药物联合治疗后传导阻滞完全逆转；

多系统管理：同步处理心衰、OSAHS、高尿酸血症及痛风。

对于 DCM 合并心力衰竭、房室传导阻滞及 OSAHS 的年轻患者，予以常规心衰治疗联合 CPAP，考虑由其自身代偿能力，可考虑暂缓安装心脏起搏器，后期随访患者药物及 CPAP 的治疗疗效，可最大程度避免手术，改善患者的预后及减轻患者经济负担。

寻找肾上腺的秘密

亢园园

上海交通大学医学院附属瑞金医院

患者基本信息：

患者为 47 岁女性，职员。

主述：

血压升高 8 年，控制不佳伴低钾血症 3 月余。

现病史：

8 年前因头痛不适发现血压升高，最高 170/100mmHg, 开始口服氯沙坦氢氯噻嗪 0.5# qd po 降压治疗，血压控制在 130/90mmHg 左右。1 年前体检上腹部 MR 发现左侧肾上腺瘤，未进一步就诊。3 月前因头痛再次测血压 180/100mmHg 就诊我科门诊，查血钾 2.98mmol/L，血醛固酮 335pg/ml，肾素 0.24ng/ml/h，调整药物左旋氨氯地平 2.5mg qd po+ 缓释异搏定 240mg qd po+ 特拉唑嗪 2mg qn po 联合降压治疗，同时予氯化钾缓释片 1.5g tid po 补钾治疗，血压控制在 130/80mmHg 左右，复查血钾 3.5mmol/l，目前换药充分，明确高血压病因入院

既往病史：

个人史：否认慢性肾病，心脏病等疾病，否认烟酒史；有高血压家族史，父母亲均有高血压病史；

生育史：已婚已育，1 子体健，否认流产史。15 岁月经初潮，47 岁自然绝经，无口服避孕药史。

病程记录：

患者换药重复后入院完善检查，排除了主动脉缩窄、肾动脉狭窄。甲亢、肾实质性疾病导致的继发性高血压，肾上腺 CTA 示左侧肾上腺稍增粗，外侧支腺瘤可能，ARR 阳性，盐水试验阳性，但是肾上腺静脉取血术（AVS）提示无优势分泌，进一步完善 1mg 以及 2mg 地塞米松抑制试验阳性，确诊为原醛合并亚临床库欣（非 ACTH 依赖性），因此我们选择用肾上腺素校正后 AVS 提示左侧优势分泌，后转入泌尿外科手术，术后患者血压完全正常，血钾正常。

检验检查记录：

心电图：正常心电图，心率 81bpm；

心脏超声：未见明显异常

颈动脉超声：未见明显异常；

尿酸 291μmol/L；尿素 4.4mmol/L；肌酐 50 umol/L；血钾 3.34 mmol/L；24h 尿蛋白 152 mg

TG 1.37mmol/L TC 4.77mmol/L HDL 0.98mmol/L LDL 2.76mmol/L；血糖：4.95-4.86 mmol/L；糖化血红蛋白：5.1%

血 F13.55pg/ml，血 ACTH 18.95pg/ml 尿 F69.69ug/dl

血肌酐 50umol/L，24 小时尿蛋白定量 152mg 略高，B 超示双肾大小正常对称

有低钾病史；血 Aldo：294-175 pg/ml; 血 Pra：0.13-0.75 ng/ml/h；血 ARR > 300，尿 aldo:18.75ug/2.3L, 尿 K 63.5mmol/L(9g/d) 原醛可能大；肾上腺 CTA：左侧肾上腺稍增粗，外侧支腺瘤可能。

鉴别诊断：

1. Liddle 综合征又称假性醛固酮增多症，为常染色体显性遗传，幼年发病，其机制为先天性肾小管遗传性缺陷致远端肾小管对钠的回吸收增加，对钾的排出增多，从而导致严重的容量型高血压合并低血钾、高尿钾、低肾素、低醛固酮、代谢性碱中毒。

2. 库欣综合征：各种原因造成肾上腺分泌过多糖皮质激素所致疾病的总称，主要包括库欣病和异位 ACTH 综合征等。库欣综合征患者高血压很常见，四成以上的患者存在低血钾。醛固酮及肾素测定正常或偏低。

3. 原发性醛固酮增多症即原醛症，是指肾上腺皮质分泌过量醛固酮，导致体内潴钠、排钾、血容量增多、肾素 - 血管紧张素系统活性受抑，临床主要表现为高血压伴低血钾，是继发性高血压最常见的原因之一，属于高醛固酮 / 低肾素代表。

其他：

无

《I 型肺动脉高压患者肺动脉去神经术治疗的突破与成效 —— 从顽疾到新生》

段娜

辽宁省人民医院

患者基本信息：

一、个人信息

姓 名： 刘跃跃

性 别：男

年 龄： 39 岁

职 业： 其他

籍 贯：辽宁省

民 族： 汉族

婚 姻： 已婚

二、个人史

生于沈阳，否认疫区、疫情、疫水接触史，否认牧区、矿山、高氟区、低碘区居住史，否认化学性物质、粉尘、放射性物质、有毒物质接触史，否认吸毒史，否认冶游史，否认吸烟、饮酒史。

三、婚育史

已婚，结婚年龄适龄，配偶健康，育有 1 子，家庭关系和睦。

四、家族史

否认家族性遗传病、精神病或类似的病史；父亲去世，死因不详，母亲健在。

主述：

胸闷气短半年余。

现病史：

患者半余年前无明显诱因偶发胸闷不适，无胸痛，未系统诊治。曾就诊于我院，完善心脏彩超等检查，诊断为“肺动脉高压”，后就诊于北部陆军总院完善右心导管检查，未行进一步治疗，今为求进一步明确诊治于我院就诊，门诊以“肺动脉高压”为诊断收入我科治疗。患者病来一般状况尚可，无畏寒发热、无咳嗽咳痰、无恶心呕吐、无反酸烧心、无头晕黑矇、无腹痛腹泻。患者近来精神可，饮食及睡眠可，大小便正常，近期体重无明显变化。

既往病史：

否认高血压病、糖尿病、脑血管病、肺部疾病及肾病病史，否认“肝炎”、“结核”、“疟疾”病史，预防接种史不详，房间隔缺损修补术后，否认外伤史，否认输血史。

病程记录：

一、一般治疗

一级护理，心内科常规护理常规。每日监测血压、心率、心律。

二、药物治疗

营养心肌：烟酰胺注射液 400mg 日一次静点；利尿：呋塞米 20mg 日一次 口服；螺内酯 20mg 日一次口服；强心：地高辛 1 片日一次两餐之间口服；控制窦性心率：伊伐布雷定 5mg 日一次口服；改善动脉粥样硬化：阿魏酸钠 1 片日一次口服；治疗肺动脉高压：他达拉非 1 片日一次口服、马昔腾坦 1 片日一次口服。

三、手术治疗

2025-04-14 于我院行冠状动脉造影检查，造影示：左冠内左主干：大致正常；前降支：大致正常，中段可见重度肌桥，血流 TIMI3 级；回旋支：大致正常，血流 TIMI3 级；右冠：大致正常，血流 TIMI3 级；结束手术。 2025-04-15 于我院行肺动脉造影 + 经皮肺动脉去神经术，使用 5F 猪尾导管行肺动脉造影后，使用 40mm 一次性使用环形肺动脉射频消融导管，依次消融 5.6.7 点。术后肺动脉平均压由术前的 65mmHg 降至 50mmHg，降幅达 23%；肺血管阻力由 15.93wood 降至 9.25wood，降幅达 41.9%; 心排量由 3.58L/min 提升至 4.32L/min。

检验检查记录：

一、实验室检查

我院化验：[2025-04-14 11:25:53]：肌钙蛋白 I:12pg/mL; 肌酸激酶同工酶 :0.37ng/mL;[2025-04-14 11:41:51]：尿酸 :470μmol/L ↑。

二、物理检查

1、2025-04-14 我院门诊心电图：窦性心律，心率 67pm，电轴右偏，逆钟向转位，ST-T 改变。

2、2025-02-27 外院肺动脉 CTA：先心病：房间隔缺损修补术后，肺动脉高压、右心室扩大。

3、心脏彩超

① 2025-04-17 我院心脏彩超：

RVOT------AO------AV----LA----RV----IVS----LV----LVPW----RA

39-----22/37/34---19----41----29----11-----48-----10----54x48；重度肺高压；右室游离壁收缩幅度减弱；右心系统及左房大，三尖瓣少 - 中等量反流；主肺动脉增宽；间接估测肺动脉压力约 90mmHg，TAPSE=16mm。EF0.59.

② 2025-05-19 我院心脏彩超：

RVOT------AO------AV----LA----RV----IVS----LV----LVPW----RA

36----22/37/34----19----40----28----11-----48-----10----50x47；重度肺高压；右室游离壁心肌搏动略减弱；右心系统及左房大，三尖瓣少量反流；主肺动脉增宽；间接估测肺动脉压力约 85mmHg，TAPSE=17mm。EF0.60。

4、6 分钟步行实验

结果为 528 米，心肺功能等级：4 级，日常活动量对应 4.88METs.

鉴别诊断：

一、左心疾病

1、左心衰竭：患者常有夜间阵发性呼吸困难、端坐呼吸等症状，心脏超声可发现左心功能不全或瓣膜病变。而肺动脉高压主要表现为活动后呼吸困难、乏力、晕厥等，心脏超声显示右心室增大、肺动脉压力升高。

2、二尖瓣狭窄：患者有典型的二尖瓣面容，即面颊紫红、口唇轻度发绀，可伴有咯血等症状。心脏超声可见二尖瓣狭窄，左心房扩大，而肺动脉高压主要表现为肺动脉压力升高和右心室改变。

二、慢性肺病和 / 或低氧血症所致肺动脉高压

慢性阻塞性肺疾病是该类 PH 最常见的病因，研究发现 COPD 相关 PH 的患病率差别较大，为 20%~91% 不等，而肺纤维化合并肺气肿并发 PH 的患病率更高，可以达到 30%~50%，8%~15% 的 IPF 患者在初次检查时即发现 mPAP ≥ 25 mmHg，而在疾病晚期和终末期 PH 的患病率更是高达 30%~50%，甚至 >60%。

三、结缔组织病相关性 PAH

15%-25% 的 PAH 与结缔组织疾病相关，最常见的是硬皮病，尽管也发生在系统性红斑狼疮、混合性结缔组织疾病、类风湿性关节炎和干燥综合征中。硬皮病患者的 PAH 患病率为 8%-14%。与其他结缔组织疾病相关性 PAH 相比，硬皮病相关性 PAH 患者的预后更差。

其他：

讨论与总结：

该患者为中年男性，既往有房间隔修补术史，近半年来因胸闷气短症状就诊于多家医院，经右心导管等相关检查，明确诊断为一型肺动脉高压。经综合评估，我院心血管病治疗中心认为该患者符合肺动脉去神经术适应症，经与患者沟通，决定实施手术治疗。

术中即刻效果显著，肺动脉平均压、肺血管阻力较术前明显降低，心输出量显著提升。患者在手术过程中未出现明显不适，术后恢复迅速，4 小时后即可下床活动。术后复查心脏超声显示，肺动脉压力由术前的 96mmHg 降至 90mmHg，呼吸困难症状明显缓解，术后第三天患者顺利出院。

肺动脉高压是一种恶性进展性肺血管疾病，以其低生存率和高猝死率被称为“心血管病中的癌症”。研究表明，未经治疗的肺动脉高压患者平均生存时间仅 2.8 年，在临床上，肺动脉高压也是导致猝死的重要原因之一。肺动脉高压患者早期可出现呼吸困难、活动耐量下降、胸闷及乏力等症状，最终可进展为右心功能衰竭甚至死亡。

肺动脉高压的传统治疗手段主要为靶向药物治疗，但由于患者个体差异、依从性及耐受性等因素，药物治疗效果常不尽如人意。肺动脉去神经术作为一种创新治疗手段，通过射频能量破坏肺动脉内膜的交感神经，抑制其过度激活，有效降低肺动脉压力和肺血管阻力，并改善肺动脉的病理性重构以及右心的结构和功能，为肺动脉高压患者提供了新的治疗选择。

从危机到生机：ExtraVAD 保驾术中急性心率骤降，双 DK CRUSH 完美收官左主干 -LAD/D1 双分叉

高晓飞

张俊杰

患者基本信息：

44 岁男性，BMI: 27.78 kg/m2，因反复心衰入院。

主述：

胸闷胸痛 1 年余，加重伴下肢水肿 1 月

现病史：

反复胸闷胸痛 1 年余，加重伴下肢水肿 1 月，夜间不能平卧。于外院造影提示：LM 体部、尾部钙化，狭窄 50-60%；LAD 近中段狭窄 90% 伴重度钙化，D1 开口狭窄 90%；LCX 开口狭窄 80%；RCA 全程弥漫斑块，偏小。考虑手术风险过高，遂转入我院。

既往病史：

高血压、2 型糖尿病、陈旧性前间壁心肌梗死（V1-V3 病理性 Q 波）、CKD5 期（规律透析 1 月）

病程记录：

经右股静脉及左股动脉置入心室辅助装置（Extra VAD） 后，经左股静脉放置漂浮导管实时监测肺动脉压力，同期经右股动脉行冠状动脉介入治疗（PCI）。7F XB 3.5 指引导管到位后，将三根工作导丝分别送至前降支（LAD）、第一对角支（D1）和回旋支（LCX）。导丝通过后 LAD 血流中断，但 Extra VAD 维持的血流动力学始终平稳。球囊预扩张 LAD 病变后，血管内超声（IVUS）显示其近段存在 270°环形钙化，钙化长度 > 5mm，遂采用 3.5mm 震波球囊反复扩张 80 次，IVUS 确认钙化环断裂。根据 DEFINITION 标准，患者同时存在左主干末端分叉病变及 LAD/D1 分叉病变，均属复杂分叉病变类型。结合患者左冠优势型、右冠细小的解剖特点，并基于 DEFINITION II 研究和 DKCRUSH 系列证据，术者决定采用 DK CRUSH 术式依次处理两处分叉病变。顺利完成 LAD/D1 分叉病变的 DK CRUSH 处理后，在左主干末端分叉进行 3.5mm 与 4.0mm 球囊对吻扩张时，患者心率自 70bpm 骤降至 45bpm。得益于 Extra VAD 支持，平均动脉压稳定维持在 70mmHg 左右，术者从容完成两处分叉的 DK CRUSH 操作。最终造影结果满意，术后 IVUS 评估达到 ULTIMATE 研究优化标准。

检验检查记录：

CRP：13.31mg/L，WBC: 5.63 x109/L, Hb: 102 g/L

ALT: 16U/L, AST: 15U/L, BUN: 15.28mmol/L, Cr: 696.60 μmol/L, Uric acid:584umol/L，P:1.59mmol/L, eGFR: 7.51ml/min *1.73 m2

TC: 2.77 mmol/L, TG: 2.17 mmol/L, HDL: 0.58mmol/L, LDL: 1.64 mmol/L

NT-proBNP: > 35000 pg/ml，BNP=3014.79pg/ml

心超：左心、右房增大，二、三尖瓣关闭不全（中度），肺动脉高压（重度），左室收缩功能减低，LVEF=36%。

胸部 CT：双侧胸腔积液；双肺水肿合并炎症，渗出性病变，轻度间质性改变。

鉴别诊断：

诊断明确，无需鉴别诊断

其他：

见山不是山—— PCI 术后急性血胸的多学科救治

李丹

中国科学技术大学附属第一医院（安徽省立医院）

患者基本信息：

患者，男性，58 岁。

主述：

胸痛一天

现病史：

患者于 2025 年 6 月 14 日因“突发胸痛 2 小时”于当地医院就诊，心电图提示 V1-V3 导联 ST 段抬高，肌钙蛋白 0.163ng/ml，建议急诊 CAG，患者拒绝，给予抗血小板、调脂治疗后胸痛缓解。6 月 15 日患者就诊我院。入院时无胸痛胸闷等不适。

血压 110/82mmHg，心率 74 次 / 分，律齐，两肺未闻及异常

既往病史：

有吸烟史 40 年，2023 年曾行右下肺肺癌手术，术后化疗 4 个疗程，有高血压病史。

病程记录：

入院诊断为不稳定型心绞痛、缺血性心肌病等，心功能 II 级，给予药物治疗。

首次 PCI 治疗前降支 CTO 失败，植入 IABP 准备。

锁骨下穿刺置管失败。

二次行右冠 PCI 治疗，术后出现持续低血压，彩超检查及 CVP 测定提示容量不足。

仔细查房后发现持续右心塌陷，及时完善肺部 CT 发现左侧急性血胸。

胸腔穿刺引流，间断引流血性积液 2600ml，输血共计 1300ml。

多学科讨论，介入探查出血点，未见锁骨下穿孔，反复探查发现左侧锁骨下动脉入口处 2 处穿孔，造影剂外渗，成功植入覆膜支架止血。

胸腔引流，保守治疗后改善，顺利出院。

检验检查记录：

CAG：LM 正常，**LAD 近段闭塞**，LCX 近端 40% 狭窄，**RCA 近段 85% 狭窄，远段 95% 狭窄**，前向血流 TIMI 2 级。

心脏彩超提示 **LVDD 69mm，LA 46mm，EF 27%**，左心室内高凝状态。

左上肢 CTA+CTV：左侧锁骨下动脉起始部造影剂外渗，考虑局部出血可能。

胸部 CT：1. 右肺及心脏术后改变，胸主动脉内气体影，左侧胸腔大量积液 (血)。2. 右肺下叶少许纤维灶；左肺散在炎症，随诊。3. 右肺多发结节，部分磨玻璃密度，密切随诊。4. 部分肋骨骨皮质扭曲。

血红蛋白，入院 157g/L，最低降至 90g/L。

鉴别诊断：

术后低血压鉴别：心包填塞？心原性休克？消化道出血？迟发性造影剂过敏？

急性血胸鉴别：锁骨下动静脉穿刺相关性穿孔？胸腔自发性出血？ IABP 相关性损伤？

其他：

本病例为 IABP 的置管操作相关的锁骨下动脉穿孔并发症，极为罕见的并发症，及时的病情观察及多学科协作，最终化险为夷，有很好的临床警示意义。

2 例不同亚型原发性醛固酮增多症患者的诊治过程

孔祥勇

中国科学技术大学附属第一医院（安徽省立医院）

患者基本信息：

CASE1 患者：女性，61 岁。

主诉：发现血压升高 15 年。

现病史：患者 15 年前发现血压升高，最高 180/100mmHg 以上，间断口服药

物治疗，未予重视。后因头晕不适多次就诊当地医院，测血压升高（曾住院治疗几次）、血钾降低、肾上腺 CT 提示占位。故来我院就诊。

首次就诊的是泌尿外科：门诊查血钾 2.91mmol/L，肾上腺 CT 增强提示：左侧腺瘤（4.5*5.1mm）。

拟手术治疗，请心内科评估。

CASE2 患者：男性，55 岁。

主诉：发现血压升高 20 余年，控制不佳 6 个月。

现病史：20 年前发现血压升高，最高 180/100mmHg 左右，偶伴有头晕，无黑朦，无头痛、心悸、出汗等，近 6 个月血压波动大，最高达 220/120mmHg，服用四种药物，血压仍控制不佳，并伴有面部潮红、血管神经性水肿。

首诊外院：侧血压明显高于正常，肾上腺 CT：左侧肾上腺外侧支增生，高血压五项（立位）：血醛固酮 220.25pg/ml，血肾素浓度 0.79pg/ml，血醛固酮 / 肾素比值（ARR）=278.8，考虑“原醛”。给予：厄贝沙坦、非洛地平缓释片、螺内酯、可乐定等药物降压。

为求进一步诊治就诊我院。

主述：

/

现病史：

/

既往病史：

/

病程记录：

/

检验检查记录：

/

鉴别诊断：

/

其他：

/

股动脉入路经导管主动脉瓣植入术并发左心室穿孔行左前外侧开胸术紧急修复

吴飞宇

浙江大学医学院附属第二医院

患者基本信息：

患者女性，74 岁，农民，浙江省金华市人。

主述：

活动后胸闷气急 1 年余，加重 2 周

现病史：

患者 1 年前出现活动后胸闷，心前区为主，持续数分钟，休息后好转，伴气急，否认胸痛、心悸、夜间胸闷发作、咳嗽咳痰、下肢水肿等不适，患者未重视，未就诊。患者近 2 周来感活动耐量较前下降，胸闷、气急程度较前加重，持续数分钟，休息后好转，阴性症状同前，患者仍未就诊。3 天前因腰背扭伤至当地医院就诊，心超提示“主动脉瓣重度狭窄伴明显钙化、升主动脉增宽”，建议上级医院就诊。患者遂至我院，门诊拟“心脏瓣膜病”收住入院。

起病来，神清，精神可，睡眠一般，胃纳可，二便无殊，体重变化不详。

既往病史：

否认高血压、糖尿病、心脏病、肾炎、传染病史、脑血管意外、慢性支气管炎等疾病史。有外伤手术史，3 天前因“腰椎骨折”，在浙江省金华市武义县第一人民医院行“L3 腰椎骨水泥填充术”，现痊愈。否认中毒、输血史、否认药物、食物过敏史，预防接种史随当地进行。

病程记录：

入院完善相关检验、检查。术前肝肾功能、BNP 等实验室指标未见明显异常。我院经胸超声心动图提示重度主动脉瓣狭窄伴轻度关闭不全（二叶式畸形，Type I 型，主动脉瓣面积 0.8cm2，主动脉瓣峰值速度 4.03 m/s，平均压力梯度 34mmHg），左室射血分数 61%，升主动脉增宽。心电门控的增强 CT 扫描显示主动脉瓣环面积为 431.4 mm2，周长为 75.8 mm，左、右冠窦融合，融合脊处可见团块状钙化，主动脉根部投照角度在右窦中心位为 70°。左主干开口高度为 9.2mm，右冠开口高度为 16.3mm。右髂总动脉中度扭曲，左髂总动脉轻度扭曲，入路血管管腔未见明显狭窄。冠状动脉在 CT 中未见明显狭窄。患者 STS 评分为 2.58%，欧洲心血管手术危险因素评分 II（EuroSCORE II）评分为 0.92%。充分考虑患者的年龄、个人需求后，心脏团队采取了经股入路的 TAVI 治疗方式。

排除禁忌后于 2025-03-18 行 TAVI。操作在全麻下进行，导丝跨瓣后猪尾导管测得左室与主动脉压力阶差为 84mmHg，予 22*40mm 球囊预扩张 1 次。在圈套器辅助下置入 Taurus Elite 26 mm 瓣膜。然而，在瓣膜跨瓣过程中，患者突发循环崩溃，血压迅速下降。我们考虑为输送过程中左心室内超硬导丝切割所致的左室破裂。快速释放瓣膜后，在超声下见到大量心包积液、心包填塞，立即进行心包穿刺引流与心脏按压，同时请心脏大血管外科进行会诊评估体外循环建立及中转开胸指征。体外循环建立，在持续引流下，患者血流动力学逐渐稳定，1 小时内心包共引流出 800mL 血性积液，复查后心包积液显著减少。然而，在体外循环转换为 ECMO 循环支持后，心包积液量再次增多，遂进行开胸探查。作左胸前外侧小切口，于第 4 肋间进胸。打开心包，见心包积液与血凝块，清除血块后可见心尖处 1.5cm 裂伤，且仍有活动性出血。予引空心脏，局部压迫固定左心尖，2-0prolene 线带垫片间断缝合两针。打结后止血效果可，冲洗心包腔，观察未见活动性出血后予止血材料压迫（图 3）。于心包后方开窗后关闭心包切口，留置左胸引流管一根。术后患者血流动力学稳定，带 ECMO 返回监护室。

ICU 期间予镇静镇痛，泰能抗感染，去甲肾上腺素维持血压，凝血酶原止血，输注血小板改善凝血功能，辅以护胃、补液、维持酸碱电解质稳定等对症治疗。患者于术后第 2 天撤去 ECMO 循环支持，第 3 天拔除气管导管与胸管。在 ICU 期间，患者血流动力学保持稳定。术后第 6 天后转至心脏监护室（CCU）。在 CCU 患者恢复良好，可下床在无陪护下进行活动，术后第 18 天出院。

检验检查记录：

1、术前检验、检查报告

术前检验：乳酸脱氢酶：270 U/L，肌钙蛋白 -T：0.019 ng/mL，同型半胱氨酸：30.4 μmol/L，D- 二聚体：1720 μg/L(FEU)，尿常规：尿潜血：+-(0.3) mg/L、尿红细胞：59 /μL。血常规、CRP、肝肾功能、电解质、传染病 4 项、血脂、糖化血红蛋白、甲状腺功能、粪常规、BNP、肿瘤筛查未见显著异常。

2025/03/17：头颅磁共振平扫 + 黑水成像：两侧脑室旁、半卵圆区多发白质高信号，右侧侧脑室旁小腔隙灶。老年性脑改变。

2025/03/17：三维超声心动图：主动脉瓣二叶式畸形（Typel 型）：重度狭窄伴轻度关闭不全，升主动脉增宽；二尖瓣、三尖瓣少量反流；室间隔基底段增厚。

2025/03/17: TAVI 术前筛查 CTA: 升主动脉增宽，主动脉瓣多发钙化，心脏增大，心包少量积液。

2025/03/17：肺功能：1、肺通气功能在正常范围；2、小气道功能障碍 ;3、肺弥散功能在正常范围；4、支气管舒张试验：阴性。

2025/03/17：床边心电图：窦性心律，T 波低平 (V2,V3,V4,V5)

2025/03/17：颈动脉、椎动脉、双侧肢体动静脉彩超检查：双侧颈动脉粥样硬化伴右侧斑块形成；双侧椎动脉未见明显异常；双侧下肢动脉粥样硬化伴多发斑块形成；左侧股总动脉前方异常分支（考虑先天发育异常）；双侧下肢深静脉未见明显异常。

2、术后检查报告：

2025/03/19：床边心电图：显著窦性心动过缓，心室内传导阻滞，下壁、前壁异常 Q 波，ST 段、T 波改变，Q-T 延长，可见起搏脉冲。

2025/03/19：超声心动图：主动脉瓣置换术后；心腔偏小，左心功能不全；微量心包积液。

2025/03/19：胸部后前位片：左肺渗出，左侧胸腔积液，心脏术后改变。

2025/03/19：胸腔彩超检查 (双侧)：所示部分左侧胸腔少量积液；右侧胸腔未见明显积液

2025/03/20：床边心电图：窦性心律，提示完全性左束支阻滞，前侧壁异常 Q 波

2025/03/21：胸部高分辨 CT 平扫：两肺渗出，两侧胸腔积液 / 血伴邻近肺组织膨胀不全，左侧少许气胸，引流管留置。心脏经导管主动脉瓣膜植入术、心脏修补术后，心脏体积增大，心包少许积液 / 血。

2025/03/21：头颅 CT 平扫：右侧顶叶斑片低密度灶，建议结合 MR+DWI 检查。

3、出院前检查报告：

2025/04/02: 三维超声心动图: 主动脉瓣 TAVR 术后，人工瓣流速、压差正常范围，升主动脉增宽；二尖瓣、三尖瓣少量反流。

2025/04/03：头颅磁共振平扫 + 黑水成像：两侧顶叶皮层下及左侧小脑半球散在腔梗，提示心源性。两侧脑室旁、半卵圆区、基底节及小脑半球多发腔隙灶。老年性脑改变。

4、随访检查报告（术后 50 天）：

2025/05/09：三维超声心动图：1. 主动脉瓣 TAVR 术后，人工瓣流速、压差正常范围（Vmax=1.64 m/s，PGmean=6 mmHg），少量瓣周漏，升主动脉近端增宽。2. 三尖瓣少量反流

2025/05/09：心脏 CT 增强扫描：影像所见：TAVI 术后复查，所示植入瓣位置可，植入瓣支架形态较规整，植入瓣后瓣叶增厚，主动脉瓣环区支架呈椭圆形，直径约 22.4mm×16.2mm，卧位心胸比约 67%，左室 EF 约 68%，右室 EF 约 36%。升主动脉增宽，直径约 45.9mm。

鉴别诊断：

1、退行性老年钙化性心脏瓣膜病：年龄相关的退行性主动脉瓣狭窄为成人最常见的主动脉瓣狭窄病因，超声心动图多见主动脉瓣钙化性病变。该病人首先考虑。

2、风湿性心脏瓣膜病：年轻患者好发，患者多有风湿热病史，抗 O 试验阳性，

超声心动图可见赘生物形成，风湿性主动脉瓣狭窄常伴反流和二尖瓣病变。

3、先天性畸形：先天性二叶瓣畸形为成人孤立性主动脉瓣狭窄的常见原因，常在 40 岁后发病；先天性四叶瓣畸形罕见，主要导致主动脉瓣反流，少部分表现为主动脉瓣狭窄。先天性畸形通过超声心动图可以鉴别。

其他：

自行复律的一例三度房室传导阻滞

刘孟华

广东省人民医院 粤西医院 （电白区人民医院）

患者基本信息：

患者，男，76 岁

主述：

“头晕伴恶心、呕吐半天”

现病史：

病人 2025 年 5 月 22 日晨起自觉头晕，眼前发黑，伴有恶心，呕吐，呕吐物为胃内容物。伴有胸闷，否认心悸，没有晕厥，在家人陪同下来本院急诊就诊，查心电图 三度房室传导阻滞，遂收治本科。

既往病史：

既往有“高血压病 2 级 很高危组”病史，未规律服药治疗。

病程记录：

入院后严密监测生命体征，同时异丙肾上腺素 1mg+0.9%NS50ml 微量泵入 2ml/h。一天后停用。

检验检查记录：

完善冠脉造影：结果示：右优势型，左主干血流正常未见狭窄，前降支近段可见斑块，狭窄 30%，中段狭窄 70%，前向血流 TIMI3 级，第一对角支 自中段病变发出，开口狭窄 90%，前向血流 TIMI3 级。回旋支内 膜不光滑，未见狭窄，前向血流 TIMI3 级，右冠脉内膜不光滑， 中段狭窄 20%，远段前向血流 TIMI3 级。

心脏彩超：各房、室腔内径不大；二尖瓣返流（轻度）；三尖瓣返流（轻度）；左心室收缩、舒张功能正常。EF71%。

5-24 动态心电图：1、窦性心律（心房率 85 次 / 分）；2、短暂的心室停搏；（有 4 次大于 3.0 秒的停搏，有 2199 次大于 2.0 秒的长 RR，其中最长为 3.68 秒，发生于 00 时 37 分）；3、偶发交界性早搏；4、偶发室性早搏伴 R on T 现象；5、偶发交界性逸搏；6、偶发室性逸搏；7、间歇性一度房室阻滞合并二度 I 型房室阻滞（呈 5:1 ~ 5:4 传导）；8、缺血型 ST-T 改变；9、V1 导联异常 q 波。

鉴别诊断：

脑动脉硬化：该病也可以出现头晕，但是脑动脉硬化心电图是正常的，本例病人心电图明确显示 三度房室传导阻滞，故可以鉴别。

其他：

患者于 5 月 27 日好转出院，

出院诊断：1. 心律失常：三度房室传导阻滞、窦性停搏；

2. 冠状动脉粥样硬化性心脏病 单支血管病变；

3. 高血压病 2 级 很高危组；

4. 高脂血症；

此患者诊断为：三度房室传导阻滞明确，住院期间完善相关检查未见导致心律失常的明确病因。期间只是使用异丙肾上腺提升心率，患者可行恢复正常心律，此种病例临床上极为少见。

四叶瓣重度主动脉瓣关闭不全 TAVR 一例

唐碧

蚌埠医科大学第一附属医院

患者基本信息：

孙 **，男，77 岁，安徽省五河县，农民，身高 158cm，体重 55Kg

主述：

活动时胸闷、气喘 2 周

现病史：

2 周前活动时出现胸闷，气喘，位于心前区，持续时间不定，休息后可好转。2025 年 3 月 15 日就诊五河县人民医院给与对症治疗缓解不明显，至我院门诊，心脏彩超提示：主动脉瓣关闭不全伴大量反流。病程中有恶心，呕吐，咳嗽，咳痰，无胸痛，晕厥，黑朦，无其他部位放射痛，否认腰痛、多饮、多尿及双下肢浮肿，体重无明显变化。

既往病史：

既往史：发现高血压病史 2 周余，最高血压 190/100mmHg，服用“沙库巴曲缬沙坦 200mg QD”，血压控制尚可。否认糖尿病，慢阻肺等病史。

病程记录：

入院后完善相关检查，给与阿司匹林 0.1g QD，氯吡格雷 75mg QD，阿托伐他汀 20mg QN，沙库巴曲缬沙坦 25mg BID，螺内酯 20mg QD，美托洛尔缓释片 23.75mg QD，达格列净 10mg QD。完成术前评估后，先行冠脉造影：未见明显异常。随行 TAVR 术（沛嘉 29mm 瓣膜），术后患者胸闷气短症状得到改善。出院带药：阿司匹林 0.1g QD，沙库巴曲缬沙坦 50mg BID，螺内酯 20mg QD，美托洛尔缓释片 23.75mg QD，达格列净 10mg QD。

检验检查记录：

1、心电图：窦性心率，左室高电压，ST 改变。

2、心脏彩超：左室舒张末期内径 55mm，LVEF 57%，主动脉瓣退行性变伴中大量反流。

3、N 端 - 脑钠肽：270pg/ml。

4、其余生化常规、心肌酶谱、肌钙蛋白、血常规、凝血常规、尿常规均未见明显异常。

5、术后动态心电图：间歇性 III 度 AVB，II 度 II 型 AVB，间歇性完全性右束支和左束支传导阻滞

6、术后心超主动脉瓣平均跨瓣压 10mmHg，无瓣周漏，主动脉瓣最大前向血流 2.15m/s

7、术后 1 月心超：主动脉瓣平均跨瓣压 9mmHg，无瓣周漏，主动脉瓣最大前向血流正常，心电图：窦性心律，ST-T 改变。

8、2025 年 6 月 29 号电话随访：无黑朦，晕厥发作，无其他不适主诉。

鉴别诊断：

1、二尖瓣狭窄：心尖区舒张中晚期杂音紧随开瓣音后，第一心音常亢进

2、Graham-Steell 杂音：由于肺动脉扩张导致相对性肺动脉瓣关闭不全时，在胸骨左缘第 2 ~ 4 肋间可闻及递减型吹风样舒张早期杂音。

其他：

蛛网膜下腔出血导致 Takotsubo 综合征合并神经源性肺水肿 1 例

杨菲菲

解放军总医院医学第四医学中心

患者基本信息：

48 岁女性

主述：

间断头痛 1 个月

现病史：

患者 1 个月来阵发剧烈头痛，曾于当地医院行颅脑 CTA 考虑多发颅内动脉瘤，为求进一步明确诊治来院就诊，门诊以“多发动脉瘤”收入院。患者目前无意识障碍，言语可，无肢体活动障碍，无恶心呕吐，无大小便失禁，无抽搐发作。

既往病史：

既往痔疮手术病史 1 个月。否认有肝炎、结核等传染病史；否认糖尿病、心脏病病史；否认其他外伤、输血史；否认药物过敏史；预防接种史不详。

病程记录：

入院诊断：颅内多发动脉瘤

病情变化：2025-03-31 21-05 患者突然意识不清，晕倒在厕所，查体：浅昏迷，自动睁眼，古测不自主活动，芷测肢体偏难，双侧瞳孔等大等圆，直径 20 mm，反射迟钝，双下肢巴氏征 (-)。颅脑 CT: 蛛网膜下腔出血，四脑室脑出血。通知主诊医师考虑：蛛网膜下腔出血，动脉瘤破裂可能性大，建议急诊手术治疗，行脑动脉造影，必要时急诊动脉瘤栓塞或者动脉瘤夹闭术。

急诊超声心动图：EF30%，左室心尖部圆隆，运动明显减弱，侧壁基底段及间隔基底段运动尚可，余左室壁运动近乎弥漫性减弱，

胸部 CT: 双肺多发对称性分布的实变影、磨玻璃密度影，边界不清，伴小叶间隔增厚，以双肺门分布为著。结合病史，考虑双肺肺水肿可能性大，双肺感染不除外，建议随诊复查。

急诊手术：2025 年 4 月 1 日 ，02:33 -2025 年 4 月 1 日 ，08:33: 全麻下行全脑血管造影术 + 左侧大脑中动脉支架辅助弹簧圈栓塞术 + 左侧颈内动脉支架辅助弹簧圈栓塞术 + 右侧颈内动脉密网支架动脉瘤栓塞术。术程顺利。

术后：术后第二日麻醉苏醒，自主呼吸可，可遵医嘱活动，给予拔除气管插管，患者诉头痛明显，恶心呕吐，考虑颅内压高及蛛网膜下腔出血刺激所导致，给予扩容，脱水，镇静止疼治疗后好转。

4-3 日复查心脏超声：EF 52%, 左室壁运动较前明显好转

4-8 复查胸部 CT: 原双肺肺水肿已完全好转。

最后诊断： **蛛网膜下腔出血 Takotsubo 综合征合并神经源性肺水肿**

检验检查记录：

头颅 CTA: 右侧颈内动脉 C6 段动脉瘤 (瘤到 8. 1mn, 瘤体大小 10.3*11.2Im), 左侧劲颈内动脉 C5 段 (瘤劲颈 2.Omm 瘤体长 2.6mm)、 左侧大脑中动脉 M1 段小动脉瘤 (瘤颈宽 2.2mm, 瘤体长 2.6mm)

急诊超声心动图 :EF30%，左室心尖部圆隆，运动明显减弱，侧壁基底段及间隔基底段运动尚可，余左室壁运动近乎弥漫性减弱，

胸部 CT: 双肺多发对称性分布的实变影、磨玻璃密度影，边界不清，伴小叶间隔增厚，以双肺门分布为著。结合病史，考虑双肺肺水肿可能性大，双肺感染不除外，建议随诊复查。

鉴别诊断：

心源性肺水肿鉴别：

1. 既往无基础心脏病

2.BNP 497pg/ml

3. 影像上典型的心源性肺水肿病灶呈蝶翼状并沿两侧肺门分布，且心源性肺水肿常可见两侧胸腔积液；而神经源性范围更大。

4. 自限性，恢复快

其他：

2 例高危外科瓣衰败后瓣中瓣处理

高晓飞

南京市第一医院

患者基本信息：

病例 1: 84 岁女性，心功能 IV 级，二尖瓣置换术后 17 年余，伴胸闷气喘半年。心脏超声提示：人工二尖瓣关闭不全（重度）。

病例 2：75 岁女性，心功能 IV 级，胸闷气喘伴下肢水肿半年余。心脏超声提示：二尖瓣生物瓣膜脱垂并中重度关闭不全。

主述：

胸闷气喘半年

现病史：

两个病例共同点：患者胸闷气喘，心功能 IV 级，既往二尖瓣置换的生物瓣膜衰败

既往病史：

病例 1 的既往史：二尖瓣置换 + 三尖瓣成形

病例 2 的既往史：二尖瓣置换 + 三尖瓣成形 + 左心耳结扎术

病程记录：

抗心衰的 GDMT 治疗，另外行经股静脉经导管二尖瓣置换。两个病例的区别是，1 例外科二尖瓣不可扩断，另外 1 例外科二尖瓣是可以扩断的。

检验检查记录：

病例 1: 心脏超声提示：人工二尖瓣关闭不全（重度）。CT 提示：模拟植入 23mm 的 S3 瓣膜，评估 LVOT 阻塞风险： 1. 二尖瓣环与主动脉环平面夹角 =116° > 105° 。2. 瓣膜与室间隔最短距离 =13.3mm>6mm。3. 最小 Neo-LVOT 面积 =521.7mm2>180mm2

病例 2: 心脏超声提示：二尖瓣生物瓣膜脱垂并中重度关闭不全。CT：模拟植入 23mm 的 S3 瓣膜，评估 LVOT 阻塞风险： 1. 二尖瓣环与主动脉环平面夹角 =128.3° > 105°。2. 瓣膜与室间隔最短距离 =6.7mm>6mm。3. 最小 Neo-LVOT 面积 =260.4mm2>180mm2

鉴别诊断：

诊断明确，无需鉴别

其他：

1 例外科二尖瓣不可扩断，另外 1 例外科二尖瓣是可以扩断的。

超越肢体无力：DES c.1024A>G 变异在心脏肌肉疾病中的复杂表型及心脏风险警示

王浏洋

重庆医科大学附属永川医院

患者基本信息：

病例 1：男性，50 岁，无业

病例 2：男性，53 岁，农民

病例 3：男性，33 岁，职员

主述：

病例 1：夜间阵发性呼吸困难伴双下肢水肿 5 天 病例 2：劳力性呼吸困难伴心悸 2 年 病例 3：下肢活动后胀痛 3 年，萎缩、无力 2 年。

现病史：

病例 1: 5 天前无明显诱因出现夜间阵发性呼吸困难伴双下肢凹陷性水肿，无胸痛、心悸，无咳嗽、咳痰，病程中逐渐加重，休息后无缓解，为寻进一步治疗就诊。

病例 2：2 年前无明显诱因出现劳力性呼吸困难，伴阵发性心悸，无胸闷、胸痛，病程中活动耐量逐渐下降，为寻进疗一步治就诊。

病例 3：3 年前出现活动后左小腿发胀感，描述为如同灌铅样，休息后改善，未特殊处理；2 年前无意间发觉左小腿变细，后右腿亦出现类似发胀感。曾至骨科就诊，行腰椎 MRI 检查未见明显异常，医师发现患者无法踞足行走，予以肌电图检查示肌源性损害，查肌酸激酶：809U/L（正常参考值：50 ~ 310U/L），为寻进疗一步治就诊。

既往病史：

病例 1：既往双下肢无力伴肌肉萎缩 13 年，曾于外院神经内科行肌电图检查提示多发周围神经损害（仅累及运动纤维），考虑“腓骨肌萎缩症”，病程中下肢无力逐渐加重，目前依赖轮椅活动。否认“高血压、糖尿病、冠心病”病史

病例 2: 既往下肢无力 15 年，未系统诊治，2 年前因心源性脑栓塞就诊于神经内科，出院后长期服用利伐沙班抗凝。否认“高血压、糖尿病、冠心病”病史

病例 3：否认“高血压、糖尿病、冠心病”病史。

病程记录：

病例 1：第一次就诊时予以利尿消肿后见双下肢明显萎缩，双下肢肌力 0 级（MRC 分级），双上肢无明显异常，患者出院后接受了呋塞米和螺内酯治疗。后患者因呼吸困难加重于一年半后再次就诊于本院，心电图提示三度房室传导阻滞，患者接受了永久性心脏起搏器植入术，并接受了利尿剂（呋塞米、螺内酯口服）、沙库巴曲缬沙坦 25 mg 每日两次和达格列净 10 mg 每日一次的治疗。他的呼吸困难和下肢水肿症状好转后出院。

病例 2：患者心电图显示阵发性心房颤动。经胸超声心动图显示左心房增大，收缩功能正常。NTproBNP 升高至 1,140 pg/ml。患者接受了利伐沙班 20 mg 每日一次、氯沙坦钾 25 mg 每日一次和达格列净 10 mg 每日一次的治疗，半月后随访患者运动耐量略有改善。

病例 3：患者予以曲美他嗪 20mg 每天三次营养心肌，心脏传导阻滞建议随访 Holter，必要时安装心脏起搏器。同时，建议患者控制体重及避免剧烈运动等减轻骨骼肌负荷。半年后随访，患者下肢无力同前，偶有胸闷症状，持续一段时间可自行缓解。

检验检查记录：

病例 1

第一次就诊

心肌损伤标志物：血清肌钙蛋白 I 0.045 ng/ml（正常参考值 <0.037 ng/ml，下同）、肌酸激酶同工酶 10 ng/ml（<2.37 ng/ml）

N 末端 B 型利钠肽前体 2248 pg/ml（<125 pg/ml）。

经胸超声心动图：弥漫性左室功能减退（左心室射血分数 47%），未见心室和心房扩张，三尖瓣及主动脉瓣轻度反流。

心电图：窦性心律， I 度房室传导阻滞，完全性右束支传导阻滞，左前分支传导阻滞。

心脏磁共振成像未见灌注异常及延迟强化异常。

冠状动脉 CT 血管造影示前降支中段轻微狭窄，余血管未见异常。

第二次就诊

心电图：III度房室传导阻滞，交界性逸搏，完全性右束支传导阻滞（如图）。

经胸超声心动图提示较前未见明显改变。

血清肌钙蛋白 I 正常范围，肌酸激酶同工酶 6.5 ng/ml，**N 末端 B 型利钠肽前体** 1170 pg/ml（<125 pg/ml）。

24 h 动态心电图：（1）窦性心律、交界性心律；（2）频发室性早搏；（3）高度、III度房室传导阻滞；（4）偶发室性逸搏；（5）完全性右束支传导阻滞；（6）ST-T 改变

病例 2

经胸超声心动图显示左心房增大，收缩功能正常。

肌酸激酶（CK）水平正常。

N 末端 B 型利钠肽前体 1140 pg/ml。

肌电图显示肌源性电生理损伤。

基因检测显示他携带家族性 DES c.1024A>G (p.Asn342Asp) 变异 .

三年后随访

经胸超声心动图随访显示左心房扩大程度变化甚微，收缩功能正常。

心电图：一度房室传导阻滞、完全性右束支传导阻滞和左前分支传导阻滞。

24 h 动态心电图：窦性心律伴阵发性房颤，伴有 17 次窦性停搏，持续时间超过 2 秒（最长为 3.6 秒），未观察到严重的房室传导阻滞。

病例 3

肌酸激酶（CK）834 U/L（<170 U/L）

血清肌钙蛋白 T 为 0.164 ng/ml（<0.03 ng/ml）

N 末端 B 型利钠肽前体为 2137 pg/ml（<125 pg/ml）。

24 h 动态心电图：窦性心律，伴有 16 次窦性停搏，持续时间超过 2 秒（最长为 2.4 秒）。**经胸超声心动图**：左心室心尖肥厚，约 15-16 毫米，收缩功能正常。

下肢肌肉 MRI 显示半腱肌、缝匠肌、股薄肌、腓骨肌和腓肠肌出现不同程度的脂肪浸润。

肌肉活检：苏木精和伊红 (H&E) 染色显示见肌纤维显著大小不等，形态不规则，较多肥大、分裂纤维，部分纤维内可见紫红色沉积物。Masson 三色染色 (MGT) 显示可见部分肌纤维内异常沉积物，结蛋白免疫组织化学呈阳性。

基因检测显示 DES c.1024A>G (p.Asn342Asp) 变异

三年后随访**经胸超声心动图**：除了心尖肥厚加重外还出现左室室间隔肥厚（心尖厚度 14-17 毫米，室间隔厚度 17-18 毫米），收缩功能正常。

鉴别诊断：

主要诊断

结蛋白病（Desminopathy）

诊断依据：患者出现的进行性肌无力伴有双下肢水肿、呼吸困难的临床表现，结合心电图上的房室传导阻滞、超声心动图提示左心室收缩功能下降、血清肌酸激酶升高、肌电图显示的肌源性损害特征，以及基因检测所发现的结蛋白基因突变，这些综合证据确诊为结蛋白病。

鉴别诊断：

1. 肌原纤维肌病（MFM）

相似点：结蛋白病本质属于 MFM 亚型，临床表现重叠。

不支持点：DES 是 MFM 最常见基因，但其他 MFM 基因（如 CRYAB、MYOT、FLNC）可致类似表型。

排除依据：基因检测仅发现 DES 变异，未检出其他 MFM 基因致病突变

2. 肢带型肌营养不良（LGMD）

相似点：肢体无力、CK 升高、肌源性肌电图、可伴心肌病

不支持点：LGMD 心脏受累房室传导阻滞少见， DES 变异非 LGMD 相关基因（如 DYSF、CAPN3 等）

排除依据：DES 基因确诊

3. 炎性肌病（多发性肌炎 / 皮肌炎）

相似点：对称性肌无力、CK 升高、肌电图肌源性损害、可累及心肌

不支持点: 典型表现为亚急性起病（非进行性数年）、自身抗体阳性（如抗 Jo-1 等）、肌活检示炎症浸润。心脏受累以心肌炎（肌钙蛋白↑）为主，房室传导阻滞罕见。

排除依据：无自身免疫证据（自身免疫抗体阴性），肌活检未提示炎症，DES 基因确诊。

其他：

详细病例资料及图片见 PPT

ECMO 辅助下高危复杂病变的 PCI 治疗病例汇报

常广磊

重庆医科大学附属第一医院

患者基本信息：

张 XX，男性，65 岁，既往体健

主述：

胸痛伴活动后呼吸困难 10 天

现病史：

10 天前突发胸痛，伴大汗，持续不缓解，未就医，自购“胃药”对症处理。逐渐出现呼吸困难，进行性加重，夜间不能平卧。急诊就诊心电图提示：V1-4 、V3R-V5R 病理性 Q 波伴 ST-T 抬高，肌钙蛋白明显升高。血常规、肝功大致正常。肾功：Urea 9.3umol/L，Crea 122umol/L。

体格检查：T 36.7℃ P 110 次 / 分 R 24 次 / 分 BP 110/80mmHg W 90 kg H 176cm 心界不大，心率 110 次 / 分，律齐，双肺闻及散在湿啰音和哮鸣音，双下肢水肿。

既往病史：

既往体检

病程记录：

入院后患者氧合不能维持先后给与 NPPV 以及 HFNC 进行呼吸支持；

血压不稳定，持续给与去甲肾上腺素、多巴胺微量泵入植入 PICCO 给与有创血流动力学监测，指导容量管理，建议植入 IABP 和 ECMO，家属拒绝；

心电不稳定，反复发生室速，室颤；反复给与电除颤；适当镇静，密切监测电解质，补充钾镁； 给与胺碘酮、利多卡因等抗心律失常药物。

其他治疗：冠心病二级预防治疗：阿司匹林 100mg qd 氯吡格雷 75mg qd 阿托伐他汀 20mg qd

低分子肝素抗凝 4000IU q12h

利尿剂：呋塞米间断静推，螺内酯 10mg qd 口服

肺部感染：哌拉西林他唑巴坦 4.5g q12h

祛痰：乙酰半胱氨酸 0.3g 雾化吸入 bid，氨溴索 30mg bid

营养支持：中长链脂肪乳、氨基酸、白蛋白等。

通便：聚乙二醇 4000 散剂

经积极治疗 1 周后，患者一般情况好转，BP 仍需要小剂量去甲肾（<0.5ug/kg/min）维持在 90/50-60mmHg，频发室早，室速仍有发作（部分为 Tdp）。

治疗 1 周后复查胸片，右肺较多实变影，复查 CT 与入院时 CT 对比: 胸腔积液减少，肺淤血和水肿仍然明显；新发气胸，双肺感染灶明显增多。

检验检查记录：

入院行心电图提示：1. 窦性心动过速；2.V1-V4,V3R-V5R 导联 Q 波形成伴 ST 段抬高

心脏彩超：左室壁搏动普遍减弱伴左室功能障碍 ,LVEF32%；左房 (40mm)、左室 (60mm)、右房 (41mm) 增大；二尖瓣中度返流

胸部 CT：肺淤血明显（红箭），双侧中到大量的胸腔积液（蓝箭）

冠脉造影提示：前降支开口闭塞（红箭），右冠近端慢性闭塞（蓝箭）

鉴别诊断：

结合患者病史及相关检查诊断：急性前壁、右室 STEMI，冠心病 Killip 分级 III 级

其他：

详见 PPT

心肌声学造影识别 NSTEMI 合并双支完全闭塞患者罪犯血管：突破心电图定位困境

邵双彤

哈尔滨医科大学附属第二医院

患者基本信息：

【患者】男，49 岁，胸痛 1 年，加重 1 日

【现病史】：患者 1 年前活动后阵发性胸痛，疼痛位于心前区，呈闷痛，范围约手掌大小，持续 3-5 分钟左右，未放射至左上肢、后背部，无咽喉紧缩感，休息后好转。病程中无咳嗽、咳痰，无恶心、呕吐，无头晕、头痛，无晕厥等，未进一步诊治。1 日前无明显诱因上述症状加重，伴双肩及后背部疼痛，伴胸闷，休息后未缓解，伴有大汗，不伴头晕头痛，不伴咳嗽咳痰，就诊于当地医院，给予对症支持治疗症状稍缓解，为求进一步诊治来我院。病程中患者饮食、二便尚可，睡眠一般。

【既往史】：高血压

【生命体征】：P:98bmp，BP:139/97mmHg

主述：

胸痛 1 年，加重 1 日

现病史：

患者 1 年前活动后阵发性胸痛，疼痛位于心前区，呈闷痛，范围约手掌大小，持续 3-5 分钟左右，未放射至左上肢、后背部，无咽喉紧缩感，休息后好转。病程中无咳嗽、咳痰，无恶心、呕吐，无头晕、头痛，无晕厥等，未进一步诊治。1 日前无明显诱因上述症状加重，伴双肩及后背部疼痛，伴胸闷，休息后未缓解，伴有大汗，不伴头晕头痛，不伴咳嗽咳痰，就诊于当地医院，给予对症支持治疗症状稍缓解，为求进一步诊治来我院。病程中患者饮食、二便尚可，睡眠一般。

既往病史：

高血压病史，否认糖尿病病史，否认其他既往病史

病程记录：

初步诊断：急性冠脉综合征

诊断依据

1、患者主因“胸痛 1 年，加重 1 日”入院

2、查体: 一般状态尚可,平车推入病房,查体合作,口唇无发绀,浅表淋巴结未肿大,双肺呼吸音清，未闻及干湿性啰音，心律齐，心率：98 次 / 分，心界不大，各瓣膜听诊区未闻及病理性杂音。腹平坦，柔软，无压痛及反跳痛，双下肢无水肿。生理反射正常，病理反射未引出。

3、既往史：高血压病史，否认糖尿病病史，否认其他既往病史

4、辅助检查：心电图检查：窦性心律，V2-5 导联 T 波倒置

鉴别诊断

1、主动脉夹层：胸痛一开始即达高峰，常放射到背、肋、腹、腰和下肢，两上肢的血压和脉搏可有明显差别，可有主动脉瓣关闭不全的表现，超声心动图、X 线或主动脉 CTA 有助于鉴别。

2、急性肺动脉栓塞：可发生胸痛、咯血、呼吸困难和休克，但有右心负荷急剧增加的表现如发绀、肺动脉瓣区第二心音亢进、颈静脉充盈、肝大、下肢水肿等，心电图示 I 导联 S 波加深，III 导联 Q 波显著，T 波倒置，胸导联过渡区左移，右胸导联 T 波倒置等改变可资鉴别。常有低氧血症，血气分析或肺动脉 CTA 有助于鉴别。

诊疗计划

1、重症监护和一般治疗，完善相关检查

2、抗血小板、调脂，抑酸、对症

3、建议行冠脉造影检查及必要时介入治疗

4、向家属交代病情

检验检查记录：

心电图检查：窦性心律，V2-5 导联 T 波倒置

超声心动图检查：心功能大致正常，左房扩大，左室前壁增厚率减低

心肌声学造影：前壁心尖段增厚率减低，侧壁中间段 - 心尖段运动减弱，心尖、侧壁基底 - 心尖段灌注延迟

冠状动脉造影：LAD 近段 100% 闭塞，LCX 近段 100% 闭塞

鉴别诊断：

主动脉夹层：胸痛一开始即达高峰，常放射到背、肋、腹、腰和下肢，两上肢的血压和脉搏可有明显差别，可有主动脉瓣关闭不全的表现，超声心动图、X 线或主动脉 CTA 有助于鉴别。

急性肺动脉栓塞：可发生胸痛、咯血、呼吸困难和休克，但有右心负荷急剧增加的表现如发绀、肺动脉瓣区第二心音亢进、颈静脉充盈、肝大、下肢水肿等，心电图示 I 导联 S 波加深，III 导联 Q 波显著，T 波倒置，胸导联过渡区左移，右胸导联 T 波倒置等改变可资鉴别。常有低氧血症，血气分析或肺动脉 CTA 有助于鉴别。

其他：

无

一例罕见的肺静脉闭塞病的诊治体会

邱家勇

广东省心血管病研究所，广东省医学科学院、南方医科大学附属广东省人民医院

患者基本信息：

男，张 XX，26 岁，江西省南昌市，2024 年 07 月 18 日就诊我院门诊

主述：

活动后胸闷、气促 1 年余

现病史：

2023 年 07 月患者无诱因出现活动后胸闷、气促，快走 500 米或爬 3 层楼即可出现气促，休息数分钟可缓解，未于重视

2024 年 03 月活动后胸闷、气促症状进行性加重，快走 300 米或爬 2 层楼即可出现胸闷、气促症状，休息 10-30 分钟可缓解

2024 年 04 月 -07 月期间就诊于多家医院完善相关检查：

-NT-proBNP：779pg/ml ↑，余血常规、肝全肾全脂全、血清蛋白电泳、自身抗体谱均未见明显异常

既往病史：

否认慢性病、传染病史。否认手术外伤史。

个人史：吸烟 7 年余，10-20 支 / 日，戒烟半年，否认饮酒嗜好；否认毒物、药物接触史，无减肥药物服用史，否认疫区旅居史

家族史：否认遗传病史，无相关疾病史

病程记录：

胸部高分辨 CT 提示二联征：双肺弥漫小叶中心型磨玻璃结节，两肺门及纵隔多发淋巴结（图 A 和 B）。经胸超声心动图：中度肺高血压（65 mmHg），右室肥厚，左室短轴切面呈“D”字型（图 C）。右心声学造影：阳性（卵圆孔未闭）（图 D）。肺功能：弥散功能重度降低。右心导管检查提示毛细血管前性肺动脉高压。进一步基因检测：EIF2AK4 基因杂合突变。患者两个位点突变，其中一个新发突变（图 E），另外一个来自健康携带的母亲（图 F）。

明确诊断为肺静脉闭塞病，卵圆孔未闭。先给予口服安立生坦单药治疗，逐渐过度到安立生坦 + 他达拉非，密切随访患者未出现肺水肿。

检验检查记录：

NT-proBNP： 426pg/ml ↑

动脉血气分析（未吸氧）：PH 7.41；PaO2 43.4mmHg ↓；PaCO2 36.9mmHg；SaCO2 78.8% ↓；HCO3-；23.4mmol/L

常规生化：WBC:8.53 ×109/L，N%:61.2 %，Plt:288 ×109/L，Hb:152g/L；ALT 45IU/L；AST 35IU/L；Alb 50g/L；Cr 68μmol/L

炎症、免疫相关及肿瘤标志物：ANA17 项（-），无 HIV、血吸虫感染证据

易栓、凝血指标：（-）

胸部高分辨 CT：双肺弥漫小叶中心型磨玻璃结节（图 A），两肺门及纵隔多发淋巴结（图 B）

超声心动图：LVEF 65%，sPAP 53mmHg，左室短轴切面呈“D”字型，右心比例增大

基因检测：发现与临床表型显著相关的 EIF2AK4 基因变异；EIF2AK4 等位基因的两个突变位点。其中一个新发突变（图 E），另外一个来自健康携带的母亲（图 F）

鉴别诊断：

特发性肺动脉高压（IPAH）？

遗传性肺动脉高压（HPAH）？

肺静脉闭塞症（PVOD/PCH）？

其他：

我们首次报道了 PVOD 中‘遗传和新发突变’双重突变模式，这表明 PVOD 可能由‘遗传和新发突变”共同引起。此病例强调了一个独特的罕见遗传特征，以及典型的胸部影像学特征，并推荐将复杂病例转诊至专业 PAH 中心进行进一步评估和治疗的必要性。

心脏结节病并血性心包积液 1 例

龚雨

山东第一医科大学附属中心医院

患者基本信息：

姓名：徐国香

出生地：山东省莱州市

性别：女

职业：退（离）休人员

年龄：65 岁

入院时间：2023-10-03 16:39

民族：汉族

记录时间：2023-10-03 16:42

婚姻：已婚

病史陈述者：患者本人

主述：

发作性胸闷 1 月余

现病史：

患者于 1 月前无明显诱因出现发作性胸闷、乏力，活动后加重。伴头晕，无黑矇、意识障碍，无发热、喘憋、呼吸困难，无咳血，无胸闷、心悸、乏力，无恶心、呕吐，无腹痛、腹胀、腹泻，无呕血、黑便，无二便失禁。至当地医院就诊，检查示“心脏超声：1. 室间隔增厚 2. 主动脉瓣退行性变并反流（轻度）3. 三尖瓣反流 4. 心包积液；甲功；促甲状腺激素 4.850uIU/ml，甲状腺球蛋白抗体 1729.346IU/ml，甲状腺过氧化物酶抗体 582.427IU/ml”，给予“心包穿刺引流”治疗，共引流血性积液 1500ml，现为求进一步诊疗，收入我科病房。

患者自此次发病以来，饮食欠佳，睡眠欠佳，规律使用“阿普唑仑”对症治疗，大小便未见明显异常，体重较前未见明显变化。

既往病史：

疾病史：既往“高血压”史 7 余年，峰值 150/90mmHg，平时规律口服“硝苯地平缓释片”，自诉血压控制可；既往“桥本甲状腺炎”史，未规律治疗。否认其他慢性病史。

传染病史：否认肝炎、结核等传染病史及密切接触史。

预防接种史：随当地。

手术史：“支气管扩张介入术后”7 年余，否认其他手术史及重大外伤史。

输血史：无输血史。

过敏史：否认药物、食物过敏史。

病程记录：

入院后完善相关检查。血细胞分析、肝功、肾功、血离子、尿常规、粪便常规未见异常。心电图检查未见明显异常。甲状腺彩超提示甲状腺弥漫性病变并部分钙化，符合桥本甲状腺炎。胸部 CT 显示双肺散在慢性炎症及纤维灶。红细胞沉降率及各项风湿免疫指标未见异常。心包穿刺引流液及流式细胞术未见淋巴瘤细胞。结核分枝杆菌核酸检测及结核菌素试验均为阴性，暂排除结核及分支杆菌感染。

患者因“血性心包积液原因待查”进行了多学科会诊。胸外科建议排除血性心包积液及主动脉夹层，提出可能的肺部肿瘤、结核及甲状腺疾病相关性，需进一步检查。血液科评估认为淋巴瘤的可能性较低，但建议进一步检查免疫球蛋白及凝血功能。肿瘤科考虑到患者的病史和相关指标，建议进行 PET-CT，以排查原发肿瘤及间皮瘤等可能性，并强调需进一步观察渗出液的炎症特征。呼吸科评估患者一般情况良好，认为感染性病因可能性低，建议检查免疫系统疾病，特别是 ANCA 及 IgG4，并进一步评估右上肺结节的性质。核医学科建议补充 PET-CT 及强化肺部 CT，明确全身病变，排查潜在的胃肠道或胰腺肿瘤。

根据多学科会诊意见完善进一步检查。胸部增强 CT 显示右肺门斑片影及双肺结节，纵隔及右侧心膈角肿大淋巴结，心包积液未见明显变化。全身 PET/CT 显示双肺门及纵隔多发 FDG 代谢增高淋巴结，腹膜后淋巴结代谢增高，心包轻度增厚并积液，心脏室间隔壁及左室心肌代谢增高，提示系统性疾病累及心脏。根据 PET/CT 结果，考虑结节病可能性较大，进一步行心脏磁共振检查。心脏磁共振显示左室不大，基底段间隔壁略增厚，左室功能未见明显异常，符合左室弥漫性心肌纤维化。右室心包增厚并延迟强化，心包积液，考虑心包炎症，提示心脏改变可能与系统性疾病相关。为进一步明确诊断行支气管镜活检，病理结果显示肺泡轻度扩张伴间质纤维增生，局灶性肉芽肿结构，不除外结节病可能。

患者右肺下叶背段肺活检上有非干酪性肉芽肿，结合 CMRI 及 PET 影像学表现，结节病诊断明确，在排除了其他可能引起心包积液的原因后，我们考虑该患者为结节病累及心包，且侵蚀心包血管导致血性心包积液。因该患者未行心脏组织活检，无法进行病理诊断，故根据 2014 年心律失常学会（HRS）提出的心脏结节病诊断标准[1]，排除结核及分枝杆菌感染后，试给予激素诊断性治疗 [0.5mg/(kg·d)]。根据患者体重，给予泼尼松 25mg/d，一月后患者症状明显缓解，逐渐减量至 15mg/d 维持。

2023 年 12 月 15 日复查 CT 显示，心包积液较前减少。于 2024 年 6 月 25 日逐渐减量至 5mg/d，复查胸部 CT 示双肺结节，较前相仿，双肺纤维灶，心包少量积液。复查 CMRI 示左室基底段间隔壁略厚，较前相仿。左室弥漫性心肌纤维化较前减轻。

检验检查记录：

2023 年 10 月 9 日胸部增强 CT 显示右肺门斑片影及双肺结节，考虑为炎性或纤维灶，纵隔及右侧心膈角肿大淋巴结，心包积液未见明显变化。

10 月 11 日全身 PET/CT 显示双肺门及纵隔多发 FDG 代谢增高淋巴结，腹膜后淋巴结代谢增高，心包轻度增厚并积液，心脏室间隔壁及左室心肌代谢增高，提示系统性疾病累及心脏。

2023 年 10 月 14 日心脏磁共振显示左室不大，基底段间隔壁略增厚，左室功能未见明显异常，符合左室弥漫性心肌纤维化。右室心包增厚并延迟强化，心包积液，考虑心包炎，提示心脏改变可能与系统性疾病相关。

2023 年 10 月 17 日行支气管镜活检，病理结果显示肺泡轻度扩张伴间质纤维增生，局灶性肉芽肿结构，不除外结节病可能。

2023 年 10 月 18 日甲状腺结节活检结果为慢性淋巴细胞性甲状腺炎。

鉴别诊断：

1. 风湿性心脏病：患者可有胸闷、喘憋、心悸、呼吸困难等心衰症状，查体可闻及心脏病理性杂音，心脏彩超及胸部 X 片有助于鉴别诊断。

2. 扩张型心肌病：患者可有胸闷、喘憋、呼吸困难等心衰表现，心脏彩超示心腔扩大、心腔壁变薄、心肌动度普遍减弱，心脏 MRI、心肌活检可助诊。

其他：

Lampoon +TMVinV 治疗二尖瓣生物瓣衰败一例

高晓飞

南京市第一医院

患者基本信息：

•78 岁男性，BMI: 21.22 kg/m2

• 主诉：二尖瓣生物瓣置换术后 17 年余，伴胸闷气喘 3 月

• 既往史：溶血性贫血 2 年，房颤病史 20 余年，胆囊结石病史 20 年余，2008 年二尖瓣生物瓣置换 + 三尖瓣成形 + 房颤射频消融术（Mdetronic 29mm Hancock）

• 查体：黄疸面容，颈静脉怒张，血压 126/67mmHg, 房颤律，心率 60 次 / 分，两肺底闻及少许细湿性啰音，心尖部可及 3/6 级 SM，双下肢轻度水肿

主述：

二尖瓣生物瓣置换术后 17 年余，伴胸闷气喘 3 月

现病史：

二尖瓣生物瓣置换术后 17 年余，伴胸闷气喘 3 月。

既往病史：

溶血性贫血 2 年，房颤病史 20 余年，胆囊结石病史 20 年余，2008 年二尖瓣生物瓣置换 + 三尖瓣成形 + 房颤射频消融术（Mdetronic 29mm Hancock）

病程记录：

患者外科手术高危，拟行经导管瓣中瓣置换，但 CT 分析提示最小 Neo-LVOT 面积 160mm2 左右，考虑患者身高 178cm，患者二尖瓣置换有流出道梗阻风险，故拟行 Lampoon 技术进行二尖瓣瓣叶切割。

顺利进行二尖瓣瓣叶切割后，成功植入 Sapein3 瓣膜，手术顺利，结果完美。

检验检查记录：

入院后超声提示：右心、左房增大，二尖瓣置换术后，人工二尖瓣脱垂并关闭不全（中重度），三尖瓣关闭不全（重度），肺动脉高压（中重度），左、右室收缩功能正常，LVEF=64%，估测 PASP =74mmHg。

鉴别诊断：

诊断明确，无需鉴别

其他：

抱歉，这个病例前几天刚刚完成，病人刚顺利出院，完整的 ppt 还没有做好，只有初稿。

超声辅助下经皮间隔支冠状动脉栓塞术治疗肥厚型梗阻性心肌病

郝潇

河北省人民医院

患者基本信息：

患者，女性，59 岁

主述：

间断胸闷、气短 8 年余，加重 10 天

现病史：

患者缘于入院 8 年余前间断出现胸闷、气短，多于活动后出现，夜间睡眠常有憋醒，曾有黑矇、大汗发作 8 次，休息数分钟缓解，就诊于当地县医院，给予对症治疗，症状可间断缓解；4 月前于当地医院行冠脉造影冠状动脉粥样硬化、心肌桥。10 天前患者再次出现上述症状加重，轻微活动即出现胸闷、气短，伴咳嗽、咳痰，自诉为血性痰，当地医院心脏彩超：室间隔基底部增厚，约 1.3cm，左室流出道流速增快，约 294cm/s，二、三尖瓣少量反流，主、肺动脉瓣少量反流，EF64%，左室舒张功能降低、收缩功能正常。为求进一步诊治来我院，以“肥厚性心肌病”收住院。

既往病史：

既往高血压病史 3 年，最高 170/100mmhg，平素口服“硝苯地平缓释片”，血压控制可。

病程记录：

入院后，给予酒石酸美托洛尔片 12.5mg 日二次、地尔硫卓缓释胶囊 90mg 日一次口服减轻左室流出道梗阻，依诺肝素 4000U 日一次皮下注射预防血栓治疗。查心脏彩超提示左室流出道严重梗阻，流速 8.3m/s，压差 280mmHg。依据患者当地冠状动脉造影，定位第一间隔支为靶血管，术中超声辅助下球囊扩张阻塞第一间隔支，见压力阶差显著下降，遂行弹簧圈栓塞第一间隔支，术前术后均行导管测压，术后导管压力阶差显著下降，患者症状明显改善。术后一个月、六个月随访，未再发作相关症状，超声提示左室流出道梗阻解除。

检验检查记录：

详见附件清单

鉴别诊断：

1）高血压导致的心肌肥厚：患者多有长期的高血压病史，心肌肥厚通常呈对称性，超声显示肥厚心肌为均匀的低回声，一般室壁厚度≤ 15 mm，室间 隔与左心室游离壁的厚度比多小于 1.3。经严格血压 控制 6~12 个月后，左心室壁肥厚程度一般可减轻或者消退。

2）主动脉瓣狭窄和先天性主动脉瓣下隔膜： 主动脉瓣狭窄中 20％ ~30％合并

不对称性心肌肥厚，心肌肥厚的程度通常相对较轻（室壁厚度 ≤ 15 mm），主动脉瓣狭窄程度常为中度以上，而 HCM 患者一般无明显的主动脉瓣病变。超声心动图 可明确病变。先天性主动脉瓣下隔膜也常合并心肌肥厚，但心肌肥厚主要表现为对称性，超声心动图 和 CMR 检查见瓣下隔膜可确诊。

3）运动员： 运动可诱发生理性心肌肥厚，心电图上可有高电压、早期复极、非特异性 ST-T 改变等，但一般无 HCM 家族史、心肺运动功能较好，超声心动图可显示左心室壁轻度均匀增厚（非对称性心肌肥 厚或者心尖肥厚罕见），可合并左心室腔内径增大，但通常不合并左心房增大和严重的左心室舒张功能异常，CMR 显示无明显心肌纤维化，终止体能训练可使肥厚程度减轻。

4）内分泌异常： 肢端肥大症时由于生长激素和胰岛素样生长因 子 -1 分泌过多，会刺激肌小节蛋白合成从而导致心肌肥厚，通常为左心室壁均匀肥厚伴有心腔扩张，且较早出现严重的收缩功能障碍，检测生长激素及生长因子水平可以鉴别。糖尿病导致的心肌病是糖尿病 患者的一种特殊心脏表现，早期可表现为左心室壁 肥厚和舒张功能障碍，并可发展为收缩功能降低和心衰 。在部分甲状腺功能减退相关的心肌病患者中，可表现有室间隔的不对称性肥厚，并可在早期规范的甲状腺激素替代治疗后恢复。

5）药物因素： 长期使用一些药物，包括羟氯喹、他克莫司和 促蛋白合成类固醇等，可以导致左心室壁肥厚，但室壁厚度很少会超过 15 mm，大部分患者左心室壁肥 厚可在停药后逆转 。

6）淀粉样变： 淀粉样变是由遗传、变性和感染等因素引起蛋白前体形成不可溶性淀粉样纤维并沉积于器官或组织细胞外，导致其结构和功能障碍的一组疾病，其中心脏是淀粉样变常累及的器官，表现为心肌肥厚和舒张功能受损。

其他：

1 例梗阻性肥厚型心肌病的诊治经过

苏柳杭

厦门大学附属心血管病医院

患者基本信息：

乐某某，男，20 岁

主述：

发现心脏杂音 19 年，间断晕厥 14 年，心悸 6 年

现病史：

缘于 19 年前患者“感冒”查体时发现心脏杂音，自诉行心脏彩超提示“心肌肥厚”，未行特殊诊治。14 年前无明显诱因出现晕厥，具体不详。9 年前于我院行心脏彩超提示：肥厚型梗阻性心肌病。9 年前无明显诱因再发晕厥，就诊我院住院治疗，入院后完善心脏彩超提示肥厚型梗阻性心肌病及二尖瓣粘液样变性，二尖瓣后叶冗长，心电图提示心房颤动，遂组织全院会诊后，患者晕厥多为活动时出现，考虑晕厥梗阻引起可能性大，但同时不能除外恶性心律失常可能，同时心脏彩超提示流出道梗阻为二尖瓣后叶粘液样变性及冗长引起，建议择期外科手术换瓣 + 肥厚室间隔切除 + 房颤手术。但患者于 2019-07-06 11:00 再发心悸伴胸痛、全身大汗，测血压 73/41、心室率 145 次 / 分，迁入 CCU 后，后予补液、降低心肌耗氧、控制心室率等对症处理后症状无法缓解，考虑患者左室流出道梗阻，导致低血压、休克，心室率加快导致心室舒张功能进一步减退、梗阻进一步加重，恶性循环，请心外科主任医师查看过患者后，遂行急诊全麻及 IABP 支持下行左室流出道疏通 + 二尖瓣置换术手术，术后心律转为窦性心律，血压逐渐恢复 90/60mmHg 左右。患者术后出现肺部感染，给予抗感染治疗，查肺部 CT 提示右侧胸腔积液，行胸腔穿刺引流术。患者于 2019-07-14 出现快室率心房颤动，给予胺碘酮、电复律均未成功，复查肝功较前明显升高，考虑药源性引起可能性大，给予保肝治疗。因药物复律、电复律均不能持续维持窦律，暂不考虑继续转复治疗，给予控制心室率、抗凝、抗感染、保肝、控制心室率治疗后，患者感染指标逐渐下降，转氨酶转为正常，心室率控制尚可。后因心悸症状较前加重，伴明显活动后气促于 2024-05-21 再次就诊我院住院治疗，门诊遂拟“肥厚型非梗阻性心肌病 持续性房颤”收住入院，自发病以来，精神、欲、睡眠尚可，二便如常，近期体重改变不详。体力较前明显下降。

既往病史：

无特殊。

家族史：母亲因“心脏病”青年猝死，否认其余亲属遗传性疾病史。 母亲有 2 个姐姐 1 个弟弟均无症状，心脏彩超均提示正常。

病程记录：

患者既往肥厚性心肌病行左室流出道疏通 + 二尖瓣置换术手术，术后反复发作房颤，入院时为持续性房颤，心室率控制欠佳，有射频消融指征，完善经食管心脏彩超排除心房血栓后于 2024-05-27 行房颤射频消融术，术后恢复窦性心律，复查动态心电图提示频发房早、频发室早，给予加用“胺碘酮”控制心室率治疗。

检验检查记录：

详见上传文件

鉴别诊断：

1. 运动员心脏（生理性心肌肥厚）：运动员长期规律锻炼可导致心脏发生适应性改变，心脏彩超大多数提示左心室壁厚度可轻度增加（通常 <15mm，偶有更高），肥厚类型多为对称性肥厚（向心性），左心室内径可增大，但收缩功能正常或超常。该类人员多数心肺运动功能良好，无心肌病家族史，基因检测阴性。停止锻炼 3 个月后心肌，肥厚程度可以减轻或消退。通常停止锻炼后心肌肥厚程度通常会显著消退 >2mm 减少或厚度 <12mm）。这是最有鉴别价值的动态观察。

2. 高血压性心脏病：该类患者心脏彩超提示左心室肥厚（常为向心性），可伴有舒张功能障碍。多数患者心肌增厚起因于长期、控制不佳的高血压。心脏彩超肥厚类型：多为对称性（向心性）肥厚，室间隔与后壁厚度比接近 1:1。非对称性肥厚（ASH）在高血压中少见。肥厚程度：通常为轻度至中度（室壁厚度 12-15mm 多见），严重肥厚（>18mm）较少见，除非合并其他因素（如 HCM）。通常无左心室流出道梗阻或 SAM 征。有效控制血压后，肥厚可部分逆转。常伴有高血压视网膜病变、蛋白尿、脑血管病史等。

3. 主动脉瓣狭窄（AS）：该类患者同样存在左心室向心性肥厚，可有心绞痛、晕厥、呼吸困难等症状，听诊有杂音（需与 HCM 梗阻型的杂音鉴别）。杂音特点呈现典型的 AS 杂音是收缩期喷射性杂音，在胸骨右缘第 2 肋间最响，向颈部传导。HCM 梗阻型杂音在胸骨左缘下段最响，很少向颈部传导，且受 Valsalva 动作、体位影响更大。心脏超声心动图是诊断 AS 的金标准，彩超可见主动脉瓣叶异常（增厚、钙化、畸形）、瓣口面积减小、跨瓣压差升高。左心室肥厚为压力负荷过重导致的向心性肥厚。AS 患者常表现为迟滞、细小的颈动脉搏动，而 HCM 患者通常正常或增强。

4. 心脏淀粉样变性（尤其是转甲状腺素蛋白型 ATTR 和轻链型 AL）：心脏彩超呈现心肌增厚（常为向心性），舒张功能障碍显著，心电图可表现为低电压（与肥厚程度不匹配）或假性心梗图形，BNP/NT-proBNP 升高。多见于老年人（尤其是 ATTR）。超声心动图可见心肌回声增强（“颗粒样闪光”）。双心室壁普遍增厚（对称性为主）。房间隔增厚。瓣膜增厚。心包积液。收缩功能后期下降（但早期可保留）。整体纵向应变（GLS） 明显受损，常表现为心尖保留的“相对心尖保留模式”。心电图表现为低电压（肢体导联 QRS 波电压 <0.5mV）或 QRS 波电压与显著肥厚程度不匹配是重要线索（HCM 通常电压显著增高）。传导阻滞更常见。心脏磁共振可见延迟钆增强（LGE）多呈弥漫性心内膜下或透壁性强化。T1 mapping 值显著升高，ECV 明显增加。心内膜心肌活检（金标准）或脂肪 / 骨髓 / 其他组织活检刚果红染色阳性也可进一步鉴别。血清 / 尿液检查可进一步鉴别心肌淀粉样变分型，AL 型需查血 / 尿免疫固定电泳、血清游离轻链；ATTR 型需测血清转甲状腺素蛋白（TTR）、必要时行骨扫描（对 ATTR 有特征性表现）。AL 型淀粉样变可有 50%~70% 患者出现肾脏受累，表现为大量蛋白尿，不伴血尿；周围神经受累表现为四肢对称性感觉及运动功能障碍、腕管综合征等，自主神经受累主要表现为位性低血压、排尿困难、排汗异常等； 累及消化系统者可出现消化不良综合征及腹泻等临床表现；还可出现巨舌、眶周紫癜等特征性软组织受累表现；此外还可出现肝脏、皮肤、眼部受累等相关症状［

5. 法布里病（Fabry Disease）：该病是 X 连锁遗传病，可导致左心室向心性肥厚（后期也可不对称），常有舒张功能障碍，心电图可有短 PR 间期。全身表现可呈现肢端感觉异常（烧灼痛）、少汗 / 无汗、血管角化瘤（皮肤红紫色丘疹）、角膜涡状混浊、蛋白尿 / 肾功能不全、早发卒中。男性患者症状重，女性携带者症状多变可较轻。超声心动图可见肥厚心肌多为向心性，但也可不对称。有时可见二尖瓣前叶轻度增厚。心脏磁共振提示 LGE 多出现在左心室基底段后外侧壁中层。男性测血清 α- 半乳糖苷酶 A 活性（显著降低），基因检测（GLA 基因突变）是诊断法布里病金标准（尤其对女性）。

6. 糖原贮积症（如 Danon 病、PRKAG2 综合征）：该病为遗传性疾病，可导致心肌肥厚。Danon 病（X 连锁）多为男性青少年起病，肥厚进展快，常伴有严重骨骼肌无力、智力发育迟缓、视网膜色素变性。心电图常表现为预激综合征（WPW）。血清肌酸激酶（CK）显著升高。PRKAG2 综合征是常染色体显性遗传性疾病，特征性三联征表现为心肌肥厚（常为向心性）、预激综合征（WPW）、进行性传导系统疾病（需起搏器）。基因检测是确诊关键，LAMP2 基因突变致 Danon 病，PRKAG2 基因突变致 PRKAG2 综合征。

7.Friedreich 共济失调：该病为遗传性疾病，可导致对称性心肌肥厚。神经系统症状可表现为进行性步态共济失调、构音障碍、深感觉丧失、腱反射消失、Babinski 征阳性，通常在儿童或青少年期起病。基因检测提示 FXN 基因内含子 GAA 重复扩增。

8. 线粒体心肌病：心脏彩超可表现为心肌肥厚或扩张。可表现为多系统受累，其中包括神经系统（癫痫、卒中样发作、肌病、眼外肌麻痹）、内分泌（糖尿病）、听力损失、视网膜病变等。血检可见乳酸升高，肌肉活检见破碎红纤维（RRF）。母系遗传模式常见。基因检测复杂。

9. 其他罕见原因：Noonan 综合征及 RASopathies： 特殊面容、身材矮小、先天性心脏病（尤其是肺动脉瓣狭窄）、发育迟缓、皮肤异常、凝血异常。心脏表现可类似 HCM（有时称为 Noonan 综合征伴多发性雀斑样痣综合征的肥厚型心肌病）。

10. 嗜铬细胞瘤：该病可表现为阵发性或持续性高血压、头痛、心悸、大汗、血糖升高。儿茶酚胺长期刺激可导致心肌肥厚（可逆性）。

11. 肢端肥大症： 生长激素过多导致内脏增大（包括心脏），多为向心性肥厚。特征性面容和肢端改变 .

其他：

巴尔通体感染导致的感染性心内膜炎合并严重贫血

汉辉

上海交通大学医学院附属瑞金医院

患者基本信息：

患者，藏族，男性，17 岁，农牧民，未婚，长期居住于西藏自治区日喀则市聂拉木县琐作乡直来村（海拔 4399 米）

主述：

咳嗽、 发热 15 天加重伴双下肢浮肿、气促 5 天

现病史：

患者自诉15天前感冒后出现阵发性咳嗽、咳痰，黄色痰，偶伴痰中带血丝，伴发热，最高体温具体不详，当时就诊于乡卫生院，给予输液治疗，具体不详，未见好转，5天前上述症状加重并出现双下肢浮肿，活动后气促症状，无乏力、胸闷、胸痛、呼吸困难、恶心、呕吐、盗汗、消瘦、腹痛、 腹胀等症状，2天前就诊于在聂拉木县医院给予药物治疗(头孢噻肟钠2g Q12h ivgtt，氨溴索30mg QD ivgtt)1天，自觉症状未见好转，故今日来我院门诊就诊，门诊以“心功能不全、感染性心内膜炎”收住院。自发病以来，患者神志清，精神尚可， 二便正常，食欲可，睡眠可，体重未见明显增减。

既往病史：

既往病史：自诉小学六年级时检查有心脏病，具体不详

吸烟史：3年，3支 / 天

病程记录：

日喀则市人民医院收治入院后，心超提示左心扩大，主动脉瓣二叶化畸形可能，无冠瓣上强回声团块（考虑赘生物可能，其他待排），主动脉瓣前向血流速度偏快并少量反流，二叶瓣前叶脱垂伴大量反流，三尖瓣少量反流；血常规提示重度贫血（Hb 56g/L）。给予输血、抗凝（低分子肝素）、抗感染（阿莫西林）、利尿（呋塞米、螺内酯）等治疗，转上海瑞金医院进一步诊疗。复查心超提示主动脉瓣病变进展，表现为重度反流，提示瓣膜穿孔可能。血检提示 Hb 下降、抗dsDNA 阳性、ANA 阳性，Coombs 阳性，血培养阴性，NGS 提示巴尔通体感染。继续予输血、抗凝、抗感染（多西环素 + 庆大霉素），激素（甲泼尼松龙）+ 静丙治疗，5天后行主动脉瓣 + 二尖瓣置换术，术后继续抗感染（多西环素 + 庆大霉素，逐步过渡为口服）、激素（甲泼尼松龙逐步减量、过渡为口服）、抗凝（华法林序贯，维持 PT-INR 2.0-3.0）及营养支持。好转后出院。

检验检查记录：

心超提示左心扩大，主动脉瓣二叶化畸形可能，无冠瓣上强回声团块（考虑赘生物可能，其他待排），主动脉瓣前向血流速度偏快并少量反流，二叶瓣前叶脱垂伴大量反流，三尖瓣少量反流；血常规提示重度贫血（Hb 56g/L）；ANA、抗 dsDNA 抗体、抗 cardiolipin IgM 抗体、Coombs 试验阳性；血培养阴性；NGS 提示巴尔通体感染

鉴别诊断：

1、系统性红斑狼疮（SLE）：SLE 患者可能出现 Libman-Sacks 心内膜炎（非感染性）；自身抗体：SLE 患者抗核抗体（ANA）、抗双链 DNA 抗体阳性，而 IE 无特异性自身抗体。1. 心脏赘生物：Libman-Sacks 赘生物多见于二尖瓣后叶，超声显示固定、扁平；IE 赘生物活动度大，易脱落导致栓塞。2. 全身表现：SLE 常伴蝶形红斑、肾炎及多系统损害，IE 则以感染中毒症状（如寒战、消瘦）为主。

2、风湿热：与 IE 均可表现为发热、关节痛及心脏受累，但存在以下差异：心脏杂音特点：风湿热多为游走性多关节炎，心脏杂音以二尖瓣和主动脉瓣反流为主，而 IE 杂音常随赘生物变化动态改变。1、实验室检查：风湿热抗链球菌溶血素 O（ASO）升高，血培养阴性；IE 血培养阳性率可达 90% 以上，血培养阴性的 IE 可进一步完善 NGS 检查。2、皮肤表现：风湿热可见环形红斑，IE 则可能出现 Osler 结节（指端痛性结节）、Janeway 损害（无痛性出血斑）等特征性体征。

其他：

一例左室辅助装置合并虚弱患者早期康复案例

宋燕新

北京大学第三医院

患者基本信息：

男性，70岁。身高 169cm，体重 49kg，BMI：17.15kg/m2。

无吸烟、饮酒史。否认早发冠心病家族史、心肌病家族史，否认其他遗传性疾病病史。

诊断“慢性心衰急性加重，扩张性心肌病”。

于 2025-04-24 09：53 入院，2025 年 5 月 7 日接受 LVAD 植入术。

主述：

胸闷、憋气伴乏力 13 年，加重 3 月

现病史：

患者 13 年前间断出现活动后胸闷、憋气伴乏力，平卧、休息 30 分钟可自行缓解，无恶心呕吐、头晕、发热、胸痛。平素无法行走超 200m，无法上楼梯，就诊于外院。诊断为“慢性心衰急性加重，扩张型心肌病”，予利尿、抗心衰、控制心率后症状缓解。2019 年患者因“室速”行 ICD 植入。3 月前患者再次出现胸闷、憋气伴乏力症状加重，就诊于外院，予卧床、对症治疗后症状缓解。现患者为进一步诊疗，入我院。

既往病史：

患者既往磺胺类药物过敏

病程记录：

患者于 2025 年 4 月 28 日接受右心导管检查，平均肺动脉压力 30mmHg。2025 年 5 月 7 日接受 LVAD 植入术。

术前及术后患者长期卧床，肌力差，营养不良，虚弱。

予左室辅助泵联合去甲肾、多巴胺等多种血管活性药物维持血压；应用 NO 降低肺动脉压；及时吸痰；输悬浮红细胞 + 血浆；保肝利胆；床旁 CRRT 治疗；泰能联合万古霉素抗炎治疗；肝素抗凝治疗。

于术后第 2 天开始早期综合康复。患者经过早期康复，肌力逐渐提高，活动能力、心理状态较前好转。

患者住院期间，活动中偶发室速，血生化显示血钾水平低，肌酐水平仍较高，营养状态仍较差。经过胺碘酮静脉泵入，口服补钾对症处理；营养科会诊，指导患者饮食，右上肢中心静脉置管，输注卡文注射液（脂肪乳氨基酸（17）葡萄糖（11%）注射液），给与静脉营养；CRRT 改善肾脏功能。

经过上述治疗，患者血钾水平、营养状态、肌酐水平都有所改善，继续康复治疗。

患者于 6 月 21 日出院，出院时患者能在助行器辅助下步行，心理评分较前改善，日常生活活动能力明显提高。

检验检查记录：

康复前

血常规：WBC 21.28（*10^9/L）↑，Neut% 94.4（%）↑，RBC 3.04（*10^12/L）↓，Hgb 96 g/L ↓，PLT 54（*10^9/L）↓

生化：ALT 22（U/L），AST 91（U/L）↑，CK 436（U/L）↑，CKMB 34（U/L）↑，LDH 442（U/L）↑，Cr 163（μmol/L）↑，K+ 3.96（mmol/L），总蛋白 52（g/L）↓，白蛋白 28（g/L）↓，NT-pro BNP 30443（ng/L）↑，TnT 1.730 ↑。凝血：PT 15.4 ↑，INR 1.44 ↑，APTT 33.3。PCT 44.4（ng/mL）↑

细菌培养：无需氧菌生长，无厌氧菌生长。

心电图：窦性心动过速；胸片：双侧肺纹理增多，双肺可见大片状、斑片状模糊影，心影增大；超声心动图：心包腔后侧方深约 30mm 无回声区；下腔静脉内径 20mm，呼吸变化率下降，血流速度 0.2m/s；PASP：26mmHg。

Barthel 指数评定量表 10 分，大便能控制，日常生活完全依赖；心理评估：广泛性焦虑量表（GAD-7）得分 20 分，重度焦虑状态；抑郁自评量表（PHQ-9）得分 15 分，中度抑郁状态。徒手肌力评估，左侧上下肢各关节肌肉群肌力 4 级；右上肢关节肌肉群肌力 2 级，右侧髋关节屈曲、膝关节伸展 3 级，踝关节背屈肌力 0 级。上下肢各关节主动关节活动度正常；右侧踝关节被动关节活动度 20°，右上肢关节被动关节活动度正常，屈髋、伸膝主动关节活动度正常。四肢肌肉萎缩明显，上臂围 19cm，小腿围 26cm。营养状态评估，MNA 调查表 7.5 分，营养不良。

康复中期

营养状态评估：MNA 调查表 9.5 分，营养不良；患者自主运动和康复训练过程中偶发室性心动过速，暂停康复；复查各项检查，结果如下血常规 WBC 12.22（*10^9/L）↑，RBC 3.77（*10^12/L）↓，Hgb 114（g/L），Plt 211（*10^9/L），Neut% 86（%）↑ 。生化 ALT 34（U/L），AST 93（U/L）↑，CK-MB 8（U/L），CK < 25（U/L），LDH 345（U/L）↑， Cr 450（μmol/L）↑，总蛋白 68.9（g/L）↓，白蛋白 34（g/L）↓，K+ 3.48（mmol/L）↓，葡萄糖 5.8（mmol/L）；NT-pro BNP 23779（ng/L）↑，PCT 0.595（ng/ml）↑。超声心动图 LVAD 术后，心包腔未见异常，下腔静脉内径 7.5mm，呼吸变化率正常。床旁胸片 双肺纹理增多，肺野透过度较前增加，心影增大。Barthel 指数评定量表 45 分，日常生活需要帮助。心理评估：焦虑量表 得分 10 分，中度焦虑状态；抑郁量表得分 10 分，中度抑郁状态。肩前屈、屈肘、伸腕肌力 V 级，髋关节屈曲、膝关节伸展、左踝背屈肌力 IV 级，右踝背屈肌力 I 级左侧各关节主动关节活动度正常，右侧上肢各关节、屈髋、伸膝主动关节活动度正常，踝背屈被动关节活动度正常。

出院前评估

患者独立坐位，T：36℃，HR：74 次 / 分，BP：96/64mmHg，R：19 次 / 分，SpO2：100%。听诊双肺呼吸音清，双肺未闻及明显干湿啰音。右上肢中心静脉置管术后。血常规：RBC 6.15（*10^9/L），RBC 2.33（*10^12/L）↓，Hgb 77（g/L）↓，Plt 89（*10^9/L）↓。生化示，总蛋白 53（g/L）↓，白蛋白 27.1（g/L）↓，Cr 92（μmol/L），K+ 4.25（mmo1/L），钠 133（mmo1/L）↓；NT-proBNP 2260（ng/L）↑。胸片 双肺纹理增多，心影增大，大致同前。超声心动图 下腔静脉内径 19mm，呼吸变化率正常，血流速度 0.5m/s。患者清醒状态，5 分问题（S5Q）=5。Barthel 指数评定量表 70 分，日常生活基本自理。心理评估：焦虑量表 得分 7 分，轻度焦虑状态；抑郁量表 得分 5 分，轻度抑郁状态。右踝背屈肌群肌力 III 级，其他肌群肌力 V 级。踝背屈主动关节活动度 10°，其他关节主动关节活动度正常。

鉴别诊断：

无

其他：

此病例为左室辅助装置患者早期康复案例，不涉及鉴别诊断内容。

CABG 术后桥血管病变的处理

郭森

郑州大学第一附属医院

患者基本信息：

患者：马 XX，男性，58 岁

生命体征：体温：36.6℃、脉搏：70 次 / 分、呼吸：19 次 / 分、血压：127/79mmHg

身高 165cm，体重 90.0Kg，BMI：33.1

体格检查：无异常发现

入院诊断：冠状动脉粥样硬化性心脏病 不稳定型心绞痛 CABG 术后 PCI 术后 心功能 II 级（NYHA 分级）

主述：

发作性心前区疼痛 9 年余，加重 1 天

现病史：

9 年前活动后出现心前区疼痛，呈压榨样，伴咽部紧缩感，持续约数分钟，休息后可缓解，遂就诊于我院，诊断为“冠心病 稳定型心绞痛 ”，行冠脉搭桥术，手术顺利，术后恢复良好。2 年前上述症状再发加重，再次就诊于我院，诊断为“不稳定型心绞痛”，行 PCI 治疗（具体不详），术后症状缓解，规律服用“阿司匹林、替格瑞洛、阿托伐他汀” 等药物治疗。1 天前上述症状再发加重，今为求进一步诊治来我院

既往病史：

无特殊

病程记录：

阿司匹林肠溶片	100mg	每晚 1 次	每次 1 片	口服
替格瑞洛片	90mg	每日 2 次	每次 1 片	口服
阿托伐他汀钙片	20mg	每晚 1 次	每次 1 片	口服
美托洛尔缓释片	47.5mg	每日 1 次	每次 1	口服

检验检查记录：

指标	实测值	正常范围	单位
PRO BNP	121	198	Pg/ml
cTN	0.018	0-0.034	μg/L
eGFR	100.069		ml/min/1.73
T-CHO	3.67	< 5.2	mmol/L
TG	1.56	< 1.7	mmol/L
LDL	2.24	< 3.61	mmol/L
HDL	0.68	> 0.91	mmol/L
ALT	30	0-40	U/L
AST	32	0-40	U/L
HbA1C	6.1	4.0-6.5	%
Hb	141	g/L	130-175
D-Dimer	0.2	mg/L	0-0.3

鉴别诊断：

无需鉴别

其他：

无

慢性心力衰竭合并急性心肌梗死

张佑俊

华东医院

患者基本信息：

患者男性，81 岁，劳模退休。

主诉：反复胸闷 , 气促 11 年 , 加重 3 天

主述：

主诉：反复胸闷 , 气促 11 年 , 加重 3 天

现病史：

现病史: 患者 11 年前反复出现胸闷、气促 , 伴夜间不能平卧 , 3 天前上述症状加重 , 伴双下肢水肿。3 天前晚上 22:00 突发胸痛 , 气促、呼吸困难 , 面色发绀 , 意识模糊 , 家属诉当时氧饱和度 70%，救护车来我院，胸痛中心测血压：150/78mmHg，吸氧后血氧 94%，心电图示：有效起搏心律。肺 CT 示：两侧胸腔积液，两下肺部分受压不张，两肺内炎症及炎症后遗灶。动脉硬化。急诊心肌酶 CKMB(-),TnT 0.031 ng/ml, D-dimer 2230ng/ml, 急诊血气：pH 7.235，pCO2 9.45kPa,pO2 6.93kPa,Hb 214g/L, 患者夜间少尿（今晨 7:00am 300ml），最低血氧 70%，予以呋塞米、注射用重组人脑利钠肽、注射用头孢米诺钠等药物对症治疗，症状缓解。现为进一步治疗收入我科。病程中，患者饮食一般，睡眠较差，大便正常，小便量少，体重无明显减轻。

既往病史：

既往史：患者既往于胸科医院行冠脉支架植入术（3 个）及安装起搏器。于同仁医院行右下肢支架植入，具体不详。患者近 2 年反复因胸腔积液入院治疗。既往有 2 型糖尿病病史多年，血糖控制不佳 ，既往有胆囊结石多年，反复阵发性胆囊炎发作。

病程记录：

1. 阿司匹林 + 硫酸氢氯吡格雷片 + 硝酸异山梨酯注射液 + 琥珀酸美托洛尔缓释片 + 他汀 + 低分子肝素
2. 抗心衰治疗：沙库巴曲缬沙坦钠片 + 注射用重组人脑利钠肽 + 呋塞米 + 螺内酯 + 琥珀酸美托洛尔缓释片 + 达格列净
3. 控制血糖：利格列汀片 + 达格列净
4. 平喘 + 化痰 +BiPAP 呼吸机
5. 心电监护 + 记 24 小时出入液量

检验检查记录：

无

鉴别诊断：

无

其他：

无

房颤合并左心耳血栓治疗一例

孔深柯

河南省胸科医院

患者基本信息：

患者，男性，60 岁

主述：

间断胸闷气短 2 年，加重 2 月。

现病史：

2 年余前活动后出现胸闷气短伴心悸，自觉呈憋闷感，休息数分钟后渐缓解，无咳嗽、咳痰，无头晕及一过性黑矇，无头痛、恶心、呕吐，遂至当地医院就诊，诊断“心力衰竭、心房颤动”，给予“利尿、控制心率等治疗后好转出院，院外未再正规治疗。2 月前胸闷气短较前加重，一般行走时即可出现胸闷气短伴心悸，就诊于当地医院行冠脉造影示”前降支、回旋支、右冠未见明显狭窄 “，行心脏彩超示：节段性室壁波动异常，左心及右房增大，主动脉瓣及二三尖瓣少量返流，左心功能低下，EF：44%，诊断为“心房颤动、心力衰竭”，后为进一步治疗于 2024-12-27 入住我院。

既往病史：

5 年前因肢体无力在当地医院诊断为“脑梗塞”，给予药物治疗后好转出院，未遗留肢体言语等后遗症。

病程记录：

患者入院后积极给予相关检查，行食道超声提示左心耳血栓，给予抗凝治疗后，3 个月后复查左心耳血栓消失，给予行房颤射频消融术及左心耳封堵术。

检验检查记录：

食道超声示左心耳血栓

鉴别诊断：

暂无。

其他：

暂无。

被束缚的心脏 --- 高血压与心肌肥厚的双重迷雾

刘飞

亳州市人民医院

患者基本信息：

患者，老年，男性，71 岁

主述：

活动后胸闷气喘 6 月

现病史：

患者 6 月前晨起散步时出现胸闷气喘症状，休息后自行缓解，持续时间半小时余，不伴胸

痛、心悸、乏力，无肩背部放射痛，无头晕、黑矇、晕厥，无双下肢水肿。无咳嗽、咳痰、咯血，无反

酸、烧心，无腹痛、恶心、呕吐，无发热。此后数天一般程度体力活动即可诱发上述病情，2 周前外院体检提示胸腔积液、球蛋白高，尿蛋白阳性，心电图示：窦性心律，V1-2ST 段略有改变 ,V4-6 导联 T 波倒置，病程中食欲差，进食少，二便如常，近 1 年来体重下降约 15kg。

既往病史：

冠心病病史、PCI 术史、乙肝小三阳、2- 型糖尿病

病程记录：

今日查房，患者休息状态下无胸闷气喘，无胸痛及肩背部疼痛，夜间可平卧，无夜间阵发性呼吸困

难；查体示：血压 119/69mmHg, 颈软，颈静脉无怒张，两肺呼吸音粗，双肺底可闻及湿罗音。心前区无隆

起，无震颤，心界不大，心率 72 次 / 分，心律齐，心音正常，胸骨左缘可闻及杂音，无心包磨擦音。腹部

膨、软，无腹壁静脉曲张，无压痛、反跳痛，肝脾未触及，两肾区无叩痛，无移动性浊音。双下肢无水

肿，神经系统检查无异常。2025-06-09 临检检验报告: * 红细胞计数 3.30x10^12/L ↓，* 血红蛋白、96.00g/L ↓，* 红细胞压积 0.311L/L ↓。2025-06-08 急诊检验报告：肌钙蛋白 I 0.088ng/ml。2025-06-08 急诊检验报告：N 端脑利钠肽前体 3007pg/ml ↑。2025-06-08 急诊检验报告：* 总蛋白 88.1g/L，球蛋白 52.3g/L。刘娟副主任医师查看患者后指出：一诊断及诊断依据：1. 冠状动脉粥样硬化性心脏病不稳定心绞痛 . 冠脉支架植入术后心功能 IV 级 (NYHA 分级)：患者老年男性，既往有冠脉支架植入术后，近 1 年反复出现活动时胸闷胸痛，持续约数分钟，休息后可逐渐缓解，近期出现稍活动即出现胸闷气喘，入院 NT-ProBNP 明显升高，2025-5 曾在外院行肺 CT 双侧胸腔积液，目前考虑上述诊断；2、肥厚型心肌病？结合患者心脏彩超诊断，进一步完善心脏 MRI 明确；3、高血压病糖尿病：结合病史，诊断明确；4、贫血高球蛋白血症：结合患者血常规，诊断明确。二、鉴别诊断：根据病史、症状、体征、辅检目前不支持急性心肌梗死、急性肺栓塞；三治疗上，患者室间隔肥厚，追问病史患者血压控制尚可，目前不排除肥厚型心肌病，进一步完善血清蛋白电泳五项免疫固定电泳 β2 微球蛋白免疫球蛋白 G 免疫球蛋白 M 免疫球蛋白 A 免疫球蛋白 E、心脏 MRI 示有无浸润性心肌病可能，治疗上继续给予抗血小板聚集、调脂、稳定斑块及减轻心脏负荷及逆转心室重构等治疗

检验检查记录：

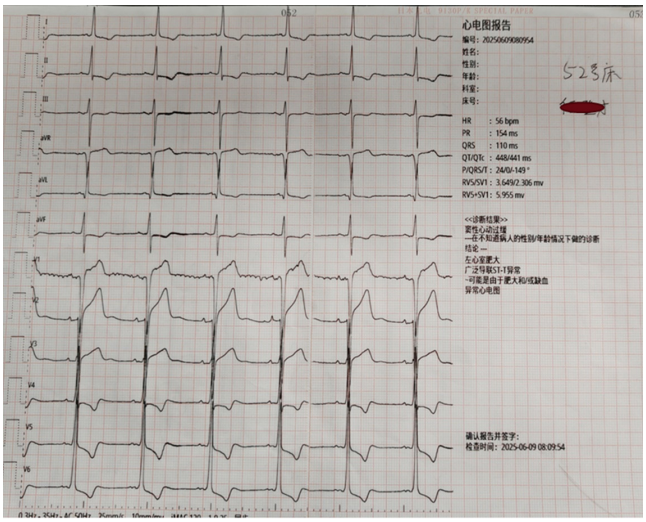

鉴别诊断：

疾病名称	特征性临床表现	支持依据	不支持依据
高血压性心脏病	早期无症状 晚期心衰症状	高血压病史多年 心电图检查结果	血压控制良好 心电监护：应用 β 受体阻滞剂后：心率下降，室内有阻滞加重 左心室壁厚度≥15mm
肥厚性心肌病	胸痛、胸闷	心电图检查结果 心脏彩超：LVDD 及 ISV 厚度：17mm	
淀粉样变	多系统受累： 心脏、肾脏等	球蛋白升高、尿蛋白阳性、贫血 心脏彩超：左室肥厚	患者心电图：左心室高电压 患者有肝炎、糖尿病仍需进一步检查，
法布雷病	感觉异常、少汗 无汗、胃肠道症状 血管角质瘤、角膜涡状混浊	尿蛋白阳性、心电图：左室高电压、传导阻滞	无上述临床表现，可能性小。

其他：

原发性甲状腺功能减退症合并心包积液、腹腔积液、自发性腹膜炎一例

程玉文

复旦大学附属华东医院

患者基本信息：

患者 40 岁男性，上海人，自由职业，离异未育

主述：

胸闷气短半年，腹痛腹泻 1 周余

现病史：

患者半年前反复出现胸闷气短，伴体力下降，辛辣刺激饮食后出现下腹部疼痛，全下腹绞痛，不伴有腹泻腹胀，未予重视，自述云南旅游时行“中医理疗”后症状缓解。1 周前无明显诱因下出现腹痛腹胀腹泻，下腹部绞痛，腹泻为黄色水样便，大便次数增多，排便不受控制。伴发热，体温最高 37.9℃。胸闷气短症状较前加重，出现乏力，夜间无法平卧，至我院就诊。

既往病史：

甲状腺功能减退症病史 15 余年，口服优甲乐治疗，已自行停药 8 年。双下肢及颜面部水肿 4 年，症状反复，未予重视。2 年前单位体检心超提示大量心包积液，未予治疗。

病程记录：

入院后立即予无创辅助通气，腹腔穿刺引流，引流出黄色伴恶臭液体，腹水常规示：李凡他试验 ++；白细胞计数 65596*10^6/L；红细胞计数 11000*10^6/L；单个核细胞 98%；多个核细胞 2%。提示自发性腹膜炎，予抗感染、利尿、护肝、护胃、营养心肌、抗凝、纠正电解质紊乱、通便、营养等对症支持治疗。入院后监测血压波动在 90~100/60~70mmHg，心率 90-110 次 / 分，治疗上予达格列净 + 螺内酯 + 伊伐布雷定 + 维立西胍抗心衰。患者重度甲状腺功能减退，内分泌科会诊建议予优甲乐一片 + 甲状腺素片一片半替代治疗，后患者频发室性心动过速，及一次尖端扭转性室速，调整替代方案为优甲乐两片，并予胺碘酮口服抗心律失常。两周患者未再发室速，继续予优甲乐一片半 + 甲状腺素两片治疗。一月余后患者气喘较前明显好转，夜间可平卧及全身水肿情况好转。复查甲状腺功能较前好转、肝肾功能恢复正常后出院。

检验检查记录：

甲状腺功能：TSH 33.1416 mU/L，FT3 < 1.6 pmol/L，FT4 < 5.2 pmol/L，TT3 < 0.31 nmol/L，TT4 < 11.7 nmol/L，肝功能：谷丙转氨酶 184.2U/L，门冬氨酸氨基转移酶 314.5U/L，总胆红素 47.7 umol/L，直接胆红素 29.1 umol/L，间接胆红素 18.6 umol/L，肾功能：肌酐：170.0 umol/L，尿素氮 16.4mmol/L。血常规：白细胞 9.8*10^9/L，红细胞 2.82*10^12/L，血红蛋白 86 g/L，血小板 161*10^9/L。电解质：钾 3.0 mmol/L，钠 3.0 mmol/L，氯 3.0 mmol/L。凝血: 凝血酶原时间 15.9 秒，纤维蛋白原降解产物 > 123.07 mg/L，D-二聚体 47.66 mg/L 。C 反应蛋白 267.41mg/L，降钙素原 3.65ng/ml，白介素 6 47.9pg/L。B 型脑钠肽：2458 pg/ml。脑钠肽前体：7049 pg/ml。糖类抗原 125（CA125） 407.5U/mL。心电图检查：1. 窦性心律 2. 偶发室性早搏 3.ST-T 段改变。心脏超声：左房、左室扩大，左室收缩活动减弱，左室收缩、舒张功能减退（LVEF：35%）；右房扩大，右室稍大，肺动脉增宽；二尖瓣反流（轻度）；

心包腔中 - 大量积液。腹部 CT 提示: 腹腔大量积液,肠系膜网膜模糊伴斑片索条影,腹膜增厚，炎性？肿瘤待排。前列腺钙化。垂体 MRI：未见明显异常。

鉴别诊断：

多浆膜腔积液的鉴别诊断：1. 感染性疾病 2. 肿瘤性疾病 3. 心血管疾病 4. 肝脏疾病 5. 肾脏疾病 6. 自身免疫性疾病 7. 其他（甲状腺功能减退症、低蛋白血症、药物反应或毒性）

其他：

扩张型心肌病 CRT-D 术后心律失常一例

古扎力奴尔·阿不拉

和田地区人民医院

患者基本信息：

患者男性，43 岁，维吾尔族，住址：新疆和田县罕艾日克乡。

主述：

发作性胸闷、气短 2 年，加重伴心悸 4 天

现病史：

患者自诉于 2 年前开始无明显诱因出现胸闷、伴气短，呈劳累性呼吸困难，于 2024 年 1 月上述症状加重伴有晕厥，在我院 CCU 住院治疗，入院后心电图提示：交界性心率，心率 51 次 / 分， 完善心脏超声提示：全心腔增大（左室舒张末期内径 67mm、左室收缩末期内径 55mm、左房 51mm、右房 57mm、右室 25mm）左室心肌运动弥漫性减弱，EF 值 35%，病情平稳后行冠脉造影术排除冠脉病变，诊断考虑为扩张型心肌病 难治性心力衰竭 心功能 IV 级，在住院期间出现持续性室性心动过速，给予药物转复，于 1 月 25 日行 CRT-D 植入术，手术过程中左室电极在冠状静脉心大静脉、心中静脉植入失败，方案改为左束支区域起搏，术后心电图提示：起搏心率，QRS：170ms，出院后正规口服五连药物，抗心律失常给予盐酸胺碘酮片口服，此次入院前 4 天无明显诱因再次出现胸闷、气短，偶有夜间阵发性呼吸困难，伴发作性心悸，紧随再次出现晕厥，CRT-D 放电后意识逐渐恢复。

既往病史：

患有先天性马蹄内足翻，其余无特殊。

病程记录：

嘱患者卧床休息，吸氧，常规改善心功能治疗口服药物包括沙库巴曲缬沙坦 25mg 每日两次口服（血压偏低），富马酸比索洛尔 2.5mg、达格列净 10mg，维利西胍 5mg，氢氯噻嗪 25mg，螺内酯 20mg 每日一次口服，对症治疗包括多巴酚丁胺强心，呋塞米利尿，患者入院后完善心电图提示：室性心动过速，抗心律失常给予盐酸胺碘酮注射液 300mg 持续泵入 2 天后患者室性心动过速未转复，停用静脉胺碘酮后改为盐酸利多卡因 200mg 静点后室速转复。停用口服胺碘酮改为美西律 150mg 每日三次口服,第三天复查 24 小时动态心电图结果提示: 窦性心律 起搏心律 偶发室性早搏（141 个 /24 小时）。

检验检查记录：

入院时心电图提示：室性心动过速，血常规提示：WBC 11.94×10^9/L，N 端 -B 型钠尿肽前提 2222pg/ml，其余无特殊异常。

鉴别诊断：

缺血性心肌病：多见于老年人，有典型的心绞痛、心肌梗死病史或心电图表现，若有左心衰竭的发作史，原发性高血压、高脂血症、糖尿病史更有助鉴别，该患者既往已行冠脉造影术提示冠脉未见明显狭窄，故不考虑缺血性心肌病。

其他：

患者于 2025 年 7 月 10 日复查心脏超声提示：全心腔增大（左心室舒张末期内径 67mm）左室心肌运动减弱 左室收缩功能减低 肺动脉增宽 起搏器术后：起搏导线表面光滑（EF 值 28%）

免疫检查点抑制剂相关心肌炎合并重症肌无力一例

章亚平

华东医院

患者基本信息：

患者男性， 75 岁，退休。

主述：

发现胃癌 1 月，腹胀纳差乏力伴肝功异常 3 天

现病史：

患者 1 月前行胃镜提示：幽门浸润型新生物，恶性肿瘤。术后病理提示：幽门腺癌，分化中等。免疫组化： MLH1（-，内对照 +）， MSH2（+）， MSH6（+）， PMS2（-，内对照 +）， HER2（1+）， PD-1（肿瘤 -，间质 1%+），PD-L1(MXR003)（CPS， Combined Positive Score， 20）， P53（++）。免疫组化结果示错配修复蛋白表达缺失，建议进一步行 MSI 分子检测。后经科内讨论，给予新辅助化疗 + 免疫治疗。 11 天前开始第 1 次化疗， 化疗方案: SOX（奥沙利铂 200mg+ 替吉奥 40mg 口服 bid ）+ 欧狄沃（纳武利尤单抗）360mg 静脉输液， Q3W。3 日前开始出现中上腹胀痛不适，夜间反复打嗝，持续性腹胀及隐痛，伴纳差乏力，入院当天（20240507）门诊查 ALT 221U/L，AST 827U/L，遂收住院。患者近 1 月来精神尚可，睡眠可，纳差，二便无殊，体重未见明显变化。

既往病史：

既往高血压病史，服用比索洛尔、厄贝沙坦和硝苯地平缓释片，血压控制良好。糖尿病病史，服用达格列净，格列齐特和吡格列酮二甲双胍片，血糖控制良好。其母有肠癌病史。

病程记录：

诊疗经过： 患者入院后完善相关检查，予还原性谷胱甘肽 + 甘草酸单铵半胱氨酸 + 门冬氨酸鸟氨酸 + 多烯磷脂胆碱保肝、抑酸护胃、头孢呋辛抗感染、营养支持等对症治疗。 入院后患者诉乏力纳差， 伴双眼睁眼困难，右眼为甚。入院后第 3 天下午患者出现胸闷，监护提示心率慢，30 次 / 分，心电图（见图 1）：1. 窦性心律 2. 室性逸博心律（心室长间歇最长 3.28 秒）3. 提示III度房室传导阻滞。查心肌酶明显升高（TnT 2.38 ng/ml， CKMB 255ng/ml，见图 2），结合患者曾行免疫治疗，考虑免疫抑制剂相关性心肌炎、免疫性肝肾功能损伤、 III房室传导阻滞。遂于当日转至 CCU 进一步治疗，转入后予以临时起搏器治疗，请神经内科、肿瘤科会诊，予大剂量甲泼尼龙抗炎 (1g*3 天 +0.5g qd)+ 丙种球蛋白 (25g qd*3 天) 治疗， 美罗培南抗感染， 积极保肝， 沙库巴曲缬沙坦 + 达格列净 + 螺内酯改善心衰，速尿利尿及抑酸护胃等对症治疗。病程中患者乏力纳差、双眼睁眼困难、吞咽困难症状仍进行性加重。 入院后第 6 天（图 3） 心电图示阵发性室性心动过速，予利多卡因治疗。患者多器官受累，积极治疗后乏力纳差、吞咽困难、呼吸困难仍进行性加重，告知家属病情极其危重，家属表示理解，并拒绝气管插管、气管切开等有创抢救措施。转归： 入院后第 8 天下午患者开始血压下降、呼吸困难、意识不清，急查血气提示呼吸性酸中毒，予 Bipap 应用，升压、呼吸兴奋剂应用、 纠酸等对症治疗， 但病情仍未见好转， 于入院后第 9 天宣告临床死亡。

检验检查记录：

生化：丙氨酸转氨酶 255.4U/L ↑，门冬氨酸转氨酶 711.9U/L ↑，门冬 / 丙氨酸 2.8 ↑,总胆红素 11.2umol/L,直接胆红素 4.9umol/L,间接胆红素 6.3umol/L，总蛋白 64.7g/L ↓，白蛋白 42.6g/L，白蛋白 / 球蛋白 1.9，碱性磷酸酶 98.2U/L,总胆固醇 5.58mmol/L,三酰甘油 1.95mmol/L ↑,葡萄糖 8.6mmol/L ↑，尿素 8.2mmol/L，肾小球滤过率估算 95ml/min，肌酐 58.0umol/L ↓，尿酸 279umol/L，钙 2.45mmol/L,磷 1.54mmol/L,谷氨酰基转移酶 25.8U/L，钾 4.40mmol/L，钠 137mmol/L，氯 97.8mmol/L，低密度脂蛋白 3.59mmol/L ↑，高密度脂蛋白 1.41mmol/L，超敏 C 反应蛋白 7.25mg/L ↑，球蛋白 22.10。

生化：丙氨酸转氨酶 164.8U/L ↑，门冬氨酸转氨酶 155.2U/L ↑，葡萄糖 11.7mmol/L ↑，尿素 14.2mmol/L ↑，肾小球滤过率估算 99ml/min，肌酐 52.6umol/L ↓，尿酸 350umol/L。

血常规：白细胞计数 14.6x10^9/L ↑，中性粒细胞百分数 92.2% ↑，红细胞计数 4.59x10^12/L，血红蛋白 143g/L，血小板计数 196x10^9/L。

心肌酶：B 型钠尿肽 250pg/ml ↑，肌钙蛋白 I 19.2486ng/ml ↑，B 型钠尿肽 346pg/ml ↑。

头颅 MRI：1、双侧额顶叶白质、基底节区少许异常信号灶，考虑脑小血管病变所致（可能为血管源性白质高信号 / 血管源性腔隙），但未见明显急性梗塞灶。2、老年脑改变。3、附见：多组副鼻窦炎症。鉴于病史，建议头颅增强检查。

肝脏，增强 磁共振检查报告：1. 胃窦壁增厚、强化，考虑：胃癌，周围多发淋巴结转移（小网膜囊一枚最大）。2. 肝脏多发异常强化灶，高度怀疑为转移瘤。3. 胰腺体尾部乏血供小灶。4. 附见：左侧肾上腺增粗。

鉴别诊断：

免疫抑制剂相关心肌炎需要与以下疾病进行鉴别诊断：

病毒性心肌炎

病因：由病毒感染引起，如柯萨奇病毒、埃可病毒等。症状：发病前 1-3 周常有病毒感染前驱症状，如发热、全身倦怠感、肌肉酸痛，或恶心、呕吐等消化道症状，随后出现心悸、胸痛、呼吸困难、水肿，甚至晕厥、猝死等心脏相关症状。检查：心肌损伤标志物如心肌肌钙蛋白、心肌肌酸激酶同工酶等升高，病原学检查可从咽拭子、粪便、血液或心包积液中分离出病毒，或检测到病毒核酸、抗体滴度升高。本患者心机损伤标志物明显升高，应考虑此病，但病史不符。

急性冠脉综合征

病因：主要是冠状动脉粥样硬化斑块破裂，继发血栓形成，导致冠状动脉阻塞。症状：典型症状为胸痛，多为压榨性、闷痛或紧缩感，可向左肩、左臂内侧等部位放射，疼痛程度较重，持续时间较长，一般超过 30 分钟，休息或含服硝酸甘油后多不能缓解。检查：心电图可出现 ST 段抬高或压低、T 波倒置等缺血性改变，心肌损伤标志物升高，冠状动脉造影可发现冠状动脉狭窄或阻塞。本患者心机损伤标志物明显升高，应考虑此病，但病史不符。

其他：

超高龄野生型转甲状腺素蛋白心脏淀粉样变一例

章亚平

华东医院

患者基本信息：

男， 98 岁，退休

主述：

纳差乏力 40 天，双下肢水肿伴气促 1 月，加重 2 周

现病史：

患者于 40 天前新冠病毒感染好转后开始出现纳差乏力，伴气促，活动后加重，双下肢逐渐出现水肿，无明显胸痛胸闷、咳嗽咳痰及发热，2 周前就诊我科门诊，心电图提示房颤，心室率 89bpm，室性早搏，异常 Q 波 (II， III, aVF)， 左前分支传导阻滞。予呋塞米、 螺内酯消肿利尿，索他洛尔 40mg bid 控制心室率等对症治疗，患者自觉症状未见明显好转。近两周气促及双下肢水肿较前加重，不能平卧，遂就诊我科急诊，查心肌酶： TnT 0.14ng/ml， CKMB 5.8ng/ml，pro-BNP 11000 pg/ml， D-dimer 6830 ng/ml，患者家属为进一步治疗，急诊以 “心功能不全” 收入我科。既往房颤病史 5 年，服用美托洛尔控制心率，利伐沙班抗凝治疗。患者近两月来纳差，精神稍差，轻度嗜睡，睡眠一般，大便正常，夜尿减少，体重未监测。

既往病史：

高血压病史 40 年，血压最高 180/90mmHg，长期服用氢氯噻嗪氯沙坦钾降压，2023-1-18 改为诺欣妥，否认糖尿病等慢性病。否认有活动后胸闷胸痛史。否认吸烟史，饮酒史 60 年，黄酒 50g/ 天，已戒酒。

病程记录：

诊断流程： 入院后查心电图提示：心房颤动伴房室连接处逸搏心律，异常 Q 波 (II， III, aVF)，左前分支传导阻滞，左胸导联低电压 (见图 1)。 心脏多普勒超声见： 左室壁增厚，左房扩大，左室舒张功能减退， GLS=-11.7%， 二维纵向应变见心尖保留现象 (见图 2)。血尿免疫固定电泳及游离轻链未见异常 (见表 1)，考虑心肌淀粉样变性，遂完善 99Tcm-PYP 心肌灌注显像，见：心肌各室壁段呈弥漫性放射性摄取，心影显示：心肌摄取浓度大于肋骨及胸骨（心肌： 226.4；肋骨： 132.1；胸骨： 193.6）（见图 3）。进一步完善腹壁脂肪活检， 镜下见纤维血管脂肪组织， 间质和血管壁见淀粉样物沉积。特殊染色： 刚果红（+）。外送 TTR 基因未见任何突变，故修正诊断为：心肌淀粉样变性（ATTRwt-CA），心力衰竭 (HFpEF)，心功能 III-IV 级，慢性心房颤动 (C5H1)，高血压 3 级 (极高危)。予活血升压 , 利尿 , 抗凝、 调脂稳斑、 改善预后、 抗感染、 解痉平喘化痰、纠正低白蛋白血症、改善前列腺症状、预防应激性溃疡等对症治疗。转归: 本患者住院期间发生心力衰竭进行性加重，消化道出血，最终因为心力衰竭死亡。

检验检查记录：

胸部 CT：两肺多发炎症，右侧胸腔中等量积液，左侧胸腔少量积液，右肺下叶部分不张，两侧小叶间隔部分可疑增厚，皮下水肿，考虑心衰所致，建议治疗后复查。

99Tcm-PYP 心肌灌注显像：影像学表现：心肌各室壁段呈弥漫性放射性摄取，心影显示：心肌摄取浓度大于肋骨及胸骨（心肌：226.4；肋骨：132.1；胸骨：193.6）影像学诊断：心肌 Tc-99m-PYP 显像弥漫性放射性摄取，心影显示，请结合临床。

鉴别诊断：

（1）AL-CA：诊断 ALCA 的必要条件是体内检测到单克隆免疫球蛋白，鉴定的方法包括血清游离轻链（free light chain，FLC）和血 清 / 尿 免 疫 固 定 电 泳（immunofixation electrophoresis，IFE）， 99Tcm 磷酸盐衍 生 物 核 素 检 查 有 助 于 CA 分 型 。

（2）肥厚性心肌病：CA 常常合并房间隔和房室瓣的增厚以及心包积液，组织多普勒显示有限制性左心室舒张功能异常，结合心电图低 QRS 波幅，有助于与肥厚型心肌病相鉴别 。

(3) 法布雷病：一种罕见的 X 连锁遗传性疾病，由于 X 染色体重编码 α- 半乳糖苷酶 A 的基因突变，导致其代谢产物三己糖神经酰胺（GL-3）和相关鞘糖脂在全身多个器官（心脏、脑部、眼部、肺部、肾脏和皮肤）大量推积所导致的临床综合征。神经系统可表现为周围神经疼痛，自主神经、CNS 均可受累，心血管系统可表现为高血压、心肌缺血、心脏瓣膜病和肥厚性心肌病，心力衰竭等。与 ATTR-CA 鉴别要点：①儿童、青年期发病较多，男性症状较重，②面部畸形，③皮肤血管角质瘤，④ α- 半乳糖苷酶 A 的活性检测，⑤血尿 GL-3 水平检测以及⑥基因检测。

其他：

机械通气联合心衰超滤脱水成功救治重症心衰一例

章亚平

华东医院

患者基本信息：

男性， 76 岁，退休。

主述：

反复胸闷气促 3 周，再发加重 2 小时

现病史：

患者于 3 周前与亲属争吵后情绪激动出现活动后胸闷，伴气促，平日活动量少，患者未予重视，外院门诊查心超示左房左室增大， LVEF 35%（具体不详），后患者自行就诊我科门诊，心电图示频发室早，室早二联律，建议患者入院进一步明确心功能不全病因，患者要求药物保守治疗，拒绝住院治疗。近期否认夜间阵发性呼吸困难，有下肢浮肿，逐渐加重， 2 小时前患者活动后突发胸闷气促加重，不能平卧，故就诊我院急诊，心率 126bpm，血压 192/119mmHg，指末氧 77%，心电图示： 1. 窦性心律， 2. 频发室性早搏， 3. 完全性左束支传导阻滞， 4. 电轴左偏。心肌酶 (-)， D 二聚体 960 ng/ml， proBNP 10300 pg/ml，急诊考虑急性左心衰，予面罩吸氧，吗啡镇静，利尿，喘定、甲强龙平喘，新活素扩管抗心衰治疗，患者症状未见明显缓解，仍端坐呼吸，指末氧不能维持，予 BiPAP 辅助通气，指末氧升至 95%，仍端坐呼吸，患者及家属为求进一步诊治，急诊拟 “急性心力衰竭” 收入我科。追问病史，患者家属代诉 3 月前新冠感染（当时有发热咳嗽咳痰）康复后遗留长期咳嗽咳痰，无发热。

既往病史：

高血压病史 15 年，血压最高 190/119mmHg，平素不规律服药， 3 周前我科门诊改为诺欣妥 100mg qd+ 倍他乐克 12.5mg bid 控制血压，自诉血压控制可。下肢静脉曲张病史多年，曾使用地奥司明治疗。否认糖尿病。吸烟史 40 年， 10 支 / 天，未戒烟。否认饮酒史。

病程记录：

诊疗经过： 入院时患者端坐呼吸， 不能平卧，查心肌酶阳性，心电图见图 1，床旁胸片（见图 2），见大片肺水肿，同时不能除外病毒性肺炎。 予无创呼吸机辅助通气， 同时予利尿、扩血管，辅以阿司匹林联合氯吡格雷双联抗板治疗，低分子肝素抗凝，阿托伐他汀稳定斑块，甲强龙抗炎，美罗培南抗感染，辅以雾化化痰护胃等治疗。但患者情绪激动，不能配合无创呼吸机，氧饱和度不能维持，复查血气分析提示呼吸衰竭加重，遂紧急行气管插管机械通气。插管后第 2 天复查胸片肺水肿明显减轻（图 2）。 第 2 天开始床边心衰超滤脱水联合利尿、扩血管等治疗，肢体浮肿逐渐消退，于入院后第 4 天拔除气管插管， 心肌酶及 BNP 均快速下降（图 3、图 4），进一步完善心超提示缺血性心肌病（图 5），遂于第 9 天完善冠脉造影 +PCI 术 : LM（-）， LAD 近中段狭窄 30-40%， TIMI 3 级，LCX 近段 30-40%， TIMI 3 级，RCA 开口处狭窄 80%，近段完全闭塞， TIMI 0 级。 RCA 植入 2 枚支架。转归：入院后第 11 天出院，出院前行 6MWT： 210 米。出院后规律服用： 阿司匹林 100mg qd、氯吡格雷 75mg qd、阿托伐他汀 20mg qn、沙库巴曲缬沙坦 50mg bid、达格列净 10mg qd、螺内酯 20mg qd、胺碘酮 200mg bid。出院后 4 个月复查心脏超声，心功能有较高水平的提升（见图 6）。

检验检查记录：

入院心电图：1. 窦性心律，2. 完全性左束枝传导阻滞，3. 室性早搏二联律，4. 电轴左偏。

鉴别诊断：

需与以下疾病进行鉴别：

1.、急性肺动脉栓塞：肺动脉栓塞常可引起晕厥、胸痛、咯血、气急和休克等症状。可通过相应病史、心电图、D- 二聚体检测及肺动脉 CT 造影有助于鉴别。本患者有胸闷气促，合并低氧血症，应考虑此病，D 二聚体检查及心电图不符。

2、急性呼吸窘迫综合征: 是其他原因所致的非心源性肺水肿，可表现为呼吸增快、大汗等症状，可行血气分析、BNP、心脏彩超等检查鉴别。

3、主动脉夹层: 可有胸部撕裂样疼痛，并伴有呼吸困难或晕厥，多有高血压病史。通过主动脉 CT 造影或磁共振主动脉显像以及超声心动图明确诊断。

其他：

异位性皮质腺瘤致难治性高血压与低钾血症一例

胡晓咏

新疆医科大学第五附属医院

患者基本信息：

年龄：45 岁 性别：男 职业：农民 身高：173 cm 体重：66 kg BMI：22.05 kg/m²

主述：

发现血压高 9 年，头晕 7 年，加重 2 天

现病史：

患者 9 年前因鼻出血在耳鼻喉科住院，发现血压高达 240/140mmHg，予 “硝苯地平控释片、卡托普利片” 等药，出院间断服上述药物，未监测血压。7 年前因头晕再次入住外院，查血钾较低，最低 1.99mmol/L, 考虑原醛，因经济原因患者拒绝行肾上腺 CT, 给予 “硝苯地平控释片、特拉唑嗪片” 等药，出院后继续服用上述药物，未监测血压。2 天前头晕较前加重，伴恶心、呕吐，呕吐 1 次，为胃内容物，测血压较高，为 180/110mmHg, 遂入我院诊治。查体：T 36.4℃，P 98 次 / 分，R 20 次 / 分，右 BP 180/104mmHg，左 BP 178/102mmHg，身高 173cm，体重 66 kg，体重指数 22.05kg/m2 ，腹围 84cm；视力粗测正常，甲状腺无肿大，颈静脉无充盈、怒张，心界略向左扩大，心率 98 次 / 分，律齐，未闻及病理性杂音，腹平软，无皮肤紫纹，未触及包块，肝脾肋下未及，腹部未闻及血管杂音，双下肢无水肿，生理反射存在，病理反射未引出。

既往病史：

既往史：无糖尿病、冠心病史，无周期性肌无力、烦渴、夜尿增多，无阵发性心悸、头痛、出汗，无腰痛、肉眼血尿，无眼睑、下肢浮肿，无睡眠打鼾。无手术外伤史。个人史：有 20 余年吸烟史，每日 10-20 支，偶尔饮酒，每次量不多。家族史：母亲患高血压，53 岁去世，死因不详，1 姐患高血压。

病程记录：

给予降压、纠正低钾（入院血钾 2.07 mmol/L）后进行内分泌评估；

检测结果：血浆醛固酮：47.61 ng/dL（↑）血浆肾素活性：0.04 ng/mL/h（↓）醛固酮 / 肾素比值（ARR）：1190，提示原醛增多症 皮质醇昼夜节律正常 排除嗜铬细胞瘤（儿茶酚胺代谢产物正常）排除 Cushing 综合征及其他内分泌疾病

影像学检查：腹部 CT 及 MRI 提示胰腺尾部与左肾上腺之间 3 cm 实性囊实混合性肿物，考虑异位肾上腺皮质腺瘤

心脏彩超：左心室肥厚，射血分数 47% 眼底检查： II 级高血压视网膜病变 脑 MRI 提示多发腔隙性脑梗死

手术治疗：行肿瘤切除术，术中未见并发症术后血压与血钾迅速恢复正常

病理诊断：肾上腺皮质腺瘤，伴局灶性髓质增生

出院后口服非洛地平缓释片单药控制血压，随访 12 个月，血压稳定（120–130/70–80 mmHg），血钾正常（3.6–4.2 mmol/L）

检验检查记录：

实验室检查：血钾：2.07 mmol/L（↓）血浆醛固酮：47.61 ng/dL（↑）血浆肾素活性：0.04 ng/mL/h（↓）同型半胱氨酸：19 μmol/L（↑）尿微量白蛋白：101.1 mg/L（↑）β2- 微球蛋白：4.78 mg/L（↑）

影像学：腹部增强 CT、MRI：胰尾与左肾上腺外侧支之间 3 cm 实性囊实肿物 心脏彩超：左心室肥厚，EF 47% 底检查： II 级高血压视网膜病变 脑 MRI：多发腔隙性脑梗死

病理与免疫组化：H&E 染色显示皮质腺瘤形态，局灶髓质增生 免疫组化：CK、Syn、CgA、S-100 等阴性，CD56 阳性，Ki-67 增殖指数低（2–3%）

鉴别诊断：

1. 原发性醛固酮增多症（PA）： 明显低钾、ARR 升高、肾上腺异常影像所支持。2. 嗜铬细胞瘤： 否定，儿茶酚胺代谢产物正常、无典型临床表现。3. 库欣综合征: 否定，皮质醇昼夜节律正常，无典型体征。4. 肾实质性高血压： 无肾功能异常或肾实质病影像学证据。5. 胰腺来源肿瘤（伪神经内分泌瘤）： 但内分泌评估阴性、免疫组化提示皮质腺瘤。

其他：

尊敬的评委老师，这是有趣且又曲折的继发性高血压的罕见病例，经过 MDT 的协作，病人的治疗和预后都得到很好的结局，希望组委会的老师可以给我们团队机会交流这个尘封已久且具有临床意义的继发性高血压的病例，让高血压这个既熟悉又陌生的疾病，为临床医生带来不一样的临床视角 - 继发性高血压。

IVL 联合旋磨治疗重度钙化病变一例

Zhou, Boda

Beijing Tsinghua Changgung Hospital

患者基本信息：

患者信息：男性，60 岁，体重 60kg。

主述：

间断胸痛 3 月余。

现病史：

患者 3 月余前在快走时出现胸痛，范围为巴掌大小，伴后背痛、胸闷，无心悸、乏力、憋喘，无头晕、头痛，无视物模糊、意识丧失，无恶心、呕吐，无咳嗽、咳血，无夜间阵发性呼吸困难、端坐呼吸，无左上肢及颈部放射痛，休息 2-3min 后自行缓解。后症状间断出现，性质同前。后就诊于我科，考虑“不稳定性心绞痛”，于 2025-01-15 行冠脉造影提示右冠状动脉近段、右冠状动脉中段、右冠状动脉远段狭窄程度 90-99%，于右冠状动脉近段、右冠状动脉中段、右冠状动脉远段分别植入 3 枚支架。于 2025-01-20 第二次行冠造提示左主干狭窄程度 30-50%，左前降支近段、左前降支中段狭窄程度 70-90%，回旋支近段、回旋支远段狭窄程度 70-90%，中间支狭窄程度 70-90%；于回旋支近段，回旋支远段植入 1 枚支架；于中间支植入 1 枚支架。术后予阿司匹林 100mg qd、氯吡格雷 75mg qd、阿齐沙坦 20mg qd、琥珀酸美托洛尔缓释 47.5mg qd、阿托伐他汀 20mg qn、依折麦布 10mg qd 等冠心病二级预防；予单硝酸异山梨酯 40mg qd、尼可地尔 5mg tid 改善症状。后患者诉症状较前明显缓解。现患者为处理剩余病变收住入院。自发病以来，患者精神可，睡眠饮食可，大小便如常，体重未见明显变化。

既往病史：

高血压 17 年，最高血压 170/90mmHg，目前规律口服阿齐沙坦 20mg qd，偶加服盐酸贝尼地平 8mg qd，阿罗洛尔 10mg qd，近期血压控制在 120-130/70-80mmHg。2 型糖尿病 14 年，餐后最高血糖可达 15mmol/L，空腹最高可达 11mmol/L，目前规律达格列净 10mg qd、阿卡波糖 50mg tid，门冬胰岛素 6IU tid、甘精胰岛素 14IU qn，近期未规律监测血糖。高胆固醇血症 10 年，目前规律口服阿托伐他汀 20mg qn、依折麦布 10mg qd，近期未规律监测血脂水平。双侧颈动脉狭窄（左侧中度狭窄、右侧重度狭窄）3 年，右颈动脉支架植入术后 3 年。

病程记录：

体格检查：体温：36.0℃，脉搏：84 次 / 分钟，呼吸：20 次 / 分钟，血压：153/71mmHg。心肺腹查体未见明显异常。

实验室检查：血常规： WBC 4.30 10^9/L ,HGB 137.00 g/L , LT 255.00 10^9/L, NEUT% 81.00 % ↑ (High)； 肾功能： Cre 67 umol/L, eGFR 95 单位 :ml/min/1.73m^2, K 4.33 mmol/L； 心脏损伤标志物：CK-MB 1.97 ng/mL, MYO 30 ng/mL, NT-ProBNP 397 pg/ml, TnT-hs 0.0106 ng/mL。

超声心动图：房间隔瘤样膨出；双房增大；主动脉瓣钙化；二尖瓣少 - 中量反流；三尖瓣中量反流；估测肺动脉收缩压增高；左室整体收缩功能正常，舒张功能减低；LVEF 65 %。

入院心电图：窦性心律不齐，房性早搏。

检验检查记录：

造影结果：

1. 左冠状动脉：左主干：狭窄程度 70-90%，TIMI III 级，有钙化；

左前降支近段、左前降支中段: 狭窄程度 90-99%, 病变长度弥漫性, TIMI III 级，有钙化；

回旋支近段：狭窄程度 30-50%，TIMI III 级，支架术后，支架内无再狭窄；

中间支：狭窄程度 90-99%，TIMI III 级；

2. 右冠状动脉：右冠状动脉近段、右冠状动脉中段可见支架影，无明显再狭窄，TIMI III 级；

图 2：冠状动脉造影结果

（三）治疗策略

进行 PCI 手术，应用 6F EBU3.5 指引导管，Runthrough 指引导丝通过 LAD 病变后，拟行 OCT 检查，但 OCT 导管难以通过 LAD 近段病变，启动旋磨治疗。经过 Finecross 微导管交换为旋磨导丝，应用 FireRaptor 冠脉旋磨系统 1.25mm 对 LAD 病变进行冠脉旋磨，转速 120000-180000rpm，共 5 次，共 15s（图 3）。

图 3：OCT 导管无法通过病变，启动旋磨治疗，进行分段旋磨

图 4：旋磨后患者诉胸痛，冠脉造影提示 LAD 血流中断

旋磨后患者诉胸痛，冠脉造影提示 LAD 血流中断（图 4）。随后出现低血压，血压最低 90/60mmHg，给予多巴胺，5 μg/kg.min，静脉泵入后血压可维持在 110/70mmHg，症状缓解；患者出现心动过缓，心率最低 50bpm，给予阿托品，0.5 mg，静脉推注后心率可恢复至 70bpm，症状缓解。

立即应用 2.0mm×20mm 预扩张球囊对 LAD-LM 病变进行预扩张，恢复冠脉血流（图 5）。

图 5：对 LAD-LM 病变进行预扩张

图 6：预扩张后 LAD 血流恢复

预扩张后造影可见 LAD 血流恢复，LAD 中段局部可见夹层影。（图 6）

对 LAD-LM 病变进行 OCT 检查，结果示可见 LAD 中段可见钙化病变，最小管腔面积 0.94mm²。（图 7）

图 7：OCT 检查可见 LAD 钙化病变，最小管腔面积 0.94mm²

由于 LAD 中段存在夹层，尽快于 LAD 中段 -LM 续贯植入 2 枚 DES（2.5mm×30mm、3.0mm×33mm），LCX 拘禁球囊技术保护边支。（图 8）

图 8：于 LAD 中段 -LM 续贯植入 2 枚 DES，LCX 拘禁球囊技术保护

LAD 中段支架内后扩张球囊无法完全膨胀，使用 3.0×12mm Shockwave 震波球囊对 LAD 近中段支架内病变进行扩张，共 80 次。IVL 治疗后，支架膨胀较前好转。（图 9）

图 9：LAD 中段支架内后扩张球囊无法完全膨胀，应用振波球囊治疗后有所改善

（四）手术结果

术后冠脉造影：

- 左冠状动脉前降支：LAD 支架通畅，无残余狭窄。（图 8）

图 10：术后冠脉造影

2. 术后腔内影像：

图 11：支架植入后前降支 OCT 检查

（六）小结

1. 该患者冠脉严重钙化，为高阻力病变，OCT 导管无法通过，迅速启动冠脉旋磨治疗。

2. 旋磨后患者出现胸痛症状，并出现低血压、心动过缓症状，冠脉造影提示 LAD 血流中断，立即进行预扩张，尽快恢复冠脉血流。

3. 复查造影提示 LAD 中段夹层影，立即植入支架覆盖，避免夹层想远处延展。

4. IVL 技术在支架膨胀不全病变中的应用，目前尚无足够循证医学证据，因此临床应用仍有待探索。

鉴别诊断：

诊断：

1. 冠状动脉粥样硬化性心脏病

不稳定性心绞痛

窦性心律

双房扩大

心功能 I 级 (NYHA 分级)

冠状动脉支架植入术后状态

2. 高血压病 2 级 (极高危)

3. 高胆固醇血症

4.2 型糖尿病

5. 左颈动脉狭窄

6. 右颈动脉支架植入术后

7. 脂肪肝

8. 反流性食管炎

其他：

IVL 治疗支架内闭塞病变一例

周博达

Beijing Tsinghua Changgung Hospital

患者基本信息：

患者信息：女性，82 岁，体重 50kg。

主述：

间断心前区不适 12 年，加重 2 周，再发胸痛 6 小时。

现病史：

患者 12 年前因心前区不适就诊外院诊断冠心病，行冠脉造影，并植入 1 枚支架（具体不详），术后规律冠心病二级预防治疗。2 周前无明显诱因出现胸痛，位于心前区，伴后背痛，外院急诊查心电图示 ST-T 改变，心肌损伤标志物升高，考虑急性非 ST 段抬高型心肌梗死。遂行急诊 PCI（2025-01-29），提示：左前降支近段狭窄 90-99%，左前降支中段狭窄 70-90%，回旋支远段狭窄 70-90%，右冠状动脉近段 100% 完全闭塞。于左前降支近段植入 1 枚支架。因患者有方差，术后予硫酸氢氯吡格雷片、利伐沙班片抗栓治疗。6 小时前（今日 8 点）患者再发胸痛，症状持续不缓解，就诊于我院急诊，心电图：心房颤动，V2-V6 导联 ST 段抬高；心肌损伤标志物：CK-MB 1.97 ng/mL，MYO 91.2 ng/mL ↑，NT-ProBNP 1397 pg/ml ↑，TnT-hs 0.0376 ng/mL ↑。考虑急性广泛前壁心肌梗死，予以阿司匹林 300mg 嚼服，为进一步诊治绕行 CCU 行急诊冠脉造影。

既往病史：

12 年前诊断高脂血症，现口服瑞舒伐他汀。高血压病 40 余年，血压最高 180/110mmHg，现口服沙库巴曲缬沙坦、苯磺酸氨氯地平治疗，平素血压多波动于 110-130/70-80mmHg。

病程记录：

体格检查：体温：36.6℃，脉搏：98 次 / 分钟，呼吸：22 次 / 分钟，血压：135/74mmHg。心肺腹查体（-）。

实验室检查：血常规：WBC 4.38 10^9/L，RBC 2.34 10^12/L ↓ (Low), HGB 87.00 g/L ↓ (Low), MCV 102.10 fL ↑ (High), MCH 37.20 pg/Cell ↑ (High), MCHC 364.00 g/L ↑ (High), PLT 255.00 10^9/L, NEUT% 81.00 % ↑ (High)；肾功能：Cre 87 umol/L, eGFR 53.617 单位 :ml/min/1.73m^2, K 4.16 mmol/L；心脏损伤标志物：CK-MB 1.97 ng/mL, MYO 91.2 ng/mL ↑，NT-ProBNP 1397 pg/ml ↑，TnT-hs 0.0376 ng/mL ↑。

检验检查记录：

（二）冠状动脉造影结果

造影结果：

1. 左冠状动脉：左前降支近段狭窄程度 100% 完全闭塞，支架术后，支架内再狭窄，TIMI 0 级；回旋支远段狭窄程度 70-90%，TIMI 3 级；

2. 右冠状动脉：右冠状动脉近段、右冠状动脉中段狭窄程度 100% 完全闭塞，TIMI 0 级；

图 2：冠状动脉造影结果

（三）治疗策略

进行急诊 PCI 手术，患者首先用 2.0mm 顺应性球囊进行扩张，恢复冠脉血流（图 3），同时进行第一次 IVUS 检查评估原支架贴壁情况，可见 LAD 近段原支架贴壁不良（图 4）。

图 3：顺应性球囊（左）扩张后，冠脉造影提示 LAD 支架内残余狭窄严重

图 4：第一次 IVUS 检查

第一次 IVUS 检查：显示 LAD 近段原支架贴壁不良，最小管腔面积 2.52mm²。（图 4）

用 2.5mm 及 3.0mm 非顺应性球囊进行扩张，但是 LAD 支架内仍残留重度狭窄，治疗效果欠佳（图 5），进行第二次 IVUS 检查评估（图 6）。

图 5：非顺应性球囊扩张（左）及冠脉造影（右）

图 6：第二次 IVUS 检查

第二次 IVUS 检查：显示 LAD 近段原支架贴壁不良，局部可见血栓影。（图 6）

使用 3.0×12mm Shockwave 震波球囊对 LAD 近段支架内狭窄病变进行扩张，共 10 次，治疗过程中患者出现室颤 1 次，立即心肺复苏，并给予 200J 非同步电除颤后患者恢复窦性心律。IVL 治疗后，支架贴壁较前好转，管腔显著扩大。（图 7）

图 7：3.0mm×12mm 振波球囊完全扩张

（四）手术结果

术后冠脉造影：

- 左冠状动脉前降支：LAD 支架通畅，无残余狭窄。（图 8）

图 8：术后冠脉造影

2. 术后腔内影像：

图 9：振波球囊扩张后前降支 IVUS 检查

下台后追溯病史，看到患者 10 天前对前降支进行介入治疗图像，可见前降支植入支架膨胀不良

图 10：患者 10 天前冠脉介入治疗图像

（六）小结

1. 该患者 10 天前于前降支植入支架，但因支架贴壁不良，发生亚急性支架内血栓，造成前降支闭塞。开通前降支后，非顺应性球囊反复扩张，前降支残余狭窄仍严重，迫不得已进行振波球囊治疗。

2. 该患者冠脉解剖复杂，RCA 为 CTO 病变，侧枝循环由 LAD 提供，对进行 IVL 治疗需慎重进行。

3. IVL 治疗过程中，需要注意血栓性病变，因为血栓经过振波球囊处理后可能会阻塞冠脉微循环。

4. IVL 技术在支架膨胀不全病变中的应用，目前尚无足够循证医学证据，因此临床应用仍有待探索。

鉴别诊断：

诊断：

1. 冠状动脉粥样硬化性心脏病

急性前壁心肌梗死

窦性心动

阵发性心房颤动（出血高危的非瓣膜性房颤）

心界不大

KillipI 级

冠状动脉支架植入术后状态

2. 高血压病 3 级 (极高危)

3. 高胆固醇血症

4. 高尿酸血症

5. 慢性阻塞性肺疾病

6. 乳腺恶性肿瘤

7. 慢性肾功能不全

8. 反流性食管炎

9. 胆囊术后

10. 中度贫血

11. 腹壁疝

12. 肠积气

13. 便秘

14. 叶酸缺乏

其他：

IVL 治疗旋磨后无法完全扩张病变一例

周博达

Beijing Tsinghua Changgung Hospital

患者基本信息：

患者信息：女性，54 岁，体重 70kg。

主述：

间断胸痛 6 年，加重 2 天。

现病史：

患者 6 年前无明显诱因出现心前区收缩样疼痛，伴胸闷、气短。外院冠脉 CTA 诊断为“冠心病”，建议置入支架治疗，患者拒绝。症状起初为 1 次 / 天，持续数分钟，后逐渐增加至 2-3 次 / 天，每次半小时左右。

既往病史：

高血压 27 年，血压控制欠佳; 糖尿病 27 年; 陈旧性脑梗死病史 2 年; 高脂血症 2 年; 吸烟史。父母及一弟一妹（42 岁发病）患有冠心病。

病程记录：

体格检查：体温：36.2℃，脉搏：93 次 / 分钟，呼吸：18 次 / 分钟，BP：148/86mmHg。心肺腹查体（-）。

实验室检查：hsTNT：0.008ng/mL；CK-MB：2.02ng/ml；NT-proBNP：304pg/mL；Scr：84μmol/L；K+：4.2mmol/L；WBC：8.62×10 ^{9} /L，N：65.2%，HGB：141.10g/L。

检验检查记录：

（二）冠状动脉造影结果

造影结果：

1. 左冠状动脉：前降支（LAD）近段严重钙化，狭窄 90%，长度约 8.9mm，钙化环 360°；对角支开口至近段 50-80% 狭窄；进行 IVUS 评估（图 3）

2. 右冠状动脉（RCA）：开口至近中段严重钙化，狭窄 70-90%，长度约 25mm，钙化环 >180°；

3. 其他：回旋支中度狭窄伴钙化，左主干末端不光滑伴钙化。

图 2：冠状动脉造影结果

A 左头位显示：B 右足位显示：C：右冠显示：

图 3：LAD 术前 IVUS 影像

A Frame425 显示：LAD 纤维斑块。

B Frame612 显示：LAD 钙化结节、纤维增生。

C Frame985 显示：LAD 最小管腔面积 1.94mm²。

D Frame1361 显示：360°环形钙化。

（三）治疗策略

2022 年 8 月第一次 PCI 手术，患者冠脉病变严重，钙化程度高，使用传统球囊扩张及旋磨治疗效果欠佳（图 4-7），因为病变局部夹层，植入 2.5mm 短支架封闭夹层后结束手术。

图 4：A、1.5mm 旋磨头 B、1.75mm 旋磨头。

图 5：A B 使用 3.25mm NC 球囊、血管仍无法完全扩张。

图 6：A 右头位、B 左头位显示、前降支中段局部夹层

图 7：A 前降支植入 2.5mm 支架

B 左头位、C 右头位，植入支架后造影

（四）第二次介入治疗

2023 年 2 月，患者因心绞痛再次住院。

根据指南和共识，FDA 批准的 Shockwave C2 冠状动脉 IVL 系统适应症严重钙化、狭窄的原发冠状动脉病变进行碎石和低压球囊扩张，采用 IVL 技术进行钙化治疗。

1. OCT 评估：OCT 显示 LAD 近段严重钙化，钙化环 360°，长度 8.9mm，最小管腔面积 0.92mm²。（图 8）

2. IVL 预处理： 使用 3.0×12mm Shockwave 震波球囊，IVL 治疗后，钙化环断裂，管腔显著扩大。（图 9-11）

图 8：2023 年 2 月术前造影

A 右头位 B 左头位 C 右足位

图 9：2023 年 2 月术前 OCT 显示：

A：LAD OCT 造影融合定位相

B：LAD 360°环形钙化，最小管腔面积 MLA1.32mm²

C：LAD 钙化厚度 1.03mm

D：LAD 360 度钙化病变长度 11.1mm。

图 10：A、B、C 使用 3.0×12mm IVL，球囊完全扩张

图 11：IVL 治疗后 OCT 检查显示

A：LAD 造影融合定位相 B：IVL 后 LAD 环形钙化断裂 C：钙化部分断裂 深度及宽度 D：纤维内膜撕裂 E：lumen 长轴图及病变长度 32.1mm

（五）手术结果

术后冠脉造影

- 左冠状动脉前降支：LAD 近段支架通畅，无残余狭窄。

图 12：2023 年 2 月左冠状动脉前降支术后造影

2. 术后腔内影像：

图 13：2023 年 2 月左冠状动脉前降支术前、术后 OCT

A:LAD 造影融合定位相 B：b 点管腔面积 C：c 点管腔面积 D：支架近端贴壁情况

图 14：术前、IVL、支架术后管腔比较

A：LAD 术前造影融合定位像 B：LAD b 点钙化 C：LAD c 点钙化 D：LAD IVL 后造影融合定位像

E：与图 B 对应位置钙化断裂 F：与图 C 对应位置钙化断裂

（六）小结

1. 该患者左右冠脉均存在严重钙化病变，传统介入方法难以有效处理，IVL 技术为严重钙化病变提供了新的解决方案。

2. IVL 通过碎石机制，能够有效断裂钙化环，显著改善管腔面积，为后续支架植入创造条件。

3. IVL 治疗后，结合 OCT 评估，确保支架贴壁良好，无明显残余狭窄，手术效果满意。

4. IVL 技术在旋磨后无法完全扩张的严重钙化病变中的应用，为复杂冠脉介入治疗提供了新的思路和方法。

鉴别诊断：

诊断：

1. 冠状动脉粥样硬化性心脏病（不稳定性心绞痛，心功能 II 级）；

2. 高血压 3 级（很高危）；

3. 2 型糖尿病；

4. 高脂血症；

5. 陈旧性脑梗死。

其他：

IVL 治疗前降支重度钙化病变一例

周博达

Beijing Tsinghua Changgung Hospital

患者基本信息：

患者信息：男性，61 岁，体重 65kg。

主述：

间断胸闷 4 年，再发加重伴胸痛 1 天。

现病史：

患者 4 年前活动后出现胸闷，范围约手掌大小，程度可忍受，休息 2 分钟后自行缓解，发作频率约 1 次 / 周。于当地医院就诊，查冠脉 CTA 示血管狭窄 65%（具体不详），诊断为不稳定心绞痛，予冠心病二级预防治疗，患者症状缓解。3 月后患者自行停用阿司匹林。患者 1 天前无明显诱因再发胸闷，伴心前区胀痛，范围约手掌大小，程度较前加重，休息 2 分钟后自行缓解 ，近 1 天发作 3 次。为求进一步诊疗于我科门诊就诊，以“不稳定性心绞痛”收入我科病房。

既往病史：

高胆固醇血症 1 年，未治疗。2 型糖尿病 1 年，未治疗。高血压病 4 年，最高血压 150/98mmHg，口服苯磺酸氨氯地平 5mg QD 降压治疗，平素未监测血压。吸烟史 30 年，每日约 10 支，未戒烟。

病程记录：

体格检查：体温：36.8℃，脉搏：54 次 / 分钟，呼吸：18 次 / 分钟，血压：124/78mmHg。心肺腹查体（-）。

实验室检查：hsTNT：0.007ng/mL；CK-MB：1.02ng/ml；NT-proBNP：105pg/mL；Scr：87μmol/L；K+：4.3mmol/L；WBC：6.55×10 ^{9} /L，N：67.2%，HGB：133.10g/L。

检验检查记录：

（二）冠状动脉造影结果

造影结果：

1. 左冠状动脉：左前降支近段、左前降支中段：狭窄 90-99%，病变长度弥漫性，TIMI III 级，有钙化；钙化（重度）；第一对角支：狭窄程度 30-50%，TIMI III 级，回旋支远段：狭窄程度 30%-50%，TIMI 3 级，血管直径 <1.5mm；

2. 右冠状动脉：右冠状动脉近段：狭窄 30-50%，TIMI III 级；

图 2：冠状动脉造影结果

A 左冠右头位 B 左冠右足位 C 右冠左前斜位

（三）治疗策略

进行 PCI 手术，患者冠脉病变严重，钙化程度高，使用切割球囊及非顺应性球囊均无法完全扩张，治疗效果欠佳（图 4-7），进行 OCT 检查评估钙化情况。

图 3：切割球囊（左）、非顺应性球囊（中）均无法完全扩张，后行 OCT 检查（右）

A：切割球囊 B：NC 球囊 C：扩张后造影

图 4：OCT 检查

A LAD 造影融合定位像

B LAD b 点钙化

C LAD c 点环形钙化 钙化厚度 1.43mm

D LAD d 点环形钙化 钙化厚度 1.37mm

E LAD 管腔长轴 Lumen 影像 钙化病变长度 18.1mm

根据指南和共识，FDA 批准的 Shockwave C2 冠状动脉 IVL 系统适应症严重钙化、狭窄的原发冠状动脉病变进行碎石和低压球囊扩张，采用 IVL 技术进行钙化治疗。

2. IVL 预处理： 使用 3.0×12mm Shockwave 震波球囊，IVL 治疗后，钙化环断裂，管腔显著扩大。（图）

图 5：3.0mm×12mm 振波球囊完全扩张

A：病变近端 IVL B：病变最狭窄处 IVL C：IVL 后造影

图 6：LAD 植入支架，Dia 主动拘禁球囊技术保护对角支

A：支架和球囊定位 B：支架和球囊同步扩张

图 7：非顺应性球囊行后扩张

A、支架及病变近端后扩 B：最狭窄处后扩

（四）手术结果

术后冠脉造影：

- 左冠状动脉前降支：LAD 近段支架通畅，无残余狭窄。（图 9）

图 8：2023 年 2 月左冠状动脉前降支术后造影

A：右头位 B：正头位

2. 术后腔内影像：

图 9：左冠状动脉前降支术后 OCT

A LAD 造影融合定位像

B LAD MSA 5.83mm²

C c 点钙化断裂

D d 点钙化断裂宽度及深度

E LAD 长轴 Lumen 像

（六）小结

1. 该患者前降支存在严重钙化病变，传统介入方法包括冠脉旋磨，IVL 技术较为简单，年轻医师容易掌握，为严重钙化病变提供了新的解决方案。

2. IVL 通过碎石机制，能够有效断裂钙化环，显著改善管腔面积，为后续支架植入创造条件。

3. IVL 治疗后，结合 OCT 评估，确保支架贴壁良好，无明显残余狭窄，手术效果满意。

4. IVL 技术在切割球囊和非顺应性球囊无法完全扩张的严重钙化病变中的应用，为复杂冠脉介入治疗提供了新的思路和方法。

鉴别诊断：

诊断：

1. 冠状动脉粥样硬化性心脏病

不稳定性心绞痛

窦性心律

心界不大

心功能 I 级 (NYHA 分级)

2. 高血压病 1 级 (极高危)

3. 高胆固醇血症

4.2 型糖尿病

5. 反流性食管炎

6. 低钾血症

其他：

酮症继发应激性心肌病

王一斐

北京清华长庚医院

患者基本信息：

64 岁女性

主述：

间断胸痛 4 年，再发 13 小时

现病史：

患者 4 年前无明显诱因发作持续心前区针扎样疼痛，放射至背部，伴恶心及呕吐胃内容物，因症状持续数小时不缓解就诊外院，心电图提示胸前导联 T 波倒置，查 cTnI 1.22ng/mL，急诊冠脉造影提示“LCX 50% 狭窄”，未干预，超声心动图提示左室各壁下 1/2 运动减低，予扩冠及冠心病二级预防治疗后患者症状缓解，治疗 1 月后复查超声心动图未见明显异常。后患者长期口服阿司匹林，自行停用氯吡格雷及阿托伐他汀，未再发作症状。13 小时前患者于休息时再次发作心前区针扎样疼痛，放射至背部，伴恶心及呕吐胃内容物，来诊。

既往病史：

患者 4 年前无明显诱因发作持续心前区针扎样疼痛，放射至背部，伴恶心及呕吐胃内容物，因症状持续数小时不缓解就诊外院，心电图提示胸前导联 T 波倒置，查 cTnI 1.22ng/mL，急诊冠脉造影提示“LCX 50% 狭窄”，未干预，超声心动图提示左室各壁下 1/2 运动减低，予扩冠及冠心病二级预防治疗后患者症状缓解，治疗 1 月后复查超声心动图未见明显异常。后患者长期口服阿司匹林，自行停用氯吡格雷及阿托伐他汀，未再发作症状。13 小时前患者于休息时再次发作心前区针扎样疼痛，放射至背部，伴恶心及呕吐胃内容物，来诊。

病程记录：

冠心病二级预防治疗及灭酮纠酸

检验检查记录：

冠脉造影：LAD：开口 - 中段 30-50% 弥漫性狭窄，远段可见约 20mm 冠脉肌桥，收缩期狭窄 70% ，TIMI-3 级；LCX：远段 50% 局限性狭窄，TIMI-3 级；RCA：近段及远段不规则病变，TIMI-3 级

尿常规：尿糖（++++），尿酮体（++）

鉴别诊断：

病毒性心肌炎

其他：

肥厚型心肌病诊断与鉴别诊断：一例纯合子女性 Fabry 心肌病诊疗过程的启示

王红

华中科技大学同济医学院附属同济医院

患者基本信息：

患者，谢某某，女性，49 岁，2024 年 3 月门诊首诊

主述：

胸闷、气促 2 年余

现病史：

现病史：胸闷、气促 2 年余，劳力明显，伴头晕、乏力，无黑矇、晕厥、肢体疼痛等，外院心脏超声提示“左室肥大”就诊我院

既往病史：

既往史及家族史：弟弟 CKD，30 岁血液透析；余无特殊

病程记录：

目前先证者及其弟弟已经开始酶学替代治疗，病情缓解或进展情况在严密随访过程中。

检验检查记录：

实验室检查提示患者心肌损伤标志物轻度增高，包括氨基末端脑钠肽前体（820.7pg/ml，正常值 < 241 pg/ml）和高敏心肌肌钙蛋白 I（21.6 pg/ml，正常值≤ 34.2pg/ml）；肾脏微量蛋白尿升高（24 小时尿微量总蛋白 292mg/24h，正常值≤ 140 mg/24h），肾功能正常。心电图提示短 PR 间期，左室高电压，下壁和侧壁导联 ST 段压低及 T 波倒置。

经胸超声心动图示，左室肥厚（室间隔 13mm，左室后壁 13mm，累及心尖部 12mm），前外侧乳头肌肥大，左房扩大（前后径 37mm）和二尖瓣轻至中度关闭不全，左室射血分数 67%。心脏磁共振检查提示左室非对称肥厚，累及心尖段及前组乳头肌，并且肥厚心肌局灶性纤维化，及左室心尖段心腔收缩期闭塞，Mapping 序列上左室心肌初始 T1 值轻度升高。

由于患者心电图表现，包括短 PR 间期以及下壁和侧壁导联 ST 段显著压低，符合 Fabry 病心电图表现，我们对患者进一步做了基因检测和干血纸片法测 a- 半乳糖苷酶（a-galactosidase A，α-Gal A）活性及脱乙酰基三己酰基鞘脂醇（globotriaosylsphingosine，Lyso-GL-3）浓度。结果提示患者 α-Gal A 活性正常值偏低水平（4.14umol/L/h，正常范围为 2.2-17.65 umol/L/h），而 Lyso-GL-3 轻度升高（7.91ng/ml，正常范围 < 1.11 ng/ml）。全外显子基因检测证实为 GLA 纯合大片段缺失变异，为疑似致病突变（ACMG 标准）；同步检出 MYLK2 基因杂合突变（错义突变，c.1691G > A），为意义未明确突变（ACMG 标准），考虑与患者表型无关。

我们随后对患者家系进行了分析并构建了本例 Fabry 病家系图（图 4B）。先证者（患者）母亲已经去世，先证者弟弟（半合子）、侄女（杂合子）和女儿（杂合子）携带与先证者一致的 GLA 大片段缺失变异，先证者父亲、儿子和 2 个侄子则未检出。先证者弟弟 α-Gal A 显著减低（0.48 umol/L/h），Lyso-GL-3 明显升高（72.70 ng/ml）；女儿 α-Gal A 正常偏低水平（2.27 umol/L/h），Lyso-GL-3 轻度升高（1.14 ng/ml）；侄女 α-Gal A 减低（1.41 umol/L/h），Lyso-GL-3 轻度升高（3.49 ng/ml），符合半合子和杂合子酶学表现

鉴别诊断：

法布雷病是一种罕见的由 GLA 基因突变导致的溶酶体贮积性遗传病。由于 GLA 基因突变致酶活性降低或缺失其代谢底物如三己糖酰基鞘脂醇（Gb3）在组织中贮积导致多脏器受损，其中心肌受损多表现为左心室肥厚（Left ventricular hypertrophy，LVH）。以左心室肥厚为表现的心肌病包括了一系列遗传、代谢或系统性疾病，其中肥厚性心肌病（Hypertrophic cardiomyopathy，HCM）为最常见的临床表型 [5]。根据指南 HCM 由于编码肌小节相关蛋白基因致病性变异导致的、或病因不明的以心肌肥厚为特征的心肌病，且需排除其他的心血管疾病或全身性、代谢性疾病引起的心室壁增厚 。HCM 的特征性超声心动图表现包括非对称的室间隔肥大和二尖瓣收缩期前运动，左心室基底段下外侧区纵向应变减少，不同于 Fabay 心肌病超声心动图表现如向心性 LVH、乳头肌肥大、“双边”现象、基底下外侧区纵向应变减少等；HCM 心脏磁共振初始 T1 值增高，而 FD 患者通常表现为初始 T1 值减低。因此在临床中考虑诊断为“肥厚型心肌病”的高危人群患者，其肥厚状态均匀型需警惕 Fabry 心肌病，但对于心脏影像学均不典型的 Fabry 心肌病患者，在诊断需要结合仔细的临床评估、家族史询问、心电图表现等多方面的考量，否则可能会被遗漏或误诊。

其他：

一例顽固性低钾患者的诊治体会

刘建根

吉林大学第二医院

患者基本信息：

患者为 50 岁中年女性，否认抽烟史及嗜酒史。母亲高血压病病史。

主述：

因发作性心悸 3 年，加重 1 个月入院

现病史：

患者缘于 3 年前无明显诱因出现心悸，无胸痛，无胸闷、气短，无头晕、乏力，无大汗，无恶心及呕吐，无意识丧失，与活动无明显相关性，自行口服药物（速效救心丸、丹参滴丸等）后效果不佳。1 个月前患者再次出现心悸，伴明显乏力，无胸痛，无胸闷、气短，无头晕，无大汗，无恶心及呕吐，无意识丧失，与劳累、情绪激动等不相关，上述症状反复发作，为求进一步诊治，遂就诊于我院。

既往病史：

发现血压升高 3 年，血压最高达 160/100mmHg，现规律口服替米沙坦、硝苯地平控释片及美托洛尔缓释片控制血压，血压控制欠佳：血压波动在 130-160/90-100mmHg 之间；糖尿病病史 4 年，现口服达格列净联合皮下注射聚乙二醇洛塞那肽注射液控制血糖，血糖控制尚可。

病程记录：

患者在治疗上给予了以下措施：患者高血压病 2 级：硝苯地平控释片 30mg 日一次 口服；替米沙坦由原来的 40mg 日一次 口服，增至 80mg 日一次 口服；美托洛尔缓释片 47.5mg 日一次 口服；患者 2 型糖尿病：监测血糖、继续目前降糖治疗；冠状动脉粥样硬化：给予阿托伐他汀抗动脉粥样硬化治疗；患者酮症考虑为营养性酮症：适当增加碳水摄入、补液（氯化钠）；电解质紊乱：给予补钾治疗（0.9% 氯化钠 250ml+10% 氯化钾 7.5ml）。

给予患者补液治疗后，患者血钾反而进一步出现了下降，血钾由原来的 3.48mmol/L 降至 3.31mmol/L。此时考虑可能是原发性醛固酮增多症？给予患者加服螺内酯 40mg 日一次 口服。因此我们给该患行肾上腺 CT 检查及激素五项（立卧位）检查。肾上腺 CT 未见肾上腺由异常改变。但是高血压五项（立位）提示：醛固酮（56.80pg/ml）和肾素（3.35pg/ml）均下降。高血压五项（卧位）提示：醛固酮及肾素均未见异常，但是血管紧张素（II）轻度升高。因此可以除外原发性醛固酮增多症的可能。

检验检查记录：

入院心电图：窦性心律，HR 96bpm，QT/QTc 360/454ms，大致正常心电图。

入院心脏彩超: LV39mm, EF60%, LA34mm, RV19mm, FS30%。主动脉瓣钙化，左室舒张功能减退。

冠脉成像 CT：冠脉成像 CT 未见冠状动脉存在中重度狭窄。

入院化验检查：CTnI 及 NT-Pro BNP 未见异常。

血常规: RBC 5.96×10^9/L，HGB 165g/L。血生化: UA416umol/L，K^+ 3.48mmol/L。尿常规：尿酮体 3+。空腹血糖 9.67mmol/L。

鉴别诊断：

醛固酮增多症可基本除外，那么还可能是什么疾病引起患者顽固性低血钾呢？患者给予补液后持续血钾下降，入院第 3 日至第 5 日血钾持续下降（2.80mmol/L，2.83mmol/L，2.77mmol/L）。

对病例特点进行总结。

1．中年女性，高血压病病史及糖尿病病史

2. 营养性酮症

3. 冠状动脉粥样硬化

4. 低钾血症：补液后反而血钾持续下降。

整体分析：

低血钾的原因包括：排出过多，摄入过少，分布异常。常见的钾排出过多原因有：消化道丢失、肾脏丢失和皮肤丢失；摄入过少的原因主要是长期饮食缺乏；分布异常主要是钾向细胞内转移。而此患者虽然平时低碳饮食，但蔬菜等相应的食物摄入并不少，因此可以基本除外摄入过少的可能；患者无腹泻和呕吐的相关病史，因此可除外消化道丢失的可能；患者日常和近期无过度出汗，因此可除外皮肤丢失的可能；因此，考虑可能肾脏丢失或皮肤丢失的可能性大。低钾血症时，钾的分布异常常常见于代谢性碱中毒时，细胞外的钾离子转移细胞中。因此我们给患者行血气分析检查，提示：pH：7.53，K+3.1mmol/L，HCO3-29.5mmol/L，HCO3std30.7mmol/L，cBase（B）6.9mmol/L，cBase（Ecf）6.4mmol/L；以上改变提示患者有代谢性碱中毒，但是患者并无可以引起代谢性碱中毒的病因，而且代谢性碱中毒可能是由低钾引起的，是果而非因。

鉴别诊断：

首先我们根据可能引起钾丢失的病因逐一分析。1、**利尿剂使用（袢利尿剂、噻嗪类），患者并无此类药物使用的病史，因此可基本除外；2、呕吐或胃液引流、腹泻，患者并无相关症状，可除外；3、原发性醛固酮增多症，结合患者肾上腺影像改变及激素改变，可除外此疾病；4、先天性肾上腺皮质增生症（CAH），往往伴随有性征的改变，而且多以青年起病，因此可基本除外。5、库欣综合征，患者无相关症状及体征，可基本除外; 6、Bartter 综合征，Bartter 综合征（Bartter syndrome，BS） 是一种罕见的遗传性肾小管疾病， 由编码或调控肾小管髓袢升支粗段和远曲小管的相关转运蛋白基因变异所致， 主要表现为盐重吸收障碍，其临床特点主要为继发性醛固酮增多症伴低血钾、低氯性代谢性碱中毒、血压正常或偏低，而且多以幼儿起病，因此可基本除外本病；7、Gitelman 综合征，是一种罕见的遗传性肾小管疾病，其临床特点主要为低钾血症、代谢性碱中毒、低镁血症、低钙尿症。临床诊断需要满足以下标准：(1) 根据患者病史排除消化道钾摄入不足或腹泻、使用利尿剂、细胞内外钾分布异常等情况；(2) 存在肾性失钾及低钾血症相关临床表现，可伴有低镁血症或低钙尿症。肾性失钾：血清钾 < 3. 0 mmol /L 时，尿钾排泄量 > 20 mmol /24 h; 或血清；钾 < 3. 5 mmol /L 时，尿钾排泄量 > 25 mmol /24 h；(3) 血压正常或偏低；(4) 代谢性碱中毒；因此该患发病症状、体征及辅助检查，与本病并不相符。8、Liddle 综合征：Liddle 综合征又称假性醛固酮增多症，是 1963 年 Liddle 等首先报告，故称为 Liddle 综合征。该病是由于肾小管上皮细胞钠通道基因突变，导致钠重吸收增加，尿钾增多，从而导致一些列的病理生理变化。本病的特征是：严重的高血压、低钾血症、代谢性碱中毒、低肾素血症。临床症状与醛固酮增多症相似，但是醛固酮分泌率很低，对螺内酯治疗无反应，对氨苯蝶啶或限盐治疗有效。结合本患者的特点，考虑患者该诊断的可能性大。**

其他：

一例以急性胸痛为表现的儿茶酚胺型心肌病的诊断和治疗带给我们的启示

刘建根

吉林大学第二医院

患者基本信息：

39 岁，青年女性，因心前区疼痛 30 分钟急诊入院，入院后患者呼吸困难持续加

重，并出现了心源性休克。

主述：

因心前区疼痛 30 分钟急诊入院

现病史：

患者缘于半小时前如厕后突然出现心前区疼痛，伴胸闷，无放散，无呼吸困难，伴头晕，伴大汗，伴恶心及呕吐，无头痛，无黑蒙及晕厥，上述症状持续不缓解，遂就诊于我院急诊。入院查体：血压 102/70mmHg, BMI：22.8Kg/m2 （体重 62Kg，身高 165cm），神清语明，平卧位，颈静脉未见怒张和异常波动，双肺呼吸音弱，双肺底可闻及湿罗音，心率 104 次 / 分，节律规整，未闻及心杂音，未闻及额外心音，未闻及心包摩擦音。

既往病史：

体健。

病程记录：

入院后给予急检心电图（图 1A）提示：I/AVL 导联 ST 段抬高（小于 0.1mv）,V4、V5、V6 导联可见 ST 段压低，T 波低平），急检高敏肌钙蛋白 0.269ng/ml 急检高敏肌钙蛋白 0.269ng/ml ↑ (0-0.08)，肌红蛋白 174.49ng/ml ↑ (0-70)，D- 二聚体 3.39mg/L ↑ (0-0.95)，考虑为急性非 ST 段抬高型急性心肌梗死，GRACE 评分 128 分，为中危风险，对患者行冠脉造影检查，可见前降支近段第一对角支开口下可见约 20-30% 狭窄，回旋支和右冠状动脉未见明显狭窄（图 2 A、B、C、D）。因此造影结果无法解释患者的症状和体征。

患者造影返回后出现呼吸困难，血压、血氧出现下降，查体：勉强平卧，患者血压 86/50mmHg，双肺可闻及水泡音，以左侧为著，心率 106 次 / 分，节律规整，未闻及心杂音。血气分析 $PO_2$60mmHg。因为患者之前 D- 二聚体升高，因此不能除外急性肺栓塞的可能，因此行肺动脉 CTA 检查，但肺动脉 CTA 检查未见肺动脉有充盈缺损和狭窄，因此可除外肺栓塞的可能。

造影返回后血常规结果回报：WBC 23.1X10^9/L，中性粒细胞百分比 87.7%，因此行胸 CT 检查，肺 CT 检查见肺间质改变，符合肺水肿的影像学变化，且患者无发热，不符合重症肺炎的表现，因此可除外感染性休克；行床头心脏彩超检查，可见射血分数 46%，左室侧壁运动减弱；继续给予患者吸氧、正压通气、多巴胺、去甲肾上腺素等支持治疗，同时 ECMO 及 IABP 备用。

次日患者临床症状在此恶化，复查肌红蛋白 53.98ng/ml (0-70)，hsTnI 1.357ng/ml ↑ (0-0.08)，NT-proBNP 7290ng/ml ↑ (0-450)，D 二聚体 0.96mg/L ↑ (0-0.95)，查床头心脏彩超可见射血分数 36%，室壁搏动减弱，以左室为著。考虑患者是不是存在爆发性心肌炎的可能，但是详细追问病史，患者否认发热、感冒、腹泻等前驱症状，同时患者肌钙蛋白升高水平不符合爆发性心肌炎的演进，同时复查心电图可以看到心电图 I/AVL 导联 ST 段已回落至基线水平 ,V4、V5、V6 导联 ST 段及 T 波也恢复至正常；心电图亦不符合爆发性心肌炎的演进，因此可以排除爆发性心肌炎的诊断。

追问患者病史时，患者自述 2 年前曾因肺部感染住院，症状表现和此次入院基本相似，都是心前区疼痛之后出现头晕、恶心等症状，症状发作前有体位变化（坐位改为立位）时突然出现上述症状。取得两年前患者入院时肺 CT 影像，发现影像表现和此次入院时肺 CT 改变基本相似，但是肺水肿程度较此次轻。调出患者肺 CT 纵隔窗，发现两次患者入院肺 CT 纵隔窗可见左肾上限有一大小约为 34X28mm 的良性肿物，考虑嗜铬细胞瘤可能性大。急检了肾上腺素和去甲肾上腺素未见异常。醛固酮 / 肾素 8.44、皮质醇（7 点 -9 点）6.695ug/dl、血管紧张素卧位 101.936pg/ml、促肾上腺皮质激素（7-9 点）29.433pg/ml、醛固酮卧位 90.165pg/ml、肾素卧位 10.678pg/ml。上述指标均在正常值范围内。行肾上腺 CT 平扫加增强可见：左侧肾上腺可见团块状软组织密度影，大小约 37mmX29mm，CT 值约为 50HU，增强扫描呈明显不均匀强化，考虑嗜铬细胞瘤可能性大。

患者入院 14 小时后，症状逐渐缓解，根据血压多巴胺、去甲肾上腺素交替减量，患者于 7 日后复查心彩超射血分数 69%，心室搏动未见异常，复查肺 CT 未见异常。

出院前给予患者 α 受体阻滞剂口服，在充分的术前准备后，患者行腹腔镜下左侧肾上腺摘除术，病理标本灰黄灰褐组织一堆，直径 5cm，切面灰褐质嫩（图 6 A）。常规光镜下可见：肿瘤细胞呈巢状、腺样排列，外周有富含血管的纤维组织和薄壁血窦分隔。瘤细胞呈多角形，胞质丰富，颗粒状，呈双嗜性。大的肿瘤细胞可见核仁，胞质空泡状。肿瘤细胞核圆形或卵圆形，核分裂罕见（图 6 B）。免疫组化结果：VI:CK(AE1/AE3)(-)、CgA（+）、Syn（+）、CD56（+）、INSM1（+）、Ki67（阳性率 3%）、S-100（部分 +）、SF-1（-）、GATA3（+）、SSTR2（+）、Rb（+）、SDHB（+）、MelanA（-）、延胡索酸水合酶（FH）(+)、calretinin（-）、α-inhibin（-）、P53（个别 +）、CK8/18（-）、WT1（-）、D2-40（-）、CD34（血管 +）。结合免疫组化及形态学结果支持嗜铬细胞瘤的诊断。

因此患者最终诊断为：嗜铬细胞瘤、嗜铬细胞瘤危象、儿茶酚胺型心肌病、心源性休克。术后 6 个月后患者随访，心彩超未见异常，心前区疼痛及头晕等症状未有发作，复查肾上腺 CT 呈左侧肾上腺摘除术后表现。该患者通过及时的手术治疗，避免了儿茶酚胺型心肌病的在此发作，避免了心血管事件的风险。

检验检查记录：

入院后给予急检心电图（图 1A）提示：I/AVL 导联 ST 段抬高（小于 0.1mv）,V4、V5、V6 导联可见 ST 段压低，T 波低平），急检高敏肌钙蛋白 0.269ng/ml 急检高敏肌钙蛋白 0.269ng/ml ↑ (0-0.08)，肌红蛋白 174.49ng/ml ↑ (0-70)，D- 二聚体 3.39mg/L ↑ (0-0.95)，考虑为急性非 ST 段抬高型急性心肌梗死，GRACE 评分 128 分，为中危风险，对患者行冠脉造影检查，可见前降支近段第一对角支开口下可见约 20-30% 狭窄，回旋支和右冠状动脉未见明显狭窄（图 2 A、B、C、D）。因此造影结果无法解释患者的症状和体征。肺动脉 CTA 检查未见肺动脉有充盈缺损和狭窄。行胸 CT 检查，肺 CT 检查见肺间质改变 (图 4 A)，符合肺水肿的影像学变化，且患者无发热，不符合重症肺炎的表现，因此可除外感染性休克；行床头心脏彩超检查，可见射血分数 46%，左室侧壁运动减弱。复查肌红蛋白 53.98ng/ml (0-70)，hsTnI 1.357ng/ml ↑ (0-0.08)，NT-proBNP 7290ng/ml ↑ (0-450)，D 二聚体 0.96mg/L ↑ (0-0.95)，床旁心脏彩超射血分数 36%，室壁搏动减弱，以左室为著。复查心电图可以看到心电图 I/AVL 导联 ST 段已回落至基线水平 ,V4、V5、V6 导联 ST 段及 T 波也恢复至正常。行肾上腺 CT 平扫加增强可见：左侧肾上腺可见团块状软组织密度影，大小约 37mmX29mm，CT 值约为 50HU，增强扫描呈明显不均匀强化，考虑嗜铬细胞瘤可能性大。患者于 7 日后复查心彩超射血分数 69%，心室搏动未见异常，复查肺 CT 未见异常（图 4 C）。出院前给予患者 α 受体阻滞剂口服，在充分的术前准备后，患者行腹腔镜下左侧肾上腺摘除术，病理标本灰黄灰褐组织一堆，直径 5cm，切面灰褐质嫩（图 6 A）。常规光镜下可见：肿瘤细胞呈巢状、腺样排列，外周有富含血管的纤维组织和薄壁血窦分隔。瘤细胞呈多角形，胞质丰富，颗粒状，呈双嗜性。大的肿瘤细胞可见核仁，胞质空泡状。肿瘤细胞核圆形或卵圆形，核分裂罕见（图 6 B）。免疫组化结果：VI:CK(AE1/AE3)(-)、CgA（+）、Syn（+）、CD56（+）、INSM1（+）、Ki67（阳性率 3%）、S-100（部分 +）、SF-1（-）、GATA3（+）、SSTR2（+）、Rb（+）、SDHB（+）、MelanA（-）、延胡索酸水合酶（FH）(+)、calretinin（-）、α-inhibin（-）、P53（个别 +）、CK8/18（-）、WT1（-）、D2-40（-）、CD34（血管 +）。结合免疫组化及形态学结果支持嗜铬细胞瘤的诊断。

鉴别诊断：

因此患者最终诊断为：嗜铬细胞瘤、嗜铬细胞瘤危象、儿茶酚胺型心肌病、心源性休克。

根据冠状动脉造影结果除外了急性心肌梗死。

根据肺动脉 CTA 结果除外了急性肺栓塞。

根据心电图和心肌酶学演变过程，除外了爆发性心肌炎。

详细过程见上述检查资料。

其他：

PADN 在 LHF-PH 患者中应用经验分享

刘建根

吉林大学第二医院

患者基本信息：

年龄： 38 岁；性别：男；身高：175cm； 体重：约 100 kg； BMI:32.65kg/m2

主述：

阵发性胸闷气短 2 年余

现病史：

患者缘于 2 年前无明显诱因突然出现心前区疼痛症状，呈闷痛，放散至后背及双臂，伴大汗，就诊于我院行心电图检查示“急性心肌梗死”，行冠脉造影，冠脉植入 4 个支架，术后发生急性心衰，经系统治疗，病情好转出院。伺候上述症状间断出现，伴胸闷气短，劳累活动时加重，休息后好转，规律口服药物治疗。今日上述症状逐渐加重，伴有头晕，周身无力，双下肢水肿，无呼吸困难，喘，无咳嗽、咳痰、咳粉红色泡沫样痰，时有腹胀症状，现为进一步诊治来到我院，门诊以“慢性心力衰竭”收入院。

入院查体: T:36.6℃, P:80 次 / 分, R: 次 / 分, BP:119/78mmHg, 双肺呼吸音清，双肺未闻及明显干湿罗音，未闻及胸膜摩擦音。心前区无隆起，未见心前区异常搏动。心尖搏动位于左测第五肋间锁骨中线外 0.5 厘米，无抬举性心尖搏动，未触及震颤。叩诊心相对浊音界稍向左下扩大，心率 80 次 / 分，节律规整，心音不弱，A2<P2，各瓣膜听诊区未闻及杂音及额外心音，未闻及心包摩擦音。双下肢无水肿。

既往病史：

否认高血压史，否认糖尿病史，否认冠心病史，无输血史，无药物、食物过敏史，预防接种史不详，无手术外伤史。。

病程记录：

患者入院后查 • 肝肾功能无异常；• 血常规：WBC:8.1*10^9，RBC: 5.03*10^12，HGB: 146 g/L, PLT: 317*10^9; •Nt-proBNP: 180pg/ml; • 凝血功能: 无异常; • 自身抗体阴性；心电图提示：窦性心律 / 不正常心电图 / 偶发室性前期收缩 / 下壁、广泛前壁心肌梗塞 / 左心房异常。心脏彩超提示：全心增大，全心功能减退，室壁运动节段异常，肺动脉高压轻度。行右心导管检查: 混合型毛细血管后肺高压。

患者入院后给与心力衰竭的 GDMT 治疗，并行 PADN 治疗。

检验检查记录：

患者入院后查 • 肝肾功能无异常；• 血常规：WBC:8.1*10^9，RBC: 5.03*10^12，HGB: 146 g/L, PLT: 317*10^9; •Nt-proBNP: 180pg/ml; • 凝血功能: 无异常; • 自身抗体阴性；心电图提示：窦性心律 / 不正常心电图 / 偶发室性前期收缩 / 下壁、广泛前壁心肌梗塞 / 左心房异常。心脏彩超提示：全心增大，全心功能减退，室壁运动节段异常，肺动脉高压轻度。行右心导管检查: 混合型毛细血管后肺高压。

鉴别诊断：

冠状动脉粥样硬化性心脏病

陈旧性下壁、前壁心肌梗死

心律失常 - 偶发室性期前收缩

心功能 II 级

肺高压（左心相关）

其他：

一共两个病例，但是只能展示一个，详情请参考 PPT。

肥厚梗阻合并房颤透析患者的新希望 -Micra 植入一例

熊雁

四川省人民医院

患者基本信息：

男，47 岁，入院查体：T 36.5℃，P 88bpm，R 20 次 / 分 BP 113/72mmHg，贫血貌，双肺未闻及明显干湿啰音，心律齐，心率 88 次 / 分，胸骨左缘可闻及杂音，双下肢无水肿。

主述：

肾移植术后 10+ 年，腹膜透析管出口处红肿 20+ 天

现病史：

肾内科现病史：10+ 年前查肌酐升高至 800+umol/L，行肾移植后多次复查肌酐仍明显升高，移植术后 2 月取出移植肾，开始血液透析，9 年前内瘘闭塞，开始行规律腹膜透析，后透析效果欠佳，行右肘窝动静脉内瘘术，后续行血液透析联合腹膜透析。20+ 天前腹膜透析管出口处出现红肿伴疼痛，伴发热，体温最高 38℃，为进一步诊治收治入院。

既往病史：

有“高血压”病史 7+ 年，血压最高达 180/ ？ mmHg，未规律服用降压药，自诉透析后血压偏低，未再服用降压药。长期房颤病史，未规范诊治。

病程记录：

入院后反复发作快心室率心房颤动，心室率 130-160bpm，发作期间出现持续低血压状态，65-78/40-46mmHg 左右，伴胸闷、气促、乏力，被迫终止血液透析。先后予以多巴胺、间羟胺维持血压，请心内科会诊后换用去甲肾上腺素升压，胺碘酮控制心率，但使用胺碘酮过程出现持续数分钟的窦缓（30-40 次 / 分），后安置临时起搏器 + 抗心律失常药物治疗，症状有所缓解。但使用胺碘酮过程中出现肝功能衰竭，被迫减量后快心室率房颤再次发作，病情加重。与患者充分沟通后，患方选择房室结消 7 融 + 永久起搏器（Micra AV）植入，手术后病情好转，规律腹透 + 血液透析出院。出院后 7 月门诊随访病情稳定，起搏器参数良好，复查心超提示梗阻消失。

检验检查记录：

入院心电图：窦性心律，心率 100bpm，入院心超：IVS 20mm 室间隔最厚 25mm，LA 52mm LVPW 14mmSAM（+）EF 0.76 入院检验：血常规：WBC 1.28*109/L、NEU 0.07 *109/L、 Hb 90g/L、 K 3.73mmol/L、Alb 28g/L、BNP：3143pg/mL；甲功：FT3 2.4pmol/L TSH 正常；心肌酶：TPI 296ng/L MYO 132ng/mL PCT：1.35ng/L

鉴别诊断：

无

其他：

我院肾内科住院患者，长期腹膜透析（不充分）+ 血液透析

Transcatheter Edge-to-Edge Repair for Tricuspid Regurgitation in Barlow-Type Tricuspid Valve Prolapse Using the DragonFly-T System

任凯达

浙江大学医学院附属第二医院

患者基本信息：

A 71-year-old female was admitted with chief complaints of chest tightness, dyspnea, and severe tricuspid regurgitation (TR) despite optimal medical treatment and was currently classified as New York Heart Association (NYHA) class II. Her medical history included primary hypertension, carotid artery plaques, lower extremity atherosclerosis, a left renal cyst, deep vein thrombosis of the lower limbs, and sleep disorders. In this case, the physical examination revealed a grade II/III holosystolic murmur auscultated along the left sternal border at the 4th and 5th intercostal spaces, with palpable lower limb edema. Transthoracic echocardiography (TTE) revealed massive TR, with bulging and prolapse of the tricuspid valve leaflets into the right atrium.

主述：

chest tightness, dyspnea, and severe tricuspid regurgitation (TR) despite optimal medical treatment

现病史：

Her medical history included primary hypertension, carotid artery plaques, lower extremity atherosclerosis, a left renal cyst, deep vein thrombosis of the lower limbs, and sleep disorders. In this case, the physical examination revealed a grade II/III holosystolic murmur auscultated along the left sternal border at the 4th and 5th intercostal spaces, with palpable lower limb edema. Transthoracic echocardiography (TTE) revealed massive TR, with bulging and prolapse of the tricuspid valve leaflets into the right atrium.

既往病史：

The patient was diagnosed with TR during a routine physical examination 10 years ago, but it was not addressed, and no treatment was initiated. Over the past year, the patient has experienced progressively increasing frequency of chest tightness and dyspnea.

病程记录：

Transesophageal echocardiography (TEE) revealed barlow-type prolapse, redundancy, and hooding of the tricuspid valve leaflets, particularly the septal leaflet (Video 1 and Figure 1A-F). The TR grade is 4+, with an effective regurgitant orifice area (EROA) of approximately 0.69 cm^2 and a regurgitant volume (RV) of 71 ml. The left ventricular wall thickness, motion, and ejection function are normal. Additionally, there was trace regurgitation of the mitral and pulmonary valves, as well as mild aortic regurgitation. Right heart catheterization (RHC) revealed a pulmonary capillary wedge pressure (PCWP) of 8 mmHg, mean pulmonary artery pressure (mPAP) of 19 mmHg, right ventricular pressure of 14 mmHg, and right atrial pressure of 7 mmHg. The cardiac output, calculated using the Fick method, was 4.7 L/min, with a pulmonary vascular resistance (PVR) of 2.34 Woods units

检验检查记录：

After admission, the patient was treated with antihypertensive, antiplatelet, and lipid-lowering therapies. Medication treatment (e.g., diuretics) was administered for TR, and while it could alleviate the patient's symptoms to some extent, it could not fundamentally relieve the chest tightness and dyspnea or effectively address the prolapsing valve leaflets. Considering the patient's advanced age and multiple comorbidities, the patient was deemed to be at high risk for undergoing isolated tricuspid valve surgery. The tricuspid valve anatomy was jointly evaluated by the multidisciplinary heart team and discussed with the patient, who decided to opt for tricuspid transcatheter edge-to-edge repair (T-TEER).

The DragonFly-T Transcatheter Tricuspid Valve Clip System (Valgen Medthch, Hangzhou, China) was selected for the T-TEER procedure. Under the guidance of DSA and ultrasound, XW0612 clip (clip width 6 mm, clip arm length 12 mm) was delivered through the femoral vein and inferior vena cava into the right atrium and then into the right ventricle, where it grasped the most pronounced prolapsing area between the anterior and septal leaflets, near the central portion of the leaflets (Video 2). After deployment, the anteroseptal regurgitation significantly decreased, with only residual regurgitation from the posteroseptal region. To address the residual posteroseptal regurgitation, a SW0609 clip (clip width 6mm, clip arm length 9mm) was selected. However, it was found that the clip arm length was insufficient to grasp the leaflets, and to avoid interaction with the first clip, the decision was made to switch to an XN0412 clip (clip width 4mm, clip arm length 12mm), which was applied in the central posteroseptal region. After deployment, the regurgitation decreased to less than 1+ (Video 3 and Figure 2A-B), and the tricuspid annulus significantly reduced in size (Figure 2C-D). The postoperative mean transvalvular gradient across the tricuspid valve was 2 mmHg, with no significant stenosis.

Afterward, the guide sheath and valve clip system were removed. The total device time was 167 minutes, the procedural time was 176 minutes, and the fluoroscopy time was 49 minutes. The procedure was successful, with the patient's symptoms relieved and no device-related complications. The patient was discharged on postoperative day 4. A pre-discharge TTE confirmed stable device placement and sustained reduction of TR.

鉴别诊断：

Rheumatic heart valve disease predominantly occurs in younger patients, who often present with symptoms such as fever, diaphoresis, and abdominal pain, along with a history of rheumatic fever, and echocardiography commonly demonstrates the presence of vegetations. Degenerative calcific heart valve disease is more common in elderly individuals, with echocardiography showing calcific lesions of the valve. In cases of congenital anomalies, auscultation may reveal vascular murmurs beneath the right clavicle, with an absence of significant ejection murmurs at the apex. Echocardiography is helpful for differential diagnosis. Considering the patient's medical history, along with the current physical examination and echocardiographic findings, there is a strong suggestion of the possibility of TR. Barlow's Disease typically affects the mitral valve, and in some cases, patients with mitral valve Barlow's disease may also exhibit similar prolapse of the tricuspid valve. However, in this patient, no significant billowing or prolapse of the mitral valve leaflets

was observed, with only trace mitral regurgitation noted , and no further diagnostic evidence suggests that the patient has Barlow's disease.

其他：

无

限制样拟表型的左心室肥厚病因何在？

宋显晶

吉林大学第二医院 (白求恩第二医院)

患者基本信息：

王某，男，67 岁

主述：

间断性胸闷气短伴双下肢水肿 10 年，加重 3 天

现病史：

10 年前活动后出现胸闷气短，伴有双下肢轻度水肿，休息后症状可减轻，无心前区疼痛，无恶心、呕吐，无晕厥及黑朦，未系统诊治。此后上述症状间断发作，性质同前，日常活动轻度受限，并逐渐加重。8 年前曾就诊于当地医院，给予心电图检查提示心房颤动，诊断为“冠心病、心衰”，给予“拜阿斯匹灵、美托洛尔、呋塞米、螺内酯“口服，症状可改善，但 活动耐力明显下降，稍活动即出现胸闷气短症状，双下肢水肿进行性加重。3 天前上述症状明显，静息下即出现胸闷气短症状，伴恶心、腹胀、头晕，无黑朦，无无呕吐，双下肢高度浮肿，故就诊于我院。门诊以“心力衰竭” 收入院。病程中，无晕厥，无发热，无咳嗽咳痰，无肢体活动及感觉障碍，进食差，睡眠尚可，尿少，24 小时尿量约 800ml，大便正常。

既往病史：

否认高血压病及糖尿病史，无吸烟及饮酒史，否认家族遗传性疾病病史

病程记录：

查 体：生命体征：T：36 ℃；P： 67 次 / 分；R： 18 次 / 分；BP：110/70 mmHg

颈静脉怒张，双肺呼吸音粗 ，两肺底可闻及湿罗音，心脏浊音正常，心率： 72 次 / 分，节律绝对不规整，第一心音强弱不等，P2>A2，各瓣膜听诊区未闻及杂音，无心包摩擦音，腹软，无压痛及反跳痛，无肌紧张，肝脏增大，剑突下 1cm ，双下肢高度浮肿，皮温皮色正常。

心电图：心肌损伤标志物：**hs-cTNI：1.1ng/ml（0-0.08）；NT-proBNP：4307.0ng/ml（0-1800）；**

血常规：血小板：94x10^9/L（125-350）x10^9/L

总胆红素：57.8umol/L（0.00-23.0）umol/l

直接胆红素：14.3ummol/l（0.00-8.0umol/l

尿蛋白：1+（阴性）

心电图：异位心律，心房颤动，II、III、AVF 呈 qS 型，V1-V4 导联 R 波递增不良，肢体导联低电压

心脏超声：主要描述：左室壁增厚，最厚处左室前壁心尖段约 19mm，静息下左室腔中部最大血流速度为 380cm/s，最大压力阶差：52mmHg；心脏超声结果提示：梗阻性肥厚型心肌病（左室腔中部），右心左房增大，左室舒张功能减退，升主动脉增宽，主动脉瓣钙化，主肺动脉增宽，肺动脉压增高（中度），三尖瓣重度返流，二尖瓣中度返流，主动脉瓣轻度返流，心包少等量积液。

电话随访：患者剧烈运动后仍感明显胸闷气短症状，乏力，无心悸，无黑朦，间断腹胀，日常活动受限。双下肢水肿（根据水肿情况自行调用利尿剂及口服补钾）

心肌损伤标志物：**hs-cTNI：1.4ng/ml（0-0.08）；NT-proBNP：4760.40ng/ml（0-1800）；**

血常规：血小板：90x10^9/L（125-350）x10^9/L

总胆红素：36.8umol/L（0.00-23.0）umol/l

直接胆红素：12.3ummol/l（0.00-8.0umol/l

尿蛋白：1+（阴性）

肾功、血糖、血脂、免疫常规、甲功三项、凝血功能、便常规：未见异常。

心电图：异位心律，心房颤动，II、III、AVF 呈 qS 型，V1-V4 导联 R 波递增不良，肢体导联低电压

心脏超声：主要描述：左室壁增厚，最厚处左室前壁心尖段约 18mm，静息下左室腔中部最大血流速度为 386cm/s，最大压力阶差：59mmHg；心肌整体纵向应变率减低，呈心尖保留征；心脏超声结果提示：梗阻性肥厚型心肌病（左室腔中部），右心左房增大，左室舒张功能减退，升主动脉增宽，主动脉瓣钙化，主肺动脉增宽，肺动脉压增高（中度），三尖瓣重度返流，二尖瓣中度返流，主动脉瓣轻度返流，心包中等量积液。

心脏核磁：双心房增大，右心室增大，室间隔心肌局部增厚，搏动减弱，伴左心室心肌及心内膜下心肌纤维化，考虑肥厚型心肌病，部分心内膜下强化，不除外合并遗传代谢性疾病，请结合基因检测，心包积液。

冠状动脉 CTA：左前降支中段 20-30% 狭窄，右冠脉近段：40-50% 狭窄，余冠脉显影清醒，未见狭窄。

心内膜心肌活检：1. 右室室间隔组织送心肌组织，心肌细胞肥大，心肌排列紊乱，部分细胞内可见脂褐色沉积，细胞核有退行性改变，核不规则，深染，部分细胞核增大，心肌间质及血管周围纤维组织增生，血管壁增厚，请结合临床；2. 特殊染色结果：刚果红染色（-），Masson 染色：（+）。

心肌病基因检测（金域检测公司）：

MYBPC3 Chr11：47364461 NM-000256.3：c1377delcp.leu460Trpfs*6 杂合致病突变

MYH6 Chr14：23854138 NM-002471.4:c.5276A>c(p.lys1759Thr) 杂 合 致病突变

法布雷疾病酶学检查：α 半乳糖苷酶 A（α-Gal A）活性检测：103.46nmol/l（参考值：>24.70）

检验检查记录：

入院前主要治疗方案：

1. 拜阿司匹灵 100mg qd，美托洛尔：23.75mg qd，阿托伐他汀：20mg qd，呋塞米 20mg qd，螺内酯 20mg qd

明确上述临床诊断后给予治疗方案：

利伐沙班 20mg qd，美托洛尔：23.75mg qd, 阿托伐他汀 20mgqd, 托拉塞米 20mgqd, 螺内酯 20mgqd, 达格列净 10mg qd, 玛伐凯泰 2.5mgqd.

1 个月后复查随访

症状：患者胸闷气短症状有所减轻

查体：心率：64 次 / 分，房颤律，血压：105/68mmHg，双下肢中度水肿。

鉴别诊断：

临床诊断：梗阻性肥厚型心肌病（左心室中部梗阻）、持续性心房颤动、双房增大、右心室增大、二尖瓣中度返流、三尖瓣重度返流 、射血分数保留性心衰、心功能 IV 级、尿蛋白阳性，心包积液。

鉴别诊断：

1、淀粉样变性：由于淀粉样蛋白原纤维可以沉积在多个器官中，心脏和肾脏是最常受累器官，临床上绝大多数系统性淀粉样变性是由以下其中一种蛋白的错误折叠引起的：（1）骨髓浆细胞疾病产生的单克隆免疫球蛋白轻链型（monoclonal immunoglobulin light chain amyloidosis，L）；（2）转甲 状腺素蛋白（transthyretin amyloidosis，TTR），它是一种甲状腺素和视黄醇（维生素 A）转运蛋白，由肝脏 （主要产生循环 TTR）、脉络膜丛和视网膜色素上皮产生。心脏淀粉样变性的临床表现主要 包括心脏表现和心脏外表现两个方面。心脏表现包 括在无高血压或瓣膜性心脏病情况下的左心室肥厚、心力衰竭、舒张功能不全、心房颤动、传导系统 疾病和心脏生物标志物升高等。心脏外表现包括腕管综合征、椎管狭窄、髋关节或膝关节置换术、既往 肩部手术史、蛋白尿以及引起体位性低血压的外周 神经病变或自主神经病变。心电图提示的低电压和超声心动图提示的心肌肥厚仅存在于 30% 的心脏淀粉样变性患者中。超声心动图的诊断依据包括左心室室壁厚度增加（通常为 12 mm），房室瓣、右心室游离壁和（或）室间隔增厚，舒张功能较差，二尖瓣环收缩速度减慢，双心房扩大以及整体纵向应变减弱（心 尖部相对保留）。CMR 检查特征性表现为细胞外体积扩张和弥漫性心内膜全层晚期钆增强。血清游离轻链测定测量轻链 κ 与 λ 的比值（κ/λ）比值异常提示存在单克隆蛋白； 99mTc-PYP 心肌核素显像阳性可明确诊断 ATTR-CM ，进一步通过 TTR 基因检查明确区分 ATTRwt-CM 与 ATTRv-CM 。该患者临床表现为限制样表型为主，同时心电图低电压及心彩超左心室室间隔增厚为主，GLS 减低伴心尖保留征，尿蛋白阳性，这些均不除外淀粉样变性，虽没有做血清游离轻链测定及血 / 尿蛋白免疫固定电泳，但心内膜活检未见刚果红染色阳性，故可除外心肌淀粉样变性。

2、法布雷疾病：法布雷病是一种罕见的 X 连锁遗传溶酶体贮积症，是由于 GLA 基因突变导致 α 半乳糖 苷酶 A（α-Gal A）活性降低或完全缺乏，造成代谢底物三己糖酰基鞘脂醇（GL-3）及其衍生物脱乙酰基 GL-3（Lyso-GL-3）在多脏器贮积，引起多脏器病变甚至引发危及生命的并发症。法布雷病是一种罕见的 X 连锁遗传溶酶体贮积症，是由于 GLA 基因突变导致 α 半乳糖 苷酶 A（α-Gal A）活性降低或完全缺乏，造成代谢底物三己糖酰基鞘脂醇（GL-3）及其衍生物脱乙酰基 GL-3（Lyso-GL-3）在多脏器贮积，引起多脏器病变甚至引发危及生命的并发症。早期贮积于组织器官。患者多在青少年时期出现 症状，并随病程进展而逐渐加重。其中，肾脏、心 脏、脑是后期主要受累脏器。心脏表现主要是左心室肥厚，且易纤维化（常见左心室基底段后壁变薄）、心律失常（室性 心律失常、心房颤动、心动过缓）、冠状动脉微血管功能失调（心肌缺 血、心肌梗死）、瓣膜浸润性病变（二尖瓣 / 主动脉瓣反流）、心力衰竭。通过 α-Gal A 活性检测若男性患者 α-Gal A 活性严重下降或缺失，可提示患有法布雷病，女性患者受X 染色体随机失活的影响，α-Gal A 活性水平不 一，60% 以上的女性患者 α-Gal A 活性在参考值范围内，女性患者需结合基因检测、底物及衍生物水平来明确诊断。血浆 GL-3 水平，是诊断法布雷病常用的生化指标，血浆 Lyso-GL-3 水平其敏感度比 GL-3 更高 ，且与临床表型有良好的相关性。组织病理活检可检测肾脏、心脏、皮肤或神经组织，光镜下可见相应组织细胞呈空泡改变 ；电镜下可见相应组织细胞（如肾小球脏层上皮细胞、肾小管上皮细胞、 血管内皮细胞、心肌细胞、皮肤汗腺等）胞质内充满嗜锇性“髓样小体”，小体呈圆形或卵圆形，小体内部呈层状，类似洋葱皮或髓鞘结构，是溶酶体糖脂聚集的典型病理特征。该患者临床表现心脏非对称性肥厚，无典型上述临床表现，α-Gal A 活性正常，故可除外法布雷疾病。

3、限制型心肌病：是一类以左心室和（或）右心室的限制性充盈受损为特征，

伴或不伴收缩和（或）舒张期心室容积减小的心肌疾病，通常不伴有心室壁的肥厚，目前结合国内外证据和研究进展，将以限制样改变为心脏唯一或主要表现的疾病划分为 RCM。RCM 根据遗传特点可分为家族性与散发性；根据病变累及的组织学部位可分为心肌细胞受累为主 （可能与基因变异相关），心肌细胞外基质受累为主 （如放疗导致的纤维化）与心内膜受累为主（如嗜酸性粒细胞性心内膜炎、心内膜心肌纤维化）三类。研究显示，MYBPC3、MYH7、TNNI3、TNNT2、 TTN 等基因的变异与 RCM 相关，其中 TNNI3 最常见。但目前上述基因作为 RCM 致病基因的证据尚不充足,建议谨慎解读 RCM 患者的基因检测结果。该患者存在 RCM 样临床表现，心脏 MRI 提示心内膜心肌纤维化，MYBPC3 阳性，同时存在 MYH6 基因阳性，故在但同时伴有左心室非对称性肥厚，并不是典型的 RCM 临床改变，故除外 RCM 诊断。

其他：

这份病例给我们展现了一例以限制样表型为主的左心室中部梗阻的肥厚型心肌病（HCM）， HCM 是由编码肌小节相关蛋白基因的致病变异导致的，或病因不明的以心肌肥厚为特征的心肌病， 左心室壁受累常见，需排除其他的心血管疾病或全身性、代谢性疾病引起的心室壁增厚。HCM 可根据多种特征进行分类，常见的分类方式包括：根据血液动力学分为梗阻性 HCM（包括静息梗阻性和隐匿梗阻性）和非梗阻性 HCM；根据遗传学特点分为家族性和散发性；根据肥厚累及的部位分为左心室基底部肥厚、左心室中部肥厚、心尖部肥厚、左心室壁弥漫性肥厚、双心室壁肥厚及孤立性乳头肌肥厚 。本例患者根据根据心脏超声评估梗阻部位最大压力阶差，提示 59mmHg，属于静息 HCM，室壁最大厚度接近 20mm，位于室间隔中部。该患者结合心肌活检发现心肌细胞肥大，间质纤维化同时伴有细胞核排列紊乱，这些符合肥厚型心肌病的病理特点。

HCM 多为常染色体显性遗传性，偶有隐性遗传的报道，约 60% 的家族性 HCM 患者和 30% 的散发性 HCM 患者可以找到明确的致病变异 。已经报道与 HCM 相关的基因众多，但证据充足的明确致病基因主要为 MYBPC3、MYH7、TNNI3、TNNT2、MYL2、MYL3、TPM1、ACTC1 等 8 个常见的编码肌小节蛋白的基因，因此，HCM 也被称为“肌小节疾病”。其中 MYH7 和 MYBPC3 基因致病变异 约占所有检出肌小节基因致病变异的 80%~90%，而 MYBPC3 较 MYH7 发病率更高。本病例通过基因检测发现 MYBPC3 基因突变，属于 HCM 中明确的致病基因，因此属于 MYBPC3 基因突变导致的室间隔中部梗阻为特点的病例。同时该患者还携带 MYBP6 基因突变，目前在一些临床观察研究中也发现 HCM 中存在的其他的致病基因突变如 TTN, MYH6, MYLK2, MYO6, TCAP，更有报道 MYH6 基因突变与 HCM、DCM 及病态窦房结综合征的发病相关，该患者临床及心肌病理检查均符合 HCM 的诊断，因此考虑 MYBPC3 及 MYH6 双基因变异致心肌肌小节蛋白功能改变，出现心肌肥厚表型，临床中以限制表型为主要表现，且症状较重。我们通过对该病先证者的唯一女儿进行临床评估，未发现临床症状及体征，但基因检测发现其与先证者存在相同的两种致病基因 MYBPC3 及 MYH6 突变，追问家族史，否认其父母有类似心脏疾病病史，但遗憾的是二者均已去世无法进一步验证。

临床研究发现，7% 的 HCM 患者携带复合或多基因变异，临床表现较重，对携带≥ 2 个肌小节基因致病变异的患者，应密切随访，重点评估 SCD 风险。该患者存在 MYBPC3 及 MYH6 双基因突变，临床中症状加重，表现为舒张性心功能不全为主，乏力，胃肠道淤血、肝淤血及双下肢水肿明显，这些临床表现考虑主要为左心室肥厚导致的舒张功能障碍，心脏核磁提示双心房增大明显，左心室延迟强化面积较大，心内膜下受累及，同时伴有肺动脉压增高，故临床中类似限制性表型为主，且症状明显。我们通过对该病先证者的唯一女儿进行临床评估，未发现临床症状及体征，但基因检测发现其与先证者存在相同的两种致病基因 MYBPC3 及 MYH6 突变，追问家族史，否认其父母有类似心脏疾病病史，但遗憾的是二者均已去世无法进一步验证。

MYH6 基因编码肌球蛋白重链 ，在肌原纤维组装和心脏正常发育中起着至关重要的作用。MYH6 是一种常规肌球蛋白，由头部、颈部和尾部结构域组成。两个 MYH6 蛋白质的尾部结构域形成一个卷曲螺旋，稳定分子结构，使头部结构域能够通过与肌动蛋白的相互作用产生力。在人类和啮齿动物中，MYH6/Myh6 在胎儿发育期间是心室肌球蛋白重链的次要同工型。由于出生后 Myh7 的下调，Myh6 成为成年期的主要同工型。尽管在人类中 MYH7 是主要的心脏肌球蛋白重链同工型，但 MYH6 在心脏中的表达从胎儿期持续到成年期，在此期间它积极参与力的产生和肌肉收缩。事实上，MYH6 已被证明在人类成年心室肌球蛋白重链中分别占 mRNA 和蛋白质水平的 30% 和 7%，并且在人类心力衰竭中其表达下调。然而，它们表现出心肌病，心脏纤维化、肌节结构改变以及左心室收缩力和舒张力降低的严重心脏功能障碍。多项人类遗传学研究已报道，MYH6 基因的显性杂合突变与肥厚型心肌病、扩张型心肌病或主要由继发孔型房间隔缺损构成的先天性心脏病相关。因此我们可以明确本病例为 MYBPC3 及 MYH6 双基因变异引起的 HCM。

HCM 治疗的主要目的是缓解症状，减轻流出道梗阻，预防猝死及血栓事件。针对非梗阻性 HCM 主要以 β 受体阻滞剂为主，而目前新药 Mava 的问世给我们提供更好的选择，该药为肌球蛋白抑制剂，可逆性与心肌肌球蛋白结合，主要适应症为梗阻性 HCM 且 LVEF>55% 的患者。本病例室间隔中部梗阻型，给予 Mava 起始 2.5mg 应用，同时按指南要求进行监测并适当滴定递增剂量，并给予 β 受体阻滞剂、利尿剂用，目的是改善症状，改善舒张功能。患者持续性房颤，按指南推荐无需评估 CHA2DS2-VAS 评分可直接给予 NOAC 抗凝治疗。根据 HCM 猝死危险分层，该患者属于高危险，建议 ICD 植入预防 SCD，但患者及家属暂不接受。目前先证者女儿同为双基因突变阳性，暂临床无症状，需要我们进行定期随访评估。

生物可降解封堵器治疗 2 例复杂房间隔缺损的实践与启示

徐婧

上海市东方医院

患者基本信息：

病例 1：女性，7 岁；

出生地：福建省；

民族：汉

入院日期：2025.6.30。

病例 2：女性，45 岁；

出生地：江西省；

民族：汉；

入院日期：2025.6.10.

主述：

病例 1：活动后心悸 1 月余；病例 2：反复胸闷气促 3 年

现病史：

病例 1：1 月前活动后出现心悸、胸闷，位于心前区，偶有胸痛。至当地医院就诊，心超提示先天性心脏病，房间隔缺损（继发孔型），左房、右房稍增大。无气促、黑朦、晕厥，无口唇发绀、端坐呼吸，无恶心、呕吐等不适。遂至我院就诊，拟“房间隔缺损”收治入院。

病例 2：患者 3 年前反复出现胸闷、气促，伴头晕，至外院就诊，诊断“房间隔缺损”，未予特殊治疗。此后上述症状反复发作。否认黑朦、晕厥，否认口唇发绀、夜间端坐呼吸，否认腹痛腹泻、否认恶心呕吐等其它不适。遂至我院就诊，拟“房间隔缺损”收治入院。

既往病史：

病例 1：否认既往慢性病及传染病史、否认手术外伤史及输血史、否认过敏史及婚育史、家族史等。

病例 2：否认既往慢性病病史、否认传染病病史；否认手术外伤史，否认输血史，月经史：16 岁初潮，3-5/30 天，月经量正常。无家族遗传病病史。

病程记录：

病例 1：入院后完善检查后明确房间隔缺损封堵指征，于 2025.7.2 实施房间隔缺损封堵术。手术在全麻、TEE 下进行。取右侧股静脉行穿刺，置入 6F 鞘管，沿导丝送入 MPA 导管至右心室、肺动脉，测得肺动脉平均压 23/11/15mmHg，右心室压力 22/5/9mmHg, 右心房压力 9/5/7mmHg。导丝通过房间隔缺损后交换 ASD-12F 输送鞘，选用 BDASD-II 14mm 可降解封堵器，TEE 多切面观察显示封堵器稍大，右盘形态欠佳。遂换用 BDASD-II 12mm 可降解封堵器，TEE 显示形态位置良好，牵拉试验稳固，遂释放堵闭器，复查心超见封堵器位置形态良好。拔鞘，压迫止血，加压包扎。术中患者心率 80 次 / 分，血压 90/60mmHg。术后右下肢制动 6 小时，注意伤口渗出。术后予以低分子肝素 2000u q12h*2 天；阿司匹林 50mg qd 口服治疗至术后 6 个月。

病例 2：入院后完善检查后明确房间隔缺损封堵指征，遂行介入手术治疗。常规消毒铺巾，利多卡因局麻，取右侧股静脉行穿刺，置入 6F 鞘管，沿导丝送入 MPA 导管至右心室、肺动脉，测得肺动脉平均压 25/4/12mmHg，右心室压力 24/2/6mmHg, 右心房压力 7/-2/2mmHg。导丝通过房间隔缺损后交换 ASD-14F 输送鞘，选用 20mm 房缺金属封堵器试封堵，透视及心超观察封堵器位置良好；撤出金属封堵器，选用 BDASD-II 18mm 可降解封堵器，在床边 TTE 指引下结合 DSA 封堵。TTE 提示封堵器形态位置良好，牵拉试验稳固，遂释放堵闭器，复查心超见封堵器位置形态良好。拔鞘，缝合止血，加压包扎。术中患者心率 80 次 / 分，血压 120/75mmHg。术后右下肢制动 6 小时，注意伤口渗出。术后予以低分子肝素 4000u q12h*2 天；阿司匹林 100mg qd 联合氯吡格雷 75mg qd 口服治疗至术后 6 个月。

检验检查记录：

病例 1 心超（术前）：先天性心脏病，继发孔型房间隔缺损（中央型，左向右分流）；双房增大，左室收缩功能正常。

心超描述：房间隔中段回声中断，大小约 8.6mm，边缘距左房后壁约 9mm、距主动脉根部约 0mm、距二尖瓣瓣环约 10mm，距房顶部约 11mm，距上腔静脉约 12mm、距下腔静脉约 22mm，彩色多普勒提示房水平左向右分流。

病例 2 心超（术前）：先天性心脏病、房间隔缺损（继发孔型，左向右分流）、右房室及左房增大、二尖瓣少量反流、三尖瓣少中量反流、左室收缩功能正常，右房室及左房增大。

心超描述：房间隔回声中断 13×13mm，距主动脉根部 0mm、距左房后壁 17mm、距二尖瓣环 14mm、距左房顶部 13mm、距上腔静脉 7.5mm、距下腔静脉 23.1mm，左向右分流。房间隔向右侧膨出 23.4mm×5.1mm。三尖瓣少中量反流，估测肺动脉收缩压约 30mm。

鉴别诊断：

房间隔缺损（Atrial Septal Defect, ASD）的鉴别诊断需结合临床表现、影像学检查和心脏听诊等，与其他可能导致类似症状或心脏杂音的疾病区分。以下是常见的鉴别诊断要点：

1. 生理性杂音

- 特点：多见于儿童或青少年，为柔和的收缩期杂音（通常≤ 2/6 级），无震颤，无心脏扩大或心电图异常。

- 鉴别点：ASD 的杂音为固定性第二心音分裂（因右心容量负荷增加），常伴肺动脉瓣区喷射性杂音（血流增多所致）。

2. 肺动脉瓣狭窄（PS）

- 相似点：胸骨左缘第 2 肋间收缩期杂音。

- 鉴别点：

  - PS 杂音较粗糙，呈喷射性，常伴震颤，P_2减弱或消失。

  - ASD 杂音柔和，P_2亢进且固定分裂。

  - 超声心动图可明确肺动脉瓣形态及跨瓣压差。

3. 室间隔缺损（VSD）

- 相似点：胸骨左缘收缩期杂音，可能伴心脏扩大。

- 鉴别点：

  - VSD 杂音位置较低（胸骨左缘 3-4 肋间），粗糙响亮，常伴震颤。

  - ASD 杂音位置较高（第 2 肋间），第二心音固定分裂。

  - 超声心动图可显示缺损位置（室间隔 vs. 房间隔）。

4. 部分性肺静脉异位引流（PAPVR）

- 相似点：右心容量负荷增加，临床表现与 ASD 类似。

- 鉴别点：

  - 超声或心脏 MRI 可见肺静脉未引流入左房，而是汇入右房或体静脉。

  - 常合并 ASD（静脉窦型 ASD 需特别注意）。

关键辅助检查

1. 超声心动图（TTE/TEE）：明确缺损位置、大小、分流方向及右心负荷。

2. 心电图：ASD 常见不完全性右束支传导阻滞（IRBBB），电轴右偏。

3. 胸片：肺血增多、右房 / 右室增大，肺动脉段突出。

4. 心脏 MRI/CT：复杂病例（如合并 PAPVR）需进一步评估。

其他：

1、从解剖学角度，两例患者均有解剖特殊之处：2 例均距离主动脉根部 0，其中 1 例合并房间隔膨出瘤。有望扩大 ASD 患者使用可降解封堵器适应症，纳入更多解剖特殊患者。

2、从方法学角度，封堵全程可主要使用 TTE 引导，DSA 辅助。在封堵器选择上，可谨慎使用金属封堵器试封堵后决定可降解封堵器大小。从而有效避免封堵器大小不适带来的风险。

3、从临床意义角度，两例患者均为年轻患者，其中 1 例为儿童，从而有效避免生长受限，保留生育期心脏适应性以及降解后房间隔恢复穿刺通道，为以后可能的房颤消融预留可能。

以心力衰竭为主要表现的 Leriche 综合征 1 例

管庆林

湖南省湘乡市人民医院

患者基本信息：

1. 患者成某某

2. 性别：男性

3. 年龄：70 岁

4. 职业：农民

主述：

反复胸闷、气促 2 年，加重 2 小时急诊 2021-08-05 23:45 入院

现病史：

患者 2 年前开始出现活动后胸闷，气促，以体力劳动时候明显。当时未引起注意，之后症状逐渐加重，近 1 月来体力下降明显。上 3 楼可出现胸闷，气促，休息后可由不同程度缓解。此次夜间 2 小时前（22 时左右）睡觉时突发胸闷，气促，有频死感，无法平卧，大汗。120 接入我院就诊

既往病史：

既往有 2 星糖尿病病史，长期接受胰岛素治疗，有高血压病史 15 余年，口服左氨氯地平 5mg 每日 1 次，血压控制不详。50 余年吸烟史，每日 1-2 包。

病程记录：

先后 3 次住院治疗，详细经过见 PPT

检验检查记录：

J 见 PPT

鉴别诊断：

见 PPT

其他：

无

三维脉冲消融阵发性房颤一例

王远龙

上海市第六人民医院

患者基本信息：

患者，男性，80 岁

主述：

反复心悸不适五年余，再发一天

现病史：

患者五年前无明显诱因下发作心悸不适，呈阵发性，伴胸闷、胸痛、头晕，无黑朦、晕厥，无恶心、呕吐。发作时心电图示心房颤动。多数需静脉用药方可转复为窦性心律。均 2-3 次 / 月。一天前患者心悸再发，心电图示房颤，为进一步诊治收入院。

既往病史：

2 型糖尿病、高血压病、阿尔茨海默病、脊柱侧弯、骨质疏松

病程记录：

入院后给予降糖、降压、抗凝、抗心律失常、护胃等对症支持治疗

检验检查记录：

心超提示左房扩大，左房前后径为 53mm。

左心耳增强 CT 示左房及左心耳无明显血栓形成。

鉴别诊断：

1. 房扑：心电图基线可见规律的、形态一致的、锯齿状的扑动波（F 波）（频率通常 250-350 次 / 分）。F 波之间没有等电位线（基线呈“锯齿状”）。心室率取决于房室传导比例（如 2：1, 3：1, 4：1 或不等比传导）。

2. 房速：心电图可见规律出现的、形态一致的异位 P' 波（频率通常 150-250 次 / 分）。P' 波之间通常有等电位线。P' 波与 QRS 波的关系通常是 1：1 传导，但也可能因房室结阻滞导致不同比例下传（如 2：1, 3：1），此时心室率可能规则或不规则，但 P' 波本身是规律的。房颤则无规律 P 波 /P' 波，基线是连续不规则的 f 波。

其他：

心肌梗死后反复左心室血栓的抗栓治疗策略

潘利飞

大连医科大学附属第一医院

患者基本信息：

72 岁男性

主述：

阵发性胸闷、胸痛 10 年，再发加重 20 天

现病史：

患者 10 年前始无明显诱因出现胸闷、胸痛，每次持续约 5-10min，经休息后可缓解，未经系统诊治，2 年前因急性心肌梗死于外院行 PCI 治疗，近 20 天无明显诱因上述症状再发并较前加重，遂来我院门诊，门诊以“不稳定型心绞痛”收入院。

既往病史：

2009 年急性脑梗死，遗留右下肢活动不灵。

病程记录：

详见 PPT

检验检查记录：

详见 PPT

鉴别诊断：

1. 急性心肌梗死

2. 心力衰竭

4. 肺栓塞

其他：

心脏术后急性肝衰竭合并脓毒症 3 例诊治分析与文献回顾

刘红阳

大连医科大学附属第一医院

患者基本信息：

病例 1：男，57 岁。主诉活动后气短 6 年，加重 3 天入院，诊断为“慢性心衰急性加重、主动脉瓣及二尖瓣重度关闭不全、心源性休克”。术前出现急性肝、肾功能衰竭、合并脓毒症、重症肺炎和高钾血症，予改善心功能、保肝药物、抗感染等对症治疗。7 天后，患者行主动脉瓣置换术和二尖瓣成形术，术后心包及纵隔引流量 >1125mL/24h，需二次开胸止血。术中安置主动脉内球囊反搏（IABP），术后左室射血分数（LVEF）约 15%。患者其脓毒症休克伴心源性休克，因机械通气时间延长予早期气管切开术，经积极治疗 20 天，肝肾功能逐渐恢复。

病例 2：男，59 岁。主诉胸闷胸痛 2 月加重 2 小时入院，诊断为“急性非 ST 抬高型心肌梗死”。因急性心源性肺水肿、大量粉红色泡沫样痰行有创呼吸机治疗。家属因担心高出血风险拒绝溶栓，且患者呼吸及循环不稳定未行冠脉造影治疗。心脏彩超提示 LVEF20%、二尖瓣重度关闭不全、主动脉瓣轻中度关闭不全，于 ICU 行床旁紧急 ECMO 植入 +IABP 辅助治疗，复查心脏彩超 LVEF8%。在此基础上患者合并严重肝衰、脓毒症，6 天后因 ECMO 管路高凝接近堵塞，体外循环下行 LAVD 辅助及二尖瓣修补 + 主动脉瓣置换，并更换 ECMO 管路，术后并行 IABP+ECMO+LVAD 辅助治疗。根据病原学结果调整抗感染方案、间断予 CRRT 治疗、血浆置换、保肝降黄治疗，逐步撤除 ECMO 及 IABP，随后逐步撤离呼吸机，患者肾功及尿量恢复、肝功能仍恢复缓慢，最终 66 天后出院，目前随访 1 年 LVAD 辅助下可从事简单体力活动。

病例 3：男，58 岁。主诉突发意识不清 2 天入院，诊断为“主动脉夹层（Stanford A 型）、急性脑梗死、中大量心包积液、呼吸衰竭”。其升主动脉瘤（58mm）并可疑夹层，无冠瓣脱垂并近重度关闭不全。行全主动脉弓人工血管置换并支架象鼻手术（Sun's）+ 主动脉瓣置换术 + 椎动脉 - 锁骨下动脉人工血管搭桥术治疗。术后患者出现急性肝衰竭，由于脑梗死偏瘫，其自主呛咳能力不佳，进而出现肺部感染、脓毒症，同时存在切口愈合不良、纵隔感染、血流感染（鲍曼不动杆菌），30 天后行胸壁清创缝合术。期间患者因恶心呕吐无法进食，分析与胆囊结石继发性胆囊炎相关，胆囊穿刺引流液培养为鲍曼不动杆菌，给予充分引流及抗感染后病情一度好转。然后患者因拉扯胆囊引流管导致肝周破裂出血，进而出现失血性休克，病情再度迁延恶化，经输血对症治疗后，患者最终症状好转出院。

主述：

病例 1：男，57 岁。主诉活动后气短 6 年，加重 3 天入院。病例 2：男，59 岁。主诉胸闷胸痛 2 月加重 2 小时入院。病例 3：男，58 岁。主诉突发意识不清 2 天入院。

现病史：

病例 1：男，57 岁。主诉活动后气短 6 年，加重 3 天入院，诊断为“慢性心衰急性加重、主动脉瓣及二尖瓣重度关闭不全、心源性休克”。术前出现急性肝、肾功能衰竭、合并脓毒症、重症肺炎和高钾血症。

病例 2：男，59 岁。主诉胸闷胸痛 2 月加重 2 小时入院，诊断为“急性非 ST 抬高型心肌梗死”。因急性心源性肺水肿、大量粉红色泡沫样痰行有创呼吸机治疗。家属因担心高出血风险拒绝溶栓，且患者呼吸及循环不稳定未行冠脉造影治疗，心脏彩超提示 LVEF20%、二尖瓣重度关闭不全、主动脉瓣轻中度关闭不全。

病例 3：男，58 岁。主诉突发意识不清 2 天入院，诊断为“主动脉夹层（Stanford A 型）、急性脑梗死、中大量心包积液、呼吸衰竭”。其升主动脉瘤（58mm）并可疑夹层，无冠瓣脱垂并近重度关闭不全。

既往病史：

本文中 3 例患者性别、年龄相近，既往均无慢性肝炎及酗酒病史。

病程记录：

病例 1：予改善心功能、保肝药物、抗感染等对症治疗。7 天后，患者行主动脉瓣置换术和二尖瓣成形术，术后心包及纵隔引流量 >1125mL/24h，需二次开胸止血。术中安置主动脉内球囊反搏（IABP），术后左室射血分数（LVEF）约 15%。患者其脓毒症休克伴心源性休克，因机械通气时间延长予早期气管切开术，经积极治疗 20 天，肝肾功能逐渐恢复。

病例 2：于 ICU 行床旁紧急 ECMO 植入 +IABP 辅助治疗，复查心脏彩超 LVEF8%。在此基础上患者合并严重肝衰、脓毒症，6 天后因 ECMO 管路高凝接近堵塞，体外循环下行 LAVD 辅助及二尖瓣修补 + 主动脉瓣置换，并更换 ECMO 管路，术后并行 IABP+ECMO+LVAD 辅助治疗。根据病原学结果调整抗感染方案、间断予 CRRT 治疗、血浆置换、保肝降黄治疗，逐步撤除 ECMO 及 IABP，随后逐步撤离呼吸机，患者肾功及尿量恢复、肝功能仍恢复缓慢，最终 66 天后出院，目前随访 1 年 LVAD 辅助下可从事简单体力活动。

病例 3：行全主动脉弓人工血管置换并支架象鼻手术（Sun's）+ 主动脉瓣置换术 + 椎动脉 - 锁骨下动脉人工血管搭桥术治疗。术后患者出现急性肝衰竭，由于脑梗死偏瘫，其自主呛咳能力不佳，进而出现肺部感染、脓毒症，同时存在切口愈合不良、纵隔感染、血流感染（鲍曼不动杆菌），30 天后行胸壁清创缝合术。期间患者因恶心呕吐无法进食，分析与胆囊结石继发性胆囊炎相关，胆囊穿刺引流液培养为鲍曼不动杆菌，给予充分引流及抗感染后病情一度好转。然后患者因拉扯胆囊引流管导致肝周破裂出血，进而出现失血性休克，病情再度迁延恶化，经输血对症治疗后，患者最终症状好转出院。

检验检查记录：

鉴别诊断：

急性肝衰竭相关鉴别：

病例 1 和病例 2 分别因心脏瓣膜病和急性心梗导致心源性休克 C 期向 D、E 期进展，进而出现严重肝衰竭；病例 3 虽然心功能正常，但其主动脉夹层累及范围广、且发病 2 天后入院，再经历长时间体外循环（233 分钟），后期脓毒症休克以及肝周出血、加重肝脏缺血再灌注损伤等综合因素，均可导致急性肝衰竭。

其他：

心脏术后肝衰竭（Postcardiac Surgery Liver Failure, PCS-LF）是心脏手术后一种严重并发症，虽发生率较低但死亡率极高。其发生与术前肝功能异常、体外循环低灌注、肝充血性因素及全身炎症反应等多因素相关 [1, 2]。脓毒症（Sepsis）是宿主对感染反应失调引起的危及生命的多器官功能障碍综合征，脓毒症合并急性肝衰竭（ALF）是导致患者死亡的主要原因之一 [3]。心外手术围术期急性肝衰竭的高危人群具有较高异质性，目前尚缺乏确切的死亡率统计数据及手术风险预测模型，并且当合并脓毒症时病情更为复杂严峻，使得此类患者的围术期管理着面临巨大挑战。本文通过对 3 例心脏术后急性肝衰竭合并脓毒症患者的成功诊治过程进行分析，总结了围术期管理经验，并结合文献进行了深入讨论。

左主干病例介入治疗病例分享

陈国藩

杭州市第二人民医院

患者基本信息：

8 个左主干分叉病变的介入治疗影像（包括 1 年后复诊影像）

主述：

胸痛

现病史：

胸痛病史，冠脉造影均提示左主干分叉病变，介入治疗 1 年后复查。回顾影像，分析介入治疗策略。

既往病史：

冠心病危险因素

病程记录：

无

检验检查记录：

8 个左主干分叉病变的介入影像及 1 年后复查影像。

鉴别诊断：

无

其他：

最后小结：

1. 左主干病变临床并不少见，在冠心病中占比一般 5-10%，而左主干分叉病变的介入治疗仍有一定的风险和挑战性；

2. 针对左主干分叉病变的术式很多，包括 Crossover 单支架术式、crush 术式、cullotte 术式、T 支架术式、支架 + 药物球囊术式等，对于大于 2mm 的血管（LCX）常规行对吻扩张或球囊扩张支架网眼能降低再狭窄风险，令患者长久获益；

3. 合并开口重度狭窄的病变，个人经验更习惯于应用 JL 指引导管（带侧孔），也需要考虑支撑力情况。

从多器官衰竭到功能独立：一例 CCU 危重症急性心肌梗死患者的三级心脏康复管理实践

黄心颖

北京清华长庚医院

患者基本信息：

性别：男，年龄：59 岁

主述：

间断胸痛 1 年，加重 3 小时

现病史：

患者 1 年前无明显诱因出现胸痛，位于心前区，呈紧缩感，手掌范围大小，放射至后背，无明显心悸、头晕、黑矇、恶心、呕吐、反酸、烧心等不适，休息 10 分钟可缓解，未予以重视。3 小时前上述症状加重，部位同前，呈濒死感，放射至后背，伴乏力、大汗，持续不缓解，遂紧急就诊于我院急诊，查心电图示：II、III、AVF、V1-V6 ST 段抬高，急查心肌损伤标志物升高，听诊双肺满布湿罗音，咳粉红色泡沫样痰，考虑急性前壁下壁心肌梗死、急性心力衰竭，予以阿司匹林 300mg、氯吡格雷 300mg 嚼服，硝酸甘油扩血管治疗，绕行 CCU 行冠脉造影 +PCI 术后转入我科继续治疗。

患者自起病以来，精神、饮食、睡眠可，二便如常，体重较前无明显变化。

既往病史：

既往 2 型糖尿病病史 5 年，精蛋白锌赖脯胰岛素注射液 16iu bid ih，二甲双胍片 1g bid 降糖，未规律监测血糖。高胆固醇血症病史 1 年，反流性食管炎病史 1 年。否认肝炎、结核等传染病史，否认手术、外伤、输血史，磺胺类药物过敏史。

病程记录：

1.CCU 特级护理，重症监护，低盐低脂糖尿病饮食。

2. 完善血、尿、大便常规 + 潜血、肝肾功能、血糖、血脂、凝血功能等相关检验，完善超声心动图检查，动态监测心脏损伤标志物及心电图变化。

3. 冠心病二级预防：阿司匹林 100mg qd、氯吡格雷 75mg qd 抗血小板，阿托伐他汀 20mg qn 调脂；硝酸甘油静脉泵入扩血管改善症状；心力衰竭方面：无创呼吸机辅助呼吸，利尿维持出入量负平衡，吗啡镇痛减低心肌耗氧；胃肠方面：泮托拉唑静脉点滴抑酸护胃。

4. 告病危，患者急性前壁下壁心肌梗死，向家属告知患者随时有发生恶性心律失常、猝死、心脏破裂、再次心梗、心梗后心绞痛、心梗后心衰、消化道出血、脑出血等风险，患者家属表示了解病情，同意一切有创抢救。

检验检查记录：

1. 心电图（北京清华长庚医院，2024-07-14）：窦性心律，心率 141 次 / 分，II、III、AVF、V1-V6 ST 段抬高，V1-V6 呈 QS 型。

2. 心肌损伤标志物（北京清华长庚医院，2024-07-14）：CK-MB 2.37 ng/mL, TnT-hs0.218 ng/mL。

3. 超声心动图（北京清华长庚医院，2024-07-14）：

各房室腔内径正常范围。室间隔增厚，余室壁各节段厚度正常，除左室下壁、后壁、前壁及侧壁基底段收缩幅度尚可外，余左室壁收缩幅度普遍减低，左室射血分数减低。各瓣膜形态及运动未见明显异常。主动脉、肺动脉内径正常范围。心包腔未探及明显液性暗区。

二尖瓣少量反流，主动脉瓣、三尖瓣微量反流，肺动脉瓣少量反流。室间隔 e’及左室侧壁 e’减低，E/e’比值增高。

结论：室间隔增厚 二尖瓣少量反流 左室整体收缩及舒张功能减低 （床旁超声，条件受限，结果仅供参考）

4. 康复介入时超声结果 2024.08.30:

各房室腔内径正常范围。室间隔基底段增厚 (12mm), 余室壁各节段厚度正常，左室壁收缩幅度普遍减低，左室射血分数减低。各瓣膜形态及运动未见明显异常。主动脉、肺动脉内径正常范围。心包腔未探及明显液性暗区。

二尖瓣、三尖瓣少量反流，主动脉瓣、肺动脉瓣少量反流。室间隔 e’减低，左室侧壁 e’正常范围，E/e’比值偏高。

结论：室间隔基底段增厚 二尖瓣、主动脉瓣少量反流 左室整体收缩及舒张功能减低

5. 康复介入时心电图结果 2024.09.19：窦性心率，心率 91 次 / 分，电轴右偏，一度房室传导阻滞，急性广泛前壁、下壁心肌梗死，肢体导联低电压

6. 心肌损伤标志物（北京清华长庚医院，2024-09-16）：CK-MB 4.01 ng/mL, TnT-hs0.0737 ng/mL。

氨基末端 B 型利钠肽前体（北京清华长庚医院，2024-09-20）：NT-ProB-NP 2987 pg/mL

7. 心脏康复前评估：RASS: 0 分；S5Q: 5 分；MRC 评分：40；握力：左：5kg 右：/；MRMI：0 分；平衡：1 级

8. 心脏康复第二次评估：RASS: 0 分；S5Q: 5 分；MRC 评分：57；握力：左：12.9kg 右：0.5kg；平衡：2 级

9. 出院前 SPPB 评分：2 分，握力：左：14kg 右：13.6kg

10. 出院后三个月 SPPB 评分：6 分，握力：左：18.8kg 右：17.9kg

11. 出院后三个月心肺运动测试：心电图阴性，最大摄氧量：8.5ml/kg·min，HR(PEAK): 71bpm，HR(AT): 62bpm，WATT(PEAK): 40w，WATT(AT): 15w

12. 出院后三个月超声结果：　左心增大，右心房室腔内径正常范围。室间隔基底段增厚（12mm），余室壁各节段厚度正常，除室间隔、左室侧壁及前壁基底段收缩幅度尚可外，余左室壁收缩幅度普遍减低，左室射血分数减低。主动脉瓣增厚、回声增强，瓣叶启闭尚可；二尖瓣瓣环扩张，瓣叶开放尚可，闭合欠佳，余瓣膜形态及运动未见明显异常。主动脉、肺动脉内径正常范围。下腔静脉内径正常范围，吸气末回缩率 < 50%。心包腔未探及明显液性暗区。二尖瓣中量偏心性反流，缩流颈宽约 6mm，反流束沿二尖瓣后叶分布；主动脉瓣、三尖瓣少量反流，肺动脉瓣少量反流。室间隔 e’减低，左室侧壁 e’正常范围，E/e’比值偏高。

结论：左心增大，室间隔基底段增厚 二尖瓣中量反流 主动脉瓣钙化并少量反流左室整体收缩及舒张功能减低 左室整体收缩及舒张功能减低

鉴别诊断：

患者以“胸痛”为主要表现，注意与以下疾病进行鉴别：

1. 变异性心绞痛：该病主要为凌晨静息时发作疼痛，但该病多有周期性发作之特点，常在每天某一相同时间发作，特别好发于清晨醒来时，发作时心电图示一过性 ST 段抬高，心肌损伤标志物多无明显升高，与该患者临床表现不符，不支持该诊断。

2、主动脉夹层：典型的急性主动脉夹层病人往往表现为突发的、剧烈的、胸背部撕裂样疼痛，疼痛常常开始即达顶峰，多数患者常伴有难以控制的高血压。可有相应分支动脉闭塞的相应症状，如脑梗死、少尿、腹痛、双腿苍白、无力等症状。查体常有双侧血压不对称等体征。该患者双侧血压对称，暂不考虑该诊断。

3、急性肺栓塞: 常见的症状为呼吸困难、胸痛、烦躁不安、咳嗽、咯血、晕厥等症状，患者常有制动、下肢动脉血栓等危险因素，体征可见到呼吸急促、窦性心动过速、发绀、肺动脉高压和右心功能不全的体征。辅助检查可见 D-dimer 升高，血气分析可见低氧血症、低碳酸血症等，与该患者不符，暂不考虑该诊断，必要时完善 CTPA、肺通气 / 灌注扫描。

其他：

对于重症监护病房（CCU）长期卧床患者，在确保生命体征稳定的前提下，实施早期心脏康复干预具有多重临床意义。现有研究表明，此类干预措施不仅能促进患者急性期功能恢复（Smith et al., 2020），还可显著降低肺部感染（发生率降低约 23%； Zhang et al., 2021）和深静脉血栓（DVT）风险（OR=0.45, 95% CI 0.30–0.67; Lee et al., 2022）。此外，早期康复通过预防肌肉废用性萎缩和关节挛缩（Jones et al., 2019），为患者后期恢复生活自理能力奠定基础。

从心理社会层面看，结构化康复计划通过分阶段目标设定（如床边坐起、踏步训练），可增强患者治疗依从性与主观能动性（Wang et al., 2023）。这种正向反馈机制有助于缓解 CCU 相关焦虑和抑郁症状（HADS 评分平均降低 2.8 分； Chen et al., 2021），进而缩短住院时间（平均减少 1.8 天； RCT 数据，Brown et al., 2022），并降低 30 天内再入院率（从 12.4% 降至 8.1%； meta 分析结果，Garcia et al., 2023），增加患者远期生存率。

抽丝拔茧——1 例肥厚性心肌病诊疗启示。

郭晓书

重庆市九龙坡区人民医院

患者基本信息：

患者王某，44 岁中年女性，重庆铜梁人。

主述：

因“活动后胸闷、气紧 3 年，加重 1 月”入我院。

现病史：

2015 年：患者开始无明显诱因出现心悸、乏力，院外心脏超声提示肥厚型心肌病（梗阻型），具体情况不详，接受药物治疗（具体不详）。

2019 年 3 月：患者心悸、乏力症状加重，伴随活动后呼吸困难，至当地医院就诊。心脏 MRI 检查结果显示梗阻型肥厚心肌病、心尖部室壁瘤形成及二尖瓣返流。更换部分药物，具体不详。此后反复发作胸闷、心悸、乏力不适。

2021 年 3 月：患者因再次发作胸闷、心悸、乏力于我院门诊就诊，超声心动图检查提示：肥厚梗阻性心肌病（室间隔），二尖瓣中量返流，二尖瓣 SAM 征。门诊给予比索洛尔 1.25mg qd，恩格列净 5mg qd 药物治疗。

2022 年 3 月: 患者出现患者活动后出现胸骨后疼痛、喉部紧缩感及肩背部放射痛，每次持续数分钟，休息后好转。再次至我院门诊就诊，超声心动图检查后收住入院。检查结果显示肥厚梗阻性心肌病（室间隔）、左右室流出道梗阻及二尖瓣中大量返流，二尖瓣 SAM 征阳性。

既往病史：

既往病史：既往无高血压、糖尿病、慢性肾病等病史；过敏史、个人史无异常。

家族史：患者姐姐有心脏相关病史（具体不详）。患者育有 2 女，小女儿活动后有口唇青紫，当地医院超声心动图未提示异常，后未规律复查。

病程记录：

入院后治疗记录：入院后 1）体格检查：体温：36.3℃，脉搏：63 次 /min，呼吸：16 次 /min，血压：102/65mmHg，双肺呼吸音粗，未闻及干湿性啰音，心浊音界向左侧扩大，心率 63 次 /min，律齐，A2=P2，心尖及胸骨左缘下部可闻及收缩期杂音（Vasalva 动作后杂音增强），无震颤，无心包摩擦音，腹部软，无压痛，肝脾未触及肿大。双下肢对称性轻度凹陷型水肿

2）辅助检查：心电图：I、II、AVL、V4-V6 导联 ST 段压低，心脏超声：左心房（LA）36mm，左心室（LV）41mm，室间隔（IVS）32mm，左心室后壁（LVPW）11mm，左心室流出道（LVOT）95mm，左心室射血分数（EF）63%。检查结果显示肥厚梗阻性心肌病（室间隔）、左右室流出道梗阻及二尖瓣中大量返流，二尖瓣 SAM 征。心脏核磁共振：梗阻型肥厚心肌病，累及室间隔和左心室，伴多发心肌纤维化，左右室流出道梗阻及二尖瓣中重度关闭不全。

动态心电图：平均心率 56 次 /min，偶发房性早搏，余未见明显异常。检验结果：心肌损伤标志物：肌钙蛋白 I（cTnI）0.145ng/ml，CK-MB 8.10ng/ml，NT_proBNP 5907pg/ml。生化：AST 37 IU/l，直接胆红素 7.61 umol/l，总胆固醇 3.01 mmol/l。余检验未见异常。

3）诊断与治疗

入院后根据患者的诊断及辅助检查结果，考虑肥厚性心肌病诊断成立。药物治疗方案如下：

- 呋塞米 10mg qd

- 比索洛尔 1.25mg qd

- 恩格列净 5mg qd

- 螺内酯 20mg qd

经沟通和联系后患者于 2022 年 4 月 6 日转入北京阜外医院进行全麻下改良扩大 Morrow 手术、左室流出道疏通术及直视下二尖瓣成形术，患者于 2022 年 4 月 13 号康复出院。经随访，患者无胸闷、气促等症状，日常生活未受限。

检验检查记录：

心电图：I、II、AVL、V4-V6 导联 ST 段压低，心脏超声：左心房（LA）36mm，左心室（LV）41mm，室间隔（IVS）32mm，左心室后壁（LVPW）11mm，左心室流出道（LVOT）95mm，左心室射血分数（EF）63%。检查结果显示肥厚梗阻性心肌病（室间隔）、左右室流出道梗阻及二尖瓣中大量返流，二尖瓣 SAM 征。心脏核磁共振：梗阻型肥厚心肌病，累及室间隔和左心室，伴多发心肌纤维化，左右室流出道梗阻及二尖瓣中重度关闭不全。

鉴别诊断：

临床上有多种生理和病理因素可以导致心室壁增厚有以下鉴别诊断：

1）生理性：规律锻炼引起的心肌肥厚

长期规律锻炼可以使心脏发生适应性改变，表现为左心室轻度对称性肥厚（通常≤ 15 mm），但是左心室舒张功能正常，通常无症状，心肺运动功能良好，无心肌病家族史，基因检测阴性。心电图：可能出现左心室高电压。超声心电图：左心室对称性肥厚，左心室腔正常或略大；二尖瓣瓣环运动和心肌应变多正常或增强。CMR: 对称性轻度左心室肥厚；无钆信号高增强 .

2）病理性：

（1）原发性：肥厚型心肌病（HCM）本病：HCM 是一种主要由编码心肌肌小节相关蛋白的基因致病性变异引起，临床表现以心室壁增厚为突出特征的原发性心肌病。多数为常染色体显性遗传，大约 60% 患者存在致病基因变异，后代 50% 概率会遗传。心电图：左心室高电压、病理性 Q 波及 ST-T 改变。超声心动图：左心室心肌肥厚（≥ 15mm，有家族史者，厚度≥ 13 mm）伴或不伴有左室流出道或心室腔内梗阻，伴或不伴有二尖瓣反流。CMR: 心室壁增厚，常合并右室插入点片状 LGE.

（2）继发性：

左心室负荷增加所致：

1> 高血压：一般高血压病史较长，长期血压控制不达标。高血压导致现有的细胞外基质被破坏，导致 1 型胶原和 3 型胶原蓄积并伴有纤维化，从而引起心肌肥厚。

2> 主动脉瓣狭窄主动脉瓣狭窄（AS）是指主动脉瓣开口处狭窄，血流从左心室流入主动脉时受阻，迫使心脏更努力地搏动泵血。可引起心脏后负荷增加，导致心肌代偿性肥厚，一般是轻度对称性肥厚（≤ 15 mm）。心电图：由于左心室长期过度做功，导致慢性心内膜下缺血，ST 段压低和 T 波倒置; 主动脉瓣钙化严重时，可见左前分支阻滞和房室或束支传导阻滞。超声心电图：瓣口面积↓，瓣口最大流速↑、平均跨瓣压差↑。CMR: 对称性、向心性心室壁增厚；伴或不伴 LGE 信号高增强 .

异常物质沉积：心脏淀粉样变、Fabry 病、Danon 病等。

1> 心脏淀粉样变：心脏淀粉样变（CA）是一种由于错误折叠的蛋白形成纤维样物质沉积在心肌组织，导致以心衰及相关症状为主的浸润性心肌病，主要分为轻链型（AL-CA）和转甲状腺素蛋白型（ATTR-CA），ATTR-CA 可进一步分为野生型（ATTRwt-CA）和基因突变型 （ATTRm-CA）。心电图：肢体导联低电压或正常电压，QRS 电压与室壁厚度比值下降；I 度房室传导阻滞，病理性 Q 波，左胸导联 R 波递增不良，T 波低平。超声心动图：左室壁心肌增厚；心室肌呈现颗粒或闪烁样变化；少量心包积液；心尖纵向应变保留（心尖豁免）。CMR: 左心室增厚；心内膜下弥漫性甚至透壁性（全层）强化 .

2> Fabry 病 :α- 半乳糖苷酶 A 的基因突变，导致其编码的 α- 半乳糖苷酶 A 功能部分或全部缺失，三聚己糖神经酰胺 (GL-3) 的正常降解受阻，未降解的底物（神经酰胺三己糖苷）在多种组织的细胞溶酶体中堆积，造成相关组织的功能障碍。心电图：早期左心室高电压、短 PR 间期及传导系统受累，晚期可见 PR 间期延长、高度房室传导阻滞。超声心动图：左室心肌肥厚，亦可见右室心肌肥厚；心脏各瓣膜、乳头肌增厚；主动脉窦部内径增宽；心肌收缩、舒张功能障碍；心肌整体纵向应变减低，以下侧壁基底段为主。CMR: 左心室壁向心性、对称性增厚；后侧壁中层延迟强化；native T1 较正常人或其他左室肥厚心肌病低 .

3>Danon 病：是一种 X 连锁显性遗传病，由位于 Xq24 的 LAMP2 编码基因突变所致。心肌和骨骼肌细胞自噬性物质和糖原沉积形成空泡 . 典型三联征表型：心肌肥厚伴遗传性 WPW、肌无力、和智力发育迟缓。心电图：窦性心律，心室预激（B 型），左心室高电压，ST-T 改变。超声心动图：心室壁异常肥厚、心室腔明显扩大、心功能减退。CMR: 左室向心性肥厚、左室游离壁广泛心内膜钆延迟强化 .

其他：

致心律失常性右室心肌病伴左心室受累一例

马连越

山东大学齐鲁医院

患者基本信息：

患者，男，59 岁

主述：

反复出现心悸、晕厥 4 年，加重 2 月

现病史：

过去 4 年反复出现心悸、晕厥，且近 2 个月症状再次频发入院。4 年前，患者无明显诱因出现阵发性心悸，伴恶心、呕吐、出汗，且多次发生晕厥。心电图（ECG）显示肢体导联 QRS 低电压、V1-V5 导联 T 波倒置；发作时心电图提示左束支传导阻滞（LBBB）形态、电轴向上的非持续性室性心动过速（VT）。经胸超声心动图（TTE）显示左心室（LV）和右心房扩大、左心室离心性肥厚、心尖部室壁瘤，左心室射血分数（LVEF）降至 32%。心脏磁共振（CMR）检查提示双心室扩大、射血分数降低（LVEF 31%，右心室射血分数 RVEF 27%），右心室游离壁局灶性“皱缩”（“手风琴征”）、心尖部轻度膨出；室间隔增厚，左心室及室间隔心肌可见弥漫性钆延迟强化（LGE），提示心肌纤维化。血清免疫固定电泳显示 M 蛋白为 3.97g/L，血清游离 κ/λ 比值正常。患者被诊断为心肌病、射血分数降低的心力衰竭（HFrEF），接受植入式心脏复律除颤器（ICD）、HFrEF 指南指导的药物治疗（GDMT）及胺碘酮（0.2g / 日）治疗。半年前，患者心悸发作，ICD 放电 4 次；2 个月前，心悸加重伴出汗，发作时心电图提示室性心动过速，动态心电图显示多源性室性早搏（22148 次 / 24 小时）

既往病史：

6 年前因胸闷行冠状动脉造影，提示冠状动脉轻度狭窄。有高血压病史及吸烟史，其兄长因不明原因猝死。

病程记录：

入院查体：血压 122/77 mmHg，心率 63 次 / 分，心脏听诊未闻及明显杂音。余体格检查未发现明显异常。入院时心电图显示类似的非持续性室性心动过速，呈左束支传导阻滞形态。血清心肌肌钙蛋白 I 轻度升高（24.31 ng/L，ULN <17.5 ng/L），而冠状动脉计算机断层扫描血管造影（CTA）排除了明显狭窄。NT-proBNP 为 126 pg/mL。血清免疫固定电泳显示 IgM 单克隆蛋白（3.97 g/L），99mTc-PYP 单光子发射计算机断层显像、血清游离轻链（κ/λ 比值正常），脂肪刚果红染色均为阴性。骨髓活检显示淋巴浆细胞浸润，刚果红染色阴性。基因检测发现桥粒芯糖蛋白 2（DSG2）变异（p.G129D 和 p.F531C）。经胸超声心动图显示左心室射血分数改善（50%），但右心室异常持续存在，包括心尖部室壁瘤、右心室壁变薄（3 mm）以及右心室面积变化分数降低（29.8%）。患者基因检测，结果显示桥粒芯糖蛋白 2（DSG2）基因杂合变异【c.386G>A（p.G129D）和 c.1592T>G（p.F531C）】，结合心脏核磁共振检查，考虑患者为致心律失常右室心肌病，累及左室。入院后完善相关检查，鉴于室性心律失常频发及 ICD 放电，建议行射频消融治疗，但患者拒绝。给予胺碘酮（0.2g / 日）控制室性心律失常，继续 HFrEF 的 GDMT 治疗。

检验检查记录：

- 血清心肌肌钙蛋白 I（cTnI）轻度升高（24.31 ng/L，参考值上限 < 17.5 ng/L），N 末端 B 型脑钠肽前体（NT-proBNP）正常（126 pg/ml）。
- 复查冠状动脉计算机断层扫描血管造影（CTA）显示左前降支近端及右冠状动脉远端轻度狭窄，排除梗阻性冠心病（图 5）。
- 血清免疫固定电泳显示 M 蛋白升高，血清游离 κ 链、λ 链轻度升高（分别为 21.42mg/L、54.11mg/L），但 κ/λ 比值正常（0.40）；骨髓检查可见小淋巴细胞伴浆细胞样 / 浆细胞分化浸润，刚果红染色阴性; 99mTc - 焦磷酸盐（PYP）单光子发射计算机断层显像（SPECT）阴性; 心肌活检刚果红染色阴性。结合上述结果及 CMR 表现，排除心脏淀粉样变性，M 蛋白升高诊断为华氏巨球蛋白血症。
- 复查 TTE 显示 LVEF 改善至 50%; 右心室（RV）心尖部局灶性室壁瘤，右心室壁变薄（最薄处 3mm），小梁回声增多（图 6，视频 1），右心室面积变化分数（RVFAC）为 29.8%，提示右心室心肌发育不良及病变持续进展。发作时心电图仍为 LBBB 形态的室性心动过速。

患者符合 2010 年工作组标准（TFC）中的多项诊断标准：①超声心动图显示 RVFAC ≤ 33%，CMR 显示 RVEF ≤ 40%；②V1-V5 导联 T 波倒置；③ LBBB 形态、电轴向上的非持续性室性心动过速。结合既往 DSG2 基因突变的检测结果，诊断为合并左心室受累的心律失常性右室心肌病（ARVC）。建议行心肌活检，但患者拒绝。

鉴别诊断：

①双心室扩大伴 LVEF 降低、心脏核磁共振显示弥漫性 钆延迟强化现象（LGE），需要与扩张型心肌病鉴别。然患者 CMR 显示室间隔增厚，与扩张性心肌病不相符; ②患者存在室性心律失常及心尖部室壁瘤，需排除心肌梗死。患者冠脉造影显示冠脉轻度狭窄，不支持心肌梗死诊断; ③左心室肥厚合并心电图肢体导联低电压，血清免疫固定电泳显示 M 蛋白升高，需鉴别心脏淀粉样变性。99mTc-PYP 单光子发射计算机断层显像、血清游离轻链（κ/λ 比值正常）阴性。骨髓活检显示淋巴浆细胞浸润，刚果红染色阴性。排除心肌淀粉样变性。

其他：

一例特殊的肺高压

彭晓宇

广东省人民医院

患者基本信息：

刘 XX，男，53 岁

主述：

反复胸闷 12 天

现病史：

患者 12 天前开始出现胸闷不适，多于活动后出现，为剑突下闷胀感，每次发作持续 2 小时，可自行缓解，逐渐出现气促、双下肢水肿，无心悸、无阵发性呼吸困难、端坐呼吸等其他不适。患者就诊于我院急诊，心电图检查提示“V1-V4T 波倒置”，高敏肌钙蛋白未见异常。完善冠脉造影：冠脉系统呈右优势型，LM 未见明显狭窄 ,LAD 未见明显狭窄，前向血流 TIMI3 级；LCX 近段狭窄约 30%，前向血流 TIMI3 级；RCA 中段狭窄约 50-60%，前向血流 TIMI3 级。术中诊断：冠状动脉粥样硬化性心脏病，单支血管病变，除外急性心肌梗死，术后急诊转入我科。自发病以来，患者目前精神状态尚可，食欲、睡眠欠佳，大、小便正常。

既往病史：

既往体健，无特殊病史。

个人史：出生原籍，无地方病或传染病流行区居住史，无毒物、粉尘及放射性物质接触史，生活习惯较规律，有吸烟史，吸烟 30 年，40 支 / 天，已戒烟 10 天。

婚育史、家族史：无特殊。

病程记录：

入院后完善心脏超声提示肺高压。

启动肺高压查因相关检查。

给予利尿、氧量等对症治疗。

检验检查记录：

心脏超声提示：右房、右室扩大，重度三尖瓣返流，肺动脉高压。

胸部 CT 提示双肺弥漫性磨玻璃影。

NT-proBNP 14063.0pg/mL ↑；

心肌损伤标志物：高敏肌钙蛋白 T 16.4pg/mL ↑；

心功酶：肌酸激酶 244U/L；肌酸激酶同工酶 MB 160.7U/L(0-25) ↑；乳酸脱氢酶 2261U/L(120-250) ↑；

肝肾功能：肌酐 120.80umol/L ↑；丙氨酸氨基转移酶 41U/L；门冬氨酸氨基转移酶 121U/L ↑；

凝血指标：血浆凝血酶原时间测定 14.80sec ↑，D- 二聚体 (比浊法) 6990ng/mL ↑（0-500）；

肿瘤指标： CA-125 42.29U/mL（0-35）↑； 神经特异性烯醇化酶 (NSE): 79.50ng/mL（0-16.3）↑，其他肿瘤指标未见异常；

风湿免疫指标：体液免疫指标：免疫球蛋白轻链 λ 0.88g/L ↓；补体 C_4 27.0mg/L ↓；补体 C_3 407.0mg/L ↓；抗核抗体谱、血管炎 5 项、血清免疫固定电泳、风湿 / 类风湿指标、抗磷脂抗体综合症筛查组合：均未见异常。炎症指标超敏 CRP(快速）： <0.5mg/L；红细胞沉降率（毛细管法）：正常；

血常规、血脂分析、糖化血红蛋白、甲状腺功能、营养指标均未见异常；

乙肝两对半：乙肝表面抗原、e 抗体、核心抗体：阳性；HBV-DNA：<2.00E+1 IU/mL。

骨髓穿刺：免疫组化提示：（骨髓活检）符合弥漫大 B 细胞性淋巴瘤累及骨髓。

鉴别诊断：

肺高压查因

第一类、动脉型肺动脉高压；

第二类、左心疾病所致肺高压；

第三类、肺病和（或）低氧血症所致肺高压；

第四类、肺动脉阻塞所致肺高压；

第五类、机制未明和（或）多因素所致导致肺高压。

其他：

结合患者检查结果，诊断淋巴瘤相关肺高压

病因治疗及随访：

2022-6-1 开始予 CHOP 方案 (环磷酰胺 + 表柔比星 + 长春新碱 + 甲泼尼龙) 化疗。

2022 年 6 月 25 日 -2022 年 11 月 4 日起续予第 1-6 周期 R-CHOP（利妥昔单抗 + 环磷酰胺 + 表柔比星 + 长春新碱 + 甲泼尼龙 + 泼尼松）+ 泽布替尼方案治疗。

4 周期、6 周期后评价达完全缓解。

胸部 CT 肺部磨玻璃影缓解。

心脏超声：肺动脉压力降至正常。

主动脉根部盲端束（RARB）室早一例

王远龙

上海市第六人民医院

患者基本信息：

患者，男性，68 岁

主述：

反复心悸不适三年余

现病史：

患者三年前无明显诱因下开始出现心悸不适，偶有胸闷，不伴胸痛，无头晕、黑朦、晕厥，无恶心、呕吐，心电图提示频发室早，动态心电图示室早 26000 余次 /24 小时，曾口服多种类抗心律失常药物，疗效欠佳，此次为进一步诊治收入院。

既往病史：

肺结节切除术后，胆囊、阑尾切除史

病程记录：

入院后完善各项辅助检查，排除绝对手术禁忌后，择期行室早射频消融术。

检验检查记录：

血常规、肝肾功能、凝血功能、心肌酶、PRO-BNP、甲状腺功能、电解质均无异常

心电图示频发室早

鉴别诊断：

1. 房早：心电图示提前出现的异形 P′波：P′波形状和窦性 P 波不同。P′波通常不是逆行性的，但若起源于心房下部，其 P′波可为逆行性。P′ -R 间期均大于 0.12s。QRS 波群的形态、时限和基本窦性心律相同。有不完全性代偿间歇。

2. 交界性早搏：心电图示提前出现的 QRS 波，其形态与窦性搏动相同。QRS 波前后可有逆行 P′波，或无逆行 P′波。若 P′波在 QRS 波前，则 P--R 间期 <0.12s；若 P- 在 QRS 波后，则 R-P- 间期 <0.20s。代偿间歇一般为完全性代偿间歇，也可为不完全性代偿间歇。

其他：

起搏器手术后的特殊心电图发现，布鲁加达综合征的异常表现？

覃佐岸

常德市第一人民医院

患者基本信息：

1 例 70 岁老年男性患者既往有“1. 心律失常 病态窦房结综合征 心脏永久起搏器术后 2. 冠状动脉粥样硬化性心脏病 Percutaneous coronary intervention（PCI）术后 3. 高血压 2 级 很高危组 ” 病史，患者因“反复胸闷伴心悸 1 周 ” 于 2022 年 10 月 30 日入院。生命体征显示 :T 36.5 ℃ P 63 次 / 分 R 20 次 / 分 BP 130/59 mmHg 。患者入院心电图提示 Brugada 波（见图 A），2022 年 11 月 03 日行冠脉造影 : 右冠优势型，前降支 : 原支架内管腔丢失 50% 左右，余无异常，行起搏器功能分析 :1. 以自身心律及 AAIR 工作方式为主。2. 起搏器基本参数未见异常，但起搏器程控记录到患者 2021 年 06 月至 2022 年 10 月共记录心房高频事件 64 阵次，持续时间 32 秒至 8 分 4 秒，平均心室率 90-176 次 / 分，共记录心室高频事件 145 阵次，持续时间 2 秒至 16 秒，平均心室率 180-229 次 / 分。因起搏器记录到多次高频心室事件，最长 16 秒，结合患者入院心电图，我们考虑患者 Brugada 综合征诊断，建议患者完善基因检测和考虑植入 ICD 治疗，预防恶性心律失常所致的心源性猝死，但患者拒绝行基因检测和 Implantable cardioverter defibrillators(ICD) 植入术。问题 : 什么原因导致患者在起搏器植入术后出现了 Brugada 波和诱发了恶性心律失常？接下来我们要怎么做？

主述：

反复胸闷伴心悸 1 周

现病史：

患者曾于 2018 年 7 月 16 日因“活动后胸闷” 第一入住我科，诊断为：1. 冠心病 心绞痛型 心功能 I 级 PCI 术 2. 高血压 1 级 高危组 3. 焦虑状态 4. 阑尾切除术后，入院后予以降压、抗栓、稳定斑块、抗冠脉痉挛、改善循环等对症支持治疗后，病情好转，于 2018 年 9 月 14 日予以办理出院。 出院后规律服药，于 2020-08-20 因“为求更换心脏起搏器”第 3 次入住我院我科，完善相关检查诊断为：1. 心律失常：心脏永久起搏器术后 2. 冠心病 PCI 术 3. 高血压 1 级 高危组 4. 焦虑状态 5. 阑尾切除术后。入院后予以抗血小板聚集，调脂、稳定斑块，降压、更换起搏器等治疗，患者术后未诉特殊不适，伤口愈合情况良好，于 2020-08-28 予以办理出院。出院后患者规律服药（氯吡格雷，阿托伐他汀，地尔硫卓等），未诉特殊不适。1 周前患者出现活动后胸闷气促，多于踩单车、快走等中等强度活动后出现，休息 10 余分钟后自行缓解，无其他部位放射，无胸痛大汗、心悸黑矇，无头晕头痛、恶心呕吐，无肢体麻木、活动障碍等其余不适，为求诊治遂再来我院，门诊以“冠心病” 第 4 次收入我科。自此次起病以来，患者精神睡眠尚可，食欲一般，大便不规律，有里急后重感，小便正常，体重减轻，具体未监测。

既往病史：

有高血压病史，服用“缬沙坦 + 盐酸地尔硫卓”降压治疗，血压控制可，有“焦虑状态” 长期服用 “盐酸帕罗西汀片” 及 “艾司唑仑片” 治疗 5. 阑尾切除术后，现未规律

服用药物，有高血压病史，最高血压 160/？ mmHg，现未服用药物，无传染病史，预防接种史随当地进行，有心脏永久起搏器植入及更换史，有冠心病 PCI 术手术史，长期服用“铝镁匹林”“氯吡格雷”，无外伤史，无输血及血制品史，无药物过敏史，无食物过敏史。

病程记录：

2022 年 11 月 3 日，冠状动脉造影显示右冠状动脉占主导地位，前降支支架狭窄 50%，无其他异常。起搏器功能分析显示窦性心律和 AAIR 起搏模式正常。然而，起搏器在 2021 年 6 月至 2022 年 10 月期间记录了 64 次心房高频事件，持续时间从 32 秒到 8 分 4 秒不等，平均心室率为 90-176bpm。此外，记录了 145 次心室高频事件，持续时间为 2-16 秒，平均心室率为 180-229 bpm。根据患者的入院心电图和起搏器数据，考虑诊断为 Brugada 综合征。尽管建议预防恶性心律失常导致的心脏死亡，但患者拒绝接受基因检测和植入式心脏复律除颤器植入。为了解决这个问题，起搏器频率降至 40 bpm，使患者恢复窦性心律。

检验检查记录：

09 月 06 日 B 型脑钠肽前体 102.00 pg/ml，超敏肌钙蛋白 I<0.010 ng/mL，血糖: 葡萄糖 9.88 mmol/L，血常规: 血红蛋白 137.0 g/L，红细胞计数 4.57 ×10^12/L，白细胞计数 4.01 ×10^9/L，中性粒细胞计数 3.14 ×10^9/L，淋巴细胞计数 0.70 ×10^9/L，电解质、肾功能、心肌酶谱未见明显异常。09 月 07 日尿常规：尿蛋白 +-，粪便隐血试验弱阳性，肝功能：总蛋白 63.6 g/L，白蛋白 37.4 g/L，血脂: 低密度脂蛋白 0.74 mmol/L，极低密度脂蛋白 1.09 mmol/L，冠脉造影: 1. 左主段（5 段）：无狭窄。2. 前降支（6-10 段）：7 段可见 80% 狭窄，8 段可见 30% 狭窄，血流 TIMI3 级。3. 回旋支（11-15 段）：无狭窄，血流 TIMI3 级。4. 右冠（1-4 段，15 段）：无狭窄，血流 TIMI3 级。

鉴别诊断：

缺血性心肌病：患者多表现为活动后气促，休息后可缓解，完善冠脉造影检查可明确。

其他：

“捉拿元凶”—— 1 例巨大冠脉瘤引发的思考

刘芮汐

重庆儿童医科大学附属儿童医院

患者基本信息：

患儿，女，11 岁 6 月

主述：

诊断不完全川崎病 8 年，发现冠脉异常 1+ 月，发热 1 天

现病史：

1) 8 年前（3+ 岁）因“发热 20+ 天”在医院甲住院治疗，诊断“不完全川崎病、冠脉扩张（LMCA:3.7mm，LAD:2.6mm）、EB 病毒感染、肝功能异常”，予以抗感染、丙球冲击、阿司匹林、谷胱甘肽治疗好转出院。出院后复查 2 次心脏超声正常，停用阿司匹林（服药时间短，具体不详），后未定期复查。

2) 2+ 月前患儿体检时发现心脏超声提示异常，遂先后于 2023.7.21 及 2023.8.8 至医院乙及医院丙就诊，彩超均提示“巨大左右冠状动脉瘤，主动脉窦部瘤样扩张、左室扩大”，遂于 2023.8.8-8.21 在医院丙住院治疗，期间予以抗凝（先后予低分子肝素、华法林）、抗板（氯吡格雷）、利尿（螺内酯 + 呋塞米）、改善心肌重构（卡托普利）等以症支持治疗，于 2023.8.21 带上述药物出院。

3）近 1+ 天出现低热，热峰 37.8，偶有单双声咳嗽，不伴皮疹、眼红、唇红、指（趾）端硬肿等表现；于 2023.9.4 收入我科。

4）患儿起病以来有多汗、活动耐量下降，无胸痛、胸闷，无浮肿、少尿，无皮肤瘀点瘀斑等出血表现。

既往病史：

既往史：

1）6 年前（5+ 岁）因“发热”于医院甲门诊部就诊，辅助检查提示三系下降、肝脾增大，骨骼涂片无阳性发现，诊断“传染性单核细胞增多症？噬血细胞综合征？”门诊予以抗感染、抗病毒等治疗 10 天，发热好转。

2）此后每年发热 1-2 次，热程 3-4 天，发热时血常规提示以三系下降为主，体温正常后血象好转。

3）1 年前（2022.10.3）因”发热、右侧颈部包块伴脓肿”在医院丙行颌下包块切除，包块活检提示组织坏死伴炎性细胞浸润。

病程记录：

入院后患儿仍有反复中高热。予抗感染（头孢唑肟），改善心肌重构（螺内酯、卡托普利、美托洛尔），营养心肌等对症治疗（因血小板低，入院初暂停了抗凝及抗板治疗）。

检验检查记录：

检验：

凝血功能：PT 15.4 秒，APTT 38.4 秒，INR 1.41。

生化指标：LDH 665(U/L)，尿素 7.8mmol/L，铁蛋白 981 ng/ml，甘油三酯 2.54mmol/L

病原体：EB CA-IgG 阳性、EB EA-IgG 阳性、EB NA-IgG 阳性。全血 EB 病毒 PCR 4.56*105（copies/ml）。

血培养、骨髓培养、T-Spot、G 实验、GM 实验、痰培养、自身抗体、抗人球蛋白试验、风湿四项、肝炎标志物 /HIV/ 梅毒均阴性。转氨酶、电解质、心肌标志物 +BNP、NK 细胞活性正常，NK 和 CTL 细胞脱颗粒功能正常。

检查：

骨髓细胞学：刺激性骨髓象伴噬血现象。

腹部超声：肝脾增大，双肾稍增大，实质回声增强，皮髓质分界欠清。

胸腹部增强 CT：双肺广泛间质性改变，双侧叶间裂增厚，双肾增大，皮髓质可见强化减低区，肝脏脾脏丰满，肝右叶钙化灶，副脾，右侧副肾动脉，盆腔少量积液，子宫较同龄儿小。四肢血管超声正常。

鉴别诊断：

1. 右侧冠状动脉瘤（中型）

2. 右侧冠状动脉血栓形成

3. 左侧冠状动脉主干瘤（巨大型）

4. 左侧冠前降支瘤（中型）

4. 左侧冠状动脉回旋支瘤（中型）

5. 缺血性心脏病

6. 主动脉窦扩张

7. 三系下降原因待查：1）上呼吸道感染 2）血液系统恶性疾病？

8. 川崎病后遗症

10. 心功能 II 级

其他：

讨论：1）患儿是否为川崎病？

2）患儿反复发热伴三系下降及肝脾肿大原因何在？

3）心脏血管病变的原因又是什么呢？

生死罗生门 ——1 例右心房占位的诊治

张文静

郑州大学第一附属医院

患者基本信息：

患者，男，64 岁，农民，于 2025 年 02 月 13 日入院。

主述：

胸闷气喘半年余，颜面部水肿 2 月

现病史：

半年余前活动后出现胸闷气喘，无胸痛，无咳嗽、咳痰、发热，无头晕、黑懵、晕厥，无腹胀、纳差，无双下肢水肿，于当地医院就诊，行动态心电图检查示：窦性心律，频发室早，短阵房速，大于 1.5s 的长 RR 间期 3394 次，建议行冠脉造影及起搏治疗，患者及家属拒绝。后就诊于我院（2024.7.22），行冠脉 CTA 检查示：前降支近中段管壁少许软斑，相应管腔约轻微狭窄，心影增大，心包积液。入院后复查动态心电图 :1. 基础心律为窦性心律 2. 频发房早 3. 短阵房速，阵发性房颤及房扑 4. 偶发室早 5. 偶发交界性逸搏 6.R-R 间期大于 2.0 秒共检出 398 次（其中大于 3.0 秒 40 次），最长 RR 间期 4.07 秒 7.ST-T 未见明显异常的动态变化 8. 心率变异性正常。诊断为“病态窦房结综合征”，于 2024 年 07 月 27 日行“双腔起搏器置入术”。术后 2 天患者出现发热，给予“舒普深”抗感染治疗 1 周，体温恢复正常。于 2024 年 08 月 06 日出院。2024.08.12 因“双下肢肿胀、双下肢紫癜”再次就诊于我院，行下肢血管超声检查示：左侧小腿肌间静脉血栓形成。肺动脉 CTA 未见明确栓塞征象。肺灌注显像示：右肺上叶部分尖段（呈亚肺段）血流灌注略减低区，考虑肺栓塞。皮肤科会诊，考虑“过敏性紫癜”，给予抗凝、糖皮质激素、控制血糖等药物治疗。院外口服“华法林”抗凝，规律监测 PT-INR，INR 稳定达标。

2024.11.07 因乏力住院，胸部 CT（2024.11.08）示：双肺多发磨玻璃影，炎性？较 2024.08.17 新见，双肺多发实性小结节，较前片部分新见，部分稍大，心包微量积液，较前减少。肺动脉 CTA（2024.11.10）示：1. 肺动脉 CTA 未见明确栓塞征象 2. 两肺多发磨玻璃影，较前 2024.11.08 范围稍大；双肺多发实性小结节，较前片变化不大。心包微量积液，双侧胸膜肥厚。继续抗凝、抗感染等治疗。2024.11.07 因乏力住院，胸部 CT（2024.11.08）示：双肺多发磨玻璃影，炎性？较 2024.08.17 新见，双肺多发实性小结节，较前片部分新见，部分稍大，心包微量积液，较前减少。肺动脉 CTA（2024.11.10）示：1. 肺动脉 CTA 未见明确栓塞征象 2. 两肺多发磨玻璃影，较前 2024.11.08 范围稍大；双肺多发实性小结节，较前片变化不大。心包微量积液，双侧胸膜肥厚。继续抗凝、抗感染等治疗。2 月前无明显诱因出现颜面部水肿，间断咯血，就诊于当地医院，将“华法林”调整为“利伐沙班”15mg bid 口服，咯血量较前减少，活动时仍感胸闷气喘。为求进一步诊治来我院，门诊以“1、颜面部水肿查因 2. 心律失常 病态窦房结综合征 双腔起搏器植入术后 3. 肺栓塞 4. 下肢肌间静脉血栓 5. 咯血”收入院。自发病以来，神志清，精神尚可，食欲正常，睡眠差，大小便正常，体重无明显变化。

既往病史：

发现血糖升高 8 个月，口服“二甲双胍维格列汀、阿卡波糖、瑞格列奈”，未规律监测血糖。无高血压病史，无脑血管疾病病史，无肝炎、结核、疟疾病史，预防接种史随社会计划免疫接种，无外伤、输血史，无食物、药物过敏史。

病程记录：

入院后给予华法林钠片 3mg 监测 INR 调整剂量（达标）→利伐沙班 20mg q.d.，阿托伐他汀钙片（立普妥）20mg 晚 1 片，富马酸比索洛尔片 1 片 q.d. →琥珀酸美托洛尔缓释片 1 片 b.i.d.，呋塞米片 20mg 早 1 片，螺内酯片 20mg 早 1 片，氯化钾缓释片 500mg 早晚各 1 片，二甲双胍维格列汀片（Ⅱ） 早晚各 1 片，阿卡波糖片 50mg 三餐前各 1 片等药物治疗。2025 年 2 月 24 日突发胸痛、呼吸困难。行胸部 CT 检查提示右侧胸腔积液。2025 年 2 月 25 日行超声引导下胸腔穿刺引流，引流液为血性。多次送检病理，病理诊断：（右侧胸水）见红细胞背景上中等量淋巴细胞、中性粒细胞、间皮细胞及组织细胞，部分细胞生长活跃，见少量片状分布的胞浆丰富且核仁明显的细胞。（胸水沉渣包埋）：见炎细胞、间皮细胞及组织细胞。镜下见异型细胞，癌不除外，靶细胞少且免疫表型表达不特异。

检验检查记录：

	第 1 次住院	第 2 次住院	第 3 次住院	第 4 次住院	
时间 项目	2024.8.5	2024.8.17	2024.11.8/10	2025.2.15	2025.3.8
胸部 CT	两肺底少许炎症，右肺中叶小结节。心包积液，双侧胸腔少量积液，双肺胸膜增厚，纵隔内多发稍大淋巴结。	双肺底少许炎症，较 2024.8.5 相仿。双肺多发结节，部分新见，考虑炎性，心影增大，心包积液，较前相仿。双肺胸膜增厚，纵隔内多发稍大淋巴结。	双肺多发磨玻璃影，炎性？较 2024.8.17 新见，双肺多发实性小结节，较前片部分新见，部分稍大。心包微量积液。双肺胸膜增厚，纵隔内多发稍大淋巴结，部分减小。	两肺多发磨玻璃影，较前 2024.11.10 增多、范围增大，建议治疗后复查；双肺多发实性小结节，较前片增多、部分增大	右心房形态不规则，局部不规则软组织影。双肺多发结节及类结节，部分较 2025.2.25 稍增大。双侧胸腔积液，右侧减少，左侧新增。
肺动脉 CTA		未见栓塞征象	未见栓塞征象	两肺多发肺栓塞	
左房 CTA				145cm3, 未见血栓	

鉴别诊断：

右房占位考虑：血栓？肿瘤？炎性？其他？

血栓：

原位？起搏导线相关？下肢静脉血栓脱落？

抗凝？溶栓？外科取栓？拔除电极？无导线起搏？

肿瘤：

支持点：心包积液病史；下肢静脉血栓；肺栓塞；下肢紫癜；肺部阴影；抗凝效果差；

不支持点：病程短、进展快，发病率低，是否考虑？

其他：

2025 年 3 月 15 日转入心外科。

于 2025 年 3 月 19 日行右心房占位活检术（明确诊断，解除梗阻）。

手术时间：2025 年 3 月 19 日 13:30-17:40

输血量：红细胞 2u，血浆 400ml，输液量 4500ml，尿量 200ml，出血 1500ml。

病理诊断：

第一次报告：

心脏肿物切除标本

（心脏肿物）梭形细胞瘤，待免疫组化及分子检测进一步明确诊断。

第二次报告：

（心脏肿物）血管肉瘤。

IVUS 指导再开放迂曲 RCA 支架术后 急性冠脉夹层闭塞一例

王剑

中国人民解放军北部战区总医院

患者基本信息：

52 岁，男性

主述：

发作性胸痛半个月，加重 6 小时

现病史：

2023-08-02 外院造影：

RCA 近段重度狭窄

PCI：于 RCA 近段置入支架 1 枚

术后返回病房后患者出现胸痛，下壁导联 ST 段抬高，返台造影提示 RCA 支架以远螺旋夹层形成

辅助检查：CK:834 U/L ↑，CK-MB:108U/L ↑ hs-TNT:1771ng/L ↑ LDL-C：4.48mmol/L ↑ Cr：83.80mmol/L

既往病史：

既往体健，否认高血压、糖尿病病史

病程记录：

入院后急诊行冠脉造影：左冠造影可见 LCX 近段、LAD 中段存在病变，RCA 近段植入支架后夹层，造影可见夹层至 RCA 远段

检验检查记录：

入院后急诊行冠脉造影：左冠造影可见 LCX 近段、LAD 中段存在病变，RCA 近段植入支架后夹层，造影可见夹层至 RCA 远段

鉴别诊断：

急性支架内血栓形成

其他：

像过山车一样的高血压

付新艳

杭州师范大学附属医院

患者基本信息：

患者女，67 岁。

主述：

因“发现血压升高 10 余年，腹痛 1 月”入院。

现病史：

患者于 10 余年前体检时发现血压升高，多次测量血压大于 140/90mmHg，最高血压不详，未规律口服降压药物。1 月前患者因腹痛在当地医院就诊，住院治疗期间予以氨氯地平控制血压，胃镜示食管裂孔疝，反流性食管炎，予以对症治疗后仍有腹痛。今患者来我院就诊，急诊科测量血压 194/131mmHg，主动脉 CTA 未见主动脉夹层，以“高血压急症 腹痛”收住我科继续治疗。

既往病史：

既往抑郁症，口服米氮平，奥氮平，盐酸文拉法辛，舍曲林

病程记录：

入院后予以降血压：比索洛尔 5mg/ 天，诺欣妥 50mg/ 天；护胃抗反流（消化科会诊）：留置胃管减压，禁食，富马酸夫诺拉生片抗反流，莫沙比利促进消化，泮托拉唑静滴护胃；抗焦虑抑郁 (精神心理科会诊)：米氮平片 2.25mg QN，奥氮平片 0.625mg QD，盐酸舍曲林 25mg BID，奥沙西泮 5mg TID；抗感染：哌拉西林钠他唑巴坦 4.5g Q8H；静脉营养支持、补钾。

检验检查记录：

辅助检查：

ü2024-12-17 本院 血常规 (急诊) 白细胞：13.81*10^9/L ↑，中性粒细胞百分数：92.4% ↑，淋巴细胞百分数：5.0% ↓；

üTNI：0.119ng/ml ↑；心肌酶谱：肌酸激酶：36U/L ↓；BNP:364.19 ↑ pg/ml;

ü 凝血常规：D- 二聚体 (D-D)：0.61mg/L FEU ↑；

ü 急诊生化：乳酸脱氢酶：357U/L ↑，钾：3.39mmol/L ↓，钠：134.4mmol/L ↓，氯：97.2mmol/L ↓，血糖：7.98mmol/L ↑，血清淀粉样蛋白 A：38.9mg/L ↑；

ü 肺部及上腹部 (CT)：提示支气管病变，肺气肿，两肺炎症；心影饱满，升主动脉增宽，主动脉壁钙化，心包局部稍厚；两侧胸膜局部稍毛糙增厚，胆囊未见明确显示，胆囊术后考虑；膀胱过度充盈，左肾周少许渗出；子宫混杂低密度灶，肌瘤？

ü2024-12-17 胸主动脉 - CTA(CT)：所示胸、腹主动脉未见明显异常，主动脉弓及降主动脉局部管壁钙化。

鉴别诊断：

血管急症（主动脉夹层夹层、肠系膜缺血）： 高血压是核心危险因素，腹痛是核心症状。

隐匿的心梗： 老年女性症状可能不典型。

嗜铬细胞瘤： 阵发性高血压 + 腹痛的组合。

胆胰疾病和憩室炎： 在老年人中常见。

其他：

此病例在临床上需抽丝剥茧，步步为营，同时需要内外科，多学科一起讨论制定治疗方案。

师出不利“逆”转得胜 ---LCX-CTO 伴 LM 重度狭窄逆向开通一例

任何

空军军医大学唐都医院

患者基本信息：

患者男性，55 岁。

主述：

间断性胸闷、气短 6 月余，加重 2 月。

现病史：

6 月前无明显诱因后出现胸闷，伴气短，位于心前区，呈一过性，不伴有心慌、出汗，无恶心、呕吐等。期间未重视，未治疗。2 月前患者劳累后再次出现上述症状并加重，表现为持续时间延长，活动耐量下降，同时夜间憋醒，后在外院就诊完善冠脉 CTA 提示重度狭窄伴钙化。为求进一步诊治，来我院以“冠心病”收住。

既往病史：

高血压病病史 8 年，血压最高时达 200/100mmHg，目前口服药物降压。2 型糖尿病病史 3 年。

病程记录：

入院后予以抗板、调脂及降压、控糖等治疗。完善相关检查后 CAG，但术中发生导管打折。经冷静处理后，应用逆向技术成功开通 LCX 闭塞血管。

检验检查记录：

血常规：WBC 7.53×109 /L、NEUT 62.4%、PLT 303×109 /L、HGB 172 g/L

肾功：Cr 70.3umol/L，eGFR 120.18ml/min

空腹血糖：6.63mmol/L

血脂：TC 6.4mmol/L、TG 2.82 mmol/L、 LDL-C 4.58mmol/L

肝功、凝血、甲功、尿便常规未见明显异常。

鉴别诊断：

无

其他：

无

心肌梗死后巨大室壁瘤患者治疗路径探寻

薛亚军

北京清华长庚医院

患者基本信息：

51 岁，男，入院时间：2022.9.26

主述：

间断胸痛、呼吸困难 5 年，加重 8 月

现病史：

患者饭后散步时突发胸闷、气短，无胸痛、心悸、黑矇、大汗等，症状持续数小时，就诊于襄阳市中医院，心电图：左前分支传导阻滞，V1-V5 导联 ST 段抬高；CK-MB 升高，诊断“急性前壁心肌梗死”。行冠脉造影结果示：前降支近段闭塞，回旋支中段 60% 狭窄，于前降支植入支架 1 枚。超声心动图: 左室增大，LV 5.9cm，室间隔增宽，节段性室壁运动异常，EF 52%。

术后予阿司匹林、替格瑞洛、沙库巴曲缬沙坦、琥珀酸美托洛尔、地高辛、呋塞米、螺内酯口服。术后患者曾出现发热，体温波动于 38.5-39℃，自觉左侧卧位时可出现胸痛，予“激素”治疗 4 天后好转。

术后第 13 天下地活动时曾再发胸闷，程度较轻，后未诉明显不适，但活动耐量明显减低，步行 100-200 米即因气短、乏力需要休息。后患者活动耐量缓慢恢复，可至耐受慢走 2000 米。

（2022-04）爬山后当晚睡觉时出现呼吸困难，不能平卧，无下肢水肿，无明显胸痛。当地医院住院诊断考虑“急性左心衰”，药物治疗后好转，出院后规律口服琥珀酸美托洛尔、沙库巴曲缬沙坦、利尿剂，间断活动时心前区针刺样疼痛、偶有后背闷痛，伴胸闷、呼吸困难、活动耐力下降，慢走 1000m 或爬半层楼即出现症状，休息数分钟好转，无夜间阵发性呼吸困难，无水肿。

（2022-07）就诊武汉亚洲心脏病医院，复查超声心动图：左房扩大、左室明显扩大，左室节段性室壁运动异常；心尖部室壁瘤形成（6.3*3.3cm），左室收缩功能间断，EF24%。左心声学造影节段性心肌组织造影剂充盈不全，提示心肌血流灌注不良；心脏磁共振：左室继发性扩张性心肌病，LA 39.5mm，LV 70.3mm；中部至心尖部左室巨大室壁瘤（9.36*5.67cm）伴附壁血栓形成，左室非活性心肌比例约 25%；左室舒张功能、收缩功能明显减低，LVEF 25%。

冠脉造影（07-13）：前降支自起始段完全闭塞。钝缘支 60% 狭窄，右冠远段 70% 狭窄，后降支 80% 狭窄，左室后支 60% 狭窄，未行介入治疗。

（2022-09）收入院 CCU，2022-09-26 行冠状动脉造影检查，结果提示：LAD 支架内再狭窄；左前降支近段：狭窄程度 100% 完全闭塞；左前降支近段介入治疗（扩张球囊）。予患者阿司匹林、替格瑞洛双联抗血小板，阿托伐他汀、琥珀酸美托洛尔缓释片、培哚普利等冠心病二级预防治疗，利尿治疗维持出入量负平衡。

既往病史：

高血压病史 10 年，血压最高 155/90 mmHg，平素规律口服琥珀酸美托洛尔，血压控制可；

高脂血症 1 年，平素规律口服阿托伐他汀。

病程记录：

LAD 供血区心肌血流灌注大范围严重受损，大室壁瘤形成（累及广泛心尖段、前壁中段和部分前壁基段、前问隔中段、部分前侧壁中段），梗死心肌为主，仅侧壁基底段及下壁基底段室壁运动良好，推测患者从血运重建术获益的可能性很小，而受益于室壁瘤切除术 + 左心室成形术的可能性也不大。

严重心室重构：左心室整体收缩功能重度受损，手术风险大。

左心室心肌机械收缩同步性极差。

检验检查记录：

血常规：HGB 113g/L，余大致正常；

肝肾功能、电解质：正常；

凝血六项：PT 12.3s，APTT 25.6s，D-dimer 2.07mg/LFEU，FDP 6.06mg/L；

心肌损伤标志物：CK、CK-MB、MYO 大致正常，NT-proBNP 1127pg/ml，TnT-hs 0.0189ng/ml；

血脂：TCHO 2.94mmol/L，TRIG 1.39mmol/L，LDL-C 1.53mmol/L；

尿酸： 289 umol/L(正常)

超声心动图

（2022-9-23，我院）左室增大，左室心尖部室壁瘤形成；二尖瓣少量反流；左室壁节段性运动异常，射血分数减低，左室射血分数 25%；左室舒张功能减低。

（2022-10-07 ，我院）左室增大，左室心尖部室壁瘤形成；左心腔内浓密自发显影；二尖瓣少量反流；左室壁节段性运动异常；左室整体收缩及舒张功能减低，左室射血分数 22 %。

动态心电图（2022-9-23，我院）

（2022-9-23）窦性心律（总心搏数 99128 次，平均心率 70 bpm）；偶发房性早搏，可见成对型房早；陈旧性广泛前壁心肌梗死；ST-T 改变符合前壁室壁瘤心电图改变。

24h 动态血压（2022-9-23，我院）

（2022-9-23）全天平均: 109/66mmHg，日间平均: 111/68mmHg，夜间平均: 105/61mmHg。

鉴别诊断：

1. 冠状动脉粥样硬化性心脏病

陈旧性前壁心肌梗死

左心室室壁瘤

窦性心律

左心扩大

心功能 II 级（NYHA 分级）

冠状劫脉支架植入术后状态

冠状动脉支架植入术后再狭窄

2. 慢性心力衰竭

3. 高血压病 1 级 很高危

4. 高脂血症

5. 轻度贫血

其他：

对于心梗后室壁瘤形成，药物治疗是基石，但预后较差，急诊 PCI 可减少心梗后室壁瘤发生率，晚期室壁瘤患者是否采用介入治疗进行再血管化存在争议

外科切除室壁瘤可部分改善预后，但围术期死亡率较高，心脏移植的迅速发展，可能成为了终末期心脏病患者最终的治疗方法

借助器械进行左室重建颇具前景，微创植入较开胸手术更具吸引力

冠脉搭桥术后 LIMA 桥血管闭塞再开通 1 例病例探讨

王海锟 Wang

第八师石河子市人民医院

患者基本信息：

男，50 岁

主述：

间断胸痛 14 年，加重 1 周

现病史：

14 年前无明显诱因间断心前区疼痛不适，每次持续 5 分钟左右自行缓解，自觉症状活动后易发作，曾就诊当地乌鲁木齐某医院，行冠脉介入治疗植入 4 枚冠脉支架（具体不详），术后症状好转。7 年前无明显诱因胸部症状再次出现，就诊于当地医院行冠脉搭桥，术后规律口服药物。2024 年 7 月胸部症状再次出现，就诊于北京当地医院考虑急性心肌梗死，急诊行冠脉介入治疗，术中植入 2 枚支架及球囊（具体不详），调整药物“阿司匹林肠溶片、硫酸氢氯吡格雷片、阿托伐他汀钙片、单硝酸异山梨酯缓释片、依洛尤单抗”诊疗。1 周前症状再发，就诊新疆医科大学第一附属医院完善冠脉 CTA 示：1. 左主干混斑，合并管腔轻度狭窄；2. 前降支近中远段支架术后，支架管壁钙斑，支架内造影剂填充欠均匀，远端血管显示纤细，支架再狭窄可能，前降支远端搭桥术后表现，血管显示断续，管腔内部分造影剂未见填充，再狭窄或闭塞可能；3. 回旋支近段支架术后，支架管壁钙斑，其内低密度充盈缺损影，再狭窄或闭塞可能，远端血管显示纤细；升主动脉与回旋支远端搭桥术后表现，管腔内造影剂未见填充，考虑桥血管闭塞；升主动脉与右冠状动脉远端搭桥术后表现；升主动脉丘状突起，考虑桥血管闭塞；4. 右冠状动脉近段混斑及软斑，合并管腔中重度狭窄，右冠状动脉中远段支架术，调整药物治疗后仍有症状间断发作，急诊以“心绞痛”收住。

既往病史：

否认病毒性肝炎、肺结核、伤寒、疟疾病史，否认高血压、糖尿病、高血脂病史，否认脑血管疾病史，否认精神病史、地方病史、职业病史。有手术史，幼年行阑尾炎手术，7 年前行冠脉搭桥术，否认外伤、输血、中毒史，否认药物、食物过敏史，预防接种史不详。

病程记录：

见 PPT 内容

检验检查记录：

见 PPT 内容

鉴别诊断：

见 PPT 内容

其他：

无

OCT 精准指导联合 QFR 处理分叉病变治疗一例

薛亚军

北京清华长庚医院

患者基本信息：

姓名：杨某某

性别：男

年龄：58 岁 1 月

婚姻：已婚

民族：汉族

职业：自由职业者

出生地：北京市市辖区昌平区

主述：

间断胸痛 14 年，加重半月 间断胸痛 14 年，加重半月

现病史：

患者 14 年前活动发作心前区闷痛，呈针扎样，范围巴掌大小，放射左侧背部，不伴大汗、心悸、头晕、头痛、恶心、呕吐、黑矇、晕厥等不适，持续 1-2 分钟，休息后症状缓解，发作频率 1-2 次周，后就诊外院完善冠脉 CTA 未见明显异常（具体不详），后症状间断发作未进一步诊治。半月前胸痛加重，性质同前，发作频率较前增加至 5-8 次天，持续时间数分钟，休息或含服速效救心丸后症状可缓解，就诊我科门诊完善心电图示“窦性心动过缓”完善冠脉 CTA 示冠状动脉粥样硬化，LAD 心肌桥，现为求进一步诊治收入我科。自发病来患者饮食睡眠可，二便正常，近期体重未见明显变化。

既往病史：

既往史： 否认高血压、糖尿病、高脂血症、脑血管病、肾病病史，否认肝炎、结核等传染病史，8 年前因左肾结石曾行输尿管支架植入术，否认外伤及输血史，否认药物、食物过敏史。

个人史：吸烟 40 年，8-10 支天，未戒；偶饮酒。否认疫区、疫水接触史。否认毒物、放射性物质接触史。

病程记录：

患者中年男性，慢性病程，急性加重，考虑不稳定性心绞痛入院，完善相关检查示: 血常规、肝肾功能、凝血、感染、甲状腺功能、糖化血红蛋白、尿酸、同型半胱氨酸未见明显异常，检查示：动态血压监测：24 小时平均血压 11870mmHg, 日间平均血压 11870mmHg, 夜间平均血压 11674mmHg。超声心动图：二尖瓣少量反流，左室整体收缩功能正常（LVEF 66%），舒张功能未见明显异常。颈动脉超声：双侧颈动脉粥样硬化斑块形成。心脏康复评定：“1. 胸痛或胸部不适明显缓解，生命体征稳定；2. 心肺耐力减低，易疲劳；3. 平衡功能正常、协调能力正常。” 除外禁忌后 2023.6.8 行冠脉造影检查示左前降支中段狭窄程度 70-90%，第一对角支 a 狭窄程度 70-90%，左前降支近段狭窄程度 50-70%，回旋支远段狭窄程度 50-70%，右冠状动脉中段、远段狭窄程度 30-50%， 考虑冠状动脉粥样硬化性心脏病，双支病变 (累及 LAD、LCX)；于第一对角支行球囊扩张保护下于前降支植入支架 2 枚，手术过程顺利，术后患者安返病房。术后继续予阿司匹林、氯吡格雷抗血小板，低分子肝素抗凝 3 天，患者冠心病明确建议控制低密度脂蛋白≤ 1.4mmolL，故高胆固醇血症诊断明确，予瑞舒伐他汀调脂稳定斑块，并加用培哚普利改善心室重构，琥珀酸美托洛尔控制心室率抑制交感激活。反酸烧心方面考虑胃食管反流，加用富马酸伏诺拉生抑酸治疗。

检验检查记录：

生 化： ALT 13.8 UL, AST 17 UL, ALP 103 UL, TBIL 8.2 umolL, DBIL 3.2 umolL, BUN 7.4 mmolL, CRE 88 umolL, eGFR 83.049 单位 mlmin1.73m^2, UA 301 umolL, K 4.63 mmolL, Na 141.2 mmolL, Cl 105.2 mmolL, CHOL 5.05 mmolL, TRIG 1.07 mmolL, HDL-C 1.42 mmolL, LDL-C 3.26 mmolL,

心肌损伤标志物： CK 175 UL, CK-MB 2.31 ngmL, MYO 39.3 ngmL, NT-ProBNP 68.1 pgml, TnT-hs 0.00536 ngmL,

甲状腺功能 T4 87.4 nmolL, Free-T4 15.9 pmolL, T3 1.61 nmolL, Free T3 4.62 pmolL, TSH 1.47 μIUmL,

糖化血红蛋白 Hb-A1c 5.5 %,

冠脉 CTA：冠状动脉粥样硬化（DA2 近段管腔中 - 重度狭窄），LAD 心肌桥

超声心动图：二尖瓣少量反流，左室整体收缩功能正常（LVEF 66%），舒张功能未见明显异常。

动态心电图：1. 窦性心律（总心搏数 89901 次 平均心率 62bpm 最慢心率 40bpm 发生于 0453 最快心率 114bpm 发生于 1308）2. 偶发房性早搏。

鉴别诊断：

1. 冠状动脉粥样硬化性心脏病

不稳定性心绞痛

窦性心动过缓

心脏不大

心功能 I 级 (NYHA 分级)

2. 冠状动脉肌桥

3. 高胆固醇血症

4. 双侧颈动脉粥样硬化 5. 反流性食管炎

其他：

血压“失控”背后的危机——一例高血压合并肾动脉狭窄与主动脉夹层的综合介入治疗与强化管理

吴皓宇

陕西省人民医院

患者基本信息：

男性， 60 岁，身高 :163cm， 体重 :80kg，BMI:30.1kg/m2。

主述：

发现高血压 10 年，血压控制不佳 1 月

现病史：

10 年前出现头晕，测血压 160/100mmHg，后多次不同日测血压均高于 140/90mmHg，最高血压 180/100mmHg，口服“厄贝沙坦、美托洛

尔”降压，血压 140/80mmg 左右。1 月前患者出现间断头痛，测血压最高 203/110mmHg，口服厄贝沙坦氢氯噻嗪片 150mg 一日一次、苯磺酸氨氯地平片 5mg 一日一次、卡维地洛片 12.5mg 一日两次，血压波动于 160/100mmHg 左右。

既往病史：

-

病程记录：

肾动脉 CTA 提示左肾动脉狭窄，主动脉 CTA 提示腹主动脉夹层。

检验检查记录：

详见 PPT

鉴别诊断：

-

其他：

对高血压患者需实施“病因 - 病变 - 靶器官”的系统评估，方能实现精准诊疗。

ECMO 联合 IABP 支持下 CHIP 介入治疗一例

王宁

北京大学国际医院

患者基本信息：

76 岁，女性

主述：

间断胸痛 18 年，加重 2 天

现病史：

详见 PPT

既往病史：

冠心病，五次 PCI 史（2004、2011、2013 、2021、2023），高血压 10 余年，糖尿病 10 余年

病程记录：

详见 PPT

检验检查记录：

详见 PPT

鉴别诊断：

详见 PPT

其他：

详见 PPT

一种新型 pVAD 支持下复杂高风险 PCI

张羽宣

浙江大学医学院附属第二医院

患者基本信息：

男性，71 岁，BMI 21.6

主述：

反复胸痛 15 年，加重 4 月

现病史：

患者 15 年前出现反复胸痛，持续性，无放射痛，无头晕头痛、无畏寒发热、无腹痛腹胀等不适，可自行缓解，未予重视。4 月余前胸痛加重，活动后明显，遂至外院就诊，2024-06-13 冠脉造影提示前降支至左主干 80-90% 狭窄，回旋支开口 90%，右冠 CTO。干 2024-06-20 行冠状动脉旁路移植术 (LIMA-LAD, 大隐静脉 -D1-LCX，大隐静脉 -RCA)。术后 1 月胸痛再发，每次持续半小时余，含服硝酸甘油后 5 数分钟可缓解，2024-08-09 冠脉造影提示桥血管闭塞。现为寻求进一步救治至我院门诊就诊，门诊拟“冠状动脉粥样硬化性心脏病”收治入院。

既往病史：

既往高血压病史 10 余年，自述血压控制可。

既往糖尿病病史 3 年，口服达格列净治疗，自述血糖控制可。

自病来，患者神志清，精神软，睡眠可，胃纳可，大小便无殊，近期体重无明显变化。

病程记录：

【检验】：

2024-09-12 10:19 血常规 (五分类): 白细胞计数 :6.8*10^9/L，血红蛋白 :147g/L，血小板计数 :223*10^9/L; 2024-09-12 10:56 凝血功能组合 (全套):D- 二器体 :370ug/L; 2024-09-12 12:50 甲状腺激素全套 : 总三碘甲状腺原氨酸 TT3:2.35 nmol/L，游离三碘甲状腺原氨酸 FT3:6.38 pmol/l;2024-09-12 13:31 肝功能常规 (省标)+ 血脂常规 (省标 / 空腹)+ 电解质常规 + 心肌功能组合 + 葡萄糖 (空腹)+ 肾功能常规 (省标): 肌钙蛋白 -T:0.016 ng/mL，肌酐 :80.04mol/L，肾小球滤过率 :85.43 ml/min，白蛋白 :41.8g/L，甘油三酯 :0.90mmol/L, 总胆固醇 :2.96 mmo1/ ↓, 低密度脂蛋白胆固醇 :1.38mmol/L，钾 :4.37mmol/L，钠 :139.9mmol/L，总胆红素 :18.7umol/L，丙氨酸氨基转移酶 :19U/L，天冬氨酸氨基转移酶 :19U/L; 2024-09-12 14:11 BNP:B 型利钠肽 :375.7 pg/mL;

【检查】：

2024/9/12: 三维超声心动图 :CABG 术后，左室心肌节段性运动异常，左心增大，左心功能减低 : 主动脉瓣中 - 大量反流 ; 二尖瓣少量反流。2024/9/13:CT 冠状动脉造影 (新双源): 冠脉搭桥术后，桥血管部分闭塞。2024/9/16: 心肌代谢存活显像 : 心肌静息灌往、葡萄糖代谢显像 (DISA 显像): 左室下壁、下侧壁心肌梗塞，梗塞区内有部分心肌存活 (占整个左心室比率为 5.8%)。2024/9/16: 静息心肌灌往显像 : 心肌静息灌往、葡萄糖代谢显像 (DISA 显像): 左室下壁、下侧壁心肌梗塞，梗塞区内有部分心肌存活 (占整个左心室比率为 5.8%)。2024/9/18: 负荷心肌灌注显像 : 药物负荷与静息下心肌血流灌注显像示 : 左室下壁及下侧壁心肌梗死，其周围存在轻度心肌缺血。2024/9/18: 浅表软组织肿块 (单部位) 彩超 : 目前右侧腹股沟所示部分未见明显异。2024/9/20: 单侧肢体动、静脉彩超 (右) 下肢 : 右侧下肢动脉粥样硬化伴多发斑块形成 ; 右侧下肢深静脉未见明显异常。2024/9/20: 肾输尿管膀胱前列腺彩超 : 左肾多发囊肿 ; 右肾、双侧输尿管、膀胱未见明显异常。

【介入及治疗】：

排除禁忌 2024-09-18 后机械辅助装置下 PCI 治疗，术中见 : 右冠中段 100% 狭窄，慢性完全闭塞性病变，可见钙化，TIMI 血流 0 级 ; 前降支近段 90% 狭窄，弥漫性病变，可见钙化，TIMI 血流 3 级 ; 回旋支近段 95% 狭窄，弥漫性病变，可见钙化，TIMI 血流 3 级 ; 左主干 50% 狭窄，分病变，可见钙化，TIMI 血流 3 级 ; 回旋支远段 100%,慢性完全闭塞性病变,血流 TIMI0 级 ;A0-SWG-DIG1 未见狭窄。前降支中段植入一枚支架、回旋支近段植入枚支架、左主干植入支架一枚，过程顺利。术后患者伤口无渗血血肿，予抗血小板、降脂稳定斑块、改善心功能、降压、降糖、护胃等对症支持治疗。

【复查】：

2024-09-20 07;55 (急诊) 血常规 +CRP: 白细胞计数 :7.9*10^9/L，全血 CRP:17.6 mg/L 个，血红蛋白 :122 g/L，血小板计数 :169*10^9/L;2024-09-20 07:37(急诊) 血生化常规 +(急诊) 肝功能 +(急诊) 心肌功能组合 : 天冬氨酸氨基转移酶 :41 U/L，肌钙蛋白 -T:0.447 ng/mL，钾 :4.35mmo1/L，钠 :139.1mmo1/L，肌酐 :63.6umo1/L，白蛋白 :36.6g/L，丙氨酸氨基转移酶 :16U/L;202409-19 12:30 血脂常规 (省标 / 空腹): 甘油三酯 :0.83mmol/L，总胆固醇 :2.89 mol/L，低密度脂蛋白胆固醇 :1.40mmol/L;2024-09-20 09:11 凝血功能组合 (全套):D- 二聚体 :350ug/L(FEU);2024-09-20 11:49BNP:B 型利钠肽 :436.6 pg/mL; 2024/9/20: 三维超声心动图 :CABG 术后，左室心肌节段性运动异常 , 左房偏大，左心功能正常低值 ; 主动脉瓣中等量反流，升主动脉增宽 ; 二尖、三尖少量反流。

检验检查记录：

【检验】：

2024-09-12 10:19 血常规 (五分类): 白细胞计数 :6.8*10^9/L，血红蛋白 :147g/L，血小板计数 :223*10^9/L; 2024-09-12 10:56 凝血功能组合 (全套):D- 二器体 :370ug/L; 2024-09-12 12:50 甲状腺激素全套 : 总三碘甲状腺原氨酸 TT3:2.35 nmol/L，游离三碘甲状腺原氨酸 FT3:6.38 pmol/l;2024-09-12 13:31 肝功能常规 (省标)+ 血脂常规 (省标 / 空腹)+ 电解质常规 + 心肌功能组合 + 葡萄糖 (空腹)+ 肾功能常规 (省标): 肌钙蛋白 -T:0.016 ng/mL，肌酐 :80.04mol/L，肾小球滤过率 :85.43 ml/min，白蛋白 :41.8g/L，甘油三酯 :0.90mmol/L, 总胆固醇 :2.96 mmo1/ ↓, 低密度脂蛋白胆固醇 :1.38mmol/L，钾 :4.37mmol/L，钠 :139.9mmol/L，总胆红素 :18.7umol/L，丙氨酸氨基转移酶 :19U/L，天冬氨酸氨基转移酶 :19U/L; 2024-09-12 14:11 BNP:B 型利钠肽 :375.7 pg/mL;

【检查】：

2024/9/12: 三维超声心动图 :CABG 术后，左室心肌节段性运动异常，左心增大，左心功能减低 : 主动脉瓣中 - 大量反流 ; 二尖瓣少量反流。2024/9/13:CT 冠状动脉造影 (新双源): 冠脉搭桥术后，桥血管部分闭塞。2024/9/16: 心肌代谢存活显像 : 心肌静息灌往、葡萄糖代谢显像 (DISA 显像): 左室下壁、下侧壁心肌梗塞，梗塞区内有部分心肌存活 (占整个左心室比率为 5.8%)。2024/9/16: 静息心肌灌往显像 : 心肌静息灌往、葡萄糖代谢显像 (DISA 显像): 左室下壁、下侧壁心肌梗塞，梗塞区内有部分心肌存活 (占整个左心室比率为 5.8%)。2024/9/18: 负荷心肌灌注显像 : 药物负荷与静息下心肌血流灌注显像示 : 左室下壁及下侧壁心肌梗死，其周围存在轻度心肌缺血。2024/9/18: 浅表软组织肿块 (单部位) 彩超 : 目前右侧腹股沟所示部分未见明显异。2024/9/20: 单侧肢体动、静脉彩超 (右) 下肢 : 右侧下肢动脉粥样硬化伴多发斑块形成 ; 右侧下肢深静脉未见明显异常。2024/9/20: 肾输尿管膀胱前列腺彩超 : 左肾多发囊肿 ; 右肾、双侧输尿管、膀胱未见明显异常。

【复查】：

2024-09-20 07;55 (急诊) 血常规 +CRP: 白细胞计数 :7.9*10^9/L，全血 CRP:17.6 mg/L 个，血红蛋白 :122 g/L，血小板计数 :169*10^9/L;2024-09-20 07:37(急诊) 血生化常规 +(急诊) 肝功能 +(急诊) 心肌功能组合 : 天冬氨酸氨基转移酶 :41 U/L，肌钙蛋白 -T:0.447 ng/mL，钾 :4.35mmo1/L，钠 :139.1mmo1/L，肌酐 :63.6umo1/L，白蛋白 :36.6g/L，丙氨酸氨基转移

酶 :16U/L;202409-19 12:30 血脂常规 (省标 / 空腹): 甘油三酯 :0.83mmol/L, 总胆固醇 :2.89 mol/L，低密度脂蛋白胆固醇 :1.40mmol/L;2024-09-20 09:11 凝血功能组合 (全套):D- 二聚体 :350ug/L(FEU);2024-09-20 11:49BNP:B 型利钠肽 :436.6 pg/mL; 2024/9/20: 三维超声心动图 :CABG 术后，左室心肌节段性运动异常 , 左房偏大，左心功能正常低值 ; 主动脉瓣中等量反流，升主动脉增宽 ; 二尖、三尖少量反流。

鉴别诊断：

患者诊断明确，无需鉴别诊断。

其他：

无

暴发性心肌炎后的顽固心衰 1 例

董佳佳

博尔塔拉蒙古自治州人民医院

患者基本信息：

患者，男，23 岁

主述：

间断胸闷气短 6 月余

现病史：

患者诉 6 个月前受凉后出现咳嗽、咳黄色黏痰，无发热，行走 500-1000 米时感胸闷、气短，休息后缓解，夜间阵发性呼吸困难，端坐呼吸，于 2023 年 12 月 20 日就诊我院急诊科，心电图提示（图 1）：窦性心动过速，左前分支传导阻滞，V1-4 导联 R 波递增不良，频发室性早搏，床旁心脏彩超提示：双房左室增大，左室室壁运动幅度明显减低，二尖瓣、三尖瓣中度反流，肺动脉压轻度增高，EF:36%,NT-proBNP：9243.70pg/ml，血常规白细胞计数 10.08×109/L，中性粒细胞 75.1%，肌钙蛋白 I 0.45ng/ml，丙氨酸氨基转移酶 97U/L，门冬氨酸氨基转移酶 133U/L，以“急性心衰”收住院，住院初步诊断为 1. 扩张性心肌病？频发室性期前收缩，心功能 IV 级，上呼吸道感染 治疗上给予抗感染、利尿、强心、扩管等对症支持治疗效果欠佳转上级医院，完善心脏 MRI 检查：左心腔增大，室壁运动普遍减弱，左室心肌前壁、侧壁、后壁及下壁，心肌层及心外膜下延迟强化，考虑为病毒性心肌炎，住院期间间断发热，完善检查诊断为甲流，给予抗病毒，免疫球蛋白，纠正心衰治疗，症状好转后出院。于 2024 年 1 月 22 日无明显诱因再次出现胸闷、气短，腹胀，干呕，端坐位呼吸，再次就诊我院，心电图提示：频发室性早搏，短阵室性心动过速，心率 103 次 / 分，QRS 波时限 120ms（图二），D- 二聚体 1.88mg/L，NT-proBNP：17166.2pg/ml，以“充血性心衰”收入院，起病以来患者神志清、精神差，小便量少，纳差，夜间高枕卧位，有夜间憋醒，端坐位呼吸。

既往病史：

无系统疾病、慢性病史

病程记录：

患者入院时体温 36.2 ℃，脉搏 110 次 / 分，呼吸 25 次 / 分，血压 100/70mmHg，神志清，急病面容，呼吸急促，端坐呼吸，双肺底可闻及干湿啰音，心界向左下扩大，律不齐，二尖瓣及三尖瓣可闻及 2/6 级收缩期吹风样杂音，腹平软，无压痛及反跳痛，无颈静脉怒张，肝颈静脉回流征阴性，双下肢轻度水肿。口服治疗给予利伐沙班 15mg 每天一次 , 托拉塞米片 5mg 每天一次 , 螺内酯 10mg 每天一次 , 氯化钾缓释片 1g 每天三次 , 沙库巴曲缬沙坦 25mg 每天两次 , 达格列净 10mg 每天一次 , 琥珀酸美托洛尔 71.25mg 每天一次 , 盐酸伊伐布雷定 2.5mg 每天一次 , 辅酶 Q10 10mg 每天三次 , 曲美他嗪 20mg 每天三次等治疗后患者症状稍改善，建议行心内膜活检进一步明确诊断，取得家属配合后，转北京阜外医院，行心肌活检提示符合愈合中的淋巴细胞性心肌炎，治疗上加用激素等对症支持治疗。随访：近半年密切随访，临床试验数据无明显改善，期间患者因心衰多次就诊，建议行心脏移植，因经济问题患者家属拒绝，根据心电图表现胸前导联 R 波递增不良，心脏核磁心肌纤维化严重，室早为多源性，射频消融效果差，经评估患者有行 ICD 或 CRT-D 适应症 .

检验检查记录：

超声心动图 :LA 50mm，LV 65mm，IVS 10mm, LVPW 9mm，RA 55*42mm，RV 29mm，EF 26%，TAPSE 15mm，S’ 7cm/s，肺动脉收缩压 41mmHg，心肌受累疾患，全心增大，二尖瓣中大量返流，三尖瓣中大量返流，心功能减低，左室心尖部血栓形成。双下肢动静脉彩超：双侧下肢动脉未见明显异常，双侧下肢深静脉血流通畅，左侧小隐静脉内血栓形成 (陈旧性 ?)。动态血压监测 ; 全天平均血压 94/57mmHg，心率 92 次 / 分，全天平均血压低 (舒张压)，收缩压昼夜节律呈非勺型，舒张压昼夜节律呈勺型。动态心电图 : 平均心率 96 次 / 分，最慢心率 82 次 / 分，最快心率 123 次 / 分，室早 17993 次，室速 161 阵，窦性心律，偶发房早，频发室早。胸部 CT 平扫提示 1. 两肺轻淤血 ; 左肺下叶小片状实变影，炎症可能 ; 双侧微少量胸腔积液。2. 心影增大。3. 肺循环高压可能。头颅 CT 平扫未见明显异常，冠状动脉 CT:1. 冠状动脉未见钙化灶 ; 冠状动脉呈右优势型 ; 各支冠状动脉主要节段未见明确狭窄，2. 全心增大，左室心肌变薄，游离壁部分心肌纤维化，左室心尖部附壁血栓形成，考虑心肌受累疾患。3. 房间隔膨凸瘤。心脏平扫磁共振 : 左心增大伴左室收缩功能重度减低，左室心肌水肿可能，心脏增强磁共振 ; 心肌多发强化，左室心尖部附壁血栓 (小) 形成，结合临床考虑心肌炎性疾患所致可能性大。静息心肌灌注显像 (SPECT)+ 心肌代谢显像 (PET):1. 左室心肌灌注及代谢弥漫不均匀性受损，以前壁心尖段及中段、侧壁为著，心肌坏死，符合心肌受累疾患改变 ;2. 左室功能评价 : 左室心腔增大，左心室各壁运动弥漫减弱，LVEF:29%。心内膜活检病理诊断：符合愈合中的淋巴细胞性心肌炎

鉴别诊断：

致心律失常性右室心肌病，自身免疫性心肌病

其他：

本案例为青年男性，急性起病，10 天前有上感病史，病情进展迅速，心电图提示窦性心律，频发室早，多发短阵室速，QRS 波时限 148ms，完全性左束支传导阻滞，心脏彩超提示全心扩大，左室收缩功能明显减退，射血分数 < 35%，心脏核磁提示心肌多发强化，左室心尖部附壁血栓 (小) 形成，行心内膜活检病理诊断：符合愈合中的淋巴细胞性心肌炎，治疗方面给予激素及规范抗心衰药物治疗，期间密切随访，临床试验数据无明显改善，期间患者因心衰多次就诊，根据心电图表现胸前导联 R 波递增不良，心脏核磁心肌纤维化严重，室早为多源性，射频消融效果差，经评估患者有行 CRT-D 适应症（IIa，B）。目前认为，各种原因导致的固有免疫过度激活及迅速触发免疫细胞大量释放炎症因子所引起的细胞因子风暴是暴发性心肌炎起病急、进展快，病情重，死亡率高的重要原因，由于机体促炎反应和抗炎反应调解失衡，从而导致机体过度免疫激活，炎症风暴形成，早期采取足够剂量糖皮质激素和足够剂量免疫球蛋白的免疫调节可以阻断发病环节，减轻炎症水肿，抗休克，缓解临床症状，挽救生命改善预后。左心室辅助装置及体外膜肺氧合作为心脏移植的过度，心脏移植仍然是目前唯一有效的长期治疗方案。由于基层医院对暴发性心肌炎的发病特点及病理生理机制认识不足，临床误诊、漏诊和延误诊断较为常见，对于暴发性心肌炎的治疗缺乏临床经验，作为基层医院对临床上发现的不明原因、病情进展迅速且常规治疗效果差的心衰。心律失常患者，因尽早通过远程会诊方式向有经验的中心提供患者信息，制定治疗方案与家属沟通后尽早开通绿色通道转诊心内膜活检，有助于早期诊断、治疗，为心脏移植提供跟多机会，争取更多时间，挽救生命，改善预后。

心肌淀粉样变 1 例

王苗

海南省人民医院

患者基本信息：

患者男性，61 岁。

主述：

反复胸闷痛 5 年，双下肢水肿、气促 1 月。

现病史：

因“反复胸闷痛 5 年，双下肢水肿、气促 1 月”于 2023 年 6 月 5 日入住海南省人民医院心血管内科病房。病程中患者水肿进行性加重，不能行走，伴气促，在外院诊断急性心力衰竭、双侧胸腔积液，给予利尿、扩血管、引流胸腔积液等治疗，但效果欠佳转来我院。

既往病史：

既往有腔隙性脑梗死病史。余无特殊。

病程记录：

患者双下肢水肿、气促，考虑急性心衰，容量负荷重，给予强化利尿治疗，合并双侧胸腔积液，行胸水常规穿刺引流，病理提示漏出液。积极查找心衰原因，完善相关检查后，最后诊断心肌淀粉样变，轻链型，建议患者转血液内科化疗，但患者拒绝，并在症状好转后出院。

检验检查记录：

详见 PPT。

鉴别诊断：

患者以心衰为主要表现，病因不明，心脏彩超提示左室壁增厚，双房增大，舒张功能不全， 心电图提示类似心肌梗死的改变，主要与肥厚型心肌病、主动脉瓣狭窄、高血压性心脏病、缺血性心肌病、法布雷病等鉴别。

其他：

一例高龄肥厚性梗阻性心肌病玛伐凯泰的治疗

张舒怡

上海市同仁医院

患者基本信息：

患者，女，83 岁。

主述：

发热伴咳嗽咳痰 1 天

现病史：

患者入院当日下午无明显诱因开始出现畏寒发热，体温最高 37.6℃，有咳嗽咳痰，痰粘不易咳出，呕吐 1 次，为胃内容物，胸闷气促，伴全身乏力，无端坐呼吸，无意识不清，无腹痛腹胀，无腹泻便秘等不适，遂于我院急诊完善检验检查，血气: 酸碱度 (pH)，7.502，↑； 二氧化碳分压 (pCO2)，5.03 KPa，； 氧分压 (pO2)，22.7 KPa，↑； 碳酸氢根离子 (HCO3-)，28.9 mmol/L，↑； 全血剩余碱 (ABE)，5.5 mmol/L，↑； 血常规: C- 反应蛋白，12.29 mg/L，↑; 白细胞，5.53 ×10^9/L，； 中性粒细胞比值，67.5 %N，； 红细胞，2.57 ×10^12/L，↓； 血红蛋白，108 g/L，↓; 红细胞压积，31.4 %，↓; 血小板，29 ×10^9/L，↓; B 型钠尿肽，

432.53 pg/ml，↑；生化：葡萄糖，11.6 mmol/L，↑；肌酐，25.7 umol/L，↓；总胆红素，24.8 umol/L，↑；直接胆红素，8 umol/L，↑；钾，2.80 mmol/L，↓；钠，134.5 mmol/L，↓；氯，96.7 mmol/L，↓；钙，2.07 mmol/L，↓；胸部 CT：两肺散在炎症，请结合临床及实验室检查，建议治疗后复查。头颅 CT：双侧基底节区、脑室旁腔隙灶，请结合临床，必要时 MR 检查。老年脑，脑室周边白质变性。考虑“社区获得性肺炎 非重症、心功能不全”；为求进一步诊治，收住我科。

既往病史：

既往高血压史 30 年余，血压最高 180/100mmHg，服用苯磺酸氨氯地平 5mg po qd，血压控制在 130/80mmHg。

既往 2 型糖尿病史 20 余年，长期胰岛素控制血糖，目前德谷门冬双胰岛素 早 15iu 晚 10iu。

既往脑梗死病史 2 次，未遗留明显肢体活动障碍，存在记忆力减退，因血小板过低暂停泰嘉 75mg qd 抗血小板聚集治疗。

既往焦虑性抑郁症病史 3 年，目前口服文拉法新 75mg qn 治疗中。

既往睡眠障碍，长期口服阿普唑仑 0.4mg qn 治疗。

既往白细胞及血小板减退 4 年病史，外院诊断为系统性红斑狼疮，目前长期口服地榆升白片、利可君治疗中。

既往曾行胆囊切除术、左侧股骨颈置换术、左侧膝关节半月板置换术。

病程记录：

患者入院后，完善相关辅助检查，予以抗感染、化痰等对症治疗，完善辅助检查期间，患者心超提示左室流出道梗阻（梗阻位于室间隔基底部，梗阻处最大压差 86mmHg，检测时心率 89 次 / 分），予以美托洛尔 47.5mg 联合地尔硫卓 90mg 控制心室率，降低心肌耗氧后出院，予以口服药物治疗。1 月后患者因乏力明显再次就诊我科，就诊时患者血压偏低 90/60mmHg 左右，遂予以停用地尔硫卓，美托洛尔减量至 23.75mg，与患者家属沟通，患者存在玛伐凯泰治疗适应证，家属同意后予以 2.5mg 口服起始，服药 3 天后监测患者肝肾功能、心衰标志物等无明显波动，予以带药出院。1 月后患者再次入院随访心超，心超提示压差较前明显下降，静息状态下左室流出道压差约 10mmHg，Valsalva 动作激发试验后压差约 21mmHg，患者一般情况较前好转，活动耐量改善。

检验检查记录：

【超声所见】

名称	测量值	参考值	
主动脉窦部内径	31	20-37mm	
左房内径	41	19-40mm	↑
左室舒张末内径	40	35-56mm	
左室收缩末内径	26	23-35mm	
室间隔厚度	12-16	6-11mm	
左室后壁厚度	11	6-11mm	
肺动脉收缩压	36	<40mmHg	
肺动脉内径	21	<27mm	

左室射血分数 (LVEF)：66.5 %

二尖瓣血流图：E/A：78.0/140；左室侧壁二尖瓣环处 DTI 测量：e'：3.6cm/s；a'：12.5cm/s；E/e'：21.7

1. 左房内径扩大，左室内径正常，基底段增厚明显，厚约 16mm，室间隔中间段、前壁、侧壁及左室心尖部均增厚，约 12-14mm，余左室壁厚度正常，室壁回声增粗，二尖瓣前叶收缩期前移，主动脉瓣收缩中期提前关闭。连续多普勒估测左室流出道峰值压差约 86mmHg（检测时患者心率 89 次 / 分），静息状态下左室壁各节段运动未见明显异常。

2. 二尖瓣后叶瓣环局部增厚，呈强回声，开放不受限，关闭时错位，彩色多普勒示二尖瓣偏心反流（沿二尖瓣后叶方向）。

3. 主动脉窦部不增宽，主动脉瓣为三叶式，瓣叶局部增厚，呈强回声，开放不受限。

4. 右房内径正常，右室内径正常，右心室舒张末内径 / 左心室舒张末内径比值 < 1，肺动脉不增宽，三尖瓣不增厚，开放不受限。右室壁整体收缩活动正常，三尖瓣环收缩期位移距离 16.1mm。

5. 心包腔内未见积液。

未见房室水平分流，可见 MR（轻中度），AR（轻度），TR（轻微）

【超声提示】

1. 左室壁增厚，提示左室流出道梗阻（梗阻位于室间隔基底部，梗阻处最大压差 86mmHg，检测时心率 89 次 / 分）

2. 左房增大

3. 主动脉瓣局灶性钙化伴轻度反流

4. 二尖瓣关闭错位，二尖瓣后叶瓣环钙化伴轻中度二尖瓣反流

5. 左室舒张功能减退

【超声所见】

名称	测量值	参考值	
主动脉窦部内径	32	20-37mm	
左房内径	43	19-40mm	↑
左室舒张末内径	45	35-56mm	
左室收缩末内径	28	23-35mm	
室间隔厚度	14	6-11mm	↑
左室后壁厚度	9	6-11mm	
肺动脉收缩压	39	<40mmHg	
肺动脉内径	21	<27mm	

左室射血分数 (LVEF)：66.98 %

二尖瓣血流图: E/A: 116.63/104.54; 左室侧壁二尖瓣环处 DTI 测量: e': 6.35cm/s；a'：7.16cm/s；E/e'：18.4

1. 左房内径扩大，左室内径正常，室间隔、左室前壁基底段至中间段室壁增厚，以室间隔基底段增厚明显约 15mm，左室心尖部各节段增厚 12-13mm，余左室壁厚度正常，静息状态下二尖瓣未见明显收缩期前移，连续多普勒估测左室流出道峰值压差约 10mmHg，Valsalva 动作激发试验后左室流出道压差约 21mmHg，静息状态下左室壁各节段运动未见明显异常。

2. 二尖瓣后叶瓣环增厚，呈强回声，开放不受限。

3. 主动脉窦部不增宽，主动脉瓣为三叶式，左冠瓣、右冠瓣局部增厚，呈强回声，开放未见明显受限，连续多普勒估测主动脉瓣峰值流速约 2.1m/s，峰值跨瓣压差约 17mmHg。

4. 右房内径正常，右室内径正常，右心室舒张末内径 / 左心室舒张末内径比值 < 1，肺动脉不增宽，三尖瓣不增厚，开放不受限。右室壁整体收缩活动正常，三尖瓣环收缩期位移距离 21.91mm。

5. 心包腔内左室后壁后方舒张期可见约 3mm 的无回声区。

未见房室水平分流，可见 MR（轻微），AR（轻微），TR（轻度）

【超声提示】

1. 提示肥厚型心肌病（静息状态下左室流出道压差约 10mmHg，Valsalva 动作激发试验后压差约 21mmHg）

2. 左房增大

3. 主动脉瓣局灶性钙化、二尖瓣后叶瓣环钙化

4. 轻度三尖瓣反流

5 微量心包积液

6. 左室舒张功能减退

鉴别诊断：

1. 急性心肌梗死：有典型缺血性胸痛与心绞痛相仿，但性质更剧烈，疼痛长达数小时，可伴有休克、心衰及心律失常，并伴有发热，反复硝酸甘油多不能缓解，心电图中面向梗死部位导联 ST 段抬高，并有 ST-T 动态演变及异常 Q 波。辅检提示白细胞计数、肌钙蛋白、肌红蛋白升高，血清心肌酶的动态曲线。该患者病史特点不符，故可排除。

1. 急性心包炎：可有严重胸痛，疼痛常常由于深呼吸或咳嗽加重，胸痛与发热同时出现，可闻及心包摩擦音，全身症状一般不如心肌梗塞严重，心电图除 AVR 导联外，其余导联均有 ST 段弓背向下的抬高，T 波倒置，无异常 Q 波出现，患者病史特点不符，故可排除。该病以心前区疼痛为主要症状，疼痛性质可尖锐，与呼吸运动有关，可因咳嗽或深呼吸时加重，疼痛也可呈压榨性，查体心浊音界扩大，心音低而遥远，大量积液可影响静脉回流，出现颈静脉怒张，超声心动图可明确诊断。心电图可出现 ST-T 改变，但无病理性 Q 波，该患者此诊断可排除。

2. 急性肺动脉栓塞：突然胸痛，气短或休克，常有急性右心负荷急剧增加表现，如 P2 亢进，右室增大，右心衰体征（发绀、颈静脉充盈、肝脏增大、双下肢水

肿等），心电图示电轴右倾，顺时针转位，肺性 P 波，S Ⅰ、Q Ⅲ、T Ⅲ，右胸及左胸 V1-3，T 波倒置，心电图改变较心肌梗塞迅速而短暂，LDH 增高，反射性核素肺通气关注扫描可助诊断。患者病史特点不符，故可排除。

3. 主动脉夹层动脉瘤：疼痛常为撕裂性，持续不缓解且胸痛一开始即达高峰，常反射到背、肋、腹、腰和下肢，双上肢的血压和脉搏可有明显差异，可有下肢暂时性瘫痪、偏瘫和主动脉瓣关闭不全体征表现，胸片、二维超声心动图、胸腔 CT 及 MRI 可资鉴别。

其他：

CRT-D 心房电极故障拔除后再植入一例

柴虹

中国人民解放军陆军军医大学第一附属医院

患者基本信息：

患者基本信息：

患者，女，69 岁；

入院时间：2025-04-20

主述：

活动后气促 4 年余，CRT-D 术后 3 年余，程控发现心房电极故障 1 月入院。

现病史：

2021.08.04 患者因“活动后胸闷、气促 3 月”来我院就诊，心电图：LBBB（QRS162ms），TTE：LVEDD67，EF=27%，确诊为扩张型心肌病、LBBB、心功能 III 级，于 2021.8.10 安置 CRT-D。

长期门诊随访，口服沙库巴曲缬沙坦、富马酸比索洛尔、恩格列净、伊伐布雷定、呋塞米、螺内酯等药物，病情稳定。

既往病史：

既往史：右乳腺 CA 行手术治疗。

个人史：无吸烟史，无饮酒史

家族史：无房颤、早发心梗病史及猝死史

病程记录：

复查胸片电极位置正常，未见脱位和磨损；

程控心房单双极感知均不能测出，起搏阈值 2v；

手术：拔除心房电极，重新植入心房电极，沿用原起搏器。

检验检查记录：

体温 :36.5℃ 脉搏 :93 次 / 分 呼吸 :14 次 / 分 血压 :110/70mmHg

查体：神清，精神可。颈静脉无充盈。双肺未闻及干湿罗音。叩诊心界临界大小。心率 93 次 / 分，律齐，各瓣膜未闻及杂音，无心包摩擦音。无异常血管征。腹部查体（-）。双下肢无水肿。

检验检查记录：

无

鉴别诊断：

无

其他：

无

快与慢的较量

王慧俐

吕梁市第一人民医院

患者基本信息：

陶某某，男，71 岁

主述：

间断性胸闷、心悸、气短 1 年

现病史：

患者 2021 年 7 月在山西省人民医院体检行动态心电图提示阵发性心房颤动，平素有间断性胸闷、心悸，气短，活动耐量轻度下降。否认头晕、黑矇、晕厥；否认腹胀、纳差；无明显乏力；未予重视。2022 年 4 月 23 日因“急性脑梗死”在神经内科溶栓治疗，行动态心电图提示阵发性心房颤动 短暂心室停搏（最长 3.692s），予抗凝、稳定斑块等对症治疗，今为进一步治疗入住我科。

既往病史：

1：	冠心病 陈旧性心肌梗死病史
2：	冠状动脉支架植入病史
3：	肾动脉支架植入病史
4：	脑梗死病史，溶栓治疗（2122 年 4 月份）
5：	阵发性房颤
6：	心室停搏（最长 3.692s）
7：	心脏查体无明显阳性体征

病程记录：

行房颤射频消融 + 左心耳封堵一站式手术

检验检查记录：

详见 PPT

鉴别诊断：

详见 PPT

其他：

肿瘤心脏病学组王慧俐委员

IgG4 相关性疾病累及冠状动脉一例

杜梦阳

阜外医院

患者基本信息：

患者男性，60 岁

主述：

间断腹痛 7 年，发作性胸闷气短 2 周

现病史：

7 年前因腹痛诊断为 IgG4 相关性疾病（自身免疫性胰腺炎，硬化性胆管炎，累及颌下腺），近 2 周无明显诱因简短胸闷。既往高脂血症、高血压病史。体格检查无明显异常，血、尿、便常规无异常，hs-cTnI 阴性，LDL-C2.82mmol/L，肝肾功能及甲状腺功能正常，IgE 499IU/ml（0-165），IgG4 6060mg/L（0-1400），炎性指标、自身抗体筛查及肿瘤标志物未见异常。心电图及超声心动图大致正常。影像学检查提示冠状动脉狭窄、局部软组织包绕。**症状体征** 发作性胸闷气短。体温 36.2 ℃，血压 127/77 mmHg（1 mm Hg=0.133 kPa），心率 62 次 /min，呼吸 18 次 /min，头颈部未触及肿大淋巴结及肿大腺体，全身未闻及血管杂音，心肺查体未见明显异常，腹部无压痛及反跳痛

既往病史：

既往有高脂血症及高血压病史。

病程记录：

结合既往 IgG4-RD 病史，血清 IgG4 水平，冠状动脉 CT 及主动脉 CT 血管周围组织包绕以及冠状动脉内超声冠状动脉周围层状增生，诊断为 IgG4-RD 累及冠状动脉。

检验检查记录：

血尿便常规未见异常，hs-cTnI 阴性，LDL-C2.82mmol/L，肝肾功能及甲状腺功能正常，IgE 499IU/ml（0-165），IgG4 6060mg/L（0-1400），炎性指标、炕核抗体 19 项、血管炎三项及肿瘤标志物未见异常。心电图及超声心动图大致正常。四肢血压未见异常。冠状动脉 CT：冠状动脉多处软组织包绕（图 1）。主动脉 CT：腹主动脉及髂动脉软组织包绕（图 2）。冠状动脉造影：前降支近段 60% 狭窄，回旋支近段 70% 狭窄，右冠状动脉近段 50% 狭窄，后降支 70% 狭窄（图 3）。血管内超声（IVUS）：冠状动脉局部管腔狭窄，外膜及以外可见纤维增生及低回声，内膜未见明显的粥样硬化斑块（包括脂质成分及坏死核心）（图 4）。

鉴别诊断：

患者肿瘤标志物为阴性，除 IgG4 及 IgE 升高外其他自身抗体均阴性，故除外肿瘤及其他自身免疫病可能。综合冠状动脉 CT、造影及 IVUS 的结果，尽管冠状动脉存在一定粥样硬化斑块，冠状动脉的狭窄是由冠状动脉周围的组织包绕增生所致，故不考虑冠状动脉粥样硬化性心脏病。

其他：

生死时速：61 岁男性左主干完全闭塞的急诊介入治疗实录

王蒙蒙

常德市第一人民医院

患者基本信息：

患者男，年龄 61 岁

主述：

胸骨后灼烧样疼痛伴大汗淋漓、背部放射痛 24 小时

现病史：

患者于 2025 年 06 月 26 日突发胸骨后灼烧样疼痛，程度中等，伴大汗淋漓及背部放射痛，无呼吸困难、恶心呕吐等。急诊就诊于当地人民医院，口服阿司匹林 300mg+ 替格瑞洛 180mg 后行冠脉造影，提示左主干完全闭塞，血栓负荷重，未能开通血管，遂转至我院。起病以来精神、食纳、睡眠尚可，二便正常。

既往病史：

既往健康，否认高血压、糖尿病、心脏病等慢性病史；吸烟史：40 余年，20 支 / 日（重要危险因素）；无药物过敏史、手术史及输血史。

病程记录：

2025-06-27 主任查房

详细告知患者家属病情，患者目前心肌梗死急性期，病情危重，随时可能出现心力衰竭、恶性心律失常、脑血管意外、应激性溃疡、心脏破裂、心跳呼吸骤停等危及生命，予以告病危，患者家属示理解，密切关注患者生命体征及病情变化；目前拟行急诊冠脉介入治疗，药物治疗上暂予阿司匹林 + 替格瑞洛抗血小板聚集、阿托伐他汀调脂、护心对症支持治疗。

2025-06-27 术后首次病程记录

患者，男性，61 岁，2025 年 06 月 27 日 18 时 54 分送手术室在局部麻醉下进行药物洗脱冠状动脉支架置入 + 主动脉球囊反搏置入术，术中处理；胸痛患者外院冠脉造影提示左主于完全闭塞带右桡动脉鞘转我院送入导管室，交换 7F 桡动脉鞘：沿鞘送 7F EBU 3.5 Guiding 导管至左冠口。沿 Guiding 送 0.014inchRunthrough NS 导丝至回旋支远段；沿 Guiding 送 Runthrough NS、Pilot 50 导丝至前降支困难；沿 Guiding 送 Sion 导丝至前降支远段远段；沿导丝送［2.5×15］mm 半顺应性球囊至回旋支开口及近段病变处，以［8-12］atm 扩张；沿导丝送［2.5×15］mm 半顺应性球囊至前降支开口及近段病变处，以［8-12］atm 扩张：沿导丝送 TuVS 分别至前降支及回旋支检查提示严重狭窄伴斑块形成; 沿导丝送[3.0×20jmm 药物支架至前降支近段稍突出左主干病变处，以［8latm 释放：稍回撤支架球囊，以［12］atm 扩张：沿导丝送 Sion black 导丝 Rewire 至回旋支远段; 沿导丝送[1.5×15]mm 球囊至回旋支开口支架网眼，以[12]atm 扩张: 沿导丝送[2.5×15]mm 球囊至回旋支开口支架网眼，以[12]atm 扩张：沿导丝送 13.5×15］mm 球囊至回旋支开口支架网眼，同时沿导丝送［3.0×15］mm 球囊至前降支开口与回旋支开口球囊构成对吻，以［8］atm 对吻扩张；沿导丝送［4.0X28］mm 药物支架至回旋支近段至左主干开口病变处，以［8］atm 释放：沿导丝送 Sion black 导丝 Rewire 至前降支远段；沿导丝送［1.5×15］mm 球囊至前降支开口支架网眼，以［12］atm 反复扩张；沿导丝送［3.0X191mm 球囊至前降支开口支架网眼处，以［12］atm 扩张；沿导丝送［3.0×15］mm 球囊至前降支开口支架网眼处；同时沿导丝送［3.5×12jmm 球囊至回旋支开口与前降支开口球囊构成对吻，以［8］atm 对吻扩张：沿导丝送［4.0×12］mm 非顺应性球囊至左主干支架内，以［16-20］atm 扩张：沿导丝送 IVUS 至回旋支远段由远及近回撤检查：支架膨胀完全、贴壁良好、支架两端无夹层血肿；再次造影示前降支、回旋支、左主干支架内未见残余狭窄，远段血流 TIMI 3 级。手术完毕，退出导丝及导管，拔除动脉血管鞘，压迫止血，加压包扎。术中用造影剂［90］ml，肝素［7000］u，术中、术后未诉特不适，安返病房，按 PCI 术后处理。

术后诊断：冠状动脉粥样硬化性心脏病

（1）急性心肌梗死（左主干闭塞）

（2）KillipI 级术后处理措施：继续抗栓、调脂、改善循环、改善心肌重塑、护胃、主动脉球囊反搏等对症治疗。

注意观察的事项：注意有无胸闷、胸痛及呼吸困难，注意复查心电图，注意生命体征。

2025-06-27 副主任查房

患者冠脉支架植入术后 + 主动脉球囊反搏植入术后返回病房，现患者无明显胸闷、胸痛，无明显呼吸困难，无心悸，精神尚可。体格检查: T:36.5°C，P:69 次 / 分，R:18 次 / 分，BP:95/57mmHg：颈静脉无充盈，双肺呼吸音清，双肺未闻及干湿啰音。心率 69 次 / 分，律齐，无杂音。腹平坦，无压痛、反跳痛，肝脾肋下未及，双下肢无水肿。四肢肌力肌张力正常，病理征（-）。副主任医师查看患者后指示：急性心肌梗死患者，起病 24 小时，左主干闭塞，目前已急诊开通左主干、前降支、回旋支，术中患者血压偏低，考虑心源性休克，予以主动脉球囊反搏辅助抗心衰治疗，但患者目前心肌梗死急性期，病情危重，随时可能出现恶性心律失常、脑血管意外、应激性溃疡、心脏破裂、心跳呼吸骤停等危及生命，家属表示知情理解病情及风险。密切监测生命体征及尿量，注意复查心电图、血气等指标，药物治疗上暂予阿司匹林 + 替格瑞洛 + 替罗非班抗血小板聚集、阿托伐他汀 + 依折麦布调脂、护胃、改善循环对症支持治疗。

2025-06-28 主任查房

患者现无胸闷、胸痛及呼吸困难，无心悸等不适，主动脉球囊反辅助循环，精神、食欲、睡眠尚可，大便暂未解，入科后尿量 1100ml。查体：T:36.6° C,P:71 改分，R:18 次 / 分，BP:93/62mmHg；颈静脉无充盈，双肺呼吸音清，双肺未闻及干湿啰音。心率 71 次 / 分，律齐，无杂音。腹平坦，无压痛、反跳痛，肝脾肋下未及，双下肢无水肿。四肢肌力肌张力正常，病理征（-）。主任医师查房后指示：患者现无明显胸闷、胸痛及呼吸困难，肺部未闻及明显啰音，昨日入科后尿量尚可，但患者目前血压仍偏低，目前多巴胺升压治疗，暂继续目前治疗方案，密切监测血压，根据血压情况逐步减最多巴胺剂量。今日完善床旁胸片检查。患者主动脉球囊反搏辅助，注意监测血小板，今日替罗非班泵完后明日开始使用肝素抗凝预防血栓形成，注意有无出血症状及体征，警惕出血，注意复查心电图。密切监测生命体征及尿量。

2025-06-29 日常

今查房，患者无胸痛及呼吸困难等不适，主动脉球囊反辅助循环，一般情况尚可，大便暂未解，24 小时尿量 1300ml。查体：体温：36.5° C，脉搏：70 次 / 分，呼吸：19 次 / 分，血压：116/65mmHg；颈静脉无充盈，双肺呼吸音清，双肺未闻及干湿啰音。心率 70 次 / 分，律齐，无杂音。腹平坦，无压痛、反跳痛，肝脾肋下未及，双下肢无水肿。处理：患者现无明显胸闷、胸痛及呼吸困难，肺部未闻及明显啰音，现血压较前上升，目前多巴胺剂量已减量，逐步停用。患者主动脉球囊反搏辅助，注意监测血小板，替罗非班使用完毕，今日开始使用肝素抗凝预防血栓形成，注意有无出血症状及体征，警惕出血，注意复查心电图。

2025-06-30 副主任查房

患者无胸痛，无呼吸困难，主动脉球囊反辅助循环，精神、食欲、睡眠尚可，大便暂未解，24 小时尿量 1850ml。查体：体温：36.5° C，脉搏：77 次 / 分，呼吸：20 次分，血压：111/70mmHg；颈静脉无充盈，双肺呼吸音清，双肺未闻及干湿啰音。心率 77 次 / 分，律齐，无杂音。腹平坦，无压痛、反跳痛，肝脾肋下未及，双下肢无水肿。四肢肌力肌张力正常，病理征（-）。副主任医师查看患者后指示：患者目前无明显呼吸困难症状，未使用血管活性药物，尿量尚可，生命体征平稳，有指征拔除 IABP，但不排除拔除 IABP 后病情加重，血流动力学不稳定、心衰可能，家属表示理解病情及风险，同意拔除 IABP。患者大便未解，加用开塞露通便。追今日复查结果。密切监测生命体征及尿量。

2025-07-01 副主任查房

患者昨日已拔除 IABP，患者现未诉胸痛、呼吸困难等不适，精神、食欲、睡眠尚可，大便暂未解，24 小时尿量 800ml。查体：体温：36.5° C，脉搏：80 次 / 分，呼吸：16 次 / 分，血压：101/66mmHg；颈静脉无充盈，双肺呼吸音清，双肺未闻及干湿啰音。心率 80 次 / 分，律齐，无杂音。腹平坦，无压痛、反跳痛，肝脾肋下未及，双下肢无水肿。四肢肌力肌张力正常，病理征（-）。处理：患者昨日已拔除 IABP，未诉呼吸困难不适，现血压及心室率控制尚可，昨日复查 BNP 较前下降，心脏彩超提示射血分数尚可，现病情较前稳定，治疗同前。

2025-07-04 副主任查房

患者无胸痛、呼吸困难等不适，一般情况尚可，大便已解，小便正常。查体：体温：36.5° C，脉搏：70 次 / 分，呼吸：20 次 / 分，血压：98/61mmHg；颈静脉无充盈，双肺呼吸音清，双肺未闻及干湿啰音。心率 70 次 / 分，律齐，无杂音。腹平坦，无压痛、反跳痛，肝脾肋下未及，双下肢无水肿，全身皮肤散在瘀点。副主任医师查房后指示：1. 患者 2025-06-27 行急诊左冠介入手术，因右冠开口异常，未行右冠造影，目前心肌梗死病情较前稳定，今完善右冠造影明确右冠是否存在病变。同时复查左冠冠脉造影评估急诊介入手术效果。余治疗继续。

2025-07-04 20:27 日常病程记录

患者今在导管室行 CAG 检查，常规消毒，铺巾，以 2% 利多卡因局麻并穿刺右桡动脉，置入 5F 鞘管，注入肝素 3000U，送入多功能冠脉造影导管分别至左右冠脉开口，注入碘海醇同时自不同体位投造，结果具体见报告，术毕退出鞘管，压迫止血，加压包扎，安返病房。

冠脉造影结果：1. 冠状动脉分布：右冠优势型；2. 左主干：

原支架内未见明显狭窄：3. 前降支：近段原支架内未见明显狭窄，近中段狭窄 50%，中段收缩期狭窄 60%，舒张期未见明显狭窄; 远段血流 TIMI3 级; 4. 回旋支: 近段原支架内未见明显再狭窄，远段血流 TIMI 3 级: 5. 右冠状动脉: 开口于左冠窦，中段狭窄 50%，远段血流 TIMI

3 级；结论与建议：1. 冠状动脉粥样硬化性心脏病：2. 建议药物治疗。

2025-07-05 患者出院

检验检查记录：

外院冠脉造影（2025-06-27）：左主干完全闭塞；

入院后完善相关检查如下：入院后急诊行血管内超声检查 + 主动脉球囊反搏植入 + 左主干支架植入术（［3.0x20］mm 药物支架至前降支近段稍突出左主干病变处、［4.0×28］mm 药物支架至回旋支近段至左主干开口病变处），术后返回 CCU 进一步治疗，完善相关检查：【检验】（2025-06-27）动脉血气：酸碱度 7.396，二氧化碳分压 35.1mmHg，氧分压 190.0mmHg1，氧饱和度 99.4%，钾离子浓度 3.80mmol/L，乳酸浓度 1.30mmol/L。（2025-06-28）血常规：白细胞计数 9.71×10~9/L，淋巴细胞百分数 12.0%，中性粒细胞百分数 79.6%，红细胞计数 4.45×10^12/L，血红蛋白浓度 132.0g/L，血小板计数 212×10^9/L：N 端脑钠肽前体 2086.000pg/ml；D- 二聚体 1.58mg/L ；促甲状腺激素 0.181uIU/mL ；凝血酶抗凝血酶 皿 复合物 17.91 ug/ml1；心肌酶：乳酸脱氢酶 663U/L ，肌酸激酶 2278U/L，肌酸激酶同工酶（活性）183.8U/L，肌红蛋白 218.0ong/ml ：血脂：高密度脂蛋白胆固醇 1.04mmol/L，低密度脂蛋白胆固醇 3.98mmol/L，甘油三酯 1.88mmol/L ，总胆固醇 5.35mmol/L ，非 HDL-C4.31mmol/L；天门冬氨酸氨基转移酶 200U/L：葡萄糖 6.61mmol/L：丙氨酸氨基转移酶 51U/L：血小板最大聚集率（ADP）27.00%、血小板最大聚集率（AA）39.00%：尿液分析：尿比重 1.050，酮体 1+；超敏肌钙蛋白 16.900ng/ml，FT3、FT4、糖化血红蛋白测定、PAP、tPAAg、TM、镁测定、电解质、肾功能、输血前常规检查大致正常（2025-06-29）血常规：白细胞计数 9.63×10^9/L，淋巴细胞百分数 10.3%，中性粒细胞百分数 79.5%，红细胞计数 4.52×10^12/L，血红蛋白浓度 131.0g/L，血小板计数 174×10~9/L。(2025-06-30) 尿液分析: 尿胆原 1+, 隐血 +; 血常规: 白细胞计数 8.77×10~9/L，淋巴细胞百分数 11.3%，中性粒细胞百分数 77.4%，红细胞计数 4.43×10^12/L，血红蛋白浓度 129.0g/L，血小板计数 163X10^9/L；肝功能：总蛋白 62.3g/L，

白蛋白 38.1g/L，天门冬氨酸氨基转移酶 64U/L：心肌酶：乳酸脱氢酶 596U/L，肌酸激酶同工酶（活性）26.3U/L：N 端脑钠肽前体 1520.000pg/ml。HCO3、肾功能、电解质大致正常。血细胞分析 - 全血细胞计数 + 五分类（2025-07-03）：白细胞计数 6.60×10~9/L，中性粒细胞百分数 65.9%，中性粒细胞绝对值 4.35×10^9/L，血红蛋白浓度 120.0g/L，血小板计数 215×10~9/L。B 型钠尿肽前体（PRO-BNP）测定：907.100pg/ml。肌钙蛋白 1 测定：0.260ng/ml。电解质常规：钾 3.75mmol/L，钠 141.30mmol/L。余血清天门冬氨酸氨基转移酶测定、血清丙氨酸氨基转移酶测定、心肌酶谱常规检查未见明显异常。【检查】心电图：1、窦性心律 2、短 PR 间期 3、电轴左偏 4、AVL 导联可见异常 Q 波 5、多导联 ST-T 改变 6、QTc 间期延长。心电图：窦性心律长 Q-T 间期 ST 段改变。胸部正侧位片：肺部炎症，心影稍大。心电图：1、窦性心律 2、ST-T 改变 3、电轴左偏。心脏彩超：升主动脉内径稍宽：MR（轻）TR（轻）。动态心电图：窦性心律（平均心率 78 次 / 分）；房性早搏 109 个；短阵房性心动过速：ST-T 改变；心率变异性减低。2025-07-04 冠脉造影结果：1. 冠状动脉分布：右冠优势型；2. 左主干：原支架内未见明显狭窄：3. 前降支：近段原支架内未见明显狭窄，近中段狭窄 50%，中段收缩期狭窄 60%，舒张期未见明显狭窄；远段血流 TIMI3 级；4. 回旋支：近段原支架内未见明显再狭窄，远段血流 TIMI 3 级：5. 右冠状动脉：开口于左冠窦，中段狭窄 50%，远段血流 TIMI3 级；结论与建议：1. 冠状动脉粥样硬化性心脏病：2. 建议药物治疗。

鉴别诊断：

主动脉夹层：突发剧烈胸背部严重撕裂样疼痛伴有呼吸困难，严重可出现心衰、晕厥甚至突然死亡，如主动脉分支闭塞，还可导致相应的脑、肢体、肾脏、腹腔脏器缺血症状；患者多伴有难以控制的高血压；无典型心电图改变，主动脉 CTA 可资鉴别。

其他：

非阻塞性心肌梗死的男性患者

臧雨奇

哈尔滨医科大学附属第二医院

患者基本信息：

男患，49 岁，主因 “入院前 8 小时突发胸痛” 收入我院。

患者入院出现阵发性胸痛，位于胸骨后，常于情绪激动后出现。每次发作持续数小时，可自行缓解，发作时伴胸闷、气短。未予重视。患者于入院 8 小时前无明显诱因出现胸痛，放散至双肩及背部伴濒死感，发作时伴胸闷、气短，伴发热，最高体温 38℃，无心悸，无咳嗽、咳痰，无头晕、头痛等。患者于当地医院就诊，行心电图检查提示心电异常，建议住院治疗。患者为求进一步明确诊断及系统治疗急诊入我院，以 " 冠心病，急性心肌梗死 " 收入院。

既往史：否认高血压、糖尿病及吸烟饮酒史。无其他既往病史。

主述：

突发胸痛 8 小时

现病史：

患者于入院 8 小时前无明显诱因出现胸痛，放散至双肩及背部伴濒死感，发作时伴胸闷、气短，伴发热，最高体温 38℃，无心悸，无咳嗽、咳痰，无头晕、头痛等。患者于当地医院就诊，行心电图检查提示心电异常，建议住院治疗。患者为求进一步明确诊断及系统治疗急诊入我院，以 " 冠心病，急性心肌梗死 " 收入院。

既往病史：

否认高血压、糖尿病及吸烟饮酒史。无其他既往病史。

病程记录：

口服药物治疗：

拜阿司匹林 100mg QD 口服

波立维 75mg QD 口服

阿托伐他汀钙片 20mg QD 口服

重症监护

改善心肌缺血

积极再灌注心肌治疗

改善心室重构

检验检查记录：

ECG 示：窦性心律，II、III、aVF 导联 ST 段有弓背抬高趋势

血清肌钙蛋白升高

心肌酶升高，离子正常

冠脉造影显示右冠中段无狭窄

OCT 显示右冠中段病变处为纤维斑块，病变处内膜增厚

鉴别诊断：

主动脉夹层

急性肺动脉栓塞

急性心包炎

心肌炎

应激性心肌病

其他：

1. 该患者为中年男性，无传统高危因素，根据实验室结果和心电图明确疾病诊断。

2. 冠脉造影无明显狭窄发现，进一步利用 OCT 探究发病部位及病变性质。

临床上，经常会遇到这样的 MI 患者：造影上无显著狭窄（DS%<50%) 病变，但肌钙蛋白升高及心电图符合 MI 诊断标准，这类患者就是非梗阻性心肌梗死（MINOCA）。

MINOCA 患者一般不会引起急性心梗的典型临床表现，因此我们在临床上容易忽略此类患者。在治疗上，我们应该针对病因进行治疗，如控制血压、血脂、血糖等危险因素，改善生活方式。同时对于已经发生心肌梗死的患者，需要采取紧急治疗措施，如抗血小板治疗、溶栓治疗等，以恢复心肌灌注和减少心肌坏死。

总之，这类特殊类型的心肌梗死我们需要足够重视，对于疑似 MINOCA 患者，应尽早进行影像学来进行诊断，明确病变类型和程度，以减少并发症和改善患者预后。

冠状动脉粥样硬化性心脏病 -- 死亡病例

车子傲

哈尔滨医科大学附属第二医院

患者基本信息：

女，69 岁；

活动后胸痛 1 个月，加重 2 天” 入住心血管内科；

伴头晕，症状持续 20 分钟，口服速效救心丸后逐渐缓解；

双侧乳腺血管瘤切除术后 20 余年；否认高血压；高血糖病史 20 年，皮下注射胰岛素治疗；脑梗病史 10 年；冠心病病史 10 年；

吸烟 50 年，平均 20 支 / 日；

冠状动脉粥样硬化性心脏病

不稳定型心绞痛

脑梗死个人史

主述：

活动后胸痛 1 个月，加重 2 天” 入住心血管内科

现病史：

头晕，症状持续 20 分钟，口服速效救心丸后逐渐缓解；

既往病史：

双侧乳腺血管瘤切除术后 20 余年；否认高血压；高血糖病史 20 年，皮下注射胰岛素治疗；脑梗病史 10 年；冠心病病史 10 年；

吸烟 50 年，平均 20 支 / 日；

不稳定型心绞痛

脑梗死个人史

病程记录：

术后患者一般状态极差、呼吸循环状态不稳定：

给予肺动脉漂浮导管穿刺置管、IABP 穿刺置管，气管插管，呼吸机辅助呼吸，生命体征仍不稳定。

后患者无明显诱因出现房颤，150J 同步电复律后无明显改善。

最终患者家属放弃心肺复苏等抢救，心电检测呈直线，血压血氧测不出，瞳孔散大光反射消失，听诊无心音。

临床死亡。

检验检查记录：

心电图、生化、入院血糖 10.54mmol/L

超声心动图

单根导管的冠状动脉造影术检查

心电及血气分析

鉴别诊断：

1. 主动脉夹层

症状特点：突发剧烈胸痛，多为撕裂样或刀割样，疼痛起始即达高峰，可放射至

背部、腹部等，常伴血压升高（部分因休克可降低）。

鉴别要点：冠心病心绞痛多为压迫性、紧缩性疼痛，常在活动后诱发，休息或含服硝酸甘油可缓解；而主动脉夹层疼痛更剧烈且持续，硝酸甘油无效。

关键检查：主动脉 CT 血管造影（CTA）可明确显示夹层撕裂部位及范围，是重要鉴别依据。

2. 急性心包炎

症状特点：胸痛多为尖锐性，与呼吸、体位相关（深呼吸、咳嗽或改变体位时加重，坐位前倾可缓解），常伴发热。

鉴别要点：冠心病心绞痛与活动相关，而急性心包炎胸痛与呼吸、体位关系更密切，且多有炎症表现（如发热、白细胞升高）。

关键检查：心电图可见广泛 ST 段弓背向下抬高，超声心动图可发现心包积液。

3. 肺栓塞

症状特点：突发胸痛、呼吸困难、咯血，常伴烦躁不安、濒死感，严重者可出现血压下降、休克。

鉴别要点：冠心病患者多有胸痛伴胸闷、出汗，而肺栓塞以呼吸困难为突出表现，且常有下肢静脉血栓等高危因素（如长期卧床、术后）。

关键检查：D - 二聚体升高（但特异性低），肺动脉 CTA 可显示肺动脉栓塞部位，心电图可出现 $S_1Q_3T_3$征。

其他：

术前评估优化：对多支血管严重病变、合并糖尿病 / 长期吸烟患者，需更严格评估手术耐受性，制定备用循环支持方案。

术中监测强化：加强术中血流动力学及心肌缺血监测（如持续 TEE），及时调整血管活性药物剂量。

术后管理重点：

严格控制血糖（避免高糖加重心肌损伤）。

早期纠正电解质紊乱（如低钙、低钾），预防心律失常。

对高风险患者提前备好抗心律失常药物及进阶循环支持设备。

寻找真凶 肌不可失

王文艳

四川省医学科学院 . 四川省人民医院

患者基本信息：

年龄：46 岁

主述：

反复心累、双下肢水肿 6+ 月，加重伴咳嗽、腹胀 20+ 天

现病史：

无晕厥胸痛，先后 2022.4 及 2022.5 于外院

先后诊断为：急性心包炎、急性心肌炎

既往病史：

否认高血压 糖尿病，血脂异常病史

否认烟酒或其他不良嗜好

家族史无特殊

病程记录：

入院后完善心电图：加速性交界性心律，偶见窦性、房性激动下传，电轴 +187° 心室内阻滞，I、aVL 见 Q 波，V1-V4 导联 r 波递增不良，ST-T 改变。心脏彩超：LA42mmLV53mm IVS9mm，RA56*55mmRV22mm，EF32%，TAPSE12 TR4.03 三尖瓣重度关闭不全，肺动脉高压，少量心包积液。心脏核磁：左室横径 55mm，右房 55*60mm，心肌稍变薄，室间隔及左室前壁线状纤维化灶，EF18%，考虑心肌病可能，未见心肌炎改变。肌电图：肌肉肌性损害。下肢肌肉核磁：肌肉可见斑片状 T1 减低，下肢肌肉水肿肿胀。

进一步完善免疫 :R0-52 阳性，抗核抗体阳性 1:100，血沉 60mm/h。MHC-1 阳性，Jo- 阴性，CD8 阴性。肌肉活检有淋巴细胞浸润。请风湿免疫科会诊，自身免疫疾病导致肌炎证据不足。进一步组织活检：电镜下见肌原纤维大部分排列基本规则，局部见肌原纤维轻度撕裂，溶解，局部线粒体轻度增多。病程中患者的出现突发意识丧失，伴有双目凝视，考虑癫痫可能大。完善脑电图提示异常。线粒体脑肌病？后完善线粒体基因全长检测未见明显可解释表型的致病基因。后复核基因检测，提示：chrm-12417CA > C，MT-ND5：c。89del，p.Asn30Thrfs*7（7000,171）. 住院期间予以利尿、超滤等对症，期间考虑是否可以心脏移植，并送配型。或 VAD 过渡到移植 BTT ？ 后病情恶化，心肾功能衰竭死亡。

检验检查记录：

体格检查：

体型瘦小 BMI 15

T: 36.5℃ P: 65 次 / 分 R:19 次 / 分 BP:90/60mmHg。

无皮损，皮疹 面容无特殊 听力减弱，视力正常

四肢肌肉发育较萎缩，无压痛

肌力正常 颈静脉可见，心界扩大

HR 65/min , 心律不齐，第一心音强弱不等，脉搏短绌，三尖瓣闻及 3 级收缩期杂音。

双下肢重度水肿

肌肉损害

神经系统主要表现有卒中、癫痫反复发作、肌阵挛、偏头痛

心肌病 心力衰竭

肾功能不全

假性肠梗阻

血常规 WBC 4.27×10E9/L N % 52.3 hs CRP 2.13

心肌酶 MYO 226 hs TnI 168ng/L CK 639 CKMB 13.5 LDH 423

肝功 AST 54

肾功 Urea12.84mmol/L Cr 93.6umol/L eGFR 63.2 K 3.9mmol/L

凝血 PT 13.5 APTT 31.2 D-Dimer 3.92

BNP 1242.9ng/ml

乳酸 2.2mmol/L

免疫： 游离轻链 K 75.9 游离轻链 λ 67.9 比值正常

甲功：FT3 2.32pmol/L TT3 0.87nmol/L anti-TPO205

鉴别诊断：

全心长大 原因？

心肌炎？

心肌病（扩张表型心肌病？）

肌酶升高其他原因？

缺血因素？

感染因素？

免疫因素？

扩张性心肌病？ 心肌炎？ 骨骼肌损害？ 多发性肌炎？肌病？ 自身免疫性肌病？

遗传性？ 代谢性？

其他：

诊断的原则

及时性

准确性

层次性

整体性

具体性

动态性

一例 HFpEF 患者的诊疗及 GDMT 原则应用病例汇报

祝珊

中国人民解放军陆军军医大学第一附属医院

患者基本信息：

患者老年女性，75 岁，身高 150cm，体重 68kg，BMI 30.2kg/m2；间断失眠

主述：

发现血压升高 17 年，阵发性胸闷、痛 8 年，反复心悸、气促 2 年

现病史：

2007 年体检时发现血压升高，最高达 180/?mmHg,，伴间断头晕，考虑 “高血压病”，间断服用“罗布麻”降压治疗。2019 年开始规律服用“苯磺酸氨氯地平（络活喜）、卡维地洛” 控制血压，血压控制在 140/90mmHg 左右。

2017 年患者无明显诱因出现胸骨下段附近的阵发性胸痛，伴闷胀感，持续约 30s 左右自行缓解，偶有发作，无夜间阵发性呼吸困难、反酸、烧心等，多次门诊就诊后诊断为房颤、ST-T 改变，冠脉造影提示: 轻 - 中度冠脉病变，肾功能提示: eGFR 波动在 35-46ml/min.L，尿酸最高时 814umol/L。行睡眠呼吸监测提示

重度阻塞性睡眠呼吸暂停低通气综合征，医嘱长期夜间佩戴呼吸机治疗，患者执行佳。长期服用“华法林、瑞舒伐他汀、琥珀酸美托洛、别嘌醇、碳酸氢钠”治疗。2022 年期间因头颅 MRI 提示“颅内微出血灶”后将华法林调整为“利伐沙班”抗凝治疗

2021 年开始，患者感胸闷、气促症状加重，表现为持续 2-3 分钟左右发作异常，伴活动后气促，休息、服用“速效救心丸 / 硝酸甘油”可缓解，此后患者反复发作上述症状，日常走平路约 200m 左右感气促，无端坐呼吸、夜间阵发性呼吸困难表现，无咳嗽、咳痰表现。2022 年 3 月于我院老年科住院，期间肺功能检查提示肺通气功能正常，乙酰胆碱激发实验阳性，同时优化调整治疗方案，给与“苯磺酸氨氯地平、富马酸比索洛尔、利伐沙班、瑞舒伐他汀、沙美特罗替卡松吸入剂”治疗心肺疾病。然患者分别于 2022 年 6 月、2022 年 8 月、2022 年 12 月、2023 年 2 月、2023 年 11 月、2023 年 12 月多次因上述症状于我院心血管内科及老年科住院治疗。2023 年 6 月将缬沙坦氨氯地平调整为沙库巴曲缬沙坦降压治疗。2023 年 12 月最后一次住院后门诊考虑 HFpEF，加用达格列净、呋塞米、安体舒通治疗。患者病情平稳，直至 2024 年 9 月患者因自行停用呋塞米后双下肢水肿，再次门诊就诊，医嘱建议继续呋塞米治疗后症状改善，于 2025 年 3 月门诊复查心脏彩超及 BNP 较前明显改善。

既往病史：

2017 年在进食“大豆”后出现双足第一趾关节疼痛伴红肿、皮温升高，结合血尿酸升高，考虑痛风。2018 年因“摔伤”导致腰椎骨折，性“骨水泥”治疗，此后诊断为重度骨质疏松，对“磺胺”过敏。

病程记录：

因患者多次住院，均有涉及轻微的方案调整，特别将重点的诊疗经过整理出来。患者于 2022 年 8 月在我科住院期间行冠状动脉造影术检查：1. 前降支造影剂滞留，近段及中段轻 - 中度狭窄 30-50%，TIMI 血流 II+ 级；回旋支造影滞留，远段轻度狭窄 20%，TIMI 血流 III- 级；3. 右冠状动脉造影剂滞留，近段及远段轻度狭窄 20%，TIMI 血流 II+ 级。完善胃镜：反流性食管炎，慢性萎缩性胃炎伴轻度肠化（C2）；期间仍给与抗凝、抑酸护胃、他汀调节血脂等治疗后出院，2023 年 6 月门诊随访期间，将患者降压药物从缬沙坦氨氯地平调整为沙库巴曲缬沙坦，2023 年 12 月最后一次住院出院后门诊考虑 HFpEF，加用达格列净、呋塞米、安体舒通治疗。患者病情平稳，直至 2024 年 9 月患者因自行停用呋塞米后双下肢水肿，再次门诊就诊，医嘱建议继续呋塞米治疗后症状改善，于 2025 年 3 月门诊复查心脏彩超及 BNP 较前明显改善。

检验检查记录：

2020.3.1 心电图：心房颤动（心室率 71 次 / 分），ST-T 改变。

2020.6.1 心电图：心房颤动（心室率 71 次 / 分），ST-T 改变。

2024.5.6 心电图：心房颤动（心室率 60 次 / 分），肢体导联低电压。

2024-09-24：心脏彩超：左房 49mm，右房 48mm，右室 22mm，EF=66%；估测肺动脉收缩压力 51mmHg；主动脉瓣轻度钙化，主动脉瓣轻度关闭不全，二尖瓣轻度反流，三尖瓣中 - 重度反流，肺动脉收缩压中度增高，肺动脉瓣轻度反流；左心室、右心室舒张功能减退。

2024-09-24：心脏彩超：左房 49mm，右房 48mm，右室 22mm，EF=66%；E 峰 =95cm/s，A 峰 =40cm/s；左房容积指数 60.4ml/m2；估测肺动脉收缩压力 32mmHg；主动脉瓣轻度钙化，主动脉瓣轻度关闭不全，二尖瓣轻度反流，三尖瓣重度反流，肺动脉稍增宽，肺动脉瓣轻度反流；左心室舒张功能减退。

2025-03-20：心脏彩超：左房 45mm，右房 46mm，右室 22mm，EF=67%；E 峰 =86cm/s，A 峰 =60cm/s；左房容积指数 42.9ml/m2；估测肺动脉收缩压力 35mmHg；主动脉瓣轻度钙化，主动脉瓣轻度关闭不全，二尖瓣轻度反流，三尖瓣中度反流，肺动脉稍增宽，肺动脉瓣轻度反流；左心室舒张功能不能确定，请结合临床。BNP 及 NT-proBNP，肌酐，尿酸的动态演变趋势及其他相关检验结果见上传图片。

肾功能显像：左肾肾小球滤过率降低（GFR 约为正常单肾低限的 69.4%）；右肾肾小球滤过功能正常。

胸片：双肺纹理增多模糊，心影增大。

鉴别诊断：

1. 反流性食管炎：患者胃镜支持诊断，但长期规范的 PPI 及促进胃肠动力药物治疗效果后患者仍反复住院。

2. 心脏神经官能症：患者有间断失眠的情况，间断服用“曲唑酮”病史，然该患者多次辅助检查 BNP 均有显著升高，症状不能归因于该病。

3. 支气管哮喘：诊断支持，然长期沙美特罗替卡松吸入治疗，症状不能缓解，BNP 升高是强不支持点。

4. 肺栓塞：活动后气促及胸痛等临床表现为支持点，DD 阴性 + 长期服用利伐沙班不支持

其他：

以急性胸痛为首发表现的颌下间隙感染合并纵隔气肿一例

邵丹

克拉玛依市中心医院

患者基本信息：

患者男性，47 岁，维吾尔族，离异，无业

入院时间： 2019 年 11 月 14 日 18:00:34

主述：

胸痛 3 小时

现病史：

患者于入院前 3 小时因情绪激动出现持续性胸痛，呈刺痛，伴胸闷、气短、大汗，无放射痛，症状持续不缓解。2019 年 11 月 14 日 16:58 我院急诊就诊，心电图示窦性心律，广泛导联 ST 段抬高，请心内科急会诊考虑“急性 ST 段抬高型心梗”，予吗啡皮下注射及抗血小板药物（波立维、阿司匹林、立普妥负荷量口服）。家属选择急诊介入治疗，签署知情同意书后行急诊冠状动脉造影术 + 左心室造影，结果显示冠状动脉未见明显狭窄 （TIMI 血流 3 级），左心室造影未见异常。术后以“胸痛待查”收住心内科 CCU。

既往病史：

高血压： 病史 5 年，未规律用药，血压控制尚可。

静脉吸毒史： 10 余年，近 2 年已戒。

手术外伤史： 1980 年因车祸致左侧股骨骨折（否认手术史）。

牙科感染：1 周前因“右侧颌下间隙感染、右侧牙槽脓肿、急性根尖周炎”输液治疗。

其他： 否认肝炎、结核、糖尿病史；无药物 / 食物过敏史。

病程记录：

1. 急诊处理

抗血小板治疗：波立维、阿司匹林、立普妥负荷量口服。

镇痛：吗啡皮下注射。

急诊介入：行单根导管冠状动脉造影 + 左心室造影（结果见检查记录）。

2. 心内科 CCU 治疗

抗感染：头孢呋辛 3.0g q12h 静点，甲硝唑 250ml q12h 静点。

支持治疗：极化液静点稳定心肌电生理，水化保护肾功能。

患者术后入 CCU 仍持续胸痛，完善 CT 检查发现右侧颌下间隙感染，纵隔气肿，患者诉 1 周前曾因牙槽脓肿、急性根尖周炎输液治疗。经口腔科、胸外科、耳鼻喉科、ICU、药学科多学科会诊后转入口腔科行急诊脓肿切开引流术，术后转入 ICU 进一步治疗。

多学科会诊：

口腔科： 诊断“颌面间隙感染”，建议急诊手术引流。

胸外科： 考虑纵隔气肿为感染产气所致，建议加强抗炎及纵隔引流。

ICU： 评估为 ASA IV 级，需术后转入 ICU 监护。

药学科： 调整抗生素为泰能（亚胺培南 / 西司他丁）0.5g q6h 静点。

3. 口腔科手术治疗

术式： 全麻下经口腔颌面部颈部探查术 + 筋膜成形术 + 皮瓣修整术 + 面神经减压术。

4.ICU 术后管理

（1）呼吸支持：患者术后因感染性休克及呼吸衰竭转入 ICU，予气管插管接呼吸机辅助通气，维持氧合（SpO_2 85%-97%）。因呼吸费力显著，调整呼吸机参数并行支气管镜检查，清除气道分泌物（黄绿色粘痰），灌洗后管腔通畅，诊断为急性支气管炎改变。

（2）抗感染治疗：联合抗生素升级：根据 PCT（降钙素原）及 CRP（C 反应蛋白）水平升高（PCT 49.53 ng/ml → 11.89 ng/ml），调整为泰能（亚胺培南 / 西司他丁）+ 万古霉素，后因肾功能不全及耐药风险改为泰能 + 利奈唑胺，覆盖革兰氏阳性球菌及阴性杆菌。

（3）血流动力学支持：去甲肾上腺素维持血压，因感染性休克导致低血压（收缩压最低至 96 mmHg），持续小剂量泵入去甲肾上腺素，血压逐步回升至 110/65 mmHg 左右。

（4）肾功能保护：连续性肾脏替代治疗（CRRT）评估：患者肌酐最高达 371.3 μmol/L，尿量减少，但因血流动力学不稳定暂未启动 CRRT，优先通过利尿剂（呋塞米）及白蛋白补充维持肾灌注。

（5）营养与代谢支持：肠内营养联合白蛋白补充：鼻饲流质饮食，补充多种维生素及微量元素，纠正低蛋白血症（白蛋白 25.6 g/L → 30.8 g/L）。

5. 患者转归方向：患者术后持续发热，血压需大剂量血管活性药物维持，感染性休克无明显改善，有创呼吸机无法脱机，家属放弃治疗签字回家。

检验检查记录：

入院时检查

1. 心电图： 窦性心律，广泛导联 ST 段抬高。

2. 实验室检查：

炎症指标： C- 反应蛋白 324.14mg/L，PCT 49.53ng/ml，白细胞 11.06×10^9 /

L，中性粒细胞 80.5%。

肾功能： 肌酐 222.5μmol/L（术后升至 371.3μmol/L）。

心肌酶： 肌钙蛋白 -T<0.05ng/mL，CK-MB 正常。

3. 影像学： 心脏超声未见明显异常，颈胸 CT 提示右侧颌下间隙感染、纵隔气肿、双肺炎症、心影增大。

术后检查

1. 实验室检查

炎症指标：

C- 反应蛋白（CRP）显著升高（324.14 mg/L → 323.05 mg/L）；降钙素原（PCT）峰值达 49.53 ng/ml，术后降至 11.89 ng/ml。

心肌酶与心肌标志物：肌钙蛋白 -T 始终未升高（<0.05 → 1.11 ng/mL），心肌酶（CK-MB、肌酸激酶）无显著升高，排除急性心肌梗死。

肾功能：入院时肌酐 222.5 μmol/L，术后升至 371.3 μmol/L。

肝功能：门冬氨酸氨基转移酶（AST）83.5 → 159 U/L，丙氨酸氨基转移酶（ALT）63.9 → 80.1 U/L，提示肝细胞损伤（可能与感染、低灌注相关）[[File]]。

血气分析：术后 pH 7.287，PaO_2 29.82 mmHg，BE -6.5 mmol/L。

2. 心电图

心电图：入院时广泛导联 ST 段抬高，术后未见动态演变。

3. 影像学检查

床旁胸片：双肺散在片状密度增高影，左肺外带弧形高密度影（胸腔积液）。

4. 支气管镜检查

镜下表现：左下叶管腔内黄绿色粘痰，灌洗后通畅，诊断为急性支气管炎改变，提示继发性肺部感染。

5. 微生物培养与药敏试验

血培养、痰培养、灌洗液培养均未检出细菌 / 真菌 / 结核杆菌，T-SPOT 阴性。

鉴别诊断：

急性心梗：患者表现为持续性胸痛、大汗及心电图广泛导联 ST 段抬高，需优先排除急性 ST 段抬高型心肌梗死（STEMI）。但冠脉造影显示冠状动脉无狭窄，左心室造影未见室壁运动异常，且肌钙蛋白 -T 及心肌酶未升高，不支持心肌坏死诊断。结合影像学与实验室检查，排除典型急性心梗，考虑 ST 段抬高可能为感染性炎症或应激反应所致

急性肺动脉栓塞 ： 患者表现为胸痛、呼吸困难及 D- 二聚体显著升高（7189.56 ng/ml），需警惕急性肺动脉栓塞。但患者无咯血、右心负荷增加表现（如颈静脉怒张、肺动脉瓣区第二心音亢进），心电图未见典型 S Ⅰ Q Ⅲ T Ⅲ改变及右胸导联 T 波倒置，结合临床表现及影像学检查，暂不支持肺动脉栓塞诊断

主动脉夹层 ： 患者胸痛呈剧烈刺痛，需鉴别主动脉夹层。但患者疼痛无放射至背部或腹部，无双上肢血压差异、主动脉瓣关闭不全杂音或神经系统症状，急诊 CT 及冠脉造影均未见主动脉内膜片或真假腔征象。结合症状特征与影像学证据，可排除主动脉夹层。

其他：

一、鉴别诊断的复杂性与必要性

1. 非心源性胸痛的鉴别难点：

年轻患者的误导性表现：本例为 47 岁男性，突发胸痛伴 ST 段抬高，典型症状易误诊为急性心梗，但冠脉造影无狭窄证据提示需警惕非心源性病因。

感染性全身炎症反应：颌下间隙感染继发纵隔气肿可导致全身炎症反应（如 CRP、PCT 显著升高），可能通过炎症因子释放间接影响心电图（ST 段抬高），需与心肌损伤鉴别。

其他需鉴别的疾病：急性心包炎：需结合心电图（广泛导联 ST 段弓背向下抬高）、心脏超声（心包积液）及肌钙蛋白水平综合判断。应激性心肌病：情绪应激诱发病史需警惕，但心脏超声未见 “章鱼篓” 样改变可排除。

二、多学科协作（MDT）的关键作用

口腔科 -ICU 联动：颌下脓肿与纵隔气肿的关联性需多学科评估，口腔科急诊手术切开引流联合 ICU 术后监护可降低死亡率（文献报道纵隔气肿死亡率达 40%-50%）。

麻醉科介入：困难气道（张口受限、颈部肿胀）需清醒气管插管，麻醉科与耳鼻喉科协作确保安全插管。

三、文献支持与局限性

1. 是否考虑合并感染性心内膜炎，诊断需依赖血培养及心脏超声，本例未明确，需后续追踪。

2. 局限性缺乏微生物培养结果，经验性抗生素选择可能存在偏差；未提及床旁超声对心功能及容量状态的动态评估，可能影响休克分型与治疗决策。

四、总结

本病例为复杂多系统疾病的典型代表，强调早期识别非心源性胸痛、多学科协作及个体化治疗的重要性，为临床实践提供重要借鉴。

一种用于清除冠脉夹层血肿的新技术——SBLP 技术

林以诺

温州医科大学附属第一医院

患者基本信息：

多个患者信息，详见幻灯片

主述：

多个患者信息，详见幻灯片

现病史：

多个患者信息，详见幻灯片

既往病史：

多个患者信息，详见幻灯片

病程记录：

多个患者信息，详见幻灯片

检验检查记录：

多个患者信息，详见幻灯片

鉴别诊断：

多个患者信息，详见幻灯片

其他：

多个患者信息，详见幻灯片

扑朔迷离的心包积液

刘逸凡

北京协和医院

患者基本信息：

患者男性，58 岁。

主述：

活动后气短半年余，双下肢水肿 2 月

现病史：

2021 年 9 月，患者无诱因出现活动后气短，逐渐加重至步行 20 米即有症状，无发热、盗汗、咳嗽、胸痛，夜间可平卧。2022 年 2 月，出现双踝以下对称性可凹性水肿。患者水肿逐渐加重，2022 年 4 月收入我院。起病以来，患者一般情况尚可，体重下降约 10kg。体格检查：体温 36.2℃，脉搏 80 次 / 分，呼吸频率 21 次 / 分，自然状态下指氧饱和度 93%-95%，右上肢血压 120/70 mmHg，左上肢血压 108/74 mmHg，双侧眼球略突出，心音低钝，余心、肺听诊无殊。腹部、淋巴结及神经查体未及明显异常，双踝以下轻度可凹性水肿。

既往病史：

既往史：否认结核病史及接触史。2019 年诊断 “脑梗死（无后遗症）、高血压、高脂血症、空腹血糖受损”，服替米沙坦、瑞舒伐他汀、二甲双胍，未监测血压、血脂、血糖。否认手术、外伤、介入、放疗及特殊用药史。个人史：否认吸烟史；饮酒 25 年，50°白酒 500 g/d，戒酒 3 年；有粉尘接触史。

病程记录：

患者入院后完善检查。血常规：白细胞 10.29×10^9/L，中性粒细胞 89.4%，血红蛋白 152g/L；尿常规正常；肝肾功能大致正常；血白蛋白 35 g/L；凝血功能、D 二聚体正常。心脏相关检查：心脏肌钙蛋白正常。N 末端 B 型钠尿肽（N-terminal Pro-Brain Natriuretic Peptide, NT-proBNP）434 pg/ml。心电图：窦性心律，心率 81 次 / 分，肢体导联低电压，前壁导联 R 波递增不良，无明显 ST-T 改变。超声心动图：中 - 大量心包积液（最深处 22mm），脏层心包絮状物沉积，主肺动脉增宽，升主动脉及主动脉窦部增宽（30 mm），主动脉瓣增厚，左心室射血分数 74%，下腔静脉宽度 16 mm，下腔静脉吸气变化率小于 50%，未见室壁运动异常。考虑心包积液可以解释患者气短、水肿、低氧、心音低钝的临床表现，需要进一步进行心包积液相关常见病因筛查，如感染性疾病、肿瘤学疾病、代谢性疾病等。感染性疾病相关检查：结核菌素皮肤试验、结核感染 T 细胞检测、梅毒螺旋体抗体、乙型肝炎抗体、丙型肝炎抗体、巨细胞病毒及 EB 病毒 DNA 阴性。炎症指标：超敏 C 反应蛋白 39.4mg/L，红细胞沉降率 23mm/h，铁蛋白 117ng/ml。胸腹部断层显像（computerized tomography ，CT）：双肺弥漫性间质病变，多发小叶间隔增厚，叶间裂增厚，牵拉性支气管扩张，少量渗出，双侧胸膜不均匀增厚，（图 3）；升主动脉、主动脉弓、降主动脉、腹主动脉管壁可疑增厚、边缘毛糙；双侧锁骨、胸骨、双侧部分肋骨、双侧肱骨近段、双侧股骨近段多发骨质密度异常；未见明确肿大淋巴结。肿瘤性疾病相关检查：外周血形态学分析未见异常；血清肿瘤标记物：癌胚抗原、鳞状细胞癌相关抗原、神经元特异性烯醇化酶、糖类标记物 19-9、糖类标记物 15-3 甲胎蛋白、β2 微球蛋白均正常。代谢性疾病相关检查：甲状腺功能正常。

患者胸腹部 CT 提示主动脉全程管壁可疑病变，因此进一步完善主动脉血管成像：

主动脉至双侧髂动脉管壁环周增厚伴轻度强化，主动脉一级分支多发受累、局部受包绕（图 1-2）；心包积液深约 1cm；双侧肾周软组织影包绕（图 2）。头增强磁共振：双侧顶部脑膜及双眼眶多发占位，蝶窦、双侧上颌窦及左侧额窦、鞍区前上及大脑镰多发异常信号占位，延髓与右侧椎动脉间异常强化灶。

综合上述检验、检查结果，患者炎症指标升高，且存在全身多系统病变，包括多浆膜腔积液、主动脉及分支管壁环周增厚、肾周软组织包绕、双肺间质性病变，以及鼻窦、脑膜、眼眶内占位。因此病因方面主要考虑可以导致多系统病变的疾病，如免疫性疾病及肿瘤性疾病。免疫性疾病相关检查：抗核抗体（antinuclear antibodies, ANA）(+)1:80，抗双链 DNA 抗体、抗可提取性核抗原（extractable nuclear antigens, ENA）抗体、抗中性粒细胞胞浆抗体（antineutrophil cytoplasmic autoantibody, ANCA）阴性；补体 C3、C4 正常；免疫球蛋白（Immunoglobulin，Ig）G 6.25 g/L，IgA、IgM 正常；血清 IgG4 正常。。为进一步评估有无肿瘤性疾病，行正电子发射断层显像（positron emission tomography-computerized tomography，PET-CT）：双侧眼球后代谢增高软组织影，最大者 1.1 cm×1.0 cm，最大标准摄取值（maximaum standard uptake value，SUVmax）7.0；双侧上颌窦代谢增高影；双肺间质性改变，代谢增高；双肾实质肿胀，代谢增高；双侧颈动脉、主动脉全程管壁增厚且代谢增高；全身骨骼多发代谢增高区（图 4），SUVmax 8.2；骶前及双侧盆壁内侧代谢增高结节；心包积液；双侧胸腔积液；全身淋巴结未见增大及放射性摄取增高。患者全身多系统病变，且病变部位代谢升高。为进一步明确诊断，拟选取 SUV 升高部位行活检。因骨活检费用较高，肾及主动脉活检风险较大，遂拟行全麻下眼眶内肿物切除活检。

在等待手术期间患者气短、双下肢水肿明显加重，夜间不能平卧。监测血压 100/60mmHg，心率 90-100 次 / 分，自然状态下指氧饱和度 90%-92%，听诊心音较前稍低。复查超声心动图：大量心包积液（最深处 28mm），脏层心包上见絮状物沉积，心脏在心包内游离状；右室舒张期塌陷状；右侧房室沟组织增厚；左心室射血分数 72%。为缓解患者症状、创造条件进行全麻手术，行心包穿刺，引出黄色微浑浊液体，约 400 ml/d。患者气短部分缓解，下肢水肿消散，血压、心率恢复基线水平，自然状态下指氧饱和度升至 95%。心包积液常规：白细胞 5-8 个 / 高倍镜视野，红细胞 9-14/ 高倍镜视野；抗酸染色、结核培养结核分枝杆菌复合群基因检测阴性；细菌、真菌、放线菌、奴卡氏菌培养阴性。患者呼吸情况改善后，行眶内肿物活检，术中可见 2.0 cm × 1.5 cm 圆形黄白色质韧肿物，与周围组织黏连紧密。活检后根据眼科活检术后的常规要求，予泼尼松 60 mg/d 治疗（服用两周后停用）。患者的心包积液引流量逐渐减少（200 ml/d → 130 ml/d → 50 ml/d），夹闭引流管后呼吸困难未再发。监测血压 110-120/70 mmHg，心率 70-90 次 / 分，自然状态下指氧饱和度 95%-96%。复查超声心动图：右侧房室沟团块样增厚，范围约 13 mm × 19 mm，少量心包积液，余大致同前。遂拔除心包引流管。眶内肿物活检病理结果：增生纤维组织中见大量泡沫样组织细胞浸润及散在多核巨细胞，另见少许小灶性分布的淋巴细胞；免疫组化：CD68、CD123（+），B-raf（+），Langerin（-），CD1a（-），IgG4（-）；分子病理结果检测到 $BRAF^{V600E}$ 突变；综合上述表现，符合 Erdheim-Chester 病（Erdheim-Chester Disease, ECD）。2022 年 6 月，患者出院，入组单臂临床试验，持续接受 BRAF 抑制剂维莫菲尼治疗。定期门诊随诊，未再发生气短及下肢水肿。2024 年 6 月，PET-CT 提示病变部位代谢活性较前降低（图 5）。2025 年 4 月，胸部 CT 显示主动脉管壁环周增厚较前略减轻、少量心包积液（图 6）。

检验检查记录：

血常规：白细胞 10.29×10^9/L，中性粒细胞 89.4%，血红蛋白 152g/L；尿常规正常；肝肾功能大致正常；血白蛋白 35 g/L；凝血功能、D 二聚体正常。心脏相关检查：心脏肌钙蛋白正常。N 末端 B 型钠尿肽（N-terminal Pro-Brain Natriuretic Peptide, NT-proBNP）434 pg/ml。心电图：窦性心律，心率 81 次 / 分，肢体导联低电压，前壁导联 R 波递增不良，无明显 ST-T 改变。超声心动图：中 - 大量心包积液（最深处 22mm），脏层心包絮状物沉积，主肺动脉增宽，升主动脉及主动脉窦部增宽（30 mm），主动脉瓣增厚，左心室射血分数 74%，下腔静脉宽度 16 mm，下腔静脉吸气变化率小于 50%，未见室壁运动异常。感染性疾病相关检查：结核菌素皮肤试验、结核感染 T 细胞检测、梅毒螺旋体抗体、乙型肝炎抗体、丙型肝炎抗体、巨细胞病毒及 EB 病毒 DNA 阴性。炎症指标：超敏 C 反应蛋白 39.4mg/L，红细胞沉降率 23mm/h，铁蛋白 117ng/ml。胸腹部断层显像（computerized tomography，CT）：双肺弥漫性间质病变，多发小叶间隔增厚，叶间裂增厚，牵拉性支气管扩张，少量渗出，双侧胸膜不均匀增厚，（图 3）；升主动脉、主动脉弓、降主动脉、腹主动脉管壁可疑增厚、边缘毛糙；双侧锁骨、胸骨、双侧部分肋骨、双侧肱骨近段、双侧股骨近段多发骨质密度异常；未见明确肿大淋巴结。肿瘤性疾病相关检查：外周血形态学分析未见异常；血清肿瘤标记物：癌胚抗原、鳞状细胞癌相关抗原、神经元特异性烯醇化酶、糖类标记物 19-9、糖类标记物 15-3 甲胎蛋白、β2 微球蛋白均正常。代谢性疾病相关检查：甲状腺功能正常。

鉴别诊断：

患者中老年男性，慢性病程，进行性加重。以活动后气短、双下肢水肿起病，检查发现心包积液。心包积液的常见病因需考虑：（1）感染性疾病：在我国最常见的引起心包积液的感染性疾病是结核，其余如柯萨奇病毒、肝炎病毒、细菌、真菌等感染也可能导致心包积液。但该患者无相关流行病学史，病程中无发热、盗汗、咳嗽、咳痰、流涕、腹痛、腹泻、尿频、尿急、尿痛等感染表现，且外周血及心包积液的病原学检查均为阴性，故诊断感染性疾病的证据不足。（2）肿瘤性疾病：患者为中老年男性，病程中体重明显下降，需考虑肿瘤性疾病的可能性。但患者的肿瘤标记物均在正常范围内，影像学检查未见占位性病变和肿大的淋巴结等特征性提示，诊断肿瘤性疾病的证据不足。（3）手术、操作、放疗相关：患者无相关病史，不作考虑。在筛查上述病因的过程中，发现了多系统病变，包括多浆膜腔积液（累及心包、胸膜）、主动脉及其一级分支管壁增厚、肾周软组织包绕、骨病变、肺间质病变，以及颅内、眼眶内、鼻窦占位行病变，诊断需考虑以下疾病：（1）IgG4 相关疾病：IgG4 相关疾病可导致心包炎、动脉周围组织增厚、肾周组织增厚、肺间质病变、炎症指标升高，与本例相似。但患者的血清 IgG4 正常，无典型的唾液腺、胰腺、淋巴结受累。因此，诊断 IgG4 相关疾病的证据不足，需要行活检进一步明确诊断。（2）淋巴瘤：患者中老年男性，为淋巴瘤的好发人群，且淋巴瘤可以导致全身多系统受累。但患者胸腹部影像学未见淋巴结及肝、脾肿大，血清 β2 微球蛋白及铁蛋白正常，诊断淋巴瘤的证据亦不足，需要进行 PET-CT 检查及活检。（3）系统性红斑狼疮（systemic lupus erythematosus, SLE）等结缔组织病：患者 ANA 阳性，炎症指标升高，存在全身多系统病变，需考虑结缔组织病，特别是 SLE 的可能性。但患者为老年男性，并非结缔组织病的好发人群；ANA 滴度较低，诊断 SLE 特异性更强的抗双链 DNA 抗体、抗 ENA 抗体阴性；无皮疹、关节受累、低补体血症等结缔组织病的常见表现，故诊断结缔组织病的证据不足。而且，结缔组织病难以解释患者的多发骨病变、主动脉及肾周的包绕性病变和眶内及颅内的占位性病变。（4）系统性血管炎：患者的炎症指标升高，存在血管受累，需考虑系统性血管炎的可能性。患者的受累血管主要为主动脉及其一级分支，应首先考虑累及大血管的血管炎，包括好发于青年患者的大动脉炎及好发于老年患者的巨细胞动脉炎。患者为老年男性，不符合大动脉炎的好发年龄和性别；亦无头痛、视物不清、间歇性下颌运动障碍、风湿性多肌痛等巨细胞动脉炎的典型表现，故大血管炎的诊断可基本除外。患者存在肺、鼻窦、眶内、脑膜病变，需考虑 ANCA 相关血管炎，特别是肉芽肿性多血管炎（granulomatosis with polyangiitis，GPA）的可能性。但患者的 ANCA 阴性，无肾小球肾炎表现，且 GPA 累及主动脉者罕见，亦难以解释多发骨受累及肾周软组织病变，故 ANCA 相关血管炎的可能性较小。组织活检亦有助于鉴别 ANCA 相关血管炎。

PET-CT 检查提示上述病变部位的代谢活性明显增高（骨骼 SUVmax 8.2），但尚不足以鉴别上述病因，故需要行活检以明确诊断。综合考虑病变的代谢活性、操作风险、经济条件、患者意愿等因素，最终行眶内肿物活检，病理检查结果符合 ECD 表现，且分子检测存在 $BRAF^{V600E}$ 突变，最终确诊 ECD。在等待活检病理结果的过程中，根据眼科活检术后的常规要求给予患者糖皮质激素治疗，患者的心包积液较前减少，亦支持 ECD 的诊断。

其他：

旋磨 + 震波处理 LM-LAD 重度钙化病变

郝鹏

首都医科大学附属北京朝阳医院

患者基本信息：

见 PPT

主述：

见 PPT

现病史：

见 PPT

既往病史：

见 PPT

病程记录：

见 PPT

检验检查记录：

见 PPT

鉴别诊断：

见 PPT

其他：

见 PPT

OCT 指导下 ROTA+IVL 处理钙化病变 PCI

李惟铭

首都医科大学附属北京朝阳医院

患者基本信息：

见 PPT

主述：

见 PPT

现病史：

见 PPT

既往病史：

见 PPT

病程记录：

见 PPT

检验检查记录：

见 PPT

鉴别诊断：

见 PPT

其他：

见 PPT

右冠状动脉痉挛致心房 P 波保留、心室停搏 1 例

杨虹波

复旦大学附属中山医院

患者基本信息：

男性，65 岁

主述：

间断胸闷胸痛 7 年，加重伴晕厥 1 次

现病史：

患者近 7 年来无明显诱因下反复出现胸闷胸痛不适，以闷痛为主，心前区明显，无放射至其他部位，发作时自行捶击胸口可缓解，发作无规律，频率不高，至今共发作 2-3 次，未予重视。2005 年发作后行 EKG 检查未见明显异常。本次于 2008.3.30 下午步行回家后突感胸痛，程度较剧烈，伴大汗及胸闷气促，急吞服 2 粒“保心丸”后症状无缓解，随即意识丧失摔倒在地，（无家属在场）数分钟后自行醒转，发现大小便失禁，症状未再有发作。2008.3.31 当地医院就诊时查心电图示窦性心动过缓，多导联 ST 压低；行动态心电图提示窦性心律，总心率 88447 次，最快心率 94 次 / 分，最慢心率 47 次 / 分，平均心率 62 次 / 分，可见房性早搏 6 次，未见长间歇，未见明显 ST 段改变；头颅 CT 未见明显异常。为进一步明确晕厥原因入院。

既往病史：

患者长期吸烟史，吸烟 40 余年，20 支 / 天，否认有高血压、2 型糖尿病、高脂血症病史。

病程记录：

患者入院后，2008-4-21 患者晨 6:50am 突发胸闷胸痛、出冷汗、头晕不适，血压 120/80mmHg，床旁心电图（图 1）见 II/III/aVF 导联 ST 段弓背向上抬高伴 I/aVL/aVR 导联 ST 段压低，长 R-R 间歇、III 度房室传导阻滞、心室停搏，并出现意识欠清，牙关紧闭，小便失禁，迅速给予胸外按压，阿托品 0.5mg 静推，2 分钟后患者意识转清，外周动脉血压 130/80mmHg，考虑长间歇为冠脉痉挛引起，予硝酸甘油 20mg 加入 500ml 生理盐水静滴，5 分钟后患者胸闷症状明显好转，复查心电图未见明显 ST-T 改变。（图 2）

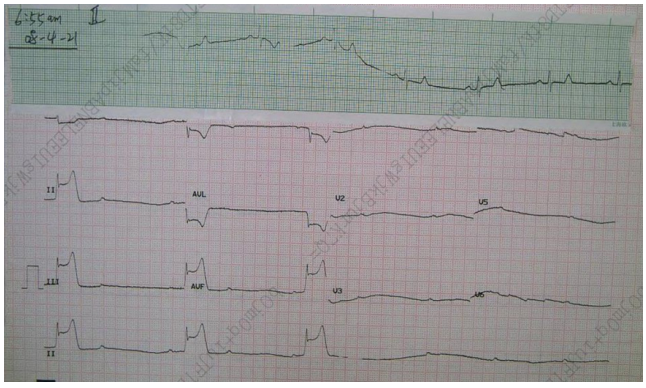

2008.4.21 予以植入临时起搏器后行冠脉造影术，见左冠脉未见明显狭窄，左前降支中段心肌桥，收缩期管腔受压 70%，舒张期不能完全恢复正常，细小左回旋支发出分支供应窦房结，右冠状动脉粗大，左室后支粗大，发出分支供应房室结，血流缓慢，注入硝酸甘油后好转。（图 3）

后予以地尔硫卓片 30mgtid+ 单硝酸异山梨酯 40mgqd+ 消心痛 5mgtid 控制心室率、抗痉挛治疗，并嘱咐患者戒烟，避免诱发冠状动脉痉挛。患者无胸闷胸痛等不适主诉，随访心电图、心肌酶谱及心肌标志物均正常。

检验检查记录：

心肌标志物正常，无发作时心电图正常。

鉴别诊断：

无。

其他：

患者两次发作晕厥，发作时伴有心电图 ST 段改变及心室停搏，考虑右冠状动脉痉挛引起恶性心律失常，积极予以药物抗痉挛治疗的基础上，于 2008.4.28 植入双腔起搏器，术后胸片提示起搏器导线位置良好，心电图提示起搏器呈 VAT 模式工作，功能良好。（图 4）患者接受抗痉挛及起搏器治疗的基础上未再有胸闷胸痛或晕厥发作，出院后门诊随访无胸痛及晕厥。

肺动脉高压治疗 1 例

陆林祥

同济大学附属东方医院

患者基本信息：

患者，女性，48 岁。

主述：

反复活动后胸闷气逼 6 年余，加重 2 月

现病史：

因“反复活动后胸闷气逼 6 年余，加重 2 月”于 2020 年 7 月 24 日入院。患者 2005 年于仁济医院诊断系统性红斑狼疮，予醋酸泼尼松龙，规律用药至今；2008 年因外伤下肢静脉血栓形成 + 肺动脉栓塞，予尿激酶 + 华法林治疗，后长期予华法林，规律用药至今；2009 年因 SLE 于北京某医院行环磷酰胺治疗 1 次（具体不详），因患者个人因素未规律治疗。

既往病史：

无高血压糖尿病高脂血症病史，无传染病家族遗传性疾病史

病程记录：

完善术前准备，排除手术禁忌症后于 2020.07..30 行右心导管检查及经皮肺动脉成形术：右房压：13/7/8mmHg， 右室压：80/11/37mmHg，肺动脉压：79/35/51mmHg。行肺动脉造影，造影示患者主肺动脉明显增宽，肺动脉及远段血管不同程度充盈缺损，以左下肺动脉、右上肺动脉尤甚。选择左肺下叶动脉为介入靶血管，故分别使用 Boston MUSTANG 3mm 外周球囊分次扩张，扩张后狭窄明显缓解，血流通畅，目标血管成形良好，狭窄血管接近原血管直径，终止手术，术后加用安立生坦 + 西地那非等靶向药物降肺动脉压治疗。

检验检查记录：

肺动脉造影 (肺动脉 CTA)(CT 增强 64 层): 两侧肺动脉栓塞，请密切随访。右肺上、下叶斑片影，右侧胸腔少量积液。注入造影剂后可见左、右肺动脉主干及分支内多发低密度充盈缺损影，管腔未见明显增宽改变。右肺上、下叶见斑片影。

心脏超声检查：右房室增大，左室内径偏小 右室壁整体运动减低 少中量三尖瓣反流 肺动脉收缩压 59mmHg 左室收缩功能正常 右室收缩功能减低。

四肢血管彩色多普勒超声 (心超室)： 双下肢动脉走行正常，血流通畅 左侧股总静脉、股浅静脉、腘静脉、胫后静脉血栓形成伴不全梗阻 右侧股浅静脉血栓形成伴不全梗阻。

术后 5 年，心脏超声提示：肺动脉收缩压 36mmHg. 生活质量明显改善。

鉴别诊断：

心脏瓣膜性疾病：二尖瓣狭窄、关闭不全等导致的肺动脉高压，心脏超声基础可以鉴别

肺部疾病：COPD、肺静脉狭窄等，肺 CTA 及肺部 CT 可以明确诊断

其他：

精神心理疾病致反复高血压急症一例

魏宇航

郑州大学第一附属医院

患者基本信息：

患者，女性，53 岁。

个人史：生于河南省漯河市，久居本地，无传染病接触史，无吸烟、饮酒、药物等嗜好，无从事有毒有害工种史，无放射性物质接触史，否认冶游史。

婚姻史：已婚，24 岁结婚，爱人体健，夫妻关系和睦，有 1 女。

月经生育史：初潮 18 岁，绝经时间 52 岁，无痛经史。

家族史：母亲已故，死于心脏病，父亲、3 哥、1 姐、1 妹健康状况良好，无与患者类似疾病，无家族性遗传病史。

主述：

发作性呼吸困难 7 小时

现病史：

发病前 7 小时进行艾灸治疗，期间突发呼吸困难，伴头晕、右侧颞部搏动性头痛、大汗，无胸闷、胸痛、心悸，无发热、咳嗽、咳痰，无腹痛、腹泻、恶心、呕吐等，持续 10 余分钟后症状逐渐自行缓解。

既往病史：

诊断“抑郁症”4 年，长期口服“黛力新”及“脑力静胶囊”治疗。否认高血压、糖尿病、脑血管病等病史。

病程记录：

入院查体: 体温 36.5℃, 脉搏 54 次 / 分, 呼吸 23 次 / 分, 血压 160/106mmHg（1 mmHg=0.133 kPa）。神志清，精神可，肺部可闻及湿啰音，心率 54 次 / 分，律齐，各瓣膜听诊区未闻及杂音，无心包摩擦音。腹部体征无异常，神经系统检查未见阳性体征。患者入院常规心电图大致正常。超敏肌钙蛋白 T：0.677 ng/mL（参考范围 0 ~ 0.1 ng/mL); 肌酸激酶同功酶质量法：11.46 ng/mL（参考范围 0 ~ 4.94 ng/mL); 乳酸脱氢酶 :254 U/L（参考范围 75 ~ 245 U/L);N 端脑钠肽前体 :1149.0 pg/mL（参考范围 0 ~ 121 pg/mL），肝功能、肾功能、凝血功能、电解质等未见异常。超声心动图示三尖瓣轻度关闭不全，左室射血分数: 61%。结合患者临床症状及心肌标志物结果，考虑急性冠脉综合征可能，进一步完善冠脉造影检查。冠脉造影示：冠脉呈右优势型，LAD 中远段可见约 50% 狭窄，前向血流 TIMI3 级；LCX 及 RCA 通畅，未见明显狭窄，前向血流 TIMI3 级。予以抗血小板聚集、调脂稳定斑块、扩冠、改善循环等治疗。5 月 30 日下午无明显诱因突发血压升高，血压 214/123 mmHg，继而出现胸闷、四肢湿冷、肺部满布湿啰音，考虑高血压急症、急性左心衰竭，心电图提示窦性心律，广泛前壁导联 T 波高尖。立即予“硝普钠”、“呋塞米注射液”、“吗啡”等药物应用后血压逐渐下降至 135/66 mmHg，临床症状逐渐缓解。复查超声心动图示左室壁节段性搏动异常，室间隔基底部增厚，EF:50%。双肾及肾血管彩超示双肾动脉阻力指数升高、左肾稍高回声。心脏磁共振示：左室室间隔稍厚，室间隔肌壁间异常强化，考虑心肌纤维化改变。头颅 MRI+MRA 未见明显异常。肾上腺 CT、肾动脉 CTA 未见异常。后患者血压正常，无不适症状，于 2019 年 6 月 3 日出院。

16 天后患者因“突发头晕头痛 1 天，加重 12 小时”再次入院。起病前无诱因突发头晕头痛，伴胸闷、气促、大汗淋漓、意识模糊，无胸痛。外院急诊心电图提示 ST 段抬高、T 波倒置，NT-proBNP：6490ng/L（参考范围 0 ~ 121 pg/mL)。转入我院急诊科后口服“阿普唑仑”后意识恢复，胸闷气促症状明显缓解。遂转入心内科。查体：体温 36.5℃，脉搏 78 次 / 分，呼吸 21 次 / 分，血压 90/63 mmHg（1 mmHg=0.133 kPa）。患者神志清，精神可，双肺呼吸音清，心率 78 次 / 分，律齐，各瓣膜听诊区未闻及杂音。腹软，无压痛，神经系统查体未见异常。后患者在院期间多次出现发作性高血压急症、急性心力衰竭，进一步完善继发性高血压筛查，肾素 - 血管紧张素 - 醛固酮立卧位检测、皮质醇节律、单胺类神经递质及代谢产物、尿儿茶酚胺类物质（肾上腺素、去甲肾上腺素、多巴胺）、24 小时尿微量白蛋白检测，均未见异常。静息门控心肌灌注显像（SPECT）示：左室心尖部及间隔心尖部灌注减低，左室整体收缩功能正常，舒张功能减低。^{131}I-MIBG 肾上腺髓质显像示：双侧肾上腺及全身其他部位摄取均正常，未见髓质活性灶。后精神医学科会诊，考虑诊断“惊恐发作”，给予“劳拉西泮”口服。随访 6 年，未再出现上述病情发作。

检验检查记录：

一、相关实验室检查：

1. 超敏肌钙蛋白 T：0.677 ng/mL（参考范围 0 ~ 0.1 ng/mL); 肌酸激酶同功酶质量法：11.46 ng/mL（参考范围 0 ~ 4.94 ng/mL); 乳酸脱氢酶 :254 U/L（参考范围 75 ~ 245 U/L);N 端脑钠肽前体 :1149.0 pg/mL（参考范围 0 ~ 121 pg/mL)，肝功能、肾功能、凝血功能、电解质等未见异常。

2. 继发性高血压筛查：肾素 - 血管紧张素 - 醛固酮立卧位检测、皮质醇节律、单胺类神经递质及代谢产物、尿儿茶酚胺类物质（肾上腺素、去甲肾上腺素、多巴胺）、24 小时尿微量白蛋白检测，均未见异常。

二、常规心电图：

动态演变（大致正常 -> 广泛前壁 T 波高尖 -> 前间壁 T 波正负双向 -> 前壁 T 波改变），无持续 ST 段抬高。

三、超声检查：

1. 超声心动图：左房增大，室间隔及左室壁增厚，左室舒张功能减低。

2. 双肾及肾动脉彩超：左肾稍高回声（考虑错构瘤），双肾动脉阻力指数增高。

四、冠状动脉造影：①冠脉分布呈右优势型。②左冠脉开口、起源、分布正常；LM 内膜光滑，LAD 内膜光滑，中远段粥样硬化伴狭窄，最重处 50%，未见明显狭窄，前向血流 TIMI3 级；LCX 内膜光滑，未见明显狭窄，前向血流 TIMI3 级；③ RCA 开口、起源、分布正常；RCA 主干及其分支未见明显狭窄。前向血流 TIMI3 级。

五、肾动脉 CTA+ 肾上腺 CT 平扫及增强扫描：双肾动脉 CTA 及双侧肾上腺未见明显异常；右肾下极稍低密度影，缺血？请结合临床；所示腹主动脉管壁散在钙斑及软斑，管腔稍变窄。

六、心脏磁共振：1. 左室室间隔稍厚，并室间隔肌壁间异常强化，考虑心肌纤维化改变 2. 左心舒张功能减低 3. 二尖瓣、三尖瓣轻度关闭不全。

七、静息门控心肌灌注显像（SPECT）示：左室心尖部及间隔心尖部灌注减低，左室整体收缩功能正常，舒张功能减低。^{131}I-MIBG 肾上腺髓质显像示：双侧肾上腺及全身其他部位摄取均正常，未见髓质活性灶。

鉴别诊断：

该病例以发作性血压升高、应激性心肌病、心力衰竭为主要临床表现，酷似嗜铬细胞瘤等临床表现。嗜铬细胞瘤起源于肾上腺髓质、交感神经节和体内其他部位嗜铬组织，肿瘤间歇或持续释放过多肾上腺素、去甲肾上腺素与多巴胺。临床表现变化多端，典型的发作表现为阵发性血压升高伴心动过速、头痛、出汗、面色苍白，部分与本病例重叠，但本例患者口服苯二氮卓类药物（阿普唑仑、劳拉西泮）后症状迅速缓解，不符合肿瘤性儿茶酚胺释放的持续性升高特征。同时嗜铬细胞瘤部分在发作期间可测定血或尿儿茶酚胺或其代谢产物 3- 甲氧基 -4- 轻基苦杏仁酸 (VMA) 有显著增高，本例患者多次发作期间 24 小时尿儿茶酚胺（肾上腺素、去甲肾上腺素、多巴胺）及其代谢产物（VMA、MN、NMN）均未升高。

其他：

该病例的讨论与核心教育意义：

1. 拓宽反复发作性高血压危象的鉴别诊断思维：

继发性高血压筛查是基石： 必须系统排查嗜铬细胞瘤、肾血管性高血压、原发性醛固酮增多症等器质性病因（本病例已完善）。

精神心理疾病是重要鉴别诊断： 当继发性病因筛查阴性，且患者有明确精神心理疾病史时，必须将精神心理因素导致的功能性心血管紊乱（如应激性心肌病、精神压力相关高血压）纳入首要考虑。本例酷似嗜铬细胞瘤，但实验室和影像学证据排除了它，最终指向精神心理源性的应激性心肌病和高血压危象。

2. 深入理解高血压急症与应激性心肌病的关联：

共同机制： 本例生动体现了交感神经过度激活、儿茶酚胺释放风暴是连接精神心理应激、高血压急症和 TTS 的核心病理生理桥梁。儿茶酚胺：导致外周血管强烈收缩→高血压危象；直接心肌毒性（尤其心尖部 β2 受体丰富）→心肌顿抑 / 收缩障碍→ TTS；在心脏储备下降基础上，后负荷剧增和心肌功能障碍共同导致急性左心衰竭。

临床表现的警示： 本例以严重高血压急症和心衰起病，伴有心电图动态变化及显著升高的 NT-proBNP（相对肌钙蛋白升高更突出），是 TTS 的重要线索，需与 ACS 仔细鉴别。

风险与处置： 高血压急症合并应激性心肌病 / 心衰时，风险极高（心源性休克、恶性心律失常）。处理需兼顾降压（硝普钠等静脉制剂）、减轻心脏负荷（利尿剂）、缓解焦虑（苯二氮卓类如劳拉西泮）及支持治疗。避免单纯依赖传统抗心绞痛 / 抗血小板药物。

3. 应激性心肌病诊断：超越典型影像，强调多维整合：

影像学价值局限： TTS 以左室心尖部或中段节段性运动减弱、基底部代偿性收缩增强为特征，形成 " 章鱼壶 " 样改变，但本例患者多次心脏超声均未发现典型室壁运动异常（仅提示 EF 短暂下降至 50%），而 SPECT 仅显示心尖部灌注减低，CMR 发现室间隔局灶纤维化。

InterTAK 评分的实用价值： 在影像不典型时，InterTAK 评分系统（本例 78 分）是强有力的辅助诊断工具，能有效整合临床特征、生物标志物、心电图和冠脉信息，提高早期识别率。

“结构 - 症状不匹配”的启示： 当严重心血管症状（高血压危象、心衰）与相对轻微的器质性影像发现不符时，应高度怀疑功能性障碍，如应激性心肌病或精神心理源性疾病。

4. 精神心理因素的核心地位与多学科协作的必要性：

关键诱因与维持因素： 本例患者（绝经后女性 + 抑郁症）是 TTS 高危人群。精神心理因素不仅是发作诱因，更可能是疾病反复和维持的核心机制（自主神经紊乱、脑 - 心轴失调）。

诊断突破口： 当心血管评估陷入困境（检查阴性、症状反复），及时的精神科会诊至关重要。抗焦虑药物（劳拉西泮）的显著疗效为诊断提供了关键验证。

治疗关键： 长期有效管理的基础是控制精神心理疾病（规范抗抑郁 / 焦虑治疗）和识别 / 管理应激源，而不仅仅是急性期的心血管对症处理。本例 6 年无复发证明了此点。

临床实践启示： 心血管医生需提高对“双心医学”的认识，建立与精神心理科协作的常规路径，尤其是在面对复杂、反复发作、检查阴性的心血管事件患者时。

本病例极具教育意义，它有力证明了严重的精神心理疾病（如抑郁症）可成为高血压危象、急性心力衰竭及应激性心肌病（TTS）的重要甚至主导诱因。强调了“身心同治”理念在心脑血管疾病领域的重要性，呼吁临床医生高度关注精神心理因素在心血管急危重症中的潜在主导作用，避免误诊漏诊，实现更精准、全面的诊疗。

冠状动脉造影后造影剂脑病 1 例

夏驭龙

北京大学第一医院

患者基本信息：

56 岁女性

主述：

间断胸闷 1 月

现病史：

主要表现为与活动无关的胸闷、胸部不适，持续时间 >15min，外院查超敏肌钙蛋白 I（hsTnI）升高，最高 124.5ng/L，复查 hsTnI 呈下降趋势为 11.8ng/L，多次查 CK-MB 均在正常范围，院前无发热、腹泻等病史。

既往病史：

基础有高血压 2 级，高脂血症，血小板增多，慢性浅表性胃炎，十二指肠球炎，结肠腺管状腺瘤术后，子宫肌瘤术后，胆囊结石，黄斑前膜，双侧颈动脉粥样硬化。有冠心病、糖尿病、高血压家族史

病程记录：

患者绝经后女性，有高血压、高脂血症、血小板增多、冠心病家族史，虽胸闷症状不典型，但症状持续时间长，且院外 hsTnI 升高，入院 hsTnI 正常，ECG 亦可见 ST-T 波改变，需警惕 ACS 可能，存在冠脉造影检查指征，患者亦存在冠脉造影的意愿，获取知情同意、除外禁忌后，于 2023-03-31 行冠状动脉造影，术中使用碘海醇，量约 20ml，术中示 LAD、LCX、RCA 均未见狭窄。术后 1.5 小时后患者出现头晕，恶心，伴干呕，血糖正常，血压 135-167/ 77-104mmHg，ECG 可见（高）侧壁 T 波改变，未见 ST 段抬高，予补液，维生素 B6、PPI 对症，后逐渐出现病理性赘述，答不切题，行为异常，造影 1 天后出现嗜睡，无法交流，伴发热，Tmax 38.9° C，多次神经科查体无明确定位体征，瞳孔等大正圆，对光反射存在，头颅 CT 平扫提示脑组织肿胀、脑水肿、可疑造影剂外渗（图 1），未见脑出血，腰穿提示颅高压（脑脊液压力 >330mm H20），病原学检查未见明确感染证据，予甘露醇脱水，后加用地塞米松抗炎，尼莫同口服，造影 2 天后神志好转，造影 3 天后神志进一步好转，但反应仍稍迟钝、左侧同位性偏盲，可正常对答，5 天后患者视野恢复正常，神志、反应、定向力、肌力均基本恢复。复查头颅 CT 提示脑水肿好转（图 1），头颅 MR 未见脑梗死、脑炎等影像学改变，可见动脉硬化性脑小血管病（图 2），脑电图未见明显异常，与神内科、神外科联合分析，考虑造影剂脑病所致神志改变、意识障碍与颅高压；TnI 升高考虑非冠脉阻塞性心肌梗死，结合患者最终患者好转后出院，出院后予患者抗血小板、降压、降脂等治疗，出院后半年随访患者无明显不适。

检验检查记录：

入院后查血常规：白细胞计数 10.00×10^9/L，血红蛋白浓度 134g/L，血小板计数 437×10^9/L，中性粒细胞百分比 81.1%，中性粒细胞计数 8.10×10^9/L；谷丙转氨酶 24IU/L，白蛋白 46.6g/L，肌酐 79.70μmol/L，估算肾小球滤过率 71.555ml/min/1.73 ㎡，钾 4.06mmol/L，CK-MB 质量 1.2ng/ml，高敏肌钙蛋白 I 9.4ng/L，钠尿肽 16.00pg/ml，超敏 C 反应蛋白 2.21mg/L，甘油三酯 1.73mmol/L，低密度脂蛋白胆固醇 2.11mmol/L，同型半胱氨酸 10.90μmol/L；糖化血红蛋白 6.20%；甲状腺功能、凝血功能未见明显异常。双肾 B 超：右肾多发囊肿，左侧肾上腺区未见占位病变，双肾动脉未见狭窄征象，腹主动脉粥样硬化。UCG：左房扩大（前后径 4.1cm），室间隔增厚（1.4cm），左室射血分数正常（73.0%），右室收缩功能正常，二尖瓣轻度反流，三尖瓣轻度反流。心脏核磁：左心室间隔增厚，最厚 17mm，未见心肌水肿表现，左心收缩功能正常。

鉴别诊断：

1、肌钙蛋白升高的鉴别：

（1）心肌缺血

- 急性冠脉综合征可能

- 其他冠脉相关原因（心律失常，毒物，冠脉介入，冠脉痉挛，冠脉栓塞，冠脉炎症，严重高血压，主动脉夹层，MINOCA 等）

- 非冠脉原因（休克，缺氧，低灌注，肺栓塞？，心胸外科手术）

（2）心肌损伤

- 合并疾病（肾衰竭，脓毒症，浸润性疾病，急性呼吸衰竭，卒中，蛛网膜下腔出血）

- 特定的病因【过劳，心脏撞击伤，电击，严重烧伤，特定药物（蒽环类、赫赛汀），一氧化碳中毒】

- 其他（应激，心肌炎？，心肌心包炎，横纹肌溶解累及心肌，肥厚型心肌病？，围产期心肌病，心衰，心脏肿瘤）

2、神志障碍的鉴别：

（1）脑血管病 - 无定位体征，无法解释脑水肿，且好转过快，但不排除合并有小的新发脑梗死，完善核磁明确

（2）脑炎 - 无前驱感染症状，脑脊液检查无相关感染证据， mNGS 基本阴性

（3）脑病

- 可逆性脑血管收缩综合症，多见于脑血管操作直接刺激血管

- 可逆性后部脑病，多见于血压剧烈波动，不支持

- 造影剂脑病可能大

其他：

无

负荷超声联合超声心肌灌注成像评估肾移植心梗患者一例

陈奕如

胡思宁

患者基本信息：

患者姓名：郑万库

性别：男

年 龄：62 岁

出生日期：1962-10-16

职业：不详

民族：汉族

国 籍：中国

出生地：不详

主述：

呼吸困难 10 天，加重 1 天

现病史：

患者 10 天前无明显诱因出现呼吸困难。发病过程中，患者伴有心悸、胸痛，伴肩背部疼痛，有双下肢水肿，无恶心、呕吐，无畏寒、发热，无咳嗽、咳痰，无头晕、头痛，无腹胀、腹泻等症状。1 天前，患者呼吸困难症状加重，伴夜间憋醒。现为求进一步诊治来我院。病程中患者饮食、大便尚可，尿量减少，睡眠一般。

既往病史：

平素健康状况：一般，无药物或食物过敏史，无输血史，有高血压病史 20 余年，最高血压达 160/100mmHg，平时口服诺欣妥治疗，血压控制尚可；有糖尿病病史 10 年平时胰岛素治疗；有乙肝病史，目前抗病毒治疗中；肾移植术后 10 年；左股骨头置换术后；左上肢动静脉瘘术后；有陈旧性心梗个人史；有心脏左室壁瘤；否认其他既往疾病史。

病程记录：

记录时间：2025-03-21 21:45

首次病程记录

病例特点：

主诉：" 呼吸困难 10 天，加重 1 天 "

1、现病史：患者 10 天前无明显诱因出现呼吸困难。发病过程中，患者伴有心悸、胸痛，伴肩背部疼痛，有双下肢水肿，无恶心、呕吐，无畏寒、发热，无咳嗽、咳痰，无头晕、头痛，无腹胀腹泻等症状。1 天前，患者呼吸困难症状加重，伴夜间憋醒。现为求进一步诊治来我院。病程中患者饮食、大便尚可，尿量减少，睡眠一般。

2、既往史及个人史：平素健康状况：一般，无药物或食物过敏史，无输血史，有高血压病史 20 余年，最高血压达 160/100mmHg，平时口服诺欣妥治疗，血压控制尚可；有糖尿病病史 10 年，平时胰岛素治疗；有乙肝病史，目前抗病毒治疗中；肾移植术后 10 年；左股骨头置换术后；左上肢动静脉瘘术后；有陈旧性心梗个人史；有心脏左室壁瘤；否认其他既往疾病史。

3、查体：体温：365℃，血压：131/69 mmHg，脉搏：77 次／分，呼吸：16 次／分。一般状态尚可，平车推入病房，查体合作，口唇无发绀，浅表淋巴结未肿大，双肺呼吸音清，未闻及干湿性啰音心律齐，心率：77 次／分，心界不大，各瓣膜听诊区未闻及病理性杂音。腹平坦，柔软，无压痛及反跳痛，双下肢轻度水肿。生理反射正常，病理反射未引出。

4、辅助检查：ECG 示：宾性心律，ST 段改变。心脏超声（大庆油田总医院 2025-03-21):

EF:38%，左室心尖部室壁瘤形成，左心整体收缩功能减低。CK-MB(2025-03-21):

10.13ng/ml; MYO(2025-03-21): 73.7ng/ml.

初步诊断：心功能不全

冠状动脉粥样硬化性心脏病

高血压

糖尿病

诊断依据：1、患者 主因 " 呼吸困难 10 天，加重 1 天 "，入病房

2、查体：双肺呼吸音清，未闻及干湿性啰音，心律齐，心率：77 次／分，心界不大，各瓣膜听诊区未闻及病理性杂音。腹平坦，柔软，无压痛及反跳痛，双下肢轻度水肿。理反射正常，病理反射未引出。

3、既往史：平素健康状况：一般，无药物或食物过敏史，无输血史，有高血压

病史 20 余年，最高血压达 160/100mmHg，平时口服诺欣妥治疗，血压控制尚可；有糖尿病病史 10 年，平时胰岛素治疗有乙肝病史，目前抗病毒治疗中；肾移植术后 10 年; 左股骨头置换术后; 左上肢动静脉瘘术后，有陈旧性心梗个人史; 有心脏左室壁瘤；否认其他既往疾病史。

4、辅助检查：ECG 示：窦性心律，ST 段改变。心脏超声（大庆油田总医院 2025-03-21):EF:38%，左室心尖部室壁瘤形成，左心整体收缩功能减低。CK-MB(2025-03-21):10.13ngml;

MYO(2025-03-21): 73.7ng/ml.

鉴别诊断: 1、主动脉夹层: 胸痛一开始即达到高峰，常放散到背、肋、腹、腰和下肢，两上肢的血压和脉搏可

有明显差别，可有主动脉瓣关闭不全的表现，超声心动图、X 线或主动脉 CTA 有助于鉴别；

2、急性肺动脉栓塞：可发生胸痛、咯血、呼吸困难和休克，但有右心负荷急剧增加的表现如发绀、肺动脉瓣区第二心音亢进、颈静脉充盈、肝大、下肢水肿等，心电图示 I 导联 S 波加深，II 导联 Q 波显著，T 波倒置，胸导联过渡区左移，右胸导联 T 波倒置等改变可资鉴别。常有低氧血症，血气分析或肺动脉 CTA 有助于鉴别。

诊疗计划：1、重症护理，心电血压血氧监护，对症吸氧，完善相关检查：

2、抗血小板、降脂、改善心肌供血，必要时抑酸、保护胃黏膜，对症；

3、建议完善冠脉造影检查，必要时介入治疗；

4、改善心室重构，控制血压、血糖等冠心病二级预防；

记录时间：2025-03-22 11:27

查房记录

患者由急诊心血管重症监护室 C 区医护人员转入 B 区，值班医师床旁查看患者，患者一般状态尚平稳，监护提示：血压 144/82mmHg 查体：双肺呼吸音清，未闻及干湿性啰音，心律齐，心率：65 次／分，心界不大，各瓣膜听诊区未闻及病理性杂音。腹平坦，柔软，无压痛及反跳痛，双下肢水肿减轻。生理反射正常，病理反射未引出。

处置：继续进一步积极治疗。

记录时间：2025-03-22 11:29

主治医师首次查房记录

查房医师：张永祥 孙艳丽

患者主诉：呼吸困难 10 天，加重 1 天

当前情况：患者一般状态尚平稳，监护提示：血压 144/82mmHg 查体：双肺呼吸音清，未闻及干湿性啰音，心律齐，心率：65 次／分，心界不大，各瓣膜听诊区未闻及病理性杂音。腹平坦，柔软，无压痛及反跳痛，双下肢水肿减轻。生理反射正常，病理反射未引出。

补充病：无

已实施的治疗措施及疗效分析: 1、重症监护，密切观察病情变化，完善相关检查等:

2、减轻心脏负荷、稳定改善心功能、保护重要脏器功能，对症支持治疗等；

3、吸氧，必要时机械辅助通气治疗；

4、进一步治疗原发病及诱因，建议必要时行冠状动脉造影检查及介入治疗；

5、必要时 CRRT 治疗；

6、向家属交代病情危重，随时有加重甚至死亡风险，该患者预后不佳。

检验检查结果：血清载脂蛋白 AI 测定 [2025-03-22 10:34:39]: ★高密度脂蛋白-胆固醇：0.85mmol/Ll ★甘油三酯：1.89mmol/L1 血细胞分析（全血细胞计数五分类和幼稚细胞）[2025-03-22 06:45:41]: ★血红蛋白测定: 114g/L!: ★血小板计数：117x10^9/L! ★白细胞计数：3.9x109/L：血清肌钙蛋白 I 测定（金标／荧光定量）组 [2025-03-22 06:32:25]: 血清肌酸激酶- MB 同工酶质量测定: 6.19ng/mL1;

诊 断：不稳定型心绞痛

冠状动脉粥样硬化性心脏病

陈旧性心肌梗死

缺血性心肌病

心功能不全

高血压

糖尿病

肾移植状态

贫血

心室壁瘤

诊断依据：1、患者 主因 " 呼吸困难 10 天，加重 1 天 "，入病房

2、查体：双肺呼吸音清，未闻及干湿性啰音，心律齐，心率：77 次分，心界不大，各重膜听诊区未闻及病理性杂音。腹平坦，柔软，无压痛及反跳痛，双下肢轻度水肿。生理反射正常，病理反射未引出

3、既往史：平素健康状况：一般，无药物或食物过敏史，无输血史，有高血压病史 20 余年，最高血压达 160/100mmHg，平时口服诺欣妥治疗，血压控制尚可; 有糖尿病病史 10 年，平时胰岛素治疗；有乙肝病史，目前抗病毒治疗中；肾移植术后 10 年；左股骨头置换术后；左上肢动静脉瘘术后；有陈旧性心梗个人史; 有心脏左室壁瘤；否认其他既往疾病史。

4、辅助检查：ECG 示：窦性心律，ST 段改变。心脏超声（大庆油田总医院 2025-03-21):EF:38%，左室心尖部室壁瘤形成，左心整体收缩功能减低。CK-MB(2025-03-21):10.13ng/ml;MYO(2025-03-21): 73.7ng/ml.

鉴别诊断的分析：1、主动脉夹层：胸痛一开始即达到高峰，常放散到背、肋、腹、腰和下肢，两上肢的血压和脉搏可有明显差别，可有主动脉瓣关闭不全的表现，超声心动图、X 线或主动脉 CTA 有助于鉴别；2、急性肺动脉栓塞：可发生胸痛、咯血、呼吸困难和休克，但有右心负荷急剧增加的表现如发绀、肺动脉瓣区第二心音进、颈静脉充盈、肝大、下肢水肿等，心电图示 I 导联 S 波加深，III 导联 Q 波显著，T 波倒置，胸导联过渡区左移，右胸导联 T 波倒置等改变可资鉴别。常有低氧血症，血气分析或肺动脉 CTA 有助于鉴别。

诊疗计划：1、重症监护，密切观察病情变化，完善相关检查等；

2、减轻心脏负荷、稳定改善心功能、保护重要脏器功能，对症支持治疗等；

3、吸氧，必要时机械辅助通气治疗；

4、进一步治疗原发病及诱因，建议必要时行冠状动脉造影检查及介入治疗；

5、必要时 CRRT 治疗；

6、向家属交代病情危重，随时有加重甚至死亡风险，该患者预后不佳。

记录时间：2025-03-22 19:01

值班医生看患者，患者状态一般，查体：血压：108/67mmHg，双肺呼吸音清，未闻及干湿性啰音，心律齐，心率 86 次／分，心界不大，各瓣膜区未闻及病理性杂音。腹平坦，柔软，无压痛及反跳痛，双下肢无水肿。生理反射正常，病理反射未引出。

处置：1、继续目前的治疗；

2、密切观察患者病情变化。

记录时间：2025-03-23 04:15

患者家属要求出院，告知家属建议患者继续住院治疗，若出院可能会出现病情反复、恶化，甚至死亡。家属知情，仍要求出院，并自愿承担上述风险，于自动转出重症监护室（CCU）知情同意书上签字。

崔销堂

处置：今日出院

检验检查记录：

鉴别诊断：

1、主动脉夹层

2、急性肺动脉栓塞

其他：

多模态影像学助力冠脉造影后罕见心房血肿的诊断：一例报告

巫凯敏

厦门大学附属心血管病医院 (厦门市心脏中心)

患者基本信息：

患者陈 XX，男，68 岁，入院日期：2024-11-01

主述：

间断胸痛 6 月余，再发 2 天

现病史：

患者 6 月余前于青海旅行步行时出现胸痛，为心前区巴掌范围闷痛，伴喘憋、乏力，服用“救心丸”并休息约 2h 后症状缓解，后就诊于当地医院，行冠脉造影示: LAD 中段 90% 狭窄，LCX、RCA 正常，遂行 LAD 支架植入术，术后规律用药。2 天前睡眠时突发胸痛，为心前区刺痛，程度剧烈，伴喘憋、乏力，就诊于当地医院，完善心电图：多导联 ST 段抬高，急诊行冠脉造影未见明显异常，考虑“变异型心绞痛”，术后完善超声心动图提示“左房占位 粘液瘤？”，建议转诊上级医院。现由 120 转诊我院急诊，完善心电图示：窦性心动过速、部分导联 ST-T 改变，床旁彩超示：左房内实性占位，致二尖瓣口梗阻，左房粘液瘤？。急诊遂以“左房占位 冠心病”收入院。患者自发病以来睡眠、食欲欠佳，精神可，近期有便秘，小便正常，体重近 1 月余下降约 2-3kg。

既往病史：

既往糖尿病病史，口服二甲双胍 0.5g bid 降糖，血糖控制可。否认吸烟、饮酒史。

婚育史、家族史无特殊。

病程记录：

老年男性，既往冠心病 冠脉支架植入术病史，表现为间断胸痛、气促、乏力，查体可闻及双下肺湿啰音，入院化验提示肌钙蛋白 T 正常，NT-proBNP 升高，心脏彩超提示：左心房占位，入院诊断考虑：1. 左心房占位待查 2. 冠心病 冠脉支架植入术后 3. 糖尿病，予双联抗血小板、降脂稳斑、利尿、降糖等药物治疗，进一步完善左心声学造影、胸部 CT 未能明确左心房占位性质，遂进一步完善胸部增强 CT 及经食道超声心动图检查，明确诊断为：左心房血肿。因血肿巨大，造成二尖瓣梗阻，决定行左心房血肿清除 / 减压术，术中可见：中量血性心包积液，心脏周围组织明显水肿，心脏胀满，沿右冠走行方向表面组织及房壁可见血肿形成，肺动脉增粗，冠脉分布正常。建立体外循环，切开右心房及房间隔，可见房间隔血肿，左房后壁可见巨大血肿形成，并向左房余各壁、二尖瓣瓣环方向、主动脉瓣下幕帘结构等蔓延，左房壁内膜明显水肿，质脆，切开左房后壁内膜一小切口，可见大量暗红色血栓流出，予吸引器清除血肿，并予生理盐水反复冲洗，发现血肿较前明显减小，遂结束手术。术后规律复查超声心动图，提示左心房血肿逐渐吸收，未再加重。患者恢复可， 顺利出院。

检验检查记录：

2024-11-01 NT-proBNP 2051 pg/mL DDimer 0.82 ug/mL 肌钙蛋白 T 47.56 pg/mL；

2024-11-01 心电图：窦性心动过速，部分导联 ST-T 改变，QTc 间期延长；

2024-11-01 超声心动图：左房内实性占位，致二尖瓣口梗阻，左房粘液瘤可能，血栓不除外 -- 建议左心声学造影。左房明显扩大，室间隔基底段增厚。轻中度三尖瓣反流；轻度肺动脉高压可能。左室整体收缩功能正常，舒张功能 II 级减退。少量心包积液。（LA 52mm AAO 34mm MPA 26mm IVS 10mm LVD 44mm LVS 30mm LVPWD 9mm EF 59%）

2024-11-01, 左心声学造影 + 心肌灌注超声检测：1、左房内充盈缺损，乏血供或无血供。2、左室整体收缩功能正常。

2024-11-01, CT 血管成像 (胸腹主动脉): 左房增大，左房及左心耳环形斑片状充盈缺损，考虑血肿可能性大，血栓待排，请结合临床。 胸腹主动脉粥样硬化，腹主动脉下段小溃疡形成。 心包少量积液。 冠脉支架植入术后。 双肺后部渗出，双侧胸腔少量积液。 肝脏、右肾多发囊性灶，双肾周渗出改变。 右侧肾上腺外侧肢局部膨隆。

2024-11-01,CT 平扫 (肺部): 左房混杂密度灶，建议增强或 CMR 进一步检查。间质性肺水肿，双肺渗出，双侧胸腔少量积液并邻近肺组织膨胀不全。双肺斑点、微结节样影，随诊。纵隔、双肺门多发淋巴结，部分饱满及钙化。心包少量积液。冠状动脉支架植入后。 甲状腺左叶稍高密度结节。

2024-11-14, 常规心电图检查 (12 导联): 心房扑动 QTc 间期延长 逆钟向转位 多导联 J 点上移伴 ST 段凹面向上抬高。

2024-11-14,CT 平扫 (肺部): 对比 2024-11-01 片： 新见心脏术后，心包微量积气，纵隔内积气、渗出。 左房密度不均，见片状稍高密度影，请随诊，并结合其他检查。 原间质性肺水肿现基本吸收，双肺渗出总体较前稍吸收，双侧胸腔少量积液并邻近肺组织膨胀不全，较前明显。 心包微量积液，较前吸收。 余大致同前。

2024-11-14, 心脏彩超 : 心房血栓清除术后：1、左房内实性回声较术前减小。2、轻度二尖瓣反流。3、轻度主动脉瓣反流；轻度三尖瓣反流。4、左室整体收缩功能正常低值；右室收缩功能减低。

鉴别诊断：

(1) 左房粘液瘤；（2）左心房血栓；（3）左房肿瘤；（4）心房血肿。

其他：

1. 心房血肿：冠脉造影 / 介入治疗罕见的并发症

2. 多模态影像学助力心房占位的鉴别诊断

3. 不同影像学方式各有优点，其中经食道彩超在左心房占位性质鉴别中具有优势。

玛伐凯泰治疗肥厚型梗阻性心肌病 超声随访 1 例

危晓玉

哈尔滨医科大学附属第二医院

患者基本信息：

患者女，41 岁

主述：

胸痛 1 月

现病史：

患者 1 月前无明显诱因出现胸痛，持续数十分钟至数小时可自行缓解，该症状 1 月内反复发作，伴胸闷，伴头痛。确诊“肥厚型梗阻性心肌病”7 年，长期服用康忻（5mg/ 次，每日 1 次），多次复查，症状改善不明显。病程中不伴乏力，无恶心呕吐，无气短，无咳嗽咳痰，为求明确诊治于今日来我院就诊。患者患病以来，饮食二便正常，睡眠精神欠佳，体重无明显改变。

既往病史：

平素健康情况良好；否认传染病史；否认手术外伤史；无输血史；有青霉素过敏史；既往有高血压病史，自述最高血压达到 160/95mmHg。

病程记录：

患者因“胸痛 1 月”入院，有肥厚型梗阻性心肌病病史 7 年，症状改善不明显，有高血压病史。完善心电图、心脏彩超、心脏磁共振、发泡实验等相关检查，诊断为“肥厚型梗阻性心肌病 高血压 2 级（高危） 心室壁瘤 心律失常 中央型房间隔缺损（卵圆孔型）”。诊断明确，给予改善心室顺应性对症治疗，建议患者应用玛伐凯泰控制病情，定期复查。

检验检查记录：

心电图：窦性心律；频发房性早搏；左室高电压；ST-T 改变

血化验：总胆固醇 5.71mmol/L ↑

超声心动图：提示心肌病 肥厚型心肌病（左室流出道隐匿梗阻，室间隔及心尖多部位肥厚） 左室舒张功能减低

心脏磁共振：1. 左室壁非对称性增厚，考虑梗阻性肥厚型心肌病（左室流出道狭窄、左室腔中部梗阻），主要累及室间隔、毗邻左室壁、侧壁心尖段及右室心尖部，心尖部室壁瘤形成，伴左室局部心肌纤维化；2. 二、三尖瓣轻度关闭不全

脑 MRI + MRA：多发腔梗，考虑左侧脑室旁小软化灶 轻度脑动脉硬化，左大脑中动脉局部显影淡

发泡实验：注射声学造影剂后，右心显影后，嘱患者 Valsalva 动作后（2-3）个心动周期左心腔内可见少量气泡回声（<10 个），提示中央型房间隔缺损（卵圆孔型）

鉴别诊断：

1、急性心肌梗死：疼痛性质剧烈，时程长，硝酸甘油不易缓解，心肌和心电图有助鉴别；

2、主动脉夹层：患者多有常年高血压病史，发病时疼痛呈撕裂样，持续不缓解，超声及主动脉 CTA 有助鉴别。

其他：

无

心内科的“血压迷局”：从直立性低血压到多系统萎缩

田佳

河北医科大学第二医院

患者基本信息：

患者 58 岁男性，河北衡水人，农民

主述：

间断头晕 1 年，加重 2 个月

现病史：

患者于 1 年前晨起站立时出现头晕，视物模糊，双下肢无力，以左下肢为著，取蹲位后症状可缓解。此后上述症状间断发作，就诊于当地医院，具体诊治不详。2 个月前上述症状较前加重，发作频繁，伴黑矇，自测血压站立位时血压低，活动耐量较前减低，低于日常体力活动时可出现胸闷、气促，无胸痛，无肩背部放射痛，无恶心、呕吐。现为行进一步诊治收入我科。

既往病史：

既往高血压 30 年，血压最高达 170/？ mmHg，间断口服降压药物，1 年前停服。前列腺增生病史多年，口服“前列通”，平素尿不尽感。否认糖尿病、高脂血症病史。否认消化性溃疡及青光眼病史，否认肝炎、结核等传染病病史。否认手术、外伤及输血史。否认食物及药物过敏史。

病程记录：

入院后查体：T36.5 ℃，P81 次 / 分，R18 次 / 分，BP 卧位 153/109mmHg、站位 70/50mmg。神清，双肺呼吸音清，未闻及干湿性啰音。心率 81 次 / 分，律齐，各膜听诊区未闻及杂音。腹软，无压痛及反跳痛，肝脾肋下未触及。双下肢无水肿。四肢肌力 V 级，肌张力正常，双侧 Babinski 征、Kernig 征阴性。

完善卧立位试验阳性，卧位血压波动于 120-155/74-109mmHg，站立位血压波动于 61-70/41-50mmHg。考虑患者以以发作性双下肢无力和直立性低血压为主要表现，需要除外下肢血管和脊髓病变。且入院后患者诉活动后间断出现胸闷，同时完善冠脉 CTA。脊髓核磁结果回报：多发椎间盘变性、多发血管瘤。进一步追问病史，患者 2 年前出现颈部僵硬，颈部前倾，患者未予以重视，1 年前夜间出现异动睡眠，表现为睡眠中大喊大叫，半年前患者出现走路不稳，脚踩棉花感，双下肢发软。完善神经系统查体: 言语含糊，颅神经阴性，四肢肌力 V 级，四肢肌张力正常，四肢腱反射对称正常，指鼻实验、跟膝胫试验不稳。考虑患者定位诊断: ①患者卧立位血压压差较大，>30mmHg，②患者既往前列腺增生病史，目前有轻微排尿困难，不能除外自主神经系统异常，患者头晕、站立不稳考虑与直立性低血压相关；②肢体共济试验阳性，轻微构音障碍，提示可能存在小脑半球病变。定性诊断：老年男性，隐匿起病，渐进性加重，同时出现自主神经系统及小脑体征，考虑为神经系统变性性疾病可能性大。因此完善头颅 MRI、MRA、SWI，提示小脑萎缩明显，出现鱼骨征；完善腰穿，除外自身免疫性中枢神经系统疾病。综上诊断为小脑型多系统萎缩。

多系统萎缩目前尚无特殊治疗方法，只能改善症状，预后不佳。①明确诊断后给予患者口服米多君，并根据血压调整剂量：初始口服米多君 2 片 / 天，卧位血压升高明显，将口服剂量减少为早上 1 片，中午半片后，卧位血压 170/100mmHg 左右，站立后能够行走，如早上改为半片，站立后自觉四肢乏力明显，行走费力，故暂时维持一天 1.5 片（早上 1 片，中午半片）的剂量。②给予患者盐酸坦索罗辛缓释胶囊 1 粒 / 晚改善排尿困难，同时考虑到坦索罗辛为 α 受体阻滞剂类药物，可能加重直立性低血压风险，告知患者及家属密切监测血压，如直立性低血压变化明显可停用。③诉患者腹带加压束腹、双下肢穿弹力袜增加静脉回心血量。

检验检查记录：

同型半胱氨酸：17.2umo1/L、

肾功能：尿素：9.60mmo1/L、肌酐 98.0μmol/L、eGFR：77.9mL/min/1.73m2、尿酸: 443.0umol/L、B2 微球蛋白: 2.50mg/L、胱抑素 C: 1.43mg/L。

血脂：碱性磷酸酶：44.0U/L、载脂蛋白：A10.96g/L。

脑脊液生化：LDH：21.73U/L，CL：126.50mmo1/L，GLU：3.61mmo1/L。

脑脊液细胞学：未见明显异常。

自身免疫性脑炎自身抗体：阴性。

叶酸：4.9ng/ml；维生素 B12：161.2pg/ml ↓

血常规、尿常规、粪便常规 + 隐血试验、电解质、凝血常规、肝功能、心肌酶、B 型钠尿肽前体、肌钙蛋白、糖化血红蛋白、血糖、甲功游离三项、术前四项未见明显异常。

XX 胸部：主动脉硬化，未见明显渗出及结节改变。

主动脉 + 冠脉 CTA 冠状动脉硬化。

颈胸腰骶脊髓 MRI：1. 颈 3-7 椎体骨质增生；颈 5-7 椎体终板炎；颈 2-7 椎间盘变性；2. 颈 5-7 椎间盘向后方突出，继发性椎管狭窄；3. 胸腰椎骨质增生，考虑胸 4、8 椎体内血管瘤可能；4. 腰 4-5 椎间盘向后突出，继发性椎管狭窄；5. 腰 3- 骶 1 椎间盘变性；6. 骶 3 椎体内血管瘤可能。

头颅 MRI、MRA、SWI：未见明显异常低信号。小脑萎缩明显，出现“鱼骨征”，脑干“十字征”未显现。

心电图：窦性心律，心室率 81bpm，II、III、aVF V4-V6 导联 ST 段压低 0.ImV，T 波倒置。

心脏、腹部大血管超声: 左房扩大，左室壁增厚，二尖瓣及主动脉瓣轻度关闭不全，左室舒张功能 I 度。EF：66.2%。LA：37mm；RA：40*46mm；LV：51mm；RV：24mm；EDV：130ml；ESV：44ml；IVS：12mm；LVPW：12mm。

下肢静脉彩超：1. 左侧股总静脉瓣膜功能不全；2. 右侧股总静脉、双侧腘静脉、双侧胫后静脉结构及血流未见异常。

下肢动脉彩超：1. 左侧股总动脉内中膜增厚，左侧腘动脉斑块形成；2. 右侧股总动脉、右侧腘动脉、双侧足背动脉结构及血流未见异常。

锁骨下动脉彩超：1. 右侧锁骨下动脉内中膜增厚，最厚处 1.2mm；2. 左侧锁骨下动脉结构及血流未见异常。

椎动脉彩超：双侧椎动脉结构及血流未见异常。

颈动脉彩超：1. 双侧颈总动脉内中膜增厚，最厚处 1.4mm，右侧颈总动脉斑块形成；2. 双侧颈内动脉结构及血流未见异常。

泌尿系彩超：1. 双肾囊肿 (右侧伴囊壁钙化)；2. 膀胱壁欠光滑；3. 前列腺增生；4. 膀胱内残余尿 74ml。

双肾动脉彩超：双肾动脉血流未见异常。

鉴别诊断：

①药物性直立性低血压：是最常见的直立性低血压类型，临床表现缺乏特异性，老年人易感性更高。可引起药物性直立性低血压的药物包括降压药（α 受体阻滞剂）、抗精神病药物、抗帕金森病药物、抗抑郁药、阿片类药物等。通过仔细询问病史，患者已停用降压药 1 年，且无应用上述药物史，可除外。

②低血容量性及其他非神经原性直立性低血压：大出血、严重腹泻和呕吐、危重症、内分泌疾病如糖皮质激素和盐皮质激素减少等均可引起血容量减少，从而导致直立性低血压。另外，营养不良、肌少症、衰弱、贫血、慢性肾功能不全、心力衰竭、缺血性心肌病可通过不同的机制导致或加重直立性低血压。详细询问相关病史，完善相关化验、心脏超声、冠脉 CTA 可除外。

③其他神经原性直立性低血压：病因复杂，是由自主神经功能障碍引得血压调节受损。原发性自主神经功能障碍包括帕金森病、多系统萎缩、路易体痴呆和单纯自主神经功能衰竭。继发性神经原性直立性低血压则包括免疫性疾病、肿瘤、感染性疾病、血管疾病、代谢性疾病、中毒、外伤、遗传性疾病等多种病因。询问相关病史，完善头颅，脊髓核磁、脑脊液检查、维生素以资鉴别。

其他：

直立性低血压（orthostatic hypotension，OH）是指在站立或体位改变超过 60°时，3 min 内出现持续收缩压下降≥ 20 mmHg 或舒张压下降≥ 10 mmHg，可伴有头昏、乏力、黑矇甚至晕厥等临床表现。神经源性直立性低血压（neurogenic OH，nOH）是 OH 的一种亚型，占所有 OH 不足 10%，但病因复杂。除了符合 OH 定义外，nOH 还出现自主神经系统功能障碍，表现为血压下降而增加的心率往往 <15 次 /min 甚至下降。原发性自主神经功能障碍一般指四种疾病，包括帕金森病、多系统萎缩、路易体痴呆和单纯自主神经功能衰竭，这些都是 α- 突触核蛋白病。继发性神经原性直立性低血压则包括免疫性疾病、肿瘤、感染性疾病、血管疾病、代谢性疾病（糖尿病，维生素缺乏等）、中毒、外伤、遗传性疾病等多种病因。

多系统萎缩（multiple system atrophy，MSA）是一种进展性的神经系统退行性疾病，平均患病率为（1.9~4.4）/10 万人，临床表现为自主神经功能障碍、帕金森综合征和小脑综合征。MSA 发病率低，诊断困难且预后不佳。本例患者为老年男性，隐匿起病，渐进性加重，同时出现自主神经系统及小脑体征，根据指南提到的诊断标准，可确诊为小脑型 MSA。

MSA 尚无特异性药物，针对 OH 的治疗目标应当以改善患者直立不耐受的症状，提升日常活动能力为中心，而非专注于将血压提升到某一程度。针对本患者，我们在明确诊断后给予患者口服米多君，并根据血压调整剂量：初始口服米多君 2 片 / 天，卧位血压升高明显，将口服剂量减少为早上 1 片，中午半片后，卧位血压 170/100mmHg 左右，站立后能够行走，如早上改为半片，站立后自觉四肢乏力明显，行走费力，故暂时维持一天 1.5 片（早上 1 片，中午半片）的剂量。由于患者轻度尿潴留，同时给予患者盐酸坦索罗辛缓释胶囊 1 粒 / 晚改善排尿困难，同时考虑到 α 受体阻滞剂可能加重直立性低血压风险，告知患者及家属密切监测血压，如直立性低血压变化明显可停用。除了药物治疗，腹带加压束腹、双下肢穿弹力袜增加静脉回心血量也可以改善 OH。经上述治疗后，患者 OH 症状明显好转，予以出院。出院后 1 年电话随访无人接听，遗憾失访。

综上，MSA 作为一种神经系统罕见病，目前尚无根治性治疗手段。该患者因 OH 首诊于心内科，极易忽略神经系统异常表现。对此，心内科医师应在常规排除药物副作用、低血容量及心原性因素后，主动开展针对 nOH 的甄别。在初诊时，应详细询问患者的自主神经症状，如晨起头晕、排尿障碍、夜间出汗或胃肠蠕动异常，并结合简易倾斜试验或 24h 动态血压监测评估血压与心率变化的时序特征；当发现患者站立后血压显著下降而心率增幅不足（通常 < 15 次 / 分），即应高度怀疑神经原性病因。此外，床旁快速筛查帕金森相关体征、共济失调或言语含糊等中枢神经受累表现，并了解既往出现的跌倒或运动迟缓史，以提高对 MSA、帕金森病等神经退行性疾病的警惕。并应及时联系神经内科共同完善查体及检查，以便早期确诊并启动对症支持治疗。通过上述简单鉴别，心内科医生可在首诊时快速识别神经源性直立性低血压，避免延误并提高治疗针对性。

房室结多径路 1 例

王建

滨州医学院附属医院

患者基本信息：

宋某某，女， 69 岁

入院时间：2024-06-02

主述：

心悸 25 年，再发 6 月

现病史：

患者约 25 年前无明显诱因出现心悸，伴出汗，持续 30 分钟，呈突发突止，未行诊治。11 年前上述症状加重，表现为发作频发，持续时间延长，就诊于我院，行电生理检查提示房室结折返性心动过速（慢快型），给予射频消融术，术后未诉不适。 6 月前患者再次出现上述症状，持续 10 分钟左右，呈突发突止，为进一步治疗就诊于我院，门诊以“阵发性室上性心动过速”收入心内科二病区。

既往病史：

既往高血压病史 6 月余，收缩压最高达 160mmHg，口服“缬沙坦 1 片 qd”治疗，血压控制可。无糖尿病、脑血管病病史。

个人史、婚育史及家族史：无特殊。

病程记录：

入院后完善相关检查，给予降压及对症治疗，期间出现心动过速发作（窄 RQS 波），行电生理检查证实为房室结多径路（慢 - 慢，快 - 慢），行射频消融后好转出院。

检验检查记录：

生化示：LDL-C 2.8mmol/L, CTNI 0.01ng/mL，余项均正常。

NT-proBNP：595.9pg/ml。

三大常规、凝血、甲功三项等检查未见异常。

鉴别诊断：

1. 窦性心动过速（ST）

2. 房室结折返性心动过速

3. 房室折返性心动过速

4. 房性心动过速（AT）

5.2:1 心房扑动（AF）

6. 相对规整的心房颤动

7. 室性心动过速（VT，希浦系统来源）

其他：

以腹胀为首发症状的未成年原发心脏血管肉瘤 1 例

张琴

重庆医科大学附属第三医院

患者基本信息：

患者，女，17 岁

主述：

腹胀 20 天，再发伴气促 3 天

现病史：

患者 20 余天前无明显诱因出现腹胀，伴有轻微腹痛，无腹泻，无呼吸困难，无胸闷、胸痛不适，无发热、畏寒、寒战，无咯血、盗汗，无端坐呼吸及夜间阵发性呼吸困难，就诊于彭水县人民医院，完善胸片提示心影明显增大。完善上腹部 CT 提示心包中 - 大量积液，原因未明，建议进一步检查，完善腹部 CT 提示胆囊壁稍增厚，胆囊窝积液，提示胆囊炎。胰腺周围、胃类及十二指肠周围筋膜增粗模糊，腹腔望谟、系膜增粗模糊。双肾尿盐沉积。肝脏脾脏未见明显异常。右侧少量胸腔积液。完善心彩超提示心包积液 (大量)(前心包厚约 10m，后心包约 19m，左侧心包厚约 18m，心尖心包厚约 15mm。2022.09.06 日就诊我科，完善心电图提示类性心动过速、电轴右偏；完善风湿 3 项、甲状腺功能 3 项、红细胞沉降率、女性肿瘤标志物 7 项、抗核抗体测定、抗中性粒细胞抗体等未见明显异常，予以利尿等治疗后复查心脏彩超提示：心包积液 (大量)，收缩期一前心包见厚约 20mm 性暗区，后心包见厚约 32m 液性暗区：舒张期 - 前心包见厚约 10m 液性暗区，后心包见厚约 26m 液性暗区。心尖四腔心切面：左室侧壁收缩期见厚约 22m 液性暗区，舒张期见厚约 15m 液性暗区；右室侧壁收缩期见厚约 20mm 液性暗区，舒张期见厚约 12m 液性暗区。于 2022-9-8 日行心包穿刺置管，共抽出约 80m1 血性心包积液，送生化常规检查，2022/9/8 胸腹水癌抗原 (CEA) 检验报告：癌胚抗原 (CA)0.56ng/m1。2022/9/8 刺液生化 5 项测定检验报告：穿刺液腺苷脱氨酶 (ADA)8.20U/L，穿刺液淀粉酶 (AMY)32.00U/L，穿刺液蛋白 (TP)51.20g/L 1 ，穿刺液糖 (CLU)2.41mmo1/L ！，穿刺液乳酸脱氢酶 (LDH)194.00U/L。2022/9/8 各种穿刺液常规检查检验报告：外观红色浑浊，红细胞计数 (RBC)1690000*106/L ，白细胞计数 (WBC)1520.00*10^6/L，单个核细胞百分比 (IMN%)34.2%，多个核细胞百分比 (PMM)65.8%。9-9 日抽出 600m1 血性心包积液，9-11 日抽出 70m1 淡红色心包积液，9-12 日末抽积液，2022/9/13 复查彩超心包积液检查报告：前心包收缩期见厚约 3m 液性暗区，后心包见厚约 5mm 液性暗区：舒张期前心包见厚约 1mm 液性暗区，后心包见厚约 2m 液性暗区。心尖四腔心切面：右室侧壁心包收缩期见厚约 9m 液性暗区，舒张期见厚约 7mm 液性暗区。剑下四腔心切面：收缩期见厚约 10mm 液性暗区，舒张期见厚约 7m 液性暗区。心包积液 (少一中量)。心包积液明显减少，考虑病毒引起非特异性心包积液可能性大。2022-09-13 症状好转后携带心包穿刺引流管出院 2022.09.15 于彭水县人民医院复查心脏彩超提示少量心包积液，故于当地医院拔除心包穿刺引流管。3 天前患者再次出现上述症状，伴剑突下疼痛、气促不适，感乏力明显，无端坐呼吸，无夜间阵发性嫗睿目吸苛傈困綮礴吞鲽夤憾芳纳，今日就诊于重庆东华医院，完善心脏彩超示：心脏各腔室大小正常，左室舒张功能减退，心包大量积液 (左心房侧 1.0cm，左心室侧 2.6cm，右心房侧 1.2cm，右心室侧 3.1cm，心尖部 2.8cm。腹部彩超提示肝胆胰脾双肾未见异常，现为求进一步诊治，门诊以 “心包积液” 收入我科。

既往病史：

无特殊

病程记录：

人院后积极完善相关检查，行床旁心包穿刺置管术，9-25 日抽取 200m1 血性心包积液化验，9-26 日抽出 540m1 血性心包积液，9-27 完善 PET-CT 结果提示：右心房近前外区域团片状代谢增高，心肌感染性病变？建议结合超声、CMR 等相关检查。心包积液、心包腔引流管。双侧少量胸腔积液，右侧明显，邻近肺组织膨胀不全。盆腔积液。9-28 日抽出 140m1 血性心包积液。9-28 重医附二院心脏磁共振 :1、右心房右前壁占位，考虑血管源性病变 (血管肉瘤 ?2、肺动脉瓣轻度关闭不全。3、心包腔中量积液。4、双侧胸腔少量积液。9-29 日心彩超 1、右房内实性占位，考虑：肿瘤性病变，血管肉瘤 ?2、肺动脉瓣局限性反流。3、心包积液 (少量)。4、双侧胸腔积液。2022/10/1 彩超腹部 (肝胆胰脾肾)(空腹) 检查报告：腹部胆囊壁毛糙。。彩超下肢深浅静脉 (双侧) 检查报告：下肢血管双侧外静脉、股总静脉、股浅静脉、股深静脉、腘静脉胫前静脉、胫后静脉、肌间静脉、大隐静脉、小隐静脉超声未见明显异常。。冠状动脉 CT 血管成像 (CTA) 检查报告：胸部 1、右心房右前壁占位，考虑肿瘤性病变，请结合临床及其他相关检查 2、左右冠状动脉开口未见明显异常，右优势型冠状动脉。3、左右冠状动脉及其分支未见确切狭窄。 4、左前降支中段走行与心肌关系稍密切，考虑壁冠状动脉 (表浅型)。5、心包少量积液心包穿刺引流后。。 X 线计算机体层 (CT) 扫描 (十六及十六层以上螺，胸部 CT 增强检查报告：胸部 1、双肺 CT 增强未见明显异常。 2、右心房右前壁占位，考虑肿瘤性病变，血管肉瘤？请结合临床及相关检查。 3、心包腔少虽积液。有手术指针，无绝对手术禁忌，于 2022-10-3 在全麻下行体外循环下右心房肿瘤切除术 + 右心房重建术 + 心脏表面临时起搏器安置术，术后予以抗感染、强心利尿、保肝等对症支持治疗，术后病理提示 :2022/10/9 手术标本检查与诊断 (每增加 1 个蜡块加收) 肿瘤根治术标本检查报告 :(右房肿瘤) 考虑脉管源性肿瘤，倾向淋巴管瘤，局部交界性不除外，待免疫组化协助诊断。

检验检查记录：

见现病史

鉴别诊断：

心力衰竭

症状相似点：心包积液和心力衰竭都可能出现呼吸困难、水肿等症状。

鉴别要点：心力衰竭通常是由于心脏泵血功能减退，导致全身组织器官供血不足，可伴有心脏结构的改变，如心室扩大等。而心包积液是心包腔内液体积聚，压迫心脏影响其功能。心脏超声检查可帮助鉴别，心包积液时可见心包腔内有液性暗区，心力衰竭时主要表现为心室壁运动异常。

肝硬化

症状相似点：肝硬化可导致腹水，出现腹胀、下肢水肿等症状，与心包积液的部分症状相似。

鉴别要点: 肝硬化主要是肝脏病变引起的，腹部超声或 CT 可发现肝脏病变和腹水，而心包积液通过心脏超声可发现心包腔内有液体。

肾功能不全

症状相似点：肾功能不全时可出现水钠潴留，导致水肿，也可能有类似心包积液的症状。

鉴别要点：肾功能不全患者通常有肾功能异常的表现，如血肌酐、尿素氮升高等，尿常规检查可发现蛋白尿、血尿等。而心包积液主要是心包腔内液体增多，通过心脏超声可明确诊断。

自身免疫性疾病

症状相似点：如系统性红斑狼疮、类风湿性关节炎等自身免疫性疾病累及心包时，可出现心包积液，同时伴有其他系统受累表现，如关节肿痛、皮疹等。

鉴别要点：自身免疫性疾病患者一般会出现多系统损伤，多种自身抗体呈阳性。通过自身抗体检测和临床表现有助于诊断。

其他：

帕金森病合并餐后低血压 1 例

张柳

新疆医科大学第五附属医院

患者基本信息：

患者石生莲，女，75 岁。

主述：

反复头晕 30 余年，胸闷、气短 2 年，加重 1 周。

现病史：

患者及家属诉患者 30 余年前无明显诱因出现阵发性头晕不适，多次测血压均大于 140/90mmHg，最高可达 180/100mmHg，为此患者就诊于当地医院，完善相关检查后明确诊断为“高血压病”，予以“苯磺酸氨氯地平片 5mg 口服 1 次 / 日”降压治疗，监测血压控制在 130/70mmHg 左右。2 年前，患者常于活动后出现胸闷、气短，间断双下肢水肿，为此多次于外院住院治疗，完善相关检查后明确诊断“慢性心功能不全”，给予降压、扩管、利尿等治疗后，病情好转出院。院外间断口服药物治疗（具体服药情况不详），头晕、胸闷、气短等不适症状仍时有反复。1 周前患者自感头晕、胸闷、气短加重，头晕多发生在餐后，自测血压，血压波动在 120-140/45-75mmHg，伴双下肢水肿，需高枕卧位，一般体力活动明显受限，伴上肢麻木，为进一步诊疗今日就诊于我院，门诊以 “高血压，慢性心功能不全” 收住。

既往病史：

平时健康情况：欠佳。既往 “冠心病” 病史 20 余年，现服用 “单硝酸异山梨酯缓释片 40mg1 次 / 日口服，阿司匹林肠溶片 0.1g1 次 / 日口服”，近 3 月胸痛的发作频率、诱因、程度及缓解方式无明显变化。既往 “帕金森病” 病史 2 年，目前服用“多巴丝肼片 0.125g3 次 / 日口服; 盐酸普拉克索片 0.25mg3 次 / 日口服”，目前运动迟缓，姿态平衡，静止性震颤及肌强直控制可。

病程记录：

初始：长效降压（苯磺酸氨氯地平片 5mg 口服 1 次 / 日）、扩管（硝酸甘油注射液 5mg 输液泵泵入 2ml/ 小时）、利尿（呋塞米注射液 20mg 静脉注射间断应用）、拮抗 RASS 系统（螺内酯片 20mg 口服 1 次 / 日）、控制心室率（琥珀酸美托洛尔片 23.75mg 口服 1 次 / 日）等治疗，同时进行改善帕金森症状（多巴丝肼片 0.125g 口服 3 次 / 日；盐酸普拉克索片 0.25mg 口服 3 次 / 日）、抗板（阿司匹林肠溶片 0.1g 口服 1 次 / 日）、调脂稳斑（阿托伐他汀钙片 20mg 口服 1 次 / 每晚）治疗。

入院后病情变化：（1）患者于入院第三日午餐后 2 小时下地活动时，出现明显头晕、乏力，随后意识模糊，无肢体抽搐、二便失禁，对发作过程无记忆。约 2h 后症状缓解。查体：神志清，精神差，不能正常对答，血压 117/57mmHg，心率 72 次 / 分，呼吸 28 次 / 分，指脉氧 95%，指尖血糖 8.0mmol/L。心肺腹查体无异常，四肢肌力正常，肌张力略增高。头颅 CT 及 MRI 均未见急性病灶，血钾 3.71mmol/L。（2）入院第四日早餐后 1h 左右再次出现上述症状，表现为明显头晕、乏力、嗜睡。反复测血压波动在 85-89/45-50mmHg 左右。约 2h 后症状缓解。发病时完善脑电图未见明显异常。

调整：患者经治疗后胸闷、气短症状好转，停用扩管、利尿治疗

（1）生活习惯调整：建议患者改变生活习惯，少食多餐，以总食量不变的每天 6 餐为最佳。餐前饮水 350-500ml，以低碳水高脂的食谱搭配为主，尽量减少葡萄糖摄入。

（2）降压药物调整：停用长效降压治疗，调整为血压高时口服短效降压药卡托普利 12.5mg。

（3）针对餐后低血压治疗：建议患者小剂量口服阿卡波糖 25mg 2 次 / 日（早、午餐）改善症状。

检验检查记录：

心电图：窦性心律。

血气分析、心梗三项未见明显异常。

血电解质：血钾 5.08mmol/L。

血常规：血红蛋白 121g/L。

心脏彩超：二尖瓣反流（少量），三尖瓣反流（少量），左室收缩功能测值正常。

颈动脉及脑动脉增强 + 重建、脑 CT、脑 MRI 未见明显脑血管病变。

24h 动态心电图提示：24h 血压均值 138/65mmHg; 白天血压均值 133/63mmHg; 夜间血压均值 163/72mmHg。血压降低的时间主要集中在 10：42 至 12：46、14：08 至 16：06、20：46 至 22：26 这三个时间段。追问患者病史，这三个时间段分别是早餐、午餐、晚餐后 2 小时内。

鉴别诊断：

1. 体位性低血压：由体位改变（如从卧位到直立位）引发，表现为站立后血压突然下降，伴随头晕、眼前发黑。

鉴别要点：症状与体位变化相关，而非进餐后发生；可通过直立倾斜试验或卧位 - 站立位转换测试确诊。

2. 餐后综合征（如倾倒综合征）：多见于胃切除术后患者，因食物快速进入小肠引发血管扩张和低血压，表现为餐后早期（15-30 分钟）的头晕、心悸、出汗、腹泻。

鉴别要点：有胃手术史，症状发生时间早且伴随消化道症状（如腹泻、腹胀）。

3. 药物性低血压：服用降压药（如利尿剂、α 受体阻滞剂）、抗抑郁药或抗帕金森病药物后，血压下降与药物作用时间相关。

鉴别要点：详细询问用药史，调整药物剂量或时间后症状可缓解。

4. 心血管疾病，如心律失常、心力衰竭：表现为持续头晕、乏力，与进餐无明确时间关联，需通过心电图、心脏超声等检查排除。

其他：

患者餐后低血压的病情（餐后头晕等）常被患者本身的基础疾病所掩盖，增加了鉴别诊断的难度。另外，患者患有帕金森病，帕金森病属于自主神经功能性疾病，笔者推测帕金森病可能加重餐后低血压的情况。

免疫检查点抑制剂相关心肌损伤合并阵发性三度房室传导阻滞 1 例

马志玲

空军军医大学西京医院

患者基本信息：

一般资料

女性、67 岁　主诉：宫颈癌III C1r 期新辅助化疗及免疫治疗后 33 天，肌肉酸痛 1 周

关键时间线：2025 年 6 月 20 日 -7 月 9 日（心电图密集监测期）

2025 年 05 月 24 日于妇科住院予以多柔比星脂质体 40mg+ 卡铂 400mg+ 斯鲁利单抗 200mg 新辅助化疗及免疫治疗

主述：

主诉：宫颈癌III C1r 期新辅助化疗及免疫治疗后 33 天，肌肉酸痛 1 周

现病史：

现病史：患者于 2025 年 04 月 22 日在西安市第三医院行宫颈活检病检提示：(宫颈多点活检) 破碎组织至少为鳞状细胞原位癌，可疑侵润。后于交大二附院病理会诊示：宫颈 CIN III级，灶状癌变，组织破碎，难以判断侵润深度。行盆腔 MRI 平扫示：子宫颈占位，右侧髂血管旁肿大淋巴结，考虑宫颈癌 (III C1r 期)。建议放化疗，患者拒绝，遂 2025 年 05 月 11 日就诊于我院门诊，行阴道镜检查 + 宫颈活检 + 阴道壁活检，病检提示：【宫颈及阴道活检标本】(宫颈) 至少鳞状上皮原位癌。(左侧阴道壁 3 点穹隆处) 鳞状上皮乳头状增生伴原位癌。行盆腔增强 MRI 示：宫颈占位，阴道上端受累，盆腔淋巴结转移可能，考虑宫颈癌 (FIGO III C1 期可能), 请结合临床，子宫肌瘤可能，双侧腹股沟区少许稍大淋巴结。行双下肢静脉超声提示：右侧小腿肌静脉内径增宽伴血栓形成 (完全充填型)。后于 2025 年 05 月 19 日于我院甲乳血管外科住院行下腔静脉滤网植入术，同时口服利伐沙班片 10mg/ 日。于 2025 年 05 月 24 日于我科住院予以多柔比星脂质体 40mg+ 卡铂 400mg+ 斯鲁利单抗 200mg 新辅助化疗及免疫治疗，同时给予补液、止吐对症治疗，化疗过程顺利。化疗后无骨髓抑制。于 2025 年 06 月 19 日出现腰部、髋关节部、双下肢疼痛不适，未服用药物。于 2025 年 06 月 22 日出现咽部疼痛不适，伴发热，最高体温 37.4℃，自服 “头孢、蓝芩口服液” 1 次。后自觉疼痛较前加重，于 2025 年 06 月 23 日出现眼睑下垂，无法自主活动，四肢无力，无胸闷、气短、心慌等，无双下肢肿胀等不适。于 2025 年 06 月 24 日就诊于我院急诊科，行心损四项及心肌酶三项结果异常 (详见报告单), 行心脏超声检查提示：心包未见明显积液；左室收缩功能正常；彩色多普勒示：主动脉瓣返流 (少量)。行心电图示：窦性心律，心率 86 次 / 分，心电图不正常，完全性右束支传导阻滞，ST、TVL、avF 抬高≤ 0.05, 请结合临床，给予人免疫球蛋白、甲泼尼龙琥珀酸钠、注射用环磷腺苷葡胺营养心肌、异甘草酸镁注射液保肝等对症治疗。后于 2025 年 06 月 25 日于心内科门诊就诊，考虑不排除病毒性心肌炎可能，给予单硝酸异山梨酯缓释片、辅酶 Q10 片、果糖二胺酸钙片对症治疗。遂门诊以 " 免疫性肌炎；免疫性心肌炎；" 收入院。

既往病史：

下肢静脉血栓 (下腔静脉滤网置入术后); 高血压病；胆囊切除术后；阑尾切除术后；肝功能异常

病程记录：

心室起搏器植入（2025-06-29）：解决 III° AVB 导致的血流动力学障碍。

糖皮质激素：重症医学科多次申请心电图，暗示启动免疫抑制治疗。

检验检查记录：

辅助检查：心肌损伤四项 (2025-06-26 本院): 肌红蛋白 2444.10ng/mL ↑，肌酸激酶 -MB 亚型质量 174.300ng/m1 ↑ ,B 型前脑尿钠肽检测 (Pro-BNP)545.80pg/m1 ↑，高敏肌钙蛋白 I 11.613ng/m1 ↑。心肌酶谱 (2025-06-26; 本院): 肌酸激酶 12772IU/L ↑，肌酸激酶 -MB 同工酶 211IU/L ↑，天门冬氨酸氨基转移酶 228IU/L ↑，乳酸脱氢酶 993IU/L ↑。(2025-06-25 本院) 急诊床旁心脏超声检查提示：心包未见明显积液；左室收缩功能正常；彩色多普勒示：主动脉瓣返流 (少量)。心肌损伤四项 (2025-06-25 本院): 肌红蛋白 2451.70ng/mL ↑，肌酸激酶 -MB 亚型质量 233.000ng/m1 ↑ ,B 型前脑尿钠肽检测 (Pro-BNP)201.50pg/m1 ↑，高敏肌钙蛋白 I 15.527ng/m1 ↑。心肌酶谱 (2025-06-25 本院): 肌酸激酶 12772IU/L ↑，肌酸激酶 -MB 同工酶 211IU/L ↑，天门冬氨酸氨基转移酶 228IU/L ↑，乳酸脱氢酶 993IU/L ↑。肝功九项 (2025-06-25 本院): 丙氨酸氨基转移酶 151IU/L ↑，天门冬氨酸氨基转移酶 273IU/L ↑，白蛋白 39.2g/L, 总胆红素 6.6μmol/L, 总蛋白 71.2g/L。血细胞分析 + 五分类 (2025-06-24 本院): 中性粒细胞百分率 0.752 ↑，红细胞计数 (8-HR)3.71X10E12/L ↓，血红蛋白 (8-HR)114g/L ↓，血小板计数 (8-HR)337X10E9/L, 白细胞计数 (8-HR)7.50X10E9/L。心脏超声检查 (2025-06-20 本院): 室间隔略增厚；主动脉硬化；左室舒张功能减低，收缩功能正常；彩色血流示：各瓣膜未见病理性返流。妇科超声检查 (2025-06-19 本院): 子宫后位，大小：6.4×4.5×3.8cm, 宫壁回声不均匀，形态不规则，轮廓清晰。子宫内膜显示不清，宫颈处见 2.1×1.5×1.5cm 实性低回声，形态不规则，边界不清，CDFI 显示可见血流信号。子宫前壁见 4.2×4.1×3.8cm 团状低回声，边界清。双侧卵巢受肠气遮挡显示不清。提示：提示：宫颈处所见：结合病史，考虑宫颈占位治疗中改变；子宫肌瘤。心电图 (2025-06-26 本院): 窦性心律；心电图不正常：完全性右束支传导阻滞；左前分支传导阻滞。

鉴别诊断：

根据病史、查体、辅助检查诊断明确。

其他：

冠脉高风险 TAVR 手术一例

高远

中国医大一院

患者基本信息：

李女士，女，69 岁，

主述：

以 “心前区及背部疼痛，端坐呼吸半个月” 为由入院

现病史：

心前区及背部疼痛，端坐呼吸半个月

既往病史：

既往史：高血压 20 余年，血压最高 180/90mmHg，口服硝苯地平血压控制在 120/60mmHg；糖尿病 10 余年，口服格列美脲、应用甘精胰岛素控制血糖；冠心病 4 年，于 LAD 及 RCA 各植入支架 1 枚

病程记录：

·查体：155cm，67.3kg，P：76bpm，BP：152/70mmHg，双肺呼吸音清，未闻及干湿啰音。心律齐，主动脉瓣听诊区可闻及 4/6 级收缩期喷射样杂音。

检验检查记录：

·cTnI 0.045ng/ml，BNP 695pg/ml

·WBC 6.33*109/L，Hb 133g/L，HCT 0.387L/L，PLT 169*109/L

·Cr 60umol/L，Urea 6.40mmol/L

·ALT 12U/L，ALP 25U/L，GGT 17U/L

鉴别诊断：

心力衰竭

缺血性心肌病

其他：

Successful treatment of pulmonary hypertension due to HIV infection and amphetamine snorting: a case report

孙翠明

中国医大一院

患者基本信息：

We report a case of HIV-positive 41-year-old Chinese man who suffered from PH with several concomitant risk factors in August 2017.

主述：

severe fatigue, worsening dyspnea, and edema of the bilateral lower extremity for a month

现病史：

In August 2017, he reported severe fatigue, worsening dyspnea, and edema of the bilateral lower extremity for a month.

既往病史：

He had a history of ventricular septal defect(VSD), which was surgically repaired at the age of 14 years, and a history of trauma and splenectomy at the age of 20 years. He was diagnosed with HIV-1 infection in September 2013 and developed severe liver abscess in November 2013.

病程记录：

His blood pressure was 130/83 mmHg, and blood oxygen saturation was 91% on room air. The N-terminal pro-B-type natriuretic peptide (NT-Pro-BNP) was 3,554 pg./mL. The chest CT scan showed an increase in pulmonary vessel diameter. Echocardiography showed mild tricuspid regurgitation with a reffux velocity of 4.6 m/s and an estimated pulmonary artery pressure of 97 mmHg. He was diagnosed with PH. To accurate evaluate the pulmonary artery pressure (PAP) and stratify PH, right heart catheterization (RHC) was recommended, but he refused due to its invasive nature. The distance of his 6-min walking test was approximately 270 m, and his cardiac function was grade III according to the World Health Organization (WHO) classiffcation (4). A combination of endothelin receptor antagonist (ERA) (bosentan) and phosphodiesterase type 5 inhibitor (PDE5I) (sildenaffl) was prescribed, but he only agreed to adopt monotherapy with sildenaffl citrate (25 mg, three times a day) due to the high price of bosentan.His HIV viral load was 4,220 copies/ml (COBAS TaqMan V2.0 RT-PCR, Roche; detection limit of 20 copies/ml) with the CD4+ T-cell count of 806/μL, while he still declined ART. The symptoms of dyspnea, fatigue, and edema were relieved gradually by undergoing sildenafil monotherapy without diuretic application.With psychosocial help, he reduced the frequency of amphetamine inhalation and was rehabilitated completely in January 2019.In April 2019, his echocardiography revealed that the reffux velocity of the tricuspid was 3.8 m/s, with an estimated pulmonary artery pressure of 68 mmHg. His plasma HIV viral load was 28,000 copies/mL, and he initiated ART (Triumeq one tablet per day, including lamivudine 300 mg, abacavir 600 mg, and dolutegravir 50 mg). The HIV viral load decreased to less than 20 copies/ml half a year affer ART. Then, he tapered sildenaffl usage (25 mg, twice daily) since November 2019. In December 2021, he was relieved of fatigue, dyspnea, and pedal edema. His physical capacity was improved, as evidenced by an increase in the distance covered during the 6-min walking test to 560 m and a decrease in NT-Pro-BNP decreased to 75 pg./mL. His cardiac function was grade I according to the WHO classiffcation. The arterial oxygen saturation was 96% in blood gas analysis performed on room air. Cardiac echo showed that the reffux velocity of the tricuspid decreased to 2.6 m/s with the estimated pulmonary artery pressure of 27 mmHg. He returned to normal work and daily life and withdrew from sildenafil subsequently.

检验检查记录：

The N-terminal pro-B-type natriuretic peptide (NT-Pro-BNP) was 3,554 pg./mL. The chest CT scan showed an increase in pulmonary vessel diameter. Echocardiography showed mild tricuspid regurgitation with a reffux velocity of 4.6 m/s and an estimated pulmonary artery pressure of 97 mmHg. The distance of his 6-min walking test was approximately 270 m, and his cardiac function was grade III according to the World Health Organization (WHO) classiffcation (4). His HIV viral load was 4,220 copies/ml (COBAS TaqMan V2.0 RT-PCR, Roche; detection limit of 20 copies/ml) with the CD4+ T-cell count of 806/μL, while he still declined ART. In April 2019, his echocardiography revealed that the reffux velocity of the tricuspid was 3.8 m/s, with an estimated pulmonary artery pressure of 68 mmHg. His plasma HIV viral load was 28,000 copies/mL, and he initiated ART (Triumeq one tablet per day, including lamivudine 300 mg, abacavir 600 mg, and dolutegravir 50 mg). The HIV viral load decreased to less than 20 copies/ml half a year affer ART. In December 2021, he was relieved of fatigue, dyspnea, and pedal edema. His physical capacity was improved, as evidenced by an increase in the distance covered during the 6-min walking test to 560 m and a decrease in NT-Pro-BNP decreased to 75 pg./mL. His cardiac function was grade I according to the WHO classiffcation. The arterial oxygen saturation was 96% in blood gas analysis performed on room air. Cardiac echo showed that the reffux velocity of the tricuspid decreased to 2.6 m/s with the estimated pulmonary artery pressure of 27 mmHg. He returned to normal work and daily life and withdrew from sildenafil subsequently.

鉴别诊断：

PAH from VSD; PAH from drug; PAH from HIV infection

其他：

复杂先心病合并 C 型主动脉弓离断一例

彭娇

武汉亚洲心脏病医院

患者基本信息：

2 月龄女患儿

主述：

发现先心病 2 月，咳嗽 1 周。

现病史：

患儿出生当天因“羊水误吸”在当地医院治疗好转。住院期间行心脏超声提示“先天性心脏病 室间隔缺损 房间隔缺损”（家属口述）。患儿出生后呼吸较促，平素吃奶时费力有停顿，易呛奶。1 周前患儿无明显诱因出现咳嗽，未行进一步诊治。自起病来，患儿精神、饮食、睡眠一般，大、小便正常，体力较差，体重正常。

既往病史：

母孕期病史不详，其他暂无。

病程记录：

患儿就诊我院门诊，门诊心电图提示：窦性心动过速。胸片：双侧肺血增多，肺无实变。气管无明确狭窄，双膈光整。肝影位于左侧膈下可能。主动脉结小、观察不清，肺动脉段饱满，心影增大。心胸比率：0.61。心脏超声：先天性心脏病：孤立右位心，室间隔缺损，房间隔缺损，动脉导管未闭，主动脉发育不良。给予维护心功能，升压，抗感染等治疗。治疗后 BNP 较前升高，进一步行增强 CT 检查示 C 型主动脉弓离断。

检验检查记录：

入院查：经胸超声心动图显示存在室间隔缺损、房间隔缺损、动脉导管未闭、主动脉发育不良 、降主动脉血流加速以及肺动脉高压（重度）。白细胞计数 3.79 10^9/L，中性粒细胞百分率 59.64%，超敏 C 反应蛋白 17.75mg/L，血清乳酸脱氢酶 304U/L，N 末端 B 型利钠肽原 >35000.00pg/ml，血清总蛋白 56.9g/L，血清白蛋白 34.5g/L，血清总胆汁酸 29.6μmol/L，血清碱性磷酸酶 322 U/L，血清前白蛋白 0.10g/L。BNP 较前升高，请行进一步检查。增强 CT 检查证实为 C 型主动脉弓中断（IAA）。动脉起始部位的远端，存在双重动脉管系依赖性循环：左侧动脉导管未闭（PDA）起源于左肺动脉，为左侧颈动脉、左侧锁骨下动脉和降主动脉供血；而右侧的 PDA 起源于右肺动脉，为孤立的右侧锁骨下动脉供血。

鉴别诊断：

1. 完全性心内膜垫缺损：多数患者在婴儿期即表现出严重的充血性心力衰竭的症状，并伴有严重的肺动脉高压，心前区隆起明显，听诊杂音响亮、粗糙，超声心动图可明确诊断。

2. 动脉导管未闭：重症动脉导管未闭并肺动脉高压，只能听到收缩期杂音，而无舒张期杂音，脉压也可不高，结合病史及彩超可排除。

其他：

无

左主干合并多支冠脉痉挛导致大面积 ST 段抬高型心肌梗死 1 例

鲍月

武汉亚洲心脏病医院

患者基本信息：

43 岁男性

主述：

胸痛 25 小时。

现病史：

患者 25 小时前发作胸痛，持续不缓解，今日至当地医院就诊，给予药物治疗，后转至我院，急诊行心电图提示下后壁导联 ST 段抬高，完善术前准备后行急诊介入手术，提示冠脉痉挛，建议药物治疗，术后收入 CCU。

既往病史：

体健，有吸烟史。

病程记录：

患者就诊我院急诊，行急诊 CAG 提示：多支冠脉痉挛，未见明显狭窄，给予抗血小板、抗痉挛、调脂稳定斑块（他汀类）及护胃等对症支持治疗

检验检查记录：

入院查：胸片：左心受累疾患，请行进一步检查。糖化血红蛋白 (NGSP) 5.80 %， 游离三碘甲状腺原氨酸 3.01 pg/ml， 游离甲状腺素 0.86 ng/dL， 促甲状腺激素 0.126 uIU/mL (↓)， 高敏肌钙蛋白 I 250.8850 ng/ml (↑)， 高敏肌钙蛋白 I-c 250885 ng/L (↑)， 白介素 -6 154.0 pg/ml (↑)， 白细胞计数 15.9 10^9/L (↑)， 中性粒细胞百分率 84 % (↑)， 淋巴细胞百分率 7 % (↓)， 红细胞计数 4.2 10^12/L (↓)， 红细胞压积 40 %， 葡萄糖测定 7.73 mmol/L (↑)， 钾测定 4.62 mmol/L， 钠测定 138.3 mmol/L， 氯测定 104.1 mmol/L， 镁测定 0.93 mmol/L， 高敏肌钙蛋白 I 80.2810 ng/ml (↑)， 高敏肌钙蛋白 I-c 80281 ng/L (↑)；白介素 -10 120.0 pg/ml (↑)， 中性粒细胞绝对值 13.4 10^9/L (↑)， 淋巴细胞绝对值 1.0 10^9/L (↓)， 单核细胞绝对值 1.5 10^9/L (↑)， 嗜酸性粒细胞绝对值 0.00 10^9/L (↓)， 嗜酸性粒细胞百分率 0.0 % (↓)， 血浆抗 Xa 活性测定 0.14 U/ml (↑)。白细胞计数 11.5 10^9/L (↑)， 中性粒细胞百分率 69 %， 淋巴细胞百分率 19 % (↓)， 红细胞计数 3.7 10^12/L (↓)， 红细胞压积 35 % (↓)， 钾测定 4.06 mmol/L， 钠测定 136.4 mmol/L (↓)， 氯测定 104.0 mmol/L， 镁测定 0.84 mmol/L， 高敏肌钙蛋白 I 30.2760 ng/ml (↑)， 高敏肌钙蛋白 I-c 30276 ng/L (↑)， 培养结果 鼻咽部正常菌群；中性粒细胞绝对值 7.9 10^9/L (↑)，单核细胞绝对值 1.4 10^9/L (↑)， 单核细胞百分率 12 % (↑)， 嗜酸性粒细胞绝对值 0.01 10^9/L (↓)， 嗜酸性粒细胞百分率 0.1 % (↓)， 血红蛋白 117 g/L (↓)， 血浆抗凝血酶活性测定 87.0 % (↓)， 血浆抗 Xa 活性测定 0.10 U/ml (↑)。

鉴别诊断：

患者胸痛原因应与以下疾病鉴别：

1、消化性溃疡：疼痛常有慢性、周期性、规律性特点，常有中上腹疼痛，多与进食有关。患者胸闷与进食无关，可能性不大。

2、食管返流或动力异常：常有烧心感，疼痛与体位改变或进食有关，食管痉挛有胸骨后持续性疼痛。患者无反酸症状，可能性不大。

3、主动脉夹层：Debakey I 型以及 II 型主动脉夹层累及冠脉时可引起急性心肌梗死，但往往受累动脉为右冠脉，故下后壁、右室心梗多见，心电图上表现为 STEMI。该患者临床上无夹层典型胸背痛特点，且查体无周围大血管杂音等体征，超声无夹层提示，综上分析，夹层不考虑。

4、冠状动脉栓塞或冠状动脉炎：结缔组织病，如 SLE、白塞氏病、大动脉炎等可同时累及主动脉瓣以及冠状动脉，但此类疾病多见于年轻女性，往往存在受系统受累，活动期多有低热等非特异性症状，该患者临床表现不支持，不考虑。

其他：

无

经导管主动脉瓣置换术中左心室游离壁穿孔引起急性心包填塞成功抢救 1 例

杨涛

昆明医科大学第一附属医院

患者基本信息：

患者女性，69 岁。

主述：

活动后胸闷、呼吸困难 1 年余。

现病史：

患者自诉 1 年来无明显诱因反复出现胸闷、呼吸困难，每次持续 10 余分钟，多于活动后出现。2024 年 12 月无明显诱因出现晕厥 1 次，约 20 分钟后自行清醒。

既往病史：

既往脑梗死病史，否认高血压、糖尿病、冠心病等慢性病史。

病程记录：

予抗血小板、利尿、改善心室重构等综合治疗，完善相关检查，确认无手术禁忌后，患者于 2025 年 3 月 27 日全麻下行 TAVI。术中反复尝试使用直头导丝跨主动脉瓣失败，遂在经食道超声心电图下采用经房间隔穿刺顺行跨瓣后抓捕导丝建立轨道。测量跨主动脉瓣压力阶差为 150mmHg，予球囊（20mm）行预扩张，同时造影评估对冠脉开口无影响后，送入 L26mm Venus-A Pro 介入瓣膜至主动脉瓣环处，超速起搏（180 次 / 分）下缓慢释放瓣膜，再予球囊行后扩张，测压提示跨瓣压 13mmHg。行主动脉根部造影，瓣膜开放良好，未影响冠脉开口，舒张期无反流，术中经食道超声心动图显示瓣膜启闭好，无瓣周漏，舒张期无反流。此时发现患者血压持续偏低，予行经胸心脏彩超提示少 - 中等量心包积液，并有增多趋势，存在心包填塞情况，立即于心尖处行心包穿刺，引流液为血性，持续引流，不能排外主动脉根部或心脏损伤，立即行股静脉穿刺置管开通静脉通道，联系血库申请输血，并立即在全麻状态下转至心脏外科行开胸探查。切开心包清除血凝块后，可见左心室游离壁活动性出血，接自体血回输及体外循环管路，予纱布压迫止血，适当减张缝合防止进一步撕裂，猪源纤维蛋白胶、可吸收止血粉、止血纱覆盖处理，间断压迫后未见活动性出血。缝合心包、留置心包引流管及纵隔引流管，术毕，返回至心脏外科 ICU。患者术后第 4 天由监护室搬回普通病房，术后 12 天好转出院。

检验检查记录：

入院心脏彩超：钙化性瓣膜病：（1）主动脉瓣极重度狭窄并极轻度关闭不全，致左房内径增大，室间隔增厚，升主动脉内径明显增宽；（2）二尖瓣轻度关闭不全。多排计算机断层扫描（multislices computed tomography，MSCT）示：主动脉瓣瓣环 22.9mm，主动脉窦 31.0mm，窦管交界 31.0mm，左室流出道 24.5mm， 左冠高度 17.7mm， 右冠高度 16.5mm，升主动脉内径 40.5mm。冠脉 CTA 各支冠状动脉未见中度及以上狭窄。出院前超声心动图：1.TAVI 术后：主动脉瓣血流正常。2. 二尖瓣钙化。3. 少量心包积液。

鉴别诊断：

梗阻性肥厚型心肌病。

其他：

多重获益–糖尿病合并多血管并发症病例

肖懿慧

西安交通大学医学院第一附属医院

患者基本信息：

男性，71 岁

主述：

发作性胸痛 4 年，加重 2 天

现病史：

4 年前快走时出现胸痛，持续约 4-5 分钟，伴心慌、出汗，休息后可缓解。于当地医院行冠脉造影示 LAD6 段狭窄约 70%，远端 TIMI 血流 3 级，出院后规律服用阿司匹林、阿托伐他汀、硝酸酯类药物，未再发作。

2 天前于夜间睡眠中突发胸痛，位于心前区，手掌大小，呈压榨性疼痛，大汗，自服硝酸甘油后症状稍缓解，2-3 小时内上述症状发作 3-4 次，每次持续约 10-15 分钟。为进一步治疗，遂来我院。

既往病史：

发现高血压 7 年，最高 180/100mmHg，目前服用倍博特，控制尚可；

1 年前脑梗死，遗留肢体活动不便

发现糖尿病 9 年，平时服用二甲双胍 + 达美康，空腹多在 7-8mmol/L，餐后未监测。

病程记录：

冠状动脉粥样硬化性心脏病

急性非 ST 段抬高型心肌梗死

心功能 1 级 (killip 分级)

2 型糖尿病

高血压 3 级

脑梗死

检验检查记录：

鉴别诊断：

无

其他：

如何选择科学的降糖方案

主动脉覆膜支架置入术治疗先天性降主动脉 - 肺静脉瘘一例并文献综述

邱接

华中科技大学同济医学院附属同济医院

患者基本信息：

患者男性，18 岁

主述：

因“间断咯血半年”入院。

现病史：

患者半年前无明显诱因出现咯血，量少，鲜红色，无发热、胸闷、气喘等不适，遂就诊于当地医院，行肺部 CT 提示先天性降主动脉 - 左下肺静脉瘘，左下肺少量感染实变伴肺泡出血、渗出，予以抗感染、止血等对症治疗，症状有所好转。出院后仍有间断咯血，性质同前。

既往病史：

无特殊

病程记录：

入院查血常规、血沉、肝肾功能、肌钙蛋白、痰培养等均未见明显异常。心电图示：窦性心律，左室肥大，广泛导联 J 点显著抬高，心室早期复极，T 波高尖。局麻下行主动脉造影术，造影示降主动脉可见有血管瘘入向左肺下叶基底段，术中于降主动脉瘘口处置入主动脉覆膜支架系统（先健 TAA2424B08）。

检验检查记录：

心脏彩超示：降主动脉 - 左下肺静脉瘘可能，左心扩大（左心房直径 41mm，左心室直径 63mm）。

胸腹主动脉 CTA 示：胸部降主动脉可见一增粗血管（直径 14-16mm）向左肺下叶基底段供血，左下肺静脉增粗并回流至左心房，左肺下叶模糊斑片影，考虑为肺泡出血，左心增大。

术后半年随访，患者未再咯血，复查心脏彩超示降主动脉 - 左下肺静脉瘘支架术后改变，左心较前明显缩小（左心房直径 32mm，左心室直径 56mm）

鉴别诊断：

肺隔离症、异常体动脉供应正常下肺基底段、肺动静脉瘘（PAVM）、弯刀综合征

其他：

1 例转甲状腺素型心脏淀粉样变超声表现

贾保霞

深圳市龙岗中心医院

患者基本信息：

男性，50 岁。

因“双眼一过性黑朦半年余，跌倒发作 21 小时”入院。

入院检查：N 末端脑利钠肽 1170(pg/ml)，高敏肌钙蛋白 T 0.037(ng/ml)，

心电图示房性心动过速、室性早搏、肢体导联低电压。

入院体格检查（–）。冠状动脉造影（-）。

主述：

双眼一过性黑朦半年余，跌倒发作 21 小时

现病史：

因“双眼一过性黑朦半年余，跌倒发作 21 小时”入院。

入院检查：N 末端脑利钠肽 1170(pg/ml)，高敏肌钙蛋白 T 0.037(ng/ml)，

心电图示房性心动过速、室性早搏、肢体导联低电压。

入院体格检查（–）。冠状动脉造影（-）。

既往病史：

既往无高血压病史，无吸烟、饮酒史。患者大哥 53 岁时因心脏肥大去世，二哥 49 岁因心脏病行手术治疗后去世，具体情况不详。

病程记录：

予氯苯唑酸抑制淀粉样沉积治疗。

检验检查记录：

1. 入院检查：N 末端脑利钠肽 1170(pg/ml)，高敏肌钙蛋白 T 0.037(ng/ml)，

心电图示房性心动过速、室性早搏、肢体导联低电压。

2. 经胸超声心动图 + 超声斑点追踪成像（图 1A-D）：心脏各腔室不大，室间隔及左室后壁厚度均为 16 mm，运动普遍减低，二尖瓣、三尖瓣轻度反流，左室射血分数（EF）34%，舒张功能减低（III 级）；左室整体纵向应变减低（LVGLS 约为– 7.1%），心尖各节段应变相对保留。TDI 示二尖瓣环间隔侧及侧壁 e' 均 <5cm/s。

3. 磁共振检查示（图 2）：左室心肌弥漫性增厚，较厚位于下壁约 17.7mm，基底段弥漫性延迟强化，左侧房室心内膜延迟强化，考虑心肌淀粉样变性（CA）。

4. 腹壁脂肪组织活检、心肌核素及基因检查，均诊断为：淀粉样变性心肌病（CA-ATTR 型）。

5.. 经皮心肌活检：确诊心肌淀粉样变性。

鉴别诊断：

1. 高血压心脏病：

●有高血压病史；心肌回声均匀，多伴有左心室腔增大

●不合并右心室壁增厚以及房室瓣增厚

2 主动脉瓣狭窄

● 主动脉瓣叶明显增厚，可伴有左室壁增厚，通常不合并右室壁增厚。

●主动脉瓣狭窄可以是 ATTR-CA 的表现之一，并存率约 6%~16%，因此对于表现为低流速低压差的重度主动脉瓣狭窄老年患者需警惕合并 ATTRwt-CA。

●左心室纵向应变是否呈现“心尖保留”有助于鉴别诊断。

3. 肥厚型心肌病

●非对称性肥厚，以室间隔为著，与左心室后壁的厚度之比 >1.5。

●心电图：左心室高电压，心前区导联 T 波倒置。

●基因检测。

其他：

一波四折，消化道大出血与急性心肌梗死此起彼伏–1 例 STEMI 合并消化道出血

陈丽远

石家庄市人民医院

患者基本信息：

患者翟某，男性，59 岁

主述：

突发胸痛 8 小时

现病史：

患者入院前 8 小时无明显诱因突发胸痛，为心前区闷痛，向肩背部放射，经休息自行缓解；入院前 3 小时活动后再次胸痛发作，性质同前，程度较前加剧，伴有大汗，恶心呕吐，自服“消心痛，速效救心丸”效果欠佳，急诊就诊于当地医院，ECG（20:24）：窦性心律，心率 91bpm，V1-V6 导联 ST 段抬高 0.2-0.5mV。予双联抗血小板药物负荷量（阿司匹林 + 替格瑞洛）嚼服后转至我院，急诊查心电图（22:35）示急性心肌梗死，肌钙蛋白 0.17ng/ ml，遂入院。

既往病史：

有“痔疮”病史，入院前间断有便血，量不详，应用“云南白药”治疗后好转。有“高血压”“2 型糖尿病”病史。

病程记录：

患者中年男性，主因持续胸痛就诊，既往“痔”病史，近期有出血。心电图示：前壁 ST 段抬高型心肌梗死，行急诊造影示冠脉三支病变，前降支介入治疗，术后 48 小时，患者出现失血性休克，紧急输血并行微创介入栓塞止血，术后吲哚布芬单药抗血小板聚集治疗，术后第 4 天再发失血性休克，再次介入栓塞止血治疗，停全部抗栓药物。查腹部增强 CT 考虑结肠癌可能。停用抗栓药物第 4 天，患者发生急性前壁 ST 段抬高型心肌梗死，行急诊介入治疗，术后吲哚布芬单药抗血小板聚集治疗。四次抢救，患者病情转危为安，查 PET-CT 考虑结肠癌。

患者出院 1 月后返院处理冠脉残余病变，术后 1 月停抗栓药物复查肠镜，未见结肠病变，复查增强 CT 未见结肠占位病变。

检验检查记录：

详见 PPT

鉴别诊断：

肺栓塞、主动脉夹层、胃食管反流

其他：

“逢堵立新”– PFO 致反常冠脉栓塞经皮肝静脉穿刺介入封堵 1 例

魏峰

西安交通大学医学院第一附属医院

患者基本信息：

患者 XXX，男，44 岁，甘肃省固原市人，职业：农民。

主述：

突发心前区疼痛 2 周

现病史：

2 周前，患者无诱因突然出现心前区疼痛，伴大汗，于当地诊断为“急性 ST 段抬高性心肌梗死（广泛前壁）”，急诊行冠脉造影示：左前降支近段闭塞，给予球囊扩张、冠脉内溶栓及血栓抽吸等治疗后，血流恢复，但管腔仍存在部分血栓，建议转院进一步治疗。

既往病史：

患者既往 2 年前于本院确诊为“布加综合征、下腔静脉及左髂静脉血栓、肺栓塞”。否认“心律失常、瓣膜病”等心脏病史，否认“高血压、糖尿病、高脂血症”等慢性病史。否认外伤、手术、输血史。吸烟 20 年，已戒烟 2 年。否认食物、药物过敏史。否认激素等特殊药物服用史及有毒物质接触史，否认家族遗传病史。

病程记录：

查体：T 36.8℃，P 76 次 / 分，R 20 次 / 分，Bp 102/74mmHg。神志清。睑结膜无苍白，巩膜无黄染。口唇无紫绀，颈静脉无充盈，甲状腺无肿大，未闻及血管杂音。胸廓对称，左肺底可闻及少量湿性啰音，未闻及胸膜摩擦音。心尖搏动位于第 5 肋间左锁骨中线内 0.5cm 处，心界不大，心率 76 次 / 分，律齐，各瓣膜听诊区未闻及杂音，无心包摩擦音。腹壁静脉充盈，腹软，肝脾肋下未触及。四肢对称无畸形，双下肢无水肿。

诊断：1. 冠脉栓塞（反常栓塞）急性 ST 段抬高型心肌梗死（广泛前壁）心功能 II 级（Killip 分级）客观评定 D；2. 卵圆孔未闭；3. 布加综合征 下腔静脉血栓形

成伴闭塞；4. 肺栓塞、左髂静脉血栓形成。

治疗：入院后给予抗凝（利伐沙班 20mg p.o qd）；抑酸（泮托拉唑 40mg ivdrip qd）；纠正心功能（诺欣妥 50mg p.o bid, 美托洛尔 23.75mg p.o qd，达格列净 10mg p.o qd, 螺内酯 20mg p.o qd）；营养心肌等治疗。同时经患者及家属同意，局麻下行经皮肝静脉穿刺 PFO 介入封堵术（图 K-L），术后继续利伐沙班（20mg p.o qd）抗凝治疗。

效果与随访：治疗 1 周，患者症状完全缓解，一般活动无明显不适。复查心动超声示 EF 52%，前间隔、左室前壁搏幅减低; 卵圆孔未闭封堵术后，封堵器形态正常，位置固定。1 月随访：无明显不适，未再发生栓塞及出血事件；1 年随访：于血管外科行下腔静脉支架植入术，未再发生栓塞及出血事件; 2 年随访: 无明显不适，未再发生栓塞及出血事件。

检验检查记录：

发病时外院心电图示：窦性心律，I、avL、V_{2-5} 导联 ST 段抬高（图 A）；心肌损伤标志物：CKMB 26.1 ng/mL（正常：0.0-4.3 ng/mL）、MYO >500 ng/mL（正常：0.0-107 ng/mL）、TNI 0.89 ng/mL（正常：0.0-0.4 ng/mL）；床旁心动超声：EF 42%，节段性室壁运动异常；急诊冠脉造影示：LAD 开口闭塞伴血栓形成（图 B）。入本院后心电图示：窦性心律，I、avL、V_{2-4} T 波倒置，V_{1-3} QS 型（图 C）；冠脉造影示：未见明显异常（图 1D）。心动超声示：EF 52%，前间隔、左室前壁搏幅减低；卵圆孔未闭 (Patent Foramen Ovale，PFO，图 E)，二、三尖瓣少量返流，少量心包积液。右心声学造影示：静息状态下右心显影后左心未见微气泡（图 F）；Valsava 动作后即刻左心内探及大量微气泡（整个心腔浑浊）（图 G）。下肢静脉超声提示：左髂外静脉血栓形成。肺动脉 CTPA: 左肺下叶后基底段肺动脉栓塞 (Pulmonary Embolism，PE) 可疑 (图 H）。下腔静脉造影示：下腔静脉闭塞伴侧枝开放（图 I）；下腔静脉及肝静脉 CTV 示: 下腔静脉肝段及肝下段血栓形成，管腔狭窄闭塞; 肝静脉血流正常 (图 J)。24 h 动态心电图：窦性心律，偶发房性早搏，未见房颤等心律失常。颈动脉超声：未见异常。头颅 CT：未见明显异常。入院实验室检查 Pro-BNP 2513pg/mL，凝血、心肌酶、血常规、肝功、肾功、血糖、血脂、电解质均正常。肿瘤、炎症、风湿、免疫、结缔组织筛查均未见异常。

鉴别诊断：

1. 冠状动脉粥样硬化性心脏病：伴有冠状动脉粥样硬化斑块，常合并高血压、高脂血症、糖尿病等动脉硬化的高危因素，冠脉造影或冠脉 CTA 可明确诊断；2. 冠状动脉痉挛：女性多见，多发生于休息状态或夜间，常有紧张、焦虑、抑郁、生气、情绪波动等诱因，冠脉造影无明显的动脉硬化及血栓表现，给予扩张冠状动脉药物后，可明显改善；3. 主动脉夹层：常有典型的撕裂样持续性胸背痛，多伴有高血压病史，CTA 可明确；4. 冠脉外压性病变：结合病史及冠脉 CTA 可明确。

其他：

本病例为国际首例局麻下经皮肝静脉穿刺 PFO 封堵术治疗反常冠脉栓塞合并布加综合征、肺栓塞、下肢静脉血栓形成的病例。

急性心肌梗死术中 IABP 支持治疗中的死亡陷阱：一例病例对比与临床反思

黄鑫

首都医科大学附属北京世纪坛医院

患者基本信息：

项目	陈顶柱	骆建平
性别	男	男
年龄	61 岁	63 岁
职业	离（退）休人员	离（退）休人员
结局	出院	死亡

主述：

1. 陈顶柱：突发意识丧失伴呼吸心跳骤停 5 小时 2. 骆建平：间断胸痛 8 小时余，意识模糊 2 小时余

现病史：

1. 陈顶柱：

患者 5 小时前（14:30）候车时突发意识丧失，伴心跳呼吸骤停，无大小便失禁、口吐白沫及角弓反张，无四肢抽搐，无意识丧失所致外伤史，后行心外按压治疗，于 12 分钟后（14：42）恢复呼吸，仍无自主意识，由 120 送至我院急诊，患者诉途中曾行除颤治疗（具体不详），急诊心电图、心肌酶示急性心梗，急诊绿色通道行冠状动脉造影检查并行 IABP 治疗后收入 CCU。自发病以来，患者意识模糊，鼻饲饮食，大小便失禁，体重无明显变化。

2. 骆建平：

患者 8 小时余前（10:00 左右）无明显诱因出现胸痛，部位位于整个前胸部，性质为闷痛，伴后背部放射痛，程度不剧烈，症状持续 10 分钟左右，自行舌下含服速效救心丸后可稍缓解。7 小时余前（13:00）左右胸痛症状再发，后至我院急诊就诊（15:22），查心电图示：窦性心律，HR 78 次 / 分，胸前导联 R 波递增不良，15:50 于我院完善胸片检查过程中自觉胸痛症状加重，并突发意识模糊，伴恶心，无呕吐，患者可触及大动脉搏动，呼吸不规整，急诊科医生立即将患者转运至抢救室，测血压为 87/58mmHg，心率 87 次 / 分，复查心电图示：窦性心律，HR 85 次 / 分，V1-V5 导联 ST 段弓背向上抬高 0.1-0.6mv，考虑“急性广泛前壁 ST 段抬高型心肌梗死”，给予静脉泵入去甲肾上腺素升压，急诊绿色通道行冠脉造影检查，结果提示：p-LAD 完全闭塞，心梗罪犯血管为 LAD，术中开通 LAD，于 LAD 病变处应用抽吸导管进行血栓抽吸并进行 PTCA 治疗，术中患者心脏机械收缩消失，给予紧急心肺复苏，同时紧急气管插管连接呼吸机辅助通气，积极抢救 40 分钟左右，患者心肌收缩略有恢复，转运至 CCU 进一步治疗。

既往病史：

项目	陈顶柱	骆建平
高血压	有	无
糖尿病	有	无
高脂血症	有	无
PCI 史	无	无
其他慢性病		

病程记录：

项目	陈顶柱	骆建平
呼吸循环支持	气管插管 + 呼吸机 +IABP	气管插管 + 升压药 + 呼吸机 +IABP
血流动力学状态	稳定	血压不稳定，持续依赖多巴胺 / 去甲肾上腺素
肾功能变化	肾前性肾功能不全，补液后好转	肾前行肾功能不全，肾功能逐步恶化
肝功能变化	AST/ALT 升高	AST/ALT 升高
消化道出血	上消化道出血（疑应激性溃疡）	明显（呕血）
感染 / 肺部变化	重症肺炎，CRP 升高，抗生素调整数次	重症肺部感染，持续发热

检验检查记录：

检查项目	骆建平	陈顶柱
心电图	V1-V5 ST 段抬高	ST 段未抬高
心肌酶峰值	肌钙蛋白 I 显著升高（195322 pg/ml）	肌钙蛋白 I 835.4 pg/mL
CRP	2.86mg/l	282.6mg/l
NT-ProBNP	490.7 pg/ml	1946 pg/ml
D 二聚体	13666ng/ml	117222ng/ml

鉴别诊断：

急性肺栓塞：临床上可出现胸痛、呼吸困难，心电图出现 S Ⅰ Q Ⅱ T Ⅲ型及 V1~V3 导联 ST 段抬高、T 波倒置，应与急性下壁、前间壁心肌梗死相鉴别。

急性心包炎：患者有胸痛、ST 段抬高，需与急性心肌梗死相鉴别。

变异型心绞痛：患者有胸痛、硝酸甘油不能缓解，ST 段抬高伴 T 波高耸，酷似急性心肌梗死。但变异型心绞痛用 Ca2+ 拮抗剂治疗有效，随着症状的缓解，ST-T 逐渐恢复正常，心肌酶谱正常范围。

其他：

我们追溯自纳入 2023 年 6 月至 2025 年 6 月于首都医科大学附属北京世纪坛急诊冠脉介入术中接受 IABP 治疗的急性心肌梗死患者 20 例，其中出院 14 例（70.0%），死亡 6 例（30.0%）。记录其出院及死亡结局，并收集年龄、SYNTAX 评分、IABP 植入后血小板计数、D- 二聚体水平及抗凝药物使用情况等指标。所有数据录入后，采用 SPSS 29.0.2.0 软件进行统计分析。连续变量以均数 ± 标准差（Mean ± SD）表示，组间比较采用 Mann-Whitney U 检验；分类变量以例数（百分比）表示，组间比较采用 Fisher 精确检验。以 $p < 0.05$ 为差异具有统计学意义，结果显示，死亡组患者的 SYNTAX 评分显著低于出院组(16.17 ± 9.24 vs 28.50 ± 12.67，$p = 0.039$)，提示病变复杂程度较低的患者反而死亡率更高。进一步分析发现，死亡组患者年龄更大（75.33 ± 7.79 vs 64.29 ± 9.03，$p = 0.026$），IABP 植入后血小板计数显著下降（90.67 ± 40.04 vs 187.69 ± 90.55，$p = 0.011$），且 D- 二聚体水平明显升高（12702.83 ± 9633.96 vs 2797.58 ± 4043.93，$p = 0.007$）。此外，死亡组中无一例患者使用抗凝药物，而出院组中有 8 例（57.1%）接受了抗凝治疗（$p = 0.042$）。上述结果提示，尽管死亡组病变负荷较轻，但高龄、IABP 植入后血小板减少、D- 二聚体升高以及抗凝治疗缺失，可能是导致死亡的关键非解剖学危险因素。因此，对于病变相对简单的患者，临床治疗过程中应在评估解剖学风险的基础上，重视全身状态、凝血功能变化及支持治疗的完善，制定更为个体化的综合治疗策略，以降低不良结局风险。

免疫检查点抑制剂相关心肌炎病例讨论

王喆

首都医科大学附属北京朝阳医院

患者基本信息：

患者，52 岁女性，2024.9.18 日住院，无烟酒嗜好，适龄婚育，育有 1 女 ，体健。已绝经。母亲 60 岁患有冠心病，73 岁心肌梗死。

主述：

发现超敏肌钙蛋白升高 8 小时

现病史：

患者 8 小时前于潘家园肿瘤医院行本周期免疫治疗给药前检查时发现超敏肌钙蛋白升高（0.374ng/ml），无胸闷、胸痛、心悸、大汗，无发热、咳嗽咳痰、呼吸困难，无头晕、头痛、黑矇等不适，进一步完善心电图示“T 波异常”（具体不详）。现为进一步诊治来我院，急诊以“非 ST 段抬高型心肌梗死”收入院。自发病以来，精神睡眠可，食欲可，二便如常，体重无明显变化。

既往病史：

2023 年 10 月因右肺中叶腺癌于当地医院行手术治疗，术后予培美曲塞 + 卡铂化疗 4 个周期（2024-2 结束）。2024-3 就诊于中国医科院肿瘤医院，考虑手术为 R1 切除，建议维持化疗及放疗。患者后续行培美曲塞维持化疗。2024-6 至 2024-7 行胸部放疗，同步进行培美曲塞 + 顺铂化疗 2 周期。2024-8-28 行第 1 周期免疫治疗：信迪利单抗 200mg 静点 1 次（每 21 天一次）。

肝功能异常，平素服用双环醇 2 片 tid、吡非尼酮 3 粒 tid 治疗。

2024-9-5 肺炎，10 日住院治疗，经静点阿莫西林及左氧氟沙星抗感染后好转出院。

否认肝炎史、疟疾史、结核史，否认高血压史、冠心病史，否认糖尿病史、脑血管病史、精神病史，否认外伤史、输血史，否认过敏史，预防接种史不详。

病程记录：

诊疗经过：入院后积极完善各项辅助检查。

治疗上 :1、患者心肌酶升高，入院完善冠脉造影显示阴性，心彩未见结构及功能改变；但术中及术后心电图显示心动过速，存在多形性室早、室速；动态心电图亦可见上述改变。结合患者既往肺癌切除术后化疗及近期免疫制剂治疗史，患者于 8-28 日首次行信迪利单抗 200mg 免疫治疗（每 21 天注射一次，9-17 因超敏肌钙蛋白升高未行治疗）。考虑诊断考虑免疫检查点抑制剂相关心肌炎可能性大，于 09-20 日转入 CCU 监护进一步治疗。请呼吸科及肿瘤科会诊，建议停用免疫治疗，给予甲强龙 280mg tid (9-20 至 9-22) 冲击治疗，患者心肌酶较前明显下降 ;09-23 至 09-25 调整甲强龙剂量为 280mg bid，于 09-26 至 09-30 将甲强龙减至 120mg qd，10-01 复查心肌酶 CKMB 较前升高，后改为 240mg qd 甲强龙静脉应用，果糖二磷酸钠及极化液营养心肌等治疗。患者完善心脏增强核磁考虑心肌炎可能，经治疗后患者心律失常症状好转，持续心电监护仅可捕捉偶发房性早搏，甲强龙 240mg 口服出院。

检验检查记录：

入院查体：血压 129/88mmHg

2024.9.19 入院检查：

肌钙蛋白 5.646ng/ml ↑，CK-MB 84.8ng/ml ↑，BNP：40pg/ml，NT-proBNP：188pg/ml，D 二聚体 0.47mg/l，总胆固醇 6.85mmol/l ↑，LDL5.33mmol/l ↑，甘油三酯 2.87mmol/l ↑，AST135u/l ↑，ALT74u/l ↑，肌酸激酶（CK）2751u/l ↑，LDH496u/l ↑，总胆红素 9.7umol/L，直接胆红素 2.8umol/L，肌酐 70.3umol/l，钠 141.2mmol/l，钾 3.3mmol/l ↓

血常规：WBC 4.27 *109/l，Hb 123g/l，PLT 174*109/l

血气分析：pH 7.44，呼碱伴代酸

尿常规、便常规及潜血（-）；PCT、CRP（-）

24.9.19 行冠脉造影，冠脉未见明显异常，术中监护术后心电监护可见多形性室早、短阵室速

甲功三项（-）；血常规、尿常规、便常规及潜血：未见明显异常

糖化血红蛋白 6.5%

24.9.19 心电图：心率 107bpm，窦性心律，频发室早、短阵室速，ST-T 改变

2024.9.20 心脏彩超诊断：左室壁运动不协调，请结合心电图；左室收缩功能尚可，舒张功能可疑减低；右室收缩功能正常

LVEF 57.5%，TAPSE 17mm

24.9.20 holter：窦性心律；偶发房早，阵发室上速（多阵次）；频发室早（多源多形），可见二联律，持续性室速（多源多形）；部分胸导电压异常减低；ST-T 改变（符合缺血性改变）；室早 114109 个，占总心搏 84.8%，有 2937 阵室性连发

治疗后检查：

24.9.23 心电图：窦性心律，ST-T 改变，室早、室速消失

2024.9.23 心脏彩超诊断：左室壁运动协调，左室收缩功能正常，舒张功能正常；右室收缩功能正常，LVEF 66%

2024.9.23 肌钙蛋白 1.377ng/ml ↑，CK-MB 29.3ng/ml ↑，BNP：241pg/ml，AST57u/l ↑

24.9.27 心脏增强核磁：诊断：左室中段间隔壁、下壁及后部纤维化改变；考虑非缺血性心肌病，结合临床不除外心肌炎改变，建议治疗后复查。左室心中段间隔壁、下壁心中层可见线样 T1 值升高；左室心中段后 IP 部心外膜可疑延迟强化灶，左室下壁可见心肌中层条线样延迟强化影。

鉴别诊断：

冠心病：CAG 阴性，可除外

肺栓塞：无相关症状体征， D-Dimer 阴性，下肢静脉无血栓，心脏彩超、心电图等无右室劳损征象，不支持

心力衰竭：无相关症状体征，BNP 40pg/ml，LVEF 57.5%，不支持

感染性疾病：无相关症状体征，血常规、CRP、PCT、肺 CT 等未见明显异常，不支持

自身免疫性疾病、心肌浸润性病变、内分泌代谢性疾病及应激性心肌病：目前证据无此倾向

其他：

一、病例特点

中年女性肺癌患者（R1 切除术后），于 2024 年 8 月 28 日首次接受信迪利单抗（ICI）治疗。20 天后（9 月 18 日）常规监测发现超敏肌钙蛋白升高（0.374ng/ml），无典型症状。入院后肌钙蛋白持续上升（峰值 5.646ng/ml），伴 CK-MB、CK 显著升高（CK 2751U/L），心电图新发多源多形性室早、短阵室速，心脏彩超提示左室壁运动不协调。冠脉造影排除冠心病，感染、心衰、肺栓塞等病因无支持证据。

二、诊断依据

1. 时间关联性：ICI 用药后 20 天出现心肌损伤标志物升高，符合 ICI 心肌炎中位发病时间（27-34 天）

2. 典型心肌损伤证据：

心肌酶动态升高（cTnI/CK-MB/CK）

新发恶性心律失常（多形性室速、室早 > 10 万次 /24h）

心脏 MRI 提示左室间隔壁、下壁心肌中层纤维化及延迟强化

3. 排除其他病因：冠脉正常、无感染 / 自身免疫 / 代谢性疾病证据

4. 治疗：大剂量甲泼尼龙（280mg tid）冲击治疗后 3 天心律失常消失，标志物下降

三、诊疗关键点

1. 早期识别：

本例于 ICI 周期前常规检测发现无症状性肌钙蛋白升高，提示用药期间定期监测心肌标志物对早期发现亚临床心肌损伤至关重要。

入院后病情迅速进展（24 小时内出现心悸 / 胸闷、室速），体现 ICI 心肌炎“隐匿起病、急剧恶化”的特点。

2. 治疗策略：

立即停用 ICI 并启动大剂量糖皮质激素（按 3 天冲击→ 3 天减量→维持方案），抗心律失常（胺碘酮）、心肌营养支持及血栓预防，多学科协作（肿瘤科会诊）优化管理 。

3. 预后警示：

本例符合重症心肌炎（3 级），病死率高达 30-50%，激素快速响应提示早期干预可改善预后，但需注意：心律失常型（早期发病）易进展为致命性室颤，即使治愈，永久禁用 ICI（指南强制推荐）

四、临床启示

1. 高危因素识别：肺癌（PD-1/PD-L1 抑制剂高使用率）、联合化疗 / 放疗史可能增加风险

2. 监测建议：

ICI 治疗前基线评估心功能，每个周期前监测肌钙蛋白、ECG（尤其首剂后 2 个月内），对无症状性肌钙蛋白升高需高度警惕，及时排查。

3. 诊断金标准：心内膜活检虽为确诊手段，但心脏 MRI（心肌中层延迟强化）已成为重要无创诊断依据。

五、总结

ICI 相关心肌炎起病隐匿、进展迅猛，本例通过肿瘤治疗常规监测发现异常，经快速鉴别诊断及激素冲击治疗成功逆转病情，凸显多学科协作与规范化管理对改善预后的核心价值。临床需建立“监测 - 预警 - 快速干预”体系以降低这一致死性并发症的风险。

被胸痛掩盖的“暗流”：嗜铬细胞瘤的 ACS 首发之谜

高英

邢台市人民医院

患者基本信息：

任某，男性，61 岁，生于邢台，久居本地，无疫水、疫源接触史；无工业、粉尘及放射线物质接触史；无烟酒嗜好；否认麻醉毒品等嗜好

婚育史及家族史：（-）

主述：

持续胸闷、气短 6 小时入院

现病史：

患者于入院前 6 小时于休息状态下出现胸闷，部位于心前区，面积约手掌大小，不向其他部位放射，自觉轻度气短，伴出汗、恶心及上腹部不适，无呕吐，无心悸，无晕厥、意识丧失，持续约 5 分钟症状减轻，但不能完全缓解。后间断出现胸闷、气短症状加重，无明显诱因，共发作 3 次，每次持续 4-5 分钟，可自行减轻。为进一步诊治入我院。

既往病史：

既往“高血压”病史 5 个月，自诉血压最高 150/90mmHg，未应用降压药物。无糖尿病、吸烟史。

病程记录：

初始诊断与治疗

结合患者症状、心电图及心肌标志物，初步诊断为：

1. 冠状动脉粥样硬化性心脏病（急性下壁、后壁心肌梗死，心功能 I 级（Killip 分级））；

2. 低钾血症。

急诊给予阿司匹林 300 mg 嚼服、替格瑞洛 180 mg 口服，补钾治疗，并急诊行冠脉造影。结果显示左前降支（LAD）肌桥，无明显狭窄或阻塞，排除典型冠状动脉闭塞性心梗。

异常表现与诊断转折

术后患者胸闷、心悸加重，监测发现血压波动剧烈：最高达 210/120 mmHg，最低骤降至 60/40 mmHg，伴心率持续增快（110-130 次 / 分）。给予美托洛尔（含服 + 口服）、硝苯地平缓释片控制心率及血压，但症状反复，且心电图显示前壁导联 ST 段压低与恢复随血压波动同步。

关键疑点：

冠脉造影无显著狭窄，无法解释心梗样心电图及症状；

血压骤升骤降伴交感兴奋（心率快、出汗），与单纯 ACS 不符；

低钾血症（儿茶酚胺可促进钾离子内流）、高血糖（10.60 mmol/L，参考值 3.9-6.1 mmol/L）提示交感过度激活。

进一步检查：肾上腺增强 CT、血儿茶酚胺、尿代谢产物

最终确诊：右侧肾上腺嗜铬细胞瘤，心肌缺血为嗜铬细胞瘤诱发。

治疗策略与转归

针对性治疗

1. 术前准备：转泌尿外科后，给予 α 受体阻滞剂酚苄明（20 mg，每日 3 次）控制血压（维持 130-150/80-90 mmHg），补充血容量纠正低血容量状态，避免术中血压骤降；

2. 手术治疗：择期行腹腔镜下右侧肾上腺肿物切除术，术中严密监测血压（肿瘤分离时血压升至 220/130 mmHg，予硝普钠控制；切除后降至 80/50 mmHg，予去甲肾上腺素及补液维持）；

3. 术后恢复：病理证实为嗜铬细胞瘤（免疫组化：CgA+、Syn+，，术后血压、心率恢复正常（血压 120/70 mmHg，心率 82 次 / 分），心电图 ST-T 段恢复正常，心肌酶及 NT-proBNP 降至正常。

检验检查记录：

心电图：窦性心动过速，下壁导联 PR 段压低，aVR 导联 PR 段抬高，下壁导联可见窄而深的 Q 波，下壁、后壁导联 ST 段抬高 0.05-0.1 mV，V1-V4 导联 ST 段压低 0.1-0.2 mV（图 1）。

心肌损伤标志物：肌红蛋白（Myo）156.98 ng/mL（参考值 0-58 ng/mL，↑），肌酸激酶同工酶（CK-MB）20.42 ng/mL（参考值 0-5 ng/mL，↑），肌钙蛋白 I（cTnI）0.20 ng/mL（参考值 0-0.3 ng/mL，正常）。

其他指标：NT-proBNP 1406.6 pg/mL（参考值 0-250 pg/mL，↑），心型脂肪酸结合蛋白（H-FABP）25.82 ng/mL（参考值 0-8 ng/mL，↑）；生化提示低钾（3.39 mmol/L，参考值 3.5-5.3 mmol/L，↓）、钠轻度降低（135.0 mmol/L）；凝血功能示 D - 二聚体 1.16 μg/ml（参考值 0-1 μg/ml，↑）

肾上腺增强 CT：右侧肾上腺区 75×44×50 mm 肿物，边界不清，增强扫描周边强化、内有低密度坏死区（图 4）；

血儿茶酚胺：肾上腺素 436 pg/ml，去甲肾上腺素 849 pg/ml（显著升高）；

尿代谢产物：去甲肾上腺素 192.5 μg/ml，香草扁桃酸（VMA）118 ng/ml（均升高）。

最终确诊：右侧肾上腺嗜铬细胞瘤，心肌缺血为嗜铬细胞瘤诱发。

鉴别诊断：

主动脉夹层：胸痛呈撕裂样剧痛，常放射至背部、腹部，血压升高为持续性，双侧上肢血压可能有明显差异。主动脉 CTA 可显示内膜片、真假腔等典型征象，与嗜铬细胞瘤的阵发性胸痛、儿茶酚胺相关血压波动及无主动脉影像学改变相区别。

其他：

总结与临床启示

1. 警惕“非典型”ACS：当胸痛患者出现血压剧烈波动（骤升骤降）、交感兴奋（多汗、心悸）、冠脉造影无显著狭窄时，需排查嗜铬细胞瘤；

2. 关键鉴别点：儿茶酚胺相关表现（发作性头痛、血糖升高、低钾）、影像学（肾上腺肿物）及生化（血 / 尿儿茶酚胺升高）是诊断核心；

3. 避免惯性思维：胸痛≠ ACS，需结合治疗反应动态评估（如本例降压后症状及心电图同步缓解），才能突破“先入为主”的诊断陷阱。

本病例提示，心内科医师需拓宽诊断视野，对“不匹配”的临床现象保持警觉，才能揭开胸痛背后的“暗流”。

春水融不动，冰消见山丛

顾崇怀

安庆市立医院

患者基本信息：

三例 RCA-CTO 伴有后三叉钝头闭塞逆向介入 non-DLMC 处理技巧

主述：

三例均为 RCA-CTO 伴出口在后三叉部位 -

现病史：

--

既往病史：

--

病程记录：

--

检验检查记录：

--

鉴别诊断：

--

其他：

幻灯片过于巨大只能上传 pdf 版本，请见谅

鲁登巴赫综合征致肺动脉高压 1 例

卓锦辉

福建医科大学附属协和医院

患者基本信息：

患者：陈某，性别：女，年龄：42 岁，职业：职员

主述：

胸闷、气促 2 年

现病史：

缘于入院前 2 年出现活动后胸闷、气促，平素爬 4 层楼即感气促，甲床青紫，曾就诊我院心外科，查 2025-02 心脏彩超示：先心，房间隔缺损（中央 + 腔静脉型），近似单心房，全心增大，二尖瓣中 - 重度反流，三尖瓣中度反流，估测肺动脉收缩压约 72mmHg，右室收缩功能减退，符合鲁登巴赫综合症。予降低肺动脉压及对症治疗后症状好转出院。出院后仍感胸闷就诊我科。

既往病史：

“心房颤动”病史 13 年，平素规律口服“比索洛尔“等药物，无心悸等不适。“甲状腺功能亢进症”病史 14 年，既往口服“丙硫氧嘧啶”，现已停药。否认吸烟、饮酒史。

病程记录：

入院后予利尿、降肺动脉压等治疗后症状缓解。行右心导管检查测肺动脉压 75/22/35mmHg，肺动脉嵌压 12mmHg，肺血管阻力 5.5WU。右房上部、中部及下部氧饱和度分别为 60%、83%、86%，上下腔静脉分别为 53%、76%，左房为 91%，肺动脉为 82%。右心导管诊断为先天性心脏病，房间隔缺损，左向右分流。肺动脉造影见肺动脉扩张，心脏明显增大，左右房为著，房间隔缺如。具有手术指征，转心外科行“房间隔缺损修补术 + 二尖瓣成形术 + 三尖瓣成形术”，术后监测肺动脉收缩压 46mmHg，食道彩超进一步评估二、三尖瓣微量反流，房间隔未见残余漏。出院后规律口服降肺动脉压等药物。

检验检查记录：

心脏彩超示房间隔缺损（中央 + 腔静脉型）大小约 54.2mm，近似单心房，二尖

瓣重度反流，三尖瓣中 - 重度反流，左房内径 60.9mm，右房内径 59.2mm，Ef 52.0%，TAPSE=15mm，s'=0.07M/S，肺动脉收缩压 94mmHg。运动心肺功能提示重度心肺功能障碍。肺功能提示小气道功能障碍，轻度弥散功能障碍。睡眠呼吸过筛提示重度低氧血症。

鉴别诊断：

1. 冠心病：多有胸闷痛等缺血性心绞痛症状，常有高血压、糖尿病、吸烟等危险因素，心电图可有 ST-T 改变，与该患者表现不符，暂不考虑。2.，慢性阻塞性肺病：患者多有长期吸烟史，常有胸闷、气促，伴慢性咳嗽、咳痰等表现，查体可见桶状胸、呼吸音减弱等，结合患者症状及肺功能检查可排除。3. 胃食管反流病：部分患者可出现胸闷、胸痛等症状，多于餐后、平卧时出现，胃镜等检查有助于鉴别，暂不考虑该病。

其他：

无

一波未平一波又起 ------ 急性心肌梗死心衰遇上急性肺栓塞病例 1 例

宋显晶

吉林大学第二医院

患者基本信息：

主诉：患者马某，男，75 岁，

主述：

因持续性胸痛胸闷 4 天，加重 1 天于 2023 年 6 月 5 日急诊就诊。

现病史：

患者 4 天前无明显诱因出现持续性心前区疼痛，呈闷痛，无放散，可耐受，伴胸闷心悸、乏力，无大汗，未诊治。入院前 1 天上述症状加重，并伴有一过性意识丧失 1 次，持续 5-10 秒钟，无抽搐，无肢体活动及感觉障碍，无尿便失禁，就诊于外院，行心电图检查提示“急性下壁心肌梗死”，为求进一步诊治转入我院。急诊以“急性心肌梗死”收入院。病程中，无发热，无咳嗽咳痰，无肢体活动及感觉障碍，无恶心、呕吐，无反酸嗳气，无尿频尿急、尿痛，饮食睡眠尚可，大便正常，近期体重无减低。

既往病史：

否认高血压病及糖尿病史，半年前患脑梗死病史，未遗留后遗症，无吸烟及饮酒史，否认家族遗传性疾病病史

病程记录：

查体：生命体征：T：36.8℃；P： 62 次 / 分；R： 18 次 / 分；在去甲肾上腺素泵注下 BP：86/58 mmHg

颈静脉无怒张，双肺呼吸音粗 ，两中下肺可闻及湿罗音，心脏浊音正常，心率：62 次 / 分，节律规整，心音弱，P2=A2，各瓣膜听诊区未闻及杂音，无心包摩擦音，腹软，无压痛及反跳痛，无肌紧张，肝脏不大，双下肢无浮肿，皮温皮色正常。

辅助检查：

6 月 5 日心肌损伤标志物外院：**hs-cTNI：26ng/ml（0-0.08），入院后我院复查 hs-cTNI：7.167ng/ml；**

CK：1178u/l（50-310）u/l，CK-MB：82u/l（0.0-25）u/l，LDH：703u/l（120-250）u/l，α- 羟丁酸脱氢酶：731u/l（72-182）u/l，

6 日 NT-proBNP：4159ng/ml（0-1800）；

6 日肝功：谷草转氨酶：172u/l(15-40)u/l，总胆红素：35.22umol/l(2-20.10)，直接胆红素：12.98umol/l（0-6.84），间接胆红素 22.24umol/l（1.71-11.97）

血脂：高密度脂蛋白胆固醇：0.87mmol/l（0.9-1.68），低密度脂蛋白胆固醇：1.79mmol/l（2.7-3.4）

血常规：白细胞：11x 10^9/L(3.5-9.5)x10^9/L，中性粒细胞：85.7%(40-75%)，淋巴细胞百分比：6.3%，中性粒细胞细胞计数：9.43x 10^9/L（1.8-6.3）x10^9/L，血红蛋白、血小板正常，

空腹血糖：14.55mmol/l（3.9-6.1）mmol/l

糖化血红蛋白：6.4%，增高，（4.6-6.2）

总胆红素：36.8umol/L（0.00-23.0）umol/l

直接胆红素：12.3ummol/l（0.00-8.0umol/l

尿糖：2+

凝血功能：D- 二聚体：0.78mg/l（0-0.5）略高；

肾功、免疫常规、甲功三项、便常规：未见异常。

6 月 5 日心电图：心率：69 次 / 分，窦性心律，不正常心电图， II、III、AVF 呈 Qr 型，ST 段抬高 0.15-0.25mv，V1-V6 导联 ST 段压低 0.05-0.2mv，V4-V6 导联 T 波浅倒置

6 月 5 日床头胸片：两肺纹理增多、紊乱，胸主动脉迂曲、增宽，两膈面光滑，肋隔角欠锐利。

6 月 6 日 血 气 分 析：PH：7，47，PCO2:24.3mmHg，PO2:72mmHg,Lac:3.1mmol/L,

6 月 8 日床头心脏超声：LV：59mm，LA：41mm，左心增大，LVEF：42%；室间隔、左室前壁、心尖运动及增厚率减低，搏动减弱，余室壁厚度及运动尚可；结果提示：室壁节段性运动异常，左心增大，左心功能减低，少量心包积液。

入院诊断：冠状动脉粥样硬化性心脏病、急性下壁 ST 段抬高型心肌梗死，Killip IV 级、2 型糖尿病、血脂异常

给与拜阿斯匹灵 300mg 负荷量，氯吡格雷 300mg 负荷量，阿托伐他汀 20mg 口服，同时给与积极补液、监测血糖。

结合该患者症状、心电图及心肌损伤标志物检查，考虑急性心肌梗死、心源性休克诊断明确，GRACE 评分 294 分，属于高危，死亡风险 >3%，符合急诊冠脉造影适应症，无禁忌症，故给予急诊冠脉造影检查，结果提示：呈均衡型，LM：正常，LAD 近段：70% 狭窄，远端给予右冠血管逆向血流，远端 TIMI 血流 3 级；LCX：正常；RCA：开口完全闭塞，远端 TIMI 血流 0 级。术中右冠大量血栓影，给予反复血栓抽吸，许欣路不 i 啊，给与非顺应性球囊扩张，再次反复抽吸，后血流恢复，血栓影消失，远端血流 TIMI3 级，建议 1 周后行则其 PCI 术。

术后患者胸痛症状减轻，但仍存在，给与比伐卢定，后替罗非班应用，并积极补液，监测血糖，术后患者血压逐渐改善，停用去甲肾上腺素，并适当给与扩冠治疗。

术后第二日 6 日，患者无明显诱因出现寒战，言语错乱，后体温升高，最高达 41℃，伴言语错乱，给以异丙嗪、地塞米松应用，持续约 20 分钟后体温恢复正常，言语正常，无肢体活动及感觉障碍，后未再出现。

术后第二日 6 日复查血常规：血常规：白细胞：9.2x 10^9/L（3.5-9.5）x10^9/L，中性粒细胞：78.5%（40-75%），淋巴细胞百分比：9.9%，中性粒细胞细胞计数：7.25x 10^9/L（1.8-6.3）x10^9/L，血小板：62 x10^9/L，血红蛋白正常。

患者血小板减少，考虑为肝素诱导的血小板减少症，未给与加用低分子肝素。

术后第三日 7 日患者胸痛症状消失，但仍有胸闷气短，无发热，无咳嗽咳痰，进食差，二便如常。查体：血压：95/59mmHg，双肺呼吸音粗，双肺底可闻及少量湿啰音，心率：95 次 / 分，节律规整，心音弱，各瓣膜听诊区未闻及杂音，双下肢无浮肿。

7 日复查心电图：心率：88 次 / 分，窦性心律，不正常心电图， II、III、AVF 呈 Qr 型，ST 段抬高 0.05mv，V1-V4 导联 R 波递增不良， V4-V6 导联 ST 段压低 0.05-0.1mv，T 波浅倒置

7 日复查 d- 二聚体：5.37mg/ml，升高（0-0.5）

检验检查记录：

治疗方案：

1. 一般监护、高流量面罩吸氧、低盐低脂糖尿病饮食、监测血糖、电解质；

2. 药物治疗：

拜阿司匹灵 100mg qd，氯吡格雷 75mg qd，阿托伐他汀：20mg qd，美托洛尔：23.75mg qd，达格列净 10mg qd 利伐沙班 15mg bid，呋塞米 20mg qd，螺内酯 20mg qd，

病情变化：患者胸闷气短症状逐渐减轻。

期间复查血小板：7 日 56x**10^9/L（125-350），8 日：81x10^9/L（125-350），9 日：109x10^9/L（125-350），10 日：122x10^9/L（125-350），14 日 281x10^9/L（125-350）**

期间复查 D- 二聚体：8 日：5.75，9 日：10.14，10 日：2.40，14 日：1.65

肿瘤标志物：未见异常

蛋白 C、蛋白 S：正常；

风湿免疫学化验：正常

术后 3 周调整利伐沙班为 20mg qd，同时停用氯吡格雷，建议 3 个月后复查肺动脉 CTA，但患者失访。

鉴别诊断：

：1、心肌梗死后并发症： 患者胸痛消失，但仍胸闷气短，呼吸困难，可平卧位，查体双肺啰音较前减轻；复查 NT-proBNP：由 6 日 4159à5546ng/ml，心脏超声提示：室壁节段性运动异常，LVEF：42%，符合心梗后心衰的诊断，但无机械性并发症，给与适当利尿、扩血管、强心、对症治疗。

2、肺动脉栓塞：该患者胸闷气短症状，心率偏快，血压偏低，D- 二聚体较前增高，不除外肺动脉栓塞可能，故给与肺动脉 CTA 检查，结果提示：右肺中叶及下叶肺动脉可见条片状低密度充盈缺损影，肺动脉干、左右肺动脉及右肺上叶肺动脉管腔显影清晰，双下肢静脉显影未见充盈缺损。故可明确急性肺动脉栓塞的诊断。

其他：

总结：这份病例给我们展现了一例急性心肌梗死合并心源性休克的病例，同时术后应用肝素后出现肝素诱导的血小板减少症（Heparin-Induced Thrombocytopenia, HIT），HIT 是一种由肝素类药物触发的免疫介导的严重不良反应，以血小板减少和血栓形成为主要特征。HIT 分 I 型和 II 型， I 型为非免疫型，发生率：约 10%-30% 使用肝素的患者，主要机制是肝素直接激活血小板，导致轻度血小板聚集，特点是血小板轻度减少（通常≥ 100×10 ^{9} /L），无症状，可自行恢复，无需停药。HIT II 型为（免疫介导型），发生率约 0.1%-5%（更高见于普通肝素 vs 低分子肝素），主要机制是肝素与血小板因子 4（PF4）结合形成复合物，触发 IgG 抗体，激活血小板和凝血系统。特点：血小板显著减少（较

基线下降≥ 50% 或绝对值 <100×10⁹/L），高血栓风险。HIT 的主要临床表现有血小板减少：通常在使用肝素后 5-14 天出现（若近期有肝素暴露史，可更快出现）；血栓形成：静脉（深静脉血栓、肺栓塞）或动脉（肢体缺血、卒中）血栓，发生率 30%-50%；其他表现可有皮肤坏死（皮下注射部位）、急性全身反应（如静脉推注后寒战、高血压）。HIT 的诊断主要通过实验室检查：免疫学检测（筛查）：ELISA 法检测抗 PF4- 肝素抗体（敏感性高，特异性较低）；功能学检测（确诊）：血清素释放试验（SRA，金标准）或肝素诱导血小板聚集试验（HIPA）。临床评分系统通过 4T's 评分（预测试概率）、血小板减少的程度和时间、血栓（新发血栓或其他后遗症）、排除其他导致血小板减少的因素、肝素暴露（与肝素使用的时间关联）。HIT 的治疗最主要的是应立即停用肝素，包括肝素冲管和肝素涂层导管；替代抗凝：避免华法林早期单用，可能加重血栓；可给与直接凝血酶抑制剂阿加曲班（Argatroban）：经肝代谢，监测 APTT，比伐卢定（Bivalirudin）常用于 PCI 或手术；可给与抗 Xa 抑制剂达那肝素（Danaparoid，部分国家可用），磺达肝癸钠（Fondaparinux，证据有限但可考虑）。当血小板恢复（≥150×10⁹/L）后，过渡至口服抗凝重叠使用华法林（维持 INR 2-3），除非活动性出血或高危手术，避免输血小板，否则可能加重血栓。

对于 HIT 伴血栓（HITT）需全剂量抗凝，若无症状但抗体阳性需密切监测，预防性抗凝存在争议。

预防与监测，应限制肝素使用时间和适应症，建议优先选择低分子肝素，对于高危人群监测血小板计数，使用肝素后第 4-14 天每 2-3 天检测，同时避免交叉反应药物如磺达肝癸钠在 HIT 中相对安全，但需谨慎。HIT 即使停用肝素，血栓事件可持续数周，HITT 死亡率可达 10%-20%，早期干预可改善预后。

该病例入院时血小板正常，术后第二日出现血小板减少，大于基线的 50%，同时伴有寒战发热，且出现急性肺动脉栓塞，虽然未对 HIT 的分型进一步检查，但结合该患者表现，考虑 II 型可能性大，治疗上患者由于患者心衰和肺栓塞同时存在，结合肺动脉 CTA 检查结果，属于分支肺动脉栓塞，考虑患者呼吸困难主要原因为心梗后心衰所致，故针对急性肺动脉栓塞的治疗给与抗凝为主，在抗凝药物选择上，考虑患者存在 HIT，故肝素及低分子肝素不适合应用，而华法林在应用早期需要与低分子肝素叠加应用，故也不适用于该患者，因此治疗上选用利伐沙班，并给与充分抗凝剂量，在治疗过程中我们严密监测患者症状，生命指正及 d- 二聚体变化，d- 二聚体逐渐下降，同时患者血小板在术后第 5 天恢复正常。

针对该病例体会，HIT II 型是肝素治疗中的严重并发症，需高度警惕血小板减少和血栓事件。诊断依赖临床评估（4T's 评分）和实验室检测，治疗核心是快速替换抗凝药物。临床医生应熟悉其表现和管理策略以避免不良结局。

KCNQ1-E115K 错义突变致长 QT 综合征 1 例

曹晨曦

郑州大学第一附属医院

患者基本信息：

患者，女，34 岁，于 2024-04-02 21:06 入院。

主述：

突发晕厥 3 小时

现病史：

3 小时前在家跳健身操时突发晕厥，摔倒在地，呼之不应，伴小便失禁，无抽搐，持续约 3 分钟，后自行恢复意识，醒后对晕厥情况无记忆，无胸闷、胸痛、大汗、心慌等，近期无发热、上呼吸道感染、腹泻等。遂至我院急诊科就诊，行心电图检查提示窦性心律，QT 间期延长；心肌损伤标志物未见异常。头颅 CT 平扫未见异常。为求进一步诊治，以“晕厥待查”收入院。自发病以来，食欲正常，睡眠正常，大小便正常，精神正常，体重无减轻。

既往病史：

既往史：无高血压、心脏疾病病史，无糖尿病、脑血管疾病病史，无肝炎、结核、疟疾病史，预防接种史随社会计划免疫接种。2 月前行“剖宫产术 + 双侧输卵管结扎术”（具体不详）。无外伤、输血史，无食物、药物过敏史。

个人史：生于河南省 - 郑州市 - 新郑市，久居当地，无疫区、疫情、疫水接触史，无牧区、矿山、高氟区、低碘区居住史，无化学性物质、放射性物质、有毒物质接触史，无吸毒史，无吸烟、饮酒史，否认冶游史。

婚育史：21 岁结婚，爱人体健，育有 1 子 2 女。

家族史：大伯 60 岁情绪激动时猝死（死因不明），其父亲和姑姑、舅舅患“脑梗死”，母亲及叔叔患“冠心病”。2 兄 1 姐及 1 子 2 女均体健，无与患者类似疾病。

病程记录：

体格检查：心率 68 次 / 分，血压 101/60mmHg，BMI=23.44kg/m2，心律齐，听诊未闻及明显心脏杂音。四肢肌力、肌张力正常，病理征阴性。辅助检查：电解质未见明显异常（钾 3.6mmol/L）；血常规未见明显异常（血红蛋白 133g/L）；低密度脂蛋白 3.02mmol/L，谷丙转氨酶 51U/L，NT-proBNP 294pg/ml，甲功、传染病、病毒全套未见异常。心脏彩超示主动脉瓣少量反流，心腔大小及功能在正常范围（EF 65%）。右心声学造影：右心造影（+），RLS 1 级。心脏 MRI：左室前侧壁远段肌壁间异常信号，考虑局灶性纤维化改变？心肌炎后遗改变？建议结合临床。冠脉 CTA：前降支中段浅表性心肌桥形成，管腔轻微狭窄。24h 动态心电图：1. 基础心律为窦性心律；全程心搏总数、平均心率及最慢心率均在正常范围；2. 偶发房性早搏；3. 部分导联 ST 段平直延长，部分导联 T 波一过性改变于快心率状态。 24h 动态血压正常。 ECG （2024-04-04） QT/QTc 间期：560/580ms（320-440ms）。

结合患者检查检验结果，初步诊断为：1. 心律失常 长 QT 综合征 偶发房早 2. 冠状动脉肌桥 3. 卵圆孔未闭。患者 QT 间期显著延长，无明确家族史，建议完善基因检测。全外显子基因检测结果提示患者为 KCNQ1 基因 c.334G > A；p.Glu115Lys 杂合变异导致相关疾病的可能性大。结合该患者的病史、心电图表型及基因检测结果，诊断为 LQTS 1 型。建议患者行运动负荷心电图检查，患者及家属拒绝，要求择期于门诊行该项检查。给予营养心肌、补钾补镁、β 受体阻滞剂等药物治疗。嘱患者日常避免剧烈活动及竞技运动，避免独自游泳或洗澡，避免情绪激动；警觉症状变化并注意监测血压、心律、心率等。建议患者出院后定期门诊复查心电图 / 动态心电图、心脏彩超等，高度警惕恶性心律失常事件，必要时考虑植入心脏复律除颤器（ICD）治疗。

检验检查记录：

电解质未见明显异常（钾 3.6mmol/L）；血常规未见明显异常（血红蛋白 133g/L）；低密度脂蛋白 3.02mmol/L，谷丙转氨酶 51U/L，NT-proBNP 294pg/ml，甲功、传染病、病毒全套未见异常。头颅 CT 平扫：未见明显异常。

心脏彩超示主动脉瓣少量反流，心腔大小及功能在正常范围（EF 65%）。右心声学造影：右心造影（+），RLS 1 级。

心脏 MRI：左室前侧壁远段肌壁间异常信号，考虑局灶性纤维化改变？心肌炎后遗改变？建议结合临床。

冠脉 CTA：前降支中段浅表性心肌桥形成，管腔轻微狭窄。

24h 动态心电图：1. 基础心律为窦性心律；全程心搏总数、平均心率及最慢心率均在正常范围；2. 偶发房性早搏；3. 部分导联 ST 段平直延长，部分导联 T 波一过性改变于快心率状态。 24h 动态血压正常。

ECG （2024-04-04） QT/QTc 间期：560/580ms（320-440ms）。

全外显子基因检测结果提示患者为 KCNQ1 基因 c.334G > A；p.Glu115Lys 杂合变异导致相关疾病的可能性大。

鉴别诊断：

晕厥待查：

一、心源性晕厥

1、其他遗传性心律失常：① Brugada 综合征（晕厥伴特征性心电图 ST 段抬高）②儿茶酚胺敏感性多形性室速（CPVT，运动 / 情绪诱发）③短 QT 综合征（QTc 缩短）。通过询问病史及心电图检查结果可鉴别。

2、获得性心律失常：①室性心动过速 / 心室颤动（如心肌梗死、心肌病引起）②高度房室传导阻滞或病态窦房结综合征（心动过缓相关晕厥）。根据心电图检查结果可进行鉴别。

3、结构性心脏病: ①肥厚型心肌病（流出道梗阻或心律失常）②主动脉瓣狭窄（劳力性晕厥）③肺栓塞（突发呼吸困难伴晕厥）。根据心脏彩超或胸部 CT 可以鉴别和排除。

二、神经反射性晕厥

1、血管迷走性晕厥：通常由疼痛、长时间站立或情绪应激诱导，开始会有恶心、出汗、视物模糊等前驱症状，发作后迅速恢复，无心律失常证据。 2、情境性晕厥：咳嗽、排尿、吞咽等特定动作诱发。

三、体位性低血压：与体位改变明确相关，无 QT 延长。自主神经功能障碍（如糖尿病、帕金森病）或药物（如利尿剂、血管扩张剂）导致体位变化时血压骤降。

四、癫痫发作：需与 LQTS 的抽搐性晕厥（如尖端扭转型室速发作）鉴别：癫痫通常伴意识丧失时间更长、发作后朦胧状态、舌咬伤或尿失禁，脑电图异常（LQTS 相关晕厥脑电图正常）。

五、代谢 / 内分泌异常

1、低血糖：出汗、饥饿感，血糖 < 2.8mmol/L。 2、电解质紊乱：如低钾血症、低镁血症（可诱发 LQTS，但本身也可致晕厥）。

主要根据心电图、诱因、家族史及发作特点相鉴别：LQTS 的核心是 QTc 延长（男性 > 450ms，女性 > 470ms），发作前常有 T 波交替或短 - 长 - 短周期。LQTS 晕厥常由运动、情绪应激或突然声音刺激（如 2 型 LQTS）诱发。多有猝死或晕厥家族史，基因检测可确诊（如 KCNQ1、KCNH2、SCN5A 突变）。心源性晕厥常无前驱症状，突发突止；神经反射性晕厥多有前驱症状。

其他：

建议患者出院后规律服用 β 受体阻滞剂，经随访，患者 2025 年 6 月情绪激动再次晕厥，建议植入心脏复律除颤器（ICD）治疗，患者拒绝。

Klinefelter 综合征合并卵圆孔未闭骑跨血栓

孙娜

哈尔滨医科大学附属第二医院

患者基本信息：

患者性别：男，年龄：44 岁，入院时间：2025 年 2 月 16 日

主述：

活动后呼吸困难 3 日

现病史：

患者活动后 3 日出现呼吸困难，伴心悸、乏力、头痛，伴咳嗽咳痰，白色粘痰。无畏寒发热，无胸痛胸闷，无黑朦、晕厥及抽搐，无腹胀纳差，无恶心、呕吐等

不适。上述症状休息 2-3 分钟后可缓解。未经系统诊治来我院就诊，门诊以“心房血栓”收治入院。患病以来，饮食、睡眠尚可，二便正常，体重无明显减轻。

既往病史：

患者平素健康情况一般，既往下肢静脉血栓病史（具体不详），无传染病史，无药物或食物过敏史，无输血史，否认高血压病史，否认糖尿病病史。

病程记录：

患者因进行性呼吸困难伴轻度头痛入院。经胸超声心动图（TTE）检测到骑跨 PFO 的血栓。我们进一步对患者动脉系统和静脉系统血栓栓塞情况进行了评估，并利用高通量全外显子组测序明确患者特殊基因型。TTE 检测到骑跨 PFO 的 43×10mm 血栓。肺动脉 CT 血管造影（CTPA）显示肺动脉主干及其双侧分支血管均有新鲜血栓。双下肢血管超声检测到腘静脉血栓形成。基于患者头痛，我们进行了脑磁共振成像，结果显示左顶叶有急性期脑栓塞病灶。主动脉和冠状动脉的 CT 血管造影未见血栓。基于高通量全外显子组测序技术揭示了该患者为 47 XXY 核型，该核型被定义为 Klinefelter 综合征，多伴有血栓形成倾向。该患者接受利伐沙班规范化抗凝治疗一个月后，复查 TTE 显示骑跨 PFO 的血栓消失。同时，CTPA 提示肺动脉主干及其分支血管血栓显著减少。随后，医疗团队对该患者进行了经导管 PFO 介入封堵治疗。

检验检查记录：

TTE 检测到骑跨 PFO 的 43×10mm 血栓。肺动脉 CT 血管造影（CTPA）显示肺动脉主干及其双侧分支血管均有新鲜血栓。双下肢血管超声检测到腘静脉血栓形成。基于患者头痛，我们进行了脑磁共振成像，结果显示左顶叶有急性期脑栓塞病灶。主动脉和冠状动脉的 CT 血管造影未见血栓。基于高通量全外显子组测序技术揭示了该患者为 47 XXY 核型，该核型被定义为 Klinefelter 综合征，多伴有血栓形成倾向。该患者接受利伐沙班规范化抗凝治疗一个月后，复查 TTE 显示骑跨 PFO 的血栓消失。同时，CTPA 提示肺动脉主干及其分支血管血栓显著减少。随后，医疗团队对该患者进行了经导管 PFO 介入封堵治疗。

鉴别诊断：

1、与房间隔缺损的鉴别：PFO 是卵圆孔未完全闭合形成的裂隙样通道，而房间隔缺损是否房间隔组织的缺损，两者在超声心动图中表现不同。PFO 可见瓣样结构，分流呈单向或双向；而房间隔缺损边缘明确，分流持续存在且血流速度较低。

2、急性冠脉综合征：胸痛、呼吸困难等症状，心肌梗死疼痛多位于胸骨后，呈压榨性，心电图可见 ST 段抬高或压低，心肌酶学升高；急性肺栓塞常见 D 二聚体升高，CT 冠状动脉和肺动脉造影可鉴别。

3、主动脉夹层鉴别：剧烈撕裂样胸背痛，伴双侧血压不对称，主动脉夹层可通过 CT 或 MRI 明确血管撕裂位置，而肺栓塞显示肺动脉充盈缺损。

4、Klinefelter 综合征的鉴别：通过临床表现、染色体核型分析、内分泌功能检测、影像学检查以及基因突变分析等多方面的评估，可鉴别 Klinefelter 综合征。在诊断过程中，应结合各项检查结果，进行综合判断，以便为患者提供准确的诊断。

其他：

本病例捕捉到 Klinefelter 综合征患者 PFO 骑跨血栓的罕见瞬间，PFO 是血栓从静脉到动脉系统的桥梁，医疗团队对患者进行了动静脉血管栓塞事件的系统评估，随后经规范化抗凝治疗后进行了经导管 PFO 介入封堵，取得了良好的治疗效果。该病例系统展示了 Klinefelter 综合征患者反常栓塞的机制。

见微知著，真相毕露 -- 肿瘤患者急性呼吸困难一例

阳全

香港大学深圳医院

患者基本信息：

李 **，74 岁 / 女；

入院日期：2023-8-29。

主述：

呼吸困难 1 周余

现病史：

患者诉 1 周余前乘坐数小时高铁后出现呼吸困难，稍事活动即可出现，休息后可部分缓解，夜间可平卧，伴有心悸、乏力、轻度水肿，未诊治。后逐渐出现咳嗽咳痰，咳少量黄痰，伴恶心呕吐、腹胀感，否认晕厥、胸痛、咯血、咳粉红色泡沫痰，否认视物模糊、偏侧肢体乏力等不适。近期患者睡眠精神差，食欲减退，大便减少，小便如常，体重无明显改变。

既往病史：

否认高血压、糖尿病、冠心病病史，否认吸烟、饮酒史，否认心肌病、猝死家族史。卵巢癌综合治疗后 2 年，目前靶向治疗中，近期服用中药，末次于 2023-7 评估病情为稳定。

卵巢癌 III 期 高级别浆液性癌，右侧附件见癌累及，腹部结节见癌

日期	2021-5	2021-6 至 2021-7	2021-7 至 2021-9	2022-2	2022-7 至 2022-12	2023-2 至 2023-8
治疗	手术	紫杉醇 卡铂 1-2 周期	紫杉醇 卡铂 3-6 周期 80% 剂量	尼拉帕利	疾病进展（颈根部、纵隔腹膜后多发肿大淋巴结） 加贝伐珠单抗 1-7 周期	贝伐珠单抗 8-15 周期
评估	---	稳定	---	进展	稳定	稳定

病程记录：

治疗：予利尿、扩血管、强心、抗凝、控制心室率、改善心室重构治疗。

病情演变：入院第 5 天，心肺功能衰竭进展迅速，抢救无效去世。

检验检查记录：

D-D 8.16 ug/ml FEU，TNT 0.04ng/ml，NT-proBNP 7368 pg/ml，胸部 CT：多发肿大淋巴结，细支气管炎，未见明显双肺实质性及间质性病变，无胸腔积液。心电图：窦性心动过速，电轴右偏，顺钟向转位，SI QIII TIII，心脏彩超：右心增大明显，左室受压，三尖瓣中度反流，双室收缩功能均有下降，这是我们当时测量的参数，可以看到，右室 70*46，右房 52*53，PASP 52，TAPSE 13mm，LVEF 40%，未见异常分流信号，下肢深静脉彩超未见血栓形成，肺动脉 CTA：右心增大 肺动脉增宽 没有见到明确的肺栓塞，肺通气灌注显像：双肺有多发节段性的缺损改变。

鉴别诊断：

急性左心衰鉴别：化疗药物所致心肌损伤、，扩张型心肌病

急性右心衰竭鉴别：右室受累原发性心肌病、右室心肌梗死、先天性心脏病、瓣膜性心脏病、肺动脉栓塞

其他：

肺肿瘤性血栓性微血管病为少见、罕见病，生前很难确诊，表型与急性肺动脉栓塞非常类似，但肺动脉 CTA 却是阴性的，可导致快速进展的心肺功能衰竭，几乎均为致命性的，目前尚无有效治疗方法，预后极差，如果肿瘤患者出现的不明原因呼吸衰竭、肺动脉高压、肺动脉 CTA 阴性等需要注意考虑到该病的可能。

深入人心 变幻莫测

阳全

香港大学深圳医院

患者基本信息：

就诊日期：2023-2-1，冯 **，68/M

主述：

反复头晕 2 月余，加重伴胸闷 9 小时

现病史：

患者 2 月前于饮酒后出现头晕、胸闷不适，伴出汗、便意，时测坐位血压为 77/44mmHg，脉搏 44-47bpm，站立如厕后呕吐、四肢冰冷、出汗、面色苍白，无晕厥，症状持续 6 小时左右缓解。近 2 月发作两次类似症状，自诉曾在外院查心电图未见明显异常。9 小时前饮酒后再发胸闷、头晕，伴血压下降，85/45mmHg 左右、脉搏 40+ 次 / 分，腹泻 2 次，为黄色成形便，呕吐胃内容物 1 次，腹泻、呕吐后症状缓解。病程中无胸痛，无头痛、晕厥、乏力，无腹痛、腹胀，无发热、咳嗽、咳痰等。

既往病史：

甲状腺结节病史多年，曾行白内障手术；否认高血压病、冠心病、糖尿病病史；吸烟史 50 年，10 支 / 天；饮酒史 30 年，1 次 150-200ml 左右，近 7-8 年偶尔饮酒；无放射性物质、毒物接触史，无心肌病、猝死家族史。

病程记录：

诊断明确考虑 AL-CA，引起心脏、肾脏、神经系统病变，予抗栓、调脂、抗浆细胞治疗、永久性心脏起搏器治疗后患者症状体征稳定，复查 TNT、NT-proBNP、尿蛋白、轻链下降。

检验检查记录：

实验室检查：血常规：WBC 12.55×10^9/L, Hb 140g/L, PLT 244×10^/L, Neu% （-）；

肾功能：CR 106umol/L，尿 PRO 3+，ERY ±，24h 尿蛋白定量 3.8g；

血脂四项：LDL-C 3.63mmol/l；

心肌标志物：CK 74 U/L，CK-MB 4.7ng/ml，TNI 0.416ng/ml，2737 pg/ml；

肝功能、HBA1C、甲状腺功能、肿瘤标志物、术前四项、凝血功能正常。

胸片：心影增大，双肺纹理增粗。

心电图：窦性心律，胸前导联 R 波递增不良，肢导联电压偏低。

心脏彩超：未见心脏扩大、室壁增厚、运动异常、LVEF 下降。

冠脉造影：冠脉左优势型，左主干未见狭窄，左前降支中段狭窄 60%，前向血流 TIMI 3 级，左回旋支，右冠动脉未见明显狭窄，前向血流 TIMI 3 级。OCT 检查提示：前降支中段纤维脂质混合斑块，局部可见微小内膜夹层，管腔狭窄最重处 MLA 约 2.95mm^2，回旋支开口 - 左主干少量纤维脂质混合斑块，内膜附着少量微小血栓，可疑巨噬细胞浸润。

病情变化：2-18 12:50 患者半卧位打电话时突感头晕伴胸闷、大汗淋漓，心率最慢 32 次 / 分，血压波动在 60-70/40+mmHg，心电图提示逸搏心律，予阿托品静脉注射，异丙肾上腺素、多巴胺微量泵入，观察无明显好转，14:20 行临时起搏器植入，2-21 拔除临时起搏；2-26 午餐饱食，傍晚排便不畅后再次出现血压、心率下降，心率 40-50 次 / 分，70-90/44mmHg，无明显头晕、胸闷不适；予异丙肾上腺素泵入后血压、心率恢复正常。

动态心动图：1. 窦性心律；起搏器术后 VVI 工作方式（频率为 65bpm），间歇性心室起搏失夺获，建议程控；2. 偶发室上性早搏：可见单发房早、成对房早、短阵房速；　偶发室性早搏：可见单发多源性室早、RonT 型室早、成对室早、短阵室速，部分室早呈二联律 ;3. 未见 ST-T 改变 ;4. 最长 R-R 间期 1.341 秒。

心脏彩超：左室 GLS 下降（10.5%），室壁各基底段应变减低，前壁、前侧壁及下侧壁中间段亦见降低，心尖段应变正常。

心脏 MRI 示：左室非血管支配分布心内膜下强化、双房壁强化，心包、双侧胸腔可见少量积液，心肌淀粉样变改变可能。

肌电图：双侧尺神经、正中神经、腓浅神经传导感觉传导功能轻度受损。

继续完善心肌淀粉样变病因筛查：

ANA ： < 1:80；

ENA 谱、C3、C4、RF、抗 Sm、SSA、SSB、抗 dsDNA、ANCA **均（-）**。

β2-mg 3.56Ug/ml;

IgA 0.64g/L ↓ ，IgG 5.45g/L ↓ ，IgM 0.33g/L ↓；

尿游离轻链定量：游离 λ 轻链 379.01mg/L ↑，游离 κ / 游离 λ = 0.1497 ↓；血清游离 κ.λ 链定量：游离 λ 轻链 214.68mg/L ↑ ↑，游离 κ 轻链 21.49mg/L ↑，游离 κ/ 游离 λ = 0.1001 ↓；

本 - 周氏蛋白：λ 轻链 , 尿 , 阳性（+）；

血清免疫固定电泳：λ 轻链 (+)。

骨穿：浆细胞占比 6.4%，浆细胞肿瘤待排；

腹壁脂肪刚果红染色阳性。

鉴别诊断：

其他：

老年男性，无明显心脏基础疾病病史，以反复血压、心率骤降伴有不明原因心力衰竭为主要表现，NT-proBNP、TNT 居高不下，伴有大量蛋白尿、肾功能受损，最后经过详尽病因查找，抽丝剥茧，诊断原发性 AL 型淀粉样变性，给予特异性化疗，目前情况良好。

特纳综合征合并复杂心血管疾病诊治： 一例以晕厥首诊的罕见病例

闫恒瑜

甘肃省人民医院

患者基本信息：

特纳综合征（Turner Syndrome, TS）作为 X 染色体缺失所致的遗传性疾病，其心血管系统并发症常被低估且严重影响患者预后。本文报道 1 例 40 岁 TS 女性，因反复胸闷、气短及晕厥就诊，系统评估发现心房扑动、继发性房间隔缺损及肺动脉高压。经射频消融、房间隔缺损介入封堵及个体化药物治疗后，患者临床症状及心功能显著改善。本例强调，TS 患者应高度重视心血管异常的早期筛查与精准干预，多学科协作的综合诊疗模式对提升 TS 患者心血管结局具有重要意义。

主述：

间断胸闷气短 1 月，加重伴晕厥 2 次

现病史：

患者于 1 月前快步行走时出现胸闷、气短不适，半月前站立时突发心悸、胸闷，并伴有意识丧失，持续数分钟，无抽搐、口吐白沫及大小便失禁等表现，未及时就诊。3 天前上述症状再次发生，外院心电图示心房扑动并完全性右束支传导阻滞（图 1），经静脉药物控制心室率后，转诊至我院，入院心电图显示房扑 2:1 传导 (图 2）。

既往病史：

既往 10 年前基因检测确诊特纳综合征（核型 45，XO，inv（9））， 未接受激素替代治疗。既往无高血压、糖尿病病史，家族中五遗传病史。患者系母亲第二胎，足月顺产，其母在妊娠期无风疹、病毒感染及服用特殊药物史。

病程记录：

1）电生理干预：行心内电生理检查证实为三尖瓣峡部依赖性逆钟向房扑（AA 间期 220ms，CS 9-10 电极 A 波领先），在三维标测模拟系统支持下，行三尖瓣环至下腔静脉峡部线性消融，术后转为窦性心律 (伴完全性右束支传导阻滞，图 3）。

2）心衰管理：术后诊断为射血分数轻度降低型心力衰竭（HFrEF，LVEF 41%），启动心衰治疗方案（螺内酯 20mg qd + 达格列净 10mg qd + 沙库巴曲缬沙坦 25mg bid）。

3）结构干预：术后 1 月行 ASD 介入封堵术（缺损直径 30mm），术后 6 分子步行实验（6MWD）提升至 378.5m，sPAP 降至 39mmHg。

4）长期随访：术后半年复查示心电图提示：窦性心动过缓，不完全性右束支传导阻滞 ST-T 改变（图 4）；LVEF 58%，sPAP 75mmHg，NT-proBNP 562.3pg/ml，6MWD 424.3m；右心漂浮导管提示肺动脉压 35/18/24mmHg，肺血管阻力（PVR）5 Wood 单位，予波生坦联合强化肺动脉高压治疗。

检验检查记录：

入院查体：P 125 次 / 分，R 20 次 / 分 BP 104/82mmHg。典型 TS 体征：身高 145cm，体重 42kg，小下颌、腭裂、低发际，扁平胸、双肘外翻、听力减低、口唇轻度发绀。心肺查体：心界向左扩大，胸骨左缘第 2 肋间闻及 3/6 级收缩期杂音，P $_2$亢进，双肺未闻及干湿啰音。心脏超声：ASD（中央型，缺损直径 30mm，房水平双向分流，左向右为主），肺动脉收缩压（sPAP）65mmHg，左室射血分数（LVEF）41%，右室扩大（RV 38mm），少量心包积液；右心导管检查：mPAP 48/22/32mmHg；子宫超声：子宫小，考虑幼稚子宫可能。垂体 MRI 检查未见明显异常；6 分钟步行试验距离（6MWD）329.5m，实验室检查：NT-proBNP: 4695pg/ml，ALT: 48.62U/L，AST: 51.21U/L，糖化血红蛋白: 6.6%，雌二醇 <10pg/ml，促卵泡激素: 31.16IU/L，黄体生成素: 8.31IU/L，孕酮: 0.19。

鉴别诊断：

首诊为复杂性特纳综合征合并房间隔缺损、心律失常和进行性右心受压；其次需与继发性肺动脉高压及进一步发展的肺血管重构型 PAH 鉴别，必要时关注 Eisenmenger 综合征的可能进展。患者既往明确行基因监测，原发病诊断明确。

本例 TS 合并孤立性房间隔缺损伴心房扑动及肺动脉高压临床罕见，诊治需整合心血管结构、电生理、肺血管病变的多维度评估。早期实施射频消融 联合 ASD 介入封堵，病配合规范化的心衰及肺动脉高压管理，可显著改善临床预后。

其他：

PPT 后续可补充

绝处逢生 -- 一例“晚期”心力衰竭患者的综合治疗实践

吴燕

交大一附院

患者基本信息：

王 XX，男，64 岁

主述：

间断胸闷、气短 26 年余，加重半月

现病史：

26 年余前安静休息时突发胸闷，伴气短、大汗，就诊于府谷县医院诊断为急性心肌梗死，给予溶栓治疗，上述症状缓解。后反复出现活动后胸闷、气短，多次就诊于当地医院给予药物对症治疗（具体不详）。

5 年余前于当地医院查心动超声示全心增大（未见报告），就诊于唐都医院行 CAG+PCI 术，RCA 植入支架 2 枚，D1 植入支架 1 枚，LAD7 段闭塞未开通，术后症状缓解不明显，快步行走即觉胸闷、气短，长期口服“托拉塞米、螺内酯、诺欣妥、达格列净、阿托伐他汀钙片、阿司匹林、单硝酸异山梨酯”等药物治疗。

3 年前始上症加重，伴四肢、颜面水肿，无胸痛、大汗，多次就诊于当地医院给予利尿、扩管等对症治疗，上症仍反复发作。

1 月前气短、水肿再次加重，就诊于我院心内科五病区查 NT-proBNP7336pg/mL，心超 EF32%，二尖瓣反流面积 17.8mm2；心电图示房扑，予以新活素等纠正心衰药物治疗，后行 CAG 示（2024-11-2）：冠心病双支病变：LAD6 段狭窄 100%，CTO；LCX11 开口处狭窄 30%-40%；RCA 2 段狭窄 70%-80%；RCA 4PD 段狭窄 95%，于 RCA 1-2 段植入支架 1 枚。术后继续口服“阿司匹林、氯吡格雷、阿托伐他汀、美托洛尔、沙库巴曲缬沙坦、恒格列净、呋塞米、螺内酯、

单硝酸异山梨酯” 等药物治疗。

2 周前再次出现气短加重，不能平卧，于当地医院住院治疗，自觉气短、胸闷、下肢水肿进行性加重，伴腹胀、纳差，为进一步诊治就诊于我院，门诊以“冠心病、心力衰竭” 收住入院。

病情加重以来，神智清，精神差，食纳差，夜休一般，小便少，大便不成形，体重未监测。

既往病史：

既往史：糖尿病史 17 年余，现口服恒格列净 10mg qd、德谷胰岛素 8U qn 降糖治疗；1 月前诊断糖尿病肾病 IV 期、糖尿病周围血管病，现口服 “参乌益肾片、百令片” 治疗。

个人史、家族史无特殊。

病程记录：

入院查体：T：36℃，P：88 次 / 分，R：20 次 / 分，Bp 90 ／ 60mmHg；身高：178cm，体重：76kg，BMI：23.98kg/m2。

急性面容，神志清醒，精神稍差，半卧位。

双下肺呼吸音低，双肺可闻湿啰音。

心界叩诊向左下扩大。心率 88 次 / 分，律齐，心音低钝，P2>A2 ，心尖部可闻及 3/6 级收缩期吹风样杂音。

腹膨隆，腹软，无压痛及反跳痛，移动性浊音阴性。

双侧胫前片状色素沉着，双下肢重度水肿。

HFrEF 急性加重期治疗：控制液体入量；临时予以左西孟旦强心、新活素扩管利尿；短期应用静脉利尿剂减轻心脏容量负荷；稳定内环境

HFrEF 的 GDMT 治疗启动顺序：

HFrEF& 房扑：心脏电复律术

HFrEF&SMR：TEER

出院后 GDMT 治疗的调整

出院 4 月复查：症状缓解、EF45%、NT-proBNP344pg/ml

检验检查记录：

辅助检查 - 心电图：房扑

心动超声：EF32%，二尖瓣大量反流

血气：PH:7.363，氧分压 98mmHg，二氧化碳分压 38.7mmHg；

NT-proBNP：11893pg/mL；高敏肌钙蛋白 T0.029ng/mL；

肾功能：肌酐 147umol/L；尿素 13.15mmol/L；eGFR 43.13ml/min/1.73m2；尿酸 431umol/L；

鉴别诊断：

心力衰竭加重的病因：心律失常、房扑以及功能性二尖瓣关闭不全导致大量反流

其他：

无特殊

隐秘在心衰背后的多发性大动脉炎

王喆

首都医科大学附属北京朝阳医院

患者基本信息：

彭某某，16 岁，女性， 2024-1-23 入院

主述：

间断咳嗽咳痰伴憋气 1 月余

现病史：

患者 1 月前无明显诱因开始出现咳嗽咳痰，为黄色血丝痰，伴活动后胸闷气短，夜间平卧受限，遂就诊于当地医院，完善肺部 CT 可见大片实变影，心影增大，肺炎支原体阳性，后患者就诊于盛京医院，考虑脓毒症，I 型呼吸衰竭，重症肺炎，甲流，给予患者阿奇霉素抗感染，止咳等治疗，患者住院期间突发急性左心衰，给予患者吸氧、呋塞米、新活素纠正心衰，达菲治疗流感。患者入院期间射血分数明显减低（LVEF=33%），给予患者达格列净、螺内酯改善心衰，倍他乐克及地高辛控制心室率，症状较前好转，但患者仍活动后憋气，夜间端坐呼吸，为进一步诊治来我院，门诊以“心功能不全” 收入我科。自起病来，患者精神、睡眠差，食欲下降，大小便正常，近一月体重下降 3.5kg。

既往病史：

2023-7-24 于中国医科大学附属第一医院行卵圆孔未闭封堵术

发现血压升高 6 个月，2023.7 住院期间测血压 110-160/72-102mmHg，考虑紧张因素，未服药治疗，血压间断升高。1 月前肺部感染、心衰住院期间血压高，给予苯磺酸地平 5mgQD，富马酸比索洛尔 7.5mgQD 治疗，回家后未监测血压。

否认吸烟、饮酒史。未婚，13 岁初潮，末次月经 2024-12-26，否认家族史。

病程记录：

诊疗经过：入院后积极完善各项辅助检查，(1) 患者入院后查体：左侧血压测不出，桡动脉搏动减弱，左侧肾动脉、锁骨下动脉听诊可闻及血管杂音，完善肺动脉磁共振 (2024-02-04) 主动脉及其分支管壁增厚、强化， 左侧颈总动脉、锁骨下动脉、双侧肾动脉管腔狭窄 符合大动脉炎表现；全脑动脉增强成

像 (2024-02-04) 左侧颈总动脉闭塞，颈内动脉多发节段性狭窄，部分近闭塞，符合大动脉炎改变；颈动脉血管超声 (2024--01-10）左侧颈总动脉管壁弥漫性增厚，左侧颈总动脉近闭塞，左侧锁骨下动脉管壁弥漫性增厚 左侧锁骨下动脉中远段闭塞符合大动脉炎改变；肾动脉超声 (2024-01-30) 右肾动脉异常所见 -- 考虑狭窄 , 左肾动脉起始段流速高 -- 狭窄待排，患者多发性大动脉炎诊断明确，患者心脏核磁 (2024-01-29) 左室下壁局部可疑灶状延迟强化，考虑局部心肌受损，心肌炎所致不除外，请结入院完善患者 1 月前甲流病史，本次入院诊断为多发性大动脉炎，不除外心肌炎与多发性大动脉炎相关，入院后给予患者维生素 C、曲美他嗪营养心肌治疗 ;(3) 心功能不全：患者入院完善心彩，射血分数明显降低 (LVEF29%)，入院后给予患者西地兰强心，呋塞米利尿，富马酸比索洛尔控制心室率治疗，螺内酯、达格列净改善心衰预后治疗；后复查心彩 LVEF38.5%。住院期间完善多学科会诊，给予患者甲强龙 40mgivgtt(2024-2-1 至 2024-2-7) 治疗，出院后继续甲泼尼龙 40mg 口服治疗，2 周后开始减量，同时给予患者甲氨蝶呤片 10mg(2024-2-5) 每周一次，第二周调整为 12.5mg 每周一次；给予激素同时给予患者补钙治疗。

检验检查记录：

心脏超声 (2024-01-29) 左心室收缩功能减低 (LVEF 29%) 左心室舒张功能减低右心室收缩功能轻度减低左心室心肌过度小梁化不除外左心增大房间隔封堵术后，房水平分流消失二尖瓣反流 (轻度) 主动脉瓣反流 (轻度) 肺动脉轻度增宽

心脏核磁 (2024-01-29) 左室舒缩功能明显减低，EF 值 31%；房间隔缺损封堵术后改变；二尖瓣及主动脉瓣可见少量返流；左室下壁局部可疑灶状延迟强化，考虑局部心肌受损，心肌炎所致不除外，请结合临床考虑。

肾动脉超声 (2024-01-30 右肾动脉异常所见 -- 考虑狭窄左肾动脉起始段流速高 -- 狭窄待排

颈部血管 (2024-01-30)：左侧颈总动脉管壁弥漫性增厚，左颈总动脉近闭塞 左锁骨下动脉管壁弥漫性增厚，左侧锁骨下动脉中远段闭塞符合大动脉炎改变，

高分辨全脑动脉管壁增强核磁 (2024-02-04) 左侧颈总动脉闭塞，颈内动脉多发节段性狭窄，部分近闭塞，可符合大动脉炎改变，请结合临床；右侧优势型椎动脉变异；双侧额叶皮层下散在少许小缺血灶。

肺动脉磁共振血管增强 (2024-02-04) 主动脉及其多发分支管壁增厚、强化，伴左侧颈总动脉、锁骨下动脉、双侧肾动脉管腔狭窄，符合大动脉炎表现；左室舒缩功能明显减低，EF 值 33.86%; 房间隔缺损封堵术后改变；二尖瓣及主动脉瓣可见少量返流；左室下壁局部可疑灶状延迟强化，考虑局部心肌受损，心肌炎所致不除外。

血常规 (2024-1-24): ★红细胞 4.76(*10^12/L)，★血红蛋白 109.00(g/L)，★红细胞压积 34.90(%)，★血小板 445(*10^9/L); 脑钠肽 346(pg/mL),

尿常规：尿红细胞 250(+++)(/μL)，尿蛋白 15(+-)(mg/dL)，动态红细胞沉降率 24(mm/h);

血 沉（2024.1.24）：22 mm/h （2-20mm/h），2024.1.31 复 查 血 沉：36mm/h

hs-CRP（2024.1.24）：15.31 mg/L（0-3mg/L），D- 二聚体（2024.1.24）：0.7mg/L，CTNI（2024.1.24）：23.8ng/L，肌酐（2024.1.24）：70 umol/L，血钾 （2024.1.24）：3.7 mmol/L，CRP：10.52mg/L

（2024.1.24）巨细胞病毒抗体 lgG 阳性，EB 病毒抗体 lgG 阳性，肺炎支原体抗体 lgG 阳性，lgM 可疑阳性

24 小时微量总蛋白尿：312mg/24h

抗 B2- 糖蛋白 1 抗体：31.01RU/ml

鉴别诊断：

1、病毒性心肌炎：临床表现取决于病变的广泛程度与部位，重者可至猝死，轻者几乎无症状。多数患者在发病前有发热、全身酸痛、咽痛、腹泻等症状。常诉胸闷、心前区隐痛、心悸、乏力、恶心、头晕。体征有心脏增大、心率改变、心音改变、杂音、心律失常、心力衰竭等。心电图常有 ST-T 改变或心律失常表现，超声心动图示心腔扩大或室壁活动异常，核素检查证实左室收缩或舒张功能减弱，血清心肌肌钙蛋白 I 或 T、CK-MB 明显增高，病原学也有相应依据。本患者发病前有甲流阳性，不除外病毒性心肌炎；

2、嗜酸性粒心包心肌病是一种罕见心脏疾病，其特征是心肌中嗜酸性粒细胞过度积聚，通畅与过敏反应、寄生虫感染和某些自身免疫病相关，患者一般会有胸痛、心悸、心力衰竭。本患者嗜酸性粒细胞无显著增高。

3、急性心包炎：可有较剧烈且持久的心前区疼痛，伴发热、胸痛在呼吸和咳嗽时加重。体征可有心包摩擦音。心电图除” AVR” 外，其余导联均有 ST 段弓背向下的抬高，T 波倒置，无异常 Q 波形成。本例患者不支持。

4、. 急性肺动脉栓塞：多表现为呼吸困难或气促，尤以活动后明显，也可有胸痛、咯血、心悸和休克。有右心负荷急剧增加的表现如肺动脉瓣区 S2 亢进、颈静脉充盈、肝大等。心电图示 I 导联 S 波加深，III 导 Q 波显著 T 波倒置。血气分析

为低氧血症，D-Dimer 可升高。CTPA 或肺动脉造影可确诊。本例患者不支持

5、扩张性心肌病：主要特征是左心室扩大引起心脏泵功能衰竭导致心力衰竭症状，扩张性心肌病症状主要包括疲劳，呼吸困难，心跳加快，胸痛等症状。本患者心功能差，不能除外。

其他：

高龄射血分数保留型心力衰竭患者高 MACE 事件一例报道

刘璐

石河子大学第一附属医院

患者基本信息：

患者男性，86 岁，丧偶，吸烟史 30 余年，每日 10 支，戒烟 20 年，否认饮酒史；父母已故，家中无遗传性疾病病史

主述：

间断胸闷、气短 20 年余

现病史：

患者 2004 年始无明显诱因出现胸闷、气憋症状，位于胸骨后，持续 3-5 分钟不等，曾就诊当地医院，完善检查后诊断冠心病，长期口服药物保守治疗，病情时有反复，可耐受；近年来患者自觉活动耐力进行性下降，未重视，2024-11-07 自觉上述症状加重，轻微活动即可诱发，并伴有乏力、心悸，11-14 日就诊我院，以“心力衰竭”收住，，查 NT-proBNP 15600pg/ml，心脏超声提示 EF67%，综上考虑诊断射血分数保留型心力衰竭 1 型。住院期间给予抗血小板、抗动脉硬化治疗，并予以沙库巴曲缬沙坦片口服纠正心衰、改善预后，病情好转，11-18 日离院复查 NT-proBNP 7579pg/ml，11.22 日门诊复查 NT-proBNP 1803pg/ml。

此后患者分别于 2024.12.02 因特异性皮炎、2024.12.19 因上呼吸道感染、2025.02.20 因腹泻、2025.04.15 因抑郁发作而诱发加重心衰住院治疗，2025.05.02 患者情绪问题未得到有效疏解，治疗依从性差，再次入院，05.04 患者呼吸心跳骤停，报病故。

既往病史：

高血压病史 30 余年；有肾功能不全病史；前列腺增生病史

病程记录：

2024-11-14 第一次入院：入院期间完善冠脉造影：冠脉分布左优势型，左主干正常，前降支近段狭窄 80%，中间支 70% 狭窄，血流 TIMI3 级，回旋支管壁不光滑，TIMI3 级，右冠浅斑块形成，未见明显狭窄，TIMI3 级；给予阿司匹林肠溶片、阿托伐他汀钙片口服抗血小板、抗动脉硬化治疗；期间双侧下肢静脉超声提示云雾状影子，D- 二聚体 1.65mg/L，与血管外科医师沟通后调整抗栓方案为利伐沙班口服，另给予沙库巴曲缬沙坦胶囊口服抑制心肌重塑、降压治疗，病情逐渐平稳，11-18 日复查 NT-proBNP 7579pg/ml，予以办理出院，11.22 日门诊复查 NT-proBNP 1803pg/ml。

2024-12-02 日第二次入院：本次心衰诱因为受凉感冒及全身皮疹，入院当日查 NT-proBNP 1936pg/ml，针对皮疹，经皮肤科医师会诊后考虑为特异性皮炎，建议甲泼尼龙 40mg 每日一次静滴；12.06 复查 NT-proBNP 6973pg/ml，双下肢轻度水肿，皮疹渐消退，予以利尿治疗，经与皮肤科医师协商后停甲泼尼龙静滴，12.08 复查 NT-proBNP 3080pg/ml，12-09 皮疹逐渐消退，病情平稳，办理出院。

2024-12-19 第三次入院：2024.12.17 日受凉感冒后患者胸闷气憋较前加重，再次入院，12.24 查 NT-proBNP 11293pg/ml，经抗感染治疗，12.27 复查 NT-proBNP 6462pg/ml。

2025-02-20 第四次入院：患者进食冰箱中隔夜果汁后出现腹泻，伴恶心、呕吐，乏力、心悸明显，就诊我院查 NT-proBNP 2582pg/ml，给予对症支持治疗好转后离院。

2025-04-15 日第五次入院：患者抑郁发作，拒绝配合治疗，情绪间断躁动不安，就诊我院查 NT-proBNP > 30000pg/ml，期间积极联系临床心理科情绪疏导，04.21 复查 NT-proBNP 25675pg/ml，04.24 病情平稳后离院。

2025-05-02 日第六次入院：自 04-24 离院返回家中后，患者治疗配合程度较差，拒绝进食，04-29 出现意识不清，05.02 再次入院，查 NT-proBNP 8649pg/ml，积极给予营养支持治疗，05-04 患者呼吸心跳骤停、意识丧失，家属拒绝一切抢救措施，报病故。

检验检查记录：

见检查检验报告单

鉴别诊断：

1、CA 同样可表现为 LVEF 保留的心力衰竭，但超声心动图常提示左心室壁均匀增厚（>12 mm）而电压低（肢体导联 QRS 振幅 <0.5 mV）的“电压 - 壁厚不匹配”，应变成像呈心尖保留的纵向应变“樱桃红点”模式，心脏磁共振显示弥漫性心内膜下延迟强化，且 99mTc-PYP/HMDP 骨闪烁显像心肌摄取阳性（提示转甲状腺素型 ATTR-CA），血清 / 尿免疫固定电泳及游离轻链检测可筛查 AL 型，最终需心外组织或心内膜活检刚果红染色证实淀粉样沉积；而 HFpEF 患者无上述特征性影像表现，且无低电压、心肌摄取异常或单克隆丙种球蛋白异常，对利尿剂反应较好但 CA 患者易出现低血压。

2、慢性阻塞性肺疾病和肺动脉高压：前者常有长期吸烟史、慢性咳痰及阻塞性通气障碍，血 BNP 正常或仅轻度升高，超声无左心室充盈压升高表现；后者则以肺动脉收缩压显著增高、右心室扩大及三尖瓣反流为特征，超声可见右心负荷过重而左心室舒张功能指标正常，且 BNP 升高幅度通常低于 HFpEF。

其他：

HFpEF 占所有心衰病例的一半以上，主要见于老年人，其中 80 岁以上人群的 HFpEF 患病率已超过 10%。过去的二十年里，虽对老年 HFpEF 的流行病学、病理生理机制、诊断治疗等方面的研究取得了显著进展，但巨大的知识空白仍然存在；高龄 HFpEF 患者多存在衰弱及多重共病的特点，年龄大于 80 岁是其首要危险因素，而目前临床试验常排除年龄 > 80 岁人群，导致高龄 HFpEF 循证治疗依据不足，无法构建准确预后评估模型。本报道患者 86 岁，合并高血压、冠心病、肾功能不全，自诊断 HFpEF 以来虽遵照指南规范药物治疗及加强共病管理，仍因多种原因导致反复入院，生活质量较差，提示临床医师对于高龄 HFpEF 的诊治模式应由“延迟性识别”转为“提前预警”，最大可能保留患者生活自理能力。值得注意的是 2025.04.15、及末次 2025.05.02 入院，心衰诱因均为抑郁发作，提示临床医师在高龄 HFpEF 的长期管理过程中，不良的心理状态亦能触发住院，造成严重心血管不良事件，不容忽视。

新四联为晚期心 - 肾 - 代谢综合征开辟一线生机

刘津

广东省人民医院

患者基本信息：

下肢水肿 3 年，反复气促 1 年，加重 2 周的 31 岁青年男性患者完善检查后提示“非梗阻性肥厚型心肌病（室间隔厚度 17mm），射血分数下降型心衰（LVEF 19%）”，合并肾脏病与高血压、肥胖、糖耐量受损，血脂异常疾病。经规范新四联治疗 1 月心功能得到显著改善（19% 升高至 55%）。BMI 28.8 kg/m^2。吸烟 10 年，20 支 / 天，未戒烟，个体户（经营烧烤摊），平素日夜颠倒。家族史：父亲祖父均有高血压病史，父亲有早发中风史，无肥厚型心肌病病史。

主述：

下肢水肿 3 年，反复气促 1 年，加重 2 周

现病史：

3 年前无明显诱因下出现双下肢水肿，无胸闷气促，无恶心呕吐，无活动后气促等不适，未伴血尿，当地就诊诊断为“肾病综合征”，予利尿、降压、降低蛋白尿等治疗后水肿消退。1 年前爬 3 层楼即可出现明显气促、夜间常喜高枕卧位，无夜间阵发性呼吸困难，余同前。2 周前患者出现咳嗽咳痰、气促，双下肢明显水肿入院。

既往病史：

既往史：高血压病史 3 年，平素未规律服药，血压 150-160/110-120 mmHg

病程记录：

利尿、抗心室重构治疗（美托洛尔缓释片 23.75mg qd、达格列净片 10mg qd、非奈利酮片 10mg qd、沙库巴曲缬沙坦钠片 100mg bid、苯磺酸氨氯地平片 10mg qd、阿托伐他汀 20mg qd。）出院带药经药物治疗 1 月后回院复查提示“LDL-c 2.2 mmol/L，Scr 170 umol/L, NT-proBNP <300 pg/ml，心脏超声：室间隔厚度 15-17mm，LVEF 55-60%”。后续上调沙库巴曲缬沙坦钠片至 200mg bid，1 年 3 次复诊心脏超声提示 LVEF 稳定在 55-60%。

检验检查记录：

入院后抽血提示 WBC 10.93*10^9/L，红细胞计数 6.54x10^12/L ↑，血红蛋白量 198g/L ↑，NT-ProBNP 为 19172.50 pg/ml，Scr 233 umol/l，肌钙蛋白 T 87.3 pg/mL ↑，HbA1c 5.70%，LDL-C3.03 mmol/L，PCR 3224 mg/dl，ACR 2611 mg/dl，风湿免疫指标、血管炎、免疫固定电泳等指标暂无特殊，完善心电图为窦性心律，窦性心律，左心室肥厚。心脏超声提示“室间隔厚度 17mm，LVEF 19%”，心脏 MR 提示“考虑浸润型心肌病可能，Fabry 心肌病？ECV 值：30%，LVEF 12 %”，行冠脉造影排除冠心病、心肌活检及基因检测排除 Fabry，未见常见肥厚型心肌病基因突变表型。

鉴别诊断：

1. 高血压性心肌肥厚，高血压病史，平素血压控制不佳；心肌肥厚多为向心性（室间隔与左室后壁厚度比值 < 1.3），伴左心室舒张功能减退；

2. Fabry 病，有心肌肥厚表现，需结合基因检测明确 GLA 基因突变导致 α- 半乳糖苷酶 A 缺乏，属 X 连锁隐性遗传。

其他：

罕见的主动脉瓣单叶畸形并重度狭窄 --- 自膨瓣成功 TAVR 全球首例报告

王勇

陆军军医大学第二附属医院（新桥医院）

患者基本信息：

李某某，男，60 岁，建筑类管理人员，重庆市九龙坡区人。

主述：

劳力性气促 10 年，加重 5 天。

现病史：

10 年前剧烈活动后出现气促，持续 10 余分钟，休息缓解，无明显胸痛、头昏、黑朦、

晕厥，未重视。因症状反复，7 年前曾就诊于我院门诊，完善心脏超声并诊断“主动脉瓣二叶式畸形并重度狭窄 ”，建议其“严格戒烟并择期行主动脉瓣置换术”，患者拒绝，未进一步就诊。近 1 年气促症状逐渐加重，爬 2-3 层楼即气促不适，并间断出现一过性头昏、黑朦。5 天前“感冒” 后喘累显著加重，并心悸、胸闷。无水肿、夜间憋醒。就诊于某三甲医院，诊断“主动脉瓣重度狭窄、慢性心衰急性加重”，建议其外科手术，患者再次拒绝并转诊于我院。

既往病史：

否认高血压、糖尿病、慢性肾病等。

病程记录：

入院血压 97/53mmHg，心率 109 次 / 分；身高 174cm，体重 57Kg。查体双上肺呼吸音减弱，双下肺闻及细湿啰音，胸骨左缘 2 肋间闻及全收缩期 4/6 级喷射样杂音，可扪及震颤；双下肢轻度凹陷性水肿。入院检验：BNP 887pg/ml，Cr 128umol/L， WBC 9.8*10^12/L ，甲功、肝功、凝血、血气分析等未见确切异常。完善心脏超声诊断主动脉瓣重度狭窄，心电图见 V1-V4 导联 R 波递增不良，ST-T 改变。胸痛三联 CTA: 冠状动脉未见确切狭窄，但主动脉瓣呈疑似单叶畸形，并升主动脉扩张，最宽处 50mm。进一步根据 CTA 对主动脉根部进行 3D 打印，清晰显示瓣叶为单叶瓣。检索文献，目前全球仅见 3 篇文献报道单叶式主动脉瓣病变行 TAVR 患者，均为球囊扩张式瓣膜（2 例经股，1 例经心尖）。反复与患者沟通 TAVR 或心外科 Bentall 术事宜，患者坚决拒绝外科手术，并要求 TAVR。经充分术前评估，于全身麻醉下行经股动脉 TAVR 术。经食道超声证实单叶瓣。未进行球囊预扩张，拟植入 VenusA L23 可回收瓣膜。因单叶瓣解剖畸形，窦底显影成马鞍状，深浅不一，术中瓣膜定位困难，多次向升主动脉及左心室移位，最终回收重释放瓣膜后瓣膜位置、功能良好。患者心衰症状缓解，术后 1 月随访良好，血压回升至 130/80mmHg，症状消失，无新发传导阻滞、瓣周漏。目前口服双抗 + 他汀 + 美托洛尔 + 沙库巴曲缬沙坦，患者持续随访中。

检验检查记录：

经胸超声显示主动脉瓣叶欠清，峰值流速 431cm/s，平均压差 47mmHg。术前 CTA(图 1A) 及 3D 打印清晰可见二叶瓣（图 1B,C）。经食道超声见单叶摆动（图 1D）并显示主动脉瓣口（图 1E）。采用圈套器辅助瓣膜跨瓣（图 1F），术中造影见瓣膜移位（图 1G），术后造影及 3D 打印可见人工瓣膜位置、形态良好（图 1H,I）。

鉴别诊断：

（1）主动脉瓣二叶式畸形并狭窄：单叶瓣很罕见（发病率约 0.02%），多在 30-50 岁发病并外科换瓣。超声及 CTA 很容易误诊为二叶式畸形，多在开胸切除原生瓣叶后，外科视角确诊单叶畸形。此患者采用 CTA、经食道超声、3D 打印等多种影像学证实单叶瓣畸形。

（2）急性冠脉综合征：患者为中老年男性，气促起病，既往有吸烟室，心电图见 V1-V4 导联 R 波递增不良，ST-T 改变。应警惕冠心病，但胸痛三联 CTA 未见冠脉病变，由此排除冠心病诊断。

其他：

主动脉瓣单叶畸形罕见（发病率约 0.02%），表现为瓣叶融合形成单一瓣口，常导致早期瓣膜退行性变，多在 30-50 岁发病，外科换瓣已被初步证实有效，但数据有限。与二叶瓣相比解剖结构更复杂，存在不对称瓣口、钙化分布不均等问题。因其解剖复杂性，单叶瓣口导致瓣膜支架难以均匀贴合，易致瓣周漏或瓣膜移位。因目前仅见 3 篇案例发表（均为球扩瓣，2 例经股，1 例经心尖），单叶瓣行 TAVR 术的经验及技术要点缺乏足够循证证据。本病例为全球首例自膨瓣成功 TAVR 全球报告，初探了自膨瓣 TAVR 在此类特殊病变中可行、有效，未来还需进一步探索此类患者的优化治疗策略及技术要点。

一例急性心肌梗死心衰失代偿期患者住院心脏康复

李茵

首都医科大学附属北京安贞医院

患者基本信息：

患者林某，男，70 岁。

主述：

发现冠心病 7 年，间断腹痛 2 周，再发加重伴憋喘 2 天。

现病史：

患者急性非 ST 段抬高型心肌梗死、急性心力衰竭抢救入院转入 CCU。病情稳定后于心衰中心继续进行治疗。治疗期间患者出现空间、时间定向障碍，日常生活能力下降，心功能稳定后为恢复患者功能请康复科会诊协助康复训练。

既往病史：

高血压 10 余年，糖尿病 10 余年，高血脂 10 余年，房颤 10 余年，陈旧性脑梗死 13 年，冠心病史 7 年，均规律服药。7 年前有十二指肠球部溃疡伴出血病史。

病程记录：

患者心功能稳定后对患者进行认知功能、上肢力量以及呼吸肌肌力训练，患者下肢彩超显示右侧股静脉不完全血栓，暂缓下肢训练，训练如下：

1. 认知功能训练：①执行功能：A. 抑制控制：彩虹字游戏。B. 任务切换：3 个手指操游戏。②记忆力训练：A. 词语记忆；B. 数字记忆；③注意力训练：删字游戏，删除一串随机数字中的某个特定的数字。④计算能力训练：加减法计算。⑤定向力训练：询问日期与地点。

2. 上肢力量训练：使用握力器与哑铃。动作过程避免 valsalva 动作。

3. 呼吸肌肌力训练：①腹式呼吸；②使用呼吸训练器。

患者在治疗中期复查下肢彩超结果显示下肢深、浅静脉通畅，与主治医生沟通后加入下肢踏车训练，所有运动应保持患者 Borg 评分保持在 11-12 分。康复介入直至患者出院。

检验检查记录：

1. 相关检查（前 / 后）：

①下肢彩超：右侧股总静脉不完全血栓 / 下肢深、浅静脉通畅；

②康复相关：

改良 Barthel 指数：71/80 分；

认知功能量表（MoCA）：19/23 分；

GAD-7 量表：2/2 分；

PHQ-9 量表：3/5 分；

PQSI 量表：8/6 分；

握力：23.7kg/22.7kg；

最大吸气肌肌力：28.7/34.31cmH_2O(31.14%/37.23%)；

最大呼气肌肌力 (MEP)：46.7/50.17cmH_2O(53.2%/57.21%)

鉴别诊断：

1. 谵妄引起的认知功能下降，可通过意识模糊评估法排除。

2. 新发脑梗引起的全身肌力下降，可通过颅脑磁共振以及头颅非增强磁共振动脉血管成像排除。

其他：

根据康复检查结果，该患者存在肌力、认知功能与日常生活能力下降的问题。因此康复的目标是维持现有的肌力与功能状态，恢复患者信心，提高患者的生活质量。患者处于心衰失代偿期，病情较重且较易发生变化，进行康复需随时关注患者生命体征与症状，并且根病情的变化及时调整康复方案。如，患者康复前存在下肢血栓，此时应暂缓下肢康复。待下肢复查结果显示无血栓后及时增加下肢的训练。此外患者夜间偶发短暂憋气症状，教患者腹式呼吸调整呼吸频率能改善其憋气症状。认知功能训练的趣味性提高了患者的依从性，下肢功能训练让从走路需要搀扶到能够完全独立行走，腹式呼吸改善憋气症状提高了患者治疗的信心。心衰失代偿期短期的康复干预极大提高了患者住院期间的生活质量。

拨开迷雾：青年 Danon 病的罕见病例分析与鉴别诊断

刘津

广东省人民医院

患者基本信息：

患者半年前无明显诱因下出现阵发性胸闷，2 月前因“兄长” 猝死于外院体检完善心脏超声提示“心肌肥厚”。予完善心脏 MR、PET-CT 检查考虑“ATTR-CR 淀粉样变”可能，同时予“氯苯唑酸钠软胶囊”治疗后患者诉明显腹胀不适。经我科心肌活检后电镜下可见溶酶体聚集形成的空泡的 Danon 样改变，最终经基因检测证实 Danon 病。

主述：

无明显诱因下出现阵发性胸闷。

现病史：

男，26 岁，半年前无明显诱因下偶现胸闷，无放射痛，持续数分钟可自行缓解，无伴大汗淋漓，无面色苍白，无明显气促，无咳嗽咳痰，无乏力，无头痛头晕，无黑矇晕厥，平素活动耐量尚可，2 月前因“兄长” 离世，于外院完善心脏超声提示“心肌肥厚”，心脏 MR、心脏核素显像检查提示“ATTR-CR 淀粉样变”可能，同时予“氯苯唑酸钠软胶囊”治疗后患者诉可伴有腹胀不适。患者为求进一步诊治入住我院我科，自起病以来精神胃纳可，大小便无明显异常。

既往病史：

既往史无特殊，自幼学习成绩较差。

病程记录：

曲美他嗪，辅酶 Q10 改善心肌能量代谢，营养心肌治疗。

检验检查记录：

外院心脏 MR、PET-CT 检查考虑“ATTR-CR 淀粉样变”可能，同时予“氯苯唑酸钠软胶囊”治疗后患者感腹胀不适。日常喜饮甜饮料，作息日夜颠倒，无工作，2 月前有“兄长” 猝死家族史。入院后生命体征正常，无明显心衰体征，查体无明显特殊，基本算数能力无异常。NT-proBNP 788 ng/L，cTNT 14 ng/L，血清游离轻链差值 <10 g/L，风湿免疫、血管炎、抗核抗体等指标无异常。动态心电图：1、窦性心动过缓；2、偶发房性早搏，偶见成对出现，偶呈短阵房性心动过速，外周神经功能：1. 未见周围神经损害。我院超声提示：左室壁增厚（13.2 mm）并心肌回声异常，考虑心肌病超声改变，左室增大，左室收缩舒张功能减低、轻度二、三尖瓣返流 LVEF 48 %。我院会诊外院心脏 CMR：左室壁弥漫性

增厚：左心室游离壁运动减弱；左心室、乳头肌、房间隔多发心肌纤维化；符合非缺血性心肌病改变，浸润性心肌病？。外院核素心肌淀粉样变显像：心肌淀粉样变显像阳性 3 级，提示转甲状腺素蛋白相关及脏淀粉样变（ATTR-CR）。我院行冠脉造影排除冠状动脉粥样硬化，腹部脂肪及心肌活检病理未见明显糖原沉积。电镜下部分肌细胞内见少数异常溶酶体聚集形成的空泡（图 1），提示 Danon 病，最终全外显子基因检测确定 Danon 含 LAMP2 突变。

鉴别诊断：

Fabry 病：心脏受累多表现为左心室肥厚（多为对称性），可伴心律失常（如传导阻滞）、冠状动脉病变，心力衰竭多为晚期表现，且常合并其他器官（如肾、脑）受累证据。

ATTR-CR: 常表现为低电压（肢体导联 QRS 波群电压 < 0.5mV，胸导联 < 0.8mV），与心肌肥厚程度不匹配，心脏超声可见左心室壁对称性或非对称性增厚，常伴有左心房扩大，室间隔及左室后壁厚度多≥ 13mm。心肌回声呈现颗粒样增强。心脏磁共振成像（CMR）：表现为室壁增厚，T1WI 序列上心肌信号强度轻度升高，T2WI 序列上信号强度变化不明显。特征性表现为钆对比剂延迟强化（LGE），多呈心内膜下或透壁性强化，也可表现为心肌内片状或弥漫性室壁内强化，有助于与其他心肌疾病鉴别。

其他：

一例升主动脉壁间血肿累及冠状动脉致心肌梗死的救治体会

殷思诺

石河子市人民医院

患者基本信息：

患者，男性，61 岁，汉族，

主述：

以“发作性胸痛 4 天。”于 2025-04-28 就诊

现病史：

4 天前始间断于提重物或劳累后感胸骨下段手掌大小范围闷痛，伴有气短、心悸、大汗，休息约 1-2 小时可缓解，上述症状反复发作，每日发作 3-4 次。10:55 就诊我院，完善心电图示：1. 窦性心律 2. 急性下壁心肌梗死 3.ST-T 改变（图 1）。急会诊后以“急性心肌梗死”收住我科。

既往病史：

患者既往患“高血压”病史 2 年，最高血压 230/？ mmHg，长期口服“苯磺酸氨氯地平 5mg 日 / 次”，平日监测血压在 150-160mmHg。

病程记录：

血压：166/101mmHg，心率 78 次 / 分，神志清楚，急性痛苦面容；双肺呼吸音清，心界不大，各瓣膜听诊区未闻及病理性杂音；腹软，无压痛反跳痛；四肢肌力、肌张力正常。实验室检查：心梗三项 (20250428): 肌钙蛋白 T 0.283 ng/ml，（正常参考范围 0 ~ 0.014ng/mL），肌酸激酶同工酶 25.460 ↑ ng/ml；NT-proBNP(20250428): 脑利钠肽前体测定 879.00 pg/ml。初步诊断：急性 ST 段抬高型心肌梗死（下壁）。胸部症状缓解，发病时间 4 天。给予抗血小板、调脂、稳斑、改善循环药物治疗。

检验检查记录：

4-30 8:58 左右无诱因突感胸骨下段手掌大小范围疼痛，性质难以描述，伴有胸闷、气短、大汗，急查心电图提示窦性心律，下壁导联 ST 段抬高（图 2a）。立即行急诊冠状动脉造影，提示右优势型，前降支中段狭窄 80%，中远段狭窄 60%，右冠近段狭窄 50%，中段斑块，远段斑块。于前降支植入 2 枚支架（GuReater 4.5* 29mm、GuReater 4.5* 29mm）图 2b）。决定立即予以经皮冠状动脉介入治疗恢复心肌的血液灌注。

4-30 13 时许患者心电监护提示：心率 40 次 / 分，血压 70/40mmHg，询问患者诉头痛。完善心电图提示：1. 显著窦性心动过缓 2. 房室脱节，窦性夺获 3. 交界性逸博心律 4. 急性下壁心肌梗死 5.ST-T 改变。立即予以去甲肾上腺素组液体泵入升压，约 20 分钟后血压上升至 90/60mmHg，心率恢复至 60 次 / 分，胸痛症状好转，经请示上级医师后，立即送介入室复查冠脉造影。

结果：冠状动脉单支病变，累及右冠；前降支原支架通畅；左室造影正常。

手术中发现操作造影导管到右冠状动脉开口困难，导管剧烈摆动（舞蹈征），反复调整后勉强到达右冠状动脉开口，行 IVUS 提示右冠开口收缩期时严重受压，局部未见冠状动脉病变及夹层。怀疑主动脉血肿。术后急诊行主动脉增强 CT 检查提示：升主动脉略显扩张，升主动脉环壁略低密度影环绕，厚约 6-7mm，主动脉期测得 CT 值约为 55-62HU。心包旁隐窝，心包内见等密度影环绕，CT 值约为 52HU。腹主动脉少许钙化斑。腹腔干、肠系膜上动脉及双肾动脉起源如常。考虑升主动脉区壁间血肿形成，心包旁隐窝及升主动脉周围少许积液 / 血。(图 4)。患者明确诊断为升主动脉壁间血肿。立即安排转院。

鉴别诊断：

主动脉夹层、肺栓塞

其他：

肥厚型梗阻性心肌病合并感染性心内膜炎 1 例

韩艳艳

解放军总医院第四医学中心

患者基本信息：

患者男性，41 岁

主述：

间断发热 1 个月

现病史：

患者于 2025 年 5 月 14 日前无明显诱因出现发热，体温最高 39.5℃，伴微汗，偶有右下肢腓肠肌酸痛，无胸闷、胸痛、咳嗽、咳痰，无头晕、头痛，无腹痛、腹泻，就诊于当地诊所，完善化验（具体不详），考虑“细菌性肺炎”，予抗感染治疗 5 天（具体不详），期间体温正常。病程期间间断发热，体温波动在 37-38℃，当地间断静脉输注抗生素治疗（具体不详）。2025 年 6 月 9 日再次发热，体温波动在 37-38℃，伴有右侧踝骨关节酸痛，当地医院化验提示：中性粒细胞百分比 82.6%， CRP 58.34mg/L，ESR 47mm/h，便潜血阳性，抗链 0、类风湿因子、抗环胍氨酸肽抗体阴性；胸部 CT：少量心包积液、脾大，考虑“肺炎”，予以“阿奇霉素、克林霉素”静脉抗感染 1 天，后“阿奇霉素”静脉抗感染 4 天，症状好转。患者为进一步诊治就诊于我院，门诊以“发热待查”收入心内科。

既往病史：

既往否认高血压病、冠心病等病史。

既往吸烟史 20 余年，约每日 20 支，已戒烟 1 年。

母亲患有肥厚型心肌病。

病程记录：

入院体格检查：体温 37.3℃，心率 84 次 / 分，血压 144/87mmHg。神志清，精神可，左侧第四手指、左足第一足趾可见甲下线状出血，双肺呼吸音清，未闻及干湿性啰音，心律规整，胸骨左缘 3-4 肋间闻及收缩期杂音，二尖瓣区闻及收缩期杂音，腹部柔软，无压痛及反跳痛，双下肢无水肿。

入院后患者低热、结合患者家族史、症状体征及相关化验检查，高度怀疑感染性心内膜炎，完善三套双侧血培养样本送检后予以经验性抗感染治疗（亚胺培南西司他丁 1g q8h）、美托洛尔控制心室率、调节肠道菌群治疗。后血培养结果回报缓症链球菌感染，青霉素、头孢曲松、万古霉素、美罗培南敏感；经食道超声提示二尖瓣赘生物，遂感染性心内膜炎诊断明确，予以静脉输注头孢曲松 2g、每日 1 次抗感染治疗。患者有肥厚型梗阻性心肌病，待心肌酶回落后，予以美托洛尔控制心室率、玛伐凯泰缓解梗阻治疗。经静脉输注敏感抗生素头孢曲松 2g、每日 1 次治疗 1 周，同时予以控制心室率、改善梗阻、调节肠道菌群等对症支持治疗后，复查心肌酶、感染指标回落，但心脏超声未见显著变化，完善药剂科会诊建议院外继续静脉输注头孢曲松抗感染治疗 1 月，同时予以美托洛尔、玛伐凯泰等药物继续院外治疗。

检验检查记录：

入院后完善检查，血常规：WBC 12.96x10^9/L, 中性粒细胞百分比 85.1%；CRP 44.6 mg/L；PCT 0.441 mg/mL，IL-6 28.50 pg/mL；ESR 38 mm/h；超敏肌钙蛋白 0.228 ng/mL，N 末端脑钠肽前体 1884 pg/mL；血培养双侧双套：缓症链球菌；尿便常规、肝肾功能、电解质、凝血功能、铁蛋白、肿瘤标记物、G 试验、GM 试验、血清呼吸道感染病原体 IGM 抗体九联、新冠病毒及支原体核酸检测、ENA 抗体、血管炎抗体、抗核抗体、抗中性粒细胞抗体、抗心磷脂抗体、体液免疫指标未见显著异常。

心电图：左室高电压，完全性左束支传导阻滞。

动态心电图：窦性心律，完全性左束支传导阻滞。

超声心动图：室间隔厚度 20mm、侧壁心尖部 16mm、左室后壁厚度 12mm、左室舒末径 46mm、射血分数 57%，左室壁非对称性肥厚，以室间隔为明显，肥厚的心肌回声粗乱，运动迟缓，余室壁运动幅度尚可，M 型显示：二尖瓣前叶 CD 段前移，SAM 征阳性；左室流出道重度梗阻（左室流出道压差 75mmHg），二尖瓣增厚、反流（少 - 中量），三尖瓣反流（少 - 中量），主动脉瓣反流（少量）。

经食道超声：考虑肥厚型梗阻性心肌病、心内膜炎不除外，左室壁非对称性肥厚，左室流出道重度梗阻 (左室流出道压差 75mmHg)，二尖瓣瓣叶弥漫增厚并少 - 中量反流，二尖瓣瓣叶异常团块影 (二尖瓣前叶者约 0.29*0.49 cm，二尖瓣后叶者大小约 0.32*0.47 cm)，三尖瓣少 - 中量反流，主动脉瓣少量反流。

心脏 MRI：1、左室壁非对称性明显增厚伴左室流出道狭窄，可符合非对称性肥厚型梗阻性心肌病影像表现。2、二尖瓣增厚冗长，二尖瓣关闭不全；主动脉瓣少许反流。3、左室下侧壁局部延迟强化。

肝胆胰脾超声：脾大（厚约 4.5cm、长径约 12.2cm）。

鉴别诊断：

患者青年男性，间断发热入院，有肥厚型心肌病家族史，查体可见甲下线状出血，胸骨旁及二尖瓣区闻及杂音，血培养提示缓症链球菌，经食道超声检出非对称性肥厚型梗阻性心肌病、二尖瓣前后叶赘生物，根据最新感染性心内膜炎诊断标准，本例符合血培养阳性、心内膜赘生物两条主要标准，有肥厚型心肌病易患因素、发热 > 38℃两条次要标准，临床诊断感染性心内膜炎。

本病需与病毒性心肌炎及风湿性疾病相鉴别。（1）病毒性心肌炎。发病前或发病时常有呼吸道或肠道病毒感染，主要受累部位在心肌，偶可累及心包，极少侵犯心内膜。发热时间短，可有关节痛但无关节炎，心尖区第一心音减低，可闻及收缩期杂音，心律失常多见；无环形红斑、皮下结节等。实验室检查白细胞多为减少或正常，血沉、CRP 均正常，补体结合试验及中和抗体阳性，心肌活检可分离出病毒。两者易于区别。（2）风湿性疾病。亦有发热和心脏病变，一种溶

血性链球菌感染所致的全身变态反应性疾病，有反复发作的倾向。此病最常侵犯青少年，发作前数天或三周往往先有链球菌咽炎或扁桃体炎病史。本病主要累及关节与心脏，其次为皮肤、浆膜、血管与脑组织等。多数病例有发热，热型多不规则,低热常见。典型的临床表现为心肌炎,对称累及大关节的游走性多关节炎(红肿热痛)，皮下结节或环形红斑(多发生于躯干和四肢近端)。急性发作时通常以关节炎较为明显，急性发作后常遗留轻重不等的心脏损害，尤以瓣膜病最为显著，形成慢性风湿性心脏病，以 20-40 岁最常见，女性多于男性。实验室检查：抗“0”> 1:500，血沉加快，C 反应蛋白阳性。该患者无上感病史、风湿免疫指标未见显著异常，暂不考虑该诊断。

其他：

房颤射频消融术后并发急性胃潴留病例 1 例

蔡磊

河北医科大学第二医院

患者基本信息：

患者金某，72 岁，女性，汉族，已婚，河北石家庄市深泽县人。

主述：

心前区不适伴视物模糊 2 年，胃胀 12 天。

现病史：

患者缘于 2 年前无明显诱因突然出现心前区不适（具体不详），伴视物模糊，不伴胸闷，无胸痛及放射痛，无气短，无恶心、呕吐，无头晕、黑曚及晕厥，症状持续约 10 分钟经休息后可缓解，就诊于当地医院，诊断为“心房颤动”，给予胺碘酮口服治疗。此后上述症状间断出现，遂就诊于我院急诊， 查 hs-cTnI+BNP+DFDimer:hs-cTnI:<0.02ng/m1 BNP: 131.4pg/mi D-Dimer:0.53mg/L，心电图：心房颤动。现为行进一步诊治收入我科。

既往病史：

既往脑梗死病史 10 年，未遗留明显后遗症。腰椎管狭窄术后 10 年。甲状腺结节切除术后 10 年，平时口服“优甲乐”治疗。高血压病史 4 年，血压最高 170/?mnHg, 平时口服“硝苯地平缓释片、马来酸依那普利片”降压，未规律监测血压。自诉冠心病病史 2 年，平时口服“阿托伐他汀、单硝酸异山梨酯”治疗。诊断心力衰竭 28 天，平时口服“呋塞米、螺内酯”治疗。否认高脂血症病史。否认糖尿病病史。否认消化性溃疡病史。否认青光眼病史。否认药物及食物过敏史。否认外伤及输血史，预防接种史不详；否认肛门、外生殖器病史。系统回顾无特殊。

病程记录：

患者入院后完善相关检验检查，未见明显禁忌症，于 15 天前行心内电生理检查 + 房间隔穿刺术 + 射频消融术。术后第 3 天，患者无明显诱因出现腹胀，伴纳差，精神差，增加胃肠动力药物后效果不佳，并出现恶心、呕吐胃内容物情况，查心电图示：心房扑动，查 CT 腹部平扫 (64 排以上) 示 :1. 胃内容物较多，请结合临床 ;2. 考虑肝脏散在囊肿 ;3. 十二指肠降段憩室 ;4. 考虑左肾囊肿 ;5. 脾周积液 ;6. 腰椎术后。综上诊断为 :1. 持续性心房颤动 心房扑动 心律失常 2. 冠状动脉粥样硬化性心脏病 3. 心力衰竭心功能 II 级 4. 高血压病 2 级 (极高危)5. 陈旧性脑梗死 6. 甲状腺结节术后 7. 腰椎管狭窄术后 8. 急性胃潴留。入院后给予依诺肝素钠抗凝，控制心率，补液营养支持，雷贝拉唑抑酸保护胃黏膜，盐酸普罗帕酮稳定心率，改善心肌代谢等综合治疗。后患者病情好转，准予出院。建议患者转入消化内科进一步处理胃潴留情况。

检验检查记录：

hs-cTnI+BNP+DFDimer:hs-cTnI:<0.02ng/m1 BNP: 131.4pg/mi D-Dimer:0.53mg/L。

心电图：心房颤动。

血钠钾氯：未见异常。

CT 胸部平扫 :1. 左肺下叶外基底段微结节，提示低危，建议年度随诊 :2. 右肺中叶条索 ;3. 两肺背侧肺组织膨胀不良 ;4. 所括肝脏散在低密度病变，请结合腹部检查。

CT 颅脑平扫 :1. 双侧放射冠、基底节区及右侧丘脑多发缺血灶 ;2. 脑萎缩。

心脏彩色多普勒超声：左房扩大，三尖瓣中度关闭不全，主动脉瓣轻度关闭不全，二尖瓣轻度关闭不全。

经食管超声心动图 :1. 主动脉瓣钙化，轻度关闭不全 2. 二尖瓣轻度关闭不全；三尖瓣中度关闭不全 3. 左心耳排空速度减低，提示左心耳功能减低 4. 左、右心耳二维 TEE+ 三维重建：左、右心耳内未探及血栓回声。

CT 腹部平扫示 :1. 胃内容物较多 ;2. 考虑肝脏散在囊肿 ;3. 十二指肠降段憩室 ;4. 考虑左肾囊肿 ;5. 脾周积液 ;6. 腰椎术后。

鉴别诊断：

1. 其他类型心律失常

2. 胃癌

3. 消化道溃疡

4. 幽门梗阻

5. 肠梗阻

其他：

房颤是临床上最常见的心律失常之一，环肺静脉隔离术被广泛认为是房颤的有效治疗方法。然而有报告指出射频消融术后胃潴留是一种罕见的心房颤动导管消融射频治疗（CA）后心脏外并发症。CA 诱发胃潴留的最可能机制是食管周围迷走神经的可逆或不可逆性损伤。胃潴留的治疗包括胃动力促进剂(如胃复安、多潘立酮、红霉素或莫沙必利)和止吐药，甚至鼻空肠营养管置入术。CA 引起的胃潴留仍然是临床医生认识不足的并发症。本文报道了房颤射频消融术后并发急性胃潴留 1 例，旨在提高心内科医师对房颤术后并发症的认识，以帮助临床医生早期识别并诊断。

回旋支旋磨一例

罗永百

西安交通大学第一附属医院

患者基本信息：

男性，75 岁

主述：

发作性胸闷 2 年，加重半月

现病史：

2年前无明显诱因出现胸闷,常于夜间休息时出现,有夜间憋醒,无明显胸痛、心慌,无大汗、头晕、黑朦等不适，未予重视：半月前无明显诱因出现上述症状加重，后常于快步行走时发作，无明显胸痛、肩背痛，无咽部紧缩感，无恶心、嗳气、反酸等不适，持续 1-2 分钟休息可自行缓解，后上述症状反复发作，遂于外院行冠脉 CTA 提示：冠脉三支病变，LAD 重度狭窄，给予“阿司匹林，瑞舒伐他汀”等药物治疗，建议进一步介入手术治疗。现为求进一步诊治遂来我院，门诊以“冠状动脉粥样硬化性心脏病”收住我科。此次病情加重以来，神志清、精神可，食纳可，大小便未见明显异常，体重无明显增减

既往病史：

否认肝炎、结核、疟疾病史，高血压史 15 年，血压最高 180/100mmHlg, 服用“苯磺酸氨氯地平 Smg1 次旧”，否认糖尿病、脑血管疾病、精神疾病史，21 年前行胆囊切除术，有磺胺类药物过敏史，无食物过敏史，无其他过敏史，预防接种史不详。

病程记录：

予以抗栓、调脂、抗心绞痛治疗，行 CAG 明确冠脉病变

检验检查记录：

CAG 提示冠脉三支钙化，CX 远端重度狭窄并钙化

鉴别诊断：

其他：

柳暗花明 -- 左心声学造影在心脏淋巴瘤诊治中的应用

王培伟

中山大学孙逸仙纪念医院

患者基本信息：

男，75 岁，退休，籍贯广东。

主述：

胸闷、呼吸困难及晕厥 1 次

现病史：

2 周前，患者无明显诱因突发黑矇、晕厥一次，意识清，偶有心悸，无四肢活动感觉障碍及呼吸困难。外院冠脉造影检查提示冠脉无明显狭窄。24 小时动态心电图检查显示：窦性心律与房颤心律交替，平均心率 61 次 / 分；检出心房颤动 1 阵，持续 2 小时 52 分钟；全天共检出大于 2 秒长 RR 间期 138 次，最长 RR 间期 3.27 秒，多为房颤伴缓慢心室率，少数为窦性停搏（图 1-A）。因此，考虑患者房颤、窦性停搏致晕厥可能，遂至我院拟行房颤射频消融治疗，必要时心脏起搏器植入。近期无发热、体重减轻、盗汗。

既往病史：

既往史、个人史无特殊

病程记录：

入院后血常规、甲状腺功能、肝肾功能检查均正常。常规经胸超声心动图检查时探及一巨大异常回声附着于左房后壁近房室沟处，大小约 50mm×67mm×19mm（图 1-B），边界较清晰，位置较固定，活动度小，难以明确肿物是原发于心房内或于心包腔内浸润性生长突入心腔；少量心包积液；余心脏结构未见明显异常。

检验检查记录：

左心声学造影检查显示肿物位于左房外侧脏层心包，向房室沟处浸润性生长并突

入左房（图 1-B ）；造影剂在左室心腔、心肌、肿物内依次显影，肿物内造影剂呈现强回声灌注显影，采用 “flash” 模式破坏微泡后肿物内造影剂又快速充填，因此考虑该占位病变可能为富含血供的恶性肿瘤。据此，临床医生为患者申请 FDG^{18}PET/CT 检查，结果提示：左房室交界处肿块（主要位于侧后壁），FDG 代谢活跃，考虑淋巴瘤与心脏肿瘤鉴别，建议活检；左颈 IV 及纵隔多发肿大淋巴结 FDG 代谢活跃，考虑转移可能（图 1-C）。患者予以肿瘤标记物（如 AFP，CEA）、HIV 相关检查，结果均为阴性。外科会诊建议胸腔镜下胸部淋巴结活检，最终病理结果为弥漫性大 B 细胞淋巴瘤 -GCB 亚型 (图 1-D)。 血液科会诊建议 R-CHOP 方 案 化 疗 (rituximab, cyclophosphamide, hydroxydaunorubicin, vincristine, and prednisone)。化疗 1 个疗程后心脏肿物明显缩小；3 个疗程后超声心动图检查未发现肿物，左心声学造影仅在左侧房室沟处隐约探及一细小回声团 (图 2)；心电图检查提示窦性心律伴正常心室律，未发现房颤或其它心律失常。出院后患者自我感觉良好，拒绝后续化疗。6 月后患者淋巴瘤复发，死于多器官衰竭。

鉴别诊断：

1. 左房血栓形成：

支持点：因患者有房颤病史，考虑左房血栓可能，

不支持点: 异常回声巨大、不位于左房血栓好发位置，活动度小，与心房边界不清。

结论：不能确定，建议进一步检查明确。

2. 黏液瘤：

支持点：位于心房后壁的巨大肿物，心包积液

不支持点：黏液瘤是原发于心脏的发病率最高的肿瘤，肿物特点不符合黏液瘤特点（有蒂连接于房间隔，活动度大等）

结论：可能性小，进一步检查明确

3. 其它心源性恶性肿瘤

支持点：位于心房后壁的巨大肿物，肿物活动度小，心包积液

不支持点：患者一般情况良好，无心外肿瘤表现，也无肿瘤恶液质表现

结论：不能确定，进一步检查明确

其他：

原发心脏淋巴瘤 (primary cardiac lymphoma, PCL) 是一种及其罕见的特殊类型淋巴瘤，目前仅有少数个案报道。据 WHO 定义，PCL 特指侵袭心肌和 / 或心包的淋巴瘤并表现与心脏相关的临床症状，可伴或不伴有其余部位淋巴结侵犯，主要累及右房及心包，其它心腔亦可受累。PCL 发病率极低，仅为 0.056%，占所有心脏原发肿瘤的 1%；该病预后差，未经治疗患者生存期不足 1 个月。PCL 好发于免疫功能低下患者，如 Epstein–Barr 病毒感染、HIV 感染者、先天性免疫功能低下或骨髓移植术后患者，偶见于免疫正常的老年男性。PCL 临床表现缺乏特异性，除体重减轻、疲劳、盗汗的淋巴瘤症状外，主要表现为肿瘤侵犯心肌、心包、冠状动脉而引起相应症状体征，如呼吸困难、胸闷、胸痛、心悸，偶见心源性休克、猝死、急性心肌梗死、心律失常、栓塞报道，同时缺乏特异的血清标记物，因此临床极易误诊为冠心病等心血管常见病，从而贻误诊治时间。PCL 恶性度高，疾病早期即可出现心外淋巴结侵犯，出现多器官衰竭。不同于其它心脏肿瘤首选外科手术，PCL 以化疗（71.8%）及免疫治疗（21.6%）为首选治疗方案，部分患者辅以手术（16.7%）及放疗 (8.2%)，经恰当治疗后中位生存期可延长至 45.4 (5.62–120.38) 个月，因此早期确诊是影响患者预后的重要因素。

左心声学造影是心脏肿物筛查的重要检查方法，具有简易、无创、无辐射、可实时显像的优点，性价比高，可多次反复应用，不受心率及心脏节律影响，心动过速或者心律不齐不影响成像质量，并可用于重症患者的床边检查。根据检查目的不同，左心声学造影可分为左心腔造影及心肌造影显像。左心腔造影采用低机械指数成像（<0.3 MI），使用造影剂后可清晰显示心内肿物与心内膜关系，并通过观察造影剂是否充填肿物区分血栓及肿瘤。心肌造影使用极低机械指数显像（<0.2 MI），持续输注造影剂对心肌及肿物显影，采用短暂的高机械指数（flash）模式破坏造影剂微泡观察再灌注的速度及数量，对比心内肿物与周围心肌组织灌注的灰度差区分肿物性质：高度血管化或恶性肿瘤具有异常丰富、扩张的新生血管，从而表现为接近或超过心肌组织回声的高灌注显像，且由于造影剂滞留出现充填快、消失慢；间质肿瘤（如粘液瘤）血供差，表现为低于心肌组织回声的低灌注显像；血栓则表现为灌注缺如的负性显影。与本病例类似，Wang S 等亦发现 PCL 在左心声学造影检查中可表现为高灌注显影，并出现造影剂滞留，导致肿物出现持续强回声显影。

经皮肺动脉瓣植入术治疗肺动脉重度反流 合并左肺动脉主干狭窄一例

柴博峰

四川大学华西医院

患者基本信息：

女 14 岁

主述：

法洛四联症术后 12 年

现病史：

12年前患者因“气短、呼吸困难”就诊于外院，诊断为“法洛四联症”并行外科手术（具体不详）治疗，术后症状明显缓解出院。出院后定期随访复查，患者生长发育较同龄儿差，使用生长激素治疗。3 月前于我院复查超声心动图示“肺动脉重度反流、左肺动脉近段狭窄（重度）、动脉导管未闭（管型）、三尖瓣少量反流等。心电图示：1、窦性心律不齐；2、完全性右束支传导阻滞；3、左房大；4、ST-T 改变。为求进一步介入干预收住我科。

既往病史：

无糖尿病、高血压、高血脂等慢性疾病。个人史、婚育史、家族史等无特殊。

病程记录：

予以抗心衰治疗。

检验检查记录：

超声心动图: 肺动脉瓣前向血流稍加速，瓣下反流 (重度)、肺动脉管腔内逆流 (重度)，左肺动脉近段狭窄 (重度)，动脉导管未闭，大血管水平连续性左向右分流，三尖瓣反流 (轻度)。双室收缩功能测值正常。

磁共振：心脏增大，右心房室增大为主。肺动脉主干、右肺动脉干增粗，左肺动脉干起始部明显狭窄。心功能数据：左心：EF:58%; EDV:118.2ml; ESV:49.4ml; SV:68.8ml. 右心室：EF:45%; EDV:262.2ml; ESV:143.6ml; SV:118.6ml。

鉴别诊断：

无

其他：

暂无

一例 F44Y 突变迟发型转甲状腺素蛋白淀粉样心肌病的病程、生化特性及长期随访

张君

中山大学附属第一医院

患者基本信息：

1. **年龄 / 性别**：74 岁男性
2. **基因型**：F44Y 杂合突变

临 床 分 期：NAC 分 期 II 期（NT-proBNP >3000 ng/L，eGFR >45mL/min/1.73m²）

主述：

呼吸困难、胸闷、双下肢水肿 21 个月。

现病史：

74 岁男性，因胸闷、气促双下肢水肿 21 个月于我院就诊。**活动、劳累后胸闷、气促**，爬 3、4 层楼后出现，休息数分钟后可缓解，伴双下肢轻度水肿，无胸痛、夜间阵发性呼吸困难，多次外院就诊，予以利尿药治疗后症状可缓解。不伴胸痛、头晕、黑矇、晕厥、胸痛、咯血、夜间端坐呼吸、泡沫尿。为求进一步诊治至我院门诊就诊。起病以来，患者精神、睡眠、胃纳可，大小便正常，体重无明显变化。

既往病史：

既往有冠心病、大疱性类天疱疮、慢性肾脏病（基线肌酐 152 μmol/L，eGFR 51 mL/min/1.73m²）

病程记录：

一、初步排查阶段：

1. **体格检查：**血压 107/53 mmHg，心率 56 次 / 分，律齐，未闻及杂音或湿啰音；小腿中段以下深浅感觉减退，双下肢中度水肿；手掌及足背可见红褐色斑片及水疱，尼氏征阴性

2. **实验室检查：**肌钙蛋白 T 为 0.069ng/mL，NT-proBNP 为 4397pg/mL，尿白蛋白为 69.1mg/L，血肌酐为 152μmol/L。

3. **心电图：**窦性心动过缓、一度房室传导阻滞、完全性右束支传导阻滞、左前分支传导阻滞。

4. **超声心动图：**左室后壁为 17mm、左室射血分数为 58%、整体纵向应变为 -16.7% 并呈 " 心尖保留 " 模式。

5. **肌电图：下肢 F 波异常。**

初步结论——高度怀疑为淀粉样变相关疾病，超声心动图的 “心尖保留” 模式提示 ATTR 相关淀粉样变可能性大。

二、病因诊断与确诊阶段：

1. **排除轻链型淀粉样变（AL）：**

- 血清蛋白电泳、免疫固定电泳、血 / 尿本周蛋白检测：均阴性
- 骨髓流式细胞学：正常

2. **通过影像学和病理活检确诊 ATTR-CM：**

- **心脏磁共振（CMR）（表 1，图 1d-f）：**

§ 左 / 右心室及室间隔弥漫性增厚

§ 心内膜下明显晚期钆增强（LGE）

§ 细胞外容积（ECV）59.7%

o **^{99}Tc-PYP 骨闪烁显像 +SPECT-CT（表 1，图 1j）：**

§ 1 小时 H/CL（心 / 对侧）比值 1.98（正常 <1.5）

§ 心肌摄取评分 3 级

o **皮肤活检（图 2）：**

§ 真皮乳头层刚果红染色阳性，甲紫染色阳性

§ 免疫组化 TTR 染色阳性（与淀粉样沉积区域对应）

§ 未见 κ 或 λ 轻链阳性染色

3. 通过基因与分子检测明确基因型和 TTR 错误折叠聚集的情况：

o 基因检测：F44Y 杂合突变（先证者），其子检测阴性

o 血清 TTR 四聚体浓度：2.16 μM（正常 >3μM）

三、治疗与随访阶段（23 个月）

初始方案：

Tafamidis（61mg qd）+ 呋塞米（20 mg qd）

治疗反应：

早期生活质量改善：1 年后 KCCQ 评分 32 → 79。

因自行减药导致心衰加重：开始治疗后 12-20 个月期间自行减药至 Tafamidis 61mg q3d，期间 NT-proBNP 达峰值 6602pg/mL，肌酐达峰值 224μmol/L。

治疗 21 个月后影像学无明显改善：CMR、超声、PYP 扫描结果与基线均无明显差异

治疗 21 个月后血清 TTR 四聚体浓度无明显升高

检验检查记录：

肌钙蛋白 T：0.069ng/mL（正常值 <0.003ng/mL）

NT-proBNP：4397pg/mL（正常值 <125pg/mL），患者自行减药期间达峰值 6602pg/mL

尿白蛋白：69.1mg/L（正常值 <20.0mg/L）

血肌酐：152μmol/L（正常值 <115μmol/L），患者自行减药期间达峰值 224μmol/L。。

心电图：窦性心动过缓、一度房室传导阻滞、完全性右束支传导阻滞及左前分支传导阻滞。

超声心动图: 左心室肥厚，左心室射血分数为 58%，GLS（整体纵向应变）为 -16.7%（正常值 <-18%），呈心尖保留型。

心脏磁共振成像：左心室、右心室及室间隔弥漫性增厚，左、右心室均有明显的晚钆增强表现，细胞外容积为 59.7%。

^{99}mTc-PYP 骨扫描及 SPECT-CT 检查：1 小时的 H/CL（心 / 对侧）比值为 1.98（正常 <1.5），视觉评分 3 级，伴有心肌摄取。

肌电图：下肢 F 波异常。

血清蛋白电泳、免疫固定、血尿中本 - 周蛋白、骨髓流式细胞术检测结果均为阴性。

皮肤活检：真皮乳头内有刚果红染色阳性及甲基紫染色阳性物质，与免疫组化检测中 TTR 染色阳性区域相对应。未发现 κ 链或 λ 链阳性染色。

基因检测：F44Y 杂合子。血清 TTR 四聚体浓度：2.16μM（正常 >3μM）。

鉴别诊断：

轻链型淀粉样变（AL）：

支持点：检验结果和超声心动图示淀粉样变导致心衰的可能性大

不支持点：血 / 尿单克隆蛋白阴性，骨髓流式正常，皮肤活检无 κ/λ 轻链沉积

结论：暂不考虑。

冠心病导致心衰：

支持点：胸闷，既往有冠心病病史。

不支持点：不伴胸痛或其他部位放射痛，疼痛程度与心衰症状严重程度不成比例。

结论：暂不考虑。

其他：

球囊扩张辅助输送系统通过卵圆孔未闭隧道的介入治疗

廖梦阳

华中科技大学同济医学院附属协和医院

患者基本信息：

性别：男

年龄：52 岁

职业：办公室职员

入院日期：2025 年 3 月 15 日

出院日期：2025 年 3 月 18 日

婚姻状况：已婚

家族史：父亲、母亲有高血压病史

主述：

反复头痛伴视物模糊 30 余年

现病史：

患者 30 年来，反复无明显诱因出现突发性剧烈头痛，伴视物模糊、恶心、呕吐，持续约 10-30 分钟后自行缓解，当地医院诊断为 " 偏头痛 "。近 1 年，患者上述症状反复发作，频率、程度较前加重，当地医院头颅 MRI 显示多发腔隙性脑梗死，TCD 提示“雨帘状右向左分流”，经食道超声提示“房间隔中部可见长约 0.8cm，宽 0.1cm 隧道”，当地医院诊断为先兆性偏头痛、卵圆孔未闭，建议行卵圆孔未闭封堵介入手术治疗。为进一步诊治来我院。病程中精神饮食睡眠可，二便如常，体重体力无明显改变。

既往病史：

否认高血压、糖尿病、高脂血症、冠心病等病史史

无吸烟、饮酒史

无药物过敏史

病程记录：

入院后完善常规检查，给予口服药物治疗：阿司匹林肠溶片 100mg qd，氯吡格雷 75mg qd

入院后第二天行卵圆孔未闭介入封堵术，手术过程如下：

1、常规消毒双侧腹股沟区域，行局部麻醉，穿刺右侧股静脉，置入 6F 血管鞘

2、在 6f MPA2 导管引导下，顺利将泥鳅导丝通过 PFO 隧道送入左上肺静脉，MPA2 导管无法跟进通过 PFO

3、将下肢血管鞘更换为 8f PFO 输送长鞘，将长鞘送至房间隔附近，以长鞘为支撑，MPA2 导管仍无法通过 PFO

4、将 MPA2 导管中的泥鳅导丝更换为 Sion blue 导丝，使用 1.5*15mm 球囊 16atm 扩张 PFO 隧道，导管仍无法通过。升级球囊为 2.0*20mm，14atm 扩张后，MPA2 导管顺利跟进通过 PFO，将导管送入左上肺静脉

5、更换加硬导丝，退出 MPA2 导管，放入长鞘内芯，顺利将 8F 长鞘通过 PFO 送入左心房

6、通过长鞘送入华医圣杰 CARDIO-O-FIX 1825 PFO 封堵器

7、术中超声验证封堵器位置、形态良好，释放封堵器，退出长鞘。常规加压包扎股静脉穿刺部位，结束手术。

检验检查记录：

外院经食道超声：房间隔中部薄弱处可见斜行裂隙，长约 0.8cm，宽 0.1cm。静息时可见 RLS I 级，Valsalva 动作后 RLS III 级

术后经胸超声心动图：封堵器位置良好，无残余分流

鉴别诊断：

动脉粥样硬化性脑梗死：患者无高血压、糖尿病、高脂血症、吸烟等危险因素，颈动脉、颅内动脉均无严重动脉粥样硬化表现

偏头痛：患者反复发生偏头痛，有视野模糊先兆表现，考虑为先兆性偏头痛可能性大

其他：

现已随访患者 3 月余，未再次发生头痛。

卵圆孔未闭介入封堵术如今已在大量医院常规开展，技术较为成熟，但仍有部分病例手术失败。输送系统难以通过 PFO 隧道是手术失败的常见原因，部分术者强行推送输送鞘导致心脏穿孔、心包填塞等严重并发症。一般而言、输送系统无法通过 PFO，多见于长隧道型 PFO，隧道中多有纤维粘连，使用球囊扩张辅助输送系统过隔，已经被中国 PFO 介入治疗专家共识推荐。球囊扩张存在房间隔撕裂风险，故应逐渐升级球囊，避免使用过大的球囊（不超过 8mm）

反复发作的心脏粘液瘤

吴子樊

武汉亚洲心脏病医院

患者基本信息：

患者女 ,27 岁，已婚，职业及工作单位不详，出生于湖北省远安县，现居湖北省远安县。

主述：

心脏术后 8 年余，再次发现心房肿物 1 年

现病史：

患者 2015 年 11 月 15 日因诊断为“右房粘液瘤”就诊于我院，完善检查后评估有手术指征，于 2015.11.17 行“微创右房粘液瘤切除 +TVP 术”，手术顺利，病检报告提示：右房粘液瘤。术后康复出院。2022 年 3 月 2 日因“活动后胸闷喘气 8 月余”，再次就诊于我院，心脏超声提示：微创右房粘液瘤切除 + 三尖瓣成形术后：右房内未见异常，左室占位（考虑粘液瘤可能，建议进一步左心声学造影检查），并于 2022 年 03 月 04 日在全麻、低温、体外循环下行 Redo- 左心室肿物切除 + 右心房肿物切除 + 手术中临时起搏器安置术，术后病检报告提示：（左室肿物、右房肿物）粘液瘤（结合病史可疑 Carney 综合征，建议进行基因检测协助诊断）。1 年前患者于外院复查再次发现心房肿物，2024.04.09 宜昌市第二人民医院超声提示：右房内异常回声（考虑粘液瘤）。建议手术治疗。现患者为进一步治疗来我院，门诊予以收住入科。起病以来，患者食欲、精神、睡眠欠佳，大、小便正常，体力较前下降，体重无改变。

既往病史：

2018 年因右侧髋关节疼痛多次就诊，2019 年诊断为股骨头坏死，于北京某医院行保守治疗，目前仍轻度活动受限，行走姿势轻度异常。2019 年诊断库欣综合征，行双侧肾上腺切除术治疗。术后激素治疗一月余，因右侧髋关节复发性疼痛自行停止激素治疗，同年因多发乳腺纤维瘤多次行外科手术切除术治疗。否认其他慢性疾病，否认其他外科手术治疗，否认食物药物过敏史。

病程记录：

患者入院后积极予以完善辅助检查，上级医师查房看病人后指示：患者病情重，建议继续完善增强 CTA 检查后讨论评估手术指征，详细告知患者及家属病情、治疗方案，商议后要求暂出院，予以办理出院。

检验检查记录：

白细胞计数 5.4 10^9/L，中性粒细胞百分率 55 %，钾测定 4.25 mmol/L，血清尿素 3.31 mmol/L ，估算肾小球滤过率 132 ml/min ，血清总胆红素 8.2 μmol/L ；超敏 C 反应蛋白 53.61 mg/L ，血清乳酸脱氢酶 251 U/L，红细胞沉降率 120 mm/1h 末， 血浆 D- 二聚体 1.313ug/ml，纤维蛋白（原）降解产物 3.51 ug/ml，血清白蛋白 38.2 g/L，血清碱性磷酸酶 153 U/L， 高密度脂蛋白胆固醇 0.76 mmol/L，乙肝表面抗体 (发光法) >1000.00IU/L， 红细胞压积 28 %， 红细胞平均体积 71 fL，红细胞平均 Hb 含量 23 pg，红细胞分布宽度 16.29 %， 血浆凝血酶原时间 13.1 S ， 国际标准化比值 1.16，部分凝血活酶时间 38.8 S， 血浆纤维蛋白原 6.49 g/L， 血浆 VIII 因子活性测定 169.3 %，钠测定 136.3 mmol/L， 血红蛋白 91 g/L， 血清前白蛋白 0.03 g/L，铁蛋白 140.1 μg/L，血清白 / 球 0.9， 血清球蛋白 42.7 g/L。心电图：窦性心律，T 波改变。心脏彩超：Redo- 左心室肿物切除 + 右心房肿物切除术后：右房腔内异常回声光团（考虑为粘液瘤可能，建议进一步检查），左室内未见异常回声。泌尿科超声：双肾、输尿管、膀胱声像图未见异常。妇科超声：子宫、附件未见明显异常。双下肢动静脉超声：双侧下肢血管未 见明显异常。

鉴别诊断：

脂肪瘤、横纹肌瘤、左房血栓、肥厚型心肌病、风湿性二尖瓣狭窄

其他：

本次就诊详细告知患者及家属病情、治疗方案，商议后要求暂出院，予以办理出院。故计划着重就 2022 年影像学检查所留存的高质量超声图像做分享和探讨。经胸超声心动图提示：左室腔内可见一大小约 3.6×2.2 厘米的中等回声瘤体反射，似附着于二尖瓣外侧乳头肌，附着面宽约 1.3 厘米，质地疏松，瘤体形态随心动周期改变，随心动周期活动度大，收缩期脱向左室流出道侧。左心声学造影提示：左室腔内可见一大小约 3.6×2.2 厘米的中等回声瘤体反射，附着于二尖瓣外侧乳头肌，附着面宽约 1.3 厘米，质地疏松，瘤体形态随心动周期改变，声学造影显示瘤体呈不均匀轻度强化，造影剂充盈强度低于正常心肌组织。经食道超声心动图可见更为清晰的肿物运动，并可生成 3D 动画以更直观观察到肿物的运动状态。CT 增强扫描可见左心室内见团块状低密度影，大小约 28mm×24.5mm，病灶似与二尖瓣相连。

IVUS 指导冠脉严重钙化病变应用 RotaTripsy 治疗 1 例

张小昊

吉林大学第二医院

患者基本信息：

67 岁女性，职业：农民

主述：

劳累性胸痛 6 个月，加重 2 天

现病史：

6 个月前劳累时出现胸骨后闷痛，休息 5-10 分钟可缓解，此后上述症状时有出现，但未影响日常生活未进一步诊断。2 天前追赶公交车时上述症状再次出现，持续约 15 分钟后缓解。

既往病史：

有高血压病史 10 余年，最高 180/100mmHg，规律口服降压药，血压控制尚可，吸烟史 30 余年，每日半包

病程记录：

入院后根据病史、体征及辅助检查，可明确诊断为冠心病、不稳定型心绞痛、心功能 I 级，高血压 3 级（很高危）。治疗上给予阿司匹林 100mg 日一次口服，氯吡格雷 75mg 日一次口服，瑞舒伐他汀 10mg 日一次口服，美托洛尔 47.5mg 日一次口服，苯磺酸氨氯地平 5mg 日一次口服，单硝酸异山梨酯 50mg 日一次口服。并于完善相关术前检查后行冠脉造影检查，冠脉造影显示 LAD 近段 80% 狭窄伴钙化，LCX 近段 50-60% 狭窄，右冠由远端至近段多处狭窄病变，中段及第一转折处可见明显充盈缺损，结合血管钙化影，考虑为钙化结节。结合患者心电图表现考虑右冠为罪犯血管，故首先选择应用 IVUS 进行评估。但 IVUS 导管不能通过中段病变，第一转折处显示为明显钙化结节。因此选择主动旋磨策略。应用 1.5mm 的磨头对右冠全程进行分段旋磨，而后行 IVUS 检查，显示右冠远端存在钙化，但不严重，中段钙化结节仍较大，旋磨消蚀有限。应用切割球囊及 NC 球囊对右冠远端进行预处理后，先于远端行支架植入，而后应用 IVL 球囊对右冠中段及第一转折处行 5 个循环的振波处理，而后植入支架，造影显示结果满意。现患者术后 1 年，门诊随访日常生活无明显心前区不适症状。

检验检查记录：

心电图显示下壁心肌缺血。心彩未见明显异常。肌钙蛋白 (-)，LDL-C 1.9mmol/L。肝肾功能及血常规凝血功能未见明显异常。

鉴别诊断：

本病常与急性心肌梗死；其他疾病引起的心绞痛：主动脉瓣狭窄、关闭不全，肥厚型心肌病，X 综合征等亦可引起心绞痛；• 肋间神经痛、肋软骨炎；心脏神经症；其他系统疾病导致的胸痛 ： 返流食管炎，消化性溃疡，颈椎病等相鉴别。该患者症状典型，有年龄、高血压及吸烟的危险因素，心电图及造影均支持不稳定型心绞痛的诊断。

其他：

CTEPH 治疗之选：保守还是介入？

崔鹏辉

长治市人民医院

患者基本信息：

女性，48 岁

主述：

劳力性气短 2+ 年，加重 1+ 月

现病史：

2+ 年前，无明显诱因出现活动后气短，初始表现为快走或爬 2 层楼梯后需要停下休息，日常活动后偶有胸闷，休息 3-5 分钟可缓解，不伴胸痛、头痛，不伴咳嗽、咳痰，不伴腹痛、腹泻等，患者就诊于当地某三甲医院，在院行冠脉造影（未见报告），诊断为“冠心病”，给予“阿司匹林 100mg 日一次口服，阿托伐他汀钙片 20mg 日一次口服”治疗，症状未明显缓解。后就诊于另一三甲医院，行肺血管 CTA 示：肺动脉干增粗，管径约 3.1cm，右肺下叶前基底段动脉管腔内见低密度充盈缺损，远端分支显影欠清，小栓子待排；左肺下叶前基底段肺动脉起始部局部管腔壁增厚，管腔狭窄。肺通气 / 灌注显像：双肺多个叶段“通气 / 灌注”不匹配，考虑肺栓塞。予“西地那非 25mg 日三次口服，利伐沙班 15mg 日一次口服”治疗，上述气短症状自觉无明显改善。入院前 1+ 月，患者自觉上述气短症状逐渐加重，爬 1 楼即感气短，偶有咳嗽，咳少量白痰，无发热、胸痛、咳血及晕厥。遂就诊于第三家三甲医院，完善心脏超声示：三尖瓣反流（轻 - 中度），肺动脉高压（重度）。给予“他达拉非 + 马昔腾坦 + 利伐沙班”治疗（具体剂量不详），自觉上述症状仍未改善。患者为求进一步诊治，遂前往我院就诊，门诊以“肺动脉高压”收入我院。自患病以来，患者精神、食欲、睡眠可，大小便如常，体重无明显变化。

既往病史：

否认既往疾病史。

病程记录：

入院查体：BP:126/60mmHg，SPO2 95%（未吸氧），颈静脉无怒张，双肺呼吸音可，未闻及明显干湿啰音。心率 80 次 / 分，律齐，各瓣膜听诊区未闻及杂音，双下肢无水肿。

完善相关辅助检查

诊断：

慢性血栓栓塞性肺动脉高压（WHO 第四组 WHO-FC III 级，中危）

肺源性心脏病

药物治疗：

利伐沙班 15mg Qd

利奥西呱 1mg tid

马昔腾坦 10mg Qd

介入治疗：

选择性肺动脉造影 + 肺动脉球囊扩张成形术（右 A8、A10）

检验检查记录：

辅助检查

动脉血气（吸氧 2L/min）：pH 值 7.43，二氧化碳分压 37mmHg，氧分压 121mmHg，氧饱和度 99.2%

NT-proBNP：563pg/mL。

血常规、肝肾功、凝血功能、甲功未见明显异常。

梅毒、艾滋、乙肝筛查未见异常。

心电图：窦性心动过缓，电轴右偏（+100°），T 波改变（II、III、aVF、V1-V6），I 导联 rS 型，aVR 导联 Qr 型。

心脏彩超：

右房增大（51 × 44 mm），右室肥大（25 mm）；

肺动脉主干及左、右分支增宽，肺动脉瓣关闭不全；

肺动脉压增高（估测肺动脉平均压约 39mmHg；TAPSE/SPAP=0.41； PVR:2.86 Wood）；

二尖瓣及三尖瓣轻度关闭不全。

肺功能检查：中度混合性肺通气功能障碍；弥散功能轻度降低。

胸片：胸廓对称，纵隔居中； 双肺纹理稍增多，双肺目前未见确切斑片影； 心影形态、大小未见确切异常；双膈面光滑，双肋膈角锐利。

胸片：胸廓对称，纵隔居中； 双肺纹理稍增多，双肺目前未见确切斑片影； 心影形态、大小未见确切异常；双膈面光滑，双肋膈角锐利。

胸部 CT：见附件 PPT。

右心导管检查：

mPAP 54 mmHg

PAWP 9 mmHg

PVR 17.3Wood U

CO/CI 3.0/2.1 L/min

SvO2 56 %

六分钟步行距离：425 米

肺通气 / 灌注显像：肺灌注显像：双肺血流灌注不均匀；双肺散在多发放射性稀疏、明显稀疏灶，请结合临床。

鉴别诊断：

1. 慢性血栓栓塞性肺动脉高压（CTEPH）

诊断依据：

临床表现：劳力性气短逐渐进展，病程较长；活动耐量下降；无显著肺部感染史或特异性系统疾病症状。

影像学支持：

肺血管 CTA：右肺下叶动脉管腔内低密度灌注缺损，左肺下叶动脉壁增厚、狭窄。

V/Q 显像：双肺多发通气 / 灌注不匹配灶，支持慢性肺动脉栓塞。

胸部 CT 示马赛克灌注征。

右心导管检查：

mPAP 54 mmHg、PVR 17.3 Wood U、PAWP 9 mmHg、SvO_2 56%，CI 2.1 L/min/m^2，提示为毛细血管性前肺动脉高压。

治疗反应： 利奥西呱 + 马昔腾坦 +BPA 治疗后症状缓解，指标改善，支持 CTEPH 诊断。

最终确诊为本病例主要诊断，同时符合 WHO PH 第四类（CTEPH）。

2. 大动脉炎相关肺动脉狭窄

诊断理由

流行病学特点：中青年女性是高发人群；本例女性 48 岁，符合易感人群。

临床表现：活动后气短，病程进展缓慢，符合大动脉炎肺动脉受累的临床特征。

肺血管 CTA 表现：左肺下叶肺动脉起始部局部管腔壁增厚、管腔狭窄——需鉴别为慢性血栓性闭塞还是血管壁炎性改变。

但否定因素包括：

无发热、乏力、体重下降等全身症状；

无上肢血压差、脉搏减弱等典型体征；

无 ESR、CRP 显著升高或免疫标志物阳性；

没有主动脉及其分支明显受累表现。

虽有一定影像支持，但缺乏系统性炎症表现，支持度不如 CTEPH。

3. 纤维性纵隔炎相关肺动脉狭窄

诊断理由：

机制特征：纤维性纵隔炎可因纵隔致密纤维组织压迫肺动脉或肺静脉，导致肺动脉高压，多累及双侧肺门部血管，或单侧肺动脉近段狭窄甚至闭塞。

影像支持：若胸部增强 CT 或 MRI 提示纵隔软组织团块、钙化，或肺门部血管“包绕性压迫”，应高度怀疑。

本例未明确提示纵隔软组织异常、钙化或主动脉旁纤维性变，影像资料中未见支持性证据。

发病年龄与临床表现可一致，但缺乏典型影像征象与病理证据。

暂不考虑该疾病诊断可能。

其他：

电解质紊乱诱发先天性长 QT 综合征尖端扭转室速发作

厉晓婷

浙江大学医学院附属邵逸夫医院

患者基本信息：

患者，女性，65 岁，浙江省杭州人，务农

主述：

反复意识丧失 2 天

现病史：

患者 2 天前因雨天路滑摔倒，自行起身后突发意识丧失，前驱自觉心跳加快，无胸闷症状，患者当时呈平卧位，睁眼张口，无肢体抽搐，无两眼上翻，无口吐白沫，无大小便失禁，家属呼喊数秒后患者有意识恢复，但仍难以发声，继续 5-6 分钟后可切题回答，呼叫 120 前往某医院就诊，测血压 174/74mmHg，查 WBC、CRP、cTNI 无殊，血钾 2.71mmol/L，血镁未测，心电图示频发室性早搏，颅脑胸部 CT 无殊，予以 0.9% NS 500ml+1g KCL+2.5mg MgSO4 补钾补镁，前列地尔 + 醒脑静改善循环治疗，于凌晨左右回家。患者 1 天前晨起扫地吃饭后自觉疲惫，拟前往卧室休息，途中再发意识丧失，发病前有心跳加快感，家属呼喊数秒钟后恢复意识，遂再次前往某医院就诊，就诊期间再次出现意识丧失，予以 CPR 后恢复意识，测脉氧 94%，心电图示室性心动过速，予胺碘酮 300mg 微泵维持，继续补钾补镁，为进一步治疗前往我院急诊，拟“意识丧失待查”收住我科。

既往病史：

既往高血压病史 20 余年，服用贝那普利片 10mg 口服 每日一次降压，自诉血压控制可；2 型糖尿病史 10 年，服用二甲双胍片 250mg 口服 每日三次 + 瑞格列奈片 0.5mg 口服 每日三次 + 阿卡波糖胶囊 50mg 口服 每日三次降糖，未监测血糖；有头痛病史数年，服用氟桂利嗪胶囊 5mg 口服 每晚一次。

病程记录：

患者意识丧失待查，入院后予以完善卧立位血压，卧位血压 143/92mmHg，立位 1 分钟 135/91mmHg， 立位 3 分钟 136/96mmHg， 立位 5 分钟 148/90mmHg，体位性低血压依据不足；心脏超声提示左室轻度增大，室间隔增厚；冠脉 CTA 提示左右冠均势型，前降支近段见少许斑块，中段及远段血管内皮光滑，未见明显狭窄，回旋支内膜光滑，未见明显狭窄，右冠远段见少许斑块；颅脑 CT 平扫提示颅内未见明显异常；肺部 CT 平扫提示两肺炎性纤维灶。两肺小叶间隔增厚；脑电图提示未见明显异常；患者心电图提示窦性心律，QTc708ms，监护提示尖端扭转性室速，予以补钾补镁，QTc 从 700ms 逐渐下降至 570ms，Schwartz LQTS 评分 >=4，进一步完善基因测，考虑先天性长 QT 综合征（LQTS1），予以普萘洛尔治疗，病情稳定后出院。

检验检查记录：

心脏超声：LA（前后径）：35.8mm IVSd：13.4mm LVIDd：53.2mm LVPWd：10mm LVIDs：31mm EDV:141ml ESV:42.7ml SV:98.3ml EF：73.3%，FS：42.7% AO：27mm AAO：36mm PA：24mm 主动脉瓣、肺动脉瓣形态、回声、活动未见明显异常。左室轻度增大，余房室内径正常。二尖瓣、三尖瓣形态、回声、活动未见明显异常。室间隔增厚，左室后壁厚度正常，呈逆向运动。左室壁活动未见异常。心脏各结构未见连续中断，心包腔内未见明显积液。CDFI: 三尖瓣口可见少量反流信号，Vmax:2.61m/s，RVSP:32mmHg，主动脉瓣口可见少量反流信号。TDI：二尖瓣环水平舒张期 E'/A' < 1.0。诊断：1. 左室轻度增大，室间隔增厚 2. 轻度三尖瓣、主动脉瓣反流 。

鉴别诊断：

1. 电解质紊乱

2. 缓慢型心律失常

3. 药物诱发的 QT 间期延长

4. 颅内高压

5. 内分泌疾病

6. 各类器质性心脏病

其他：

急性心肌梗死后精神障碍 1 例

马越

北京大学第三医院

患者基本信息：

52 岁 / 女

入院日期：2024-11-09 18:41

主述：

胸闷、恶心、呕吐 4 小时

现病史：

4 小时前患者无明显诱因出现胸闷，伴恶心、呕吐胃内容物 1 次，无血性或咖啡色物质，无胸痛、呼吸困难、心悸，无发热、咳嗽、咳痰、咯血，无头晕、黑朦，无苍白、大汗，持续不缓解，就诊于我院急诊，心电图示 II、III、aVF、V7-V9、V3R-V5R 导联 ST 段抬高，查心肌损伤标志物示全血肌钙蛋白 I 测定 15(ng/mL) ↑，肌酸激酶同工酶 300(ng/mL) ↑，诊断急性下壁后壁右室心肌梗死，予阿司匹林 300mg、替格瑞洛 180mg 口服，行急诊冠脉造影示 RCA 大量血栓，血栓抽吸后植入支架 1 枚，由于术中血压下降，最低 82/60mmHg，给予多巴胺持续静脉泵入，术后予替罗非班、尼可地尔持续静脉泵入，收入心血管内科重症监护病房。

既往病史：

既往史

高血压、脂肪肝

个人史、家族史

无吸烟、饮酒史

否认早发冠心病家族史、心肌病家族史，否认其他遗传性疾病病史

病程记录：

冠心病二级预防

阿司匹林 100mg QD

替格瑞洛 90mg BID

阿托伐他汀 20mg QN

依诺肝素 4000IU Q12H

因血压低暂缓 ARNI/ACEI/ARB 类药物及 β 受体阻滞剂

右心功能不全、心原性休克

根据心功能积极补液

小剂量多巴胺、去甲肾上腺素泵入

预防应激性溃疡、消化道出血

雷贝拉唑 10mg QD

检验检查记录：

血常规：白细胞 7.19*109/L，Net% 90.7% ↑，Net 6.52*109/L ↑

凝血：FDP 10.6ug/ml ↑，D- 二聚体 1.84ug/ml ↑

心肌损伤标志物：NT-proBNP 3410pg/ml ↑，TnI 15ng/ml ↑，CK-MB 300ng/ml ↑，MYO 900ng/ml ↑

肝肾电解质：AST 527U/L ↑，Cr 72umol/L，K 4.45mmol/L

血气分析：pH 7.45，PO2 136.6mmHg，PCO2 22.6mmHg，实际碳酸氢根 16.2mmol/L，Lac 4.16mmol/L ↑

尿常规：尿蛋白 +

鉴别诊断：

脑血管病

造影剂脑病

中枢神经系统感染

系统性疾病

其他：

“冠脉血栓 + 狼疮脑病” 同时起病的活动性狼疮，罕见病例

经房间隔穿刺途径无射线消融左侧旁道并发短暂性全面遗忘症一例

陈奕帆

温州医科大学附属第二医院

患者基本信息：

病例资料

患者，女，28 岁，因“反复阵发性心悸 2 年”曾查心电图示“阵发性室上性心动过速”。拟行导管射频消融术入院。完善各项检查未见异常后，局麻下行心内电生理检查为左侧隐匿性旁路。遂经右股静脉行 1 次房间隔穿刺，将 SL1 鞘管置入大头电极，在二尖瓣环 2 点钟找到靶点，予 35W，42 度，17ml/min，消融 1.2 秒后旁道阻断，巩固消融 60S X3 次，观察 20 分钟再次心内电生理检查未见异常，手术成功。术中 ACT280 秒，肝素用量 3000IU。术中生命征稳定，无诉不适。但手术快结束时发现患者反复询问医生：“现在在哪里、为什么躺在这里及目前在做什么”等。即便多次告知后还是不能记住，仍反复询问。不能记起术前一段时间（约 2-3 周内）的事情及住院手术的全过程，却能正确回忆工作单位名称、爱人姓名等。急诊测血糖、血气分析显示正常，床边心超未见心包液性暗区。神经内科会诊进行神经系统详细体格检查，除时间、地点定向障碍，顺向性记忆障碍外，无其他阳性体征。急诊 MRI 未见明显异常，考虑为短暂性全面遗忘症（transient global amnesia，TGA）。返回病房 5 小时后患者开始能部分回忆及复述近期事件，此后呈进行性好转。次日上午完全恢复。但对记忆丧失期间发生的事仍失忆。6 个月后电话随访，患者完全正常且无再发失忆，但仍不能回忆手术全过程。

讨论

本例诊断标准符合由 Hodges 和 Warlo 提出的 TGA 修订标准：(1) 突然发病，发作时必须有目击者；(2) 发作时神经功能障碍仅限于重复询问及遗忘；(3) 记忆丧失表现为一过性，在 24 h 内缓解；(4) 发病后记忆力可完全恢复，唯独发作期间的经历不能想起，形成记忆空洞，这是患者遗忘发作留下的唯一症状；(5) 无其它重要神经系统症状和体征。目前认为其发病机制可能为血管性因素，因此改善脑循环及代谢是主要治疗方式。临床上需与短暂性癫痫性失忆、短暂性脑缺血发作、谵妄、心因性遗忘等鉴别。TGA 通常预后良好。本例发作持续时间约为 5 小时，经对症处理，24 h 内自行完全缓解。

主述：

反复阵发性心悸 2 年

现病史：

患者 2 年来反复出现心悸心慌、伴胸闷等不适症状，为突然发作突然停止特点，而且发作频率逐渐增加，每次发作持续的时间逐渐延长。最近一次持续约 2 小时，在当地医院查心电图提示“室上性心动过速”。无黑矇晕厥，无胸痛冷汗，无下肢浮肿。今为求进一步诊治来我院住院治疗。

既往病史：

既往体健

病程记录：

入院后予完善各项检查未见异常，予术前准备后，局麻下行心内电生理检查和无射线下导管射频消融术。术中右心室起搏见 CS 3、4 极 逆传 A 波最早，提示左侧隐匿性旁路。遂经右股静脉行 1 次房间隔穿刺，将 SL1 鞘管置入大头电极，在二尖瓣环 2 点钟找到靶点，予 35W，42 度，17ml/min，消融 1.2 秒后旁道阻断，巩固消融 60S X3 次，观察 20 分钟再次心内电生理检查未见异常，手术成功。术中 ACT280 秒，肝素用量 3000IU。术中生命征稳定，无诉不适。但手术快结束时发现患者反复询问医生：“现在在哪里、为什么躺在这里及目前在做什么”等。即便多次告知后还是不能记住，仍反复询问。不能记起术前一段时间（约 2-3 周内）的事情及住院手术的全过程，却能正确回忆工作单位名称、爱人姓名等。急诊测血糖、血气分析显示正常，床边心超未见心包液性暗区。神经内科会诊进行神经系统详细体格检查，除时间、地点定向障碍，顺向性记忆障碍外，无其他阳性体征。急诊 MRI 未见明显异常，考虑为短暂性全面遗忘症（transient global amnesia，TGA）。返回病房 5 小时后患者开始能部分回忆及复述近期事件，此后呈进行性好转。次日上午完全恢复。但对记忆丧失期间发生的事仍失忆。6 个月后电话随访，患者完全正常且无再发失忆，但仍不能回忆手术全过程。

检验检查记录：

心超、MRI 未见异常

鉴别诊断：

以下疾病进行鉴别：1 短暂性癫痫性失忆：TEA 是一种罕见的颞叶癫痫，其特征是局部发作，表现为反复发作的短暂性孤立记忆丧失。但癫痫的特点主要包括持续时间短、多次发作等，本例发作持续时间约为 5 小时，从中午开始，以单一事件的形式出现且没有其他运动障碍的表现，不符合。2. 短暂性脑缺血发作 (TIA)。没有其他局灶性神经功能缺损的孤立性失忆症在 TIA 或中风中可以表现出来，但临床上较罕见。仅局限于海马或丘脑的单侧脑卒中可能会出现以暂时性失忆的唯一或主要表现，然而脑部 CT 或磁共振成像 (MRI) 会显示相关部位的缺血损伤，而在 TGA 患者中，脑部的 CT 扫描通常是正常的，本例 MRI 检查未见明显的异常，因此不考虑该病。3. 谵妄，谵妄在老年患者中相对常见，但通常表现出更普遍的意识混乱和注意力不集中。本例对答切题，注意集中没有表现出谵妄的注意力持续时间缩短和情绪起伏类型特征。不考虑该病。4. 心因性遗忘，心因性遗忘与 TGA 之间也容易混淆。但心因性遗忘更突出的表现是记忆的丧失，而本例除了记忆的丧失外还有突出表现为新信息的学习和接受不能，这与心因性遗忘之间也有所差别。

其他：

无

“硬骨头克星”——旋磨联合 IVL 治疗重度钙化病变 1 例

马越

北京大学第三医院

患者基本信息：

姓名：王 **

62 岁 / 男性

入院日期：2024-02-23

主述：

活动后胸闷 3 个月，加重 2 周

现病史：

3 月前活动后出现胸闷，多于快走时出现，休息数分钟后好转，发作频率约 1 次 / 周，无明显胸痛、心悸，无恶心、呕吐，无呼吸困难、下肢水肿，未予重视。

2 周前上述症状加重，程度、性质同前，发作频率 3-5 次 / 周，就诊于我院门诊，心电图运动平板试验阳性 (+)，且运动过程中胸闷症状再发，考虑缺血可能性大，为进一步评估冠脉情况收入院。

既往病史：

既往史：

高血压 20 年，血压最高 170/110mmHg，替米沙坦 80mg、美托洛尔 47.5mg 降压，血压维持在 130-140/90-100mmHg

高脂血症 3 年，阿托伐他汀 20mg、非诺贝特 10mg 降脂

个人史：

吸烟 40 年，3-5 支 / 天，未戒烟

家族史：

早发冠心病家族史 弟弟 50 岁患冠心病

病程记录：

抗血小板

• 阿司匹林 100mg Qd

• 替格瑞洛 90mg Bid

降脂

• 瑞舒伐他汀 10mg Qn

• 非诺贝特 10mg Qd

降压

• 替米沙坦氢氯噻嗪 40/12.5mg Qd

• 美托洛尔 47.5mg Qd

抗心绞痛

• 单硝酸异山梨酯 20mg Bid

检验检查记录：

血常规：白细胞 5.16(*10^9/L)，红细胞 4.35*10^12/L)，血红蛋白 137(g/L)，血小板 241(*10^9/L)，中性粒细胞百分数 54.4(%)，中性粒细胞绝对值 6.07(*10^9/L)

凝血：凝血酶原时间 9.9(秒)，凝血酶原活动度 113.0(%)，活化部分凝血活酶 33.6(秒)，D- 二聚体定量 <0.15(μg/ml)

生化: 丙氨酸氨基转移酶 25(U/L), 天门冬氨酸氨基转移酶 29(U/L), 肌酐 (酶法) 78(umol/L)，估算的肾小球滤过率 90(ml/min/1.73m^2)，尿酸 532(μmol/L) ↑，甘油三酯 5.59mmol/L ↑，低密度脂蛋白胆固醇 3.15mmol/L ↑，脂蛋白 a 28mg/L

心肌损伤标志物：NT-proBNP 55(pg/ml)，肌钙蛋白 T 0.021(ng/mL)，肌酸激酶同工酶 MB 7(U/L)

血糖：HbA1c 5.8(%)

术前免疫、电解质、甲功：未见明显异常

鉴别诊断：

冠状动脉性心脏病

不稳定型心绞痛

心界不大

心律齐

心功能 I 级（NYHA 分级）

高血压病 3 级（极高危）

高尿酸血症

高脂血症

其他：

复查高危钙化病变介入治疗 1 例，应用了旋磨技术、震波技术，在腔内影像学指导下进行介入治疗

经导管二尖瓣缘对缘修复术治疗急性心梗导致二尖瓣前叶脱垂

厉晓婷

浙江大学医学院附属邵逸夫医院

患者基本信息：

患者，女性，73 岁，浙江杭州人，公司退休人员

主述：

胸痛 3 天，乏力 2 天

现病史：

患者 3 天前晨起出现胸痛，向左腋下放射，疼痛不剧，持续 2 小时，伴乏力、冷汗，自服丹参片后好转，无心悸，无意识丧失，无头晕等不适，患者未予重视，后胸闷胸痛未再发作。患者 1 天前活动后出现乏力不适，休息后可缓解，伴纳差，有头晕，无食物选择，无明显胸闷、胸痛，自测血压低，后乏力程度较前逐渐加重，余性质同前，遂至我院急诊，测血压 73/47mmHg，乳酸 (LAC) 1.75mmol/L，急诊肌钙蛋白 I 28.946ng/mL，肌酸激酶 -MB 同工酶活性 39IU/L，心电图提示高侧壁异常 Q 波，高侧壁、前壁、侧壁 ST 段抬高，心超示预估 EF：40% 左右，二尖瓣前叶脱垂伴中重度关闭不全可能，考虑急性 ST 段抬高型心肌梗死，心源性休克，入 EICU 监护治疗。

既往病史：

既往高血压 20 余年，糖尿病 10 余年。

病程记录：

入 EICU 后予无创呼吸机辅助通气，多巴胺 + 重酒石酸去甲肾上腺素持续使用维持血压，哌拉西林他唑巴坦 4.5g 8 小时一次 抗感染治疗，阿司匹林肠溶 0.1g 每日一次 + 替格瑞洛片 90mg 每日二次抗血小板，阿托伐他汀 40mg 每晚一次降脂稳斑，辅以利尿、控制血糖、电解质平衡、护胃等对症治疗，并拟进一步行 CRRT 脱水稳定内环境。2025-05-26 主任床边查房，考虑患者急性心梗、二尖瓣脱垂，大剂量血管活性药物维持下血压仍难以维持，拟急诊行经皮二尖瓣钳夹术 (MitraClip)，予行床边气管插管，送急诊手术。于 2025-05-26 行冠状动脉造影术，术中见 “左冠状动脉：左主干未见明显狭窄，前降支、未见明显狭窄，中间支近段起闭塞，回旋支、钝缘支内膜光滑，未见明显狭窄病变。右冠状动脉：右冠近段 50% 狭窄”，选友德邦 2.25*25mm 药物球囊中间支贴壁释放 60s，手术结束后行 TEER 治疗，置入德晋 Dargonfly XW0612 夹子 2 枚，德晋 Dargonfly SN0409 夹子 1 枚钳夹二尖瓣瓣叶，二尖瓣返流程度减轻，予以留置 IABP 送入 ICU。转入 CCU 后继续抗血小板、降脂稳斑、抗感染、扩冠、护肝、降糖、营养支持等对症支持治疗。2025-05-29 予拔除 IABP，2025-05-30 予拔除气管插管，序贯高流量吸氧，给氧浓度 45%。动态复查心肌酶、心电图及心脏超声等。2025-06-02 予拔除胃管，改半流及糖尿病饮食，停胰岛素持续泵入，改德谷胰岛素针 12iu 皮下注射 每晚一次 + 阿卡波糖片 100mg 口服 每日三次控制血糖。病情稳定后于 2025-06-03 转入 CCU，予以心电监护，吸氧，低盐低脂糖尿病饮食，治疗上继续予抗血小板、匹伐他汀 2mg 每晚一次降脂稳斑、瑞卡西单抗降脂治疗，沙库巴曲缬沙坦钠片 50mg 口服 每日一次改善心功能，头孢克洛缓释片 0.375g 口服 每日二次抗感染，德谷胰岛素针 + 阿卡波糖片控制血糖，辅以抑酸护胃等治疗。患者入院后血糖波动，请内分泌科会诊多次调整降糖方案。目前予德谷门冬双胰岛素 12-10 iu 每天两次 + 达格列净 100mg 每天三次降糖，监测血糖。住院期间患者无明显胸闷胸痛等再发，2025-06-06 复查心超提示双平面法 EF:59.0%，二尖瓣轻度反流，监测心肌酶、BNP 逐渐下降，复查动态心电图见少量室性早搏，末次复查 BNP 875pg/mL，高敏肌钙蛋白 I 83ng/L，予带药出院。

检验检查记录：

心脏超声：LVIDd:53mm LA:55*49*48mm Teich 法 EF:65% 双平面法 EF:55% 主动脉瓣增厚，回声增粗增强；肺动脉瓣、三尖瓣形态、回声、活动未见明显异常。左心增大，右房室内径正常。二尖瓣 2 区前叶长约 24mm（直线测量，可能低估），后叶长约 12mm，前叶 A2 区、部分 A1 收缩期向左房侧脱入，脱入高度约 4.7mm，前叶上可见一长约 5mm 的飘带样回声，呈连枷样运动，连枷宽约 16mm，关闭时前后叶不能闭合，可见细小裂隙。二尖瓣瓣环距卵圆窝上缘约 40mm。画迹法二尖瓣口面积 4.4c ㎡。室间隔基底段增厚，厚约 12.4mm，室间隔及左室后壁呈逆向运动。左室下侧壁下段、前侧壁中下段、下壁中下段运动减弱，余左室壁活动未见异常。心脏各结构未见连续中断，心包腔内未见明显积液。CDFI: 二尖瓣口舒张期血流频谱分析：Vmax：1.7m/s，PPG：11.8mmHg，MPG：4.4mmHg，二尖瓣口可见大量偏心性反流信号，沿后叶及左房后侧壁走行，反流主要来源于 2 区略偏 1 区，反流颈宽约 13mm，反流汇聚区半径 17.4mm，EROA：1.37c ㎡，反流量：125ml。三尖瓣口可见少量反流信号。TDI：二尖瓣环水平舒张期 E'/A' < 1.0。左室舒张功能：二尖瓣口血流频谱 E 峰 V:177cm/s， E/A=2.5，二尖瓣环水平舒张期 LatE'=13.1cm/s，MedE'=6.6cm/s, 平均 E/E'=18。右室收缩功能：TAPSE：18.7mm，三尖瓣环 S' 峰：11cm/s。下腔静脉内径约 20mm，随呼吸变化率约 40%。诊断：1. 二尖瓣前叶腱索断裂伴前叶 (A2 区、累及部分 A1 区) 脱垂，二尖瓣重关闭不全（DMR 4+,Carpentier 分型 II b） 2. 左心增大，室间隔基底段增厚；左室壁节段性运动异常伴左室收缩功能正常低值，左室舒张功能障碍III级 3. 主动脉瓣退行性变伴轻度反流 4. 轻度三尖瓣反流 5. 下腔静脉呼吸变化率减低

鉴别诊断：

1. 急性心肌梗死机械并发症二尖瓣脱垂

2. 二尖瓣脱垂合并急性心肌梗死

其他：

小球囊开启大希望

廖梦阳

华中科技大学同济医学院附属协和医院

患者基本信息：

性别 / 年龄：男，62 岁

职业：离退休，文职岗位退休

入院时间：2025 年 1 月 16 日

主述：

反复胸闷乏力 2 年余

现病史：

患者 2 年前无诱因出现胸闷、乏力，持续难以缓解，活动后加重，常伴有剧烈咳嗽、心悸、头晕。外院诊断为 " 冠心病 "，行冠脉介入治疗，置入支架 3 枚（LAD），术后症状未改善。2025 年 1 月以来，上述症状加重，咳嗽咳痰，伴发热，活动受限制，难以平卧。来我院就诊，心脏彩超提示：右心扩大、左室受压，三尖瓣重度关闭不全，重度肺动脉高压。肺动脉 CTA 提示双肺多发肺动脉段充盈缺损。考虑为" 慢性血栓栓塞性肺动脉高压 "，收入院拟行 BPA 治疗。

起病后，精神饮食睡眠差、二便如常、体重体力下降。

既往病史：

诊断为冠心病，行介入治疗 8 月余，术后规律药物治疗

否认高血压、糖尿病、COPD 等病史

既往无明确 VTE、APE 病史，无肿瘤、风湿等疾病

病程记录：

患者入院后精神、饮食差，端坐呼吸，反复发热、咳黄痰。BP96/60mmHg，HR117bpm，血氧饱和度 81%（不吸氧）94%(吸氧后)

入院后完善自免全体、易栓症筛查、血培养等检查。给予美罗培南、头孢哌酮舒巴坦等抗生素治疗约半月，另给予艾多沙班 60mg qd 抗凝治疗，马昔腾坦 10mg qd、利奥西呱 0.5mg tid 降肺动脉压力治疗，间断利尿。为 BPA 手术创造条件。

于 2025.2.5 行 BPA 手术。考虑患者手术耐受性较差，本次手术仅选择了左下肺的 3 给肺动脉段和右下肺的 1 个肺动脉段使用 2.0*20mm 版顺应性球囊进行扩张（8-16atm）。约 1.5 小时左右，患者咳嗽较剧烈，血氧饱和度降至 81%，遂立即终止手术。术后患者一般情况可，术后 3 天，患者诉呼吸困难较前明显减轻。

2025.4.17 患者再次入院行 BPA 治疗，本次患者精神好，活动无明显受限。本次入院手术时间约 2 小时，对所有明显狭窄肺动脉段进行扩张，根据血管直径选择非顺应性球囊进行扩张。术后患者未诉不适，手术结束时血氧饱和度 91%。

患者通过 2 此 BPA 心功能从 WHO IV 级恢复至 I 级，心脏结构基本正常，拟于 7 月复查肺动脉造影、右心导管。

检验检查记录：

2025.1.17 肺动脉 CTA：慢性肺气肿，双肺多发炎症改变，散在钙化结节。右肺下叶前、外、后段、左侧上叶尖后段，左侧下叶背段、前、外、后段多发条状充盈缺损

鉴别诊断：

冠心病：虽确诊，但与患者症状不符合，介入治疗无效，考虑于患者严重呼吸困难无关

肺部疾病：患者合并有肺气肿，但无二氧化碳潴留，肺功能于严重呼吸困难、重度肺动脉高压不符合，考虑为 CTEPH 合并肺部疾病

特发性肺动脉高压：肺动脉 CTA 等影像学提示多发肺栓塞

其他：

本例 CTPEH 患者入院时心功能极差，且合并严重肺部感染，通过积极的抗感染、抗凝、PAH 靶向治疗，为 BPA 创造手术机会。

CTEPH 患者第一次 BPA 手术往往是心功能最差的时候，一般再次 BPA 时心功能都较前有所改善，手术耐受较前提高，因此第一次 BPA 的手术策略尤为重要。本中心第一次 BPA 手术原则是选择导管容易到位、导丝容易通过的肺动脉段进行扩张，一般选择 2.0*20 版顺应性球囊进行扩张，尽快结束手术，避免发生并发症，再次 BPA 时会根据血管直径选择较大的非顺应性球囊进行充分扩张。曹云山教授近期发表的论文支持了本中心的初次 BPA 策略，文章中提到通过 2.0*20mm 球囊扩张的血管 1 个月后会发生自发扩张，初次 BPA 使用小球囊扩张的策略有效的减少了肺水肿和机械并发症的发生，同样可以降低患者肺循环阻力、改善心功能，为再次手术创造有利条件，改善患者远期预后。

暴发性心肌炎救治 1 例

崔晓

浙江大学医学院附属第一医院

患者基本信息：

男，55 岁，急诊入院。

主述：

发热伴胸闷气促 3 天

现病史：

患者 3 天前无明显诱因下出现发热，最高体温 39.0℃，无畏寒寒战，自服退烧药布洛芬退热，伴胸闷气促，无胸痛咯血，无咳嗽咳痰，有恶心呕吐，呕吐胃内容物，具体量不详，纳差，稍有腹胀，无腹痛腹泻，无四肢抽搐，无大小便失禁，昨至当地卫生院输液治疗，具体药物不详，症状未见改善，遂至我院急诊就诊。

入院体格检查：T 36.5℃　P 108bpm　R 19bpm　BP 82/63mmHg，BMI：24kg/m2，神清，精神软。颈静脉无充盈。双肺呼吸音粗，闻及少许湿啰音。叩诊心界不大。心率 108 次 / 分，心律不齐，各瓣膜未闻及病理性杂音，无心包摩擦音。无异常血管征。腹部查体（-）。神经生理反射存在，病理反射未引出。脑膜刺激征阴性。双下肢无可凹性水肿。

既往病史：

无高血压、高脂血症、糖尿病、肾病等病史。

个人史：无吸烟、饮酒习惯

家族史：父母已故，年龄原因不详。无遗传病家族史。

病程记录：

一、于急诊抢救室会诊

1、建议重症监护室会诊，评估 ECMO 指征；

2、建议急诊冠状动脉造影及临时起搏器植入；

3、考虑患者暴发性心肌炎可能，经知情同意后尽快早期加用甲泼尼龙 500mg qd 静滴、丙种球蛋白 10-20g qd 静注；

4、合并用药：异丙肾上腺素静脉微泵提升心率，去甲肾上腺素静脉微泵维持血压，谷胱甘肽静滴护肝，泮托拉唑静滴抑酸护胃。

二、急诊冠状动脉造影及临时起搏器植入：

先行临时起搏器植入，冠状动脉造影示：左主干未见明显狭窄；左前降支中段 40% 狭窄，TIMI3 级；左回旋支未见明显狭窄；右冠中段 50% 狭窄，TIMI3 级。

三、ICU 诊治：

1、PICCO 示低排高阻，心源性休克明确；

2、甲泼尼龙 500mg QD 静滴 *3 天 + 丙种球蛋白 20g QD 静注 * 3 天，后序贯以甲强龙 40mg Q8H*3 天，40mg Q12H*3 天，甲强龙 40mg QD 静滴，后逐步过度至甲强龙 4mg QD 口服；

3、合并用药：去甲肾上腺素、多巴酚丁胺静脉微泵维持血压；利多卡因控制频发室早、短阵室速；头孢呋辛、更昔洛韦经验性抗感染；重组人脑利钠肽改善心衰、呋塞米利尿及对症补钾；低分子量肝素预防性抗凝等。

4、完善多种病原学检测未见明显异常。

四、病情监测：

1、患者心律逐步稳定，室速发作逐步减少；

2、2024-10-13 拔除临时起搏器，未再发高度房室传导阻滞。

3、监测肌钙蛋白逐步下降，复查心超逐步改善：2025-10-08，LVEF20%；2025-10-09，LVEF40%；2025-10-15，LVEF 52%。

2024-10-14 转入心内科，继续甲强龙抗炎及低分子量肝素抗凝等。

2024-10-15 突发胸闷气促，血压一过性不稳定，文丘里面罩吸氧氧合尚可。

急诊肺动脉 CTA：右肺动脉主干、两侧肺动脉分支多发栓塞。

五、病情转归：

2024-10-15 转回 ICU；

经血管外科及呼吸内科会诊，予依诺肝素 1.5 支 Q12H 抗凝；

完善易栓症筛查结果无殊。

继续抗炎抗凝等治疗，后患者病情逐步稳定，带药出院。

检验检查记录：

一、急诊检查：

2024-10-05

血常规：白细胞计数 5.89 *10E9/L，中性粒细胞 (%) 76.6 % ；

血生化: 超敏 C 反应蛋白 12.06 mg/L，谷丙转氨酶 84 U/L，谷草转氨酶 220 U/L，肌酐 137 μmol/L，尿素 12.29 mmol/L ；

D- 二聚体：1050 ug/L FEU；

肌钙蛋白 I：36.13 ng/mL；

心肌酶：乳酸脱氢酶 786 U/L 羟丁酸脱氢酶 699 U/L 磷酸肌酸激酶 1166 U/L 肌酸激酶同工酶 194 U/L；

NT-proBNP 6690 ng/L；

血气分析：Lac 2.9 mmol/L，pH 7.41，pO2 97.7mmHg，pCO2 30.2mmHg，HCO3- 19.2 mmol/L，BE -4.1。

心电图及心电监护提示多种心律失常，时呈高度房室传导阻滞、加速性室性自主心律。

超声心动图（床旁）：左室壁节段性运动异常，左室收缩功能不全（估测 LVEF: 30%），左室舒张功能减退，二三尖瓣轻度返流。各房室大小正常范围，室壁不厚。

全腹 CT 平扫（上中下腹平扫）：胆囊炎。 附见：脂肪肝。脾脏稍大。盆腔少量积液。心包少量积液。食管裂孔疝可能。腹膜后淋巴结稍大。

二、入院后检查：

监测肌钙蛋白逐步下降，复查心超逐步改善：2025-10-08，LVEF20%；2025-10-09，LVEF40%；2025-10-15，LVEF 52%。

2025-10-15 急诊肺动脉 CTA：右肺动脉主干、两侧肺动脉分支多发栓塞。

病原学检测、易栓症相关筛查无殊。

鉴别诊断：

1、急性心肌梗死：主要通过冠脉造影与暴发性心肌炎进行鉴别，同时结合 CMRI、炎症因子等综合评估。

2、脓毒性心肌病：该类患者早期有明确的细菌感染灶、血白细胞显著升高及其他全身表现，血培养或病原学检查的阳性发现有助于鉴别。

3、普通急性心肌炎：急性心肌炎心功能受损明显较轻，临床症状较暴发性心肌炎轻，无明显血流动力学障碍和严重的传导异常，细胞因子水平增高不显著，尤其是 sST2 水平 <780 nmol/L；病情可长期迁延而成为慢性心肌炎或心肌病改变。

4、应激性心肌病：可能有心理应激作为诱因，嗜铬细胞瘤交感危象时也可模拟强烈应激而诱发应激性心肌病。冠脉造影没有固定狭窄，合理治疗能迅速康复。

其他：

总结与反思：

1、暴发性心肌炎诊断治疗均需迅速果断；

2、暴发性心肌炎诊疗以生命支持治疗为中心，极早期给予足剂量激素及免疫球蛋白同样非常重要，本次患者除临时起搏器及 CRRT 外，未使用气管插管及 ECMO、IABP 等机械循环呼吸支持治疗，治疗效果佳，恢复较好；

3、暴发性心肌炎的 VTE 预防需高度关注，本例患者预防性抗凝基础上仍发生肺栓塞，带来额外挑战。

4、暴发性心肌炎的短期预后与长期预后，康复期是否需长期使用改善心衰预后药物，值得进一步研究。

一例终末期心衰合并肺动脉高压患者的综合治疗。

秦小腾

山东大学齐鲁医院

患者基本信息：

刘 **，女，59 岁，2024 年 6 月 11 日入院。

主述：

阵发性咳嗽伴胸闷、憋气 11 年余，腹胀 4 月余。

现病史：

患者 11 余年前无明显诱因出现阵发性咳嗽，伴胸闷、憋气，当地医院诊断为“心力衰竭”，给予药物治疗。后患者于山东省立医院多次就诊调整药物，症状控制较稳定。4 年前患者于我院住院期间出现阵发性室性心动过速，给予电复律及药物治疗。3 年前患者劳累后出现胸闷、憋气，伴双下肢明显水肿，我院查心超示 LVEF0.13，心尖部血栓形成。患者自 2021 年至 2023 年因心衰发作于我院 8 次住院。4 个月前患者无明显诱因出现腹胀、纳差、尿量减少，活动时有心悸、气短等不适症状，为行进一步治疗收入我院。患者本次发病以来，饮食差、睡眠欠佳，小便量少，大便未见明显异常，体重无明显增减。

既往病史：

下肢静脉曲张病史数年，否认高血压、糖尿病等慢性病史。

病程记录：

1. 入院后给予抗凝、改善心肌重构、利尿、强心等治疗，患者憋喘明显，腹部膨隆，腹胀严重，稍活动即感心悸、气短，少尿，病情加重转入 ICU，给予腹腔穿刺引流、强心、改善肾功能等治疗后好转，患者憋喘、腹胀减轻，尿量逐渐恢复，血压趋于稳定，患者于 2024-6-17 转至 CCU 病区。

2. 在 CCU 住院期间给予患者充分药物治疗，考虑到患者终末期心衰诊断明确，左室辅助装置植入指征明确，家属对 LVAD 十分积极，同时考虑到患者右心功能较差，手术风险高，对患者进行充分的术前评估和优化右心功能后，于 2024-7-12 行 LVAD 植入术 + 主动脉瓣生物瓣膜置换术 + 三尖瓣成形术 + 左心耳结扎术。

3. 术后出现持续 2 个月的无尿，下腔静脉显著增宽且塌陷率几乎消失，多浆膜腔积液，考虑患者为右心功能差所致，给予患者 CRRT、曲前列尼尔降肺压、强心、抗感染、营养支持等综合治疗。

4. 患者 2024-9-14 首次有尿，尿量 50ml，后尿量逐渐增多，至 2024-9-23 彻底脱离 CRRT，血压趋于稳定，2024-10-8 出院。术后复查恢复良好，日常活动基本不受限。

检验检查记录：

2024-6-13 心脏彩超

2024-6-26 右心导管

2024-6-27 心脏彩超

2024-7-4 冠状动脉造影

鉴别诊断：

心衰鉴别：左心衰、右心衰、全心衰

无尿鉴别：肾前性、肾性

其他：

检查报告详见 PPT

大动脉炎合并坏疽性脓皮病及桥粒斑蛋白基因突变致青年顽固性高血压一例报告

肖雨倩

山东第一医科大学附属中心医院

患者基本信息：

姓名：王帅

出生地：山东省济南市

性别：男

职业：学生

年龄：19 岁

入院时间：2024-05-27

民族：汉族

记录时间：2024-05-27

婚姻：未婚

病史陈述者：患者本人

主述：

皮肤破溃 6 年余，血压升高伴头痛 1 周。

现病史：

患者 6 年前因颜面部多发红色肿物伴部分肿物破溃流脓，难以愈合，当地医院多次予以清创换药效果欠佳，前往烧伤科予以创面扩创术并行二期植皮封闭创面，仍有反复破溃。考虑患者在严格抗感染前提下，存在反复低热，多次细菌培养结果阴性，请皮肤科会诊，完善皮肤组织病理活检，结果示：符合坏疽性脓皮病。根据病史、皮疹表现、皮肤组织病理及治疗反应，考虑 PAPA 综合征。住院期间规律服用醋酸泼尼松、环孢素软胶囊、异维 A 胶丸、溴隐亭治疗，治疗效果可。2 年前患者因自行停用环孢素后出现右下肢溃疡加重，排除相关禁忌给予司库奇尤单抗注射液治疗。患者后间断出现腰腹部不适，2022.09.04 于我院完善腹部 CT（图 1）提示腹主动脉上段瘤样扩张、肠系膜上动脉边缘模糊，后行腹主动脉强化 CTA 示腹主动脉及部分分支管壁增厚，壁间血肿可能，渗出性改变可能。请风湿免疫科会诊，根据影像学表现，确诊为“大动脉血管炎”，给予激素及环磷酰胺治疗，症状控制可。现患者规律应用 “强的松激素及阿达木单抗注射液”治疗，患者皮损及症状好转。患者 1 周前午睡醒来后测血压明显升高并自觉头痛剧烈，呈持续性，伴发热，体温最高 38.1℃，为进一步治疗收入我院治疗。

既往病史：

既往否认高血压、糖尿病、冠心病等慢性病病史。2020 年因“面颈部溃疡”于我院烧伤科行“创面扩创术、二期植皮封闭创面”，否认食物及药物过敏史。个人史、婚育史、家族史未见明显异常。

病程记录：

患者头痛明显，伴有体温升高，炎性指标高、血细胞沉降率加快，考虑大动脉炎病情活动期，院内给予甲泼尼龙 (80mg/ 次，1 次 /d) 联合免疫抑制剂甲氨蝶呤（10mg/ 次，1 次 /qw）治疗，体温降至正常水平。患者头痛未见明显改善，血压持续升高，最高血压 203/139mmHg，考虑高血压急症。完善颅脑相关检查，排除脑出血等相关病变，同时予以硝酸甘油联合硝苯地平对症处理，血压控制欠佳。考虑患者青年起病，发病时间短，起病初期即表现出恶性高血压且血压难以控制，完善肾动脉磁共振提示双肾动脉重度狭窄醛固酮且肾素水平较正常值明显偏高。于 2024 年 6 月 3 日组织多学科会诊，邀请高血压科、血管外科、影像科等多个学科协助诊疗。高血压科会诊考虑患者继发性醛固酮升高，导致血压持续升高难以控制，建议：1. 完善肾图尿微量白蛋白及 24 小时蛋白尿评估肾脏功能 2. 予以螺内酯拮抗 RAS 系统，抑制血管纤维化。3. 治疗上首选钙离子拮抗剂，β 受体阻滞剂，α 受体阻滞剂，中枢降压药物联用，在评估肾功能后谨慎使用

ACEI 类降压药。4. 必要时转入血管外科手术干预。血管外科会诊：患者双肾动脉狭窄，右肾动脉重度狭窄，建议开通血管通路。医学影像学会诊：结合肾动脉 MRA 及主动脉 MRA；腹腔干，肠系膜上动脉，双肾动脉重度狭窄，右肾动脉起始部重度狭窄，次全闭塞。符合大动脉炎表现。建议：情况允许时行主动脉 CTA 检查。由于内科治疗效果差且合并严重肾动脉狭窄，与手术外科积极沟通后，评估目前患者大动脉炎控制良好且肾功基本正常，可耐受手术。于 2024 年 6 月 4 号转入血管外科行肾动脉造影（图 4），在超声引导下穿刺进入左侧股动脉，置入 5F 短鞘，0.035 导丝配合猪尾导管行腹主动脉、肾动脉造影示，双肾动脉狭窄，右侧为重，肠系膜上动脉闭塞，引入 coper 导管，选入右肾动脉，造影示：右肾动脉起始段狭窄严重，后更换 7F 短鞘，配合肾动脉 Cuiding 导管定位病变位置，引入 6-40mm 球囊进行扩张，扩张后示狭窄病交段较前改善。Coper 导管配合 0.035 导丝选入双侧颈动脉造影示，双侧颈动脉通畅，无道影剂滞留，血流通畅，遂结束手术。2025 年 6 月 7 日再次复查：白细胞计数 14.82×109/L、单核细胞计数 0.7×109/L、中性粒细胞计数 9.99×109/L、中性粒细胞百分比 67.4%，超敏 C 反应蛋白 1.29mg/L，血细胞沉降率 16 mm/h，肌酐 65μmol/L、尿素 6mmol/L；肾动脉 B 超示右侧肾动脉起始处球囊术后、对比前期超声流速明显好转。术后患者血压得到有效控制，血压维持至 BP150/100mmHg，血沉及 C 反应蛋白较前有明显好转。药物治疗方案调整如下: 1. 抗凝治疗: 利伐沙班(10mg/ 次，1 次 /d)，氯吡格雷 (75mg/ 次，1 次 /d)。2. 免疫调节治疗：甲泼尼龙减量至 (48mg/ 次，1 次 /d)，甲氨蝶呤 (10mg/ 次，1 次 /qw)，阿达木单抗注射液 (40mg/ 次，1 次 /q2w)。3. 降压方案：培哚普利 (8mg/ 次，1 次 /d)，氨氯地平 (10mg/ 次，1 次 /d)，美托洛尔 (47.5mg/ 次，1 次 /d)。术后完善全外显子基因检测(检测编号: N018693)，检出 DSP 基因 c.8417C>T(p.Ala2806Val) 杂合错义突变（图 X），ACMG 证据条目为 PM2（人群频率极低）+PP3（生物信息学预测有害），评级为 ' 临床意义未明 2 级。可导致致心律失常性右室心肌病（Arrhythmogenic Right Ventricular cardiomyopathy，ARVC）、扩张型心肌病（Dilated Cardiomyopathy, DCM）、隐性致死性棘层松解性大疱性表皮松解症（lethal acantholytic epidermolysis bullosa，LAEB）等。可解释患者皮肤病变及心电图右束支阻滞。

检验检查记录：

血细胞分析：白细胞计数 11.07×109/L、单核细胞计数 0.75×109/L、中性粒细胞计数 6.89×109/L、中性粒细胞百分比: 65.6%，超敏 C 反应蛋白: 48.58mg/L，血细胞沉降率： 32mm/h，免疫球蛋白定量测定：免疫球蛋白 A4.34g/L、免疫球蛋白 G16.4g/L, 血离子分析：钾 2.86mmol/L、氯 97 mmol/L，高血压五项：醛固酮 754pg/ml、肾素 156uIU/ml, 血浆醛固酮 / 肾素活性比值（plasma aldosterone/plasma renin concentration，ADRR）4.83, 尿离子分析（24 小时）： 24 小时尿钠 317.1mmol/24h、尿氯 265.7mmol/24h、24 小时尿醛固酮 25.8ug/24h，性激素六项：催乳素 23.27ng/Ml，血凝血常规六项：活化部分凝血酶时间 40.43s、纤维蛋白原 6.32g/L，肾功能：肌酐 58μmol/L、尿素 4 mmol/L; 降钙素原、风湿系列 16 项、肝功未见明显异常。心电图: 1. 窦性心律 2. 不完全性右束支阻滞图形（图 2）。肾上腺 CT：1. 双侧肾上腺 CT 平扫未见明显异常，必要时进一步检查 2. 脂肪肝 3. 腹主动脉近端局部稍增宽。颈部血管彩超（含锁骨下动脉）示右侧椎动脉先天发育细、右侧椎动脉频谱异常（官腔局部狭窄闭塞可能）。双肾及肾动脉 + 肾上腺彩超示双侧肾动脉起始处狭窄（右侧：重度；左侧：中度）。腹主动脉及肾动脉磁共振（图 3）示腹主动脉及其分支多发管壁环形增厚并不同程度狭窄：腹主动脉局部环形增厚、管腔轻度狭窄；右肾动脉起始部重度狭窄或次全闭塞，左肾动脉起始部重度狭窄；右肾动脉分支血管较对侧略细并稀疏，提示左肾血流灌注较对侧减低可能；腹腔干起始部重度狭窄；肠系膜上动脉近段重度狭窄可能，以远血流信号略显稀疏、消失；考虑大动脉炎。颅脑磁共振、脑电图未见明显异常。

鉴别诊断：

· 原发性醛固酮增多症 (原醛症): 由肾上腺醛固酮瘤或增生引起。常伴有低血钾（或正常低限）、乏力、肌无力、夜尿增多。血浆醛固酮 / 肾素比值显著升高是筛查关键，确诊需行盐水负荷试验等。影像学（肾上腺 CT/MRI）可能发现腺瘤或增生。无血管炎表现。

原发性高血压：最常见的高血压类型，多见于中老年人，常有家族史。通常起病隐匿，进展缓慢。对于年轻患者（尤其 <30 岁）出现的中重度高血压，应高度警惕继发性原因，包括大动脉炎。 原发性高血压无大动脉炎的特征性血管病变、无脉、血管杂音及全身炎症表现。

系统性红斑狼疮：可引起狼疮性肾炎导致肾实质性高血压，也可引起血管炎。但 SLE 有特征性的多系统表现 (皮疹、关节炎、浆膜炎、肾脏、血液系统、神经系统、抗核抗体谱阳性等），其血管炎通常累及中小血管而非大动脉。

肾实质性高血压：通常由慢性肾小球肾炎、慢性肾盂肾炎、多囊肾、糖尿病肾病、狼疮性肾炎等。有明确的肾脏病史（蛋白尿、血尿、肾功能异常）。高血压通常是疾病进展的结果，而非早期或唯一表现。尿液检查（蛋白尿、血尿、管型尿）、肾功能（血肌酐、尿素氮升高）、肾脏超声（结构异常）常有阳性发现。通常无大动脉炎特征性的血管杂音、无脉或不对称血压。

其他：

一步之遥–– 冠状动脉 - 主动脉夹层 1 例

张国勇

首都医科大学附属北京同仁医院

患者基本信息：

老年男性，76 岁

因拟行右冠介入治疗入院

主述：

间断胸闷 15 年，加重 1 年余

现病史：

15 年前始自觉劳累及情绪激动后感胸骨后闷痛，自行休息约 3-5 分钟后可完全缓解，就诊于当地医院，行冠脉 CTA 提示：冠心病、右冠狭窄约 50-60%、左冠狭窄约 40-50%（具体不详），予以输液等治疗。院外坚持规律服用阿司匹林肠溶片 1 年，后自行停药。后上述症状反复间断发作，未作规律治疗。1 年前始自觉上述症状较前明显加重，发作频率较前明显增加。为求进一步诊治，3 月前就诊于我院，行冠脉造影提示左主干 + 三支病变，术中尝试开通右冠 CTO 病变未成功；后给予规律冠心病二级预防用药。今为行进一步介入治疗，再次就诊于我院门诊。门诊以 “冠心病” 收入科。

既往病史：

高血压病史 10 余年，血压最高 150/90mmHg，规律服用药物治疗，血压控制可。2 型糖尿病病史 5 年，目前口服药物加胰岛素治疗，院外未规律监测，血糖控制情况不详。高脂血症病史 1 年，规律口服降脂药物治疗。反流性食管炎病史 1 年。

病程记录：

患者入院后给予强化抗血小板、降脂、降压、降糖等药物治疗。完善血常规、生化、凝血、免疫、甲功等相关检验，完善胸片、心电图、心脏超声等相关检查。排除禁忌后。行冠脉造影，于术中开通右冠 CTO，并植入支架 2 枚。术中出现右冠开口 - 近段、开口 - 右冠窦 - 主动脉夹层，复查床旁心脏超声未见异常。次日复查血常规、凝血、心肌酶、BNP、心脏超声较前均无明显异常。拟复查主动脉 CTA，患者拒绝。

检验检查记录：

血常规、生化、凝血、免疫、甲功等相关检验；

胸片、心电图、心脏超声等相关检查。

鉴别诊断：

患者诊断明确，无需鉴别

其他：

经食道超声诊断左心耳血栓致反复心肌梗死 1 例

李世川

重庆市荣昌区人民医院

患者基本信息：

患者男，70 岁

主述：

胸痛 5 月，再发伴气促 3 小时

现病史：

入院前 5 月，患者无明显诱因出现胸痛不适，为胸骨中下段续性压榨样疼痛，伴肩背部放射痛，伴大汗淋漓、濒死感。就诊于荣昌区中医院，行心电图：窦性心律、左房负荷过重、偶发房性早搏、偶发室性早搏、V1-V4 导联 ST 段抬高、电轴左偏。予以阿司匹林 300mg、氯吡格雷 300mg 嚼服后转入我院，行心电图提示抬高 ST 段回落，查肌钙蛋白 I 34.54ng/ml。急诊行冠状动脉造影提示：冠状动脉右冠优势型；左冠主干未见明显狭窄；前降支血管最远段细小，最远段闭塞；回旋支血管未见明显狭窄，TIMI3 级；右冠血管未见明显狭窄，TIMI3 级（图 1）。行前降支球囊扩张成形术，冠脉内推注硝酸甘油及盐酸替洛非班后，造影前降支远段未显影，予以刺破球囊至前降支远段推注硝普钠 100ug 后，造影提示前降支远段隐约显影，TIMI2 级。院外规律口服冠心病二级预防药物。入院前 3 小时 (2024-06-05 06:00)，患者晨起出现胸痛再发伴气促不适，伴大汗淋漓、濒死感，遂急诊至我院，心电图：窦性心律，III、aVF 导联轻微上抬，查 cTnI 提示 0.47ng/ml。

既往病史：

既往有高血压、风湿性心脏病、慢性支气管炎伴肺气肿病史，长期吸烟史。

病程记录：

①患者因 “突发胸痛 1+ 小时” 于 2024 年 1 月 9 日于我院心内科住院治疗，冠脉造影提示前降支远端闭塞，行前降支远端 PTCA 术，术后口服 “阿司匹林肠溶片 100mg 每日一次、替格瑞洛 90mg 每日二次、阿托伐他汀 20mg 每晚一次、缬沙坦 80mg 每日一次、琥珀酸美托洛尔缓释片 47.5mg 每日一次”，后因心力衰竭加用 “呋塞米 20mg 每日一次、螺内酯 20mg 每日二次”。②患者因 “胸痛 5 月，再发伴气促 3 小时” 于 2024 年 6 月 5 日再次于我院心内科住院治疗，冠脉造影提示右冠远端闭塞，考虑冠状动脉栓塞可能，予以口服 “华法林（逐渐滴定至靶计量）、氯吡格雷 75mg 每日一次、阿托伐他汀 20mg 每晚一次、缬沙坦 80mg 每日一次、琥珀酸美托洛尔缓释片 23.75mg 每日一次、呋塞米 20mg 每日一次、螺内酯 20mg 每日二次”，皮下注射依诺肝素 40mg 每日二次 (前 3 天)。③患者病情好转后于 6 月 11 日完善经食道超声明确左心耳血栓，停用氯吡格雷、阿托伐他汀钙片，予以口服华法林抗凝。

检验检查记录：

急诊行冠脉造影：冠状动脉右冠优势型；左冠主干未见明显狭窄；前降支血管未见明显狭窄，TIMI3 级；回旋支血管未见明显狭窄，TIMI3 级；右冠血管近中段至远段未见明显狭窄，第一后降支远段细小，远段闭塞，左室后支远段细小，远段闭塞。完善相关检查：（2024-01）NT-proBNP 1092.4pg/ml、肌钙蛋白 I 34.54ng/ml。电解质、肝肾功、血常规、C 反应蛋白、血脂、肝肾功、甲功、糖化血红蛋白未见明显异常。心电图：窦性心律，偶发房性早搏，左室高电压。心脏彩超：左房增大（前后径 55mm）、二尖瓣中度狭窄伴中度反流。(2024-

06）DD 聚 体 1mg/L、cTnI 0.47ng/ml、NT-proBNP 4186.3pg/ml。 复 查 cTnI 6.56ng/ml。心电图：窦性心律，III、aVF 导联轻微上抬。心肌酶谱：肌酸激酶 415.30U/L ↑、肌酸酶同工酶 66.3U/L ↑。血常规、C 反应蛋白、凝血功能、肝肾功、电解质、大小便常规、大便隐血未见明显异常。胸片：1. 心影增大；2. 慢性支气管炎、肺气肿征象； 3. 右侧胸腔积液。心脏彩超：左房增大（前后径 52mm）、二尖瓣增厚伴钙化，重度狭窄伴轻度反流。经食道超声 :1. 左心耳充盈及排空速度明显减低；2. 左心耳尖部弱回声附着，考虑血栓可能。多次完善动态心电图未见心房颤动。

鉴别诊断：

冠状动脉栓塞是记性心肌梗死一个重要的非动脉粥样硬化性原因，其表现与动脉粥样硬化性急性冠脉综合征相似。仅凭症状、心电图、心肌酶学变化和冠状动脉造影很难将冠状动脉栓塞与急性心肌梗死其他原因鉴别。

其他：

造影剂致急性喉头水肿 ECMO 下零造影剂救治一例

刘慧敏

哈尔滨医科大学附属第二医院

患者基本信息：

男患，76 岁

主述：

发作性胸闷胸痛半月

现病史：

半月前因胸闷胸痛于当地医院行 CAG，提示三支病变，为行进一步治疗来我院

既往病史：

高血压病 20 余年，血压控制不佳；糖尿病病史 9 年，胰岛素治疗

病程记录：

造影时发生过敏反应，出现喉头水肿，心脏骤停，ECMO 支持下零造影剂完成 PCI。

检验检查记录：

心电图 心脏彩超

鉴别诊断：

急性心梗

其他：

无

经导管封堵预激综合征导管消融术后左房左室瘘一例

何芊蓓

四川大学华西医院

患者基本信息：

男，30 岁

主述：

胸痛、肩颈部疼痛 1 月余

现病史：

患者于入院前 1 月无明显诱因出现左侧胸痛，向左肩颈部放射，为阵发性隐痛，无发热，无头晕、头痛，黑蒙、晕厥，无咳嗽、咳痰，呼吸困难，无恶心、呕吐、反酸等。2024-10-18 在我院行相关检查提示：MYO、CTnT、CK-MB、PRO-BNP、肝肾功能、血常规、血脂等未见明显异常。为进一步诊治来我院就诊。

既往病史：

扩心病病史 4 年余，预激综合征射频消融术后 4 年余。无糖尿病、高血压、高血脂等慢性疾病。

病程记录：

入院后行经导管封堵左房左室瘘，手术顺利完成。

检验检查记录：

术前超声心动图：左房 - 左室通道 左室收缩功能测值正常。

术前 CT：左心房下方（食管前）现大小约 2.7cmX2.0cm 突起，局部与左心经腔相连，请结合临床及其他检查。CTA：左心室增大，心脏房室间隔连续。房室连接及心脏大动脉连接术见异常。左心耳未见明品充盈缺损，室间及左心室心肌未见增厚。肺动脉主干、左右肺动脉及其分支未见明显狭容及扩张，未见充盈缺损。肺静脉左右各两支主干汇入左房。左心房内未见充盈缺损。右肺中叶内段小结节，长径约 0.3cm，多系炎性结节，请随诊。右肺下叶后基底段胸膜下小钙化灶。

术后超声心动图：左室假性室壁瘤 - 左房瘘封堵术后 3 天 封堵器旁未见明显分流 左室收缩功能测值正常

术后 CT：CTA：左心房下份环状高密度影伴放射状伪影，周围结构品示不清；左心室增大，心脏房室间隔连续。房室连接及心脏大动脉连接来见异常。左心耳未见明显充盈缺损，室间隔及左心室心肌未见增厚。肺动脉主干、左右肺动脉及其分支术见明品狭窄及扩张，未见充盈缺损。肺静脉左右各两支主干汇入左房。左心房内来见充盈缺损。

鉴别诊断：

患者既往病史及导管消融术史明确，超声心动图及增强 CT 均提示“左房左室瘘”。

其他：

从“出血倾向”到“冠脉血栓”——一例血友病 A 合并急性心肌梗死的治疗挑战

黄德华

广东省阳江市人民医院

患者基本信息：

姓名：陈文仁

性别：男性

年龄：71 岁

职业：缝纫工

婚姻状况：已婚

吸烟史 40 余年，1 包水烟烟丝 / 周（约 20 支香烟 / 日）；无酗酒史。

家族史：外公有血友病病史，父亲生前有 2 次脑梗塞病史（发病年龄约 70-75 岁间）；母亲有高血压、脑出血病史（发病时间约 70+ 岁）。共 5 个兄弟姐妹（3 个弟弟，2 个姐姐）；其中大姐有“胃癌”病史（已去世）；二姐有冠心病病史，曾植入冠脉支架；其中一个弟弟有胃癌病史（已去世），另一个弟弟有血友病病史（自杀过世）。

主述：

突发胸闷 4 小时。

现病史：

患者于 2025 年 4 月 15 日 19:30 洗澡后坐着看电视时突发胸闷，呈压迫感，非撕裂样，无放射痛，与呼吸运动无关，持续不缓解，伴出汗，休息后无好转。无呼吸困难，无咳嗽、咳痰、咯血，无腹痛、呕吐，无呕血、黑便，无晕厥、黑朦，无头晕、头痛，无单侧肢体肿痛，无抽搐，无发热。20:26 送至阳江市人民医院急诊。

既往病史：

血友病 A 病史 60 余年，曾出现多部位、多器官出血，如皮肤黏膜出血、下肢肌肉出血、肾出血、牙龈及舌出血，曾多次输血治疗，平素不规律使用“人凝血因子Ⅷ”替代治疗；末次用药为半月前因右上肢出血接受 “人凝血因子Ⅷ” 800 IU 治疗。目前已多关节变形、步态异常。高血压病史多年，最高收缩压 160mmHg，未规律服药及监测血压。否认糖尿病、脑梗死、脑出血、消化道出血、心脏病病史。

病程记录：

初始用药：阿司匹林肠溶片 300mg 、氯吡格雷片 300mg、瑞舒伐他汀钙片 20mg。

病情沟通：患者有急诊再灌注治疗指征，但患者合并血友病，有溶栓禁忌，优选 PCI 治疗，患者及家属急诊签字（21:00）不同意冠脉介入治疗。

再次评估：21:40 入院 CCU，21:41 复查心电图如右图。胸闷症状未完全缓解，请血液内科会诊建议术前静滴人凝血因子Ⅷ（1200IU ）降低出血风险，再次与患者沟通后同意手术（23：00）。

冠脉介入：冠脉呈右优型，LM 未见明显狭窄，LAD 管壁不整，D1 近段狭窄 50%，D2 近段狭窄 80%，TIMI 血流 3 级；LCX 中段次全闭塞，远段次全闭塞，TIMI 血流 3 级；RCA 管壁不整，TIMI 血流 3 级。于 LCX 远段及近段病变处分别予淇济 2.25×20mm、淇济 2.5×20mm 药物球囊予 8atm 释放 60s, 复行造影示血管成形佳，远段残余狭窄 30%,TIMI 血流 3 级。

术后用药：铝镁匹林片（1 片 po qd）、氯吡格雷（75mg po qd）、瑞舒伐他汀钙片（10mg po qd）、依折麦布（10mg po qd）、雷贝拉唑钠肠溶片（10mg po qd）。

病情转归：2025-04-18（术后第 3 天）病情好转，转入心内科普通病房；2025-04-21 出院。

随访情况：2025-4-26 至 2025-04-30 反复腹痛，考虑“腹腔出血”，急诊补充人凝血因子Ⅷ针。

2025-05-13 血液科门诊：血尿，再次补充人凝血因子Ⅷ针。

2025-05-19 心内科门诊：近 1 周反复血尿，因出血问题患者已自行停用所有心血管药物。团队讨论后继续服用他汀、依折麦布、叶酸片等药物，停用铝镁 匹林、氯吡格雷。

2025-05-21 至 2025-05-26 因“血尿”于血液科住院，补充凝血因子Ⅷ、止血对症治疗。

2025-06-17 心内科门诊：未再发出血，无胸痛症状，病情平稳。

检验检查记录：

实验室检查：

心肌酶谱：2025-04-15CK(肌酸激酶)367U/L，CK-MB(肌酸激酶同工酶)70.1U/L。

血脂：CHOL(总胆固醇)4.78mmol/l，TG(甘油三酯)2.00mmol/l，HDL(高密度脂蛋白胆固醇)0.90mmol/l，LDL-C(低密度脂蛋白胆固醇)2.99mmol/l，ApoA1(载脂蛋白 A1)1.09g/L，ApoB(载脂蛋白 B)1.12g/L，ApoA1/ApoB0.97，Lp-a(脂蛋白 a)203.3mg/L。

2025-04-16 N 端 -B 型钠尿肽原 (NT-proBNP)283.5pg/ml，肌钙蛋白 I(cTnI)43.80ng/ml。

凝血功能：2025-04-15 PT(凝血酶原时间)10.7Sec，Fib(纤维蛋白原)4.79g/L，APTT(活化部分凝血活酶时间)87.4sec。

凝血因子：凝血因子Ⅷ活性 （Ⅷ:C）14.70%（参考区间 50-150%）。

血常规：WBC(白细胞总数)11.07*10^9/L，Neu#(中性粒细胞数目)9.23*10^9/L，RBC(红细胞总数)4.09*10^12/L，HGB(血红蛋白)119g/l，HCT(红细胞比积)37.5%，PLT(血小板总数)231*10^9/L。

活化血小板功能：CD41 膜糖蛋白（CD41+/CD61+）99.84%，CD61 膜糖蛋白（CD61+/PLT）97.64%，CD42a 膜糖蛋白（CD42a+/CD61+）16.80% ↓，CD42b 膜糖蛋白（CD42b+/CD61+）99.92%，活化血小板（CD62P+/CD61+CD41+）1.31%，血小板 - 白细胞聚集（CD61+/CD45+）36.17% ↑。

易栓症基因检测：2 个风险因子。

1.NM_000602.5(PAI-1):c.-820G[(4_5)] (-675 4G/5G)。PAI-1 基因上游 2KB 内 (820) 位置的基因多态性，G 碱基的杂合缺失，该基因多态性跟体内纤溶酶原激活物抑制剂 -1(PAI-1) 水平显著相关，可能会导致纤溶系统功能抑制。

2.NM_005957.5(MTHFR):c.665C>T (p.Ala222Val)。MTHFR 基因 665 位置的碱基由 C 替换为 T，导致 222 位置的氨基酸由丙氨酸替换为缬氨酸，为杂合错义突变，基因突变导致叶酸生成不足，同型半胱氨酸含量相应增加，引起血管内皮损伤，血栓形成。

其他：HCY(同型半胱氨酸)12.7umol/L；CRP(C 反应蛋白) 15.82mg/l；UA（尿酸）412umol/L；HbA1c(糖化血红蛋白)5.7%

影像学检查：

心脏彩超：各房室不大，左室收缩功能正常（LVEF 69%），左室舒张功能减弱（ I 级）。

胸片：双下肺透亮度减低，可见散在条索状、斑片状阴影。

鉴别诊断：

1. 主动脉夹层（排除：无撕裂样胸痛、血压对称，影像学不支持）。

2. 肺栓塞（排除：无长期卧床、外科手术、恶性肿瘤等高危因素，无咯血、呼吸困难，D- 二聚体正常）。

3. 应激性心肌病（排除：否认近期情绪或躯体应激事件，心脏超声未表现为心尖球样扩张，冠脉造影提示冠脉有闭塞病变）。

其他：

追根溯源–血压难降，乏力背后的真相?

张芙溶

哈尔滨医科大学附属第二医院

患者基本信息：

男患，42 岁，身高 177cm，体重 86kg，BMI：27.5kg/m2

主述：

陈发性头晕 8 年，加重 1 个月

现病史：

患者于 8 年前无明显诱因出现血压高伴头晕，无乏力、气短，无咳嗽咳痰、无恶心呕吐、口服硝苯地平缓释片，可自行缓解，近 1 个月患者血压波动，控制不佳，上述症状反复发作，持续不缓解，伴头晕，心悸，伴乏力，偶伴气短。病程中饮食睡眠差，二便尚可。

既往病史：

既往强直性脊柱炎 23 年

病程记录：

门诊：患者自述肾上腺腺瘤，近期口服合心爽、可多华

泌尿系超声：提示前列腺轻大伴钙化形成，双肾、双肾血流、膀胱未见明显异常。卡托普利试验（+），ADRR ，遂入院诊治。

入院时：T:36.5℃，P:70 次 / 分，RR:18 次 / 分，BP:185/114mmHg

身高 177cm，体重 86kg，BMI：27.5kg/m2

自备肾上腺 CT：右侧肾上腺占位 1.0cm

检验检查记录：

皮质醇 8：00ACTH8:00, 皮质醇 16：00ACTH16:00,AVS,

鉴别诊断：

非醛固酮所致盐皮质激素过多综合征，Liddle 综合征，伴高血压、低血钾的继发性醛固酮增多症

其他：

无

ICD 植入治疗冠状动脉痉挛所致恶性心律失常一例

潘军

河北医科大学第二医院鹿泉院区

患者基本信息：

患者男性，69 岁，活动后胸闷、胸痛 5 年余，间断晕厥 3 个月入院。5 年前曾因心绞痛于右冠状动脉植入支架一枚。近 3 个月来，患者多次出现不明原因晕厥，住院期间患者再次出现晕厥，动态心电图记录到 II、III、avF、V5、V6 导联一过性抬高，随后出现室性心动过速及心室颤动，后能自行转复窦性心律，转复前有一过性停搏，复查冠脉造影未见冠脉狭窄，结合患者症状及其相关检查，考虑右冠状动脉痉挛所致恶性心律失常，最终采取植入 ICD 联合药物治疗。

主述：

活动后胸闷、胸痛 5 年余，间断晕厥 3 个月

现病史：

患者 5 年前开始出现活动后胸闷、胸痛症状，位于胸前区，向咽喉部放射，含服“速效救心丸”后能缓解，后于当地医院就诊，查冠状动脉造影并于右冠状动脉植入支架一枚（具体不详）。近 3 个月来，患者共发生 3 次一过性晕厥，每次发作前均有胸闷症状，含服“速效救心丸”不能缓解，伴有心悸、头晕症状，持续数分钟后出现一过性晕厥，晕厥数分钟后可自行苏醒，伴有大小便失禁，多次因晕厥就诊，未能明确病因。患者入院前 7 天再次出现晕厥，性质同前，于我科住院治疗。

既往病史：

既往无高血压、糖尿病病史，抽烟史 30 余年，约 40 支 / 日。

病程记录：

给予患者“阿司匹林肠溶片、替格瑞洛、琥珀酸美托洛尔缓释片、盐酸地尔硫卓片、单硝酸异山梨酯缓释片、尼可地尔片、阿托伐他汀钙片”等治疗，患者于入院第 3 天 14 时 44 分时再次出现胸闷症状，伴有心悸、头晕及乏力症状，12 分钟后出现晕厥，患者面色青紫，双眼上吊，身体抽搐，持续 45 秒左右恢复自主意识，Holter 记录仪成功记录发作时心电图回顾当地动态心电图记录：14 时 45 分 55 秒患者心电图 II、III、avF、V5、V6 导联 ST 段呈下斜型抬高 1.3mV（图 6），15 时 13 分 55 秒心电图提示室性心动过速（图 7），15 时 14 分 47 秒出现心室颤动（图 8），15 时 15 分 37 秒心电图由心室颤动转为停搏，6 秒后自行恢复窦性心律（图 9）。患者于入院第 4 天复查冠脉造影示：LM 未见异常，LAD 散在斑块浸润，未见有意义狭窄，LCX 散在斑块浸润，未见有意义狭窄。RCA 中段可见支架影，支架内未见狭窄（图 2-5）。结合患者症状、心电图表现及冠状动脉造影结果，提示右冠状动脉 CAS 所致恶性心律失常，停用琥珀酸美托洛尔缓释片，于入院后第 7 天行埋藏式心脏复律除颤器（ICD）植入治疗，加用盐酸地尔硫卓缓释胶囊 90mg BID，晕厥未再发作，1 周后出院。

检验检查记录：

心电图：窦性心律，大致正常心电图。血常规、肝功能、肾功能、电解质、心肌损伤标志物、BNP 均正常。头颅 MR 可见腔隙性梗死，颅脑动脉硬化。心脏超声、颈动脉、椎动脉、锁骨下动脉提示斑块，未见狭窄。

鉴别诊断：

1. 肺栓塞

2. 其他类型恶性心律失常

其他：

膀胱肿瘤患者肌酶持续升高 1 例 -- 免疫检查点抑制剂相关肌炎

张恒亮

河南科技大学第一附属医院

患者基本信息：

患者，宋 **，男，69 岁，农民。

主述：

确诊膀胱多发高级别浸润性尿路上皮癌 2 月余

现病史：

入院前 2 月余 (2024-05-20 左右) 患者因体检发现膀胱多发占位前来我院，先于我院介入科行（2024-5-30）左侧髂总动脉“经皮动脉支架置入术”，术后转入泌尿外科，于 2024-06-06 在全麻下行“经尿道膀胱肿瘤诊断性电切术”，术

后给予对症治疗后出院，术后病理示：（膀胱）浸润性尿路上皮癌，考虑为低分化的神经内分泌癌。建议患者行膀胱根治性切除术及左侧输尿管肿瘤根治术，患者及家属要求保守治疗，于 2024-7-6 行“特瑞普利单抗 + 吉西他滨 + 顺铂”抗肿瘤治疗一周期，化疗联合免疫治疗后患者出现骨髓抑制，于当地医院给予皮下注射粒细胞集洛刺激因子升白治疗。于 2024-7-23 行“特瑞普利单抗”治疗一周期。治疗期间曾自行口服“中药红豆杉”抗肿瘤。入院前 4 天（2024-08-06）患者无明显诱因出现胸闷、呼吸困难。2024-8-10 就诊于我院泌尿外科，拟行肿瘤术后序贯治疗。

既往病史：

有糖尿病病史 2 年，未规律服药，血糖未规律监测。

病程记录：

患者胸闷及呼吸困难于平卧位加重，端坐或侧卧位减轻，心电图示：频发室性早搏，完右。心脏彩超提示：左房增大，升主动脉增宽，三尖瓣少量反流，EF 55%。

血清肌钙蛋白 I 测定 :1.14ng/ml，肌红蛋白 :1751.1ng/ml，肌酸激酶同工酶 :90.2ng/mL，B 型钠尿肽 (BNP) 测定 :1080.00pmol/L，尿素 :10.2mmol/L，血清肌酐 :125μmol/L。急诊血常规：白细胞数目 (WBC):6.67x10^9/L，血红蛋白 HGB:104g/L，血小板数目 PLT:212x10^9/L。

考虑患者心肌酶升高，临床心功能差，不排除急性冠脉事件导致的心衰，于入院当天转我科继续诊治。

查体：血压 128/80mmHg，心率 105 次 / 分，呼吸 23 次 / 分，氧饱和度 85% 左右，神志清楚，查体合作。双上睑下垂，双肺可闻及湿啰音，心律齐，各瓣膜未闻及杂音，双下肢无水肿。

检验检查记录：

日期	8/10/2024	8/12/2024	8/13/2024
肌酐（umol/L）	125	130	124
尿素 (mmol/L)	10.2	9.3	9.1
BNP(pmol/L)	1080		
肌酐蛋白 i（ng/ml）	1.14		1.23
肌红蛋白（ng/ml）	1751.1		772.2
CK（U/L）		6350	5939
CK-MB(ng/ml)	90.2	149.4	156.7

入科后心肌酶进行性升高，常规心衰治疗后，尿量可，呼吸困难无改善。甲状腺功能异常，发病第 3 天开始伴有上睑下垂加重，下肢无力及肌肉酸痛进行性加重。

两次复查心脏彩超左房轻度增大（38m），左室（53mm）。左室壁运动欠协调。EF 56%。

胸部 CT：心包少量积液，胸腔少量积液，双肺渗出，未发现胸腺肿瘤等。

肌电图：隔神经重度损伤， 胸透提示隔肌功能正常。

鉴别诊断：

急性冠脉综合征？

重症肌无力？

副肿瘤综合征？

心力衰竭？

心肌炎？肌炎？

格林 - 巴利综合征？

横纹肌溶解？

肺栓塞？

化疗药物相关？

中药“红豆杉”相关？

胸腺肿瘤？

其他：

免疫检查点抑制剂（immune checkpoint inhibitors, ICIs）在实体肿瘤治疗中饱受青睐，其所致免疫相关不良事件（immune-related adverse events，IRAEs）发生率约为 4.2%。ICIs 相关肌炎的发生率 < 1%。但随着 ICIs 应用的增加，ICIs 相关肌炎的个案报道和病例系列报道越来越多。

跨越冠心病的思维定式：心脏结节病带来的诊断启示

杨兴丽

哈尔滨医科大学附属第二医院

患者基本信息：

男患，64 岁

主述：

阵发性胸闷胸痛 11 年，加重 1 个月

现病史：

患者于入院前 11 年于快步行走及上楼时出现阵发性胸闷胸痛，位于心前区，每次发作持续数分钟，服速效救心丸后可缓解。入院前 1 个月上述症状持续时间增长，偶有阵发性头晕，每次发作持续数十分钟后可自行缓解，伴有气短、喘憋、咳嗽、咳痰，无夜间憋醒、无端坐呼吸、无头疼、无视物旋转。病程中偶心悸、乏力、恶心，无畏寒发热，无呕吐、腹泻，无黑朦、晕厥及抽搐，无腹胀、纳差等其他不适主诉。现为求进一步治疗于我院就诊，病程中睡眠、饮食、二便尚可。

既往病史：

有糖尿病 10 余年，自行注射来得时每晚 24 单位，诺和锐 3 次 / 日、每次 10 单位，有高血压病史 10 余年，口服厄贝沙坦 75mg 每日 1 次，比索洛尔 5mg 每日 1 次，无吸烟饮酒史，否认家族遗传病史，自述 2022 年行冠脉造影无异常。

病程记录：

低盐低脂饮食

抗血小板、降脂、扩张冠脉等对症治疗

降压、控制血糖治疗

神经内科、内分泌科会诊

择期完善冠脉造影必要时支架植入

完善心脏核磁、风湿免疫系列化验

检验检查记录：

血常规：白细胞 8.8*109/L，中性粒细胞 76.6%，红细胞 5.13*1012/L，血红蛋白 169g/L，血小板 145*109/L；尿常规：蛋白质 1+，尿微量白蛋白测定 150mg/L，尿肌酐测定 17.7mmol/L，蛋白 / 肌酐 8.5mg/mmol，红细胞 3/HPF，比重 1.022，PH 5.5；粪便隐血试验阴性；

生化：未见明显异常，CK：54U/L，LDH:177U/L，CKMB:2.8ug/L，CRP：1.6mg/L，甲功正常，HbA1c：8.7%；

血气分析：PH7.42，PCO2：38mmHg，PO2：99mmHg，Lac:2.4mmol/L，HCO3-:24.1mmol/L，BE:-0.3mmol/L，SPO2：98%，钙 1.54mmol/L，钾：4.8mmol/L；

cTnI：1.457ug/L，MYO：372，CKMB：6.6，NT-proBNP :1057pg/mL；

凝血功能：未见明显异常

心脏彩超：左房扩大，左室壁增厚，右室壁增厚，考虑心肌病可能；主动脉弹性减低，室间隔心尖段及左室心尖部运动幅度减低，二尖瓣轻度反流，左室舒张功能不全 (I- II 级)，左室收缩功能减低。少量心包积液。

冠脉 CTA：左前降支近段钙化及非钙化斑块，管腔中度狭窄，左前降支中段心肌桥，壁冠状动脉无有意义狭窄回旋支中远段造影剂充盈欠佳，考虑中 - 重度狭窄主肺动脉内径 :3.08cm

心脏核磁：双房、左室增大，左室双期功能减低，非缺血性心脏病，左室壁多节段受累，受累心肌散在纤维化，左室壁局部水肿，考虑心脏结节病左室间隔壁中段脂肪沉积，二尖瓣、三尖瓣及主动脉瓣少量反流心包少量积液

鉴别诊断：

①缺血性心肌病：关键鉴别点在于冠状动脉解剖评估。冠脉造影显示非阻塞性病变，且 CMR/PET 显示非冠脉分布区（基底部为主）的异常有助于 CS 诊断。

②特发性扩张型心肌病：与 CS 相比，DCM 患者传导阻滞发生率较低， LGE 多呈线性中壁强化（不同于 CS 的斑片状）， FDG-PET 无局灶性摄取，女性比例较低

③致心律失常性右室心肌病（ARVC）：主要累及右心室（CS 多为左心主导），典型表现为右室脂肪浸润和室壁变薄，基因检测有助于确诊（桥粒蛋白突变）。

④心脏肿瘤：钙化性无定形肿瘤（CAT）：罕见（占原发性心脏肿瘤 2.5%），由钙化结节嵌入纤维蛋白基质构成，超声显示带蒂肿块，CT 可见高密度钙化，好发于左心系统（不同于本病例的右房 CAT）。

其他：

慢性血栓栓塞性肺动脉高压患者介入诊断和治疗 1 例

冯克福

安徽省立医院

患者基本信息：

患者，男，75 岁，

主述：

活动后气急胸闷 2 月

现病史：

患者，男，75 岁，因“活动后气急胸闷 2 月”于 2025 年 2 月 222 日入院，患者自诉入院前 2 月出现活动较前受限，休息后缓解，无胸痛和晕厥。

既往病史：

高血压病史 1 年余，慢性阻塞性肺病病史 10 余年

病程记录：

临床诊断：急性肺栓塞、COPD、高血压病。入院后给予吸氧、利伐沙班抗凝、控制血压和改善心室重构治疗。患者正规治疗 3 月，自诉仍有活动后气急胸闷症状，复查肺动脉造影提示 LA10 近中段闭塞，给予 BPA 治疗，术中 2.5/15mm 球囊扩张后远端血管未显影，指引导管至闭塞病变远端超选择造影可见血管显影（图 1）。IVUS 检查提示管腔内血栓性病变，血栓密度接近纤维化组织（图 2）。

检验检查记录：

入院后完善相关检查：血常规、NT-proBNP、心肌坏死标记物、肝肾功能、甲状腺功能、免疫组合、肿瘤全套、抗核抗体全套、血管炎相关抗体等均未见明显异常。UCG 示 LA 41mm，LVEDD 56mm，LVEF 67%，sPAP 72mmHg。ECG: 窦性心律。CTPA; 左下叶后基底段低密度充盈缺损，肺气肿。肺 ECT 提示左下肺内基底段灌注缺损。右心导管检查：导管路径未见异常，mPAP 24mmHg，SvO2 60%，PVR 3.03woods，CI 2.7L/min.m2，结论：毛细血管前性肺动脉高压。肺动脉造影提示 LA10 近中段闭塞。

鉴别诊断：

结合患者病史特点，可排除左心功能不全、内分泌性疾病、血液性疾病、神经肌肉性疾病导致活动耐量下降。

其他：

慢性血栓栓塞性肺动脉高压（CTEPH）的病理特征是机化的血栓阻塞肺动脉，伴随非阻塞部位的小血管病变 [1]。2016 年 Kawakami 等 [2] 首次提出了 CTEPH 五种造影分型：环状狭窄、网状病变、次全闭塞病变、完全闭塞病变和迂曲病变。其中完全闭塞病变是未溶解的血栓慢性机化导致整个血管完全闭塞，迂曲病变多为血管长期闭塞后自身侧支循环形成所致，完全闭塞病变和迂曲病变治疗难度大，并发症发生率较高 [3]。理论上，近期闭塞血管其腔内组织较松软，在介入治疗过程中，导丝更容易通过病变组织，随着闭塞时间延长，血管腔内红色血栓发生纤维化，组织病变更加复杂，手术成功率降低。因此，对于闭塞病变，尽早介入治疗，能够提高开通血管成功率，但由于血栓机化过程尚不明确，如果手术时间过早，可能会出现本例病变情况，因此，延长抗凝治疗时间等待血栓充分机化且尚未发生完全纤维化可能是介入治疗的最佳时机，但急性肺栓塞抗凝治疗后多久接受介入治疗的时间窗尚需进一步研究。当然，本例患者腔内检查存在局限性，对于完全闭塞的血栓性病变给予 OCT 检查可能更好观察血栓病变性质。

参考文献

1、Delcroix M,Torbicki A,Gopalan D,et al.ERS Statement on Chronic Thromboembolic

Pulmonary Hypertension.Eur Respir J. 2021-06-01;57(6).

2、Kawakami T, Ogawa A, Miyaji K, et al. Novel angiographic classification of each vascular lesion in chronic thromboembolic pulmonary hypertension based on selective angiogram and results of balloon pulmonary angioplasty[J]. Circ Cardiovasc Interv, 2016, 9(10): e003318.

3、Lang IM, Andreassen AK, Andersen A, et al. Balloon pulmonary angioplasty for chronic thromboembolic pulmonary hypertension: a clinical consensus statement of the ESC Working Group on Pulmonary Circulation and Right Ventricular Function[J]. Eur Heart J, 2023, 44(29): 2659-2671.

Treat-repair 策略治疗房间隔缺损相关性肺动脉高压 1 例

冯克福

安徽省立医院

患者基本信息：

患者，女，28 岁，因“活动后气急胸闷 1 周伴晚孕”于 2024 年 11 月 21 日入院，

主述：

活动后气急胸闷 1 周伴晚孕

现病史：

患者本次因活动后呼吸困难 1 周伴晚孕（孕 38+2 周）拟入院妊娠，入院后会阴保护下分娩分娩出一活婴。患者分娩前已存在胸闷症状，但能耐受，分娩后即刻呼吸困难加重，血氧饱和度 88%-90%，转至 ICU，给予利尿、呼吸机辅助呼吸治疗症状少改善。

既往病史：

自诉既往体健，无高血压、糖尿病等慢性病史，2020 年足月顺产一男婴。

病程记录：

患者分娩前已存在胸闷症状，但能耐受，分娩后即刻呼吸困难加重，血氧饱和度 88%-90%，转至 ICU，给予利尿、呼吸机辅助呼吸治疗症状少改善，急诊完善相关检查，临床诊断：房间隔缺损相关性肺动脉高压，I 型呼吸衰竭、WHO 心功能Ⅳ级，给予改善心功能、安立生坦、他达拉非和曲前列尼尔治疗后病情稳定出院。

患者正规治疗 3 个月后再次入院，复诊 UCG：LA 35mm，LVEDD 41mm，sPAP 54mmHg，房间隔缺损（II 孔型，左向右分流）、肺动脉高压（中度）。右心导管检查：mPAP 31mmHg，PVR 2.94woods，Qp/Qs 2.23。结论：房间隔缺损，毛细血管前性肺动脉高压。2025 年 2 月 28 日行房间隔封堵术，术后复查 UCG 提示 sPAP 44mmHg，继续给予安立生坦、他达拉非和曲前列尼尔和改善心功能治疗，院外加用司来帕格逐步替代曲前列尼尔，定期门诊复诊，患者多次复查 UCG 提示 sPAP 正常，曲前列尼尔逐渐减量并停用，继续应用安立生坦、他达拉非和司来帕格和改善心功能治疗，患者病情稳定，择期复查右心导管。

检验检查记录：

2024 年 11 月 22 日

急诊 UCG：LA 25mm，LVEDD34mm，sPAP80mmHg，房间隔缺损（II 孔型，双向低速分流）、重度肺动脉高压。ECG：窦性心动过速，电轴右偏。CTPA 排除急性肺栓塞。

2025 年 2 月 22 日，正规治疗 3 个月后

UCG：LA 35mm，LVEDD 41mm，sPAP 54mmHg，房间隔缺损（II 孔型，左向右分流）、肺动脉高压（中度）。

右心导管检查：mPAP 31mmHg，PVR 2.94woods，Qp/Qs 2.23。结论：房间隔缺损，毛细血管前性肺动脉高压。

2025 年 2 月 28 日行房间隔封堵术，术后复查 UCG 提示 sPAP 44mmHg，

鉴别诊断：

结合患者病史特点，可排除急性肺栓塞、左心衰竭、DIC 等导致严重呼吸困难。

其他：

先天性心脏病相关性肺动脉高压（CHD-PAH）不同于特发性肺动脉高压，早期肺动脉主要表现为血管中膜增厚、正常非肌性小动脉肌性化等可逆性病变，即以动力性肺动脉高压为主，如果未能尽早关闭缺损，体肺分流持续损伤肺血管，触发血管内膜发生丛状病变，造成肺血管床不可逆性重构，演变为阻力性肺动脉高压，导致部分患者失去手术时机 [1]。Takaya

等 [2] 研究发现，Treat-repair 策略对于处理 CHD-PAH 血流动力学状态处于动力性和阻力型之间“灰色地带”患者具有重要临床价值。本例患者初诊时为房间隔缺损伴双向分流的重度肺动脉高压患者，经 Treat-repair 策略治疗后为患者创造手术机会，术后患者病情稳定。由于目前尚无明确区分动力性或阻力型肺动脉高压的方法，Qp/Qs 和 PVR 是评价血管病变的替代指标，该指标与预后关系存在不确定性 [1]。而且指南推荐的评估方法多来自于回顾性研究，尚缺乏高质量循证医学证据，因此，对于房间隔缺损相关肺动脉高压患者的矫正术需谨慎，且术后需要规律靶向药物应用。

参考文献

1、Jone PN,Ivy DD,Hauck A,et al.Pulmonary Hypertension in Congenital Heart Disease: A Scientific Statement From the American Heart Association.European Heart Journal，Circ Heart Fail. 2023;16(7):e000080. DOI: 10.1161。

2、Takaya Y, Akagi T,Sakamoto I,et al.Efficacy of treat-and-repair strategy for atrial septal defect with pulmonary arterial hypertension. Heart 2022;108(5):382-387.

一例 Takotsubo 综合征的病例报告

张璐

石河子市人民医院

患者基本信息：

67 岁女性

主述：

突发胸闷、气短 1 天，加重 2 小时余

现病史：

患者于 1 天前无明显诱因出现胸闷、气短症状，无胸痛、大汗，未在意未进行诊治，2 小时前突感上诉症状加重，为求进一步诊治就诊我院急诊科，完善心电图提示“前壁导联 st-t 改变”，急诊以“急性冠脉综合征”收入我科。

既往病史：

既往否认高血压、糖尿病、脑血管病史。

病程记录：

入院后急诊完善冠脉造影提示：右冠优势型，LAD：近段斑块，RCA：中段斑块。给予阿司匹林抗板治疗，阿托伐他汀调脂稳斑，辅酶 q10 改善心肌代谢。

检验检查记录：

心电图：广泛导联 ST-T 改变，心脏彩超：左室壁运动不协调：前间隔（心尖段 + 中间段）、前壁（心尖段 + 中间段）及心尖部运动较周围室壁明显减弱，左室收缩功能减低（EF：44%）。冠脉造影：右冠优势型，LAD：近段斑块，RCA：中段斑块。脑利钠肽前体测定：812pg/ml，肌钙蛋白 T：0.113ng/ml，肌红

蛋白：26.87ng/ml，肌酸激酶同工酶：2.44ng/ml，病毒相关检查：巨细胞病毒抗体 IgM<5.0U/ml，巨细胞病毒抗体 IgG 测定 >180.0U/ml，单纯疱疹病毒抗体 1=2 型 IgG 测定 27.3U/ml，风疹病毒抗体 IgG 测定 16.1U/ml，血常规、肝肾功、甲功、ENA、CCP、离子均正常。12 小时后复查患者肌钙蛋白 T 降至 0.050ng/ml，肌红蛋白、肌酸激酶同工酶均降至正常范围，2024 年 7 月 20 日复查脑利钠肽前体测定 74.4pg/ml。心脏核磁: 1、左心室收缩功能轻度减低（LVEF 46.86%,CO 4.01L/min ，EDVi 64.73ml/m2）。 2、主动脉瓣及二尖瓣轻度关闭不全。3、左心室前壁中段及心尖部前壁运动减弱。增强扫描：心肌首过灌注未见确切异常强化，延迟扫描未见确切高信号显示。2024 年 7 月 19 日复查心电图 T 波较前部分导联已恢复。6 月后（2025 年 1 月 10 日）复查心脏彩超：室间隔及左室壁各节段厚度正常，运动协调，收缩幅度正常。1 年后（2025 年 7 月）复查心电图：窦性心律，正常心电图。

鉴别诊断：

与心绞痛鉴别: 疼痛特点: 心绞痛多为压榨性胸痛, 持续数分钟（一般 <20 分钟），休息或含服硝酸甘油可缓解；心梗疼痛更剧烈，持续时间 >30 分钟，且药物无法缓解。心电图表现：心绞痛无 ST 段持续性抬高或压低，无病理性 Q 波；心梗可出现 ST 段动态演变（如抬高或压低）及病理性 Q 波。心肌酶学：心绞痛无心肌酶（如肌钙蛋白、CK-MB）显著升高，而心梗患者心肌酶呈典型升高曲线。

其他：

携带 TTR 基因 S77F 突变的迟发型转甲状腺素蛋白心肌淀粉样变一例

陈梓航

中山大学附属第一医院

患者基本信息：

年龄 / 性别：73 岁男性

基因型：S77F

主述：

反复胸闷 7 年，再发伴气促 2 月。

现病史：

患者 7 年前无明显诱因开始出现活动后胸闷，无咳嗽、咳痰。2 月前胸闷症状较前加重，平静状态下也有胸闷、气促，有端坐呼吸、夜间憋喘，伴双下肢凹陷性水肿，偶有咳嗽，咳白痰，无发热，无头晕，无腹痛、腹泻。

既往病史：

阵发性心房颤动

冠状动脉粥样硬化性心脏病

前列腺增生

病程记录：

一、初步排查阶段：

1、体格检查：BP94/61mmHg。双肺闻及少量湿性啰音，第一心音强弱不等，心律绝对不齐，双下肢中度浮肿

2、实验室检查：NT-proBNP 1037pg/ml，高敏肌钙蛋白 T 58.8pg/ml

3、心电图：肢体导联低电压、心房颤动、间歇性三度房室传导阻滞

4、超声心动图：III级舒张功能障碍，双心房扩大，严重向心性左心室肥厚（厚度 16mm），心肌内斑点状回声（提示淀粉样变性）

5、肌电图：感觉和神经运动功能障碍，多发性周围神经损伤

初步结论：

二、病因诊断与确诊阶段：

1、排除轻链型淀粉样变（AL）：

血清游离轻链检测、血清 / 尿蛋白免疫固定电泳：均为阴性

2、通过影像学和病理活检确诊 ATTR-CM：

99mTc-PYP 骨闪烁显像：Perugini 3 级；1 小时 H/CL（心 / 对侧）比值 1.51，3 小时 H/CL（心 / 对侧）比值 1.43

心肌活检：淀粉样物质沉积（刚果红染色阳性），免疫组化证实沉积蛋白为 TTR

3、通过基因明确基因型：

基因检测：S77F 杂合突变

三、治疗阶段

患者拒绝治疗

检验检查记录：

·NT-proBNP 1037pg/ml，高敏肌钙蛋白 T 58.8pg/ml

·心电图：肢体导联低电压、心房颤动、间歇性三度房室传导阻滞

·超声心动图：III级舒张功能障碍，双心房扩大，严重向心性左心室肥厚（厚度 16mm），·心肌内斑点状回声（提示淀粉样变性）

·肌电图：感觉和神经运动功能障碍，多发性周围神经损伤

·99mTc-PYP 骨闪烁显像：Perugini 3 级；1 小时 H/CL（心 / 对侧）比值 1.51，3 小时 H/CL（心 / 对侧）比值 1.43

·心肌活检：淀粉样物质沉积（刚果红染色阳性），免疫组化证实沉积蛋白为 TTR

鉴别诊断：

鉴别诊断：

1、轻链型淀粉样变（AL）；

支持点：检验结果、超声心动图均提示淀粉样变导致心衰可能性大。

不支持点：血清游离轻链检测、血清 / 尿蛋白免疫固定电泳均为阴性。

结论：暂不考虑。

2、心动过速心肌病

支持点：房颤伴快速心室率，NT-proBNP 水平升高。

不支持点：超声心动图提示无收缩功能障碍，有舒张功能障碍，有室壁肥厚。

结论：暂不考虑。

其他：

ECMO 支持下二叶瓣实战

翁浩宇

北京大学第一医院

患者基本信息：

63 岁男性，急诊入院

主述：

活动后气短 1 年，加重一月就诊

现病史：

1 年前患者出现活动相关气短，就诊于外院提示 EF 35%，全心扩大，主动脉瓣重度狭窄合并中度关闭不全，二尖瓣轻 - 中度流，对症治疗后患者好转，外院建议患者行瓣膜置换，患者拒绝。1 月前患者出现轻微活动后明显喘息，夜间不能平卧，双下肢水肿，进行性加重。急诊查 ALT 344IU/ L , AST 481IU/ L , Scr 197.2umol/ L ,K 5.56mmol/ L , CK - MB 4.0ng/ ml , TnI 172.7ng/ L , BNP >4967.0pg/ ml。血常规： WBC 17.54*10^9/L, Hb 132g/ L , Plt 754*109/L, NE %90.1%, CRP 8.89mg/ L。ABG : pH 7.42,PC0224mmHg, P02 151mmHg, Lac 4.1mmol/ L ,HC03-15.6mmol/ L。

既往病史：

既往高血压，血压未规律监测。否认其余病史。否认吸烟饮酒史。

病程记录：

入院后完善相关检查：EF 15.3%，左室舒张末内径 7.2cm，室间隔厚度 1.3cm，主动脉瓣二叶畸形，左 - 无融合，主动脉瓣口峰值流速 423cm/s，峰值压差 72.4mmHg，平均压差 43.1mmHg，瓣口面积 0.97cm^2。予以去甲肾上腺素、多巴酚丁胺、新活素泵点，无创呼吸机辅助通气，利尿后患者症状稍好转，逐渐减停血管活性药物。后除外禁忌后在 ECMO 支持下行 TAVR 术。手术顺利，患者血流动力学稳定，逐渐撤除 ECMO，康复出院。

检验检查记录：

3 月后患者复查超声心动：EF 58.8%，左室舒张末内径 5.7cm，室间隔厚度 1.6cm，主动脉瓣口峰值流速 310cm/s，峰值压差 38.6mmHg，平均压差 17.8mmHg，瓣口面积 1.8cm2。

鉴别诊断：

缺血性心肌病

高血压心脏病

扩张型心肌病

其他：

“钙化三剑客”对一例冠脉搭桥术后患者的治疗价值

王连旭

哈尔滨医科大学附属第二医院

患者基本信息：

陈某，女，78 岁

查体：体温：36 ℃，脉搏：65 次 / 分，呼吸：19 次 / 分，血压：119/61mmHg。

主述：

心悸 4 年。

现病史：

现病史：患者 4 年前出现心悸，不伴心前区及左臂部放射痛和咽部紧缩感，不伴出汗、乏力，无恶心、呕吐，无头晕、头痛，无咳嗽、咳痰。症状持续约 10 余分钟，于休息后逐渐缓解，未予重视及系统治疗。现为求进一步诊治来我院治疗。患者患病以来，饮食二便正常，睡眠欠佳。

既往病史：

既往史：冠脉搭桥术后 9 年；糖尿病 20 年，肌注胰岛素治疗；心房颤动 4 年。

病程记录：

7 月 5 日完善相关检查后确诊：不稳定型心绞痛；冠状动脉粥样硬化性心脏病；心脏搭桥术后; 糖尿病; 心功能不全。综合以上情况，决定决定对患者行 CAG 治疗，必要时行 PCI 治疗。

7 月 7 日手术治疗，术中发现患者前降支近段、右冠状动脉中段完全闭塞，回旋支近段次全闭塞，TIMI 血流 2。本次罪犯病变为 LCX，分别在回旋支远端、回旋支至左主干处置入 2 枚支架，并行 IVUS 腔内影像学辅助检查，术后患者体征平稳，返回心血管重症监护室。

术后第一日（7 月 8 日），患者生命体征平稳，无不适主诉，于 13 点拔除 IABP，术区加压包扎，规律口服双抗、利尿等改善心功能，维持窦性心律的药物。

7 月 9 日查房，患者无不适，术区恢复良好，复查心电图无异常变化，转入心内科普通病房。

7 月 10 日，行有氧训练，心肺功能康复评定，好转出院。

检验检查记录：

高敏肌钙蛋白：49.2ng/L

BNP：2274pg/ml

肌酸激酶：65U/L

肌酸激酶同工酶：11.1U/L

国际标准化比值：1.01

肝肾功离子，凝血象，血常规均正常

心脏超声、下肢血管超声

鉴别诊断：

急性心肌梗死：急性心肌梗死是血管急性闭塞导致的心肌细胞坏死，发作症状重、疼痛持续时间长，伴有其他全身症状，如焦虑、烦躁、大汗，甚至恶心、呕吐，心电图出现动态演变伴心肌酶升高。

主动脉夹层：主动脉夹层是致命性的急性大血管病变，表现为突发后背部、胸背部撕裂样疼痛，疼痛刚开始即达到高峰。患者多伴随高血压、动脉粥样硬化等高危因素，通过主动脉 CTA 可以鉴别。

反流性食管炎：反流性食管炎与饮食、体位有关，通过冠脉造影、胃镜相鉴别。

肋间神经痛：肋间神经痛通常表现为肋软骨有压痛。

心脏神经官能症：心脏神经官能症患者常诉胸痛，但对于短暂刺痛或持续性隐痛，喜欢时不时深呼吸或叹气样呼吸，且血管造影中不能有明显阳性发现。

其他：

”钙化三剑客“治疗的意义：患者病变复杂，主血管闭塞，且存在搭桥病史。因此，选择何种方式通开血管显得极为重要。术中根据患者一般情况及血管情况，最终再 IABP 辅助下行冠状动脉内膜高速旋磨术，经皮冠状动脉粥样斑块切除术，振波球囊术，并置入 2 枚支架。患者术后体征平稳，好转出院。

生死时速：一例心脏性猝死的救治

游洁芸

上海市东方医院（同济大学附属东方医院）

患者基本信息：

患者，男性，64 岁。

主述：

持续性胸痛 10 小时。

现病史：

患者入院前 10 小时出现持续性胸痛，伴背部放射痛、出汗，无发热，无咳嗽、咳痰，无恶心、呕吐，无黑矇、晕厥，无腹胀、腹痛，无头晕、头痛，症状持续不能缓解。遂于今晨 06:30 来我院就诊，查心电图（06:40）提示：1、窦性心律 2、S-T 段异常（aVR、V1、V2 水平 / 上斜抬高 0.5-2.0mm，II、III、aVF、V4、V5、V6 水平压低 1.0-3.0mm）。06:42 患者于急诊抢救室突发意识丧失，呼之不应，急诊心电监护室颤。予 200J 双向非同步电除颤一次，积极给予肾上腺素 1mg 静脉推注 2 次，2 分钟后患者恢复窦性心律，意识恢复，复查心电图提示频发室早，短阵室速，ST-T 较前无动态改变。急诊血气未见异常。继续予可达龙 150mg 静脉推注 +300mg 静脉推泵改善心律。并予阿司匹林 100mg+ 倍林达 90mg 嚼服，开通绿色通道行急诊冠脉造影。现为求进一步诊治，收治入院。

既往病史：

入院前 8 个月及 5 个月因 “不稳定性心绞痛” 择期行 PCI 术，于 LAD 近中段植入支架共 2 枚；高血压、脑梗死病史；吸烟史 2 年，10 支 / 天。

病程记录：

患者入院后反复出现室颤，持续 CPR+ 多次电除颤 + 机械通气 + 肾上腺素 / 去甲肾上腺素维持，ECMO 支持下完成冠脉造影，植入 IABP。

急诊冠脉造影示前降支非支架节段 70-80% 狭窄，回旋支全程纤细，右冠未见闭塞及狭窄。造影未见支架内血栓形成及斑块破裂征象，与既往冠脉影像资料相比，本次造影过程中，冠脉血管全程纤细，考虑冠脉痉挛所致。

术后予 ECMO+IABP 辅助（ECMO 流量 3.0L/min，IABP 心电 1:1 触发），机械通气，去甲肾 0.2ug/kg/min 维持循环，丙泊酚镇静 + 咪达唑仑充分镇静，胺碘酮 1mg/min+ 艾司洛尔 0.2mg/kg/min 抗心律失常，钾镁泵维持。但仍反复室速室颤发作，逐步滴定抗痉挛药物（硝酸酯类、贝尼地平、地尔硫卓、尼可地尔、他汀）。第 7 天起室性心律失常逐步控制，心功能逐步改善，第 7 天撤除 ECMO，第 8 天拔除气管插管，第 11 天拔除 IABP。本例患者因冠脉痉挛导致心搏骤停，发病时心电图见明显 ST 段抬高，有冠心病基础，属于高危患者，第 27 天行 ICD 植入术，第 31 天出院。

检验检查记录：

入院时检查结果：

1、心电图：窦律，ST 段改变（前壁、下壁导联压低，aVR 导联抬高）；

2、心超：左室壁节段运动异常，左室收缩功能减低，未见明显心包积液，EF30%；

3、心肌酶：NT-proBNP 714.9 ng/L ↑，cTnT 0.608 ng/mL ↑，CK-MB 9.07 ng/mL ↑，Myo 698.4 ng/mL ↑；

4、血气分析：K 3.5 mmol/l，Lac 5.8 mmol/l ↑。

鉴别诊断：

急性心肌梗死、主动脉夹层、急性肺动脉栓塞、暴发性心肌炎、急性心包炎、原发性心肌病急性加重、其他引起胸痛的疾病。

其他：

病例亮点：

1. 心原性猝死患者死亡率极高，国内外指南均指出，院外心脏骤停复苏成功的 STEMI 患者，包括未确诊但高度怀疑心肌缺血的患者，应当尽快接受冠脉造影检查及可行的干预。在临床实践中，不同于常规的心梗患者救治，心肺复苏后患者往往在急诊间就已接受机械通气等有创辅助，对这部分患者实施急诊冠脉造影检查和治疗过程中往往需要动用更多的人力，包括搬运及心内科以外其他科室医护协助等。这就需要相关医疗单位有充分的预案，在短时间内能集结心内科、呼吸科、麻醉科、心外科、重症医学等学科医护，多学科团队作战，来应对这类情况，以避免治疗的延误。东方医院心脏团队中包括了心内、心外、重症医学等科室，对相应情况可以快速响应，也在心脏重症患者救治方面积累了大量的经验。

2. VA-ECMO 已越来越多的应用于心脏重症患者的救治，对于出现有效循环不能维持、组织灌注不足、代谢紊乱的患者，应当尽早应用 ECMO 辅助以改善全身组织供血及代谢，后者是休克患者救治的重要组成部分。鉴于 VA-ECMO 应用本身增加心脏后负荷，应用于心原性休克患者时建议常规和 IABP 联合使用，以最大程度降低心脏后负荷。ECPR 的实施同样需要一个能快速反应、合作熟练的心脏团队，与此同时，ECMO 应用后的管理与快速植入同样重要，以避免器械本身带来的并发症。

3. 冠状动脉痉挛在临床并不少见，但因冠脉激发试验较少进行，其通过冠脉血管大小的直观改变来最终确诊的并不多。医生往往根据临床症状、心电图改变和非激发试验下的冠脉造影结果（需排除有血流动力学意义的固定狭窄，个别病例在造影过程中可见导管刺激导致的冠脉痉挛表现）等方面判断患者是否存在冠脉痉挛因素所导致的临床症状。鉴于痉挛本身可导致缺血症状外，血管痉挛也是促发斑块破裂的重要原因，而后者是 ACS 发病的主要原因。因此，在临床工作中应当重视对冠脉痉挛的诊治，以预防猝死等严重不良后果。冠脉痉挛的治疗原则已在文中加以叙述，对于已应用地尔硫卓、硝酸酯类等一线药物干预后症状仍反复出现的患者，可贝尼地平、尼可地尔等二线治疗药物，往往可以更好的控制症状，但需要密切随访患者的血压及心率情况。ICD 植入本身并非冠脉痉挛患者治疗的推荐，但其在猝死二级预防中具有重要的价值。本例患者住院的后一阶段中在药物下未在有室性心律失常发作，为更好的二级预防，出院前给予了 ICD 植入。

4. 冠脉病变快速进展在这一患者中表现突出，首次 PCI 治疗 3 个月后因症状复发再次造影检查，发现其前降支开口部位明显狭窄加重并有血栓迹象，并再次予以支架植入治疗。斑块破裂及后续局部血栓形成，在造影影像下即表现为前降支开口部位的明显狭窄，临床上表现为胸痛复发。而冠脉痉挛则可能是导致斑块破裂的重要原因，其他可能导致病变进展加速的因素，如前次操作损伤等，若无急性血栓形成，一般不会在 3 个月的时间里让狭窄明显加重。本例患者在末次急诊造影时可见前降支开口部位支架和中段支架支架的自身冠脉血管段有痉挛表现，对于这一段支架未覆盖血管节段的斑块情况及性质，急诊未行影像学检查。后续我们会密切临床随访，必要时可考虑再次冠脉造影并进行 OCT 等腔内影像学检查以评估其风险程度。

“药物性高血压急症”遇上“肾上腺危象”：一剂“民间秘方”引发的风暴

Haojie Yan

中国人民解放军总医院心血管医学部

患者基本信息：

***，男，50 岁

主述：

头痛 1 天

现病史：

患者于 2024 年 4 月 4 日无明显诱因出现头痛，伴头晕、嗜睡，在家自测血压最高 220/110mmHg，服用止痛药物后出现恶心，呕吐 2 次，不伴视物不清、抽搐、肢体瘫痪、失语等伴随症状。4 月 5 日 7：00 就诊于我院急诊，测血压 200/123mmHg，给予乌拉地尔降压治疗后收入院。

既往病史：

既往史：（1）否认高血压（常自测血压）和心脑血管疾病病史

（2）荨麻疹病史 1 年，口服药物治疗 6 个月（民间药物，具体成分不详）

个人史和家族史

（1）吸烟史 10 年，每日 60 支

（2）饮酒史 10 年，每周 2-3 次，每次约 150g

（3）母亲患有高血压病

体格检查：（1）心率：99 次 / 分，血压：166/113mmHg，体重：115kg，BMI：36.3

（2）嗜睡状态，神志清楚，对答切题

（3）全身皮肤可见片状色素沉着，皮肤发硬，球结膜水肿

（4）甲状腺大小正常，未触及包块和震颤，

（5）双肺呼吸音清，未闻及干湿罗音

（6）心尖搏动正常，心界叩诊正常范围，心率 99 次 / 分，律齐，各瓣膜听诊区未闻及病理性杂音，周围血管征 (-)

（7）腹型肥胖，余无明显腹部阳性体征，

（8）生理反射正常，病理反射未引出

病程记录：

诊疗过程：心电、血压以及脉氧饱和度监测

降压治疗：盐酸乌拉地尔注射液、硝普钠持续泵入

厄贝沙坦片 150mg 口服 1/ 日

非洛地平缓释片 5mg 口服 1/ 日

纠正电解质紊乱：15% 氯化钾

10% 氯化钠

口服枸橼酸钾溶液

请神经内科、内分泌科急会诊，完善检查查找继发性高血压线索

辅助检查结果：肾上腺 CT：双侧肾上腺 CT 扫描未见异常

血清皮质醇：0am 582.6nmol/L，8am 1196.41nmol/L，4 pm 1022.49nmol/L

血浆促肾上腺皮质激素: 0am 2.49pmol/L, 8am 15.8pmol/L, 4pm 1.87pmol/L

24 小时尿皮质醇 5290.4nmol/L

病情变化：中午突然谵妄状态，躁动，查体欠合作。

心电监护：血压波动于 160-180/100-115mmhg，心率 80-90 次 / 分

急查血常规：白细胞计数 12.71×10^9/L、中性粒细胞 87.2%

急查血生化：葡萄糖 9.84mmol/L、钠 117.0mmol/L、氯化物 82.5mmol/L、钾 3.55mmol/L

联合会诊 -1：内分泌科：诊断考虑抗利尿激素不适当分泌综合征和肾上腺皮质功能不全可能。建议：1. 监测血、尿电解质，注意稀释性低钠血症、水中毒，记 24 小时出入量，在维持血容量正常情况下，避免过多入量。2. 肾上腺皮质功能不全诊断不排除，可以酌情给予氢化可的松。

神经内科：考虑弥漫性脑损伤，存在脑水肿。建议：1. 行颅脑 CT 检查；2. 必要时行脑脊液检查并测压；3. 应用白蛋白 20g 与甘油果糖 250ml 交替应用，给予脱水治疗；4. 纠正低钠低氯血症。

神经内科复诊：头颅 CT 考虑存在脑水肿，但未见脑出血、脑梗塞、脑部占位等影像学改变。

联合会诊后治疗方案调整：经口气管插管，呼吸机辅助呼吸，静脉给予呋塞米，人血白蛋白注射液，甘油果糖氯化钠注射液

联合会诊 -2：心血管内科、内分泌科、神经内科、风湿科、呼吸科、血液科

明确诊断：肾上腺危象 代谢性脑病 继发性高血压 低钠低氯血症

制定治疗方案：

①激素替代治疗：氢化可的松琥珀酸钠 100mg 1/ 日

②纠正脑水肿：甘油果糖 50mg，1 次 /12 小时，白蛋白 10g，1 次 /12 小时

③持续镇静，呼吸机辅助呼吸

检验检查记录：

化验检查：

（1）白细胞计数 12.51×109/L，中性粒细胞 87.1%

（2）血浆 D- 二聚体 0.82μg/mL

（3）钾 3.00mmol/L，钠 120.2mmol/L，氯化物 85.0mmol/L，葡萄糖 9.89mmol/L，总胆固醇

（4）5.18mmol/L, 低密度脂蛋白胆固醇 3.43mmol/L，肝肾功能正常

（5）动脉血气：PO2 75mmHg，PCO2 32mmHg，pH 7.44，Lac 1.3mmol/L

心电图：窦性心律，心率 107 次 / 分，肢体导联和胸前导联 T 波低平，可见 U 波

胸片：老年性心肺改变

颅脑 CT：颅脑 CT 平扫未见明显异常

超声心电图：左心室舒张末期内径 45mm，左心室收缩末期内径 31mm，室间隔 13mm，左心室后壁 11mm，左心室射血分数 60%，缩短分数 32%，左心房前后径 39mm，上下径 58mm，左右径 36mm，E/A<1，结论：室间隔增厚，左心室舒张功能减退

鉴别诊断：

高血压病 3 级（极高危）

高血压急症

继发性高血压待排

电解质紊乱

低钾血症

低钠血症

低氯血症

其他：

恶疾潜藏心脏处，青春未尽心已殇：心脏滑膜肉瘤一例

张成龙

中南大学湘雅医院

患者基本信息：

邓某，男，29 岁，未婚，工人

主述：

反复胸闷 7 月，加重伴呼吸困难 1 月余

现病史：

患者于 7 月前反复胸闷，就诊于外院，检查提示“心包积液”，经保守治疗后症状好转。1 月前出现症状加重，并出现呼吸困难，伴咳嗽，平卧及体力劳动时加重，无咳痰，无胸痛，无发热，无下肢水肿，遂来我院就诊，门诊行胸部 CT 示心脏右前方 - 上腹部囊实性肿块，性质待定。遂入院治疗。患者自起病以来精神、饮食、睡眠欠佳，二便正常，体重未见明显增减。

既往病史：

无特殊慢性病史。

病程记录：

入院体查：一般情况：体温 36.5℃ 脉搏 77 次 / 分 呼吸 20 次 / 分 血压 104/79mmHg。发育正常，神志清楚，自主体位。全身浅表淋巴结无肿大。颈静脉无充盈。胸廓无畸形，胸骨无压痛。双肺呼吸音清晰，未闻及明显干、湿啰音。心前区无隆起，未触诊到心尖搏动，无震颤，无心包摩擦感。心界扩大，难以叩诊到正常心界。心律齐，心音遥远，未闻及杂音，无额外心音，无心包摩擦音，无异常血管征。腹部平软，无压痛及反跳痛，移动性浊音阳性。双侧下肢无凹性水肿。

为明确肿块性质并减轻压迫症状，行心包病损切除术 + 心包剥脱术：术中探查见心包腔巨大囊性包裹，心脏受压明显，其内大量血性及淡黄色积液，腔内众多分隔条状物，心包膈面及侧面以及膈肌上有多个大小不等的实质性肿块，边界不清。膈肌可见 4*5cm 的破口与腹腔相通。打开心包腔，清除积液及分隔组织，剥离心脏前面及膈面的心包解除心脏压迫。

手术病理：（心包）梭形细胞肿瘤，细胞显轻 - 中度异型，局灶伴坏死，倾向软组织来源，待慢石蜡及免疫组化明确类型。免疫组化结果：CD34（-），Ki67（约 20%+），STAT6（-），S-100（-），SMA（-），Desmin（-），SOX10（-），Myogenin（-），MYOD1（-），Bcl-2（+），CD99（+），INI1（+），SMARCA4（+），EMA（-），CD117（-），Dog-1（-），CK-Pan（-），CD5（-），P63（-），WT1（-），MUC4（-），TdT（-），NTRK（+），Vimentin（+）。分子病理结果：SS18（FISH）（发生断裂）。结论：（心包肿物、纵隔肿物）梭形细胞恶性肿瘤，结合免疫组化及 SS18 基因检测结果符合滑膜肉瘤 。

23-6-28 入住我院肿瘤化疗科，6-29 行异环磷酰胺 2g d1-3 化疗；

后患者失访。

检验检查记录：

血常规：血红蛋白 122 g/L ↓，HCT 38.1% ↓；大小便常规正常；

NT-proBNP 495 pg/mL ↑；

肝肾功能、甲功三项、凝血功能、hs-cTnI、心肌酶、E7A、血糖、血脂正常；

ANA、血管炎三项、免疫全套、狼疮全套正常；

T-SPOT 正常；ESR 正常；PCT 0.06 ng/ml ↑；

新 C12：CA 125 65U/ml ↑；

心电图：1. 窦性心律；2. 不完全性右束支传导阻滞；3. 胸导联 QRS 波低电压；4. 电轴右偏；5. T 波改变。

心脏彩超：右房、右室受压偏小；右室舒张受限。右室游离壁、右侧房室沟处探及不规则巨大囊性包块（153x108mm），其内可见大量不规则分隔条状回声，呈蜂窝状改变，内回声欠均匀，部分分隔内回声稍强，可见絮状回声。

彩超肝胆脾胰（组合）：肝大、脾大；右肝钙化灶，腹腔积液；**左上腹腹腔包裹性积液；**前列腺区囊肿；双侧胸腔少量积液。

2023-3-20 检查项目 :CT 胸部 (肺及纵隔) 平扫增强三维成像

检查所见：心脏右前方 - 上腹部见巨大囊实性分隔性病变，大部分为液体成分，其内见散在壁结节实性成分，平扫 CT 值约 53HU，增强后 CT 值约 104HU，邻近右心房分界欠清，右心房、右心室明显受压变扁，纵隔明显左移，肝左外叶受挤压，与胃壁相贴。右中肺内段、左上肺、双下肺可见多发条索、斑片状密度增高灶，右侧胸腔内见少量积液，右肺膨胀不全。纵隔内淋巴结显影欠清。余增强后未见明显异常强化灶。肝右叶可见斑点状钙化灶。上腹部大网膜混浊。

检查提示：

1. 心脏右前方 - 上腹部囊实性肿块，性质待定。建议腹腔盆腔增强进一步检查。

2. 右侧胸腔少量积液，双下肺少许炎症，左下肺外压性肺不张。

3. 左腹部大网膜混浊。

23-3-19CT 腹部盆腔平扫双期增强三维成像

检查所见：

左侧中上腹部囊实性占位肿块，较大横截面约 160x88mm，病灶似与纵隔相连，平扫 CT 值约 15-36HU，增强扫描病灶内分隔可见强化，病灶内低密度区未见明显强化；病灶占位导致肝脏及周围胃肠管受压移位。胆内容物密度增高。左肾下极见一类圆形低密度无强化灶，长径约 6m，CT 值约 12HU。双侧肾乳头区另可见多个斑点状高密度灶，边缘模糊。脾脏、胰腺未见明显异常密度灶及异常强化灶。肝脏未见明显异常强化灶。肠系膜及大网膜增厚、混浊。肠系膜及腹膜淋巴结增大，大者短径约 6mm。腹、盆腔积液。右侧胸腔积液。

检查提示：

1. 左侧中上腹 - 纵隔占位灶，性质待定，假性粘液瘤？

2. 胆囊内容物密度增高，意义待定，造影剂？

3. 双侧肾乳头多发钙化可能。

4. 左肾囊肿。

5. 肠系膜及大网膜增厚、混浊，考虑脂膜炎可能；腹盆腔积液，肠系膜及腹膜后淋巴结增大。

6. 右侧胸腔积液。

鉴别诊断：

粘液瘤？淋巴瘤？

其他：

病例图像和视频资料详见 PPT

残肾动静脉瘘致心力衰竭并肺动脉高压一例

王皓辰

广东省医学科学院

患者基本信息：

70 岁女性，广东佛山人，汉族，离退休。

主述：

体力下降伴双下肢水肿 1 年余。

现病史：

患者 2024-01 起开始出现活动耐量下降，表现为平地行走 50-100m 及出现气促，无法爬楼，夜间无法平卧，胃纳差，伴双下肢水肿。当地医院予抗心衰、利尿等治疗后症状稍好转。1 年前（2024-06）患者再次出现胸闷伴下肢水肿，就诊于湘乡市人民医院，查超声心动图示：LVEF 51%，左房、右心增大，肺动脉高压（中度）。后再次因症状加重，表现为反复活动后气促，夜间阵发性呼吸困难，尿少，于 2024-09 就诊于广东省人民医院南海医院，心电图提示阵发性房颤，行冠脉造影未见异常，右心导管提示肺动脉高压（未见报告单），予他达拉非 20mg qd、安立生坦 5mg qd 双联靶向治疗，胺碘酮 0.2g qd、利伐沙班 15mg qd、利尿、补铁、护肾等治疗。因症状加重于 2024-12、2025-02、2025-04 于广东省人民医院南海医院住院治疗，查 Hgb 波动于 89-106g/L，Cr 波动于 160.5-262umol/L，NT-ProBNP 波动于 1859-19943pg/ml。2025-04-28 超声心动图示：LVEF 61%，左心、右房增大，三尖瓣返流，估测肺动脉收缩压 59mmHg。以肺动脉高压、阵发性心房颤动收入院。

既往病史：

30 余年前因“肾炎”行左侧肾全切术，术后未规律复查；15 年前因“胆囊结石”行胆囊切除术；否认高血压病史；否认脑梗塞史；否认慢性肺气肿病史；否认风湿性心脏病史；否认冠心病史；否认心梗病史；否认肝炎病史；否认结核病史；否认其他传染病史；否认输血史；否认外伤史；否认中毒史；无过敏史。

病程记录：

入院查体：

神志清楚，发育正常，营养良好，面容与表情安静，体位自主，检查合作。Bp：98/ 47 mmHg，神志清晰，无特殊面容，颈静脉正常，双肺呼吸音清，未闻及干湿性啰音，无心前区隆起，相对浊音界无扩大，心率：66 次 / 分，心律齐，各瓣膜听诊区未闻及杂音，双下肢轻度浮肿。腹部柔软，腹部无压痛、反跳痛，腹部无局部隆起，腹部未触及搏动性包块，无压痛、反跳痛。

检验结果：

NT-ProBNP 1340 pg/mL，Hb 95g/L，PLT 166*10^9/L，WBC 4.78*10^9/L，Scr 186mmol/L，肝功能未见异常。

检查结果：

心电图：窦性心律，未见明显异常。

超声心动图：左心、右房增大，左、右室壁运动正常，主肺动脉增宽，左肺动脉开口内径 18mm，右肺动脉开口内径 22mm，房室间隔未见中断，下腔静脉内经 19mm，随呼吸运动塌陷率小于 50%；三尖菲返流，彩束面积 3.6cm2，估测肺动脉收缩压 61 mHg。

肺静脉 CT 增强：未见异常。

诊断：

肺动脉高压，心房颤动，心功能 3 级、慢性肾脏病 4 期。

药物治疗：

安立生坦 5mg qd、利奥西呱 1mg tid，呋塞米 20mg qd，螺内酯 20mg qd，

下一步治疗：

按计划行房颤射频消融术，同时为明确血流动力学，行右心导管检查。术中测肺动脉血氧饱和度为 85%，下腔静脉血氧饱和度 94%，PAP 50/18/32mmHg，PAWP 15/6/11mmHg，使用 Fick 法计算 PVR 2.04 WoodU，肺循环血流量（Qp）10.29 L/min，体循环血流量（Qs）5.53 L/min，Qp/Qs=1.86，诊断毛细血管前性肺动脉高压，考虑存在大量左向右分流，但患者本身并不存在房间隔缺损，遂复测股静脉血氧饱和度为 79%，判断分流位于股静脉与肝静脉之间，但患者本身肾功能极差（eGRF 23.96mL/（min*1.73m2））， 术前已经接受了肺动静脉增强 CT，不适合短期内再进行血管造影，故先行环肺静脉电隔离术处理心房颤动。术后复习病史，考虑患者的动静脉分流最有可能来自于左肾残存的动静脉，查体在左侧腹靠近脐周可闻及显著收缩期血管杂音，完善左肾动静脉超声检查，见左肾静脉走形扭曲，腹主动脉与肠系膜上动脉夹角左侧左肾静脉扩张，左肾动脉末端与左肾静脉末端相互交通，交通口处宽约 0.6cm，考虑动静脉瘘。在经过 2 个月的护肾、利尿、降肺动脉压治疗后，完善主动脉全程 CT，明确诊断左肾动静脉瘘，遂转入血管外科，计划主动脉植入覆膜支架，完全阻断左肾动脉血供，以达到封闭分流的目的。

检验检查记录：

血常规、电解质、肝功能、凝血功能：未见明显异常

肾功能：Scr 186mmol/L，eGFR 23.96mL/（min*1.73m^2）

肾动静脉超声：左肾静脉走形扭曲，腹主动脉与肠系膜上动脉夹角左侧左肾静脉扩张，内径：1.7cm，左肾动脉起始段内径 0.6cm，远端扩张，走形扭曲，内径约 0.9cm，左肾动脉末端与左肾静脉末端相互交通，交通口处宽约 0.6cm。CDFI：腹主动脉与肠系膜上动脉夹角左侧左肾静脉可见左肾动脉血流瘘入。

右心导管检查：PAP 50/18/32mmHg，PAWP 15/6/11mmHg，使用 Fick 法计算 PVR 2.04 WoodU，肺循环血流量（Qp）10.29 L/min，体循环血流量（Qs）5.53 L/min，Qp/Qs=1.86，诊断毛细血管前性肺动脉高压，考虑存在大量左向

右分流。

鉴别诊断：

对于肺动脉高压进行病因诊断：

1、特发性：该患者存在左肾动静脉瘘（AVF），导致高动力性分流（Qp/Qs=1.86），可解释 PAH，不支持特发性。

2、药物 / 毒素相关 PAH（如芬氟拉明、安非他命）：无相关用药史。

3、结缔组织病相关 PAH（如系统性硬化症、SLE）：风湿免疫指标阴性，无雷诺现象、皮疹或关节炎，可能性低。

4、先天性心脏病相关 PAH（如房缺、室缺、动脉导管未闭）：超声及 CT 未见心内分流，但 AVF 导致类似血流动力学改变（左向右分流→肺循环超负荷）。

5、门脉高压相关 PAH：无肝硬化、脾大或门静脉血栓证据。

其他：

继发性肾动静脉瘘占肾动静脉瘘的 70%-75%，主要报道的病因包括医源性因素、创伤、肿瘤、炎症。肾脏切除术后继发的肾动静脉瘘并不罕见，不同于原发性肾动静脉瘘，且因肾脏切除常无血尿，其临床症状因瘘口大小不同而各异，以心血管症状、体征为主，如腹部杂音、高血压、心脏扩大、充血性心力衰竭等，常首诊于心血管科。所以对肾外伤或手术后出现心力衰竭、高血压者，应排查肾动静脉瘘。当动静脉瘘分流严重时，动脉系统血液直接从瘘口由肾动脉返回下腔静脉内，导致回心血量增加。而长期静脉回心血流量增加可引起充血性心力衰竭、肺血管阻力升高、肺动脉压力升高。所幸在解除分流后，患者的症状通常可以好转。

负性重构致冠脉破裂一例

邓熠

遵义医科大学附属医院

患者基本信息：

63 岁，男患，长期吸烟史；

主述：

因“劳力性胸痛 4 月，加重 1 周”入院

现病史：

患者男性，63 岁，因“劳力性胸痛 4 月，加重 1 周”入院。4 月前出现活动后胸闷，胸痛，以胸骨中下段明显，持续数分钟，休息后可缓解；无肩背部放射痛，无心悸，气促；曾就诊于当地县医院，考虑“冠状动脉粥样硬化性心脏病”，未进一步治疗，1 周前上述症状加重，遂就诊于我院。入院查体：体温 36.5° C，血压 152/92mmhg，心率 102 次 / 分，呼吸 18 次 / 分；神志清楚，对答切题；心界不大，心音有力，未闻及额外心音及心脏杂音，双下肢无水肿；四肢肌力及肌张力正常，生理反射存在，病理反射未引出。

既往病史：

既往发现血压升高 5^{+} 年，最高血压达 180/80mmhg，一直予以“苯磺酸左旋氨氯地平”控制血压，自诉血压控制可；同期发现血糖升高，予以“二甲双胍”控制血糖，未规律监测血糖，无“手术、外伤”史；

病程记录：

住院期间给予冠心病二级预防，控制血压等治疗，结合患者症状、体征、辅助检查，故进一步行冠状动脉造影检查，并根据冠状动脉造影检查决定进一步治疗方案。CAG:LM 未见明显狭窄；LAD 近段狭窄 30%，中远段节段性狭窄，最重狭窄 90%；LCX 远段狭窄 90%；RCA 细小，未见明显狭窄；

手术策略及过程：根据病史、辅助检查决定对左冠行介入治疗，并使用 IVUS 进行指导；经桡动脉送入 EBU3.5 指引导管至左冠口，Runthough 导丝通过病变至 LAD 远段，Sion 导丝通过病变至 LCX 远段，分别行对 LAD 及 LCX 行 IVUS 件检查：根据 IVUS 结果决定先行 LAD 行介入治疗，送入 2.5×20mm 球囊扩张 LAD 病变处，经 LAD 中远段至近段植入 3.0×29mm、3.5×29mm 药物支架两枚；继以 3.5×15mm 非顺应性球囊予以支架内及支架连接处扩张塑形；

继续送入 3.0×10mm 切割球囊于 LCX 病变处 10-12atm 扩张，继取 3.5×21mm 药物支架于 LCX 病变处以 10atm 释放，随后造影发现造影剂外渗，立即予以 3.5×15mm 非顺应性球囊于 LCX 近段行封堵，并送入雅培 3.5×19mm 覆膜支架植入 LCX 破裂处，再次复查造影仍可见造影剂外渗，再送入自制 3.5×12mm 覆膜支架，复查造影无造影剂外渗。

检验检查记录：

生化检查：高敏肌钙蛋白 T 20.63ng/L（正常参考值 < 14ng/L）；B 型尿钠钛前体 100ng/L（正常参考值小于 125ng/L），总胆固醇 3.64mmol/L（正常参考值小于 5.2mmol/L）、低密度脂蛋白 2.43mmol/L（正常参考值小于 3.15mmol/L）；随机血糖 9.3mmol/L；血常规、肝功能、肾功能未见异常；

心电图： 窦性心动过速；心脏彩超（LAS 37mm、IVSD 9mm、LVD 57mm、PA 21mm、RVD 27mm、RAS 34mm、EF 56% ）结论：左心增大；主动脉瓣毛躁；无冠瓣钙化反流；二尖瓣轻度反流；三尖瓣轻度反流。

CAG:LM 未见明显狭窄；LAD 近段狭窄 30%，中远段节段性狭窄，最重狭窄 90%；LCX 远段狭窄 90%；RCA 细小，未见明显狭窄。

鉴别诊断：

无

其他：

高原地区肺动脉高压一例

朱芳一

青海省心脑血管病专科医院

患者基本信息：

26 岁藏族女性

主述：

活动后胸闷、气喘 3 年，再发伴咳嗽、咳痰 10 天。

现病史：

患者自诉于 3 年前受凉感冒后出现胸闷、气喘症状，伴咳嗽，咳痰，痰呈白色粘痰，量少，易咳出，胸闷、气喘症状症状在活动后发作明显，因不影响正常生活故未予重视，逐渐出现乏力症状，活动耐量逐渐下降。入院前 10 天受凉感冒后胸闷、气喘症状再发并加重，伴咳嗽、咳痰，咳呈白色粘痰，量少，不易咳出，尤以夜间咳嗽症状发作明显，自觉发热（当时未测体温），伴双下肢轻度浮肿，纳差、乏力明显，夜间尚能平卧，偶有头晕，无明显恶心、呕吐，无胸痛、咯血等症状，活动耐量进一步减低，平路快步行走 50 米胸闷、气喘症状即可出现。

既往病史：

既往否认高血压、糖尿病等慢性病史；无关节肿胀、疼痛史；无皮肤红斑、皮疹及反复口腔溃疡史；否认肝炎、结核等传染病病史，无外伤、手术史，无吸烟、饮酒等不良嗜好。

个人史：5 年前生育 1 女婴，无自然流产史，无手术及输血史，无服用避孕药物及减肥药物史。

病程记录：

入院诊断：

肺动脉高压（中高危组）

先天性心脏病

房间隔缺损

心功能 II 级（NYHA 分级）

大动脉炎

细菌性肺炎

低氧血症

加用双联靶向药物治疗：一氧化氮途径药物：西地那非片（20mg tid po），内皮素受体拮抗剂：马昔腾坦片 （10mg qd po）

检验检查记录：

NT-proBNP 883.5pg/mL

PCT 0.061ng/mL

CRP 9.16mg/L

D- 二聚体 0.55ug/mL FEU

肾功示：尿素氮 3.56mmol/L，肌酐 52umol/L

血常规：淋巴细胞百分比 43.9%，红细胞计数 5.84*10^12/L 血红蛋白测定 123g/L，血小板计数 392*10^9/，白细胞计数 4.21*10^9/L

血气分析（鼻导管氧流量 3L/min）：PH 7.42，二氧化碳分压 34.00mmHg，氧分压 73.00mmHg，氧饱和度 94.4%。

心脏超声：

1. 先天性心脏病、房间隔缺损（中断约 18mm），房水平双向分流，左向右为主。

2. 三尖瓣大量返流，返流速度：556cm/s。

3. 估测动脉高压收缩压 139mmHg，平均压 >77mmHg。

4. 右心增大，左室短轴呈“D 字型”，右房：左右径 54mm，上下径 55mm。右室：前后径 34mm，左右径 58mm。下腔吸气萎陷率小于 50%

鉴别诊断：

大动脉炎

纤维素性纵隔炎

肺动脉缺如

其他：

嗜铬细胞瘤所致高血压 1 例

陈璐

首都医科大学附属北京同仁医院

患者基本信息：

• 女，29 岁，2024-03-25 入院

主述：

间断头痛、心悸 2 周余

现病史：

•2 周余前无明显诱因间断感头痛、心悸，伴出汗较多，自测血压升高（具体不详），无恶心、呕吐，无胸痛、胸痛，无头晕、视物模糊，无黑矇、晕厥，无脸变圆红、皮肤紫纹增多，无少尿、水肿、泡沫尿，无乏力。后（2024-03-09）就诊于中国中医科学院广安门医院，行心电图示“窦性心动过速，心率 129 次 / 分，异常心电图”，考虑“心悸、心脾两虚证”，予“炒白术、党参、黄芪、当归、灸甘草、茯神、远志、炒酸枣仁、广木香、龙眼肉、生姜、大枣、牡蛎、麦冬”等中药治疗 2 周，自觉上述不适无明显缓解。平素下午至夜间自觉无头痛、心悸时测血压 130/90mmHg，具体不详。3 天前上述不适再发，至我院门诊测血压 167/134mmHg（左上肢），心率 149 次 / 分，予“硝苯地平片”血压可较前下降，具体不详。今为进一步诊治，门诊以“高血压”收入院。

• 自发病以来，精神可，饮食可，夜眠欠佳，平素情绪紧张，失眠多梦，未应用助眠药物。两便如常，体重无明显变化。身高 170cm，体重 52kg，BMI 17.99kg/m2。

既往病史：

•3 年余前于我院诊断“雄激素性脱发”，曾予“米诺地尔酊外用、活力苏口服液口服及二硫化硒洗剂外用”；

•2 年余前曾因“荨麻疹”于我院皮肤科就诊。

• 近期应用叶酸片 1 片 / 日。【备孕】

•否认冠心病史，否认肝炎、结核、疟疾病史，否认糖尿病、脑血管疾病、精神疾病史，否认手术、外伤、输血史，阿奇霉素过敏，否认食物及其他药物过敏史，预防接种史不详。

病程记录：

入院后完善相关化验检查，血儿茶酚胺 3 项（入院）甲氧基去甲肾上腺素 2916.4pg/ml ↑，甲氧基肾上腺素 18.2pg/ml，3- 甲氧基酪氨 28.1pg/ml ↑，多巴胺 80.3pg/ml ↑，去甲肾上腺素 9419.7pg/ml ↑，肾上腺素 <32.40(pg/ml)；血儿茶酚胺 3 项（次日晨起）：甲氧基去甲肾上腺素 4650.8pg/ml ↑，甲氧基肾上腺素 21.7pg/ml，3- 甲氧基酪氨 37.3pg/ml ↑，多巴胺 100.8pg/ml ↑，去甲肾上腺素 14030.8pg/ml ↑，肾上腺素 <32.40pg/ml，皮质醇 +ACTH 节律正常，醛固酮卧立位试验提示卧位及立位肾素升高，肾上腺 B 超提示“右肾上腺肿物，结合病史考虑嗜铬细胞瘤可能”，肾上腺增强 CT 提示“右侧肾上腺区富血供病变，嗜铬细胞瘤可能性大”，自身免疫相关筛查均阴性，考虑患者高血压原因为继发性高血压，结合病史考虑嗜铬细胞瘤可能性大，予哌唑嗪 1mg 每日 3 次治疗，血压较前下降；监测心率偏快，加用酒石酸美托洛尔 25mg 每日 2 次治疗，心率较前下降，患者消瘦，尿酮体阳性，遵临床营养科会诊意见予低脂普食、安素补充肠内营养，复查尿酮体转阴。现患者病情相对平稳，要求出院，请示上级医师予自动出院。

检验检查记录：

详见幻灯片

鉴别诊断：

（一）原发性高血压？继发性高血压待除外：患者血压明显升高，伴心动过速，否认高血压家族史，由于高血压病因比较复杂，并且此患者病史不明确，故需要从病因角度进一步鉴别诊断。

1、嗜铬细胞瘤: 是继发性高血压中较少见的一种，以阵发性高血压为特征，发作时，血压可从正常范围急骤上升至很高水平，伴有头痛、面色苍白、出汗、心动过速等，可持续数分钟至数小时，多以情绪波动、触及肿瘤部位、体位改变等为诱因。可完善血儿茶酚胺明确。患者血压升高伴心动过速，需警惕本病可能，但否认血压急骤升高，注意监测血压、心率；

2、肾实质性高血压：是引起高血压的常见原因，可见于慢性肾小球肾炎、糖尿病肾病、慢性肾盂肾炎、结缔组织病、多囊肾、肾移植术后等，此患者无上述疾病病史，故需要进一步行肾功、肾脏 B 超等检查加以诊断或排除；

3、肾血管性高血压：指单侧或双侧肾动脉主干或分支狭窄引起，可由大动脉炎、纤维肌性发育不良或动脉粥样硬化所致，查体上腹部未闻及血管杂音或伴有其它部位动脉粥样硬化的表现，给予查双肾动脉 B 超，必要时行肾动脉造影以除外；

4、原发性醛固酮增多症：是由于肾上腺皮质肿瘤或增生，分泌过多的醛固酮引起的综合征，高血压是其主要的临床表现，伴有肢体无力或麻痹，常呈周期性发作，实验室检查表现为血钾降低、尿钾增多，血和尿醛固酮增加，此患者无上述特点，可能性不大。入院后可查血钾、血管活性物质系列、肾上腺超声等以除外。

其他：

• 患者规律应用酚卞明，后于外院住院（2024-05-08 至 2024-05-20），于 2024-05-15 全麻下行腹腔镜右肾上腺嗜铬细胞瘤切除术，术后病理提示嗜铬细胞瘤，已停用药物，血压正常。

纸上得来终觉浅，绝知此事要躬行 ----“无复流”病例一例

俞帅

上海市东方医院

患者基本信息：

患者：王 XX，出生地：上海；

性别：女性，职业：退休

年龄：67 岁，婚姻：已婚

入院日期：2023.4.24

主述：

反复胸痛 1 月

现病史：

患者近 1 月无明显诱因下反复出现胸痛，位于胸骨后，呈压迫感，含服硝酸甘油 10 分钟左右症状减轻，否认放射痛，否认咳嗽咳痰，否认咯血，否认反酸烧心，否认气促，否认呼吸困难

既往病史：

既往高血压史 10 余年，血压最高 160/100mmHg，服用诺欣妥 100mg qd 降压，平日未规律监测血压；

有冠心病史，10 年前在外院行 PCI 术，植入支架一枚（具体不详）；

否认其他慢性疾病史。

病程记录：

患者入院后根据病情完善检查，予以阿司匹林、氯吡格雷、单硝酸异山梨酯、阿托伐他汀、比索洛尔、诺欣妥等药物，择期完善冠脉造影检查：前降支近段 90% 局限性狭窄，回旋支未见明显狭窄，第一钝缘支近段 50% 节段性狭窄；右冠近中段见原植入支架，支架内 70-80% 再狭窄; 先对前降至行 PCI 术，植入 3.0*16mm 支架一枚，术后 1 个月，对右冠支架内再狭窄病变进行干预时，术中发生后降支无复流，先后使用硝普钠（100ug*15 次）、铭复乐（4mg）、替罗非班（10ml*2 次）、2.0*15mm 预扩球囊扩张、微导管内注射硝普钠等方法仍无法改善无复流，遂使用抽吸导管抽吸，抽吸出淡黄色块状物质

检验检查记录：

实验室检查结果：

2023.4.24 血常规、肾功能、电解质、D 二聚体、凝血功能、CK-MB、cTnT、NT-proBNP 均在正常范围 .

2023.4.25 天门冬氨酸氨基转移酶 98.3U/L, 丙氨酸氨基转移酶 149U/L。

2023.4.25 TC 3.94mmol/L,TG 1.21mmol/L,HDL 1.03mmol/L,LDL 2.53mmol/L, NHDL 2.91mmol/L, LP(a) 20nmol/L。

特殊检查结果：

2023.4.24 心电图未见明显异常。

2023.2.24 心内结构及血流未见明显异常。

鉴别诊断：

胸痛的鉴别诊断：肺栓塞、主动脉夹层、气胸、心包炎、反流性食管炎等

无复流：微循环栓塞、缺血 - 再灌注损伤、冠状动脉介入操作诱发的血管痉挛收缩、个体易患性

其他：

造影图像较大，无法完全上传

经导管二尖瓣缘对缘修复术治疗急性心梗后二尖瓣腱索断裂致心源性休克合并多器官衰竭 1 例

金震

北部战区总医院

患者基本信息：

男，74 岁。

主述：

阵发性心前区不适 25 年，突发胸闷气短 21 天。

现病史：

患者于 25 年前始无明显诱因自觉偶有心前区不适，就诊于当地医院考虑为“冠心病”，未检查及治疗，每年体检心脏超声提示左心大，瓣膜轻度反流（具体不详），间断自行服用“阿司匹林”、“稳心颗粒”。患者于 2025 年 3 月 21 日 14:00 无明显诱因突发胸闷气短，伴周身大汗，症状持续不缓解，2025-03-22 就诊于当地医院，完善相关化验检查，诊断为“急性非 ST 段抬高型心肌梗死”，给予对症治疗后症状缓解，4 月 3 日行冠脉造影示：LM 正常，LAD 动脉硬化改变；LCX 动脉硬化改变；RCA 近段 100% 闭塞，可见血栓影，血流 TIMI0 级，经其同意，

行右冠病变 PCI，于右冠病变处经球囊扩张后复查造影右冠全程见大量血栓影，血流 TIMI1-2 级。此后继续药物对症治疗。4 月 11 日复查心脏超声提示二尖瓣后叶脱垂伴重度关闭不全，建议转至上级医院进一步治疗。现为进一步治疗收入心内科监护室。

既往病史：

阵发性房颤病史 5 年，未系统抗凝治疗；10 余年前行下肢静脉曲张手术，10 年前胃出血病史，原因不详；

病程记录：

急性非 ST 段抬高型心肌梗死后 13 天冠脉介入未成功，转诊至我院时心源性休克合并肺、肾等多器官衰竭：急性肺水肿、严重低氧血症，气管插管呼吸机辅助通气，伴大剂量血管活性药物联合主动脉内球囊反搏（IABP）治疗，伴快速房颤。急性肾损伤，无尿，需连续肾脏替代治疗 CRRT。代谢性酸中毒，严重肺内感染，持续发热。经食道超声证实二尖瓣后叶腱索断裂伴重度反流（平均跨瓣压差 44mmHg），射血分数（EF）45%。经过 6 天多器官器械支持治疗后在全麻下行经导管二尖瓣缘对缘修复术（TEER），经食道超声引导，房间隔高位穿刺后送入二尖瓣夹系统（型号 XW0612）于左房，调节输送系统使夹子垂直指向二尖瓣 2 偏 3 区脱垂最大处且夹臂垂直于二尖瓣对合缘。补夹第二枚 SN0409。术后即刻超声：二尖瓣反流程度从 5+ 降至 1+，平均跨瓣压差为 2mmHg。术后临床指标显著改善：术后即刻停用 IABP，24 小时内成功脱离呼吸机，48 小时停用血管活性药物及 CRRT。下肢静脉超声提示血栓形成，肺通气灌注扫描提示右肺三个亚段肺栓塞。感染得到控制后出院。

检验检查记录：

经食道超声：二尖瓣后叶腱索断裂伴重度反流（平均跨瓣压差 44mmHg），射血分数（EF）45%。下肢静脉超声提示血栓形成，肺通气灌注扫描提示右肺三个亚段肺栓塞。

鉴别诊断：

诊断明确

其他：

急性心梗合并二尖瓣腱索断裂致心源性休克伴多脏衰的危重病例临床治疗方法有限且疗效欠佳，治愈病例极少。本案例证实 TEER 技术通过解剖精准修复与即时血流动力学纠正，可有效逆转继发于急性二尖瓣脱垂致心源性休克。在合并多脏器衰竭的危重状态下，外科手术治疗风险极大，因此 TEER 治疗成为打破 " 心脏 - 肺 - 肾 " 交互衰竭恶性循环的关键；其中心功能的即刻恢复是其他器官功能逆转的前提。本例术后平均跨瓣压差从 44mmHg 急剧下降至 2mmHg，迅速消除肺水肿的病理基础，同时心输出量提升使肾灌注压恢复，改善肾脏功能。若无二尖瓣反流的及时纠正，药物合并器官支持治疗难以阻断多脏器衰竭进程。同时，TEER 为外科高危心衰患者开辟了安全有效的替代路径，为挽救终末期器官功能争取关键治疗窗口期。

以“头痛”为单一症状的急性心梗 1 例

俞帅

上海市东方医院

患者基本信息：

患者：薛 XX，出生地：上海

性别：男 性，职　业：退休

年龄：72 岁，民　族：汉族

婚　姻：已婚

入院日期：2025.5.25

主述：

持续头痛 14 小时

现病史：

患者 14 小时前（2025 年 5 月 24 日 19 点 30 分）无明显诱因下出现头痛，为整个头部钝痛，症状持续不能缓解，否认头晕，否认视物旋转，否认恶心呕吐，否认视物模糊，否认颈部僵硬感，否认黑朦晕厥，否认四肢抽搐，否认意识障碍，否认胸闷胸痛，否认气促，否认呼吸困难，遂于 5 月 25 日 9 点 50 分至我院神经内科急诊，神经系统查体未引出明显阳性体征，头颅 CT 提示：1. 左侧颞叶、双侧基底节区、半卵圆中心多发缺血灶，请结合临床及 MRI 检查。2. 老年脑、脑白质变性。3. 双侧筛窦、上颌窦炎、左侧蝶窦炎。神经内科排除急性脑卒中遂转至急诊内科急查心电图（10 点 19 分）：1、房颤（快室率）2、符合超早期下壁 + 侧后壁心肌梗塞的心电图改变 3、室性早搏（见右室后壁图）4、S-T 段异常（aVR、V1、V2、V3、V4、V3R、V4R、V5R 水平压低 0.5-5.0mm），心内科急会诊后考虑急性心肌梗死，开通急诊绿色通道，行急诊冠脉造影检查。10 点 35 分心梗三项 +NT-proBNP:NT-proBNP 1060ng/L，CK-MB 29.75 microg/L，TNT 0.162microg/L，MYO 486 microg/L。

既往病史：

患者有支气管哮喘病史 10 余年。

否认其他慢性疾病史。

长期吸烟史，吸烟 50 年，20 支 / 天

病程记录：

根据患者急诊心电图及心梗三项结果考虑急性心肌梗死，急诊予以阿司匹林肠溶片 300mg、替格瑞洛 180mg 负荷后行急诊冠脉造影提示：右优势型，左主干未见明显狭窄；前降支近段至远段 50-70% 弥漫性狭窄，血流 TIMI3 级；回旋支近段 100% 完全闭塞，血流 TIMI0 级；右冠状动脉近段 50-60% 节段性狭窄；右冠状动脉远段 60-70% 节段性狭窄，后降支中远段 70% 节段性狭窄，血流 TIMI3 级。对回旋支行 PCI 术，植入 2.5*18mm XIENCE Alpine 支架一枚，术后安返 CCU，继续双抗、他汀调脂、诺欣妥抑制心肌重构、比索洛尔降低心肌耗氧等治疗。患者术后头痛症状即刻缓解，始终无胸闷胸痛、放射痛等临床表现。

检验检查记录：

2025.5.25 急诊头颅 CT：1. 左侧颞叶、双侧基底节区、半卵圆中心多发缺血灶，请结合临床及 MRI 检查。2. 老年脑、脑白质变性。3. 双侧筛窦、上颌窦炎、左侧蝶窦炎，请结合临床。

2025.5.25 急诊心电图：1、房颤（快室率）2、符合超早期下壁 + 侧后壁心肌梗塞的心电图改变 3、室性早搏（见右室后壁图）4、S-T 段异常（aVR、V1、V2、V3、V4、V3R、V4R、V5R 水平压低 0.5-5.0mm。）

2025.5.25 急诊床旁心超：左室壁节段运动异常，室间隔基底段增厚，主动脉窦部增宽，主动脉瓣钙化，二尖瓣少量反流，三尖瓣中量反流 肺动脉收缩压 49mmHg，未见明显心包积液，左室收缩功能减低

2025.5.25 急诊胸部 CT：1. 肺气肿，两肺慢性炎症，两肺多发小结节，复查；两上胸膜增厚钙化。2. 左肺下叶背段支气管扩张伴感染，建议随诊复查。3. 主动脉及部分冠状动脉硬化。4. 心包积液。

2025.5.25 心梗三项 +NT-proBNP:NT-proBNP 1060ng/L，CK-MB 29.75 microg/L，TNT 0.162microg/L，MYO 486 microg/L。

鉴别诊断：

该患者以“头痛”就诊，入院前至出院时始终无胸闷胸痛、放射痛等症状，因此，在急诊就诊时并未先完成心电图检查，鉴别诊断主要围绕头痛展开，如：1. 血管性头痛；2. 精神性头痛；3. 紧张性头痛；4. 颅内占位病变或高低颅压；5. 脑膜刺激性头痛；6. 中度、代谢等系统性疾病导致的头痛；7. 颅内、外结构性疾病；8. 外伤性头痛。此外，该患者房颤，需排除有无栓子脱落导致的脑栓塞亦可导致头痛。急诊时血压较高，最高达 203/110mmHg，需排除高血压导致的头痛。

其他：

拿什么拯救你，年轻而颤动的心–青年学生心脏骤停的原凶

周乐群

北京大学第三医院

患者基本信息：

男性，22 岁，大学本科在读学生；主因“11 小时前呼吸心跳骤停”，2024-09-21 入院

主述：

11 小时前呼吸心跳骤停

现病史：

患者 11 小时前（2024-09-20 14：17）平稳骑行电动车时突然倒地，14：20 被群众发现意识丧失不能触及大动脉搏动，随即开始胸外按压及人工呼吸，并呼叫 120。约 14：30 左右 120 到场行气管插管并持续心肺复苏。14：39 转运至邻近医院，昏迷、大动脉搏动未触及，心电示波直线，予持续胸外按压、肾上腺素注射及有创呼吸机辅助通气等治疗，期间反复发作室颤，予可达龙静滴、多次电除颤等治疗。血气分析示 PH7.0，$PaCO_2$ 63mmHg，PaO_2 50mmHg，HCO_3 18mmol/L，K 5.2 mol/L，LaC 13.4 mmol/L。15：57 恢复自主循环，心电监护提示窦性心律，心率 100~110 次 / 分，血压 120~130/70~80mmHg。经气管插管可吸出鲜红色血痰，患者躁动、四肢不自主活动。颅脑 CT 未见明显异常；肺 CT 示双肺渗出性改变、双下肺膨胀不全，未见明显胸廓畸形；双下肢超声示双下肢动脉及静脉未见血栓形成；心电图提示 II、III、aVF，V2-V6 导联 ST 段上斜型压低。于 20：54 转至我院急诊科，心电监护提示窦性心律、心率 78 次 / 分，血压 110/74mmHg，SpO_2 100%（持续有创机械通气 FiO_2 50%），昏迷，双侧瞳孔直径 4mm，对光反射迟钝。双肺呼吸音粗，双下肺可闻及湿啰音。心律齐，各瓣膜区未闻及明显杂音。腹部柔软，压之无痛苦表情，双下肢无水肿。血气分析（FiO_2 50%）：pH 7.312，$PaCO_2$ 42.5mmHg，PaO_2 73.2mmHg，K 3.14mmol/L，LaC 5.28mmol/L；N 端 -B 型钠尿肽前体 619（pg/mL），全血肌钙蛋白 I 测定 14（ng/mL）；肌酸激酶同工酶 MB 192（U/L）↑，肌酸激酶 1722（U/L）↑；D- 二聚体定量 12.56（μg/ml）；丙氨酸氨基转移酶 88（U/L），天门冬氨酸氨基转移酶 260（U/L），尿素 6.08（mmol/L），钾 2.62（mmol/L），肌酐 111（umol/L）。心电图：II、III、aVF、V2~V6 导联 ST 段压低；超声心动图：左室前壁、前间壁中段 - 心尖段运动减低；二尖瓣增厚，二尖瓣前叶脱垂伴反流（轻度），黏液样变性待明确，LVEF52%（2-D）。为进一步诊治收入院。

体格检查：

体温 36.3℃，脉搏 88 次 / 分，呼吸 16 次 / 分，血压 105 / 72mmHg。

有创呼吸机辅助通气，模式 A/C，Vt 490mL，PEEP 6cmH2O，f 16 次 / 分，FiO2 50%

镇静状态，瞳孔等大同圆直径 4mm，对光反射迟钝；

颈无抵抗，双肺呼吸音清，双下肺闻及少量细湿啰音，无胸膜摩擦音。

心前区无隆起，心尖搏动正常，心浊音界正常，心率 88 次 / 分，律齐，心音低钝，各瓣膜区未闻及明显杂音，无心包摩擦音。

腹平软，肠鸣音 2 次 / 分，双下肢无浮肿。

双侧 Babinski 征阴性。

既往病史：

（1）既往史：1 月前上呼吸道感染后有轻微腹泻症状，1~2 日未用药自行好转。无冠心病、高血压、糖尿病、高脂血症、心肌病病史。平素体力活动无不适。（2）个人史：久居俄罗斯，4 年前居住于北京。平素喜熬夜，每日睡眠 6~8 小时，无吸烟史，无毒物滥用史。（3）家族史：否认心肌病家族史，否认猝死家族史。弟弟漏斗胸行手术治疗。

病程记录：

诊疗经过：

1. **采用心脏骤停后综合治疗策略：**

（1）心脏骤停后脑保护：目标体温管理——亚低温治疗；目标体温 35℃，9 月 21—24 日；目标温度 36℃，9 月 24—26 日。神经元特异性烯醇化酶：57.5ng/mL（9 月 20 日），36.1ng/mL（9 月 22 日），24.6ng/mL（9 月 25 日）；9 月 24 日复查颅脑 CT：提示灰白质分界欠清，考虑存在轻度脑水肿，给予减轻脑水肿药物：糖皮质激素抗炎、甘露醇脱水。

（2）对症支持治疗：镇静、镇痛、肌松；气管插管接有创呼吸机（9 月 21—29 日）：根据血气情况调节参数。抗感染治疗，给予亚胺培南 + 万古霉素，逐渐降级抗生素。静脉营养支持，应激性溃疡预防。肝肾功能、凝血功能监测，对症治疗。维持水电解质酸碱平衡。

2. **抗心律失常治疗：**

入院当日仍有短阵室速（9 月 21 日 06：44），应用胺碘酮静脉泵入 15 小时。目标温度达成后，复查 ECG QTc 较前延长（421ms → 493ms），停用胺碘酮，监测无室早或室速。9 月 26 日 05：23，再发短阵室速，亚低温程序已经结束，复查 QTc 缩短（493ms → 418ms），艾司洛尔静脉泵入后序贯美托洛尔 12.5mg bid；胺碘酮静脉泵入后序贯口服；Holter（9 月 27—28 日）：平均心率 91bpm，最慢心率 57bpm，最快心率 111bpm，房性早搏 350 个，室性早搏 16 个。

3. **心脏骤停后综合治疗效果：**

9 月 26 日停亚低温治疗，停镇静镇痛肌松药物；9 月 27 日患者昏睡状态，疼痛刺激后可睁眼，不能按照指令完成动作；9 月 28 日患者神志清，精神虚弱，可按照指令完成眼球活动等简单动作；9 月 29 日拔除气管插管，患者可以正确对答，遗忘发病前后经历；9 月 30 日拔除胃管，经口进食无不适；10 月 1 日拔除尿管，四肢及躯干肌力逐渐恢复。

4. **预防恶性事件再发的特殊治疗**

10 月 15 日完成皮下 ICD 植入，口服胺碘酮 0.2g qod，后病情好转出院。出院程控无室性心律失常发作，ICD 未放电。出院后 2 个月病情稳定，停用胺碘酮治疗，换位美托洛尔缓释片 47.5mg qd 抗心律失常

检验检查记录：

心电图：窦性心律 II、III、aVF、V2-V6 导联 ST 段压低

超声心动图：左室前壁、前间壁中段 - 心尖段运动减低；二尖瓣增厚，二尖瓣前叶脱垂伴反流（轻度），黏液样变性待明确，LVEF52%（2-D）

冠脉 CTA：LAD 中段浅肌桥，其余冠状动脉血管未见明显狭窄；各冠状动脉起源未见明显异常

心脏增强磁共振：左房、左室增大（舒张末内径 58mm）；收缩期可见二尖瓣后叶根部与左室心肌分离，距离最大约 8mm；二尖瓣脱垂，可见反流信号——二尖瓣环分离、脱垂、反流；左心室乳头肌肥大，前组、后组乳头肌局灶性延迟强化；T1 Mapping 及 T2 Mapping 正常，无心肌炎、心肌梗死表现

Holter（9-27 至 28 日）：平均心率 91bpm，波动在 57bpm-111bpm。房早 350 个，室早 16 个

鉴别诊断：

青年患者猝死病因分析：

青年猝死心源性原因为最常见原因，但由于事发突然，外院迅速完善了能够容易做的检查，基本排除了肺源性，脑源性猝死的相关疾病。包括：**a. 肺栓塞**：由于患者不存在血栓形成的高危因素，在给予呼吸机支持后氧合迅速得以纠正，同时双下肢静脉超声未显示血栓形成，超声心动图也未见右心扩大，肺动脉高压等表现，所以可排除肺栓塞导致的猝死。**b. 急性脑血管病**：患者既往体健，并且颅脑 CT 未见出血等明显异常。因此，肺栓塞以及脑血管疾病导致的猝死可以被排除。对于年轻且无既往疾病史的患者发生猝死，通常心源性原因也是最常见的，因此针对该例患者心源性猝死的可能原因进行了如下分析：

①心肌炎：由于患者在猝死前 1 个月出现过上呼吸道感染后的轻微腹泻（1~2d），未治疗自行好转。鉴于此情况，首先考虑该患者是否为心肌炎所致猝死。然而，患者为恶性心律失常起病，上呼吸道感染后并未见重症心肌炎常见的乏力、疲劳、胸闷、心悸等常见表现。同时从患者入院后的病情监测，未经针对重症心肌炎的激素治疗病情相对平稳，以及对感染相关指标进行筛查均为阴性，心脏核磁未提示心肌炎常见的心肌水肿、延迟强化等表现，所以排除心肌炎导致猝死的可能。

②冠状动脉病变相关，如冠脉起源异常或心肌梗死：a. 冠脉起源异常：由于患者冠脉 CTA 显示 LAD 中段浅肌桥，其余冠状动脉血管未见明显狭窄；各冠状动脉起源未见明显异常。故排除冠脉起源异常等畸形导致的猝死。且患者并没有常见的冠脉起源异常等畸形导致的在运动中因为心肌严重缺血导致的猝倒过程，也不支持冠脉畸形的诊断。b. 急性心肌梗死：患者入院后心肌酶谱虽然表现为心肌梗死的酶学曲线过程，但是该酶学为持续心肺复苏 1 小时 40 分钟后的结果，不能排除严重低灌注所致，参考价值不大；同时复苏后患者心电图没有提示大面积心肌梗死常见的异常 Q 波，T 波倒置等动态演变过程，UCG 心脏的节段性室壁运动异常以及射血分数迅速恢复等临床表现，均不提示该患者是由冠脉功能学异常主要指的是冠脉痉挛，所导致的心肌梗死。故患者无冠状动脉病变相关原因导致猝死。

③其他严重的结构性心脏病：患者的超声心动图没有提示肥厚性心肌病、主动脉瓣严重狭窄、扩张性心肌病等相应表现，因此基本排除由结构性心脏病导致的猝死。

④心律失常：心律失常是年轻患者猝死的重要原因。由于患者出现持续性多形性室性心动过速、室颤，入院后监测也发现了两次室速，故考虑室速室颤等这一恶性心律失常是导致患者猝死的主要原因。病因鉴别主要分为两方面，**一方面为遗传性心律失常**，比如长、短 QT 综合征，Brugada 综合征，早复极综合征等，但患者没有猝死家族史，心电图不具备特殊 ECG 表型，全外显子基因筛查无特殊提示，排除遗传性心律失常综合征导致的室性心动过速、室颤后猝死的情况。**第二方面，存在少见心脏疾病导致心律失常。**该患者入院超声心动图提示二尖瓣前叶冗长伴脱垂，存在轻度二尖瓣反流，因为查体未闻及心脏杂音，并未引起重视，但 9 月 25 日查体时发现患者心尖部可闻及收缩期 2/6 级吹风样杂音；9 月 26 日心尖部可闻及收缩晚期喀喇音，其后可闻及 2/6 级吹风样杂音，左侧卧位时明显。鉴于此体征明显变化，故将二尖瓣脱垂与室性心律失常联系起来，并进行文献检索，提示 Barlow 综合征可以有相关表现，遂请超声心动图再次检查，结果提示二尖瓣前叶后叶脱垂伴轻度反流、二尖瓣环分离以及二尖瓣黏液样变性，符合 Barlow 综合征的 UCG 表现。因此，怀疑该患者为二尖瓣黏液样变性伴脱垂及室性心律失常病因——Barlow 综合征。

针对二尖瓣黏液样变性及脱垂，也鉴别了其他原因导致的可能性，如自身免疫性疾病、风湿性疾病、退行性疾病等，患者无既往病史，自身免疫抗体等化验均不提示疾病，基本可除外。其他一些与基因遗传相关结缔组织疾病，如 Marfan 综合征，Loeys-Dietz 综合征，Ehlers-Danlos 综合征，成骨不全症和成人多囊肾等疾病。但患者无上述疾病典型临床表现，全外显子基因测序无提示，可排除上述疾病。因此，最终考虑 Barlow 综合征，即二尖瓣黏液样变性伴脱垂、二尖瓣环分离，导致室性恶性心律失常。结合心脏磁共振结果提示，二尖瓣瓣环存在扩大、分离，二尖瓣前后瓣叶均脱垂；此外，从左室基底到心尖段存在延迟强化，主要出现在前后组乳头肌；该患者延迟强化部位可以解释多个起源形态不同的室速起始部位。患者心肌多发延迟强化提示纤维化改变，可能与二尖瓣组织脱垂，在长期牵拉、疲惫等状态下出现纤维化改变。

其他：

二尖瓣脱垂是最常见的瓣膜疾病，人群患病率为 0.6%-2.4%，通常被视为良性病变，但近年来“心律失常型二尖瓣脱垂复合体”作为室性心律失常甚至心原性猝死的潜在原因逐渐被重视 。Barlow 综合征（表现为显著的二尖瓣分离）被认为是恶性 MVP 综合征的“红旗”，提示高风险，需加强风险分层 。病理和心脏磁共振研究证实二尖瓣脱垂与左心室纤维化（28%-37%）相关，纤维化常位于二尖瓣环附近基底部左心室壁（包括乳头肌、下侧壁和下壁），而乳头肌中壁延迟强化（LGE）或左心室下基底段片状非缺血性纤维化与复杂性室性心律失常相关 。此外，细胞外容积（ECV）定量或增强后 T1 值提示的间质心肌纤维化与复杂性室性心律失常风险增加相关 。然而，并非所有二尖瓣分离均与室性心律失常相关，提示局部纤维化可能呈进展性，需密切监测二尖瓣脱垂患者（尤其伴显著黏液样变性者）的电生理和形态学特征 。二尖瓣脱垂患者心律失常高危指标包括：下壁或侧壁导联 T 波倒置；频发、多形性室性早搏（PVC）及后续非持续性室速（NSVT），其 PVC 形态多起源于乳头肌、二尖瓣环或左心室基底部；二尖瓣环分离；冗长瓣叶；左心房扩大；左心室射血分数≤ 50%；心脏磁共振提示乳头肌或瓣环区域延迟强化 。临床实践中，并非所有二尖瓣脱垂患者均会发生室性心律失常，但存在上述高危指标时，应保持警惕，建议行动态心电图监测以筛查心律失常并进行风险分层，及时动态心电图监测未提示严重室性心律失常，必要时仍建议行心脏磁共振全面评估心肌纤维化情况和心律失常风险 。

嗜铬细胞瘤所致继发性高血压 1 例

陈璐

首都医科大学附属北京同仁医院

患者基本信息：

• 女性，43 岁，2022-10-10 入院

主述：

间断头痛 2 周余

现病史：

•2 周余前于劳累后出现头痛，伴双眼眶胀痛、颈项不适，感恶心，无头晕、呕吐，无视物旋转、视物模糊，无言语不利、肢体活动障碍，无胸痛、胸闷，无心悸，无咳嗽、咳痰，先后就诊于神经内科及我科，测血压最高为 170/109mmHg，考虑高血压病，予苯磺酸氨氯地平及松龄血脉康胶囊口服降压。患者每日晨起测血压，仅于收缩压≥ 150mmHg 和（或）舒张压≥ 100mmHg 时口服苯磺酸氨氯地平 5mg，用药后监测血压维持于 135/95mmHg 水平。1 周余前进一步完善肾动脉彩超未见明确狭窄征象，行肾上腺平扫 CT 示“右侧肾上腺区占位性病变”。3 天前上午于外出活动时再次出现头痛，无恶心、呕吐，无视力下降，无言语不利、肢体活动障碍，无胸痛、心悸等，测血压 150+/105mmHg，口服苯磺酸氨氯地平 5mg 及松龄血脉康胶囊 3 粒。21:00 复测血压仍为 150+/105mmHg，再次口服苯磺酸氨氯地平 5mg。现为进一步诊治，以“高血压”收入我科。

• 自发病以来，精神可，睡眠可，食欲可，二便如常，近期体重无明显变化。

既往病史：

• 半月来间断于爬 3 层楼后出现前正中胸痛，无放射痛，无胸闷、心悸，休息约 5min 后缓解，未予重视诊治。

• 曾于 711 医院行肺 CT 示右肺下叶钙化灶，外院考虑陈旧性肺结核。

•2020 年发现 ALT、AST 升高，超过正常值 3 倍以上，于佑安医院就诊，予保肝治疗后转氨酶恢复正常，同时就诊期间发现门静脉增宽，未予特殊处理。

• 家族史：母亲于 45 岁时诊断高血压，外祖父、外祖母、舅舅均患高血压。

病程记录：

患者入院后完善常规检查，结合既往血压测量数值等情况，考虑高血压病诊断。该患者为中年女性，急性起病，血压升高程度相对严重，需警惕继发性高血压可能。进一步行心脏彩超未见明显异常，行肾动脉彩超未见明显狭窄征象。患者既往肾上腺平扫 CT 示右侧肾上腺占位，进一步行肾上腺增强 CT 示右侧肾上腺区占位性病变，考虑腺瘤可能性大。结合内分泌科及泌尿外科会诊意见，考虑目前肾上腺占位性质尚不明确，需手术切除完善病理检查以助明确，暂加用盐酸特拉唑嗪 2mg qn，监测血压波动于 120-140/90-95mmHg 水平，心率波动于 90-105 次 / 分。目前血儿茶酚胺 3 项结果未归，患者病情相对稳定，请示上级医师准予出院。出院后结果回报阳性，患者后续于泌尿外科住院。

检验检查记录：

详见幻灯片

鉴别诊断：

有关高血压的鉴别诊断：

1、原发性高血压：是以体循环动脉压升高为主要临床表现的心血管综合征，高血压诊断主要根据诊室测量的血压值，采用经核准的水银柱或电子血压计，测量安静休息坐位时上臂肱动脉部位血压，一般需非同日测量三次血压值收缩压均≥ 140mmHg 和（或）舒张压≥ 90mmHg 可诊断高血压。根据该患者既往血压测量数值，考虑高血压诊断明确，需进一步除外继发性高血压的情况以助明确。

2、继发性高血压：是指由某些确定的疾病或病因引起的血压升高，其主要病因包括：

（1）肾实质性高血压：最常见，包括肾小球肾炎、糖尿病肾病、慢性肾盂肾炎、多囊肾和肾移植后等多种肾脏病变引起的高血压。该患者既往无肾脏疾病、糖尿病、泌尿系感染等病史，无泡沫尿、血尿史，考虑肾实质性高血压可能性小，可进一步完善肾功能、肾脏彩超等检查以助明确。

（2）肾血管性高血压：是单侧或双侧肾动脉主干或分支狭窄引起的高血压，如多发性大动脉炎、肾动脉纤维肌性发育不良多见于青少年。但该患者查体时于腹部未闻及血管杂音，既往肾动脉彩超未见明确狭窄征象，暂不考虑肾血管性高血压可能。

（3）原发性醛固酮增多症：是肾上腺皮质增生或肿瘤分泌过多醛固酮所致，以长期高血压伴低血钾为特征。该患者肾上腺 CT 可见右侧肾上腺占位，入院后需复查完善电解质、完善卧立位醛固酮测定、肾上腺增强 CT 等检查以助明确。

（4）其他可引起继发性高血压的疾病: 如嗜铬细胞瘤、皮质醇增多症、主动脉缩窄，可进一步完善肾上腺增强 CT、皮质醇节律测定、超声心动图等以助除外。

其他：

•2022-10-24 于我院泌尿外科住院，2022-11-11 在全麻下行腹腔镜右肾上腺切除术，术后病理提示嗜铬细胞瘤。患者现未应用降压药物，监测血压平稳。

罕见的右冠状动脉瘤伴附壁血栓形成合并右冠状动脉–左心室瘘

李振华

哈尔滨医科大学附属第二医院

患者基本信息：

患者男性，70 岁，因胸闷行 CT 检查怀疑心脏前方巨大囊肿就诊。他的病史有双下肢水肿，高血压病、脑梗死病史。入院时，实验室检查结果显示 N 端 B 型利钠肽前体（NT-proBNP）（1231 pg/ mL），心肌酶指标均正常。进一步的心脏检查，包括心脏超声和冠状动脉三维成像。超声心动图表现提示为右冠状动脉囊性扩张和冠状动脉左心室瘘。冠状动脉三维成像显示右冠状动脉局部管腔轻微狭窄，同时伴有动脉瘤形成，右冠状动脉内形成了附壁血栓，并且与左心室之间出现了一个异常的通道（瘘管），主动脉硬化，同时伴有附壁血栓形成以及多发性溃疡。

主述：

体检发现肺门区肿块 4 天

现病史：

患者 4 天前因右侧肢体无力、吞咽困难就诊于珲春市人民医院，完善检查时发现右肺门区肿块，当地医院诊断心包囊肿、脑梗死，建议至上级医院进一步治疗。病程中患者无明显不适，自觉肢体无力，今患者为求进一步治疗来我院，门诊以“先天性心包囊肿”为诊断收治入院病程中患者无咳嗽、无咳痰、无咯血、无胸闷、无胸痛、无黑蒙、晕，无腹胀，睡眠、饮食未受明显影响，二便正常，体重无明显变化。

既往病史：

高血压 10 年，不规律口服硝苯地平缓释片、厄贝沙坦氢氯噻嗪片；脑梗死病史 4 天现右侧肢体无力。

病程记录：

入院后病情变化症状：患者精神可，无胸闷、胸痛，右侧肢体无力较前改善（肌力 4+ 级）。夜间可平卧，活动后稍气促。体征：BP 140-160/80-90 mmHg（调整降压药后），双肺底湿啰音减少，心律齐，双下肢无水肿。治疗经过：心功能改善：呋塞米 20mg qd，调整为托拉塞米 10mg bid（尿量 1500-2000ml/ 日）；血压控制：硝苯地平控释片 30mg qd; 抗栓 / 冠心病：阿司匹林 100mg qd（术后将联用氯吡格雷）；肾功能保护：停用 NSAIDs

检验检查记录：

实验室检查结果显示 N 端 B 型利钠肽前体（NT-proBNP）（1231 pg/ mL），心肌酶指标均正常。

进一步的心脏检查，包括心脏超声和冠状动脉三维成像。超声心动图表现提示为右冠状动脉囊性扩张和冠状动脉左心室瘘。冠状动脉三维成像显示右冠状动脉局部管腔轻微狭窄，同时伴有动脉瘤形成，右冠状动脉内形成了附壁血栓，并且与左心室之间出现了一个异常的通道（瘘管），主动脉硬化，同时伴有附壁血栓形成以及多发性溃疡。

鉴别诊断：

1. 先天性心包囊肿：患者体检发现右肺门区肿块，心脏彩超及主动脉 CTA 可予以鉴别。

2. 主动脉夹层：患者多有高血压病史，突发剧烈胸痛，呈撕裂样，持续不缓解，心脏彩超及主动脉 CTA 可予以鉴别。

3. 主动脉瓣病：患者可有类似心绞痛症状，偶伴晕厥，查体可闻主动脉瓣区心脏杂音，心脏彩超及冠脉检查可鉴别。

其他：

一例 ATTR 型心肌淀粉样变的诊治

张舒怡

上海市同仁医院

患者基本信息：

男，64 岁，退休

主述：

反复胸闷气促 2 年，加重伴头晕 1 天。

现病史：

患者 2 年前反复出现胸闷气促，就诊中山医院，完善相关检查（具体不详），考虑诊断限制性心肌病，给予琥珀酸美托洛尔缓释片治疗，后期患者因心跳偏慢停用。1 月前因胸闷不适至仁济医院就诊，予诺新妥 25mg bid 治疗。患者昨天自觉胸闷加重，伴头晕，乏力明显，有四肢麻木，自测血压 59/36mmhg，收入心衰专科进一步诊治。

既往病史：

患者近 1 年反复出现腹泻，7-8 次 / 天，水样便，就诊华山医院完善胃镜示慢性糜烂性胃炎，肠镜未见异常，给予护胃及止泻治疗后效果不佳，近 1 年体重下降 10kg。

否认高血压、糖尿病史。

病程记录：

患者入院后完善相关辅助检查，予以托拉塞米改善容量负荷，倍他乐克控制心室率，诺欣妥抑制心肌重构，左西孟旦强心治疗，病程中患者出现血压低，予以停用影响血压药物。患者心超提示限制型心肌病可能，予以完善血清免疫固定电泳、心脏增强 MR、基因检测，考虑患者为转甲状腺素蛋白淀粉样。予以调整药物治疗方案后出院。

检验检查记录：

心脏 mr: 左室心肌收缩减弱，舒张受限，心室壁增厚，厚度约 18mm，左房右房稍大。心肌灌注扫描显示各部分心肌均匀强化，心内膜下未见充盈缺损。延迟扫描左心室壁、右心室壁见弥漫性强化。诊断：1. 左右心室壁弥漫性病变，考虑淀粉样变性可能，请结合临床。2. 左房及右房稍大，左室壁增厚，左心功能不全，少量心包积液

唇腺活检：病理诊断：唾液腺萎缩消失，纤维及脂肪组织增生，伴散在淋巴细胞、浆细胞浸润，局灶结合特染考虑淀粉样变性。

鉴别诊断：

1. 肌小节蛋白编码基因突变导致的 HCM ？

2. 糖原贮积病？（LAMP2/PRKAG2）

3.Fabry 病？（α- 半乳糖苷酶 A 酶活性）

4. 线粒体疾病？（核 DNA 或线粒体 DNA 突变）

5. 系统性淀粉样变？（轻链型 / 转甲状腺素蛋白）

6. 高血压引起的心肌肥厚?

7. 冠心病合并心肌肥厚?

其他:

一例甲亢导致急性冠脉综合征

王海锟

石河子市人民医院

患者基本信息:

患者李志莲，女性， 80 岁，汉族

主述:

发作性胸闷、胸痛 20 年，胸骨后烧灼感 1 月。

现病史:

患者及家属诉：20 年前始每慢步行走 10 余米即感胸闷、气短、乏力，偶感胸骨中段手掌大小范围针刺样疼痛发作，多次就诊于我院。2010 年 12 月 28 日曾于我科住院行“冠脉造影提示：左主干（-）；前降支开口斑块，近中段内膜不光滑，第一对角支开口斑块 60% 狭窄，中段 80% 狭窄；回旋支开口斑块远段 90% 狭窄；右冠近中段内膜不光滑，斑块浸润”。2011 年 1 月 14 日于前降支行 PCI 术，术后规律服药。2021 年 4 月、9 月 15 日、2025 年 5 月于我科住院诊断“1. 急性非 ST 段抬高型心肌梗死 陈旧性心肌梗死 冠状动脉支架植入后状态 KillipI 级”，拒绝冠脉介入诊疗。间断感胸骨后烧灼感，于我科住院诊断“急性非 ST 段抬高型心肌梗死 KillipII 级 冠状动脉支架植入后状态 陈旧性心肌梗死”，经治疗后患者胸痛症状减轻，拒绝行 PCI 治疗，出院后规律服药。近 1 月患者夜间平卧后感胸骨后烧灼感，伴反酸，坐起后好转，日间慢步活动未诉特殊，就诊我院门诊，门诊以“冠心病”收入。

既往病史:

有“高血压”病史 30 年，血压最高 220/100mmHg ，长期口服“沙库巴曲缬沙坦钠片 50mg 一日两次、酒石酸美托洛尔片 12.5mg 一日两次”，血压波动在 120-110/80-70mmHg。有“2 型糖尿病”病史 3 年，长期使用达格列净片 10mg 一日一次口服，阿卡波糖胶囊 50mg 一日三次口服，未监测血糖。无吸烟、饮酒史。

病程记录:

2025 年 6 月 21 日夜间突发胸闷、胸痛，复查心电图较前动态演变，急诊行冠脉介入治疗，于右冠植入三枚支架，术后患者全身不适，持续心动过速、持续性房颤、非持续性室速、低血压状态、发热，经积极抗感染、补液、抗休克、控制心室率治疗后患者逐渐出现昏迷、休克无法纠正，根据血压逐渐调整多巴胺、多巴酚丁胺、去甲肾上腺素泵速，停面罩吸氧，改为高流量吸氧，反复与患者家属沟通病情，告知目前病情危重，治疗困难，死亡风险极高，预后极差，患者家属表示理解，拒绝心肺复苏、气管插管、电除颤、转重症医学科、呼吸机支持等措施，拟予以肾上腺素静推，经积极抢救患者大动脉搏动消失，呼吸心跳停止，报病故。

检验检查记录:

急诊行冠脉造影提示：前降支开口 50% 狭窄，近→中段 80% 弥漫狭窄伴钙化，D1 原支架内轻度内膜增生，回旋支开口 90% 狭窄伴钙化，近段 100% 闭塞，右冠全程钙化，近中 60% 狭窄，中→远段多处狭窄 90%，PDA 100% 闭塞，PLA 70% 狭窄。术中于右冠病变处使用震波球囊扩张，植入三枚支架（GuReater 2.75/24mm、firebird2 3.0/33mm、GuReater3.0/15mm）。TSH: 促甲状腺激素 <0.01 ↓ uIU/mL，心梗三项：肌钙蛋白 T 0.102 ng/ml，肌红蛋白 77.760 ↑ ng/ml，肌酸激酶同工酶 7.900 ↑ ng/ml，血脂四项：总胆固醇 1.56 ↓ mmol/L，高密度脂蛋白 0.75 ↓ mmol/L。血分析五分类：白细胞计数 15.76 ↑ 10^9/L，红细胞计数 3.26 ↓ 10^12/L，血红蛋白 97 ↓ g/L，红细胞压积 31.1 ↓ %，IL-6+PCT: 白介素 6 测定 344.00 ↑ pg/ml，降钙素原 0.81 ↑ ng/ml，超敏 C 反应蛋白：超敏 C 反应蛋白 >5.00 ↑ mg/L，全量程 C 反应蛋白 10.83 ↑ mg/L，电解质：钾 5.57 ↑ mmol/L，甲乙型流感抗原检测阴性。血分析五分类：白细胞计数 17.66 ↑ 10^9/L，血红蛋白 89 ↓ g/L，红细胞压积 28.4 ↓ %，凝血全项：凝血酶原时间 -RP 16.40 ↑ 秒，国际标准化比率 -RP 1.52 ↑ ，ABO 血型及 RHD 联合测定 :ABO 血型系统正反鉴定 A 型 ，Rh 血型系统 D 鉴定 D 阳性 (CCee) ，A-TPO+A-TG+ 甲五：游离三碘甲状腺原氨酸 12.50 ↑ pmol/L，游离甲状腺素 >100.00 ↑ pmol/L，三碘甲状腺原氨酸 3.82 ↑ nmol/L，甲状腺素 205.00 ↑ nmol/L，促甲状腺激素 <0.01 ↓ uIU/mL，肾四 + 肝八：丙氨酸氨基转移酶 108.00 ↑ U/L，天门冬氨酸氨基转移酶 113.00 ↑ U/L，白蛋白 26.30 ↓ g/L，球蛋白 18.30 ↓ g/L，尿素 15.60 ↑ mmol/L，肌酐 167.70 ↑ umol/L，尿酸 667.00 ↑ umol/L，新冠核酸检测阴性。呼吸道病原体八项阴性。

鉴别诊断:

急性心包炎：前胸持续性锐痛，随呼吸或体位变化加剧，可伴发热。心电图示多导联 ST 段弓背向下抬高（非区域性），心肌酶轻度升高但无动态变化；心脏超声可见心包积液。

主动脉夹层：突发撕裂样剧痛，范围广泛（可放射至背部、腹部），持续不缓解，常伴血压骤升或双侧脉搏不对称。心电图无 ST 段抬高 / 压低，心肌酶正常；确诊依赖急诊增强 CT 或血管造影。

其他:

无

IVUS 指导下左主干介入治疗一例

王中良

邢台医学院第二附属医院

患者基本信息:

患者中年男性，58 岁，病例号：004357

主述:

主因间断胸闷、胸痛 1 年，加重 20 天入院

现病史:

患者 1 年前，常用活动或劳累后出现胸闷、胸痛，咽中如有物堵塞，胸中窒闷、疼痛，位置在胸骨后，阵发性反复发作，每次发作几分钟、十几分钟，时间不等，未予正规诊治。20 天前，患者胸闷、胸痛症状加重，发作较前频繁，持续时间延长，并向左上肢放射，含服硝酸甘油可缓解，遂于我科住院，诊断“不稳定型心绞痛 冠心病”，并行冠脉造影示左主干 + 三支病变，拒绝行冠脉搭桥治疗，RCA 置入支架 2 枚，术后规律口服阿司匹林、替格瑞洛等药物治疗。今为进一步处理左冠病变来院。

既往病史:

高血压病史 5 年，血压最高 180/100mmHg，平时口服硝苯地平控释片治疗，血压控制可；2 型糖尿病病史 5 年，平时口服二甲双胍、格列美脲治疗，血糖控制不详。无外伤史，无“肝炎、结核”等传染病史，无输血史。

病程记录:

完善术前检查，行 IVUS 指导下左主干介入治疗。

检验检查记录:

心电图：窦性心律，T 波低平倒置。心脏彩超：左房前后径 41mm、左室舒张末前后径 51mm、射血分数 64%。血常规 WBC 7.5*10~9/L、HGB 150g/L、PLT 132*10~9/L

肝功能 ALT57U/L ↑、AST 27U/L

血脂 LDL-C 1.09mmol/L、甘油三酯 TG1.97mmol/L ↑

空腹血糖 6.46mol/L、糖化血红蛋白 6.7% ↑

心肌酶未见异常

NTpro-BNP<100pg/ml

凝血、电解质、肾功能、甲功未见异常

鉴别诊断:

患者诊断明确，无需鉴别

其他:

OCT 指导急性心肌梗死斑块破裂非支架植入治疗患者一例

李顺子

哈尔滨医科大学附属第二医院

患者基本信息:

患者，性别：男，年龄：40 岁，国籍：中国，民族：汉族，婚姻状况：已婚。

主述:

阵发性胸痛 20 天，加重 1 小时。

现病史:

患者 20 天前无明显诱因开始出现阵发性胸痛，呈心前区烧灼性疼痛，范围约手掌大小，未放散至后背、双肩及左上肢，待续数分钟至半小时不等，可自行或舌下含服的硝酸甘油缓解，伴有大汗。气短、无咳嗽、咳痰，无恶心、呕吐，无头晕，头痛等，本予重视，患者下入院前 1 小时 突发胸痛，呈持续性压榨样，疼痛程度较重，未放散至后背，双肩及左上肢，作大汗、气短，无咳嗽、咳痰，伴恶心、呕吐一次，呕吐物为胃内存物，无头笼，头痛等，急呼 120，行心电图提示下壁心肌梗死，给予拜阿斯匹灵 300mg 口服 随急送入我院， 以“冠心病急性心肌梗死”收入院、病程中患者饮食，二便尚可，睡眠欠佳 .

既往病史:

有自述发现高血压 10 天余，未服用降压药物，否认糖尿病病史，有既往有吸烟史 20 年，每天约 30 支，未戒烟；既往有饮酒史 20 年，未戒酒 .

病程记录:

手术治疗：患者首次入院时，ECG 示 II、III、AVF、V3R-5R 导联 ST 段抬高，诊断为 STEMI，行冠脉造影示右冠近端 90% 狭窄，TIMI 血流：3 级；行 OCT 示右冠近段狭窄、斑块破裂伴大量白色血栓血栓；因为 OCT 示患者管腔较大，斑块破裂较小，所以考虑行双抗药物保守治疗。

患者术后一月，行冠脉造影示右冠脉 70% 狭窄，TIMI:3 级；行 OCT 示右冠脉近段狭窄，斑块破裂，含机化血栓，红血栓。

患者术后一年，行冠脉造影示右冠脉 40%，TIMI:3 级，行 OCT 示右冠脉近段狭窄斑块愈合，血栓消失。

药物治疗：术前双抗用药：拜阿斯匹林、氯吡格雷

术后用药：

1 拜阿斯匹灵 .

. 替格瑞洛片：90/mg

3. 琥珀酸美托洛尔缓释片：23.75/mg

4. 阿托伐他汀钙片：20/mg

5. 培哚普利叔丁胺片：2/mg

检验检查记录：

ECG 示：窦性心律，II、III、AVF、V3R-5R 导联 ST 段抬高

造影结果：右冠脉近端 90% 狭窄

OCT 示：右冠狭窄伴斑块破裂，管壁附着白色血栓

血清肌钙蛋白 I：7.789ug/L ↑

B 型钠尿肽前体：63pg/mL

肌酸激酶同工酶质量：31ug/L

鉴别诊断：

1. 主动脉夹层

2. 急性肺动脉栓塞

其他：

花季少年——因何安上起搏器？

朱桐彤

哈尔滨医科大学附属第二医院

患者基本信息：

1、主诉：间断胸闷 1 年，胸痛 5 天。

2、男患，26 岁，10 年前疑似心肌炎病史、无吸烟饮酒史、无药物过敏史、无手术外伤史

4、查体：体温：36.5° C，血压：135/60 mmHg，脉搏：42 次 / 分，呼吸：22 次 / 分。一般状态尚可，平车推入病房，查体合作，口唇无发绀，浅表淋巴结未肿大，双肺呼吸音清，未闻及干湿性啰音，心律齐，心率：42 次 / 分，心界不大，各瓣膜听诊区未闻及病理性杂音。腹平坦，柔软，无压痛及反跳痛，双下肢无水肿。生理反射正常，病理反射未引出

5、辅助检查：ECG 示：交界性逸搏心律

主述：

间断胸闷 1 年，胸痛 5 天。

现病史：

患者 1 年前熬夜后出现阵发性胸闷，呈持续性，无胸痛，未放射至左上肢、后背部，无咽喉紧缩感，休息后症状好转。病程中无发热、无咳嗽、咳痰，无腹泻，无恶心、呕吐，无头晕、头痛，无晕厥等，未进一步诊治。5 天前患者无明显诱因出现胸痛，呈持续性，伴大汗，无恶心呕吐，不伴头晕头痛，不伴咳嗽咳痰，自行口服心宝、辅酶 q10 后未见好转，于我院就诊，ECG 提示：逸搏心律、ST-T 改变，心率最低约 39 次 / 分，行冠状动脉造影检查，未见明显异常，给予对症支持治疗，并建议起搏器植入治疗，患方表示拒绝后出院。患者出院后胸痛仍间断发作，现为求进一步诊治来我院。病程中患者饮食、二便尚可，睡眠一般。

既往病史：

10 年前疑似心肌炎病史、无吸烟饮酒史、无药物过敏史、无手术外伤史

病程记录：

详见检查文件

检验检查记录：

详见检查文件

鉴别诊断：

主动脉夹层、急性冠脉综合征、风湿免疫病等

其他：

无

PCI 后的高风险 TAVR

向睿

重庆医科大学附属第一医院

患者基本信息：

女性 71 岁，

主诉：反复胸痛 3 年以上，再发加重 3 周

既往史：入院前 3 年 +，患者无诱因出现左右前胸壁压榨性疼痛、双上肢麻木，持续 2-3 分钟后可自行缓解，夜间疼痛至苏醒有心悸，于其他医院就诊，完成冠状动脉造影提示：左主干无明显狭窄，前降支近段后血管闭塞，血管狭窄 70-85%，血流正常。后予以“氢氯吡格雷、阿司匹林、曲美他嗪、阿托伐他汀”等药物治疗。有所缓解建议上级医院进一步就诊。遂于我院行冠脉造影提示后在前降支植入 2 枚支架。

现病史：反复胸痛胸闷加重，再次行冠状动脉造影术提示：左右冠状动脉原支架血流通畅，未见明显狭窄

个人史：无特殊

婚姻史、家族史无特殊

主述：

主诉：反复胸痛 3 年以上，再发加重 3 周

现病史：

反复胸痛胸闷加重，再次行冠状动脉造影术提示：左右冠状动脉原支架血流通畅，未见明显狭窄

既往病史：

既往史：入院前 3 年 +，患者无诱因出现左右前胸壁压榨性疼痛、双上肢麻木，持续 2-3 分钟后可自行缓解，夜间疼痛至苏醒有心悸，于其他医院就诊，完成冠状动脉造影提示：左主干无明显狭窄，前降支近段后血管闭塞，血管狭窄 70-85%，血流正常。后予以“氢氯吡格雷、阿司匹林、曲美他嗪、阿托伐他汀”等药物治疗。有所缓解建议上级医院进一步就诊。遂于我院行冠脉造影提示后在前降支植入 2 枚支架。

病程记录：

病人入院后，完善冠脉的头部 CTA 检查，进一步冠脉造影完成

排除其他问题，进行 TAVR 检查及手术

冠脉支架衍伸至窦里，手术困难，风险极高

[illegible]记录：

鉴别诊断：

所见：左房内径增大，主动脉瓣增厚，主动脉瓣收缩期湍流速度约为 263cm/s，舒张期探及中 - 重度反流，测算瓣口面积约 1.1cm2。另探及二尖瓣、三尖瓣轻度反流。余未探及明显异常。

提示：

左房增大

主动脉瓣病变伴中度狭窄及中重度关闭不全

左室肥厚伴顺应性减退

其他：

冠脉行支架保护的 TAVR

向睿

重庆医科大学附属第一医院

患者基本信息：

性别：女 年龄 :77 岁年

民族：汉族　婚姻状况：已婚

主 诉：胸闷、心悸 1 月

现病史 :1 月前，患者无明显诱因出现胸闷，心悸，安静休息下也可诱发，以剑突下为主，持续时间大约 2 分钟，无放射痛、无恶心、呕吐，无呼吸困难，无黑曦、晕厥，现患者为进一步诊治入我院，门诊以“主动脉重度狭窄”收入我科。患者本次发病以来食欲正常，神志清醒，精神尚可，睡眠尚可，大便正常，小便正常体重无明显变化。

主述：

主 诉：胸闷、心悸 1 月

现病史：

现病史 :1 月前，患者无明显诱因出现胸闷，心悸，安静休息下也可诱发，以剑突下为主，持续时间大约 2 分钟，无放射痛、无恶心、呕吐，无呼吸困

既往病史：

无特殊

病程记录：

病人入院后完成 TAVR 相关术前检查，窦相对小，支架冠脉风险高，术中进行两侧冠脉保护，支架释放时完成冠脉保护，最后植入瓣膜，两侧冠脉显影

检验检查记录：

超声检查及 TAVRCT 检查

鉴别诊断：

主动脉瓣重度狭窄伴中度关闭不全二尖瓣、三尖瓣中度反流，PASP:70mmig

左房增大

左室肥厚伴舒张功能减退。

其他：

泛血管团队合作下利用左室辅助装置保驾的 CHIP 患者冠脉介入治疗

黄安安

浙江大学医学院附属第二医院

患者基本信息：

患者老年男性，缺血性心肌病，冠脉双支重度狭窄伴严重钙化，合并左心功能不全及多重泛血管疾病

主述：

反复胸闷气促 6 年，再发加重 1 周

现病史：

患者于 6 年前出现反复胸闷气促，活动后为甚，休息后逐渐缓解；2 年前在我院就诊，冠脉造影提示右冠 CTO、前降支 90% 狭窄、回旋支全程 95% 狭窄，于右冠近段植入支架，后续出院后仍右胸闷气促发生，2023 年外院复查冠脉造影提示左主干 50% 狭窄，前降支、回旋支最重 99% 狭窄伴严重钙化，予口服药物保守治疗；1 周前再发胸闷气促，伴咳嗽咳痰、咳痰，外院胸 CT 提示支气管炎、肺气肿，两肺感染，予以抗感染、抗心衰、利尿消肿、抗血小板等治疗，胸闷气促较前稍好转，现为求进一步诊疗，拟“心力衰竭、缺血性心肌病”收住入院。

既往病史：

原发性高血压、陈旧性脑梗死、甲状腺结节、脂肪肝

病程记录：

入院后完善相关检查，给予抗血小板、他汀及 PSCK9i 调脂、呋塞米及螺内酯利尿、美托洛尔 / 达格列净改善心室重构等治疗，泛血管团队 MDT 评估患者整体手术策略，最后拟先由血管外科团队完成左侧髂动脉支架植入术后保证股动脉入路通畅，随后沿左侧股动脉入路植入左心室辅助装置完成后续冠脉介入治疗。

检验检查记录：

辅助检查：1. 心脏超声：EF: 27.8%，左室心肌节段性运动异常，左心增大，左心功能不全；主动脉瓣退行性变少量反流；二尖瓣少量反流，二尖瓣后叶瓣环及腱索钙化灶；三尖瓣少量反流。

2. 颈动脉、椎动脉超声：左侧颈动脉粥样硬化伴多发斑块形成，左侧颈内动脉起始段溃疡斑块考虑、双侧颈内动脉狭窄（左侧中 - 重度狭窄，右侧重度狭窄）、右侧椎动脉闭塞、左侧椎动脉起始段重度狭窄考虑，远段流速减低。

3. 双下肢动静脉超声：双侧下肢动脉粥样硬化性闭塞、双侧股浅动脉闭塞考虑。

4. CT 全主动脉造影：胸 - 腹主动脉全段及其分支粥样硬化，局部溃疡形成，双侧髂内动脉局部闭塞，余管腔轻中度狭窄

5. 头颅 CT：左侧额顶叶软化灶，左侧侧脑室扩张，左侧中脑体积缩小，老年性脑改变，椎动脉钙化。

鉴别诊断：

诊断明确

其他：

1 年后复查心超提示：EF：38.7%，LVIDd：6.44 cm LA：4.16 cm。

该病例是在经我院泛血管中心团队综合分析、团队共同下完成的复杂高危 PCI 一例，通过血管外科团队对髂动脉支架植入，从而为后续冠脉 PCI 治疗提供血管入路，左心室辅助装置能够顺利植入，为后续 PCI 治疗保驾护航；在 PCI 过程中有了左心室辅助装置，使得术者能够很好的利用冠脉高速旋磨、震波等技术，顺利开通前降支，从而最终使得患者心功能得到明显改善。

左主干三支病变支架植入术中 IVUS 导管嵌顿导致支架毁形器械缠绕 1 例

田野

贵州省人民医院

患者基本信息：

患者，男，68 岁

主述：

因“反复胸痛 1 + 月，再发 3 + 天”入院。

现病史：

因“反复胸痛 1 + 月，再发 3 + 天”入院。1 月前因胸痛与当地医院 CAG 示：左主干 + 三支血管病变，于右冠脉植入支架 3 枚症状缓解出院。3 天前因再发胸痛入院。

既往病史：

2 型“糖尿病”10 年；“左侧面瘫”6 年。　　无高血压及脑血管病史。

病程记录：

入院后予以积极抗血小板聚集，调脂，稳定斑块治疗，

检验检查记录：

心 电图：窦性心律（心室率 63bpm）。

外院 CAG：左主干及三支血管弥漫病变

RCA 支架术后

术前 UCG: 左室舒张功能减退，三尖瓣轻度返流

肺　CT: 胸膜轻度增厚。

肌钙蛋白轻度升高：0.075ug/L

鉴别诊断：

与急性心肌梗死鉴别的要点在于，患者无剧烈的胸痛，无病理性 Q 波形成。

其他：

LVAD 术后重度 AR 经颈动脉入路 TAVR 病例分享

洪旭林

浙江大学医学院附属邵逸夫医院（浙江省邵逸夫医院）

患者基本信息：

• 患者，男，73 岁，178 cm/ 69Kg，BMI 21.8 Kg/m2

主述：

反复胸闷 10 年余，再发 1 月

现病史：

• 患者 10 年余前开始出现反复胸闷气急，初始活动后明显，后静息时也有症状，活动耐量显著下降，2021.9 诊断“扩张型心肌病、频发室性心动过速”，行药物治疗 + 双腔 ICD 植入术，术后仍反复发作胸闷、双下肢水肿、夜间不能平卧等症状，2024.4 行体外循环下左心室辅助装置（LVAD）植入，同时予心脏移植登记。

既往病史：

无

病程记录：

• 入院后实验室检查：Hb 139 g/L，Plt 127000 /uL，Cr 142 μmol/L，BNP 3683 pg/mL，AST 30 IU/L，ALT 17 IU/L，Uric 432.3 umol/L，Alb 36.1 g/L

• 合并用药：美托洛尔缓释片 47.5mg QD，沙库巴曲缬沙坦 50mg BID，维力西呱 2.5mg QD，华法林 1.5mg QD，托伐普坦 7.5mg QD，螺内酯 20mg QD

检验检查记录：

左室 LVAD 置入术后

主动脉瓣反流	重度
反流颈	6.7mm
LVIDd	64.9mm
EF	16.8%
二尖瓣反流	中度
三尖瓣反流	重度

鉴别诊断：

诊断明确，无需鉴别

其他：

无

开弓没有回头箭——入路极度扭曲 TAVR 手术一例

洪旭林

浙江大学医学院附属邵逸夫医院（浙江省邵逸夫医院）

患者基本信息：

77 岁，男性。

主述：

反复胸闷 3 余年，再发伴胸痛 10 天入院。

现病史：

反复胸闷 3 余年，再发伴胸痛 10 天入院。

既往病史：

PCI 术后 3 年，植入支架 1 枚

病程记录：

反复胸闷 3 余年，再发伴胸痛 10 天入院。

检验检查记录：

肌酐：88umol/L，血红蛋白：137g/l

TNI（-），BNP：155 pg/ml

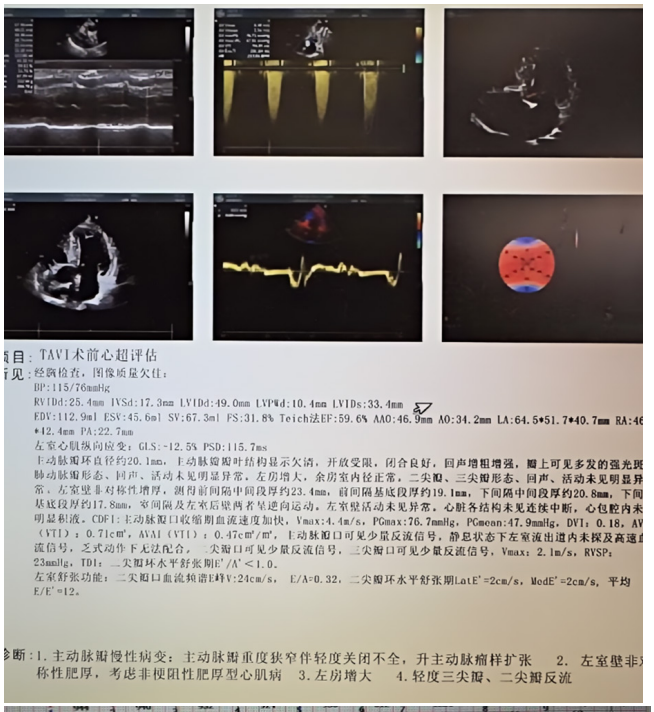

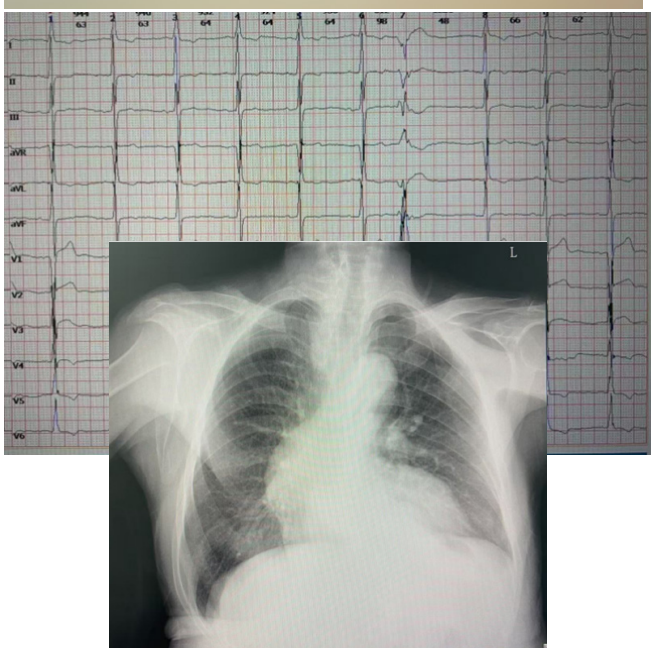

鉴别诊断：

诊断明确，无需鉴别

其他：

无

一波三折，冠脉狭窄之外，警惕心尖陷阱！

穆洋

解放军总医院第六医学中心

患者基本信息：

刘 X，男，73 岁。饮酒史多年。

主述：

间断活动后胸闷、气短 9 年余，加重 1 周

现病史：

患者于 2016 年 2 月无明显诱因出现活动后胸闷、气短，无胸痛，无肩背部放射痛，无恶心呕吐，休息后缓解，就诊于当地医院，行冠脉造影发现前降支中段 70% 狭窄，右冠近段狭窄 80%，中段狭窄 50-60%，遂于右冠近段植入支架 1 枚，出院后规律用药症状好转。近 1 周，胸闷、气短症状再发，当地医院行冠脉 CT 发现前降支中段中度狭窄，回旋支中段中重度狭窄，右冠近段支架内内膜增生。为行进一步检查入我院

既往病史：

高血压病 10 余年，糖尿病 5 年。

病程记录：

入院后给予降压、降糖、调脂及支持对症治疗，完善冠脉造影检查提示前降支 70% 狭窄，余血管未见明显狭窄。心电图检查结果提示胸部导联深倒置 T 波。进行超声心动图检查发现患者主动脉瓣中度狭窄，室间隔中段及心尖段肥厚，同时在负荷试验过程中存在左室腔中部梗阻，提示患者不仅存在冠脉问题，同时存在心肌病变，后完善心脏磁共振检查，结果发现除了肥厚的心肌表现外，还存在着左室心尖部室壁较薄，并形成室壁瘤。最后诊断“肥厚型梗阻性心肌病伴心尖部室壁瘤形成（左室腔中部梗阻）”。诊断明确后给予玛伐凯泰治疗，继续观察梗阻变化情况，目前还在随访中。

检验检查记录：

超声心动图提示：主动脉瓣中度狭窄伴轻度关闭不全，左房扩大，肥厚型梗阻性心肌病（左室腔中部梗阻），二、三尖瓣轻度反流，肺动脉压轻度升高。

心脏磁共振：肥厚型心肌病（左室中部肥厚），心尖部室壁瘤形成；左房扩大。

心电图：窦性心律 ST-T 改变 左室高电压

鉴别诊断：

1、冠心病：患者既往有冠心病病史，并植入支架，本次发病冠脉 CT 提示狭窄加重，不除外再次发现冠脉缺血可能，但入院后造影提示仅为中度狭窄；

2、肥厚型心肌病：患者 ECG 提示前壁导联广泛深倒 T 波，与一般的心肌缺血 T 波倒置表现不同，但既往无相关诊断，需完善超声心动图检查及心脏磁共振，明确诊断；

3、应激性心肌病：患者胸闷气短表现，起病急，且情绪焦虑，不除外发生应激性改变可能，需冠脉造影及心脏磁共振明确诊断。

4、瓣膜性心脏病：患者超声心动图提示主动脉瓣瓣膜中度狭窄，不除外狭窄导致心肌肥厚可能。

其他：

血常规正常，肝功、肾功、血脂正常，空腹血糖 8.14mmol/L，BNP 236pg/ml

免疫检查点抑制剂相关心肌炎后并发三度房室传导阻滞，到底何时植入永久起搏器

张弛

北京清华长庚医院

患者基本信息：

86 岁老年女性，神智清、精神可，饮食、睡眠正常，大便、小便正常，体重无明显变化

基本信息：双膝、右髋关节置换术后 10 年。否认传染病史、外伤史、输血史、过敏史、疫区接触史、毒物或放射性物质接触史、烟酒史。月经婚育史：已绝经，已婚，育有 1 子 1 女，配偶及子女体健。家族史：否认早发心血管病家族史或其他遗传病史。

查体：双下肺细湿啰音，心脏 (-)、颈静脉怒张 (-)、腹部查体 (-)、双下肢水肿 (-)

主述：

胸闷喘憋 1 天

现病史：

1 天前患者无明显诱因出现喘憋，伴大汗，自测心率约 40 次 / 分，否认胸闷、胸痛、心悸、头晕、黑矇、恶心、呕吐、腹痛、腹胀等不适，持续约半小时后自行缓解。至我院急诊查心肌损伤标志物示 CK-MB 70.8 ng/mL，MYO 1396 ng/mL，TnT-hs 0.344 ng/mL；NT-ProBNP 993 pg/ml。心电图示三度房室传导阻滞、完全性右束支传导阻滞。超声心动图示 LVEF 65%

既往病史：

1、慢性阻塞性肺疾病 4 年，规律吸入布地格福 2 吸 bid

2、子宫恶性肿瘤、腹腔继发恶性肿瘤 1 年余，2024-4-23 开始联合化疗 + 靶向药物抗肿瘤，后因药物性肝损伤停用，并于 1 月前（2024-8-13）首次使用信迪利单抗 200mg 治疗 1 次，2 周前自觉左侧眼睑下垂

3、高血压病 5 月余，规律口服硝苯地平控释片 30mg qd

病程记录：

1、请肿瘤科会诊评估宫颈癌病情后，考虑诊断为免疫治疗相关性心肌炎，同时合并三度房室传导阻滞，遂停用抗肿瘤治疗 “信迪利单抗”

2、免疫抑制方面：持续给予吗替麦考酚酯 0.5g bid；初始给予甲泼尼龙静脉抗炎，期间逐渐过渡至甲泼尼龙口服；间断静脉注射免疫球蛋白

3、心律方面：入院后随即植入临时起搏器，6 周后心肌炎控制后，更换为永久起搏器

4、肺部感染方面：根据患者痰培养结果予头孢曲松 2g qd 抗感染，联合复方磺胺甲恶唑 0.96g tiw 预防 PCP；同时给予药物雾化吸入从而化痰、扩张气道

检验检查记录：

入院时急诊查

心肌酶：CK-MB 70.8 ng/mL，MYO 1396 ng/mL，TnT-hs 0.344 ng/mL，**NT-ProBNP** 993 pg/ml，**PCT** 0.145 ng/mL，**D-dimer：**0.48 mg/LFEU

ECG：三度房室传导阻滞

UCG ：LVEF 65%，左房增大，室间隔增厚，主动脉瓣钙化并少量返流，二尖瓣环后叶瓣环钙化并少量返流，左室整体收缩功能正常，舒张功能减低

双下肢血管超声：未见明显异常

鉴别诊断：

1、急性心梗: 患者以突发胸闷起病，查血见心肌损伤标志物升高，且患者具有高龄、高血压等冠心病高危因素，故需考虑急性心梗。但心电图未见缺血表现，复查肌钙蛋白未见动态演变，故暂排除心脏急性缺血事件

2、急性心衰：患者以突发胸闷憋喘起病，故需排除急性心衰。但入院时查体未见心衰的相关瘀血性体征，NT-pro BNP 未见明显升高（不同年龄段的正常范围不同），且心脏超声未见心功能下降，故暂排除急性心衰

3、急性肺栓塞：患者以突发胸闷喘憋起病，且既往宫颈癌病史，可能会导致血液高凝状态，故需考虑急性肺栓塞。但入院时查体未见相关症状、体征，查凝血提示 D-dimer 阴性，动脉血气未见明显低氧血症、低碳酸血症，下肢血管超声未见静脉血栓，故暂排除急性肺栓塞

其他：

提供此病例的临床意义：

重点在于更换为永久起搏器的时间点选择：（1）对于部分患者来说，停止免疫检查点抑制剂后，药物相关并发症诸如三度房室传导阻滞有恢复的可能性，但等待时间尚无定论。（2）这部分患者为癌症患者，生存期可能较短，但更换起搏器的手术花费较高。（3）心肌炎急性期的心肌水肿，以及这部分患者易出现感染，故植入永久起搏器有较大的手术风险。综合以上因素，到底需要等待多久后更换为永久起搏器，这一临床决策目前并没有医学共识或指南提供相关指导，故通过提供临床案例，以填补这方面的治疗经验空缺。

负荷超声心动图联合心肌声学造影辅助诊断 MINOCA 病因一例

王文涛

哈尔滨医科大学附属第二医院

患者基本信息：

x 性别：女；

年龄：57 岁；

主诉：胸痛 1 日

现病史：1 日前无明显诱因出现胸痛，持续约 10 分钟，放射至后背部，伴有胸闷气短，伴有大汗、乏力，伴有头晕，伴有腹胀。

既往史：高血压

入院生命体征：P：78bmp，BP：143/84mmHg

主述：

胸痛 1 日

现病史：

患者 1 天前无明显诱因出现阵发性胸痛，疼痛位于心前区，呈闷痛，范围约手掌大小，持续约 10 分钟左右，放射至后背部，无咽喉紧缩感，伴有胸闷气短，伴有大汗、乏力，伴有头晕，伴有腹胀，病程中无咳嗽、咳痰，无腹痛腹泻，无恶心、呕吐，无头痛，无晕厥等，为求进一步诊治来我院。病程中患者饮食、二便尚可，睡眠一般。

既往病史：

高血压病史，口服厄贝沙坦治疗

病程记录：

1、重症护理，心电血压血氧监护，对症吸氧，完善相关检查，

2、抗血小板、降脂、改善心肌供血、抑酸保护胃黏膜（阿司匹林、氯吡格雷、阿托伐他汀、雷贝拉唑）

3、完善冠脉造影检查

4、改善心室重构，摔制血压等冠心病二级预防

5、完善负荷超声心动图联合心肌灌注、左心室造影检查

6、向家属交代病情

检验检查记录：

1、心电图检查：I、avL 病理性 Q 波；R 波递增不良

2、冠状动脉造影检查：左主干、前降支、回旋支以及右冠状动脉管腔通畅，未见明显狭窄

3、负荷超声心动图联合心肌灌注、左心室造影检查：冠状动脉储备功能异常

鉴别诊断：

主动脉夹层：胸痛一开始即达到高峰，常放散到背、肋、腹、腰和下肢，两有明显差别，可有主动脉瓣关闭不全的表现，超声心动图、X 线或主动脉 CTA 有助于鉴别。

急性肺动脉栓寒：可发生胸痛、咯血、呼吸困难和休克，但有右心负荷急剧增加的表现如发绀、肺动脉瓣区第二心音亢进、颈静脉充盈、肝大、下肢水肿等，心电图示 I 导 S 波加深，III 导 Q 波显著，T 波倒置，胸导联过渡区左移，右胸导联 T 波倒置等改变可鉴别。常有低氧血症、血气分析或肺动脉 CTA 有助于鉴别。

其他：

表现为肺动脉高压的先天性门体静脉分流

马明远

山东大学齐鲁医院

患者基本信息：

男，20 岁

主述：

活动后胸闷 10 余年，加重半月余

现病史：

患者 10 余年前学龄期即出现活动后气短，活动耐力低于同龄人，不能参加剧烈活动，8 岁时于当地医院行超声心动图提示心脏扩大 (患者母亲口述)，未特殊检查。半月前于我院行超声心动图检查示超声心动图示 :LA40mm,LV 55mm,RV22mm,LVEF 73%, 估测 sPAP 83mmHg，提示 : 左心扩大、肺动脉增宽、主动脉瓣返流轻度、二尖瓣返流轻度、三尖返流中度。活动耐力可，能登 5 楼。无复发性口腔溃疡、光过敏、脱发，无喜蹲踞、无特殊药物应用史。外院诊断为特发性肺动脉高压并给予安立生坦治疗，症状无改善，今为求系统诊疗收入我科，患者近半月饮食睡眠好，大小便无异常，体重无明显变化。

既往病史：

患者幼年发育正常，无喜蹲踞，无光过敏、脱发，无复发性口腔溃疡，无口干、眼干，无骨关节疼痛等。自发病以来，饮食睡眠可，大小便无异常，体重无明显减轻。过敏性紫癜病史 1 年余，现遗留有双下肢皮肤色素沉着。否认脑血管病、糖尿病、高血压等慢性病病史。

病程记录：

PAH 排因检查：甲状腺功能、风湿免疫系列及肺功能无异常；肺动脉 CT 血管成像（CTA）及心脏结构 CT 排除肺栓塞及心脏大血管畸形。阳性检查结果为胆红素显著升高: 总胆红素（TBIL）47.6 μmol/L（参考值 5.0-21.0）、直接胆红素（DBIL）12.8 μmol/L（参考值 <6.0）、间接胆红素（IBIL）34.8 μmol/L（参考值 2.0-15.0）；腹部超声显示肝门静脉增宽（13mm），提示门脉高压。右心导管检查测肺动脉压（pulmonary arterial pressure, PAP）59/24/40 mmHg、肺小动脉楔压（pulmonary capillary wedge pressure, PCWP）11 mmHg、心输出量（cardiac output, CO）9.4 L/min、肺血管阻力（pulmonary vascular resistance, PVR）3.1 Wood 单位（WU），符合毛细血管前肺动脉高压诊断。患者合并门静脉增宽和胆红素异常增高，进一步行门静脉 CTA，提示门静脉左支与肝静脉异常交通形成。最终诊断：先天性肝内门静脉 - 肝静脉瘘、肺动脉高压。行门静脉 - 肝静脉瘘介入封堵术。术后 3 个月运动耐力恢复正常，超声心动图提示 sPAP 降至 49mmHg、左室内径缩至 49mm，TBIL（19.1 μmol/L）、DBIL（9.0 μmol/L）、IBIL（10.1 μmol/L）同步下降，停用安立生坦。术后 14 个月复查

sPAP 41mmHg、左室直径 45mm。术后 4 年随访患者持续稳定、日常活动不受限。

检验检查记录：

血常规 WBC 3.76*10^9/L、PLT 121*10^9/L、HGB 143g/L

ESR 2mm/h

肝功 ALT 20U/L、AST 26U/L

TBIL 47.6umol/L、DBIL 12.8umol/L、IBIL 34.8umol/L

UA 311umol/L、GLU 4.83mmol/L

动脉血气分析：pH 7.49，PaO2 87mmHg，PaCO2 37mmHg，SaO2 97%（右上肢）

动脉血气分析：pH 7.46，PaO2 70mmHg，PaCO2 41mmHg， SaO2 95%（右下肢）

PR3-ANCA 6.99U/ml 、MPO-ANCA 1.45U/ml

体液免疫系列：C3 0.496g/l 、C4 < 0.071g/l

IgG、IgA、IgM、IgE1 未见异常

NT-proBNP < 70pg/ml

凝血系列、肾功、血生化、心肌酶、风湿系列、甲功、肿瘤系列、铁蛋白、尿便常规、乙肝标志物、丙肝、HIV 未见明显异常

6 分钟步行距离：640m

肺通气功能正常

睡眠呼吸监测正常

鉴别诊断：

CHD-PAH：患者幼年起病、超声心动图提示左心扩大，应排除 CHD-PAH。患者超声心动图及心脏结构 CT 均未发现心脏、大血管水平异常分流，可以排除 CHD-PAH。

左心疾病相关肺动脉高压（LHD-PH）：患者有左心扩大，应排除左心疾病如左心衰竭、左心瓣膜病等导致的肺动脉高压。此类患者常有夜间阵发性呼吸困难、端坐呼吸等症状，心脏超声可发现左心功能不全或瓣膜病变。该患者病史及超声心动图均不支持。

其他：

有惊无险–导丝被卡死后…

王小东

上海东方医院（同济大学附属东方医院）

患者基本信息：

患者，女性，79 岁，2024 年 08 月 12 日 14:02 入院

主述：

恶心呕吐 3 周

现病史：

患者 3 周前无明显诱因下出现恶心呕吐，伴纳差、乏力，无胸闷胸痛，12 天前于外院复查心肌标志物未及明显异常。今日就诊我院，急查 CNTI 0.3ng/ml ↑，BNP 3734.0pg/ml ↑，肌红蛋白 36.0ng/ml，肌酸激酶同工酶 2.53ng/ml，心超提示左室壁节段性运动异常，左室心尖部室壁瘤形成，EF67%

既往病史：

高血压病史 30 年；2 型糖尿病病史 30 年

病程记录：

完善检查，药物治疗，择期冠脉造影

检验检查记录：

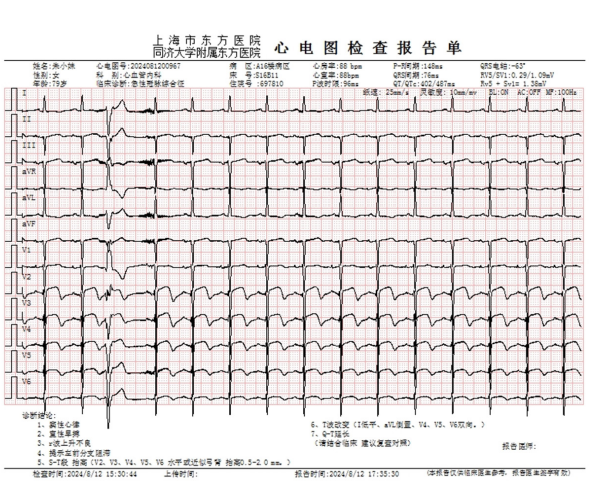
上海市东方医院 心电图检查报告单
同济大学附属东方医院

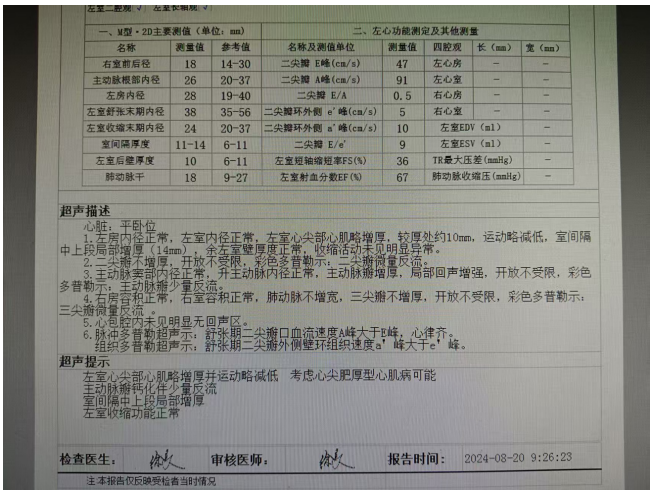
一、M型·2D主要测值（单位：mm）			二、左心功能测定及其他测量				
名称	测量值	参考值	名称及测值单位	测量值	四腔观	长（mm）	宽（mm）
右室前后径	18	14-30	二尖瓣 E峰(cm/s)	47	左心房	–	–
主动脉根部内径	26	20-37	二尖瓣 A峰(cm/s)	91	左心室	–	–
左房内径	28	19-40	二尖瓣 E/A	0.5	右心房	–	–
左室舒张末期内径	38	35-56	二尖瓣环外侧 e'峰(cm/s)	5	右心室	–	–
左室收缩末期内径	24	20-37	二尖瓣环外侧 a'峰(cm/s)	10	左室EDV（ml）		–
室间隔厚度	11-14	6-11	二尖瓣 E/e'	9	左室ESV（ml）		–
左室后壁厚度	10	6-11	左室短轴缩短率FS(%)	36	TR最大压差(mmHg)		–
肺动脉干	18	9-27	左室射血分数EF(%)	67	肺动脉收缩压(mmHg)		–

超声描述

心脏：平卧位
1.左房内径正常，左室内径正常，左室心尖部心肌略增厚，较厚处约10mm，运动略减低，室间隔中上段局部增厚（14mm），余左室壁厚度正常，收缩活动未见明显异常。
2.二尖瓣不增厚，开放不受限，彩色多普勒示：二尖瓣微量反流。
3.主动脉窦部内径正常，升主动脉内径正常，主动脉瓣增厚，局部回声增强，开放不受限，彩色多普勒示：主动脉瓣少量反流。
4.右房容积正常，右室容积正常，肺动脉不增宽，三尖瓣不增厚，开放不受限，彩色多普勒示：三尖瓣微量反流。
5.心包腔内未见明显无回声区。
6.脉冲多普勒超声示：舒张期二尖瓣口血流速度A峰大于E峰，心律齐。
组织多普勒超声示：舒张期二尖瓣外侧壁环组织速度e'峰大于e'峰。

超声提示

左室心尖部心肌略增厚并运动略减低 考虑心尖肥厚型心肌病可能
主动脉瓣钙化伴少量反流
室间隔中上段局部增厚
左室收缩功能正常

检查医生： 审核医师： 报告时间：2024-08-20 9:26:23

注:本报告仅反映受检者当时情况

鉴别诊断：

诊断明确，无需鉴别

其他：

无

妊娠合并重度肺动脉高压 1 例

夏驭龙

北京大学第一医院

患者基本信息：

33 岁女性

主述：

停经 32+5 周，憋气 2 周，加重 10 天

现病史：

平素月经规律，LMP 2024-08-14，规律产检，EDC：2025-05-21，产检心电图：窦性心律、V1 导呈 Rs 型，NT 正常，无创 DNA 低风险，排畸彩超未见胎儿结构异常，OGTT（-），胎动正常。2 周前无明显诱因出现憋气，平地走路 10m 出现，休息后可好转，伴胸部紧缩感、咳嗽、咳白痰，无胸痛，10 天前加重，偶出现夜间无法平卧，坐起后好转。近 10 余天因腹痛、阴道流血，予保胎治疗，日间活动量极少，卧位时间长，出现下肢水肿。昨日再次因阴道流血就诊于同仁医院，予硫酸镁治疗后阴道流血好转，并予地塞米松促胎肺成熟，hsTnI 24.6ng/L，BNP 965pg/ml，D-Dimer 1.13mg/L。ABG：pH 7.455，PaCO2 24mmHg，PaO2 62mmHg，Lac 2.1mmol/L，HCO3- 16mmol/L。超声心动图：右心扩大，TAPSE 13mm，中度三尖瓣关闭不全，肺动脉高压（估测收缩压 59mmHg），肺动脉扩张，左室腔 D 字型，LVEF 69%，少量心包积液。下肢血管超声：深静脉未见 DVT，动脉未见管腔狭窄。为进一步诊治收入院。精神、饮食可，近期睡眠不佳，大小便如常，孕期体重增加 9Kg

既往病史：

既往史、个人史、婚育史：桥本甲状腺炎、一过性甲亢，目前已好转。前庭功能障碍。妊娠期铁缺乏，曾补铁治疗。否认高血压、糖尿病、慢性肾脏病、出血病史。否认外伤史、输血史。否认药物、食物过敏史。2019 年剖宫产分勉一男婴，3900g，体健。未怀孕时活动量正常。家族史：父母均患高血压，奶奶患“冠心病”，否认其他家族遗传病史及类似疾病史

病程记录：

1. 心脏方面：患者育龄期女性，主要临床表现为憋气，BNP 965pg/ml,D-Dimmer 升高、I 型呼吸衰竭，超声心动图示肺动脉收缩压升高、右心扩大，经全市会诊讨论考虑患者妊娠合并严重肺动脉高压明确，猝死高危。入院后复查超声心动示左心功能正常，未见先心病征象，完善自身免疫疾病谱、感染筛查、下肢血管超声等检查未见明显异常，CTPA 未见肺栓塞征象，考虑肺动脉高压原因不明，I 型可能大，影像学提示 PCH 不除外。予经鼻高流量吸氧支持，术前尝试曲前列尼尔泵入联合西地那非口服，并间断利尿改善容量负荷、加强营养支持、小剂量血管活性药物泵入等治疗，监测患者血流动力学稳定，基础心率降低，BNP、NT-proBNP 水平较入院前显著改善，复查超声心动示右心功能略改善。04-06 患者因宫缩明显、经全市会诊讨论后行急诊剖宫产术终止妊娠，术前留置股动静脉鞘管并备 ECMO 保驾，手术顺利，术后继续加强容量管理，予持续 NO 吸入扩血管（逐渐减少用量），并根据血压将西地那非滴定至 20mgtid，曲前列尼尔逐渐过渡为皮下泵入（17.5ng/kg/min），去甲肾上腺素逐渐暂停，监测患者循环相对稳定，无憋气症状，BNP 逐渐下降 64pg/ml，6MWT 230m。

2. 产科方面：患者孕 32 周【+5 天，G2P1，头位，未产】，因重度肺动脉高压、心功能 IV 级，经全市会诊后建议控制病情后尽快终止妊娠，以降低围术期母体风险。住院期间予地塞米松促肺成熟，硫酸镁胎儿脑保护，定期行胎心监护未见明显异常，拟 4-7 行剖宫产术，围术期予 ECMO 备用。但患者 4-6 下午自觉宫缩明显，联系产科，请多学科急会诊后决定急诊剖宫产术终止妊娠。完善术前准备后患者 2025-4-6 下午于手术室腰硬联合麻醉下行子宫下段剖宫产术 +

双侧子宫动脉结扎术，于 18:41 娩一活婴，女，2300g，羊水清，Apgar 评分 1 分钟 10 分，5 分钟 /10 分钟均为 10 分，胎盘胎膜全，手术顺利，术中出血 300ml。术后监测子宫复旧良好，恶露不多，伤口情况良好。予芒硝外敷，溴隐亭 2.5mg bid 抑乳治疗。

3. 感染方面：患者间断咳嗽咳痰，PCT 升高，CT 示双肺多发磨玻璃密度，呼吸道感染不除外，予筛查新冠病毒、甲乙流病毒、肺炎支原体抗体 (-)，痰 tNGS 见卡他莫拉菌 (序列数 4563，相对丰度 0.7%)，血 tNGS 见粪肠球菌 (序列数 192，相对丰度 3.5%)，结合痰 tNGS 结果予头孢克洛口服 (4-2 至 4-6)，监测体温正常，炎症指标稳定。患者剖宫产术后出现低热及炎症指标波动，尿培养可见铜绿假单胞菌，予头孢哌酮钠舒巴坦钠 3gq8h 抗感染治疗，对症雾化、化痰，后监测患者体温正常，炎症指标较前下降。

4. 其他方面 :1) 甲功：患者桥本甲状腺炎病史，入院复查甲功提示低 T3 综合征，请内分泌科会诊，考虑符合目前疾病状态，暂不予特殊干预，待病情稳定后择期复查。2) 营养方面：患者入院前喘憋，营养欠佳，入院后查尿酮体间断阳性，内分泌会诊考虑饥饿性酮体可能大，予补液治疗后好转，现患者恢复半流食，口服瑞能补充营养，监测尿酮体阴性。3) 凝血方面：患者剖宫产术后，有抗凝指征，术后予血栓弹力袜及下肢驱动泵治疗预防血栓，监测血色素稳定后 4-7 起予那屈肝素 0.3mlqn 抗凝治疗。4) 肾脏方面：患者否认慢性肾脏病史，入院尿常规提示血尿 (均一红细胞)、蛋白尿 (微量)，请肾内科会诊考虑近期尿检异常与心脏原发病相关可能大，暂不考虑合并肾小球疾病，继续监测尿蛋白，警惕围术期肾损害。5) 患者电解质紊乱，予积极纠正，保证血钾 4.0mmol/L 以上。

检验检查记录：

血常规：WBC 8.22*109/L, Hb 118g/L, Plt 114*109/L, NE% 86.7%

生化 :ALT 69IU/L, AST 36IU/L, Alb 32.9g/L, ALP 108IU/L, Tbil 19.4umol/L, Dbil 6.5umol/L, Scr 57.9umol/L, eGFR 116.731ml/min/1.73m2, UA 441umol/L, BUN 3.75mmol/L, K 4.00mmol/L, Na 135.7mmol/L, CO2 16.5mmol/l, LDL-C 1.92mmol/L

凝血：PT 11.9s, APTT 24.1s, D-Dimer 0.19mg/L

炎症指标：PCT 1.19-1.38ng/ml, CRP、IL-6 正常

ABG: 低氧血症已纠正（80-117mmHg），Lac 降至正常

免疫球蛋白、补体、自身抗体谱、ANCA、血小板抗体、Cooms试验、狼疮抗凝物、磷脂抗体未见明显异常

甲状腺功能：T3 0.58、FT3 2.78，余在正常范围

CTPA 未见肺栓塞征象，PCH 不除外

鉴别诊断：

肺动脉高压病因鉴别：

1、动脉性肺动脉高压

2、左心疾病所致肺动脉高压

3、肺部疾病和（或）低氧所致肺动脉高压

4、慢性血栓栓塞性肺动脉高压和（或）其他肺动脉阻塞性病变所致肺动脉高压

5、未明和（或）多因素所致肺动脉高压

结合该病人辅助检查结果，考虑该患者为动脉性肺动脉高压

其他：

无

转甲状腺素蛋白心脏淀粉样变一例

许文静

华中科技大学同济医学院附属协和医院

患者基本信息：

62 岁男性患者，汉族

主述：

头晕呕吐 5 小时

现病史：

患者 5 小时前无明显诱因出现头晕、呕吐伴大汗淋漓，无胸闷、胸痛、黑朦、晕厥、气促、心慌等不适，无肢体感觉、活动异常，于外院就诊发现 TNI 升高，特来我院就诊。

既往病史：

高脂血症病史 5 年，服用阿托伐他汀 20m qd 治疗；脂肪肝病史 5 年；糖尿病 4 年，口服阿卡波糖 50mg tid，达格列净 10mg qd；双下肢麻木感 2 年

病程记录：

入院时体检：体温 36.3 °C，脉搏 85bpm，呼吸 20bpm，血压 149/81mmHg。神志清楚，营养状态、体型正常。颈静脉无怒张，肝颈回流征 (-)，双肺呼吸音清，未闻及干湿啰音，心律齐，未闻及明显杂音，双下肢无水肿。入院后给与抗血小板、调脂等治疗，行冠脉造影检查提示前降支狭窄 30%，行心脏超声提示室壁增厚，行心肌磁共振检查提示浸润性心肌病（心肌淀粉样变），行 99mTc-PYP SPECT/CT 断层融合显像提示室间隔显像剂弥散性浓聚，SQA 评级为 3 级，考虑 ATTR 型心肌淀粉样变。行遗传性心血管疾病全外显子组检测发现 TTR;NM_000371.3:c.302C>T(p.Ala101Val) 变异，给与氯苯唑酸 61mg qd 口服。出院后间断随访，在服用氯苯唑酸 14 个月时复查心电图为正常心电图表现，完全性右束支阻滞已恢复，但复查超声心动图仍有室壁增厚。患者未再出现恶心、呕吐、头晕等体位性低血压表现。

检验检查记录：

心电图提示完全性右束支传导阻滞，动态心电图提示窦性心律，偶发室性早搏，二度一型房室传导阻滞，交界性逸博。超声心动图提示 LA 4.6cm，LV 4.3cm，IVS 1.5cm，RA 3.1cm，RV 3.5cm，EF 62%，左室壁增厚，其中室间隔 1.5cm，下侧壁 1.3cm，二尖瓣轻中度关闭不全。

鉴别诊断：

1. 急性冠脉综合征：患者头晕、呕吐伴全身大汗，外院查 TNI 升高，且既往有糖尿病史，应考鉴别于急性冠脉综合征

2. 急性心肌炎：患者 TNI 升高，且发病突然，应鉴别于急性心肌炎

3. 肺栓塞

4. 急性主动动脉综合征

其他：

血小板增多症合并心脏破裂

俞帅

上海东方医院（同济大学附属东方医院）

患者基本信息：

男性，77 岁

主述：

新冠感染后 1 个月，咳嗽 2 周

现病史：

患者入院 1 个月前感染新冠，自测新冠抗原为阳性，自行服药治疗，2 周前患者出现咳嗽，无发热，无胸闷气促，无胸痛，无肩背部放射痛，无腹胀腹痛，无头晕头痛，无恶心呕吐等不适。于 2023 年 01 月 30 日 16 时 41 分入住我院。

既往病史：

高血压病史 10 余年，血压最高 150/100mmHg，平素未服药，自诉血压控制可。1 月前感染新冠。

病程记录：

D1 2023-01-30

• 重要检查：BNP 595 pg/mL，hs-cTnI 0.283 ng/mL，PLT 669×10 ^{9} /L；ECG：前壁 ST 段抬高；胸 CT：病毒性肺炎表现

• 转入 CCU 监护，抗感染 + ACS 对症，暂不抗栓

D2 2023-01-31

• 心超：巨大心尖室壁瘤（≈ 44 × 35 mm）、EF ≈ 40 %、中量心包积液

• 继续 ACS 对症、升级抗菌，仍停抗栓

D3 2023-02-01

• 开始术前血流动力学监测与支持

D5 2023-02-03

• JAK2-V617F 阳性，PLT 峰值 846×10 ^{9} /L

• 请血液科会诊，诊断原发性血小板增多症，启动羟基脲 0.25 g qd

D6 2023-02-04（手术）

• 术中证实破口 + 附壁血栓

• 手术：室壁瘤切除 + Dor 成形 + 左室取栓 + 临时起搏器

D7 2023-02-05

• 拔除气管插管

D8 2023-02-06

• 突发言语不清，口角向左歪斜，头颅 MRI：急性左侧脑梗死

• 抗栓调整：替格瑞洛 90 mg bid + 利伐沙班 10 mg qd；羟基脲继续

D9-D19 02-07 ~ 02-17

• PLT 逐降至 471×10 ^{9} /L；无再出血 / 栓塞

D20 2023-02-18

• 病情稳定，办理出院

检验检查记录：

院前化验（2023-01-30）：

心梗 +BNP：B 型钠尿肽 595.000 pg/mL，肌酸磷酸激酶同工酶 1.84 ng/mL，高敏肌钙蛋白 I 0.283 ng/mL。

院前心电图（2023-01-30）：

窦性心律，偶发房性早搏，异常 Q 波，ST 段抬高，T 波改变。

院前胸部 CT 报告（2023-01-30）（口述）：

病毒性肺炎渗出改变

院前化验（2023-01-30）：

D- 二聚体 6.32 ug/ml

肾功能 + 电解质：肌酐 (干化学) 177 umol/L，电解质未见明显异常

肝功能：丙氨酸氨基转移酶 68U/L，天门冬氨酸氨基转移酶 61U/L

C 反应蛋白 44.74 mg/L，降钙素原 0.010 ng/mL

血常规：白细胞计数 22.87 10^9/L, 中性粒细胞 75.9%, 淋巴细胞 10.1% 偏低，红细胞计数 3.76 10^12/L, 血红蛋白测定 115 g/L, 血小板计数 669 10^9/L

入院化验（2023-01-30）：

心梗三项 +pro-BNP：B 型钠尿肽前体 3874.000 ng/L，肌酸磷酸激酶同工酶 2.850 ng/mL，高敏肌钙蛋白 0.157 ng/mL， 肌红蛋白 143.800 ng/mL

D- 二聚体 5.990 mg/L

肾功能 + 电解质：肌酐 (干化学) 178.40 umol/L，电解质未见明显异常

C 反应蛋白 42.42 mg/L，降钙素原 0.093 ng/mL，白细胞介素 6 15.260 pg/mL

血常规：白细胞计数 21.66 10^9/L, 中性粒细胞百分率 80.4 %, 淋巴细胞百分率 9.4 % 偏低，中性粒细胞绝对数 17.42 10^9/L, 淋巴细胞绝对数 2.04 10^9/L，红细胞计数 4.04 10^12/L, 血红蛋白测定 120.0 g/L, 红细胞比积测定 36.9 %, 平均红细胞体积 91.3 fL，平均血红蛋白含量 29.7 pg，平均血红蛋白浓度 325.0 g/L，红细胞分布宽度 13.4 %，血小板计数 755 10^9/L

心彩超（2023-01-31）：

左室壁节段性运动异常

左室心尖部室壁瘤形成

左室心尖部可疑异常回声，建议左心声学造影排除附壁血栓可能

室间隔中上段增厚

主动脉窦部及升主动脉增宽，主动脉瓣钙化

三尖瓣少量反流

中量心包积液（局部较多）

左室收缩功能低

JAK2 V617F 基因定性（2023-02-01）：

阳性

鉴别诊断：

1. 急性前壁心肌梗死

支持点：区域性 ST 抬高，hs-cTnI 明显升高，心超出现巨大前壁室壁瘤

不支持点：暂无

结论：不能排除，予以 ACS 对症治疗

2. 病毒性心肌炎

支持点：近期感染病史，胸 CT 病毒性肺炎影

不支持点：心电图呈局灶前壁改变而非散在 ST-T；超声为节段性室壁运动异常而非弥漫性；缺乏心肌炎典型电压降低

结论：证据不足，暂不考虑

3.Dressler 综合征（心包炎型）

支持点：梗死后第 2-3 周易发

不支持点：发病过早；心包积液量多且血性；超声示破口

结论：证据不足，暂不考虑

其他：

该病例存在以下创新点：

1. 超声预警直通手术

床旁超声发现室壁瘤 + 心包积液即绕过常规流程，直接启动手术准备，突破传统诊疗路径。

2. 一站式心室重建

单次手术完成室壁瘤切除 +Dor 成形 + 取栓 + 起搏器植入，避免分期手术风险。

3. 基因导向精准诊断

及时进行 JAK2 检测，将血小板增多从应激反应提升为 ET 诊断，改变治疗策略。

4. 创新三联抗栓方案

首创” 利伐沙班 + 替格瑞洛 + 羟基脲” 组合，同时应对破裂出血风险和 ET 血栓风险。

5. 围术期抗栓桥接优化

快速从低分子肝素过渡到 DOAC，避免阿司匹林，实现出血风险最小化的个体化抗栓。

求因之路–低弥散相关肺动脉高压

李慧婷

上海市肺科医院

患者基本信息：

基本情况：女性，65 岁，农民。

入院日期：2025-02-25

个人史：无吸烟、饮酒史，无疫区、疫水、野生动物及禽类接触史。

婚育史：适龄结婚，配偶体健。

生育史：2-0-0-2，育有 2 子，儿子体健。

月经史：16 岁 4-6 天 /28-30 天 50 岁。

家族史：否认家族遗传病史。

主述：

活动后气促 2 年，加重 2 月。

现病史：

2022 年 1 月开始出现活动后气促，否认咳嗽、咳痰、咯血，否认发热、晕厥等，患者未重视，也未进一步诊疗。2024 年 10 月，自觉气促明显加重，当地医院就诊，查胸部 CT 示：间质性病变，心脏超声检查提示：中重度肺动脉高压，肺功能检查提示：轻度限制性通气功能障碍，重度弥散功能障碍。外院完成右心导管检查，结果提示：肺动脉压力正常，肺血管阻力增高，但具体结果不详，外院考虑 “间质性肺病、肺动脉高压”，予尼达尼布 150mg qd 抗纤维化，利奥西呱 2mg tid 靶向降压治疗 2 月，病情无明显好转，仍有逐步加重趋势，2025 年 2 月 25 日为进一步诊疗收入我科。自发病以来，患者精神、食欲差，二便正常，体重有下降，具体不详。

既往病史：

既往史：无特殊，否认 “伤寒、结核” 等传染病史，否认 “高血压、心脏病、糖尿病” 史，否认手术、外伤史，否认输血史，否认食物、药物过敏史，预防接种史不详。

病程记录：

入院后诊治：

1. 肺动脉高压靶向降压：利奥西呱更换为他达拉非 20mg qd po

2. 利尿补钾：

托拉塞米片 10mg qd po

螺内酯片 20mg bid po

氯化钾缓释片 1.0g tid po

3. 化痰：

乙酰半胱氨酸片 0.3 po tid

4. 激素：强的松 10mgpo qd，对症护胃

但持续治疗 1 月后，患者仍觉症状改善不明显，且诊断不明确。

检验检查记录：

入院后辅助检查：

2025-02-26 血气分析检验报告：pH7.457，二氧化碳分压 29.50mmHg，氧分压 41.80mmHg，血红蛋白总量 14.90g/dL，氧饱和度 80.30%。

2025-02-27 尿常规检验报告：葡萄糖 +-，蛋白质 +-，

2025-02-27 血凝检验报告: 凝血酶原时间 12.60sec，国际标准化比值 (INR)1.13，D- 二聚体 0.41mg/L（-）。

2025-02-27 血常规检验报告：血红蛋白 135.0g/L，红细胞计数 4.48*10^12/L，白细胞计数 4.48*10^9/L，血小板 324*10^9/L，超敏 C 反应蛋白 5.9mg/L。

2025-02-27 血凝检验报告：降钙素原 <0.05ng/ml。

2025-02-27 心肌四联检验报告：肌红蛋白 <21.00ng/ml，末端前 B 型钠尿肽 643.3pg/mL，肌钙蛋白 T0.008ng/ml，肌酸激酶同工酶 1.230ng/ml。

2025-02-27 血沉检验报告：红细胞沉降率 24.0mm/H。

2025-02-27 生化检验报告：谷丙转氨酶 13.5IU/L，谷草转氨酶 17.2IU/L，谷草转氨酶同工酶 6.8IU/L，总蛋白 62.6g/L，白蛋白 38.2g/L，肌酐 34.9umol/L，总胆固醇 5.46mmol/L,低密度脂蛋白 3.65mmol/L,视黄醇结合蛋白 22.1mg/L，

2025-02-27 微生物检验报告：荧光染色抗酸杆菌【阴性 (-)】:。

2025-02-27 HIV 梅毒检验报告: HIV，梅毒，肝炎阴性，放免疫: 肿瘤标志物阴性。

2025-02-27 微生物检验报告：真菌（1-3）β 葡聚糖 :<37.5。

2025-02-27 总 IGE 检验报告：免疫球蛋白 IgG3.91g/L，免疫球蛋白 IgA10.00g/L，免疫球蛋白 IgM0.25g/L。

2025-02-27 过敏原检验报告：总 IgE73.20kUA/L，食物性过敏源 0.46kUA/L，烟曲霉 0.06kUA/L，吸入性过敏源 0.14kUA/L，链格孢 0.00kUA/L，霉菌混合 0.10kUA/L。

2025-02-27 唾液酸化糖链检验报告：糖链抗原 724.82U/mL。

2025-02-27 呼吸道病毒九项检验报告：阴性。

2025-02-27 风湿 + 白介素检验报告： 阴性。

2025-02-27 双下肢静脉：双侧下肢深静脉未见明显血栓形成。

2025-02-27 腹部彩超：肝内实性结节，考虑血管瘤。

2025-02-27 心脏彩超：1. 中度肺动脉高压（估测肺动脉收缩压 63mmhg）；重度三尖瓣关闭不全，轻度肺动脉瓣关闭不全 2. 微量心包积液。

2025-02-26 心电图报告检查结论：正常心电图。

2025-02-26 FGN 检查报告：20 ppb

2025-02-26 FGN 检查报告：肺通气功能轻度减退（限制性）残气正常，肺总量减低，残总比正常，弥散功能重度减退，气道阻力增高（见下图）。

2025-02-26 FGN 检查报告（IOS 通气报告）：外周气道阻力正常，中央气道阻力正常（见下图）。

2025-02-26 FGN 检查报告（呼吸肌力测定）：最大吸气压减低，最大呼气压正常，P0.1 增高。（见下图）

2025-2-26 6 分钟步行距离： 330m。

2025-02-26 两肺纹理增多增粗，请结合临床及 CT（见下图）。

2025-02-27 CT 检查报告：1. 双肺散在少许炎症，建议抗炎后复查。 2. 双肺数枚小结节，建议随诊。3. 双肺气肿。 4. 纵隔部分淋巴结增大。5. 附示，肝脏低密度灶，建议进一步检查。 6.CTPA 未见明显充盈缺损。（见下图）

2025-03-03 MR 检查报告：1. 右室收缩运动轻度减弱，肺动脉增宽，请结合临床。2. 左右肺动脉主干远端血流放缓。3. 心肌纤维化。4. 心包积液。

2025-03-03 ECT 检查报告：两肺散在性血流灌注受阻，两肺血流灌注与通气显像较匹配。

2025.3.4 右心导管检查：毛细血管前性肺动脉高压；肺动脉造影未见明显异常。（见下图）

鉴别诊断：

1. 肺静脉闭塞症 PVOD ？

2. 结缔组织病 CTD ？

3. 间质性肺病 ILD ？

4. 肺气肿合并肺纤维化 CPFE ？

5.POMES 综合征?

其他：

《初发心衰遇上巨大心室血栓：青年维吾尔族患者规范化管理的成功范例》

张爱梅

石河子大学第一附属医院

患者基本信息：

患者男性，35 岁，未婚，吸烟史 10 余年，每日 10 支，戒烟 1 月，饮酒年限 15 年，饮酒量 250ml/ 日，已戒酒 1 月；家中无遗传性疾病病史。

主述：

间断胸闷、气短 10 天，加重伴双下肢水肿 3 天。

现病史：

患者自诉 2025 年 5 月初劳累及受凉感冒后出现胸闷、气短不适，伴腹胀、纳差、咳嗽，无痰，患者未重视，未进一步诊治。此后活动耐量进行性下降，步行 100 米即可诱发。3 天前患者再次受凉后胸闷、气短加重，伴有咳嗽、咳痰，痰为黄色粘痰，并出现双下肢水肿，范围至双下肢腹股沟及阴囊，夜间不能平卧，夜间阵发性呼吸困难，故以“1、急性心力衰竭 ,2、高血压病 3 级（极高危）,3、糖尿病急性心力衰竭” 收住院。

查体：体温 :36.6℃，脉搏 :135 次 / 分，呼吸 :22 次 / 分，血压 :160/110mmHg，颜面口唇无紫绀，双眼巩膜无黄染，双侧颈静脉充盈，双肺呼吸音粗，两肺可闻及散在湿性啰音，两肺下野呼吸音减弱，心前区无隆起及凹陷，心尖搏动范围弥散，可见抬举样搏动，未触及细震颤及心包摩擦感，叩诊心界增大，听诊心率 135 次 / 分，律不齐，未闻及早搏，未闻及心脏杂音，可闻及第三心音奔马律，腹部膨隆，移动性浊音阳性，无压痛及反跳痛，肝脾肋下未扪及，双下肢及阴囊重度未见水肿，皮肤破溃处可见清亮组织液渗出。

既往病史：

既往高血压病史 6 年余，血压最高 200/140mmHg，未治疗，糖尿病病史 4 年，未监测血糖，未治疗。

病程记录：

2025 年 05 月 13 日首次入院：患者急性全心衰竭，合并严重水钠潴留，入院后给予氧气吸入、持续心电、血氧饱和度监测，急查血气分析、血常规、肝肾功、电解质、心肌酶、肌钙蛋白 T、NT-proBNP、血凝肝肾功等检查。给予呋塞米 20mg、托拉塞米 10mg 静推利尿减轻心脏负荷，新活素静脉泵入抑制心肌重塑、抑制交感神经系统、RAAS 系统等对症治疗。患者血压偏高，多波动在 180-190/120-130mmHg，予以硝普钠、乌拉地尔静脉泵入降压，维持血压在 140-150/100-110mmHg；患者血糖控制欠佳，入院血糖 20.97mmol/L，糖化血红蛋白 15.7%，予以人胰岛素静脉泵入调整血糖；降钙素原、C 反应蛋白、中性粒细胞水平偏高，予以哌拉西林钠他唑巴坦钠抗感染治疗。入院诊断：1、急性心力衰竭；2、高血压病 3 级（极高危）；3、高血压性心脏病；4、高血压急症；5、新功能Ⅳ级；6、肺部感染；7、2 型糖尿病；8、低蛋白血症。

5 月 14 日：心脏彩超提示心室**附壁血栓（3.3cm×2.3cm）**，予以利伐沙班 20mgQD 抗凝，高血压急症，予以硝普钠泵入降压，降压方案调整为：苯磺酸氨氯地平片 5mgqd 联合诺欣妥 100mg,bid 降压。患者 NT-proBNP 水平高（29451pg/ml），且双下肢及阴囊重度水肿，予以托拉塞米静脉泵入积极利尿治疗对症；血脂偏高，给予阿托伐他汀钙 1 片 QN 对症降脂治疗；患者餐前餐后血糖均偏高，且糖化血红蛋白指标为 15.7%，血酮体弱阳性，请内分泌科医师会诊制定降糖方案；血小板、红细胞水平偏高，请血液科医师会诊进一步明确诊断；患者白细胞、中性粒、降钙素原等感染指标均偏高，完善肺 CT 提示右肺中叶局灶慢性炎症，予以哌拉西林他唑巴坦对症抗感染治疗。患者水钠潴留严重，据出入量动态调整给药剂量，维持负平衡在 2000-3000ml。

5 月 15 日：降糖方案调整为联合甘精胰岛素 12U 睡前皮下注射、门冬胰岛素三餐前各 6 单位皮下注射、桑枝总生物碱 50mgTid 口服; 患者白蛋白水平偏低（22g/L），予以人血白蛋白对症静脉滴注处理，同时请营养科会诊给予营养支持。

5 月 16 日：患者心电监测提示基础心率偏快，加用地高辛 0.125gQD 控制心室率;

5 月 17 日：联合伊伐布雷定 5mgBid 口服控制心室率，降低心肌耗氧量； 加用芪苈强心 4 粒 Tid，调整诺欣妥剂量至 200mgBid；停用哌拉西林他唑巴坦。

5 月 19 日：患者水钠潴留较前减轻，停用呋塞米注射液，换用呋塞米口服片剂 20mgBid; 患者转氨酶偏高，不除外药物不良反应，停用达格列净及阿托伐他汀; 复查人血白蛋白为 28.5g/L。

5 月 21 日: 患者住院期间因经济原因拒绝完善冠状动脉造影、心脏核磁，骨髓穿刺、心肌病相关基因筛查等，要求单纯药物保守治疗，患者心衰指标 NT-proBNP 水平降低大于 50%（5 月 14 日：29451pg/ml，5 月 19 日：10047pg/ml），提示治疗有效，但该指标仍高，提示远期预后不良。目前患者水钠潴留明显缓解（体重从 70kg 下降至 53kg），胸腔积液减少（5 月 14 日：6cm；5 月 19 日：1.9cm）且无腹腔积液，患者目前无特殊不适，治疗有效，报出院，嘱其门诊规律随诊。出院诊断：1、全心衰竭；2、高血压性心脏病伴心力衰竭；3、低蛋白血症；4、左心室附壁血栓形成；5、高血压急症；6、高血压病 3 级（极高危）；7、2 型糖尿病；8、胸腔积液等。

出院带药方案：利伐沙班 20mgQD，沙库巴曲缬沙坦钠 200mgBid，苯磺酸氨氯地平片 5mgQD，呋塞米片 20mgBid，螺内酯 20mgQD，氯化钾 0.5gTid，盐酸依伐布雷定 5mgBid，富马酸比索洛尔 1.25mgQD，甘精胰岛素 14U 睡前皮下注射，门冬胰岛素三餐前各 8 单位皮下注射，桑枝总生物碱 1 粒，三餐前口服。

5 月 28 日门诊随访：心电图提示 HR：81 次 / 分，胸腔彩超提示胸腔积液为 0.9cm，丙氨酸氨基转移酶 102U、L，天门冬氨酸转移酶 68U/L，白蛋白 41.2，NT-proBNP: 6295pg/ml，**心脏彩超: EF=34%，心室血栓: 1.9cm×1.9cm**，用药方案调整为富马酸比索洛尔 2.5mgQD，呋塞米 20mgQD，氯化钾 0.5gQD，余方案同前。

6 月 25 日门诊随诊：胸腔彩超提示**双侧胸腔未见积液**，丙氨酸氨基转移酶 20U/L，天门冬氨酸转移酶 28U/L，白蛋白 42.4g/L，NT-proBNP：9083pg/ml，**心脏彩超：EF=49%，心室未见血栓**，用药方案调整为：停用呋塞米、氯化钾、富马酸比索洛尔、苯磺酸氨氯地平片，加用达格列净片 10mgQD，比索洛尔氨氯地平片 5mg/5mgQD，余方案同前。

检验检查记录：

见检查检验报告单

鉴别诊断：

1、肺源性心脏病：肺、心功能代偿期 此期主要是慢阻肺表现。慢性咳嗽、咳痰、气促，活动后可感心悸、呼吸困难、乏力和劳动耐力下降。体检可有明显肺气肿征，听诊多有呼吸音减弱，偶有干、湿性啰音，下肢轻微浮肿，下午明显，次晨消失。心浊音界常因肺气肿而不易叩出。心音遥远，但肺动脉瓣区可有第二心音亢进，提示有肺动脉高压。三尖瓣区出现收缩期杂音或剑突下示心脏搏动，多提示有右心室肥大。部分病例因肺气肿使胸膜腔内压升高，阻碍腔静脉回流，可见颈静脉充盈。又因膈下降，使肝上界及下缘明显地下移，应与右心衰竭的肝淤血征相鉴别。肺心病患者常有营养不良的表现。

2、支气管哮喘：本病多见于青少年有过敏史，发作时不一定强迫坐起，咳白色粘痰后呼吸困难常可缓解，肺部听诊以哮鸣音为主，而心衰以夜间阵发性性呼吸困难，多见于老年高血压或冠心病病人，发作时必须坐起，肺部有干湿性啰音，甚至咳粉红色泡沫痰。

其他：

本例患者的成功治疗表明，对于首发心衰合并心室血栓且伴有重度水肿的患者，及时有效的利尿治疗可迅速缓解症状，为后续治疗创造有利条件。规范的药物治疗方案结合按时随诊管理，能够显著改善患者心功能，促进心室血栓的溶解，提高患者预后。然而，在治疗过程中也暴露出一些问题，如心衰病因未系统筛查以及血小板计数增高、BNP 反复和感染指标升高等原因不明的情况。

在今后的临床工作中，应重视心衰患者的病因筛查，制定个体化的治疗方案。同时，要密切关注患者治疗过程中的各项指标变化，对于异常情况及时进行深入分析和处理，以提高心衰患者的整体治疗水平，改善患者的生活质量。此外，加强对患者及家属的健康教育，提高其对疾病的认知和自我管理能力，也是促进患者康复的重要环节。

一例以晕厥为首发表现的精原细胞癌颈部转移

马丽

甘肃省人民医院

患者基本信息：

继发于精原细胞瘤颈部转移灶压迫颈动脉窦引发的反射性晕厥属于罕见肿瘤并发症。我们报告了一例 35 岁男性患者，以突发晕厥为特征性表现，伴头晕及乏力。通过多种影像学评估（颈部软组织 MR、全身 PET-CT 及 24 小时心电监测）揭示左颈 III-V 区肿大淋巴结及软组织肿物、窦性心动过缓、窦性停搏。患者在入院后完善相关检查，明确晕厥病因，进行针对性治疗，使症状不再复发。本文描述了使用多种影像学诊断的过程，并讨论了临床特征、病理生理机制及管理中的挑战。全面文献回顾阐明了该病症的罕见性、诊断误区。

主述：

间断头晕乏力 2 月，晕厥一次

现病史：

患者于 2 月前无明显诱因感头晕、乏力，以午间时段为著，当时未予重视。入院前 6 小时，突发晕厥 1 次，无口吐白沫及四肢抽搐，无大小便失禁，持续数秒钟意识恢复，自感明显乏力伴恶心不适，遂就诊于我院。

既往病史：

2 月前因精原细胞瘤接受左侧睾丸切除术，术后未进行化疗及放疗。

病程记录：

入院时测 BP 119/64mmHg，HR 60 bpm，常规心电图检查：心室率 43 bpm，窦性心动过缓、ST-T 改变（图 1）。急诊进行冠状动脉造影 + 左心室造影 + 升主动脉造影均未见明显异常（图 2）。需要关注的是，因患者术中心率持续在 35-40 bpm 之间，遂经股静脉植入临时起搏器维持心率在 60bpm（图 3）。病情相对稳定后，行动态心电图检查示：总心搏 82749 个，平均心率 62 bpm，最快心率 98 bpm（07:02），最慢心率 35 bpm（12:02），其中短暂心室停搏 1 次、约 3.5 秒（ 11:50）（图 4），窦性停搏 21 次、最长约 2.4 秒，以中午为甚，ST-T 改变。入院后积极完善相关检查，提示符合精原细胞瘤淋巴结转移。积极与肿瘤内科会诊讨论后，给予 BEP 方案治疗：盐酸博莱霉素 (Bleomycin) 20mg 肌肉注射 D2、9、16，依托泊苷 (Etoposide) 130mg 静滴 D1-3；顺铂 (Cisplatin) 30mg 静滴 D1-5。规律化疗 9 个周期后，患者再无晕厥发作，咽喉部哽噎感消失，复查动态心电图：窦性心律，总心搏 113974 个，平均心率 82 bpm，最快心率 126 bpm（01-21 07:21），最慢心率 48 bpm（01-21 05:31）。ST-T 改变。复查 PET-CT 显示：原左颈、左锁骨区、上纵隔、腹膜后、右侧肩胛骨等 FDG 高代谢病变消退，提示治疗有效（完全缓解）。

检验检查记录：

颈部彩色多普勒提示：左侧锁骨上窝可见多个低回声肿物，大者 33*16mm，形态规则，边界清，CDFI：内见血流信号。颈部软组织核磁检查：前上纵隔内主动脉弓上见大小约 7.9x5.6x11.6cm 实性软组织影，增强扫描呈轻 - 中度强化，病灶内见小片状低强化区，病灶边界较清，病灶包绕左侧颈动脉、左锁骨下动脉，气管受压右移，向上沿左侧颈部间隙生长，周围肌肉软组织水肿；左侧颈部间隙见多发增大淋巴结影。右侧颈部肌肉软组织层次清晰，未见明显异常强化灶（图 5）。PET-CT 检查结果提示：左颈 III-V 区、左侧锁骨区、上纵隔多发肿大淋巴结及软组织肿物、腹主动脉左侧软组织肿物，FDG 摄取异常增高；右侧肩胛骨髓腔 FDG 摄取增高（图 6A-B），以上改变考虑恶性肿瘤性病变，结合病史考虑睾丸肿瘤性病变转移可能。进而行病理活检：左锁骨上淋巴结活检提示：淋巴组织中可见异性成分，结合临床病史及本次免疫组织化学染色结果：符合精原细胞瘤淋巴结转移。

鉴别诊断：

1、神经介导的反射性晕厥：是由交感或迷走神经反射异常引起周围血管扩张和 / 或心动过缓造成的晕厥。依据传出路径分为交感性或迷走性反射性晕厥。当反射性晕厥以直立位血管收缩反应降低导致低血压为主要机制时，为血管抑制型；当以心动过缓或心脏收缩能力减弱为主要机制时，为心脏抑制型；这两种机制均存在时为混合型。年轻人的血管迷走性晕厥 (vasovagal syncope, VVS) 常为典型、单纯性的 VVS。老年人出现的反 射性晕厥常伴有心血管或神经系统异常，表现为直立位或餐后低血压，这种反射性晕厥是病理性的，主要与药物相关的自主神经系统代偿反射受损和原发性或继发性自主神经功能衰竭相关。VVS 是 最常见的晕厥类型。

2、0H 及直立不耐受综合征：当自主神经系统对血管张力、心率和心脏收缩力的调节功能存在缺陷时，在直立位，血液过多存留于内脏和下肢血管， 造成回心血量减少、心输出量下降、血压明显降低，又称直立不耐受综合征。与反射性晕厥相比，自主神经功能衰竭时，交感神经反射通路传出活动慢性受损，而出现自主神经系统对血管张力、心率和心肌收缩力的调节功能异常导致晕厥。体位性心动过速综合征 (POTS) 是直立不耐受综合征的另一种类型，发病机制尚不清楚。可能与自主神经系统功能紊乱、低血容量、肾上腺素活性升高、去适应作用、焦虑、过度紧张等因素有关。表现为站立时出现头晕、心悸、震颤、全身乏力、视野模糊、运动不能耐受等。反射性晕厥和自主神经功能衰竭的病理生理过程完全不同，但二者的临床表现常有相同之处，有时会造成鉴别诊断的困难。

3、心原性晕厥：心原性晕厥包括心律失常或器质性心血管疾病所致晕厥，为第 2 位常见原因，危险性最高、预后较差。心律失常所致晕厥是最常见的心原性晕厥类型，心律失常发作时伴血流动力学障碍，心输出量和脑血流量明显下降引起晕厥。影响发作的因素有心率的快慢、心律失常类型、左心室功能、体位和血管代偿能力，尤其是压力感受器对低血压的反应性高低。器质性心脏病所致晕厥多见于老年患者，当大脑需要的供血量超过心脏的供血能力，如果相应的心输出量增加不足则可引起晕厥。部分患者可同时存在反射机制，如阵发性房性心动过速、病态窦房结综合征、肥厚型心肌病、下壁心肌梗死和主动脉瓣狭窄患者可同时存在神经反射机制、心输出量减少和心律失常。

其他：

主动脉压迹部位房性心动过速导管消融 1 例

罗斌

首都医科大学附属北京同仁医院

患者基本信息：

患者田 **，女，63 岁，以“间断心悸伴心前区不适 1 月余，加重 2 天”为主诉于 2025-7-1 入院。既往“胆囊炎”5-6 年。否认高血压、糖尿病等其他病史。入院肝肾功电解质、血常规未见异常，心超未见异常。入院心电图示窦性心律频发房早，短阵房速，v1+，下壁导联 +。

主述：

间断心悸伴心前区不适 1 月余，加重 2 天”为

现病史：

1 月余前感冒、流涕好转后出现心悸、心前区不适，位于咽部至剑突下之间，伴憋气，多于平卧位时出现，坐起后可减轻，每阵持续数分钟左右，曾口服美托洛尔 1/4 片 bid 等药物效果不佳。2 天前起发作较前频繁，性质同前，就诊于我院门诊，行心电图提示心律失常，为进一步诊治收入院。自发病以来，精神食欲睡眠可，大小便正常，近半年体重增加 5kg。

既往病史：

• 既往史：“胆囊炎”5-6 年。否认高血压、糖尿病等其他病史。

病程记录：

入院后完善相关检查，给以电生理检查 + 导管消融治疗（具体见 word 文档）

检验检查记录：

心电图诊断为房性心动过速

鉴别诊断：

根据心电图房速，诊断明确无需鉴别诊断

其他：

无

甲亢患者感染 EB 病毒至心功能急剧下降一例

田倪妮

昆明市第一人民医院

患者基本信息：

患者男性，44 岁，主因“心悸半年，阵发性胸痛 2 天”入院。患者既往有甲状腺功能亢进病史 10 年，平素口服“甲巯咪唑片”治疗，近半年来停用“甲巯咪唑片”，有“2 型糖尿病”病史，平素口服“二甲双胍肠溶片 3 次 / 日”治疗。近半年来感到心悸，发作时持续数小时或者数小时不等，门诊行心电图提示“频发室性早博”，考虑“胸痛、室性早博”收住心内科。入院时体格检查：体温 36.5℃，脉搏 107 次 / 分，R18 次 / 分，血压 137/95mmHg；双肺呼吸音粗糙，未闻及明显干湿啰音。心界稍向左扩大，心律不齐，闻及早搏 8-10 次 / 分不等。双下肢无浮肿。

主述：

心悸半年，阵发性胸痛 2 天

现病史：

近半年来感到心悸，发作时持续数小时或者数小时不等， 门诊行心电图提示 “频发室性早博”，考虑 “胸痛、室性早博” 收住心内科。

既往病史：

既往有甲状腺功能亢进病史 10 年，平素口服“甲巯咪唑片”治疗，近半年来停用“甲巯咪唑片”，有 “2 型糖尿病” 病史，平素口服 “二甲双胍肠溶片 3 次 / 日” 治疗。

病程记录：

入院后给予口服“甲巯咪唑片”，给予“莫西沙星”抗感染，“美托洛尔缓释片”及“稳心颗粒” 控制心律失常治疗一周后。

检验检查记录：

复查相关指标发现 CT 上心脏明显扩大，感染加重，胸腔积液（图 3 B），心脏彩超上心脏扩大明显，射血分数降低明显 (EF 降至 42.5%，左心房 37mm, 左室舒张末内径 57mm)。甲状腺术前准备完善（口服甲巯咪唑 1 周）后考虑心功能下降明显，急性冠脉事件不能排外，完善冠状动脉造影术提示冠脉正常（见图 2A、B）。

鉴别诊断：

1. 肋间神经痛；2. 带状疱疹；3. 主动脉夹层。

其他：

因为写了个 WORD 版本打算投稿杂志，后面看医学会的病例分享行不行？ PPT 没有来得及做的，**全文在上传检查文件 2.**

GDMT 逆转高龄心衰患者完全性左束支阻滞 1 例

李兴红

松阳县人民医院

患者基本信息：

患者宋弟弟，女，92 岁，松阳县人。

主述：

活动后胸闷气促 2 年，再发 3 天

现病史：

入院 2 年前，患者出现活动后胸闷气促，超声心动图提示左室舒张末内径（Left Ventricular End-Diastolic Diameter，LVDD）54mm，左房内径（Left Atrial Diameter，LAD）35mm，左室射血分数（Left Ventricular Ejection Fraction，LVEF）30%，二尖瓣中度反流；心电图显示窦性心律，CLBBB，QRS 时限 164ms。诊断为慢性心力衰竭，给予厄贝沙坦、琥珀酸美托洛尔缓释片、呋塞米、螺内酯治疗，但患者出院后 1 个月自行停药。3 天前患者胸闷气促症状再发，休息后缓解，夜间可平卧，遂来院。

既往病史：

8 年前因肋骨骨折住院，查心电图提示完全性左束支传导阻滞（CLBBB），QRS 时限 156ms，当时超声心动图提示无殊。否认其他基础疾病及家族遗传病史，否认吸烟饮酒史。

病程记录：

初始方案：呋塞米片 20mg qd、螺内酯片 20mg qd、氯沙坦钾片 25mg qd，心衰症状控制后加用琥珀酸美托洛尔缓释片 23.75mg qd，三个月逐步滴定至患者能够耐受的靶剂量：氯沙坦 50mg qd、琥珀酸美托洛缓释片尔 47.5mg qd。

检验检查记录：

心电图提示 CLBBB，QRS 时限 180ms。超声心动图显示 LVDD 78mm，LAD 39mm，LVEF 24%，二尖瓣中重度反流。冠脉 CTA 提示：前降支轻中度狭窄。胸部 CT：左心增大，心包少量积液，两侧胸腔积液，肺水肿改变，考虑心衰可能。N 端 -B 型钠尿肽前体（N-terminal pro-B-type Natriuretic Peptide，NT-proBNP）15212pg/ml。血常规、CRP、肝肾功能、电解质、甲状腺功能、肿瘤标志物、急诊心肌酶等大致正常。

鉴别诊断：

患者 92 岁老年女性，以活动后胸闷气促症状入院，体检提示两肺闻及湿啰音、心界左下扩大、心尖部收缩期杂音 ,NT-proBNP 显著升高（15212pg/ml），超声心动图显示 LVDD 显著扩大（78mm）、LVEF 24%, 胸部 CT 提示左心增大、肺水肿改变，因此慢性心力衰竭（射血分数减低型，HFrEF）诊断明确。2012 年至 2020 年多次心电图均显示持续性 CLBBB，无频率依赖性改变，诊断完全性左束支传导阻滞（CLBBB）明确。

该患者诊断难点在于 CLBBB 与心衰的因果关系：本例患者 CLBBB 持续 8 年后出现心衰，且治疗后 CLBBB 消失伴心功能恢复，支持 CLBBB 导致心肌病的假说。

鉴别诊断：1. 冠状动脉粥样硬化性心脏病：患者无心绞痛、心肌梗死病史，心衰症状与缺血事件无关，冠脉 CTA 显示前降支仅轻中度狭窄，且 GDMT 显著改善心功能，不支持缺血性心肌病的不可逆损伤机制。2. 心脏瓣膜病：患者心超提示二尖瓣中重度反流，但瓣膜结构正常，考虑左室扩大导致的继发性改变，经 GDMT 后反流程度减轻至消失，进一步支持功能性反流。

其他：

患者出院后 1 年复查超声心动图提示 LVDD 43mm，LVEF 67%，二尖瓣无反流。心电图提示窦性心动过速，QRS 时限 102ms。胸部 CT 复查心影未见明显增大。出院后 2 年复查超声心动图提示 LVDD43mm，LAD 30mm，LVEF 62%，二尖瓣轻度反流。心电图提示窦性心律，QRS 时限 112ms。随访第 3 年（2023 年），患者 95 岁，因新冠病毒感染去世。

无冠窦房速 1 例引发的思考

马铮

首都医科大学附属北京同仁医院

患者基本信息：

患者田某某，女，76 岁，住院号：01376212，入院时间：2025 年 7 月 1 日

主述：

间断心悸伴心前区不适 1 月余，加重 2 天

现病史：

1 月余前感冒、流涕好转后出现心悸、心前区不适，位于咽部至剑突下之间，伴憋气，多于平卧位时出现，坐起后可减轻，每阵持续数分钟左右，曾口服美托洛尔 1/4 片 bid 等药物效果不佳。2 天前起发作较前频繁性质同前，就诊于我院门诊，首次心电图提示：心律失常、心房颤动，复查心电图提示窦性心律，为进一步诊治收入院。

既往病史：

慢性胆囊炎 5 年。

病程记录：

入院诊断：

心律失常

阵发性心房颤动

房性心动过速

频发房早

慢性胆囊炎

诊断依据：心律失常 - 阵发性心房颤动、房性心动过速、频发房早：患者老年女性，近 1 月余间断出现心悸、心前区不适、憋气，平卧位可加重、每阵持续数分钟，近 2 天发作较前频繁，心电图提示房颤与窦律交替出现，入院后监护发现频发房早及房性心动过速发作，诊断成立。

检验检查记录：

入院后完善检查，心电监护提示窦性心律与房颤交替，简短出现房性心动过速及频发房早。入院查甲状腺功能未见异常。超声心动提示左房前后径 32mm，三尖瓣轻度关闭不全，LVEF 60%。

鉴别诊断：

1）窦性心动过速：窦性心律的频率超过 100 次 / 分，受多种因素影响，生理性包括情绪、体位、体力活动、体温及药物等引起，病理性包括心脏器质性病变引起，常见于心功能不全时心脏代偿性变化，其他疾病如甲亢、贫血、外伤等刺激引起，且多数窦过速为逐渐增快或逐渐减慢，兴奋迷走神经不能中止，而阵发性室上速常为突发突止，刺激迷走神经可中止。

2）房性心动过速：通常见于器质性或缺血性心脏病，慢性阻塞性肺病，电解质平衡失调或药物毒性反应，包括心房内折返、自主性心动过速和触发性心动过速，心房节律规则，每个 P 波后有 QRS 波群，形态通常与窦性时相同，PR 间期正常或延长，均可行射频消融术治疗。

3）心房扑动：多数为 2:1 房室传导，心室率 140-160 次 / 分，心电图表现为规则的锯齿形扑动波，兴奋迷走神经可是心室率减慢，多数通过心电图可明确鉴别。

其他：

多旁道预激综合征消融一例

聂俊刚

南昌大学第一附属医院

患者基本信息：

患者姓名：唐某某

年龄：57

性别：女

主述：

心悸 30 余年，加重 1 年

现病史：

心悸 30 余年，加重 1 年，伴头痛头晕，伴轻微胸痛胸闷， 近一年加重，服药后未见明显好转，心电图提示心室预激。

既往病史：

3 年前下肢车祸行手术治疗

病程记录：

入院后行电生理检查 + 射频消融术，提示多旁道。

检验检查记录：

见 PPT

鉴别诊断：

诊断清楚，无需鉴别。

其他：

心房颤动合并冠状动脉栓塞 1 例

梁美玲

茂名市中医院

患者基本信息：

患者李某某，男性，71 岁

主述：

反复心悸、胸闷 1 年余

现病史：

患者 1 年余前反复出现心悸、胸闷，心悸呈阵发性，每次持续时间长短不等，胸闷位于胸骨后，呈憋闷感，无胸痛，无出汗，无头晕、黑蒙，无恶心、呕吐，无肢体偏瘫，无言语不利，曾多次在我院行心电图检查提示心律失常，阵发性心房颤动，予控制心室率，抗凝等对症治疗后，心悸、胸闷症状能缓解。患者于 2025 年 2 月 24 日突发胸痛，位于胸骨后，伴出汗，无心悸，胸痛无向他处放射，当时在我科住院，诊断 急性非 ST 段抬高型心肌梗死，行冠脉造影提示 RCA 中段狭窄 30%，PLV1 远端闭塞，无前向血流。结合患者阵发性心房颤动病史，考虑为冠状动脉栓塞引起 PLV1 闭塞，由于远端血管管腔直径小、器械难以到达病变远端等原因，介入治疗存在困难，且效果不确定，药物治疗可能是更适宜的治疗方案，予抗凝治疗；平时仍有心悸发作，为进一步治疗，收入我科。自起病以来，胃纳、睡眠一般，大小便正常。

既往病史：

否认高血压、糖尿病，否认家族类似病史。

病程记录：

1、冠心病二级预防及抗凝治疗

2、脉冲电场消融术

检验检查记录：

2025.2.24 CKMB40.5U/L，cTN I 1131ng/ml

心电图提示窦性心律

2025.2.24 CAG：冠脉系统呈右优势型，LM 未见明显狭窄，LAD 中段狭窄 30%，LCX 近中段狭窄 20-30%，RCA 中段狭窄 30%，PLV1 远端闭塞。

2025.5.27 心脏彩超提示：节段性室壁运动异常，主动脉瓣钙化伴轻度狭窄，二三尖瓣轻度关闭不全，左室稍大，轻度肺动脉高压，目前左心舒张功能减低，收缩功能未见明显异常。

2025.6.12 心脏 CT 增强：各房室腔内未见明确血栓形成

鉴别诊断：

冠状动脉粥样硬化性心脏病

其他：

既往研究认为，冠状动脉栓塞为少见病乃至罕见病，但有研究显示冠状动脉栓塞在急性心肌梗死中占到 2.9%，在急性 ST 段抬高型心肌梗死中占 4.3%

经胸或食管的超声心动图、冠状动脉造影等检查对冠状动脉栓塞的诊断及判断栓子来源有重要的意义。

血管内超声或 OCT 等冠状动脉腔内影像学能很好地明确有无冠状动脉斑块破裂或侵蚀，对冠状动脉栓塞的鉴别和排除有重要的意义。

心肌桥合并冠脉痉挛致急性心肌梗死 1 例

李兴红

松阳县人民医院

患者基本信息：

患者女性，64 岁，家住浙江丽水松阳县，农民。于 2025 年 6 月 19 日胸痛流程入院。

主述：

突发胸痛 18 小时。

现病史：

患者 18 小时前无明显诱因下开始出现胸痛，为心前区，初为隐痛，间歇约数分钟至数十分钟缓解，与活动关系不大，7 小时开始症状加重，呈持续性不缓解，向背部放射，有出汗、心悸，伴右上肢麻木，无胸闷，无恶心呕吐，无咳嗽咳痰。送至我院急诊就诊，查心电图提示窦性心律，V2-V3 导联 ST 段略抬高。予以胸痛一包药使用后症状缓解。15 分钟后复测心电图 V2-V3 导联 ST 段回落。心肌酶示 CKMB14.26ng/ml，肌钙蛋白 I0.87ng/ml，肌红蛋白 76.0ng/ml。冠脉 CTA：LAD7 段局部心肌桥形成。拟 “急性冠脉综合征” 收住。

既往病史：

既往有高血压病史 10 余年，不规律用药，有慢性乙肝病史，长期服用恩替卡韦分散片抗病毒治疗。否认其他疾病史及家族史。

病程记录：

入院后复测心肌酶进行性升高，复查心电图提示下壁导联 Q 波，V1-V5 导联 T 波倒置，急诊行冠脉造影提示前降支中段心肌桥，收缩期压缩 70%, 对角支 70-80% 狭窄，前向血流 TIMI3 级，右冠脉近段 40% 狭窄，前向血流 TIMI3 级。心超：轻度二尖瓣、三尖瓣反流。予以阿司匹林片、氯吡格雷片、单硝酸异三梨脂片、阿托伐他汀片使用。症状未再发作。

检验检查记录：

心脏 MRI：左室中远段室间隔心内膜下心肌水肿、缺血、纤维化，考虑缺血性心肌病（左前降支供血区域受累可能）。

鉴别诊断：

1. 冠脉内自溶：患者以胸痛为主诉入院，有高血压病史，结合心电图心肌酶表现，需考虑，但冠脉造影提示血管内未见易损斑块，可能性不大。2. 应激性心肌病：患者无明显应激因素，心超、冠脉造影也没有应激性心肌病提示。

其他：

患者出院后随访未再胸痛发作。

扩张性心肌病合并重度冠状动脉肌桥 1 例

黄浩

茂名市中医院

患者基本信息：

患者梁某，男，27 岁。汉族，未婚，职业农民，现住广东省茂名市茂南区。

主述：

反复胸闷、气短 2 年余，加重 2 天

现病史：

缘患者于 2 年余前反复于活动时出现胸闷发作，位于胸前区，呈憋闷感，无明显胸痛，伴间中气促，无出汗，无心悸，无头晕头痛，无咳嗽、咳痰，无恶心、呕吐，无尿频、尿急、尿痛等不适，休息后症状持续数分钟至半小时缓解，遂至外院就诊，完善心脏彩超考虑扩张型心肌病，予以相关治疗（具体不详）后症状改善，后症状反复，多次至外院及我院诊疗。2023-12-29 因胸闷气促再发至我院住院治疗，诊断扩张型心肌病、心功能 3 级，予以减轻心脏负荷、利尿、降低心肌耗氧量，改善心室重构及其他对症治疗后症状好转，出院后规律服药。此后曾多次因肺部感染诱发急性心力衰竭入住我科，曾建议患者行 CRTD 治疗，但因经济困难，不同意行 CRTD 治疗，均予药物保守治疗，胸闷、气短缓解后出院。患者于近 2 天自觉气短、胸闷较前加重，气短发生频率较前增多，持续时间较前增长，今为进一步诊治，遂至我院门诊就诊，门诊行心电图提示窦性心律，室性早搏，完全性左束支传导阻滞（QRSD 217ms），左室高电压，ST-T 改变。门诊拟 “慢性心力衰竭急性加重 扩张型心肌病 心脏增大 窦性心律 心功能 3 级” 收入院。入院时症见：患者神清，精神一般，床旁活动稍胸闷气促，无明显胸痛，汗多，偶有心悸，无肢体浮肿，胃纳可，眠差，小便可，大便质稀，5-6 次 / 日。

既往病史：

冠状动脉肌桥病史，LAD 收缩时狭窄 95%。既往桥本甲状腺炎病史，甲功未见异常。否认肝炎、结核、疟疾病史，否认高血压病史，否认糖尿病、脑血管疾病、精神疾病史，有手术史曾行眼角膜切除术及扁桃体切除术（具体不详），无输血史，否认食物、药物过敏史，预防接种史不详。

病程记录：

入院后治疗上予单硝酸异山梨酯注射液静脉泵注扩管，呋塞米及螺内酯口服利尿，美托洛尔缓释片及盐酸伊伐布雷定片口服控制心室率，达格列净片口服改善心功能，芪苈强心胶囊口服强心等抗心衰治疗。因患者间中胸痛发作行冠脉造影提示 LAD 肌桥，收缩时狭窄 95%，逐步加大 β 受体阻滞剂用量症状有改善。

检验检查记录：

2023 年 12 月 25 日外院心脏彩超结果：符合左室心肌致密化不全心肌病超声改变，全心扩大，左室收缩功能明显减低（EF19%），重度二尖瓣返流，中度三尖瓣返流，中度肺动脉高压（55mmHg）。2024 年我院冠脉造影提示：LAD 远段可见肌桥形成，收缩时狭窄 95%。2024-02-29 冠脉造影：冠脉系统呈左优势型，开口未见明显异常，LM 未见明显狭窄，LAD 远段可见肌桥形成，收缩时狭窄 95%，LCX 未见明显狭窄，RCA 未见明显狭窄，血流均为 TIMI3 级，诊断：冠脉肌桥。入院 NT-proBNP 3715pg/mL，出院前复查 NT-proBNP 2215pg/mL

鉴别诊断：

急性心肌梗死

1)、支持点：患者因“反复胸闷、气短 2 年余，加重 2 天”入院，近 2 天自觉气短、胸闷较前加重，气短发生频率较前增多，持续时间较前增长。2023-12-25 广东省人民医院行心脏彩超：符合左室心肌致密化不全心肌病超声改变；全心扩大，左室收缩功能明显减低（EF19%）；重度二尖瓣返流，中度三尖瓣返流，中度肺动脉高压（55mmHg）。2024-02-29 冠脉造影：冠脉系统呈左优势型，开口未见明显异常，LM 未见明显狭窄，LAD 远段可见肌桥形成，收缩时狭窄 95%，LCX 未见明显狭窄，RCA 未见明显狭窄，血流均为 TIMI3 级，诊断：冠脉肌桥。

2)、不支持点：无明显胸闷痛发作。

3)、结论：完善肌钙蛋白等进一步排除。

其他：

思考讨论：

1. 患者心肌病的原因是由于心肌桥长期引起心肌缺血导致缺血性心肌病还是原发的扩张型心肌病；

2. 患者心肌病的治疗是否只是原来经典方案就行还是要加上改善心肌缺血的药物如盐酸曲美他嗪等；

3. 患者的后继治疗除了 CRTD 和心脏置换术是否还有其他出路。

部分型无顶综合征合并冠状静脉窦闭锁引流入永存左上腔静脉封堵 1 例

蒲俊舟

首都医科大学附属北京安贞医院

患者基本信息：

患者，女性，54 岁。

主述：

站立后胸闷憋气 2 年加重半年

现病史：

患者自诉近 2 年来出现站立后胸闷憋气，近半年来症状加重，行家庭吸氧治疗。

既往病史：

否认高血压，糖尿病，高脂血症病史

病程记录：

平卧位血气血氧饱和度 96%，站立位血气血氧饱和度 92%。

经食道超声心动图 + 右心声学造影提示：卵圆孔未闭，大量右向左分流，永存左上腔静脉。

冠状动脉造影时发现，冠状静脉窦显影后，左上腔随即显影，同期右心房未见明确显影。

行右心导管检查 QP/QS=1.0。冠状静脉窦造影示：冠状静脉窦闭锁，大量造影剂经永存左上腔静脉，汇入无名静脉引流入上腔静脉。同时少量造影剂经冠状静脉无顶口分流入左心房。

尝试同期封堵 PFO 及冠状静脉 - 左心房交通。

手术经过：

1、 穿刺右侧股静脉，同时送入两枚 6F 导管鞘；

2、 将导丝经腔静脉送入冠状静脉窦，再送至左心房送达左上肺静脉；

3、 经另一个穿刺鞘送入 MPA1 导管 + 抓捕器抓捕

4、 建立腔静脉轨道后，经永存左上腔侧送入 JR 4.0guiding 至下腔静脉

5、 于缺损处植入 8mm AVP II 封堵器一枚

6、 再交换输送鞘至左心房

7、 尝试缺损处植入雅培 18/25 封堵器，无法稳固于缺损处，更换 12mm 华医 ASD 封堵器，仍无法稳固植入，最终更换 16mm ASD 封堵器

8、 植入后超声提示位置形态良好，周围结构未受影响

9、 再造影示无顶综合征封堵满意，无明显残余分流，冠状静脉窦可见少量细小分支汇入右心房内显影，患者心电图无异常改变，无不适症状。

检验检查记录：

尝试同期封堵 PFO 及冠状静脉 - 左心房交通。

手术经过：

1、 穿刺右侧股静脉，同时送入两枚 6F 导管鞘；

2、 将导丝经腔静脉送入冠状静脉窦，再送至左心房送达左上肺静脉；

3、 经另一个穿刺鞘送入 MPA1 导管 + 抓捕器抓捕

4、 建立腔静脉轨道后，经永存左上腔侧送入 JR 4.0guiding 至下腔静脉

5、 于缺损处植入 8mm AVP II 封堵器一枚

6、 再交换输送鞘至左心房

7、 尝试缺损处植入雅培 18/25 封堵器，无法稳固于缺损处，更换 12mm 华医 ASD 封堵器，仍无法稳固植入，最终更换 16mm ASD 封堵器

8、 植入后超声提示位置形态良好，周围结构未受影响

9、 再造影示无顶综合征封堵满意，无明显残余分流，冠状静脉窦可见少量细小分支汇入右心房内显影，患者心电图无异常改变，无不适症状。

鉴别诊断：

动脉导管未闭：胸骨左缘第二三肋间全期机械样杂音，影像学以肺门影增宽，肺血增多，左心扩大为主，暂不支持诊断；

肺动脉瓣狭窄：胸骨左缘第三四肋间粗糙的收缩期杂音，P2 减弱或未及，心脏正位相肺动脉段直立样突出，肺血减少表现表现，暂不支持诊断；

其他：

超声诊断成人 Shone 综合征 1 例

苏秀秀

上海交通大学医学院附属瑞金医院

患者基本信息：

患者女，72 岁

主述：

胸闷、腹胀伴下肢浮肿 3 月

现病史：

患者 3 月前出现胸闷、腹胀、下肢浮肿，活动后气促伴上背部疼痛，活动耐量减低，否认黑矇晕厥。2 月前于当地医院就诊，拟“肺炎、心力衰竭”收治，住院期间查心超示左房增大，左室肥厚，二尖瓣钙化、瓣膜冗长、脱垂待排，主动脉瓣中度反流，EF 58%；查胸部 CT 示两肺炎症，两侧胸腔少量积液，两肺少许纤维灶，主动脉及冠脉钙化，永存左上腔静脉；查心电图示窦性心律，频发室早；查血管超声示双侧颈动脉斑块形成，轻度狭窄，双侧下肢动脉斑块形成，轻度狭窄，双侧下肢深静脉未见异常。予以头孢曲松抗感染，美托洛尔控制心率，呋塞米、螺内酯利尿减负，氯吡格雷抗血小板，阿托伐他汀调脂，缬沙坦改善心肌重构等治疗，患者胸闷、腹胀、下肢浮肿有改善，活动后仍有气促。现为求进一步治疗收入院。

既往病史：

50 年前因主动脉狭缩窄行手术治疗，具体不详

病程记录：

二尖瓣置换 + 主动脉瓣置换 + 房间隔缺损修补术

检验检查记录：

经胸超声心动图可见二尖瓣前后叶及腱索冗长，腱索仅附着于后侧乳头肌，呈 " 降落伞样 " 改变，瓣叶增厚，回声增强，开放受限，后叶活动度较大，关闭时后叶局部及部分腱索脱向左房，二尖瓣重度反流。主动脉瓣呈三叶型，重度反流。房间隔中部可见回声中断 (5mm)。降主动脉起始处收缩期最大流速约 2.2m/s。超声诊断：先心，Shone 综合征可能，降落伞样二尖瓣，二尖瓣狭窄伴重度关闭不全；房间隔缺损（继发孔型）；主动脉缩窄术后，主动脉瓣重度关闭不全。术中探查证实二尖瓣前后叶腱索均附着于后乳头肌呈降落伞样，瓣叶多发脱垂，二尖瓣重度关闭不全；房间隔缺损；主动脉瓣重度关闭不全，与超声诊断一致。患者行二尖瓣置换 + 主动脉瓣置换 + 房间隔缺损修补术，术后超声复查二尖瓣及主动脉瓣无明显反流，前向血流速度无明显异常。

鉴别诊断：

风湿性二尖瓣狭窄

其他：

Shone 综合征是一种少见先天性心脏病，由二尖瓣瓣上环、降落伞型二尖瓣、主动脉瓣下狭窄、主动脉缩窄 4 种左心畸形构成，分为完全型和不完全型，完全型为 4 种畸形同时出现，极为少见，不完全型为具备 2-3 种畸形，临床以不完全型多见，多合并室间隔缺损、永存左上腔静脉、动脉导管未闭、房间隔缺损等其他畸形。本例患者符合不完全型 Shone 综合征的诊断。目前广义定义 Shone 综合征为以左心系统流入道和流出道多个水平梗阻为特征的复杂心脏畸形。根据患者在左心系统多水平梗阻程度不一，轻者可不需治疗，严重者多在幼年发病，需要手术治疗，并且因为发育引起植入物和受体的不匹配可能需要进行多次手术。Shone 综合征患者多数预后较好，手术死亡率与二尖瓣病变的严重程度、室壁肥厚程度及多次手术相关。本例患者年轻时因主动脉缩窄行手术治疗，本次因出现心衰症状入院行双瓣置换 + 房间隔缺损修补术，手术后症状明显缓解，预后较好。

超声心动图作为一种无创、简便的方法能在术前明确诊断，准确评估病变的严重程度，并能在术后进行随访，对于 Shone 综合征的诊断和治疗具有很好的指导作用。

十年误诊迷雾，一纸基因寻真--法布雷病心肌病的曲折诊断启示

张海琳

福建医科大学附属第一医院

患者基本信息：

姓　名：陈某某

性　别：男

籍　贯：福建福清

年　龄：70 岁

主述：

胸闷、气喘 10 年余，加重半年。

现病史：

10 年前频感胸闷、气喘，走路、爬楼后加重，偶伴头痛，休息可缓解，于外院查冠脉 CTA 阴性。

6 年前就诊我院，查心脏彩超提示：左室壁非对称性增厚，考虑“非梗阻性肥厚型心肌病”。

期间均予以β受体阻滞剂、ARB等治疗，症状改善不明显，期间多次复诊，均考虑“肥心”。

半年前症状加重，伴间歇性腹痛、腹胀，偶有肢体麻木、疼痛。拟“心肌肥厚”收入院。

既往病史：

既往史：既往体质一般。高血压 10 余年，血压最高 170/90mmHg，规律服用“琥珀酸美托洛尔 47.5mg qd，坎地沙坦酯片 8mg qd”，目前控制在 130/80mmHg。有“慢性胃炎、多发性肝囊肿、脂肪肝”等病史。

个人史：吸烟 15 年，10 支 / 日，已戒烟 3 月。

家族史：父母年老已故（具体死因不详），有 2 哥、2 姐、2 妹，大哥已故（具体死因不详），家族中是否有类似病史不详。

病程记录：

70 岁男性，福建省福清市人。反复胸闷、气促 9 年余，加重半年。期间多次就诊心内科诊断为肥厚型非梗阻性心肌病，予“利尿、抗心脏重构”等治疗后症状仍反复发作，偶有肢体麻木疼痛，近半年症状加重，伴右上腹疼痛。经过详细的鉴别诊断，最终明确为法布雷病心肌病，给予阿加糖酶治疗后好转。

检验检查记录：

心脏彩超提示左室肥厚，最厚处 2.48cm，LVEF 值正常，舒张功能减退，二维应变提示整体纵向应变减低，以前外侧壁明显。BNP 108ng/L，TNI 阴性。血尿免疫电泳见异常 M 蛋白（IgM-κ）。血清免疫固定电泳：IgM、κ 在 γ 区可见异常浓集区带，4.8%。PYP 显像阴性。骨穿：未见明显形态异常浆细胞。骨髓流式：可见 0.61% 异常成熟单克隆 B 淋巴细胞和 0.02% 异常单克隆浆细胞。全身 PET-CT 未见代谢异常增高灶。肌电图可见：双下肢 SSR 异常。心脏增强磁共振：左心室最厚处约 2.9cm，室间隔、左室前壁、部分侧壁可见延迟钆强化，局部可见 T1 mapping 值降低。心肌活检：心肌细胞空泡化改变，刚果红染色（-），甲苯胺蓝染色（+）。心肌电镜：可见髓样小体。α-GLA A 24.6 nmol/L（轻度降低），Lyso-GL 3 4.06nmol/L（明显升高），基因检测检出 GLA 基因致病的半合子变异，NM_000169.3:c.640-801G>A。

鉴别诊断：

和其他类型心肌病进行鉴别，如肥厚型心肌病、心肌淀粉样变性等。

其他：

左心室肥厚的鉴别诊断一直是临床诊疗中的一大难题。提高对该疾病的早期识别意识，并建立多学科联合的规范化筛查流程，对于左心室肥厚相关疾病的精准诊治而言，具有至关重要的意义。

法布雷病心肌病作为一种罕见的代谢性心肌病，在福建省的发病率处于全国较高水平。然而，目前福建省在该病的整体诊治水平方面仍存在不足，有待进一步提升。由于法布雷病心肌病早诊早治对于预防心源性猝死起着关键作用，因此加强相关诊疗能力的建设刻不容缓。

此次分享的这个病例：一名患者被误诊长达 10 余年的法布雷病患者，住院期间发现 M 蛋白，一度疑似心肌淀粉样变性，患者接受了一系列全面且完整的检查，包括心脏超声、心脏磁共振、血液学检查、核素显像、心肌活检以及基因检测等。经过这些细致的检查，最终得以明确诊断。希望通过分享这个病例，能够为更多医院的医生提供启示，促使大家更加重视罕见心肌病的筛查工作，从而为患者争取更早的诊断和更有效的治疗。

髓母术后又遇嗜铬，青年血压何以控

李静媛

山东大学齐鲁医院

患者基本信息：

本报告描述了一名 23 岁青年女性出现不受控制的高血压的病例，既往脊髓血管母细胞瘤、胰腺多发囊肿病史，再发嗜铬细胞瘤，遗传分析提示患者存在较为少见的 VHL 外显子缺失突变。本病例强调在高血压及多器官肿瘤患者中应高度重视遗传综合征，系统性评估、规范的家系调查及基因检测，对患者治疗决策至关重要。

主述：

右眼视物模糊伴头晕 1 周

现病史：

一位 23 岁青年女性，因“右眼视物模糊伴头晕 1 周”就诊于眼科，眼底照相及 OCT 检查提示右眼高血压性视网膜病变并黄斑水肿，左眼视神经病变。于门诊测量血压达 200/120mmHg，既往未监测血压。入院后，团队在积极控制血压的同时，系统筛查继发性高血压因素。

既往病史：

患者 4 年前曾因进行性右下肢无力合并感觉减退，就诊于神经科，查体：右下肢肌力 II 级，左下肢肌力 III 级，双下肢浅感觉减退，右踝以下深感觉减退，双下肢腱反射减退，病理反射未引出。磁共振检查提示 T2-T5 水平椎管内占位，病灶上下方脊髓空洞形成。之后接受髓内肿物切除术，术后病理证实为脊髓血管母细胞瘤，浸润脊髓组织（WHO I 级）。术后神经功能逐渐恢复，目前双下肢肌力、感觉均正常。

病程记录：

体格检查、心电图、心脏超声均未见异常。CT 提示：（1）右肾上腺区存在一最大截面积约 5.9×4.9cm 的肿块，与右肾上腺分界不清，中心见片状坏死无强化区。（2）胰腺肿大，弥漫分布囊性低密度灶，考虑多发囊肿。（3）双肾动脉管腔未见明显狭窄及扩张征象。

检验检查记录：

化验提示，血管紧张素转换酶、醛固酮、肾素、皮质醇等激素水平均正常，去甲肾上腺素（31.58nmo1/L，参考值 0-5.17）、甲氧基去甲肾上腺素（22.55nmo1/L，参考值 0-0.17）显著升高。18F-fluorodeoxyglucose (18^{F}-FDG)-PET testing 结果提示右侧肾上腺区肿块高度不均匀摄取 FDG 的影，SUVmax 15.3；胰腺见多发无明显 FDG 摄取的囊样低密度灶。复习患者 5 年前影像资料提示：胰腺多发囊肿，双侧肾上腺大小形态未见异常。

患者胰腺多发囊肿较前明显进展，血糖水平正常，血脂持续偏高（低密度脂蛋白胆固醇 5.81mmol/L， 总胆固醇 7.35mmol/L），淀粉酶、脂肪酶水平升高，提示胰腺外分泌功能受损。

经多学科会诊，考虑右侧肾上腺占位性质为嗜铬细胞瘤可能性大，建议患者酚苄明口服（10mg po q12h）3 周后，行外科手术治疗。继续随访胰腺情况，目前无手术指征。由于患者年纪轻且存在多器官肿瘤，考虑遗传性综合征的可能性，同时完善基因检测。

3 周后患者接受腹腔镜下右肾上腺切除术，术后病理证实为嗜铬细胞瘤。基因检测结果提示：患者 VHL 基因第 3 外显子 c.340_343del（p.Val114Serfs*8）杂合缺失变异，根据 ACMG 指南，该变异初步判定为致病性变异。

术后 1 月随访患者，未应用降压药情况下，血压一直维持在正常，视物模糊情况较前明显改善。

鉴别诊断：

肾上腺 tumor 的鉴别诊断包括：功能性肾上腺瘤（醛固酮瘤、皮质醇瘤、嗜铬细胞瘤）、 非功能性肾上腺肿瘤（肾上腺腺瘤，肾上腺皮质癌、转移性肿瘤）、肾上腺囊肿、出血等。

根据患者年龄、血管母细胞瘤以及高血压病史，诊断重点集中于评估功能性肾上腺瘤及转移性肿瘤。

其他：

暗藏玄机的 T 波

陈俊陪

荣昌区人民医院

患者基本信息：

男，71 岁

主述：

反复胸痛 1 周，加重 11 小时；

现病史：

入院 1 周前，患者无明显诱因出现胸痛，为心前区绞痛，程度尚可忍受，每次持续半小时左右，可自行缓解，症状反复出现，入院 11 小时前，患者无明显诱因再次出现胸痛，性质同前，程度剧烈，伴右上肢放射痛，伴大汗淋漓，每次可持续半小时至数小时不等，伴活动后气促，休息后可缓解。为求进一步诊治，于零晨来我院就诊。

既往病史：

“高血压”病史 10+ 年，长期口服降压药物（具体不详）治疗，未规律监测血压变化；有“慢性支气管”病史 5+ 年；无“糖尿病、慢阻肺、肾病”等慢性疾病史；自诉既往有“肺结核”病史，已治愈；否认“肝炎、伤寒”等急慢性传染病史。

病程记录：

无

检验检查记录：

D- 二聚体 0.35mg/L；指血糖：7.6mmol/L

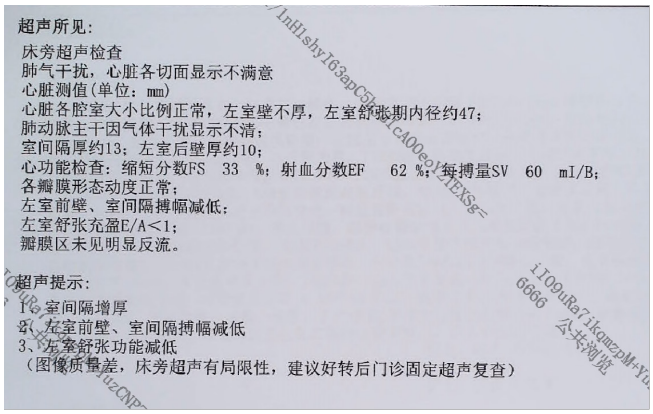
超声所见：
床旁超声检查
肺气干扰，心脏各切面显示不满意
心脏测值(单位：mm)
心脏各腔室大小比例正常，左室壁不厚，左室舒张期内径约47；
肺动脉主干因气体干扰显示不清；
室间隔厚约13；左室后壁厚约10；
心功能检查：缩短分数FS 33 %；射血分数EF 62 %；每搏量SV 60 mI/B；
各瓣膜形态动度正常；
左室前壁、室间隔搏幅减低；
左室舒张充盈E/A<1；
瓣膜区未见明显反流。

超声提示：
1、室间隔增厚
2、左室前壁、室间隔搏幅减低
3、左室舒张功能减低
（图像质量差，床旁超声有局限性，建议好转后门诊固定超声复查）

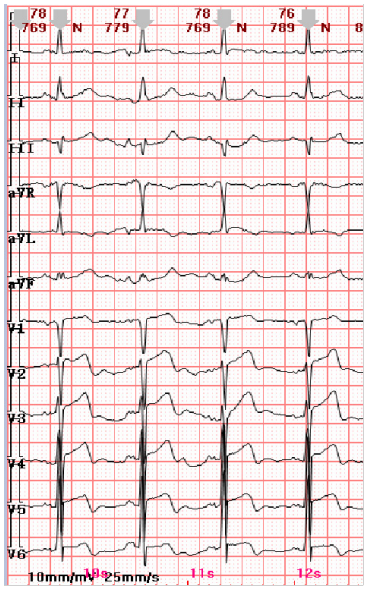

鉴别诊断：

一、心尖肥厚型心肌病

心尖部心肌肥厚，可出现胸痛症状，心电图有倒置Ｔ波，与 Wellens'综合征相似。但心尖肥厚型心肌病倒置Ｔ波出现在Ｖ４～Ｖ６导联，常伴有Ｖ４～Ｖ６导联Ｒ波电压增高。心脏超声和心脏磁共振检查有利于鉴别。

二、脑血管意外的心电图异常

脑血管意外时交感神经兴奋，可导致心肌细胞直接损伤及冠状动脉痉挛，引起心电图巨大Ｔ波倒置。这种Ｔ波常宽大畸形伴有ＱＴ间期明显延长，结合病史易于鉴别。

三、肺栓塞

肺栓塞时引起肺动脉压升高，右室负荷过重导致Ｖ１～Ｖ３导联Ｔ波倒置，易误为Ｗｅｌｌｅｎｓ　Ｔ波征。

二者主要区别为：①Ｗｅｌｌｅｎｓ　Ｔ波征患者心电图往往有Ⅰ、ａＶＬ导联Ｔ波倒置；急性肺栓塞心电图则为下壁导联（尤其是III导联）Ｔ波倒置。②Ｗｅｌｌｅｎｓ　Ｔ波征患者的心电图Ｖ１导联Ｔ波不倒置或浅倒置，Ｔ波即使倒置，形态也不对称，而肺栓塞心电图Ｖ１导联Ｔ波倒置常见，且Ｔ波是对称倒置。

四、应激性心肌病

本病是指由各种应激情况导致的心尖部球形扩张伴室壁运动障碍，表现为突发胸痛、心电图多导联Ｔ波倒置，但有心电图ＳＴ段抬高，ＱＲＳ波群异常、心肌酶升高，冠状动脉造影正常，可与Ｗｅｌｌｅｎｓ　Ｔ波征患者相鉴别。

五、假性Ｗｅｌｌｅｎｓ　Ｔ波征

一般来讲，Ｗｅｌｌｅｎｓ　Ｔ波征具有指向ＬＡＤ严重狭窄病变的特异性。但有时这种特征性的心电图改变，并非ＬＡＤ狭窄所致，此时称为假性Ｗｅｌｌｅｎｓ Ｔ波征。有报道心肌桥可致假性Ｗｅｌｌｅｎｓ　Ｔ波征；冠状动脉痉挛也能引起假性Ｗｅｌｌｅｎｓ　Ｔ波征，特别是吸食可卡因、大麻、苯环已哌啶等毒品的患者。也有报道硫酸吗啡控释片导致假性Ｗｅｌｌｅｎｓ综合征，并认为此种改变与制剂，而不是药品本身有关。邱景伟等报告１例双硫仑样反应患者诱发Ｗｅｌｌｅｎｓ　Ｔ波征；Ｇｒａｕｔｏｆｆ等报告了１名诊断为急性胆囊炎患者，心电图呈Ｗｅｌｌｅｎｓ　Ｔ波征，原因不明。

Ｍｉｇｌｉｏｒｅ等[３５]对４种不同情况下，包括心肌桥、冠状动脉夹层、胆囊炎、Ｔａｋｏｔｓｕｂｏ综合征具有Ｗｅｌｌｅｎｓ　Ｔ波征心电图表现的患者，进行增强心肌核磁共振显像，结果显示Ｔ波倒置区域存在心肌水肿，且当心电图Ｔ波异常消失时，心肌水肿也消散，提示心肌水肿可能导致心肌细胞复极化不均从而产生特征性Ｔ波改变。

其他：

无

室间隔破裂封堵术后三尖瓣腱索断裂、乳头肌脱垂 1 例

何丽婷

昆明医科大学第一附属医院

患者基本信息：

性别：男

年龄：64 岁

主诉：胸闷、呼吸困难，伴颜面部、双下肢不肿 2 月

既往史：外伤致肺部感染史

入院时间：2024 年 8 月 14 日

主述：

颜面部、双下肢水肿 1 月

现病史：

患者 6 月份摔倒后致肺部损伤，并于昭通市第二人民医院就诊及定期复诊 :2024-07-31 患者无明显诱因下出现面部及下肢水肿，面部水肿晨起明显，下午时水肿缓解：下肢水肿下午不缓解，伴胸闷、呼吸困难，无胸痛、无咳嗽咳痰、无头晕、黑朦，患者未服药治疗，水肿持续不缓解遂于 2024-08-07 日至当地民医院就诊，外院子完善心超彩超示 :1、后间隔中段回声中断，结合病史考虑室间隔穿孔可能性大 ;2、室水平左向右高速分流；3、双房及右室增大：4、三尖瓣大量反

流 :5、少 - 中量心包积液 ;NT-ProBNP:1380Pg/ml, 外院子惠者相关治疗 (具体不详) 后患者水肿较前好转，外院建议患者进一步上级医院就诊进行室间隔缺损的诊疗，遂患者为求进一步诊疗至我院就诊，门诊以“室间隔缺损”收住我科·病程中患者精神良好，二便正常，睡眠佳，近期体重无明变化；

既往病史：

2024-6 摔倒史

病程记录：

排外相关禁忌后，于 2024-8-15 至我院心内科行“室间隔穿孔修补术”，术后复查心脏彩超提示：三尖瓣前叶重度脱垂，细小腱索断裂及部分乳头肌撕裂可能）；2. 三尖瓣重度关闭不全致右房（50*60mm）、右室 (45*43*59mm) 扩大，右室舒张功能不全 II 级，右室肺动脉收缩耦联指数低危。3. 室间隔肌部缺损封堵术后：未见残余分流；遂联系心外科转至心外科 ICU 病房，因患者头颅 MRI 提示急性脑梗期，存在手术禁忌，暂未手术。2024-10-11 患者为行进一步手术治疗，再次至我院就诊，门诊以“三尖着关闭不全“收住心外科。病程中患者精神良好，二使正常，睡眼佳，近期体无重无明显变化 -。

入院后完善术前准备，于 2024-10-21 行“三尖瓣成形术 + 右心房减压术 + 体外循环辅助开放性心脏手术 + 关胸术”，术后患者生存质量良好，术后 6 月复查心超较前明显改善。

检验检查记录：

2024-7-31 当地医院心超：1、后间隔中段回声中断（断端约 10mm，过隔血流峰值流速约 411cm/s），结合病史考虑室间隔穿孔可能性大；2、室水平左向右高速分流：3、双房及右室增大 :4、三尖瓣大量反流：5、少 - 中量心包积液；冠脉造影未见明显狭窄；

2024-7-31 当地医院冠脉造影：各冠脉未见狭窄；

2024-8-15 我院入院心超：1. 室间隔中下段过隔分流（后间隔距心尖约 15mm 处组织连续中断，断端约 12mm，过隔血流峰值流速 5.6 m/s，压差 126mmHg），左房（34mm）、左室 (左室舒张末内径 55mm) 内径增大；

2. 中度肺动脉高压（64mmHg，三尖瓣反流速度：3.8m/s），主动脉内径增宽，右房 (45*59mm)、右室 (42*35*80mm) 内径增大；

2024-8-16 室间隔介入手术后第一天：1. 三尖瓣前叶疏松、毛躁，于收缩期明显脱向右房，可见细小腱索，长约 6.5mm，于整个心动周期于右房右室间甩动，呈“连枷样”改变，另一细小腱索末端可见稍强回声附着，大小约 8.5*4.7mm，瓣环扩大，CDFI 示：收缩期大量反流，反流缩流经 13mm（三尖瓣前叶重度脱垂，细小腱索断裂及部分乳头肌撕裂可能）；2. 三尖瓣重度关闭不全致右房（50*60mm）、右室 (45*43*59mm) 扩大，右室舒张功能不全 II 级，右室肺动脉收缩耦联指数低危。3. 室间隔肌部缺损封堵术后：未见残余分流；

2024-10-28 三尖瓣成形术后第 8 天心超：各房室内径恢复至正常范围；三尖瓣成形术后：瓣膜少量反流；先心病室间隔肌部缺损封堵术后：封堵器下缘细小残余分流（近心尖处约 2mm）；

2025-4 三尖瓣成形术后半年复查心超：三尖瓣成形术后 + 先心病室间隔肌部缺损封堵术后：1）三尖瓣少量反流；2）封堵器上缘细小残余分流；

鉴别诊断：

1. 先心病 室间隔缺损；

2. 心梗后室间隔破裂；

其他：

系统性红斑狼疮合并心衰的精准化管理 --- 多模态监测与 CRRT- 血浆置换协同治疗

张玉媛

新疆维吾尔自治区人民医院

患者基本信息：

患者 30 岁女性

体温：38.4℃ 脉搏：122 次 / 分 呼吸：28 次 / 分 血压：111/73 mmHg

神志清楚，贫血貌。

左侧眼部明显肿胀，不能睁眼，左侧面部肿胀，皮温升高，有触痛感，全身皮肤粘膜未见黄染及出血点，全身浅表淋巴结未触及肿大。

双肺呼吸音清，双下肺未闻及湿性啰音。

心律齐，各瓣膜听诊区未闻及杂音。

腹平软，未触及压痛，无反跳痛，肝脾肋下未触及，Murphy 征（-），肠鸣音正常

双下肢中度水肿，末梢皮温可，无花斑。神经系统查体未见异常

主述：

面部、下肢水肿 2 月，左侧眼部肿胀 1 天

现病史：

2 月前无明显诱因出现颜面部水肿，并逐渐出现双下肢水肿，呈轻度凹陷性水肿，水肿情况在劳累时加重，休息后有所缓解，当地医院治疗后好转出院（具体不详）；3 周前上述症状再次出现，有胸闷、气短，夜间可平卧，遂再次就诊于当地医院完善相关检查明确诊断：系统性红斑狼疮，狼疮肾炎，给予激素、免疫制剂、利尿等治疗，但胸闷、气短仍存在，活动耐量下降，夜间需高枕卧位；1 天前无明显诱因出现左侧眼部及面部肿胀，有红肿热痛等不适，伴食欲减退，乏力，发热，最高体温 39.3℃；为进一步诊治就诊我院

既往病史：

系统性红斑狼疮病史 3 周，羟氯喹 200mg 2 次 / 日，泼尼松 45mg 1 次 / 日，吗替麦考酚酯胶囊 0.75mg 2 次 / 日药物治疗

病程记录：

入院后予以去甲肾上腺素：0.09ug/kg/min；亚胺培南注射液 500mg q6h；万古霉素注射液 0.5g q12h；甲硝唑氯化钠注射液 500mg q12h；静住人免疫球蛋白注射液 20g q；甲泼尼龙注射液 40mg qd；泮托拉唑注射液 40mg qd；双环醇片 25mg tid；重组人脑利钠肽注射液；沙库巴去缬沙坦片 50mg bid；呋塞米注射液 20mg bid；尿毒清颗粒 +α 酮酸片护肾，碳酸氢钠碱化尿液，双环醇片护肝，50% 葡萄糖 + 胰岛素降钾，人血白蛋白注射液纠正低蛋白血症，输注悬浮红细胞纠正贫血，依诺肝素钠注射液抗凝预防下肢血栓形成。

予以 CRRT 清除肌酐、超滤、纠正电解质紊乱，1 次双膜及 3 次单膜血浆置换以清除系统性红斑狼疮致病因子

第一天：患者端坐呼吸，胸闷、气短明显，左眼部及面部明显肿胀，无法睁眼，皮温略高，有触痛；双肺可闻及湿性啰音；腰腹部及双下肢水肿明显。

高流量吸氧状态（流速 60L/min，氧浓度 50%）T：38.5℃，血流动力学不稳定，入院 2 小时尿量：200mlBNP：>5000.00 ↑ pg/mL，K+ 5.71 ↑ mmol/L，Cr 326.20 ↑ umol/LPiCCO 提示低排高阻，心源性休克结合患者心脏彩超，考虑全心衰竭，肺循环、体循环淤血严重同时合并感染性休克

予以床旁 CRRT 清除肌酐、脱水减轻机体容量负荷及纠正电解质紊乱

第 2 天：患者胸闷、气短略好转，左眼部及面部仍肿胀。血管活性药物下调趋势，高流量吸氧状态（流速 60L/min，氧浓度 50%）24 小时出入量：-700-1000ml/日，超滤量：2000ml/ 日，尿量：100ml/ 日 T：37.0-38.1℃，感染指标仍较高（WBC 30.62 → 33. 68 10^9/L，PCT： 64.96 → > 100 ↑ ng/mL，IL-6：1323.00 → > 1000 pg/ml，LAC：6.66 → 1.22 mmol/L）贫血较前纠正（Hb 61 → 80.00 g/L）BNP：>5000.00 ↑ pg/mL 下腔静脉宽约 17mm，picco 提示详见 PPT，予以床旁 CRRT 联合 HA-380 灌流吸附炎症介质; 完善眼眶 CT 等检查，明确左眼眶蜂窝织炎，眼科会诊，妥布霉素地塞米松眼液 :0.1ml 左眼 qid， 妥布霉素地塞米松眼膏 :0.1mg 左眼 q2h。

第 4-6 天：胸闷、气短好转，左侧颜面部红肿较前局限，可轻度睁眼。停用血管活性药物

高流量吸氧状态（流速 40L/min，氧浓度 45%）24 小时出入量：-1000-1500ml/日，超滤量：2500ml/ 日，尿量：800-1000ml/ 日

T：36.3-37.4℃，感染指标下降趋势（WBC 11.32 10^9/L，PCT：34.99 ng/mL，IL-6：5.74 pg/ml）BNP：>5000.00 ↑ pg/mL 血培养：化脓链球菌；撤除 PiCCO，针对患者系统性红斑狼疮，继续给予患者甲泼尼龙控制病情，静注人免疫球蛋白 5 天达疗程后停用

第 7 天：胸闷、气短好转，左侧颜面部红肿较前局限，可睁眼。高流量吸氧状态（流速 35L/min，氧浓度 40%）尿量较前恢复，1200ml/ 日 T 正常范围，感染指标下降趋势（WBC 9.65 10^9/L，PCT：5.41 ng/mL，IL-6： < 5.00 pg/ml）BNP：>4887.2 ↑ pg/mL 血小板进行性下降（PLT 131.00 → 21.00 10^9/L），临床表现改善，无明确厌氧菌感染证据，停用甲硝唑 + 万古霉素抗炎；因体内明确存在化脓性感染病灶，针对 SLE，暂不予环磷酰胺免疫抑制治疗；血小板下降，血红蛋白下降不明显，需排除药物作用可能性，停用万古霉素后继续观察血小板变化情况。

第 8 天：BNP：>5000.00 ↑ pg/mL，加强呋塞米利尿减轻心脏容量负荷；静息心率偏快，加用富马酸比索洛尔控制心室率降低心肌氧耗。血小板进行性下降，原因考虑：患者狼疮 SLEDA 评分 20 分处于重度活动，考虑存在 SLE 活动继发血栓性微血管病（TMA）有无药物相关性血小板减少？目前已停用万古霉素，暂停用依诺肝素抗凝，完善抗血小板抗体。狼疮对外周血影响？完善骨髓穿刺

第 9-11 天：感染较前控制，改为头孢曲松钠抗感染。针对 SLE，甲泼尼龙注射液 400mg 3 天 ,1 次双膜及 3 次单膜血浆置换以清除系统性红斑狼疮致病因子

第 12 天：患者胸闷、气短明显缓解，下肢水肿减轻

第 13-15 天：甲泼尼龙 200mg 静点 3 天后昨日开始减量至 80mg 每日 1 次；激素冲击治疗结束后给予足量激素联合环磷酰胺控制原发病

第 16 天：好转出院

检验检查记录：

血气分析：PH 7. 31，PaCO2 29. 0mmHg，PaO2 149. 00 mmHg

血常规：WBC 30. 62 ↑ 10^9/L，Hb 61.00 g/L，PLT 131.00 10^9/L，N% 92. 80 ↑ %，

CRP 143. 15 ↑ mg/L

IL-6：1323.00 ↑ pg/ml，PCT： 64.96 ↑ ng/mL，LAC：6.66 ↑ mmol/L

心肌损伤标志物：TnI 4.039 ↑ ng/mL，TnT 0.545 ↑ ng/mL，MYO 514.40 ↑ ng/ml，

CK 1260.00 ↑ U/L，CK-Mb 4.57 ng/ml

BNP：>5000.00 ↑ pg/mL

肝 功 能：TBIL 19.12 umol/L，ALB 28.51 ↓ g/l ，ALT 94.00 ↑ U/L，AST 75.00 ↑ U/L，GGT 32. 00 U/L，ALP 53. 00 U/L

肾功能：BUN 20.73 ↑ mmol/L，Cr 326.20 ↑ umol/L，UA 646.38 ↑ umol/L

电解质：K+ 5.71 ↑ mmol/L，Na+ 130.00 ↓ mmol/L，Cl- 104.40 mmol/L，Ca2+1.95 ↓ mmol/L，P 2.29 ↑ mmol/L

凝血功能：PT 19.6 ↑秒，PA 46 ↓ %，INR 1.78 ↑ INR，FIb 4.41 ↑ g/L，

APTT 35.80 ↑秒，D-Dimer 10.267 ↑ mg/L

贫血四项：促红细胞生成激素 193.90 ↑ mIU/mL，维生素 (B12) 277.00 pg/mL，叶酸 >23.40 ↑ ng/mL，铁蛋白 >1500.00 ↑ ng/mL

淋巴细胞亚群分析：淋巴细胞计数（CD45 计数） 586.10 ↓ 个 /μL，CD3 总 T 细胞百分比 53.42 ↓ %，CD4 辅助 / 诱导 T 细胞百分比 13.69 ↓ %，CD19B 淋巴细胞百分比 40.82 ↑ %，CD4/CD8 0.35 ↓

急诊尿常规 + 沉渣：尿白细胞 1+ ↑ ，尿蛋白质 4+ ↑ ，尿葡萄糖 3+ ↑ ，尿胆红素 1+ ↑ ，尿隐血 3+ ↑ ，白细胞计数 267.90 ↑ 个 /μL，红细胞计数 62.60 ↑ 个 /μL，上皮细胞计数 77.00 ↑ 个 /μL，管型 29.92 ↑ /μL，黏液丝 3.81 ↑ 个 /μL，透明管型 9.59 ↑ /μL，非鳞状上皮 14.30 ↑ 个 /μL

ds-DNA 全套 +ENA 抗体谱 + 抗核抗体：ANA(抗核抗体 IgG 型) +++ ，抗体滴度 (IIF) 1: 1000 ，荧光模型 (IIF) 均质型 ，抗 dsDNA 抗体 IgG 型 (IIF) 阳性 (+)1:10 ↑ ，抗 dsDNA 抗体 IgG 型 184.30 ↑ U/mL，抗 dsDNA 抗体 IgG 型 (IBT) + ↑ ，抗 Histones 抗体 IgG 型 (IBT) + ↑

单项补体（C1q）+ 抗 β2- 糖蛋白 1+ 抗核小体抗体：抗补体 C1q 抗体 IgG 型 49.80 ↑ AU/mL，抗核小体抗体 IgG 型 105.70 ↑ RU/mL

类风湿因子 (RF) 测定、抗链球菌溶血素、抗环瓜氨酸肽、抗角蛋白抗体、抗核周因子抗体 APF、ANCA 全套、抗肾小球基底膜抗体均未见明显异常

头 + 胸 + 腹部 CT：1. 额面部软组织肿胀，左侧眼睑周围为著；

2. 全组副鼻窦炎；

3. 左肺上叶纤维硬结灶；

4. 心包积液，双侧胸腔积液，双下肺部分膨胀不全；

5. 心影重度增大，心腔、大血管腔密度减低 - 考虑贫血，

6. 双侧颈根部、腋窝、肺门及纵隔内多发增大淋巴结；

7. 腹水，扫及胸腹壁皮下水肿。

心脏彩超：全心略大

下腔静脉略增宽并固定

室壁整体运动不协调且减弱

三尖瓣口中大量反流

二尖瓣口轻度反流

少量心包腔积液

LVEF：38%

鉴别诊断：

诊断明确

其他：

该患者病情极为复杂，系统性红斑狼疮重症活动期并发脓毒血症、感染性休克及心源性休克，导致多脏器功能障碍。在治疗过程中，需在维持心功能的同时兼顾其他脏器支持，但治疗策略之间存在诸多矛盾和挑战。一方面，患者同时存在脓毒血症、感染性休克以及心源性休克。在进行补液容量复苏时，需警惕诱发肺水肿、加重心脏负荷以及导致心功能进一步恶化；此外，患者还合并肾功能不全，过度脱水利尿可能加重肾前性肾损伤；在药物治疗方面，也需在疗效与副作用之间进行动态平衡，例如，利尿剂长期使用可能导致耐药，肾小管钠重吸收增加，需联合托伐普坦或超滤治疗，但过度超滤又可能引起低血压或血栓形成；去甲肾上腺素可改善心功能减少液体负荷，但也加重心脏后负荷与氧耗及增加急性肾损伤风险。另一方面，患者处于 SLE 重度活动期且合并重症感染，在使用免疫抑制剂和激素治疗时，虽然能够控制 SLE 的病情进展，但存在感染进一步加重的风险，因此，我们采用双重血浆置换快速清除自身抗体，在控制 SLE 活动的同时，尽可能降低感染风险。综上，对于此类血流动力学不稳定且多脏器功能衰竭的重症患者，精准管理及治疗至关重要，我们采用脉搏指示连续心排量监测（PiCCO）精准评估心脏前后负荷、心肌收缩力等参数，并结合床旁超声心动图实时评估心脏结构和功能、机体容量状态以及无创血流动力学监测，通过整合各项血流动力学参数及检查结果，指导和及时调整治疗方案，优化多脏器功能支持，以期达到最佳治疗效果，改善患者的预后。

具体讨论详见 PPT

肺动脉瘤合并肺动脉夹层：一例病例报告及文献综述

张展

甘肃省人民医院

患者基本信息：

患者，女，56 岁。

主述：

突发胸痛 12 小时，伴进行性呼吸困难

现病史：

患者于 12 小时前无明显诱因突发胸痛，胸痛呈压榨性，无放射痛及体位相关性，伴随活动耐力急剧下降（NYHA IV 级）及口周发绀。面罩吸氧（FiO_2 0.5）下指脉氧饱和度 90%。否认咯血、晕厥及下肢水肿。入院查体：体温 36.3℃，脉搏 74 次 / 分，呼吸频率 19 次 / 分，双侧上肢血压显著不对称（右上肢 187/112 mmHg，左上肢 137/76 mmHg）。口唇及颜面发绀，右肺中下野闻及中等量湿性啰音，左肺呼吸音清晰。心界向左扩大，心音遥远，未闻及明确病理性杂音。无颈静脉怒张及下肢水肿。行心电图检查提示窦性心律，电轴右偏，V1 导联 R 波优势，V2-V6 导联 ST 段压低伴 T 波倒置，急诊 CT 主动脉成像示肺动脉改变，考虑肺动脉瘤并夹层形成 2. 右肺动脉干起始部管壁欠规整，少许附壁血栓、肺动脉壁炎性改变，心肌标志物二项：NT-proBNP：2800pg/ml、hsTnI：0.01ng/ml，心肌酶未见明显异常。为进一步诊治，以“肺动脉瘤、肺动脉夹层”收住大血管外科。入院后经胸超声心动图：1. 主肺动脉、肺动脉融合部及左右肺动脉明显增宽 2. 双房、左室增大，以左心增大为著 3. 主动脉窦部及升主动脉、主动脉弓增宽 4. 肺动脉压力增高 (mPAP=55mmHg)5. 中量心包积液；传染病及自身抗体检查均为阴性。入院 3h 后患者突发意识不清，呼之不应，心电监护显示无脉性电活动，经持续心肺复苏 45 分钟无效，宣告临床死亡。

既往病史：

既往高血压病史 8 年（最高 190/110 mmHg），接受非规范化降压治疗，未规律监测血压。

病程记录：

入院 3h 后患者突发意识不清，呼之不应，心电监护显示无脉性电活动，经持续心肺复苏 45 分钟无效，宣告临床死亡。

检验检查记录：

血常规：白细胞 （WBC）15.26×10^9 /L；红细胞（RBC）:7.74×10^{12} /L；血红蛋白（HGB）:217g/L，心肌标志物：NT-proBNP 2800 pg/ml，hsTnI 0.01 ng/ml；生化全套、心肌酶、传染病、自身抗体全套未见明显异常。心电图：窦性心律，电轴右偏，V1 导联 R 波优势，V2-V6 导联 ST 段压低伴 T 波倒置。急诊 CT 主动脉成像：肺动脉高压 ，考虑肺动脉瘤并夹层形成，右肺动脉干起始部管壁欠规整，少许附壁血栓；心脏增大，心包少量积液。经胸超声心动图：主肺动脉及左右肺动脉明显增宽，双房及左室增大，肺动脉压力增高（mPAP=55 mmHg），中量心包积液。

鉴别诊断：

肺动脉瘤合并肺动脉夹层需与多种疾病进行鉴别诊断：①肺动脉栓塞表现为突发胸痛和呼吸困难，但增强 CT 显示充盈缺损而非血管壁分层，且 D- 二聚体显著升高；②主动脉夹层虽有类似撕裂样胸痛和血管壁分层表现，但疼痛多位于前胸并向背部放射，CTA 显示破口多位于主动脉瓣上 4cm 内；③肺炎 / 胸膜炎虽可出现胸痛和呼吸困难，但伴有发热等感染症状，听诊可闻及湿啰音或胸膜摩擦音；④冠心病急性发作时心电图可见 ST-T 动态改变，心肌酶谱升高，冠脉造影可明确诊断；⑤肺血管炎多伴有多系统受累表现和炎症指标升高，血管壁增厚但无明确分层；⑥原发性肺动脉肿瘤在影像学上表现为占位性病变而非血管壁分层。临床需结合病史、症状、影像学特征及实验室检查综合判断。

其他：

无

利伐沙班治疗右心房电极血栓失败后的处理策略：1 例报道

王博雯

甘肃省人民医院

患者基本信息：

患者女性，65 岁。

主述：

射频消融联合起搏器植入术后 6 年，起搏器升级术后 3 年，再发房扑 1 周

现病史：

患者 6 年前因“阵发性房颤、房扑合并高度房室传导阻滞”于我院行射频消融联合永久性双腔起搏器植入术（左束支起搏）。3 年前因“阵发性心悸伴晕厥”就诊于我院，行心电图检查提示：室性心动过速，行超声心动图检查提示：LVEF=33%，再次于我院将原双腔起搏器升级为心脏再同步治疗除颤器（左束支起搏联合右室除颤电极），术后恢复良好，病情稳定出院。此次入院 1 周前感胸闷、气短伴心悸，于我院门诊行心电图检查提示：心房扑动，拟行二次射频消融术，经食道超声心动图 (TEE) 检查，结果提示：右房电极异常回声（大小约 10*3.5mm）。入院后经胸超声心动图未见右房电极异常回声。追问病史，房扑复发时间不明，1 周前出现症状，且未服用抗凝药物。近期无发热，实验室检查未见炎症标志物升高。血培养亦未见细菌生长。结合临床症状及相关化验检查结果，考虑电极赘生物为血栓可能性大，遂给予利伐沙班 20mg QD 抗栓治疗。患者出院后 1 月复查 TEE 显示右房电极异常回声无变化，停用利伐沙班，改用华法林抗凝，INR 维持至 2.0-3.0，房扑自行转复。出院 3 月后复查时，TEE 显示原电极异常回声变长，增至 18*3.8mm，上调华法林剂量，INR 调至 2.5-3.0。院外定期我院门诊监测 INR。6 月时复查，TEE 显示原电极赘生物消失。

既往病史：

既往多次介入手术病史，患者 6 年前因“阵发性房颤、房扑合并高度房室传导阻滞”于我院行射频消融联合永久性双腔起搏器植入术（左束支起搏）。3 年前因“阵发性心悸伴晕厥”就诊于我院，行心电图检查提示：室性心动过速，行超声心动图检查提示：LVEF=33%，再次于我院将原双腔起搏器升级为心脏再同步治疗除颤器（Cardiac Resynchronization Therapy Defibrillator，CRT-D）（左束支起搏联合右室除颤电极）。

病程记录：

结合临床症状及相关化验检查结果，考虑电极赘生物为血栓可能性大，遂给予利伐沙班 20mg QD 抗栓治疗。患者出院后 1 月复查 TEE 显示右房电极异常回声无变化，停用利伐沙班，改用华法林抗凝，INR 维持至 2.0-3.0，房扑自行转复。出院 3 月后复查时，TEE 显示原电极异常回声变长，增至 18*3.8mm，上调华法林剂量，INR 调至 2.5-3.0。

检验检查记录：

我院门诊行心电图检查提示：心房扑动，拟行二次射频消融术，经食道三维超声心动图检查，结果提示: 右房电极异常回声（大小约 10*3.5mm）。为进一步诊治，收入我科。入院心电图：心房扑动，心室起搏心律（VVI）。入院经胸超声心动图未见右房电极异常回声。

患者出院后 1 月复查时 3D-TEE 显示右房电极异常回声无变化，停用利伐沙班，改用华法林抗凝，INR 维持至 2.0-3.0，房扑自行转复。出院 3 月后复查时，3D-TEE 显示原电极异常回声变长，增至 18*3.8mm，上调华法林剂量，INR 调至 2.5-3.0。院外定期我院门诊监测 INR。6 月时复查，3D-TEE 显示原电极赘生物消失。

鉴别诊断：

结合既往病历报道与本例患者临床资料，考虑该患者右房电极附着物为血栓的依据有：1、患者无发热等全身感染表现，炎症指标未见异常；2、TEE 检查时血栓常显现为中 - 低回声的不规则团块或呈条索状，通常活动性较差，且最大的特点是变化大，尤其是在抗凝治疗之后，会明显变小甚至消失。而感染性赘生物常呈团块状、息肉状或绒毛絮状中等强度回声，直接附着于瓣膜、室壁、室间隔残端、动脉壁上或有蒂相连，随血流于心腔内或大动脉内摆动，边缘多模糊，呈蓬草样或毛刺状改变，内部回声多不均匀。

其他：

无

Lunderquist guidewire technique Simplifies Extremely Tortuous Access in Transfemoral Transcatheter Aortic Valve Replacement

艾丽菲热·艾合买提

新疆维吾尔自治区人民医院

患者基本信息：

Computed tomography scan before TAVR shows extreme tortuosity of the right and left femoral arteries (Figure1A-Figure 1C). Considering the patient's age, symptom, and significant burden of comorbidities, the heart team members opted to proceed with transfemoral TAVR. The left femoral artery was punctured as the main approach, and the long guidewire was difficult to ascend and the vessel was tortuous（Figure 2A）. To address this, a super-smooth guidewire was utilized to facilitate placement of a 6F pigtail catheter, enabling the exchange to a Lunderquist guidewire positioned in the aortic sinus (Figure 2B- Figure 2D). After straightening the access vessel, the long guidewire was successfully exchanged, and two ProGlide suture devices were pre-embedded at the femoral artery puncture site for vascular closure (Figure 2E). The ultra-smooth guidewire is re-inserted and delivered to the aortic sinus, facilitating the delivery of a 5F pigtail catheter to assist in exchanging for the Lunderquist guidewire. The arterial sheath and catheter were carefully withdrawn, and the Edwards 14F arterial sheath was successfully introduced with slow and controlled advancement. Intraoperative coronary angiography showed 90-95% stenosis in the middle section of the Left anterior descending（LAD）, and one stent was placed in the LAD. Combined with the results of preoperative CT and balloon dilatation, the Edward 26 prosthetic valve was selected and fitted to the delivery system and sent to the left ventricle via a stiffened guidewire.Under the guidance of DSA and ultrasound-assisted localization, the valve was gradually deployed (Figure 2F). Initial DSA imaging revealed suboptimal valve frame expansion with mild paravalvular leakage. Subsequent post-dilation using the original balloon was performed. Follow-up aortic root angiography confirmed mild paravalvular leakage and unobstructed flow in the right and left coronary arteries.

主述：

Chest tightness and shortness of breath for more than 5 years

现病史：

Computed tomography scan before TAVR shows extreme tortuosity of the right and left femoral arteries (Figure1A-Figure 1C). Considering the patient's age, symptom, and significant burden of comorbidities, the heart team members opted to proceed with transfemoral TAVR. The left femoral artery was punctured as the main approach, and the long guidewire was difficult to ascend and the vessel was tortuous（Figure 2A）. To address this, a super-smooth guidewire was utilized to facilitate placement of a 6F pigtail catheter, enabling the exchange to a Lunderquist guidewire positioned in the aortic sinus (Figure 2B- Figure 2D). After straightening the access vessel, the long guidewire was successfully exchanged, and two ProGlide suture devices were pre-embedded at the femoral artery puncture site for vascular closure (Figure 2E). The ultra-smooth guidewire is re-inserted and delivered to the aortic sinus, facilitating the delivery of a 5F pigtail catheter to assist in exchanging for the Lunderquist guidewire. The arterial sheath and catheter were carefully withdrawn, and the Edwards 14F arterial sheath was successfully introduced with slow and controlled advancement. Intraoperative coronary angiography showed 90-95% stenosis in the middle section of the Left anterior descending（LAD）, and one stent was placed in the LAD. Combined with the results of preoperative CT and balloon dilatation, the Edward 26 prosthetic valve was selected and fitted to the delivery system and sent to the left ventricle via a stiffened guidewire.Under the guidance of DSA and ultrasound-assisted localization, the valve was gradually deployed (Figure 2F). Initial DSA imaging revealed suboptimal valve frame expansion with mild paravalvular leakage. Subsequent post-dilation using the original balloon was performed. Follow-up aortic root angiography confirmed mild paravalvular leakage and unobstructed flow in the right and left coronary arteries.

既往病史：

without

病程记录：

without

检验检查记录：

Intraoperative coronary angiography showed 90-95% stenosis in the middle section of the Left anterior descending（LAD）, and one stent was placed in the LAD.

鉴别诊断：

without

其他：

胸痛合并肌钙蛋白升高，都是心梗惹的祸？

张睿

北京清华长庚医院

患者基本信息：

女性

63 岁

主述：

胸痛 13 小时

现病史：

•13 小时前患者安静休息时无明显诱因突发恶心、呕吐胃内容物，伴心前区针扎样疼痛及灼烧感，范围约手掌大小，放射至后背部，持续不缓解，否认呼吸困难、大汗、濒死感

•8 小时前（2020-11-10 16:00）就诊我院急诊，测得血压 139/93mmHg，心电图示：窦性心律，胸前导联 R 波递增不良，心脏损伤标志物： TnT-hs 0.033->0.255 ng/mL

• 患者起病以来，精神、饮食、睡眠可，体重无明显变化，大小便如常

既往病史：

4 年前曾有心梗病史，药物治疗

高血压 40 年，最高血压 220/90mmHg，口服厄贝沙坦氢氯噻嗪 1#qd、硝苯地平控释片 30mgqd 控制血压，血压控制在 120-140/60-70mmHg

2 型糖尿病病史 12 年，口服二甲双胍 500mgtid、阿卡波糖 50mgtid、胰岛素皮下注射治疗，2 月前自行停用胰岛素皮下注射，血糖控制差

高脂血症 4 年，未规律口服他汀类药物调脂治疗

2 周前患者左侧膝关节摔伤，近期活动受限

子宫切除术后 10 年，乳腺结节切除术后

“庆大霉素”药物过敏史，否认其它药物及食物过敏史

否认吸烟饮酒史

已婚，育有 1 子，配偶及儿子体健

否认早发心血管疾病史及猝死家族史，否认家族性遗传病

病程记录：

查体：体温：36.6℃，脉搏：92 次 / 分钟，呼吸：17 次 / 分钟，左上肢血压：133/83mmHg，右上肢血压：126/83mmHg，SPO2 99%

神志清，精神可，体型肥胖，颈静脉无怒张，双肺未及干湿罗音，心率 92 次 / 分，律齐，各瓣膜听诊区未闻及病理性杂音，腹部可见陈旧性手术瘢痕，腹软，无压痛及反跳痛，肝脾肋下未触及，肝颈静脉回流征（-）。左侧膝关节活动受限，双下肢轻度可凹性水肿

补充病史：患者 4 年前无明显诱因出现恶心、呕吐，伴心前区针扎样疼痛，放射至后背部,程度可忍受,伴有喘憋、双下肢水肿,症状持续不缓解,就诊于安贞医院、急查心电图提示窦性心律、胸前导联 T 波倒置，心脏损伤标志物 cTnI 1.22ng/ml，随机血糖 21-22mmol/L，尿酮体 2+，诊断为“急性非 ST 段抬高型心肌梗死、糖尿病酮症酸中毒”，急诊冠状动脉造影提示“LCX 50% 狭窄”，超声心动图示左室各壁下 1/2 运动减低，给予药物治疗后患者症状迅速缓解，出院后 1 月复查超声心动图示左室壁活动未见异常。院外规律口服阿司匹林、氯比格雷（1 年后自行停用）、阿托伐他汀（自行停用）治疗。患者自述期间未再发作胸闷、胸痛等不适，运动耐量正常

药物治疗：心脏方面：阿司匹林 100mgqd、氯吡咯雷 75mgqd、瑞舒伐他汀 20mgqn、琥珀酸美托洛尔 23.75mgqd（11-14 日因心率偏慢停用）、厄贝沙坦 150mgqd；静脉补钾补镁治疗。降糖方面：三餐前阿卡波糖 50mgtid、重组人胰岛素 8 单位 tid、甘精胰岛素 20 单位 qn、卡格列净 100mgqd

检验检查记录：

急诊冠脉造影：LAD 开口 - 中段 30%~50% 弥漫性狭窄，LAD 远段可见长约 20mm 冠状动脉肌桥，收缩期缩窄 70%，LCX 中段不规则，远段 50% 局限性狭窄；RCA 近段及远段不规则病变

心电图：心率 50bpm，QTc=472ms

超声心动图：左房增大，左室心尖部球囊样膨出；二尖瓣少量反流；左室射血分数减低 (LVEF=46%)

心肌断层显像：静息心肌灌注显像未见明显异常，左心室收缩功能正常

鉴别诊断：

1. 胸痛待查

急性心肌梗死

急性心肌炎

肺栓塞

主动脉夹层

2.2 型糖尿病

糖尿病酮症

3. 高血压 3 级，很高危

4. 高脂血症

5. 睡眠呼吸暂停低通气综合征（中度）

6. 子宫切除术后

其他：

急性心梗导致二尖瓣乳头肌断裂合并心源性休克救治 1 例

张彬

六安市人民医院

患者基本信息：

患者，女，55 岁，农民。

主述：

反复胸闷半月，加重 1 天

现病史：

患者半月前开始出现胸闷，活动时加重，休息后稍缓解，未重视，1 周前至我院急诊查心电图及胸部 CT 未见特殊异常，予以对症处理后离院。1 天前出现胸闷加重再次至我院急诊，查心肌酶、D- 二聚体阴性，动脉血气：低氧血症，心电图：窦性心律，ST-T 改变，心超：左室壁阶段性运动异常（左室下壁及后壁基底段），左房室增大，左室收缩、舒张功能下降，二尖瓣前叶 A2 区腱索断裂：重度二尖瓣反流，轻度主动脉瓣反流，轻度三尖瓣反流，肺动脉高压。心内科及心外科会诊后拟“心脏瓣膜病、冠心病”收心脏外科病房。

既往病史：

既往体健，否认高血压、糖尿病、冠心病、高脂血症等病史，否认外伤、吸烟、饮酒史。

病程记录：

1. 心电监护、吸氧、多巴胺及硝酸甘油泵入改善心功能、头孢呋辛抗感染及对症处理

2.2-21 15：30 出现血氧饱和度逐渐下降至 80%，血压下降至 60/40mmHg，予以气管插管及去甲肾上腺素升压，血氧渐升至 93%，血压渐升至 95/60mmHg，转 ICU 进一步治疗。

3.2-22 予以大剂量去甲肾上腺素及多巴酚丁胺维持血压，联合硝酸甘油、新活素及间断利尿剂减轻心脏负荷，头孢哌酮舒巴坦抗感染

4.2-23 升级亚胺培南抗感染，仍需大剂量血管活性药物维持循环，院内 MDT 讨论外科手术或内科介入干预瓣膜及冠脉缺血。

5.2-24 行 TEER+CAG+LCX-PCI 术

6. 术后继续予以抗凝（那屈肝素钙注射液 4100IU，皮下注射 q12h）、双联抗血小板（铝镁匹林片（ II)114mg qd、替格瑞洛 90mg bid）、他汀（阿托伐他汀 20mg qd）调脂稳定斑块药物应用，呼吸循环支持，纠正内环境紊乱，抗感染（2-25 加用替考拉宁覆盖球菌，3-2 再次降级头孢哌酮舒巴坦钠抗感染，3-7 痰培养提示肺炎克雷伯杆菌、嗜麦芽窄食单胞菌，根据药敏实验，加用左氧氟沙星抗感染）及对症处理，3-8 转心内科普通病房，3-14 停抗生素，3-20 好转出院。

检验检查记录：

2025-2-15 血常规、CRP、肾功能、CK-MB、CK 均正常范围。胸部 CT：右肺上叶、左肺下叶实性结节。

2025-2-21 血常规: 白细胞 13.42*109/L，血红蛋白 145g/L，血小板 311*109/L; D- 二聚体 0.82ug/ml，肌钙蛋白 I2.31ng/ml，CK-MB15U/L，CK123IU/L，肌红蛋白 165.7ng/ml，BNP374.5pg/ml；动脉血气：PH7.397，氧分压 48.2mmHg，二氧化碳分压 40.1mmHg，碳酸氢根浓度 23.7mmol/L，乳酸盐 2.2mmol/l；肾功能、电解质、凝血功能基本正常；胸片：两肺渗出伴感染，请结合临床。心电图：窦性心律，ST-T 改变，心超：左室壁阶段性运动异常（左室下壁及后壁基底段），左房室增大，左室收缩、舒张功能下降，二尖瓣前叶 A2 区腱索断裂：重度二尖瓣反流，轻度主动脉瓣反流，轻度三尖瓣反流，肺动脉高压。

鉴别诊断：

- **1. 支气管哮喘**：多见于青少年，有过敏史，常在春秋季节发作。发作时双肺可闻及典型哮鸣音，咳出白色黏痰后呼吸困难常可缓解。而心衰导致的“心源性哮喘”多见于中年以上有器质性心脏病的患者，发作时必须坐起，重症者肺部有干、湿性啰音，甚至咳粉红色泡沫痰。测定血浆 BNP 水平对鉴别有较大参考价值，BNP 大于 100pg/mL 时，并且患者出现气促、呼吸困难或活动后胸闷等症状时，多考虑为心力衰竭。2. **慢性阻塞性肺疾病（COPD）**：有长期吸烟史、慢性咳嗽和呼吸困难病史，常伴有喘息、呼吸音减弱，肺功能检查显示阻塞性通气功能障碍，胸部 X 线片或 CT 可显示肺气肿等改变。心衰患者主要表现为胸闷、气短、咳嗽、咳痰等症状，还会伴随端坐呼吸、肝肿大、下肢水肿等症状、体征。

3. 心包积液、缩窄性心包炎：心包积液患者可出现奇脉，无杂音，心浊音会随着体位发生改变；缩窄性心包炎患者也会出现奇脉，无杂音，且心界略大。而右心衰竭容易出现心脏杂音或肺气肿的情况。可通过超声心动图、心脏磁共振以及患者病史等方面进行鉴别。**肺栓塞**：多在活动时出现憋气、胸闷、呼吸困难、胸痛等症状，听诊时肺部一般没有啰音。而左心衰患者一般在饮水过多或劳累的情况下，容易出现呼吸困难、喘息等症状，还会咳出粉红色泡沫痰，肺部能听到湿啰音。D- 二聚体升高、肺血管增强 CT 示血管栓塞等有助于肺栓塞的诊断。

其他：

顽固性高胆固醇血症一例

来晏

上海市同济医院

患者基本信息：

患者女性，首诊 2023 年，44 岁

主述：

头晕 2 年余，加重 2 月

现病史：

2 年前出现反复头晕，外院颈部 CTA 提示双侧颈动脉狭窄，头颅 MRA 未见明显异常。于我院神经外科住院治疗。平时有活动后胸闷不适，无明显胸痛。

既往病史：

既往高血压史 5 年，血压最高达 180mmHG, 口服硝苯地平控制片降压治疗，血压未规律监测

既往发现高脂血症 2 年，目前间断口服瑞舒伐他汀 10mg

病程记录：

冠状动脉左主干钙化斑块形成伴管腔轻度狭窄；左冠状动脉前降支近段钙化斑块及混合斑块形成，伴管腔重度狭窄；回旋支管壁多发软斑块形成，伴管腔中度狭窄；右冠状动脉管壁多发钙化及软斑块形成，管腔重度狭窄

检验检查记录：

u 查体：营养状态良好，手肘部可见明显黄色素瘤

uTC：17.53mmol/L ；LDL 11.7 mmol/L；HDL 2.35mmol/L；LP（a）923.5mgLL； TG 2.6mmol/L

u 心肌损伤标志物：阴性

u 肝肾功能、电解质、血常规、凝血功能均正常

u 心电图：未见异常

u 心超：左房增大，二尖瓣后叶钙化，升主动脉斑块形成，主动脉瓣及瓣环钙化，左室舒张功能中度减退，左室各节段收缩活动未见异常， EF 65%

鉴别诊断：

患者造影提示双侧颈内动脉重度狭窄伴病变不稳定，分别在 2024 年 9 月、12 月行双侧颈内动脉支架植入术

其他：

u 给予他汀 + 依折麦布 +PCSK9 抑制剂（依洛尤单抗 140mg q2w）强化降脂治疗

u 给予阿司匹林 + 替格瑞洛抗栓治疗

u 缬沙坦氨氯地平降压

u 比索洛尔控制心室率

患者诊断为家族性高胆固醇血症，但在药物治疗中，使用他汀 + 依折麦布无效，PCSK9 无效，小分子 RNA 药物一度有效，但后期仍未能明显降低低密度脂蛋白胆固醇。

u 患者 2 年前发现血脂明显升高，曾服用他汀治疗，但因服用他汀后复查 LDL 无明显下降，甚至有时有升高趋势，因此未规律服用

u 使用他汀 + 依折麦布 +PCSK9 方案 1 月后复查 LDL 12.6mmol/l

u 不降反升？

u 结合患者既往服用他汀 LDL 有升高趋势，停用他汀，继续使用 PCSK9+ 依折麦布，1 月后复查 LDL 11.0mmol/L，后多次复查 LDL 在 10-11mmol/L

GDMT 下一例心衰患者的治疗历程

杨爽

重庆医科大学附属永川医院

患者基本信息：

76 岁，男性

主述：

反复气促 3- 年，加重 4 月

现病史：

3- 年前患者活动时感气促，休息后缓解，我院门诊行心脏彩超：左房、左室增大，EF 减低；冠脉 CTA 未见明显异常，到当地医院治疗，期间多次因气促加重当地住院治疗，出院后平时长期服用药物治疗（呋塞米、螺内酯、美托洛尔片）。4 月前受凉后静息时感气促，伴夜间阵发性呼吸困难，在我院住院治疗，治疗效果不佳，建议患者行 CRT-D 治疗，患者表示拒绝，症状稍缓解后出院。院外规律服用呋塞米、螺内酯、美托洛尔缓释片、沙库巴曲缬沙坦、达格列净、地高辛。患者仍稍活动后感气促，为进一步诊治入院治疗。

既往病史：

否认高血压、糖尿病病史，否认甲亢、贫血、肾脏疾病病史。已戒烟、戒酒 4 年，子女健，无家族性心脏病病史。

病程记录：

呋塞米 20mg qd

螺内酯 20mg qd

比索洛尔 1.25mg qd

沙库巴曲缬沙坦 25mg bid

达格列净 10mg qd

检验检查记录：

心脏彩超：EF 32%

LVD 82mm

LAD 52mm

二尖瓣中度反流

鉴别诊断：

缺血性心肌病

其他：

经左侧肱动脉行主动脉内球囊反搏辅助下经右侧肱桡动脉联合入路逆向开通冠脉慢性完全闭塞一例

徐承义

武汉亚洲心脏病医院

患者基本信息：

患者男，74 岁，工人，身高 168cm，体重 69Kg。因“胸闷 4 年，加重 1 月”于 2025 年 2 月 14 日入院。

主述：

胸闷 4 年，加重 1 月

现病史：

患者于 4 年前发作胸闷，位于中段胸骨后，与劳力相关，性质不清，多持续数分钟可缓解，未诊治。2 年前某日重体力劳动时发作严重胸痛，，位于心前区，压榨性，持续约 3 小时逐步减轻，伴心悸、出汗，亦为诊治。1 月前反复发作胸闷，位于胸骨后，绞痛，轻微活动亦可诱发。1 月 21 日于当地医院住院治疗，期间冠状动脉造影结果显示，左主干末端狭窄 80%，前降支 (1eft anteriorde scending，LAD) 中段狭窄 70%，左回旋支 (1eft circumflex artery，LCX) 开口次全闭塞，右冠状动脉 (right coronary artery，RCA) 近段次全闭塞，中段完全闭塞。拟在在主动脉内球囊反搏（intra-aortic balloon pump，IABP）下行经皮冠状动脉介入治疗 (percutaneous coronary intervention,PCI) 开通 RCA 慢性完全闭塞病变（coronary chronic total occulusion，CTO），术中下肢动脉造影结果显示，右侧股动脉闭塞，左侧髂总动脉开口闭塞。尝试正向开通 RCA CTO 失败，RCA 远段血肿形成。现为进一步治疗来我院。

既往病史：

既往有高血压病史，口服沙库巴曲缬沙坦 100mg QD 治疗；脑梗死病史。

病程记录：

入院后完善大血管 CT 造影，结果显示左侧髂总、左侧髂内、双侧髂外弥漫性闭塞，右侧髂内动脉重度狭窄至闭塞，腹壁侧枝动脉开放；右侧髂总动脉多发溃疡，见图 2C。该患者左主干病变合并三支血管病变，Syntax 评分 31 分，且 RCA 中段 CTO 病变首次介入治疗失败，左心室射血分数 32%，治疗上血运重建方案首选冠状动脉旁路移植术（coronary artery bypass grafting,CABG），次选 PCI 方案。患者拒绝 CABG，选择 PCI 治疗。该基础心功能差，左心室射血分数 32%，冠状动脉无保护左主干病变合并 CTO 病变，PCI 治疗风险高，术中需机械循环辅助，结合患者外周血管特点，选择经左侧肱动脉穿刺植入 IABP 球囊导管（transbrachial artery insertion of IABP，TBA-IABP），并在 IABP 辅助下分期介入治疗，一期处理 RCA CTO 病变，择期处理左冠状动脉。RCA CTO 首次介入治疗失败，并远段血肿形成，再次介入正向开通 CTO 病变可能性小，需使用逆向导丝技术，拟经右侧桡动脉路径使用 6 Fr 指引导管经左冠状动脉行对侧造影或使用逆向导丝技术开通 RCA CTO，经右侧肱动脉路径使用 7Fr 指引导管前向尝试开通 RCA CTO 病变。2025 年 2 月 17 日行介入治疗，术中首先经左侧肱动脉路径行 TBA-IABP，见图 4。穿刺右侧桡动脉及肱动脉，分别置入 6 Fr 及 7 Fr 血管鞘，先后经 6 Fr 及 7 Fr 送 EBU 4.0 及 AL 1.0 指引导管至左主干开口和 RCA 开口。术中尝试开通 RCA CTO 病变失败，随即采取逆向导丝技术开通 RCA，并在血管内超声（intravascular ultrasound,IVUS）指导下植入 4 枚药物洗脱支架 [2.5 mm×23 mm、3.0 mm×33 mm、3.5 mm×33 mm、3.5 mm×29 mm，Firebird，上海微创医疗器械 (集团) 有限公司]，见图 6。择期处理前降支和回旋支，术中在 IVUS 指导下于 LAD 中段至 LM 开口植入 2 枚药物洗脱支架 [3.0 mm×29 mm、3.5 mm×29 mm，Firebird，上海微创医疗器械 (集团) 有限公司]，LCX 开口病变行球囊扩张成形术。

患者术后恢复良好，无路径血管并发症，无胸闷、胸痛等缺血性胸痛症状。术后 3 个月随访，无胸痛等缺血症状以及呼吸困难等心力衰竭症状。复查超声心动图示，结果显示，左心室扩大 (舒张末期内径 5.4 cm)；左室节段性室壁运动异常；左心室射血分数 41%。

检验检查记录：

急诊室检查资料显示，N 末端 B 型脑钠肽前体 6650.6pg/ml (正常值 0~125 pg/ml)；高敏肌钙蛋白 I 0.211 ng/ml(正常值 0~0.01 ng/m1)。全血细胞计数、肝功能、肾功能均正常。超声心动图示：左房扩大；左心室扩大（舒张末期内径 6.1 cm）；左室节段性室壁运动异常；二尖瓣轻度关闭不全；左心室射血分数 32%。

住院期间大血管 CT 造影，结果显示左侧髂总、左侧髂内、双侧髂外弥漫性闭塞，右侧髂内动脉重度狭窄至闭塞，腹壁侧枝动脉开放；右侧髂总动脉多发溃疡

鉴别诊断：

无特殊。

其他：

无特殊。

运动诱发心跳骤停合并冠状动脉起源异常 1 例

贺行巍

同济医院

患者基本信息：

患儿，女，14 岁

主述：

突发心跳骤停 1 小时余

现病史：

患儿于课间跑步时突发晕厥、抽搐，继而意识丧失。现场心电图示室颤，紧急行电除颤及 CPR，恢复自主心跳后转入本院急诊。既往无明显基础疾病史，体格健康。

既往病史：

无糖尿病、高血压等慢性病史，无传染病及外伤手术史。曾因“头晕”就诊，外院心超提示二尖瓣、三尖瓣轻度关闭不全。

病程记录：

入院体征：T 36.5℃，P 130 次 / 分，R 20 次 / 分，BP 76/45 mmHg（去甲肾上腺素维持），SpO_2 97%。急查心电图提示室颤，高敏心肌肌钙蛋白 I 明显升高（>50000 pg/mL）

初步诊断：呼吸心跳骤停，冠状动脉起源异常，急性非 ST 段抬高型心肌梗死（NSTEMI）

治疗：初期采用呼吸机辅助通气、IABP 辅助循环、抗感染等对症支持治疗。完善检查明确诊断后，**行开胸冠状动脉血管成形术**：术中探查发现左冠及右冠均开口于右冠状窦，左冠经壁冠状动脉移行至左冠窦；经切开并重塑壁冠状动脉，改善左冠起源及通道；手术顺利，术后复查通畅，未再发心律失常或低灌注表现。

检验检查记录：

冠状动脉 CTA：左冠状动脉（LM）异常起源于右冠状窦，走形经主动脉与肺动脉之间，LM 局部中度狭窄，LAD 中段心肌桥。**冠脉造影 +IVUS**：左冠开口异位，LM 体部狭窄约 70%，IVUS 显示 LM 受压，MLA 约为 4.75 mm^2。**心脏 MRI**：左心室弥漫性水肿，心外膜下强化灶，提示心肌缺血 / 损伤。

鉴别诊断：

1. 心肌炎；2. 急性心肌梗死（川崎病冠脉受累）3. 恶性心律失常

其他：

AMI 左主干分叉病变合并心源性休 PCI 一例

李辉

双鸭山双矿医院

患者基本信息：

女性，68 岁 间断胸痛、胸闷 3 天，加重伴大汗 6 小时

患者于入院前 3 天出现胸骨后闷痛，伴有周身轻微出汗，可放射至后背部，含

硝酸甘油后缓解，3 天来症状逐渐加重。入院当日上午 7 时再发胸痛，含药后约 20 分钟缓解。下午 13 时胸痛再次加重伴大汗，恶心，未呕吐，持续 1 小时不能缓解，14 时到当地医院就诊，诊断急性心肌梗死合并低血压，并给予行急诊冠脉造影示左主干 + 三支病变，给予去甲肾上腺素及多巴胺升压后建议转往上级医院进一步治疗。16:23 病人到达我院。胸闷、胸痛，恶心，呕吐，呕吐物为胃内容物，无咖啡色胃液呕出，

危险因素：糖尿病病史 5 年，二甲双胍缓释，空腹 7mmol/L 左右，高血压病史 7 年余，最高 160/90mmHg, 硝苯地平缓释片每日 1 片，血压 140-150/70-80mmHg 左右。

查体：周身冷汗淋漓，面色苍白，脉搏：108 次 / 分 呼吸：22 次 / 分 血压：80/50mmHg(多巴胺 15ug/kg.min、去甲肾上腺素 20ug/min) 双肺闻及散在湿罗音，心率 110 次 / 分，节律不齐，可闻及早搏，

双下肢不肿。

主述：

间断胸痛、胸闷 3 天，加重伴大汗 6 小时

现病史：

患者缘于入院前 3 天开始间断出现胸痛，胸闷，位于胸骨后中段，活动量增多及静息均可发作，每次持续 10 分钟左右可自行好转，可放射至后胸背部，周身轻微出汗，近 3 天每日可发作 1-2 次，持续时间逐渐延长，最长达 20 分钟，今日上午 7 时许疼痛再发时曾口服丹参滴丸 3 丸，未到医院就诊。6 小时前 (2024.06.19.13 时许) 突发胸痛伴大汗，伴有胸闷、气短，恶心，未呕吐，持续 1 小时余不能缓解，于 15 时许到宝清县人民医院就诊，考虑急性心梗，抗聚及抗凝治疗，给予留置尿管，并给予行急诊冠脉遣影示左主干 + 三支病变，伴有心源性休克状态，建议转往上级医院行 PCI 治疗，在当地医院住院期间及转运途中给予多巴胺及去甲肾上腺素维持血压。家属陪同下急转至我院。18:23 病人入我院时周身湿冷大汗，面色苍白，恶心，呕吐，呕吐物为胃内容物，无咖啡色胃液呕出，18:25 测量血压 60/40mmHg, 立即将多巴胺调至 30ug/kg.min 泵入，去甲肾上腺素调至 0.4ug/kg.min 泵入，18:29 行心电图示窦性心律，AVR 导联 ST 段抬高 .2mv,V2-V6 导联 ST 段压低 0.2-0.5mv 不等，室早，考虑急性心梗合并心源性休克，血管未通死亡率高达 80%, 充分与家属沟通建议立即行急诊 IABP 支持下冠脉介入治疗，进一步开通血管，并充分交代手术目的及疾病风险，完善术前准备。拟急诊局麻下行冠脉介入治疗。患者本次发病以来无发热，咳嗽，咳白痰，无腹痛，无肢体功能障碍，平素饮食及睡眠可，二便自主。

既往病史：

一般健康状况：一般状况一般

手术史：有手术史；双眼青光眼术后 10 余年。

输血史：无输血史

传染病史：2022.12 有 “新型冠状病毒” 传染病史，自愈。

外伤史：无外伤史

预防接种史；不详

食物或药物过敏史：无药物过敏史；无食物过敏史

疾病史：既往糖尿病病史 5 年，二甲双胍缓释片 1 片日一次口服，空腹多 7mmol/L 左右，餐后不监测。高血压病史 7 年余，最高 160/90mnHlg, 硝苯地平缓释片每日 1 片口服，血压多 140-150/70-80mmHg 左右。

病程记录：

诊疗计划：1.CCU 入院护理常规，重症监护。

2. 病重，绝对卧床。

3. 吸氧，心电，血氧饱和度，血压监测。

4. 强化抗血小板聚集 (阿司匹林 100mg 日一次口服，替格瑞洛 90mg 日二次口服), 抗动脉硬化 (阿托伐他汀钙 20mg 日一次口服), 抗凝 (低分子量肝素钙 4100 单位日 2 次皮注), 抗休克，升压，强心 (多巴胺 30ug/kg.min 泵入，去甲肾上腺素 4ug/kg.min 泵入中)。

5. 完善床旁心脏超声，血常规，血生化，心肌酶，BNP 等化验。

6. 急诊行冠脉介入治疗。

7. 动态观察心电图及心肌损伤标志物变化。

8. 充分与患者及家属沟通病情。

检验检查记录：

. 查体：入院时 18:25BP60/40mmHg(多巴胺 18ug/kg.min 泵入，去甲肾上腺素 0.4ug/kg.min 泵入中),18:30 复测血压 80/50mmHg(多巴胺 30ug/kg.min 泵入，去甲肾上腺素 0.4ug/kg.min 泵入中), 神志淡漠，呼吸急促，双肺闻及散在湿罗音，未闻及哮鸣音，心界叩诊无扩大，心率 98 次 / 分，节律不齐，可闻及早搏，26 次 / 分，心音正常，无杂音。腹部平坦，无腹部压痛，双下肢无浮肿。

3. 辅助检查: 2024.06.19.18:29ECG: 窦性心律，AVR 导联 ST 段抬高 0.2mv,V2-V6 导联 ST 段压低 0.2-0.5mv 不等，室早。床旁超声: EF47%, 左室壁节段性运动异常，左室收缩、舒张功能减低，主动脉瓣退行性改变伴少重返流，二尖瓣大量这流。TNI ^{0} .18ng/,I^{1}4.Z/ ，mDD.TlB,proBNP1444.71pg/ml。

鉴别诊断：

鉴别诊断：1. 主动脉夹层：多有高血压史，疼痛呈突发剧烈撕裂样痛，双上肢III压及脉博可有左刑，心屯无明显特征性改变，主动脉增强 CT 可助诊，该病人可排除之。

2. 急性肺动脉栓塞：肺动脉大块栓塞常可引起胸痛，气短和休克，但有右心负荷急剧增加的表现。如右心室急剧增大、肺动脉瓣区搏动增强和该处第二心音亢进、三尖瓣区出现收缩期杂音等。发热和白细胞增高出现也较早。心电图示心电轴右偏，I 导联出现 S 波或原有的 S 波加深，II1 导联出现 Q 波和 T 波倒置，AVR 导联出现高 R 波，胸导联过渡区向左移，右胸导联 T 波倒置等，与心肌梗死的变化不同，可资鉴别。

其他：

心脏激动顺序异常与心衰 一例完全性左束支传导阻滞性心肌病患者的诊治体会

高峰

清华大学附属北京清华长庚医院

患者基本信息：

马某，男 /62 岁，工人（电焊工）

入院时间：2021 年 9 月 22 日

主述：

劳力性胸闷 2 周

现病史：

2 周前开始，常于轻度体力活动后出现胸闷，休息约 10 分钟可缓解，不伴胸痛、出汗、咳嗽、咳痰、咯血，不伴尿少、浮肿、夜间阵发性呼吸困难。

既往病史：

既往史：

发现心电图异常 18 年（2003 年开始）

近 10 年来工厂每年体检心电图异常

高血压病史 10 年，最高达 160/100mmhg，未规律服药

个人史：无吸烟饮酒史

病程记录：

入院后明确诊断为心功能不全，患者表现为心脏扩大、射血分数下降，给予心衰规范化药物治疗，同时给予双腔永久起搏器植入术，患者心衰好转出院，出院后随访，患者射血分数明显提升

检验检查记录：

重要检查包括心电图、动态心电图、多次心脏彩超、冠脉造影等

鉴别诊断：

心功能不全

缺血性心肌病?

扩张型心肌病?

左束支阻滞性心肌病?

高血压性心脏病失代偿期?

.....

高血压病

其他：

这是一例完全性左束支传导阻滞性心肌病患者，患者行双腔永久起搏器植入术 (左束支起搏)，获得射血分数明显提升

双侧冠状动脉瘤样扩张合并冠状动脉 - 肺动脉瘘、房间隔膨胀瘤 1 例

文丹

遵义医科大学

患者基本信息：

50 岁，男患

主述：

突发胸闷、胸痛 1 天

现病史：

患者于家中，突发胸闷、胸痛 1 天，休息后不能缓解，无四肢乏力，无咳嗽咳痰，无外伤。

既往病史：

发现高血压 10 年，最高血压 180/85mmHg，规律治疗。既往史：高血压 10 年，最高血压 180/85mmHg，规律治疗。8 年前突发右上肢无力，外院诊断脑出血，

具体情况不详。

病程记录：

急诊入院，进入胸痛中心，行心电图、实验室检查、冠脉造影等相关检查，未发现急性心肌梗死依据。对患者行对症治疗后好转，完善其他影像学检查，胸部 CT 平扫。冠状动脉 CTA 及超声检查，患者无手术意愿，遂签字出院。

检验检查记录：

心电图提示完全性右束支阻滞。

检验提示心肌酶（-），D 二聚体（-），超敏肌钙蛋白（-）。

胸部 CT 平扫提示前纵隔占位性病变。

冠状动脉 CTA 提示左右冠状动脉弥漫扩张，多发动脉瘤形成，左侧冠状动脉最宽处约 33mm，右侧冠状动脉最宽出约 18mm；冠状动脉 - 肺动脉瘘，肺动脉起始部左侧壁与扩张左冠状动脉交通。房间隔膨出瘤。

心脏超声提示先天性心脏病: 左、右冠状动脉瘤; 左冠状动脉 - 肺动脉瘘; 左心增大; 主动脉窦部及升主动脉增宽；三尖瓣及主动脉瓣轻度反流；心包腔微少量积液。

冠状动脉造影提示左冠状动脉主干见巨大冠状动脉瘤，大小约 18x25mm；左前降支近中远段全程瘤样扩张，TIMI 血流 3 级；左旋支近远段全程瘤样扩张，TIMI 血流 3 级；右冠状动脉开口见巨大冠状动脉瘤，大小约 18x27mm，近中远段全程瘤样扩张，TIMI 血流 3 级。

鉴别诊断：

急性心肌梗死，患者急性起病，症状符合，既往史高血压 10 年、脑出血病史。但心电图、实验室检查及冠脉造影不支持。

其他：

本例最终诊断为：①冠状动脉瘤样扩张并左侧巨大冠状动脉瘤，依据左侧冠状动脉扩张最宽处 33mm，> 20mm，定义为巨大冠状动脉瘤。Markis 分型为 I 型，即双支或三支冠状动脉弥漫性扩张。②冠状动脉瘘，即冠状动脉与心腔或其他血管（冠状静脉、肺动脉）之间存在异常通道，是一种少见的畸形，发病率 1.3%，本例患者开口位置位于肺动脉，即为 Sakarupare III型。③房间隔膨胀瘤，是少见的先天性房间隔发育异常性疾病，由于先天性房间隔发育薄弱，在心脏负荷因素的作用下向低压侧膨隆而形成气球样的瘤样膨出，故称房间隔膨出瘤或房间隔瘤样膨出。见图 1

冠状动脉瘤样扩张、冠状动脉瘘、房间隔膨胀瘤均是少见的心血管疾病，同时出现在一个患者中，较为罕见。从病理基础上，冠状动脉瘤样扩张患者可以分为三组，动脉粥样硬化组、炎症组以及非炎症组，患者无心肌缺血及炎症浸润的临床证据，影像学血管无斑块形成，基于所获得临床资料可排除动脉粥样硬化组、炎症组，考虑非炎症组。非炎症组包括介入操作相关、感染、毒物中毒、先天性均可造成冠状动脉异常扩张，结合患者合并冠状动脉肺动脉瘘及房间隔膨胀瘤，考虑先天性因素所致可能性大。

一例大动脉转位单心室姑息治疗 20 年患者长期生存随访

刘栩含

四川大学华西医院

患者基本信息：

女，20 岁，自由职业，汉族

主述：

气促 2+ 年，加重 7 月

现病史：

患者入院前 2+ 年，无诱因出现气促，伴全身乏力，活动耐力下降，剧烈运动后症状加重，蹲下或休息后缓解。7 月前上述症状加重，伴咳嗽、颜面水肿，无双下肢水肿，于当地医院对症治疗后无好转。遂就诊于我院。

既往病史：

6 月龄时发现先天性心脏病。否认传染病及过敏史，无手术及过敏史，无外伤史，无吸烟、饮酒、吸毒史。

病程记录：

2024/3/2-2024/10/19: 他达拉非 + 曲前列尼尔 20ng/kg.min

2024/10/19- 至今：马昔腾坦 10mg qd+ 他达拉非 20mg qd

其他药物：倍他乐克 23.75mg qd，螺内酯 20mg qd，呋塞米 20mg qd，安达唐 10mg qd

检验检查记录：

凝血常规、甲功、肝功能、肾功、血脂、血糖、肿瘤标志物、乙肝、丙肝、梅毒、HIV 为阴性

nt-bnp 595-173

（心电、心彩超、ct、磁共振影像 / 右心导管报告在附件里）

鉴别诊断：

1. 血栓形成

肺栓塞：血栓脱落导致肺栓塞，表现为突发呼吸困难、胸痛、咯血、低氧血症。除上述表现外，是导致肺血管阻力急性升高和 Fontan 循环急性失代偿的重要原因。

脑卒中 / 外周动脉栓塞： 新发神经功能缺损或肢体疼痛 / 缺血症状。

需与与循环衰竭鉴别， 血栓栓塞常导致急性或亚急性症状恶化。

2. 特发性肺动脉高压：结合影像学明确先心病诊断。若 TPG 显著升高（>10-12 mmHg），需警惕继发性肺血管病变（如血栓栓塞、肺血管重塑），而非 IPAH。

其他：

全球首例 VenusP 瓣膜开窗治疗复杂肺动脉病变

王皓辰

广东省人民医院

患者基本信息：

19 岁女性，大学生，广东惠州人。

主述：

法洛四联症术后 10 余年，体力下降 1 年

现病史：

患者 19 年前（10 月龄）接受了法洛四联症外科根治术，10 年前因为肺动脉瓣重度返流，行外科肺动脉瓣置换术。近一年患者再次出现体力下降，只能爬 2 层楼，2024-9-19 经胸超声提示肺动脉瓣生物瓣中 - 重度狭窄并中度返流。

既往病史：

先心病手术史：2006 年（10 月龄）行 “法洛四联症” 矫治术。2010-10 发现左肺动脉狭窄，先后两次行肺动脉球囊扩张成形术。2015 年发现肺动脉瓣重度返流，行肺动脉生物瓣膜置换术（23mm 肺动脉生物瓣膜）。2017 年发现左肺动脉再狭窄，行左肺动脉支架植入术（9mm*25mm 金属裸支架）。否认高血压病史；否认脑梗塞史；否认慢性肺气肿病史；否认风湿性心脏病史；否认冠心病史；否认心梗病史；否认肝炎病史；否认结核病史；否认其他传染病史；否认输血史；否认外伤史；否认中毒史；无过敏史。

病程记录：

入院查体：

T:36.3℃，P:80 bpm，R:20 次 / 分，BP：112/66mmHg, 体重：52kg，身高：159cm，BMI 20.56kg/m2。神志清晰，无特殊面容，口唇无紫绀，颈静脉无怒张。双肺呼吸音清，未闻及干湿性啰音。胸壁可见纵行手术瘢痕，无心前区隆起，相对浊音界无扩大，心率：80 次 / 分，心律齐，肺动脉瓣听诊区收缩期喷射性杂音、舒张期递减型杂音。无双下肢浮肿，周围血管征阴性。

诊断：

法洛四联症术后、肺动脉瓣膜置换术后、肺动脉瓣生物瓣衰败、肺动脉瓣狭窄、肺动脉瓣关闭不全；左肺动脉支架植入术后；右心功能不全。

下一步诊疗计划：

该患者因法洛四联症术后、肺动脉瓣生物瓣衰败（中 - 重度狭窄合并中度反流）伴活动耐力下降、右心功能下降，符合手术指征。根据 2020 年 ESC 成人先心病指南推荐，在解剖合适的情况下，首选 TPVI，并且患者多次开胸手术，再次开胸风险极高，因而 TPVI 成为了唯一可选手术方式。由于患者多次手术，且左肺动脉支架脱出，根据三维重建模型，制定以下手术策略：1、将左肺动脉支架重新扩张，改善左肺动脉血供；2、将准备植入的肺动脉瓣架开侧孔，保证左肺动脉血流通畅；3、将肺动脉瓣架在右肺动脉释放；4、使用后扩球囊充分塑形瓣架。

手术过程：

右心导管检查 + 肺动脉造影术：经右股静脉血管鞘送入 6F PIG 导管，测右肺动脉压力 31/7/14 mmHg，主肺动脉压力 31/10/16 mmHg，右心房压力 14/1/4 mmHg，右心室压力 53/-6/13 mmHg。行肺动脉造影示：肺动脉瓣置换术后改变，肺动脉瓣大量返流（图 6-1），左肺动脉支架置入术后改变，左肺动脉狭窄。于左肺动脉支架内以 12.0mm*40mm 球囊扩张，复查肺动脉造影示左肺动脉支架植入部分内径较前明显增宽。以电烧灼器于人工肺动脉瓣膜支架覆膜部分上部多处开窗。经加硬导丝送 P24-25 人工肺动脉瓣膜至肺动脉瓣位置释放。复查肺动脉造影示：人工肺动脉瓣膜释放定位良好，瓣膜支架腰部（原肺动脉瓣水平）稍见狭窄。以 23mm 非顺应性球囊扩张人工肺动脉瓣膜，再次复查肺动脉造影示：肺动脉瓣返流消失，瓣叶活动良好，未见瓣周漏，瓣架固定良好。冠状动脉造影示左冠状动脉血流通畅，人工瓣膜未对左冠状动脉形成挤压。手术顺利。

术后药物治疗：

1. 术后立即启用低分子量肝素桥接华法林治疗（目标 INR 2.0 ~ 3.0）。

2. 使用呋塞米利尿，保证每日出量在 2000mL 以上，平衡量 -500mL 以上。

3. 预防性使用广谱抗生素，加强护理。

预后：

目前患者术后半年规律随诊，肺动脉瓣膜功能正常，心功能恢复至 I 级。

检验检查记录：

Hb 113g/L，PLT 305*10^9/L，WBC 5.72*10^9/L，NT-ProBNP 58 pg/mL，肌钙蛋白 T 3.1pg/mL，肝肾功能未见异常。

心电图：完全性右束支传导阻滞，ST-T 改变。

超声心动图：室间隔修补处完整，未见分流。右心扩大，流出道疏通良好，右室流出道流速 0.6m/s。肺动脉瓣生物瓣置换术后，瓣叶活动显示不清，前向血流明显加速，关闭可见瓣内返流。主肺动脉血流通畅，右肺动脉增宽，内径约 19mm，主肺动脉及左肺动脉近段可探及支架反射，肺动脉端开口内径：7.6mm，左肺动脉支架远端显示不清。肺动脉瓣返流，彩束面积 7.4cm2。

肺动脉 CTA：法洛四联症术后，心室及右房扩大，主肺动脉及右肺动脉粗大，左肺动脉支架植入术后改变。

运动心肺测试：运动耐量严重下降，运动心肺等级 C 级。

鉴别诊断：

1. 感染性心内膜炎：

支持证据：患者既往植入心脏生物瓣膜，存在易感因素。

排除证据：无发热、超声心动图未见赘生物。

2. 肺栓塞：

支持证据：右心负荷增加。

排除证据：无典型症状（胸痛、呼吸困难、低氧）。

其他：

右室流出道 - 肺动脉功能障碍常表现为肺动脉返流及肺动脉狭窄，获得性病变中，常见于右室流出道重建术后的患者，在我国常见于法洛四联症手术后。因为我国旧的术式常采用跨肺动脉瓣补片扩大修补右室流出道 - 肺动脉，其患者大部分在往后十余年逐渐发展为重度肺动脉瓣返流，进而造成右心室功能不全，最终导致右心衰竭。

对于右室流出道重建术后并发中重度或重度 RVOTD 的患者，TPVI 可以改善患者 RVOTD 相关的症状，逆转患者右心室重构，改善患者心功能。对于需要行肺动脉瓣置换且解剖合适的患者，优先选择 TPVI，对于解剖不合适的患者，应考虑外科肺动脉瓣置换。对于带瓣血管通道患者，更多地选择球囊扩张肺动脉瓣；对于自体流出道患者，更多地选择自膨胀肺动脉瓣。TPVI 适合于合并有 RVOT 狭窄的先心病外科矫治术后并发的中重度或重度 PR，伴或不伴有 RVOT 梗阻，解剖学适合，有 RVOTD 相关临床症状患者。当患者无相关临床症状但符合以下条件：解剖学适合，且伴有右心室扩大、三尖瓣反流、合并严重 ROVT 梗阻、严重或进行性右心室功能下降或猝死高危因素等 1 种以上的情况时，同样推荐。

对于适合进行 TPVI 的患者，肺动脉 CT 和心脏 MR 是不可缺少的影像学检查，可以通过对肺动脉的三维重建，精确评估其形态及大小，制定详细的手术策略。相较于外科手术，TPVI 可以减少患者一生中的开胸次数，延迟下一次开胸，减少手术时间，降低手术风险及创伤。对于既往多次开胸，再次开胸高风险的患者，TPVI 是其唯一的选择。

以先天性白内障、肥厚型心肌病及高乳酸血症为主要表现的 Sengers 综合征一例

林曼欣

厦门大学附属心血管病医院

患者基本信息：

患者男童，12 岁（出生日期 2010-11-29），2023-05-19 首次入院。

主述：

上腹痛伴气促 5 日

现病史：

患者 5 日前无诱因出现持续性上腹痛（疼痛性质描述不清），位于剑突下及脐上区域，程度较剧烈，发作时伴气促，腹胀、纳差，否认头晕、头痛、黑矇、意识丧失及肢体活动障碍，否认胸闷，胸痛及肩背放射痛，否认咳嗽、咳痰、咯血，否认恶心、呕吐、腹泻、黑便等表现，因上述症状不缓解就诊当地医院，完善心脏彩超提示：左右室壁增厚，轻中度三尖瓣反流，中度肺动脉高压（LVD:64mm，LVEF20％），心电图提示：窦性心律，左室高电压，多导联 T 波改变，NT-proBNP 13369pg/mL，cTNI 4.05ng/L，考虑“肥厚型心肌病、心功能不全”，为求进一步治疗转诊我院，急诊以“心肌肥厚 肥厚型心肌病待排 心功能不全 腹痛待查”收入 CCU 病区。自发病以来患者精神、睡眠差，大便如常，尿量约 1000-1500mL/d。

既往病史：

既往史：5 月龄时发现先天性白内障，2 岁半时行晶状体植入术。8 年前曾行心脏彩超提示心肌肥厚、心脏扩大，未进一步诊治。否认高血压、糖尿病、高脂血症等慢性病史。否认传染病、外伤、输血史，否认药物过敏史。

个人史：足月剖宫产第 3 胎，无窒息史，目前小学六年级，生长发育顺序似同龄儿，平常活动耐量差，否认烟、酒、放射物质及毒物接触史。

家族史：姐姐 17 岁高中生，1 岁时发现白内障并行晶状体植入术，9 岁时发现心肌肥厚，目前 LVEF60％，因乏力小学起停上体育课，目前活动耐量差，智力正常。哥哥 15 岁初中生，体健，未行系统体检，智力正常。父母体健，非近亲结婚。爷爷、奶奶、姥姥、姥爷均体健。

病程记录：

[第一次我院诊治经过]

患者 2023-05-19 至 2023-05-27 首次就诊于我院并收住 CCU，临床表现为肺部感染、心衰失代偿（体循环、肺循环淤血），多次复查心脏彩超提示心肌肥厚、心脏扩大，心功能重度减退（LVEF20-27%），诊断肥厚型心肌病、病因待查，予头孢曲松 2g qd、呋塞米 20mg qd、琥珀酸美托洛尔缓释片 23.75mg qd、诺欣妥 25mg bid、螺内酯 20mg qd、达格列净 10mg qd 及平喘、祛痰、保肝、抑酸护胃、胸腔穿刺引流、对症支持等治疗，期间完善相关检验检查结合病史除外冠心病、瓣膜病、高血压、内分泌异常及药物因素相关的心肌肥厚，考虑患者发病年龄小，家族有先天性白内障、心肌肥厚病史，遗传性疾病相关可能性大，予送检基因检测结果未归，建议进一步完善心脏 MR 检查，考虑患者心衰终末期，建议评估心脏移植，家属要求转诊中国医学科学院阜外医院进一步诊治。

[阜外医院诊治经过]

患者 2023-05-30 至 2023-06-16 就诊于中国医学科学院阜外医院，完善相关检验检查进一步除外了淀粉样变、法布雷病、自身免疫性疾病及代谢性疾病等，期间予抗心衰等治疗效果欠佳。2023-06-01 患者基因检测结果回报 AGK 基因突变，考虑线粒体心肌病、Sengers 综合征诊断明确，予调整药物方案：托拉塞米 5mg bid、螺内酯 20mg bid、沙库巴曲缬沙坦 12.5mg bid、琥珀酸美托洛尔缓释片 23.75mg qd、醋酸泼尼松龙 10mg bid、碳酸钙 D3 0.6g qd、骨化三醇胶丸 0.25μg qd、辅酶 Q10 10mg bid、乙酰半胱氨酸 600mg bid、果糖二磷酸钠 10ml bid、牛磺酸 0.4g tid、左卡尼汀 10mg bid、硒酵母片 70mg qd。经上述治疗患者病情未见明显改善，多次复查超声心动图提示 LVEF20-29%。

[第二次我院诊治经过]

外院出院后患者未再规范诊治随访，心功能持续恶化，2023-10-28 因感染诱发心衰加重、心源性休克合并多脏器功能衰竭再次就诊我院并收住 CCU，住院期间治疗方案如下：

1）抗感染治疗：头孢哌酮钠舒巴坦钠 3g q12h

2）营养心肌、保护线粒体功能：辅酶 Q10、维生素 B1&B2、硒酵母片、左卡尼汀、牛磺酸、碳酸钙 D3、

骨化三醇滴丸、乙酰半胱氨酸、果糖二磷酸钠口服液

3）抗心衰、强心、升压：口服及静脉呋塞米、托拉塞米、螺内酯利尿，间断应用吗啡并予去甲肾上腺素、

多巴胺、多巴酚丁胺、奥普力农、地高辛、西地兰等药物维持循环，因患者低血压未能加用 β 受体阻滞剂、ARNI，因患者低龄未能加用 SGLT2i

4）脏器支持：多烯磷脂酰胆碱、谷胱甘肽保肝，雷贝拉唑抑酸护胃等

5）营养支持、康复治疗

患者线粒体心肌病、心衰终末期诊断明确，尽管经积极治疗血流动力学仍持续恶化、循环难以维持，监测乳酸进行性升高，最终因循环衰竭于 2023-11-02 14:02 宣告临床死亡。

检验检查记录：

【基因检测】

患者 AGK 基因变异：① NM_018238.4: Intron7: c.424.3C > G，母源（致病突变）② NM_018238.4: Exon12: c.871C > T，父源（致病突变）

【超声心动图】

左心扩大，左室壁运动幅度减低，左室壁增厚，考虑肥厚型心肌病。轻中度二三尖瓣反流，中度肺动脉高压，左室整体收缩功能明显减低，舒张功能减退，右室收缩功能减退。（EF:20%, IVS:15.8mm, LVD:58mm, LA:41mm, E/e’:18, PASP:58mmHg）

【动态心电图】

全天总心搏：136241 次，平均心室率 97 次 / 分，房性早搏：99 次 / 全天；室性早搏：30 次 / 全天。

【外院检查】

①腹部彩超：肝、胆、胰、脾结构及血流未探及明显异常。

②肾上腺彩超：未见异常。

③颈动脉彩超：未见异常。

④双下肢动静脉彩超：右侧股总动脉内中膜增厚。双下肢静脉未见异常。

⑤心脏 CT：左心室增大，其内肌小梁增多紊乱，考虑心肌受累疾病可能。

⑥颅脑 CT：未见异常。

【心脏 MRI】

心脏MRI结果： 左室增大伴收缩功能明显减退，左右室壁增厚

心脏增强MRI结果： 左室增大伴收缩功能明显减退，左室心肌广泛异常强化，不除外遗传代谢性疾病可能

具体描述：

左室增大，左室舒张末期66mm，室间隔及毗邻左心室增厚，以室间隔增厚为著（**IVS 16-20mm**，左室下壁10-11mm），室间隔肌壁间可见条状T2 STIR高信号，提示心肌水肿。左室内肌小梁明显增多，前后组乳头肌粗大，左室心肌舒张顺应性减低，收缩功能明显减退，左室流出道通畅，未见收缩期梗阻征象，右房、室不大，右侧室壁增厚，未见脂肪浸润，未见梗阻征象，右室收缩功能减退 (PASP:26mmHg)，主肺动脉20mm，开主动脉内径19mm，二尖瓣可见少量反流信号，主动脉瓣及三尖瓣未见反流信号，心包无增厚，少许心包积液。

左心功能：	**EF：20%**	CO：5.33L/min	EDV：320.76ml	EDVI：238.74ml/m^2
右心功能：	**EF：46.75%**	CO：5.32L/min	EDV：137ml	EDVI：102ml/m^2

鉴别诊断：

我院及外语就诊期间已除外冠心病、瓣膜病、高血压、内分泌异常、药物因素、淀粉样变、法布雷病、自身免疫性疾病及代谢性疾病相关的心肌肥厚。

其他：

极低 EF 值 ecmo 辅助下 36.7mm 极大瓣环 TAVR 一例

马文帅

空军军医大学第二附属医院

患者基本信息：

患者男性 68 岁

主述：

胸闷 1 年，加重 2 月

现病史：

患者 1 年前开始出现活动后胸闷、气短，休息后可缓解，劳累后加重，未诊治。2 周前出现咳嗽、咳痰，伴流涕，再发胸闷，部位性质大致同前，频率、持续时间较前增加，伴大汗淋漓，无关节疼痛，遂至当地医院就诊，完善心脏超声提示主动脉瓣狭窄 (未见报告)，给予输液及口服药物治疗 (具体不详)，咳嗽、咳痰等症状缓解，胸闷无明显改善，现为进一步诊治，就诊我科门诊，查超声提示“主动脉瓣重度狭窄，主动脉瓣赘生物”，以“心脏瓣膜病 主动脉瓣重度狭窄”收入院

既往病史：

否认高血压 糖尿病

病程记录：

入院后给与纠正心力衰竭

ECMO 辅助下高危 TAVR 治疗

检验检查记录：

超声提示：

主动脉瓣钙化，考虑重度狭窄伴轻度关闭不全，主动脉异常回声附着

主动脉窦部及升主动脉内径增宽

左室壁运动普遍减低

左室大

室壁增厚

心包积液 (少量)

左室收缩功能减低

鉴别诊断：

与冠心病鉴别，冠状动脉造影可明确

其他：

极低 EF 值 ecmo 辅助下 36.7mm 极大瓣环 TAVR 一例

左束支起搏逆转终末期肥厚型心肌病一例

林曼欣

厦门大学附属心血管病医院

患者基本信息：

男性，73 岁，以“劳力性气促 6 年，加重伴夜间阵发呼吸困难 10 天”入院。

主述：

劳力性气促 6 年，加重伴夜间阵发呼吸困难 10 天

现病史：

患者 6 年前开始出现劳力性气促，2 年前就医查心脏彩超显示 LVD81mm，LVEF37%，IVS 12mm，LVPWD 13mm。开始服用“坎地沙坦，美托洛尔及螺内酯”治疗，但症状仍进行性加重，后改为“螺内酯、美托洛尔缓释片、呋塞米、沙库巴曲缬沙坦钠”治疗，入院前 10 天出现气促加重，伴夜间阵发性呼吸困难及双下肢水肿，为进一步诊治入院。

既往病史：

既往有高血压病史，有长期吸烟史。患者有 2 个儿子及 1 个女儿，其中 1 个儿子有高血压病史，体检发现“心肌肥厚”。无猝死家族史。

病程记录：

患者 73 岁老年男性，临床以劳力性气促 6 年、活动耐量进行性下降为主要表现，超声心动图提示心肌肥厚（IVS12mm、LVPWD12mm），LVEF 26%，心电图提示合并完全性左束支传导阻滞、QRS 时限 185ms，通过详细筛查排除了常见心肌肥厚继发病因后考虑肥厚型心肌病扩张期，优化 GDMT 治疗效果欠佳，因经济原因患者拒绝 CRT-D、接受了 CRT-P 治疗， 术中成功进行了希氏束起搏及左束支起搏，术后心电图提示 QRS 时限缩短至 105ms、电学再同步成功，随访 3 月患者心功能显著恢复（NYHA 分级改善），超声心动图提示 LVEF 回升至 54%，术后 1 年随访，心功能维持良好、电极参数稳定，超声显示持续逆重构。

检验检查记录：

实验室检查：NT-proBNP' 3881p/mL；其他实验室检查未见异常（血常规、血气分析、凝血功能、高敏肌钙蛋 T、肝肾功、血脂、甲状腺功能、糖化血红蛋白未见异常）。心电图：窦性心律，左心室高电压， **Sv_1+Rv_5=5.6mv ；** 完全性左束支阻滞，QRS 时限 185ms。胸片显示心胸比例 0.58。心脏彩超： IVS/LVPWD 12mm/12mm；LVEDD 81mm,EF 26%；冠脉造影检查未见冠脉狭窄。进一步行基因检测，全外显子组测序（含线粒体）未检出与临床表型高度相关的基因变异，但检出 4 个突变位点：SCN5A:NM_198056.3:exon16:c.2773A>G :p.I925V；NM_182914.3:c.2646+2T>G；

GAA:NM_000152.5:exon14:c.1935C>A:p.D645E；

FHOD3:NM_025135.5:exon12:c.1388G>A:p.R463Q

鉴别诊断：

诊断：肥厚型心肌病扩张期（DHCM），心力衰竭，心功能 III-IV 级，完全性左束支阻滞；高血压病。鉴别诊断：已除外冠心病、瓣膜病、内分泌异常、药物、淀粉样变、法布雷病、自身免疫性疾病及代谢性疾病等可能导致心肌肥厚的疾病。

其他：

肥厚型心肌病出现左室扩大及射血分数下降时提示已进入终末期，伴随完全性左束支阻滞是预后不良的重要因素，既往研究表明双心室起搏对于此类患者效果不佳。本例为 LBBP-CRT 在 HCM 终末期伴 LBBB 患者中实现超反应性心脏逆重构和功能恢复的首例报道，提示 LBBP 技术能有效纠正电学不同步，优于传统双心室起搏，可为类似难治性心衰患者提供新的选择。

胸闷气促为哪般？按图索骥 追根溯源

游洁芸

上海市东方医院（同济大学附属东方医院）

患者基本信息：

男性，65 岁。

主述：

突发胸闷气促 1 天。

现病史：

突发胸闷气促 1 天。

既往病史：

房颤病史 10 余年，未规律抗凝，长期阿司匹林抗血小板。高血压病史 5 年，血压最高 160/90mmHg，长期口服氨氯地平治疗，血压控制可。吸烟史 20 余年，每天半包，戒烟 7 年。

病程记录：

1. 入院后心电图分析及诊断：基础节律为房颤律，且心室率较快（100-130 次 / 分）；I 导联可见 S 波，III 导联可见 T 波倒置；胸前导联 T 波倒置，且倒置幅度以 V1-V2 为中心递减，并伴有下壁导联 T 波倒置；V1 导联 QRS 波终末可见类似右束支阻滞的小 r 波。综合以上心电图特点，并结合其他临床信息，我们优先考虑的诊断是急性肺栓塞。立即完善肺动脉 CTA，结果提示骑跨于左右肺动脉主干上巨大血栓栓塞，同时左房内可见大片充盈缺损，考虑血栓且伴有机化表现。完成心超检查，提示左房内巨大血栓形成，右室扩大、收缩活动减弱，肺动脉压力升高（PASP 49mmHg），左室收缩功能正常（EF 56%）。完成下肢血管 B 超检查，可见右侧腘静脉血栓形成。至此，患者此次急性起病的罪魁祸首推断为下肢深静脉血栓脱落所致的急性肺动脉栓塞。检查同时发现的左房血栓考虑为陈旧性，可能与患者长期房颤未正规抗凝有关，是否与此次症状加重或促发因素之一，需要在治疗中进一步随访。

2. 急性肺栓塞危险分层及治疗：该患者简化 PESI 评分 1 分（心率≥ 110 次 / 分），心肌损伤标志物升高，右室功能受损，但血流动力学尚稳定，危险分层属中高危。我们即刻对其启动溶栓治疗，采用 rt-PA 50mg/2 小时的静脉溶栓方案。考虑到患者动静脉系统多发血栓，我们对其应用了低分子肝素联合华法林的高强度抗凝方案。溶栓后患者指脉氧恢复至 98-100%，心室率降低至 70-80 次 / 分，即刻

心电图可见 V1 导联 QRS 终末部小 r 波消失，提示右心系统后负荷减轻或解除，溶栓有效。溶栓后第三天复查心超右室明显缩小，肺动脉高压消失，但左房血栓无明显变化。多次随访心超左房血栓亦无明显变化，且基底较宽，活动度差。溶栓后第三天复查下肢 B 超，右下肢深静脉血栓消失。

3. 进一步查证病因：持续性房颤未正规抗凝的患者临床上并不少见，但左房形成如此巨大的血栓却十分罕见，况且该患者甚至还出现了静脉系统的血栓，这背后是否隐藏着我们还未了解的病因？为此，我们进一步完善了自身抗体及免疫相关检查，结果发现该患者心磷脂抗体 IgG 和 IgM 以及狼疮抗凝物阳性。同时结合患者动静脉多发血栓的临床表现，最终诊断为抗磷脂抗体综合征。根据 INR 水平逐渐调整华法林剂量，INR 稳定后患者平稳出院，建议终身抗凝，密切随访。

检验检查记录：

1. 心电图：房颤、ST-T 变化；

2. 心肌酶：cTnT 0.082 → 0.098ng/ml ↑，CK-MB 及 MYO 正常，NT-prpBNP 2219ng/L ↑；

3. D-Dimer 5.7 mg/L ↑；

4. 血常规、炎症指标、肝肾功能、电解质未见明显异常；

5. 急诊胸部 CT 平扫：左房扩大、左房内可见异常密度影（占位？血栓？）。

鉴别诊断：

急性心肌梗死、主动脉夹层、急性肺动脉栓塞、暴发性心肌炎、急性心包炎、原发性心肌病急性加重、其他引起胸痛的疾病。

其他：

病例亮点：

1. 心电图是极具价值的无创诊断工具，掌握心血管急危重症患者的心电图特征性表现及原理有助于早期识别和诊断疾病，为患者获得及时准确的治疗赢得时间。

2. 系统性静脉溶栓作为中高风险急性肺栓塞患者治疗选择的效果和全性较高，但对于存在血流动力学障碍等情况的高风险患者，应积极采取导管取栓及局部溶栓等措施。

3. 对于存在多发血栓的肺栓塞患者应注意排查有无获得性因素，如易栓症、自身免疫性疾病等。虽然 DOAC 抗凝管理较为方便，安全性较高，但华法林仍是目前 APS 患者的首选且唯一的抗凝治疗方案。

急性心包炎合并代谢相关脂肪性肝病的诊治 1 例

王琨璐 Wang

河北医科大学第二医院

患者基本信息：

患者，男性，32 岁，自由职业者

主述：

心前区疼痛 2 周，间断发热 10 天，气短 3 天

现病史：

患者 2 周前劳累后出现心前区针刺样疼痛，NRS 评分 3-4 分，未向肩背部放射，症状持续存在，平卧时加重，坐位时减轻，未予重视。10 天前患者夜间受凉后出现发热，体温最高 37.8℃，伴畏寒、乏力，持续 10 余小时体温自行降至正常，此后每日均出现发热，程度及规律同前。3 天前患者出现频繁干咳，影响睡眠，伴气短、喘憋，伴食欲下降，自测新冠核酸抗原为阴性，口服莫西沙星 0.4g 1/ 日，症状无明显好转，于 2024-11-11 入院。

既往病史：

病毒感染史：5 年前于美国生活期间曾患传染性单核细胞增多症，曾 2 次感染新冠病毒。代谢相关病史：痛风病史 7 年，脂肪肝、肝损害 3 年，高脂血症 2 年，发现胰岛素抵抗半年，发现肾损害 4 个月。

病程记录：

针对患者急性心包炎，给予甲泼尼龙琥珀酸钠静点（80mg*1 天 --60mg*5 天 --40mg*4 天）、醋酸泼尼松口服（30mg*2 天 --20mg*2 天），静注人丙种球蛋白 20g*2 天，同时给予抗病毒、控制心率、营养心肌等治疗；针对患者代谢相关脂肪性肝病，给予异甘草酸镁、多烯磷脂酰胆碱胆碱保肝，熊去氧胆酸降低胆红素；针对患者代谢综合征、痛风，给予低盐低脂低嘌呤饮食，非布司他片 20mg 1/ 日口服，治疗期间保证热量供给，监测血糖、体重变化。

检验检查记录：

心电图：窦性心动过速；心脏超声：中量心包积液；心脏 MR 平扫 + 强化：考虑心包炎，心包积液（中度），左、右心室轻度舒张受限；胸部 CT：两肺散在少许小条索，心包较多积液，所扩不均匀脂肪肝或肝损害。

化 验： 心 肌 酶：hs-CRP 9.9mg/L，Myo 127.6ng/ml，LDH 278.9U/L；CK-MB、cTnI、BNP 未见异常；血常规：WBC 11.77*10^9/L，NE 63.60%；ESR 49mm/h，CRP 70.80mg/ L；EBV NA IgG、EBV VCA IgG：>50.00AU/ ml，血培养、病毒筛查、结核及自身免疫等未见异常。

代 谢 相 关 检 查： 肝 功 能：TBIL 50.09umol/L，DBIL 14.64umol/L，IBIL 35.45umol/L，ALT 116.4U/ L，ALP 177.0U/L，γ-GGT 453.0U/L； 血脂：TC 5.25mmol/L，TG 0.99mmo1/L，LDL-C 3.41mmol/L； 肾 功 能：Cr 97.3μmol/L，UA 320.6μmol/L；FibroScan：CAP 360dB/m，E 21.1kPa；代谢成分测定：REE 2165 Kcal/day，RQ 0.86，REE/Pred 92%。

鉴别诊断：

主要诊断：1. 急性心包炎 病毒性心包炎可能性大，2. 肝损害 代谢相关脂肪性肝病，3. 代谢综合征 高脂血症 胰岛素抵抗 肥胖，4. 痛风，5. 肾损伤

鉴别诊断：

1. 结核性心包炎：是结核杆菌感染引起的心包疾病，主要表现为长期低热、盗汗、疲乏无力、胸痛、呼吸困难等症状，心包积液量常较大，易发展为慢性，形成缩窄性心包炎。

2. 缩窄性心包炎：是心肌瘢痕形成以及随之发生的心包囊正常弹性丧失的结果，表现为心脏的收缩和舒张功能受限，心功能减退，全身血液循环障碍，多是由结核性、化脓性、创伤性、非特异性、尿毒症性、红斑狼疮性心包炎引起，肿瘤、放射、心脏手术等因素引起的心包炎也可发展为缩窄性心包炎。患者常表现为发热、胸痛、腹胀、下肢肿胀、疲乏、食欲不振等。

其他：

病情转归：治疗第 3 天患者体温降至正常，此后上述症状逐渐好转，出院前 BMI 降至 38.50kg/m^2，复查血沉、CRP 降至正常，心脏超声示心包积液消失，心电图示部分导联 T 波低平倒置，共住院 14 天。院外口服布洛芬 200mg 3/ 日 *1 个月，同时予以护胃、营养心肌、保肝等治疗，患者未再出现不适，规律随访中。

关键词：急性心包炎；代谢相关脂肪性肝病；代谢综合征；肥胖

与死神赛跑：百米冲刺 or 马拉松？——1 例心梗后心脏破裂的诊疗与思考

游洁芸

上海市东方医院（同济大学附属东方医院）

患者基本信息：

男性，74 岁。

主述：

突发胸痛 5 小时。

现病史：

患者入院前 5 小时（约 11：00）出现持续性胸痛，伴背部放射痛、出汗，无发热，无咳嗽、咳痰，无恶心、呕吐，无黑矇、晕厥，无腹胀、腹痛，无头晕、头痛，症状持续不能缓解。遂于 15:38 来我院就诊，查心电图（15:38）提示：窦律，完右，下壁异常 Q 波，符合超早期前壁心肌梗死心电图改变；心肌酶（16:20）提示 TnI 1.03ng/ml，CK-MB 93.76ng/ml， NT-ProBNP 274ng/l。

既往病史：

高血压病史 30 余年，最高血压 190/100mmHg，糖尿病病史 2 年。否认青光眼、慢性支气管炎、胃溃疡、胃出血病史。长期吸烟史。

病程记录：

PCI 术后 1.5 小时（发病约 8 小时）患者突发大汗，呼之有反应，对答不能，瞳孔对光反射存在，血压 84/40mmHg，呼吸急促，颈静脉怒张，双肺呼吸音粗，闻及干湿啰音，心率 100 次 / 分，律齐，心音遥远，腹平软，无压痛，反跳痛，肝脾肋下未及，双下肢无浮肿，穿刺部位伤口无渗血，动脉搏动弱。床旁心超提示大量心包积液。立即予急诊心包穿刺引流，去甲肾 + 多巴胺维持循环，肾上腺素反复静推，气管插管 + 机械通气 + 补液扩容 + 亚低温保护，床旁植入 ECMO（转速 3620 转 / 分，流量 3.05L/min），急诊开胸探查 + 心脏破裂修补。术后经历了凝血异常、活动性出血、ECMO 膜前血栓、体循环低灌注、急性肾损伤、多重耐药菌感染、消化道出血、脱机困难等困境，经 ECMO、机械通气、血管活性药物、输血、抗感染、气道护理、营养支持等积极抢救与治疗，病情好转。术后 4 个月随访，无不适主诉，LVEF56%。

出院诊断：1. 冠心病 急性 ST 段抬高型前壁心肌梗死 PCI 术后 左室游离壁破裂 心脏破裂修补术后 ECMO 术后 心源性休克 心功能 IV 级（Killip）2. 高血压病 3 级 很高危 3. 2 型糖尿病 4. 肺部感染（鲍曼不动杆菌、烟曲霉）5. 贫血 6. 低蛋白血症 7. 高脂血症 8. 高钠高渗血症（已纠正）9. 凝血功能异常 10. 肝肾功能异常（已纠正）11. 消化道出血 应激性溃疡。

检验检查记录：

1. 心电图提示急性前壁心肌梗死。

2. 心肌酶：BNP 274 ng/L，CK-MB 93.76 ng/mL，TNI 1.03 ng/mL。

3. 血 生 化：Scr 83.20μmol/L，ALT 31.00U/L，K 3.86mmol/L，Na 141.87mmol/L

4. 血常规: RBC 4.91×10^12/L，HCT 44.0%，WBC 13.10×10^9/L，Hb 152.0g/L，PLT 226×10^9/L，N 79.7%。

5. 急诊冠脉造影提示：前降支近段节段狭窄 50-70%；前降支中段完全闭塞，血流 TIMI0 级；回旋支中段分叉处节段性狭窄 70%，血流 TIMI3 级；右冠状动脉远段血管外瘪影，斑块破裂征象，血流 TIMI3 级。前降支中段病变处植入 3.0×18mm 药物洗脱支架一枚。

鉴别诊断：

再发心肌梗死、主动脉夹层、急性肺动脉栓塞、暴发性心肌炎、急性心包炎、原发性心肌病急性加重、其他引起胸痛的疾病。

其他：

不同寻常的膀胱肿瘤——副神经节瘤

刘淼

山东第一医科大学附属中心医院

患者基本信息：

姓 名：王建光　出生地：山东省烟台市招远市
性 别：男　职业：农民
年 龄：52 岁　病史陈述者：患者本人（本人）
婚 姻：已婚　入院日期：2025 年 05 月 08 日 10 时 23 分
民 族：汉　记录日期：2025 年 05 月 08 日 14 时 13 分

主述：

发作性心慌 5 年余，血压升高 1 年余，加重 1 月

现病史：

患者 5 年前开始出现阵发性心慌，多于小便后时出现，持续约 3-5 分钟，休息后缓解，伴乏力，偶有头痛，无头晕，无胸闷、胸痛，无大汗，无恶心、呕吐，无腹痛、腹泻，无尿频、尿痛、排尿困难等症状，患者未在意。1 年前上述症状发作时，自测血压增高多在 130-140/95-100mmHg 之间，未予重视；近 1 月来患者上述症状发作时自测血压，最高达 240/140mmHg, 休息后缓解。曾就诊于“招远县人民医院”，行化验检查示: “醛固酮 174pg/ml, 肾素 4pg/ml, 血钾 5.5mmon/L; 甲状腺功能三项：未见异常；泌尿系 B 超：右肾囊肿；肾上腺 CT：左肾上限及其结合部稍粗；”。诊断为“高血压病”，被推荐就诊于我院。

患者自发病以来，神志清，精神可，大小便无明显异常，体重无明显变化。

既往病史：

既往健康状况一般，慢病病史：有：“右肾囊肿”病史，否认“糖尿病、冠心病”等病史，传染病史： 否认“肝炎、结核、伤寒”等传染病及接触史。 手术史：否认 疾病史 (含外伤): 否认 输血史 : 无 过敏史 : 否认 （药物、食物过敏史，）预防接种史：预防接种史不详。

病程记录：

患者入院后完善相关辅助检查，晨起血儿茶酚胺检测示：血去甲肾上腺素 1941.9pg/ml，去甲变肾上腺素 599.2pg/ml. 入院症状发作两次，发作时血压 180-190/110-120mmHg，心率 110-120 次 / 分。发作时血儿茶酚胺检测：去甲变肾上腺素 225pg/ml、250pg/ml。颅脑及盆腹腔 MRI 示：膀胱占位。全身 PET/CT 示：膀胱左侧壁软组织结节，FDG 代谢无明显增高，131 I-MIBG 摄取明显增高，考虑为副神经节瘤，未发现有转移病灶，随转入泌尿外科行手术治疗，手术顺利，术后患者恢复好，未再发生心慌、头疼，血压高等症状。

检验检查记录：

院外检查：化验检查结果：“醛固酮 174pg/ml, 肾素 4pg/ml, 血钾 5.5mmon/L; 甲状腺功能三项：未见异常；

泌尿系 B 超：右肾囊肿；肾上腺 CT：左肾上限及其结合部稍粗；

入院检查：晨起血儿茶酚胺检测示：血去甲肾上腺素 1941.9pg/ml，去甲变肾上腺素 599.2pg/ml.

发作时血儿茶酚胺检测：去甲变肾上腺素 225pg/ml、250pg/ml。

颅脑及盆腹腔 MRI 示：膀胱占位。

全身 PET/CT 示：膀胱左侧壁软组织结节，FDG 代谢无明显增高，131 I-MIBG 摄取明显增高，考虑为副神经节瘤，未发现有转移病灶

鉴别诊断：

1. 原发性高血压：原发性高血压与嗜铬细胞瘤均可出现高血压症状，但原发性高血压的血压波动较小，且多无阵发性发作的特点，影像学检查也不会发现肿瘤病灶。

2. 甲状腺功能亢进症：甲状腺过度分泌甲状腺素，甲状腺素是一种能够加速身体代谢的激素，过度分泌会导致心跳加快、胸部发闷等症状，可伴有血压升高，但一般收缩压增高，舒张压降低，脉压差增大。

3. 心动过速性心律失常：患者多有阵发性心慌，多伴有胸闷、憋气等，可有血压增高，心率多较快，心率大于 130 次以上，心率快到一定程度可出现血压低，心电图可鉴别。

其他：

1 例诊治一波三折的淀粉样变性心肌病

周乐群

北京大学第三医院

患者基本信息：

患者为 46 岁男性，主因“腹胀 2 月，呼吸困难伴活动耐量下降 1 月”来诊。

主述：

腹胀 2 月，呼吸困难伴活动耐量下降 1 月

现病史：

2 月前患者间断腹胀伴乏力，无胸闷、胸痛、呼吸困难、心悸，无咳痰、尿少，自行服用胃药后无好转。1 月前呼吸困难伴活动耐量下降，行走 50m 出现四肢乏力，伴气短，双下肢重度水肿，夜间高枕卧位。就诊当地医院，测血压低，脑钠肽 1070.72pg/ml（<125），肌钙蛋白 I 0.492mg/ml（<0.023），肌酐 106.1umol/L，超声心动图：左室壁不均匀增厚，左房、右房增大，升主动脉增宽，肺动脉高压 PASP42mmHg，左室舒张功能减退，左房压 18mmHg 增高，LEVF 56%，少量心包积液。诊断为舒张性心力衰竭 肥厚性心肌病可能，急性非 ST 段抬高型心肌梗死可能，予阿司匹林、替格瑞洛抗血小板，瑞舒伐他汀、依洛尤单抗降血脂，单硝酸异山梨酯扩血管，布美他尼、呋塞米利尿，沙库巴曲缬沙坦、螺内酯改善预后，经治疗后患者症状较前好转，可爬 3 层楼，无气促、喘憋等。为求进一步诊治、明确病因收入我科。患者自发病以来，精神欠佳，睡眠差，食欲差，夜尿增多，伴尿中泡沫。大便干结，3-4 天 1 次。体重下降约 20 斤。

体格检查：体温 36.3℃ 脉搏 101 次 / 分 呼吸 22 次 / 分 血压 98 / 74mmHg，双肺呼吸音清，未闻及干湿性罗音，律齐，心音有力，A2>P2，各瓣膜听诊区未闻及杂音，未闻及心脏附加音，无心包摩擦音。腹部柔软，无压痛，双下肢无浮肿。

既往病史：

其他病史：吸烟 20 余年，每日 20 支；饮酒 20 余年，每周 2 次，每次 200mL 56°白酒。高血压家族史。否认心肌病家族史，否认猝死家族史。否认早发冠心病家族史。

辅助检查：脑钠肽 1070.72pg/ml（<125），肌钙蛋白 I 0.492mg/ml（<0.023），肌酐 106.1umol/L，超声心动图：左室壁不均匀增厚，左房、右房增大，升主动脉增宽，肺动脉高压 PASP42mmHg，左室舒张功能减退，左房压 18mmHg 增高，左室射血分数 56%，少量心包积液。

病程记录：

第一阶段：心力衰竭病情分析：

患者临床表现为腹胀、活动耐量下降、下肢水肿等右心衰症状。病情逐渐加重出现：劳力性呼吸困难、夜间阵发性呼吸困难、高枕卧位等左心衰症状。化验脑钠肽升高，左室射血分数 56%，考虑全心衰竭诊断明确，为射血分数轻度下降的心衰。结合病程此次心衰加重的诱因是：劳累和容量负荷过重。

进一步完善辅助检查：心电图：窦性心律，V3-6 导联 ST 段压低、T 波双向，肢体导联低电压。多次复查心电图 ST-T 段无动态演变。超声心动图：左室壁运动弥漫减低 左房增大 左室壁增厚（LVMI 126.09g / m2） 升主动脉增宽 二尖瓣反流（中度） 三尖瓣反流（轻度） PASP: 28mmHg 左室舒张功能减退 左房压增高 LAP:19mmHg LVEF 46%（2-D） 下腔静脉内径及呼吸变化率正常；左室心肌应变明显减低 左室整体 GLS-6.7% (APLAX GLS-7.0%, 4CH GLS -5.9%, 2CH GLS-7.2%)。Holter：窦性心律，平均 93bpm（80-113bpm），偶发房早、成对房早，偶发室早（14/108230）、短阵室速（1 阵，自行终止、患者无症状），R 波递增不良，ST-T 改变。胸片：双肺纹理增多。TnT 0.14(ng/ml) ↑（<0.1），CKMB(mass) 12.1(ng/ml) ↑（<5.6），CK 188(U/L) ↑（<135），LDH 279(U/L) ↑（<246）；NT-proBNP 8144(pg/ml) ↑（<900）； 血常规：WBC 12(*10^9/L) ↑（3.5-9.5），Hb 147(g/L)，N% 70.9(%)； 生化：ALT 55(U/L) ↑（<35），Alb 41.2(g/L)，BUN 10.09(mmol/L) ↑（<2.5-6.1），K 4.66(mmol/L)，Cr 119(umol/L) ↑（46-92），Ca 2.4mmol/L；尿常规：尿糖 4+，尿酮体 -，尿蛋白 -；血脂：TC 2.73(mmol/L)，TG 1.43(mmol/L)，HDL-c 0.76(mmol/L) ↓，LDL-c 1.66(mmol/L)，Lp(a) 970(mg/L) ↑；Glu 6.6(mmol/L) ↑，HbA1c 7(%) ↑；颈动脉超声：双侧颈动脉粥样硬化斑块形成；冠脉 CT 未见血管严重狭窄；心脏磁共振检查：左室、右室壁、房间隔弥漫增厚（左室最厚为室间隔中段约 20mm，右室最厚为游离壁约 10mm），伴双室壁、双房壁弥漫延迟强化，符合心肌淀粉样变性；左房增大；左室、右室运动弥漫减低，左室、右室收缩功能下降（LVEF 37%，RVEF 33%）；心包少量积液。

综上，考虑心力衰竭病因为心脏淀粉样变性。

第二阶段：心脏淀粉样变性明确诊断及分类：根据诊断依据，患者有典型的心脏症状，心电图低电压表现，超声提示弥漫室壁增厚、舒张功能减退，纵向应变减弱伴有心尖保留征。磁共振提示心室壁弥漫延迟强化，肌钙蛋白持续低血平升高，伴有 NT-proBNP 升高。心脏外合并自主神经功能异常及体位性低血压，考虑心脏淀粉样变性诊断明确。心脏淀粉样变性根据沉积的物质不同，常见的包括 AL 型和 ATTR 型，还有一些其他更少见的类型。这些疾病发病率非常低，均为罕见病。按照诊断流程图，我院完善血清及尿免疫球蛋白固定电泳未见单克隆蛋白形成。焦磷酸盐显像，心脏 / 对侧肺比值是 1.8，大于 1.5；视觉摄取 2 级。心肌活检：刚果红染色提示为淀粉样物质沉积，免疫组化染色显示以 TTR 蛋白为主。结合临床及影像学，符合 ATTR 型淀粉样变性心肌病。免疫组化：CD3（散在极个别 +），CD20（-），CD68(KP1)（散在个别 +），κ（弱 +，与血管中阳性信号相比较弱，考虑为非特异性着色），λ（-），TTR(Prealbumin)（间质强 +）。

综上，考虑 ATTR 型心脏淀粉样变性。

第三阶段：修正诊断

血 清：κ 1048.97mg/L（3.30-19.40），λ 12.21mg/L（5.71-26.30），κ/λ 85.9107（0.2600-1.6500）

通过血液科、病理科、核医学科在内的多学科会诊，继续完善骨髓穿刺 + 活检：血液病免疫分型：骨髓中见 6.76% 异常浆细胞。骨髓细胞学检查：骨髓增生活跃，考虑多发性骨髓瘤。骨髓病理：浆细胞数量增多，主要呈散在分布，仅个别灶浆细胞数量大于 10 个。免疫组化结果：MPO（粒系 +），CD61（巨核系 +），CD71（红系 +），CD3（少量 +），CD20（少量 +），κ（+），λ（-），CD138（+），CD56（个别 +），CyclinD1（+）。结论：（骨髓）κ 限制性表达，结合形态及

免疫组化结果符合浆细胞异常增生。（送外院会诊）心肌胶体金免疫电镜标记：κ（+++），λ（-），TTR（±）；结论：（心肌）符合淀粉样变（AL-κ 型）。基因检测：未发现与淀粉样变性相关有意义的致病基因。

综上，患者存在多发性骨髓瘤，且心脏淀粉样变性是轻链型的。PYP 的阳性结果可能是由于轻链蛋白存在导致的假阳性。患者心力衰竭原因为 AL 型的心脏淀粉样变性，存在系统性的淀粉样变性。

治疗上，心脏方面主要为抗心衰治疗。原发病方面，血液科规律化疗，采用 PCD 方案化疗，应用两个疗程后患者心衰再次加重。再次多学科会诊建议应用达雷妥尤单抗，其联合环磷酰胺 + 硼替佐米 + 地塞米松（Dara-CyBorD）显著提高血液学缓解率（≥ VGPR），部分患者心脏功能改善（NT-proBNP 下降）（ANDROMEDA 研究，2020）。但患者及家属因经济原因未用药。最终患者因心力衰竭去世。从出现心力衰竭症状到死亡仅 6 个月。

检验检查记录：

心电图：窦性心律，V3-6 导联 ST 段压低、T 波双向，肢体导联低电压。多次复查心电图 ST-T 段无动态演变。超声心动图：左室壁运动弥漫减低 左房增大 左室壁增厚（LVMI 126.09g / m2） 升主动脉增宽 二尖瓣反流（中度） 三尖瓣反流（轻度） PASP: 28mmHg 左室舒张功能减退 左房压增高 LAP:19mmHg LVEF 46%（2-D） 下腔静脉内径及呼吸变化率正常；左室心肌应变明显减低 左室整体 GLS-6.7% (APLAX GLS-7.0%, 4CH GLS -5.9%, 2CH GLS-7.2%)。Holter：窦性心律，平均 93bpm（80-113bpm），偶发房早、成对房早，偶发室早（14/108230）、短阵室速（1 阵，自行终止、患者无症状），R 波递增不良，ST-T 改变。胸片：双肺纹理增多。TnT 0.14(ng/ml) ↑（<0.1），CKMB(mass) 12.1(ng/ml) ↑（<5.6），CK 188(U/L) ↑（<135），LDH 279(U/L) ↑（<246）；NT-proBNP 8144(pg/ml) ↑（<900）； 血常规：WBC 12(*10^9/L) ↑（3.5-9.5），Hb 147(g/L)，N% 70.9(%)； 生化：ALT 55(U/L) ↑（<35），Alb 41.2(g/L)，BUN 10.09(mmol/L) ↑（<2.5-6.1），K 4.66(mmol/L)，Cr 119(umol/L) ↑（46-92），Ca 2.4mmol/L；尿常规：尿糖 4+，尿酮体 -，尿蛋白 -；血脂：TC 2.73(mmol/L)，TG 1.43(mmol/L)，HDL-c 0.76(mmol/L) ↓，LDL-c 1.66(mmol/L)，Lp(a) 970(mg/L) ↑；Glu 6.6(mmol/L) ↑，HbA1c 7(%) ↑；颈动脉超声：双侧颈动脉粥样硬化斑块形成；冠脉 CT 未见血管严重狭窄；心脏磁共振检查：左室、右室壁、房间隔弥漫增厚（左室最厚为室间隔中段约 20mm，右室最厚为游离壁约 10mm），伴双室壁、双房壁弥漫延迟强化，符合心肌淀粉样变性；左房增大；左室、右室运动弥漫减低，左室、右室收缩功能下降（LVEF 37%，RVEF 33%）；心包少量积液。

血清及尿免疫球蛋白固定电泳未见单克隆蛋白形成。焦磷酸盐显像，心脏 / 对侧肺比值是 1.8，大于 1.5；视觉摄取 2 级。心肌活检：刚果红染色提示为淀粉样物质沉积，免疫组化染色显示以 TTR 蛋白为主。结合临床及影像学，符合 ATTR 型淀粉样变性心肌病。免疫组化：CD3（散在极个别 +），CD20（-），CD68(KP1)（散在个别 +），κ（弱 +，与血管中阳性信号相比较弱，考虑为非特异性着色），λ（-），TTR(Prealbumin)（间质强 +）。

继续完善骨髓穿刺 + 活检：血液病免疫分型：骨髓中见 6.76% 异常浆细胞。骨髓细胞学检查：骨髓增生活跃，考虑多发性骨髓瘤。骨髓病理：浆细胞数量增多，主要呈散在分布，仅个别灶浆细胞数量大于 10 个。免疫组化结果：MPO（粒系 +），CD61（巨核系 +），CD71（红系 +），CD3（少量 +），CD20（少量 +），κ（+），λ（-），CD138（+），CD56（个别 +），CyclinD1（+）。结论：（骨髓）κ 限制性表达，结合形态及免疫组化结果符合浆细胞异常增生。（送外院会诊）心肌胶体金免疫电镜标记：κ（+++），λ（-），TTR（±）；结论：（心肌）符合淀粉样变（AL-κ 型）。基因检测：未发现与淀粉样变性相关有意义的致病基因。

鉴别诊断：

患者临床表现为腹胀、活动耐量下降、下肢水肿等右心衰症状。病情逐渐加重出现：劳力性呼吸困难、夜间阵发性呼吸困难、高枕卧位等左心衰症状。化验脑钠肽升高，左室射血分数 56%，考虑全心衰竭诊断明确，为射血分数轻度下降的心衰。结合病程此次心衰加重的诱因是：劳累和容量负荷过重。

分析患者心衰的病因：

（1）冠心病、心肌梗死：患者有男性、长期大量吸烟史、高脂血症、糖尿病等多种冠心病危险因素，此次起病心电图有 ST-T 段改变，肌钙蛋白升高，需要考虑冠心病、心肌梗死导致心衰，但患者无典型胸痛症状，心电图及心肌酶学不符合心梗动态演变过程，超声心动图未见室壁节段性运动异常。仍然需要进一步完善冠脉评估并动态监测心电图及酶学变化协助诊断。

（2）心肌病：患者超声提示室壁不均匀增厚，但无高血压病相关证据；结合病史，为右心衰首先起病，需警惕心肌病，尤其是浸润性心肌病，或致心律失常右室心肌病。但患者否认既往病史及家族史，仍需进一步完善检查评估。

（3）代谢性 / 自身免疫性疾病等：这些疾病也可导致右心衰，患者无症状及既往病史，入院完善相关检查协助评估。

结合后续辅助检查结果，考虑心力衰竭病因为心脏淀粉样变性。

患者有典型的心脏症状，心电图低电压表现，超声提示弥漫室壁增厚、舒张功能减退，纵向应变减弱伴有心尖保留征。磁共振提示心室壁弥漫延迟强化，肌钙蛋白持续低血平升高，伴有 NT-proBNP 升高。心脏外合并自主神经功能异常及体位性低血压，考虑心脏淀粉样变性诊断明确。

分析心脏淀粉样变性类型：心脏淀粉样变性根据沉积的物质不同，常见的包括 AL 型和 ATTR 型，还有一些其他更少见的类型。这些疾病发病率非常低，均为罕见病。

按照诊断流程图，我院完善血清及尿免疫球蛋白固定电泳未见单克隆蛋白形成。焦磷酸盐显像，心脏 / 对侧肺比值是 1.8，大于 1.5；视觉摄取 2 级。心肌活检：刚果红染色提示为淀粉样物质沉积，免疫组化染色显示以 TTR 蛋白为主。结合临床及影像学，符合 ATTR 型淀粉样变性心肌病。免疫组化：CD3（散在极个别 +），CD20（-），CD68(KP1)（散在个别 +），κ（弱 +，与血管中阳性信号相比较弱，考虑为非特异性着色），λ（-），TTR(Prealbumin)（间质强 +）。

综上，考虑患者未 ATTR 型心脏淀粉样变性。

外送检查：血清：κ 1048.97mg/L（3.30-19.40），λ 12.21mg/L（5.71-26.30），κ/λ 85.9107（0.2600-1.6500）

通过血液科、病理科、核医学科在内的多学科会诊，继续完善骨髓穿刺 + 活检：结合形态及免疫组化结果符合浆细胞异常增生。（送外院会诊）心肌胶体金免疫电镜标记：κ（+++），λ（-），TTR（±）；结论：（心肌）符合淀粉样变（AL-κ 型）。

综上，患者存在多发性骨髓瘤，且心脏淀粉样变性是轻链型的。PYP 的阳性结果可能是由于轻链蛋白存在导致的假阳性。患者心力衰竭原因为 AL 型的心脏淀粉样变性，存在系统性的淀粉样变性。

其他：

患者诊断一波三折，不放过任何一个有问题的细节，通过多个角度反复验证，最终明确心肌淀粉样变性类型，为下一步治疗赢得时间。但患者对常规治疗效果不佳，随着对系统性淀粉样变性研究进展，可以应用达雷妥尤单抗，其联合环磷酰胺 + 硼替佐米 + 地塞米松（Dara-CyBorD）显著提高血液学缓解率（≥ VGPR），部分患者心脏功能改善（NT-proBNP 下降）（ANDROMEDA 研究，2020）。但遗憾的是，我们的患者及家属因经济原因未用药。最终患者因心力衰竭去世。从出现心力衰竭症状到死亡仅 6 个月。

通过这个病历我们可以看到，对于心衰、心肌病的诊断，尤其是这种罕见病，是非常困难的。我们要有抽丝剥茧的耐心，刨根问底的决心，和多学科会诊的齐心，才能形成合力，为患者明确诊断，精准制定个性化治疗方案，赢得更好的治疗机会，改善预后。

迷雾重重的心原性休克–免疫检查点抑制剂相关心肌炎 1 例

周乐群

北京大学第三医院

患者基本信息：

男性，60 岁；间断胸痛 1 周，15 小时前意识丧失，于 2023-10-22 入院

主述：

间断胸痛 1 周，意识丧失 15 小时

现病史：

n 1 周前，患者无明显诱因前胸持续性闷痛，伴束带感，活动时明显，休息不能缓解，活动耐力下降。口服“速效救心丸”后症状有好转。伴呃逆、恶心、呕吐、乏力、纳差、嗜睡，无发热、咳嗽、咳痰，无晕厥、黑矇，无下肢水肿、尿量减少。

n 1 天前，患者仍感胸痛，伴心悸、头晕、大汗，症状进行性加重，出现腹泻、排水样便，无发热、腹痛。就诊于外院，查肌钙蛋白 T（Troponin T，cTnT）TnT 0.027 ng/mL（正常值 < 0.014 ng/mL），血清钠 116.5 mmol/L ↓。头、胸部计算机断层扫描（Computed Tomography，CT）未见明显异常，建议转上级医院。

n 16 小时前，患者症状加重，呼叫救护车测血压 76/50 mmHg，心率 116 次 / 分。心电图示：窦性心律，V4-6 导联 ST 段压低、T 波倒置。转入急诊后测血压 66/47 mmHg，外周血氧测不出。

n 15 小时前患者就诊过程中突发意识丧失，大动脉搏动消失。立即进行胸外按压，气管插管接有创呼吸机辅助通气，心电示波为心室颤动，除颤 1 次转复窦性心律，持续心肺复苏 9 分钟后自主循环恢复，神志恢复可简单对答，血压仍测不出。予快速补液，大剂量血管活性药物升压。

n 床旁超声心动图提示心包压塞表现，引流出橘色心包积液 200 mL。

应用大剂量多巴胺、间羟胺、去甲肾上腺素三种药物泵入，血压仍难以维持至 90/60 mmHg 以上。考虑“心原性休克”，行体外膜肺氧合（Extracorporeal Membrane Oxygenation，ECMO）循环辅助支持。

l 体格检查：（ECMO 循环辅助支持，转速 3545 rpm，流量 2.91 L/min；气管插管接有创呼吸机辅助通气，模式 A/C-VC，潮气量 480 mL，呼吸频率 12 次 / 分，给氧浓度 30%，呼气末正压 4 cmH_2O；去甲肾上腺素 1.5 μg/kg/min，多巴胺 12.5 μg/kg/min）体温 36.0℃，脉搏 98 次 / 分，呼吸 25 次 / 分，BP 116/100 mmHg。双侧球结膜水肿，双侧瞳孔等大等圆，直径 4 mm，对光反射迟钝。双肺呼吸音清晰，可闻及湿性啰音，下肺呼吸音减低。心界不大，心音低钝，律齐，各瓣膜听诊区未闻及杂音，无心包摩擦音。腹软，按压未见痛苦表情，肠鸣音减弱，2 次 / 分。双下肢无水肿

l 体格检查：（ECMO 循环辅助支持，转速 3545 rpm，流量 2.91 L/min；气管插管接有创呼吸机辅助通气，模式 A/C-VC，潮气量 480 mL，呼吸频率 12 次 / 分，给氧浓度 30%，呼气末正压 4 cmH_2O；去甲肾上腺素 1.5 μg/kg/min，多巴胺 12.5 μg/kg/min）体温 36.0℃，脉搏 98 次 / 分，呼吸 25 次 / 分，BP 116/100 mmHg。双侧球结膜水肿，双侧瞳孔等大等圆，直径 4 mm，对光反射迟钝。双肺呼吸音清晰，可闻及湿性啰音，下肺呼吸音减低。心界不大，心音低钝，律齐，各瓣膜听诊区未闻及杂音，无心包摩擦音。腹软，按压未见痛苦表情，肠鸣音减弱，2 次 / 分。双下肢无水肿

既往病史：

l 既往史

n 20 个月前发现左下肢腘窝处纤维肉瘤，行手术治疗后复发，10 个月前再次手术切除并行左膝关节置换术。10 个月前开始化疗联合靶向治疗，方案为前 4 次盐酸多柔比星+替雷利珠单抗(Programmed Death-1 inhibitor,PD-1 抑制剂)，后 2 次单用替雷利珠单抗。末次化疗时间为 3 个月前，肿瘤治疗已足疗程。

n 2 个月因“胸痛”住院，诊断为冠心病、急性非 ST 段抬高型心肌梗死（Acute Non-ST Segment Elevation Myocardial Infarction，NSTEMI）。行冠脉造影示：LM（Left Main Coronary Artery，LM）管状狭窄 30%-40%，LAD（Left Anterior Descending Artery，LAD）开口狭窄 90%，LCX（Left Circumflex Artery，LCX）及 RCA（Right Coronary Artery，RCA）正常。在血管内超声（Intravascular Ultrasound，IVUS）指导下对 LAD 开口病变行切割球囊治疗后植入支架 1 枚，术后复查 IVUS 示支架贴壁良好。

2 个月前住院期间出现淡漠、乏力、低钠血症（血清钠最低 125 mmol/L），血皮质醇、促肾上腺皮质激素（Adrenocorticotropic Hormone，ACTH）降低，甲状腺功能异常，考虑免疫检查点抑制剂（Immune checkpoint inhibitors，ICIs）相关垂体功能减退，予强的松 5mg qd 治疗。出院后患者未规律服药，未定期随诊。

l 辅助检查：

n 急诊心电图：窦性心动过速，广泛导联 ST 段压低，T 波双向或倒置。

n 实验室检查：N 端 -B 型钠尿肽前体（NT-proBNP） 1100 pg/mL ↑，全血肌钙蛋白 I 测定 0.05 ng/mL ↑（正常值 < 0.023 ng/mL）；肌酸激酶同工酶 MB（CKMB） 32 U/L ↑（正常值≤ 24 U/L），肌酸激酶 171 U/L ↑（正常值 55-170 U/L），钾 3.59 mmol/L，钠 120.9 mmol/L ↓，氯 92.1 mmol/L ↓，肌酐 133 μmol/L ↑（正常值 53-130μmol/L）。乳酸 5.6mmol/L ↑。

超声心动图：心包压塞表现，左室壁运动弥漫减低，左室射血分数（Left Ventricular Ejection Fraction，LVEF）35%；下腔静脉内径正常，呼吸变化率减低。

病程记录：

患者为 60 岁男性，急性病程，表现为进行性加重的胸痛，伴有意识模糊逐渐加重，突发室颤、呼吸心跳骤停，经复苏及心包穿刺引流后仍为严重低血压状态、补液治疗效果不佳，需要大剂量升压药物维持血压。心电图示广泛导联 ST 段压低，超声心动图提示心包压塞及左室功能减低，肝肾功异常，血乳酸升高，诊断心原性休克，予 ECMO 支持治疗。但患者心原性休克原因尚不清楚，复苏后顽固性低血压也难以完全用心原性休克解释。

结合化验检查，考虑心原性休克诊断。但患者既往诊断 ICIs 相关垂体损伤未治疗，此次起病出现顽固性低血压伴严重低钠血症，根据皮质醇节律、甲状腺功能等化验指标，考虑此次存在 ICIs 相关肾上腺皮质功能减退，加重低血压、休克的进程。

进一步完善相关检查评估病因：

心脏增强磁共振：左室前壁、室间隔中段 - 心尖段室壁运动幅度略减低；心包无增厚，心包少量积液；左室各壁心肌 Native T1 值弥漫升高，延迟扫描示左室前壁、室间隔中段 - 心尖段及左室侧壁中段见心内膜下延迟强化，局部透壁，前组乳头肌受累，符合陈旧性心肌梗死表现，同时符合 ICIs 相关心肌炎影像改变。

总结本次病例特点：患者曾接受替雷利珠单抗（PD-1 抑制剂）治疗，且曾发生 ICIs 相关垂体功能减退，此次乏力、淡漠、顽固性低钠等表现提示皮质功能异常；距离首次应用 PD-1 抑制剂 9 个月，距离末次应用 3 个月，符合 ICIs 相关心肌炎发生的时间窗。临床表现为乏力、胸痛、低血压等急性心包炎、心包压塞症状，室颤，炎症指标升高，左室功能减低。影像学表现为心脏磁共振示左室壁运动异常，心肌 Native T1 值弥漫升高，延迟强化符合 ICIs 相关心肌炎影像改变。应用糖皮质激素后心功能快速回升，炎症指标回落，心肌酶迅速降至正常。综合考虑，患者心原性休克的具体病因为 ICIs 相关心肌炎。

治疗上，1. 支持治疗：（1）呼吸循环支持：ECMO、气管插管、升压治疗。（2）对症支持：抗感染、化痰、保肝、维持水电解质平衡。（3）冠心病二级预防：阿司匹林联合氯吡格雷双联抗血小板治疗，阿托伐他汀降脂、稳定斑块。2. 病因治疗：（1）糖皮质激素：按照醋酸泼尼松 2mg/kg 治疗后序贯减量原则，起始予甲泼尼龙静脉 120mg 每日一次治疗 7 日，后减量为甲泼尼龙静脉 80mg 每日一次治疗 3 日，减量为甲泼尼龙静脉 40mg 每日一次维持 7 日。后评估病情稳定，减量为甲泼尼龙口服 36 mg/ 日，每周减量 4 mg，减量至 4 mg 每日一次维持。（2）免疫球蛋白：丙种球蛋白 200mg/kg 治疗 4 天。3. 监测：（1）心功能监测：LVEF 从 35% 逐渐恢复至 70%。（2）炎症指标监测：IL-6 等炎症指标逐渐下降。（3）内分泌监测：电解质水平恢复正常，精神好转。

急性期予 ECMO、气管插管、升压治疗等维持生命体征，辅以抗感染、化痰、保肝、维持水电解质平衡等对症支持治疗。予糖皮质激素、丙种球蛋白抗炎治疗，后序贯逐渐减量糖皮质激素并小剂量维持。经抗炎治疗后超声心动图评估 LVEF 在 10 日内从 35% 回升至 70%，撤除 ECMO，维持冠心病二级预防口服药物治疗。出院时无胸部不适，活动耐力逐渐增加，精神状态好。复查心肌酶、电解质均在正常范围。

出院诊断：

1. 心原性休克

   免疫检查点抑制剂相关心肌炎（重症）

2. 免疫检查点抑制剂相关肾上腺皮质功能减退

3. 心律失常 - 心室颤动

4. 冠状动脉性心脏病、冠状动脉支架置入术后

5. 电解质紊乱 - 低钠血症 低氯血症

6. 心脏骤停后综合征 - 急性肾功能不全、急性肝功能不全、胰腺损伤、凝血功能异常

7. 纤维肉瘤术后、化疗后

8. 左侧膝关节置换术后

检验检查记录：

入院后进行休克评估的相关检查。

心电图：广泛导联 ST 段压低，T 波双向或倒置，窦性心动过速。

心包积液化验：多核为主渗出液，穿刺液常规示细胞总数 26574 个 /uL，白细胞数 7574 个 /uL，多核细胞百分比 94%。穿刺液生化示腺苷脱氨酶 18 U/L，葡萄糖 5.4 mmol/L，总蛋白 50.8 g/L，白蛋白 28.8 g/L，乳酸脱氢酶 1098 U/L。

实验室检查：

2023-10-22：N 端 -B 型钠尿肽前体 1860 pg/mL ↑，全血肌钙蛋白 I 0.57 ng/mL ↑；丙氨酸氨基转移酶 196 U/L ↑，天门冬氨酸氨基转移酶 425 U/L ↑，肌酸激酶同工酶 MB 63 U/L ↑，肌酸激酶 597 U/L ↑，乳酸脱氢酶 855 U/L ↑； 钾 3.84 mmol/L， 钠 125.8 mmol/L ↓， 氯 93.2 mmol/L ↓， 肌酐 138 μmol/L ↑，淀粉酶 429 U/L ↑。

凝血功能：凝血酶原时间 20.2 s ↑，凝血酶原活动度 46% ↓，国际标准化比值 1.88 ↑，纤维蛋白原 4.62 g/L ↑，纤维蛋白降解产物 71.4 μg/mL ↑，D-二聚体 9.54 μg/mL ↑。

炎症指标：白介素 6 > 2500 pg/mL ↑。

内分泌功能检查：

甲状腺功能：总三碘甲状腺原氨酸 0.50nmol/L ↓，总甲状腺素 6.70nmol/L，游离三碘甲状腺原氨酸 1.13pmol/L ↓，游离甲状腺素 0.94pmol/L，促甲状腺激素 1.87μU/mL。

皮质醇节律（地塞米松 10mg/ 日应用 1 日）：早 8 点 ACTH 1.5 pg/mL，皮质醇 4.7 μg/dL; 下午 4 点 ACTH 1.5 pg/mL,皮质醇 4.1 μg/dL; 夜间 0 点 ACTH 1.5 pg/mL，皮质醇 3.4 μg/dL。

病毒病原体化验：阴性。

双下肢静脉超声：未见血栓形成。

心脏增强磁共振：左室前壁、室间隔中段 - 心尖段室壁运动幅度略减低；心包无增厚，心包少量积液；左室各壁心肌 Native T1 值弥漫升高，延迟扫描示左室前壁、室间隔中段 - 心尖段及左室侧壁中段见心内膜下延迟强化，局部透壁，前组乳头肌受累，符合陈旧性心肌梗死表现，同时符合 ICIs 相关心肌炎影像改变。

鉴别诊断：

低血压原因：

（1）心原性休克：患者为中老年男性，急性病程，表现为胸痛加重、意识模糊、四肢末梢冷，严重低血压且快速大量补液后仍低。伴随急性心包压塞（超声心动图示心包积液，引流出 200 mL 心包积液）、左室射血分数显著下降（LVEF 35%），出现室颤等恶性心律失常，血乳酸升高，肝肾功能异常。结合上述表现，考虑心原性休克。

（2）肾上腺皮质功能减退：患者既往诊断 ICIs 相关垂体损伤未治疗，此次起病出现顽固性低血压伴严重低钠血症，根据皮质醇节律、甲状腺功能等化验指标，考虑此次存在 ICIs 相关肾上腺皮质功能减退，加重低血压、休克的进程。

心原性休克病因鉴别：

1. 急性心肌梗死：2 月余前行冠脉造影，并在 IVUS 指导下行介入治疗。术后未发作缺血性胸痛等症状，且心肌酶及心电图动态变化与单纯冠心病不符，未再次行血运重建心功能快速回升，可除外冠脉新发缺血导致心原性休克。

2. 病毒性心肌炎：病原学检查阴性，不支持此诊断。

3. 心肌病或瓣膜病：无既往病史，超声心动图无相应表现，不支持此诊断。

4. 肺栓塞：无难以纠正的低氧血症病史，无右心负荷过重等表现，不支持此诊断。

其他：

1. **肿瘤化疗与放射病科：**免疫检查点抑制剂相关心肌炎有以下特点：（1）发生率低但致死性高：免疫治疗相关心血管并发症主要包括心肌炎、心力衰竭、心房颤动、心包积液和冠心病等；其中，发生心肌炎、缺血性心脏病及心力衰竭的患者预后最差，死亡率超过 40%。不同的 ICI 药物出现心脏毒性比例不同，抗细胞毒性 T 淋巴细胞相关蛋白 4（Anti-Cytotoxic T-Lymphocyte-Associated Protein 4，抗 CTLA-4）出现心脏相关不良反应为 20%，抗 PD-1 出现心脏相关不良反应为 69.4%，抗程序性死亡配体 1（Anti-Programmed Death-Ligand 1，抗 PD-L1）出现心脏相关不良反应为 10.6%。关于国产 ICI 的回顾性研究显示，我国 ICI 相关心肌炎发生率约为 1.05%。（2）发病时间不固定：1）ICIs 治疗所致心脏毒性可能发生于肿瘤免疫治疗过程中的任一阶段：中位时间为接受 ICIs 治疗后第 27 天，其中 76% 出现在治疗后 6 周内，81% 的心肌炎发生在用药后 3 个月内；不仅可以出现在药物使用早期或中期 (<90 天)，在晚期及治疗后 (90 ~ 454 天) 亦可出现，且晚发心肌炎患者较早发患者出现心脏衰竭的比例更高。2）ICIs 相关心肌炎的发病时间早于其他器官的免疫不良反应，但心血管相关死亡和全因死亡在两组间并无差异。3）ICIs 治疗所致心力衰竭事件中约一

半发生在 ICIs 治疗终止后的几个月内。ICIs 的心脏毒性可能发生于治疗过程中的任何阶段，故在 ICIs 治疗中进行全程心脏毒性评估与监测具有重要意义。（3）. 与药物种类及剂量相关：抗 PD-1 抗体治疗的心脏不良事件更多，联合用药可能增加严重性。

2. **心血管内科：**应当警惕 ICIs 相关心脏毒性：尤其在治疗早期（6 周内）及停药后数月内，必要时定期检测各个内分泌腺体功能。当出现非典型的临床表现时，例如患者未非冠心病或心律失常高风险人群，但出现严重冠心病、心房颤动、室性心律失常、缓慢性心律失常等，需警惕为 ICI 相关心脏毒性。在诊疗过程中，尤其重视症状与体征，发现可疑表现后需要进一步完善检查仔细甄别，同时评估其他免疫治疗相关损害情况。. 及时诊断后应当早期应用糖皮质激素，可显著改善预后。免疫治疗患者需全程心脏监测与心内科、肿瘤科、内分泌科等多学科管理。

3. **内分泌科：**应用 ICI 治疗过程中内分泌腺体易受损伤，需要定期监测。抗 PD-1 抗体可诱发垂体炎，导致 ACTH 分泌不足，进而引起继发性肾上腺皮质功能不全。正如本例患者的特点，ICI 相关肾上腺皮质功能减退往往起病隐匿，在出现神志改变、严重低钠血症、严重低血压时应该尽早筛查。治疗上，应该进行紧急糖皮质激素替代治疗，而非单纯升压治疗，糖皮质激素兼具抗炎与替代双重作用。此后需要长期进行糖皮质激素替代治疗。ICI 相关心肌炎治疗时需大剂量激素冲击，但需同步监测电解质及血压波动，避免相对性肾上腺皮质功能不全加重。ICI 相关垂体损伤常为永久性，需终身激素替代（>80% 患者无法恢复），需要定期随访电解质情况（尤其血钠）、晨间皮质醇、ACTH，每 3 月进行复查。若出现应激事件，如感染、手术等情况下，替代治疗的糖皮质激素剂量加倍，避免肾上腺危象。

青年教师的反复晕厥之谜

李燕秋

重庆医科大学附属第三医院

患者基本信息：

张 X，男，47 岁，化学教师

主述：

反复黑矇、晕厥 20 年，再发 1 周

现病史：

患者 18 岁开始出现第一次晕厥发作，每年发作 1-2 次，发作前有均有强烈的排便感，随之晕厥发作，持续数十秒至 1 分钟后可自行苏醒，伴有大汗淋漓。每次发作时患者体位不固定，躺下后不能阻止晕厥的发作。近 2 年发作频率较前增加；曾多次外院就诊，多次完善脑电图、动态心电图均未见异常。本次就诊 1 周前出现晕厥 1 次，后有持续头晕症状，我院门诊动态心电图: 窦性心律（平均 59 次 / 分，最慢 41 次 / 分，最快 137 次 / 分）；最长 RR 间期 2.203 秒；II°I 型房室传导阻滞。为进一步治疗门诊以 “晕厥待查” 收入我科住院治疗。

既往病史：

无烟酒史；无家族遗传病史、家族中无猝死病史及类似病史。

病程记录：

心脏迷走神经节消融术。

检验检查记录：

阿托品试验阴性、直立倾斜试验（+）

鉴别诊断：

恶性心律失常

其他：

随访术后无晕厥

LOT-CRT 治疗房颤、完左心衰 1 例

李燕秋

重庆医科大学附属第三医院

患者基本信息：

女性，79 岁

主述：

心悸 4 年，加重伴气促 1 周

现病史：

2018 年患者开始出现阵发性心悸，持续数分钟至数小时可缓解，心电图提示为阵发性心房颤动；患者未规律服药。外院冠状动脉造影检查排除冠心病。近 1 周心悸症状反复发作，伴有活动后气促，伴有夜间阵发性呼吸困难。

既往病史：

否认糖尿病、高血压等；否认烟酒史。

病程记录：

1. 住院用药：新活素、呋塞米、西地兰，症状较快缓解后启用 “新四联” 方案

2. 出院带药：沙库巴曲缬沙坦钠 50mg bid

达格列净片 10mg qd

琥珀酸美托洛尔缓释片 23.75mg qd

螺内酯片 20mg qd

利伐沙班片 15mg qd

3. 其它治疗：房颤射频消融术？心外科换瓣？ CRT？ TAVR？→患者无手术治疗意愿

检验检查记录：

肝功能、肾功能、甲状腺功能、心肌损伤标记物、

血常规、凝血功能、尿常规、大便常规、大便隐血（-）。

鉴别诊断：

急性心肌梗死后心力衰竭

其他：

后续再次住院

基层医院一例疑难心肌病诊断探索

张少沛

河北省第一荣军优抚医院

患者基本信息：

患者张某，男，67 岁，退休人员

主述：

间断腹部胀满 2 年，气短 1 个月

现病史：

2 年前患者无明显诱因出现进食后腹部胀满，无恶心呕吐，无腹痛、腹泻，曾于当地及石家庄、北京多家医院就诊，给予药物治疗，患者诉症状均能减轻，但复发间隔逐渐缩短。1 月前患者出现气短症状，并快速加重，稍有活动即出现气短，休息可缓解，无胸痛、 咯血、黑矇、晕厥。

既往病史：

既往史：既往高血压病史 20 年，最高 180/?mmHg, 现口服硝苯地平缓释片 II，1 片 / 日，自诉血压 140-150/80-90mmHg 水平，否认冠心病、糖尿病病史。

个人史：无吸毒史，无酗酒史，吸烟史 40 余年，10 支 / 天，已戒烟 3 年。

婚育史：已婚，配偶及子女体健。

家族史：父母已故，否认两系三代家族遗传病、精神病、传染病及类似疾病史。

病程记录：

2025-5-24 于 13 时 04 分接到检验科报告危急值 :CK-B14.11ng/ml，考虑患者可能存在轻微心肌损伤，给予保护心肌等药物治疗处理，2025-5-25 于 9 时 28 分接到检验科报告危急值 :CK-IB12.86ng/m1，肌钙蛋白 I1.12(ng/m1); 患者 CK-B 较前回落，肌钙蛋白较前升高，患者生命体征平稳，心室率较前减慢，症状改善，未诉胸痛、胸闷、心悸，考虑与患者心肌病需氧供氧失衡相关，给予利尿、高流量吸氧处理；患者尿蛋白 3+，进一步查 24 小时尿蛋白定量。结合患者既往病史、院前检查、入院病情、辅助检查，诊断 :1. 肥厚性心肌病 心力衰竭 心功能III级，多浆膜腔积液，心律失常 房性早搏，2.I 型呼吸衰竭，3. 肺动脉高压重度，4. 低钾血症，5. 高血压病 3 级 极高危。患者昨日利尿效果不佳，拟今日加强利尿治疗，观察电解质变化；患者指脉氧偏低，考虑心肺氧合能力欠佳，必要时呼吸科会诊。既往病史 (2024 年邢台市人民医院等诊断腹主动脉、髂动脉溃疡) 提示腹主动脉、动脉夹层表现，补充诊断腹主动脉夹层，继续控制血压、利尿、纠正电解质紊乱等治疗，患者病情仍重，向家属交代，尤其是动脉夹层存在，暂不予抗凝抗血小板治疗，患者 D 二聚体升高，不能除外微小血栓等高凝状态，患者心肌肥厚为近 2 年新发变化，肥厚型心肌病可能性较小，考虑法布雷病及心肌淀粉样变可能性较大，继续进一步检查，目前先给予减轻心负荷、抗感染等治疗。2025-5-30 复查心脏、胸水彩超：患者心包积液较前减少，胸水未见明显减少，但症状改善，考虑患者右心衰病情重，体环淤血较重，虽利尿较多，但仍需继续利尿减轻负荷。淀粉样变及法布雷查结果：血氢链 K6.0g/L ↑，血氢链入 1.4g/L，比值 4.29 个；血 Igm 入阳性；尿氢链 K42.2mg/L ↑，尿氢链入 9.56 个，尿 IgG m 蛋白阳性，考虑多发性骨髓瘤淀粉样变不除外，患者血氧饱和度仍较低，氧流量 4L/min 状态下经皮指脉氧仍波动在 89-90%，给子高流量氧气吸入辅助通气治疗。同患者及家属沟通后于 2025-5-31 行骨髓穿刺 + 活检，送检结果提示: 患者外院及本院骨髓检查结果暂不支持血液病诊断，法布雷病也不支持，患者病情好转，要求出院，告知其心肌肥厚考虑心肌淀粉样变可能性大，建议其前往北京等地上级医院进一步明确病因及治疗，患者及家属表示知情，签字出院。

检验检查记录：

2025-5-24NT PrOBNP:13278PG/ML;2025-05-24 心肌三项 :CK-MB14.11ng/ml； 钾离子 :3.37mmol/L; 肌酐 107umol/L; 谷丙 92.7U/L, 谷草 58.2U/L; 血小板、红细胞、白细胞未见明显异常，中性粒百分比 80.9%，中性粒计数 6.70*10/L;2025-05-24 血气分析 (检验科):PH 值 7.450 ，动脉血氧分压 53(mmHg) ↓，动脉血二氧化碳分压 26.4(mmHg) ↓，乳酸 1.75(mmo1/L)+;2025-05-24 凝血四项：国际标准化比值 1.40 个，凝血酶原时间 16.80(S) ↑，D- 二聚体测定 1.34(mg/L) ↑ ;2025-05-24 下肢动静脉超声：左侧髂外动脉近端瘤样扩张 双下肢动脉内 - 中膜增厚伴斑块形成 可视双下肢深静

脉未见明显血栓 双下肢皮下软组织水肿 ;2025-5-24 门诊心脏超声 : 右心增大 (右房左右径 :52mm; 右室前后径 :28m) 心肌回声异常室间隔及左室壁增厚 (左室后壁厚度 :17m; 室间隔厚度 :17mm) 室壁运动幅度欠协调左室舒张功能减低 二尖瓣中度关闭不全 三尖瓣重度关闭不全 主、肺动脉瓣轻度关闭不全 肺动脉高压 (估测肺动脉压约 114mmHg) 心包积液 (中等量), 肺部 CT 可见双侧胸腔积液, 左侧少量，右侧中大量。

2025-5-25 心电图：1. 窦性心律不齐，2.T 波改变（V1-5），3.QTc 间期延长，4. 肢导低电压；心肌三项：肌红蛋白 88.0(ng/m1) ↑，肌钙蛋白 11.12(ng/m1) ↑，肌酸激酶同工酶 12.68(ng/mL) ↑；2025-05-25 尿有型成分分析：尿蛋白 3+；2025-5-25 电解质：氯 114mmol/L ↑，二氧化碳 16.4mmol/L ↓；甲功五项无异常。泌尿系彩超：双肾实质回声增强，左肾肾盂分离

左侧输尿管上段稍增宽，前列腺增大伴钙化。腹腔积液彩超：腹腔积液。

2025-05-26 消化道肿瘤筛查无异常

2025-05-27 便常规：隐血试验弱阳性；24h 尿蛋白定量：24h 尿蛋白 1.13g/24h ↑；复查电解质：氯 113mmol/L ↑，二氧化碳 20mmol/L ↓；痰细菌培养未见细菌。

2025-5-28 胸腔积液彩超：右侧深约 11.0cm，左侧液深约 3.1cm，双侧胸腔积液。腹部彩超：肝脏外形增大、肝右静脉增宽–淤血肝待排，胆囊壁增厚–考虑继发性改变，胆囊多发息肉样变，腹腔积液。

2025-5-29 心脏彩超：右心增大 (右房左右径 43mm，右室前后径 28mm)，室间隔及左室壁增厚心肌回声较致密 (左室后壁厚度 14mm，室间隔厚度 15mm)，运动幅度欠协调。

2025-5-30 血氢链 K6.0g/L ↑, 血氢链入 1.4g/L, 比值 4.29 个 ; 血 Igm 入阳性 ; 尿氢链 K42.2mg/L ↑，尿氢链入 9.56 个，尿 IgG m 蛋白阳性

2025-05-31 血清四项：乙肝表面抗体 487.144(mIU/mL) ↑，乙肝 e 抗体 0.761(PEIU/mL) 个，余未见异常；复查心肌三项、电解质无明显异常

2025-06-01 心肌酶：胆碱酯酶 3531(U/)，白蛋白 24.64(g/L) ↓，白球比 0.7 ↓，前白蛋白 94.22(mg/1)，乳酸脱氢酶 276(0/):2025-06-01 红细胞沉降率测定 (ESR) 仪器法：血沉 31(mm/h)+;2025-06-01 降钙素原检测：降钙素原 (PCT) 0.07(ng/m);2025-06-01 C- 反应蛋白测定 (全血快速定量): 白细胞 7.51(10~9/L)，淋巴细胞百分比 14.20(%) ↓，单核细胞百分比 10.40(%) ↑，红细胞 3.77(10~12/L) ↓，血红蛋白 108(g/L) ↓，红细胞压积 32.00(%) ↓，血小板 224(10~9/)，C 反应蛋白 6.60(mg/L) 个

2025-6-3 胸腔积液彩超：右侧深约 5.4cm，左侧液深约 2.8cm，双侧胸腔积液。腹部大血管彩超：超腹主动脉内中膜增厚，下腔静脉塌陷率约 20%。2025-6-3 骨髓活检 :IHE 及 PAS 朵色示骨储增生大致正常 (40%)，粒红比例大致正常，系各阶段细胞可见，镜下所见 : 以中幼及以下阶段细胞为主，红系各阶段细胞可见，以中晚幼红细胞为主，巨核细胞数量及形态大致正常，2-4 个 /HPT，以分叶核为主 ; 少量小淋巴细胞及浆细胞散在分布，网状纤维染色 (F-0 级)。刚果红 (-)。

流式细胞检音 : 标本中可见单克隆浆细胞占有核细胞的 0.15%

2025-6-6 腹部大血管彩超：腹主动脉内中膜增厚，下腔静脉塌陷率约 36%。

2025-6-8 NT PrOBNP:2667PG/ML

鉴别诊断：

1. 扩张型心肌病 : 可以有活动后胸闷、气喘，但心脏超声可见全心增大、室壁运动减弱、室壁变薄。该患者超声可除外。

2. 急性心肌梗死 : 患者常有胸闷、胸痛、心悸、气短等症状，含服药物无效，症状逐渐加重，可有恶心、出汗，严重可出现心源性休克，心电图可见动态 ST-T 缺血改变，时间窗内出现心肌坏死标记物升高 ; 该患者症状不符，暂不考虑

其他：

受限于医院条件以及患者及家属的意愿，没有进一步行诊断性检查操作明确患者是否为淀粉样心肌病。我科仍建议患者前往专业机构进一步检查明确诊断并治疗，并定期随访。

“睡”出来的心脏病

孟玮

哈尔滨医科大学附属第二医院

患者基本信息：

59 岁男患

主述：

阵发性心悸 20 年，加重 4 月

现病史：

患者 20 年前无明显诱因反复出现阵发性心悸，自觉心跳快且不规则，初发频率约每年数次，每次持续数十分钟至数小时不等，可自行缓解，未诊治；近 4 个月心悸发作频率显著增加至每周 1-2 次，持续时间延长至 6-12 小时 / 次，最长 24 小时，发作时伴胸闷、活动后气促及乏力，需口服美托洛尔 (剂量) 部分缓解，但无法完全控制，同时服用利伐沙班抗凝治疗；病程中持续存在夜间睡眠打鼾，家属观察有呼吸暂停现象（鼾声中断伴呼吸停止数十秒，每小时数次），伴夜间憋醒、晨起口干头痛及日间嗜睡；病程中无胸痛、晕厥、咯血、夜间阵发性呼吸困难及双下肢水肿。

既往病史：

痛风，高血压，嗜烟酒

病程记录：

第 1 日：仍有心悸，BP 130/80mmHg，HR 118 次 / 分 (房颤律)，SpO_2 93%（未吸氧），双肺无啰音，双下肢无水肿。处置：控制心率、抗凝治疗，完善心脏彩超、holter、甲功、电解质，同时完善睡眠呼吸监测，经食道超声；

第 2 日：心悸缓解，心率 90-100 次 / 分，冠脉 CTA：轻度狭窄。 UCG：左房扩大（40.4mm）左室壁非对称性肥厚，考虑肥厚非梗阻性心肌病，BNP 升高，血糖、血脂高，肌酐、尿酸高。处置：睡眠呼吸监测；

第 3 日：PSG 回报：重度 OSA，AHI：37.6，最低血氧：37%，经食道超声未见血栓；处置：CPAP 压力滴定

第 4 日：CPAP 压力滴定因幽闭恐惧症失败；处置：面更换鼻枕，日间脱敏；

第 5 日：压力滴定成功，患者自觉日渐嗜睡明显好转，同时给予房颤射频消融治疗，转为窦律。

检验检查记录：

冠脉 CTA：轻度狭窄。

UCG：左房扩大（40.4mm）左室壁非对称性肥厚，考虑肥厚非梗阻性心肌病，

BNP 升高，血糖、血脂高，肌酐、尿酸高。

holter：房颤，室早 2772

重度 OSA，AHI：37.6，最低血氧：37%

鉴别诊断：

心房扑动：典型心电图表现为规则锯齿状 F 波（心房率 250-350 次 / 分），心室率多规则。不支持点：本例心电图已明确为房颤（f 波伴 RR 间期绝对不齐）。

慢性肺病 / 肺栓塞：D- 二聚体升高、血气示低氧血症，可伴咯血、胸痛。排除：D- 二聚体阴性，血气正常，无呼吸系统症状。

其他：

法布雷病心肌病合并房颤的冷冻消融治疗 1 例

李远翥

重庆医科大学附属第一医院

患者基本信息：

患者，女性，50 岁，因“反复心前区闷痛 6 年，加重伴心悸 1 d”于 2021 年 9 月 24 日入院。

患者以反复心前区闷痛为主要表现，呈阵发性，活动后加重，休息后缓解，伴心悸、乏力，不伴夜间憋醒、下肢水肿。20 年前母亲因“心脏疾病”去世。

主述：

反复心前区闷痛 6 年，加重伴心悸 1 天

现病史：

患者 6 年前起无明显诱因反复出现心前区闷痛，阵发性发作，活动后加剧，休息后缓解，不伴夜间憋醒、下肢水肿等。患者 4 年前于外院就诊，心脏彩超示左心室增厚（14 mm），动态心电图示窦性心动过缓、频发房性早搏、短阵房性心动过速。冠状动脉造影提示左侧冠状动脉回旋支细小，余血管造影未见明显异常。给予“参松养心胶囊”等治疗后，症状稍缓解，但仍反复发作。入院 1 d 前上述症状再次发作，程度较前明显，伴心悸，自觉心跳不整齐，为进一步诊治来我院急诊。急诊心电图提示“心房扑动”，以“心律失常”收入心血管内科住院。

既往病史：

患者 4 年前于外院诊断“慢 - 快综合征”，否认高血压、糖尿病、冠状动脉粥样硬化性心脏病史。

病程记录：

患者入院后予以胺碘酮 600 mg 微量泵泵入转律，达比加群酯 110 mg、2 次 / d 口服抗凝，呋塞米 20 mg 隔日一次利尿，后转为窦性心律。但患者心悸症状反复发作，窦性心律时心率慢，不宜使用抗心律失常药物预防心房颤动、心房扑动发作。和患者沟通后行“双侧肺静脉冷冻消融术”。

检验检查记录：

入院后完善相关检查，血气分析、血常规、肝肾功、凝血功能、电解质、血脂未见明显异常；心肌损伤标志物：肌钙蛋白 I 0.27 ng/ml（升高 15 倍）、N 端脑钠肽前体 3910 pg/ml。

心电图：患者入院后心电图提示：心房扑动 2-3:1 下传；恢复窦性心律后的心电图提示窦性心动过缓，左室肥厚；患者再次发作时心电图提示快速心室率房颤；患者冷冻消融术后心电图转为窦性心律。

心脏彩超：左室射血分数 65%，室间隔舒张末厚度 15 mm，左室后壁舒张末厚度 15 mm，心尖部最厚处 18 mm，左室舒张功能减退。

动态心电图：窦性 + 异位心律，总心室率 75902 次，最快心室率 136 次 /

min，最慢心室率 36 次 /min，平均心室率 53 次 /min，多源性室上性早搏 3401 次，室性早搏 2 次，最长 R-R 间期为 2.14 s。

动态血压：24 h 平均血压 120/72 mmHg，白天平均血压 121/72 mmHg，夜间平均血压 118/72 mmHg。

心脏核磁共振：心尖部及左心室中部壁弥漫性增厚，心尖处明显，舒张期最厚处约 21 mm，考虑肥厚型心肌病可能。

基因检测：GLA 基因突变伴 α- 半乳糖苷酶 A（Alpha-galactosidase A, α-Gal A）活性降低，酶代谢底物脱乙酰基三己糖酰基鞘脂醇（Globotriaosylsphingosine, Lyso-GL-3）浓度增高。

鉴别诊断：

1. 肥厚型心肌病：患者心室肥厚，需与肥厚型心肌病鉴别，但肥厚型心肌病多以室间隔不对称肥厚为主，该患者室间隔和左室后壁均匀增厚，不符合典型的肥厚型心肌病的心脏彩超特征；2. 高血压性心脏病：高血压常导致室间隔和左室后壁均匀性增厚，但该患者无高血压病史，其入院后的动态血压也未提示高血压，故可排除；3. 其他引起左室肥厚的疾病如淀粉样变、主动脉瓣狭窄、运动员心脏等，结合该患者的病史和辅助检查可除外。

其他：

本例为首例未接受 ERT 的法布里病患者经冷冻消融成功控制房颤的报道。分子机制研究通过 SWISS-MODEL 模拟及 JAMDA 分子对接证实：E358del 突变导致 α- 半乳糖苷酶 A 结构关键位点（W236/S276/D335/N408）构象改变，显著削弱其与底物 Gb3 的结合能力（JAMDA 评分：野生型 -3.80 vs 突变体 -4.80，P<0.05）。患者表现为迟发型心脏局限型法布里病（50 岁起病且无经典全身症状），冷冻消融术后 2 年维持窦律，提示该技术可作为 ERT 禁忌或拒绝患者的替代治疗方案。

Congenitally Corrected Transposition of the Great Arteries with Altered Structure

Gebremichael Mekonnen Hailemichael 范翼展 何美娇

哈尔滨医科大学附属第一医院

患者基本信息：

A 51-year-old male with a history of tobacco and alcohol use for 30 years, as well as a history of Atrial Fibrillation for 5 years

主述：

Dyspnea following physical exertion for one week

现病史：

A 51-year-old male presented to the Emergency Department with a chief complaint of dyspnea following physical exertion for one week. The patient reported experiencing nocturnal dyspnea, with relief being felt while assuming an upright position. Two days ago, the patient exhibited worsened shortness of breath, leading to multiple awakenings during the night. This was followed by feelings of fatigue, dizziness and peripheral edema.

既往病史：

A history of tobacco and alcohol use for 30 years, as well as a history of Atrial Fibrillation for 5 years

病程记录：

The bradycardia required pacing. However, it was hypothesized that there was a SA node damaging characteristics from the calcified RCA. Following a consensus discussion in the cardiology department, patient was promptly referred to the catheterization laboratory for Coronary Angiography (CAG) initially, while ensuring their safety through the use of a temporary pacemaker. Fortunately, there was no stenosis of the RCA detected. Therefore, the patient had the placement of a permanent pacemaker with dual chamber leads after three days in order to facilitate the elimination of anticoagulant and antiplatelet medications used during CAG and to sustain sinus rhythm. In addition, the patient received recombinant human brain natriuretic peptide, furosemide, and empagliflozin to stabilize their condition while in the hospital. Upon discharge, the patient was prescribed Sacubitril Valsartan/Angiotensin Receptor Neprilysin Inhibitor, Empagliflozin and Rosuvastatin to manage their symptoms.

检验检查记录：

The patient exhibited elevated concentrations of Cardiac Troponin I (cTnI) (686 pg/ml, reference range: 0-32.4pg/ml) and N-Terminal prohormone Brain Natriuretic Peptide (NT-proBNP) (3794pg/ml, reference range: 0-300pg/ml). The ECG test confirmed the presence of Atrial fibrillation along with a complete Atrioventricular (AV) block. In addition, the patient's Chest X-ray displayed a dextrorotatory enlarged heart with consolidation, indicating the presence of cardiomegaly and possibility of pulmonary edema. The echocardiography showed that the patient's aorta was positioned anteriorly and the pulmonary artery posteriorly. The echocardiogram additionally identified the presence of a tricuspid valve connecting the left atrium to the right ventricle, and a mitral valve connecting the right atrium to the left ventricle. Furthermore, the Doppler echocardiogram revealed a significant Tricuspid Regurgitation (TR), raising suspicion of congenitally corrected transposition of the great arteries (ccTGA) as the underlying condition and heart failure as the trigger for dyspnea. However, the morphological right ventricle's ejection fraction remained preserved at 54%. To establish a proper diagnosis, a CT Angiography (CTA) of the heart, pulmonary arteries and coronary arteries was selected by the treating physician. CTA of the heart showed a dextral orientation with intact atrial and interventricular septum. Moreover, abnormal atrioventricular connections were present along with the transposition of the left and right ventricles with the great arteries. The pulmonary arteries were also located posterior to the aorta. This confirmed ccTGA. Meanwhile, the CTA of the Pulmonary arteries exhibited some dilatation, CTA of the coronary arteries revealed a calcification in the Right coronary artery (RCA)

鉴别诊断：

Acute coronary syndrome; Sick sinus-node syndrome

其他：

心脏“别墅户型”，大空间到让您无依无靠！

李艳杰

上海市胸科医院

患者基本信息：

女，75 岁。身高：150 cm，体重：35 kg，职业：离退休，民族：汉族，出生地：上海，婚姻：已婚，国籍：中国，户籍：上海。

主述：

二尖瓣置换术后 12 年，反复胸闷气急 2 周

现病史：

患者 12 年前因反复活动后胸闷不适查心超：“风心病，联合瓣膜病变：二尖瓣重度狭窄，主动脉瓣中度狭窄伴轻度反流，三尖瓣中重度反流伴中重度肺动脉高压，LVEF 78%，双房增大，右室增大”。2013-3-26 于我院全麻体外下行 DVR+TVR+ 消融术后（置换瓣膜均为生物瓣膜）。2023.6.20 因交界性逸搏于我院行起搏器植入术（经导管植入式无导线起搏系统 MC1VR01，单腔，美敦力，兼容 MRI）。近 2 周来患者无明显诱因下出现反复胸闷气急不适，伴双下肢水肿，无明显咳嗽咳痰、头晕头痛、胸痛、腹痛腹胀、乏力纳差等症状，夜间平卧时亦有胸闷不适，现为进一步诊治收住入院。

既往病史：

2013 年行心脏生物瓣膜置换术，2023 年行心脏起搏器植入，否认高血压、糖尿病病史和药物过敏史。

病程记录：

入院后完善相关检查，评估病情。予抗凝、利尿、扩冠、平喘、化痰、无创正压通气、改善心功能等综合治疗。经详细心脏超声、心脏 CTA 评估后于 2025-05-27 全麻下行经导管二尖瓣瓣中瓣植入，术后患者恢复良好，胸闷气急等症状较前明显好转出院。

检验检查记录：

2025-05-07 心电图：心房颤动，心室按需型起搏（VVI 起搏）70bpm。

2025-05-08 冠脉 CTA：LAD 近段管壁局限性钙化斑块，管腔轻度狭窄；中段局部显影欠清。RCA 远段管壁局限性钙化斑块，管腔轻度狭窄。附见心脏明显增大。二尖瓣、主动脉瓣及三尖瓣术后。升主动脉增宽。肺高压。请结合临床。2025-05-09 胸片：心脏术后，心影增大。

2025-05-23 腹部彩超：肝内实质病灶，血管瘤可能，胆囊结石，左肾囊肿，肝门部门静脉、脾静脉未见明显异常，胰、脾未见明显异常。

2025-05-27 心脏超声：二尖瓣、主动脉瓣及三尖瓣生物瓣置换术后， 二尖瓣生物瓣功能异常， 二尖瓣生物瓣反流（重度）。

2025-05-28 心脏超声：二尖瓣位生物瓣瓣中瓣术后，主动脉瓣及三尖瓣生物瓣置换术后随访， 三尖瓣位生物瓣功能异常，肺高压，升主动脉增宽，左室壁节段性收缩活动异常，右室壁收缩活动未见明显异常。

鉴别诊断：

1. 感染性心内膜炎：感染性心内膜炎可导致心脏瓣膜损害，出现赘生物。患者常有发热、寒战、皮肤瘀点等表现。血培养常阳性，超声心动图可发现瓣膜上的赘生物。

2. 老年性退行性瓣膜病：随着年龄增长，瓣膜发生退行性变，常见于主动脉瓣。患者多无明显症状，或仅有轻微的心悸、气短。超声心动图可显示瓣膜钙化、增厚等改变。

3. 心肌病：心肌病如扩张型心肌病、肥厚型心肌病等，可能影响心脏的整体功能，导致类似心脏瓣膜病的症状。但心肌病主要是心肌本身的病变，通过心肌活检、心脏磁共振等检查可与心脏瓣膜病鉴别。

其他：

患者老年女性，体质瘦弱（术前体重：34kg），二尖瓣生物瓣膜衰败，双房显

著增大（右房：109 cm X 73 cm，左房内径：56 cm）；由于解剖条件较差（双房大、心室内径正常），无法常规行经导管二尖瓣瓣中瓣植入，选择经股动静脉建立全轨道将球扩瓣送至二尖瓣瓣环，顺利完成介入手术。

复杂腹主动脉瘤介入治疗 1 例

王亚松

中国人民解放军北部战区总医院

患者基本信息：

患者，男，57 岁，发作性腹痛一个月，外院复查 CTA 提示肾下腹主动脉瘤，瘤体直径 5.8cm，长度 12.5cm，为进一步诊治。就诊于我院，既往有冠心病史 15 年，曾行 PCI 植入冠状动脉支架 4 枚，冠状动脉药物球囊扩张成形术 2 次。目前患者无心衰症状，既往高血压病史 20 余年，，血压最高 180/110mmHg，血压控制一般，高脂血症 10 余年。现应用英克司兰控制血脂，血脂控制一般，无吸烟、饮酒史

l 患者影像学特征

① 瘤体直径大 58mm

② 病变长度长 125mm

③ 若按照常规低肾动脉（右肾）动脉为基准测量瘤颈，瘤颈长度约 20mm，但是梯形瘤颈变化过大，低肾动脉下沿主动脉 21.6mm，低肾动脉下沿 10mm 处主动脉 27mm，低肾动脉下沿 20mm 处主动脉 30.6mm

④ 左髂总动脉近端直径 16.7mm，中段直径 14.7mm，远端直径 14.1mm

⑤ 右髂总动脉近端直径 19.5 mm；中段 20.2mm；远端 15mm

⑥ 双侧股动脉钙化，左侧更为显著。

⑦ 右肾动脉开口向上，直径 5.7mm，左肾动脉近段 20%~30% 狭窄

l 根据上述所描述的患者腹部血管特点，拟采取以下手术策略，

① 延长瘤颈铆定区，防止内漏。采用肾动脉“烟囱支架”术式。

② 右肾动脉口部至腹主动脉植入肾动脉支架，内侧植入腹主动脉覆膜支架，最终对吻扩张

③ 左侧股动脉钙化严重。采取右侧股动脉作为支架主体入路，尽量防止左侧股动脉缝合并发症。

④ 入路选择为采用右肱动脉进行主动脉造影及肾动脉支架植入，双侧股动脉为腹主动脉“人字形”支架植入入路。

l 手术流程

① 穿刺：患者取平卧位，双侧腹股沟区、下腹部及右侧肱动脉术区常规消毒、铺巾。穿刺双侧股动脉术区，预埋 ProGlide 血管缝合器，置入 10F 动脉鞘，穿刺右侧肱动脉术区，置入 6F 动脉鞘。

② 首先进行肾动脉支架预埋：经加长超滑导丝推送 JR 3.5 6F 指引导管至右肾动脉开口，送导丝顺利通过右肾动脉开口至其远端，经导丝推送 BLUE 5.0mmx18m 支架至右肾动脉近段。

③ 腹主动脉覆膜支架主体植入：于右股动脉经导丝送 6F”黄金猪尾型”导管顺利至降主动脉，精准测量，交换 260mm 支架专用加硬导丝，退出右股动脉 10F 动脉鞘，经加硬导丝推送 Medtronic ENBF 3216C170EE 覆膜支架主体至右肾动脉下沿水平，造影定位后。先逐节释放覆膜支架主体至左侧分支释放处，固定支架主体部分。

④ 术前测量右肾动脉内径 5.7mm，拟植入 BLUE 5.0mmx18m 支架，调整右肾动脉支架近端与覆膜支架上端平齐，以 20ATM 释放肾动脉支架，留置支架球囊于原位备用。

⑤ 左侧分支覆膜支架植入：左侧支架长度 120mm，远端直径 16mm，左股动脉经导丝送 6F 右冠造影导管穿覆膜支架主体顺利至降主动脉，经导管交换 260mm 支架专用加硬导丝，退出左股动脉 10F 动脉鞘，经左股动脉加硬导丝推送 Medtronic ENLW1616C120EE 覆膜支架分支，与支架主体重叠 30mm，后撤支架系统，固定止血，复查造影显示支架扩张满意

⑥ 释放覆膜支架主体：释放剩余部分支架主体，造影示支架远端进入右髂总动脉，长度约 10mm，髂总锚定长度不足，决定远端再次植入 1 覆膜支架，经右股动脉加硬导丝推送 MedtronicENLW1616C95EE 覆膜支架分支（覆膜支架长度 95mm，直径 16mm），近端定位于右髂总动脉末端，造影示支架膨胀良好。

⑦ 球囊后扩张：经硬导丝送 Medtronic AB46 球囊至腹主动脉及左、右髂动脉覆膜支架内行后扩张，其中肾动脉支架球囊与腹主动脉腹膜支架近端对吻扩张，先各自扩张，最后对吻扩张，其他重叠处及远端扩张。主动脉造影示支架膨胀良好。

⑧ 入路处置：右股动脉缝合后搏动良好，左股动脉缝合后搏动较弱。进行选择性造影示左髂外动脉夹层，股动脉闭塞。股动脉有自身侧支形成，有前向血流。经右股动脉入路行闭塞处球囊扩张后，造影示残余狭窄夹层，最后植入 VI-ABAHN 8mmX10cm 带膜支架。双球囊后扩，因支架直径大，选用两大口径球囊（Emerge 3.0mmX15mm 球囊、Quantum 5.0mmX12m 球囊）扩张。

⑨ 肱动脉鞘管于术后 30 分钟后拔除，压迫止血 20 分钟。包扎固定。

⑩ 穿刺口无感染、出血，动脉搏动良好。

主述：

发作性胸痛 15 年， 发作性腹痛 1 月余

现病史：

患者男，57 岁，发作性腹痛一个月，外院复查 CAT 提示下腹主动脉瘤，瘤体直径 5.8cm，长度 12.5cm，为进一步诊治就诊于我院

既往病史：

冠心病史 15 年，曾行 PCI 植入冠状动脉支架 4 枚，冠状动脉球囊扩张成形术 2 次。目前患者无心绞痛症状，既往高血压病史 20 余年，血压最高 180/110mmHg，血压控制尚可高血脂症 10 余年，现应用英克司兰控制血脂。无吸烟、饮酒史

病程记录：

入院情况：患者因“发作性胸痛 15 年，发作性腹痛 1 月余”为主诉入院。1. 中老年男患，既往高血压、高脂血症病史；2. 患者 2010 年起多次出现心肌梗死，多次行冠状动脉介入治疗，仍有胸痛间断性发作，近 1 个月，患者自觉腹痛，2025 年 6 月 3 日于外院行胸腹主动脉 CTA 示：腹主动脉瘤伴腹壁血栓形成。今为行进一步诊治，门诊以“腹主动脉瘤”收入院。3. 查体：BP:150/89mmHg，双肺听诊呼吸音清，未闻及干湿啰音，心率：75 次 / 分，律齐，各瓣膜听诊区未闻及病理性杂音，双下肢无水肿。4. 入院心电图示：窦性心律， II 、III、AVF 导联呈病理性 q 波。

入院诊断：1. 腹主动脉瘤 2. 冠状动脉粥样硬化性心脏病 2.1 陈旧性前间壁心肌梗死 2.2 冠状动脉支架植入术后 3. 高血压 3 级 很高危 4. 高脂血症

诊疗过程：入院后给予抗血小板聚集、降压、调脂、稳定斑块等治疗；2025-06-09 行主动脉造影：肾动脉下腹主动脉瘤，瘤体直径 58mm，瘤颈短。延长锚定区，右肾动脉植入 BLUE 6×18mm 支架，于腹主动脉支架主体呈“烟囱型”，右侧上 Medtronic ENLW 1616C95EE，左侧接 Medtronic ENLW 1616C120EE，无内漏，左股动脉缝合后造影见左股动脉夹层闭塞，植入 GORE 公司 VBHR081002 覆膜支架。现患者生命体征相对平稳，要求出院，请示上级医师准予出院。

出院诊断：1. 腹主动脉瘤 2. 冠状动脉粥样硬化性心脏病 2.1 陈旧性前间壁心肌梗死 2.2 冠状动脉支架植入术后 3. 高血压 3 级 很高危 4. 高脂血症

出院情况：患者无胸闷、气短及心前区疼痛，双肺呼吸音清，未闻及干湿啰音，律齐，各瓣膜听诊区未闻及病理性杂音。术区好，无血肿及渗出。请示上级医师准予出院。

出院医嘱：

1. 保持心情愉悦，避免情绪激动、剧烈运动、过度劳累、熬夜、精神过度紧张，避免受凉感冒。作息规律，低盐低脂饮食，减轻体重，戒烟酒，避免被动吸烟，保持大便通畅。避免行磁共振检查。

2. 继续药物治疗：

1）抗血小板凝集：阿司匹林肠溶片 100mg（1 片），1/ 日，长期；替格瑞洛片（倍林达）90mg（1 片），口服，2/ 日，至 PCI 术后 1 年；服用期间注意皮肤粘膜有无出血倾向，如有出血倾向请及时就诊；服用期间若出现停服或漏服将会增加心肌梗死、支架血栓甚至危及生命的风险！

2）调脂、稳定斑块：阿托伐他汀钙片（立普妥）20mg，口服，1/ 晚，低密度脂蛋白控制在 1.4mmol/L，服药期间注意定期检查肝功、如出现肌肉疼痛、肌肉无力、肝酶升高等情况请停药就医；

3）控制血压、改善心室重构：沙库巴曲缬沙坦 100mg，口服，2/ 日； 注意监测血压，根据血压调整用药，血压控制在 130/80mmHg 即可，避免过低；若血压< 100/60mmHg，应逐渐减量至停药。

3. 出院每 6 个月复查胸腹主动脉 CTA，此后每年复查胸腹主动脉 CTA，定期复查血常规、凝血、便潜血、肝肾功、血脂、离子、心脏超声及心电图。

4. 有症状时复查造影，病情变化随诊。

检验检查记录：

详见 PPT

鉴别诊断：

与血管疾病鉴别：主动脉夹层：假性动脉瘤：穿透性主动脉溃疡：

与急腹症鉴别：急性胰腺炎：肠梗阻：肾结石：

与其他腹部疾病鉴别：腹主动脉周围炎：腹型霍奇金淋巴瘤：腹主动脉分叉处恶性肿瘤：

其他：

详见 PPT

大动脉炎合并主动脉瓣关闭不全 1 例

欧尾妹

厦门大学附属心血管病医院

患者基本信息：

患者女，52 岁

主述：

体检发现异常 10 年，反复胸闷 1 年余，再发 3 天

现病史：

缘于 10 年前体检时心脏彩超提示“中度主动脉瓣反流“，4 年前复查心脏彩超提示”重度主动脉瓣反流“，否认胸闷痛、气喘乏力等不适。1 年余前无明显诱因开始出现胸闷，伴头晕，自诉活动后症状可缓解，无心悸、气促，无头晕、黑朦及晕厥，无恶心、呕吐，无咳嗽、咳痰等，未诊治。此后上述症状反复发作，8 个月前再次出现胸闷、头晕，就诊我院，查心脏彩超示“重度主动脉瓣反流”，颈动脉彩超示“双侧颈动脉球部狭窄（70-99%），右侧颈内动脉几近闭塞；双侧颈外动脉狭窄”，肾动脉彩超示“双肾动脉狭窄”，2024-8-22 行冠脉造影检查示：冠脉起源未见异常，右冠优势型；LM 未见异常；LAD 未见异常，TIMI 3 级；LCX 未见异常，TIMI 3 级；RCA 近段可见粥样硬化斑块，TIMI 3 级。肾动脉造影示：左肾动脉近段狭窄 50%，右肾动脉近段狭窄 50%。结合病史，考虑” 大动脉炎 “，建议规律药物治疗。3 天前活动后再发胸闷不适，呈紧缩感，伴双侧下颌及左肩放射痛，测得血压显著升高，予降压药口服半小时后上症缓解，不伴咳嗽、咳痰，无面色苍白、大汗，无头晕、头痛、黑矇、晕厥等不适，今为复查再诊我院门诊，完善检查提示 “重度主动脉瓣反流；腹主动脉肝后段狭窄（峰值压差 87mmHg）、中度肺动脉高压可能，N 端 -B 型钠尿肽测定 5205 ng/L”，遂以 “ 大动脉炎，主动脉瓣关闭不全” 收入院

既往病史：

大动脉炎病史 19 年，未规律治疗；肾动脉狭窄、腹主动脉狭窄病史 10 年；高血压病史 3 年，长期服用” 沙库巴曲缬沙坦、螺内酯、氨氯地平 “，后因肌酐、血钾上升，改为 “氨氯地平、阿罗洛尔”

病程记录：

患者中年女性，既往有大动脉炎等病史，以“体检发现异常 10 年，反复胸闷 1 年余，再发 3 天” 为主诉入院，入院后完善相关检查，彩超提示左室扩大、重度主动脉瓣关闭不全，于 2025-5-15 行右心导管检查提示毛细血管后混合性肺动脉高压，合并多发性大动脉炎、经动脉严重狭窄，外科风险高危，经结构组医师团队评估，有行经导管 TAVR 指征，结合患者及其家属意愿，于 2025-5-21 行全麻下经心尖 TAVR 手术，术后复查心脏彩超提示主动脉瓣人工瓣膜位置及功能正常，好转出院。术后 1 月复查心脏彩超提示主动脉瓣人工瓣膜位置及功能正常，症状明显改善。

检验检查记录：

NT-proBNP：5205 ng/L　hs-CTNT: 14.7 ng/L，ESR：6.5 mm/H（2024-9-3：17mm/H），hs-CRP：1.01 mg/L，肝、肾功能、电解质、凝血功能、糖化血红蛋白、甲功、感筛未见异常。

2025-5-13 术前彩超：重度主动脉瓣关闭不全，腹主动脉肝后段狭窄（峰值压差 87mmHg），升主动脉、肺动脉增宽，左心扩大，左室壁增厚，中度肺动脉高压可能

轻度三尖瓣反流，轻度二尖瓣反流，左室整体收缩功能正常，舒张功能减退。

2025-5-15 右心导管检查：右房 15/5（9），右室 53/7（28），肺动脉 53/27（37），肺小动脉楔压 32/8（25），主动脉压为 111/75（87）mmHg。计算 QP/QS=1，肺总阻力 10.75wood，肺小阻力 3.49wood，CI=2.63 L.min-1.m-2

1，肺总阻力 10.75wood，肺小阻力 3.49wood，CI=2.63 L.min-1.m-2

鉴别诊断：

风湿性心脏病，缺血性心脏病，扩张性心脏病，

其他：

BECARE 技术开通 CTO 一例

陈根锐

西京医院

患者基本信息：

76 岁 男性

主述：

间断胸痛 5 年，加重半年

现病史：

患者于 5 年前无明显原因出现胸痛不适，每次持续 10-20 分钟，以劳累后为著，休息可缓解，一直未重视及诊治，半年前胸痛症状加重，静息也可发作，就诊于当地医院，行 CAG 后提示 :RCACTO（严重钙化）、LAD 严重狭窄（严重钙化）。建议 CABG，患者拒绝，当地医院于 LAD 中段植入 1 枚支架，近端因严重钙化，高压球囊扩张失败，为进一步介入治疗，遂来我院。

既往病史：

高血压病史 20 年，最高 160/110mmHg，口服降压药物，血压控制可

病程记录：

患者于 5 年前无明显原因出现胸痛不适，每次持续 10-20 分钟，以劳累后为著，休息可缓解，一直未重视及诊治，半年前胸痛症状加重，静息也可发作，就诊于当地医院，行 CAG 后提示 :RCACTO（严重钙化）、LAD 严重狭窄（严重钙化）。建议 CABG，患者拒绝，当地医院于 LAD 中段植入 1 枚支架，近端因严重钙化，高压球囊扩张失败，为进一步介入治疗，遂来我院。

检验检查记录：

心电图：II III AVF ST 段压低，T 波倒置

鉴别诊断：

患者于 5 年前无明显原因出现胸痛不适，每次持续 10-20 分钟，以劳累后为著，休息可缓解，一直未重视及诊治，半年前胸痛症状加重，静息也可发作，就诊于当地医院，行 CAG 后提示 :RCACTO（严重钙化）、LAD 严重狭窄（严重钙化）。建议 CABG，患者拒绝，当地医院于 LAD 中段植入 1 枚支架，近端因严重钙化，高压球囊扩张失败，为进一步介入治疗，遂来我院。

其他：

无

经导管二尖瓣 “环中瓣” 植入术 1 例

席子惟

首都医科大学附属北京安贞医院

患者基本信息：

男性，64 岁

主述：

发现二尖瓣关闭不全 30 余年，二尖瓣修复术后 2 年

现病史：

患者 30 余年前体检发现 “二尖瓣关闭不全”，未规律随访。2 年前出现间断心前区不适，就诊于我院，查超声心动图示 LVEF68%，LVEDD 55mm，二尖瓣前后叶脱垂，二尖瓣关闭不全（重度），行外科 CABG （SVG-LAD, SVG-DI-OM）+ 二尖瓣成形术（Edwards 520034#）+ 三尖瓣成形术 + 卵圆孔未闭缝合术。3 天前患者复查超声心动图示 CABG+ 二、三尖瓣成形 + 卵圆孔未闭修补术后，左房增大，肺动脉及分支增宽，二尖瓣反流（重度）。为求进一步治疗来我院。

既往病史：

存在高血压病史 6 年，存在阵发性心房颤动病史、甲状腺功能减低 2 年。

病程记录：

术前讨论

患者既往曾行 CABG+ 二、三尖瓣成形 + 卵圆孔未闭修补术，二次外科开胸手术风险较高，可考虑行经导管二尖瓣 “环中瓣” 植入术。

既往植入 Edwards Physio II 34，true IA 616 mm^2，该成形环形态、尺寸如下图所示。Physio II 为半刚性完全环，透视下可显影。

经导管二尖瓣置换术专用器械尚处在临床试验阶段，目前临床中常用 Edwards SAPIEN 3 经导管主动脉瓣系统。29mm Edwards SAPIEN 3 经导管心脏瓣膜在 Physio II 34mm 成形环中的形态如下图所示。

检验检查记录：

入院检查: Bp 130/76 mmHg，身高 171cm，体重 62 kg。双肺未闻及干湿性啰音，心率 75 次 / 分，律齐，二尖瓣瓣听诊区可闻及收缩期 2/6 级杂音，双下肢无水肿。Cr 72.6umol/L，eGFR 95.08ml/min×1.73m2，Hb 130 g/l，PLT 81*10^9/L，BNP 142 pg/ml。

入院后经食道超声心动图：左室收缩末期内径 38mm，舒末内径 58mm，LVEF 62%，左房 47*48*60mm，右房 39*52mm，二尖瓣瓣环回声增强，二尖瓣对合点后移，对合不良，以 3 区和后交界区为著，二尖瓣房侧大量反流信号，VC-width 6mm，EROA 0.44cm^2，Rvol 88ml。 三尖瓣瓣环回声增强，收缩期房侧少量反流信号。

鉴别诊断：

-

其他：

术者心得

1. 使用 Edwards SAPIEN 3 瓣膜行经导管二尖瓣瓣膜置换术（TMVR）需要一个着陆区来锚定瓣膜，主要用于外科手术高危的人工生物瓣膜衰败（瓣中瓣 MViV）、二尖瓣瓣环成形术后（环中瓣 MViR）的患者，或存在二尖瓣瓣环钙化（ViMAC）的患者，既往有研究显示 TMVR 手术中 ViV 占比 78%，ViR 占比 11.7% ，ViMAC 占比 10.3%，比较不同 TVMR 的术后 30 天内死亡率发现，VIV<vir<vimac（J Am Coll Cardiol. 2021;78(23):2326-2353.）；

2. MViR 是否可行取决于成形环的成圆能力和锚定能力，MViR 要求经导管瓣膜与成形环之间有超过 270 度的贴合以提供充分的锚定作用，并降低瓣周漏风险；因此包括 Edwards GeoForm、Metronic Profile 3D 等偏心的刚性完全环可供锚定但却难以成圆，会导致 THV 膨胀不全、变形和瓣周漏则并不适宜行 MViR；而柔性不完全环可成圆但却无法提供有效支撑；半刚性完全环则较为理想；

3. 术前需谨慎评估二尖瓣植入人工瓣膜后的流出道梗阻风险。通常二尖瓣人工瓣膜植入后新 LVOT（neo-LVOT）的面积会较术前明显减小，器械形态及与主动脉瓣的相对位置关系是影响 LVOT 梗阻风险的重要因素，目前认为 neo-LVOT 面积小于 1.9 cm^2 时，梗阻风险较高；

4. MViV 和 MViR 术中房间隔穿刺是非常重要的一步，房间隔的穿刺位置可直

接影响手术的难度与风险，与 TEER 手术不同的是，MViV 和 MViR 的理想穿刺点通常是下、后位，穿刺点高度距离二尖瓣环至少 3.5cm（Ann Cardiothorac Surg. 2021;10(1):96-112.）；

6. 术前充分了解既往成形环和人工瓣膜的特征与形态，通过影像综合评估患者的解剖特征，对 MViV 和 MViR 术来说至关重要。

可操控鞘管联合新型穿刺导丝在下腔静脉迂曲患者中成功实施经房间隔穿刺术一例

陈桐帅

山东大学齐鲁医院

患者基本信息：

患者老年女性，73 岁

主述：

反复心悸 2 年余，加重半年。

现病史：

患者 2 年余前无明显诱因出现间歇性心悸，未予重视，未系统治疗。近半年心悸明显加重，呈持续性，伴活动后乏力，无晕厥、胸痛等不适。门诊心电图提示持续性房颤，拟行射频消融治疗。

既往病史：

有高血压病史 10 年，规律服药控制尚可。无冠心病、糖尿病、脑卒中病史。无手术史，否认过敏史。

病程记录：

患者在局麻与深镇静下接受持续性房颤射频消融术。初次经右侧股静脉使用 SL1 鞘管进行房间隔穿刺失败，造影显示右侧股静脉严重迂曲。改用对侧股静脉进鞘至下腔静脉，推进 BRK 穿刺针时遇阻，且患者主诉腰背部疼痛。针拔出后可见其多处弯曲，提示下腔静脉显著迂曲。

随后尝试使用 8.5 Fr 可操控鞘管（CARTO VIZIGO ™）联合新型房间隔穿刺导丝（AccuSafe ™），鞘管顺利经右股静脉进入下腔静脉，并在 ICE 引导下成功对准卵圆窝。导丝轻推穿刺后自动形成 “J 形” 远端结构，顺利进入左上肺静脉，随后将鞘管推进至左心房。手术顺利完成，术中无并发症，术后 2 个月随访未见房颤复发或相关并发症。

检验检查记录：

心电图：持续性房颤，心室率快（图 1）

术中造影: 右侧股静脉及下腔静脉严重迂曲(图 2A),BRK 穿刺针严重弯曲变形(图 2B)

ICE 检查: 鞘管及导丝定位至卵圆窝 (图 3B) , J 形导丝顺利进入左房及肺静脉 (图 3D)

肺静脉造影：显示 Vizigo 鞘管顺利进入左房并完成肺静脉显影（图 4）

鉴别诊断：

1. 房颤伴左房血栓（术前经影像排除）

2. 先天性心脏病（否认相关病史及超声心动图支持）

3. 心脏结构性疾病导致的房性心律失常（术前心超未见明显结构异常）

其他：

反复室颤，缘由几何？

张睿

北京清华长庚医院

患者基本信息：

患者李 XX，64 岁，男性，2022 年 6 月 25 日经急诊入心脏监护室

主述：

发作性意识丧失 4 年，再发 1 天

现病史：

患者 4 年前晚餐后休息中有坐位转为立位行走时出现晕厥，晕厥前否认活动、饮酒、情绪激动、排尿等，家属诉发作时有跌倒，双眼上翻、牙关紧闭、四肢抽搐，持续数分钟意识自行恢复，否认二便失禁，否认头晕、黑矇，否认心悸，否认胸闷、胸痛等不适，就诊潞河医院完善检查示低钾血症（具体不详），头颅 CT 提示陈旧性脑梗死，予补钾治疗后出院。1 天前（2022-6-24 17:00）患者家中休息时无明显诱因出现晕厥，伴跌倒，持续约半分钟，后患者意识自行恢复，诉腰痛就诊我院，因患者为封控区人员入发热门诊进行诊疗，完善血电解质提示低钾血症、低镁血症(Mg 0.70 mmol/L, K 3.09 mmol/L),心肌损伤标志物 TnT-hs 0.0319 ng/mL, 心电图示波窦性心律，QTc 间期延长（511 ms）未见明显 ST-T 改变，CT 提示腰椎压缩性骨折，予对症止痛、补钾、补镁治疗，8 小时前心电监护过程中（2022-6-25 5:00）患者出现一过性意识丧失，心电监护提示室颤，颈动脉无法触及，双上肢强直，口唇发绀，即刻行床旁胸外按压，后患者意识恢复，心率恢复窦性心律，未诉明显胸痛、胸闷、憋气等不适，现为求进一步诊治收入我科。自发病来，患者饮食欠规律，睡眠可，二便正常，近期体重未见明显变化。

既往病史：

既往史：发现血压升高 5 年余，BPmax160/100mmHg，未监测血压，未用药。发现脑梗死 5 年，否认四肢活动不利、言语不利等后遗症，曾口服脑心通、银杏叶片治疗。4 年前诊断酒精依赖，曾就诊安定医院行戒断治疗 2 月，后患者规律口服精神类药物（具体不详），未戒酒。高脂血症时间不详，曾口服他汀类药物降脂，后自行停药。否认糖尿病、肾病病史，否认肝炎、结核等传染病史，3 年前外伤左手第四、第五手指缺如，否认其他外伤、手术及输血史，否认药物、食物过敏史。

个人史、婚育史、家族史：吸烟 35 年，20 支 / 天，未戒，饮酒 30 年，每日折合酒精 90g/ 天。否认家族遗传病史、猝死史，早发心脏病史。

病程记录：

2022-6-25 14:58、14:59 心电监护示 2 阵**尖端扭转型室速**，每阵持续 4s，后自行转复窦性心律，心室率 75 次 / 分，患者无心悸等不适主诉，血压 170/90mmHg。15:00 心电监护示**室性心动过速后出现室颤**，血压测不出，患者双眼上翻，牙关紧闭，四肢抖动，肌张力明显增高，考虑阿 - 斯综合征，立即予心肺复苏，先后予非同步 120j 电除颤 4 次，除颤后患者窦性心律无法维持，予患者急查血气、肝肾功能、心肌损伤标志物，并予利多卡因 0.1g 静脉注射后 10mg/min 静脉泵入，后患者转复窦律。血结果回报： K(Blood Gas) 2.69 ↓ (Low) mmol/L, 继续静脉补钾治疗。除颤后患者躁动不能配合治疗，期间仍有间断室早、室速均自行转复，为保护气道配合治疗，行镇静镇痛，气管插管保护气道，外接有创呼吸机辅助通气，后患者镇静状态，持续丙泊酚、右美托咪定镇静，利多卡因静脉泵入抑制室性心律失常发生，氯化钾静脉泵入补钾，可维持窦性心律。

治疗

1. 心律失常：完善全外显子基因检测后除外先天性长 QT 综合征，鉴于患者长期饮酒及应用精神类药物，考虑酒精相关低钾血症、低镁血症所致获得性长 QT 综合征可能性大，进而导致室性心动过速、室颤引起晕厥。予对症补钾、补镁治疗，监测血钾及 QTc，避免使用延长 QTc 药物；

2. 缺血性心脏病：患者老年男性，有高血压、高脂血症、脑梗、长期大量吸烟的 ASCVD 高危因素，监测心肌损伤标志物可见 CK-MB，MYO 及 cTnT 升高伴动态变化，需警惕急性冠脉综合征，且患者长期饮酒，需考虑酒精性心肌病可能，予依诺肝素抗凝，拟完善冠脉 CTA、或心肌 MRA 评估心脏情况，后因患者间断烦躁，不能配合，嘱患者出院后继续精神病专科治疗，待患者病情稳定后再次入院行冠脉造影评估病情；心功能方面，患者左心增大；左室整体收缩及舒张功能减低（左室射血分数 :33 %），考虑射血分数减低型心力衰竭诊断成立，予螺内酯、沙库巴曲缬沙坦治疗，后因患者血钾偏高暂停；

3. 精神方面：患者间断烦躁、言语错乱、不能配合医嘱，结合既往长期饮酒病史，考虑酒精戒断综合征，请回龙观医院精神病专科医生会诊，考虑酒精所致精神障碍，予地西泮 10mg tid，逐渐减量，辅以维生素 B1 营养神经治疗；

4. 感染方面：患者住院期间监测感染指标提示 CRP 持续升高，结合胸部影像学及痰培养考虑肺部感染，先后予特治星、头孢呋辛酯抗感染；

5. 血栓方面：患者下肢静脉超声提示双小腿肌间静脉血栓，CTPA 未提示肺动脉血栓形成，予低分子肝素抗凝治疗，出院后与利伐沙班 20mgQD 抗凝治疗。

检验检查记录：

1.ECG（2022-06-26）：窦性心动过缓，QT 间期延长（QTc 627ms）

2.24h 动态心电图（2022-7-5）： 1. 窦性心律（总心搏数 94204 次 平均心率 65bpm 最慢心率 46bpm 发生于 08:02 最快心率 121bpm 发生于 11:44）；2. 偶发房性早搏，可见成对型房早及短阵二联律；3. 短阵房性心动过速（共 1 阵 4 次 / 阵 频率 100bpm）；4. 偶发室性早搏；5. 可见 ST 段改变（心率增快时 ST 段呈水平型下移约 0.1mv, 持续时间 > 1 分钟）；6.QT 间期延长（最长 QT 间期 520ms QTc487ms 发生于 8:02)。

3.24h 动态血压（2022-7-5）：24 小时平均血压 100/64mmHg，心率 68 次 / 分，平均动脉压 76mmHg；

4. 全腹部 (上腹 + 下腹 + 盆腔)CT 扫描：不均匀脂肪肝，双肾小结石或肾动脉钙化，前列腺钙化

5. 头颅 CT：头颅 CT 平扫未见明显出血及骨折，请结合临床，必要时复查，腔隙性脑梗死，脑白质脱髓鞘改变，鼻窦炎。

6. 超声心动图：左心增大（左房 39*56*37mm，左室舒张末径：58 mm），左室整体收缩及舒张功能减低（LVEF 33%）。

7.CTPA：CTPA 未见明确肺栓塞。

鉴别诊断：

患者主因反复意识丧失入院，鉴别诊断方面需与：急性心肌梗死、肥厚型心肌病、心律失常、晕厥、肺栓塞、脑血管疾病、癫痫发作及颅内占位鉴别

其他：

Stanford A 型主动脉夹层诱发显著 T 波倒置：病例报告

王春玲

甘肃省人民医院

患者基本信息：

33 岁男性，因突发剧烈胸痛 6 小时就诊于会宁县人民医院急诊科。

主述：

突发胸痛 6 小时。

现病史：

一名 33 岁男性患者因突发剧烈胸痛 6 小时就诊于会宁县人民医院急诊科。其胸痛向背部、腰部及右下肢放射，并伴发右侧肢体轻偏瘫。患者有 6 年未控制的高血压病史。急诊查体示血压 174/78 mmHg，双上肢血压对称；双侧股动脉、胫后动脉及足背动脉搏动可触及且左右对称；体温正常。

既往病史：

患者既往高血压病史 6 年，未规律口服降压药物治疗。

病程记录：

入院后完善十二导联心电图示窦性心律伴室性早搏二联律：aVR 导联 T 波直立，I、II、III、aVL、aVF 及 V1-V6 导联广泛 T 波倒置，提示心肌缺血（图 1A、1B）。实验室检查：白细胞计数 12.9×10 ^{9} /L（参考值 4.0-10.0×10 ^{9} /L），D-二聚体 2.34 mg/L（参考值 <0.50mg/L）；心肌酶谱示肌钙蛋白正常，B 型利钠肽 724 pg/mL（参考值 0-100 pg/mL），肌红蛋白 220 ng/mL（参考值 0-107 ng/mL）；肾功能示肌酐 187 μmol/L（参考值 44-97 μmol/L），血清电解质提示低钾血症。基于胸痛症状及广泛导联 T 波倒置，临床拟诊急性冠脉综合征（ACS），给予抗血小板负荷量后遂急诊行冠状动脉造影，未见阻塞性冠状动脉病变。2020 年 12 月 7 日复查心电图示 I、II、III、aVL、aVF 及 V1-V6 导联 T 波倒置程度减轻（图 1C）。经胸超声心动图示升主动脉扩张（直径 38mm），左心室壁增厚，室壁运动弥漫性减低，其中心尖部运动弱于基底部，左心室射血分数 40%（图 2）。行胸腹 CT 血管造影确诊 Stanford A 型主动脉夹层（累及升主动脉至降主动脉），夹层未累及冠状动脉、双侧颈总动脉及左锁骨下动脉（图 3）。遂转入兰州大学第一医院进一步诊治。

检验检查记录：

入院后完善十二导联心电图示窦性心律伴室性早搏二联律：aVR 导联 T 波直立，I、II、III、aVL、aVF 及 V1-V6 导联广泛 T 波倒置，提示心肌缺血（图 1A、1B）。实验室检查：白细胞计数 12.9×10 ^{9} /L（参考值 4.0-10.0×10 ^{9} /L），D- 二聚体 2.34 mg/L（参考值 <0.50mg/L）；心肌酶谱示肌钙蛋白正常，B 型利钠肽 724 pg/mL（参考值 0-100 pg/mL），肌红蛋白 220 ng/mL（参考值 0-107 ng/mL）；肾功能示肌酐 187 μmol/L（参考值 44-97 μmol/L）。给予抗血小板负荷量后遂急诊行冠状动脉造影，未见阻塞性冠状动脉病变。2020 年 12 月 7 日复查心电图示 I、II、III、aVL、aVF 及 V1-V6 导联 T 波倒置程度减轻（图 1C）。经胸超声心动图示升主动脉扩张（直径 38mm），左心室壁增厚，室壁运动弥漫性减低，其中心尖部运动弱于基底部，左心室射血分数 40%（图 2）。行胸腹 CT 血管造影确诊 Stanford A 型主动脉夹层（累及升主动脉至降主动脉），夹层未累及冠状动脉、双侧颈总动脉及左锁骨下动脉（图 3）。

鉴别诊断：

急性心肌梗死： 患者均有突发胸痛 / 胸闷、呼吸困难、心电图 ST 段抬高或压低 /T 波倒置、心肌酶（肌钙蛋白、CK-MB）升高、左心室功能不全的表现。但是冠脉造影： 急性心梗通常可见明确的冠状动脉阻塞性病变（血栓、斑块破裂）。应激性心肌病冠脉造影通常正常或仅有轻度非阻塞性病变。应激性心肌病的心肌酶升高幅度通常低于同等程度心功能不全的急性心梗。急性心梗的心电图改变通常与特定冠脉供血区域一致，并随时间有特征性演变（如 Q 波形成）。应激性心肌病的 ST 段抬高常更弥漫，T 波倒置更深更广泛，且不出现病理性 Q 波（少数例外）。应激性心肌病特征性的心室中部和心尖部运动减弱 / 消失，而基底部运动代偿性增强（“章鱼篓” 样改变）。急性心梗的室壁运动异常通常与阻塞冠脉的供血区域一致（如左前降支阻塞导致前壁心尖部运动异常）。 应激性心肌病的室壁运动异常和心功能通常在数天至数周内显著改善或完全恢复，而急性心梗的恢复较慢且常遗留局部室壁运动异常。

其他：

一石二鸟–TEER 令 SAM 更美好！

李艳杰

上海市胸科医院

患者基本信息：

性别：男，年龄：69 岁，职业：离退休，民族：汉族，出生地：上海，婚姻：已婚，国籍：中国

主述：

胸闷气促半年余

现病史：

患者半年前起无明显诱因下出现反复胸闷气促不适，活动后加重。2 月前患者无明显诱因出现咳嗽、咳痰、咳血丝痰、盗汗等不适，2025-6-1 外院 CT 检查：右肺下叶占位，右肺门增大，右肺中叶支气管闭塞，右肺中叶肺不张。纵隔淋巴结肿大。考虑性质不清。2025-06-11 我院行肺穿刺活检明确肺占位性质。心超提示肥厚梗阻性心肌病，二尖瓣后叶瓣下腱索断裂伴脱垂可能，二尖瓣反流（中重度）；心电图：快房颤。予抗凝、控制心室率等治疗。

既往病史：

否认高血压、糖尿病、脑卒中等病史。

病程记录：

入院后完善相关检查，予以抗凝、控制心室率、利尿等治疗。评估病情，于 2025-07-03 全麻下行冠脉造影 + 经皮二尖瓣钳夹术：CAG 示 LAD 近段混合斑块，管腔 50% 狭窄; 中段心肌桥; LCX、RCA(-); 后成功实施二尖瓣钳夹术（Dragonfly 0612 夹合器）。术后复查心超提示轻微二尖瓣反流，SAM 明显减轻，效果满意。患者胸闷气促症状明显改善。

检验检查记录：

2025-06-09 肺 CT：右肺下叶肿块，考虑恶性病变可能。两肺慢性炎症，两肺上叶陈旧性病灶可能。右肺中叶实变不张。两肺泡性气肿。右肺门及纵隔肿大淋巴结影。两侧胸膜局部增厚。右侧胸腔少量积液。

2025-06-10 经胸心脏超声：肥厚型梗阻性心肌病声像图改变， 梗阻水平位于左室流出道，二尖瓣后叶瓣下腱索断裂伴脱垂可能，二尖瓣反流（中重度） 建议 TEE 进一步检查，升主动脉增宽，心包积液（少量），左室壁节段性收缩活动异常。

2025-06-12 经食道心脏超声：二尖瓣后叶瓣下腱索断裂伴脱垂，二尖瓣反流（中重度），梗阻性肥厚型心肌病。

2025-06-13 CT 报告：LAD 近段混合斑块，管腔中度狭窄；中段心肌桥。RCA 近、远段非钙化斑块，管腔中度狭窄。右后降支（R-PDA）非钙化斑块，管腔轻度狭窄。

鉴别诊断：

1. 缺血性心肌病：患者多存在心绞痛或心肌梗死病史多年，多出现活动后胸闷或夜间呼吸困难等心力衰竭症状，超声心动图示左室心腔扩大，EF 降低。行冠脉造影个明确诊断。

2. 退行性瓣膜病：可有心功能不全症状，有心脏杂音，无风湿热病史，心超检查可发现瓣膜病，心脏扩大，可鉴别。

其他：

该病例为二尖瓣 P3 脱垂合并 HOCM，1 区 SAM 但无明显反流，二尖瓣反流主要来源于 3 区；实施 TEER 有效解决 P3 脱垂和二尖瓣反流，并改善 SAM，患者获益显著。

多位点起搏间期的个体化优化新方法

刘元伟 Liu

清华大学附属北京清华长庚医院

患者基本信息：

患者，男性，83 岁

主述：

活动后气短 1 年余，加重 10 天

现病史：

患者 1 年前开始出现活动后胸闷、气短，下肢水肿，外院诊断为 “冠心病、心力衰竭”，给予优化心衰、抗栓、冠心病药物治疗症状减轻。10 天前开始出现咳嗽、咳痰、活动后气短加重，不能平卧，下肢水肿加重，并出现端坐呼吸，夜间阵发性呼吸困难。入院查体：BP130/72mmHg, 颈静脉充盈，双肺呼吸音粗，右下肺可闻及散在干、湿啰音。心界左大，心率 66 次 / 分，心律齐，未闻杂音及心包摩擦音，腹软，肝脾肋下未触及，双下肢轻度水肿。辅助检查：超声心动图：LVEDD 58mm，二尖瓣返流（中 - 大量），室壁节段性运动异常（下壁），左室收缩明显不同步，左室射血分数（LVEF）29%。心电图（图 1）：窦性心律，完全性左束支传导阻滞 (CLBBB)，QRS 172ms。胸片：右肺炎症，阻塞性炎症待除外，双侧胸腔积液。冠脉造影提示：LAD 远段局限性狭窄约 50%。NT-proBNP 3170pg/ml。

既往病史：

高血压 10 余年，慢性阻塞性肺疾病 10 余年

病程记录：

根据 2013ESC 器械置入指南，患者扩张性心肌病，心功能 III 级，完全性左束支传导阻滞，QRS > 150ms，左室射血分数 29%，具有心脏再同步化起搏及心脏复律除颤器（CRT-D）I 类指征。于 2017 年 2 月 27 日行 CRT-D 置入术，手术成功，顺利将左室四极导线置入左室侧静脉（图 1A）。设置 LV1（D1-P4）和 LV2（M3-RVcoil）左室双部位起搏。术后即刻默认设置为 LV1 → LV2 → RV 各领先 5ms（图 1B）。术前心电图 QRS 间期（图 1C）为 172ms，术后即刻心电图（图 1D）QRS 间期缩短为 146ms。患者左束支传导阻滞，但是右束支仍有传导功能，为充分利用患者自身生理性传导，改善心脏同步化治疗，进行了 CRT-D 个体化优化，具体如下：首先设置较长 AV 间期，避免心室起搏，经程控仪打印心房、左室和右室腔内图（图 2A），分别测量 A-RV（此例为 262ms）及 RV-LV 间期（此例 60ms）。分别调整 AV 间期（150ms-300ms）及 VV 间期（5-60ms），记录 12 导联心电图，心电图 QRS 间期最小时的参数作为优化参考值，结果发现设置 PAV250ms，SAV225ms，LV1-LV2 间期 5ms，LV2-RV 间期 45ms 时 QRS（124ms）最窄（图 2C）。

检验检查记录：

随访 3 个月，患者心衰症状消失，复查超声心动图: LVEDD 54mm，二尖瓣返流（微量），左室射血分数（LVEF）51%。NT-proBNP 523pg/ml。

鉴别诊断：

患者慢阻肺病史，需要鉴别肺心病。患者胸片未见明显肺动脉段突出，超声心动图全心扩大未见明显肺动脉高压，不支持肺源性心脏病诊断。

其他：

右位心合并内脏转位的室性早搏消融一例

刘元伟 Liu

清华大学附属北京清华长庚医院

患者基本信息：

患者，女性，47 岁

主述：

活动后胸闷、气短，下肢水肿 1 年

现病史：

1 年前频发心悸不适，伴气短、下肢水肿，体格检查：双肺清，肺底少量湿罗音。颈静脉充盈。心界扩大，右侧心音，心率 85 次 / 分，频发室早，各瓣膜听诊区未及明显病理性杂音，双下肢轻度水肿。 1 月前动态心电图提示频发室早 34595 次 /24h (31%) 非持续性室速。胸片和腹部 CT 提示右位心和内脏转位。心电图(左右手反接): 窦律,频发室早。超声心动图: LVEF 31% 和左室扩大 (LVEDd 59mm)。冠脉造影：未见明显冠脉狭窄。

既往病史：

胆结石

病程记录：

患者中年女性，慢性病程，反复气短水肿入院，颈静脉充盈，心界扩大，超声心动图提示心脏扩大，EF31%，心功能不全明确。患者室早负荷 31%，过高的室早负荷可以导致心动过速心肌病，可以表现为心衰，这类心衰在室早消融后心功能可以恢复，借此可以和原发性心肌病引起的心衰鉴别。但是，原发性扩张性心肌病也可以导致心衰，室早，但往往是多形性室性早搏。目前患者心悸气短明显，心功能下降，室早负荷 31%，具有射频消融指征。术后随访心功能恢复情况，如果心功能恢复则支持心动过速心肌病诊断。完善术前准备后，择期行心内电生理检查及射频消融。在三维标测系统 Ensite Velocity 导航行右室流出道三维建模及激动标测，于右室流出道后间隔标测到最早心室激动，提前体表 QRS44ms，起搏标测完全匹配，设置 43℃ , 30W，放电 5 秒室早消失。手术成功。

检验检查记录：

动态心电图提示频发室早 34595 次 /24h (31%) 非持续性室速。胸片和腹部 CT 提示右位心和内脏转位。心电图（左右手反接）：窦律，频发室早。超声心动图：LVEF 31% 和左室扩大 (LVEDd 59mm)。冠脉造影：未见明显冠脉狭窄。

鉴别诊断：

患者室早负荷 31%，过高的室早负荷可以导致心动过速心肌病，可以表现为心衰，这类心衰在室早消融后心功能可以恢复，借此可以和原发性心肌病引起的心衰鉴别。但是，原发性扩张性心肌病也可以导致心衰，室早，但往往是多形性室性早搏。

其他：

IVUS 指导冠状动脉自发夹层（SCAD）导致急性前壁 ST 段抬高型心肌梗死治疗一例

邓熠

遵义医科大学附属医院

患者基本信息：

女性，36 岁。

主述：

因“突发胸痛 3 天，加重 3 小时”入院

现病史：

3 天前不明诱因出现胸痛，以胸骨中下段为主，疼痛数分钟，休息后可缓解。3 小时前上述症状再发加重，胸痛持续不缓解，伴有大汗淋漓。

既往病史：

既往否认“高血压、糖尿病”病史。无吸烟、饮酒史。无吸毒、长期口服避孕药史。G2P2，无多胎妊娠史。家族中无特殊疾病史

病程记录：

诊治过程

急诊冠脉造影：经胸痛中心网络平台会诊后绕行急诊科直接送人导管室行急诊 CAG，结果示：LM 未见狭窄；LAD 近段未见狭窄，中段可见血管管腔细小，TIMI 血流 0-1 级，TIMI 血流 1 级；LCX 未见未狭窄，TIMI 血流 3 级；RCA 未见明显狭窄，TIMI 血流 3 级。

急诊 PCI 过程：选用 6F EBU3.5 指引导管，送入 Runthough 导丝通过病变至 LAD 远段，结合急诊造影结果反复注入硝酸甘油，狭窄未减轻，除外冠脉痉挛；LAD 中段后血管弥漫细小，结合右冠及回旋支管壁光滑，考虑 LAD 病变不能除外壁内血肿可能，拟进一步行 IVUS 检查。沿导丝送入 Opticross OCHD60mhz IVUS（Boston）导管行前降支检查，结果提示 LAD 中段至远段可见弥漫性血肿，未见血栓影及斑块破裂征像。结合病史该患为年轻女患，冠心病易患因素少，结合病史，体征，冠脉造影结果以及 IVUS 结果，目前考虑自发性冠状动脉夹层（SCAD），中段至远段弥漫性血肿，TIMI 血流 0-1 级，根据 SCAD 管理的处理原则，拟采用切割球囊治疗，必要时行支架植入术（见图 3）。沿 Runthough 导丝送入 boston 切割球囊 2.25×10mm 以 6-10atm 反复多次扩张，可见 LAD 血流较前改善并见夹层，暂不予以支架植入，术后较前缓解，生命体征平稳，安返病房，予以双联抗血小板治疗。

检验检查记录：

体格检查: T 36.5°, Bp 120/72mmhg , HR72 次 / 分 , R 18 次 / 分 , 无颈静脉怒张，双侧颈动脉无血管杂音。心界不大，心律整齐，心音无增加或减弱，各瓣膜听诊区未闻及病理性杂音、额外心音及心包摩擦音。双肺呼吸音清晰，未闻及干湿啰音。腹部平软，全腹部无压痛、反跳痛及肌紧张，肝颈静脉回流征阴性，腹部无血管杂音。四肢脉搏对称，无搏动减弱。双下肢无水肿。

辅助检查：生化检查：高敏肌钙蛋白 T 124ng/L（正常参考值 < 14ng/L）；B 型尿钠钛前体 100ng（正常参考值小于 125ng/L），总胆固醇 3.64mmol/L（正常参考值小于 5.2mmol/L）、低密度脂蛋白 2.43mmol/L（正常参考值小于 3.15mmol/L）；随机血糖 9.3mmol/L；血常规、肝功能、肾功能未见异常。心电图：V1-V6 导联 ST 段弓背向上抬高。心脏彩超：左心增大（LVD 54mm ,EF52%），二尖瓣轻度反流，三尖瓣轻度反流。

鉴别诊断：

1. 主动脉夹层

2. 肺栓塞

其他：

全球首例机器人辅助经股动脉入路经导管主动脉瓣置换术

陈翔

厦门大学附属心血管病医院

患者基本信息：

患者男性，70 岁，汉族，身高 168cm，体重 61kg，婚育史正常

主述：

反复活动后气促 5 年余，加重 1 周

现病史：

缘于入院前 5 年余无明显诱因出现活动后气促，快走 200 米后感气促不适，无咳嗽、咳痰，无咯血，无夜间阵发性呼吸困难及端坐呼吸，无腹胀及双下肢浮肿，无昏厥及抽搐等其他不适，就诊当地医院，完善相关检查，诊断“主动脉瓣狭窄”明确，具有外科手术指征，但患者当时拒绝手术，暂予药物治疗，期间仍反复发作，入院前 1 周无明显诱因出现上述症状加重，稍活动即感气促明显，伴咳嗽、咳痰，伴端坐呼吸，无咳粉红色泡沫痰，无胸痛、咯血，无腹胀、双下肢浮肿，无头晕、黑朦，无昏厥及抽搐等其他不适，今为进一步诊治，就诊我院，门诊拟 " 心脏瓣膜病 : 主动脉瓣狭窄 心功能 III 级。" 收治入院。自发病以来，患者精神、食欲、睡眠尚可，大小便尚正常，体重无明显变化。

既往病史：

无高血压、糖尿病

曾行眼角膜手术

病程记录：

患者入院后予抗心衰、利尿、营养心肌等对症支持治疗，完善相关检查，诊断“主动脉瓣狭窄”明确，具有外科手术指征，但患者心功能差，病情重，手术风险较大，患者家属暂不予考虑外科手术治疗；经与患者家属充分沟通 TAVR 手术相关事项，告知术中、术后可能出现的风险、意外、并发症等，患者家属表示理解并同意手术，于 2025.4.2 行机器人辅助下 TAVR 手术，术后患者胸闷、气促不适较前明显缓解，复查超声示主动脉人工瓣位置及功能正常，1 周后出院。

检验检查记录：

检验：总蛋白 58.50 ↓ g/L 白蛋白 34.90 ↓ g/L 球蛋白 23.60 g/L 丙氨酸氨基转移酶 23.0 U/L 天门冬氨酸氨基转移酶 28.3 U/L γ- 谷氨酰基转移酶 17.7 U/L 总胆红素 8.6 umol/L 甘油三酯 1.17 mmol/L 总胆固醇 2.71 mmol/L 高密度脂蛋白胆固醇 0.73 ↓ mmol/L 低密度脂蛋白胆固醇 1.71 mmol/L 载脂蛋白 -A1 0.79 ↓ g/L 载脂蛋白 -B 0.66 g/L 血糖 8.55 mmol/L 肌酸激酶 -MB 同工酶活性 9.4 U/L 尿素 5.90 mmol/L 肌酐 87.6 umol/L 尿酸 276.2 umol/L 肾小球滤过率 76.76 ↓ mL/(min*1.73m2); 高敏肌钙蛋白 T 58.8 ng/L N 端 - B 型钠尿肽测定 1334 ↑ ng/L; 白细胞计数 5.50 10^9/L 中性粒细胞计数 4.15 10^9/L 淋巴细胞计数 0.65 ↓ 10^9/L 单核细胞计数 0.49 10^9/L 红细胞计数 3.67 ↓ 10^12/L 血红蛋白 105 ↓ g/L 血小板计数 255 10^9/L;ABO 血型 O 型 RH(D) 阳性 ; 其余凝血功能、D- 二聚体、甲状腺功能、ESR、术前传染病筛查、尿常规、粪常规未见明显异常。

检查：

2025-04-08 动态心电图：总采集时长：1：窦性心律为主导心律，平均心率：57bpm ，最慢心率：44 bpm。 最快心率：82 bpm。 分析的心搏总数：81529 个。 2：最长 RR 间期：1464 毫秒。 3：房性早搏有 68 次 / 全天，其中有 57 次单发房早， 有 1 阵房性二联律，4 次成对房早和 1 阵房速，房早心搏数占比：0.09% 。 4：室性早搏有 17 次 / 全天，其中 8 次单发室早，有 1 阵室速，室早心搏数占比：0.03% 。 5：符合左心室大心电图表现，II、III、aVF、I、

V5-V6 导联 ST 段水平或下斜型压低 0.05-0.1mV，II、III、aVF、I、V4-V6 导联 T 波低平、负正双向或倒置，请结合临床。 6：心率变异性正常。DC 轻度减低。心脏彩超：主动脉瓣 TAVI 术后：1、主动脉人工瓣位置及功能正常，少量瓣周反流。2、轻度二尖瓣反流。3、左房扩大；左室壁增厚。4、左室下后壁运动幅度减低。5、左室整体收缩功能减低，舒张功能减退。6、少量心包积液。CT 平扫：与前片（2025-03-21）对比： 新见主动脉瓣术后改变。 左侧少量气胸。 间质性肺水肿，双肺渗出，双侧胸腔积液，较前吸收。 心包积液较前吸收。 气管内粘液栓基本吸收。 双侧胸腔置管、右侧深静脉置管影。 新扫及肝内多发高密度影，肝内胆管结石或钙化灶可能。 余大致同前。老年性脑改变，脑白质疏松可能，建议必要时 MR 检查。 颅底动脉钙化。 副鼻窦黏膜稍增厚。 --- 与前片（2025-03-25）对比，大致同前相仿。膀胱置管后，腔内密度增高，考虑造影剂滞留。 前列腺饱满并钙化。 双侧髂动脉粥样硬化。 左侧髋臼骨岛可能。 双侧腹股沟少许渗出。 左臀部皮下小结节。肝内多发囊性灶。 肝内多发钙化灶或肝内胆管结石。 胆囊、双肾密度增高，考虑造影剂滞留。 双侧肾上腺局部饱满，左侧肾上腺外侧肢可疑小圆形低密度影，微小腺瘤不除外，建议进一步检查。食管裂孔稍增宽。 结肠多发小憩室。 腹主动脉粥样硬化。 L5 椎体小骨岛。心脏彩超（术前）:1、主动脉瓣重度狭窄并中重度关闭不全。2、轻度三尖瓣反流；中度肺动脉高压可能。3、轻度二尖瓣反流。4、左心扩大；左室壁整体运动幅度普遍减低。5、左室整体收缩功能减低，舒张功能III级减退。6、少量心包积液。--建议 3DTEE 进一步检查。 2025-03-25CT 平扫 (颅脑): 老年性脑改变，脑白质疏松可能，建议必要时 MR 检查。 颅底动脉钙化。 副鼻窦黏膜稍增厚。 双下肢彩色多普勒检查；双下肢动脉内中膜增厚伴多发斑块形成。双下肢静脉彩色多普勒检查未见明显异常。 腹部彩超 :1、肝内多发钙化灶；肝囊肿。2、胆、胰、脾未见明显异常。 颈动脉系统彩超 :1、双侧颈动脉内中膜增厚伴斑块形成。2、右侧锁骨下动脉斑块形成。2025-03-24 CT 血管成像 (TAVI 升主动脉筛查)(术前): 可疑主动脉二瓣叶畸形，主动脉瓣增厚并多发钙化，瓣膜黏连，收缩期开放受限，舒张期关闭不全。 冠状动脉粥样硬化。 前降支中段浅肌桥。 靶区： 左心增大，心包少量积液。 肺气肿；双侧胸腔少量积液，并邻肺部分膨胀不全，双肺多发渗出。 肝内小囊性灶及钙化灶。 主动脉硬化。可疑主动脉二瓣叶畸形，主动脉瓣增厚并多发钙化，瓣膜黏连，收缩期开放受限，舒张期关闭不全。左心增大，心包少量积液。 胸腹主动脉及其分支动脉粥样硬化，腹主动脉下段小溃疡灶。双肾双动脉供血。 肝动脉变异。 左侧髂内动脉开口中度狭窄。 靶区：肺气肿；双肺多发渗出，两侧胸腔少量积液。肝内囊性灶及钙化灶。前列腺点状钙化。结肠憩室。脊柱稍侧弯。 2025-03-22 动态心电图 + 变异性 :1: 窦性心律为主导心律。最快心率是 109bpm, 发生于 05:44。最慢心率是 66bpm, 发生于 05:10。平均心率是 82bpm, 分析的心搏数为 106513 个。最长 RR 间期是 1.078 秒 , 发生于 05:10:01。 2: 房性早搏有 1244 次 / 全天。其中有 1209 次单发房早 , 有 2 阵房性三联律 , 有 4 次成对房早和 7 阵房速。 3: 室性早搏有 55 次 / 全天。 4: 符合左心室大心电图表现 ,II、aVF、I、aVL、V5-V6 导联 ST 段呈水平或下斜型压低 0.05-0.2mV, 伴 T 波负正双向或倒置 , 请结合临床。5: 心率变异性中度减低。心率减速力轻度减低。2025-03-21 CT 平扫 (肺部): 左心增大，主动脉瓣、二尖瓣钙化，心包少量积液。冠脉、主动脉钙化。间质性肺水肿，双肺多发渗出，右肺中叶、双肺下叶膨胀不全，双侧胸腔中等量积液。 左肺上叶前段结节，请随诊。 肺气肿。 气管内粘液栓。 肝脏小类圆形低密度影，囊肿可能。 脊柱稍侧弯，胸 8 椎骨稍变扁。

鉴别诊断：

1. 肥厚型心肌病：室间隔显著不对称肥厚导致左心室流出道动力性梗阻（收缩期二尖瓣前叶前向运动 - SAM 现象加重梗阻），需鉴别杂音性质（常为收缩期喷射性杂音，但受 Valsalva 动作、体位影响大），超声心动图可见室间隔肥厚、SAM 征、左心室流出道压力阶差。

2. 主动脉缩窄：严重的主动脉缩窄也可引起左心室肥厚和心绞痛等症状，鉴别点如下：上肢高血压、下肢低血压 / 脉搏减弱 / 消失（股动脉搏动延迟或消失），胸骨旁或肩胛间区连续性或收缩期杂音，侧支循环体征（胸壁杂音、搏动）。

3. 其他导致左心室流出道梗阻的罕见原因：

感染性心内膜炎赘生物：大的赘生物可造成功能性梗阻。

主动脉窦瘤破裂：破入右心系统时，大量左向右分流可掩盖狭窄体征，或瘤体本身造成梗阻。

左心肿瘤：如左心室粘液瘤，可脱垂至流出道造成梗阻。

大动脉炎（Takayasu arteritis）：可累及升主动脉或主动脉弓，导致管腔狭窄。

严重的主动脉粥样硬化：非常罕见导致显著血流动力学梗阻。

其他：

梦魇之息：睡眠呼吸暂停与肺高血压的秘密

何慧玉

哈尔滨医科大学附属第二医院

患者基本信息：

男患，44 岁

主诉：打鼾，乏力一年

现病史：患者入院前 1 年无明显诱因出现乏力，伴有出汗，气短，夜间有憋醒，偶有胸闷、胸痛。于当地医院行辅助检查提示肺动脉高压。为求明确诊治来我院就诊。

既往史：有高血压病数年，应用药物不详。否认其他既往疾病。

体格检查：体温：36.20℃　脉搏：93 次 / 分　呼吸：20 次 / 分　血压：128/100mmHg，BMI: 44.08kg/m2

主述：

打鼾，乏力一年

现病史：

患者入院前 1 年前无明显诱因出现持续性乏力，日常行走 200 ~ 300 m 即需停下休息，伴全身大汗，气短， 夜间睡眠 7 h 内可憋醒 2 ~ 4 次，需坐位或站立 5–10 min 方能缓解，近 3 个月出现劳力性胸痛，位于胸骨后，持续 1–3 min，休息可缓解，无放射痛。无发热、咯血、双下肢水肿、晕厥及意识障碍。当地县医院查心脏彩超提示“肺动脉收缩压约 60 mmHg”，建议上级医院进一步诊治。未系统治疗，仅间断口服“降压药”（具体不详）。症状进行性加重，遂来我院。

既往病史：

有高血压病数年，应用药物不详。否认其他既往疾病，否认食物药物过敏史，吸烟史：20 支 / 日 × 20 年，饮酒史：白酒 250 mL/ 日 × 15 年，近 1 个月减量；否认家族遗传病史，否认传染病史。

病程记录：

44 岁男性，主诉打鼾、乏力 1 年。既往有数年高血压病史，用药不详。入院查体：BP：128/100 mmHg，BMI 为：44.08kg/m²。查体：神清语明，双肺呼吸音粗，未闻及明显干湿啰音，心前区无隆起，叩诊心脏相对浊音界无明显扩大，心律齐，未闻及瓣膜杂音，其余查体无阳性体征。患者自备心脏彩超提示：肺动脉高压。心脏超声提示三尖瓣反流速度峰值最高达 2.10m/s，推算肺动脉收缩压为 28mmHg。双下肢彩超未见明显异常。实验室检查显示 NT-proBNP 402pg/ml 升高，糖化血红蛋白 6.8% 和总胆固醇 5.76mmol/L 也升高。血气分析（未吸氧）显示 pH 值为 7.33，PCO_2 为 68mmHg，PO_2 为 48mmHg，BE 为 7.4mmol/L，SO_2 为 80%，提示为 II 型呼吸衰竭。心电图显示肺型 P 波及电轴右偏。睡眠呼吸监测结果显示重症阻塞性睡眠呼吸暂停低通气综合征，存在重度夜间血氧下降（氧减指数 74.0/h，最低 SpO_2 为 30%）。右心导管检查进一步明确肺动脉高压情况，平均肺动脉压为 28mmHg，肺毛细血管压为 9mmHg，肺血管阻力为 4.2 Wood 单位。最终诊断为睡眠呼吸暂停低通气综合征相关肺高压、II 型呼吸衰竭、高尿酸血症、高脂血症、3 级高血压（高危）。患者接受呼吸机治疗，并服用西地那非片（20mg，tid）。经过长期持续无创正压通气治疗后，患者乏力症状有所改善。

检验检查记录：

心脏超声提示三尖瓣反流速度峰值最高达 2.10m/s，推算肺动脉收缩压为 28mmHg。实验室检查显示 NT-proBNP 402pg/ml 升高，糖化血红蛋白 6.8% 和总胆固醇 5.76mmol/L 也升高。血气分析（未吸氧）显示 pH 值为 7.33，PCO_2 为 68mmHg，PO_2 为 48mmHg，BE 为 7.4mmol/L，SO_2 为 80%，提示为 II 型呼吸衰竭。心电图显示肺型 P 波及电轴右偏。睡眠呼吸监测结果显示重症阻塞性睡眠呼吸暂停低通气综合征，存在重度夜间血氧下降（氧减指数 74.0/h，最低 SpO_2 为 30%）。右心导管检查进一步明确肺动脉高压情况，平均肺动脉压为 28mmHg，肺毛细血管压为 9mmHg，肺血管阻力为 4.2 Wood 单位。血常规、尿常规、肝肾功、离子、凝血、双下肢超声、免疫学筛查未见明显异常。

鉴别诊断：

结缔组织病相关肺高压：免疫学筛查阳性，出现雷诺现象、皮疹、关节痛等表现，出现 SLE、硬皮病等所致肺高压。

慢性血栓栓塞性肺高压：有急性肺栓塞史；双下肢彩超出现血栓，D- 二聚体明显升高；CTPA 和 V/Q 提示灌注缺损。

其他：

这是一例以「打鼾 + 乏力」首诊、最终经规范化流程确诊为重度 OSA 相关第 3 类肺高压的中年肥胖男性，其鉴别重点在于排除左心病、CTEPH 和特发性 PAH，治疗以持续气道正压通气（CPAP）联合西地那非为核心，随访症状明显改善，提示对任何不明原因肺高压患者必须常规筛查睡眠呼吸障碍。

BAT 技术辅助横位心 AS TAVR1 例

胡健强

唐都医院

患者基本信息：

女性，汉族，76 岁、体重 62 KG, 身高 158 cm。

主述：

间断胸闷、气短 3 年，加重 1 周

现病史：

患者 3 年前始出现间断胸闷、气短不适症状，多于“快走，爬坡”等活动后出现，伴有心慌、头晕不适，无明显胸痛，无大汗，无恶心、呕吐等不适，休息后可缓解，患者当时未重视，未明确诊治，此后患者间断出现上述胸闷、气短、心慌、头晕等不适症状。1 周前夜间无明显诱因出现上述症状，自觉症状较前加重，坐位可减轻，于当地诊所就诊，药物治疗效果不佳，症状逐渐加重，活动耐力进行性下降，2 天前至渭南市第一医院就诊，查心脏彩超提示：主动脉瓣重度狭窄，药物治疗后稍好转，现为进一步诊治，遂来我院门诊就诊，门诊以“主动脉瓣重度狭窄“收入院。

既往病史：

患者过去体质身体一般。发现高血压病史 5 年，血压最高 160/110mmHg，平素服用降压药物治疗，具体不详，平素未监测血压。疾病史：否认“糖尿病”“冠心病”等病史。

病程记录：

入院后完善化验检查，于 2025-04-08 在心内科导管室行 TAVR+PCI+CAG+ 临时起搏器置入术。常规体位造影示 :LAD 近中段狭窄 80%，获窄长度 20mm，D1 口狭窄 60%，狭窄长度 5mm，D2 近段狭窄 75%，狭窄长度 10mm，TIMI 血流 3 级 :LCX 近段狭窄 30%，狭窄长度 10mm，TIMI 血流 3 级：RCA 中段狭窄 50%，狭窄长度 15mm，TIMI 血流 3 级。余冠脉血管未见明显异常。结论：冠心病。经患者家属同意后于 LAD 病变处植入 3.5*26 支架 1 枚。于主动脉瓣植入 23mm 人工瓣膜 1 个。手术成功，术后给予预防感染、抗血小板、营养支持、抑制心室常规、改善心功能等治疗，现症状好转，无特殊不适。

检验检查记录：

2025-03-29 外院心脏彩超：主动脉瓣重度狭窄，升主动脉瘤样扩张，左心右房增大，左室整体收缩功能减低，心包少量积液。左心室收缩功能、舒张功能减低。彩色血流：二尖瓣中量反流。入院后完善检查：血气分析 :pO_2 73.7mmHg；尿液分析 + 沉渣: 尿白细胞 *1+, 尿糖定性 *3+; 甲功: 三碘甲状腺原氨酸 * 1.20nmol/L，游离三碘甲状腺原氨酸 *3.82pmol/L，甲状腺素 *118.00nmol/L；卡式血型鉴定 :ABO 血型鉴定 B 型，RH(D) 血型鉴定阳性；NT-proBNP：1150.00pg/mL；心肌损伤标志物 :TnI 0.053ng/mL；阿司匹林药效及出血风险评估检测 (全血): 胶原 / 二磷酸腺苷 152.0s；(他汀类) 化学药物用药指导基因检测 E3/E4；(氯吡格雷) 化学药物用药指导基因检测 *2*2; 凝血系列检查 :D- 二聚体 (定量)*1.020ug/mL；感染八项、肝功、电解质、肾功、C- 反应蛋白测定、血常规、血脂七项、肌酸激酶未见明显异常。腹部彩超 : 右肾大小正常，肾囊肿，肝、胆、胰、脾、左肾大小正常，图像未见异常。心脏彩超：主动脉瓣钙化并重度狭窄，左房大，左室内径正常高值，升主动脉扩张，降主动脉显示不清，心包积液 (少量)，二尖瓣轻度关闭不全，左室舒张功能减低。全主动脉 CTA:1、全主动脉血管成像示：动脉瓣区所见，符合重度狭窄；升上动脉增宽：主动脉弓、主动脉、左颈总动脉及锁骨下动脉开口段、腹主动脉、双侧髂总动脉、右侧髂内动脉、左侧髂外动肽管壁散在混合斑、钙斑，局部管腔轻度狭窄；2、原始图像示：右肺上叶尖段模糊阴影，多考虑炎性病变；右肺上叶下舌段少量渗出；右肺上叶前段小结节，考虑 Lung-RADS 2 类；纵内及右侧肺门区淋巴结增大；左肾囊肿；升结肠及结肠肝曲管腔扩张不佳，管壁结构显示不清左侧臀部皮下钙化灶；3、右侧岛叶腔隙性脑梗死；双侧侧脑室旁脑白质脱髓鞘；左侧上颌窦及双侧筛窦炎。

鉴别诊断：

1、缺血性心肌病：支持点：患者有间断发作胸闷、气短症状；不支持点：患者听诊主动脉瓣区可闻及收缩期杂音，考虑主动脉瓣狭窄明确，可进一步行冠脉造影检责协助鉴别；

2、慢性肺栓塞：本病多见于长期卧床、创伤、肿瘤思者，常为胸闷、胸痛、气急，可体有量展、暖、血痰，胸片见肺部阴影，D2 聚体阳性，肺动脉注及肺动脉造影检查可以明确。支持点，有胸闷、气短症状发作。不支持点：患者无“长期卧床、创伤、手术”等肺检危险因素，无明显呼吸困难，未见肺栓 ST 段典型心电图表现，如肺型 P 波，暂不支持，可进一步完普血气分析、D 二聚体、下肢静脉超声，必要时行肺动脉 CTA 协助鉴别。

其他：

跨越漫漫长路：应用 ADR 技术开通前向及逆向尝试失败的复杂 CTO 病变

张明明

空军军医大学第二附属医院心血管内科

患者基本信息：

黄某，男，42 岁，农民。

生于河南省，无疫区居住史，无冶游史，无饮酒史，有吸烟史，已戒烟，无放射物、毒物接触史。无疫区接触史，无不洁饮食史，无传染病史，地方病接触史 : 无地方病病史，预防接种史不详。

已婚，生育 : 育 1 子 1 女，配偶健康状况良好。

父母已故，兄弟姐妹健康状况良好，子女健康状况良好。家族中无传染病、遗传性疾病史。

体温 :36.3℃，脉搏 :96 次 / 分，呼吸 :18 次 / 分，血压 :106/70mmHg。

查体: 心前区 : 无隆起，心尖搏动 : 心尖搏动有力，位于左侧锁骨中线内侧 0.5cm，无搏动弥散，震颤 : 未触及震颤，相对浊音界 : 正常，心率 :96 次 / 分，心律 : 律齐各瓣膜听诊区杂音 : 各瓣膜听诊区未闻及杂音。

(2024.11.25 本院) 心电图 : 窦性心律、心率 70 次 / 分、V1-V6ST 段压低；

心肌损伤示 :CK-MB2.39ng/ml ↑、cTnI0.164ng/ml ↑ 、Myo128ng/ml ↑

主述：

间断胸闷、气短 1 月

现病史：

患者自诉于 1 月前无明显诱因出现胸痛，位于心前区，呈憋痛，向左上肢及左上颌放射，症状持续不缓解，与进食无关，与体位无关，偶有胸闷、心悸，无左肩背部放射痛，无气短、胸痛、无头晕、头痛，无恶心、呕吐、无呼吸困难、无咳嗽、咳痰、无一过性黑朦、晕厥等症状，在本院诊断为“急性心肌梗死”，行冠状动脉造影结果 : 前降支近段 100% 闭塞；回旋支远段 100% 闭；中间支窄程度 80%，狭窄长度 20mm; 右冠状动脉近段狭窄程度 80%，狭窄长度 15mm; 右冠状动脉中远段窄程度 80%，狭窄长度 10mm; 间隔支近段狭窄程度 80%，狭窄长度 5mm; 结论 : 冠心病，于 LCX 远段及中间支近段各植入 1 枚药球，出院后有气短、乏困不适，今为进一步处理剩余闭塞病变，遂来我院门诊，门诊查心电图 : 窦性心律、心率 78 次 / 分、V1-V6ST 段压低 (2024.12.29 唐都医院); 门诊遂以“冠心病、PCI 术后” 收治入院。患者目前精神好，体力正常，食欲正常，睡眠正常，体重无明显变化，大便正常，排尿正常。

既往病史：

患者过去体质体健。疾病史：既往有 “糖尿病” 病史 2 年余，口服” 盐酸二甲双胍缓释片” 控制血糖，自诉血糖控制不佳。传染病史：否认肝炎、结核、疟疾等传染病史。预防接种史；预防接种史不详。过敏史：否认药物、食物过敏史。手术史 :20 余年前因脊结核行外科手术 (具体不详)。外伤史 : 否认外伤史。输血史 : 否认输血史。中毒史 : 否认中毒史。

病程记录：

2024.11.25 因急性心梗行冠状动脉造影结果 : 前降支近段 100% 闭塞（CTO 病变）; 回旋支远段 100% 闭塞（心梗病变）; 中间支窄程度 80%，狭窄长度 20mm; 右冠状动脉近段狭窄程度 80%，狭窄长度 15mm; 右冠状动脉中远段窄程度 80%，狭窄长度 10mm; 间隔支近段狭窄程度 80%，狭窄长度 5mm; 结论 : 冠心病，于 LCX 远段及中间支近段各植入 1 枚药球。

2024.12.31 前降支近段窄程度 100%; 间隔支近段狭窄程度 50%，狭窄长度 15mm; 中间支近段狭窄程度 30%，狭窄长度 15mm; 回旋支远段狭窄程度 30%，狭窄长度 15m; 右冠状动脉中远段狭窄程度 80%，狭窄长度 10mm; 右冠状动脉远段狭窄程度 75%，狭窄长度 20mm; 右冠发育细小。

结论 : 冠心病，于 LAD 近中段共植入 2 枚支架。应用 ADR 技术开通前向及逆向尝试失败的前降支复杂 CTO 病变。

检验检查记录：

心脏彩超：心功能大致正常。LDL-C2.74；2 型糖尿病患者糖化血红蛋白 10.1

鉴别诊断：

主动脉夹层：患者无刀割样、针刺样或撕裂样疼痛，D- 二聚体正常，超声提示无主动脉夹层。

肺栓塞：患者无咳嗽、咳血、呼吸困难和胸痛等症状，D- 二聚体正常，血气分析正常。

其他：

1. 患者三支病变，前降支近段 100% 闭塞（CTO 病变）; 回旋支远段 100% 闭塞（心梗病变）; 中间支窄程度 80%，狭窄长度 20mm; 右冠状动脉近段狭窄程度 80%，狭窄长度 15mm; 右冠状动脉中远段窄程度 80%，狭窄长度 10mm; 间隔支近段狭窄程度 80%，狭窄长度 5mm。属于极高危人群。

2. 前降支近段 100% 闭塞，病变钙化严重，长 CTO 病变。

3. 前向及逆向尝试失败的前降支复杂 CTO 病变，耗时 2 个小时。尝试 ADR 技术 10 分钟开通 CTO 病变完成支架植入。效率高。

4.IVUS 提示长钙化 CTO 病变。

冠脉造影术后脾动脉瘤破裂失血性休克 1 例

周睿

常州市第四人民医院

患者基本信息：

患者 79 岁，女性，

主述：

胸闷伴随上腹部不适 1 月

现病史：

患者 1 个月前开始无诱因反复出现胸闷感，位于心前区，伴随胸骨中上段胀痛感，无下颌及肩背部放射痛，无恶心及呕吐，无反酸、嗳气，症状持续数分钟可自行缓解，患者进食差，当地医院诊断胃炎，治疗效果不佳，建议到上级医院行冠心病检查，病人遂由门诊以 “心绞痛” 收入心内科，过程中病人睡眠可、饮食不佳、无腹痛及呕血、黑便。

既往病史：

胃部肿瘤术后病史多年，胆囊结石病史

病程记录：

入院病人上腹部轻压痛，首先完善肝胆胰脾超声及全腹部 CT 平扫，提示胆囊结石，未明确有脾动脉瘤，老年女性，胸闷主诉，心电图缺血改变，考虑冠心病，入院第三天排除手术禁忌症行冠脉造影：回旋支远端 50-60% 狭窄及右冠近端 50%，远端 60-70% 狭窄，术中有迷走反射，一过性心率慢、血压低，给予阿托品及间羟胺升压处理后血压稳定。

病情变化；返回病房病人血压仍低，但没有明显急腹症表现，值班医生考虑术中迷走反射继续给予补液升压，后患者自述腹痛、腰疼，监护血压偏低，补液升压抑酸对症（胆囊结石、胃肿瘤病史），后查体全腹部压痛，腹部膨隆，完善腹部超声及 CT：提示腹腔出血，急诊造影提示脾动脉破裂出血，行弹簧圈栓塞失败后剖腹探查，见腹腔大量出血及凝血块，量约 2500ml, 打开小网膜，见胰腺上缘脾动脉瘤破裂，直径 3*3cm，活动出血，行脾脏 + 胰尾切除，术中自体血回输，病人术前、术中及术后低血压，失血性休克，术后转入 ICU，给予继续输血浆、冷沉淀、凝血酶原复合物、血小板，升压、止血，抗炎等处置，病人出血量大，

期间输血量惊人，一过性缺血缺氧脑病，终经 14 天抢救病人症状逐渐好转，22 日胰腺上下缘引流多，淀粉酶明显增高，考虑胰漏转肝胆外科治疗后出院。

检验检查记录：

术前全腹部 CT 扫描（2023-12-09）：胃底高密度，胆囊新发结石，原胆囊颈结石较前相仿，双肾囊肿

冠脉造影（2023-12-12）：回旋支远端 50-60% 狭窄及右冠近端 50%, 远端 60-70% 狭窄

病理：脾脏红髓白髓萎缩，脾门血管内膜及内膜下水肿、出血、局灶血管壁厚薄不均，伴周围组织大量出血。

入院全腹部 CT 扫描（2023-12-12）：盆腹腔大量积液（血），胃底高密度，胆囊新发结石，原胆囊颈结石较前相仿，双肾囊肿

术后腹部 CT 扫描（2023-12-15）：脾脏、胰尾切成术后，盆腹腔大量积液（血）较前增多，胃底高密度，胆囊新发结石，原胆囊颈结石较前相仿，双肾囊肿，**（2023-12-15）：**盆腹腔大量积液（血）较前减少**（2023-12-25）：**盆腹腔大量积液（血）较前吸收，肝周积液较前增多，两肺膨胀不全，双肺低积液减少。(2024-1-3) 脾脏、胰尾切成术后，较前吸收，肝周积液较前增多，胆囊体积增大，周围渗出，考虑胆囊炎。

鉴别诊断：

围术期低血压病人都要进行如下检查血常规，心电图，心脏彩超 1. 血压低伴心率慢，心电图未提示下壁心梗及胸痛，考虑迷走反射，尤其有疼痛刺激，精神紧张者。心电异常考虑下壁心梗或主干闭塞，弯曲血管如果支架后改变形态过度牵来会导致病人迷走发射。

2. 血压低伴心率快：

休克–心源性：Ci 小于 3，中心静脉压大于 15，心电提示广泛前壁或左主干闭塞，ST（支架内血栓）

脉压差小，心率快，明显憋气，发绀，考虑急性心包填塞，彩超可以证实

伴随喉痒，皮疹，暖休克，顽固休克要考虑造影剂过敏，有报道第一次无过敏第二次过敏迟发型 IV 型变态反应，肾上腺素，激素有效。

心肌血肿（干性填塞）间隔或心内膜下血肿彩超可以证实，症状休克表现，喘憋但肺清晰

容量不足：禁食，造影剂高渗利尿，术前或术中应用 CCB 等药物，术中失血

穿刺股动脉者–血压低伴随腰痛提示后腹膜血肿，下肢局部大血肿，养成习惯术后股动脉造影，及时发现穿刺血管并发症。

桡动脉途径：出现低血压、气短要警惕纵膈血肿可能，尤其在治疗右冠脉病变时的低血压。容易漏诊，习惯导管床 AP 位踩脚透视看看。

术中低血压导管并发症：GC 堪顿，急性 AR，主干血管夹层等，有经验术中容易第一时间发现，及时处理。

二 . 腹部动脉瘤破裂：心血管患者围术期充分抗栓，术中血压波动，搬动等因素均可促发肝血管瘤、脾动脉瘤破裂出血，低血压好要警惕急腹症失血性休克。

其他：

该患者抢救期间输血量惊人：冰冻血浆 25820ml, 血小板：3 单位，凝血因子：1161 单位，少白细胞红细胞悬液：1700 单位

背景与目的：冠脉造影后脾动脉瘤破裂临床报道少见，当其破裂时早期单纯出现血压低易被漏诊或误诊。笔者对 1 例造影后脾动脉瘤破裂病例的临床表现及影像学特点、诊断及治疗措施等方面进行分析总结，以期拓展心血管医生对临床低血压疾病诊疗思路。

方法：对 1 例脾动脉瘤破裂前后的临床表现、诊疗过程及预后进行回顾性分析，并结合国内外文献，总结脾动脉瘤的临床和影像学特点、诊断及治疗方法探索。

结果：患者以“胸闷伴随上腹部不适 1 月为主要表现就诊，既往有胃部肿瘤术后病史，入院完善肝胆胰脾超声及全腹部 CT 平扫，提示胆囊结石，未明确有脾动脉瘤。老年女性，胸闷主诉，心电图缺血改变，考虑冠心病给予行冠脉造影检查，术中低血压、术后持续低血压直到出现腹痛症状，急诊造影提示脾动脉瘤破裂，失血性休克，介入栓塞失败后外科脾切除，术后经积极抢救休克后出院。

结论：脾动脉瘤为临床少见疾病，未破裂时可无明显临床表现，发生隐匿，临床表现缺乏特异性，发病率男女 1；4，尤其妊娠期女性多见，腹部外伤、手术可为病因，表现为消化系疾病或破裂后休克多见报道。随着心血管介入技术广泛发展，冠脉造影已经作为冠心病有创常规检查，术中血流动力学变化及抗凝，会促进病人原有动脉血管瘤破裂，出血更凶险，而且围术期低血压更多想到介入并发症相关，破裂早期往往就是低血压，无明显急腹症表现，脾动脉瘤诊断须综合临床表现、腹部 CT 血管造影及数字减影血管造影检查，介入处理脾动脉瘤栓塞并发症高，大的破裂口往往栓塞无效，外科止血是该病治疗的有效手段。

众里寻“PA”千百度

朱彬

哈尔滨医科大学附属第二医院

患者基本信息：

男患，59 岁；个人史、家族史：无特殊

主述：

血压升高 10 年，头晕头痛 10 日

现病史：

10 年前发现血压升高，最高 220/120mmHg，口服硝苯地平控释片 30mg，厄贝沙坦 150mg，血压控制在 140~150/90~100mmHg。5 年前血压控制欠佳，厄贝沙坦改为厄贝沙坦氢氯噻嗪，测血压 130/85mmHg。10 日前无明显诱因头晕、头痛，血压 160~170/100~110mmHg。有睡眠打鼾、呼吸暂停及白日嗜睡、乏力，无黑朦、晕厥，无腹泻、恶心、呕吐。

既往病史：

甲状腺癌行甲状腺切除术，否认糖尿病病史，无烟酒嗜好

病程记录：

完善生化、血气分析、血细胞分析、D- 二聚体、BNP、HCY、甲状腺功能、尿便常规、肝功、肌酶谱等，控制血压对症，筛查继发性高血压的病因等检查

检验检查记录：

心脏彩超：EF：65%，左心房：41.6mm 室间隔厚度：13.4mm，左室后壁厚度：13.2mm 二尖瓣口 E/A：0.7，左室舒张功能不全（I-II 级）

肾上腺 CT: 双侧肾上腺略粗，局部略呈结节样 右侧膈肌脚旁类圆形影，建议结合其他检查

冠脉 + 主动脉 CTA：右肾动脉开口非钙化斑块，无狭窄 LAD 近段钙化斑块，轻度狭窄

ABI：四肢血压升高、对称，ABI 正常、baPWV 升高

PSG：重度阻塞性睡眠呼吸暂停：AHI：62.1/h，血氧饱和度：最低 30%，平均 80%，CT 90：67.4%，CT 80：60.9%

肺 CT：双肺小结节，最大 4mm。双肺间质性改变

动态血压监测：24 小时：SBP 和 DBP 均升高（156/91 mmHg）白天清醒时段：SBP 和 DBP 均升高（162/94 mmHg）夜间睡眠时段: SBP 和 DBP 均升高（139/85 mmHg）起床后清晨时段：SBP 和 DBP 均升高（179/111 mmHg）昼夜节律：SBP 和 DBP 昼夜节律正常

鉴别诊断：

1、主动脉夹层：胸痛一开始即达到高峰，常放散到背、肋、腹、腰和下肢，两上肢的血压和脉搏可有明显差别，可有主动脉瓣关闭不全的表现，超声心动图、x 线或主动脉 CTA 有助于鉴别；

2、急性肺动脉栓塞：可发生胸痛、咯血、呼吸困难和休克，但有右心负荷急剧增加的表现如发绀、肺动脉瓣区第二心音亢进、颈静脉充盈、肝大、下肢水肿等，心电图示 I 导联 S 波加深，III 导联 Q 波显著 ,T 波倒置，胸导联过渡区左移，右胸导联 T 波倒置等改变可资鉴别。常有低氧血症，血气分析或肺动脉 CTA 有助于鉴别。

3、脑梗塞：头晕头痛，常伴肢体活动障碍，头 CT 可鉴；

4、嗜铬细胞瘤：阵发性血压升高伴心动过速，头痛、出汗、面色苍白，肾上腺 CT 可鉴别。

其他：

重症肌无力导致肺高血压 1 例报告

刁嘉康

广东省医学科学院 广东省人民医院

患者基本信息：

姓名：黄 XX

性别： 女性

年龄：34 岁

职业：自由职业者

工作单位：无

婚姻：已婚

民族：汉族

病史报告者：患者本人

入院 (室) 时间：2025-06-04 15:06:57

记录时间：2025-06-04 15:53

主述：

上肢乏力、消瘦 5 年余，双下肢水肿 1 年

现病史：

患者于 5 年余前无明显诱因出现上肢乏力，主要表现为双上肢抬举无力，呈“晨轻暮重”，伴胃纳差，2020 至 2021 年间体重自 45kg 降至 40kg，当时未查超声心动图，曾间断服用中药。1 年余前患者出现双下肢水肿，就诊于外院，予利尿及中药治疗后下肢水肿稍好转，具体不详。后仍反复有双下肢水肿。2025-05 因下肢水肿就诊于外院，查 Hgb154g/L，NT-proBNP 652pg/ml，超声心动图示：右房右室增大，三尖瓣关闭不全，估测肺动脉收缩压 71mmHg。肺动脉 CTA 示：左右肺动脉主干及其分支显影良好，管腔未见充盈缺损，肺动脉主干扩张 34mm。考虑“慢性心力衰竭、重度肺动脉高压”，予利尿等治疗后出院。目前患者诉快走或爬楼梯 1-2 层时即出现气促。目前用药（2025-05-26 始）：利奥西呱 1mg Tid、安立生坦 5mg qd。现患者为进一步诊治来诊。发病以来，患者精神、睡眠尚可，食欲一般，大小便正常，体重减轻如上述。

既往病史：

否认高血压病史；否认高脂血症病史；否认糖尿病病史；否认脑梗塞史；否认慢性肺气肿病史；否认风湿性心脏病史；否认冠心病史；否认心梗病史；否认房颤病史；否认肝炎病史；否认结核病史；否认其他传染病史；否认输血史；否认外伤史；否认手术史；否认中毒史；过敏史无。

病程记录：

患者入院后行动脉血气分析示：pH 7.13，$PaCO_2$ >115 mmHg，PaO_2 280 mmHg，提示 II 型呼吸衰竭。超声心动图检查提示中度肺动脉高压（PH），估测肺动脉收缩压（PASP）为 65 mmHg。右心导管检查测得平均肺动脉压（mPAP）为 32 mmHg，肺血管阻力（PVR）为 3.17 Wood U，平均肺动脉楔压（mPAWP）为 12 mmHg。胸部计算机断层扫描（CT）未见肺栓塞或间质性肺病征象，亦无胸腺增生表现。肌电图（EMG）显示左侧副神经及双侧面神经重复神经电刺激（RNS）呈阳性。神经肌肉病自身抗体谱检测显示抗肌肉特异性受体酪氨酸激酶（MuSK）抗体阳性。综合上述结果，诊断为重症肌无力、肺高血压及 II 型呼吸衰竭。

鉴于患者肺血管阻力处于低值范围，考虑其肺高血压主要继发于 II 型呼吸衰竭所致的低氧血症（即第 3 类肺高血压），遂逐步减量并停用肺动脉高压靶向药物。在神经科指导下，治疗方案包括：溴吡斯的明 30 mg 每日三次改善神经肌肉接头传导，缓解肌无力症状、阿托品 0.15 mg 每日一次拮抗溴吡斯的明的毒蕈碱样不良反应、艾加莫德 α400 mg 每周一次（静脉注射）免疫调节、甲泼尼龙 4 mg 每日一次（口服）低剂量免疫抑制，针对重症肌无力原发病治疗。同时予双水平正压通气（BiPAP） 辅助呼吸，以改善通气功能。

检验检查记录：

2025-05-22 外院肺动脉 CTA：1、未见明确肺栓塞征象；2、肺动脉主干增宽（管径约 34mm），提示肺动脉高压可能，请结合临床相关检查。

2025-06-05 右心导管检测: 平均肺动脉压（mPAP）32 mmHg，肺血管阻力（PVR）3.17 Wood U，平均肺动脉楔压（mPAWP）12mmHg，考虑毛细血管前性肺高血压。

2025-06-10 肌电图：1、左侧副神经、左右面神经 RNS 阳性，左侧尺神经 RNS 阴性；2、考虑左侧三角肌有类肌源性损害。

2025-06-11 超声心动图: 1、中度肺动脉高压（PASP 估测 65mmHg），原因待查；2、重度三尖瓣返流；3、轻度二尖瓣返流。

2025-06-11 神经肌肉自身抗体相关抗体谱检测：抗 AChR-Ab 抗体阴性，抗 MuSK-Ab 抗体阳性（滴度 1:100）。

鉴别诊断：

1、左心疾病相关肺动脉高压

支持依据：存在右心功能不全表现：双下肢水肿反复 1 年余，超声心动图示右房右室增大、三尖瓣关闭不全，NT-proBNP 升高（652pg/ml），符合心力衰竭特征。

排除依据：肺动脉 CTA 未见左心相关异常：无左心室扩大、二尖瓣病变等影像学证据。

结论：暂不考虑。

2、慢性血栓栓塞性肺动脉高压（CTEPH）

支持依据：双下肢水肿反复 1 年，活动耐量下降（快走或爬 2 层楼梯气促），符合 CTEPH 的慢性进展特征；。

排除依据：肺动脉 CTA 明确显示左右肺动脉主干及分支无充盈缺损，无血栓栓塞直接证据，不符合 CTEPH 的典型影像学表现。

结论：暂不考虑

3、慢性阻塞性肺疾病（COPD）相关肺动脉高压。

支持依据：快走或爬楼梯时气促，可能与气道阻塞导致的通气功能下降相关；5 年间体重从 45kg 降至 40kg，符合 COPD 长期慢性炎症导致的营养不良。

排除依据：无慢性咳嗽、咳痰、喘息病史，肺动脉 CTA 未提示肺气肿、支气管扩张等 COPD 典型改变。

结论：暂不考虑

其他：

心肌炎后快速进展性心衰的隐藏病因：MYZAP 变异

胡雷

四川大学华西第二医院

患者基本信息：

13 岁青少年女性，起病急、病程短

主述：

因咳嗽 5 天，胸闷、胸痛 1 天入院

现病史：

入院前 5 天，患者无明显诱因出现轻度咳嗽咳痰，频率不剧，伴恶心、大汗淋漓，无发热、气促、发绀等，至当地诊所“打针”治疗 3 天，具体不详，治疗后无明显好转；入院前 1 天，患儿仍有咳嗽、恶心症状，性质同前，并出现胸闷、胸痛，伴气促、呼吸困难、声嘶，遂至县人民医院就诊，检验学检查提示 CK > 1000U/L，CK-MB550.8U/L，cTnI > 50ng/ml，超声提示左房增大，左室壁运动幅度减低，左室收缩功能降低，心包腔微 - 少量积液，考虑“暴发性心肌炎”可能，予甲泼尼龙、果糖二磷酸钠治疗后无明显好转；转至市人民医院就诊，测得血压最低为 77/58mmHg，检验学检查提示 CK2306.8U/L，CK-MB220.9U/L，hs-cTnI98840.3ng/ml，NT-proBNP4209.63pg/ml，心电图提示前壁 ST 段抬高，T 波改变，考虑“暴发性心肌炎”，予多巴酚丁胺、甲泼尼龙琥珀酸钠、呋塞米、大剂量维 C 等治疗后病情稍好转，血压上升至 94/68mmHg，由急诊入 PICU

既往病史：

既往病史无特殊

病程记录：

予多巴酚丁胺强心、哌拉西林及甲泼尼龙抗感染治疗

检验检查记录：

心肌酶升高：CK-MB：52.69ug/L；CK：1173U/L

肌钙蛋白显著升高：> 25000ng/L(入院时) → 12622ng/L → 3569ng/L → 140ng/L(出院时复查)

BNP 显著升高：1200.53pg/L (入院时) → 762.84pg/L → 193.53pg/L → 340.79pg/L(出院时复查)

心电图: 常规 -ST 段改变 (II III aVF V2-V6 ST 段轻度上抬); 动态 - 加速性房性逸博、室早

超声心动图：左房稍大，心功能基本正常（LVEF=52 → 55 → 62%）

冠脉 CTA：未见明显异常

心脏磁共振：心肌水肿、广泛的早期强化和延迟强化

鉴别诊断：

急性左心衰

急性心包炎

急性冠脉综合征

其他：

1 月后，患者因咳嗽 3 天，胸痛、腹痛伴乏力半天，咯血 5 次再次入院，超声心动图提示左心增大、心尖圆顿（LA=32mm、LV=45mm），左室收缩功能测值减低（EF=35%），全外显子测序发现 MYZAP 基因点变异

支架内旋磨治疗心衰肾衰，低 EF 值的右冠慢性闭塞病变 1 例

梁长彬

中国医科大学附属第一医院

患者基本信息：

男性，65 岁。

主述：

主诉：因“活动后气短 6 个月加重 1 周”入院。

现病史：

23 年（2002 年）前因急性前壁，下壁心梗，植入 1 枚支架（位置不详），1 年后症状再发，再次植入 1 枚支架（位置不详）。04 年转至心外科行冠脉搭桥，16 年（09 年）前因心动过缓植入单腔起搏器，后仍有症状。09 年前再次植入支架 1 枚。6 个月前因心衰住院，行 CRT-D 植入，1 个月前因房颤行射频消融及左心耳封堵。近 1 个月出现轻微活动后胸闷气短症状，口服“速效救心丸”可稍有缓解，偶有夜间憋醒。病来无发热，无腹痛腹泻，无尿频尿急尿痛，无下肢水肿，睡眠和饮食一般，精神及体力差，体重无明显改变。

既往病史：

糖尿病 35 年，口服阿卡波糖，胰岛素注射，血糖控制可。

脑梗 10 年，右侧偏盲，无运动及语言功能障碍。

糖尿病肾病 3 年。一侧肾萎缩，孤立右肾。

40 年吸烟史，戒烟 5 年。

病程记录：

入院后给予指南指导的标准抗心衰治疗，并给予双联抗血小板治疗，他汀联合依折麦布强化降脂治疗后，准备择期进行冠脉造影评估，术前进行水化治疗。造影提示内乳动脉 - 前降支桥血管通畅，大隐静脉 - 回旋支桥通畅，右冠近段及支架内完全闭塞。向家属交代病情后进行介入治疗，正向反复调整 Gaia I,Gaia III,Conquest，最终以 CP12 导丝，在 LIMA 桥血管逆向造影指导下通过血管远端，但各种微导管及球囊均无法通过病变，最终经微导管交换为旋磨导丝，先后以 1.25mm,1.5mm 旋磨头对支架内进行旋磨，每个旋磨头平均 5-6 次通过病变。后充分球囊预处理后共植入 3 枚支架。术后 1 个月复查支架通畅良好。

检验检查记录：

查体：172cm，62kg，P：60bpm，BP：104/85mmHg，半卧位，双肺呼吸音粗，肺底可闻及湿啰音。

入院生化：NT-Pro BNP：10657ng/ml，血 cr:300umol/L，肌钙蛋白正常。血常规：Hb:105g/L. 低密度脂蛋白：0.83mmol/L.

鉴别诊断：

主要和以下几种疾病鉴别诊断

1. 急性心肌梗死

疼痛特点：急性心肌梗死的疼痛更为剧烈，持续时间更长，可伴有心律失常、心力衰竭等严重并发症。不稳定型心绞痛疼痛程度较重，但一般不会出现心肌梗死那样剧烈的疼痛和严重并发症。

心电图改变：急性心肌梗死的心电图可出现 ST 段抬高和病理性 Q 波。不稳定型心绞痛的心电图多为 ST 段压低、T 波倒置，但不出现病理性 Q 波。

心肌损伤标志物：急性心肌梗死患者的心肌损伤标志物如肌红蛋白、肌钙蛋白等明显升高。不稳定型心绞痛患者的心肌损伤标志物可轻度升高，但一般不会像急性心肌梗死患者那样显著升高。

2. 主动脉夹层

疼痛特点：主动脉夹层的疼痛常为撕裂样或刀割样，可放射至背部、腹部等部位。不稳定型心绞痛的疼痛部位和性质与稳定型心绞痛相似，但疼痛程度更剧烈，持续时间更长。

辅助检查：主动脉夹层的心电图和胸部 X 线检查有助于诊断，可发现主动脉增宽等异常。不稳定型心绞痛的心电图和胸部 X 线检查一般无特异性改变。

3. 肺动脉栓塞

疼痛特点：肺动脉栓塞的疼痛多为胸膜炎性胸痛，伴有呼吸困难、咯血等症状。不稳定型心绞痛的疼痛主要为胸部闷痛、压迫感等，一般不伴有咯血症状。

辅助检查：肺动脉栓塞的心电图、胸部 X 线检查和肺动脉造影有助于诊断。不稳定型心绞痛的心电图和胸部 X 线检查一般无特异性改变。

4. 急腹症

疼痛特点：如急性胰腺炎、胆囊炎、胃溃疡穿孔等疾病也可出现类似心绞痛的症状，但疼痛部位和性质与不稳定型心绞痛有所不同。急腹症的疼痛通常位于上腹部或右上腹等部位，可伴有恶心、呕吐、腹胀、腹泻等症状。

辅助检查：通过详细的病史采集、体格检查和相关辅助检查，如腹部超声、CT 等，有助于明确诊断。

其他：

A boy with chest tightness and dyspnea

文凌仪

四川大学华西第二医院

患者基本信息：

A 13-year-old boy

主述：

Chest tightness and dyspnea for 20 days

现病史：

A 13-year-old boy was admitted for reporting chest tightness and dyspnea

既往病史：

The patient had no prior history of cardiovascular disease

病程记录：

No special treatment

检验检查记录：

Physical examination revealed no abnormalities. Laboratory tests showed elevated cardiac troponin I at 13.267 ug/L (reference range 0-0.14 ug/L). ECG showed sinus rhythm with mild ST segment elevation (0.1 mv). A coronary CT angiography was performed and found right coronary artery dominance, anomalous origin of the right coronary artery (RCA) from the left coronary sinus accompanied by mild ostial stenosis (< 50%). Cardiovascular magnetic resonance (CMR) was then performed for further assessment, and showed subepicardial edema and fibrosis on lateral wall of left ventricle, from the basal to apical slices. No myocardial perfusion abnormalities were found in corresponding myocardial segments

鉴别诊断：

Myocarditis

Cardiac amyloidosis

Acute myocardial infarction

Acute pericarditis

其他：

Acute myocardial infarction (AMI) and myocarditis can present with similar clinical manifestations but they can also be differentiated using CMR. In addition to exhibiting characteristics of myocardial inflammation, patient with AMI also shows myocardial perfusion impairment in segments supplied by the culprit vessel. In this case, the patient differs from AMI in two aspects: (1) myocardial injuries located in segments supplied by left coronary artery rather than right coronary artery, as well as inferior wall of left ventricle; (2) no myocardial perfusion impairment found in the corresponding myocardial segments. Overall, CMR is a useful tool to differentiating myocardial infarction with non-obstructive coronary arteries from myocarditis

青少年中主动脉综合征合并难治性高血压一例报告及分析

熊昌

广东省人民医院

患者基本信息：

性别：男性；年龄：19 岁；职业：学生。

主述：

发现血压升高 2 周

现病史：

19 岁，男，2 周前无明显诱因出现咳嗽，伴咳黄白色痰，后逐渐在快步上坡、上楼 2-3 时出现呼吸困难症状，休息后可自行缓解，入当地医院就诊测量血压收缩压 180+mmHg，后多次测量并测四肢血压均升高。外院诊断为“高血压”，予利尿降压等治疗后转入我院。颈静脉无充盈，双侧颈动脉可闻收缩期杂音，左锁骨下可闻及收缩期杂音，心界向左下扩大，心律齐，主动脉瓣第二听诊器可闻及舒张期 4/6 级叹息样杂音，向心尖传导，毛细血管搏动征、水冲脉、枪击音（+），肩胛区可闻及血管杂音；双下肺可闻及散在湿罗音，左肺可闻及哮鸣音；腹部未闻及血管杂音，双侧股动脉、腘动脉、足背动脉无明显异常；可见轻度杵状指。

既往病史：

既往史：支气管扩张病史 5 年，有高血压病史详见现病史，生活习惯不规律，无烟酒史，无冶游史。家族史：姐姐因肠肿瘤去世，具体不详；否认高血压家族史。

病程记录：

治疗随病情变化调整，先后予氨氯地平 10mg qd、沙库巴曲缬沙坦 200mg qd、多沙唑嗪 4mg qd、依伐布雷定 7.5mg bid、地尔硫卓 30mg tid、泼尼松 25mg qd、甲氨蝶呤 10mg qw、达格列净 10mg qd、呋塞米 20mg。

检验检查记录：

入院后抽血提示 WBC 8.17*10^9/L，血红蛋白量 172g/L，NT-ProBNP 206.7 pg/ml，肌钙蛋白 T 11.3 pg/mL，C 反应蛋白 15.42mg/L；PCT 0.25ng/mL；肌酸激酶 250U/L；肌酸激酶 -MB 同工酶 14.6U/L；体液免疫指标：轻链 λ 0.79g/L；风湿免疫指标：CRP、ESR 等炎症指标不高，HLA-B27 阴性；无抗核抗体阳性；抗 KU 抗体弱阳性。

完善检查排除原发性醛固酮增多症、嗜铬细胞瘤、皮质醇增多症、肾实质性病变、OSAS 引起的高血压。

完善心电图为窦性心动过缓；左心室高电压；ST 段改变。

心脏超声提示“LVEF64%，升主动脉 44mm，符合大动脉炎超声改变，胸降主动脉内径变窄，血流加速，升主动脉扩张”；

PET-CT 提示“升主动脉、降主动脉 - 腹主动脉交界处扩张；主动脉弓中段 - 腹主动脉上端变细；升主动脉 - 腹主动脉上段、双侧肾动脉分支多发钙化，糖代谢未见增高；左肾梗塞可能性大；头臂干、左侧颈总动脉起始处周围脂肪间隙欠清晰，糖代谢增高，不除外动脉炎。”

心血管全外显子基因提示：未检测到与受检者临床表型相关的单核苷酸序列变异、短插入缺失变异和拷贝数变异及线粒体基因组变异。

鉴别诊断：

1. 大动脉炎

支持点：PET-CT 提示头臂干、左侧颈总动脉起始处周围脂肪间隙欠清晰，糖代谢增高，不除外动脉炎。查体发现多处血管杂音，符合大动脉炎的临床表现。炎症指标（如 C 反应蛋白）升高。

不支持点：风湿免疫指标（如 HLA-B27、抗核抗体）不支持其他风湿性疾病。

2. 原发性高血压

支持点：患者有高血压病史，血压显著升高。

不支持点：患者为年轻患者，出现难治性高血压，且伴有其他系统性表现（如心脏杂音、血管杂音），不符合典型原发性高血压的表现。

3. 继发性高血压（如肾动脉狭窄、嗜铬细胞瘤、原发性醛固酮增多症等）

支持点：患者出现难治性高血压，需考虑继发性高血压的可能。

不支持点：完善检查已排除原发性醛固酮增多症、嗜铬细胞瘤、皮质醇增多症、肾实质性病变、OSAS 引起的高血压。

综上所述，患者的主要诊断倾向于中主动脉综合征（大动脉炎可能）。

其他：

变应性支气管肺曲霉病合并 Kounis 综合征 1 例

张云烨

杭州师范大学附属医院

患者基本信息：

患者，女，77 岁。因“反复咳嗽咳痰伴气急 7 年余，再发伴加重 2 天”入院。患者 7 年余前受凉后出现咳嗽咳痰，咳少许黄白粘痰，伴活动后喘息胸闷，入院完善胸部 CT 提示两肺炎性病变考虑，肺功能提示重度阻塞性通气功能障碍，诊断为“慢性阻塞性肺病伴急性加重”，予“头孢唑肟、左氧氟沙星”抗感染，“甲泼尼龙琥珀酸钠”抗炎治疗后好转出院。出院后口服“孟鲁司特”、吸入“舒利迭”控制，间断复发住院治疗数次。2 天前患者感咳嗽咳痰较强加重，静息时即有胸闷气促入院。既往变应性支气管肺曲霉病（ABPA）、支气管哮喘、肺恶性肿瘤个人史。否认食品药物过敏史，否认烟酒嗜好，否认家族遗传史。

主述：

反复咳嗽咳痰伴气急 7 年余，再发伴加重 2 天

现病史：

患者 7 年余前受凉后出现咳嗽咳痰，咳少许黄白粘痰，伴活动后喘息胸闷，入院完善胸部 CT 提示两肺炎性病变考虑，肺功能提示重度阻塞性通气功能障碍，诊断为“慢性阻塞性肺病伴急性加重”，予“头孢唑肟、左氧氟沙星”抗感染，“甲泼尼龙琥珀酸钠”抗炎治疗后好转出院。2 天前患者感咳嗽咳痰较强加重，静息时即有胸闷气促入院。

既往病史：

既往变应性支气管肺曲霉病（ABPA）、支气管哮喘、肺恶性肿瘤个人史。

病程记录：

患者入院后完善相关检查，结合患者嗜酸性粒细胞明显增高，胸部 CT 提示右肺支气管扩张伴实变较前增多，既往 ABPA 病史，初步诊断为“ABPA、慢性阻塞性肺病伴有急性加重，支气管哮喘，肺恶性肿瘤个人史”。予哌拉西林他唑巴坦钠针 4.5g Q12H 静滴抗感染，甲基强龙针 40mg QD 微泵静推抗炎，盐酸溴己新 4mg BID 微泵静推化痰，孟鲁司特钠片 1 片 QN 口服降低气道高反应性治疗。次日患者仍感明显胸闷气促，查肌钙蛋白 I：1.693ng/ml，复查常规心电图：窦性心动过速，下壁 ST 段轻度抬高，V4-V6、下壁导联 T 波倒置。考虑为 NST-ACS，予低分子肝素 4000IU Q12H 皮下注射抗凝，氯吡格雷 75mg QD 口服抗血小板，阿托伐他汀 20mg QN 口服调脂稳斑治疗。4 小时后患者出现端坐呼吸，胸闷气促明显，吸氧条件下 SPO2 95%，复查肌钙蛋白 I：2.041 ng/ml，B 型钠尿肽：1150.78 pg/ml，血气分析：65.60mmHg，乳酸 2.5mmol/l。常规心电图提示：窦性心动过速，下壁 ST 段轻度抬高，V4-V6、下壁导联 T 波倒置，超声心动图提示：室壁运动幅度普遍减低（中断至心尖段明显）、主动脉瓣轻中度返流、左室收缩功能降低。考虑合并“急性冠脉综合征、急性左心衰”转至 ICU 进一步治疗，临时加用米力农针 20mg 微泵静推强心，单硝酸异山梨酯 40mg 微泵静推舒张冠脉，同时予高流量及无创呼吸机交替给氧，盐酸伊曲康唑 0.2g Q12H 口服抗真菌治疗。入院第 2 天完善真菌检测 PCR：烟曲霉、黄曲霉、念珠菌等均阴性，过敏原测定：点青 / 分支孢 / 烟曲 / 交链孢霉 5.60kU/l,IgE（总）2148.00IU/m，多次复查肌钙蛋白 I 及心电图见。入院第 3 天行冠脉造影：左主干未见明显下载，前降支近段轻度粥样硬化，20% 狭窄，远段肌桥，对角支未见明显狭窄，TIMI 血流 3 级；回旋支、钝圆支未见明显狭窄，TIMI 血流 3 级；右冠近段粥样硬化，20-30% 狭窄，后降支、左室后支未见明显狭窄，TIMI 血流 3 级。

检验检查记录：

入院检查：

SCRP、血气分析正常范围，血常规：嗜酸性粒细胞百分数：20.7%，嗜酸性粒细胞绝对值 1.71*10^9，急诊生化：肌酸激酶 210u/l，肌酸激酶同工酶 5.73ng/ml，肌红蛋白 130.1ug/l。B 型钠尿肽：132.85pg/ml。常规心电图：窦性心律。胸部高分辨率 CT：两肺多发炎性改变及条索灶，两肺部分支气管扩张，右肺中叶部分支气管中断伴实变影，左肺术后改变，主动脉壁及冠脉钙化，两侧胸膜局部增厚，纵隔稍增大淋巴结。

冠脉造影：

左主干未见明显下载，前降支近段轻度粥样硬化，20% 狭窄，远段肌桥，对角支未见明显狭窄，TIMI 血流 3 级；回旋支、钝圆支未见明显狭窄，TIMI 血流 3 级；右冠近段粥样硬化，20-30% 狭窄，后降支、左室后支未见明显狭窄，TIMI 血流 3 级。

鉴别诊断：

需与以下疾病鉴别：1）应激性心肌病：存在严重应激诱因，超声显示心尖球样扩张，冠脉造影阴性，但左室造影呈“章鱼壶”样改变，肌钙蛋白轻中度升高（通常 <10 倍正常值），BNP 显著升高；2）嗜酸性粒细胞性心肌炎：嗜酸性粒细胞浸润损伤心肌，血嗜酸性粒细胞水平高，肌钙蛋白水平高，持续时间长，冠脉造影阴性，确诊依赖心肌活检出现嗜酸性粒细胞浸润及心肌坏死；3）急性心肌梗死：心电图缺血或者梗死改变，肌钙蛋白阳性，冠脉造影阳性。以应激性心肌病或嗜酸性粒细胞性心肌炎为代表的一类疾病以损伤心肌细胞为主，肌钙蛋白水平通常没有快速升高快速下降的特点，存在其他特异性改变，而急性心肌梗死则通过冠脉造影能明确鉴别。

其他：

心大的年轻人：NSTEMI 引发的严重心衰 1 例

郑雅璇

北京清华长庚医院

患者基本信息：

患者中年男性，38 岁

主述：

间断胸闷、胸痛 5 月，加重 1 天

现病史：

患者 5 月前出现活动后及夜间胸闷，休息及坐位可缓解，伴心前区胸痛，有左前臂放射痛、后背放射痛，无头晕、头痛、咳嗽、咳痰等，未规范诊治，1 月前出现胸闷程度加重，具体表现为爬楼梯困难，未规范诊治，今日因咳嗽、胸闷就诊呼吸内科完善心电图可见 ST 改变， TnT-hs 0.0342 ng/mL,NT-ProBNP 5023 pg/ml, 入急诊内科，予以扩冠、利尿治疗后患者胸闷症状好转，现患者为求进一步诊治收入我院 CCU。患者起病以来，饮食可，睡眠良好，精神良好，体重无明显变化，大小便正常。

既往病史：

糖尿病 10 余年，平素口服二甲双胍 0.5g bid 及阿卡波糖 50mg tid 降糖治疗，平素未规律监测血糖，否认高血压、结核，否认外伤史、手术史、输血史、药物及食物过敏史。

病程记录：

入 CCU 后查氨基末端 B 型利钠肽前体 3458pg/ml ↑，肌钙蛋白 T- 高敏 0.04ng/mL ↑， 床旁超声心动图：左室射血分数：13 %，左心及右房增大，室间隔及左室侧后壁增厚，主动脉瓣钙化，少量反流，二尖瓣少量反流，少 - 中量心包积液，左室整体收缩及舒张功能减低，右室整体收缩功能减低。入院后测血压 200/110mmHg，予硝酸甘油扩冠、乌拉地尔降压、呋塞米利尿治疗，并予琥珀酸美托洛尔缓释片 23.75mg qd 减缓心肌重构，停用硝酸甘油后加用氨氯地平 2.5mg qd 降压治疗。明确病因，症状缓解后完善冠脉造影，行介入治疗。

检验检查记录：

查血常规：白细胞计数 5.74×10^9/L，红细胞计数 5.39×10^12/L，血红蛋白量 152g/L，血小板计数 211×10^9/L，中性粒细胞绝对值 3.37×10^9/L，C 反应蛋白（全血）16.74mg/L ↑，心肌损伤标志物四项 -1（检验科 ,CK/CKMB/hs-CTNT/MYO)（急),N 端 -B 型钠尿肽前体 (NT-ProBNP) 测定：* 氨基末端 B 型利钠肽前体 3458pg/ml ↑，* 肌钙蛋白 T- 高敏（急）0.04ng/mL ↑， 床旁超声心动图：左室射血分数：13 %，左心及右房增大，室间隔及左室侧后壁增厚，主动脉瓣钙化，少量反流，二尖瓣少量反流，少 - 中量心包积液，左室整体收缩及舒张功能减低，右室整体收缩功能减低。入院后测血压 200/110mmHg。2025-04-07 转入普通病房。入院查 ECG：窦性心律，电轴左偏，P 波异常；超声心动图（2025-04-07）：左室后壁厚度：11 mm，左室射血分数：14 %，左室后壁的心包积液：10 mm，左室心尖部室壁瘤形成，左室腔内占位，血栓可能性大，少量心包积液，左室整体收缩及舒张功能减低；右心功能：三尖瓣少量反流，右室整体收缩功能减低。复查心肌损伤标志物：肌酸激酶 40U/L ↓，肌钙蛋白 T- 高敏 0.0432ng/mL ↑，氨基末端 B 型利钠肽前体 1281pg/ml ↑，血常规：C 反应蛋白（全血）3.58mg/L，白细胞计数 7.28×10^9/L，红细胞计数 6.44×10^12/L ↑，血红蛋白量 179g/L ↑。动态血压：24H 平均血压 114/73mmHg，白天平均血压 117/76mmHg，夜间平均血压 105/64mmHg；动态心电图：1. 窦性心律（总心搏数 109712 次，平均心率 80bpm，最快心率 111bpm，发生于 04-09 04:58:34，最慢心率 63bpm，发生于 04-09 00:39:36）2.P 波异常 3. 偶发房性早搏 4. 偶发多形室性早搏，可见成对型室早 5. 间歇性室内阻滞（与快频率相关）6.ST-T 改变；双侧椎动脉超声未见明确异常；双侧颈动脉超声：右侧颈动脉分叉处斑块形成；肝胆胰脾超声未见明显异常。血常规：白细胞计数 8.04×10^9/L，红细胞计数 6.68×10^12/L ↑，血红蛋白量 185g/L ↑，中性粒细胞绝对值 5.14×10^9/L，C 反应蛋白（全血）3.65mg/L，肾功能：尿素（急）19.5mmol/L ↑，肌酐 126umol/L ↑，评估肾小球滤过率 61.927，钾 3.97mmol/L 氨基末端 B 型利钠肽前体 1548pg/ml ↑，肌钙蛋白 T- 高敏（急）0.0264ng/mL ↑。超声心动图（2025-04-11）：左室射血分数：21 %，左室后壁心尖处可见大小约 26mm*16mm 强回声团块。左室后壁（11mm）及侧壁（12mm）增厚。超声心动图（2025-04-14）：左室射血分数：22 %；左室下后壁心尖处可见一强回声团块，形态不规则，大小约 27mm*17mm。于 2025-04-15 行冠脉造影提示：左前降支中段、第二对角

支：狭窄程度 100% 完全闭塞，回旋支远段：狭窄程度 50-70%，右冠状动脉后降支：狭窄程度 <30%，未行介入治疗。术后复查血：WBC 8 10^9/L ↑ (High), RBC 6.37 10^12/L , HGB 177 g/L , HCT 51.2 % , RDW-SD 38.50 fl ↓ (Low), LY# 1.55 10^9/L ↑ (High), 术后肾功能：UREA 11.6 mmol/L, Cre 125 umol/L, eGFR 62.527 , K 3.95 mmol/L , 心肌酶： CK 52 U/L, CK-MB 0.935 ng/mL, MYO 31.9 ng/mL, TnT-hs 0.0227 ng/mL。ECG：窦性心律，左束支传导阻滞。

鉴别诊断：

1. 病毒性心肌炎

2. 扩张型心肌病

3. 高血压性心脏病

4. 缺血性心脏病

其他：

蜂毒的警示：严重二尖瓣管不不全 1 例

郑雅璇

北京清华长庚医院

患者基本信息：

62 岁 老年男性

主述：

间断劳累后憋气 10 年，突发头晕 4 天

现病史：

患者于 10 年前开始于劳累后出现憋气，程度较轻微，休息后可缓解，体力活动轻度受限，不伴头晕、心悸、不伴胸闷、胸痛、夜间阵发呼吸困难、端坐呼吸，不伴反酸、烧心等症状。患者未予重视，未就诊，期间未规律体检。4 天前患者意外受马蜂蛰咬后出现头晕、跌倒，伴乏力、大汗，否认胸闷、胸痛、意识丧失，就诊于我院急诊，完善 BNP 197 pg/ml，头颅 CT 未见明显异常。心电图示窦性心律，电轴轻度左偏，ST 段改变。进一步就诊我科门诊，完善超声心动图提示左房增大，二尖瓣后叶脱垂，重度关闭不全（LVEF64%），考虑“二尖瓣重度关闭不全”收入我科。患者自发病以来精神饮食尚可，睡眠不佳，大小便正常，体重较前未见明显变化。

既往病史：

高血压病 5 年，最高血压 180/95mmHg，未治疗；高胆固醇血症 5 年，未治疗。否认其他长期慢性病史，否认心律失常史、其他系统疾病史、传染病史、手术外伤史、输血史、药物及食物过敏史。

病程记录：

完善疾病筛查，为明确病因行冠脉造影检查除外缺血性心脏病，行 MitraClip（二尖瓣钳夹术）改善瓣膜闭合功能

检验检查记录：

血常规：CRP(B) 1.23 mg/L, WBC 12.99 10^9/L, HGB 173 g/L, PLT 263 10^9/L, NEUT# 10.62 10^9/L, LY# 1.96 10^9/L, NEUT% 81.8 %, LY% 15.1 %,

心肌损伤标志物： NT-ProBNP 197 pg/ml, TnT-hs 0.00678 ng/mL,

肝 肾 功：ALT 14.5 U/L, AST 29.2 U/L, ALB 47.2 g/L, Cre 92 umol/L, eGFR 76.523 ml/min/1.73m^2, GLU 6.44 mmol/L, K 4 mmol/L,

糖化： Hb-A1c 5.3 %,

血脂： CHOL 4.73 mmol/L, TRIG 0.73 mmol/L, HDL-C 1.52 mmol/L, LDL-C 2.84 mmol/L,

术前感染、凝血、甲状腺功能、尿酸均未见明显异常。

肝胆胰脾超声：肝外胆管增宽，胰管增宽。

颈部血管超声：双侧颈动脉粥样硬化斑块形成；双侧椎动脉超声未见明确异常。

超声心动图：左房增大；二尖瓣后叶脱垂，重度关闭不全；主动脉瓣少量反流；三尖瓣少量反流，估测肺动脉收缩压增高；左室整体收缩功能正常，舒张功能减低（LVEF64%）

经食道超声心动：[超声所见]: 左房增大，左心耳内未探及异常回声物附着，左心耳排空速度正常（58cm/s）。房间隔连续性完整，未探及明确回声中断。二尖瓣前叶正常、长度 26mm，二尖瓣后叶冗长、卷曲、回声增强，长约 21mm，收缩期 P2 区及部分 P3 区脱向左房侧，以 P2 区为主，脱垂宽度 14mm，脱垂高度 5mm，前后叶对合高度 5mm。二尖瓣环前后径 32mm，左右径 30mm。二尖瓣重度反流，缩流颈宽度 6mm。余心内结构及血流同经胸超声心动图。[结论]: 二尖瓣病变 粘液样变性可能性大; 后叶 P2 区及部分 P3 区脱垂; 二尖瓣重度关闭不全；左房增大。

动态心电图：1. 窦性心律 (总心搏数 91149 个 , 平均心率 65bpm, 最慢心率 46bpm, 发生于 02:29. 最快心率 118bpm, 发生于 08:29.)2. 偶发房性早搏，可见成对型、未下传型房早 3. 短阵房性心动过速 (2 阵 ,3–4 次 / 阵 , 最快频率 127bpm)4. 心率快时 , 可见 ST–T 改变。

动态血压：24h 平均 146/77mmHg，白日平均 146/78mmHg，夜间平均 148/74mmHg。

冠脉造影：【结果】 冠状动脉起源及分布：正常，右优势型；既往未行介入治疗；左前降支近段、左前降支中段狭窄程度 30-50%，TIMI III 级，回旋支近段、回旋支远段狭窄程度 <30%，TIMI III 级，右冠状动脉近段、右冠状动脉中段狭窄程度 30-50%，TIMI III 级

鉴别诊断：

1. 风湿性心脏病（链球菌感染后引发免疫反应导致二尖瓣瓣叶粘连、钙化、增厚）

2. 感染性心内膜炎（心菌感染瓣叶形成赘生物）

3. 心肌缺血或梗死（左室乳头肌因冠脉供血不足发生坏死、纤维化）

4. 左心室扩大（长期高血压、扩心病导致左室扩张）

5. 先天性因素

其他：

打破常规：围手术期肺动脉高压危象中的 ECMO 新策略

张弛

北京清华长庚医院

患者基本信息：

37 岁青年女性，神智清、精神可，饮食、睡眠正常，大便、小便正常，体重无明显变化

基本信息：否认手术史、传染病史、外伤史、输血史、过敏史、疫区接触史、毒物或放射性物质接触史、烟酒史。婚育史：已婚，育有 1 子 1 女，配偶及子女体健。家族史：否认早发心血管病家族史或其他遗传病史。

主述：

间断胸闷 2 月余

现病史：

患者 2 月余前产后间断胸闷，就诊于外院查指脉氧下降至 87-88%；心脏超声示（2025-1-27）：先天性心脏病复合畸形：室间隔膜肌部大缺损（22.2mm×20.4mm， 室水平双向分流 ，以左向右分流为主，左向右分流占比 54.97% ），动脉导管未闭（ 2.5mm， 动脉水平双向分流，左向右分流为主），右室前壁增厚，右室流出道异常增厚肌束，右室流出道流速稍快，左房增大（67.2mm×35mm），肺动脉高压（重度），肺动脉瓣中度反流，主肺动脉明显扩张。 现患者为求进一步诊治收入我院

既往病史：

既往体健

病程记录：

1、完善右心导管术 + 右心室造影：

PVR 11.7，Qp/Qs1.51，诊断：肺动脉高压 毛细血管前性

2、行手术治疗：室间隔缺损组织补片修补术 + 动脉导管未闭切断缝合术 + 房间隔开窗术 + 体外膜肺氧合

（1）手术发现：

吸氧前：外周无创血压 131/77mmHg， 心率 70-75bpm； 肺动脉压 102/55(75)mmHg；

吸氧后：外周无创动脉压：132/78mmHg，心率 79-75bbpm；肺动脉压 93/46(67)mmHg。

（2）手术经过：

在术中发现卵圆孔未闭，直径约 3 mm。在完成室间隔缺损的补片修补及房间隔造口术后，经食道超声心动图（TEE）显示显著的右向左房分流。患者表现出难以脱离体外循环，提示围手术期肺动脉高压危象。

为应对此情况，采用了一种新型的静脉 - 左心房体外膜肺氧合（V-LA ECMO）模式。通过左侧股静脉置入一枚 17F 引流管，同时经右侧股静脉置入一枚 19F 回流管，该导管穿过房间隔并定位于左心房内。该方法实现了血液直接回流至左心房，有效减轻右心负荷，同时维持系统性氧合与灌注

3、经过 21 天的体外膜肺氧合支持治疗后，患者成功脱离 ECMO，肺动脉压力降至 40/30 mmHg，病情明显好转并出院

[illegible]记录：

外院心脏超声（2025-01-27）：先天性心脏病复合畸形：室间隔膜肌部大缺损（ 22.2mm×20.4mm， 室水平双向分流 ，以左向右分流为主，左向右分流占比 54.97% ），动脉导管未闭（ 2.5mm， 动脉水平双向分流，左向右分流为主），右室前壁增厚，右室流出道异常增厚肌束，右室流出道流速稍快，左房增大（67.2mm×35mm），肺动脉高压（重度），肺动脉瓣中度反流，主肺动脉明显扩张

鉴别诊断：

需鉴别：动脉导管未闭、主动脉 - 肺动脉窗

均属于左向右分流性先天性心脏病，通过心脏超声、术中探查可进行鉴别

其他：

提供此病例的临床意义：术中使用的是一种全新的 ECMO 方式，并且对于围术期肺动脉高压危象的患者来说，这种方式较好的规避了常规 V-A 或 V-V ECMO 的部分不足之处，以下为详细说明：

1. 静脉 - 左心房体外膜肺氧合（V-LA ECMO）

V-LA ECMO 是一种全新的 ECMO 插管模式，其特点为：通过股静脉引流静脉血，并直接回输至左心房。与传统的静脉 - 静脉体外膜肺氧合（V-V ECMO）相比，V-LA ECMO 能更有效地减轻右心室的前负荷; 同时，不同于静脉 - 动脉体外膜氧合（V-A ECMO），它能改善冠状动脉灌注并降低左心室后负荷。

鉴于其在生理上的优势，V-LA ECMO 可能为围手术期发生严重肺动脉高压危象的患者，尤其是需右心室功能支持者，提供一种具有前景的替代方案。

2. 扩展应用的潜在适应证

该插管方式在存在左向右心腔内分流，且伴有肺动脉高压和右心功能不全的患者中，可能具有特殊的临床价值。例如：患有**动脉导管未闭（PDA）或主动脉 - 肺动脉窗**等先天性心脏病的患者。

瞰见钙化 磨道开路 IVUS 指导下旋磨处理重度钙化病变一例

纪兆乐

空军军医大学唐都医院

患者基本信息：

患者男性，55 岁。

主诉：间断性胸闷、气短 6 月余，加重 2 月。

现病史：6 月前无明显诱因后出现胸闷，伴气短，位于心前区，呈一过性，不伴有心慌、出汗，无恶心、呕吐等。期间未重视，未治疗。2 月前患者劳累后再次出现上述症状并加重，表现为持续时间延长，活动耐量下降，同时夜间憋醒，后在外院就诊完善冠脉 CTA 提示重度狭窄伴钙化。为求进一步诊治，来我院以“冠心病”收住。

既往史: 高血压病病史 8 年，血压最高时达 200/100mmHg，目前口服药物降压。2 型糖尿病病史 3 年。

个人史：长期吸烟，20 支 / 日。

家族史：无

体格检查：血压 125/90mmHg、心率 71bpm。律齐，各瓣膜区未闻及异常杂音。

主述：

间断性胸闷、气短 6 月余，加重 2 月

现病史：

6 月前无明显诱因后出现胸闷，伴气短，位于心前区，呈一过性，不伴有心慌、出汗，无恶心、呕吐等。期间未重视，未治疗。2 月前患者劳累后再次出现上述症状并加重，表现为持续时间延长，活动耐量下降，同时夜间憋醒，后在外院就诊完善冠脉 CTA 提示重度狭窄伴钙化。为求进一步诊治，来我院以“冠心病”收住。

既往病史：

高血压病病史 8 年，血压最高时达 200/100mmHg，目前口服药物降压。2 型糖尿病病史 3 年。

病程记录：

患者入院后给予抗血小板，调脂等对症治疗后，择期行冠脉造影提示三支中重度病变，伴严重钙化，IVUS 指导下行旋磨处理并植入支架。

检验检查记录：

心电图示：窦性心律，ST-T 缺血性改变。心脏超声示：EF0.69，升主动脉钙化，左房略大，主动脉瓣钙化

鉴别诊断：

诊断明确

其他：

FFR 联合 OCT 指导 PCI 一例

王芳芳

空军军医大学唐都医院

患者基本信息：

郭 XX, 男，67 岁，2025-4-7 入院

主诉：间断胸痛 2 年，再发 1 周。

现病史：2 年前活动后胸痛，就诊于外院行冠脉造影并于植入支架 (具体情况不详)，术后规律用药。近 1 周来再次出现胸痛。于 4 月 7 日入院，

既往史：有高脂血症及糖尿病病史，否认“高血压、慢性肾病 ^ 病史。否认肝炎、肺结校、疟疾、菌痢等传染病史。否认输血史，否认外伤史，预防接种史不详，无过敏史。

危险因素：高脂血症、2 型糖尿病、慢性心力衰竭。

主述：

间断胸痛 2 年，再发 1 周。

现病史：

2 年前活动后胸痛，就诊于外院行冠脉造影并于植入支架 (具体情况不详)，术后规律用药。近 1 周来再次出现胸痛。于 4 月 7 日入院，

既往病史：

有高脂血症及糖尿病病史，否认“高血压、慢性肾病 ^ 病史。否认肝炎、肺结校、疟疾、菌痢等传染病史。否认输血史，否认外伤史，预防接种史不详，无过敏史。

病程记录：

完善血常规及生化检查 , 并安排行冠脉造影及 PCI 治疗 .

检验检查记录：

心电图：心电图：1. 窦性心律 2. T 波异常。

心脏超声 : 左房、左室大；左室后壁、部分下壁陈旧性心梗改变，三尖瓣、二尖瓣轻度关闭不全左室收缩功能减低，EF=39%；

鉴别诊断：

肺栓塞 胆囊炎等

其他：

该病例为介入手术病例 , 详见上传 PPT

莫让“原醛”成为漏网之鱼：高血压患者筛查的重要性

张盈璨

哈尔滨医科大学附属第二医院

患者基本信息：

基本信息：女性，53 岁

主诉：激动后心慌 1 年，加重 3 个月

病史：心慌时伴出汗、乏力，偶有心前区刺痛，休息后 10 分钟缓解，当地医院诊断为室早，口服美西律好转后停药。新冠感染后心慌加重，伴胸背钝痛、乏力、头晕头痛、咳嗽咳痰、头颈板紧

既往史：高血压 5 年，最高 200/118mmHg，平素口服维拉帕米控制在 130/80 mmHg。腔梗、高脂血症、低钾血症病史。否认糖尿病病史，无吸烟史、饮酒史。否认家族遗传病史。

入院生命体征：BP 164/94mmHg，心率 56 次 / 分，心律齐

主述：

激动后心慌 1 年，加重 3 个月

现病史：

患者于入院前 1 年于激动后出现心慌，心慌时伴出汗、乏力，偶有心前区刺痛，休息后 10 分钟缓解，当地医院诊断为室早，口服美西律好转后停药。于入院前 3 月于新冠感染后心慌加重，伴胸背钝痛、乏力、头晕头痛、咳嗽咳痰、头颈板紧。患者病程以来，一般状态尚可，精神尚可，饮食睡眠尚可，二便正常，体重无明显减轻。

既往病史：

高血压 5 年，最高 200/118mmHg，平素口服维拉帕米控制在 130/80 mmHg。腔梗、高脂血症、低钾血症病史。否认糖尿病病史，无吸烟史、饮酒史。否认家族遗传病史。

病程记录：

入院后完善血常规、生化、心肌酶、醛固酮、肾素、皮质醇指标 ，完善冠脉 CTA、肾上腺 CT、肺 CT、泌尿系和肾血管彩超、holter 及心电图检查，给予肾动脉造影及冠脉 CAG，口服沙库巴曲缬沙坦钠片一日一次，一次 100mg po

检验检查记录：

1. 冠脉 CTA:

•LM 及 LAD 近中段：钙化及混合斑块，管腔轻微狭窄

•RCA 多发钙化斑块，管腔轻微狭窄

•D2 中段心肌桥，壁冠状动脉未见有意义狭窄，近段钙化及非钙化斑块，管腔轻微狭窄

2. 肾上腺 CT:

• 左侧肾上腺局部增粗，考虑为肾上腺增生可能

3. 胸部 CT

• 双肺结节、局限性肺气肿，钙化灶。右下叶间质改变，左肺斑索。双侧胸膜略厚

• 左心室大

4. 泌尿系 + 肾血管三维超声

• 双肾及双肾血管、膀胱未见明显异常

鉴别诊断：

1. 肾实质性高血压

包括急慢性骨小球肾炎，糖尿病性胥病慢性肾盂肾炎，多衷胥和肾移植后等多种肾脏病变引起的高血压，是最常见的继发性高血压。所有肾脏疾病在终末期肾病阶段 80% ~ 90% 以上有高血压。肾实质性高血压的发生主要是由于肾单位大量丢失，导致水钠潴留和细胞外容量增加，以及肾脏 RAAS 激活与排钠激素减少。高血压又进步升高肾小球内袁压力，形成恶性循环，加重肾脏病变。

2. 肾血管性高血压

肾血管性高血压是单侧或双侧肾动脉主干或分支狭窄引 | 起的高血压。常见病因有多发性大动脉炎，肾动脉纤维肌性发育不良和动脉粥样硬化，前两者主要见于青少年，后者见于老年人。肾血管性高血压的发生是由于肾血管狭窄，导致肾脏缺血，激活 RAAS。凡进展迅速或突然加重的高血压，均应怀疑本症。本症大多有舒张压中、重度升高，体检时在上腹部或背部肋脊角处可闻及血管杂音。大剂量快速静脉肾盂造影、多普勒超声、放射性核素肾图有助于诊断，肾动脉造影可明确诊断和狭窄部位。

4. 嗜铬细胞瘤

嗜铬细胞瘤起源于肾上腺髓质、交感神经节和体内其他部位嗜铬组织，肿瘤间歌或持续释放过多肾上腺素、去甲肾上腺素与多巴胺。

临床表现变化多端，典型的发作表现为阵发性血压升高伴心动过速、头痛出汗、面色苍白。在发作期间可测定血或尿儿茶酚胺或其

代谢产物 3- 甲氧基 -4- 羟基苦杏仁酸 (VMA)，如有显著增高，提示嗜铬细胞瘤。超声、放射性核素、CT 或碰共振可作定位诊断。

其他：

确定诊断：

I. 原发性醛固酮过多症

II. 高血压 3 级（很高危）

III. 心律失常

IV. 频发性室性期前收缩

以心律失常为表现的结节病 1 例

jjj_xy

西安交通大学第一附属医院

患者基本信息：

中年女性，56 岁。职业：教师。

主述：

间断咳嗽、胸痛半年

现病史：

半年前无明显诱因出现干咳，伴前胸部持续性疼痛；偶有胸闷、气短；无发热、盗汗、乏力、关节及肌肉疼痛；无心慌、黑懵、恶心、呕吐。就诊于当地医院，完善胸部 CT 平扫示：纵隔及双肺门多发肿大淋巴结，双肺散在实性结节；肿瘤标志物未见明显异常。考虑肺部感染，予以抗感染及平喘治疗，患者自觉咳嗽较前减轻，胸痛无好转。遂于 2025 年 3 月就诊于我科。肺动脉 CT 血管造影示双肺门、纵隔多发软组织结节、肿块，部分融合，多考虑肿大淋巴结影。左右主气管管腔稍狭窄，两肺上叶多发小结节。两下肺间质性改变并少许间质性炎症。超声支气管镜引导纵隔 7 组、4R 组、4L 组淋巴结针吸活检结果示：纤维素性渗出物中见淋巴细胞及肉芽肿形成，未见坏死。细胞学检查结果示未见恶性细胞，可见淋巴细胞、柱状细胞。分子病理检测示结核分枝杆菌复合群（MTBC）核酸检测阴性。心电图示窦性心律，心率 97 次 / 分，室性早搏。心动超声示 EF68%，左室舒张末内径 48mm，左室收缩末内径 31mm，左室后壁厚度 8mm。左室舒缓功能减低。心肌酶、B 型脑钠肽前体、肌钙蛋白 I 未见明显异常。肺动脉、肺功能、支气管舒张试验、呼出气一氧化氮测定未见明显异常。考虑诊断为：1. 纵隔淋巴结肿大；2. 双肺炎性肺结节。患者干咳，考虑肿大淋巴结压迫气道、肺间质性改变刺激气道所致，给予复方福尔可定止咳对症处理，胸痛建议心血管内科或疼痛科就诊，余予以盐酸莫西沙星抗感染治疗。出院后患者仍有咳嗽，咳白色泡沫痰，伴心慌、胸闷，于外院复查胸部增强 CT 可见：纵隔内及双肺门多发增大淋巴结；双肺散在实性结节灶，较前变化不著；双肺下叶炎症，左肺上叶小叶间隔增厚。心包腔少量积液。动态心电图可见窦性心律，总心搏 129579 次，最快心率 153bpm，最慢心率 69bpm，平均心率 92bpm，室性早搏总数（15638 次，12.07%，双源）。最长 RR 间期 1.199 秒。再次就诊于我科。自发病以来，神志清、精神可，食欲、夜休一般，二便正常，体重半年来下降 10kg。

既往病史：

既往有焦虑症病史 30 年，长期口服帕罗西汀 20mg/ 日抗焦虑。

26 年前行剖腹产手术。

糖耐量减低病史 4 年，监测空腹血糖波动于 7mmol/L 左右，餐后 2 小时血糖波动于 10mmol/L 左右。

否认结核、甲状腺、心脏病史，否认药物、食物过敏史。

无化学性物质、放射性物质、有毒物质接触史。

无吸烟史。

否认家族性遗传病史。

病程记录：

入院后予以比索洛尔 5mg QD，稳心颗粒 5g TID 控制心率对症治疗。

结节病诊断明确后，调整治疗方案为：泼尼松 30mg/ 日，辅以护胃、补钙、稳定心室率对症治疗。

检验检查记录：

浅表淋巴结超声：右侧锁骨上窝淋巴结肿大。右侧锁骨上窝可见一淋巴结，大小约 9.0×6.5mm，边界清，形态饱满，皮髓质分界不清。余双侧颈部、双侧腋窝、双侧腹股沟区、腹主动脉及下腔静脉周围未探及明显异常肿大淋巴结。于超声引导下行右锁骨上窝淋巴结穿刺，病理结果回报：少许纤维脂肪及骨骼肌组织。

肝胆胰脾超声：胆囊壁毛糙，胆囊息肉。

甲状腺超声: 甲状腺左叶钙化灶。甲状腺左叶可见一强回声斑点，余腺体回声均匀。

心动超声：EF73%，左室舒张末内径 46mm，左室收缩末内径 26mm，左室后壁厚度 8mm。二尖瓣增厚伴少量反流，左室舒缓功能减低，心包积液（微量）。

心脏核磁 1.5T 平扫: 1. 心脏形态及运动未见明显异常，建议必要时增强扫描。2. 左心室远段侧壁心肌过度小梁化，二尖瓣少量反流；心包少量积液。

冠状动脉 CT 血管造影：1. 冠状动脉未见明确斑块征象，管腔未见明显狭窄。2。心包少许积液。

	结果	参考值范围
甲胎蛋白（ng/mL）	3.63	0-7
癌胚抗原（ng/mL）	2.06	0-5
神经元特异性烯醇化酶（ng/mL）	14	0-16.3
细胞角蛋白片段（ng/mL）	1.69	0-3
总 IgE（IU/mL）	< 17	0-100
红细胞沉降率（mm/h）	7	0-20
降钙素（pg/mL）	1.01	0-6.4
谷草转氨酶（U/L）	15	13-35
谷丙转氨酶（U/L）	13	7-40
碱性磷酸酶（U/L）	73	50-135
γ- 谷氨酰转肽酶（U/L）	57	7-45
总胆红素（umol/L）	8.6	3.4-17.1
直接胆红素（umol/L）	0.4	0-3.4
间接胆红素（umol/L）	8.2	0-17.1
胆碱酯酶（U/L）	7578	4650-10440
尿素（mmol/L）	5.68	2.6-7.5
肌酐（umol/L）	53	41-73
尿酸（umol/L）	221	155-357
胱抑素 C（mg/L）	1.150	0.6-1.55
eGFR（mL/min/1.73m^2）	102.22	> 90
乳酸脱氢酶（U/L）	174	120-250
肌酸激酶（U/L）	< 20	40-200
肌酸激酶同工酶（U/L）	12.25	0-24
B 型脑钠肽前体（pg/mL）	234	0-125
血清肌钙蛋白 I（pg/mL）	< 2	0-15.7
高敏肌钙蛋白 T（ng/mL）	< 0.003	0-0.014
红细胞计数（10×10^{12}/L）	4.89	3.8-5.1
血红蛋白（g/L）	139	115-150
白细胞计数（10×10^9/L）	8.35	3.5-9.5
中性粒细胞计数（10×10^9/L）	6.74	1.8-6.3
淋巴细胞计数（10×10^9/L）	1.24	1.1-3.2
血小板计数（10×10^9/L）	387	125-350
嗜酸细胞计数（10×10^9/L）	0.00	0.02-0.52

鉴别诊断：

1. 肺结核：由结核分枝杆菌 感染引起。主要临床症状为低热、盗汗、乏力、消瘦、咳嗽、咯血。病理特征性病变为干酪样坏死性肉芽肿。确诊依赖于病理组织中找到抗酸染色阳性（Ziehl-Neelsen 染色）的结核杆菌或通过分子生物学 /PCR 检测到结核杆菌 DNA。

2. 致心律失常性右室心肌病 ： 主要是一种遗传性心肌病，多数病例为常染色体显性遗传。主要临床表现为室性心律失常，如室性早搏、非持续性或持续性室性心动过速。多达 90% 的 ARVC 患者可能在心电图上出现复极化或去极化异常。最常见的发现是 V1–V3 导联 T 波倒置，无右束支传导阻滞。ε 波的存在仍然是诊断的主要标准。

其他：

以心律失常为表现的结节病 1 例

加雪莹 殷艳蓉

摘要： **目的** 结节病是一种病因不明的罕见肉芽肿性炎症性疾病，25%-50%的病例累及心脏。本文报道 1 例以心律失常为表现的心脏结节病中年患者，探讨其诊断方法与治疗策略。**方法** 56 岁女性因“干咳、胸痛半年”就诊。动态心电图可见室性早搏（总数 15638 次，12.07%，双源）。心动超声示 EF73%，左室舒张末内径 46mm，左室收缩末内径 26mm，左室后壁厚度 8mm。二尖瓣增厚伴少量反流，左室舒缓功能减低，心包积液（微量）。心脏核磁 1.5T 平扫：左心室远段侧壁心肌过度小梁化，二尖瓣少量反流；心包少量积液。胸部增强 CT 可见：纵隔内及双肺门多发增大淋巴结；双肺散在实性结节灶；双肺下叶炎症，左肺上叶小叶间隔增厚；心包腔少量积液。支气管镜淋巴结针吸活检结果示纤维素性渗出物中见淋巴细胞及肉芽肿形成，未见坏死。于 2025 年 6 月 28 日予以泼尼松 30mg/日治疗，截至 2024 年 7 月 15 日，患者干咳较前好转，偶有胸痛。目前持续随访中。**结果** 文献检索 PubMed(2022-2025)，纳入 234 例心脏结节病的病例分析显示：心脏结节病常见的表现包括传导阻滞、室性心律失常或左心室功能障碍。心肌磁共振成像诊断心脏结节病具有高灵敏度（95%）和特异性（85%）。结节病患者中 60%的死亡归因于心脏受累。**结论** 早期识别心脏结节病高危患者，并及时干预治疗至关重要。临床亟需制定心律失常分层管理策略。

关键词： 心脏结节病；心律失常；病例报道；文献复习

手机号：15535439179

Email：j1553543@163.com

单位：西安交通大学第一附属医院

抗磷脂综合征合并反复下壁 STEMI 1 例

霍黎明

北京大学人民医院

患者基本信息：

男，35 岁，汉族，籍贯北京

主述：

皮肤瘀点 3 个月，胸痛、胸闷 17 小时

现病史：

3 个月前，患者无明显诱因出现四肢瘀点，16 天前因口腔血疱门诊就诊，实验室检查发现血小板显著减少 (2×109/L)，抗核抗体 (1:80)、狼疮抗凝物和抗心磷脂抗体阳性。经过地塞米松、人免疫球蛋白及间歇性血小板输注治疗后，血小板计数恢复至 56×109/L，随后治疗加入了海曲泊帕和强的松。17 小时前，患者突发左侧胸部持续性疼痛伴胸闷，急诊检查显示肌钙蛋白升高 (hsTNI 1011pg/ml，正常值 <17.8pg/ml)，12 导联心电图示 III、aVF 导联 ST 段抬高，初步诊断为急性下壁 ST 段抬高型心肌梗死，经阿司匹林 + 氯吡格雷抗板负荷抗板后，收入心脏监护病房。

既往病史：

银屑病史 16 年，间断服用中药 (具体不详) 治疗；代谢相关脂肪性肝病病史 1 年，转氨酶升高，间断服用保肝药；发现桥本甲状腺炎 1 周；否认高血压、糖尿病病史；否认病毒性肝炎、结核病史及其密切接触史；痔疮术后 8 年，肛瘘术后 7 年；无外伤史，有血小板、人免疫球蛋白输注史，头孢皮试阳性，否认食物过敏史，预防接种史按计划进行。

病程记录：

患者入院后的冠脉造影未见明显心外膜血管狭窄及血栓表现，但是存在冠脉微循环功能障碍，结合心电图及心肌损伤标志物动态演变过程、心脏增强磁共振延迟强化特点，确诊为急性下壁 ST 段抬高型心肌梗死。进一步结合自身免疫及血液病相关化验检查，除外结缔组织病、感染性疾病及血液系统肿瘤后，最终诊断为原发性抗磷脂综合征。初步治疗给予患者氯吡格雷、低分子肝素抗栓及羟氯喹免疫调节治疗，心梗病情得到一定程度的控制，但血小板计数持续下降（住院期间最低 8×109/L）。为避免出血事件，遂停用抗栓药物，并恢复糖皮质激素、海曲波帕治疗，但是患者住院期间胸痛复发并伴有心肌损伤标志物、心电图动态演变，提示再发心梗（患者本人拒绝复查冠脉造影）。经心内科、风湿免疫科、血液科、药学部等多学科联合会诊后，考虑原发性抗磷脂综合征并发急性冠脉综合征（ACS）明确，aGAPSS 评分复发血栓事件和急性心肌梗死风险 > 10 分 [2]，充分评估血栓及出血风险后，决定采用甲泼尼龙（40mg qd）序贯泼尼松 (40mg qd) 口服、利妥昔单抗（首次 200mg，500mg×3 次）免疫调节，依诺肝素序贯华法林 (4.5mg qd) 及氯吡格雷 (75mg qd) 等抗栓治疗，辅以保肝及预防感染。患者胸痛症状缓解，血小板计数趋于稳定后出院。

检验检查记录：

入院血小板计数正常（182×109/L），转氨酶升高（丙氨酸氨基转移酶 96U/L，天门冬氨酸氨基转移酶 41U/L），高尿酸血症（尿酸 548umol/L），抗磷脂综合征（凝血象及血栓相关化验未见明显异常，抗核抗体 1:80，狼疮抗凝物、抗心磷脂抗体阳性、抗 β2 糖蛋白 1 抗体阴性），血液病相关检验提示血小板数量减少且未见恶性增殖现象（骨髓增生III级，骨髓有核细胞数不少，巨核细胞成熟障碍，血小板量少；骨髓免疫学、细胞遗传学及分子生物学检查未见明显异常。），感染相关化验（新型冠状病毒核酸阳性，呼吸道病毒、肠道病毒、血培养及非典型病原体检查阴性），蛋白尿（24 小时尿蛋白 140mg），急性下壁 ST 段抬高型心肌梗死(hsTNI 峰值 11673.4pg/ml,心电图示III、aVF 导联可见病理性 Q 波)，心脏 MR 增强扫描示左心室中远段下壁、中段下室间隔、室间隔延迟强化），冠状动脉微循环功能障碍（冠脉造影示主要心外膜血管未见明显狭窄；LAD、LCX 及 RCA 定量血流分数阴性，造影衍生微循环阻力指数阳性）。

鉴别诊断：

血栓再通、系统性红斑狼疮、原发性血小板减少性紫癜

其他：

患者出院后，定期心血管内科及风湿免疫科规律随诊，未再次出现胸痛、胸闷等症状，无皮肤黏膜及内脏出血表现。出院 4 个月后，患者免疫指标有所改善，进行了第 4 次利妥昔单抗 500mg 治疗，继续泼尼松联合羟氯喹治疗原发病。出院 6 个月后，免疫指标保持稳定，利妥昔单抗输液间隔延长至每半年 1 次。出院 1 年后，患者心肌损伤标志物、抗磷脂抗体均阴性，超声心动图未见明显异常，予利妥昔单抗 500mg 再次强化治疗，继续维持泼尼松 5mg/7.5mg 隔天联合羟氯喹 200mg bid 治疗，同时继续氯吡格雷 75mg qd 联合华法林 4.5mg qd 抗栓，及预防骨质疏松和调脂稳定斑块的治疗。

精于术，慈于心，带来” 心” 希望 ---- 一例双腔起搏器升级为 CRT-P DCM 病例

孙兴华

庆阳市人民医院

患者基本信息：

患者：张 XX，女，54 岁。

主述：

阵发性头晕、胸闷、气短 10 年，加重 1 月。

现病史：

患者于 10 年前受凉后出现阵发性头晕、胸闷、气短，体力活动后加重，经休息后可缓解，无黑朦，无意识障碍，无胸痛，无咳嗽，无恶心、呕吐等症状，后逐渐出现阵发性呼吸困难，伴双下肢水肿，伴腹胀，就诊于当地医院，行冠脉造影后，诊断为“III° AVB、扩心病”，给予治疗后 (具体不详) 症状无明显缓解，后就诊于我院，行永久性心脏起搏器（双腔）植入术，术后规律服用“呋塞米、螺内酯、美托洛尔”等药物治疗，上症时轻时重，反复发作，多次就诊。1 月前无明显诱因上症加重，伴双下肢水肿，伴腹胀，伴夜间不能平卧休息，无胸痛，无咳嗽、咳痰等不适，无晕厥，无肢体活动障碍，今为进一步诊治，遂我院就诊，门诊查 pro-BNP 2000pg/ml，起搏器电池即将耗竭；门诊以“1. 心律失常：三度房室传导阻滞、起搏器电池耗竭 ;2. 扩张性心肌病：心功能 III 级”收入院。自病情加重以来，患者神志清，精神欠佳，饮食及睡眠欠佳，小便量减少，大便如常。

既往病史：

平素体质一般。否认“高血压”“糖尿病”等特殊疾病史。否认肝炎、肺结核、疟疾、菌痢等传染病史。预防接种史不详。无过敏史。无输血史。

病程记录：

1. 扩张型心肌病

心脏扩大

心功能 III 级（NYHA 分级）

2. 心律失常

III 度房室传导阻滞

3. 起搏器电池耗竭

检验检查记录：

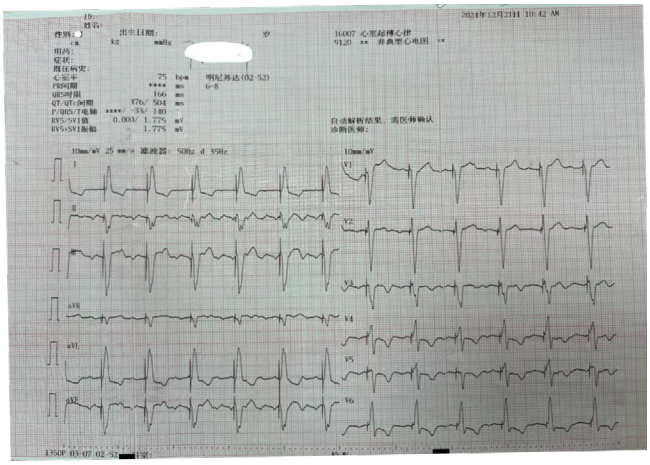

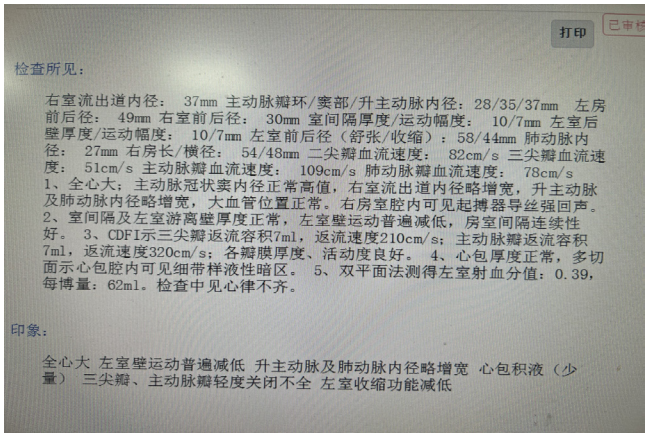

鉴别诊断：

扩张型心肌病（DCM）or 起搏器诱导的心肌病（PICM）

建议升级为三腔起搏器

其他：

消失的激动去哪儿了?

玄研华

辽宁省人民医院

患者基本信息：

男性，57 岁

主述：

反复心悸 5 天

现病史：

5 天前开始发作心悸，外院诊断“室上速”，药物治疗好转，但仍反复发作，来诊。

既往病史：

无高血压、糖尿病、冠心病等病史

病程记录：

行心脏电生理检查及射频消融术

检验检查记录：

心电图、心脏超声、血尿化验

鉴别诊断：

室上速

房速

房扑

其他：

主动脉内漂浮球囊联合 IVUS 处理右冠开口病变 1 例

汪永生

合肥市第一人民医院

患者基本信息：

Ø 患者，王 X 传，男性，57 岁

主述：

胸痛 1 周

现病史：

患者近 1 周来无明显诱因反复发作胸痛，部位胸骨中下段，成人手掌范围大小，部位深在，呈压榨性疼痛，向左肩放射，起先每次持续 3-5 分钟，可自行缓解，未予重视及就医。3 天前中午用力大便再发胸痛，程度加重，伴大汗淋漓，持续 30 分钟左右逐渐缓解，仍未就医，后间断发作，伴活动耐力下降及胸闷气促。今为进一步诊治，就诊我院心内科门诊，拟 “ACS” 收住院。病程中一般情况可，食欲减退、精神差，二便正常。

既往病史：

Ø 既往病史: 高血压病史 10 年，口服“施慧达、美托洛尔缓释片”治疗; 否认糖尿病、脑梗塞、慢性肾病等病史；吸烟 30 年，20 支 / 日

病程记录：

1、A.S.A 100mg qd+300mg st!

2、替格瑞洛 90mg bid+180mg st!

3、阿托伐他汀 20mg qn

4、美托洛尔缓释片 47.5mg qd

5、诺欣妥 100mg qd

6、那曲肝素钠 4100U ih q12h

检验检查记录：

Ø 实验检查：心肌损伤标志物：CK-MB<30.0u/l, cTnI：2.17ng/mL，Myo<30.0ng/ml，NT-pro-BNP：1612.42pg/ml。

Ø 血 常 规：WBC:10.34*109/L，RBC:4.75*1012/L，HB:143g/L，PLT:262*109/L；

Ø 生化：ALT 39U/l，Cr:82.8umol/L，K：3.51mmol/L，GLU：8.44mmol/L，LDL-C：1.94mmol/L。HbA1c:6.3%。

ØECG: 窦性心律，III、avF 导联异常 Q 波伴 ST 段损伤型改变，前壁导联 r 波递增不良。

鉴别诊断：

1. 气胸

2. 肺栓塞

3. 反流性食管炎

4. 急性心包炎

其他：

/

一例新发的 LDLR 突变

苏鹏宇

华北理工大学附属医院

患者基本信息：

患者张娟，女，30 岁，自由职业者，已婚已育。

主述：

发现血脂升高 3 年余

现病史：

患者 3 年前体检时发现血脂异常，自诉总胆固醇最高达 10mmo/L（未见具体报告单），后自行通过饮食调节，至当地医院查血脂胆固醇波动在 8-11mmol/L，均未见详细报告单。1 年前至我院心血管代谢病中心就诊，完善颈动脉超声未见内膜增厚及动脉硬化等，予以阿托伐他汀钙 20mg 1 次 / 日，后复查血清总胆固醇仍高于正常值，遂加用依折麦布 10mg 1 次 / 日，后复查血清总胆固醇 4.0-5.6mmol/L，LDL-C 2.3-3.6mmol/L，半年前至我院完善全外显子组测序提示 LDLR 突变，且为新发突变（详见报告单），经基因确诊为家族性高胆固醇血症。患者 2 月前自行停药，近日于当地医院查血清总胆固醇 10mmol/L，为控制血脂再次至我院心血管代谢病中心门诊。

既往病史：

既往体健，无高血压、糖尿病、冠心病等慢性病史，无吸烟饮酒史。

病程记录：

1 年前至我院心血管代谢病门诊就诊，予以阿托伐他汀钙 20mg 1 次 / 日，后复查血清总胆固醇仍高于正常值，遂加用依折麦布 10mg 1 次 / 日。

检验检查记录：

血脂：总胆固醇 10.34mmol/L，低密度脂蛋白胆固醇 7.46mmol/L，高密度脂蛋白胆固醇 1.39mmol/L，甘油三酯 1.39mmol/L。全外显子测序结果显示，患者存在 LDLR >c.97del（p.Gln33SerfsTer173）位点突变，该突变位点为新发位点，尚未报道，未经过细胞功能验证，但综合考虑后其致病性仍判定为可能致病（见报告单）。患者超声报告结果为自诉，未提供报告单。

鉴别诊断：

甲状腺功能减退症：甲状腺功能减退症患者常伴有明显的甲状腺功能异常症状，如疲劳、体重增加、皮肤干燥等，而本例患者仅表现为血脂异常明显，且降脂治疗有效，无体重增加、皮肤干燥等表现，可进行鉴别。

植物固醇血症：FH 和植物固醇血症都以 LDL-C 极度升高、早发冠心病及全身黄色瘤为典型表现，植物固醇血症也是由基因突变所致，但二者的致病基因不同。本例患者已通过基因检测鉴别。

其他：

本文作者为血脂异常学组委员。

R-R 间期不等的窄 QRS 心动过速： 室上速 or 其他？

玄研华

辽宁省人民医院

患者基本信息：

女性，68 岁

主述：

反复心悸 2 年

现病史：

2 年前开始反复心悸，自觉心动过速，卵巢癌需化疗，但因心动过速发作频繁，无法化疗，为行射频消融术来诊

既往病史：

2019 年患卵巢癌

病程记录：

心脏电生理及射频消融术

检验检查记录：

心电图、心脏超声、血尿便化验

鉴别诊断：

室上速

房颤

其他：

梗阻性肥厚型心肌病合并妇科肿瘤诊治一例

孙美珠

解放军总医院第四医学中心

患者基本信息：

53 岁女性

主述：

胸闷伴咽部紧缩感 1 年余，加重伴喘憋 1 小时

现病史：

患者 1 年余前无明显诱因出现胸闷伴咽部紧缩感，症状持续数分钟，与活动无明显关系，休息后可缓解。2025-1-17 就诊当地，诊断为梗阻性肥厚型心肌病 阵发房颤。03-06 就诊于阜外医院，给予呋塞米 10mg 1/ 日，螺内酯 20mg 1/ 日，利伐沙班 15mg 1/ 日，酒石酸美托洛尔 25mg 2/ 日，患者规律用药。2025 年 1 月因“自然绝经 1 年后间断阴道出血”于当地妇幼保健院行宫腔镜下取环加诊刮术，术后病理示：（宫腔）增殖期改变子宫内膜，部分区域见低分化腺癌，考虑浆液性腺癌。3-13 为行妇科手术以“子宫恶性肿瘤”收住我院妇科，住院期间因家事情绪激动，随即出现胸闷、喘憋、端坐呼吸，症状持续加重，血压逐渐下降，经我科医生会诊，考虑“梗阻性肥厚型心肌病 阵发房颤 急性左心衰”，为进一步诊治转入 CCU。

既往病史：

高血压；子宫内膜低分化浆液性腺癌 II 期

病程记录：

患者入科时房颤伴快室率，血流动力学不稳定，予 150J 同步电除颤后转复窦性心律。给予利伐沙班 20mg 1/ 日、富马酸比索洛尔 2.5mg 1/ 日、胺碘酮 200mg 3/ 日、雷贝拉唑钠肠溶片 20mg 1/ 日、水飞蓟宾葡甲胺片 100mg 3/ 日。经妇科、肿瘤科、麻醉科多学科会诊，考虑患者目前心源性猝死风险高，暂无法耐受手术麻醉及抗肿瘤治疗（化疗、靶向及免疫治疗），待心脏情况相对稳定后再行手术治疗。针对肥厚性心肌病流出道梗阻，患者及家属拒绝行外科室间隔减容术和经皮室间隔减容术，给予玛伐凯泰胶囊 2.5mg 1/ 日，症状缓解后出院。

检验检查记录：

血常规：白细胞 13.66×10^9/L、中性粒细胞百分比 73.1%、红细胞 5.13×10^{12}/L、血红蛋白 152g/L、血小板 332×10^9/L；生化：ALT58.1U/L、尿素 13.78mmol/L、尿酸 612umol/L、肌酐 136umol/L；心梗三项：肌钙蛋白 I 0.082ng/ml、肌红蛋白 317ng/mL、CK-MB 12.2ng/mL；NT-ProBNP 22387pg/ml；甲功七项阴性。血气分析：pH 7.359、二氧化碳分压 33.6mmHg、氧分压 156mmHg、氧饱和度 99.7%、乳酸 3.0mmol/L。

心电图：房颤，心室率 145 次 / 分，完全性右束支传导阻滞。

超声心动图：考虑诊断肥厚型梗阻性心肌病；左室壁弥漫性明显增厚；左室流出道梗阻；LVEF62%，室间隔厚度 28mm, 左室后壁厚度 23mm，左室侧壁厚度 25mm，左室舒末径 42mm，左室收末径 28mm，左房前后径 47mm，左室流出道流速 4.2m/s，压差 74mmHg。

冠脉 CTA：左室壁普遍明显均厚、以室间隔为著；符合冠脉粥样硬化（CAD-RADS 2 级）改变，左前降支中段见混合斑块，管腔狭窄程度约 25%-49%。

心脏核磁：梗阻性肥厚型心肌病，左室壁明显增厚，以室间隔为著，左房增大，建议对比增强扫描进一步评估心肌组织特征；二尖瓣关闭不全（中度）；主肺动脉增宽。

鉴别诊断：

高血压性心脏病；法布雷病

其他：

免疫检查点抑制剂引起的以心肌炎为首发症状的多系统衰竭

彭鑫

湘潭市中心医院

患者基本信息：

性别年龄：男，56 岁

入院日期：2022-08-05

入院方式：平车

这个病例是一位 56 岁的男性患者，2 月前确诊为右肺鳞癌 T4N3M1c（肺、脑转移），基因检测提示 PD-L1 表达阳性，TPS:40%，在外院参加了晚期非小细胞肺癌的临床试验，先后 2 次予以“盐酸安洛替尼 + 帕博利珠单抗 / TQB2450 注射液”抗肿瘤治疗，在抗肿瘤治疗之前，患者有慢性阻塞性肺疾病、酒精性肝硬化和高血压病史，除此之外，没有其他自身免疫性疾病。

主述：

胸闷、心悸 1 天，晕厥 1 次

现病史：

2022.8.4 中饭后无明显诱因出现胸闷、心悸不适，伴头晕，皮温低，间断干咳，在家自测血压 66/32mmHg，卧床休息，未予重视。

8.5 早晨 6:50 再次出现胸闷不适，突然晕倒 1 次，摔倒在地，持续数秒后苏醒。

当地医院就诊：TNI > 2000ng/L，CK-MB 62.7U/L；ECG 示室性心动过速，利多卡因药物复律，复查 ECG 示窦性心律、室性早搏；冠脉造影未见阻塞性病变。

既往病史：

既往史

右肺鳞癌病史 2 月

高血压病史 1 年，服硝苯地平缓释片 每天一片，未监测血压

COPD、酒精性肝硬化

个人史

吸烟 30 年，2 包 / 天

饮酒 30 年，5 两 / 天

家族史

无遗传病史和类似病史

病程记录：

在完成第二次治疗后 1 周，患者出现了严重的心肌炎表现，临床表现主要为胸闷、心悸、晕倒等，生命体征不平稳，血压呈休克状态，入住我院 CCU。入院生命体征如下：T：36.5℃ P：189bpm R：20bpm BP：82/54mmHg（去甲肾维持），心电图提示室性心律失常，实验室检查提示心肌损伤标志物显著升高，hs-TNT:2.220ng/ml(正常值在 0.003-0.014 之间),NT-proBNP:11162pg/ml（正常 <900），心肌酶：CK：415IU/L（正常值在 25-195 之间）CK-MB：61.4IU/L（正常值在 2-25 之间）。入院时超声心动图提示左室射血分数为 EF 55%，左心整体纵向应变（LVGLS）降低（-14.2），外院冠脉造影未见明显异常，心脏磁共振提示心肌弥漫性水肿，左室侧壁心肌少许坏死（图 1），因为家属拒绝，我们没有进一步做心内膜活检。但根据其典型的临床症状和实验室相关检查，经过多学科会诊考虑免疫检查点抑制剂相关心肌炎（危重型），我们停用了抗肿瘤相关治疗，并且予以大剂量甲泼尼龙冲击治疗，患者的心律失常在我们经过药物和电复律之后约 26 小时恢复窦律（图 2），我们同时对该患者进行了抗休克及抗心衰等治疗，患者心衰控制、心肌酶较前动态下降，我们认为患者的心肌炎得到了较好的控制。

检验检查记录：

心肌损伤和心衰标志物

hsTnT 2.22 ng/ml（0-0.014）

CK 415 U/L（25-195），CK-MB 64.1 U/L（2-25），CK-MB/CK 15.4%

NT-proBNP 11162 ng/mL（0-900）

常规和生化检验

血常规：WBC 10.14×109 /L，Hb 151g/L，PLT 261×109 /L

肝功能：ALT 37.5U/L，AST 59 U/L

肾功能：Cr 144 umol/L

血糖、血脂、凝血功能、D 二聚体、甲亢三项、术前四项：无异常

鉴别诊断：

病毒性心肌炎

其他：

见 PPT

孤独” 右心衰 - 最熟悉的陌生人

彭鑫

湘潭市中心医院

患者基本信息：

张某，43 岁女性，超市员工。

主述：

因“反复活动后气促 1 年余，下肢浮肿 1 月” 入院。

现病史：

现病史：患者 1 年余前开始出现活动后气促，大约爬 3 层楼后感气促不适，静息状态下无明显气促，易乏力，偶感心悸，自觉心跳加快，无胸闷胸痛，无咳嗽咳痰等其他特殊不适。1 月前无明显诱因出现下肢浮肿，休息时明显，活动后减轻，活动后症状大致同前，外院完善心脏彩超，提示右心扩大及重度三尖瓣返流（报告不全），遂来我院就诊。

既往病史：

既往史：既往体健，否认“糖尿病、高血压、冠心病、慢性肺部疾病” 等病史，既往无结缔组织疾病病史，无静脉血栓或栓塞病史，无 HIV、肝炎、结核病史，无烟酒等不良嗜好。

家族史：无遗传性心脏病病史，无肺动脉高压家族史，无其他遗传病家族史。

婚育史：已婚已育，育有 1 女，女儿体健。

病程记录：

先天性心脏病？× 完善心脏彩超未见先心病，无双向分流

肺栓塞？×

瓣膜性心脏病？？ 风湿免疫检查阴性，三尖瓣返流考虑继发性可能大，不排除心脏瓣膜病引起，手术治疗是否有效?

缺血性心肌病 ?× 结合动态心电图、心脏核磁等检查未见明显心肌缺血

心肌病？？

肺动脉高压 ?× 完善肺动脉测压不高

肺源性心脏病 ?× 无肺源性基础疾病，肺动脉压不高

罕见性右肥厚性心肌病？继发性心脏瓣膜病?

检验检查记录：

血常规：血小板 95 10^9/L，余正常。

肝功能：总胆红素：28.8umol/L，直接胆红素 19.1umol/L

NT-proBNP：757pg/ml

肾功能、心肌酶学、甲功三项、凝血功能、D 二聚体、电解质、TNT、CRP、尿常规及粪便常规均大致正常

风湿免疫检查均为阴性

鉴别诊断：

肥厚梗阻性心肌病

其他：

无

继发性高血压：隐匿性颈动脉体瘤一例

郭天晨

首都医科大学附属北京安贞医院

患者基本信息：

患者男性，48 岁

主述：

1 月前因头痛测血压升高，最高 170/110mmHg，无头晕、胸闷、胸痛、心悸、大汗、乏力等，发现血压高前无发热、咽痛、血尿、泡沫尿，自行监测血压 150/110mmHg 左右。

现病史：

病程中患者无毛发增多、满月脸、水牛背、悬垂腹、向心性肥胖、紫纹、多血质、痤疮；无阵发性血压升高、头痛、心悸、大汗、面色苍白或潮红；无乏力、腹胀，无周期性麻痹、夜尿增多、血尿、泡沫尿；有打鼾，有呼吸暂停，无白天嗜睡；无黑棘皮征，无下肢水肿。

既往病史：

既往高脂血症病史，长期大量吸烟史，父母及 1 兄均患高血压。

病程记录：

患者行手术治疗，术中予完整切除，术后病理提示颈动脉体瘤 / 副神经节瘤。患者术后无不适，仅口服比索洛尔 2.5mg qd，血压控制良好。颈动脉体瘤又称化学感受器瘤，属于副神经节瘤，临床多表现为颈部下颌角下方无痛性肿块，患者多有局部血管、气管及神经压迫症状，少数患者的肿瘤具有神经内分泌活性，可分泌儿茶酚胺，引起心悸、头晕、高血压及发热等症状。本例患者高血压起病，但无明显发作性心悸、头晕不适及局部压迫症状，手术切除后血压明显好转。

检验检查记录：

体格检查见左侧颈部下颌角下方局部隆起，质软无压痛，完善继发性高血压相关筛查提示血多巴胺、3- 甲氧基酪胺，24 小时尿 3- 甲氧基酪胺升高超过正常上限 2 倍（以上结果均予复查）；头颈部核磁提示颈动脉鞘内侧占位性病变

鉴别诊断：

考虑良性神经源性肿瘤，1、神经鞘瘤；2、颈动脉体瘤；3、不除外副节瘤。颈部增强 CT+ 三维成像：左侧颈动脉鞘区占位，考虑颈动脉体瘤可能性大。

其他：

中华医学会
CHINESE MEDICAL ASSOCIATION
1915

CSC
Chinese Society of Cardiology